EUROPEAN WATER RESOURCES ASSOCIATION

10th WORLD CONGRESS

on Water Resources and Environment

"Panta Rhei"

5-9 July 2017
Athens, Greece



PROCEEDINGS

Editors

George Tsakiris
Vassilios A. Tsihrintzis
Harris Vangelis
Dimitris Tigkas



Athens, 2017

EUROPEAN WATER RESOURCES ASSOCIATION

10th WORLD CONGRESS

on Water Resources and Environment

"Panta Rhei"

5-9 July 2017
Athens, Greece



PROCEEDINGS

Editors

George Tsakiris
Vassilios A. Tsihrintzis
Harris Vangelis
Dimitris Tigkas

Athens, 2017

Aegis

Presidency of the Hellenic Republic

Organising Bodies

Principal Organiser

National Technical University of Athens
School of Rural and Surveying Engineering
Centre for Assessment of Natural Hazards
and Proactive Planning

Cooperating Organisation

Environmental and Water Resources Institute
American Society of Civil Engineers

DISCLAIMER: Although this book of proceedings has been compiled with utmost care, the Editors cannot be held responsible for any misprints and/or omissions. The options expressed by the authors are not necessairily endorsed by the Association.

Cite this publication as follows:
Tsakiris G., Tsihrintzis V.A, Vangelis H., Tigkas D. (eds.) 2017. Panta Rhei. Proceedings of the 10th World Congress of EWRA on Water Resources and Environment, 5-9 July 2017, Athens, Greece

© 2017 European Water Resources Association

Sponsors







Prince Sultan Bin Abdulaziz
International Prize for Water



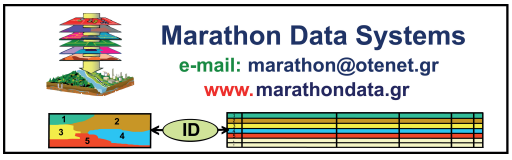








Prince Sultan Bin Abdulaziz
International Prize for Water
Recognizing Innovation
Invitation for Nominations
8th Award
(2018)
Creativity Prize
Surface Water Prize
Groundwater Prize
Alternative Water Resources Prize
Water Management & Protection Prize
Nominations open online
until 31 December 2017
www.psipw.org
e-mail: info@psipw.org

Organising and Scientific Committee

Tsakiris G. (chairman)	National Technical University of Athens
Karatzas G.	Technical University of Crete
Loukas A.	University of Thessaly
Safiolea E.	National Technical University of Athens
Tigkas D.	National Technical University of Athens
Tsihrintzis V.A.	National Technical University of Athens
Vangelis H.	National Technical University of Athens

International Scientific Committee

Batelaan O.	Flinders University, Australia
Boulos P.	Innovyze, USA
Cancelliere A.	University of Catania, Italy
Canters F.	Free University of Brussels, Belgium
Chau K.W.	Hong Kong Polytechnic University, Hong Kong
Christodoulou S.	University of Cyprus, Cyprus
Franchini M.	University of Ferrara, Italy
Garrote L.	Technical University of Madrid, Spain
Grafton R.Q	Australian National University, Australia
Harmancioglu N.B.	Dokuz Eylül University, Turkey
Iglesias A.	Technical University of Madrid, Spain
Karnib A.	Lebanese University, Lebanon
Kavouras M.	National Technical University of Athens, Greece
Khalili D.	Shiraz University, Iran
Kindler J.	Warsaw University of Technology, Poland
Koutsoyiannis D.	National Technical University of Athens, Greece
Loucks D.P.	Cornell University, USA
Maia R.	University of Porto, Portugal
O'Connell P.E.	Newcastle University, UK
Pahl-Wostl C.	Osnabrück University, Germany
Pereira L.S.	University of Lisbon, Portugal

Reddy J.	Indian Institute of Technology Bombay, India
Savic D.	University of Exeter, UK
Sechi G.	University of Cagliari, Italy
Schumann A.	RUHR – University of Bochum, Germany
Shatanawi M.	University of Jordan, Jordan
Shiau J.T.	National Cheng Kung University, Taiwan
Srivastava P.	NASA, USA
Starrett S.K.	Kansas State University, USA
Simonović S.P.	Western University, Canada
Singh V.P.	Texas A & M University, USA
Srdjevic B.	University of Novi Sad, Serbia
Tanyimboh T.	University of Strathclyde, Scotland/UK
Tayfur G.	Izmir Institute of Technology, Turkey
Todini E.	University of Bologna, Italy
Tortajada C.	Institute of Water Policy, Singapore
van Oel P.	Wageningen University, The Netherlands

National Scientific Committee

Angelakis A.	National Agricultural Research Foundation
Angelides P.	Democritus University of Thrace
Antonopoulos V.	Aristotle University of Thessaloniki
Argialas D.	National Technical University of Athens
Baltas E.	National Technical University of Athens
Bellos C.	Democritus University of Thrace
Dercas N.	Agricultural University of Athens
Dalezios N.	University of Thessaly
Giakoumakis S.	National Technical University of Athens
Hrissanthou V.	Democritus University of Thrace
Ioannidis Ch.	National Technical University of Athens
Kalavrouziotis I.	Open University of Greece
Kangalou I.	Democritus University of Thrace
Kerkides P.	Agricultural University of Athens
Kanakoudis V.	University of Thessaly
Katsifarakis K.	Aristotle University of Thessaloniki

Kaleris V.	University of Patras
Latinopoulos P.	Aristotle University of Thessaloniki
Laspidou C.	University of Thessaly
Loizidou M.	National Technical University of Athens
Mantoglou A.	National Technical University of Athens
Nalbantis I.	National Technical University of Athens
Papadopoulou M.	National Technical University of Athens
Papamichael D.	Aristotle University of Thessaloniki
Remoundaki E.	National Technical University of Athens
Sakellariou–Makrantonaki M.	University of Thessaly
Stamou A.	National Technical University of Athens
Tzimopoulos C.	Aristotle University of Thessaloniki
Yannopoulos St.	Aristotle University of Thessaloniki
Yannopoulos P.C.	University of Patras
Zouboulis A.	Aristotle University of Thessaloniki

Editors' Preface

This volume of Proceedings includes the papers presented at the 10th World Congress of the European Water Resources Association (EWRA) on Water Resources and Environment "Panta Rhei". "Panta Rhei" is the saying of the famous Greek philosopher Heraclitus meaning that everything flows. The Congress was held in Athens, Greece, 5-9 July 2017.

The Congress was set under the aegis of the Presidency of the Hellenic Republic, and it is part of the celebrations for the 100 years from the establishment of the School of Rural and Surveying Engineering and the 180 years from the foundation of the National Technical University of Athens. Also, the Congress coincides with the 30-year anniversary of WATER RESOURCES MANAGEMENT, the journal of EWRA published by Springer. Furthermore, for the first time the Congress is co-organized by the Environmental and Water Resources Institute of the American Society of Civil Engineers, in an effort to establish a constructive dialogue between Europe and America on water resources and environmental issues.

The task of the organisation of the Congress was undertaken by the Centre for the Assessment of Natural Hazards and Proactive Planning and the Laboratory of Reclamation Works and Water Resources Management of the School of Rural and Surveying Engineering of the National Technical University of Athens.

The aim of the Congress was the presentation of timely scientific research and studies by engineers and scientists on topics concerning Water Resources and the Environment. Other aims were the exchange of information, experiences and achievements in water resources and environmental protection, evaluation of new technologies, and presentation of innovative ideas for the protection of water resources and the environment. The Congress comprised the following nine specialised conferences:

I. Advances in Hydrological Processes
II. Climate and Water Resources
III. Water Resources Management
IV. Droughts and Water Scarcity
V. Water Quality and Environmental Processes
VI. Urban Water Networks
VII. Agricultural Water Management
VIII. Groundwater Hydrology and Contamination
IX. Legislation and Policies

These nine conferences cover a wide range of cutting edge topics on water resources and the environment. The final papers presented in each of the above conferences will comprise a number of Special Issues of the journal EUROPEAN WATER, which will be published in 2017. There were also 11 invited speeches in various topics of water resources and the environment which are included in the Special Issue of the journal WATER RESOURCES MANAGEMENT "Facets of Modern Water Resources Management" which was published in June 2017 (Vol. 31, Issue 10). Other presentations, such as those in the Round Table, the session of demonstration papers, and the seminars are not included in this volume.

The total number of authors contributing to this volume was 1046 coming from more than 50 countries of the world.

The editors would like to thank:

- The authors of the papers for contributing and sharing their own expertise.
- The reviewers of the papers for ensuring high scientific standards for the presentations.
- The sponsors of the conference for their financial support.
- All conference participants for their involvement in the exchange of knowledge, which is the essence of this Congress.

George Tsakiris
Vassilios A. Tsihrintzis
Harris Vangelis
Dimitris Tigkas

TABLE OF CONTENTS

I. Advances in Hydrological Processes 1

Water depth-damage functions for flood direct tangible damage evaluation in built-up areas in Sardinia (Italy) 3
S. Frongia, A.Ruiu and G.M. Sechi

On urban inundation and damage modelling 11
A. Radice' A. Bettiga, R. Figueiredo and D. Molinari

Flood risk and flood processes in a changing environment 19
A.H. Schumann and S. Fischer

Numerical modeling of Samsun Mert River floods 27
A. Ulke, N. Beden, V. Demir and N.Menek

Flood Directive implementation in Greece: Experiences and future improvements 35
P. Dimitriadis, A. Tegos, A. Petsiou, V. Pagana, I. Apostolopoulos, E. Vassilopoulos, M. Gini, A. Koussis, N. Mamassis, D. Koutsoyiannis and P. Papanicolaou

Spatial variability of flood source areas using "unit flood response" method 43
M. Rezaei, M. Vafakhah and B. Ghermezcheshmeh

Evaluation of flood management plan on Cilemer river basin, Indonesia 49
D. Indrawati,Y. Suryadi, D.P. Saputro, I. Taufik and M.B. Adityawan

Cluster analysis and classification of storm events at Rethymno 57
N. Martzikos, A. Lykou, C. Makropoulos and V. Tsoukala

Daily runoff estimation in Musi river basin, India, from gridded rainfall using SWAT model 63
V. Jothiprakash, C. Praveenkumar and M. Manasa

Distributed rainfall runoff modeling over Krishna river basin 71
S. Nandi and M.J. Reddy

Application of HEC-HMS for the event and continuous simulation in high-altitude scarcely-gauged catchment under changing climate 77
M. Azmat, M.U. Qamar, S. Ahmed, E. Hussain, M. Umair

Prediction and validation of turbulent flow around a cylindrical weir 85
N.G. Soydan, O. Şimşek, M.S. Aköz

Time series analysis of water characteristics of streams in Eastern Macedonia – Thrace, Greece 93
T. Papalaskaris and G. Kampas

Application of Bayesian algorithm in continues streamflow modeling of a mountain watershed 101
S. Sadeghi-Tabas, S.Z. Samadi and B. Zahabiyoun

Impact of extreme events on watershed dynamics 109
J. Kim, M. Dwelle, A. Warnock, V. Ivanov and N. Katopodes

A decision support system for urban stormwater drainage management 115
F. De Paola, M. Giugni, F. Pugliese, P. Romano

Modelling of a combined sewer system and evaluation of mitigation measures using SWMM 123
I.M. Kourtis, V.A. Tsihrintzis, E.A. Baltas

WRF-PDM: Prognostic approach for discharge prediction in ungauged catchment 131
P.K. Srivastava, T. Islam, G. Petropoulos, M. Gupta

Estimation of the Muskingum routing coefficients by using fuzzy regression 135
M. Spiliotis and L. Garrote

A simple model for low flow forecasting in Mediterranean streams 143
K. Risva, D. Nikolopoulos, A. Efstratiadis and I. Nalbantis

Influence of precipitation and land cover changes in a Mediterranean mountain watershed (Guadalaviar River, Spain) 151
I. Melendez-Pastor, E.I. Hernández, J. Navarro-Pedreño, I. Gómez, M.B. Almendro-Candel

An implementation of a water balance model in the Evrotas basin 157
P.G. Marinou, E.G. Feloni, O. Tzoraki and E.A. Baltas

Multivariate modelling of meteorological droughts 165
E. Iliopoulos, V. Tsakiris, H. Vangelis, D. Tigkas and G. Tsakiris

Evaluation of different global optimization algorithms for calibration of a daily hydrological model . 173
H. Khozeymehnezhad, S. Sadeghi-Tabas, M. Pourreza-Bilondi

Ungauged drainage basins: Investigation on the basin of Peneios River, Thessaly, Greece 181
V. Gourgoulios and I. Nalbantis

Effect of land cover/use change on soil erosion assessment in Dubracina catchment (Croatia) 189
N. Dragicevic, B. Karleusa and N. Ozanic

Development of flood and mudflow events for the spatio-temporal risk assessment of networks 197
J. Hackl, M. Heitzler, J.C. Lam, B.T. Adey and L. Hurni

Site suitability analysis of soil and water conservation structures in watershed using GIS 205
D.G. Regulwar and R.M. Ambhore

Imputation of erosivity values under incomplete rainfall data by machine learning methods 211
K. Vantas and E. Sidiropoulos

Impact of restoration measures in a densely urbanised area: The case of Buenos Aires 219
I.M. Arzuaga, G. Navarro′ and S.V. Viñes

Snowcover monitoring with MODIS product 10A2 225
S. Karalis, G. Karakostas and I. Katsios

Presenting the mathematical model to determine retention in the watersheds 233
S Shamohammadi and A. Sharifi

Considering data uncertainty in the water and sanitation sector: Application to large number of alternatives and criteria 241
F. Ezbakhe, A. Pérez-Foguet

Hydrological modelling of low flows for operational water resources management 249
L. Vasiliades, G. Sarailidis and A. Loukas

A network model simulation proposal for river basin management plans (RBMPs) in Turkey 257
S. Burak, H. Bilge and D. Dernek

Assessment of bedload transport in gravel-bed rivers with a new fuzzy adaptive regression 263
M. Spiliotis, V. Kitsikoudis and V. Hrissanthou

Modeling and optimization control of a hybrid water system 271
H. Mu, T. Rauschenbach, D. Karamanzia and N. Cai

Experimental and numerical simulation of the flow over a spillway 279
A. Serafeim, L. Avgeris, V. Hrissanthou and K. Bellos

Methodological framework to estimate the coastal sediment supply of the island beaches 287
I. Kontogeorgos, O. Tzoraki*, N. Moutafis, Th. Hasiotis and A. Velegrakis

Influence of river routing methods on integrated catchment water quality modelling 293
A. Moreno Rodenas, V. Bellos', J. Langeveld, F. Clemens

Definition of critical support area revisited 299
I. Papageorgaki and I. Nalbantis

Integration of rain gauge errors in radar-rain gauge merging techniques 305
F. Cecinati, A. Moreno Ródenas and M. A. Rico-Ramirez

Effect of varying calibration scenarios on the performance of a hydrodynamic sewer model 313
F. Tscheikner-Gratl, P. Zeisl, C. Kinzel, J. Leimgruber, T. Ertl, W. Rauch and M. Kleidorfer

Surrogate modelling for simplification of a complex urban drainage model 319
M. Mahmoodian', J.P. Carbajal, V. Bellos', U. Leopold, G. Schutz and F. Clemens

Multivariate autoregressive modelling and conditional simulation of precipitation time series for urban water models 325
J.A. Torres-Matallana', U. Leopold and G.B.M. Heuvelink

A simplified methodology for flood simulation in urban catchments 333
V. Bellos', I.M. Kourtis and V.A. Tsihrintzis

Comparison of different rainfall-runoff models performance: A case study of Liqvan catchment, Iran 341
N. Sadeghi Louye and M. Rahimi Jamnani

Model selection techniques in SWAT-based hydrological modelling 349
B. Asl-Rousta, S. Jamshid Mousavi and M. Ehtiat

Identification of potential locations for groundwater pumping and recharge to minimize the impact of floods and droughts in the Ganges basin 355
L. Surinaidu, D. Kumar, U. Amarasinghe and M.J. Nandan

II. Climate and Water Resources 363

The effect of storage under climate change in Southern European basins 365
A. Granados, L. Garrote, A. Sordo-Ward and F. Martin-Carrasco

Assessment of climate-change impacts on precipitation based on selected RCM projections 373
D.J. Peres, M.F. Caruso and A. Cancelliere

Evaluating the water resources and operation of the Boukan dam in Iran under climate change 381
F. Emami and M. Koch

Turkish Water Foundation (TWF) statistical climate downscaling model procedures and temperature projections 389
I. Dabanlı and Z. Şen

Influence of the geographic location of dams on spring daily flows magnitude during the 2007-2008 La Niña event (Québec, Canada) 397
A.A. Assani and A. Pothier-Champagne

An informational entropy application to test the goodness of fit of probability functions 403
T. Baran, F. Barbaros, A. Gül and G. Onuşluel Gül

A snow variability analysis in Iran in relation to global warming and climate change 409
T. Raziei, I. Bordi′ and L.S. Pereira

Hydrological and water temperature modelling for dam decommissioning and climate change studies 417
S.J. Dugdale′, A. St-Hilaire′ and R.A. Curry

Assessment of impact of climate change on streamflows using VIC model 425
A. Treesa, J. Das and U. Nanduri

Weather generator utilization in climate impact studies: Implications for water resources modelling 433
M.W. Gitau, S. Mehan and T. Guo

Causes of dimming/brightening in Greece and implications on reference evapotranspiration 441
G. Kitsara, G. Papaioannou and P. Kerkides

Using Weather Research and Forecasting (WRF) model for extreme precipitation forecasting in an Andean region with complex topography 449
G. Yáñez Morroni, J. Gironás′, M. Caneo and R. Delgado

Impact of climate change on irrigation need and groundwater resources in Pinios Basin 455
A. Panagopoulos, F. Herrmann, V. Pisinaras and F. Wendland

Investigations of trends in meteorological time series 463
M. Zeleňáková, P. Purcz, D.C. Diaconu, B. Pius, H. Hlavatá and M.M. Portela

Generation of daily synthetic flows for Switzerland 471
M.M. Portela, A.T. Silva, A.C. Santos′ and B. Schaefli

Impact of climate change on inflows using refined precipitation and temperature scenarios 481
J. Vieira and M.C. Cunha

Spatial analysis of large atmospheric oscillations and annual precipitation in lake Urmia basin 489
B. Vaheddoost

Seasonal and annual trend analysis of meteorological data in Sanliurfa, Turkey 497
V. Gümüş, N.G. Soydan, O. Şimşek, H.M. Algin, M.S. Aköz and K. Yenigun

Quantile regression based method for investigating rainfall trends associated with flooding and drought conditions 503
Y. Xuan, S. A. Abbas, X. Song and D.E. Reeve

Parametric study of trends in flood stages over time in the regulated Guadalquivir River (years 1910-2016) 511
P. Bohorquez and J.D. Del Moral-Erencia

Effects of climate and land use changes on runoff extremes 519
D. Pumo, E. Arnone, A. Francipane, V. Noto and G. La Loggia

Forecasting of geophysical processes using stochastic and machine learning algorithms 527
G.A. Papacharalampous, H. Tyralis and D. Koutsoyiannis

Reliability estimation of rainwater catchment system using future GCM output data (case study: Birjand city) 535
A. Jafarzadeh, M. Pourreza Bilondi, A. Khashei-Siuki, A. Aghakhani Afshar, M. Yaghoobzadeh

WSMN: An in-situ monitoring network for soil moisture monitoring in West Wales, UK 543
G.P. Petropoulos and J.P. McCalmont

Uncertainty in estimated water cycle determined with atmospheric budget, water budget and total water storage 549
M. Birylo

Seasonal mean Baltic Sea level change in coastal zone 557
K. Pajak and M. Birylo

A simple scaling procedure to assess the impact of climate change on extreme precipitation 565
A. Forestieri, E. Arnone and L.V. Noto

Analysis of rainfall trend in southern Italy through the application of the ITA technique 571
T. Caloiero, R. Coscarelli and Ennio Ferrari

Climate change mitigation and adaptation plan for West Athens 579
V. Krommyda

Spatiotemporal evaluation of reanalysis and in-situ surface air temperature over Ethiopia 587
T.W. Tesfaye, C.T. Dhanya and A.K. Gosain

An investigation of the use of Sentinel-2 data for mapping wetlands: A case study from Greece 595
A. Chatziantoniou, G.P. Petropoulos, E. Psomiadis

On the use of climate-flood links and CMIP5 projections to predict flood hazard under climate change scenarios 601
A.T. Silva, M.M. Portela and M. Naghettini

III. Water Resources Management 609

On the barriers to adapt to less water under climate change in Mediterranean countries 611
Ana Iglesias, Luis Garrote

Sensitivity analysis of a probabilistic flood inundation mapping framework for ungauged catchments 619
G. Papaioannou, A. Loukas, L. Vasiliades and G.T. Aronica

Using cross-over analysis to support water user discussion about investments in water sources for irrigation 627
M.J. Nikkels″, J.H.A. Guillaume, P. Leith, N.J. Mendham, P.R. van Oel and H. Meinke′

Simulation and optimization of hydraulic-hydrologic complex system (case study in Iran) 635
Ramin Mansouri, Hassan Torabi Pudeh, Mohammad Zounemat-Kermani, Ali Karbakhsh

Evaluation and development of spatial decision support system 643
H. Alrayess and A. Ulke

Integrated water resources management in agro-economy using linear programming: The case of lake Karla basin, Greece 651
A. Alamanos, S. Xenarios, N. Mylopoulos and P. Stålnacke

A land accounting system for integrated water resources management 659
G.E. Bariamis, E.A. Baltas, V.A. Tsihrintzis and M.A. Mimikou

Prospects for sustainable water resources management within the River Djetinja catchment 667
B.B. Matić and Z. Simić

Towards the optimization of water resource use in the Upper Blue Nile river basin 673
A.-T. Stamou and P. Rutschmann

Indexing vulnerability of an embankment reach against breaching: A remote sensing and hydrodynamic based study 679
B. Talukdar, A. Baid and R. Das

Algiers water issue: Key indicators for a diagnosis of water resources carrying capacity 685
M. Naimi Ait-Aoudia′ and E. Berezowska-Azzag

The seismic risk of new and existing dams 693
P.N. Psarropoulos

Water, energy and food nexus: The Q-Nexus model 701
A. Karnib

Small zoned earthfill dam simplified design with 3D solid modeling techniques 711
D. Myronidis

Different design techniques in determining reservoir capacity 719
H. Alrayess, U. Zeybekoglu and A. Ulke

Geo-Information analysis of the mini hydropower potential in the Liguria Region 729
A. Palla, I. Gnecco, P. La Barbera, M. Ivaldi and D. Caviglia

Trade-off between environmental flow policy and run-of-river hydropower generation in Mediterranean climate 737
A. Kuriqi, A.N. Pinheiro, A. Sordo-Ward and L. Garrote

Effects of crop pattern changes on hydroelectric power generation in Gediz river basin 745
C.P. Çetinkaya and M.C. Günaçtı

GIS based analytic hierarchy process in determination of suitable site for water storage 753
I. Ahmad and M.K. Verma

Water resources management and lack of water in the Zayandehroud river basin, Iran 761
A. Sharifi and R. Mirabbasi

Effect of land use change on flood extent in the inflow stream of lake Paralimni, Cyprus 769
C. Sophocleous and I. Nalbantis

Robust prioritization for SEA with the missing data 777
D. Park

Research on conjunctive use of surface water and groundwater for managed aquifer recharge (MAR) at the River Nestos Delta, Greece 781
L. Avgeris, D. Karasogiannidis, I. Gkiougkis, F. Pliakas, T. Tzevelekis, K. Bellos and I. Diamantis

Land accounting perspective on water resources management 789
G.T. Paschos, G.E. Bariamis and E.A. Baltas

Environmental flow assessment through integrated approaches 795
M. Tegos, I. Nalbantis and A. Tegos

Sustainable management of water resources to safeguarding drinking water – The Water-Guard Project 803
S. Taskaris, I. Boskidis and P. Symeonidis

IV. Droughts and Water Scarcity 811

Drought management and policy: Changing the paradigm from crisis to risk management 813
D.A. Wilhite

Near-real time hydrological drought monitoring in the European Drought Observatory 821
C. Cammalleri, J. Vogt, and P. Salamon

Modification of the Palmer Drought Severity Index for Mediterranean environments: Model and application 827
A. Paulo, D.S. Martins, P. Paredes, R.D. Rosa, L.S. Pereira

Climate change and water valuation in Souss-Massa region: Management and adaptive measures 835
L. Bouchaou, R. Choukr-Allah, A. Hirich, M.S. Ennasr, M. Malki, H. Abahous, B. Bouaakaz and A. Nghira

Analysis of drought severity in Seyhan river basin 843
G. Onusluel Gul and A. Kuzucu

Coastal aquifer response to drought scenarios: The case of Rhodes island 851
H. Vangelis, G. Kopsiaftis, D. Tigkas and V. Christelis

Comparison of hedging rule curves depending on available water and current storage in reservoir operation under droughts 859
S. Lee, Y. Jin and P. Jinhyeog

Monitoring drought in Shiraz, Iran, using Reconnaissance Drought Index (RDI) and Standardized Precipitation Index (SPI) 865
S. Ansarifard and S.A. Shamsnia

Regional drought analysis for derivation the drought SAF curve using bivariate copula in the Lake Urmia basin, Iran 873
M. Montaseri, B. Amirataee and H. Rezaie

Assessing the use of SPI in detecting agricultural and hydrological droughts and their temporal cyclicity: Some Slovakian case studies 881
M.M. Portela, A.T. Silva, J.F. Santos, M. Zeleňáková and H. Hlavatá

Peak drought severity time analysis of Cheongmicheon watershed using meteorological and hydrological drought index 889
S.H. Kim and E.-S. Chung

Wavelet transform based trend analysis for drought variability over 566 stations in India 895
M.K. Goyal and A. Sharma

Frequency and severity of dry spell phenomenon in Ghezala Dam reservoir (Tunisia) 903
M. Mathlouthi and F. Lebdi

Drought analysis with SPI index and entropy 911
T. Baran, U. Guner Bacanli and F. Dikbas

Long-term variation of PDSI and SPI computed with reanalysis products 919
D.S. Martins, A.A. Paulo, C. Pires and L.S. Pereira

Water shortage characterisation for surface water systems with storage 927
I. Nalbantis

Sustainable management of rainwater harvesting systems: A case study of semi-arid area 933
M. Nanekely and M. Scholz

The effect of reservoir networks on drought propagation 941
P.R. van Oel, E.S.P.R. Martins and A.C. Costa

Low flow conditions evaluation within the western Morava river basin 947
Z. Simić and B.B. Matić

Stochastic generation of low stream flow data of Perigiali Stream, Kavala city, NE Greece 953
T. Papalaskaris and T. Panagiotidis

Crop pattern modification for long term mitigation planning against persisting droughts 961
V. Tsakiris, D. Tigkas and H. Vangelis

Characterization of drought in Italy applying the Reconnaissance Drought Index 967
R. Zucaro, C. Antinoro and G. Giannerini

SPI analysis over Greece using high resolution precipitation gridded datasets 973
E.G. Feloni, K.G. Kotsifakis, P.T. Nastos and E.A. Baltas

System based multivariate drought characterisation for surface water 981
I. Nalbantis and G. Tsakiris

Drought Identification and Trend Analysis in Peloponnese, Greece 989
K. Saita, I. Papageorgaki and H. Vangelis

V. Water Quality and Environmental Processes 995

Unusual river turbidity and water quality hysteresis in the most urbanised catchment in the UK 997
D.M. Lawler

Pyrosequencing analysis of ammonia oxidizing bacteria in municipal activated sludge system 1003
O.O. Awolusi, S. Kumari and F. Bux

Evaluation of membranes as promising technique for reclamation and reuse of wastewater 1011
B. Maryam, S. Ustun and H. Buyukgungor

The effect of polymer concentration on electrospun PVDF membranes for desalination by direct contact membrane distillation 1017
S.B. Armand, A. Fouladitajar, F.Z. Ashtiani and M. Karimi

High performance functionalized MWCNT/PES membrane for oil-in-water treatment 1023
S.M. Abedan Dehkordi, F. Zokaee Ashtiani and A. Fouladitajar

Purification of Humic acids contained simulated wastewater using membrane ultrafiltration 1029
S. Saha and C. Das

Removal of diclofenac in drinking water with fenton process 1037
S. Ustun Odabasi and H. Buyukgungor

CFD-aided modelling for hydrodynamic analysis of biological reactor 1043
S. Manenti, S. Todeschini, M.C. Collivignarelli and A. Abbà

Bimetal doping on TiO_2 for photocatalytic water treatment: A green route 1049
V. Rao and A.K. Golder

CFD modelling of wind effect on rectangular settling tanks of water treatment plants 1057
A. Gkesouliand A. Stamou

Investigation of preparation conditions of Nano-SiO_2 embedded PES membranes for producing clean water from wastewater 1065
A. Fouladitajar, M.B. Ghandashtani and F.Z. Ashtiani

Understanding the anaerobic fluidized membrane bioreactor for wastewater treatment 1071
J. Wang, A.G. Fane and J.W. Chew

Moving towards a water-sustainable chemical industry: Novel water recovery processes..... 1075
G. Kolliopoulos, E. Shum, J. Marial and V.G. Papangelakis

Biological treatment of a low strength domestic wastewater in a membrane bioreactor 1083
A. Bezirgiannidis, N. Marinakis, S. Ntougias and P. Melidis

Influence of clay lens on contaminant transport in unconfined coastal aquifers..... 1087
B. Sharma, D.S. Rishi, B.K. Mudai and R.K. Bhattacharjya

Application of nanostructured materials in fluoride removal from contaminated groundwater 1093
S. Bhattacharya

Distribution and assessment of heavy metals and physicochemical parameters in riverine basin.... 1101
M. Khalilzadeh Poshtegal, S.A. Mirbagheri and M. Noury

Desalination and alternative water resources 1109
N.X. Tsiourtis

Source separation technologies, opportunities for sustainable wastewater management..... 1117
T. Zinati Shoa, M. Barjenbruch and A. Wriege-Bechtold

Assessing ecological flow conditions for wetlands fed from ungauged stream reaches..... 1125
A. Gül, K. Ayyıldız, F. Barbaros and T. Baran

Evaluation of streamflow habitat relationships using habitat suitability curves and HEC-RAS..... 1133
Christina Papadaki, Vasilis Bellos, Maria Stoumboudi, George Kopsiaftis and Elias Dimitriou

Simulation of organics and nitrogen removal from wastewater in constructed wetland..... 1141
M. Taheriyoun and M. Rad

Assessing the source of nitrate and heavy metals in groundwater resources of Abarkooh plain, central Iran..... 1149
M. Meraat, H. Jafari and A. Qishlaqi

Case studies investigating hydraulic parameters in full-scale constructed wetlands 1157
V.G. Ioannidou and J.M. Pearson

Modelling of nickel dynamics in vertical subsurface flow constructed wetlands using a System Thinking Environment 1165
C. Defo and R. Kaur

Multi-criteria evaluation of wastewater treatment technologies in constructed wetlands 1171
B. Srdjevic, Z. Srdjevic and K. Suvocarev

Assessment at mid-Black Sea coast of Turkey for recovery valuable heavy metals from sediments..... 1179
A.Şimşek and G. Bakan

Evaluation of clogging in HSF pilot-scale CWs using tracer experiments..... 1185
G.D. Gikas, V.A. Papaevangelou, K. Moutsopoulos and V.A. Tsihrintzis

Earth Observation based monitoring in Natura-2000 sites, providing ecosystem services for their adaptive management 1191
A. Zouboulis, A. Tsirika, E. Terzopoulou, G. Skoufas, I.-D. Adamakis, S. Kyriakidis, V. Liakopoulos, N. Tziolas and G. Zalidis

Water quality estimation in Greek lakes from Landsat 8 multispectral satellite data..... 1199
E. Kontopoulou, P. Kolokoussis and K. Karantzalos

Assessment of the environmentally minimum lake level based on morphological features 1205
C. Doulgeris, P. Georgiou, A. Apostolakis, D. Papadimos, Di. Zervas, O. Petriki, D. Bobori, D. Papamichail, V. Antonopoulos, C. Farcas and P. Stålnacke

Critical review of adaptation strategies for the restoration of Lake Koronia 1211
D. Malamataris, E. Kolokytha, I. Mylopoulos and A. Loukas

Evaluating the ecological restoration of a Mediterranean reservoir..... 1217
P. Sidiropoulos, M. Chamoglou and I. Kagalou

Adaptive management of Koronia ecosystem based on external-internal dynamics..... 1225
E. Ntonou, C. Mitraki, V.A. Tsihrintzis, T.L. Crisman and G.C. Zalidis

A comparative study of water quality in a highly frequented seacoast in Albania..... 1233
E. Hamzaraj, P. Lazo, A. Paparisto and R. Bami

Performance of direct contact membrane distillation for simulated dyeing wastewater treatment 1239
M. Lou, L. Ding, F. Zhao, F. Li, C. Ma, Q. Tianand Y. Liu

Stable isotopes (dD & dO) and major ion chemistry of surface waters in Tajikistan, arid Central Asia..... 1245
Q. Li, J. Wu and H. Zeng

New, energy saving, cleaning procedures in MBR systems 1253
L. Lintzos, K. Chatzikonstantinou, N. Tzamtzis and S. Malamis

Comparative study of the environmental state of Ohrid and Prespa Lakes, Albania 1261
A. Shehu, M. Vasjari, S. Duka, L. Vallja and N. Broli

Water quality in Osumi, Devolli and Shkumbini rivers, using benthic invertebrates..... 1269
B. Pepa, A. Paparisto, E. Keci and E. Halimi

Assessment of pollution pressure over water bodies in Thessaly region 1275
D. Dinouli, P.T. Nastos and A. Papaioannou

Study of contamination of the transboundary river Kura in Georgia..... 1283
E. Bakradze, G. Kuchava andL. Shavliashvili

Biodiversity indices and nutrient load assessment in Ishmi River, Albania, during 2012-2013..... 1289
E. Keçi, B. Pepa, A. Paparisto and S. Duka

Possibility of artificial beach nourishment using crushed limestone aggregate 1295
S. Juradin, M. Rajkovic and M. Vranjes

The impact of drinking water on the prevalence of *H. Pylori* in humans in Elbasan, Albania 1301
S. Mali, L. Vrushi and N. Hila

Groundwater contamination from uninsulated sewage tanks in an eastern Hungarian settlement 1305
T. Mester, G. Szabó, G. Karancsi and D. Balla

Linkages between physicochemical status and hydromorphology in Greek lakes under WFD policy..... 1311
E. Mavromati, I. Kagalou, D. Kemitzoglou, A. Apostolakis and V. Tsiaoussi

Relationship between water yield and water quality in broadleaf forested watersheds 1319
F. Gokbulak, Y. Serengil,I. Yurtseven, B.U. Erdogan, M.S. Ozcelik, S. Ozhan and K. Sengonul

Water quality model of Alibeykoy watershed and LID implementation 1325
S. Gulbaz and C.M. Kazezyılmaz-Alhan

Change of land use and soil coverage in the area of influence of natural national park Los Nevados 1331
D.A. Patino Rincon, S.A. Camargo, D. Rey, J.J. Velez and J. Zambrano

Comparison of two habitat modeling approaches for the determination of the ecological flow 1339
G. Papadonikolaki, A. Stamou, E. Dimitriou, M.-D. Bui and P. Rutschmann

Annual sediment yield prediction by means of three soil erosion models at the basin scale 1345
K. Kaffas, V. Hrissanthou

Bioavailability of metals in soils irrigated by synthetic wastewater: Metal speciation 1353
S.I. Korfali and H. Karaki

Finding a sustainable balance in the water food nexus – Socio-economic transformation in an agricultural catchment 1361
M. Roobavannan, J. Kandasamy, S. Pande, S. Vigneswaran and M. Sivapalan

Assessing the quality of bottled water brands using a new water quality index 1369
V. Tsakiris, D. Alexakis and V.A. Tsihrintzis

GIS-based spatial decision support system for the optimum siting of offshore windfarms 1375
E. Sourianos, K. Kyriakou and G.A. Hatiris

Development of an updated water quality index based on legislation and experts' opinion 1383
F. Iakovidou, E. Trikoilidou, G. Samiotis, A. Stamos, L. Tsikritzis and E. Amanatidou

Water management in nuclear power plant using advanced low-temperature systems 1393
G. Zakrzewska - Kołtuniewicz

Productivity analysis based on fuzzy logic on paddy area irrigated by varied water sources 1399
B. Aydin and Y. Ahi

Wastewater treatment by solar air gap multi-stage membrane distillation 1407
I.J. Siddique, R. Bahar, S. Ibrahim and M.H.F. Al Hazza

VI. Urban Water Networks 1411

Efficient parallel evolutionary optimization algorithm applied to a water distribution system 1413
T.T. Tanyimbohand A.G. Seyoum

Modeling and optimization control of a hybrid water system 1421
H. Mu, T. Rauschenbach, D. Karamanzia and N. Cai

Using bayesian networks for risk assessment of real losses in water distribution systems 1429
M. Tabesh, N.R. Faghihi, A. Roozbahani, R. Heidarzadeh and B. Roghani

Diagnosis of water pipeline systems by frequency domain analysis 1437
M. Ferrante and C. Capponi

Reliability-based design of water distribution networks considering mechanical failures 1445
S. Sirsant and M.J. Reddy

Stochastic gradient methods for the optimization of water supply systems 1453
A.A. Gaivoronki, J. Napolitano and G.M. Sechi

Spectral analysis and topological and energy metrics for water network partitioning of Skiathos island 1461
A. Di Nardo,M. Di Natale, C. Giudicianni, C. Laspidou , F. Morlando, G.F. Santonastaso and D. Kofinas

Waterloss detection in streaming water flow timeseries using change-point anomaly methods..... 1467
S.E. Christodoulou, E. Kourti and A. Agathokleous

Towards resilient water networks by using resilience key performance indicators 1473
D. Ayala-Cabrera, O. Piller, J. Deuerlein and M. Herrera

Data mining for household water consumption analysis using self-organizing maps..... 1481
A.E. Ioannou, D. Kofinas, A. Spyropoulou and C. Laspidou

Incorporating uncertainty in the design of water distribution systems 1487
M. Spiliotis and G. Tsakiris

Pressure dependent analysis for managing contaminant propagation in water supply systems..... 1495
M. Zafari, M. Tabesh and S. Nazif

Evolution of water supply infrastructures of Thessaloniki city, Hellas, through centuries 1503
S. Yannopoulos,A. Kaiafa-Saropoulou, E. Gala-Georgila and E. Eleftheriadou

Water demand management in Europe: Reducing household water consumption in four cities from 1995 to 2015..... 1511
M. Stavenhagen, C. Tortajada and J. Buurman

Impact of water pricing policy and climate change on future water demand in Volos, Greece 1519
N. Mylopoulos, C. Fafoutis, S. Sfyris and A. Alamanos

Domestic water demand forecasting for Makkah, Saudi Arabia..... 1527
M.F.M. Abushammala and A.K. Bawazir

The role of rainwater harvesting on providing vegetation water requirement in arid and semi-arid regions 1535
M.T. Dastorani, B. Kouhzad, A. Sepehrand A. Talebi

Robustness and vulnerability assessment of water networks by use of centrality metrics 1543
A. Agathokleous, C. Christodoulou and S.E. Christodoulou

The role of domestic rainwater harvesting systems in storm water runoff mitigation..... 1551
I. Gnecco, A. Palla and P. La Barbera

Water efficiency indicators studies and energy applied to real water distribution system of south of Minas Gerais - Brazil..... 1559
F.G.B. Silva, F.R. Soares, M.R. Andrade and D.O. Sant´Ana

Relationship between Hazen-William coefficient and Colebrook-White friction factor: Application in water network analysis..... 1567
M. Niazkar, N. Talebbeydokhti and S.H. Afzali

VII. Agricultural Water Management 1575

Accuracy of daily PM-ET_o estimations with ERA-Interim reanalysis products 1577
P. Paredes, D.S. Martins, J. Cadima, C. Pires and L.S. Pereira

Proving the contribution of a seasonal shallow water table to evapotranspiration..... 1585
G. Bourazanis, I. Argyrokastritis and P. Kerkides

Temporal variation of reference evapotranspiration and regional drought estimation using SPEI method for semi-arid Konya closed basin in Turkey 1593
A.S. Anli

Calculation of the irrigation water needs spatial and temporal distribution in Greece..... 1601
K.X. Soulis and D.E. Tsesmelis

Daily transpiration of a single sessile oak measured by the tissue heat balance method 1609
M.S. Ozcelik

Impact of climate change on water footprint of wheat, rice and potato (case study: Iran)..... 1615
M. Montaseri and N.R. Majd

Water buyback in agriculture: What can we expect?..... 1623
C.D. Perez-Blanco and C. Gutierrez-Martin

Sustainability assessment of agricultural production through causal loop diagrams..... 1631
R. de Vito, I. Portoghese, A. Pagano, R. Giordano, M. Vurro and U. Fratino

Estimation of crop water requirements using remote sensing for operational water resources management..... 1637
J. Tzabiras, M. Spiliotopoulos and A. Loukas

Economic productivity of irrigation water and the closure of a river basin in Southern Spain..... 1645
A. Exposito and J. Berbel

Parameterization of "canopy resistance" and estimation of hourly latent heat flux over a crop..... 1653
A. Margonis, G. Papaioannou, P. Kerkides and G. Bourazanis

A methodology to determine the productivity - reliability curve as a tool for improving water management in the agricultural sector..... 1661
A. Chavez-Jimenez, A. Granadosand L. Garrote

Water Footprint for cotton irrigation scenarios utilizing CROPWAT and AquaCrop models..... 1669
M. Zoidou, I.D. Tsakmakis, G.D. Gikas and G. Sylaios

Mathematical analyses of water management's effects on rice productions: A case study of Mae Kuang Udom Thara Dam, Thailand..... 1675
C. Likasiri and E. Duangdai

Correction and sensitivity analysis of Hargreaves - Samani model in the estimation of the reference evapotranspiration (case study: Gonabab city in Iran)..... 1681
A. KhasheiSiuki, F. Sarvari and M. PourrezaBilondi

Pollution control by agroforestry systems: A short review..... 1689
G. Pavlidis and V.A. Tsihrintzis

Spatial interpolation of potential evapotranspiration for precision irrigation purposes..... 1695
N. Malamos, I.L. Tsirogiannis, A. Tegos, A. Efstratiadis and D. Koutsoyiannis

The effect of Yazd wastewater on forage quantity and quality of *Atriplex lentiformis*..... 1703
A.A. Karimian and M. Ebrahimi

Spatial and temporal assessment of potential soil erosion over Greece..... 1707
A.P. Kazamiasand M. Sapountzis

Water availability and requirements for precision agriculture in vulnerable agroecosystems..... 1715
N.R. Dalezios, N. Dercas, N.V. Spiropoulosand E. Psomiadis

Modelling sustainable smart islands using harmony search: A water-energy nexus initiative in Greece..... 1723
I. Kougias, S. Szabo, A. Nikitas and N. Theodossiou

Multi-objective optimization for irrigation deficit through cascade reservoirs..... 1731
M.U. Rashid, S.S. Haider, M. Latif and N.A. Raja

Irrigation with highly saline water: A new innovative water treatment system evaluated for vegetable production in greenhouse..... 1739
A. Gertsis and K. Zoukidis

Irrigation water pricing in the countries of the OECD – Modern trends and critical review: The Greek case..... 1747
I. Giannopoulou, E. Eleftheriadou and S. Yannopoulos

Irrigation of walnut trees in the vicinity of Hisareyn - Gölcük / Kocaeli, Turkey 1755
F. Dokmen, Y. Ahi and D.D. Koksal

Soil water electrical conductivity determination based on the salinity index concept 1759
G. Kargas, P. Mougiou, A. Petsetidi and P. Kerkides

Assessing the vulnerability of water for agricultural use to climate change: The case of Cyprus 1767
D. Charchousi, M.P. Papadopoulou, K. Spanoudaki, D. Alexakis, C. Giannakopoulos and A. Karali

Utilizing earth observation systems towards the implementation of Nexus approach for achieving sustainable water management at a river basin scale 1773
G. Zalidis

Evaluation of the water footprint and water use efficiency in a high density olive (*Olea europea* L.) grove system 1779
A. Gertsis, K. Zoukidis and A. Mavridis

Regulation and mitigation services of forests as the components of urban resilience 1787
B. Uygur Erdogan

Wastewater treatment and reuse for irrigation as alternative resource for water safeguarding in Souss-Massa region, Morocco 1795
M.Malki, L. Bouchaou, I. Mansir, H. Benlouali, A. Nghira and R. Choukr-Allah

Bioenergy water footprints, comparing first, second and third generation feedstocks for bioenergy supply in 2040 1803
P.W. Gerbens-Leenes

VIII. Groundwater Hydrology and Contamination 1811

Space-time modelling of aquifer level using novel geostatistical tools 1813
E.A. Varouchakis, P.G. Theodoridou and G.P. Karatzas

Artificial neural networks and particle swarm optimization based model for the solution of groundwater management problem 1819
S. Gaur, A. Dave, A. Gupta, A. Ohri, P.K.S. Dikshit and S.B. Diwedi

Vulnerability of groundwater to pollution using three different models in Halabja Saidsadiq basin, Iraq 1827
T.O. Abdullah, S.S. Ali, N.A. Al-Ansari and S. Knutsson

Artificial intelligence and regression analysis in predicting ground water levels in public administration 1835
G.N. Kouziokas, A. Chatzigeorgiou and K. Perakis

Ground water risk management using dynamic bayesian networks and PROMETHEE method 1841
A. Roozbahani, E. Ebrahimi and M.E. Banihabib

Analytical solutions to groundwater flow around wells using discharge potential 1849
S. Korkmaz

Management of coastal hydrosystems through the application of free and open source software tool FREEWAT 1857
M. Perdikaki, C. Pouliaris, I. Borsi, R. Rossetto and A. Kallioras

Modifying SINTACS method to assess groundwater vulnerability and pollution risk to nitrate 1863
G. Busico, N. Colombani, E. Cuoco, M. Mastrocicco, M. Sirna and D. Tedesco

Application of head-guided zonation method to delineate groundwater vulnerability zones in a data-scarce catchment 1869
D.K.S.Y. Klaas, M.A. Imteaz and A. Arulrajah

Impact of land-use change on a multilayer aquifer in south-eastern coast of Caspian Sea 1873
I. Karimirad, K. Ebrahimi and S. Araghinejad

Hydrochemical and qualitative assessment of natural water spring in southern Italy 1881
S. Gaglioti, E. Infusino, T. Caloiero and G. Callegari

Mechanism of controlling seawater intrusion at coastal aquifers using subsurface barrier 1889
R. Shafiee, S.S. Mehdizadeh and A.S. Gooya

Long term monitoring of aquifer salinization processes in a physical analog model 1895
N. Colombani, B.M.S. Giambastiani and M. Mastrocicco

A three dimensional modeling approach to groundwater management in Paharpur canal command area, Dera Ismail Khan, Pakistan 1899
A. Khan, A. Qadir, M. Zafarand T. Khan

Hydrogeological and hydrochemical regime of fissured rocks in Pelion massif (E. Thessaly) 1905
E. Dikarou, G. Migiros, G. Stamatis, K. Serelis and A. Solomonidou

Updated groundwater vulnerability evaluation at a coastal aquifer system in NE Greece 1913
G. Eminoglou, I. Gkiougkis, A. Kallioras and F.-K. Pliakas

Use of remote sensing and electrical resistivity tomography to determine Tidsi spring recharge and underground drainage 1919
M. Hssaisoune, S. Boutaleb, L. Bouchaou, M. Benssaou and T. Tagma

Environmental impacts of urbanization in hydrogeological systems 1925
A. Mitropapas, A. Panagopoulos, G. Karatzas and A. Kallioras

A two-dimensional analytical model for tide-induced groundwater fluctuation in leaky aquifers 1933
M.-H. Chuang and H.-D. Yeh

Pumping optimization in coastal aquifers: Comparison of sharp interface and density dependent models 1941
G. Kopsiaftis, V. Christelis and A. Mantoglou

Towards sustainable management of groundwater: A case study of semi-arid area, Iraqi Kurdistan region 1949
M. Nanekely, M. Scholz and S. Qarani Aziz

Assessing groundwater use in irrigation districts with multiple resources (MIGRAD) 1957
D. Zingaro, I. Portoghese, A. Pagano, R. Giordano and M. Vurro

Using groundwater flow simulation of the Chania Plain area to propose a proper irrigation plan 1965
C. Goumas, Z.Dokou, G.G.Morianou, N.N.Kourgialas and G.P. Karatzas

Sustainable use of groundwater for irrigated agriculture: A case study of Punjab, Pakistan 1973
G.Z. Hassan and F.R. Hassan

Physics-based and data-driven surrogate models for pumping optimization of coastal aquifers 1979
V. Christelis and A. Mantoglou

Phreatic / confined flows in polygons: Dupuit-Forchheimer model versus potential solutions 1987
A.R. Kacimov, A. Al-Maktoumi and Y.V. Obnosov

Comparison of SGD rate between northern-southern coastlines of the Persian Gulf using RS 1995
M. Farzin, A. Nazari Samani, S. Feiznia, G.A. Kazemi and I. Golzar

Groundwater flow simulation in confined aquifer by meshless element free Galerkin method 2003
T. Pathania and A.K. Rastogi

IX. Legislation and Policies 2011

Sustainable restoration of the Urmia lake: History, threats, opportunities and challenges 2013
M. Soudi, H. Ahmadi, M. Yasi and S.A. Hamidi

Measuring sustainable delivery of water, sanitation and hygiene services at the household level: Does the measure matter? 2021
R. Giné-Garriga and A. Pérez-Foguet

Water market and its effects on the sustainable management of water resources in Chile 2029
Nicole Kretschmer, Ricardo Oyarzun, Pablo Alvarez, Jose Arumi

Prototype observatory facilitating integrated coastal zone management at municipal level 2037
N. Kokkos, V. Kaplakis, V. Pissinaras and G. Sylaios

Legislative framework for drinking water (re)sources monitoring in the Adriatic region 2043
B. Karleusa and B. Matic

Ecological flows and the Water Framework Directive implementation: An effective coevolution? .. 2051
Vanessa Ramos, Nuno Formigo, Rodrigo Maia

Underground taming of floods in the Ganges basin: Technologies, institutions and policies 2061
V. Ratna Reddy, S.K. Rout and P. Pavelic

Environmental crimes in the water sector 2069
L. Segato, W. Mattioli, N. Capello and M. Migliorini

Grounded theory methodology and public participation in water management 2077
Z. Srdjevic, N. Funamizu, B. Srdjevic and R. Bajcetic

The Non-Conventional Water Resources (NCWR) programme in north Mediterranean 2083
M. Antonakopoulou, K. Toli, V. Constantianos, and M. Scoullos

Towards 3D modelling of public law restrictions in water bodies 2091
D. Kitsakis and I. Papageorgaki

A road map for resolving conflicts in dam's administration: The case of Peiros - Parapeiros dam in Greece 2099
M.V. Podimata and P.C. Yannopoulos

A perspective to wastewater legislation in European Countries and Turkey 2107
H.T. Gultas, A.H. Orta and Y. Ahi

I. Advances in Hydrological Processes

Proceedings of the 10th World Congress of EWRA 'Panta Rhei', 5-9 July 2017, Athens, Greece
© 2017 *European Water Resources Association*

Water depth-damage functions for flood direct tangible damage evaluation in built-up areas in Sardinia (Italy)

S. Frongia*, A.Ruiu and G.M. Sechi
DICAAR – Dept. of Civil and Environmental Engineering and Architecture, University of Cagliari, Italy
* *e-mail: frongiasara@tiscali.it*

Abstract: Flash floods occurring in the Mediterranean area lead to investigate on relevant damages caused by floods in Sardinian territory (Italy). The Flood Directive 2007/60/EC, requiring a cost-benefit analysis for the definition of mitigation measures, should be supported by appraisals of flood damages. Actual study background recognises the use of water depth-damage functions as key elements in decision-making evaluation of authorities. Flood damage functions are still not available for Italy and should be developed considering the regional territory. This paper revises the Joint Research Centre Model approach (Huizinga H.J., 2007) for Sardinian region and provides water depth-damage functions for direct tangible damage assessment. Historical data on flood damages were collected considering two recent events. The first event occurred the 22nd October 2008 in Capoterra town, in the South-East of the region, where it caused damages in structures of residential and touristic area for millions of Euros, and 4 victims; the second event occurred the 18th November 2013 in the North-East area determining damages in multi-storey buildings in Olbia town and 13 victims. The collected data were statistically studied considering the possibility of fitting relations between water depth and expected damage data using a Pearson III probability distribution. The water depth-damage functions show different trends due to building types in the two studied areas. The procedure was subsequently implemented considering synthetically generated flood events in order to estimate the expected mean annual damage values due to flooding in prone areas and to verify economic efficiency of planned mitigation measures.

Key words: Water depth-damage functions, flood damage estimation, Pearson III probability distribution, JRC Model validation

1. INTRODUCTION

Modelling the flood damages in quantitative economic terms is a field of study currently under development and improvement by researchers as essential requirement defining mitigation measures. Methodologies and software for the appraisal of losses in human, property, financial, and social impacts caused by natural hazards have been recently developed (Scawthorn C. et al., 2006). Among them reaserchers are mainly working using HAZUS-MH, FLEMO Model, Damage Scanner, Flemish Model, Multi Coloured Manual, Rhine Atlas and Joint Research Centre Model (Jongman B. et al., 2012), (MCM Model, 2005), (Huizinga H.J., 2007).

Usually, in the bibliography, the categorisation of damage is divided in the two classes of tangible and intangible damage, when the losses can or not be economically quantifiable and, subsequently, each class is divided in direct and indirect damage when the loss is respectively caused or not by a direct contact with the flood flow. The present work is focused on the evaluation of the direct component of the tangible flood damage by applying the water-depth damage approach achieved in the Joint Research Centre report: JRC Model, (Huizinga H.J., 2007). The main aim of the research is the identification of the economic amount of flood losses caused by the contact of the water with elements distributed in the territory. In fact, quantification of losses under existing conditions is valuable for understanding and communicating the importance of hazards and determining factors contributing to the risk (Scawthorn C. et al. 2006). The evaluation of flood damage in quantitative economic terms is a relevant issue assuming decision for stakeholders and government authorities who take advantages of these studies to optimize allocation of financial resources.

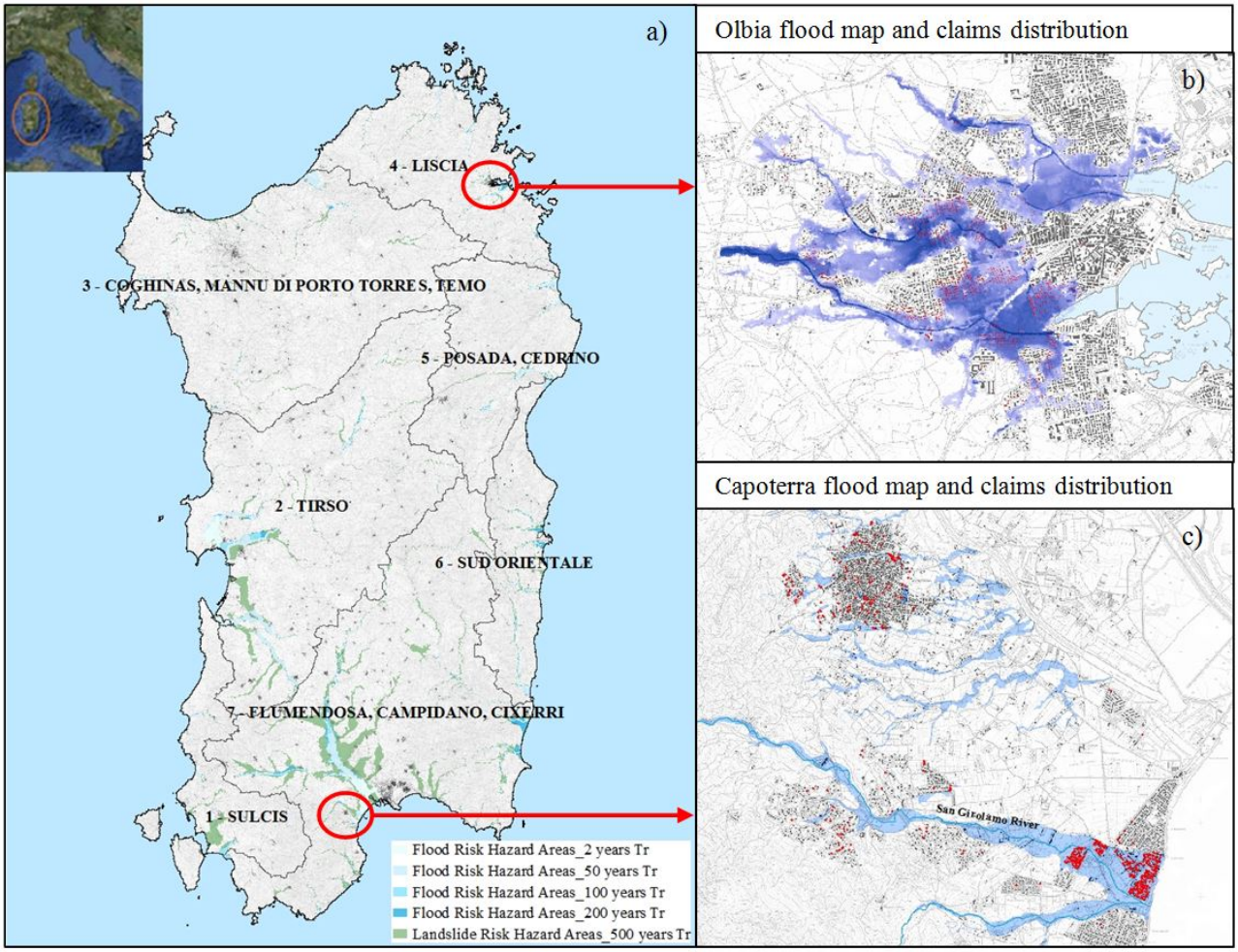

Figure 1. a) Location of Olbia and Capoterra council territory and hydrogeological risk areas defined in the Regional Flood Plan PSFF; b)Flood map of the 19th November 2013 event in Olbia and damage claims distribution; c)Flood map of the 22nd October 2008 event in Capoterra and damage claims distribution

The peculiarities, arose studying locally the territory to determine regional water depth-damage curves, lead to collect and analyse the database of refunds claimed after significant floods registered in Sardinia (Italy) in October 2008 and November 2013. The research examined two different urbanised areas, aiming to obtain regional representative water depth-damage functions and to allow a comparison with the JRC water depth-damage function for residential land use territories. The two study-cases are localised along the Eastern coast of the Sardinian region, as it is possible to observe in Figure 1a. Olbia town residential losses, in the North-East coast, are mainly related to multi-storey buildings, while Capoterra residential dwellings are mainly family houses of one or two floors located in the South-East of the Sardinian coast.

The available damage-claims database have been analysed taking into account uncertainties related with potential errors in data collection, limitations on water depth information and on building/inventory conditions. As a first step, results obtaining water depth-damage functions have been compared with the JRC curve and give back differences mainly due to the structural dwelling typologies. Subsequently, the research considers synthetically generated flood events in order to estimate uncertainty and reliability in the damage evaluations considering mean values of the damage in flood prone areas. This second step evaluation has been developed considering a Pearson III probability distribution to fit observed damage values.

2. WATER DEPTH-DAMAGE CURVE EVALUATION FOR THE SARDINIAN TERRITORY

2.1 Methodology elaboration and applicability on the Sardinian territory

The starting point in analysing potential flood losses is the quantification of the flood hazard using hydraulic models (Scawthorn C. et al., 2006),(Frongia S. et al, 2015),(Appelbaum S.J.and A.M.ASCE, 1985),(Smith D.I., 1994),(Pistrika A.K. and Jonkman S.N., 2010),(Tsakiris G., 2014). This information makes aware of the potential extension of the flood and, consequently, of the values of the hydraulic parameters involved in the flood damage evaluation modelling. The approach here used for Sardinian territories appraises the magnitude of the damages caused by a flood relating water depths to flood losses. Usually, the losses, expressed in €/m^2, increase proportionally with the water depth and reach the maximum value of damage at a predefined water level. The behaviour of the damage associated to flood water depth changes in function of the land use category under analysis.

Mainly, we refer to JRC Model approach (Huizinga H.J., 2007) that considers the territory organised in five land use categories (residential, commercial, industry, road network and agriculture). Accurated studies on water depth-damage curves have been already developed in some European Country and allowed Huizinga H.J. to define "harmonised" water depth-damage curves theoretically applicable to the whole European territory making available a general process for the flood damage evaluation. JRC Model considers the economic situation of the Countries to appreciate the maximum damage value caused by a maximum flood level of 6 metres. Nevertheless, studies undertaken to obtain the "harmonized" curves show a high difference between the values collected by each country: these aspects underline the necessity to validate the JRC functions country by country and, possibly, more deeply, at meso-scale level of regional territory.

The analysis in the present research considers collected data of damages caused by floods on residential territory in Sardinian region (Italy). The evaluation of water depth-damage function takes advantages of the refund data collected by regional and council authorities after the flood events of the 22nd October 2008 that hit the territory of Capoterra town, and of the 18th November 2013 registered in the territory of Olbia town. Both of the floods have been caused by intense precipitation rainfell in short time and reaching in few hours 350 mm of rain, in Capoterra territory, and 440 mm in Olbia territory.

The flood event registered in Capoterra town, South-East of the Sardinian territory (Figure 1c), has been modelled with the 2D hydraulic model MIKE (RAS-Vol.1, 2015). The MIKE model allows to evaluate the water depth level registered mainly in the suburban areas close to the coast where the most part of the damages have been caused by the overflow of San Girolamo River. Capoterra council office made available a sample of residential refunds consisting in 758 damage records. Each damage record has been georeferenced and associated with the relative built area acquired by Capoterra council cadastral map after a crosschecking process with the Google Street tool. Subsequently an accurate check process on data, the record number in the sample decreases to 329 records. The database clean-up was checked on the association of claim data with flood map. Mainly data refusal depends on lack of information of water depths that are not available everywhere in the flooded area; or in some cases the required damage values were evaluated too high according with dwelling typology and refund limits. Figure 1c shows that the area where the flood has been localized: along San Girolamo River close to the coast.

The damages registered in Olbia territory after the flood of the 18th November 2013 have been provided by the Sardinian Civil Protection and by the Olbia Council office that supplied also the reconstruction of the flood map modelled with the 2D hydraulic model FEST-RS (Mancini M., 2014). The crosschecked of the two samples provided by the Sardinian Civil Protection and Olbia Council office led to consider 1325 records of claim localised inside the built area; buildings were identified using the cadastral map of Olbia. As in previous case, the Olbia residential claims have been related with the flood map obtained by the reconstruction of the flood event in order to

associate at each claim data the maximum water depth occurred. As in the previous case, subsequently an accurate check process on data, the sample size decreased from 1325 to 989 data. Figure 1b shows claims distribution in the urbanized area of Olbia town and the flood map.

3. DATABASES STATISTICAL VALIDATION

Capoterra and Olbia claims database are characterised by data consisting in the economic evaluation of the damage, expressed in €/m^2, and the related water depth, expressed in metres. The two samples have been categorized in classes of water depth of 0.5 m and for each class the mean value of the damage and its standard deviation have been calculated. Starting from mean values of each class, for Capoterra the obtained water depth-damage curve is described by a linear trend till the water depth reaches 0.5 metres and follows a trend interpolated with a polynomial of 3rd degree, as shown in Figure 2. The behaviour of mean data of damage collected by the event registered in Olbia town is defined by a linear trend reaching 0.5 m of water depth and proceeds with an exponential trend. The Olbia water depth-damage curve is reported in Figure 2, as well as the JRC evaluated function for the Italian country.

Differences between these curves need some comments. Firstly, the dissimilarities are related to the maximum water depth value that for these flooding zones do not exceeded 3 metres. Moreover, the differences are related to different type of urbanization: Capoterra residential dwellings are mainly family houses located in the South-East of the Sardinian coast, the houses are one or two floor buildings and damages are consistent just starting from few decimetres of water depth. Olbia town residential losses, in the North-East coast, are mainly related to multi-storey buildings and damages become more and more significant, as the water depth is growing. The same behaviour can be shown from the JRC curve; grater values here evaluated can be related to intrinsic buildings values. Uncertainties related with the mean values evaluation of these economic damages can be significant.

These uncertainties can be related to different factors: above all to different economic values of buildings, moreover, to the appraise of the level of damages determined inside building (including inventories) and due to limitation considering only the water depth as hydraulic parameter representative of the flood to define the damage value. Further evaluations can also be done considering the sum of mean and standard deviation values of each sub-sample (Frongia S. et al., 2015).

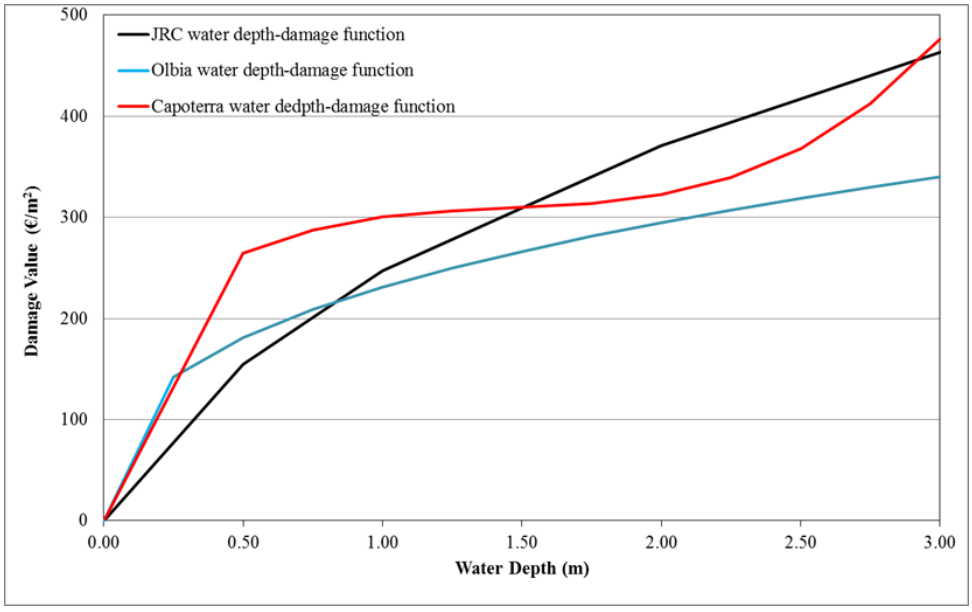

Figure 2. JRC, Capoterra and Olbia water depth-damage functions for residential territory

Here, in a deeper analysis, a statistical study has been focused on fitting the occurrence probability of the damage inside each class of the depth-damage sample. Unfortunately, only the sample of damage claims provided by Olbia flood event has proper size to completely develop this kind of analysis.

The damage sample, inside each class of water depth, has been fitted considering a Pearson III probability distribution, also called Gamma probability distribution, given by the following Equation (1):

$$p(x \mid a,b) = \frac{1}{b^{\alpha}\Gamma(a)} x^{\alpha-1} e^{-\frac{x}{b}} \tag{1}$$

where: damages are $x \in [0,\infty)$, b is scale parameter and a shape parameter of the distribution and $\Gamma(a)$ is the Gamma function:

$$\Gamma(a) = \int_0^{\infty} e^{-t} t^{a-1} dt \tag{2}$$

After the test of fitness was positively achieved for each water depth class, a procedure of synthetically generation of damages due to flood events has been implemented. The observed vector of damage values has been examined using the *gamfit* function of the Matlab library to obtain the maximum likelihood estimates of the gamma distribution parameters and to achieve in the *parmhat* output. *Parmhat* output consists in a vector of two elements, a and b^{-1}, that are the Gamma probability distribution parameters for each class, as shown in Table 1.

Table 1. Pearson III parameters for Olbia sub-samples of damage values

	Olbia	
Steps of h (m)	**a**	**b^{-1}**
0.0 < h ≤ 0.5	1.2886	50.0154
0.5 < h ≤ 1.0	1.5310	69.9979
1.0 < h ≤ 1.5	1.8619	80.4843
1.5 < h ≤ 2.0	2.3337	75.8464

A Montecarlo generation process has been then implemented in a Matlab script. The procedure generates a random matrix of probability, N x M size, of damage values, inside the considered class. The N rows of the matrix are equal to the size of the observed values of each class; the M columns are equal to the number of randomly generated events inside each class, set here equal to 1000. Considering the a and b parameters obtained for each class and the randomly generated probability value p (0:1), the matrix of the synthetically generated damage was created with the Matlab *gaminv* function that works according with the inverse gamma probability function:

$$x = F^{-1}(p \mid a,b) = \{x : F(x \mid a,b) = p\} \tag{3}$$

Matlab *gaminv* function determines damage values for the generated matrix of probability values. For each class, the script calculates again the mean and the related standard deviation. Moreover, the *quantile* function estimates the damage values with exceedance probability of 2.5%, 25%, 50%, 75% and 97.5%. This investigation can be useful to define the reliability of the damage evaluations and related level of uncertainty. Obtained results are given in Figure 3 showing the quantile amplitude, growing with the water depth.

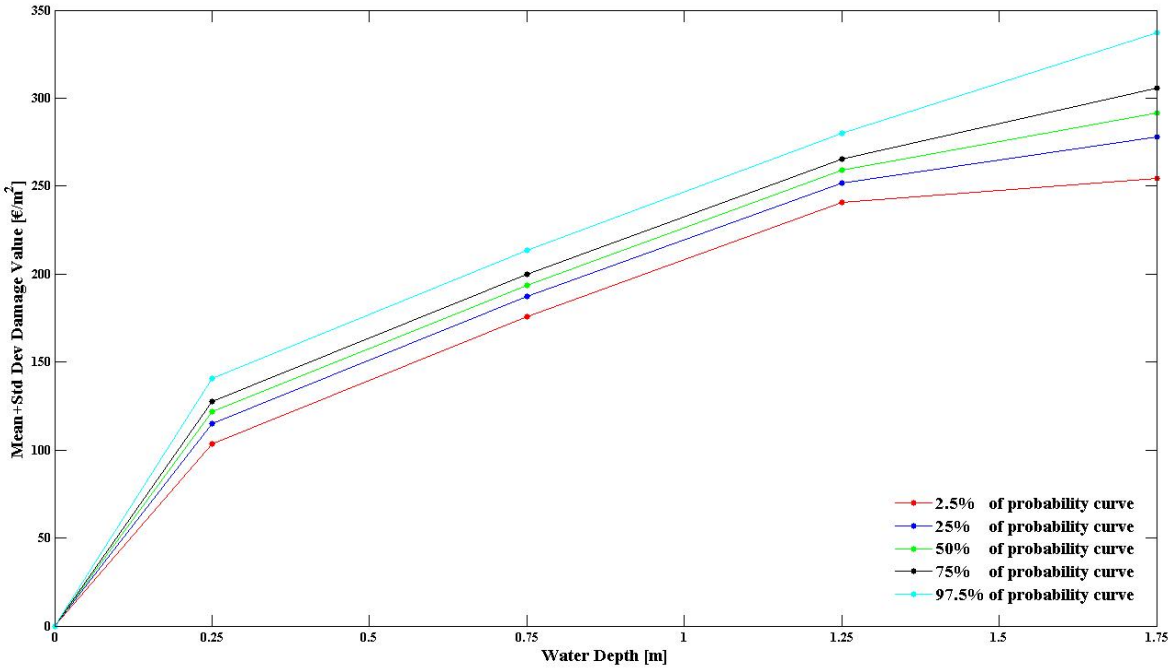

Figure 3. Curves of Olbia claim sample with probability to be exceeded at level of 2.5%, 25%, 50%, 75% and 97.5%

4. RESULTS AND CONCLUSIONS

The analysis here reported was developed with the aim of defining residential water depth-damage curves for Sardinian territory studying data collected after the floods happened in the urbanised areas of Capoterra and Olbia. Obtained results allowed a comparison with the residential water depth-damage curve proposed in the JRC Model. Nevertheless, JRC water depth-damage curves are the result of an harmonisation process of curves collected in several European Countries marked by a significant heterogeneity in building typologyes. The building typologyes are characterised many types of dwellings surely very different considering each country and territory peculiarityes and features. This aspect pinpoints the uncertainty in JRC possibility of application evaluating residential water depth-damage function.

The need to consider specific damage function has been investigated: Capoterra buildings in the suburban coastal area could be defined as villa one or two floor typology for which the most part of the damages are determined by low water depth; Olbia town dwellings are mainly many floor houses and block of flats lived by different families. This dissimilarity reflects differences on the trend of the water depth-damage curves. The difference with JRC evaluated function for the Italian country are significant and underline the necessity to develop specific curves for specific territories, even considering the only residential use.

More studies in depth have been done considering Olbia database to evaluate level of reliability in damage evaluations using this water-depth damage approach: a statistical procedure for uncertainty estimation level was developed by a Montecarlo generation, fitting frequencies in each water-depth class of damages by a Pearson III probability distribution.

5. ACKNOWLEDGEMENTS

Authors gratefully acknowledge Sardinia Regional Government for the financial support, particularly for Sara Frongia PhD scholarship grant (P.O.R. Sardegna F.S.E. Operational Programme of the Autonomous Region of Sardinia, European Social Fund 2007-2013-Axis IV Human Resources, Objective l.3, Line of Activity l.3.1.)

REFERENCES

Appelbaum S.J.and A.M.ASCE. (1985). Determination of Urban Flood Damages. J. Water Resources Planning and Management , 269-283.

Bellos V. and Tsakiris G. (2015). Comparing various methods of building representation for 2D flood modelling in built-up areas. Water Resources Management , 379-397.

Frongia S., Liberatore S. and Sechi G.M.(2015). Flood Damage Risk Assessment Optimizing a Flood Mitigation System. 9th WORLD CONGRESS OF EWRA "Water Resources Management in a Changing World: Challenges and Opportunities". Istanbul.

Huizinga H.J. (2007). Flood Damage Functions for EU member states. Joint Research Centre.

Jongman B., Kreibich H., Apel H., Barredo J.I., Bates P.D., Feyen L., Gericke A., Neal J., Aerts J.C.J.H. and Ward P.J. (2012). Comparative flood damage model assessment: towards a European approach. Natural Hazards and Earth System Sciences, 3733-3752.

Mancini M. (2014). Studio di variante al Piano Stralcio per l'Assetto Idrogeologico (PAI) e del quadro delle opere di mitigazione del rischio idraulico nel territorio comunale di Olbia.

MCM Model. (2005). The Benefits of Flood and Coastal Risk Management: A Handbook of Assessment Techniques. Flood Hazard Research Centre (FHRC). Middlesex University Press.

Merz B., Kreibich H., Thieken A., and Schmidtke R.(.(2004). Estimation uncertainty of direct monetary flood damage to buildings. Natural Hazards and Earth System Sciences, 153-163.

Notaro V., De Marchis M., Fontanazza C.M., La Loggia G., Puleo V., Freni G.(2014). The effect of damage functions on urban flood damage appraisal. Science Direct - Elsevier, 1251-1260.

Pistrika A. (2014). Flood Depth-Damage Functions for Built Environment. Environ. Process., 553–572.

Pistrika A.K. and Jonkman S.N. (2010). Damage to residential buildings due to flooding of New Orleans after hurricane Katrine. Natural Hazards , 413-434.

Price R.K. and Vojinovic Z. (2008). Urban flood disaster management. Urban Water Journal , 5 (3), 259-276.

RAS-Vol.1. (2015). Piano di Gestione del Rischio Alluvione-Documentazione sui principali eventi alluvionali recenti in Sardegna-Volume 1.

Scawthorn C., ASCE F., Blais N., Seligson H., Tate E., Mifflin E., Thomas W., Murphy J., and Jones C. (2006). HAZUS-MH Flood Loss Estimation Methodology. I: Overview and Flood Hazard Characterization. Natural Hazard Reviw ASCE, 60-71.

Scawthorn C., ASCE F., Flores P., Blais N., Seligson H., Tate E., Chang S., Mifflin E., Thomas W., Murphy J., Jones C., and Lawrence M.(2006). HAZUS-MH Flood Loss Estimation Methodology. II. Damage and Loss Assessment. Natural Hazards Review ASCE, 72-81.

Smith D.I. (1994). Flood Damage Estimation- A review of urban stage-damage curves and loss functions. Water SA, 231-238.

Tsakiris G. (2014). Floods risk assessment: concepts, modelling, applications. Natural Hazards and Earth System Sciences, 1361-1369.

Proceedings of the 10th World Congress of EWRA 'Panta Rhei', 5-9 July 2017, Athens, Greece
© 2017 *European Water Resources Association*

On urban inundation and damage modelling

A. Radice[1*], A. Bettiga[1], R. Figueiredo[2] and D. Molinari[1]
[1] *Politecnico di Milano, Milan, Italy*
[2] *Scuola Universitaria Superiore di Pavia, Pavia, Italy*
[*] *e-mail: alessio.radice@polimi.it*

Abstract: Flood risk results from a complicated interplay of natural and anthropic factors. Therefore, risk modelling and assessment may require different modelling tools, related to individual facets of the problem. These may be organized in a chain where each model represents a ring. The interfaces among the single modelling rings represent a most critical part of the analysis that must be added to the inherent criticalities and uncertainties of each modelling step. In this work a prototypal case-study in northern Italy (the town of Sondrio, that is prone to flood risk by the Mallero river) is considered. A 100-year synthetic river flood was simulated and an outflow hydrograph was accordingly computed in an earlier study. The present work considered the further rings of the chain. A two-dimensional wave flooding the town was numerically modelled, simulating building blocks as impermeable obstructions. Different configurations of the blocks were considered within a sensitivity analysis of the modelling result to the geometric description. Hazard indicators were obtained and transferred to the following modelling ring. Flood-induced damages to buildings, considered proxies for the flood risk, were computed by a recently developed synthetic model, that provides absolute damage values based on a component-by-component analysis of physical damages to residential buildings. In the described sequential procedure, the hydraulic analysis served as a support for the following risk assessment. Therefore, the results of the sensitivity analysis for the hydraulic model were not useful per se but rather with reference to their implications for the quantification of damage and thus of risk.

Key words: Urban flood, risk assessment, two-dimensional wave, damage model

1. INTRODUCTION

Assessment of environmental risks requires consideration of both hazard and vulnerability factors, the former and the latter being mostly related with natural processes and anthropic items, respectively. One way to handle the job is to organize several modelling modules into a chain. For example, Apel et al. (2006) developed a "complete flood disaster chain from the triggering event down to its various consequences". In such a sequential approach, feedback effects are typically discarded to maintain the modelling chain as simple as possible. Furthermore, different degrees of complexity can be used for the single modelling modules. In all cases, however, key aspects of the study are the identification of the parameters needed in each modelling ring and the capability of the previous rings to furnish their values to the following ones.

This work documents an application of hydraulic risk modelling to a mountainous town situated in Northern Italy. The complete chain was actually split into two parts, with the first one (related with hydro-geologic processes, flash flood in the river and embankment overtopping) developed in an earlier study (Radice et al., 2016) and the following part (related with urban flood propagation and consequent damage to property) developed in this manuscript. Therefore, here two consecutive modelling rings were considered. Following the idea that transfer of information is a key aspect to be taken into account, the objective and main point of interest of the present study was not in the single modelling modules, but rather in assessing the sensitivity of the second module to the implementation of the first one.

2. PRESENTATION OF THE CASE-STUDY

This manuscript considers the town of Sondrio in Northern Italy as a prototypal case-study for

application of urban flood and damage modelling. Sondrio (Figure 1) is a 22,000-people town lying on an alluvial fan at the foot of the Valmalenco Valley (350 km^2 wide) in Northern Italy. The fan was created by the Mallero River, which is the main water course of the Valmalenco, with a length of about 25 km. The river enters Sondrio just downstream of a sharp right-ward bend and crosses the town in its last 2 km before flowing as a tributary into the Adda River, which is the major stream of the Valtellina Valley. Elevation in Valmalenco ranges between 280 and 4,050 m a.s.l.; ground elevations in Sondrio are in the range of 280 to 310 m a.s.l., approximately. The position of Sondrio at the foot of a mountainous catchments leads to the presence of significant ground slopes in the town.

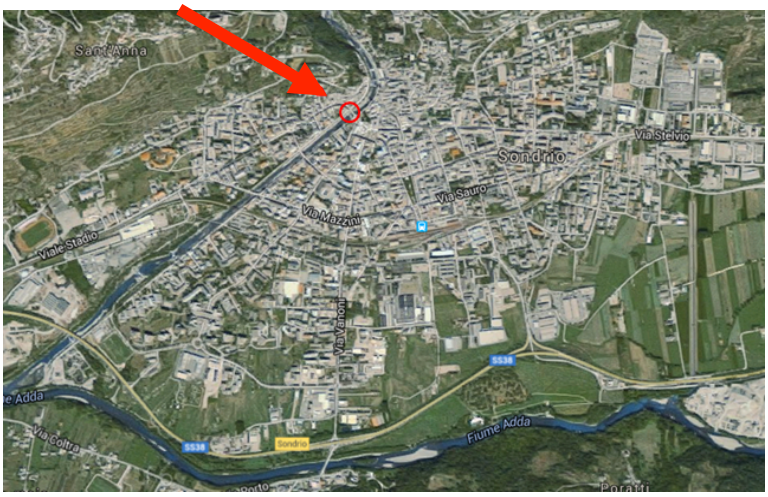

Figure 1. Aerial photograph of Sondrio, with indication of the outflowing location used in the model.

A major flash flood of the Mallero River occurred in 1987. During that event, the town was fortunately not inundated. However, in the following years a major concern of local authorities was stimulated by the event and several studies were performed to assess the flood hazard endangering the town. Thanks to this, different kinds of data are available, making this place a suitable case-study. The authors of the present manuscript have performed in the last years several studies of the hydro-graphic basin morphology (Longoni et al., 2016), river hydro-morphologic processes under different flood scenarios (Radice et al., 2013 and 2016; Radice and Elsayed, 2014), flood damages and existing flood management tools (Menoni et al., 2012; Molinari et al., 2013 and 2014).

3. HAZARD SCENARIO AND MODELLING CHAIN

A back analysis of the 1987 event showed that, as in other flood events taking place in the twentieth century, the flood hazard for the town was exacerbated by the intense sediment transport in the Mallero River during a flash flood. The transported sediment typically tends to deposit in the in-town reach, due to a much reduced slope of this reach compared to the slopes in the upstream portion of the river. Records of the 1987 flood reported aggradation depths up to 5 m in the in-town reach (for reference, one should consider that the bank height is around 5 to 8 m in the same reach).

The expected phenomenology described above clarifies that any assessment of the flood hazard for the town of Sondrio would require analysis of all the hydro-geologic processes taking place in the hydro-graphic basin, which eventually determine the river hydraulics in the in-town reach that is situated in the final portion of the river. Risk modelling can be organized into a chain comprehending at least (i) hydrologic models for the flood hydro-graph, (ii) models for sediment production in the catchments, (iii) hydro-morphologic models for the river flow and sediment transport, (iv) hydraulic models for the outflowing discharge hydro-graph and (v) for the propagation of a flood wave into the town and (vi) models for expected damages, considered as proxies for the hydraulic risk.

This manuscript considers rings (v) and (vi) of the chain above. The town is flooded with a water hydro-graph that was determined by Radice et al. (2016) as a result of a 100-year flood in the river, corresponding to a 60-hours flash flood peaking at 650 m^3/s. A location where outflow from the river into the town would be most likely was determined (circled in Figure 1), and a flooding hydro-graph was estimated as having a duration of 25 hours and a peak discharge of 140 m^3/s. This hydro-graph is used here as a condition for the following modelling rings.

4. TOOLS AND RESULTS FOR FLOOD AND DAMAGE MODELLING

The urban flood was modelled using the depth-averaged model implemented in River2D (Steffler and Blackburn, 2002). The flood-induced damages were estimated using the INSYDE model by Dottori et al. (2016). This section briefly describes the modelling procedures and the quantitative outputs.

4.1 Urban flood

River2D implements a finite-element solver of the shallow-water equations. In this model, the ground geometry is discretized using an unstructured mesh with triangular elements. Bed resistance is modelled using a Chezy equation while lateral stresses are modelled by an eddy-viscosity approach. The fixed-bed model considers both surface and groundwater flow. Boundary conditions are expressed in terms of a water hydro-graph at an inflow location and a water elevation at an outflow location. These inflow and outflow locations must be defined as portions of the boundary of the computational domain. Consistently with this brief description, the parameters to be chosen by the user are the mesh size, equivalent roughness height, eddy viscosity, transmissivity (T) and storativity (S) of the ground, inflow and outflow locations and boundary conditions. The result of the computation is in terms of spatial maps of several hydraulic properties (water elevation and depth, velocity, and others), or temporal evolution of these properties at some monitoring points.

In the absence of guidelines for the application to a urban flood, the performance of the model was first verified with reference to a laboratory experiment of Soarez-Frazão and Zech (2008), where an idealized city made of 5 × 5 square-based obstacles was impacted by a dam-break wave. Each obstacle was 0.3 × 0.3 m and streets were 0.1 m wide. This experiment is a unique benchmark for two-dimensional models, that was used as a reference also by Petaccia et al. (2010) and Xia et al. (2011). A negative water depth must be used as a downstream boundary condition to mimic the propagation of the wave over an initially dry bed. Buildings can be simulated by impermeable obstructions. For this experimental case, best results were obtained with a model parameterization limiting the groundwater flow ($T = 0.1$ m^2/s, $S = 0.001$).

Also for the propagation of the two-dimensional wave flooding the town, groundwater flow was prevented by suitable parameterization of soil transmissivity and storativity (that were the same as for the idealized town above). Incorporating single buildings into the geometric description would have been unfeasible, therefore building blocks were considered and, similarly to the idealized town, they were simulated by impermeable obstructions. Two different configurations of the blocks were considered within a sensitivity analysis of the modeling result to the geometry used in the numerical simulations (Figure 2). In a first situation (geometry 1 henceforth), the street width was increased to somehow compensate the use of completely impermeable blocks, whilst in a second realization (geometry 2) the obstruction opposed to the flow was more pronounced. With geometry 1 the two-dimensional solver was able to capture the town flooding and the water recession, whereas for geometry 2 solver crash was not avoidable and the recession phase could not be

satisfactorily modelled. Spatial distributions of instantaneous and maximum water depth and velocity were obtained, in the first case together with distributions of water residence time. The modelling approach was more sophisticated than that used by Apel et al. (2006) who determined the contour of the flooded area by a purely topographical method (by comparing characteristic water depth with the ground elevation) and than that used by ISMES (1988) and ISMES and CAE (1988) who, for the same case-study considered in this work, modelled streets as a network of one-dimensional channels.

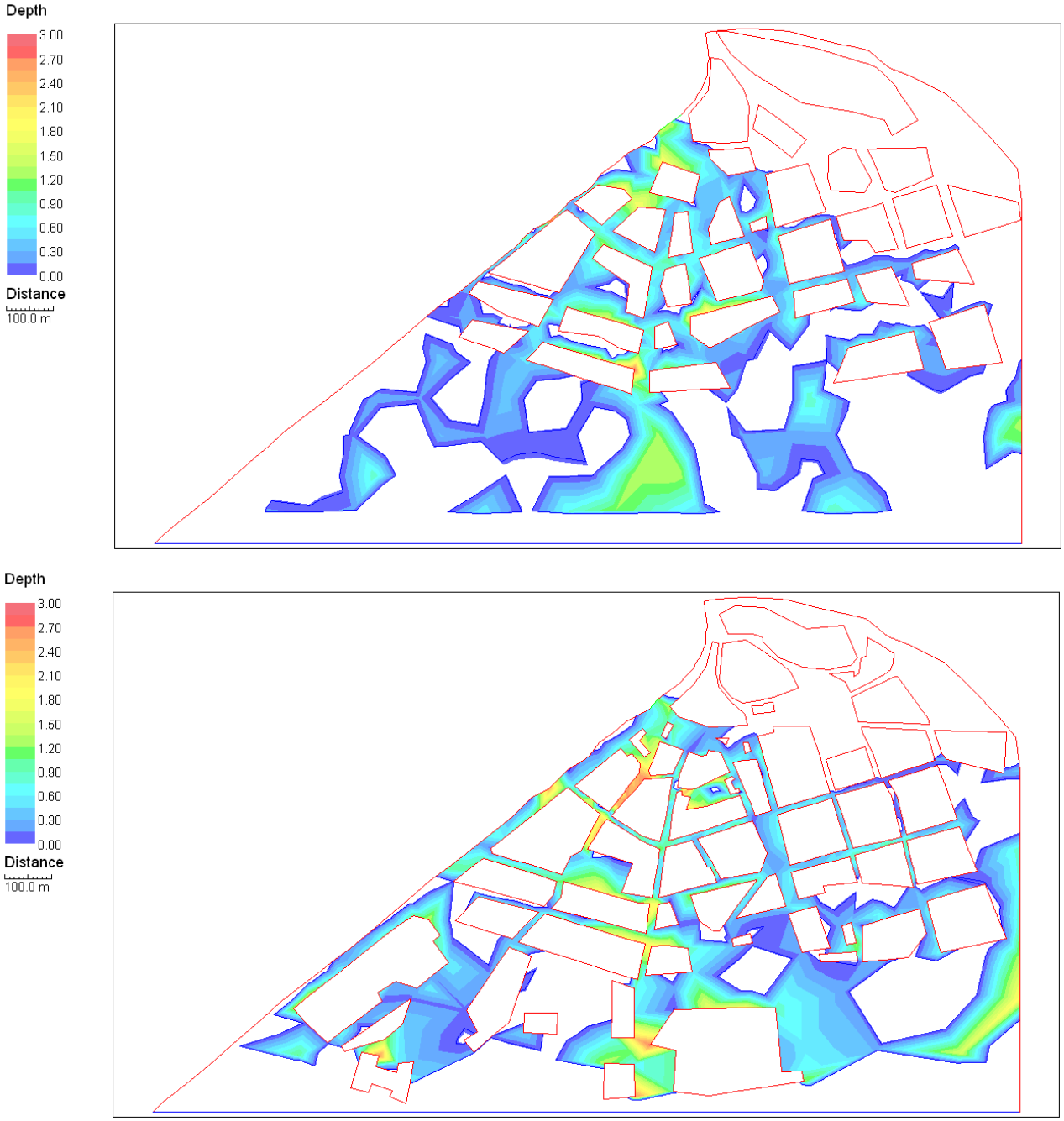

Figure 2. Results for the two-dimensional wave propagation into the town: water depth at peak of inundation for geometry 1 (top) and geometry 2 (bottom).

4.2 Damages

Flood-induced damages to buildings, considered proxies for the flood risk in the investigated

scenario, were computed by a recently developed synthetic model, INSYDE (Dottori et al., 2016). This model, that is for the time being suitable to residential areas, provides absolute damage values based on a component-by-component analysis of physical damage to buildings, including costs for removal and replacement of damaged items and plants, structural reconstruction, cleanup and finishing. Absolute damages can be converted into relative ones dividing the model output by the expected cost for building replacement with an analogous one. The model was validated with reference to data for 300 buildings hit by a 2010 flood in Veneto Region, Italy. Parameters to be input to the model include hazard factors (water depth and velocity at peak, duration of inundation, and sediment concentration and water quality as additional parameters) and vulnerability factors (including, among others, the type of building, plan area, number of levels, presence of basement, year of construction, level of maintenance, and building value per m^2).

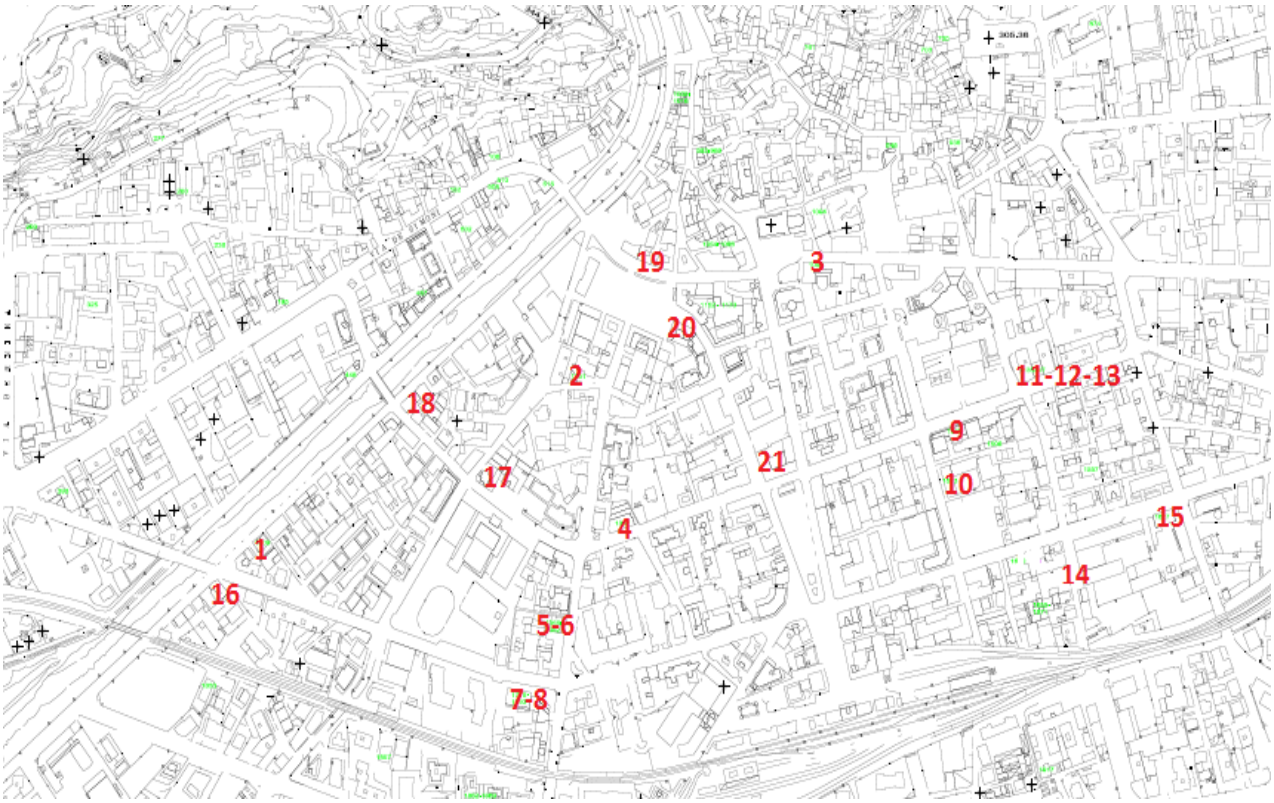

Figure 3. Location of sample buildings.

The properties of 21 sample buildings (Figure 3) were surveyed in the spring of 2016 to determine the minimum set of vulnerability parameters to be input to the model. Hydraulic parameters (water depth and velocity at the peak of inundation, duration for which an item was flooded) were derived from the hydraulic models as those for closest location to the building, or by spatial interpolation. Obviously these parameters could be obtained if they were provided by the model (for example, it was mentioned above that only for geometry 1 the model could be run until the end of the inundation providing the duration of the flood for each building). In case a parameter value was not available, the default value assumed in the INSYDE model was used. Results of the damage assessment are depicted in Figure 4 by a histogram plot of the relative damage. Different damage estimations were obtained for geometry 1 when using only the water depth, or the water depth and velocity, or all the three hydraulic parameters. A major effect sensitivity was detected to the use of duration. Moreover, changing the geometry description to version 2, the damage for some buildings switched from zero (flood not arriving there) to some value, demonstrating the major effect of the geometric description.

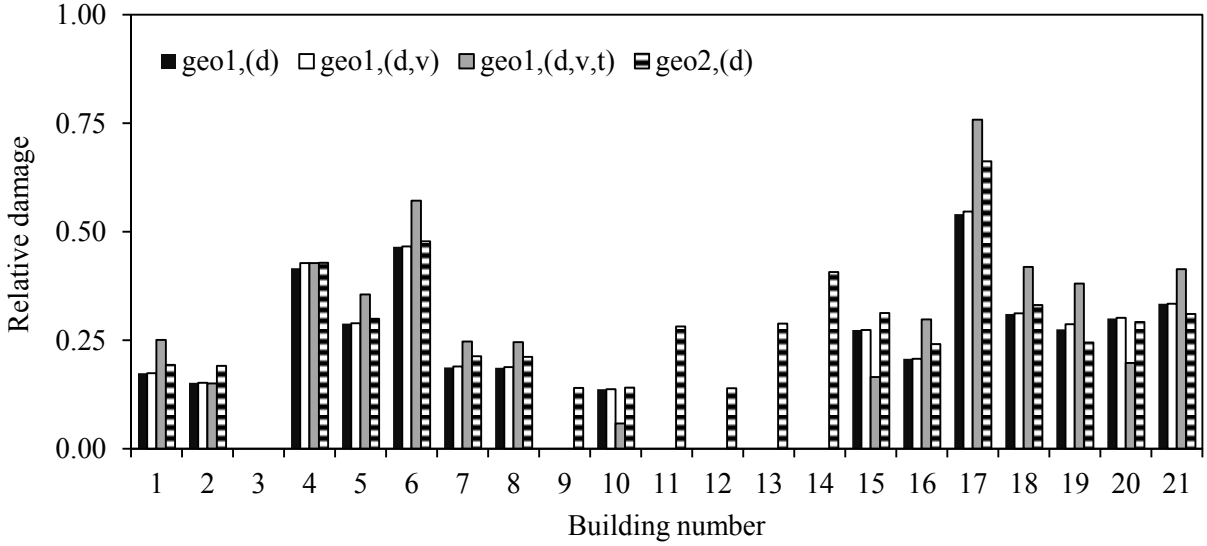

Figure 4. Sensitivity analysis of damage modelling to hydraulic parameters (geometry 1 or 2, using: d = *depth;* d,v = *depth and velocity;* d,v,t = *depth, velocity and flood duration).*

5. CONCLUDING DISCUSSION

In the described sequential procedure, the hydraulic analysis serves as a support for a final risk assessment in terms of expected damage to buildings. Therefore, the result of a sensitivity analysis for the hydraulic model is not discussed *per se* but rather with reference to its implications for the quantification of damage. For example, the damage model used in the present work considers the water residence time as a major factor impacting the absolute damage. Following this, a key feature of a hydraulic model would be represented by its capability to provide a value for such a parameter, and this target should be privileged when running the hazard evaluation. Second, it was found that changing the geometric description of the building blocks could change the water paths up to a level where a building that is completely safe with a certain description can be significantly damaged with another description.

The use of sensitivity analysis was the only possibility to characterize robustness of the results in the absence of appropriate validation data, since fortunately Sondrio was never flooded in recent times. Guidelines for the hydraulic model application were derived from a validation for a laboratory experiment, thus with a huge change of scale.

A major limitation of the present work is related with the prevention of groundwater flow by model parameterization. On the one hand, this sounds reasonable in consideration of the mostly impermeable urban context. On the other hand, it should be borne in mind that in a urban flood the surface flow largely interacts with the sewage system. In principle, even in the absence of a coupled solver for flow over the surface and in the sewer, some coupling could have been obtained also by a different setting of ground transmissivity and storativity. This was not done in the present work because, in the above-mentioned absence of real data, it would have been a mere tentative.

The geometric model used in this work was quite coarse and many specific aspects (e.g. Bazin et al., 2016) were also overlooked. However, the minimum resolution to be used in these kinds of models is an open debate (e.g. Apel et al., 2009; Dottori et al., 2013). On another hand, a high detail would be requested by analyses of the expected damage at the micro-scale (that is considering individual buildings). Combination of an affordable hydraulic modelling with a detailed damage assessment calls for spatial interpolation of hazard indicators, an operation that is not straightforward and can introduce mistakes. Interpolation would also be needed at a further step of the modelling, to convert the damage values obtained for single scattered buildings into a meso-scale damage assessment. This is also a still open issue that shall be addressed by future research.

ACKNOWLEDGMENTS

This work was partially supported by Fondazione Cariplo, through the project "Flood-IMPAT+: an integrated meso & micro scale procedure to assess territorial flood risk". A. Babaee and M. Izadifar are gratefully acknowledged for contributing to the present study during their M.Sc thesis in Civil Engineering for Risk Mitigation at the Politecnico di Milano.

REFERENCES

Apel, H., Aronica, G. T., Kreibich, H., Thieken, A. H., 2009. Flood risk analyses – how detailed do we need to be? Natural Hazards, 49(1): 79-98.

Apel, H., Thieken, A. H., Merz, B., Blöschl, G., 2006. A probabilistic modeling system for assessing flood risks. Natural Hazards, 38(1-2): 79-100.

Bazin, P.-H., Mignot, E., Paquier, A., 2016. Computing flooding of crossroads with obstacles using a 2D numerical model. Journal of Hydraulic Research, 55(1): 72-84.

Dottori, F., Di Baldassarre, G., Todini, E., 2013. Detailed data is welcome, but with a pinch of salt: Accuracy, precision, and uncertainty in flood inundation modeling. Water Resources Research, 49(9): 6079-6085.

Dottori, F., Figueiredo, R., Martina, M., Molinari, D., Scorzini, A. R., 2016. INSYDE: A synthetic, probabilistic flood damage model based on explicit costa analysis. Natural Hazards and Earth System Sciences Discussions, 16: 2577-2591.

ISMES, 1988. Modello di simulazione dell'inondazione in Sondrio: mappe di inondazione. ISMES, Bergamo (in Italian).

ISMES, CAE, 1988. Piani di allarme connessi alla situazione di rischio idrometeorologico nella Val Malenco. Lineamenti per un piano di intervento per la protezione della città di Sondrio. ISMES, Bergamo (in Italian).

Longoni, L., Ivanov, V. I., Brambilla, D., Radice, A., Papini, M., 2016. Analysis of the temporal and spatial scales of soil erosion and transport in a mountain basin. Italian Journal of Engineering Geology and Environment, 16(2): 17-30.

Menoni, S., Molinari, D., Parker, D., Ballio, F., Tapsell, S., 2012. Assessing multifaceted vulnerability and resilience in order to design risk-mitigation strategies. Natural Hazards, 64(3): 2057-2082.

Molinari, D., Ballio, F., Handmer, J., Menoni, S., 2014. On the modeling of significance for flood damage assessment. International Journal of Disaster Risk Reduction, 10(PA): 381-391.

Molinari, D., Ballio, F., Menoni, S., 2013. Modeling the benefits of flood emergency management measures in reducing damages: A case study on Sondrio, Italy. Natural Hazards and Earth System Sciences, 13(8): 1913-1927.

Petaccia, G., Soarez- Frazão, S., Savi, F., Natale, L., Zech, Y., 2010. Simplified versus detailed two-dimensional approaches to transient flow modeling in urban areas. Journal of Hydraulic Engineering, 136(4): 262-266.

Radice, A., Elsayed, S. M., 2014. Hydro-morphologic modelling for different calamitous scenarios in a mountain stream. Proc. River Flow 2014, VII International Conference on Fluvial Hydraulics, Lausanne, Switzerland.

Radice, A., Longoni, L., Papini, M., Brambilla, D., Ivanov, V. I., 2016. Generation of a design flood-event scenario for a mountain river with intense sediment transport. Water, 8(12): 597.

Radice, A., Rosatti, G., Ballio, F., Franzetti, S., Mauri, M., Spagnolatti, M., Garegnani, G., 2013. Management of flood hazard via hydro-morphological river modelling. The case of the Mallero in Italian Alps. Journal of Flood Risk Management, 6(3): 197-209.

Soares- Frazão, S., Zech, Y., 2008. Dam-break flow through an idealised city. Journal of Hydraulic Research, 46(5): 648-658.

Steffler, P. M., Blackburn, J., 2002. River2D – Two-dimensional depth averaged model of river hydrodynamics and fish habitat. University of Alberta, www.river2d.ca.

Xia, J., Falconer, R. A., Lin, B., Tan, G., 2011. Modelling flash flood risk in urban areas. Proceedings of the ICE, Water Management, 164(WM6): 267-282.

Proceedings of the 10th World Congress of EWRA 'Panta Rhei', 5-9 July 2017, Athens, Greece
© 2017 *European Water Resources Association*

Flood risk and flood processes in a changing environment

A.H. Schumann* and S. Fischer
Ruhr- University Bochum, Institute of Hydrology and Water Management, D-44801 Bochum, Germany
** e-mail: andreas.schumann@rub.de*

Abstract: Driven by the EU- Flood Directive, flood risk management became one of the focusing points of water policy. Flood risk means the combination of the probability of a flood event with its adverse consequences. Unfortunately, the consequences of a changing environment on floods are hidden by high uncertainties about the stochastic behavior of flood inducing processes and their possible changes. Tools, which are able to combine statistical assessments with deterministic considerations, are rare. In this presentation, the problem of instationarity is discussed to demonstrate the need to close the gap between stochastic and deterministic flood hydrology. Some methodological tools will be presented which are useful for this purpose.

Key words: Floods, multivariate statistics, timescales, flood types, peak over thresholds

1. INTRODUCTION

In the last 25 years, floods moved into the focus of European water management. This resulted from a large number of catastrophic events that happened in the last 25 years in several parts of Europe. The political goal of flood management was propagated in the European Flood Directive (EFD), which aims to reduce the likelihood of flooding as well as its harmful consequences. By definition flood risk management has to consider the eventuality of flood damages, even if the causing floods would have "a low probability" or belong in the category of "extreme event scenarios" (European Commission 2007). According to the Merriam- Webster Dictionary the word "management" means not only the act of managing: "the conducting or supervising of something" but also the "judicious use of means to accomplish an end". In this sense flood risk management is aimed at managing whole flooding systems by their catchments in an integrated way that accounts for all of the potential interventions that may alter flood risk (Sayers et al. 2002). At this extended spatial scale, their effects on local, regional and supra-regional flood risks may differ and often depend on event-specific interactions between tributaries and the alterations of floods by other interventions in the flood regime, which may differ in their impacts between events also (Schumann, 2017). However, if the specification of effective measures for flood management is essential, assessments and comparisons of economic efficiencies are also indispensable. With regard to the stochasticity of floods, this efficiency of flood protection measures depends strongly on the exceedance probabilities of design floods. The economic aspects of flooding can be assessed using the Expected Annual Damage (EAD) concept [e.g. (Chow et al. 1988)]. The reduction of damage costs by flood management depends on the choice of the design, which is selected to adapt the system, but also on the expected changes of the damage curve after adaptation (Rosbjerg 2017). Both problems mentioned above, the improved characterisation of hydrological loads to specify the performance of flood management measures and the estimation of flood probabilities under consideration of the multivariate flood characteristics, demand new methodological approaches in flood statistics. It is insufficient to specify floods by the exceedance probabilities of their peak flow only. The variability between flood events with similar peaks, but different hydrograph and volumes or the spatial differences of flood formation between events becomes more and more relevant if we try to characterize options and limitations of flood management in a more realistic way than by single design floods only.

2. MULTIVARIATE OR PROCESS-BASED STATISTICS?

For flood retention, the assessment of flood volumes for design floods, which are statistically specified by the exceedance probability of their peak flows, is essential. One main application of copulas is to support the sizing of a design flood to consider the dependencies between peak and volume ((De Michele et al. 2005; Shiau et al. 2006; Klein et al. 2010)). With copulas, a joint distribution of correlated random variables can be expressed as a function of the univariate marginal distributions. Copulas allow modeling of the dependence structure of two (or more) random variables. This structure often shows a variability over the range of flood peaks, which is an indicator for different flood processes. To analyze these differences, the "flood timescale" that was proposed by (Gaál et al. 2012) can be applied. It is the quotient of the flood volume and flood peak. In another study (Gaál et al. 2015) analyzed the consistency of the peak–volume relationship quantified by the Spearman rank correlation coefficient for a large sample of watersheds in Austria. The main conclusion of this study is that a mix of different flood types reduces the consistency between flood peaks and volumes. The authors explain a weak dependence in the high alpine catchments by the mix of flood types, including long-duration snowmelt, synoptic floods and flash floods, which are a characteristic of these regions. An important conclusion of this publication is that climate-related factors are more important than catchment-related factors in controlling the consistency between peaks and volumes. We use these results to go a step further. By an analysis of the correlation between peaks and volumes, we differentiated the monthly flood peaks by groups, which characterize certain types. In Fig. 1 an example is given.

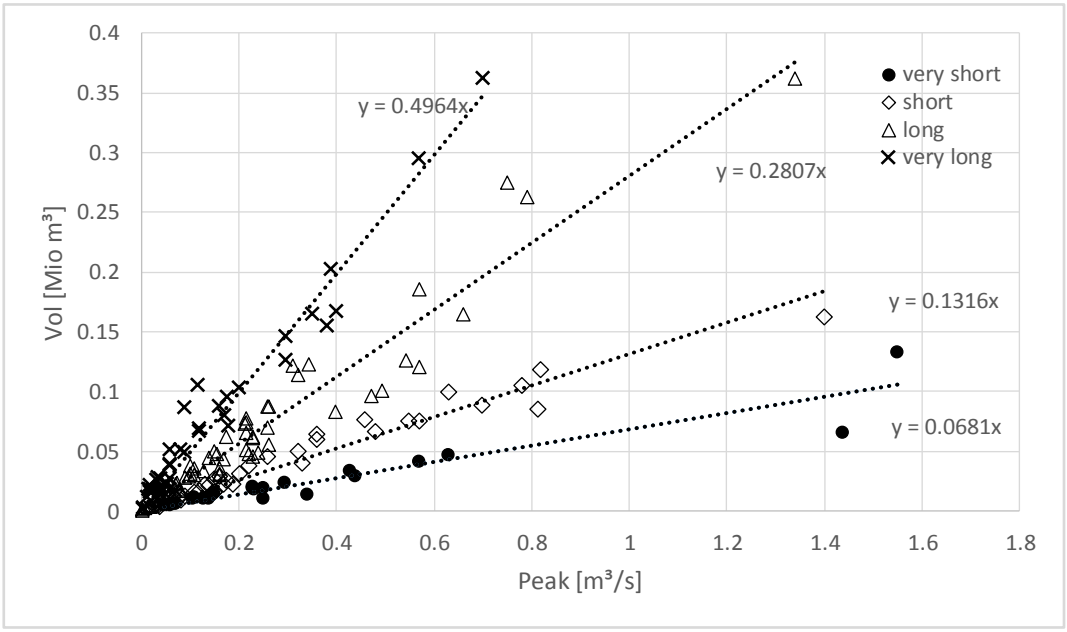

Figure 1. Relationships between peak and volume (direct runoff only) for floods at the gauge Derenburg/ Hellbach in Germany.

According to the timescale we differentiated into four groups from "very short" to "very long". There are some accumulations of short events in the months June to August (convective storms) and of very long events in March to April (snowmelt). However, the most of the floods happen in different seasons of the year. This result is similar to the experience of other authors (Brunner et al. 2016). As a result, we can separate samples of flood peaks according to their event-type. With a POT- approach, where different thresholds are used for the different flood types, probability distribution functions can be estimated for all of these samples. These distributions can be combined by a methodology, which was proposed by (Zhou et al. 2016). This mixing POT-model is an extension to the classical POT-models using the Generalized Pareto distribution (see e.g. Fischer and Schumann, 2016). The common distribution of the n_t different event types is given by:

$$F(x) = 1 - \sum_{i=1}^{n_t} \left(1 - G_i(x;\theta_i,u_i)\right)\left(1 - F_i(u_i)\right)\omega_i \quad (1)$$

where G_i is the Generalized Pareto distribution with parameter θ_i fitted to event type i exceeding a threshold u_i and F_i is the marginal distribution of this event type. The weighting ω_i corresponds to the probability of occurrence of the event type. It estimates the joint distribution of flood peaks under consideration of the frequencies of events of certain types. In total, we get a statistics of yearly flood peaks but also the probabilities that a flood peak is caused by a certain flood type and the expected values of the flood volumes. Compared with the multivariate copula-based approach, this differentiation of the entity of observed floods into flood types improves our opportunities to specify the upper reach of the copula under consideration of physical boundaries and a shift of flood type frequencies within the range of observations. Examples are given in Fig. 2 und 3.

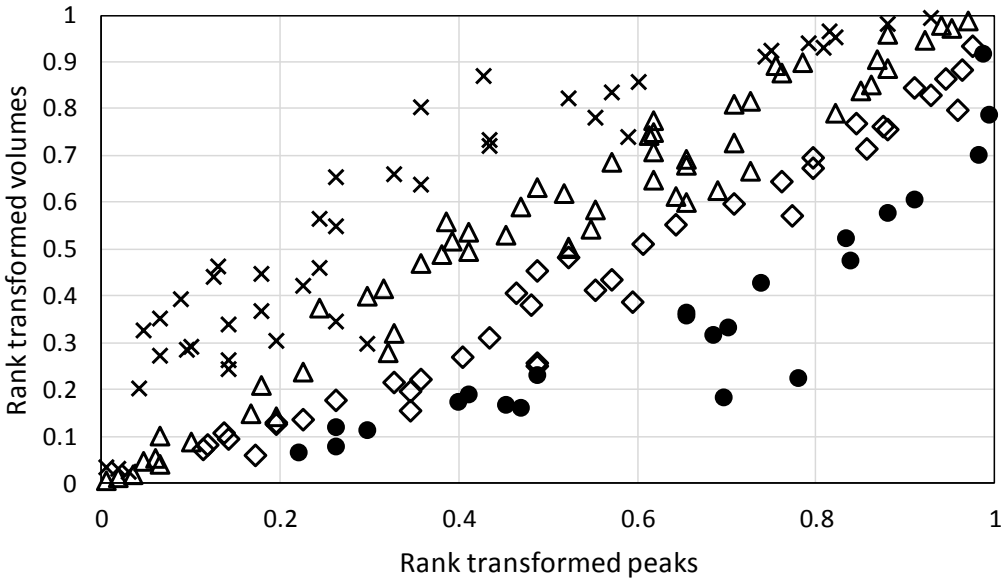

Figure 2. Scatter plot of rank transformed volumes above rank transformed peaks for flood events at the gauge Derenburg/ Hellbach in Germany. The marking of flood types is the same as in Fig. 1

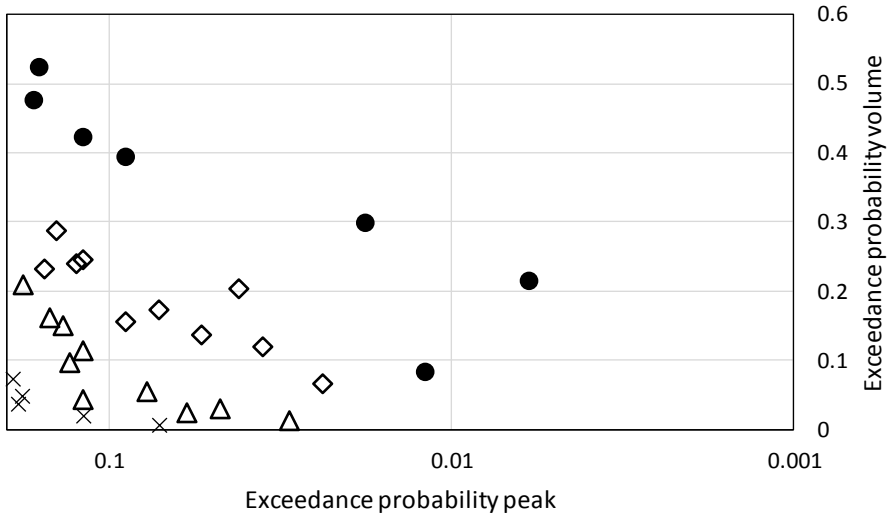

Figure 3. The variety of flood volumes for the highest flood events of all four types, gauge Derenburg/ Hellbach

It can be seen that in the range of peaks with exceedance probabilities above 0.1, estimated from

all events above the thresholds, the categories “very short” and “short” floods are much more represented than events belonging to the long categories. The volumes of these events have higher exceedance probabilities. It has to be emphasized that the mixed POT- approach results in annual flood probabilities, which are nearly the same as derived from the classical Annual Maxima Series (AMS) by application of the Generalized Extreme Value distribution and a parameter estimation with L- moments. By the proposed methodology, it becomes possible to specify the dominating flood type for this catchment and to consider this result in flood regionalization.

3. CHANGING FREQUENCIES OF FLOOD TYPES

The characteristics of flood types become highly relevant for impact assessments of climatic change. The relevance of global warming on snowmelt and rain-on-snow floods is obvious and was discussed in several studies (e.g. (Köplin et al. 2014; Støren et al. 2012; Köplin et al. 2014; Vormoor et al. 2015)). But also changes of other climatic characteristics as the frequencies of large-scale circulation pattern (Jacobeit 2003) or of the soil moisture state (Nied et al. 2014) could have impact on flood statistics. Such changes could affect the frequencies of floods with specific types only. Especially for tropical extreme events observations reveal a distinct link between rainfall extremes and temperature, with heavy rain events increasing during warm periods and decreasing during cold periods (Allan und Soden 2008). Flash floods could happen more often caused by short and intensive rain events in the summer. How an increase of frequencies of short but intensive rainfall events would affect the flood statistics in summer will be demonstrated in the following. For this study, we use the “maximum Winter-Summer-Types approach” (WST) (Fischer et al., 2016). It is based on a subdivision of the year in a summer and a winter period. By multiplication of non-exceedance probabilities in winter and summer, the probability of a flood peak can be estimated. The annual maximum is, in any case, the maximum of the summer or winter annual maximum. Vice versa, if the annual maximum X_A does not exceed some value x, then the summer and winter annual maximum must not exceed this value. Thus, the annual non-exceedance probability can be estimated multiplicatively from the probabilities of winter X_W and summer X_S peaks (Todorovic and Rouselle, 1971):

$$P\left(X_A \le x\right) = P\left(X_S \le x\right) \cdot P\left(X_W \le x\right) \tag{2}$$

As described above, several flood types could be identified for both seasons by their timescales. With regard to the question raised above, we differentiate here between long and short summer events only. The statistics of winter events will not be modified. For this purpose, the seasonal mixing model was extended to a model that considers the different distributions of winter and summer floods as well as the differences between short and long summer events. Considering several flood types (long and short floods) in summer demands a statistical mixing model to specify the resulting flood probabilities in summer. The maximum mixing model benefits from the fact that the non-exceedance of a summer flood peak x demands that it is not exceeded by any short or long flood event in this half-year. Thus, the multiplicative approach of Todorovic and Rouselle (1971) can be applied as follows:

$$P\left(X_A \le x\right) = \left(P\left(X_{S,l} \le x\right) \cdot P\left(X_{S,s} \le x\right)\right) \cdot P\left(X_W \le x\right) \tag{3}$$

where $X_{S,s}$ and $X_{S,l}$ are the flood peaks of short and long summer runoffs.

For flood peaks in winter we know the complete sample. This is not the case if we differentiate summer maxima into short and long summer floods. As only a member from one of both groups is the maximum of the summer half-year, we know just the highest summer flood per year which can be characterized by a long or by a short timescale. Smaller values are overlaid. To estimate the distributions of long and short flood events, we have to correct the statistical parameters of both

subsamples. For this purpose we applied a method of "filling" both data series.

It can be shown by statistical simulations that maxima series resulting from two different distributions are always dominated by the distribution that has the larger location parameter. If all other parameters (scale and shape) are equal, shares of this dominating series of approximately 97% can be obtained. If the other series has a larger scale, this relation is diminished, but the series with the larger location parameter still dominates the maxima series (about 80%). The shape parameter has only a small influence on the shares of the two distribution functions in this series. This leads to the following procedure to adjust statistical parameters. The shares are estimated by counting the number of events belonging to one or the other distribution that occur in the maxima series. As only a member from one of both groups is the maximum of the summer half-year, we only know the highest summer flood per year which can be characterized by a long or by a short timescale. We estimated the location parameter μ_S of the whole summer annual maxima series. We know that the event type with a higher share in this sample determines this parameter. For this part of the sample we used the location parameter μ_S, for the other part which has a relative share RS (with RS<0.5) we replaced the location parameter with $(RS+0.5)\cdot\mu_S$. The more equal the shares of both event types within the summer series, the more equal both location parameters are to the location parameter of the summer series. To replace the missing values, we can use the fact that for the subseries that dominates the summer annual maxima, the missing values scatter around the parameter μ_S, because none of the overlaid events belongs to the sample of large events, which were observed. No events from the right tail occur in the series of missing values (these are already included in the non-overlaid series), so we can assume that these are distributed symmetrically. There is no option to estimate the variance of this subsample directly. Relatively large events are possibly overlaid by large events belonging to the other subsample. That is why we considered a spectrum around the location parameter to introduce an artificial variance. We used the robust estimator MAD (median absolute deviation) to estimate this variance from the known part of this series which is based on the median of each subsample. Within the interval $[RS\cdot\mu_S\text{-MAD}; RS\cdot\mu_S\text{+MAD}]$ resp. $[\mu_S\text{-MAD}; \mu_S\text{+MAD}]$ the missing values in the two subsamples were chosen from a uniform distribution. Further details are given in (Fischer et al., 2016).

In our case study the increased frequency of short and intensive rain events in summer results in a higher frequency of floods with high peaks and short timescales. This leads to a reduced skew but a higher location and scale of the distribution of such events since the mid of the distribution increases. That is, the right tail of the distribution becomes "more probable". Simultaneously the location of the long summer is reduced since the long events have less magnitude. The proposed statistical model can consider such changes. To demonstrate this we use an example of the flood statistics at the gauge Berthelsdorf, which is located at the Freiberger Mulde River in Germany. The relationship between short and long flood events at gauge Berthelsdorf is 0.4 to 0.6. We invert this relationship now. As a result the parameters of the distributions of flood peaks in summer are changed. For short events we've got a reduced skew but a higher location and scale of the distribution, for long events the location was reduced since the long events have less magnitude. The modification of the mean μ, standard deviation σ and skewness ξ are shown in Table 1.

Table 1. Parameters of the GEV distribution for short and long summer events at the gauge Berthelsdorf/ Freiberger Mulde under assumed climatic change

	Current conditions		**Climate change scenario**	
	summer (short)	summer (long)	summer (short)	summer (long)
μ	11.718	14.307	12.7	10.307
σ	3.988	7.416	6	7.416
ξ	0.752	0.32	0.7	0.32

With these parameters, short and long summer series were simulated and combined via the maxima to obtain a series of half- years maxima in summer. The simulated series of winter and

summer floods were combined to a simulated annual maximum series, which is needed for the statistics of annual flood peaks. To compare the changes of return periods under the climate change scenario, the annualities of the five largest observed floods (note that these were summer events) are listed in Table 2.

Table 2: Estimated annualities of the five largest floods at the gauge Berthelsdorf/Freiberger Mulde before and after an assumed climatic change

	Current conditions		**Climate change scenario**	
HQ [m³/s]	**AMS**	**Maximum WST**	**AMS**	**Maximum WST**
68.2	11	17	10	11
120	35	62	35	34
122	41	64	36	35
140	55	83	50	44
360	476	375	461	198

It becomes obvious how the increased frequency of short summer floods, which are critical for the flood regime in this watershed, results in decreased return periods. For the highest observed flood (360 m^3/s) peak, which was caused by a short summer event in the year 2002, the return periods estimated with the AMS model would not change. Using the seasonal approach and considering more frequent events of this type in summer, the WST approach estimated higher exceedance probabilities. For this flood event, the return period would be halved.

4. CONCLUSIONS

The basic assumption of flood statistics is that the observations are homogeneous, i.e., subject to a common set of forces. This is often not the case. Snow-, rain-on-snow, convective or synoptic rain flood events are mixed in annual series of maxima. If the different types are separated, we gain a better understanding about the main impacts on hydrological aspects of flood risk assessments. Floods can be specified by multiple event characteristics (peak, volume, hydrograph). This can be useful for planning of flood protection measures, e.g. for retention facilities. But also aspects of climate variabilities, which affect only some flood types, could be considered in a better way. In this sense, process knowledge can improve and adapt flood statistics to new challenges.

REFERENCES

Yapo, P. O., Gupta, H. V., Sorooshian, S., 1998. Multi – objective global optimisation for hydrologic models. Jurnal of Hydrol.; 204: 83-97.

Allan, Richard P.; Soden, Brian J. (2008): Atmospheric warming and the amplification of precipitation extremes. In: Science (New York, N.Y.) 321 (5895), S. 1481–1484. DOI: 10.1126/science.1160787.

Brunner, Manuela I.; Viviroli, Daniel; Sikorska, Anna E.; Vannier, Olivier; Favre, Anne-Catherine; Seibert, Jan (2016): Flood type-specific construction of synthetic design hydrographs. In: Water Resour. Res. DOI: 10.1002/2016WR019535.

Chow, Ven T.; Maidment, David R.; Mays, Larry W. (1988): Applied hydrology. New York: McGraw-Hill (McGraw-Hill series in water resources and environmental engineering), 1988

De Michele, C.; Salvadori, G.; Canossi, M.; Petaccia, A.; Rosso, R. (2005): Bivariate Statistical Approach to Check Adequacy of Dam Spillway. In: J. Hydrol. Eng 10 (1), S. 50–57. DOI: 10.1061/(ASCE)1084-0699(2005)10:1(50).

European Commission (2007): Directive 2007/60/EC of the European Parliament and of the Council of 23 October 2007 on the assessment and management of flood risks. Online available under http://ec.europa.eu/environment/water/flood_risk/index.htm

Fischer, S.; Schumann, A.H. (2016) Robust flood statistics - comparison of classical annual maxima and Peak over Threshold approaches, Hydrological Science Journal, 61 (3), 457-470, 2016, DOI:10.1080/02626667.2015.1054391

Fischer, Svenja; Schumann, Andreas; Schulte, Markus (2016): Characterisation of seasonal flood types according to timescales in mixed probability distributions. In: Journal of Hydrology 539, S. 38–56. DOI: 10.1016/j.jhydrol.2016.05.005.

Gaál, L.; Szolgay, J.; Kohnová, S.; Hlavčová, K.; Parajka, J.; Viglione, A. et al. (2015): Dependence between flood peaks and volumes: a case study on climate and hydrological controls. In: Hydrological Sciences Journal 60 (6), S. 968–984. DOI: 10.1080/02626667.2014.951361.

Gaál, Ladislav; Szolgay, Ján; Kohnová, Silvia; Parajka, Juraj; Merz, Ralf; Viglione, Alberto; Blöschl, Günter (2012): Flood timescales: Understanding the interplay of climate and catchment processes through comparative hydrology. In: Water Resour. Res. 48 (4), S. n/a. DOI: 10.1029/2011WR011509.

Jacobeit, J. (2003): Links between flood events in central Europe since AD 1500 and large-scale atmospheric circulation modes. In: Geophys. Res. Lett. 30 (4). DOI: 10.1029/2002GL016433.

Klein, Bastian; Pahlow, Markus; Hundecha, Yeshewatwsfa; Schumann, Andreas (2010): Probability Analysis of Hydrological Loads for the Design of Flood Control Systems Using Copulas. In: J. Hydrol. Eng. 15 (no. 5), S. 360–369.

Köplin, N.; Schädler, B.; Viviroli, D.; Weingartner, R. (2014): Seasonality and magnitude of floods in Switzerland under future climate change. In: Hydrol. Process. 28 (4), S. 2567–2578. DOI: 10.1002/hyp.9757.

Nied, Manuela; Pardowitz, Tobias; Nissen, Katrin; Ulbrich, Uwe; Hundecha, Yeshewatesfa; Merz, Bruno (2014): On the relationship between hydro-meteorological patterns and flood types. In: Journal of Hydrology 519, S. 3249–3262. DOI: 10.1016/j.jhydrol.2014.09.089.

Rosbjerg, Dan (2017): Optimal adaptation to extreme rainfalls in current and future climate. In: Water Resour. Res. DOI: 10.1002/2016WR019718.

Sayers, P. B.; Hall, J. W.; Meadowcroft, I. C. (2002): Towards risk based flood hazard management in the UK. In: Proceedings of the ICE, Civil Engineering 150 (5), S. 36–42. DOI: 10.1680/cien.150.5.36.38631.

Shiau, Jenq-Tzong; Wang, Hsin-Yi; Tsai, Chang-Tai (2006): Bivariate Frequency Analysis of Floods Using Copulas. In: Journal of the Americal Water Resources Association (Paper No. 05145), S. 1549–1564.

Støren, Eivind N.; Kolstad, Erik W.; Paasche, Øyvind (2012): Linking past flood frequencies in Norway to regional atmospheric circulation anomalies. In: J. Quaternary Sci. 27 (1), S. 71–80. DOI: 10.1002/jqs.1520.

Vormoor, K.; Lawrence, D.; Heistermann, M.; Bronstert, A. (2015): Climate change impacts on the seasonality and generation processes of floods - projections and uncertainties for catchments with mixed snowmelt/rainfall regimes. In: Hydrol. Earth Syst. Sci. 19 (2), S. 913–931. DOI: 10.5194/hess-19-913-2015.

Zhou, Xiao-Yi; Schmidt, Franziska; Toutlemonde, François; Jacob, Bernard (2016): A mixture peaks over threshold approach for predicting extreme bridge traffic load effects. In: Probabilistic Engineering Mechanics 43, S. 121–131. DOI: 10.1016/j.probengmech.2015.12.004.

Proceedings of the 10th World Congress of EWRA 'Panta Rhei', 5-9 July 2017, Athens, Greece
© 2017 *European Water Resources Association*

Numerical modeling of Samsun Mert River floods

A. Ulke[1], N. Beden[2*], V. Demir[3] and N.Menek[4]
[1] *Department of Civil Engineering, Faculty of Engineering, Ondokuz Mayis University, Samsun,Turkey*
[2] *Department of Construction, Kavak Vocational School, Ondokuz Mayis University, Samsun,Turkey*
[3] *Department of Civil Engineering, Faculty of Engineering, Karatay University, Konya, Turkey*
[4] *Department of Chemistry, Faculty of Arts and Science Ondokuz Mayis University, Samsun, Turkey*
[*] *e-mail: neslihan.beden@omu.edu.tr*

Abstract: Floods are considered one of the most important natural disasters after earthquakes in Turkey. As a result, there is currently great public interest in this issue and it is necessary to intensify research activities in order to understand natural disasters better and to reinforce risk management. The effect of climate change on meteorological events causes an increase in extreme events such as excessive precipitation in some regions. An extreme natural event becomes a disaster when it has a large impact on human settlements and activities. Study area Samsun city is placed in the north of Turkey in the middle of Blacksea region where Kizilirmak and Yesilirmak rivers poured deltas. Samsun with a height of 735 mm mean annual precipitation is above the national average. Samsun is exposed to flooding every two to three years. In this study, flood risks of Samsun Mert river downstream area determinate with numerical modeling method. Numerical analysis has become the most basic tool recently used in modeling floods. Numerical model selection for studies provides advantages in developing and changing the solutions with time. Hydrological models were also created corresponding to 100 and 500 year return period floods. 1D and 2D hydrodynamic modeling was created with MIKE powered by DHI software; MIKE 11 and MIKE 21.

Key words: Flood modeling, MIKE 11, MIKE 21, Samsun, Turkey

1. INTRODUCTION

In recent years the economic damage from flooding has greatly increased due to rapid urbanization coupled with possible climate change impacts. The Intergovernmental Panel on Climate Change (IPCC) special report on managing the risks of extreme events and disasters emphasized that continuation of the observed Earth warming would change the frequency, severity and spatial pattern of climatic extremes (Field and Ed 2012; Cheng et al. 2014). The effect of climate change on meteorological events causes an increase in extreme events such as excessive precipitation in some regions. Extreme rainfall increases the influenceability against floods and causes extra stresses on infrastructure systems.

Nowadays flood inundation maps are essential for urban planning, urban renewal, disaster insurance rates, urgent action plans and environmental protection. Inundation maps depend on the numerical solution of shallow depth flow equations using topographical data, cross-sections along the channel and the discharges having different return periods. The flood problem is not a recent issue neither for Turkey nor for other countries. Therefore, the need for the flood protection and flood management are not new too (Akyurek et al. 2015).

Numerical analysis has become the most basic tool recently used in modeling floods. Numerical model selection for studies provides advantages in developing and changing the solutions with time. Therefore, changes in the model conditions, such as riverbed rehabilitation or structural adjustments, affect model result accuracy directly since flood model represents the present situation of the river and the study area.

Hydraulic modeling of floods is affected by many uncertainty sources like input data, model

structure, model parameters etc. Besides several factors in each source of uncertainty affect the flood modelling process and mapping results that increase or decrease the uncertainty of outcome (Papaioannou et al. 2016). There are many studies in literature about flood modelling and flood mapping (Ahmed 2010; Webster et al. 2014; Delaney et al. 2015; Papaioannou et al. 2016).

The aim of this study is to modeling of Mert River floods and to obtain flood inundation maps for floods of different return periods.

2. STUDY AREA

Study area Mert River is located in the center of Samsun shown in Figure 1. The geographic location of the study area is between Latitude 41.279 and Longitude 36.352. The Mert River, which is about 7.0 kilometers long, flows into the Black Sea. There are six highway bridges and a pedestrian bridge over the river. First three bridges are located in the Black Sea coastline and provide transport between cities. Structural features of the bridges are given in Table 1. In July 2012, the city of Samsun experienced important flooding, shown in Figure 2012. Mert River flooding occurred over a majority of the study area; impact on transportation networks and other technical infrastructures, damaging homes, displacing residents, and taking lives (Ulke et al 2013). There is the E22A062 Corak Gaging Station on the Mert River with a 740 km^2 precipitation area and average annual total discharge value for the 2007-2012 period is 137,59 hm^3. The selected watershed maximum precipitation is 70.8 mm in November, the minimum precipitation is 29.4 mm in August, and the annual average precipitation is 674.8 mm. Flood values of different return periods and annual instant maximum flows that calculated with SCS unit hydrograph method obtained from the Turkish General Directorate of State Hydraulic Works and given in Table 2. Also manning roughness coefficients that computed by Cowan's method (Cowan, 1956), are obtained from the Turkish General Directorate of State Hydraulic Works.

3. METHODOLOGY

3.1 MIKE 11-One Dimensional Hydraulic Model

MIKE 11 is a professional engineering software package for the simulation of flows, water quality and sediment transport in rivers, channels and other water bodies. MIKE 11 HD applied with the dynamic wave description solves the vertically integrated equations of conservation of continuity and momentum (the 'Saint Venant´ equations). The solution of the equations of continuity and momentum is based on an implicit finite difference scheme developed by Abbott and Ionescu (1967) (DHI 2016a). Hydraulic structures (*e.g.* bridges, weirs, culverts) are defined with MIKE 11 and flow above that structures can be calculated. The equations of continuity and momentum, as used by MIKE 11 are presented Equation 1 and 2.

$$(dq/dx)+(dA_{fl}/dt) = q_{in} \quad (1)$$

$$(dq/dt)+(d(\alpha q^2/A_{fl}))/dx+gA_{fl}(dh/dx)+(gq|q|)/(C^2A_{fl}R) = 0 \quad (2)$$

In this equations the meaning of the notations are; A; flow area (m^2), q; lateral flow (m^2/s), h; depth above datum (m), C; Chezy resistance coefficient ($m^{1/2}/s$), α; momentum distribution coefficient, x; Cartesian coordinates, g; acceleration due to gravity (m/s^2).

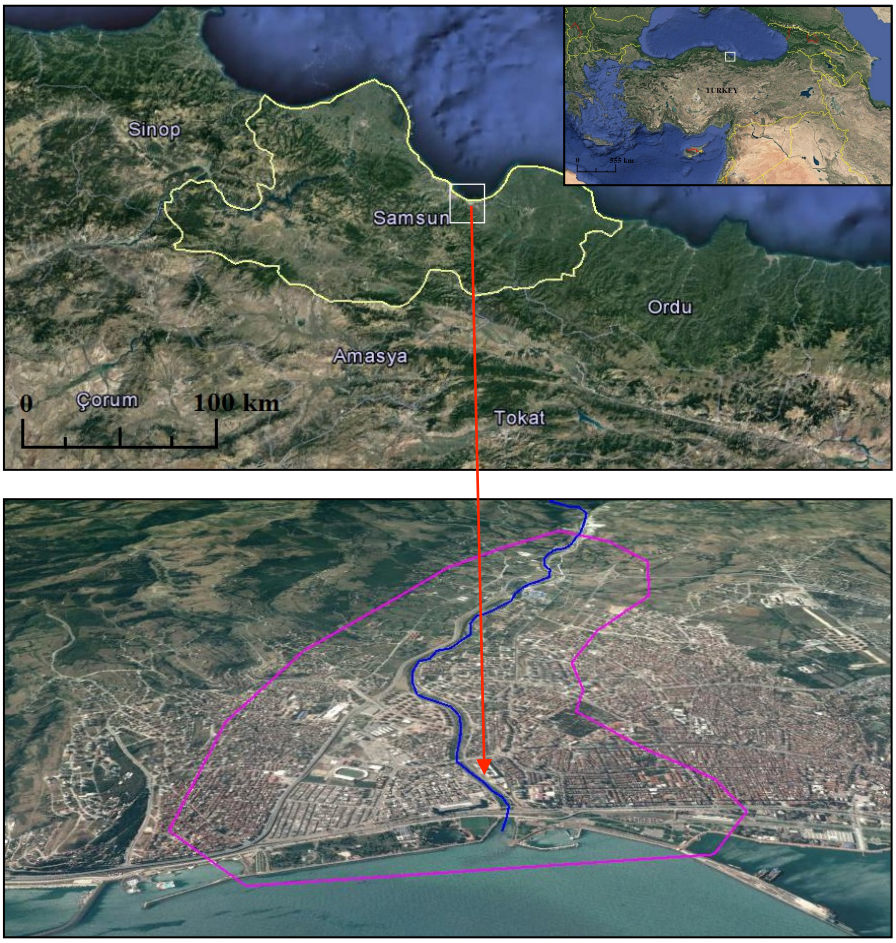

Figure 1. Study area.

Table 1. Bridges on Mert River

Km (from downstream)	*Code*	*Upper elevation*	*Bottom elevation*	*Bridge deck thickness(m)*
0+260	*(C1)*	*4.05*	2.35	1.70
0+300	*(C2)*	*3.50*	2.50	1.00
0+350	*(C3)*	*3.80*	3.00	0.80
0+400	*(C4)*	*4.00*	3.10	0.90
1+000	*(C5)*	*7.00*	5.40	1.60
1+800	*(C6)*	*5.90*	4.40	1.50
2+150	*(C7)*	*14.70*	13.50	1.20
4+500	*(C8)*	*21.40*	19.90	1.50

Table 2. Flood values of different return periods of Mert River.

Return Periods	*5*	*10*	*25*	*50*	*100*	*500*	*1000*	*10000*
Discharge (m^3/s)	*296.0*	*441.3*	*552.3*	*719.4*	*863.9*	*1029.1*	*1453.3*	*2660.0*

3.2 MIKE 21-Two Dimensional Hydraulic Model

MIKE 21 Flow Model FM is a new two-dimensional modeling system based on a flexible mesh approach for free surface flows. The Hydrodynamic Module is the basic computational component of the entire MIKE 21 Flow Model FM modeling system. The Hydrodynamic Module is based on the numerical solution of the two-dimensional shallow water equations - the depth- integrated incompressible Reynolds-averaged Navier-Stokes equations. Thus, the model consists of continuity,

momentum, temperature, salinity and density equations. In the horizontal domain, both Cartesian and spherical coordinates can be used. However, being a general modeling system for 2D and 3D free surface flows it may also be applied for studies of inland surface waters, e.g. overland flooding and lakes or reservoirs (DHI 2016b).



Figure 2. 2012 Samsun flood disaster

4. APPLICATION

4.1 Mapping

The required digital elevation model (DEM) was created from 1/1000 scale topographical contour lines and supported with the field measurements at the study area. The obtained (x, y, z) point values were used to create a combined DEM. Bathymetry term is used for the DEM as a model map of MIKE (Bozoglu 2015).

4.2 1D Modeling

In this study flood analysis carried out along the river line with the networks created both structured and unstructured. The river cross-sections have been created every 50 m. Considering the location of structures and topography of river, the sections have been taken in 20-30 m intervals in some places. For 7013 m river network, 150 cross-sections have been generated. The capacity of the river banks was evaluated with one-dimensional model.

4.3 2D Modeling

MIKE 21 model compares model inundation on study area with different discharge volumes. 2D model inputs are; bathymetry of the area, defined input and output discharge points, Manning's roughness coefficient, boundary conditions and some other default calculation effects (density,

viscosity, precipitation etc.) MIKE 21 FM is a flexible mesh model and uses triangular mesh for model calculations. DEM was transformed to flexible mesh with Mesh Generator interface in MIKE. Triangular mesh for the model was created from these elevation values. With flexible mesh, variable sized elements can be defined for multiple parts of the maps. Thus variable sizes of mesh elements provide advantages for modeling. The riverbed was created with small area size quadrilateral compared to the remaining parts.

5. RESULTS

5.1 MIKE 11 Model Results

The flow rate according to the results of one-dimensional model tends to spread over the urbanized regions beyond the floodplain. Since the model to be used for the solution purposes is 2D modeling. Structured and unstructured results of Mert River profile for Q100 and Q500 discharges are shown in Figures 3 and 4. As shown in Figure 3(b) and 4(b), structures attenuate the cross sections and increased the water level during both the discharges of Q100 and Q500.

The flow rate according to the results of one-dimensional model tends to spread over the urbanized regions near the floodplain. Here result in maps of Q100 and Q500 maximum water depth with structures and without structures, Figure 5.

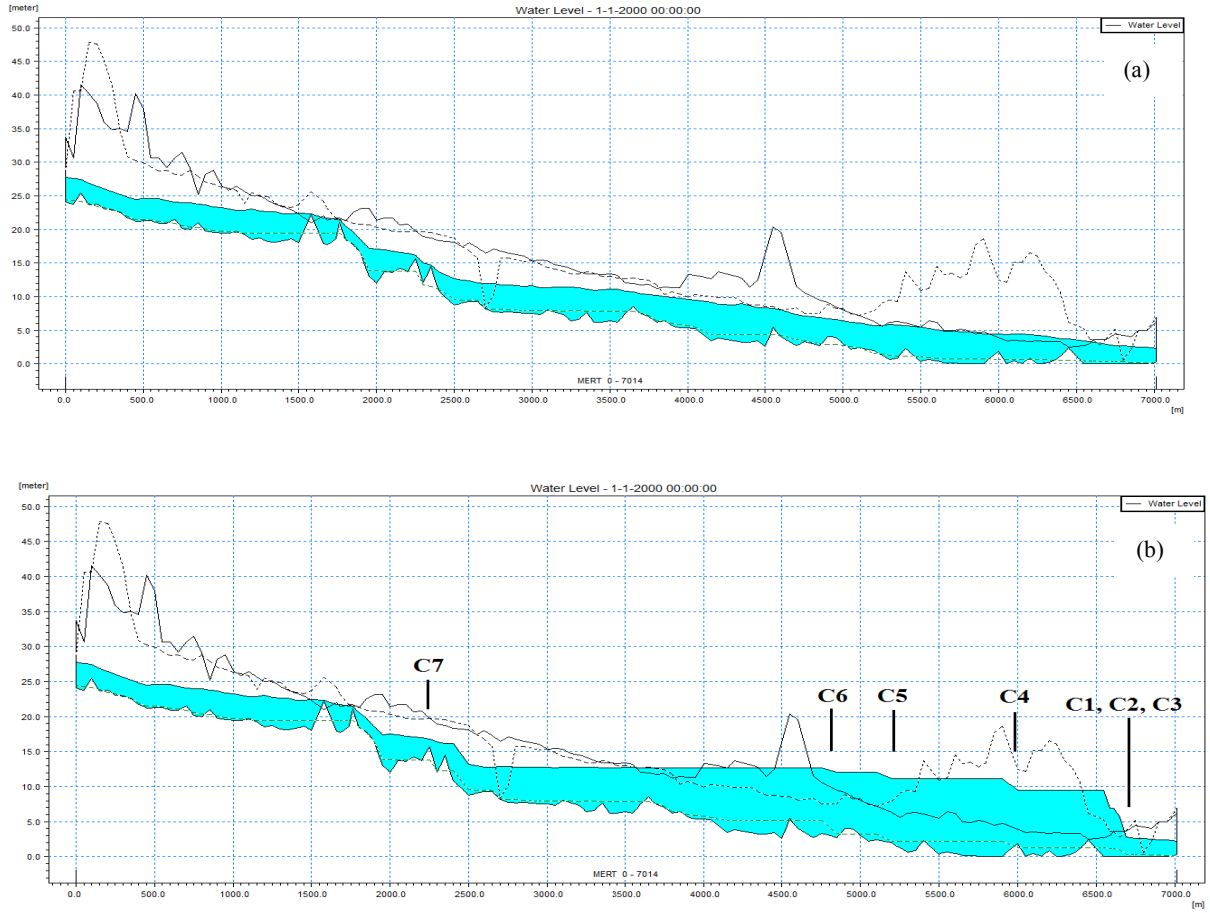

Figure 3. River profile for Q100 (a) without structures, (b) with structures

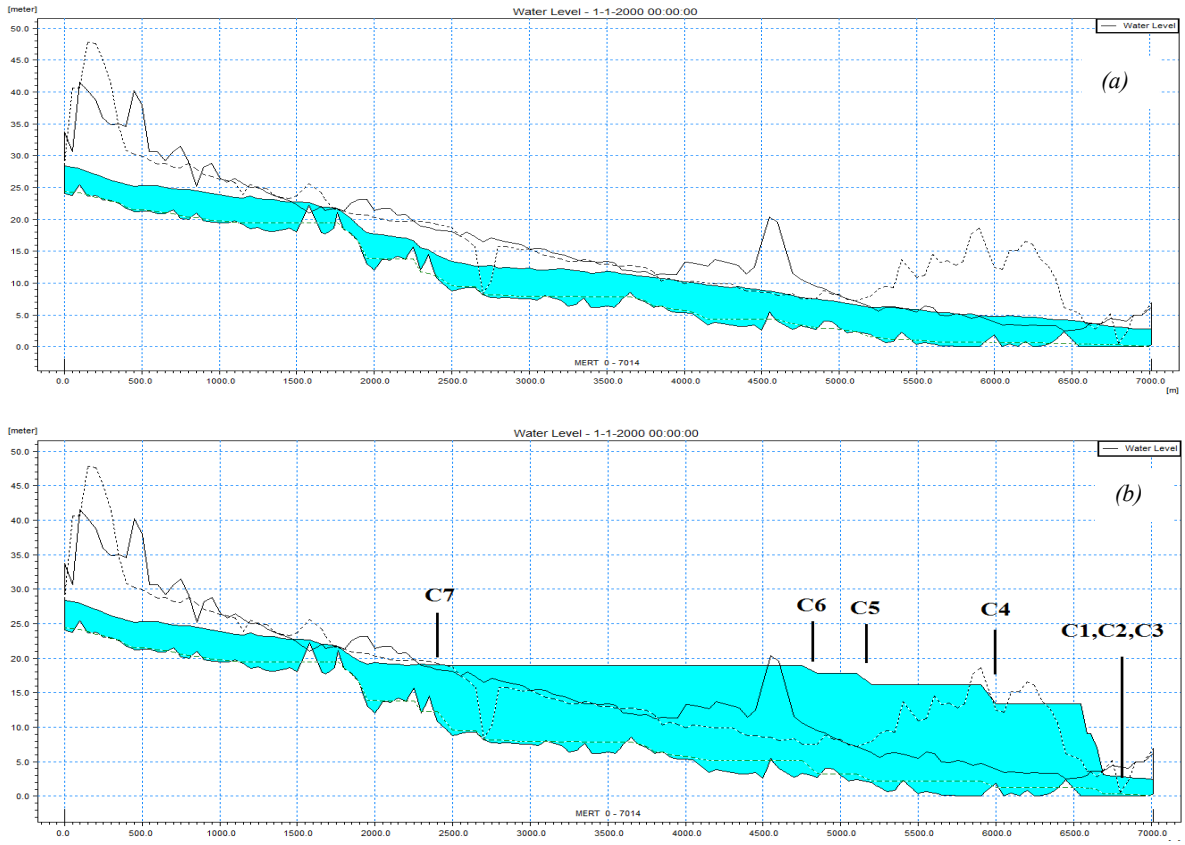

Figure 4. River profile for Q500 (a) without structures (b) with structures

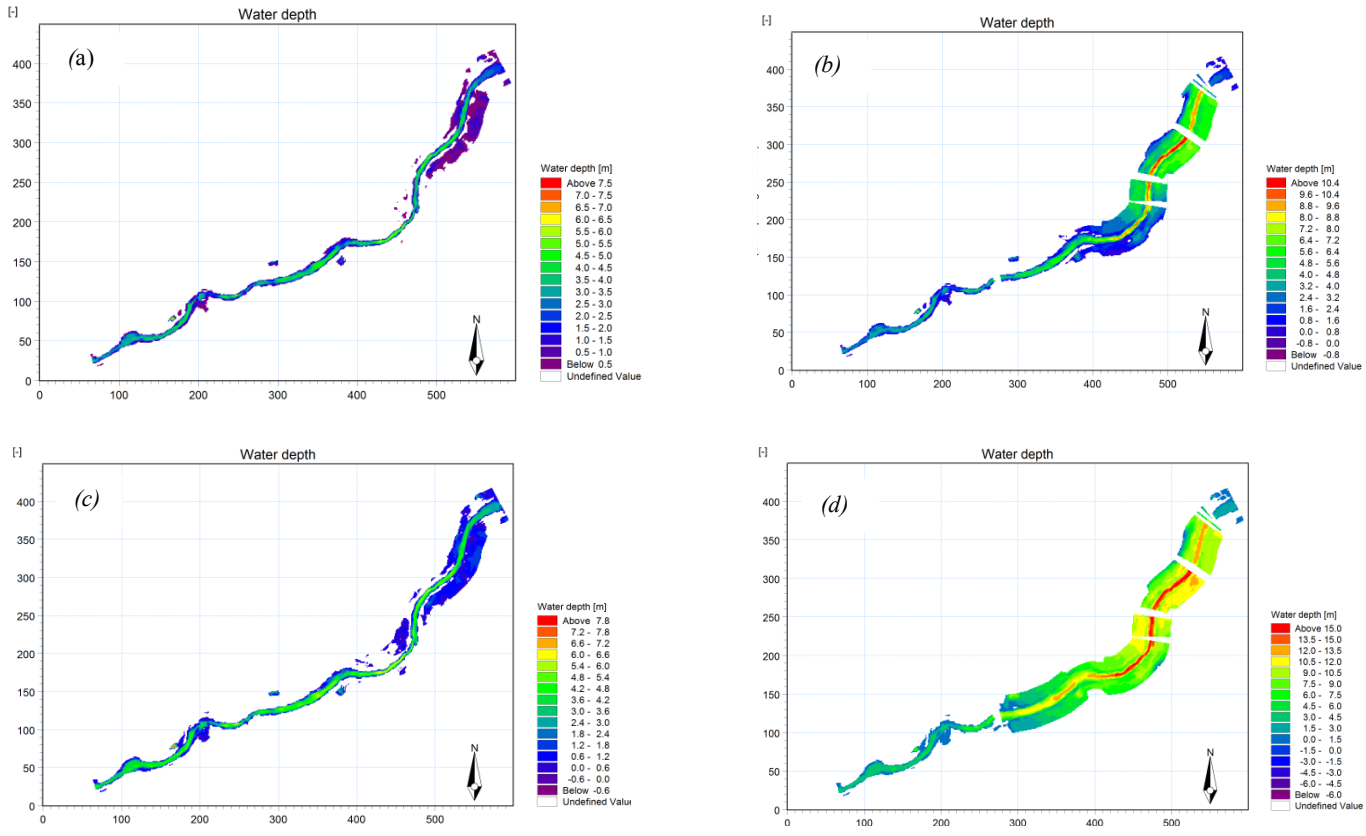

Figure 5. 1D results for Q100 maximum water depth ((a); without structures, (b) with structures), for Q500 maximum water depth ((c); without structures, (d) with structures)

5.2 MIKE 21 Model Results

The cross-sections along the river do not pass the Q100 and Q500 discharges in the one-dimensional hydrodynamic model. If water levels overcome river banks, one-dimensional hydrodynamic model perceives water as a water column and elevates the water column along the defined sections. In this case, one-dimensional model become meaningless, therefore a two-dimensional model should be used to shown flood inundation in the study area realistically.

2D model's output flood inundation map for Q100 and Q500 are seen in Figure 6. The figures show that study area is under threat of flood disasters. It is expected that downstream of the Mert River where the industrial area is located will suffer great damage from floods.

It is clear that the results obtained in 2D studies are more detailed than 1D study results. One dimensional model applicable for river channels, floodplains, however, two-dimensional models running entire boundaries that user choose.

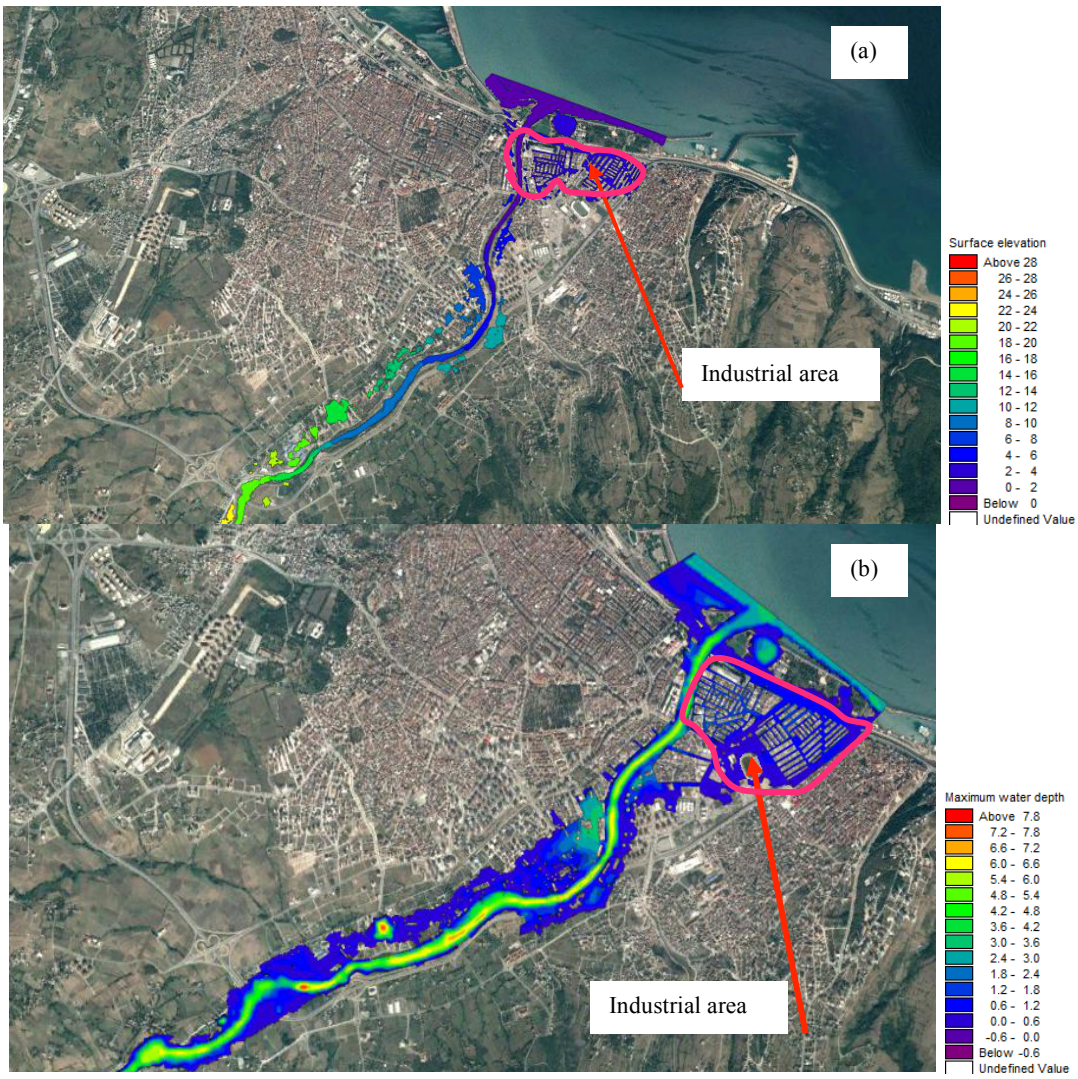

Figure 6. 2D results on study area (a) Q100 maximum water depth (b) Q500 maximum water depth

6. CONCLUSIONS

The flood inundation maps demonstrated that some areas, from the upstream to downstream of the Mert River basin, are highly affected from 100 year and 500 year return period events. Through Q100 discharge, the maximum water depth reached 7.25 m and affected urban area was approximately 60 % in the downstream of the Mert River. In addition, over 1000 buildings were

affected by this flood. The largest inundations are seen in the industrial area at the right side of the river. There isn't a certain measurement for Mert River at 2012 flood hazard. The recent and recorded event that caused damage in the Mert River was the flood event that took place on 1967. At this time there wasn't a field measurement about the fill rate of the river or the flood marks at the reference structures, therefore the model calibration cannot be carried out preferred. Also; there have been many changes that affect the inflow on the land, and interventions have been made in the floodplain. All these factors are taken into account, there is no valuable data available for model calibration from past flood reports. Limitation of this study is the calibration of the models.

As a result, in order to ensure safety during the floods that may occur in the study area, there must be taken preventive precautions. Sand accumulations should be cleaned periodically to prevent the rise of thalweg level in downstream where the river merged with the sea. Especially since the first four bridges negatively affected the water profile in one-dimensional model, existing bridges should be reviewed. Sediment accumulation, environmental wastes and excavation wastes along the riverbed may cause detention of inflow. Thus the riverbed should be cleaned. With all that upstream master plans should be an overhaul for Mert River basin.

ACKNOWLEDGMENTS

The authors would like to thank the DHI Turkey Office for the provision of the full edition packages of MIKE powered by DHI software and also Turkish General Directorate of State Hydraulic Works Samsun Office for obtaining data.

REFERENCES

Abbott, M.B., Ionescu, F.1967. On the numerical computation of nearly-horizontal flows, Journal of Hydraulic Research, 5, 97-117.

Ahmed, F., 2010. A hydrodynamic model for the Lower Rideau River. Natural Hazards, 55, 85-94.

Akyurek, Z., Bozoglu, B., Surer, S., Mumcu, H., 2015. Upstream structural management measures for an urban area flooding in Turkey. Proc. IAHS, 370, 45–50.

Bozoglu, B., 2015. 1-D and 2-D flood modeling studies and upstream structural measures for Samsun City Terme District. Master of Science Thesis, Middle East Technical University, 140.

Cheng, L., AghaKouchak, A., Gilleland, E., Katz, R.W.,2014. Non-stationary extreme value analysis in a changing climate. Climatic Change 127:353–369.

Cowan, W.L., 1956. Estimating hydraulic roughness coefficients: Agricultural Engineering, v. 37, no. 7, p. 473-475.

Danish Hydraulic Institute., DHI (2016a). MIKE 11 A modelling system for rivers and channels, Reference Manual, Danish Hydraulic Institute.

Danish Hydraulic Institute., DHI (2016b). MIKE 21 Flow model FM, hydrodynamic module Reference Manual, Danish Hydraulic Institute.

Delaney, P., Qiao, Y., Mereu, T., Lorrain, N., 2015. Using detailed 2D urban floodplain modelling to inform development planningin mississauga, on. 22nd Canadian Hydrotechnical Conference, "Water for Sustainable Development: Coping with Climate and Environmental Change",12 pages.

Field, C. B.,Ed. 2012. Managing the risks of extreme events and disasters to advance climate change adaptation: special report of the intergovernmental panel on climate change.Cambridge University Press.

Papaioannou, G., Loukas, A., Vasiliades, L., Aronica, G.T., 2016. Flood inundation mapping sensivity to riverine spatial resolution and modelling aproach. Natural Hazards, 83, S117-S132.

Ulke, A., Uslu, A., Beden, N., 2013. Historical Chronology of Samsun City Floods and 2012 Year Samsun Flood (In Turkish). Taskin ve Heyelan Sempozyumu 2013, 555-564.

Webster, T., McGuian, K., Collins, K., MacDonald, C., 2014. Integrated river and coastal hydrodynamic flood risk mapping of the La Have river estuary and town of Bridgewater, Nova Scotia, Canada. Water, 6, 517-546

Proceedings of the 10th World Congress of EWRA 'Panta Rhei', 5-9 July 2017, Athens, Greece
© 2017 *European Water Resources Association*

Flood Directive implementation in Greece: Experiences and future improvements

P. Dimitriadis[1*], A. Tegos[1], A. Petsiou[1], V. Pagana[1], I. Apostolopoulos[1], E. Vassilopoulos[2], M. Gini[3], A. Koussis[4], N. Mamassis[1], D. Koutsoyiannis[1] and P. Papanicolaou[1]

[1] *Department of Water Resources and Environmental Engineering, Faculty of Civil Engineering, National Technical University of Athens.*

[2] *YPODOMI – Consulting Engineers Ltd*

[3] *Special Secretariat for Water, Ministry of Environment and Energy.*

[4] *Director of Research, Emeritus, National Observatory of Athens Hydraulics, Hydrology, Hydrogeology, Water Resources Engineering, Science & Management.*

[*] *e-mail: pandim@itia.ntua.gr*

Abstract: The implementation of the European Directive 2007/60 is a crucial step towards the development of a sophisticated flood management plan for the main River Basin Districts by including any necessary structural measures. For this reason, extensive hydrological and hydraulic analysis is needed under the ubiquitous uncertainty which cannot be eliminated by numerical models. In this study, we present our experience from the directive implementation and we discuss structural components of uncertainty in the flood modelling practice mostly related to the river network. We propose and review some of the most efficient engineering practices by examining issues like: (a) the consistency and accuracy of the required input data of the topography such as the Digital Elevation Model, cross-sectional measurements of the river and maps of land use; (b) the uncertainty components related to the hydrological SCS-CN framework and other hydrological methods for the determination of the input hydrograph; (c) the theoretical framework of each hydraulic model such as the scheme dimension (1d, 2d or coupled 1d/2d), the type of solution of the numerical scheme (explicit or implicit), the boundary conditions and the type of discretization (grid or section-based); (d) the uncertainty components related to the flood inundation modelling, such as the roughness coefficient at the river and floodplain; (e) the necessity of validation data such as the flow discharge, the flood inundation area, and the velocity measurements.

Key words: European Directive 2007/60; flood modelling, uncertainty, river geometry, roughness coefficient

1. INTRODUCTION

The optimum design of flood protection works has been the primary target in Europe due to the occurrence of extreme flood events in the last decades (Tsakiris et al. 2009). However, the large uncertainty in the prediction of flood inundation extending from the hydrological and hydraulic input (Efstratiadis et al., 2014) to the inundation algorithms (Dimitriadis et al., 2016) has shifted the primary target to flood risk management rather than protection as described in the EU Directive 2007/60 (Mostert and Junier, 2009). The Directive implementation highlights the need to quantify the uncertainty of the most important parameters included in the estimation of the flood risk and hazard maps, and by also offering the opportunity, through the experiences gained and identified difficulties, to suggest possible improvements. In this study, we present our experience from the directive implementation in a main River Basin District (Central Makedonia GR10). We present our methods used to construct the flood maps for high flood risk zones (Fig. 1) and how we tackle several practical issues mostly related to: (a) the consistency and accuracy of the required input data of the topography such as the Digital Elevation Model, cross-sectional measurements of the river and maps of land use (section 2.1); (b) the uncertainty components related to the hydrological SCS-CN framework and other hydrological methods for the determination of the input hydrograph (section 2.2); (c) the theoretical framework of the hydraulic models used, i.e., the 1d HEC-RAS and quasi-2d FLO-2d, such as the scheme dimension, the type of solution of the numerical scheme, i.e.,

implicit and explicit, respectively, the boundary conditions and the type of discretization, i.e., section-based and grid-based, respectively (section 2.3); (d) the uncertainty components related to the flood inundation modelling, such as the flow hydrograph (Di Baldassarre and Montanari, 2009) and roughness coefficient of the river and floodplain (Dimitriadis et al., 2016); (e) the necessity of validation data such as the flow discharge, the flood inundation area, and the velocity measurements, so as to be able to verify the model output but to also justify any adopted assumptions related to the input parameters and methods. Additionally, in section 3, we present two applications, one following the standard methodology for the construction of flood risk maps and one including a sensitivity analysis for the most uncertain river parameters, in case of limited or inadequate information of the river geometry and surface material, an common case in Greece as compared to other European countries. Finally, in section 4, we conclude our analysis and we discuss on the structural components of uncertainty in the flood modelling practice along with suggestions for a possible future improvement.

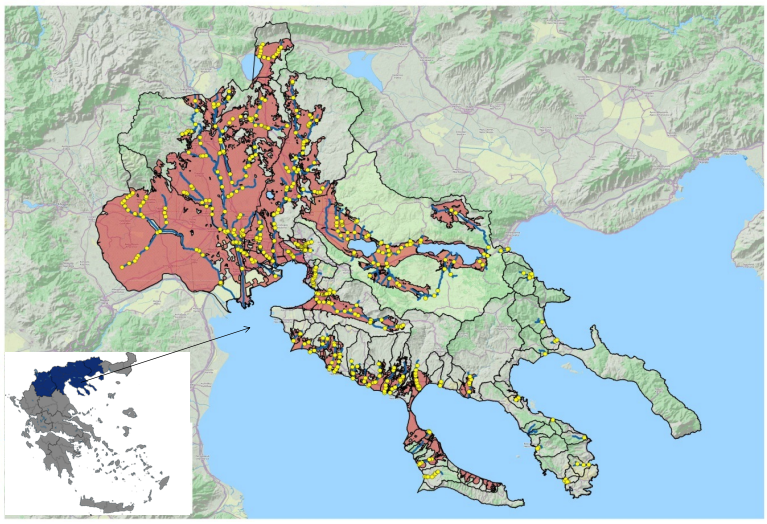

Figure 1: High risk flood zones (purple areas), technical works (yellow points) and river network (blue lines) of the GR10 basin located at central Makedonia, Greece.

2. EFFICIENT ENGINEERING PRACTICES

2.1 Topographical input data

Topographical data is one of the preliminary input data for the hydrological and hydraulic study of a river basin. It describes the morphology of the study area and therefore, all model output and plotted maps are highly dependent on the accuracy of the land survey. For a detailed analysis on the sensitivity of the spatial resolution and method to the flood inundation modelling can be seen in Papaioannou et al. (2016). Usually, for the floodplain area a coarse Digital Elevation Map (DEM) is used, whereas for the area along and at the banks of the river a more detailed survey is usually acquired. In the current study, the applied DEM is provided by the National Cadastre and Mapping Agency S.A., with a pixel size of 5x5m^2. An important feature is that the analysis of the DEM is more accurate near the coastline where there is a potentially higher flood risk. Particularly, in these areas a finer pixel size is often used, i.e., 1x1m^2.

In order to improve the uncertainty of the DEM, actual field topographical measurements are conducted, especially near the river network (i.e., cross-sections), at areas of environmental importance and interest, and near technical works (Fig. 1), such as bridges, levees, dams etc., that are of great importance for the flood risk management. Another way to improve the accuracy of the DEM would be to use satellite data extracted from satellite images of larger discreet ability by

assigning the pixel size of the imagery, however this method is very expensive since high cost equipment is required. Therefore, the applied DEM in the hydrological and hydraulic analysis is usually reconstructed based on some field measurements obtained from Survey Engineers. Afterwards, the pixel is resized according to the needs of the flood propagation model for the conduction of the hydrological and hydraulic analysis of the river basin. This process is aimed to keep both the stability of the used model and the sufficient spatial resolution for the optimum simulation of the hydrological process and the spatiotemporal evolution of the flood inundation map.

2.2 Hydrological modelling

For obtaining the input flow hydrograph we follow the standard hydrological method of estimating the ombrian curves through the General Extreme Value distribution (e.g., following the methodology described in Koutsoyiannis et al., 1998):

$$i(d) = \frac{a(T)}{(d + 0.076)^{0.686}} \tag{1}$$

where i is the rainfall intensity (mm/hr), d is the rainfall duration (hr), T is the return period (years) and a is a function of T , usually of the form $a_1(T^{a_2}\text{-}a_3)$, with a_1, a_2 and a_3 parameters determined by the historical rainfall data of the area of interest and the isohyetal map (spatial distribution of rainfall).

Additionally, we estimate the hyetograph through the alternative block method for the return periods of 50 and 100 years (best and moderate case scenarios) and through the worst profile method for the 1000 years return period (worst case scenario). These three scenarios are further processed for the evaluation of the input flow hydrogrpah by a rainfall-runoff model, such as the SCS-CN one implemented through the HEC-HMS (www.hec.usace.army.mil/software/hec-hms/).

2.3 Hydraulic models for flood inundation

After the construction of the DEM and the flow hydrograph, we select the type of the hydraulic model for the flood inundation, i.e., one-dimensional (1d), two-dimensional (2d) or quasi-2d (a brief mathematical description of 1d, quasi-2d and 2d algorithms can be found in Tsakiris and Bellos, 2014). Particularly, in cases where the flooded volume is propagated mostly by the river and not by the floodplain, 1d models are applied (such as HEC-RAS), following the standard procedure of model building, simulation and validation (e.g., Lazaridou et al., 2004). A detailed review on the hydrological Muskingum flood routing models can be found in Koussis (2009) and of the determinants of hydraulic modelling choices for free-surface flow that are based on the interplay between flow characteristics and cross-scale and scale-independent views can be found in Cheviron and Moussa (2016).

In cases where the lateral momentum of the flow is no longer negligible compared to the longitudinal one, a 2d model should be applied. However, since 2d hydraulic models (or of higher dimensions) usually have a larger numerical burden and, as a consequence, are more time-consuming, quasi-2d (or else coupled 1d/2d) models are often preferred (Bates and Roo, 2000; Papaioannou et al., 2016).

After selecting the type of model, the type of discretization (i.e., cross-sectional based or grid-based models), the nature of the numerical scheme (i.e., explicit or implicit or mixed), the boundary conditions (e.g., with the preservation of depth or velocity etc. at the various boundaries; cf. Domeneghetti et al, 2013) as well as various model parameters (with some being physical-based while others behaved as black-boxed) still need to be determined depending on the information we have on the area and on the behaviour of the selected model. All the aforementioned choices will

have an effect on the flood inundation output and therefore, on the flood risk management.

2.4 River parameters

An additional advantage of the aforementioned quasi-2d models is that they enable the use of Monte-Carlo analysis, a necessity when the observed and measured data are limited or when the applied parameters, model algorithms and model boundary conditions are expected to be unknown or of high uncertainty. An interesting and unavoidable feature of all models is that they are prone to discretization errors and thus, even if the topography and all the hydrological and hydraulic parameters are well determined, still there would be a fraction of uncertainty related to the selected model algorithm. An illustration of this characteristic based on benchmark experiments (i.e., where the geometry and all parameters related are known in detail) can be found in Dimitriadis et al, (2016). Since the uncertainty components related to the flood inundation are numerous, and even a broad Monte-Carlo analysis could be impractical in terms of time cost, a decision needs to be taken towards the estimation and sensitivity analysis of the parameters with the larger weight of uncertainty at the model output. Such parameters (from the highest to the lowest standardized uncertainty) are the model algorithm, the river roughness coefficient and that of the floodplain (obtained from the land use as instructed by Corine, 2000; http://geodata.gov.gr/en/dataset/corine-2000), the input flow hydrograph, the longitudinal and transverse slope of the river and floodplain and the model resolution (Dimitriadis et al., 2016). Note that the former result is based on specific benchmark experiments, parameter range and model algorithms. Although the river parameters (i.e., roughness coefficient and geometry) seem to have a large effect on the flood inundation, it can sometimes be highly-expensive or even devious to measure them in field, especially in rough topographies of during severe flood events. This can be tackled by applying a sensitivity analysis, as in the case of the flow hydrograph.

2.5 Validation data

The data collection for validation purposes is an important task in flood modelling since, however sophisticated the analysis may be, limited validation could lead to unjustified actions such as model over-fitting, adoption of non-physically-based algorithms and unnecessary use of assumptions with only a minor contribution to the flood risk map. The validation data should include flow hydrographs that initiated particular flood events (e.g., obtained from operational gauging stations), flood inundation maps resulted from these events (e.g., using satellite images), and other important characteristics of the events such as velocity measurements (e.g., through installation of broad river network measuring devices) and roughness coefficients (e.g., from geological surveys). However, since recording in field can be sometimes impractical (or even impossible) during extreme (or even moderate) flood events, especially in rough topographies (and policies) as in Greece, the application of sensitivity analyses (e.g., Horritt and Bates, 2002; Dimitriadis et al., 2016) can be rather crucial.

3. APPLICATION

In this section, we present two applications, one following a standard practice for the assessment of flood risk maps and one including additional components of uncertainty particularly related to the river network.

3.1 Axios river basin with current practices

Following the processes described in previous sections for the Axios river (the longest river

crossing the Makedonia basin GR-10), we construct the DEM following the methods explained in sect. 2.1 (e.g., by including information from studies of technical works in the area, land use maps and more detailed topographical surveillances), we estimate the flow hydrographs for return periods of 50, 100 and 1000 years and for a best, moderate and worst case scenario, as described in sect. 2.2. For this particular basin, since a quasi-2d model is required, we select the freeware FLO-2d (www.flo-2d.com/) raster-based model that has an explicit-central finite difference scheme and is more suitable for large grid cell size. In Fig. 2, we present the output flood hazard map for the moderate case scenario.

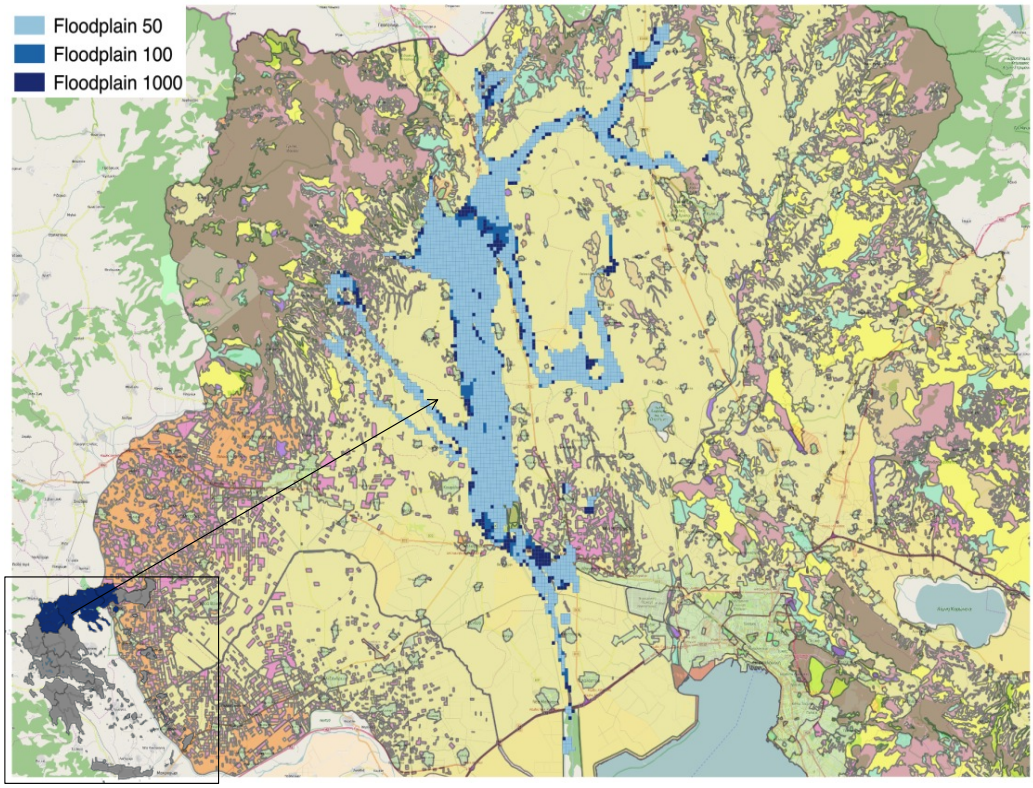

Figure 2. Flood inundation map for the Axios river basin for the moderate case scenario and for various return periods

3.2 Penios river basin with a proposed practice

The 40 km length of a fraction of the Penios river, located at Thessaly in Greece, extends from the Ali Efenti (upstream) to Amygdalia (downstream) gauging station (Fig. 3). In this application, we perform a Monte-Carlo analysis to account for the uncertainty of some additional components often met in ungauged basins and characterized by limited or inadequate information (Efstratiadis et al., 2014), such as the river width, depth and roughness coefficient. We apply the steady flow of 750 m^3/s determined from Oikonomou et al. (2013) as the best fit of an observed extreme flood inundation occurred in 28/1/2003. Thus, we generate 50 synthetic spatial timeseries for each river parameter following a log-normal distribution (Domeneghetti et al., 2013), with mean and standard deviation for the river width and depth as indicated by the DEM and by also preserving the correlation of the original data, and for the roughness coefficient within 0.025–0.03 and with a coefficient of variation 20–35% (Hydraulic Engineer Center, 1986). In Fig. 3, we illustrate how the model simulation can be improved by a sensitivity analysis of the river components. Particularly, the observed but not-simulated area (pink zone) as estimated from the original steady flow scenario can be somehow explained by the uncertainty of the river components (in Fig. 3, we only show the 50% water depth quartile by a brown zone).

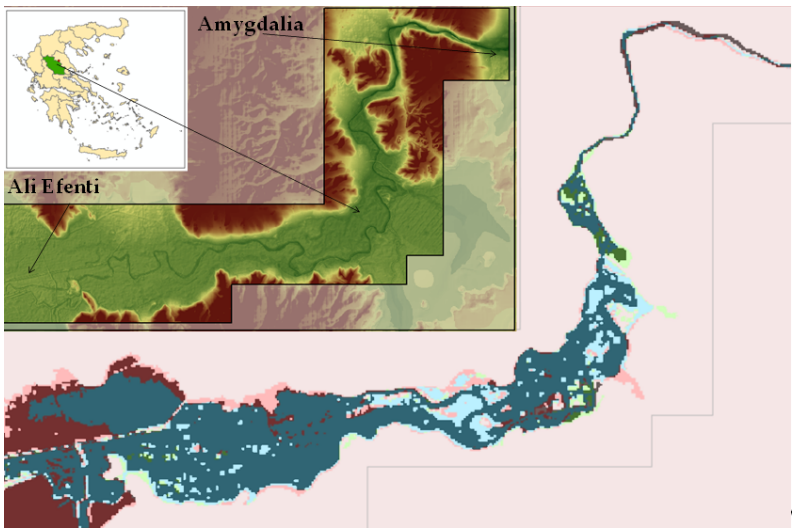

Figure 3: Location and topography of the study area, the best fitted simulated flood inundation for river geometry as estimated from the 5×5 DEM and for a constant 0.03 roughness coefficient (light blue zone is the observed and simulated by the model area, green zone is the non-observed but simulated area, pink zone is the observed but not-simulated area), the brown zone is the 50% water depth quartile, as estimated from the sensitivity analysis, and the dark blue is the mixture of light blue and brown colours.

4. CONCLUDING REMARKS

Some of the most uncertain parameters in flood inundation modelling that are often neglected or inadequately measured are the river geometry and roughness coefficient. While the former is usually obtained from a coarse DEM, the latter, in most cases, is considered as constant for the whole length of the river. In this study, we illustrate how the exerting uncertainty from these sources (along with additional hydrological and hydraulic sources such as input hydrograph and numerical schemes) can be quite large in cases of limited measurements or inadequate information on the river geometry and surface material. Therefore, a proposed engineering practice could be to always perform sensitivity analyses for all the parameters included in the flood risk framework but especially for the ones related to the river network (such as width, depth and roughness).

REFERENCES

Bates, P.D., and De Roo, A.P.J., 2000. A simple raster-based model for flood inundation simulation. *J. Hydrol.* 236(1), 54–77.

Cheviron, B., and Moussa, R., 2016. Determinants of modelling choices for 1-D free-surface flow and morphodynamics in hydrology and hydraulics: a review. *Hydrol. Earth Syst. Sci.*, 20, 3799-3830.

Di Baldassarre, G., and Montanari, A., 2009. Uncertainty in river discharge observations: a quantitative analysis. *Hydrol. Earth Syst. Sci.*, 13, 913–921.

Dimitriadis, P., Tegos, A., Oikonomou, A., Pagana, V., Koukouvinos, A., Mamassis, N., Koutsoyiannis, D., and Efstratiadis, A., 2016. Comparative evaluation of 1D and quasi-2D hydraulic models based on benchmark and real-world applications for uncertainty assessment in flood mapping. *Journal of Hydrology*, 534, 478–492.

Domeneghetti, A, Vorogushyn, S, Castellarin, A, Merz, B, Brath, A. 2013. Probabilistic flood hazard mapping: effects of uncertain boundary conditions. *Hydrology and Earth System Sciences*, 17: 3127–3140.

Efstratiadis, A., Koussis, A. D., Koutsoyiannis, D., Mamassis, N., 2014. Flood design recipes vs. reality: can predictions for ungauged basins be trusted? Nat. Hazards Earth Syst. Sci., 14, 1417–1428.

Horritt, M. S., & Bates, P. D., 2002. Evaluation of 1D and 2D numerical models for predicting river flood inundation. *Journal of Hydrology*, 268(1-4), 87-99.

Hydraulic Engineering Center, 1986. Accuracy of Computed Water Surface Profiles, *U.S. Army Corps of Engineers*, Davis, CA.

Koussis, A.D., 2009. Assessment and review of the hydraulics of storage flood routing 70 years after the presentation of the Muskingum method. *Hydrological Sciences Journal* 54 (1), 43-61.

Koutsoyiannis, D., Kozonis, D., and Manetas, A., 1998. A mathematical framework for studying rainfall intensity-duration-frequency relationships, *Journal of Hydrology*, 206 (1-2), 118–135.

Lazaridou, P. L., Daniil, E. I., Michas, S. N., Papanicolaou, P. N., Lazarides, L. S., 2004. Integrated environmental and hydraulic desigh of Xerias river, Corinthos, Greece, training works. *Water, Air and Soil Pollution*: Focus 4, 319–330.

Mostert, E., and Junier, S.J., 2009. The European flood risk directive: challenges for research. *Hydrology and Earth System Sciences Discussions*, 6(4), 4961-4988.

Oikonomou, A., Dimitriadis, P., Koukouvinos, A., Tegos, A., Pagana, V., Panagopoulos, P., Mamassis, N., and Koutsoyiannis, D., 2013. Floodplain mapping via 1D and quasi-2D numerical models in the valley of Thessaly, Greece, *European Geosciences Union General Assembly 2013*, Geophysical Research Abstracts, Vol. 15, Vienna, EGU2013-10366, doi:10.13140/RG.2.2.25165.03040, European Geosciences Union.

Papaioannou, G., Loukas, A., Vasiliades, L., Aronica, G.T., 2016. Flood inundation mapping sensitivity to riverine spatial resolution and modelling approach, *Natural Hazards*, 83(1):117–132.

Tsakiris, G., Nalbantis, I, Pistrika, A., 2009. Critical Technical issues on the EU flood directive. *Eur Water*, 25(26):39–51.

Tsakiris, G, Bellos, V., 2014. A numerical model for two-dimensional flood routing in complex terrains. *Water Resour. Manag.* 28(5):1277–1291.

Proceedings of the 10th World Congress of EWRA 'Panta Rhei', 5-9 July 2017, Athens, Greece
© 2017 *European Water Resources Association*

Spatial variability of flood source areas using "unit flood response" method

M. Rezaei[1], M. Vafakhah[1*] and B. Ghermezcheshmeh[2]
[1] *Faculty of Natural Resources Tarbiat Modares University, Iran*
[2] *Soil Conservation and Watershed Management Research Institute, Iran*
[*] *e-mail: vafakhah@modares.ac.ir*

Abstract: In current study, two major aims were considered including investigation of the application of distributed ModClark model in flood hydrograph simulation and determination of Flood Source Area (FSA) in distributed and sub-watershed condition in the Khanmirza watershed, Iran. Toward this attempt, at first, inputs of the model were extracted by ArcGIS 9.3 and then model was calibrated and validated. In next step, in order to determine FSA for cell units and sub-watersheds, by applying unit flood reaction method, at first, design rainfall with return periods of 25, 50, and 100 years at the Aloni station were extracted and then influence of each cell and sub-watershed on the output hydrograph in the outlet of the watershed were obtained. The results of model based on comparison between equal-width discharges show that at validation step, the model simulated the flood hydrograph with high precision with root mean square error, efficiency coefficient, and R2 of 1.53, 0.89, and 0.74, respectively. Also, according to the results of the current study, based on the flood volume relative error, peak discharge, base time, and time to peak, ModClark model had lower error in predicting the flood volume and peak discharge. The final results showed that FSA increases in sub-watersheds from downstream to upstream, while it doesn't follow any distribution in cell units. Also, the statistically significant positive linear correlation was found between FSA and Curve Number (CN) values of each cell.

Key words: Flood, ModClark Model, Distributed Modeling, Cellular Automation

1. INTRODUCTION

Flood is a sudden happening and quick and destructive event that causes annually death and financial sensible and insensible damages in different parts of the world and Iran. Usually, flood management can be done through four stages: prediction, preparation, prevention and damage assessment (Konadu and Fosu 2009). The rainfall–runoff response is strongly dependent on soil, vegetation and topographic characteristics of the watershed (Miller *et al.* 2002)**.** Although flood hazard (or risk) reduction attacks the flood problem at the source by seeking to prevent large flow downstream (Smith and Ward 1998), the key to the success of these efforts is to identify and prioritize headwater areas with respect to flood generation at the outlet (Saghafian and Khosroshahi 2005). Identification of the FSA and its cumulative contribution at the basin's outlet has been carried out using the hydrological models (Saghafian and Khosroshahi 2005; Roughani *et al.* 2007; Saghafian *et al.* 2010). Saghafian and Khosroshahi (2005) proposed the ''Unit Flood Response'' approach to identify and quantitatively prioritize FSA required for flood control planning**.** The approach was originally applied in a semi-distributed manner so that a subwatershed map of flood index could be obtained. However, a fully distributed approach was only realized without actual implementation. A number of studies have attempted to calibrate and apply the distributed hydrologic models (Braud *et al.* 1998; Ajami *et al.* 2004; Knebl *et al.* 2005; Ghavidelfar *et al.* 2011). Many studies have been carried out on the impact of landuse change on the flood peak at the watershed's outlet using HEC-HMS model (Wan and Yang 2007; Saghafian *et al.* 2006; Ali *et al.* 2011; Sanyal *et al.* 2014).

The aim of current study is: (1) to identify and quantitatively prioritize FSA for cell units and sub-watersheds, by applying unit flood response method, and (2) to investigate the relationship

between landuse, hydrologic soil groups and slope percent with FSA classes. The results of this study have direct implications for flood management practices that are undertaken to reduce the peak inflow to reservoirs during storm events.

2. STUDY AREA

The study area is located in the southeast of Chaharmahal and Bakhtiari Province, Iran. The application site lies between the latitudes 31° 22′ 24″ N to 31° 37′ 30″ N, and the longitudes 50° 55′ 00″ E to 51° 18′ 03″ E with 391.16 km^2 in area (Fig. 1). The topographical elevation of the study area varies between 1,729 and 2,955 m above sea level (a.s.l.) with average elevation of 2,342m. The watershed comprises of five tributary subwatersheds and two intermediate subwatersheds. The watershed is governed by the dry and warm Mediterranean climate, mainly covered by agricultural areas in the mid and downstream, forest and rangeland in the upstream areas, and it has heavy soils. The watershed is equipped with Zarinderakht hydrometric station at the main outlet **(**Sadeghi and Mizuyama 2007).

For the digital elevation model (DEM) creation, 1:25,000 topographic maps were digitized in ArcGIS 9.3. The contour interval of the elevation map was 10 m. DEM was generated by contour interpolation on a 25 m cell size**.** The physiographic characteristics of all subwatersheds are summarized in Table 1.

Table 1 Physiographic characteristics of the Khanmirza sub watersheds

Subwatershed	(km^2) Area	Area (%)	Slope(%)	Mean Elevation (m)	Distance from outlet (km)
1	60.66	15.60	8.34	2071	0
2	38.84	9.99	5.37	2109	6.47
3	74.52	19.17	3.39	2042	16.40
4	55.49	14.27	10.19	1965	16.60
5	83.12	21.38	2.76	2030	16.60
6	46.85	12.05	1.11	1921	6.47
7	32.12	8.26	7.67	2135	6.47

Available maps of land use and hydrologic soil groups were also imported into the GIS. About 40% of the watershed area consists of class B, 31% of the watershed area consists of class C and 29% consists of class D soil groups. The major land use type of the study area consists of agriculture and covers almost 43.12 % of it.

In Khanmirza region, a strong correlation was found between precipitation and elevation. So, this relationship can be used further to assess the design rainfall. Mean annual precipitation data (some 30-year period) that collected from inside and outside stations of Khanmirza watershed were also used.

3.METHODOLOGY

3.1 ModClark model

In this study, ModClark model was selected to translate the excess precipitation of the watershed. This model is a linear, quasi-distributed transform method that is based on the Clark conceptual unit hydrograph. ModClark model eliminates time-area curve and instead uses a separate travel time index for each grid cell (Feldman 2000). The travel time distribution follows from this relationship (Kull and Feldman 1998):

$$t_{cell} = T_c \frac{l_{cell}}{l_{max}} \quad (1)$$

where, t_c is the time of concentration for the watershed, time of concentration was computed by using the Natural Resources Conservation Service (NRCS) equation (USDA SCS 1972), l_{cell} is the travel distance from the cell to the outlet, and l_{max} is the travel distance from the cell furthest to the outlet.

Excess rainfall of each grid cell is accomplished using the NRCS method (USDA SCS 1972), then this excess rainfall lagged based on the travel time to the outlet. Travel time is calculated for each grid cells and scaled to overall watershed time of concentration, then the lagged runoff from each grid cell is routed through the linear reservoir using Eq. (2) to take account of the effects of watershed storage. It is a linear, quasi-distributed transform method based on the Clark conceptual unit hydrograph. Storage coefficient R is estimated as the discharge at the inflection point on the recession limb of the hydrograph divided by the slope at the inflection point (Viessman *et al.* 1972).

$$O(t) = C_a I = C_b O(t-1) \tag{2}$$

where, $C_a = \Delta t / R + 0.5\Delta t$; $C_b = 1 - C_a$; O(t)=ordinate of an Instantaneous Unit Hydrograph (IUH) at time t; I=ordinate of translation hydrograph for interval t−1 to t; R=storage coefficient for linear reservoir; and t=time interval for which the IUH is defined.

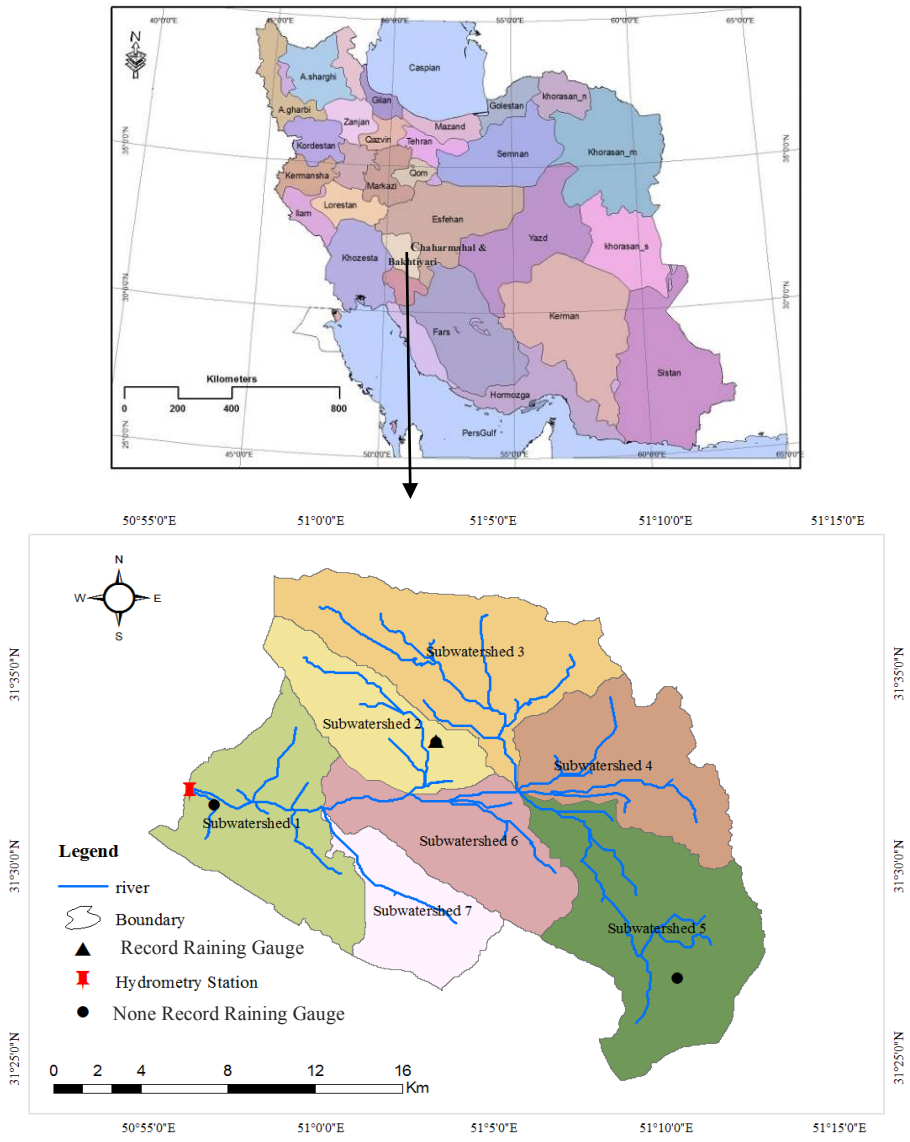

Fig. 1 Map of subwatersheds boundary, stream network and location of hydrometric station of the study area

Flood hydrographs recorded at Zarinderakht hydrometric station and the corresponding rainfall events measured at some 5 rain gauge stations inside and outside of the Khanmirza watershed were accumulated in order to calibrate and validate the model. The ModClark model was calibrated and validated with eight events. Of the eight selected events, five events were used for calibration and three for validation. Model parameters (time of concentration, uniform initial abstraction and storage coefficient) were calibrated based on the first data group with percent error in peak discharge as the criteria and then validated against the second data group, and the agreement between observations and, finally forecasted flood was evaluated based on relative error (RE), root mean square error (RMSE) and Nash-Sutcliffe efficiency criteria (CE).

The effect of each square cell (unit) and subwatershed on the flood peak discharge at the outlet (priority determination of FSA) and the relationship between landuse, hydrologic soil groups and slope percent with FSA classes in the surface of the Khanmirza watershed used the "unit flood response" approach. The unit flood response approach can be used to standardise the contributions of subwatersheds and cell unites to the peak flow and determined FSA (Saghafian and Khosroshahi 2005; Saghafian *et al.* 2010). The unit flood response approach ranks each subcatchment and square cell (unit) on the basis of their contribution to the flood generation at downstream areas of the watershed and is expressed as:

$$f_i = \frac{\Delta Q_i}{A_i} \tag{3}$$

where, f ($m^3\ s^{-1}\ km^{-2}$) is unit area flood index, ΔQ_i is the peak outlet discharge difference between the base scenario and the simulation when the ith cell unit is removed (in m^3/s) and A_i is the cell area (if the cell is entirely inside the watershed boundary) or the area of the part of the cell that is inside the watershed (for boundary cells).

In order to identify and quantitatively prioritize FSA for cell units and subwatersheds, a design rainfall depth for the 25, 50 and 100 return periods was selected using the intensity– duration–frequency (IDF) curve at Aloni station near the watershed centroid assuming the watershed concentration time as duration. The spatial distribution of design rainfalls was determined based on the correlation between average annual rainfall depth and ground elevation. Therefore, the regression equation between the average annual rainfall and elevation was applied on the watershed DEM map and was later non- dimensionalized relative to the spatially averaged annual rainfall.

In order to calculate f, a cell (unit) and particular sub-watershed was disabled while keeping the connectivity of the streams intact for the entire model. In the next step, this model was run (without the contribution of the cell (unit) and disabled sub- watershed) and the f values for that particular cell (unit) and sub- watershed were derived by subtracting the peak flow of the modified model from the peak flow of the model that incorporates all cell (unit) and sub- watersheds. The FSA maps divided into five classes (Very low, low, moderate, high, very high) based on the f value of each return period. Then, the relationship between landuse, hydrologic soil groups and slope percent with FSA classes of each return period were identified according to percentage of their areas using the intersect table in ArcGIS 9.3 environment.

4. RESULTS AND DISCUSSION

The model simulated the flood hydrograph with high precision with root mean square error, efficiency coefficient, and R^2 of 1.52, 0.91, and 0.74, respectively. Also, according to the results, based on the flood volume relative error, peak discharge, base time, and time to peak, reveals a good match between the observed and simulated volumes and flood peaks.

In Fig. 2 the result of the Raster flood index map of the 100 return period is presented, that includes five hazard classes (very low, low, moderate, high, very high). In all return periods, it is indicated that the north and north-western parts of the watershed located in the very low and low

flood map classes and the south-east and central parts of the watershed located in the very high and high flood map classes.

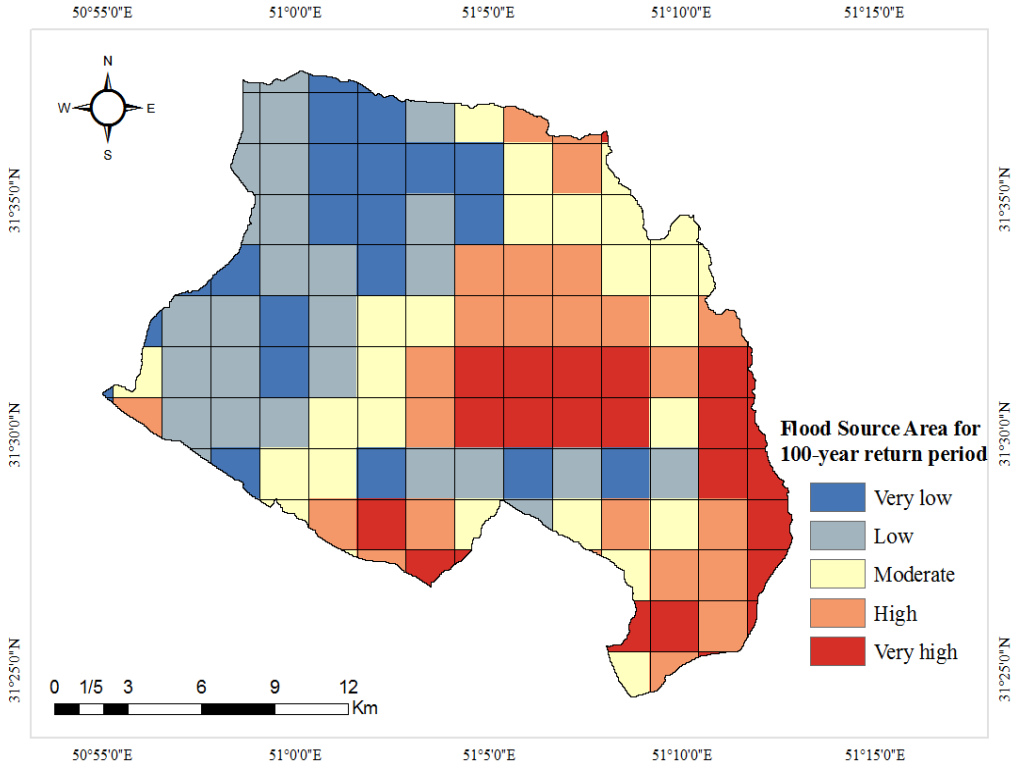

Fig. 2 FSA map for 100 year return period

The percentage area of different classified FSAs in the slope classes showed considerable percentage area of the all flood index classes located in the 0-5 slope class. This result between slope classes with FSA is likely to be dependent on slope low in Khanmirza watershed and other factors. The intersection results of the classified FSA with the hydrologic soil groups for the 25- and 50-year return periods indicated that the class D of soil group had the highest contribution (64.78 percent) in very high class and class B of soil group had the highest contribution in high and very low classes in classified FSA. In the case of, the 100-year return period 39.73% of the very high class has class B of soil group and also, class B of soil group from 58.1% of the very low class. The results of the intersected classified FSA (all return periods) with the land use map showed that in the all return periods increase in forest surfaces leads directly to decreased flood, and increase in forest-cliff , dryland and range land surfaces leads directly to increased flood. These results indicate that there is a certain overlap and congruence between landuse and FSA. In other words, proportionately forest-cliff, dryland and range land surfaces located in very high areas of FSA and such areas are to be addressed and further prioritized in flood management.

5. CONCLUSIONS

In current study, identify and quantitatively prioritize FSA were quantified for cell units and sub-watersheds, by applying "Unit Flood Response" method and the relationship among landuse, hydrologic soil groups and slope percent with FSA classes was quantified through simulating the flood hydrographs of the Khanmirza watershed by using ModClark hydrologic model. Overall, the results of model based on comparison between equal-width discharges showed that in validation step, the model simulated the flood hydrograph with high precision. Also, results reveal a good match between the observed and simulated flood volumes and flood peaks, respectively. Also, the

results indicated that FSA increases in sub-watersheds from downstream to upstream, whereas, it doesn't follow any distribution in cell units.

REFERENCES

Ajami NK., Gupta H., Wagener T., Sorooshian S. (2004) Calibration of a semi-distributed hydrologic model for streamflow estimation along a river system. J Hydrology. 298(1–4):112–135.

Ali M, Jamal Khan, Aslam I. Zahiruddin Khan 2011. Simulation of the impacts of land-use change on surface runoff of Lai Nullah Basin in Islamabad, Pakistan. Landscape and Urban Planning, 102(4): 271–279.

Braud I., Fernandez P., Bouraoui F., 1998. Study of the rainfall-runoff process in the Andes region using a continuous distributed model, Journal of Hydrology, 3(4): 155-171.

Ghavidelfar, S., Alvankar, S. R., & Razmkhah, A. (2011). Comparison of the lumped and quasi-distributed Clark runoff models in simulating flood hydrographs on a semi-arid watershed. Water Resources Management, 25(6), 1775-1790.

Knebl, M.R., Yang, Z.L., Hutchinson, K., Maidment, D.R., 2005. Regional scale flood modeling using NEXRAD rainfall, GIS, and HEC-HMS/RAS: a case study for the San Antonio River Basin Summer 2002 storm event. J. Environ. Manag. 75, 325–336.

Konadu D.D., Fosu C. 2009. Digital elevation models and GIS for watershed modelling and flood prediction–a case study of Accra Ghana, Appropriate Technologies for Environmental Protection in the Developing World. Springer, 325-332.

Kull D.W., Feldman A.D. 1998. Evaluation of Clark's unit graph method to spatially distributed runoff. Journal of Hydrologic Engineering, ASCE, 3: 9-19.

Miller S N., Kepner W G., Mehaffey M H., Hernandez M., Miller R C., Goodrich D C., Devonald K., Heggem D T., Miller, W P. 2002. Integrating landscape assessment and hydrologic modeling for land cover change analysis. Journal of the American Water Resources Association, 38(4): 915-929.

Natural Resources Conservation Service (NRCS), 1972. National Engineering Handbook, Section 4, Hydrology. U.S. Government Printing Office.

Roughani, M., Ghafouri, M., Tabatabaei, M., 2007. An innovative methodology for the prioritisation of sub-catchments for flood control. Int. J. Appl. Earth Obs. Geoinf. 9, 79–87.

Sadeghi SHR, Mizuyama T (2007) Applicability of the modified universal soil loss equation for prediction of sediment yield in Khanmirza watershed, Iran. Hydrol Sci J 52(5):1068–1075

Saghafian B., and Khosroshahi M. 2005. Unit response approach for priority determination of flood source areas, Journal of Hydrologic Engineering, ASCE, 10(4): 270-277.

Saghafian B., Ghermezcheshmeh B., Kheirkhah M. M. 2010. Iso-flood severity mapping: a new tool for distributed flood source identification, Natural Hazards, 55: 557–570.

Sanyal J., Densmore A L., Carbonneau P. 20014. Analysing the effect of land-use/cover changes at sub-catchment levels on downstream flood peaks: A semi-distributed modelling approach with sparse data, Catena 118 (2014) 28–40.

Smith, K., & Ward, R. (1998). Floods: physical processes and human impacts. John Wiley and Sons Ltd.

USACE (2000) HEC-HMS Technical Manual, Hydrologic Engineering Center. Davis, CA, 187 p.

Viessman w. 1977: Introduction to hydrology, Harper and row, p. 760.

Wan, R., Yang, G., 2007. Influence of land use/cover change on storm runoff—a case study of Xitiaoxi River Basin in upstream of Taihu Lake watershed. Chin. Geogr. Sci. 17 (4), 349–356.

Proceedings of the 10th World Congress of EWRA 'Panta Rhei', 5-9 July 2017, Athens, Greece
© 2017 *European Water Resources Association*

Evaluation of flood management plan on Cilemer river basin, Indonesia

D. Indrawati[1*],Y. Suryadi[2], D.P. Saputro[3], I. Taufik[4] and M.B. Adityawan[2]
[1] *Departement of Civil Engineering, Universitas Jenderal Achmad Yani-Cimahi, PO.BOX 148 Cimahi, West Java, Indonesia*
[2] *Water Resources Development Center, Institut Teknologi Bandung, Jalan Ganesha 10, Bandung, West Java, Indonesia*
[3] *Laboratory of Fluid Mechanics, Departement of Civil Engineering, Institut Teknologi Bandung, Jalan Ganesha 10, Bandung, West Java, Indonesia*
[4] *Public Works and Public Housing Regional Office, Banten Province*
[*] *e-mail: dian.indrawati@lecture.unjani.ac.id*

Abstract: As one of the significant rice barn in Indonesia, Banten Province faces serious problems related to flood disaster which occurs in several paddy fields on the rainfall season, especially on January until March. One of the critical area which is oftenly flooded is Cilemer River Basin around Cilemer River. This river flows through 94.3 km with 56.957 Ha area of its river basin. The disaster causes an average loss of approximately USD 4.33 million every year, and an additional losses of morale due to the disruption of the community activities in the flood area. A flood management was proposed in a previous study by the local government, based on a 1D model. The total cost is approximately USD 16.196 Million, mainly to construct levees and to normalize the river. Unfortunately, this river basin is maintained by the province under a limited budget. Therefore, stake holders had studied and issued a flood management plan to divide the construction in three stages. the middlestream, downstream, and upstream of this river basin. In this study, the plan was evaluated in order to find a more effective solution, with a lower cost. The evaluation was conducted using a coupled 1D-2D model. The model is used to simulate the flood based on 2, 5, 10, and 25 years of return periods. The flood discharge was calculated based on five rainfall stations, Mandalawangi, Pasir Wangi, Pagelaran, Sanghiang Damar, dan Kadubera stations. The model was used to obtain the inundation maps for each return period, following each stage of the flood management plan. The results show that the completion of the second stage has successfully reduced the flooding, up to a 25 years return period.

Key words: Cilemer, flood management, adaptive structural engineering, 2D Modelling

1. INTRODUCTION

Banten Province is one of the rice barn in Indonesia. Unfortunately, the rice paddy field in several areas are facing problem from flood in the rainy season. The flood causes an annual loss of approximately USD 4.35 million per year shown on Figure 1. This value was estimated based on Economic Commission for Latin America and the Caribbean (ECLAC) method for the period of 2007 to 2015.

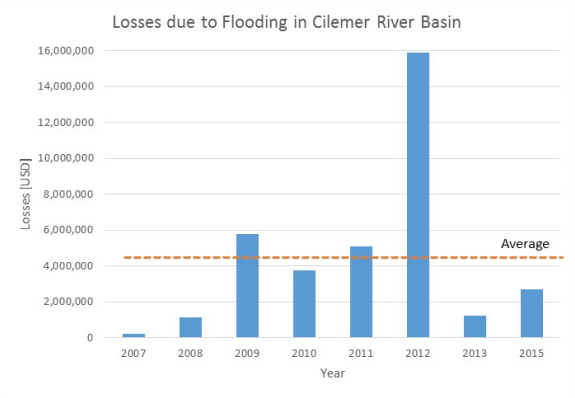

No	Year	Losses (USD)
1	2007	191,731
2	2008	1,134,423
3	2009	5,764,231
4	2010	3,734,115
5	2011	5,093,738
6	2012	15,903,731
7	2013	1,227,692
8	2015	2,686,154

Figure 1 Losses due to Floodng in Cilemer River Basin

The flooding requires an immediate action in order to minimize the loss. The local government conducted a study and proposed a flood management plan. The study was conducted using a 1D model for simulating the inundation in Cilemer River Basin. The proposed plan costs about to USD 16.196 Million, mainly to construct levees and to normalize the river.

The Cilemer River and River Basin is maintained by the Province that faces limited budgetting. Hence, the proposed solution was divided into three stages as ilustrated in Figure 2. Each of the stage varies in cost. The cost for the first, second and third stages are USD 6.72 Million, USD 5.49 Million, and USD 3.97 Million, respectively. The first stage is in the middle of the stream with a length of approximately 6.757 km, the second stage in the downstream, approximately 5.634 km long, and the last one is in the upstream, 8.356 kmlong.

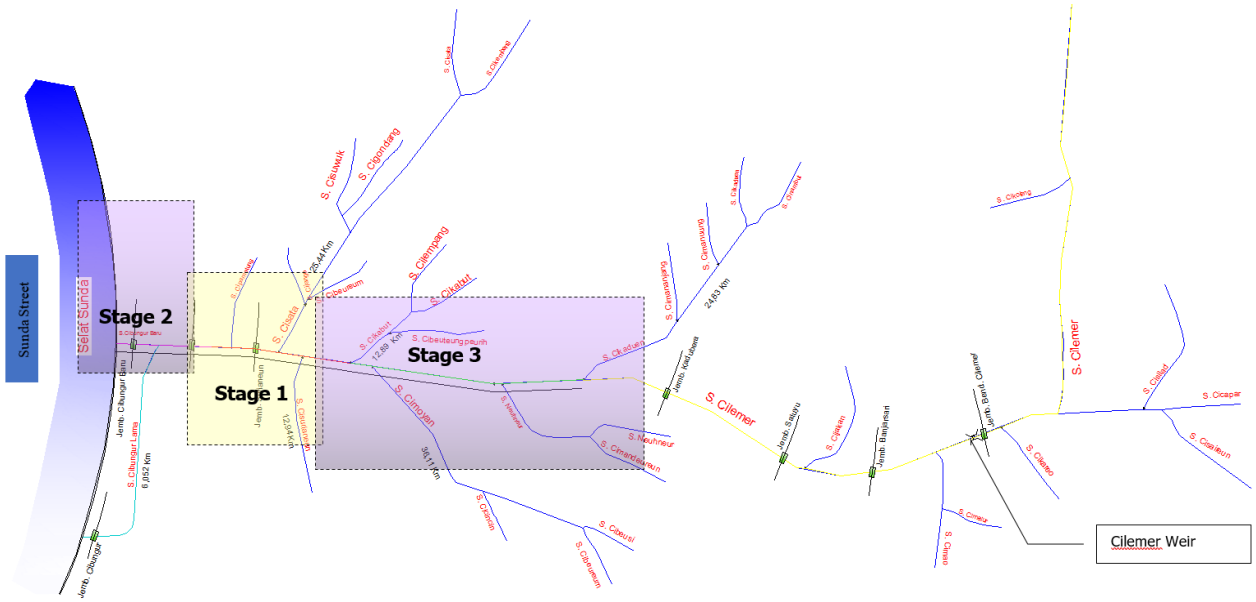

Figure 2 Schematic of Cilemer River

This proposed plan may face social problems. It requires a large sum of land acquisitions that may cause resistance from the locals. Thus, the local government requires an evaluation of the proposed plan to find a more effective way to solve the flooding.

The local government conducted their study using a one dimensional hydrodynamic model. The 1D approach is commonly used for flood simulation. However, the accuracy of this approach may not be sufficient in some cases (Lin et al., 2006). The interaction between the river and the overland flow cannot be properly simulated using a 1D model. In this case, a 2D approach is more accurate, as it is shown in previous studies for modeling the flood in in upper Citarum River Basin (Suryadi, 2008; Indrawati, 2011). A 2D model was successfully used to simulate a high-magnitude outburs flood in Kverkfjoll, Iceland (Carrivick, 2005). Flooding in urban area was also studied using a 2D based Shallow Water Equation (Mignot et al., 2005). However, a full 2D model may be time consuming and temperamental in term of stability. Therefore, a coupled 1D-2D model was proposed. The method combines the effectiveness of a 1D approach in the river, while taking the full advantage of a 2D approach for the overland flow. This method was used and tested for large and complex river system with good results (Lin et al., 2006; Patro et al., 2009; Giles and Moore, 2010).

The Cilemer River Basin is large and therefore, a coupled 1D-2D model is more appropriate for simulating the flood. In this study, the method was used to evaluate the proposed flood management plan in order to obtain a better solution for the flooding in Cilemer River Basin.

2. METHODOLOGY

This study employs a coupled 1D-2D model. The 1D model was used to simulate the flow in the river. On the other hand, the 2D model was used to simulate the overland flow. Both models are coupled using MIKEFLOOD (MIKEFLOOD, 2010).

The 1D model is based on the well known Saint Venant Equations, as follows:

Continuity Eq.
$$\frac{\partial Q}{\partial x} + \frac{\partial A}{\partial t} = q \tag{1}$$

Momentum Eq.
$$\frac{\partial Q}{\partial t} + \frac{\partial\left(\alpha \frac{Q^2}{A}\right)}{\partial x} + gA\frac{\partial h}{\partial x} + \frac{gQ|Q|}{C^2 AR} = 0 \tag{2}$$

where Q is discharge (m^3/s), A is the flow area (m^2), q is the lateral flow (m^2/s), h is the height above datum (m), C is the Chezy coefficient ($\sqrt{m}/s$), R is the hydraulic or resistance radius (m) and α is the momentum distribution coefficient which is dimensionless.

The 2D model is based on the following equations:

Continuity Eq.
$$\frac{\partial \varsigma}{\partial t} + \frac{\partial p}{\partial x} + \frac{\partial q}{\partial y} = \frac{\partial d}{\partial t} \tag{3}$$

Momentum Eq. For X-Direction
$$\frac{\partial p}{\partial t} + \frac{\partial\left(\frac{p^2}{h}\right)}{\partial x} + \frac{\partial\left(\frac{pq}{h}\right)}{\partial y} + gh\frac{\partial \varsigma}{\partial x} + \frac{gp\sqrt{p^2+q^2}}{C^2h^2} - \frac{1}{\rho w}\left[\frac{\partial\left(h\tau_{xx}\right)}{\partial y} + \frac{\partial\left(h\tau_{xy}\right)}{\partial x}\right] + \Omega_q - fVV_x + \frac{h}{\rho w}\frac{\partial\left(p_\alpha\right)}{\partial x} = 0 \tag{4}$$

Momentum Eq. For Y-Direction
$$\frac{\partial p}{\partial t} + \frac{\partial\left(\frac{p^2}{h}\right)}{\partial y} + \frac{\partial\left(\frac{pq}{h}\right)}{\partial x} + gh\frac{\partial \varsigma}{\partial y} + \frac{gp\sqrt{p^2+q^2}}{C^2h^2} - \frac{1}{\rho w}\left[\frac{\partial\left(h\tau_{yy}\right)}{\partial y} + \frac{\partial\left(h\tau_{xy}\right)}{\partial x}\right] + \Omega_p - fVV_y + \frac{h}{\rho w}\frac{\partial\left(p_\alpha\right)}{\partial y} = 0 \tag{5}$$

where ζ is the surface elevation (m), d is time varying water depth (m), h is water depth (m), p is the flux density in x-direction (m^2/s), q is flux density in y-direction (m^2/s), C is Chezy resistance coefficient ($\sqrt{m}/s$), g is the gravity acceleration (m/s^2), V, V_x, V_y are the wind speed and the components in the x and y direction (m/s), f is the wind friction factor (dimensionless), Ω is the Coriolis parameter (/s), $p\alpha$ is the atmospheric presure (kg/ms^2), ρw is the water density (kg/m^3), x and y are the space coordinates (m), t is time (s), and τ_{xx}, τ_{xy}, τ_{yy} are the components of effective shear stress (m^2/s^2).

The boundary condition on the upstream is the flood discharge and hydrograph, and the downstream is the tidal level. The model was simulated by changing the upstream boundary condition for several return periods. The flood discharge was estimated using Syntetics Hydrograph Nakayashu. The method is commonly used in the Ministry of Public Works, Indonesia, since 1976. The peak discharge is given as:

$$Q_p = \frac{AR_a}{3.6\left(0.3T_p + T_{0.3}\right)} \tag{6}$$

where Q_p is peak discharge (m^3/s), R_a the unit rainfall (mm), T_p is time between rainfall start to peak (mm), $T_{0.3}$ the declining time until 30% of peak discharge and A the river basin area to the river outlet.

The rainfall data was obtained from 5 measurement stations. They area Mandalawangi, Pasir Wangi, Pagelaran, Sanghiang Damar, dan Kadubera stations. The regional rainfall was obtained using the Polygon Thiessen method. This rainfall was further analyzed to estimate the return period rainfall, for calculating the flood discharge.

3. CILIMER RIVER BASIN

The delineation of Cilimer River Basin was conducted based on the Digital Elevation Model (DEM), provided by the Geospatial Information Agency (BIG). This river basin has 569.57 km^2 area with the main river is Cilemer river of approximately 94.30 km long.

Administratively, Cilemer River Basin is dominated by counties in Pandeglang District (74.99%) and Lebak District (24.75%), while the rest is located in Serang district (0.26%). Topographically, 77.38% of the total area is flat, which is typical for a lowland area. Rocks and soil in Cilemer River Basin are mostly derived from Brecciated Lava unit (Qhv) (27.04%) and Alluvium (Qa) (23.65%). This condition leads to a high probability of erosion on the upstream and sedimentation on the downstream of river basin.

The River Basin can be divided into 7 (seven) sub river basins listed on Table 1 and shown on Figure 3. There are five rainfall stations that influence Cilemer River Basin, Mandalawangi, Pasir Wangi, Pagelaran, Sanghiang Damar, dan Kadubera stations, as shown on Figure 3.

Table 1 Sub River Basin in Cilemer

	Cilemer Hulu	Cikadeun	Cimoyan	Cikobut	Cisurianeun	Cisata	Cilemer Hilir
River Length (km)	69.0	24.0	36.1	12.8	12.9	25.4	8.5
River Basin Area (km^2)	243.24	79.89	105.88	26.03	21.00	62.89	27.78

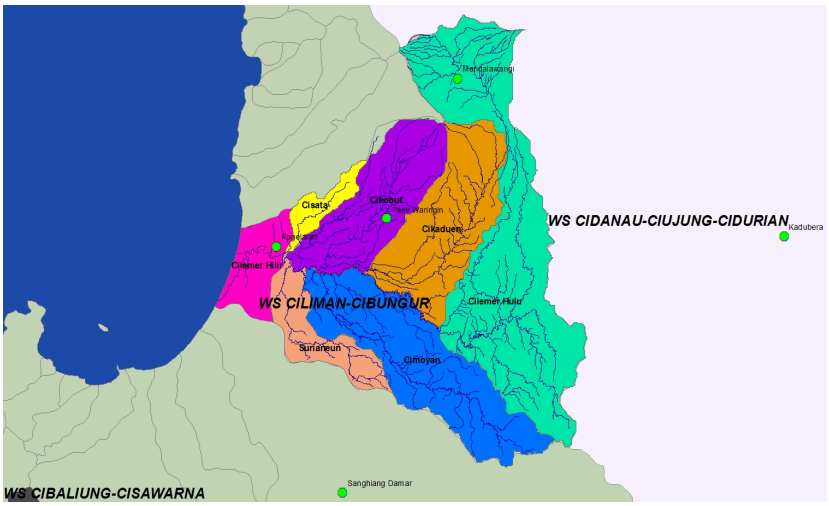

Figure 3 Cilemer River Basin

4. HYDROLOGICAL MODELING

Based on Nakayashu SUH, flood discharge was estimated per sub river basin, for 2, 5, 10, and 25 years of return periods. The results show that the flood discharge varies from 170 m^3/s in Cisurianeun sub river basin until 670 m^3/s in Cilemer Hulu sub river basin as shown on Figure 4 below.

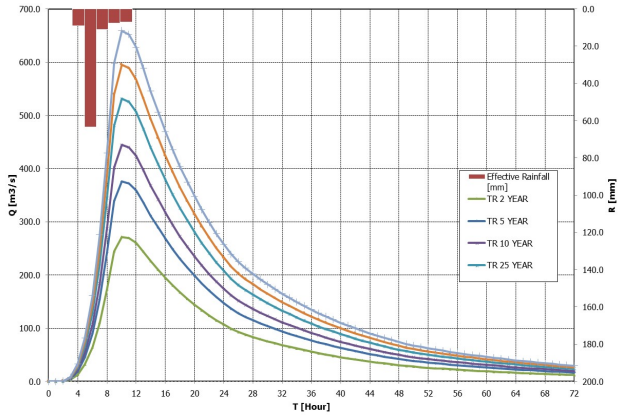

(a) Cilemer Hulu Sub River Basin

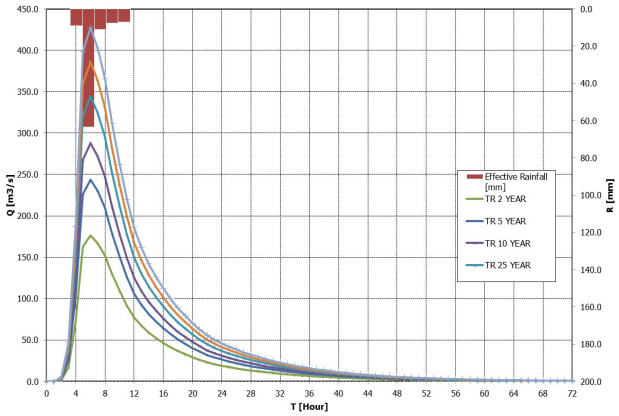

(b) Cikaduen Sub River Basin

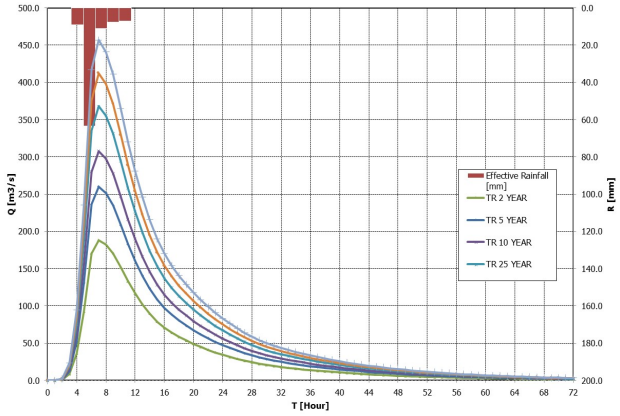

(c) Cimoyan Sub River Basin

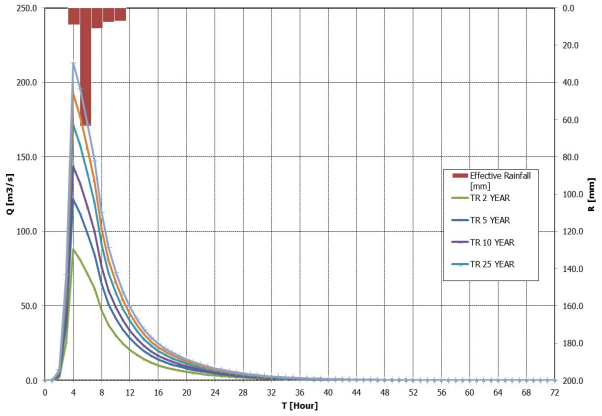

(d) Cikobut Sub River Basin

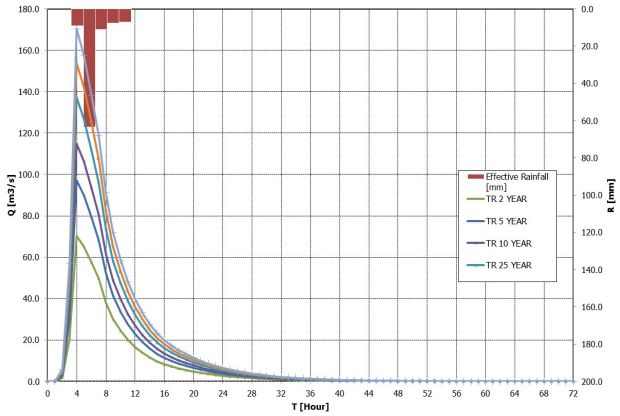

(e) Cisurianeun Sub River Basin

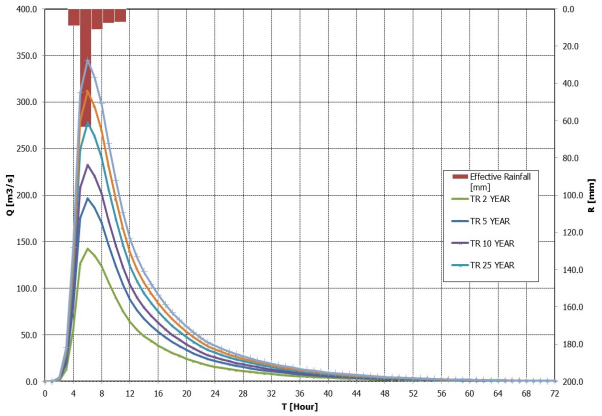

(f) Cisata Sub River Basin

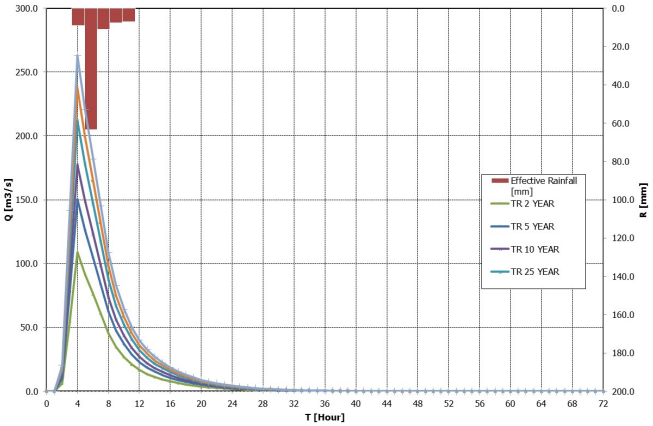

(g) Cilemer Sub Hilir River Basin

Figure 4 Discharge in Several Sub River Basin

5. FLOOD MANAGEMENT PLANNING

At present, the average width of Cilemer river varies from 32 to 40 meters. Public Works and Public Housing Regional Office of Banten Province plans to increase the river capacity gradually. The construction is divided into 3 stages, with a total of 7 (seven) segments, which are listed below.

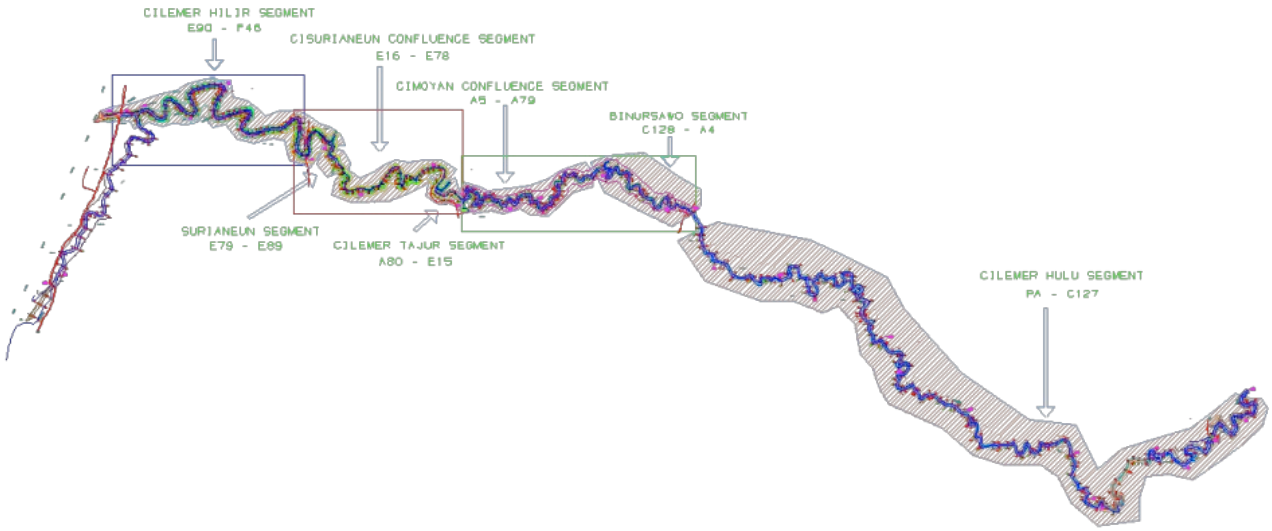

Figure 5 Segmentation of Flood Management in Clemer River

Table 2 River Improvement Planning

Stages	Segementation	Width (m)	Height (m)	Length (km)
-	Cilemer Hulu Segment PA-C127	18.00	3.00	24.973
Stage 3	Binursawo Segment C128-A4	30.00	4.00	26.535
	Cimoyan Tributaries Segment A5-A79	34.00	4.00	4.485
Stage 1	Cilemer-Tajur Segment A80-E15	46.00	4.00	1.317
	Cisurianeun Tributaries Segment E16-E78	52.00	4.00	2.615
	Surianeun Segment E79-E89	64.00	4.00	1.163
Stage 2	Cilemer Hilir Segment E90-F46	70.00	4.00	7.895

6. FLOOD MODELING

The model is used to simulate the effectiveness of the solution at each stage to decrease the flooding in Cilemer River Basin. There are three scenarios, existing, first stage, and a combination of first and second stages.

The model input are the topography data, river network and cross sections, the flood discharge, and the tidal level. The river network and cross section were used in the 1D river model. The topography data are uses in the 2D overland flow model, with a 50 m x 50 m grid size. A maximum tide level (HWL) of +0.82 m is used as the boundary condition at the downstream. The upstream boundary condition is the estimated flood discharge, as given in the previous section.

The inundation maps of the existing condition for the flood discharge with return periods of 2, 5, 10, and 25 years is shown in Figure 6.

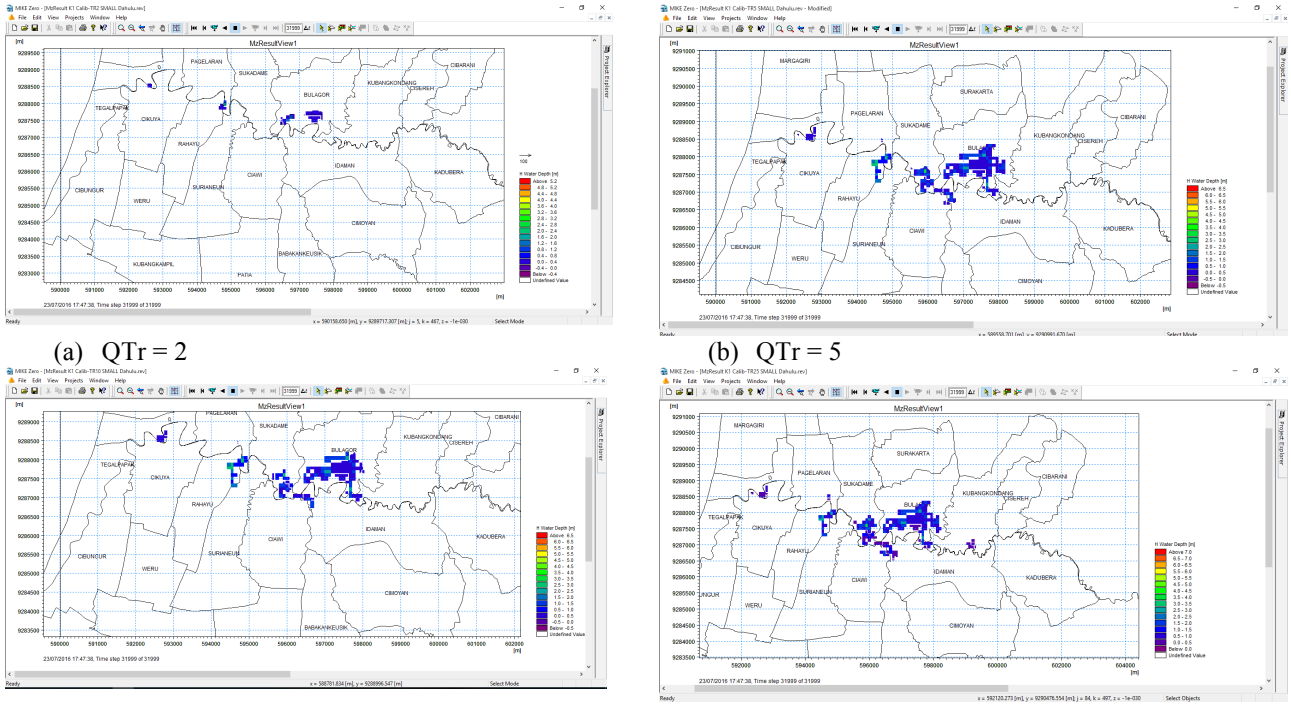

(a) QTr = 2 (b) QTr = 5

(c) QTr = 10 (d) QTr = 25

Figure 6 Inundation Map, Existing

Based on the simulation results for the existing condition, inundated area for a 2 year return period is located in Bulagor, Pagelaran, Rahayu, Cikuya dan Tegalpapak Villages, with a total area of approximately 95.75 Ha and an average depth of approximately 0.43 m. The inundated area and depth gets higher with the return period. Sukadame, Idaman, Ciawi, and Surianeun Villages, are inundated with a total area of approximately 574.75 Ha and an average depth of approximately 0.75 m, for a 5 year returns period. The area and depth for 10 and 25 years return periods are 600.50 Ha, 0.75 m, and 668.00 Ha 0.98 m, respectively.

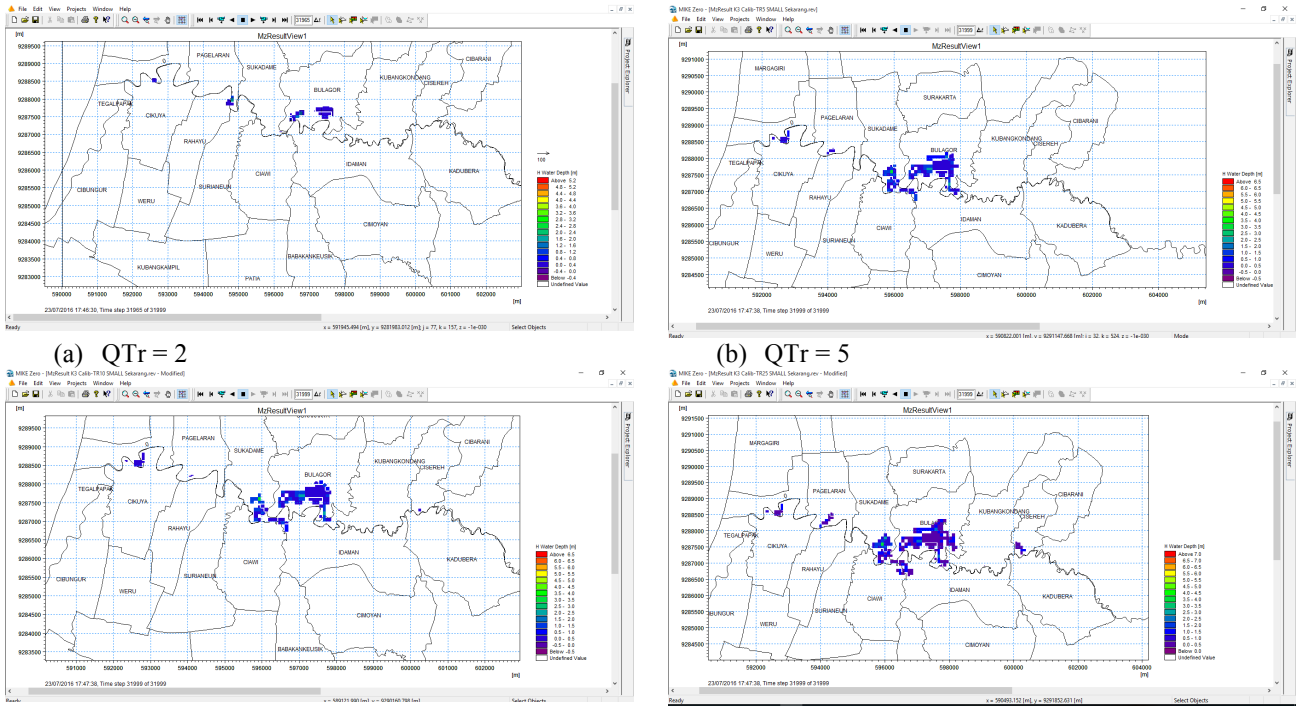

(a) QTr = 2 (b) QTr = 5

(c) QTr = 10 (d) QTr = 25

Figure 7 Inundation Map, Stage 1

The model shows the decreasing of the flood inundation following the completion of stage 1 as shown in Figure 7. The inundated area for a 2 years return period is located in Bulagor, Pagelaran, Rahayu, Cikuya dan Tegalpapak Villages with a total area of approximately 197 Ha and an average depth of approximately 0.35 m. The inundated area for the 5, 10, and 25 years return periods are 350.25 Ha, 435.25 Ha, and 628.75 Ha, respectively. The inundation depth for the same return periods are 0.63 m, 0.64 m, and 0.76 m, respectively.

There are no inundation following the completion of stage 2. Therefore, it should be highlighted here that there is no need for constructing stage 3.

7. CONCLUSION

In this study, a coupled 1D-2D model was used to evaluate the flood management plan in Cilemer River Basin. The study indicates that the flooding in Cilemer River Basin, up to a 25 years return period, can be reduced to none after completing the second stage of the proposed flood management plan. Therefore, there is no need to spend an extra USD 3.97 Million to complete the third stage.

This study has not considered the inundation due to local drainage system. It is possible that the local inflow and flooding may contribute to the overall flooding in Cilemer River Basin, especially because of the flat contour. In addition, a sediment transport related study in this river should be conducted. They should be studied further to support the flood management plan in Cilemer River Basin.

ACKNOWLEDGEMENTS

This study is supported by the Project Study of Performance Evaluation Flood Management on Cilemer River Basin in 2016 and SID Cilemer River Treatment (Cibungur) in 2008 by Public Works and Public Housing (d.h Water Resources and Housing) Regional Office of Banten Province.

REFERENCES

Carrivick,. J.L., 2005 ‘Application of 2D hydrodynamic modelling to high-magnitude outburst floods: An example from Kverkfjoll, Iceland’ Journal of Hydrology 321:187-199.

Gilles D. and M. Moore (2010) ‘Review of Hydraulic Flood Modeling Software used in Belgium, The Netherlands, and the United Kingdom’, Int. Perspectives in Water Resource Management, IIHR, Hydroscience & Engineering University of Iowa.

Indrawati, Dian., Studi Pengembangan Model Jaringan Syaraf Tiruan untuk Indeks Banjir Berdasarkan Fungsi Karakteristik Hidrotopografi dan Spot Banjir Secara Spasial (Studi Kasus DAS Citarum Hulu), Thesis, 2011

Lin B., J.M. Wicks, R.A. Falconer and K. Adams (2006) ‘Integrating 1D and 2D hydrodynamic models for flood simulation’ Water Management, Vol. 159, pp. 19-25.

Mignot, E., Paquier, A., Haider, S., 2005. Modelling floods in a dense urban area using 2D shallow water equations. Journal of Hydrology : 327 : 186-199

MIKE 11 (2011) ‘A Modelling System for River and Channels’, Reference Manual, DHI Water & Environment.

MIKE 21 (2011) ‘Flow Model, Hydrodynamic Module’, Scientific Documentation, DHI Water & Environment.

MIKE FLOOD TUTORIAL (2010) ‘Salmon and Trout Rivers Exercise’, HydroEurope, DHI Water & Environment.

Patro S., C. Chatterjee, S. Mohanty, R. Singh and N.S. Raghuwanshi (2009) ‘Flood Inundation Modeling using MIKE FLOOD and Remote Sensing Data’ J. Indian Soc. Remote Sens., Vol. 37, pp. 107-118.

Suryadi, Yadi., Pengaruh hujan terhadap debit puncak hidrograf inflow, luas genangan, kedalaman genangan dan waktu genang dalam menentukan indeks banjir, Dissertation, 2008

Proceedings of the 10th World Congress of EWRA 'Panta Rhei', 5-9 July 2017, Athens, Greece
© 2017 *European Water Resources Association*

Cluster analysis and classification of storm events at Rethymno

N. Martzikos[1*], A. Lykou[2], C. Makropoulos[2] and V. Tsoukala[1]
[1] *Laboratory of Harbor Work, National Technical University of Athens, Athens, Greece*
[2] *Laboratory of Hydrology & Water Resources Utilization, National Technical University of Athens, Athens, Greece*
[*] *e-mail: nmartzikos@central.ntua.gr*

Abstract: Coastal urban areas, shorelines, ports and coastal structures are being increasingly threatened by violent hydro - meteorological phenomena such as storms, especially nowadays due to climate change and the climate variability. An extended analysis of storm events in Rethymno city of Crete Island, is attempted, under the frames of PEARL (Preparing for Extreme And Rare events in coastaL regions) an undergoing EU funded project. The aim of this paper is to present an integrated analysis of storm events and their thresholds by enhancing the storm definition for this location and finally to classify them by means of clustering methods. The storm is usually defined as the event exceeding a minimum significant wave height with a certain minimum duration, but the thresholds for the wave height, the duration and the calm period between two successive storms vary depending on the area of interest. Investigating extreme historical storm events and their future projections, the thresholds are defined as 90th percentile of the data set rather to describe the most rare events, checking simultaneously the independence between two successive events. Since the thresholds are selected, a storm's definition is created and the storm events are classified into five classes, depending on their severity. The classification is accomplished with cluster analysis based on the storm energy and the storm period. The different clustering algorithms and methods (hierarchical, k-means, partitioning around medoids and fuzzy clustering) are validated via appropriate indices and the results are presented, checking also their impacts on the coastal area.

Key words: extreme events, storms, classification, clustering evaluation

1. INTRODUCTION

Storm events are one of the most destructive natural hazards which affect low-lying coastal areas and they are responsible, among others, for urban coastal flooding (Costas et al., 2015). The destructiveness of these extreme events depends on their energy and their duration, while due to climate change they are of great importance for many scientists over the past decades. PEARL is an undergoing EU funded project "Preparing for Extreme And Rare events in coastaL regions" which examines the case study of Rethymno city of Crete Island. Extreme storm events at Rethymno cause wave overtopping affecting the stability of breakwaters as well as the safety of human population and the coastal economic activity, as evidenced the last years.

In this study an analysis of storm events and their thresholds is attempted with the main purpose to present an integrated storm classification through clustering methods and their evaluation, extending in this way the previous study of Tsoukala et al. (2016).

2. DATA

The available data in this study were projections of the wave climate to the future which were derived by SWAN wave model (Booij et al. 1999; Ris et al. 1999), a model which was set up and used in the context of the research project: "Estimating the effects of Climate Change on SEA level and WAve climate of the Greek seas, coastal Vulnerability and Safety of coastal and marine structures - CCSEAWAVS", (Prinos, 2014) and discussed thoroughly by Athanassoulis et al. (2015) and Tsoukala et al., (2016). The wind data used for the hindcast and climate simulations were proceeded by using a dynamical down-scaling approach of the atmospheric simulations

conducted with the regional model RegCNET (Pal et al., 2007), driven by hindcast carbon dioxide emissions during 1960-2000 while integrating AR4-A1B emission scenarios for the period 2000-2100 (Vagenas et al. 2014; Velikou et al. 2014). Those simulations consisted of 3-hourly timeseries of various wave parameters in deep waters, i.e. the significant wave, the spectral peak wave period, the wave direction (Figure 1).

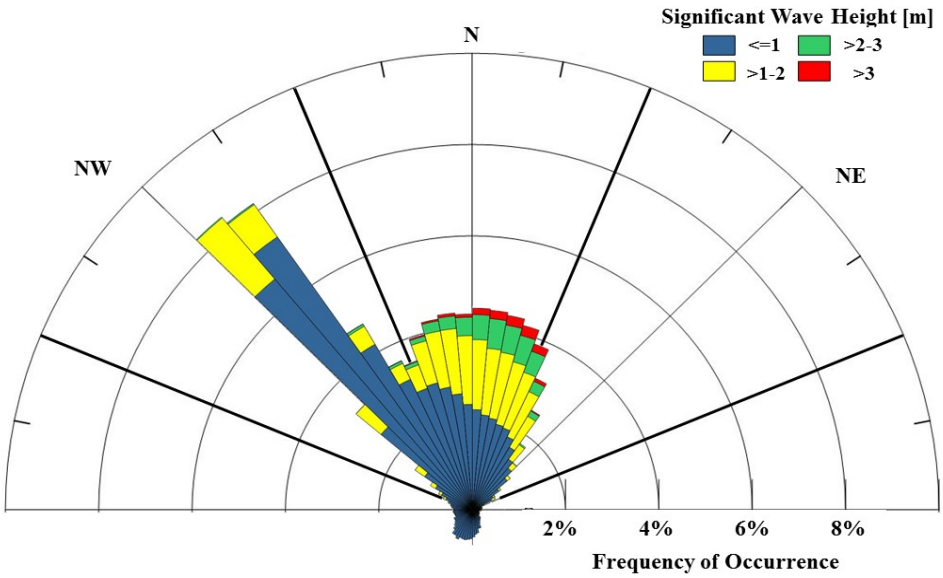

Figure 1. Direction wave occurrence with associated significant wave height at Rethymno, for the period 1960-2000.

3. METHODOLOGY

3.1 Storm Thresholds

Lin-Ye et al., (2016) explicitly state that a storm determination should include the storm intensity, the thresholds of H_S, the minimum duration, as well as the calm period between two consecutive storm events. Considering the storm as an extreme event which rarely occurs, the significant wave height's threshold is defined as the 90th percentile of the data set, as it has already been proposed by previous studies (Rangel-Buitrago and Anfuso, 2011; Eastoe et al., 2013; Bernardara et al., 2014). Thus, taking into account the wave predictions from hindcast data, it is confirmed that the 10% of the total wave data exceed the threshold of 2 m for the significant wave height (H_S).

The duration of a storm event is defined as the time period in which the H_S remains over the threshold (Boccotti, 2000). Contrary to previous studies, where the minimum duration of a storm event is determined without a clarification (see also Table 1.), in this study the minimum duration is estimated to be 9 hours, following again the rule of 90th percentile, having already discarded all the single occurrences with duration of 3 hours.

Regarding the calm phase or the inter-arrival time (De Michele et al, 2007; Corbella and Stretch, 2012) between two consecutive storms, it is of great importance to investigate the independence of two events. For this purpose all the events with inter-arrival time not exceeding 48 hours are checked out about their correlation, estimating Kendall's tau and Spearman's rho statistic test. The p-value should be lower than 0.05 in order to reject the null hypothesis of having dependent events. The results show that the correlation has no evident trend concerning the duration between two events, but the first low p-values are indicated for the calm phase of 18 hours. According to this threshold the events which are developed at time interval less than 18 hours, are considered as the same storm event.

Based on the above analysis and for the specific area of Rethymno, a storm event is defined as an extreme wave event which has a significant wave height over the threshold of 2 m, for a minimum duration of 9 hours and a minimum inter-arrival time of 18 hours from the next event. In this way the definition presented by Tsoukala et al. (2016) for the same location is extended.

Next, the data are sorted by wave direction, creating three categories for North, Northeast and Northwest incident waves at the Rethymno coast. As shown in Figure 1, the waves of these directions have the highest frequencies of occurrence and additionally as vertically incident waves they are considered of high-risk for the coastal zone (Allsop et al., 2008). It should be noted that the direction of a storm event is identified with the mean direction of each event, while the standard deviation and the coefficient of variation show that there are no big fluctuations around the mean.

3.2 Storm Clustering

Following the definition of the storm energy (Eq. 1) as it was proposed by Dolan and Davis (1992, 1994) and was also used by Mendoza et al. (2011) and Kokkinos et al. (2014) for the Mediterranean Sea, a classification of storm events can be derived with a cluster analysis.

$$E = \int_{t_1}^{t_2} H_s^{\,2}\, dt \tag{1}$$

In previous studies, hierarchical agglomerative cluster analysis was carried out with Ward's method (Kokkinos et al., 2014) or average linkage method (Dolan and Davis, 1992, 1994; Mendoza et al. 2011), using the euclidean distance between two objects and the energy content as a classification variable.

In this study the cluster analysis is based upon the energy and the average peak period, with aim to associate a storm event with the most important variables, i.e. H_S, duration and T_P and finally to classify a total of 563 and 1463 storm events respectively for two periods: 1960 - 2000 (past climate) and 2000 - 2100 (future climate). The classification is accomplished into five classes, trying to have an agreement with previous studies but especially with Dolan-Davis Scale and the Saffir-Simpson Hurricane Wind Scale (Dolan and Davis, 1992) which are used extensively by many scientists and organizations (Kelman, 2013).

However many studies in Computer Science (de Morsier, et al., 2015; Arbelaitz et al., 2013; Jain, 2010; Halkidi, et al., 2001) have proposed a lot of indices in order to evaluate the clustering results and find the optimum method. An integrated analysis consequently is conducted for the purpose of clarifying the clustering procedure.

First, before trying to find patterns in our data it is necessary to investigate if it is highly clusterable. The Hopkins Statistic value (Banerjee and Dave, 2004) indicates, especially if it is lower than 0.05, that there are clusters in our data and so it is worth to proceed. Next for the validation of clustering methods, the connectivity, Dunn and silhouette indices are estimated. The connectivity (Handl, et al., 2005) indicates the degree of clusters' association and should be closer to zero. Dunn index (Dunn, 1974) is intended to specify the density of clusters and how well-seperated they are; Dunn value should be maximized. The Silhouette Width (Kaufman and Rousseeuw, 2005) is the mean of each Silhouette value which estimates the degree of confidence in a specific cluster, when the values are close to one indicate well clustered data without outliers. Correspondingly many measures evaluate the stability of a clustering results removing one column at each time and comparing the results. Thus the average proportion of non-overlap (APN), the average distance (AD), the average distance between means (ADM), and the figure of merit (FOM) are also estimated as they were proposed and described by Datta and Datta, (2003), while small values for all of them are preferred.

All the above estimations are carried out by R (R Core Team, 2016) and mainly based on specific packages of Brock et al., 2008; Maechler, 2016; Kassambara and Mundt, 2016. Here the typical cluster algorithms which are examined are Hierarchical Agglomerative clustering, K-means, Fuzzy and Partitioning around Medoids, for all the clustering methods (i.e. Ward, Single –

Complete and Average linkage) and for two types of distance Euclidean and Manhattan. At this stage authors would like to highlight that a detailed description of clustering procedure and their methods is absent in this study, prompting the reader for an extensive study to basic books (i.e. Theodoridis and Koutroumbas, 2009) and references therein.

The results show that the optimum clustering algorithm is the Hierarchical Agglomerative, having always the best combination of all examined indices. In addition, the Euclidean distance indicates in any case better results than Manhattan, contrary to the clustering method which differs according to the direction of the storm events.

More specifically, for the period of 1960-2000, the storm events clustered by:

- Average linkage for N direction
- Single linkage for NE direction
- Ward method for NW direction.

And for the period of 2000-2100 the storm events clustered by:

- Single linkage for N direction
- Average linkage for NE direction
- Ward method for NW direction.

4. STORM CLASSIFICATION

In conclusion, the use of foregoing clustering methods contributes to a well-developed storm classification for past and future wave climate and for each direction N, NE, NW. The storm events are classified into five classes depending on their severity, (I - Weak, II - Moderate, III - Significant, IV - Severe, V - Extreme). All the results for the period 1960-2000 are described below in Tables 1-3 in association with the wave height, the wave peak period and the duration for each storm class.

Table 1. Storm events and their characteristics for the period 1960-2000 North wind direction

Storm Class	Significant Wave Height [m]		Peak Period [s]			Energy [m^2h]			Duration [h]	Events
	max	mean	min	max	mean	min	max	mean	mean	
I	3.12	2.18	4.99	9.67	7.26	36.27	135.38	81.16	16.31	183
II	4.09	2.40	5.25	9.16	7.50	137.14	269.91	198.83	32.68	122
III	4.47	2.57	5.71	9.34	7.71	274.26	472.79	345.54	49.25	84
IV	5.26	2.89	4.84	10.36	7.95	490.10	981.40	652.01	72.10	60
V	6.31	3.45	5.28	10.82	8.38	1173.10	1862.63	1517.76	114.86	14

Table 2. Storm events and their characteristics for the period 1960-2000 Northeast wind direction

Storm Class	Significant Wave Height[m]		Peak Period [s]			Energy [m^2h]			Duration [h]	Events
	Max	mean	min	max	mean	min	max	mean	mean	
I	2.82	2.13	5.31	7.93	7.07	37.27	105.83	67.65	14.36	28
II	2.88	2.29	5.90	9.45	7.36	122.66	213.85	167.83	30.94	16
III	3.70	2.49	5.83	8.81	7.45	239.86	310.29	270.45	41.45	11
IV	4.15	2.93	5.85	9.02	7.88	361.34	442.05	411.76	44.25	4
V	4.29	2.99	6.27	9.09	7.92	504.73	698.02	582.86	60.75	4

Table 3. Storm events and their characteristics for the period 1960-2000 Northwest wind direction

Storm Class	Significant Wave Height [m]		Peak Period [s]			Energy [m^2h]			Duration [h]	Events
	Max	mean	min	max	mean	min	max	mean	mean	
I	3.02	2.18	6.56	8.97	7.71	39.02	93.41	61.53	12.16	19
II	3.55	2.39	5.45	9.15	7.59	113.66	154.41	134.19	21.90	10
III	3.80	2.58	4.74	9.48	7.89	173.55	204.20	191.25	26.25	4
IV	4.38	2.88	4.62	10.34	8.35	273.85	287.91	280.88	30.00	2
V	4.24	3.19	6.19	9.64	6.19	404.12	404.12	404.12	36.00	1

5. STORM IMPACTS

Finally in order to connect the storm classes with their impacts (Coco et al., 2014; Del Rio et al., 2012; Almeida et al., 2012) the wave data of each storm event is used by MIKE21 PMS so as to simulate the wave propagation into shallower water regions and estimate the corresponding nearshore wave characteristics, giving also their spatial evolution in the coastal zone of Rethymno. With purpose to study unfavourable sea states, one storm event of class V for each direction is selected for simulation and then the mean wave overtopping is estimated, in one known structure section.

6. CONCLUSION

An integrated analysis of storm events at Rethymno was investigated in this study and a storm classification by means of clustering methods was also examined. The significant wave height and the inter-arrival period thresholds were estimated according to the 90th percentile rule, in order to describe rare and extreme events, such as storms. Consequently a new definition of storm event for the coastal zone of Rethymno was derived. Well-known clustering algorithms and their methods were validated using many indices which are generally used in computer and data science community for the cluster results evaluation. All the above analysis and procedure should be used by anyone who wants to cluster wave data in any specific area. Finally numerical simulations could be used as a tool in order to associate the storm impacts with each class.

ACKNOWLEDGMENTS

This study is part of Mr. Martzikos' PhD thesis which is co-funded through the Action: «Enhancing the Human Research Potential through the Implementation of Doctoral Research» of the Operational Programm «Human Resources Development, Education and Lifelong Learning» of NSRF 2014-2020, co-financed by the European Social Fund and the Greek Government. The research leading to these results has also received partial funding from the European Union Seventh Framework Programme (FP7/2007-2013) under Grant agreement n° 603663 for the research project PEARL (Preparing for Extreme And Rare events in coastaL regions). The research and its conclusions reflect only the views of the authors and the European Union is not liable for any use that may be made of the information contained herein.

REFERENCES

Allsop, W., T. Bruce, T.A. Pullen, J.W. Van der Meer., 2008. Direct hazards from wave overtopping-the forgotten aspect of coastal flood risk assessment? In: 43rd Defra Flood and Coastal Management Conference, 1-3 July 2008, Manchester University. ID code: 215.

Almeida, L.P., Vousdoukas, M.V., Ferreira, O., Rodrigues, B.A., Matias, A., 2012. Thresholds for storm impacts on an exposed sandy coastal area in southern Portugal, Geomorphology, 143–144: 3–12

Arbelaitz, O., Gurrutxaga, I., Muguerza, J., Pérez, J., Perona, I., 2013. An extensive comparative study of cluster validity indices. Pattern Recognition, 46(1): 243-256

Athanassoulis, G.A., Belibassakis, K.A., Gerostathis, Th.P., Kapelonis, Z.G., 2014. Application of SWAN wave model for climatic simulation of sea condition at coastal areas of the Mediterranean. In: 6th Panhellenic Conf. Coastal Zones Manage. Improvement, 24-27 November 2014, Athens, Greece: 345-364.

Banerjee, A., Dave, R., 2004. Validating clusters using the Hopkins statistic. IEEE International Conference On Fuzzy Systems (IEEE Cat. No.04CH37542), doi: 10.1109/fuzzy.2004.1375706

Bernardara, P., Mazas, F., Kergadallan, X., L., Hamm, 2014. A two-step framework for over-threshold modelling of environmental extremes. Nat. Hazards Earth Syst. Sci. 14: 635-647.

Boccotti, P., 2000. Wave mechanics for ocean engineering. Elsevier Oceanography Series. Elsevier Science, Amsterdam:183-184

Booij, N., Ris, R.C., Holthuijsen, L.H., 1999. A third-generation wave model for coastal regions: 1. Model description and validation. Journal of Geophysical Research, 104(C4): 7649.

Brock, G., Pihur, V., Datta, S., Datta, S., 2008. clValid: An R Package for Cluster Validation. Journal of Statistical Software, 25(4): 1-22

Coco, G., Senechal, N., Rejas, A., Bryan, K., Capo, S., Parisot, J. et al., 2014. Beach response to a sequence of extreme storms. Geomorphology, 204: 493-501

Corbella, S., Stretch, D.D., 2012. Predicting coastal erosion trends using non-stationary statistics and process-based models. Coastal Engineering, 70: 40-49.

Costas, S., Ferreira, O., Martinez, G., 2015. Why do we decide to live with risk at the coast?. Ocean & Coastal Management, 118: 1-11

Datta, S., Datta, S., 2003. Comparisons and validation of statistical clustering techniques for microarray gene expression data. Bioinformatics 19(4): 459-466.

De Michele, C., Salvadori, G., Passoni, G., Vezzoli, R., 2007. A multivariate model of sea storms using copulas. Coastal Engineering 54: 734-751.

De Morsier, F., Tuia, D., Borgeaud, M., Gass, V., Thiran, J., 2015. Cluster validity measure and merging system for hierarchical clustering considering outliers. Pattern Recognition, 48(4): 1478-1489

Del Rio, L., Plomaritis, T.A., Benavente, J., Valladares, M., Ribera, P., 2012. Establishing storm thresholds for the Spanish Gulf of Cádiz coast. Geomorphology, 143–144: 13–23

Dolan, R., Davis, R.E., 1992. An intensity scale for Atlantic coast northeast storms. J. Coast. Res., 8(4): 40-853

Dolan, R., Davis, R.E., 1994. Coastal storm hazards. J. Coast. Res., (SI 12): 103-114

Dunn, J.C., 1974. Well separated clusters and fuzzy partitions. Journal on Cybernetics, 4: 95-104.

Eastoe, E., Koukoulas, S., Jonathan, P., 2013. Statistical measures of extremal dependence illustrated using measured sea surface elevations from a neighbourhood of coastal locations. Ocean Eng., 62: 68-77.

Halkidi, M., Batistakis, Y., Vazirgiannis, M., 2001. On Clustering Validation Techniques. Journal of Intelligent Information Systems 17: 107

Handl, J., Knowles, K., Kell, D., 2005. Computational cluster validation in post-genomic data analysis. Bioinformatics, 21(15): 3201-3212.

Jain, A. K., 2010. Data clustering: 50 years beyond K-means. Pattern Recognition Letters, 8: 651-666

Kassambara, A., Mundt, F., 2016. factoextra: Extract and Visualize the Results of Multivariate Data Analyses. R package version 1.0.3., https://CRAN.R-project.org/package=factoextra

Kaufman, L., Rousseeuw, P., 2005. Finding Groups in Data: An Introduction to Cluster Analysis (1st ed.). Hoboken: John Wiley & Sons, Inc., Chapter 2: 68.

Kelman, I., 2013. Saffir-Simpson Hurricane Intensity Scale. In: Bobrowsky, P. T., 2013. Encyclopedia of Natural Hazards. Springer Netherlands: 882-883

Kokkinos, D., Prinos, P., Galiatsatou, P., 2014. Assessment of coastal vulnerability for present and future climate conditions in coastal areas of the Aegean Sea. In: Paper Presented at the 11th Inter-national Conference on Hydroscience & Engineering: Hydro-Engineering for Environmental Challenges, http://vzb.baw.de/e-medien/iche-2014/PDF/15%20Mini-Symposium%20Impacts%20of%20Climate%20Change/15_04.pdf.

Lin-Ye, J., Garcia-Leon, M., Gracia, V., Sanchez-Arcilla, A., 2017. A multivariate statistical model of extreme events: An application to the Catalan coast. Coastal Engineering, 117: 138-156

Maechler, M., Rousseeuw, P., Struyf, A., Hubert, M., Hornik, K., 2016. cluster: Cluster Analysis Basics and Extensions. R package version 2.0.4.

Mendoza, E.T., Jiménez, J.A., Mateo, J., 2011. A coastal storms intensity scale for the Catalan sea (NW Mediterranean). Nat. Hazards Earth Syst. Sci., 11(9): 2453-2462

Pal, J., Giorgi, F., Bi, X., Elguindi, N., Solmon, F., Rauscher, S. et al., 2007. Regional Climate Modeling for the Developing World: The ICTP RegCM3 and RegCNET. Bulletin Of The American Meteorological Society, 88(9): 1395-1409

Prinos, P., 2014. Climate change effects on the Greek seas and coastal areas - the research project THALIS-CCSEAWAVS. In: 6th Panhellenic Conference on Coastal Zones Management and Improvement, 24-27 November 2014, Athens: 315-324.

R Core Team, 2016. R: A language and environment for statistical computing. R Foundation for Statistical Computing, Vienna, Austria, https://www.R-project.org/.

Rangel-Buitrago, N., Anfuso, G., 2011. An application of Dolan and Davis (1992) classification to coastal storms in SW Spanish littoral. J. Coast. Res., SI 64: 1891-1895.

Ris, R.C., Holthuijsen, L.H., Booij, N., 1999. A third-generation wave model for coastal regions: 2. Verification. J. Geophys. Res., 104 (C4): 7667-7681

Theodoridis, S., Koutroumbas, K., 2009. Pattern recognition (4th ed.). London: Academic Press.

Tsoukala, V., Chondros, M., Kapelonis, Z.G., Martzikos, N., Lykou, A., Belibassakis, K., Makropoulos, Ch., 2016. An integrated wave modelling framework for extreme and rare events for climate change in coastal areas - the case of Rethymno-Crete, Oceanologia, 58 (2): 71-89

Vagenas, C., Anagnostopoulou, C., Tolika, K., 2014. Climatic study of the surface wind field and extreme winds over the Greek seas. In COMECAP 2014. Abstracts and e-contributions. 12th International Conference on Meteorology, Climatology and Physics of the Atmosphere, Heraklion 28–31 May 2014. Hereklion, Crete: Crete University Press: 283–288.

Velikou, K., Tolika, K., Anagnostopoulou, C., Tegoulias, I., Vagenas, C., 2014. High resolution climate over Greece: assessment and future projections. In: 12th International Conference on Meteorology, Climatology and Atmospheric Physics (COMECAP 2014), Heraklion.

Proceedings of the 10th World Congress of EWRA 'Panta Rhei', 5-9 July 2017, Athens, Greece
© 2017 *European Water Resources Association*

Daily runoff estimation in Musi river basin, India, from gridded rainfall using SWAT model

V. Jothiprakash*, C. Praveenkumar and M. Manasa
Indian Institute of Technology Bombay, Mumbai 400076, India
* *e-mail: vprakash@iitb.ac.in*

Abstract: The main objective is to assess the spatial water availability in Musi river basin, India from gridded rainfall data and compare the results with the observed discharge data. Musi River passing through Hyderabad, India being one of the major sub basins of Krishna River and is catering various demands. In the recent past, it is suffering from severe spatial and temporal water availability problem. Thus, there is a need to quantify the spatial and temporal runoff availability in the Musi River for better water management. The spatial and temporal runoff has been estimated using Soil Water Assessment Tool (SWAT) model with the available data. The SWAT model has been developed and validated with India Meteorological Department (IMD) gridded rainfall data as one of the inputs and the daily runoff data observed at Dharmacherla (runoff data obtained from WRIS website of Central Water Commission (CWC)) as the model output. A rigorous calibration, sensitivity and uncertainty analyses are being carried out using SWAT-CUP. The obtained results are evaluated using performance measures such as Coefficient of determination (R^2), Nash-Sutcliff Efficiency (NSE), Mean Absolute Error (MAE), and Percent bias (PBias). It is found that the results obtained from SWAT model are satisfactory. Based on the present study it may be concluded that SWAT model can be used to generate spatial and temporal runoff from IMD gridded rainfall data in Musi River Basin.

Key words: *IMD gridded rainfall, Musi River India, Soil Water Assessment Tool, Spatial and temporal water availability, SWAT-CUP*

1. INTRODUCTION

Water is one of the most important natural resources which support the survival of living organisms on earth. Rainfall is a primary cause of water existence on the land surface and is also a major input in hydrological models to quantify surface flow. Soil and Water Assessment Tool (SWAT) developed by Arnold *et al*. (1998) is a widely used semi-distributed hydrological model for estimating surface flow at catchment level. SWAT model is applied at different geographical locations of the earth for quantifying daily surface flow (Hernandez et al. 2000; Saha *et al*. 2014; Gamvroudis *et al*. 2015; Szcześniak and Piniewski 2015; Uniyal *et al*. 2015; Yen *et al*. 2015; Kim *et al*. 2016). It is reported that rainfall is a spatially distributed phenomenon which may not be represented by traditional rain gauges because of its course spatial distribution at catchment level (Xu *et al*. 2014). Therefore, representation of rainfall data in a gridded format with high resolution is needed for modeling surface flow. Previous studies also show the use of gridded rainfall data to estimate surface flow using SWAT model (Vu *et al.* 2012). Hence, there is a need to understand the applicability of the SWAT model for the prediction of runoff with gridded rainfall data.

There are two ways to quantify surface flow using SWAT model, (i) with curve number (CN) method and (ii) with physically based Green and Ampt method (GA). Yang *et al*. (2016) showed that daily runoff estimation using GA method is better. But GA method needs sub-daily rainfall data for runoff estimation which is highly difficult to get at the catchment scale. Therefore, in the present study CN method is used to estimate daily surface flow. SWAT model is a comprehensive model and relies on several parameters varying widely while transforming rainfall into runoff. Calibration process becomes complex and computationally extensive since the number of parameters is substantial. However, with the help of sensitivity analysis, it is possible to reduce the number of parameters by not considering non-sensitive parameters for calibration, which in turn can

give results relatively in shorter time. SWAT Calibration and Uncertainty Program (SWAT-CUP) is the calibration, validation and sensitivity analysis of SWAT model.

2. STUDY AREA

The study area Musi basin lies between 78^0 to 79^0 44' east longitudes and 16^0 40' to 17^0 50' northern latitudes and has an area about 10,885 km^2. Musi River is a tributary of the Krishna River in the Deccan Plateau flowing through Telangana state in India. It originates in Anantagiri Hills near Vikarabad in Ranga Reddy district, 90 km to the west of Hyderabad and flows due east. It finally joins Krishna river after traveling a length of 240 Km in Nalgonda district at Vadapally.

3. HYDROLOGICAL MODELLING OF MUSI SUB BASIN USING SWAT

SWAT model is used for hydrological modelling of Musi basin where watershed delineation and hydrological response unit definition are to be carried out. Digital Elevation Model (DEM), soil map, land use and land cover map, and slope map are given as inputs to the SWAT model. DEM is used to delineate the watershed. Soil map, land use/land cover map and also slope maps used to create Hydrological response units (HRU's).

Figure 1 shows that the Musi basin is divided into 98 sub-basins by using stream network and outlet point present in Dharmacherla. SWAT model was simulated to generate runoff by using gridded weather data obtained from India Meteorological Department (IMD). The simulated data is calibrated using manual calibration helper followed by SWAT-CUP by adjusting the parameters.

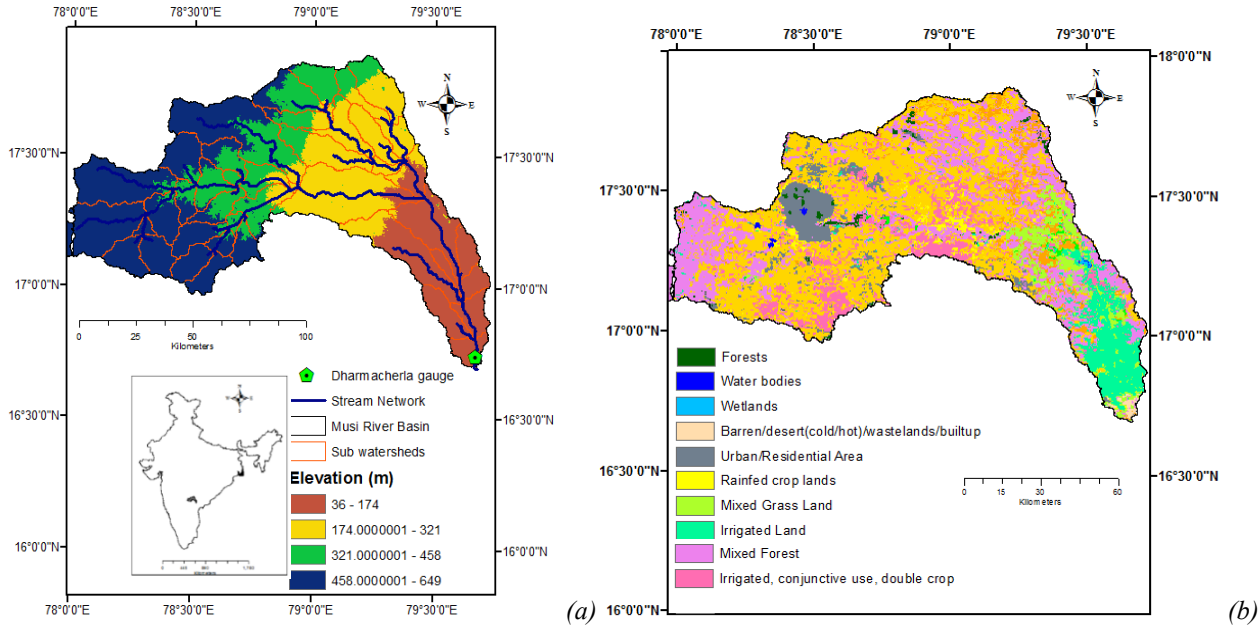

Figure 1. Location (a) and land use (b) maps of Musi basin

3.1 Database preparation

SWAT model primarily requires the following input data for the hydrologic simulation of runoff.

3.1.1 Climate data

SWAT requires climate data in daily time step for weather generation. The climate data includes information on the location of the weather station (latitude and longitude), daily values of precipitation (mm), maximum and minimum air temperature (^{o}C). India Meteorological Department (IMD) gridded precipitation data of 0.25^{0}x0.25^{0} resolution and temperature data of 1x1 degree resolution has been used.

3.1.2 Runoff data

The stream gauge measured by Central Water Commission (CWC) department located at Dharmacherla at the basin outlet is used for SWAT model calibration. The daily runoff time series has been collected from India-WRIS portal (*www.india-wris.nrsc.gov.in/wris.html*) for a period from 01 January 2001 to 31 May 2012 and the observed runoff is shown in the Figure 2(a). There seems to be one outlier which is 5 times of the nest maximum. Figure 2(b) shows the observed runoff after excluding that outlier. This data has been used in the further SWAT model.

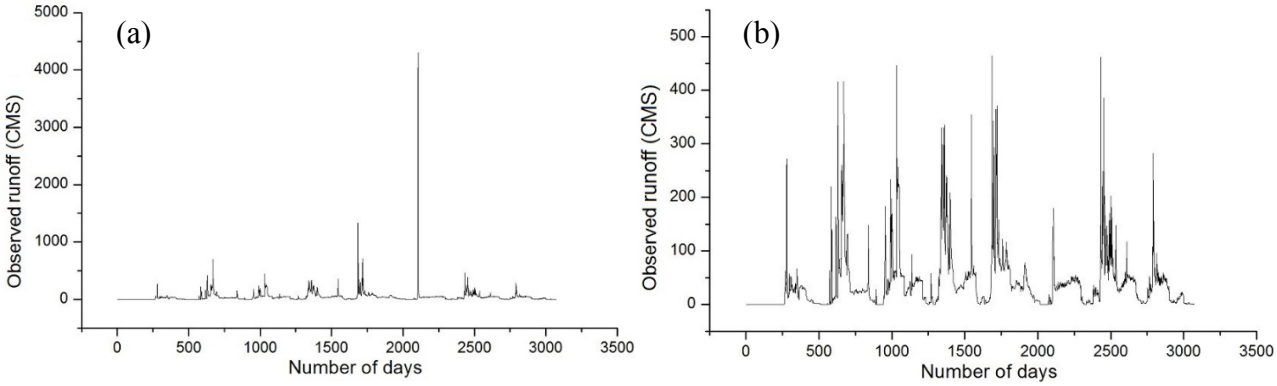

Figure 2. Time series for observed runoff a) original data, b) excluding peak runoff

3.1.3 Digital Elevation Model (DEM)

A 30m resolution digital elevation model has been downloaded from Bhuvan website (*http://bhuvan.nrsc.gov.in/data/download/index.php*). Different elevation bands can be seen from Figure 1. The high values are the locations of higher elevations located in Western Ghats and is shown in Figure 1.

3.1.4 Land Use and Soil map

Land use land cover map has been downloaded from the website *www.swat.tamu.edu* which is of 1km x 1km resolution for Indian data sets and has been used in this study. From the map (Figure 1b), it can be observed that there are around 10 classes of Land use. The types of land cover present in the watershed are shown in the Figure 1(b). Soil map of the Musi river basin has been downloaded in raster format from the website *www.swat.tamu.edu*. The Musi river consists of three different soil classes namely, silty loam, rocky/sandy loam, and fine sandy loam, however majority of the basin lies in rocky/sandy load type of soil.

3.1.5 HRU map

Hydrological response units (HRU) are the regions with homogenous land use, soil and topographical characteristics. SWAT requires the land use map, soil map and slope classification

map for creating HRU. From SWAT overlay analysis nearly 341 HRU's were generated.

4. RESULTS AND DISCUSSION

The above collected, analysed and generated data has been used to simulate the runoff from Musi basin using SWAT model. As an initial step a sensitivity analysis has been carried out.

4.1 Sensitivity analysis

Sensitivity analysis is performed using the SUFI-2 algorithm of SWAT-CUP. The parameter producing the highest average percentage change in the objective function value is ranked as most sensitive.

SWAT-CUP uses the SWAT input files and runs the SWAT simulations by modifying the given parameters. Model calibration and validation are challenging and to a certain degree it is a subjective step in a complex hydrological model. SWAT model of Musi watershed was calibrated and validated using measured daily river discharge available at Dharmacherla.

The optimized parameters of the Musi watershed will be very important in representing the entire watershed and analyzing the water distribution under natural conditions. The Dharmacherla has the discharge data for the period 2001-2012 and the same has been used in the SWAT simulation. The first three years were used as a warm-up period to mitigate the effect of unknown initial conditions, which were subsequently excluded from the analysis. Hence, we divide the discharge data into two periods: a calibration (2004–2009) and a validation period (2010–2012). Based on the built in sensitivity analysis tool in SWAT (*Neitsch et al., 2002*), nine most sensitive parameters were identified. Nevertheless, it is concluded that other parameters are also considered to be important for SWAT simulation in the Musi watershed. After performing rigorous manual calibration, we feed initial values to SWAT-CUP after which sensitivity analysis is performed to get the best fitted values of the parameters. The Table 1 shows the parameter values prior to the usage of the SWAT-CUP and final values of the parameters after incorporating the sensitivised value obtained from the SWAT-CUP sensitivity analysis. The 14 parameters sensitivity analysis results are shown in Table 1. They represent the minimum and maximum values between which the parameters are changed in a SWAT-CUP sensitivity analysis to get the best fitted value of the parameters.

Table 1. Comparison of initial and final values of the parameters used in SWAT-CUP

Parameter Name	Parameter Description	Initial values	Final values	Minimum value	Maximum value
A__CH_K2.rte	Effective channel hydraulic conductivity, mm/hr	0.0000	55.16	55.0	65.0
R__CN2.mgt	Curve Number	77.000	76.81	76	82
V__OV_N.hru	Manning's N	0.1500	3.59	3.50	4.5
V_SURLAG.bsn	Surface runoff lag coefficient, mm/hour	4.0000	20.36	19.0	21.0
V__ESCO.bsn	Soil evaporation compensation factor	0.9500	0.67	0.63	0.68
V__RCHRG_DP.gw	Groundwater recharge	0.0500	0.18	0.0	0.2
R__SOL_K (...).sol	Saturated hydraulic conductivity	3.6634	-0.006	-0.04	0.0
V__GW_DELAY.gw	Ground water delay, days	31.000	57.50	55.0	60.0
A__GWQMN.gw	Threshold depth for ground water flow to occur, mm	1000.0	927.7	920.0	930.0
V__GW_REVAP.gw	Ground water evaporation coefficient	0.0200	0.082	0.08	0.11
V__EPCO.bsn	Plant uptake compensation factor	1.0000	0.89	0.85	0.9
V__ALPHA_BF.gw	Base flow recession factor, days	0.0480	0.08	0.08	0.09
R__SOL_AWC (...).sol	Available water capacity, m/m	0.1211	0.47	0.47	0.49
V__SOL_BD (...).sol	Moist bulk density (Mg/ m3)	1.5090	1.21	1.20	1.4

Table 2. Performance measures

Performance measure	Calibration	Validation
R^2	0.50	0.48
NSE	43 %	44 %
MAE (m^3/sec)	21.39	15.238
Pbias (m^3/sec)	-4.40	12.5

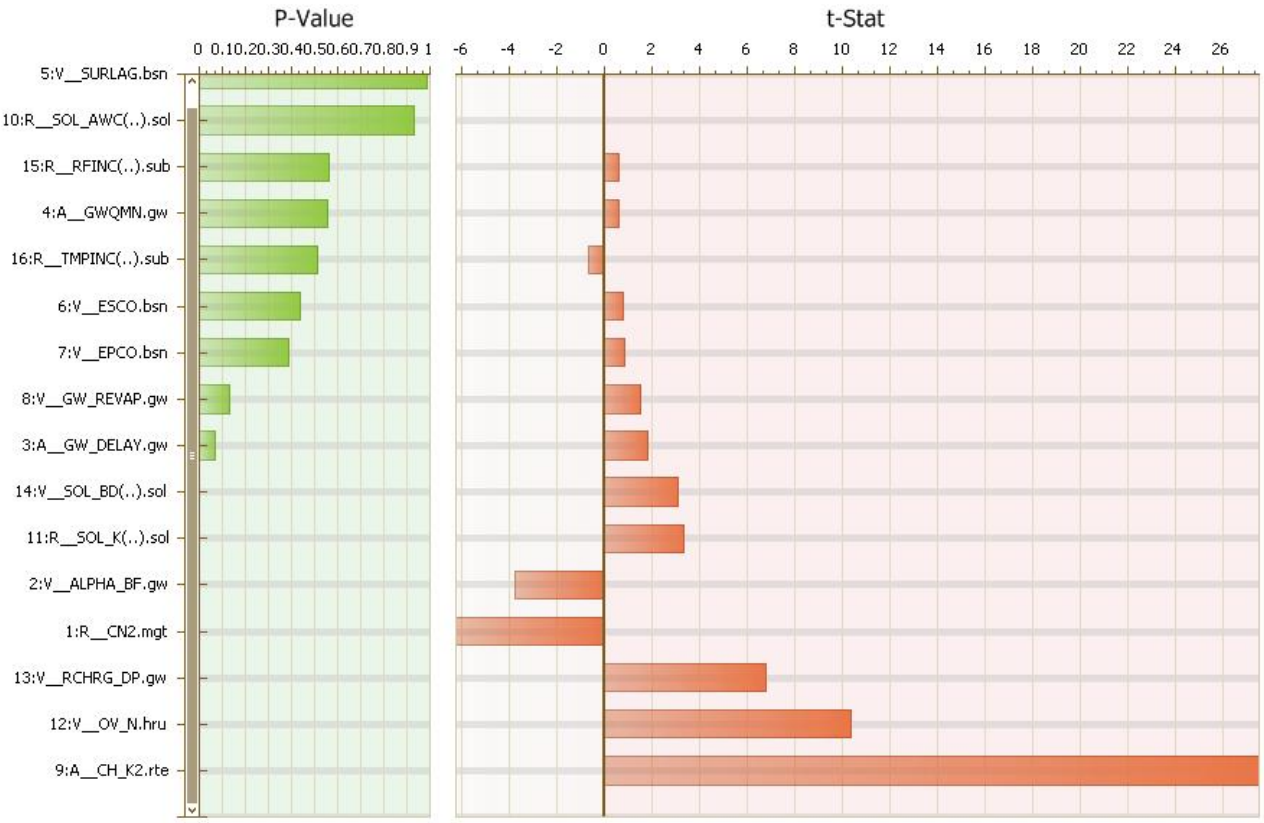

Figure 3. Sensitivity analysis of the SWAT model parameters used in Musi basin

4.2 Global sensitivity analysis

The sensitivities given above are resulted estimates of the average changes in the objective function. This gives relative sensitivities based on linear approximations and, hence, only provides partial t-stat value (larger in absolute values are more sensitive). P-values determined the significance of the sensitivity. A value close to zero has more significance. In Figure 3, it can be seen that the most sensitive parameters are CH_K2, OV_N, RCHRG_DP, CN2, ALPHA_BF, SOL_K and SOL_BD.

4.3 Calibration and Validation of Musi basin using SWAT-CUP

The SWAT hydrologic model was calibrated using observed inflow at Dharmacherla. The calibration procedure involved the adjustment of the SWAT parameters by using SWAT-CUP such that the resulting stream flows matched the observed inflows at Dharmacherla between the period 2004 and 2009 and validation was carried out between the period 2010 and 2012.

Before going to calibration of the model, there is a need to perform uncertainty analysis and sensitivity analysis. This has been carried out by using 14 parameters as shown in Table 1. All parameters except Surface Runoff Lag Coefficient (SURLAG) and Soil Available Water Capacity

(SOL_AWC) are observed to be most sensitive parameters. The SWAT model was again simulated with these sensitivised parameters to obtain the daily discharge. The time series and scatter plot of observed and SWAT resulted runoff during calibration and testing period at basin outlet (Dharmacherla) are shown in Figures 4 and 5, respectively.

The performance of SWAT model has been analyzed based on the graphical representation as well as on the basis of various statistical parameters such as Nash Sutcliff Efficiency (NSE) and regression coefficient (R^2). The value of NSE ranges between -∞ and 1, values between 0.4 and 1.0 are viewed as acceptable levels of performance. The regression coefficient (R^2) describes the proportion of the total variance in the observed data that can be explained by the model. The closer the value of R^2 to 1, the higher is the agreement between the simulated and the measured flow. The statistical performance during calibration period is R^2=0.5, NSE=43%; and during validation R^2 and NSE values are 0.48 and 44% respectively, this shows that the resulted runoff statistics are in acceptable range for daily simulation. The performance measures of SWAT model during calibration and validation are given in Table 2. The performance measures R^2 and NSE have been discussed in detailed above. Mean Absolute Error (MAE) value obtained is not very high considering the number points that are considered for the analysis. Pbias shows that the simulated flow is over estimated in case of calibration and under estimation in case of validation. However, for a daily catchment area based runoff, the results are seems to be in acceptable range.

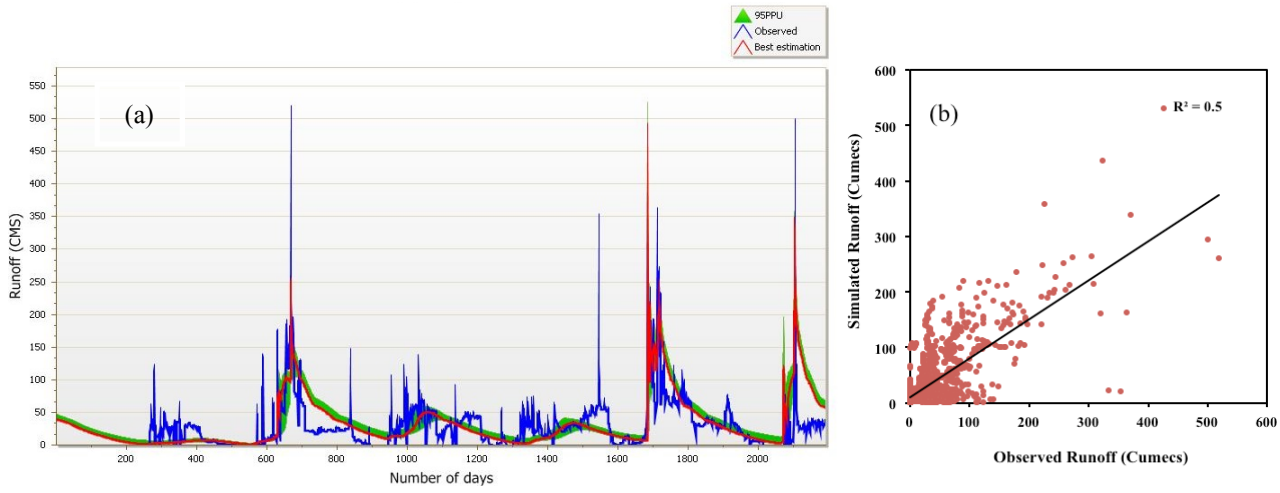

Figure 4. a) Time series and b) scatter plot of observed and SWAT simulated runoff during calibration period

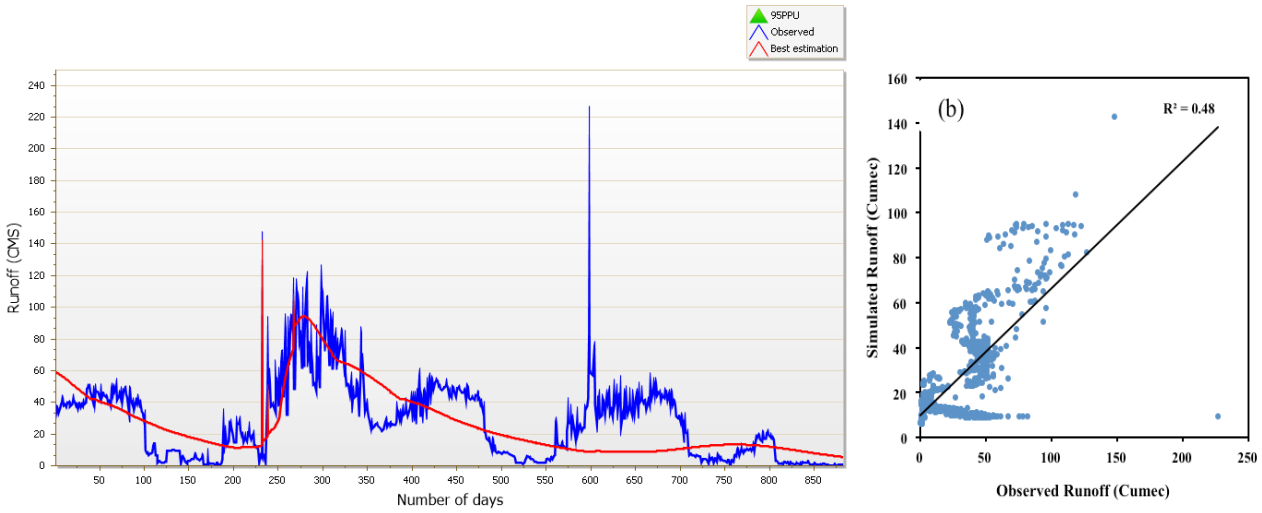

Figure 5. a) Time series and b) scatter plot of observed and SWAT simulated runoff during validation period

5. CONCLUSION

In the present study, a physical process based SWAT model has been developed for the Musi river basin. The Arc SWAT interface of SWAT model has been successfully used for exploring hydrological characteristics of Musi basin. The automatic watershed delineation at HRU level clearly shows the basic features like land use, soil and slope have an effect on the hydrology of the catchment. SWAT-CUP advance calibration and uncertainty analysis tool has been used for automatic calibration of stream flow measurement on daily basis for the period from 2004 to 2012 using the SUFI-2 procedure. The sensitivity analysis adopted for calibration shows variations between parameter values which had been initialized for model calibration on daily basis. After considering all the uncertainties like inconsistency in the observed flow data and with only one outlet available, the SWAT model is a good result for daily simulated flow. The developed SWAT model was calibrated and the results obtained are in acceptable ranges of R^2 and NSE values of 0.5 and 0.43 during calibration. In the case of validation too, the results obtained are in acceptable ranges of R^2 and NSE values of 0.48 and 0.44. The R^2 and NSE for daily calibration more than 0.4 indicate that model gives good results which mean the results obtained are satisfactory.

REFERENCES

Arnold, J. G., Srinivasan, R., Muttiah, R. S., & Williams, J. R. (1998). Large area hydrologic modeling and assessment part I: Model development1.

Gamvroudis, C., Nikolaidis, N. P., Tzoraki, O., Papadoulakis, V., & Karalemas, N. (2015). Water and sediment transport modeling of a large temporary river basin in Greece. Science of the Total Environment, 508, 354-365.

Hernandez, M., Miller, S. N., Goodrich, D. C., Goff, B. F., Kepner, W. G., Edmonds, C. M., & Jones, K. B. (2000). Modeling runoff response to land cover and rainfall spatial variability in semi-arid watersheds. In Monitoring Ecological Condition in the Western United States (pp. 285-298). Springer Netherlands.

Kim, S., Noh, H., Jung, J., Jun, H., & Kim, H. S. (2016). Assessment of the Impacts of Global Climate Change and Regional Water Projects on Streamflow Characteristics in the Geum River Basin in Korea. Water, 8(3), 91.

Neitsch, S. L., Arnold, J. G., Kiniry, J. R., Williams, J. R., & King, K. W. (2002). Soil Water Assessment Tool theoretical documentation. Version 2000. Texas Water Resource Institute, college station, Texas. TWRI Report. TR-191.

Saha, P. P., Zeleke, K., & Hafeez, M. (2014). Streamflow modeling in a fluctuant climate using SWAT: Yass River catchment in south eastern Australia. Environmental earth sciences, 71(12), 5241-5254.

Szcześniak, M., & Piniewski, M. (2015). Improvement of hydrological simulations by applying daily precipitation interpolation schemes in meso-scale catchments. Water, 7(2), 747-779.

Uniyal, B., Jha, M. K., & Verma, A. K. (2015). Assessing climate change impact on water balance components of a river basin using SWAT model. Water Resources Management, 29(13), 4767-4785.

Vu, M. T., Raghavan, S. V., & Liong, S. Y. (2012). SWAT use of gridded observations for simulating runoff-a Vietnam river basin study. Hydrology and Earth System Sciences, 16(8), 2801.

Xu, X., Li, J., & Tolson, B. A. (2014). Progress in integrating remote sensing data and hydrologic modeling. Progress in Physical Geography, 38(4), 464-498.

Yang, X., Liu, Q., He, Y., Luo, X., & Zhang, X. (2016). Comparison of daily and sub-daily SWAT models for daily streamflow simulation in the Upper Huai River Basin of China. Stochastic Environmental Research and Risk Assessment, 30(3), 959-972.

Yen, H., White, M. J., Jeong, J., Arabi, M., & Arnold, J. G. (2015). Evaluation of alternative surface runoff accounting procedures using SWAT model. International Journal of Agricultural and Biological Engineering, 8(3), 64-68.

Proceedings of the 10th World Congress of EWRA 'Panta Rhei', 5-9 July 2017, Athens, Greece
© 2017 *European Water Resources Association*

Distributed rainfall runoff modeling over Krishna river basin

S. Nandi* and M.J. Reddy
Department of Civil Engineering, Indian Institute of Technology Bombay, Mumbai 400076, India
* *e-mail: ce.saswata@gmail.com*

Abstract: Floods can have catastrophic consequences and can have effects on the economy, environment and people. It initiates comprehensive assessment and forecasting of possible flooding events, which is typically carried out using hydrological models. Thus, the main objective of this study was to present a distributed hydrological model, namely Variable Infiltration Capacity (VIC) model for simulating the hydrological variables over Krishna River Basin, India and evaluating its performance by comparing with observed datasets. The main advantages of the VIC model compared to other physically based hydrological models, are the variable infiltration curve, which implement a nonlinear function of the fractional grid cell area to scale the maximum infiltration for enabling runoff calculations for sub grid-scale areas and the parameterization of baseflow using a nonlinear recession curve. Meteorological forcing at 0.5 degree by 0.5 degree spatial resolution from 1980 to 2005 over the basin were used to run the model at a daily time step. The model showed an acceptable performance during calibration and validation with Nash-Sutcliffe efficiency (NSE) = 0.34 and coefficient of determination (R^2) = 0.60 for calibration and NSE = 0.42 and R^2 = 0.68 for validation periods. The results from VIC model shows that it can handle large-scale variability, however it has a tendency to overestimate the streamflow in the downstream portion possibly due to not considering the effect of storage structures in the present model.

Key words: Hydrological model, VIC, Streamflow

1. INTRODUCTION

Water is vital for agricultural, industrial, domiciliary and ecological purposes. Although the earth is made up of 71% of water, the amount of freshwater available for human use is very less. Water resources management requires a system approach, which includes all of the hydrological components, its linkage and interactions amongst all the components. Understanding the hydrology of a watershed is crucial for managing hydrological extremes (floods and droughts), through proper forecasting of hydrological variables.

The Krishna river basin is one of the major river basin in India. It ranks fourth considering annual discharge, and it is regarded as fifth largest basin in terms of surface area in India. The Krishna River is flowing over the states of Maharashtra, Karnataka, Telangana and Andhra Pradesh, and providing freshwater (75% dependable water) of 58.3 km^3 (Sathish 2012). However, the hydrology of this river basin is changing rapidly due to human interventions on the environment, including land use and land cover change, irrigation, flow regulation etc. (Biggs *et al*. 2007). In last few decades, the Krishna River Basin has also witnessed high rainfall and consequent floods during monsoon. Hydrological models were developed and applied to look at these consequences on water resources by large number of researchers (Bergstorm *et al*. 1998; Kite *et al*. 1999; Arnell 1999). Some of the past studies have noted that advanced basin scale hydrological models can contribute for better water resource management (Smakhtin 2006; Biggs *et al*. 2007), which is also very relevant to Krishna river basin.

In this paper, in order to represent the spatial variability of important land surface characteristics in River Basin, the VIC (3L) model, a distributed hydrological model, which is used widely by different researchers, is presented to simulate the runoff and other hydrological processes in Krishna River Basin. The VIC model was developed by Wood *et al*. (1992) and upgraded to the VIC-2L model by enhancing the water and energy balance algorithms by Liang *et al*. (1994). In the VIC-3L

model, the spatial distribution of rainfall is also considered and the parameterization of soil moisture and land surface thermal fluxes are integrated for simulating runoff and hydrographs precisely. In a recent study, Reddy *et al*. (2016) studied the effect of climate change impacts on crop water balance in lower Krishna River Basin of South India by VIC-3L model.

One of crucial tasks for hydrologist is to estimate the various hydrologic variables for water policy making, flood regulations, hydropower plants and in various other watershed management works that utilizes rainfall-runoff models to produce synthetic flood flows from rainfall data. Therefore, the goal of this study is to develop a general framework to perform hydrologic simulation by the application of a distributed hydrological modeling over Krishna River basin.

2. DECRIPTION OF VIC HYDROLOGICAL MODEL

VIC is a semi-distributed land surface hydrologic model that consider the interaction of atmosphere, vegetation and soil, the dynamic change of water and energy flux. One distinguishing characteristic of the model is that it represents vegetation heterogeneity using multiple vegetation tiles in a single grid cell, multiple soil layers with variable infiltration, and non-linear drainage from a lower soil moisture zone (base flow)(Wood *et al*. 1992; Liang *et al*. 1994). For vegetation tiles, evapotranspiration is calculated according to the Penman–Monteith equation (Liang *et al*. 1994), adding the canopy layer evaporation and vegetation transpiration. The Horton infiltration curve is employed to account for the sub-grid variability of soil infiltration functionality under various soil types land covers.

As the VIC-3L model generates the runoff depth in each grid cell, a standalone routing scheme is required for routing of the model simulated runoff via channel network to the outlet of the basin. The routing scheme that was presented by Nijssen *et al*. (1997) is used in the study. This routing model transports the grid cell surface runoff simulated by means of the VIC-3L model inside every grid cell to the outlet of that grid cell and then into the river network. The routing within a grid cell makes use of a Unit Hydrograph theory and the channel routing makes use of the linearized Saint-Venant equations.

3. MODEL APPLICATION

3.1 Study area and data used

The Krishna River Basin, located in southern India, lies between 73°15′ to 81°20′ E and 13°5′ to 19°20′ N (Fig. 1) with a total basin area of 258,912 km^2. The river originates in the Western Ghats at an elevation of about 1337 m, just north of a town called Mahabaleshwar at about 64 Km from the Arabian Sea, and flows for about 1400 km before reaching the Bay of Bengal. The average annual rainfall is 850 mm (spatially varying 500–2000 mm); the maximum temperature varies between 20° C and 42°C and the minimum temperature between 8° and 30°C.

The VIC model requires various forcing files, which includes meteorological, soil parameter, vegetation parameter and vegetation library files. This vegetation parameter and vegetation library data is used to differentiate between various land cover types. This vegetation datasets are collected from Hydro Group at University of Washington (Weedon *et al*. 2011) at a one kilometer spatial resolution and consists of 11 totally different land cover classes. Soil data is based on soil textures of FAO (1995) and obtained from the same source. For gridded weather data, this study uses the dataset prepared for VIC at $0.5^o \times 0.5^o$ spatial resolution for the period 1980 to 2005 by the University of Washington Climate Impacts Group (Maurer *et al*. 2002). Daily observed streamflow of the Krishna River at Wadenapally station was taken from the WRIS-India for model calibration.

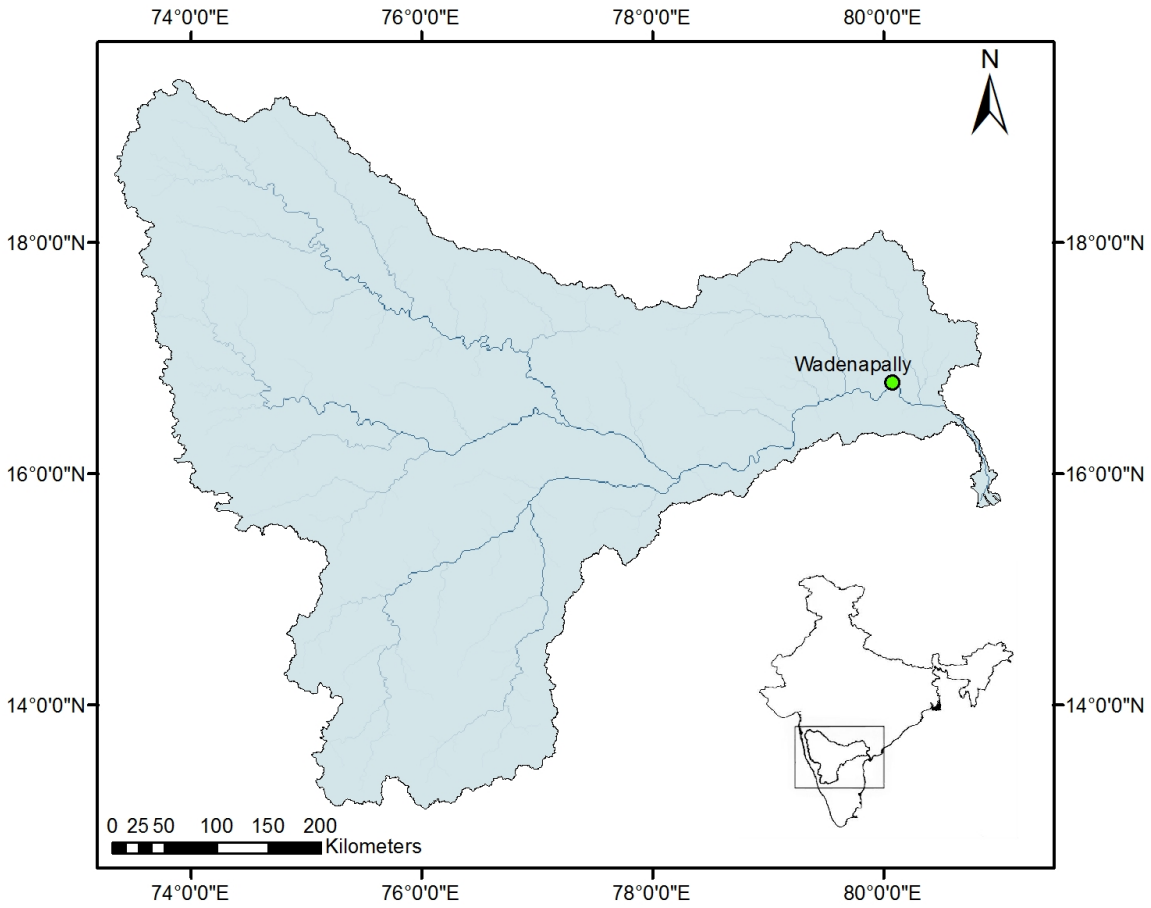

Figure 1. Krishna River Basin

3.2 Model implementation

Data are collected from the mentioned sources and extracted for the study area. Both the VIC model and the standalone routing model are run on Linux platform. All hydrological simulations were performed at daily time step in water balance mode. Routing model was assigned to compute the daily series of the streamflow at Wadenapally station of the Krishna River Basin. Streamflow is an effective measure of hydrologic response in the river basin. Hence, observed streamflows are considered as the most important parameters for comparison of the model and understanding the model capabilities. Given that, the size of the modelled study area is large, monthly averages were used to compare simulated and observed streamflow. The observed discharges of Wadenapally hydrological station are used in model calibration.

3.3 Model calibration and validation

Physically based VIC hydrological model has several parameters that need to be adjusted. Generally, six parameters are approached for calibration (Lohmann *et al*. 1998): i) the infiltration parameter (b_{infit}), that regulates the separation of rainfall into direct runoff and infiltration (a lower b_i offers higher infiltration and yields less surface runoff); ii) d_2 and d_3, that are the thickness of second and third soil layer and have an effect on the available water for transpiration and baseflow respectively (thinner soil depths have faster runoff reaction); iii) W_s, D_s and D_{smax} are the parameters for baseflow and also are finalized via calibration. W_s represents the fraction of most soil moisture content of the third soil layer at which non-linear baseflow occurs, D_s represents the fraction of largest baseflow speed and D_{smax} represents the highest baseflow speed. These three baseflow

parameters decide how fast the stored water in the third soil layer is departed as baseflow (Liang *et al.*1994). The calibration procedure here involves manual adjustment of these six parameters values to achieve best fit results. During model validation, calibrated parameters were taken as input along with other known parameters and the performance of the VIC model were evaluated using Coefficient of determination (R^2) and Nash–Sutcliffe efficiency (NSE) by the following equations:

$$R^2 = \frac{\left(\sum_{i=1}^{n}\left(O_i - \overline{O}\right)\left(S_i - \overline{S}\right)\right)^2}{\sum_{i=1}^{n}\left(O_i - \overline{O}\right)^2 \times \sum_{i=1}^{n}\left(S_i - \overline{S}\right)} \quad (1)$$

$$NSE = 1 - \frac{\sum_{i=1}^{n}\left(O_i - S_i\right)^2}{\sum_{i=1}^{n}\left(O_i - \overline{O}\right)^2} \quad (2)$$

where O_i and S_i are the observed and simulated values, n is the total number of paired values, $\overline{O}$ is the mean observed value.

4. RESULTS AND DISCUSSION

The VIC model using the Lohman routing scheme was applied to the Krishna river basin to simulate the streamflow during the period of 1980 to 2005. The meteorological forcing series was divided into two part (i.e., 1980-1884 and 1995-2005) for evaluating the streamflow before and after the rapid irrigation project expansion and dam construction**.** The calibration period was chosen from 1/1/1980 to 31/12/1989, in which the model was manually calibrated using standard calibration measures. Calibration was performed for the monthly mean streamflow. During calibration, value of coefficient of determination was 0.604 and the value of Nash Sutcliffe model Efficiency (NSE) was obtained as 0.34. A yearly average simulated flow of 968 m^3/s vs a yearly average observed flow of 756 m^3/s were also obtained during calibration. So, there is clearly some overestimation in model simulated flow values. For simulated and observed flows, the standard deviations were obtained as 1008 m^3/s and 1259 m^3/s respectively. It indicates the averaging out of extreme flow values in VIC model. Details of the calibrated parameter values and their range used for calibration are given in the Table 1. Comparison of monthly average runoff between calibrated simulated streamflow and observed streamflow is shown in the Figure 2a.

Table 1. Details of the calibrated parameter values

Parameter	***units***	***Range***	***Calibrated value***
b_{infilt}	*index*	*0.00001–0.4*	*0.01*
D_s	*fraction*	*0.0–1.0*	*0.2*
D_{smax}	*mm/day*	*1-40*	*5*
W_s	*fraction*	*0.0–1.0*	*0.99*
d_2	*meters*	*0.3-2.5*	*0.7*
d_3	*Meters*	*0.2-4.5*	*2.1*

After model calibration, next five years (1990-1994) were chosen for model validation. Comparison of monthly average runoff for validation period is shown in the Fig. 2b. During validation, values of coefficient of determination and NSE were estimated as 0.68 and 0.42 respectively. Mean and standard deviation of simulated flows were 963 and 1187 m^3/s, while for observed flow they were 1019 and 1353 m^3/s for the validation time. From the results presented in Fig. 2b, is was noticed that the model is performing quite well during validation period.

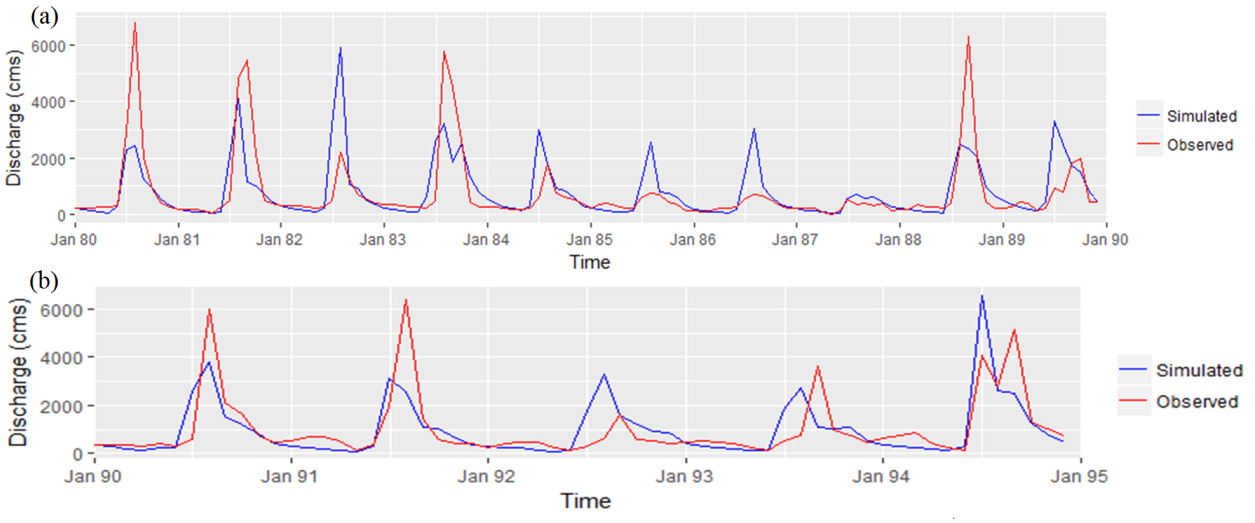

Figure 2. Comparison of VIC generated streamflow with observed streamflow during (a) calibration (1980-1989) and (b) validation (1990-1994)

According to CWC report (1999), Krishna river basin's mean annual runoff was found to be 57 km^3 (29% of rainfall) or 1807 m^3/s for 1901-1990, which is around twice of the simulated average annual runoff for the basin (968 m^3/s). It has been reported that rapid dam construction and irrigation project expansion resulted 54.5 km^3 of total live reservoir storage by the twenty century, which is also nearly equal to annual discharge of Krishna river basin (Biggs *et al*. 2007). Even in the present study, when the calibrated model was operated for 1995 to 2005, it showed a poor performance with coefficient of determination and NSE as 0.5 and -4.2 respectively. It can be shown (Fig.3) that, after 1995 most of year were having significantly less discharges, even in the monsoon periods. Annual average of simulated flow during this period was 1129 m^3/s, while the observed annual flow decreased to 460 m^3/s. Without significant changes in rainfall, discharges were reduced due to the effect of various storage structures. This might attributed to the degradation of model performance due to not considering this storage structures effects within the model.

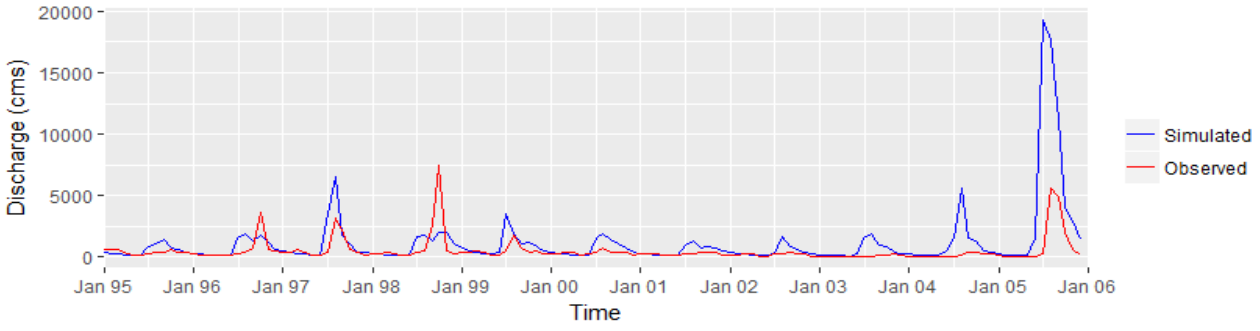

Figure 3. Comparison of VIC generated streamflow with observed streamflow during 1995-2005

4. CONCLUSION

In this study, a framework for applying the VIC-3L model to conduct hydrological simulations over the Krishna River Basins is described. Daily forcing data for the period of 1980 to 2005 are prepared grid-wise at $0.5^o \times 0.5^o$ spatial resolution along with the vegetation and soil dataset and then the VIC-3L model is applied to each of the 93 grids of Krishna river basin. Comparison of monthly streamflow at Wadenapally in the Krishna River Basin shows a moderate agreement between model simulated and observed flows.

However, it is also found that in the Krishna river basin, the large number of storage structures (i.e., total 660 dams) is effecting the natural stream and play an important role in altering the flow hydrographs. These storage structures are also found to be responsible for minimization of peak annual flood, which leads to reduction in flood damages. However, it is expected that in order to obtain a better hydrologic simulation in Krishna river basin using VIC hydrologic model, the effect of storage structure should be incorporated in the model.

REFERENCES

Arnell, N. W., 1999. A simple water balance model for the simulation of streamflow over a large geophysical domain. Journal of Hydrolog. 217(3): 314-355.

Bergstrom, S., and Graham, L. P., 1998. On the scale problem in hydrological modeling. Journal of Hydrology 211(1), 253-265.

Biggs, T., Gaur A., Scott, C., Thenkabail, P., Gangadhara, R. P, Gumma, M. K., Acharya, S., and Turral, H., 2007. Closing of the Krishna Basin: irrigation, streamflow depletion and macroscale hydrology. International Water Management Institute 111: 17-32.

Central Water Commission, 1999. Reassessment of water Resources potential of India. Ministry of Water Resources, Government of India.

Kite, G. W., and Haberlandt, U., 1999. Atmospheric model data for macroscale hydrology. Journal of Hydrology 217(3): 303-313.

Liang, X., Lettenmaier, D. P., Wood, E. F., and Burges, S. J., 1994. A Simple hydrologically Based Model of Land Surface Water and Energy Fluxes for GSMs. Journal of Geophysical Research 99: 415-428.

Lohmann, D., Raschke, E., Nijssen, B. and Lettenmaier, D.P., 1998. Regional scale hydrology: II. Application of the VIC-2L model to the Weser River, Germany. Hydrological Sciences Journal *43*(1): 143-158.

Maurer, E. P., Wood, A. W., Adam, J. C., Lettenmaier, D. P., and Nijssen, B., 2002. A Long-Term Hydrologically Based Dataset of Land Surface Fluxes and States for the Conterminous United States. *Journal of Climate* 15(22): 3237–3251.

Nijssen, B., Lettenmaier, D. P., Liang, X., Wetzel, S. W., and Wood, E. F., 1997. Streamflow simulation for continental-scale river basins. Water Resources Research *33*(4): 711-724.

Pichuka, S., Prasad, R., Maity, R. and Kunstmann, H., 2017. Development of a method to identify change in the pattern of extreme streamflow events in future climate: Application on the Bhadra reservoir inflow in India. Journal of Hydrology: Regional Studies *9*: 236-246.

Reddy, K. S., Kumar, M., Maruthi, V., Lakshminarayana, P., Vijayalakshmi, B., Umesha, B., and Reddy, Y. V., 2016 Climate change impacts on crop water balance of maize in lower Krishna River Basin of South India. Current Science 111(3): 565-570.

Sathish, S., 2012. Changing Paradigms of River Valley Settlements-krishna River Valley. International journal of Social Science & Interdisciplinary Research 1(7): 145-154.

Smakhtin, V. Y., 2006. An assessment of environmental flow requirements of Indian river basins. International Water Management Institute 107: 6-17.

Weedon, G.P., Gomes, S., Viterbo, P., Shuttleworth, W.J., Blyth, E., Österle, H., Adam, J.C., Bellouin, N., Boucher, O. and Best, M., 2011. Creation of the WATCH forcing data and its use to assess global and regional refere nce crop evaporation over land during the twentieth century. Journal of Hydrometeorology *12*(5): 823-848.

Wood, E. F., Lettenmaier, D. P., and Zartarian, V. G., 1992. A land-surface hydrology parameterization with subgrid variability for general circulation models. Journal of Geophysical Research 97: 2717-2728.

Proceedings of the 10th World Congress of EWRA 'Panta Rhei', 5-9 July 2017, Athens, Greece
© 2017 *European Water Resources Association*

Application of HEC-HMS for the event and continuous simulation in high-altitude scarcely-gauged catchment under changing climate

M. Azmat[1*], M.U. Qamar[2], S. Ahmed[1], E. Hussain[1], M. Umair[3]
[1] *School of Civil and Environmental Engineering (SCEE), National University of Sciences and Technology (NUST), H-12, Islamabad, Pakistan.*
[2] *Deaprtment of Irrigation and Drainage, Faculty of Agricultural Engineering, University of Agriculture, Fasialabad, Pakistan.*
[3] *Water Resources and Remote Sensing Laboratory, Department of Water Resources, Graduate School of Water Resources, Sungkyunkwan University, Suwon 440-746, Republic of Korea.*
[*] *e-mail: azmat@igis.nust.edu.pk*

Abstract: Aim of this study was to examine the most suitable combination of different methods (transfer and loss) provided by a standard rainfall-runoff model (HEC-HMS), used for the event based and continuous streamflow simulation, in a high-altitude (snow- and glacier-fed) scarcely-gauged Jhelum River catchment (western Himalayan), under potential changing climate scenarios. The observed and remotely sensed Tropical Rainfall Measuring Mission (TRMM) data were utilized to simulate daily streamflows. Further, the land use land cover layers were utilized as input data to design initial curve numbers (CN) of the study area. The model were calibrated during 2000-2007 and validated during 2007-2012, for different combinations of transfer (Snyder Unit Hydrograph and Clark Unit Hydrograph method) and loss methods for event based (Soil Conservation Service Curve Number (SCS-CN) and Green and Ampt) and for continuous simulation (Soil Moisture Accounting (SMA) and deficit and constant loss method) for the selection of most suitable combination to forecast the daily streamflow under potential climate change scenarios. Overall, all the combinations performed within the acceptable range with least NS coefficient of 0.76 for event based and 0.68 for continuous simulation. The combination of Green and Ampt and Clark UH for event based and SMA and Snyder UH for continuous simulation showed best efficient results than any other combination, in high-altitude scarcely-gauged catchment. Further, the hypothetical climate change scenarios showed a significant increase of annual streamflows (21.87%) of the Jhelum River catchment by the increase of 20% precipitation in comparison with 3 ^{o}C temperature increase (10.79%).

Key words: HEC-HMS, Event based, Continuous simulation, Hydrological Modelling

1. INTRODUCTION

The application of hydrological models with accurate formulation is essential for the simulation and forecasting of streamflows in catchments characterized by high-altitude with limited data issues to manage the hydrological extremes such as droughts and floods, in relation with climate change. The hydrological models can be categories into rainfall-runoff and snowmelt-runoff models. The rainfall-runoff models showed their importance because of provision to incorporate snowmelt-runoff and can simulate both source of runoff i.e. rainfall or snowmelt (Azmat et al. 2016). However, the rainfall-runoff models are less efficient in high-altitude watersheds (Martinec J 2008). In hydrological modelling the quality of climate data and selection of simulation methods significantly affects the accuracy of outcomes which further leads to the uncertainty in hydrological predictions under changing climate (De Silva et al. 2013). Therefore, the selection of appropriate methods by considering catchment characteristics is always been challenging for the hydrological community.

The Hydrologic Engineering Center–Hydrologic Modelling System (HEC–HMS) developed by the U.S. army Corps of Engineers, is a well-known rainfall-runoff model used for the dendritic watershed modelling, offers several methods for the modelling on lumped and distributed basis. This model is seldom calibrated and validated for the high-altitude Pakistani watersheds and essential to examine under local input data issues. The calibration of hydrological models by

employing local observed or remotely sensed data is in fact useful to improve accuracy of predictions (Halwatura and Najim 2013).

The HEC-HMS offers total nine different loss and seven transfer methods to simulate streamflows and few of them are specifically designed for event based simulations, while others are for continuous simulation. Several researchers (Azmat et al. 2015; De Silva et al. 2013; Halwatura and Najim 2013; Shahid et al. 2016) have been applied HEC-HMS for the event based and continuous simulation by employing different methods. However, this study is an attempt to check the efficiency of different combinations of loss and transfer methods available in HEC-HMS model for event based and continuous simulation by the integration of remotely sensed data. Subsequently, a most efficient combination was applied to investigate the impact of climate change on streamflows of the Jhelum River basin.

2. STUDY AREA

This study was carried out in the Jhelum River basin originates from Northern Pakistan, a sub-basin of the Indus Basin, having an area of 33,867 km^2 up to Mangla dam located in Azad Kashmir, Pakistan. Due to transboundary river catchment, more than 50% catchment area is situated in India which is considered as ungauged part of the catchment because of data collection issues (Azmat et al. 2015). The elevation of the study area ranges between 300- 6182 m a.s.l. (mean elevation~ 2094 m a.s.l.) and only four (4) stations area located above the mean elevation. The Jhelum River basin is mainly a snow-fed catchment with slightly covered by perennial glaciers, approximately 3% (>5000 m a.s.l.) of the total area, as confirmed by the hypsometric analysis.

3. METHDOLOGY

3.1 Hydrometeorological Data

The observed daily precipitation and temperature data were obtained from Water and Power Development Authority (WAPDA), and Pakistan Meteorological Department (PMD) for eleven (11) stations located within the boundary of Pakistani border, spanning 2000-2013. While, the daily streamflow data at Mangla dam were made available over the period of 2000-2013 from Surface Water Hydrology Project of WAPDA (SWHP-WAPDA).

3.2 Remotely sensed data

3.2.1 Precipitation data

Further, to cover the ungauged part of the catchment, two remotely sensed (Tropical Rainfall Measuring Mission (TRMM) and ERA-interim datasets were evaluated for the integrity in comparison with observed data. We utilized 3B42 version 7 daily precipitation at spatial resolution of 0.25°x0.25°. TRMM data were extracted at seven points located in ungauged part of the catchment. This dataset have been tested and successfully used by Azmat et al. (2016), in Jhelum River basin.

3.2.2 Topographic, soil and land use data

The Advance Spaceborne Thermal Emission and Reflection Radiometer (ASTER) global digital elevation model (GDEM) was utilized in this study to estimate physical characteristics such as

catchment area, reach length and slope etc. The project was generated by the integration of ASTER GDEM with the HEC-GeoHMS (an extension of ArcGIS).

The curve number values estimation is mainly based on the soil type and LULC information, therefore, both information were integrated for further analysis. In order to obtain the LULC data, the information extraction was performed by using data provided by two (European Space Agency (ESA) and classify images of Landsat 8) different agencies which further compared to assess the difference between both datasets. The comparison between the information obtained from both datasets was performed by considering ESA data as a reference because this data have been successfully used by Adnan et al. (2016), for this region. The results for both datasets were found very similar, therefore, the information extracted from Landsat 8 images were finally used to compute the initial Curve Number values with help of guidelines given in National Engineering Handbook of Hydrology (USDA-NRCS 2007). The soil types for the study basin was extracted by using Digital Soil Maps of World prepared by Food and Agriculture Organization (FAO) of the United Nations, during 2007 (FAO 2007).

3.3 HEC-HMS model application

HEC–HMS a standard rainfall-runoff model detail discussed by Azmat et al. (2016) and De Silva et al. (2013). In this study, event and continuous simulations by employing HEC-HMS was carried out on semi-distributed basis and the study catchment was divided into twenty two (22) sub-basins by using HEC-GeoHMS. To examine the event based simulation efficiency of the model, two flood events were selected in a year (one from each season i.e. winter (Sep-March) and summer (April-August)) during 2000-2007. The selection of events during different seasons was associated with the investigation of model capability for the simulation of events occurred during snow accumulation and monsoon season (extreme rainfall events). The event based calibration was carried out during 28 July–08 August 2000 and 07 July–26 July 2005, for summer season and 21–28 Feb. 2000 and 08 –19 Feb. 2005, for winter season. While, the validation was performed during 07 July–19 July, 2006 and 21 June–19 July, 2007, for summer season, and 23–05 March 2006 and 01–13 Dec. 2007, for winter season. Further, the calibration and validation for the continuous simulation was performed during April 2000–March 2007 (5 years) and April 2007–March 2012 (5 years), respectively.

The model was applied by using different combinations of loss and transfer methods available in HEC-HMS in order to examine the most suitable combination for event and continuous streamflow simulation in high-altitude scarcely-gauged catchment (Table 1). The selection of loss and transfer method was chosen by considering their specific application i.e. event or continuous. In this study, we employed two loss methods i.e. Green and Ampt and Soil Conservation Services (SCS) Curve Number (CN) for event based, while, soil moisture accounting (SMA) and deficit and constant for continuous simulation. Further, two different transfer methods i.e. Snyder Unit Hydrograph and Clark Unit Hydrograph, were adopted for both event and continuous simulations, as adopted by Azmat et al. (2015).

Further, to incorporate snowmelt contribution, the model offers temperature index and gridded temperature index method. The gridded temperature index method is complicated and its application is limited in scarcely-gauged catchments, therefore, temperature index method was adopted in this study. The optimized range and detail of source of initial parametric values is given in Table 1.

Further, the model efficiency was evaluated by using three well-known statistical descriptors such as normalized objective function (NOF), the Nash–Sutcliffe efficiency (NS), and the

percentage bias (δb).

3.4 Climate change scenarios

The climate change hypothetical scenarios were established by considering outcomes of previous studies for this region such as Akhtar et al. (2008); IPCC (2014). In this study, two scenarios were considered for the climate change analysis, as follows:

First, for the precipitation scenarios we considered an increase by 10 and 20%, while decrease by 10%, in base precipitation (2000-2005). Second, an increase by 2 and 3 ^{o}C, while decrease by 2 ^{o}C, in base temperature.

Table 1: Range of estimated and calibrated values for the calibration and validation of event based and continuous streamflows, for the twenty two (22) sub-basins of Jhelum River basin.

Parameter	Range of Optimized values	Source of Initial Values
Soil Moisture Accounting (SMA) Loss Method		
Canopy storage (mm)	7.5 – 20	HEC-HMS Help manual (Scharffenberg and Fleming 2006)
Surface storage (mm)	8 – 12	HEC-HMS Help manual (Scharffenberg and Fleming 2006)
Max infiltration (mm/h)	8 – 10	GIS data (Landsat 8)
Imperviousness	21 – 30	GIS data (Landsat 8)
Soil storage (mm)	28 – 55	FAO soil data
Tension storage (mm)	15 – 30	HEC-HMS Help manual
Soil percolation (mm/h)	25 – 50	FAO soil data
Ground water 1 storage (mm)	125 – 200	Calibration trail and error
Ground water 1 percolation (mm/h)	1.0 – 1.50	Calibration trail and error
Ground water 1 coefficient (h)	80 – 200	Calibration trail and error
Ground water 2 storage (mm)	140 – 180	Calibration trail and error
Ground water 2 percolation (mm/h)	1.0 – 1.50	Calibration trail and error
Ground water 2 coefficient (h)	1.0 – 1.50	Calibration trail and error
Deficit and Constant Method		
Initial Deficit (mm)	10 – 35	HEC-HMS Help manual (Trail and Error)
Constant Rate (mm/hr)	0.30 – 3.25	HEC-HMS Help manual (Trail and Error)
Impervious (%)	18 – 35	GIS data (Landsat 8)
Curve Number Method		
Initial Abstraction (mm)		Trail and error
Curve Number	41.85 – 49.39	GIS and FAO data (Trail and error)
Green and Ampt Method		
Initial loss (mm)	2 – 8	GIS data (Landsat 8), Calibration trail and error
Moisture deficit	0.21 – 0.58	FAO soil data and De Silva et al. (2013), (trial and error method)
Suction head (mm)	195.39 – 225	FAO soil data and De Silva et al. (2013), (trial and error method)
Conductivity (mm/h)	2.5 – 3.0	FAO soil data and De Silva et al. (2013), (trial and error method)
Impervious (%)	25 – 35	GIS data (Landsat 8), Calibration trail and error
Snyder UH Transfer Method		
Standard Lag (hr) Peaking Coefficient	2.98 – 23.66	US Soil Conservation Service equation for time of concentration
Clark UH Transfer Method		
Time of Concentration (hr)	4.23 – 36.22	SCS log equation, Calibration trail and error
Storage Coefficient (hr)	8.41 – 35.63	
Temperature Index Method		
Px Temperature (^{o}C)	2.5 – 3.0	HEC-HMS help (constant for each sub-basin but varies over simulation time window)
Base Temperature (^{o}C)	0	HEC-HMS help (constant for each sub-basin but varies over simulation time window)
Lapse Rate (^{o}C /100 m)	-0.65 – -0.15	By using observed temperature data (WAPDA)
Degree Day Factor (DDF) (mm/ ^{o}C-day)	4.2 – 7.4	Extract from previous studies conducted on Himalayan Range (Azmat et al. 2016)
Evapotranspiration (mm/month)	3.0 – 78	By using Hamon method

4. RESULTS AND DISCUSSION

This study suggests the best suitable combination of methods offered by HEC-HMS for the simulation of event and continuous based streamflows to improve the modelling efficiency.

4.1 Event based simulations

The extreme events during winter and summer of 2000 and 2005 were selected for the event based streamflow simulations. Table 2 depicted that the model performed efficient during calibration and validation period with least values 0.22, 0.86 and 13.59 of NOF, NS and δb (%), respectively, for the calibration of summer season (28–08, August 2000) by employing C3 (SCS CN and Snyder UH) combination. However, during winter season (21 – 28 Feb. 2000) the model performed slightly less efficient for the extreme events with least NOF, NS and δb (%) values of 0.21, 0.84 and 14.17, respectively, by employing C3 combination. The results showed that the C2 (Green and Ampt and Clark UH) combination showed best simulation efficiency with values 0.12, 0.96 and 10.18 of NOF, NS and δb (%), respectively, during both calibration periods of summer season (07–26 July, 2005). The results obtained during validation period showed slightly poor efficiency of HEC-HMS with highest NS coefficient value of 0.86 during summer season (07–19 July, 2006) for C2 combination. Moreover, Figure 1 showed a substantial difference in streamflows during winter and summer season. It observed that the HEC-HMS reproduce streamflows efficiently against observed by employing all the combinations, however, C2 produced best results. Overall, it noticed that the HEC-HMS performed slightly less efficient during winter with comparison of summer season. This may be associated with low efficiency of the HEC-HMS with the simulation of snowmelt runoff. During winter season, the precipitation occurs in low elevation part of the catchment generate runoff, however, in high elevation part, the precipitation occurrence in form of solid snow resulting delay in hydrological response.

4.2 Continuous streamflow simulation

The results for the calibration and validation of continuous streamflow by employing different combinations of loss (SMA and Deficit and Constant) and transfer (Snyder UH and Clark UH) is presented in Table 2. The results showed that the HEC-HMS performed fairly well with least NS coefficient value of 0.75 and 0.68 during calibration and validation period, respectively. Although, the simulation efficiency for all combinations were found very similar, however, C5 (SMA and Snyder UH) combination was found most efficient during both calibration and validation with NS coefficient value of 0.78 and 0.73, respectively. Figure 2 depicted that the HEC-HMS reproduce streamflows fairly well against observed during both summer and winter season. The streamflows during winter season are not substantial in comparison with summer season, nevertheless, few non exiting peaks against observed data were produced by HEC-HMS by employing C5 combination in contrast to C7. However, it observed that the C5 combination performed slightly better to reproduce rapid streamflow peaks in comparison with C7 (Deficit and constant and Clark UH). The similar results were found for C6 and C8 combinations. Overall, during summer season, the simulated streamflows were overestimated under all combinations. This may be associated with the limitation of HEC-HMS which is poor to properly capture some rapid streamflow peaks generated by extreme rainfall events and snowmelt generated runoff. Since, the Jhelum River basin is influenced by two precipitation patterns (monsoon and westerlies circulations), therefore, the streamflow generate by rainfall are overlapped by snowmelt runoff particularly during early summer season.

Table 2: Statistical descriptors for the event based and continuous streamflow simulation by using different combinations of loss and transfer methods, at Mangla dam.

Event Based Simulation			NOF	NS	δb (%)	NOF	NS	δb (%)
For Calibration Events			Summer Events			Winter Events		
			28 July – 08 August 2000			21 Feb. – 28 Feb. 2000		
C1	Green and Ampt	Snyder UH	0.20	0.88	17.43	0.21	0.85	12.48
C2	Green and Ampt	Clark UH	0.18	0.94	11.82	0.14	0.91	10.18
C3	SCS CN	Snyder UH	0.22	0.86	13.59	0.21	0.84	14.17
C4	SCS CN	Clark UH	0.20	0.92	12.28	0.15	0.86	10.87
			07 July – 26 July 2005			08 Feb. – 19 Feb. 2005		
C1	Green and Ampt	Snyder UH	0.20	0.87	12.12	0.22	0.85	12.48
C2	Green and Ampt	Clark UH	0.12	0.96	10.18	0.11	0.93	9.48
C3	SCS CN	Snyder UH	0.17	0.89	12.42	0.18	0.85	11.57
C4	SCS CN	Clark UH	0.13	0.93	10.55	0.14	0.90	10.38
Average for Validation Event			07 July – 19 July 2006			23 Feb. – 05 March 2006		
C1	Green and Ampt	Snyder UH	0.26	0.81	13.63	0.32	0.78	15.67
C2	Green and Ampt	Clark UH	0.16	0.86	12.17	0.24	0.83	13.65
C3	SCS CN	Snyder UH	0.25	0.78	19.35	0.36	0.76	15.39
C4	SCS CN	Clark UH	0.23	0.80	16.66	0.36	0.76	16.33
Continuous Simulation		Calibration April 2000 – March 2005						
C5	SMA	Snyder UH	0.40	0.78	21.27	–	–	–
C6	SMA	Clark UH	0.42	0.77	22.39	–	–	–
C7	Deficit and Constant	Snyder UH	0.44	0.75	25.63	–	–	–
C8	Deficit and Constant	Clark UH	0.42	0.76	24.21	–	–	–
		Validation April 2007 – March 2012						
C5	SMA	Snyder UH	0.45	0.73	31.33	–	–	–
C6	SMA	Clark UH	0.48	0.70	32.51	–	–	–
C7	Deficit and Constant	Snyder UH	0.46	0.72	30.28	–	–	–
C8	Deficit and Constant	Clark UH	0.49	0.68	32.88	–	–	–

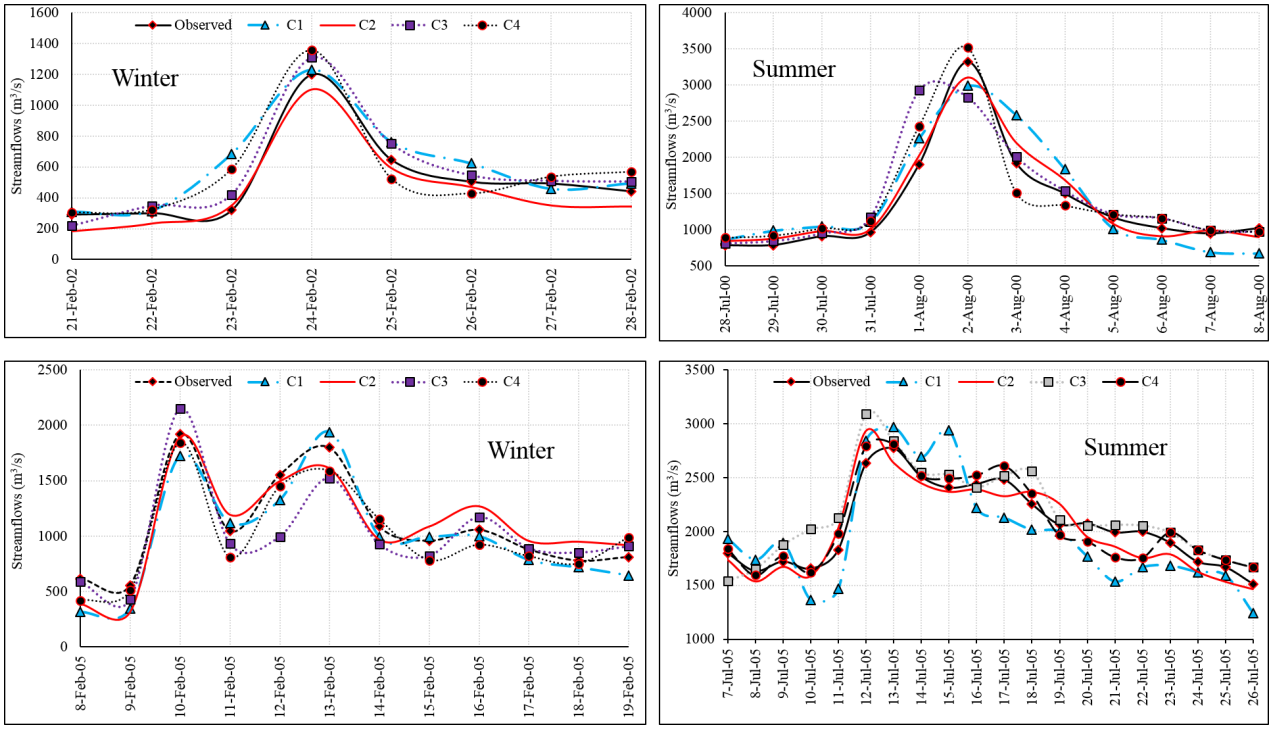

Figure 1: Observed and event based simulated streamflow for the combination of C1, C2, C3 and C4 at Mangla dam (Jhelum River basin), during the calibration periods.

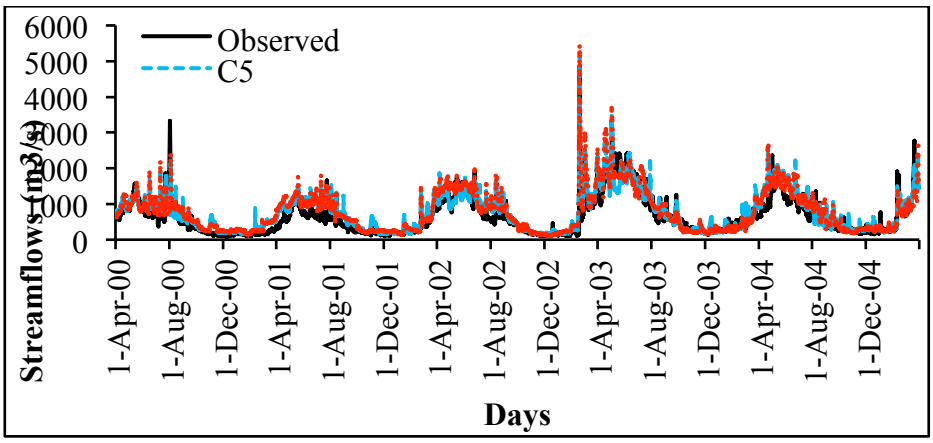

Figure 2: Observed and continuous daily simulated hydrograph for the combination of C5 and C7 at Mangla dam (Jhelum River basin), during the calibration period of five (5) years (April 2000 – March 2005).

4.3 Impact of climatic variations on streamflows

The impact of climate change on streamflow was investigated under hypothetical scenarios of change in precipitation and temperature by employing calibration period of C5 (SMA and Snyder UH) combination, as shown in Figure 3. A significant change was observed by the change of climate variables. It observed that the winter streamflows were significantly influenced by the change in temperature as compare to summer. This change is slightly different in case of change in precipitation. With the increase of 10% (P+10%) and 20% (P+20%) precipitation, the streamflows during summer season were found increased by 16.96% and 22.82%, respectively. With the decrease in precipitation by 10% (P-10%), the streamflows were found decreased by -22.18% during summer season. This may be associated with fact that the HEC-HMS is largely sensitive to the precipitation and less to the temperature. Therefore, the model response fairly well to the precipitation change. Moreover, the Jhelum River basin is mainly influenced by the monsoon precipitation pattern and slightly by westerlies circulation, therefore, a slight increase in precipitation could largely effects the summer streamflows. Figure 3 depicted that the increase in precipitation by 10 and 20% resulting significant increase in streamflow during June, July and August (summer months).

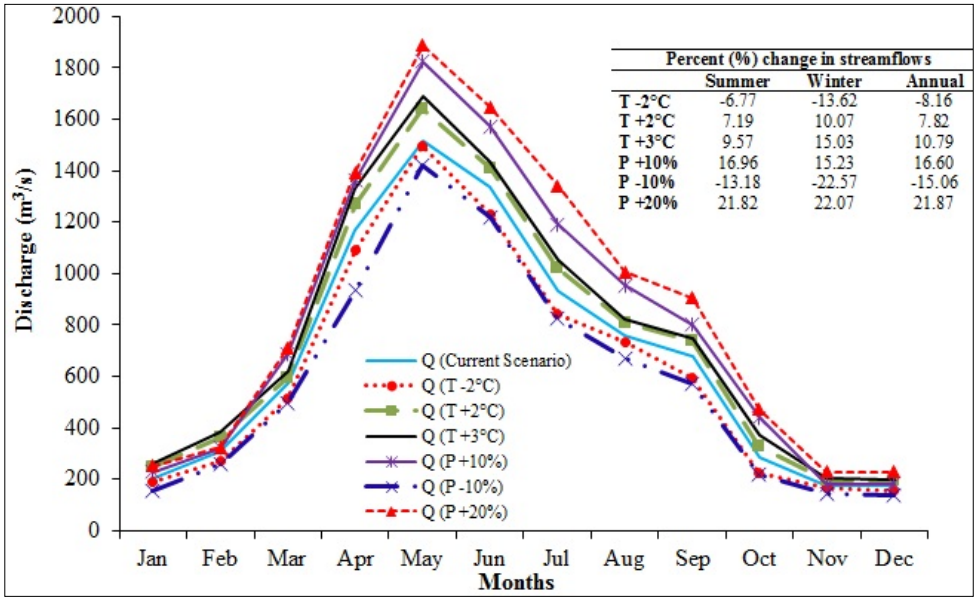

Figure 3: Percent change in streamflows under different hypothetical scenarios of change in precipitation and temperature.

5. CONCLUSIONS

This study suggests that the combination of different loss and transfer methods are effective to improve the continuous and event based hydrological modelling in a high-altitude scarcely-gauged catchment. The application of different combinations shows the capability of HEC-HMS to reproduce streamflows by the integration of different datasets of soil and land use land cover to improve the parametrization of the model. Moreover, the remotely sensed TRMM (3B42) precipitation data could be useful alternative for the scarcely-gauged Himalayan catchments. The climate change analysis shows a significant change in streamflows by the change in climate variables, in Jhelum River basin. Moreover, the Jhelum River streamflow is mainly responded by monsoon rainfall as compare to temperature during the end summer months, therefore, a significant increase in streamflow is expected in future.

REFERENCES

Akhtar M, Ahmad N, Booij MJ (2008) The impact of climate change on the water resources of Hindukush–Karakorum–Himalaya region under different glacier coverage scenarios. J Hydrol 355(1):148–163

Azmat M, Choi M, Kim T-W, Liaqat UW (2016) Hydrological modeling to simulate streamflow under changing climate in a scarcely gauged cryosphere catchment Environmental Earth Sciences 75:1-16

Azmat M, Laio F, Poggi D (2015) Estimation of water resources availability and mini-hydro productivity in high-altitude scarcely-gauged watershed Water Resources Management 29:5037-5054

De Silva M, Weerakoon S, Herath S (2013) Modeling of Event and Continuous Flow Hydrographs with HEC–HMS: Case Study in the Kelani River Basin, Sri Lanka Journal of Hydrologic Engineering 19:800-806

FAO (2007) Digital Soil Map of World, Version 3.6. Retrieved from http://due.esrin.esa.int/globcover/

Halwatura D, Najim M (2013) Application of the HEC-HMS model for runoff simulation in a tropical catchment Environmental modelling & software 46:155-162

Martinec J RA, Roberts R (2008) SRM snowmelt runoff model user's manual. New Mexico State University, Las Cruces

Shahid MA, Boccardo P, Usman M, Albanese A, Qamar MU (2016) Predicting peak flows in real time through event based hydrologic modeling for a trans-Boundary River catchment Water Resources Management:1-18

Scharffenberg WA, Fleming MJ (2006) Hydrologic modeling system HEC-HMS: User's manual. US Army Corps of Engineers, Hydrologic Engineering Center,

IPCC Core Writing Team, Pachauri RK, Meyer LA (2014) Contribution of working groups I, II and III to the fifth assessment report of the intergovernmental panel on climate change. Climate Change 2014: Synthesis Report. IPCC, Geneva

Proceedings of the 10th World Congress of EWRA 'Panta Rhei', 5-9 July 2017, Athens, Greece
© 2017 *European Water Resources Association*

Prediction and validation of turbulent flow around a cylindrical weir

N.G. Soydan, O. Şimşek*, M.S. Aköz
Cukurova University, Civil Engineering Department, Adana, Turkey
* *e-mail: oguzsimsek@cu.edu.tr*

Abstract: Weirs are commonly used for regulating, controlling and measuring the flow in a river or an open channel. When a weir is constructed across a river, sediment deposition occurs in the upstream of the structure and this can affect the function and efficiency of the weir. If these structures can be designed to pass sediment, the performance of the weir will not change over time because of sediment accumulation. In this study, the characteristics of turbulent flow around a cylindrical weir placed at a distance from the bed are investigated experimentally and numerically. The governing equations of the two-dimensional turbulent flow is solved numerically by using ANSYS Fluent. The volume of fluid (VOF) method is used to compute the free surface of the flow. Grid Convergence Index (GCI) is performed to examine the effect of the selected grid structure on the numerical results. In the numerical simulations, Renormalization Group k-ε, Shear Stress Transport k-w and Reynolds Stress turbulence closure models are employed. The numerical results for the turbulent flow characteristics are compared with the experimental data obtained by Laser Doppler Anemometer measurements in a laboratory channel. Experimental validations of the velocity field and free surface profiles show that the computations by using the turbulence models are successful in predicting the turbulent flow characteristics around a cylindrical weir placed at a distance from the bed.

Key words: Cylindrical Weir, Laser Doppler Anemometer, Open Channel Flow, Turbulence Model, VOF

1. INTRODUCTION

In open channel flow, weirs are commonly used for flow control and discharge measurement. Cylindrical weir is a construction which has many advantages such as stable overflow pattern, easy discharge, simple design and lower cost. Also, it has larger discharge capacity than the sharp crested and broad crested weirs (Chanson and Montes 1998). The flowing water in an open channel, transports sediment particles and these particles accumulate at the gate inlets and behind the weir structures. This can lead to overflowing of the water with narrowing the channel width, may cause the stability of the structure to deteriorate and reduce the measurement accuracy. Therefore, Majcherek (1984) first suggested an idea of combined-free over-under flow on a weir-gate. By using a model where weirs and gates are combined, sedimentation effects can be minimized. If the weir structure placed at a distance from the bed, it could be able to control the sediment transport and water level at the same time. While some attention has been focused on this topic, it has not yet been studied in detail experimentally and numerically. Chanson and Montes (1998), studied the circular weir overflows, with eight cylinder sizes, for several weir heights and for five types of inflow conditions experimentally. They stated from the range of the experiments that the cylinder size, the weir height D/R and the presence of an upstream ramp had no effect on the discharge coefficient, flow depth at crest, and energy dissipation. They concluded that the discharge measurements with circular weirs are significantly affected by the upstream flow conditions. Bhattacharyya and Maiti (2004), studied the vortex shedding around a cylinder and the Karman vortex street behind a cylinder experimentally and numerically. At Reynolds number up to 1400, the interaction of wall boundary layer on the vortex shedding has been investigated for different gap ratios. The governing equations of the unsteady flow are discretized by finite volume method. It has been found that the strength of the positive vortices arising from the lower side of the cylinder reduces with the decrease of gap height. Castro-Orgaz, et al. (2008), examined the hydraulics of circular crested weirs by using generalized one dimensional model based on the critical flow in

curvilinear motion which was developed by themselves. The predictions obtained from the models compared with the experimental results. They stated that the discharge coefficient increases when the streamline effects are included. Severi, et al. (2015), experimentally studied on discharge coefficient variation of combined-free over-under flow on a cylindrical weir-gate. For varied geometrical dimensions of the weir-gate under hydraulic conditions of over, combined and under flows, many experiments were carried out. They used the Buckingham Phi theorem to correlate the discharge coefficient to the effective dimensionless hydraulic and geometrical arguments. They stated that the developed empirical relationships for over, combined and under flows presented good coincidence with experimental results within the limitations of the runs.

In this study the characteristics of flow over and under a cylindrical weir is investigated experimentally and numerically. The governing equations of the weir flow are solved by using ANSYS-Fluent program based on the finite volume method. In the numerical analysis Renormalization Group k-ε (RNG), Shear Stress Transport k-ω (SST) and Reynolds Stress Model (RSM) were used. The velocity field of the flow is measured by means of Laser Doppler Anemometry technique. The velocity field and free surface profiles of the weir flow are presented and discussed.

2. EXPERIMENTAL SET-UP

Experiments were conducted in a glass-walled, hydraulically smooth laboratory channel that was 0.30 m wide, 0.30 m deep and 8.00 m long. As may be seen in Figure 1, a smooth-surface cylindrical weir with D=0.16 m diameter was placed at 5 m distance from the beginning of the channel and 3 cm above the channel bed. The free surface profile of three-dimensional flow around a cylindrical weir was measured by using limnimetry. The velocity field around the weir was obtained by using one dimensional Laser Doppler Anemometry. The Reynolds number in the upstream region of the flow is calculated as 135575. The flow in the upstream of the channel is subcritical, with a Froude number of 0.254. The experiment is performed for a flow rate of 0.0317 m^3/s.

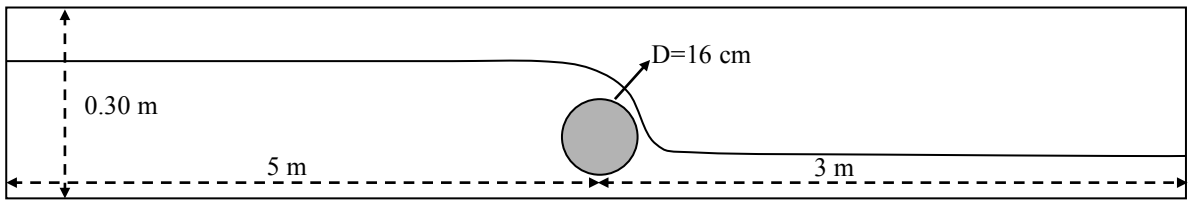

Figure 1. Schematic view of open channel flow with cylindrical weir

3. FORMULATION AND NUMERICAL MODELING

3.1 Governing equations

The 2D Reynolds-averaged continuity and Navier-Stokes equations (RANS) were used to theoretically simulate the present open channel flow. For an incompressible, Newtonian fluid flow these equations can be expressed as

$$\frac{\partial \overline{u}_i}{\partial x_i} = 0 \tag{1}$$

$$\rho\left(\frac{\partial \bar{u}_i}{\partial t}+\bar{u}_j\frac{\partial \bar{u}_i}{\partial x_j}\right)=\rho g_i-\frac{\partial \bar{p}}{\partial x_i}+\mu\frac{\partial^2 \bar{u}_i}{\partial x_j^2}+\frac{\partial \tau_{ij}}{\partial x_j} \quad (2)$$

In Eqs. (1) and (2), u_i is velocity component in x_i-direction, g_i is gravity, p is pressure, μ is dynamic viscosity, ρ is fluid density, t is time, $\tau_{ij}(=-\rho\overline{u_i'u_j'})$ is the turbulence stress. The turbulence stresses are obtained from the linear constitutive equation formulated by Boussinesq:

$$\tau_{ij}=-\rho\overline{u_i'u_j'}=\mu_t\left(\frac{\partial \bar{u}_i}{\partial x_j}+\frac{\partial \bar{u}_j}{\partial x_i}\right)-\frac{2}{3}\rho k\delta_{ij} \quad (3)$$

In Eq. (3) u_i' and u_j' is horizontal and vertical velocity fluctuation, respectively, μ_t is turbulent viscosity, k $(=\overline{u_i'u_i'}/2)$ is the turbulent kinetic energy and δ_{ij} is Kronecker delta. The models used for the calculation of the turbulent viscosity in Eq. (3) are:

1. Renormalization-group *k-ε* (RNG) (Yakhot, et al. 1992),
2. Shear Stress Transport *k-ω* (SST) (Menter 1994),
3. Reynold Stress Model (RSM) (Launder, et al. 1975)

3.2 Solution domain, boundary and initial conditions

The geometry of the solution domain and the boundary conditions are shown in Figure 2. At the air-filled upper boundary of the solution domain, the pressure p =0. At the inlet boundary, the flow velocity was u = 0.40 m/s, and v =0. The outlet boundary was a free over fall at the outlet boundary where p = 0. All of the wall boundaries were set as stationary, i.e. non-slip wall. The viscosity dominated near-wall region was dealt with the enhanced two-layer wall treatment.

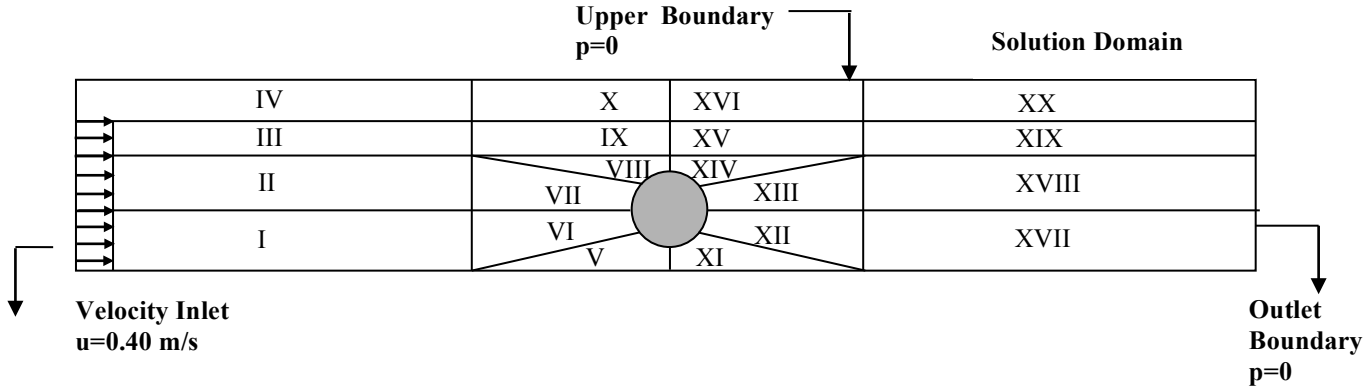

Figure 2. Geometry of solution domain and boundary conditions

In the numerical modeling, SIMPLE (Semi-implicit method for pressure-linked equations) algorithm was used for velocity-pressure coupling which is designed specifically for transient simulations (Patankar and Spalding 1972). First-order upwind discretization scheme was used for the momentum, turbulent kinetic energy and dissipation equations; and in the discretization of pressure term PRESTO (Pressure staggered option) algorithm was employed (Patankar 1980). In the computations, the residual error as a convergence criterion was within 10^{-4} for all the computed variables (u, v, w, k, ε).

In this study, VOF method is used to determine the free surface of the flow field in the numerical simulations. The VOF method renders the shape and location of a constant-pressure free surface boundary of the flow field. It uses a filling process to determine which cell in the meshing volume is filled and which one is emptied (Hirt and Nichols 1981).

3.3 Computational Grid

The resolution of the computational discretization of the solution domain is important for an ultimate grid-independent solution. For the purpose of designing a suitably-spaced computational grid system, structured grids of different local cell concentrations were tested. Considering the flow characteristics for the present interaction problem, the solution domain was divided into 20 regional sub-domains. Due to the increasing velocity gradient, the density of discretization was intentionally increased towards the solid boundary by compressing the grid system. Three grid systems with different density, Grid 1 (coarse), Grid 2 (medium) and Grid 3 (fine), were used to examine the effect of the grid size on the accuracy of the numerical results. Fine grid which is adopted for the final design of the computational grid system, containing 20 sub-domains, is seen in Figure 3. The discretization error of the computational domain was estimated using a Grid Convergence Index (GCI) for the three-grid comparisons (Roache (1998), Çelik, et al. (2008)). The predicted errors in the velocity due to discretization for the fine-grid solutions were found within 2% which is well acceptable for the verification of computed results. Therefore, the solution obtained on the fine mesh given in Figure 3 can be accepted as grid-independent.

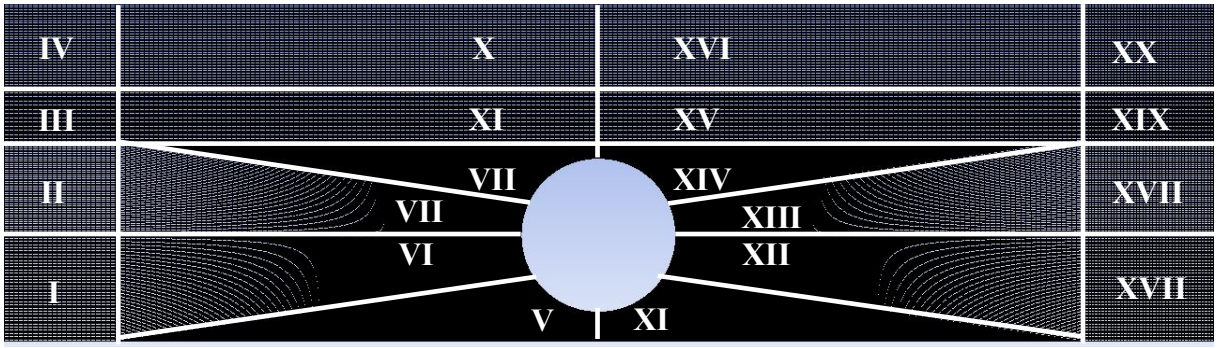

Figure 3. Sub-domains of computational grid

4. RESULTS AND DISCUSSION

In the comparisons of computed velocity profiles from different turbulence closure models with those of experiments, mean square error (MSE) and mean absolute relative error (MARE) values were used as a quantitative evaluation criterion. MSE and MARE of measured and predicted velocity profiles in the channel is expressed as

$$MSE = \frac{1}{N}\sum_{n=1}^{N}(v_m - v_p)^2 \tag{4}$$

$$MARE = \frac{1}{N}\sum_{n=1}^{N}\left|\frac{v_m - v_p}{v_m}\right| x100 \tag{5}$$

where v_m and v_p are measured and computed mean horizontal velocities, respectively along the solution domain and N is the total number of velocity profiles. The results of MSE and MARE values calculated for the velocity profiles from the different turbulence closure models are given in Table I. From the table, it can be seen that according to the mean MSE and MARE values the most successful turbulence model in predicting the velocity field around the cylindrical weir is RNG turbulence model. RNG model shows superior performance in the upstream, downstream and upper region of the cylindrical weir among the used models. Figure 4 shows the experimental x velocity distribution around the cylindrical weir. From the figure, the stagnation region effect on the x velocity profile can be clearly seen in the upstream region. The jet flow formation under the

cylindrical weir, the effect of streamline curvature over the weir and the distribution of the velocity profile in the wake region behind the circular weir are also clearly evident from the figure. The graphical comparisons of the horizontal velocity profiles between the experimental data and numerical predictions using the turbulence models in the upstream and downstream region of the cylindrical weir were also given in Figure 5. It can be clearly seen that all the turbulence models show discrepancies with the experimental measurements near the wall region in the upstream region of the weir. In the downstream region the poor agreement between the experimental and numerical velocity profiles can be clearly seen.

Table 1. MSE and MARE values for the horizontal velocity profiles at different sections for the turbulence models

x(cm)	RNG		RSM		SST	
	MARE	**MSE**	**MARE**	**MSE**	**MARE**	**MSE**
420	7.119	0.001	8.568	0.001	7.732	0.001
468	7.201	0.001	8.971	0.001	7.837	0.001
484	7.908	0.002	10.828	0.004	8.802	0.003
487	9.131	0.004	13.752	0.007	11.062	0.005
490	15.085	0.006	21.124	0.012	17.796	0.008
491	21.858	0.012	28.172	0.021	24.942	0.016
492	17.594	0.017	24.414	0.030	20.908	0.023
494	42.672	0.157	47.106	0.176	44.487	0.164
500	12.445	0.047	18.210	0.102	15.261	0.071
506	58.068	0.161	72.709	0.195	64.214	0.165
508	58.242	0.065	77.153	0.092	59.858	0.070
510	482.380	0.132	547.640	0.160	495.058	0.138
512	59.117	0.131	65.305	0.156	60.383	0.134
514	40.339	0.186	42.423	0.201	39.341	0.179
516	28.654	0.160	31.272	0.187	28.336	0.157
525	30.673	0.246	33.253	0.283	30.711	0.243
548	26.840	0.203	28.762	0.229	27.274	0.206
Mean	**54.431**	**0.090**	63.510	0.109	56.706	0.093

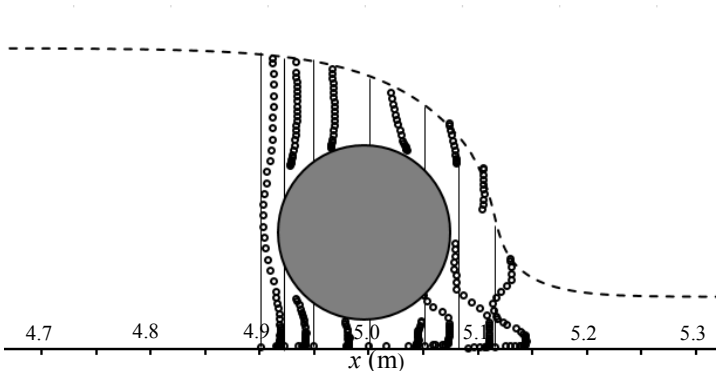

Figure 4. Experimental x velocity distribution around the cylindrical weir

Figure 6 gives the measured and computed free surface profiles from the VOF method along the channel by the three turbulence models used in this study. As may be seen from the figures, the computed flow profile using all turbulence models show good agreement with the measured profile throughout the solution domain. In the upstream and downstream regions, the differences between the predictions and measurements can be clearly seen from the figure. In the weir region turbulence models show good agreements with the measurement. Figure 7 shows the plan view of the x and y velocity components obtained from RNG turbulence model in the weir region. From the contours of x velocity, the stagnation point in front of the weir is clearly seen. Also, the wake region in the downstream region where the maximum pressure and minimum velocity occurs can be seen. The maximum values of the x velocity component are located under the cylindrical weir where the jet flow occurs. The contours of y velocity show where the two dimensional flow is prominent. The maximum y velocity occurs where the flow goes over the weir as expected.

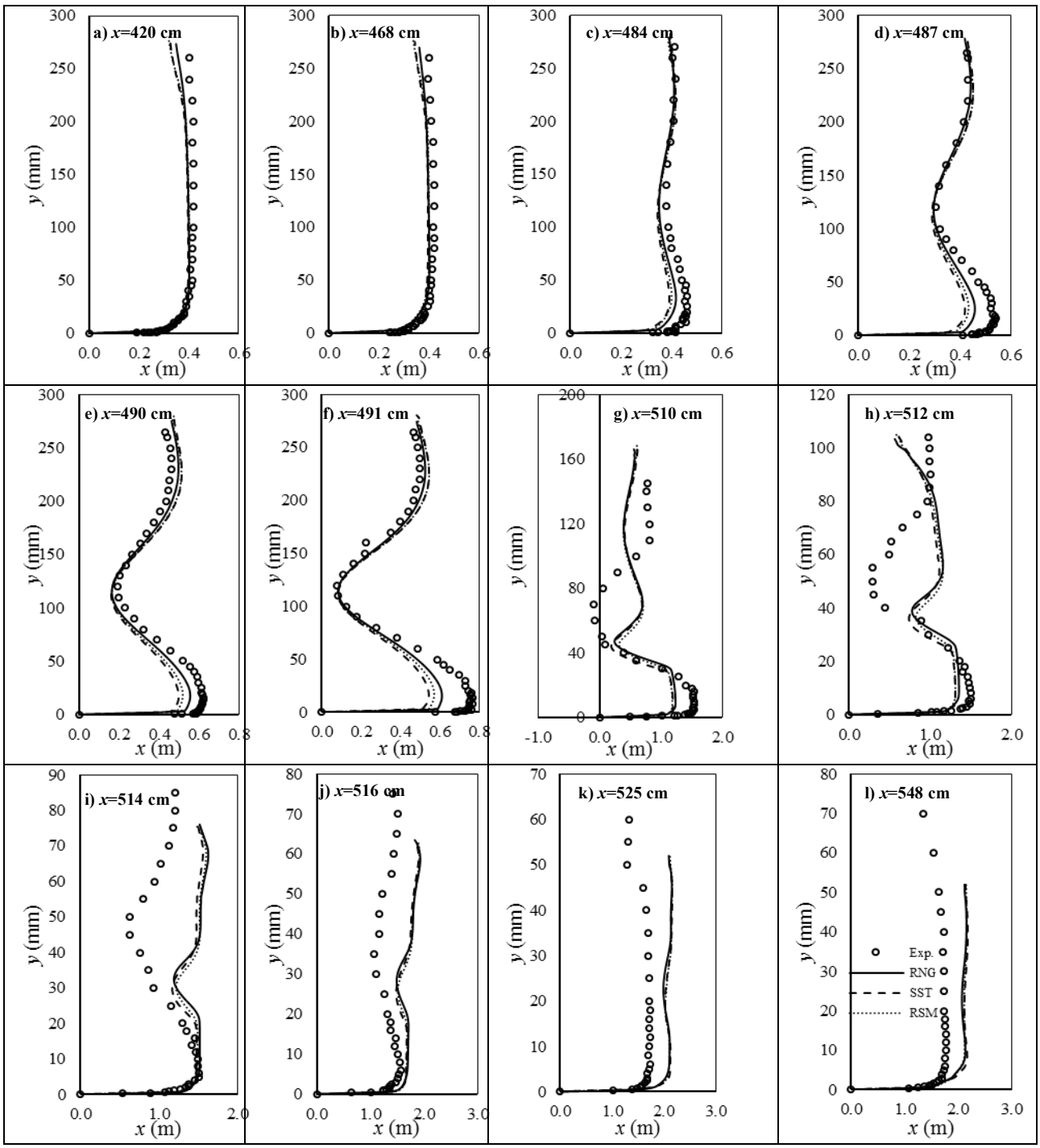

Figure 5. The experimental and predicted horizontal velocity profiles obtained by the three different turbulence closure models for selected sections

Figure 8 gives the streamline patterns and velocity vectors of the flow field around the cylindrical weir obtained from RNG turbulence model which is found to be the most successful model in this study. As may be seen from the streamline patterns and velocity vectors, RNG turbulence model predict successfully the stagnation region in the upstream face, jet flow under the weir, streamline curvature effect over the weir and the wake region behind the weir successfully. Figure 9 gives the numerical turbulence kinetic energy (TKE) and the pressure distribution along the channel and around the cylindrical weir obtained from RNG turbulence model. It can be clearly seen from the patterns of turbulence kinetic energy contours that the maximum value of the turbulence kinetic energy is calculated under the cylindrical weir where the jet flow occurs. It is also seen that the highest value of turbulence intensity reaches its maximum value in the region

close the channel bed downstream of the weir and then gradually decreases towards the water surface. It can be said that turbulence kinetic energy in the supercritical flow region is higher than that of the subcritical region. The pressure in the wake region is negative due to the flow separation. The maximum values of pressure take place in the upstream region of the channel. The point where the pressure passes from the positive to negative is clearly seen from the figures. Maximum dimensional pressure value in the flow field is calculated as $p/0.5\rho u^2$ =30.38 in the upstream channel bed.

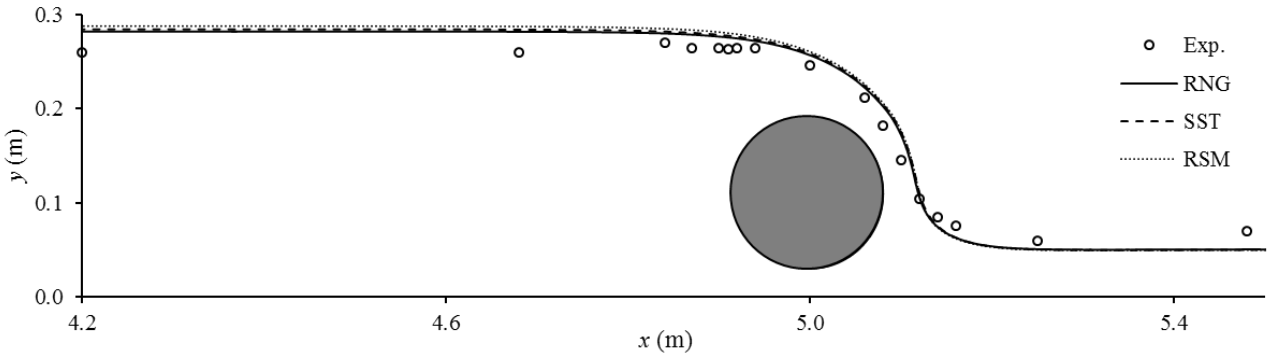

Figure 6. The experimental and predicted free surface profiles obtained from three turbulence models

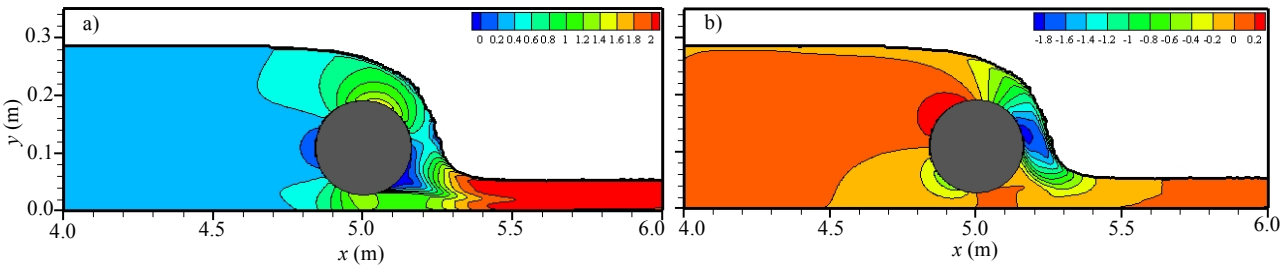

Figure 7. Numerical x velocity (a) and y velocity (b) distributions obtained from RNG turbulence model

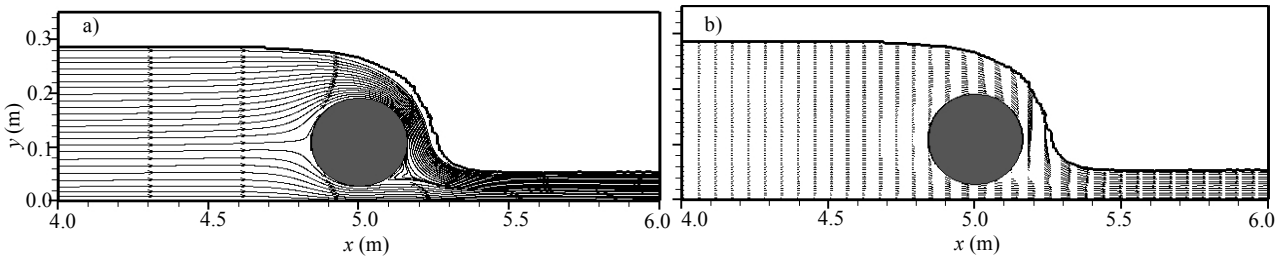

Figure 8. Numerical time averaged patterns of streamlines (a) and distribution of velocity vectors (b) by RNG

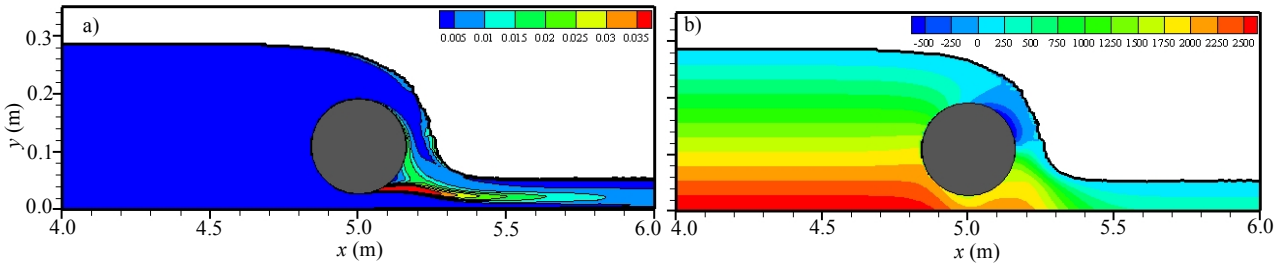

Figure 9. Numerical TKE (a) and pressure distribution (b) obtained from RNG turbulence model

5. CONCLUSION

An open channel flow over and under a cylindrical weir was analysed numerically and experimentally. The experimental velocity profiles were measured in a laboratory channel by using Laser Doppler Anemometry. The numerical results based on the CFD analyses for the same conditions with the experiments were validated by the laboratory measurements. Using the Renormalization Group k-ε, Shear Stress Transport and Reynolds Stress Model, the governing equations of the flow were solved by the Finite Volume Method. The MSE and MARE statistics of the velocity profiles were used as a criterion for the quantitative analysis of results obtained from the turbulence closure models. From the comparisons of the experimental and numerical results, the simulations using Renormalization-Group k-ε provide better predictions for the horizontal velocities compared to the other turbulence closure models. The stagnation point in the upstream region of the weir, the streamline effect over the weir and the wake region in the downstream region of the cylindrical weir were obtained successfully experimentally and numerically. It can be concluded that the flow characteristics obtained from the RNG turbulence model estimates the flow characteristics over and under a weir successfully.

REFERENCES

Bhattacharyya, S., Maiti, D., 2004. Shear flow past a square cylinder near a wall. International Journal of Engineering Science; 42(19):2119-2134.

Castro-Orgaz, O., Giráldez, J., Ayuso, J., 2008. Critical flow over circular crested weirs. Journal of Hydraulic Engineering; 134(11):1661-1664.

Chanson, H., Montes, J. S., 1998. Overflow characteristics of circular weirs: Effects of inflow conditions. Journal of irrigation and drainage engineering; 124(3):152-162.

Çelik, I. B., Ghia, U., Roache, P. J., Freitas, C. J., 2008. Procedure for Estimation and Reporting of Uncertainty Due to Discretization in CFD Applications. Journal of Fluids Engineering-Transactions of the Asme; 130(7).

Hirt, C. W., Nichols, B. D., 1981. Volume of Fluid (Vof) Method for the Dynamics of Free Boundaries. Journal of Computational Physics; 39(1):201-225.

Launder, B. E., Reece, G. J., Rodi, W., 1975. Progress in the development of a Reynolds-stress turbulence closure. Journal of Fluid Mechanics; 68(03):537.

Menter, F. R., 1994. 2-Equation Eddy-Viscosity Turbulence Models for Engineering Applications. Aiaa Journal; 32(8):1598-1605.

Patankar, S. V., 1980. Numerical heat transfer and fluid flow. Washington: Hemisphere Pub. Corp.

Patankar, S. V., Spalding, D. B., 1972. A calculation procedure for heat, mass and momentum transfer in three-dimensional parabolic flows. International Journal of Heat and Mass Transfer; 15(10):1787-1806.

Roache, P. J., 1998. Verification of Codes and Calculations. Aiaa Journal; 36(5):696-702.

Severi, A., Masoudian, M., Kordi, E., Roettcher, K., 2015. Discharge coefficient of combined-free over-under flow on a cylindrical weir-gate. ISH Journal of Hydraulic Engineering; 21(1):42-52.

Yakhot, V., Orszag, S. A., Thangam, S., Gatski, T. B., Speziale, C. G., 1992. Development of Turbulence Models for Shear Flows by a Double Expansion Technique. Physics of Fluids a-Fluid Dynamics; 4(7):1510-1520.

Proceedings of the 10th World Congress of EWRA 'Panta Rhei', 5-9 July 2017, Athens, Greece
© 2017 *European Water Resources Association*

Time series analysis of water characteristics of streams in Eastern Macedonia – Thrace, Greece

T. Papalaskaris[1*] and G. Kampas[2]
[1] *Department of Civil Engineering, Democritus University of Thrace, Kimmeria Campus, 67100 Xanthi, Greece*
[2] *Deputy Head of Water Directorate of Eastern Macedonia - Thrace, 65404 Kavala, Greece*
[*] *e-mail: tpapalas@civil.duth.gr*

Abstract: Water is one of the most important sources of water on earth supporting the existence of the majority of living organisms. Time series analysis, modeling and forecasting constitutes a tool of paramount importance with reference to a wide range of scientific purposes both in meteorology and hydrology (e.g. precipitation, water quality, humidity, temperature, solar radiation, floods and draughts). The present research applies the Box-Jenkins approach, employing SARIMA (Seasonal Autorregressive Integrated Moving Average) model to perform short term forecasts of maximum monthly water temperatures Nestos River at the junction with its trans-boundary tributary, Despatis River, at the specific location called Nestos River – Gefira Despati, situated within the range of Paranesti area, Drama Prefecture, Region of Eastern Macedonia-Thrace, North-Eastern Greece, North-Eastern Mediterranean Basin, modeling past maximum monthly water temperatures time series components structure and predicting future quantities in accordance to the past ones. The model which is mostly fit to both describe the past water quality data and thus generate the most reliable future forecasts is selected and rated by means of the (BIC-), (MAPE), (MAE) and (RMSE) model evaluation criteria. The conclusions of this research will provide local authorities (e.g. Water Directorate of Eastern Macedonia – Thrace, General Secretariat for Civil Protection, European Center for Forest Fires, Deputy Governor of Agricultural Economy, daily fire risk maps designers, hydraulic, irrigation and environmental engineers, city inhabitants, farmers etc., biologists, fish scientists etc.) valuable data in order to develop strategic plans, policies and appropriate use of available water resources within the Region of Eastern Macedonia-Thrace.

Key words: Water temperature time series forecasting; auto regressive moving average models; trend; seasonality; SARIMA models

1. INTRODUCTION

Water temperature is undoubtedly world over considered as one of the most important water quality indicator. It is a significant water quality and environmental aspect because it essentially controls the range of kinds and types of aquatic life, determines the maximum dissolved oxygen density in the water, and affects the rate of chemical and biological reactions. It can be affected both by natural causes, (e.g. sun, precipitation, surface run-off, groundwater and upstream headwaters inputs, reciprocal transmissions of heat to the air and heat received or transmitted by evaporation or condensation) as well as by artificial causes (e.g. discharge of cooling water and/or heated industrial effluents, alterations to streams shading due to agriculture and water harvesting, urban development and climate change).Water temperature in streams and rivers changes over time much shorter time in comparison to those of lakes. Their seasonal and diurnal water temperatures are much more closely connected with the specific atmospheric temperature patterns, established within the surrounded area climate, in accordance with the size and origin of those natural watercourses than do those of lakes. A variety of statistical procedures are often employed to forecast rainfall amounts. In warm water streams the temperatures should not exceed 31.67 ^{o}C, whilst at the same time in cold water streams the temperatures should not exceed 20.00 ^{o}C, since often heat occurring during summer can provoke fish kills, especially those inhabiting stream ponds due to the fact that the more the stream water temperature increases, the less dissolved oxygen (crucial for aquatic life survival) is available into the stream water. One of the most common methods for time series data analysis is that which was developed within the general concept of stochastic hydrology, also known with the name of ARIMA (Autoregressive Integrated Moving

Average) (Box and Jenkins, 1970). ARIMA modeling procedure has been applied the world over on a significant number number of not only financial but additionally, hydrological time series data in order to forecast rainfall data, water reservoir inflow/outflow discharge patterns as well as river flows and river water characteristics modeling (Bari et al., 2015; Papalaskaris et al., 2016).

2. METHODOLOGY

2.1 Study area

With the view to investigate maximum monthly temperature patterns in Despatis river, a trans-boundary stream, originating in Bulgaria and discharging into Nestos River, daily recorded observations from the only one available, operating conventional gauging station (location name: "Nestos River – Despatis Bridge") which records dissolved oxygen, water conductivity, water temperature, turbidity, pH, O.R.P. (oxidation reduction potential) and water level, located at 41.404956° N and 24.100250° E (WGS84 coordinates), were analyzed, which started its operation by the 1st of April 2013 covering a time interval period of 3 years and 3 months (1st of April 2013 - 31st of July 2016) as depicted in Figure 1.

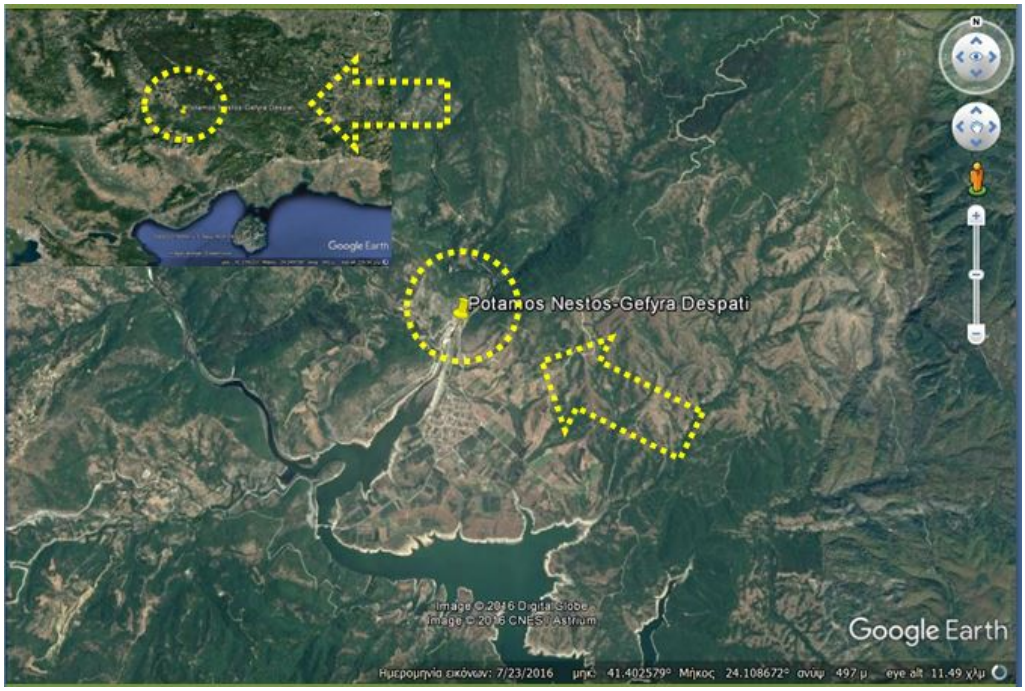

Figure 1. Nestos River- Despatis Bridge water quality gauging station, Paranesti area, Drama Prefecture, Greece (Source: Google Earth).

2.2 The Box-Jenkins model-building procedure

The statisticians Box and Jenkins (1970) developed a modeling method, primarily for financial time series analysis, dealing with stationary time series, and fitting either autoregressive moving average (ARMA) or autoregressive integrated moving average (ARIMA) or seasonal autoregressive integrated moving average (SARIMA) models with the view to discover the most appropriate match of a time series data to previous values of the same time series, with the view to perform future predictions and forecasts. The model-building procedure incorporates the following successive stages (Box and Jenkins, 1970; Abdul-Aziz et al., 2013).

2.2.1 Model identification and selection

Verifying the stationarity of the variables, tracing and locating seasonality if exists, within the time series data under investigation (situation which can be treated by seasonal differencing) and interpreting charts of autocorrelation and partial autocorrelation functions of the time series data under examination with the view to conclude which autoregressive or moving average constituent would be the most appropriate to take place in the model.

2.2.2 Model parameters estimation

Using calculation procedures in order to assay the most competent coefficients for the preferable ARIMA model, in most cases, by means of computation methods like either maximum likelihood estimation or least-squares estimation.

2.2.3 Model checking and forecasting

By examining whether the elaborated model complies with the requirements of a stationary univariate process, namely, the residuals should be independent between each other and exhibit constancy in terms of mean and variance along the entire length of the time series, as the time passes by; this can be carried out by plotting the mean and variance of residuals over time and executing a Ljung-Box test or/and charting autocorrelation and partial autocorrelation functions of the residuals as a means to verify whether the model we built best fit our time series data or not.

2.3 Type of ARIMA models

2.3.1 Autoregressive (AR) and Moving Average (MA) models

In an autoregression model, we forecast the variable of interest using a linear combination of past values of the variable. The term autoregression indicates that it is a regression of the variable against itself (Tamura, 2004; Hyndman and Athanasopoulos, 2012; PennState Eberly College of Science, 2017). Thus an autoregressive model of order p can be written as,

$$y_t = c + \varphi_1 \times y_{t-1} + \varphi_2 \times y_{t-2} + \cdots + \varphi_p \times y_{t-p} + e_t \quad (1)$$

where c is a constant and e_t is white noise. This procedure resembles a multiple regression but with lagged values of y_t as predictors. Reference is made to this type of model as an AR(p) model.

2.3.2 Autoregressive-Moving-Average (ARMA) models

Instead of using past values of the forecast variable in a regression process, a moving average model uses past forecast errors within a regression-resembling model building (Hyndman and Athanasopoulos, 2012),

$$y_t = c + e_t + \theta_1 \times y_{t-1} + \theta_2 \times y_{t-2} + \cdots + \theta_q \times y_{t-q} \quad (2)$$

where e_t is white noise. We make reference to this type of model as an MA(q) model.

2.3.3 Seasonal (ARIMA) models

ARIMA models possess also the ability to model seasonal data of a great extent. A seasonal ARIMA model, or so- called SARIMA model, is generated by incorporating supplementary seasonal components in the ARIMA models we have already mentioned above, and it can be written in the following form (Hyndman and Athanasopoulos, 2012; Nau, 2017):

$$\text{ARIMA } (p,d,q,)\ (P,D,Q,)_m \tag{3}$$

with p=non-seasonal (AR) order, d=non-seasonal differencing, q=non-seasonal (MA) order, P=seasonal (AR) order, D=seasonal differencing, Q=seasonal (MA) order, and where m=number of periods per season or in other words, time interval of repeating seasonal behavior. The seasonal components of the model are written by means of uppercase letters, whilst, on the contrary, we write the non-seasonal components of the model via lowercase letters. The seasonal portion of the model is comprised of components greatly resembling the non-seasonal terms of the model, yet they include backshift operators of the seasonal period. The additional seasonal components are multiplied through a simple way with the non-seasonal components of the model.

3. RESULTS

Primordial time series analysis was carried out dealing with maximum monthly temperature data recorded from 01.04.2013 to 31.07.2016 employing the Box-Jenkins ARIMA model-building procedure.

3.1 Primordial data analysis

By definition, a time series is considered non-stationary, when its values mean and variance either do not exhibit stability over time in terms of mean and variance; The ACF and PACF charts inspection can also provide clues of trend and seasonality existence (Senter, 2008; Abdul-Aziz et al., 2013). We selected to specify 38 autocorrelation lags concerning the maximum monthly water temperature data although Box and Jenkins (1970) suggested that the estimated autocorrelations would be calculated for k=0,1,…k, was not larger than N/4 (40/4=10) series data. Seasonality often results to non-stationary time series owing to the fact that the average values along different parts of the time series occurring within the seasonal time interval differ from the average values along other segments of the same time series. A practical rule, usually employed, while interpreting an ACF chart is if there are designed autocorrelation bars that are larger in value than two standard errors apart from the zero mean, then they suggest proxy of autocorrelation which is statistically significant. The ACF plot reveals alternative positive and negative values, decaying to zero, suggesting the use of an autoregressive model (Smith, 2015). In Figure 3, there are three charted autocorrelation values, at lags 1, 2 and 3, that either extend more (or close to) than two standard errors from the mean, represented by the zero value whilst the two continues lines designed above and below the zero mean stand for the approximate 95% confidence limits.

Visually inspecting, an anticipated conventional 6-month seasonal pattern, following a cyclical pattern between the summer period during which the recorded water temperature values are at their highest levels, and the winter period during which the water temperature values reach its lowest levels, can be definitely both traced and recognized.

Furthermore it should be noted that the performance of the time series analysis in the spectral domain, and after having examined the spectral density graph, proved that the largest seasonal pattern takes place at approximately 12.00-months time intervals, instead of 6-months intervals (Senter, 2008). Hence, we conclude that charting the ACF plot the seasonality pattern is unfolded which couldn’t be discovered by the simple linear equation describing the linear trend line

associated with the original raw maximum monthly recorded water temperature data. This pattern can be easily identified in the following Figure 4, focusing on the high peak at close the frequency 0.1.

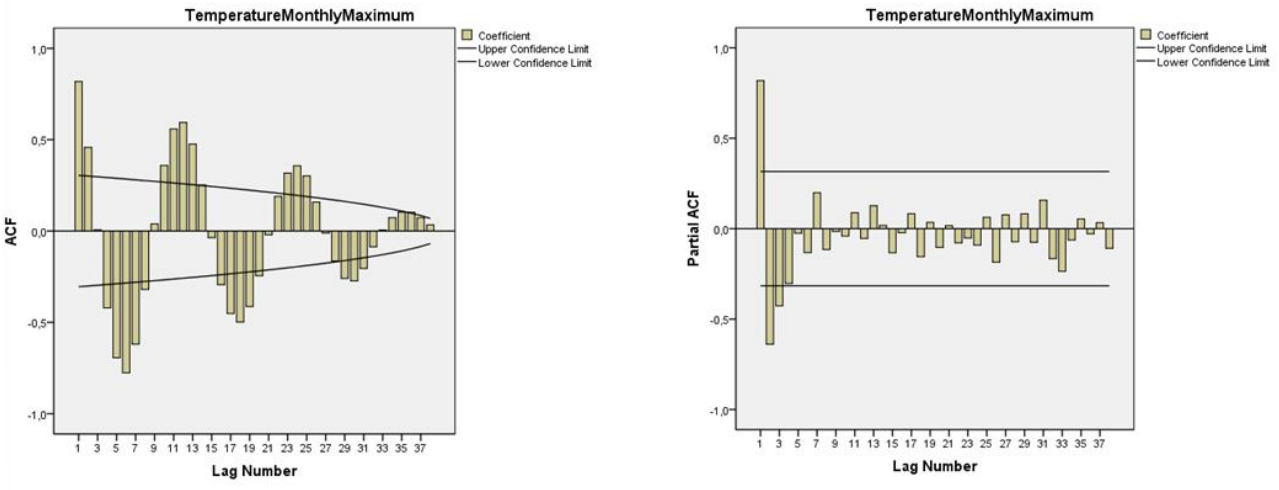

Figure 3. ACF and PACF charts of the raw data of the original observed maximum monthly water temperature, at Nestos River – Gefira Despati - Paranesti area station, Drama Prefecture, Greece.

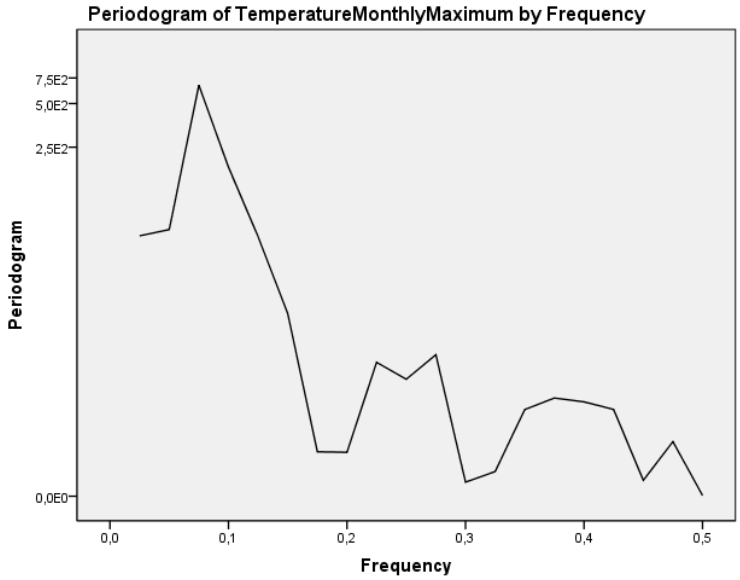

Figure 4. Spectral density chart of the raw data of the original observed maximum monthly water temperature, at Nestos River – Gefira Despati - Paranesti area station, Drama Prefecture, Greece.

3.2 Data stationarity check

The Augmented Dickey-Fuller Unit Root Test, expressed within three different models, was employed and applied on the entire maximum monthly recorded water temperature time series data with the view to investigate and verify whether the rainfall time series is stationary or not. The Figure 5, depicts the outcomes of the test: In the first model (intercept only), the test statistic value -5.140 is lower in value than critical values, -3.655, -2.961 and -2.613 all at 1%, 5% and 10% correspondingly; moreover, the regression coefficient L1 is negative in value (L1=-0.8365932), hence, we can accept the model as a valid one. In the second model (trend and intercept), the test statistic value -5.329 is lower in value than critical values, -4.251, -3.544 and -3.206 all at 1%, 5% and 10% in consequence; in addition, the regression coefficient L1 is once again negative in value

(L1=-0.8677031), consequently, the model can be definitely considered as a valid one. In the third and last model (neither trend nor intercept), the test statistic value -2.830 is lower in value than critical values, -2.638, -1.950 and -1.606 all at 1%, 5% and 10% successively; furthermore, the regression coefficient L1 is once again for this last model negative in value (L1=-0.3478649), therefore, the model can be definitely accepted as a valid one. Evidently, after having performed, examined and checked all three different Augmented Dickey-Fuller Unit Root Tests we concluded in all cases that we reject the null hypothesis H_0, and we accept the alternative hypothesis H_1, which declares that the variable Y (maximum monthly recorded water temperature) is stationary and does not have a unit root.

```
. dfuller Y, regress lags(0)

Dickey-Fuller test for unit root                   Number of obs   =        39

                               ---------- Interpolated Dickey-Fuller ---------
                  Test         1% Critical       5% Critical      10% Critical
               Statistic           Value             Value             Value
------------------------------------------------------------------------------
 Z(t)             -5.140            -3.655            -2.961            -2.613
------------------------------------------------------------------------------
MacKinnon approximate p-value for Z(t) = 0.0000

------------------------------------------------------------------------------
         D.Y |      Coef.   Std. Err.      t    P>|t|     [95% Conf. Interval]
-------------+----------------------------------------------------------------
           Y |
         L1. |  -.8365932   .1627485    -5.14   0.000    -1.166353   -.5068334
             |
       _cons |   46.90517   11.95831     3.92   0.000     22.67534    71.13501
------------------------------------------------------------------------------
```

Figure 5. ADF test applied on the raw data (intercept only) of the original observed maximum monthly water temperature, at Nestos River – Gefira Despati - Paranesti area station, Drama Prefecture, Greece.

3.3 Data differencing (seasonality)

Although the ADF test applied on the maximum water temperatures recorded monthly time series of the raw data revealed it is a stationary time series, after examining the ACF chart depicted in the Figure 3, we considered that the time series data should be seasonally differenced, (due to a few spikes cut the 95% confidence limits), by order D=1, in order to eliminate seasonality (Senter, 2008; Abdul-Aziz et al., 2013).

3.4 Model identification

As soon as several tests concerning the maximum monthly recorded water temperatures have been completed a few candidate models were considered that best meet the criteria and we finally concluded that the seasonal ARIMA (SARIMA) $[(0,1,0)X(0,1,0)_{12}]$ is considered the most suitable one appearing to have the highest R-squared (R^2) (0.853), whilst simultaneously the least Normalized B.I.C. (1.586), M.A.P.E. (17.077), M.A.E. (1.820), Root Mean Squared Error (R.M.S.E.) (2.079) (Senter, 2008; Abdul-Aziz et al., 2013) .

3.5 Model adequacy and diagnostic tests

By examining in Figure 6 the autocorrelation and partial autocorrelation charts of the residuals we verify that there aren't any bar peak values that significantly extend beyond the two continuous lines, plotted above and below the zero mean which imply the approximate 95% confidence limits (Abdul-Aziz et al., 2013; Bari et al., 2015).

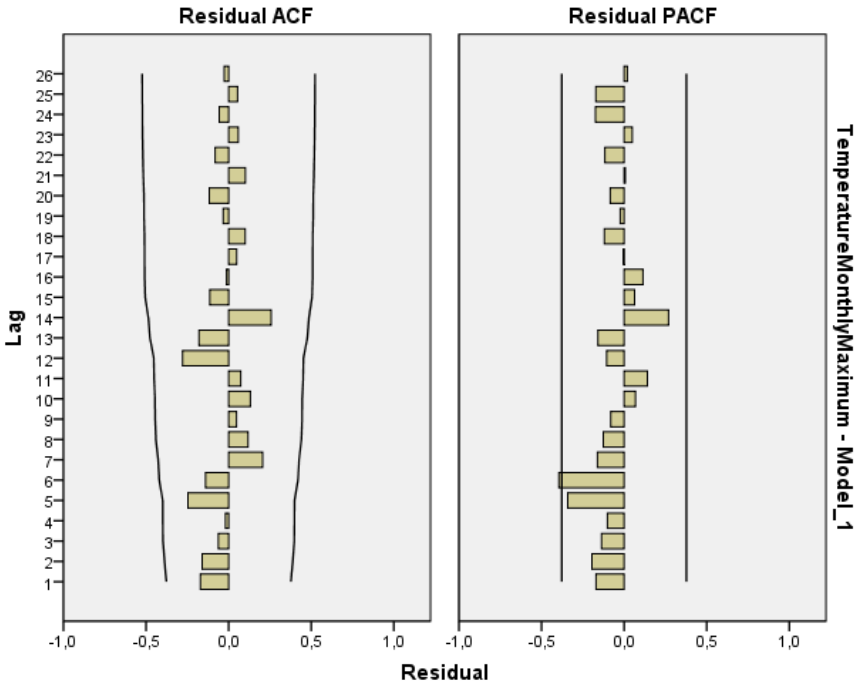

Figure 6. ACF and PACF charts of SARIMA [(0,1,0)X(0,1,0)$_{12}$] model Residuals, at Nestos River – Gefira Despati - Paranesti area station, Drama Prefecture, Greece.

3.6 Forecasting future values

In the Table 1 are depicted the forecasted values :

Table 1. Forecasted values of SARIMA [(0,1,0)X(0,1,0)$_{12}$] model, at Nestos River – Gefira Despati - Paranesti area station, Drama Prefecture, Greece.

SARIMA Model	Aug 2016	Sep 2016	Oct 2016	Nov 2016	Dec 2016	Jan 2017	Feb 2017	Mar 2017	Apr 2017	May 2017	Jun 2017	Jul 2017
Forecast	21.84	19.47	15.61	12.05	7.39	5.42	10.06	10.70	16.53	19.37	23.31	24.14

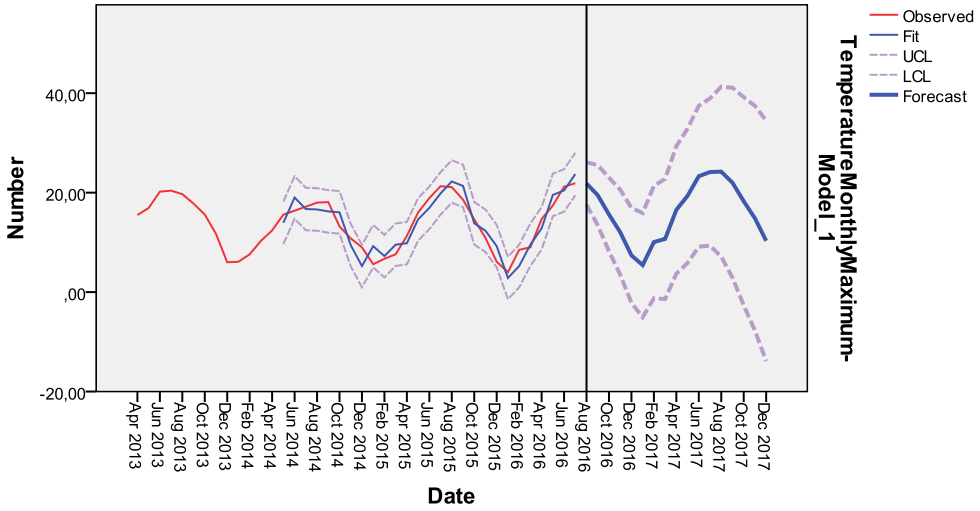

Figure 7. Forecast chart of SARIMA [(0,1,0)X(0,1,0)$_{12}$] model Residuals, at Nestos River – Gefira Despati - Paranesti area station, Drama Prefecture, Greece.

The observed, fit and forecast values as well as the upper and low confidence levels with

reference to the finally selected SARIMA $[(0,1,0)X(0,1,0)_{12}]$ model, are all summarized within the chart illustrated by Figure 7 (Senter, 2008; IBM Corporation, 2011; Abdul-Aziz et al., 2013; Bari et al., 2015).

4. CONCLUSIONS

The stream flow water maximum monthly temperature patterns, observed at Nestos River, Gefira Despati, Paranesti Region gauging station have been studied using the Box-Jenkins (SARIMA) model methodology. Adaili water temperature record spanning the period of April 2013 – July 2016 has been used to develop the most fit model. After having examined a group of candidate SARIMA models and having compared them based on several statistical criteria (e.g. R-squared, B.I.C., M.A.E., M.A.P.E., R.M.S.E.) we concluded that SARIMA $[(0,1,0)X(0,1,0)_{12}]$ model best fits the maximum recorded monthly water temperature data of Nestos River – Gefira Despati, Paranesti area, Drama Prefecture, NE Greece, for the period 01.04.2013-31.07.2016. The study reveals that the Box-Jenkins (SARIMA) model methodology could be implemented as a suitable tool to simulate the maximum monthly water temperature at Nestos River, Gefira Despati, Paranesti Region gauging station for the up-coming months (up to July 2017). Although, undoubtedly, the operation time span can be considered relatively short in order to come up with secure conclusions, the continuous future gauging station operation will feed the modeling procedure with more raw data in an attempt to develop a more adequate model. The results achieved for water temperature forecasting will assist scientists and decision makers to develop policies concerning river pollution, fish farming, river fauna and flora sustainability etc.

REFERENCES

Abdul-Aziz A.R., Anokye M., Kwame A., Munyakazi L. and Nsowah-Nuamah N.N.N. (2013). Modeling and forecasting rainfall pattern in Ghana as a seasonal ARIMA process: The case of Ashanti Region. *International Journal of Humanities and Social Science*, 3 (3), 224-233.

Bari S.H., Rahman M.T., Hussain M.M. and Ray S. (2015). Forecasting monthly precipitation in Sylhet City using ARIMA model. *Civil and Environmental Research*, 7 (1), 69-77.

Box G.E.P. and Jenkins G. (1970) (Revised edition: 1976). *Time Series Analysis: Forecasting & Control*, Holden-Day Publishments, San Fransisco, pp. 1-575 (in English).

Hyndman R.J., G. Athanasopoulos. (2012) 8.3: Autoregressive models. Available from: https://www.otexts.org/fpp/8/3 [Accessed 17th January 2016].

Hyndman R.J., G. Athanasopoulos. (2012) 8.4: Moving average models. Available from: https://www.otexts.org/fpp/8/4 [Accessed 17th January 2016].

Hyndman R.J., G. Athanasopoulos. (2012) 8.9: Seasonal ARIMA models. Available from: https://www.otexts.org/fpp/8/9 [Accessed 17th January 2016].

IBM Corporation (1989, 2011). *IBM SPSS Forecasting 20*, p. 95 (in English).

Nau R. (2017) ARIMA Models for time series forecasting. Available from: https://people.duke.edu/~rnau/seasarim.htm [Accessed 17th January 2016].

Papalaskaris T., Panagiotidis T. and Pantrakis A. (2016). Stochastic monthly rainfall time series analysis, modeling and forecasting in Kavala city, Greece, North-Eastern Mediterranean Basin. *Proceedings 2nd International Conference on Efficient & Sustainable Water Systems Management toward Worth Living Development ("2nd E.W.a.S. 2016")* (eds. V. Kanakoudis, G. Karatzas and E. Keramaris), Chania, Crete, Greece, 2016, Theme F: Hydrology, ID 064.

Papalaskaris T., Panagiotidis T. and Pantrakis A. (2016). Stochastic monthly rainfall time series analysis, modeling and forecasting in Kavala city, Greece, North-Eastern Mediterranean Basin. *Procedia Engineering*, 162, 254-263.

PennState Eberly College of Science. (2017) 2.1: Moving Average Models (MA models). Available from: https://onlinecourses.science.psu.edu/stat510/node/48 [Accessed 17th January 2016].

Senter A. (2008) Time series analysis. Available from: http://userwww.sfsu.edu/efc/classes/biol710/timeseries/timeseries1.htm [Accessed 17th January 2016].

Smith M. J. (2015) ARMA and ARIMA (Box-Jenkins) models. Available from: http://www.statsref.com/HTML/index.html?arima.html [Accessed 17th January 2016].

Tamura H. (2004) Chapter 6: Autoregression. Available from: http://faculty.washington.edu/htamura/qm500/king/Ch06.pdf [Accessed 17th January 2016].

Proceedings of the 10th World Congress of EWRA 'Panta Rhei', 5-9 July 2017, Athens, Greece
© 2017 *European Water Resources Association*

Application of Bayesian algorithm in continues streamflow modeling of a mountain watershed

S. Sadeghi-Tabas[1*], S.Z. Samadi[2] and B. Zahabiyoun[1]
[1] *Department of Civil Engineering, Iran University of Science and Technology (IUST), Tehran-Iran*
[2] *Department of Civil and Environmental Engineering, University of South Carolina, Columbia, South Carolina-USA*
[*] *e-mail: s_sadeghitabas@civileng.iust.ac.ir*

Abstract: Appropriate prediction of streamflow at mountain region poses substantial challenges to any hydrology modelling system. In this type of watershed, the rainfall-runoff process is typically rapid; thus, a key approach for a successful simulation is how to reduce the uncertainty and error in simulation. The focus of this study is on parameter and predictive uncertainty estimation of a semi-distributed hydrology model (i.e., ARNO). The ARNO model is coupled with the DiffeRential Evolution Adaptive Metropolis (DREAMzs) algorithm to calibrate fifteen hydrological parameters. Analysis suggests that DREAM efficiently reduced the uncertainty associated with modelling and performed best during moderate to moderately high flow. The 95 prediction uncertainty (95 PPU) bracketed most high and medium flows. Overall, application of DREAM algorithm to the ARNO model identified the uncertainty associated with the maximum soil moisture storage and the routing model components. ARNO parameter uncertainty largely depends on the complexity, and variability of streamflow records, and the simplicity of its lumped formulation. These results provide useful insights into the complexities of surface flow simulation and demonstrate the importance of reducing parameter and predictive uncertainty of a rapid response hydrologic system.

Key words: Parameter Uncertainty Assessment, ARNO, DREAMzs, Continuous Simulation, Mountainous Watershed

1. INTRODUCTION

Rainfall-runoff models are widely used in hydrology to simulate river basin water quantity and play an important role in management of water resources. It is an accepted fact that a hydrological model prediction, should not be deterministic, most-probable representation, but should also explicitly include an estimate of uncertainty. Uncertainty in model predictions arise from measurement errors associated with the system input (forcing) and output, model structure errors due to the aggregation of spatially distributed real-world processes into a mathematical model, initial conditions and measurement errors cause by in situ observations that can be collectively considered as data errors. Realistic assessment of these various sources of uncertainty provide reliable information to decision makers and practitioners and help to manage water resources in different hydrological systems.

In order to estimate predictive uncertainty of the hydrologic models, infer the parameters, and predict model outputs, various methodologies may be adopted, including first-order approximation, state-space filtering, multi model averaging, and various Bayesian approaches. Among these approaches, Bayesian algorithms have been widely used in hydrology for statistical inference of parameters and model predictive uncertainty. Under Bayes theorem, posterior distribution combines the data likelihood with the prior distributions of parameters, narrow parameter space and predict the uncertainty.

Recently, a new Markov chain Monte Carlo (MCMC) sampler, namely DREAMzs (DiffeRential Evolution Adaptive Metropolis algorithm), was used under a Bayesian framework as an efficient and robust sampler in hydrologic modeling. Compared to the generalized likelihood uncertainty estimation (GLUE), the main advantage of DREAM (using MCMC simulation) is separating the effects of input (forcing), parameters and model structural uncertainties from total predictive uncertainty (Vrugt et al., 2009b). DREAMzs is based on the original DREAM algorithm (Vrugt et

al., 2009a) that was modified for an efficient estimation of the posterior probability density function of parameters o to address high-dimensional posterior exploration problems.

This study linked DREAMzs with for a semi-distributed conceptual continuous rainfall-runoff model (ARNO). The ARNO model, which derives its name from its first application to the ARNO River, is a semi-distributed conceptual continuous rainfall-runoff model. The soil moisture balance module of this model is taken originally from the Xinanjiang model (Zhao, 1977), in which the spatial distribution of the soil moisture capacity is expressed in the form of a probability distribution function. Later, the original Xinanjiang model scheme was modified by Todini (1988), by allowing the soil moisture to be depleted not only by evapotranspiration, as in the original Xinanjiang model, but also by drainage into the river network and percolation into the water table. This modified ARNO model were adopted by several scholars (e.g. Franchini, 1996; Khazaei et al., 2011 & 2013; Adams, 2015).

This study makes a comprehensive evaluation about the parameter and predictive uncertainty of daily streamflow in mountainous catchment from Iran. Special attention is paid: 1) model setup, parameterization and choice of calibration parameters, 2) definition of performance criteria and likelihood function, and 3) prediction of parameter and predictive uncertainty for daily streamflow simulation of the ARNO model. We are especially concerned with identifying potential regionalization relationships, correlating parameter sensitivity and uncertainty with site characteristics and analyzing posterior probability density functions of sensitive parameters.

2. METHODOLOGY

2.1. Study Area

The Karaj River Basin (KRB) is located in the mountainous region of Alborz province (51°03′ to 51°36′ longitude and 35°53′ to 36°10′ latitude) with a drainage area of 840 sqkm. AmirKabir Dam (Karaj Dam), one of the most important water resources of Tehran province, has been constructed on the Karaj River. Karaj River annual mean flow rate at its entrance to the Karaj Dam is 450×106 m3; additionally 8.2 and 1450 CMS (cubic meter per second) in this location were measured, respectively as minimum and peak annual temporal flow rates. This dam supplies water for municipal and cultural uses and electrical energy generation. It has been located 23 km north of Karaj and 63 km northwest of Tehran, and is under operation since 1963.

2.2. Hydrology Model

ARNO continuous rainfall-runoff model developed by Todini, (1988) and is used to simulate daily runoff in this study. This model is broadly used in water management, low flow, and real-time flood forecasting studies in different parts of the world. In ARNO, the basin is composed of an infinite number of elementary areas, each of which has a different soil moisture capacity. The spatial distribution of the soil moisture capacity is expressed in the form of a probability distribution function. Soil moisture content is fed by rainfall that infiltrates into the soil and is depleted by evapotranspiration, drainage and percolation. For each of the elementary areas with different soil moisture capacity and different soil moisture content, the continuity of mass is simulated over time. Basin runoff is the integral of the runoff of elementary areas, transferred to the outlet of the basin via a routing module (Todini, 1996). The upper and the lower bounds that define the prior uncertainty ranges of the ARNO parameters are listed in Table 1. More details on the ARNO model are described by Todini (1996).

Table 1: The ARNO parameters used in this study

Parameter's Number	Parameter	Dimension and Symbol	Lower Bound	Upper Bound
1	Convectivity coefficient for the Hillslope	C1 [m/s]	1	3
2	Diffusivity coefficient for the Hillslope	D1 [m^2/s]	10	1000
3	Length of the path traveled by water to reach the channel	DX1 [km]	10	100
4	Convectivity coefficient for the channel	C2 [m/s]	1	3
5	Diffusivity coefficient for the channel	D2 [m^2/s]	100	10000
6	Length of the channel reach	DX2 [km]	1000	100000
7	Average volume of soil moisture storage	Wm [mm]	50	600
8	Moisture content threshold value in drainage calculation	SOL (or Wd) [mm]	0	300
9	Moisture content threshold value below which the percolation is negligible	SOL1 (or Wi) [mm]	0	100
10	A shape factor for the curve of soil moisture vs saturated areas	b	0.01	1
11	Maximum drainage that should be expected when the soil is completely saturated	Dmax [mm per time unit]	0	10
12	A drainage parameter	Dmin	0	10
13	Maximum percolation should be expected when the soil is completely saturated	PERC (or Is) [mm per time unit]	0	5
14	Exponent used to represent drainage when saturation is not reached	CESP (or c)	1.5	5
15	Initial volume of soil moisture storage	W0 [mm]	0	10

2.3. DREAMzs Algorithm

DREAMzs, proposed by Schoups and Vrugt (2010), is based on the original DREAM algorithm (Vrugt et al. 2009a). This newest approach uses sampling from an archive of past states to generate candidate points in each individual chain and requires only three parallel chains to summarize the posterior distribution. DREAMzs does not require outlier detection and removal; it maintains a detailed balance at every single step in each of the parallel chains (Schoups and Vrugt 2010). In addition, DREAMzs contains a snooker update to generate jumps beyond parallel direction updates (ter Braak and Vrugt 2008) in order to increase the diversity of the candidate points. The snooker axis runs through the states of two different chains, and the orientation of this jump is different from the parallel direction update, utilized in DREAM (Laloy and Vrugt 2012). The algorithmic implementation of the snooker update within the context of the differential evolution Markov chain (DE-MC) method was proposed by ter Braak (2006). More discussion on this algorithm is provided by Schoups and Vrugt (2010) and Laloy and Vrugt (2012).

2.4. Likelihood Function of DREAMzs Model

Performance of each set of parameters in predicting the observed model may be evaluated by a likelihood measure (He et al., 2010). In literature, many authors defined and evaluated various likelihood functions based on the maximum absolute residual (Keesman and van Straten 1989); inverse error variance with a shape factor (Beven and Binley 1992), an auto-correlated Gaussian error model (Romanowicz et al. 1994); Nash-Sutcliffe efficiency criterion with shape factor T, as well as the exponential transformation of the error variance with shaping factor T (Freer et al. 1996); the maximum likelihood function (Makowski et al. 2002); minimum mean square error (Wang et al. 2005) and normalized root mean square error (RMSE; Izady et al. 2015).

In order to assess the uncertainty of ARNO, Sum of Square Error (SSE) was chosen as the likelihood function (Eq. 1).

$$L(\theta_i \mid O) = \sum_{j=1}^{n} (O_j - Y_j(\theta_i))^2 \tag{1}$$

where θ_i is the ith set of parameters, $Y_j(\theta_i)$ is the jth type of model output (simulated stream flow) under θ_i set of parameters, O is the observed stream flow, Oj is the jth observation of O, N is the number of parameter sets, and M is the number of observations.

2.5. Performance Criteria

In this research, two indices were used to quantify the goodness of calibration/uncertainty performance: a P-factor (the maximum value is 100%), which is the percentage of data bracketed by a 95% prediction uncertainty band (95PPU; Vrugt et al., 2009b; Hamraz et al, 2015; Pourreza-Bilondi et al, 2016; Pourreza-Bilondi and Samadi, 2016; Nourali et al., 2016), and R-factor [or d-factor; Eqs. (2) and (3)], which is the average width of the uncertainty band divided by the standard deviation of the corresponding measured variable (the minimum value is zero; Abbaspour et al., 2007). Theoretically, the value for the P-factor ranges between 0 and 100%, while the R-factor ranges between 0 and infinity. A P-factor of 1 and R-factor of 0 is a simulation that exactly corresponded to measured data. The average thickness of the 95PPU band or the R-factor are estimated in every run and the best simulation can be judged based on the simulation with almost observed and modeled data located inside the 95% band with the highest P-factor and the least R-factor.

$$\bar{d}_x = \frac{1}{k} \sum_{i=1}^{k} (X_U - X_L) \tag{2}$$

$$R - Factor = \frac{\bar{d}_x}{\sigma_x} \tag{3}$$

where $\bar{d}_x$ denotes the average distance between the upper and the lower 95PPU; X_U and X_L represent the upper and lower boundaries of 95PPU; and σ_x is the standard deviation of the measured data. As all uncertainties in the conceptual model and inputs are reflected in the measurement, bracketing most of the measured data in the predictive 95PPU ensures that uncertainty is depicted by the parameter uncertainty (Pourreza-Bilondi et al., 2016).

The total uncertainty index (TUI) is also calculated based on the P-factor and R-factor for each flood event (Eq. (4)).

$$TUI = \frac{P_{Factor}}{R_{Factor}} \tag{4}$$

After running rainfall-runoff model with DREAMzs algorithm, simulated flow obtained from the best set of parameters (with maximum likelihood function or minimum objective function) compared with observed streamflow. Statistical indicators including RMSE (Eq. (5), Kling-Gupta Efficiency (KGE, Eq. (6)) (Gupta et al., 2009), and Nash- Sutcliffe (NSE, Eq. (7)) criteria were used to compare the performance of calibration.

$$RMSE = \sqrt{\frac{1}{n}\sum_{i=1}^{n}\left(Qo_i - Qs_i\right)^2} \tag{5}$$

$$KGE = 1 - \sqrt{(\mathrm{cc}-1)^2 + (\alpha-1)^2 + (\beta-1)^2} \tag{6}$$

$$NSE = 1 - \frac{\sum_{i=1}^{n}\left(Qs_i - Qo_i\right)^2}{\sum_{i=1}^{n}\left(Qo_i - \overline{Qo}\right)^2} \tag{7}$$

where Qo_i is the observed discharge, $\overline{Qo}$ is the mean value of observations, Qs_i is the simulated discharge, n is the number of observations, cc is the linear correlation coefficient between Qo and Qs, α is the ratio of standard deviation of Qs to standard deviation of Qo, and β is the ratio of the mean of Qs to mean of Qo. The smallest possible RMSE along with KGE and NSE close to 1, represent a better performance of likelihood function.

2.6. Convergence of the Sampled Chains

The convergence of a DREAMzs run can be monitored with the R statistic (Gelman and Rubin 1992), which determines convergence to the stationary posterior distribution. Based on the R statistic, DREAMzs was efficient at traversing the parameter space by quickly achieving convergence at a stationary posterior distribution (R-stat < 1.2). In other words, DREAMzs convergence for each of the ARNO parameters (including routing and basin parameters) was achieved after approximately 43,000 iterations.

2.7. Parameter Uncertainty and Posterior Distribution

Posterior density responses of the model parameters were visually investigated and the marginal posterior densities were constructed using fifteen model parameters (figure 1). This plot is created using the top 10 % of the total samples that retains as behavioral parameter sets. The x-axis in each graph is fixed to the prior range of each individual parameter to facilitate comparison of model optimized parameters.

Best parameters values is also recognized with blue symbol (×). Analysis suggests that allocation of some parameters such as C1 and C2; DX1 and DX2 possibly either arriving to similar distributions or at least very close to each other for several parameters. Also marginal distribution of several parameters (e.g. SOL, b and Dmin) showed normal distribution over time. Moreover, it can be seen that PERC parameter value is approximately close to zero meaning that much of overland flow contributed to surface runoff. Therefore, groundwater module had no contribution to runoff generation. High degree of variability in some model parameters, e.g. moisture content threshold value below which the percolation is negligible (Wi) and initial volume of soil moisture storage (W0), along with other channel and soil properties reflect the fact that these parameters were insensitive and contributed more uncertainty in modeling.

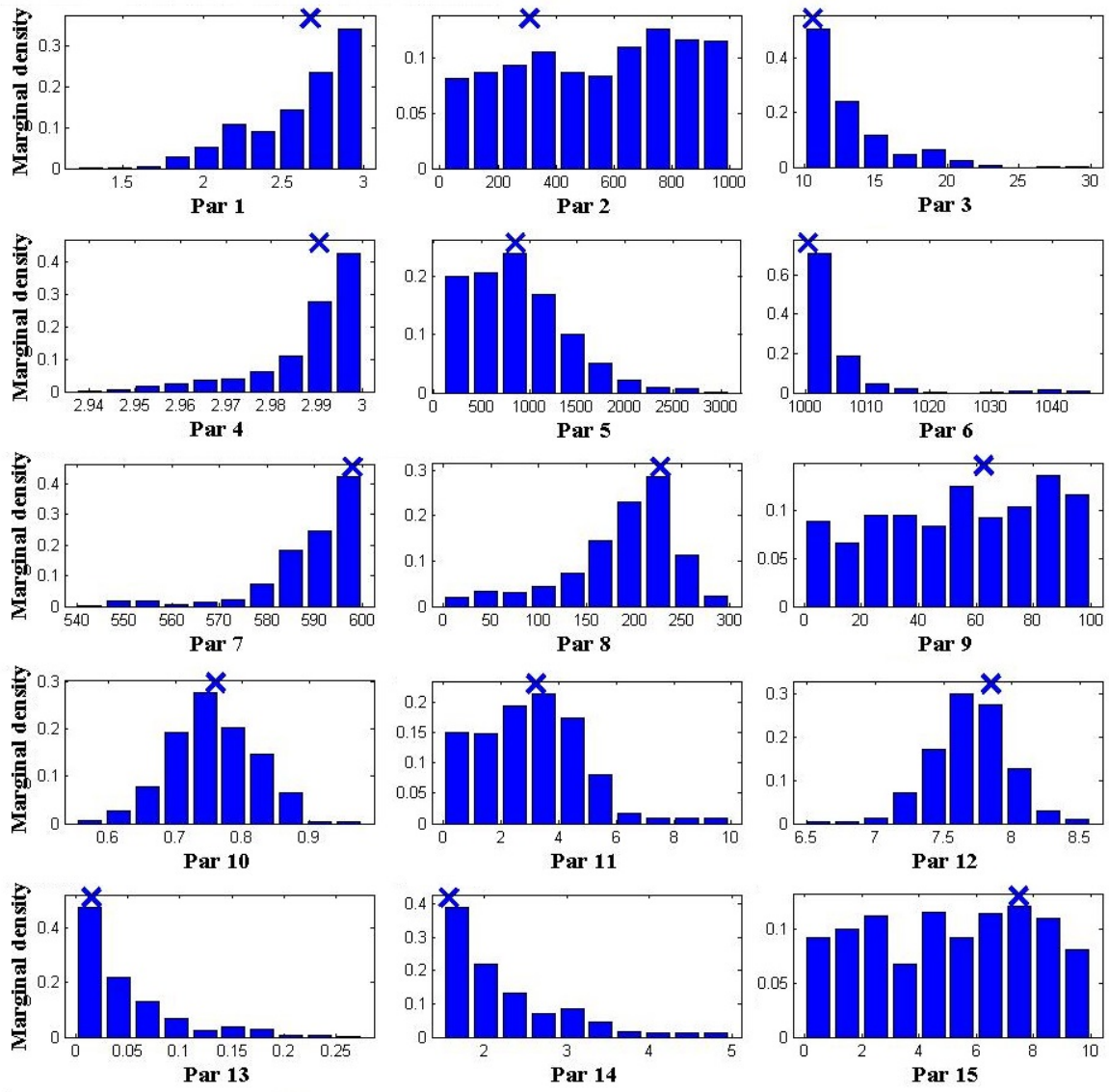

Figure 1: Marginal posterior probability distributions of fifteen ARNO parameters computed by DREAMzs

2.8. Predictive uncertainty

Figure 2 shows the observed data (dots), a 95 % parameter uncertainty due to posterior distribution of the parameter estimates (green shaded area) and a 95% hydrograph predictive uncertainty associated with the total uncertainty (greyshaded area) in the DREAMzs sampler. X-axis represents time equal to seven years from Sep-2002 to Oct-2008. Based on figure 2, 95% total prediction uncertainty ranges may bracket most of the observed flows.

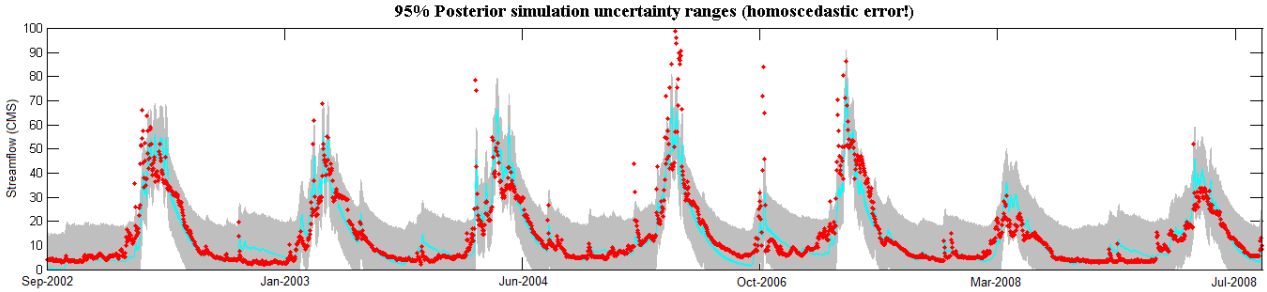

Figure 2: 95% total and parameter prediction uncertainty ranges of daily streamflow in the DREAMzs algorithm

Summary results and the performances of DREAMzs simulation are provided in Table 2. By calculating uncertainty assessment indicator (P-factor), 95% parameter uncertainty covers greater than 95% of observed data, but 95% total prediction uncertainty bounds are quite wide (figure 2) which is an indication of considerable uncertainty in the model structure and measured input data.

Table 2: Uncertainty and calibration performance criteria of the DREAMzs simulation

Uncertainty Criteria	*Total Uncertainty*	*Parameter Uncertainty*	*Performance Criteria*	*Best Value*
P-Factor%	*96.83*	*7.08*	*KGE*	*0.81*
R-Factor	*1.92*	*0.05*	*RMSE*	*7.23*
TUI	*50.41*	*135.2*	*NSE*	*0.76*

Green region in figure 2 (corresponding to parameter uncertainty) does not bracket observed streamflow data (P-factor=7%). The gaps between the uncertainty bounds of parameter and the observed data may be originated from uncertainties in observational input–output data (forcing data) and structural inadequacy of model which is indicating that model structure and observation measurements are needed to be improved in order to achieve more accurate predictions as recommended by Laloy et al (2010).

The R-factor and TUI values showed that the parameter uncertainty bound is highly efficient but it's not biased and skewed (P-Factor approximately 7%) that this could be due to disregarding rainfall data error while it may be dominant in many catchments (especially in mountainous regions) due to significant spatial and temporal variability of rainfall fields. It seems that rainfall forcing error should be considered in uncertainty assessment of ARNO model in future works. Ignoring errors of the input variables affects the structure of parameter uncertainty and confidence limits of the parameters in calibration of hydrologic models, and may lead to biased predictions (Kavetski et al., 2006a). Overall, considering all performance criteria, including RMSE, KGE and NSE, results showed that DREAMzs algorithm represents a good performance in calibration and uncertainty assessment of the ARNO model in mountainous region. More research is needed to understand the rainfall-runoff processes in rapid response watershed. However, the outputs of this research will help to understand modeling deficiencies and improve simulation in this type of region.

Since ARNO was unable to skillfully capture the magnitude of base flow contribution, the authors argue that subsurface module of this model can be improved significantly to better simulate streamflow records in time of no rainfall events.

REFERENCES

Abbaspour, K. C., et al. (2007). "Modelling hydrology and water quality in the pre-alpine/alpine Thur watershed using SWAT." J. Hydrol., 333(2): 413–430.

Adams, R., 1995. Assessing the performance of the NELUP hydrological models for river basin planning. Journal of Environmental Planning and Management, 38(1): 53-76.

Beven K, Binley A (1992) The future of distributed models: model calibration and uncertainty prediction. Hydrol Process 6:279–298. doi:10.1002/hyp.3360060305

Franchini, M., 1996. Use of a genetic algorithm combined with a local search method for the automatic calibration of conceptual rainfall-runoff models. Hydrological Sciences Journal, 41(1): 21-39.

Freer J, Beven K, Ambroise B (1996) Bayesian estimation of uncertainty in runoff prediction and the value of data: an application of the GLUE approach. Water Resour Res 32(7): 2161–2173. doi:10.1029/95WR03723

Gupta, H.V., Kling, H., Yilmaz, K.K., Martinez, G.F., 2009. Decomposition of the mean squared error and NSE performance criteria: implications for improving hydrological modeling. J. Hydrol. 377 (1), 80–91.

Gelman, A., and Rubin, D. B. (1992). "Inference from iterative simulation using multiple sequences." Stat. Sci., 7(4), 457–472.

Hamraz, B., Akbarpour, A., Pourreza-Bilondi, M. and Sadeghi-Tabas, S., 2015. On the assessment of ground water parameter uncertainty over an arid aquifer. Arabian journal of geosciences, 8(12): 10759-10773.

He, J., Jones, J.W., Graham, W.D., Dukes, M.D., 2010. Influence of likelihood function choice for estimating crop model parameters using the generalized likelihood uncertainty estimation method. Agric. Syst. 103: 256–264.

Izady A, Davary K, Alizadeh A, Ziaei AN, Alipoor A, Joodavi A, Brusseau ML (2014) A framework toward developing a groundwater conceptual model. Arab J Geosci 7:3611–3631. doi:10.1007/s12517-013-0971-9

Kavetski, D., Kuczera, G., Franks, S.W., 2006a. Bayesian analysis of input uncertainty in hydrological modeling: 1. Theory. Water Resour. Res. 42: W03407, doi: 10.1029/2005WR004368.

Keesman K, van Straten G (1989) Identification and prediction propagation of uncertainty in models with bounded noise. Int J Control 49(6): 2259–2269.

Khazaei, M.R., Zahabiyoun, B., Saghafian, B. and Ahmadi, S., 2014. Development of an automatic calibration tool using genetic algorithm for the ARNO conceptual rainfall-runoff model. Arabian Journal for Science and Engineering, 39(4), pp.2535-2549.

Khazaei, M.R., Zahabiyoun, B. and Saghafian, B., 2012. Assessment of climate change impact on floods using weather generator and continuous rainfall□runoff model. International Journal of Climatology, 32(13): 1997-2006.

Laloy, E., and Vrugt, J. A. (2012). "High-dimensional posterior exploration of hydrologic models using multiple-try DREAM (ZS) and high performance computing." Water Resour. Res., 48(1): 1–18.

Laloy, E., Fasbender, D., Bielders, C.L., 2010. Parameter optimization and uncertainty analysis for plot-scale continuous modeling of runoff using a formal Bayesian approach. J. Hydrol. 380: 82–93.

Makowski, D., Wallach, D. and Tremblay, M., 2002. Using a Bayesian approach to parameter estimation; comparison of the GLUE and MCMC methods. Agronomie-Sciences des Productions Vegetales et de l'Environnement, 22(2): 191-204.

Nourali, M., Ghahraman, B., Pourreza-Bilondi, M. and Davary, K., 2016. Effect of formal and informal likelihood functions on uncertainty assessment in a single event rainfall-runoff model. Journal of Hydrology, 540: 549-564.

Pourreza-Bilondi, M., Samadi, S.Z., Akhoond-Ali, A.M. and Ghahraman, B., 2016. Reliability of Semiarid Flash Flood Modeling Using Bayesian Framework. Journal of Hydrologic Engineering, p.05016039.

Pourreza-Bilondi, M. and Samadi, S.Z., 2016. Quantifying the uncertainty of semiarid flash floods using generalized likelihood uncertainty estimation. Arabian Journal of Geosciences, 9(13), p.622.

Romanowicz R, Beven KJ, Tawn J (1994) Evaluation of predictive uncertainty in non-linear hydrological models using a Bayesian approach. In: Barnettand V, Turkman KF (eds) Statistics for the environment: water related issues. Wiley, NewYork, pp 297–317

Schoups, G., Vrugt, J. A., Fenicia, F., and Van de Giesen, N. C. 2010. Corruption of accuracy and efficiency of Markov chain Monte Carlo simulation by inaccurate numerical implementation of conceptual hydrologic models. Water Resour. Res., 46: W10530.

ter Braak, C. J. F., and Vrugt, J. A. (2008). "Differential evolution Markov chain with snooker updater and fewer chains." Stat. Comput., 18(4), 435–446.

Todini, E.: Il modello afllussi deflussi del fiume Amo. Relazione Generale dello studio per conto della Regione Toscana, in Tech. Report. Bologna (1988)

Todini, E.: The ARNO rainfall-runoff model. J. Hydrol. 175(1–4), 339–382 (1996)

Vrugt, J.A., ter Braak, C.J.F., Diks, C.G.H., Robinson, B.A., Hyman, J.M., Higdon, D., 2009a. Accelerating Markov Chain Monte Carlo simulation using self-adaptative differential evolution with randomized subspace sampling. Int. J. Nonlin. Sci. Numer. Simul. 10 (3), 273–290.

Vrugt, J.A., ter Braak, C.J.F., Gupta, H.V., Robinson, B.A., 2009b. Equifinality of formal (DREAM) and informal (GLUE) Bayesian approaches in hydrologic modeling? Stoch. Environ. Res. Risk Assess. 23 (7), 1011–1026.

Wang X, He X, Williams JR, Izaurralde RC, Atwood JD (2005) Sensitivity and uncertainty analyses of crop yields and soil organic carbon simulated with EPIC. Trans ASAE 48(3):1041–1054. doi:10.13031/2013.18515

Zhao, R.J.: Flood forecasting method for humid regions of China. East China College of Hydraulic Engineering, Nanjing (1977)

Proceedings of the 10th World Congress of EWRA 'Panta Rhei', 5-9 July 2017, Athens, Greece
© 2017 *European Water Resources Association*

Impact of extreme events on watershed dynamics

J. Kim[1], M. Dwelle[2], A. Warnock[3], V. Ivanov[2] and N. Katopodes[2*]
[1] *Department of Civil and Environmental Engineering, Sejong University, Seoul, Republic of Korea*
[2] *Department of Civil and Environmental Engineering University of Michigan, Ann Arbor, USA*
[3] *SRI International, Menlo Park, CA, USA*
[*] *e-mail: ndk@umich.edu*

Abstract: This paper presents the methodology for a quantitative assessment of the impact of extreme events on watershed morphology and dynamics. By linking some key factors of erosion to land morphology and biota, a quantitative measure of the sustainability of aquatic life is also presented. The integrated watershed-morphology model is used to perform a formal sensitivity analysis of land dynamics to various hydrologic changes at the drainage basin level. Finally, by running simulation scenarios over long term periods, it is possible to establish quantitative measures of the trade-offs between the ecosystem services provided by water within a watershed.

Key words: Climate change; watershed dynamics; Numerical models; Erosion; Sedimentation

1. INTRODUCTION

Long-term effects of land use practices and extreme weather phenomena lead to erosion and sedimentation processes that are responsible for many undesirable changes to the ability of the land to sustain microbial life and produce food. Every isolated event has an irreversible impact on the land due to the potential for erosion that ignites a sequence of events whose scale increases with time. Variations in watershed headwater land use, as well as climate change, directly affect the local runoff and erosion processes, and the related ecosystem services. The process-scale dynamics of hill-slope-channel erosion and streamflow sediment yield are well understood, being strongly affected by the spatial heterogeneity in soil and bedrock, vegetation cover, and topography. The rainfall-runoff mechanism is the primary driver of these dynamics, exhibiting high heterogeneity over a number of spatial and temporal scales and a strong dependence on antecedent conditions. Consequently, changes in watershed headwater land use, as well as changes in key forcing elements of the hydrologic cycle may alter the characteristics of local runoff production and erosion processes. This, in turn, may lead to the adverse effects of excessive sedimentation and unstable hydrology of estuarine and wetland habitats.

Even if alternative scenarios for watershed management were available, it would be impossible to quantitatively assess how long it would take to restore a watershed to its original state and provide relevant uncertainty bounds. Additionally, the transfer of qualitative interpretations from one watershed to another is not meaningful, as most of the information derived is site specific, and the underlying physical and ecological components are difficult to scale. It is therefore clear that physical processes occurring in the headwater drainage basin are critical, and need to be considered for meaningful and robust evaluations. A predictive sensitivity analysis model is needed to quantify each of the processes involved, to explain how past practices have led to the present state, as well as to offer alternative land use approaches for the future. Such a tool would be also capable of interpreting anticipated perturbations in the hydrological cycle as a result of deviations from mean climate.

We present a method that can overcome these difficulties by coupling a high resolution land morphology model with a large scale watershed model. The two models are mathematically compatible, thus there is high confidence that their integrated results will provide a unique method

for the investigation of both extreme and long-term changes due to flood and drought.

2. MODEL DESCRIPTION

The primary tool used for hydrologic assessment is the tRIBS-OFM model (Kim et al, 2012). The model is also capable of simulating erosion and sedimentation (Kim et al, 2013). The fundamental development for the hydrologic processes is due to Ivanov et al (2008). The overland flow dynamics was originally developed by Bradford and Katopodes (1999) and later converted to an unstructured grid by Begnudelli and Sanders (2006).



Figure 1. Computational grid.

A key feature of the model is the collocation of the computational grids for the hydrologic and hydrodynamic modules. As shown in Fig. 1, the Voronoi cells of the hydrologic model are mapped onto the Delaunay triangles of the overland flow model, thus coupling the two processes by means of the runoff volume at the cell center. This allows a two-way transfer of information from between the erosion and sedimentation module and the precipitation and energy flux input of the integrated model. This represents the precise mechanism by which the sensitivity analysis can be performed by seamless transfer of adjoint data from the downstream end to the headwaters of the watershed.

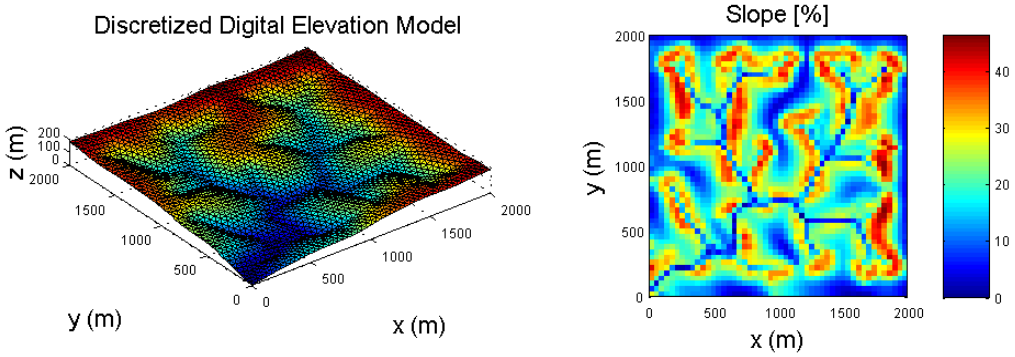

Figure 2. Watershed model.

A typical depiction of a watershed is shown in Fig. 2, in which a digital elevation model is used to characterize the morphological elements of the terrain. The soil erosion model was originally proposed by Hairsine and Rose (1992), and later modified by Sander et al (1996). The current model also includes modules that capture the subgrid effects of land resistance (Kim et al, 2012), and the dynamic switch between dynamic and kinematic waves introduced by Warnock et al (2014).

The input climate data are introduced using the downscaling approach is due to Fatichi et al (2015). GCM projections are consistently downscaled using the weather simulator. It generates a hydro-meteorological series with prescribed characteristics in which the interdependencies between key states are preserved, e.g. change in precipitation occurrence will have an effect on cloudiness,

incoming short- and longwave radiation, and air temperature. The foregoing projections can be accounted for by modfiying the parameters of the Poisson arrival model and nudging the deterministic temperature component to reflect either positive or negative trends. Seasonal interdependencies can then be further tuned. An atmosphere radiative transfer model is used that treats two shortwave bands, VIS and NIR, separately allowing one to estimate fluxes for clear sky conditions. Cloudy sky conditions are also accounted for by suitable parameterizations. Terrain effects are introduced using geometric information on local topographic aspect and slope.

Air temperature is assumed to be the sum of two variables: a deterministic and a random variate. The deterministic component is determined based on an empirical method that attributes temporal variation of the air temperature to the divergence of radiative and eddy heat fluxes. In essence, the deterministic temperature increment is regressed on several hydro-meteorological variables such as the site Sun position, a factor of cloudiness, and incoming longwave radiation. The random variate is approximated by a first order Markov process. For air humidity, the model converts the minimum daily temperatures to dew point temperature using information on daily potential evaporation and degree of aridity of the region. Since dew point temperatures typically exhibit low variability during the day, daily values suffice for our modeling purposes. Finally, wind speed is introduced as an independent process. Skewed hourly wind speed data are generated using a first order Markov model where the random term forces skewness on the results of the autoregressive model. Using the generated runoff and eroded particles as input, the transport model simulates the redistribution of sediment both as bedload and as suspended load across the basin drainage network. The long-term simulations allow the representation of characteristic hydro-geomorphic seasonal dynamics. Thus, at the framework back-end, this will provide the necessary information for the evaluation of rates of change of stream and estuary morphology that will be translated to changes in aquatic habitat quality.

3. SENSITIVITY ANALYSIS

A formal sensitivity analysis is conducted based on the adjoint equation method developed by Sanders and Katopodes (2000). The integrated watershed-estuary-habitat model is used to perform a systematic study of the factors affecting aquatic life in wetlands and estuaries. The precise impact of climatic change or alternative land practices at the watershed level can be quantitatively assessed if one system parameter is varied while all others remain constant. The effect of such variation on a specific target, e.g. habitat component, represents the sensitivity of the habitat to each parameter change.

The proposed model provides the ideal means for performing such an analysis using the best possible physical description of the system. However, in cases where the impact of a parameter variation requires several years to manifest itself in the habitat, tedious computations are needed to obtain the relevant sensitivity information. These must be then repeated for each parameter that can potentially affect the target process. Adjoint sensitivity analysis allows us to compute the same impact information extremely efficiently without repetitive runs of the model. By running the adjoint model in the reverse time direction, all sensitivity data for a given habitat component can be computed by a single simulation of the direct and one of the adjoint model, regardless of the number of parameters affecting the target component. Remarkably rich information can be thus retrieved very efficiently, and parameters that have insignificant impact on the habitat can be securely excluded from further studies.

4. DISCUSSION OF RESULTS

The fundamental hypothesis of the present study is that erosion and sedimentation constitute a chain of information that links hydrologic processes to estuarine morphology. Although this is intuitively evident, there is no quantitative estimate of the causes and relative impact of the stressors

that cause these changes. Therefore, computational scenarios have been developed to demonstrated the relation between hydrologic inputs and estuarine or wetland changes. The present scenarios have focused on precipitation changes, local temperature, and wind data. Soil properties have also been included in th study, but not as a direct sensitivity indicator.

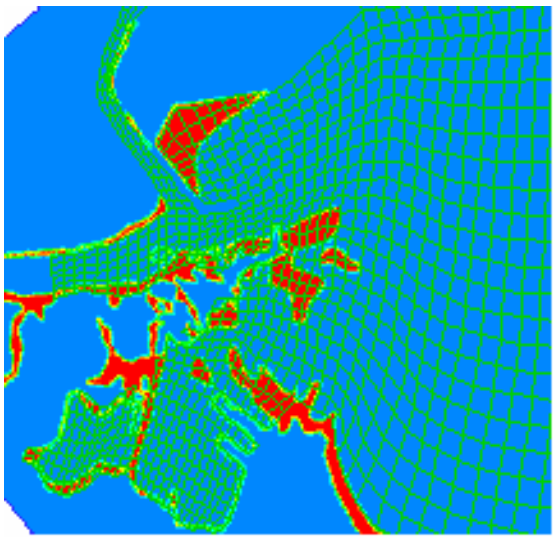

Figure 3. Sensitivity of Deposition areas in Muskegon River estuary.

The sensitivity analysis identifies areas of potential deposition in a study area, such as the one shown in Fig. 3. Then, the model tries to identify the individual sensitivities of a unit change in estuarine depth to unit changes in the parameters of the study. Trial runs eliminate parameters with low sensitivity, thus allowing subsequent runs to focus on those parameters that have a larger impact on sedimentation.

The results of this study provide overwhelming evidence that soil moisture conditions, as affected by the infiltration process, subsurface redistribution in the unsaturated-saturated zones, and evapotranspiration are the antecedent conditions with the highest sensitivity. In areas susceptible to erosion, the locally produced event-scale runoff is then translated into sediment yields. Diffusive erosion processes due to rain-splash, freeze-thaw, bioturbation, and wet-dry cycles represent lower frequency phenomena responding to seasonal and long-term dynamics. This extreme drought followed by extreme precipitation is therefore the mechanism with the highest sensitivity to changes in aquatic biota in estuaries and wetlands. The proposed model is capable of providing spatially distributed information on the specific areas of a given watershed that are susceptible to erosion to which estuarine dynamics show high sensitivity. It is believed that this information may be of value to engineers and planners that can then take measures to prevent these changes.

REFERENCES

Begnudelli, L., and B. F. Sanders (2006), Unstructured grid finite-volume algorithm for shallow-water flow and scalar transport with wetting and drying, *Journal of Hydraulic Engineering-ASCE*, *132*(4), 371-384.

Bradford, S. F., and N. D. Katopodes (1999), Hydrodynamics of turbid underflows. I: Formulation and numerical analysis, *Journal of Hydraulic Engineering-ASCE*, *125*(10), 1006-1015.

Fatichi, S., Rimkus, S., Burlando, P., Bordoy, R., Molnar, P., (2015). High-resolution distributed analysis of climate and nthropogenic changes on the hydrology of an Alpine catchment. J. Hydrol. 525, 362–382.

Hairsine, P. B., and C. W. Rose (1992), Modeling water erosion due to overland flow using physical principles: 1. Sheet flow, *Water Resources Research*, *28*(1), 237-243.

Ivanov, V.Y., R.L. Bras, and E.R. Vivoni, *Vegetation-hydrology dynamics in complex terrain of semiarid areas: 1. A mechanistic approach to modeling dynamic feedbacks.* Water Resources Research, 2008. 44(3).

Kim, J., Ivanov, V. and Katopodes, N.D., " Modeling erosion and sedimentation coupled with hydrological and overland flow processes at the watershed scale," *Water Resources Research,* Volume 49, Issue 9, pages 5134-5154, September 2013

Kim, J., V.Y. Ivanov, and N. Katopodes, "Hydraulic resistance to overland flow over vegetated surfaces," *Water Resources Research*, 48, 10, 2012.

Kim, J, Warnock, A., Ivanov, V. and Katopodes, N.D., " Coupled modeling of hydrologic and hydrodynamic processes including overland and channel flow," *Advances in Water Resources,* 37, 104-126, 2012

Sander, G. C., P. B. Hairsine, C. W. Rose, D. Cassidy, J. Y. Parlange, W. L. Hogarth, and I. G. Lisle (1996), Unsteady soil erosion model, analytical solutions and comparison with experimental results, *J. Hydrol.*, *178*(1-4), 351-367.

Sanders, B.F. and Katopodes, N.D., (2000) “Sensitivity Analysis of Shallow Water Flow by Adjoint Method, Journal of Engineering Mechanics, Vol. 126, No. 9, pp. 909-919.

Warnock, A., Kim, J., Ivanov, V., and Katopodes, N., "Self-Adaptive Kinematic-Dynamic Model for Overland Flow," *Journal of Hydraulic Eng*ineering, 140(2), 169-181, 2014.

Proceedings of the 10th World Congress of EWRA 'Panta Rhei', 5-9 July 2017, Athens, Greece
© 2017 *European Water Resources Association*

A decision support system for urban stormwater drainage management

F. De Paola*, M. Giugni, F. Pugliese, P. Romano
Department of Civil, Architectural and Environmental Engineering. University of Naples Federico II, Naples, Italy
* *e-mail: depaola@unina.it*

Abstract: In the last decades, urban pluvial floods are occurring with increasing frequency all over the world, including developed countries (e.g. Italy) due to factors mainly referable to Climate and Land Use Changes (coupled with urbanization and increasing population). Urbanization is typically accompanied by increases in impervious surfaces, compaction of soils, and modifications to vegetation. This results in increased surface runoff, increased runoff velocity and stream erosion, decreased time of concentration of watersheds, and decreased water quality, due to water contamination from suspended sediments, heavy metals, hydrocarbons, nutrients, and pathogens. In the context of Urban Water Management, a useful role can be represented by innovative approaches, implementing optimization techniques and new technologies for Low Impact Development (LID) type of stormwater Best Management Practices (BMPs) for urban runoff control. The main goal of these strategies should be the improvement of the resilience of the cities against the increase of the storm water flows and the risk of flooding (urban flash floods). In this paper a Decision Support System for the identification of the best strategy for adapting to climate and land use changes is presented. This System allows to identify the most useful BMPs, among the usual ones in the technical literature (i.e. detention ponds, infiltration trenches, pervious pavement, green roofs, etc.). In particular the System interfaces a simulation model (SWMM5.1) with an optimization module (Harmony Search) able to identify the best combination of BMPs to adequately reduce flood peak discharges and volumes.

Key words: Best Management Practices, Low Impact Development, SWMM 5.1, Harmony Search, Urban Drainage Systems, Optimization Algorithms

1. INTRODUCTION

During the last decades, urban floods events have increased in frequency and intensity, as a consequence of the ongoing Climate and Land Use changes. Mitigation and adaptation to the in-development forcing are intended as one of the most pressing and, at the same, difficult challenges to deal into the field of the urban drainage system management, especially for developing countries, where the uncontrolled and indiscriminate expansion of both the urban centres and the related socio-economical activities is evolving.

Recent studies pointed out how the excessive runoff, caused by the significant increments of impervious surfaces (such as building roofs, parking area, roads), is causing uncontrolled flooding in urban areas, increasing the deterioration of water quality in receiving water bodies (Khan et al., 2006; Dietz, 2007). However, the urbanization represents an in-progress phenomenon with global interest in many countries, predicting to reach in 2050 percentages of 80% and 75% of areas having levels of urbanization greater than 50% and 75%, respectively (DESA, 2015). Among these countries, China represents one of the most pregnant examples, with an urbanization rate, intended as the ratio between the population living in urban areas and the overall population, increasing from 12.5% in 1952 up to 60%, predicted in 2020 (Wei, 2012). This trend is strongly impacting on the natural ecosystems, predicting more severe future configurations (Du et al., 2012; Hager et al., 2013). Stormwater drainage management is undergoing significant changes, moving from operative approaches mainly based upon flood mitigation and health protection to others strongly addressed to environmental, social and economical considerations (Fletcher et al., 2015). Specifically, one of the most interesting challenge for engineering research regards the definition of innovative environmental criteria to limit and face the detrimental impacts of urbanization. Among them, the application of LID-BMPs (Low Impact Development-Best Management Practices) technologies to

control and manage the stormwater runoff quality and quantity (Davis, 2005; Field et al., 2006) represents a recognized environmental technique for measurement, control and management of quali-quantitative stormwater runoff in a cost-effective manner (US EPA, 2004). To this category, bioretention cells, porous pavements, green roofs, vegetative swales, rooftop gardens and infiltration trenches are included, having different removal efficiencies, costs, environmental impacts and disposal capacities.

Due to the recent application, and still yet not complete knowledge about the performances of various technologies in urban areas, with unavoidable uncertainties in their uses (Li et al., 2013), the definition of LID-BMPs effectiveness and suitability results a complex but unavoidable step in the field of the urban runoff control planning. Furthermore, the planning process related to the application of LID-BMPs techniques is strictly correlated to urban master planning, land use, landscape, drainage system and water pollution planning, for the selection of the most appropriate practices, able to accomplish the required development goals and objectives, in compliance with the socio-economical constraints, guaranteeing, at the same time, the effectiveness of costs, sizing and placement selection (Cheng et al., 2009; Jia et al., 2012; Barbosa et al., 2012). In this field, several urban runoff simulation and optimization tools (Elliot and Trowsdale, 2007), such as SUSTAIN (System Urban Stormwater Treatment and INtegration), were implemented to perform analyses on LID-BMPs applications (US EPA, 2009; Lee et al., 2012; Fletcher et al., 2013; Mao et al. 2016), which use represents a suitable combination of LID-BMPs techniques in urban areas, as a function of the available cost resources.

To this aim, in the present paper the implementation of a Decision Support System (DSS) to LID design for urban stormwater drainage development was analyzed and discussed. An interface between the Harmony Search meta-heuristic algorithm (Geem et al., 2001) and the EPA SWMM 5.1 solver was implemented for optimal design of LID-BMPs practices.

The Harmony Search was widely applied in the field of hydraulic engineering both for optimization of water supply systems (Geem et al., 2002; Geem, 2006; De Paola et al., 2016a) and urban drainage systems (De Paola et al., 2015, 2016b), resulting strongly competitive for searching for optimal solutions in short computational times (De Paola et al., 2016c).

2. A DECISION SUPPORT SYSTEM MODEL TO DESIGN LID-BMPS IN STORMWATER DRAINAGE SYSTEMS: THE CASE-STUDY OF FUORIGROTTA (NA)

This work was devoted to the definition of benefits connected to the application of LID-BMPs practices in stormwater drainage systems to manage and control the urban flow, aiming at both decreasing the total volume of rainfall water drained into urban stormwater systems and reducing the urban flooding risk.

Case-study in question regarded a sub-area located in the Fuorigrotta district in Naples (IT), bounded by exploiting the natural limits, set by both buildings and natural orographic configuration. The boundary limit is constituted by Via Terracina in the northern side, by Posillipo Hill in the est and south sides and by the Mostra d'Oltremare building in the west side. The investigated study area was equal to 1.89 km^2 with perimeter of 6975 m.

2.1 Urban-operational analysis by using a GIS software

Territorial analyses were performed by using the UTM WGS84 33N multi-precision topographic geo-database, available from the Campania Region Authority, in reference to year 2004. To update the actual urban territorial configuration, specific analyses were performed, in reference to the considered area, analysing the land use, its intended use, the pervious and impervious surface partition, the urban traffic density and the location of urban areas, potentially reliable to be converted into LID-BMP practices. A GIS model was applied to define the properties of each point

of interest, combined with a Digital Terrain Model (DTM), made available from the Campania Region Authority.

2.2 The urban stormwater system of Fuorigrotta (NA) basin. Modelling in SWMM 5.1

The urban stormwater system of the Fuorigrotta (NA) basin was built in 1950, undergoing to multiple integrations during the following years. The main sewer was composed of the Arena Sant'Antonio sewer to convey the rainwater, whereas the Cuma outflowing stream collects the wastewaters.

As a result of the study about the functioning of the sewer system, two hydrographic basins were defined, named *North Basin* and *South Basin*, respectively (Fig. 1). The sewers, which compose the *North Basin*, totally flow into the Arena Sant'Antonio main sewer, whereas the main sewer in Via Diocleziano conveys all the water volumes coming from the *South Basin*. This configuration is exclusively referred to the rainfall volumes, because the wastewaters are conveyed into the Cuma main sewer. The model in SWMM 5.1 consisted of a significant simplification, which brought to model the solely main sewers, located downstream the two abovementioned basins and connected through a final node.

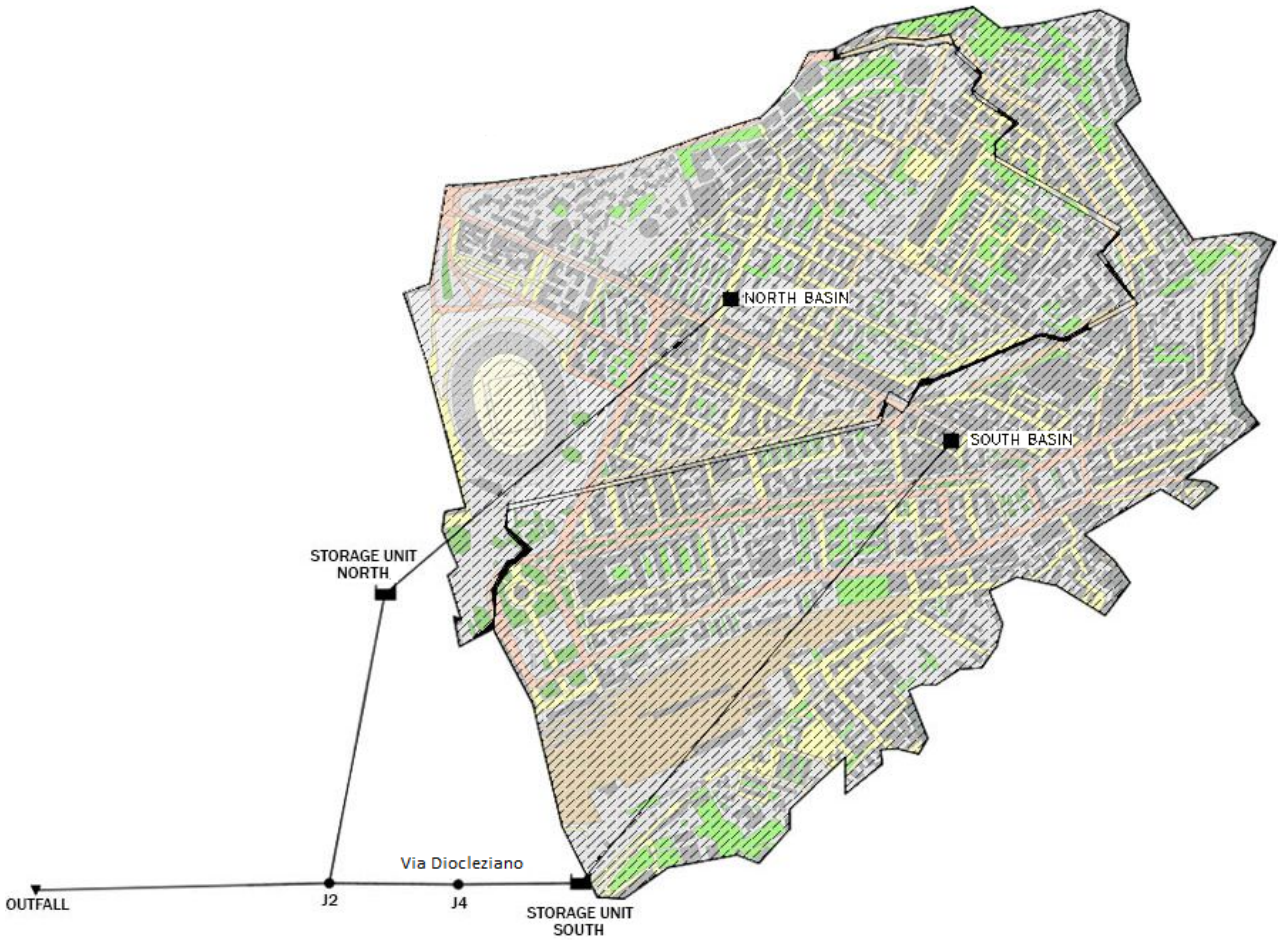

Figure 1. SWMM model of Fuorigrotta (NA) basin.

The above described configuration defined the so-called "Baseline Scenario" which represented the rainwater configuration before the introduction of LID-BMP practices.

An interface between the hydraulic solver SWMM 5.1 and the Harmony Search meta-heuristic code was implemented, according to the operative procedure summarized in the flow-chart in Fig. 2.

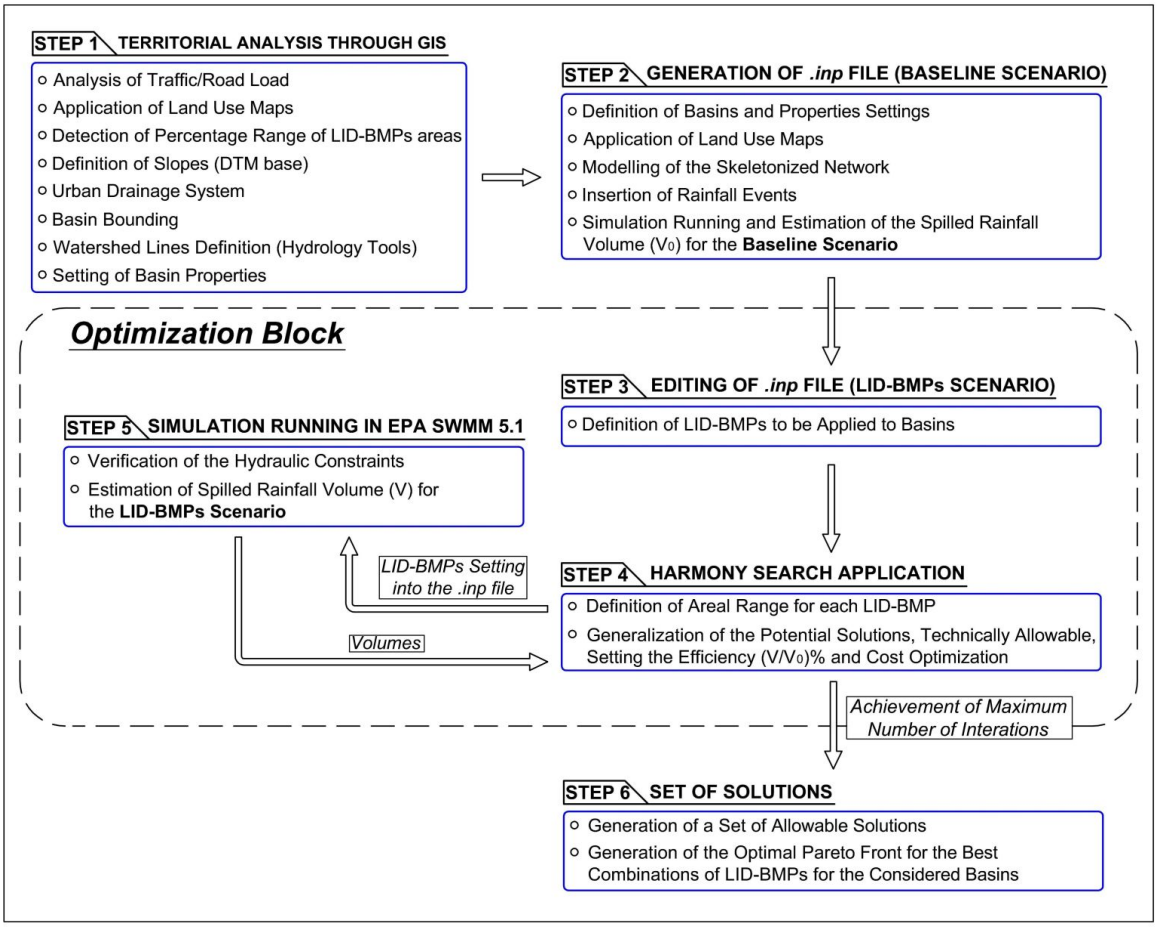

Figure 2. Flow-chart of the applied procedure to design the LID-BMPs applications.

2.3 Design of LID-BMPs by using the Harmony Search algorithm

Simulations were performed as a function of 18 rainfall events, which historical rainfall data were provided by the Basin Authority of Campania Centrale, in reference to 6 durations. Three return periods were accounted for, equal to 5, 10 and 20 years, and spilled volume V_0, referred to the Baseline Scenario, was calculated in order to estimate the improvements obtainable by applying LID-BMPs in terms of spilled volume reduction with respect to the Baseline Scenario V/V_0. A critical duration d = 1 h was considered for simulations.

Considered LID-BMP practices, among those available in SWMM 5.1, were porous pavements, bioretention and roof garden. The choice was done as a consequence of the analysis of the land use map about the availability of the potentially convertible areas in the studied zone. A storage unit was also set for each final node of the basins, fixing a maximum potential capacity of 1'000 m^2 (Fig. 2). In the following Table 1, set input properties are summarized to calculate the LID-BMPs extension.

Table 1. Setting parameters of LID-BMPs.

	North Basin	South Basin
Area (m^2)	821'400	1'072'700
Width (m)	4'086.6	6'476.4
Impervious Surface (%)	92.90	81.40
Bioretention Max Area (m^2)	66'184.25	199'955
Green Roof Max Area (m^2)	11'505.05	141'851.5
Porous Pavement Max Area (m^2)	383'629.05	419'552.9

For both each LID-BMP type and final storage units, the maximum potential areas were set (Table 1) and simulations were run, by considering 10'000 iterations. A maximum allowable total cost was fixed. Unitary cost for each LID-BMP practice was evaluated according to Zheng (2013). Three levels of simulations were performed, by varying the volume ratio V/V_0 with respect to the Baseline Scenario in the ranges: (a) 100-77%; (b) 77-47% and (c) 47-34%. A total of 30'000 solutions, in terms of costs and volume V/V_0 rate, were found, defining the Pareto Front, on which the dominant solutions were included. Thus, they represented the solution, referring to which, for a fixed cost, the volume reduction was maximized; conversely, for a fixed volume rate V/V_0, they defined the relative minimum costs (Fig. 3).

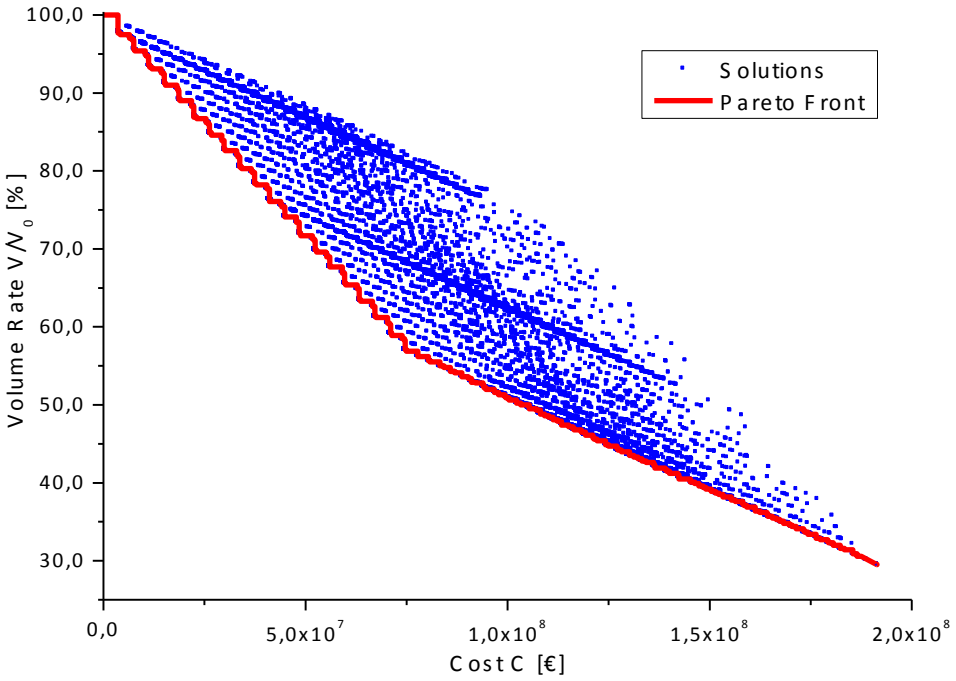

Figure 3. Cost-volume solutions and Pareto Front.

2.4 Solution selection and data validation

The developed model can be intended as a DSS (Decision Support System) because it allows to define the optimal design of LID-BMP practices, as a function of the available economic budget.

In reference to the considered case-study, a maximum budget in the range 50-55 millions € was set and a maximum volume rate V/V_0 equal to 70% to choose the optimal solution. With reference to the *North Basin*, areas converted into porous pavements were equal to 269'155.5 m^2, whereas bioretention areas had extension of 65.21 m^2. Green roofs were not considered for the selected solution. Concerning the *South Basin*, porous pavements were designed for an area of 294'291.2 m^2, whereas neither bioretention nor green roof practices were included into the solution. Conversely, a storage unit of 113.26 m^2 was considered for the South Basin.

It is interesting to point out that the evaluation of the required volume rate V/V_0 has to be accomplished by taking into account also the geological composition of the considered site. In the studied case-study, the soil was mainly constituted by loose pyroclasts, which could determine significant compaction if strongly imbibed.

The repetition of the 18 simulations was performed in order to compare results of the Baseline Scenario and of the LID-BMPs ones. Moreover, a further simulation comparison between pre/post LID-BMP scenarios was performed by considering the historical rainfall event which involved the Fuorigrotta (NA) district on 15/09/2011, clustered in two intense showers with a mean intensity larger than 50 mm/h. It corresponded to a return period of 500 years, causing damages estimated in

about actualized 240 millions €. This last comparison was useful to quantify the environmental and economic improvements, obtainable by applying LID-BMPs practices, when catastrophic events occur. Specifically, a volume rate V/V_0 equal to 68.3% was estimated.

3. CONCLUSIONS

In this work the implementation of a Decision Support System to manage urban stormwater systems was presented and discussed. The model was implemented by combining the Harmony Search meta-heuristic code with the SWMM 5.1 hydraulic solver, aiming at defining the optimal design of LID-BMP practices in urban stormwater systems. The case-study of Fuorigrotta (NA) urban basin was analyzed, with reference to the installation of porous pavements, bioretention and roof gardens, with the aim of reducing the flooded urban areas when high rainfall events occur. Analysis of both the orographic configuration and the land use and definition of areas potentially convertible in LID-BMPs was developed by using a GIS software. The model was able to define the solution which, for a fixed available budget, maximizes the reduction of flooded volume. Conversely, having chosen a technical threshold of flooded volume, it allows to quantify the required budget. Comparison between pre and post intervention scenarios pointed out the reliability of the developed model to estimate the reachable environmental and economic benefits of LID-BMPs, in case of extreme rainfall events.

REFERENCES

Barbosa, A. E., Fernandes, J. N., David, L. M., 2012. Key issues for sustainable urban stormwater management. Water Res.; 46 (20): 6787-6798.

Cheng, M. S., Zhen, J. X., Shoemaker, L., 2009. BMP decision support system for evaluating stormwater management alternatives. Front. Environ. Sci. Eng. China; 3(4): 453-463.

Davis, A.P., 2005. Green engineering principles promote low-impact development. Environ. Sci. Technol.; 39(16): 338A-344A.

De Paola, F., Galdiero, E., Giugni, M., Pugliese, F., 2015. Sustainable development of stormwater systems in Africa cities considering climate change. Proc. Eng., 119, 1181-1191.

De Paola, F., Galdiero, E:, Giugni, M., 2016a. A jazz-based approach for optimal setting of pressure reducing valves in water distribution networks. Eng. Opt., 48(5), 727-739.

De Paola, F., Giugni, M., Pugliese, F., 2016b. A harmony-based tool for urban drainage systems. Water Manage. (in press).

De Paola, F., Fontana, N., Giugni, M., Marini, G., Pugliese F., 2016c. An application of the Harmony-Search Multi-Objective (HSMO) optimization algorithm for the solution of Pump Scheduling problem. Proc. Eng.; 162: 494-502.

DESA Department of Economic and Social Affairs of the United Nations (2015). World Urbanization Prospects: The 2014 Revision, (ST/ESA/SER.A/366)

Dietz, M. E., 2007. Low impact development practices: a review of current research and recommendations for future directions. Water Air Soil Pollut.; 186(1-4): 351-363.

Du, P. F., Jia, H. F., Yu, S. L., 2012. Urban watershed management under rapid urbanization. Front. Environ. Sci. Eng.; 6(5): 595.

Elliott, A. H., Trowsdale, S. A., 2007. A review of models for low impact urban stormwater drainage. Environ. Model. Softw.; 22: 394-405.

Field, R., Struck, S. D., Tafuri, A. N., Ports, M. A., Clar, M., Clark, S., Rushton, B., 2006. BMP Technology in Urban Watersheds: Current and Future Directions. ASCE, Reston, VA, ISBN 0-7844-0872-6.

Fletcher, T. D., Andrieu, H., Hamel, P., 2013. Understanding, management and modeling of urban hydrology and its consequences for receiving waters: a state of the art. Adv. Water Resour.; 51: 261-279.

Fletcher, T. D., Shuster, W., Hunt, W. F., Ashley, R., Butler, D., Arthur, S., Trowsdale, S., Barraud, S., Semadeni-Davies, A., Bertrand-Krajewski, J-L., Mikkelsen, P. S., Rivard, G., Uhl, M., Dagenais, D., Viklander, M., 2015. SUDS, LID, BMPs, WSUD and more – The evolution and application of terminology surrounding urban drainage. Urban Water J.; 12(3): 525-542.

Geem, Z. W., Kim, J. H., Loganathan, G. V., 2001. A new heuristic optimization algorithm: Harmony Search. Simul.; 76: 60-68.

Geem, Z. W., Kim, J. H., Loganathan, G. V., 2002. Harmony search optimization: application to pipe network design. Int. J. Model. Sci. Comp.; 22(2): 125-133.

Geem, Z. W., 2006. Optimal cost design of water distribution networks using harmony search. Eng. Opt.; 38(3): 259-280.

Hager, G. W., Belt, K. T., Stack, W., Burgess, K., Grove, J. M., Caplan, B., Hardcastle, M., Shelley, D., Pickett, S. T., Groffman, P. M., 2013. Socioecological revitalization of an urban watershed. Front. Ecol. Environ.; 11(1): 28-36.

Jia, H. F., Lu, Y. W., Yu, S. L., Chen, Y. R., 2012. Planning of LID-BMPs for urban runoff control: the case of Beijing Olympic Village. Sep. Purif. Technol.; 84: 112-119.

Khan, S., Lau, S. L., Kayhanian, M., Stenstrom, M. K., 2006. Oil and grease measurement in highway runoff-sampling time and event mean concentrations. J. Environ. Eng.; 132(3): 415-422.

Lee, J. G., Selvakumar, A., Alvi, K., Riverson, J., Zhen, J. X., Shoemaker, L., Lai, F. H., 2012. Awatershed-scale design optimization model for stormwater best management practices. Environ. Model. Softw.; 37: 6-18.

Li, H., Harvey, J. T., Holland, T. J., Kayhanian, M., 2013. The use of reflective and permeable pavement strategies for heat island mitigation and stormwater management. Environ. Res. Lett.; 8, 015023.

Mao, X., Jia, H., Yu, S.L., 2016. Assessing the ecological benefits of aggregate LID-BMPs through modelling. Ecol. Model., (in press).

US EPA, 2004. The Use of Best Management Practices (BMPs) in Urban Watersheds. EPA/600/R-04/184, Washington, DC.

US EPA, 2009. SUSTAIN-a Framework for Placement of Best Management Practices in Urban Watersheds to Protect Water Quality. EPA/600/R-09/095. Office of Research and Development, Cincinnati, OH.

Wei, Y. H. D., Liefner, I., 2012. Globalization, industrial restructuring, and regional development in China. Appl. Geogr.; 32(1):102–105.

Zheng, Z., 2013. Development of a stormwater low impact development planning tool. Thesis for the degree of Master of Applied Science in the Program of Civil Engineering, Ryerson University, Toronto, Ontario, Canada.

Proceedings of the 10th World Congress of EWRA 'Panta Rhei', 5-9 July 2017, Athens, Greece
© 2017 *European Water Resources Association*

Modelling of a combined sewer system and evaluation of mitigation measures using SWMM

I.M. Kourtis[1*], V.A. Tsihrintzis[1], E.A. Baltas[2]
[1] *Centre for the Assessment of Natural Hazards and Proactive Planning & Laboratory of Reclamation Works and Water Resources Management, School of Rural and Surveying Engineering, National Technical University of Athens, 9 Iroon Polytechniou St., Zografou 15780 Athens, Greece.*
[2] *Department of Water Resources Hydraulic and Maritime Engineering, School of Civil Engineering, National Technical University of Athens, 9 Iroon Polytechniou St., Zografou 15780 Athens, Greece.*
[*] *e-mail: gkourtis@central.ntua.gr*

Abstract: Pluvial flooding is often unavoidable and unexpected and can only be mitigated with the design and implementation of appropriate measures. This study presents the analysis, the modelling, the identification of deficiencies in terms of capacity, the location of areas where flooding may occur, and the design of mitigation measures of a part of the combined sewer system of Athens (Zone D, Ano Patisia, Kypseli). The developed hydrologic and hydraulic model was based on the EPA Storm Water Management Model (SWMM5) software. The alternating block method was used to develop storm hyetographs. Floods of various return periods, i.e., 2, 5, 10, 25, 50 and 100 years, were tested. The mitigation measures examined, included, the enlargement of sewer sizes and the sizing of detention ponds parallel to the network. The results indicated that in case of sewer enlargement, the drainage capacity of the combined sewer system increases by 61%, while in the case of installation of detention ponds, the peak discharge at the exit of the system reduces by 29%. Overall, it was found that SWMM is a useful and easy to apply tool in testing the adequacy of existing drainage systems and the design of mitigation measures. SWMM can be used effectively for the simulation of urban drainage systems, and by comparing existing and proposed solutions, it can be a very useful tool for testing mitigation measures even for areas where there is no flow monitoring.

Key words: combined sewer system; urban drainage; SWMM; flooding mitigation; detention ponds

1. INTRODUCTION

Urbanization is one of the main factors of flooding. Extreme flooding events occur in cities with an increasing frequency mainly due to urbanization. During the last century, the city of Athens has experienced a significant number of inundation incidents (Pistrika et al., 2014; Bathrellos et al., 2016).

In this paper, the analysis, the modelling and the identification of deficiencies in terms of capacity of the combined sewer system in Zone D (Ano Patisia, Kypseli) of Athens are presented. The SWMM model was implemented. The modelling aimed to assess the capacity of this combined drainage system, to locate nodes/areas with flooding problems, and to propose measures of solving the problems. Mitigation measures modeled with SWMM included enlargement of sewer sizes and sizing of detention ponds.

2. MATERIALS AND METHODS

2.1 Case Study Area

The combined sewer system of Athens comprises a set of conduits and facilities that collect and drain the combined flow of stormwater and wastewater. It is divided into subcatchments, namely B, C, D, E, F, Z1, Z2, I-H, H1, H2 and Th as shown in Fig. 1. The wastewater drains in the Central

Sewerage Pipeline (CSP), while the stormwater drains in Kifisos River and in the stream of Prophet Daniel.



Figure 1: Subcatchments of the combined sewer system of Athens

The subcatchment examined was D (89 ha), which is located in the region of Ano Patisia, Kypseli (Athens, Greece). The combined sewer system is located in a highly urbanized area. The network consists of 112 nodes and 79 combined sewer pipes with a total length of 5 km. The drainage system comprises either egg-shaped pipes with depths ranging from 0.9 m to 2.4 m, or circular pipes with diameters ranging from 0.3 m to 0.6 m. In Figure 2, one can see the land use, the sewer network and the boundary of the study area.

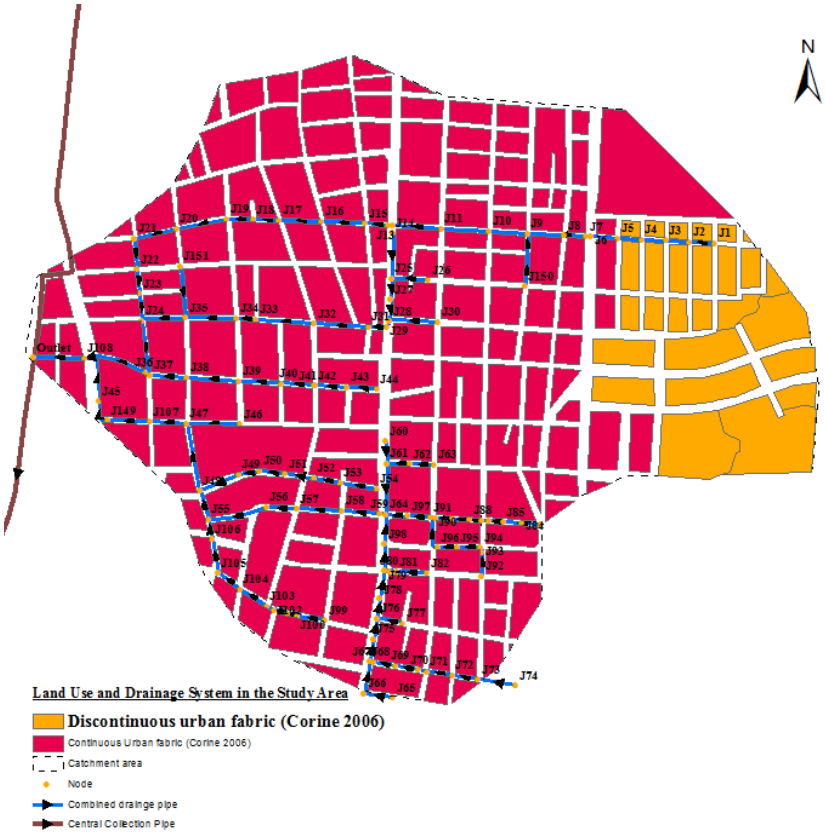

Figure 2: Land use and drainage system in the study area

2.2 SWMM Model

SWMM is a fully dynamic rainfall-runoff simulation model employing in hydraulic computations the momentum, mass and energy conservation laws (Rossman, 2010). SWMM can be used in the design, analysis and planning of drainage systems, in estimating the effects of urbanization and in continuous hydrologic simulation in urban areas (e.g., Zhu et al., 2016; Salvadore et al., 2015; El-Sharif and Hansen, 2001; Park et al., 2008; Smith et al., 2005; Hsu et al., 2000; Selvalingam et al., 1987; Jang et al., 2007). Moreover, SWMM can also be used for the simulation of runoff quality in urban areas (e.g., Rossman, 2010; Tsihrintzis and Hamid, 1998; Tsihrintzis et al., 1995; Ouyang et al., 2012).

2.3 Mitigation Measures

Conventional stormwater measures rely on construction interventions in order to collect, as quickly as possible, and transport the runoff to the receiving water bodies. Conventional measures are used mainly for controlling flood runoff events (Damodaram et al., 2010). In our study, a set of scenarios was modeled, using SWMM, to test the effectiveness of conventional measures in reducing flooding compared to the existing conditions. Scenarios included the enlargement of sewer sizes and the design of detention ponds along the sewer system.

Enlargement of sewers: The first mitigation measure examined and modeled with SWMM, was the enlargement of the sewer sizes of the system, in order to increase drainage capacity. The enlargement of the sewers size was examined in the entire drainage network to increase the capacity in order for the system to be able to carry the runoff of rainfalls with return periods up to ten years. The sizing and the simulation of the combined drainage network was carried out using SWMM software for different rainfall durations (1, 2, 3, 6, 12 and 24 h) for the 10-year return period.

Detention ponds: The next measure examined was the construction of detention ponds, at available empty parcels of lands closely located to the drainage network. Detention ponds are excavated reservoirs, which are dry during low flow periods. They provide temporary storage of stormwater runoff for peak attenuation and also, if specially designed, may offer water quality enhancement.

3. RESULTS AND DISCUSSION

Mitigation measure scenarios were simulated and compared with the existing conditions of the study area. As the site is ungauged, the existing condition scenario and the mitigation scenarios were simulated using the following IDF curve (Mimikou et al., 2000):

$$i = 15.39T^{(0.276)}d^{(-0.725)} \quad (1)$$

The simulation took place for six synthetic design storms of 10-year return period and durations: 1-hour (24.06 mm), 2-hours (35.16 mm), 3-hours (39.80 mm), 6-hours (47.56 mm), 12-hours (57.55 mm) and 24-hours (69.63 mm). The rainfall distributions for the synthetic design storms were developed using the Alternating Block Method (USBR, 1977).

3.1 Existing condition

The simulation of the existing condition for the six storms revealed that in two nodes the water surpassed the height of the curb and 48 pipes had a filling ratio greater than 0.8. Fig. 3 presents the rainfall and the produced hydrograph at the exit of the combined drainage system for return period of 10 years and for duration of 1 h. The peak discharge was estimated at about 18.3 m^3/s and the

time of peak at 36 min. The total volume of water that the dual drainage system (sewers and roads) was not able to drain was 261 m^3. In total, 61 % of the pipes of the combined drainage system had a filling ratio greater than 0.8. However, none of those pipes belonged to the central collector pipe of the combined drainage system, so the Greek Technical Specifications (Presidential Degree 696/74) were not violated.

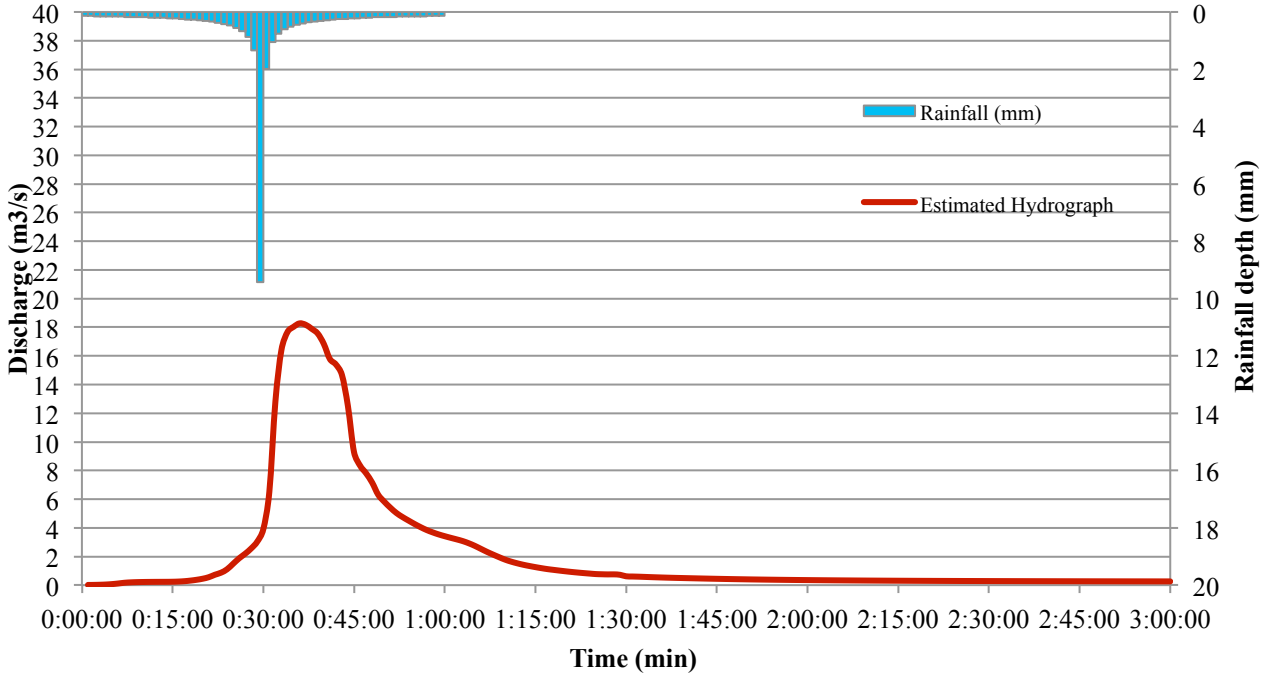

Figure 3: The 10-year, 1-hour rainfall, and the derived hydrograph at the exit of the combined sewer system under existing conditions

3.2 Scenario 1: Sewer enlargement

Under this scenario, in total, 60 of the 79 pipes of the modeled drainage system were selected for enlargement. After the enlargement, the diameter of the circular pipes ranged from 0.4 m to 1.2 m, while the height of the rectangular pipes ranged from 1.05 to 2.4 m and their width ranged from 1.2 m to 3.0 m. The sewer enlargement took place using the trial-and-error method in SWMM model. After the changes, the system was simulated and none of the pipes had a filling ratio greater than 0.8. Moreover, the major system (surface roads) did not operate. Fig. 4 presents the discharge (m^3/s) at the exit of the combined drainage system of Zone D of Athens before and after the sewer enlargement for the 10-year return period and duration of 1 h storm. It can be observed that the peak discharge increased from about 18.3 m^3/s to 29.4 m^3/s, and this is because, after the enlargement of the sewers, the combined drainage system was able to drain all the runoff produced. On the other hand, the peak time essentialy remained the same, 00:34:00 and 00:36:00, respectively. It should be noted that the peak at the exit increases; so, on one hand local flooding is resolved but, on the other hand, the impact on the downstream receiving CSP and Kifisos River should be also examined.

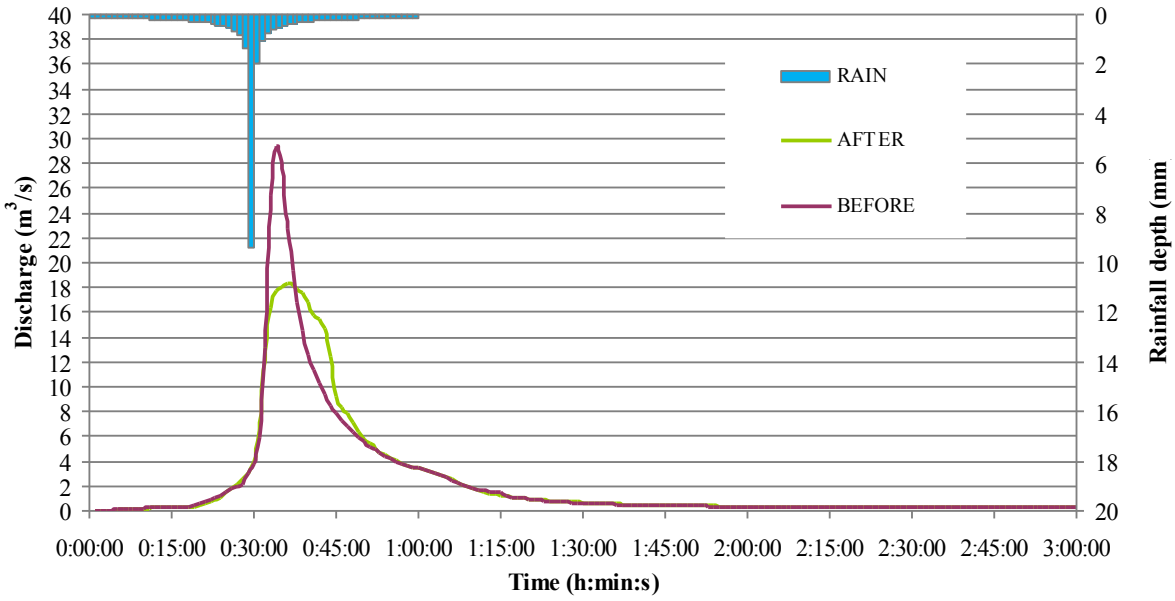

Figure 4: Detail of the hydrograph of the 10-year, 1-hour storm at the exit of the combined sewer system before and after the sewer enlargement (Scenario 1)

3.3 Scenario 2: Detention ponds

In total, 29 detention ponds were designed with depths ranging from 0.5 m to 3.0 m and volume capacities ranging from 10 m^3 to 1042 m^3. According to the results, the detention ponds reduce the peak discharge at the outlet of the combined drainage system by 29%, from about 18.3 m^3/s to 13.0 m^3/s. As a result, no node is flooding, the filling ratio of the pipes is less than 0.8 and no surface flow occurs on the major roads for return periods up to 10-years and any storm duration. Fig. 5 shows the discharge at the exit of the system for the 10-year return period and duration of 1 h storm, before and after the installation of the detention ponds. The volume of flooding was computed by SWMM at 261 m^3, for the whole study area, before the installation of the detention ponds while after the installation there was no flooding.

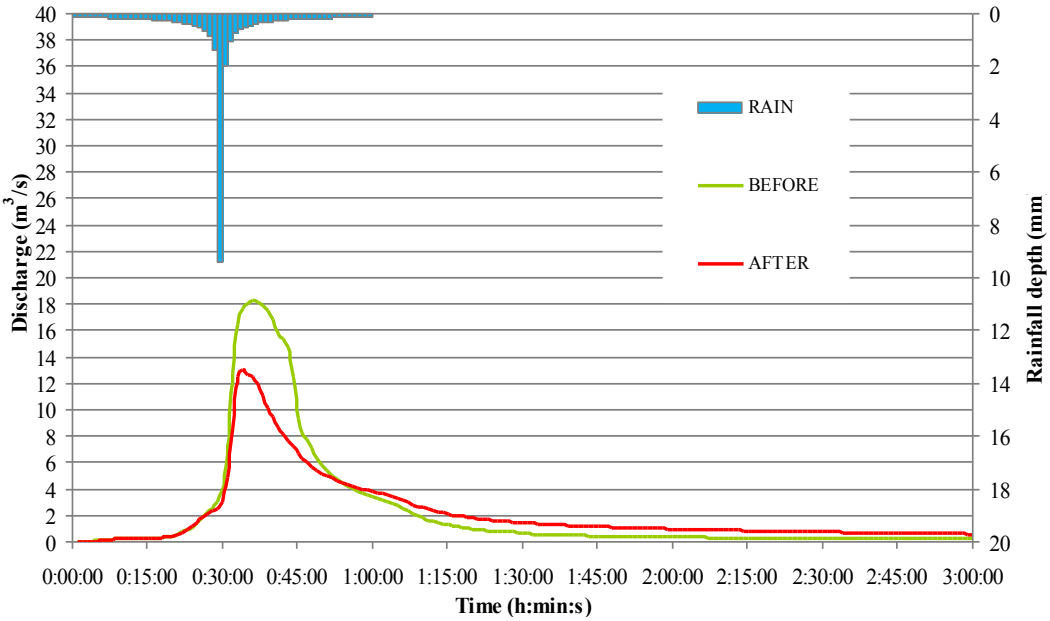

Figure 5: Detail of the hydrograph of the 10-year, 1-hour storm at the exit of the combined sewer system before and after the implementation of the detention ponds (Scenario 2)

From the model results, it is clear that in the case of sewer enlargement the drainage capacity of the combined sewer system increases by 61%, while in the case of installation of detention ponds the peak discharge at the exit of the system reduces by 29%. In the first case, 60 pipes (from 79 combined sewer pipes) must be replaced, while in the second scenario 29 detention ponds must be installed at various parts of the drainage system. For both solutions, major earthwork must be undertaken. The construction of detention ponds next to the combined sewer system is very difficult to be implemented because of the significant number required and the great cost (land acquisition, construction, etc.) and the inconvenience that this entails. Thus, it may be unrealistic. In future research, additional scenarios combining sewer enlargement and minimizing detention ponds should be tested and an optimization to minimize cost should be considered.

4. CONCLUSIONS AND RECOMMENDATIONS

This paper has presented the analysis, simulation and proposal of conventional measures for the combined drainage network of Zone D of Athens. SWMM model was selected for the hydrologic and hydraulic simulation. Overall, the SWMM is a useful and easy to apply tool in testing the adequacy of existing drainage systems and the design of mitigation measures. Moreover, SWMM can be used effectively for the simulation of pluvial flooding, and, by comparing existing and proposed solutions, it can be a very useful tool to test mitigation measures even for a region there has been no flow monitoring.

Focusing on the combined sewer system of Athens, some ideas can be proposed for further research. The first one is the analysis and the modelling of all the Zones of the combined sewer system. The second one is the implementation of rainfall runoff monitoring in major systems. Moreover, other measures could be proposed, such as Low Impact Development (LID) or Best Management Practices (BMPs), which should be examined and evaluated. Finally, it is essential to identify the best methodologies for the selection of the optimum combinations between the various mitigation measures, which would be able to achieve sustainability goals at the minimum cost.

ACKNOWLEDGEMENTS

The authors would like to thank the Athens Water Supply and Sewerage Company (EYDAP S.A.) for supplying background information on the combined drainage network of Athens.

RERERENCES

Bathrellos G.D., Karymbalis E., Skilodimou H.D., Gaki-Papanastassiou K., Baltas E.A., 2016. Urban flood hazard assessment in the basin of Athens Metropolitan city, Greece. Environmental Earth Sciences, 75(4): 1-14

Damodaram C., Giacomoni M.H., Prakash-Khedun C., Holmes H., Ryan A., Saour W., Zechman E.M., 2010. Simulation of combined best management practices and low impact development for sustainable stormwater management. Journal of the American Water Resources Association, 46(5): 907-918

El-Sharif A., Hansen D., 2001. Application of SWMM to the flooding problem in Truro, Nova Scotia. Canadian Water Resources Journal, 26(4): 439-459

Hsu M.H., Chen S.H., Chang T.J., 2000. Inundation simulation for urban drainage basin with storm sewer system. Journal of Hydrology, 234(1): 21-37

Jang S., Cho M., Yoon J., Yoon Y., Kim S., Kim G., Kim L., Aksoy H., 2007. Using SWMM as a tool for hydrologic impact assessment. Desalination, 212(1): 344-356

Lee S.B., Yoon C.G., Jung K.W., Hwang H.S., 2010. Comparative evaluation of runoff and water quality using HSPF and SWMM. Water Science and Technology, 62(6): 1401-1409

Ouyang W., Guo B., Hao F., Huang H., Li J., Gong Y., 2012. Modeling urban storm rainfall runoff from diverse underlying surfaces and application for control design in Beijing. Journal of Environmental Management, 113: 467-473

Park S.Y., Lee K.W., Park I.H., Ha S.R., 2008. Effect of the aggregation level of surface runoff fields and sewer network for a SWMM simulation. Desalination, 226(1): 328-337

Pistrika A., Tsakiris G., Nalbantis I., 2014. Flood depth-damage functions for built environment. Environmental Processes, 1(4), pp.553-572

Rossman L.A., 2010. Storm water management model user's manual, version 5.0. Cincinnati, OH: National Risk Management Research Laboratory, Office of Research and Development, US Environmental Protection Agency 276p.

Salvadore E., Bronders J., Batelaan O., 2015. Hydrological modelling of urbanized catchments: A review and future directions. Journal of Hydrology, 529: 62-81

Selvalingam S., Liong S.Y., Manoharan P.C., 1987. Use of RORB and SWMM models to an urban catchment in Singapore. Advances in Water Resources, 10(2): 78-86

Smith D., Li J., Banting D., 2005. A PCSWMM/GIS-based water balance model for the Reesor Creek watershed. Atmospheric Research, 77(1): 388-406

Tsihrintzis V. A., Hamid R., Fuentes H.R., 1995. Calibration and verification of watershed quality model SWMM in subtropical watersheds. Proceedings of the First International Conference on Water Resources Engineering, ASCE, San Antonio, Texas, August 14-18: 373-378

Tsihrintzis V.A., Hamid R., 1998. Runoff quality prediction from small urban catchments using SWMM. Hydrological Processes, 12(2): 311-329

USBR (U.S. Bureau of Reclamation) 1977. Design of Arch Dams, U.S. Government Printing Office, Denver

Zhu Z., Chen Z., Chen X., He P., 2016. Approach for evaluating inundation risks in urban drainage systems. Science of the Total Environment, 553:1-12

Proceedings of the 10th World Congress of EWRA 'Panta Rhei', 5-9 July 2017, Athens, Greece
© 2017 *European Water Resources Association*

WRF-PDM: Prognostic approach for discharge prediction in ungauged catchment

P.K. Srivastava[1*], T. Islam[2], G. Petropoulos[3], M. Gupta[4]
[1] *Institute of Environment and Sustainable Development, Banaras Hindu University, Varanasi, India*
[2] *NASA Jet Propulsion Laboratory, Pasadena, CA, USA*
[3] *Department of Geography and Earth Sciences, University of Aberystwyth, UK*
[4] *Department of Geology, University of Delhi, India*
[*] *e-mail: prashant.just@gmail.com*

Abstract: In this study, the mesoscale model WRF (Weather Research & Forecasting model) is used for dynamical downscaling of European Centre for Medium Range Weather Forecasts (ECMWF) ERA interim reanalysis global datasets for obtaining hydro-meteorological variables. The WRF estimated precipitation and Evapo-transpiration are then used as input data for the Probability Distributed Model (PDM) for discharge prediction. For performance evaluation of the integrated framework, objective function like Nash Sutcliffe Efficiency (NSE) is used. Analysis of NSE indicates values of 0.85 and 0.82 during the calibration and validation respectively for the combination observed rainfall and station based reference Evapotranspiration (ETo). On the other hand, a marginally lower performance is reported by the combination Observed Rainfall and WRF based ETo (NSE_{cal}= *0.82;* NSE_{val}= *0.80*), while a very poor performance is reported by the combination Rainfall and ETo when both derived from WRF (NSE_{cal}= *0.58;* NSE_{val}= *0.06*). The overall analysis suggests that the WRF-PDM can be used for discharge prediction in the absence of ground based measurements. This study provides valuable information to the hydro-meteorologist on downscaled weather variables from global datasets and its applicability to rainfall-runoff modeling for river discharge prediction.

Key words: WRF-PDM, GLUE, Rainfall-runoff, Discharge, Sensitivity Analysis and Uncertainty Estimation

1. INTRODUCTION

Precipitation and Reference Evapotranspiration (ETo) are considered as two important key variables for rainfall runoff modelling (Shukla and Mintz, 1982). The WRF model is used by many researchers in last decade and found to be promising for regional applications and development of operational numerical weather prediction (Lo *et al.*, 2008; Givati *et al.*, 2011). Recently, efforts have been made to estimate ET and precipitation using Weather Research and Forecasting model (WRF) (Bukovsky and Karoly, 2009; Skok *et al.*, 2010).

Among hydrological models, the lumped rainfall runoff model PDM (Probability Distributed Model) has been widely used in many parts of the world with satisfactory performances (Srivastava *et al.*, 2013). PDM model is developed by the UK Centre for Ecology and Hydrology by Moore in (Moore, 2007). The PDM model uses long records of flow and rainfall and provides a highly effective representation of the runoff generation process (Srivastava *et al.*, 2014). Because of its high performance it is also used in this study for discharge esatimation.

In purview of the above, the main aim of this study is to examine the performance of WRF-PDM framework for discharge prediction with different input data conditions derived from global reanalysis datasets using WRF and station based measurements. This type of study is important to understand the model performances and their suitability for discharge prediction especially for ungauged catchments.

2. MATERIALS AND METHODOLOGY

The Brue catchment is located in the south-west of England and used as a case study in this work. The flow and rainfall datasets are provided by Environment agency, UK, while meteorological datasets are provided by the British Atmospheric Data Centre *(*BADC), UK. The hourly datasets from August 2010 to January 2012 are used for calibration and validation of the model. The global European Centre for Medium Range Weather Forecasts (ECMWF) ERA interim reanalysis data is used as forcing for Weather Research and Forecasting (WRF) model (http://www.ecmwf.int/). The latest WRF model is used in this study with the Advanced Research WRF (ARW) dynamic core (Powers, 2007; Schwartz *et al.*, 2009). The WRF model is centered over the Brue catchment with three nested domains (D1, D2 and D3). The innermost high resolution domain (D3) is used in this study. The outputs of WRF i.e. precipitation and ET are used as inputs in the lumped rainfall runoff model PDM (Probability Distributed Model) for discharge prediction. Total five PDM parameters --C_{max} (maximum store capacity), b (exponent of pareto distribution), g (groundwater recharge time constant), K_f (fast flow component) and K_s (slow flow component) are used for model calibration.

3. RESULTS AND DISCUSSION

The WRF estimated precipitation and ETo are used as input for the Probability Distributed Model (PDM) for discharge prediction. Total three input data conditions are designed for assessing the WRF-PDM performance for discharge prediction as shown in Table 1.

Table 1. Different combinations used in this study

S.No.	Input conditions	Combinations
1	Set1	Observed Rainfall and Station based ETo
2	Set2	Observed Rainfall and WRF based ETo
3	Set3	Rainfall and ETo both from WRF

Sensitivity analysis is performed on the locally conditioned PDM model parameters C_{max}, b, g, K_f and K_s. After optimizing the PDM model parameters, the discharge by using the different combinations are estimated and the hydrographs are presented in Fig. 2.

The performance is depicted in terms of Taylor diagram as shown in Fig.3. It provides a simpler way of presenting the model performances using the graphical interface by summarizing how closely the model simulated results match with the observations. The performances between the two datasets are quantified in terms of their correlation, their centered root-mean-square difference and the standard deviations. In calibration, poorest performance can be seen in case of set3, while set1 and set2 are mostly similar in prediction discharge. During the validation, the worst performance is reported by set3 and better in case of set1 and set2.

The analysis of objective function Nash Sutcliffe Efficiency (NSE) indicates values of 0.85 and 0.82 during the calibration and validation respectively (set-1). On the other hand, a marginally lower performance are reported by set-2 (NSE_{cal}= 0.82; NSE_{val}= 0.80), while a very poor performance is reported by set-3 (NSE_{cal}= 0.58; NSE_{val}= 0.06). The lower performance of set3 can

be attributed to the poor simulation of WRF precipitation, which indicates that more work is needed on improvement of parameterization schemes for discharge prediction.

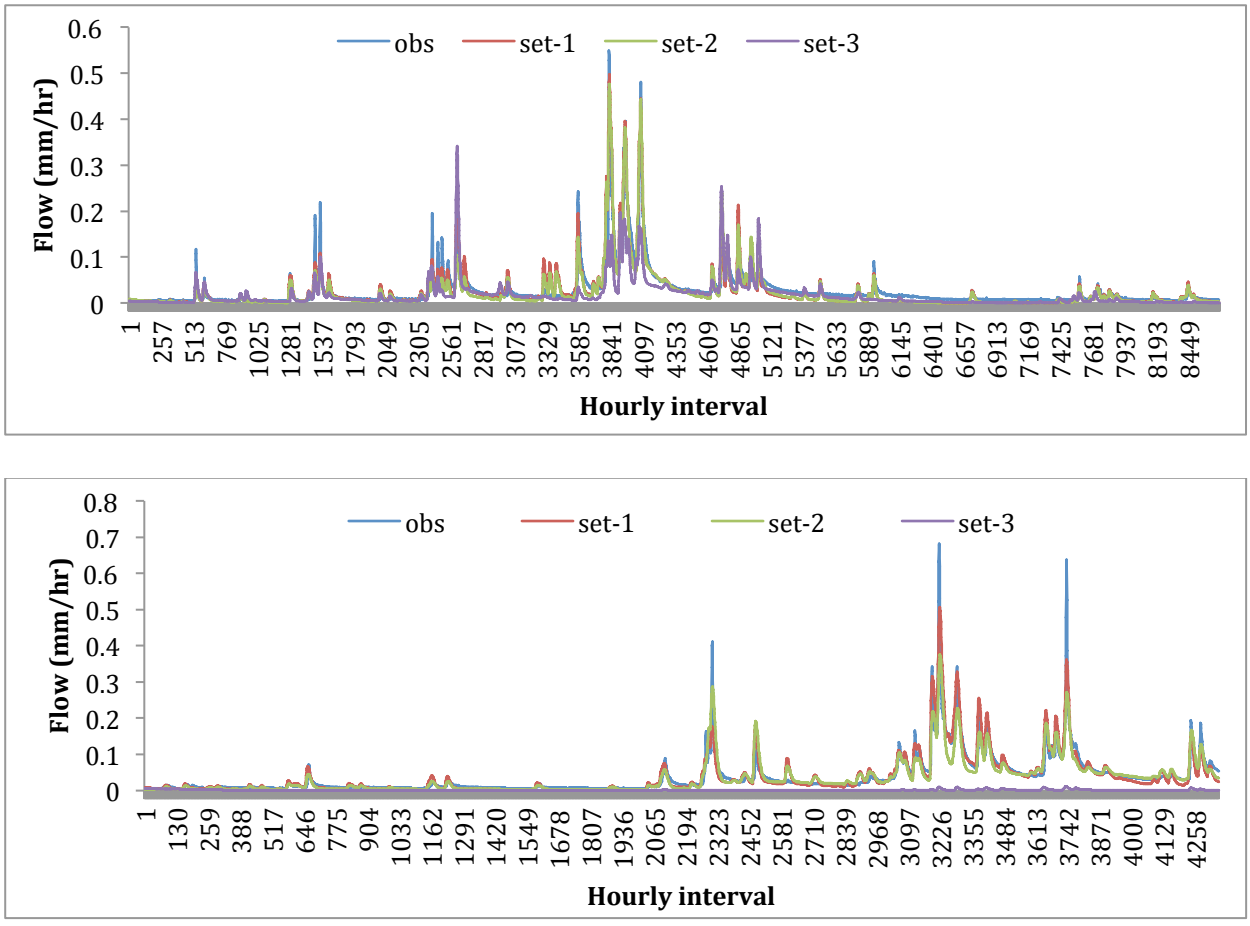

Fig. 2 Hydrographs obtained by using different combinations: (a) Calibration; (b) Validation

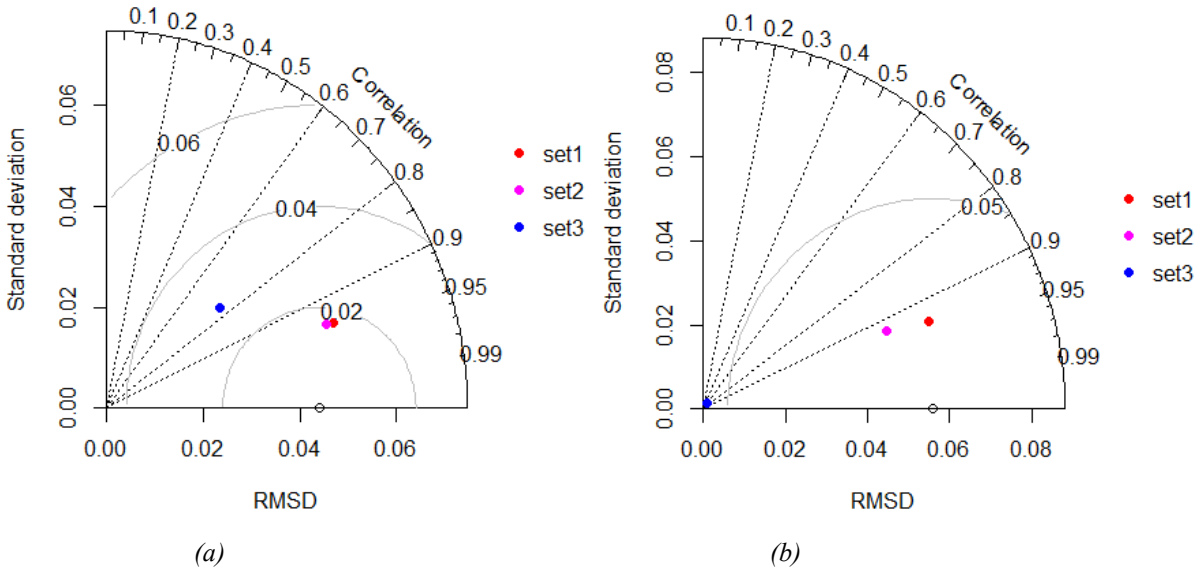

Fig.3 Taylor diagram showing the performance of different combinations: (a) Calibration; (b) Validation

The overall analysis suggests that the estimates in the predicted discharge using the WRF derived ET have comparable performance with the ground based observed datasets and hence

promising for the discharge prediction in the absence of ground based measurements of ET.

4. CONCLUSIONS

The over application of WRF indicates that it is able to downscale the global data into much finer resolutions in space and time for hydro-meteorological applications. Further, it can be used in integration with PDM model for prediction of discharge. The different datasets used in this study indicates that the WRF downscaled meteorological variables can be used for ET. Further the quality of ET derived is better than the WRF simulated precipitation, which is also reflected by the simulated discharge. The overall analysis indicates that the WRF precipitation is least useful for discharge prediction and therefore better schemes or forcing are needed for precipitation. On the other hand, ET is giving satisfactory performance, when used with observed rainfall. This study can provide hydrologists with valuable information on downscaled weather variables from global datasets and its applicability for rainfall-runoff modeling.

ACKNOWLEDGMENT

The authors would like to thank the Commonwealth Scholarship Commission, British Council, United Kingdom and Ministry of Human Resource Development, Government of India for providing the necessary support and funding for this research. The authors would like to acknowledge the British Atmospheric Data Centre, United Kingdom for providing the ground datasets.

REFERENCES

Bukovsky, M.S., Karoly, D.J., 2009. Precipitation simulations using WRF as a nested regional climate model. Journal of applied Meteorology and Climatology 48, 2152-2159.

Givati, A., Lynn, B., Liu, Y., Rimmer, A., 2011. Using the WRF model in an operational streamflow forecast system for the Jordan River. Journal of Applied Meteorology and Climatology 51, 285-299.

Lo, J.C.F., Yang, Z.L., Pielke, R.A., 2008. Assessment of three dynamical climate downscaling methods using the Weather Research and Forecasting (WRF) model. Journal of Geophysical Research: Atmospheres 113.

Moore, R., 2007. The PDM rainfall-runoff model. Hydrology and Earth System Sciences Discussions 11, 483-499.

Powers, J.G., 2007. Numerical prediction of an Antarctic severe wind event with the Weather Research and Forecasting (WRF) model. Monthly Weather Review 135, 3134-3157.

Schwartz, C.S., Kain, J.S., Weiss, S.J., Xue, M., Bright, D.R., Kong, F., Thomas, K.W., Levit, J.J., Coniglio, M.C., 2009. Next-day convection-allowing WRF model guidance: A second look at 2-km versus 4-km grid spacing. Monthly Weather Review 137, 3351-3372.

Shukla, J., Mintz, Y., 1982. Influence of land-surface evapotranspiration on the earth's climate. Science 215, 1498-1501.

Skok, G., Tribbia, J., Rakovec, J., 2010. Object-based analysis and verification of WRF model precipitation in the low-and midlatitude Pacific Ocean. Monthly Weather Review 138, 4561-4575.

Srivastava, P.K., Han, D., Ramirez, M.R., Islam, T., 2013. Appraisal of SMOS soil moisture at a catchment scale in a temperate maritime climate. Journal of Hydrology 498, 292-304.

Srivastava, P.K., Han, D., Rico-Ramirez, M.A., Islam, T., 2013 Machine learning techniques for downscaling SMOS satellite soil moisture using MODIS land surface temperature for hydrological application Water Resour Manage.

Srivastava, P.K., Han, D., Rico-Ramirez, M.A., Islam, T., 2014. Sensitivity and uncertainty analysis of mesoscale model downscaled hydro-meteorological variables for discharge prediction. Hydrological Processes 28, 4419-4432.

Proceedings of the 10th World Congress of EWRA 'Panta Rhei', 5-9 July 2017, Athens, Greece
© 2017 *European Water Resources Association*

Estimation of the Muskingum routing coefficients by using fuzzy regression

M. Spiliotis[1*] and L. Garrote[2]
[1] *Democritus University of Thrace, School of Engineering, Department of Civil Engineering, Section of Hydraulics, 12 Vasilissis Sofias Str., 67100 Xanthi, Greece*
[2] *Department of Civil Engineering: Hydraulics, Energy and Environment, Technical University of Madrid, ETSI Caminos. C/ Prof. Aranguren s/n 28040 Madrid, Spain*
[*] *e-mail: m.spiliotis@gmail.com*

Abstract: The Muskingum model is a popular method to analyse the flood routing. Most of the methodologies for estimating the parameters of the routing are based on the distance between observed outflows and estimated outflows. In this work, for the first time, the parameters for a linear Muskingum model are determined by following a different principle. The coefficients is proposed to be determined based on the fuzzy linear regression principles. Therefore the scope of the fuzzy calibration is to assess the Muskingum routing parameters as symmetric fuzzy triangular numbers so that all the observed data must be included in the produced fuzzy band aiming at its minimum. This formulation leads to a constrained optimization problem with unknown variables the centres and the widths of the Muskingum routing coefficients. Instead of the identification of the parameters K, x, the problem is oriented to the determination of the coefficients C1 and C2. Based on the problem itself the constant term of the usual regression model has been eliminated. In order to reduce the fuzzy band a proposed mixed goal programming fuzzy regression analysis is also used. Thus, the produced fuzzy band can be reduced by enabling some observed data to be near the produced fuzzy curve. In any case the maximum observed outflow must be included within the produced fuzzy band.

Key words: Fuzzy Regression, Fuzzy sets and logic, Goal programming, Parameter estimation, Muskingum routing equation

1. INTRODUCTION

The Muskingum model is a popular method to analyse flood routing based on the continuity equation and a simplified version of the dynamics equation. Most of the methodologies for estimating the routing parameters are based on the comparison between observed and estimated outflows. Several techniques have been developed to achieve the calibration of the Muskingum routing parameters by using traditional optimization techniques (e.g. Stephenson, 1979), more advanced optimization techniques by using heuristing optimization processes (e.g. Ouyang et al., 2014).

In this work, for the first time, the parameters for a linear Muskingum model are determined by following a different principle. The coefficients are proposed to be determined based on a fuzzy linear regression model. Therefore the scope of the fuzzy calibration is to assess the Muskingum routing parameters as fuzzy numbers so that all the observed data must be included in the produced fuzzy band aiming at its minimum.

2. METHODOLOGY

The methods applied in this paper are presented in this section. The widely used Fuzzy Linear Regression Analysis is presented first. Next the Muskingum routing coefficients are calculated by using the fuzzy linear regression model of Tanaka. Finally, a novel method based on fuzzy regression enhanced by goal programming is proposed in this work in order to determine the Muskingum routing coefficients.

2.1 Fuzzy Linear Regression analysis

Fuzzy models are a useful approach to investigate complex physical phenomena such as the interconnection between adjacent watersheds (Tsakiris et al., 2006), the rainfall-runoff process, etc. The Fuzzy linear regression has been shown to be a useful tool to express functional relationships between variables, especially when data are not sufficient in number (Ganoulis, 1994). In contrast to the statistical regression, the fuzzy regression analysis has no error term since the uncertainty is incorporated in the model by means of fuzzy numbers (Spiliotis and Bellos, 2016).

Fuzzy regression analysis assumes a fuzzy functional relationship between the dependent and independent variables (Papadopoulos and Sirpi, 1999). The input data may be crisp or fuzzy. In this work the input data are considered to be crisp numbers. Firstly the fuzzy linear regression method, which was developed by Tanaka (1987), is examined. According to this approach, the problem of fuzzy linear regression is finally formulated as a constrained optimization problem. Additionally, by using symmetrical fuzzy triangular numbers, the problem is transformed into a linear programming problem (Tanaka et al., 1989, Tsakiris et al., 2006, Kitsikoudis et al., 2016 & Spiliotiis and Bellos, 2016). An ambiguous point in the formulation is that according to Tanaka et al., 1987 methodology, all the data must be included in the regression model.

The fuzzy linear regression model proposed by Tanaka, 1987 and Tanaka et al., 1989 has the following form:

$$\tilde{Y}_j = \tilde{A}_0 + \tilde{A}_1 x_{1j} + \ldots \tilde{A}_i x_{ij} + \ldots. + \tilde{A}_n x_{nj},$$

$$\text{with } j = 1, \ldots, m,\ i = 1, \ldots, n \tag{1}$$

where n is the number of independent variables, m is the number of data, and $\tilde{A}_i = (a_i,\ w_{c_i})_{TR}$ are symmetric fuzzy triangular numbers selected as coefficients (Fig. 1), which have the following membership function:

$$\mu_{Ai}(\alpha_i) = \begin{cases} 1 - \dfrac{|\alpha_i - a_i|}{w_{c_i}}, & if \quad a_i - w_{c_i} \le \alpha_i \le a_i + w_{c_i} \\ 0, & otherwise \end{cases} \tag{2}$$

where a_i and w_{c_i} are the centres and the widths of the fuzzy coefficients, respectively. The general definition of fuzzy numbers can be found in Klir and Yuan, 1995.

However, the constant term in our problem has no physical meaning and hence, it is omitted:

$$\tilde{Y}_j = \tilde{A}_1 x_{1j} + \ldots \tilde{A}_i x_{ij} + \ldots. + \tilde{A}_n x_{nj} \tag{3}$$

The model of fuzzy linear regression produces a fuzzy band which is calculated based on the extension principle of fuzzy sets and logic. In general, the extension principle enables us to define the crisp functions on a fuzzy domain and consequently the extension principle can be used in order to define the algebraic operations between fuzzy sets (e.g. Klir and Yuan, 1995). If the input data are crisp numbers, then the model of fuzzy linear regression can be interpreted mathematically by multiplying fuzzy numbers and crisp numbers as well as adding the fuzzy numbers. In case that the coefficients are fuzzy triangular numbers, the linearity remains also in the total regression output.

According to fuzzy arithmetic, the function Y_j has the following centre ($y_{a,j}$) and semi-width ($y_{c,j}$) (Tanaka, 1987):

$$\textit{Centre:} \qquad y_{a,j} = a_1 x_{1j} + \ldots + a_i x_{ij} + \ldots. + a_n x_{nj} \tag{4.a}$$

Semi- width: $$y_{c,j} = w_{c_1} |x_{1j}| + ... + w_{c_i} |x_{ij}| + ... + w_{c_n} |x_{nj}| \quad (4.b)$$

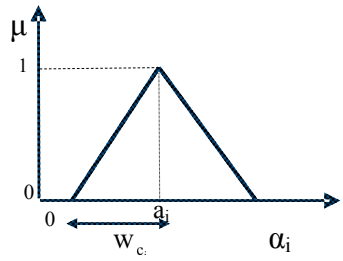

Figure 1. Fuzzy triangular symmetrical number.

The α – cut set, which is a crisp set, of a fuzzy number A represented by $[A]_\alpha$, is defined for $0 < \alpha \leq 1$ as follows (Klir and Yuan, 1995):

$$[A]_\alpha = \{x | \mu_A(x) \geq \alpha, x \in \Re\} \quad (5)$$

In case of α = 0, the definition of the α- cut (Eq. 5) is slightly changed, without the equality, to include the zero-cut which can be named also as the support set (Kitsikoudis et al., 2016, Buckley and Eslami, 2002, Spiliotis et al., 2016).

According to the conventional fuzzy linear regression model, the centres and the widths of the fuzzy coefficients could be determined by solving a linear programming problem with an objective function which can minimize the total spread of the fuzzy outputs, on condition that all the data given from the historical sample outputs y_j should be included in the estimated function Y_j, that is:

$$\mu_{Yj}(y_j) \geq \alpha, \; j = 1,\ldots,m, \quad (6)$$

where μ_Y is the membership function of Y_j (Papadopoulos and Sirpi, 1999 & Kitsikoudis et al., 2016).

The above constraints arise from the concept of inclusion, the definition of which is provided below (e.g. Spiliotis and Bellos, 2016):

Definition: The inclusion of a fuzzy set A to the fuzzy set B with the associated degree $0 \leq \alpha \leq 1$ is defined as follows:

$$[A]_\alpha \subseteq [B]_\alpha \quad (7)$$

The above definition can also be used in order to apply fuzzy regression analysis in cases where the data are not crisp (as in this text), but fuzzy.

Based on the previous description, the fuzzy linear regression analysis is reduced to the estimation of the fuzzy coefficients $A_j = (a_i, \; w_{c_i})_L$, *i=1,...,n* that minimizes the total spread of the fuzzy output subject to the constraints:

$$J = \min \left\{ \sum_{j=1}^{m} \sum_{i=1}^{n} w_{c_i} |x_{ij}| \right\} \quad (8)$$

As mentioned before, the constant term of the fuzzy regression is eliminated due to the fact that in the examined problem, it has no physical meaning. Hence, by selecting the α-cut to check for the inclusion property and by using are symmetric fuzzy triangular numbers, the problem of selecting

the coefficients of the regression model leads to the following linear optimization problem:

$$J = \min\left\{\sum_{j=1}^{m}\sum_{i=1}^{n} w_{c_i}\left|x_{ij}\right|\right\} \tag{9.a}$$

subjects to:

$$y_j \geq \sum_{i=1}^{n} a_i x_{ij} - (1-\alpha)\sum_{i=1}^{n} w_{c_i}\left|x_{ij}\right| \tag{9.b}$$

$$y_j \leq \sum_{i=1}^{n} a_i x_{ij} + (1-\alpha)\sum_{i=1}^{n} w_{c_i}\left|x_{ij}\right| \tag{9.c}$$

$$w_{c_i} \geq 0 \tag{9.d}$$

where $i=1,...,n$ and $j=1,...,m$. Where n is the number of independent variables and m is the number of available data.

2.2 Estimation of the Muskingum routing coefficients by using the fuzzy regression model of Tanaka, 1987

In case that the relationship between storage and flow through a reach is linear, the Muskingum storage relationship can be written as:

$$S = K\left[xI + (1-x)Q\right] \tag{10}$$

where I is the inflow rate to the reach, Q is the outflow rate from the reach, K the storage time constant for the reach and x a weighting factor that varies between 0 and 0.5 (Viessman and Lewis, 1996).

The mass balance equation can be expressed in discrete form as follows:

$$\frac{(I_1 + I_2)}{2}\cdot\Delta t - \frac{(Q_1 + Q_2)}{2}\cdot\Delta t = (S_2 - S_1) \tag{11}$$

By combining Eqs. 10 and 11 the Muskingum routing equation is achieved:

$$Q_2 = C_0 I_2 + C_1 I_1 + C_2 Q_1 \tag{12}$$

where

$$C_0 = \frac{-(Kx - 0.5\Delta t)}{K - Kx + 0.5\Delta t},$$

$$C_1 = \frac{(Kx + 0.5\Delta t)}{K - Kx + 0.5\Delta t}$$

$$C_2 = \frac{(K - Kx - 0.5\Delta t)}{K - Kx + 0.5\Delta t}$$

It is obvious that $C_0 + C_1 + C_2 = 1$. (13)

A direct method of calibrating the Muskingum routing parameters can be achieved based on the fuzzy linear regression. Instead of the identification of the parameters *K, x,* the problem is oriented to the determination of C_1 and C_2 parameters. Therefore the scope of the fuzzy calibration is to assess the parameters C_1 and C_2 (as fuzzy numbers) so that all the data must be included in the produced fuzzy band aiming at its minimum width. The parameters C_1 and C_2 are considered to be fuzzy symmetrical triangular numbers, instead of crisp numbers.

After rearranging the Muskingum routing equation at time interval *j,* the examined fuzzy regression and by taking into account that $C_0 + C_1 + C_2 = 1$, will be the following:

$$\tilde{C}_1\left(I_j - I_{j+1}\right) + \tilde{C}_2\left(Q_j - I_{j+1}\right) = \left(Q_{j+1} - I_{j+1}\right) \tag{14}$$

This form, but without fuzziness, was investigated by Stephenson, 1979. The fuzzy linear regression-based model of Tanaka can be used to estimate the coefficients. Consequently, the fuzzy coefficients can be determined by solving the following constrained optimization problem:

$$\mathrm{J} = \min\left\{\sum_{\mathrm{j}=1}^{\mathrm{m}}\left(w_{\mathrm{c}1}\left|I_j - I_{j+1}\right| + w_{\mathrm{c}2}\left|Q_j - I_{j+1}\right|\right)\right\}$$

s.t.

$$\begin{aligned}
&\mathrm{a}_{\mathrm{c}1}\left(I_j - I_{j+1}\right) + \mathrm{a}_{\mathrm{c}2}\left(Q_j - I_{j+1}\right) + (1-a)\left(w_{c1}\left|\left(I_j - I_{j+1}\right)\right| + w_{c2}\left|Q_j - I_{j+1}\right|\right) \geq \left(Q_{j+1} - I_{j+1}\right) \\
&\mathrm{a}_{\mathrm{c}1}\left(I_j - I_{j+1}\right) + \mathrm{a}_{\mathrm{c}2}\left(Q_j - I_{j+1}\right) - (1-a)\left(w_{c1}\left|\left(I_j - I_{j+1}\right)\right| + w_{c2}\left|Q_j - I_{j+1}\right|\right) \leq \left(Q_{j+1} - I_{j+1}\right) \\
&w_{c1},\ w_{c2} \geq 0
\end{aligned} \tag{15}$$

where $\mathrm{a}_{\mathrm{c}1}$, $\mathrm{a}_{\mathrm{c}2}$ and w_{c1}, w_{c2} the central values and the semi-widths of the fuzzy coefficients $\tilde{C}_1$ *and* $\tilde{C}_2$. In addition where *m* is the number of data, whilst *n=2* (number of independent variables). The term $\left(Q_{j+1} - I_{j+1}\right)$ is considered as dependent variable. Thus, the produced fuzzy band with respect of the auxiliary independent variables $\left(I_j - I_{j+1}\right)$, $\left(Q_j - I_{j+1}\right)$must contain all the available data.

2.3 Estimation of the Muskingum routing coefficients by using the fuzzy regression model enhanced by goal programming

Fuzzy linear regression is heavily influenced by the presence of outliers, which can extremely increase the uncertainty of the model (e.g., Peters 1994). Subsequently, several researchers attempted to modify the rigid inclusion constraints of the widely used fuzzy linear regression of Tanaka, 1987 (Kitisikoudis et al., 2016). Here, we propose a modification of the fuzzy linear regression model enhanced with goal programming which is proposed by Kitsikoudis et al., 2016, based on the nature of the examined problem itself. The main idea is the use of the distance (error), d_j^+, which is associated with the over-estimation of the left-hand boundary and another distance measure (error), d_j^-, which is associated with the under-estimation of the right-hand boundary. As in goal programming extension (Appendix I), the proposed method enables the overstepping of the fuzzy boundaries at some points. Obviously, the model aims at minimizing the overstepping as well as the sum of the fuzzy spread. Therefore the extreme sensitivity of the original fuzzy regression model of Tanaka due to some "outliers" is reduced significantly by following the proposed

methodology.

The basic model remains the same:

$$\tilde{C}_1\left(I_j - I_{j+1}\right) + \tilde{C}_2\left(Q_j - I_{j+1}\right) = \left(Q_{j+1} - I_{j+1}\right)$$

However, a divergence (error) is permitted for each inequality constraint (A.II):

$$\begin{aligned} &\mathrm{a}_{c1}\left(I_j - I_{j+1}\right) + \mathrm{a}_{c2}\left(Q_j - I_{j+1}\right) + \left(1-a\right)\left(w_{c1}\left|I_j - I_{j+1}\right| + w_{c2}\left|Q_j - I_{j+1}\right|\right) + d_j^- \geq \left(Q_{j+1} - I_{j+1}\right) \\ &\mathrm{a}_{c1}\left(I_j - I_{j+1}\right) + \mathrm{a}_{c2}\left(Q_j - I_{j+1}\right) - \left(1-a\right)\left(w_{c1}\left|I_j - I_{j+1}\right| + w_{c2}\left|Q_j - I_{j+1}\right|\right) - d_j^+ \leq \left(Q_{j+1} - I_{j+1}\right) \\ &w_{c1}, w_{c2} \geq 0 \end{aligned} \tag{16.a}$$

Finally, the scope of the final optimization problem is to minimize the total spread of components of the unit hydrograph as well as the sum of the error (distance) terms d_j^+, d_j^-:

$$\mathrm{J} = \min\left\{w_1 \cdot \sum_{\mathrm{j}=1}^{\mathrm{m}}\left(d_j^+ + d_j^-\right) + w_2 \cdot \left(\sum_{j=1}^{m}\left(w_{c1}\left|I_j - I_{j+1}\right| + w_{c2}\left|Q_j - I_{j+1}\right|\right)\right)\right\} \tag{16.b}$$

in which, $d_j^+, d_j^-, w_1, w_2 \geq 0$ (16.c)

By using the weight w_1, the divergence from the fuzzy band is penalized, while, by using the weight w_2, the spread of the produced fuzzy band is penalized (Kitsikoudis et al., 2016).

3. CASE STUDY

The case study is based on the inflow and outflow rate hydrographs exhibiting linear characteristics (Viessman and Lewis, 2003 & Al-Humoud and Esen, 2006). The data can be found at Al-Humoud and Esen, 2006. By following the traditional approach of Tanaka, 1987 with α =0 (that is, the zero-cut), the following curve is produced:

$$\left(0.0133,\ 0.7964\right)_{TR} \cdot \left(I_j - I_{j+1}\right) + \left(\ 0.5174,\ 0.0624\right)_{TR} \cdot \left(Q_j - I_{j+1}\right) = \left(Q_{j+1} - I_{j+1}\right) \tag{17}$$

where the first number in the bracket shows the central value and second value denotes the semi-width of the fuzzy symmetrical triangular number. Unfortunately, the calculation of the *K, x* parameters based on the central values of C_1 and C_2 can not be achieved. It is easy to find the value of Q_{j+1} from Eq.17 because I_{j+1} is a crisp number. Figure 2 presents the outflow rate and the predicted fuzzy band for the same variable based on Eq. 17. Indeed, all the observed data are included in the produced fuzzy band. However, the fuzzy band is rather wide for some time steps and hence, the model can be characterised as not so functional.

Subsequently, the fuzzy regression method enhanced by goal programming is implemented for α=0 and the following curve is produced:

$$\left(0.4723,\ 0.2977\right)_{TR} \cdot \left(I_j - I_{j+1}\right) + \left(\ 0.4523,\ 0.06802\right)_{TR} \cdot \left(Q_j - I_{j+1}\right) = \left(Q_{j+1} - I_{j+1}\right) \tag{18}$$

As it can be seen from Figure 3, even if, a small region does not belong to the produced fuzzy band, the maximum observed outflow belongs to the produced fuzzy band and in general, the predicted fuzzy band simulates the observed outflow. The spread of the fuzzy band is reduced almost to one half. Another interesting point of view, is that based on the central values of the

parameters C_1 and C_2, K and x can be calculated (K= *1.69* and x = *0.21*). These values are not far from these from the least square method.

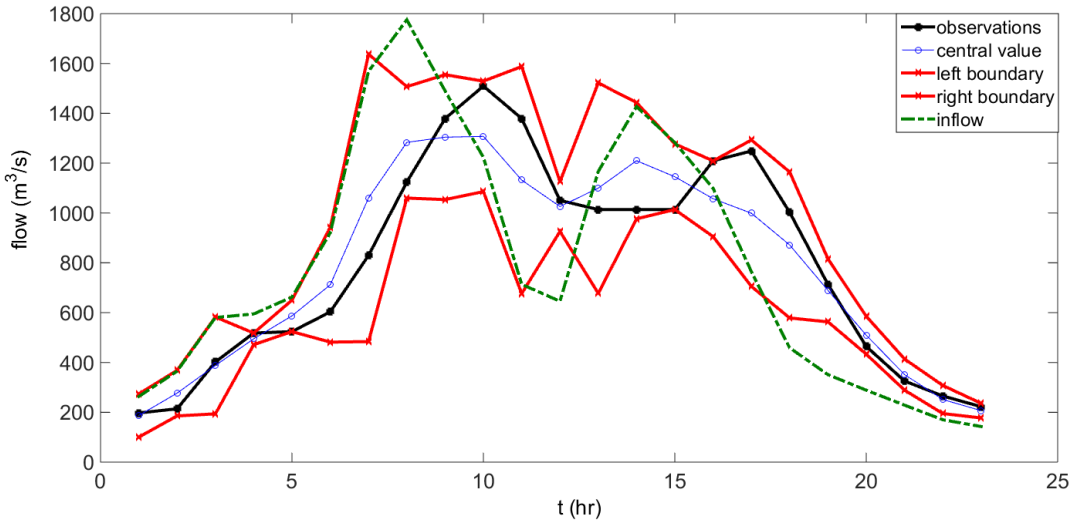

Figure 2. Inflow and outflow hydrographs (data) and the predicted fuzzy band based on the Tanaka fuzzy linear regression model.

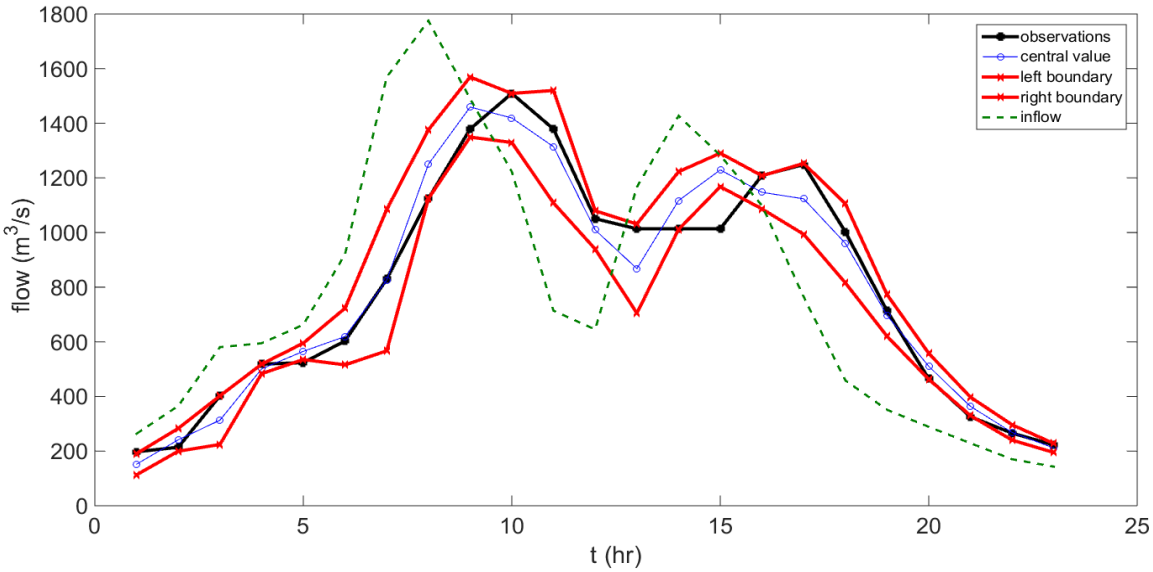

Figure 3. Inflow and outflow hydrographs (data) and the predicted fuzzy band based on our proposed method of fuzzy regression enhanced by goal programming.

4. CONCLUSIONS

The consideration of a fuzzy version for the Muskingum routing model, instead of the usual precise (crisp) model, is closer to our uncertain understanding of nature. Thus, based on the Tanaka, 1987 method, the fuzzy linear regression is implemented to determine the Muskingum routing parameters. Based on the Tanaka model, the Muskingum routing parameters are determined as symmetric fuzzy triangular numbers, so that all the observed data must be included in the produced fuzzy band aiming at its minimum.

However, the implementation of the Tanaka, 1987 method creates several problems, the most prominent among those being the large width of the produced fuzzy band. We have shown with our work that the determined fuzzy band can be significantly reduced, without a general cancelling of

the inclusion property of the fuzzy regression, by using a goal programming based hybrid fuzzy regression approach.

REFERENCES

Al-Humoud, J. and Esen, I., 2006. Approximate Methods for the Estimation of Muskingum Flood Routing Parameters. Water Resources Management; 20: 979–990.

Ganoulis, J., 1994. Engineering Risk Analysis of Water Pollution Probabilities and Fuzzy Sets. VCH..

Kitsikoudis, V., Spiliotis, M. and Hrissanthou, V., 2016. Fuzzy regression analysis for sediment incipient motion under turbulent flow conditions. Environmental Processes; 3(3): 663–679.

Klir G. and Yuan B.T., 1995. Fuzzy Sets and Fuzzy Logic Theory and its Applications. Prentice Hall.

Ouyang, A., Li, K., Truong, T.K., Sallam, A.and Sha E., 2014. Hybrid particle swarm optimization for parameter estimation of Muskingum model. Neural Comput & Applic; 25: 1785–1799.

Papadopoulos, B. and Sirpi, M., 1999. Similarities in fuzzy regression models. Journal of Optimization Theory and Applications; 102(2): 373 – 383.

Peters, G., 1994. Fuzzy linear regression with fuzzy intervals. Fuzzy Sets Syst; 63: 45-55.

Spiliotis, M. and Bellos, C., 2015. Flooding risk assessment in mountain rivers. European Water; 51: 33-49.

Stephenson, D., 1979. Direct optimization of Muskingum routing coefficients. Journal of Hydrology; 41: 161-165.

Tanaka H., Hayashi I. and Watada J., 1989. Possibilistic linear regression analysis for fuzzy data, European Journal of Operation Research; 40(3): 389- 396.

Tanaka, H., 1987. Fuzzy data analysis by possibilistic linear models. Fuzzy Sets Syst; 24(3):363–375.

Tsakiris, G., Tigkas, D. and Spiliotis, M., 2006. Assessment of interconnection between two adjacent watersheds using deterministic and fuzzy approaches. European Water; 15/ 16: 15- 22.

Viessman, Jr., W. and Lewis, G.L., 2003. Introduction to Hydrology, Pearson Education, Inc., Upper Saddle River, New Jersey, USA.

Zimmermann, H.J., 1996. The extension principle and Applications.In Fuzzy Set Theory and Its Applications, Kluwer Academic Publishers, 53 – 67.

APPENDIX

In general terms, one of the most popular conventional forms of goal programming is the following:

$$\begin{cases} \max \sum_{j=1}^{m} \left(d_j^- + d_j^+ \right) \\ \left(AX \right)_j + d_j^- - d_j^+ = b_j \left(\text{to express the} \text{"} \cong \text{"} \right), \\ \text{other constraints} \end{cases} \tag{A.I}$$

In which the term $\left(AX \right)_j + d_j^- - d_j^+ = b_j$, expresses the jth soft equality constraints. The divergence from the equity constraint is measured by the corresponding distances d_j^- and d_j^+.

However, we can extend the cases that we can use the goal programming when there are inequalities which are enabled to be partially (softly) satisfied. In this case, we can also use the goal programming approach by using only one distance of divergence for each equality constraint as follows (Kitsikoudis et al., 2016):

$$\begin{aligned} &\left(AX \right)_j - d_j^+ \le b_j \ \left(\text{to express the} \text{"} \lesssim \text{"} \right) \\ &\left(AX \right)_j + d_j^- \ge b_j \ \left(\text{to express the} \text{"} \gtrsim \text{"} \right) \end{aligned} \tag{A.II}$$

In the same way with the conventional goal programming, the objective function is the sum of the inequality diversions.

Proceedings of the 10th World Congress of EWRA 'Panta Rhei', 5-9 July 2017, Athens, Greece
© 2017 *European Water Resources Association*

A simple model for low flow forecasting in Mediterranean streams

K. Risva[1], D. Nikolopoulos[2], A. Efstratiadis[2] and I. Nalbantis[1*]
[1] *School of Rural and Surveying Engineering,, National Technical University of Athens, Greece*
[2] *School of Civil Engineering, National Technical University of Athens, Greece*
[*] *e-mail: nalbant@central.ntua.gr*

Abstract: Low flows commonly occur in rivers during dry seasons within each year. They often concur with increased water demand which creates numerous water resources management problems. This paper seeks for simple yet efficient tools for low-flow forecasting, which are easy to implement, based on the adoption of an exponential decay model for the flow recession curve. A statistical attribute of flows preceding the start of the dry period is used as the starting flow, as for example the minimum flow of early April. On the other hand, the decay rate (recession parameter) is assumed as a linear function of the starting flow. The two parameters of that function are time-invariant, and they are optimised over a reference time series representing the low flow component of the observed hydrographs. The methodology is tested in the basins of Achelous, Greece, Xeros and Peristerona, Cyprus, and Salso, Italy. Raw data are filtered by simple signal processing techniques which remove the effect of flood events occurring in dry periods, thus allowing the preservation of the decaying form of the flow recession curve. Results indicate that satisfactory low flow forecasts are possible for Mediterranean basins of different hydrological behaviour.

Key words: dry period; recession rate; Savitzky-Golay filter; benchmark function; Monte Carlo calibration; uncertainty

1. INTRODUCTION

The World Meteorological Organization (WMO) (1974) defines low flow as the river discharge during prolonged dry weather. Actually, low flows are periodic phenomena and integral components of the river regime. Particularly, in Mediterranean catchments exhibiting significant variability across seasons, baseflow is the major, and occasionally the sole component of river hydrographs during dry periods. Therefore, low-flow estimations, in terms of magnitude, frequency and duration, are essential premise in solving numerous water engineering and management problems.

The literature reports multiple attempts for low-flow modelling, including hydrograph recession techniques, stochastic autoregressive functions, physically-based models, and data-driven approaches (Smakhtin, 2001). A typical concept is the linear reservoir model that represents the recession limb of a hydrograph as the outflow from a tank of infinite storage capacity, implementing the groundwater storage. The model is linear since outflow is expressed as a constant fraction of storage, thus resulting to an exponential decay function.

This article investigates the use of the above approach as a forecasting tool for the dry-period recession, using daily flow data retrieved at the first half of April. Key objective is providing a parsimonious model of acceptable predictive capacity, which can be implemented for operational purposes (e.g., annual irrigation planning). The model is evaluated at four rivers with different low-flow dynamics, namely Achelous (Greece), Salso (Italy), and Xeros and Peristerona (Cyprus).

2. OUTLINE OF METHODOLOGY

2.1 Model assumptions

Generally, a hydrograph is separated into rising limbs, reflecting increases in discharge from

precipitation events, and recession limbs, representing delayed flow due to processes in the saturated and unsaturated zone. Particularly, low flows during the dry period are mostly attributed to groundwater responses, which can be well represented as outflows from a linear reservoir. Under this assumption, the low flow component of the dry-period hydrograph of a specific year j can be modelled by an exponential decay:

$$q_{jt} = q_{0j} \exp(-k_j\, t) \tag{1}$$

where q_{0j} is the low flow at the beginning of the dry period of year j, t is the day index, and k_j is a recession parameter, associated with the macroscopic hydrological behaviour of the aquifer. Here, eq. (1) is applied in discrete form, using a daily time interval, flows are expressed in m^3/s, and the time is considered in days, while k_j is expressed in inverse daily units. The start and end of the dry period, the initial flow q_{0j}, and the recession parameter k_j is varying across hydrological years. In the remaining text the index j is omitted when unnecessary.

For convenience, we consider a *reference time horizon* of six months, from April 15th to October 15th, which is a reasonable assumption for the maximum duration of the dry period in Mediterranean rivers. Moreover, after preliminary investigations, we decided taking as initial discharge, q_{0j}, the minimum flow value of the first two weeks of April. Thus, for each year j, q_{0j} is a priori determined based on observed flow data, in contrast to the recession coefficient k_j, which is inferred through calibration, i.e. by fitting eq. (1) to the observed dry-period hydrograph.

2.2 Derivation of adjusted low flow data

For a given record of daily discharge data between April 15th and October 15th, and a given q_{0j}, the estimation of k_j is far beyond a typical calibration problem, since the duration of the dry period is not constant, while the dry-period hydrograph contains both rising and recession limbs, as well as individual peaks. Therefore, for each year, it is essential to extract the low flow component from the total hydrograph; these data are next referred to as *adjusted low flows*. In order to construct the adjusted data from observed flows, while also determining the effective length of the dry period, conventionally starting at April 15th, we employ a multi-step processing procedure, as illustrated in Fig. 1 and outlined next.

Step (a): The dry-period hydrograph exhibits both large- and small-scale fluctuations; the former are due to flood events whereas the latter are generally induced by random errors of the monitoring instruments (e.g., stage recorders), also resulting to local minima that do not have physical meaning. In order to remove such effects and obtain a smoothed hydrograph, we employ the numerical filter introduced by Savitzky and Golay (1964), which allows increasing the signal-to-noise ratio without greatly distorting the signal. This is achieved by replacing raw values by new ones, which are computed from a moving polynomial fitted to $2n + 1$ neighbouring points, with n being at least equal to the order of the polynomial. This is handled similarly to a weighted moving average, since the coefficients of the smoothing procedure remain constant.

Step (b): We define the beginning and end of the dry period, and its last flow value, q_{jn}. First, using as cut-off threshold the initial flow, q_{0j}, we seek for the last flow value being greater than q_{0j}; the date with that value denotes the actual beginning of the dry period, whereas observed flows for previous dates are ignored within model fitting. Next, we calculate the average flows over 15-day intervals and their first differences until October 15th. Moving backwards in time, we examine whether the flow trend changes from negative to positive, which marks the end of the dry period.

Step (c): We remove all flow values above the line joining q_{0j} with q_{jn}, i.e.

$$q_{jt} = q_{0j} - (q_{0j} - q_{\mathrm{n}j})\, t \,/\, n_j \tag{2}$$

since the negatively exponential low flow model (1) is by construction below this line. In eq. (2), n_j is the number of days between April 15th and the end of the dry period of year j.

Step (d): We reduce the flow peaks remaining below the theoretical upper threshold (2), considering small-scale flood events of typical duration up to two days. In this context, we apply twice a cut-off procedure comprising the identification of all local flow maxima over the dry period, which are next set equal to the value of the previous day. The remaining flows between q_{0j} with q_{nj} comprise the adjusted low flow sample, used in fitting eq. (1). This is generally non-continuous and contains much less values than the length n_j, since all important local flood events are removed.

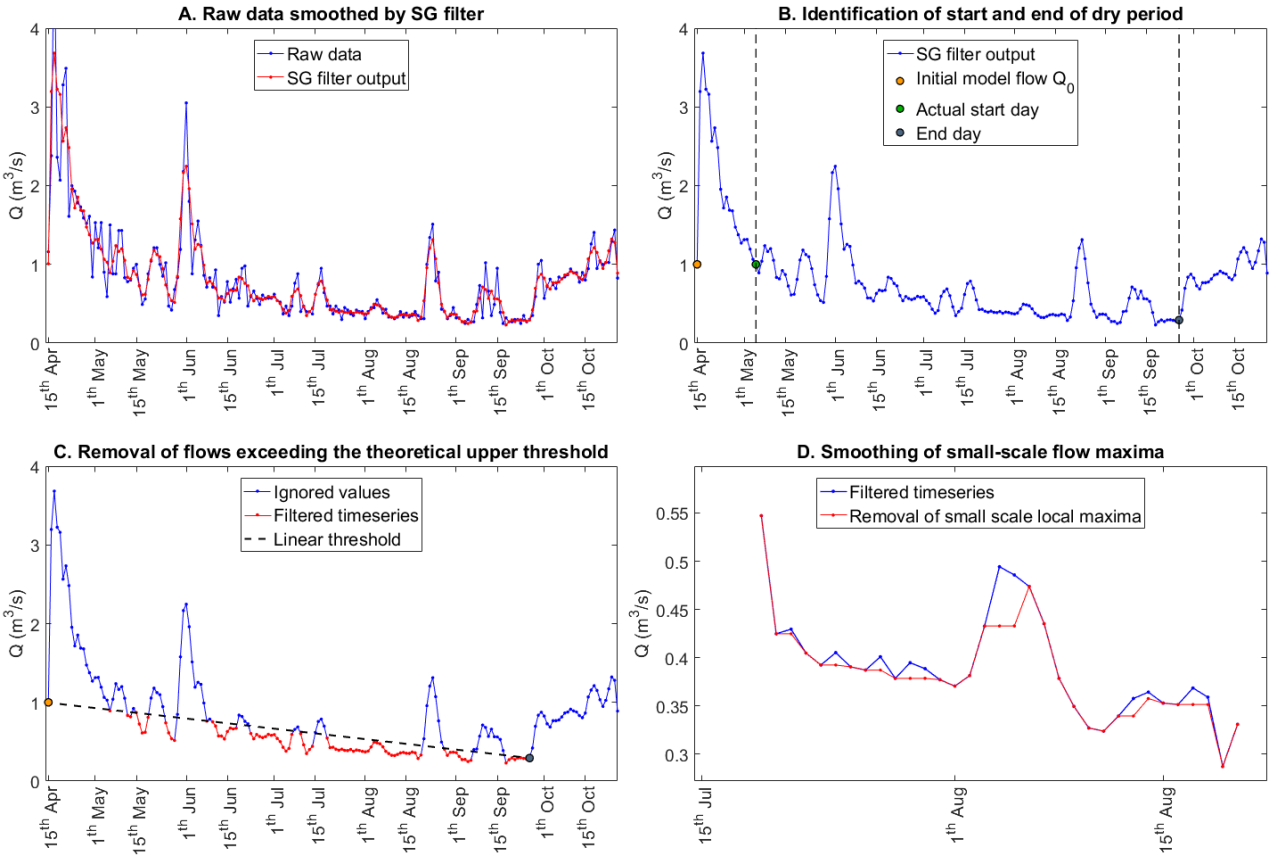

Figure 1: Example of extracting adjusted flow data from daily hydrographs; SG stands for Savitzky- Golay

2.3 Model calibration

For each year j, a one-dimensional calibration problem is solved, to identify the value of k_j that ensures the optimal fitting of eq. (1) to the adjusted data. Our objective function is a modified expression of efficiency (MEF), using as benchmark the expected flows over the reference period. This is of key importance, since the well-known Nash-Sutcliffe efficiency would compare the simulated values against the average flow, thus providing unrealistically high model performance. Apparently, the average is far from being representative of the river regime during the dry period, which exhibits a non-stationary behaviour due to the systematic flow decrease. This shortcoming has been widely discussed in the literature (e.g., Pushpalatha *et al.*, 2012).

Initially, we considered as benchmark not the overall mean flow over the reference time horizon but the mean flow value of each individual day, as well as the median, which is generally a better estimator than the mean, since the dry-period flows are highly skewed. However, due to noise effects, the two benchmarks (particularly the mean) exhibit random fluctuations, which are not desirable (Fig. 2). To remove such effects, we introduced three stepwise exponential functions that were fitted to the daily means and medians, as well as the lower envelope of medians. The latter is the most representative of the river regime during the dry period, and thus it was finally used as benchmark within calibrations.

2.4 Model formulation in forecast mode

The initial formulation of the low-flow simulation model (1), considering an annually varying recession coefficient, has limited practical usefulness, as we seek the development of a forecasting tool with parameters that are known in advance, before issuing a forecast. For employing eq. (1) in forecast mode, we need a formula for estimating the annual value of parameter k_j, based on easily retrievable information that is available before the start of the dry period (similar to q_{0j}, which is estimated on the basis of early April flows). In this respect, also accounting for the outcomes of preliminary calibrations, we tested the application of a linear relationship between k_j and q_{0j}, i.e. $k_j = a\ q_{0j} + b$, where a (s m^{-3} d^{-1}) and b (d^{-1}) are regional parameters, i.e. constant for each basin and independent of the year index j. Hence, the model in forecast mode is now written:

$$q_{jt} = q_{0j} \exp[-(a\ q_{0j} + b)\ t] \tag{3}$$

In order to obtain parameters a and b, we examine two procedures. First, we use a set of already calibrated values of k_j and fit a linear regression equation against the independent variable q_{0j}. By accepting the assumptions of the least squares approach, the slope and intercept of the regression model are optimal estimators of a and b. Alternatively, parameters a and b are considered as control variables of a global optimization problem, asking for fitting eq. (3) to the entire set of reference flow data (in contrast to eq. (1), where different values of k_j are obtained by calibrating against the low flows of each dry period).

For both procedures, the model performance was assessed in terms of modified efficiency through the calibration period, while its predictive capacity was assessed by calculating MEF across an independent data period (validation).

2.5 Uncertainty analysis

A renowned shortcoming of the classical calibration-validation paradigm, known as split-sample test, is the dependency of the model performance on the length and time window of the data sample. This may introduce significant uncertainty, not only to the model performance but also to the optimized parameter values.

In order to account for such uncertainties within the estimation of parameters a and b, we employed a Monte Carlo calibration-validation scheme. For both procedures, we calibrated a and b against 1000 randomly selected subsets (not necessarily continuous) over the whole period of adjusted low flows, and validated against the remaining subsets (a constant validation period of 10 years was systematically considered). For all results (parameter values and performance criteria) we estimated their average and standard deviation.

3. STUDY AREAS

The methodology was tested at four rivers of different scale (one large and three small) and hydrological regime (Risva, 2016). Their key characteristics as well as the corresponding daily average and median flows across the reference time horizon, are depicted in Fig. 2. Low flow regimes of the selected rivers are different. Specifically, Achelous, which produces the highest annual runoff in Greece (950 mm), retains significant discharge, while the departure of the mean daily flow from the median is practically negligible from May to August. In contrast, in Salso River there are large deviations between means and medians, since the dry period flows exhibit substantial asymmetry due to occasional yet quite severe flood events. Finally, in the two Cyprian rivers there are also systematic differences between means and medians, until the mid-summer; in particular, from early July, Xeros River retains a practically constant baseflow, while in Peristerona the flow is interrupted.

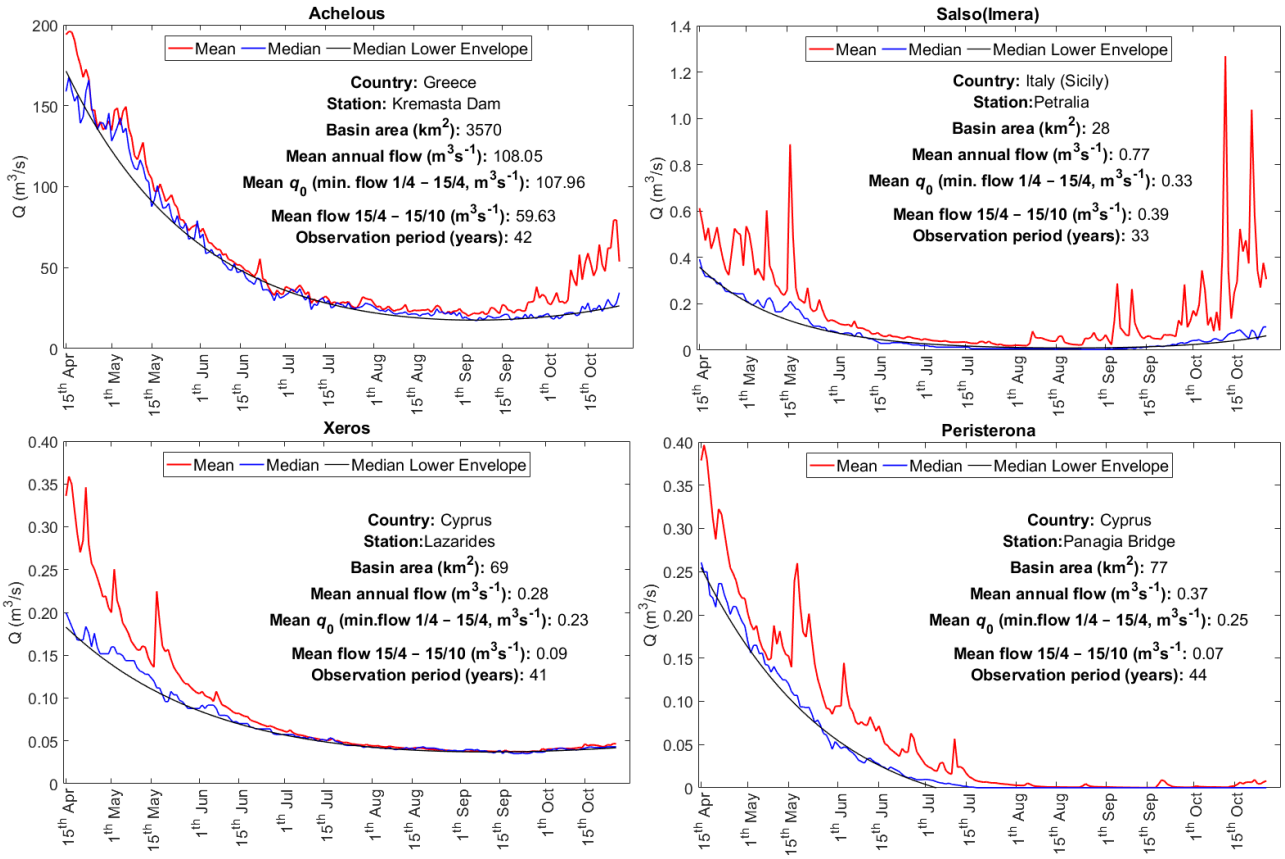

Figure 2: Synoptic information for case studies, plots of daily average and median flows from April 15th to October 15th and benchmark models fitted to the lower envelope of medians.

4. RESULTS AND DISCUSSION

Key results for all rivers are summarized in Table 1. The two parameter estimation approaches (regression-based and global optimization-based) are employed within a Monte Carlo context.

For the first approach, we demonstrate the optimized MEF considering eq. (1), with optimally fitted parameters k_j per calibration sample, and eq. (3), with a and b estimated through a posteriori regression between the optimized values of k_j and q_{0j}; in the last case, MEF refers to calibration and validation samples, and the full data sample (in forecast mode). Moreover, we show the optimized values of a and b, as well as the coefficient of determination (r^2) of the linear regression. Finally, using as typical starting flow the mean q_{0j} (average of minimum early April flows over the entire data period) we provide the corresponding recession rate, k. It is interesting to note that even a low correlation between k and q_0 may yield a satisfactory predictive capacity, as shown for Salso and, particularly, for Peristerona.

Regarding the second approach, we show MEF values for the calibration and validation samples, and the full data sample (forecast mode), the optimized parameters a and b, and the average recession rate, k.

By comparing MEF in forecast mode, it seems that both procedures ensure similar predictive capacity, which is reasonable, since the average recession rates are almost identical (except for Salso). However, in Achelous and Salso, the two approaches are not equivalently robust, as indicated from the variability of MEF. In such cases, we suggest selecting the parameterization ensuring the lowest uncertainty.

Characteristic examples of model fitting in forecast mode are given in Fig. 3. The model is absolutely consistent with the anticipated hydrological behavior of each river, which is well-represented by the average recession rate. As shown in Table 1, the lowest rate refers to Achelous, i.e. a large river with permanent flow, while the highest rate refers to Peristerona, which allows

reproducing the intermittent regime of this river.

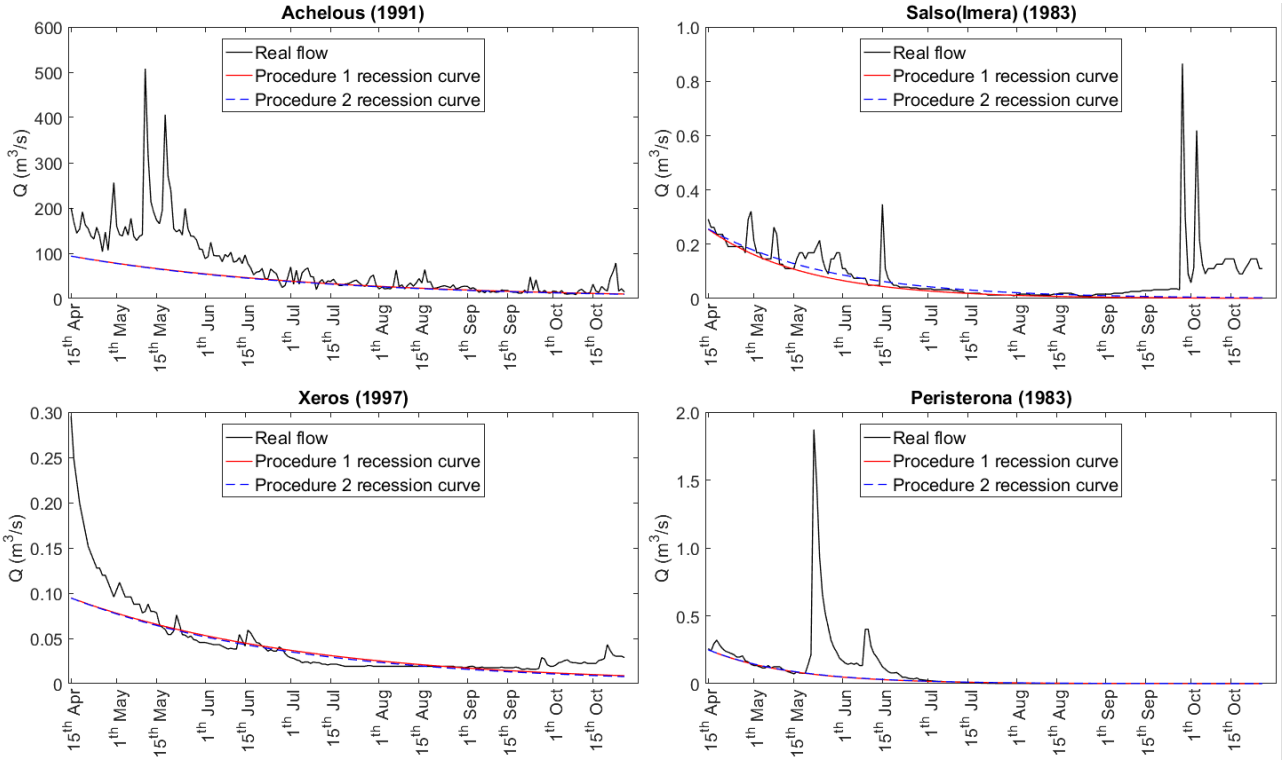

Figure 3: Examples of forecasted low flows through the two parameter estimation procedures (1: regression, 2: global optimization) against the observed hydrographs over the reference period (15/4 to 15/10).

Table 1. Summary of model results (means out of 1000 simulations and standard deviations, in parentheses)

River name	Achelous	Salso (Imera)	Xeros	Peristerona
Parameter estimation through regression between k and q_0				
MEF, local calibration	0.643 (0.035)	0.790 (0.026)	0.889 (0.017)	0.831 (0.016)
Coefficient of determination, r^2	0.771 (0.028)	0.073 (0.029)	0.437 (0.031)	0.083 (0.019)
Parameter a (mm^{-1} d^{-1})	0.0034 (0.0001)	0.0052 (0.0011)	0.0204 (0.0012)	-0.0179 (0.0023)
Parameter b (d^{-1})	0.0037 (0.0002)	0.0244 (0.0014)	0.0098 (0.0003)	0.0400 (0.0009)
Recession rate k (d^{-1}) for mean q_0 (mm)	0.0126 (0.0003)	0.0297 (0.0018)	0.0157 (0.0005)	0.0350 (0.0011)
MEF, calibration	0.523 (0.044)	0.441 (0.070)	0.787 (0.032)	0.721 (0.021)
MEF, validation	0.496 (0.124)	0.414 (0.195)	0.752 (0.146)	0.713 (0.078)
MEF, forecast mode	0.523 (0.029)	0.437 (0.008)	0.788 (0.006)	0.721 (0.006)
Parameter estimation through global optimization				
Parameter a (mm^{-1} d^{-1})	0.0030 (0.0003)	0.0074 (0.0033)	0.0159 (0.0035)	-0.0170 (0.0070)
Parameter b (d^{-1})	0.0049 (0.0009)	0.0170 (0.0040)	0.0109 (0.0012)	0.0390 (0.0028)
Recession rate k (d^{-1}) for mean q_0 (mm)	0.0129 (0.0011)	0.0245 (0.0052)	0.0155 (0.0016)	0.0342 (0.0034)
MEF, calibration	0.529 (0.036)	0.483 (0.076)	0.800 (0.035)	0.725 (0.020)
MEF, validation	0.484 (0.143)	0.320 (0.196)	0.729 (0.173)	0.692 (0.113)
MEF, forecast mode	0.525 (0.006)	0.438 (0.084)	0.794 (0.006)	0.718 (0.004)

5. CONCLUSIONS

Low flow dynamics in Mediterranean rivers can be well approximated using the linear reservoir concept, which implies the determination of two parameters, i.e. the starting flow and the recession rate (respectively denoted as q_{0j} and k_j in eqs (1)-(4)). Our analyses indicated that the former can be easily defined as the lowest daily flow during early April, while the latter can be expressed as a linear function of q_0. In this respect, we can build a simple yet effective low flow forecasting model, by determining the slope and intercept of the above function, based on historical flow data.

Key innovations of the proposed framework are the extraction of the adjusted flow data from the total hydrograph, requiring a series of sequential transformations of the original data (smoothing,

peak removal, etc.), the selection of the lower envelope of daily medians as benchmark flows to be used within calibrations, and the stochastic implementation of calibrations, which allows quantifying the uncertainty of parameters and performance measures.

The case studies indicated that the proposed methodology is suitable for both large and small basins, producing both permanent and intermittent runoff. The strong advantage of the model is its parsimony, not only in terms of parameters but also in data requirements, since, after calibration, the sole input is the starting flow q_0. This makes the model easy to apply in an operational context, so as to provide reliable estimations of surface runoff during dry seasons.

REFERENCES

Pushpalatha, R., Perrin, C., Le Moine, N., Andréassian, V., 2012. A review of efficiency criteria suitable for evaluating low-flow simulations. J. Hydrol.; 420-421: 171–182.

Risva, K., 2016. Model development for low flow estimations in river basins across the Mediterranean. Diploma thesis, School of Rural and Surveying Engineering, National Technical University of Athens.

Savitzky, A., Golay, M. J. E., 1964. Smoothing and differentiation of data by simplified least squares procedures. Analyt. Chem.; 36(8): 1627–39.

Smakhtin, V. U., 2001. Low flow hydrology: a review. J. Hydrol.; 240(3): 147–186.

World Meteorological Organization (WMO), 1974. International Glossary of Hydrology.

Proceedings of the 10th World Congress of EWRA 'Panta Rhei', 5-9 July 2017, Athens, Greece
© 2017 *European Water Resources Association*

Influence of precipitation and land cover changes in a Mediterranean mountain watershed (Guadalaviar River, Spain)

I. Melendez-Pastor*, E.I. Hernández, J. Navarro-Pedreño, I. Gómez, M.B. Almendro-Candel
Department of Agrochemistry and Environment, University Miguel Hernández of Elche, Av/ Universidad s/n Edifico Alcudia, 03202 Elche, Spain
* *e-mail: imelendez@umh.es*

Abstract: In this study the influence of recent (1984-2014) precipitation patterns and land cover changes in the water flow of the Guadalaviar River basin were analysed. The watershed is located in the southern Iberian Range (Spain) and is characterized by medium-high altitude (880-1849 m), extensive forest areas and low population density. This region is located in the confluence of the Tagus, Ebro and Turia great basins. The climate varies from cold continental sub-Mediterranean to mountain climate. Land cover maps were obtained from supervised classification of satellite imagery. Precipitation and water flow time series were obtained from official public institutions. Land covers dynamics in the study area seems to be more strongly influence by the process of rural abandonment than climatic variables. The expansion of shrubs and pine forest at expense of agricultural land is a quite slow process and the influence of short-term climate variability was not clearly revealed. The statistical analysis of precipitation and water flow time series anomalies revealed different water regimens and intense drought periods. A strong relationship between water flow and precipitation variability was evident for the portion of the river with a natural water flow. The significant relationship between precipitation and water flow after a reservoir was disrupted. Forestland expansion did not evidence a clear influence on precipitation or water flow patterns. However, other land cover changes (shrub vs. dryland agriculture) seemed to be greatly affected by precipitation variability along with other socio-economic factors.

Key words: Climate variability, land cover changes, Mediterranean mountain, remote sensing

1. INTRODUCTION

Climate variability and land cover changes have been identified as relevant factors affecting water flow dynamics in river watersheds (Wei et al. 2013). Climate change is affecting the hydrologic cycle by the intensification of extreme events (droughts and floods) and the increase of differences between dry and wet regions (Famiglietti and Rodell 2013). On the one hand, land cover changes influence many aspects of the water cycle such as the evapotranspiration, soil's water holding capacity, precipitation interception by vegetation stands and runoff parameters (Zhang et al. 2014). On the other hand, land cover changes not only affect the amount of water transported by rivers, but also their quality (Khare et al. 2012). Many research efforts are being focused in the determination of the influence of climate and land cover changes as drivers of water flow (Guo et al. 2016; Li et al. 2016) and quality (Delpla and Rodriguez 2014) worldwide.

In the case of the Iberian Peninsula, there are evidences that suggest a general trend of lower water flow in Spanish natural water courses (Martínez-Fernández et al. 2013). Several studies have shown the influence of land cover changes on the water flow from rivers (Morán-Tejeda et al. 2011; Lana-Renault et al. 2011), and the joint influence of climate and rural abandonment in surface hydrology of mountain areas (Beguería et al. 2003; Otero et al. 2011). Within the context of the province of Teruel (South of the Iberian Range, Spain), the Guadalaviar River (upper basin of the Turia River) is one of the main watersheds. Its basin encompasses most of the region of the "Sierra de Albarracín" and limits with the head of the Tagus. It is a watershed with remarkable sociocultural and environmental values, very low population density (about 3 inhabitants/km^2) and a dynamics of land cover changes induced by rural abandonment (Melendez-Pastor et al. 2014). The

ecological status of the river is good and the river water is used by some traditional irrigation systems and as water supply from the "Arquillo de San Blas" reservoir.

The objective of this study was the analysis of the influence of precipitation variability and land cover changes in the Guadalaviar River's water flow. Time series of precipitation and water flow, along with several land cover maps obtained from satellite imagery (1984-2014) were employed.

2. MATERIAL AND METHODS

The study area comprises the Guadalaviar River watershed with a total area of 845.6 km^2, a mean altitude of 1366 m a.s.l. and average slope of 9.6 degrees. The delimitation of the study area was based on the analysis of a 1:25,000 digital elevation model (Figure 1), provided by the Spanish National Geographic Institute (IGN). The basin was divided in three parts: upper, middle and lower. The water gauging stations of Tramacastilla limits the upper sub-basin, from this point to Arquillo de San Blas the middle sub-basin, and from this point to the confluence of Alfambra River and Guadalaviar the lower sub-basin. This is the starting point of the Turia River. The water gauging stations Yearbook Information System provided water flow data. Precipitation time series (1967-2014) from nine meteorological stations were also employed. Meteorological stations were located within or surrounding the study area at altitudes ranging from 920 m in San Blas to 1519 m in Guadalaviar. The State Agency of Meteorology (AEMET) provided precipitation time series.

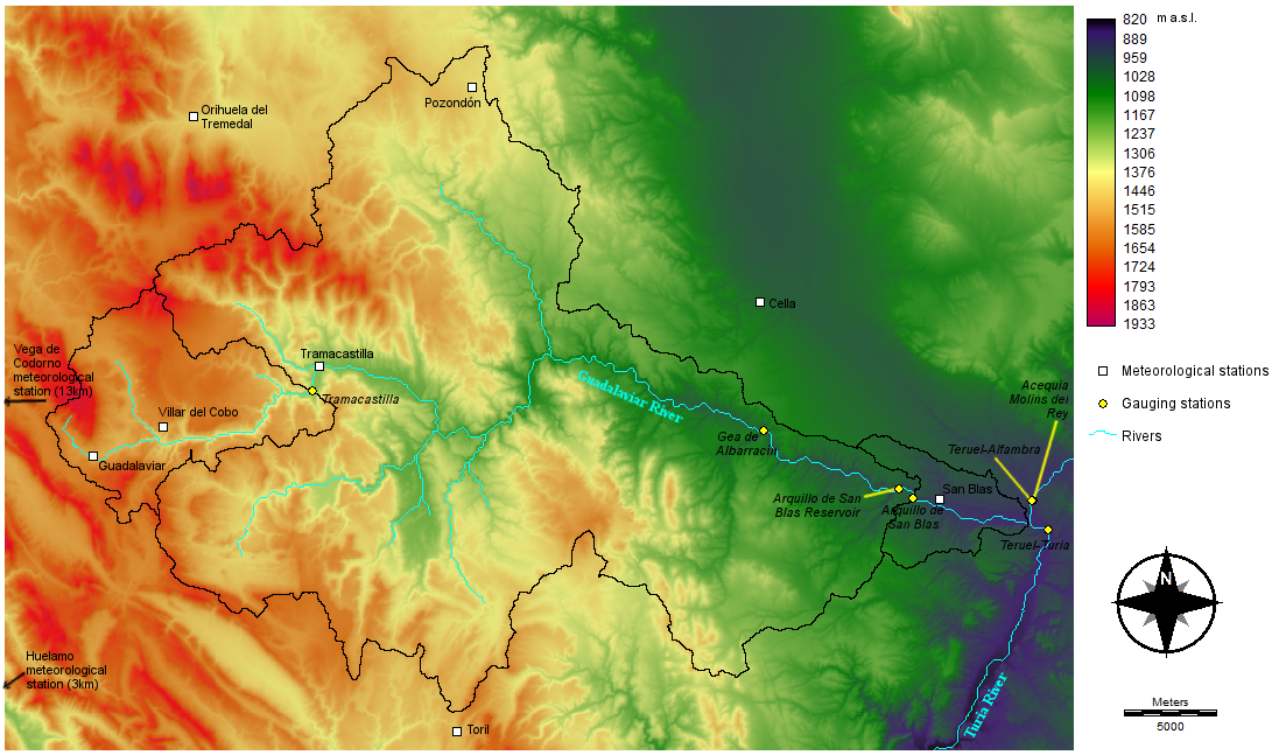

Figure 1. Digital elevation model of the study area. Meteorological and gauging stations are shown. Upper, middle and lower catchments are also shown.

Land cover maps were obtained from Landsat satellite images (summers of 1984, 2000 and 2014). The images were acquired from Landsat 5, 7 and 8 respectively. For this reason, an intensive pre-processing procedure including geometric, radiometric and atmospheric correction was done according to Melendez-Pastor *et al*. (2014). Field survey, aerial images and historical maps helped for the development of a training and test areas database. A total of 427 sampling points were considered. Those sampling points were located at unambiguous land cover classes for each date. A random division of the training (2/3) and test areas (1/3) dataset was performed. Seven land cover classes (i.e., pine forest, oak forest, rangeland, irrigation/river forest, drylands agriculture, water

bodies and urban) that are representative of the entire study area and associated with different land cover were identified. The maximum likelihood classifier was applied to the non-urban areas (urban areas were previously masked because they are very small).

Precipitation and water flow time series were analysed for four different periods, namely 1967-1984, 1984-2000 and 2000-2014 and for the total length of the time series (1967-2014). Time series anomalies were computed for a monthly basis. The time series anomaly (z-score) was computed using the following expression:

$$z = \frac{x_i - \mu}{\sigma} \quad (1)$$

where x_i is the time series value for a given moment i, and μ and σ are respectively the mean value and the standard deviation value of the time series. When the z-score is negative, it indicates below-normal water flow conditions and when it is positive it indicates above normal water flow conditions thereby pointing to wet seasons or periods. Spearman rank correlation test was employed to analyse the relation between precipitation and water flow anomalies time series for the four time periods.

The influence among land cover changes, precipitation variability and water flow variations was evaluated for the upper and middle basins. Land cover changes were computed for the periods 1984-2000 and 2000-2014. Average precipitation maps for the periods 1967-1984, 1984-2000 and 2000-2014 were computed by developing multiple regression models combining precipitation data, altitude, aspect and geographical location. Average precipitation and water flow changes for the periods 1984-2000 and 2000-2014 were obtained and compared with the corresponding land cover changes.

3. RESULTS AND DISCUSSION

Average water flow of the Guadalaviar River (1967-2014) was 0.68 m^3/s for the upper basin (until Tramacastilla gauging station) and 1.37 m^3/s for the middle basin (limited by Arquillo de San Blas gauging station). Maximum water flow values were obtained for winter in both locations. A more intense variability between winter and summer was observed for the middle basin gauging station. Water flow just before the confluence of the Guadalaviar River with its major tributary (Alfambra) is unavailable. The development of the precipitation maps allowed the estimation of average precipitation and standard deviation for the upper (829±98 mm), middle (570±113 mm) and lower (375±12 mm) basins. The lower portion of the study area is relatively plain (altitude ranging from 880 to 1129 m a.s.l.) and small, with a cold continental sub-Mediterranean climate and intensively occupied by urban areas. The middle basin is the most extensive and diverse, with a mean altitude of 1354 m a.s.l. (ranging from 932 to 1849 m a.s.l.). The upper basin is basically mountainous, with a mean altitude of 1586 m a.s.l. (ranging from 1261 to 1845 m a.s.l.).

The first part of the research was focused in the analysis of the relations between precipitation and water flow at representative locations along the watershed. Three weather stations representative of the sub-basin were selected. The Guadalaviar village weather station was selected for the upper basin, and the Tramacastilla and San Blas weather stations were selected for the middle and lower basins respectively. Water flow was available for gauging stations located very close to the last two villages. Spearmanere similar for the three weather stations due to their time series anomalies were significantly correlated for all time periods. Intense precipitation events are usually associated to Atlantic fronts (Gobierno de Aragón 2007) thus explaining a great part of the correlations between the time series and the differences between the upper and western locations and the lower basin. Summer storms are very important too and even more frequent for the more mountainous areas. Water flow pattern for both locations were also significantly correlated for all

time periods but with quite low significance values. The lower gauging station (Arquillo de San Blas) is located after the reservoir and its water flow is technically controlled according to water demands for irrigation and water supply. The Tramacastilla gauging station is monitoring a natural water flow region. It seemed relevant for the correlations between water flow and precipitation. The influence of precipitation in the upper and middle basins in the natural water flow river is significant for all time periods. Future scenarios of climate change in the region could lead to serious impacts on water management and river ecology (López-Moreno et al. 2013) thus requiring the development of strategic plans to minimize future environmental and socio-economic problems.

Table 1. Spearman rank correlation matrix between time series of precipitation and water flow anomalies. The maximum values for each cross between locations is in bold.

		Time periods	Precipitation			Water flow	
			Guadalaviar	**Tramacastilla**	**San Blas**	**Tramacastilla**	**Arquillo de San Blas**
Precipitation	**Guadalaviar**	TOTAL		0.730**	0.455**	0.379**	0.011 ns
		1967-1984		0.708**	0.325**	**0.441****	0.008 ns
		1984-2000		0.756**	**0.559****	0.420**	-0.089 ns
		2000-2014		**0.773****	0.445**	0.233**	0.110 ns
	Tramacastilla	TOTAL	0.730**		0.645**	0.331**	**0.143****
		1967-1984	0.708**		0.540**	**0.406****	0.124 ns
		1984-2000	0.756**		**0.725****	0.289**	0.074 ns
		2000-2014	**0.773****		0.658**	0.234**	0.111 ns
	San Blas	TOTAL	0.455**	0.645**		**0.111***	0.094 ns
		1967-1984	0.325**	0.540**		0.030 ns	0.112 ns
		1984-2000	**0.559****	**0.725****		0.128 ns	0.147 ns
		2000-2014	0.445**	0.658**		0.128 ns	0.062 ns
Water flow	**Tramacastilla**	TOTAL	0.379**	0.331**	**0.111***		0.241**
		1967-1984	**0.441****	**0.406****	0.030 ns		0.273**
		1984-2000	0.420**	0.289**	0.128 ns		0.204*
		2000-2014	0.233**	0.234**	0.128 ns		**0.298****
	Arquillo San Blas	TOTAL	0.011 ns	**0.143****	0.094 ns	0.241**	
		1967-1984	0.008 ns	0.124 ns	0.112 ns	0.273**	
		1984-2000	-0.089 ns	0.074 ns	0.147 ns	0.204*	
		2000-2014	0.110 ns	0.111 ns	0.062 ns	**0.298****	

Significance levels: **: $p \leq 0.01$; * : $p \leq 0.05$; ns : not significant

The second part of the research was focused in the analysis of land cover changes. Land cover maps were obtained from satellite images for the years 1984, 2000 and 2014. Major land covers in the upper basin are forest (48.5% in 2014) and rangeland areas (37.3% in 2014) that are frequently employed by cattle for grazing. The presence of dryland agriculture areas is less prominent (11.2% in 2014). The importance of rangeland increased in the middle basin (44.4% in 2014) due to the presence of poorer soils, lower precipitations and higher human activities pressure. Forest (38.2% in 2014) and dryland agriculture (14.4% in 2014) areas are very important too. The lower basin is dominated by the presence of dryland and irrigation agriculture (63.0% and 9.7% respectively), rangeland (12.5% in 2014) and urban areas (8.5 % in 2014). The importance of forest (6.3% in 2014) in the lower sector of the Guadalaviar River watershed is very limited.

The general trend was the expansion of rangeland and forest areas at expense of dryland agriculture. This general process has been observed for the this region (Melendez-Pastor et al. 2014) and similar Spanish mountainous areas (Arnaez et al. 2011) and it is related with the process of rural abandonment. However, this general pattern was slightly different for three sub-basins. Land covers and land uses in the lower basin are very influenced by the nearby urban area of Teruel city. Land cover dynamics in this portion of the study area are quite limited. Moreover, the middle and upper basins exhibited more intense land cover changes although their population is drastically reducing and migrating to the nearby cities (Melendez-Pastor et al. 2014).

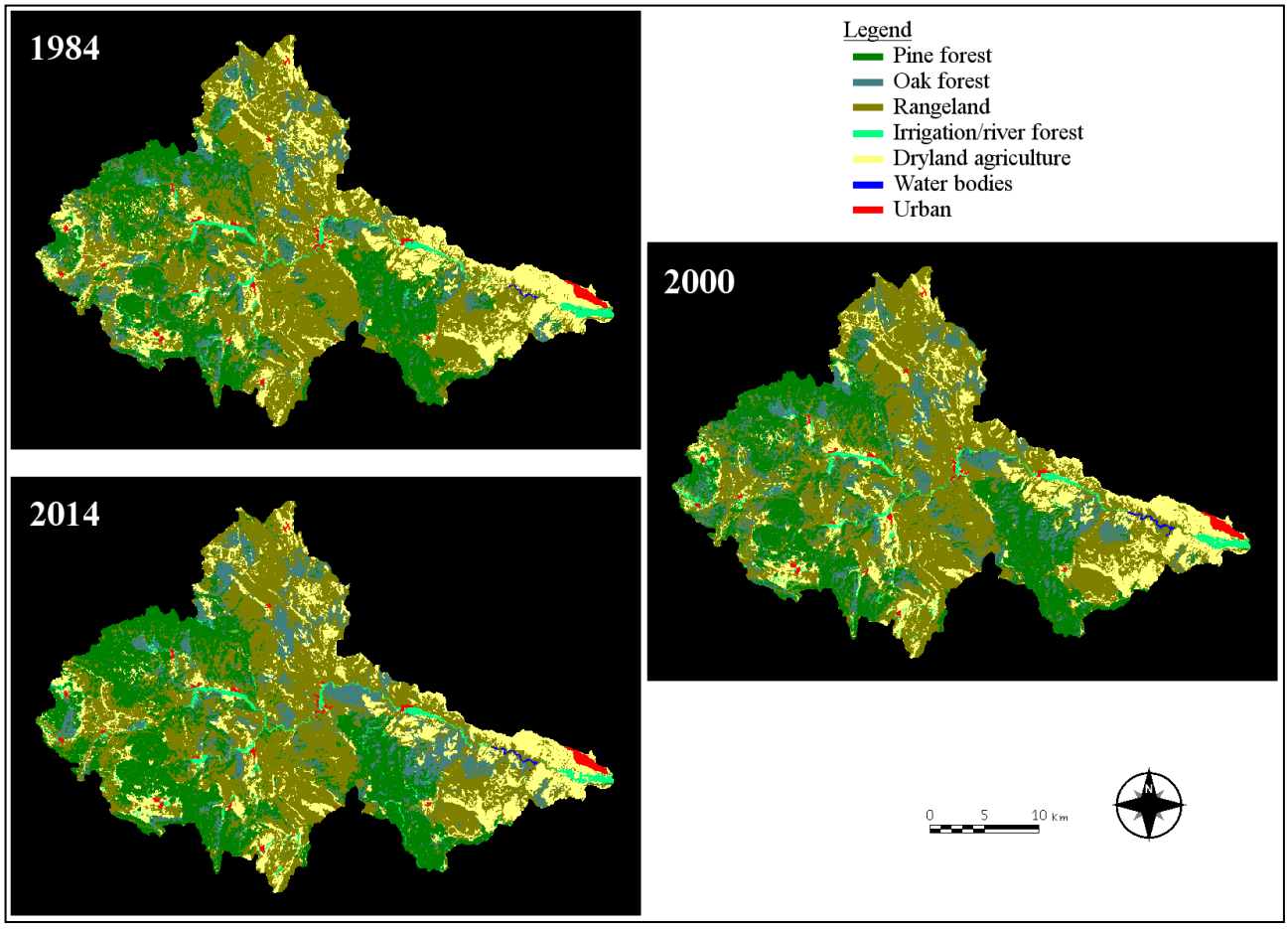

Figure 2. Land cover maps for 1984, 2000 and 2014.

Finally, the relation among land cover, water flow and precipitations changes was assessed. Land cover changes from 1984 to 2000 and 2000 to 2014 were related with comparable average precipitation and water flow changes (the period 1980-2000 respect to 1967-1984 and the period 2000-2014 respect to 1980-2000). These changes were analysed for the middle and upper basins where land cover, precipitation and water flow data were available. The upper basin experienced an almost synchronized reduction of water flow and precipitation in the first period (about -6%) and a notable increase in the second one (more than 20%). Land cover dynamics was characterized by a reduction of dryland agriculture and the corresponding increase of natural areas (forest + rangeland) in the first period. The increase of precipitation and water flow in the second period was associated with an increase of dryland agriculture at the expense of shrubs developed in temporally abandoned fields in the previous period. Forest areas continued their expansion dynamics. The middle basin water flow was controlled by the water level regulation at the reservoir and its association with the other variables was uncertain. Precipitation patterns were similar to the upper basin and land cover changes were dominated by the continuous expansion of forest and rangeland (with less intensity) at the expense of agriculture lands. This process of forestland expansion implies an homogenization and simplification of the landscape, with negative effects from the reduction in biodiversity and landscape variety and positive effects due to land re-vegetation that contributes to reducing soil degradation (Lasanta-Martínez et al. 2005). Also, the importance of water yield in headwaters is crucial to understand the evolution of water resources in major rivers (Morán-Tejeda et al. 2010). Our results area in accordance with previous studies at mountainous, densely forested areas (López-Moreno et al. 2013; Li et al. 2016) that suggested that the overall influence of land cover changes in water flow is less evident that the effect of precipitation variability for the whole study area.

4. CONCLUSIONS

This study analysed the influence of land cover, water flow and precipitations changes in the headwater of the Turia River. The Guadalaviar River watershed was characterized by a process of rural abandonment that implied an important expansion of forestland especially in the more inaccessible mountainous areas. The relationship between water flow and precipitation was highly evident for the portion of the river with a natural water flow. A reservoir in the lower portion of the river greatly affected the relationship between precipitation and water flow. The process of forestland expansion did not evidence a great influence on precipitation or water flow patterns. However, other land cover changes (shrub vs. dryland agriculture) seemed to be greatly affected by precipitation variability along with other socio-economic factors previously studied.

ACKNOWLEDGEMENTS

This study was funded by the *Instituto de Estudios Turolenses* (IET). The authors thank the AEMET for providing the climate data used in the study. We also acknowledge the U.S. Geological Survey for providing the Landsat satellite imagery.

REFERENCES

Arnaez, J., Lasanta, T., Errea, M. P., Ortigosa, L., 2011 Land abandonment, landscape evolution, and soil erosion in a Spanish Mediterranean mountain region: The case of Camero Viejo. Land Degrad Dev; 22:537–550.

Beguería, S., López-Moreno, J. I., Lorente, A., Seeger, M., García-Ruiz, J. M. (2003) Assessing the effect of climate oscillations and land-use changes on streamflow in the central Spanish Pyrenees. Ambio; 32:283–286.

Delpla, .I, Rodriguez, M. J., 2014 Effects of future climate and land use scenarios on riverine source water quality. Sci Total Environ; 493:1014–1024.

Famiglietti, J. S., Rodell, M., 2013. Water in the Balance. Science; 340:1300–1301.

Gobierno de Aragón, 2007. Atlas Climático de Aragón [*Climate Atlas of Aragón*]. Gobierno de Aragón: Zaragoza, Spain

Guo, J., Su, X., Singh, V., Jin, J., 2016. Impacts of Climate and Land Use/Cover Change on Streamflow Using SWAT and a Separation Method for the Xiying River Basin in Northwestern China. Water; 8:192.

Khare, Y. P., Martinez, C. J., Toor, G. S., 2012. Water quality and land use changes in the Alafia and Hillsborough river watersheds, Florida, USA. J Am Water Resour Assoc; 48:1276–1293.

Lana-Renault, N., Latron, J., Karssenberg, D., Serrano-Muela, P., Regüés, D., Bierkens, M. F. P., 2011. Differences in stream flow in relation to changes in land cover: A comparative study in two sub-Mediterranean mountain catchments. J Hydrol; 411:366–378.

Lasanta-Martínez, T., Vicente-Serrano, S. M., Cuadrat-Prats, J. M., 2005. Mountain Mediterranean landscape evolution caused by the abandonment of traditional primary activities: A study of the Spanish Central Pyrenees. Appl Geogr; 25:47–65.

Li, Y., Chang, J., Wang, Y., Jin, W., Guo, A., 2016. Spatiotemporal impacts of climate, land cover change and direct human activities on runoff variations in the Wei River Basin, China. Water; 8:220.

López-Moreno, J. I., Zabalza, J., Vicente-Serrano, S. M., Revuelto, J., Gilaberte, M., Azorin-Molina, C., Morán-Tejeda, E., García-Ruiz, J. M., Tague, C., 2013. Impact of climate and land use change on water availability and reservoir management: Scenarios in the Upper Aragón River, Spanish Pyrenees. Sci Total Environ; 493:1222–1231.

Martínez-Fernández, J., Sánchez, N., Herrero-Jiménez, C. M., 2013. Recent trends in rivers with near-natural flow regime: The case of the river headwaters in Spain. Prog Phys Geogr; 37:685–700.

Melendez-Pastor, I., Hernández, E. I., Navarro-Pedreño, J., Gómez, I., 2014. Socioeconomic factors influencing land cover changes in rural areas: The case of the Sierra de Albarracín (Spain). Appl Geogr; 52:34–45.

Morán-Tejeda, E., Ceballos-Barbancho, A., Llorente-Pinto, J. M., 2010. Hydrological response of Mediterranean headwaters to climate oscillations and land-cover changes: The mountains of Duero River basin (Central Spain). Glob Planet Change; 72:39–49.

Morán-Tejeda, E., Ceballos-Barbancho, A., Llorente-Pinto, J. M., López-Moreno, J. I., 2011. Land-cover changes and recent hydrological evolution in the Duero Basin (Spain). Reg Environ Chang; 12:17–33.

Otero, I., Boada, M., Badia, A., Pla, E., Vayreda, J., Sabaté, S., Gracia, C. A., Peñuelas, J., 2011. Loss of water availability and stream biodiversity under land abandonment and climate change in a Mediterranean catchment (Olzinelles, NE Spain). Land use Policy; 28:207–218.

Wei, X., Liu, W., Zhou, P., 2013. Quantifying the Relative Contributions of Forest Change and Climatic Variability to Hydrology in Large Watersheds: A Critical Review of Research Methods. Water; 5:728–746.

Zhang, T., Zhang, X., Xia, D., Liu, Y., 2014. An Analysis of Land Use Change Dynamics and Its Impacts on Hydrological Processes in the Jialing River Basin. Water; 6:3758–3782.

Proceedings of the 10th World Congress of EWRA 'Panta Rhei', 5-9 July 2017, Athens, Greece
© 2017 *European Water Resources Association*

An implementation of a water balance model in the Evrotas basin

P.G. Marinou[1], E.G. Feloni[1*], O. Tzoraki[2] and E.A. Baltas[1]
[1] *Department of Water Resources and Environmental Engineering, School of Civil Engineering, National Technical University of Athens, 5 Iroon Polytechniou, 157 73, Zofrafou, Attiki, Greece*
[2] *Marine Sciences Department, School of Environment, University of the Aegean, Greece*
[*] *e-mail: feloni@chi.civil.ntua.gr*

Abstract: This research paper focuses on the implementation of the "abcd" water mass balance model in Evrotas River Basin for the runoff simulation. The study area, which is located in Greece and more specifically at SE. Peloponnese, is the Evrotas river basin, covering a total area of 1739 km2 with its main watercourse of 90 km length. The model is performed in four subbasins of Evrotas; Oinountas (the outlet of which is in Kladas station), Rasina I (up to the Koumousta Station), Rasina II (up to the station located at the Rasina Airport) and Vivari (up to Sellasia station). The first three subbasins were studied on a daily step for an entire water year (2009-2010), while the later one on a monthly basis for a five-year period (2006-2009). The model's calibration was accomplished by the calculation of the Nash-Sutcliffe coefficient (N-S); for the estimated and the measured discharges. The performance of the "abcd" model was good for monthly flows simulation (N-S=0.82 for Vivari subbasin) and adequately in the daily interval application (N-S>0.62). Additionally, a sensitivity analysis in the parameters of the model is provided, establishing the different results per subbasin.

Key words: water balance, "abcd" model, Evrotas, sensitivity analysis

1. INTRODUCTION

Hydrologic modeling has become an indispensable tool for the assessment, management, and use of water resources. For hydrologists, such models are especially useful in the evaluation of assumptions and theories about the dominant hydrologic processes in a basin (Al-Lafta et al., 2013). Watershed models are powerful tools for simulating the effect of watershed processes and management on soil and water resources. However, no comprehensive guidance is available to facilitate model evaluation in terms of the accuracy of simulated data compared to measured flow and constituent values.

The "abcd" model was originally introduced by Thomas (1981) and Thomas et al. (1983) and it is a simple, nonlinear watershed model which accepts precipitation and potential evapotranspiration as input, producing streamflow as output. Internally, the model also represents soil moisture storage, groundwater storage, direct runoff, groundwater outflow to the stream channel and potential evapotranspiration. The "abcd" model has been used in a large number of hydrologic applications, especially in America (indicatively: Martinez et al., 2010; Al-Lafta et al., 2013).

This work therefore aims to study the hydrologic regime of four different watersheds, namely Oinountas (Kladas station), Rasina I (Koumousta station), Rasina II (Airport station) and Vivari by the use of the "abcd" hydrologic model. These subbasins are located in a complicated hydrogeologically and geomorphologically basin, the Evrotas River Basin (Tzoraki et al, 2011 and 2013). At the same time, this work intends to illustrate the different characteristics per subbasin through a sensitivity analysis in the model's parameters. In this work, the model was initially implemented using monthly time series for Vivari basin for a period of four hydrologic years. However, the suitability for the daily water balance simulation was examined, and, for this reason, the "abcd" model was also performed for the daily timeseries in three subbasins and for a whole hydrologic year. These subbasins are Oinountas (Kladas), Rasina I (Koumousta) and Rasina II (Airport).

2. STUDY AREA AND DATA USED

2.1 Description of the region

Evrotas River, as many rivers in the Mediterranean region, is a temporary river with intermittent flow in the main stream and many tributaries. Evrotas basin (Figure 1) is located in the south-eastern Peloponnese (Greece) in the Prefectures of Laconia and Arcadia, covering an area of 2410 km^2, with a main stream length of 90 km (up to Vrontamas karst). The population of the region has reached 66000 inhabitants and the largest town is Sparta with 18000 inhabitants. The basin has a Mediterranean climate with mild or cold winters and prolonged hot and dry summers, with a mean annual temperature of 18.5˚C at the town of Sparta. Monthly mean temperatures in the meteorological station of Sparta are typically 10.3˚C in winter and 27.6˚C in summer. The basin is bounded by the Taygetos (2407 m) and Parnonas (1940 m) mountains from which numerous intermittent streams discharge into the river network. The main tributaries are the Oinountas, Magoulitsa, Gerakaris, Kakaris, Rasina, Mariorema, Xerias (Querner et al., 2016). By using GIS technics, it was found that the 40% of the basin area is above 600 m elevation, the 45% between 150 and 600 m, and the 15% <150 m.

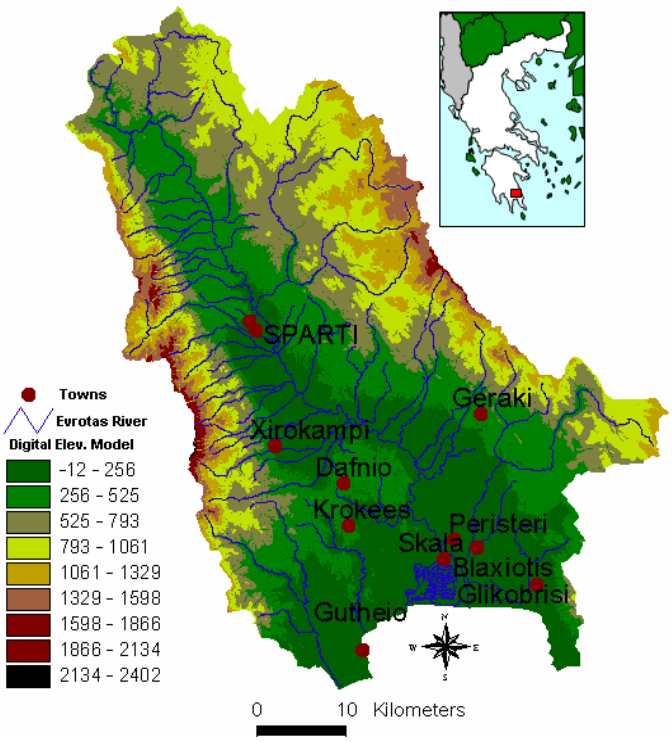

Figure 1. Location of the Evrotas river basin

Concerning the land cover type, approximately the 59% of the surface is forest, bareland or grassland, the 40% is covered by agricultural uses and only the 1% is urban. More specifically and according to CORINE (2012), the land cover classes are scrub and herbaceous vegetation associations (60.8%), forests (16.0%), heterogeneous agricultural areas (15.0%), permanent crops (6.5%), open spaces with little or no vegetation (1.1%), urban fabric (0.3%), arable land (0.1%) and the rest (0.2%) are industrial, commercial and transport units, mine, dump and construction sites and artificial, non-agricultural vegetated areas. The geological structure of the area mainly consists of limestone (49%) and schist (29%). The valley is filled with fluvial sediments of different ages and alluvial deposits are covering the river floodplain area. Taygetos and Parnonas mountains are mainlykarstic, but with areas of impermeable formations. A unit of low-transmissivity alluvial fans, restricted adjacent to the east edge of the Taygetos mountains, comprise significant water storage.

Taygetos karst has high transmissivity (1.16×10^{-8}–1.16×10^{-9} m^2 d^{-1}) and recharges the alluvial fans and associated aquifer north-west of the town of Sparta. The unsaturated zone in this region is between 20–30 m depth, with hydraulic conductivity varying between $8.1 \times 10^{-12} – 9.2 \times 10^{-10}$ md^{-1} (Antonakos and Lambrakis, 2000). The Sparta aquifer is penetrated by numerous wells used to provide water for irrigation. Long sections of the river have intermittent flow, influenced by the local geology, low rainfall, abstraction and high evaporation. The river discharge has declined markedly in recent decades. In a total river network of 5143 km length, the 3.5% has permanent flow, the 4.5% is intermittent and the 92% of the stream network has rain-generated flow which is episodic and appears only during a rain event. The largest change is in the period between 1980 and present and is the result of irrigating olives. A comparison between the current situation and the natural one in 1900 leads to the conclusion that currently 79% of the stream network is in a poor hydrological and ecological condition due to human influence (Querner et al., 2016). The main causes of desiccated river bed are the steep topography of the terrain, the karst geology and groundwater abstraction for irrigation (Gamvroudis et al., 2015).

2.2 Data

The "abcd" water balance model was implemented is four subbasins and at various temporal scales, given the existing data limitations and the large area of the watershed. In this study, data used for processing generated from the meteorological and hydrological stations which are located in the region (Figure 2a). There are six stage recording stations on the Evrotas and its tributaries. Two of these, at Vrontamas and Vivari, are on the main river; two are on the Oinountas and two on the Rasina tributary. Vrontamas station is the oldest one, providing flow data since 1973 on a monthly basis, while the Kladas and the Rasina hydrometric stations provide daily runoff data since 2008 and 2009, respectively.

Daily precipitation has been measured since 1970 at six stations: Ellos (4 m elevation), Riviotissa (163.5 m), Vrontamas (280 m), Perivolia (490 m), Sellasia (590 m) and Vasaras (646 m) (Thiessen polygons in Figure 2b).

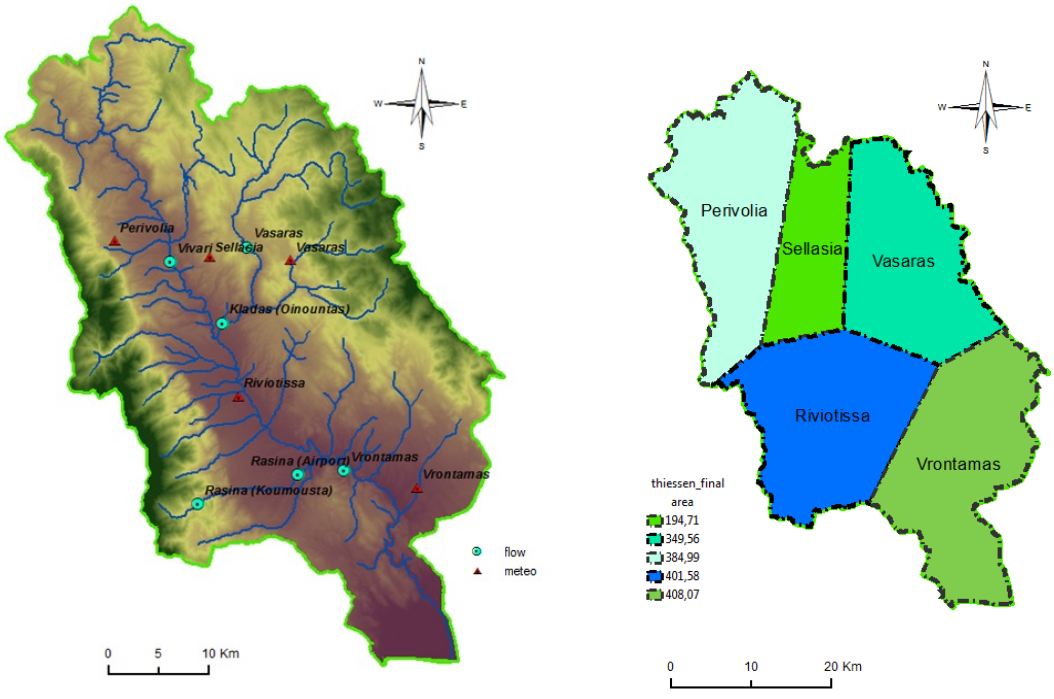

Figure 2. (a) Meteorological (red triangles) and stage recording (blue circles) stations in Evrotas river basin, (b) Thiessen polygons of the 5 rain gauge stations in Evrotas river basin.

According to these stations measurements for the hydrologic years 1969-2011, mean annual precipitation in the region varies between 565 mm (Vrontamas) and 1341 mm (Perivolia). Two temperature stations located within the basin were used to drive the hydrologic model using daily data. These stations are Riviotissa and Sellasia which have been in operation since 1966. Temperature time series in a daily time step of Sellasia station were used for the two subbasins of Oinountas (Kladas) and Vivari, while the temperature data of Riviotissa were used for the other two subbasins of Rasina. The data of wind speed and relative humidity received by the meteorological station of Sparta for the period of 1974 - 2004, provided by the Hellenic National Meteorological Service. As the station of Sparta did not provide sunshine data, for model processing purposes the only available time series of relative sunshine (in hr) was at the station of Kalamata (HNMS), which was finally used. In a Geographic Information System (GIS), thematic maps of the hydrological network, geology, type of soil, and slopes were created and analysed in order to estimate the specific characteristics of the whole basin.

3. METHODOLOGY

For modeling purposes, the main physiographic characteristics were estimated for each sub-basin, including drainage area, mean elevation and also spatially discretization of the basin, using the ArcGIS 10 interface.

In this paper, the application of the "abcd" water balance model is studied, by implemented it on both a daily and a monthly basis. For the estimation of mean areal rainfall, the Thiessen method was applied (Figure 2b). The individual weights are multiplied by the station observation and the values are summed to obtain the areal average precipitation. Evapotranspiration is a process depending on solar radiation, air temperature, relative humidity and wind speed. In this study, daily and monthly evapotranspiration time series was estimated using the FAO Penman-Monteith method (FAO-PM). This method is recommended, as the standard ET_0 method, with which the evapotranspiration of a hypothetical reference vegetated field is unambiguously determined (Allen et al., 1998). The method has been reported to be able to provide consistent ET_0 values in many regions and climates (Allen et al., 2005; Allen et al., 2006) and it has long been accepted worldwide, as a good ET_0 estimator when compared with others methods, especially for daily computations (e.g. Chiew et al., 1995; Jacobs and Satti, 2001; Temesgen et al., 2005). Concerning the available hydrological data, which were used for the hydrologic modeling, those in a daily time step refer to the water year 2009 - 2010 for Oinountas (Kladas), Rasina I (Koumousta), Rasina II (Airport) subbasin, while those in a monthly time step (for Vivari subbasin) are provided for the period 2006-2009.The four subbasins are presented in Figure 4.

The "abcd" model is schematically comprised of two storage compartments: soil moisture and groundwater (Figure 3). The soil moisture storage (S) receives water from precipitation (P) and loses water through potential evapotranspiration (ET), surface runoff (DR) and groundwater recharge (GR). The groundwater compartment gains water from recharge and loses water as discharges. The total streamflow is the sum of surface runoff from the soil moisture and groundwater discharge.

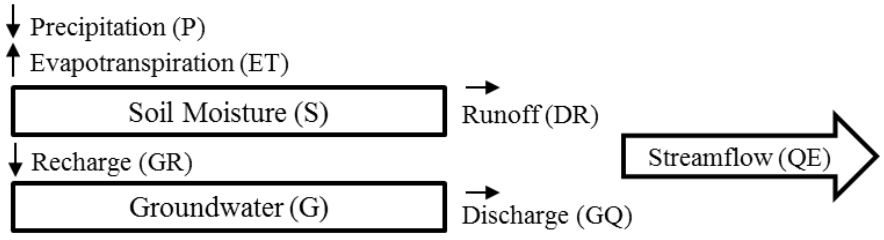

Figure 3. Streamflow simulation by Thomas (1981) - "abcd" model

There are four parameters governing the model behavior:
a: controls the amount of runoff and recharge that occurs when the soil is not saturated.
b: controls the saturation level of the soil.
c: defines the ratio of groundwater recharge to surface runoff.
d: controls the rate of groundwater discharge.

The calibration of the model parameters was based on the maximization of the Nash-Sutcliffe coefficient value (Nash and Sutcliffe, 1970) via the Excel Solver.

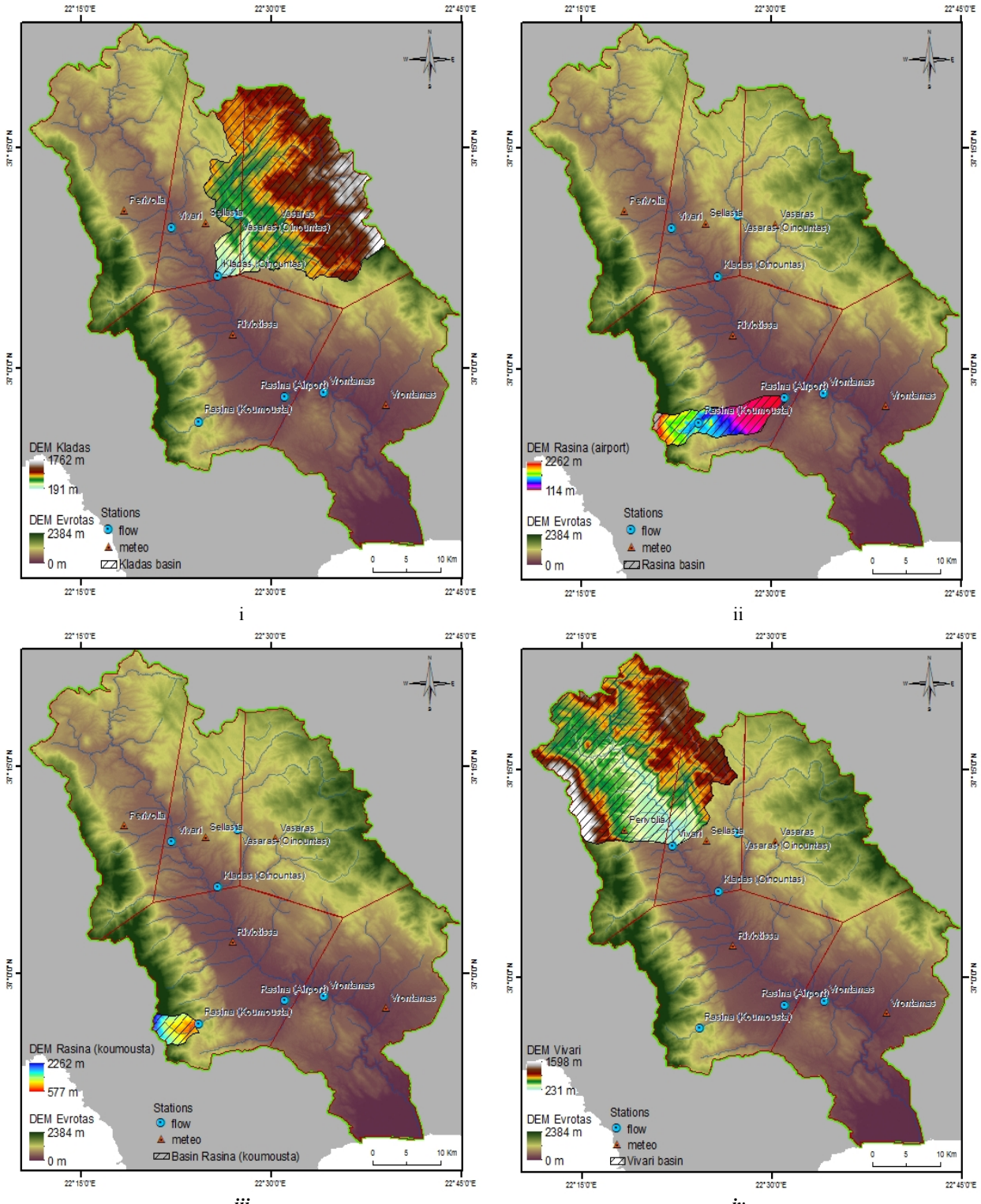

Figure 4. (i) Oinountas (Kladas) subbasin, (ii) Rasina II (Airport) subbasin, (iii) Rasina I (Koumousta) subbasin, (iv) Vivari subbasin

Additionally, in order to demonstrate the different characteristics per subbasin, a one-factor-at-a-time (OAT/OFAT) sensitivity analysis was carried out in the model parameters specifically and separately for each subbasin. In order to quantify what effect produces a change in the model parameters to the efficiency coefficient (EC), the sensitivity was estimated by altering the optimal values of one parameter in equal percentages (Figure 6) and calculating the change in one output (e.g., mean discharge).

4. RESULTS

Results reveal that in both daily and monthly application of the "abcd" model, the values of N-S efficiency coefficient are satisfactory. More specifically, Nash index is greater than 0.6 in all cases; with its best values (>0.8) in Kladas and Vivari subbasins, providing a reliable model, proper for all subbasins (see EC values in Table 1).

Table 1. Values of basic parameters for each subbasin after calibration of the model

Parameter	Oinountas (Kladas)	Rasina I (Koumousta)	Rasina II (Airport)	Vivari
a	0.9995	0.9662	0.8852	0.9906
b	732.30	995.99	503.92	1500.00
c	0.41	0.95	0.90	0.77
d	0.00	0.00	0.00	0.00
S_0	312.88	210.03	180.35	100.00
G_0	50.00	80.00	80.00	40.00
EC (N-S)	0.85	0.71	0.62	0.83

Figure 5 presents the observed versus simulated discharges for (a) Kladas, (b) Rasina I (Koumousta), (c) Rasina II (Airport) and (d) Vivari stage recording stations, for the step of calibration. The fit between the simulated and the observed discharge denotes adequate agreement, as indicated by the values of the EC.

Regarding to the sensitivity analysis, the simulation output that has been controlled over the sensitivity analysis was the change of the average discharges, by changing one-at-a-time model parameter (Figure 6). The results of sensitivity analysis are concentrated as follows:

- The amount of runoff and recharge that occurs when the soil is not saturated (parameter a) and the saturation level of the soil are the most crucial parameters for Kladas basin, while the contribution to the river of the groundwater storage (parameter c) is found to be lower (0.40) than the rest subbasins.
- For the Rasina basins (I-Koumousta, II-Airport), the most important parameter affecting the model is the fraction of streamflow coming from groundwater (parameter c), while change in the potential evapotranspiration and soil water storage does not entail significant change.
- The Vivari basin seems to be more "sensitive" for an up to 30% increase or decrease of the value of the parameter a, while with further percentage reduction in parameters the most critical parameter is c. The potential evapotranspiration and storage of soil moisture (parameter b) seems to be a minor factor at that location.
- The initial value of G(0) [not shown] and S(0) seems not to affect any model.

5. SUMMARY AND CONCLUSIONS

The "abcd" water balance model implementation in four subbasins of Evrotas River and in monthly and daily temporal scale showed a satisfactory agreement with field observations. The discharge simulation can be characterized as adequate, taking into account the use of a simplistic model.

- Sensitivity analysis in the parameters a, b, c, d, S(0), G(0) reveals that, in all cases, either parameter 'a' or 'c' is the most crucial.

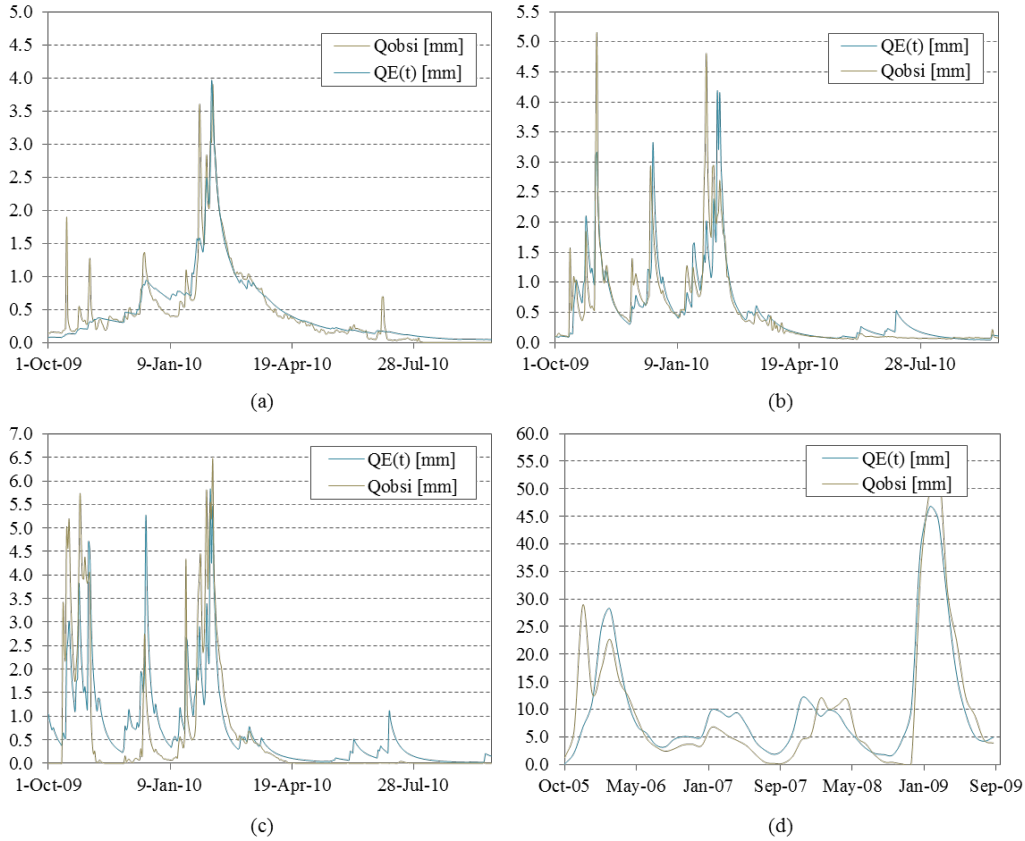

Figure 5. Simulated and observed discharge for (a) Kladas (daily runoff data), (b) Rasina I (Koumousta) (daily runoff data), (c) Rasina II (Airport) (daily data) and (d) Vivari stations (monthly runoff data)

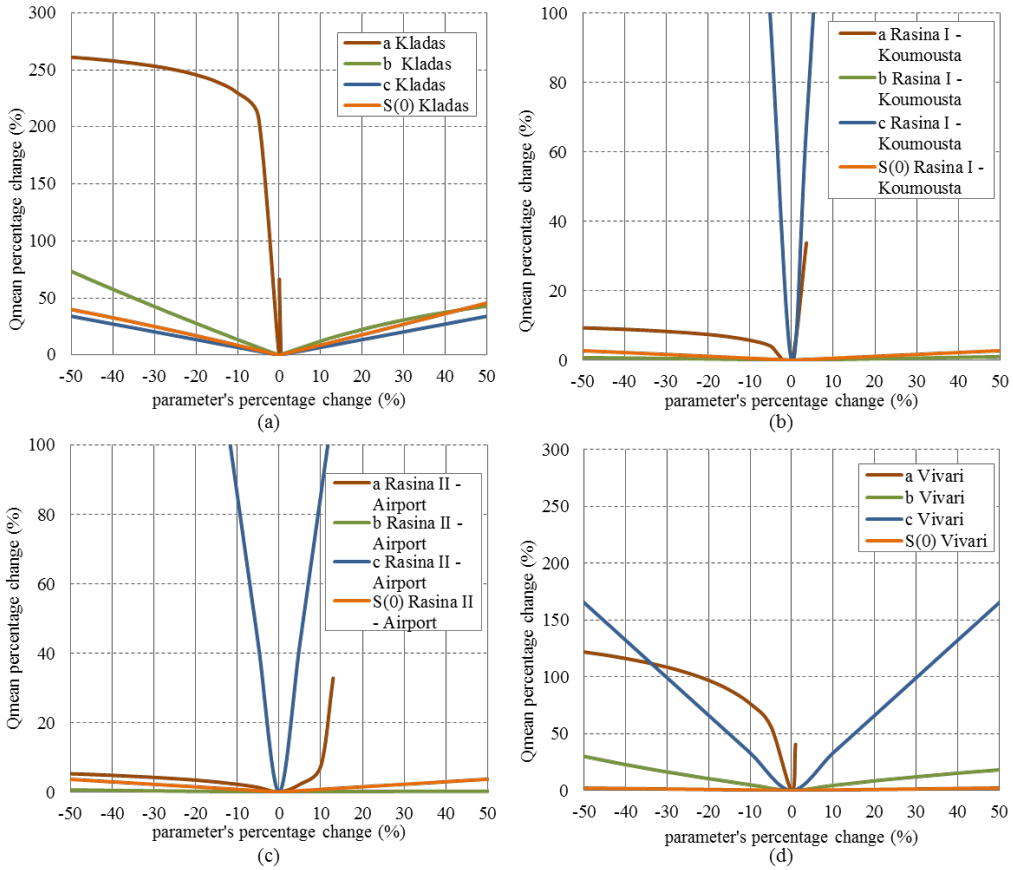

Figure 6. OAT Sensitivity analysis results for the subbasins of (a) Kladas, (b) Rasina I (Koumousta), (c) Rasina II (Airport) and (d) Vivari

- As expected, Rasina I and Rasina II seem to follow similar patterns, however, in Rasina I, which is a mountainous basin, parameter ‘a’ is comparatively more important.
- Concerning future research, additional daily flow data should be taken into account, an aspect that may give a more reliable simulation output, as in the current research the model applied to just one hydrological year. Moreover, extra performance indicators can be introduced for the evaluation of the “abcd” model's suitability in both temporal scales for the examined area.

REFERENCES

Al-Lafta, H.S., Al-Tawash, B.S. and Al-Baldawi, B.A., 2013. Applying the “abcd” Monthly Water Balance Model for Some Regions in the United States. Advances in Physics Theories and Applications Volume, 25, pp.36-47.

Allen, R.G., Pereira, L.S., Raes, D. and Smith, M., 1998. Crop evapotranspiration-Guidelines for computing crop water requirements-FAO Irrigation and drainage paper 56. FAO, Rome, 300(9), p.D05109.

Allen, R.G., Clemmens, A.J., Burt, C.M., Solomon, K. and O’Halloran, T., 2005. Prediction accuracy for projectwide evapotranspiration using crop coefficients and reference evapotranspiration. Journal of Irrigation and Drainage Engineering, 131(1), pp.24-36.

Allen, R.G., Pruitt, W.O., Wright, J.L., Howell, T.A., Ventura, F., Snyder, R., Itenfisu, D., Steduto, P., Berengena, J., Yrisarry, J.B. and Smith, M., 2006. A recommendation on standardized surface resistance for hourly calculation of reference ET o by the FAO56 Penman-Monteith method. Agricultural Water Management, 81(1), pp.1-22.

Antonakos, A. and Lambrakis, N., 2000. Hydrodynamic characteristics and nitrate propagation in Sparta aquifer. Water Research, 34(16), pp.3977-3986.

Chiew, F.H.S., Kamaladasa, N.N., Malano, H.M. and McMahon, T.A., 1995. Penman-Monteith, FAO-24 reference crop evapotranspiration and class-A pan data in Australia. Agricultural Water Management, 28(1), pp.9-21.

Gamvroudis, C., Nikolaidis, N.P., Tzoraki, O., Papadoulakis, V. and Karalemas, N., 2015. Water and sediment transport modeling of a large temporary river basin in Greece. Science of the Total Environment, 508, pp.354-365.

Jacobs, J.M., Satti, S.R. and Fitzgerald, J.M., 2001. Evaluation of reference evapotranspiration methodologies and AFSIRS crop water use simulation model. Publ. SJ2001-SP8. Available online at http://www.sjrwmd. com/programs/outreach/pubs/ techpubs/sj2001-sp8. pdf (Verified 20 October, 2003).

Martinez, G.F. and Gupta, H.V., 2010. Toward improved identification of hydrological models: A diagnostic evaluation of the “abcd” monthly water balance model for the conterminous United States. Water Resources Research, 46(8).

Nash, J.E. and Sutcliffe, J.V., 1970. River flow forecasting through conceptual models part I—A discussion of principles. Journal of hydrology, 10(3), pp.282-290.

Temesgen, B., Eching, S., Davidoff, B. and Frame, K., 2005. Comparison of some reference evapotranspiration equations for California. Journal of irrigation and drainage engineering, 131(1), pp.73-84.

Thomas, H.A., 1981. Improved methods for national water assessment. Report WR15249270, US Water Resource Council, Washington, DC.

Thomas, H.A., Marin, C.M., Brown, M.J. and Fiering, M.B., 1983. Methodology for water resource assessment, report to US Geological Survey. Rep. NTIS, pp.84-124163.

Tzoraki, O., Papadoulakis, V., Christodoulou, A., Vozinaki, E., Karalemas, N., Gamvroudis, C. and Nikolaidis, N.P., 2011. Hydrologic modelling of a complex hydrogeologic basin: Evrotas River Basin. In Advances in the Research of Aquatic Environment (pp. 179-186). Springer Berlin Heidelberg.

Tzoraki, O., Nikolaidis, N.P., Keldjsen, T., Cooper, D., Gamvroudis, C., Gallart, F., Froebrich, J., Querner, E., 2013. Flood Generation and Classification of a semi-arid Intermittent Flow Watershed: Evrotas river, Intl. J. River Basin Management Vol. 11, No. 1, pp. 1–16

Querner, E.P., Froebrich, J., Gallart, F., Prat, N., Cazemier, M., Tzoraki, O., 2016. Simulating stream flow variability in temporary streams using a coupled groundwater – surface water model. Hydrological Sciences Journal, Vol. 1, Issue 1, 2 January 2016, Pages 146-161 doi: 10.1080/02626667.2014.983514

Proceedings of the 10th World Congress of EWRA 'Panta Rhei', 5-9 July 2017, Athens, Greece
© 2017 *European Water Resources Association*

Multivariate modelling of meteorological droughts

E. Iliopoulos[1], V. Tsakiris[2], H. Vangelis[1], D. Tigkas[1] and G. Tsakiris[1*]
[1] *Centre for the Assessment of Natural Hazards and Proactive Planning, School of Rural and Surveying Engineering, National Technical University of Athens, Greece*
[2] *Department of Civil and Environmental Engineering, Imperial College London, United Kingdom*
[*] *e-mail: gtsakir@central.ntua.gr*

Abstract: Drought is conventionally expressed as meteorological, hydrological and agricultural, dependent on the affected system and the variables used in the analysis. The main dimensions of the meteorological drought, apart from severity, are the duration of the event and the spatial extent of the affected area. The study presented in this paper attempts to perform frequency analysis for the pairs severity-duration and severity-areal extent, using 2D-Archimedean Copulas. The Gumbel-Hougaard, the Clayton and the Frank families of copulas have been tested. The proposed methodology is applied to the eastern part of the island of Crete- Greece. The area under study is divided in 1328 squares of 4km^2 each. The sample of 30 years of precipitation and temperature data from 9 meteorological stations is reproduced 9 times. The Reconnaissance Drought Index is used for estimating the severity of each drought event. The duration is represented by the number of years under drought, whereas the areal extent is estimated by the number of squares under drought. The proposed methodology proves to be simple and practical and can contribute to more realistic decisions on measures against droughts by authorities and stakeholders.

Key words: Meteorological droughts, multivariate modelling, marginal probability distributions, drought severity, Reconnaissance drought index, Crete island

1. INTRODUCTION

Drought is a recurrent natural hazardous phenomenon affecting most parts of the world. Drought is conventionally expressed as meteorological, hydrological and agricultural, dependent on the affected system and the variables used in the analysis. The main dimensions of the meteorological drought are the severity and duration of the event, and the spatial extent of the affected area. Thus, for the frequency analysis it is appropriate to take into account all the three dimensions.

The study presented in this paper attempts to perform frequency analysis of the pairs "severity-duration" and "severity-areal extent" using 2D-Archimedean Copulas. Using meteorological data from the eastern part of the island of Crete, the 2D Gumbel-Hougaard, the Clayton and the Frank families of copulas have been tested.

2. BASIC NOTIONS

Droughts, as several other natural hazards, are multidimensional phenomena. Since drought episodes are stochastic in nature, numerous studies have been reported analysing droughts using probabilistic theories (Gupta and Duckstein 1975; Kendall and Dracup 1992; Rossi et al. 1992; Vangelis et al. 2011; Bonaccorso et al. 2015; and many others). There are several studies in the literature analysing the various dimensions of drought (e.g. Dalezios et al. 2000; Reddy and Ganguli 2012; Kim et al. 2011; Reddy and Singh 2014; Saghafian et al. 2003; Shiau and Modarres 2009; Todisco et al. 2013). Most of these studies have analysed droughts either as univariate phenomenon or they have analysed each drought characteristic separately. In this context, the double frequency analysis seems more appropriate provided that the probability distributions (marginal distributions), describing each of the variables (dimensions) analysed, belong to the same family of probability

distributions.

It is easily understood that it is most unlikely that the both dimensions of drought (e.g. severity and duration or severity and areal extent) follow the same type of probability distribution in all possible applications. As has been shown in many occasions, the drought variables follow different probability distributions. Therefore, to overcome this problem, the copula approach can be implemented. As known copulas are functions joining univariate distribution functions from any family into a single multivariate distribution function. From the first introduction of copulas by Sklar (1959), several important studies have been published with applications in various fields, among which is also hydrology (Salvadori et al. 2007 and Genest and Favre 2007). Interesting applications on droughts have been also made by Shiau (2006), Yusof et al. (2013), Chen et al. (2013), Bazrafshan et al. (2015), Huang et al. (2015), Vergni et al. (2015) and others.

There are several types of copula functions, which are described in books (e.g. Nelsen 1999). The most popular copulas for hydrologic analysis are those of the Archimedean family, which are characterised by their simple structure and strong representativeness (Huang et al. 2015; Tsakiris et al. 2015).

3. APPLICATION

The application presented in this paragraph is partially based on the data used in a recent paper (Tsakiris et al. 2016). The area studied is the eastern part of the island of Crete which is one of the main drought prone areas of Greece. The area was divided into 1328 squares of 4 km^2 each. The monthly meteorological data, concerning precipitation and temperature, collected from 9 stations in the area, cover the period of 30 years (1962-1991). The meteorological data were transferred to the center of the squares using the method of inverse distance (Wei and McGuiness, 1973). As a result, annual series of data were produced, creating 2 matrices 1328 x 30.

The available data were reproduced for additional 270 years using a simple stochastic process (AR 1). The synthetic time series for areal average precipitation and potential evapotranspiration are presented in Figures 1 and 2.

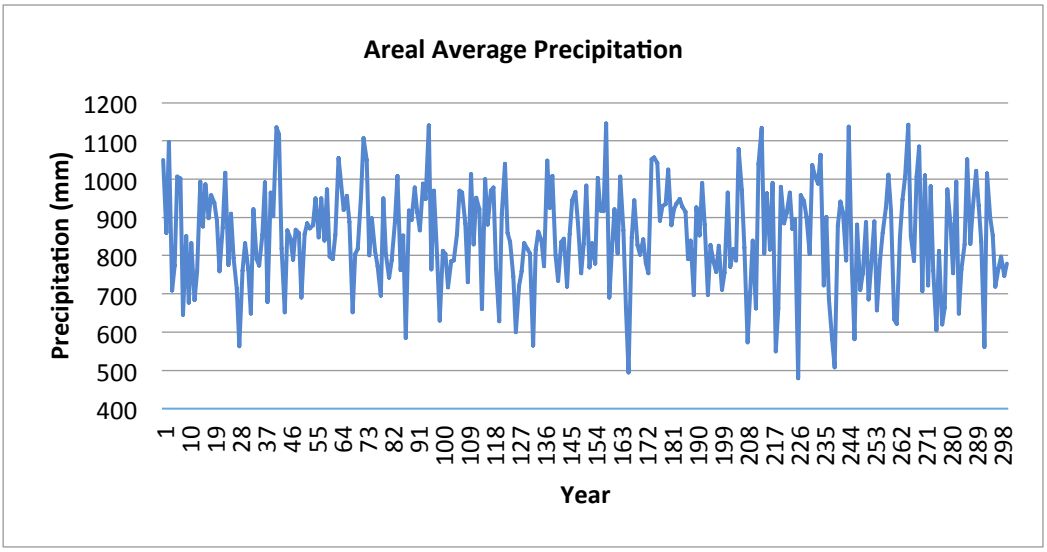

Figure 1. The annual precipitation of the area generated from the 30-year sample

Regarding the dimensions of drought (severity, areal extent and duration) were calculated for all 300 years. The severity was estimated using the Reconnaissance Drought Index (RDI; Tsakiris et al. 2007). As known, RDI has three expressions, using precipitation and potential evapotranspiration data. The areal extent is represented by the total number of squares under drought whilst duration by the number of consecutive years under drought. Figures 3 and 4 depict the severity and areal

extent whereas the duration dimension is presented in tables not presented in this short version of the paper.

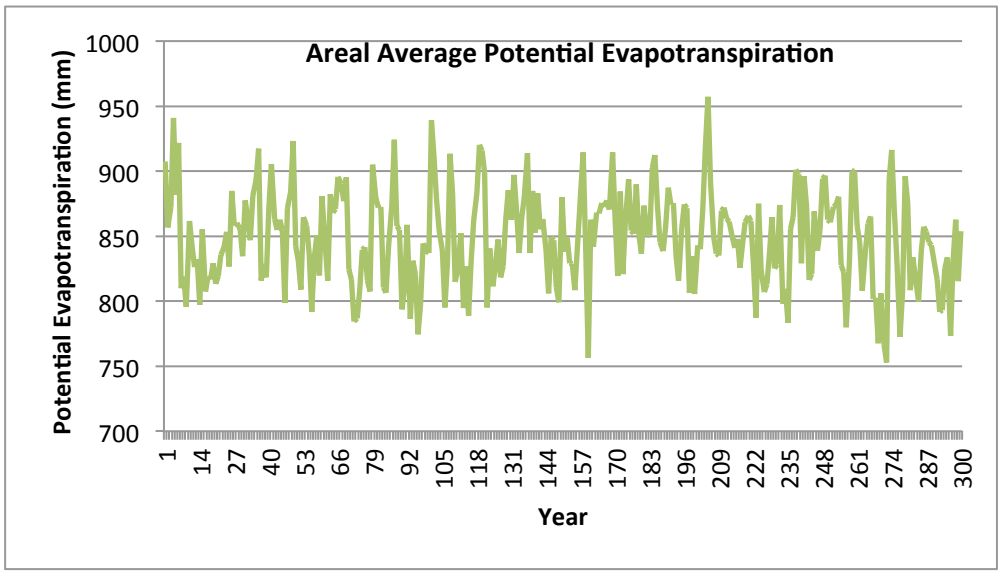

Figure 2. The annual potential evapotranspiration of the area generated from the 30-year sample

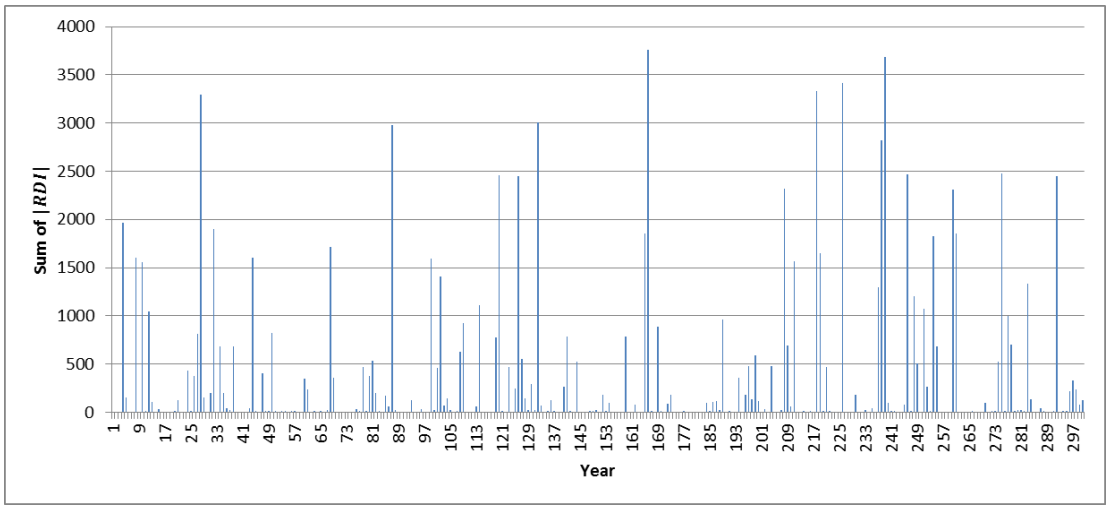

Figure 3. The severity of drought for the 300 years represented by the sum of absolute RDI values

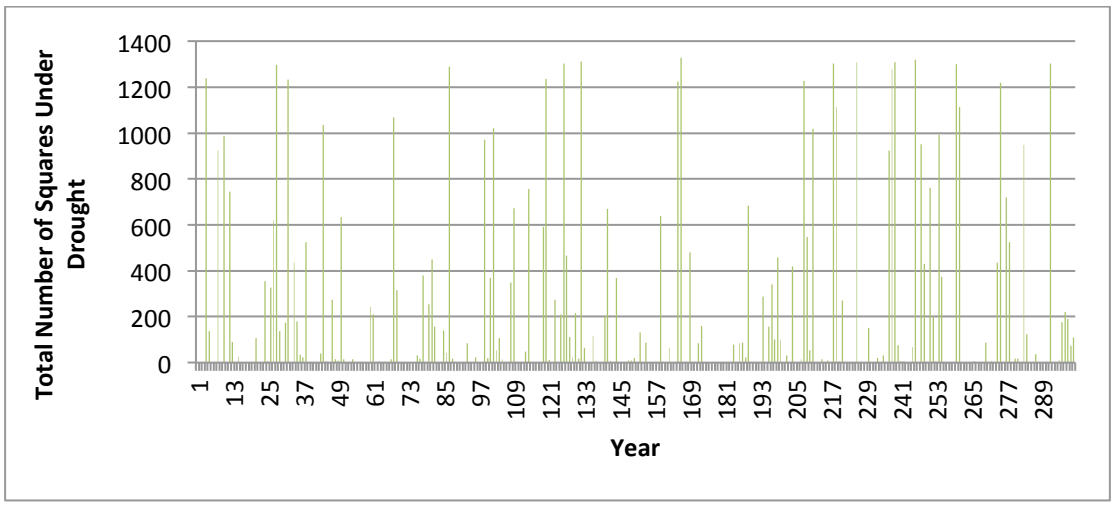

Figure 4. The areal extent for the 300 years represented by the total number of squares under drought

The multivariate modelling of droughts was achieved by using 2D Archimedean copulas for the pairs severity-duration, and severity-areal extent. The copulas used, are the Gumbel-Hougaard, the Clayton and the Frank, with equations presented in Table 1.

Table 1. Joint probability function of Archimedean copulas

Archimedean Copula	Joint Probability Distribution Function
Gumbel–Hougaard	$F_{x,y} = C_\theta(F(X),F(Y)) = \varphi^{-1}\left(\varphi(F(X)) + \varphi(F(Y))\right) = \exp\left\{\left[(-lnF(x))^\theta + (-lnF(Y))^\theta\right]^{\frac{1}{\theta}}\right\}$
Clayton	$F_{x,y} = C_\theta(F(X),F(Y)) = \varphi^{-1}\left(\varphi(F(X)) + \varphi(F(Y))\right) = \left\{\left[(F(x))^{-\theta} + (F(Y))^{-\theta} - 1\right]^{\frac{1}{\theta}}\right\}$
Frank	$F_{x,y} = C_\theta(F(x),F(y)) = -\theta^{-1}\ln\left\{1 + \frac{\left(e^{-\theta F(x)} - 1\right)\left(e^{-\theta F(y)} - 1\right)}{e^{-1} - 1}\right\}$

The parameter θ was estimated through the Kendall's τ as shown in Table 2 for all three Archimedean copulas (Tsakiris et al. 2016). The following table gives the expressions of the generator φ and the Kendall's τ,for the above most popular Archimedean families, such as Gumbel-Hougaard, Clayton and Frank.

Table 2. The generator and Kendall's τ, for the three most popular Archimedean families

Family	Generator φ	Kendall's τ
Gumbel-Hougaard	$\left(-\ln\left(t\right)\right)^\theta$	$1 - \frac{1}{\theta}$
Clayton	$\left(t^{-\theta} - 1\right)/\theta$	$\frac{\theta}{\theta + 2}$
Frank	$-\ln\left(\frac{e^{-\theta t} - 1}{e^{-\theta} - 1}\right)$	$1 - \frac{4}{\theta} + \frac{4D_1\left(\theta\right)}{\theta}$

In Table 2, $D_1\left(\theta\right) = \int_0^\theta \left(\frac{x}{\theta}\right) \Big/ \left(e^x - 1\right) dx$, which is the first Debey function.

4. RESULTS AND DISCUSSION

For the construction of Archimedean copulas for the pairs severity - areal extent and severity - duration, the following results were derived (Table 3).

Table 3. Parameter θ estimation through Kendall's τ

Pair	Kendall's τ	$\theta_{Gumbel\text{-}Hougaard}$	$\theta_{Clayton}$	θ_{Frank}
Severity-Areal Extent	0.598	2.488	2.975	1.420
Severity-Duration	0.191	1.236	0.472	1.380

Based on the results of Frechet-Hoeffding test, it was concluded that Frank copula was unsuitable for modelling the set of data used whereas Gumbel- Hougaard copula seems to perform more successfully.

The 3D graphs presented on the Figures 5 and 6 illustrate the Gumbel- Hougaard copulas for the pair Severity-Areal Extent and the Severity-Duration, respectively. Similarly, 3D graphs have been produced for the Clayton copulas for the same pairs, respectively.

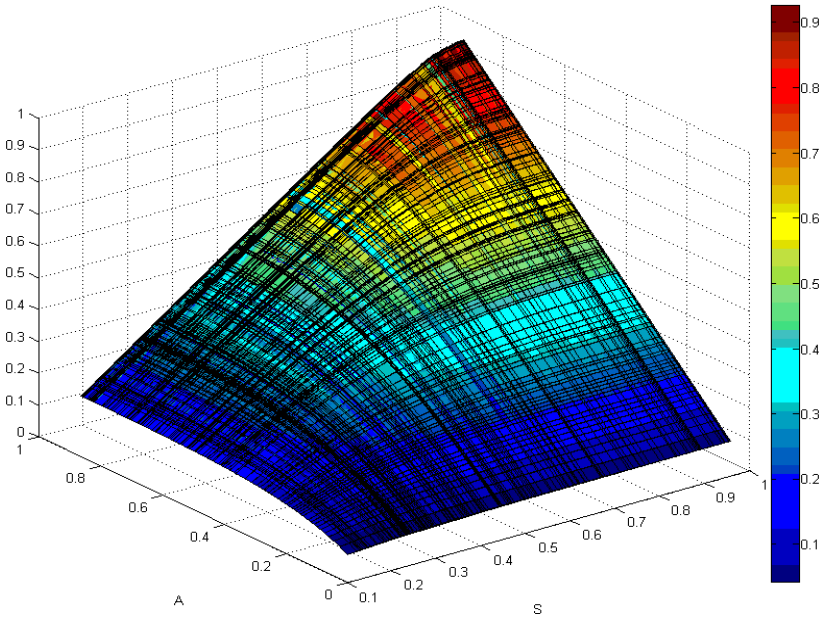

Figure 5. Gumbel – Hougaard copula for Severity – Areal Extent

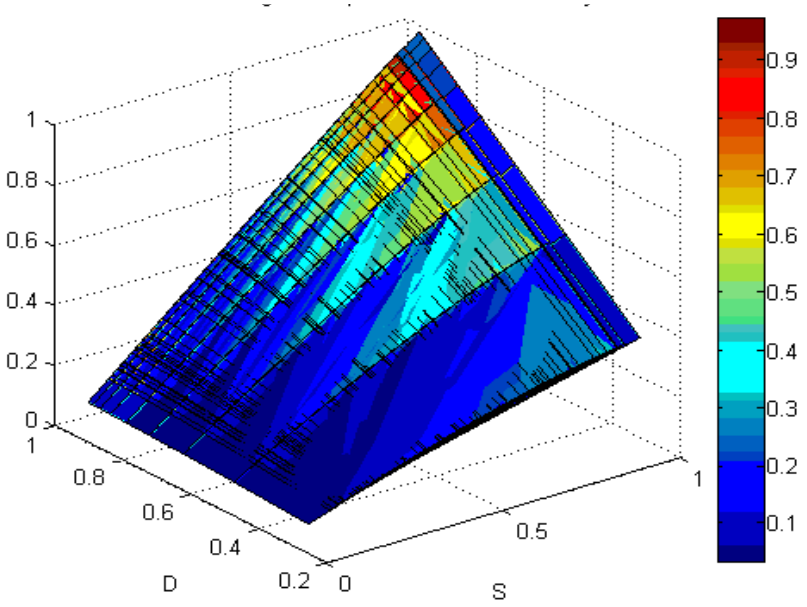

Figure 6. Gumbel – Hougaard copula for Severity – Duration

Finally, Figures 7 and 8 show a convenient way for calculating the joint probability for both pairs severity-areal extent and severity-duration. In the graphs S stands for severity (represented by absolute RDI value), *A* for the areal extent (represented by the total number of squares under drought), and *D* for the duration (in years).

5. CONCLUDING REMARKS

Using the Archimedian copulas, the joint distribution functions were derived for the pairs of drought events, severity-areal extent and severity-duration. It is concluded that by this 2D frequency analysis, a more comprehensive assessment of droughts can be achieved. As a result, the proposed approach can assist authorities and stakeholders to base their preparedness planning on more secure information by considering more than one dimension of drought.

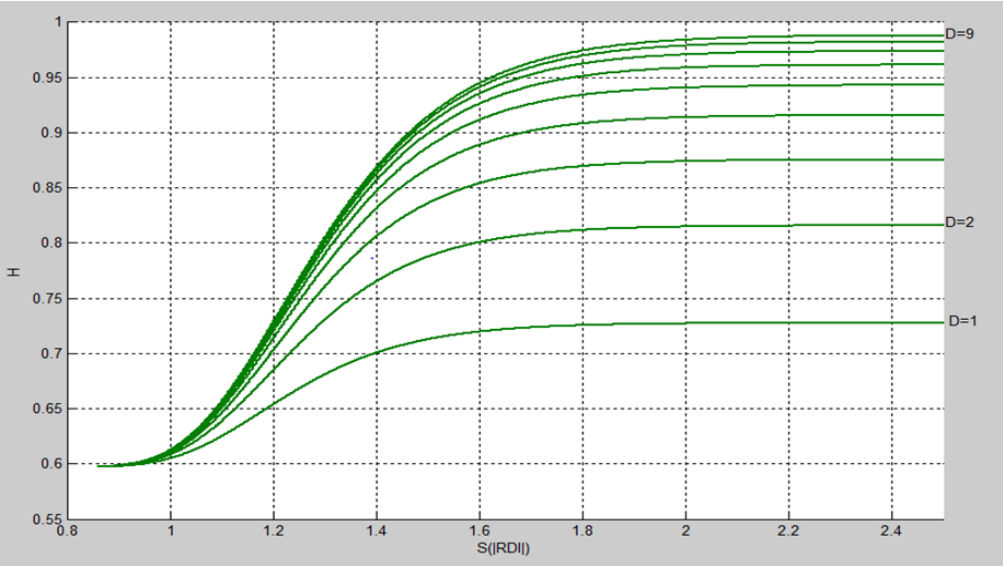

Figure 7. Joint cumulative probability distribution H for Severity – Duration

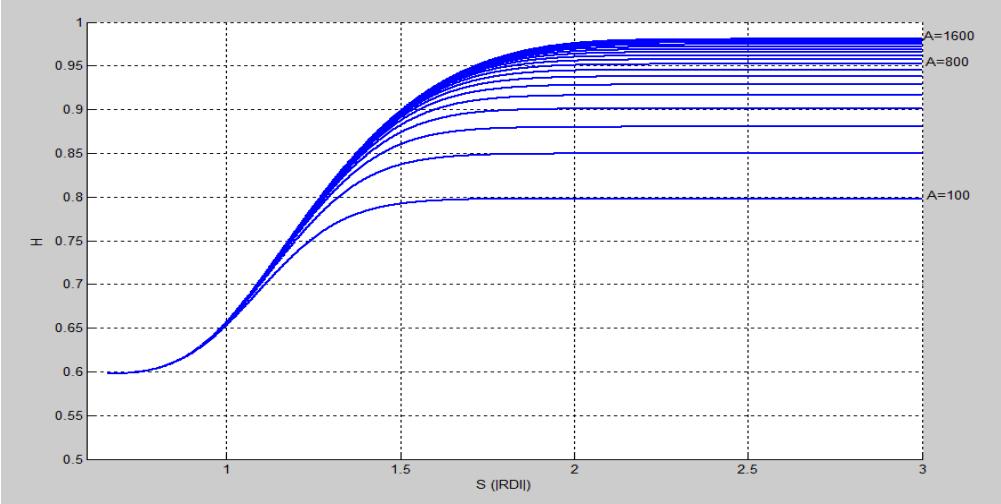

Figure 8. Joint cumulative probability distribution H for Severity – Areal extent

REFERENCES

Bazrafshan J, Nadi M, Ghorbani K (2015) Comparison of Empirical Copula-Based Joint Deficit Index (JDI) and Multivariate Standardized Precipitation Index (MSPI) for Drought Monitoring in Iran. Water Resources Management 29(6):2027-2044

Bonaccorso B, Peres D, Castano A, Cancelliere A (2015) SPI-based probabilistic analysis of drought areal extent in Sicily. Water Resources Management 29:459-470

Chen L, Singh VP, Guo S, Mishra AK, Guo J (2013) Drought analysis using copulas. Journal of Hydrologic Engineering 18(7):797-808

Dalezios NR, Loukas A, Vasiliades L, Liakopoulos E (2000) Severity-duration-frequency analysis of droughts and wet periods in Greece. Hydrological Sciences Journal 45(5):751-769

Ganguli P, Reddy J (2012) Risk assessment of droughts in Gujarat using bivariate copulas. Water Resources Management 26:3301-3327

Genest C, Favre AC (2007) Everything you always wanted to know about copula modeling but were afraid to ask. Journal of Hydrologic Engineering 12(4):347-368

Gupta VK, Duckstein L (1975) A stochastic analysis of extreme droughts. Water Resources Research 11(2):221-228

Huang S, Huang Q, Chang J, Chen Y, Xie Y (2015) Copulas-based drought evolution characteristics and risk evolution in a typical arid and semi-arid region. Water Resources Management 29(5):1489-1503

Reddy M, Ganguli P. (2012) Application of copulas for derivation of drought severity–duration–frequency curves. Hydrological Processes 26(11):1672-1685

Kendall DP, Dracup JA (1992) On the generation of drought events using an alternating renewal reward model. Stochastic Hydrology and Hydraulics 6(1):55-68

Kim DH, Yoo C, Kim TW (2011) Application of spatial EOF and multivariate time series model for evaluating agricultural drought vulnerability in Korea. Advances in Water Resources 34(3):340-350

Nelsen RB (1999) An introduction to copulas. Springer-Verlag, Berlin - New York

Reddy MJ, Singh VP (2014) Multivariate modeling of droughts using copulas and meta-heuristic methods. Stochastic Environmental Research and Risk Assessment 28(3):475-489

Rossi G, Benedini M, Tsakiris G, Giakoumakis S (1992) On regional drought estimation and analysis. Water Resources Management 6(4):249-277

Saghafian B, Shokoohi A, Raziei T (2003) Drought spatial analysis and development of severity-duration-frequency curves for an arid region. International Association of Hydrological Sciences 278:305-311

Salvadori G, De Michele C, Kottegada NT, Rosso R (2007) Extremes in Nature. An approach Using Copulas. Water Science and Technology Library, Springer, vol. 56

Shiau JT (2006) Fitting drought duration and severity with two-dimensional copulas. Water Resources Management 20:795-815

Shiau JT, Modarres R (2009) Copula-based drought severity-duration-frequency analysis in Iran. Meteorological Applications 16(4):481-489

Singh K, Singh VP (1991) Derivation of bivariate probability density functions with exponential marginals. Stochastic Hydrology and Hydraulics 5(1):55-68

Sklar A (1959) Fonctions de répartition à n dimensions et leurs marges. Publ. Inst. Statist. Univ. Paris 8:229-231 (in French)

Song S, Singh VP (2010a) Frequency analysis of droughts using the Plackett copula and parameter estimation by genetic algorithm. Stoch Environ Res Risk Assess 24(5):783–805

Song S, Singh VP (2010b) Metaelliptical copulas for drought frequency analysis of periodic hydrologic data. Environ Res Risk Assess 24(3):425–444

Tigkas D, Vangelis H, Tsakiris G, 2015. DrinC: a software for drought analysis based on drought indices. Earth Science Informatics 8(3):697-709

Todisco F, Mannocchi F, Vergni L (2013) Severity–duration–frequency curves in the mitigation of drought impact: an agricultural case study. Natural Hazards 65(3):1863-1881

Tsakiris G, Nalbantis I, Vangelis H, Verbeiren B, Huysmans M, Tychon B, Jacquemin I, Canters F, Vanderhaegen S, Engelen G, Poelmans L, De Becker P, Batelaan O (2013) A System-based Paradigm of Drought Analysis for Operational Management. Water Resources Management 27(15):5281-5297

Tsakiris G, Pangalou D, Tigkas D, Vangelis H (2007a) Assessing the Areal Extent of Drought. Proceedings of EWRA Symposium “Water Resources Management: New Approaches and Technologies”, Chania - Greece, 14 - 16 June 2007, pp. 59-66

Tsakiris G, Pangalou D, Vangelis H (2007b) Regional Drought Assessment Based on the Reconnaissance Drought Index (RDI). Water Resources Management 21(5):821-833

Tsakiris G, Vangelis H (2005) Establishing a drought index incorporating evapotranspiration. European Water 9-10:3-11

Tsakiris G, Kordalis N, Tsakiris V (2015) Flood Double Frequency analysis: 2D-Archimedean copulas vs bivariate probability distributions. Environmental Processes 2(4):705-716

Tsakiris G (2017) Drought risk assessment and management. Water Resources Management 31:3083–3095

Tsakiris G, Kordalis N, Tigkas D, Tsakiris V and Vangelis H (2016) Analysing drought severity and areal extent by 2D Archimedean copulas. Water Resources Management 30(15):5723-5735

Vangelis H, Spiliotis M, Tsakiris G (2011) Drought Severity Assessment Based on Bivariate Probability Analysis. Water Resources Management 25(1):357-371

Vangelis H, Tigkas D, Tsakiris G (2013) The effect of PET method on Reconnaissance Drought Index (RDI) calculation. Journal of Arid Environments 88:130-140

Vergni L, Todisco F, Mannocchi F (2015) Analysis of agricultural drought characteristics through a two-dimensional copula. Water Resources Management 29(8):2819-2835

Wei TC, McGuinnes JL (1973) Reciprocal distances squared method. A computer technique for estimating areal precipitation. U.S. Department of Agriculture, ARS-NS-8, 1-23

Weiss G (2011) Copula parameter estimation by maximum-likelihood and minimum-distance estimators: a simulation study. Computational Statistics 26(1):31-54

Yusof F, Hui-Mean F, Suhaila J, Yusof Z (2013) Characterisation of drought properties with bivariate copula analysis. Water Resources Management 27(12):4183-4207

Zelenhastic E, Salvai A (1987) A method of streamflow drought analysis. Water Resources Research 23(1):156-168

Proceedings of the 10th World Congress of EWRA 'Panta Rhei', 5-9 July 2017, Athens, Greece
© 2017 *European Water Resources Association*

Evaluation of different global optimization algorithms for calibration of a daily hydrological model

H. Khozeymehnezhad[1*], S. Sadeghi-Tabas[2], M. Pourreza-Bilondi[1]
[1] *Department of Water Engineering, University of Birjand, Birjand, Iran*
[2] *Department of Civil Engineering, Iran University of Science and Technology (IUST), Tehran, Iran*
[*] *e-mail: hkhozeymeh@birjand.ac.ir*

Abstract: Hydrological Modelling can be a highly complex problem, particularly due to difficulties caused by multiple dominant discharge states. Since manual adjustment of parameters is a time-consuming and labour-intensive task, automatic calibration techniques are generally required to obtain reasonable estimates of model parameters. Thus, in this research we aim to compare and assess calibration of a conceptual daily rainfall-runoff model (Hymod) with three global optimization methods (GOMs). Also, a case study (Karaj River Basin) was selected to assess and present the results. Calibration was carried out based on four performance criteria (KGE, NS, R2 and RMSE) with three year periods for all three optimization methods. KGE, as a new extension of the widely used Nash–Sutcliffe efficiency (NSE) was applied in this study to analyse different components which constitute NSE. Results indicated that particle swarm optimization (PSO) may be significantly more efficient and robust and will be able to simulate daily runoff with better performance criteria. Thus this method is able to obtain optimal values more accurately and in a faster manner for the five parameters of hydrological models within a multidimensional parameter space, which could provide the best fit between observed and simulated runoff.

Key words: Optimization Methods, Rainfall-Runoff Model, Karaj River Basin

1. INTRODUCTION

Due to recent significance of catchment management, a crucial need has emerged for sufficient information and accurate estimation of rainfall and runoff in catchments. Considering this, various conceptual models have been presented. These models are comprised of certain parameters which must be estimated in accordance with observed data. Accurate estimation of these parameters is of significant importance such that future studies and researches are highly dependent on exactly how these parameters are estimated. One way for calibrating these models is to use auto-calibration (optimization algorithms) methods which are more accurate and faster than trial and error methods.

Optimization is considered as one of the main economical and management tools commonly used in various scenarios. The reason of these algorithms are famous is that on one hand they require a constant and fixed amount of resources and decreasing amounts in certain cases whereas on the other hand, demands and requirements are rapidly increasing. Many of these kinds of methods are influenced by nature and are based on one of various methods of random search. For this reason, they are known as evolutionary algorithms (EAs). Although these algorithms cannot ensure achieving global optimums, however, they can find a close to optimum solution with a high chance of success. The objective function in evolutionary algorithms is an informed function and the decision space is investigated intelligently. Usually, an objective function is computed for a combination of decision variables which result in various magnitudes and are used to achieve optimum solution.

Amongst well-known examples of evolutionary algorithms for optimization include Particle Swarm Optimization (PSO), Hybrid Genetic Algorithm and PSO (H-GA&PSO), and Firefly Algorithm. In this regard, Fan et al. (2006) proposed a method based on a combination of the simplex method with GA and PSO. Cao and Zahara (2007) applied a GA-PSO combination method for a multi-modal function. The floating genetic algorithm proposed by Wang and Qiu (2005) was

used for this method and mutation was determined using PSO. Then, an elitist policy was used to increase evolution rate. Also, Ghaderi et al. (2006) used SCE algorithm for performing auto-calibration of a rainfall-runoff model. Zhang et al. (2008) investigated the application of five optimization techniques; SCE, GA, PSO, Differential Evaluation (DE), and Artificial Immune Systems (ASI) for calibrating a hydrological model. Results indicated that GA performed better than all other algorithms for more than 2000 times model executions. However, for less than 2000 times model executions, PSO algorithm had better performance. Thus, considering computational complexity and time, PSO was preferred as the optimum method. Borhani and Farahmandfar (2011) calibrated a rainfall-runoff model using Honey-bees Mating Optimization (HBMO) and GA algorithms and eventually results were then compared and analysed.

This study proposes to perform a comprehensive analysis of five common optimization methods including: PSO, H-GA&PSO and Firefly to compare and assess calibration of a conceptual daily rainfall-runoff model (Hymod) for a river basin: Karaj located in Iran.

2. MATERIALS AND METHODS

2.1 Geographical location of study region

2.1.1 Karaj River Basin

The Karaj River Basin (KRB) is located in the mountainous region of Alborz province (51°03′ to 51°36′ longitude and 35°53′ to 36°10′ latitude) with a drainage area of 840 km^2 (Fig 1). AmirKabir Dam (Karaj Dam), one of the most important water resources of Tehran province, has been constructed on Karaj River. Karaj River annual mean flow rate at its entrance to Karaj Dam is 450×106 m^3; additionally 8.2 and 1450 CMS in this location were measured, respectively as minimum and peak annual temporal flow rates. This dam supplies water for municipal and cultural uses and electrical energy generation. It has been located 23 km north of Karaj and 63 km northwest of Tehran, and is under operation since 1963.

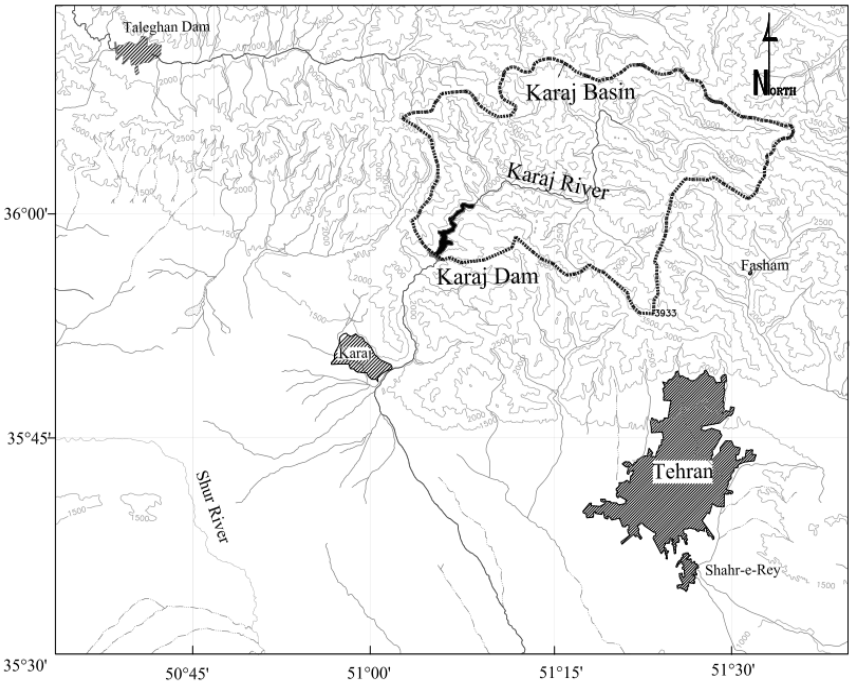

Figure 1. Geographical location of Karaj river basin, Iran

2.2 Evolutionary Optimization Algorithms

One method for model calibration is the use of auto-calibration methods (optimization algorithms) which are faster and more accurate than trial and error approaches. Optimization algorithms can be divided in two main categories; local search and global search. Local search algorithms are not suited for multi-modal functions since they may only be able to find local optimums. Thus we cannot ensure finding global optimum in these conditions (Liu, 2007).

On the other hand, global search algorithms are considered appropriate methods for multi-modal functions, especially for finding global optimum. Thus, researches in the area of optimizing calibration procedures for conceptual rainfall-runoff models are tended towards global search algorithms. Some common methods used for global search are investigated in this study. General methodology for all global search methods is finding a relatively wide range of possible values for each parameter. Then, a finite series of parameters are produced by the optimization algorithms. Each series is performed on the rainfall-runoff model. Performance of each series is evaluated according to the following criteria: correlation coefficient, Nash-Sutcliff coefficient, Mean Square Error, etc. The algorithm then iterates and model evolves until finally it converges and global optimum is found.

2.2.1 Particle Swarm Optimization Algorithm

The PSO algorithm was first proposed by Candy and Aberhart (1995). The algorithm is based on collective behaviour and is influenced by the orderly fashion of movement amongst nests of birds and fishes. Like other evolutionary techniques, the PSO algorithm starts with an initial population including potential solutions to be explored as part of the search space. Each particle has a velocity vector which can change the current position of that particle. In other words the velocity vector shows the direction that a certain particle will move towards. This mechanism is used to explore the search space.

2.2.2 Hybrid Genetic Algorithm & Particle Swarm Optimization

Meta-heuristic methods such as GA and PSO, influenced by nature and natural procedures are quite capable in obtaining the optimum cloud (range), for instance PSO has a high convergence rate and rapidly determines a cloud (space) containing optimum solution. Also, amongst other merits of these two algorithms are global search procedure in GA and local search in PSO, which in combination increase the accuracy of finding an optimal solution. Thus, a combinatory algorithm containing both merits of GA and PSO algorithms was proposed. This new procedure was named H-GA&PSO. Considering the capabilities of this new procedure, the scope for researches in this field is a rather vast one. The tableau for this algorithm is as follows:

1. Produce random initial population
2. Evaluate fitness of each particle
3. Register particle with best fitness
4. Update position of current and best global particle
5. Determine whether global and local optimums have changed. If so, go to step 7, otherwise, continue
6. Since global and local optimums have no changes, must escape local optimum (GA mutation is used for escaping local optimum)
7. Update all particles
8. Evaluate fitness of all particles
9. If maximum number of generations (evaluations) reached, then terminate algorithm, otherwise go to step 3.

2.2.3 Firefly Algorithm

The firefly algorithm is considered a swarm-based heuristic algorithm and was proposed by Yang for purposes of solving limited optimization problems. This algorithm is influenced by the behaviour of fireflies in nature. This procedure uses a population-based iterative approach with various factors (called fireflies). These fireflies are allowed to investigate the cost function space in a more efficient way compared to randomly distributed search procedures. Intelligent optimization techniques assume that the solution to a given optimization problem can be considered as a factor (firefly) where each firefly has a brightness level corresponding to its fitness. Consequently, each firefly can attract other fireflies (despite their gender) in order to explore the search space in a more efficient manner.

The firefly algorithm is based on three main principles, which are themselves influenced by the actual behaviour of fireflies in nature. These principles are as follows:

All fireflies are androgynous and are attracted to brighter fireflies.

The brightness of a firefly is dependent on its fitness. Also, brightness may drop as distance between two fireflies' increases. If a firefly cannot find a brighter firefly than itself, it moves randomly.

Brightness of a firefly is indicated using objective function (Yang, 2009).

This algorithm is based on creating global relations between particles and is thus, more suited for multi-modal optimization problems.

2.3 Rainfall-Runoff Model

Various models can be used for simulating rainfall-runoff procedure. All of these models require a minimum amount of observational data in order to simulate rainfall and runoff procedures. The model chosen for this study was the conceptual Hymod model for simulating output discharge scaled to daily time period. In order to perform calibration on the model using evolutionary algorithms, model parameters have been chosen as decision variables. Range of decision variables used in this study are provided in Table 1.

Table 1. Range of parameters for Hymod rainfall-runoff model.

Parameter (unit)	Symbol	Minimum	Maximum
Maximum humidity storage of basin (mm)	Cmax	1	500
Spatiality of soil humidity storage	Bexp	0.1	2
Distribution factor between two humidity storages	Alpha	0.1	0.99
Shelf life in laminar flow tank (day)	Rs	0.001	0.1
Shelf life in fast water tank (day)	Rq	0.1	0.99

The Hymod model has been previously used in various researches (Boyle, 2000, Vrugt et al., 2003, Wang and Qiu, 2005.) due to its high accuracy, simplicity, and low computational complexity.

2.4 Model Evaluation Criteria

In order to evaluate and assess the proposed model, the four Kling Gupta Efficiency (KGE) (Gupta et al., 2009) Nash-Sutcliff coefficient, Root Mean Square Error, and R-Square coefficient were used. The formulas for each of these criterions are shown below:

$$KGE = 1 - \sqrt{(cc-1)^2 + (\alpha-1)^2 + (\beta-1)^2} \tag{5}$$

$$R^2 = 1 - \frac{\sum_{i=1}^{N}(Qo_i - Qs_i)^2}{\sum_{i=1}^{N}(Qo_i - \overline{Qo})^2} \quad (6)$$

$$RMSE = \sqrt{\frac{1}{n}\sum_{i=1}^{n}(Qo_i - Qs_i)^2} \quad (7)$$

$$NSE = 1 - \frac{\sum_{i=1}^{n}(Qs_i - Qo_i)^2}{\sum_{i=1}^{n}(Qo_i - \overline{Qo})^2} \quad (8)$$

where Qoi indicates observed discharge, Qsi indicates simulated discharge, $\overline{Qo}$ shows average observed discharge, n is the number of observed data, , cc is the linear correlation coefficient between Qo and Qs, α is the ratio of standard deviation of Qs to standard deviation of Qo, and β is the ratio of the mean of Qs to mean of Qo.

3. RESULTS

The Hymod model was used and executed 500 times for each optimization algorithm. Firstly, decision variables (model parameters) were randomly sampled from the specified range and optimization algorithms were then executed and optimum parameters were obtained. Optimum parameters obtained for each algorithm are shown for each basin in Table 2.

Table 2. Optimum parameters obtained by optimization algorithms for Karaj river basin

Method	**Rq**	**Rs**	**Alpha**	**bexp**	**Cmax**
PSO	0.10	0.01	0.10	0.45	500
Hybrid GA&PSO	0.37	0.01	0.10	0.49	500
FireFly	0.10	0.001	0.14	1.50	327.95

Using values provided in above table, simulation parameters of daily discharge for Hymod model were calculated for each algorithm and for basin during calibration period. Resulting observational hydrograph of daily rainfall and discharge in a three year period are shown in figure 2 for basin.

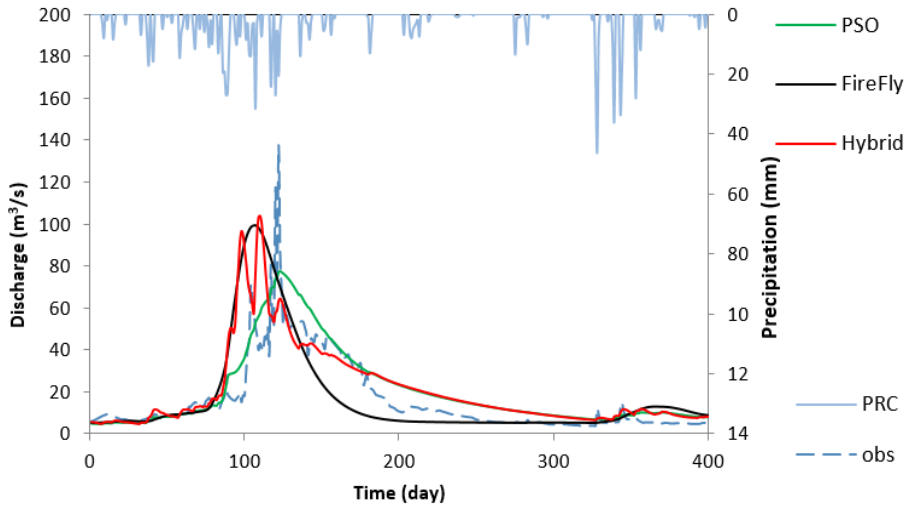

Figure 2. Observed and simulated daily discharge for Hymod model during calibration period using various algorithms for Karaj river basin (2006-2008)

In order to perform validation of optimum parameters (calibration period), a 2-year period was chosen for each basin. Observational and simulated hydrographs for the validation period are shown in figures 3 for Karaj river basin.

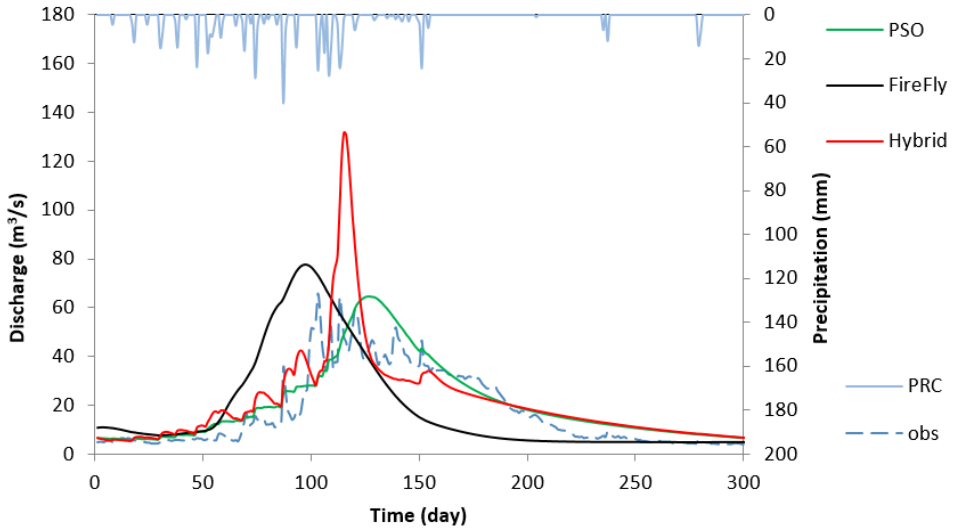

Figure 3. Observed and simulated daily discharge for Hymod model during validation period using various algorithms for Karaj river basin (2002-2003)

Also, simulated and observed discharge values using Kling Gupta, Root Mean Square Error, R-Square and Nash-Sutcliff criteria for evaluation are provided in Table 3.

Table 3. Comparison of simulated and observed discharge using model evaluation criteria for Karaj river basin

Period	***Method***	***NSE***	***RMSE***	***R2***	***KGE***
Calibration	PSO	0.64	8.04	0.68	0.82
	Hybrid GA&PSO	0.36	10.64	0.50	0.70
	Firefly	0.17	12.27	0.40	0.61
Validation	PSO	0.78	6.55	0.79	0.84
	Hybrid GA&PSO	0.54	9.55	0.65	0.73
	Firefly	0.10	13.34	0.33	0.57

As can be seen from Table 3, PSO had better results compared to H-GA&PSO and Firefly algorithms for both calibration and validation periods. These results indicate the superiority of the former algorithms in determining optimum parameters of Hymod rainfall-runoff model. This conclusion has also been achieved by various other related researches (investigating the application of PSO and SCE in calibrating hydrological models) (Chang et al., 2013, Matott et al., 2012, Wu et al. 2013, Zhang et al., 2008, Zhang et al., 2011). PSO is generally preferred due to its ability to perform direct searching and random searching and other advantages in the parameter space. These advantages clearly show why this algorithm is preferred (Zhang et al., 2008).

Convergence rate (convergence to optimum solution) for all studied algorithms were approximately the same with no significant difference. The main reason for this (as mentioned by Shawn et al. (2013)) is the small number of parameters. In the present study, H-GA&PSO had a relatively higher convergence rate, since according to Cheng et al. (2013). H-GA&PSO has the advantages of both GA and PSO.

4. CONCLUSION

Considering that the main problem in using river models is in fact the high number of parameters and lack of physical understanding of these parameters, or in other words difficulties in calibrating parameters, the present study proposed to investigate the performance of three optimization algorithm; PSO, H-GA&PSO and Firefly in estimating optimum parameters for Hymod rainfall-runoff model for Karaj river basin. The algorithms were assessed in two phases of calibration and validation. During calibration, a 3-year period was selected for assessing daily discharge. After calibration, validation was performed using independent observational data and suitable parameter series, which resulted from the previous phase (calibration).

After investigating results and evaluation criteria, it was concluded that PSO was relatively better evaluated than other algorithms. The ability to directly find optimum solutions along with concurrent random selection of parameters from available space, made this algorithm (PSO) stand out amongst others in regards to performance. Also, H-GA&PSO algorithm had higher convergence compared to other algorithms which is indicative of combining the advantages of both GA and PSO.

REFERENCES

Borhani, Darian, A.R., and Z., Farahmandfar, 2011. Calibration of Rainfall-runoff models using MBO algorithm. the Iranian Society of Irrigation and Water Engineering 1 (4): 60-71.

Boyle, D.P., 2000. Multicriteria calibration of hydrologic models.Ph.D. Dissertation, Department of Hydrology and Water Resources, University of Arizona, Tucson.

Chang, J. X., Bai, T., Huang, Q., and D. W., Yang, 2013. Optimization of Water Resources Utilization by PSO-GA. Water Resources Management, 1-16.

Fan, S.K.S., Liang, Y.C., and E., Zahara, 2006. A genetic algorithm and a particle swarm optimizer Hybridized with Nelder-Meat simplex search. Computer & Industrial. Engineering, 50: 401-425.

Gupta, H.V., Kling, H., Yilmaz, K.K., and G.F., Martinez, 2009. Decomposition of the mean squared error and NSE performance criteria: Implications for improving hydrological modeling, Journal of Hydrology, 377(1-2): 80-91.

Haddad, O.B., Ashofteh, P.S., Ali-Hamzeh, M. and Mariño, M.A., 2015. Investigation of Reservoir Qualitative Behavior Resulting from Sudden Entry of Biological Pollutant. Journal of Irrigation and Drainage Engineering, 141(8), p.04015003.

Kao, Y.T., and E., Zahara, 2007. A hybrid genetic algorithm and a particle swarm optimization for multimodal functions. Applied Soft Computing. 8 (2): 849-857.

Kennedy, J., and R., Eberhart, 1995. Particle Swarm Optimization. Proc. Of the International Conference on Neural Networks, Perth, Australia, IEEE, Piscataway, 1942-1948.

Liu, S., Butler, D., and R., Brazier, 2007. Using genetic algorithms to calibrate a water quality model. Science of the Total Environment. 374 (2-3): 260-272.

Matott, L. S., Tolson, B. A., and M., Asadzadeh, 2012. A benchmarking framework for simulation-based optimization of environmental models. Environmental Modelling and Software, 35: 19-30.

Qaderi, K., Mohammad, Vali Samani, J., Eslami, H.R., and B., Saghafian, 2006. Automatic calibration of a rainfall-runoff model using SCE optimization method. Iran Water Resources Research, 2(2): 39-52.

Shawn, M., Beth, H., Camden, R., Christine, B., and A., Shirmin, 2013. Telescoping strategies for improved parameter estimation of environmental simulation models. Computers and Geosciences, 60: 156-167.

Vrugt, J.A., Gupta, H.V., Bouten, W., and S., Sorooshian, 2003. A Shuffled Complex Evolution Metropolis algorithm for optimization and uncertainty assessment of hydrologic model parameters. Water Resource Research, 39(8):1201.

Wang, F., and Y., Qiu, 2005. A modified particle swarm optimizer with roulette selection operator. Proc. Nat. Lang. Process. Knowl. Eng., 765-768

Wu, Y., Liu, S., Li, Z., Dahal, D., Young, C. J., Schmidt, G. L., and J., Oeding, 2013. Development of a generic auto-calibration package for regional ecological modeling and application in the Central Plains of the United States. Ecological Informatics.

Yang., X.S, ,2009. Firefly algorithm for multimodal optimization in proceedings of the stochastic Algorithms,Foundations and Applications. (SAGA 109). 5792 of Lecture notes in Computer Sciences Springer

Zhang, X., Srinivasan, R., Arnold, J., Izaurralde, R. C., and D., Bosch, 2011. Simultaneous calibration of surface flow and baseflow simulations: a revisit of the SWAT model calibration framework. Hydrological Processes, 25(14): 2313-2320.

Zhang, X., Srinivasan, R., Zhao, K., and Van M., Liew, 2008. Evaluation of global optimization algorithms for parameter calibration of a computationally intensive hydrologic model. Hydrological Process. 23(3), 430-441.

Proceedings of the 10th World Congress of EWRA 'Panta Rhei', 5-9 July 2017, Athens, Greece
© 2017 *European Water Resources Association*

Ungauged drainage basins: Investigation on the basin of Peneios River, Thessaly, Greece

V. Gourgoulios and I. Nalbantis*
Centre for the Assessment of Natural Hazards and Proactive Planning & Laboratory of Reclamation Works and Water Resources Management; School of Rural and Surveying Engineering; National Technical University of Athens, Athens, Greece
* *e-mail: nalbant@central.ntua.gr*

Abstract: The effect on flow prediction accuracy of the lack of streamflow data is investigated. For this a testing framework is set up which involves three stages. In the first stage a deterministic physics-based distributed rainfall-runoff model is calibrated. The selection of this model category is dictated by the will to minimise the number of parameters that need calibration. These parameters are the "sensitive parameters" which primarily affect simulated flows. All other parameters are set to their default values or values based on hydrologic experience. The Nash-Sutcliffe Efficiency (NSE) is selected as the metric of model performance. In the second stage the basin is considered as ungauged and sensitive parameters are synthetically generated using the uniform distribution. Thus a frequency distribution of NSE is obtained. The third stage involves the comparison of simulated flows obtained in the first two stages of analysis. The Precipitation-Runoff Modelling System, version IV (PRMS-IV) is selected as the simulator of hydrological processes. The system subdivides the basin into Homogeneous Recharge Units (HRUs). The test basin was the Peneios river basin at the gauging station of Sarakina. This is located in the Thessaly Water District, central Greece and has an area of 1076 km2. Results indicated that the sensitive parameters of the model are seven in number. Upper extreme values of the distribution of NSE in the case with the ungauged basin were found to be close to values of the calibrated model, whereas the mean NSE was lower by 34%.

Key words: Ungauged basins; Precipitation-Runoff Modelling System (PRMS); Homogeneous Recharge Units; Peneios river

1. INTRODUCTION

Very often hydrologists are faced with ungauged basins in the sense that no streamflow records are available in them. As a result, modelling of hydrological processes in these basins becomes problematic. In response to the challenge regarding flow prediction in ungauged basins the International Association of Hydrological Sciences (IAHS) launched the international initiative known as "Predictions in Ungauged Basins" or PUB (Hrachowitz et al., 2013). The initiative covered the decade 2003-2012 and it was aimed at formulating and executing scientific programs that would achieve progress in predictions in ungauged basins. It was recognised that this requires changing the traditional paradigm that involves empiricism and model calibration into a new paradigm that focuses on extending the theoretical knowledge regarding the hydrological processes of the studied system. The change of paradigm would allow the improvement of existing models as well as the development of new models that effectively account for the variability of hydrological processes in both time and space. In the new paradigm, hydrology is the main scientific domain having interfaces with geology, topography, ecology and climatology. The accomplishments of PUB are related to the heterogeneity of data and processes, models and the associated uncertainty, basin classification and new hydrological theory. Within the general framework for hydrological modelling as this was set by the PUB Initiative, a modelling experiment is carried out with the aim to objectively respond to the question "What is the expected reduction of model performance if a basin is considered as ungauged?". The methodology towards this aim is outlined in section 2. The effort is focused on a gauged basin presented in section 3. Section 4 is devoted to results, while some conclusions are included in section 5.

2. METHODOLOGY

2.1 General

Starting from the general goal of this work, it is natural to limit our scope to conceptual and physics-based models, since these are generally assumed to represent physical processes through their structure and parameterisation. This fact created the general belief that, in order to achieve a certain level of predictive power, such models require less information on basin response than do empirical models. Also, our scope is limited to the daily time step. The selected model that fulfils the above requirements is briefly described in sub-section 2.2, while its calibration is discussed in sub-section 2.3. The full setting of our modelling experiment is outlined in sub-section 2.4.

2.2 The rainfall-runoff model

In this work we use the well-known Precipitation Runoff Modelling System (PRMS) (Leavesley et al., 1983) developed and maintained by U.S. Geological Survey (USGS). PRMS is classified as a distributed model which, in addition, is physics-based. It divides the study basin into a number of Hydrological Response Units (HRUs) as do also other models such as HYDROGEIOS (Efstratiadis et al., 2008) and the Soil Water Assessment Tool (SWAT (Arnold et al., 1999). Hydrological processes in each one of the HRUs are considered homogeneous and are simulated using physical laws or empirical relationships (Markstrom et al., 2015). Water is moving between storage elements representing various forms of water storage. The outputs from these elements contribute to the total basin flow. Precipitation (rainfall or snowfall) that is not intercepted by vegetation reaches the soil zone or the impervious zone. Surface, sub-surface and groundwater flow contribute to the total basin flow. The model employs five types of spatial units, i.e., the basin as a whole, river segments, HRUs, lakes and sub-basins. PRMS uses 17 "processes" that correspond to physical processes or to procedures for data management. The processes are the following: (1) Basin Definition; (2) Cascading Flow Process; (3) Solar Table Process; (4) Time Series Data; (5) Temperature Distribution; (6) Precipitation Distribution; (7) Combined Climate Distribution; (8) Solar Radiation Distribution; (9) Transpiration Period; (10) Potential Evapotranspiration; (11) Canopy Interception; (12) Snow; (13) Surface Runoff; (14) Soil-Zone; (15) Groundwater; (16) Streamflow; (17) Summary. These processes are implemented using 36 modules.

2.3 Model calibration

Model calibration is performed manually through a series of repeated simulations. The simulated daily streamflows obtained on output are aggregated into monthly streamflows which are then compared to observed monthly streamflows. The well-known Nash-Sutcliffe Efficiency (NSE) metric is used for the evaluation of model performance. This is expressed as

$$\mathrm{NSE} = 1 - \frac{\sum_{t=1}^{N} \left(Q_t - \mathrm{QS}_t\right)^2}{\sum_{t=1}^{N} \left(Q_t - \overline{Q}\right)^2} \tag{1}$$

where Q_t is the observed streamflow in month t with mean equal to $\overline{Q}$, QS_t is the simulated streamflow, and N is the number of observations.

2.4 The modelling experiment

A framework for a modelling experiment is set up which is comprised of the following steps: (1) In a preliminary stage, the PRMS model is run with the purpose to identify model parameters which exert a significant influence on simulated streamflows; these are called the 'sensitive' parameters, whereas the remaining parameters are the 'insensitive' parameters and are henceforth set to their default values; (2) the model is calibrated and validated using the NSE criterion of equation 1 applied on hydrological data from the basin selected for study; up to now the basin is considered as gauged; (3) the sensitive parameters are considered as unknown quantities that are modelled as random variables following the uniform distribution within the parameter intervals given by Markstrom et al. (2005); (4) a set of N combinations of sensitive parameters is randomly generated using Monte Carlo simulation; (5) by setting the insensitive parameters equal to their default values as proposed by Markstrom et al. (2005), N different full parameter sets are formed; this approach is inspired from the well-known GLUE method (Beven and Binley, 1992) and has been used also in uncertainty analysis (e.g., Nalbantis and Lymperopoulos, 2012); (6) the model is run N times, each one corresponding to one of the above N parameter sets; (7) NSE is computed for each model run, which results in a sample of N NSEs; (8) statistics of the latter are compared to the NSE value of step 2 (in validation). Evidently, in steps 3 through 6 the study basin is considered as ungauged.

3. STUDY BASIN AND DATA

3.1 The study basin

The Peneios river basin is the main river basin of the Thessaly Water District in central Greece. It covers an area of 9448 km^2 out of 13153 km^2 of the district as a whole. In this work we have chosen a headwater sub-basin of the Peneios river with its outlet at the Sarakina hydrometric station. The test basin is located in the North-western part of the entire Peneios basin. Its hypsometry and hydrographic network are shown in Fig. 1.

The Peneios river basin at Sarakina has a surface area of 1076.1 km^2 and mean ground elevation equal to 823.1 m. Its minimum, maximum and median ground elevation is 171.90 m, 2169.01 m and 785.00 m respectively.

3.2 Data used

Daily precipitation depths were collected for seven raingauges within and in the vicinity of the basin. These were provided by the National Bank for Meteorological and Hydrological Information, (Hydroscope) maintained by the Special Secretariat for Water, Ministry of Environment and Climate Change of Greece. Data were processed so as to remove statistical inhomogeneity and gaps (Gourgoulios, 2016). Daily maximum and minimum air temperatures were used for the assessment of potential evapotranspiration using the Hargreaves method (Hargreaves and Samani, 1985) and data from the station Megali Kerasia. Monthly streamflows for the period from January 1959 to February 1985 were employed which have been obtained from raw data of the Sarakina hydrometric station (Nalbantis and Koutsoyiannis, 1997). The Digital Elevation Model (DEM) of the study area was provided by the National Cadastre and Mapping Agency of Greece at the resolution of 5 m. The basin DEM allowed obtaining the spatial distribution of ground elevation (Fig, 1) and ground slope (Fig. 2). Land cover data was obtained from the EU project known as CORINE 2000. Land cover categories within the basin were found to be 19 in number, while the total number of categories in the project is 44. Categories were grouped to form the five land cover categories required by PRMS IV (Fig. 3).

The intersection of ground slope and land cover map layers provided us with the HRUs. Then all

HRUs with an area below 1.5 km^2 were attached to adjacent HRUs to obtain 199 HRUs in the final model configuration.

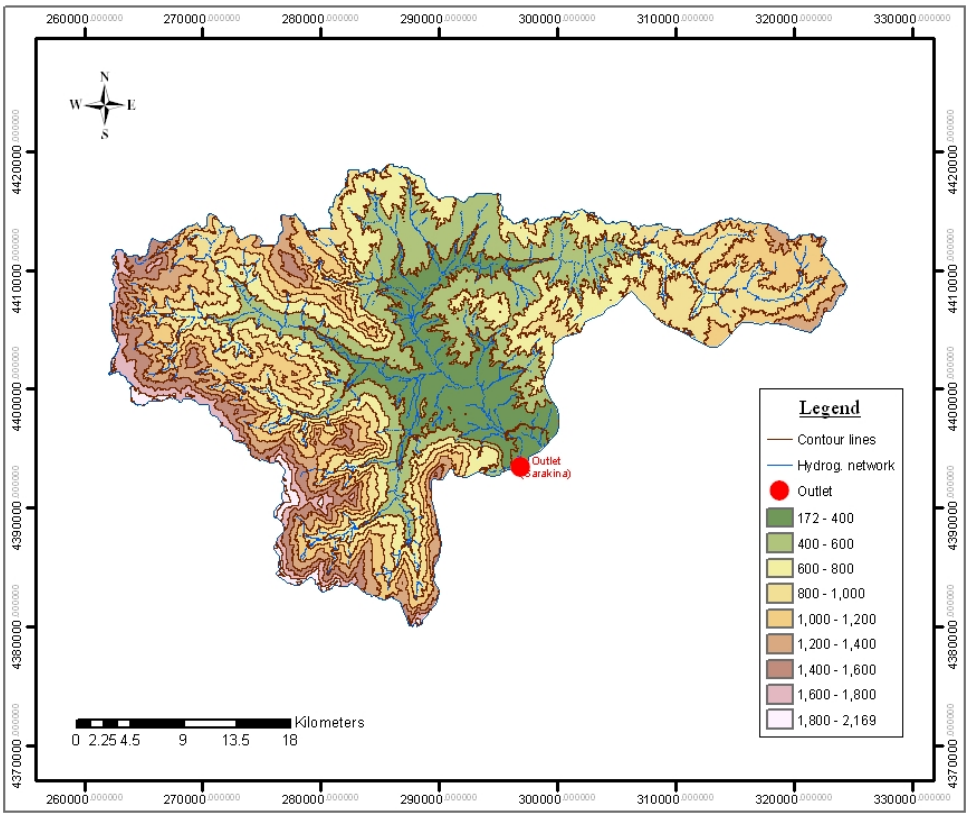

Figure 1. The Peneios river basin at Sarakina.

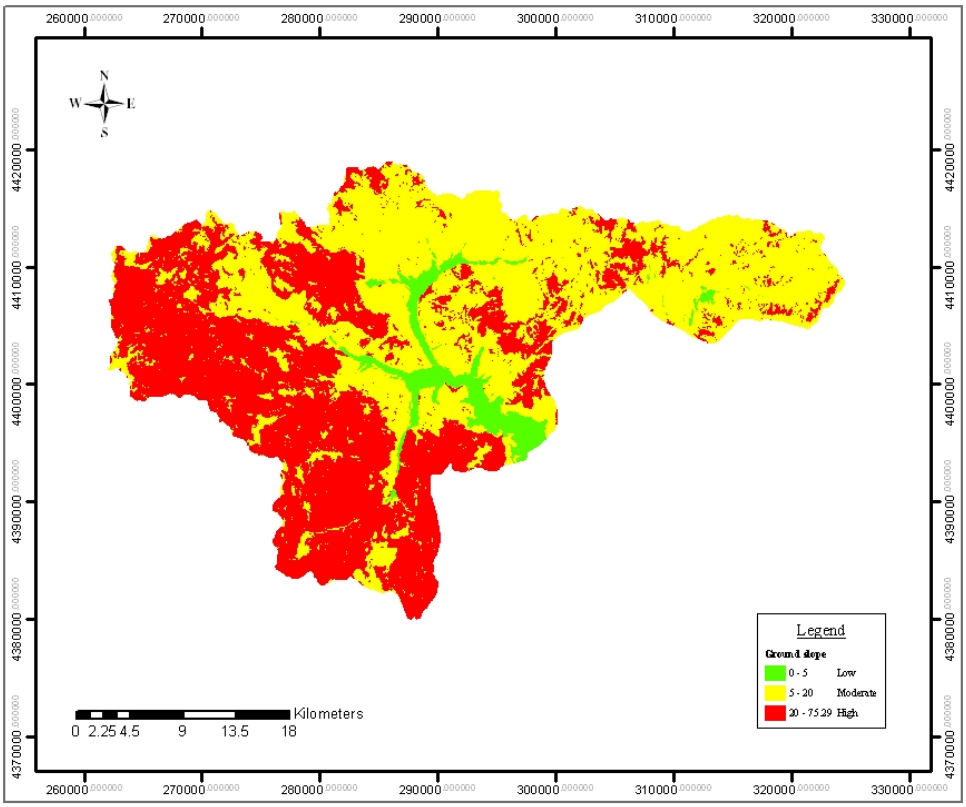

Figure 2. Ground slope in the Peneios river basin at Sarakina.

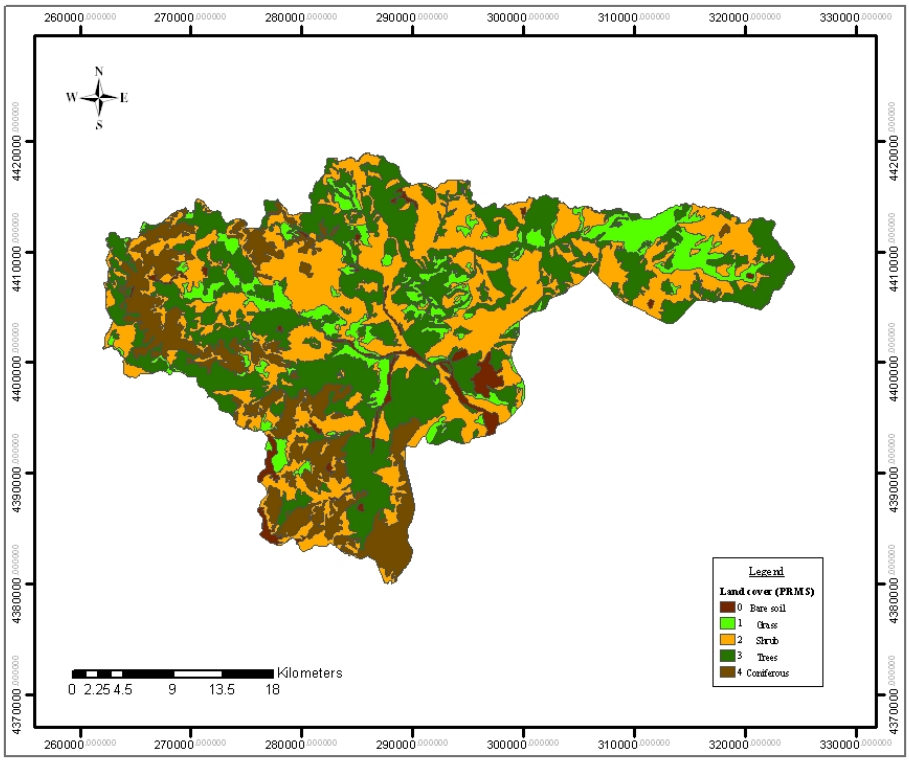

Figure 3. PRMS land cover categorisation in the Peneios river basin at Sarakina.

4. RESULTS

4.1 Case with gauged basin

Preliminary model runs showed that, for our test basin, only seven out of the 41 model parameters can be classified as sensitive (step 1 of modelling experiment). These are hs_krs, smidx_coef, smidx_exp, soil_moist_max, soil_rechr_max, soil2gw_max, and ssr2gw_rate. For detailed explanation of parameters the reader is asked to refer to Markstrom et al. (2005).

In step 2 of sub-section 2.4, the model is calibrated using daily series of observed precipitation and air temperature for the period from October 1973 to September 1980, i.e., seven hydrological years. Also, the hydrological year 1972-73 is used as a warm-up period. The methodology described in sub-section 2.3 is followed, which gave NSE = 0.553. Model validation is performed on data from the period from October 1980 to September 1985, while NSE was found equal to 0.531, a value which is close to that of the calibration. This indicates some level of model robustness, although the model performance can be characterised as low. The simulated and observed streamflows are depicted in Fig. 4.

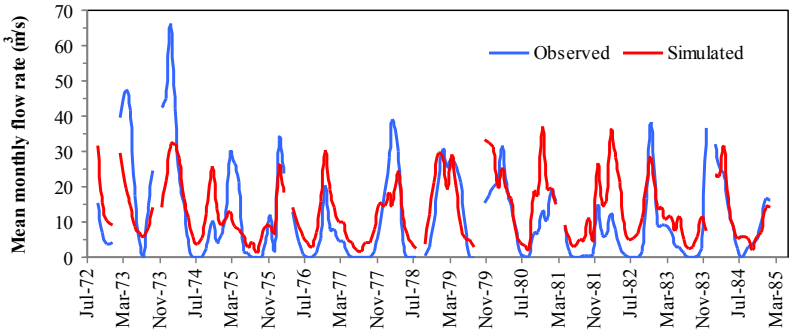

Figure 4. Observed and simulated monthly streamflows in the Peneios river basin at Sarakina

4.2 Case with ungauged basin

Steps 3 through 7 of the modelling experiment of sub-section 2.4 are executed using a number of sensitive parameter sets equal to 100. Statistics of NSEs for the generated parameter sets are given in Table 1. As seen in this table, the bulk of NSE quantiles is well below the value of NSE obtained in validation (step 2), whose probability of non-exceedance is between 0.95 and 0.975.

Table 1. Quantiles of NSE in the case with ungauged basin

Probability of non-exceedance	*NSE quantile*	*Difference from NSE in validation (%)*
0.025	0.201	-62.2
0.05	0.275	-48.2
0.1	0.305	-42.6
0.25	0.324	-39.0
0.5	0.364	-31.5
0.75	0.411	-22.6
0.9	0.462	-12.9
0.95	0.501	-5.7
0.975	0.579	9.0

5. CONCLUSIONS

In this work a simple approach was followed with the purpose to objectively assess the possible loss in performance of a rainfall-runoff model in the case that the model is applied to an ungauged basin. Our investigations revealed the following:

1. Since, in ungauged basins, the model structure should faithfully represent hydrological processes, a complex model of the conceptual type was necessarily chosen, which was PRMS.
2. To simplify the treatment of model parameters in the case with an ungauged basin, the parameter set was partitioned into sensitive and non-sensitive parameters based on their influence on simulated runoff. Then, stochastic simulation was applied only to the sensitive parameters; these were found to be seven in number out of a total of 41.
3. Although the model efficiency in the case with a gauged basin (in validation) was rather poor, this efficiency is expected to be highly improbable (within the upper 5% of efficiency distribution).
4. If, in the case of an ungauged basin, multiple model runs are performed, the median value of model efficiency is expected to be lower than the efficiency of the calibrated model (case with gauged basin) by about 34%.
5. It is therefore confirmed that extra information is required to reduce the above-mentioned loss of model efficiency before attempting to exploit runoff predictions of an uncalibrated model of the type tested in this work.

ACKNOWLEDGEMENTS

The authors wish to thank the personnel of the National Cadastre and Mapping Agency of Greece for providing the ground elevation data.

REFERENCES

Arnold, J. G., Williams, J. R., Srinivasan, R., King, K. W., 1999. Soil and Water Assessment Tool.

Beven, K., Binley, A., 1992. The future of distributed models: model calibration and uncertainty prediction. Hydrological Processes; 6(3): 279-298.

Efstratiadis, A., Nalbantis, I., Koukouvinos, A., Rozos, E., Koutsoyiannis, D., 2008. HYDROGEIOS: a semi-distributed GIS-based hydrological model for modified river basins. Hydrology and Earth System Sciences; 12(4): 989–1006.

Gourgoulios, V., 2016. Ungauged drainage basins: Investigation on the basin of Pineios River at Sarakina, Thessaly. Diploma Thesis, School of Rural and Surveying Engineering, National Technical University of Athens, Athens, Greece, 133 pages.

Hargreaves, G. H., Samani, Z. A., 1985. Reference crop evapotranspiration from temperature. Applied Engineering in Agriculture; 1(2): 96–99.

Hrachowitz, M., Savenije, H. H. G., Blöschl, G., McDonnell, J. J., Sivapalan, M., Pomeroy, J. W., Arheimer, B., Blume, T., Clark, M. P., Ehret, U., Fenicia, F., Freer, J. E., Gelfan, A., Gupta, H. V., Hughes, D. A., Hut, R. W., Montanari, A., Pande, S., Tetzlaff, D., Troch, P. A., Uhlenbrook, S., Wagener, T., Winsemius, H. C., Woods, R. A., Zehe, E., Cudennec, C., 2013, A decade of Predictions in Ungauged Basins (PUB)-a review. Hydrological Sciences Journal; 58(6): 1198–1255.

Leavesley, G. H., Lichty, R. W., Troutman, B. M., Saindon, L. G., 1983. Precipitation-Runoff Modeling System: User’s Manual. U.S. Geological Survey Water Resources Investigation Report 83- 4238.

Markstrom, S. L., Regan, R. S., Hay, L. E, Viger, R. L., Webb, R. M., Payn, R. A. LaFontaine, J. H., 2015. PRMS-IV, the Precipitation-Runoff Modelling System, Version 4. Techniques and Methods 6-B7, Reston, Virginia, USA.

Nalbantis, I., Koutsoyiannis, D., 1997. Upgrading and updating of hydrological information of Thessalia. Report 4, pp. 78, Department of Water Resources, Hydraulic and Maritime Engineering, National Technical University of Athens, Athens (in Greek).

Nalbantis, I., Lymperopoulos, S., 2012. Assessment of flood frequency after forest fires in small ungauged basins based on uncertain measurements. Hydrological Sciences Journal; 57(1): 52-72.

Proceedings of the 10th World Congress of EWRA 'Panta Rhei', 5-9 July 2017, Athens, Greece
© 2017 *European Water Resources Association*

Effect of land cover/use change on soil erosion assessment in Dubracina catchment (Croatia)

N. Dragicevic*, B. Karleusa and N. Ozanic
Facullty of Civil Engineering University of Rijeka, Croatia
* *e-mail: nevena.dragicevic@uniri.hr*

Abstract: The assessment of erosion intensity and sediment production using Erosion Potential Method was made for the Dubračina catchment, Croatia. During the extensive research and data collection, several data sources for the land cover/use map were available: Spatial Plan, Corine database and Landsat images. Landsat data source was included in the study to provide a more up-to-date and higher resolution assessment and was available also for various time periods. Different information sources imposed the need to choose one data source as the most appropriate through the acknowledgement of their differences and the effect on the model outputs. The analysis presented in this paper also includes the change in erosion intensity and sediment production between the past and the present time. For this purpose, the land cover categories for Dubračina catchment were derived from the Landsat images. The most noticeable spatial change in erosion intensity between the two-time series is on sub-catchments Slani Potok and Mala Dubračina, where the area affected by excessive erosion was found to increase from the past to present time. The overall decrease in average values for the sediment production is noted from the past to present time but this change in values was not found to be significant, in contrast to the change in the spatial distribution visible on the maps.

Key words: Erosion Potential Method, soil erosion, erosion intensity, erosion sediment production, various data sources, changes in time, land cover/use

1. INTRODUCTION

Water erosion can occur in all types of soil at different rates and in different forms (Merritt et al., 2003). The most important elements (e.g. Morgan, 2005) that influence the rate of water erosion are climate, soil, topography, vegetation cover and anthropogenic factors.

The need for the information on soil erosion (Merritt, 2003), at temporal and spatial scales describing the sediment pattern throughout the catchment and its associated quantities, is increasing due to various demands from stakeholders and decision makers in spatial as well as soil and water conservation planning.

Within this paper, erosion assessment for the Dubračina catchment, Croatia, was made using the Erosion Potential Method for the past and present time. The emphasis is given on choosing the appropriate input data from various information sources for soil protection parameter that is based on land cover/use categories.

Applied erosion monitoring methods on the Dubračina catchment are presented and include the verification of the Landsat-derived land cover map for the present time and the erosion coefficient (intensity) map.

2. METHODODOLOGY AND INPUT DATA DESCRIPTION

2.1 Erosion Potential Method

The Erosion Potential Method - EPM (Gavrilović method) is based on erosion field research conducted in 1960`s in the Morava River Catchment area in Serbia (Gavrilović, 1972). The method

was modified through the years by various authors (Dragičević et al., 2016). Today, the method encompasses erosion mapping, sediment quantity estimation, and torrent classification and has, since 1968, been extensively applied to erosion and torrent-related problems in the Balkan countries (Gavrilović et al., 2008).

Erosion model discussed within this paper is based on the EPM method and used to provide two main outputs (de Vente and Poesen, 2009) the total annual volume of detached soil W_a (Equation 1) and the erosion coefficient Z (Equation 3).

$$W_a=T*P_a*\pi*sqrt(Z^3)*F \quad (1)$$

$$T=sqrt(T_0/10+0.1) \quad (2)$$

$$Z=Y*X_a*(\varphi+sqrt(J_a)) \quad (3)$$

where:
W_a - total annual volume of detached soil (m^3/year)
T - temperature coefficient (-)
P_a - average annual precipitation (mm)
Z - erosion coefficient (-)
F - study area (km^2)
T_0 - average annual temperature (^oC)
Y - soil erodibility coefficient (-)
X_a - soil protection coefficient (-)
φ - coefficient of type and extent of erosion (-)
J_a - average slope of the study area (%)

2.2 Case study: Dubračina catchment

The EPM was applied on Dubračina catchment, Croatia (Figure 1). The catchment has an area of 43 km^2 and is characterised by steep slopes in its lower and upper part, with an elevation difference of 920 m and a complex soil structure. High annual rainfall, steep topography and variable geology contribute to its land instability features such as landslides and excessive erosion processes. Although most of its tributaries tend to dry out during the summer period, during the rainy period, considerable flow oscillations are very common.



Figure 1: Distribution of the Dubračina catchment sub-catchments

The overall catchment can roughly be divided into an upper karstic part with steep slopes and active sediment movement, and a lower Flysch as a less permeable area. The complex geological structure, special valley cross section with distinct and steep slopes affected by erosion, local landslides and torrents are the reasons why this area has been known for many years as an area of potential erosion hazard.

2.3 Input data and data sources

Erosion intensity and sediment production for the Dubračina catchment using the EPM were assessed for two time periods: the past (1961-1990) and the present (1991-2020). The input data that differs for both time-series are as follows:

- Average annual precipitation,
- Average annual temperature,
- Soil protection coefficient.

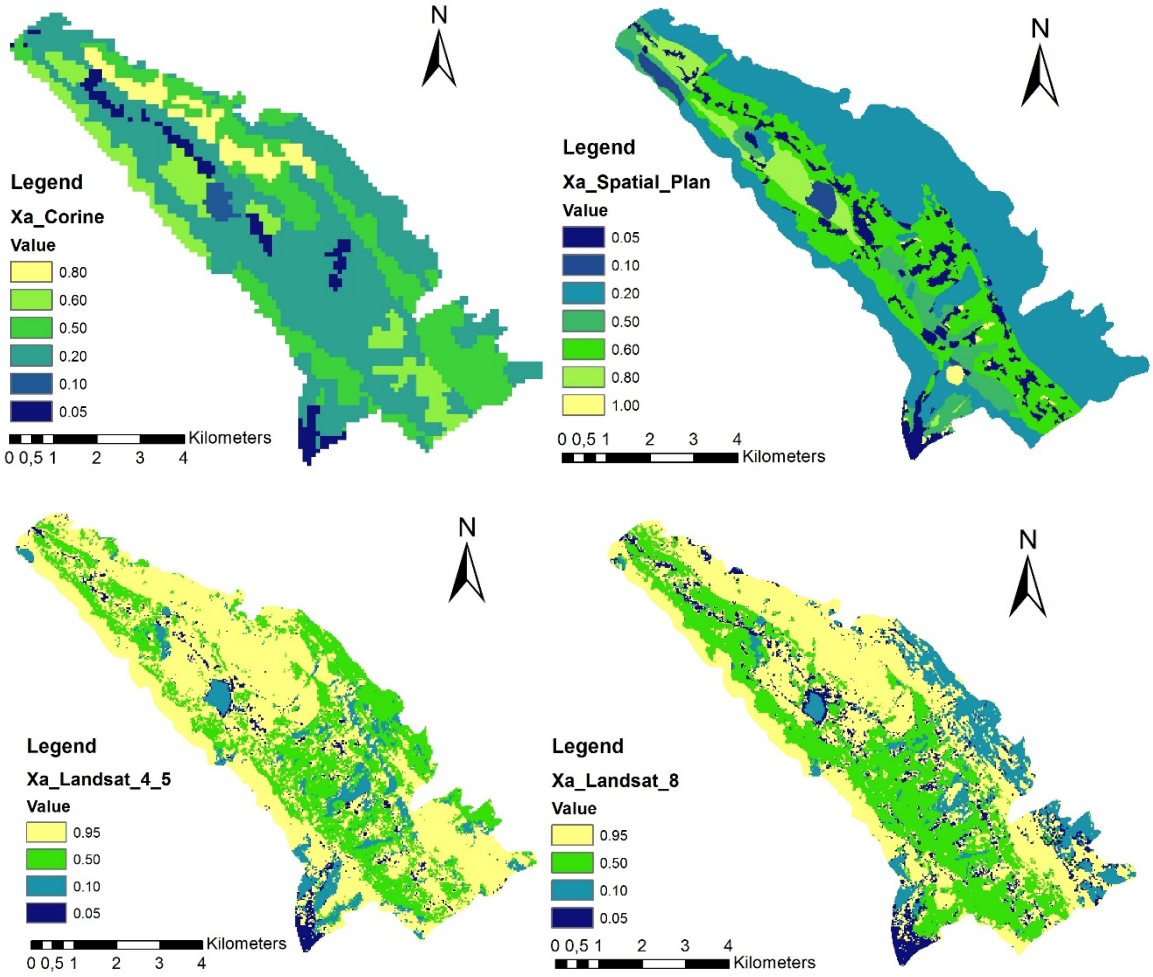

Figure 2: Soil protection coefficient based on different land cover/use maps

The spatial distributions of precipitation and temperature, with a resolution of 1000x1000 m, were obtained from the Croatian Meteorological and Hydrological Service for the time period of 1961 to 1990. Both the average annual temperature and the average annual precipitation for the town of Crikvenica were found to increase for the period from 1991 to today compared to the period of 1961 to 1990 (by 0.9°C and 55.9 mm) (Dragičević et al., 2017). Based on this changes and on the assumption that the spatial distribution pattern remains the same throughout the catchment, the spatial distribution maps for these parameters were derived also for the time period from 1991 to 2020. The soil erodibility coefficient is based on a pedological map of Primorsko-

Goranska County, with a scale of 1:100 000. The soil protection coefficient is based on land cover/use categories for the Dubračina catchment. Land cover/use maps were available from three different data sources:

- The Corine land cover map (1:100,000) developed by the European Commission (EC) in 2006,
- the Spatial Plan of land use (1:25,000) developed by the local government in 2004 and
- Landsat data.
- The Landsat data source provided two datasets, one for each time period:
- Landsat 4,5 with a cell size of 30x30 m from August 1984 representing the past time period 1961-1990 and
- Landsat 8 with a cell size of 15x15 m from August 2013 representing the present time period 1991-2020.

To facilitate Landsat data processing, based on supervised classification, the software ERDAS Imagine 2014 was used and six land cover classes were recognised: water, urban area, medium dense vegetation, bare rock, bare soil to rare vegetation and dense vegetation.

Furthermore, LIDAR data were used to generate a digital elevation model with a 2x2-m cell size spatial resolution. The coefficient of type and extent of erosion was based on the Spatial Plan map of known erosion-affected areas (scale 1:25,000).

3. RESULTS

3.1 Model output deviation due to land cover/use source change

In the case of Dubračina River catchment, where there was no previous existence of information database, during the extensive research and data collection, the authors have come across several data sources for the same parameter – soil protection coefficient. The need to choose one as the most appropriate has stressed the need to properly evaluate each data source and acknowledge the difference between them. That was made by the comparison of model outputs W_a and Z obtained using a different data source, each time, as a model input for soil protection parameter. The deviations in input datasets for soil protection parameter and derived model output values are shown in Table 1.

Table 1: Model uncertainty shown in percent change in the model output

Data source	Change in Soil protection coefficient dataset in comparison to Landsat 8 dataset [%]	Change in model output values in comparison to model outputs (Z_I and $W_{a.I}$) obtained using Landsat 8 dataset	
		[%Z_I]	[%Wa.I]
Spatial Plan	-45.5	-46.0	-46.9
Corine database	-45.0	-45.0	-44,7
Landsat 4,5	-2.5	+9.9	+9.8

As shown in Table 1, the comparison was made using Landsat 8 data source as the base input data in a model for X_a parameter. The similar difference in oscillation from basic model scenario using both Spatial plan and Corine database can be found in the similar approach used while creating these two datasets (both took into account topographic maps of the area). In contrast to them, the Landsat datasets are based on remote sensing technology obtained from the classification of earth satellite images. Below is a comparison of soil protection coefficient based on Landsat 8 scene (presenting basic scenario) with those obtained using different data sources for land cover/use input data. This parameter, when based on Corine dataset, deviates by 45% in relation to that based on Landsat 8 dataset. The 45% change in dataset causes 44.7% change in total annual volume of the soil model output and 45% change in erosion coefficient output. This parameter affects the model outputs greatly, and according to sensitivity analysis conducted by Dragičević et al. (2017) is

classified as one with very high sensitivity to model.

In was noted that the Corine dataset was unchanged in the 10 year time difference for the area of Dubračina catchment, while the difference in land cover is obvious in Landsat satellite images. Thus, the Corine dataset in considered less reliable for this case study. Landsat dataset is chosen as most relevant for further model estimations also due to its highest resolution and detail in comparison to the other two data sources.

3.2 Past to present change in erosion assessment for the Dubračina catchment

The erosion coefficient, which indicates the erosion intensity in the catchment and the total annual volume of the detached soil, which indicates the overall erosion sediment production on an annual basis, were derived in a form of maps for the Dubračina catchment. For each output parameter (Z, W_a), two maps were generated (Figure 3), one representing the past (1961-1990) and the other representing the present (1991-2020). The maps showing the change between the time series for Z and W_a are also presented in Figure 3, which clearly indicates the areas of increase/decrease in the values.

The most noticeable spatial change in erosion coefficient was recorded around the Slani Potok and Mala Dubračina sub-catchments, where the area encompassed by excessive erosion ($Z \geq 1.0$) has increased from the past to the present. The change in the mean values between the past and the present is approximately 9%, showing an overall decrease in erosion intensity in the catchment over the years, with greater changes noted on the sub-catchments Kučina, Leskovnik, Slani Potok, Mala Dubračina and Ričina Tribaljska.

Similar changes are observed on the spatial distribution map representing the total annual volume of the detached soil, between the time periods. The average change in values throughout the catchment is found to decrease by 3% between the past and the present: in the past, the average value of the detached soil in the catchment was 15.64 m^3/cell/year, which is equivalent to 1564 m^3/km^2/year, and in the present time, the value is 15.12 m^3/cell/year or 1512 m^3/km^2/year. Based on these values, it can be concluded that this change is not significant; however, when the map showing the spatial distribution of its values (Figure 3) and the change in W_a per sub-sub-catchment is considered, sub-catchments of Leskovnik, Ričina Tribaljska, Slani Potok, Mala Dubračina and Kučina contribute the most to the overall change in W_a values; they all exhibit values that increase/decrease by up to several times the average values for the entire catchment.

The calculated value for the total annual volume of the detached soil for the present time is 64 810.75 m^3/catchment/year, and that for the past is 67 072.91 m^3/catchment/year, corresponding to an overall decrease in erosion production by 3.3. Overall, the average erosion coefficient for the Dubračina catchment in present time is 0.25, which classifies it as an area of slight erosion. Nevertheless, although the overall classification categorises the erosion processes in the catchment as slight, the maximum values reach 4.189, which is more than 4 times higher than the defined boundary value for the excessive erosion class.

4. MODEL VERIFICATION

The land cover maps derived from the Landsat images were verified using the visual land survey method and observing twenty on-site locations. The verification refers to the land cover map for the present time (1991-2020). For each location, GPS coordinates were noted, as were photographic documentation of the site. In addition to that, the descriptive observation notes of the onsite and close surrounding vegetation cover were noted as well. The observation was made in July 2016 to correspond to the same year period for which the land cover for the present time was made (August 2013). For each location, observation notes were compared in the ERDAS Imagine software to the land cover category derived from the Landsat data. The observed vegetation cover on the chosen location corresponded well to those obtained with the Landsat 8 image land cover classification.

For the same locations, visual signs of erosion processes, such as the presence of soil loss, gully formation, or sediment deposition on the site or in the river bed, are noted and compared with the erosion coefficient values that define the erosion intensity categorisation for each chosen location. Very good results were obtained from the comparison of the field survey and the erosion coefficient obtained using the EPM model for the present time series. Most of the observed points (eleven) correspond to very slight erosion, six points correspond to slight erosion, and one point corresponds to each of medium, severe and excessive erosion. In some points, the erosion coefficient was found to correspond to very slight to slight erosion, and some sediment yield was noted within the river beds. These sediments are the result of erosion processes in the upper part of the sub-catchments and not the location itself.

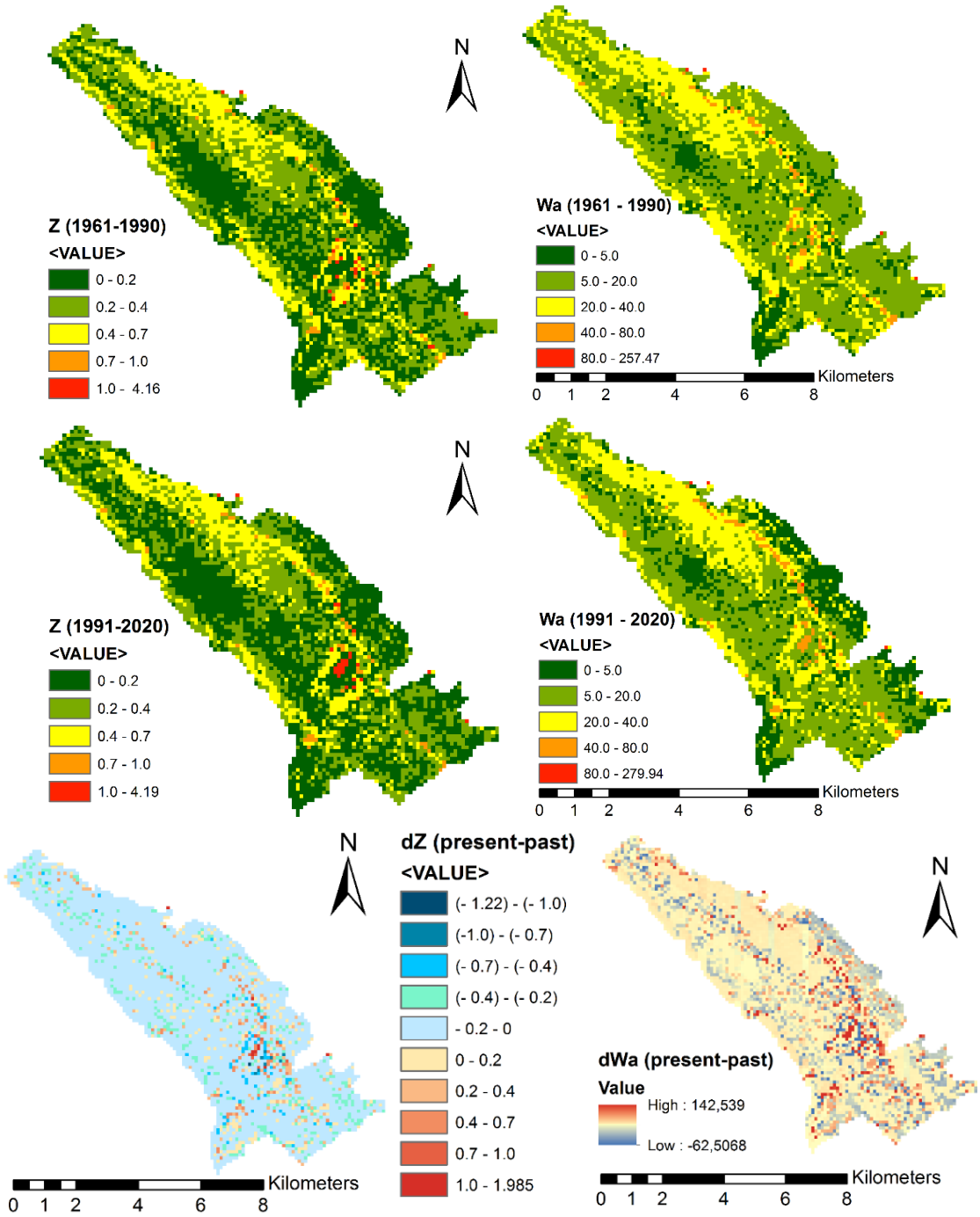

Figure 3: Model outputs: erosion coefficient and total annual volume of the detached soil [m^3/cell/year] for past and present time and the differences between time periods

5. CONCLUSION

The analysis indicates that when changing the data source, significant changes to the model outcome value (up to approximately 47% as shown on Dubračina River catchment study area) can occur. Such changes depend on detailed preliminary research and data gathering.

Landsat data was chosen as the most appropriate input data on which Soil protection coefficient is based due to its highest resolution and reliability.

The estimated values and maps derived by the EPM presented in this paper include outputs for the erosion coefficient (intensity) and the total annual volume of the detached soil for the past and present time. The most noticeable spatial change in the erosion coefficient between the time series is located near the Slani Potok and Mala Dubračina sub-catchments, where the area affected by excessive erosion was found to increase from the past to present. The overall decrease in the average values of the total annual volume of the detached soil is noted from the past (15.64 m^3/cell/year) to present (15.12 m^3/cell/year) time; however, this change in these values was not found to be significant, in contrast to the change observed in the spatial distribution visible on the maps.

The model output erosion intensity and land cover map for the present were verified using a visual survey monitoring method and a GPS device. All verifications revealed good results, and the high accuracy of the derived maps was confirmed.

ACKNOWLEDGMENT

This research was conducted within the University of Rijeka funded projects: "Development of New Methodologies in Water and Soil Management in Karstic, Sensitive and Protected Areas" (13.05.1.3.08) and "Hydrology of water resources and risk identification of flooding and mudflows in the karst areas" (13.05.1.1.03.) as well as Croatian-Japanese project "Risk identification and Land-Use Planning for Disaster Mitigation of Landslides and Floods in Croatia" funded by the Ministry of Science, Education and Sports of the Republic of Croatia and Japanese Government and "Hydrology of Sensitive Water Resources in Karst" (114-0982709-2549) project financed by the Ministry of Science, Education and Sports of the Republic of Croatia.

REFERENCES

Merritt W.S., Letcher R.A., Jakeman A.J., 2003. A review of erosion and sediment transport models. Environmental Modelling & Software. 18: 761-799.

Morgan R. P., 2005. Soil Erosion & Conservation. Oxford, United Kingdom: Blackwell Science Ltd.

Gavrilović S., 1972. Inženjering o bujičnim tokovima i eroziji. Izgradnja. special issue: 1-292.

Gavrilovic Z., Stefanovic M., Milovanovic I., Cotric J., Milojevic M., 2008. Torrent classification - base of rational management of erosive regions. In: IOP Conference Series: Earth and Environmental Science 4 (1): 1-8.

Dragičević N., Karleuša B., Ožanić N., 2016. A review of the Gavrilović method (Erosion Potential Method) application. GRAĐEVINAR. 68 (9): 715-725.

de Vente, J. and Poesen, J. (2005): Predicting soil erosion and sediment yield at the basin scale: scale issues and semi-quantitative models. Earth-Science Reviews. 71 (1-2): 95-125.

Dragičević N., Karleuša B., Ožanić, N., 2017. Erosion Potential Method (Gavrilović Method) Sensitivity Analysis. Soil and Water Research. 12 (1): 51-59.

Proceedings of the 10th World Congress of EWRA 'Panta Rhei', 5-9 July 2017, Athens, Greece
© 2017 *European Water Resources Association*

Development of flood and mudflow events for the spatio-temporal risk assessment of networks

J. Hackl[1*], M. Heitzler[2], J.C. Lam[1], B.T. Adey[1] and L. Hurni[2]
[1] *Institute of Construction and Infrastructure Management, Swiss Federal Institute of Technology (ETH), Zürich, Switzerland*
[2] *Institute of Cartography and Geoinformation, Swiss Federal Institute of Technology (ETH), Zürich, Switzerland*
[*] *e-mail: hackl@ibi.baug.ethz.ch*

Abstract: Networks such as transport, water and power are critical lifelines to society. Network managers plan and execute interventions to guarantee their operational state under various circumstances, including after the occurrence of (natural) hazard events. Creating an intervention program demands knowing the probable network-related consequences (i.e., risk) of the various stochastic hazard events that could occur. The way such events are simulated has implications on (i) the overall computational cost of the entire risk assessment, which increases as the complexity of the network of interest increases, (ii) the accuracy of the individual risk estimations, as well as (iii) the quantified uncertainty of resulting risk estimations. To support network managers in their task to assess network-related risks, a method is presented here to develop rainfall-triggered hazard events, namely riverine flood events and mudflow events. The method enables the generation and simulation of hazard events that (i) are of a specific modeller-defined return period, enabling the characterization of the uncertainty of risk estimation for given return periods, and (ii) change over space and time, leading to the spatio-temporal estimation of network-related risk. The method is designed for network managers, and therefore, integrates computationally-efficient models that can be quickly coupled, and require data that is generally available or can be easily obtained or estimated, without impacting the integrity of the results. An example is presented to illustrate the application of the method to develop flood and mudflow events to be used in the assessment of risk for a road network in Switzerland.

Key words: Risk assessment, probabilistic modelling, natural hazards, flood, mudflow

1. INTRODUCTION

Managers of transport, water, power and other networks need methods that support decisions on maintenance, repair, retrofit, renewal and other infrastructure management interventions. Since their networks are spatially distributed and have temporal attributes (e.g., traffic flow, water demand and electricity consumption vary throughout the day), managers understand that independent and dependent disruptive events could occur in one or multiple points within the network, and manifest at different times for various lengths. As a result, each possible scenario will lead to a different set of consequences in terms of restoration costs and loss of level of service. In particular, managers, whose networks are exposed to (natural) hazards, are in need of probabilistic methods that can support the quantification of probable consequences, here referred to as risks, along with their uncertainty, by considering the various stochastic ways hazard events could manifest.

A number of research works has put forward methods, models and support systems in response to these needs. These works cover a wide area of contributions, from those solely concerned with assessing the probable costs of restoration (e.g., Padgett et al. (2010) for the transport sector due to earthquake hazard events) to assessing the probable loss of service (e.g., Hackl et al. (2015) for the transport sector due to flood hazard events). There are also works that have investigated the effects of cascading events (e.g., Kiremidjian et al. (2007) for the transport sector with respect to liquefaction and landslide hazard events due to ground shaking) and a large set of stochastic events (i.e., over 1000; e.g., ERN-AL (2012) for the water sector due to earthquake hazard events). Methods that integrate these various important elements are still needed to support the management of networks. Furthermore, there is a need to expand methods related to the assessment of

consequences due to spatio-temporal hazard events such as hydro-meteorological hazards as a large majority of the literature focuses on geological hazards, specifically earthquakes, which are often simulated as sudden events with only spatial characteristics.

The probabilistic method presented here supports the numerical estimation of risk while reducing the computational cost of modelling a complex system, which comprises the continuous, non-linear interaction between a network and its surrounding environment, using peer-reviewed simplified models. As a result, the method supports the simulation of a large set of hazard events and the subsequent quantification of the uncertainty of risk results. The method is solely concerned with rainfall-triggered hazard events, specifically riverine flood events as well as mudflow events, which are modelled as events that change over space and time. The application of the method is illustrated by an example of a road network in Switzerland.

2. PROBABILISTIC METHOD

The presented probabilistic method was constructed using the iterative process described in Adey et al. (2016). The detailed quantitative and computer-supported models used to estimate network-related risk are described in Hackl et al. (2016) and Heitzler et al. (2016). In this paper, the focus lies on the *hazard module* (i.e., the modelling of the different rainfall-triggered events and their interactions over space and time).

The environmental conditions, whose data is generally available (e.g., terrain, hydrological network, gauge station data), can be approximated (e.g., precipitation fields Sigrist et al. (2012)), or can be collected through inventory (e.g., geological features), and hazard events, which could possibly impact the network, are defined through the hazard module that is illustrated in Figure 1 using Business Process Model and Notation (BPMN). Each specific event, which should be considered in the risk assessment, is described by a so-called *model*, which is in this context a peer-reviewed model (i.e., understood to be accurate given the assumptions and limitations of each of those models) with unambiguously-defined input and output interfaces. Inputs are either provided via external input (e.g., user inputs, geo data, historical data) or via internal input (i.e., by using outputs of other models generating compatible datasets). Hence, each model interacts with other models by receiving and delivering information (i.e., processed data). This dynamic interaction is also shown in Figure 1.

Most network managers are mainly interested in the additional loads impacting their critical structures, and therefore, need to have the capability to select hazard events based on the periodicity of the manifested site-specific loads, as opposed to being primarily concerned with the preceding source rainfall events leading to those loads. The presented probabilistic method accounts for this particular need by enabling the selection of the hazard events based on the return period of interest related to loads at a specific site. This selection is achieved through a calibration process (Figure 1). In this process, a random rainfall event is produced, and the corresponding discharge values are computed. Should the obtained discharge value at a location of interest be in the 50-percentile of the discharge values calculated for that specific location using gauge data and for the desired return period, the simulation continues; otherwise, the rainfall event gets calibrated, and the evaluation process starts again.

In order to provide a computationally-efficient and accurate estimation of risk, the structures of the models and of the modelling environment in which the models are embedded have to be adapted for the specific context and needs of a network manager. For example, the hazard module illustrated in Figure 1 describes two hazard events: riverine flood events and mudflow events. Both hazards are triggered by a rainfall event, which causes additional discharge in the rivers and an increase in surface-water flow.

Once the models and data are assembled appropriately, the modelling environment can be used to perform simulations. The inputs for the simulation may be defined by the network manager or potentially automated when performing multiple runs (e.g., by sampling a certain distribution using

Monte Carlo methods). The results of a simulation represents the outcome of a so-called *scenario*, which is one possible sequence of events based on a set of initial conditions.

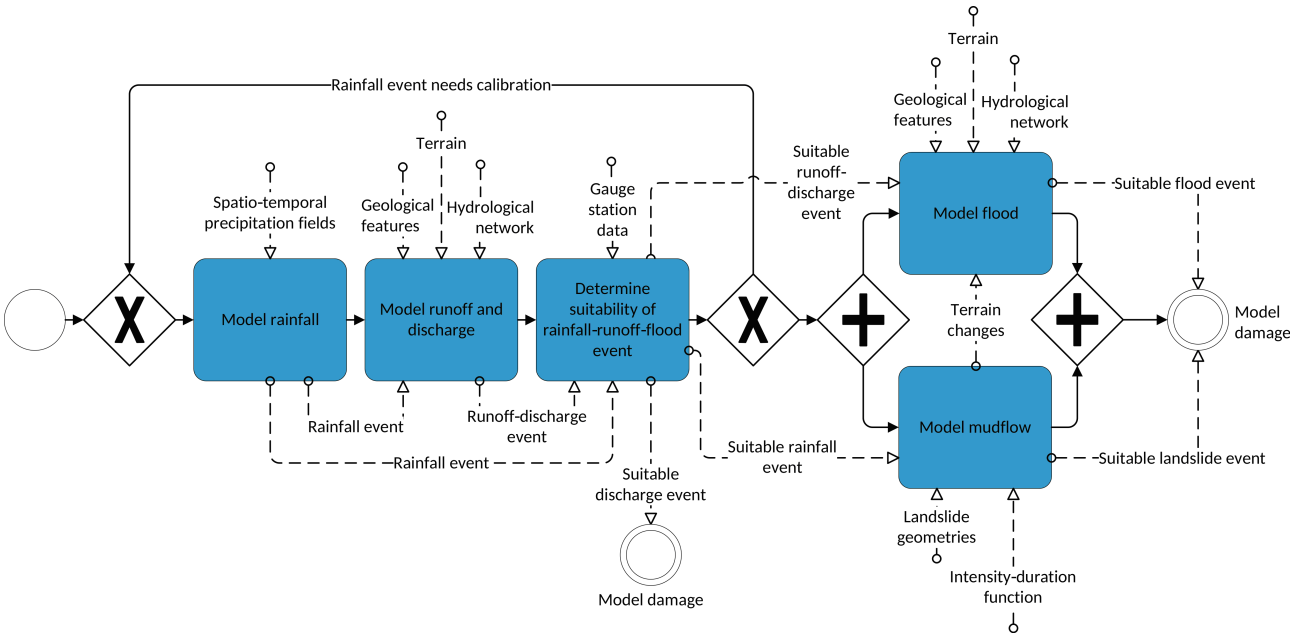

Figure 1. Hazard module for rainfall-triggered events.

The use of stochastic inputs allows to express the uncertainties related with the environmental conditions. For example, the use of a random spatio-temporal precipitation field allows to consider uncertainties related to the rainfall event. These uncertainties propagate through the entire hazard module, and will be passed on to succeeding models (i.e., damage model and consequence models for costs of restoration and loss of level of service), influencing the estimated risks. Instead of single risk values for a specific return period, a distribution of risk can be obtained.

3. EXAMPLE

3.1 Introduction

An example is included here to illustrate the application of the method described to determine the probable environmental conditions surrounding road networks and the resulting riverine flood events and mudflow events, for the Rhine Valley area around Chur, Switzerland in the Canton of Grisons (Figure 3.B) This area was suspected to have an unacceptable level of road network-related risk due to riverine floods as well as mudflows. Historical records and previous studies suggested that the heavy rainfalls in this area have the potential to result in the listed hazard events. The road network in the area of study, which is considered to play an important role in the economy of the eastern part of Switzerland, consists of 32 km of high speed roads, 559 km of local roads, and 92 bridges, with many of these objects exposed to the hazards of interest. A detailed description of the area in the context of the example can be found in Hackl et al. (2016).

3.2 Application of method

To describe the environmental conditions and hydro-meteorological hazard events, the model shown in Figure 1 was utilized. This model included five defined sets of activities:

1. The rainfall events were generated based on the spatio-temporal precipitation fields of the RdisaggH-Dataset (Wüest et al., 2010). This dataset was reduced to the extent of the target

area, and regridded to conform to the target extent and resolution. Based on a predetermined start date and duration, the corresponding subset from the spatio-temporal precipitation catalogue was extracted. The fields of this catalogue subset were then normalized according to the maximum rainfall amount over the considered time period. Afterwards, each normalized value was multiplied by a randomized precipitation volume. Once a precipitation volume was assigned to each dataset, the datasets themselves were normalized. By multiplying the assigned precipitation volume for a given time step to that precipitation field, the actual amounts of rainfall were determined.

2. The runoff volume was computed from the volume of rainfall that was considered to be intercepted, infiltrated, stored, evaporated, or transpired. Therefore, the ModClark model (Kull and Feldman, 1998) was used to estimate the discharge during the rainfall event. This model explicitly accounts for translation and storage, where the storage was determined through a linear reservoir model. Translation was accounted for through a grid-based travel-time model. The grid was superimposed on the watershed. For each cell of the grid representation of the watershed, the distance to the watershed outlet was specified. Translation time to the outlet was computed. The area of each cell was specified, and from this, the volume of inflow to the linear reservoir for each time interval was computed as the product of area and rainfall excess. This excess was computed for each cell using the watershed data extracted from the GIS model. Each cell's excess was then lagged to the basin outlet according to the cell's travel time. Next, individual lagged cell outflows were routed through a linear reservoir, with a lag time due to natural storage effects. The lagged and routed outflows were then summed, base flow was added, and the watershed's outlet hydrograph was produced.
3. The rainfall and the runoff model were used together to determining whether the resulting discharge scenario corresponded to the discharge value of a desired return period, which was estimated based on available gauge data. If the desired return period was not achieved, the rainfall event was calibrated (i.e., up-scale, down-scale of predetermined spatio-temporal precipitation fields), and the analysis was performed again.
4. A simple 1D model was used and justified by the relatively large size of the investigated area (approximately 20 km) and the need of a model that would require relatively little computation time to run simulations. In particular, a steady and gradually varied flow in open channels was considered. The required discharge and stage data were acquired by the hydrological model, described above, using rainfall data as an input, rather than being measured by gauge stations. The outputs of interests were the velocity, shear stress, and water depth in each cross-section of the rivers, which could be used for estimating the effects on network objects such as bridges, ramps, and dams.
5. Also due to computational constraints, the design of the mudflow model was kept simple, considering only predetermined areas of potential landslides (Losey and Wehrli, 2013). In total, 54 potential mudflows were considered for the target area. Because the duration of landslides to occur usually is in the range of seconds to minutes while the time step of the simulation was one hour, the dynamic process itself was not modelled. For each time step, an iteration was performed over all triggering locations. For each location, the respective values were extracted from the precipitation field, and used as input for the intensity-duration function (Rickenmann, 1999): $T=32 \cdot D^{-0.72}$, where T was the threshold that caused the mudflow to be potentially triggered when exceeded, and D was the duration of the rainfall event in the triggering location. The output of this model for each time step was a digital elevation map (DEM), whose elevation values were updated according to the heights of the triggered landslides at a given time step.

The major source of randomness was introduced by the directionality of the spatio-temporal precipitation fields and the scaling of these. In the considered scenarios, the initial condition that the network manager could freely chose was limited to the return period(s) of the flood. This feature

was of particular importance to support scenario selection for infrastructure management applications (e.g., assess the performance of a network with respect to a given return period) and the quantification of the uncertainty of probable consequences for a desired return period.

In total, 1,180 simulations were conducted: 20 simulations for each of the return periods between 1 and including 9 years as well as 100 simulations for each of the return periods of 10, 25, 50, 100, 250, 500, 1,000, 2,500, 5,000 and 10,000 years - such selection enables the generation of a loss exceedance curves (i.e., functional representations of cost of restoration or monetized loss of level of service over return periods). Depending on the return period, rainfall patterns with different durations were calculated. For return periods smaller than 100 years, the rainfall patterns had a duration of 7 to 13 hours, for periods between 100 and 1,000 years. Patterns had a duration between 10 and 16 hours, and for patterns greater than 1,000, they had a duration between 13 and 19 hours. The durations of the resulting flood events varied greatly and were in the range of 20 to 30 hours.

3.3 Software and hardware

The code used in the determination of the risk was programmed in Python. Since most network managers use geographic information systems (GIS), a GIS interface was developed to facilitate the import and export of data. Furthermore, the program code was optimized for massively parallel computing in order to reduce the computational time of the optimization process (i.e., each simulation ran on a designated CPU, and therefore, an increase in the amount of CPUs, increases the number of simulations). The computation of the scenarios was conducted on a 4 x10 Core Intel Xenon E5-2690v2 3.0Ghz, 384GB DDR2 server running on Ubuntu 14.04 64bit operating system. Overall, the real-time computational time for all hazard events amounted to approximately 2 days.

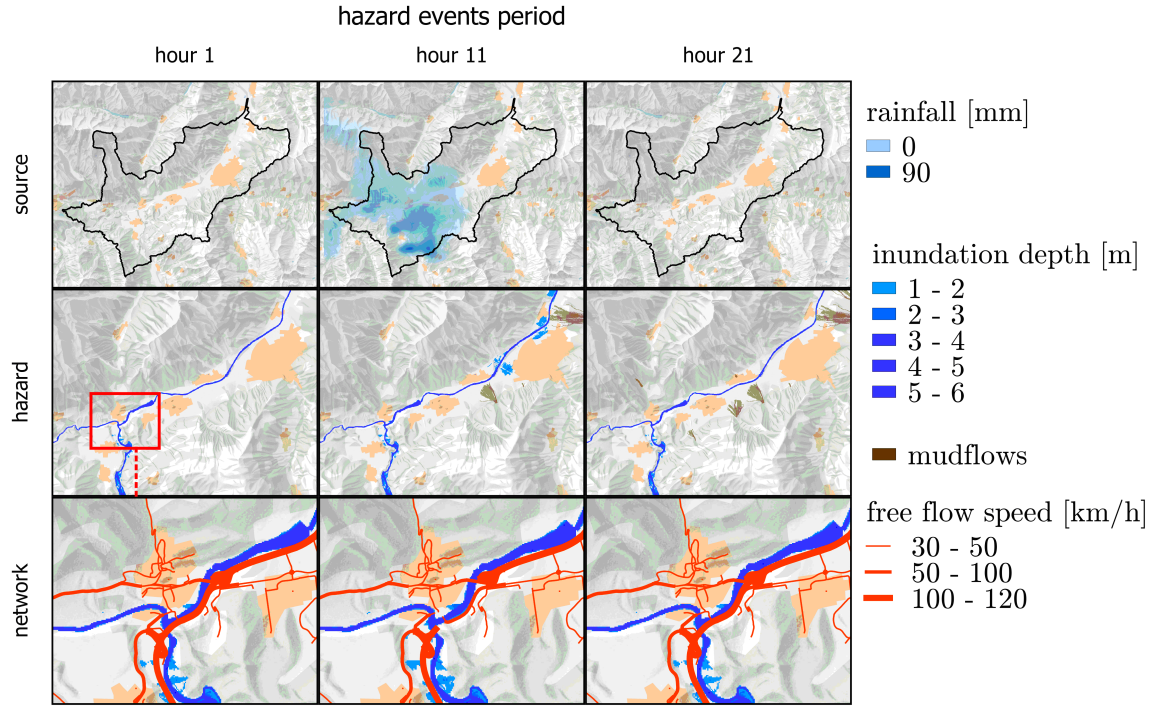

Figure 2. Changes over time for as specific simulation run.

3.4 Results

Figure 2 shows how the rainfall, the flood and the mudflow events, and the consequences on the road network change over time for one specific simulation run. While the beginning of the

simulation (hour 1) corresponds to a period before the hazard events occur, hours 11 and 21 correspond to periods during and at the end of the hazard events, respectively. In addition to the evolution of the flood event over time, the triggering of different mudflow events can be observed, which can be used in a later processing step to estimate the probable consequences on the network, which in this case are changes of free flow speed on the inundated and damaged road network.

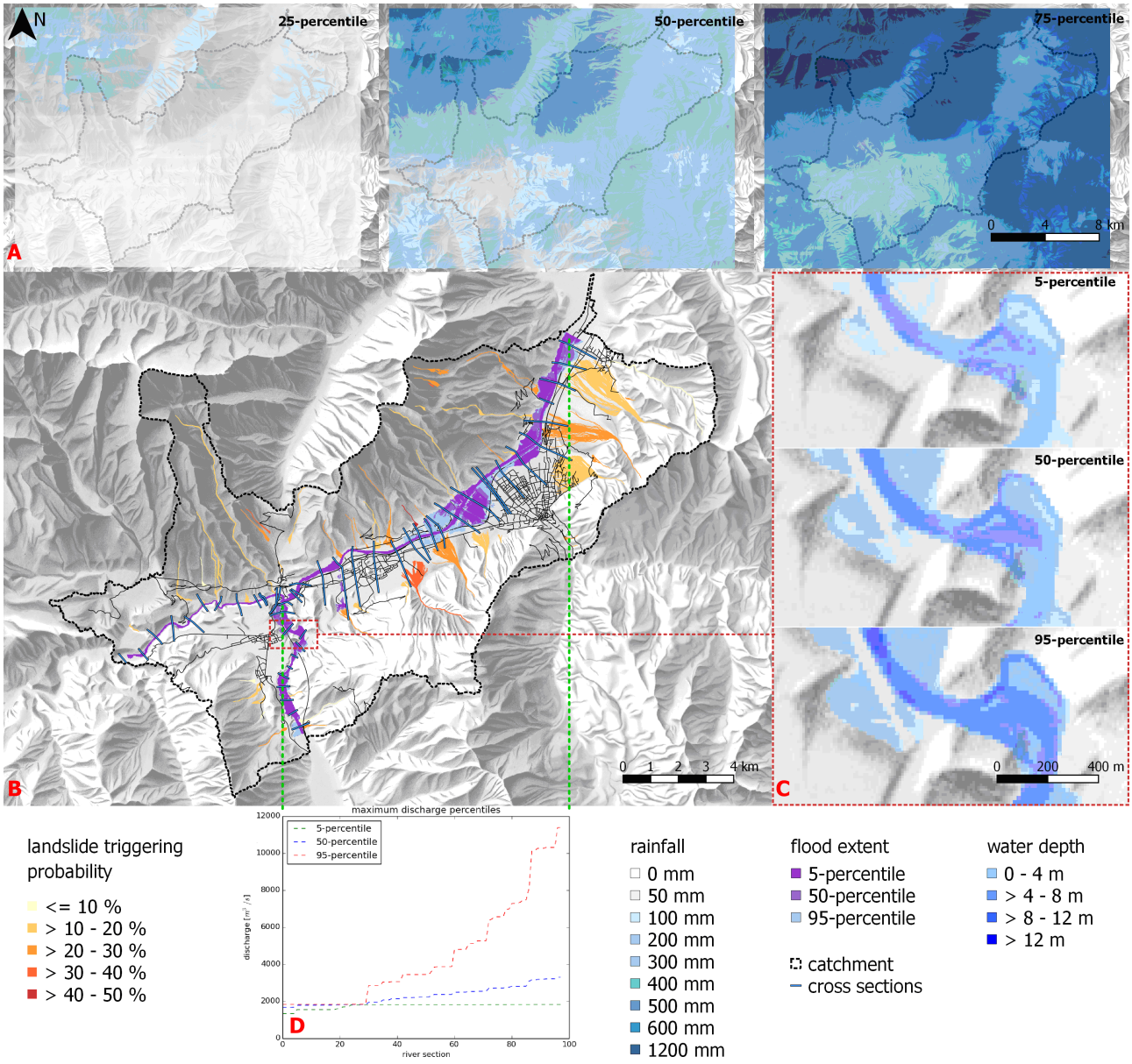

Figure 3. Aggregated simulation for a return period of 500 years.

The aggregated simulation results for a scenario with a return period of 500 years are illustrated in Figure 3. Figure 3.A shows the 25, 50 and 75-percentile of precipitation fields, where darker areas indicate more intense rainfall. An overview of the area is given in Figure 3.B. In this figure, the hazard events of interest are also presented, specifically the 5, 50 and 95-percentile of possible inundation depths and the location of possible mudflows color-coded according to their probability of occurrence. Figure 3.C zooms into a particular area. The expected discharge along the river is illustrated in Figure 3.D. It can be observed that the, 5, 50 and 95-percentile values are approximately 1,800 m^3/s at section 30, because in the chosen scenario this value corresponds to the targeted discharge value of the 500 year flood event at a the predefined gauging station located in that section.

4. CONCLUSIONS

The probabilistic method introduced here supports the modelling of the environmental conditions and hazard events impacting networks. As defined here, hydro-meteorological hazards such as riverine flood events and mudflow events change over space and time. With the decomposition into peer-reviewed models, this complexity was reduced, which resulted in a decrease of the overall computational cost of the entire risk assessment and allowed to quantify the uncertainty of resulting risk estimations. Therefore, network manager rely on computationally-efficient models that can be quickly coupled, and require data that is generally available or can be easily obtained or estimated, without impacting the integrity of the results. When an increased level of detail is required of any model, this could be achieved at a computational cost.

The method was implemented in the context of an example that aimed at stochastically simulating spatio-temporal rainfall events that caused flood and mudflow events. The results of this application are of significance to risk assessments for networks. For example, besides temporary inundation, flood events can cause scour to selected bridges that play a key role in communicating two sides of a city. Also, mudflow events can cause permanent damage to road sections that are critical due to lack of redundancy (e.g., alternative routes). Despite the virtues of the probabilistic method presented here, there is still work to be done in the development of flood and mudflow events to support network managers in calculating network related risk. Future work may focus on enhancing the hazard module described in the example to output refined results. This may include improving the determination of the time periods for the rainfall events and the intensity-duration function that triggers the mudflow events. Furthermore, given the need to determine the uncertainties related with the results, it is necessary to further explore the adequate distribution of the inputs and initial conditions. Further work could also consider an enhancement to account for the uncertain calculated discharge values in the calibration process.

REFERENCES

Adey, B. T., J. Hackl, J. C. Lam, P. van Gelder, P. Prak, N. van Erp, M. Heitzler, I. Iosifescu-Enescu, and L. Hurni (2016, Jan). Ensuring acceptable levels of infrastructure related risks due to natural hazards with emphasis on conducting stress tests. In K. Kobayashi (Ed.), *1st International Symposium on Infrastructure Asset Management (SIAM2016)*, Kyoto, Japan, pp. 19–29.

Consorcio Evaluación de Riesgos Naturales América Latina, E.-A. (2012). Tomo i: Perfil de riesgo catastrófico, medidas de mitigacin y proteccin financiera. caso sedapal y emapica. Report, Programa de Agua y Saneamiento del Banco Mundial.

Hackl, J., B. T. Adey, M. Heitzler, and I. Iosifescu-Enescu (2015). An overarching risk assessment process to evaluate the risks associated with infrastructure networks due to natural hazards. *Special Issue of International Journal of Performability Engineering on Transport System Safety, Risk and Asset Management* 11(2).

Hackl, J., M. Heitzler, J. C. Lam, B. T. Adey, and L. Hurni (2016). Final model, methodology and information exchange. Deliverable 4.2, Novel indicators for identifying critical, INFRAstructure at RISK from Natural Hazards (INFRARISK). grant agreement No. 603960, 224 pages.

Heitzler, M., J. C. Lam, J. Hackl, B. T. Adey, and L. Hurni (2016, Dec). Improved visualization of risk related to network infrastructure. *9th International Forum on Engineering Decision Making (IFED),* Stoos, Switzerland..

Kiremidjian, A., J. E. Moore, Y. Fan, O. Yazlali, N. Basoz, and M. Williams (2007). Seismic risk assessment of transportation network systems.

Kull, D. and A. Feldman (1998). Evolution of clark's unit graph method to spatially distributed runoff. *Journal of Hydrologic engineering* 3(1), 9–19.

Losey, S. and A. Wehrli (2013). Schutzwald in der schweiz: Vom projekt silvaprotect-ch zum harmonisierten schutzwald. Final report, Bundesamt für Umwelt (BAFU), Bern, Switzerland.

Padgett, J. E., R. DesRoches, and E. Nilsson (2010). Regional seismic risk assessment of bridge network in charleston, south carolina. *Journal of Earthquake Engineering* 14(6), 918–933.

Rickenmann, D. (1999). Empirical relationships for debris flows. *Natural Hazards* 19(1), 47–77.

Sigrist, F., H. R. Künsch, and W. A. Stahel (2012, dec). A dynamic nonstationary spatio-temporal model for short term prediction of precipitation. *The Annals of Applied Statistics* 6(4), 1452–1477.

Wüest, M., C. Frei, A. Altenhoff, M. Hagen, M. Litschi, and C. Schär (2010). A gridded hourly precipitation dataset for Switzerland using rain-gauge analysis and radar-based disaggregation. *International Journal of Climatology* 30(12), 1764–1775.

Proceedings of the 10th World Congress of EWRA 'Panta Rhei', 5-9 July 2017, Athens, Greece
© 2017 *European Water Resources Association*

Site suitability analysis of soil and water conservation structures in watershed using GIS

D.G. Regulwar* and R.M. Ambhore
Department of Civil Engineering, Government College of Engineering, Aurangabad, Maharashtra State, India
* *e-mail: regulwar@gmail.com*

Abstract: The planning of conservation measures to conserve water and soil resources taking hydrological planning unit as watershed is considered to be effective. Optimum utilization of natural resources like land, water, soil, vegetation, resources conservation measures and integrated development of the area along with the improvement in quality of lives of people are the main objective of watershed management program. In this study an attempt has been made for selection of the most suitable sites for water and soil conservation structures in GP IV watershed of Aurangabad district in Maharashtra, India using QGIS. Delineation of the catchment area is carried out after georeferencing them. The IRS LISS-III satellite imagery of Sillod study area is used and LULC classes have been derived from it. A soil map is obtained from National Bureau of Soil Survey and Land use planning, Nagpur, India. The slope map and drainage maps are obtained from SRTM Digital Elevation Model. The various thematic maps such as LULC map, soil map, drainage map, slope map are laid over each other and optimal allocation of check dams are proposed for construction according to guidelines for selecting suitable site for water harvesting structures according to Integrated Mission for Sustainable Development (IMSD) Govt. of India. For suggesting soil conservation structures site locations considering slope parameter, slope was divided into eight classes and accordingly structures are suggested for classes. The water balance study was also done for same watershed with monthly average temperature and precipitation data using Thornthwaite Mather model.

Key words: Geographic Information System, watershed management, soil conservation, water conservation

1. INTRODUCTION

Watershed management includes the conservation of natural resources like soil, water and increase the social and economical status of people living in the watershed. Soil and water conservation structures and its position in the watershed is key factor in efficient watershed development program. Constructing water conservation structures at suitable sites will not only conserve the runoff water optimally but also prevent huge investment on the unproductive structures.

Water harvesting structures are extremely important to conserve precious natural resources like soil and water, which is depleting day by day at alarming rate (Singh et al., 2008). There are always strong links between soil conservation and water conservation measures (Subasini et al., 2016). Classification of land according to its capability class is very much important for identification of the area for appropriate soil conservation measure for effective planning and management of watershed (Srivastava et al., 2010). Sillod watershed area in Maharashtra state, India is taken for the study and GIS is used as tool for suggesting water conservation structures and water balance study is carried out for same area using Thornthwaite Mather model. Soil conservation measures are suggested for arable and non arable land.

2. STUDY AREA

The study area of GP IV watershed is located in the Sillod Taluka of Aurangabad district Maharashtra state,India.The study area comes in the region of longitudes of 75°45' to 75°70' E and

latitudes of 20°37’ to 20°51’ N with geographical area of 195.052 km².

3. MATERIALS USED

For preparation of thematic maps firstly watershed maps of Aurangabad district is taken to extract study area.SRTM DEM is taken for deriving slope maps. Soil map is taken from NBSS Nagpur and then georeferenced. Weather data is taken for the year 2013. All the data and maps are firstly georeferenced and digitize for further work.

4. METHODOLOGY

4.1 Water Balance study

Water balance study for the watershed for each month is done with the use of TM model using data of daily precipitation and monthly mean temperature. The water balance of a small area can be expressed as:

$$P = I + AET + OF + \delta SM \quad (1)$$

where: P = Precipitation
I = Interception
AET = Actual evapotranspiration
OF = Overland flow
δSM = Change in soil moisture

In this study ground water parameter is not considered while doing monthly water balance study. TM model is widely used because it is simple, empirical and convenient and the ET determined by TM model is based on average temperature and length of day (Michel, 1978). Data required for running TM model for monthly water balance and indirectly calculating runoff in watershed are mean monthly temperature, soil textures and their water holding capacities, root zone depth of different soil types which we get from NBSS soil bulletin.

There are three types of soil present in the watershed viz, Clayey soil, Clayey loam and rocky outcrops clayey soil. Soil depth and water holding capacities of these types are get from NBSS soil bulletin data. According to this various components of water balance equation is calculated to get overland flow by using data of rainfall and temperature.

4.1.1 Calculation of PET

For the calculation of PET, firstly monthly heat index for each month is calculated by the equation:

$$j = (t_n/5)^{1.514} \quad (2)$$

where, t_n =mean temperature of nth month, j = Month heat index

Annual heat index (J) is calculated by the following equation:

$$J = \sum_1^{12} j \quad (3)$$

PET is calculated with the following equation:

$$PET = 16 \times (10t_n / J)^a \quad (4)$$

where, PET = Potential Evapotranspiration, t_n =monthly mean temperature, J = Annual heat index, a is cubic function of J and it is calculated as:

$$a = 0.49 + (1.79 \times 10^{-2} \times J) - (7.711 \times 10^{-5} \times J^2) + (6.751 \times 10^{-7} \times J^3) \quad (5)$$

In this study PET is calculated for the 12 months for the year 2013 then difference of Precipitation and Potential evapotranspiration (P-PET) is computed for each month.

4.1.2 Calculation of Soil moisture

For the calculation of soil moisture:
If P < PET for any month then Soil moisture is considered as full water holding capacity of soil
If P > PET then equation is:

$$(\text{Soil moisture})_n = (\text{Soil moisture})_{n-1} \times e^{(\text{P-PET}/\text{ Soil moisture full})} \quad (6)$$

where, n = n^{th} month
By applying these conditions to all the months of the year and soil moisture is calculated. The change in soil moisture is calculated from the successive months beginning from end of wet season (Table 1).

4.1.3 Calculation of Actual Evapotranspiration (ET)

For the calculation of actual evapotranspiration following two criterias considered:
If P > PET, then ET = PET
If P < PET, then ET = P + change in soil moisture.

The deficit exists only during the months, when precipitation is less than potential evapotranspiration. Excess surplus moisture is termed as runoff and percolation and in the water balance equation is assumed to become stream flow (Q) (Table 1). Similar table is prepared for the other two soil types viz, Clayey Loam and clayey soil and the runoff and runoff volume is computed for the watershed.

Table 1. Long term monthly water balance for Rock outcrops clayey soil with water holding capacity 168mm

	Precipi-tation	Average Day Temp	Monthly Heat Index	Annual Heat Index	a	PET	P-PET	Soil Moisture	Change in Soil Moisture	ET	Surplus	Deficit
January	0	21.30	8.98	137.19	3.24	66.52	-67	56	-27	27	0	93.52
February	4	24.22	10.89	137.19	3.24	100.70	-97	31	-25	29	0	121.71
March	2	27.12	12.93	137.19	3.24	145.25	-143	13	-18	20	0	161.25
April	0	30.06	15.11	137.19	3.24	202.69	-203	4	-9	9	0	211.69
May	0	32.94	17.36	137.19	3.24	272.78	-273	0.8	-3.2	3.2	0	275.98
June	408	26.78	12.69	137.19	3.24	139.42	269	168	0	139	269	0
July	496	23.66	10.52	137.19	3.24	93.44	403	168	0	93	403	0
August	474	23.06	10.12	137.19	3.24	85.91	388	168	0	86	388	0
September	231	24.17	10.86	137.19	3.24	100.07	131	168	0	100	131	0
October	147	23.31	10.29	137.19	3.24	89.07	58	168	0	89	58	0
November	5	21.78	9.28	137.19	3.24	71.49	-66	113	-55	60	0	121.49
December	3	19.99	8.16	137.19	3.24	54.21	-51	83	-30	33	0	81.21
Σ			**137.19**								**1249**	

4.2 Water conservation structures

The data of Sillod watershed is obtained from the sources and firstly the maps are extracted for

our region after georeference and then prepared in digital format using Geographic Information System. The flowchart for preparation of thematic maps is as shown in the figure 1 below,

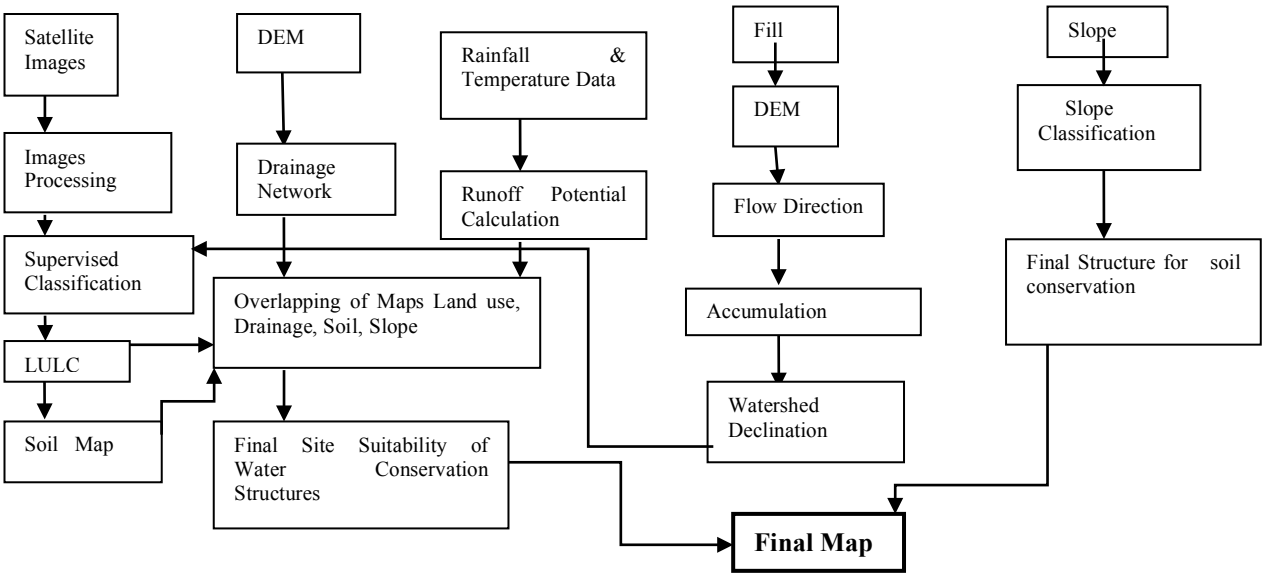

Figure 1. Flow chart of methodology for site suitability of Soil and Water conservation structures

Check dams are suggested according to the following guidelines given by IMSD:

(i) The slope should be less than 15 per cent.
(ii) The land use may be barren, shrub land and riverbed.
(iii) The infiltration rate of the soil should be less.
(iv) The type of soil should be sandy clay loam.

4.3 Soil conservation structures

For suggesting soil conservation structures in the arable and non arable land study area is divided into 8 land capability classes as per land AISLUO(1970) the classification of slope is as per shown in Figure 3.

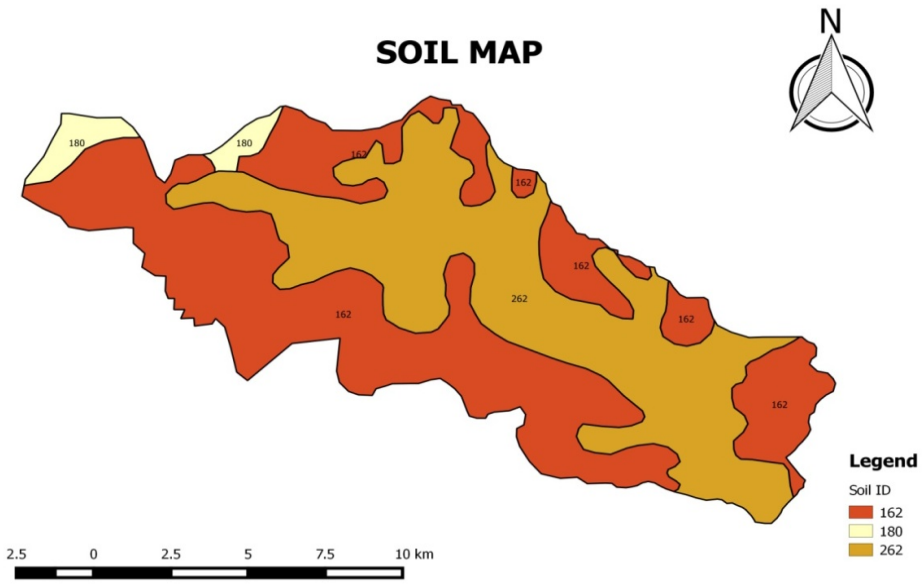

Figure 2. Soil map

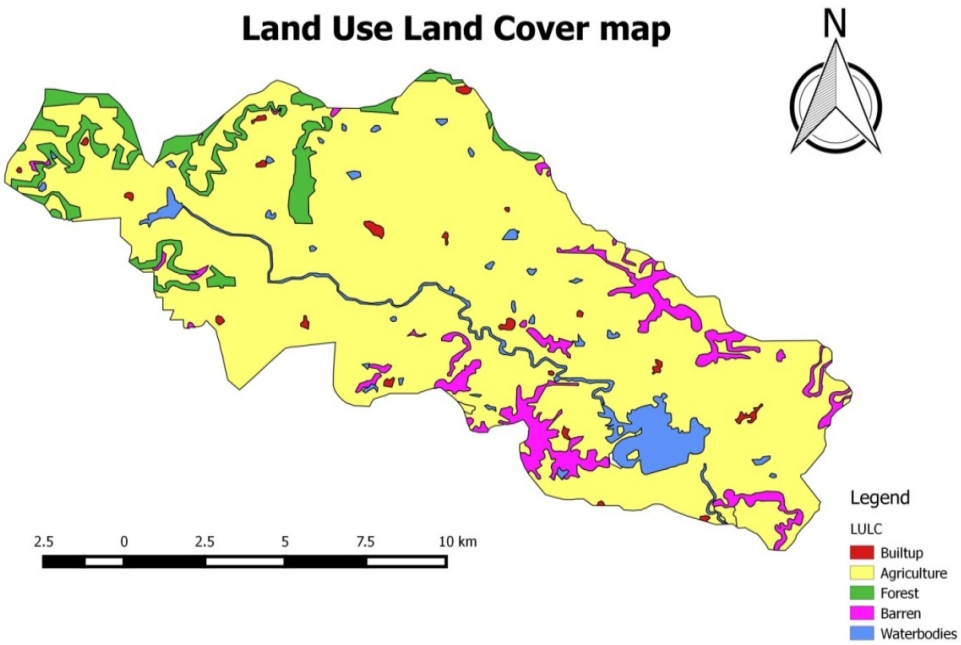

Figure 3. Land cover map

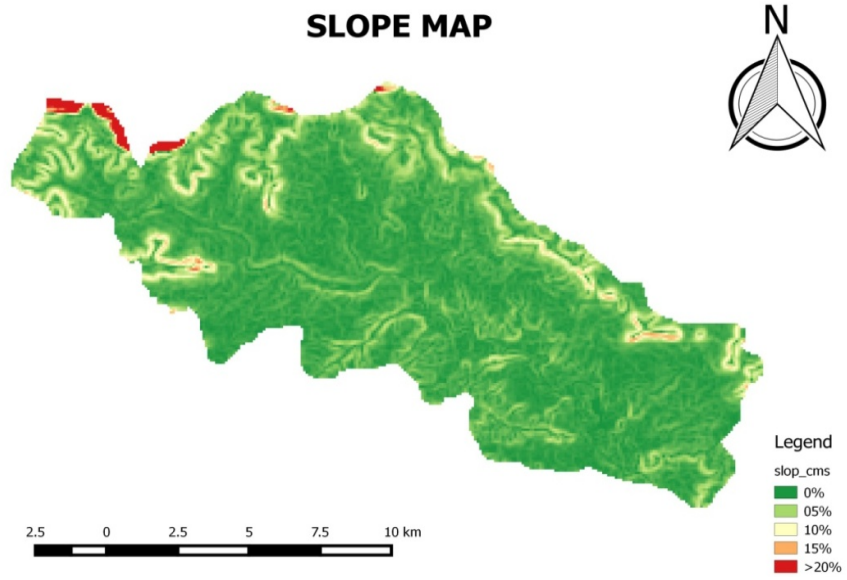

Figure 4. Slope Map

5. CONCLUSION

5.1 Water balance study

The water balance study is done using the TM model for each month for the Sillod watershed in Aurangabad India. The runoff for the year 2013 was found to be 1249 mm and the total runoff volume for the watershed is 243 Mm^3 (Table 1).

5.2 Soil conservation structures

By classifying the study area into 8 land capability classes considering the slope parameter soil conservation structure contour bunding is suggested for class I to IV i.e. for arable lands. The main

aim to provide soil conservation structure in this type of arable land is reducing erosion while keeping desired soil moisture. Contour trenching should provide in the non arable land that is for land capability class V to VIII. The main aim for providing these structures in non arable land region is to reduce the runoff velocity and infiltration of water to increase the groundwater table.

5.3 Sites for check dams

All the thematic maps such as Land use land cover, soil map, slope map and stream network are overlayed and cross operation has been done using GIS and best suitable location for check dams are suggested in the study area and 15 sites for check dams are proposed in the GPIV watershed. The final map of suitable site location is as shown in Figure 4.

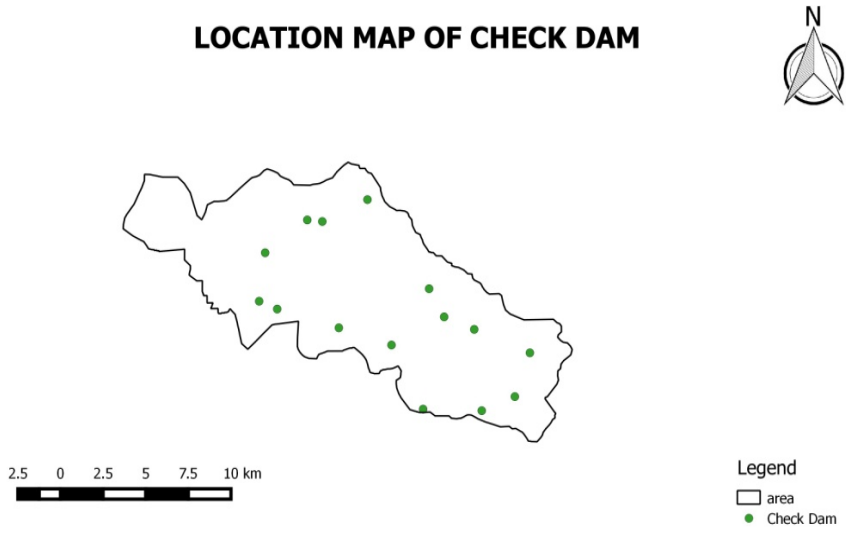

Figure 5. Final map showing suitable location of check dams

REFERENCES

Singh J.P., Singh D., Litoria P.K., 2009. Selection of Suitable Sites for Water Harvesting Structures in Soankhad Watershed, Punjab using Remote Sensing and Geographical Information System (RS&GIS) Approach- A Case Study. J. Indian Soc. Remote Sens; 37: 21–35.

Srivastava R.K., Sharma H.C., Raina A.K., 2010. Suitability of soil and water conservation measures for watershed management using geographical information system. Journal of soil and water conservation; 9(3):148-153.

Subasini A., Shanmugasundram K., Ravikumar V., 2016. Optimal allocation of check dam using remote sensing and geographical information system – a new approach. American Research Thoughts; 2(6):31-42.

Michael A.M., 1978. Irrigation: Theory and Practice.Vani Educational Books.

AISLUSA, 1990. Watershed Atlas of India, Department of Agriculture and Cooperation. All India Soil and Land use Survey, IARI campus, New Delhi.

Proceedings of the 10th World Congress of EWRA 'Panta Rhei', 5-9 July 2017, Athens, Greece
© 2017 *European Water Resources Association*

Imputation of erosivity values under incomplete rainfall data by machine learning methods

K. Vantas and E. Sidiropoulos*
Faculty of Engineering, Aristotle University of Thessaloniki, Greece
* *e-mail: nontas@topo.auth.gr*

Abstract: In this article, a comparison is presented of empirical equations to machine learning methods for the estimation and imputation of rainfall erosivity values, associated with significant amounts of rainfall measurements that are missing in the available recording rain gauge data of the Greek Hydroscope database. The empirical equations are mainly based on exponential relations between erosivity and rainfall, while the machine learning methods employed in this paper are feed-forward neural networks with Bayesian regularization and ridge regression with nonlinear transformation. The data came from 81 measuring stations of the Ministry of the Environment and Energy. In the employed algorithms, the output was the weekly cumulative erosivity value, which resulted from processing the data of all rain gauges and pluviographs, while the input data consisted of the weekly cumulative rainfall, the month, the co-ordinates and the elevation of the station, as well as the number of days for which the rainfall was recorded. For validation, a method of nested cross-validation was employed. The machine learning methods gave significantly better results compared to the empirical equations, thus reducing the effects of estimating R from only weekly rainfall records.

Key words: machine learning, missing values, imputation, rainfall erosivity

1. INTRODUCTION

The soil loss problem of Greece dates back to prehistoric times (Vita-Finzi, 1969; Van Andel and Zangger, 1990), while during the last fifty years it has been aggravated due to the intensification and mechanization of the agricultural sector (Boardman and Poesen, 2006). In the year 2001, the Hellenic National Action Plan against Desertification was enacted, in which it was recognized that the country is inflicted by the phenomenon of desertification. The most significant process responsible for soil loss in Greece is related to rainfall erosivity.

The evaluation of rainfall erosivity is essential for the assessment of the soil loss risk, and the difficulty in small scale modelling has led to more tractable rainfall indices, such as the coefficient R of the Universal Soil Loss Equation (USLE), (Wischmeier and Smith, 1978). The computation of R requires pluviograph data for the determination of 30 minutes' maximum intensities of storms over time periods of more than 20 years (Renard and Freimund, 1994). In order to deal with the lack of such data, several models have been developed based on rainfall measurements at various time steps, on spatial parameters and on climatological data, such as maximum precipitation etc. (Diodato and Bellocchi, 2007; Angulo-Martínez and Beguería, 2009).

Pluviograph data, although available to a great extent in Greece, suffer from significant proportions of missing values. This fact necessitated imputation of the erosivity values that resulted from the data, so as to finally estimate R on a countrywide basis. For this imputation both empirical equations and machine learning methods were employed and comparisons between these two approaches are presented in this paper.

The problem of infilling hydro-meteorological data in general has been dealt within the literature, in terms of local averages (Pappas et al., 2014) and in relation to various forms of neural networks (Coulibaly and Evora, 2007; Nkiaka et al., 2016). Imputation in relation to erosivity is scarce. A recent publication (Diodato et al., 2017) concerns reconstruction of time series from

coarser rainfall records. The use of machine learning methods, such as Neural Networks can be found in the recent literature on the subject of rainfall prediction (Hellman et al., 2012; Sharma and Goyal, 2016), but not in relation to the special issue of erosivity, as presented in this paper.

2. DATA AND METHODS

2.1 Constitution of the data set

The data utilized in the analysis were taken from the Hydroscope Database (Koutsogiannis et al., 1995) and came from 81 meteorological stations of the Ministry of the Environment (Figure 1). The time series comprised a total of 2,333 years of pluviograph records with a time step of 30 minutes for the time period from 1953 to 1997, including the corresponding rain gauge 24-hour measurements with average record length 28 years. The time series were checked for gross errors and cleaned from noise that was due to the initial digitization of the pluviometers' bands. Missing values were marked out in a consistent way. In the pluviograph data, the percentage of these values was 44% on average, while the corresponding value in the rain gauges' data was 7%.

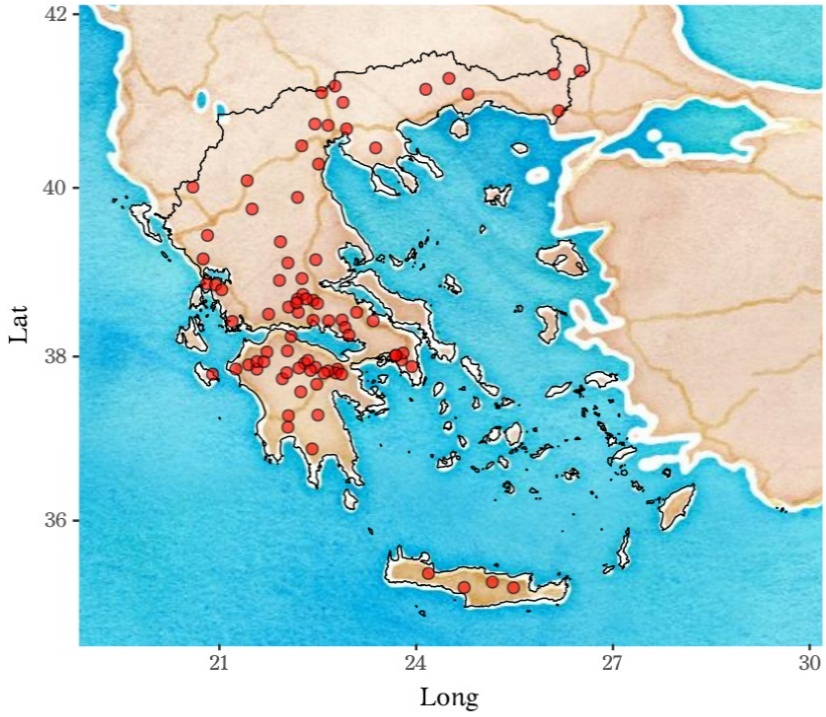

Figure 1. Meteorological stations.

For the above described data, it was deemed useful to change the time step and aggregate the data into weekly values, because 57% of the recordings were associated with storms occupying time periods covering parts of more than one calendar day, although only 17% of the storms had duration of more than 24 hours. Under the time step of one week, it was found out that 80% of the values emanated from a single storm. The storms that were crossed temporally by two consecutive weeks were assigned to the first of the two weeks. They comprised only 7% of the data. Thus, through the use of weekly instead of daily values, divisions of storms due to time-step were prevented.

2.2 Extraction of rainfall erosivity

The R coefficient (MJ.mm/ha/h/yr) is defined as the long-term average of the product of the

kinetic energy of a storm and the maximum 30 min intensity (Brown and Foster, 1987):

$$R = \frac{1}{n}\sum_{j=1}^{n}\sum_{k=1}^{m_j}\left(EI_{30}\right)_k \tag{1}$$

where n is the number of years with rainfall records, m_j the number of storms during year j and EI_{30} the erosivity of storm k. The erosivity EI_{30} (MJ.mm/ha/h) is equal to:

$$EI_{30} = \left(\sum_{r=1}^{m} e_r v_r\right) I_{30} \tag{2}$$

where e_r is the energy of rainfall (MJ/ha/mm) and v_r the rainfall depth (mm) for the time interval r of the hyetograph, which has been divided into r = 1, 2, ..., m subintervals, such that each one of these is characterized by constant rainfall intensity. The quantity e_r is calculated for r from the relation:

$$e_r = 0.29 \cdot \left(1 - 0.72e^{-0.05 i_r}\right) \tag{3}$$

where i_r is the rainfall intensity (mm/h). The rules that apply in order to single out the storms causing erosion and to divide rainfalls of large duration are: (a) A rainfall event is divided into two parts, if its cumulative depth for duration of 6 hours at a certain location is less than 1.3 mm and (b) A rainfall is considered erosive, if it has a cumulative value greater than 12.7 mm or if during a time period of 15 mins a cumulative value of at least 6.4 mm is recorded.

2.3 Solution methods

The erosivity imputation problem is set up as a scheme of statistical learning, consisting of (a) data representing features of the studied physical processes, (b) measured outcomes of the same processes and (c) numerical models that simulate the physical processes as closely as possible based on the data of (a) and (b).

2.3.1 Outcomes and features

The outcomes, denoted as $y^{(i)}$, where (i) is the index of a sample consisting of m = 20,603 values, represented weekly cumulative rainfall erosivity, as it resulted from the pertinent calculations based on the data of all pluviographs. The features included the weekly cumulative rainfall P of erosive events, the month to which the above individual m values are referred, the longitude, latitude and altitude of the meteorological stations and the number of the days of the week (one, two, three or more), for which rainfall is recorded. Depending on the model used, a different subset of input variables was used.

2.3.2 Validation of models

A number of models were evaluated for the imputation problem, accompanied each time by a suitable algorithm. In all cases the estimation of the out-of-sample error and the optimal hyperparameters of the used models was performed using nested cross validation. In the outer cross validation, the data were divided into 10 sections for the purpose of estimating the out-of-sample error. In the inner cross validation, every set of the outer training was divided again into 10 sections in order to select the optimal hyperparameters of the models. The division of the data into sections

was executed on a yearly basis, so that sets of equal sizes could be formed. The coefficient of determination R^2 was used as a measure of the error:

$$R^2 = 1 - \frac{\sum_{i=1}^{m} \left(h\left(x_{test}^{(i)} \right) - y_{test}^{(i)} \right)^2}{\sum_{i=1}^{m} \left(\hat{y}_{train} - y_{test}^{(i)} \right)^2} \tag{4}$$

thus, each model was compared with a simplistic one which was equal to the average of the training set values $\hat{y}_{train}$.

2.4 Models and algorithms

2.4.1 Nonlinear least squares models

Two alternative exponential models (Richardson et al., 1983; Yu and Rosewell, 1996) were tried, given by Equations (5) and (6) and leading to optimal adjustments of two respective hypotheses, NLLS1 and NLLS2:

$$h_\theta(x) = \theta_0 \cdot P^{\theta_1} \tag{5}$$

$$h_\theta(x) = \theta_0 \left(1 + \theta_1 \cos\left(\frac{\pi}{6}(m - \omega) \right) \right) \cdot P^{\theta_2} \tag{6}$$

where ω is the month with the largest median of the y values as it derived from the training data and θ_0, θ_1 and θ_2 the parameters of the two hypotheses. The latter were determined by minimizing the following objective function by the trust region reflective method (Coleman and Li, 1994, 1996):

$$J(\theta) = \frac{1}{2m} \sum_{i=1}^{m} \left(h_\theta(x^{(i)}) - y^{(i)} \right)^2 \tag{7}$$

2.4.2 Ridge regression with nonlinear transformation

The hypothesis LR tried was the following:

$$h_\theta(x) = \theta_0 + \sum_{j=1}^{17} x_j \cdot \theta_j \tag{8}$$

where x_j, j=1, 2, ..., 17 stands for the input data and θ_j, for the parameters of the linear regression to be determined. The input data x were the normalized values of log(P), Long, Lat, Alt, 11 binary values for the corresponding month and 2 binary values representing the rainy days. The normalizing transformation of the data was the following:

$$N\left(x^{(i)} \right) = \frac{x^{(i)} - \bar{x}}{sd(x)} \tag{9}$$

where $\hat{x}$ denotes average and sd(x) standard deviation. The parameters θ_j were determined from the minimization of the following objective function by means of the conjugate gradient algorithm

(Nocedal and Wright, 2006):

$$J(\theta)=\frac{1}{2m}\sum_{i=1}^{m} w^{(i)}\left(h_\theta\left(x^{(i)}\right)-y^{(i)}\right)^2+\frac{\lambda}{2m}\sum_{j=1}^{n}\theta_j^2 \quad (10)$$

The regularizing hyperparameter λ prevented overfitting of the model to the training data (Abu-Mostafa et al., 2012). The weight of sample i, $w^{(i)}$ was set equal to $w^{(i)} = y^{(i)}/\max(y)$ so that higher y values had proportionately larger weights and z = log(y) was the nonlinear transformation of the outcome. The optimal value of $\lambda = 3\cdot10^{-7}$ resulted from a vector of values $\mathbf{\Lambda} = [10^{-9}, 3\cdot10^{-8}, 10^{-8}, ...,1]$.

2.4.3 Feed-forward neural networks with Bayesian regularization

Neural networks as powerful regression tools try to mimic the function of the human brain (Bishop, 1995). The learning algorithm used here is Bayesian regularization back-propagation, in combination with the Levenberg-Marquart method (Moré, 1978). Regularization and feature selection are automatically incorporated and the whole algorithm yields a network with good generalizing abilities (MacKay, 1992; Foresee and Hagan, 1997).

The architecture of the neural networks included one hidden layer with a linear output. The training of the networks was performed by the method of early stopping (Wang et al., 1994) by utilizing a random validation set consisting of 10% of the training data, so as to avoid overfitting of the neural networks. In order to prohibit negative values, the network output results were bounded based on the smallest outcome value of the training data. The input data x were the normalized values of P, Long, Lat, Alt, eleven binary values representing the month and two binary values representing the number of rainy days.

The hypothesis NNET employed consisted in the ensemble averaging of 20 neural networks, in order to deal with the inherent instability of neural networks due to locally optimal solutions for their parameters. The number of hidden neurons was treated as a hyperparameter of the algorithm and it was finally determined as l = 30 from a vector of possible values L = [20, 25, 30, 35, 40].

3. RESULTS

The comparison of the algorithms was based on the work Demšar (2006), Garcia and Herrera (2008) and García et al. (2010) on the use of non-parametric methods for the evaluation of results of machine learning algorithms, because parametric hypothesis testing methods (pairwise t-test and ANOVA) were not deemed suitable due to the nature of the algorithms. The procedure employed for hypothesis testing made use the statistical programming language R (R Core Team, 2016).

The mean ranking of the algorithms is given on the basis of the 10 values of R^2 that resulted from the outer nested cross validation and is: NLLS1 = 3.9, NLLS2 = 3.0, LR = 1.8 and NNET = 1.3 with median values of R^2: 0.46, 0.50, 0.61 and 0.65 respectively. Figure 2 shows the box plots of the error measures, where the superior performance of NNET is demonstrated.

The Friedman test (Friedman, 1937) was performed, in order to determine whether an algorithm has a systematically better or worse performance. The obtained p-value $1.7\cdot10^{-5}$ indicated that the null hypothesis of all the algorithms perform the same could be safely rejected. Then post-hoc tests followed for all possible pairs of algorithms using the Wilcoxon signed rank test (Wilcoxon, 1945). Because of the multiple pair wise tests, the p-values that resulted were adjusted using Benjamini and Hochberg method (1995), which controls the false discovery rate. The results are given in Table 1, where it is shown that there were statistically strong evidences that the machine learning algorithms outperformed parametric methods. Between LR and NNET there were statistical evidences that the latter performed better.

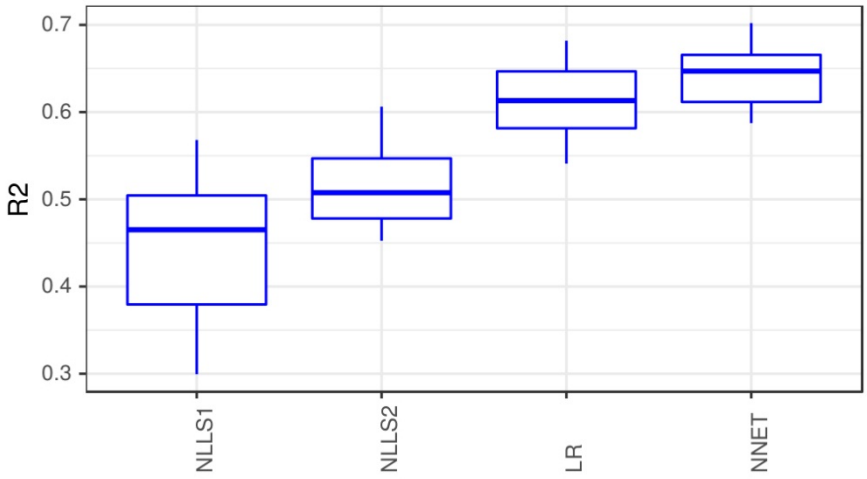

Figure 2. Outer cross validation R^2 boxplots.

Table 1. Adjusted Wilcoxon signed rank test p-values by Benjamini and Hochberg method.

	NLLS1	***NLLS2***	***LR***
NLLS2	*0.011*		
LR	*0.004*	*0.006*	
NNET	*0.004*	*0.004*	*0.064*

3. CONCLUSIONS

Because of the significant percentage of missing values in the time series, the use of the existing pluviograph data only would lead to an underestimation of R values. For this reason, a number of algorithms were employed for the imputation of erosivity values. From the performance evaluation of the algorithms by descriptive analysis and statistical inference, it was concluded that the presented machine learning algorithms outperformed the classical methods of estimation via parametric equations, reducing the effects of estimating R from weekly rainfall records. The NNET algorithm, besides having the best performance, presented the additional advantage of not necessitating prior knowledge of the form of its nonlinearity, in contrast to other tested algorithms.

REFERENCES

Abu-Mostafa, Y. S., Magdon-Ismail, M. and Lin, H.-T. (2012), Learning from data, Vol. 4, AMLBook Singapore.

Angulo-Martínez, M. and Beguería, S. (2009), 'Estimating rainfall erosivity from daily precipitation records: A comparison among methods using data from the Ebro Basin (NE Spain)', Journal of Hydrology 379(1), 111–121.

Benjamini, Y. and Hochberg, Y. (1995), 'Controlling the false discovery rate: A practical and powerful approach to multiple testing', Journal of the Royal Statistical Society. Series B (Methodological) 57, 289–300.

Bishop, C. M. (1995), Neural Networks for Pattern Recognition, Oxford University Press.

Boardman, J. and Poesen, J. (2006), Soil Erosion in Europe, Wiley Online Library.

Brown, L. and Foster, G. (1987), 'Storm erosivity using idealized intensity distributions', Trans. ASAE 30(2), 379–386.

Coleman, T. F. and Li, Y. (1996), 'An interior trust region approach for nonlinear minimization subject to bounds', SIAM Journal on Optimization 6(2), 418–445.

Coleman, T. and Li, Y. (1994), 'On the convergence of Reflective Newton Methods for Large-scale Nonlinear Minimization Subject to Bounds vol. 67', Ithaca, NY, USA: Cornell University.

Coulibaly, P. and Evora, N. (2007), 'Comparison of neural network methods for infilling missing daily weather records', Journal of hydrology 341(1), 27–41.

Demšar, J. (2006), 'Statistical comparisons of classifiers over multiple data sets', Journal of Machine Learning Research 7(Jan), 1–30.

Diodato, N. and Bellocchi, G. (2007), 'Estimating monthly (R) USLE climate input in a Mediterranean region using limited data', Journal of Hydrology 345(3), 224–236.

Diodato, N., Borrelli, P., Fiener, P., Bellocchi, G. and Romano, N. (2017), 'Discovering historical rainfall erosivity with a parsimonious approach: A case study in Western Germany', Journal of Hydrology 544, 1–9.

Foresee, F. D. and Hagan, M. T. (1997), Gauss-Newton approximation to Bayesian learning, in ‘International Conference on Neural Networks, 1997.’, Vol. 3, IEEE, pp. 1930–1935.

Friedman, M. (1937), ‘The use of ranks to avoid the assumption of normality implicit in the analysis of variance’, Journal of the American Statistical Association 32(200), 675–701.

García, S., Fernández, A., Luengo, J. and Herrera, F. (2010), ‘Advanced nonparametric tests for multiple comparisons in the design of experiments in computational intelligence and data mining: Experimental analysis of power’, Information Sciences 180(10), 2044–2064.

Garcia, S. and Herrera, F. (2008), ‘An extension on “Statistical Comparisons of Classifiers over Multiple Data Sets” for all Pairwise Comparisons’, Journal of Machine Learning Research 9 (Dec), 2677–2694.

Hellman, S., McGovern, A. and Xue, M. (2012), Learning ensembles of Continuous Bayesian Networks: An application to rainfall prediction, in ‘Intelligent Data Understanding (CIDU), 2012 Conference on’, IEEE, pp. 112–117.

Koutsogiannis, D., Tsakalias, G., Christofidis, A., Manetas, A., Sakelariou, A., Maurodimou, P., Papakostas, N., Mamasis, N., Nalbandis, I. and Ksanthopoulos, T. (1995), HYDROSCOPE: Creation of a National Databank for Hydrological and Meteorological Information, Technical report, National Technical University of Athens.

MacKay, D. J. (1992), ‘Bayesian interpolation’, Neural Computation 4(3), 415–447.

Moré, J. J. (1978), The Levenberg-Marquardt algorithm: Implementation and theory, in ‘Numerical Analysis’, Springer, pp. 105–116.

Nkiaka, E., Nawaz, N. and Lovett, J. (2016), ‘Using self-organizing maps to infill missing data in hydro-meteorological time series from the Logone catchment, Lake Chad basin’, Environmental monitoring and assessment 188(7), 1–12.

Nocedal, J. and Wright, S. J. (2006), ‘Conjugate Gradient Methods’, Numerical Optimization pp. 101–134.

Pappas, C., Papalexiou, S. M. and Koutsoyiannis, D. (2014), ‘A quick gap filling of missing hydrometeorological data’, Journal of Geophysical Research: Atmospheres 119(15), 9290–9300.

R Core Team (2016), R: A Language and Environment for Statistical Computing, R Foundation for Statistical Computing, Vienna, Austria.

Renard, K. G. and Freimund, J. R. (1994), ‘Using monthly precipitation data to estimate the R-factor in the revised USLE’, Journal of Hydrology 157, 287–306.

Richardson, C., Foster, G. and Wright, D. (1983), ‘Estimation of erosion index from daily rainfall amount’, Transactions of the ASAE 26(1), 153–156.

Sharma, A. and Goyal, M. K. (2016), ‘Bayesian network for monthly rainfall forecast: A comparison of K2 and MCMC algorithm’, International Journal of Computers and Applications 38(4), 199–206.

Van Andel, T. H. and Zangger, E. (1990), Landscape stability and destabilisation in the prehistory of Greece, in ‘Proceedings of the INQUA/BAI symposium on the impact of ancient man on the landscape of the Eastern Mediterranean region and the Near East’, Vol. 12, pp. 139–157.

Vita-Finzi, C. (1969), The Mediterranean valleys: Geological changes in historical times, Vol. 165, University Press.

Wang, C., Venkatesh, S. S. and Judd, J. S. (1994), ‘Optimal Stopping and Effective Machine Complexity in Learning’, Advances in Neural Information Processing Systems 6, 303–310.

Wilcoxon, F. (1945), ‘Individual comparisons by ranking methods’, Biometrics Bulletin 1(6), 80–83.

Wischmeier, W. H. and Smith, D. D. (1978), Predicting rainfall erosion losses-A guide to conservation planning, USDA, Science and Education Administration.

Yu, B. and Rosewell, C. (1996), ‘An assessment of a daily rainfall erosivity model for New South Wales’, Soil Research 34(1), 139–152.

Proceedings of the 10th World Congress of EWRA 'Panta Rhei', 5-9 July 2017, Athens, Greece
© 2017 *European Water Resources Association*

Impact of restoration measures in a densely urbanised area: The case of Buenos Aires

I.M. Arzuaga[1], G. Navarro[1,2] and S.V. Viñes[1*]
[1] *Universidad Católica Argentina, Facultad de Ciencias Fisicomatemáticas e Ingeniería, Buenos Aires, Argentina.*
[2] *CONICET, Argentina*
[*] *e-mail: susanavines@yahoo.com.ar*

Abstract: In the Metropolitan Area of the Buenos Aires City (AMBA) does not exist regulation which prioritizes the need to preserve water reservoirs and still less to generate them to compensate for the growing anthropization of the territory and to mitigate the effects of climate change. The objective of this work is to evaluate the impact of altering the morphology of a sub basin of the Las Tunas stream, tributary of Lujan River, belonging to the "Pampa Ondulada Bonaerense" territory. The hydrological analysis was performed and the topographic characteristics of the basin were generated in HEC-HMS model, obtaining flow rates in different morphological situations. The input and output system flow rates are calculated using rainfall-runoff and flow-through procedures. The histogram method (for a given frequency of occurrence of the event) has been selected, which specifies the temporal distribution of precipitation intensity during the storm. The results indicated a lamination of the peak of the flooding in more than fifty percent with only preserving less than five percent of the study area to generate a temporary reservoir, which reveals the need to protect natural reservoir areas or generate them, in order to restore in the basins the hydrogeomorphological conditions precedent to anthropization. This reservoir becomes even more necessary when considering the effects of Climate Change on runoff due to the increase in precipitation intensity of extreme events.

Key words: Hydrogeomorphological Basin, Runoff, Climate Change

1. INTRODUCTION

The population growth in the Metropolitan Area of the Buenos Aires City (AMBA) shows the incessant transformation of rural land into urbanized areas with industrial areas, private neighborhoods and slums chaotically located. This situation alters the runoff on basins due to variations in the topography and waterproofing of it.

Alterations on the meteorological parameters, lead by climate change (Viñes, 2014), causes variations in the values that must be adopted for the design of the infrastructure, in order to reduce the risks of its obsolescence. Therefore, appears the need to attenuate floods to preserve populated areas waters below the intervention.

The objective of this work is to evaluate the impact of altering the morphology of a sub basin in Las Tunas stream, establishing comparative advantages that arise from modeling different morphological conditions (Verstappen et al., 1991). These situations are generated by simulations on the HEC-HMS Model. The simulations are carried out with the objective of seeking compensation for the constant increase of the runoff, caused by the alteration of the natural hydrogeomorphological conditions in the basins (Campo de Ferreros et al., 1999). Its purpose is to generate an alternative morphological situation that mitigates the undesirable effects of anthropization and Climate Change (Torrero, 2016).

2. METHODOLOGY

2.1 Model

Based on the characteristics of the system and the available information, the HEC-HMS

Simulation Model of the U. S. Army Corps of Engineers Research Center, located in Davis, California, is selected.

The HEC - HMS Model is designed to simulate surface runoff resulting from a precipitation event, by representing the basin as a system of interconnected components.

As final results of the modeling process, a direct runoff hydrographs is obtained for several sub-areas and the flow hydrographs at predetermined locations on the basin.

The hydrographs obtained by the software are used directly or in conjunction with other software packages for studies of water availability, urban drainage, flow projection, impacts of future urbanization, landfill projects on dams, flood damage reduction, among others.

The components that take part of the model are classified into two types, Surface Runoff Component and Stream Flow component. The first one is for a subarea and is used to represent the movement of water on the surface of the terrain towards the river channels. The input data in this component is a precipitation plot. Excess rain is calculated by subtracting infiltration and losses. The second one is used to represent the movement of crescent waves through a channel. The input data for this component is the upstream hydrograph, which results from the individual or combined contributions of the subarea runoff, the flow movement, or the shunts. This hydrograph is transported downstream using the characteristics of the channel.

2.2 Study area

The modeling carried out corresponds to the basin of the Las Tunas stream, belonging to the Darragüeira - Las Tunas basin (Cabral, 2015).

The Darragüeira - Las Tunas basin flows into the Reconquista River Relief Channel, and includes a contribution area of 30.9 km2, which comprises part of the Malvinas Argentinas department (departments: Malvinas Argentinas, Los Polvorines, Pablo Nogués and Villa de Mayo) and the Tigre department (departments: Lopez Carmelo and El Talar).

The basin of the Las Tunas stream, on the other hand, has an approximate area of 1334 hectares (with closure in the tracks of the General Bartolomé Mitre train line). In the interior of the land, the stream unloads its waters on a lagoon of 17,400 square meters. Figure 1 schematizes the extension of the study basin.

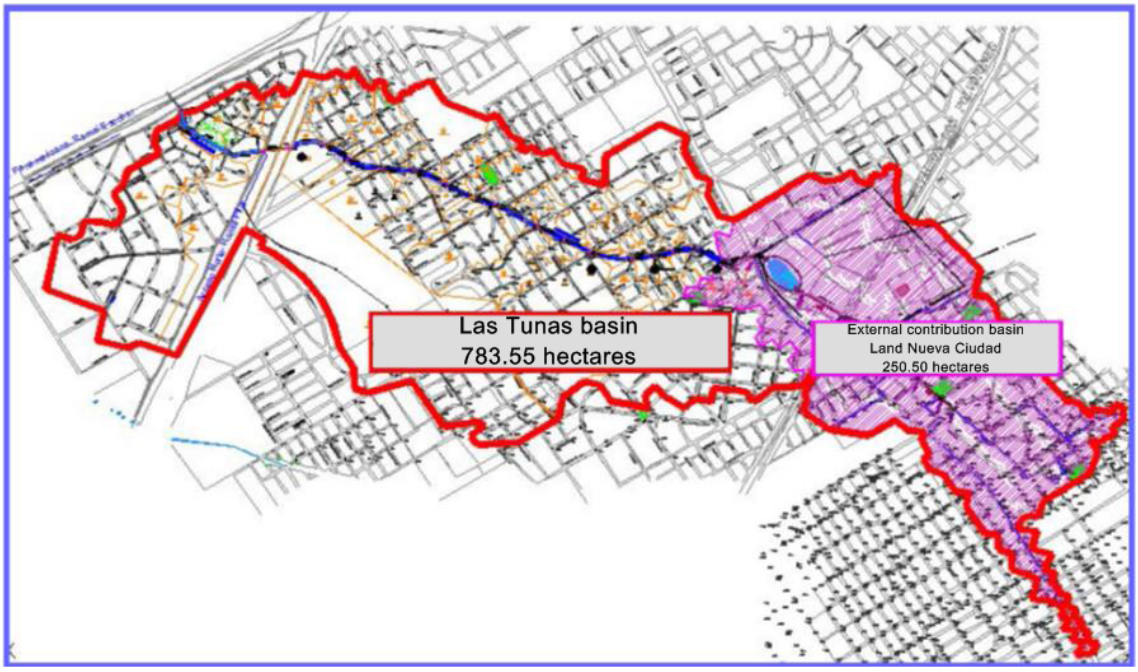

Figure 1. Darragüeira-Las Tunas basin with closure in the collector Ramal Escobar Sur, Buenos Aires province, Argentina

2.3 Model set up

In relation to the hydrological model of the basin, four types of elements are adopted, which can be seen in Figure 2. The main basin is divided into 10 sub-basins elements, which are defined by its extension area (measured in km2). Respecting to junction elements, three confluences are adopted that receive the irrigation flow of the different sub-basins. The confluence No. 1 receives flow from the sub-basins 8, 9 and 10. The confluence No. 2 receives the flow of the sub-basins 4, 5, 6 and 7. Finally, the confluence No. 3 receives the flow of the Sub-basins 2 and 3.

Concerning to reach element, three waterworks are adopted. The first one receives the irrigation flow accumulated at confluence No. 1, and ends at the confluence No. 2. The second one does the same with the flow of the confluence No. 2 and ends at the confluence No. 3. Finally, the third route takes the flow of confluence No. 3 and flows directly into the lagoon.

The last element is a lagoon, a reservoir type. This element receives the accumulated flow along the entire basin through the third conduit, as well as the irrigation flow of the sub-basin 1 in which the lagoon is located.

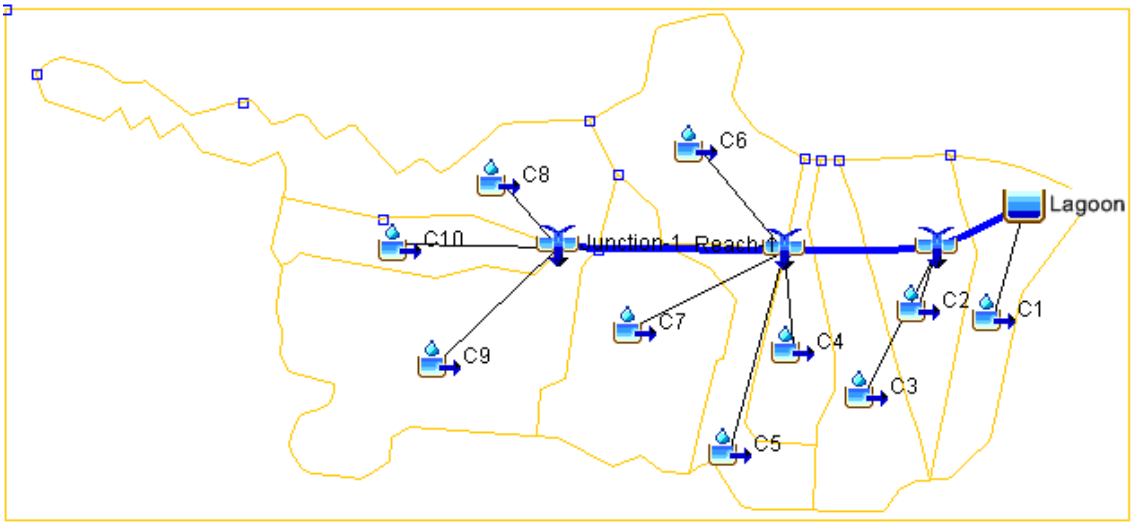

Figure 2. Scheme of the study basin model in the HEC-HMS software, with the different elements that compose it.

Each sub-basin is characterized by the area covered by each one, and other parameters that define the hydrology of each one, such as the concentration time (TC), the percentage of impermeability, the initial flow rate and the initial loss. Table 1 presents the data adopted.

In the case of the lagoon, the modeling requires a characterization of it by an Elevation-Area relation and an Elevation-Discharge relation. For this, the proposal for the lagoon is to maintain its current surface area of approximately 17,400 square meters, with a water height of 0.75 meters for a target level of water of 18.00 meters IGN (National Geographic Institute), making a slope 1: 8 from the bottom up quota 20,20 m (Level for 100 years of Recurrence). This covers an area of 27,760 square meters within the park.

The discharge of the Lagoon will be carried out by a rectangular concrete conduit of 2.00 m of base and 1.20 m of internal height, and quota of 18.00 m IGN to maintain the objective level.

For the determination of precipitation events, a design storm, derived from statistical studies of maximum short-term rainfall, is used (Kolhyari et al., 1992). This study describes the relation between precipitation intensity, frequency of occurrence and duration of precipitation. These are the so-called I-D-F (Intensity, Duration, Frequency) curves (Table 2).

For the election of IDF parameters, the duration of the storm is assumed in 1 hour. In (Silveira et al., 2014) we found that for these short storms, a rise in the intensity due to Climate Change is found, and is for these cases that the use of small reservoirs is taking value. The other parameter to be chosen is the frequency, which is assumed in intervals of 5 minutes, compatible with the time of

generation of the peak of the flood in this type of watersheds and with similar surfaces of the Buenos Aires suburban area.

Table 1. Hydrological parameters of the sub-basins.

Basin	Area (km^2)	Initial flow ($m^3/s/km^2$)	TC lag (min)	Initial Loss (mm)	Constante rate (mm/HR)	Imp %
C1	0.152	0.0059	14.5	0.508	3.556	16
C2	0.172	0.0059	12	0.508	3.556	60
C3	0.174	0.0059	12.25	0.508	3.556	26
C4	0.103	0.0059	5.62	0.508	3.556	31
C5	0.143	0.0059	6.77	0.508	3.556	55
C6	0.198	0.0059	10.77	0.508	3.556	55
C7	0.26	0.0059	6.12	0.508	3.556	50
C8	0.274	0.0059	17.23	0.508	3.556	55
C9	0.363	0.0059	12.08	0.508	3.556	61
C10	0.105	0.0059	7.62	0.508	3.556	55

Table 2. I-D-R curves.

Duration (hrs)	Frequency (min)								
	2	**5**	**10**	**20**	**50**	**100**	**500**	**1000**	**5000**
0.5	27.4	36.1	41.8	47.2	54.3	59.6	71.9	77.2	89.4
1	34.1	**46.0**	53.8	61.4	71.1	78.4	95.3	102.6	119.5
3	51.2	68.8	80.4	91.6	106	116.8	141.9	152.6	177.6
6	62.1	83.1	97.0	110.3	127.6	140.6	170.5	183.3	213.2
12	73.7	103.1	122.7	141.4	165.6	183.8	225.7	243.8	285.6
24	78.7	114.6	138.4	161.2	190.7	212.8	264.0	285.9	336.9

The location of the precipitation bars has been carried out under the methodology of Alternate Blocks (Chow et al., 1998), with maximum precipitation in the central position of the storm (Figure 3).

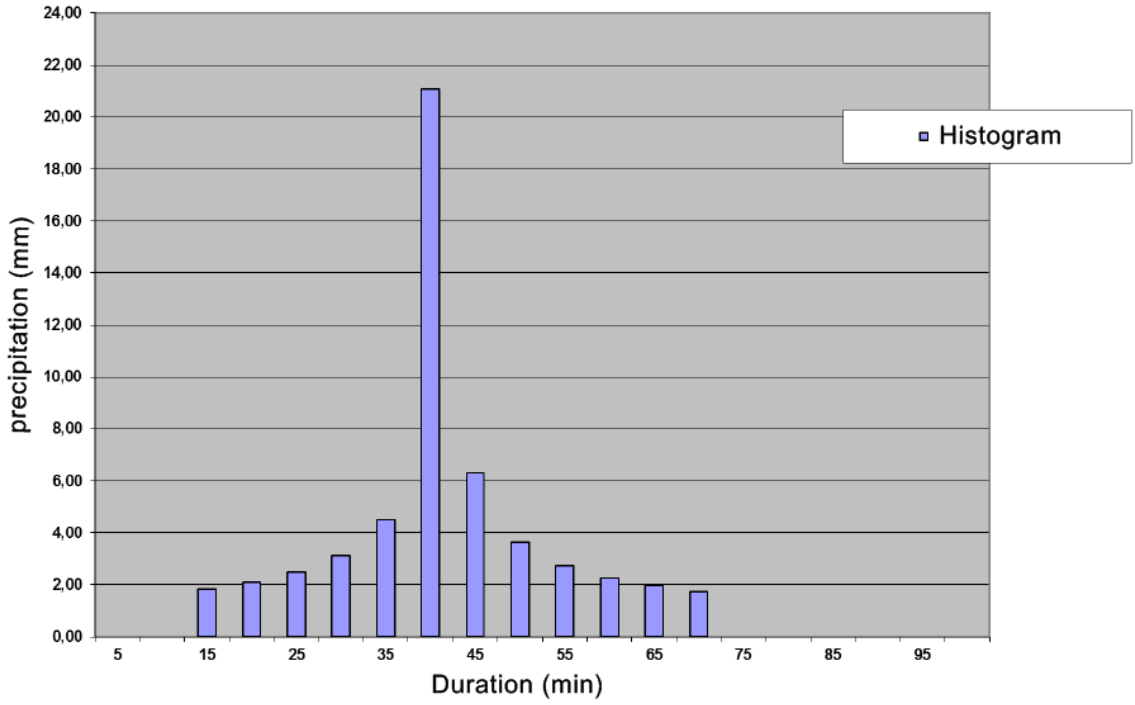

Figure 3: Input diagram.

3. RESULTS

Finally, the model results in the variation in time of the storage / elevation volume of the lagoon, and the flow of the lagoon output (Figure 4). These values can be used as input data for the next stage, in which are used to model the course of the stream between the lagoon and the highway near the studied area.

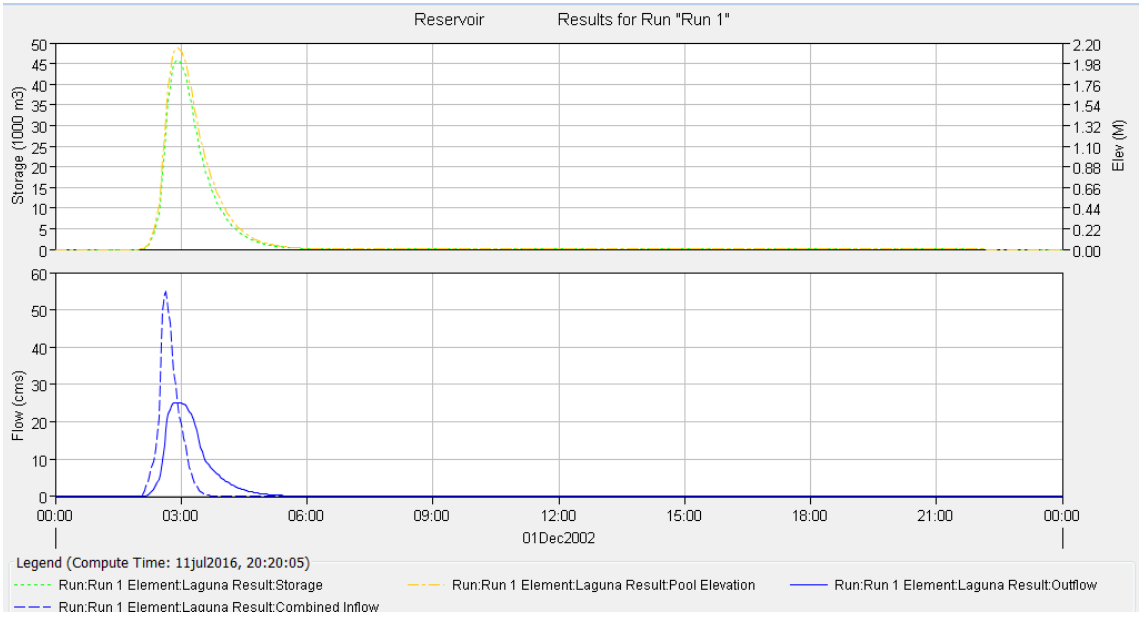

Figure 4. Laguna result curves.

The model shows an attenuation (laminating) of a peak of flood of approximately 60m^3/s to 25 m^3/s with only invading an area of 3 hectares.

The culverts of the Panamericana highway are designed for a 10-year recurrence and a flow of 19 m^3/s with a relief provided, in the case of the Las Tunas stream.

Eliminating the lagoon would almost increase three times the design flow, with the consequent increase in the dimensions of these elements of road infrastructure.

4. CONCLUSIONS AND RECOMMENDATIONS

It is possible to mitigate the devastating effects of runoff peaks that occur during rainfall events.

Preserve 5% percent of the surface of the study area generates an attenuation of 50% of the peak of the runoff. Therefore, for streams with similar characteristics to those of the Las Tunas stream, which belongs to the "Pampa Ondulada Bonaerense" territory of the Province of Buenos Aires, it is clear to recommend green areas with temporary facilities. These can be removed in anticipation of rainfall events that exceed the infiltration and runoff capacity of the basins in ordered to not affect the inhabitants of the basin. This should be a priority criterion in land use planning.

In the particular case of the Las Tunas stream, in the modeled area it is recommended to optimize the discharge operation with the bottom discharger of the lagoon and gates.

REFERENCES

Cabral, G. A., 2011. Saneamiento Hidráulico Nueva Ciudad. Municipio de Malvinas Argentinas, Buenos Aires, Argentina.

Campo de Ferreros, A., Piccolo, M.C., 1999. Hidrogeomorfología de la Cuenca de Rio Quequén Grande, Argentina. Papeles de Geografía, 29: 35-46.

Chen, C. L., 1983. Rainfall intensity-duration-frequency formulas. Journal of Hydraulic Engineering, 109(12), 1603-1621.

Chow, V.T., Maidment, D.R. and Mays, L.W., 1998. Hidrología Aplicada. McGraw- Hill, Santa Fe de Bogotá,584 pp.

Kolhyari, C., Gorde, I., 1992. Rainfall Intensity, Duration, Frequency. Journal of Hydraulics Engineering , vol 118, N°2, EEUU.

Silveira, L., Usera, G., Alonso, J., Scavone, M., Chreties, C., Perera, G., & González, M., 2014. Nuevas curvas intensidad-duración-frecuencia de precipitación para el departamento de Montevideo, Uruguay. Agrociencia Uruguay, 18(1), 113-125.

Torrero, M. P., 2016.Comentarios a la carta Laudato Si, Cap.XII,El Agua ,fuente de vida, Biblioteca Testimonial del Bicentenario, Buenos Aires, Argentina

Verstappen, H. T., Zuidam, R. V., Meijerink, A. M. J., & Nossin, J. J., 1991.The ITC system of geomorphologic survey: a basis for the evaluation of natural resources and hazard.

Viñes, S., 2014. Proyecto de Inversión 2014. Análisis del Cambio Climático sobre las Obras de Ingeniería Civil. Facultad de Ciencias Fisicomatemáticas e Ingeniería. UCA. Buenos Aires, Argentina

Proceedings of the 10th World Congress of EWRA 'Panta Rhei', 5-9 July 2017, Athens, Greece
© 2017 *European Water Resources Association*

Snowcover monitoring with MODIS product 10A2

S. Karalis*, G. Karakostas and I. Katsios
Technological Educational Institute of Athens (TEI Athens), Faculty of Technological Applications, Department of Civil, Surveying and Geoinformatics Engineering, 12243 Egaleo, Greece
* *e-mail: skaralis@teiath.gr*

Abstract: Snow is a valuable water resource that is sometimes neglected. Apart from being the primary water feeder for snow-fed rivers and streams allowing them a perennial flow regime and thus benefitting biodiversity and satisfying human water needs, snow also supports local economy in areas where winter tourism is an important source of income. One of these areas in Greece is the Kalavryta region where a large ski center is situated on the northern slopes of Chelmos (Aroania) mountain, one of the taller mountain ranges of Northern Peloponnese (2355 m), the name of which meant actually "snowy mountain". This research aimed at the monitoring of the snow cover of watersheds of Northwestern Peloponnese with the purpose to use time series of snow cover data (in the form of Snow Depletion Curves) as input to a Snow Melt Model. The entire time series (10 water years) of the MODIS 8-day composite snow product MOD10A2 was downloaded and processed. The overall purpose was to understand the hydrologic regime of Vouraikos river, a small perennial river outflowing in the Gulf of Corinth, and quantify the different mass balance terms, particularly the contribution of snowmelt. The well-known Snowmelt Runoff Model (SRM), a conceptual hydrological model based on the degree-day method was used for the simulations with good results. For the purpose of streamlining of the analysis, a toolbox was created in ArcGIS for skipping the time-consuming tasks of reprojecting, clipping and reclassifying.

Key words: Snow Cover Depletion Curves, SRM model, Modis Snow products, Northern Peloponnese, Hydrologic regimes, GIS

1. INTRODUCTION

Understanding snow processes is significant to water resources management in regions where snow accumulation and ablation influence the surface water cycle. In this research, our impetus has been the integration of the snow accumulation and melting processes in the hydrology of the Vouraikos river basin. Vouraikos is a small, perennial stream outflowing in the Gulf of Corinth, with its headwaters in the steep slopes of Chelmos and Erymanthos mountains of Northwestern Peloponnese.

The melting of snow and ice is assumed to be related to air temperature as long as air temperature is above a critical threshold, usually close to the melting point of ice. This is the basis of the so called degree-day methods for the melting of snow and ice, in which the total daily melt is equated to a coefficient times the temperature difference between the mean daily temperature and a base temperature. This coefficient, a proportionality ratio, is termed the degree-day coefficient. Rather than assuming a steady value, this coefficient varies both in time and place, reflecting the more complicated nature of snowmelt thermodynamics, so, in practical modelling, it is treated as a time series.

The use of a temperature index to predict daily rates of snowmelt is accepted to be a considerable simplification of the full energy balance. But, in the context of basin-scale modelling, the theoretical superiority of an energy balance method is outweighed by its excessive data requirements (Rango and Martinec, 1995). Indeed, the application of an energy balance approach requires knowledge of many energy data terms that are rarely available. In contrast, models based in the degree-day methods are much more modest in input data requirements and also more computational simple. According to Hock (Hock, 2003) degree-day models are widely used for four reasons: (1) wide availability of air temperature data, (2) relatively easy interpolation and

forecasting possibilities for air temperature, (3) computational simplicity and (4) generally good model performance despite their simplicity.

1.1 The SnowMelt Runoff Model and the Snow Depletion Curves (SDC)

One of the first degree-day models is the Snow Melt Runoff Model (SRM). SRM originated with Jaroslav Martinec, and has undergone substantial development since 1975 in collaboration mainly with Al Rango. SRM was developed specifically to predict snowmelt runoff and has been extensively applied to snowmelt modelling in mountainous terrain and, more recently, to climate-change scenarios (Abudu et al., 2012).

The basin is subdivided into elevation zones, typically extending over 400 to 500 meters of elevation difference each. Runoff from all elevation zones is added together before routing, so location is not taken into account in the model (except with the form of a time Lag coefficient). Daily time step is used and snow melt in each zone is predicted from air temperature, any rainfall is added on, and the total new water is routed through a single store. The equation used in the most recent version of the model (Martinec et al., 2008) is the following:

$$Q_{n+1} = \left[\mathrm{Cs}_n a\left(T_n + \Delta T\right)S_n + \mathrm{Cr}_n P_n\right]\frac{A \times 10\,000}{86\,400}\left(1 - k_{n+1}\right) + Q_n k_{n+1} \tag{1}$$

where the subscript n denotes time in days. In equation (1), Q_{n+1} (m^3/s), the daily average discharge on day $n + 1$, is calculated as the sum of three quantities from the preceding day n:

- snowmelt calculated as the product of the degree-day factor α ($cm°C^{-1}\ d^{-1}$), the representative zonal degree-days ($T + \Delta T$) (°C d^{-1}), the ratio S of the SCA (snow covered area) to the total basin area A (km^2), and the snowmelt runoff coefficient Cs;
- precipitation contributing to runoff (cm), calculated as the product of measured precipitation P and the rainfall runoff coefficient Cr;
- discharge on the previous day Q_n, weighted by the recession coefficient $k_{n+1} = xQ_n^y$ where x and y are two empirical parameters.

The term ($T + \Delta T$) represents the extrapolated degree-day calculated at the hypsometric average elevation of the zone from the degree-days measured at the meteorological stations. The snowmelt and rainfall runoff coefficients Cs and Cr are defined, respectively, as those fractions of snowmelt and rainfall that become streamflow. The recession coefficient on day $n + 1$, k_{n+1}, is defined as the ratio of streamflow on day n+1 to that on day n when there is no input of runoff. The factor 10,000/86,400 converts cm $km^2\ d^{-1}$ to m^3/s.

Equation (1) is applied separately to each zone and the discharges are summed. In addition to the five parameters (Cs, a, Cr, x and y) and input data appearing in equation (1), the other parameters are the Temperature Lapse Rate, the critical temperature for melting (Tf) and for the snowfall/snowmelt partition (Tc), i.e. the temperatures, respectively, above which snow starts melting and precipitation falls as snow.

As it can be seen from equation (1), boundary conditions besides Precipitation and Temperature are the time series of Snow Covered Area (SCA) in each zone, also termed Snow Depletion Curves (SDCs). The basis of this approach is that patterns of disappearing snow cover are similar year after year. However, the SDC for a particular basin can vary from year to year because of differences in the amount of winter snow accumulation and melting conditions. The same initial SCA can correspond to differing amounts of stored snow. The higher the Snow Water Equivalent (SWE), the more slowly the SCA will decline under the action of a given temperature series.

2. STUDY AREA AND AVAILABLE DATA

As mentioned previously, this study is concerned with Vouraikos river basin (~280 km^2), located in northern Peloponnese in central Greece. Vouraikos trunk follows a SSW/NNE direction and discharges after a course of about 30 km into the Gulf of Corinth, forming the alluvial fan of Diakofto (Figure 1).

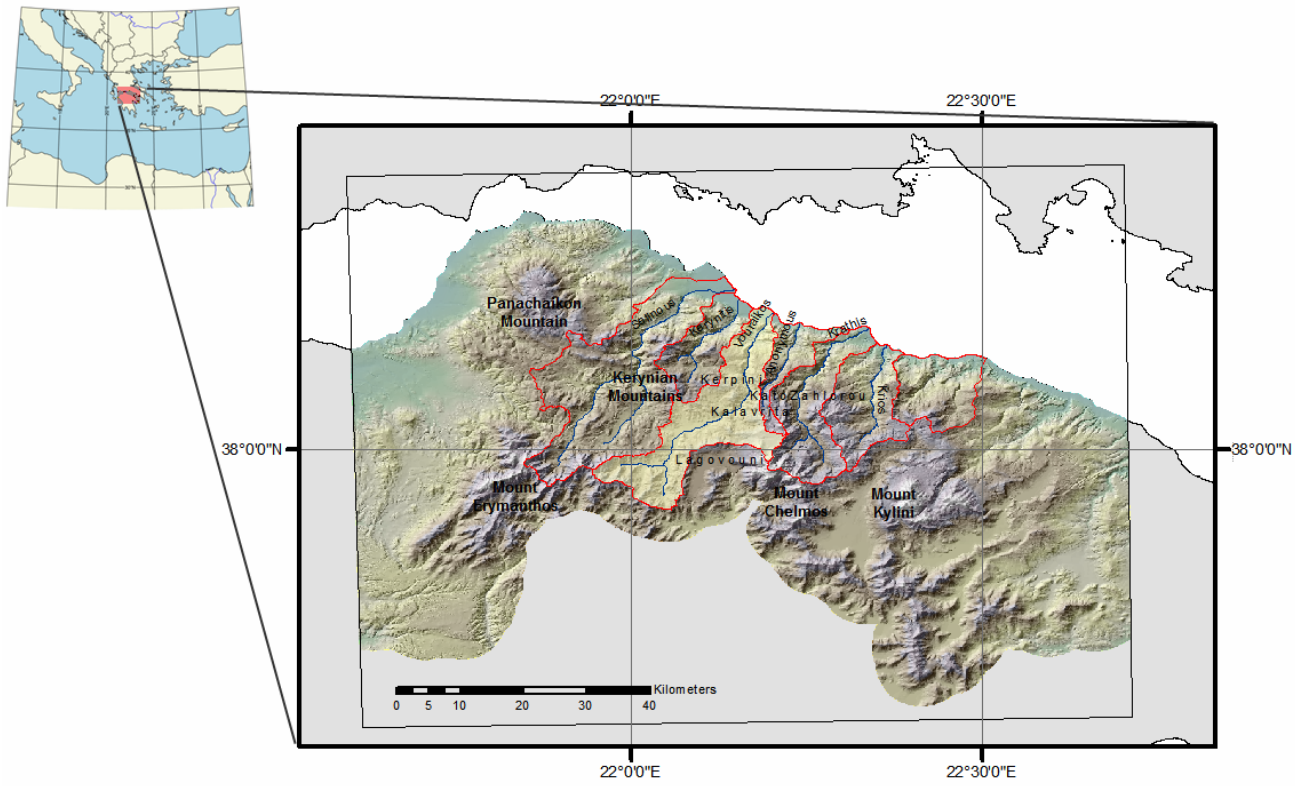

Figure 1: Map of the extended study area. The box within the right panel is the mask used to extract snow statistics from the reclassified MODIS product

Thanks to the Greek Public Electricity Corporation (DEH), a host of good quality hydrological and meteorological data are available for Vouraikos basin. A stream gauging station, just upstream from the village of Zachlorou, is recording stage from 1980 to present. DEH is also operating three rain stations, recording daily precipitation in Kalavryta, Lagovouni and Kerpini (Figure 3). Observations regarding snow fall are also available from Kerpini station, while temperature is recorded in Kalavryta station.

The MODIS snow and sea ice products (http://modis-snowice.gsfc.nasa.gov/) are available at a variety of resolutions and projections to serve different user groups (Hall et al., 2002), and are distributed through the National Snow and Ice Data Center (NSIDC) in Boulder, Colorado. Snow maps are available at 500 m resolution on a sinusoidal projection (Hall and Riggs, 2007). In our study we used the MOD10A2 product. This data set is an 8-days composite that reports the maximum snow cover during an eight day period in 1200 x 1200 km tiles. 505 files in HDF format from 2004041 to 2015025 were downloaded and processed (Figure 2).

For studying the hydrology of the basin we made use of other MODIS Terra products relevant to the vegetation dynamics and the energy balance of the territory. Subsets (temporal and spatial) summaries of such variables like Potential and Actual Evapotranspiration, Vegetation indices like NDVI, EVI, LAI along with phenological observations are available for downloading (ORNL DAAC https://daac.ornl.gov/).

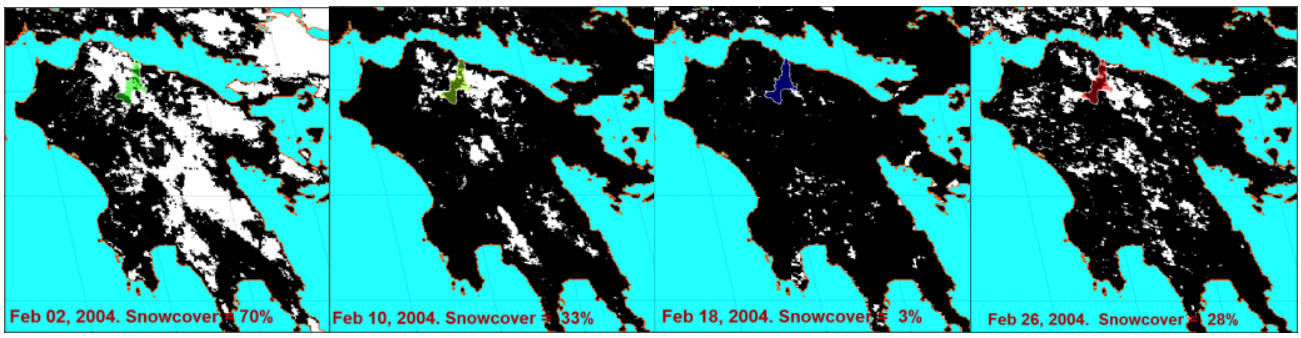

Figure 2: Four consequent snapshots of the snow – no snow raster cover over the Peloponnese, developed from the original MODIS product. Percentages of snow cover refer to Vouraikos basin, located in the North. It can be seen that after depletion in the 18th of February a new snow fall replenished the snow cover of the territory

3. METHODS

For automating the procedure we developed a toolbox in ArcGIS (available at http://users.teiath.gr/skaralis/). This toolbox accomplishes the GIS tasks of reading the HDF file, reprojecting (from sinusoidal MODIS to UTM -WGS84), cropping the area of interest and reclassifying the 11 values of the original raster to a snow-no snow raster of a particular date.

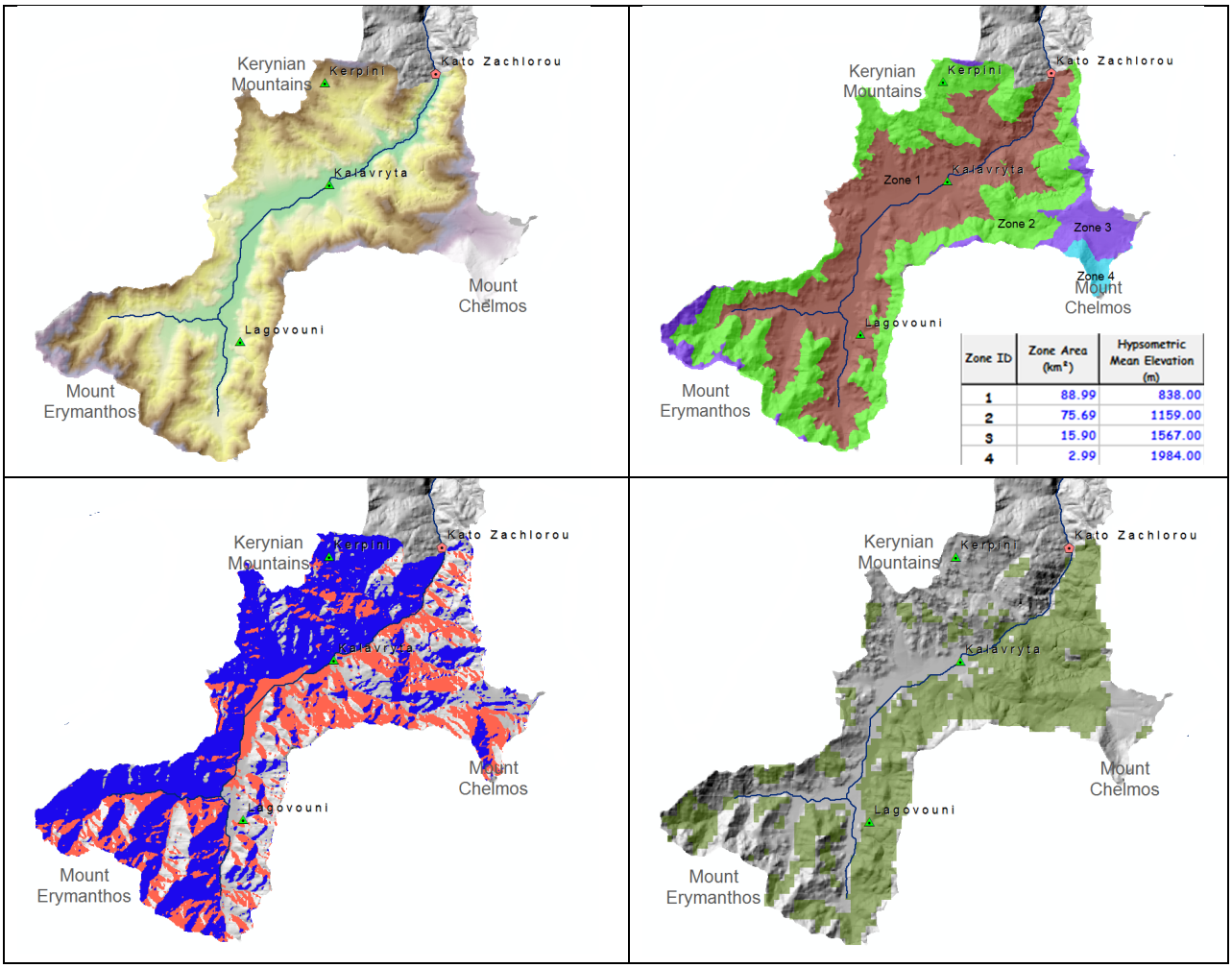

Figure 3: The study area. The zoning is illustrated in the upper-right panel. The two upper zones represent only about 25% of the area. The bottom left panel shows the aspect of the terrain split in two major categories: Blue colours signify slopes facing SE while red-grey colours signify slopes facing NW. In the bottom right panel the forested area of the basin is shown. Note that NW facing slopes are also the forested ones.

For the GIS analysis (extracting time series of mask and zonal statistics) we used the functionality of the "spatial" packages of R language (R Development Core Team, 2008).

Precipitation was estimated with a Thiessen polygon scheme, and the average daily temperature of Kalavryta Station was used as the temperature record. Lapse rate was taken to be 0.7°C / 100m (Nikas, 2004) with base altitude the elevation of the Station (710 m). No precipitation lapse rate was taken into consideration. Discharge was calculated from stage with our own rating curve. Gaps in the stage recordings (the most prolonged being an 8 month period from February to September 2013) were filled with the use of IHACRES rainfall – runoff "data-driven" model (Littlewood et al., 1993). Energy terms were calculated with a USGS program called Thornthwaite Water Balance Model, an implementation of the Thornthwaite – Mather Water Balance concept, operated by a user interface. It calculates long term monthly values of the water – energy budget (McCabe and Markstrom, 2007).

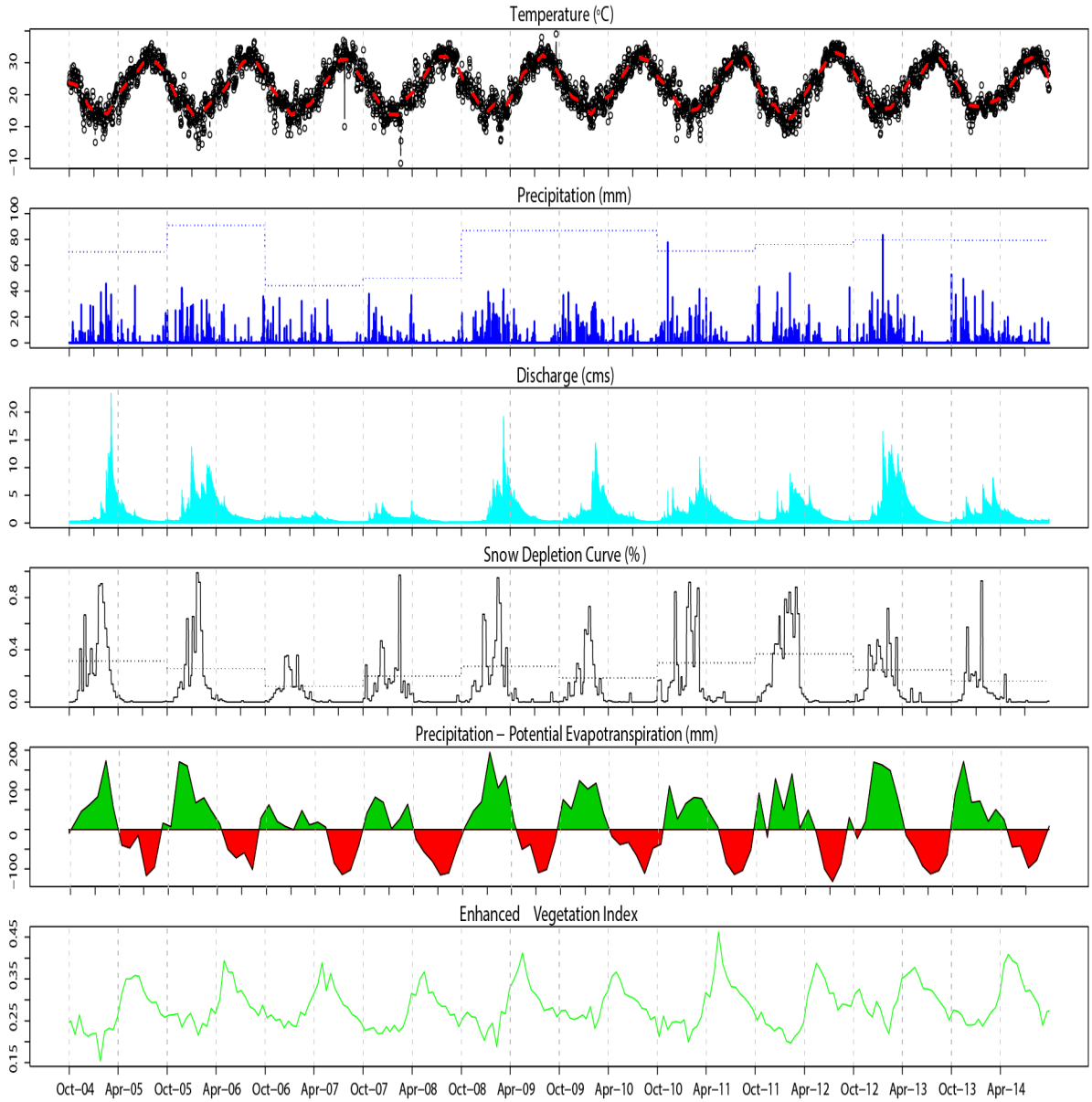

Figure 4: The yearly marches of environmental variables for the entire period of 10 water years (2004-2005 to 2013-2014). Thin dotted horizontal lines depict average monthly values for precipitation (for each water year), and snow coverage (for 6 months). It is interesting to note that despite the fact that the last 3 years have been rich and about equal in precipitation, the snow areal coverage is diminishing

The study of the yearly marches and phenology reveal a maximum of ET in May (when EVI peaks). Then, while the basin starts drying, it falls suddenly and reaches its minimum in July, to

locally peak again in early September when the rain period begins. The yearly patterns can shift for a 30-45 days period. From the Thornthwaite budget, it appears that the period of minimum water content of the basin is the months of August – September, but the low flow periods continue deep into December and often January. It is then when the water deficit is replenished after the start of the rainy season (August-September), and the severe rainfalls start to give noticeable runoff. On February and March melting of snow starts producing runoff, furnishing the background of augmented discharge and frequent floods, on top of it.

3.1 SMR Simulations

SMR simulations performed well. After experimenting with the values of the various parameters and their yearly distribution in the first 2 years, validation in the next years gave R^2 in the range of 0.60 to 0.90, while the volume difference was no larger than 25%. Generally, different sets of coefficients should be used depending on whether a dry or a wet year is simulated. It appears that the snow melt accounts for a 10-15% of the total runoff, concentrated in February, March, April, and sometimes May.

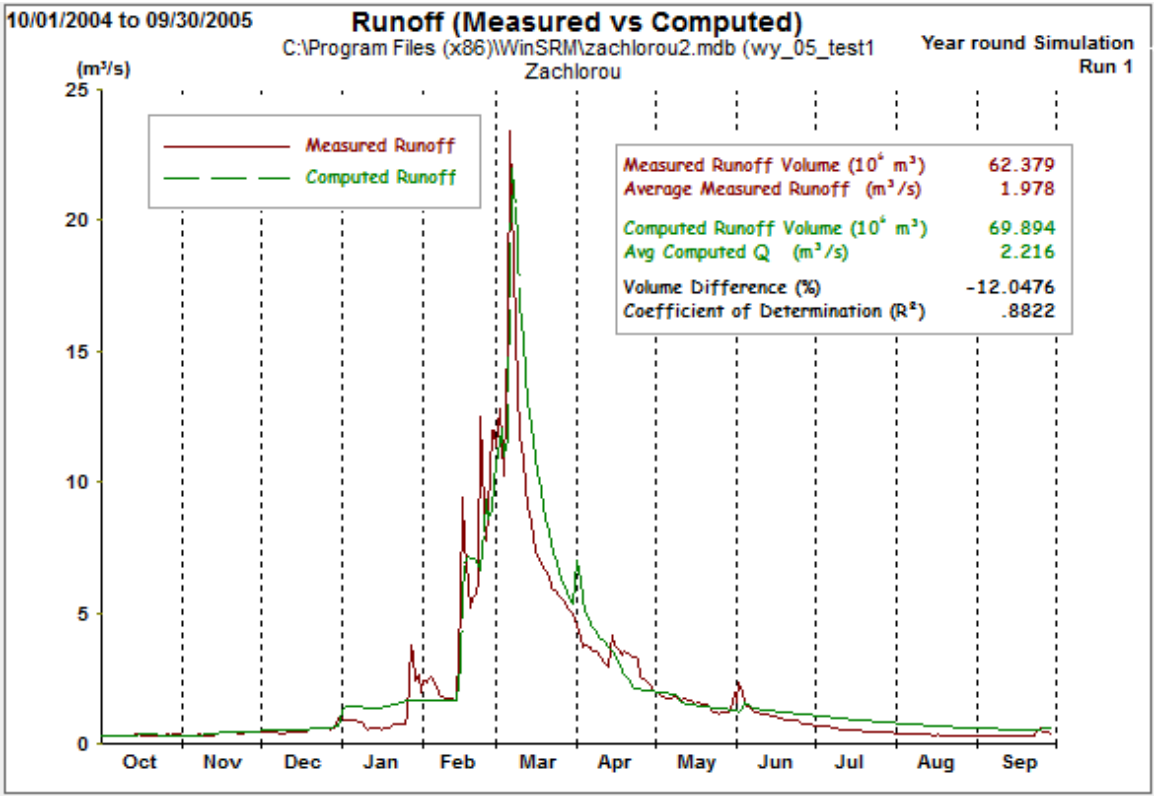

Figure 5: Simulation results with SRM for the first water year of record, 2004-2005. Simulation results verify the hydrological functioning of the basin and substantiate the water budget calculations

3. CONCLUSIONS

Conceptual snowmelt runoff models such as SRM, fed by good quality data and remote sensing measurements, provide a valuable resource for estimating basin runoff and thus informing water resource management decisions. With a minimum effort in the "calibration" procedure it is possible to get good indices of model behavior. Despite the crude measurements of the snow coverage, given the small size of the catchment compared to the resolution of the snow raster, the spatial extent and timing of the snowpack was convincingly described. Further improvement and refinements can be made by incorporating land cover (forest or not) and/or aspect in the zoning, for applying different

parameter values to them.

The hydrological regime of a river summarizes all its hydrological characteristics and its variations, and it is defined by its discharge variations. The hydrological regime of Vouraikos is rather a simple regime (one maximum, one minimum and one mode of alimentation) with the existence of two distinct seasons. More particularly, Vouraikos fits to a pluvio-nival (snow) regime characterized by significant inter-annual variations.

AKNOWLEDGMENTS

This study is a part of the PhD research of the first author. I would like to thank my professor, Efthymios Karymbalis for his undiminished encouragement and support. The authors wish to thank the hydrological department of DEH and especially the head of the office of Hydrology, MSc Eng. J. Kouvopoulos, for making the data available and discussing them with us, while giving us some very informed advices.

REFERENCES

Abudu, S., Cui C.L., Saydi M., King J.P, 2012. Application of snowmelt runoff model (SRM) in mountainous watersheds: A review. Water Science and Engineering, 5(2):123-136

Hall, D.K., and Riggs, G.A., 2007. Accuracy assessment of the MODIS snow products. Hydrological Processes 21, 1534–1547.

Hall, D.K., Riggs, G.A., Salomonson, V.V., DeGirolamo, N.E., Bayr, K.J., Jin, J.M., 2002. MODIS snow-cover products. Remote Sensing of Environment 83, 181–194

Hock, R. 2003. Temperature index melt modelling in mountain areas. Journal of Hydrology 282, 1-4, 104-115.

Littlewood I.G, Down K., Parker J.R., Post D.A., 1997. The PC version of IHACRES for catchment-scale rainfall streamflow modelling: User Guide. Institute of Hydrology, Australia.

Martinec J., Rango A. & Roberts R.T., 2008. Snowmelt Runoff Model (WinSRM) Users' Manual, 19-39. New Mexico State University Press.

McCabe, G.J., and Markstrom, S.L., 2007. A monthly water-balance model driven by a graphical user interface: U.S. Geological Survey Open-File report 2007-1088, 6 p.

Nikas K., 2004. Hydrogeological conditions of the North Eastern part of Achaia Prefecture (in Greek). PhD Thesis, University of Patra, School of Geology.

Rango, A. & Martinec, J. ,1995. Revisiting the degree-day method for snowmelt computation. Water Resour. Bull. 31(4), 657-669.

R Development Core Team, 2008. R: A language and environment for statistical computing. R Foundation for Statistical Computing, Vienna, Austria. ISBN 3-900051-07-0, http://www.R-project.org.

Proceedings of the 10th World Congress of EWRA 'Panta Rhei', 5-9 July 2017, Athens, Greece
© 2017 *European Water Resources Association*

Presenting the mathematical model to determine retention in the watersheds

S Shamohammadi and A. Sharifi*
Department of Water Enginerring, Faculty of Agriculture, Shahrekord University, Sharekord, Iran
* *e-mail: areza_sharifi@yahoo.com*

Abstract: This paper presents a new mathematical model for computation of retention potential (S) based on the principle concepts of SCS-CN model. In the Mathematical model, not only rainfall-runoff concepts in SCS-CN model are precisely represented in a mathematical form, new concepts, called "maximum retention" and "total retention" are introduced, and concepts of potential retention capacity, maximum retention, and total retention have been separated from each other. In the proposed model, actual retention (F), maximum actual retention (Fmax), total retention (S), maximum retention (Smax), and potential retention (Sp), for the first time clearly defined. As a result, Sp is not a variable. It is a function of morphological characteristics of the watershed. Indeed, based on the mathematical relation of conceptual curve of SCS-CN model, the proposed model provides a new method for the computation of actual retention in watershed and it simply determined runoff based on. In the corresponding relations, in addition to Precipitation (P), Initial retention (Ia), cumulative values of actual retention capacity (F), total retention (S), runoff (Q), antecedent moisture (M), potential retention (Sp), total retention (S), we introduced Fmax and Fmin referring to maximum and minimum actual retention, respectively. The advantages of the modified version versus the original model include better precision, higher performance, easier calibration and speed computing.

Key words: Model, mathematical, retention, watershed, SCS

1. INTRODUCTION

All rainfall-runoff models and in a broader sense, hydrological models are simplified the characteristics of the real-world system (Moradkhani and Sorooshian, 2009). Planning for containment, flood management, protection of the quality and proper utilization of them require proper and accurate understanding of rainfall-runoff modeling. One of the most important challenges for hydrologists is the selection of a rainfall-runoff model which can simulate a wide range of runoff properly (Chow et al., 1988). Therefore, evaluation of the retention methods enjoys a particular importance in hydrological modeling. Chow et al. (1988) have divided retention methods into two categories: the first category is those methods which are based on hydrological and morphological characteristics of the watershed such as C.N method and the second category is the methods based on rainfall-runoff observed data (Tramblay et al., 2010). Cordery (1987) divided retention methods into five groups: the relative retention method, continuous retention with a fixed rate (φ), initial - continuous retention with a fixed rate, curve or diffusion equation and curve number method. The selection and calibration of each of these methods depend on the type of available data and the process of runoff production.

2. S.C.N.-C.N. RAINFALL-RUNOFF MODEL

The curve number method was presented by the Soil Conservation Service (SCS) to calculate the depth of surface runoff. This method is an event-based model, and often has several advantages for real-time and operational applications (Cordery, 1987). This model only needs information at event scale and does not use the full time series (Tramblay et al., 2010). The application of curve number method (S.C.S.-C.N.) is very common and widely used because of the simplicity of it. This model

uses three A.M.C levels namely dry, average and wet for estimating the antecedent moisture conditions (A.M.C). There a lot of studies using this method in order to predict the runoff in all over the world such as SCS, 1993.

2.1 S.C.S.-C.N. model hypotheses

S.C.S. runoff model is based on a hypothesis which is resulted from the conceptual curve of Fig. 1 and is shown as (1).

$$\frac{F}{S}=\frac{Q}{P-I_a} \tag{1}$$

where F is actual retention; S is retention potential or the maximum difference between rainfall and runoff from since start of rainfall; Q is runoff depth; P is total depth of rainfall and I_a is is the primary absorption (retention). All parameters are in mm.

On the other hand, we can always write:

$$F+I_a=P-Q \tag{2}$$

And as a result, runoff depth, Q is obtained from combination of (1) and (2) as model (3):

$$Q=\frac{(P-I_a)^2}{P-I_a+S} \tag{3}$$

S value, based on curve number (C.N) which itself depends on soil characteristics, land use, agricultural operations and antecedent soil moisture is obtained based on the (4) C.N and S depend on inherent characteristics of the watershed and are independent of the amount of rainfall.

$$S=\frac{25400}{CN}-254 \tag{4}$$

Also, in the S.C.S.-C.N. Model, the initial absorption amount is introduced as coefficient (20%) of potential retention (S). This coefficient is as $I_a = \lambda S$ where $\lambda = 0.2$. In addition, if the amount of rainfall and runoff is available from one watershed, the parameter S, using (3), is written as (5) (Chow et al. 1998):

$$S=\frac{1}{2\lambda^2}\left(2\lambda P-\lambda Q+Q-\sqrt{\lambda^2Q^2-2\lambda Q^2+4\lambda PQ+Q^2}\right) \tag{5}$$

The above equations also include cumulative runoff and rainfall at scale event. Additionally, Fig. 1 has been proposed for theoretical explanation of S.C.S.-C.N. rainfall - runoff model (Xiao et al. 2011).

Fig. 1 shows runoff depth as a function of rainfall in a long time. As shown in Fig. 1, at the end of initial retention (I_a), runoff begins immediately in a form of a curve and comes close to a straight line with a slope of 45 degrees.

2.2 Disadvantages of S.C.S.-C.N. Model

Several drawbacks have been propounded by various researchers on the S.C.S.-C.N. Model. The use of discrete data instead of continuous ones, use of rainfall regardless of its duration, and time-

consuming of field operations process such as measurement of soil penetration in order to calculate the C.N and S (Muhammad et al. 2015).

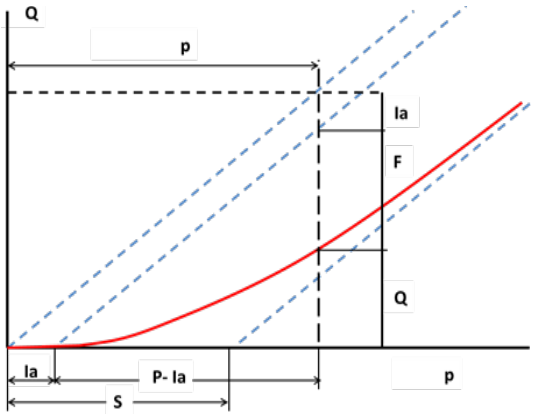

Figure 1: The relationship between cumulative rainfall and cumulative runoff (Zhi-Hua et al., 2009)

As it has been brought up in definitions of S.C.S.-C.N. method and shown in Fig. 1, S value is the retention potential of watershed and is a fixed number. In fact, the S value is related to state in which the depth of rainfall reaches its maximum possible value. In other words, S value occurs only when F value has reached its maximum level (Berthet, 2009).

Thus, with regard to the above concept, during the rainfall and since the initial absorption finishes, the values of F, Q & P are variable, and S and I_a parameters will be fixed. As a result, hypothesis (1) which is written as (1) does not provide boundary conditions of Fig. 1; because when the amounts of rainfall come close towards I_a, (P-I_a goes to zero) Q and F values come close to zero, but S value remains constant that has been defined by relation (7), and principally is unrelated to rainfall changes (only depends on inherent characteristics of the watershed).

$$Lim_{\varepsilon \to 0} \frac{\varepsilon}{S} = Lim_{\varepsilon \to 0} \frac{\varepsilon}{\varepsilon} \Rightarrow 0 \neq 1 \tag{6}$$

And according to Fig. 1, relation (1) can be written as (7).

$$Lim_{p \to Ia} (\frac{F}{S}) = Lim_{p \to Ia} (\frac{Q}{P - I_a}) \tag{7}$$

In fact, the strengths of the S.C.S. model is not mathematically correct, because mathematically it is not possible that in a proportion (1) three parameters (P- I_a & Q, F) become variable but S remains constant.

Additionally, (5) that is resulted from (3), has the following drawbacks:

1. The value of S in this equation is as a function of rainfall and runoff and it changes by rainfall change. This issue is not compatible with the definition of S in the S.C.S.-C.N. model (S value depends on morphological characteristics and is independent of rainfall).
2. The value of S obtained through this method, is valuable only for one quite similar rainfall, not other rainfall.

3. THE INTRODUCTION OF MODIFIED MODEL

This model is usable for areas having watershed with sufficient statistic. Currently, most of the countries in the world have such watersheds and their numbers will increase in the future. So it seems that such models in the future will enjoy a wide application domain in the world.

This model, in fact, is the mathematical relation of S.C.S.-C.N. conceptual curve that calculates the amounts of watershed actual retention by offering a new method and accordingly runoff is calculated simply. For more precise application of the model, the following concepts are defined separately.

3.1 Definitions

In a rainfall (P), after the completion of initial retention phase (I_a), the cumulative amount of actual retention (F), total retention (S) and runoff (Q) increase dynamically by increase in depth of rainfall (Fig. 1).

- The rainfalls selected for new model have identical antecedent moisture (M).
- The retention potential of watershed (Sp) is dependent on the inherent characteristics of the watershed and is independent of the amount of rainfall, whereas total retention (S) is variable.
- S_{max} and F_{max} are defined as the watershed's maximum retention and watershed's maximum actual retention respectively.

The relationships between parameters used in the new model are shown as follows:

$$P=S+Q$$

$$S=F+I_a$$

$$S_{max}=F_{max}+I_a$$

$$S_p=S_{max}+M$$

If another rainfall does not occur 5 days prior to the rainfall (soil becomes dry before rainfall) then = 0, in this case, the initial retention will reach to its maximum rate (I_{am}), thus $I_a = I_{am}$. In such a case, the maximum retention would be assumed as the potential retention.

Fig. 1 amply demonstrates the value of S will increases dynamically by increase in P, Q and F values, until it eventually reaches its maximum value. We must distinguish between this retention and potential retention which is independent of rainfall and is dependent on the characteristics of the watershed (S_p).

4. PRESENTATION OF A MATHEMATICAL MODEL

In order to offer a new model, with regard to the definitions listed above, Fig. 1 has been modified as Fig. 2.

As shown in Fig. 2, in the range of $I_a<P$, the gradient of function F and gradient of function Q are defined as relations 8 and 9:

$$\frac{dQ}{dP}=\frac{F}{F_{max}} \tag{8}$$

$$\frac{dF}{dP}=\frac{k_{sh}}{k_{sh}+(P-I_a)} \tag{9}$$

In this relation, k_{sh} is a coefficient which depends on morphological characteristics of the watershed. The rest of the parameters have been previously defined.

On the other hand, based on the principle of the law of conservation of mass we can always write:

$$(P\text{-}I_a)=F+Q \text{ or } P=I_a+F+Q \quad (10)$$

And by taking the derivative of both sides of the (10) with respect to rainfall, we will have:

$$\frac{d(P\text{-}I_a)}{dP}=\frac{dF}{dP}+\frac{dQ}{dP} \quad (11)$$

As a result:

$$1=\frac{dF}{dP}+\frac{dQ}{dP} \quad (12)$$

By combining (8), (9) and (12), the relation (13) is obtained:

$$1=\frac{k_{sh}}{k_{sh}+(P\text{-}I_a)}+\frac{F}{F_{max}} \quad (13)$$

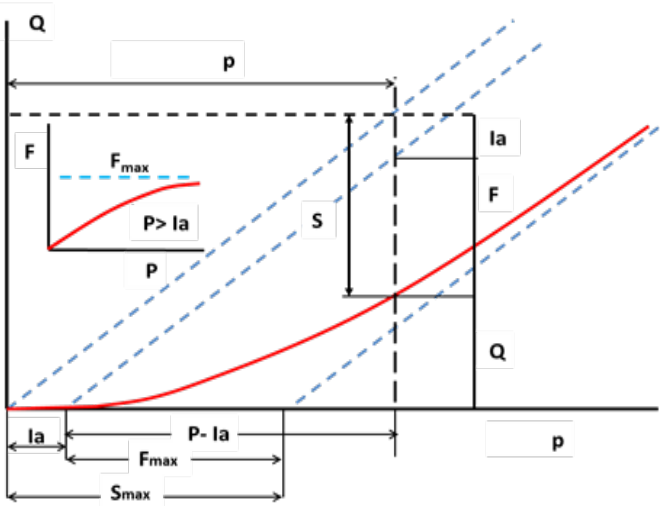

Figure 2: The relationship between cumulative runoff, cumulative rainfall and retention parameters

Therefore, by displacement of equation parameters, relation (14) is obtained to calculate the actual retention.

$$F=F_{max}\frac{(P\text{-}I_a)}{k_{sh}+(P\text{-}I_a)} \quad (14)$$

The method for solution of (14) is as follows:

(a) I_a could be calculated using the previous conventional methods. But one suggestion is that using establishment of linear regression relation between the amounts of rainfall (P) and runoff (Q) in the watersheds having rainfall - runoff statistics (rainfall data versus runoff data) I_a value (initial absorption) is calculated from the cross of line with rainfall axis (P). The other conventional methods

(b) To calculate the parameters F_{max} and k_{sh} we do as follows:

1. The rainfall (p) and runoff (Q) data of watershed are prepared and listed in a table in two separate columns.
2. In the third column of the table, by having I_a, P- I_a values are calculated.
3. Using (14) and corresponding values of P- I_a and F and using software such as Mat lab, k_{sh} and F_{max} values are calculated.

Then by having K_{sh} and F_{max} values, per amount of rainfall, we can calculate the amount of actual retention for similar watersheds. Also, total retention value (S) can be calculated from relation (15) per separate rainfall. Fig. 3 shows the relationship between cumulative rainfall and retention parameters.

$$S=I_a+F_{max}\frac{(P-I_a)}{k_{sh}+(P-I_a)} \tag{15}$$

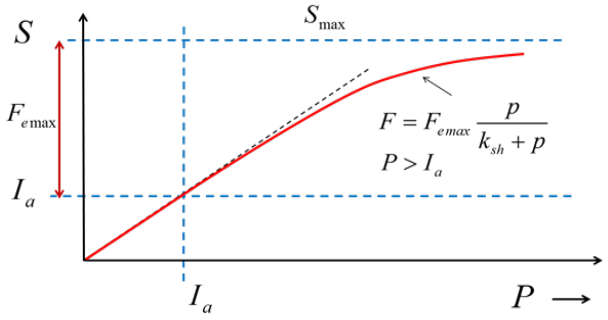

Figure 3: The relationship between cumulative rainfall and retention parameters

In the model (15), with regard to the definitions in section 2, S value is variable and can be calculated per any separate amount of rainfall (with the same antecedent moisture). The relations (16) and (17) show that the cumulative value of S in any case can be as a function of the watershed initial and actual retention (this relation in S.C.S. classic method is just possible for retention potential state and is a fixed value).

$$S=I_a+F \tag{16}$$

$$S_{max}=I_a+F_{max} \tag{17}$$

Also, with regard to variability of S value runoff amount for each rainfall can be obtained using the relation (18).

$$Q=P-S \tag{18}$$

By combining the (15) and (18), the amount of runoff (Q) is directly obtained from relation (19).

$$Q=P-[I_a+F_{max}\frac{(P-I_a)}{k_{sh}+(P-I_a)}] \tag{19}$$

Whenever the goal is to obtain Q_{max} (maximum runoff), I_a= 0 is the better choice.

For example, when the antecedent moisture of a certain rainfall reaches its maximum amount (saturated soil), with the onset of rainfall, runoff is created and relation (19) is written as relation (20).

$$Q_{max}=P-F_{max}\frac{P}{k_{sh}+P} \tag{20}$$

Whenever the purpose is calculation of the watershed's potential retention, a simple way is that rainfall chosen for the model should be with an antecedent dry moisture; then, $I_a = I_{am}$ and it will have a maximum amount .In this case, maximum retention will became as the watershed's potential retention.

The results of the use of modified model in the Kasilian, Amameh and Roodzard watersheds in Iran showed the model enjoys good efficiency.

REFERENCES

Berthet L., Andreassian V., Perrin, C., Javelle, P., 2009. How crucial is it to account for the antecedent moisture conditions in flood forecasting? Comparison of event-based and continuous approaches on 178 catchment", Hydrol. Earth Syst. Sci. Discuss., 6:1707-1736.

Chow, V. T., Maidment, D. R., Nays, L. W., 1988. Applied Hydrology, New York: McGraw-Hill.

Cordery, I., 1987. Storm losses and design rainfall excess I Australian rainfall and runoff, a guide to flood estimation. Institution of Engineers, Australia, 117-126.

Moradkhani, H., Sorooshian S., 2009. General review of rainfall-runoff modelling: model calibration data assimilation and uncertainty analysis. Advanced Water Resource, 28(2): 135-147.

Muhammad, A., Geon-woo, M., Jae-hyun, A., Tae-woong, K., 2015. Investigation of S.C.S.-C.N. and its inspired modified models for runoff estimation in South Korean watersheds. Journal of Hydro Environment Research, 1-12.

S.C.S., 1993. Hydrology, National Engineering Handbook, Supplement A, Section 4, Soil Conservation Service USDA. Washington, DC.

Tramblay, Y., Bouvier, C., Martin, C., Didon-Lescot, J., Todorovik, D., Domergue, J., 2010. Assessment of initial soil moisture conditions for event-based rainfall-runoff modelling. Journal of Hydrology, 387: 176-187.

Xiao, B., Wang, Q., Fan, J., Han, F.P., Dai, Q. H., 2011. Application of the S.C.S.-C.N. model to runoff estimation in a small watershed with high spatial heterogeneity, Soil Science Society of China, 21(6): 738-749.

Yapo, P. O., Gupta, H. V., Sorooshian, S., 1998. Multi – objective global optimisation for hydrologic models. Jurnal of Hydrol.; 204: 83-97.

Zhi-Hua, Sh., Li-Ding, Ch., Nu-Fang, F., De-Fu, Q., Chong-Fa, C., 2009. Research on the S.C.S.-C.N. initial abstraction ratio using rainfall-runoff event analysis in the three Gorges Area, China. Catena, 77: 1-7.

Proceedings of the 10th World Congress of EWRA 'Panta Rhei', 5-9 July 2017, Athens, Greece
© 2017 *European Water Resources Association*

Considering data uncertainty in the water and sanitation sector: Application to large number of alternatives and criteria

F. Ezbakhe*, A. Pérez-Foguet
Research group on Engineering Sciences and Global Development, Department of Civil and Environmental Engineering, Barcelona School of Civil Engineering (ETSECCPB), Universitat Politècnica de Catalunya
* *e-mail: fatine.ezbakhe@estudiant.upc.edu*

Abstract: Priority-driven and target-focused management of water and sanitation services is essential to achieve long-term sustainability. However, in the context of water and sanitation, statistical uncertainty is an inevitable feature, as surveys are the primary sources of the information used in the decision making process. Therefore, it needs to be considered to have a greater confidence in the decisions made based on the collected data. Outranking approaches provide an opportunity to handle imprecision and uncertainty characteristic of water management problems. In particular, ELECTRE-III uses pseudo-criteria to consider uncertainty in the decision-maker's preferences, but does not take into account statistical uncertainty. A new interpretation of ELECTRE-III, in which pseudo-criteria are linked to the data uncertainty, is presented in the paper. The modified outranking approach (E3M) is used to evaluate water and sanitation services in Kenya and rank its 338 subdistricts according to their performances on 9 different criteria. E3M proved to be an effective ranking tool, providing a detailed hierarchy between the subdistricts, even when dealing with hundreds of alternatives. However, a quadratic dependence between the number of subdistricts ranked and the computational cost of the method was found, indicating that for larger number of alternatives (order of thousands), the time required would rise to the order of hours. Future work should focus on optimising the method's algorithm and allowing its scalability to thousands of alternatives.

Key words: ELECTRE III; Data uncertainty; Water and Sanitation; Multiple criteria decision-making; Non compensatory

1. INTRODUCTION

Sustainability of water and sanitation services has become a central element in the post-2015 development agenda (Sachs 2012, UN-Water 2014), being now considered fundamental for long-term human and environmental well-being. However, achieving sustainable services can be a complex task, as it concerns all levels of planning (local, regional, global) and contexts (economic, social, environmental) (UNEP 2011). To tackle this complexity, countries have adopted integrated approaches for the management of water and sanitation resources (UN-Water 2012). In addition, to provide more efficient services, countries have developed more decentralised structures (Ribot 2002, Parker & Tsur 2012), shifting decision-making responsibilities to local authorities.

This new way of water and sanitation planning requires improved data systems with robust and reliable information (Medema et al. 2008). Such information can be collected from different sources, from monitoring networks to knowledge-based systems and surveys (Timmerman et al. 2000). In the context of water and sanitation services, household surveys are key sources and consist in standard questions that assess the state of facilities and practices (JMP 2006). As in other types of surveys, the sampling strategy used dictates the reliability of the data (UN 2005) and thus introduces statistical uncertainty in the data. This uncertainty becomes more significant when data is collected at lower administrative levels, as larger samples are needed to cover all smaller areas (Giné-Garriga et al. 2013). Therefore, statistical uncertainty must be considered when data is used to support water and sanitation management decisions.

Multi-criteria decision making provides an opportunity to address uncertainties characteristic of water management problems (e.g. problem formulation, objective identification, preference setting, etc.) (Jakeman et al. 2006, Lerner et al. 2011). Methods based on the outranking approach (i.e.

building outranking relations by pairwise comparison of alternatives) have gained significant interest in the water sector (Roy et al. 1992, Duckstein et al. 1994, Bella et al. 1996, Raju et al. 2000, Trojan & Morais 2012, Kumar et al. 2016). In particular, ELECTRE-III uses pseudo-criteria as means of handling imprecision and uncertainty in the decision-maker's preferences (Roy 1991). However, in the standard ELECTRE-III, the statistical uncertainty related to the data is not considered in the pseudo-criteria. Therefore, a new version of ELECTRE-III is needed to make dealing with data uncertainty less challenging for decision and policy makers. A recent contribution was made to address this drawback (Ezbakhe & Pérez-Foguet, 2017), in which a new interpretation of the outranking model was proposed. In the new approach, denominated as E3M, the pseudo-criteria were linked to statistical uncertainty (i.e. confidence intervals of survey's estimates). E3M proved to be a simple but effective ranking and prioritising tool applicable to a small number of communities. However, outranking methods are considered to be impractical when it is applied to rank more than tens of alternatives (Pereira & Duckstein 1993, Joerin et al. 2001).

This paper is an extension of the previous work and focuses on the scalability of E3M. The aim is to explore the suitability of the method when dealing with hundreds of administrative subunits. In Section 2, a brief overview of the E3M method and the case study are presented. In Section 3, the uncertainty of the case study's data is analysed. Next, E3M is applied to rank the subdistricts considering this uncertainty, first at a district level (i.e. in each district) and then at a country one (i.e. in all districts conjointly). The paper finished presenting the main conclusions found.

2. METHODS

2.1 New interpretation of ELECTRE-III (E3M)

ELECTRE-III consists of two phases: (i) construction of the outranking relation between each pairs of alternatives and (ii) exploitation of the previous outranking relations to produce an order of all alternatives. In this section, only an overview of the pseudo-criteria is given. The comprehensive description of the method can be found elsewhere (Roy 1978).

When applying ELECTRE III, for each criterion considered (c_i), every alternative is compared to the others in order to assess the outranking relation "alternative *a* is at least as good as alternative *b*" (i.e. *a* outranks *b*). To measure the credibility of this assertion, pseudo-criteria are used, which consist in three threshold values: indifference (q_i), preference (p_i) and veto (v_i). Depending on the difference value between the two alternatives' performances, $g_i(a)$ and $g_i(b)$, four outranking situations can take place: (i) *a* and *b* are considered to be indifferent ($g_i(a)-g_i(b)<q_i$), (ii) *a* is weakly preferred over *b* ($q_i \leq g_i(a)-g_i(b)<p_i$), (iii) *a* is strongly preferred over *b* ($p_i \leq g_i(a)-g_i(b)<v_i$) and (iv) *b* cannot be preferred over *a* ($g_i(a)-g_i(b) \geq v_i$).

These thresholds can be re-interpreted by expressing them in terms of the upper and lower limits of the confidence intervals of the alternatives. Consequently, if alternative *b* falls into the confidence interval of alternative *a*, they cannot be differentiated; but if their intervals do not overlap, alternative *b* can be preferred over *a*. The new definition of the method's thresholds is represented in Figure 1.

The binomial proportion confidence intervals of the alternatives ($p(a)_{upper,i}$ and $p(a)_{lower,i}$) are calculating according to the Clopper-Pearson method (Clopper & Pearson 1934), which is a function of the survey results (number of answers that meet the criterion and total number of answers) and the confidence level α (of 80% in the present study). The method has been implemented in R software (v3.3.1) in a standard laptop (2.6GHz Intel Core i5).

2.2 Case study

In 2006, the Government of Kenya and UNICEF Programme of Cooperation "Acceleration of

Water Supply and Sanitation towards Reaching Kenya's Millennium Development Goals (2006 – 2011)" was launched to increase the access to water and sanitation in 21 rural districts (divided in a total of 338 sub-districts). In 2009, a comprehensive baseline was established to evaluate the impact of this initiative at mid-term. 9 different criteria were assessed: (c1) access to improved water sources (c2) access to improved sanitation facilities, (c3) water quality inspection, (c4) point-of-use water treatment, (c5) water quality, (c6) time used to collect water, (c7) operational status of water source, (c8) individual responsible for collecting water and (c9) domestic water consumption. Data was collected at a household level in each subdistrict. A complete description of the scope and implementation of the survey is detailed elsewhere (Giné-Garriga et al. 2013).
E3M was used to analyse the state of Kenya's subdistricts regarding the 9 water-related criteria. The method was applied to rank these administrative units at a district level (ranking the subdistricts district by district) and country level (ranking all Kenya's subdistricts).

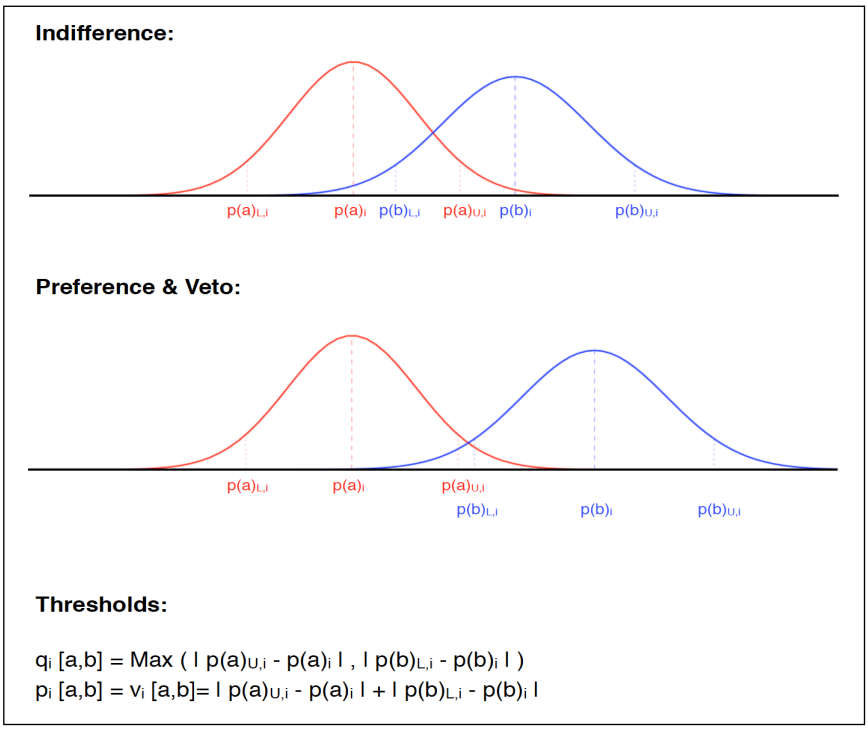

Figure 1. Definition of E3M's thresholds linked to confidence interval of alternatives.

3. RESULTS AND DISCUSSION

In this section, the usefulness of the E3M as a prioritisation and decision-making tool is demonstrated. First, the data's uncertainty is analysed to illustrate the difficulty entailed in its ranking. Next, the method is used to rank the subdistricts at a district level (i.e. applied in each district separately) in order to determine its effectiveness. Finally, the method is used at a country level (i.e. to all districts indistinctly) with the aim of evaluating its suitability for a large number of administrative units.

3.1 Analysis of data uncertainty

Information related to the different water and sanitation criteria was collected at a household level through a structured questionnaire. Values of 0-1 were given to the households depending on whether they met the criterion's condition (1) or not (0). This provided the proportions of households in each of the 338 subdistricts that verified the criterion (p_i), with their respective confidence intervals ($p_{L,i}$, $p_{U,i}$). Figure 2 illustrates these estimates in each district (identified with

its enumeration areas, EA) for the criterion of access to improved water sources.

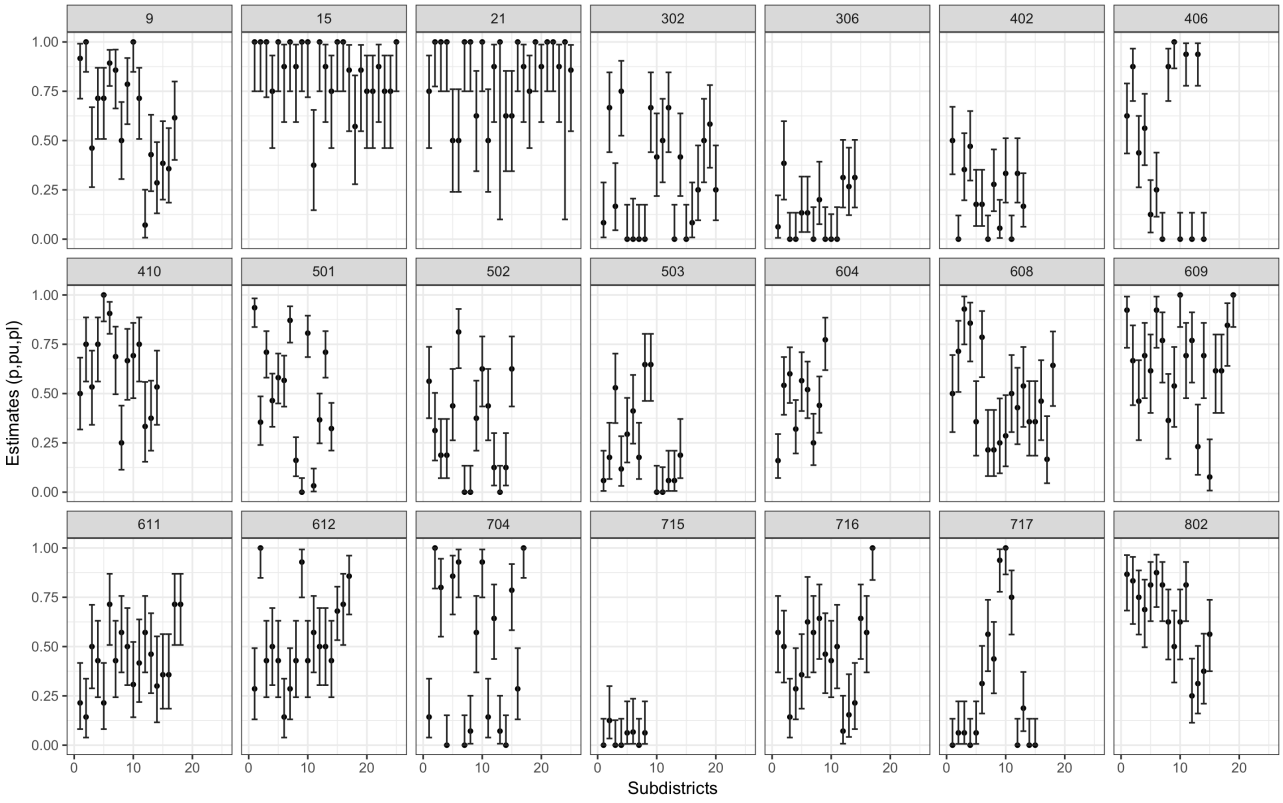

Figure 2. Estimated proportions and confidence intervals of subdistricts (p_i ,$p_{L,i}$, $p_{U,i}$) in the 21 districts for access to improved water sources.

Since small sample sizes were selected for the implementation of local surveys, large lengths of confidence intervals were obtained. As a result, the subdistricts' confidence intervals overlapped, making their ranking a challenging task. It becomes evident that a tool such as E3M, where statistical uncertainty is considered in the analysis, is needed.

3.2. Application of E3M at district level

The E3M method was applied to each one of the 21 rural districts of the Kenyan case study in order to analyse the state of its subdistricts. In each district, the subdistricts were ranked based on their performance regarding the different criteria. At first, only two criteria were considered (c1 and c2), then the outranking tool assessed all criteria. The number of ranks obtained (i.e. the number of positions within the hierarchy) and the ranking effectiveness (i.e. percentage of ranks obtained over the maximum possible, which corresponds to a ranking where each subdistrict is placed in a different position) is presented in Table 1.

When only two criteria were evaluated, E3M was able to provide a detailed ranking of the subdistricts, resulting in most cases in a total of ranks of more than 50% of the maximum possible. This did not happen in just two districts, EA-015 and EA-021, where their 25 subdistricts had a similar performance in terms of access to improved water and sanitation.

When all criteria were considered, the ranking changed in two manners. For most districts, taking more criteria into account entailed a more complete information of the subdistricts conditions, as it was easier to discriminate between them. Consequently, more criteria resulted in more ranks and a higher ranking effectiveness. However, for various districts, the consideration of additional criteria did not help the outranking process. This was the case of EA-604 and EA-612 (which remained the same) and EA-501, EA-503, EA-608, EA-609, EA-611 and EA-716 (which

decreased in 1-2 ranks). The drop could be attributed to the fact that their subdistricts' performances were indistinguishable for two pairs of criteria: (i) time used to collect water and individual responsible for the fetching, and (ii) water quality and domestic water consumption. Nevertheless, even in these cases, the ranking effectiveness exceeded 50%.

Table 1. Ranking of sub-districts at district level

District		Nº Sub-districts	Nº Ranks		Ranking effectiveness (%)	
			2 criteria	9 criteria	2 criteria	9 criteria
EA-009	Kitiu	17	9	11	53	65
EA-015	Kieni	25	5	10	20	40
EA-021	Molo	25	10	17	40	68
EA-302	Kwale	20	10	14	50	70
EA-306	Garissa	14	7	12	50	86
EA-402	Isiolo	13	7	10	54	77
EA-406	Tana River	14	8	9	57	64
EA-410	Wajir	14	7	8	50	57
EA-501	Waest Pokot	14	10	9	71	64
EA-502	Turkana	15	11	11	73	73
EA-503	Busia	14	10	9	71	64
EA-604	Kisumu	9	5	5	56	56
EA-608	Bondo	18	12	8	67	44
EA-609	Siaya	19	15	13	79	68
EA-611	Kajiado	18	12	10	67	56
EA-612	Nyando	17	12	12	71	71
EA-704	Rachuonyo	17	10	12	59	71
EA-715	Mwingi	8	4	5	50	63
EA-716	Uasin Gishu	17	11	10	65	59
EA-717	Mandera	15	10	11	67	73
EA-802	Marsabit	15	10	11	67	73

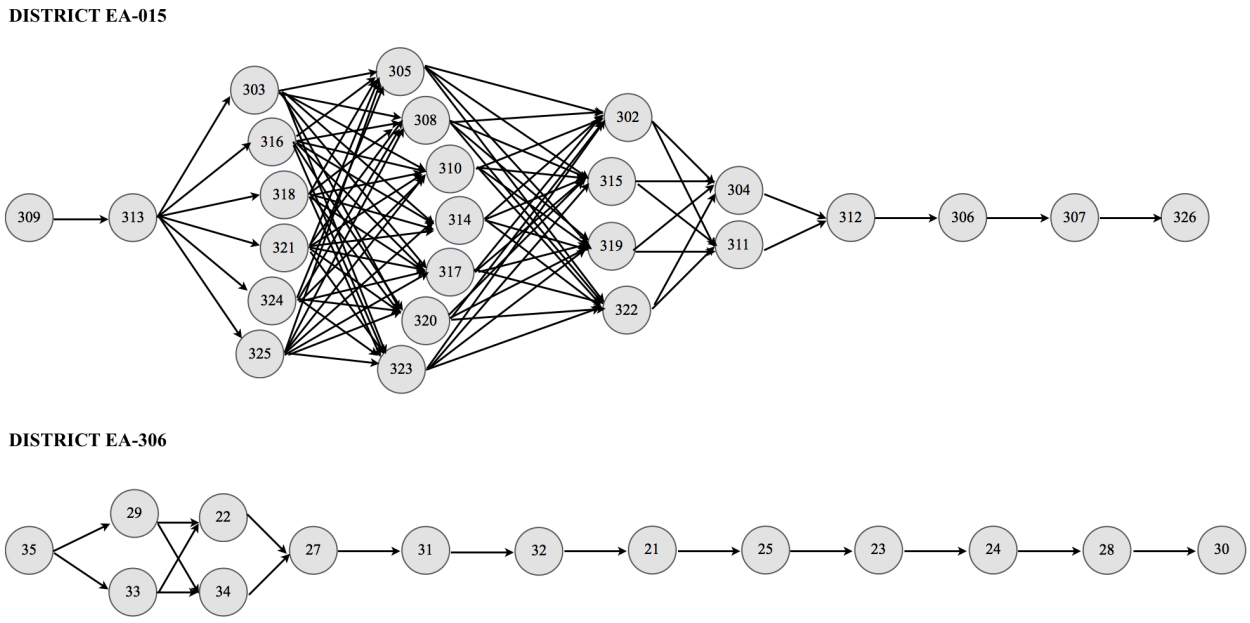

Figure 3. District level ranking in districts EA-015 and EA-306 regarding all criteria.

The difference in ranking effectiveness is illustrated in Figure 3, where districts EA-015 and EA-306 are represented with their ranked subdistricts for all criteria. While E3M provided a poor ranking of subdistrict in EA-015 (its 25 subdistricts were ranked in 10 different positions), for EA-306, the result was more precise (14 subdistricts in 12 ranks). This shows that the effectiveness of E3M for ranking at a district level depends on the data (if subdistricts perform homogeneously, it would be difficult to state that one is better than the others).

3.3 Application of E3M at country level

To determine the suitability of E3M as a prioritisation tool at a country level (with hundreds of administrative subunits), it was applied to all subdistricts jointly. The number of subdistricts evaluated progressively increased (50, 100, 200 and 338) to assess the number of ranks obtained and the computational cost required in each case. At first, only two criteria were considered (access to improved water sources and access to improved sanitation facilities). Then two hygiene-related criteria were added (water quality inspection and point-of-use water treatment). Finally, the analysis was undertaken with all criteria. The results are illustrated in Figure 2.

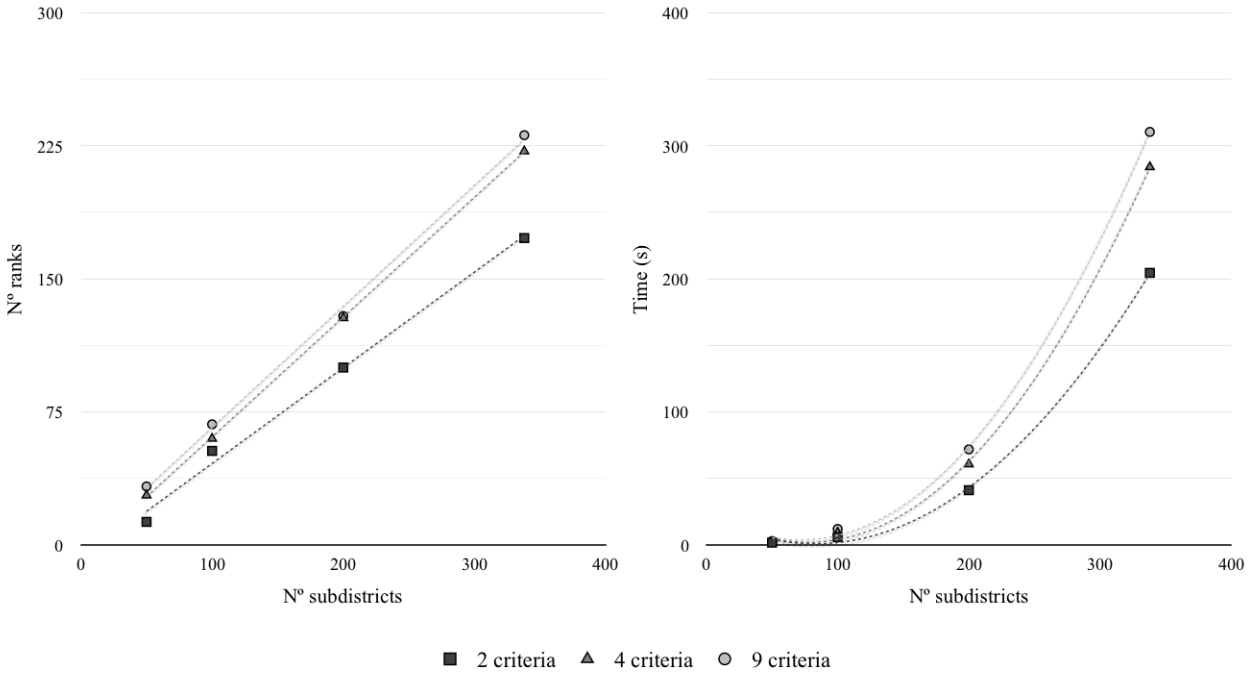

Figure 4. Ranking of sub-districts at country level.

The number of ranks obtained increased linearly with the number of subdistricts evaluated, for all groups of criteria (R^2 value of 0.9938, 0.9999 and 0.9983, respectively). However, it did not translate in an linear increase of ranking effectiveness. For the two criteria evaluation, E3M ranked the 50, 100, 200 and 338 subdistricts in 13, 53, 100 and 173, respectively. Except the first increase in the number of subdistricts (i.e. from 50 to 100), in which the effectiveness increased from 26 to 53%, in the rest it remained constant. The same happened when considering four and nine criteria. The reason of this lied in the data: since many subdistricts performed similarly, it was not possible to conclude that their performances were different.

On the other hand, the time required to execute E3M algorithm followed a second order polynomial function (R^2 value of 0.9989, 0.9991 and 0.9993 with 2, 4 and 9 criteria, respectively). The method's outranking algorithm performs loops of n x n x m, being n the number of subdistricts and m the number of criteria considered. Therefore, it performs n^2 operations. Doubling the input

amount of subdistricts increases the number of operations by a factor of four, which explains the quadratic time dependence. It can be thus concluded that E3M is suitable when dealing with hundreds of alternatives.

4. CONCLUSIONS

Statistical uncertainty is an inevitable feature of water and sanitation services management, as surveys are the primary sources of the information used in the decision making process. Sampling strategies lead to high levels of uncertainty present in the data, which complicates its use for prioritisation and targeting purposes. Therefore, to measure water and sanitation services and identify those sector areas and communities most in need, statistical uncertainty needs to be considered.

The paper employs a new version of the outranking method ELECTRE-III, E3M, in which pseudo-criteria are expressed in terms of estimates' confidence intervals. The method was used to rank Kenya's 338 subdistricts in regards to their performance on 9 water and sanitation related criteria. The subdistricts were ranked first at a district level (i.e. district by district). E3M provided an effective ranking of the administrative subunits, being able to establish a detailed hierarchy between the subdistricts. Then, a country level analysis was selected (i.e. to all districts indistinctly), in which 50, 100, 200 and 338 subdistricts were compared. The number of ranking positions and the computational time used was analysed. The first followed a linear increase with number of subdistricts, showing that E3M remained effective even when ranking hundreds of units. On the other hand, the computational time presented a quadratic increase. For a larger number of alternatives (order of thousands), the method's time shoots to the order of hours.

Consequently, this modified ELECTRE-III approach was found effective at taken statistical uncertainty into account in prioritisation and ranking tasks, even when the number of administrative units to be evaluated was hundreds. However, with 1,000 or 2,000 subdistricts, the method is expected to have an impractical computational cost of 1 and 4.4 hours, respectively. Future work should focus on optimising the algorithm to decrease its time complexity and allow its scalability to thousands of alternatives.

REFERENCES

Bella, A., Duckstein, L. and Szidarovszky, F., 1996. A multicriterion analysis of the water allocation conflict in the upper Rio Grande basin. Applied Mathematics and Computation, 77(2-3), pp.245-265.

Clopper, C., Pearson, E.S., 1934. The use of confidence or fiducial limits illustrated in the case of the binomial. Biometrika, 26 (4), pp. 404-413

Duckstein, L., Treichel, W. and Magnouni, S.E., 1994. Ranking ground-water management alternatives by multicriterion analysis. Journal of Water Resources Planning and Management, 120(4), pp.546-565.

Ezbakhe, F., Pérez-Foguet, A., 2017. Water, sanitation and hygiene multi-criteria decision-making: An improved approach for including uncertainty of surveyed data. Water Resources Management. Under Review.

Giné-Garriga, R., Jiménez-Fernández, A., Pérez-Foguet, A., 2013. Water–sanitation–hygiene mapping: An improved approach for data collection at local level, Science of The Total Environment, 463–464, pp. 700-711

Jakeman, A.J. , Giupponi C., Karssenberg D., Hare M.P., Fassio A., Letcher R.A., 2006. Integrated management of water resources: concepts, approaches and challenges. Sustainable Management of Water Resources. Edward Elgar

Joerin, F., Thériault, M. and Musy, A., 2001. Using GIS and outranking multicriteria analysis for land-use suitability assessment. International Journal of Geographical information science, 15(2), pp.153-174.

Joint Monitoring Programme (JMP), 2006. Core questions on drinking-water and sanitation for household surveys. Geneva/New York: WHO/UNICEF

Kumar, V., Del Vasto-Terrientes, L., Valls, A. and Schuhmacher, M., 2016. Adaptation strategies for water supply management in a drought prone Mediterranean river basin: application of outranking method. Science of the Total Environment, 540, pp.344-357.

Lerner, D.N., Kumar, V., Holzkämper, A., Surridge, B.W. and Harris, B., 2011. Challenges in developing an integrated catchment management model. Water and Environment Journal, 25(3), pp.345-354.

Medema, W., McIntosh, B. and Jeffrey, P., 2008. From premise to practice: a critical assessment of integrated water resources management and adaptive management approaches in the water sector. Ecology and Society, 13(2): 8.

Parker, D.D. and Tsur, Y., 2012. Decentralization and coordination of water resource management (Vol. 10). Springer Science & Business Media.

Pereira, J.M. and Duckstein, L., 1993. A multiple criteria decision-making approach to GIS-based land suitability evaluation. International Journal of Geographical Information Science, 7(5), pp.407-424.

Raju, K.S., Duckstein, L. and Arondel, C., 2000. Multicriterion analysis for sustainable water resources planning: a case study in Spain. Water Resources Management, 14(6), pp.435-456.

Ribot, J.C., 2002. Democratic decentralization of natural resources. In Beyond Structural Adjustment The Institutional Context of African Development (pp. 159-182). Palgrave Macmillan US.

Roy, B., 1978. ELECTRE III: Algorithme de classement base sur une representation floue des preferences en presence de criteres multiples. Cahiers de CERO, 20 (11), pp. 3-24.

Roy, B., 1991. The outranking approach and the foundations of ELECTRE methods. Theory and decision, 31(1), pp.49-73.

Roy, B., Slowinski, R. and Treichel, W., 1992. Multicriteria programming of water supply systems for rural areas. Journal of the American Water Resources Association 28(1), pp. 13-31.

Sachs, J.D., 2012. From millennium development goals to sustainable development goals. The Lancet, 379(9832), pp.2206-2211.

Timmerman, J.G., Ottens, J.J. and Ward, R.C., 2000. The information cycle as a framework for defining information goals for water-quality monitoring. Environmental management, 25(3), pp.229-239.

Trojan, F. and Morais, D.C., 2012. Prioritising alternatives for maintenance of water distribution networks: a group decision approach. Water Sa, 38(4), pp.555-564.

United Nations, 2005. Household surveys in developing and transition countries (Vol. 96). United Nations Publications - Department of Economic, United Nations. Statistical Division, & National Household Survey Capability Programme. Chicago

UNEP, 2011. Towards a green economy: pathways to sustainable development and poverty eradication. United Nations Environment Programme. Paris, France

UN-Water, 2012. Status Report on the Application of Integrated Approaches to Water Resources Management for Rio+20. Status Report on Integrated Water Resources Management

UN-Water, 2014. A Post-2015 Global Goal for Water: synthesis of key findings and recommendations from UN-Water.

Proceedings of the 10th World Congress of EWRA 'Panta Rhei', 5-9 July 2017, Athens, Greece
© 2017 *European Water Resources Association*

Hydrological modelling of low flows for operational water resources management

L. Vasiliades*, G. Sarailidis and A. Loukas
Department of Civil Engineering, University of Thessaly, Pedion Areos, 38334 Volos, Greece
* *e-mail: lvassil@civ.uth.gr*

Abstract: Hydrological modelling of low flows is performed in this study for operational water resources management. The HBV hydrological model is used to simulate, reconstruct and extent the observed discharges to a complete 30-year daily simulated discharge dataset at Yermasoyia river, Cyprus. Calibration and validation techniques are used to assess the validity of the hydrological model for low flow modelling. Low flows simulated and observed characteristics are estimated and compared using the monthly varying threshold approach. Then, the monthly threshold method and the inter-event time and volume criterion (IC) is applied to derive independent sequences of low-flow events. Severity-duration-frequency (SDF) curves of low flows are developed based on the annual maximum severities for fixed durations at 30, 60, 90, 180 and 360 days. The best theoretical probability distribution is then selected for each threshold method based on individual probabilistic analysis, and finally the SDF curves for the study threshold are derived to quantify the relationship among the severities, durations, and frequencies. Hence, based on typical simulated drought characteristics (deficit volume and duration), this study develops quantitative relationships for low flows among drought parameters using monthly varying threshold levels.

Key words: hydrological droughts, low flows, hydrological modelling, low flow indices, severity–duration–frequency (SDF) curves, streamflow deficits, threshold level method

1. INTRODUCTION

Droughts are generally considered as periods with insufficient precipitation, soil moisture and water resources for sustaining and supplying the socio-economic activities of a region (Mishra and Singh, 2010). The American Meteorological Society (2004) adopted a four-type drought classification system based on the nature of the water deficit. According to this classification, meteorological, hydrological and agricultural droughts are considered environmental droughts, and they are defined as periods with insufficient amounts of precipitation, river flow or groundwater, and soil moisture, respectively. The fourth drought type is the socio-economic drought, which is related to the failure of water resources systems to meet the water demands. Droughts are long-term phenomena affecting large regions causing significant damages both in human lives and economic losses. Droughts are the costliest natural disaster of the world and affect more people than any other natural disaster (Wilhite, 2000). In the past few years, major drought events have been recorded in Ethiopia, Australia, United States, Eurasia, Middle East, and southern Europe (IPCC, 2012; AghaKouchak et al., 2013).

Streamflow drought properties have been extensively analysed for the design of hydrotechnical projects and water resources planning and management during the last two decades. Information on the magnitude and frequency of low flows is very important for streamflow drought analysis at operational level in public water supply systems. The objective of this study is to model hydrological droughts for operational water resources management. Hydrological droughts are estimated using rainfall-runoff models and low flow analysis techniques. It should be noted that a low flow event may not necessarily be a drought event. Low flows are usually seasonal-periodical events that are integral parts of the hydrograph, while droughts are caused by abnormal lack of precipitation and water resources (Tallaksen and van Lanen, 2004). The methodology is developed and demonstrated for volume deficits using probabilistic analysis on a semi-arid catchment in

Cyprus. The probabilistic analysis provides an overall characterization of the basin concerning the drought events and is oriented to long term drought management and infrastructure (i.e. reservoirs) design and operation.

2. STUDY AREA

The study basin is the Yermasoyia watershed, which is located on the southern side of mountain Troodos of Cyprus, roughly 5 km north of the city of Limassol. The watershed area is 157 km^2 and its elevation ranges from 70m up to 1400m. Most of the area is covered by typical Mediterranean-type forest and sparse vegetation. A reservoir with storage capacity of 13.6 hm^3 was constructed downstream of the mouth of the watershed in 1969 for irrigation and municipal water supply purposes (Hrissanthou, 2006). The climate of the area is of Mediterranean maritime climate, with mild winters and hot and dry summers. Precipitation is usually generated by frontal weather systems moving eastwards. Average basin-wide annual precipitation is 640 mm, ranging from 450 mm at the low elevations up to 850mm at the upper parts of the watershed. Mean annual runoff of the Yermasoyia River is about 150 mm, and 65% of it is generated by rainfall during winter months. The river is usually dry during summer months. The peak flows are observed in winter months and produced by rainfall events. Good-quality daily precipitation, maximum and minimum temperature for a period of 30 years (1969-1998) from Limassol meteorological station were used in this study. Potential evapotranspiration values are estimated with the Hargreaves equation (Hargreaves and Samani, 1985; Allen et al., 1998). Furthermore, 11 years of daily streamflow data (October 1986–September 1997) were available for the Yermasoyia watershed. Further details of the Yermasoyia watershed could be found in recent studies (Hrissanthou, 2006; Loukas and Vasiliades, 2014).

3. METHODOLOGY

The objective of this study is to derive hydrological drought severity-duration-frequency (SDF) curves using low flows estimated from a rainfall-runoff model and analysed with the threshold level method. Low flow severity is defined as the total water deficit volume to the target threshold for a given drought duration. A conceptual rainfall-runoff model following the structure of the HBV model (Parajka et al., 2007) is used to reconstruct and extent the observed discharges to a complete 30-year daily simulated discharge dataset at Yermasoyia watershed.

In this study, a semi-distributed conceptual model, HBV, was chosen for hydrologic simulation of the rainfall runoff process. The motivation of choosing this particular model is that the model was used in previous studies and showed a good performance in this watershed (Paraskeuas et al., 2015). The model runs on daily values of precipitation, temperature and estimates of potential evapotranspiration. Flow observations are used for calibration and validation of the model. The model contains routines for snow accumulation and melt, soil moisture accounting, runoff generation and a routing procedure. The snowmelt routine of the HBV model is based on the degree-day approach. It is based on air temperature, with a water holding capacity of snow which delays runoff. The soil moisture routine of the model controls runoff formation, accounts for soil field capacity and change in soil moisture storage due to rainfall/snowmelt and evapotranspiration. The excess water from the soil moisture zone transforms to runoff in the response routing. The response function of the model consists of two reservoir – one upper nonlinear, one lower linear, and one transform function. The runoff is computed by adding the contribution from the upper and lower reservoir, and the generated runoff is routed through a transformation function in order to get a proper shape of the hydrograph at the outlet of the watershed.

The 15 parameters of the HBV model need to be calibrated in order to provide model output that closely resembles observed data as it is a conceptual model. In this study, the first 6 years of runoff data (from 1986 to 1992) were used to calibrate the hydrologic model and the last 5 years of data

(1992-1997) were used to validate the model. The Nash-Sutcliffe model efficiency on square root flows was used as the objective function of the optimisation process (Krause et al., 2005). The square root transformation of the flow values leads to the flattening of peaks and the low flows are kept more or less at the same level. As a result the influence of the low flow values is increased in comparison to the flood peaks resulting in an increase in sensitivity, similarly to the logarithmic transformation (Krause et al., 2005). The calibration of the model was performed automatically using the Self-Organising Migrating Algorithm (SOMA) optimisation algorithm (Zelinka, 2004). The SOMA is a general-purpose, stochastic optimisation algorithm. The approach is similar to that of genetic algorithms, although it is based on the idea of a series of migrations by a fixed set of individuals, rather than the development of successive generations. It can be applied to any cost-minimisation problem with a bounded parameter space, and is robust to local minima.

The HBV simulated discharges are then analysed with the monthly varying threshold level method in the estimation of derived streamflow deficits and durations. In monthly varying threshold, there are twelve different thresholds, one for each month. The threshold for January results from the values of flow of January for the entire period of record. The monthly 50th percentile values of the flow duration curve are selected as the threshold choices which are suitable for semiarid catchments where zero runoff occurs during summer months (Sarailidis et al., 2015). Then, the inter-event time and volume criterion (IC) is applied to derive independent sequences of low-flow events (Tallaksen et al., 1997). According to IC method two events are pooled if: (a) they occur less than a predefined number of days, t_{min}, apart (the inter-event time (τ_i) is less than t_{min}) and; (b) the ratio between the inter-event excess volume (s_i) and the preceding deficit volume, v_i, is less than a critical ratio, p_i. The adjacent deficits are then pooled if the aforementioned requirements are fulfilled. The pooled deficit characteristics (d_{pool}, d_i, d_{i+1} in days), (v_{pool}, v_i, v_{i+1} in mm) can be calculated as follows:

$$d_{pool} = d_i + d_{i+1} + \tau_i \quad (1)$$

$$v_{pool} = v_i + v_{i+1} - s_i \quad (2)$$

The IC method was tested on two Danish rivers with contrasting flow regimes and it was found that the optimal values of the pooling criteria were t_{min} = 5 days and p_i = 0.1 (Tallaksen et al., 1997). Sensitivity analysis is applied for accurate estimation of the method parameters. Finally, the HBV-simulated SDF curves are developed based on the annual maximum severities for fixed durations at 30, 60, 90, 180 and 360 days. Based on individual probabilistic analysis, the best theoretical probability distribution is selected and then the SDF curves are developed to quantify the relationship among the severities, durations, and frequencies or return periods. These curves also integrate the return period–duration curve to quantify the extent of the threshold method. Hence, this study developed quantitative relationships among drought parameters based on typical drought characteristics (deficit volume and duration) and monthly varying threshold levels.

4. APPLICATION AND RESULTS

4.1 Hydrological Modelling of Low Flows

The methodology described above was applied to simulate flows at the outlet of the watershed using the HBV rainfall runoff model and to evaluate hydrological model accuracy. Three more evaluation metrics apart from the square root transformation of NSE (NSE(√Q)) were employed for model evaluation: the runoff volume error (Vol. Error in %); the root mean square error between the simulated and the observed flow values (RMSE) and the Nash-Sutcliffe model efficiency (NSE). Table 1 presents the evaluation metrics for calibration and validation periods and for the complete period with the observed runoff data. Furthermore, Table 2 presents the comparison of the

streamflow deficits for the observed and simulated flows for the period 1986-1997 (11 years). The observed and simulated streamflow deficits are calculated using the monthly varying threshold level method, according to which a deficit is defined as a period when the flow is below a predefined discharge (Yevjevich, 1967). In this study the IC pooling method was used in the observed and simulated flow timeseries. The IC method is preferred from other pooling methods since it produces more reliable results (WMO, 2008; Sarailidis et al., 2015). Default values as suggested were used in the IC method to eliminate the problem of having short duration drought events (Tallaksen et al., 1997). Deficit duration is defined as the period of time (d_i), when the flow is below the threshold. Deficit volume (v_i) is defined as the sum of discharges for the corresponding deficit duration, and deficit intensity (or severity) is defined as the ratio between the volume and the duration of deficit, and finally, the last characteristic is the minimum flow of a deficit. Based on Table 2 the HBV model is reproduce quite satisfactorily the observed runoff timeseries since the observed and modelled streamflow deficits have similar statistical characteristics. Hence, it could be used to extent and produce simulated streamflow series for the complete period of analysis 1969-1998.

Table 1. Evaluation metrics for assessing the accuracy of the HBV model

	NSE(√Q)	NSE	Vol. Error (%)	RMSE
Calibration Period (Oct 1986-Sep 1992)	0.92	0.87	-1.26	0.32
Validation Period (Oct 1992-Sep 1997)	0.89	0.82	-6.34	0.32
Complete Period (Oct 1986-Sep 1997)	0.91	0.86	-2.69	0.32

Table 2. Comparison of observed and simulated streamflow deficit characteristics for the period 1986-1997

Characteristic	Observed	HBV modelled
Number of drought events per year	3.55	3.48
Mean drought duration (d)	83.34	83.40
Mean drought deficit (mm)	26.77	23.89
Mean drought intensity (or severity) (mm/d)	0.24	0.22

4.2 Streamflow Deficits Analysis

The HBV simulated flow timeseries were used for hydrological drought modelling of low flows with the monthly varying threshold level method. The monthly 50th percentile values of the simulated flow duration curve are selected as the threshold choices which are suitable for semiarid catchments where zero runoff occurs during summer months. Then, the inter-event time and volume criterion (IC) is applied to derive independent sequences of low-flow events. Sensitivity analysis is applied for accurate estimation of the IC model parameters. Figure 1 presents the results of this analysis for IC model parameters ($3 \leq t_{min} \leq 15$ and $5 \leq p_i \leq 15$). Application of the sensitivity analysis showed that the inter-event time and volume criterion is an unbiased pooling method and there is no subjectivity in the choice neither of days of pooling nor of the ratio of volumes. This is reflected in Figure 1, where there is a good convergence of the different periods of days of pooling, and a good convergence of the three different ratios of pooling. The IC method with t_{min} =5 days and p_i=10% is selected to estimate the duration and the deficit volume or severity of the identified simulated drought events. Using the monthly varying threshold level method, deficits characteristics were derived for the monthly Q50 quantiles. Most streamflow deficits occur in winter months and in wet season (October-March) which is valuable information because deficits that occur in wet season are very important for water resources management in the study area (Fig. 2).

The knowledge of future volume of deficits is very important for the design of hydro-technical projects. In this study, a probabilistic analysis of maximum volumes of deficits was done for return periods 10, 20, 30, 50, 100, 250 and 500 years. In order to incorporate the influence of drought duration, annual maximum volumes were extracted for selected drought durations (30, 60, 90, 180, 360 days) for each hydrological year.

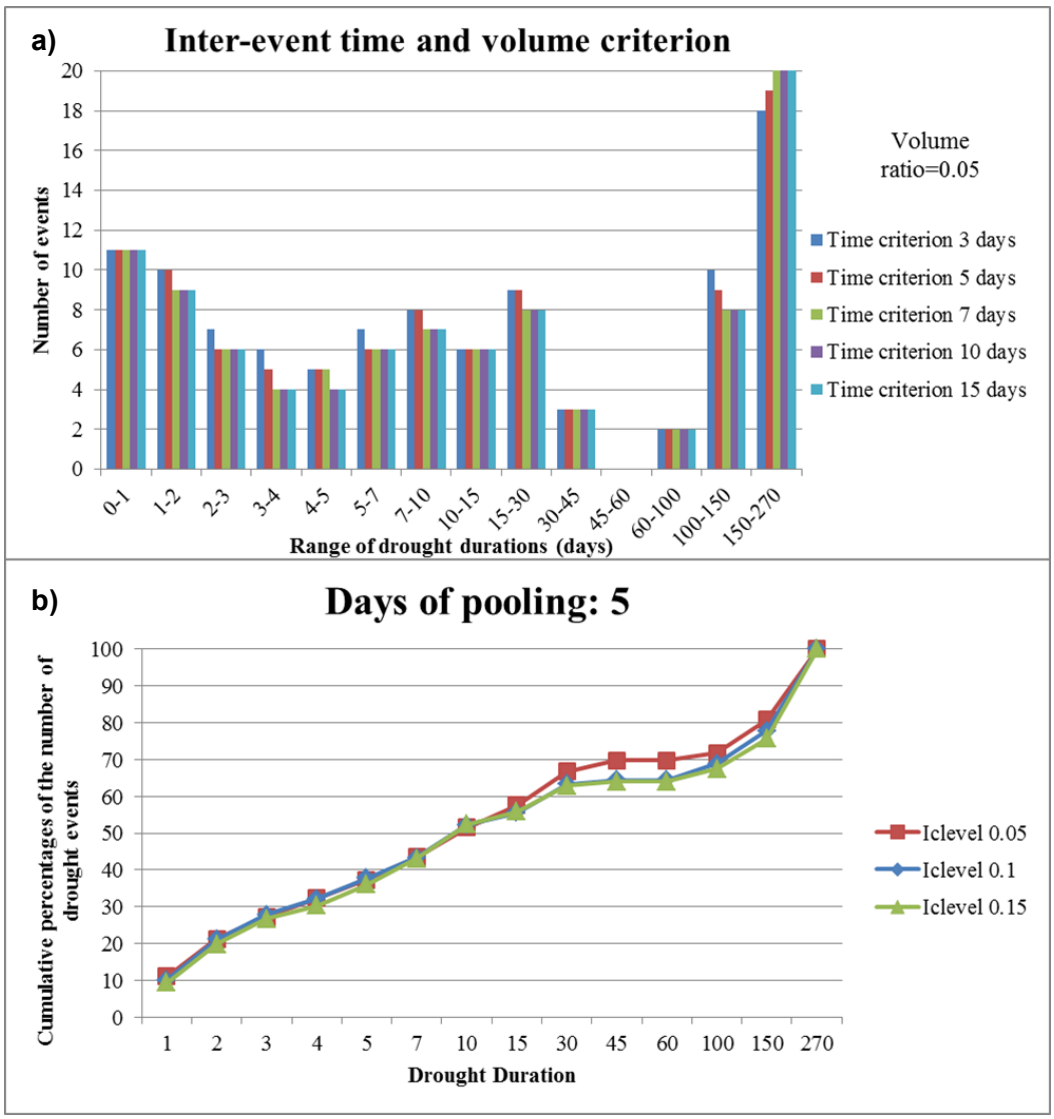

Figure 1. Sensitivity of the inter event time and volume criterion method: a) the effect of inter event time on low flow events and b) the effect of volume criterion on the estimated low flow events

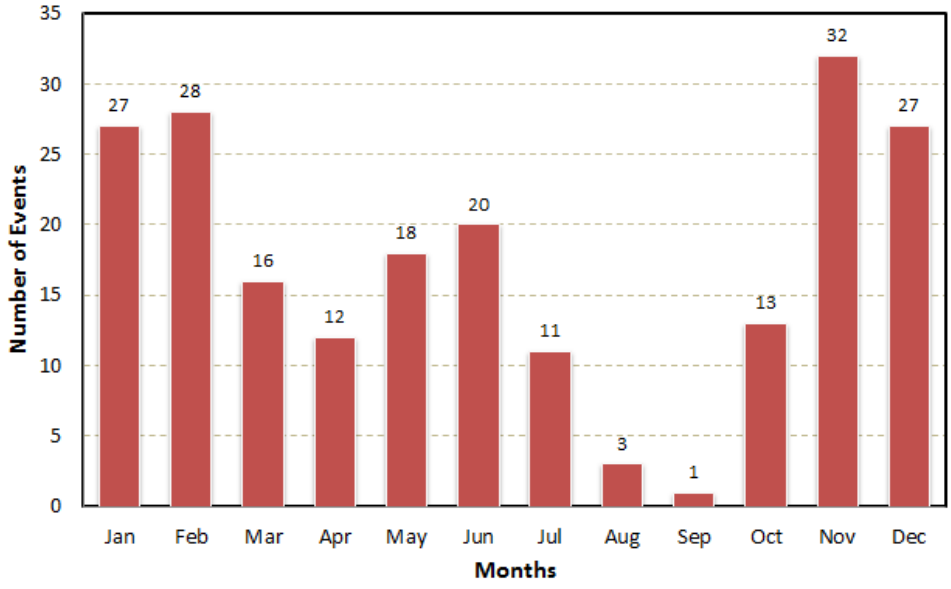

Figure 2. Estimated number of drought events for each month using the monthly varying threshold method

Several theoretical probability distributions were fitted to the extracted annual maximum volume deficits and the fitted theoretical distributions were evaluated with the use of Kolmogorov-Smirnov test. Results show that annual maximum volume deficits are best represented with the Pareto probability distribution (with L-moments estimated parameters) for the study durations. Figure 3a shows fitting of Pareto distribution to annual maximum volume deficits. Then, the Pareto distribution is used for estimation of volume deficits at typical return periods of 10, 20, 30, 50, 100, 250, and 500 years and the creation of volume deficit-duration-frequency curves, as shown in Figure 3b.

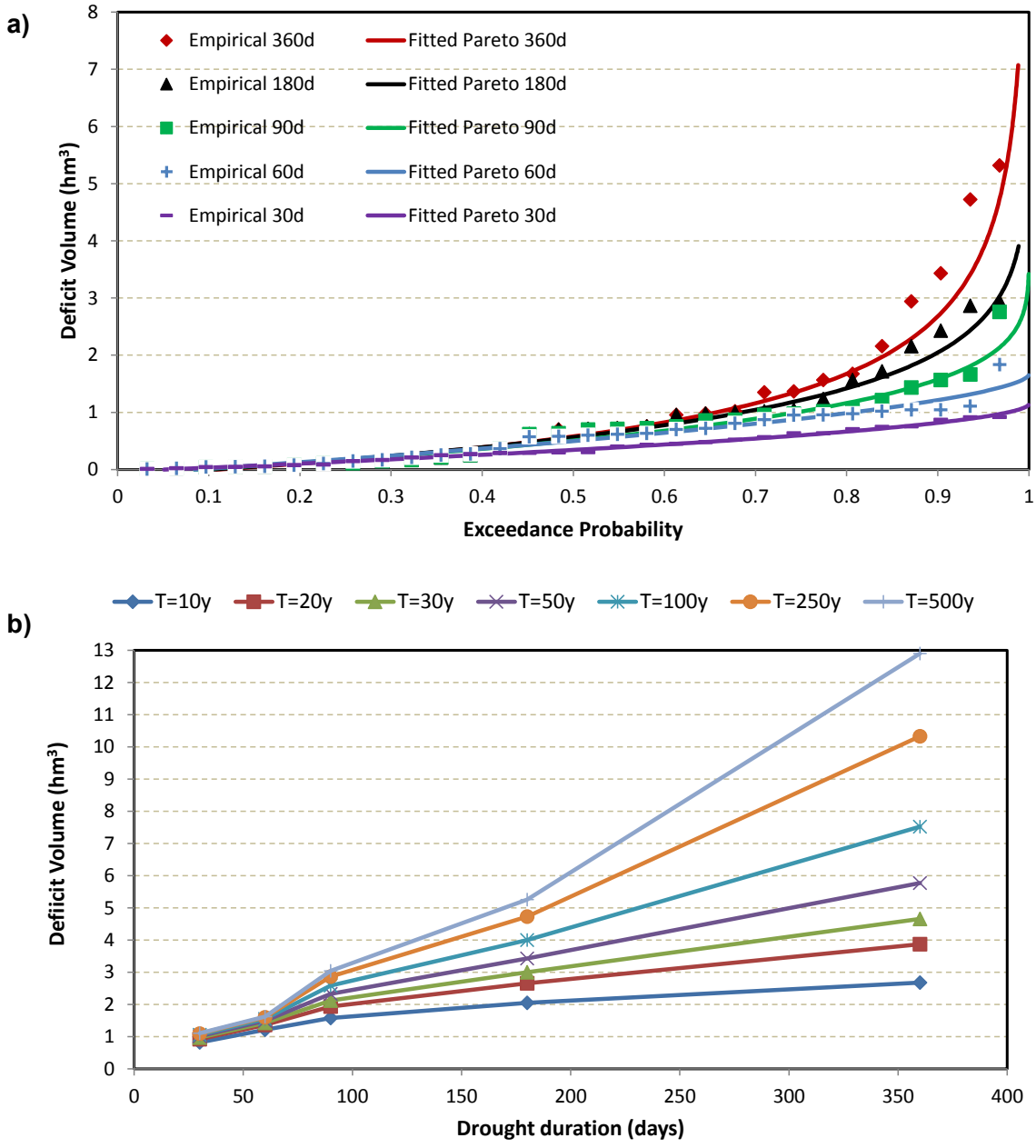

Figure 3. a) Fitting of Pareto theoretical distribution to annual maximum volume deficits for the study durations and b) Development of volume deficit-duration-frequency curves

5. CONCLUDING REMARKS

Hydrological modelling of low flows for operational water resources management is examined in this study. The HBV hydrological model is able to simulate accurately the observed low flow for

the study watershed and it could be used as an operational tool to create synthetic discharge timeseries. Low flow events created with the use of the hydrological model and the monthly varying threshold approach are used to model streamflow characteristics. Severity-duration-frequency (SDF) curves of low flows are developed based on the annual maximum severities for fixed durations at 30, 60, 90, 180 and 360 days. Hence, based on typical simulated drought characteristics (deficit volume and duration), this study developed quantitative relationships for operational management of low flows.

REFERENCES

Agha Kouchak, A., Easterling, D., Hsu, K., Schubert, S., Sorooshian, S., (eds.), 2013. Extremes in a Changing Climate: Detection, Analysis and Uncertainty. Water Science and Technology Library, Vol. 65, Springer: Netherlands.

Allen, R. G., Pereira, L. S., Raes, D., Smith, M., 1998. Crop Evapotranspiration - Guidelines for Computing Crop Water Requirements. FAO Irrigation and Drainage Paper No. 56, Food and Agriculture Organization of the United Nations, Rome.

American Meteorological Society (AMS), 2004. Statement on meteorological drought. Bull. Am. Meteorol. Soc.; 85: 771-773.

Hargreaves, G. H., Samani, Z. A., 1985. Reference crop evapotranspiration from temperature. Applied Engrg. in Agric.; 1(2): 96-99.

Hrissanthou, V., 2006. Comparative application of two mathematical models to predict sedimentation in Yermasoyia reservoir, Cyprus. Hydrol. Process.; 20: 3939-3952.

Intergovernmental Panel on Climate Change (IPCC), 2012. Managing the Risks of Extreme Events and Disasters to Advance Climate Change Adaptation. A Special Report of Working Groups I and II of the Intergovernmental Panel on Climate Change [Field, C.B., V. Barros, T.F. Stocker, D. Qin, D.J. Dokken, K.L. Ebi, M.D. Mastrandrea, K.J. Mach, G.-K. Plattner, S.K. Allen, M. Tignor, and P.M. Midgley (eds.)]. Cambridge University Press, Cambridge, UK, and New York, NY, USA, 582 pp.

Krause, P., Boyle, D. P., Bäse, F., 2005. Comparison of different efficiency criteria for hydrological model assessment. Advances in Geosciences; 5: 89-97.

Loukas, A. Vasiliades, L., 2014. Streamflow simulation methods for ungauged and poorly gauged watersheds. Nat. Hazards Earth Syst. Sci.; 14: 1641-1661.

Mishra, A. K., Singh, V. P., 2010. A review of drought concepts. J. Hydrol.; 391(1-2): 202-216.

Parajka, J., Merz, R., Blöschl, G., 2007. Uncertainty and multiple objective calibration in regional water balance modelling: case study in 320 Austrian catchments. Hydrol. Process.; 21(4): 435-446.

Paraskeuas, I., Vasiliades, L., Loukas, A., 2015. A generic framework for the identification of hydrological droughts through the propagation of runoff generation mechanisms in semi-arid catchments. Geophysical Research Abstracts EGU General Assembly; 17: EGU2015-14075.

Sarailidis, G., Vasiliades, L., Loukas, A., 2015. The quantification of the threshold level method on low flows studies. E-proceedings of the 14th International Conference on Environmental Science and Technology (CEST 2015), 5-7 September 2015, Rhodes Island, Greece, 5 pp.

Tallaksen, L. M., Madsen, H., Clausen, B., 1997. On the definition and modelling of streamflow drought duration and deficit volume. Hydrolog. Sci. J.; 42(1): 15-33.

Tallaksen, L. M., Van Lanen, H. A. J., 2004. Hydrological Drought: Processes and Estimation Methods for Streamflow and Groundwater. Developments in Water Science 48, Elsevier Science B.V., Amsterdam, the Netherlands.

Wilhite, D.A., 2000. Drought as a Natural Hazard: Concepts and Definitions. In Drought: A Global Assessment, Wilhite D.A., ed. Dordrecht, NL: Routledge.

World Meteorological Organization (WMO), 2008. Manual on Low Flow Estimation and Prediction. Operational Hydrology Report no. 50, WMO no. 1029, World Meteorological Organization, Geneva, Switzerland.

Yevjevich, V., 1967. An Objective Approach to Definitions and Investigations of Continental Hydrologic Drought. Hydrology Paper No. 23, Colorado State Univ., Fort Collins, Colorado.

Zelinka, I., 2004. SOMA - self-organizing migrating algorithm. In New Optimization Techniques in Engineering, G.C. Onwubolu & B.V. Babu (eds.), Vol. 141, pp. 167-217, Springer.

Proceedings of the 10th World Congress of EWRA 'Panta Rhei', 5-9 July 2017, Athens, Greece
© 2017 *European Water Resources Association*

A network model simulation proposal for river basin management plans (RBMPs) in Turkey

S. Burak[1*], H. Bilge[2] and D. Dernek[1]
[1] *Istanbul University, Institute of Marine Sciences and Management, Istanbul-Turkey*
[2] *Kadir Has University, Faculty of Engineering and Natural Science, Istanbul-Turkey*
[*] *e-mail: sburak@istanbul.edu.tr*

Abstract: Turkey is a negotiating candidate country with the EU. Although Turkey has been developing its water resources policy taking into account of the present and future water needs of its growing population, developments at global level and the on-going EU accession process, it stands at a critical threshold value with regard to its per capita water demand and is expected to become a water-stressed country beyond 2030. Moreover, climate change impacts on water resources lead to irregularities in the flow regime, which constitutes an additional severe burden on water management Already heavy population in water scarce-regions has necessitated water transfer from adjacent basins. This management approach requires a comprehensive decision support system taking into account different situations. In this study, we aim to use a network simulation model within the Greater Istanbul Metropolitan Area that has been facing a heavy population increase caused by local immigration since the 1970's. We run the algorithm repeatedly for different random realizations of estimated inputs and we show that existing water resources are sufficient until 2040 with the projected demand, providing that existing resource conditions remain unchanged. Also the model results show that significant changes in resource replenishment, which may be generated by natural and anthropogenic adverse impacts, will draw back the horizon year of 2040.

Key words: Istanbul water supply system, water supply security, water transfer

1. INTRODUCTION

The city of Istanbul straddles two continents linked by three bridges and two undersea crossings at present. Its boundaries lie between 28°10′ and 29°40′ East longitudes and 40°50′ and 41°30′ North latitudes and extends to the Black Sea, both sides of the Golden Horn and Istanbul Strait (Bosphorus) on the Asian and European continents as shown in Figure 1a (UCTEA CEE, 2014).

The Greater Metropolitan Municipality of Istanbul, with its settlement area covering 5400 km^2 and a population of approximately 15 million, is a coastal mega city that has been attracting immigrants for many centuries. Natural growth and immigration resulted in exacerbated urbanization from the 1970s.

Yet the city does not have large rivers within its administrative boundaries that would ensure a reliable water supply. These socio-geographic and hydrologic constraints have given rise to significant challenging management issues since the 16th century. Heavy population increase caused by local immigration has resulted in a sharp rise in water demand since the 1970's. In response to this situation the State Hydraulic Works (DSI) and Istanbul Water and Sewerage Administration (ISKI) have launched comprehensive water resources development projects aiming at finding viable solutions in order to meet immediate and future demands. Water transfer from adjacent river basins and related management plans have been part of these remedial actions. During recent decades this solution has found widespread implementation in many water-scarce regions all over the world (Gohari et al., 2013). Similarly, water managers adopted this solution for the Istanbul water supply system.

This study presents a network model that is run in order to assess the water supply system for the near future, taking into account water resources within Istanbul, together with the Melen Project stipulated in the latest master plan as the most reliable resource external to Istanbul.

2. METHODOLOGY

Recent decades have seen widespread use of systems analysis to help manage water resources. (Harou et al., 2009).

In the present work, the basins of the creeks located in Istanbul and that of Istranca located in to the West are considered as a single basin and the total capacity of all the reservoirs is modelled by a single node, as shown in Figure 1a and 1b. In the same line, all water treatment systems are united in a single node. As it can be seen from Figure 2, the water supply system is supplemented directly or indirectly by the Yesilcay and Melen rivers located to the East of the city, some 100 km and 200 km respectively. For the purposes of global dynamics we consider these as a single external input to the Istanbul water supply system.

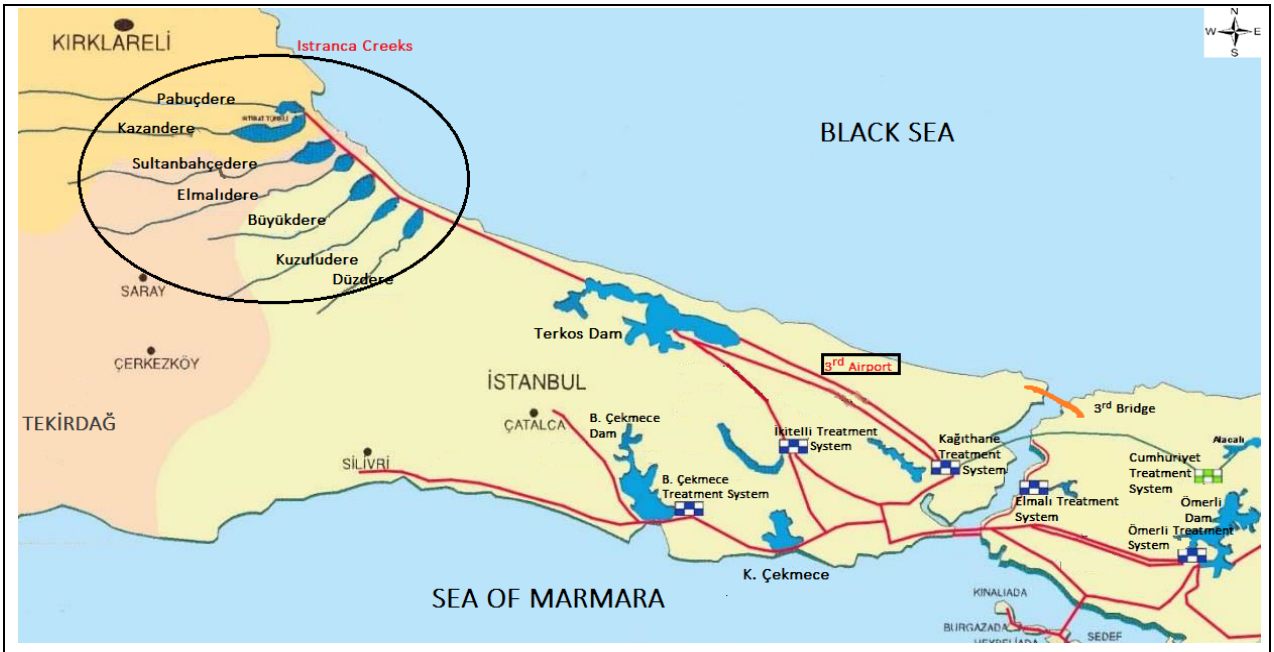

(a) Istanbul water resources (UCTEA CEE, 2014)

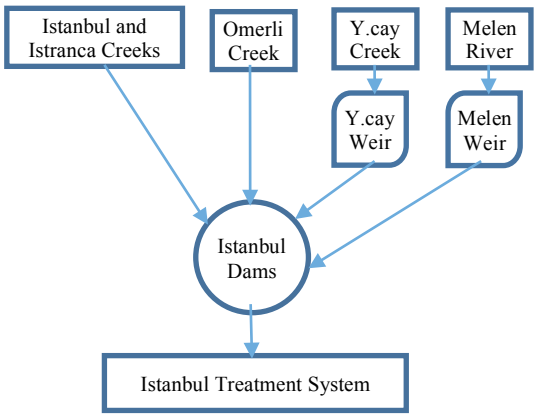

(b) Schematic diagram of Istanbul water supply system

Figure 1. Istanbul water resources and water supply system

The system composed of water catchment basins, reservoirs and water treatment plants is modelled as a network, as depicted in Figure 2. Additional updated data are gathered from ISKI and exchanges are made with ISKI officials (ISKI, 2015).

The major water supply at present is via the Yesilcay and Melen regulators. Omerli and Terkos dams that are located respectively in the Asian and European parts of the city are the main local

water supply. As shown in the figure, these major dams are interconnected to smaller ones that act as backup systems. Treated water is transferred to the various parts of the city. The network model for the detailed system will be investigated in an optimization framework in future works.

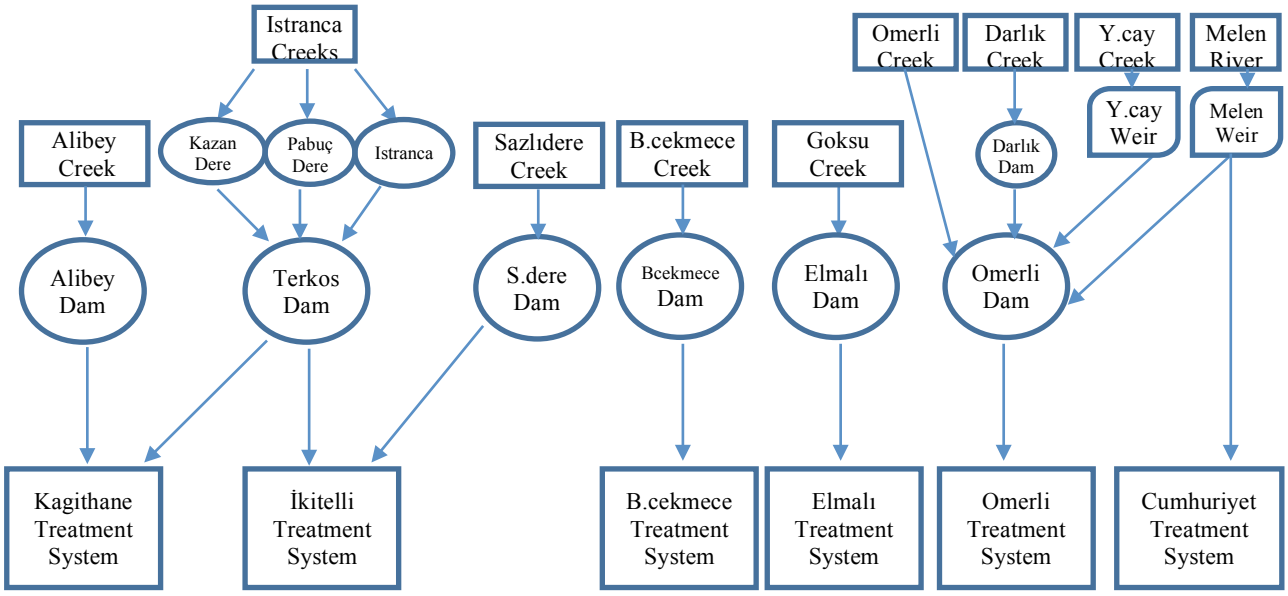

Figure 2. The detailed structure of the Istanbul water supply system

3. OVERVIEW OF THE CURRENT MASTER PLAN FOR ISTANBUL METROPOLITAN AREA

The current Master Plan entitled "Istanbul Water Supply, Sewerage and Drainage, Sewage Treatment and Disposal Master Plan Study" was launched in 1993 in order to replace the DAMOC Master Plan which became obsolete following the city's rapid expansion trend. Urbanisation spread towards rural areas, beyond planned urban boundaries, affecting the Omerli Water Catchment Basin in particular. This was due to meteoric migration into the Istanbul Metropolitan Area, driven by unforeseen socio-economic issues.

A severe drought in 1990, together with relatively dry periods with below average rainfall over the next few years resulted in extreme water shortages in Istanbul. Heavily rising demand due to population increase worsened the already difficult supply conditions, leading to rationing of water supplies throughout the city and in some areas water cuts lasting several days.

The water supply report of the master plan reviews existing infrastructure, together with the current status of planning for Istanbul and key factors that affect further infrastructure development. Water demand projections are then established for the Master Plan period, and an assessment made of the water resources available to satisfy those demands (IMC, 1999).

With the completion of ongoing resource development projects on the European side of Istanbul, there will be no further significant resources to exploit in order to satisfy rising water demands in that part of the city. Accordingly, future water resources development focuses mainly on the Asian side of the Bosphorus where DSI proposes to exploit the resources of the Melen River. This project, known as the Buyuk Melen System, will secure Istanbul's water demand throughout the Master Plan period until 2040. In 1991, a study was undertaken which established the feasibility of the Buyuk Melen System and made recommendations about the sizing and staging of the works. A primary task of the Master Plan was to verify the 1991 study and to update the proposals made in the light of new data available and the latest projections of population and water demand.

As part of this review, hydrological data has been re-evaluated and the safe yields of sources have been re-assessed. In addition, the conjunctive use of the various water resources serving Istanbul has been modelled to indicate the possible benefit that carefully managed source operation could bring in

terms of both increasing available supplies and in delaying the future development of new sources. A preliminary assessment has been made of groundwater sources. Water quality aspects of both ground and surface sources have also been considered.

Details of the existing water resources in Istanbul are presented in Table1.

Table 1. Details of Existing Water Resources (IMC, 1999; ISKI, 2017; DSI,2017)

Characteristics of Catchment Areas and Reservoirs	**European Side**				**Asian Side**		
	Terkos	Alibeyköy	B.Çekmece	Sazlıdere	Ömerli	Darlık	Elmalı
1. Drainage area (km2)	619	160	622	165	621	207	76
2. Mean Annual Rainfall (mm)	750	837	700	627	880	880	-
3. Mean Annual Inflow (Mm^3/a)	163	54	219	49,2	236	108	32
4. Average runoff coefficient (%)	35	40	50	47	45	59	-
5. Reservoir							
5.1 Gross capacity	187	36	182	-	357	113	11.7
5.2 Dead storage (Mm^3)	42	1	20	-	122	6	0.2
5.3 Effective capacity (Mm^3)	162,241	34,143	148,943	88,730	235,371	107,500	9,600
5.4 Fully supply level (E.M)	4.5	30	6.3	48	62	52	67.5
5.5 Min. Operating level (E.M)	-1.00	11	0.8	-	46	21	37.5
5.6 Reservoir area at F.S.L (km2)	39.0	3.0	36	-	22.4	7.0	1.2
6. Nominal annual draught (safe yield) Mm^3/a	142	36	70	-	220	97	14.7

In this work we focus our study on a quantitative approach and present several scenarios based on various resources regardless of policy decisions.

4. THE NETWORK MODEL

Let $U_i>0$ and $Y_i>0$ be respectively the net input to the reservoirs and the net water demand during year i. We use the realized and the potential water demand values for the years 1955-2040, as given in Table 2, to project Yi beyond 2040 up to 2100 in terms of a sigmoidal model that can be applied in our research (Carrillo, 2003).

The output of the simulation depends crucially on the precision of the estimation of the water demand. In order to obtain reliable results for future planning the sigmoidal projection curve should be updated as needed, using current values.

The net input to the reservoirs, U_i, is modelled as a Gaussian random variable with mean and standard deviation computed from ISKI data. The adjustments for various drought scenarios and anticipated irregularities can be done by modifying the mean and the standard deviation, respectively.

Let W_i be the amount of water present in the reservoirs at the beginning of year i. Clearly, $0<W_i<W_0$ where W_0 is the total capacity of the reservoirs. We denote by X_i the water withdrawn from (positive sign) or added to (negative) the storage volume of the reservoirs during the year i. Let V_i be the amount of water input from external basin. V_i has to be less than the maximum yield of these sources, V_m. We will call U_i and V_i as local and external inputs respectively.

The algorithm given below stops when $W< - W_0$.

- If $U_i>Y_i+(W_0-W_i)$, then we use the local input only to meet the water demand, to fill the reservoirs and we discharge any surplus.
- If $U_i+Y_m>Y_i+(W_0-W_i)$, we use the local and external input to meet the water demand and to fill the reservoirs but there is no discharge.
- If $U_i+Y_m<Y_i+(W_0-W_i)$, we use the local and the maximal external input to partially meet the water demand and supplement it from the reservoirs.

Table 2. Potential water demand for Greater Istanbul (DSI, 1991)

Year	Population (1000)	Net Per Capita Demand (l/c/d)	Net Water Demand (million m³/year)	Unaccounted for Water (%)	Gross Water Demand (million m³/year)
1955	1 527	112	62	50	124
1960	1 874	120	82	50	164
1965	2 285	129	108	50	216
1970	3 020	138	152	48	292
1975	3 923	148	212	46	393
1980	4 787	159	278	44	496
1985	5 936	170	368	42	634
1990	7 475	182	497	40	828
1995	8 780	195	625	37	992
2000	10 110	212	782	34	1 185
2005	11 395	231	961	32	1 413
2010	12 584	244	1 121	30	1 601
2015	13 728	250	1 253	28	1 740
2020	14 683	255	1 367	26	1 847
2025	15 492	263	1 487	24	1 957
2030	16 120	270	1 589	22	2 037
2035	16 601	276	1 672	21	2 116
2040	16 963	284	1 758	20	2 198

We run the algorithm described above repeatedly for different random realizations of estimated input U_i., as presented in Figure 3. During the earlier phase at which the Yesilcay and Melen system was not operational, the fluctuations in the left end of the Figure 3 represent those in the local input U_i. During the intermediate period extending up to 2040, the Yesilcay and Melen systems and local input are sufficient to run the system without any net withdrawal from the storage capacity of the reservoirs, as anticipated in the Master Plan. But beyond that period, based on our sigmoidal projection, the system starts to fail, in the sense that during certain years, there is a net withdrawal from the storage capacity.

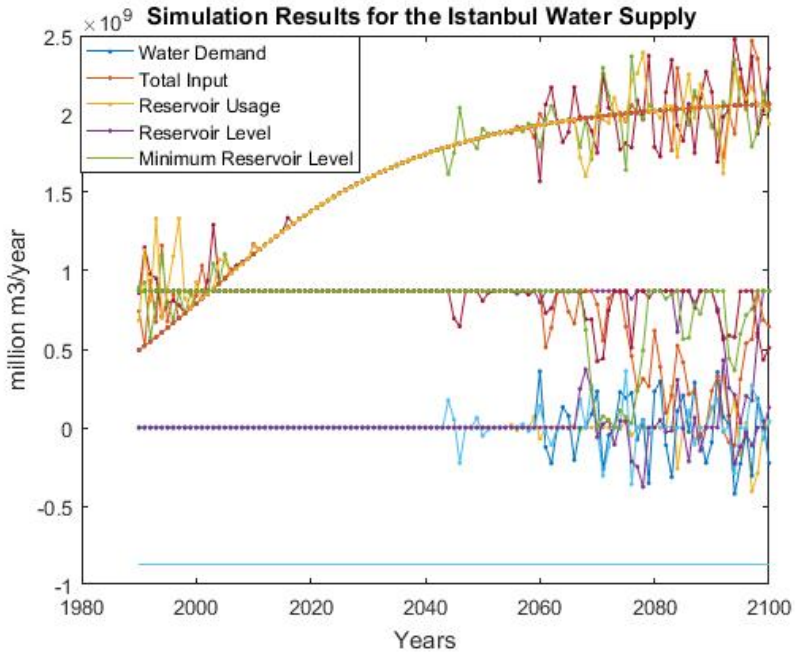

Figure 3. Simulation results for the Istanbul water supply system.

5. CONCLUDING REMARKS

The Master Plan assumes that prevailing conditions in the future will inevitably be different from

the ones projected throughout the given period. Therefore it has been emphasized that regular reviews should be made of the planning proposals in order to take account of demographic, economic, legislative and urban development changes in future years. Depending upon the extent and pace of change, reviews may be needed as frequently as every ten years on average. Applying this model gives us an assessment of the future situation and corresponding water demand and supply conditions.

Unpredictable issues like the severe hazard generated by the 1999 earthquake have been a reason for the development of the city to the north and northwest, where ground conditions are more suitable for housing. This new direction in urban expansion, followed by the construction of a third bridge across Istanbul Strait and the location of a new airport to the northwest may generate new urban expansion in this area.

The model results show that existing water resources will be sufficient until 2040, according to projected demand, providing that existing resource conditions remain unchanged. Also the model results show that significant changes in resource replenishment which may be generated by natural and anthropogenic adverse impacts will bring forward the horizon year of 2040. These impacts can be enumerated as follows:

- severe repeated droughts and extremes,
- anthropogenic impact on resource yield mainly caused by urbanisation to the detriment of forest areas,
- changes in run-off patterns within water catchment basins in Istanbul and in the external basins supplying water to Istanbul due to natural and anthropogenic hazards

In conclusion, first of all, water resource planning must continue to promote the diversification of Istanbul's water resources to help reduce the vulnerability of the city to future drought periods. Second, regardless of supply-sided water resource development, it is obvious that management policy decisions (e.g. minimising water losses, conserving resources by controlling demand, promoting reuse where practically feasible) have to be taken into account in the process. Third, in the case of water supply to Istanbul, all sustainable policy decisions must be applied by a common agreement and consensus among all stakeholders. Also compensation measures with regard to water quantity and quality must be discussed with the users of the adjacent basins (i.e. Melen River, in particular) in order to avoid other alarming water shortage situations, as occurred in 1990.

ACKNOWLEDGMENT

This project is supported by the Istanbul University Scientific Research Projects Coordination Unit.

REFERENCES

Carrillo, M. (2003). Growth, life cycle and dynamic modelling. Mathematical and Computer Modelling of Dynamical Systems, 9(2), 121-136.

DSI, (1991). Feasibility study for the Buyuk Melen System (Stage 1), Reference 5.

DSI, (2017). http://www.dsi.gov.tr/baraj-arama Access date: 17/02/2017.

Gohari, A., Eslamian, S., Mirchi, A., Abedi-Koupaei, J., Bavani, A. M., & Madani, K. (2013). Water transfer as a solution to water shortage: a fix that can backfire. Journal of Hydrology, 491, 23-39.

Harou, J. J., Pulido-Velazquez, M., Rosenberg, D. E., Medellín-Azuara, J., Lund, J. R., & Howitt, R. E. (2009). Hydro-economic models: Concepts, design, applications, and future prospects. Journal of Hydrology, 375(3), 627-643.

IMC Istanbul Master Plan Consortium, 1999. Istanbul water supply, sewerage and drainage, sewage treatment and disposal master plan study, Final Report, Water supply, Vol 2, Part A.

ISKI, (2015). Activity report, Istanbul Metropolitan Municipality; 281, (in Turkish).

ISKI, (2017). Dam detail diagrams, http://www.iski.istanbul/web/tr-TR/baraj-detay-grafikleri Access date: 22/02/2017.

UCTEA Chamber of Environmental Engineering, (2014). Technical determination report on water basins of Istanbul European side, Istanbul branch. 6, (in Turkish).

Proceedings of the 10th World Congress of EWRA 'Panta Rhei', 5-9 July 2017, Athens, Greece
© 2017 *European Water Resources Association*

Assessment of bedload transport in gravel-bed rivers with a new fuzzy adaptive regression

M. Spiliotis[1*], V. Kitsikoudis[2] and V. Hrissanthou[1]
[1] *Division of Hydraulic Engineering, Department of Civil Engineering, Democritus University of Thrace, Kimmeria Campus, Xanthi 67100, Greece*
[2] *Division of Hydraulics, Department of Civil Engineering, Istanbul Technical University, Maslak 34469, Istanbul, Turkey*
[*] *e-mail: mspiliot@civil.duth.gr*

Abstract: Bedload transport in gravel-bed rivers exhibits notable differences with increasing discharge. For low discharges, the bedload consists mainly of sand and fine gravel, originating from the upstream, while the surface armor layer remains intact. For high discharges, approximately for bankfull flows, the armor layer breaks up and the bedload, which increases considerably, comprises gravel from the surface layer as well as finer material from the subsurface layer. However, this transition occurs gradually, and for this range of discharges the contribution of each bedload transport mechanism is unclear. An adaptive fuzzy based regression is proposed in this article to include this no constant behaviour of the discharge-bedload relation. For low discharges, until a fuzzy threshold, a conventional (crisp) relation between bedload transport and discharge is established, while for high discharges, a curve with sharper slope must be derived to fit the bedload data. Between these curves and for a discharge range where the armor layer gets disrupted, the Sugeno theory of expert systems is used, that is, each fuzzy rule with a corresponding curve holds to some degree. Instead of the usual trial and error method, a two-phase training optimization based method to achieve this adaptive curve is proposed. The training method is a couple between the heuristic Particle Swarm Optimization method and the conventional regression method. In the present study, the proposed methodology is implemented on discharge-bedload data from several gravel-bed rivers from mountain basins of Idaho, U.S.A.

Key words: Armor layer, bedload transport, fuzzy rules, fuzzy sets and logic, Particle Swarm Optimization

1. INTRODUCTION

Sediment transport in steep gravel-bed streams is a complicated phenomenon that needs to be quantified for engineering design, habitat protection, and river management and restoration, among others. However, sediment transport prediction within tolerable error margins in such streams remains highly problematic (Gomez and Church, 1989) and site-specific (Barry et al., 2004; Kitsikoudis et al., 2014), and constitutes a challenge for engineers and geomorphologists. This is particularly owed to the fact that the incipience of sediment motion may occur for a relatively wide range of flow conditions and there is not a single threshold for specified flow conditions (Buffington and Montgomerry, 1997; Kitsikoudis et al., 2016). This is attributed to the near-bed turbulence (e.g. Diplas et al., 2008), sediment exposure and protrusion to the flow (e.g. Kirchner et al., 1990), and relative depth (e.g. Recking, 2009).

Natural gravel-bed rivers are usually poorly sorted and characterized by a wide range of sediment sizes. These rivers tend to self-organize and form an armor layer, which is a coarse surface layer overlying a finer sublayer (Parker and Klingeman, 1982). This has direct implications on the boundary layer hydrodynamics and, consequently, the bedload transport. In general, the break-up of the armor layer leads to different phases of bedload transport with distinct sediment properties. Ryan et al. (2002) implemented a piecewise regression to show these different bedload transport trends. For flows that cannot entrain the coarse armor layer, the bedload comprises sand and fine gravel from the interstices among the coarse grains or from sediment patches. For intense flows that occur in floods, the armor layer breaks up and the bedload consists of the coarse particles that constitute the armor layer and the finer sediment from the subsurface layer. Ryan et al. (2002)

marked the break-up of the armor layer with a single point, which causes an abrupt change in the sediment transport trend, to facilitate the calculations. However, the break-up of the armor layer is a phenomenon that occurs gradually. Firstly, the coarse particles that are more exposed to the flow and are subject to increased turbulent shear stresses, are more likely to be entrained. As the flow gets more intense, the probability of entrainment is increased for particles less exposed to the flow, until an upper limit where the whole surface layer is in motion. In this article, an adaptive fuzzy based regression is proposed to include this no constant behaviour. For low discharges, until a fuzzy threshold, a conventional (crisp) relation between bedload transport and discharge is established, while for high discharges, a curve with sharper slope must be derived to fit the bedload data. Between these curves and for a discharge range where the armor layer gets disrupted, each fuzzy curve holds to some degree. Therefore, it can be suggested that the proposed method emanates from the physical problem itself.

2. PROPOSED ARCHITECTURE OF THE FUZZY RULE BASED SYSTEM

A widely used form of the fuzzy rule based system is the following:

Ru (λ): If x_1 is A_1^λ and x_2 is A_2^λ … and x_N is A_N^λ

then $y_\lambda = a_{\lambda 0} + a_{\lambda 1} x_1 + ... + a_{\lambda N} x_N$ (1)

where A_N^λ is a fuzzy set in Universe $U_i \subset R$, λ is the order of the rule, $(x_1, x_2, ..., x_N)^T \in U$ are the input variables. Let L be the number of the fuzzy rules, that is, $\lambda = 1, \ldots, L$ and let N be the number of the independent variables. By using the extension principle and the weighted average defuzzification formula, the final single output is (Chen and Pham, 2001; Botzoris and Papadopoulos, 2015):

$$y = \frac{\sum_{\lambda=1}^{L} \left[\left(\mu_{1,\lambda}(x_1) \wedge ... \wedge \mu_{N,\lambda}(x_N) \right) \left(a_{\lambda 0} + a_{\lambda 1} x_1 + ... + a_{\lambda N} x_N \right) \right]}{\sum_{\lambda=1}^{L} \left(\mu_{1,\lambda}(x_1) \wedge ... \wedge \mu_{N,\lambda}(x_N) \right)} \quad (2)$$

where μ is the membership function which characterizes the fuzzy set and takes values into the closed interval between zero and one (Tsakiris et al., 2006). As $\wedge$, the fuzzy intersection is symbolized.

Many scientific articles are based on the Matlab toolbox which is based on the ANFIS systems. However, even if the errors remain within acceptable range, sometimes the rational and logical basis of the application is erroneous (Sen, 2010). In contrast, in the proposed method, the problem itself modulates the structure of the expert system. Indeed, by using the fuzzy logic, the couple between the linguistic variables and numerical methods can be achieved and hence, more smart numerical models can be established.

In the proposed model, only one variable has the ability to derive the use of the proper linear relation. Thus, this variable (discharge) takes only two linguistic values (high and low) which correspond to quantitative fuzzy sets. In addition, in this application, only two rules exist (one with each linguistic value). Consequently, there are two regions without uncertainty where only one regression equation is activated. However, between two crisp regions (Fig. 1) there is a grey region where both rules are activated to some degree. Furthermore, a semi-static structure is supposed. That is, even if the starting points and the ending points are unknown, the shape of the membership functions μ_1 and μ_2 will follow the structure of Fig.1. Based on Fig. 1, it is obvious, that only two rules are modulated, whilst in fact the grey region (fuzzy region) is between β_1 and β_2. In the middle of the distance between the parameters, the two membership functions μ_1 and μ_2 are equal to 0.5.

Let only one input variable (discharge), x. For given variables β_1 and β_2, the final output y for the input x is given as follows:

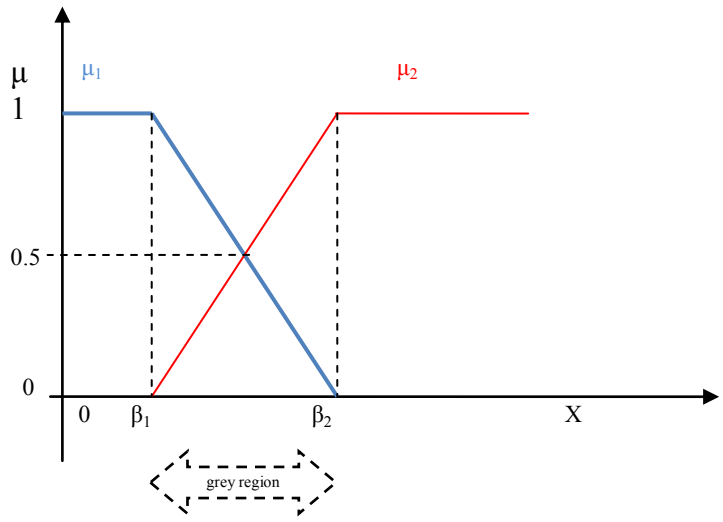

Fig. 1: Architecture of the fuzzy rules

$$y = \frac{\mu_1(x)(a_{10}+a_{11}x)+\mu_2(x)(a_{20}+a_{21}x)}{\mu_1(x)+\mu_2(x)} = \frac{\mu_1(x)}{\mu_1(x)+\mu_2(x)}a_{10} + \frac{\mu_2(x)}{\mu_1(x)+\mu_2(x)}a_{20} + \frac{\mu_1(x)x}{\mu_1(x)+\mu_2(x)}a_{11} + \frac{\mu_2(x)x}{\mu_1(x)+\mu_2(x)}a_{21} \quad (3)$$

The produced smart regression model is suitable to study the bedload transport in gravel-bed rivers which exhibits notable differences with increasing discharge. For low discharges, the bedload discharge consists mainly of sand and fine gravel, originating from the upstream, while the surface armor layer remains intact. For high discharges, approximately for bankfull flows (Ryan et al., 2002), the armor layer breaks up and the bedload, which increases considerably, comprises gravel from the surface layer as well as finer material from the subsurface layer. However, this transition occurs gradually, and for this range of discharges the contribution of each bedload transport mechanism in the total bedload transport is unclear.

The training of the proposed model is achieved based on a two-phase approach. Let the thresholds β_1 and β_2 be known. Assuming that a set of M input-output data is given, the following linear system of algebraic equations is concluded:

$$\boldsymbol{\Lambda}\cdot\boldsymbol{\theta} = \mathbf{b}$$

$$\boldsymbol{\Lambda} = \begin{bmatrix} \frac{\mu_1(x^1)}{\mu_1(x^1)+\mu_2(x^1)} & \frac{\mu_2(x^1)}{\mu_1(x^1)+\mu_2(x^1)} & \frac{\mu_1(x^1)x^1}{\mu_1(x^1)+\mu_2(x^1)} & \frac{\mu_2(x^1)x^1}{\mu_1(x^1)+\mu_2(x^1)} \\ \cdots\cdots & & & \\ \frac{\mu_1(x^M)}{\mu_1(x^M)+\mu_2(x^M)} & \frac{\mu_2(x^M)}{\mu_1(x^M)+\mu_2(x^M)} & \frac{\mu_1(x^M)x^M}{\mu_1(x^M)+\mu_2(x^M)} & \frac{\mu_2(x^M)x^M}{\mu_1(x^M)+\mu_2(x^M)} \end{bmatrix}$$

$$\boldsymbol{\theta} = \begin{bmatrix} a_{10} & a_{20} & a_{11} & a_{21} \end{bmatrix}^T$$
$$\mathbf{b} = \begin{bmatrix} y_1 & \dots & y_M \end{bmatrix}^T \quad (4)$$

Based on the usual least squares method, the optimal coefficients **θ*** can be determined:

$$\boldsymbol{\theta}^{*} = \left[\boldsymbol{\Lambda}^{\mathrm{T}} \cdot \boldsymbol{\Lambda}\right] \boldsymbol{\Lambda}^{\mathrm{T}} \mathbf{b} \tag{5}$$

The successfulness of the model is measured on the basis of the standard error between the observed and the predicted data resulting from the applied model:

$$E = \left(\mathbf{b} - \boldsymbol{\Lambda} \cdot \boldsymbol{\theta}^{*}\right)^{\mathrm{T}} \cdot \left(\mathbf{b} - \boldsymbol{\Lambda} \cdot \boldsymbol{\theta}^{*}\right) \tag{6}$$

Thus, in case that the thresholds β_1 and β_2 are known, the constant terms of the linear relations can be determined by following a least squares approach.

The entire training method is a couple between the heuristic Particle Swarm Optimization (PSO) method and the conventional regression method. The application of the conventional regression method is presented above. According to the first phase, a population of possible solutions is modulated. Each possible solution contains only the unknown thresholds β_1 and β_2. For each candidate solution (the values of β_1 and β_2), the above analysis of the usual regression model is running and hence, the optimal coefficients and the standard error E are calculated. Finally, the thresholds with the minimum error (Eq. 6) are chosen after a selected number of iterations.

3. PARTICLE SWARM OPTIMIZATION METHOD AND THE PROPOSED LEARNING PROCESS

Particle Swarm Optimization (PSO) is a stochastic global optimization method based on the simulation of social behavior. As in Genetic Algorithms (GA), PSO exploits a population of candidate solutions to probe the search area. Therefore, the Particle Swarm Optimization (PSO) algorithm can be characterized as one of the population based algorithms (Parsopoulos and Vrahatis, 2002). Although PSO is an effective and widely used method, it is also much simpler than several other evolutionary algorithms (e.g. GA), due to the fact that it does not contain the crossover and mutation operations in the original version (Spiliotis, 2014).

PSO can deal with nonlinear optimization problems in non-convex domains (Ostadrahimi, 2012). Each candidate solution is called a particle, and the set of potential solutions in each iteration creates the '*swarm*' (Papadopoulos et al., 2011; Spiliotis et al., 2016). A '*swarm*' has a dimension *N′*, in which *N′* is the number of the potential solutions. Each potential solution is comprised of *D* variables, in which *D* is the dimension of the problem (Spiliotis et al., 2016).

More analytically, the population dynamics in PSO simulates the behavior of a "*birds flock*", where social sharing of information takes place and individuals benefit from the discoveries and previous experience of all other companions during their search for food. Thus, two variants of the PSO algorithm were developed considering either a local neighbourhood or a global neighbourhood. In the former, the partial optimum of the particle is usually applied (Spiliotis, 2014). In the latter, each particle moves towards its best previous position and towards the best particle in the whole swarm (Eberhart et al., 1996; Parsopoulos and Vrahatis, 2002; Spiliotis et al., 2016).

Several modifications to the original version of the PSO method of Kennedy and Eberhart (1995) have been proposed, such as the adaptation of inertia term and the consideration of the maximum velocity (e.g. Poli et al., 2007). The basic PSO algorithm is presented below (e.g. Shi et al., 1998; Poli et al., 2007):

Algorithm 1 Original PSO

1: Initialize a population array of particles with random positions and velocities on *D* dimensions in the search area.

2: *Loop*

3: For each particle, evaluate the desired optimization fitness function in *D* variables.

4: Compare particle fitness evaluation with its best previously visited position (p_i). If the current value is better than p_i, then set p_i equal to the current value.

5: Identify the particle in the neighbourhood with the best success so far, and assign its index to the variable p_g.

6: Change the velocity and position of the particle according to the following equation

$$\begin{cases} \overset{r}{\upsilon}_i(t+1) = \omega\overset{r}{\upsilon}_i + c_1\rho_1(\ )\cdot\left(\overset{r}{p}_i - \overset{r}{x}_i(t)'\right) + c_2\rho_2(\ )\cdot\left(\overset{r}{p}_g - \overset{r}{x}_i(t)'\right) \\ \overset{r}{x}_i(t+1)' = \overset{r}{x}_i(t)' + \overset{r}{\upsilon}_i(t+1) \end{cases} \quad (7)$$

7: If a criterion is met (usually a sufficiently good fitness or a maximum number of iterations), exit loop.

8: *End loop*

where $\rho()$ is a vector of random numbers uniformly distributed in the open interval 0,1 that is generated at each iteration and for each particle, p_i is the best previously visited position of the ith particle (partial optimum) and p_g is the global best previously visited position of all particles (global optimum). Furthermore, the term $c_1\rho_1(\ )\cdot\left(\overset{r}{p}_i - \overset{r}{x}_i'\right)$ that associates the particle's own experience with its current position, is weighted by the constant c_1, and is called individuality (cognitive acceleration). The term $c_2\rho_2(\ )\cdot\left(\overset{r}{p}_g - \overset{r}{x}_i'\right)$ is associated with the social interaction between the particles of the swarm and weighted by the constant c_2, and is called sociality (social acceleration). For the standard PSO, the coefficients c_1 and c_2 were allowed to take values in the interval 1.5 to 2.5 (Papadopoulos et al., 2011; Spiliotis et al., 2016).

To summarize the learning process, at first, a swarm of possible solutions is randomly created. Each possible optimum solution (member of the swarm) contains only the values of the β_1, β_2 parameters of the membership functions. Then, based on the architecture of the membership functions of Fig. 1, the training process is activated, and the values of the constant terms of the regression curves, $\boldsymbol{\theta}^*$ and the error function, *E,* are finally determined. Subsequently, the algorithm returns to the PSO process in order to compare the solutions and to re-find the global optimum and the partial optimum for each possible solution. Finally, the new position of each member of the swarm is determined and the process is repeated for the new swarm.

The process is finished when the maximum number of iterations occurs. The reason for which a conventional optimization toolbox is not used, is that the formulation of the two rules follows a very no conventional form. The membership functions are not differentiable functions at the critical points (β_1 and β_2).

4. CASE STUDY

The proposed methodology is tested in several mountainous gravel-bed streams from Idaho, U.S.A., with the utilized data originating from an extensive field campaign (King et al., 2004). Firstly, the bedload data for Big Wood River are studied. A curve between the bedload transport rate, *mg* (output variable) and the discharge, *Q* (input variable) is achieved based on the proposed methodology with two fuzzy rules and the architecture of Fig. 1. Practically, from Fig. 2 it is evident that the optimum heuristically based solution is achieved after the 10th iteration. According to the proposed methodology, the square error, *E*, is equal to 8.9721 which is significantly smaller than the square error of the usual linear regression (*E*= 17.2510).

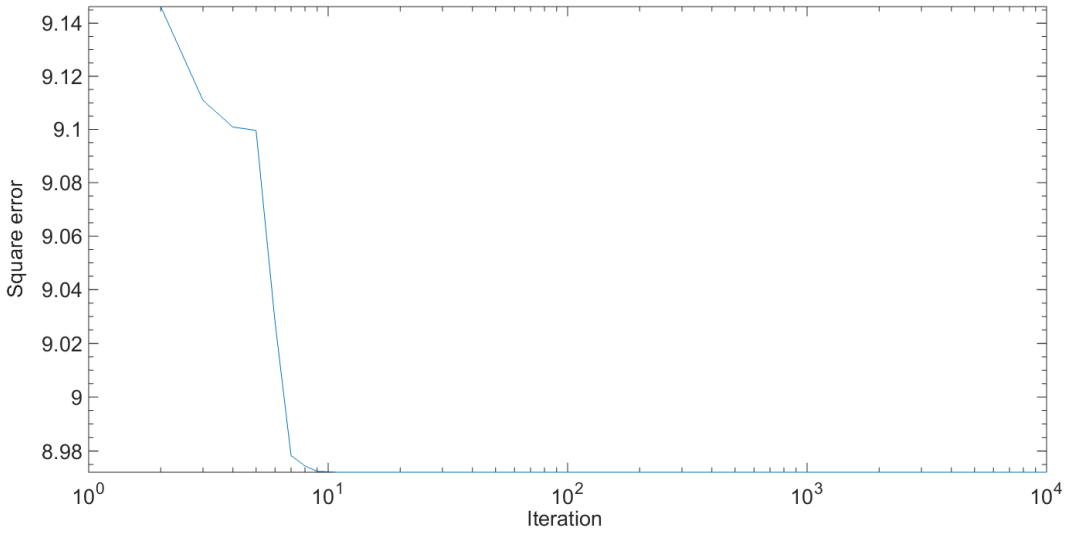

Fig. 2: Squared error as a function of the number of iterations for Big Wood River

The coefficient of efficiency E' proposed by Nash and Sutcliffe (1970) is defined as one minus the sum of the squared differences between the predicted and observed data normalized by the variance of the observed values (Krause et al., 2005):

$$E' = 1 - \frac{\sum_{i=1}^{M} \left(O_i - mg_i\right)^2}{\sum_{i=1}^{M} \left(O_i - \bar{O}_i\right)^2} \tag{8}$$

where M is the number of data, the symbol O refers to the observed data (bedload transport rate), while the symbol mg to the predicted data.

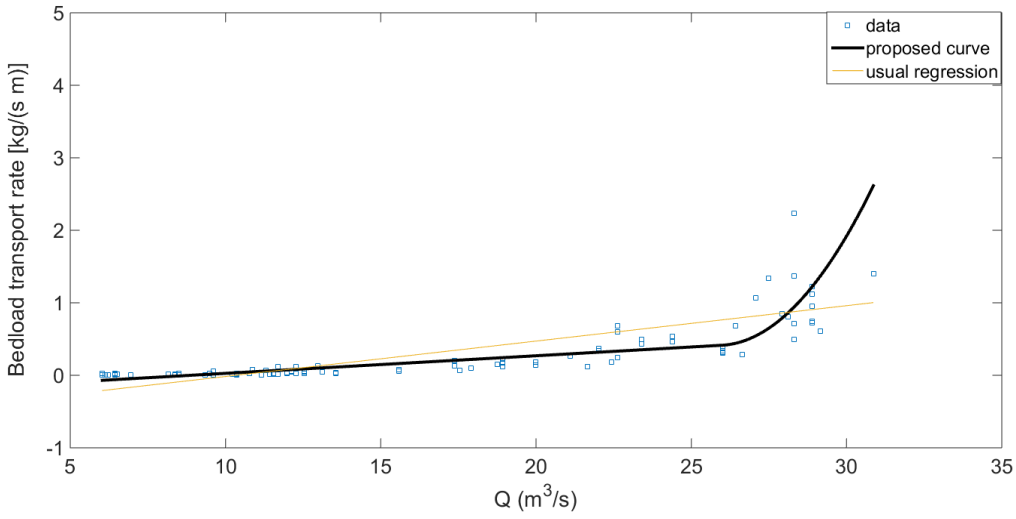

Fig. 3: Data, usual crisp linear regression and the produced (crisp) curve for Big Wood River

The error E' is equal to 0.7183 which is close to unity (perfect result). The thresholds β_1 and β_2 are equal to 25.9952 m^3/s and 30.8654 m^3/s. The (crisp) relation between the bedload transport rate, mg, and the discharge, Q, is the following:

$$mg(Q) = \frac{\mu_1(Q)}{\mu_1(Q)+\mu_2(Q)}(-0.2151)+\frac{\mu_2(Q)}{\mu_1(Q)+\mu_2(Q)}(-11.3331)+\frac{\mu_1(Q)}{\mu_1(Q)+\mu_2(Q)}0.0242\cdot Q+\frac{\mu_2(Q)}{\mu_1(Q)+\mu_2(Q)}0.4519\cdot Q \quad (9)$$

The first two terms are referred to the constant terms and the last two are referred to the coefficients of the independent variable. The two rules are fired according to the corresponding ratio of the membership functions. For example, for the first rule, it is fired according to the ratio: $\frac{\mu_1(Q)}{\mu_1(Q)+\mu_2(Q)}$.

In case of the Fourth of July Creek (Fig. 4), the parameters β_1 and β_2 are between 3.0076 m^3/s and 3.0599 m^3/s which means that the fuzzy area (where the behavior is changed) is rather small, and the coefficient of efficiency of Nash and Sutcliffe is equal to 0.7755. However, the fact that the generated curve is not monotonic in case of the Fourth of July Creek, highlights the data-driven nature of this technique and the necessity for high quality representative data. The curves in Fig. 3 exhibit the expected monotonic form, contrary to Fig. 4. This is attributed to the fact that in the grey region, within the two linear regression curves, there are more available points for the proper training of the suggested model. This grey area corresponds to infrequent high discharges that induce the break-up of the armor layer.

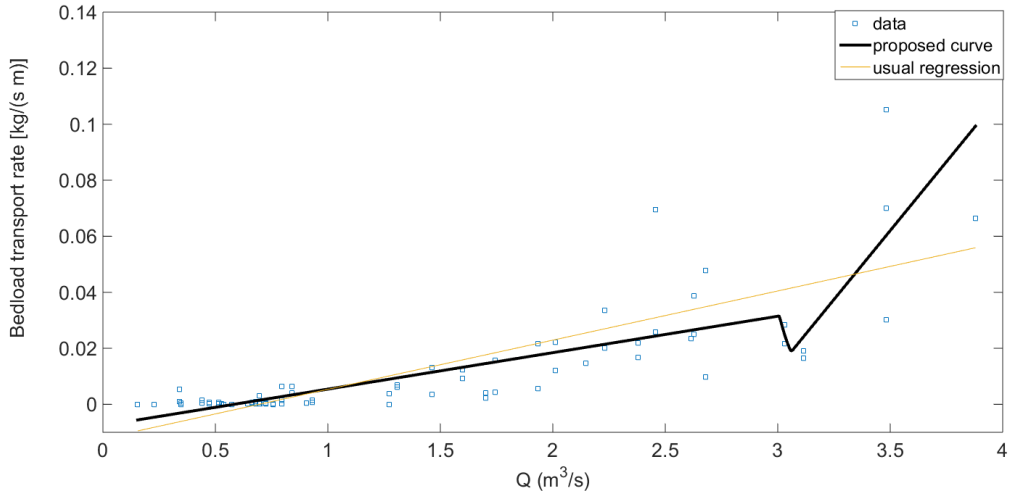

Fig. 4: Data, usual crisp linear regression and the produced (crisp) curve for Fourth of July Creek

Another interesting point which must be clarified, is that the calculated curve is a crisp relation (without uncertainty as the fuzzy regression model of Tanaka (1987), see also Tsakiris et al., 2006; Kitsikoudis et al., 2016), although elements of fuzzy sets and logic are used to construct the model. In fact, the fuzziness is implemented in the grey region between the critical points.

5. CONCLUSION

A smart fuzzy regression is produced based on fuzzy rules (with a given architecture) combined with the conventional linear regression. The training is based on the coupling between the PSO and the conventional linear regression. The method is successfully applied in order to determine the bed load transport rate as a function of the discharge in selected gravel-bed streams. After several running processes it is concluded that many times the break-up of the armor layer can be identified between two parameters in case they are neighboured and hence the model can automatically detect such a physical process. However, this does not happen in all cases, even if the training process can be characterized as successful.

REFERENCES

Barry, J.J., Buffington, J.M. and King, J.G., 2004. A general power equation for predicting bed load transport rates in gravel bed rivers. Water Resources Research; 40(10): W10401.

Botzoris, G. and Papadopoulos, B., 2015. Fuzzy Sets. Sofia Publications, Thessaloniki (in Greek).

Buffington, J.M. and Montgomery, D.R., 1997. A systematic analysis of eight decades of incipient motion studies, with special reference to gravel-bedded rivers. Water Resources Research; 33(8): 1993-2029.

Chen, G. and Pham T.T., 2001. Introduction to fuzzy sets, fuzzy logic, and fuzzy control systems. CRC Press LLC.

Diplas, P., Dancey, C.L., Celik, A.O., Valyrakis, M., Greer, K, and Akar, T., 2008. The role of impulse on the initiation of particle movement under turbulent flow conditions. Science; 322(5902): 717-720.

Gomez, B. and Church, M., 1989. An assessment of bed load sediment transport formulae for gravel bed rivers. Water Resources Research; 25(6): 1161-1186.

King, J.G., Emmett, W.W., Whiting, P.J., Kenworthy, R.P. and Barry, J.J., 2004. Sediment transport data and related information for selected coarse-bed streams and rivers in Idaho. Gen. Tech. Rep. RMRS-GTR-131. Fort Collins, CO: U.S. Department of Agriculture, Forest Service, Rocky Mountain Research Station, 26 p.

Kirchner, J.W., Dietrich, W.E., Iseya, F. and Ikeda, H., 1990. The variability of critical shear stress, friction angle, and grain protrusion in water-worked sediments. Sedimentology; 37(4): 647-672.

Kitsikoudis, V., Sidiropoulos, E. and Hrissanthou, V., 2014. Machine learning utilization for bed load transport in gravel-bed rivers. Water Resources Management; 28(11): 3727-3743.

Kitsikoudis, V., Spiliotis, M. and Hrissanthou, V., 2016. Fuzzy regression analysis for sediment incipient motion under turbulent flow conditions. Environmental Processes; 3(3): 663–679.

Krause, P. Boyle, D.P. and Bäse, F., 2005. Comparison of different efficiency criteria for hydrological model assessment. Advances in Geosciences; 5: 89–97.

Nash, J.E. and Sutcliffe, J.V., 1970. River flow forecasting through conceptual models, Part I - A discussion of principles. Journal of Hydrology; 10: 282–290.

Ostadrahimi, L., Mariño, M. and Afshar, A., 2012. Multi-reservoir Operation Rules: Multi-swarm PSO-based Optimization Approach. Water Resources Management; 26(2): 407-427.

Papadopoulos, K., Papagianni, C., Gkonis, P., Venieris, I., and Kaklamani, D., 2011. Particle Swarm Optimization of Antenna Arrays With Efficiency Constraints. Progress in Electromagnetics Research M; 17: 237-251

Parker, G. and Klingeman, P.C., 1982. On why gravel bed streams are paved. Water Resources Research; 18(5):1409-1423.

Parsopoulos, K.E. and Vrahatis, M.N., 2002. Recent Approaches to Global Optimization Problems Through Particle Swarm Optimization. Natural Computing; 1 (2-3): 235-306.

Poli, P., Keenedy, J. and Blackwell, T., 2007. Particle swarm optimization. Swarm Intelligence; 1(1): 33-57.

Recking, A., 2009. Theoretical development on the effects of changing flow hydraulics on incipient bed load motion. Water Resources Research; 45(4): W04401.

Ryan, S.E., Porth, L.S. and Troendle, C.A., 2002. Defining phases of bedload transport using piecewise regression. Earth Surface Processes and Landforms; 27(9): 971-990.

Sen Z., 2010. Fuzzy logic and Hydrological Modelling. CRC Press, Taylor and Francis Group.

Shi, Y. and Eberhart, R.C., 1998. A modified particle swarm optimizer. Proceedings of IEEE International Conference on Evolutionary Computation; pp. 69–73.

Spiliotis M., 2014. A Particle Swarm Optimization (PSO) heuristic for water distribution system analysis. Water Utility Journal; 8: 47-56.

Spiliotis, M., Mediero, L. and Garrote, L., 2016. Optimization of Hedging Rules for Reservoir Operation During Droughts Based on Particle Swarm Optimization. Water Resources Management; 30(15): 5759–5778.

Tanaka, H., 1987. Fuzzy data analysis by possibilistic linear models. Fuzzy Sets and Systems; 24(3): 363–375.

Tsakiris, G., Tigkas, D. and Spiliotis, M., 2006. Assessment of interconnection between two adjacent watersheds using deterministic and fuzzy approaches. European Water; 15/ 16: 15- 22.

Proceedings of the 10th World Congress of EWRA 'Panta Rhei', 5-9 July 2017, Athens, Greece
© 2017 *European Water Resources Association*

Modeling and optimization control of a hybrid water system

H. Mu[1*], T. Rauschenbach[2], D. Karamanzia[2] and N. Cai[1]
[1] *Fraunhofer Beijing Representative Office, Landmark Tower II 0611, Chaoyang, Beijing, PR. China*
[2] *Advanced System Technology (AST) Branch of Fraunhofer IOSB, Am Vogelherd 50, 98693 Ilmenau, Germany*
[*] *e-mail: muh@fraunhofer.com.cn*

Abstract: In most deltas, rivers and channels compose to a water network system. Different water conservancy projects, such as pumping stations, sluices, and barriers are constructed in the water system. These water conservancy projects change the natural water flows, i.e. the direction of a water flow is no longer controlled by the natural terrain, but by the difference in the state of the water heads between sluice gates. Even the flow of the rivers is not clear anymore. The water system influenced by a discrete state control has evolved into a complex hybrid water system. The conventional way to manage such a water system is to monitor water level changes and to control different sluice gates based on experience. However, such management is challenging and causes a serious loss of energy and resources. Therefore, a model-based optimal scheduling process is expected in practice. Unfortunately traditional hydrological models are unable to model hybrid water systems totally. Interdisciplinary research is needed, especially inheriting some approaches from the field of automation technology. This paper models a complex hybrid water system with a scheduling optimization approach. The definition "virtual tank" is introduced to solve the bi-directional flow problem of the hybrid water system. Scheduling processes in short or midterm periods are optimized with the Model Predictive Control Method (MPC). The modeling and optimization approaches are demonstrated in a case study – Smart flood control in the hybrid water network area of Jiangyin, PR China.

Key words: Bi-directional flow, Hybrid water system, MPC-MLD optimisation, Water network modelling

1. INTRODUCTION

Artificial water conservancy projects, such as pumping stations, sluices, and barriers, densely cover a plain river network area. They change the natural hydrologic dynamic flow and form a hybrid water system (Definition of Hybrid Water System see chapter 2). The water flow in the river is no longer caused by the natural terrain, but by the difference in the water level of sluices on the ends of the river. Changing the state of a sluice causes a change in the water flow situation. Therefore, for the management of water resource scheduling, not only the dynamic change of the continuous variable should be considered, but also the discrete event caused by opening and closing the sluices should be analyzed. In order to solve such complex hybrid water systems, two concepts are developed and implemented in this work:

1. With the introduction of an innovated concept, the "virtual tank", the modeling process for the dynamic flow changes based on state changes (sluice gate open or closed) in hybrid water systems can be solved. The modeling not only provides a visual simulation, which makes it easy for decision makers to understand the water situation, but also provides a basement for optimal scheduling.
2. Model Predictive Control (MPC) Method based on Mixed Logical Dynamic (MLD), is applied to solve the optimization scheduling in short and midterm periods. The system can calculate and deliver suggestions for control strategies in time, based on the weather forecast and scenario definition.

The goal of this study is to set up scenarios with short-term regional hydrological changes, i.e. heavy precipitation in a short timeframe. The hybrid water system is then modelled to forecast the water situation. According to the limiting conditions of engineering projects (dams, gates, sluices,

barriers) and optimization objectives for scheduling, the management strategies are then determined by the MPC-MLD approach. This paper refers to some research results of Delft University of Technology in Netherlands (van Ekeren, 2011), but the models have been redefined in this work with the innovated concept called the "virtual tank", and was implemented as a large scale research in a dense river network area of Yangzi delta in Jiangyin (987.5km^2), Jiangsu Province, PR China.

2. METHODOLOGY

2.1 Modelling

First of all, we must define the term "hybrid system". The term "hybrid system" originates from Cybernetic science. In this system, not only do dynamic continuous variables exist, but also discrete state events. A hybrid water system is a special reflection in water resources management. Figure 1 shows a typical hybrid water system with natural river flow, sluices, etc.

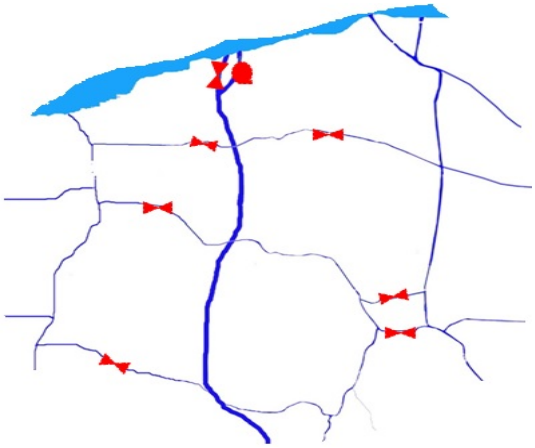

Figure 1: A typical hybrid water system

In Figure 1, only the big river in the north is still flowing relatively natural in the entire river system. Sluice gates are densely constructed on other rivers. Due to the opening and closing of these sluice gates, the water level, the flow activity, and the direction of water are changed actively. Therefore, in order to simulate the actual interactions of the hydrological dynamic variables, i.e. the river flow, and the discrete state variables caused by opening and closing pump stations and sluice gates, this paper introduces an innovated concept of the virtual tank. A virtual tank can be applied at two different application levels:

1. The intersection of two or more channels is assumed to be a virtual tank. Neighboring virtual tanks are connected by channel between them. For the flow calculation the Chézy model is introduced as follows:

$$f_{chézy}\left(x_i(k), x_j(k)\right) = A_{c,ij}\left(x_i(k), x_j(k)\right) C_{ij} Sign(x_j - x_i) \times \sqrt{\frac{R_{ij}\left(x_i(k), x_j(k)\right)|(x_j - x_i)|}{l_{ij}}} \quad (1)$$

where x_i and x_j are the water level of two virtual tanks i and j $A_{c,ij}\left(x_i(k), x_j(k)\right)$ is the minimum section area of flow $q_{ij}\left(x_i(k), x_j(k)\right)$ C_{ij} is roughness coefficient, $R_{ij}\left(x_i(k), x_j(k)\right)$ is hydraulic radius of flow $q_{ij}\left(x_i(k), x_j(k)\right)$, l_{ij} is the length of the connection between i and j. $Sign(x_j - x_i)$ express the flow direction.

The model calculates the flow direction in each time interval. When the calculated value is positive the flow is the same as the initial direction of flow; when it is negative the flow is in the opposite direction. Figure 2 shows the structure of the first concept of the virtual tank.

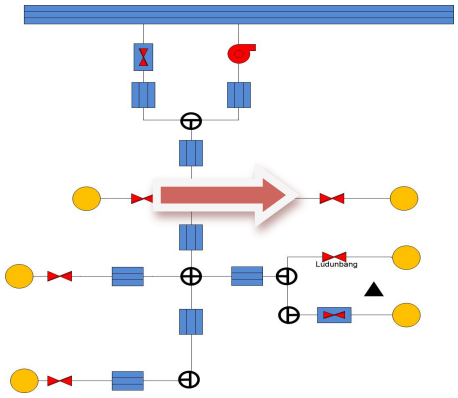

Figure 2 : Structure of the first description of the model based on the virtual tank

This application is good for modeling of river networks considering the time discrete state changes. This enables a clear expression of the water situation. It can be used for testing the control strategies, river flood control, and water diversion management.

2. The second application of the virtual tank concept is at a higher level in considering the catchment area, the administrative area, and the river channel characteristics. The study area is divided into a set of submodel areas, each partition is assumed to be a virtual tank. Both neighboring partitions, i.e. virtual tanks, are connected by a main channel in between. Figure 3 shows an expression of the second application of the concept of a virtual tank:

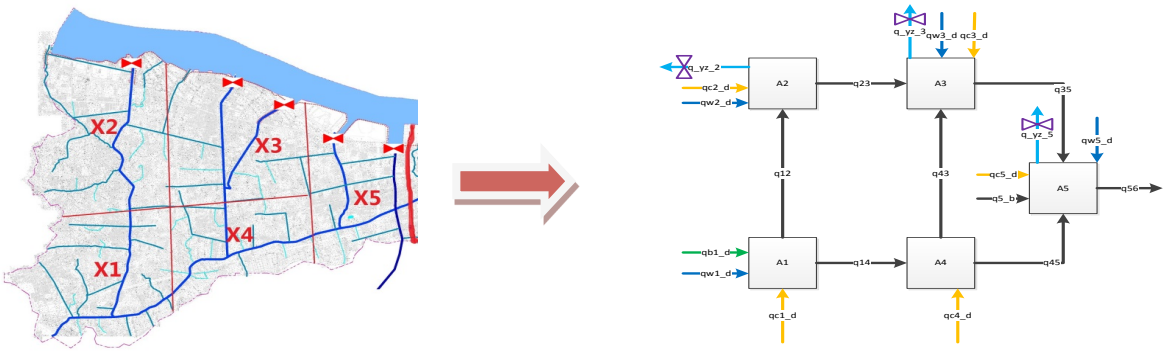

Figure 3: Higher level of the application of a virtual tank

This application is suitable for modelling of large regions. The region is divided into different sub-regions (virtual tanks). All tanks were modelled at lower level and their behaviours were analysed. This method can express the impact on each model area caused by the rainfall and runoff. It has a profound significance for flood control in the whole region.

Based on the concept of the virtual tank, a hybrid water system can be modeled. Take Figure 3 for example. This water system consists of 3 sluices and 5 virtual tanks, which are connected by main channels in between. Some additional inflows to the virtual tanks are also considered respectively. The state of each tank is represented by the water level. According to the mass balance principle, the change of the water level in the discretized time step k+1 is described as follows:

Virtual Tank A1:

$$X_1(k+1) = \frac{Ts}{A_{s1}}\left[q_{b1\_d}(k) + q_{w1\_d}(k) + q_{c1\_d}(k) - q_{12}\left(X_1(k), X_2(k)\right)\right] + X_1(k) \quad (2)$$

Virtual Tank A2:

$$X_2(k+1) = \frac{Ts}{A_{s2}}\left[-q_{yz\_2}\left(X_2(k), Yz\_L_2(k), u_2(k)\right) + q_{w2\_d}(k) + q_{c2\_d}(k) + q_{12}\left(X_1(k), X_2(k)\right) - q_{23}\left(X_2(k), X_3(k)\right)\right] + X_2(k) \quad (3)$$

The Virtual Tank A3 to A5 expressed in the same way, where k is the discrete time step, Ts is the sample time; A_{si} (i=1,2,….,5) is the surface area of the water surface in each tank; $X_i(k)$ (i=1,2,…,5) is the water level of each corresponding virtual tank at k time step; $q_{ci\_d}(k)$ (i=1,2,3,4,5) is the disturbance inflow due to the precipitation and transpiration; $q_{w1\_d}(k)$, $q_{w2\_d}(k)$, $q_{w3\_d}(k)$, $q_{w5\_d}(k)$ are the inflows due to the water supply from the external river; $q_{b1\_d}(k)$, $q_{5\_b}(k)$ are the disturbance inflows from the boundaries; $q_{yz\_2}\left(X_2(k), Yz\_L_2(k), u_2(k)\right)$, $q_{yz\_3}\left(X_3(k), Yz\_L_3(k), u_3(k)\right)$, $q_{yz\_5}\left(X_5(k), Yz\_L_5(k), u_5(k)\right)$ are flows between the large north river and the local channels, which controlled by the sluices; and $q_{12}\left(X_1(k), X_2(k)\right)$, $q_{23}\left(X_2(k), X_3(k)\right)$, $q_{43}\left(X_4(k), X_3(k)\right)$, $q_{35}\left(X_3(k), X_5(k)\right)$, $q_{14}\left(X_1(k), X_4(k)\right)$, $q_{45}\left(X_4(k), X_5(k)\right)$ *and* $q_{56}\left(X_5(k), X_6(k)\right)$ are the flows between two connected tanks, this is equivalent to $q_{ij}\left(X_i(k), X_j(k)\right)$ in the Chézy formula (van Ekeren, 2010), and can be expressed as:

$$q_{ij}\left(x_i(k), x_j(k)\right) = f_{chézy}\left(x_i(k), x_j(k)\right) \quad (4)$$

$$f_{chézy}\left(x_i(k), x_j(k)\right) = A_{c,ij}\left(x_i(k), x_j(k)\right) C_{ij} Sign\left(x_j - x_i\right) \times \sqrt{\frac{R_{ij}\left(x_i(k), x_j(k)\right)\left|\left(x_j - x_i\right)\right|}{l_{ij}}} \quad (5)$$

The section area variable $A_{c,ij}\left(x_i(k), x_j(k)\right)$ and the hydraulic radius $R_{ij}\left(x_i(k), x_j(k)\right)$ are the functions of the water level. Their values are inflected according to the change in water level between the two tanks in each time step. The section area variable h_{mean} is approximated with the average value of x_i, x_j. Under this kind of approximation, the area of the cross section and the hydraulic radius are only related to the channel parameters (b the width of the channel and m the slope):

$$A_{c,ij}\left(x_i(k), x_j(k)\right) = (b + m \times h_{mean}) \times h_{mean} \quad (6)$$

wetted perimeter calculation formula:

$$P_{c,ij}\left(x_i(k), x_j(k)\right) = b + 2 \times h_{mean}\sqrt{1 + m^2} \quad (7)$$

It follows that the hydraulic radius can be calculated as:

$$R_{ij}\left(x_i(k), x_j(k)\right) = \frac{A_{c,ij}\left(x_i(k), x_j(k)\right)}{P_{c,ij}\left(x_i(k), x_j(k)\right)} = \frac{A_{c,ij}\left(x_i(k), x_j(k)\right)}{b + 2 \times h_{mean}\sqrt{1+m^2}} \quad (8)$$

The flows $q_{yz\_2}\left(X_2(k), Yz\_L_2(k), u_2(k)\right)$, $q_{yz\_3}\left(X_3(k), Yz\_L_3(k), u_3(k)\right)$, $q_{yz\_5}\left(X_5(k), Yz\_L_5(k), u_5(k)\right)$ are described by the formula of Chézy, the difference here is that a key variable $u_i(k)$ is added, which represents the state of corresponding sluices, therefore the formula can be rewritten as:

$$q_{yz\_i}\left(X_i(k), Yz\_L_i(k), u_i(k)\right) = u_i(k)\, f_{chézy}\left(x_i(k), Yz\_L_i(k)\right) \quad (9)$$

where,

$Yz\_L_i(k)$ is the water level of the north river (see Figure 2), and the state of the sluice is given by

$$u_i(k) = \begin{cases} 0 & if\ the\ sluice\ closed\ at\ the\ time\ k \\ 1 & otherwise \end{cases} \quad (10)$$

Now, all the variables are defined. Through the time series of the input data (the disturbance inflows) and static state data, the water level output data can be calculated under the conditions of the initial data. Then virtual tank model parameters $(A_{c,ij}\left(x_i(k), x_j(k)\right), l_{ij})$ can be inferred backwards by comparing the actual levels of output data.

2.2 Optimization using MPC based on MLD

MPC (Model Predictive Control) originates from the process industry, but nowadays MPC is used in many different fields. In water resources management, especially in dealing with water hybrid systems, MPC is quite new. MPC as a technology of Advanced Process Control (APC) is based on a prediction model. Several models could be selected for the hybrid system, such as Hybrid Automata, Petri Net, Piece Wise Affine, and MLD (mixed logical dynamical). Because the virtual tank model can be easily extended to the MLD model, the MLD model is selected here. (Zhang, 2007),

An MLD system has these well-known expressions:

$$\boldsymbol{X}(k+1) = \boldsymbol{A}(k)\boldsymbol{X}(k) + \boldsymbol{B}_1(k)\boldsymbol{U}(k) + \boldsymbol{B}_2(k)\boldsymbol{\delta}(k) + \boldsymbol{B}_3(k)\boldsymbol{Z}(k) + \boldsymbol{B}_4(k)\boldsymbol{D}(k) \quad (11)$$

$$\boldsymbol{Y}(k) = \boldsymbol{C}(k)\boldsymbol{X}(k) + \boldsymbol{D}_1(k)\boldsymbol{U}(k) + \boldsymbol{D}_2(k)\boldsymbol{\delta}(k) + \boldsymbol{D}_3(k)\boldsymbol{Z}(k) + \boldsymbol{D}_4(k)\boldsymbol{D}(k) \quad (12)$$

$$\boldsymbol{E}_1(k)\boldsymbol{X}(k) + \boldsymbol{E}_2(k)\boldsymbol{U}(k) + \boldsymbol{E}_3(k)\boldsymbol{\delta}(k) + \boldsymbol{E}_4(k)\boldsymbol{Z}(k) + \boldsymbol{E}_5(k)\boldsymbol{D}(k) \le \boldsymbol{G} \quad (13)$$

The expression shows a MLD system which is defined as a linear relation consisting of continuous variables and binary variables, where, X is the state of the system, Y is the output variable of the system, U is defined as input vector and is a control variable of the system, Y and U have the same structure like X. δ is the logical statement of the system : $\delta \in \{0,1\}^{r_l}$; Z is the auxiliary continuous statement: $z(k) = x(k) * \delta(k),\ z(k) \in \Re^{r_c}$; D represents disturbance variables. $z(k)$ Equation is nonlinear, therefore some inequality constraints have to be defined (van Ekeren, 2010):

$$z(k) \le M\delta(k) \quad (14)$$

$$z(k) \ge m\delta(k) \quad (15)$$

$$z(k) \le x(k) - m\left[1 - \delta(k)\right] \quad (16)$$

$$z(k) \ge x(k) - M\left[1 - \delta(k)\right] \quad (17)$$

In the case study, M is defined as the maximum possible value of the state of virtual tank, and m is the minimum possible value of the virtual tank. The relation (2), (3) are multiple expressions, and the part of the nonlinear flow functions are piecewise smooth. In practice, it is impossible to get an analytic solution, which requires the use of multiple linear regression algorithms. Therefore, linearization operations have to be conducted. For example, the part $q_{12}(X_1(k), X_2(k))$ after linear regression can be written as $a_{12}X_1(k) + b_{12}X_2(k)$, where a_{12} and b_{12} as regression coefficients can be obtained by the unconstrained nonlinear multivariable optimization method (in this work fminunc function in Matlab was used to obtain the coefficients). The approximated linear functions used for

MLD are presented in the following:

$$X_1(k+1) = \frac{Ts}{A_{s1}}\left[q_{b1\_d}(k) + q_{w1\_d}(k) + q_{c1\_d}(k) - a_{12}X_1(k) - b_{12}X_2(k)\right] + X_1(k) \quad (18)$$

$$X_2(k+1) = \frac{Ts}{A_{s2}}\left[-a_{yz_2}z_2(k) - b_{yz\_2}Yz\_L_2(k)\delta_2(k) + q_{w2\_d}(k) + q_{c2\_d}(k) + a_{12}X_1(k) + b_{12}X_2(k) - a_{23}X_2(k) - b_{23}X_3(k)\right] + X_2(k) \quad (19)$$

2.3 Optimization

For the optimization, the objective function and some constraints have to be defined. There are two kinds of objectives, $J_i(\tilde{x}_i(k))$ and $\mathrm{J_k}\left(\tilde{\delta}_\mathrm{k}(\mathrm{k})\right)$. $J_i(\tilde{x}_i(k))$is the objective function for water level of each virtual tank, the water level have to stay in the safety region, r_{i1} is the unsafe level, $\mathrm{r_{i2}}$ is the dangerous level, which can cause flood disaster. λ_{i1}, λ_{i2}, λ_{i3} are cost factors, $\mathrm{e_{max,i1}(k)}$ and $\mathrm{e_{max,i2}(k)}$ are the exceedances of reference water level $\mathrm{r_{i1}}$ and $\mathrm{r_{i2}}$ respectively; $\mathrm{e_{i3}(k)}$ is a binary auxiliary variable, which shows whether or not the water level has been exceeded.

$$J(k) = J_1(\tilde{x}_1(k)) + J_2(\tilde{x}_2(k)) + J_3(\tilde{x}_3(k)) + J_4(\tilde{x}_4(k)) + J_5(\tilde{x}_5(k)) \quad (20)$$

$$J_i(\tilde{x}_i(k)) = \lambda_{i1}e_{max,i1}(k) + \lambda_{i2}e_{max,i2}(k) + \lambda_{i3}e_{i3}(k) \text{ (i=1,2,3,4,5)} \quad (21)$$

$$e_{max,i1}(k) = \max(\max(\tilde{x}_i(k)) - r_{i1}, 0) \quad (22)$$

$$e_{max,i2}(k) = \max(\max(\tilde{x}_i(k)) - r_{i2}, 0) \quad (23)$$

$$e_{i3}(k) = \begin{Bmatrix} 1 \; if \; e_{max,i2}(k) > r_{i2} \\ 0 \; if \; e_{max,i2}(k) \le r_{i2} \end{Bmatrix} \quad (24)$$

The minimization of this cost function is reformulated into the following equivalent form:

$$\min J_i(\tilde{x}_i(k)) = \min(\lambda_{i1}e_{max,i1}(k) + \lambda_{i2}e_{max,i2}(k) + \lambda_{i3}\delta_{i3}(k)) \quad (25)$$

$\mathrm{J_k}\left(\tilde{\delta}_\mathrm{k}(\mathrm{k})\right)$ represents the objective function for sluices. The first term denotes the cost of closing the sluices, the second term stand for the cost of changing the state.

$$J_k\left(\tilde{\delta}_k(k)\right) = \lambda_{k1}\sum_{j=1}^{N}[1 - \delta_k(k+j-1)] + \lambda_{k2}\sum_{j=1}^{N}|\delta_k(k+j-1) - \delta_k(k+j-2)| \quad (26)$$

The minimization of the first part is rewritten as follows:

$$\min \lambda_{91}\sum_{j=1}^{N}[1 - \delta_9(k+j-1)] = \min -\lambda_{91}\sum_{j=1}^{N}\delta_9(k+j-1) \quad (27)$$

The minimization of the second part is :

$$\min \lambda_{92}\sum_{j=1}^{N}|\delta_9(k+j-1) - \delta_9(k+j-2)| = \min \lambda_{92}\sum_{j=1}^{N}p_j \quad (28)$$

$\boldsymbol{\lambda}$ is a weighting factor, $\mathrm{p_j}$ are continuous auxiliary variables. Considering the objective functions and constraints, the optimization problem can be solved by the MILP (linear programming mixed-integer) method.

$$\min \mathbf{c}^{\mathrm{T}}\boldsymbol{\theta} \tag{29}$$

$$\boldsymbol{G\theta} \leq \mathbf{h} \tag{30}$$

where C is a matrix of the weight coefficients; $\boldsymbol{\theta}$ is the matrix of the optimal target factors.

3. CASE STUDY

The area of the case study is located in the Yangtze River Delta in Middle East of china. The area has a flat terrain, with dense river network, and each river (Channel) has more than one water conservancy project. North of the area is the Yangtze River. The water level of Yangtze River is affected by the upstream runoff and tide factors of the downstream. Therefore, along the Yangtze River not only dams were built for the flood protection, but also in the crossing between local rivers and the Yangtze River a set of gates were constructed for the management of navigation and controlling of the river water level, and exchanging the water between local rivers and the Yangtze. In some special positions two-way water pump stations were constructed for flood and drought control. Within the local river network, different kinds of sluices were constructed for the easy management of wateruse. Because of the artificial structure, the natural water system has evolved into a complex hybrid water system. In this case study, the model region is divided into 19 virtual tanks, and contains six Yangtze River gates, eight river control sluices and a pumping station (consist of five 20m^3/s two-way pumps).

3.1 Scenario description

The rainfall forecast for the next three days from 09:00 on 10.Aug.2016 to 15:00 on 13.Aug.2016 shows a lot of rain (especially, there is a heavy rainfall with 210mm on 10.Aug.). Figure 4 give the overview of the rainfall situation.

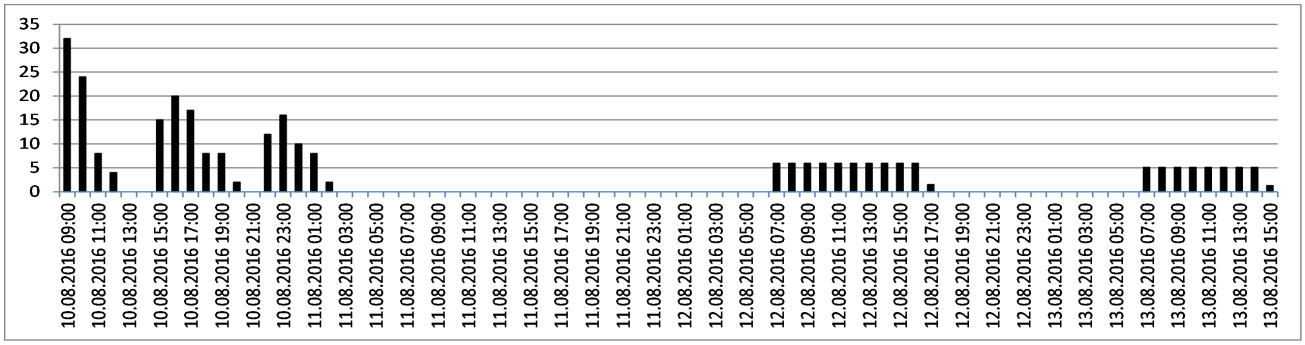

Figure 4: Precipitation forecast

The control goals are shown in Table 1.

Table 1: Control goals

Submodel	Risk water level	Flood water level
Virtual Tank 03	3,4m	4,0m
Virtual Tank 04	3,3m	4,2m
Virtual Tank 05	3,4m	4,1m

The whole system was compiled and run under the MATLAB environment. The simulation model shows you how the water level changed through the control from experience (see Figure 6, the dotted line). It shows very clearly that after one day of the heavy rainfall the water level can

cause a flood, the operation plan is not suitable for this heavy rain event, it has to be optimized.

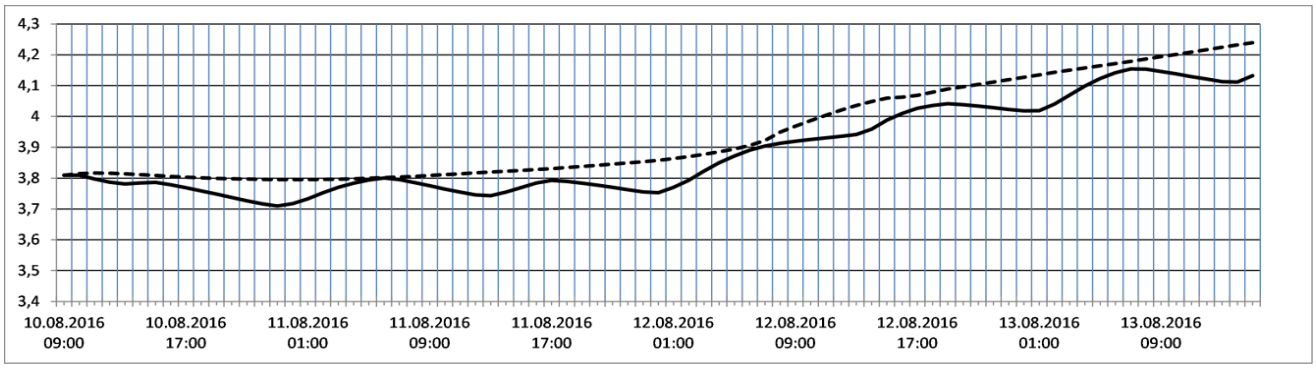

Figure 5: Water level on A03 with empirical operation and optimization

The solid line in figure 5 shows the new operation plan for Gate(YZ-03) using the optimization model. There are two significances in this figure: on one hand, it is very clear that the water situation using the optimization control is be much better than from the expert experience, the risk of flood would be belayed about 8 hours (look the quadrangle), in this time humans can take a lot of counter measures and actions against the flood; and on the other hand, the optimization calculate within a defined time period, in this time period the water level could be also reached the risk level of flood, therefore, the optimization process should be renewed by the actual water situation, so that the modified optimized control plan would be suggested.

4. CONCLUSIONS

In this study, the model of a hybrid water system based on Visual Tank concept is established. The theory of the solution for bi-directional flow in hybrid water system is discussed. A water resources scheduling optimization system for hybrid water system was developed based on MPC-MLD optimization method. MPC-MLD is a well-known approach from cybernetics area, but very fresh application in hybrid water systems. This method can support the target of flood control, drought or environmental diversion in complex river networks for in short-term period. This work provides a new method to solve the optimization scheduling problem. In the future research, the special water policy of water resources protection will be implemented in MPC-MLD method. The optimization will be made more efficient und fit for the practical applications.

REFERENCES

Karimanzira D., H. Mu, H. Linke, and T. Rauschenbach. 2011., Water resources and environmental management of Cities in the Beijiang river basin: A pilot project. The 8th international conference on urban watershed management.

Mu H., T. Rauschenbach, D. Karimanzia. 2013., Modeling and Control of Bi-Directional Water Flow with Application to the Taihu Lake Basin. Global Perspective on Engineering Management.

Pfuetzenreuter T., and Th. Rauschenbach. 2007. A Simulation Library for an Integrated Water Resources Management.

van Ekeren H., 2010., Master of Science Thesis - Hybrid Model Predictive Control of the Rhine-Meuse delta. Delft University of Technology

van Ekeren H., R.R. Negenborn, P.J. van Overloop, and B. De Schutter, 2011., Hybrid model predictive control using time-instant optimization for the Rhine-Meuse Delta. IEEE International Conference on Networking.; 15(2):215-220

Zhang P. 2007., Mater of Engineer Thesis - Model Predictive Control for Hybrid Systems Based on Mixed Logic Dynamical Model. Jilin University

Proceedings of the 10th World Congress of EWRA 'Panta Rhei', 5-9 July 2017, Athens, Greece
© 2017 *European Water Resources Association*

Experimental and numerical simulation of the flow over a spillway

A. Serafeim*, L. Avgeris, V. Hrissanthou and K. Bellos
Department of Civil Engineering, Democritus University of Thrace, Kimmeria Campus, 67100 Xanthi, Greece
* *e-mail: athanseraf@hotmail.com*

Abstract: This paper presents the results of modeling the flow over a side-mounted Ogee type spillway using experimental and CFD (Computational Fluid Dynamics) methods, specifically Ansys - CFX. This research aims to use CFD model to validate the simulation of the flow over an Ogee type spillway which is installed in the Hydraulics Laboratory of Democritus University of Thrace. To achieve this pressure-based, transient simulation of the flow which involves an interaction between liquid water and air, the Volume of Fluid (VoF) and the standard "κ-ε" turbulence numerical models, with standard wall functions, were used, which simulate the free surface of two-phase flow and the flow turbulence, respectively. Three individual meshes with different density in computational cells were created (coarse, medium and dense) using prismatic and tetrahedral elements. Numerical results of the volume fractions, velocity and water depths were plotted for various positions across the spillway and were discussed through a validation process by comparing the CFD model results with the results obtained from physical model. Even though some slight differences between numerical and experimental results were revealed, the graphical trends of the numerical results remain reasonably similar for all experimental tests, and had a close correlation to those achieved in the physical model.

Key words: Ogee type spillway, experimental simulation, numerical simulation, CFD, Ansys Fluent, VoF

1. INTRODUCTION

There are plenty methods to determine the water flow conditions at hydraulic structures. One way of achieving this determination is to conduct field measurements. However, this method is time consuming and sets as a premise the existence of the structure. An alternative method is the use of experimental simulations which require large buildings to be installed, and the installation and the maintenance of the model might be proved expensive. Finally, the most inexpensive and least time consuming method for determining the water flow conditions is the numerical simulation by using Computational Fluid Dynamics (CFD) (Kanyabujinja, 2015 and Kumcu, 2017). This method, besides the need of a powerful computer, has not any specific constraints, and is one of the most promising methods to validate the flow conditions observed either during field measurements or during laboratory experiments.

The general purpose of this paper is the investigation of water flow conditions over a side-mounted Ogee type spillway by using experimental and CFD methods. The experimental model, built in the Hydraulics Laboratory, Department of Civil Engineering, Democritus University of Thrace, and the CFD Ansys Fluent software were used to determine the flow conditions over the spillway at the dam of Berkeche stream, in Ain Temouchent province, Algeria.

The project was tested for three water flow rates, corresponding to different recurrence intervals. The physical model was constructed using the similarity law of Froude – Manning, and the results from the numerical simulation arose by using the multiphase model Volume of Fluid (VoF) in combination with the κ-ε turbulence model.

2. EXPERIMENTAL METHOD

2.1 Experimental set-up and similarity functions

Experiments were carried out by Avgeris et al. (2015) in a built-in model, in Hydraulics Laboratory of Civil Engineering Department, Democritus University of Thrace. This project consists of the reservoir, the spillway, the side collection canal, the transfer canal, the stilling basin and the tailrace. The experimental model was tested for three flow rates; 245 m^3/s, 500 m^3/s and 670 m^3/s corresponding to recurrence intervals of 100, 1000 and 5000 years, respectively (Table 1).

The construction of the model and the laboratory tests were performed with a 1:50 scale between the model and the prototype and in accordance with the similarity law of Froude – Manning. A full geometric and dynamic similarity between prototype and model can only be achieved when the Froude and Reynolds numbers are equal. However, for free surface flows, the inertial and gravitational similarities could be achieved if the equality of Froude number is maintained and Reynolds number is greater than 2000. Therefore, by choosing the equality of Froude number as a criterion of dynamic similarity, a satisfactory representation of the water depths, the hydrostatic pressures and the flow conditions can be achieved (Bellos, 2010). To achieve this similarity, the following Equations (1) – (4) were used:

$$Q_r = L_r^{2.5} \tag{1}$$

$$V_r = L_r^{\frac{1}{2}} \tag{2}$$

$$t_r = L_r^{\frac{1}{2}} \tag{3}$$

$$n_r = L_r^{\frac{1}{6}} \tag{4}$$

where Q_m and Q_p are the water flow rates in the model and the prototype, respectively, Q_r is the flow rate scale (Q_m/Q_p), L_r is the length scale, V_r is the velocity scale, t_r is the time scale, and n_r is the Manning coefficient scale.

By applying the scale 1:50, the ratio of model lengths to prototype lengths is:

$$L_r = 1/50 \tag{5}$$

Consequently, based on the above equations, the scales Q_r, V_r and t_r obtain the following values:

$$Q_r \approx 1/17700 \tag{6}$$

$$V_r \approx 1/7 \tag{7}$$

$$t_r \approx 1/7 \tag{8}$$

In Table 1, the model values Q_m are also given.

2.2 Experimental measurements

Measurements of water flow rate, water depth and pressure were made at several sections along the experimental set-up, including the reservoir, the spillway and the stilling basin. However, this

paper deals only with the spillway and water flow conditions over it. Specifically, instantaneous measurements of the water flow depth in the downstream side collection canal were performed.

Table 1. Recurrence interval and water flow rates of the prototype (Q_p) and the model (Q_m)

Recurrence interval [years]	Q_p [m^3/s]	Q_m [m^3/s]	Q_m [l/s]
100	245	0.014	13.86
1000	500	0.028	28.28
5000	670	0.038	37.90

3. NUMERICAL METHOD

3.1 Numerical model simulation

Computational Fluid Dynamics (CFD) is a computer-based tool that is used to represent and analyze systems that involve fluid flow, heat transfer and chemical reactions, by using numerical methods that are based on partial differential equations describing these systems (Versteeg and Malalasekera, 2007). CFD techniques are governed by a number of differential equations which must be solved in each control volume, and their fundamental principles remain similar to those applicable to the experimental model. These equations include mass conservation or continuity, momentum and energy equations, also known as the Navier - Stokes equations.

In order to transform a real hydraulic structure into a computable model, Ansys Fluent software was used. Ansys Fluent is a CFD package created by Ansys Inc., which is based on finite volume method and uses the Volume of Fluid (VoF) methods and the standard "κ-ε" turbulence numerical models to simulate the free surface flow and the flow turbulence, respectively (Fluent, 2009).

3.2 Geometry and mesh

CFD model geometry was built with the same dimensions of the physical model (Figure 1-[1]), by using the Ansys design modeler. In the geometry builder, both surface and body were frozen to allow a fluid flow to pass through the modeling domain.

The accuracy of a CFD solution depends upon the number of cells in the mesh. In order to analyze the fluid flow, the domain had to be split into smaller cells within which the governing equations would be solved. The areas of high solution interest have been meshed up with the finer mesh, while the coarser mesh was implemented in areas with less solution interest. The main features of interest in the numerical domain are the spillway crest, the downstream side collection canal where the turbulent phenomenon occurs, and the region of interface between the two phases (water and air).

For the 3D model, three individual meshes with different density in computational cells were created (coarse, medium and dense) using prismatic and tetrahedral elements (Figure 1-[2]). According to Ansys Inc. (2008), the list of quality criteria for mesh metric includes: element quality, aspect ratio, Jacobean ratio, warping factor, parallel deviation, maximum corner angle, skewness, and orthogonal quality. In this work, computational cell skewness has been adopted. Cell skewness is defined as the measured difference between the shape of the cell and the shape of an equilateral cell of equivalent volume. Highly skewed computational cells can reduce the accuracy and stability of the solution. The range of equisize skewness lies between 0 and 1 where cell skewness should not exceed 0.98. For all cases, computational cells (mesh) had equisize skewness less than 0.24 which indicates a good quality of mesh.

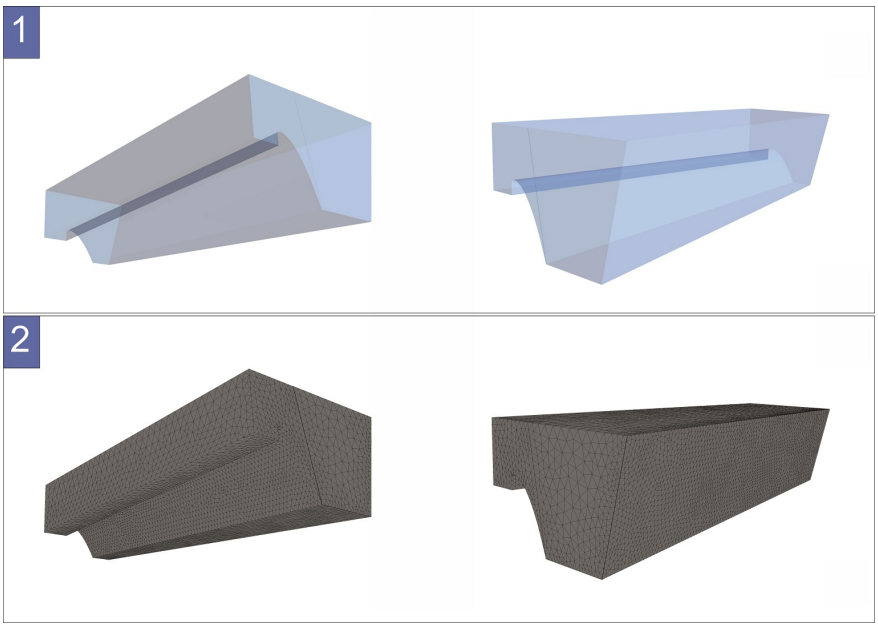

Figure 1. [1]: Three - dimensional CFD model geometry, SW and SE view. [2]: Three - dimensional CFD model mesh, SW and SE view.

3.3 Multiphase modeling

Multiphase modeling is a technique which simulates flow in the simultaneous presence of different phases. All three phases (gas, liquid and solid) are identifiable with a distinct particular inertial response to an interaction with the flow and the potential field. There are four main categories of multiphase flows; gas-liquid, gas-solid, liquid-solid and three-phase flows (Murrone and Villedieu, 2011). Such complex systems have been made possible with the availability of two broad approaches for the numerical calculation, namely Euler-Euler (Volume of Fluid model or VoF model) and Euler-Lagrange (Discrete Phase Model) approaches. The Volume of Fluid model (VoF) was chosen to simulate the multiphase flow. Two Eulerian phases, air and water, were defined as primary and secondary phase, respectively.

4. RESULTS

The investigations conducted in the physical and numerical modeling were focused on the validation of the flow conditions over an Ogee type spillway from the physical modeling through a comparison of results obtained for equivalent flow rates of CFD modeling.

In the spillway model, water surface profiles of each flow rate were investigated along the spillway chute from upstream to downstream of the spillway. It should be noted that the water surface profiles obtained along the spillway refer to the flow depth measured in the downstream side collection canal. The water profiles are presented in Figures 2-[1], 2-[2] and 2-[3] and the constant line represents the readings obtained through physical modeling, while the solid fills of the charts demonstrate the results obtained through CFD modeling.

Three individual surface planes where created for the detailed display of the numerical results. The exact locations are 0.1, 0.6 and 1.1 meters from the upper side of the spillway.

In the spillway numerical analysis, volume fractions cases for both primary and secondary Eulerian phases were examined. The secondary phase (fluid tap water) volume fraction results are presented in Figures 3-[1], 3-[2] and 3-[3].

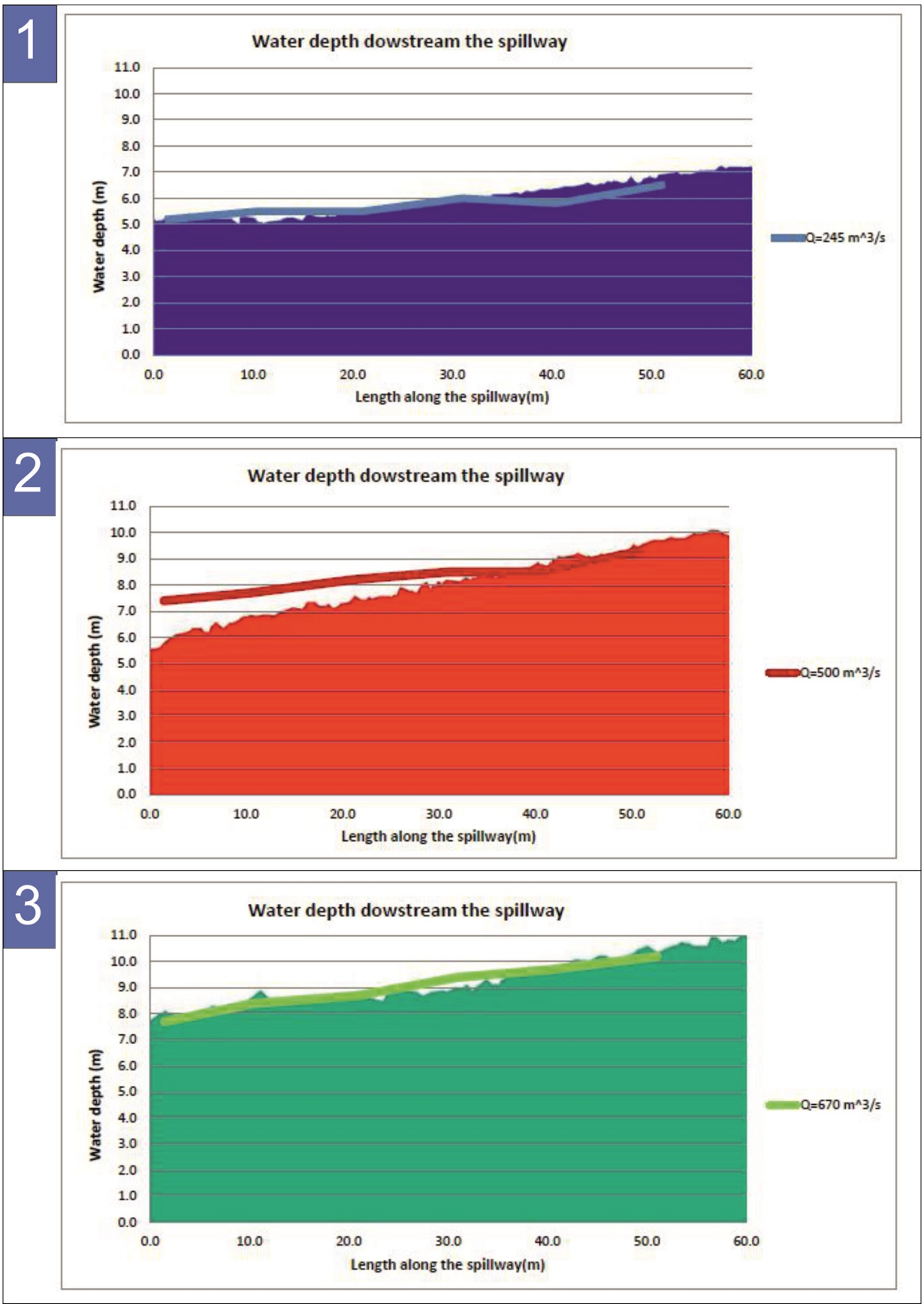

Figure 2. A comparison of water profiles downstream of the spillway which were formed through the experimental and numerical simulation for flow rate: [1] 245 m^3/s, [2]: 500 m^3/s, [3]: 670 m^3/s.

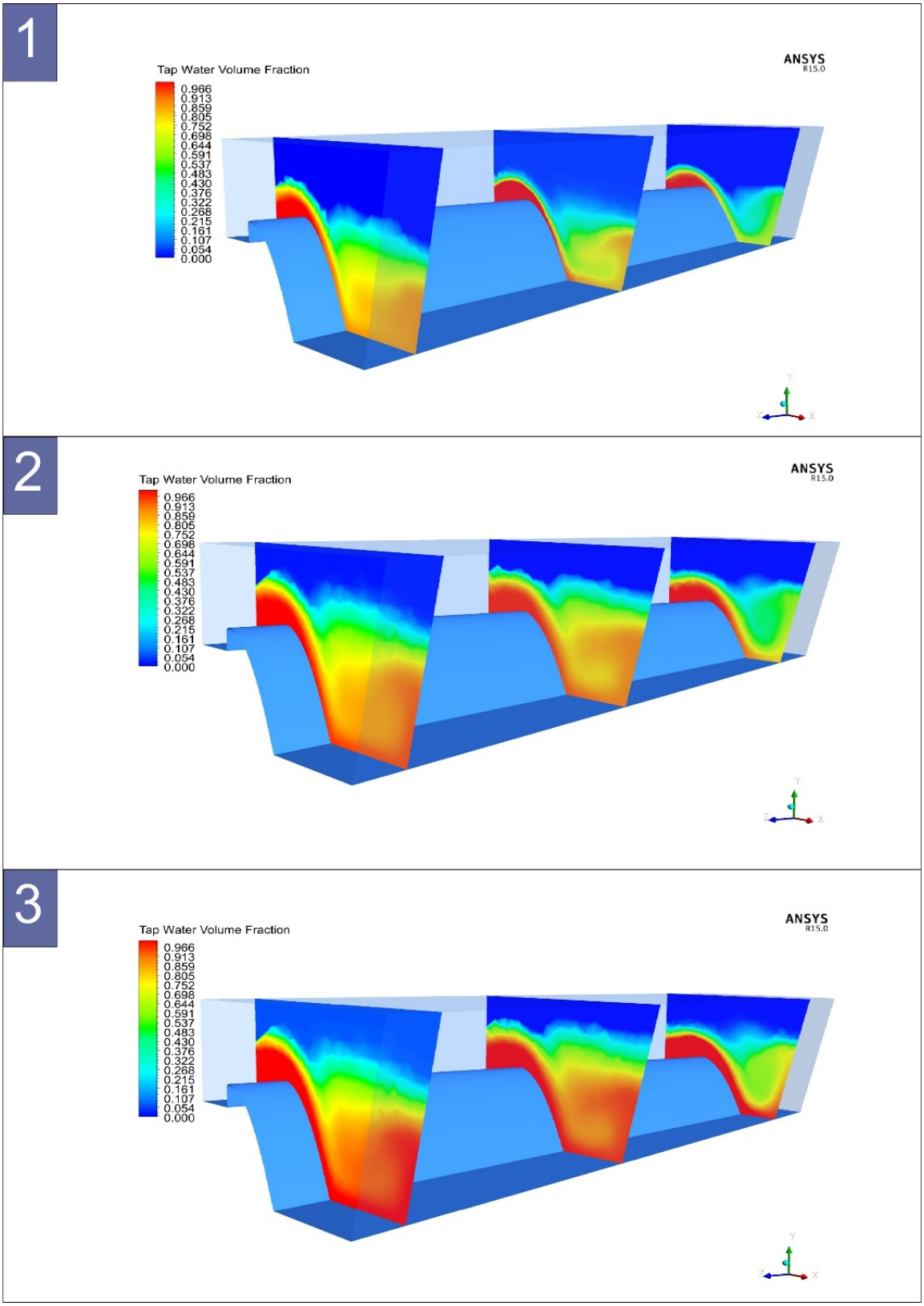

Figure 3. Numerical water volume fraction distribution (density contours) on the spillway for flow rate: [1] 245 m^3/s, [2]: 500 m^3/s, [3]: 670 m^3/s.

The numerical velocity results are presented in Figures 4-[1], 4-[2] and 4-[3]. The highest velocity value was 1.986 m/s.

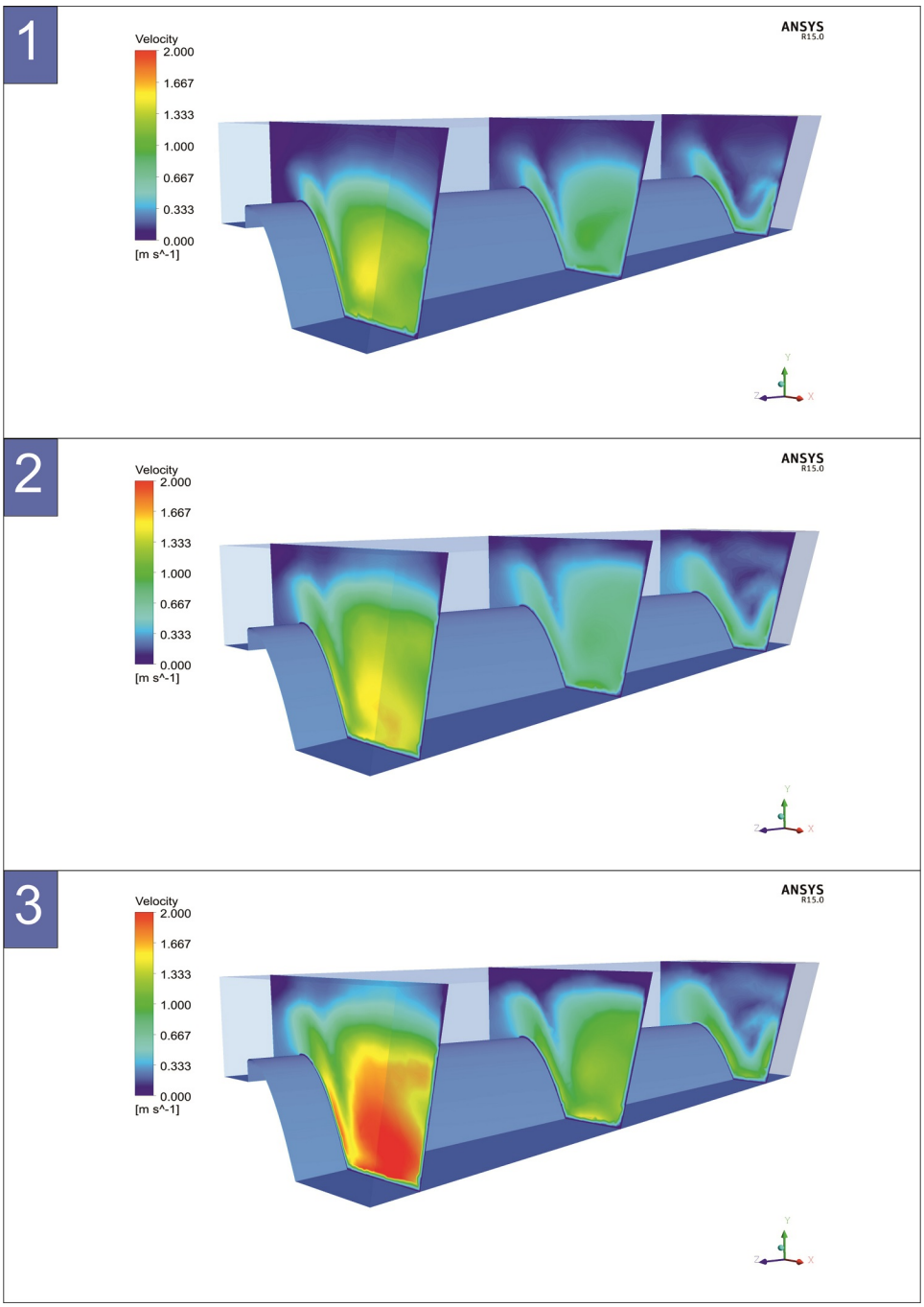

Figure 4. Numerical velocity distribution (density contours) on the spillway for flow rate: [1] 245 m^3/s, [2]: 500 m^3/s, [3]: 670 m^3/s.

5. CONCLUSIONS

A study of flow interaction with scaled model of a side-mounted Ogee shape spillway was presented. A fully three-dimensional CFD model was set up and the numerical model was validated against experimental information. Most of the simulation results are found to be in reasonable agreement with the experimental ones. The outcomes of the simulations permitted the evaluation of the designed structures.

The study of the flow surcharge at different flow rates indicated that the water surface profiles obtained from CFD modeling are similar to the physical model.

Numerical results of water volume fraction and velocity are reasonable and interrelated both with water profiles downstream of the spillway.

Based on the numerical results, the design of the Ogee shape spillway was found to be appropriate for all simulation conditions. Although physical model studies may be more expensive and time consuming than computational modeling, they are still crucial for providing data for numerical model calibration and validation studies. The unique combination of computational expertise with physical flow modeling can be applied in order to provide cost effective, practical solutions to spillway flow problems. Thus, CFD modeling can be used as a complementary tool along with physical modeling to solve complex flow problems of spillways.

REFERENCES

Avgeris, L., Bellos, V., Xiloudis, N., Papalexopoulos, V., Bensasson, A. and Bellos, K., 2015. Experimental simulation of spillway at Berkeche dam. Proceedings of the 3rd Joint Conference, 13th Conference of the Greek Hydrotechnical Association, 9th Conference of the Greek Committee for Water Resources Management and 1st Conference of the Hellenic Water Association, Athens, Greece, 10-12/12/2015, pp. 403-410 (in Greek).

Bellos, K., 2010. Open-Channel Hydraulics. Department of Civil Engineering, Democritus University of Thrace, Xanthi, Greece (in Greek).

Fluent, 2008. Ansys Fluent 6.3 User's guide. Ansys Inc., USA.

Fluent, 2009. Ansys Fluent 12.0 Theory Guide, S.1. Ansys Inc., USA.

Kanyabujinja, P. N., 2015. CFD Modelling of Ogee Spillway Hydraulics and Comparison with Physical Model Tests. Master of Engineering Thesis, Stellenbosch University, Stellenbosch, Western Cape, South Africa.

Kumcu, S. Y., 2017. Investigation of Flow Over Spillway Modeling and Comparison between Experimental Data and CFD Analysis. KSCE Journal of Civil Engineering, March 2017, Volume 21, Issue 3, pp 994–1003.

Murrone, A. and Villedieu, P., 2011. Numerical Modeling of Dispersed Two-Phase Flows. Aerospace Lab.

Versteeg, H. and Malalasekera, W., 2007. An introduction to Computational Fluid Dynamics: The finite volume method. Prentice Hall, Harlow, England.

Proceedings of the 10th World Congress of EWRA 'Panta Rhei', 5-9 July 2017, Athens, Greece
© 2017 *European Water Resources Association*

Methodological framework to estimate the coastal sediment supply of the island beaches

I. Kontogeorgos, O. Tzoraki*, N. Moutafis, Th. Hasiotis and A. Velegrakis
Department of Marine Science, University of the Aegean, University hill, 81100 Mytilene, Greece
* *e-mail: rania.tzoraki@aegean.gr*

Abstract: A new framework is developed to guide the assessment of the sediments deposition from the upland and upstream areas to the island beaches. The study of the coastal sediment supply of the insular river basins includes as the main processes the collection and analysis of meteorological and geomorphological data, the assessment of the climate trends, the use of erosion models to estimate the sediment 'output' of the various management scenarios including the effect of the climate change on the erosion processes. Important step in this procedure is the selection of the mathematical tool to estimate the erosion process considering the data availability. The widely used USLE equation is suggested for beaches that are not connected to any river. In case of beaches that are fed with sediment by an upstream river, a combination of a semi-distributed hydrologic and a hydraulic model is suggested. This framework was applied in Eressos beach, Lesvos, Greece with a drainage basin of the order of about 57 km2, 26 km2 of which are drained through Halandra stream to the Eressos reservoir (total capacity 2.76 Mm3). Only 17% of the produced sediment is reaching the marine environment, since 73% of the produced sediment is retained in the riverbed and into the Eressos reservoir. The findings of the current study show that the application of the developed framework and the combination of various modelling tools may close the uncertainty produced by the limited or absence of erosion monitoring.

Key words: erosion, beaches, SWAT, HEC-RAS, sediment

1. INTRODUCTION

Beaches are critical components of the coastal system as they provide a buffer against marine flooding to backshore coastal ecosystems and assets (Neumann et al., 2015) and, at the same time, have high earning potential. Tourism, an economic sector that contributes an estimated 5 % of the Global Gross Product and about 6 – 7 % of the global employment (Hall et al., 2013) has been increasingly associated with beach recreational activities according to the 'Sun-Sea-Sand-3S' tourism model (Phillips and Jones, 2006). Several beaches in the Aegean face serious erosion problems such as the eastern tip of the Rhodes island (Anagnostou et al., 2011) and Eressos beach in Lesvos (Velegrakis et al., 2008). Beach erosion problems have intensified in recent decades due to climate change impact (Monioudi et al., 2017), raising the need for a better understanding of the sediment transport processes especially at the river mouths and the adjacent beaches.

The fragmentation of insular watersheds, the intermittent flow character for the majority of the rivers and the lack of monitoring create severe problems in estimating the terrestrial sediment budget. This work therefore aims to develop a methodology to estimate the coastal sediment supply of the island beaches of Aegean Archipelago with emphasis on ungauged or limited data watersheds. The developed methodological framework was applied to estimate the coastal sediment supply of Eressos beach, Lesvos, Greece.

2. METHODOLOGY

2.1 Methodological framework

This methodological framework is an attempt to display the processes involved in sediment transport to serve as a guideline for the estimation of the inland contribution to the beach sediment budget in the islands of Aegean Sea. A complete, integrated approach on beach sediment budget management involves the coastal sediment transport estimation, its combination with the coastal morphological analysis output for the assessment of the erosion trend, the design and implementation of a management plan to address the impacts using multi-criteria analysis of different scenarios, and the subsequent monitoring and revision of the management plan (Figure 1). The inland part includes (a) the data collection, (b) the selection of the appropriate modelling tools or a combination of them and (c) the projection of future climatic trends as important integrated parts in the analysis, synthesis, description and future projection of the inland erosion rate and sediment transport.

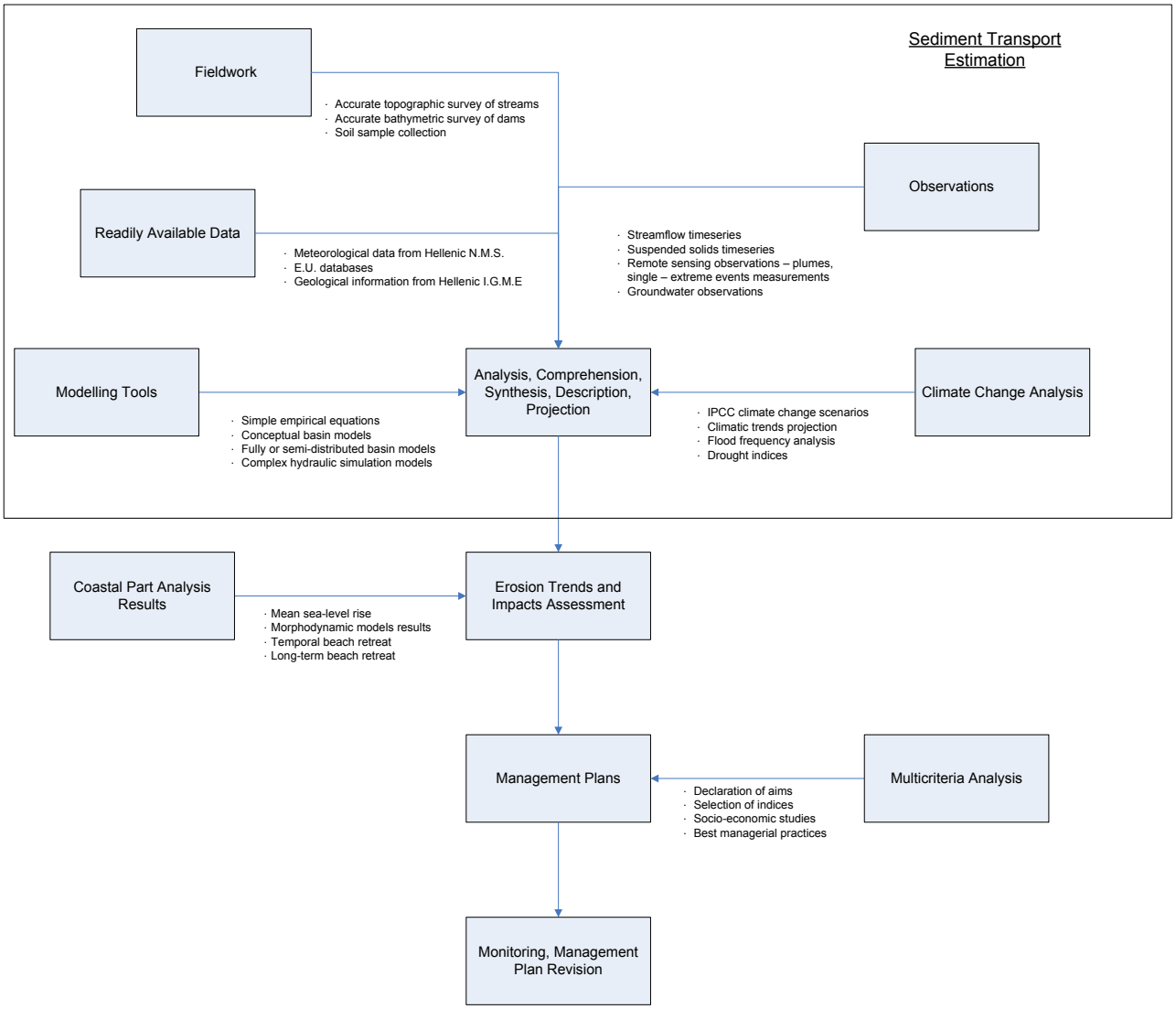

Figure 1. Conceptual framework for the estimation of the coastal sediment supply, beach erosion and management plan implementation.

The first step, (a) data collection, includes the collection of available spatial, meteorological,

hydrological and sediment data, and the additional fieldwork to fill in or evaluate them. Meteorological data are available from the Hellenic National Meteorological Service (N.M.S.), while other meteorological stations operators, such as universities, collect data with less availability for the public. Spatial information (satellite data, digital elevation models, soil maps, land-use and land-cover maps) is mainly available through the EU inventories (http://www.copernicus.eu/, http://www.eea.europa.eu/data-and-maps/data/eu-dem, http://esdac.jrc.ec.europa.eu/, http://land.copernicus.eu/pan-european/corine-land-cover/clc-2012) as well as national data inventories, i.e. such as maps published by the Institute of Mineral and Geological Exploration (IGME) and Geographical Military Service. Additional fieldwork may be carried out, such as topographic surveys of the basin and riverbed, collection of soil samples and recording of streamflow and suspended sediments observations, if possible. Installation of automatic level loggers is suggested to measure water level at high frequency and a series of monthly discharge measurements to construct the rating curves for every station. The flashy character of many streams exposes the instruments at high risk. In case of a reservoir inside the basin it is highly recommended as a site for monitoring.

The second step (b) is the selection of the appropriate mathematical model. Model selection is strongly depended on the studied problem and the available data. Mathematical tools include simple empirical erosion models, simplified conceptual river basin models, advanced hydraulic models, fully and semi-distributed models and models for reservoir siltation.

Simple empirical models consist of simple empirical equations, require less data, give estimates at monthly and annual scales, often approach more accurately complex river basin models, and are preferred for small runoff basins (runoff surface <10 km^2) homogeneous in terms of topographical relief, soil types and land use. Universal Soil Loss Equation (USLE) is a widely used empirical model to estimate soil loss caused by surficial run off in small scale, low gradient areas (Wischmeier and Smith, 1965) and has been used since in various situations (Fistikoglu and Harmancioglu, 2002; Pandey et al., 2007).

Hydraulic river simulation models (i.e. HEC-RAS) require, in addition to the available meteorological data, detailed topographic data of the river bed and the riparian area and the sediment grain size characteristics. Hydraulic models can provide reliable estimates of the sediment processes (erosion/deposition) along the main river corridor providing necessary information for decision making on restoration projects and constructions works.

River basin models (i.e. SWAT, HSPF) require spatial data, DEM, land-use and soil maps, and meteorological information that are readily available in various spatial resolutions from European Union databases. They require discharge measurements at daily scale or lower and at least monthly suspended sediment measurements that are often unavailable for calibration and validation purposes. In case of an ungauged basin, model parameter values may be calibrated for a neighborhood, gauged basin, sharing similar characteristics, with available observations and then transferred in the ungauged basin.

Hydraulic and hydrologic model results can be combined for an effective and integrated estimation of the hydrological and sediment transport processes. They give the possibility to run various scenarios related to land-use and agricultural management practices and the effect of climate change and can provide reliable estimates of flow and sedimentation trends.

In case of reservoir presence, specialized isotope techniques can be used to track terrestrial sediments from soil sources to freshwater systems and extract the sedimentation rate of the reservoir (Porto et al., 2014). This type of fieldwork demands special laboratory equipment, but may be significant in the verification of annual model results in the absence of available monitoring data of the catchment area.

The third step (c) concerns the study of climatic trends. At this stage, meteorological time series from global and regional models may be inserted in calibrated hydrologic models for future streamflow and sediment transport predictions under different scenarios. The results may be used for flash flood analysis and their impact on sediment transport. Flood frequency analysis, employs different kinds of methods such as the use of stochastic methods, Bayesian analysis and traditional

statistical distributions such as the log – Pearson Type III, the Generalized Extreme Value (GEV) and Extreme Value Type EV1 (Gumbel).

These three steps are combined in the data analysis, the comprehension of the processes, the synthesis of the processed results, the description of the current state and future projection of hydrological processes, erosion rate and sediment transport for the estimation of the inland sediment transport in the downstream beach (Figure).

2.2 Study area

The study area is the drainage area of Eressos, Lesvos, Greece. Located in the southwest (SW) part of the island of Lesvos, 52 km away from the capital of the island, Mytilene (Figure 2). The drainage basin of Eressos is 57km^2, 26 km^2 of which are drained through Halandra stream to the Pythari reservoir with a total capacity 2.76 Mm^3, located approximately 2.5 km east of Eressos village and about 5km NE from the beach. Parts of the river and the estuary are susceptible to intense flood events, while Eressos beach, downstream, displays negative sedimentary balance. This study is focused on the flood and sediment transport characteristics of the two main river branches, Karasaris and Halandra streams, both of which play an important role in sediment deposition in Eressos beach.

3. RESULTS – DISCUSSION

The results from the hydraulic analysis showed that the Halandra stream experiences calm/river flow in general, however at the junction point of the two tributaries, where the flow passes from subcritical to critical and rainfall events with short return period lead to serious flood events. Sediment deposition is observed in a small plateau downstream the reservoir and in the river estuary which forms a shoreline consisted of a natural sand edge. The plateau downstream the reservoir operates as sediment trap during both low and high flows, while the sand barrier retains sediment in lower flows and breaks during flush floods (Figure 2), enhancing the formation of river plumes in the sea. This behaviour was also validated by the video images.



Figure 2. Riverbed change for peak discharges with return period 2, 100, 1000 yr, scale from blue to red shows high erosion to high deposition.

Hydrology, erosion and sediment transport was modelled on a daily time-step for the period 2009/09/01 - 2016/08/31 (Figure 3), including a three-year warm-up period for two scenarios, with reservoir and without the reservoir operation. SWAT hydrological calibration was transferred from a neighborhood calibrated basin, however irrigational demands, affecting the reservoir water storage, were calibrated using the water level records of the reservoir for the periods 2014/05/07 – 2014/10/10 and 2015/12/05 – 2016/06/19 (Figure 3). Reservoir water height, corresponding to full

capacity, differs for each period, because the water level logger was placed at different altitude each time. Considering personal communication with the reservoir operators, reporting that the irrigation demand ranges from 0.7 to 1.2 Mm3 of water during the summer season, SWAT tends to underestimate the irrigation needs from 0.6 to 0.7 Mm3.

SWAT estimates an erosion rate of 8 t/ha – yr that generates 45 kt/yr of sediment, out of which only 17% is the coastal sediment supply. The sediment generated by the reservoir drainage area was predicted 5.7 kt/yr by the SWAT model, whereas the reservoir siltation rate was estimated around 14.5 kt/yr. However, the modelled erosion rate appears to be underestimated when compared with the siltation rate of the reservoir resulting from the detailed topographic surveys. Finally, the comparison of the two scenarios outputs (with and without reservoir) shows that the reservoir retains only the 2% of the coastal sediment and high sediment volumes are retained in the small plateau downstream of the reservoir and in the NATURA area of the river delta.

These simulation results contain a great degree of uncertainty since they have not been compared with suspended sediment observations and only the hydrological part of the model has been calibrated. Nevertheless, they provide an estimation of the erosion and deposition processes within the basin, as well as an estimate of the percentage of sediment that eventually ends up at the beach. HEC-RAS results, validated by the river plume images, are exposing the two sediment traps along the riverbed supporting the results of the SWAT hydrological analysis.

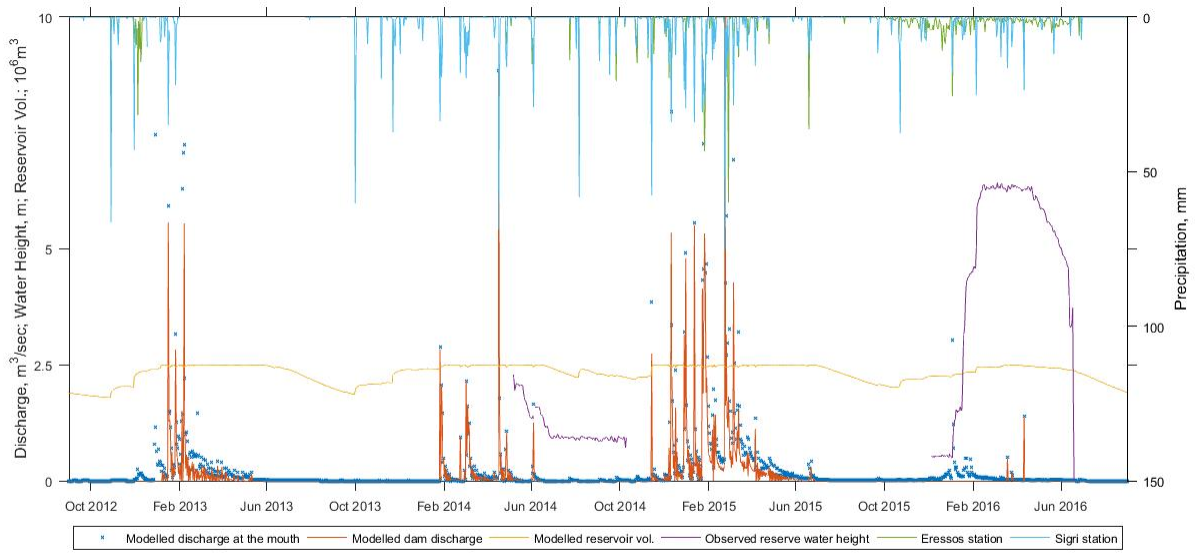

Figure 3. Modelled discharge results at the mouth of the river and the dam vs precipitation, and comparison of modelled reservoir storage vs observed water reservoir water height. (water height corresponds to different altitude for each period)

4. CONCLUSIONS

HEC-RAS incorporating detailed riverbed topographical data, has revealed two sediment deposition sites along the riverbed, the estuary area which operates as a sediment trap in low-flow cases and a small plateau downstream of the reservoir. The combination of HEC-RAS with river plume images and the precipitation records allowed an initial estimate of the threshold from which the stream ceases to function as a sediment trap and releases sediment to the sea.

SWAT managed to adequately model the hydrology of Eressos basin despite the lack of observed data and produced an initial estimate of the hydrologic regime and the erosion behaviour of Eressos basin. Both models show that the river delta behaves as a sediment trap, and its effect in sediment trapping appears to be more important than the reservoir.

A series of the steps proposed in the framework were utilized successfully to overcome the absence of monitoring and reduce the uncertainty. Finally, the need to combine different approaches

and the systematic monitoring of river systems is helpful to reduce the uncertainty in flood estimation and sediment transport.

AKNOWLEDGEMENTS

The current work is supported by the ERA-Beach Project, http://erabeach.aegean.gr/.

REFERENCES

Anagnostou, C., Antoniou, P.F., Hatiris, G.A., 2011. Erosion of a depositional coast in NE Rhodos island (SE Greece) and assessment of the best available measures for coast protection. Journal of Coastal Research SI 64, 1316–1319.

Ballabio, C., Panagos, P., Monatanarella, L., 2016. Mapping topsoil physical properties at European scale using the LUCAS database. Geoderma 261, 110–123. doi:10.1016/j.geoderma.2015.07.006

Bouraoui, F., Benabdallah, S., Jrad, A., Bidoglio, G., 2005. Application of the SWAT model on the Medjerda river basin (Tunisia). Physics and Chemistry of the Earth 30, 497–507. doi:10.1016/j.pce.2005.07.004

Brunner, G.W., 2016. HEC-RAS River Analysis System, Hydraulic Reference Manual, Version 5.0 (No. 69). U. S. Army Corps of Engineers, Hydrologic Engineering Center, Davis, CA.

Cook, A., Merwade, V., 2009. Effect of topographic data, geometric configuration and modeling approach on flood inundation mapping. Journal of Hydrology 377, 131–142. doi:10.1016/j.jhydrol.2009.08.015

Fistikoglu, O., Harmancioglu, N.B., 2002. Integration of GIS with USLE in assessment of soil erosion. Water Resources Management 16, 447–467. doi:10.1023/A:1022282125760

Gassman, P.W., Reyes, M.R., Green, C.H., Arnold, J.G., 2007. The Soil and Water Assessment Tool: Historical Development, Applications, and Future Research Directions. Transactions of the American Society of Agricultural and Biological Engineers 50, 1211–1250. doi:10.13031/2013.23637

Glavan, M., White, S., Holman, I.P., 2011. Evaluation of river water quality simulations at a daily time step–Experience with SWAT in the Axe Catchment, UK. CLEAN–Soil, Air, Water 39, 43–54. doi:10.1002/clen.200900298

Hall, C.M., Scott, D., Gössling, S., 2013. The Primacy of Climate Change for Sustainable International Tourism. Sustainable Development 21, 112–121. doi:10.1002/sd.1562

Maingi, J.K., Marsh, S.E., 2002. Quantifying hydrologic impacts following dam construction along the Tana River, Kenya. Journal of Arid Environments 50, 53–79. doi:10.1006/jare.2000.0860

Monioudi, I.N., Velegrakis, A.F., Chatzipavlis, A.E., Rigos, A., Karambas, T., Vousdoukas, M.I., Hasiotis, T., Koukourouvli, N., Peduzzi, P., Manoutsoglou, E., others, 2017. Assessment of island beach erosion due to sea level rise: the case of the Aegean archipelago (Eastern Mediterranean). Natural Hazards and Earth System Sciences 17, 449–466. doi:10.5194/nhess-17-449-2017

Neitsch, S.L., Arnold, J.G., Kiniry, J.R., Williams, J.R., 2011. Soil and Water Assessment Tool Theoretical Documentation Version 2009 (No. 406). Texas Water Resources Institute, College Station, Texas.

Neumann, B., Vafeidis, A.T., Zimmermann, J., Nicholls, R.J., 2015. Future Coastal Population Growth and Exposure to Sea-Level Rise and Coastal Flooding-A Global Assessment. PloS one 10, e0118571. doi:10.1371/journal.pone.0118571

Panagos, P., 2006. The European soil database. GEO: connexion 5, 32–33.

Pandey, A., Chowdary, V.M., Mal, B.C., 2007. Identification of critical erosion prone areas in the small agricultural watershed using USLE, GIS and remote sensing. Water Resources Management 21, 729–746. doi:10.1007/s11269-006-9061-z

Phillips, M.R., Jones, A.L., 2006. Erosion and tourism infrastructure in the coastal zone: Problems, consequences and management. Tourism Management 27, 517–524. doi:10.1016/j.tourman.2005.10.019

Porto, P., Walling, D.E., Alewell, C., Callegari, G., Mabit, L., Mallimo, N., Meusburger, K., Zehringer, M., 2014. Use of a 137Cs re-sampling technique to investigate temporal changes in soil erosion and sediment mobilisation for a small forested catchment in southern Italy. Journal of Environmental Radioactivity 138, 137–148. doi:10.1016/j.jenvrad.2014.08.007

Tóth, B., Weynants, M., Nemes, A., Makó, A., Bilas, G., Tóth, G., 2015. New generation of hydraulic pedotransfer functions for Europe. European journal of soil science 66, 226–238. doi:10.1111/ejss.12192

Velegrakis, A., Vousdoukas, M., Andreadis, O., Adamakis, G., Pasakalidou, E., Meligonitis, R., Kokolatos, G., 2008. Influence of dams on downstream beaches: Eressos, Lesbos, Eastern Mediterranean. Marine Georesources and Geotechnology 26, 350–371. doi:10.1080/10641190802425598

Velegrakis, A.F., Trygonis, V., Vousdoukas, M.I., Ghionis, G., Chatzipavlis, A., Andreadis, O., Psarros, F., Hasiotis, T., 2015. Automated 2D shoreline detection from coastal video imagery: an example from the island of Crete, in: Remote Sensing, T.I.C. on, Environment (RSCy2015), G. of the (Eds.), ProceedingsSPIE. doi:10.1117/12.2192687

Williams, J.R., 1995. Computer Models of Watershed Hydrology, in: Singh, V.P. (Ed.), Water Resources Publications, Highlands Ranch, CO, pp. 909–1000.

Wischmeier, W.H., Smith, D.D., 1965. Predicting Rainfall - Erosion Losses from Cropland East of the Rocky Mountains, Guide for Selection of Practices for Soil and Water Conservation (No. 282). U.S. Deparment of Agriculture, Agricultural Research Service, Washington, DC.

Proceedings of the 10th World Congress of EWRA 'Panta Rhei', 5-9 July 2017, Athens, Greece
© 2017 *European Water Resources Association*

Influence of river routing methods on integrated catchment water quality modelling

A. Moreno Rodenas[1*], V. Bellos[2,3], J. Langeveld[1], F. Clemens[1]
[1] *Water Management Department, Technishe Universiteit Delft, The Netherlands*
[2] *CH2M, UK*
[3] *School of Rural and Surveying Engineering, National Technical University of Athens, Greece*
[*] *e-mail: a.m.morenorodenas@tudelft.nl*

Abstract: Compliance with the water framework directive (2000/60) in urbanised catchments requires effective water management strategies. Integrated catchment modelling (ICM) represents a key tool in the decision making process. ICM evaluate pollution dynamics by linking urban drainage infrastructure, wastewater treatment facilities and receiving water bodies. Within this set of linked sub-models the river model structure plays an important role. River hydraulic characteristics directly influence water quality processes (e.g. dilution of pollutant loads, pollutant residence time or reaeration dynamics). Several approaches exist in order to simulate flow routing phenomena. In general, these approaches can be categorised in hydraulic or hydrological routing methods. In this paper, we investigate the effect of river flow model structure on dissolved oxygen simulations. Specifically, three methods were compared: a simple hydrological storage method (SM), the fully mass-conservative Variable Parameter McCarthy-Muskingum Method (VPMM) and the solution of the full form of the one-dimensional Shallow Water Equations (1D-SWE). First, the comparison is performed in a simple benchmark case study in order to define the most sensitive parameters for the derived results. Second, the two hydrological methods are implemented in a real world case study for the Dommel catchment (the Netherlands), which is simulated using the software WEST for integrated urban water systems. Based on the results, it seems that the selection of river routing method can be a relevant factor, which should be carefully addressed.

Key words: Integrated Catchment Modelling, river routing, Muskingum method, water quality, WEST software

1. INTRODUCTION

Integrated Catchment Modelling (ICM) aims to simulate the links between several complex subsystems, such as urban drainage networks, rural hydrology, wastewater treatment plants (WWTP) and water bodies (Solvi, 2006). In the context of the ICM, both water quantity and quality parameters can be simulated. This paper discusses the influence of hydrological-simplified river routing methods in ICM structures for dissolved oxygen simulations. Two hydrological routing methods were tested: i) Storage Method (SM), in which the river is represented as a sequence of tanks-in-series and ii) Variable Parameter McCarthy-Muskingum Method (VPMM). The two routing schemes were implemented in a series of synthetic experiments, which represent different geometrical configurations of a river channel. Water quantity outputs (flow and water depth) were compared against the solution of the one-dimensional Shallow Water Equations (1D-SWE). This was considered as a validation process to describe the behaviour of the hydrological representation. Additionally, SM and VPMM methods were applied to a real case study: an urbanised catchment located in the river Dommel (the Netherlands). Model results were compared with observed data for both water quantity and quality.

2. RIVER ROUTING

2.1 Storage Method (SM)

The SM can be classified as a conceptual hydrological model. The river channel is discretised in

a series of tanks with a given length and cross-section. The volume conservation equation is applied to every tank with specified stage-discharge relationship, which defines the outflow at any given time.

$$\frac{dV}{dt} = Q_{in} - Q_{out} \tag{1}$$

$$Q_{out} = \frac{1}{n} A R_H^{\frac{2}{3}} \sqrt{S} \tag{2}$$

where V is the ith tank's volume state, Q_{in} is the incoming flow, n is the Manning's coefficient, A is the section's wet area, R_H is the hydraulic radius and S is the longitudinal slope.

2.2 Varying Parameters McCarthy Muskingum

The VPMM method is based on the Muskingum method (Cunge, 1969) and was developed by Perumal and Price (2013). The classical form of Muskingum method accepts two parameters (x and k), which are dependent on the input hydrograph conditions. Although the geometry of the channel is considered as stationary, the input hydrograph is not. Additionally, in real-world simulations, both water quantity and water quality simulations are often performed in long-time series. Therefore, they are subjected to several input hydrographs with different characteristics. In the context of the VPMM method, these two Muskingum parameters are automatically determined through an algorithm based on the geometry and the dynamics of the river. Additionally, VPMM compensates for the non-conservation of mass phenomena observed at the Muskingum scheme. A full description of the method can be found at Perumal and Price (2013).

3. SYNTHETIC EXPERIMENTS

Two synthetic experiments were generated in order to evaluate each model structure. Figure 1 shows the set-up of the hypothetical case study. The first experiment implemented the routing of an input hydrograph along a trapezoidal channel of 40 km with a steady slope (corresponding to sections S_1.1, S_1.2 and S_3 from Figure's 1 scheme). The solutions rendered by SM and VPMM were compared against the 1D-SWE results, derived from the well-known HEC-RAS hydraulic software (HEC, 2016).

The river section geometry was tested in 9 configurations (E1-E9 shown at Table 2). This served to test the behaviour of the hydrological model implementations against values of four parameters: the width of the channel (W), the embankment's slope (z), the Manning coefficient (n) and the channel slope (S). The second experiment was implemented in order to investigate the effect of rapidly varying lateral inflows (often seen in urban drainage discharges). In this experiment, the full set-up was used.

Input hydrographs were defined according to the Equation (3) (NERC, 1975). Table 1 summarises the parameters used in both of the experiments. The solution scheme was obtained at three space discretisation levels (500 m, 1000 m and 2000 m). Table 2 presents a quantitative assessment for the flow routing comparison with the 1D-SWE, whereas a graphical comparison is provided at Figure 2. It should be mentioned that the space step for the numerical solution through the HEC-RAS software was 100 m. Figure 3 depicts the results from Experiment 2. It is also noted that both methods (VPMM and SM) showed a mass conservative behaviour.

$$Q(t) = Q_{base} + \left(Q_{peak} - Q_{base}\right)\left[\frac{t}{t_{peak}} exp\left(1 - \frac{t}{t_{peak}}\right)\right]^{\beta} \tag{3}$$

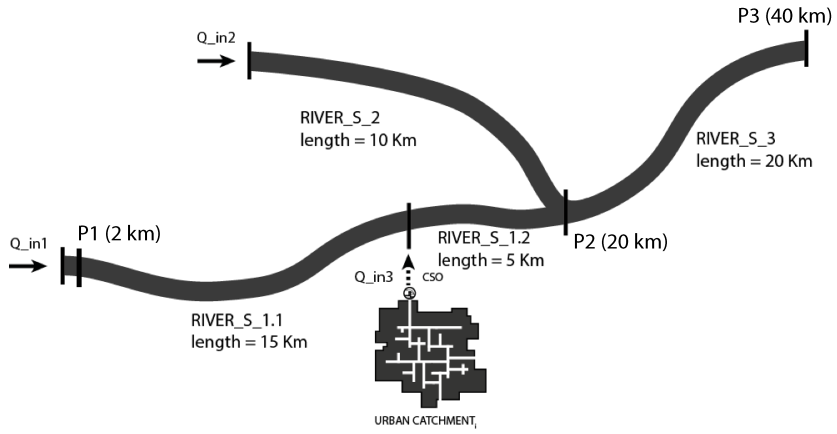

Figure 1. Synthetic set-up of the hypothetical case-study: Experiment 1 attends only to the main river section (S_1.1, S_1.2, S_3) and Experiment 2 is composed by the full set-up.

Table 1. Hydrograph shape parameters

	Q_{base}	Q_{peak}	t_{peak}	beta	dt(s)	Duration
Q_in1_**Experiment1**	5	15	48	10	3600	10 days
Q_in1_**Experiment2**	5	15	48	10	3600	10 days
Q_in2_**Experiment2**	2	8	35	10	3600	10 days
Q_in3_**Experiment2**	1	8	40	200	3600	10 days

Table 2. Nash-Sutcliffe efficiency (%) (NSE) and Root Mean Square Error (RMSE) for the selected parameter combinations and spatial discretisation (L).

Setup	***Geometry***				***VPMM***						***SM***					
	W	***S***	***z***	***n***	***L=500 m***		***L=1000 m***		***L=2000 m***		***L=500 m***		***L=1000 m***		***L=2000 m***	
	(m)	***(%)***	***(-)***	***($s/m^{1/3}$)***	*NSE*	*RMSE*	*NSE*	*RMSE*	*NSE*	*RMSE*	*NSE*	*RMSE*	*NSE*	*RMSE*	*NSE*	*RMSE*
E1	*5*	*0.20*	*1*	*0.035*	*99.99*	*0.03*	*99.99*	*0.03*	*99.99*	*0.03*	*99.87*	*0.08*	*99.85*	*0.08*	*99.76*	*0.01*
E2	*10*	*0.20*	*1*	*0.035*	*99.99*	*0.06*	*99.99*	*0.06*	*99.98*	*0.06*	*99.52*	*0.15*	*99.50*	*0.15*	*99.35*	*0.17*
E3	*5*	*0.050*	*1*	*0.035*	*99.70*	*0.08*	*99.71*	*0.07*	*99.75*	*0.07*	*98.40*	*0.18*	*99.03*	*0.13*	*99.63*	*0.07*
E4	*10*	*0.050*	*1*	*0.035*	*99.76*	*0.08*	*99.79*	*0.07*	*99.85*	*0.06*	*98.90*	*0.17*	*99.34*	*0.13*	*99.52*	*0.12*
E5	*10*	*0.025*	*1*	*0.035*	*98.18*	*0.19*	*98.25*	*0.19*	*98.41*	*0.18*	*90.74*	*0.41*	*93.63*	*0.32*	*96.98*	*0.19*
E6	*10*	*0.050*	*5*	*0.035*	*99.79*	*0.08*	*99.82*	*0.08*	*99.88*	*0.07*	*98.91*	*0.16*	*99.55*	*0.11*	*99.41*	*0.16*
E7	*10*	*0.050*	*1*	*0.040*	*99.63*	*0.09*	*99.67*	*0.08*	*99.75*	*0.07*	*98.53*	*0.19*	*99.19*	*0.14*	*99.51*	*0.11*
E8	*10*	*0.050*	*1*	*0.060*	*99.00*	*0.15*	*99.08*	*0.14*	*99.25*	*0.12*	*94.69*	*0.32*	*97.27*	*0.21*	*99.13*	*0.10*
E9	*10*	*0.050*	*1*	*0.080*	*98.27*	*0.18*	*98.38*	*0.17*	*98.63*	*0.16*	*88.62*	*0.43*	*94.11*	*0.29*	*98.39*	*0.11*

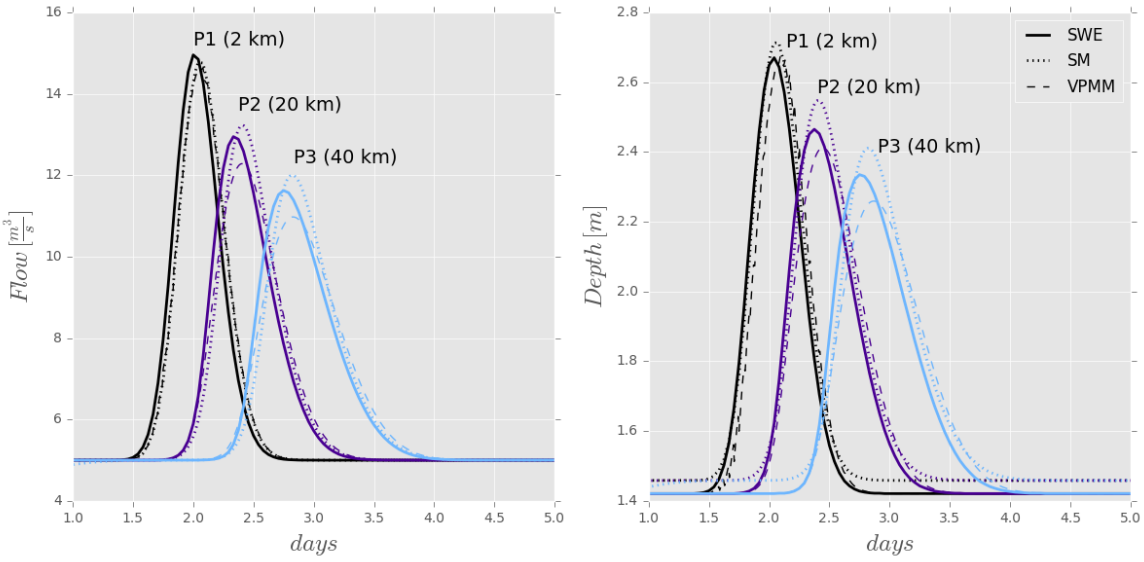

Figure 2. Comparison of flow and depth simulated at several locations along the channel (distances from channel's upstream boundary). Parameter combination E9 with 1000 m spatial discretization.

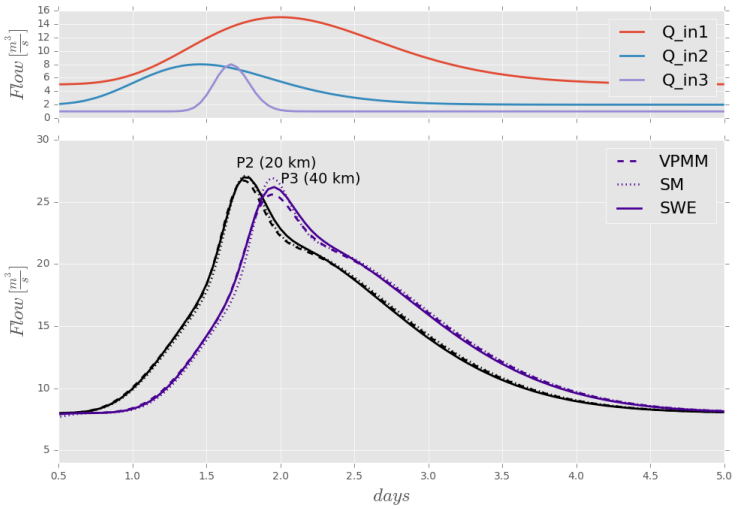

Figure 3. Routing in Experiment 2. Above is shown the 3 input hydrographs. Bellow the flow propagated at 2 sections of the river (corresponding to P2 and P3).

4. DOMMEL CATCHMENT

The performance of SM and VPMM methods was further tested in a real-world case study: the river Dommel (the Netherlands). This river stretch receives the discharge of about 200 combined sewer overflow (CSO) structures and of a wastewater treatment plant (WWTP) of 750,000 p.e, detailed information can be found at Langeveld et al. (2013). The simulator was composed by ~130 km of river tributaries represented by VPMM and SM routing schemes. Each section was conceptualised as tank of 800 m to 2000 m of length, with averaged section geometry from field measurements. Lateral inflows were characterised by monitoring data from CSOs and from the effluent of the WWTP. River base-flow from rural connected catchments was estimated from hydrological modelling.

The biochemical processes included in the model involved: degradation of biodegradable organic matter, nitrification, respiration from macrophytes, sedimentation of particulate organic matter and sediment oxygen consumption. The two methods (VPMM and SM) were implemented in the modelling software WEST (MIKE-DHI). The numerical solver used was a stiff scheme CVODE on a Tornado kernel (Hindmarsh and Petzold, 1995; Claeys et al., 2007) this allowed to perform efficient long-term simulations in which the dynamic state is continuously varying.

A first qualitative manual fitting was performed followed by a global optimization of Nash-Sutcliffe efficiency for flow simulated-monitored data. The parameters used were Manning's coefficient (n=0.078 s/m$^{1/3}$ for the SM method, and n=0.081 s/m$^{1/3}$ for the VPMM method) along with a re-scaling factor for the rural input hydrographs (which SM k_f=0.92 for the SM method and k_f=0.68 for the VPMM method). The later was necessary for fitting the base flow level at the river.

Literature parameter values where used to describe the dissolved oxygen processes. Followed by a global optimization of calibration parameters to fit in dissolved oxygen dynamics in detail. Figure 4 provides a graphic description of the simulated-measured comparison.

5. DISCUSSION

The river Dommel is characterised by low slopes and flow velocities. As far as the magnitude of the flow is concerned, the Dommel can be characterised as a medium river (4-20 m^3/s). The river flow is highly influenced by the connected urban areas and the WWTP effluent. This generates rapidly varying flows for a low-sloped river channel, which is characterized by highly diffusive flow patterns. Muskingum routing methods are known for their ability to simulate the diffusive term

of wave propagation. In this study we compared the performance of a simplistic routing process (SM) with a more complex hydrological model structure (VPMM). The comparison was performed through a series of synthetic experiments, and showed low discrepancies in a range of geometries. However, as it can be seen at Table 2, SM's performance rapidly decreased with the defined tank length for highly rough sections (E8 and E9). This should be taken into account during the process of model design.

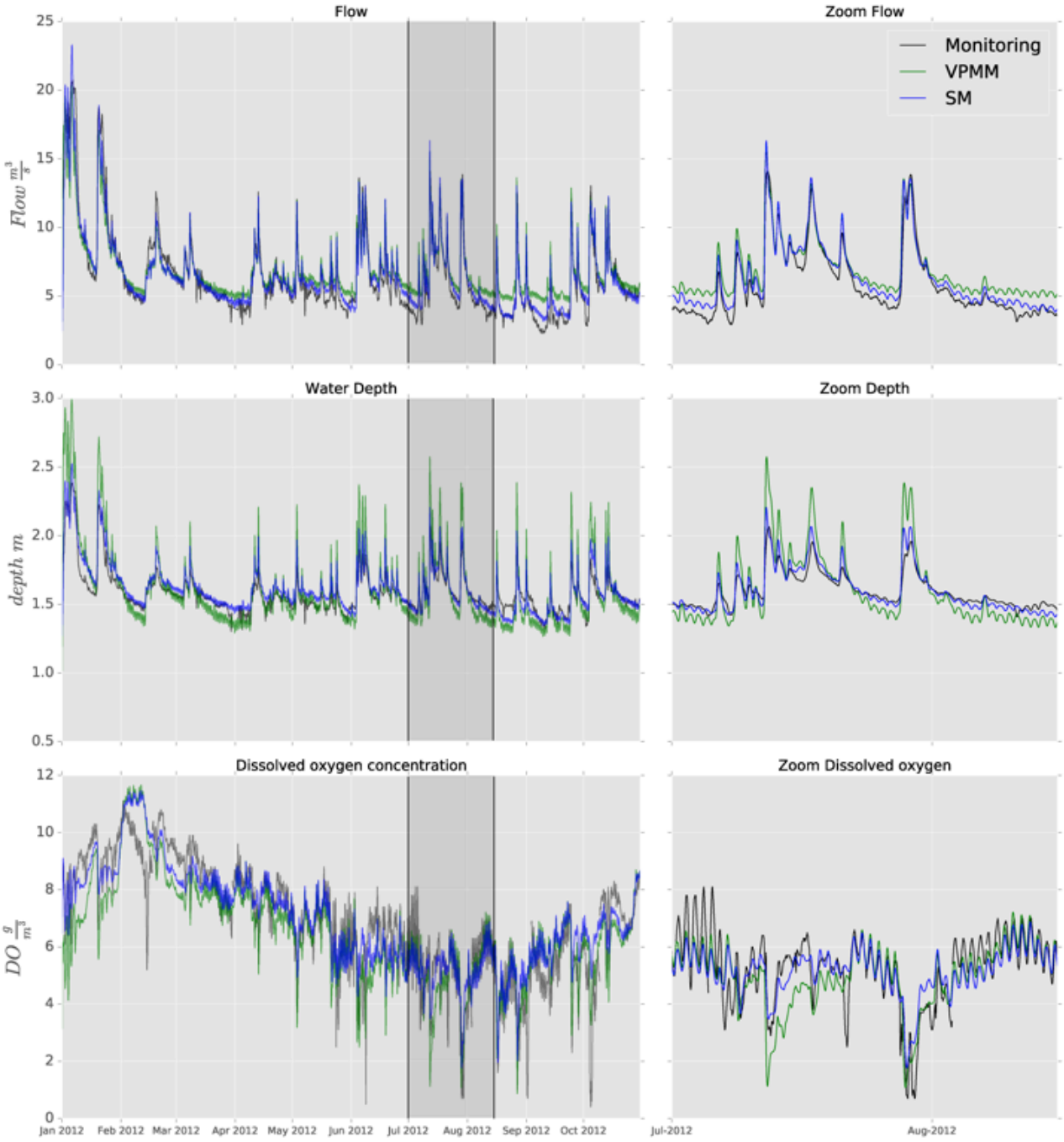

Figure 4. Comparison of monitoring data, VPMM and SM simulations for flow, water depth and dissolved oxygen at the outlet of the Dommel catchment (~17 km downstream of the WWTP). In the left side: the dynamics for January to October of 2012. In the right side: a detail for two events between the 01-Jul-2012 and the 15-Aug-2012.

The comparison of the routing methods for the real case study showed an equivalent performance when matching flow peaks. However, VPMM produced a systematic overestimation of base-flow. VPMM produced also, a higher fluctuation of averaged hydraulic depth, which in turns affects water quality processes (as reaeration potential or sedimentation). The main difference

between the two model structures was apparent in the fitting of the reaeration coefficient (which relates section's depth-velocity with a reaeration potential) and of the degradation constant for fast biodegradable matter. In this case, the increase of complexity in the model structure (represented by the VPMM) didn't lead to a better performance than a simpler storage-discharge relationship.

This misfit is probably is due to the presence of structures in the river body, which are not accounted in the model structure. The VPMM implementation for the Dommel river rendered three time slower simulations that the corresponding with the SM method. Additionally, certain combination of parameter-hydrograph input generates numerical instabilities, which can hamper the use of automated calibration or parameter sampling schemes.

6. CONCLUSION

In this paper, the influence of the river routing method at the water quality parameters is examined, using both a synthetic experimental set-up and a real-world case study.

As far as the SM method is concerned, although its simplicity, the ability to reproduce diffusion is highly depended on the spatial discretisation used for the representation of the computational domain. This issue should be appropriately addressed in the model design process.

On the other hand, the VPMM method does not depend on the space step and can sufficiently reproduce the diffusive phenomena of the flow. However, in real world case studies in which flow is characterised by great complexity, human structures and low flow velocities, the VPMM method does not perform better, even though the method is more physically consistent than the SM method.

It seems that the hydrological routing method used in conceptual integrated catchment structures can have an impact in the flow routing pattern, which is transferred to dissolved oxygen patterns. Therefor the selection of model structure should be carefully assessed and tested in a case study basis.

ACKNOWLEDGEMENTS

This research was done as part of the Marie Curie ITN – Quantifying Uncertainty in Integrated Catchment Studies (QUICS) project. This project has received funding from the European Union's Seventh Framework Programme for research, technological development and demonstration under grant agreement no. 607000.

REFERENCES

Cunge, J. A., 1969.On the subject of a flood propagation method (Muskingum method). Journal of Hydraulic Research, 7(2): 205-230.

Filip H.A. Claeys, Peter Fritzson, Peter A. Vanrolleghem, 2007. Generating efficient executable models for complex virtual experimentation with the Tornado kernel. Water Science and Technology Sep, 56 (6), 65-73, DOI: 10.2166/wst.2007.581.

Hindmarsh, A. C., and Petzold, L. R., 1995. Algorithms and software for ordinary differential equations and differential-algebraic equations. Computers in Physics, 9, 148-155.

Hydrologic Engineering Centre (HEC), 2016. HEC-RAS River Analysis System, Hydraulic Reference Manual, Version 5.0, US Army Corps Of Engineers.

Langeveld, J. G., Benedetti, L., de Klein, J. J. M., Nopens, I., Amerlinck, Y., van Nieuwenhuijzen, A., Flameling T., van Zanten O., Weijers, S. 2013. Impact-based integrated real-time control for improvement of the Dommel River water quality. Urban Water Journal, 10(5), 312-329.

Natural Environment Research Council (NERC), 1975. Flood Routing Studies, in Flood Studies Report, col. III, Institute of Hydrology, Wallingford, UK.

Perumal, M. and Price R. K., 2013. A fully mass conservative variable parameter McCarthy-Muskingum method: Theory and verification. Journal of Hydrology, 502, 89-102.

Solvi A.-M. 2006. Modelling the sewer-treatment-urban river system in view of the EU Water Framework Directive, PhD Thesis, Ghent University, Belgium.

Proceedings of the 10th World Congress of EWRA 'Panta Rhei', 5-9 July 2017, Athens, Greece
© 2017 *European Water Resources Association*

Definition of critical support area revisited

I. Papageorgaki* and I. Nalbantis
Laboratory of Reclamation Works and Water Resources Management; School of Rural and Surveying Engineering, National Technical University of Athens, Athens, Greece
* *e-mail: ino@central.ntua.gr*

Abstract: Selecting the upslope contributing area threshold for channel initiation, herein termed as the Critical Support Area (CSA), is known to be crucial for extracting the hydrographic network from a Digital Elevation Model (DEM). Commonly, an arbitrary quantity is selected which is constant in both time and space. This study is aimed to investigate the spatio-temporal variation of CSA based on information from conventional maps. Specifically, maps at the scale 1:50000 for a Greek river basin are used to identify stream heads and the corresponding values of CSA for two seasons of the hydrological year: the wet and dry season. A DEM with a cell size of about 30 m is used for tests, which is based on the Shuttle Radar Topography Mission (SRTM). A Geographic Information System (GIS) is employed for data processing. For each stream head indicated on the map, raw data are extracted, which include CSA and statistics (mean and standard deviation) of the ground slope, square root of ground slope and height above the nearest drainage point (HAND) A variety of linear regression models were tested using untransformed data by regressing CSA on one or more of the remaining variables. No statistically significant relationship was found, which led us to propose the basin-wide median CSA for each season of the year as the best selection. The proposed CSAs are compared to the constant CSA of the common approach using multiple basin-wide geomorphometric characteristics.

Key words: Critical Support Area (CSA), upslope contributing area threshold for channel initiation, hydrographic network, Digital Elevation Model (DEM), geomorphometry

1. INTRODUCTION

Nowadays due to the availability of Digital Elevation Models (DEMs), the extraction of hydrographic networks and catchment delineation are typically performed in an automatic way. Identifying the extent of a hydrographic network based on a DEM is known to be of primary geomorphic and hydrologic importance (Montgomery and Dietrich, 1989; Montgomery and Foufoula-Georgiou, 1993). The hydrographic network affects the simulated hydrologic response of a catchment, which implies that the accurate estimation of stream heads is important for accurate runoff prediction.

The upslope contributing area threshold, herein referred to as the Critical Support Area (CSA), is the critical quantity that allows the extraction from DEMs of useful hydrological information. CSA is commonly selected as a constant quantity without consideration of its variation in time and space. Diverse methods have been proposed for automatically extracting channel networks from DEMs (O'callaghan and Mark, 1984; Tarboton et al., 1991; Band and Moore, 1995), the most common being the adoption of a value of CSA as the minimum drainage area required for a channel to initiate (Band, 1986; Morris and Heerdegen, 1988; Tarboton et al., 1988). In practice, this value is often selected on the basis of visual similarity between the hydrographic network extracted from a DEM and the blue lines depicted on topographic maps.

In this work, a mapped stream network from conventional maps is compared to a stream network derived from a DEM with a spatial resolution of 30 metres obtained from the Global Shuttle Radar Topography Mission (SRTM). The spatial variation of CSA is investigated by examining relationships between CSA and geomorphometric characteristics. Also, the temporal variation of CSA is investigated by adopting two seasons within each hydrological year: (i) the wet season in which both perennial and intermittent streams are considered, and (ii) the dry season in which only

perennial streams are assumed to be present.

2. METHODOLOGY

2.1 General

As mentioned in the Introduction, in this work, relationships between the Critical Support Area (CSA) and various geomorphometric characteristics are sought, with the purpose to better define CSA in practical applications. The examined geomorphometric characteristics include: (i) the average ground slope; (ii) the standard deviation of ground slope; (iii) the average of the square root of ground slope; (iv) the standard deviation of the square root of ground slope; (v) the mean value of Height Above the Nearest Drainage (HAND); (vi) the standard deviation of HAND. All the above quantities refer to the upslope contributing area.

As also mentioned in the Introduction, in this study, the hydrographic network is considered as a dynamic feature of a drainage basin by focusing on two extreme situations: a first one for the wet season of the hydrological year and a second one for the dry season.

A Geographic Information System (GIS) is employed for data processing by implementing processing steps as a model in ModelBuilder. All datasets, i.e., conventional maps at the scale 1:50000 and the SRTM DEM data are projected in the same reference coordinate system so as to limit errors. Data pre-processing ensures that topographic depressions and flat areas are filled and each grid cell is linked to the catchment outlet by means of an uninterrupted flow path.

The employed methodology involves four steps. Step 1 involves the digitization of heads of perennial and intermittent streams from projected conventional maps. In step 2, the above mentioned information regarding the location of stream heads is transferred from the used map to the DEM-based hydrographic network using a snapping procedure. The need for such procedure arises from data geo-referencing and the imperfect ability of the DEM to accurately represent topography. The procedure ensures the selection of cells with high accumulated flow as the representations of channel heads. Step 2 is executed twice, i.e., separately for each season, using a vector-to-raster conversion. For all selected cells, the upslope contributed area is defined and the corresponding values of CSA are computed.

In step 3, a number of geomorphometric characteristics are assessed which are given in sub-section 2.2 and serve as the explanatory variables in a regression analysis with the upslope contributing area being the dependent variable. Only linear relationships are considered. Their statistical significance is checked using the well-known F-test. In this work, we provide the determination coefficient R^2, the value of F and the related probability, denoted as "significance of F" which is compared to a critical small value.

In step 4 of the methodology the final values for CSA are selected and the implications thereof on CSA-dependent basin-wide geomorphometric characteristics described in sub-section 2.2.

2.2 Geomorphometric characteristics

The definition of the employed geomorphometric characteristics of hydrological interest is necessary. This is given next.

Ground slope (Burrough and McDonell, 1998) is computed for the upslope contributed area for each stream head in the catchment, while the mean value and standard deviation of slope are selected to represent the frequency distribution of this variable. Slope is commonly computed in units of degrees as follows:

$$\text{Slope} = 57.29578 \times \tan^{-1} \sqrt{G_x^2 + G_y^2} \tag{1}$$

where G_x and G_y are terrain gradients in the x and y direction respectively.

The height above the nearest drainage point (HAND) is a new terrain feature than normalizes DEMs according to the vertical distances relative to drainage channels (Nobre et al., 2011; Papageorgaki and Nalbantis, 2013). HAND is calculated for each DEM cell, as the elevation difference from the nearest cell belonging to the drainage network, following the flow direction path. Evidently, HAND is directly affected by errors in the definition of the stream network.

The calculation of the upslope area depends on the way the accumulated area of upstream cells is routed to one or more downstream cells. In this work, the D8 flow direction algorithm (Jenson and Domingue, 1988) is used which involves conveying the area of each cell to its neighboring cell lying in the steepest downslope direction.

Basin-wide geomorphometric characteristics used for comparisons are the mean and standard deviation of stream slope, square root of stream slope, and HAND, as well as the total stream length.

3. STUDY AREA AND DATA

3.1 Description of the study area

One drainage basin was selected for tests, which is presented in Figure 1. Its watercourse is a tributary of the Acheloos River known as Krikeliotis River. The basin is located in western mainland Greece and has an area of 88.8 km^2. It is characterized by a mountainous topography, with a mean ground elevation of 1296 m and an average ground slope of 20.2 degrees.

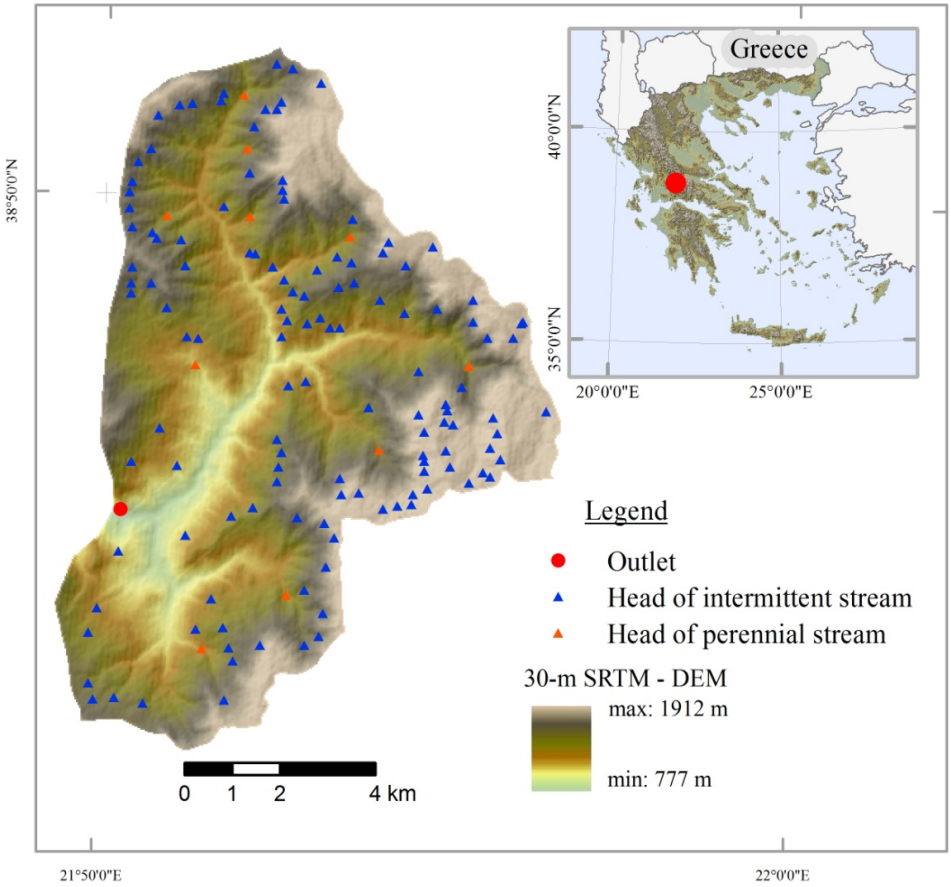

Figure 1. The study basin

3.2 Data used

Two kinds of spatial information are used for the definition of the Critical Support Area. These include the following: (i) conventional maps at the scale 1:50000 covering the study area; and (ii) an 1-arc-second Global coverage Shuttle Radar Topography Mission (SRTM) DEM. The National Aeronautics and Space Administration (NASA) and the National Geospatial-Intelligence Agency (NGA) of the United States of America participated in an international project to acquire radar data which were later used to create the first near-global set of land elevations. The 1-arc-second Global SRTM product offers worldwide coverage of void filled data at the resolution of 30 m. It was tested in previous studies with regard to its accuracy and reliability (Nalbantis et al., 2017).

4. RESULTS

The methodology described in section 2 was applied to data presented in section 3. In the data preparation stage, it was revealed that the snapping distance required to achieve a successful transfer of information on stream heads from maps to the DEM-based hydrographic network was 120 to 150 m. The upslope contributing areas for the two seasons of the year were regressed on data for variables indicated in sub-section 2.2. Only cases with one and two explanatory variables were tested due to the small sample size, which was particularly restrictive for the dry season. Results are summarized in Table 1. By adopting the significance level of 0.05, only one regression relationship was found to be significant. Specifically, for the dry season and when using the mean and standard deviation of square root of ground slope, the significance of F fell below 0.05. Despite this fact, in this work, we consider that the sample size is very low (equal to 8), and we do not accept the regression relationship that was identified. In view of the fact that, in general, no significant dependence of the upslope contributing area to geomorphometric characteristics was found, we adopt the median value for this area for each season separately. For comparison purposes we examine also a third value for CSA which is the mean of the two CSAs for the two seasons. The implication on the basin-wide geomorphometric characteristics of sub-section 2.2 is shown in Table 2. A visual comparison of the hydrographic networks resulting from the various selected values of CSA is made in Figure 2. It is evident that the selected value of CSA exerts a significant influence on all geomorphometric characteristics selected for testing, the largest repercussion being observed for the total stream length.

Table 1. Results of regression analysis for the upslope contributing area using various explanatory variables

Explanatory variables	Dry season			Wet season		
	R^2	F	Significance of F	R^2	F	Significance of F
Mean ground slope	0.278	2.31	0.179	0.000	0.01	0.920
Mean of square root of ground slope	0.319	2.81	0.145	0.000	0.01	0.918
Mean HAND	0.204	1.54	0.261	0.025	2.10	0.151
Mean ground slope, Std of ground slope	0.683	5.39	0.057	0.057	2.48	0.090
Mean of square root of ground slope, Std of square root of ground slope	0.730	6.75	0.038	0.046	1.96	0.147
Mean HAND, Std of HAND	0.365	1.43	0.322	0.035	1.47	0.236

Std = standard deviation

Table 2. Basin-wide CSA-dependent geomorphometric characteristics as functions of the selected value of CSA

Geomorphometric characteristic	CSA of dry season	CSA of wet season	Average CSA
Mean stream slope (^{o})	7.25	14.92	8.27
Mean of square root of stream slope (^{o})$^{0.5}$	2.56	3.74	2.74
Mean HAND (m)	4.40	5.87	4.77
Std of stream slope (^{o})	4.31	6.28	4.73
Std of square root of stream slope (^{o})$^{0.5}$	0.81	0.94	0.85
Std of HAND (m)	5.26	7.16	5.59
Total stream length (m)	34265	246571	44973

Std = standard deviation

5. CONCLUSIONS

In this work the variation in both space and time of the upslope contributing area threshold for channel initiation, denoted as the Critical Support Area (CSA), was investigated with the purpose to assist the procedure for its selection. Results of our investigation allow for drawing the following conclusions:

- Conventional maps at coarse spatial scales (e.g., 1:50000) can be useful in providing information about stream heads and consequently about CSA.
- No statistically significant relationship was found between the CSA values from maps and typical geomorphometric characteristics such as the ground slope, square root of ground slope, and height above the nearest drainage point (HAND); it is therefore proposed to select the median value of CSA from maps by ignoring the spatial variation of CSA.
- As far as the temporal variation of CSA, heads for ephemeral and perennial streams allowed for roughly distinguishing between values of CSA for the wet and dry season of the hydrological year.
- It was demonstrated that selecting the CSA based on map information by simultaneously considering its temporal variation is crucial for assessing typical geomorphometric characteristics that depend on CSA.

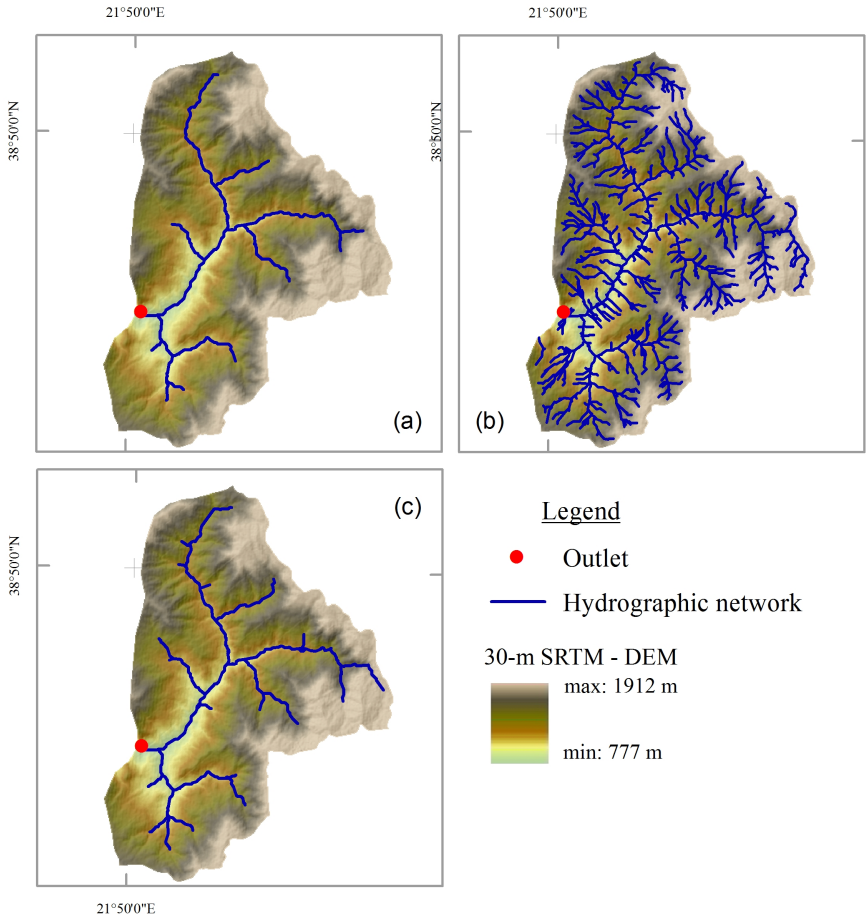

Figure 2. The hydrographic network of the study basin obtained by adopting (a) the dry season median CSA, (b) the wet season median CSA, and (c) the average of the two values

REFERENCES

Band, L. E., 1986. Topographic partition of watersheds with digital elevation models. Water Resources Research; 22 (1): 15–24.

Band, L. E., Moore, I. D., 1995. Scale: landscape attributes and geographical information systems. Hydrological Processes; 9 (3-4): 401-422.

Burrough, P. A., McDonell, R. A., 1998. Principles of Geographical Information Systems. Oxford University Press, New York, 190p.

Jenson, S. K., Domingue, J. O., 1988. Extracting Topographic Structure from Digital Elevation Data for Geographic Information System Analysis. Photogrammetric Engineering and Remote Sensing; 54 (11): 1593-1600.

Montgomery, D. R., Dietrich, W. E., 1989. Source areas, drainage density, and channel initiation, Water Resources Research; 25 (8): 1907–1918.

Montgomery, D. R., Foufoula-Georgiou, E., 1993. Channel network source representation using digital elevation models. Water Resources Research; 29 (12): 3925–3934.

Morris, D. G., Heerdegen, R. G., 1988. Automatically derived catchment boundaries and channel networks and their hydrological applications. Geomorphology; 1 (2): 131–141.

Nalbantis, I., Papageorgaki, I., Sioras, P., Ioannidis, C., 2017. Effect of uncertainty in Digital Surface Models on the extent of inundated areas. Hydrological Processes; 31 (9): 1760–1775.

Nobre, A. D., Cuartas, L. A., Hodnett, M., Rennó, C. D., Rodrigues, G., Silveira, A., ... Saleska, S., 2011. Height Above the Nearest Drainage–a hydrologically relevant new terrain model. Journal of Hydrology; 404 (1): 13-29.

O'callaghan, J. F., Mark, D. M., 1984. The extraction of drainage networks from digital elevation data. Computer vision, graphics, and image processing; 28: 323–344.

Tarboton, D. G., Bras, R. L., Rodriguez-Iturbe, I., 1988. The fractal nature of river networks. Water Resources Research; 24 (8): 1317-1322.

Tarboton, D. G., Bras, R. L. Rodriguez-Iturbe, I., 1991. On the extraction of channel networks from digital elevation data. Hydrological Processes; 5 (1): 81-100.

Papageorgaki, I., Nalbantis, I., 2013. Hydrological landscape classification based on digital elevation models and orthophotos. In: EGU General Assembly Conference Abstracts; 15: 9867.

Proceedings of the 10th World Congress of EWRA 'Panta Rhei', 5-9 July 2017, Athens, Greece
© 2017 *European Water Resources Association*

Integration of rain gauge errors in radar-rain gauge merging techniques

F. Cecinati[1*], A. Moreno Ródenas[2] and M. A. Rico-Ramirez[1]
[1] *University of Bristol, Department of Civil Engineering*
[2] *Technische Universiteit Delft, Water Management Department*
[*] *e-mail: fc14509@bristol.ac.uk*

Abstract: Kriging interpolation methods are often applied without considering measurement uncertainty, but rarely rain gauge uncertainty is negligible. The most used technique to consider measurement uncertainty in Kriging is to include a nugget effect in the variogram model. The nugget is a measurement of the variance that one can expect between two measurements at short distance. Including a nugget in the variogram model is appropriate when the uncertainty is stationary in space; if a time variant variogram is not used, the uncertainty is considered stationary in time as well. This is not the case for rain gauge interpolation, because rain gauge uncertainty is proportional to the rainfall rate, which is highly variable in space and time. Kriging for Uncertain Data (KUD) is a technique proposed in literature to solve this problem, modifying the nugget effect for each time step and for each measurement point. Nevertheless, the application to rain gauge interpolation showed that the methodology is not stable in certain conditions. Several factors can affect the performance: the position and the number of rain gauges, their accuracy, spatial characteristics of the rainfall field, rainfall intensity, or the relative position of peaks compared to the rain gauge position. This work investigates the performance of KUD with three synthetic experiments, simulating the variation of rainfall spatial variability, rain gauge density, and rain gauge accuracy. The results suggest that rain gauge density in relation to the rainfall variability plays an important role in the performance of KUD.

Key words: rain gauge interpolation, kriging, kriging for uncertain data

1. INTRODUCTION

Rain gauge measurements are probably the most used source of rainfall information for hydrological applications. Often rain gauge interpolations are accomplished neglecting measurement uncertainties (AghaKouchak et al., 2010; Ciach et al., 2007; Dai et al., 2014; Germann et al., 2009; Rico-Ramirez et al., 2015; Villarini and Krajewski, 2009). Rain gauge uncertainty is reduced when temporal accumulation is performed, when more expensive high-accuracy devices are used and when the data is correctly managed and calibrated (Habib et al., 2004, 2008; Molini et al., 2005; Nešpor and Sevruk, 1999; Sevruk, 1996). Ideally, accurate and dense rain gauge networks should be used for hydrological applications, especially at urban scale, when high spatial resolutions is required (Schilling, 1991). In reality, rain gauge networks, especially high-accuracy device networks, are rarely sufficiently dense. To improve the spatial resolution, rain gauge networks with different accuracy characteristics are often integrated (Peleg et al., 2013; Villarini et al., 2008). The integration of accurate and less accurate rain gauges networks is often unavoidable to reach a sufficient density and measurement uncertainty cannot be neglected. Additionally, rain gauge uncertainty is proportional to the rainfall rate, thus highly variable in space and time (Ciach, 2003; Habib et al., 2001).

Kriging interpolation methods provide rainfall estimations with associated variance, offering a starting platform for uncertainty estimation. The nugget effect in the variogram model is a way to represent the rain gauge measurement uncertainty (Clark, 2010), but it assumes homoscedasticity, therefore the uncertainty is modelled uniform in space. If a time invariant variogram is used, the modelled uncertainty may be modelled uniform in time as well (Cressie, 1993). De Marsily, (1986), proposes an approach named Kriging for Uncertain Data (KUD) to use a different nugget for different measurement points. The formulation is refined by Mazzetti and Todini, (2009). However,

we are not aware of KUD applications to rain gauge interpolation and of its performance evaluation.

This work studies the application of KUD to the interpolation of rain gauge measurements. The formulation in this work is a simplification of Mazzetti and Todini, (2009). Since the application to real case studies does not allow to vary the factors affecting the KUD performance, here synthetic tests are used. The application of KUD is compared to standard ordinary kriging (OK) in three synthetic tests to investigate the effect of different factors on the KUD performance.

2. METHODOLOGY

2.1 Kriging for Uncertain Data (KUD)

In ordinary kriging, the interpolation at each point x_0 is a weighted average:

$$\hat{R}(x_0) = \sum_{\alpha=1}^{n} w_\alpha \cdot R(x_\alpha) \tag{1}$$

where $\hat{R}(x_0)$ is the interpolated rainfall in x_0, $R(x_\alpha)$ are the rain gauge measurements at locations x_α, n is the number of rain gauges, and w_α are kriging weights, estimated through the kriging system:

$$\begin{cases} \sum_{\alpha=1}^{n} w_\alpha(x_0) = 1 \\ \sum_{\alpha=1}^{n} w_\alpha(x_0) \cdot C(x_\beta - x_\alpha) + \mu = C(x_\beta - x_0) \quad \beta = 1, \dots, n \end{cases} \tag{2}$$

where x_α and x_β are generic rain gauge locations and μ is the Lagrange parameter (Cressie, 1993). $C(d)$ is the covariance function that describe the covariance between measurements at two different locations, as function of their distance d.

Equation 2 can be written in matricial form:

$$\boldsymbol{W} = \boldsymbol{C}^{-1} \cdot \boldsymbol{D} = \begin{bmatrix} w_1 \\ w_2 \\ \vdots \\ w_n \\ \mu \end{bmatrix} = \begin{bmatrix} C_{11} & C_{12} & \dots & C_{1n} & 1 \\ C_{21} & C_{22} & \dots & C_{2n} & 1 \\ \vdots & \vdots & \ddots & \vdots & \vdots \\ C_{n1} & C_{n2} & \dots & C_{nn} & 1 \\ 1 & 1 & \dots & 1 & 0 \end{bmatrix}^{-1} \cdot \begin{bmatrix} C_{10} \\ C_{20} \\ \vdots \\ C_{n0} \\ 1 \end{bmatrix} \tag{3}$$

where $\boldsymbol{W}$ is a vector containing the kriging weights and the Lagrange parameter, $\boldsymbol{C}$ is the covariance matrix, where elements C_{ij} are the short notation for $C(x_i - x_j)$, and $\boldsymbol{D}$ is a vector containing the elements C_{i0} , i.e. the covariance function applied to the distances between each measurement point x_i and the prediction point x_0.

The covariance function used in this work has an exponential form:

$$C(d) = \begin{cases} c + c_0 & for\ d = 0 \\ c - c\left(1 - exp\left(-\frac{3d}{r}\right)\right) & for\ d > 0 \end{cases} \tag{4}$$

where c is the sill, r is the effective range, and c_0 is the nugget. The nugget effect can be interpreted as measurement uncertainty (Clark, 2010) and using this formulation it appears only at distance *d=0*.

The conventional modelling of measurement uncertainty is done assuming a spatially and often temporally invariant nugget effect in the definition of the covariance function, which is then applied to all the elements of Equation 3. The KUD approach instead assumes $c_0 = 0$ in the covariance function definition; then it modifies the diagonal of the covariance matrix $\boldsymbol{C}$ at each time step, so that each element C_{ii} is substituted with:

$$C_{ii} = c + c_{0i} \quad (5)$$

where c_{0i} is the nugget corresponding to the uncertainty associated to the ith rain gauge, i.e. the estimated measurement variance. Applying the operation at each time step, the measurement uncertainty is modelled variant in space and in time.

2.2 Synthetic tests

The performance of KUD is expected to be affected by many factors. In particular the performance is evaluated considering three factors: 1) the spatial variability of the precipitation field, represented by the range of the covariance function; 2) the density of measuring points; 3) the accuracy of measurement points. To investigate the impact of these factors on the KUD performance three synthetic experiments are carried out. The experiments are designed to reproduce a possible case study in which a certain number of accurate rain gauges are complemented with a certain number of less accurate rain gauges.

2.2.1 Setup for all the experiments

Synthetic Gaussian fields θ, are generated with given mean $m = 1$ and variogram sill $s = 0.1$ using unconditional Gaussian simulations on a 106 by 106 pixels grid. Although the experiment is unitless, pixels can be representative of a square kilometre, and the field values to rainfall intensity in [mm/h]. Each realisation of θ is sampled by more or less accurate rain gauge simulators that sample the field θ obtaining measurement values that contain errors. The measurement value is drawn from a Gaussian distribution with mean equal to the true θ value; accurate simulators use a standard deviation equal to 5% of the true θ value, while less accurate simulators use a standard deviation equal to 20% of the true θ value. For KUD, the nugget c_0, which is a measurement of variance, is the square of the error standard deviation. This model is realistic for different rain gauges types and reproduce the proportionality of the errors to the rainfall intensity, as observed in real rain gauges (Ciach, 2003; Habib et al., 2001). The rain gauge position changes randomly for every realisation of θ.

Once the fields are measured by the rain gauge simulators, both KUD and standard OK are performed and compared, as explained in section 2.3.

The three synthetic experiments are designed as follow:

2.2.2 First synthetic experiment: field spatial variability

The first experiment aims at assessing what is the impact of the rainfall spatial variability on the KUD performance. The range parameter is varied, using values of 10, 30, 50, 80 and 100 pixels. For each value, 500 realisations of θ are made and sampled. 10 accurate sampling points and 10 less accurate ones are used and their position is randomly sampled from a uniform distribution in the domain for each realisation.

2.2.3 Second synthetic experiment: rain gauge density

The second experiment assesses the impact of rain gauge density, for a given spatial variability of rainfall. The test compares the use of 4, 10, 20, 40, and 80 rain gauges in the domain, divided evenly between highly accurate measuring points and less accurate ones. 500 realisations are made for each of the values, changing the position of the measuring points randomly at each realisation.

2.2.4 Third synthetic experiment: sampling point accuracy

The third experiment looks at the impact of the relative number of accurate and less accurate rain gauges. 30 sampling points are used for all realisations, divided unevenly between accurate and less accurate ones. In particular the accurate/less accurate combinations are (5/25, 10/20, 15/15, 20/10, 25/5).

Table 1. Overview of the three experimental setups

	Experiment 1	Experiment 2	Experiment 3
Tested variable	Range	Total number of rain gauges (RG)	Ratio between accurate and less accurate rain gauges
Tested values	Range = (10, 30, 50, 80, 100)	Number of RG = (4, 10, 20, 40, 80)	Ratio = (5/25, 10/20, 15/15, 20/10, 25/5)
Number of realisation	500 for each range value	500 for each tested number of rain gauges	500 for each tested rain gauge ratio
Number of accurate rain gauges	10	2, 5, 10, 20, 40	5, 10, 15, 20, 25
Number of less accurate rain gauges	10	2, 5, 10, 20, 40	25, 20, 15, 10, 5
Range value [pixels]	10, 30, 50, 80, 100	50	50
Sill [-]	0.1	0.1	0.1
Mean [-]	1	1	1

2.3 KUD performance evaluation

In all the experiments, the performance of KUD is compared in the same way. Each time a realisation is done and sampled, the synthetic measurements are interpolated both with KUD and with standard OK, obtaining the fields θ_{KUD} and θ_{OK} respectively. An evaluation score β is then calculated as follow:

$$\beta = \sqrt{E\{(\theta - \theta_{OK})^2\}} - \sqrt{E\{(\theta - \theta_{OKUD})^2\}} \quad (5)$$

where the spatial mean $E\{\}$ is calculated throughout the pixels. β is designed to be positive when KUD performs better than OK and negative when OK performs better than KUD. A β value is calculated for each realisation, therefore 500 β values are calculated for each tested parameter.

Rainfall is not Gaussian in reality and the use of Gaussian fields may improve kriging performances. Nevertheless, both KUD and OK are affected in the same way and the use of a differential indicator assures that this assumption does not alter the results.

3. RESULTS

For each experiment, the average β, together with the 10% and 90% quantiles obtained out of the 500 realisations are presented. Additionally, the number of realisations with positive or negative β, indicating the number of times KUD outperforms or underperforms OK, are reported.

The results are summarised in Figure 1.

4. DISCUSSION

The results reported in Figure 1 show some interesting outcomes. The first thing to notice is that in none of the analysed configurations KUD performs consistently better or consistently worse than OK throughout the 500 realisations. This suggests that each combination of rain gauges configuration, error sampling, and rainfall field behave in a different way. The reason for this is that

KUD tends to smooth the field, giving less weight to the less accurate measurements. This has a positive effect if indeed the introduced error overestimates a peak or underestimate a low. Instead, the effect is counterproductive when it results in smoothing peaks and lows that were correctly estimated. When a sufficient number of measuring point is available, in relation to the field spatial variability, KUD is able to better estimate the direction of the errors and correct them, thanks to the comparison to adjacent measuring points; if instead the rain gauges are too sparse, in relation to the spatial variability of the field, KUD may result in a loss of spatial information.

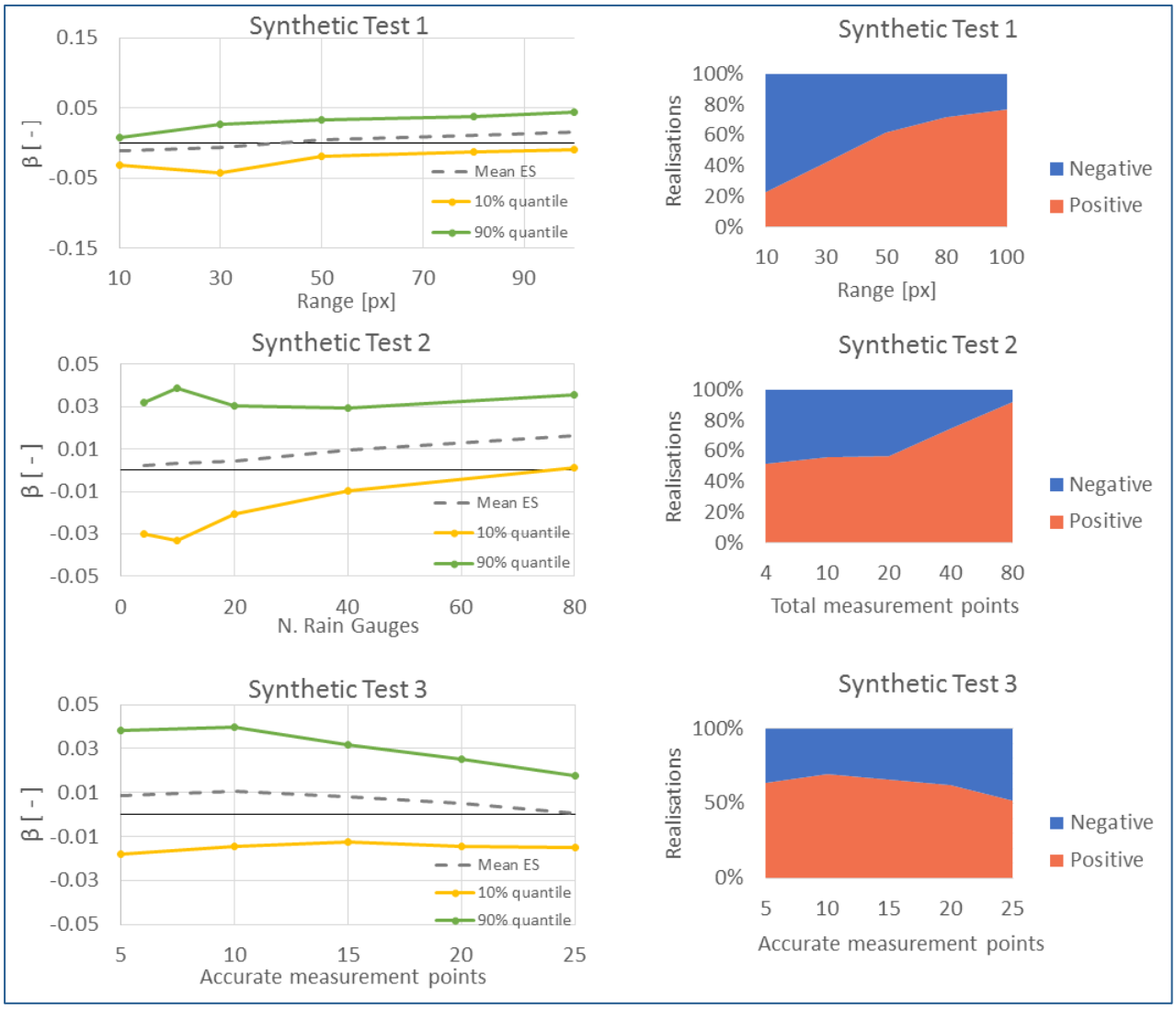

Figure 1. For each experiment, two plots are reported; the ones on the left show the mean, and the 10% and 90% quantiles of the β values. The plots on the right show how many times KUD outperforms OK (positive β) and how many times instead OK outperforms KUD (negative β). In the bottom panels, where the results of the third experiment are reported, the "x" axis reports only the number of accurate rain gauges, and it must be kept in mind that a corresponding number of less accurate rain gauges is present, such that they sum up to 30.

The results of the first experiment, reported in the top plots of Figure 1, show that KUD performs better when a high range value is used. In such a situation the fields θ are smoother and a lower number of rain gauges is sufficient. This experiment suggests that KUD could perform better in interpolating rain gauges when the studied rainfall event is stratiform, and worse when the field is convective.

The results of the second experiment, reported in the central panels of Figure 1, show that KUD performs better with a higher rain gauge density. The reason for this behaviour is again that a higher number of rain gauge allows us to have a correct spatial sampling of the field, identify highs and lows more precisely and balancing out the measurement errors. Another interesting feature that can

be observed in the second experiment is that the variability of outcomes, represented by the difference between the 10% and 90% quantile, becomes lower for higher rain gauge densities. This means that the KUD and OK results tend to converge to a better estimation of the field.

Finally, the third experiment suggests that KUD performs better than OK when the rain gauges have a more variable accuracy, when the difference between the number of accurate and less accurate rain gauges is lower. The KUD method is able to give a higher weight to the good measurements, and a lower weight to the less accurate ones. When the sampling points have a more uniform accuracy, this advantage is less important, and the two methods perform more similarly, i.e. the β mean is closer to zero. Again the distribution is narrower for a higher number of accurate rain gauges indicates that more accurate measurements result in a convergence of KUD and OK results.

5. CONCLUSIONS

The work presented in this paper investigates the applicability of Kriging for Uncertain Data (KUD) to rain gauge interpolation, in order to take into account the measurement errors and their variability in space and time. The investigation is conducted by means of three synthetic experiments, in which random Gaussian fields correlated in spaces are generated to represent rainfall, and are sampled with rain gauge simulators, able to reproduce a realistic error structure in the measurements. The interpolation performed with KUD is compared to the interpolation done with the standard Ordinary Kriging (OK) algorithm. The comparison is done for multiple realisations of the Gaussian field, and for multiple rain gauge positions, varying factors that influence the KUD performance. In particular, the spatial variability of the field is studied in the first experiment, the rain gauge network density in the second, and the relative accuracy of the rain gauges in the third.

The presented work is not a complete and comprehensive overview of all the possible factors that can influence the KUD performance in rain gauge interpolation, the use of Gaussian fields is an approximation, and temporal correlation is not considered. However, the experiment results give some insight in the KUD properties, its strengths and its weaknesses. The following conclusions are drawn:

1. The use of KUD is advisable only if a sufficient rain gauge density is available, in relation to the rainfall field spatial variability. If the rain gauge network is too sparse, or the rainfall field decorrelation distance too short, the KUD performance drops.
2. KUD is particularly recommended when the used rain gauges have a variable accuracy, because it is able to give a higher weight to more accurate rain gauges.
3. The more accurate and dense the measurements are, the more KUD and OK estimates tend to converge, and KUD seems to outperform OK.
4. The strength and the limitation of KUD is the fact that it tends to smooth the field, in particular in the surroundings of less accurate measurements. If a sufficient sampling is performed, the smoothing primarily targets the deviation due to errors; if instead the spatial information is too sparse, the smoothing may affect real rainfall field features, like peaks and lows, and the quality of the estimation drops.

Given the above mentioned conclusions, the use of KUD is in general recommended, because it tends to outperform the standard OK algorithm in most of the situations, but there are conditions in which it is counterproductive. In particular, it is not advisable for sparse rain gauge networks, coupled with convective rainfall events.

Although the experiment is tailored to rain gauge rainfall interpolation, the conclusions can be interesting for the application of KUD to other fields as well.

ACKNOWLEDGEMENTS

This work was carried out in the framework of the Marie Skłodowska Curie Initial Training Network QUICS. The QUICS project has received funding from the European Union's Seventh Framework Programme for research, technological development and demonstration under grant agreement no 607000. We would like to thank Prof. Gerard B.M. Heuvelink for the geostatistical feedback.

REFERENCES

AghaKouchak, A., Habib, E., Bárdossy, A., 2010. Modeling Radar Rainfall Estimation Uncertainties: Random Error Model. J. Hydrol. Eng. 15, 265–274. doi:10.1061/(ASCE)HE.1943-5584.0000185

Ciach, G.J., 2003. Local Random Errors in Tipping-Bucket Rain Gauge Measurements. J. Atmos. Ocean. Technol. 20, 752–759.

Ciach, G.J., Krajewski, W.F., Villarini, G., 2007. Product-Error-Driven Uncertainty Model for Probabilistic Quantitative Precipitation Estimation with NEXRAD Data. J. Hydrometeorol. 8, 1325–1347. doi:10.1175/2007JHM814.1

Clark, I., 2010. Statistics or geostatistics? Sampling error or nugget effect? J. South. African Inst. Min. Metall. 110, 307–312.

Cressie, N.A.C., 1993. Statistics for Spatial Data.

Dai, Q., Han, D., Rico-Ramirez, M., Srivastava, P.K., 2014. Multivariate distributed ensemble generator: A new scheme for ensemble radar precipitation estimation over temperate maritime climate. J. Hydrol. 511, 17–27. doi:10.1016/j.jhydrol.2014.01.016

De Marsily, G., 1986. Quantitative Hydrogeology.

Germann, U., Berenguer, M., Sempere-Torres, D., Zappa, M., 2009. REAL – Ensemble radar precipitation estimation for hydrology in mountainous region. Q. J. R. Meteorol. Soc 135, 445–456. doi:10.1002/qj.375

Habib, E., Ciach, G.J., Krajewski, W.F., 2004. A method for filtering out raingauge representativeness errors from the verification distributions of radar and raingauge rainfall. Adv. Water Resour. 27, 967–980. doi:10.1016/j.advwatres.2004.08.003

Habib, E., Krajewski, W.F., Kruger, A., 2001. Sampling Errors of Tipping-Bucket Rain Gauge Measurements. J. Hydrol. Eng. 6, 159–166. doi:10.1061/(ASCE)1084-0699(2001)6:2(159)

Habib, E.H., Meselhe, E. a., Aduvala, A. V., 2008. Effect of Local Errors of Tipping-Bucket Rain Gauges on Rainfall-Runoff Simulations. J. Hydrol. Eng. 13, 488–496. doi:10.1061/(ASCE)1084-0699(2008)13:6(488)

Mazzetti, C., Todini, E., 2009. Combining Weather Radar and Raingauge Data for Hydrologic Applications, in: Flood Risk Management: Research and Practice. Taylor & Francis Group, London.

Molini, A., Lanza, L.G., La Barbera, P., 2005. The impact of tipping-bucket raingauge measurement errors on design rainfall for urban-scale applications. Hydrol. Process. 19, 1073–1088. doi:10.1002/hyp.5646

Nešpor, V., Sevruk, B., 1999. Estimation of wind-induced error of rainfall gauge measurements using a numerical simulation. J. Atmos. Ocean. Technol. 16, 450–464. doi:10.1175/1520-0426(1999)016<0450:EOWIEO>2.0.CO;2

Peleg, N., Ben-Asher, M., Morin, E., 2013. Radar subpixel-scale rainfall variability and uncertainty: lessons learned from observations of a dense rain-gauge network. Hydrol. Earth Syst. Sci. 17, 2195–2208. doi:10.5194/hess-17-2195-2013

Rico-Ramirez, M. a., Liguori, S., Schellart, a. N. a., 2015. Quantifying radar-rainfall uncertainties in urban drainage flow modelling. J. Hydrol. 528, 17–28. doi:10.1016/j.jhydrol.2015.05.057

Schilling, W., 1991. Rainfall data for urban hydrology : what do we need? Atmos. Res. 27, 5–21.

Sevruk, B., 1996. Adjustment of tipping-bucket precipitation gauge measurements. Atmos. Res. 42, 237–246. doi:10.1016/0169-8095(95)00066-6

Villarini, G., Krajewski, W.F., 2009. Empirically based modelling of radar-rainfall uncertainties for a C-band radar at different time-scales. Q. J. R. Meteorol. Soc. 1438, 1424–1438. doi:10.1002/qj

Villarini, G., Mandapaka, P. V., Krajewski, W.F., Moore, R.J., 2008. Rainfall and sampling uncertainties: A rain gauge perspective. J. Geophys. Res. 113, D11102. doi:10.1029/2007JD009214

Proceedings of the 10th World Congress of EWRA 'Panta Rhei', 5-9 July 2017, Athens, Greece
© 2017 *European Water Resources Association*

Effect of varying calibration scenarios on the performance of a hydrodynamic sewer model

F. Tscheikner-Gratl[1*], P. Zeisl[2], C. Kinzel[2], J. Leimgruber[3], T. Ertl[4], W. Rauch[2] and M. Kleidorfer[2]
[1] *Sanitary engineering, Delft University of Technology, P.O. Box 5048, 2600 GA Delft, The Netherlands*
[2] *Unit of Environmental Engineering, University of Innsbruck, Technikerstrasse 13, Innsbruck 6020, Austria*
[3] *Institute of Urban Water Management and Landscape Water Engineering, Graz University of Technology, Stremayrgasse 10/I, Graz 8010, Austria*
[4] *Institute of Sanitary Engineering and Water Pollution Control (SIG), University of Natural Resources and Life Sciences, Muthgasse 18, Vienna 1190, Austria*
[*] *e-mail: F.Tscheikner-Gratl@tudelft.nl*

Abstract: Case studies concerning urban water management tend to be large, prestigious cities which have the financial and human resources to participate in research projects. This bears the risk that research outcomes are biased towards large municipalities. Consequently, the aim of this paper is to discuss calibration of a hydrodynamic model for the representative example of a small municipality. To exemplify the uncertainties immanent to the calibration process 17 scenarios - differing in assumptions for calibration - were estimated. The performance of the different scenarios was assessed using a hydrodynamic sewer model. The occurring flooding volume from the urban drainage system elicited by the rainfall data sets used as well as the combined sewer overflow was compared for the different scenarios and rain measurements. The different calibration scenarios proved to result in high deviations in the performance of the hydrodynamic model. It can be seen, that the selection of the applied calibration data is a very sensitive decision in the modelling process. The variations show that model calibration is of utmost importance. The differences in performance can lead to different outcomes design and decision-making processes possibly leading to higher volumes, which is not cost-effective, or to underestimation of the needs that will result in lacking robustness and malfunctioning of the network.

Key words: calibration, urban drainage, uncertainties

1. INTRODUCTION

Discrepancies between the simulated and the measured system behaviour of urban drainage models are unavoidable, due to unavoidable uncertainties. These can be caused by the simplification of the real physical interrelationships inherent to modelling as well as by difficulties to identify the necessary model parameters. Hence, the calibration process is a crucial and fundamental component of the model development process, unquestioned from a scientific point of view (Muschalla et al., 2009).

However, in engineering practice uncalibrated or insufficiently calibrated models are still used, with data availability often being the limiting factor. Calibration usually requires sampling campaigns, which in turn can increase the economic cost of the projects up to an unachievable level (Freni et al., 2009). Calibration uncertainties relate to the data used for calibration and their selection, and to the calibration methods (Leonhardt, 2015). They source in measurement errors for both, inputs and outputs, the selection of appropriate calibration input and output datasets, the applied calibration algorithms and the objective functions used in the calibration process (Deletic et al., 2012).

Case studies of urban water management studies in scientific literature are often large, prestigious cities, which have the financial, and human resources to participate in research projects. They are selected for providing a good data background as e.g. measurement data over the last years and/or the required infrastructure for further data collection and management. Such case studies are not always representative for the entire situation of the living environment in a country. At least,

there is the risk that research outcomes are biased towards large municipalities (Tscheikner-Gratl et al., 2016a).

Consequently, the aim of this paper is to discuss calibration of a hydrodynamic model for the representative example of a small Austrian municipality (15,000 inhabitants). For this purpose, the hydrodynamic drainage model of this case study was calibrated based on different calibration scenarios (different number of calibration events, different rainfall input). Additionally, varying precipitation data of the surrounding area using an uncalibrated model plus the various calibrated models was used to analyse influences of input data uncertainties.

2. METHODS

The analysed case study in this paper is a small municipality with 15,000 inhabitants in Tyrol, Austria (Kleidorfer et al., 2014; Muschalla et al., 2015; Tscheikner-Gratl et al., 2016a; Tscheikner-Gratl et al., 2016b). The urban drainage network consists of only 14 km of combined sewers, 67 km of wastewater sewers and 24 km of stormwater sewers. These stormwater sewers have 28 outfalls into the receiving water bodies, while in comparison only three combined sewer overflows (CSO) exist. In total, a catchment area of 95.31 hectare is connected to the combined sewer system. For model calibration and validation, precipitation was measured over the period of one year at three sites (rain gauges 1-3) in the catchment area and the water level at one site near the inflow to the wastewater treatment plant. This measurement setup also represents limited data availability, inherent to smaller operators due to limited budget.

The performance of different scenarios was assessed using the Storm Water Management Model (SWMM) software tool (Gironás et al., 2010). For the calibration of the hydrodynamic model a genetic algorithm implemented in PC-SWMM (James et al., 2002) was applied. For calibration data, measurements of rainfall at three locations within the municipality and water levels at the catchment outflow of the 10 strongest rainfall events, which occurred in the measurement period of one year, were chosen.

To exemplify the uncertainties immanent to the calibration process 17 scenarios - differing in assumptions for calibration - were used. The first scenario was the base scenario (00) without calibration. Then a calibration for each rainfall event took place individually (scenarios 01 – 10). Further, the model was calibrated using the entire rain series (11). For the next scenarios (12 -14) the rain series was used for calibration with only data from one of the three available rain gauges (1-3) respectively. Furthermore, the model was calibrated under the assumptions of a systematic 30% error of the water level monitoring data (+30% for scenario 15 and -30% for scenario 16) using again the entire rain series (like in scenario 11) to show the influence of measured calibration data uncertainties.

The Nash-Sutcliffe efficiency NSE (Nash and Sutcliffe, 1970) was chosen as the objective function to compare measured and predicted water levels. NSE is a measure to compare time series. It ranges from $-\infty$ to 1 (perfect match). After calibration, the remaining rainfall events were simulated and model performance for the individual calibration scenarios was evaluated. For this purpose, the absolute deviation of the NSE of each model (00 - 11) for every rainfall event to its best fit (which is always the scenario calibrated on that rainfall event) was calculated and summed up to get a cumulative measure. This verifies that scenario 11 (calibration on all ten events) shows the best overall performance and can therefore be used as reference scenario. For more details, see Tscheikner-Gratl et al. (2016a).

To show the influence of rainfall measurement uncertainties in comparison with the calibration scenario uncertainties, we compared the model results using two different precipitation data sets (1 year) of the Austrian Central Institute for Meteorology and Geodynamics (ZAMG) from the nearest measurement sites available (ZAMG1 10km from the catchment and ZAMG2 30km) with using our own measurements. Consequently, the occurring flooding volume from the urban drainage system elicited by the rainfall data sets used as well as the combined sewer overflow (CSO) was compared for the different scenarios and rain measurements.

3. RESULTS AND DISCUSSION

Figure 1 shows the variations of predicted flooding volume for the five measured rainfall series (RG 1 – 3 and ZAMG 1 and 2) when applying the 17 different calibration scenarios. It is notable that not all rain data sets (RG 1 and ZAMG 2) elicited flooding, while ZAMG 1 caused 3946 m³ of flooding for calibration scenario 15 in the observation period of 1 year. This illustrates also the variations in rainfall, even in a small though mountainous region. Even variations between the measurement points within a radius of 30 km are notable, hinting the variability of spatial precipitation distribution (Muthusamy et al., 2017). Furthermore, Figure 1 shows that for the rainfall data RG 2 in scenario 15, which elicits the most flooding, only 30% of the flooding occurs compared to the rainfall data of ZAMG 1 and in average over all scenarios only 8%. For RG 3 it is even less with 3% in average and 10% in scenario 15.

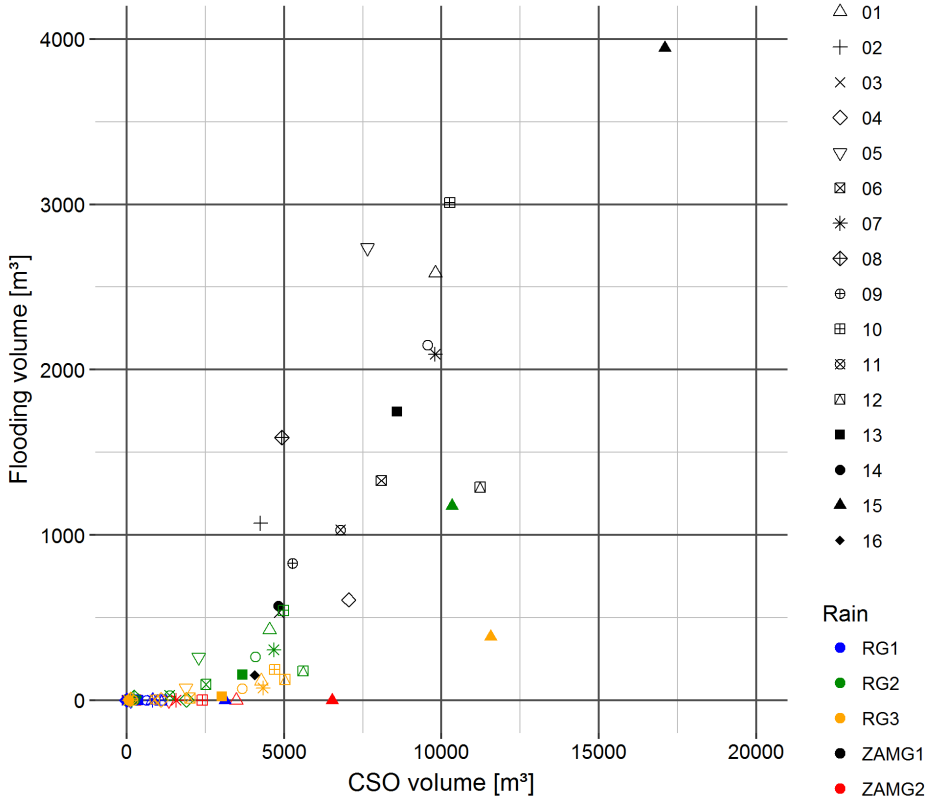

Figure 1. Flooding volume and CSO volume for measured 1 year rain series (RG 1 -3 and ZAMG 1 and 2) and the different calibration scenarios.

It also shows the variability of the results concerning the calibration scenarios, which are in the same scale as the before mentioned differences for rainfall data. For the same rainfall series (ZAMG 1) the scenarios can cause differences of up to 90%. Even if we neglect the obvious effect of a scenario assuming a systematic 30% error of the depth monitoring data (scenario 15 and 16), we can observe differences of up to 60% between calibration on one single rain event (e.g. between scenario 03 and 10). The flooding volume alone could however be misleading without taking into account other network data. The observed flooding volume can be regulated by combined sewer overflows (CSO).

By assuming scenario 11 to be the reference scenario (Tscheikner-Gratl et al., 2016a) and subdividing the scenarios in terms of deviation of the flooding and CSO volume for the rain set that elicits the most flooding ZAMG 1, the effect of calibration is easy to see (see Figure 2). The other rain series (RG 3 and RG 2) result in very low flooding volumes (5 and 30m^3) for scenario 11 and the deviations are therefore even higher.

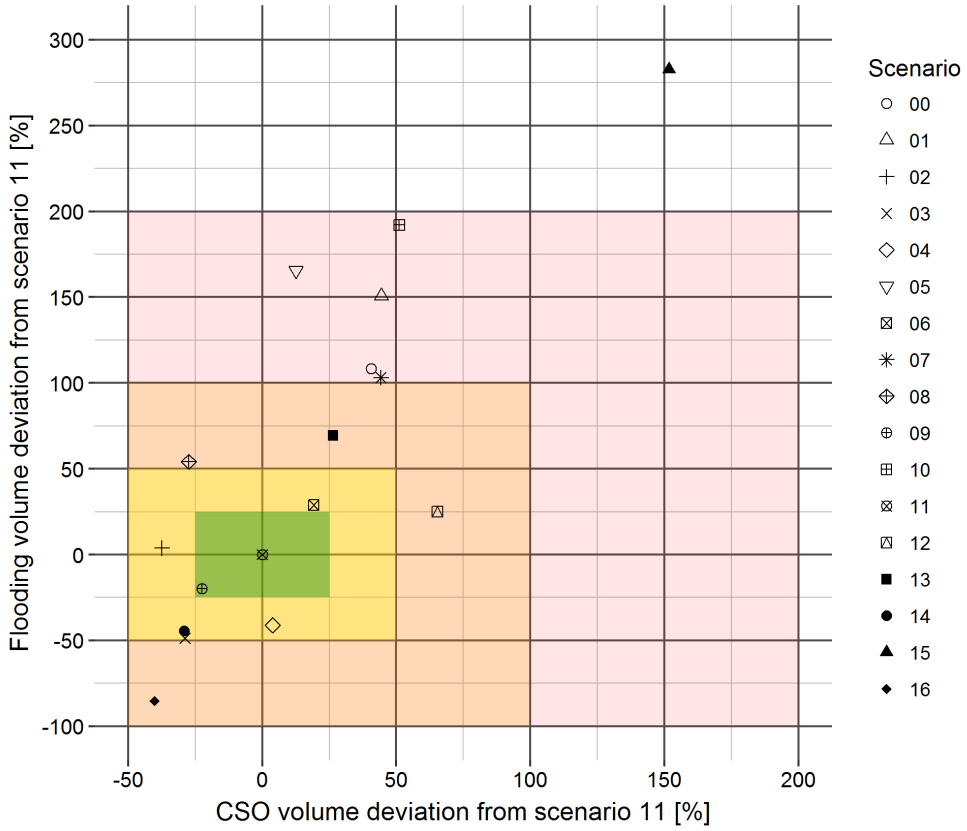

Figure 2. Flooding volume and CSO volume deviation from scenario 11 for measured 1 year rain series ZAMG 1

Only one scenario (09) shows low (less than 25%) deviation from the reference scenario in terms of flooding and CSO volume. Medium deviation (less than 50%) can be observed in 5 scenarios (02, 03, 04, 06 and 14). Other scenarios show high (up to 100% for scenarios 08, 12, 13 and 16) and very high (up to 200% for scenarios 00, 01, 05, 07, 10 and 15) deviations. Scenario 15 deviated even more. That shows that these scenarios with very high deviations perform even worse than an uncalibrated model (00) or at least not better for the rainfall ZAMG 1. Furthermore, it can be seen that these scenarios stem mainly from choosing an inappropriate rainfall event for calibration or from systematic errors in calibration data measurements. Interestingly the overestimation of these data (scenario 15) elicits a lot more effect on the flooding volume than the underestimation (scenario 16). This seems to be caused by plausibility restrictions in the calibration process (Tscheikner-Gratl et al., 2016a).

4. CONCLUSION

It can be seen, that the selection of the applied calibration data is a very sensitive decision in the modelling process. The variations show that model calibration is of utmost importance. The differences in performance can lead to different outcomes in design and decision-making processes. Subsequently this results in larger pipe diameters or higher storage volumes, which are not cost-effective, or in underestimation of the needs, which will result in lacking robustness and malfunctioning of the network (e.g. urban flooding).

The necessity of calibration also shows the importance of measurement data available in sufficient quantity and quality. It can be seen that spatial distributed rainfall measurement is advisable to minimize the uncertainties stemming from differences in rain intensities and distribution, which also occur in relatively small areas, especially in mountainous regions.

Further details can be found in Tscheikner-Gratl et al. (2016a) and Tscheikner-Gratl et al. (2016b).

REFERENCES

Deletic, A., Dotto, C. B. S., McCarthy, D. T., Kleidorfer, M., Freni, G., Mannina, G., Uhl, M., Henrichs, M., Fletcher, T. D., Rauch, W., Bertrand-Krajewski, J.-L., and Tait, S. (2012) Assessing uncertainties in urban drainage models. Physics and Chemistry of the Earth, 42–44, 3–10. DOI: 10.1016/j.pce.2011.04.007.

Freni, G., Mannina, G., and Viviani, G. (2009) Assessment of data availability influence on integrated urban drainage modelling uncertainty. Environmental Modelling and Software, 24(10), 1171–1181. DOI: 10.1016/j.envsoft.2009.03.007.

Gironás, J., Roesner, L. A., Rossman, L. A., and Davis, J. (2010) A new applications manual for the Storm Water Management Model (SWMM). Environmental Modelling & Software, 25(6), 813–814. DOI: 10.1016/j.envsoft.2009.11.009.

James, W. R. C., Wan, B., and James, W. (2002) “Implementation in PCSWMM using Genetic Algorithms for auto calibration and design- optimization” in E. W. Strecker and W. C. Huber (eds.), 9th International Conference on Urban Drainage (9ICUD). Portland, OR, USA, 1–10.

Kleidorfer, M., Tschiesche, U., Tscheikner-Gratl, F., Sitzenfrei, R., Kretschmer, F., Muschalla, D., Ertl, T., and Rauch, W. (2014) Von den Daten zum Modell: Anforderungen an hydraulische Entwässerungsmodelle in kleinen und mittleren Gemeinden. Wiener Mitteilungen, 231, J1–J14.

Leonhardt, G. (2015) *Development and Application of Software Sensors and Reverse Models for Urban Drainage Systems*, innsbruck university press. ISBN: 978-3-902936-70-7.

Muschalla, D., Schuetze, M., Schroeder, K., Bach, M., Blumensaat, F., Gruber, G., Klepiszewski, K., Pabst, M., Pressl, A., Schindler, N., Solvi, A. M., and Wiese, J. (2009) The HSG procedure for modelling integrated urban wastewater systems. Water Science and Technology, 60(8), 2065–2075. DOI: 10.2166/wst.2009.576.

Muschalla, D., Sulzbacher, R. M., Leimgruber, J., Maier, R., Ertl, T., Neunteufel, R., Kretschmer, F., Kleidorfer, M., and Tscheikner-Gratl, F. (2015) *Auf effizientem Wege von den Daten zum Modell (DatMod): Sanierungs- und Anpassungsplanung von kleinen und mittleren Kanalnetzen*, Bundesministerium für Land- und Forstwirtschaft, Umwelt und Wasserwirtschaft. [online] https://www.bmlfuw.gv.at/service/publikationen/wasser.html.

Muthusamy, M., Schellart, A., Tait, S., and Heuvelink, G. B. M. (2017) Geostatistical upscaling of rain gauge data to support uncertainty analysis of lumped urban hydrological models. Hydrology and Earth System Sciences, 21, 1077–1091. DOI: 10.5194/hess-2016-279.

Nash, J. E. and Sutcliffe, J. V (1970) River Flow Forecasting Through Conceptual Models. Journal of Hydrology, 10, 282–290. DOI: 10.1016/0022-1694(70)90255-6.

Tscheikner-Gratl, F., Zeisl, P., Kinzel, C., Leimgruber, J., Ertl, T., Rauch, W., and Kleidorfer, M. (2016a) Lost in calibration: why people still don’t calibrate their models, and why they still should – a case study from urban drainage modelling. Water Science and Technology, 74(10), 2337-2347. DOI: 10.2166/wst.2016.395.

Tscheikner-Gratl, F., Zeisl, P., Kinzel, C., Leimgruber, J., Ertl, T., Rauch, W., and Kleidorfer, M. (2016b) “Uncertainties in hydrodynamic modelling regarding rainfall measurements and calibration” in Proceedings of the Computing and Control for the Water Industry Conference (CCWI 2016). Amsterdam, The Netherlands.

Proceedings of the 10th World Congress of EWRA 'Panta Rhei', 5-9 July 2017, Athens, Greece
© 2017 *European Water Resources Association*

Surrogate modelling for simplification of a complex urban drainage model

M. Mahmoodian[1,2*], J.P. Carbajal[3], V. Bellos[4,6], U. Leopold[1], G. Schutz[5] and F. Clemens[2]
[1] *Luxembourg Institute of Science and Technology, Belval, Luxembourg*
[2] *Technical University of Delft, Delft, The Netherlands*
[3] *Swiss Federal Institute of Aquatic Science and Technology, Eawag, Switzerland*
[4] *CH2M, Swindon, UK*
[5] *RTC4Water, Belval, Luxembourg*
[6] *National Technical University of Athens, Athens, Greece*
[*] *e-mail: mahmood.mahmoodian@list.lu*

Abstract: Urban drainage modelling typically requires development of highly detailed and complex models due to the nature of the underlying drainage processes. This makes activities such as model calibration, uncertainty quantification analysis and usage in real-time control (RTC) challenging and computationally expensive. The focus of this paper is to develop a surrogate model to simplify and accelerate a complex model, and make it available for RTC in future studies. Hence, only the output of the model which is relevant for RTC is considered. Surrogate models may lead to larger uncertainties in the model predictions but can significantly decrease simulation runtime. Therefore, quantification of this uncertainty is addressed here as well. We use the detailed InfoWorks ICM software as the simulator for surrogate modelling. The case study area is within the Haute-Sûre catchment in Luxembourg. First, we ran the InfoWorks ICM model to produce a dataset of inputs and outputs of the simulator. Second, a surrogate model is developed based on this data. The surrogate model is able to give an estimation of the wastewater volume in the storage tank which can be used to control the combined sewer overflow (CSO) volume. The preliminary results show that the introduced surrogate model provides a reliable method to decrease model complexity and runtime significantly. It also allows for a simple quantification of the uncertainty induced by model simplification for different simulations. However, further investigation is required to find the optimum model simplification in this regard.

Key words: Surrogate modelling, urban drainage, combined sewer overflow (CSO), uncertainty

1. INTRODUCTION

Most of the urban drainage systems which have been constructed during the 19th and 20th centuries are classified as Combined Sewer Systems (CSS) (Burian 1999), which means that the sewer network combines the runoff produced after a rainfall event with wastewater produced from households and industry. One significant disadvantage for this kind of drainage systems, is that during rain events with high precipitation, parts of the wastewater may overflow and spill into the receiving water body before passing through the wastewater treatment plant (WWTP). This event, which is known as Combined Sewer Overflow (CSO), can cause serious environmental impacts on the receiving waters and its ecosystems (see e.g. Toffol 2006).

One way of tackling this problem is to take advantage of a dynamic management approach such as model based Real-Time Control (RTC) to increase the performance of the urban drainage system. In a model-based RTC, the simulator is run several times, and frequently, to produce predictions of the outcomes of many reasonable actions, therefore a computationally expensive simulator may hinder the application of RTC. Hence, we need fast simulators, even if this entails larger uncertainties in the predictions. There are two main strategies to achieve a fast model (Asher et al. 2015): a) to develop a simple, conceptual model tailored to RTC (e.g. Mahmoodian et al. 2016); b) to simplify/reduce the already existing computationally expensive models to construct the so-called surrogate models (e.g. Carbajal et al. 2016; van Daal-Rombouts et al. 2016).

In this paper, we combine these two approaches in a hybrid way. The strategy for developing a surrogate model or emulator consists of the following steps: a) identification of the variables to be

emulated; b) development of a simplified model in which every component contributing to the variables identified in step (a), is replaced by a function; and c) definition of these functions, which can be ad hoc or based on training data obtained with the detailed simulator.

2. MATERIALS AND METHODS

In this study, our main focus is the CSO locations in the urban drainage system. The components such as WWTP or the receiving water body are not considered here. We apply the strategy described previously, to construct an emulator for the dynamics of the volume in a storage tank and the overflow of a CSO weir. These two are the variables of interest as required by the step a) of the strategy. The detailed simulator used herein is a model of an urban catchment located in the area of Nocher-Route-Dahl, Luxembourg which includes these structures (tank with weir). Step b) requires the development of a simplified model. For the case of the storage tank, an intuitive model is given by the mass balance equation:

$$\frac{dV}{dt} = D(t, d_c) + R(t, \alpha, \tau) - P(t, p_c) - C(t, V_{max}, \alpha, \tau) \quad (1)$$

where V is the storage tank volume, and is driven by an inflow and an outflow. The inflow is composed of the dry weather flow (D) and the inflow generated by rainfall (R). The outflow is composed of the outflow generated by a pump (or a controllable valve) installed in the storage tank (P) and the CSO volume which overflows through the weir (C). Next, we give the explicit expression of each component.

The wastewater inflow depends on several properties of the catchment (e.g. population), and is characterised by a daily pattern. Since this pattern is well identified, it can be described by:

$$D(t, d_c) = d_c d(t) \quad (2)$$

where $d(t)$ is the daily pattern unit waveform of wastewater flow and d_c is a scaling constant (equal to 0. 66L/s in the specific case study).

The R component is the inflow to the tank due to rainfall. This function aims at implementing a short-cut for the transformations that the upstream network, to which the tank is connected, apply on the runoff flowing into the pipes. Two major transformations are the delay introduced by the upstream network physical properties (e.g. lengths, slopes, etc.) and the scaling of the rain-to-runoff process. Herein we learn this function from training data provided by the detailed simulator playing the role of a virtual but reference reality implemented using the InfoWorks ICM® software. We use this simulator to obtain the inflow to the tank when the rain events have a constant intensity and a predefined duration. The training data consists of 40 different constant rainfall intensities (from 2.5 to 100mm/h with a 2.5mm/h step) with a 4-hour duration. The reasons why we use these synthetic rainfall scenarios are: 1) The available observed rainfall data are not representing the worst case scenarios (high intensities and long durations); and 2) In this way, it is possible to analyse the relationship between rainfall characteristics and the system response in a simpler approach. It is noticed that the function is independent from duration of the rainfall. In this conditions, the inflow to the storage tank volume depends only on the rainfall intensity r and a lag τ in a linear way, and not in the duration of the rainfall. Therefore, R is defined as follows:

$$R(t, \alpha, \tau) = \alpha r(t - \tau) \quad (3)$$

where the value of α obtained from the training data is 0.294 (it is noted that r is in mm/h, t and τ is in min and R is in m^3), whereas the lag as τ=30min. The lag for the case study is defined based on cross-correlation analysis of the rainfall time series (input) and tank volume and CSO time series (output).

The P component is the pump flow, which depletes water from the tank at a constant discharge

determined by the manufacturer. Therefore, P takes the value 0 (pump is off) or p_c (pump is on). In this study, p_c has a value of 6 L/s.

The C component is the CSO volume which overflows through a weir when the storage tank volume reaches the maximum capacity V_{max}. The equation of the flow over the weir should be in the following form:

$$C(t, C_D, L, A, V_{max}) = \begin{cases} \frac{C_D g^{\frac{1}{2}} L}{A^{3/2}} (V(t) - V_{max})^{\frac{3}{2}} & if V \geq V_{max} \\ 0 & otherwise \end{cases} \quad (4)$$

where C_D is the discharge coefficient of the weir, g is the gravitational acceleration, L is the length of the weir and A is the area of the tank.

However, due to the integration scheme weir overflow is significantly overestimated. Therefore, C is calculated from the training data, similar to R:

$$C(t, V_{max}, a, \tau) = \begin{cases} ar(t - \tau) & if V \geq V_{max} \\ 0 & otherwise \end{cases} \quad (5)$$

3. RESULTS

As it was mentioned earlier, the purpose of developing an emulator in this study was to be able to apply it for prediction of output with real (unseen) inputs. Hence, in this section we are going to use the emulator for prediction of storage tank and CSO volumes using a real rainfall time series recorded by a rain gauge located in the catchment during October of 2007 until December of 2009 and compare them with the corresponding results derived by the InfoWorks. Figure 1 shows the comparison between the emulator and the simulator for three indicative events, taken from the entire time series, for both of storage tank and CSO volume.

As it can be observed in Figure 1a, the emulator, at the current stage of development, is able to capture the ascending part of storage tank volume in a considerably high accuracy. This part is related to tank filling stage. More importantly, the peaks are emulated correctly as well. The latter is more important in our future model-based RTC application, because if we can predict accurately the time in which the tanks in the network would fill up during or after a potential rainfall event, we can use this information to manipulate the actuators of the network (e.g. pumps or control valves) in an optimised way to avoid or mitigate possible CSO events.

According to Figure 1b, the emulator is able to capture the large CSO events (first row) relatively better than the smaller events. Although, the time period of CSO events, is predicted accurately in all three cases.

At the current stage of development, the main problem with the emulator is that it depletes the storage tank faster than the simulator. Since the CSO component is estimated relatively well and its volume is much less than the storage tank volume, this problem must be related to the simplification of P component of the emulator which is the pumping outflow. This can be a result of the fact that the simulator does not use the pump's maximum capacity (6 L/s) during all the time steps in which the pump is on. More investigation is going to be done regarding this issue to improve the emulator.

For quantification of uncertainty induced by model simplification, the Normalised Root Mean Squared Error (NRMSE) is calculated between the results derived by the emulator and the simulator for both of storage tank and CSO volumes in respect to time. NRMSE is derived via dividing RMSE by the range of the variable (storage tank or CSO volume). This can be considered as a simple structural uncertainty quantification. The normalised RMSE, for the storage tank volume is found equal to 0.072, whereas for the CSO volume 0.002, correspondingly. This indicates that the emulator gives better results regarding CSO volume prediction and, in fact, this aspect is more interesting for us regarding future RTC system design. Although, a better comparison would be done by comparing the simulator and emulator results with real measured data, if available. In addition to the RMSE, an effort is made to define the distribution of the residuals between the emulator and the simulator. Figure 2 shows these distributions.

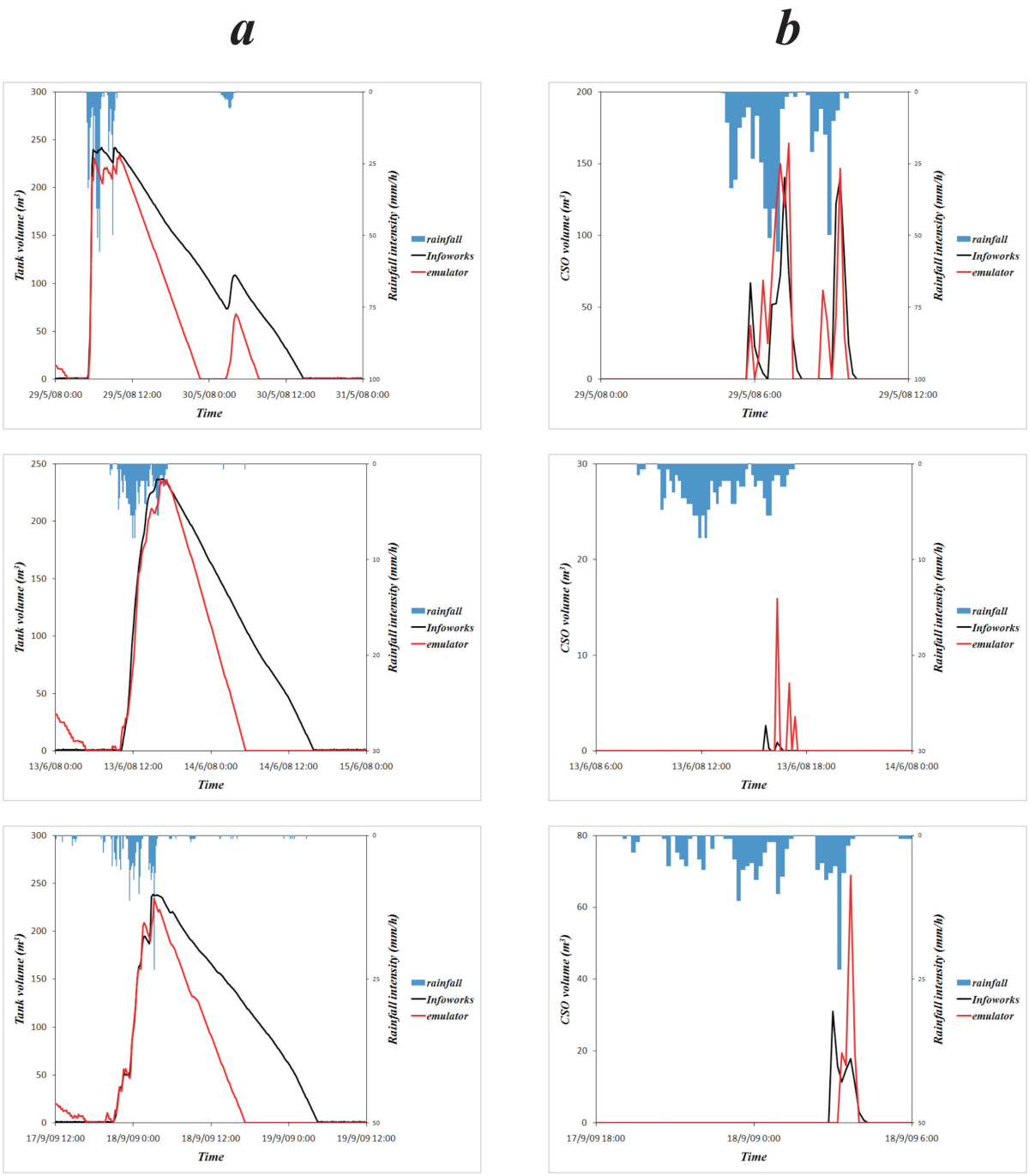

Figure 1. Comparison between emulator and simulator: a) for the storage tank volume; b) for the CSO volume.

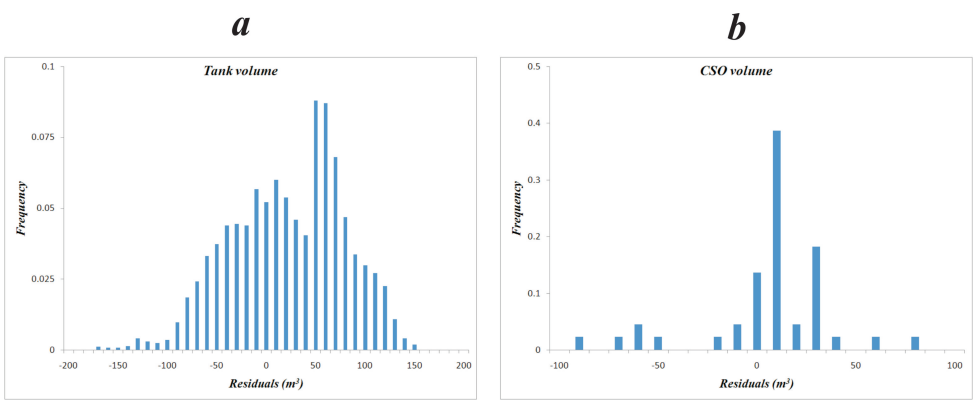

Figure 2. Distribution of the residuals between emulator and simulator: a) for the storage tank volume; b) for the CSO volume

4. CONCLUSIONS

Herein, we developed an emulator for the emulation of a storage tank volume and CSO flow in the downstream part of an urban catchment at Nocher-Route-Dahl in Luxembourg. The component functions of the emulator were learnt using simulations from a detailed model implemented in InfoWorks. The emulator provides satisfactory results in terms of speeding up the simulations. As an example, the speed up it provides on a 2-years-long time series of observed values is approximately 1300 (i.e. the emulator is 1300 times faster than the simulator). This would be an interesting aspect regarding application of the emulator for RTC purpose, in which we are required to speed up the optimisation process by employing faster models.

In contrast with some previous studies, in which the input was the inflow to the storage tank or WWTP (e.g. Mahmoodian et al. 2016 and Vanrolleghem et al. 2005), the surrogate herein uses rainfall measurements (or forecasts) as inputs. This will provide an RTC system with longer reaction time to compute the optimal control actions and the consequent behaviour of the system actuators.

The simplistic emulation approach which is introduced in this study, is on its early stage of development. The approach would get more complex for more detailed case studies with several inputs and outputs of interest in various locations within the sewer network. In future steps, we will focus on producing more precise results and reducing the uncertainty induced by model simplification. Finally, we will develop the surrogate model to consider wastewater quality modelling in addition to its quantity modelling to be applied in RTC practices.

ACKNOWLEDGMENTS

This research was done as part of the Marie Curie ITN – Quantifying Uncertainty in Integrated Catchment Studies (QUICS) project. This project has received funding from the European Union's Seventh Framework Programme for research, technological development and demonstration under grant agreement no. 607000. JPC received funding from the EmuMore Project URL: kakila.bitbucket.io/emumore.

REFERENCES

Asher, M. J., Croke, B. F. W., Jakeman, A. J., Peeters, L. J. M., 2015. A review of surrogate models and their application to groundwater modeling. Water Resources Research, 51(8): 5957–5973.

Burian, S. J., Nix S. J., Durrans R. S., Pitt R .E., Fan C., Field R., 1999. Historical Development of Wet Weather Flow Management. Journal of Water Resources Planning and Management,125: 3-13.

Carbajal, J. P., Leitão, J. P., Albert, C., 2016. Appraisal of data-driven and mechanistic emulators of nonlinear hydrodynamic urban drainage simulators. Environmental Modelling and Software, 92: 17-27.

Van Daal-Rombouts, P., Sun S., Langeveld J., Bertrand-Krajewski J., Clemens F., 2016. Design and performance evaluation of a simplified dynamic model for combined sewer overflows in pumped sewer systems. Journal of Hydrology, 538: 609–624.

Innovyze, 2017. InfoWorks ICM. Available at: http://www.innovyze.com/products/infoworks_icm/.

Mahmoodian, M., Delmont, O.,Schutz, G., 2017. Pollution-based model predictive control of combined sewer networks, considering uncertainty propagation. International Journal of Sustainable Development and Planning, 12(1): 98–111.

Toffol, S., 2006. Sewer system performance assessment – an indicators based methodology. Universität Innsbruck.

Vanrolleghem, P. A., Benedetti, L., Meirlaen, J., 2005. Modelling and real-time control of the integrated urban wastewater system. Environmental Modelling and Software, 20(4): 427-442.

Proceedings of the 10th World Congress of EWRA 'Panta Rhei', 5-9 July 2017, Athens, Greece
© 2017 *European Water Resources Association*

Multivariate autoregressive modelling and conditional simulation of precipitation time series for urban water models

J.A. Torres-Matallana[1,3*], U. Leopold[2] and G.B.M. Heuvelink[3]

[1] *Luxembourg Institute of Science and Technology, Department for Environmental Research and Innovation, Chemical Pollution Control and Impact Assessment Unit, 41 Rue du Brill, L-4422, Belvaux, Luxembourg. E-mail: arturo.torres@list.lu*

[2] *Luxembourg Institute of Science and Technology, Department for Environmental Research and Innovation, eScience Unit, 41 Rue du Brill, L-4422, Belvaux, Luxembourg*

[3] *Wageningen University and Research Centre, Soil Geography and Landscape Group, PO Box 47, 6700AA, Wageningen, The Netherlands*

[*] *e-mail: arturo.torres@list.lu*

Abstract: Precipitation is the most active flux and major input of hydrological systems. Precipitation controls hydrological states (soil moisture and groundwater level), and fluxes (runoff, evapotranspiration and groundwater recharge). Hence, precipitation plays a paramount role in urban water systems. It controls the fluxes towards combined sewer tanks and the dilution of chemical and organic compounds in the wastewater. Furthermore, small catchments (i.e., areas of about 20 ha) have a fast response to precipitation. Therefore, catchment average precipitation is a key component in urban water models. However, average catchment precipitation is not always accurately known when measured at rain gauges, because the location of the gauge might be outside the catchment boundaries or does not reflect the entire catchment. The objective of this paper is to develop a method to estimate the precipitation in a catchment given a known precipitation time series at a location outside of the catchment, while quantifying the uncertainty associated with the estimation. We developed a multivariate autoregressive time series model for conditional simulation of precipitation time series. The case study is a small sub-catchment (16.5 ha) in Luxembourg. The time series of precipitation outside of the sub-catchment are available for two stations and cover the year 2010. We calibrated the model using the R-package 'mAr' and applied the developed conditional simulation algorithm to generate multiple realisations of precipitation time series. The results show that the proposed method is suitable to estimate time series of precipitation at ungauged sites and can quantify the associated uncertainty.

Key words: multivariate model, autoregressive model, precipitation uncertainty, input uncertainty, time series simulation

1. INTRODUCTION

Precipitation is the most important flux and major input of hydrological systems. Precipitation controls hydrological states as soil moisture and groundwater level, and fluxes as runoff, evapotranspiration and groundwater recharge (Guan *et al.*, 2009). Hence, precipitation plays a paramount role in urban water systems. It controls the fluxes towards storage tanks of combined sewer overflows (CSOs) and the dilution of chemical, organic and biological compounds in the wastewater. Furthermore, small catchments (i.e. areas of about 20 ha or smaller) have a fast response to precipitation input. Therefore, catchment average precipitation is a key component in urban water models. However, average catchment precipitation is not always accurately known when measured at rain gauges, because the location of the gauges might be outside the catchment boundaries or do not reflect the entire catchment at one location.

The objective of this paper is to develop and present a method to estimate the precipitation in a specific catchment given a known precipitation time series in a location outside of the catchment under analysis, while also quantifying the uncertainty associated with the estimation. After model implementation, simulated precipitation time series can then be used in urban water models for Monte Carlo uncertainty propagation analysis to reach more robust results for urban water system design and associated potential environmental and economic impacts.

2. MATERIALS AND METHODS

2.1 Multivariate autoregressive time series modelling

The set-up of the case study provides two measured time series of precipitation, one at the rain gauge 1, *RM(t)*, inside the catchment, and one outside the catchment, rain gauge 2, *RM2(t)* (see Figure 1). However, we need to estimate the precipitation at the sub-catchment level, *R(t)*. We model the precipitation in the sub-catchment as:

$$R(t) = RM(t) \cdot \delta(t) \tag{1}$$

where $\delta(t)$ is defined as the ratio of *RM(t)* and *R(t)*, the statistical properties of which are derived using measured time series of *RM(t)* and *RM2(t)*. We assume that *R(t)*, *RM(t)* and $\delta(t)$ are log-normally distributed stochastic processes, so that:

$$\log[R(t)] = \log[RM(t)] + \log[\delta(t)] \tag{2}$$

which we write as :

$$LR(t) = LRM(t) + L\delta(t) \tag{3}$$

LR(t), *LRM(t)* and $L\delta(t)$ are modelled using a first-order multivariate autoregressive process model. Given Equation 3, we only need to model *LRM(t)* and $L\delta(t)$ as (Luetkepohl, 2005):

$$\begin{bmatrix} LRM(t+1) \\ L\delta(t+1) \end{bmatrix} = \begin{bmatrix} \mu_R \\ \mu_\delta \end{bmatrix} + \begin{bmatrix} A_{11} & A_{12} \\ A_{21} & A_{22} \end{bmatrix} \left(\begin{bmatrix} LRM(t) \\ L\delta(t) \end{bmatrix} - \begin{bmatrix} \mu_R \\ \mu_\delta \end{bmatrix} \right) + \begin{bmatrix} \varepsilon_R(t+1) \\ \varepsilon_\delta(t+1) \end{bmatrix} \tag{4}$$

where $\mu_R = \mathrm{E}(LRM)$; $\mu_\delta = \mathrm{E}(L\delta)$; A_{11}, A_{12}, A_{21}, A_{22} are the coefficients of the autoregressive (AR) model; ε_R and ε_δ are zero-mean, normally distributed white noise processes.

We need to calibrate this model, i.e. estimate the parameters μ_R, μ_δ, A_{11}, A_{12}, A_{21}, A_{22}, σ_R^2, σ_δ^2 and $\rho_{R\delta}$, where $\sigma_R^2 = \mathrm{Var}(\varepsilon_R)$, $\sigma_\delta^2 = \mathrm{Var}(\varepsilon_\delta)$, and $\rho_{R\delta}$ is the correlation between ε_R and ε_δ. The parameters σ_R^2, σ_δ^2 and $\rho_{R\delta}$ are needed to account for cross-correlation. We use the R package 'mAr' (Barbosa, 2015) to calibrate the model given the two time series *LRM* and $L\delta$. For this, we derive $L\delta$ by taking the difference of *LRM* and *LRM2*, in other words we assume that the time series *RM* and *R* have similar multivariate behaviours as time series *RM* and *R*. Note that the rain gauge associated with time series *RM2(t)* is about the same distance from the first rain gauge as the sub-catchment.

We derive a time series of δ by dividing the *RM* data by the *RM2* data, for times when both $RM > 0$ and $RM2 > 0$, i.e. we create a bivariate time series of *RM* and δ. Next, we generate time series *LRM(t)* and $L\delta(t)$ by taking log[*RM(t)*] and log[*RM2(t)/RM(t)*].

2.2 Conditional time series simulation

Given the calibrated model we need to simulate from $L\delta(t)$. This simulation should be conditional to *LRM*. We define:

$$X_1(t) = LRM(t) - \mu_R; \qquad \varepsilon_1(t) = \varepsilon_R(t) \tag{5}$$

$$X_2(t) = L\delta(t) - \mu_\delta; \qquad \varepsilon_2(t) = \varepsilon_\delta(t) \tag{6}$$

and therefore we have:

$$\begin{bmatrix} X_1(t+1) \\ X_2(t+1) \end{bmatrix} = \begin{bmatrix} A_{11} & A_{12} \\ A_{21} & A_{22} \end{bmatrix} \begin{bmatrix} X_1(t) \\ X_2(t) \end{bmatrix} + \begin{bmatrix} \varepsilon_1(t+1) \\ \varepsilon_2(t+1) \end{bmatrix} \tag{7}$$

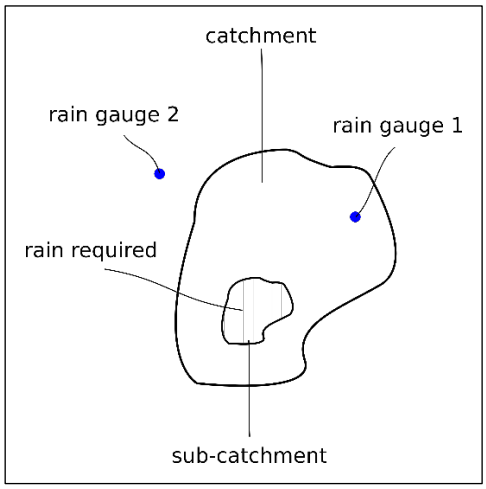

Figure 1. Schematic definition of the case study set-up. Rain gauge 1 = RM(t); rain gauge 2 = RM2(t); rain required = R(t)

At each time step we need to simulate $X_2(t+1)$ given $X_1(t)$, $X_1(t+1)$ and $X_2(t)$. If we assume $\rho_{R\delta} = 0$, then $X_2(t+1)$ is given by:

$$X_2(t+1) = A_{21} \cdot X_1(t) + A_{22} \cdot X_2(t) + \varepsilon_2(t+1) \tag{8}$$

where $X_1(t)$, $X_2(t)$, A_{21}, A_{22} are known, and $\varepsilon_1(t+1)$ is a normally distributed white noise process with mean 0 and variance σ_2^2. If we assume $\rho_{R\delta} \neq 0$, this case is not straightforward, because $X_1(t+1)$ and $X_2(t+1)$ are also 'directly' correlated so that $X_1(t+1)$ has to be included in the conditional distribution. We can write:

$$Y = \begin{bmatrix} X_1(t) \\ X_1(t+1) \\ X_2(t) \\ \hline X_2(t+1) \end{bmatrix} = \begin{bmatrix} Y_1 \\ Y_2 \end{bmatrix} \tag{9}$$

with

$$Y_1 = \begin{bmatrix} X_1(t) \\ X_1(t+1) \\ X_2(t) \end{bmatrix}; \qquad \text{and} \qquad Y_2 = \left[X_2(t+1)\right] \tag{10}$$

Y follows a multivariate normal distribution with mean vector μ and variance-covariance matrix Σ (Box *et al.,* 2008):

$$Y = \begin{bmatrix} Y_1 \\ Y_2 \end{bmatrix} \sim N\left(\begin{bmatrix} \mu_1 \\ \mu_2 \end{bmatrix}, \begin{bmatrix} \Sigma_{11} & \Sigma_{12} \\ \Sigma_{21} & \Sigma_{22} \end{bmatrix} \right) \tag{11}$$

where μ_1 = 3x1, μ_2 = 1x1, Σ_{11} = 3x3, Σ_{12} = 3x1, Σ_{21} = 1x3, Σ_{22} = 1x1. Solving Equation 11, we then

know:

$$\{Y_2|Y_1 = a\} \sim N\left(\mu_2 + \Sigma_{21} \cdot \Sigma_{11}^{-1} \cdot (a - \mu_1), \qquad \Sigma_{22} - \Sigma_{21} \cdot \Sigma_{11}^{-1} \cdot \Sigma_{12}\right) \tag{12}$$

so we can simulate from $Y_2 = X_2(t+1)$ by sampling from this conditional normal distribution. Therefore, we need to derive vector $[\mu_1, \mu_2]$ and the variance-covariance matrix Σ. The first is straightforward because we centred X_1 and X_2 on zero:

$$\begin{bmatrix} \mu_1 \\ \\ \mu_2 \end{bmatrix} = \begin{bmatrix} 0 \\ 0 \\ 0 \\ 0 \end{bmatrix} \tag{13}$$

Regarding the calculation of the variance-covariance matrix Σ, we assume stationarity for variances and covariances, not depending on time, so the initial effect fades out. Therefore, we can define:

$$\sum = \begin{bmatrix} C_{11} & C_{12} & C_{13} & |C_{14} \\ \\ C_{21} & C_{22} & C_{23} & |C_{24} \\ \\ C_{31} & C_{32} & C_{33} & |C_{34} \\ - & - & - & - \\ C_{41} & C_{42} & C_{43} & |C_{44} \end{bmatrix} \tag{14}$$

We can demonstrate that the components of the Σ matrix are defined as:

$$C_{11} = C_{22} = \frac{A_{12}^2}{1 - A_{11}^2} \cdot \frac{A_{21}^2\sigma_1^2 + \sigma_2^2}{A_{11}^2 + A_{11}^2A_{22}^2 - A_{12}^2A_{21}^2} + \sigma_1^2 = \mathrm{Var}(X_1) \tag{15}$$

$$C_{33} = C_{44} = \frac{A_{21}^2\sigma_1^2 + \sigma_2^2}{A_{11}^2 + A_{11}^2A_{22}^2 - A_{12}^2A_{21}^2} = \mathrm{Var}(X_2) \tag{16}$$

$$C_{13} = C_{31} = C_{24} = C_{42} = \frac{A_{11}A_{21}\mathrm{Var}(X_1) + A_{12}A_{22}\mathrm{Var}(X_2) + \rho\sigma_1\sigma_2}{1 - A_{11}A_{22} - A_{12}A_{21}} = \mathrm{Cov}(X_1, X_2) \tag{17}$$

$$\rho\sigma_1\sigma_2 = \mathrm{Cov}(\varepsilon_1, \varepsilon_2) \tag{18}$$

$$C_{12} = C_{21} = A_{11}\mathrm{Var}(X_1) + A_{12}\mathrm{Cov}(X_1, X_2) = \mathrm{Cov}[X_1(t+1), X_1(t)] \tag{19}$$

$$C_{34} = C_{43} = A_{21}\mathrm{Cov}(X_1, X_2) + A_{22}\mathrm{Var}(X_2) = \mathrm{Cov}[X_2(t+1), X_2(t)] \tag{20}$$

$$C_{23} = C_{32} = A_{11}\mathrm{Cov}(X_1, X_2) + A_{12}\mathrm{Var}(X_2) = \mathrm{Cov}[X_1(t+1), X_2(t)] \tag{21}$$

$$C_{14} = C_{41} = A_{21}\mathrm{Var}(X_1) + A_{22}\mathrm{Cov}(X_1, X_2) = \mathrm{Cov}[X_2(t+1), X_1(t)] \tag{22}$$

2.3 Case study

The case study is located at Goesdorf, a small sub-catchment (16.5 ha) of the Haute-Sure system in the Northwest of Luxembourg. We know the time series of precipitation outside of the Goesdorf sub-catchment at two locations: Dahl (around 2 Km from the CSO tank Goesdorf) and Esch-sur-Sure (around 3.5 Km from the CSO tank Goesdorf). The time series of precipitation provided by the

Luxemburgish *Administration des services techniques de l'agriculture* (ASTA)*, covers the year 2010 with measurements at 10 minutes resolution. The precipitation stations are provided with Lambrecht 15188 tipping bucket rain gauges with a resolution of 0.1 mm per tip, and a surface of the round reception area of 200 cm^2. We have 52,556 observations for each time series. The total precipitation at Esch-sur-Sure is 658.6 mm, and 758.7 mm at Dahl. The time series of precipitation were validated by the Observatory for Climate and Environment (OCE) of the Luxembourg Institute of Science and Technology (LIST).

3. RESULTS

3.1 Multivariate autoregressive time series modelling

Two observed ASTA time series, Esch-sur-Sure and Dahl (Figure 2), were used for the calibration of the multivariate autoregressive model. Before we could calculate of $\delta(t)$ (Eq. 1) we applied a Daniell Kernel (R Core Team and contributors worldwide, 2017) to smooth the time series and avoid the sudden tipping bucket effect in the measurements (Table 1). Only those values of precipitation above 0.1 mm were smoothed. Then, the time series were filtered and posteriorly computed the ratio between them. The filter creates two new time series for the cases where the value of precipitation is higher than 0.01 mm for both time series to compute the ratio. The length of the resulting filtered time series was 6,454 observations. Finally, the ratio between the time series was computed.

Table 1. Daniell Kernel for smoothing the observed time series of precipitation

Index	Factor
-2	0.1111
-1	0.2222
0	0.3333
1	0.2222
2	0.1111

We defined the log-transform of the observed filtered time series, $LRM(t)$, and the ratio, $L\delta(t)$, and checked the normality assumption. The log-transform of the time series is fairly normal for the observed, $LRM(t)$, and the ratio, $L\delta(t)$, time series. Also, we checked the autocorrelation function (ACF) of these time series and both follow a similar pattern.

Given the $LRM(t)$ and $L\delta(t)$ we calibrated the multivariate autoregressive model for order one (Equation 4) using the 'mAr' R-package. Table 2, summarises the calibrated parameters of the model.

3.2 Conditional time series simulation

Upon calibration of the multivariate autoregressive model, we proceeded with the conditional simulation of Y_2 or $X_2(t+1)$ (Equation 12). For this, we compute the Σ matrix given the parameters of the model (Table 2). Table 2 also presents the calculated values of the components of Σ.

Once the components of Σ matrix are calculated, we developed an algorithm for simulating Y_2 given the known values of Y_1 i.e. $X_1(t)$, $X_1(t+1)$ and $X_2(t)$. Then, we added the mean to the time

* http://www.asta.etat.lu

series Y_2, backtransformed the lognormal values to compute the required precipitation time series at the sub-catchment *R(t)* according to Equation 1. Figure 3 shows the observed, *RM(t)* at Esch-sur-Sure, and the simulated, *R(t)* at Goesdorf, precipitation time series of the case study.

Table 2. Calibrated parameters of the multivariate autoregressive model for LRM(t) and Lδ(t) and components of Σ

Parameter	Value	Component	Value
μ_R	2.8550080	C_{11}	0.00639559
μ_δ	0.1019426	C_{33}	0.00388534
A_{11}	0.9564952	C_{13}	-0.00135028
A_{12}	0.0397994	C_{12}	0.00617109
A_{21}	0.0242934	C_{34}	0.00339810
A_{22}	0.8830385	C_{23}	-0.00144617
σ_R^2	0.0724132	C_{14}	-0.00103698
σ_δ^2	0.0795191		
$\rho_{R\delta}$	-0.0387570		

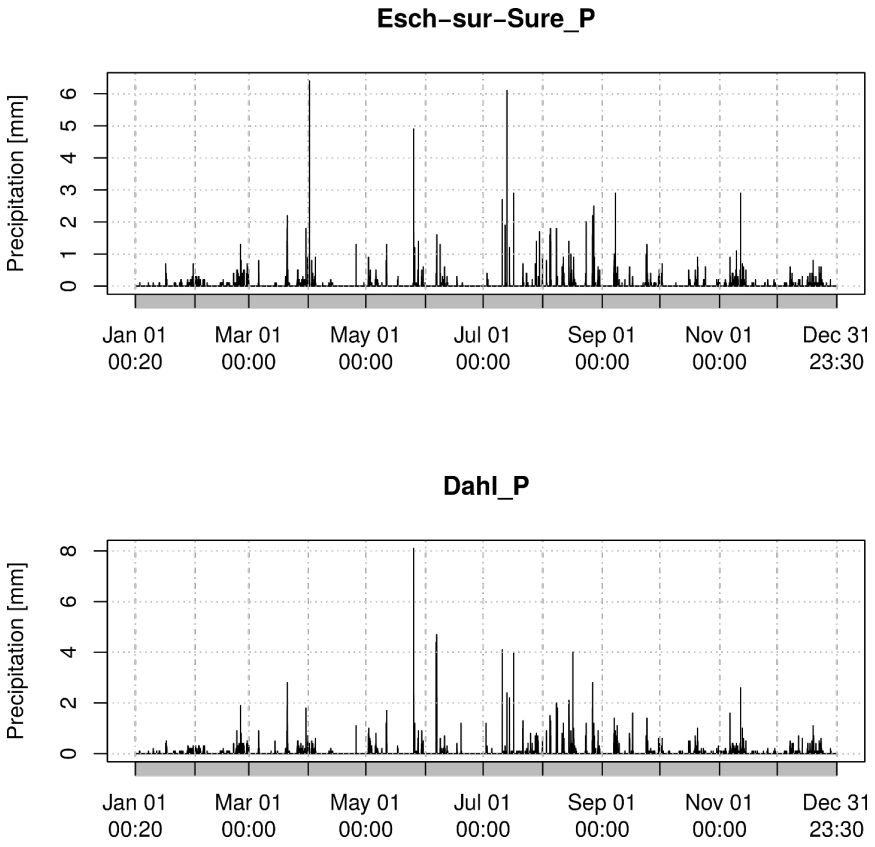

Figure 2. Observed precipitation time series of the case study: Esch-sur-Sure and Dahl.

4. DISCUSSION

According to McMillan *et al*. (2011), traditional calibration methods do not take into account input error, which leads to bias in parameter estimation and possible misleading model predictions. Several studies have proposed precipitation multipliers for overcoming this issue and taking into account precipitation input uncertainty in hydrological model calibration and prediction (McMillan *et al.*, 2011; Leta *et al.*, 2015; Del Giudice *et al.*, 2016). Based on data from a dense gauge and radar network, McMillan *et al.* (2011) validated and confirmed the suitability of a multiplicative error model. Moreover, they showed that the lognormal multiplier distribution is a good approximation to the true error characteristics.

We proposed a multivariate autoregressive model for conditional simulation of input precipitation based on a multiplicative error model in the lognormal distribution. This method is essentially the same as the application of a Kalman filter/smoother (Kalman, 1960; Webster and Heuvelink, 2006). From a mathematical-statistical point of view we addressed the same principle of Kalman filter, i.e. to compute the conditional probability distribution given the available time series at each time step, sample from it and move to the next time point. Despite the goodness of the proposed method, some cases show an overestimation of the simulated precipitation, mainly due to high values of the ratio for the multiplicative factor $\delta(t)$. This behaviour is also recognised by McMillan *et al*. (2011), who stated that the multiplicative factor used in their study "*does not capture the distribution tails, especially during heavy rainfall where input errors would have important consequences for runoff prediction*"

Note also that we ignore the change-of-support effect because the sub-catchment area is much greater than a point. Future research may address this issue of support.

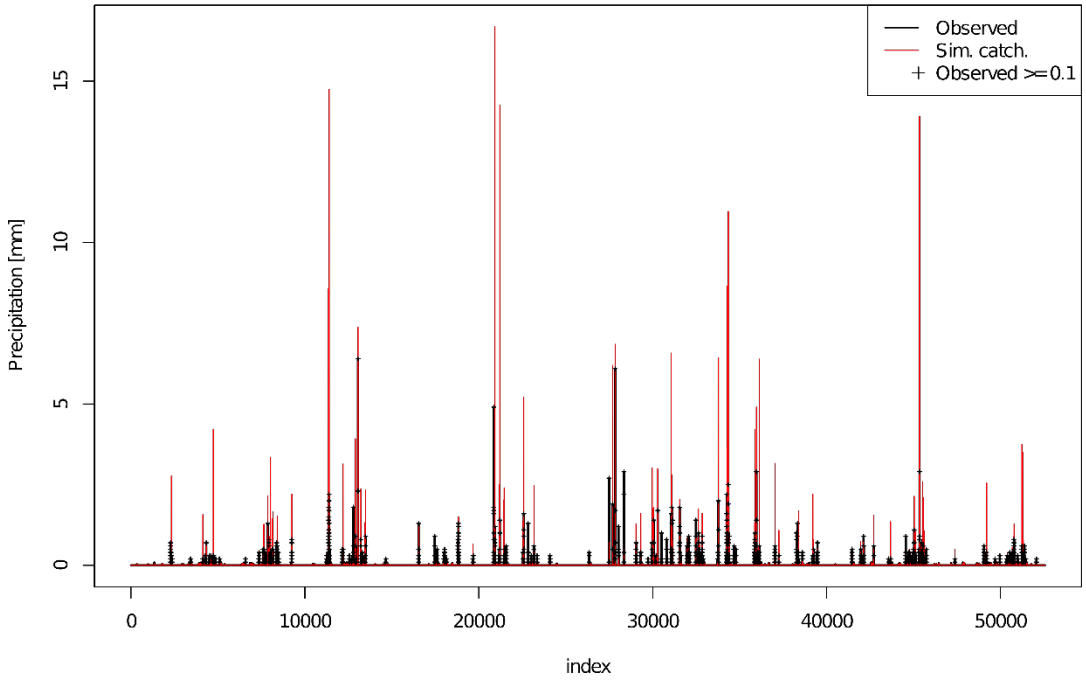

Figure 3. Observed and simulated precipitation time series of the case study: simulation at Goesdorf.

5. CONCLUSIONS

Catchment average precipitation is a major driving force and key component in urban water models. However, average catchment precipitation is not always accurately known when measured at rain gauge, because the location of the gauge might be outside the catchment boundaries or do not reflect the entire catchment at one location. To overcome this issue, we developed a method to estimate the precipitation in a catchment given a known precipitation time series in a location outside of the catchment, while quantifying the uncertainty associated with the estimation. A first-order multivariate autoregressive model for conditional simulation of input precipitation based on a multiplicative error model was proposed. This method is essentially the same as the application of a Kalman filter/smoother. Although the goodness of the proposed method, some cases show an overestimation of the simulated precipitation due to high values of the ratio for the multiplicative factor. This behaviour is also recognised in the literature.

The simulated precipitation time series can be used in urban water models for uncertainty propagation analysis to reach more robust results for urban water system design and associated potential environmental and economic impacts.

ACKNOWLEDGEMENTS

The work presented is part of the QUICS (Quantifying Uncertainty in Integrated Catchment Studies) project. This project has received funding from the European Union's Seventh Framework Programme for research, technological development and demonstration under grant agreement No. 607000, and the Luxembourg Institute of Science and Technology (LIST). The authors thank to the Luxemburgish *Administration des services techniques de l'agriculture* (ASTA) for the time series of precipitation provided, and to the Observatory for Climate and Environment (OCE) of the LIST for its technical support.

REFERENCES

Barbosa S.M. 2015. Package 'mAr': Multivariate AutoRegressive analysis. The Comprehensive R Archive Network, CRAN, 1.1-2 edition.

Box G.E.P., Jenkins G.M., Rinsel G.C., 2008. Time series analysis: forecasting and control, 4th ed., John Wiley & Sons, Inc.

del Giudice D., Albert C., Rieckermann J., Reichert P. 2016. Describing the catchment-averaged precipitation as a stochastic process improves parameter and input estimation. Water Resources Research, 52(4):3162-3186, doi: 10.1002/2015wr017871.

Guan H., Wilson J.L., Xie H. 2009. A cluster-optimizing regression-based approach for precipitation spatial downscaling in mountainous terrain. Journal of Hydrology, 375(3-4):578-588, doi: 10.1016/j.jhydrol.2009.07.007.

Kalman R.E. 1960. A new approach to linear filtering and prediction problems. Transactions of the American Society of Mechanical Engineers: Journal of Basic Engineering, 82D, 35–45.

Leta, O.T., Nossent, J., Velez, C., Shrestha, N.K., van Griensven, A. and Bauwens, W., 2015. Assessment of the different sources of uncertainty in a SWAT model of the River Senne (Belgium). Environmental Modelling & Software, 68:129-146.

Luetkepohl H., 2005. New Introduction to Multiple Time Series Analysis. Springer.

McMillan, H., Jackson, B., Clark, M., Kavetski, D. and Woods, R., 2011. Rainfall uncertainty in hydrological modelling: An evaluation of multiplicative error models. Journal of Hydrology, 400(1):83-94.

R Core Team and contributors worldwide, 2017. The R Stats Package. The R Project for Statistical Computing, 3.5.0 edition. https://stat.ethz.ch/R-manual/R-devel/library/stats/html/00Index.html.

Webster, R. and Heuvelink, G.B.M., 2006. The Kalman filter for the pedologist's tool kit. European Journal of Soil Science, 57(6):758-773.

Proceedings of the 10th World Congress of EWRA 'Panta Rhei', 5-9 July 2017, Athens, Greece
© 2017 *European Water Resources Association*

A simplified methodology for flood simulation in urban catchments

V. Bellos[1,2*], I.M. Kourtis [2] and V.A. Tsihrintzis[2]
[1] *CH2M, UK, vasilis.bellos@ch2m.com*
[2] *Centre for the Assessment of Natural Hazards and Proactive Planning & Laboratory of Reclamation Works and Water Resources Management, School of Rural and Surveying Engineering, National Technical University of Athens, 9 Iroon Polytechniou St., Zografou 15780 Athens, Greece*
[*] *e-mail: vasilis.bellos@ch2m.com*

Abstract: A simplified methodology for urban flooding simulation is proposed, combining the use of detailed, physically-based hydrodynamic models and the Unit Hydrograph theory. The methodology comprises the following steps: a) Unit Hydrograph derivation using a two-dimensional, physically-based detailed model; b) calculation of the losses in order to determine the effective rainfall depth; c) flood event simulation using the principle of the superposition. In this study, the above methodology is implemented in a, small urban catchment located in the city of Athens (Greece). The model used for the first step is FLOW-R2D. For the second step, the well-known SWMM software is used in order to determine losses, which comprise, runoff to the sewers of the system, initial abstraction, surface ponding, and, of less significance, infiltration. In order to derive a magnitude of the uncertainty of the results of the proposed method, an ensemble of 100 Unit Hydrographs is derived. The parameters which were modified in order to produce this ensemble were the Manning coefficients in the two friction zones (residential and urban open space areas). For the sampling, the Latin Hypercube technique was adopted. It is found that although the uncertainties to the derived results has to be taken into account, the proposed methodology can be a fast and efficient way to cope with the dynamic flood simulation in an urban catchment.

Key words: urban flooding, FLOW-R2D model, SWMM software, unit hydrograph

1. INTRODUCTION

The urban hydrology is of great importance (Jha et al., 2012), as the risk for people and properties from flooding is high (Tsakiris, 2013; Pistrika et al., 2014), and is increasing over the last few decades. Although there is a significant progress in the field of rural hydrology, urban hydrology modelling is still characterised by many weaknesses, due to the complexity of the urban environment, the number of the processes involved in the urban water cycle, and because phenomena are highly influenced by the dynamics and the spatial variability of the rainfall event.

The methodology presented herein is based on a previous work by Bellos and Tsakiris (2016), in which a physically-based hydrodynamic model was used coupled with the hydrological Unit Hydrograph theory, in an attempt to simulate the runoff of a real flash flood event in a rural catchment. Although the catchment was located in the north suburbs of Athens and its major part was rural, it still had a significant built-up area. In the present study, this methodology is extended in order to be implemented at the urban scale.

2. MATERIALS AND METHODS

The methodology consists of the following steps: a) Unit Hydrograph derivation using a detailed numerical model based on the full form of the two-dimensional Shallow Water Equations (2D-SWE); b) calculation of the losses in order to define the effective rainfall depth; c) flood simulation using the principle of superposition.

The losses in the rural scale are mainly dominated by infiltration. However, in the urban scale, the losses are mainly due to the runoff diverted in the sewers of the system, and the initial

abstraction (interception, ponding and wet surface), and to a lesser degree due to the infiltration phenomenon.

The numerical model used in Unit Hydrograph derivation is the FLOW-R2D model (Tsakiris and Bellos, 2014), whereas for losses SWMM (Rossman, 2010) is used.

2.1 FLOW-R2D model

The FLOW-R2D is an in-house numerical model, which solves the 2D-SWE using the Finite Difference Method through a modification of the McCormack numerical scheme. FLOW-R2D has been applied in the urban environment (Bellos and Tsakiris, 2015a) and in several case studies (Bellos and Tsakiris, 2015b; Papadaki et al., 2016).

2.2 SWMM software

EPASWMM5 is a fully dynamic rainfall-runoff simulation model, employing in hydraulic computations the momentum, mass and energy conservation laws (Rossman, 2010). SWMM was primarily developed for urban areas and can be used in the design, analysis and planning of drainage systems, and in simulation of runoff quality (e.g., Zhu et al., 2016; El-Sharif and Hansen, 2001; Hsu et al., 2000; Tsihrintzis and Hamid, 1998).

2.3 Case Study Description and Application

The case study consists of a small urban catchment located in the centre of Athens (Greece), in a neighbourhood called Kypseli. The area is highly populated and characterised by dense urban development (multi-story buildings and generally limited open space). However, in the specific, drainage area, there exist some open spaces due to the existence of hills at the upper part of the drainage area. Figure 1 presents a satellite view of the urban catchment and the location of the urban open space. It should be mentioned that this is one of the few Greek areas in which a combined sewer system is still in operation.



Figure 1.Catchment boundaries of the case-study and location of the open urban space (National Cadastre & Mapping Agency of Greece, www.ktimatologio.gr).

Based on the combined drainage network characteristics and the hydrologic and hydraulic conditions, the area in SWMM was delineated into 7 subcatchments. The network consists of 26 nodes and 25 combined sewers, with a total length of about 1.1 km. The sewer network comprises

both egg-shaped conduits (with characteristic depths ranging from 0.9 m to 1.20 m), or circular pipes with diameter of 0.40 m.

3.RESULTS AND DISCUSSION

3.1 Unit hydrograph derivation using FLOW-R2D

Due to the fact that the computational domain is a built-up area, the dominant element of the simulation is the way in which the buildings are represented. There are several ways for representing the buildings in the relative literature (e.g., Abderrezzak et al., 2008; Bellos, 2012). In the specific study, due to the fact that the Digital Terrain Model (DTM) is relatively coarse, in order to represent the complexity of the city infrastructure, the computational domain was classified in two friction zones: a) the residential area; and b) the urban open space.

In order to have a magnitude of the uncertainties of the proposed method, one hundred (100) Unit Hydrographs were derived using different combinations of Manning coefficients for the two friction zones. The sampling was made using the Latin Hypercube Sampling technique, assuming that the Manning coefficient in the main urban area ranges from 0.02 to 0.05 s/m$^{1/3}$, whereas in the forest area it ranges from 0.03 to 0.08 s/m$^{1/3}$. Regarding the input data, the DTM consisted of a grid with a resolution of 5 x 5 m. 10-min Unit Hydrographs were derived, hence the input rainfall had an intensity of 1.67 mm/h. Regarding the required parameters, based on passed experience (Bellos and Tsakiris, 2016), the time step was determined as Δt=0.001 s, the threshold which distinguishes the wet and dry cells as h_{dry}=0.0001 m and the diffusion factor as ω=0.99.

For mass conservation purposes, each of the derived Unit Hydrographs is multiplied by a correction factor which is determined dividing the volume of the water entered in the computational domain through rainfall by the volume of the water of the Unit Hydrograph (Bellos and Tsakiris, 2016).

It should be mentioned that the derivation of each Unit Hydrograph required about one day of computational budget. The derivation of 100 Unit Hydrographs would be very difficult unless a High Performance Computing (HPC) platform was used. In this work, the HPC platform of the Computational Centre of the National Technical University of Athens was used, which consists of a cluster with 24 cores.

3.2 Effective rainfall calculation using SWMM

The calculation of losses is performed using the SWMM software. The various required parameters of the model are calibrated against observed data recorded in the urban drainage system. The observed data are obtained from a storm event which occurred on the 24th of February, 2006 (Antonaropoulos and Associates, 2006). The following parameters were used in a manual calibration: the width of the subcatchments, the percentage of the impervious area in each subcatchment of the system, the Manning coefficients, the initial abstraction depths of the pervious and impervious areas, and the Manning coefficient on the sewer system. Table 1 presents the calibrated values of these parameters. The range of these parameters refers to the 7 subcatchments, in which the drainage area is divided. In Figure 2, the comparison between the simulation results derived by the SWMM and the measured data is shown. A good comparison is shown in terms of magnitude of peak, and general shape of the predicted hydrograph.

Due to the fact that during this event no flooding is observed on the surface of the catchment, a 6 h-duration synthetic storm was generated in order to test the proposed methodology. The hypothetical storm comprises two parts: a first part in which the rainfall intensity is low, called Event 1, and a second part in which the rainfall intensity is high, called Event 2 (Figure 3). Figure 4 presents the losses due to the runoff diverted into the sewers of the system, the infiltration and the

initial abstraction, assuming that the several required parameters of SWMM take the values derived in the calibration phase.

Table 1. Calibrated parameters for the SWMM software

Parameter	Calibration
Width (m)	82 ~ 918
Impervious area (%)	13 ~ 77
Manning coefficient of the impervious area ($s/m^{1/3}$)	0.015
Manning coefficient of the pervious area ($s/m^{1/3}$)	0.2
Initial abstraction of the impervious area (mm)	2.54
Initial abstraction of the pervious area (mm)	6.51
Manning coefficient of the sewer system ($s/m^{1/3}$)	0.013

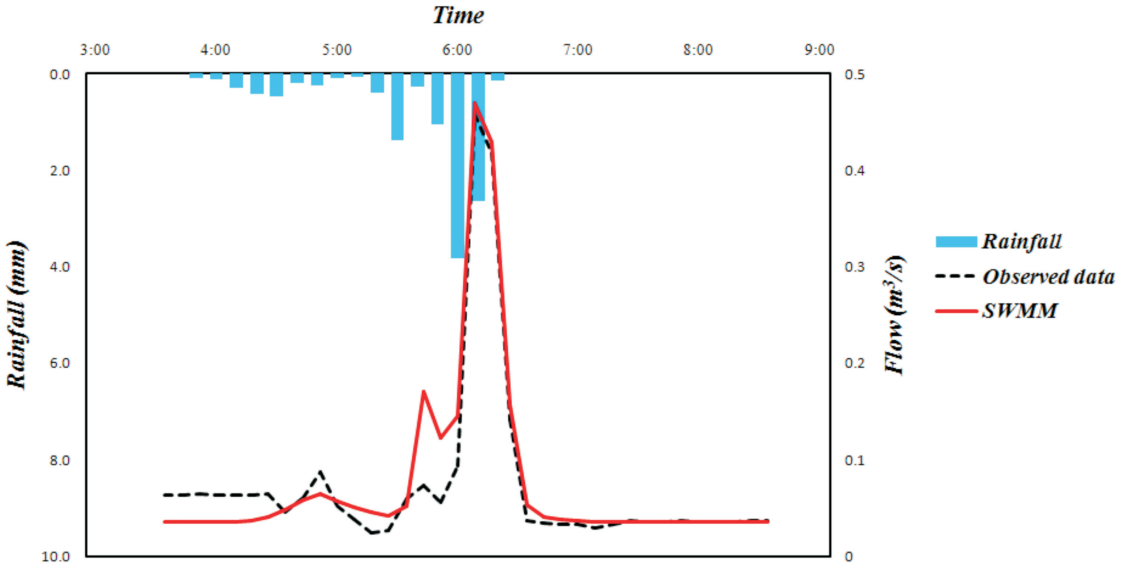

Figure 2.Comparison of measured and predicted by SWMM hydrographs during the calibration phase

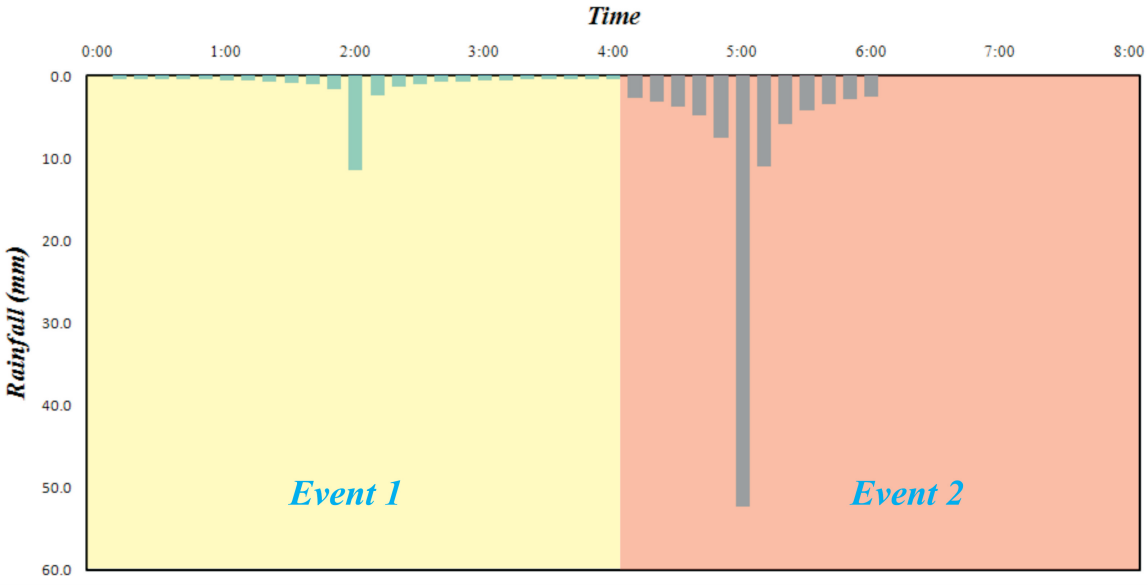

Figure 3.Hypothetical storm with two subsequent events of low and high intensity

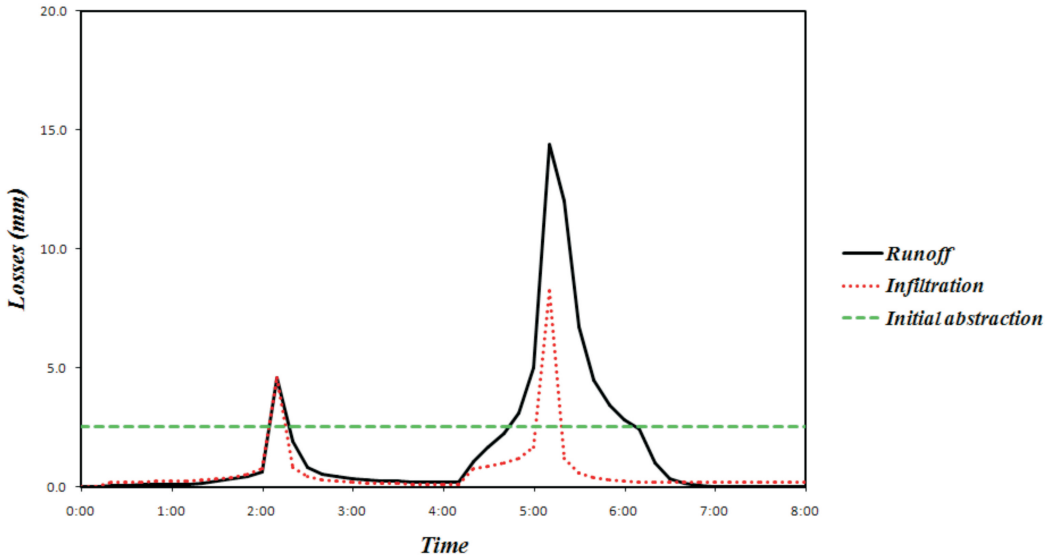

Figure 4. Predicted losses by SWMM

3.3 Flood simulation

Using the principle of superposition, an ensemble of 100 flood simulation events was derived. Figure 5 presents the band of 95% confidence of the solution, whereas Figure 6 presents the box-whisker plots of the two flood peaks of the hypothetical storm, for both Events.

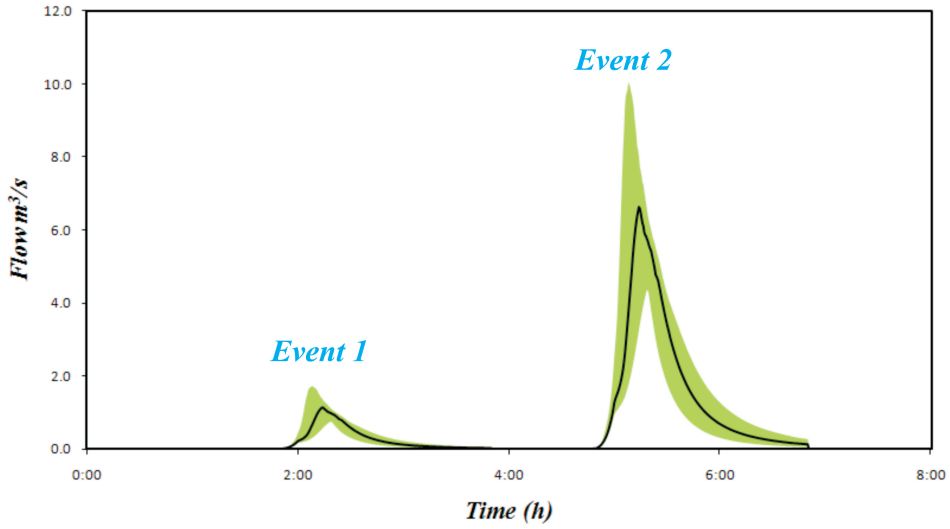

Figure 5. Uncertainty band of the urban flooding using the proposed methodology

It can be noticed (Figure 6) that as far as the peak of the flood events is concerned, significant uncertainties exist, and hence, the range of the Manning coefficients is of high importance. Besides, the uncertainty band is greater for Event 2 than Event 1. Probably this is due to the fact that the second event is characterised by more intense rainfall, and therefore, is more dynamically affected. One disadvantage of the methodology is that with the given computational power, the methodology can be implemented in relatively small catchments. However, the proposed methodology can be a useful, fast tool in the decision making process, flood warning schemes, etc., in comparison with the time consuming physically-based, 2D models, whereas it can cope with the dynamics of the flooding occurring on the catchment surface, in comparison with the typical 1D/1D urban drainage models, which consist of 1D simulation both in surface and drainage flow (Kourtis et al., 2017).

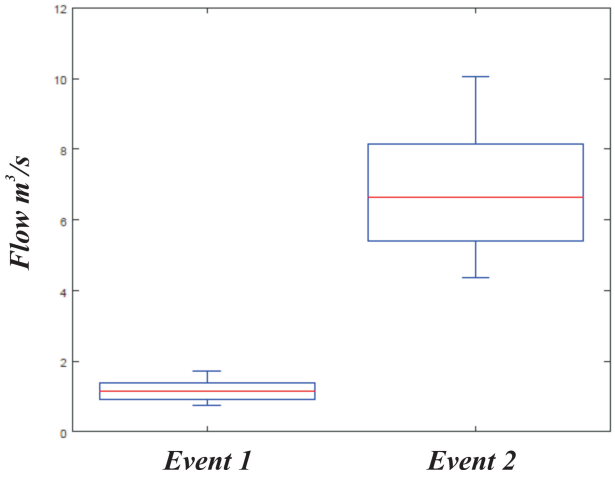

Figure 6. Box-whisker plot of the flood peaks, for the two events of the hypothetical storm

Although there are several values for the Manning coefficients in the relative literature, it is found that most times in the real world applications of these coefficients are significantly higher than those of the literature (Jarrett, 1985; Christelis et al. 2016), due to the fact that they compensate for the various energy losses occurring in real world flood events. Therefore, a careful strategy should be adopted for the selection of these values, coupling the modeller's experience and existing data, in order to either perform a calibration phase, or narrowing the range of values.

4. CONCLUSIONS

A new simplified methodology, combining physically-based hydrodynamic models and the hydrological Unit Hydrograph theory, is presented for urban flooding simulation. Uncertainties are noticed in the derived results due to the Manning coefficients, which probably are increased as the flood is more dynamically affected. Despite this fact, and adopting a more careful strategy for friction modelling, the method can simulate the dynamics of the flood on the catchment surface with a fast and efficient way, and therefore, it can be a useful tool in decision making processes.

ACKNOWLEDGMENTS

This research was done as part of the Marie Curie ITN – Quantifying Uncertainty in Integrated Catchment Studies (QUICS) project. This project has received funding from the European Union's Seventh Framework Programme for research, technological development and demonstration undergrant agreement no. 607000. Besides, acknowledgments are expressed to A. M. Rodenas for his useful advice in statistics and to the Computer Centre of NTUA for the access provided to the computer facilities.

REFERENCES

Abderrezzak, K., Paquier, A., Mignot, E., 2008. Modelling flash flood propagation in urban areas using a two-dimensional numerical model. Natural Hazards, 50: 433-460.

Antonaropoulos, P. and Associates, 2006. Technical Report: Demonstration of a European Knowledge Management Framework for a Procedure on Waste-Water Asset Management (Contract Nr. IPS-2001-42115) – Application of the Hydroplan Methodology in the Pilot Area of Athens, EYDAP S.A, (in Greek).

Bellos, V., 2012. Ways for flood hazard mapping in urbanised environments: A short literature review. Water Utility Journal, 4: 25-31.

Bellos, V., Tsakiris, G., 2015a. Comparing various methods of building representation for 2D flood modelling in built-up areas. Water Resources Management, 29(2): 379-397.

Bellos, V., Tsakiris, G., 2015b. 2D Flood Modelling: the case of Tous dam break. Proceedings of 36th IAHR World Congress, 28/6-3/7, the Hague, the Netherlands. (e-proceedings).

Bellos, V., Tsakiris, G., 2016. A hybrid method for flood simulation in small catchments combining hydrodynamic and hydrological techniques. Journal of Hydrology, 540: 331-339.

Christelis, V., Bellos, V., Tsakiris, G., 2016. Employing surrogate modelling for the calibration of a 2D flood simulation model. Proceedings of 4th IAHR Congress, 'Sustainable Hydraulics in the Era of Global Change', edited by S. Erpicum, B. Dewals, P. Archambeau, M. Pirotton, Liege, Belgium: 727-732.

El-Sharif, A., and Hansen, D., 2001. Application of SWMM to the flooding problem in Truro, Nova Scotia. Canadian Water Resources Journal, 26(4): 439-459.

Hsu M.H., Chen S.H., Chang, T.J., 2000. Inundation simulation for urban drainage basin with storm sewer system. Journal of Hydrology, 234(1): 21-37.

Jarrett, R., 1985. Determination of roughness coefficients for streams in Colorado. Water Resources Investigation Report 85-4004, US Geological Survey.

Jha, K. A., Bloch, R., Lamond, J., 2012. Cities and Flooding: A guide to integrated urban flood risk management for the 21st century. The World Bank Publications.

Kourtis, I. M., Bellos, V., Tsihrintzis, V. A., 2017. Comparison of 1D-1D and 1D-2D urban flood models. In Proceedings of the 15th International Conference on Environmental Science and Technology (CEST 2017), 31/08-02/09 2017, Rhodes, Greece.

Papadaki, C., Bellos,V., Ntoanidis, L., Dimitriou, E., 2016. Comparison of West Balkan adult trout habitat predictions using a Pseudo-2D and a 2D hydrodynamic model. Hydrology Research, nh2016352.

Pistrika, A., Tsakiris, G., Nalbantis, I., 2014. Flood depth-damage functions for built environment. Environmental Processes 1(4): 553–572.

Rossman L. A., 2010. Storm Water Management Model User's Manual, Version 5.0. Cincinnati, USA.

Tsakiris, G., 2013. Flood risk assessment: concepts, modelling, applications. Natural Hazards and Earth System Sciences, 2(1): 261-286.

Tsakiris, G., Bellos, V., 2014. A numerical model for Two-Dimensional Flood Routing in Complex Terrains. Water Resources Management, 28(5): 1277-1291.

Tsihrintzis V. A. and Hamid R., 1998. Runoff quality prediction from small urban catchments using SWMM. Hydrological Processes, 12(2): 311-329.

Zhu Z., Chen Z., Chen X., He P., 2016. Approach for evaluating inundation risks in urban drainage systems. Science of the Total Environment, 553: 1-12.

Proceedings of the 10th World Congress of EWRA 'Panta Rhei', 5-9 July 2017, Athens, Greece
© 2017 *European Water Resources Association*

Comparison of different rainfall-runoff models performance: A case study of Liqvan catchment, Iran

N. Sadeghi Louye[1*] and M. Rahimi Jamnani[2]
[1] *Dept. of Irrigation and Drainage Engineering, College of Abureyhan, University of Tehran, Pakdasht, Iran.*
[2] *Dept. of Irrigation and Reclamation Engineering, Faculty of Agriculture Engineering and Technology, College of Agriculture and Natural Resources, University of Tehran, Karaj, Iran.*
[*] *e-mail: nazaninsadeghi@ut.ac.ir*

Abstract: A vast part of Iran is located in arid and semiarid areas. In these localities, rainfall is typically meagre, irregular and highly variable. The precipitation variability in these areas causes uncertainties in runoff prediction. The mutual interaction between the climatic parameters including temperature, precipitation, evaporation, wind and etc. and hydrological factors like streamflow, concentration time, permeation and others has rendered the relationship between rainfall and runoff take a nonlinear and undetermined form. The objective of the present study is the simulation rainfall-runoff process via taking advantage of two conceptual models, namely HEC-HMS and IHACRES and three other empirical approaches models Including Artificial Neural Network (ANN), Multiple Linear Regression (MLR) and Simple Linear Regression (SLR); moreover, The models' performance has also been compared regarding the Liqvan River in Iran. Monthly time series data of Streamflow and Meteorological data were applied for the duration of 1972 to 2004. The R2, RMSE, Te and MAE indices are used to achieve desired model. IHACRES model showed a desirable performance in estimating the normal streamflow but the peak streamflows are overestimated. Similar to IHACRES, HEC-HMS model does not makes adequate performance in estimating the peak streamflows despite the fact that the HEC-HMS overall performance was better. MLR model could simulate the normal flow but peak streamflows are underestimated. Due to the simplicity of the SLR model, its simulation performance was unacceptable. ANN model provides more appropriate estimations in terms of peak streamflows in comparison to the other models. Also In total, the results of the evaluation showed that the ANN model was more accurate (R2= 0.80, RMSE= 0.29, Te= 0.004, MAE=0.003).

Key words: Rainfall-Runoff Simulation, Artificial Neural Network, HEC-HMS, IHACRES, Liqvan Catchment

1. INTRODUCTION

A vast part of Iran is located in arid and semiarid areas. In these localities, rainfall is typically meager, irregular and highly variable (Ahrens, 2003). The precipitation variability in these areas causes uncertainties in runoff prediction. In practice, the complex models often do not provide more accurate runoff predictions relative to simpler and less detailed ones (Bahat et al., 2009).

Estimating catchment streamflow is of a great importance because the deficiency in streamflow can lead to financial losses and its excess, in the form of flood, can cause financial as well as life losses. The necessity to appropriately predict the river flows in engineering constructions, river management, the surface water reservoir management and flood warning systems is tangibly felt. Also, the simulation of the river flows for the purpose of getting aware of the prospective river flow rates are among the significant and applied issues in water resources management (Fathabadi et al., 2009).

The mutual interaction between the climatic parameters including temperature, precipitation, evaporation, wind and etc. and hydrological factors like streamflow, concentration time, permeation and others has rendered the relationship between rainfall and runoff take a nonlinear and undetermined form. The objective of the present study is the simulation rainfall-runoff process via taking advantage of two conceptual models, namely HEC-HMS and IHACRES and three other empirical approaches models Artificial Neural Network (ANN), Multiple Linear Regression (MLR) and Simple Linear Regression (SLR); moreover, The models' performance has also been compared

regarding the Liqvan River in Iran.

There are numerous studies performed in relation to the rainfall-runoff process simulation as well as various methods comparisons. Lallahem and Mania (2002) offered an appropriate method based on artificial neural network for large-scale problems and longtime intervals and compared theirs with the other methods. Dastorani et al., (2009) made use of artificial neural network along with other models for rebuilding the current discharge data and they concluded the superiority of the neural network results in comparison to the correlation and normal ratio methods. Asati and Rathore, (2012) developed an autoregressive model, MLR and ANN for a complex non-linear relationship between rainfall as input data and output as runoff, without considering the nature of process and compared the performance of each model. Yaghoubi and Massah Bavani (2014) compared three models of HVB, HEC-HMS and IHACRES in A'azam Harat catchment in Iran. HVB model proved to be displaying the best performance and HEC-HMS exhibited the lowest performance.

2. MATERIALS AND METHODS

2.1. Study area

Liqvan Catchment, with an area of 76 km^2, is located in the southern section of the city of Tabriz in Iran and it originates from the northern foothill of Sahand Mountain. It continues its route towards north after joining the tributary branches and, as the main drainage system of the catchment, finally, discharges to AjiChai River. Geographically, it is located in 38º,01', 30" to 37º,43',30" of the Northern latitude and 46º,31',35" to 46º,22',00" of the Eastern latitude. The position of Liqvan catchment and also Liqvan station has been shown in Figure 1.

Liqvan Catchment has a dry and cold climate. The catchment height reaches to an average value of 2675 meters and its average annual precipitation is 318 mm. The slope is 25 percent on average and the main waterway expose a slope of 9 percent. Geologically, the Floor and sides of the river bed are made of tuffs and according to the characteristic features of such material the waterway basin shows low permeability.

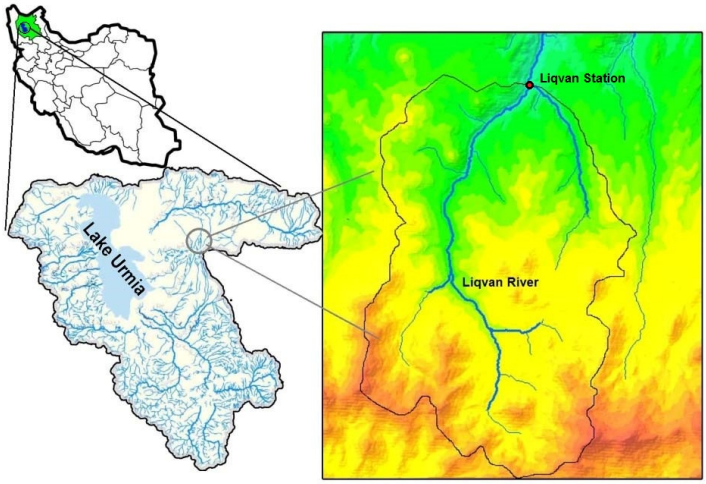

Figure 1.General location of Study Area.

2.2. IHACRES

IHACRES is an integrated metric-conceptual model for the simulation of the precipitation-runoff (Jakeman et al., 1990). IHACRES model is applied for the simulation of the runoff in catchments

for which the precipitation and temperature data have been recorded incessantly. The model, as observed in Figure 2, is consisted of two nonlinear and linear associated parts which are, respectively, used to calculate the losses and transform the effective precipitation to runoff.

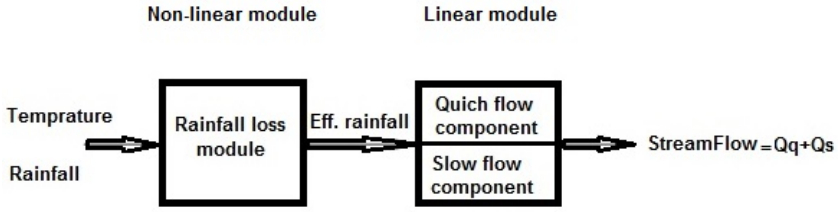

Figure 2. Linear, nonlinear and the output part of IHACRES model.

2.3. HEC-HMS

HEC-HMS (The Hydrologic Engineering Center—the Hydrologic Modeling System) is a physically based distributed model, designed to simulate the rainfall-runoff processes of dendritic catchment systems. The model is capable of simulating the catchment in accordance with various climatic conditions. HEC-HMS model takes hydrological elements such as catchment boundaries, sub-catchment and etc**.**, the waterways connection points and drainage points as its inputs and it requires climate data, soil type, vegetative cover and casualties in every sub-catchments (Scharffenberg & Fleming, 2010). HEC-HMS includes three main components: Basin model, Meteorological model, and Control specifications. The basin model stores the physical datasets describing the basin properties and the meteorological model includes precipitation, evapotranspiration, and snowmelt data. The time span of a simulation is controlled by control specifications including a starting date and time, ending date and time, and computation time step (Anderson et al., 2002).

In the present study, SCS-CN method has been used for modeling the intensity of losses. In Figure 3, the land use map for Liqvan sub-catchments was determined by taking advantage of Landsat satellite images from July 2004. Then, ArcHydro toolbox was applied to delineate the Curve Number (CN) map by making use of soil specifications and land use map of study area.

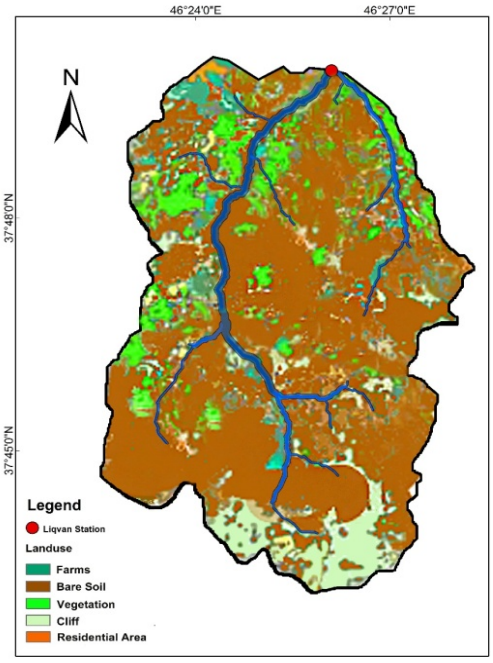

Figure 3.Land use map of the study area.

2.4. Artificial Neural Network

Artificial Neural Networks (ANN) is a simple model of human's brain. An ANN is nonlinear mathematical structure that has ability to show the nonlinearity process for communicating between inputs and outputs of any system. This network is training with present data in learning process and can be used for future prediction. Each network has been formed from one input layer, one output layer and one or more hidden layer. Neurons of each layer are connected to next layer by weights (Akbarpour & Rahnama, 2006).

2.5. Multiple Linear Regression

Regression analyses are among the oldest statistical techniques used in hydrology. Multiple Linear Regressions (MLP) represent a mathematical equation expressing one random variable as being correlatively related to another random variable, or to several random variables. The regression equation may be any function that can be fitted to a set of points of observed variables (Sobri et al., 2002). Regression analysis is a statistical technique for creating a linear relationship between the dependent and independent variables. It aims at predicting the dependent variable from the independent variable. Multivariate linear regression equation is as stated below:

$$Y_i = c_0 + \sum_{j=1}^{n} a_j X_{ij} \quad (1)$$

where, α is the regression parameters, X is the independent variables, c is the equation fixed constant and Y is the regression equation.

2.6. Simple Linear Regression

Linear Regression is the simplest regression model (SLR) which was frequently used in the past. In SLR model, the Equation below is applied to create a relationship between the dependent and independent variables.

$$y = Ax + B + \varepsilon \quad (2)$$

where, Y_i is the dependent variable and x is the independent variable and ε is the error.

2.7. Data Used in the Models

Monthly Streamflow and climate data from March 1972 through March 2004 were used from Liqvan station. Precipitation data (mm) and temperature data (ºC) are inserted as input variables for the runoff simulation and the streamflow (cubic meters per second) data are used for assessing IHACRES and ANN models accuracy. Also, wind speed, sun radiation, precipitation and temperature data were used for HEC-HMS and MLR models; In addition, the precipitation data was used in SLR model.

2.8. Performance Criteria

To achieve desired optimal model, correlation of determination (R^2), root mean square error (RMSE), total error (T_e) and mean absolute error (MAE) are used in current study.

3. RESULTS

For IHACRES, Simulation results in calibration stage are as presented in Table 1.

Table 1. IHACRES Calibrated coefficients.

C	τ_w	f	τ_{ref}	I	P
0.00093	7	3.5	2	0	1

To run HEC-HMS3.5, hydrological elements including catchment, sub-catchments and waterways network, waterways connection point and the model's output point were determined by making use of ArcHydro, and the sub-catchments characteristics are summarized in Table 2.

Table 2. Sub-catchments characteristics.

sub-basin	**1**	**2**	**3**	**4**
Slope (%)	12.3	8.4	7.0	4.0
Concentration Time (hr)	25.5	36.4	47.6	64.8
Lag Time (hr)	15.3	21.8	28.6	38.9

Land use map and soil specifications were used to generate the curve number map which is illustrated in Figure 4.

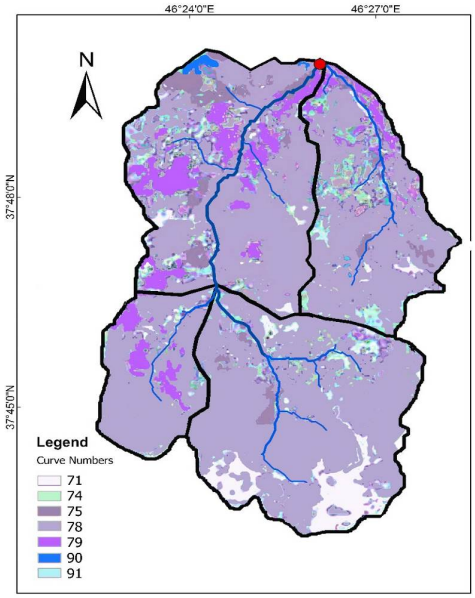

Figure 4.Liqvan catchment Curve Number map.

The generated Neural Network possesses two input layers due to having two inputs, namely precipitation and temperature. Ten neurons have been considered for the neural network and 25 years of data were applied for training and the remaining were used for testing. Also, the determination coefficients (R2) for training, validation and test stages were 0.77, 0.94 and 0.73, respectively.

In MLR Model, According to the results obtained and also based on the finding that the minimum and maximum temperatures do not show a high correlation (Pierson's correlation coefficient approaching unity), daily mean temperature as well as a new parameter extracted through multiplying maximum temperature by minimum temperature were applied (Tmm).

Based on the investigations performed on the three parameters, namely R^2, Cp and PRESS, and using two methods of ENTER and STEPWISE, the equation presented in Table 3 was accepted as

the final equation. It's accepted, based on the fact that it offers the least values for Cp and PRESS and a maximum value for R2 and also because its Durbin-Watson value was above 1 and it had VIFs below 10.

Table 3. Accepted equation of MLR model

Inputs	Equation	Press	Cp	VIF	
P,T, R, Tmm	Q=-0.031+0.009*P+0.038*T+ 0.095*W+0.001*Tmm+0.003*R	121	6	P	1.2
				T	1.5
				W	2.6
				Tmm	6.6
				R	5.8

MLR Model validation was carried out for the years from 2002 to 2004 and the relative error value (RE) and RMSE were obtained 0.58 and 0.51, respectively which is indicative of a high error level of the model. According to the results obtained from SLR model simulations, PRESS was found 177 for this model which is indicative of a lack of optimum ability of the model for simulations. Figure 5 shows the determination coefficient (R^2) of observed and simulated values of each model. The evaluation performances of models have been summarized in the Table 4 and Figure 6 also exhibits the simulated and observed streamflow acquired by models.

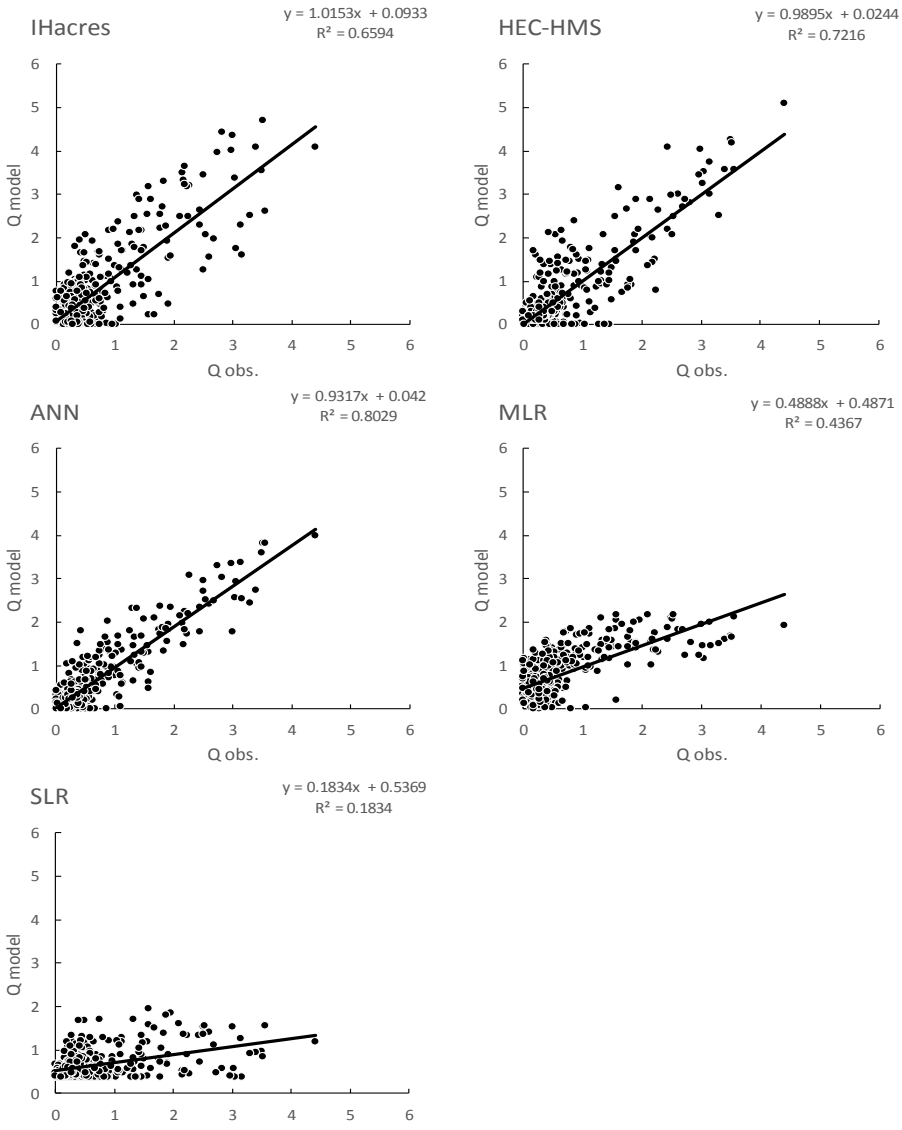

Figure 5.The determination coefficient of each model.

Table 4.Summarized models evaluation indices.

Model	RMSE	R^2	TE	MAE
ANN	0.29	0.80	0.004	0.003
HEC-HMS	0.41	0.72	0.026	0.017
IHACRES	0.43	0.66	0.157	0.103
MLR	0.57	0.45	0.229	0.430
SLR	0.44	0.18	0.022	0.450



Figure 6.The simulated and observed streamflow time series of models.

4. DISCUSSION AND CONCLUSIONS

According to Figure 6, it is evident that the IHACRES does not show a high competency in

simulating the peak streamflows. It displays a favorable performance in estimating the normal streamflow but as it is seen the peak streamflows are overestimated. Similar to IHACRES, HEC-HMS model does not makes adequate performance in estimating the peak streamflows despite the fact that the overall performance is better. ANN model provides more appropriate estimations in terms of peak streamflows in comparison to the other models and the shape of the simulated streamflow generally follows the observed streamflow. MLR model does not have the ability to simulate the peak streamflows and it shows better performance in simulating the normal streamflow. And as expected, SLR model is not suitable for simulating. SLR model leads to a severe underestimation of peak streamflows.

According to the Table 5, the highest determination coefficient goes to the neural network and it is indicative of the higher accuracy of the model output. This is because the neural network is trained based on the observed flow. Artificial Neural network model also indicates the lowest RMSE among the extant models which shows the ANN model is more accurate.

After ANN model, HEC-HMS exhibits the better performance. The weaknesses of HEC-HMS model can be explained as model considers fixed values for physical parameters regarding the various flood incidents during simulation period (Ia and CN). In other words, the change in the land use resulting from the human activities brings about an uncertainty in curve number (CN).

IHACRES model shows relatively promising results and its weakness is predominantly due to the complicacy of the climatic behavior. The low number of the parameters required by the model as inputs can be pointed out as the advantages of this model.

MLR model outperforms SLR model due to its taking more input parameters into consideration, though both of the models showed weaker performances in comparison to the other models because of considering the runoff behavior as linear.

ACKNOWLEDGEMENTS

The authors hereby, would like to express gratitude to Iran's Meteorological Organization and the East Azarbayjan Regional Water Authority both of which greatly assisted us in accomplishing the paper.

REFERENCES

Ahrens, C.D., 2003. Meteorology Today: An Introduction to Weather, Climate, and the Environment. Brooks Cole, Thomson Learning.

Akbarpour, M., Rahnama, M., 2006. Simulation of rainfall-runoff process by ANNs and HEC-HMS model. Dams and Reservoirs, Societies and Environment in the 21st Century, vol.2, 783-786.

Anderson, M.L., Chen, Z.Q., Kavvas, M.L., Feldman, A., 2002. Coupling HEC-HMS with atmospheric models for prediction of watershed runoff. Journal of Hydrology Eng, Vol.7, 312–318.

Asati, S.R., Rathore, S.S., 2012. Stream Flow Prediction Using Soft Computing Technique. International Journal of Lakes & Rivers, Vol.5, No.1, 7-22.

Bahat, Y., Grodek, T., Lekach, J., Morin, E., 2009. Rainfall–runoff modeling in a small hyper-arid catchment. Journal of Hydrology, 373(1-2), 204-217.

Dastorani, M.T., Moghadamnia, A., Piri, J., Rico-Ramirez, M., 2009. Application of ANN and ANFIS Models for Reconstructing Missing Flow Data, Journal of Environmental Monitoring and Assessment. Vol.166, 421–434.

Fathabadi, A., Salajegheh, A., Mahdavi, M., 2009. Streamflow Forecasting Using Neuro-Fuzzy and Time Series Methods. Iran-Watershed Management Science & Engineering, Vol.2, 21-30.

Jakeman, A.J., Littlewood, I.G., Whitehead, P.G., 1990. Computation of the instantaneous unit hydrograph and identifiable component flows with application to two small upland catchments, Journal of Hydrology, Vol.117, 275-300.

Lallahem, S., Mania, J., 2002. A non-linear rainfall- runoff model using neural network technique. Mathematical and Computer Modeling, 37:1047-1061.

Scharffenberg, W, Fleming, M., 2010. Hydrologic modeling system HEC-HMS v3.2 user's manual. USACEHEC, Davis.

Sobri, H., Nor Irwan, A., Amir, H., 2002. Artificial Neural Network Model For rainfall-runoff relationship, Journal of Teknology, Vol.37, 1-12.

Yaghoubi, M., Massah, A., 2014. Sensitivity analysis and comparison of capability of three conceptual models HEC-HMS, HBV and IHACRES in simulating continuous rainfall-runoff in semi-arid basins. Journal of Earth and space physics, Vol.2, 153-172.

Proceedings of the 10th World Congress of EWRA 'Panta Rhei', 5-9 July 2017, Athens, Greece
© 2017 *European Water Resources Association*

Model selection techniques in SWAT-based hydrological modelling

B. Asl-Rousta[1*], S. Jamshid Mousavi[1] and M. Ehtiat[2]
[1] *School of Civil and Environmental Engineering, Amirkabir University of Technology (Tehran Polytechnic), Tehran, Iran*
[2] *College of Engineering,Civil Engineering Group, Ardakan University, Yazd, Iran*
[*] *e-mail: roosta.hoda@aut.ac.ir*

Abstract: Hydrological modeling is subject to issues of simplicity vs. complexity and accuracy vs. uncertainty. This recognition has led to a growing tendency among hydrologist to postulate several alternative hydrological models for a given problem. In this case, model selection techniques can be used as effective yet practical just-in-time approaches to rank these candidate models and select the 'best' one among them and/or attempt to construct a set of 'good' models. SWAT (soil and water assessment tool) is one of the most comprehensive large-scale watershed models with a large number of parameters capable of evaluating hydrologic processes, so its calibration is challenging. This study aims to investigate the efficiency of AIC model selection criterion for selecting a "good" calibration setting. To predict water discharge at Sirwan River Basin outlet, a SWAT model of the basin has been set-up. Depending on the number of calibration parameters and observation data, different calibration settings have been built using sequential uncertainty fitting (SUFI) approach. The calibration settings were compared then against Nash Sutcliff, P-Factor and R-factor statistics, as well as AIC model selection criterion. Results showed that a good calibration setting is the one with less number of observations according to the AIC.

Key words: hydrological modeling, SWAT, calibration, model selection criteria

1. INTRODUCTION

Hydrological modelling plays a critical role in assessing water resources problems. During the last decades, several physically based distributed hydrological models have been emerged and applied to simulate the basin wide hydrological processes. Some of the models include System Hydrologic Europeen (SHE) (Abbott at al. 1986a, b), Variable Infiltration Capacity (VIC) (Liang et al. 1994), and Soil and Water Assessment Tool (SWAT) (Arnold et al. 1998).

SWAT is a physics-based model with the ability of predicting the impact of land-management practices on water, sediment, and agricultural chemical yields in watersheds with varying soil, land use, and management conditions (Neitsch et al. 2011). Due to the complex nature of the hydrological processes, SWAT contains a large number of parameters, the value of some of which cannot be measured directly and should be estimated through the calibration. Indeed, the agreement between the simulated and the observed data is measured through the calibration by evaluating one or more objective functions (Zhang et al. 2008).

Characteristics of a calibration setting depend on the purpose of the study (Gong et al 2012). Several studies have focused on single-gauge calibration for the hydrological modeling (Li et al. 2010, Sudheer et al. 2011, Bitew et al. 2012). Multiple gauges-based calibration has been documented by Abbaspour et al. (2007), Migliaccio and Chaubey (2007), and Faramarzi et al. (2015), among others. Finally, several authors have successfully applied multi-objective formulations for the calibration (White and Chaubey (2005), Bekele and Nicklow (2007), Ahmadi et al. (2014)).

Model selection offers a way to draw inferences from a set of multiple competing models. These criteria discriminate among models based on how closely they reproduce hydrologic observations using maximum likelihood estimates of model parameters (favoring models that reproduce observed behavior most closely) and how many such parameters they contain (penalizing models that contain many) (Ye et al. 2008). The Akaike information criterion (Akaike, 1973) is among the

most widely used criteria for model selection that estimates the Kullback–Leibler information lost by approximating full reality with the fitted model.

In this paper, SWAT model was applied to hydrologically simulate *Sirwan* River basin in Iran. In order to calibrate the model, several calibration settings were built, and an attempt was made to evaluate the impact of the number of observations as well as the number of calibration parameters on the calibration results according to AIC criteria.

The remainder of the paper is organized as follows: materials and methods are described in Section 2. Section 3 discusses results and discussion, and Section 4 describes the conclusions.

2. MATERIALS AND METHODS

2.1 Study area

With an area of about 9515 km2, Sirwan river basin, is located in west of Iran (Fig. 1). It lies between 46°1′-48 °N and 34°43′-35°48′ E, where topography is complex, in that altitude varies from 3273 m to 601 m, according to the ASTER DEM (NASA and JPL 2009). Sirwan is mostly mountainous and the heterogeneous climate conditions make the hydrological modeling challenging in the basin.

2.2 SWAT model setup

The National Centers for Environmental Prediction's Climate Forecast System Reanalysis (CFSR) daily weather data (precipitation and temperature) with the resolution of 38 km have been used as input to SWAT (Saha et al. 2010). SWAT required spatial data including digital elevation model (DEM), soil map, and land cover data were driven from the Advanced Spaceborne Thermal Emission Reflection Radiometer (ASTER) DEM dataset (NASA and JPL 2009), at the resolution of 30 m 30 m, the digital soil map of the world (FAO 1995), and the Iranian Ministry of Energy, respectively. Precipitation, maximum and minimum temperature have been considered for 13 stations, from 1981 to 2012. In order to account for orographic effects of each subbasin on precipitation, temperature and solar radiation, five elevation bands were assigned to each subbasin. SWAT built 39 subbasins and 707 HRUs for the Sirwan basin, and it simulated the streamflow for a period of 32 years from 1981 to 2012, considering the first three years as the warm-up.

2.3 Calibration settings

For the calibration of SWAT model, SUFI-2 calibration and uncertainty analysis method (Abbaspour et al. 2004) was used, utilizing SWAT-CUP software. The period of 1985 to 2003 was chosen to perform the calibration, in which a variety of the hydrological conditions/extremes had been occurred within the watershed. Moreover, during this time period the flow was almost natural and just Gheshlagh Dam (Fig. 1) had been operating. The following 9 years i.e., 2004-2012 were considered for the validation. The Nash and Sutcliffe (NS) statistics (Nash and Sutcliffe 1970), the P-Factor (the fraction of measured data bracketed by the 95PPU band) and R-factor (the ratio of the average width of the 95PPU band and the standard deviation of the measured variable) indices (Abbaspour et al. 2004, Abbaspour et al. 2007) were used in this study to evaluate the calibration. As the objective of the study was to evaluate different calibration settings utilizing AIC model selection criterion, two basic scenarios were defined, based on each of which four calibration settings were built. Overall, 8 settings were built for the calibration of the *Sirwan* river basin. The scenarios are:

Scenario 1: To consider the outlet site (gauge) for the calibration. Since in the Sirwan basin the Gheshlagh dam had been operating during the calibration time period, we had to consider the

observed data of the sites 3 and 4 (Fig 1) in the calibration (objective function) to capture the physical characteristics of the dam upstream.

Scenario 2: To consider sites located in the middle of the *Sirwan*'s tributaries in addition to the outlet site. We selected sites that were not nested and were not hydrologically connected (Table 2).

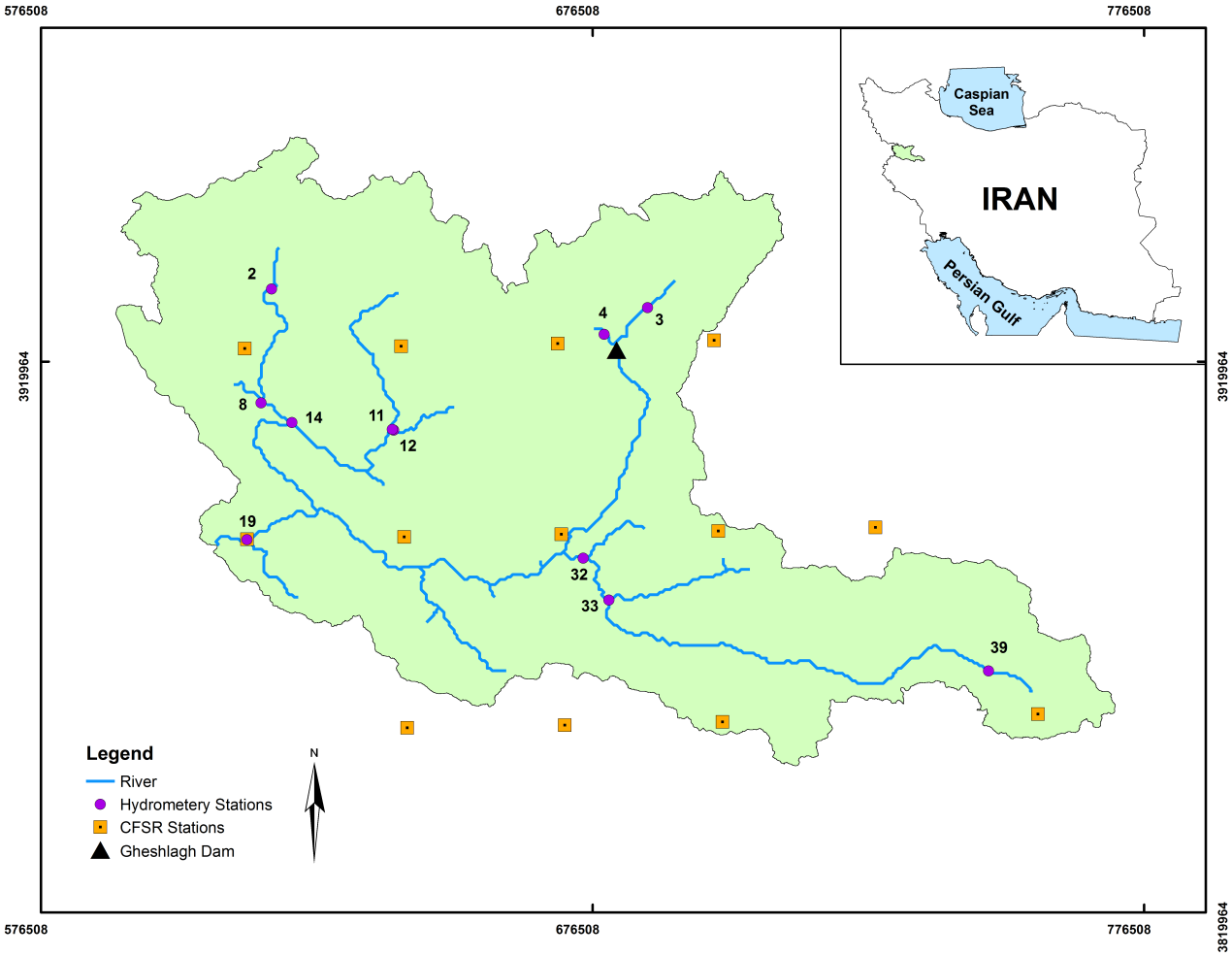

Figure 1. Study area.

For the settings built according to the basic scenarios, 28 commonly used parameters (Abbaspour et al. 2007) were considered for the calibration of discharge, and their values were initially set according to the guidelines provided by SWAT developers (Arnold et al. 2012a). These parameters and their definition can be found in Table 1. We examined each scenario for two cases and built 4 calibration settings; in the first case (Combined), we built a calibration setting considering all the sites mentioned in Table 2 in one model. In the second case (Separate), we calibrated the area upstream of each site separately. Then, we aggregated calibrated parameters into one setting. Then, we performed one-at-a-time sensitivity analysis, reduced the number of the parameters and built another 4 settings based on the sensitive parameters. After building calibration settings, AIC model discrimination criterion (Eq. 1) was used for ranking and evaluating the set of 8 settings and also making some beneficial inferences.

$$AIC = -2 \log(\mathcal{L}) + [2K] \quad (1)$$

where K is the number of parameters; $\mathcal{L}$ is maximum likelihood of the model.

Table 1. Calibration parameters

Parameter Name	Definition	Sensitive or not
v__ALPHA_BF.gw	Baseflow alpha factor	Yes
v__GW_DELAY.gw	Groundwater delay time	Yes
v__GW_REVAP.gw	Groundwater "revap" coefficient	Yes
v__GWQMN.gw	Threshold depth of water in the shallow aquifer required for return flow to occur	Yes
v__REVAPMN.gw	Groundwater “revap” coefficient	
r__CN2.mgt	Initial SCS runoff curve number for moisture condition II	Yes
v__CH_N2.rte	Manning's "n" value for the main channel	
v__CH_K2.rte	Effective hydraulic conductivity in main channel alluvium	Yes
r__SOL_AWC().sol	Available water capacity of the soil layer	Yes
r__SOL_K().sol	Saturated hydraulic conductivity	
r__SOL_BD().sol	Moist bulk density	Yes
r__SLSUBBSN.hru	Average slope length	
v__OV_N.hru	Manning’s “n” value for overland flow	
v__CANMX.hru (FRST)	Maximum canopy storage for the landuse "FRST"	
v__CANMX.hru (FRSE)	Maximum canopy storage for the landuse "FRSE"	
v__CANMX.hru (FRSD)	Maximum canopy storage for the landuse "FRSD"	
v__CANMX.hru (PAST)	Maximum canopy storage for the landuse "PAST"	
v__SFTMP.bsn	Snowfall temperature	Yes
v__SMTMP.bsn	Snowmelt base temperature	Yes
v__SMFMN.bsn	Melt factor for snow on December 21	Yes
v__SMFMX.bsn	Melt factor for snow on June 21	Yes
v__ESCO.bsn	Soil evaporation compensation factor	
v__EPCO.bsn	Plant uptake compensation factor	
v__SNOCOVMX.bsn	Minimum snow water content that corresponds to 100% snow cover	Yes
v__TIMP.bsn	Snow pack temperature lag factor	Yes
v__SURLAG.bsn	Snow pack temperature lag factor	
v__PLAPS.sub	Precipitation lapse rate	Yes
v__TLAPS.sub	Temperature lapse rate	Yes

Table 2. Characteristics of calibration settings

Calibration Setting	Basic Scenario	Sites considered in the calibration	Combined (C) or Separate (S)	Sensitivity Analysis	Number of observed data considered in the calibration	Number of calibration parameters	Calibration time (min)	Calibration Residual Sum of Squares (RSS)	Validation Residual Sum of Squares (RSS)
Setting1	Scenario1	3, 4, 19*	C	No	684	30[a]	711	528345.1	392117.7
Setting2	Scenario2	3, 4, 8, 14, 19, 32	C	No	1368	30[a]	584	388143.9	139920.3
Setting3	Scenario1	3, 4, 19	S	No	684	30[a]	1076	577833.6	212510.3
Setting4	Scenario2	3, 4, 8, 14, 19, 32	S	No	1368	30[a]	2446	417220.2	153447.6
Setting5	Scenario1	3, 4, 19	C	Yes	684	18[a]	375[e]	557576.1	181235.4
Setting6	Scenario2	3, 4, 8, 14, 19, 32	C	Yes	1368	18[a]	763	414032.2	161490.1
Setting7	Scenario1	3, 4, 19	S	Yes	684	18[a]	1786	612368.9	194964.6
Setting8	Scenario2	3, 4, 8, 14, 19, 32	S	Yes	1368	18[a]	3141	339383.0	141555.4

* site 19 is the outlet

$\Delta AIC = AIC_i - AIC_{min}$ can be used in order to rank the competing settings (Burnham & Anderson 2004). The weight of evidence or the probability that setting i is the best model is given by:

$$w_i = \Pr(\text{model}_i \mid \text{data}) = (\exp(-0.5\Delta AIC_i))/(\sum^{R}_{j=1}(\exp(-0.5\Delta AIC_j))) \quad (2)$$

where i=1.2.….R, and R is total number of settings. These weights have a value between 0 to 1, with the sum equals 1 for all settings in the candidate set.

3. RESULTS AND DISCUSSION

The objective of the hydrological simulation of this study was to estimate discharge at the outlet (site 19). Therefore, 8 different calibration settings were built considering various number of observations, and parameters to find settings which better simulate discharge at the outlet. We have considered all sites in the validation procedure, but analysed the evaluation criteria for the outlet (Table 3). Low validation NS value for settings 1 (column 7 in Table 3), i. e. 0.13, shows the poor performance of this setting in simulating the outlet discharge. Close validation NS values of other settings which assert a good calibration (NS>0.55, R-factor<1.5, P-factor>0.5) (Moriasi et al. 2007), suggests the consideration of other criteria rather than NS and P-factor and R-factor for evaluation of the settings. Hence, AIC model selection criterion has been utilized to evaluate and rank calibration settings excluding setting1 (Tables 3).

Results presented in Table 3 show that setting5 is prioritized as the most preferred setting, followed by setting7 and setting3. Therefore, if the watershed is calibrated under measures considered in setting5, a good simulation with a low error value and reasonable calibration effort will be achieved. Comparison of the results presented in Table 3 shows that according to AIC, consideration of 3 sites (Scenario1) in the calibration is preferred to consideration of 6 sites (Scenario2). In fact, settings with fewer observations are prior to ones with more observations. It also can be inferred from Table 3 that except for settings 2 and 6, settings with less parameters are prior to settings with more parameters.

Table 3. Statistical indices, Δ and w_j values for the outlet (site19)

	calibration			validation			AIC			
	p-factor	r-factor	NS	p-factor	r-factor	NS	Value	Δ	w_j	Rank
1	2	3	4	5	6	7	8	9	10	11
Setting1	0.94	1.09	0.86	0.93	1.2	0.13	N/A	N/A	N/A	N/A
Setting2	0.84	1.03	0.86	0.82	1.05	0.74	3416	1388	0.00	5
Setting3	0.88	1.13	0.82	0.7	1.16	0.55	2062	35	0.00	3
Setting4	0.81	0.54	0.85	0.59	0.52	0.69	3458	1431	0.00	7
Setting5	0.94	1.32	0.85	0.89	1.25	0.64	2027	0	1.00	1
Setting6	0.94	0.83	0.85	0.85	0.83	0.67	3430	1403	0.00	6
Setting7	0.74	0.82	0.84	0.46	0.64	0.6	2055	28	0.00	2
Setting8	0.89	0.65	0.88	0.87	0.7	0.73	3312	1285	0.00	4

4. CONCLUSION

The purpose of this study was to choose a "good" calibration setting which had low error value as well as low reasonable calibration effort. To do so, 8 calibration settings considering different number of observations and calibration parameters were built using SUFI 2 algorithm, to calibrate SWAT hydrological model of *Sirwan* river basin in Iran. The set of settings were then evaluated according to NS, P-factor and R-factor statistics. The results showed these statistics were not sufficient for the judgment of the calibration settings since their values all asserted good calibration (according to guidelines provided by Moriasi et al. (2007)). In this respect, model selection techniques can be of great advantage. Therefore, AIC model selection criteria were applied to rank the settings. According to AIC, settings with less number of observations and were preferred to the others.

REFERENCES

Abbaspour K, Johnson C, Van Genuchten MT (2004) Estimating uncertain flow and transport parameters using a sequential uncertainty fitting procedure Vadose Zone Journal 3:1340-1352

Abbaspour KC et al. (2007) Modelling hydrology and water quality in the pre-alpine/alpine Thur watershed using SWAT Journal of hydrology 333:413-430

Abbott M, Bathurst J, Cunge J, O'connell P, Rasmussen J (1986a) An introduction to the European Hydrological System—Systeme Hydrologique Europeen,"SHE", 2: Structure of a physically-based, distributed modelling system Journal of hydrology 87:61-77

Abbott MB, Bathurst JC, Cunge JA, O'Connell PE, Rasmussen J (1986b) An introduction to the European Hydrological System—Systeme Hydrologique Europeen,"SHE", 1: History and philosophy of a physically-based, distributed modelling system Journal of hydrology 87:45-59

Ahmadi M, Arabi M, Ascough JC, Fontane DG, Engel BA (2014) Toward improved calibration of watershed models: Multisite multiobjective measures of information Environmental Modelling & Software 59:135-145

Akaike H (1974) A new look at the statistical model identification IEEE transactions on automatic control 19:716-723

Arnold J, Kiniry J, Sirinivasan R, Williams J, Haney E, Neitsh S (2012) SWAT input–output documentation, version 2012. Texas Water Resource Institute. TR-439

Arnold JG, Srinivasan R, Muttiah RS, Williams JR (1998) Large area hydrologic modeling and assessment part I: Model development1. Wiley Online Library,

Bekele EG, Nicklow JW (2007) Multi-objective automatic calibration of SWAT using NSGA-II Journal of Hydrology 341:165-176

Bitew MM, Gebremichael M, Ghebremichael LT, Bayissa YA (2012) Evaluation of high-resolution satellite rainfall products through streamflow simulation in a hydrological modeling of a small mountainous watershed in Ethiopia Journal of Hydrometeorology 13:338-350

Burnham KP, Anderson DR (2004) Multimodel inference understanding AIC and BIC in model selection Sociological methods & research 33:261-304

FAO G (1995) Digital Soil Map of the World (GeoLayer), 18 Feb 2014 edn.,

Faramarzi M, Srinivasan R, Iravani M, Bladon KD, Abbaspour KC, Zehnder AJ, Goss GG (2015) Setting up a hydrological model of Alberta: Data discrimination analyses prior to calibration Environmental Modelling & Software 74:48-65

Gong Y, Shen Z, Liu R, Hong Q, Wu X (2012) A comparison of single-and multi-gauge based calibrations for hydrological modeling of the Upper Daning River Watershed in China's Three Gorges Reservoir Region Hydrology Research 43:822-832

Li Z, Shao Q, Xu Z, Cai X (2010) Analysis of parameter uncertainty in semi-distributed hydrological models using bootstrap method: A case study of SWAT model applied to Yingluoxia watershed in northwest China Journal of Hydrology 385:76-83

Liang X, Lettenmaier DP, Wood EF, Burges SJ (1994) A simple hydrologically based model of land surface water and energy fluxes for general circulation models Journal of Geophysical Research: Atmospheres 99:14415-14428

Migliaccio KW, Chaubey I (2007) Comment on Cao W, Bowden BW, Davie T, Fenemor A. 2006.Multi-variable and multi-site calibration and validation of SWAT in a large mountainous catchment with high spatial variability'. Hydrological Processes 20 (5): 1057-1073 Hydrological Processes 21:3226

Moriasi DN, Arnold JG, Van Liew MW, Bingner RL, Harmel RD, Veith TL (2007) Model evaluation guidelines for systematic quantification of accuracy in watershed simulations Trans Asabe 50:885-900

NASA, JPL (2009) ASTER Global Digital Elevation Model [Data set].

Nash JE, Sutcliffe JV (1970) River flow forecasting through conceptual models part I—A discussion of principles Journal of hydrology 10:282-290

Neitsch SL, Arnold JG, Kiniry JR, Williams JR (2011) Soil and water assessment tool theoretical documentation version 2009. Texas Water Resources Institute,

Sudheer K, Lakshmi G, Chaubey I (2011) Application of a pseudo simulator to evaluate the sensitivity of parameters in complex watershed models Environmental Modelling & Software 26:135-143

White KL, Chaubey I (2005) Sensitivity analysis, calibration, and validations for a multisite and multivariable swat model1. Wiley Online Library,

Ye M, Meyer PD, Neuman SP (2008) On model selection criteria in multimodel analysis Water Resources Research 44

Zhang X, Srinivasan R, Van Liew M (2008) Multi-site calibration of the SWAT model for hydrologic modeling Transactions of the ASABE 51:2039-2049

Proceedings of the 10th World Congress of EWRA 'Panta Rhei', 5-9 July 2017, Athens, Greece
© 2017 *European Water Resources Association*

Identification of potential locations for groundwater pumping and recharge to minimize the impact of floods and droughts in the Ganges basin

L. Surinaidu[1*], D. Kumar[1], U. Amarasinghe[2] and M.J. Nandan[1]
[1] *CSIR-National Geophysical Research Institute (NGRI), Hyderabad, India*
[2] *International Water Management Institute (IWMI), Colombo, Sri Lanka*
[*] *e-mail: suryangri@gmail.com*

Abstract: Floods and droughts are very frequent in the Ganges basin that flows across four countries namely Nepal, India, Bangladesh and Bhutan. In the monsoon season, floods are causing damage to huge property, agriculture and loss for many lives. On the other hand in the non-monsoon season, downstream areas mostly in Bangladesh and Indian territories are facing acute water shortage for agriculture and navigation. During the last four decades, many studies were conducted by various researchers to understand the impact of groundwater pumping and recharge on floods and droughts. The results indicated that creating subsurface storage during the non-monsoon season by extracting groundwater and storing flood water during the rainy season can reduce the impact of both floods and droughts in the basin. Identification of such locations is very critical and detailed information is not available. In the present study, attempts were made to identify potential locations in Ramganga sub-basin of the Ganges for pumping, recharge and both pumping-recharge by integrating pertinent hydrological and hydrogeological information using Arc GIS. The analysis results revealed that in the Ramganga sub-basin, 14,515 km^2 area is suitable for groundwater pumping in the non-monsoon with simultaneous recharge in monsoon and 8,419 km^2 area is highly potential for immediate groundwater recharge. The implementation of the technique can increase the basin ecosystem service by increasing groundwater availability and river flows while reducing impacts of floods and droughts with huge potential to implement elsewhere in the similar kind of river basins.

Key words: Ganges basin, Ramganga, recharge, floods, groundwater pumping, Arc GIS

1. INTRODUCTION

River Ganges and its tributaries formed a large flat and fertile lands in India and Bangladesh. It flows mainly through Nepal, India, Bangladesh and Tibet (China) that covers 10,86,000 km^2 (http://india-wris.nrsc.gov.in/). The lands are very fertile with abundant water resources and suitable climate that creates developed agriculture based civilization. On the other hand, monsoonal floods are causing loss of life, property, crops, infrastructure, etc. However, in the nonmonsoon season surface water flows are not sufficient to meet minimal water requirement for navigation and irrigation mostly in the downstream parts of Ganges those are Bangladesh and India between Haridwar and Allahabad during December to May. On an average Ganga basin receives 1 million cubic meters (MCM)/km^2. Of this, 30% is evaporation, 20% seepage to sub-surface and remaining 50% is available as surface runoff. In all tributaries of Ganges has flooding characteristics with 0.5-2 km width of river banks. This active flood plain floods every year (http://nmcg.nic.in /hydrology.aspx).

Therefore, Revelle and Lakshminarayana (1975) have suggested pumping groundwater near rivers in non-monsoon to create subsurface storage that can fill during monsoon by natural infiltration and river seepage. He also suggested that in the non-monsoon season the stored water can seep towards the rivers that can increase dry season flows. During last four decades, a lot of water resource development has taken place. Now the scenario has been changed and it is required to implement distributed recharge with pumping that can minimize the impact of floods (Surinaidu et al. 2016). In the present study, an effort has been made to identify the potential locations for recharge and groundwater pumping by considering high resolution hydrogeological data base for

the Ramgana sub-basin basin that methodology can be up scaled to the basin scale.

2. GEOLOGY AND HYDROGEOLOGY

Ramganga is the first major tributary that joins the Ganges River, which is having a catchment area of 25086 km2 (Figure 1). The topographic elevation of the Ramganga sub-basin varies from 1,000 to 3,071 m above mean sea level (amsl) in the northern part. The river falls to an elevation less than 360 m amsl after entering the alluvial Ganga Plains. In the plains, the topography ranges from 360 m in Bijnor District to 124 m in Hardoi District in the south. The river flows through the states of Uttarakhand (formerly Uttaranchal) and Uttar Pradesh and has a total length of 595 km. (Water Resources Information System of India [http://www.india-wris.nrsc.gov.in]). The average annual rainfall from 1996 to 2010 in the Ramganga Sub-basin was 923 mm, with a minimum of 506 mm in 1997 to a maximum of 1,221 mm in 1998. The basin receives 90% of the rainfall during the monsoon period from July to September (Surinaidu et al. 2016).

The geology of Ramganga basin consists of a variety of lithologies such as inner lesser Himalaya comprises of bedrocks belonging Damtha and Tejam groups and Berinag Formation. The upper parts of the basin (Almora, Garhwal, and Nainital) is Crystallines defined by a variety of schists, micaceous quartzites and gneisses. The lower parts below foothills (Bijnor to Hardoi) filled by Holocene, Quaternary and the Precambrian age alluvium. The detailed geology of the Ramganga sub-basin has explained by Asthana et al. 2015. The subsurface lithology in the Ramganga was indicated clay with silt and sand on the surface and it is underlaid by sand with gravel and boulders with varying proportion (Surinaidu et al. 2016).

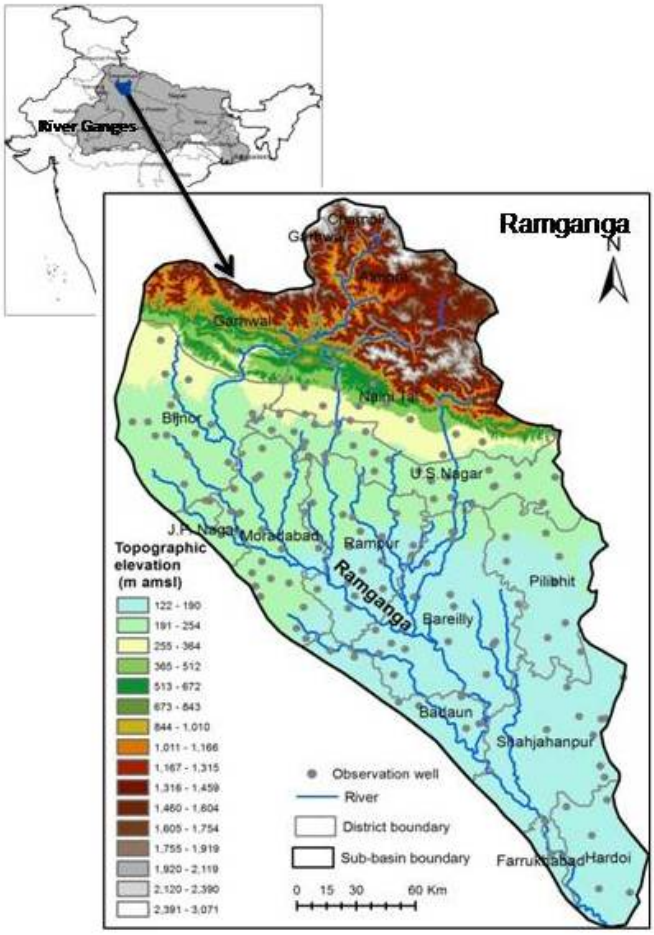

Figure 1. Location of the Ramganga sub-basin and streams with stream order

3. DATA AND METHODOLOGY

GIS techniques have been used by many researchers to identify potential groundwater zones in different river basins (Daiman and Gupta, 2015). The data has been collected from a different organization such as district groundwater boards and web based information. In the present study, integrated GIS technology has been used to generate various thematic maps viz., geology, lineaments, slope, drainage, land use-land cover, soils, annual rainfall and groundwater level. The maps were converted into raster format using the spatial analysis tools and then all thematic layers were reclassified (figure 2 and figure 3).Subsequently, the weighted overlay analysis method was used to assign suitable weights (ranking system) on their hierarchy of importance and integrated all thematic layers in the process of identification of groundwater recharge areas, and to facilitate the demarcation of potential zones for groundwater recharge and groundwater pumping. The weights assigned to the different layers have considered according to Raymond et al. (2009). The final product shows very poor to very good locations for groundwater recharge (Fig. 4). On the other hand, poor zones for groundwater recharge is highly potential for groundwater pumping.

4. RESULTS

The collected information has been analyzed and reclassified using Arc GIS. The weights and ranks have been assigned based on their importance for groundwater recharge. The following layers have been considered in the integrated analysis.

4.1 Land use and land cover

In the present area land use and the land cover map is extracted from IWMI global land use maps (http://waterdata.iwmi.org/Applications/GIAM2000/). The distribution of different land use patterns in the area is shown in figure 2a. The major land use pattern in the Ramganga basin is agriculture lands followed by forest lands. In the analysis of recharge locations, urban lands and existing water bodies were given low priority and forest and agriculture lands were given high priority (Fig. 2a and Table 1).

4.2 Soil Type

The Ramganga sub-basin is occupied by alluvial soils that can have good recharge and water retention capacity. Distribution of different soil types are presented in Figure 2b. Ustifluvents, typichaplaquepts and fluent soils are given greater priority for recharge and other soils less priority in the analysis.

4.3 Topography and Slope

Slope index was derived from the DEM (ASTER 30m resolution) to find the ratings for recharge, it was reclassified and given priority for more recharge for less slopes and less or nil priority for greater slopes. The spatially distributed slope map was presented in Figure 2c. The generated slope ranges from 1-2% in the plains and whereas in uplands it is >6% (Fig. 2c and Table 1). Since there are no major variations in slope in the plains, the slope has been neglected in the analysis.

4.4 Rainfall

Rainfall is the principle source of all groundwater aquifers. Rain fall distribution is attempted by taking 12 stations data distributed across the area from 2000-2010. The average rainfall varies from 575 mm to >1400 m. The high rainfall high priority and low rainfall low priority was given in the area (Figure 2d and Table 1). However, rainfall recharge depends on several other factors such as

topography and hydrogeological conditions.

Lineaments:

Lineaments are preferential pathways for infiltration and retention of more water. Hence, major lineaments are extracted from (http://www.india-wris.nrsc.gov.in) and prepared lineament density map. The high density facilitates more recharge and good potential for groundwater, so that, greater preference for high dense lineaments and low preference for low density lineaments. The spatially distributed lineament map is presented in (Figure 3a and Table 1).

Table 1. Range of different thematic layers and its ranking based on priority in the Ramganga R-Ranking

Drainage density (/km^2)		**Groundwater level in m (bgl)**		**Lineament /Km^2**		**LULC**		**Rainfall (mm)**		**Slope**	
Range	R	Range	R	Range	R	Range	R	Range	R	Range	R
0.0-0.2	9	2.13-3	1	0-0.01	1	Urban	0	575-600	2	0-1	6
0.2-0.4	8	3-4	2	0.01-0.03	2	Forest Evergreen	0	600-750	6	1-2	5
0.4-0.6	7	4-5	3	0.03-0.05	3	Forest Deciduous	1	750-900	7	2-3	4
0.6-0.8	6	5-6	4	0.05-0.1	4	Forest Mixed	1	900-1050	7	3-4	3
0.8-1	5	6-7	5	0.1-0.15	5	Pasture	7	1050-1200	8	4-6	2
1-1.2	4	7-8	6	0.15-0.25	6	Range Grasses	7	1200-1300	8	>6	1
1.2-1.4	3	8-10	7	0.25-0.35	7	Range Brush	7	1300-1400	8		
1.4-1.6	2	10-15	8	0.35-0.45	8	Water	0	>1400	9		
1.6-1.98	1	>15	9	0.45-0.7	9	Snow	0				
						Agricultural Land Generic	9				

4.5 Groundwater

In the groundwater analysis, observation records of 150 wells for 10 years (2000-2010) were considered. Then, the average pre-monsoon water level map is prepared. In the study area, groundwater level fluctuations are varying from <3 m to > 15 m in pre-monsoon. The greater groundwater depths have given high priority for groundwater recharge and whereas areas having less groundwater depths are considered for potential locations for groundwater pumping (Fig 3b and Table 1).

4.6 Geology

Geology plays a greater role in occurrence and movement of groundwater and recharge capacity with different well yields. Hence geology layer is integrated for identification of both pumping and managed aquifer recharge locations. The geology map indicated that the Ramganga sub-basin filled by alluvial sediments and the uplands are covered by crystalline rock formations (Fig 3c).

4.7 Drainage

The drainage of the study is derived from the analysis of ASTER 30 m resolution DEM data. The drainage density map was prepared using the spatial analysis tool in Arc GIS. The drainage density values thus obtained were reclassified to prepare a drainage density map of the study area. In general, drainage represents geological and lithological characteristics of the area, more drainage represents hard rocks and more runoff with poor recharge and low drainage density is good to recharge and low runoff. The high ranks for less drainage density and low ranks for high drainage density are considered in the study. The spatial distribution of drainage density map is presented in (Figure 3d and Table 1)

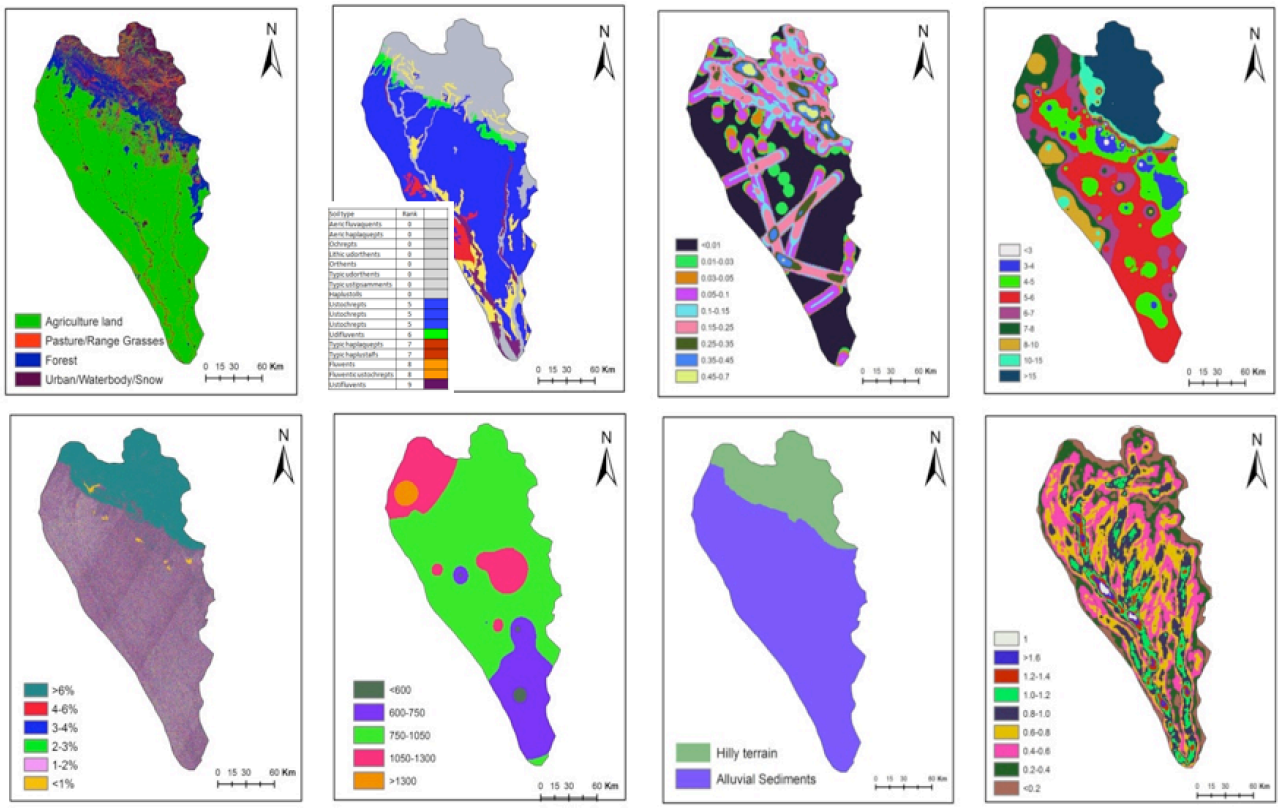

Figure 2. Reclassified thematic layers of Ramganga for identification of recharge and pumping

5. DISCUSSION

The potential unmet water demand in the Ramganga sub-basin is estimated under two scenarios by Amarasinghe et al. 2016. The first scenario assumed that irrigation will be provided to all irrigable area in the Rabi season (November to March) and hot-weather season (March to June). The second scenario assumes that irrigation will be provided to all cropped areas in the Rabi and hot-weather season. The estimated potential unmet demand under the two scenarios ranges from 2.5 to 3.3 Bm3. However, due to water supply constraints, the potentially reliable unmet water demand in the Ramganga sub-basin is about 2.5 Bm3. Muthawatte et al. 2015 have estimated runoff from the Ramganga sub-basin 10.1 Bm3 (75% dependable flows), and approximately 83% of this runoff is occurring during the rainy season. It contributes to 7% of the total inflow from the upstream areas to the regularly flood-stricken Bihar, which is located in the middle part of the Gangas River Basin (Muthuwatta et al. 2015). However, to meet the maximum unmet agricultural water demand in the Ramganga sub-basin only require capturing 33% of the monsoon flows. Surinaidu et al. 2016 have suggested that 4 m subsurface storage could be created by pumping of 0.25 Bm3/yr by the year 2020. If the flood waters stored in sub-surface that can minimize the flood impact on downstream and increase the dry season flows. The high hydraulic conductivities of aquifers in the Ganga basin can increase the base flows to the rivers in the dry season after storing the water in the monsoon. In order to store flood waters, there should be storage in the aquifers. For this, aquifer should be explored for groundwater pumping. However, in some places of the basin storage space is already available. Hence, identification of locations for both recharge and pumping is the trivial task.

The groundwater recharge depends on several factors such as soils, geology, hydrogeology and rainfall. It is essential to integrate all of these thematic layers to identify potential locations for both groundwater recharge and pumping. In the present study the integration of various thematic layers has been carried out using Arc GIS. The weights and ranks with a total score of each thematic layer are presented in Table 2. The slope will have great importance in groundwater recharge and hence highest weight 20 was given. But in the Ramganga slope variations in the plains are almost

negligible that varies from 1-2% so that it has given low rank 1. Geology, groundwater depths, and rainfall are major driving factors in the basin for recharge, so that these layers are assigned highest weight of 15 then drainage density was given 10. The highest rank was given layers based on their importance for recharge viz., LULC, geology, groundwater levels, rainfall, soil, drainage density and lineament density.

The final integrated map for identifying recharge and pumping is obtained by multiplying of the ranks and weights of the layers then the summing of all pixel values of the different classes. The final product for identifying potential recharge and pumping locations are presented in Figure 4 which indicated that 7526.8 km^2 and 1192.7 km^2 area in the Ramganga is having good to very potential groundwater recharge. The recharge structures can be selected based on local hydrogeological conditions. However, the poor recharge areas mean the areas having shallow groundwater tables in the Ramganga and these locations can be potential zones for further groundwater pumping. In the Ramganga 1852km^2 area is highly suitable for groundwater pumping. In addition 14515 km^2 area is also suitable for groundwater pumping but this needs to be filled up by means of artificial recharge during the monsoon season (Fig. 4). The additional pumped out water can bring the additional area under irrigation or can increase the intensity of the irrigation. The subsurface storage can be filled with monsoon rains/flood water that minimizes floods in the downstream and increases water accessibility in the basin.

Table 2. Integration of different thematic layers and overall ranking and Weight

Thematic layer	Weight	Rank	Total Score
LULC	15	9	135
Soil	5	5	25
Slope	20	1	1
Rainfall	15	7	105
Lineament density	5	2	10
Groundwater levels	15	8	120
Geology	15	9	135
Drainage density	10	4	40
Total	100		571

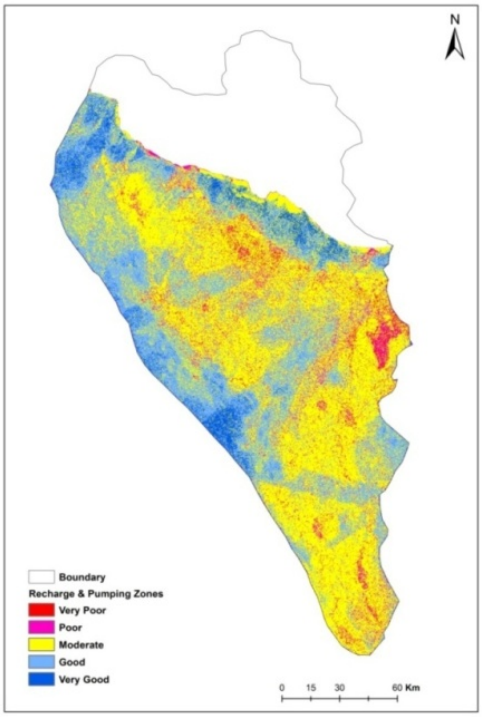

Figure 4. Hot spot locations for both pumping and recharge in the Ramganga (Very poor - 273.2 km^2, Poor-1579 km^2, Moderate -14515 km^2, Good - 7526.8 km^2, Very good - 1192.7 km^2)

Notes:

- Hilly portion was excluded in the analysis
  Immediate pumping can be implemented in very poor to poor regions that covers 1852 km^2
  Start with groundwater pumping than recharge in an area of 14515 km^2 (Moderate)
- Area should start with recharge first and highly potential for immediate recharge is 8719 km^2 (Good to very good)

6. CONCLUSIONS

The Ramganga sub-basin receives an average annual rainfall of 930 mm/year. The most upstream parts of the basin are highly elevated >2000 m amsl. The downstream areas are low elevated <190 m amsl and flat terrain. The Ramganga plains have very less slope with 1-2% with Gangetic alluvial deposits with a lot of scope for groundwater recharge. Most of the basin is covered by agricultural and then forest lands. The well managed conjunctive utilization of land and water resources can create ample scope for creating additional subsurface water storage that can bring additional land under irrigation. In the Ramganga basin, 1852 km^2 is available for additional groundwater pumping, in addition, 14515 km^2 is also available for groundwater pumping but groundwater recharge should also be initiated after creating sub-subsurface storage by pumping. The groundwater recharge should be implemented and 8719 km^2 of land is highly potential for immediate groundwater recharge.

ACKNOWLEDGEMENTS

This research study was undertaken as part of the CGIAR Research Program on Water, Land and Ecosystems (WLE) by the International Water Management Institute (IWMI).

REFERENCES

Revelle, R., Lakshminarayana, V.1975. The Ganges water machine. Science 188(4188): 611-616.

Surinaidu, L., Muthuwatta, L., Amarasinghe, U.A., Jain, S. K., Ghosh, N.C., Sudhir K. and S. Singh 2016. Reviving the Ganges Water Machine: Accelerating surface water and groundwater interactions in the Ramganga Sub-basin. Journal of Hydrology, 10.1016/j.jhydrol.2016.06.025

Asthana, A. K. L., Gupta, A.K., Luirei, K., Bartarya, S. K., Rai, S. K., Tiwari, S. K. 2015. A

Quantitative Analysis of the Ramganga Drainage Basin and Structural Control on Drainage Pattern in the Fault Zones, Uttarakhand. Journal Geological Society Of India. 86, 9-22

Daiman, A., Gupta, N.2015. Identification of groundwater recharge zones and rainwater harvesting sites using geo-informatics: A case study of Karwan watershed in Sagar district of Madhya Pradesh, Journal of Geomatics, Vol.9(2), 198-202

Raymond, A., Duraiswami, D.V., Shetty, V. 2009. Geospatial mapping of potential recharge zones in parts of Pune City. Journal Geological Society of India, 73:621–638

Amarasinghe, U.A., Lal Mutuwatta, Lagudu Surinaidu, Sumit Anand, and S. K Jain. 2016. Reviving the Ganges Water Machine. Potential. Hydrol. Earth Syst. Sci. 20, 1085–1101

Muthuwatta, L., Amarasinghe, U., Sood, A., Surinaidu, L. 2015. Identifying potential areas for augmenting sub-surface water storage in the ganges river basin, hydrol. Earth syst. Sci. Discuss., 12, 9741-9763

II. Climate and Water Resources

Proceedings of the 10th World Congress of EWRA 'Panta Rhei', 5-9 July 2017, Athens, Greece
© 2017 *European Water Resources Association*

The effect of storage under climate change in Southern European basins

A. Granados*, L. Garrote, A. Sordo-Ward and F. Martin-Carrasco
Department of Civil Engineering: Hydraulics, Energy and Environment. Technical University of Madrid, Spain
** e-mail: a.granados@upm.es*

Abstract: The dominant strategy to address water resources variability and uncertainty in water-scarce regions is the development of reservoir storage. This paper presents an analysis of the role of storage in water availability in Southern Europe as a strategy for climate change adaptation. Water availability is computed for 16 basins under current and future climate scenarios. Climate scenarios cover the full array of projections made under the SRES and RCP emission scenarios with a variety of regional climate and hydrologic models. Water availability is analysed as a function of emission scenario, changes in mean annual flow, changes in variability and reservoir storage. A total of 16 model runs were computed for the reference scenarios and 35 model runs for the climate change scenarios. Results were analysed under the hypothesis of equiprobability of all scenarios, comparing the probability distribution of water availability under reference conditions to that under climate change. The results show significantly different behaviours in the group of basins analysed. For basins with large storage values the reductions of water availability were similar to the reductions of mean annual flow. For basins with less storage, the probability distributions of reductions tend to differ, with increased uncertainty for availability. The role of storage was further analysed through a sensitivity analysis performed obtaining water availability under current and future conditions with variable values of reservoir storage, ranging from 25% to 200% of current values. The results show that uncertainty under climate change is reduced for basins with large storage values.

Key words: Water resources, climate change, water availability, reservoir storage

1. INTRODUCTION

Many studies have addressed the potential impact of climate change on hydrology and water resources and the corresponding adaptation measures (Arnell, 1999; Vörösmarty et al., 2010; Krysanova et al., 2010). Future scenarios for Southern Europe suggest a progressive decay of mean annual runoff and changes in seasonal and inter-annual variability which may threaten sustainability of current water uses. The development of reservoir storage has been the dominant technical strategy to fight hydrologic variability and uncertainty in this region. A significant investment in dam construction was made during the second part of the 20th century in Southern European countries. The current availability of reservoir storage enables advanced water management schemes and is perceived as a valuable asset to facilitate climate change adaptation. In this paper we present an analysis of the role of storage in water availability in Southern Europe as a possible strategy for climate change adaptation. We perform a comparative study of the impacts of climate change on water availability in 16 representative basins of Southern Europe. The study is focused on the analysis of three critical factors in regulated water resources systems: streamflow variability, storage capacity and water availability.

2. DATA AND METHODS

2.1 Area under analysis

The area under analysis is composed of 16 major river basins in Southern Europe that are shown in Figure 1. The area is divided in a number of subbasins, following the "Hydro1k" data set (EROS,

2008). The original subbasins were processed to eliminate basins too small (less than 1000 km^2), which were merged to neighbouring basins. The reservoir storage volume in every subbasin was obtained from the ICOLD World Register of Dams (ICOLD, 2003). We selected dams in the register with more than 5 hm^3 of storage capacity, excluding dams managed only for hydropower. All dams located in a given subbasin were grouped in an equivalent reservoir adding the storage volume and flooded area. The main characteristics of the basins considered in this study are shown in Table 1.

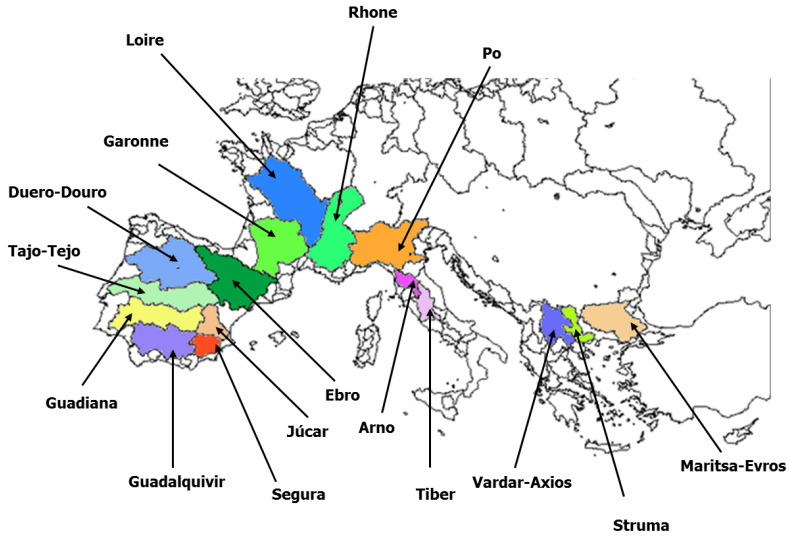

Figure 1. Southern European basins considered in this study.

2.2 Current and future runoff scenarios

The analysis performed in this work is based on three previous studies that include Southern European basins.

The study by (Gonzalez-Zeas et al., 2014) used the output of regional climate models from the PRUDENCE project (Christensen et al. 2007) in emission scenarios A2 and B2. The study compared the projections made by eight RCMs nested in a single global model, referred to as HadAM3H, in current (1960-1990) and future (2070-2100) time slices.

The study by (Garrote et al., 2015a) analysed the major Mediterranean river basins of Europe. Naturalized streamflow was obtained from the results of the regional climate models of the ENSEMBLES project (Hewitt and Griggs, 2004), using several transient model runs available for the time period from 1960 to 2100 produced by three RCMs under emission scenario A1B. Three time slices were considered: historical (1960-1990), short term (2020-2050) and long term (2070-2100)

The study by (Garrote et al, 2015b) analysed 1261 subbasins covering the entire territory of Western Europe. Naturalized streamflow was obtained from the results of the application of the PCRGLOBWB model (van Beek and Bierkens, 2009) to the Inter-Sectorial Impact Model Intercomparison Project (Warszawski, et al., 2014). The PCRGLOBWB model was forced with five global climate models under historical conditions and climate change projections corresponding to four Representative Concentration Pathways scenarios: RCP2P6, RCP4P5, RCP6P0 and RCP8P5. Two time slices were considered in this analysis: historical (1960-1999) and long-term projection (2060-2099).

A total of 16 model runs were available for the historical period (eight model runs from the PRUDENCE project, three model runs from the ENSEMBLES projects and five model runs from the PCRGLOBWB model. In order to assess the quality of the hydrological projections, time series obtained in the current scenario are compared to the best estimate available for runoff under current conditions. This study used the annual surface runoff layer of the UNH/GRDC dataset (Fekete et

al., 2004) as a reference to compare the results obtained at the working scale of each RCM. For the long-term projection a total of 35 model runs were available: eight runs corresponding to the A2 scenario, four runs corresponding to the B2 scenario, three runs for the A1B scenario, five runs for RCP2P6 scenario, five runs for RCP4P5 scenario, five runs for RCP6P0 scenario and five runs for RCP8P5 scenario.

Table 1. Basic characteristics of the basins analysed in this study

Basin	Basin Area (A) (10^3 km^2)	Mean Annual Flow (MAF) (km^3/yr)	Storage Volume (V) (km^3)	MAF/A	S/MAF
Arno	10.30	4.22	0.07	0.41	0.02
Po	84.73	46.46	0.93	0.55	0.02
Loire	115.91	30.43	0.73	0.26	0.02
Tiber	17.31	8.58	0.36	0.50	0.04
Garonne	79.67	26.30	1.81	0.33	0.07
Rhone	88.43	42.71	3.72	0.48	0.09
Struma	16.81	2.36	0.23	0.14	0.10
Douro	96.24	18.39	3.48	0.19	0.19
Vardar-Axios	22.73	5.19	1.17	0.23	0.23
Ebro	84.90	14.16	4.63	0.17	0.33
Guadalquivir	54.96	8.51	6.29	0.15	0.74
Maritsa-Evros	52.60	3.97	3.57	0.08	0.90
Tagus	69.73	9.66	8.88	0.14	0.92
Jucar	21.83	1.02	2.58	0.05	2.53
Guadiana	60.85	4.34	14.19	0.07	3.27
Segura	17.55	0.14	1.14	0.01	8.36

2.3 Water availability analysis

Potential Water Availability (PWA) is estimated with WAAPA model (Garrote et al., 2011). This model simulates the operation of a water resources system with several reservoirs. WAAPA main components are inflows, reservoirs and demands, all linked to points in the river network. The model computes the amount of water supplied to demands from a system of reservoirs accounting for ecological flows and evaporation losses. Input data are monthly inflows in relevant points of the river network, monthly required environmental flow in every reservoir, monthly demand values sorted by priority with the corresponding return flow, monthly maximum and minimum capacity, storage-area relationship and monthly evaporation rates in every reservoir and reservoir initial storage. All reservoirs in the basin are coordinated to satisfy the set of demands, drawing water preferably from reservoirs located upstream. The results are the following set of time series: monthly volumes supplied to each demand, monthly storage values and monthly values of spills, environmental flows and evaporation losses in every reservoir. Demand reliability can be computed from this output applying any conventional procedure.

WAAPA can obtain potential maximum water availability for a given reliability criterion through an iterative scheme that changes global demand values until the reliability criterion is met with a given precision. In this study, PWA is estimated by considering only one type demand present in the system, with constant monthly distribution. Ecological flows are specified as the 10% percentile of the monthly marginal distribution. System performance is evaluated as gross volume reliability. Water availability is obtained for 92% volume reliability.

3. RESULTS AND DISCUSSION

3.1 Climate projections

Climate projections were taken from the runoff variable of RCM models in the PRUDENCE and

ENSEMBLES projects and of the PCRGBLOBWB model. Mean and coefficient of variation of annual flows were computed for each basin during the historical period and during the long term projection. Changes in the long term projection were estimated taking the control period as a reference, applying the following expressions:

$$\Delta MAF = \frac{MAF_{PROJ} - MAF_{HIST}}{MAF_{HIST}} \quad ; \quad \Delta CV = \frac{CV_{PROJ} - CV_{HIST}}{CV_{HIST}} \tag{1}$$

where MAF is Mean annual flow, CV is coefficient of variation and the sub-indices HIST and PROJ refer to the historical period and to the long-term projection.

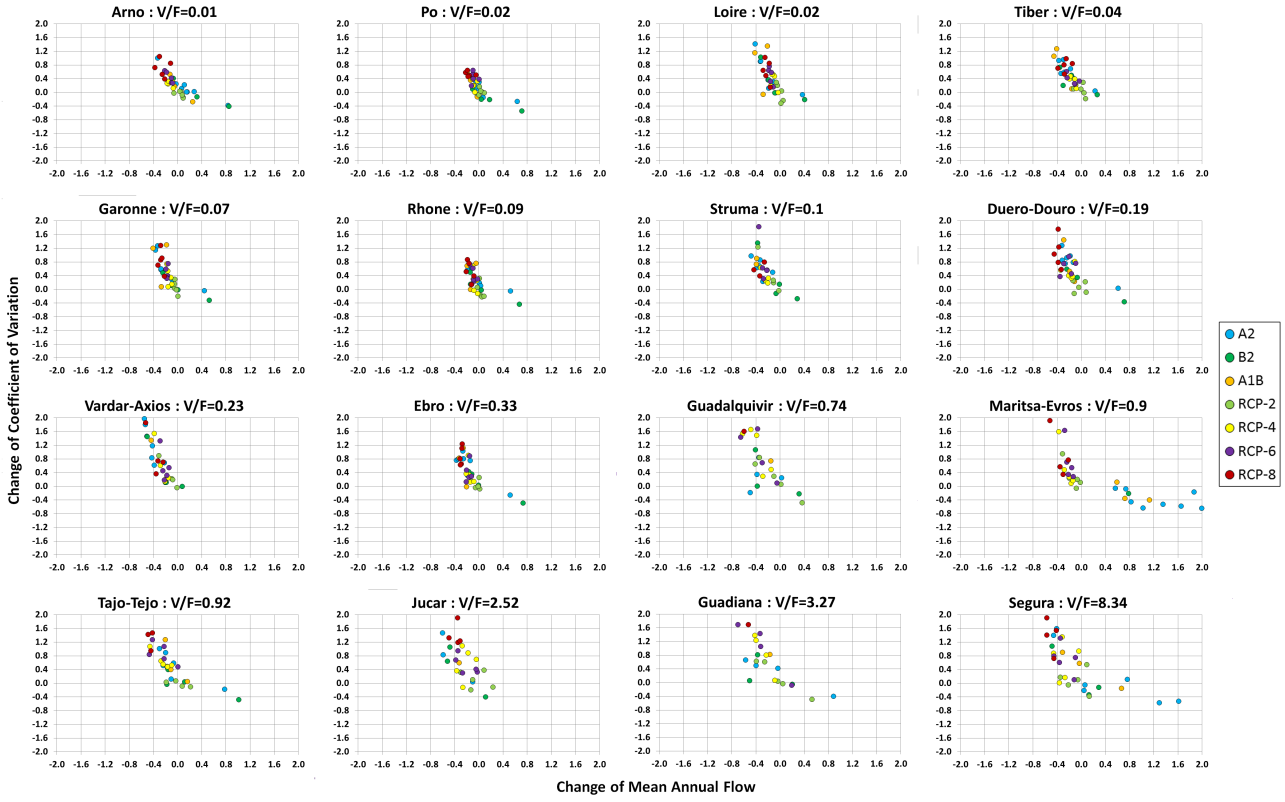

Figure 2. Relative changes in Mean Annual Flow and Coefficient of Variation of Annual Flow for the 35 available projections in the 16 basins under study.

Figure 2 compares the relative changes in MAF and CV for the 35 available projections in the 16 basins under study. Figure 2 shows a general tendency of reduction of MAF and increase of CV in most basins with clear implications for water availability. This tendency is stronger for A2 and RCP8 emission scenarios and for basins with larger storage capacity that are already facing strong hydrologic irregularities. It can also be seen that expected changes in CV are much larger than changes in MAF, with many basins reaching extreme values close to 2. The basins showing more extreme projections are Maritsa-Evros, Guadiana and Segura.

3.2 Water availability

Potential Water Availability (PWA) was computed for the historical period and for the long-term projection in the 16 basins under analysis using the WAAPA model. The results are shown in Figure 3, which presents the estimated cumulative probability distribution function of PWA in the historical period and in the long-term projection based on the assumption that all model runs are equiprobable. The corresponding emission scenario is identified for each model run available in the

long-term projection. The results show a large uncertainty in the estimation of PWA, both in the historical and in the projection periods. There is no apparent correlation between the emission scenario and the projected PWA. Values corresponding to different emission scenarios are mixed and the most extreme scenarios (A2 and RCP8) do not always produce the minimum values for PWA. It should be noted that all model runs available in the historical period were corrected for bias with respect to the GRDC estimation of MAF and therefore the uncertainty in PWA is only due to the different seasonal and interannual variability produced by each model run, because all share the same MAF value. Unfortunately, the skill of the models to reproduce current hydrological conditions in the basins cannot be evaluated because there are no available global data sets on interannual streamflow variability.

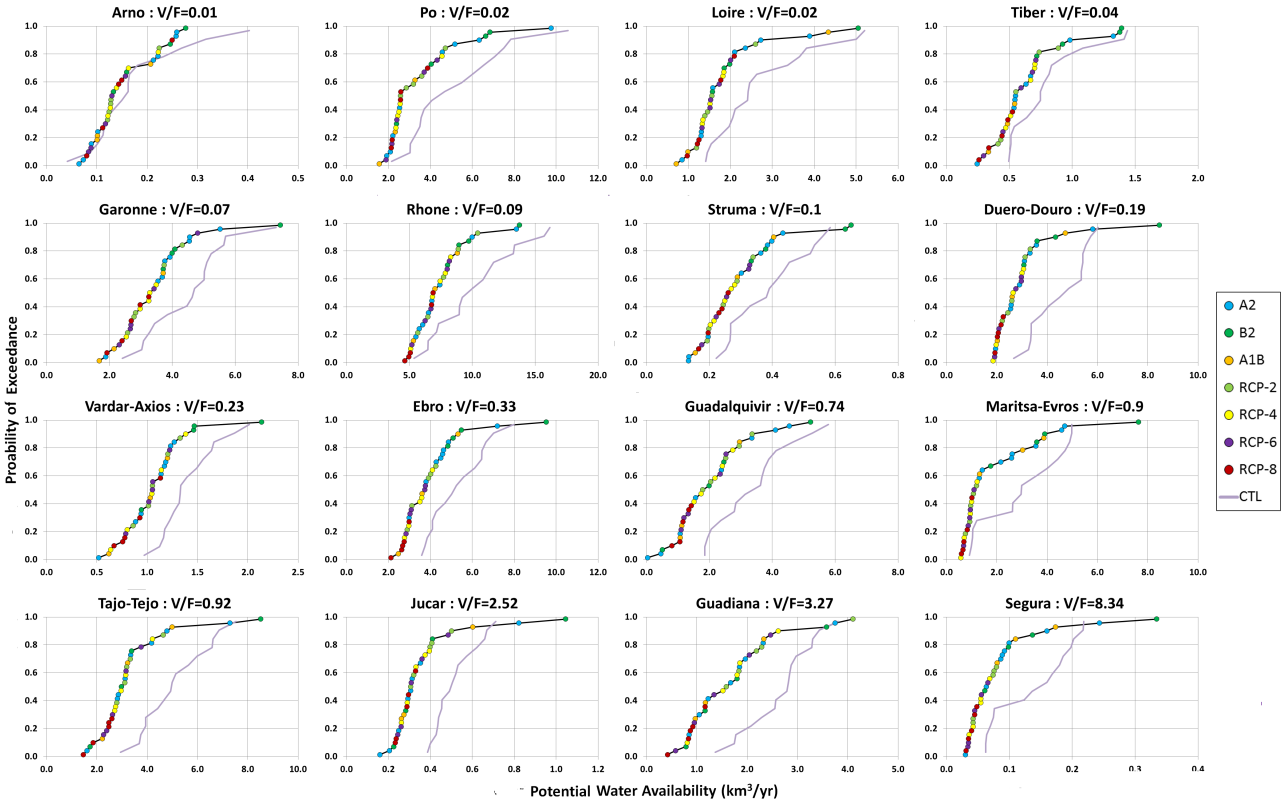

Figure 3. Estimated cumulative probability distribution function of potential water availability (km^3/yr) in the historical period (CTL: 16 model runs) and in the long-term projection (35 model runs) in the 16 basins under study.

According to model results water availability is expected to decrease significantly in all basins, although the uncertainties in PWA estimation are much larger than the expected average decrease due to large model uncertainty. The most significant reductions are projected for the basins of South Western Europe: Guadiana, Guadalquivir and Segura.

The estimated changes in PWA are compared to estimated changes in MAF in Figure 4. In this figure the probability distributions of changes are estimated from the comparison of values obtained in the long-term projection and the control period for the same model, applying the following expressions:

$$\Delta MAF = \frac{MAF_{PROJ} - MAF_{HIST}}{MAF_{HIST}} \quad ; \quad \Delta PWA = \frac{PWA_{PROJ} - PWA_{HIST}}{PWA_{HIST}} \tag{2}$$

where MAF is Mean Annual Flow, PWA is Potential Water Availability and the sub-indices HIST and PROJ refer to the historical period and to the long-term projection.

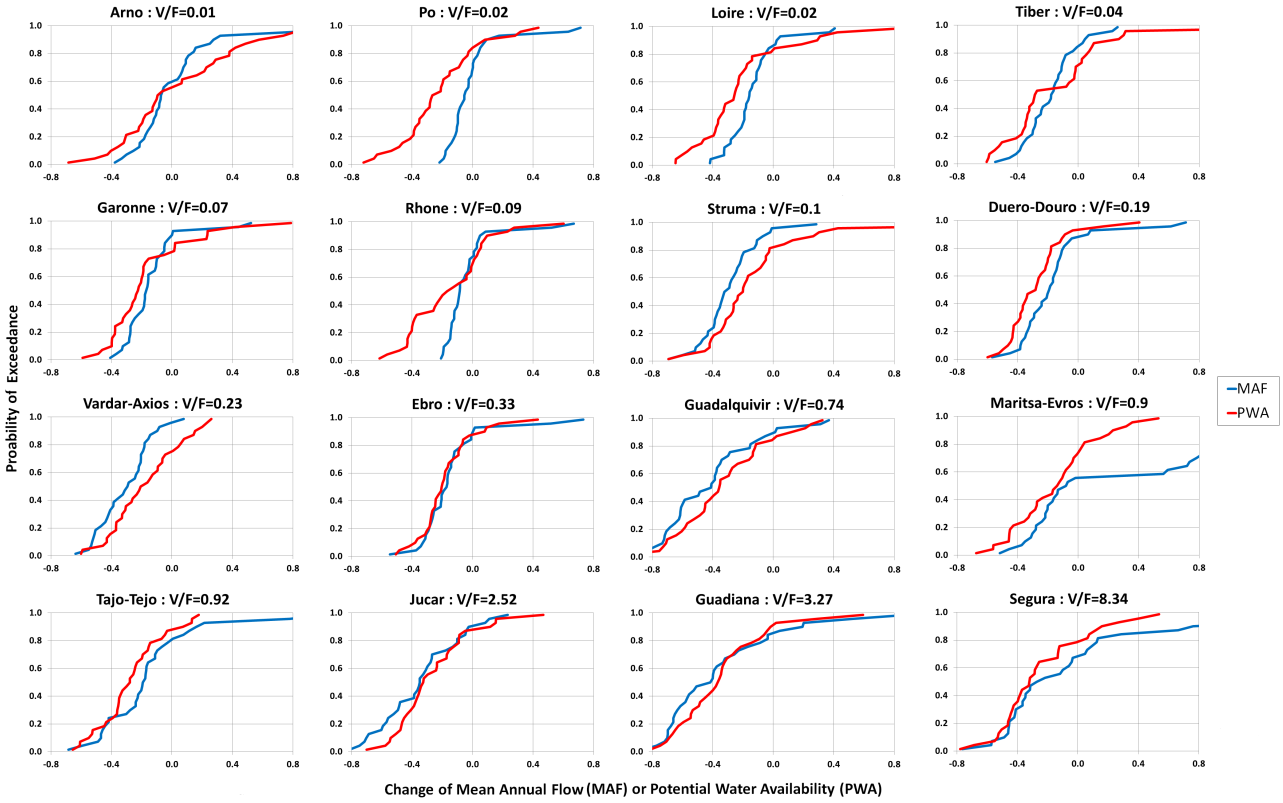

Figure 4. Estimated cumulative probability distribution function of changes in Mean Annual Flow and changes in Potential Water Availability for the 16 basins under analysis.

The analysed basins show a wide range of behaviours. For some basins, like Ebro, the distributions of expected changes in MAF and PWA are very similar. For other basins, like Struma, Vardar-Axios or Guadalquivir the expected reductions in PWA are less than the expected reductions in MAF, suggesting that the availability of reservoir storage tends to dampen the effect of climate change. In a third group of basins, the probability distributions of MAF and PWA cross each other, producing a larger variability in PWA than in MAF. This effect may be due to the changes in variability, which directly affect water availability. Finally, some basins like Duero-Douro present larger expected reductions in PWA than in MAF.

3.3 The influence of storage

In order to assess the influence of reservoir storage on changes of water availability we conducted the water availability analysis for different storage volumes. We asummed variable reservoir volumes of 25%, 50%, 75%, 100%, 125%, 150% and 175% of current storage and computed water availability in current and future scenarios in the 16 basins. The results obtained were fitted to normal probability distributions, assuming that all scenarios computed are equally likely. The results are shown in Figure 5 which presents the probability distribution of changes in MAF (blue line) and PWA for different storage values in coloured lines from brown (25% of current storage volume) to green (175% of current reservoir storage). The results show variable sensitivity to storage in the different basins analysed. Some basins, like Arno, or Maritsa-Evros, showed very little sensitivity while others, like Po, Tiber, Struma or Guadalquivir presented significant differences in behaviour depending on the storage volume assumed.

A remarkable effect shown in Figure 5 is that the uncertainty on changes in MAF seems to grow as reservoir storage grows. Basins with largest reservoir storage, like Guadiana or Segura, show much larger uncertainty on changes in MAF than basins with relatively small storage capacity, like Arno, Po or Loire. This effect is likely due to the fact that reservoir storage has been developed in

basins where hydrologic variability is larger. In fact, the difference in uncertainty between changes in MAF and changes in PWA, which is very high in basins with small storage, is progressively reduced as basin storage increases.

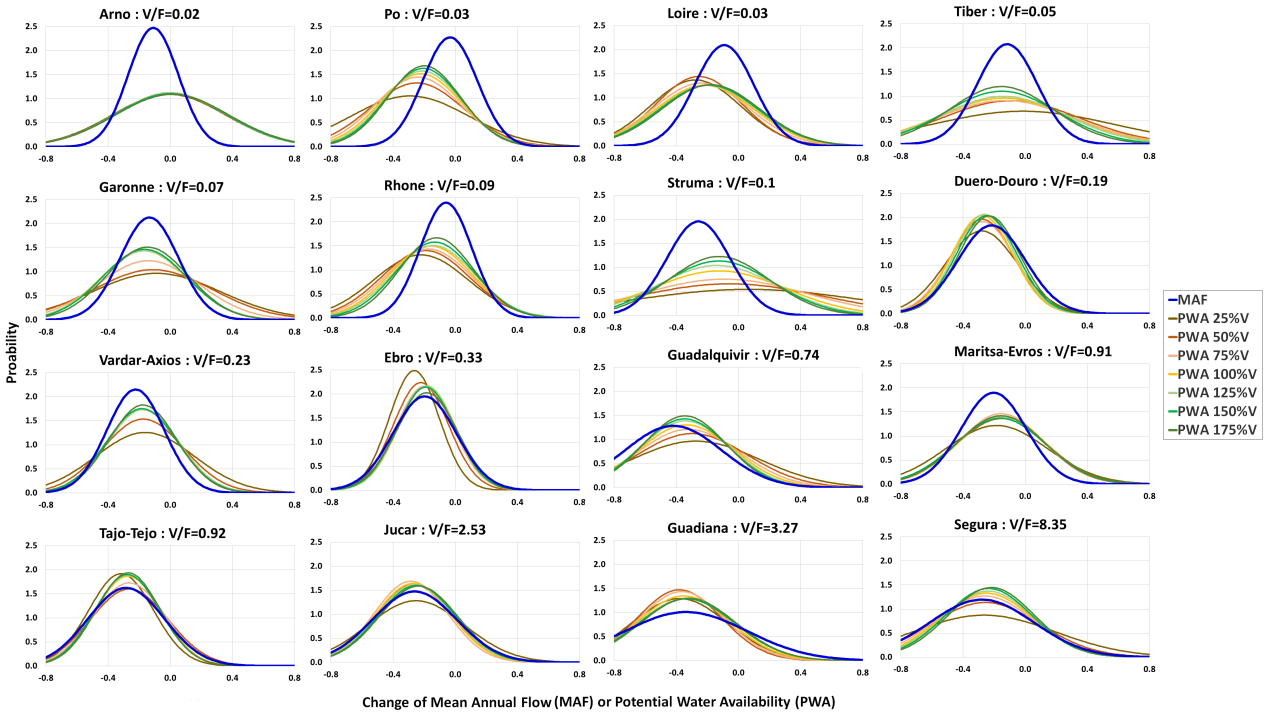

Figure 5. Probability distribution of changes of Mean Annual Flow and Water Availability for different storage values (from 25% to 175% of current storage volume) in the 16 studied basins.

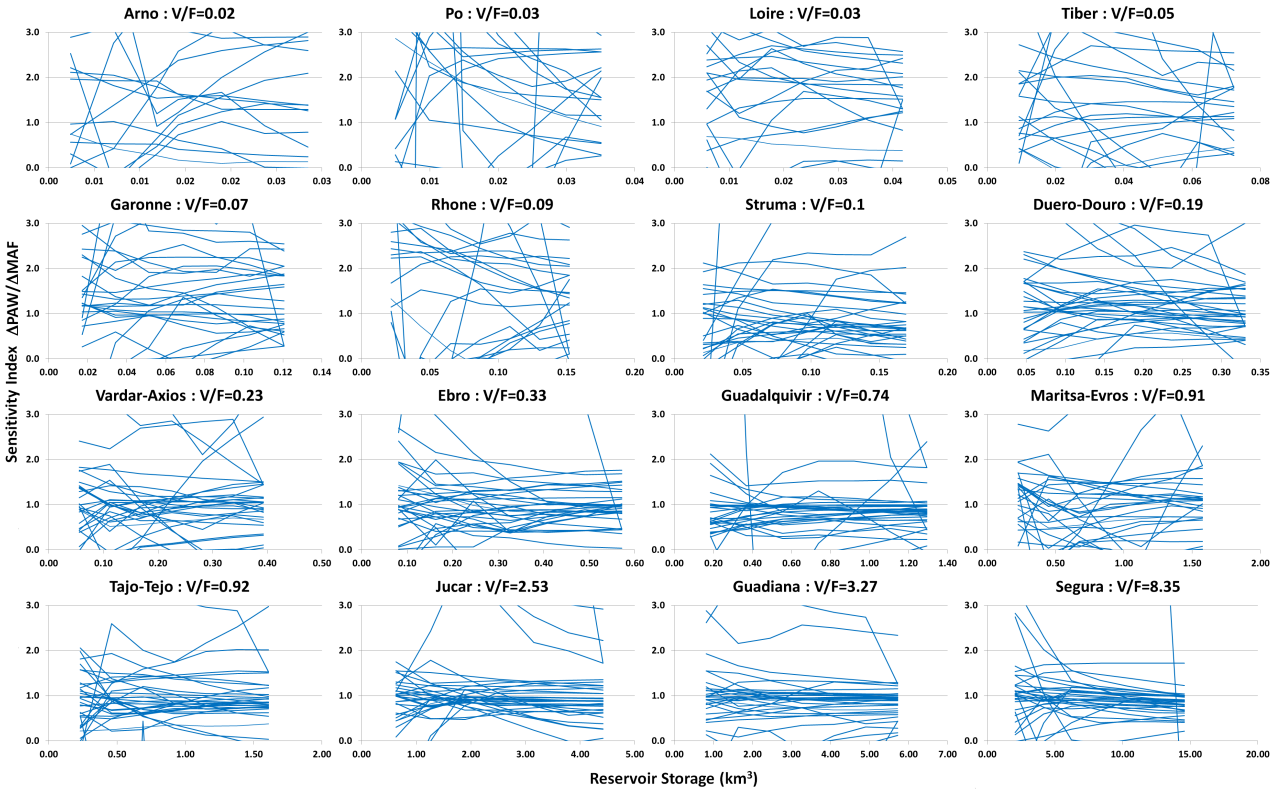

Figure 6. Probability distribution of changes of Mean Annual Flow and Water Availability for different storage values in the studied basins.

The influence of reservoir storage on the elasticity of water availability was analyzed by computing a sensitivity index, defined as the ratio between the change in PWA and the change in MAF. Figure 6 presents the value of this ratio as a function of reservoir storage in each basin for all available projections. The large variability obtained reflects the complex interplay between the variables that determine water availability: hydrologic regime, storage volume, changes in MAF and changes in variability. Figure 6 shows that as reservoir storage grows across basin locations the variability of the sensitivity index is significantly reduced, which suggests that reservoir storage plays a critical role in attenuating the effects of climate change on water availability.

4. CONCLUSIONS

Projected changes in hydrologic regime and water availability were analysed in 16 basins in Southern Europe applying the WAAPA model to streamflow obtained from 35 climate projections under 7 emission scenarios. Climate projections suggest a significant reduction of mean annual flow and an even stronger increase in hydrologic variability in most basins. This implies a corresponding reduction in potential water availability, with variable results across basins depending on hydrologic regime and reservoir storage. Overall, a consistent picture emerges, although model uncertainty is larger than the expected reduction of water availability. The analysis of the influence of reservoir storage on the basin response to climate change showed the complex interplay between hydrologic regime, reservoir storage and water availability. Basins with large storage values showed reductions of water availability comparable to the reductions of mean annual flow. For basins with less storage, the probability distributions of reductions tend to differ, with increased uncertainty for availability. The role of storage was further analysed through a sensitivity analysis of water availability to reservoir storage, with values ranging from 25% to 200% of current storage values. The results showed that uncertainty under climate change is reduced for basins with large storage values.

REFERENCES

Arnell, N. W., 1999: The Effect of Climate Change on Hydrological Regimes in Europe. Global Environmental Change 9:5

Christensen, J. H., T.R. Carter, M. Rummukainen and G. Amanatidis, 2007: Evaluating the performance and utility of regional climate models: the PRUDENCE project. Climatic Change, 81, 1-6

EROS, USGS, 2008: HYDRO1k Elevation Derivative Database. Tech. rept. U.S. Geological Survey Center for Earth Resources Observation and Science (EROS). http://eros.usgs.gov/products/elevation/hydro1k.html-97

Fekete, B. M., Vörösmarty, C. J., and Grabas, W., 2004: High-resolution fields of global runoff combining river discharge and simulated water balances, Global Biogeochem. Cycles, 16(3), 1042.

Garrote L.; Iglesias, A.; Martin-Carrasco, F.; Mediero, L. 2011: WAAPA: a model for water availability and climate change adaptation policy analysis. Proceedings of the EWRA Conference 2011

Garrote L., A. Iglesias, A. Granados, L. Mediero, F. Martin-Carrasco, 2015a: Quantitative Assessment of Climate Change Vulnerability of Irrigation Demands in Mediterranean Europe. Water Resources Management, Volume 29, Issue 2, 325-338.

Garrote L.; Granados, A.; Iglesias, A., 2015b: Assessing water availability in Europe: a comparative study. Proceedings of the EWRA Conference 2015

González-Zeas D., L. Garrote, A. Iglesias, A. Granados, A. Chávez-Jiménez, 2014: Hydrologic Determinants of Climate Change Impacts on Regulated Water Resources Systems. Water Resources Management. Volume 29, Issue 6, pp 1933-1947.

Hewitt, C. D. and Griggs, D. J., 2004: Ensembles-based predictions of climate changes and their impacts. Eos, Vol. 85, No. 52, pp 566

ICOLD, 2004: World Register of Dams. International Commission on Large Dams

Krysanova, V.; Dickens, C.; Timmerman, J. et al., 2010: Cross-Comparison of Climate Change Adaptation Strategies Across Large River Basins in Europe, Africa and Asia. Water Resour Manage 24:4121

van Beek L.P.H., Marc F.P. Bierkens, 2009: The Global Hydrological Model PCR-GLOBWB: Conceptualization, Parameterization and Verification. Department of Physical Geography. Utrecht University.

Vörösmarty, C. J.; McIntyre, P. B.; Gessner, M. O. et al., 2010: Global threats to human water security and river biodiversity. Nature 467:555

Warszawski L, et al., 2014: The Inter-Sectoral Impact Model Intercomparison Project (ISI–MIP): Project framework. Proc Natl Acad Sci USA 111:3228–3232

Proceedings of the 10th World Congress of EWRA 'Panta Rhei', 5-9 July 2017, Athens, Greece
© 2017 *European Water Resources Association*

Assessment of climate-change impacts on precipitation based on selected RCM projections

D.J. Peres*, M.F. Caruso and A. Cancelliere
University of Catania, Department of Civil Engineering and Architecture
* *e-mail: djperes@dica.unict.it*

Abstract: Regional climate models (RCMs) are essential to perform climate change impact studies. At the state of the art, many RCM products have limited accuracy, which reduces the reliability of climate change impact assessments. Bias correction techniques are commonly applied to obtain modified RCM data that are more consistent with observations. Nevertheless these techniques have been criticized by some researchers, for their limited physical basis. In this study we propose a different approach, suitable when a relatively high number of different RCM simulations are available for the region of interest. The proposed approach consists in first evaluating the available RCM datasets by measures of agreement with observed data, and then to perform climate change impact assessment only with those RCM data complying with certain accuracy requirements. The approach is applied to assess potential future changes of precipitation in Sicily. To this aim, daily data sets of the Euro-CORDEX initiative are used for both intermediate and extreme greenhouse gas concentration emission scenarios (RCP 4.5 and RCP 8.5). Changes in future precipitation are computed in terms of widely-used standard climate indices (ETCCDI), and statistical tests are applied to assess statistical significance of changes. Analysis of the accuracy of RCM data indicates that only 4 out of the 14 RCMs have limited biases. The ensemble of these four RCM models predicts an overall decrease of mean annual rainfall, as well as an increase of the maximum length of number of consecutive dry days, suggesting a potential future increase of water shortage problems and droughts in the studied region.

Key words: Climatic projections; EURO-CORDEX; Global warming; global circulation models; natural hazards

1. INTRODUCTION

Climate change due to uncontrolled greenhouse emissions is claimed to induce increases in water-related risks (IPCC, 2014). Future impacts of greenhouse emissions on climate can be assessed by perturbing global circulation models (GCM) with different emission scenarios defined at the international level (representative concentration pathways, RCPs). The 250-600 km spatial resolution of GCMs is increased by dynamical downscaling techniques, which yield regional climate model (RCM) products that can be used for an assessment at national or sub-national levels. Both GCM and RCM temperature and precipitation data are generally affected by significant biases, which can be spotted from comparisons with observations in the reference (past) period. When observations and climate model data are both available for the area of interest, it is an established practice to correct the climate model data, so they result more consistent with observations. This sort of calibration procedure has however some practical and theoretical downsides and it is not fully defendable from a physical standpoint since it can violate mass conservation principles (Ehret *et al.*, 2012). In this paper we propose a different approach consisting in evaluating available RMCs on the basis of their ability to reproduce current climate, and then to perform the climate change impact assessment only by the set of more accurate models. This implies to implicitly assume that models that these models will be also the most accurate in predicting the future scenario. Here we apply this procedure with the aim of assessing future changes of precipitation in Sicily.

2. METHODOLOGY

The first phase of the methodology is aimed at deriving the set of most reliable RCM models. Hence the accuracy of each RCM in reproducing the observation in the baseline period (here assumed as 1971-2000) is assessed. Then, metrics of the goodness of reproduction are computed and only the models with metrics above fixed thresholds are considered for further analyses. We consider performance metrics based on the relative errors (computed on a cell basis) of the mean annual precipitation:

$$e_i[\%] = \frac{\bar{P}_i^{(m)} - \bar{P}_i^{(o)}}{\bar{P}_i^{(o)}} \tag{1}$$

where e_i is the relative error [%], $i = 1, \ldots, N_c$ identifies the grid cell, $\bar{P}_i^{(m)}$ is the historical annual average precipitation estimated by the model in the *i*th cell [mm]; $\bar{P}_i^{(o)}$ is the annual average precipitation observed in the *i*-th cell [mm].

Several indices can be computed based on these errors over a region of interest. Here we consider the mean error and the percentage of cells with relative error less than a certain amount. More specifically, only models with absolute mean error less than 15% and for which at least half of the cells have errors less than 25% are retained.

Once the reduced ensemble of models complying with the fixed accuracy requirements is defined, we assess climate change impacts on precipitation in terms of indicators suggested by the Expert Team on Climate Change Detection and Indices (ETCCDI) of the CCL/CLIVAR Working Group on Climate Change Detection, which can be classified based on the type of information they provide:

- Central tendency/cumulative amounts: the total annual precipitation and the mean daily intensity (SDII) belong to this category
- High-rainfall extremes: represent periods of intense rainfall, and are thus related to floods.
- Indices of this group include: Rx1day, Rx5day, R10mm, R20mm, R95p, R99p, CWD
- Low-rainfall extremes: indicate presence of prolonged periods of dryness or low rainfall, and are connected to droughts. In our analyses we consider the maximum number of consecutive days of dryness (CDD).

The reader is referred to the ETCCDI website (http://etccdi.pacificclimate.org/indices.shtml) for definitions of the indices mentioned above. To study the impact of climate changes, for each RCM of the selected ensemble, the ETCCDI indices are computed for the historical and for three periods (2021-2050; 2041-2070; 2061-2090), in each emission scenario (RCP 4.5 and RCP 8.5). Then the variation of the index as the difference between its value in the future period and in the historical reference period is computed to quantify the changes for each RCM of the ensemble. Results given by the various models are then combined by testing the significance and the concordance of the projected changes. The Wilcoxon-Mann-Whitney test (see Helsel and Hirsch, 1992) has been applied to assess statistical significance of changes. This test has been applied in its one-sided version at a significance level of 10%, in testing for either positive or negative changes. Consequently, this means that the no-variation case corresponds to a two-sided test with 20% level of significance.

Once the test has been applied then the concordance has been assessed. In particular, model can be *concordant* in predicting an increase, a decrease, or no-variation if a given percentage (>50%) of the models give significant changes in the same direction. Otherwise, models can be *disconcordant*, or the changes can be *not significant*. The results have been synthesized through the use of the so-called climate signal maps (Pfeifer, 2015), indicating the ensemble mean of variation by the color of the cell, and the direction of significant and concordant changes by an upward (positive) or downward (negative) arrow or a dash (stable, unchanged conditions) or a question mark (non-

significant or discordant), respectively.

3. APPLICATION

The proposed procedure has been applied to assess potential future changes of precipitation in Sicily (Italy). For the validation of RCM climate models, daily rainfall grids have been derived from the observational dataset of the regional water observatory of Sicily, including a set of 508 rain gauges (which however worked in different and non-overlapping periods), being the most accurate available covering the historical reference period (1971-2000).

Table 1 lists the fourteen models from the EURO-CORDEX initiative (Jacob et al., 2014), providing climate products at the resolution of 0.11 degrees (approximately 12.5 km). As reported in the table, six different institutes produce the data, and the different datasets may be obtained by the same regional downscaling model (RCM) applied to a different global circulation model (GCM). For brevity, in this study the different models are identified with the institution's acronym followed by the GCMs.

Table 1. Ensemble of regional climate models from the EURO-CORDEX initiative considered in this study. Models selected based criterion A and B are reported in bold font (see text).

ID	Acronym	Institute	GCM	RCM	Ensemble member	Ranking	
						Crit. A	Crit. B
1	**EC-EARTH (DMI)**	CLMcom	**CNRM-CM5**	**CLMcom-CCLM4-8-17**	**r1i1p1**	**4**	**7**
2	**MPI-ESM-LR (CLMcom)**		**EC-EARTH**	**CLMcom-CCLM4-8-17**	**r12i1p1**	**5**	**6**
3	CNRM-CM5 (CLMcom)		HadGEM2-ES	CLMcom-CCLM4-8-17	r1i1p1	14	12
4	CNRM-CM5(SMHI)		MPI-ESM-LR	CLMcom-CCLM4-8-17	r1i1p1	12	9
5	EC-EARTH (SMHI)	CNRM	CNRM-CM5	CNRM-ALADIN53	r1i1p1	6	4
6	MPI-ESM-LR (SMHI)	DMI	EC-EARTH	DMI-HIRHAM5	r3i1p1	9	10
7	**EC-EARTH (KNMI)**		**NorESM1-M**	**DMI-HIRHAM5**	**r1i1p1**	**3**	**3**
8	EC-EARTH (CLMcom)	IPSL -INERIS	IPSL-CM5A-MR	IPSL-INERIS-WRF331F	r1i1p1	8	2
9	CNRM-CM5 (CNRM)	KNMI	EC-EARTH	KNMI-RACMO22E	r1i1p1	13	14
10	**NorESM1-M (DMI)**		**CNRM-CM5**	**SMHI-RCA4**	**r1i1p1**	**2**	**1**
11	IPSL-CM5A-MR (IPSL)	SMHI	EC-EARTH	SMHI-RCA4	r12i1p1	1	8
12	IPSL-CM5A-MR (SMHI)		HadGEN2-ES	SMHI-RCA4	r1i1p1	10	13
13	HadGEM2-ES (CLMcom)		IPSL-CM5A-MR	SMHI-RCA4	r1i1p1	11	11
14	HadGEM2-ES (SMHI)		MPI-ESM-LR	SMHI-RCA4	r1i1p1	7	5

4. RESULTS

4.1 Evaluation and selection of the EURO-CORDEX models

Figure 1 shows box-plots of the relative errors in mean annual precipitation for each RCM. The box-plots depict the distribution over the different cells of the error in each cell computed by Eq. (1), so the outliers represent grid cells with extreme relative errors. For some models, huge relative errors can be present in certain cells; for one model (model 3), errors reach 1000%, which means that the difference between RCM and observed mean annual precipitation is 10 times the observed

precipitation itself (see model 3, CNRM-CM5 CLMcom); and though this may occur in some specific grid cells, still 25% of the cells exhibit errors above 200%. Furthermore, the mean and spreading of errors are large for a significant portion of data also for other models (see models 9 and 13). Some models present a narrower spreading of the error, but still significant biases (such as models 12 and 14). Models 1, 2, 7, 10 and 11 have limited bias (absolute value less than 15%). Half of the models (1, 2, 5, 7, 8, 10 and 14) have narrow error spreading, that is the relative error of at least the 50% of cells is less than 25 % in absolute value. Last two columns of Table 1 present the ranking of each model based on criterion A (absolute value of mean of the relative errors), and criterion B (proportion of cells having an absolute value of relative error less than 25%).

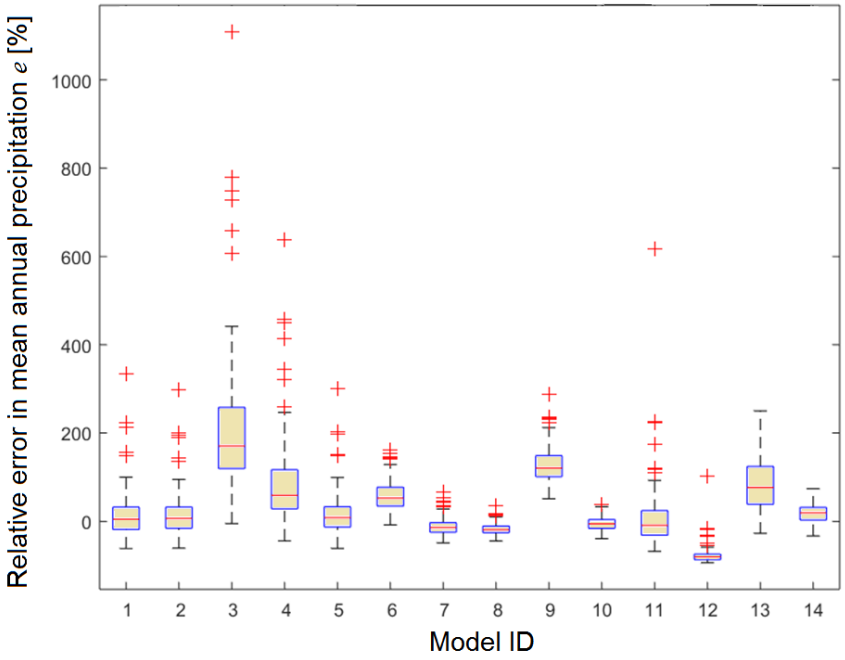

Figure 1. Box-plot of the relative errors in mean annual precipitation for each EURO-CORDEX model. Each box-plot refers to the distribution of errors between model and observed precipitation in Sicily during the reference period 1971-2000.

Only four out of 14 models fulfill the quality criteria: model 1: CNRM-CM5 (SMHI); model 2: EC-EARTH (SMHI); model 7: CNRM-CM5 (CLMcom); and model 10: MPI-ESM-LR (CLMcom). This ensemble of models has been considered for assessing the changes in precipitation induced by the two scenarios RCP 4.5 (intermediate emissions) and RCP 8.5 (high emissions). In particular, signal climate maps have been derived, and are shown in the ensuing parts of this paper. This signal climate maps report concordance in either a positive (increase) or negative direction (decrease), or no-variation if at least 3 out of 4 models indicate the same direction of changes and these are significant according to the Wilcoxon-Mann-Whitney rank sum test. Variations are computed with respect to the rainfall data given by the corresponding RCM in the baseline period 1971-2000.

4.2 Changes in mean annual precipitation

Figure 2a shows for three future time periods (2021-2050, 2041-2070, 2061-2090), changes in total annual rainfall in Sicily related to RCP4.5 and 8.5 emission scenarios. For the first emission scenario, models agree in predicting a reduction of the total annual precipitation over Sicily, which however is significant and concordant only in some parts of mid-western and north-eastern areas of the region, where the amount of the decrease of may reach 100 mm. Nevertheless, for a larger portion of the region significant changes are either discordant (periods 2021-2050 and 2061-2090) or indicate no changes (period 2041-2070).

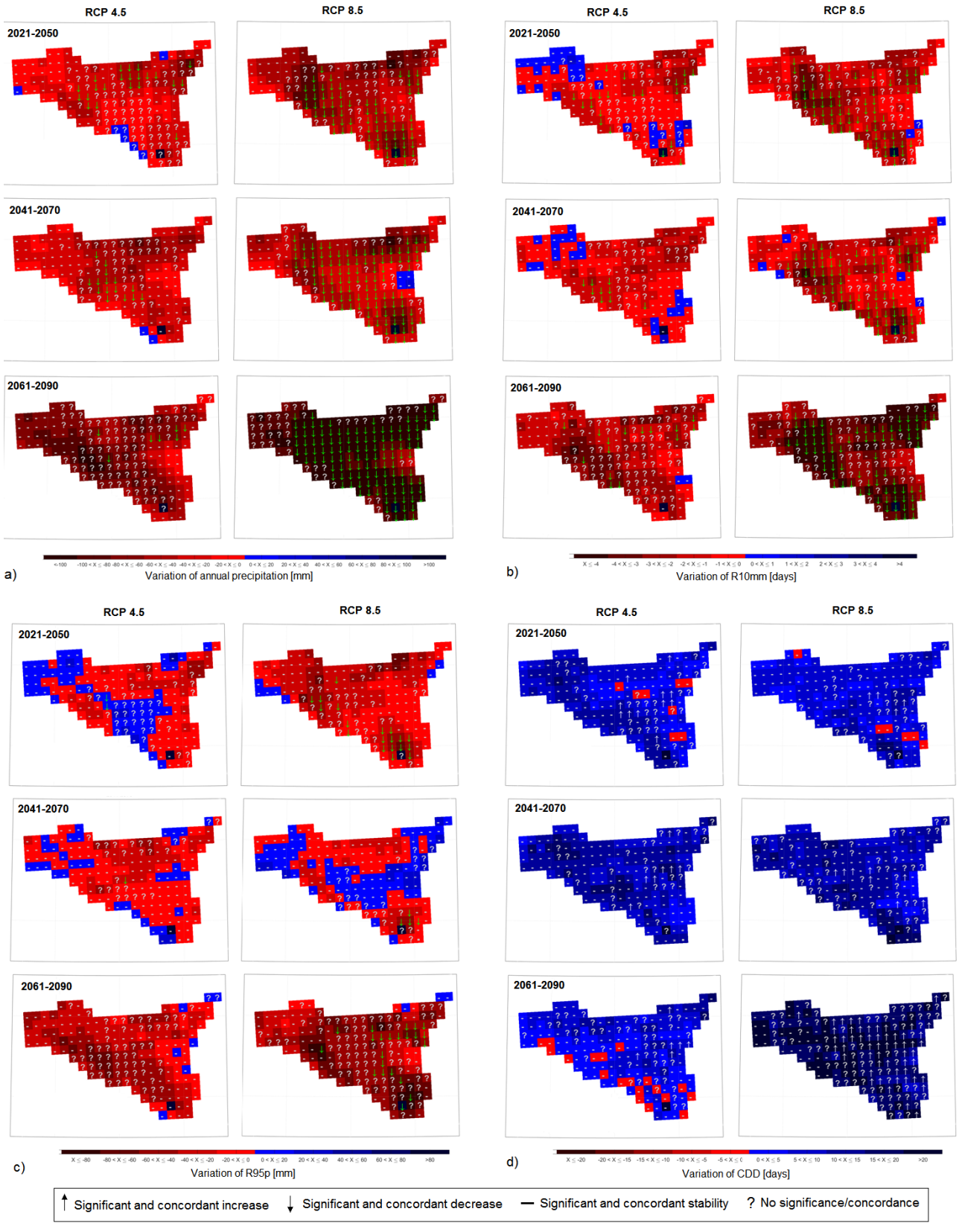

Figure 2: Climate signal maps relatively to the two emission scenarios (RCP 4.5 and RCP 8.5) and three future temporal horizons. Variations are computed respect to reference period 1971-2000. Map for: a) total annual precipitation, b) R10mm, number of days with precipitation exceeding 10 mm, c) R95p, rainfall exceeding 95% percentile of reference-period daily precipitation, and d) CDD, maximum number of consecutive dry days.

On the other hand, for RCP 8.5, climate models agree in predicting, for the period 2021-2050, a reduction of total annual precipitation almost over the entire region, with the exception of western

Sicily and of some other sparse areas in the central-north part. In the period 2061-2090, reductions of more than 100 mm are predicted for a large portion of the cells. It may be concluded that the high emission scenario may produce a reduction of yearly-accumulated precipitation with potential water scarcity problems and more severe droughts in the future.

4.3 Changes in high-rainfall extremes

Figure 2b shows the climate signal maps relative the number of days with intense precipitation, (R10mm) defined as the number of days in a year with precipitation greater than 10 mm. As can be seen from the maps, the ensemble mean indicates a decrease of R10mm, with reductions amount to a few (3-4) days in the period, for both RCPs. However, for RCP4.5 the changes are seldom significant or concordant, with the exception of some sparse areas in the eastern or south-central parts of the island. For the RCP8.5 scenario, projections have a clearer trend, and indicate a reduction of R10mm in all central and almost all eastern parts of the region. Changes are clear for period 2061-2090, where R10mm variations can exceed 4 days.

Regarding the highly extreme precipitation amounts *R95p* (Figure 2c), no clear variations are indicated by the models. The ensemble mean shows that in the period 2021-2050 tends to indicate mainly a decreases, but mostly the changes are not significant or concordant, unless for few cells. Indeed changes are significant in the case of the high emission scenario and periods 2041-2070 and 2061-2090, where significant decreases of *R95p* can be up to 40-60 mm in a significant portion of Sicily.

4.4 Changes in low-rainfall extremes

Changes in the number of the maximum number of consecutive dry days (CDD) are shown in Fig. 2d. For both emission scenarios, models predict mostly an increase of CDD. The ensemble mean indicates, approximately 5-10 days of increases in many parts of Sicily. Again, only a limited portion of the island has significant changes for RCP4.5, being a non-variation the most frequent case in this scenario. Also, as for the other indices, in the RCP8.5 scenario, changes are high and significant for the last period, where the ensemble mean can indicate a variation up to 15-20 days.

5. CONCLUSIONS

Assessment of climate change is subject to a significant degree of uncertainty. Our application has shown that regional climate model products may be affected by significant errors (up to 1000% in some areas) in reproducing the precipitation regime in Sicily. Nevertheless, among the considered EURO-CORDEX ensemble, a limited, but still significant, portion of the models (4 out of 14) have limited errors, and can thus be used to assess changes in rainfall induced by greenhouse emissions. The application has shown also that while the ensemble mean may indicate high variations of a given climatic feature (as represented by one or more ETCCDI standard indices), at the same time changes can be discordant or non-significant. Notwithstanding these uncertainties, there are some significant and concordant changes for the studied region. The analyses indicate more clear variations in the RCP8.5 scenario respect to the RCP4.5, even though qualitatively they are similar. Specifically, models indicate a reduction of annual rainfall even higher than 100 mm for the high-emission scenario in period 1961-2090. An increase in the number of dry days per year is also predicted quite clearly, which is again more significant for the RCP8.5 scenario than the RCP4.5, and can reach up to 20 days. Changes in heavy precipitation are less significant, and models are mostly concordant in predicting no variation respect the reference climate (1971-2000). Indeed, some significant decreases are predicted. Overall, analysis of the selected ensemble of EURO-CORDEX high-resolution RCMs suggests an increase of water shortage issues and

droughts. On the other hand, results seem to do not support the hypothesis of an increase of heavy-rainfall triggered hazards induced by climate change, such as floods. This is somehow in agreement with trend analysis performed on observed time series in Sicily, that indicate no significant changes in extreme rainfall (Bonaccorso et al., 2005; Arnone et al., 2013), with the exception of short time scales (one hour or less). Thus, to assess variations at the sub-daily scale may be useful for a better understanding of potential impacts of climate change on floods, especially for small catchments with concentration times less than few hours. This task may be accomplished by temporal downscaling of RCM daily products.

REFERENCES

Arnone, E., Pumo, D., Viola, F., Noto, L. V., and La Loggia, G., 2013. Rainfall statistics changes in Sicily. Hydrol. Earth Syst. Sci., 17, 2449-2458, doi:10.5194/hess-17-2449-2013.

Bonaccorso, B, Cancelliere, A., Rossi, G., 2005. Detecting trends and extreme rainfall series in Sicily. Adv Geosci 2:7–11

Ehret, U., Zehe, E., Wulfmeyer, V., Warrach-Sagi, K., Liebert, J., 2012. HESS Opinions "Should we apply bias correction to global and regional climate model data?". Hydrology and Earth System Sciences 16 (9), 3391- 3404.

Helsel, D., R., and Hirsch, R, M, 1992. Statistical methods in water resources. Elsevier.

IPCC, 2014. Climate Change 2014: Synthesis Report. Contribution of Working Groups I, II and III to the Fifth Assessment Report of the Intergovernmental Panel on Climate Change. IPCC, Geneva, Switzerland, p. 151.

Jacob, D., et al., 2014. EURO-CORDEX: new high-resolution climate change projections for European impact research. Regional Environmental Change 14.2: 563-578.

Pfeifer, S., et al., 2015. "Robustness of ensemble climate projections analyzed with climate signal maps: seasonal and extreme precipitation for Germany." Atmosphere 6.5: 677-698.

Proceedings of the 10th World Congress of EWRA 'Panta Rhei', 5-9 July 2017, Athens, Greece
© 2017 *European Water Resources Association*

Evaluating the water resources and operation of the Boukan dam in Iran under climate change

F. Emami* and M. Koch
Department of Geotechnology and Geohydraulics, University of Kassel, Germany
* *e-mail: farzad.eee@gmail.com*

Abstract: The operating policies of a reservoir dam in a river basin are dependent on the upstream river's inflow. As the latter may be affected by impacts of climate change which, in turn, may alter the water supply for the various stakeholders in the basin, studies to this regard are of utmost importance to ensure the sustainable development of the future water resources in the areas. Here we present the case study of the Boukan dam, located on the Zarrine river, highlighted as the main inflow source of Lake Urmia, which is the largest inland wetland of Iran and the largest lake in Middle East. Firstly the calibrated rainfall-runoff model SWAT is used to predict the various flow components of the Zarinne river for the historical and future periods until 2049, using downscaled input precipitation predictors of three RCP-scenarios captured from one of the projections of the CMIP5-GCM ensemble, the CESM1-CAM5-model. These streamflow scenarios are then employed in the MODSIM water management model to simulate the present-day and future available water resources of the basin and to determine the optimal operation of the Boukan dam, based on some prioritization of the water allocation for the various water use sectors in the basin. Finally, the impacts of climate and demand changes on the dam operation are evaluated by comparing future and historical MODSIM-simulated average water budget and supply/demand ratio (SDR) for the three CESM-model scenarios. In summary, the results show that the region will face more intensive water shortages in the future, owing to climatic change and increasing demands.

Key words: Climate Change, SWAT, MODSIM Water Management Model, Reservoir Dam Operation, Lake Urmia, Iran

1. INTRODUCTION

Climate change can worsen an already existing water shortage as an additional pressure factor in some regions of the world, as it may lead to increased rainfall variability and global warming (Bates et al., 2008). Specifically, the Western Asia and Middle East countries, such as Iran, which have already been experiencing a fragile arid or semiarid environment over many decades, are most vulnerable to a changing climate, not to the least due to increasing population pressure requiring more agricultural food production (Abbaspour et al., 2009). It is thus of no surprise that the unsustainable development of agricultural demands in Iran has intensified the already existing water crisis there as an external driver.

As water resources become further stressed due to the impacts of climate change and increasing demands, it is of a strategic importance to evaluate the various components of the water resources system, such as the efficiency of reservoir dams, in order to detect the appropriate operation strategies to mitigate such hydrologic changes.

Although many studies investigated the impacts of climate change on the water cycle (i.e. Abbaspour et al., 2009), fewer studies have focused on the evaluation of the water supply of a river basin due to the impacts of climate change (Emami, 2009; Ashraf Vaghefi et al., 2015).

The wetland of Lake Urmia, as the largest inland wetland of Iran and the largest lake in the Middle East, which is mainly fed by the head waters of the Zarrine river, has been tremendously diminishing in recent years which may lead to some drastic socio-ecological repercussions in that region (Aghakouchak et al., 2015). Thus it seems undeniable that the water supply system of the lake freshwater resources and also the unsustainable development of the region should be adjusted to allow for the restoration of the lake and so, hopefully, lead to a decrease of the water stress in the

basin region (Emami and Koch, 2017).

In a recent previous study of the authors (Emami and Koch, 2017), QMAP (quantile mapping)-downscaled precipitation from a projection of the CMIP5- project for a particular climatic scenario has been employed, together with SDSM- downscaled temperatures of the HADCM3 GCM-model, as input drivers for the Soil and Water Assessment Tool (SWAT), a widely used distributed rainfall-runoff watershed model (Neitsch et al., 2001), to simulate the streamflow changes of the river basin and the inflow of the dam.

The present study, as a continuation, will use this calibrated SWAT-model to predict the flow components in the historical and future periods until 2049, based on three new RCP-scenarios of precipitation captured from the latest projections of CMIP5-GCM ensemble with a better atmospheric grid resolution. This predicted streamflow will then be employed in the water management model MODSIM to simulate the present-day and future available water resources of the basin and the best operation of the dam in the wake of upcoming climate change in the basin.

2. DESCRIPTION OF THE STUDY AREA

The Zarrine river basin (ZRB), with an area of about 11,000 km^2, is located in the southern part of Lake Urmia in west Azerbaijan province between 45° 46‘ E to 47° 23‘ W longitude and 35° 41‘ S to 37° 44‘ N latitude. The river basin system contains 24 hydrometrical stations and there is one operating dam on the Zarrine River, Boukan Dam, as the biggest and most important dam of the basin, together with the diversion dam, Nouroozloo, located downstream.

The average annual temperature in the ZRB varies between 8 and 12 °C and the rainfall is situated in the range of 200 - 850 mm/a.

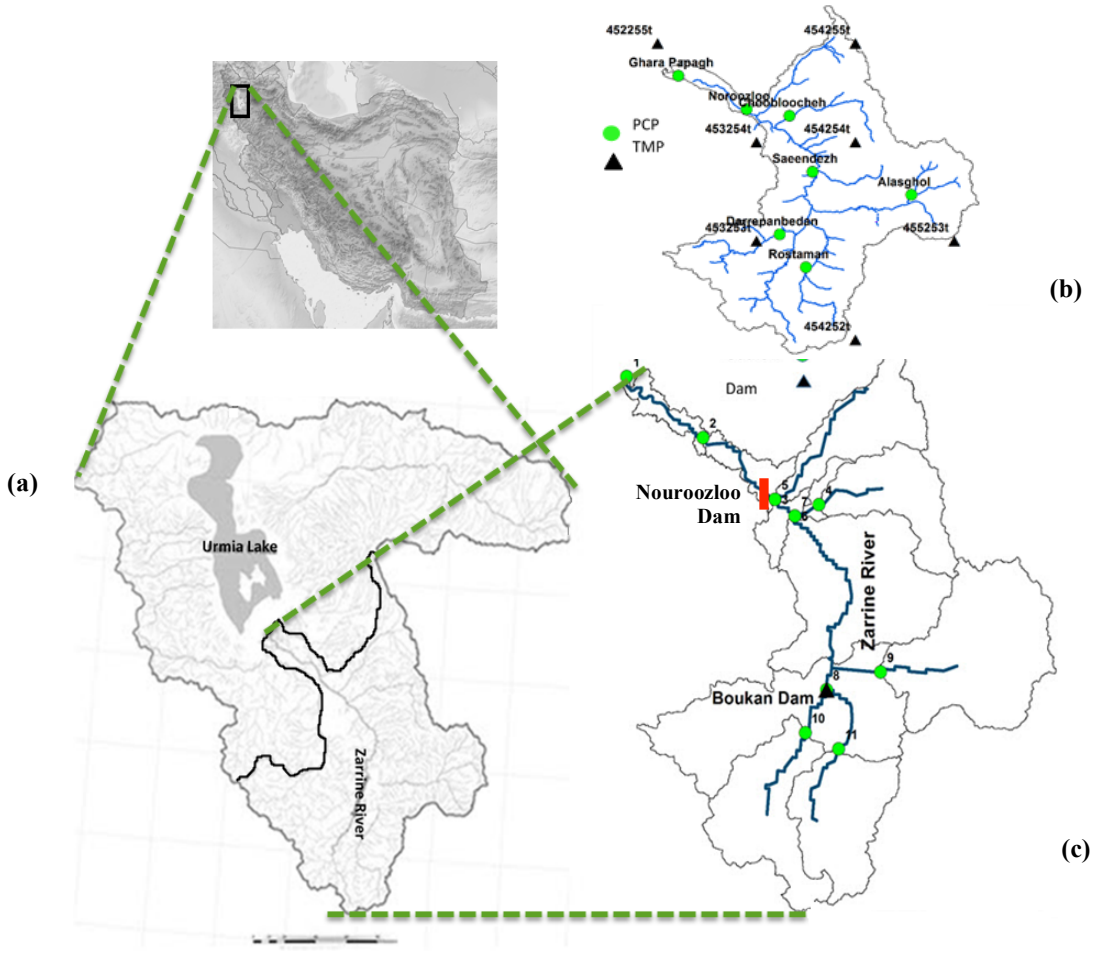

Figure 1. Map of the ZRB in Iran (a), with sub-basins and location of climatic stations (b) and selected outlets (c)

3. MATERIALS AND METHODS

3.1 Downscaling of climate predictors from GCM-RCP projections

For the future prediction of the precipitation, daily predictors from five available GCM-models from the CMIP5 project series, based on their good spatial resolutions and output availability, are captured for three RCP scenarios (2.6, 4.5 and 8.5) for a 35-year period, 2015 to 2049.

These GCM-predictors are then downscaled with a non-parametric quantile mapping model (Gudmundsson et al., 2012), using robust empirical quantiles (Package QMAP in the $R^{©}$- software environment) and provided by the "ccafs-climate" data portal (Navarro-Racines and Tarapues-Montenegro, 2015), are assessed and then the best fitted model with the lowest biases is selected for generating the future downscaled precipitation predictors for further hydrological modelling. The QMAP downscaling method removes the systematic bias of all statistical moments of the distributions of the raw GCM-predictors compared with those of the historical observations. Of course, likewise to all statistical downscaling methods, it is assumed also in this method that the historical biases will be the same in the future.

Historical and future minimum and maximum daily temperatures, also previously used in the concurrent study of Emami and Koch (2017), are SDSM- (Wilby et al., 2002) downscaled predictors from the Hadley center's HADCM3 GCM-model, as employed in the IPCC Fourth Assessment Report (AR4) for the extreme emission scenario (SRES) A2 (promoting further regional economic development) and the more benevolent B2 (with emphasis on an ecologically sustainable development). For further details the reader is referred to Emami and Koch (2017).

3.2 SWAT-hydrological modeling and MODSIM water resources decision modeling

Using the downscaled climate predictors of previous section in the hydrologic model SWAT, streamflow and other relevant hydrological parameters of the ZRB, namely, the inflow into the Boukan dam are simulated for the three climate (RCP) scenarios. Details of the setup and calibration and validation of the SWAT-model used, with some minor differences from the present application, are discussed in Emami and Koch (2017).

In the subsequent, final step, the river basin (water resources) decision model, MODSIM (Labadie, 1995), is applied to assess the impact of future predicted climatic change on the dam operation and water supply by incorporating the output of the previously modelled SWAT-streamflow as input drivers into this model.

MODSIM simulates the optimal water allocation in a river basin through a sequential solution of the following generalized network flow optimization problem, namely, a minimization of the water allocation costs, for each time period, under the constraint that the mass balance all over the network is satisfied. Mathematically this optimization problem can be cast in the following form:

$$minimize \ \sum_{\ell \epsilon A} c_\ell q_\ell \tag{1}$$

subject to:

$$\sum_{\ell \epsilon O_i} q_\ell - \sum_{k \epsilon I_i} q_k = b_{it}(q) for\ all\ nodes\ i \epsilon N \tag{2}$$

$$\imath_{\ell t}(q) \leq q_\ell \leq \ u_{\ell t}(q) for\ all\ links\ \ell \epsilon A \tag{3}$$

where A is the set of all links in the network; N is the set of all nodes; O_i is the set of all links originating at node I (i.e., outflow links); li is the set of all links terminating at node i (i.e., inflow links); q_ℓ is the integer valued flow rate in linkℓ; c_ℓ is the cost weighting factor, or priority number per unit flow rate in linkℓ; $l_{\ell t}$ and $u_{\ell t}$ are the lower and upper bound on flow in link ℓ at time t.

4. RESULTS AND DISCUSSION

4.1 Downscaled climate variables

To predict the future daily precipitation the QMAP- downscaled outputs of five GCM-models of the CMIP5- project are evaluated for the historical period 1977 to 2005, using the quantile bias (QB_t), defined as the ratio of the downscaled monthly precipitation to that of the observed one above a specified percentile *t*, wherefore the 5%, 50% and 75% percentiles are usually used (Mehran et al., 2014). In addition the root mean square error (*RMSE*), and the coefficient of determination (R^2) are computed as further performance criteria. The results are listed in Table 1 for the RCP2.6 scenario. Similar tables were set up for the other two RCPs, 4.5 and 8.5, and are not shown here.

As can be seen from the table, CESM1_CAM5 (Community Earth System Model (CESM) with RCP #1 = RCP2.6, with the Community Atmosphere Model (CAM), version 5) has overall the best performance. As this holds also for the RCP4.5 and 8.5 precipitation scenarios, output of the model CESM, i.e. CESM1, CESM2 AND CESM3, are used in the later hydrological analysis.

The results of Table 1 indicate that for all GCM-models the quantile bias QB_t of the downscaled precipitation is decreasing numerically from values close to 1 at at the 25% quantile to values QB_t <1 at higher (50 and 75%) quantiles, i.e. the downscaled precipitation underestimates the observed one during the historical period, particularly, for extreme precipiation. Nevertheless, as all seven stations have R^2 -values between 0.42 and 0.51 and RMSE between 21-56mm/m for the CESM1-model scenario, the recorded historical precipitation in the region is rather well mimicked by the downscaled one. It should be noted that because of its high resolution (0.94^o x 1.25^o), all three CESM-model precipitation variants have lower bias and better performance than the MPI-ESM-LR model used previously by Emami and Koch (2017) for precipitation downscaling in the ZRB.

Table 1. Statistical evaluation of the QMAP-downscaling precipitation performance of five selected CMIP5- GCM-models under climate scenario RCP2.6 for relative to the observations. Best model is highlighted in gray.

Station	Statiscal Paramet	CCCMA_CANESM2	CESM1_CAM5	MPI_ESM_MR	MRI_CGCM3	NIMR_HADGEM2	QBt	CCCMA_CANESM2	CESM1_CAM5	MPI_ESM_MR	MRI_CGCM3	NIMR_HADGEM2
Alasghol	**R2**	0.29	0.45	0.39	0.39	0.42	**25%**	1.00	1.00	0.99	0.99	0.98
	RMSE	43.5	36.1	37.1	36.1	35.7	**50%**	0.82	0.81	0.81	0.79	0.78
							75%	0.56	0.66	0.58	0.60	0.62
Choobloocheh	**R2**	0.41	0.51	0.43	0.35	0.52	**25%**	1.00	1.00	0.99	1.00	0.98
	RMSE	35.7	30.1	32.4	34.6	29.2	**50%**	0.82	0.84	0.82	0.79	0.83
							75%	0.70	0.70	0.61	0.59	0.61
Darre Panbedan	**R2**	0.41	0.42	0.37	0.38	0.40	**25%**	0.99	0.99	1.00	1.00	0.98
	RMSE	35.8	35.2	36.3	36.5	34.6	**50%**	0.83	0.84	0.82	0.84	0.79
							75%	0.69	0.66	0.66	0.60	0.60
Rostaman	**R2**	0.33	0.43	0.34	0.35	0.35	**25%**	1.00	1.00	1.01	1.01	0.97
	RMSE	64.1	56.0	59.2	58.3	57.9	**50%**	0.82	0.82	0.80	0.80	0.80
							75%	0.60	0.62	0.61	0.57	0.54
Noroozloo	**R2**	0.32	0.45	0.38	0.30	0.45	**25%**	1.00	1.00	0.99	1.01	0.98
	RMSE	33.0	29.0	30.5	32.7	28.5	**50%**	0.80	0.84	0.83	0.78	0.81
							75%	0.62	0.67	0.60	0.56	0.63
Saeendezh	**R2**	0.32	0.43	0.43	0.27	0.42	**25%**	1.00	1.00	0.99	1.00	0.99
	RMSE	33.6	29.1	28.6	32.6	28.2	**50%**	0.83	0.81	0.84	0.78	0.80
							75%	0.61	0.71	0.68	0.56	0.60
Ghara Papagh	**R2**	0.40	0.45	0.45	0.32	0.33	**25%**	1.00	1.00	0.99	0.99	0.97
	RMSE	22.3	21.0	20.7	22.5	22.9	**50%**	0.83	0.84	0.82	0.82	0.78
							75%	0.65	0.68	0.63	0.52	0.53

4.2 Impact of climate change on inflow of the dam and reservoir operation

For evaluating the impact of climate change on dam operation, the downscaled climate variables are applied to the calibrated SWAT-model to simulate the future inflow of the dam changes in the time period of 2019 to 2049, as the downscaled predictions of the CMIP5-scenario models CESM1/2/3 start from 2015 and the SWAT- model uses a warm-up period of 4 years.

Fig. 2 shows the SWAT-simulated inflow of the dam for the historical and future time periods using the downscaled precipitation of the scenario-models CESM1, CESM2 and CESM3. Each of the latter were run with both A2- and B2- temperature scenarios – with only minor differences - and the average of two computed for the final evaluation of the dam's inflow as shown in the figure. One can notice from Fig. 2, that the future inflow of the more extreme CESM2- model scenario is lower than that of CESM1 (as well as CESM3). On the other hand, the inflow fluctuations of CESM1 are stronger than those of the other two models. Compared with the average annual streamflow into the dam of the historical reference period, that of the future CESM1- and CESM3-scenario will be increased by 33 and 14%, respectively, but reduced by 8% for the CESM2-scenario. Moreover, the average maximum monthly inflow will increase by 3% for CESM1, but will decrease by 27 and 3% for CESM2 and CESM3, respectively.

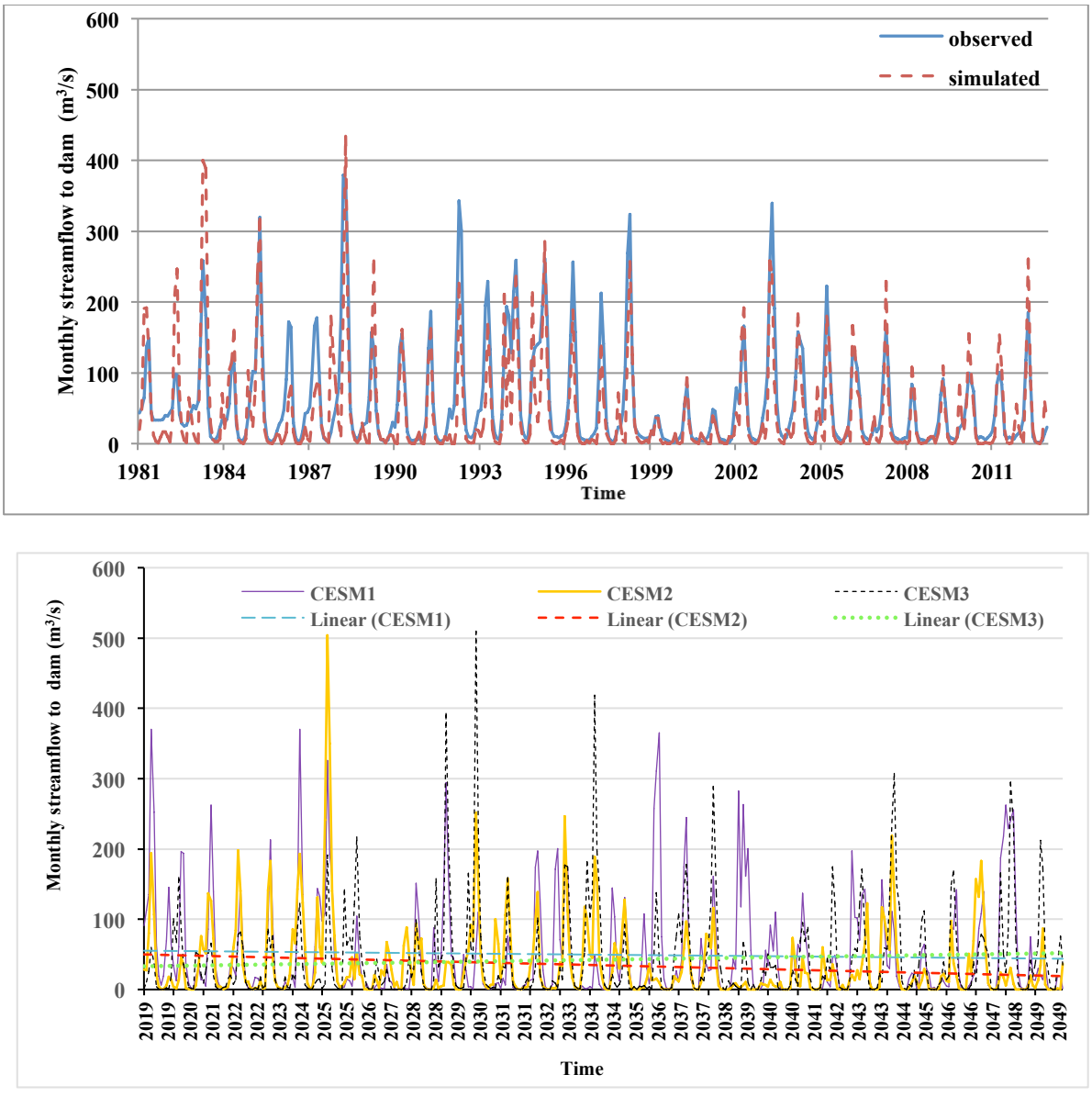

Figure 2. Observed and SWAT-simulated streamflow (inflow of the Boukan Dam) for historical period 1981- 2012 (top) predicted inflows of the dam for CESM1(RCP2.6), CESM2 (RCP4.5) and CESM3 (RCP8.5), with linear trend (bottom)

4.3 MODSIM simulated optimal water allocation

Finally, the water management of the Boukan dam for optimal water allocation in its downstream areas are modelled by means of MODSIM, using the schematic water network structure as sketched in four panels of Fig. 3 and the SWAT-simulated streamflow to the dam and from the tributaries along the Zarrine river as input.

Fig.3 depicts the various SWAT-MODSIM simulated annual, cumulative inflow and outflow water volumes for the different demand categories - which are in order of decreasing priority: potable (Pot), industrial (Ind), environmental (Env), fishery, agricultural (Agr) demands and filling the reservoir - along the ZRB- network for the historical (1981 to 2012) and the three future (2019 to 2059) CESM-model scenarios, discussed previously. Also indicated are the average annual water demands for the corresponding simulation periods, wherefore values of the future demands, which sum up to a total increase of 21% - mainly due to a doubled drinking water demand, and a 5% agricultural demand growth, together with a gradual increase of water demands in other sectors (Fesenduz fishery and Legzi pumping transfer) - were taken from Iran ministry of Energy administration reports. Assumptions in all these MODSIM-models include constant removal from the - already nowadays stressed - groundwater aquifers and, depending on the agricultural section, a 5 to 10 % return flow from irrigation demands to the subsurface.

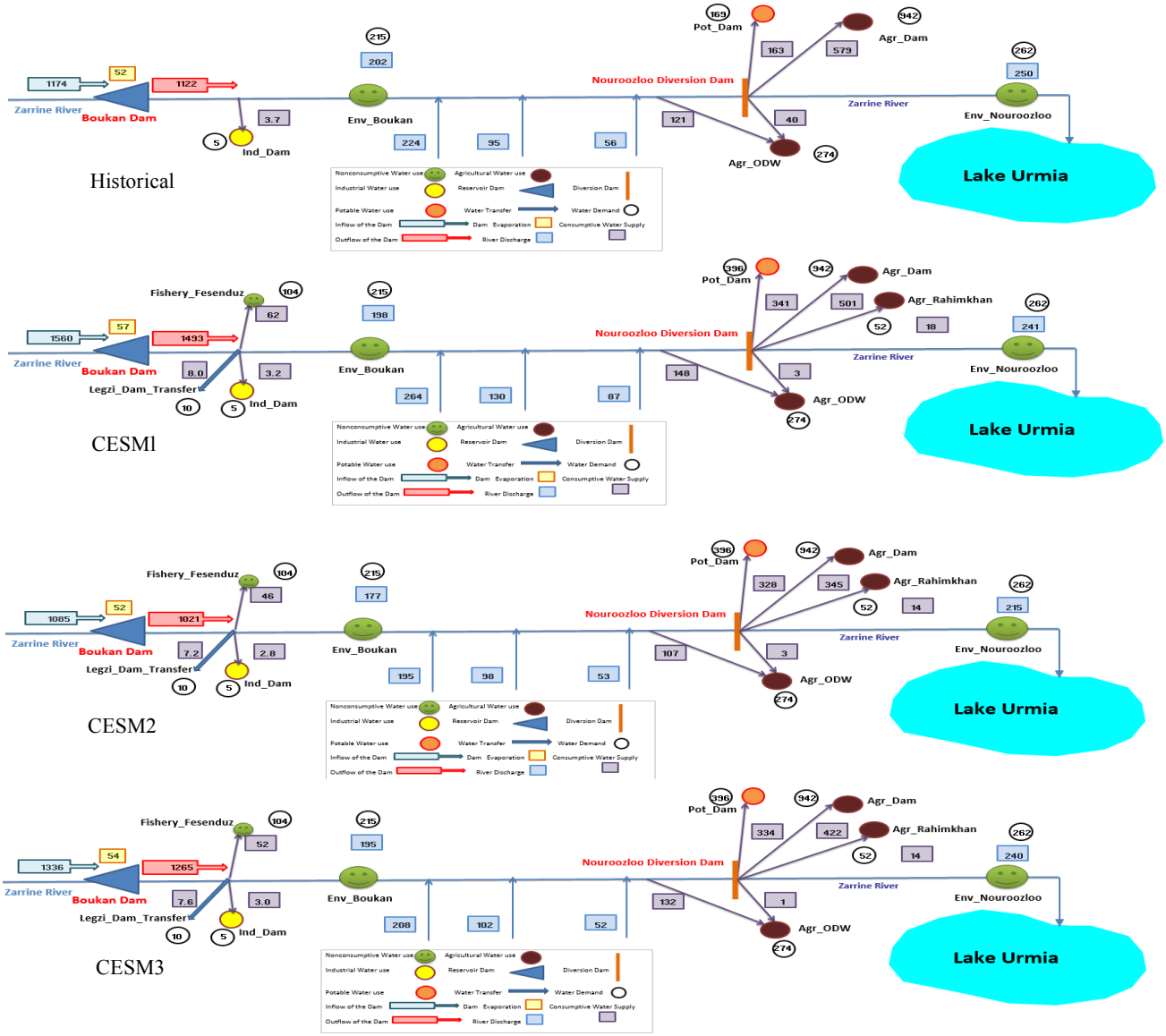

Figure.3. MODSIM- water use network of the ZRB starting with the Boukan dam and ending at Lake Urmia, with annual volumes (MCM) of different water demand sectors and MODSIM-simulated supplies for historical (top) and future period for climate prediction scenarios of CESM1, CESM2 and CESM3.

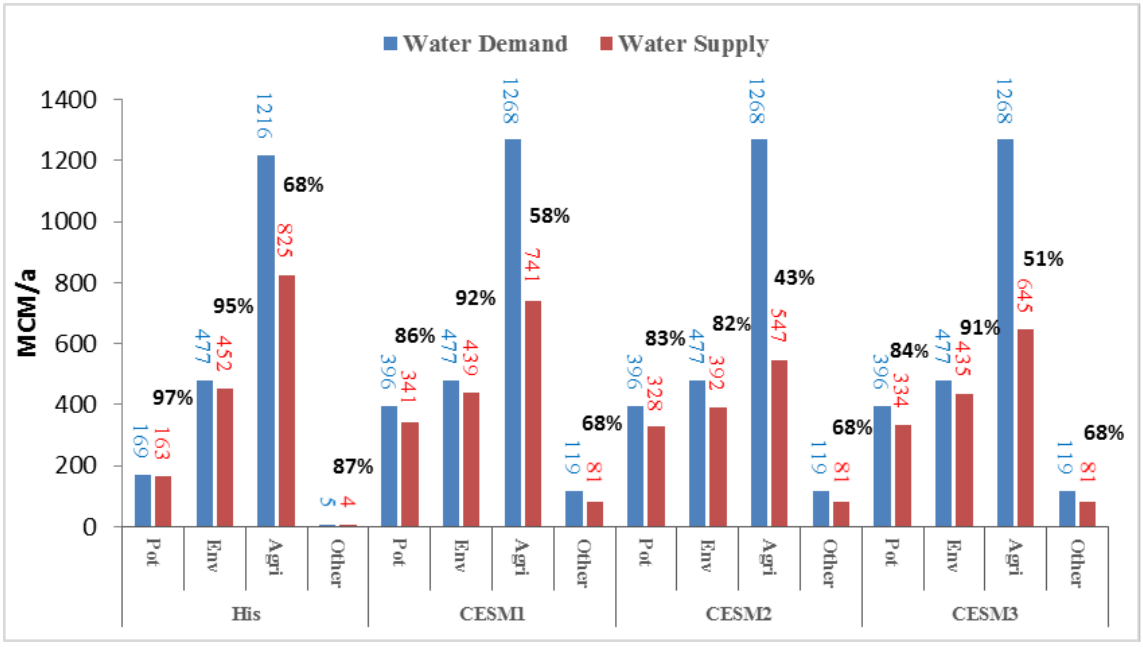

Figure 4. Barplots of the total ZRB- water annual demands (MCM/a), the corresponding MODSIM – simulated supply and the corresponding supply/demand ratio SDR (in percent) for the various water use sectors, as for the historical and the three future climate scenarios.

The MODSIM- simulated annual water budget numbers indicated in Fig. 3 for the different water sectors for the historical period and the three future model scenarios unveil that on average the future available water resources predicted with the CESM1- (RCP2.6) and CESM3 (RCP8.5) scenarios will increase, but decrease for the CESM2 scenario (RCP4.5). More specifically, the inflow and outflow of the dam in the CESM1 and CESM3 scenarios will rise by 33% and 14%, respectively. For CESM1, the inter-basin flows will, in addition, also increase by 28%, while they will experience a 3% decrease for CESM3. In contrast, for the CESM2-model scenario, inflow and outflow of the dam as well as the inter-basin flows will all fall by 9%.

The separate water demand/supply components along the ZRB network as depicted in Fig. 3 and discussed above, are accumulated for the totality of the ZRB in Fig. 4. From these values the ratio of water supply to demand, SDR, has been computed and listed as well. Thus, one can notice from Fig. 4 that the total basin SDR in the various water use sectors will be decreased in the future as follows: For potable water, it will decline from historic 97% to future 83-86%, depending on the scenario; for the agricultural demands it will drop from 68% to 43-58%; and for other types of demands it will dip by 19%, while SDR of the environmental water rights will drop by 3% - 13%.

In conclusion, all three climate scenarios investigated, indicate growing water resource deficits in the ZRB in the future, with the CESM2- scenario showing the strongest and CESM1 the weakest adverse effects. And because increasing water demands are another significant contributing factor to this upcoming water crisis, there will be the necessity for limiting the development of future demands and/or having recourse to an alternative water planning, such as a hedging rule or a deficit irrigation plan for the region.

5. CONCLUSIONS

The impact of changing climate on inflows and operation of the Boukan dam in the ZRB is investigated using a basin-wide hydrologic model (SWAT), in conjunction with a water management model (MODSIM). The hydrological model is driven by downscaled (quantile mapping) climate predictors from the CESM_CAM5 GCM, with three future scenarios, RCP2.6, RCP4.5 and RCP8.5. Although both the RCP2.6- and RCP8.5- scenario models predict an optimistic increase of the future available water in the basin, this increase cannot cover the future

growth of the demands. Very pessimistic is the RCP4.5 – scenario model which predicts even a decrease of the future inflow to the Boukan dam. This peculiar result may hint of some uncertainties in the GCM model prediction of the precipitation.

The water allocation optimization results by means of MODSIM using the historical prioritization of the various water use sectors, together with a gradual increase of the demands, indicate an endangerment of the water supply for the drinking water sector and of the environmental rights, as the most important priorities; with the water crisis further exacerbated by the development of agricultural and other demands.

This study also shows that the add-on of a water management model to a hydrological model results in a powerful simulation tool that is able to serve for sustainable river basin management and the output can be used further to support better water decision making systems.

REFERENCES

Abbaspour K.C., Faramarzi M., Ghasemi S.S., Yang H., 2009. Assessing the Impact of Climate Change on Water Resources of Iran, Water Resour. Res.; 45, W10434.

AghaKouchak A., Norouzi H., Madani K., Mirchi A., Azarderakhsh M., Nazemi A., Nasrollahi N., Farahmand A., Mehran A., Hasanzadeh E., 2015. Aral Sea syndrome desiccates Lake Urmia: Call for action, J. Great Lakes Research; 41: 307–311.

Ashraf Vaghefi, S., S. J. Mousavi, K. C. Abbaspour, R. Srinivasan, Arnold J. R., 2015. Integration of hydrologic and water allocation models in basin-scale water resources management considering crop pattern and climate change: Karkheh River Basin in Iran. Reg. Environ Change; 15:475-484.

Bates B.C., Kundzewicz Z.W., Wu S. and Palutikof J.P., 2008. Climate Change and Water. Technical Paper of the Intergovernmental Panel on Climate Change. Geneva: IPCC Secretariat. 210 pp.

Emami F., 2009. Development of an algorithm for assessing the impacts of climate change on operation of reservoirs, Master of Science Thesis, University of Tehran.

Emami F., Koch M., 2017. Modeling the Projected Impact of Climate Change on Boukan Dam Inflow and Water Availability in the Zarrine River Basin of Iran. „River Basins“- 2017 International SWAT Conference Warsaw, Poland, 28th-30th June.

Gudmundsson, L., Bremnes, J. B., Haugen, J. E., & Engen-Skaugen, T., 2012. Technical Note: Downscaling RCM precipitation to the station scale using statistical transformations - a comparison of methods. Hydrol. Earth Syst. Sci., 16(9), 3383–3390.

Labadie J.W., 1995. MODSIM: river basin network flow model for conjunctive stream-aquifer management. Program user's manual and documentation, Colorado State University.

Mehran A, AghaKouchak A, Phillips T., 2014. Evaluation of CMIP5 continental precipitation simulations relative to satellite observations. J Geophys. Res.; 119: 1695−1707.

Navarro-Racines C.E., Tarapues-Montenegro J.E., 2015. Bias-correction in the CCAFS-Climate Portal: A description of methodologies. Decision and Policy Analysis (DAPA) Research Area. International Center for Tropical Agriculture (CIAT). Cali, Colombia.

Neitsch S. L., Arnold J. G., Kiniry J. R., Williams J. R., 2001. Soil and Water Assessment Tool - Theoretical Documentation - Version 2005, Grassland, Soil and Water Research Laboratory, Agricultural Research Service and Blackland Research Center, Texas Agricultural Experiment Station, Temple, TX.

Wilby, R. L., Dawson C. W., Barrow E. M., 2002. SDSM- a decision support tool for the assessment of regional climate change impacts, Envir. Model. Soft. 17, 147–159.

Proceedings of the 10th World Congress of EWRA 'Panta Rhei', 5-9 July 2017, Athens, Greece
© 2017 *European Water Resources Association*

Turkish Water Foundation (TWF) statistical climate downscaling model procedures and temperature projections

I. Dabanlı* and Z. Şen
Istanbul Medipol University, School of Engineering and Natural Sciences, Civil Engineering Department, 34810, Istanbul, Turkey
** e-mail: idabanli@medipol.edu.tr*

Abstract: The Turkish Water Foundation (TWF) statistical climate downscaling model is further developed and implemented to a set of monthly temperature observations. The TWF model is structured by two phases as spatial and temporal downscaling of Global Circulation Model (GCM) scenarios. The TWF model takes into consideration the regional dependence function (RDF) for spatial structure and Markov Whitening Process (MWP) for temporal features of the records. The impact of climate change on monthly temperatures is employed by downscaling Intergovernmental Panel on Climate Change – Special Report on Emission Scenarios (IPCC-SRES) A2 and B2 emission scenarios from Max Plank Institute (EH40PYC) and Hadley Centre (HadCM3). The main purposes are to explain the TWF statistical climate downscaling model procedures and to expose the validation tests, which are rewarded in same specifications as "very good" for all stations in the Akarcay catchment that is in the west central part of Turkey. It is, therefore, possible to say that the TWF model has reasonably acceptable skill for highly accurate estimation regarding standard deviation ratio (SDR), Nash–Sutcliffe efficiency (NSE) and percent bias (PBIAS) criteria. Regarding validated model, temperature predictions are generated from 2011 to 2100 by using 30-year reference observation period (1981-2010). Temperature arithmetic mean and standard deviation have less than 5% error for EH40PYC and HadCM3 SRES (A2 and B2) scenarios.

Key words: Climate change, downscaling, TWF model

1. INTRODUCTION

Climate change impacts on different regions warn people about future climate features especially climate change projections under different scenario perspectives. Increases in extreme events like flood, drought, and heat waves triggered great interest on climate change in the past few decades (Laflamme et al., 2015). Recent surveys indicate that mean temperature temporal trend has been increasing over the Mediterranean and Middle-east and all over the world as well. Temperature distribution varies depending on regional features of country both spatially and temporally. Also, similar spatial and temporal variability has been observed in Turkey (Piras et al., 2016). The climate of Turkey is vulnerable to impacts of warm Mediterranean air born movements in summer and cold climate periods due to Balkan's air movements in winter. Hence, assessment of climate change impacts is very important for agriculture, economy, society, water resources, hydropower generation, and human activities (Huang et al., 2017).

Global climate change assessment is reported periodically in each five-year by IPCC (Intergovernmental Panel on Climate Change). The TAR (Third Assessment Report) is released by the IPCC with a different set of SRES (Special Report on Emissions Scenarios) in 2000. The SRES research group classified scenarios into four narrative storylines as A1, A2, B1, and B2, for the evaluation of global effects due to greenhouses gasses and aerosol emissions during the 21st century. The technological, social, demographic and environmental developments are described for each storyline by Nakicenovic et al. (2000).

The AR4 (Fourth Assessment Report) offers several GCMs (General Circulation Models), which can be employed under the control of the different climate research centres to produce simulated climate data based on different scenarios. The AR5 (Fifth Assessment Report) includes future climate change impacts of final CMIP5 (Coupled Model Inter-comparison Project, Phase 5).

Although, the AR5 is one of the developed scenarios, including human activities, i.e. RCP4.5 and RCP8.5 (Representative Concentration Pathways), there are no significant differences between the SRES and the AR5 scenarios. Therefore, both SRES and AR5 scenarios can be used for different analyses of future climate change projections (Torres and Marengo, 2013).

The downscaling process can be defined as a reduction in large-scale (coarse) model scenario data to a finer resolution. This process involves empirical relationship derivations between GCM (predictors) to regional scale variables (predictands). Dynamical and statistical downscaling procedures are frequently employed in scientific researches (Kerr et al., 2016). On the other hand, dynamical and statistical mixture downscaling procedures are also available in the literature. Dynamical or statistical downscaling procedure transforms coarse specification of the GCM variables to regional scale variables such as temperature (Muchuru et al., 2015). Several dynamical and statistical downscaling models have been developed in literature to adjust from sparse GCM output data scales to regional scales (Rashid et al., 2016). Similar to Mehrotra and Sharma (2005) study, diverse range of statistical models has been employed by many researchers (Yuan et al., 2017). The coarse-scale climate and regional scale time-lagged parameters, as precipitation and temperature, are common focus points of statistical downscaling, which is simulated by climatic and regional scale functions (Vu et al., 2016).

There are two main purposes in this paper; (1) to investigate the impact of climate change on temperature by assessing variations from observations to possible future projections using the four SRES emissions model outputs; (2) to underline the value of TWF (Turkish Water Foundation) statistical downscaling model.

2. STUDY AREA AND DATA

Akarcay is a closed basin located in the central western part of Turkey at the intersection of the Aegean, Central Anatolian, and Mediterranean regions between the geographical coordinates 30° 02'-31° 51' E longitudes and 38° 04'-39° 09' N latitudes as seen in Figure 1. It consists of two sub-basins as the Upper-Akarcay, where Akarcay River spills to Eber Lake and another one, Lower-Akarcay within the Aksehir Lake basin.

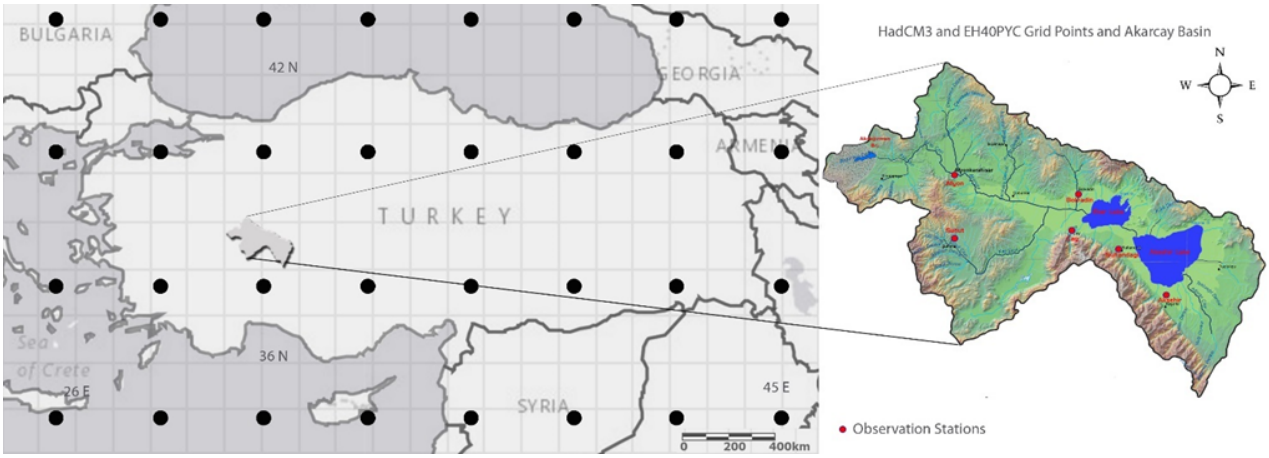

Figure 1. GCMs data grid points over Turkey and Akarcay basin location on Turkey mainland with physical features.

Six observation stations (Afyon, Suhut, Bolvadin, Cay, Sultandagi, and Aksehir) are chosen for downscaling studies. The 30-year records from 1981 to 2010 are considered as the reference period. The monthly mean temperature data are obtained from Hadley Centre for Climate Prediction (England) and the Max Planck Institute for Meteorology (MPI-M) (Germany) models for A2 and B2 SRES scenarios between 1981 to 2100.

3. METHODOLOGY

3.1 TWF statistical downscaling model

The TWF (Turkish Water Foundation) statistical downscaling model is employed for determining climate change impacts over Akarcay basin in Turkey. Initially, RDF (Regional Dependence Function) is used to set relationships between each observation gauge and other gauges. Hence, it is possible to obtain the relationship between distance and regional correlation coefficient like illustrated in Figure 2 (Şen, 2009a).

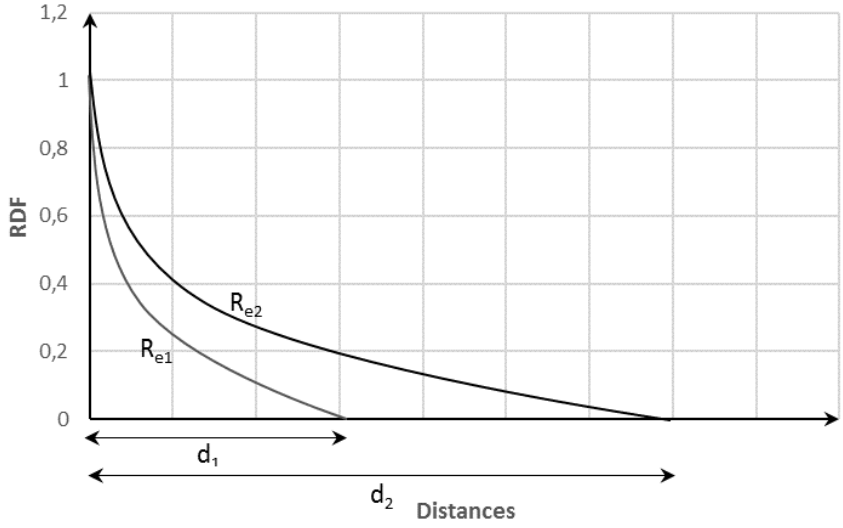

Figure 2 Theoretical RDF and distance relationship graph.

The general expression of the RDF, R_e, is given as follows (Şen, 2009b):

$$R_e = \sum_{i=1}^{n} \left(\frac{w_i}{\sum_{i=1}^{n} w_i} \right) R_i \tag{1}$$

where w_i is weight coefficient and R_i is the rainfall variable.

3.1.1 Point cumulative semi-variogram model (PCSV)

The basis of the RDF consists the cumulative semi-variogram (CSV) and point cumulative semi-variogram (PCSV) methods, which help to obtain spatially finer resolutions (Şen, 2009a; Şen and Öztopal, 2001; Öztopal, 2006). The least squares regression method is used to obtain the best curve fitting between the RDF data scatter and the most convenient mathematical model. According to the relationship in Figure 2, the mathematical function of Z, for the RDF appears in the form of an exponential expression as follows:

$$Z = ae^{-bd} \tag{2}$$

where *a* and *b* are the model parameters and *d* is the distance.

3.1.2 Markov whitening process (MWP)

The MWP is preferred due to its simplicity, fast calculation, and preserving correlation coefficient flexibly rather than any other stochastic processes. The MWP is constituted by the white noise (independent) process and first-order Markov process. The best suitable temporal autocorrelation coefficient can be determined randomly by independent process combination. The MWP combination, Z_t the value is calculated by using the following equation:

$$Z_t = X_t + \beta\eta_t \tag{3}$$

where X_t is a first-order Markov process value; η_t is the independent (whitening) process value, and finally, β is a parameter that shows contribution of the independent process rate on the overall MWP. The left-hand side of this equation shows the adjusted scenario data and right side; X_t is for the raw scenario data which are transferred to the record points as a result of downscaling by RDFs. The term, $\beta\eta_t$, consists adjustments that can be applied to the downscaled scenario data at the same location of the recorded time series.

4. IMPLEMENTATION AND RESULT

The Akarcay catchment with six stations is selected for the application of the statistical downscaling model and future projection generations. The TWF downscaling model provides the variety of future projections both in local point and regional scales. The downscaled scenario raw data and observations are described by Gamma cumulative distribution function (CDF) as presented in Figures 3 for EH40PYC (A2-B2) scenarios at Afyon station.

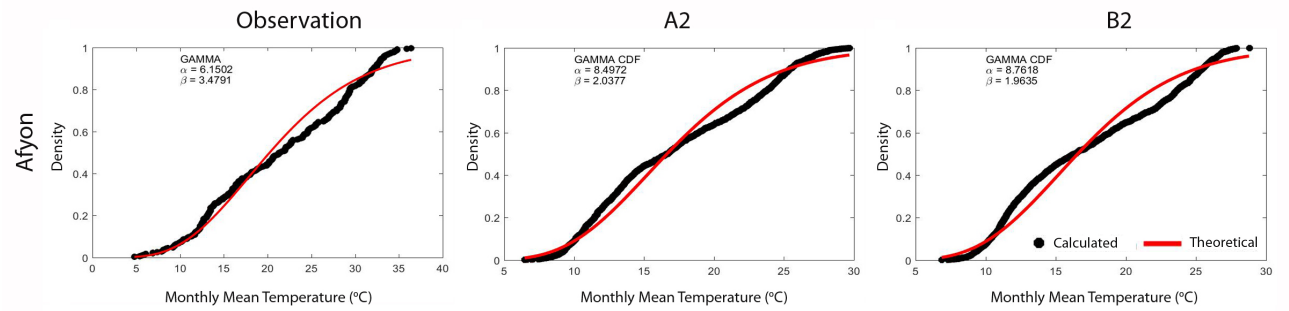

Figure 3 Theoretical and calculated Gamma CDF for EH40PYC scenarios and observations.

The most important characteristic of TWF model is protecting correlation similarity between observations and predictions. The MWP is applied after achieving RDF and point cumulative semi-variogram models on downscaled raw data to preserve correlation similarity and provide coherence between observations and downscaled data. Figure 4 shows explicitly the visual relationship between observation and projections clearly for Afyon station. The dashed red lines refer to the harmony after the PCSV calculations. The basic idea about the MWP that is the addition of the random compounds on the raw scenario series so as to get more consisted the scenario data. Critical question at this step is how can the best random variable be selected? The logical and simple answer is that the random compounds with various standard deviations should be examined until the sum of error square differences yields to minimum value. Then, the best correlated random compound can be added to scenario data.

Figure 4 indicates lags (2 to 24) versus correlation coefficient for all scenarios to illustrate the cyclical manner of scenario data. In general, relationship shape is expected to be harmonic because of the monthly periodicity.

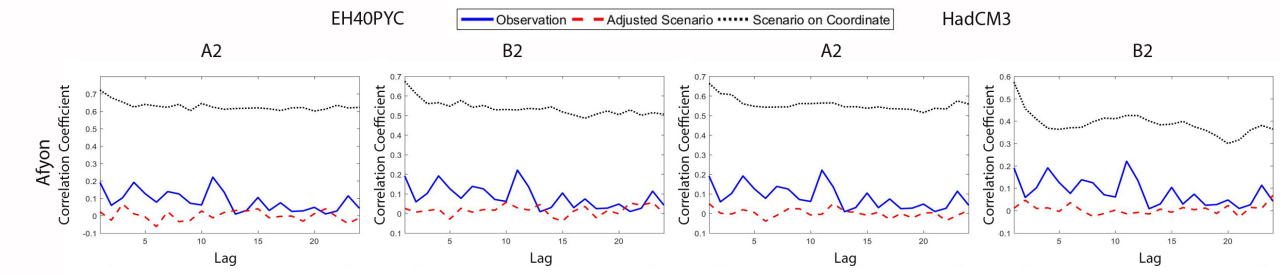

Figure 4 Correlation coefficient relationship among the observation, the raw scenario on point and new adjusted scenario illustrations.

It is obviously seen in Figure 4, if the downscaled raw scenario data cannot be adjusted by MWP, the harmony will disappear between recorded time series and projection data. Hence, the adjusted scenario data coherence is obtained by means of MWP calculations. The correlation coefficient relationship between observation and raw scenario on coordinate and new adjusted scenario can be easily distinguishable. The consistency between new adjusted scenario which is obtained from MWP and observation proves the reliability and vitality of MWP.

Another important step in the TWF downscaling model is the similarity confirmation of monthly mean temperature between observations and predictions. After the correlation coefficient adjustment achieved, mean monthly temperature temporal variation consistency processes are employed. Though, significant coherence has already been observed between scenarios on coordinate and observations prior to MWP, new adjusted time series exposes better fit as presented in Figure 5 for Afyon station.

Two essential parameters (correlation coefficient and monthly mean temperature) and standard deviation coherence preservation between observations and predictions, makes the TWF model better steady. Furthermore, the TWF procedure allows random fluctuations of temperature estimation while preserving these three parameters.

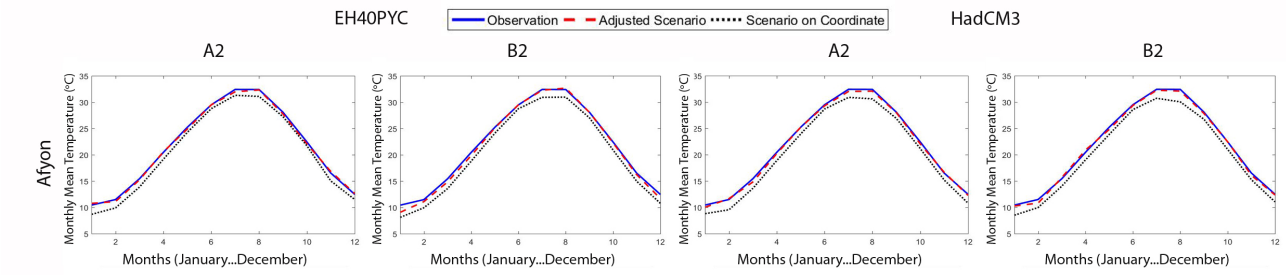

Figure 5 Monthly mean temperature relationship among the observation, the raw scenario on the coordinate and new adjusted scenario.

The monthly mean temperature projection at each station is presented in Figure 6. The highest temperature values around 25 ˚C are expected at Sultandagi station while the lowest one is estimated around 25 ˚C at Afyon station in the summer (significantly in August) season. In other seasons, model results indicate no significant differences between station temperature averages.

Stochastic characters of temperature, make long-time predictions rather hard in monthly scale. This means that monthly temperature estimation accuracy is expected to be low if it is compared on the annual scale. However, drought risk especially agricultural (3-6 months) drought should be assessed by monthly mean predictions due to the significant differences in each month. To obtain more reliable results, annual time series of predicted scenario data are presented in Figure 7. One of the most important features in this graph is that obvious decreasing trend can be seen for each projection. As seen in Figure 7, predicted temperature differences between 2010 and 2100 are 0.36 ˚C and 0.34 ˚C for HadCM3-A2 and HadCM3-B2, respectively. The extreme annual hottest (coldest) years are predicted around 2090s-12.40 ˚C (2040s-11.10 ˚C) for EH40PYC-A2 scenario

and around 2045s-12.45 ˚C (2025s-11.15 ˚C), for the EH40PYC-B2 scenario. Similarly, The extreme annual hottest (coldest) years are estimated around 2050s-12.50 ˚C (2035s-11.10 ˚C) for HadCM3-A2 scenario and around 2035s-12.40 ˚C (2080s-11.00 ˚C), for the HadCM3-B2 scenarios.

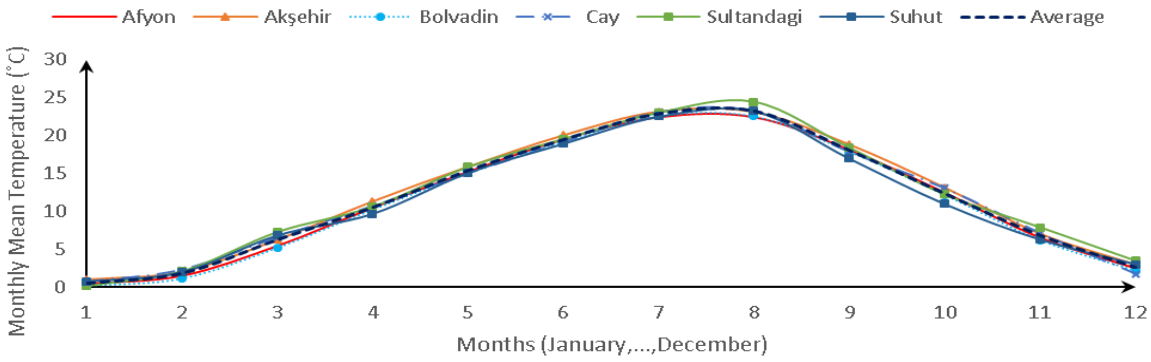

Figure 6 Monthly Mean temperature predictions between 2011 to 2100.

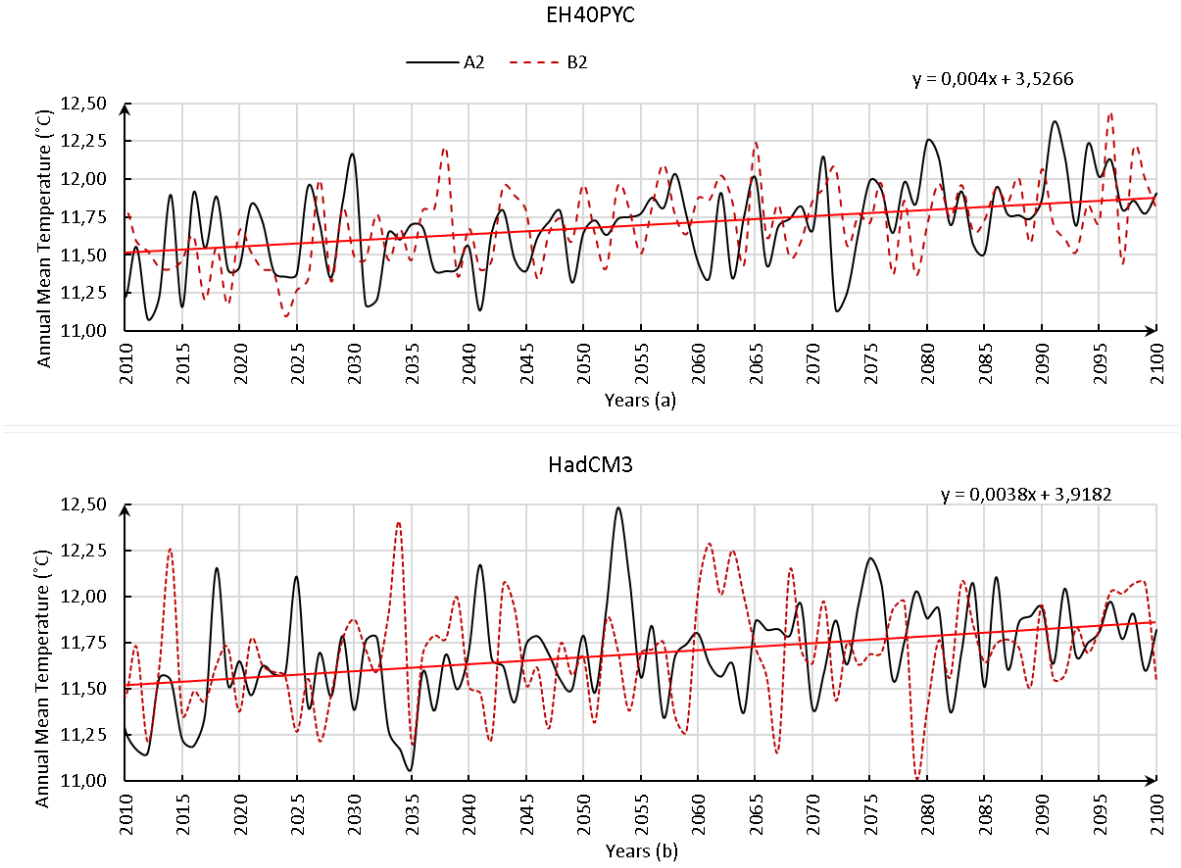

Figure 7 Annual mean temperature predictions between 2011 to 2100.

4.1 Validation of TWF Model

The validation of the model is one of the essential step for climate and hydrology researches. The Nash–Sutcliffe efficiency (NSE) (Nash and Sutcliffe, 1970), Percent Bias (PBIAS) between the observations and downscaled scenarios, and standard deviation ratio (SDR) are selected to evaluate the TWF model validation. For validation assessment, monthly mean observation and prediction data (i=1, 2, …, 12) are selected by considering the basis of the TWF model.

Table 1 Classification of validation test scores (Moriasi et al., 2007)

Performance Rating	SDR	NSE	PBIAS (%)
Very good	$0.00 \leq SDR \leq 0.50$	$0.75 < NSE \leq 1.00$	$\pm 1.00 \leq PBIAS \leq \pm 10$
Good	$0.50 < SDR \leq 0.60$	$0.65 < NSE \leq 0.75$	$\pm 10 \leq PBIAS < \pm 15$
Satisfactory	$0.60 < SDR \leq 0.70$	$0.50 \leq NSE \leq 0.65$	$\pm 15 \leq PBIAS < \pm 25$
Unsatisfactory	$SDR > 0.70$	$NSE < 0.50$	$PBIAS \geq \pm 25$

Validation test results are listed in Table 2 with observation and scenarios means and standard deviations. As expected all test scores rewarded as "very good" based on Table 1. Consequently, the TWF model is validated perfectly if the three well-known test results are taken into consideration.

Table 2 Classification of validation test scores.

	Observation			A2					B2				
Stations	μ	σ	GCM	μ	σ	NSE	SDR	PBIAS (%)	μ	σ	NSE	SDR	PBIAS (%)
Afyon	11,40	8,14	EH40PYC	11,29	8,02	1,00	0,04	0,93	11,05	8,50	1,00	0,07	3,02
			HadCM3	11,18	8,11	1,00	0,04	1,88	11,23	8,15	1,00	0,04	1,50
Aksehir	12,09	8,15	EH40PYC	11,84	8,31	1,00	0,06	2,03	11,95	8,21	1,00	0,04	1,12
			HadCM3	11,91	8,37	1,00	0,05	1,47	11,91	8,36	1,00	0,05	1,46
Bolvadin	11,21	8,25	EH40PYC	11,01	8,21	1,00	0,04	1,80	11,06	8,31	1,00	0,04	1,32
			HadCM3	10,94	8,38	1,00	0,05	2,42	10,99	8,34	1,00	0,05	1,94
Cay	11,72	8,14	EH40PYC	11,63	8,03	1,00	0,05	0,73	11,59	8,02	1,00	0,04	1,13
			HadCM3	11,59	8,20	1,00	0,04	1,11	11,53	8,14	1,00	0,04	1,64
Sultandagi	12,06	8,20	EH40PYC	11,95	8,31	1,00	0,03	0,92	11,93	8,13	1,00	0,04	1,11
			HadCM3	12,05	7,94	1,00	0,05	0,14	11,96	8,12	1,00	0,04	0,86
Suhut	11,35	7,91	EH40PYC	11,20	8,00	1,00	0,03	1,31	11,25	7,98	1,00	0,04	0,89
			HadCM3	11,26	7,91	1,00	0,03	0,83	11,29	7,91	1,00	0,02	0,56
Average	11,64	8,13		11,49	8,15	1,00	0,04	1,30	11,48	8,18	1,00	0,04	1,38

5. DISCUSSION AND CONCLUSION

In this study, the regional dependence function (RDF)-based statistical downscaling procedure is applied for downscaling monthly temperatures from GCM SRES scenarios. The theoretical basis of the TWF model depends on two distinctive parts, which are combined in a harmonic behavior for adjusting the predictions with local ground observations. The first part considers the spatial behavior of the hydro-meteorological variables through the innovative RDF, which provides predictions on the gauge coordinate basis from GCM coarse produced grid point data to finer resolutions. Another ingredient of the TWF model is for temporal adjustment through the Markov whitening process (MWP), which is necessary for adjusting the serial structure temporal coherence of scenario data to the observations. Due to the stochastic behavior of temperature, it is hard to predict in daily scales. The optimal scale to estimate future rainfall should be monthly, and therefore, the TWF model is based on monthly temperature projections.

The TWF downscaling model is applied to obtain monthly temperature projections until 2100 in the Akarcay catchment by using reference period between 1981 and 2010. The future projections' mean temperature and standard deviation under the light of EH40PYC and (HadCM3) A2 (B2) SRES scenarios are obtained as 11.49˚C (11.48˚C) and 8.15 ˚C (8.18 ˚C) in Akarcay basin, respectively. The preservation of effective spatial dependence together with the temporal character of observations has the major importance in the TWF model. Consequently, the TWF model performs highly accurate results regarding SDR, NSE, and PBIAS validation tests. The validation of the TWF model results is rewarded as "very good" in all stations.

ACKNOWLEDGMENTS

This study is supported by The Scientific and Technological Research Council of Turkey (TUBITAK) with grand number 1059B141501044. The corresponding author would like to thank

TUBITAK for its support and Assist. Prof. Dr. Ahmet ÖZTOPAL for valuable contributions this study. Also, the authors wish to thank Turkish State Meteorological Service (TSMS) for the supply of long-term monthly mean climatic variables.

REFERENCES

Huang, J., Chen, X., Xue, Y. et al., 2017. Changing characteristics of wet/dry spells during 1961–2008 in Sichuan province, southwest China. Theor Appl Climatol.127(1): 129-141.

Kerr, G. H., DeGaetano, A. T., Stoof, C. R. et al., 2016. Climate change effects on wildland fire risk in the Northeastern and Great Lakes states predicted by a downscaled multi-model ensemble. Theor Appl Climatol., doi: 10.1007/s00704-016-1994-4

Laflamme, E. M., Linder, E., Pan, Y., 2015. Statistical downscaling of regional climate model output to achieve projections of precipitation extremes. Weather and Climate Extremes, 12: 15-23

Mehrotra, R., Sharma, A., 2005. A nonparametric nonhomogeneous hidden Markov model for downscaling of multi-site daily rainfall occurrences. J. Geophys. Res. 110: D16108

Moriasi, D.N., et al., 2007. Model Evaluation Guidelines for Systematic Quantification of Accuracy in Watershed Simulations. Transactions of the ASABE, 50: 885-900.

Muchuru, S., Landman, W. A., Dewitt, D. G., 2015. Prediction of inflows into Lake Kariba using a combination of physical and empirical models. International Journal of Climatology, 2581: 2570–2581.

Nakicenovic, N. et al., 2000. Special Report on Emissions Scenarios: A Special Report of Working Group III of the Intergovernmental Panel on Climate Change, Cambridge University Press, Cambridge, U.K., 599 pp. Available online at: http://www.grida.no/climate/ipcc/emission/index.htm

Nash, J. E., Sutcliffe, J. V., 1970. River flow forecasting through conceptual models Part I – a discussion of principles. J. Hydrol. 10(3): 282–290.

Öztopal, A. 2006. Artificial neural network approach to spatial estimation of wind velocity data. Energy Conversion and Management, 47(4): 395–406.

Piras, M., Mascaro, G., Deidda, R., Vivoni, E. R., 2016. Impacts of climate change on precipitation and discharge extremes through the use of statistical downscaling approaches in a Mediterranean basin. Science of the Total Environment, 543: 952–964.

Rashid, M. M., Beecham, S., Chowdhury, R. K., 2016. Statistical downscaling of rainfall: a non-stationary and multi-resolution approach. Theoretical and Applied Climatology, 124(3-4): 919–933.

Şen Z., 2009a. Spatial modeling principles in earth sciences. Springer, Dordrecht, 351 pp.

Şen Z., 2009b. Precipitation downscaling in climate modeling using a spatial dependence function. Int J Glob Warm 1(1–3): 29–42.

Şen, Z., Öztopal, A., 2001. Assessment of regional air pollution variability in Istanbul. Environmetrics, 12(5): 401–420.

Torres, R. R., Marengo, J. A.,2013. Uncertainty assessments of climate change projections over South America. Theoretical and Applied Climatology, 112(1–2): 253–272.

Vu, M. T., Aribarg, T., Supratid, S., Raghavan, S. V., Liong, S. Y., 2016. Statistical downscaling rainfall using artificial neural network: significantly wetter Bangkok? Theoretical and Applied Climatology, 126(3–4): 453–467.

Yuan, Z., Yang, Z., Yan, D. et al., 2017. Historical changes and future projection of extreme precipitation in China. Theor Appl Climatol. 127(1): 393-407.

Proceedings of the 10th World Congress of EWRA 'Panta Rhei', 5-9 July 2017, Athens, Greece
© 2017 *European Water Resources Association*

Influence of the geographic location of dams on spring daily flows magnitude during the 2007-2008 La Niña event (Québec, Canada)

A.A. Assani* and A. Pothier-Champagne
Department of Environmental Sciences, University of Quebec at Trois-Rivières, 3351 Boulevard des Forges, Trois-Rivières, Québec, G9A 5H7, Canada
* *e-mail: Ali.Assani@uqtr.ca*

Abstract: The 2007-2008 La Niña event was characterized by an abnormally snowy 2008 winter and an abnormally rainy 2008 spring in Quebec. These abnormally wet conditions led to abnormally high spring flows. The goal of the study was to test whether the geographic location of dams affects spring flows (April to June) released downstream from these structures. We compared flows measured downstream from two dams located in the upper portion (Gouin and Châteauvert) and two others located in the lower portion (Taureau and La Gabelle) of the watershed of the Saint-Maurice River (44,000 km²), one of the main tributaries of the St. Lawrence River in Quebec. This comparison using several statistical tests revealed that spring flows are abnormally high downstream from dams located in the lower watershed, but abnormally low downstream from dams in the upper watershed. This difference between the two portions of the watershed is due to the fact that, to control flooding in the lower watershed, much more water derived from snowmelt and rainfall was stored in reservoirs located in the upper part of the watershed, leading to extreme hydrological drought despite abnormally high winter snowfall and spring rainfall.

Key words: La Niña, spring flows, floods, extreme hydrological drought, reservoir, dam, Kruskal-Wallis test, Saint-Maurice

1. INTRODUCTION

There are two theses in the science literature about the relationship between climate and flows downstream from dams. The first thesis, which may be referred to as the "flow independence and homogeneity thesis", holds that climate has little or no impact on flows downstream from dams (flows are independent of climate) (e.g., Lopez-Moreno et al., 2009; Poff et al., 2007). This leads to flow homogeneity downstream from dams, regardless of climate conditions in the area where these dams are built (Poff et al, 2007). On this, Poff et al. (2007) noted that "by strongly modifying natural flow regimes, dams have the potential to reduce these natural regional differences and thus impose environmental homogeneity across broad geographic scales". The second thesis contends that flows downstream from dams are also affected by climate ("flow dependence and heterogeneity thesis"), so that there are significant links between the temporal variability of flows and that of climate downstream from dams, among other places (e.g., Fortier et al.,2010; Naik and Jay, 2011).

The existence of these two theses, which have never been confronted in the science literature, raises the following fundamental question: how could climate affect flows downstream from some dams, but not downstream from others? The influence of numerous factors could be invoked to answer this question, including dam management mode, the type of hydrological variable analyzed, the spatio-temporal scale of analysis, the geographic location of the dams and reservoirs in a given watershed, the size of the watersheds, dam and reservoir characteristics, etc. The fundamental question which the study addresses is the following: does an extreme hydrologic event such as flooding (exceptionally high spring freshet of 2008) produce the same hydrological impacts downstream from all dams located in the same climate setting and in the same watershed? According to the first thesis, the independence and homogeneity thesis, flows downstream from all dams in a given watershed and in the same climatic setting should be homogeneous, i.e. flooding should occur downstream from all dams. According to the second thesis, flows downstream from

dams located in the same watershed and the same climate setting may be heterogeneous depending on the human and/or physiographic factors (climate-independent factors) that influence them. The goal of this study is to confront these two theses for the first time by comparing spring daily flows released downstream from four dams located in the same watershed, the Saint-Maurice River watershed in Quebec, and the same climate setting during the 2007-2008 La Niña event.

2. METHODOLOGY

2.1 Choice of gauging stations

One of the main tributaries of the St. Lawrence River on its north shore, the Saint-Maurice River, drains a 44,000 km^2 area (Fig. 1). To analyze the effects of the geographic location of reservoirs and hydroelectric power plants on spring flows, three reservoirs and one power plant were selected. Two of these reservoirs are located in the upper part of the watershed. These are the Gouin (Watershed surface area: 9473 km²; Total storage capacity: 14200 ha) and Châteauvert (Watershed surface area: 456 km²; Total storage capacity: 3200 ha) reservoirs. The former was built in the headwaters of the Saint-Maurice River proper and is the largest reservoir in the watershed. The latter was built on the Manouane River, one of the main tributaries of the Saint-Maurice River. The Taureau reservoir (Watershed surface area: 4070 km²; Total storage capacity: 9505 ha), on the Matawin River, and the La Gabelle power plant (watershed surface area: 42223 km²; Total storage capacity: 300 ha), on the Saint-Maurice River, both located in the lower part of the watershed, were also selected. The La Gabelle power plant is located near the confluence of the Saint-Maurice and St. Lawrence Rivers. The choice of these four dams is based on the existence of continuous daily flow data going back to the time they were built.

Aside from flows measured downstream from dams, spring flows and winter (from January to March) and spring (from April to June) precipitation (the results of precipitations are not presented in this article) measured at the Saint-Michel-des-Saints station (1390 km²), as well as spring flows in the Vermillon River (2670 km²), one of the main tributaries of the Saint-Maurice River, were also analyzed. The Saint-Michel-des-Saints station is located upstream from the Taureau reservoir on the Matawin River (lower portion of the watershed), whereas the Vermillion River station is located in the upper part of the watershed.

It is important to point out that flows measured at the Saint-Michel-des-Saints station are not affected by the Taureau reservoir (Assani et al., 2002) and that this station is the reference hydroclimate station for the Saint-Maurice watershed (e.g., Assani et al., 2002). Thus, flow measurements at these two stations reflect natural hydroclimate conditions in the Saint-Maurice River watershed. Data on amount of snow for 2008 were taken from a Quebec-scale map (http://www.mddelcc.gouv.qc.ca/climat/surveillance/precipitation-neige2007-2008.pdf).

2.2 Analysis of flow data

To highlight the effect of dam location on spring flows during the 2007-2008 La Niña event, we compared flows measured during the spring of 2008 (April to June) with those measured in the spring of 2007 and mean spring daily flows calculated over a 30 year period (1979-2008) downstream from these four dams and in natural rivers (Matawin station upstream from the dam and Vermillon station). Four hydrological variables were used for this comparison: monthly averages (April, May, and June) of spring flows calculated from daily flows, monthly maximum daily flows (Max; highest daily flow measured over a month), monthly minimum daily flows (Min; lowest daily flow measured over a month) and the total number of days without flow release (zero flow) downstream from a dam or reservoir (ZFD). Monthly average values were compared using the analysis of variance (ANOVA) with a single classification criterion parametric test and the

Kruskal-Wallis non-parametric test. The other three variables were not compared using a statistical test because only one value is measured for each of these three variables each month. Finally, it should be mentioned that the 2007-2008 La Niña event was one of the most intense observed during the 2000 decade. It started around summertime and continued until December 2007 in the Tropical Pacific Ocean. From a hydrologic standpoint, the impacts of El Niño and La Niña events are mainly observed during the following spring in Quebec. This is why we refer to it as the 2007-2008 La Niña. Flow data measured at the Saint-Michel-des-Saints and Vermillon stations were taken from the website of the Ministère de l'Environnement du Québec's Centre d'expertise hydrique (http://www.cehq.gouv.qc.ca/, viewed on May 20, 2014). As for flows measured downstream from the dams, the data were kindly provided by Hydro-Québec, which manages these dams.

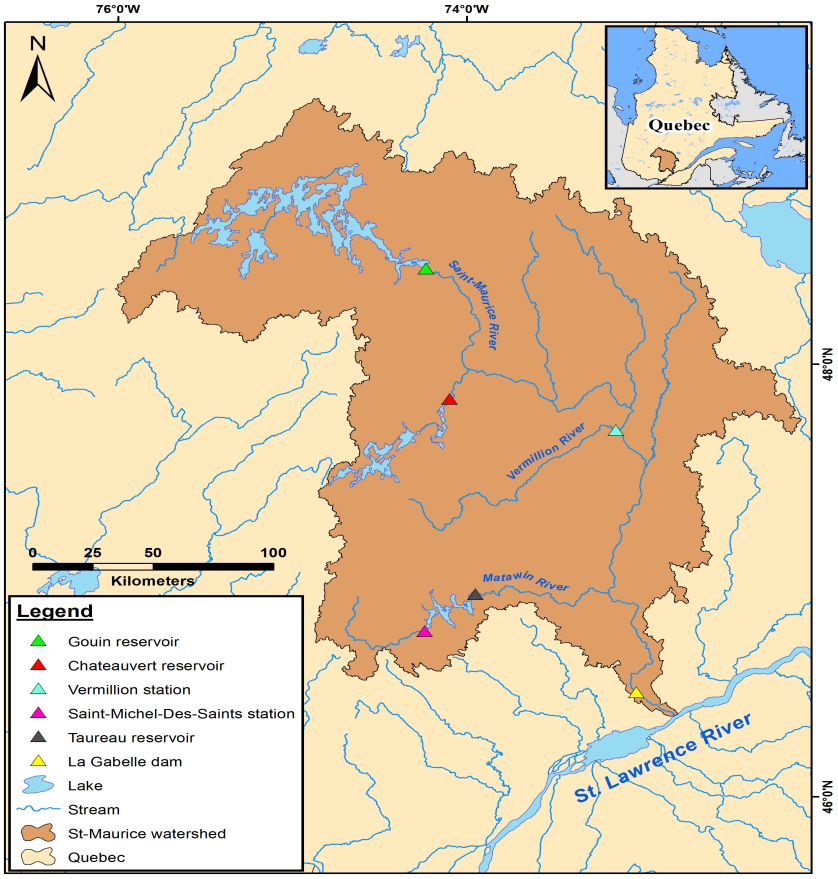

Figure 1. Location of studied dams and flow-gauging stations in the Saint- Maurice River watershed.

3. RESULTS AND DISCUSSION

3.1 Analysis of spring daily flows in pristine station

We compared spring daily flows measured at the Saint-Michel-des-Saints station (Matawin River) and on the Vermillon River (Table 1). It may be seen that mean values of spring daily flows for 2008 (La Niña year) were systematically higher than those measured in 2007 and over the 30-year period for both rivers. As far as monthly maximum daily flows are concerned, they were higher than those measured the previous spring (2007) only in April and May at the Saint-Michel-des-Saints station, but for all three spring months in the Vermillon River (Fig. 2). Finally, the same trend is observed for minimum daily flows, which were higher in spring 2008 than in spring 2007, except in April at the Saint-Michel-des-Saints station. Thus, in natural rivers, the relatively high amounts of winter snow and spring rain produced much higher spring daily flows in 2008 than in

2007. Such exceptionally high spring flows were observed in many watersheds in Quebec in 2008, and led to extensive flooding and numerous landslides (e.g., http://ici.radio-canada.ca/regions/est-quebec/2008/05/04/003-transport-ferroviaire_n.asp.).

Table 1. Comparison of spring daily flows (m^3/s) in two pristine stations and downstream from four dams in the Saint-Maurice River watershed

Dams	Mean			Maximum			Minimum			ZFD	
	2007	2008	1979-2008	2007	2008	1979-2008	2007	2008	1979-2008	2007	2008
April											
Vermillon	73.7	158.2a	91.7	205.9	314	403	19.7	31.6	85.2	0	0
Matawin (upstream from dam)	63.2	90a	64.9	172	218.2	236.2	16.7	12.5	49.3	0	0
Gouin	168.9	65.7a	55.4	398.6	334.1	398.6	6.6	6.4	6.4	0	0
Châteauvert	24.1	11.8a	26.5	79.7	53.1	153	0	0	0	18	21
Taureau	7.2	29.3a	37.7	38.9	84.7	245	0	0	0	24	11
La Gabelle	895	1449a	1019	1735	3200	3050	560	431	752	0	0
May											
Vermillon	63.2	93.7b	105.6	150.4	233.8	337	30.7	42.1	74	0	0
Matawin (upstream from dam)	49.3	61.5b	59	140.1	171.2	240	18.4	29.3	46.3	0	0
Gouin	189.1	14.2a	35.8	401.6	99.6	401.6	6.7	6.7	0	0	0
Châteauvert	9.8	0a	16.7	38	0	221	0	0	0	15	31
Taureau	9.3	97.9a	49.3	68.3	151	453	0	0	0	24	2
La Gabelle	824	1274a	1221	1515	2998	3871	549	681	1841	0	0
June											
Vermillon	45.9	74.8a	45.2	95.9	111.1	145	26.9	39.5	49.5	0	0
Matawin (upstream from dam)	29.1	38.4a	25.6	58.6	55.6	70.4	14.7	29.2	30.8	0	0
Gouin	133.1	43.8a	88.4	300.2	169.3	583	6.8	6.8	0	0	0
Châteauvert	43.8	17.8a	26.6	88.5	31.6	158	10.2	0	0	0	0
Taureau	77.4	116.5a	59.3	118.8	246	246	0	52	0	0	0
La Gabelle	620	796a	652	1034	1216	2530	301	564	852	0	0

a = the mean value of flows for 2008 (La Niña year) is statistically different from those for the other two periods at the 5% level; b = the mean value of flows for 2008 (La Niña year) is statistically different from those for 2007 at the 5% level. ZFD = Number of zero-flow days.

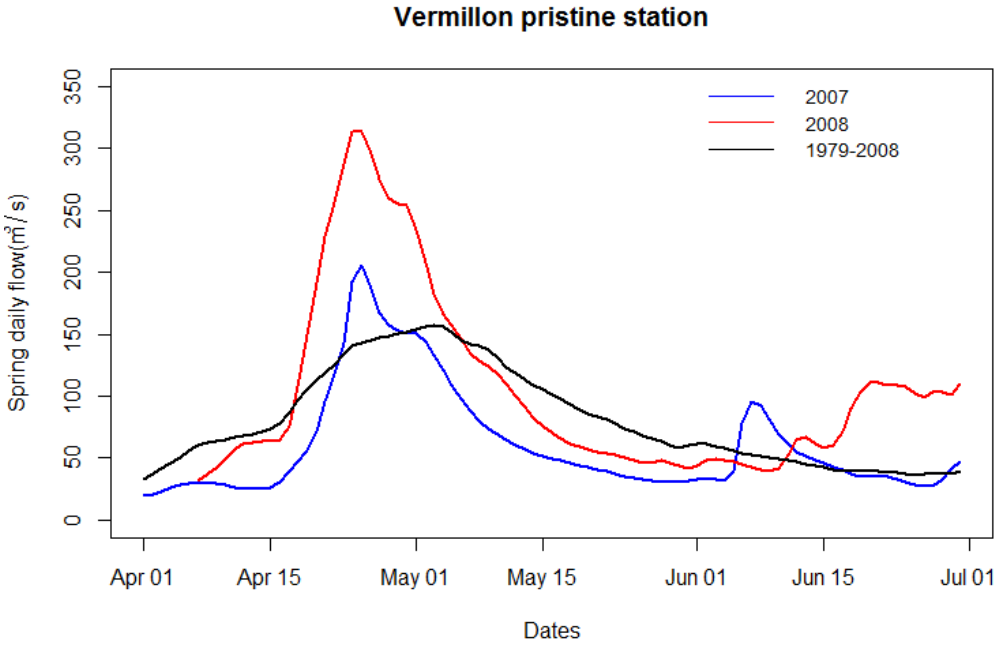

Figure 2. Comparison of spring daily flows at the Vermillon station.

3.2 Comparison of the spatio-temporal variability of spring daily flows downstream from dams

Data for the four hydrological variables measured downstream from the dams are shown in Table 1. As far as mean daily flows are concerned, they were much lower in 2008 than in 2007 downstream from the Gouin (Fig. 3) and Châteauvert reservoirs located in the upper watershed. In fact, downstream from the Châteauvert reservoir, the mean daily flow for the month of May was zero. In other words, no water was released during that whole month. In contrast, these flows were much higher in 2008 than in 2007 downstream from the Taureau reservoir (Fig. 4) and the La Gabelle power plant located in the lower watershed. The same trend is also observed for maximum daily flows. For minimum daily flows, there is very little difference between dams and, therefore, between the upper and lower portions of the watershed. Finally, the comparison of the total number of days with zero flow downstream from the dams reveals that zero flows occur only downstream from the two reservoirs built on tributaries, namely the Châteauvert reservoir on the Manouane River and the Taureau reservoir on the Matawin River. In spring 2008, the number of days with zero flow was higher than in spring 2007 downstream from the Châteauvert reservoir for the months of April and May, whereas the opposite was true downstream from the Taureau reservoir, located in the lower watershed.

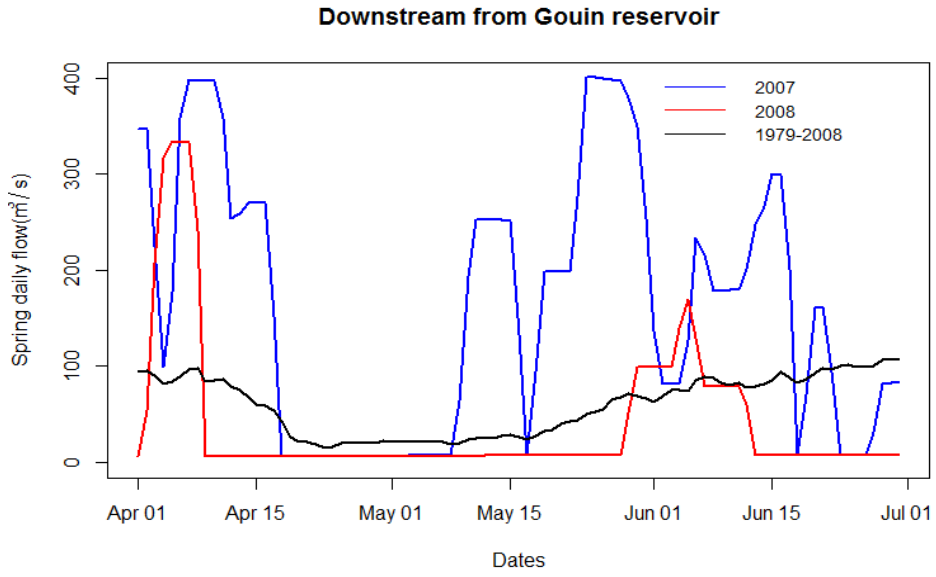

Figure 3. Comparison of spring daily flows at the downstream from Gouin reservoir on the St. Maurice River.

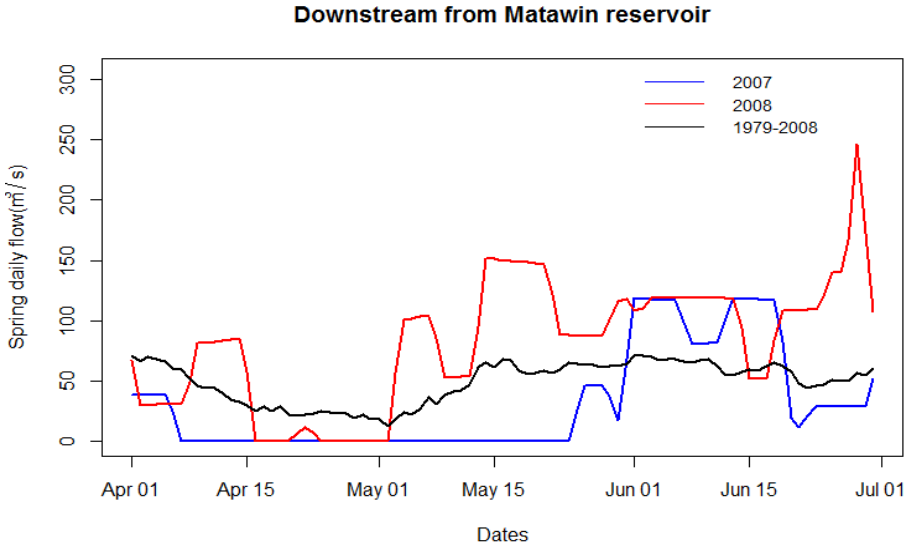

Figure 4. Comparison of spring daily flows at the downstream from Taureau reservoir on the Matawin River.

The results highlight the marked difference in amount of flows released downstream from dams between the upper and lower portions of the watershed during the spring of 2008. Thus, downstream from both reservoirs located in the upper watershed, spring flows were lower in 2008 than in 2007. In fact, there was an extreme hydrological drought downstream from the Châteauvert reservoir during the months of April and May even as a very strong freshet was occurring in natural rivers in the area. In contrast, downstream from both dams located in the lower watershed, spring flows were much higher in 2008 than in 2007. This difference in observed flows between the two parts of the same watershed is due to the fact that the winter and spring of 2008 were much snowier and rainier than in 2007. To avoid serious flooding along the Saint-Maurice River, nearly all water derived from snowmelt and rainfall was stored in reservoirs in the upper portion of the watershed, while large amounts of water were released downstream from dams located in the lower watershed. This led to an abnormally severe hydrological drought in the upper watershed despite abnormally high snowfall and rainfall. These results clearly highlight the influence of dam location on the relationship between spring flows and climate conditions. Dams located in the upper watershed produced an extreme hydrological drought in the spring of 2008 despite very wet conditions (abundant snow in winter and rain in the spring) which prevailed in the watershed, whereas those located in the lower watershed were characterized by very wet conditions.

4. CONCLUSION

The relationship between streamflow downstream from dams and climate is very complex due to the influence of numerous factors. Among these factors, the location of a dam in a relatively large watershed can be crucial during extreme hydroclimate events. The 2007-2008 La Niña event was characterized by a very snowy winter and rainy spring in the Saint-Maurice River watershed. Despite these abnormally wet hydroclimatic conditions, however, spring flows were not homogeneous downstream from all dams and reservoirs in this watershed. To mitigate the effects of the spring freshet resulting from these large amounts of snow and rain in the lower part of the watershed, large amounts of water were stored in reservoirs in the upper part of the watershed, leading to a very intense hydrological drought downstream from these reservoir, and inhibiting a correlation between the exceptionally wet climate conditions and spring flows. This lack of correlation is not observed over the whole watershed, however. The study shows for the first time that both the climate-dependent flow and climate-independent flow theses for flows downstream from dams may be valid in a single watershed depending on the geographic location of the dams. It is important to take this factor into account when predicting extreme flows during extreme hydrological events in the Saint-Maurice River watershed.

REFERENCES

Fortier, C., Assani, A.A., Mesfioui, M., Roy, A.G. 2011. Comparison of the interannual and interdecadal variability of the heavy flood characteristics upstream and downstream from dams in inversed hydrologic regime: case study of Matawin River (Québec, Canada). River Res. Applic.; 27: 1277-1289.

Lopez-Moreno, J.I., Vicente-Seranno, S.M., Begueria, S., Garcia-Ruiz, J.M., Portela, M.M., Almeida, A.B. 2009. Dam effects on drougths magnitude and duration in a transboundary basin: the Lower River Tagus, Spain and Portugal. Water Resourc. Res.; 45: W02405, doi: 10.1029/2008WR007198.

Naik, P.K., Jay, D.A. 2011. Distinguishing human and climate influences on the Columbia River : changes in mean flow and sediment transport. Journal of Hydrol.; 404: 259-277.

Poff, N.L., Olden, J.D., Merrit, D.M., Pepin, D.M. 2007. Homogenization of regional dynamics by dams and global biodiversity implications. PNAS; 104: 5732-5737.

Proceedings of the 10th World Congress of EWRA 'Panta Rhei', 5-9 July 2017, Athens, Greece
© 2017 *European Water Resources Association*

An informational entropy application to test the goodness of fit of probability functions

T. Baran[1], F. Barbaros[2*], A. Gül[3] and G. Onuşluel Gül[4]
Dokuz Eylul University, Faculty of Engineering, Department of Civil Engineering, Izmir, Turkey
[*] *e-mail: filiz.barbaros@deu.edu.tr*

Abstract: Increasing population, higher levels of human and industrial activities have affected the water resources in last decades. In addition, per capita demand for water in most countries is steadily increasing as more and more people achieve higher standards of living. Researchers should have more information about water resources as using and managing water resources efficiently. So, getting much and quick information had a great importance in water resources planning and management; and consequently, the determination of the characteristics of water resources had more importance. For this purpose, useful and easily applicable methods are searched to get optimum results and several test techniques are investigated to get much more information from the available water resources data. In the presented study, Informational Entropy method is introduced as an alternative test method to test the goodness of fit of probability functions. Presented study gives a brief detail on the applicability of Informational Entropy as a goodness of fit tool. For this purpose, mean precipitation data for 60 stations in Turkey are investigated. Results by testing the goodness of fit of probability functions by entropy-based method show that Informational Entropy can be applied for fitting the probability function according to the investigated datasets.

Key words: Informational Entropy, Probability Analysis, Trend Analysis

1. INTRODUCTION

Efficient use of water resources is stated as a must by research results. For this purpose, getting much and quick information about water resources had become an important topic and therefore, more useful and easily applicable methods have to be researched. The presented study consists of two parts. The first part is to determine the global climate change effect in temperature and precipitation data in selected stations by using trend analysis. For this purpose, 9 different data series are used in gaging stations of İzmir (temperature and precipitation data, 49 years), Güre (precipitation data, 28 years), Salihli (temperature data, 31 years), Gediz (precipitation data, 29 years), Kula (precipitation data, 60 years) and Adana (temperature and precipitation, 49 years). All meteorological data are provided from State Meteorological Works - DMI.

The second part is to test the best fit of probability distribution function of precipitation data in Turkey. For this purpose, 60 gaging stations having long-term precipitation data are investigated which located in major cities in Turkey. In probability analysis, the best fitting probability distribution is investigated by Chi-square test and Informational Entropy method.

2. INFORMATIONAL ENTROPY

2.1 Need for measuring the information content of hydrologic processes

All attempts towards an efficient development of water resources within technical and economic perspectives require data and information on the quality and quantity of such resources. Accordingly, measuring and evaluating hydrologic processes that represent time-variant characteristics of water resources is highly significant. It is up to the planner to extract the

maximum amount of information from these series and to determine the required parameters for the design and operation of water resources systems. The planner is not only concerned with the availability of data but also with the proper delineation of data collection networks. This is due to fact that collection processing and acquisition of hydrologic data require a significant amount of labor and investment. Thus, it is highly important that collected data bring *new* information.

Considering the limited financial resources to be allocated to monitoring of data, emphasis must be put on the optimum selection of spatial of and temporal monitoring frequencies. The collected data must also be assured to meet the objectives of water resources planning and development. Consequently, it may be stated that an objective criterion in needed to determine the amount of information conveyed by observed data since all activities towards the planning of water resources rely on data and information contained in available observations.

Entropy is a measure of the degree of uncertainty of random hydrological process. Since the reduction of uncertainty by means observations is equal to the amount of information gained, the entropy criterion indirectly measures the information content of a given series of data.

The entropy concept known as the Mathematical Communication Theory or Information Theory seems to offer such a criterion and appears to bring appropriate solutions to the aforementioned problems in water resources engineering. In the area of hydrology and water resources, a range of applications of entropy has been reported during the last decades. In the entropy-based parameter estimation, the distribution parameters are expressed in terms of the given information (Singh, 1998).

Baran (1993) has defined entropy as *the variation of information content instead of as reduction of uncertainty ≡ amount of information gained.* The method is demonstrated on the series of the monthly observations of selected stream gaging stations. The results confirm that the new entropy definition leads to results that are more reliable and can be effectively used for the solution of water resources engineering problems related to uncertainty and information. The mathematical formulation developed does not depend on the use of discretizing intervals so that a single value for the variation of information can be obtained. Furthermore, the new definition introduces tolerance limits for the entropy function, which makes it possible to compare the uncertainty of various hydrologic processes with different magnitudes and different probability structures (Bozoglu and Baran, 2010; 2012)

2.2 The role of the entropy concept in evaluation of hydrologic data

In mathematically communication theory, the concept of and the measure for information content has been derived from statistical and probabilistic principles. Within this respect, the theory has also been referred to as *Statistical Communication Theory*.

Mathematical communication theory analyzes the statistical structure for information of a series of numbers, sings or symbols that make up a communication signal, without considering all their kind, meaning, value or any other subjective characteristics. The term *information content* here refers to the capability of signals to create communication, and the basic problem is the generation of correct communication by sending a sufficient amount of signals, leading neither to any loss nor to repetition of information (Cherry, 1957; Pfeiffer, 1965).

Shannon has considered that average information content of the source is more significant than described per each symbol. In this case, Shannon considers that the source is made up of independent and discrete signs or symbols which occur with probabilities p_n (n=1, …, N). Consequently, Shannon defined the information content of a message sent by the transmitter as:

$$H(n) = -\sum p_n \log p_n \tag{1}$$

with units as (bit/symbol). The further named the information content H(n) as entropy (Shannon & Weaver, 1949) as his definition is similar to the entropy function described in statistical mechanics (Cherry, 1957; Pierce, 1961; Pfeiffer, 1965).

Hydrologic processes must be observed to achieve optimum decisions regarding the design and operation of water resources systems. On the other hand, data collection practices must also be realized on an optimum basis in delineation of *what, where, when* and *how long* to measure (Baran, 1993). Planners after use the terms *expected information, increase of information,* or *deficiency of information* and relate their design parameters to the information conveyed by available data. Information has often been expressed indirectly in terms of statistical parameters such as variance, standard error or correlation coefficient instead of quantitative terms (Harmancioglu and Singh, 1998).

The main difficulty associated with the applicability of the entropy concept in hydrology is the lack of a precise definition for the case of continuous variables. According to Baran (1993), a new definition describes the concept, not as an absolute measure of information but as a measure of *variation of information.*

2.3 Variation of information entropy for testing the goodness of fit

For investigated *Variation of Information* [$H(X/X^*)$], basic statistical parameters are calculated and then the range of each data set and maximum entropy are calculated by equations (2) and (3), respectively.

$$H_{\max} = \log R \tag{2}$$

$$R = b - a \qquad a < x < b \tag{3}$$

Marginal entropy is calculated by equation (4) and then informational entropy $H(X/X^*)$ is calculated by equation (5).

$$H(X) = \log\sqrt{2\pi} + \log\sigma + 1/2 \tag{4}$$

$$H\left(X / X^*\right) = H(X) - H_{\max} \tag{5}$$

For the half range value, replacing the appropriate values in Eq. (4)., one obtains the acceptable entropy value for normal probability density function as equation (6) using normal logarithms.

$$H\left(X / X^*\right)_{cr} = 0.6605 \tag{6}$$

When the entropy $H(X/X^*)$ of the variable which is assumed to be normal, remains below the above value, one may decide that the normal probability density function is acceptable and that sufficient amount of information has been collected about the process (Baran, 1993; Baran and Barbaros, 2015).

If the a posteriori distribution function is selected as lognormal $LN(\mu_y, \sigma_y)$, the variation of information for the variable x can be determined as equation (7). Here, since lognormal values will be positive, one may consider –a=0. Then the acceptable value of $H(X/X^*)$ for the lognormal distribution function will be as in equation (8).

$$H\left(X / X^*\right) = \log\left|2Sinh(a\sigma_y)\right| - \log\sigma_y - 1.4189 \tag{7}$$

$$H\left(X / X^*\right) = a\sigma_y - \log\sigma_y - 1.4189 \tag{8}$$

One may observe here that, no single constant value exists to describe the confidence limit for lognormal distribution. Even if critical halfrange is determined, the confidence limits will vary according to the variance of the variable. However, if the variance of x is known, one can compute the confidence limits (Baran, 1993; Bozoğlu and Baran, 2010; Baran and Bacanli, 2006, 2007 a and b).

3. AVAILABLE SITUATION AND DATA

There are different climates in various parts of Turkey due to irregular topography. In the Taurus Mountains, it is close to the shore and rain clouds cannot penetrate the interior of the country. As the

rain clouds pass over the mountains and reach Central Anatolia, they do not have an important ability to produce rain. The North Black Sea Mountains and the Caucasus Mountain keep the rain cloud, which is why the region is affected by the long and very cold winters and continental climate. In the eastern mountains, minimum temperatures between -30°C and -38°C are observed and can snow for 120 days a year. Winter often passes through heavy snowfall. The villagers in this area can remain isolated for several days during the winter storms (DMI, 2002; Bacanli, et. al., 2008; 2010).

In Turkey, summers are hot and dry; temperatures are above 30°C. Although spring and autumn usually pass slightly, abrupt hot and cold changes in the area are frequent in both seasons. Annual average precipitation is about 500-800 mm; actual quantities are determined by elevation. Annual average precipitation in Turkey is shown in Figure 1.

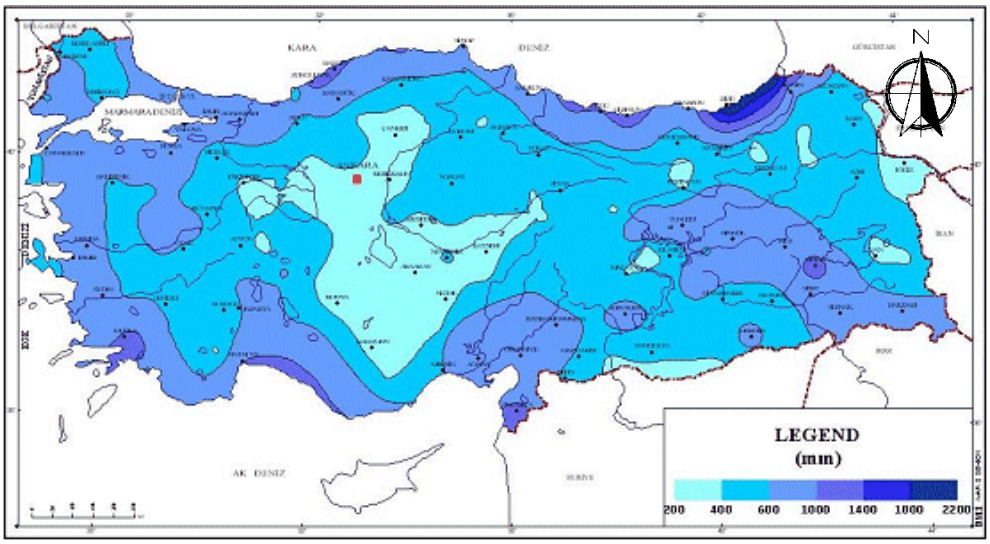

Figure 1. Annual average precipitation of Turkey.

Western Anatolia has a mild Mediterranean climate with an average temperature of 9°C in winter and 29°C in summer. Similar climatic conditions are observed on the southern coast of Anatolia. The climate of Anatolian Plateau is a systematic climate. There is a big temperature difference between day and night. The average temperature in summer is 23°C and winter is -2°C. The climate in the Black Sea region is wet and moist (summer 23°C, winter 7°C). There is a long winter in Eastern Anatolia and Southeastern Anatolia, and there is snow from november to the end of april (average temperature in winter is -13°C and 17°C in summer). The long-term average temperature of Turkey is shown in Figure 2.

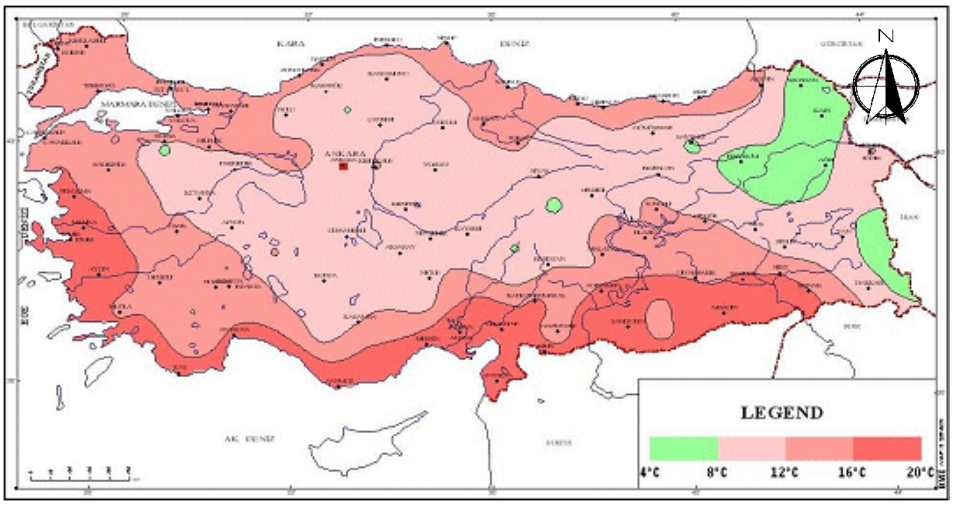

Figure 2. Long term mean temperature of Turkey.

All meteorological data are provided from State Meteorological Works - DMI. In the presented study, precipitation and temperature data of 60 DMI Gaging Station in Turkey are investigated. The observed period of Precipitation Gaging Stations - PGS is from January 1950 to December 1998. The altitudes, latitudes and mean values in the observed period of investigated PGS are executed.

In trend analysis, both the temperature and precipitation data are performed by parametric and non-parametric methods. Some selected gaging stations and different data series investigated in detail are Izmir (temperature and precipitation data, 49 years), Güre (precipitation data, 28 years), Salihli (temperature data, 31 years), Gediz (precipitation data, 29 years), Kula (precipitation data, 60 years) and Adana (temperature and precipitation, 49 years). All these data are provided from DMI and investigated in trend analysis.

4. TREND AND PROBABILITY ANALYSIS

In the presented study, average monthly and annual temperature and precipitation data are analyzed in detail using the available 9 different data sets for 6 districts. Izmir, Güre, Salihli, Gediz, Kula and Adana, which have long-term temperature and precipitation data, are investigated for trend in both parametric and non-parametric methods. The annual mean precipitation datasets which located in major cities are also performed by both parametric and non-parametric methods in trend analysis. Both Spearman-Rho and Mann-Kendall non-parametric tests are performed and the results showed there are no significant trends for the performed data.

The best fitting Probability Distribution Function (PDF) is searched for each precipitation gaging station. For this purpose, prior parameters – the basic statistics (mean, standard deviation, skewness, and excess coefficients) are calculated and the parameters for best fitting PDF for Chi-square Test are executed.

For the following step, each precipitation gaging stations are investigated in terms of *Informational Entrop*y and prior statistical parameters are calculated. Basic parameters and equation results to determine the *Informational Entropy* are executed for 60 major cities and obtained the "*Suitable*" result each for the case. This is expected as suitable for normal distribution when executing the total precipitation data and suitable for lognormal distribution if there is skewness. The results are given only for the 8 example cities of 60, for normal and lognormal distributions in Table 1 and 2, respectively.

Table 1. Results of Informational Entropy Method for Normal Distribution

	Average	Range	Hmax	Hx	H(XIX')	Test
Adapazarı	817.87	585.9	6.37	6.29	0.08	Suitable
Adıyaman	732.37	694.4	6.54	6.64	-0.09	Suitable
Afyon	425.25	403.4	6.00	5.87	0.13	Suitable
Amasya	454.30	293.8	5.68	5.74	-0.05	Suitable
Ankara	396.64	410.6	6.02	5.79	0.23	Suitable
İzmir	678.63	746.8	6.62	6.54	0.08	Suitable
Manisa	731.26	732.4	6.60	6.54	0.05	Suitable
Zonguldak	1222.32	847.3	6.74	6.67	0.07	Suitable

Table 2. Selected Summarized Results of Informational Entropy Method for Log Normal Distribution

	Hmax	Hx	H(XIX')	Hcr	Test
Adapazarı	6.37	5.16	1.21	3.01	Suitable
Adıyaman	6.54	5.95	0.59	2.19	Suitable
Afyon	6.00	4.98	1.02	2.57	Suitable
Amasya	5.68	4.65	1.03	2.94	Suitable
Ankara	6.02	4.88	1.14	2.60	Suitable
İzmir	6.62	5.84	0.78	2.22	Suitable
Manisa	6.60	5.77	0.82	2.35	Suitable
Zonguldak	6.74	5.53	1.22	3.05	Suitable

5. CONCLUSIONS

In trend analysis, the aim is to determine the effect of global climate change on temperature and precipitation. For this purpose, 9 different data sequences were examined. It is noted that the selected data stations having long term observations (annual total precipitation) and also affected by urbanization or agricultural facilities. The results show that there is no significant trend in the data series investigated except for rainfall data at Güre and Gediz stations. On the other hand, it should be noted that even it is stated as there is no trend in annual precipitation data, performed trend analysis in detail for selected stations' monthly precipitation data show the significant trend.

In the probability analysis, the best fitting probability distribution was investigated and it was found that most Precipitation Gaging Stations - PGSs are suitable for normal and lognormal distributions. Normal and Log-normal distributions are considered only in the Information Entropy method. Similar results were obtained for goodness of fit testing by both Informational Entropy and Chi-Square Method. The results for these stations should be investigated by further specified studies. Consequently, the presented application of Informational Entropy method can be stated as one of the effective tools to evaluate hydrological data besides the other testing methods and it can be stated as a potential tool to be used in investigating climate change effects and in decision making processes.

REFERENCES

Bacanli, Ü. G., Dikbas, F., Baran, T., 2008. Drought analysis and a sample study of Aegean Region, 6th International Conference on Ethics and Environmental Policies, Italy.

Bacanli, Ü. G., Dikbas, F., Baran, T. 2010. Kuzey Ege Bölgesi için meteorolojik kuraklık analizi, 6th National Hydrology Congress, Denizli.

Baran, T., 1993. Hidrolojik Süreçlerin Bilgi İçeriğindeki Değişim Miktari olarak Entropi Tanimi, Dokuz Eylül University, The Graduate School of Natural and Applied Sciences, Department of Civil Engineering, Department of Hydraulic – Hydrology and Water Resources, Ph. D. Thesis (Advisor: N. Harmancioglu), 153 p.

Baran, T., Bacanli, Ü.G., 2006. Evaluation of Suitability Criteria in Stochastic Modeling, European Water, 13-14, pp. 35-43.

Baran, T., Bacanli, Ü.G., 2007 (a). An Entropy Approach for Diagnostic Checking in Time Series Analysis, WaterSA, V.33, No. 4, pp. 487-496.

Baran, T., Bacanli, Ü.G., 2007 (b). Evaluation of Goodness of Fit Criterion in Time Series Analysis, Digest 2006, V.17, pp. 1089-1102.

Baran T., Barbaros F., 2015. Testing the Goodness of Fit by Informational Entropy, European Water Resources Association 9th World Congress, İstanbul.

Bozoglu, Ö. T, Baran, T., 2010. Gediz havzası örneğinde beklenen aylık toplam yağışların entropi yöntemiyle tayini, 6th National Hydrology Congress, Denizli.

Bozoglu, Ö. T., Baran, T., 2012. Determination of Expected Value for Monthly Total Precipitation by Entropy Based Method, 10th International Congress on Advances in Civil Engineering, Ankara.

Cherry, C., 1957. On Human Communication: A Review, A Survey and A Criticism. Massachusetts, the Technology Press of Massachusetts Institute of Technology, 333 p.

DMI, 2002. Turkish State Meteorological Service web site, www.mgm.gov.tr

Harmancioglu, N, Singh, V. P., 1998. Entropy in Environmental and Water Resources. In: Herschy R. W. and Fairbridge R. W. (eds) Encyclopedia of Hydrology and Water Resources, Kluwer, Dordrecht, Netherlands, pp. 225-241.

Pierce, 1961. Symbols, Signals and Noise: The Nature and Process of Communication. New York, Harper and Row Publisher INC.

Pfeiffer, P. E., 1965. Concept of Probability Theory. New York, McGraw-Hill Book Company, 399 p.

Shannon, C.E., Weaver, W. 1949. The mathematical theory of communication. Urbana, University of Illinois Press.

Singh, V. P., Fiorentino, M., 1992. Entropy and Energy Dissipation in Water Resources, Springer, 595 p.

Singh, V. P., 1998. Entropy-Based Parameter Estimation in Hydrology, Dordrecht, Kluwer Academic Publishers, 364p.

Proceedings of the 10th World Congress of EWRA 'Panta Rhei', 5-9 July 2017, Athens, Greece
© 2017 *European Water Resources Association*

A snow variability analysis in Iran in relation to global warming and climate change

T. Raziei[1*], I. Bordi[2,4] and L.S. Pereira[3]
[1] *Soil Conservation and Watershed Management Research Institute (SCWMRI), Agricultural Research, Education and Extension Organization (AREO), Tehran, Iran*
[2] *Department of Physics, Sapienza University of Rome, Rome, Italy*
[3] *LEAF- Landscape, Environment, Agriculture and Food Research Center, Universidade de Lisboa, Instituto Superior de Agronomia, Lisbon, Portugal*
[4] *Interuniversity Consortium for the Physics of the Atmosphere and Hydrosphere (CINFAI), Rome, Italy*
[*] *e-mail: tayebrazi@yahoo.com*

Abstract: NOAA/NESDIS weekly Snow Cover Extent (SCE) and the reanalysis ERA-Interim monthly snow depth (SD) and density (SDR) time series are used to evaluate temporal snow variability in Iran. The possible linkage with climate warming is also investigated by analysing the time variation of SCE, air temperature (T) and frequency of snow occurrences at 14 selected observatories distributed over the country. Snow water equivalent (SWE) is estimated based on SD and SDR and then converted into SCE by classifying grid boxes with SWE greater than 1 mm as snow-covered grids, so that they are comparable with NOAA SCE data. The percentage of snow-covered grids to the whole ones over Iran is taken as an indicator for snow variability and climate change. For the time variability analysis, the winter season and each individual winter month are considered. Results for both datasets do not fully agree in showing the same time variability of the percentage of snow-covered grids. NOAA/NESDIS SCE data have no trend, while ERA-Interim SCE show a downward trend for winter (also evident in March) that is not statistically significant. Similarly, the time series of the frequency of snow days observed at stations are characterized by a not statistically significant downward trend. In winter, an inverse relationship is found between SCE variability/snow frequency occurrences and T in almost all stations, suggesting a possible link between the observed behaviour in the reanalysis SCE and the increasing T. However, the non-statistically significance of trends makes the relationship not robust and necessary of further investigations with longer time series.

Key words: Snow, climate change, SCE, SWE, NOAA/NESDIS, ERA-Interim, Iran

1. INTRODUCTION

Snow is an important hydrological variable since it serves as a water source in many regions of the world. An example is given by Iran where the mountainous regions act as a water supplier for its surrounding arid and semi-arid areas. Typically, in Iran snow amount and coverage display a large interannual variability, very likely because of complex interactions between the mountain barriers and atmospheric circulation (Greenland, 2005). Thus, any changes in the snow areal coverage and amount may have important adverse hydrological and environmental effects also because snow plays a crucial role in agricultural and water management strategies in the country.

Many studies indicate that rising temperature has caused redistribution and variations of snow cover at watershed scales in the Northern Hemisphere (NH), High Asia, and mid-latitude mountains (McCabe and Wolock, 2009; Lopez-Moreno et al., 2009). Hence, a detailed understanding of historical changes in snow amount and areal extent in the target area may shed light on the effects of climate variability and change.

Groisman et al. (1994) found a substantial retreat in snow coverage of the NH during the second half of the 1972–1992 period and suggest that the retreat during spring (April–May) has contributed to increases in air temperature during spring months through positive radiative feedbacks. Frei and Robinson (1999) also identified a connection between the NH snow coverage and atmospheric circulation variability during 1972–1994. They also found relations between atmospheric

circulation and snow extent in North America and indicate that the latter is associated with the longitudinal position of the North American ridge, while over eastern North America is associated with a meridional oscillation of atmospheric pressure. Brown (2000) studied NH snow cover area using snow depth observations for the period 1915–1997 and found a substantial change in March that could be due to the increases in temperature in that month.

As mentioned above, although there is evidence for snow cover decrease at a hemispheric scale in response to recent warming, the picture is more complex for mountain regions of the world (e.g., Alps, Himalaya, Alborz and Zagros mountains in Iran) where snow cover trends are characterized by large regional and altitudinal variations (Brown and Petkova, 2007). Laternser and Schneebeli (2003) found a gradual increase in the mean snow depth, the number of snowfall days, and the duration of continuous snow cover in the Swiss Alps for the period 1931–1980, followed by a statistically significant decrease since the early 1980s. Similarly, an increasing trend has been found in snow cover over the mountainous regions of Poland during the last half of the 20th century (Falarz, 2004) although Petkova et al. (2004) found statistically significant trends in snow cover in Bulgaria. In Slovakia, snow cover decreases were observed for areas below critical elevations (Vojtek et al., 2003).

The purpose of the present paper is to evaluate the variability of snow cover and occurrences in Iran also in relation to the climate change, in order to provide preliminary information on snow variability. Since snow is an integral of water resources in the country changes in the snow amount and areal extent can directly affect policies of water resources management; a comprehensive study on the temporal changes of snow cover and amount in response to climate change is also important for water planning strategies.

2. DATA AND METHODS

Data used in this study include the NOAA/NESDIS weekly Snow Cover Extent (SCE), ERA-Interim monthly snow depth (SD) and density (SDR) time series, the monthly frequencies of snow occurrences and the mean monthly temperature (T) of 14 synoptic stations distributed over the mountainous areas of Iran.

The most recently released NOAA/NESDIS weekly SCE, which is mainly based on the longest available satellite-derived time series of snow charts produced from the analysis of primarily optical satellite imagery (Robinson et al., 1993), is used. SCE data, maintained and housed at the Rutgers University Global Snow Lab (Brown and Robinson, 2011), were used herein, since they are widely used by the climate community and have been subject to several evaluations (Wang et al., 2005; Brown et al., 2007; Derksen and Brown, 2012). The time period considered for the present analysis is 1966–2015.

The ECMWF SD and SDR data from the ERA-Interim reanalysis with a 0.75-degree horizontal resolution and covering the time period from 1979 to the present have been also used (Dee et al., 2011). For the present analysis, SD data have been converted into snow water equivalent (SWE). ERA-Interim is based on a 12-h four-dimensional variational data assimilation (4D-Var) system with a horizontal resolution of approximately 80 km and with 60 vertical levels. This reanalysis incorporates several improvements with respect to the previous reanalysis ERA-40, which include improved horizontal resolution, the use of a variational bias correction to better handle satellite data biases, advances in model physics, background errors, data quality control, and radiative transfer modelling (Dee and Uppala 2009).

At the ECMWF, SD and SDR are first estimated by the forecast model based on Douville et al. (1995) and then updated based on a Cressman analysis of station observations of snow depth and snow cover fraction (when available) provided by satellite data (Drusch et al., 2004). The SWE at ERA-Interim grid points were computed using the SD and SDR variables, to be used subsequently for extracting SCE. Furthermore, the monthly total of days with snow occurrences and the mean monthly temperature of 14 stations located at the mountainous areas of Iran were considered for the analysis. The selection of stations was based on the records' length and the frequency of snow

occurrences (i.e., a long data record with less than 5% missing values and the frequency of snow occurrences at that station relatively high).

Although the snow occurrence in October, November, and April is not unusual in many parts of western and northern mountainous areas of Iran, this analysis is focused on December–March (DJFM) season during which the probability of snow occurrences is the highest all over the country. The time period considered for the analysis of temperature and snow days is 1951–2014 and 1951–2010, respectively.

In this analysis the computed SWE at ERA-Interim grid points were converted into SCE by classifying the grid boxes with SWE greater than 1 mm as snow covered (e.g., Drusch et al., 2004). Thereafter, the percentage of SCE of Iran for the DJFM season and for each individual winter months was computed for both NOAA/NESDIS and ERA-Interim data sets.

Trends of the NOAA/NESDIS and ERA-Interim SCE time series relative to the DJFM season and the four individual winter months were evaluated by fitting a linear least square trend. Similarly, the time series of the mean temperature and the total number of days with snow occurrences relative to the winter season and individual months were examined to uncover if a relationship exists between SCE time series (NOAA/NESDIS and ERA-Interim) and observations represented by the number of snow days as well as the mean monthly temperature observed at the 14 selected stations.

3. RESULTS

Figure 1 shows the time variability of the SCE relative to the DJFM season, derived from NOAA/NESDIS (Fig. 1a) and ERA-Interim (Fig. 1b) data sets, respectively. As can be seen, the NOAA/NESDIS snow cover extent fluctuates around the mean and does not exhibit any trend. Based on this figure the percentage of SCE in Iran in DJFM season varies between 20 and 25 percent. Differently, the percentage of winter SCE represented by the Era-Interim data set (Fig. 1b) may vary between 10 and 20 percent. Figure 1b also shows an evident downward trend that, being statistically significant at an alph level 0.05, explains about 30% ($R^2 = 0.3$) of the total variance of the SCE time series. Time variability of the SCE relative to December, January, February, and March were also assessed separately (not shown) and no significant trend was found, nonetheless, March exhibited a sharper decreasing trend. In both seasonal and monthly time scales, no agreement was found between the SCE time series of both datasets that could be related to their different spatial resolution and data source; in particular, NOAA/NESDIS data is likely not able to capture the snow cover variability of the mid-latitudes mountainous areas as they are mostly patchy. This is supported by the study of Drusch et al. (2004), which showed that the fractional snow cover below 40%–50% (at 500 m resolution) may not be correctly detected by algorithms based on visible and infrared measurements. Therefore, it can be stated that the area of grid boxes affected by snow is likely underestimated or not well captured by the NOAA/NESDIS product.

As shown in Fig. 2, the time variability of the frequency of snow occurrences in DJFM season, observed at the stations also exhibits no evidence of trends. However, the time series are characterized also by high-frequency fluctuations that indicate highly variable snow occurrences at the stations. It is evident that all the stations are vulnerable to long-term events of snow occurrences deficit. Similar results were also obtained when monthly snow occurrences were analyzed for the selected stations. However, a not statistically significant negative trend was found for March at a few stations (not shown), which is in agreement with the result obtained for the same month using the ERA-Interim data set.

Figure 3 shows the time variability of mean DJFM temperature for the selected stations. Some stations show a slight tendency towards warmer period, however, no one exhibits a statistically significant trend. The observed trend is more evident for Kermanshah, Mashhad, Khoramabad and Tehran for which the R^2 is between 0.1 and 0.2. Time series of mean monthly temperature for December, January, February, and March reveal similar patterns of not statistically significant trends (not shown). However, the observed increasing trend in March is much more pronounced at

all the considered stations, albeit not significant. The observed increasing trend of mean monthly temperature in March could be related to the observed decreasing trend of SCE in the same month, as represented by the ERA-Interim data set (not shown).

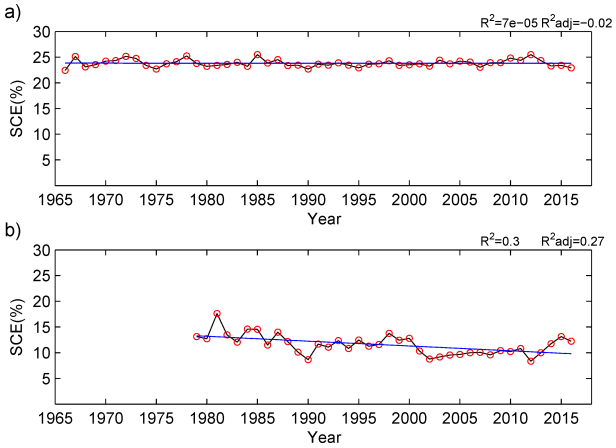

Fig. 1 Time variability of the DJFM SCE in Iran derived from a) NOAA/NESDIS and b) ERA-Interim dataset; in blue the associated linear least squares fits.

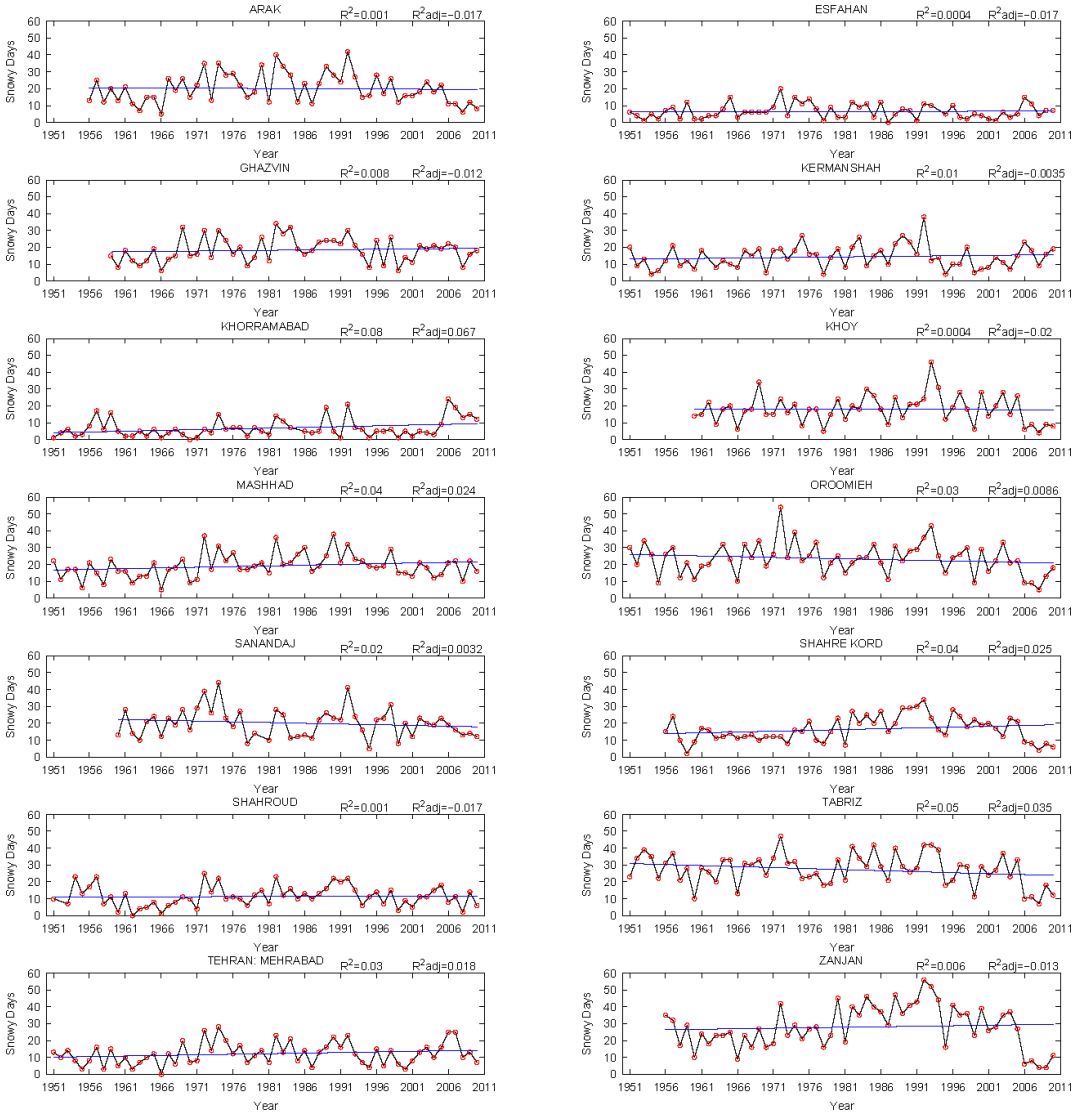

Fig. 2 Time variability of the frequency of DJFM snow occurrences observed at the selected synoptic weather stations and the associated linear least squares trends.

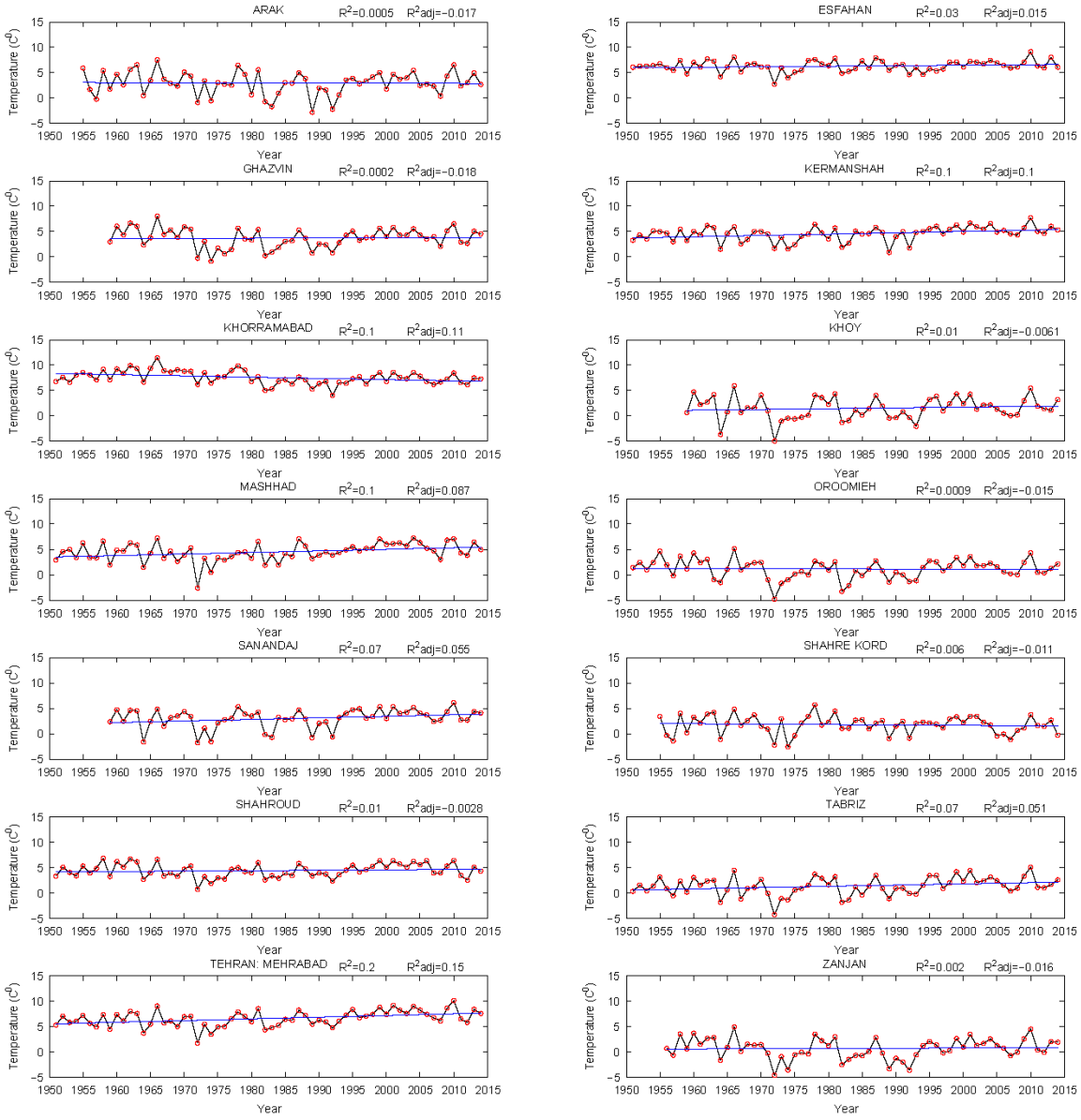

Fig. 3 Time variability of mean daily temperature of the DJFM season observed at the selected synoptic weather stations and the associated linear least squares trends.

4. CONCLUSION

The time variability of SCE for DJFM season in Iran was evaluated by using NOAA/NESDIS and ERA-Interim datasets. The NOAA/NESDIS snow cover extent showed no trend, but a slight downward trend, although not statistically significant, was found using the ERA-Interim. Similar results were found when winter months were considered separately. No agreement was found between the SCE time series of NOAA/NESDIS and ERA-Interim datasets that could be partly related to their different spatial resolutions and data source.

Time variability analysis of the frequency of snow occurrences in DJFM season observed at 14 selected stations also exhibited no evidence of trends. The mean DJFM temperature in most of the stations showed a slight tendency towards warmer periods, not statistically significant. The observed increasing trend was more pronounced in March at all stations, but still not statistically significant. The observed increasing trend of mean monthly temperature in March could be related to the observed decreasing trend of the SCE in the same month, as represented by ERA-Interim

As stated by Madani et al. (2016), not statistically significant trend has been observed in average

precipitation over Iran during the past three decades. In line with this statement, the frequency of snow occurrences in different parts of the mountainous areas of Iran showed not statistically significant trend; time series are characterized by high-frequency fluctuations which make the snow occurrences at the selected stations highly variable and sites vulnerable to long-term snow deficit events.

Many Iranian people and scientists believe that the amount and frequency of snow have changed in Iran due to the global warming and climate change. There is also a common perception among people that the air temperature in recent decades has increased in the country. Based on this perception, climate change is continuously blamed for inducing the increasing water scarcity in the country. It is also called into question for justifying and reasoning the rapid shrinkage of the Lake Urmia in northwestern Iran as well as the frequent occurrence of different environmental challenges such as droughts, air quality issues in major cities, dust storms and the extinction of some endangered species (Madani et al., 2016). However, in contrast to this common belief, neither a statistically increasing trend in the air temperature nor a decreasing trend in the frequency of snow days in Iran was found to justify such environmental problems.

Although this study is considered as a preliminary research on snow variability in the country, results clearly suggest that no significant changes occurred in the air temperature and the number of snow days in the selected stations. Therefore, changes in precipitation, snow events, and air temperature, if any, seem to be not enough to explain the increasing water crises and related environmental problems in the country. The lack of agreement found between the NOAA/NESDIS and ERA-Interim data sets can be considered as a limitation of this study that needs further checks with other datasets and/or observations. The lack of ground snow depth measurements for the selected stations to be used in the analysis can be considered as the second major limitation of the study. Very likely, the snow depth data could better represent changes in the snow water equivalent in the country than the number of snow days used in the present analysis. An in-depth analysis of snow variability by taking into account the aforementioned limitations will be topic for future research. Furthermore, future efforts should be devoted to investigate the possible application of innovative sensors for monitoring dynamic changes of snow and ice, like radio-frequency identification (RFID) tags (e.g., Greco et al., 2015) or microwave mini-radar (e.g., Bertoldo et al., 2015).

REFERENCES

Bertoldo, S., Allegretti, M., Greco, G., Lucianaz, C., 2015. Extreme rain events analysis using X-band weather radar, Proc. Of 2015 International Conference on Electromagnetics in Advanced Applications, ICEAA 2015, pp. 157–160, doi: 10.1109/ICEAA.2015.7297094

Brown R, Derksen C, Wang L 2007. Assessment of spring snow cover duration variability over northern Canada from satellite datasets, Remote Sens Environ 111: 367–381.

Brown R, Robinson D, 2011. Northern Hemisphere spring snow cover variability and change over 1922–2010 including an assessment of uncertainty, Cryosphere, 5: 219–229.

Brown RD, 2000. Northern Hemisphere snow cover variability and change, 1915–1997. J Climate., 13: 2339–2355.

Brown RD, Petkova N, 2007. Snow cover variability in Bulgarian mountainous regions, 1931–2000. Int J Climatol 27: 1215–1229.

Dee D P, Uppala S, 2009. Variational bias correction of satellite radiance data in the ERA-Interim reanalysis. Q J R Meteorol Soc 135: 1830–1841.

Dee DP et al. 2011. The ERA-Interim reanalysis: configuration and performance of the data assimilation system. Q J R Meteorol Soc 137: 553–597.

Derksen C, Brown R, 2012. Spring snow cover extent reductions in the 2008–2012 period exceeding climate model projections. Geophys Res Letters 39: L19504.

Douville H, Royer JF, Mahfou J F, 1995. A new snow parameterization for the Meteo-France climate model. Part I: validation in stand-alone experiments. Climate Dynamics, 12 (1): 21–35.

Drusch M, Vasiljevic D, Viterbo P, 2004. ECMWF's global snow analysis: assessment and revision based on satellite observations. J Appl Meteorol Climatol, 43 (9): 1282–1294.

Falarz M, 2004. Variability and trends in the duration and depth of snow cover in Poland in the 20th century. Int J Climatol 24: 1713–1727.

Frei A, Robinson DA, 1999. Northern Hemisphere snow extent: regional variability 1972–1994. Int J Climatol 19:1535–1560.

Greco, G., Lucianaz, C., Bertoldo, S., Allegretti, M., 2015. Localization of RFID tags for environmental monitoring using UAV, Proc. of 2015 IEEE 1st International Forum on Research and Technologies for Society and Industry, RTSI 2015, pp. 480–483, doi:10.1109/RTSI.2015.7325144

Greenland D, 2005. Mountain climates. In Encyclopedia of World Climatology, Oliver JE (ed.). Springer: Dordrecht, pp 517–523.

Groisman PY, Karl TR, Knight RW, 1994. Changes of snow cover, temperature, and radiative heat balance. J Climate 7:1633–1656.

Laternser M, Schneebeli M, 2003. Long-term snow climate trends of the Swiss Alps (1931–99). Int J Climatol 23: 733–750.

Madani K, AghaKouchak A, Mirchi A, 2016. Iran’s Socio-economic Drought: Challenges of a Water-Bankrupt Nation, Iranian Studies, 49(6): 997-1016.

McCabe GJ, Wolock D M, 2009. Recent Declines in Western U.S. Snowpack in the Context of Twentieth-Century Climate Variability, Earth Interact., 13, 1–15.

Petkova N, Koleva E, Alexandrov V., 2004. Snow cover variability and change in mountainous regions of Bulgaria, 1931–2000. Meteorologische Zeitschrift, 13: 19–23.

Robinson D, Dewey K, Heim R, 1993. Global snow cover monitoring: An update, Bull Am Meteorol. Soc 74: 1689–1696.

Vojtek M, Fasko P, Stastny P, 2003. Some selected snow climate trends in Slovakia with respect to altitude. Acta Meteorologica Universitatis Comenianae, 32: 17–27.

Wang L, Sharp M, Brown R, Derksen C, Rivard B, 2005. Evaluation of spring snow covered area depletion in the Canadian Arctic from NOAA snow charts, Remote Sens Environ 95: 453–463.

Proceedings of the 10th World Congress of EWRA 'Panta Rhei', 5-9 July 2017, Athens, Greece
© 2017 *European Water Resources Association*

Hydrological and water temperature modelling for dam decommissioning and climate change studies

S.J. Dugdale[1,3], A. St-Hilaire[2,3] and R.A. Curry[2]
[1] *School of Geography, Earth and Environmental Sciences, University of Birmingham, Birmingham B15 2TT, United Kingdom*
[2] *Canadian Rivers Institute, University of New Brunswick, Fredericton, NB, Canada*
[3] *Presenter and corresponding author: INRS-ETE, University of Québec, Québec City, G1K 9A9, Canada*
[*] *e-mail: andre.st-hilaire@ete.inrs.ca*

Abstract: The Mactaquac Dam and Generating Station, a 672 MW run-of-the-river hydroelectric facility located on the Saint John River, Canada, will have to be decommissioned or reconstructed by 2030. In order to simulate the impact of reservoir emptying (drawdown) and climate change on the thermal regime of the lower reaches of the river, the CEQUEAU hydrological and water temperature model was used. The model was successfully calibrated and validated for both flow and water temperature, with Nash coefficients ranging from 0.63 to 0.86 for flow and RMSE ranging between 0.74°C and 1.3°C for temperature. Subsequently, different drawdown and climate change scenarios were simulated using the calibrated models. Median value of maximum water temperature in the river is expected to increase by 2-3°C by 2100, regardless of the dam reconstruction scenario.

Key words: CEQUEAU, hydrological model, water temperature, dams, climate change

1. INTRODUCTION

A number of dams have outlived their intended duration and/or are no longer serving their initial purposes. Their presence in many riverscapes has been recognized as a potential threat to aquatic ecological communities for decades (Grant, 2001). The large number of aging dams in North America and Europe has resulted in the development of a number multidisciplinary studies related to dam removals (e.g. Manatawny Creek study: Bushaw-Newton et al. 2002, Elwha River: Duda et al. 2011). In Eastern Canada, this science is in its infancy and the first major research endeavour on dam removal is currently underway on the Saint John River drainage basin in New Brunswick. The dam replacement/removal decision is to be taken among three possible options: repowering the station with a new powerhouse and spillway, rebuilding the spillway only, or removing all parts of the dam/station. One key component of this study is the implementation of a major modelling effort to simulate the possible impacts of these future management options. In addition, the modelling exercise allows for the investigation of the possible impacts of climate change on the hydrology and thermal regime of the system. This paper focuses on the hydrological/water temperature modelling component of MAES. The main objectives are: 1) to investigate the sensitivity of the model to its discretization module (i.e., the size of elementary hydrological units used in the model); 2) to simulate the most probable drawdown scenario and to investigate its potential impact on the water temperature regime of the river; and 3) to investigate the possible impacts of climate change on flows and temperature on the lower Saint John River.

2. METHODS

2.1 CEQUEAU Hydrological and water temperature model….

The hydrological component of CEQUEAU (Morin and Couillard 1990) decomposes the

drainage basin into Elementary Hydrological Units (EHU) of equal area (called "whole squares"). For each EHU, altitude, percentage of forest cover and the percentage of EHU covered by lakes and wetlands are required as inputs. Required meteorological inputs include daily solid and liquid (or total) precipitation, as well as maximum and minimum daily air temperature.

The CEQUEAU water temperature model is based on heat budget calculations. Water temperature (T_w; °C) is calculated as the ratio of the enthalpy (H; MJ) over the product of water volume (V; m^3) and water specific heat capacity (θ = 4.187 MJ/(m^3·°C)):

$$T_w = (H/(V\,\theta)) \tag{1}$$

Change in H at each time step (ΔH) is calculated on the simulated water volume on each EHU by summing the following heat fluxes: incoming short wave radiation, net longwave radiation, latent heat loss (evaporation), sensible heat lost or gained through convection, heat advected from upstream and lost to downstream by water movement, heat fluxes from local runoff, interflow and groundwater input. To perform these calculations, solar radiation, pressure, wind velocity and cloud cover are also required.

2.2 Implementation and model calibration

Flow routing and physiographic information required as model inputs were extracted and computed using an automated GIS tool developed by the first author (Dugdale et al. 2016). Following the application of this algorithm, 650 EHUs of 100 km^2, were initially defined and further divided into 1389 partial squares.

The model boundary conditions (flow and temperature) were imposed at the outflow of the Mactaquac Dam. Reservoir water temperatures associated with this outflow (temperature at a reservoir depth of 7m) were simulated using a simple non-linear regression (Mohseni et al., 1998) with air temperature (14-day moving average, measurements taken at Environment Canada Climate station 8102536) as the predictor. Once calibrated, the model produced high R^2 (0.98) and low RMSE (0.64 °C).

Meteorological inputs used by the hydrological model were gathered from 44 Environment Canada weather stations in or close to Saint John River basin for the period 1983 – 1994, the longest period with concomitant data. This period was divided in two sub-periods, seven years for calibration and four years for validation. A block bootstrap approach was used to test different periods for calibration and validation. Model parameters were initially adjusted by hand and subsequently the CMA-ES automatic calibration algorithm (Hansen and Ostermeier, 2001) was applied. Model performance was evaluated using the Nash Sutcliffe coefficient (Nash and Sutcliffe, 1970; Equation 2), the root-mean-square error (RMSE; Equation 3) and the bias (bias; Equation 4).

$$NTD = 1 - \frac{\sum_{i=1}^{n}(Q_{obs,i}-Q_{sim,i})^2}{\sum_{i=1}^{n}(Q_{obs,i}-\bar{Q}_{obs})^2} \tag{2}$$

$$\%\mathrm{RMSE} = \frac{\left(\frac{1}{n}\sum_{i=1}^{n}(Q_{obs,i}-Q_{sim,i})^2\right)^{0.5}}{\bar{Q}_{obs}} \times 100 \tag{3}$$

$$Bias = \frac{1}{n}\sum_{i=1}^{n}(Q_{obs,i} - Q_{sim,i}) \tag{4}$$

where $Q_{obs,i}$ and $Q_{sim,i}$ are the observed and simulated mean discharges respectively on day i and $\bar{Q}_{obs}$ is the mean observed discharge for the entire study period with a length of n days.

The thermal model was calibrated by comparing observed and simulated daily mean temperatures using temperature observations from a thermograph moored in 2011 and 2012 at a the Maugerville station, a few km downstream of Fredericton. Initial model calibration was conducted

by hand and subsequently optimised using the Tabu Search algorithm (Zheng & Wang, 1996). Validation was completed using water temperature time series recorded in 2014 in the main stem of the Saint John River at Fredericton. Simulations were also inspected against temperature records from tributaries of the Saint John River (Nashwaak and Keswick Rivers). The RMSE, which is the most common performance metric used to assess thermal models, was used to compare observed and simulated water temperature time series.

2.3 Drawdown scenarios

The reservoir drawdown scenario for the Mactaquac headpond that was considered in the models consists of four stages: 1) An initial (~1 month) drawdown following the spring freshet, 2) a ~5 month period with no drawdown in order to demolish the existing sluiceway, 3) a second ~1 month drawdown lowering the level to its pre-impoundment state and 4) a slow final drawdown draining the remainder of the headpond over a period of 29 months.

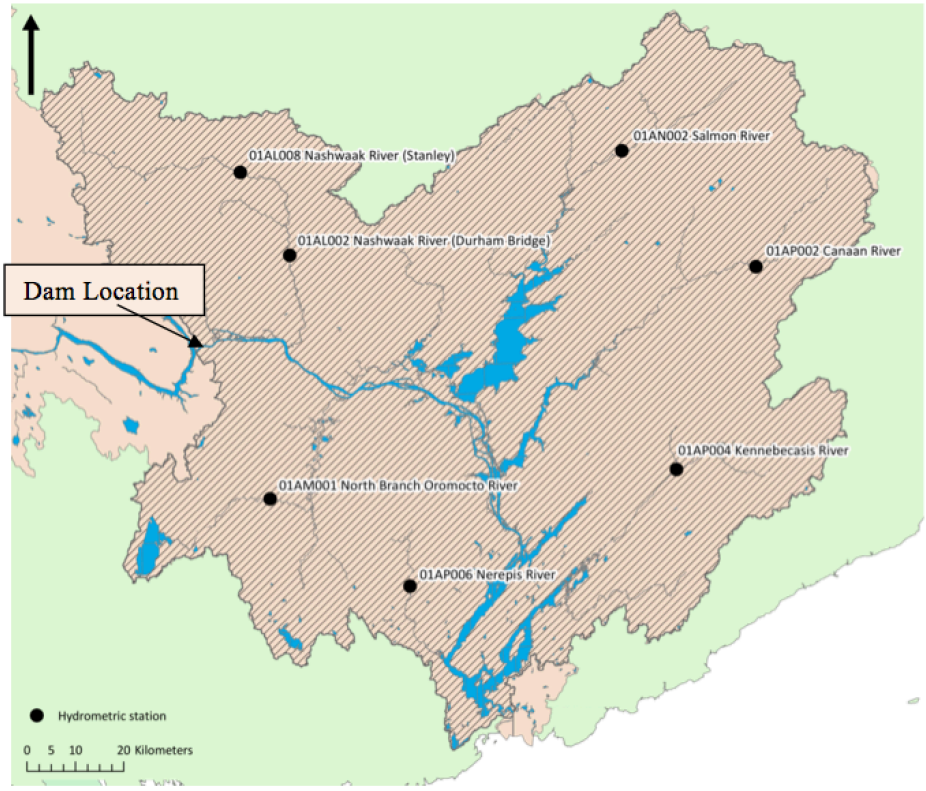

Figure 1. Map of the Lower SaintJohn River drainage basin showing the location of hydrometric gauging stations on the main tributaries.

Emptying the Mactaquac dam reservoir would therefore involve the release of a large volume of hypolimnetic water from the Mactaquac headpond. River temperatures associated with this drawdown scenario were modelled using CEQUEAU by imposing headpond outflows and temperatures at the upstream-most partial square. The model was then used to simulate water temperatures downstream of this point corresponding to varying meteorological conditions and facilitating comparison with a baseline time series of simulated temperatures from the recent past (2010-2014).

Drawdown scenarios were constructed using meteorological data from 1995 to 2014. A scenario includes 36 months and thus the historical time series were divided in sub-periods (i.e. 1995-1997, 1996-1998, etc.) starting from 7 days after the peak freshet discharge event during the first year of each scenario. In total, 15 drawdown simulations were performed.

2.4 Climate change scenarios

Meteorological inputs to the hydrological and water temperature models were extracted from 11 simulations generated by regional climate models (RCM) driven by global climate models (GCM) at the RCM boundaries. A number of more or less pessimistic greenhouse gas (GHG) scenarios were selected with a view to encompassing the range of variability in projected temperature and precipitation change. CEQUEAU flow and water temperature simulations associated with these climate change scenarios were subsequently generated and compared to the reference period.

3. RESULTS

3.1 Validation of hydrological and water temperature models

The simulated flows during the various validation periods show good agreement with observations on tributaries of the Saint John River located downstream of the dam, as shown by the NTD Values (all ≥ 0.6) reported in Table 1.

Table 1. Mean performance statistics for all block bootstrapped 4-year validation periods

Station	Nash-Sutcliffe coefficient	RMSE	%Bias
Nashwaak at Durham Bridge	0.86	16.28	0.66
Nashwaak at Stanley	0.84	7.64	1.35
North Branch Oromocto at Tracy	0.71	10.11	-0.19
Nerepis River near Fowlers Corner	0.76	6.31	-0.35
Salmon River at Castaway	0.70	14.39	-0.98
Canaan River at East Canaan	0.62	10.52	-1.48
Kennebecasis River at Apohaqui	0.60	17.85	-3.16

An example of observed vs. simulated flows from the Nashwaak River (Figure 2) also shows strong concordance. Some of the peak discharge values were poorly simulated. However, given that the emphasis in this modelling project is on water temperature and that the highest values of temperature occur during low flow periods, the impact of peak flow underestimation on thermal modelling is minimal.

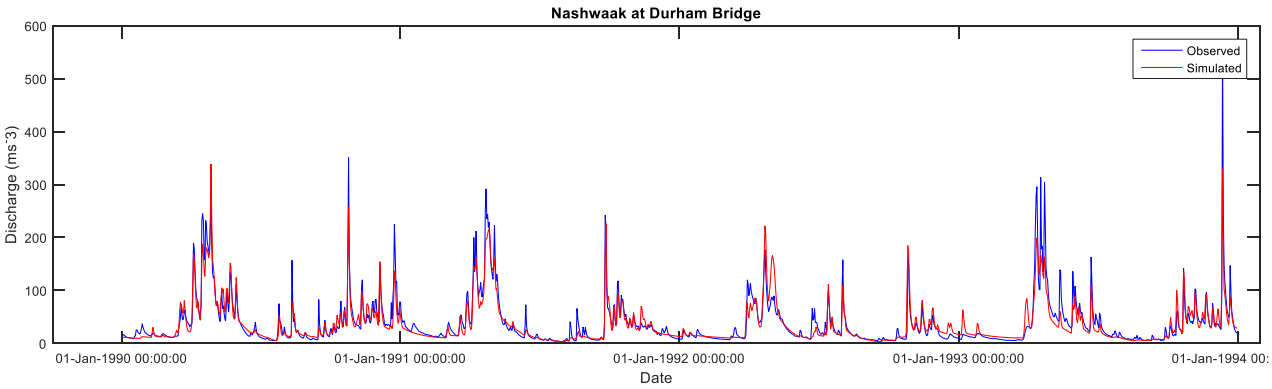

Figure 2. Observed and simulated hydrographs for gauging station at Durham Bridge on Nashwaak River showing good model fit (Nash-Sutcliffe coefficient = 0.86).

Similarly, the thermal model performed quite well (RMSE < 1.0 °C on the main river in the summer and RMSE < 1.4 °C on tributaries; see Table 2).

Table 2. RMSE for four temperature sites within the lower Saint John River watershed

Station	Summer RMSE (°C)	Annual RMSE (°C)
Saint John River at Fredericton	0.74	0.97
Saint John River at Maugerville	0.98	1.19
Nashwaak River at Marysville	1.39	1.12
Keswick River at Keswick	1.32	1.27

3.2 Thermal modelling and reservoir drawdown/climate change scenarios

Water temperature time series were simulated using meteorological inputs for 14 different three-year periods (Figure 3). Simulated water temperatures during the first year of the drawdown event (mean = 9.8 °C, maximum 23.1 °C) are similar to current temperatures downstream of the dam (mean = 10.9 °C, max = 23.0 °C). As the river returns to more 'natural' conditions during Phases 2 and 3, the possibility for higher summer maximum temperature than baseline increases (23.9 °C) and the mean temperature decreases (9.0 °C) compared to the reference period, presumably because more 'natural' conditions can result in an increase of days with water temperature < 5° C.

A number of temperature metrics deemed ecologically relevant, especially for stenotherm fish were calculated for the reference period (Table 3) and from the time series shown in Figure 5 for all three possible Mactaquac dam outcomes (rebuilding the dam and power house, rebuilding the dam only, or restoring the natural river). We selected a modelling threshold of 23°C based on the temperature tolerances of Atlantic Salmon (temperature threshold between $T_{minimum}$ = 20°C and $T_{critical}$ = 25°C; Breau 2013) which is an endangered species in the river.

Comparison of Tables 3 and 4 show that minimum summer temperatures will likely decrease, while maximum temperatures will remain fairly constant.

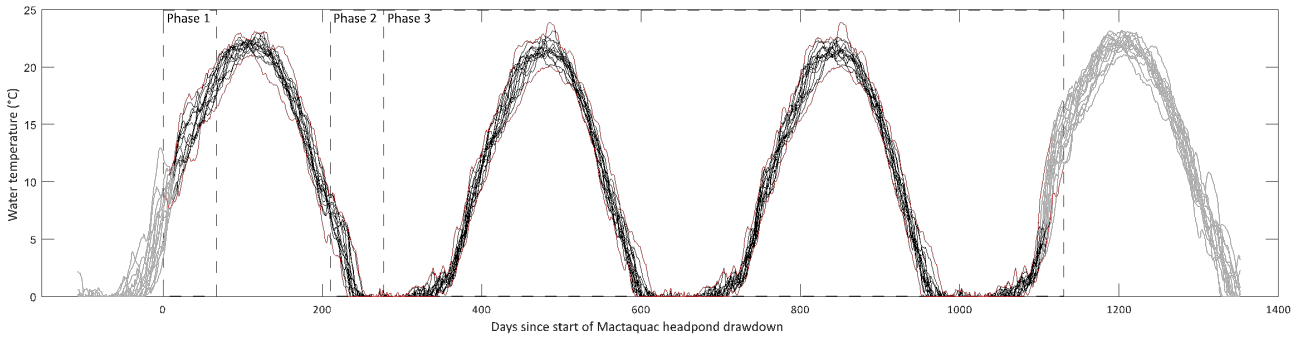

Figure 3. Temperatures generated by Mactaquac headpond drawdown for 11 different meteorological scenarios. Red lines represent upper and lower range of temperatures; grey lines represent temperatures outside of the drawdown scenario computed during model spin-up/spin-down.

This general decrease in temperature is reflected by the number of degree hours associated with the various drawdown scenarios, which also indicates that the thermal loading of the Saint John River will be lower during the drawdown than under current conditions.

Table 3. Water temperature metrics for the Saint John River near Fredericton for the reference period 2010-2014

Year	Annual mean temp. (°C)	Annual maximum temp. (°C)	Standard deviation (°C)	No. degree hours (>0 °C)	Minimum July – August temp. (°C)	No. of days ≥23 °C
2010	11.2	23.0	7.9	4085.5	18.9	0
2011	11.0	22.4	8.3	4007.6	20.1	0
2012	11.1	22.8	8.4	4051.2	21.3	0
2013	10.7	22.9	8.5	3901.2	19.6	0
2014	10.5	23.0	8.7	3820.1	20.7	1
Mean	10.9	22.8	8.4	3973.1	20.1	0.2

Table 4. Water temperature metrics for the Saint John River near Fredericton for the 15 different drawdown scenarios

Year	Annual mean temp. (°C)	Annual maximum temp. (°C)	Standard deviation (°C)	No. degree hours (>0 °C)	Minimum July – August temp. (°C)	No. of days ≥23 °C
(1995-1997)	9.81	22.61	8.71	3579.5	18.55	0
(1996-1998)	9.34	21.75	8.46	3410.1	18.71	0
(1998-2000)	9.52	21.87	8.45	3473.4	17.45	0
(1999-2001)	9.97	22.59	8.61	3639.9	17.09	0
(2000-2002)	10.45	22.35	8.93	3814.6	19.80	0
(2001-2003)	9.29	21.08	8.14	3390.4	15.88	0
(2002-2004)	10.52	23.09	8.72	3839.1	19.36	4
(2003-2005)	9.26	22.50	8.65	3378.8	16.26	0
(2004-2006)	9.98	23.01	8.69	3642.9	17.74	1
(2005-2007)	9.62	22.32	8.31	3510.8	16.10	0
(2008-2010)	10.17	22.21	8.53	3712.9	17.84	0
(2009-2011)	9.40	22.04	8.13	3432.3	16.91	0
(2010-2012)	9.99	23.11	8.44	3646.4	17.24	5
(2011-2013)	9.96	22.97	8.83	3634.0	18.02	0
(2012-2014)	10.71	22.39	8.60	3910.4	19.17	0
Mean	9.87	22.39	8.55	3601.0	17.74	0.67

Figure 4 clearly shows that most climate change scenarios predict an increase in mean and maximum temperatures of nearly 2°C on average for the 2100 future horizon. However, restoring the river to its natural state leads to greater variability in expected mean annual temperature and minimum summer temperature.

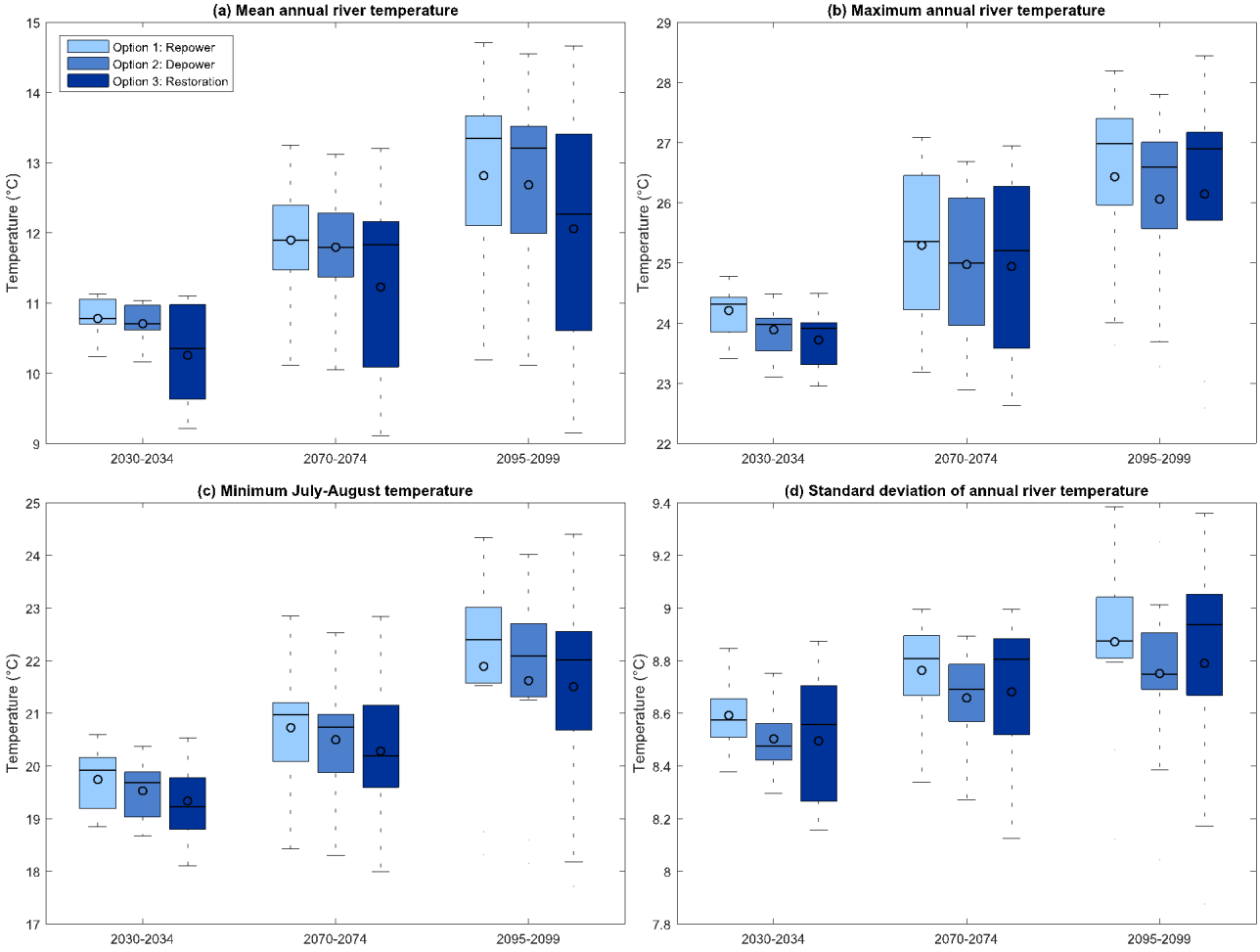

Figure 4. Variability in projected water temperature metrics for the Saint John River near Fredericton for a range of future climate scenarios (see table 2)

4. CONCLUSION

The modelling results summarized in this paper and the effort currently underway as part of MAES (hydrodynamic, sediments, fish habitat) are crucial to the decision-making process of NB Power, the facility that owns the dam. The CEQUEAU model was used to determine provide future hydrological and thermal scenarios according to the different possible outcomes associated with dams decommissioning or reconstruction. Our results indicate that temperature increases predicted for the horizon 2100 may be problematic for stenotherm fish in the river system. A rise in minimum temperatures may mean shorten recuperation periods for fish that were thermally stressed during the day, for instance. Incorporating these predicted water temperature scenarios in fish habitat models appears to be the next logical step to further investigate such potential impacts.

ACKNOWLEDGEMENTS

The MAES project is funded by NSERC and NB Power.

REFERENCES

Breau, C. 2013. Knowledge of fish physiology used to set water temperature thresholds for inseason closures of Atlantic salmon (Salmo salar) recreational fisheries. DFO Can. Sci. Advis. Sec. Res. Doc. 2012/163. iii + 24 p.

Bushaw-Newton, K., D. D. Hart, J. E. Pizzuto, J. R. Thomson, J. Egan, J. T. Ashley, T. E. Johnson, R. J. Horwitz, M. Keeley, J. Lawrence, D. Charles, C. Gatenby, D. A. Kreeger, T. Nightengale, R. L. Thomas, D. J. Velinsky. 2002. An integrative approach towards understanding ecological responses to dam removal. The Manatawny Creek study. J. of Am. Wat. Res. Assoc., 38 (6): 1581–1599.

Grant, G. 2001. Dam removal: Panacea or Pandora for rivers? Hydrol. Process., 15: 1531–1532. DOI: 10.1002/hyp.473

Duda, J.J., J.A. Warrick, and C.S. Magirl, eds., 2011. Coastal habitats of the Elwha River, Washington – Biological and physical patterns and processes prior to dam removal. U.S. Department of the Interior, U.S. Geological Survey. 110 pages.

Dugdale, S., A. St-Hilaire, R.A. Curry. 2017. Automating drainage direction and physiographic inputs to the CEQUEAU hydrological model: sensitivity testing on the lower Saint John River watershed, Canada. Journal of Hydroinformatics, 9(3): 469-492

Hansen, N., & Ostermeier, A. (2001). Completely Derandomized Self-Adaptation in Evolution Strategies. Evolutionary Computation, 9, 159-195

Khakbaz, B., Imam, B., Hsu, K., & Sorooshian, S. (2012). From lumped to distributed via semi-distributed: Calibration strategies for semi-distributed hydrologic models. Journal of Hydrology, 418–419: 61-77

Morin, G. and D. Couillard, 1990. Predicting river temperatures with a hydrological model. Encyclopedia of Fluid Mechanics, 10, Gulf Publishing Company, Hudson, Texas, 171-209.

Mohseni, O., Stefan, H.G., & Erickson, T.R. (1998). A nonlinear regression model for weekly stream temperatures. Water Resources Research, 34, 2685-2692

Nash, J.E., & Sutcliffe, J.V. (1970). River flow forecasting through conceptual models part I — A discussion of principles. Journal of Hydrology, 10, 282-290

Zheng, C., & Wang, P. (1996). Parameter structure identification using tabu search and simulated annealing. Advances in Water Resources, 19, 215-224

Proceedings of the 10th World Congress of EWRA 'Panta Rhei', 5-9 July 2017, Athens, Greece
© 2017 *European Water Resources Association*

Assessment of impact of climate change on streamflows using VIC model

A. Treesa, J. Das and U. Nanduri*
National Institute of Technology, Warangal, 506004, India
* *e-mail: mahesh@nitw.ac.in*

Abstract: Climate change, a change caused by human activities and natural variability, will have significant impact on frequency of extreme climatic events including intense storms, heavy rainfall, droughts, and an alarming rise in sea level. The purpose of this work is to study the effect of climate change on the streamflow pattern of Wainganga river basin by analysing the monsoon and non-monsoon flows for the near future (2020-2044). Variable Infiltration Capacity (VIC), a physically based macro-scale hydrological model is calibrated for optimum parameter sets obtained by trial and error method using observed meteorological data from India Meteorological Department (IMD) and observed streamflow from Central Water Commission (CWC). Statistically downscaled six Global Circulation Models (GCMs) have been used to predict the future global climatic Representative Concentration Pathways (RCPs) scenario 4.5 for the future time scale. The specific conclusions derived from the study reveals that the low flows as described by all the models have gone above the lower extreme of the observed streamflow during monsoon season. The high flow values in the monsoon as per the models are almost similar to that of the observed, except for two models. However, high flows during non-monsoon season show a significant increment as compared to the original series. Frequency analysis of ensemble mean of all the GCMs gives a similar return level for different return period as observed.

Key words: Climate change, Frequency analysis, GCM, Streamflow, VIC model, Wainganga river basin

1. INTRODUCTION

With the increase in impact of changing climate, it is essential to quantify the consequences at river basin scale for better and efficient planning and management of water resources (Das and Umamahesh, 2016). Therefore modelling the climate impact incorporates the simulation of Global Circulation Models (GCMs), tools those are designed to project the future changes in the atmospheric variables considering dynamic behaviour of the greenhouse gases at a larger scale (> 10^4 km^2) (Ghosh and Mujumdar, 2008). However, these projections are not suitable to assess the impact at regional scale (Bates et al., 1998) and it leads to downscale the coarser scale projections to the finer scale by applying the downscaling technique. The alternation in the atmospheric circulation due to climate change in the form of change in fluxes of moisture and energy has immediate and prolonged effects on the land surface hydrology. In addition, Nijssen et al., (2001a) stated that though the present ecosystems and human activities are well adapted to the present climate, but with the pace of changing climate they may become more vulnerable. Hence, attempts have been made to evaluate the adverse effect on land hydrology for better risk management. Dan Yan et al (2015) assessed the impact of climate change on the seasonal and extreme discharge of Pearl River in China and resulted in increased magnitude of high flows in the downstream part of the basin. Similarly Lu et al. (2013) examined the mean monthly and annual flows over Huang-Huai-Hai region of China and found that runoff is more sensitive to the rainfall than temperature. The change due to anthropogenic activity in the form of land use change is evaluated by Dadhwal et al. (2010) over River Mahanadi of India and found an increase in the streamflow from 1972 to 2003 as a result of decrease in forest cover.

The broad objective of the present study focuses to assess the climate change impact on the seasonal variations on the streamflow in Wainganga Sub-basin of Godavari River and the specific objectives are presented as follows.

- Calibration and validation of three layer Variable Infiltration Capacity (VIC-3L) hydrologic model with respect to observed streamflow to obtain best match between observed and simulated streamflow.
- Downscaling meteorological forcings for the period 2020-2044 using change factor method.
- Simulation of future streamflow using downscaled meteorological forcings.
- Assessment of impact of climate change on streamflow for the future period.

2. STUDY AREA AND DATA USED

Wainganga, which means 'Arrow of Water', is one of the major tributaries of the Godavari River. The Wainganga sub-basin (Figure 1) occupies the area between latitudes 19^0 30' N and 22^0 40'N and longitudes 78^0 0'E and 81^0 0' E and about 16.45% of the total area of Godavari River basin. The annual precipitation varies between 900 mm to 1600 mm with most of the precipitation during south-west monsoon (June to October). The minimum winter temperature fluctuates from 7° C to 13°C and maximum summer temperature varies from 39° C to 47°C. The area is predominantly covered by fine and medium texture soil with clay and clayey loam as the principal soil types. The land use pattern mostly occupied with crop land and forest land.

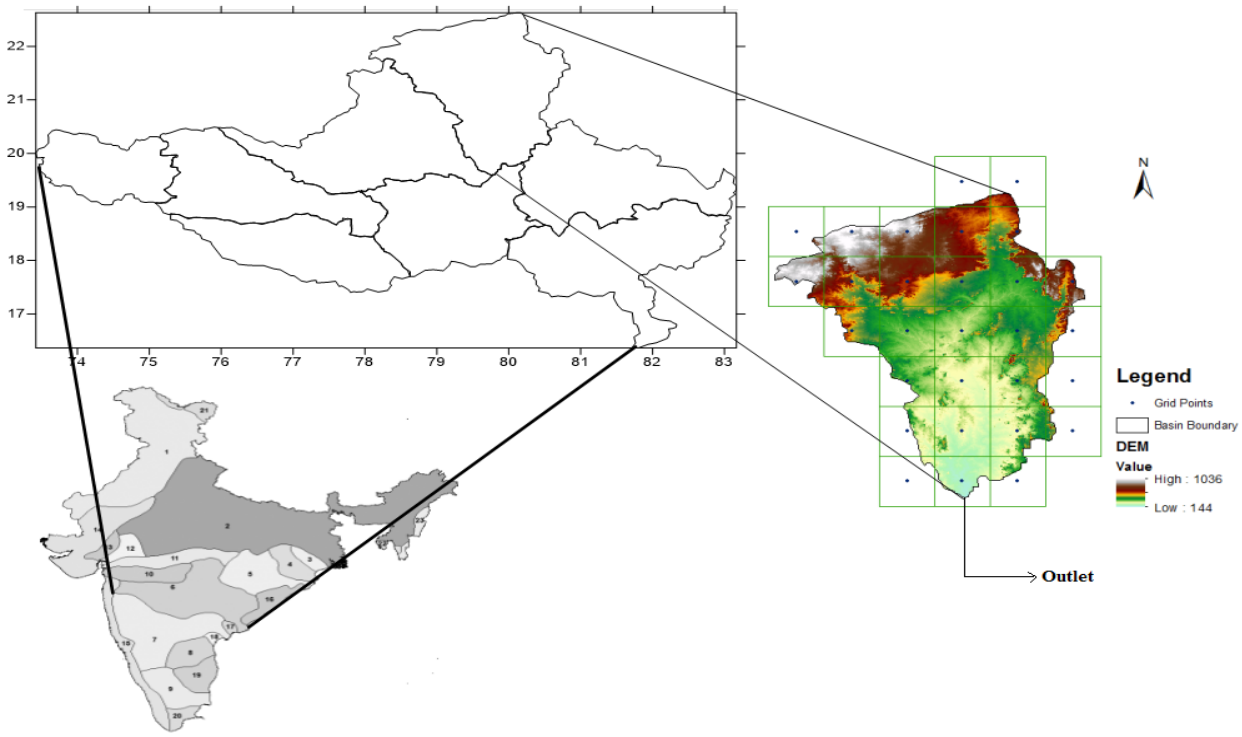

Figure 1. Location of the study area.

To calibrate and validate the VIC-3L model different meteorological variables are acquired from various sources. Meteorological variables such as precipitation, maximum and minimum temperature are obtained from the high resolution (0.5^o*0.5^o) India Meteorological Department (IMD) gridded dataset from 1971-2005. The wind velocity for the same duration is prepared by using the data provided by the Princeton University (Sheffield et al., 2006). The observed streamflow data at the outlet of the Wainganga basin is procured from Central Water Commission (CWC), Hyderabad. To evaluate the effect of climate change on streamflow in the near future (2020-2044), the climatic variables are downloaded from the six different GCMs under the Representative Concentration Pathways 4.5 (RCP4.5) scenario.

3. METHODOLOGY

To achieve the broad objective of the study the methodology is categorised into different stages. Initially the hydrologic model is calibrated and validated using the observed meteorological data. Next, the coarser resolution GCM outputs are downscaled to the finer resolution using statistical downscaling. Then the calibrated model is forced with the downscaled GCM outputs to project the streamflow during 2020-2044.

3.1 VIC-3L - An Overview

The VIC model (Liang et al., 1994; Liang et al., 1996) is a macro-scale hydrological model, which simulates water and energy storages and fluxes. It is a grid based semi distributed hydrological model which quantifies the dominant hydro-meteorological process taking place at the land surface atmospheric interface. It incorporates spatially distributed parameters describing topography, soils, land use, and vegetation classes.VIC can accept any combination of daily or sub-daily meteorological variables. At minimum, VIC requires daily precipitation, minimum temperature, maximum temperature and wind speed to generate the streamflow. The VIC-3L is the modification of the VIC-2L by adding one extra thin surface layer for better representation of the bare soil evaporation process. Initially, the VIC generates runoff at each grid point, soling the water and energy balance equations, covering the study area accounting the heterogeneity in the land use and soil type. Then, it routs the generated runoff to the outlet of each grid point and finally to the outlet of the basin based on the stream network using the routing model (Chawla and Mujumdar, 2015) developed by Lohmann et al. (1998).

3.2 Statistical Downscaling – Change Factor Method

A variety of methods are available to estimate values of meteorological variables at future times and at spatial scales that are appropriate for local climate change impact assessment. Change Factor (CF) or delta method is commonly used to project the change in the climatic variables at regional scale. CF is one of the simplest methods to project the future changes modelled by GCM. Screening of potentially suitable predictors is not needed as the predictand and predictor need to be the same variable.

There are two types of change factors, namely, additive or multiplicative. The additive change factor is computed by taking the arithmetic difference between a GCM variable derived from simulation carried over the historical period and derived from a future climate scenario at a GCM grid point. The future modelled values are obtained by adding this difference to the observed local variable. This method is usually used for modelling temperature (Anandhi et al., 2011). The multiplicative change factor is obtained by taking the ratio between GCM variable derived from future climate scenario and that derived from current climate simulation. The modelled future value is obtained by multiplying the change factor with the observed local variable. This change factor is usually used for modelling precipitation (Anandhi et al., 2011).

In the present study, Change Factor method is used for downscaling climatic variables from 6 GCMs. In the CF method, typically, monthly ratios are constructed for both the historical and future series, and climate change scenarios for precipitation, maximum temperature, minimum temperature and wind velocity are produced. For constructing the climate change scenario of each GCM, the equations used are:

$$\Delta P_i = \frac{\overline{P}_{GCM,FUT,i}}{\overline{P}_{GCM,BASE,i}} \quad (1)$$

$$\Delta T_i = \overline{T}_{GCM,FUT,i} - \overline{T}_{GCM,BASE,i} \quad (2)$$

$$\Delta W_i = \frac{\overline{W}_{GCM,FUT,i}}{\overline{W}_{GCM,BASE,i}} \quad (3)$$

where, ΔP_i, ΔT_i, ΔW_i are the change factors for precipitation temperature and wind velocity respectively; $\overline{P}_{GCM,FUT,i}$,$\overline{T}_{GCM,FUT,i}$,$\overline{W}_{GCM,FUT,i}$ are the long term average of precipitation, temperature and wind velocity simulated by the GCM in the future periods per month ($1 \leq i \leq 12$) respectively and $\overline{P}_{GCM,BASE,i}$,$\overline{T}_{GCM,BASE,i}$,$\overline{W}_{GCM,BASE,i}$ are the long term average of precipitation, temperature and wind velocity simulated by the GCM in the base period for each month ($1 \leq i \leq 12$) respectively.

After calculating the change factors for different variables (Eq. 1-3), the change factor method is used to downscale the data. For obtaining time series of future temperature scenarios, the respective change factor is added to the corresponding observed values. Similarly the time series of future precipitation scenarios are obtained by multiplying the climate change factor to the observed values. In this study CanESM2, IPSL-CM5A-MR, MIROC-ESM, ACCESS1-0, GISS-E2-R and GFDL-ESM2M model data are considered for downscaling, the equations used are:

$$P_i = P_{OBS} \times \Delta P_i \quad (4)$$

$$T_i = T_{OBS} + \Delta T_i \quad (5)$$

$$W_i = W_{OBS} \times \Delta W_i \quad (6)$$

where, P_{OBS}, T_{OBS}, W_{OBS} indicate observed IMD precipitation, temperature and wind velocity time series (daily) in the baseline period; P, T, W indicate time series of the future climate scenarios of precipitation, temperature and wind velocity respectively and ΔP, ΔT, ΔW indicate the respective climate change factors.

Change factor methodology is used to calculate the future climatic scenario of precipitation, maximum and minimum temperature and wind velocity for each grid cell. This downscaled meteorological data obtained is used as an input to the VIC model for simulating the future streamflow.

4. RESULTS AND DISCUSSION

4.1 Model Calibration and Validation

In the calibration process the optimum value of the parameters are obtained by the iterative method to make better agreement with the observed series. In the present study we have calibrated the model by altering different combination of parameters such as; the depths of second and third layer (d_2, d_3); three baseflow parameters (D_s, D_m, W_s); and infiltration parameter (b_{inf}). The efficiency of the model is examined by the Nash- Sutcliffe coefficient (E), and Correlation coefficient(R).

For analysis, the historical data of 35 years from 1971-2005 is divided into 2 sets, i.e. 25-year data and 10-year data. The 25-year data is then divided into 4 sets, i.e., 1971-1995, 1973-1997, 1975-1999 and 1978-2002, which are used for the calibration process. Subsequently the 10-year data is used for the model validation. Out of the above sets considered for both calibration and validation, the set that yields the maximum correlation coefficient and NSE value is taken as the baseline period for climate change analysis. Various calibrations, within the range specified for

each parameter by Xie et al., (2007), have been done in order to obtain the optimum value for each of the calibration parameters. Out of these calibration and validation sets we have found better E and R values for the calibration period 1978-2002 i.e., 0.909 (R) and 0.816 (E). And for the validation during (1971-1977) we have obtained 0.911 (R) and 0.772 (E), whereas during (2003-2005) we have resulted 0.86 and 0.4 for R and E respectively. The comparison between the observed and simulated is presented in Figure 2.

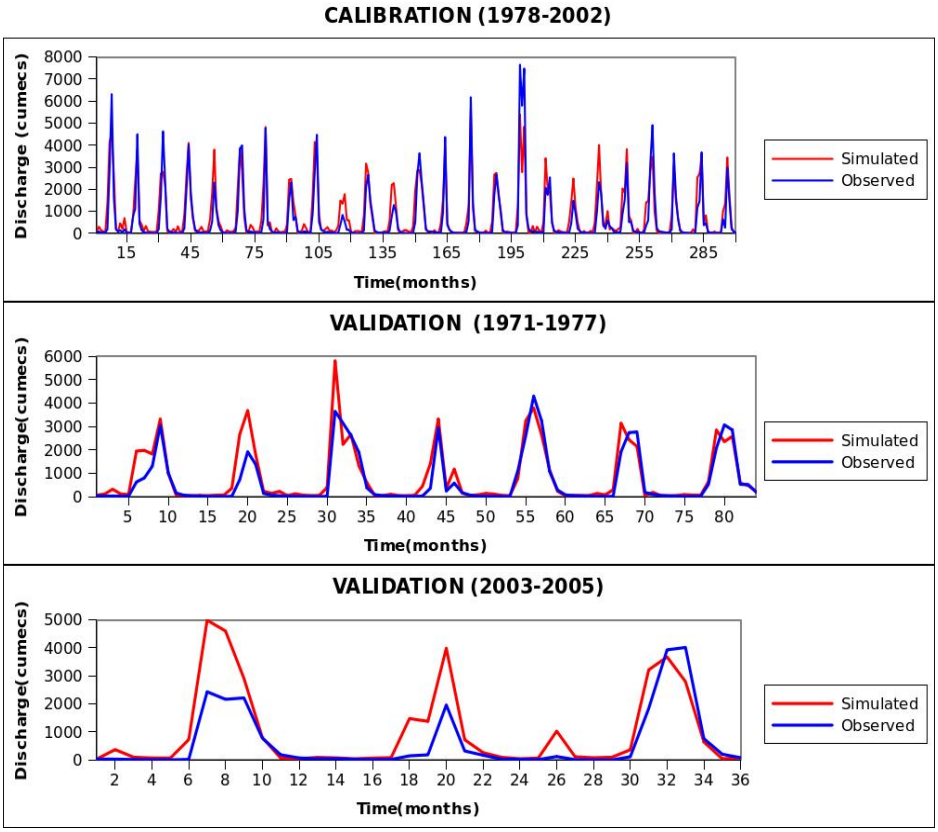

Figure 2. Comparison of monthly streamflow for the calibration and validation periods.

4.2 Impact Analysis on Streamflow

With the calibrated and validated VIC-3L model the downscaled atmospheric forcings from different 6 GCMs are given as an input to the model to project the streamflows during 2020-2044. To analyse the impact of climate change, an annual scale is divided into two main seasonal components (i.e. monsoon and nonmonsoon). The monsoon flow comparison between the baseline and future is presented in Figure 3. Along with the each GCM an ensemble mean is also calculated to minimize the uncertainty associated with each GCM.

From the Figure 3, it can be noted that the lower extreme of monsoon flow as described by all the models have gone above the lower extreme of the observed monsoon streamflow. On comparing the results of lower extreme values obtained from the GCM Models, it can be seen that CanESM2, IPSL-CM5A-MR, MIROC-ESM and GFDL-ESM2M yield similar values. ACESS1-0 model predicts the smallest lower extreme value. The higher extreme values as per the models are almost similar to that of the observed values.IPSL-CM5A-MR and MIROC-ESM models predicted similar values which are less than the observed value and GFDL-ESM2M predicts the smallest of all the values. It is also seen that the GISS model clearly overestimates the values of both the higher and lower extreme flow. However, the ensemble mean suggests that there is no significant increase in the monsoon flows in the near future. Similarly the flows in the non-monsoon season are compared with observed and plotted in Figure 4.

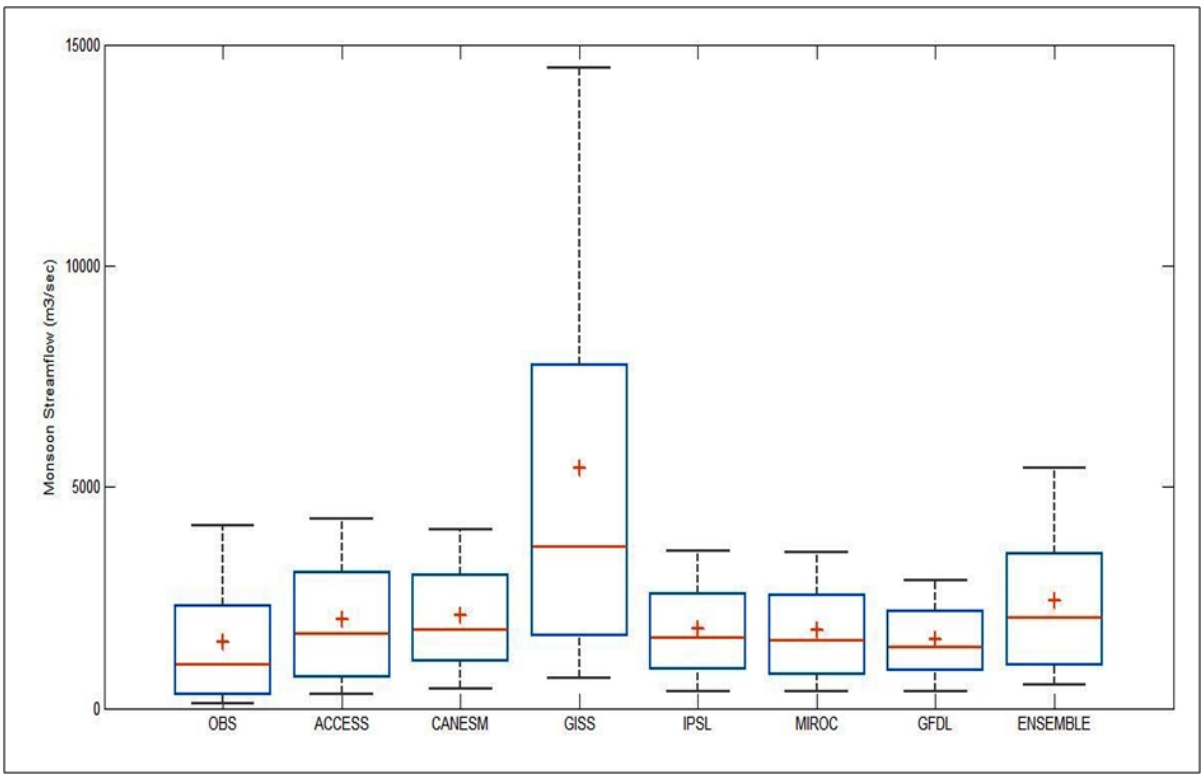

Figure 3. Comparison between the observed and future simulated monsoon flows.

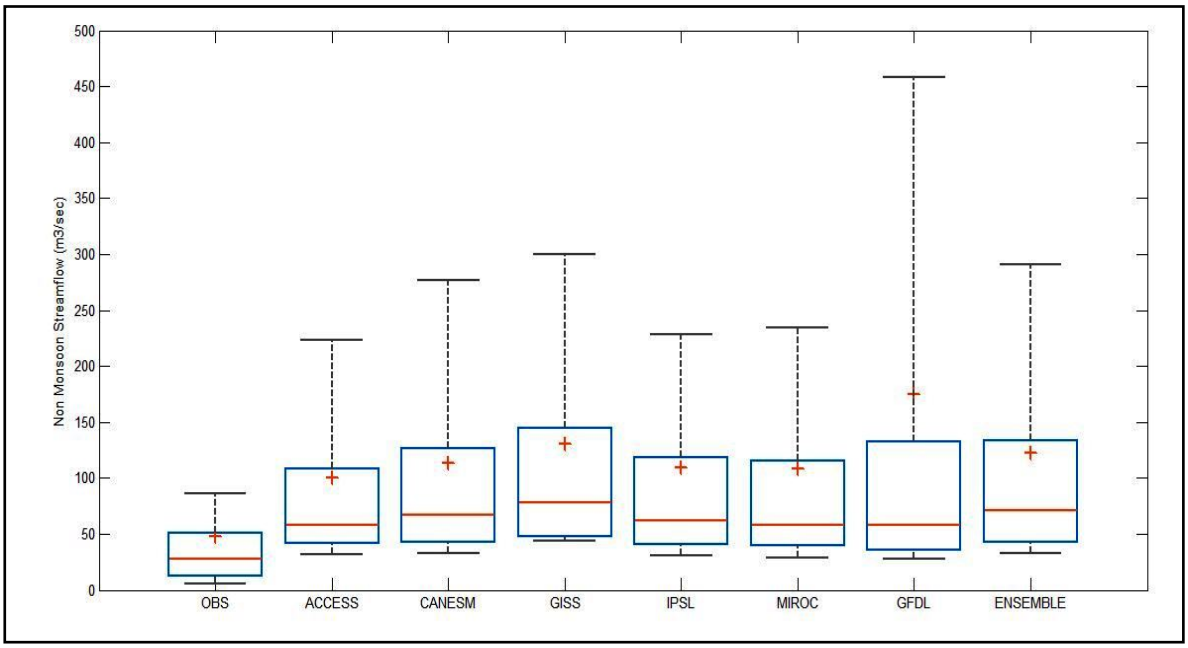

Figure 4. Comparison between the observed and future simulated non- monsoon flows.

Figure 4 depicts the box plot for the non-monsoon season. Here also, the low flows described by the models are all greater than the observed, the highest low flow being recorded by GISS-E2-R. ACCESS1-0, CanESM2, IPSL-CM5A-MR, MIROC-ESM and GFDL-ESM2M predicted similar values. However, there is greater variation in the case of high flow. It can be seen that higher extreme flow predicted by all the models are greater than the observed high flow. It is also interesting to note that the models ACCESS1-0, IPSL-CM5A-MR and MIROC-ESM share an almost similar plot. Furthermore, the ensemble mean of all the models projects a substantial increase in the non-monsoon flow unlike the monsoon flows. In order to evaluate the change in the

return levels under different return period frequency analysis is performed assuming the General Extreme Value (GEV) distribution. The obtained results are shown in Figure 5.

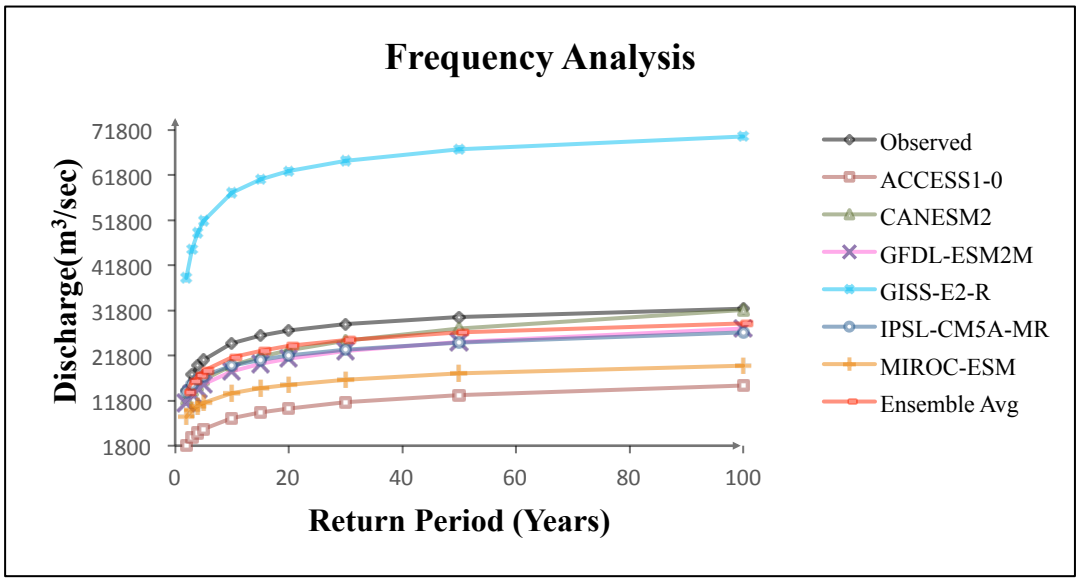

Figure 5.Frequency analysis for different return periods.

It can be observed that the discharge-return period relationship varies much with the type of GCM model used. While the data obtained from ACCESS 1-0 and MIROC-ESM give an underestimated discharge for different return periods, data from GISS-E2-R overestimates the discharge values. Results from CANESM2, GFDL-ESM2M and IPSL-CM5A-MR give discharge-return period relationship closely resembling the observed relationship between discharge and return period.

5. SUMMARY AND CONCLUSIONS

In this study VIC-3L model is used to simulate historic as well as future streamflow of Wainganga River Basin. To analyse the impact of climate change on streamflow six GCM Models are considered under RCP4.5 scenario. Change factor methodology is adopted to downscale the GCM data. The downscaled meteorological variables are used to predict the streamflow for a period of 2020-2044. Frequency analysis is also carried out to analyse the discharge- return period relationship.

The specific conclusions derived from the study are summarized below:

- There are no significant variations in the monsoon flows are observed except the GISS-E2-R model. Whereas, the monsoon flows will remain constant with slight variations in the upper extreme as suggested by the ensemble average of all the six GCMs.
- For the non-monsoon period the streamflow is significantly increasing with upper and lower extremes.
- The return levels for different return periods show a decrease in the return levels for all the return periods except GISS-E2-R model.

REFERENCES

Anandhi, A., Frei, A., Pierson, D. C., Schneiderman, E. M., Zion, M. S., Lounsbury, D., Matonse, A. H., 2011. Examination of change factor methodologies for climate change impact assessment. Water Resources Research; 47.

Bates, B. C., Charles, S. P., Hughes, J. P., 1998. Stochastic downscaling of numerical climate model simulations. Environmental Modelling & Software; 13: 325-331.

Chawla, I., Mujumdar, P. P., 2015. Isolating the impacts of land use and climate change on streamflow. Hydrology and Earth System Sciences; 19: 3633-3651.

Das, J., Umamahesh, N. V., 2016. Downscaling Monsoon Rainfall over River Godavari Basin under Different Climate-Change Scenarios. Water Resources Management; 30: 5575-5587.

Dhadwal, V. K., Aggarwal, S. P., Mishra, N., 2010. Hydrological simulation of Mahanadi river basin and impact of Land use / land cover change on surface runoff using a macroscale hydrological model. ISPRS TC VII Symposium – 100 Years ISPRS, Vienna, Austria, IAPRS, Vol. XXXVIII, Part 7B.

Ghosh, S., Mujumdar, P. P., 2008. Statistical downscaling of GCM simulations to streamflow using relevance vector machine. Advances in Water Resources; 31: 132-146.

Liang, X., Lettenmaier, D. P., Wood E. F., 1996. One-dimensional statistical dynamic representation of subgrid spatial variability of precipitation in the two-layer variable infiltration capacity model. Journal of Geophysical Research; 101: 21403-21422.

Liang, X., Lettenmaier, D. P., Wood E. F., Burges, S. J., 1994. A simple hydrologically based model of land surface water and energy fluxes for general circulation models. Journal of Geophysical Research; 99: 14415-14428.

Lohmann, D., Raschke, E., Nijssen, B., Lettenmaier, D. P., 1998. Regional scale hydrology: I. Formulation of the VIC-2L model coupled to a routing model. Hydrological Sciences Journal; 43: 131-141.

Lu, G., Xiao, H., Wu, Z., Zhang, S., Li, Y., 2013. Assessing the Impacts of Future Climate Change on Hydrology in Huang-Huai-Hai Region in China Using the PRECIS and VIC Models. Journal of Hydrologic Engineering; 18: 1077-1087.

Nijssen, B. N., O'Donnell, G. M., Lettenmaier, D. P., Wood, E. F., 2001a. Predicting the Discharge of Global Rivers. Journal of Climate; 14: 3307-3323.

Sheffield, J., Goteti, G., Wood, E. F., 2006. Development of a 50-Year High-Resolution Global Dataset of Meteorological Forcings for Land Surface Modeling. Journal of Climate; 19: 3088-3110.

Xie, Z., Yuan, F., Duan, Q., Zheng, J., Liang, M., Chen, F., 2007. Regional Parameter Estimation of the VIC Land Surface Model: Methodology and Application to River Basins in China. Journal of Hydrometeorology; 8: 447-467.

Yan, D., Werners, S. E., Ludwig, F., Huang H. Q., 2015. Hydrological response to climate change: The Pearl River, China under different RCP Scenarios. Journal of Hydrology: Regional Studies; 4: 228-245.

Proceedings of the 10th World Congress of EWRA 'Panta Rhei', 5-9 July 2017, Athens, Greece
© 2017 *European Water Resources Association*

Weather generator utilization in climate impact studies: Implications for water resources modelling

M.W. Gitau*, S. Mehan and T. Guo
Department of Agricultural and Biological Engineering, Purdue University, 225 S. University St. West Lafayette, IN. 47907
* *e-mail: mgitau@purdue.edu*

Abstract: Weather generators are increasingly used in water resources studies, and more so with current concerns on climate change and its implications on the water resource. In general, generated weather data should go beyond matching values with observed data to mirroring statistical properties of observed data. With the use of generated data in future-cast studies, it is additionally important that generated data capture anticipated variabilities in climate. The generators, thus need to be evaluated prior to being applied in new areas and/or those with climate characteristics distinct from those in which they were developed. Furthermore, considering the stochasticity of weather, it is important that several realizations be generated to capture the range of variability in climate. We present some considerations based on experience with three commonly used climate generators: CLIGEN, LARS-WG, and WeaGETS. We then present a discussion on realizations and their impacts on the suitability of generated data. Finally, we discuss implications for water resources modelling.

Key words: Weather generators, statistical properties, realizations, modelling, water resources

1. INTRODUCTION

Weather generators are increasingly used in water resources studies to: provide model input, particularly where observed data are not consistent or available in sufficient quantities and consistence for modelling (Yu 2003, Fodor et al. 2013, Lemann et al. 2016); develop datasets for ungauged stations (Fodor et al. 2013); obtain localized predictions based on observed data (Al-Mukhtar et al. 2014); downscale from coarse resolution predictions (Semenov and Barrow 1997, Fatichi et al. 2011, Farzanmanesh et al. 2012); and provide flexibility needed for Monte Carlo simulations. Daily weather data are needed to run hydrologic, water quality, and crop-growth models. Thus, in addition to evaluating generated values on a daily time scale, it is especially important that these values also mirror the statistical properties (Semenov and Barrow 1997, Chen et al. 2012) and other essential characteristics of observed data. We discuss some important considerations in this regard with examples from work done with three commonly used generators CLIGEN (Nicks et al. 1995), LARS-WG (Racsko et al. 1991), and WeaGETS (Chen et al. 2012).

2. CONSIDERATIONS FOR WEATHER GENERATOR UTILIZATION

2.1 Selection of base time period from which to parameterize the generator

Parameterization generally involves obtaining average characteristics computed on a monthly or bi-weekly time period. The length of observed input data from which parameters are generated (base time period) is, therefore, important as it translates to the nature of the parameters. For example, considering a 75-year record and comparing daily precipitation values averaged on a monthly basis across the entire dataset to those obtained on a 25-year and 10-year basis (Figure 1a):

1) For 25-year means, the period from 1966-1990 had lower mean daily values than that computed across the dataset while mean values were higher in 1991-2015; 2) For 10-year means, values were higher in 1941-1960 and 2011-2015 and generally lower in 1961-2000 than values obtained across the dataset. Means for the period 2011-2015 were substantially higher than those for all other periods, although these means were only calculated for the first 5 years of the decade and patterns might vary once a complete 10-year dataset is available. Ideally, a longer base period should provide a better representation of climate; for example, a 20-year period is recommended to provide a suitable set of input parameters (Semenov and Barrow 1997). However, variations inherent in different time periods and data lengths, as shown in Figure 1a, imply that the selection of base time period could well translate into an overestimation or under estimation of expected values. Furthermore, data from a more recent albeit shorter time period would be better suited for future-cast predictions than historical data over a longer time period. Thus, a longer period is not necessarily better; a more suitable approach to selecting a base time period would be to analyse the data for trends and select periods in which the data are either consistent or show consistent trends.

2.2 Determining the length of the generated dataset

With a base time period selected or determined, oftentimes simulated values are obtained for a time period equal to the base time period- for example, 55 years (Min et al. 2011) and 30 years (Hayhoe and Stewart 1996). However, at times data are generated for a period less than or greater than the base time period e.g. 10-year simulation from 20-year base data (Al-Mukhtar et al. 2014) and 300-year simulation from 30-year data (Kou et al. 2007), respectively. Commonly used generators generally produce weather time series of a specified length X which are not necessarily matched in a pair-wise fashion with the base input data. Where the length of generated data is equal to that of the base data, such a pairwise relationship might be assumed. However, if the length of the generated data (Y) is shorter than X, generated data could represent any of the many different potential combinations of time series each of length Y (Figure 1b: X=30, Y=20). This might present a challenge where data are generated for use with modelling applications, and especially when model outputs are used in parameter optimization. A challenge may also present where data are extrapolated beyond the length of the base input data. This is sometimes done, for example, to evaluate what-if scenarios for factors other than climate, in which case the desire is to fix the climate data to a certain or prevailing pattern so as not to confound the analysis. With extrapolating beyond the base data, pertinent changes and variabilities might not be captured, for example in Figure 1b where there is a discernible increase in daily mean values.

2.3 Utilizing a suitable number of realizations

Because weather generators produce random outputs, it is unlikely that any two simulation runs will produce the same output, pointing to the need for multiple realizations. The number of realizations used based on current literature varies from one (Farzanmanesh et al. 2012, Fan et al. 2013, Al-Mukhtar et al. 2014) through 100 (Min et al. 2011) to 1000 (Brisson et al. 2015). In some cases, generated data have been obtained for a large number of years and then divided into a number of different sets, for example 300 years divided into ten sets each 30 years in length (Kou et al. 2007). Based on a comparison of LARS-WG output for 50 realizations each of length 50 years with the corresponding values obtained from one realization 2500 years in length split into 50 sets of length 50 years (pseudo-realizations), the choice of method did not seem to make a difference for maximum and minimum temperatures, and standard deviation of precipitation (Figure 2). Mean

precipitation was, however, better represented with 50 realizations based on which it was possible to capture observed values. With the pseudo-realizations, the entire dataset was a reflection of the single realization (in this case an underestimation) and errors were simply propagated across the dataset. The same picture might be expected if the realization had resulted in an overestimation of values thus the need for several realizations to better capture the range of variability in climate, and especially so when looking at possible future climate. A comparison of 1, 25, 50, and 100 realizations showed that 25 realizations were sufficient to represent the essential characteristics of observed data. Results from 50 realizations were generally not different from those obtained using 25 realizations and there was no advantage of going over 50 realizations.

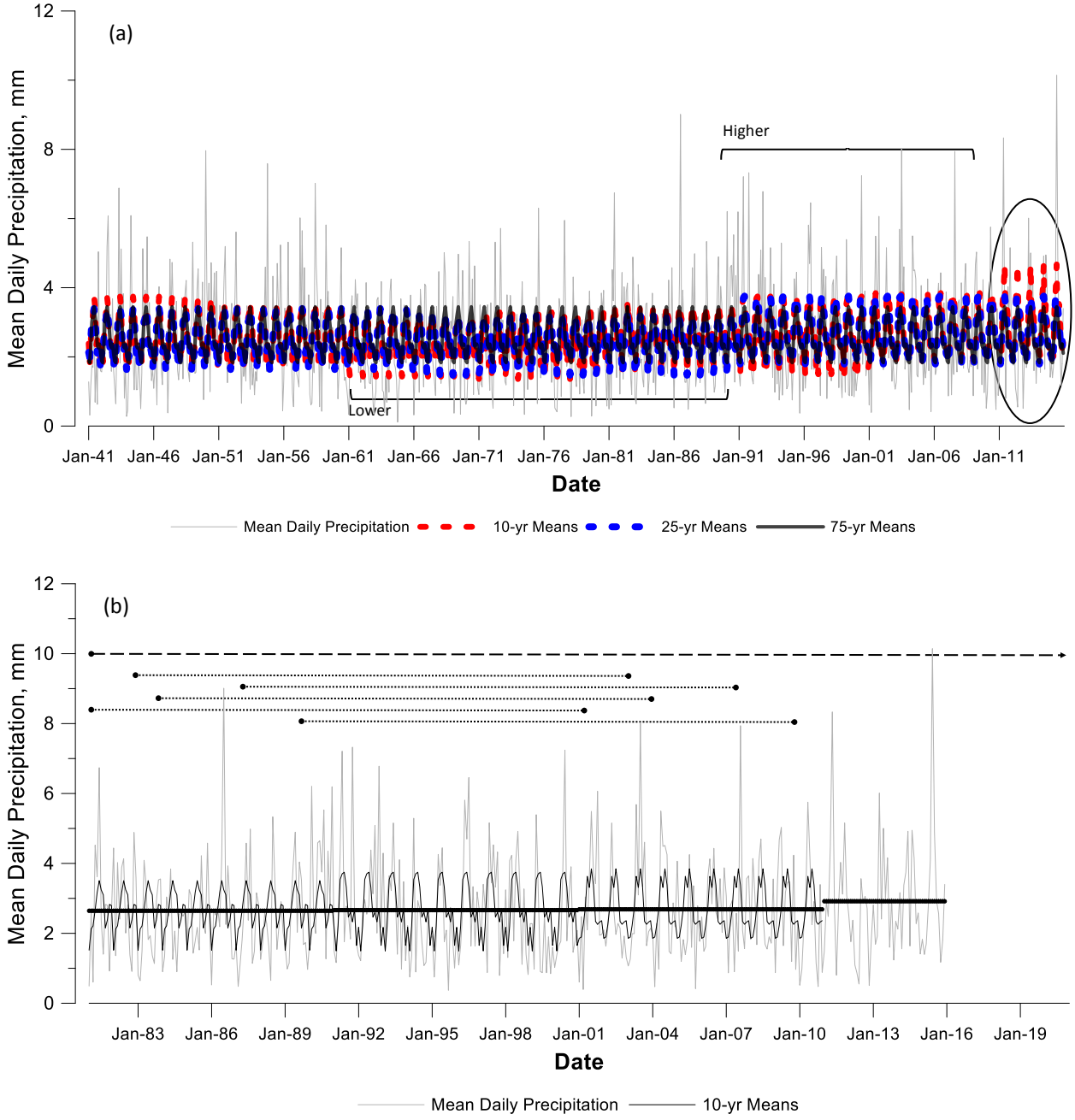

Figure 1. Fort Wayne, Indiana daily time series showing: a) variations in data during 1941-2015; and, b).30-year base time period (1981-2010) with possible representation of a 20-year time period (dotted) and extrapolation beyond the base time period (dashed).

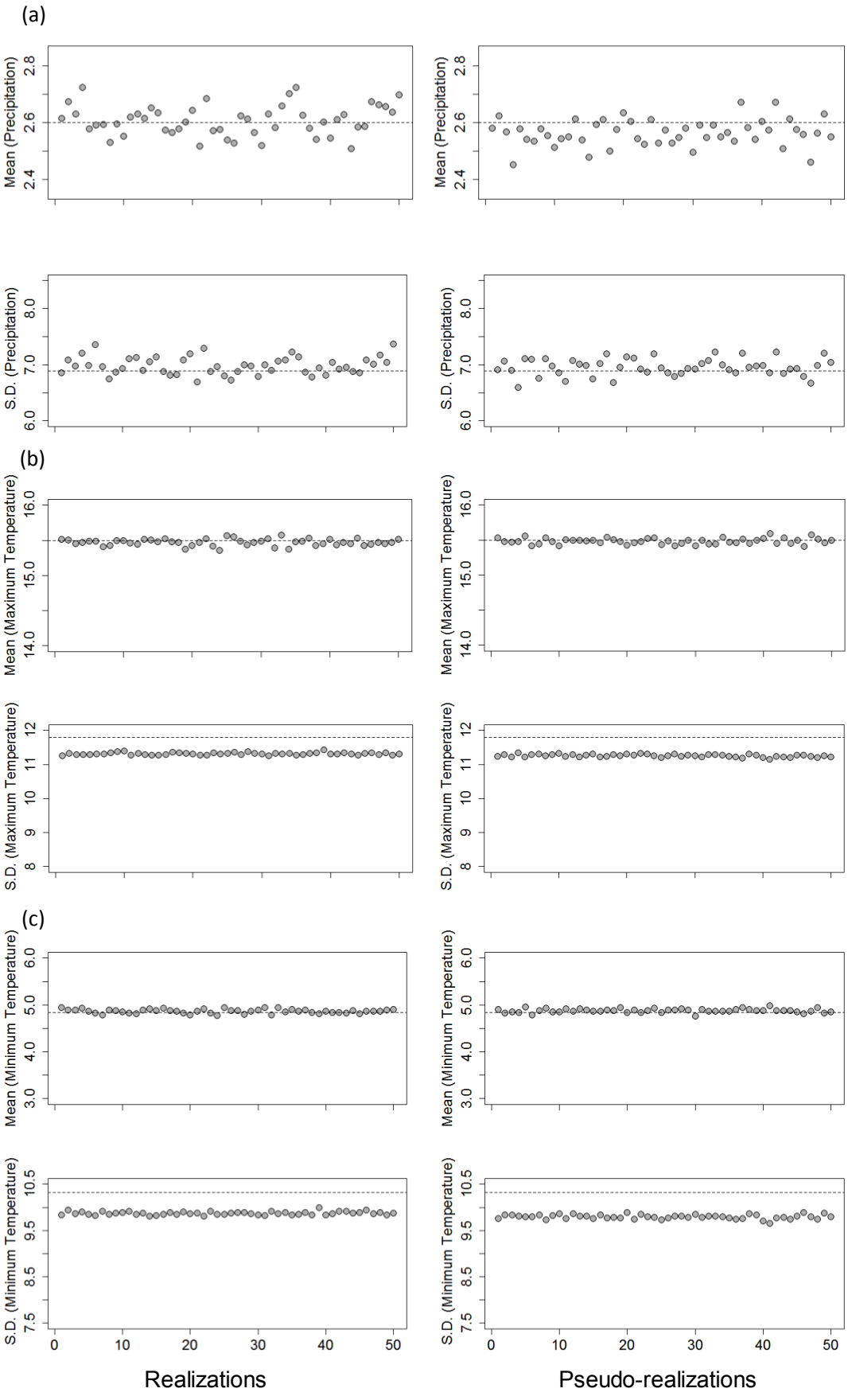

Figure 2. Use of realizations in simulating weather data I) results from 50 realizations each of length 50 years; II) results from 1 realization length 2500 years with data split into 50 equal parts each length 50 years (pseudo-realizations). Dotted line shows respective observed data value computed for a period of 50 years.

2.4 Representation of essential characteristics of observed climate

Primary statistical properties of observed data include daily mean, standard deviation, skewness, kurtosis, and percentiles. e.g. (Zhang and Garbrecht 2003, Min et al. 2011, Chen and Brissette 2014). Generally, there needs to be some reasonable agreement between observed and simulated data at this point since values are aggregated. Other essential characteristics include the minimum and maximum values and inter-annual variations. A detailed knowledge of wet and dry spells (including sequences, monthly distributions, and lengths) is important for water resources allocation and distribution, and water management planning in general. This information is also important for crop management. Temperature characteristics are also important as they influence components of the hydrologic cycle, in particular evapotranspiration. They also influence the nature of precipitation and whether it is more likely to fall as rain or snow (particularly where snow-melt hydrology is of importance). Other characteristics that are important include those related to the growing season. In the U.S. midwest for example, corn is an economically important crop; ideal temperatures for corn growth are 20-25 °C. Adverse impacts occur when temperatures rise above 35 °C or drop below 10 °C. Thus, depending on the intended use of the synthetic data, it is also important that the generators are able to capture the variety of associated characteristics (Table 1).

Table 1. Example weather generator performance for select stations in Indiana, Michigan and Ohio

	Fort Wayne, IN			Adrian, MI			Norwalk, OH		
	Obs†	**CLIGEN**	**LARS-WG**	**Obs†**	**CLIGEN**	**LARS-WG**	**Obs†**	**CLIGEN**	**LARS-WG**
Max Precipitation	111.8	147.0	111.5	120.4	171.3	120.8	229.1	277.6	228.4
Max Temperature, °C	41.1	45.4	38.8	40.0	45.6	37.6	39.4	45.4	37.5
Min Temperature, °C	25.6	31.9	25.6	24.4	30.5	24.2	26.1	32.2	25.3
% days with Min Temp ≤ 0.5 °C‡	34.8	34.8	36.2	39.5	39.8	41.5	35.6	35.6	37.6
Wet Sequences Count	18.0	24.0	24.0	39.0	38.0	45.0	14.0	27.0	19.0
Dry Sequence Count	213.0	279.0	223.0	191.0	225.0	178.0	230.0	284.0	231.0
% days with Max Temp > 35 °C*	0.4	8.7	0.2	0.3	7.3	0.2	0.2	7.8	0.2
% days with Mean Temp <10 °C*	47.3	47.1	47.6	49.7	50.7	51.1	48.3	48.4	49.0

†Observed; ǂ precipitation more likely to fall as snow; *impacts on corn growth

Statistical tests of significance (t- and F-test) have been used to compare synthetic data to observed data (Kou et al. 2007, Min et al. 2011, Chen and Brissette 2014). For output other than temperature and aggregated precipitation data, assumptions of normality and equal variances inherent in these tests are violated. These violations are, however, likely to be of little consequence when sample sizes are large (Ott and Longnecker 2015). Several authors have called to question the validity of standard tests of significance, e.g. (Cohen 1977, Kirk 1996, D'Errico 2009) and especially so when sample sizes are large (Royall 1986, McBride 2002, Denis 2003). Thus, care must be taken in using and interpreting results from such tests. Alternatives to significance testing have been suggested including equivalence testing, effect sizes, confidence intervals, and graphical techniques (Cohen 1977, Lecoutre et al. 2001, Denis 2003, Ngatia et al. 2010). Where more than a single realization is generated, visual comparisons become especially important as these allow a more detailed examination of the data where numerical presentation of the data would be overwhelming. The K-S test has been used to check that datasets come from the same distribution, e.g. (Hayhoe and Stewart 1996, Zhang and Garbrecht 2003, Fan et al. 2013, Al-Mukhtar et al. 2014). This test has been found to work better than the χ^2 test (Massey Jr 1951).

2.5 Implications for water resources modelling

Precipitation is the primary driver in water resources applications and how well precipitation is represented ultimately impacts the ability to model other aspects of water resources. Temperature is

also important due to its impacts on components of the hydrologic cycle and implications for crop growth as previously discussed. Generator selection for water resources modelling will largely depend on study or project objectives. In that regard, the suitability of generated data with respect to simulated water resource responses also needs to be determined. The use of multiple realizations in water resources modelling will generate large datasets, presenting specific challenges related to analysis of output. If the purpose is to obtain a single climate dataset for use as model input, then the performance of individual realizations will help find the best fitting set. This simplifies the analysis of output. If, however, the data have been extrapolated beyond the base input data, have been generated for a period shorter than the base time period, or the interest is in future-cast scenarios, individual realizations need to be maintained in order to capture the possible range of variability in climate. This may present additional challenges with respect to computational efficiency and the handling of model output especially with distributed models. A high-throughput computing framework has been used to perform over 43,000 model runs resulting from a combination of weather realizations and pollutant control practice scenarios (Gitau et al. 2012). Today facilities to handle such runs and associated data output are more readily available.

3. DISCUSSION AND CONCLUSIONS

With the increasing use of weather generators in water resources applications, it is important that the generators be evaluated for their suitability for the area in which they would be applied. In particular, the generators need to be evaluated for their ability to represent statistical properties and essential characteristics of observed data in addition to matching values. The choice of characteristics to evaluate will largely depend on the intended use for the synthetic output. Other important considerations include the base time period from which input parameters will be generated and the length of the synthetic data relative to the base time period. Generally, a number of realizations are needed in order to capture the range of variability in climate. However, the number of realizations will be of no consequence for a particular weather variable if the generator is incapable of simulating that variable relative to observed data. The use of weather realizations in water resources modelling studies could potentially be computationally expensive and produce large datasets all of which will likely require computing resources beyond the standard workstation. There is the need to determine how the effectiveness of a weather generator in simulating climate variables translates to effectiveness with respect to simulated water resource responses.

REFERENCES

Al-Mukhtar, M., Dunger, V. and Merkel, B. (2014). Evaluation of the climate generator model CLIGEN for rainfall data simulation in Bautzen catchment area, Germany. Hydrology Research 45(4-5): 615-630.

Brisson, E., Demuzere, M., Willems, P. and van Lipzig, N.P. (2015). Assessment of natural climate variability using a weather generator. Climate Dynamics 44(1-2): 495-508.

Chen, J., Brissette, F. and Leconte, R. (2012). WeaGETS– a Matlab-based daily scale weather generator for generating precipitation and temperature. Procedia Environmental Sciences 13: 2222-2235.

Chen, J. and Brissette, F.P. (2014). Comparison of five stochastic weather generators in simulating daily precipitation and temperature for the loess plateau of China. International Journal of Climatology 34(10): 3089-3105.

Cohen, J. (1977). Statistical power analysis for the behavioural sciences (rev. Ed.). New York: Academic.

D'Errico, G.E. (2009). Issues in significance testing. Measurement 42(10): 1478-1481.

Denis, D.J. (2003). Alternatives to null hypothesis significance testing. Theory & Science 4(1): 21.

Fan, J.C., Yang, C.H., Liu, C.H. and Huang, H.Y. (2013). Assessment and validation of CLIGEN-simulated rainfall data for northern Taiwan. Paddy and Water Environment 11(1-4): 161-173.

Farzanmanesh, R., Abdullah, A.M., Shakiba, A.R. and Amanollahi, J. (2012). Impact assessment of climate change in Iran using LARS-WG model. Pertanika Journal of Science & Technology 20(2): 299-311.

Fatichi, S., Ivanov, V.Y. and Caporali, E. (2011). Simulation of future climate scenarios with a weather generator. Advances in Water Resources 34(4): 448-467.

Fodor, N., Dobi, I., Mika, J. and Szeidl, L. (2013). Applications of the MVWG multivariable stochastic weather generator. The Scientific World Journal 2013.

Gitau, M.W., Chiang, L.C., Sayeed, M. and Chaubey, I. (2012). Watershed modeling using large-scale distributed computing in condor and the soil and water assessment tool model. Simulation 88(3): 365-380.

Hayhoe, H. and Stewart, D. (1996). Evaluation of CLIGEN and WXGEN weather data generators under Canadian conditions. Canadian Water Resources Journal 21(1): 53-67.

Kirk, R.E. (1996). Practical significance: A concept whose time has come. Educational and Psychological Measurement 56(5): 746-759.

Kou, X., Ge, J., Wang, Y. and Zhang, C. (2007). Validation of the weather generator CLIGEN with daily precipitation data from the loess plateau, China. Journal of Hydrology 347(3): 347-357.

Lecoutre, B., Lecoutre, M. P. and Poitevineau, J. (2001). Uses, abuses and misuses of significance tests in the scientific community: Won't the Bayesian choice be unavoidable? International Statistical Review 69(3): 399-417.

Lemann, T., Zeleke, G., Amsler, C., Giovanoli, L., Suter, H. and Roth, V. (2016). Modelling the effect of soil and water conservation on discharge and sediment yield in the upper Blue Nile basin, Ethiopia. Applied Geography 73: 89-101.

Massey Jr, F.J. (1951). The Kolmogorov-Smirnov test for goodness of fit. Journal of the American Statistical Association 46(253): 68-78.

McBride, G.B. (2002). Statistical methods helping and hindering environmental science and management. Journal of Agricultural, Biological, and Environmental Statistics 7(3): 300.

Min, Y.M., Kryjov, V.N., An, K.H., Hameed, S.N., Sohn, S.J., Lee, W.J. and Oh, J.H. (2011). Evaluation of the weather generator CLIGEN with daily precipitation characteristics in Korea. Asia-Pacific Journal of Atmospheric Sciences 47(3): 255-263.

Ngatia, M., Gonzalez, D., San Julian, S. and Conner, A. (2010). Equivalence versus classical statistical tests in water quality assessments. Journal of Environmental Monitoring 12(1): 172-177.

Nicks, A., Lane, L. and Gander, G. (1995). Weather Generator. USDA-Water Erosion Prediction Project hillslope profile and watershed model documentation. NSERL Report (10): 2.1-2.22.

Ott, R.L. and Longnecker, M.T. (2015). An introduction to statistical methods and data analysis. Thomson Learning, Inc. Duxbury, Pacific Grove, CA., Nelson Education.

Racsko, P., Szeidl, L. and Semenov, M. (1991). A serial approach to local stochastic weather models. Ecological Modelling 57(1-2): 27-41.

Royall, R.M. (1986). The effect of sample size on the meaning of significance tests. The American Statistician 40(4): 313-315.

Semenov, M.A. and Barrow, E.M. (1997). Use of a stochastic weather generator in the development of climate change scenarios. Climatic Change 35(4): 397-414.

Yu, B. (2003). An assessment of uncalibrated CLIGEN in Australia. Agricultural and Forest Meteorology 119(3): 131-148.

Zhang, X. and Garbrecht, J.D. (2003). Evaluation of CLIGEN precipitation parameters and their implication on WEPP runoff and erosion prediction. Transactions of the ASAE 46(2): 311-320.

Proceedings of the 10th World Congress of EWRA 'Panta Rhei', 5-9 July 2017, Athens, Greece
© 2017 *European Water Resources Association*

Causes of dimming/brightening in Greece and implications on reference evapotranspiration

G. Kitsara[1], G. Papaioannou[1*] and P. Kerkides[2]
[1] *National and Kapodistrian University of Athens, Department of Physics, Greece*
[2] *Agricultural University of Athens, Department of Natural Resources Development and Agricultural Engineering, Greece*
[*] *e-mail: gpapaioa@phys.uoa.gr*

Abstract: Many studies continue to investigate, in a changing climate, the decadal changes of surface solar radiation (SSR) known as Global Dimming/Brightening phenomenon (GDB) and its underlying causes. Contributing to the ongoing debate on whether GDB is global or just local phenomenon, this study analyses the temporal changes of Sunshine Duration (SD) measurements (as a proxy of SSR), for various areas in Greece, during the period 1968 to 2012. In addition to the temporal changes in aerosol concentrations and cloud cover (CL), changes in precipitable water (PW) and the effect of urbanization are also investigated as possible causes of GDB. Anomaly CL and PW series examined according to their time evolution are subsequently used to remove the CL effect and detect causes of GDB linked to atmospheric aerosols. Moreover, the population density index is used to quantify the impact of urbanization on GDB. The consistency of SSR trends with the trends of reference evapotranspiration (ET) and their impact on changes in the hydrological cycle has hardly been studied until now. In order to investigate the implication of GDB in ET changes, anomaly ET series, are estimated by the Reference Evapotranspiration Model for Complex Terrains (REMCT), which has already been tested and locally calibrated in Greece, for the same time period. The results show that the ET temporal changes rather follow the SD ones, indicating the GDB effect in the ET changes in Greece.

Key words: Global Dimming/Brightening phenomenon, Sunshine Duration, population density index, Reference Evapotranspiration Model for Complex Terrains

1. INTRODUCTION

Many researchers have confirmed GDB phenomenon, namely the widely observed decline of SSR (Dimming) between 1950s and 1980s and its subsequent recovery until around 2000, (Brightening) in many parts of the world (e.g. Stanhill and Cohen, 2001; Wild, 2009), while mixed trends are shown afterwards (Wild, 2009; 2016). Possible causes of GDB are associated with temporal changes in aerosol or/and CL (Stanhill and Cohen, 2001; Wild, 2009). Changes in concentrations and optical properties of aerosols due to the direct/indirect aerosol effect are considered as the most likely factor explaining SSR variations (e.g. Wild, 2009; 2016). Water vapor also influences SSR and although the magnitude of its impact is reported as substantially small, should not be ignored (Ohmura, 2009; Wild, 2009).

Some studies have argued that GDB is dominated by the large air polluted urban sites and thus, is more of a local rather than a global phenomenon. In addition, the possible impact of urbanization on GDB has recently come to the light (Wang et al., 2014; Imamovic et al., 2016; Tanaka et al., 2016). In order to infer the influence of urbanization on SSR, many studies have used population density data, as proxies of air pollution level (Alpert and Kishcha 2008; Stanhill and Cohen, 2009).

Changes in SSR affecting the energy available at the surface to drive evaporation are considered as a potential impact of GDB on the water cycle (Wild and Liepert, 2010). Evaporation paradox, the decrease of pan evaporation (Epan) under global warming, has been explained by the decreasing SSR during dimming phase (Stanhill and Cohen, 2001; Roderick at al., 2009). Moreover, the decrease from 1950s and the recently reported increase after mid-1980s of Epan (Ogolo, 2011) or ET (Papaioannou et al., 2011; Zhao et al., 2015) mainly follow the SSR trends, underlying the impact of GDB on changes in the hydrological cycle, but further investigation is needed.

As a first objective, this study aims to contribute to the recent debate on whether the observed SSR changes are global or just local phenomenon, by detecting GDB phenomenon in Greece, using SD measurements as a proxy of SSR during the period 1968-2012. The second objective is to detect possible causes of GDB during the same period. Besides investigating changes in aerosols or cloud cover, effects of PW changes and the impact of urbanization (taking into account population density indices) especially during dimming period, are also examined. The third objective is to investigate GDB impact on ET. The consistency of SD trends with the trends of ET estimates by the REMCT model or measurements of Epan at a non-urbanized site are tested.

2. DATA AND METHODS

2.1 Data sets

Daily measurements of SD and CL, obtained from the National Meteorological Service for 13 stations (evenly distributed across the country, Figure 1) are used for analysing long-term changes in SSR and detect the GDB phenomenon in Greece, during the period 1968-2012. Daily SD is considered as a 'proxy' of SSR (Stanhill and Cohen, 2005) and daily CL is used for removing the cloud cover-related variability from the SD measurements. Additionally, column integrated water-vapour (PW) daily NCEP/NCAR reanalysis products extracted for the pixel in which the 13 stations are located, are also employed for detecting causes of GDB linked mainly to changes in water-vapour.

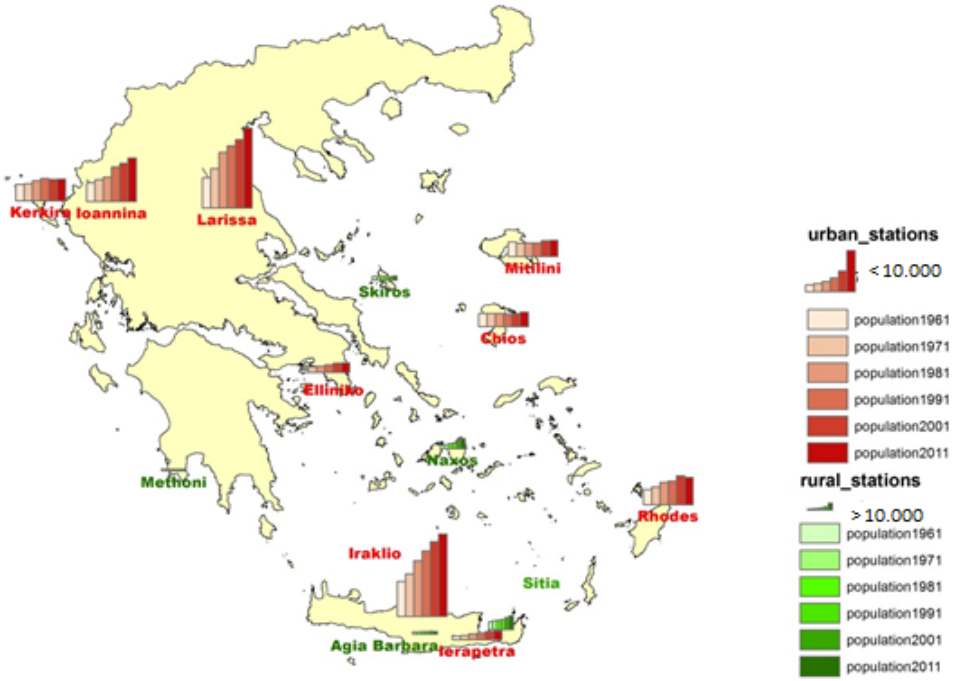

Figure 1. Stations of the study and population change based on census from 1961 to 2011.

Municipality population data, obtained from the Hellenic Statistical Authority (http://www.statistics.gr/el/statistics/pop) are used for indicating any effect of urbanization on SD.

Monthly values of precipitation, mean and maximum air temperature for the 13 stations are used for estimating monthly ET from REMCT model (Diodato and Bellocchi, 2007), for the period 1968-2012. Daily Epan measurements of Agia Barbara station obtained from the Institute of Land Reclamation of Crete are also used for investigating the GDB impact on evaporation in a non-urbanized area.

The years 2005, 2006, 2007 and 2008 are excluded from the analysis, due to a gap in the quality control of the data supplied by the National Meteorological Service.

2.2 Methods

2.2.1 Causes of GDB

In order to address the question of whether GDB is local or a larger scale phenomenon, the 13 stations are separated into two groups: urban and rural. Municipalities and communes of Greece are characterized as urban when having 10000 or more inhabitants in the largest population center (http://unstats.un.org/unsd/demographic/sconcerns/densurb/Defintion_of%20Urban.pdf) and as rural or semirural, when the population is less than 2000 or between 2000 and 9999, respectively (https://www.statistics.gr/documents/20181/1210503/methodological_note_census_coverage_survey_final.pdf).

For detecting GDB and its possible causes, anomalies of annual SD and CL or PW values for each station are computed, as relative deviations from their corresponding 1971-2000 mean, during 1968-2012. Annual mean series are calculated by averaging the 13 stations considered 'as a whole'. In order to remove the cloud effect and detect causes of GDB linked to atmospheric aerosols, the residuals SD time series are calculated from the linear regressions of SD and CL anomalies for each station.

Population data are assumed as a proxy for anthropogenic activity, especially during the dimming period, which is characterized by limited air quality regulations. For quantifying the possible impact of urbanization on SD changes, the population density (PD) index, already used in several studies (e.g. Imamovic et al., 2016; Tanaka et. al., 2016) is calculated as:

$$PD=TP/LA \tag{1}$$

where, TP is the total population and LA is the land area of each municipality (km^2).

2.2.2 Impact of GDB on ET changes

In order to investigate the effects of GDB in ET, annual ET anomaly values are estimated, as relative deviations from their 1971-2000 mean, for the 13 stations, for the period 1968-2012. REMCT model is selected for estimating ET in Greece, since its model parameters for various groups of stations have been locally calibrated and it has been independently validated from available Epan measurements (Papaioannou et al., 2011). Especially, the model has been also verified in the urban area of Athens (Kitsara et al., 2013). The REMCT model estimates ET as:

$$ET_{DB} = \frac{R_{so}}{\lambda} \cdot (T + 17.8) \cdot (\sqrt{T_{\max} - ref(T_{\min})} - f(w) \cdot Rd) \cdot f(c\lim) \tag{2}$$

where R_{so} is the mean monthly extraterrestrial solar radiation (MJ m^{-2} d^{-1}), λ is the latent heat of vaporization (MJ kg^{-1}), T or T_{max} is the mean monthly or the mean monthly maximum air temperature (°C) respectively, Rd is the number of rainy days in a month ($month^{-1}$), ref(T_{min}) is a reference minimum air temperature (°C) and f(clim) and f(w) are semi-empirical functions.

Since Epan measurements incorporate the influence of radiation, atmospheric humidity and wind speed, trends of annual Epan measured at the non-urbanized area of Agia Barbara are also computed, for the period 1970-2007.

The analysis is furthermore accomplished by applying the best fits, from first order to third order, to the yearly time series of the mentioned SD or PW or residual SD or ET anomalies or Epan values.

3. RESULTS

3.1 Causes of GDB

In order to detect GDB and its causes, annual SD and residual SD or PW anomaly series, either for all stations (as averaged from the 13 stations) or for the selected urban (Iraklio) or rural (Methoni) station are shown in Figure 2 as a, b or c, respectively. Annual SD anomaly series for all stations (black bold line) show a negative trend up to minimum at the early 1980s (dimming period), a recovery until early 2000 (brightening period) and a stabilization phase until the end of the considered period (Figure 2a). Temporal changes of SD anomaly series, selected to represent urban or rural areas (noted with red or green bold line, respectively) have shown the same dimming/brightening periods. The evolution of annual CL anomaly series for all stations has been found as decreasing until late1980s, followed by an increase until 2012 not explaining the obvious decrease/increase in SD. Thus, the residual SD series are obtained from the linear regressions of SD and CL anomalies and their time evolution is presented either for all stations, considered as averages from the 13 stations, (bold black line) or for the selected urban (red bold line) or rural (green bold line) station in Figure 2b. The residual SD series for all stations show a clear decrease from the beginning of the study period up to early 1980s with a subsequent recovery until mid-2000 and a phase of stabilization thereafter. The residual SD anomaly series for urban or rural sites, although similar in shape, as compared to the evolution of the residuals SD series for all stations, indicate the reversal from dimming to brightening a little bit earlier, around 1980. A clear decrease in residual SD series is detected between 1991 and 1992 especially at the urban station, probably due to Pinatubo volcanic eruption (June 1991). Additionally, the effect of water-vapour changes in GDB is examined and the time evolutions of PW anomalies for all stations (or urban or rural station), are shown in Figure 2c (black or red or green bold line, respectively). PW anomalies decreasing from 1968 up to early 1980s (or 1980), remaining stable until mid-2000s (or 2000, respectively) and rather decreasing thereafter cannot explain SD variation.

PDs (as a proxy of local air pollution) are employed for investigating the possible effect of urbanization on the observed SD changes. Figure 1 shows the population per decade at municipality basis for the 13 sites (with urban or rural and semirural sites, noted with red or green color, respectively) and Figure 2d shows the changes in PDs in the 13 municipalities. Red and green lines indicate urban and rural stations, respectively. PDs are obviously increased for the majority of the urban stations, during the first decades of the study (1961-1981) and they are stabilized, during the last decade. In contrast, PDs of the rural areas attain lower values and remain unchanged through the years. The PDs of the selected urban (Iraklio) or rural (Methoni) station are shown in dashed lines in Figure 2d. Large PDs in Iraklio (among the biggest Greek cities) change through the years, while low PDs in Methoni remain almost the same.

3.2 Impact of GDB on ET changes

The impact of GDB on ET is examined by investigating the consistency of SD trends with ET trends. Annual time evolutions of anomalies of ET_{DB}, for all stations (as averaged from 13 sites) or for the selected urban or rural station, for the period 1968-2012 are shown in Figure 3a (black or red or green bold line, respectively). A negative trend up to minimum around the late 1970s, then a recovery until mid-2000 and a slight decrease until the end of the study period is observed. Similar variations of ET_{DB} anomalies are observed for urban or rural stations, except during the period after the mid-2000, when they continue to rise in rural sites but slightly decrease in urban ones.

To enhance the results for the effect of GDB on evaporation, temporal variation of annual Epan measurements from 1970 up to 2007, for the rural area of Agia Barbara (which has a stable population around 2000) and annual SD series from the closest site of Tympaki are presented in Figure 3b. Annual Epan series highlighted the dimming period from 1970 up to early or mid-1980s

and the brightening period thereafter until 2007, in accordance with the results of ET_{DB}. It is indicated that even in the non-urbanized site of Agia Barbara, the GDB is still observed, probably related to the background aerosols.

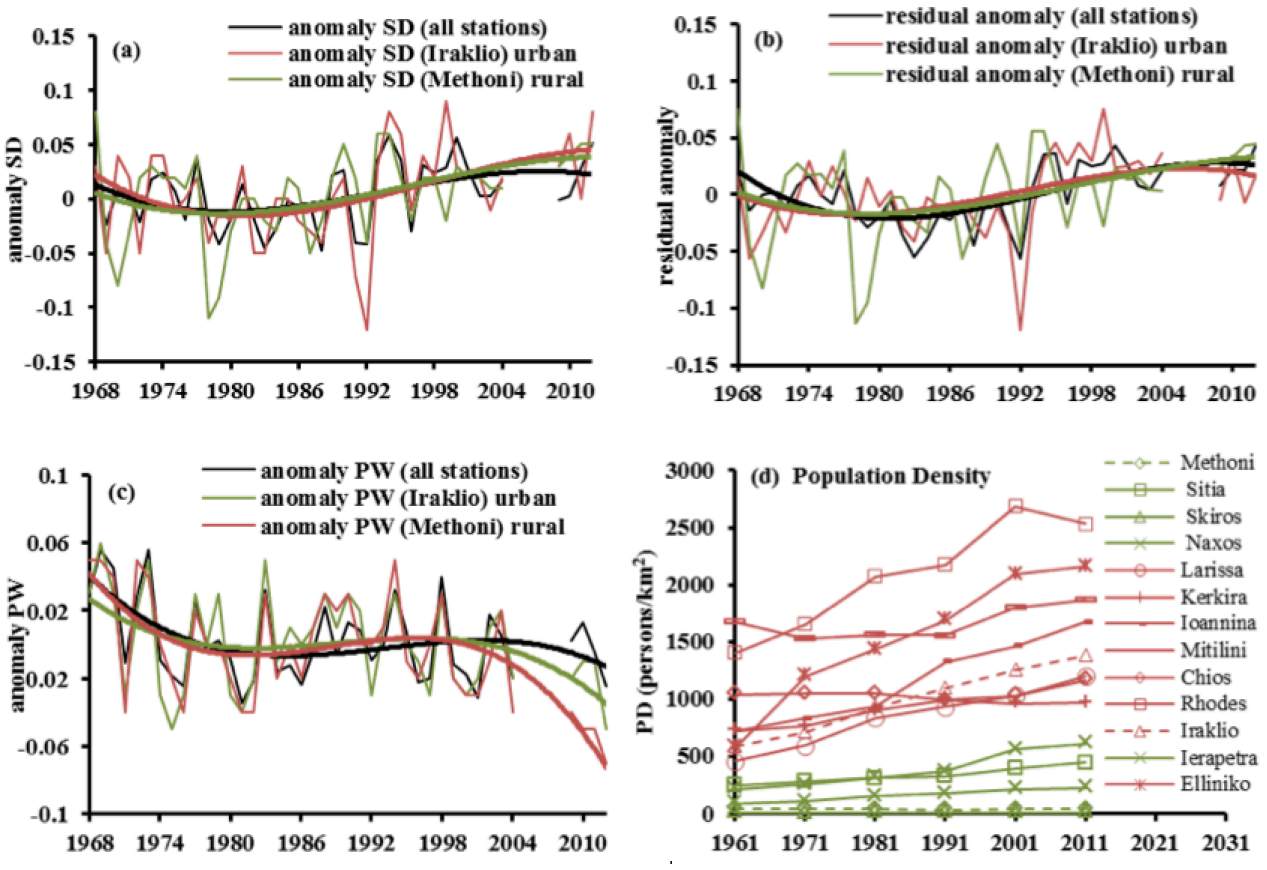

Figure 2. Annual time evolution of (a) SD anomaly,(b) residuals estimated from the linear regression between SD anomaly and CL anomaly and (c) PW anomaly for all stations or the selected urban (Iraklio) or rural (Methoni) station, during the period 1968-2012. Changes of population density index in urban (red line) or rural (green line) stations in Greece since 1961 (d).

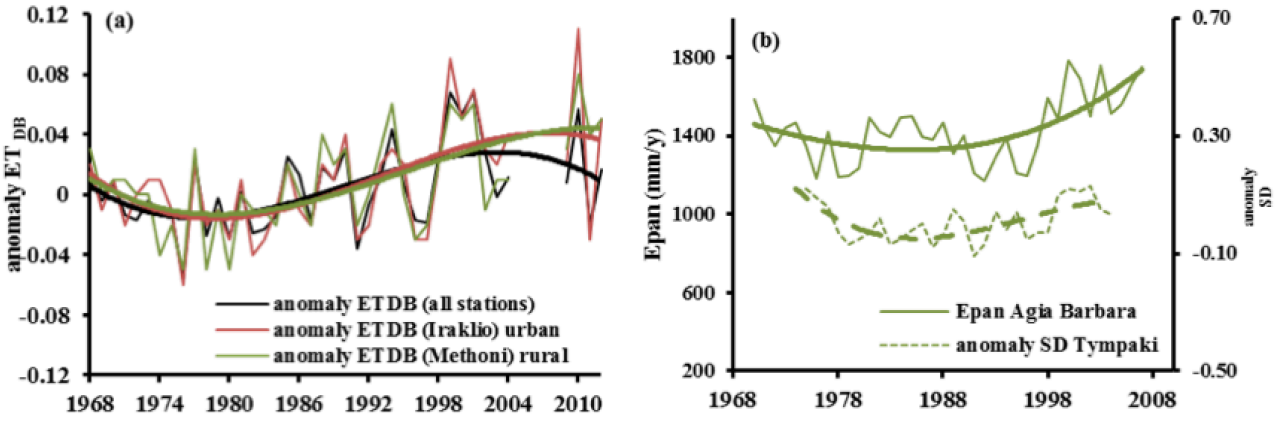

Figure 3. Annual time evolution of (a) ET anomalies for all stations or the selected urban (Iraklio) or rural (Methoni) station, during 1968-2012, (b) Epan values in Agia Barbara (1970-2007) or SD anomalies in Tympaki (1974-2004)

4. DISCUSSION AND CONCLUSIONS

Dimming is detected in Greece, from 1968 to early-1980s, while afterwards brightening is observed until mid-2000 and seems to level off thereafter, in general accordance with studies based

on SD trends in Europe (e.g. Manara et al., 2015). Thus, GDB might be regarded, as not a local phenomenon.

PW and CL changes were found as not attributing to the phenomenon. After removing cloud effect annual residual SD series highlighted the same GDB periods, in urban and rural sites, pinpointing that dimming is mainly linked to aerosols changes (e.g. Norris and Wild, 2007). Furthermore, brightening is consistent with the reduction of local aerosols, due to air-quality control measures taken all over European Union (Streets et al., 2006).

PD indices have shown that any urbanization was mainly occurred, during the dimming period, but SD anomalies decline during the dimming phase in both urban and rural sites. During the brightening phase, SD recovery happened not only in the rural areas, which is supposed to be unaffected from urbanization and local pollution, but also in the urban stations in agreement with results referred by Wang et al. (2014). This suggests that local air pollution did not play a role in causing GDB, in agreement with the findings of Tanaka et al. (2016), for Japan or Imamovic et al. (2016), for Europe.

Annual ET_{DB} anomalies show a negative trend until the late 70s and then a partial recovery until mid -2000s, for all stations or both the selected urban or rural station, being in general coincidence with the annual evolution of SD anomalies and pointing out the GDB effect on ET changes. This is in agreement with similar results reported by Papaioannou et al. (2011), Kitsara et al. (2013), Zhao et al. (2015). The effect of SD trends on ET_{DB} trends is furthermore supported by Epan trends in the rural area of Agia Barbara, following the changes of SD anomalies (obtained from the nearest Tympaki station), underlying that GDB is due to background air pollution transported from long distance polluted areas, through long-range transport (Ramanathan et al., 2007).

This study suggests that the GDB in Greece is not restricted to urban areas but is also detected in rural areas in accordance with other studies (Wang et al., 2014; Imamovic et al., 2016) and probably caused by large scale changes in background aerosols (Tanaka et al., 2016).

ACKNOWLEDGEMENTS

The authors wish to express their thanks, to the National Meteorological Service of Greece and the Institute of Land Reclamation of Crete, for providing the data.

REFERENCES

Alpert, P., Kishcha, P., 2008. Quantification of the effect of urbanization on solar dimming. Geophys. Res. Lett.; 35: L08801, doi:10.1029/2007GL033012.

Diodato, N., Bellocchi, G., 2007. Modeling reference evapotranspiration over complex terrains from minimum climatological data. Water Resour. Res.; 43: W05444.

Imamovic, A., Tanaka, K. , Folini, D., Wild, M., 2016, Global dimming and urbanization: did 5 stronger negative SSR trends collocate with regions of population growth?. Atmospheric Chemistry and Physics; 16:2719-2725.

Kitsara, G., Papaioannou, G., Papathanasiou, A., Retalis A., 2013. Dimming/brightening in Athens: Trends in Sunshine Duration, Cloud Cover and Reference Evapotranspiration. Water Resour. Manage; 27: 1623-1633.

Manara, V.,. Beltrano, M.C., Brunetti, M., Maugeri, A., Sanchez-Lorenzo, C., Simolo, Sorrenti, S., 2015. Sunshine duration variability and trends in Italy from homogenized instrumental time series (1936–2013). J. Geophys. Res.Atmos.; 120: doi:10.1002/2014JD022560.

Norris, J.R., Wild, M., 2007. Trends in aerosol radiative effects over Europe inferred from observed cloud cover , solar ‘’dimming ,’’ and ‘brightening’. J. Geophys. Res.; 112:D08214, doi:10.1029/2006JD007794.

Ohmura, A., 2009.Observed decadal variations in surface solar radiation and their causes. J. Geophys. Res.;114: D00D05, 10.1029/2008jd011290.

Ogolo, E.O., 2011. Regional trend analysis of pan evaporation in Nigeria (1970 to 2000). J. Geogr. Reg. Plann., 4, 10,566-577.

Papaioannou, G., Kitsara, G., Athanasatos, S. 2011. Impact of global dimming and brightening on reference evapotranspiration in Greece,.J. Geophys. Res.; 116: DO9107, doi:10.1029/ 2010JD015525.

Ramanathan, V., Li, F., Ramana, M.V., Praveen, P. S., Kim, D., Corrigan, C. E., Nguyen, H., Stone, E. A., Schauer, J. J.,Carmichael, G. R., Adhikary, B., Yoon, S. C., 2007. Atmospheric brown clouds: Hemispherical and regional variations in long-range transport, absorption, and radiative forcing. J. Geophys. Res.;112:D22S21,10.1029/2006jd008124.

Roderick, M. L., Hobbins, M. T. , Farquhar, G. D., 2009. Pan evaporation trends and the terrestrial water balance. II. Energy balance and interpretation. Geogr. Compass; 3(2): 761–780.

Stanhill, G., Cohen, S., 2001. Global dimming: A review of the evidence for a widespread and significant reduction in global radiation with discussion of its probable causes and possible agricultural consequences. Agric. For. Meteorol.; 107:255-278.

Stanhill, G., Cohen, S., 2005. Solar radiation changes in the United States during the twentieth century: Evidence from sunshine duration measurements,.J. Climatol ;18: 1503-1512.

Stanhill, G., Cohen, S., 2009. Is solar dimming global or urban? Evidence from measurements in Israel between 1954 and 2007. J. Geophys. Res.; 114: D00D17, doi: 10.1029/2009JD011976.

Streets, D. G., Y. Wu, M. Chin M., 2006. Two-decadal aerosol trends as a likely explanation of the global dimming/brightening transition. Geophys. Res. Lett.; 33: L15806, doi:10.1029/2006GL026471.

Tanaka, K., Ohmura, A., Folini, D., Wild, M., Ohkawara, N., 2016. Is global dimming and brightening in Japan limited to urban areas?, Atmos. Chem. Phys. Discuss.; doi:10.5194/acp-2016-559.

Wang, K., Ma, Q. Wang, X., Wild, M., 2014. Urban impacts on mean and trend of surface incident solar radiation. Geophys. Res. Lett.; 41: 4664–4668.

Wild, M., 2009. Global dimming and brightening: A review. Geophys. Res. Lett.; 114:D00D16, doi: 10.1029/JD011470.

Wild, M., Liepert, B., 2010. The Earth radiation balance as driver of the global hydrological cycle, Environ. Res. Lett.; 5:025003, doi:10.1088/ 1748-9326/5/2/025203.

Wild, M., 2016. Decadal changes in radiative fluxes at land and ocean surfaces and their relevance for global warming. WIREs Clim Change;7:91, 107. doi: 10.1002/wcc.372

Zhao, N.A., Xiaofan, Z., Huaiwei, S., 2015. Impact of global dimming on reference evapotranspiration in Hai River basin, China. Remote Sensing and GIS for Hydrology and Water Resources, IAHS Publ.; 368: doi:10.5194/piahs-368-287-2015.

Proceedings of the 10th World Congress of EWRA 'Panta Rhei', 5-9 July 2017, Athens, Greece
© 2017 *European Water Resources Association*

Using Weather Research and Forecasting (WRF) model for extreme precipitation forecasting in an Andean region with complex topography

G. Yáñez Morroni[1*], J. Gironás[1,2], M. Caneo[3] and R. Delgado[3]
[1] *Departamento de Ingeniería Hidráulica y Ambiental, Pontificia Universidad Católica de Chile, Chile*
[2] *Centro de Investigación para la Gestión Integrada de Desastres Naturales (CIGIDEN), Centro de Desarrollo Urbano Sustentable (CEDEUS) y Centro UC de Cambio Global.*
[3] *Dirección Meteorológica de Chile (DMC)*
[*] *e-mail: gjyanez@uc.cl*

Abstract: The Weather Research and Forecasting (WRF) model is broadly used for weather prediction and research due to its good performance, but atmospheric conditions simulation over complex topography is not always optimal. Consequently, WRF has an ineffectiveness resolving Chilean mountainous terrain and foothills, precisely the site where some of the main cities are located and the most extreme rainfall events take place. This work uses a mixed physic scheme to enhance initial forecasts made by Chilean Weather Agency (DMC): testing it over vertical levels, PBL (planet boundary layer), microphysics and lead time in the computational simulations. Even when the steep topography difficult the storm peak amount, and to a lesser degree, the exact storm beginning prediction, WRF do predict properly the N-hours with the biggest amount of rainfall (5 hours corresponding to Quebrada de Ramón's time of concentration) and the temperatures during the event. Finally, a Lin et al. or WSM 6-class microphysics was chosen as the best in this event, but further testing in more storms in this region is required.

Key words: flash flood, numerical weather predictors, WRF, extreme rainfall events, Andean mountain

1. INTRODUCTION

Hydro-meteorological disasters have been a severe problem, specifically in Latin America and the Caribbean region, where ~90.000 people have died and 150 million people were injured over the last 30 years. Furthermore, this type of disaster has caused more than 120 billion dollars of economic losses (EM-DAT, 2016). The occurrence of flash floods, avalanches or extreme rainfall events is highly variable in time, and their disruptive impacts over the region increase when the events concentrate in relatively short periods of time. The Andes Mountains are a very influential geographical accident, where urbanization takes place in its foothill areas. The city of Santiago, in central Chile (Figure 1), is in the Andean front range. Here extreme precipitation events usually cause floods. Their effects can be significant increased by the lack of urban planning and the massive alteration of the natural drainage system. Concurring high temperatures during these events increase the possibility of having significant floods as liquid precipitation takes place in areas in which snow usually occurs.

Reducing or preventing natural disaster via forecasting is one of the main goals of numerical weather predictors (NWP) models. Usually the use of NWP also considers a downscaling process through a statistical or dynamical approach. Currently, the accuracy exhibited by downscaled NWP results enables forecasting hydro-meteorological hazards. This becomes a priceless opportunity for avoiding damages in cities, and implementing preventative actions and mitigation schemes.

The objectives of this work are: i) to enhance initial WRF forecasts made by DMC over mountainous regions using a mixed physics scheme, and ii) to test it over vertical levels (PBL, planet boundary layer), microphysics and lead-time in the computational simulations. The prediction of beginning of the storm events, its peak, and the N-rainiest hours will be used to define the best microphysical scheme. Therefore, it will be used for evaluating the WRF performance over complex Andean topography.

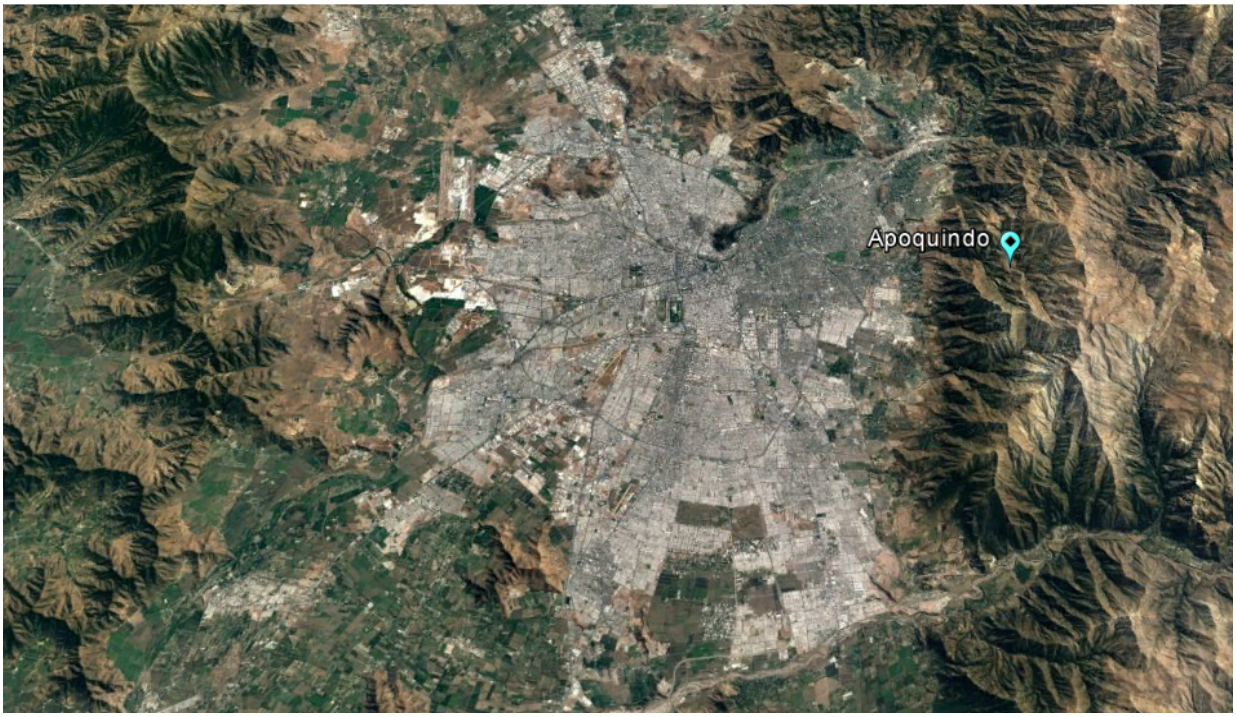

Figure 1. Santiago (33.5°S; 70.7°W) and Apoquindo meteorological station

2. APRIL 2016 EXTREME STORM EVENT

In April 13 – 18, 2016, Chile's central valley was affected by an extreme rainfall event. During the storm, a precipitation of 108 mm in 24 hours was measured at the Apoquindo rain gauge, located in the Andean Front Range at an elevation of 1625 m. (Figure 1). This frontal system moved from north to south, with negative anomalies in atmospheric pressure and geopotential height at 500 hPa, and negative values of 50 m. (Figure 2a). Satellite images (not included) showed an important moisture contribution advected from lower latitudes, which incorporated more precipitable water into the system. Furthermore, a coupled subtropical and polar jet stream intensification at 250 hPa also took place (Figure 2b). The highest wind intensities (i.e. positive anomalies of 35 m/s in the wind vectors) were in the nucleus of the system over central Chile, which favoured cloudiness development (Figure 2b).

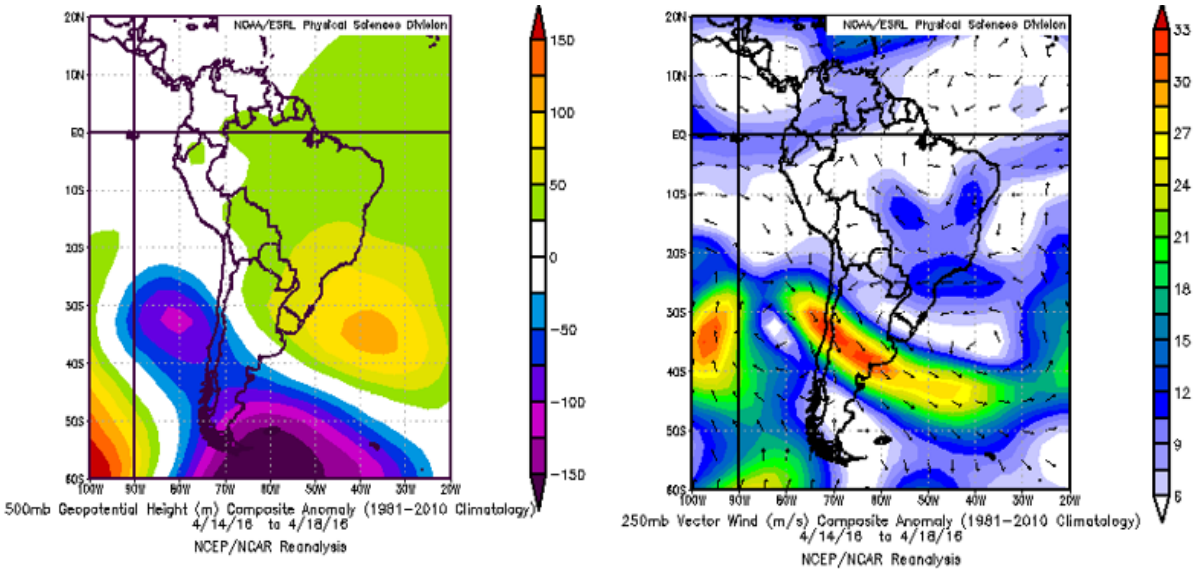

Figure 2. Composite anomaly for 500 mb geopotential height (a) and vector wind (b) during the storm event.

All these factors led to an enhanced event, which concurred with the zero-degree isotherm or freezing level being above 3000 m. These conditions originated a large contribution of liquid precipitation at relatively high temperatures. The previous produced significant flow rates in the front range watersheds of the area. In fact, in April 16th the Santiago's main river, Mapocho River, flooded the central part of this city, causing severe economic losses. This flood took place when the total flow capacity was reduced by a highway construction nearby the river bed at the time.

3. WRF SIMULATIONS AND PHYSICAL SCHEMES

Simulations of the event were performed using ARW-WRFv3.5, a state-of-the-art mesoscale NWP model suitable for a wide range of studies in weather simulation, prediction and forecasting. WRF uses scalar conservation and compressible non-hydrostatic Euler equations, applied over the terrain. The model follows vertical coordinates with variable grid density. WRF system and its code is maintained by the National Center for Atmospheric Research (http://www.mmm.ucar.edu/wrf/users). Four nested domains of 54, 18 and 6 km grids were implemented using a Lambert Projection with the central point located on Santiago (33.5°S; 70.7°W).

Good agreements in simulating temperature and wind speed proved the benefits of a finer resolution of the grid. Although Saide et al. (2011) recommended 39 vertical levels for the area of interest, we finally used 50 equidistant levels. Thus the atmospheric conditions during the storms, particularly the dew temperature, were better simulated (Figure 3).

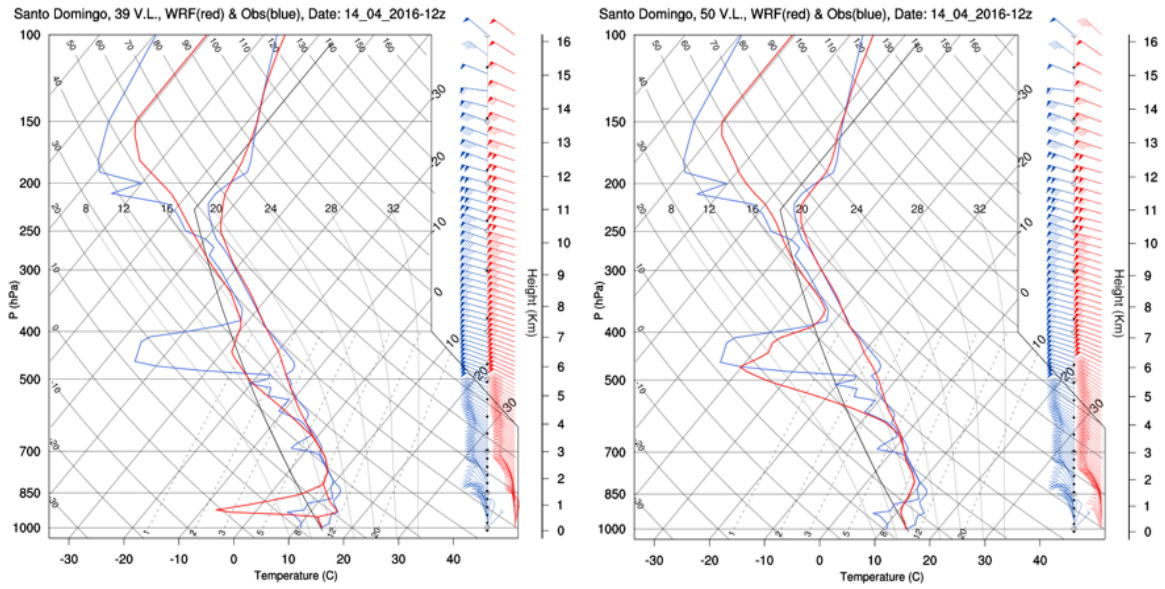

Figure 3. Skew-T plot for San Antonio, Chile. Simulation made with 39 vertical levels (left) and 50 (right)

The difficulty to simulate rainfall events near mountainous areas motivated us to implement a modelling ensemble to improve the forecast. Such approach has been commonly implemented in several studies before. This has been useful for capturing the forecasting uncertainty and for improving the physics parametrization (e.g., Ruiz et al., 2010; Evans et al., 2012; Kim et al., 2013; Katragkou et al., 2015; Dimitrova et al., 2015; Ekström, 2016). In this work, 17 simulations were performed in the study of vertical levels, PBL, MP and lead-time sensitivity.

A brief PBL physical scheme's ensemble was made, in which we tested USGS and MODIS land data, and FNL and GFS weather input data (not shown). The simplest PBL scheme was initially adopted (i.e. 5 – Layer), but Noah and NoahMP schemes were also tested to represent the storm. Eventually MODIS data and NoahMP scheme were found to be the most appropriate for depicting

surface variables. FNL data was not considered due to its inoperability in real time rain forecast.

4. MODEL EVALUATION IN MOUNTAINOUS REGION

The Apoquindo gauge was chosen to evaluate the WRF simulations. Simulations testing MP schemes were performed with WSM-3class, Lin et al. and WSM 6-class. Furthermore, the lead-time of the forecast was studied by considering simulation starting dates in April 12, 13 or 14. Figure 4a shows that none of the schemes can predict accurately the storm event, as there is a lag between the observed and simulated rainfall storm peaks (i.e. WRF forecasts this storm peak 48 h before it takes place). This issue is also identified from the values of IoA (refined Index of Agreement) for different lags (Figure 4b).

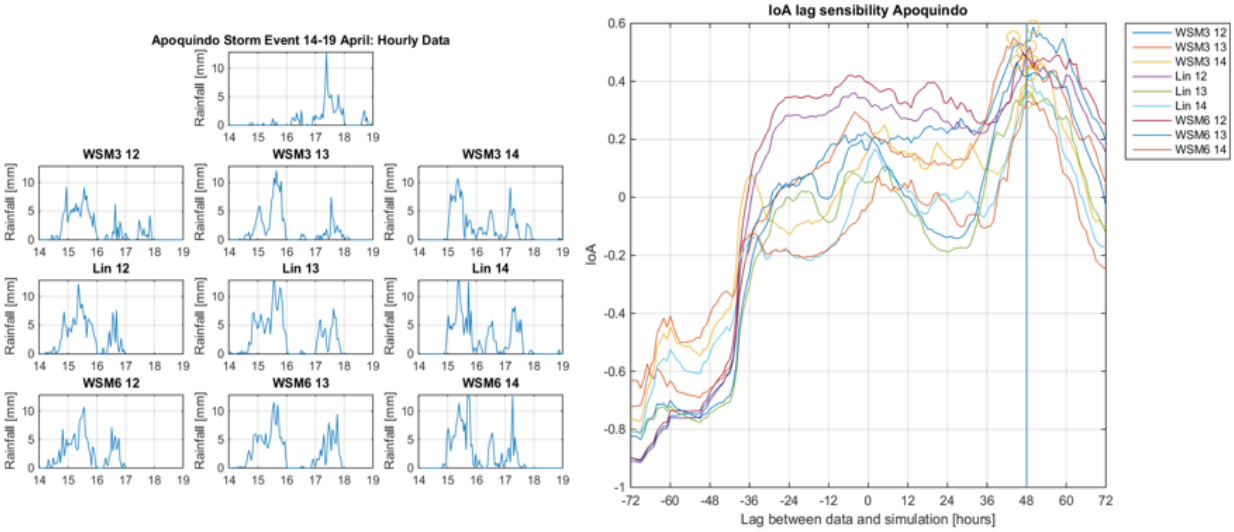

Figure 4. (a) Observed and forecasted ensemble rainfall time series. (b) IoA index sensitivity to lag between observations and simulated data. The maximum IoA value for all ensemble members is reached 48 hours after, i.e., WRF forecast the storm peak 2 days before.

This WRF shortcoming is relevant even when the whole ensemble is considered, making clear that the precipitation event model prediction is 48 hours out of phase. With a 1 mm threshold in hourly rainfall definition, the complete ensemble was analysed in Apoquindo gauge, considering that WRF predicted a rainy hour whenever the probability of rain occurrence exceeded 0.5 for the ensemble (Figure 5).

The definition of probable rainy events doesn't improve using the whole ensemble rather than choosing only one scheme as the optimal: this lag is explained on account of the precipitation event complex configuration. Temperature in Apoquindo gauge is poorly estimated before the main rainfall event (i.e. there are differences of 4°C). However, this error reduces significantly during the storm, as the observed temperature series often runs between the 25th and 75th percentiles of the ensemble (Figure 5).

Despite WRF poorly predicts the dynamics of this storm event, the duration and total rainfall amount were properly simulated using the Lin and WSM6 schemes, due to its refined treatment of microphysics processes. Figure 6 shows the cumulative precipitation during the consecutive rainiest N-hours (N=1, 2... 10), (Figure 6a), and the corresponding mean absolute error (MAE) of the temperature (Figure 6a). Note that the Lin and WSM6 schemes started in April 13 and 14 perform very well in simulating the cumulative amount of precipitation in consecutive hours. Here the errors were smaller than 15% (Figure 6a). Moreover, the schemes also predict the concurring temperatures with a MAE smaller than the 2°C tolerance threshold (dashed line, Figure 6b).

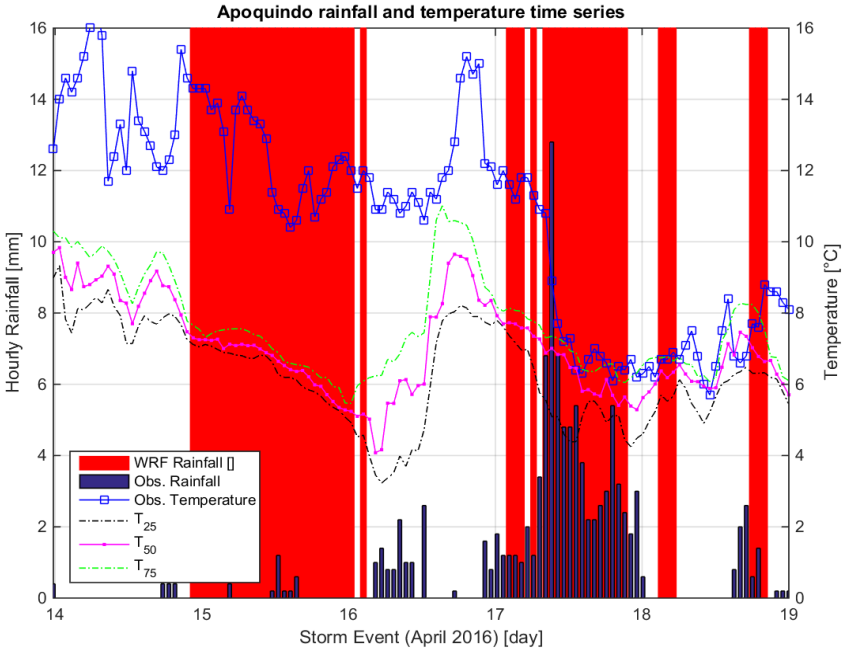

Figure 5. Apoquindo's observed rainfall and temperature time series. Red stripes indicate rain as the probability of having rain in the ensemble exceeds 0.5. Temperature time series includes 25, 50 and 75 percentiles for the ensemble forecast

This is relevant as the proper simulation of temperature is critical in the prediction of occurrence of liquid or solid precipitation in mountainous regions. The vertical blue line in Figures 6a and 6b marks the time of concentration of the Quebrada de Ramón watershed (approximately 5 h). This time is very relevant as it corresponds to the time at which the entire watershed is contributing to the runoff. Thus, these simulations eventually would allow having good estimations of the flow discharges, which in turn facilitates the implementation of an early warning system.

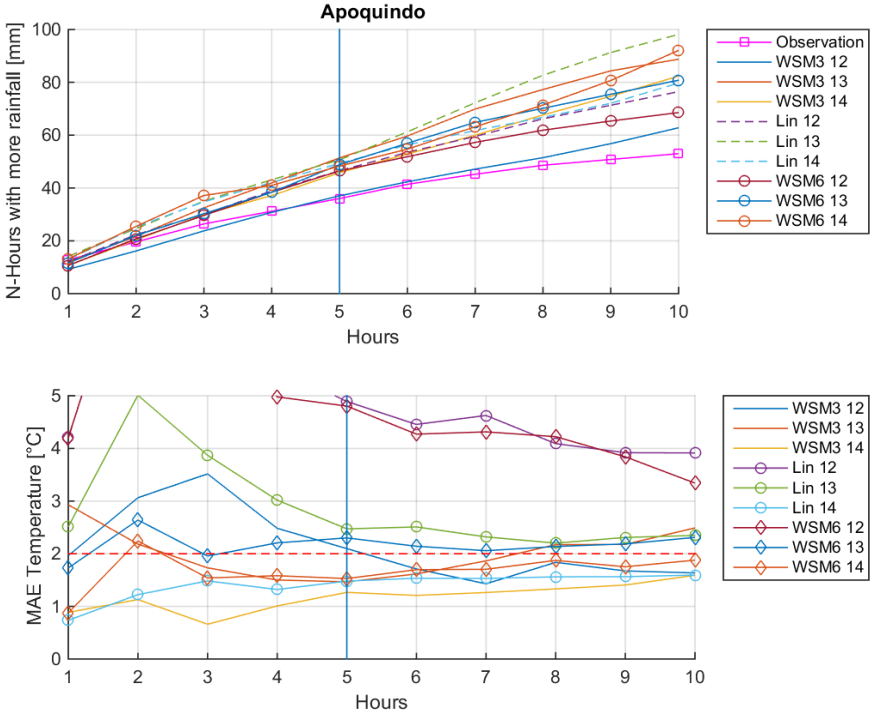

Figure 6. Observed and simulated cumulative precipitation during the consecutive rainiest N-hours (a). Corresponding mean absolute error for the simulated temperature (b). The vertical blue line corresponds to the time of concentration (~5h) of Quebrada de Ramón watershed, while the vertical dashed line at 2°C represent tolerance threshold.

5. CONCLUSIONS

This work presents the use of WRF to forecast extreme precipitation in an Andean region with complex topography. The model predicts the storm and its beginning with 48 hours lag in its peak. The previous was despite the microphysical scheme used, with obvious differences in rain amounts. WRF simulated successfully the cumulative precipitation for the rainiest N-hours of the storm together with the concurring temperature during these hours.

In addition, the microphysics ensemble proved that Lin et al. and WSM 6-class schemes provided more realistic amounts of rainfall, even when overestimation occurred sometimes. Let us recall that these schemes presented a refined treatment of the rain processes. More investigation is needed to assess WRF and improve its parameterization to properly represent the time development of rainfall events in highly complex reliefs. These additional researches could include more storms in the same area or additional downscaling techniques.

REFERENCES

EM-DAT, 2016. The International Disaster Database, Centre for Research on the Epidemiology of Disasters (CRED), School of Public Health, Université Catholique de Louvain, Belgique

Ekström, M, 2016. Metrics to identify meaningful downscaling skill in WRF simulations of intense rainfall events, Environmental Modelling & Software 79, 267-284.

Evans, J. P., M. Ekstrom, and F. Ji, 2012: Evaluating the performance of a WRF physics ensemble over South-East Australia. Climate Dyn., **39**, 1241–1258.

Dimitrova, R., Silver, Z., Zsedrovits, T., Hocut, C. M., Leo, L. S., Di Sabatino, S., & Fernando, H. J., 2015. Assessment of Planetary Boundary-Layer Schemes in the Weather Research and Forecasting Mesoscale Model Using MATERHORN Field Data. Boundary-Layer Meteorology, 1-21.

Katragkou, E., García-Díez, M., Vautard, R., Sobolowski, S., Zanis, P., Alexandri, G., Cardoso, R. M., Colette, A., Fernandez, J., Gobiet, A., Goergen, K., Karacostas, T., Knist, S., Mayer, S., Soares, P. M. M., Pytharoulis, I., Tegoulias, I., Tsikerdekis, A., and Jacob, D., 2015. Regional climate hindcast simulations within EURO-CORDEX: evaluation of a WRF multi-physics ensemble, Geosci. Model Dev., 8, 603-618, doi:10.5194/gmd-8-603-2015.

Kim, J.-H., D.-B. Shin, and C. Kummerow, 2013: Impacts of a priori databases using six WRF microphysics schemes on passive microwave rainfall retrievals. J. Atmos. Oceanic Technol., 30, 2367–2381, doi:10.1175/JTECH-D-12-00261.1.

Peña, H., 2016. Desafíos de la seguridad hídrica en América Latina y el Caribe, Comisión Económica para América Latina y el Caribe (CEPAL), LC/L.4169, Santiago de Chile

Saide, P.E., Carmichael, G.R., Spak, S.N., Gallardo, L., Osses, A.E, Mena-Carrasco, M.A., Pagowski, M., 2011. Forecasting urban PM10 and PM2.5 pollution episodes in very stable nocturnal conditions and complex terrain using WRF–Chem CO tracer model, Atmospheric Environment, 45(16), 2769-2780.

Ruiz, J. J., C. Saulo, and J. Nogués-Paegle, 2010: WRF Model sensitivity to choice of parameterization over South America: Validation against surface variables. Mon. Wea. Rev., 138, 3342–3355, doi:10.1175/2010MWR3358.1.

Proceedings of the 10th World Congress of EWRA 'Panta Rhei', 5-9 July 2017, Athens, Greece
© 2017 *European Water Resources Association*

Impact of climate change on irrigation need and groundwater resources in Pinios Basin

A. Panagopoulos[1*], F. Herrmann[2], V. Pisinaras[1] and F. Wendland[2]
[1] *Hellenic Agricultural Organization, Soil and Water Resources Institute, 57400 Sindos, Greece*
[2] *Forschungzentrum Juelich GmbH, Agrosphere Institute (IBG-3), D-52425 Juelich, Germany*
[*] *e-mail: panagopoulosa@gmail.com*

Abstract: Initially an area-differentiated modelling of groundwater recharge in River Pinios Basin (Greece) was carried out for the reference period 1980–2000 based on the mGROWA model using daily precipitation data from 57 meteorological stations and average temperature data from 17 stations as climatic input data. After checking the plausibility of the related model results the model was applied to assess the impacts of climate change on groundwater recharge. For this purpose bias-corrected projected climate data from an ensemble of climate models driven by several general circulation models for the projected periods 2020–2050 and 2050–2080 have been used as input data. Results of all RCM–GCM combinations indicate a considerable decrease in groundwater recharge with variable rates between the applied projected periods.

Key words: water balance, climate change impact assessment, water availability

1. INTRODUCTION

Pinios Basin is considered as one of the highest productive regions of the country, located in Thessaly (central Greece) with total surface area of approximately 11.000 km^2. In the plain areas of Pinios Basin, intensive agricultural activities have frequently led to environmental pressures related to water resources. According to the latest official water resources management plans that were compiled in accordance to the WFD, a number of characterized water systems within the basin have been assessed as being either at risk of becoming at poor status, or are already at poor status (Hellenic Ministry for the Environment, Energy and Climate Change, 2014). Over 85% of the totally available water resources (both surface and groundwater) are used by agricultural activities. Groundwater levels are strongly controlled by the seasonal exploitation of the resources over the summer irrigation period, mainly exercised by numerous shallow but mainly deep wells that reach 400m.

Due to lack of coordinated water resources management policies in the past, signs of over-exploitation were documented and a notable negative water balance has been established in the last 3 decades (Alexandridis et al., 2014). In an attempt to restore documented quality and quantity issues, the Hellenic Special Secretariat for Water has approved an integrated management plan for the river basin (Hellenic Ministry for the Environment, Energy and Climate Change, 2014). Nevertheless, a detailed and updated area differentiated quantification of the renewable total water quantities (i.e. total runoff) and groundwater quantities (i.e. groundwater recharge) respectively, has not been provided so far although these water quantities are needed for the implementation of a sustainable water resources management plan, which adapts water use and demand to the renewable water quantities. This lack of information is attempted to be covered via the application of two water balance models in Pinios river basin, i.e. GROWA (Kunkel & Wendland, 2002) and mGROWA (Herrmann et al., 2015).

The first goal, the GROWA application, is the determination of the mean long-term renewable water quantities, i.e. the runoff distributions (status quo analyses) and their further development until 2080 (climate change impact assessment). The second goal, the mGROWA application, is the

consideration of the inner-annual variability of renewable water quantities and their further development. This issue has become more important during the last years with regard to the assessment of the impact of both, the actual climate and climate change on the available water resources. The consideration of the inner-annual distribution of water quantities can be regarded as a prerequisite for both, adapting the actual water management in Pinios river basin to the inner-annual variability of renewable water quantities and taking the climate change induced development of the inner-annual available water volumes into account for the implementation of a sustainable water resources management plan, which adapts future water use and demand to the renewable water quantities.

2. STUDY AREA

Pinios Basin is characterized by highly diversified geological, hydrological and hydrogeological conditions. The climate is typical Mediterranean (Alexandridis et al., 2014). Mean annual precipitation is 791mm and mean annual temperature is 14.6 °C. Precipitation is distributed mostly during the cold season, without any significant precipitation during the hot summer at the plains of the basin.

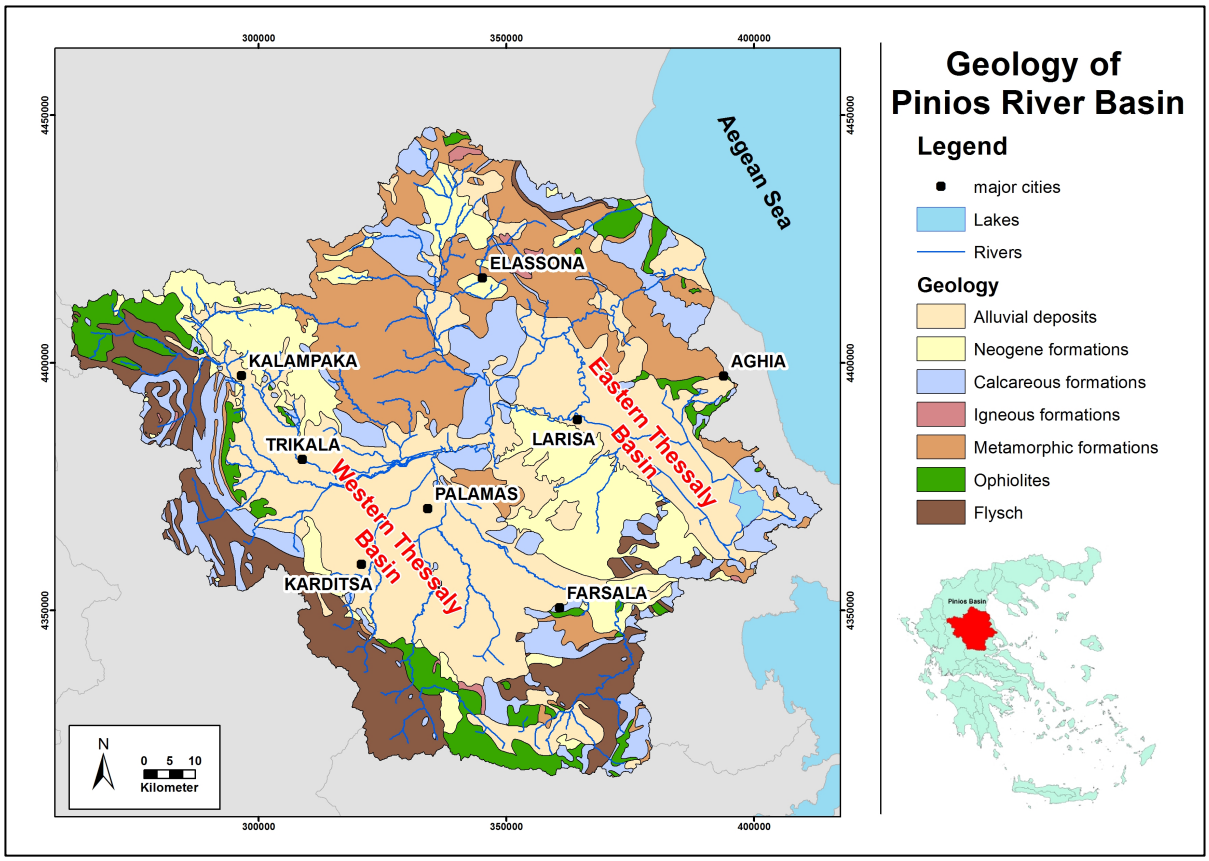

Figure 1. Geological regime of Pinios River Basin

The wider region is tectonically active and fault and fold tectonics control its geological evolution (Figure 1). A rugged topographic relief that reaches altitudes of over 2000m bounds the basin, whereas the plains are characterized of quasi-flat topographic surfaces that extend from almost 200m down to the sea-level. Geologically, the area is structured by metamorphic rocks of the alpine orogeny. Extensive outcrops of schists and karstified limestones and marbles delineate the plains and form the bedrock of the basin, whereas ophiolites of considerable spatial extent also exist, predominantly along the western and southeastern margins. The high degree of karstification of the carbonate rocks give rise to extensive aquifers of high potential that control the

hydrogeological evolution of the region through numerous springs and lateral crossflows that recharge the alluvial aquifer systems of the plains. Groundwater resources exploitation is focused on the two main and the smaller peripheral alluvial basins, and also on the karstified systems. Surface water from the rich hydrologic network cover considerable part of irrigation demands especially at the western plain of the basin.

3. METHODOLOGY

GROWA is an empirical model, which displays a minimal temporal resolution of one year (Kunkel & Wendland, 2002). It has been used in numerous water balance studies in and outside Germany since the beginning of the 2000s (Wendland et al., 2003; Herrmann et al., 2009; Panagopoulos et al., 2015). The mGROWA model (Herrmann et al., 2015) emerged from the water balance model GROWA and can be classified as a deterministic grid-based distributed hydrological water balance model. This implies a description of hydrological processes reflecting the fundamental laws of physics (in particular hydro- and thermodynamics) in a simplified, approximate manner. In addition this concept involves in general a certain degree of empiricism. mGROWA has been developed for determining water balance variables including groundwater recharge in large areas (river basins, Federal States etc.) under present and possible future climate conditions. The mGROWA modelling concept was rigorously aligned to both, the spatial resolution of the data commonly available for hydrological modelling and the necessity to obtain spatially and temporally highly resolved patterns of water balance variables for the local and regional groundwater management.

Within the basic part, the hydrological processes at the earth's surface and in the root zone of soil are simulated. In particular, soil moisture dynamics including percolation water movement, capillary rise from groundwater to the root zone, actual evapotranspiration and total runoff generation are calculated in daily time steps. For the simulation of soil moisture dynamics, the multi-layer soil water balance model BOWAB (Engel et al., 2012) is integrated. Herein, the common water balance equation is solved. Grass reference evapotranspiration is calculated using the Penman-Monteith-equation (Allen et al., 1998) and soil moisture dependency of evapotranspiration is considered by the Disse-equation (Disse, 1995). Additionally, mGROWA calculates the water balance for impervious surfaces (e.g. sealed surfaces in urban areas) and open water surfaces using approaches adapted to the specific storage characteristics.

4. RESULTS

4.1 GROWA model results for reference period 1980-2002

Water balance modeling was performed based on a series of long-term average climatic and hydrological data for a reference period of 23 years (1980-2002) and in a spatial resolution of 100 by 100 m. Results for total runoff are illustrated in Figure 2, from which it can be seen that average annual total runoff levels vary between < 50 mm/a and > 1000 mm/a. Overall, a decrease trend is captured from the mountainous to the plains areas and also from the west to the east, which is in good agreement with the analyzed distribution of precipitation and evapotranspiration. In general, low levels of total runoff (less than 200 mm/y) occur at nearly 70% of the total Pinios basin.

The reliability of the calculated area-differentiated runoff levels was validated by comparing real long-term (measured) discharge values with the ones calculated by GROWA model for 12 gauging stations that exhibit a fair spatial distribution over the study area. The measure of validity was based on the coefficient of determination (R2) between these two values which is nearly 0.92 indicating satisfactory matching between observed and simulated discharge values.

4.2 GROWA model results for climate change impact assessment until 2080

Against the background of the good model performance for the actual reference period, GROWA has been applied in order to assess the potential impacts of climate change in the hydrologic regime of Pinios River basin. For this purpose GROWA model was applied with bias-corrected precipitation and temperature data from four regional climate models (RCMs) for the projected periods 2020–2050 (period A) and 2050–2080 (period B). Bias correction was performed using the linear scaling approach. Following, four RCMs from the various models of ENSEMBLES project (van der Linden & Mitchell, 2009), under A1B scenario have been applied: a) HIRHAM5, hereafter referred as HA driven by ARPEGE GCM, b) RACMO2, driven by ECHAM5 GCM, c) REMO, hereafter referred as REE, driven by ECHAM5 GCM and d) RCA3, hereafter referred as RH, driven by HadCM3 GCM. The performance of the aforementioned RCM-GCM combinations were found to be adequate for the representation of precipitation and temperature variation in several Mediterranean basins (Deidda et al., 2013).

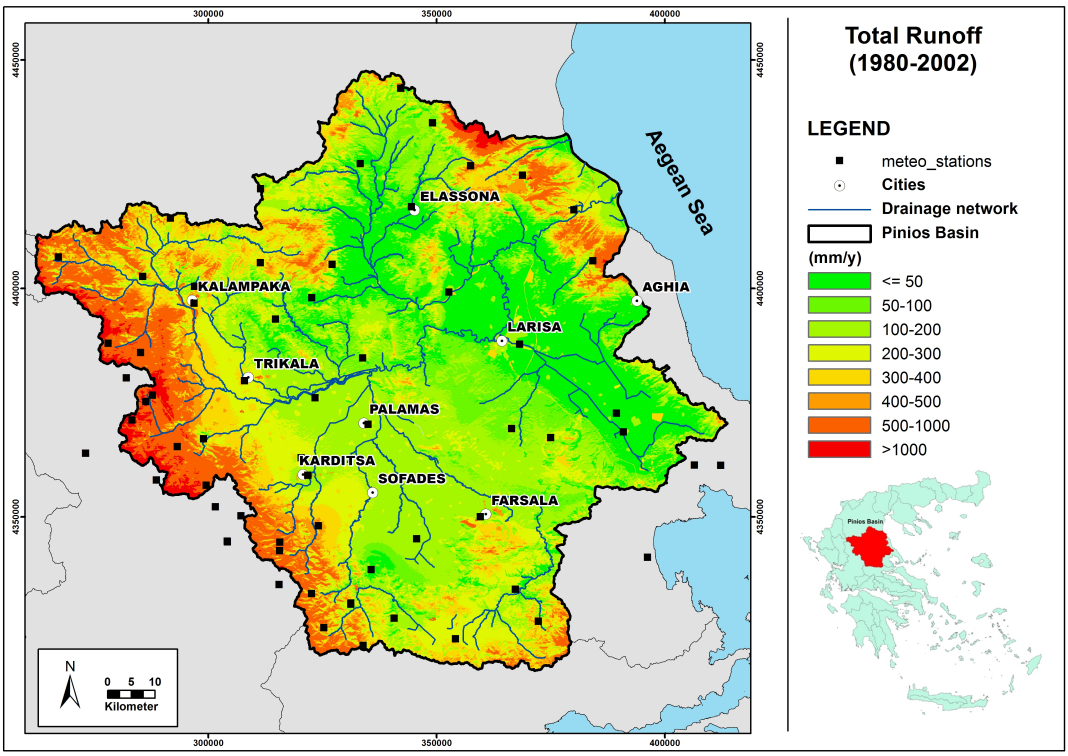

Figure 2. Average annual total runoff in Pinios River basin for the period 1980-2002 based on GROWA

Evaluation of climate data for the actual reference period has shown that mean annual precipitation is 791 mm and mean annual temperature is 14.6°C (see red columns in Figure 3). For both projection periods considered, all projections indicate increment in mean annual temperature and decrement in mean annual precipitation, except from RH models, which indicate for period A an increment in mean annual precipitation by 85 mm (or 12%) when compared to the reference period and a negligible change for period B when compared to the corresponding value for the reference period (see Figure 3).

The impact of the changes in precipitation and temperature on total runoff are shown in Figure 4. Results showed that all RCM–GCM combinations lead to a considerable decrease in total run-off (Qt) with variable rates between the examined projected periods. With simulated climatic data input from HA, RA, and REE, a significant impact to the overall water budget is forecasted, as the total amount of Qt is decreased by 46 to 66% until 2080. On the contrary, when Qt was simulated with climatic data from RH, smoother rates were exhibited due to smaller variations of precipitation and

temperature from the reference period and the relevant Qt reduction by the end of the projection (2080) is 22% only. Generally, the relevant variations in Qt values are greater during period A (compared to reference period) than in period B (compared to period A). In this way, the greatest reduction of Qt (62%) from the reference period was forecasted for period A (2020–2050), and was simulated when GROWA model run with input data from HA model, which indicated greater decrements in precipitation and increments in temperature. On the contrary, projected Qt results with RH models input are by far more optimistic compared to the other three models, and the final overall decrement is significantly smaller (22%) with nearly constant variation rate for both projection periods.

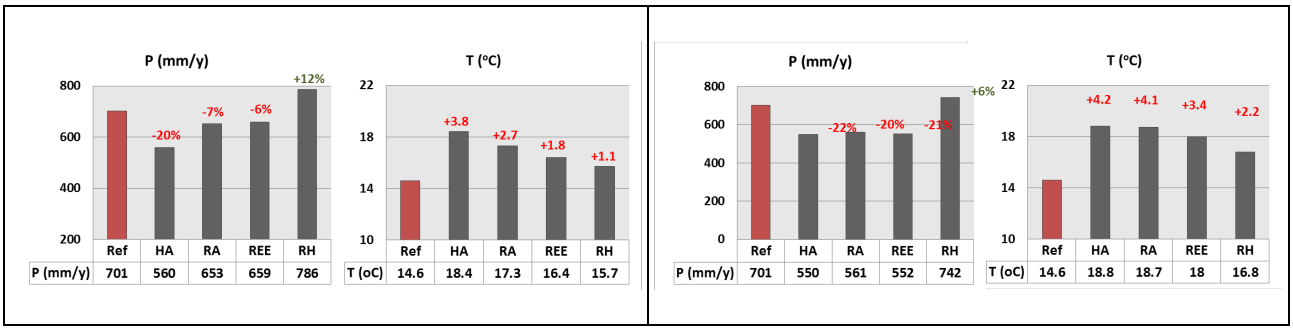

Figure 3. Projections of mean annual precipitation and mean annual temperature for period A (2020-2050, left) and period B (2050–2080, right)

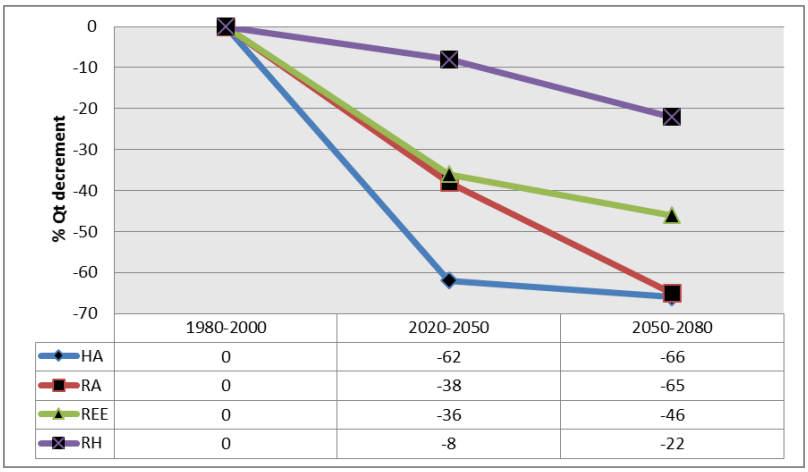

Figure 4. Percentages of Qt decrement for four RCM–GCM combinations in respect to the reference period.

Due to the limited temporal resolution of the GROWA model, the inner annual variability of runoff generation and groundwater recharge is not represented. Therefore, possible shifts or shortenings of the runoff and groundwater recharge generation periods and quantities within one year cannot be represented. The consideration of inner annual shifts or shortenings however, is an important prerequisite in order to support and justify reliable recommendations for adapting the regional (ground-) water management to the changed inner-annually available water volumes. In order to analyze how far runoff generation and the available water resources are influenced by an inner annual shift / changes due to climate change (precipitation, temperature), runoff generation simulations have been repeated based on the mGROWA model.

4.3 Preliminary mGROWA model results for reference period 1971-2000

For the Pinios river basin a grid size of 100 m (1 hectare) was chosen for the mGROWA simulations, whereas all input parameters remained unchanged with the exception of the climate

data which was applied in daily time steps. Mean monthly based total runoff levels are shown in Figure 6 for the observed reference period 1971-2000.

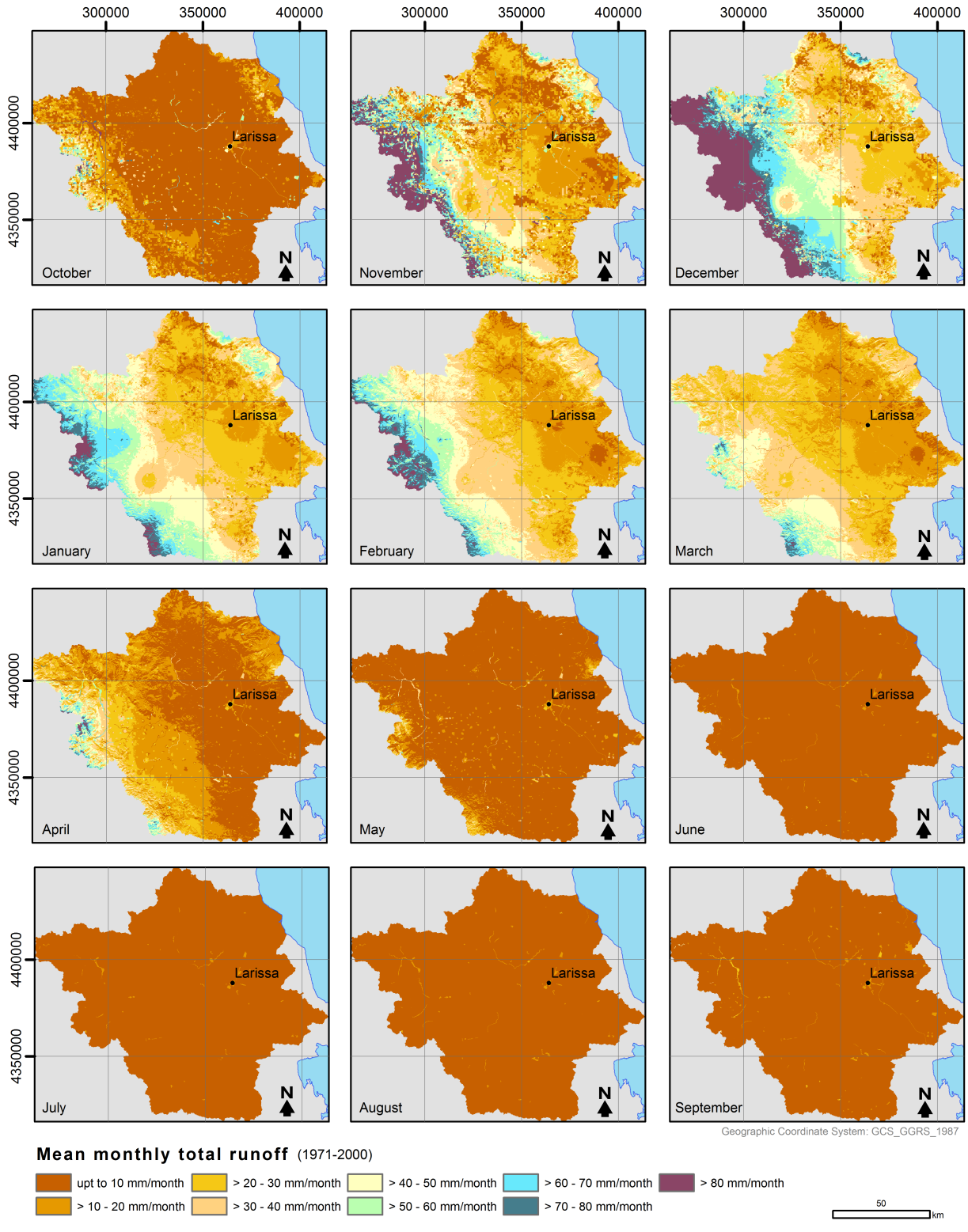

Figure 6. Average simulated monthly net runoff levels (1980-2002) based on mGROWA

Due to the pronounced spatial gradients of decreasing precipitation and increasing reference evapotranspiration from the mountainous areas to the plains, total runoff levels in the basin generally decrease in the same direction. Hence, runoff levels >400 mm/a only occur in the mountainous regions (especially along the western-southwestern part of the basin), whereas runoff

levels in the plains of the basin are significantly lower. With regards to the inner-annual variability, Figure 5 shows that runoff generation is restricted to the period November to March, whereas runoff generation in the rest of the year is negligible.

5. CONCLUSIONS AND OUTLOOK

GROWA model results provide a reasonable overview of the actual mean water availability and its projected evolution towards a reduced water budget. The temporally high resolution mGROWA results demonstrate that at present runoff generation is restricted to the periods November to March. In order to analyze shifts / shortenings of the inner-annual runoff generation periods it is foreseen to run the mGROWA model based on climatic input data from RCMs in high temporal resolution.

In the context of climate change impact assessments, the mGROWA model results can be of utmost importance, as they provide a representative measure for the available water quantities under climate change conditions. The projected climate effects on runoff generation can be used for the long-term strategic planning of water resources as they are an appropriate framework to design and implement an integrated set of measures in the direction of adaptation and preparedness, so that the anticipated impacts from climate change can be minimized and controlled in due time.

Presented model results should not conceal the fact that there is lack of input data, the existence of which would improve the robustness of assessed water quantities implementation of regionally adapted and efficient water management strategies. Lack of reliable time series from the existing runoff monitoring network reduces the accuracy of the quantified renewable water resources. So does the existence of only one climate station (Larissa station) within the basin equipped with the sufficient sensors from which data can be used to perform potential evapotranspiration calculations using accurate methods. Moreover, lack of vegetation specific parameters additionally impedes the model-based determination of actual evapotranspiration rates with high accuracy.

Against this background it is part of the overall strategy of a research cooperation between the Hellenic Agricultural Organization, Soil and Water Resources Institute and Forschungzentrum Juelich GmbH, Agrosphere Institute (IBG-3) to set up a hydrologic observatory in Agia basin, a 10 km^2 sub-catchment of Pinios River basin. In this test site state-of-the-art devices are installed with the aim to improve the climatic data base, to determine vegetation specific evapotranspiration parameters and to quantify the lateral groundwater inflow into the basin from adjacent mountainous areas. The parameters derived and lateral groundwater flow rates assessed with the help of the state-of-the-art devices will then additionally be used in the entire Thessaly basin, e.g. in the model-based assessment of sustainably available water resources based on the mGROWA model.

REFERENCES

Alexandridis T.K., Panagopoulos A., Galanis G., Alexiou I., Cherif Y., Chemin Y., Stavrinos E., Bilas G., Zalidis G.C. (2014): Combining remotely sensed surface energy fluxes and GIS analysis of groundwater parameters for irrigation system assessment. Journal of Irrigation Science, 32, 127-140.

Allen R.G., Pereira L.S., Raes D., Smith M. (1998): Crop evapotranspiration - Guidelines for computing crop water requirements. FAO - Food and Agriculture Organization of the United Nations.

Deidda R., Marrocu M., Caroletti G., Pusceddu G., Langousis A., Lucarini V., Puliga A., Speranza A. (2013): Regional climate models' performance in representing precipitation and temperature over selected Mediterranean areas. Hydrology and Earth System Sciences, 17(12), 5041-5059.

Disse M., 1995. Modellierung der Verdunstung und der Grundwasserneubildung in ebenen Einzugsgebieten. Fakultät für Bauingenieur- und Vermessungswesen der Universität Fridericiana zu Karlsruhe.

Engel N., Müller U., Schäfer W. (2012): BOWAB - Ein Mehrschicht-Bodenwasserhaushaltsmodell. GeoBerichte - Landesamt für Bergbau. Energie und Geologie, 20, 85-98.

Hellenic Ministry for the Environment, Energy and Climate Change-Special Secretariat for Water (2014): Compilation of Management Plan for the River Basins of Thessaly Water district (GR08)-Management Plan. Athens, 252 p.

Herrmann F., Jahnke C., Jenn F., Kunkel R., Voigt H-J., Voigt J., Wendland F. (2009): Groundwater recharge rates for regional groundwater modelling: a case study using GROWA in the Lower Rhine lignite mining area, Germany. Hydrogeology Journal, 17-8, 2049 – 2060.

Herrmann F., Keller L., Kunkel, R., Vereecken H., Wendland F. (2015): Determination of spatially differentiated water balance components including groundwater recharge on the Federal State level – A case study using the mGROWA model in North Rhine-Westphalia (Germany). Journal of Hydrology: Regional Studies, 294-312.

Kunkel R., Wendland F. (2002): The GROWA98 model for water balance analysis in large river basins - the river Elbe case study. Journal of Hydrology, 259, 152-162.

Panagopoulos A., Arampatzis G., Tziritis E., Pisinaras V., Herrmann F., Kunkel R., Wendland F. (2016): Assessment of climate change impact in the hydrological regime of River Pinios Basin, central Greece. Desalination and Water Treatment, 57(5), 2256 – 2267.

van der Linden P., Mitchell J.F.B. (2009): ENSEMBLES: Climate Change and its Impacts: Summary of Research and Results from the ENSEMBLES Project. Met Office Hadley Centre, UK, p. 160.

Wendland F., Kunkel R., Tetzlaff B., Dörhöfer G. (2003): GIS-based determination of the mean long-term groundwater recharge in Lower Saxony. Environmental Geology, 45, 273-278.

Proceedings of the 10th World Congress of EWRA 'Panta Rhei', 5-9 July 2017, Athens, Greece
© 2017 *European Water Resources Association*

Investigations of trends in meteorological time series

M. Zeleňáková[1*], P. Purcz[2], D.C. Diaconu[3], B. Pius[4], H. Hlavatá[5] and M.M. Portela[6]
[1] *Department of Environmental Engineering, Technical University of Košice, Košice, Slovakia*
[2] *Department of Applied Mathematics, Technical University of Košice, Košice, Slovakia*
[3] *Department of Meteorology and Hydrology, University of Bucharest, Bucharest, Romania*
[4] *Department of Hydrology and Water Management, Nicolas Copernicus University, Toruń, Poland*
[5] *Slovak Hydrometeorological Institute, Košice, Slovakia*
[6] *Department of Civil Engineering, Technical University of Lisboa, Lisboa, Portugal*
[*] *e-mail: martina.zelenakova@tuke.sk*

Abstract: The present study performs the temporal trend analysis of the meteorological variables time-series in chosen climatic stations in Poland, Slovakia and Romania during period of 1962 (1967 in Poland)–2015. Climatic stations are situated in Carpathian Mountains area which has a humid continental climate with cold winters, no dry season, warm summers and strong seasonality. The Carpathians consist of a chain of mountain ranges that stretch in an arc from the Czech Republic (3%) in the northwest through Slovakia (17%), Poland (10%), Hungary (4%) and Ukraine (11%) to Romania (53%). The highest range within the Carpathians is the High Tatras, on the border of Slovakia and Poland, where the highest peaks exceed 2,600 m. The second-highest range is the Southern Carpathians in Romania, where the highest peaks exceed 2,500 m. Trend of long-term data of average temperature, precipitation, relative humidity and wind speed were investigated. The Mann–Kendall (MK) test and the Theil–Sen approach (TSA) were applied to quantify the significance of trend and magnitude of trend. Prior to the application of statistical tests, the pre-whitening technique was used to eliminate the effect of autocorrelation of precipitation data series. The application of the above-mentioned analysis has shown significant increasing trend mainly for temperature in the study area. The other investigated variables have shown increasing as well decreasing trends, but not significant at significance level of 95%.

Key words: precipitation; temperature; relative humidity; wind speed; Mann Kendall test

1. INTRODUCTION

The detection of trends in meteorological data is essential for the assessment of the impacts of climate variability and change on the water resources (Sarkar et al., 2012). The major possible effects of climate change may include variability in water resources, increase desertification, loss of biodiversity and changes in agricultural productivity (Burlando and Rosso, 2002). Changes in precipitation patterns are very important for water resources managers to deal with the water resources planning and management. Variations in precipitation over daily, seasonal, annual, and decadal timescales influence water resource systems (Ampitiyawatta and Shenglian, 2009). The recent emphasis on integrated catchment planning and unifying EU directives has led to considerable research interest in the study of hydrology systems and climate. The major pressures on the European water are water pollution, water scarcity (including droughts), floods and modification to water bodies (Tsakiris, 2015).

The objective of presented study is to investigate trends in meteorological time series in climatic stations in Carpathians, exactly in Poland, Slovakia and Romania. Annual and seasonal trends in average temperature, precipitation, relative humidity and wind speed were detected by Mann-Kendall statistical test.

The Carpathians climate change was investigated eg. in Hlásny et al. (2016). They strived to identify the main regional climate change hot-spots and evaluate the distribution of climatically exposed land-use types and ecosystems. The authors adopted a methodology based on change trajectories in a multidimensional climate space. Three hot-spots were in the Western Carpathians

(Czech Republic, Slovakia, and Hungary), two were in Ukraine, and three were in the Romanian and Serbian Carpathians. Analysis of inter-climate model variability indicated that the level of confidence in hot-spot position and magnitude differed among hot-spots. In addition to identifying a large-scale regional pattern of climate change, their results showed that there are sub-regions with remarkably high climate exposure. The hot-spot distribution in lower elevations suggests that Carpathian ecosystems in water-limited environment may be particularly exposed to climate change.

2. STUDY AREA

The situation of the Carpathians (Fig. 1), on the boundary line between western and eastern Europe, is reflected in the features of their climate, which in winter is governed by the inflow of polar-continental air masses arriving from the east and northeast, while during other seasons oceanic air masses from the west predominate.

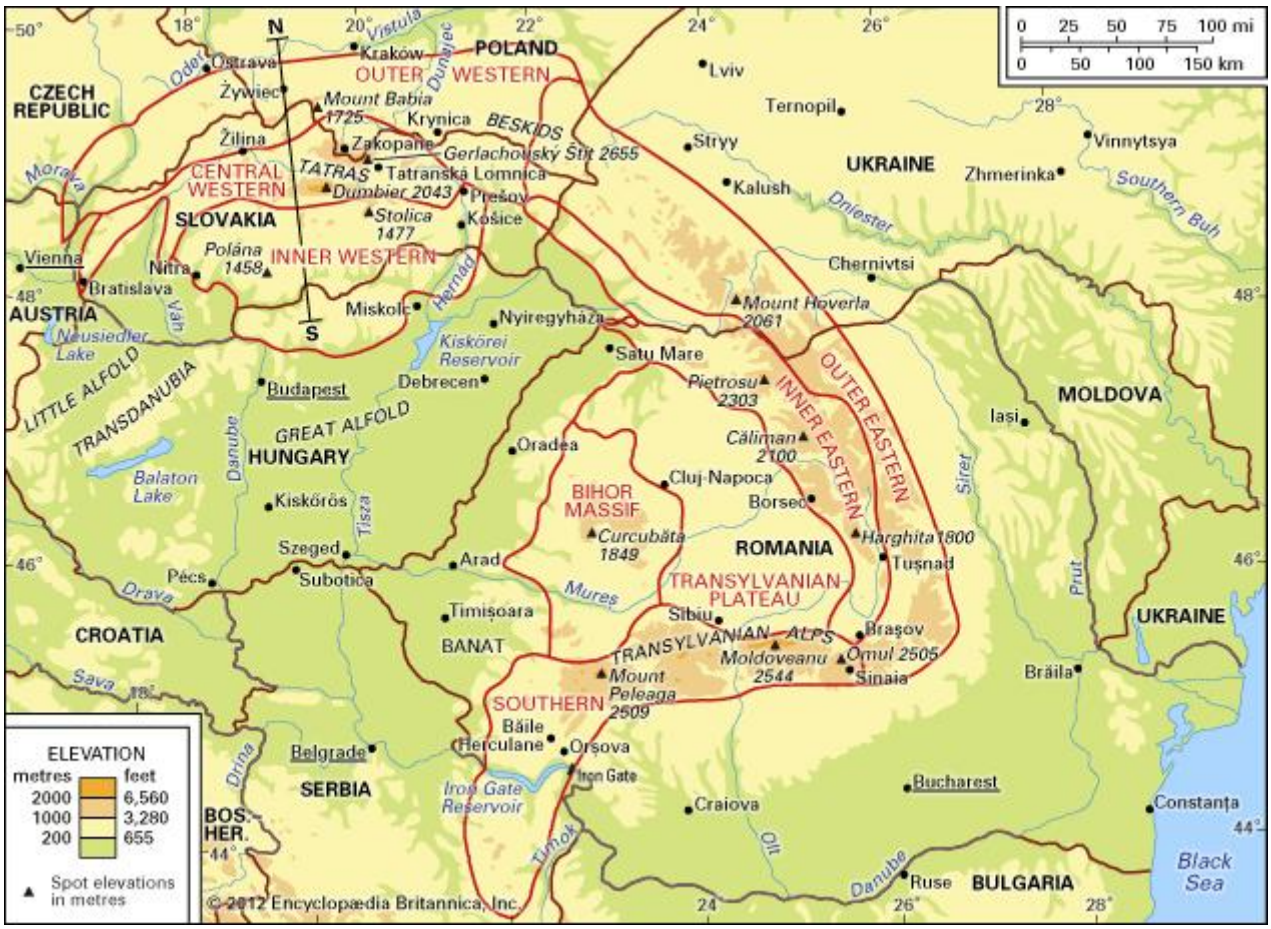

Figure 1. Regional division of the Carpathian Mountains (Encyclopedia Britannica, Inc.).

The Carpathians thus possess certain features of a continental climate, although from the viewpoint of relief they constitute a sort of island amid the surrounding plains, where the climate is much drier. In winter, temperature inversion, in which the low depressions retain very cold air while the mountaintops show relatively high temperatures, is a common occurrence throughout the Carpathians. In some depressed areas, notably the Transylvanian Plateau, the total annual precipitation is less than 24 inches (600 millimetres), while precipitation in the mountains at 2,600 feet (800 metres) above sea level is about 45 inches, and on the highest massifs it reaches 65 to 70 inches. The mean annual and monthly air temperatures vary according to altitude above sea level but by no means at constant rates (Kondracki, 2009).

For the Polish part of the Carpathians, a series of climatic types and stages has been distinguished; and with slight modification these may be applied to the whole Carpathian mountain range. The range of mean temperatures is 6 °C in the northeast to 10 °C in the southwest, but individual readings in Poland's regions vary widely by season. On the highest mountain peaks, the mean temperature is below 0 °C. The average annual precipitation for the whole country is 600 mm (23.6 in), but isolated mountain locations receive as much as 1,300 mm (51.2 in) per year. In winter about half the precipitation in the lowlands and the entire amount in the mountains falls as snow (IMGW, 2005). Among the geographical factors influencing Poland's climate, it is relief that plays the most important role. Its impact manifests itself in the spatial variability to air temperature, solar radiation and precipitation between various parts of Poland (Błażejczyk and Matzarakis, 2007). An interesting results regarding the climate change especially in Poland we can found in (Kaczmarek, 2003; Kundzewicz et al., 2005; Przybylak et al., 2005; Lupikasza, 2010; Gadek and Leszkiewicz, 2012; Bogawski and Bednorz, 2014 Marszelewski and Pius, 2016) and many others.

The territory of Slovakia is in the light of global climate classification in the northern temperate climatic zone with a regular alternation of four seasons and variable weather, with a relatively even distribution of rainfall throughout the year. In Slovakia, according to the Slovak Hydrometeorological Institute (SHMI), are sometimes in average less than 600 mm of precipitation per year. Temperature conditions of Slovakia are diverse and vary from place to place thanks to a relatively large variability of altitude. The lowest air temperature in the period 1961-2010 was as low as -36.0 °C in Plaveč (1963) and the highest air temperature in the same period was as high as -36.0 °C in Hurbanovo. The minimum value of the relative air humidity is most frequently measured in April, which is related to the quick rise of the air temperature and frequent outbreaks of cold air masses with a low amount of water vapour to Slovakia. In the summer the relative air humidity reaches its annual maximum mostly in the mountains. The highest values of annual average wind speed in the interval 5.5 – 9.5 $m.s^{-1}$ were recorded in the top parts of the mountains alongside the Carpathians belt. The mean annual wind speed in the lowlands in Slovakia reaches from 2.5 to 3.5 $m.s^{-1}$. Conditions of the general circulation of the atmosphere in winter half-year cause an increase of windiness in most parts of Slovakia with a maximum in spring; in the summer half-year the windiness is smaller (SHMI, 2015). The climate in Slovakia was investigated in Hlavcova, et al. (2002); Vojtek et al. (2003); Pekarová and Szolgay (2005); Gaál et al. (2012); Lapin et al. (2012); Štefunková et al. (2014); Velísková et al. (2014); Portela et al. (2015); Zeleňáková et al. (2015); Čistý et al. (2016) and others.

Romania has a climate which ranges from temperate to continental. The average annual temperature is 11 °C (51.8 °F) in the south and middle-south and 8 °C (46.4 °F) in northeast. Rainfall receive more than 1,010 mm (39.8 in) of precipitation each year in mountainous areas. Annual precipitation averages are about 635 mm (25 in) in central Transylvania and only 381 mm (15 in) at Constanta on the Black Sea (Micu et al., 2014). There are many studies investigating climate and climate changes in Romania eg. Mares et al. (2005), Bîrsan et al. (2012), Croitoru et al. (2012), Croitoru et al. (2013), Prăvălie et al. (2013), Birsan (2015), Matei et al. (2016), Pintilii et al. (2017).

3. STATISTICAL ANALYSIS

The meteorological data series for trend analysis were obtained from Institute of Meteorology and Water Management in Poland (8 climatic stations), Slovak Hydrometeorological Institute (7 climatic stations) and National Institute of Meteorology and Hydrology in Romania (5 climatic stations).

The Mann–Kendall (MK) test (Kendall, 1975), (Mann 1945) is a rank-based nonparametric test for assessing the significance of a trend, and has been widely used in hydro-meteorological trend detection studies (Lettenmaier et al., 1994), (Burn, 2002), (Pauling and Paeth, 2006), (Partal and Kahya, 2006), (Sayemuzzaman and Jha, 2014) (Johnes et al., 2015).

Many tests for the detection of significant trends in meteorologic time series can be classified as

parametric and non-parametric methods. The Mann–Kendall (MK) test (Kendall, 1975), (Mann, 1945) is a rank-based nonparametric test for assessing the significance of a trend, and has been widely used in hydro-meteorological trend detection in many studies.

In this study non-parametric Mann-Kendall test is used for the detection of the trend in a time series. Mann-Kendall test is following statistics based on standard normal distribution (Z), by using Eq.(1).

$$Z = \begin{cases} \dfrac{S-1}{\sqrt{Var(S)}} & if \quad S>0 \\ 0 & \text{if} \quad S=0 \\ \dfrac{S+1}{\sqrt{Var(S)}} & if \quad S<0 \end{cases} \tag{1}$$

$$S = \sum_{k=}^{n-1} \sum_{k+i}^{n} \text{sgn}(x_j - x_k) \tag{2}$$

$$\text{sgn}\left(x_j - x_k\right) = \begin{matrix} +1 & if\,(x_j - x_k) & >0 \\ 0 & if\,(x_j - x_k) & =0 \\ -1 & if\,(x_j - x_k) & <0 \end{matrix} \tag{3}$$

$$Var(S) = \left[n(n-1)(2n+5) - \sum_{i=1}^{m} t_i(t_i-1)(2t_i+5) \right] / 18 \tag{4}$$

where n is the number of data points, m is the number of tied groups (a set of sample data having the same value).

According to this test, the null hypothesis H0 states that the depersonalized data (x_1, …, x_n) is a sample of n independent and identically distributed random variables. The alternative hypothesis H1 of a two-sided test is that the distributions of x_k and x_j are not identical for all $k, j \leq n$ with $k \neq j$. The significance level is chosen as $\alpha = 0.05$ and $Z_{\alpha/2}$ is the value of normal distribution function, in this case $Z\alpha/2 = 1.95996$. Hypothesis H0 - no trend is if ($Z < Z_{\alpha/2}$) and H1 - there is a trend if $Z > Z_{\alpha/2}$. Positive values of Z indicate increasing trends, while negative values of Z show decreasing trends.

The magnitude of the trend was determined using Sen`s estimator. Sen's method assumes a linear trend in the time series and has been widely used for determining the magnitude of trend in hydro-meteorological time series (Sen, 1968), etc. In this method, the slopes (β) of all data pairs are first calculated by

$$\beta = Median\left((x_j - x_k)/(j-k)\right) \tag{5}$$

for $i = 1, 2, ..., n$, where x_j and x_k are data values at time j and k ($j > k$), respectively and N is a number of all pairs x_j and x_k. A positive value of β indicates an upward (increasing) trend and a negative value indicates a downward (decreasing) trend in the time series.

4. RESULTS AND DISSCCUSSION

In this study, programme developed in Microsoft Excel was used to generate the algorithm of non-parametric method.

Monthly meteorological data series for the 54 years period, from 1962-2015 for Slovakia and Romania and for 49 years period, from 1967-2015, were considered for trend detection. In the Sen's

method the slope of all the data points are calculated and their median value is the Sen's estimator of slope. The trend analysis was done for the whole year from November to October (XI –X) in the study area.

Bold values in Table 1 indicate statistical significance at 95% confidence level as per the Mann–Kendall test (+ for increasing and − for decreasing).

Table 1. Meteorological time series trends in climatic stations in Carpathians region

	Climatic station	Average Temperature		Precipitation		Relative Humidity		Wind speed	
		Z	β	Z	β	Z	β	Z	β
Poland	Kielce	1,456463	0,001826	-1,25137	-0,00027	-0,49824	-0,00069	**2,195307**	**0,000284**
	Krakow	1,547663	0,001900	-1,23792	-0,00028	-1,64475	-0,00223	-0,22338	-3,5E-05
	Lodz	1,475796	0,001846	-0,62096	-0,00012	-0,88573	-0,00152	**-4,45260**	**-0,00078**
	Lublin	1,320294	0,001733	-0,38392	-7,7E-05	-1,00046	-0,00139	**-2,65635**	**-0,00041**
	Poznan	1,528330	0,001905	0,911366	0,000173	-0,67811	-0,00122	**-5,11496**	**-0,00084**
	Suwalki	1,420319	0,001946	0,463773	9,63E-05	-0,60036	-0,00089	**-6,05175**	**-0,00123**
	Torun	1,466970	0,001893	-0,16790	-3,5E-05	**-2,00324**	**-0,00346**	**-4,58919**	**-0,00050**
	Ziel_Gora	1,405190	0,001761	0,152770	3,20E-05	1,405190	0,001761	**-2,58448**	**-0,00033**
Slovakia	Bratislava	**1,829910**	**0,002083**	-0,01924	-0,00012	**2,951209**	**0,000389**	**-4,81344**	**-0,00751**
	Hurbanovo	1,459258	0,001724	0,634257	0,003785	**-4,67519**	**-0,00053**	-1,23022	-0,00184
	Sliac	1,633375	0,001923	-0,46313	-0,00319	**-2,31303**	**-0,00023**	**-3,47917**	**-0,00490**
	Telgart	1,473456	0,001546	1,353517	0,012530	1,116255	0,000167	-0,12872	-0,00015
	Kamenica	1,431608	0,001614	-0,44258	-0,00294	**-4,09567**	**-0,00040**	**-1,94312**	**-0,00233**
	Kosice	**1,779842**	**0,002095**	0,016253	0,000118	**-9,17085**	**-0,00145**	**-3,74258**	**-0,00769**
	Poprad	1,500358	0,001678	0,655554	0,004467	**-9,66966**	**-0,00171**	-0,87488	-0,00097
Romania	Brasov	0,409279	0,002480	0,409279	0,001305	-0,40528	-0,00083	-0,69085	-9,4E-05
	In. Buzaului	0,480489	0,003106	0,480489	0,001332	**4,088972**	**0,007969**	**-4,76438**	**-0,00061**
	Sinaia	-0,19274	-0,00193	-0,19274	0,001489	**-2,76831**	**-0,00424**	**-9,57763**	**-0,00189**
	Buzau	0,754432	0,004422	0,754432	0,001411	**-1,74956**	**-0,00400**	**2,621527**	**0,000370**
	Ploiesti	0,985866	0,006368	0,985866	0,001492	-1,37280	-0,00297	**2,223330**	**0,000215**

Regarding the temperature trends in climatic stations in Carpathians region we can conclude that although all climatic stations prove increasing trends only Bratislava and Kosice station prove significant increasing trend (Table 1).

There are no significant trends in precipitation in all investigated climatic stations, although the stations situated in the north Carpathians (Poland) prove more decreasing trends in precipitation than the stations situated in the south Carpathian (Romania) which is in contrary with Fifth Assessment Report of the Intergovernmental Panel on Climatic Changes. Mentioned Report concluded that precipitation has generally increased over latitudes north of 30 over the period of 1900–2005 (Stocker et al., 2013).

Regarding the relative humidity and the wind speed, there are mostly a significant decreasing trends. Although some stations – Bratislava (Slovakia) and Intorsura Buzaului (Romania) proved a significant increasing trends of relative humidity and stations – Kielce (Poland), Buzau and Ploiesti (Romania) proved a significant positive trend in wind speed. It is an interesting results that need the further investigations in trends of meteorological time series.

5. CONCLUSION

The Carpathians are the largest European mountain range and harbour exceptional biodiversity. Its distance from the Atlantic Ocean (from 620 to 1,240 miles) and the influence of the intervening masses of the Alps and the Bohemian Massif cause diminished precipitation in the Carpathians. However, recent and anticipated changes in climate along with rapid social and economic development suggest that the region's values may not be sustained (Kondracki, 2009). Most of the recent studies about climate change suggest that the behaviour of some of the climatological variables has already changed and will continue to change towards increasing or decreasing magnitudes and frequencies, depending on the type of variable. Increased rainfall and floods are expected in some regions while other regions will experience smaller rainfall and longer droughts,

meaning water scarcity. Mountains are generally richer in atmospheric precipitation than the plane areas. Rainfall in general is increasing with altitude of approximately 50-60 mm at 100 meters of the high. Air masses have a different dependency of air temperature from the altitude, mostly expressed by a significant decrease about 0.6 °C per 100 m. The relative air humidity increases irregularly with increasing altitude in general. Its lowest values are usually recorded in lowlands during the whole year, except from the winter months, when frequent temperature inversions cause the air humidity decrease to the lowest level in stations with altitude above 900 m a. s. l. Wind speed is changeable during the year.

Trend analysis for meteorological time series is an important and popular tool for better understanding the effects of climate variation and anthropogenic activities. The Mann-Kendall test coupled with the Sen's slope was applied to identity the significant trends, as well as the increasing or decreasing trend and the magnitude of those trends.

The results achieved for meteorological time series revealed more frequent increasing trends in temperatures, no trends in precipitation and significant decreasing trends in relative humidity and wind speed in investigated climatic stations in Carpathians.

ACKNOWLEDGMENT

This paper was written thanks to support from project VEGA 1/0609/14. This work has been supported by the Slovak Research and Development Agency by supporting the project SK-PT-0007-15.

REFERENCES

Ampitiyawatta, A. D., Shenglian, G., 2009. Precipitation trends in the Kalu Ganga basin in Sri Lanka. The Journal of Agricultural Science; 4(1)Sarkar, A., Singh, R. D., Sharma, N., 2012. Climate variability and trends in part of Brahmaputra river basin. India Water Week 2012 – Water, Energy and Food Security: Call for Solutions, New Delhi.

Birsan, M. V., 2015. Trends in Monthly Natural Streamflow in Romania and Linkages to Atmospheric Circulation in the North Atlantic. Water Resour Manage; 29: 3305.

Bîrsan, M., Zaharia, L., Chendeş, V., Brănescu, E., 2012. Recent trends in streamflow in Romania (1976–2005). Romanian Rep Phys; 64(1): 275–280.

Błażejczyk, K., Matzarakis, A., 2007. Assessment of Bioclimatic Differentiation of Poland Based on the Human Heat Balance. Geographia Polonica; 80(1): 63-82.

Bogawski, P., Bednorz, E., 2014. Comparison and Validation of Selected Evapotranspiration Models for Conditions in Poland (Central Europe). Water Resour Manage; 28: 5021.

Burlando, P., Rosso, R., 2002. Effects of transient climate change on basin hydrology. 1. Precipitation scenarios for the Arno River, central Italy. Hydrological Processes; 16(6): 1151–1175.

Burn, D. H., Hag Elnur, M. A., 2002. Detection of hydrologic trends and variability. Journal of Hydrology; 255: 107-122.

Čistý, M., Becová, A., Celar, L., 2016. Analysis of Irrigation Needs Using an Approach Based on a Bivariate Copula Methodology. Water Resour Manage; 30: 167.

Croitoru, A. E., Holobaca, I. H., Lazar, C., Moldovan, F., Imbroane, A., 2012. Air temperature trend and the impact on winter wheat phenology in Romania. Clim Chang; 111(2): 393–410.

Croitoru, A. E., Piticar, A., Dragotă, C. S., Burada, D. C., 2013. Recent changes in reference evapotranspiration in Romania. Global Planet Change; 111: 127–137.

Gaál, L., Szolgay, J., Kohnova, S., Parajka, J., Merz, R., Viglione, A., Bloschl, G., 2012. Flood timescales: Understanding the interplay of climate and catchment processes through comparative hydrology. Water Resources Research; 48: 21.

Gadek, B., Leszkiewicz, J., 2012. Impact of climate warming on the ground surface temperature in the sporadic permafrost zone of the Tatra Mountains, Poland and Slovakia. Cold Regions Science and Technology; 79–80: 75–83.

Hlásny, T., Trombik, J., Dobor, L. Barcza, Z., Barka, I., 2016. Future climate of the Carpathians: climate change hot-spots and implications for ecosystems. Reg Environ Change; 16(5): 1495-1506.

Hlavcova, K., Kalas, M., Szolgay, J., 2002. Impact of climate change on the seasonal distribution of runoff in Slovakia. Slovak Journal of Civil Engineering; 10(2): 10-17.

IMGW, 2005. Atlas klimatu Polski [Atlas of Climate of Poland], Instytut Meteorologii i Gospodarki Wodnej (IMGW), Warszawa, 116p.

Johnes, J. R., Schwartz, J. S., Ellis, K. N., Hathaway, J. M., Jawdy, C. M., 2015. Temporal variability of precipitation in the Upper Tennessee Valley. Journal of Hydrology: Regional Studies; 3: 125–138.

Kaczmarek, Z., 2003. The Impact of Climate Variability on Flood Risk in Poland. Risk Analysis; 23: 559–566.

Kendall, M. G., 1975. Rank Correlation Measures. Charles Griffin, London.

Kondracki, J. A., 2009. Carpathian Mountains. Online: https://www.britannica.com/place/Carpathian-Mountains.

Kundzewicz, Z. W., Ulbrich, U., Brücher, T. Graczyk, D., Krüger, A., Leckebusch, G. C., Menzel, L., Pińskwar, I., Radziejewski, M., Szwed, M., 2005. Summer Floods in Central Europe – Climate Change Track? Nat Hazards; 36: 165.

Mann, H. B., 1945. Non-parametric tests against trend. Econometrica; 13: 245-259

Mares, C., Mares, I., Stanciu, A., 2005. Extreme climatic events in the precipitation time series in Romania and their impact in the Danube inferior basin. Geophys. Res. Abstracts; 7, 07106.

Marszelewski, W., Pius, B., 2016. Long-term changes in temperature of river waters in the transitional zone of the temperate climate: a case study of Polish rivers. Hydrological Sciences Journal; 61 (8).

Matei, M., Laslo, L., Ciobotaru, N., Musat, C., Madalina, B., Raischi, M., Gyorgy, D., 2016. Assessment of pressures caused by climate changes on wetlands in Romania based on MAES framework. International Journal of Environmental Science http://iaras.org/iaras/journals/ijes

Micu, D. M., Dumitrescu, A., Cheval, S., Birsan, M. V., 2014. Climate of the Romanian Carpathians: Variability and Trends. Springer.

Lapin, M., Basták-Durán, I., Gera, M., Hrvol’, J., Kremler, M., Melo, M., 2012. New cli¬mate change scenarios for Slovakia based on global and regional general circulation models. Acta Met. Univ. Comen.; 37: 25-74.

Lettenmaier, D. P., Wood, E. F., Wallis, J. R., 1994. Hydro-climato-logical trends in the continental United States, 1948–88. Journal of Climate; 7: 586–607.

Lupikasza, E., 2010. Spatial and temporal variability of extreme precipitation in Poland in the period 1951–2006. Int. J. Climatol.; 30: 991–1007.

Partal, T., Kahya, E., 2006. Trend analysis in Turkish precipitation data. Hydrological Processes; 20: 2011–2026.

Pauling, A., Paeth, H., 2006. On the variability of return periods of European winter precipitation extremes over the last five centuries. Clim. Past Discuss.; 2: 157–189.

Pekarová, P., Szolgay, J., 2005. Assessment of Climate Change Impact on Selected Components of the Hydrosphere and Biosphere in the Hron and Vaáh River Basins. VEDA, Bratislava; 419-492.

Pintilii, R. D., Andronache, I., Diaconu, D.C., Dobrea, R.C., Zeleňáková, M., Fensholt, R., Peptenatu, D., Drăghici, C. C., Ciobotaru, A. M., 2017. Using Fractal Analysis in Modeling the Dynamics of Forest Areas and Economic Impact Assessment: Maramureș County, Romania, as a Case Study. Forests; 8, 25.

Portela, M. M., Zeleňáková, M., Santos, J. F., Purcz, P., Silva, A. T., Hlavatá, H. 2015. A comprehensive drought analysis in Slovakia using SPI. European Water; 51: 17-33.

Prăvălie, R., Peptenatu, D., Sîrodoev, I., 2013. The impact of climate change on the dynamics of agricultural systems in South-Western Romania. Carpathian Journal of Earth and Environmental Sciences; 8(3): 175–186.

Przybylak, R., Majorowicz, J., Wójcik, G., Zielski, A., Chorążyczewski, W., Marciniak, K., Nowosad, W., Oliński, P., Syta, K., 2005. Temperature changes in Poland from the 16th to the 20th centuries. Int. J. Climatol.; 25: 773–791.

Sayemuzzaman, M., Jha, M. K., 2014. Seasonal and annual precipitation time series trend analysis in North Carolina, United States. Atmospheric Research; 137: 183–194.

Sen, P. K., 1968. Estimates of the regression coefficient based on Kendall’s tau. Journal of the American Statistical Association; 63: 1379–1389.

SHMI, 2015. Klimatický atlas Slovenska. [Climate atlas of Slovakia]. Slovak Hydrometeorological Institute (SHMI), Banská Bystrica, 228 p.

Štefunková, Z., Hlavčová, K., Lapin, M., 2014. Runoff change scenarios based on regional climate change projections in mountainous basins in Slovakia. Contributions to Geophysics and Geodesy. 43(4): 327–350.

Stocker, T. F. et al., 2013. Climate Change 2013: The Physical Science Basis. Working Group I, Fifth Assessment Report of the Intergovernmental Panel on Climatic Change`s (IPCC), Cambridge University Press, UK.

Tsakiris, G., 2015. The status of the European Waters in 2015: a Review. Environ Process; 2: 543-557.

Velísková, Y., Sokáč, M., Halaj, P., Koczka Nara, M., Dulovičová, R., Schugerl, R., 2014. Pollutant spreading in a small stream: A case study in Mala Nitra canal in Slovakia. Eviron Process; 1: 265-276.

Vojtek, M., Faško, P., Šťastný, P., 2003. Some selected snow climate trends in Slovakia with respect to altitude. Acta Met. Univ. Comenianae; 32: 17-27.

Zeleňáková, M., Portela, M. M., Purcz, P., Blišťan, P., Silva, A. T., Hlavatá, H., Santos J. F., 2015. Seasonal and spatial investigation of trends in precipitation in Slovakia. European Water; 52: 35-42.

Proceedings of the 10th World Congress of EWRA 'Panta Rhei', 5-9 July 2017, Athens, Greece
© 2017 *European Water Resources Association*

Generation of daily synthetic flows for Switzerland

M.M. Portela[1*], A.T. Silva[1], A.C. Santos[1,2] and B. Schaefli[3]
[1] *IST, CERIS-Civil Engineering Research and Innovation for Sustainability, Lisbon University, Portugal*
[2] *École Polytechnique Fédérale de Lausanne, ECHO-Laboratory of Ecohydrology, Switzerland*
[3] *Faculty of Geosciences and Environment, Institute of Earth Surface Dynamics (IDYST), University of Lausanne, Switzerland*
[*] *e-mail: maria.manuela.portela@tecnico.ulisboa.pt*

Abstract: The generation of synthetic flow series is a common tool to quantify the uncertainty and natural variability of the river flow regime, namely in stochastic problems related to water resources, whose solutions depend on the values of the streamflows and their temporal pattern. Uncertainties in hydrological data analysis reflect both the inability to quantify the phenomena and underlying processes, and the variable nature of hydrological events. While the former uncertainties are largely beyond the control of most end-users of hydrological data, the latter can be reduced if more information is made available. As the size of the samples becomes smaller, their capability to describe the natural variability of the hydrological systems decreases, thus increasing the uncertainty of the hydrological data-based modelling. In the previous framework, this paper presents an application of a two-level approach recently developed for the method of fragments to obtain synthetic daily flows by direct disaggregation of annual flows at 23 Swiss river gauge stations, covering a wide range of rainfall- and snowfall-driven discharge regimes. The results showed that the approach preserves the historical statistical characteristics not only of the annual and daily flows, to which is applied, but also of the monthly flows obtained indirectly, by accumulation of daily flows.

Key words: Daily flow; disaggregation modelling; method of fragments; Switzerland

1. INTRODUCTION

Uncertainties in hydrological data analysis reflect both the inability to quantify the phenomena and underlying processes, and the intrinsic variable nature (in time and space) of hydrological events (Kundzewicz, 1995, Yen, 2002). While the first uncertainties are largely beyond the control of most of the end-users of hydrological data, the prediction uncertainty due to natural variability can be reduced if more information is made available. As the size of the samples becomes smaller, their capability to describe the natural variability of the hydrological systems diminishes, thus increasing the uncertainty of the hydrological data-based modelling.

Quantifying the uncertainty due to the intrinsic stochastic nature of a hydrological process becomes even more crucial when facing stochastic design problems, whose solutions depend on the values of the hydrological variables themselves but also on their temporal pattern. This is the case if streamflows are used for long-term planning, design, and operation of many water resources systems, including the optimization of the operation rules of artificial reservoirs, or their simulation under alternative inflow scenarios, the evaluation of water supply reliability and assessment of water resource risk related issues, among others.

For many decades, synthetic flow series have played a major role among the several quantitative methods for incorporating the uncertainty and variability due to the random nature of the sequences of streamflows (Thomas & Fiering, 1962, Matalas, 1967, Valencia & Schaake, 1973, Salas *et al.*, 1980, Stedinger & Vogel, 1984, Stedinger *et al.*, 1985, Srinkanthan & McMahon, 2001, McMahon & Adeloye, 2005, Lee *at al.,* 2007, Silva & Portela, 2012, Portela & Silva, 2016). Under the assumption of hydrological stationarity, the synthetic streamflow series are alternative hydrological events that mimic the historical samples by preserving their empirical structure, in terms of statistical properties and probabilities of occurrence (McMahon & Adeloye, 2005, Acharya & Ryu, 2014)

The generation of synthetic flows with a stochastic model based on historical flow records uses two main approaches (Salas *et al*., 1980, Santos, 1983): (i) a one-level approach through the generation of streamflows at the required time level by applying an appropriate model directly to that level; or (ii) a two-level approach comprehending the generation of annual flows using a suitable model (generally of statistical nature), followed by the disaggregation of those annual flows into flows at the required time level. The first approach may be suitable for the simpler problem of generating seasonal or monthly flows, but not for daily flows, while the second approach can be applied to any time level. It also has the advantage of preserving the historical statistical properties at both the upper time level (year) and the lower time level to which the flows are disaggregated (season, month or day), as well as the additive property (also known as the summability criteria), meaning that the generated flows at the lower time level yields the generated flows at the upper time level (Valencia & Schaake, 1973, Santos, 1983, Silva, 1992, Santos & Salas, 1992).

One of the simplest disaggregation models is the method of fragments developed by Svanidze, (1964) and widely discussed by several authors (Srinkanthan & McMahon, 2001, McMahon & Adeloye, 2005, Guimarães & Santos, 2011, Silva & Portela, 2012). The method uses a purely deterministic approach based on the resampling of short duration fragments obtained from a historical sample, followed by the scaling of those fragments to match annual sums. Each fragment refers to one year and is a dimensionless or standardized sequence of flows at the lower time level (season, month or day).

The method requires the clustering of the fragments into classes whose number and definition are its most important features, although unsolved until recently (Silva & Portela, 2012). In order to provide a reproducible, but theoretically sound procedure to define the classes, Portela & Silva, 2016, proposed classes such that the difference between the non-exceedance probabilities of the two boundary annual flows that define any class is constant (classes equally-spaced in terms of the difference between the non-exceedance probabilities). For that purpose and starting with a fixed number of classes, *C*, with fixed amplitude of 100/*C* %, *C* is progressively reduced by one until all the classes have at least one fragment. After each reduction of the number of classes by one, the new values of the constant probability amplitude and of the annual flows that define the boundaries of the different classes are recomputed, followed by the re-allocation of the fragments into the C-1 new classes. This procedure is repeated until there are no empty classes.

This paper presents the results from the enhanced method of fragments developed by Portela & Silva, 2016, to the direct disaggregation of annual streamflows into daily streamflows at several river gauge stations of Switzerland. The synthetic monthly streamflow series at each location were obtained by accumulating the daily flows, thus ensuring the additivity between the synthetic flows at any two-time levels (day or month versus year and day versus month).

The assessment of the performance of the method utilized the comparison of statistical characteristics: the synthetic series are representative alternative sequences if they preserved the historical statistics of the streamflows.

If *M* synthetic series are generated, the comparison of a given sample series' historical statistic, θ (the mean, the standard deviation and the skewness coefficient of the annual flow or of each daily or monthly flow), with the corresponding synthetic series' statistics $\hat{\theta}^{(m)}$ $\left(m = 1,2,...,M\right)$, can be made by obtaining the mean ($\overline{\hat{\theta}}$) and the standard deviation ($s_{\hat{\theta}}$) of $\hat{\theta}^{(m)}$ and by establishing a confidence interval at level $(1-\alpha)$ for θ (Salas *et al.*, 1980):

$$\left]\overline{\hat{\theta}} - z_{1-\alpha/2}\, s_{\hat{\theta}}; \overline{\hat{\theta}} + z_{1-\alpha/2}\, s_{\hat{\theta}}\right[\tag{1}$$

where $z_{1-\alpha/2}$ is the $1-\alpha/2$ quantile of the normal standard distribution, α being the significance level. If the statistics estimated from the historical data, θ, lies within the interval of eq. 1, it is considered to be preserved by the synthetic series.

Additionally, for each day and month, a nonparametric analysis was carried out based on the representation of the historical statistic, θ, along with the average of $\hat{\theta}^{(m)}$, $\bar{\hat{\theta}}$, and with the following empirical quantiles, $q_{\hat{\theta}\beta}$, computed based on the ranking of the M values of $\hat{\theta}^{(m)}$: $\beta = 2.5\%$, $\beta = 25.0\%$, $\beta = 75.0\%$, and $\beta = 97.5\%$.

2. DATA - SERIAL INDEPENDENCE OF THE ANNUAL FLOWS

The main types of river regimes in Switzerland can be classified according to their main drivers as pluvial, snow-dominated and glacier regimes (Musy & Hingy, 2011, Hänggi & Weingartner, 2012). In the pluvial regime, the behavior of discharges is driven mainly by precipitation and evapotranspiration. This regime is predominant in the Plateau and Jura regions, located in the North. In the snow-dominated regime, snow accumulates intra-annually and the peaks of discharge tend to occur by the end of spring, when snow melts. Finally, in the glacier regime, the main driver of discharge production is snow- and ice melting, and snow accumulation occurs inter-annually at the highest altitudes of the catchment. These two last regimes occur in the Alps region, with certain climatic differences between the North and South of the Alps.

In order to represent the diversity of the river regimes, 26 river gauge stations under natural conditions were selected (Table 1) and the daily discharges obtained from the Swiss Federal Office for Environment (FOEN).

Table 1. Identification and general characteristics of the river gauge stations.

River gauge station		River regime classification	Hydrological region	Area covered by glacier (%)	Watershed area (km^2)	Mean annual discharge (m^3/s)(1)	Altitude		Period with daily flow data	
Code	Name						Mean	Outlet section	Starting date	Ending date
2112	Sitter, Appenzell	Nival de transition	Plateau and Jura	0.0	74.2	3.48	1252	769	01-01-1912	30-06-2015
2126	Murg, Wängi	Pluvial inférieur		0.0	78.0	1.85	650	466	01-01-1954	31-05-2015
2159	Gürbe, Belp, Mülimatt	Pluvial supérieur		0.0	117.0	1.73	837	522	25-02-1922	
2161	Massa-Blatten bei Naters	a-Glaciaire	Alps	65.9	195.0	13.81	2945	1446	01-01-1931	30-06-2015
2179	Sense, Thörishaus, Sensematt	Nivo-pluvial préalpin	Plateau and Jura	0.0	352.0	9.07	1068	553	01-01-1928	
2206	Melera, Melera (Valle Morobbia)	Nivo-pluvial méridional	South of Alps	0.0	1.1	0.05	1419	944	01-01-2005	
2244	Krummbach, Klusmatten	Nival méridional		3.0	19.8	0.77	2276	1795	01-01-1995	
2251	Rotenbach, Plaffeien, Schweinsberg	Nival de transition	Plateau and Jura	0.0	1.7	0.08	1454	1275	01-09-1961	
2268	Rhone, Gletsch	a-Glaciaire	Alps	52.2	38.9	2.87	2719	1761	01-01-1956	
2276	Grosstalbach, Isenthal	Nival alpin		9.3	43.9	1.79	1820	767	10-02-1956	
2299	Alpbach, Erstfeld, Bodenberg	b-Glaciaire		27.7	20.6	1.62	2200	1022	14-01-1960	31-05-2015
2308	Goldach, Goldach, Bleiche	Pluvial supérieur	Plateau and Jura	0.0	49.8	1.39	833	399	01-01-1974	
2319	Ova da Cluozza, Zernez	Nivo Glaciaire	Alps	2.2	26.9	0.79	2368	1509	28-06-1961	
2327	Dischmabach, Davos, Kriegsmatte	b-glacio nival		2.1	43.3	1.71	2372	1668	24-07-1963	30-06-2015
2356	Riale di Calneggia, Cavergno, Pontit	Nival méridional	South of Alps	0.0	24.0	1.42	1996	890	01-01-1967	
2366	Poschiavino, La Rösa	Nival méridional		0.4	14.1	0.55	2283	1860	01-01-1970	
2374	Necker, Mogelsberg, Aachsäge	Nivo-pluvial préalpin	Plateau and Jura	0.0	88.2	3.27	959	606	01-01-1972	31-05-2015
2430	Rein da Sumvitg, Sumvitg, Encardens	b-Glacio nival	Alps	6.7	21.8	1.49	2450	1490	15-09-1977	30-06-2015
2432	Venoge, Ecublens, Les Bois	Pluvial jurassien	Plateau and Jura	0.0	231.0	4.15	700	383	01-01-1979	
2471	Murg, Murgenthal, Walliswil	Pluvial inférieur		0.0	207.0	3.50	637	419	26-06-1980	31-05-2015
2480	Areuse, Boudry	Pluvial jurassien		0.0	377.0	11.70	1060	444	01-01-1904	30-06-2015
2603	Ilfis, Langnau	Nivo-pluvial préalpin		0.0	188.0	5.38	1051	685	01-04-1989	31-05-2015
2605	Verzasca, Lavertezzo, Campiòi	Nivo-pluvial méridional	South of Alps	0.0	186.0	10.76	1672	490	01-09-1989	
2608	Sellenbodenbach, Neuenkirch	Pluvial inférieur	Plateau and Jura	0.0	10.5	0.22	615	515	12-09-1990	30-06-2015
2609	Alp, Einsiedeln	Nivo-pluvial préalpin		0.0	46.4	2.24	1155	840	27-02-1991	
2610	Scheulte, Vicques	Pluvial jurassien		0.0	72.8	1.54	785	463	01-01-1992	31-05-2015

(1) - The units for river gauge stations 2206 and 2251 are l/s

As mentioned, the applied approach combines a random generation process at the annual level which requires that the annual flows are i.i.d. random variables, i.e., without temporal serial correlation. In order to identify the 12-month period compatible with the randomness assumption, the lag-1 autocorrelation coefficient, r_1, was computed for each station, assuming that the 12-months period starts in each calendar month, provided that complete series of 12 months could be obtained. However, even for an independent series, r_1 can differ from zero due to the variability of the natural flow regime. To decide if a given value of r_1 differs significantly from zero, the

probability limits for the serial correlation of an independent series were computed for the confidence level of 95%, by applying the Anderson test (Anderson, 1941).

The results thus achieved rejected the assumption of serial temporal independence of the annual flows in the gauge stations 2161, 2430 and 2471, regardless of the starting month of the 12-months period. Accordingly, those stations were discarded. For the remaining 23 stations, only the periods of 12-months starting in January, February and November always ensured the serial temporal independence of the annual flows. Just for the sake of simplifying, the civil year was adopted at the annual level. Figure 1 presents some of the characteristics of the annual flows in those stations, as well as the schematic locations of the stations.

River gauge station		Watershed area	Period (ending on 31-12-2014)		Annual series						
					Mean annual flow depth	Volume			Natural logarithms[2]		
Code	Name	(km^2)	Starting date	Number of years, *N*	(mm)	Mean (10^6 m^3)[1]	Standard deviation (10^6 m^3)[1]	Skewness coefficient (-)	Mean (-)	Standard deviation (-)	Skewness coefficient (-)
2112	Sitter, Appenzell	74.2	01/01/1912	103	1507.2	111.8	21.6	0.33	18.51	0.20	-0.20
2126	Murg, Wängi	78.0	01/01/1954	61	732.4	57.1	11.9	0.50	17.84	0.20	0.11
2159	Gürbe, Belp, Mülimatt	117.0	01/01/1923	92	707.9	82.8	19.2	0.08	18.20	0.24	-0.46
2179	Sense, Thörishaus, Sensematt	352.0	01/01/1928	87	768.6	270.5	58.1	-0.04	19.39	0.23	-0.56
2206	Melera, Melera (Valle Morobbia)	1.1	01/01/2005	10	1291.6	1.4	0.6	0.68	14.08	0.44	-0.09
2244	Krummbach, Klusmatten	19.8	01/01/1995	20	1231.8	24.4	5.2	1.10	16.99	0.20	0.46
2251	Rotenbach, Plaffeien,	1.7	01/01/1962	53	1627.5	2.8	0.6	-0.18	14.81	0.23	-0.62
2268	Rhone, Gletsch	38.9	01/01/1956	59	2240.6	87.2	11.0	0.14	18.28	0.13	-0.26
2276	Grosstalbach, Isenthal	43.9	01/01/1957	58	1288.1	56.5	8.2	0.09	17.84	0.15	-0.19
2299	Alpbach, Erstfeld, Bodenberg	20.6	01/01/1961	54	2422.3	49.9	5.9	-0.01	17.72	0.12	-0.31
2308	Goldach, Goldach, Bleiche	49.8	01/01/1974	41	874.0	43.5	9.7	1.44	17.57	0.21	0.64
2319	Ova da Cluozza, Zernez	26.9	01/01/1962	53	910.7	24.5	4.2	0.28	17.00	0.17	-0.20
2327	Dischmabach, Davos, Kriegsmatte	43.3	01/01/1964	51	1238.9	53.6	7.8	-0.18	17.79	0.15	-0.49
2356	Riale di Calneggia, Cavergno, Pontit	24.0	01/01/1967	48	1838.3	44.1	10.5	0.47	17.57	0.24	-0.25
2366	Poschiavino, La Rösa	14.1	01/01/1970	45	1238.6	17.5	4.1	0.77	16.65	0.23	-0.23
2374	Necker, Mogelsberg	88.2	01/01/1972	43	1168.2	103.0	16.1	0.43	18.44	0.16	-0.01
2432	Venoge, Ecublens, Les Bois	231.0	01/01/1979	36	566.6	130.9	33.9	-0.28	18.65	0.29	-1.02
2480	Areuse, Boudry	377.0	01/01/1904	111	1023.0	385.7	89.3	-0.24	19.74	0.26	-0.89
2603	Ilfis, Langnau	188.0	01/01/1990	25	902.7	169.7	33.9	0.02	18.93	0.21	-0.39
2605	Verzasca, Lavertezzo,	186.0	01/01/1990	25	1825.0	339.4	93.0	-0.32	19.60	0.31	-1.09
2608	Sellenbodenbach, Neuenkirch	10.5	01/01/1991	24	651.4	6.8	1.9	0.56	15.70	0.28	-0.17
2609	Alp, Einsiedeln	46.4	01/01/1992	23	1523.2	70.7	14.1	0.39	18.05	0.20	0.16
2610	Scheulte, Vicques	72.8	01/01/1992	23	679.6	49.5	15.2	0.30	17.67	0.32	-0.23

(1) - The units for river gauging stations 2206 and 2251 are 10^3 m^3.

(2) - For annual volumes expressed in cubic meters per second, except for river gauging stations 2206 and 2251, where the volumes are expressed in litters.

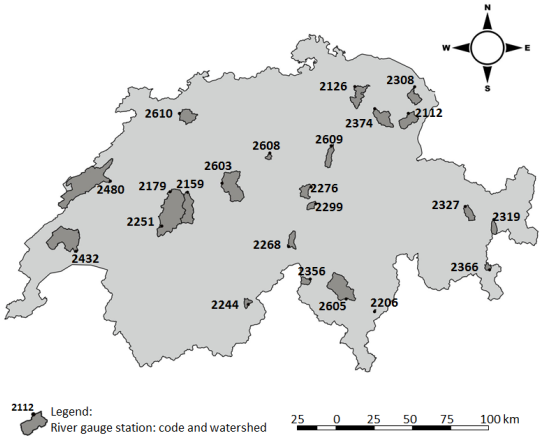

Figure 1. 23 river gauge stations with uncorrelated annual flows. General characteristics of the annual flows. Schematic location of the stations.

To assess the suitability of the statistical model applied at the annual level – the log-Pearson III distribution – three statistical goodness-of-fit tests were applied for the 5% significance level: the Anderson-Darling (AD), Kolmogorov-Smirnov (KS) and Pearson chi-squared (CSQ) tests (Naghettini, 2017). Figure 2 shows the boxplots of the 23 resulting p-values for each test, as well as the rejection rates (which correspond to the rejection of 1 out of 23 samples in each test). Since the obtained rejection rates are close to the expected type-I error probability (*i.e.*, 5%), we opted to keep all the 23 samples.

3. RESULTS

The two-level approach was applied to each of the 23 samples to generate M=5000 synthetic annual and daily flow series, each with the length N of the historical series to which it corresponds

(see Figure 1 for *N*). The previous number of *M* synthetic flow series verifies the smallest indicated by Guimarães & Santos, 2011, for storage-yield related problems. The maximum number of classes was *C*=10 (Portela & Silva, 2016).

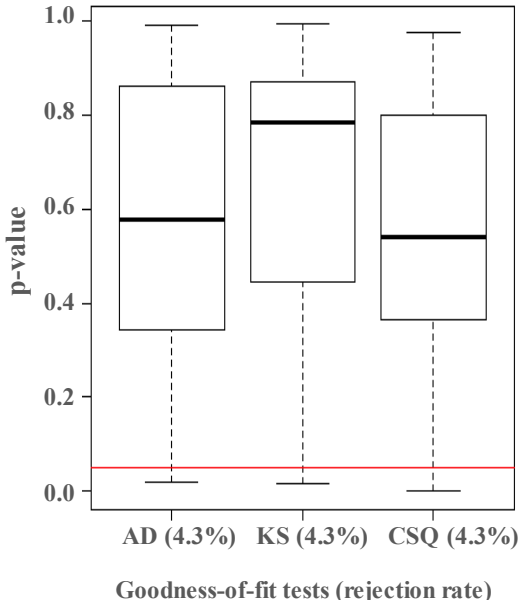

Figure 2. Boxplots of the p-values of the Anderson-Darling (AD), Kolmogorov-Smirnov (KS) and Pearson Chi-squared goodness-of-fit tests applied to test the suitability of the log-Pearson type III to the 23 annual streamflow samples.

Regarding the performance of the approach, Table 2a) shows the number of days without preservation of the historical statistical characteristics, as well as the final number of equally spaced classes resulting from the re-allocation of the empty classes. The characteristics at the annual and monthly levels were always preserved.

Table 2. Performance of the model (occurrences outside the allowed limits are highlighted by shaded cells)
a) Number of days without preservation of each one of the historical statistical characteristics.

River gauge station		Effective number of classes	Number of days without preservation of a historical statistical parameter		
Code	Name		Mean	Standard deviation	Skewness coefficient
2112	Sitter, Appenzell	10	0	0	0
2126	Murg, Wängi		0	0	0
2159	Gürbe, Belp, Mülimatt		0	0	0
2179	Sense, Thörishaus, Sensematt		0	0	0
2206	Melera, Melera (Valle Morobbia)	4	0	0	0
2244	Krummbach, Klusmatten	8	0	1	1
2251	Rotenbach, Plaffeien, Schweinsberg	10	0	0	0
2268	Rhone, Gletsch		0	0	0
2276	Grosstalbach, Isenthal		0	0	0
2299	Alpbach, Erstfeld, Bodenberg		0	0	1
2308	Goldach, Goldach, Bleiche		0	0	0
2319	Ova da Cluozza, Zernez		0	0	1
2327	Dischmabach, Davos, Kriegsmatte		0	0	0
2356	Riale di Calneggia, Cavergno, Pontit		0	0	0
2366	Poschiavino, La Rösa		0	0	0
2374	Necker, Mogelsberg, Aachsäge		0	0	1
2432	Venoge, Ecublens, Les Bois		0	1	1
2480	Areuse, Boudry		0	0	0
2603	Ilfis, Langnau		0	0	0
2605	Verzasca, Lavertezzo, Campiòi		0	0	1
2608	Sellenbodenbach, Neuenkirch	9	0	0	0
2609	Alp, Einsiedeln	10	0	0	0
2610	Scheulte, Vicques	9	0	1	1

b) Numbers of days, months and years where each sample series' statistics, q, was not contained in the centered empirical quantile ranges of 50% (from $q_{\hat{\theta}0.25}$ to $q_{\hat{\theta}0.75}$) and 95% (from $q_{\hat{\theta}0.025}$ to $q_{\hat{\theta}0.975}$).

River gauge station		Centered empirical range of 50%									Centered empirical range of 95%								
		Daily level			Monthly level			Annual level			Daily level			Monthly level			Annual level		
Code	Name	Average	Standard deviation	Skewness coefficient	Average	Standard deviation	Skewness coefficient	Average	Standard deviation	Skewness coefficient	Average	Standard deviation	Skewness coefficient	Average	Standard deviation	Skewness coefficient	Average	Standard deviation	Skewness coefficient
2112	Sitter, Appenzell	0	20	24	0	0	2	0	0	1	0	0	0	0	0	0	0	0	1
2126	Murg, Wängi	93	80	93	2	3	4	0	0	1	0	0	0	0	0	0	0	0	0
2159	Gürbe, Belp, Mülimatt	9	31	40	0	0	1	0	0	1	0	0	0	0	0	0	0	0	1
2179	Sense, Thörishaus, Sensematt	58	89	91	0	1	3	0	0	0	0	0	0	0	0	0	0	0	0
2206	Melera, Melera (Valle Morobbia)	66	51	117	2	1	6	0	0	0	0	0	0	0	0	0	0	0	0
2244	Krummbach, Klusmatten	77	131	85	2	3	1	0	0	0	0	1	0	0	0	0	0	0	0
2251	Rotenbach, Pfaffeien, Schweinsberg	64	82	93	3	2	3	0	0	1	0	0	0	0	0	0	0	0	0
2268	Rhone, Gletsch	31	55	109	0	4	3	0	0	1	0	0	0	0	0	0	0	0	1
2276	Grosstalbach, Isenthal	48	63	79	1	2	1	0	0	1	0	0	0	0	0	0	0	0	0
2299	Alpbach, Erstfeld, Bodenberg	119	141	141	1	4	2	0	0	1	0	0	0	0	0	0	0	0	1
2308	Goldach, Goldach, Bleiche	143	125	136	4	3	4	0	0	0	0	0	5	0	0	0	0	0	0
2319	Ova da Cluozza, Zernez	94	169	97	3	4	3	0	0	0	0	0	2	0	0	0	0	0	0
2327	Dischmabach, Davos, Kriegsmatte	70	61	101	1	1	2	0	0	1	0	0	0	0	0	0	0	0	1
2356	Riale di Calneggia, Cavergno, Pontit	50	102	104	1	4	1	0	0	0	0	0	0	0	0	0	0	0	0
2366	Poschiavino, La Rösa	106	132	177	3	6	7	0	0	0	0	0	5	0	0	0	0	0	0
2374	Necker, Mogelsberg, Aachsäge	103	115	100	4	4	3	0	0	0	0	0	1	0	0	1	0	0	0
2432	Venoge, Ecublens, Les Bois	134	119	113	2	4	3	0	0	0	0	0	2	0	0	0	0	0	0
2480	Areuse, Boudry	59	74	91	2	3	4	0	0	0	0	0	2	0	0	0	0	0	0
2603	Ilfis, Langnau	101	97	124	3	3	2	0	0	1	0	0	0	0	0	0	0	0	0
2605	Verzasca, Lavertezzo, Campioi	161	158	137	5	7	1	0	0	0	0	0	0	0	0	0	0	0	0
2608	Sellenbodenbach, Neuenkirch	69	85	102	1	2	3	0	0	0	0	0	0	0	0	0	0	0	0
2609	Alp, Einsiedeln	61	80	70	0	3	3	0	0	0	0	0	0	0	0	0	0	0	0
2610	Scheulte, Vicques	138	100	123	4	1	4	0	0	0	0	0	2	0	0	0	0	0	0

Table 2b shows the results from the non-parametric analysis. For each gauge station and statistic, the table shows the mean annual number of days, months and years where the sample series' statistic, θ, was not contained in the centered empirical quantile ranges of 50% (from $q_{\hat{\theta}0.25}$ to $q_{\hat{\theta}0.75}$) and 95% (from $q_{\hat{\theta}0.025}$ to $q_{\hat{\theta}0.975}$) obtained from the M=5000 synthetic flow series. Per definition, for the 50% centered empirical quantile, the number of occurrences lying outside the empirical quantile range should not exceed around 182, 6 and 0 for the daily, monthly and annual level, respectively. The equivalent values for the 95% centered empirical quantile are approximately 18, 1 and 0. The numbers of occurrences that exceeded the previous reference values are highlighted in Table 2b) by shaded cells.

Figure 3 exemplifies the comparison between statistical characteristics derived from the samples and from the M=5000 synthetic flow series, based on the gauge stations of Rhone, Gletsch (2268), Poschiavino, La Rösa (2366) and Areuse, Boudry (2480), with different hydrological regimes.

The figure compares day-by-day, for the daily level, and month-by-month, for the monthly level, a given historical statistical characteristic, θ, with the average that results from the M=5000 synthetic flow series for the same statistical characteristic, $\overline{\hat{\theta}}$. Only the averages and the standard deviations were considered in the figure because nothing in the model accounts for the skewness coefficients, which makes their analysis spurious. The figure also includes the results of the non-parametric analysis, namely the number of days and months where θ was not contained in the centered empirical quantile ranges of 50% and 95%, represented by #50% and #95%, respectively. Finally, the figure includes the mean annual maximum absolute difference, Max, between the j values of θ and of $\overline{\hat{\theta}}$, expressed in percentage of θ, with j=365, at the daily level, and j=12, at the monthly level.

4. CONCLUSIONS

Although the method of fragments is well known, its application to the generation of synthetic streamflow series is not as popular as its simplicity would suggest. The authors believe that this is mostly due to the lack of objective criteria to define the classes into which the fragments are grouped in order to introduce a relationship between those fragments and the overall temporal flow pattern.

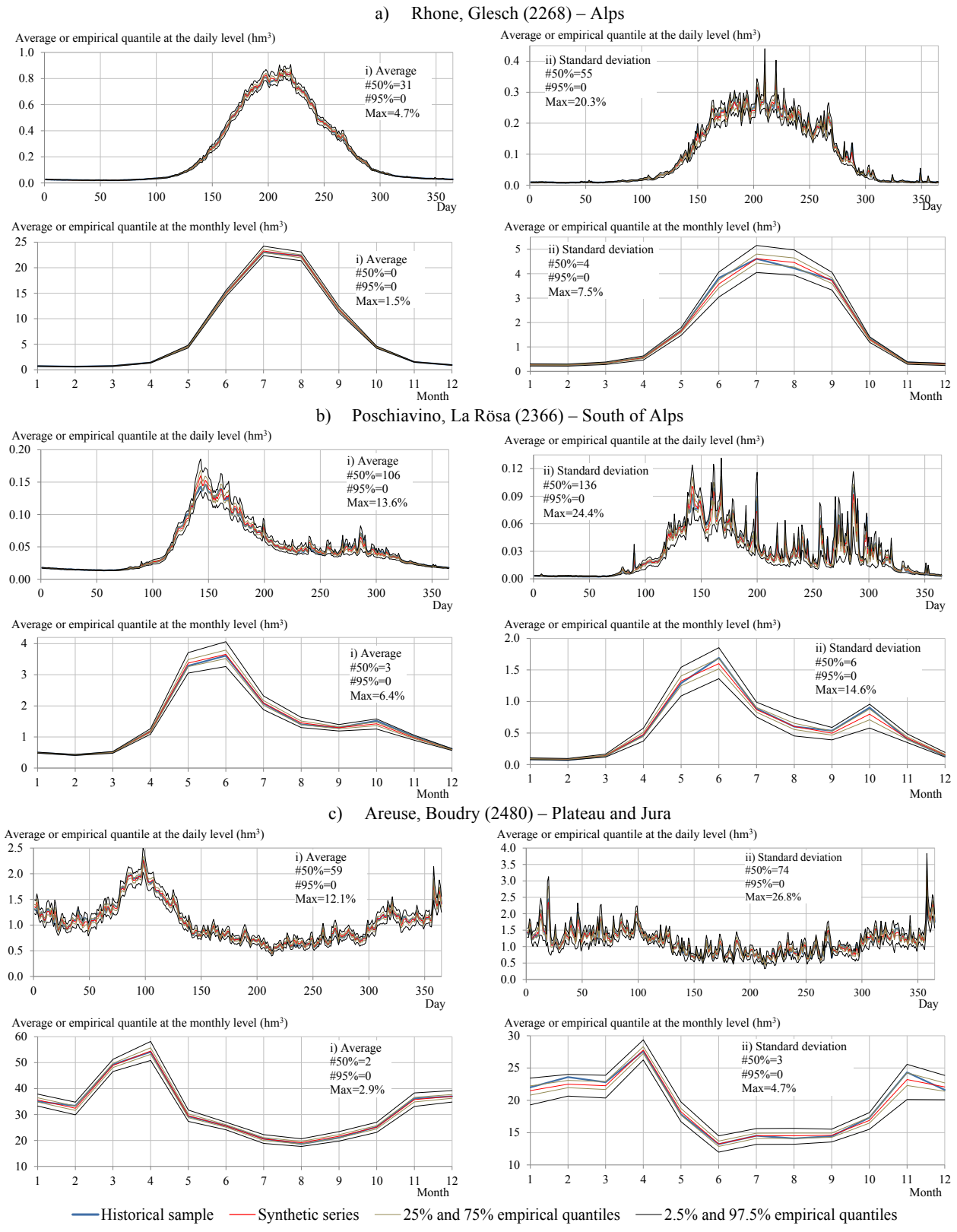

Figure 3. Gauge stations of Rhone, Gletsch (2268), Poschiavino, La Rösa (2366) and Areuse, Boudry (2480). Parameters of the historical and synthetic series and results from the non-parametric analysis. #50% and #95% refer to the mean annual number of months and days were the statistics was not contained in the centered empirical quantile ranges of 50% (from $q_{\hat{\theta}0.25}$ to $q_{\hat{\theta}0.75}$) and 95% (from $q_{\hat{\theta}0.025}$ to $q_{\hat{\theta}0.975}$), respectively. Max refers to the mean annual maximum absolute difference between the j values of a given historical statistical characteristic and the average that results from the M=5000 synthetic flow series for the same statistical characteristic (j=365, at the daily level, and j=12, at the monthly level).

Aiming at exploring the capabilities of the method and following the work of Silva (2010), on the application of the method to generate synthetic monthly flow series, Portela & Silva (2016), developed a new criterion to define the classes of fragments as equally spaced probability intervals. The application of the method based on this criterion to several Portuguese rivers proved to be very robust even in its unprecedented use to generate synthetic daily flow series by direct disaggregation of annual flows. This fact suggested the pertinence of analyzing the adequacy of the model to hydrological constraints different from those prevailing in Portugal, which is precisely the contribution of the present paper.

The results obtained for the Swiss rivers clearly confirm the overall good performance of the two-level streamflow generation model. In fact, except for a few cases related to the skewness coefficient and the standard deviation, most of the historical statistical characteristics at all the time levels were preserved.

The results at the monthly level are particularly noticeable because the synthetic monthly flows were obtained by simple accumulation of the synthetic daily flows. It is important to mention that the preservation of the means and standard deviations is a consequence of the formalism of the method, namely at the daily level to which it is applied. However, the preservation of those characteristics also at the monthly level and the unexpected remarkable preservation of the skewness of most of the daily and monthly flows without requiring any additional treatment make the approach particularly attractive.

A robust and integrated tool, as the one presented, that delivers alternative sequences of flows that simultaneously accounts for the stochastic nature of the river flows at different time levels and for their temporal variability, is particularly suitable to address the uncertainty due to the random nature of the river regime, which, obviously needs further research.

REFERENCES

Acharya, A. & Ryu, J., 2014. Simple Method for Streamflow Disaggregation. Journal of Hydrologic Engineering; 19(3), 509–519. Doi: 10-1061/(ASCE)HE.1943-5584.0000818.

Anderson, R.L., 1941. Distribution of serial correlation coefficients. The Annals of Mathematical Statistics, 8(1):1-13.

Guimarães, R., & Santos, E.G., 2011. Principles of stochastic generation of hydrologic time series for reservoir planning and design: a case study. Journal of Hydrologic Engineering, 16(11):891-898. Doi: http://dx.doi.org/10.1061/(ASCE)HE.1943-5584.0000375.

Hänggi, P., & R. Weingartner (2012), Variations in discharge volumes for hydropower generation in Switzerland, Water Resources Management, 26(5): 1231-1252.

Kundzewicz, Z.W., 1995. Hydrological uncertainty in perspective. In New uncertainty concepts in hydrology and water resources, Kundzewicz ZW (ed.), International Hydrology Series, Cambridge University Press: Cambridge; 3–10.

Lee, D., Salas, J.D., Boes, D., 2007. Uncertainty analysis for synthetic streamflow generation. World Environmental and Water Resources Congress 2007:1-11. Doi: 10.1061/40927(243)417

McMahon, T.A., & Adeloye, A., 2005. Water resources yield. Littleton, CO. Water Resources Publications.

Matalas. N.C., 1967. Mathematical assessment of synthetic hydrology. Water Resources Research; 3(4): 937–945. Doi: 10.1029/WR003i004p00937

Musy, A., and C. Higy (2004), Hydrologie 1 - Une science de la nature, Presses polytechniques et universitaires romandes, PPUR, Lausanne.

Naghettini, M., 2017. Statistical Hypothesis Testing. In Fundamentals of Statistical Hydrology (pp. 251-309). Springer International Publishing.

Portela, M.M. & Silva, A.T., 2016, Disaggregation modelling of annual flows into daily streamflows using a new approach of the method of fragments. Water Resources Management. doi:10.1007/s11269-016-1402-y.

Yen, B.C., 2002. System and component uncertainties in water resources. In risk, reliability, uncertainty, and robustness of water resources systems, Bogardi JJ, Kundzewicz ZW (eds), International Hydrology Series. Cambridge University Press: Cambridge; 133–142.

Salas, J.D., Delleur, J.W., Yevjevich, V., Lane, W.L., 1980, Applied modeling of hydrologic time series. Water Resources Publication. ISBN 0918334373, 9780918334374.

Santos, E.G., 1983. Disaggregation modeling of hydrologic time series. PhD Thesis, Colorado State University, Colorado, USA.

Santos, E.G., & Salas, J.D., 1992. Stepwise disaggregation scheme for synthetic hydrology. Journal of Hydraulic Engineering; 118(5):765–784. Doi: http://dx.doi.org/10.1061/(ASCE)0733-9429(1992)118:5(765).

Silva, M.M., 1992. Daily step-disaggregation model. Application to daily flow synthetic generation. SPRUCE. Statistics in Public Resources and Utilities, and in Care of the Environment, Lisbon, Portugal.

Silva, A.T., & Portela, M.M., 2012. Disaggregation modelling of monthly streamflows using a new approach of the method of fragments. Hydrological Sciences Journal; 57(5): 942-955. Doi:10.1080/02626667.2012.686695.

Srinkanthan, R., & McMahon, T.A., 2001. Stochastic generation of annual, monthly and daily climate data: a review. Hydrology and Earth System Sciences; 5(4): 653–670. Doi: 10.5194/hess-5-653-2001

Stedinger, J.R., Lettenmaier, D.P., Vogel, R.M., 1985. Multisite ARMA(1,1) and disaggregation models for annual streamflow generation, Water Resources Research; 21(4):497–509. Doi: 10.1029/WR021i004p00497.

Stedinger, J.R., & Vogel, R.M., 1984. Disaggregation procedures for generating serially correlated flow vectors. Water Resources research; 20(1): 47–56. Doi: 10.1029/WR020i001p00047.

Svanidze, G.G., 1964. Osnovy rascheta regulirovaniya rechnogo stoka metodom Monte-Karlo. Izd. Akad. Nauk GSSR, Tbilisi (in Russian).

Thomas, H.A. & Fiering, M.B., 1962, Mathematical synthesis of streamflows sequences for the analysis of river basins by simulation. In Design of water systems, A. Mass et al., eds., 459-493, Cambridge, Massachusetts, Harvard University press.

Valencia, D.R., & Schaake, J.C.Jr., 1973. Disaggregation processes in stochastic hydrology. Water Resources Research; 9(3):580–585. Doi: 10.1029/WR009i003p00580.

Proceedings of the 10th World Congress of EWRA 'Panta Rhei', 5-9 July 2017, Athens, Greece
© 2017 *European Water Resources Association*

Impact of climate change on inflows using refined precipitation and temperature scenarios

J. Vieira* and M.C. Cunha
MARE – Marine and Environmental Sciences Center, Department of Civil Engineering, University of Coimbra, Portugal
* *e-mail: jvieira@dec.uc.pt*

Abstract: The modification of the natural inflows on watersheds due to future climate change is of great concern to environmental and water resource managers. Long-term sectorial impact studies on water supply planning require realistic assessment of future climate change on the basin scale. High spatial resolution scenarios have been developed from coupling Atmospheric-Ocean General Circulation Models (AOGCM) with Regional Climate Models (RCM). Furthermore, evidence of bias in the output of AOGCM-RCM has prompted many researchers to refine already downscaled data to make model output more realistic at local scale. In this study, one calibrated hydrological (Temez) model is used to evaluate the modification of the natural inflows from different precipitation and temperature projections for the period 2071-2100 to Odeleite reservoir-dam, located in the south of Portugal. Bias correction is made using the well-known delta change method which uses changes in average values from simulated data for the control period and the scenario period to correct observed values. The results indicate significant differences in the runoff for each RCP depending on the AOGCM-RCM. The decrease of the natural inflows under RCP 4.5 is between -10% and -2%. Under RCP 8.5, the decrease of the natural inflows is much higher between -44% and -24%.

Key words: Climate change, AOGCM-RCM, bias correction, surface hydrology, hydrological modelling

1. INTRODUCTION

The sensitivity of the hydrological cycle to the meteorological variables, in particular precipitation and temperature, demand reliable climate-change projections for impact studies. The use of hydrological models for estimating the runoff in watersheds requires high spatial resolution meteorological input data. Consequently, global climate scenarios produced from Atmospheric-Ocean General Circulation Models (AOGCM) with a resolution of approximately 100-250 km are inadequate for most hydrological assessment studies (e.g., Christensen et al., 2007; Fowler et al., 2007).

From the progress on Regional Climate Models (RCM), AOGCM forced by RCM offer today a physically realistic approach for downscaling to 10-50 km, which is a scale more appropriate for examining the impacts of climate change on runoff or groundwater recharge (e.g., Berg et al., 2012; Teutschbein and Seibert, 2012; Lafon et al., 2013; Pulido-Velazquez et al., 2015). However, AOGCM-RCM simulations often show significant kind of biases in relation to the observed climate and significant variation in relation to the projections for the future periods. One recommendation for impact studies is to use different AOGCM-RCM simulations together with bias correction methods (e.g., Teutschbein and Seibert, 2012; Camici et al., 2014).

The main purpose of this paper is to present one first estimation of the changes in the natural inflows to Odeleite reservoir-dam, located in the south of Portugal by using AOGCM-RCM simulations available more recently from the EURO-CORDEX project. Details of the methodology used in this study are given in section 2. The results are discussed in section 3. Conclusions are drawn in the last section.

2. METHODOLOGY

The methodology adopted for the analysis of climate change impacts on natural inflows in a scenario or future period is summarized in Figure 1. First AOGCM-RCM climate simulations are selected for the region of interest. Then, for each simulation, raw monthly precipitation (P) and temperature (T) data are statistical downscaled using the well-known delta change method to get bias-corrected time series. In the last step, the refined data for the future period is used as input data in a hydrological model previously calibrated to estimate the modified natural inflows.

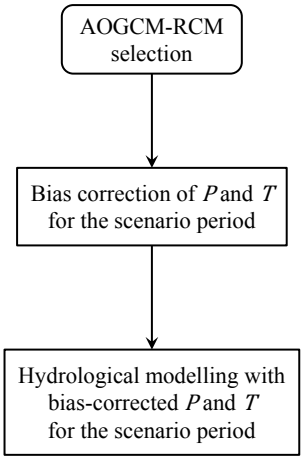

Figure 1. Simplified flowchart for the determination of climate change impacts on natural inflows.

2.1 AOGCM-RCM selection

The EURO-CORDEX project (http://www.euro-cordex.net/) is one of the programmes sponsored by the World Climate Research Program (WRCP) to organize an internationally coordinated framework to produce improved regional climate change projections for all land regions world-wide. Under this programme, ensemble AOGCM-RCM climate simulation with a resolution of 0.11 (~12.5 km) and 0.44 degree (~50 km) are provided for the European domain. The climate projections from the EURO-CORDEX project are based on multiple dynamical and empirical-statistical downscaling models forced by multiple global climate models from the Coupled Model Intercomparison Project Phase 5 (CMIP5) for different Representative Concentration Pathways (RCP) scenarios of greenhouse gas concentration trajectories in the atmosphere.

2.2 Delta change method

The underlying idea of the well-known delta change method is to use changes in average values from AOGCM-RCM simulated data for the control period and the scenario period to correct observed values (the observed values and the simulated data for the control period should be coincident in time). For the future scenario, the AOGCM-RCM simulated anomalies between that scenario and the control time series are superimposed upon the observed time series. Here, the anomalies are computed on a monthly basis:

$$\delta_{P,k} = \frac{\bar{P}_{sim\_s,k}}{\bar{P}_{sim\_c,k}} \tag{1}$$

$$\delta_{T,k} = \bar{T}_{sim\_s,k} - \bar{T}_{sim\_c,k} \tag{2}$$

where $\bar{P}_{sim\_s,k}$ ($\bar{T}_{sim\_s,k}$) and $\bar{P}_{sim\_c,k}$ ($\bar{T}_{sim\_c,k}$) are average monthly precipitation (temperature) values provided by one AOGCM-RCM for the future (sim_s) and the control period (sim_c), respectively. Then, the anomalies $\delta_{P,k}$ and $\delta_{T,k}$ are used as correction factors. A multiplicative correction is applied to the observed values of precipitation, where as an additive correction is made to adjust temperature:

$$P_{fut,ky} = P_{obs,ky} \times \delta_{P,k} \tag{3}$$

$$T_{fut,ky} = T_{obs,ky} + \delta_{T,k} \tag{4}$$

where $P_{obs,ky}$ ($T_{obs,ky}$) is the observed value (obs) of precipitation (temperature) for month k in year y of the time series, and $P_{fut,ky}$ ($T_{fut,ky}$) is the adjusted value of precipitation (temperature) for the scenario period (fut) for month k in year y of the time series.

All time series (obs, sim_c, sim_s and fut) have the same extent (e.g., 30 years). The same past period is covered by obs and sim_c (e.g., 1971-2000), and the same future period is covered by sim_s and fut (e.g., 2071-2100).

The main drawback of the delta change method is that it does only account for potential future changes in average values (Teutschbein and Seibert, 2012; Camici et al., 2014). Changes in climate variability (e.g., number of wet days vs. dry days) and in statistical properties (e.g., skewness), remain unchanged.

2.3 Hydrological model

The Temez model (Temez, 1977) is a simplification of the classic Stanford Watershed Model (SWM). Both models implement an aggregated approach to simulate the rainfall-runoff processes occurring on a watershed. The formulation of the Temez model includes only four parameters that need to be calibrated (the SVM includes 24 parameters that need to be determined): maximum soil holding capacity (H_{max}); maximum infiltration rate (I_{max}); runoff coefficient (C); and aquifer discharge coefficient (α). Estrela et al. (1999), Vaz (2010) and Paredes et al. (2014) present typical, minimum and maximum values for each parameter. The other two inputs are precipitation and potential evapotranspiration, and the main output is specific runoff (runoff per unit drainage area).

The Temez model is readily applied to small and medium watersheds in which there is some homogeneity regarding climatic, edaphological and geological characteristics. For larger watersheds, the spatial domain can be divided in sub-basins and, thus, allowing to implement a semi-aggregated approach. The model is usually run with a monthly time step although any other temporal discretization (e.g., hourly, daily or annual) can be used.

3. CASE STUDY

3.1 Introduction

The modification of the natural inflows was analysed for Odeleite reservoir-dam (Figure 2), located in the south of Portugal. The watershed of Odeleite reservoir is 348 km^2. This infrastructure is the main water source of an important multi-purpose water system for urban use and irrigation. The storage of water for future use is fundamental in a region in which the precipitation is low, intermittent and concentrated in a short winter, followed by a long and dry period.

The hydrological (Temez) model was calibrated with historic stream flows from December 1960 to June 2006 at Monte dos Fortes gauging station in a previous study (Nunes et al. 2009). This gauging station (drainage area = 284 km^2) is located upstream of Odeleite reservoir as indicated in Figure 2.

The natural inflows to the Odeleite dam were estimated using the specific runoff provided from the application of the Temez model calibrated for the single gauging station existing in the watershed multiplied by the drainage area of the reservoir. Monthly areal precipitation and temperature were computed through the Thiessen polygon method by using meteorological stations within the region (Figure 2). Average potential evapotranspiration determined by the Penman-Monteith method was considered by combining monthly temperature data with average monthly values of air humidity, radiation and wind speed for the calibration period.

For the bias correction step, the period 1971-2000 was selected as representative of the present-day climate in accordance with the use of EURO-CORDEX data.

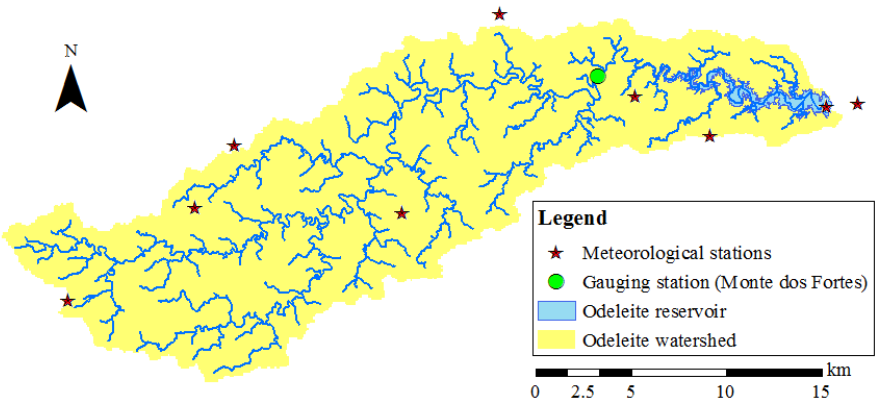

Figure 2. Study area and monitoring network.

3.2 AOGCM-RCM

In this study, three AOGCM-RCM simulations from the EURO-CORDEX project with a resolution of 0.11 degree were selected and combined with the two RCP scenarios defined for the IPCC AR5 report (RCP 4.5 and RCP 8.5) to evaluate potential impacts of climate change on the natural inflows to the Odeleite reservoir-dam for the period 2071-2100. Under RCP 4.5, aggregated greenhouse gas emissions peak around 2040, then decline. Under RCP 8.5, emissions continue to increase throughout the 21st century (Meinshausen et al., 2011).

The AOGCM-RCM used here correspond to the three simulation in which the same RCM (RCA4) was combined with different AOGCM (CNRM-CERFACS-CNRM-CM5, ICHEC-EC-EARTH and MPI-M-MPI-ESM-LR, in short, CNRM, ICHEC and MPI, respectively) in the project "Local Warning Website" (LWW – http://portaldoclima.pt/en/). The LWW is a project from a programme operated by the Portuguese Environment Agency on adaptation to climate change. Generally, the LWW has its main goal the increase of the capacity to assess vulnerability to climate change, to raise awareness and education on climate change in Portugal, and the LWW portal allows users to access weather data from selected simulations.

3.3 Results

3.3.1 Bias correction of AOGCM-RCM

The bias correction of the precipitation and temperature for the period 2071-2100 was carried out in accordance with the procedure described in section 2.2.

Figure 3 shows the changes in monthly precipitation under the two RCP scenarios (4.5 and 8.5). Under RCP 4.5, the increase in precipitation forecast in some autumn or winter months is not enough to counteract a decrease in the annual precipitation. Under RCP 8.5, the projections are fairly consistent for the decrease of precipitation in most months. Table 1 shows the average annual

values for all simulations. Less reduction in precipitation are projected by CNRM simulations for the two RCP scenarios. The reduction in annual precipitation is between -75.6 mm (-10 %) and -13.2 mm (-2 %) under RCP 4.5, and -207.8 mm (-28 %) and -117.9 mm (-16 %) under RCP 8.5.

The changes in temperature are consistent in the three AOGCM-RCM simulations for the two RCP scenarios (Figure 4). The variation of the average annual temperature is between +1.7ºC (+11 %) and +1.9ºC (+12 %) under RCP 4.5, and +3.4ºC (+21 %) and +3.7ºC (+22 %) under RCP 8.5 (Table 2).

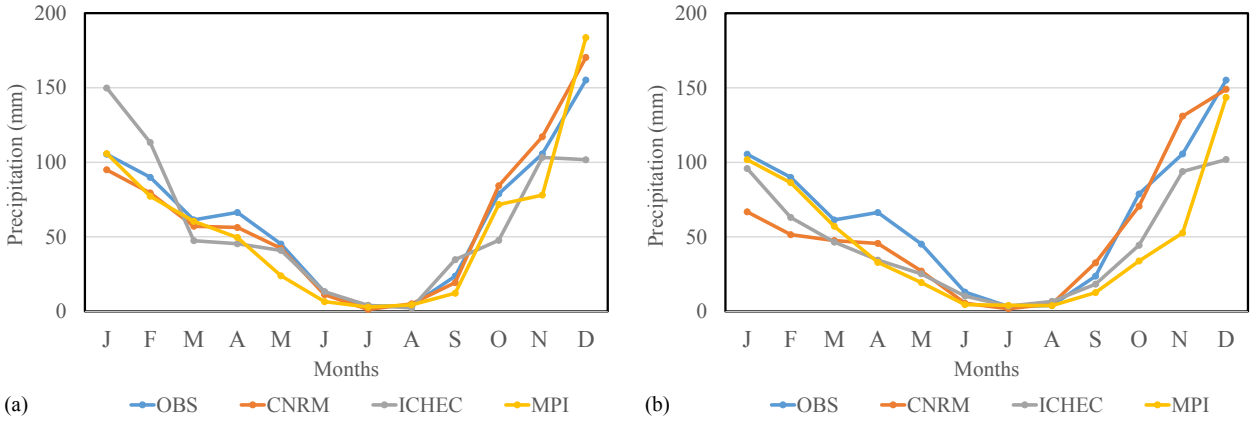

Figure 3. Comparison between the average monthly precipitation (mm) of the observed values in 1971-2000 (OBS) and the three selected AOGCM-RCM simulations (CNRM, ICHEC and MPI) for the period 2071-2100: (a) RCP 4.5 and (b) RCP 8.5.

Table 1. Comparison between the average annual precipitation (mm) of the observed values in 1971-2000 (OBS) and the three selected AOGCM-RCM simulations (CNRM, ICHEC and MPI) for the period 2071-2100 under RCP 4.5 and RCP 8.5.

Time series		**Average annual precipitation (mm)**	
OBS		751.8	
		RCP 4.5	**RCP 8.5**
AOGCM-RCM	CNRM	738.6	633.9
	ICHEC	703.9	544.0
	MPI	676.2	552.6

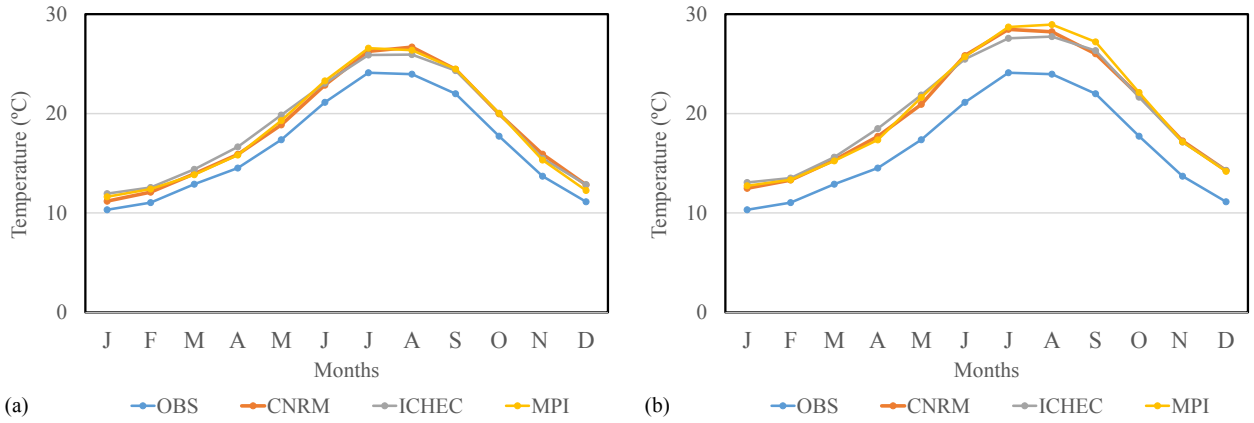

Figure 4. Comparison between the average monthly temperature (ºC) of the observed values in 1971-2000 (OBS) and the three selected AOGCM-RCM simulations (CNRM, ICHEC and MPI) for the period 2071-2100: (a) RCP 4.5 and (b) RCP 8.5.

Table 2. Comparison between the average annual temperature (ºC) of the observed values in 1971-2000 (OBS) and the three selected AOGCM-RCM simulations (CNRM, ICHEC and MPI) for the period 2071-2100 under RCP 4.5 and RCP 8.5.

Time series		Average annual temperature (ºC)	
OBS		16.7	
		RCP 4.5	**RCP 8.5**
AOGCM-RCM	CNRM	18.4	20.1
	ICHEC	18.6	20.2
	MPI	18.4	20.4

3.3.2 Potential evapotranspiration

Potential evapotranspiration and precipitation are the two meteorological input data of the hydrological model (section 2.3) used in the case study. The potential evapotranspiration for the period 2071-2100 under the two RCP scenarios was determined by the Penman-Monteith method combining the temperature given from the application of the delta change method (Figure 4 and Table 2) with historical monthly values of air humidity, radiation and wind speed. The increase in potential evapotranspiration is higher in summer months (Figure 5). Annually, the potential evapotranspiration increases 5% under RCP 4.5 and 10% under RCP 8.5 (Table 3).

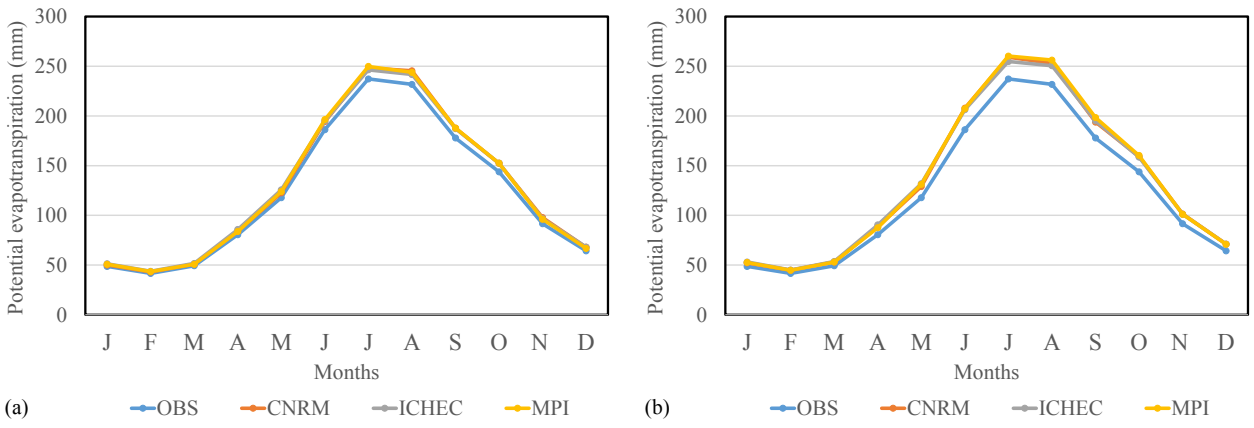

Figure 5. Comparison between the average monthly potential evapotranspiration (mm) for the period 1971-2000 (OBS) and the three selected AOGCM-RCM simulations (CNRM, ICHEC and MPI) for the period 2071-2100: (a) RCP 4.5 and (b) RCP 8.5.

Table 3. Comparison between the average annual potential evapotranspiration (mm) for the period 1971-2000 (OBS) and the three selected AOGCM-RCM simulations (CNRM, ICHEC and MPI) for the period 2071-2100 under RCP 4.5 and RCP 8.5.

Time series		Average annual potential evapotranspiration (mm)	
OBS		1470	
		RCP 4.5	**RCP 8.5**
AOGCM-RCM	CNRM	1544	1613
	ICHEC	1546	1611
	MPI	1546	1623

3.3.3 Inflows to the Odeleite reservoir

Figure 6 shows the average monthly natural inflows to the Odeleite reservoir estimated with the Temez model. In Figure 6, the inflows for the period 1971-2000 are compared with the minimum, average and maximum values obtained from using the bias-corrected precipitation and temperature/potential evapotranspiration for the period 2071-2100 (sections 3.3.1 and 3.3.2). The uncertainty is significant under the two RCP.

Under RCP 4.5 (Figure 6a), all climate change projections lead to a decrease of the average inflows in spring months (March, April and May). In the other months, the modified natural inflows given from using different AOGCM-RCM simulations do not show the same relation (higher or below) with the inflows for the period 1971-2000. On other hand, natural inflows calculated with ICHEC bias-corrected input data are the highest in January and February and the lowest in December from using the three different AOGCM-RCM simulations. From Figure 3a, it can be seen that those modified inflows are closely related with the modification of the precipitation regime. The rainfall projections from ICHEC simulation for the period 2071-2100 are significant higher than the observed values in January and February and the lowest in December. In the period of one year, the three AOGCM-RCM simulations anticipate a decrease of the average annual inflows between -10.0 hm^3 (-10%) with ICHEC and -1.8 hm^3 (-2%) with CNRM (Table 4).

Under RCP 8.5 (Figure 6b), the average inflows decrease in all months and AOGCM-RCM except in November with CNRM. But the magnitude of the reductions is different from using the different input data. In the period of one year, the three AOGCM-RCM simulations lead to a decrease of the average annual inflows between -43.6 hm^3 (-44%) with ICHEC and -23.9 hm^3 (-24%) with CNRM (Table 4).

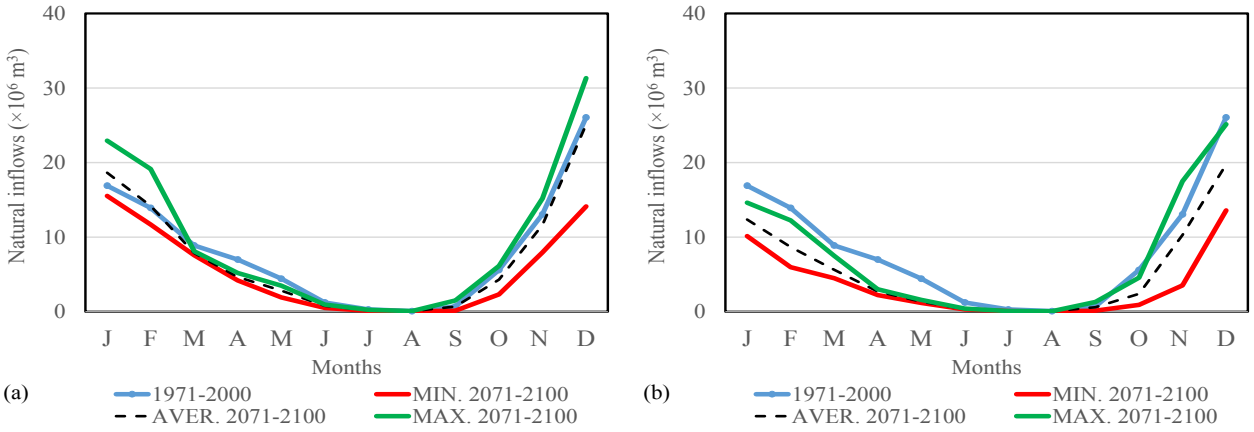

Figure 6. Comparison between the average monthly natural inflows (1 hm^3 = 10^6 m^3) estimated for the period 1971-2000 and minimum, average and maximum values for the period 2071-2100: (a) RCP 4.5 and RCP 8.5.

Table 4. Comparison between the average annual natural inflows (1 hm^3 = 10^6 m^3) estimated for the period 1971-2000 and to the period 2071-2100 under RCP 4.5 and RCP 8.5.

Time series		**Average annual inflows (hm^3)**	
OBS		98.2	
		RCP 4.5	**RCP 8.5**
AOGCM-RCM	CNRM	96.4	74.3
	ICHEC	88.2	54.6
	MPI	88.5	64.0

4. CONCLUSIONS

In this paper, it has been applied a modelling approach for estimating the changes in the natural inflows of watersheds. The methodology consists in a sequence of steps: selection of AOGCM-RCM simulations, bias correction (or statistical downscaling) of meteorological data and hydrological modelling one the future scenario.

The approach was applied to evaluate future natural inflows (2071-2100) to Odeleite reservoir-dam under two emission scenarios (RCP 4.5 and 8.5). Three AOGCM-RCM were used and bias correction was made with the well-known delta change method. The results indicate significant differences in the runoff for each RCP depending on the AOGCM-RCM used. The decrease of the natural inflows under RCP 4.5 is between -10% and -2%. Under RCP 8.5, the decrease of the natural inflows is much higher between -44% and -24%.

Subsequent studies will be pursued with other AOGCM-RCM and bias correction methods as these two factors are two important sources of uncertainty in climate change projections and in impact studies for the water sector.

ACKNOWLEDGEMENTS

This study had the support of Fundação para a Ciência e Tecnologia (FCT), through the strategic project UID/MAR/04292/2013 granted to MARE.

REFERENCES

Berg, P., Feldmann, H., Panitz, H. J., 2012. Bias correction of high resolution regional climate model data. Journal of Hydrology, 448: 80-92. doi: 10.1016/j.jhydrol.2012.04.026

Camici, S., Brocca, L., Melone, F., Moramarco, T., 2014. Impact of climate change on flood frequency using different climate models and downscaling approaches. Journal of Hydrologic Engineering, 19(8):04014002. doi: 10.1061/(Asce)He.1943-5584.0000959

Christensen, J. H. et al., 2007. The Physical Science Basis. Contribution of Working Group I to the Fourth Assessment Report of the Intergovernmental Panel on Climate Change. Edited by: Solomon et al., Cambridge University Press, Cambridge, United Kingdom and New York, NY, USA.

Estrela, T., Cabezas, F., Estrada, F., 1999. La evaluación de los recursos hídricos en el Libro Blanco del Agua en España [The evaluation of the water resources in the White Paper of Water in Spain]. Ingeniería del Agua, 6(2): 125-138

Fowler, H. J., Blenkinsop, S., Tebaldi, C., 2007. Linking climate change modelling to impacts studies: recent advances in downscaling techniques for hydrological modelling. International Journal of Climatology, 27(12): 1547-1578. doi: 10.1002/joc.1556

Lafon, T., Dadson, S., Buys, G., Prudhomme, C., 2013. Bias correction of daily precipitation simulated by a regional climate model: a comparison of methods. International Journal of Climatology, 33(6): 1367-1381. doi: 10.1002/joc.3518

Meinshausen, M. et al., 2011. The RCP greenhouse gas concentrations and their extensions from 1765 to 2300. Climatic Change, 109(1-2): 213-241. doi: 10.1007/s10584-011-0156-z

Nunes, L. M. et al., 2009. Projecto OPTEXPLOR – Relatório Final [Project OPTEXPLOR—Final report]. Universidade do Algarve, IMAR-Universidade de Coimbra, CVRM-IST, Faro, Portugal.

Paredes, J., Solera, A., Andreu, J., Lerma, N., 2014. Herramienta EvalHid para la evaluación de recursos hídricos [EvalHid tool for the evaluation of water resources]. Technical Manual v1.1, Universidad Politécnica de Valencia, Valencia, Spain.

Pulido-Velazquez, D., Garcia-Arostegui, J. L., Molina, J. L., Pulido-Velazquez, M., 2015. Assessment of future groundwater recharge in semi-arid regions under climate change scenarios (Serral-Salinas aquifer, SE Spain). Could increased rainfall variability increase the recharge rate? Hydrological Processes, 29(6): 828-844. doi: 10.1002/hyp.10191

Temez, J. R., 1977. Modelo matemático de transformación precipitación-aportación. [Rainfall-runoff mathematical model]. Asociación de Investigación Industrial Eléctrica (ASINEL), Madrid, Spain.

Teutschbein, C., Seibert, J., 2012. Bias correction of regional climate model simulations for hydrological climate-change impact studies: Review and evaluation of different methods. Journal of Hydrology, 456:12-29. doi: 10.1016/j.jhydrol.2012.05.052

Vaz, J., 2010. Modelos de transformação da precipitação em escoamento à escala mensal: aplicação a três casos de estudo em Moçambique [Rainfall-runoff models at a monthly timescale: application to three case studies in Mozambique]. MSc Thesis, Instituto Superior Técnico, Universidade de Lisboa, Lisbon, Portugal.

Proceedings of the 10th World Congress of EWRA 'Panta Rhei', 5-9 July 2017, Athens, Greece
© 2017 *European Water Resources Association*

Spatial analysis of large atmospheric oscillations and annual precipitation in lake Urmia basin

B. Vaheddoost
Department of Civil Engineering, Istanbul Technical University, Turkey
e-mail: vaheddoostb@itu.edu.tr

Abstract: Precipitation is the main phenomenon that brings water from the surface of the oceans to the land surface all around the world. Oscillation of large atmospheric patterns, happening in oceans however is proved to have a great effect on the pattern of precipitation based on spatiotemporal and geographical properties of the region. Lake Urmia, as a wetland of international importance and the world's second largest hyper-saline lake is dealing with water shortage basin wide. Due to importance of studying behaviour of major role players in the basin, effect of several well-known large atmospheric oscillations namely, North Atlantic Oscillation (NAO), El Nino/Southern Oscillation (ENSO), Atlantic Multidecadal Oscillation (AMO), Arctic Oscillation (AO), Indian Ocean Dipole (IOD), Southern Annular Mode (SAM) and Pacific Decadal Oscillation (PDO) were investigated by means of zero-lagged cross-correlation projected on heat maps on the basin. Considering 95% confidence limit in the analysis, it is observed that the PDO, ENSO, IOD and SAM oscillations have significant correlations with annual precipitation. In addition, harmonic means of annual precipitation, Euclidian distance and mutual information coefficient were used in comparison with cross-correlation patterns in order to define the most effective oscillations. It is concluded that ENSO oscillation pattern has the most similar pattern with harmonic mean of annual precipitation while the PDO has the major effect across the basin.

Key words: Lake Urmia, large atmospheric oscillation, precipitation, spatial analysis

1. INTRODUCTION

Lake Urmia is one of the most important hyper-saline lakes in the world and a terminal lake for migrant birds. Precipitation as the cornerstone of lake hydrological cycle is being fed by water evaporated from large bodies of water around the world. Large atmospheric oscillations are periodic or quasi-periodic cycles associated with climate patterns like atmospheric temperature, sea surface temperature, precipitation etc. which usually change as inter-annual and/or multi-annual patterns. The most well-known oscillation are North Atlantic Oscillation (NAO), El Niño/Southern Oscillation (ENSO), Atlantic Multidecadal Oscillation (AMO), Arctic Oscillation (AO), Indian Ocean Dipole (IOD), Southern Annular Mode (SAM) and Pacific Decadal Oscillation (PDO).

NAO is a weather phenomenon happening in North Atlantic Ocean causing changes in atmospheric pressure at sea level between the Icelandic low and the Azores high. El Niño is happening due to warming water surface in the eastern tropical Pacific Ocean by the sun. Together with La Niña, it pushes the limits of two out of three states of the constantly changing ENSO oscillation that can affect weather patterns around the globe. AMO is also a climate oscillation which is effective on the sea surface temperature in North Atlantic Ocean. AO or also called Northern Annular Mode/Northern Hemisphere Annular Mode (NAM) is an index of the non-seasonal sea-level pressure variating in the north of the 20˚ northing latitude. IOD, also known as the Indian Niño, is an irregular pattern of oscillation in the sea-surface temperatures in which the western Indian Ocean becomes alternately warmer and then colder than the eastern part of the ocean. SAM oscillation, also known as Antarctic oscillation (AAO) or Southern Hemisphere Annular Mode (SHAM) is a low-frequency mode of atmospheric variability of the southern hemisphere. PDO, is a long-lived oscillation very similar to the El Niño pattern in Pacific climate variability, while the two climate oscillations have similar spatial climate fingerprints, they have

very different temporal behaviour.

There are several studies about the effect of these oscillations on precipitation, in which Marchane et al. (2016) and Pavia et al. (2016) are among those who investigated the effect of large atmospheric oscillations on precipitation recently. The structure and characteristics of annual precipitation in Lake Urmia basin was detailed by Vaheddoost and Aksoy (2017); also Alipour (2006), Hassanzadeh et al. (2012), Delju et al. (2013), Tabari et al. (2013), Ghajarnia et al. (2015), Alizadeh-Choobari et al. (2016), Fathian et al. (2016) and Fazel et al. (2017) studied precipitation characteristics in Lake Urmia Basin. However, the effect of large atmospheric oscillations in Lake Urmia basin was not studied in details. Although the effect of these oscillations on annual precipitation around the world is too coarse to be detailed at annual time interval, a multi-annual analysis can also reveal the effect of major role players within the basin. In this study, precipitation data recorded in 53 meteorological stations across the basin from 1981 to 2011 are used. Time series of 31 years of recorded data are compared with annual time series of NAO, ENSO, AMO, AO, IOD, SAM and PDO oscillations.

2. DATA

Data used in this study are total annual precipitation of 53 stations sharing 31 years of common record length from 1981 to 2011. A comparison over similarities between total annual precipitation characteristics and major atmospheric oscillations is aimed in this study. As Vaheddoost and Aksoy (2017) concluded, Box and Whiskers plots of selected stations show existence of outliers within the data which cause in positive asymmetry over distributions (Figure 1).

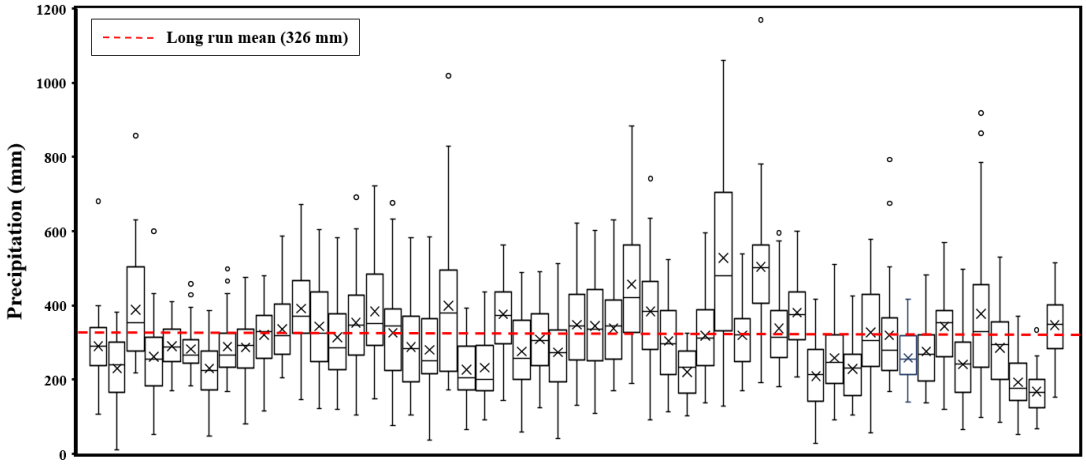

Figure 1. Box and Whiskers plot of annual precipitation in stations over Lake Urmia basin.

Time series of the stations were compared with the annual time series of selected oscillations provided from National Oceanic and Atmospheric Administration of United States (NOAA, 2015). Zero-lag cross-correlation between annual precipitation over the basin crossed with oscillation time series in which ENSO, SAM, IOD and PDO showed significant linear correlation with precipitation. This significance boundary was considered based on 95% confidence limit over 31 years as ±0.35 to define the degree of significance in analysis.

Most of the oscillations are effective in western and south-western parts of the basin. It is found that NAO, has no major effect on the basin, while there are a few hot spots with insignificant positive cross-correlation in south-west, west and east of the lake. The same analysis can be associated with AO and AMO oscillations which have positive effect mostly on south-west, south and east of the lake. PDO however, has a major and significant effect on precipitation in west, centre and south parts of the basin. On the other hand, analysis for IOD and SAM shows more effective and positively correlated precipitation in eastern side of the basin.

3. METHODS USED

To define and track the degree of similarity and concordance between each pair of station-oscillation time series, several methods are used. Harmonic mean of annual precipitation in each station is used to reduce the effect of interdependence in time and space over time series. Harmonic mean tends toward the least elements of the data set (i.e. compared to the arithmetic mean) to mitigate the impact of large outliers and aggravate the impact of small ones. The degree of graphical concurrency is measured by the match of hotspots over heat map and iso-height map. Considering time series analysis, the most common metric is the Euclidean distance which measures the length of a vector between *x* and *y* as

$$\left|D_{xy}\right|_t = \sqrt{\left(x_t - y_t\right)^2} \tag{1}$$

where $|D_{xy}|_t$ is the distance between time series *X* and *Y* at time *t*. Analysis between harmonic mean of precipitation and oscillation time series are both standardized, to be used as a measure of comparison. Results of this comparison are shown on heat maps over basin, while stations with lower Euclidean distance shows more similarities with the atmospheric oscillations. Mutual information coefficient (MIC) is also used to determine the amount of information attainable within the data. Mutual information contains information about all linear and nonlinear dependence in time.

There are sophisticated methods of calculating mutual information coefficient while a simple one is suggested by Gel'fand and Yaglom (1957) as

$$MIC = \frac{-\log\left(1 - r_{xy,t}^2\right)}{2} \tag{2}$$

where $r_{xy,t}$ is the cross-correlation coefficient between annual precipitation and atmospheric oscillation. Results of this analysis are also shown on heat map over basin.

4. RESULTS AND DISCUSSION

4.1 ENSO

Results of Euclidean distance, mutual information and overlaying harmonic mean on cross-correlation between annual precipitation and ENSO time series are shown in Figure 2.

Figure 2a shows that the dissimilarity between annual precipitation and ENSO time series is lower in western and southern coasts of the lake. Since these stations have significant correlation with ENSO time series, it is almost confident to say that, irregular break through is caused by ENSO in these stations. Figure 2b also shows the distribution of mutual information coefficient across the basin. It does not contain a lot of information as the variation changes in the range of 0.07 to -0.05. There is also a hot spot in the northern hillside of the mount Sahand (3707 m above sea level) which shows a low distance in comparison with other parts of the basin. These results are also in concordance with Figure 2c, which shows that harmonic mean (Contour map) of the annual precipitation is graphically similar to cross-correlation (heat map).

4.2 SAM

The same analysis as used in the analysis of similarities in ENSO oscillation is carried out to track down the similarities between the two-time series. Figure 3 shows the results of comparison

between SAM and annual precipitation time series across the Lake Urmia basin.

Figure 3a shows that the Euclidean distance is high everywhere while eastern and western parts of the basin shows more similarities. It also shows that the distance between precipitation and SAM oscillation is very high over Lake Urmia. Hence, precipitations over the lake are not following the same order. Two hot spots with the least distance in Figure 3a can be confirmed in Figure 3b. One of these hot spots is located on the summit of mount Sahand and the other one is located near the basin border in south-west. Figure 3c, shows the harmonic mean contour map on the cross-correlation heat map, while the similarity between two patterns is not significant graphically. There is a shift to the left while the general pattern is not preserved.

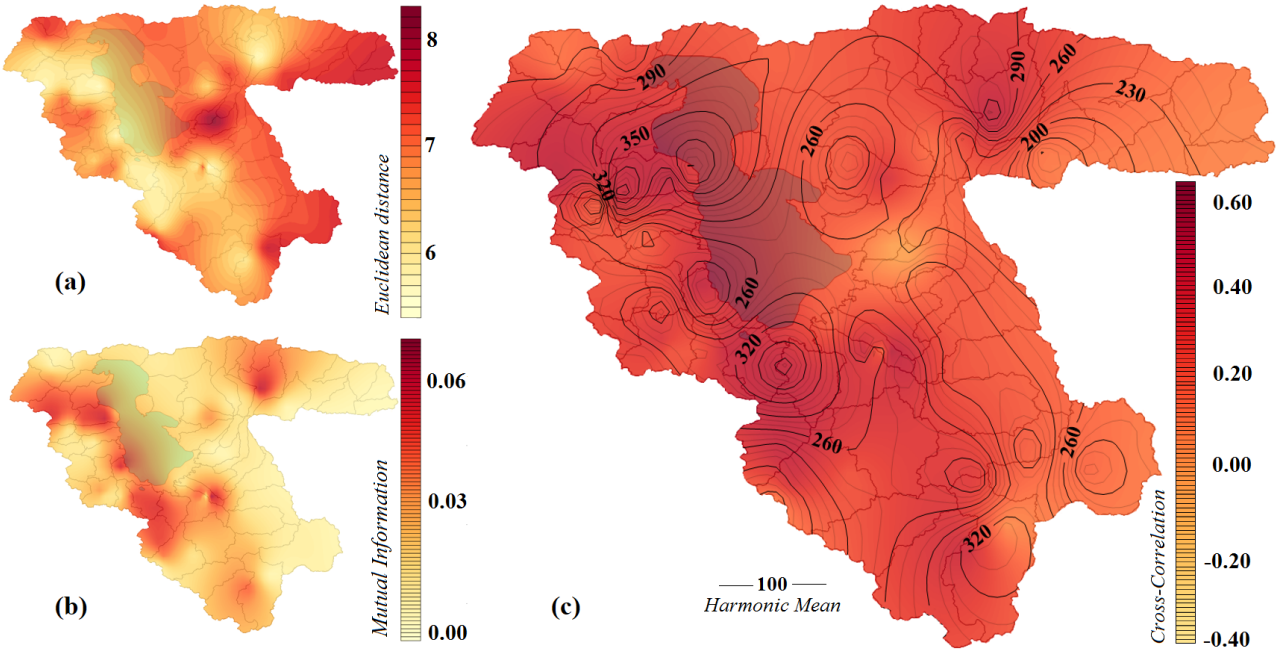

Figure 2. Analysis of ENSO oscillation over basin by (a) Euclidean distance, (b) mutual information coefficient and (c) overlaying harmonic mean on cross-correlation heat map.

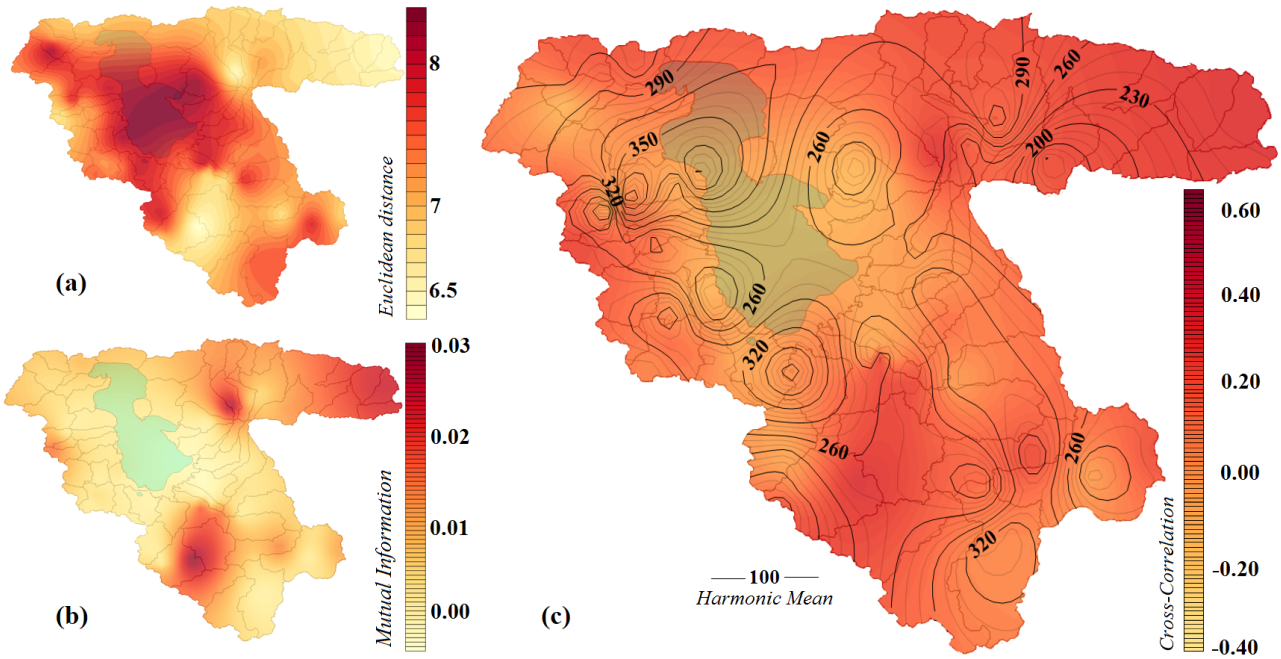

Figure 3. Analysis of SAM oscillation over basin by (a) Euclidean distance, (b) mutual information coefficient and (c) overlaying harmonic mean on cross-correlation heat map.

4.3 IOD

The same analysis as used for ENSO and SAM oscillation comparatively is used for tracking the patterns of similarities (Figure 4).

Figure 4a shows that the similarities between annual precipitation and IOD time series is higher in eastern and southern parts of the basin. Mutual information however, shows that summit of mount Sahand is also affected by IOD oscillation (Figure 4b). It should be underlined that the hot spot associated with the southern part of the basin in mutual information is shifted to the north according to Euclidean distance map (Figure 4a) or contain similarities with much more distant length (similarities). Hence, eastern parts of the basin contain more information interconnected with IOD oscillation. Figure 4c, also shows that IOD oscillation has similarities with harmonic mean of the annual precipitation.

4.4 PDO

Figure 5, shows that the harmonic mean and PDO oscillation have a perfect graphical match while almost all of the hotspots are crossed over cross-correlation patterns. In addition, it is obvious that the PDO oscillation is effective mostly in western and southern parts of the Lake Urmia basin.

Euclidean distance shows that the highest similarities can be tracked in the western side of the basin (Figure 5a). There are also a few similarities in northern, western and southern hillside of the mount Sahand. Figure 5b shows that the disturbed pattern of annual precipitation in north-west, south –west and south of the basin. It demonstrates that the uncertainty associated with annual precipitation in western and southern parts of the basin can be related to the PDO oscillation. Figure 5c, however shows more hotspots in western parts of the basin.

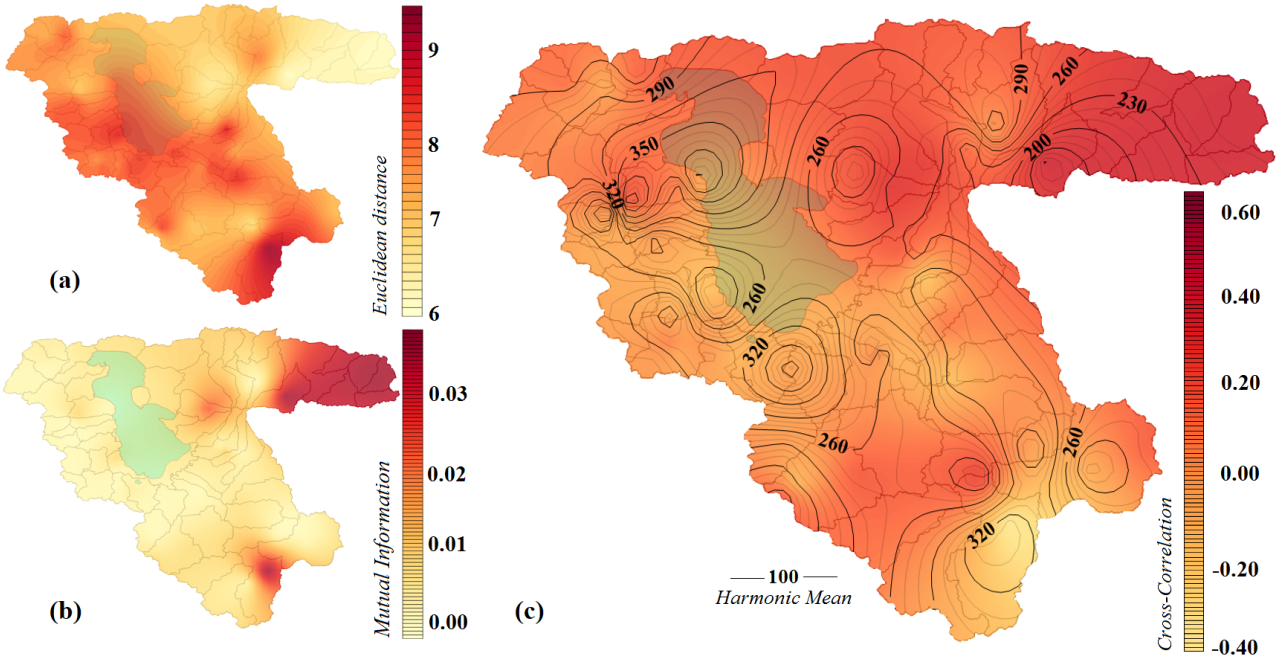

Figure 4. Analysis of IOD oscillation over basin by (a) Euclidean distance, (b) mutual information coefficient and (c) overlaying harmonic mean on cross-correlation heat map.

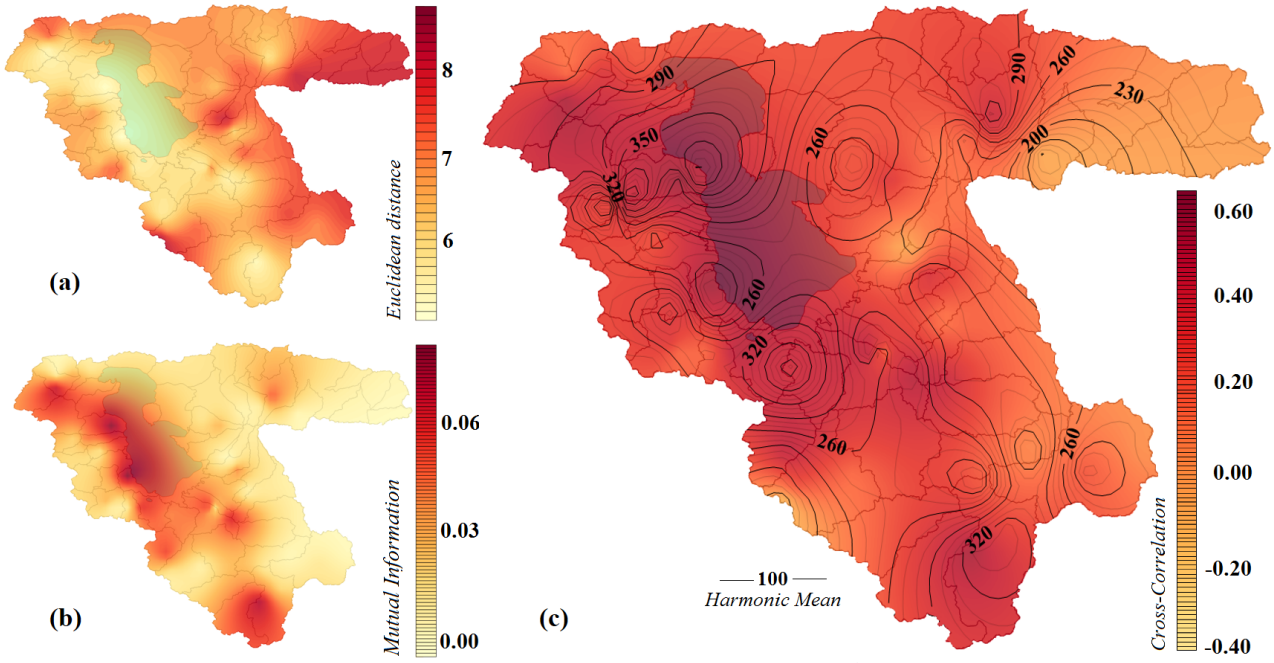

Figure 5. Analysis of PDO oscillation over basin by (a) Euclidean distance, (b) mutual information coefficient and (c) overlaying harmonic mean on cross-correlation heat map.

5. CONCLUSION

Similarities between annual precipitation and large atmospheric patterns of NAO, ENSO, AMO, AO, SAM, IOD and PDO are studied using cross-correlation, Euclidean distance and mutual information coefficient. Results of these analysis are expressed using heat map and contour map over Lake Urmia basin. It is concluded that ENSO, SAM, IOD and PDO have the most effect at annual scale on the precipitation over the basin. Results indicate that the harmonic mean has the most graphical similarities with cross-correlation of annual precipitation and PDO oscillation. It is also obvious that Euclidean distance and mutual information express more information in comparison with other similarity metrics such as Pearson correlation coefficient. Therefore, IOD and SAM oscillations in the eastern and ENSO and PDO oscillations in western and southern parts of the basin are effective.

REFERENCES

Alipour, S. (2006). Hydrogeochemistry of seasonal variation of Urmia Salt Lake, Iran. Saline systems 2(1): 1. DOI: 10.1186/1746-1448-2-9.

Alizadeh□Choobari, O., Ahmadi□Givi, F., Mirzaei, N., and Owlad, E. (2016). Climate change and anthropogenic impacts on the rapid shrinkage of Lake Urmia. International Journal of Climatology 36: 4276–4286. DOI: 10.1002/joc.4630.

Delju, A. H., Ceylan, A., Piguet, E., and Rebetez, M. (2013). Observed climate variability and change in Urmia Lake Basin, Iran. Theoretical and applied climatology 111(1-2): 285-296. DOI: 10.1007/s00704-012-0651-9.

Fathian, F., Aliyari, H., Kahya, E., and Dehghan, Z. (2016). Temporal trends in precipitation using spatial techniques in GIS over Urmia Lake Basin, Iran. International Journal of Hydrology Science and Technology 6(1): 62-81. DOI: 10.1504/IJHST.2016.073883.

Fazel, N., Berndtsson, R., Uvo, C. B., Madani, K., & Kløve, B. (2017, in press) Regionalization of precipitation characteristics in Iran's Lake Urmia basin. Theoretical and Applied Climatology, 1-11. DOI: 10.1007/s00704-017-2090-0

Gel'fand, I.M., Yaglom, A.M. (1957). Calculation of amount of information about a random function contained in another such function. American Mathematical Society Translations: Series 2. 12: 199–246. English translation of original in Uspekhi Matematicheskikh Nauk 2 (1): 3-52.

Ghajarnia, N., Liaghat, A., and Arasteh, P. D. (2015). Comparison and evaluation of high resolution precipitation estimation products in Urmia Basin-Iran. Atmospheric Research 158: 50-65.

Hassanzadeh, E., Zarghami, M., and Hassanzadeh, Y. (2012). Determining the main factors in declining the Urmia Lake level by using system dynamics modeling. Water Resources Management 26(1): 129-14. DOI:10.1007/s11269-011-9909-8.

Marchane, A., Jarlan, L., Boudhar, A., Tramblay, Y., and Hanich, L. (2016). Linkages between snow cover, temperature and rainfall and the North Atlantic Oscillation over Morocco. Climate Research 69(3): 229-238. DOI:10.3354/cr01409.

National Oceanic and Atmospheric Administration (NOAA). (2015). Climate Indices: Monthly Atmospheric and Ocean Time Series. http://www.esrl.noaa.gov/psd/data/climateindices/list/. Accessed 15 Jun 2015

Pavia, E. G., Graef, F., and Fuentes□Franco, R. (2016). Recent ENSO–PDO precipitation relationships in the Mediterranean California border region. Atmospheric Science Letters 17(4): 280-285. DOI: 10.1002/asl.656

Tabari, H., Nikbakht, J., and Talaee, P. H. (2013). Hydrological drought assessment in North-western Iran based on streamflow drought index (SDI). Water resources management 27(1): 137-151. doi:10.1007/s11269-012-0173-3.

Vaheddoost, B., and Aksoy, H. (2016, in press). Structural characteristics of annual precipitation in Lake Urmia basin. Theoretical and Applied Climatology (-): 1-14. DOI: 10.1007/s00704-016-1748-3.

Proceedings of the 10th World Congress of EWRA 'Panta Rhei', 5-9 July 2017, Athens, Greece
© 2017 *European Water Resources Association*

Seasonal and annual trend analysis of meteorological data in Sanliurfa, Turkey

V. Gümüş[1*], N.G. Soydan[2], O. Şimşek[2], H.M. Algin[1], M.S. Aköz[2] and K. Yenigun[2]
[1] *Harran University, Civil Engineering Department, Sanliurfa, Turkey*
[2] *Cukurova University, Civil Engineering Department, Adana, Turkey*
[*] *e-mail: gumus@harran.edu.tr*

Abstract: Global rising temperature has become more of an issue among societies and governments worldwide due to the environmental changes and climate warming. In this regard, the trend analysis of hydro-meteorological variables (such as precipitation, temperature, wind speed, humidity etc.) provides reliable outcomes for a better planning and management of water resources. Historical data possess time dependent characteristics that are generally being affected by climate variability and changes. For this reason, it is vitally important to scrutinize the changes in hydro-meteorological parameters for water supply management. In this study, minimum temperature (MiT), maximum temperature (MaT), mean temperature (MeT), mean humidity (MH), mean wind speed (MWS) and total precipitation (TP) data are obtained for the period from 1975 to 2015 for Sanliurfa region which is an important agricultural area located at the southern east of Turkey. According to the meteorological data, the trend analysis is carried out using non-parametric Mann Kendall and Spearman's Rho tests. Sen's slope trend method is employed for detecting the slopes of trend. The beginning years for the trend of the stations which present statistically significant trend are estimated using Mann-Kendall Rank Correlation test. Accordingly, the variations in hydro meteorological data in Şanlıurfa province during 1975 to 2015 have been examined in detail.

Key words: Sanliurfa region, Trend Analysis, Mann-Kendall Test, Spearman's Rho Test, Sen's slope

1. INTRODUCTION

Climate change can be described as major variations in the average climate in long terms. Although the climate change is taking place on a global scale, its effects are generally varying from region to region (Trajkovic and Kolakovic, 2009). For this reason, the trend analysis on the meteorological variables represents an important task in determining the climate change and water resources planner. In recent times many researchers have given great importance to the trend analysis for the hydro-meteorological variables due to climatic changes. A number of studies have been conducted to identify trends in climate change occurred worldwide. (Erlat and Türkeş, 2012, Sayemuzzaman et al., 2015, Chowdhury et al., 2015, Adarsh and Janga Reddy, 2015, Mohsin and Gough, 2009, Madsen et al., 2014). However, most of these studies have focused only on temperature and precipitation variations. Bahadır and Özdemir (2011) carried out the statistical analysis on the changes in the watershed climate and the level of Iznik Lake to determine the trend analysis. For the determination of the relationship between the climate elements and the variations in the lake elevation, the correlation and the regression analyses were carried out. The trend inclinations were determined using Quadratic and Linear Trend models. As a result, it was estimated that according to the trend analysis carried out in order to determine the level changes of Iznik lake, the lake level may decrease approximately 30 cm until the year of 2025. Altın et al. (2012) examined the variations in precipitation and temperature data from 1975 to 2007 for the 33 stations at the borders of the Central Anatolian Region. According to the Mann-Kendall test results, it was stated that the intensity of rainfall decreases in winter and spring, and increases in summer and autumn. Gocic and Trajkovic (2013) analysed the annual and seasonal trends of seven meteorological variables for the twelve weather stations in Serbia during 1980-2010. The non-parametric Mann-Kendall and Sen's methods were used to determine the trend in weather data.

They stated that the results of using the Mann-Kendall and Sen's tests demonstrated the good agreement of performance in detection of the trend for meteorological variables. Kisi (2015) performed a trend analysis of monthly pan evaporations by using recently developed innovative trend analysis (ITA) method for the six different locations in Turkey. They investigated the monthly trends of pan evaporation by non-parametric Mann–Kendall (MK) method. According to ITA and Mann-Kendall method results, the trends for six locations were estimated. Wu and Qian (2016) investigated the trends in annual and seasonal rainfall at the 14 rainfall stations in Shaanxi Province, China, using the methods of ITA, Mann–Kendall test and linear regression analysis. The aim of their study was to evaluate the results from ITA with the Mann-Kendall test and linear regression analysis and to identify the statistical significant trends.

In this study, the trend analysis on the six meteorological variables (i.e. minimum temperature-MiT, maximum temperature-MaT, mean temperature-MeT, mean humidity-MH, mean wind speed-MWS and total precipitation-TP) for Sanliurfa station located in the southeast of Turkey. It is performed for seasonal and annual data. The non-parametric Mann-Kendall and Spearman's Rho tests are used to determine the significant trend. Sen's slope trend method is used to determine the slopes of trend. The beginning years for the trend of the stations which present the significant trend are determined using the Mann-Kendall Rank Correlation test.

2. MATERIALS AND METHODS

2.1 Study area and data

Since Sanliurfa region is having important characteristics for the economic and social developments in Turkey, this region is selected in this study to determine the trend of the meteorological variables for this region.



Figure 1. Study Area

The 41-year (1975-2015) monthly mean, maximum and minimum temperature, wind speed, humidity and total precipitation values from Sanlıurfa station obtained from Turkish State Meteorological Service and used to determine the seasonal and annual trend analysis. The seasonal and annual mean values of the meteorological variables are given in Table 1.

Table 1. The seasonal and annual mean values of the meteorological variables

	MeT (°C)	MiT (°C)	MaT (°C)	MWS (m/s)	MH (%)	TP (mm)
Winter	6.82	-1.62	17.10	1.24	69.18	225.8
Spring	16.70	5.34	29.65	1.67	54.14	131.6
Summer	30.66	18.60	41.58	2.19	33.70	5.7
Autumn	19.95	9.54	32.43	1.43	49.27	79.5
Annual	18.53	7.96	30.19	1.63	51.57	443.8

2.2 Methods

In this study, the Mann–Kendall test (Mann, 1945, Kendall, 1948) and Spearman's Rho test (Yue and Wang, 2002) are used to determine statistically significant trend for the meteorological variables. These tests are popular and reliable non-parametric tests for the hydro-climatological time series and widely used worldwide. Since the Mann–Kendall and Spearman's Rho tests requires time series to be serially independent, in order to remove the serial correlation from the data sets, Von Storch and Navarra (1995) have suggested to pre-whiten the time series data in advance. Therefore, the serial correlation is tested before applying the Mann–Kendall and Spearman's rho tests. The detail of this procedure is given in Gocic and Trajkovic (2013).

The Mann–Kendall rank correlation test is used to determine the trend-initiating year. This test does not take differences in magnitude of the values into account, it only counts the number of consecutive values where the value increases or decreases compared with the prior values (Yenigün ve ark. 2008). The true slope in terms of the per unit time is estimated by adopting a following non-parametric procedure developed by Sen (1968) for the case of a linear trend (Kahya and Kalaycı, 2004, Yenigün et al., 2008).

3. RESULTS

Figure 2 provides the Lag-1 serial correlation coefficients for the considered parameters of mean, maximum and minimum temperature, wind speed, humidity and total precipitation (denoted as MeT, MiT, MaT, MWS, MH and TP, respectively) based on the seasonal and annual periods. The bold lines in Figure 2 represents the probability limits on the correlogram for an independent series of r_1. Figure 2 shows both positive and negative serial correlation for all variables. Figure 2 indicates that the positive serial correlation is determined to be significant in all meteorological variables except TP, and the corresponding negative serial correlation is obtained for only the summer session of TP values. The trend analysis is undertaken using the pre-whitened time series, in order to remove serial correlation from the data sets.

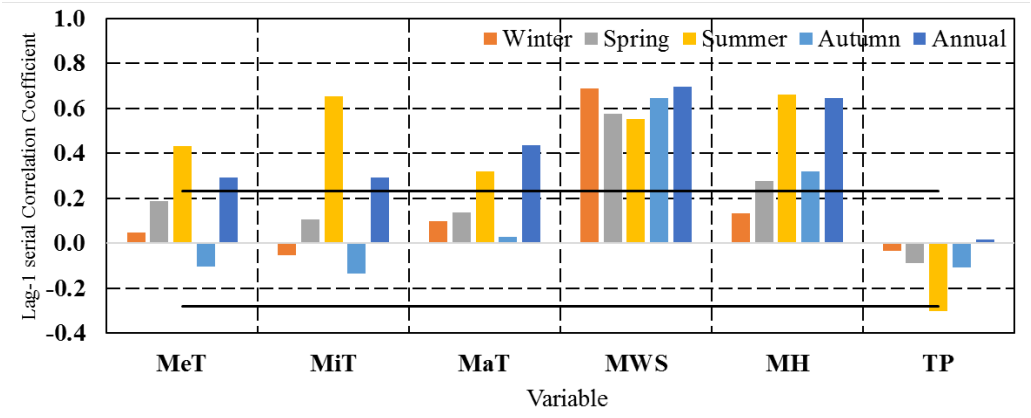

Figure 2. Lag-1 serial correlation coefficient for the seasonal and annual parameters of MeT, MiT, MaT, MWS, MH and TP (the bold line represents the probability limits on the correlogram for an independent series, r_1)

The results of Mann–Kendall and Spearman's rho tests are given in Figure 3. According to the figure, it can be stated that both methods provide the same results, except MeT for winter considering the statistically significant trends at 5% significant level. Figure 3 demonstrates that a positive trend at a 5% significance level is determined in all seasons and annual temperatures values except MeT and MiT for winter. The negative trend at 5% significance level is detected only for MH in the spring period. According to Figure 3, the significant positive trend for TP is only determined in the summer period.

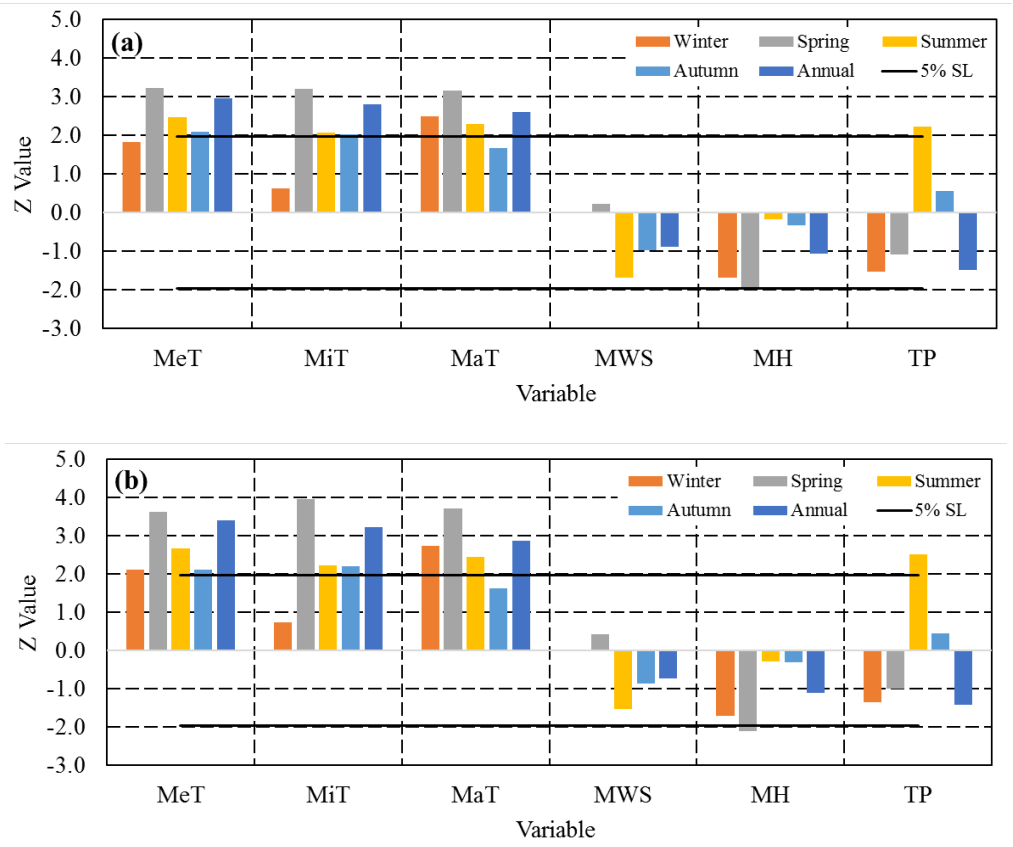

Figure 3. The results of trend analysis (a) Mann–Kendall test (b) Spearman's rho test

Figure 4 shows the linear slope values calculated by using Sen's Trend slope method on the meteorological data. Accordingly, the highest change for MeT is obtained in the spring season with 0.053 C/year, while the lowest value is observed in the autumn with about 0.022 C/year. According to Figure 4 (b), the highest change of the MiT values is determined at summer as 0.08 C/year. In Figure 4 (c), it is also determined for MaT, similar to the results for MeT, the highest change is set at 0.061 C/year in the spring period and the lowest change is set as 0.025 C/year in the autumn period. According to Figures 4 (d-f) the highest changes are determined as -0.014 m/s/year in the summer period for MWS, -0.152 m/s/year in the spring for MH and -1.5 mm/year in the annual data for TP.

Table 2 shows the trend initiate years determined by the Mann-Kendall rank correlation test for the six meteorological variables for Sanlıurfa station. According to the results, the beginning years for the trend variations are between 1979-1987 for winter, 1988-2010 for spring, 1978-1995 for summer, 1993-2007 for autumn and 1993-2003 for annual values. Additionally, the increasing trend of the temperature starts especially from the middle of 1990s and the early 2000s.

The graphs of $u(t)$ -$u'(t)$ obtained by the Mann-Kendall rank correlation test for the temperature values are given in Figure 5. It shows that the increasing trend is clearly visible at 5% significance level.

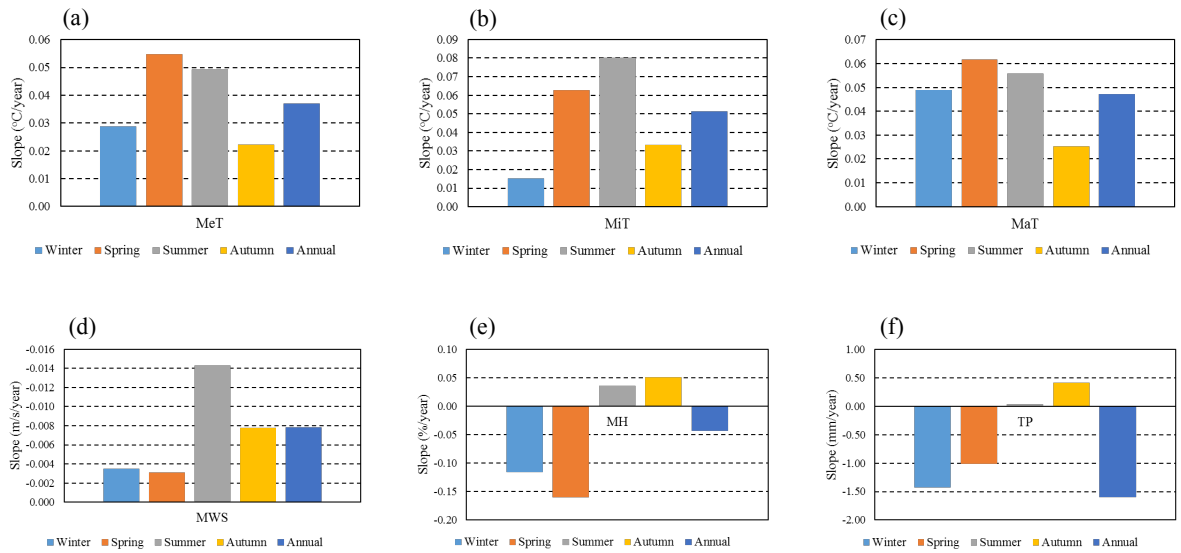

Figure 4. The linear slopes of (a) MeT (b) MiT (c) MaT (d) MWS (e) MH (f) TP

Table 2. The beginning year of the trends according to the Mann-Kendall rank correlation test

	Winter	Spring	Summer	Autumn	Annual
MeT	1979	2001	1995	1993	2003
MiT		1994	1991	2007	1997
MaT	1987	1988	1995	1994	1993
MWS			1980		
MH	1983	2010			
TP			1978		

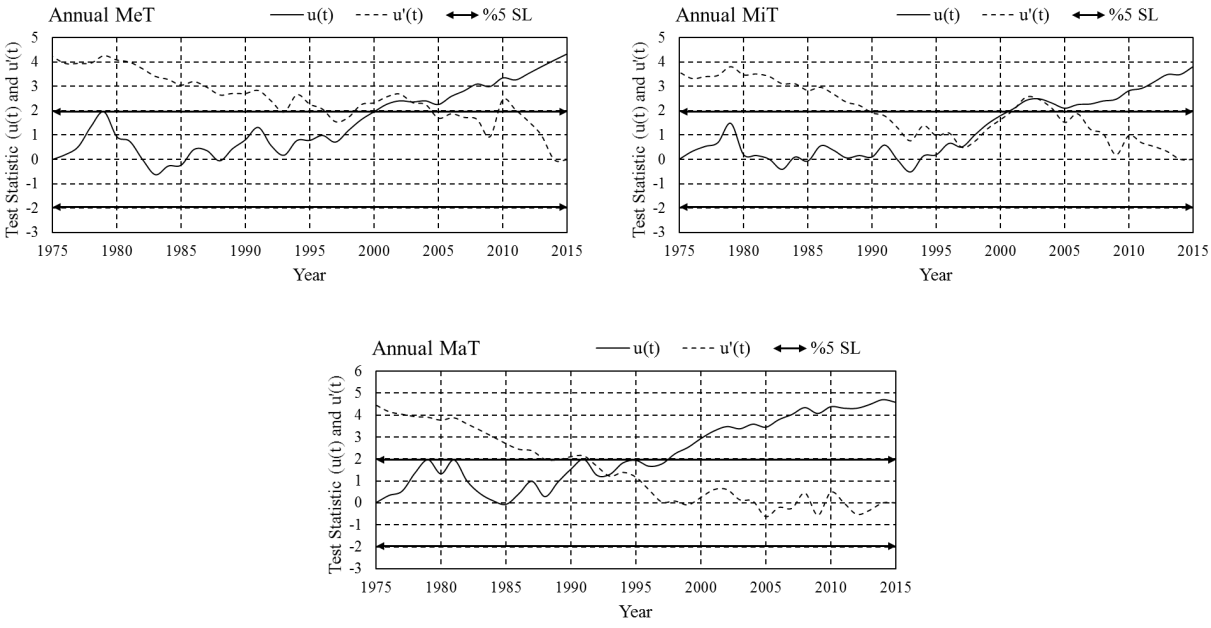

Figure 5. The Mann-Kendall rank correlation results of (a) (b) (c)

4. CONCLUSION

Based on the findings from the presented study, the following conclusions may be drawn:

- Both positive and negative serial correlation are determined for all variables. The trend analysis is undertaken using the pre-whitened time series in order to remove serial correlation from the data sets.
- The Mann–Kendall and Spearman's rho tests give the same results for 5% significant level. The positive trend at a 5% significance level is determined in all seasons and annual temperatures values except MeT and MiT for winter. Negative trend at 5% significance level is detected only in MH for Spring period.
- The highest change for MeT is obtained in the spring season with 0.053 C/year, while the lowest value is observed in the autumn period with about 0.022 C/year. According to Figure 4 (b) the highest change for the MiT values is determined at summer period about 0.08 C/year. In Figure 4 (c), it is also determined for MaT, similar to the results for MeT, the highest change is set at 0.061 C/year in the spring period and the lowest change was set at 0.025 C/year in the autumn period.
- The highest changes are determined 0.053 C/year in the spring period for MeT, 0.08 C/year in the summer period for MiT, 0.061 C/year in the spring period for MaT, -0.014 m/s/year in the summer period for MWS, -0.152 m/s/year in the spring period for MH and -1.5 mm/year in the annual data for TP.
- The increasing trend of the temperature starts especially from the middle of 1990s and the early 2000s.

REFERENCES

Adarsh, S. and Janga Reddy, M. 2015. Trend analysis of rainfall in four meteorological subdivisions of southern India using nonparametric methods and discrete wavelet transforms. International Journal of Climatology, 35: 1107-1124.

Altın, T. B., Barak, B. and Altın, B. N. 2012. Change in Precipitation and Temperature Amounts over Three Decades in Central Anatolia, Turkey. Atmospheric and Climate Sciences, 02: 107-125.

Bahadır, M. and Özdemir, M. A. 2011. Climate Trend Analysis of the Level Changes of Iznik Lake in Turkey. Journal of Biology and Life Sciences, 2: 4-13.

Chowdhury, R. K., Beecham, S., Boland, J. and Piantadosi, J. 2015. Understanding South Australian rainfall trends and step changes. International Journal of Climatology, 35: 348-360.

Erlat, E. and Türkeş, M. 2012. Analysis of observed variability and trends in numbers of frost days in Turkey for the period 1950-2010. International Journal of Climatology, 32: 1889-1898.

Gocic, M. and Trajkovic, S. 2013. Analysis of changes in meteorological variables using Mann-Kendall and Sen's slope estimator statistical tests in Serbia. Global and Planetary Change, 100: 172-182.

Kahya, E. and Kalaycı, S. 2004. Trend analysis of streamflow in Turkey. Journal of Hydrology, 289: 128-144.

Kendall, M. G. 1948. Rank correlation methods, Griffin: London, England.

Kisi, O. 2015. An innovative method for trend analysis of monthly pan evaporations. Journal of Hydrology, 527: 1123-1129.

Madsen, H., Lawrence, D., Lang, M., Martinkova, M. and Kjeldsen, T. R. 2014. Review of trend analysis and climate change projections of extreme precipitation and floods in Europe. Journal of Hydrology, 519: 3634-3650.

Mann, H. B. 1945. Nonparametric tests against trend. Econometrica: Journal of the Econometric Society: 245-259.

Mohsin, T. and Gough, W. A. 2009. Trend analysis of long-term temperature time series in the Greater Toronto Area (GTA). Theoretical and Applied Climatology, 101: 311-327.

Sayemuzzaman, M., Jha, M. K. and Mekonnen, A. 2015. Spatio-temporal long-term (1950-2009) temperature trend analysis in North Carolina, United States. Theoretical and Applied Climatology, 120: 159-171.

Sen, P. K. 1968. Estimates of the Regression Coefficient Based on Kendall's Tau. Journal of the American Statistical Association, 63: 1379-1389.

Trajkovic, S. and Kolakovic, S. 2009. Wind-adjusted Turc equation for estimating reference evapotranspiration at humid European locations.

Von Storch, H. and Navarra, A. 1995. Analysis of Climate Variability-Applications of Statistical

Techniques. Springer-Verlag, New York; 334.

Wu, H. and Qian, H. 2016. Innovative trend analysis of annual and seasonal rainfall and extreme values in Shaanxi, China, since the 1950s. International Journal of Climatology.

Yenigün, K., Gümüş, V. and Bulut, H. 2008. Trends in streamflow of the Euphrates basin, Turkey. Proceedings of the Institution of Civil Engineers - Water Management, 161: 189-198.

Yue, S. and Wang, C. 2002. The influence of serial correlation on the Mann–Whitney test for detecting a shift in median. Advances in Water Resources, 25: 325-333.

Proceedings of the 10th World Congress of EWRA 'Panta Rhei', 5-9 July 2017, Athens, Greece
© 2017 *European Water Resources Association*

Quantile regression based method for investigating rainfall trends associated with flooding and drought conditions

Y. Xuan[1], S. A. Abbas[1*], X. Song[2] and D.E. Reeve[1]
[1] *Energy & Environment Research Group, Zienkiewicz Centre for Computational Engineering ZCCE, College of Engineering, Swansea University, Bay Campus, Swansea SA1 8EN, UK*
[2] *School of Resources and Geosciences, China University of Mining and Technology, Xuzhou 221116*
[*] *e-mail: 802170@swansea.ac.uk*

Abstract: Conducting trend analysis of climatic variables is one of the key steps in many climate change impact studies in which the trend is often checked against aggregated variables. In addition, there is a strong need to explore the trend of data in different regimes. The quantile regression (QR) based method fits this need very well as it can reveal temporal dependencies of the variable in question, not only for the mean value, but also for its quantiles. As such, tendencies revealed by the QR will be immensely helpful in practice where different mitigation methods need to be considered for various level of severities. In this study, the linear quantile regression method is employed to analyse the long-term trend of rainfall records in two climatically different regions: The Dee river catchment in the UK with daily rainfall data over 1970-2004 and the Beijing metropolitan area in China with monthly rainfall data from 1950 to 2012. Two quantiles are used to represent extreme wet condition (98% quantile) and severe dry condition (2% quantile). The results show that the quantile regression is able to reveal the patterns of both extremely wet and dry conditions of the areas. The clear difference between the trends at chosen quantiles manifests the utility of using QR in this context.

Key words: climate change, trend analysis, rainfall, quantile regression

1. INTRODUCTION

Trend analysis of climatic variables such as precipitation, temperature and river flows has been reported in many recent studies, especially in the area of climate change impact and adaptation. Methodologically, ordinary linear regression is commonly used as a starting point for identifying the trend. Non-parametric methods, such as Mann-Kendall test (Mann, 1945; Kendall, 1975) are also widely adopted to further confirm the trend at given confidence level. One of such examples is given in Song et al. (2014).

One of the major drawbacks of this method is that the trend it manifests is often expressed as mean value of the given climatic variables conditionally on time. While it is very useful in general, it fails to gain insights into how the events associated with more extreme values other than the mean vary with time. For example, water managers would be more concerned with the trends of severe storms or extreme dry spells than those of 'mean' conditions.

The quantile regression (QR) method (Koenker & Bassett, 1978; Koenker, 2005), on the other hand, extends the ordinary linear regression method so that it can explain how the quantiles of response variables are conditioned on the input variables; as such offers a new window through which different regimes of the response variables can be examined in details. Since quantiles are often a convenient measure of data departing from their mean and hence loosely being associated with the rarity of those values, it becomes very convenient to use QR to reveal the trend of 'extreme' events as indicated by different quantiles. A more vigorous approach to linking QR with extreme value distribution can be referred to Cai and Reeve (2013).

In this paper, we present a study of using QR to identify the rainfall trends in two drastically different climate regions: The Dee catchment in the UK and the Beijing Metropolitan area in China. Focus is set on the trend of both extremely wet and dry conditions as they are of great value as far

as flood risk management and water resources management are concerned. We use a higher quantile 0.98 to represent the extreme wet condition – where severe flooding may occur; and a lower quantile 0.02 for the extreme dry condition where prolonged droughts may be induced. We further show that the spatial distribution of such trends can also help produce a coherent, detailed structure to serve flood risk and water management purposes.

2. STUDY AREAS

We selected two drastically different climate regions in this study – the River Dee catchment in the UK and the Beijing metropolitan area in northern China. The Dee river in the UK originates from the mountainous area of Snowdonia in North Wales and flowing east to the Wales-England border with a total length of 113 km and a catchment area of 2,215 km^2 as shown in Figure 1.

The annual rainfall over the Dee catchment ranges from 650 mm in the downstream area to the east e.g. Chester city, to 1,200 mm in the upstream in the west. Daily rainfall records from the 13 rain gauges in the vicinity of the catchment over a period of 35 years (1970-2004) are used in this study. Figure 1 shows the catchment elevation as well as the locations of the rain gauges and their annual rainfall distributions.

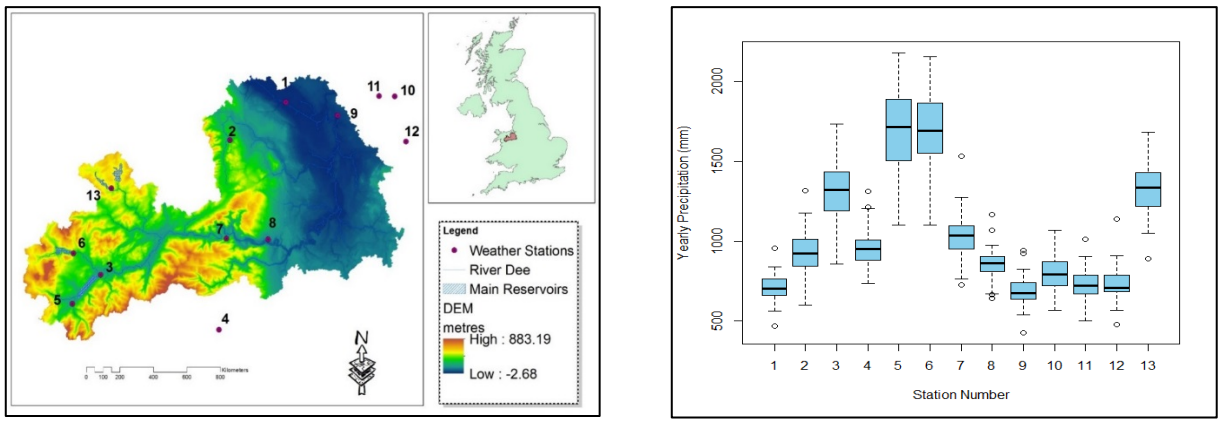

Figure1. The Dee catchment and the locations of the 13 Rain Gauges (left) and Annual Rainfall Distributions at the Locations (right)

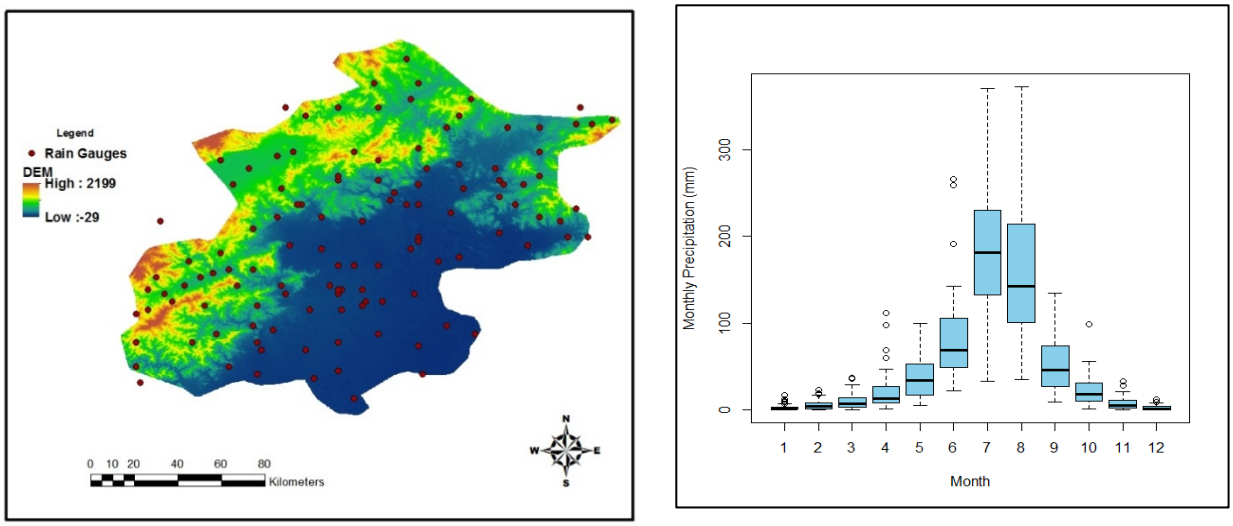

Figure2. The Beijing Metropolitan Area with Location of the Rain Gauges (left) and the Annual Rainfall Distributions at the Locations (right).

In contrast, the area of metropolitan Beijing is far larger (16,410 km^2) yet with a similar layout of topography with its west and north (68% in area) having elevation 1000-1500 m, while the central and south-east parts are just 20-60 m above the sea level. Climate wise, this area is rather opposite to the Dee catchment, as it has a monsoon-driven humid continental climate which has cold and dry winters and hot hummed summers. Monthly rainfall over the entire region was obtained over the period of 1950-2012. The areal rainfall is aggregated from the observation of a relatively dense rain gauge network (more than 100 gauges) as seen in Figure 2. The variation of monthly rainfall over the region as well as the distribution (histogram) of annual rainfall are shown in Figure 2.

3. METHODOLOGY

3.1 Linear quantile regression

The quantile regression is a powerful extension to the ordinary linear regression in a sense that the quantiles of given response variables are conditioned on independent variables. There are plenty of resources over the derivation of QR in the literature, e.g., Koenker & Bassett, (1978), Koenker (2005). A quick recap is presented here for illustration purposes.

First, considering Y is a random response variable with cumulative distribution function $CDF\ F_Y(y) = P(Y \leq y)$, the τ-*th* quantile of Y can be expressed as:

$$Q_\tau(Y) = inf\{y: F_Y(y) \geq \tau\} \tag{1}$$

where $0 < \tau < 1$ is the quantile level and $Q_\tau(Y)$ is decreasing function of τ (i.e. $Q_{\tau 1}(Y) < Q_{\tau 2}(Y)$ for $\tau_1 < \tau_2$ **).** The linear conditional quantile function used in this study can be expressed as follow:

$$Q_\tau(Y \mid x) = X^\tau \beta(\tau) \tag{2}$$

where x is the vector of dependent variable; $\beta(\tau)$ is the vector of parameters associated with the τth quantile. Statistically speaking, each quantile of the conditional distribution in linear quantile regression is characterised by an individual hyper-plane and for individual set of observation (i.e. x and y) the parameters of can be estimated by:

$$\hat{\beta}(\tau) = \arg\min_\beta \sum_{i=1}^{n} \rho_\tau\{y_i - x_i^T \beta\} \tag{3}$$

where ρ_τ is loss quantile function and can be presented as follow:

$$\rho_\tau = \begin{cases} u(p-1) \text{ if } u < 0 \\ up \text{ if } u \geq 0 \end{cases} \tag{4}$$

The difference between the absolute observed variable y_i and the corresponding τ-*th* quantile $y_\tau(x_i)$ is given as a weight of $(1-p)$ if the observed variable is below quantile plane, otherwise a weight of p is given.

3.2 Significance test of the linear trends

A warranted question related to any trend analysis is whether such trend is statistically significant. For quantile regression, bootstrap methods are developed to test the significance of the fit. Discussion of this topic goes beyond the scope of this paper and readers can refer to the relevant references mentioned in Koenker et al. (2016) for further details. The analysis in this study is conducted using the R package *quantreg* which has integrated both the fitting methods as well as

the significance test method.

3.3 Choice of the quantiles

Another advantage of using QR in trend analysis is due to the natural link between quantiles and the random events they represent. Certainly, such relationship is dependent on the underlying probability distribution. In order to overcome the unnecessary difficulties of fitting yet another distribution model, the widely used plotting method can be used to estimate such link. One of the plotting position formula is given by Gringorten (1963).

$$P = \frac{r-0.44}{n+0.12} \tag{5}$$

where r is the rank of the data and n is the sample size. By using this formula, the higher quantile 0.98 (lower quantile 0.02) of the rainfall records can roughly be linked to an event of wet condition (dry condition) with a frequency of 1 in 64 years. Of course, such estimate is not always accurate but nonetheless indicates a 'mildly' extreme event.

4. RESULTS AND DISCUSSIONS

For the Dee catchment, daily rainfall records from the 13 rain gauges were aggregated into monthly and yearly datasets upon which the linear trend of 0.98 and 0.02 quantiles are produced at each rain gauges, before being interpolated over the catchment using Inverse Distance Weighted (IDW) method.

As shown in Fig. 3, there is a basin-wide positive trend at 0.98 quantiles. There is also a clear spatial pattern associated with this overall positive trend with strong gradients (>20mm/year) in the western area gradually decreasing to the east flat area (~ 3mm/year, Fig. 3a). In addition, the trends at 10 out of 13 rain gauges are statically significant. However, the trend at 0.02 quantile is not as uniform, with an increasing trend to the west and southwest and a rather negative trend covering the rest part. It is worth noting that for the lower quantile, the trends shown at most gauges are not significant (Fig. 3b); however, those stronger negative trends indeed are significant. In other words, the catchment is shown to be even wetter for the extreme conditions (especially in the west) but only the northeast part becomes significantly dryer for the extreme dry conditions.

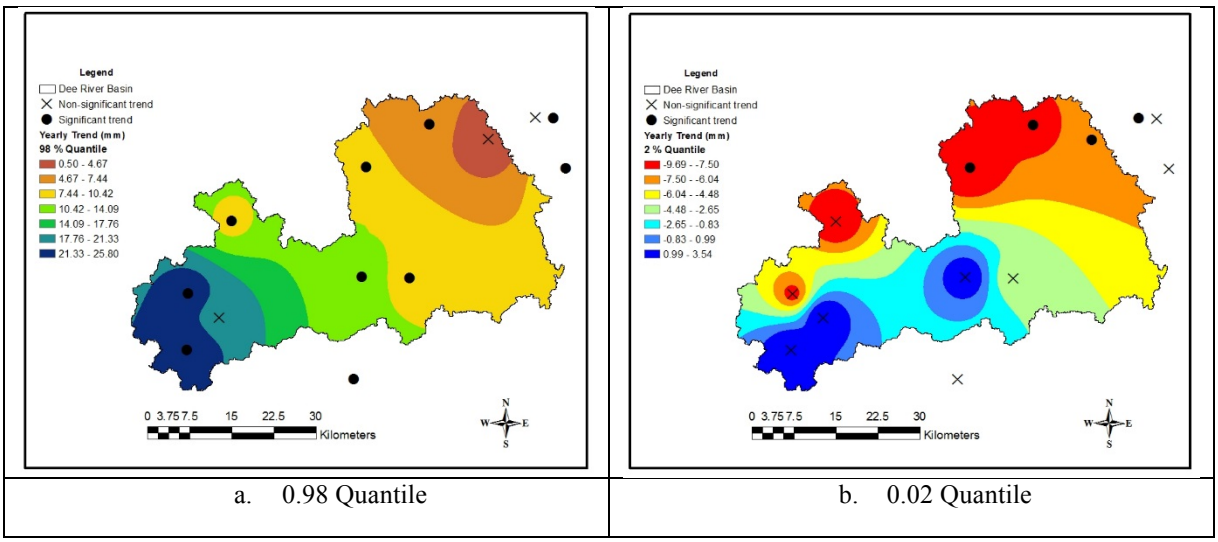

a. 0.98 Quantile

b. 0.02 Quantile

Figure3. Spatial Distribution of the trend of annual rainfall over the Dee catchment.

On monthly time scale, the trend of winter months (November, December and January), together

with the combination of these three months (winter trend) are shown in Fig. 4.

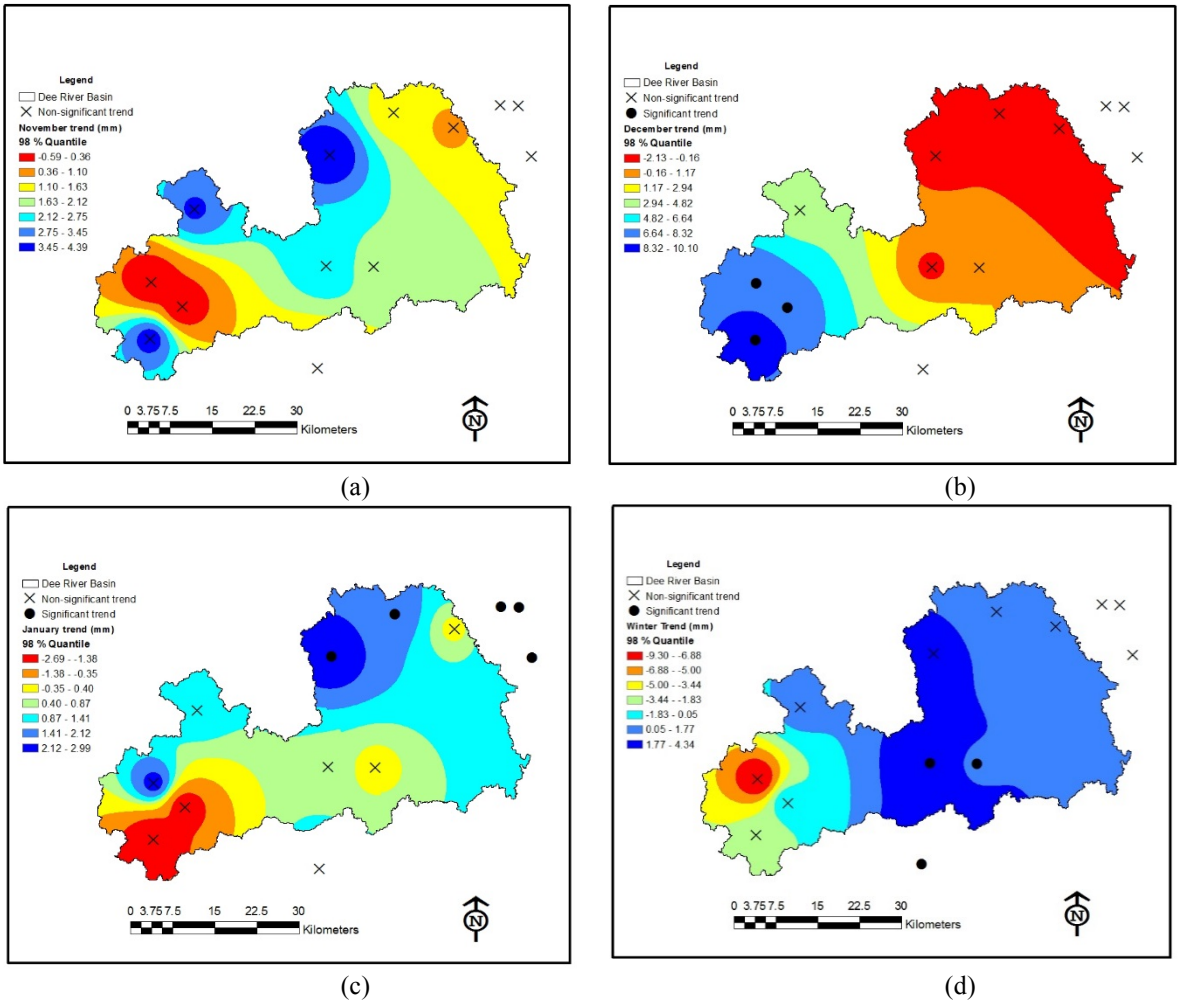

Figure 4. Spatial distribution of monthly rainfall of winter months in the Dee catchment (a November, b December, c January and d November – January)

The trends of November, January and winter (aggregation of November, December and January) appear to have a similar pattern with an increasing trend in the mid and the downstream part of the Dee river basin and decreasing trends in the upstream as shown in Fig. 4a, 4c and 4d. Interestingly, December has an opposite pattern as illustrated in Fig. 4b. It is remarkable that in general winter months do not have statically significant trends at most gauges.

For the metropolitan area of Beijing, monthly areal rainfall over the period of 1950-2012 is analysed with regard to its annual areal rainfall for typical winter and summer months (January and winter) and two seasons (DJF and JJA). The trends are expressed as the gradient of the lines fitted using linear quantile regression with various quantile levels. Table 1 shows the slopes of these fits as well as the test results of significance. Above all, a clear decrease trend at 0.98 quantile of both annual and summer rainfall is identified. For July while in general decreasing trends are found for a range of different quantiles (lower than 98%), the trend of 98% quantile does show an ascending trend, although this trend is not statistically significant, due to the fact that there are only a few years in late 1990s in which July witnessed higher amount of monthly rainfall. This revelation is very important as it implicates a more volatile climate. For the lower end of the quantiles, none of the trends at 0.02 quantile appear to be significant, which is also coincident with rather flat gradients.

Table 1. Slope and P-value of Trend Results in Beijing Area

Months	Quantile	Gradient	P-value
Yearly	0.98	-5.131	0.00002
	0.02	0.023	0.97802
July	0.98	0.272	0.83851
	0.02	0.123	0.91564
	0.35	-1.378	0.00919
	0.50	-1.201	0.05000
	0.75	-2.063	0.05081
January	0.98	-0.137	0.32575
	0.02	0.000	1.00000
	0.30	-0.012	0.00008
Summer (JJA)	0.98	-5.985	0.00318
	0.02	-1.175	0.27748
Winter (DJF)	0.98	0.140	0.44956
	0.02	0.000	1.00000

The variation of trends conditional on the selected quantiles is shown in Fig. 5. The uncertainty bands of the slopes reveal that, for summer, there are increasing trends for quantiles blow 0.5 and decreasing for those above 0.5, but the trends seem to go up for quantiles larger than 0.8. The implication is that overall the summer rainfall tends to be more stable around its median, the heavy rainfall events may become more extreme. For winter, the gradient tends be more flat and centred around 0. In view of the significance test, it is not yet decisive to conclude any significant trends for winters.

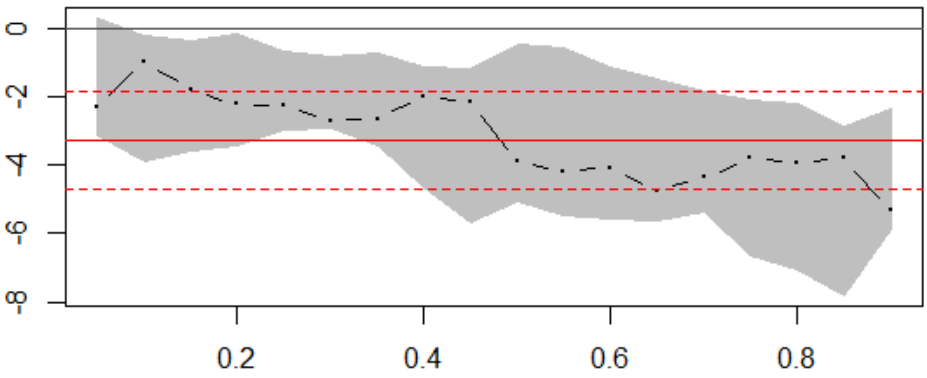

(a)

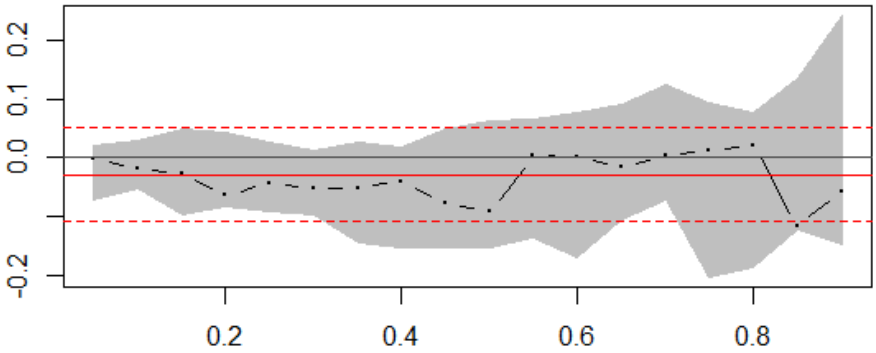

(b)

Figure 5. Confidence Band of the gradient (mm/year) of the fitted lines using summer (a) and winter (b) Seasons in Beijing. The horizontal axes are quantiles and the vertical axes refer to the gradient of the trend lines; the red lines represent the confidence bands of the fits using ordinary linear regression.

5. CONCLUSION

In this study, we demonstrate a new, quantile regression based method for analysing the trend in climatic variables. Long-term rainfall data from two drastically different climate regions is investigated focusing on the trends of the data close to 'extreme' regimes, in order to link them to the events of interests. It can be concluded that:

1. The QR based trend analysis can provide far more detailed information with respect to the quantity in question. This is particularly useful for water managers who are more concerned with extreme values rather than the averaged one;
2. This method can help build a comprehensive picture of climatic variables in terms of their variation over time at different magnitude/frequency;
3. The involvement of quantile brings an extra benefit that bridges the trend analysis with frequency, which implies great potential of its use in studying climate change impact on engineering design without having to assume data stationarity.

Certainly, more studies are needed to improve the method with respect to the problems found in this study, which include but are not limited to:

1. A better link between quantiles and event frequency (return period) in the context of trend analysis.
2. The method needs to be refined further to be more reliable on lower quantiles. It has been found that most trends of quantile 0.02 are insignificant, but this may not be true as lower end of the data suffer from larger errors and zero values may as well interfere with the process.

ACKNOWLEDGEMENT

We would like to thank British Atmospheric Data Centre, Natural Resources Wales and Beijing Water Authority for their assistance in data collection. The PhD scholarship for S. Abbas from the Higher Committee for Education Development in Iraq (HCED) is also kindly acknowledged.

REFERENCES

Bayissa, Y., Moges, S., Xuan, Y., Van Andel, S., Maskey, S., & Solomatine, D. et al. (2015). Spatio-temporal Assessment of Meteorological Drought under the Influence of Varying Record Length: The Case of Upper Blue Nile Basin, Ethiopia. Hydrological Sciences Journal, 1-16. DOI: 10.1080/02626667.2015.1032291

Cai, Y. & Reeve, D. (2013). Extreme Value Prediction via a Quantile Function Model. Coastal Engineering, 77, 91-98. DOI: 10.1016/j.coastaleng.2013.02.003

Gringorten, I. I. (1963). A plotting rule for extreme probability paper. Journal of Geophysical Research, 68(3), 813-814.

Kendall, M. G. (1975). Rank Auto-correlation Methods. Charles Griffin, London.

Koenker, R. & Bassett, G. (1978). Regression Quantiles. Econometrica, 46(1), 33. DOI:10.2307/1913643

Koenker, R. (2005). Quantile Regression (No. 38). Cambridge university press.

Koenker, R., Portnoy, S., Ng, P. T., Zeileis, A., Grosjean, P., & Ripley, B. D. (2016). Package 'quantreg'.

Mann, H. B. (1945). Nonparametric Tests Against Trend. Econometrica: Journal of the Econometric Society, 245-259. DOI:10.2307/1907187

Song, X., Zhang, J., AghaKouchak, A., Roy, S., Xuan, Y., & Wang, G. et al. (2014). Rapid urbanization and changes in spatiotemporal characteristics of precipitation in Beijing metropolitan area. Journal of Geophysical Research: Atmospheres, 119(19), 11,250-11,271. DOI: 10.1002/2014jd022084

Proceedings of the 10th World Congress of EWRA 'Panta Rhei', 5-9 July 2017, Athens, Greece
© 2017 *European Water Resources Association*

Parametric study of trends in flood stages over time in the regulated Guadalquivir River (years 1910-2016)

P. Bohorquez* and J.D. Del Moral-Erencia
Área de Mecánica de Fluidos, Departamento de Ingeniería Mecánica y Minera, CEACTierra, Universidad de Jaén, Campus de las Lagunillas, 23071 Jaén
* *e-mail: patricio.bohorquez@ujaen.es*

Abstract: The present study aims to report on the trends in flood hazard over time in the Guadalquivir River (Southern Spain), one of the most affected rivers by climate change in Europe. A complex physical scenario is drawn in the near future due to the interaction of long-term rainfall predictions and the reduction in channel capacity in this intensively regulated river. During the studied period, that extends between the years 1910 and 2016, the three hydropower stations Marmolejo, Valtodano and Mengíbar have operated along the selected stretch of 70 km length. Less frequent wet periods but concentrated in heavy rainfall events have developed, provoking unexpected exceptional floods in urban areas as a consequence of the increase in sediment supply from unregulated tributaries and the altered fluvial regime at high stages. A parametric study has been conducted in order to quantify the relative influence of the factors controlling the flood stages, namely: in-channel sedimentation and encroachment of riparian vegetation. Instrumental and non-systematic hydrological data were combined to lengthen flood records and reconstruct the spatial patterns of rare and extreme events, a technique common in paleohydrology. The conclusions of this study reveal that the integrated water resource management in the Guadalquivir River Basin, which is strongly influenced by political economy factors, needs to be reconsidered in order to avoid the increase in impact of flood in the near future.

Key words: Guadalquivir River, backwater effect, silted-up reservoir, paleohydrology, vegetation encroachment

1. INTRODUCTION

The present study aims to identify the factors that have increased the flood risk vulnerability in urban areas near the Guadalquivir River since the very beginning of the electric era in Southern Spain. A stretch of the river flowing over three dams (Mengíbar, Valtodano and Marmolejo), two towns (Mengíbar and Villanueva de la Reina) and one city (Andújar), among other smaller villages, was selected as the study site because it has suffered an unexpected increase in flood stage over time after river impoundment (see Figure 1). As a matter of fact, exceptional floods with characteristic river discharges in the range of 700-2000 $m^3 \cdot s^{-1}$ occurred between the years 2009 and 2013 (economic losses amounted to 149 M€). The extents and impacts of the inundations were much lower during the periods 1920-1930 and 1960-1970 for similar discharges.

We show for the first time that the vulnerability to flooding risk have raised in the Upper Guadalquivir River because of the synergistic effects of increasing the sediment budget from the basin and the decrease in channel capacity during the regulated river regime, which has led to the infilling of dam reservoirs, the aggradation of the main channel and the colonization of slackwater deposits by woody vegetation. This situation arose mostly due to the complexity of water resources management and water policy in the Guadalquivir Basin (Bhat and Blomquist, 2004) that allowed the use of the 87% of the water resources (4000 hm^3/year) to irrigation (CHG, 2013) and introduced great pressures in the fluvial ecosystem. By studying the temporal evolution of the stage and the drainage capacity of the river channel between the years 1910 and 2016, we characterise the increase in flood risk vulnerability after river impoundment.

The problematic at hand is important worldwide. For instance, Slater, Singer and Kirchner (2015) highlighted the importance of the reduction in channel capacity that increased the flood frequency across the United States. Also, Naylor et al. (2017) showed that the hydrogeological

counterpart cannot be neglected in flood risk vulnerability studies in an age of climate extremes. Indeed, we have already shown that the long-term evolution of vegetation (>50 years) acts as a geomorphic driver of flood hazard through the encroachment of the main channel in Southern Spain (Bohorquez et al., 2014; Bohorquez, 2016).

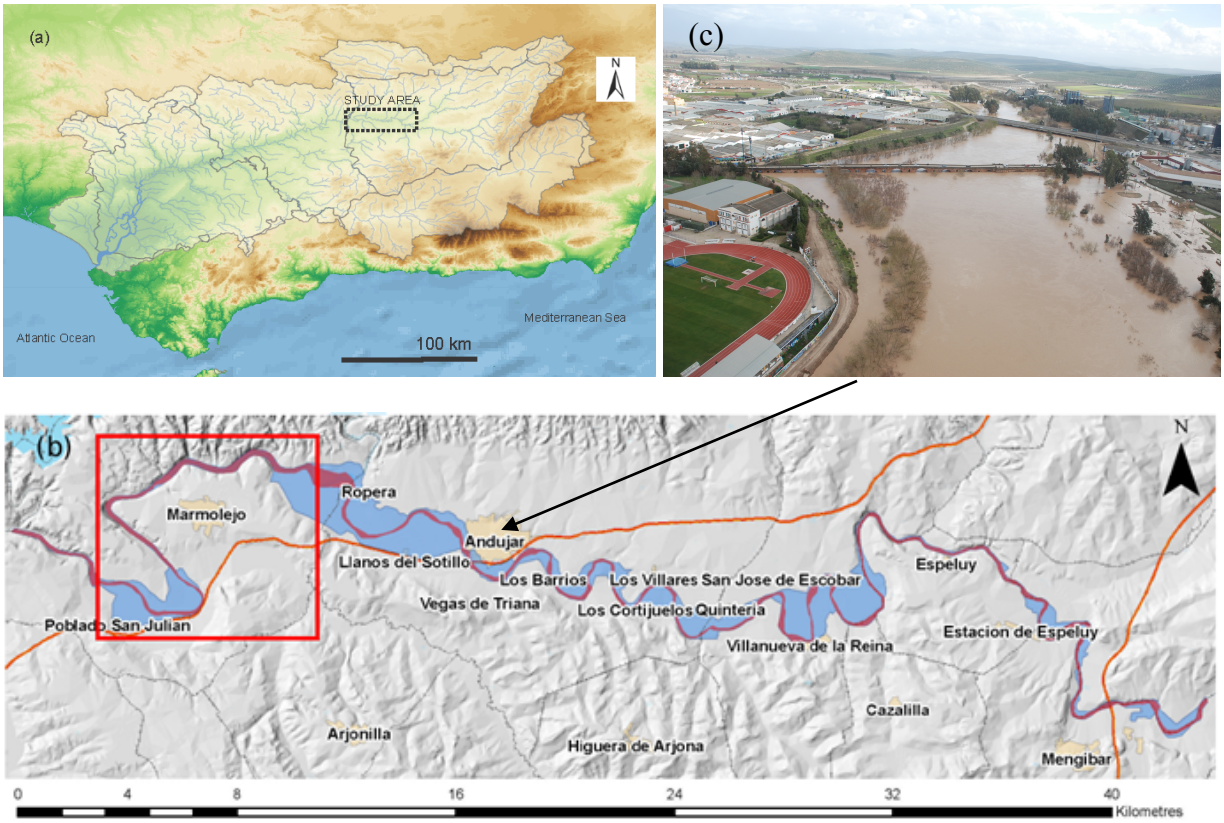

Figure 1. (a) Location of the study site in the Guadalquivir River Basin (Spain). (b) Study site (flow from right to left): the main channel of the Guadalquivir River is depicted in red, inundated areas the date of 24th February 2010 are coloured in blue, urban areas are labelled in black and highways are highlighted in orange. (c) The photograph shows the inundated areas near the Roman bridge in Andújar city. A detail description and simulation of the floods occurred in the boxed area in panel (b) was presented in Bohorquez (2016).

2. STUDY AREA

The field area is situated along a stretch of the Guadalquivir Valley in Southern Spain, upstream of the border of the provinces of Jaén and Córdoba (Figure 1a). The fluvial regime is typically Mediterranean, showing a summer drought period with minimum water levels and highest values in winter and spring. The complex topography of the surrounding landscapes, the large size of the drainage area (19.546 km^2) and the different climate influences of the Mediterranean Sea and the Atlantic Ocean favour the occurrence of heavy precipitation events and floods (Bohorquez et al., 2014). Indeed, flooding is the most damaging type of natural disaster in this area with economic losses per province ranging between 200 and 1200 M€ (Barredo et al., 2012).

In this work, we extend the flood risk analysis presented by Bohorquez (2016) along the river reach Marmolejo-San Julian (see squared area in Figure 1b) up to Mengibar dam, which is located 70 km upstream of Marmolejo dam. In the middle reach, the morphology of the river is characterised by a train of meanders. Unpaired terraces were formed by the incised channel across its floodplain, which is intensively used by the human activity. In the upstream and downstream boundaries, the river flows across confined valleys. There, two dams operated since 1910 and 1916 (Mengíbar and Marmolejo dams, respectively).

Between the two dams, the meanders in mixed sand-mud that developed in the lower terrace

(elevated 5-6 m above the thalweg) reduced the mean bed slope from 0.12% (straight channel configuration) to 0.072% (meandering set-up). The bed is made of clasts and rounded coarse gravels with grain diameters in the range of 6-40 cm. The bed slope in the meandering morphology (0.072%) tends to the downstream valley slope (0.076%), which clearly indicates the existence of a downstream hydraulic control of the meanders dynamics by the confined valley in Marmolejo (Seminara, 2006). The meanders are stable as they did not migrate even during the past wet periods (years 1920-1930 and 1960-1970) when the peak water discharges reached values between 1400 and 3000 $m^3 \cdot s^{-1}$. Stable meander dimensions are given in Table 1. The bankfull stage was determined from the proto-floodplain (top of the point bar surface) that supports woody vegetation. These values are useful to determine the channel capacity before the instrumental era.

Table 1. Characteristic values of the geometrical properties of the meanders (M) located upstream of Andújar city, see Figure 1b. The streamwise distance was measured using Mengíbar dam as the origin of reference. L=length, L_m=axial wavelength, P=sinuosity (L/L_m), A=amplitude, B=bankfull width, H=bankfull depth

	M1	**M2**	**M3**	**M4**	**M5**
Start (km)	20.0	26.6	33.7	37.8	41.8
End (km)	26.6	31.8	37.8	41.8	46.7
L (m)	6600	5200	4100	4000	4900
L_m (m)	2600	1950	2700	2150	2720
P	2.5	2.7	1.5	1.9	1.8
A (m)	1500	1550	1400	1500	1450
B (m)	100-250	175	166	159	156
H (m)	5.7	6.2	5.5	6.4	6.9

The channel planform has experienced negligible changes after impoundment (i.e., in the period 1910-2016), but the main channel has suffered the following major changes (Bohorquez et al., 2014; Bohorquez, 2016): the channel slope has decreased up to vanish along the reach of 15 km length upstream of Marmolejo dam due to reservoir sedimentation; lateral bars in sand-mud have developed in multiple locations of the river because of the increase in sediment supply from non-regulated tributaries and changes in land-use; finally, vegetation encroachment has developed as a consequence of river flow regulation during droughts. All these factors led to a substantial reduction in channel capacity, as described below.

3. RESULTS

3.1 Pre-impoundment bankfull discharge: regime based capacity

The analysis of channel form provides a context for interpretation of past changes in the fluvial environment. We adopt the following two methods to quantify the water discharge responsible for sculpting the meanders into the lowest sand-mud terrace: first, the algebraic equations by Dury (1976) were selected from the available equations in the paleohydrology literature (Williams, 1984); second, results from regime based equations by Yalin and da Silva (2001) linking the bankfull dimensions of the channel and the water discharge served to verify the first method.

Dury (1976) empirically derived a couple of one-parameter equations correlating the meander wavelength L_m and the water discharge Q. These relations were based on the analysis of multiple meandering rivers with characteristic water discharges lower than 4100 $m^3 \cdot s^{-1}$ and read:

$$L_m = 54.34\, Q^{0.5} \text{ and } L_m = 35.695\, Q^{0.55} \quad (1)$$

Substituting the wavelength values from Table 1 into (1), one obtains that the water discharge

ranges between 2023 and 2168 $m^3 \cdot s^{-1}$.

Alternatively, Yalin and da Silva (2001) reviewed all the available regime-data before 1990 and showed that the bank full dimensions of the collected rivers satisfy the following set of equations:

$$L_m = 54.34Q^{0.5}\ ,\quad h = (\alpha_B{}^2\, Fr)^{-\frac{1}{3}} \left(\frac{Q\, v_{*,cr}}{g}\right)^{\frac{1}{3}},\quad Fr = c^2\, S_0\ ,\quad c = \frac{h^{1/6}}{n\sqrt{g}}\,. \tag{3}$$

In (3), the parameter α_B depends on the roughness of the river and the sediment properties, $v_{*,cr}$ denotes the critical velocity for the inception of sediment motion, and Fr is the Froude number. Both parameters can be eliminated from (3), leading to the classical Manning (or Chezy) equation for a uniform flow in a channel with rectangular cross section $\{B, h\}$, bed slope S_0 and roughness parameter n (or c):

$$L_m = 54.34Q^{0.5} \quad \text{or} \quad Q = c\, B\, \sqrt{g\, S_0}\, h^{\frac{3}{2}}\,. \tag{4}$$

The main advantage of (4) is that it incorporates the roughness coefficient n (or c) explicitly. The Manning's roughness was calibrated in Bohorquez (2016) at the foot of Marmolejo dam by comparing the measured rating curve and the simulated one using the two-dimensional Saint-Venant equations. In the situation of pre-vegetation encroachment, n=0.035 $s \cdot m^{-1/3}$. Evaluating (4) with the mean thalweg slope S_0=0.076%, the mean bankfull width B=184 m and a bankfull flow depth in the range of 4-5 m, it yields $1460 \leq Q \leq 2118$ $m^3 \cdot s^{-1}$. Note that the upper bound is in close agreement with Dury's solution: $2023 \leq Q \leq 2168$ $m^3 \cdot s^{-1}$.

By increasing the Manning's roughness up to 0.06 $s \cdot m^{-1/3}$ in the situation of post-vegetation encroachment, we obtain a reduction in channel capacity from 1460 (2118) to 852 (1236) $m^3 \cdot s^{-1}$ for the bankfull flow depth h=4 (5) m. This result is consistent with the recent inundations of the floodplains at the low water discharges of 800-1070 $m^3 \cdot s^{-1}$ due to the presence of vegetation encroachment and the colonisation of sediment bars.

3.2 Post-impoundment bankfull discharge: flow competence

Another fundamental approach to retrodict past channel and flow conditions from geomorphic considerations is the flow competence criterion (Jacobson, O'Connor and Oguchi, 2003). It takes advantage of empirical relations between flow strength and the largest size of clasts transported by the flow. Recently, Alexander and Cooker (2016) reviewed the algebraic formulas relating the boulder size and the flow velocity and showed the utility to retrodict past flow conditions.

Fieldworks were conducted between January and March 2017 in order to locate coarse gravel and boulder deposits. Gravel bars and exposed gravel substrates were found out in two locations (Figure 2): in the fourth meander (M4), downstream of Valtodano dam; and, in front of the bridge in Villanueva de la Reina.

In both locations, the diameter of largest rounded clast was approximately $d \equiv 0.4$ m. There were also modern concrete debris of 1 m but the shape was planar. Using Clarke's method in a steady regime, the flow velocity required to transport the rounded clast is $V = 3.7\ d^{0.478} = 2.4$ $m \cdot s^{-1}$. However, Clarke's equation typically overestimates the flow velocity. Alexander and Cooker found out a lower velocity of 0.9 $m \cdot s^{-1}$ by setting a lower friction factor between the boulder and the bed. Assuming bankfull conditions in Valtodano dam, and using the value of the wetted area at this location (885 m^2), we get Q = 796 $m^3 \cdot s^{-1}$. This result is consistent with the water discharge Q = 1070 $m^3 \cdot s^{-1}$ measured in February 2010. Unfortunately, we did not found out any larger boulder evidence of older floods.

Comparing the flow competence result (Q = 796 $m^3 \cdot s^{-1}$) and the regime based discharge ($852 \leq Q \leq 1236$ $m^3 \cdot s^{-1}$), we corroborate that the actual capacity of the river channel has notoriously

decreased. In the present configuration, bankfull conditions are achieved with a much lower water discharge than during the years previous to flow regulation ($1460 \leq Q \leq 2118$ $m^3 \cdot s^{-1}$).

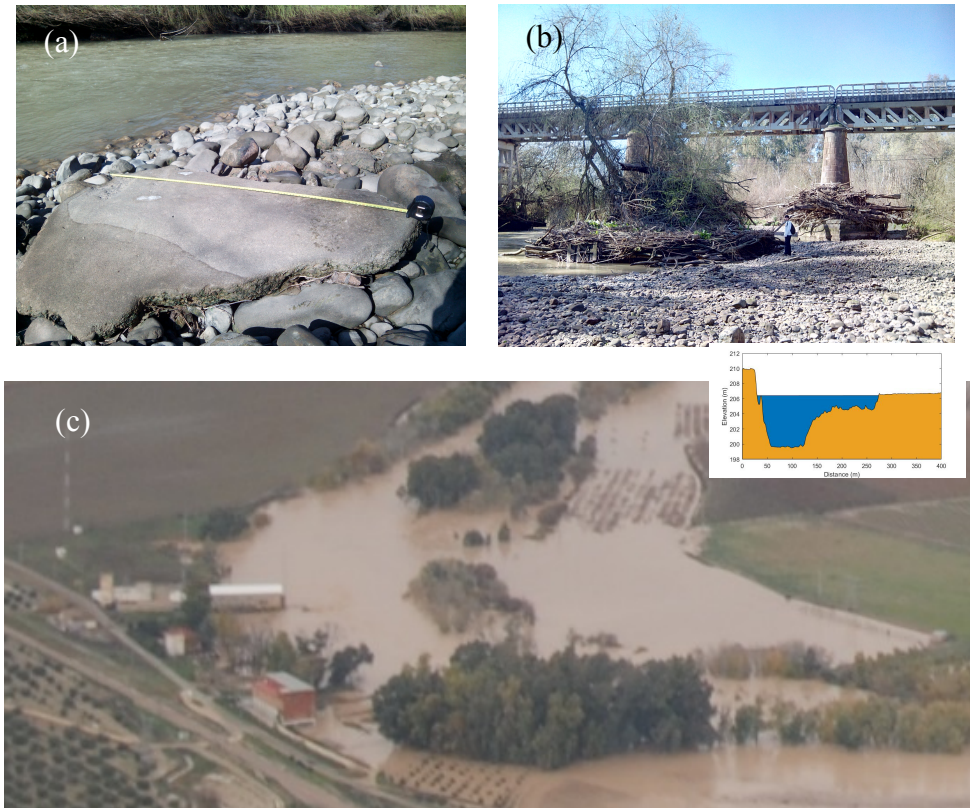

Figure 2. (a) Photograph of the largest boulder found downstream of Valtodano dam. (b) Coarse gravels and woody debris in the bridge of Villanueva de la Reina, see the guy for the scale. (c) Image of the overtopped Valtodano dam in December 2010. The inset shows the shape of the cross section and the wetted area in bank full condition.

3.3 Changes in flood stage over time

Systematic recording of daily average water discharge in Spain began in 1911 with the publication of the annual review of gauge stations. Later, hourly average values have been provided by the national net for real-time hydrologic monitoring since the year 1989. Local records are available at three hydropower stations near Marmolejo during different periods. Gauging records could be merged into a single series because of the proximity of the three stations. In Mengíbar, the gauge station is located 650 m downstream of the dam. Interestingly, it was inundated during modern floods (2009-2013), when in-situ measurements had to be taken manually. Other damages occurred during extreme floods as dams were overtopped in multiple occasions (e.g., see Figure 2c).

In the absence of systematic measurements, the water stage was retrodicted from historical imagery. Hence, imagery was collected from the following sources to lengthen flood records of extreme events: in situ photographs (1906–2013), aerial photographs from helicopter surveys (2009–2013) and sequences of orthophotos (1945–2013). Using these data, fieldworks were conducted with the main aim of positioning the highest watermark from the photos by using a modern laser Leica DISTO^{TM} S910 (Swiss technology); next, rating curves were obtained by correlating the date and time of the photo with the inferred flood stage and the water discharge.

Figures 3a and 3b summarise the results on the stage-discharge curves at Marmolejo and Mengíbar dams since 1912 and 1910, respectively. In both cases, we observe an increase of the stages through time that is particularly evident during the most recent floods (years 2009-2013).

In Mengíbar (Figure 3c), we found flow depths as deep as 12.3 m with the water discharges of,

approximately, 2000 $m^3 \cdot s^{-1}$. Such extreme values occurred in the inundation of the year 1963 which is remembered as the most catastrophic inundation of the last century. The rest of floods in the period 1912-2009 were less severe and exhibited flow depths lower than 10.6 m with water discharges smaller than 1577 $m^3 \cdot s^{-1}$. Surprisingly, the maximum stage during the period 2010-2013 was 9.7 m with the water discharge 670 $m^3 \cdot s^{-1}$. The ensuing stage is of the same order of magnitude than in the 1924 flood that nearly doubled the water discharge (1577 $m^3 \cdot s^{-1}$). Furthermore, the flow depths corresponding with the water discharge 670 $m^3 \cdot s^{-1}$ were 9.7 m and 6.7-7.5 m in the periods 2009-2013 and 1912-2009, respectively. Such an increase in the flow stage at the same water discharge is due to the development of an island, currently colonised by non-flexible riparian vegetation, that substantially increases the local head losses in this reach of the Guadalquivir River.

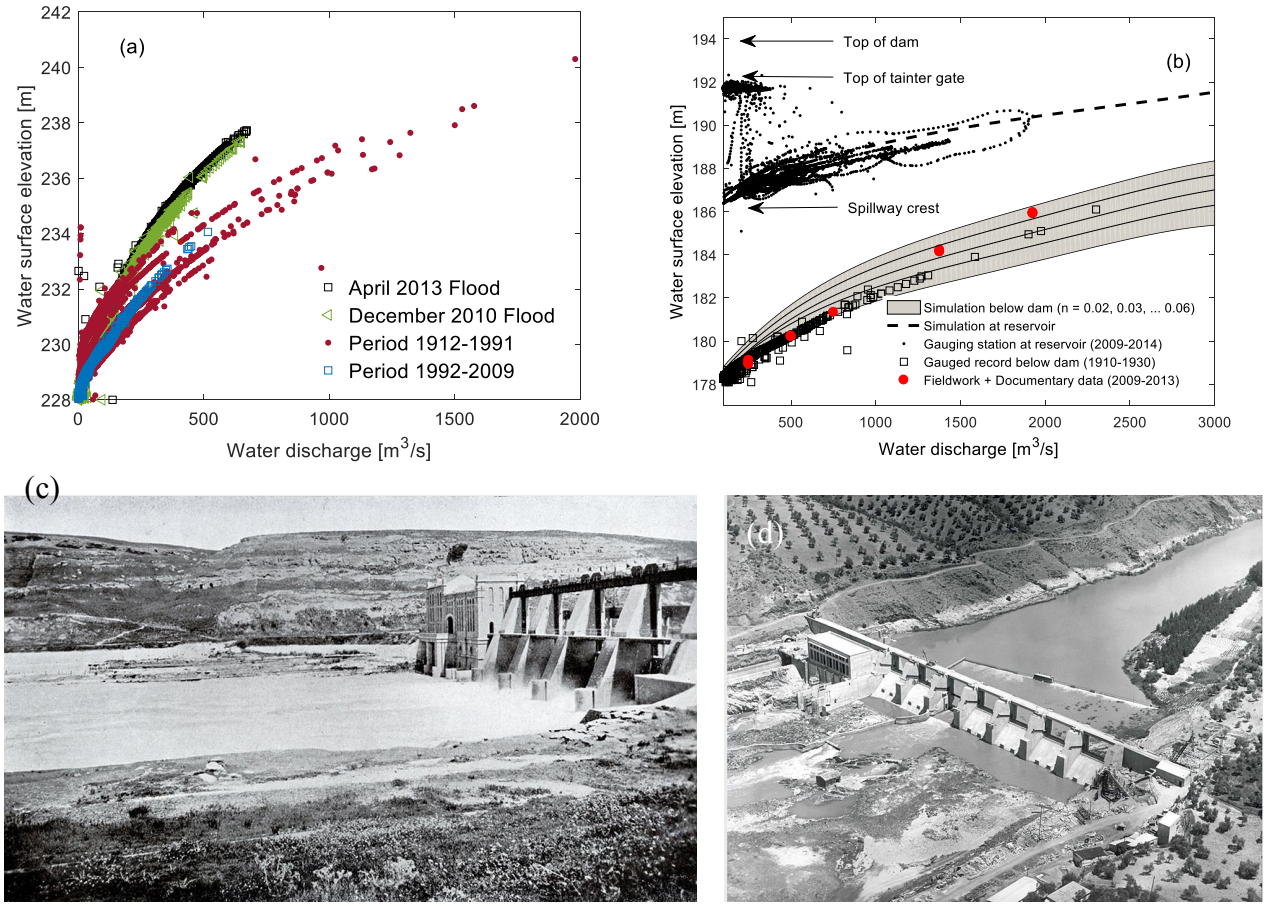

Figure 3. Rating curves: (a) at the foot of Mengíbar dam; (b) in the reservoir and at the foot of Marmolejo dam. (c) Mengíbar dam in 1916 and (d) Marmolejo dam in 1962. The characteristic dimensions of Mengíbar dam are: height = 12.2 m, crest length = 150 m, top of vertical rising sluice gate = 239.7 m, outlet channel elevation = 227.5 m, reservoir capacity = 2.4 Hm^3 and design flood = 3700 $m^3 s^{-1}$. The characteristic dimensions of Marmolejo dam are: height = 20 m, crest length = 230 m, spillway crest = 186.2 m, top of tainter gate = 191.73 m, outlet channel elevation = 175.35 m, reservoir capacity = 13 Hm^3 and design flood = 3450 $m^3 s^{-1}$.

This effect could be appreciated in the rating curves downstream of Marmolejo dam (Figure 3d). As a matter of fact, the rating curve of the most recent floods (years 2009-2013) lies above that of the period 1910-1930 for $Q \geq 1300$ $m^3 \cdot s^{-1}$. Two-dimensional numerical simulations using a standard version of the shallow water equations over fixed beds were performed in Bohorquez (2016) by means of DassFlow-Shallow 2.0 (Monnier et al., 2016). The simulated rating curve is depicted in solid line in Figure 3b with Manning's roughness of $0.02 \leq n \leq 0.06$ $s \cdot m^{-1/3}$. They serve to show that vegetation encroachment provoked 10% deeper floods at the water discharge of 2000 $m^3 \cdot s^{-1}$, which implied an increase in Manning's roughness coefficient from 0.04 to 0.055 $s \cdot m^{-1/3}$.

4. CONCLUSIONS

In this work, we revisited the current risk of flooding in the Guadalquivir River since the year 1910 by accounting for reduction in channel capacity. This factor clearly competes with the observed reduction in peak water discharges during modern floods.

Our results contrast to the flood hazard projections by Alfieri et al. (2015) and EEA (2017) based on a global analysis of one-in-a-century river floods in a scenario of climate change in southern Spain. Previous studies only considered the climate counterpart in relation to the flood risk analysis of the Guadalquivir River. On the one hand, we corroborated the present reduction in streamflows. On the other hand, we showed that the channel capacity in natural conditions previous to flow regulation was much larger than nowadays observed. The increase in Manning's roughness coefficient due to vegetation encroachment after river impoundment led to the reduction in channel capacity from 2100 to 852 $m^3 \cdot s^{-1}$. Vegetation encroachment developed during drought periods after upstream river impoundment, provoking the underpredicted increase in flood risk.

In addition to the obvious inundation of the floodplain at much lower river discharges, we found out a positive feedback between reduction in channel capacity, channel infilling, reduction of bed slope and channel squeezing. Consequently, a complex physical scenario is drawn in the near future due to the interaction of long-term rainfall predictions and the reduction in channel capacity in this intensively regulated river.

ACKNOWLEDGMENTS

This work was supported by the Spanish Ministry of Economy and Competitiveness (MINECO/FEDER, UE) under Grant SEDRETO CGL2015-70736-R and the PhD scholarship BES-2016-079117 (MINECO/FSE, UE) by the Spanish National Programme for the Promotion of Talent and its Employability (call 2016). P.B. acknowledges the earlier support by Caja Rural Provincial de Jaén and University of Jaén under Grant UJA2014/07/04.

REFERENCES

Alexander J., Cooker M. J., 2016. Moving boulders in flash floods and estimating flow conditions using boulders in ancient deposits. Sedimentology, 63: 1582-1595.

Alfieri L., Burek P., Feyen L., Forzieri G., 2015. Global warming increases the frequency of river floods in Europe. Hydrology and Earth system sciences, 19(5), 2247-2260.

Barredo J., Saurand D., Llasat M., 2012. Assessing trends in insured losses from floods in Spain 1971–2008. Natural Hazards and Earth System Sciences, 12, 1723-1729.

Bhat A., Blomquist W., 2004. Policy, politics, and water management in the Guadalquivir River Basin, Spain. Water Resources Research, 40(8), W08S07.

Bohorquez P., 2016. Paleohydraulic reconstruction of modern large floods at subcritical speed in a confined valley: proof of concept. Water, 8, 567.

Bohorquez P., Aranda V., Calero J., García-García F., Ruiz-Ortiz P., Fernández T., Salazar C., 2014. Floods in the Guadalquivir River (Southern Spain), in Proceedings of the International Conference on Fluvial Hydraulics, River Flow 2014 (eds. Schleiss A., Cesare G., Franca M. and Pfister M.). CRC Press/Balkema: Leiden, The Netherlands; pp. 1711-171.

CHG, 2013. Plan Hidrológico de la Demarcación Hidrográfica del Guadalquivir; MAGRAMA: Madrid, Spain.

Dury G. H., 1976. Discharge prediction, present and former, from channel dimensions, Journal of Hydrology, 30(3), 219-245.

European Environment Agency, 2017. Climate change, impacts and vulnerability in Europe 2016: An indicator-based report. EEA Report No 1/2017, doi:10.2800/534806.

Jacobson R. B., O'Connor J. E., Oguchi T., 2003. Surficial geological tools in fluvial geomorphology, in Tools in Fluvial Geomorphology (eds. Kondolf G. M. and Piégay H.), John Wiley & Sons, Ltd, Chichester, UK.

Monnier J., Couderc F., Dartus D., Larnier K., Madec R., Vila J.P., 2016. Inverse algorithms for 2D shallow water equations in presence of wet dry fronts. Application to flood plain dynamics. Advances in Water Resources, 97, 11-24.

Naylor L. A., Spencer T., Lane S. N., Darby S. E., Magilligan F. J., Macklin M. G., Möller I., 2017. Stormy geomorphology: geomorphic contributions in an age of climate extremes. Earth Surf. Process. Landforms, 42: 166-190.

Seminara G., 2006. Meanders, Journal of Fluid Mechanics, 554, 271-297.

Slater L. J., Singer M. B., Kirchner J. W., 2015. Hydrologic versus geomorphic drivers of trends in flood hazard. Geophysical Research Letters, 42, 2014GL062482.

Williams G. P., 1984. Paleohydrologic equations for rivers, in Developments and Applications of Geomorphology (eds. Costa J.E. and Fleisher P. J.), Springer-Verlag: New York, pp. 343-367.
Yalin M. S., da Silva A. M. F., 2001. Fluvial Processes, IAHR Monograph, IAHR: Delft, The Netherlands.

Proceedings of the 10th World Congress of EWRA 'Panta Rhei', 5-9 July 2017, Athens, Greece
© 2017 *European Water Resources Association*

Effects of climate and land use changes on runoff extremes

D. Pumo*, E. Arnone, A. Francipane, V. Noto and G. La Loggia
DICAM, Università degli Studi di Palermo, Italy
* *e-mail: dario.pumo@unipa.it*

Abstract: This work proposes a modeling framework for the analysis of alterations in the watershed hydrological response and, more specifically, in runoff extremes, induced by climate change and urbanization. A weather generator and a cellular automata land-use change model are used to generate hypothetical scenarios accounting for relevant trends at the global scale. Such scenarios are successively considered to force a spatial-distributed hydrological model, which simulates, at high time-resolution, most of the key hydrological variables at the basin scale. The framework is applied to the *Peatcheater Creek at Christie* basin (OK, USA). The considered climate alterations are negative and positive variations in mean annual precipitation, obtained by different configurations of rainfall intensity and frequency, and simultaneous increase in temperature. Urbanization is conceptualized by an increase in the fraction of impervious areas within the basin. The analysis of the hydrological response simulated under the different scenarios, shows how the considered perturbations, acting separately or combined, may significantly alter the runoff generation mechanisms, resulting in relevant alterations of the extreme runoff events intensity and their associated return period.

Key words: hydrological change, climate change, urbanization

1. INTRODUCTION

The alterations induced in many basins' hydrological processes by natural or anthropogenic perturbations are commonly referred to as "hydrological changes". The analysis of the hydrological changes and their interacting triggering factors are high-priority research objectives, also defined within the *Panta Rhei* decade 2013-2022. Climate change and urbanization are among the most recurrent causes for hydrological changes at the global level. While the former is surely one of the most studied causes in recent literature (e.g., Francipane et al., 2015; Pumo et al., 2016), the latter represents a potential driver for hydrological changes still rather unexplored.

In this direction, this work aims to investigate possible alterations in the generation of basin scale runoff extremes due to these two types of perturbation acting singularly or in a combined manner. Specifically, we analyzed the peaks over threshold (POT) for the daily runoff and annual peaks of hourly runoff (HAP). Such indicators have been computed on the runoff time series for the river basin of the *Peatcheater Creek at Christie* (OK, USA), obtained by forcing a physically-based and spatial-distributed hydrological model by different hypothetical scenarios (combination of different synthetic climate schemes and land use maps).

2. METHODOLOGY

The proposed modeling framework involves the combined use of a land-use change model, a weather generator and a spatial-distributed hydrological model, briefly described below.

2.1 Land-use change model

We specifically developed a Land-Use Change Model (LUCM) with the aim to reproduce possible future land-use maps which take into account the increase of urbanization. The model

belongs to the class of probabilistic cellular automata models, based on: i) the consideration of the basin as a grid of regular cells; ii) the definition of an initial status (*urban* or *not-urban*) at any cell; iii) the iterative generation of a new grid at each successive temporal step according to time invariant fixed rules that determinate the new status in each cell as a function of its previous status and the status of the cells in its neighborhood. At each iteration, a value of probability of being urbanized (*urbanization probability*) is first associated to each *not-urban* cell and, successively, a new grid is generated starting from the previous one and replacing the cells with a higher *urbanization probability* by "new" *urban* cells.

The model considers an urban expansion criterion, according to which urban areas tend to expand around pre-existing urban zones following gentler slopes. The *urbanization probability* of each cell, in fact, depends on: 1) the slope (higher probability to cells with lower slope); 2) the total number of contiguous *urban* cells (i.e., within the Moore neighborhood, including the cells on a two-dimensional square lattice 3x3 around the analyzed cell); 3) the total number of *urban* cells in the neighborhood (i.e., within the extended Moore neighborhood, including the cells on a square lattice 7x7).

The model requires a raster map of slope and the initial status (*urban* or *not-urban*) of each cell within the basin. Model parameters are: the temporal horizon (generally equal to the simulation time of the application); the operative time step for new grids generation (e.g., 1 year); the projected future fraction of urban areas after the selected temporal horizon. A linear trend in built-up areas increase is assumed, so that urban expansion results constant year by year.

2.2 Weather generator and hydrological model

A weather generator is used to generate stationary climate schemes of current or possible future conditions. Specifically, we adopted the *Advanced WEather GENerator*, AWE-GEN (Fatichi et al., 2011), which is a statistical hourly stationary model capable to reproduce statistical properties of several weather variables (i.e., precipitation, cloudiness, radiation, temperature, and wind speed).

The adopted hydrological model is the *TIN-based Real-time Integrated Basin Simulator* - tRIBS (Ivanov et al., 2004a and 2004b). It explicitly considers the spatial variability of land-surface descriptors and uses an adaptive multiple resolution approach, based on a triangulated irregular networks (TIN), to solve basin hydrology at very high temporal (i.e., hourly) and spatial (10-100m) resolutions, simulating most of the natural hydrological processes. Moreover, it simulates the interactions of the fluxes inside the surface soil layers (i.e., unsaturated zone and water table) and reproduces four different mechanisms of runoff generation.

3. CASE STUDY

A synthetic experiment is here carried out on the real case of *Peacheater Creek at Christie* (OK, USA), one of the basins originally used to calibrate and validate the tRIBS model. A 100m Digital Elevation Model (Fig. 1a), and information available from other previous works (e.g., Vivoni et al., 2004), have been retrieved and used to characterize the spatial distribution and the properties of soils and land cover, as well as the geomorphologic characteristics of the basin.

The basin's area is 64 km^2, with mean elevation of 328 m a.s.l. and slopes from 2% to 40%. The vegetation is a mixture of forest grasslands and cropland-urban areas with an impervious fraction estimated in about 1.6%. The predominant soil is made of gravelly silt loams. Precipitation and temperature are characterized by scarce seasonally, with mean annual values approximately equal to 1,160 mm/year and 14.6°C, respectively.

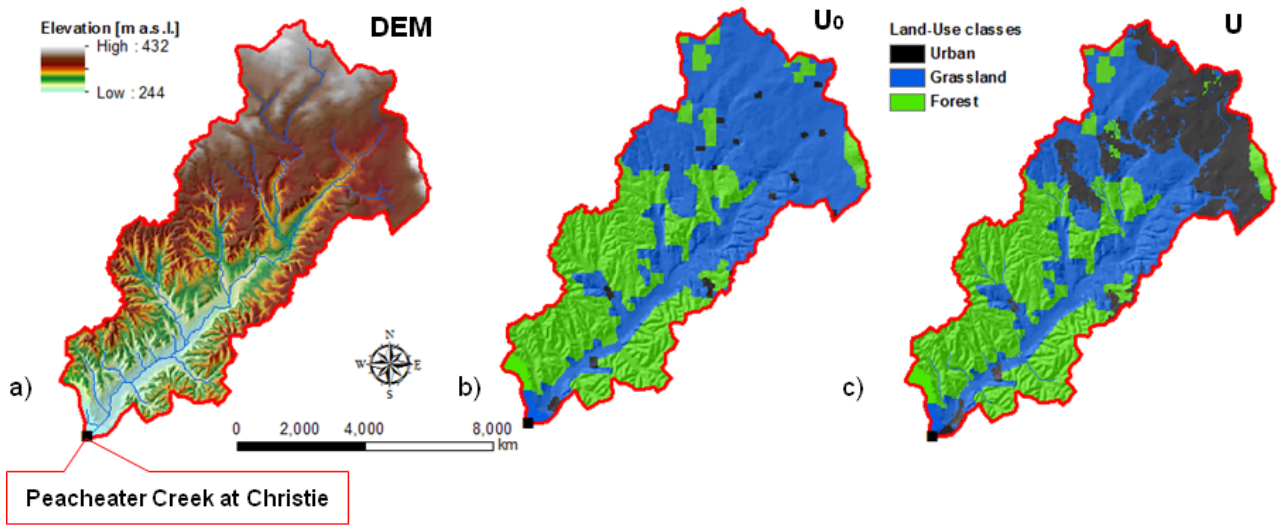

*Figure 1. DEM and stream network for Peacheater Creek at Christie (**a**). Land Use Maps: observed current map U_0 (**b**) and urbanized map (U) derived by the LUCM (**c**)*

3.1 Land Use Maps

The hydrological model is applied considering two different land use maps: the current map (U_0) and the altered map (U). In particular, U_0 (Fig. 1b) is the observed land use map and considers the same classification (i.e., *forest*, *grassland* and *urban*) and parameterization of Ivanov et al. (2004b).

The U map (Fig. 1c) is a possible future map obtained through the LUCM by increasing the fraction of impervious areas (replacing *not-urban* cells, previously classified as *forest* or *grassland*, with "new" *urban* cells). The working resolution is the same of the DEM (i.e., 100 m) from which the slope map has been derived. The used temporal horizon is equal to 100 years while the operative time step for new grids generation is equal to 1 year.

The urbanization process is highly variable in space and time and depends on a variety of local factors (e.g., socio-economic attractiveness, political, social, and geographical context, etc.). In view of the purposes of this work, we have imposed a percent increment of urban areas up to the 25% after 100 years, consistently with some trends observed in many fast developing regions of the world (e.g., Gumindoga et al., 2014).

3.2 Climate schemes and generation of different synthetic scenarios

Different, 30-year long, stationary climate schemes have been generated by using the AWE-GEN: the first is a reference period relative to the current conditions (*Baseline*), while the others represent possible future conditions obtained considering different climate change projections. The considered trends in the generation of each future climate scheme are not representative of projections specific for the area under analysis, but rather widespread limit conditions projected at the global level. In particular, climate changes considered for the generation of future climate schemes consist in relevant negative and positive trends in the Mean Annual Precipitation (MAP) and a simultaneous increase in temperature, according to some "highly probable" projections by the IPCC-5AR (IPCC, 2013). Other climate variables are assumed to maintain the observed statistical properties.

The *Baseline* has been created inferring the AWE-GEN climate parameters from hourly data recorded from 1992 to 1998 at the *Fayetteville* weather station (close to the basin: 36°1'N, 94°166'W).

Temperature time series for future climate schemes have been generated considering an increase (+2.6 °C) for the mean annual temperature. Two opposite limit conditions have been considered

with regard to the generation of the precipitation time series for future schemes: a negative trend (*CN*), consisting in a reduction by the 25% of the MAP, and a positive trend (*CP*), consisting in an increment by the 25% of the MAP. Four different types of climate scheme, characterized by different rainstorm characteristics, have been generated for both the *CN* and *CP* conditions:

A. variation in MAP exclusively due to an equal percent variation in the frequency of rainstorms (-25% for CN_A and +25% for CP_A);

B. variation in MAP entirely due to an equal percent variation in the mean intensity of rainstorms (-25% for CN_B and +25% for CP_B);

C. variation in MAP resulting by the application of an equal percent variation to both the rainstorm frequency and intensity (i.e., -13.4% for the CN_C and +11.8% for the CP_C);

D. variation in MAP due to an increase of the mean rainstorm intensity by the 50% for both the CN_D and CP_D and a consequent reduction of the frequency (-50% for CN_D and -16.67% for CP_D).

A total of 18 different stationary scenarios have been obtained by combining the 2 land use maps derived by the LUCM and the 9 climate schemes generated by the AWE-GEN. A code is here used to identify each scenario, with the first part referring to the climate scheme (*Baseline*, CN_i, or CP_i, with i=A, B, C, or D) and the second to the considered land use map (U_0 or U).

4. RESULTS

4.1 Analysis of the peaks over threshold

Peaks of daily runoff are analyzed in terms of mean annual percentage of days with runoff exceeding a fixed threshold (Peaks Over Threshold - POT). This last has been selected equal to the daily runoff value associated to the 90th percentile under the reference scenario (*Baseline*-U_0), i.e. the value that is currently exceeded for less than 36 days per year (i.e., 1.98 mm/day). The results are synthesized by the histogram in Fig. 1a, where the POT (% over the year) values are reported for each scenario; the variation with respect to the current value, expressed in terms of difference (Δ) in mean annual number of days with runoff over the selected threshold, is also reported by the label on the top of each bar.

Climate perturbation has a dominant role in determining hydrological changes, even if the role of land use change is not marginal, especially under the CN_i schemes. When only land use changes are considered (*Baseline*-U_2), the POT slightly increases.

When only negative climate trends are considered (scenarios with climate schemes CN_i and the U_0), the POT drastically reduces, with even 22 (i.e., CN_B) days per year less with runoff over threshold with respect to the reference scenario. Comparing the cases CN_B-U_0 and CN_D-U_0 it can be noticed that, at equal MAP, a higher POT is associated to the last case, whose mean rainstorms intensity is higher. When only positive climate trends are considered (scenarios with climate schemes CP_i), the POT significantly increases, with Δ ranging from 10 (i.e., CP_B and CP_D) to 19 (i.e., CP_A) days. The *CP* scheme associated to the scenario with the highest POT is that corresponding to the highest mean frequency and the lowest mean intensity of rainfall events (i.e., CP_A).

The combined application of climate and land use perturbations leads to contrasting effects on peaks generation, depending on the climate scheme considered. The effect due to the urbanization tends to smooth the reduction in the POT induced by the MAP reduction under the CN_i, especially for the climate scheme A, while it tends to exacerbate the increment in the POT caused by the MAP increment under the CP_i, especially for the scheme D. The only exception is the case under the CP_A, where POT and Δ are almost the same for both the U_0 and the U maps: in this case, an increment in

the rainstorms frequency with unaltered intensity produces similar effects on daily runoff peaks considering both a fraction of impervious areas of the 1.6% and the 25%.

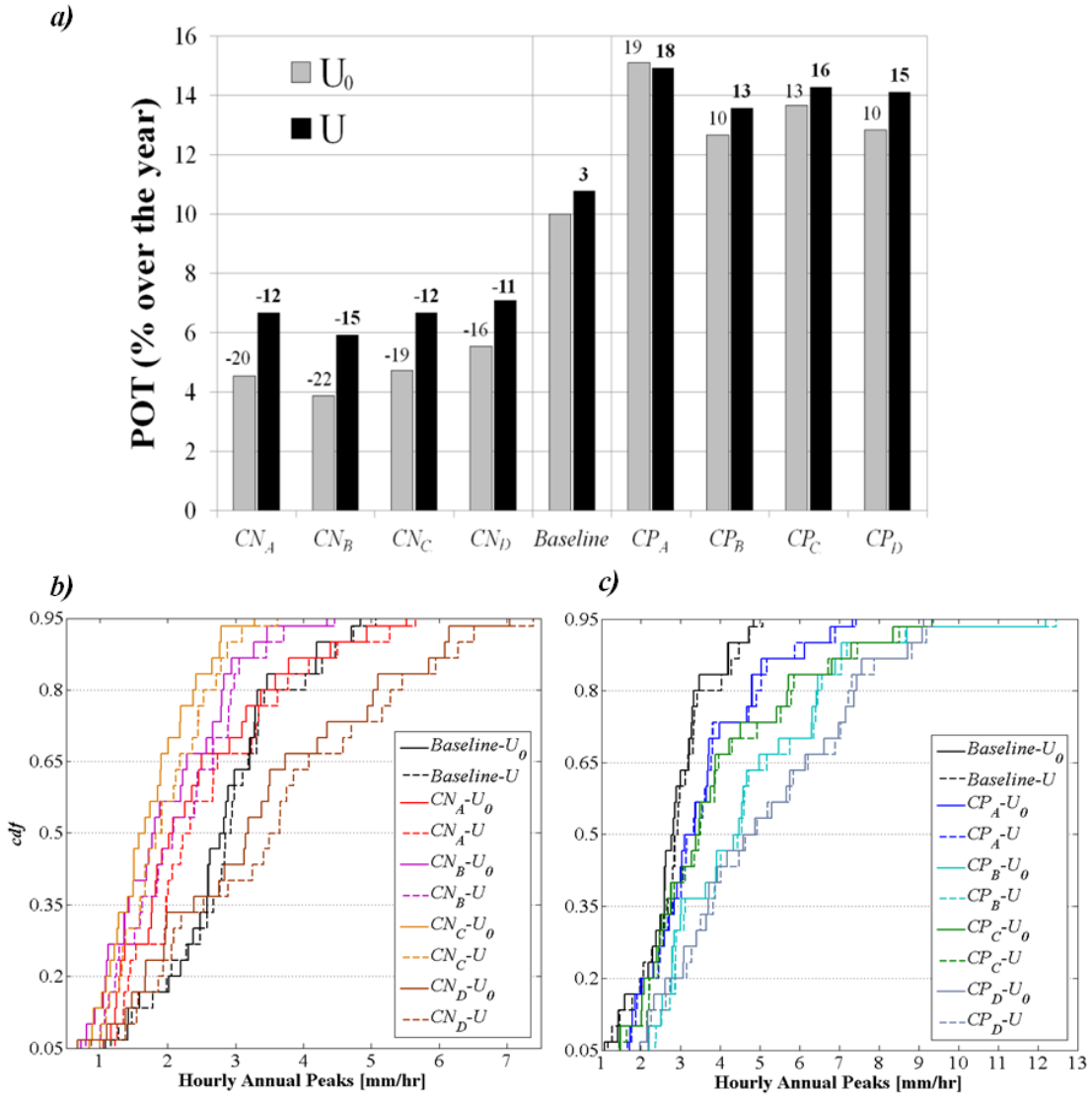

Figure 2. (a) Days per year with flow over threshold: POT (% over the year) reported by the histogram bars and variation Δ (days) with respect to the current scenario (labels). Cumulative distribution functions (cdfs) of annual peaks of hourly runoff (HAP) derived from the hourly runoff time-series under the different scenarios considering the CN_i (b) and the CP_i (c) climate schemes

From our results it is then presumable that the POT is highly sensitive to rainfall intensity in conditions of limited MAP (e.g., *CN* scenarios), while, when MAP is higher (e.g., *CP* scenarios), rainfall frequency may have a predominant role in influencing the POT.

4.2 Analysis of the annual peaks of hourly runoff

Figure 2 also shows the cumulative distribution functions (*cdfs*) of the Hourly Annual Peak (HAP) of runoff for each scenario. The upper and lower tails are not represented, focusing only on the probability domain from 5% to 95% and neglecting, then, possible outliers.

Under unaltered land use map, MAP reduction for the CN_i-U_0 scenarios (Fig. 2b) induces, except for the CN_D-U_0, a drastic reduction of HAP especially for the more extreme values (upper tail of the *cdfs*). For instance, under the CN_C-U_0, both the mean and the median are reduced with respect to the

Baseline-U_0 by about the 40%. Alterations induced by the CP_i-U_0 scenarios (Fig. 2c) result in higher HAP, with mean and median increased, on average, by the 56.6% and 39.2%, respectively. Under unaltered climate (i.e., *Baseline*), the urbanization process induces not negligible increments in HAP values (mean and median increase by about the 3.6%).

The coupled application of climatic and land use changes implies a partial compensation of the effects on hourly runoff extremes for the case under climate schemes CN_i, while, in the case of positive trends in climate (under climate schemes CP_i), the effects of two perturbations are overlapping. It is worth emphasizing that the percent variations in HAP induced by the simultaneous application of the two perturbations are significantly different (lower in absolute value) from those resulting from the sums of the percent variation singularly induced by climate and land use changes.

Changes on HAP due to the consideration of a reduction in MAP with an increment in rainfall intensity (CN_D-U_0) are comparable to those induced by an increment in MAP through the only increment in rainfall frequency and unaltered rainfall intensity (CP_A-U_0). The two cases, characterized by markedly different values of MAP, exhibit similar HAP, with almost overlapping *cdfs*. When the U map is considered, the two cases (i.e., CN_D-U and CP_A-U) result even more similar with each other, with lower discrepancies for all the statistics.

Also with regard to the only other case under CN_i conditions where rainfall intensity is not reduced, i.e., the CN_A-U_0, the upper part of the *cdf* (Fig. 2b) is basically unaltered with respect to the *Baseline*-U_0, demonstrating that changes in HAP, especially for what concerns the more extreme values, are highly sensitive to changes in rainstorm intensity rather than to changes in mean annual rainfall and, sometimes (as in the case CN_D-U_0), an increment in rainfall intensity could totally mask the effects on extreme hourly runoff due to a reduction in MAP.

The relevant sensitivity of hourly runoff peaks to rainfall intensity is also confirmed by the analysis of the cases under CP_i schemes; from Fig. 2c it is possible to observe how the raise in HAP is directly proportional to the trend magnitude applied to the rainstorm intensity. Simulations under the CP_D are, in fact, those showing the most severe variation in terms of HAP with respect to the *Baseline*-U_0, with a percent increment for the median of the *cdf* equal to 65.6% and 67.8% under the maps U_0 and U, respectively.

The analyzed perturbations have then a relevant impact on runoff extremes. For example, the extreme hourly runoff associated to the 90th percentile under the *Baseline*-U_0 (i.e., about 4 mm/hr corresponding to a return period of 10 years) would be much more recurrent under the scenario CP_D-U (where it is characterized by a return period of only 2 years), while the HAP under the CP_D-U having a return period of 10 years would be more than two times (i.e., 9.2 mm/hr) the current value (Fig. 2c). Under scenarios considering CN_i schemes, the events with a return period of 10 years are reduced in magnitude for climate schemes with reduction in rainfall intensity (up to 2.7 mm/hr for the CN_B-U_0), it is almost unaltered for the schemes with unaltered rainfall intensity (CN_A) under both the U_0 and U, while it is significantly increased for climate schemes with increased rainfall intensity (up to 6.3 mm/hr for the CN_B-U). Thus, under drier annual precipitation conditions, extreme runoff events are particularly sensitive to the rainfall characterization, resulting increasing with rainstorm intensity, especially under more impervious land use conditions.

5. CONCLUSIONS

Climate changes and urbanization, acting separately or combined, may significantly alter the basin scale runoff generation mechanisms with evident modifications in runoff extremes. Our results have highlighted a strong not-linearity in the basin response to the change factors that makes the superposition principle scarcely applicable. With regard to the considered trends, climate changes have a clear predominant role in altering the main characteristics of runoff extremes. A careful characterization of rainstorm events seems to be a crucial aspect in such a kind of studies. Urbanization, whose effects results more evident when finer time-scales of analysis (i.e., hourly) are adopted, tends to smooth the effects due to the consideration of negative climate trends, while the

opposite behaviour results under positive climate trends. Many of the evidences from this study can be explained looking at the modifications induced by the two perturbations here considered to the runoff components partitioning. Our simulation has shown how urbanization induced a major production of the fastest component of runoff, the surface runoff for infiltration excess mechanism, and the same has been observed for climatic schemes with increased rainstorms intensity. An increased relative weight of such component with respect to the other implies an increase of the intensity of the runoff peaks.

REFERENCES

IPCC. Climate change 2013. The physical science basis. Contribution of Working Group I to the fifth assessment report of the Intergovernmental Panel on Climate Change. Cambridge University Press, Cambridge, United Kingdom and New York, NY, USA, 2013

Ivanov, V.Y., Vivoni, E.R., Bras, R.L., Entekhabi, D., 2004a. Catchment hydrologic response with a fully-distributed triangulated irregular network model. Water Resour. Res., 40(11), W11102

Ivanov, V.Y., Vivoni, E.R., Bras, R.L., Entekhabi, D., 2004b. Preserving high-resolution surface and rainfall data in operational-scale basin hydrology: a fully-distributed physically-based approach. J. Hydrol., 298 (1-4): 80-111

Fatichi, S., Ivanov, V.Y., Caporali, E., 2011. Simulation of future climate scenarios with a weather generator. Adv. Water Resour., 34 (4): 448-467

Francipane, A., S. Fatichi, V. Y. Ivanov, and L. V. Noto (2015), Stochastic assessment of climate impacts on hydrology and geomorphology of semiarid headwater basins using a physically based model, J. Geophys. Res. Earth Surf., 120, 507–533, doi:10.1002/2014JF003232.

Gumindoga, W., Rientjes, T., Shekede, M.D., Rwasoke, D.T., Nhapi, I., Haile, A.T., 2014. Hydrological impacts of urbanization of two catchments in Harare, Zimbabwe. Remote Sens., 6 12544-12574; doi:10.3390/rs61212544

Pumo, D., Caracciolo, D., Viola, F., Noto, L.V., 2016. Climate change effects on the hydrological regime of small non-perennial river basins. Science of the Total Environment, 542 (Part A): 76-92; doi:10.1016/j.scitoten.2015.10.109

Vivoni, E.R., Ivanov, V.Y. Bras, R.L., Entekhabi, D., 2005. On the effects of triangulated terrain resolution on distributed hydrologic model response, hydrological Processes, doi: 10.1002/hyp.5671

Proceedings of the 10th World Congress of EWRA 'Panta Rhei', 5-9 July 2017, Athens, Greece
© 2017 *European Water Resources Association*

Forecasting of geophysical processes using stochastic and machine learning algorithms

G.A. Papacharalampous*, H. Tyralis and D. Koutsoyiannis
[1] *Department of Water Resources and Environmental Engineering, School of Civil Engineering, National Technical University of Athens, Iroon Polytechniou 5, 157 80 Zografou, Greece*
* *e-mail: papacharalampous.georgia@gmail.com*

Abstract: We perform an extensive comparison between four stochastic and two machine learning (ML) forecasting algorithms by conducting a multiple-case study. The latter is composed by 50 single-case studies, which use time series of total monthly precipitation and mean monthly temperature observed in Greece. We apply a fixed methodology to each individual case and, subsequently, we perform a cross-case synthesis to facilitate the detection of systematic patterns. The stochastic algorithms include the Autoregressive order one model, an algorithm from the family of Autoregressive Fractionally Integrated Moving Average models, an Exponential Smoothing State Space algorithm and the Theta algorithm, while the ML algorithms are Neural Networks and Support Vector Machines. We also use the last observation as a Naive benchmark in the comparisons. We apply the forecasting methods to the deseasonalized time series. We compare the one-step ahead as also the multi-step ahead forecasting properties of the algorithms. Regarding the one-step ahead forecasting properties, the assessment is based on the absolute error of the forecast of the last observation. For the comparison of the multi-step ahead forecasting properties we use five metrics applied to the test set (last twelve observations), i.e. the root mean square error, the Nash-Sutcliffe efficiency, the ratio of standard deviations, the index of agreement and the coefficient of correlation. Concerning the ML algorithms, we also perform a sensitivity analysis for time lag selection. Additionally, we compare more sophisticated ML methods as regards to the hyperparameter optimization to simple ones.

Key words: Stochastic algorithms, machine learning algorithms, multiple-case study, cross-case synthesis, multi-step ahead forecasting, one-step ahead forecasting, time lag selection, hyperparameter optimization

1. INTRODUCTION

Machine learning (ML) algorithms are widely used for the forecasting of geophysical processes as an alternative to stochastic algorithms. Popular ML algorithms are the rather well established Neural Networks (NN) and the new-entrant in most scientific fields Support Vector Machines (SVM). The latter was presented in its current form by Cortes and Vapnik (1995; see also Vapnik, 1995, 1999). The large number of the relevant applications is imprinted in Maier and Dandy (2000) and Raghavendra and Deka (2014).

As a result, the research in geophysical sciences often focuses on comparing stochastic to ML forecasting algorithms. The comparisons performed are usually based on single-case studies (e.g. Koutsoyiannis et al., 2008; Valipour et al., 2013), which offer the benefit of studying the phenomena in detail as also in their context and thus can provide interesting insights. On the other hand, single-case studies do not allow generalizations in any extent (Achen and Snidal, 1989). Generalizations could be derived by examining a sufficient number of different cases, as implemented in Papacharalampous et al. (2017). Within the latter study large-scale computational experiments based on simulations are conducted to compare several stochastic and ML methods regarding their multi-step ahead forecasting properties. A statistical analysis is performed and the results are presented accordingly.

Here we conduct a multiple-case study composed by 50 individual cases, each of them based on geophysical time series data from Greece. We apply a fixed methodology to each individual case for the comparison between several stochastic and ML methods regarding their one-step ahead and multi-step ahead forecasting properties. Concerning the ML methods, we also perform a sensitivity

analysis for time lag selection. Additionally, we compare more sophisticated ML methods as regards to the hyperparameter optimization to simple ones. Finally, we perform a cross-case synthesis to facilitate the detection of systematic patterns. We believe that the multiple-case study method can be useful for the comparative assessment of forecasting methods, as it can provide a form of generalization named "contingent empirical generalization", while retaining the immediacy of the single-case study method (Achen and Snidal, 1989).

2. DATA AND METHODS

2.1 Time series

We use 50 time series of total monthly precipitation and mean monthly temperature observed in Greece. We select only those with few missing values (blocks with length equal or less than one). Subsequently, we use the Kalman filter algorithm from the zoo R package (Zeileis and Grothendieck, 2005) for filling in the missing values. We use the deseasonalized time series for the application of the forecasting methods for the improvement of the forecasting quality, as suggested in Taieb et al. (2012). The deseasonalization is performed using a multiplicative model of time series decomposition.

The basic information about the time series is provided in Table 1. To describe the long-term persistence of the deseasonalized time series, we estimate the Hurst parameter H for each of them using the maximum likelihood method (Tyralis and Koutsoyiannis, 2011) implemented with the HKprocess R package (Tyralis, 2016).

2.2 Forecasting methods

We use four stochastic and two ML forecasting algorithms. The stochastic algorithms include the Autoregressive order one model (AR(1)), an algorithm from the family of Autoregressive Fractionally Integrated Moving Average models (auto_ARFIMA), an Exponential Smoothing State Space algorithm (BATS) and the Theta algorithm. The ML algorithms are Neural Networks (NN) and Support Vector Machines (SVM). We also use the last observation as a Naive benchmark in the comparisons. We apply the stochastic algorithms using the forecast R package (Hyndman and Khandakar, 2008; Hyndman et al., 2016) and the ML using the rminer R package (Cortez, 2010, 2015). The Naive, AR(1), auto_ARFIMA and BATS algorithms apply Box-Cox transformation to the input data before fitting a model to them.

While the stochastic forecasting methods are simply defined by the stochastic algorithm, the ML methods are defined by the set {ML algorithm, hyperparameter selection procedure, time lags}. We compare two procedures for hyperparameter selection, i.e. predefined hyperparameters or defined after optimization, and 21 regression matrices, each using the first n time lags, $n = 1, 2, \ldots, 21$. The hyperparameter optimization is performed with the hold-out method.

Hereafter, we consider that the ML models are used with predefined hyperparameters and that the regression matrix is built only by the first time lag, unless mentioned differently. We use two ML forecasting methods (one for each algorithm) in the comparisons conducted between stochastic and machine learning. We also use 42 forecasting methods (21 for each algorithm) to perform a sensitivity analysis for time lag selection and four ML forecasting methods (two for each algorithm) for the investigation of the effect of the hyperparameter optimization.

2.3 Metrics

Regarding the one-step ahead forecasting properties, the assessment is based on the absolute error (AE) of the forecast of the last observation. For the comparison of the multi-step ahead

forecasting properties we use the Root Mean Square Error (RMSE), the Nash-Sutcliffe efficiency (NSE), the ratio of standard deviations (rSD), the index of agreement (d) and the coefficient of correlation (Pr) applied to the test set. These metrics quantify the forecasting methods' performance according to several criteria related to the accuracy, the capture of the variance and the correlation between the forecasted and their respective observed values. For the definitions of the metrics NSE, d and Pr the reader is referred to Krause et al. (2005), while for the definition of the rSD to Zambrano-Bigiarini (2014).

Table 1. Time series examined. The Hurst parameter H is estimated for the deseasonalized time series.

s/n	Process	Code	Location	Station id	Reference	Start	End	Length (months)	H
1	Precipitation	prec_1	Agrinion	16672000	Peterson and Vose (1997)	Jan 1956	Dec 1987	384	0.48
2		prec_2	Alexandroupoli	16627000		Jan 1951	Dec 1990	480	0.59
3		prec_3	Aliartos	16674000		Jan 1907	Dec 1990	1008	0.53
4		prec_4	Anogeia	16754001		Jan 1919	Dec 1939	252	0.52
5		prec_5	Anogeia	16754001		Jan 1950	Dec 1979	360	0.53
6		prec_6	Araxos	16687000		Jan 1949	Dec 2000	624	0.51
7		prec_7	Athens	16714000		Jan 1860	Dec 1881	264	0.48
8		prec_8	Athens	16714000		Jan 1887	Dec 2005	1428	0.53
9		prec_9	Athens	16716000		Jan 1929	Dec 1945	204	0.52
10		prec_10	Fragma	16715001		Jan 1926	Dec 1990	780	0.54
11		prec_11	Heraklion	16754000		Jan 1946	Dec 1990	540	0.50
12		prec_12	Igoumenitsa	16641001		Jan 1951	Dec 1990	480	0.49
13		prec_13	Ioannina	16642000		Jan 1951	Dec 1990	480	0.58
14		prec_14	Kalamata	16726000		Jan 1956	Dec 1970	180	0.51
15		prec_15	Kalo Chorio	16756001		Jan 1950	Dec 1984	420	0.50
16		prec_16	Kastelli	16760001		Jan 1949	Dec 1976	336	0.55
17		prec_17	Kerkyra	16641000		Jan 1952	Dec 1996	540	0.51
18		prec_18	Kythira	16743000		Jan 1951	Dec 1973	276	0.48
19		prec_19	Kos	16742000		Jan 1958	Dec 1990	396	0.49
20		prec_20	Kozani	16632000		Jan 1955	Dec 1987	396	0.57
21		prec_21	Larissa	16648000		Jan 1951	Dec 1997	564	0.55
22		prec_22	Lemnos	16650001		Jan 1951	Dec 2000	600	0.52
23		prec_23	Methoni	16734000		Jan 1951	Dec 1991	492	0.49
24		prec_24	Milos	16738000		Jan 1951	Dec 1990	480	0.57
25		prec_25	Mytilene	16667000		Jan 1952	Dec 1990	468	0.55
26		prec_26	Naxos	16732000		Jan 1955	Dec 1971	204	0.46
27		prec_27	Patra	16689000		Jan 1901	Dec 1984	1008	0.52
28		prec_28	Sitia	16757000		Jan 1960	Dec 1983	288	0.56
29		prec_29	Skyros	16684000		Jan 1955	Dec 1987	396	0.50
30		prec_30	Thessaloniki	16622000		Jan 1931	Dec 1997	804	0.58
31		prec_31	Thessaloniki	16622002		Jan 1961	Dec 1970	120	0.56
32		prec_32	Trikala	16645001		Jan 1951	Dec 1990	480	0.56
33		prec_33	Tripoli	16710000		Jan 1951	Dec 1985	420	0.53
34	Temperature	temp_1	Araxos	16687001	Lawrimore et al. (2011)	Jan 1951	Dec 1980	360	0.66
35		temp_2	Athens	16714000		Jan 1858	Dec 1975	1416	0.67
36		temp_3	Athens	16714000		Jan 1989	Dec 2001	156	0.68
37		temp_4	Athens	16716000		Jan 1951	Dec 2012	744	0.65
38		temp_5	Heraklion	16754000		Jan 1950	Dec 2015	792	0.69
39		temp_6	Kalamata	16726000		Jan 1956	Dec 2015	720	0.74
40		temp_7	Kerkyra	16641000		Jan 1951	Dec 2016	792	0.67
41		temp_8	Larissa	16648000		Jan 1899	Dec 2016	1416	0.64
42		temp_9	Lemnos	16650000		Jan 1951	Dec 1998	576	0.75
43		temp_10	Methoni	16734000		Jan 1951	Dec 1972	264	0.59
44		temp_11	Methoni	16734000		Jan 1975	Dec 2000	312	0.61
45		temp_12	Patra	16689000		Jan 1951	Dec 1989	468	0.69
46		temp_13	Samos	16723000		Jan 1955	Dec 1969	180	0.64
47		temp_14	Samos	16723000		Jan 1974	Dec 2003	360	0.64
48		temp_15	Souda	16746000		Jan 1961	Dec 2015	660	0.71
49		temp_16	Thessaloniki	16622000		Jan 1892	Dec 2016	1500	0.71
50		temp_17	Thessaloniki	16622001		Jan 1961	Dec 1970	120	0.67

2.4 Methodology outline

We conduct 50 single-case studies by applying a fixed methodology to each time series (see Section 2.1), as explained subsequently. First, we split the time series into a fitting and a test set. The latter is the last observation for the one-step ahead forecasting experiments and the last 12 observations for the multi-step ahead forecasting experiments. Second, we fit the models to the deseasonalized fitting set, within the context determined by each forecasting method (see Section 2.2), and make predictions corresponding to the test set. Third, we add the seasonality to the predicted values and compare them to their corresponding observed using the metrics (see Section 2.3). Finally, we conduct the cross-case synthesis presented in Section 3 to demonstrate similarities and differences between the single-case studies conducted.

3. RESULTS AND DISCUSSION

We visualize the results within and across the individual cases using heatmaps. For the quantitative form of the latter graphs, as well as for Figures S1 and S2, the reader is referred to the Supplementary material, which is available at: http://dx.doi.org/10.17632/p8sw8pzkcd.3.

As regards the heatmaps of the present study, they are formed under the following conditions: a) the darker the colour the better the forecasts and b) the scaling is performed in the row direction. White color rows indicate that no scaling is taking place. The latter happens when the forecasting methods under comparison perform equally well regarding the criterion tested.

In Figures S1 and 1 we present the heatmaps formed for the comparison between the stochastic and two of the ML forecasting methods on precipitation and temperature time series data respectively. As we observe, the results of the single-case studies vary significantly. We also observe that in every individual case examined the following applies. There is no best or worst forecasting method regarding all the criteria set simultaneously. In other words, none of the forecasting methods is uniformly better or worse than the rest. The former observations apply equally to the stochastic and the ML forecasting methods, while it is noteworthy that the Naive benchmark is as competent as the forecasting methods regarding all the criteria set.

The observations outlined above are particularly important, because they reveal that the forecasting quality is subject to limitations. Each forecasting method has some specific theoretical properties and, due to the latter, it performs better or worse than other forecasting methods regarding specific criteria and in specific cases. Thus, the conduct of a single-case study using fewer criteria would have led to a very different overall picture. We note that the metrics RMSE and NSE give almost the same information about the forecast quality regarding the multi-step ahead forecasting experiments, a fact that does not apply to any other pair of metrics.

It is also interesting that the forecasting methods AR(1) and auto_ARFIMA are the least proper to use on precipitation data, while they are competent on the temperature time series data. This is actually a systematic pattern, which can be explained, when tracing back to the single-case studies using precipitation time series data. In more detail, those two forecasting methods predict zero precipitation in contrast to the rest, as a result to the zero precipitation observations in the summer months.

Finally, by studying the numerical results we note that the forecasts for temperature are remarkably better than the forecasts for precipitation. This may be explained by the fact that the variability in temperature is more regular than that in precipitation.

In Figures 2 and S2 we present the heatmaps formed for the sensitivity analysis on the time lags in time series forecasting using the NN and the SVM algorithms respectively. In both figures we observe significant variations in the results across the individual cases, in an extent that it is impossible to decide on a best or worst ML forecasting method among the single-case studies. Regarding the SVM algorithm (Figure S2), we observe no systematic patterns and the variations seem to be rather random, while for the case of the NN algorithm (Figure 2) we observe that the left parts of the heatmaps are smoother with no white cells.

(1) one-step ahead forecasting - AE (2) multi-step ahead forecasting - RMSE (3) multi-step ahead forecasting - NSE
(4) multi-step ahead forecasting - rSD (5) multi-step ahead forecasting - d (6) multi-step ahead forecasting - Pr

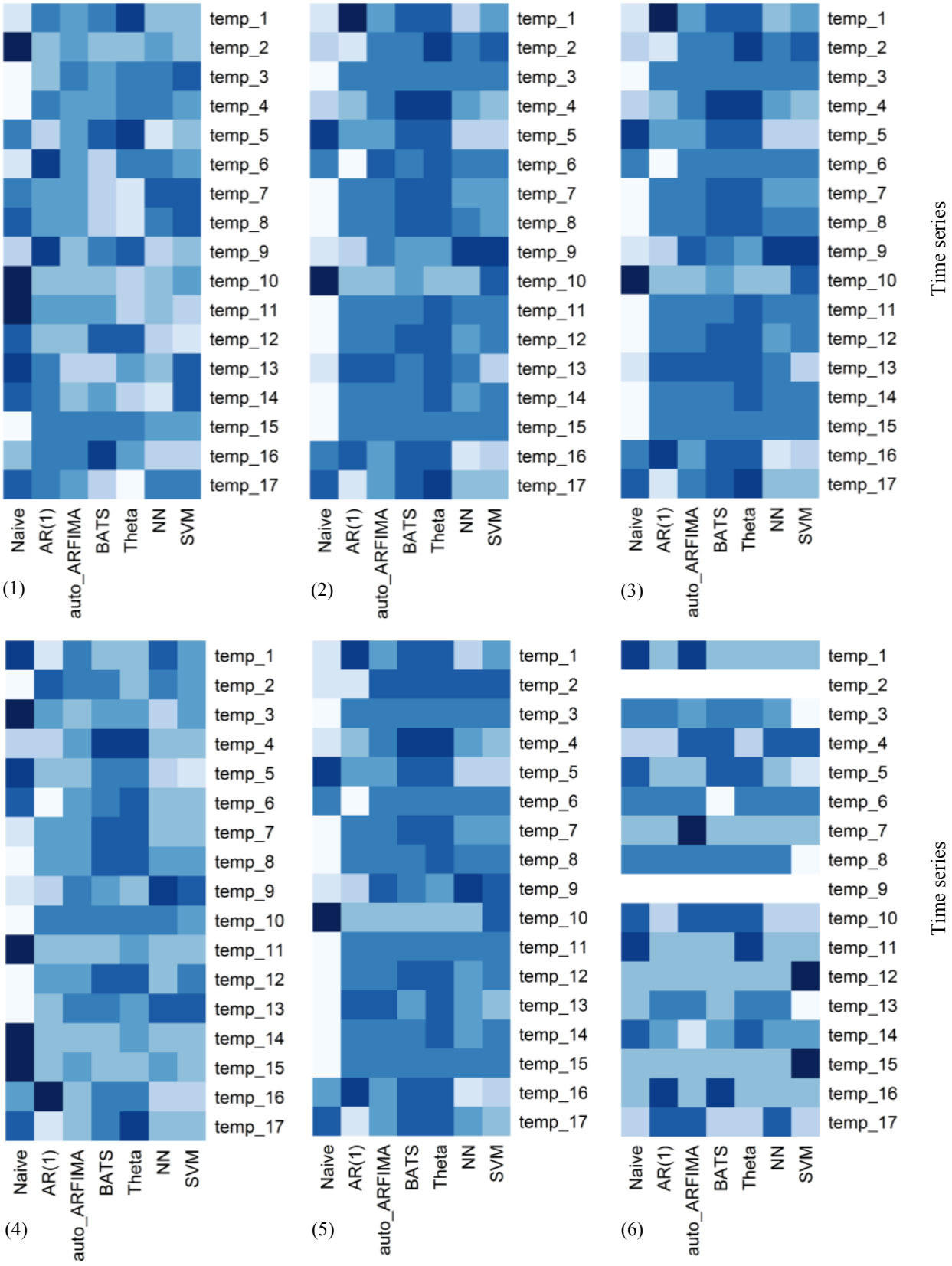

Figure 1. Heatmaps for the comparison between stochastic and ML methods on temperature time series.

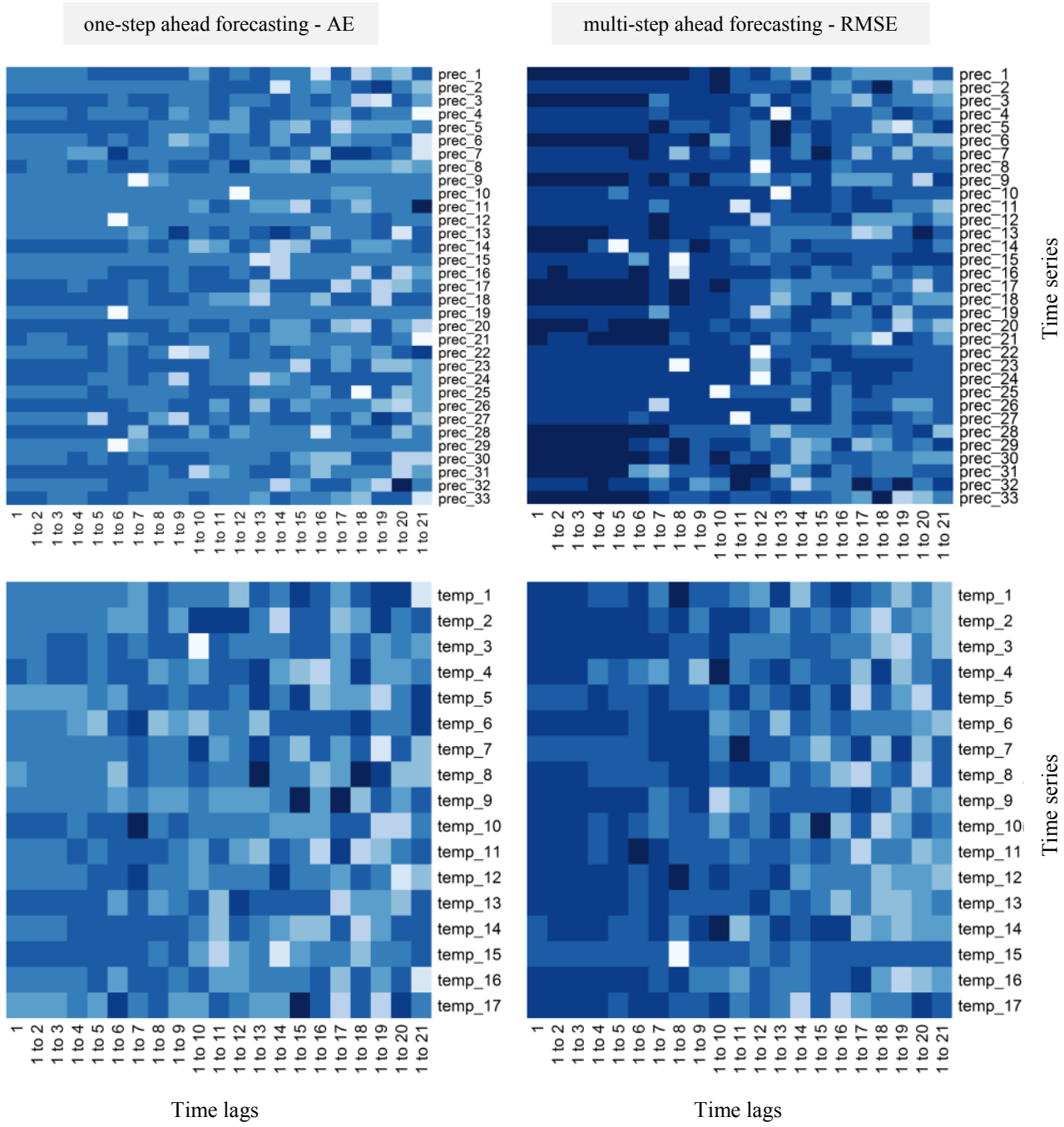

Figure 2. Heatmaps for the sensitivity analysis on the time lags in time series forecasting using the NN algorithm.

In Figure 3 we present the heatmaps formed for the investigation of the effect of the hyperparameter optimization. The results vary across the single-case studies in a rather random manner, which indicates that the hyperparameter optimization does not necessary lead to better forecasts for the NN and SVM algorithms.

4. CONCLUSIONS

The multiple-case study conducted must be encountered as a contingent empirical evidence on several issues that have drawn the attention in the field of time series forecasting. The findings suggest that the stochastic and ML methods can perform equally well, but always under limitations. The best forecasting method depends on the case examined and the criterion of interest, while it can be either stochastic or ML. However, the ML methods are computationally intensive. Regarding the time lag selection, the best choice seems to depend mainly on the case, while the ML algorithm

might has also some effect. Finally, for the algorithms used in the present study hyperparameter optimization does not necessarily lead to better forecasts.

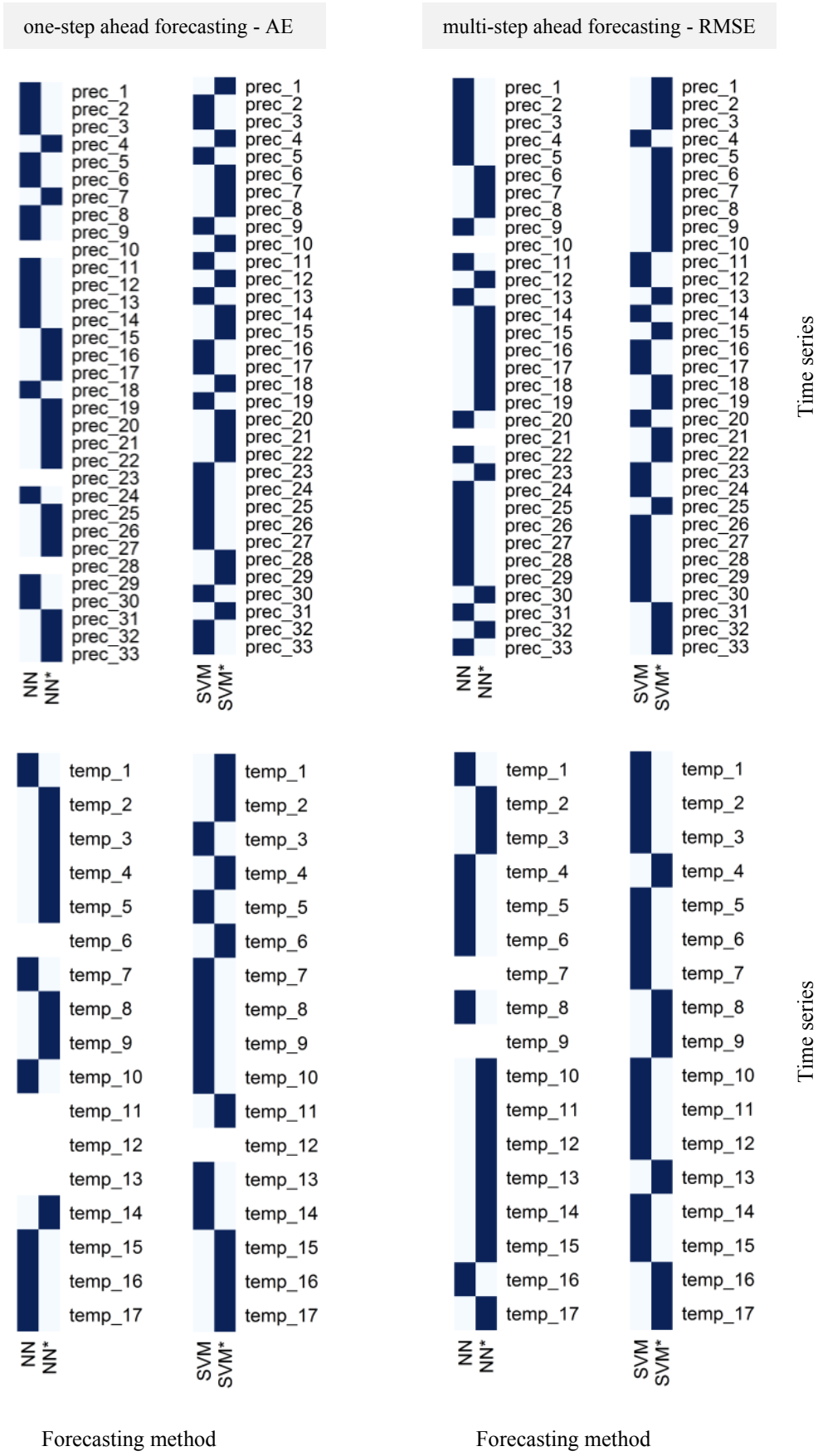

*Figure 3. Heatmaps for the investigation of the effect of hyperparameter optimization on the forecast quality. The symbol * in the name of a forecasting method denotes that the model’s hyperparameters have been optimized.*

REFERENCES

Achen, C. H., Snidal D., 1989. Rational deterrence theory and comparative case studies. World Polit.; 41(2): 143-169. doi:10.2307/2010405

Cortes, C., Vapnik, V., 1995. Support-vector networks. Mach. Learn.; 20(3): 273-297. doi:10.1007/BF00994018

Cortez, P., 2010. Data mining with neural networks and support vector machines using the R/rminer tool. In: Perner P (eds) Advances in Data Mining. Applications and Theoretical Aspects. Springer Berlin Heidelberg, pp 572-583. doi:10.1007/978-3-642-14400-4_44

Cortez, P., 2015. rminer: Data mining classification and regression methods. R package version 1.4.1. https://cran.r-project.org/web/packages/rminer/index.html

Hyndman, R. J., O'Hara-Wild, M., Bergmeir, C., Razbash, S., Wang, E., 2016. forecast: Forecasting functions for time series and linear models. R package version 7.1. https://CRAN.R-project.org/package=forecast

Hyndman, R. J., Khandakar, Y., 2008. Automatic time series forecasting: the forecast package for R. J. Stat. Softw.; 27(3): 1-22. doi:10.18637/jss.v027.i03

Koutsoyiannis, D., Yao, H., Georgakakos, A., 2008, Medium-range flow prediction for the Nile: a comparison of stochastic and deterministic methods. Hydrolog. Sci. J.; 53(1). doi:10.1623/hysj.53.1.142

Krause, P., Boyle, D. P., Bäse, F., 2005. Comparison of different efficiency criteria for hydrological model assessment. Adv. Geosci.; 5: 89-97

Lawrimore, J. H., Menne, M. J., Gleason, B. E., Williams C. N., Wuertz, D. B., Vose, R. S., Rennie, J., 2011. An overview of the Global Historical Climatology Network monthly mean temperature data set, version 3. J. Geophys. Res.; 116(D19121). doi:10.1029/2011JD016187

Maier, H. R., Dandy, G. C., 2000. Neural networks for the prediction and forecasting of water resources variables: a review of modelling issues and applications. Environ. Model. Softw.; 15(1): 101-124. doi:10.1016/S1364-8152(99)00007-9

Papacharalampous, G. A., Tyralis, H., Koutsoyiannis, D., 2017. Comparison of stochastic and machine learning methods for multi-step ahead forecasting of hydrological processes. Journal of Hydrology. In review

Peterson, T. C., Vose, R. S., 1997. An overview of the Global Historical Climatology Network temperature database. Bull. Am. Meteorol. Soc.; 78(12): 2837-2849. doi:10.1175/1520-0477(1997)078<2837:AOOTGH>2.0.CO;2

Raghavendra, N. S., Deka, P. C., 2014. Support vector machine applications in the field of hydrology: a review. Appl. Soft Comput.; 19: 372-386. doi:10.1016/j.asoc.2014.02.002

Taieb, S. B., Bontempi, G., Atiya, A. F., Sorjamaa, A., 2012. A review and comparison of strategies for multi-step ahead time series forecasting based on the NN5 forecasting competition. Expert Syst. Appl; 39(8): 7067-7083. doi:10.1016/j.eswa.2012.01.039

Tyralis, H., 2016. HKprocess: Hurst-Kolmogorov Process. R package version 0.0-2. https://cran.r-project.org/web/packages/HKprocess/index.html

Tyralis, H., Koutsoyiannis, D., 2011. Simultaneous estimation of the parameters of the Hurst–Kolmogorov stochastic process. Stoch. Env. Res. Risk.; 25(1): 21-33. doi:10.1007/s00477-010-0408-x

Valipour, M., Banihabib, M. E., Behbahani, S. M. R., 2013. Comparison of the ARMA, ARIMA, and the autoregressive artificial neural network models in forecasting the monthly inflow of Dez dam reservoir. J. Hydrol.; 476: 433-441. doi:10.1016/j.jhydrol.2012.11.017

Vapnik, V. N., 1995. The nature of statistical learning theory, first edition. Springer-Verlag New York. doi:10.1007/978-1-4757-3264-1

Vapnik, V. N., 1999. An overview of statistical learning theory. IEEE Trans Neural Netw; 10(5): 988-999. doi:10.1109/72.788640

Zambrano-Bigiarini, M., 2014. hydroGOF: Goodness-of-fit functions for comparison of simulated and observed hydrological time series. R package version 0.3-8. https://cran.r-project.org/web/packages/hydroGOF/index.html

Zeileis, A., Grothendieck, G., 2005. zoo: S3 infrastructure for regular and irregular time series. J. Stat. Softw.; 14(6): 1-27. doi:10.18637/jss.v014.i06

Proceedings of the 10th World Congress of EWRA 'Panta Rhei', 5-9 July 2017, Athens, Greece
© 2017 *European Water Resources Association*

Reliability estimation of rainwater catchment system using future GCM output data (case study: Birjand city)

A. Jafarzadeh[1], M. Pourreza Bilondi[1*], A. Khashei-Siuki[1], A. Aghakhani Afshar[2], M. Yaghoobzadeh[1]
[1] *Dept of Science and Water Engineering, University of Birjand, Iran*
[2] *Dept of Water Engineering, Faculty of Civil Engineering, University of Tabriz, Tabriz, Iran*
[*] *e-mail: Mohsen.pourreza@birjand.ac.ir*

Abstract: Due to climate condition of arid area, a major part of rainfall will be out of reach in the form of flash floods and a few percent recharged to groundwater aquifers. Therefore in order to reach to a sustainable development, water resource management based on rainwater harvesting systems (RWHS) will be inevitable. The main aim of this study is reliability assessment of RWHS for future. In first step, monthly rainfall may be simulated using GCMs outputs in historical and future periods. Then data is downscaled spatially through BCSD for 20 grid points around of Birjand rain-gauge station. Monthly rainfall for this station is interpolated by ordinary kriging method during future period automatically and then top GCMs are selected. Finally using interpolated monthly rainfall time series, reliability assessment of RWHS may be examined in different roof area and storage tank capacity. Results indicate that a range of reliability of was estimated 0.05-0.45 RWHS in historical period and this range will be raised in future period based on simulated monthly rainfall corresponding to the top GCMs. That's why a significant volume of household water demand can be satisfied by relying on RWHS. Also variation of reliability of RWHS showed that reliability of RWHS under 2.6rcp will be more than 8.6rcp in future period generally.

Key words: rainwater harvesting, climate change, reliability, kriging

1. INTRODUCTION

Water Scarcity is largest challenge that most of regions faced with today especially in developing countries. Hence research activates to find non-conventional water resources have increased. Rainwater harvesting system (RWHS) is considered as one of major technics that can save rainwater for domestic or agriculture uses (Traboulsi and Traboulsi, 2015) and has a long tradition for thousands of years (AbdelKhaleq and Ahmed, 2007).

In recently year climate change has caused significant effects on meteorological and hydrological components. Many studies relating to climate change effects in arid and semi-arid regions revealed that amount of rainfall have decreased in these regions (Tabari and Talaee, 2011). Since precipitation is main driver in RWHS, Shift in its quality and quantity can change operation of these systems efficiently. Therefore some researches in recent years aimed to evaluate assessment of RWHS and climate change effects on them.

Some of studies about climate change effects on RWHS covered performance assessment of rainwater harvesting as adaptation strategy (Pandey et al, 2003; Salas et al, 2009; Amin et al, 2013). Some of other studies survey change of rainwater harvesting yield based on rainfall variation which mainly affected through climate change (Ogungbenro and Morakinyo, 2014). Also there are studies that concerned climate change effects on reliability of RWHS for supply household water demand. This part of literature has been performed by a few studies incorporated future uncertain rainfall event in estimating reliability of a RWHS (Basinger et al. 2010). The main objective of this study is to determine reliability of RWHS and optimal size of storage tank influenced by climate change effects in dry climate.

2. STUDY AREA

Birjand city is center of Southern Khorasan province. This city with dry and cold climate is putted in east of Iran (fig. 1). The annual average precipitation, temperature, relative humidity, and pan evaporation are 170 mm, 16.5 °C, 37 %, and 2250 mm, respectively.

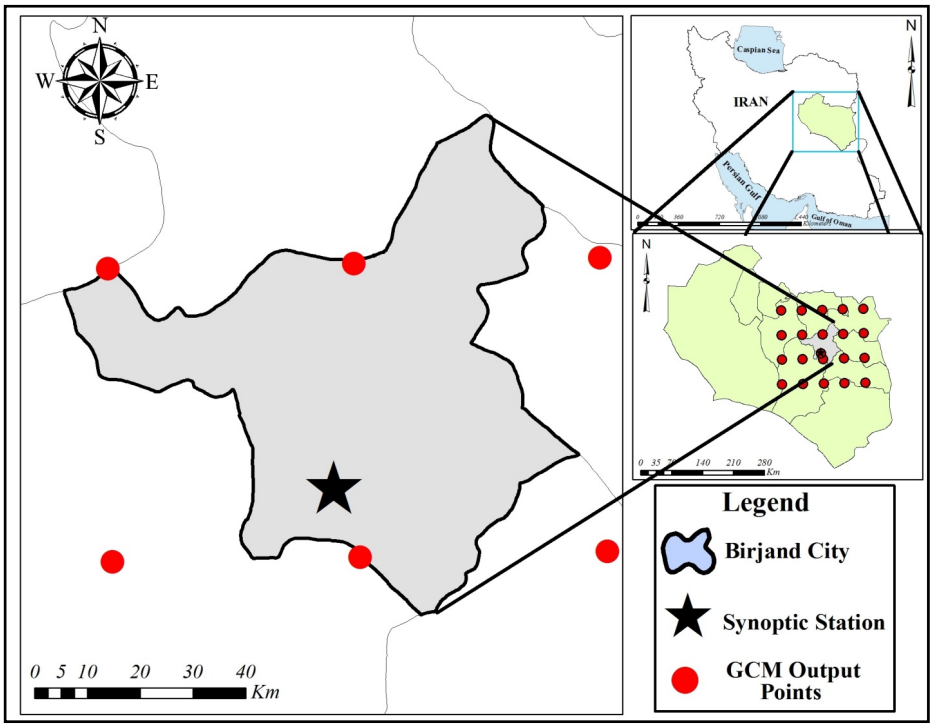

Figure 1. Location of the study area

3. MATERIAL AND METHOD

3.1 Monthly rainfall time series from projected climate

Rainfall data time series for future pattern is obtained from monthly rainfall output from GCMs in the Coupled Model Intercomparison Project 5 (CMIP5). In this study were used from GCMs under 2.6rcp and 8.6rcp which have more adaptation to condition of dry climate in east of Iran (Afshar et al, 2016) which have been listed in detail in Table 1.

Table 1. Details of GCMs used in this study

Model name	Organization
HadGEM2-ES	MOHC, Met Office Hadley Centre, UK
GFDL-CM3	NOAA, Geophysical Fluid Dynamics Laboratory, USA
GFDL-ESM2M	
GFDL-ESM2G	
MIROC5	MIROC, Centre for Climate System Research, Japan
MIROC-ESM	
MIROC-ESM-CHEM	
IPSL-CM5A-LR	IPSL, Institute Pierre Simon Laplace, France
IPSL-CM5A-MR	
NorESM1-M	NCC, Norwegian Climate Centre, Norway
BCC-CSM1.1	BCC, Beijing Climate Centre, China
CSIRO-Mk3.6.0	CSIRO-QCCCE, Commonwealth Scientific and Industrial Research Organization, Australia
CCSM4	NCAR, National Center for Atmospheric Research, USA
CESM1(CAM5)	NSF-DOE-NCAR, Community Earth System Model Contributors

3.2 Downscaling

Due to low resolutions of GCMs, their outputs are not suited to simulation of climate components at a specific location such as meteorological gauge (Duan and Mei, 2014). Concerning this issue downscaling process are performed to convert climate data from GCMs grid points to local point (Farajzadeh et al, 2014). In this study monthly rainfall of GCMs were obtained for historical (1992-2005) and future (2017-2030) periods from the Downscaled CMIP3 and CMIP5 Climate and Hydrology Projections Website and then downscaled by BCSD method. Frist applications of BCSD are related to estimation of long-term hydrology parameters (Wood et al, 2002). More details about BCSD are presented in studies of Wood et al, (2002). The rainfall was extracted for 20 points around of case study station.

3.3 Automating of Kriging interpolation method

Monthly rainfall for Birjand rain-gage station obtained by ordinary kriging interpolation method automatically and described in this section in detail.

3.3.1 Short description of kriging method

Kriging is a strong geostatistical tool for interpolation and extrapolation which was based on regionalized variables (Cressie, 1993). First application of this technology was limited to exploration of new streaks of specific minerals. Calculating semi-variograms ($\gamma^*(h)$ in Equation 1) as a basic geostatistical measure is applied to determine the rate of change of a regionalized variable along a specific orientation.

$$\gamma^*(h) = \frac{1}{2 \times N(h)} \sum_{1}^{N(h)} [Z(X_\alpha + h) - Z(X_\alpha)]^2 \quad (1)$$

where N(h) is number of points with the distance h, and is the point value. More details about kriging operation are demonstrated in study Biau et al, (1999).

3.3.2 Application of kriging in this study

Monthly rainfall time series for Birjand rain gauge interpolated by BCSD output points as observation data points which located around. We evaluated experimental variogram firstly (equation 1) and then the best theoretical variogram selected amongst linear, spherical, Gaussian and exponential for each months. Finally weight of neighboring points estimated by equation 2 and monthly rainfall for Birjand rain-gauge obtained for all used GCMs (table 1).

3.4 Performance Criteria

Identification of best GCMs for a given study region performed by testing downscaled GCM output against historical rainfall. Some performance criteria used for assessment of GCMs listed below (see equations 2 to 5).

$$PBIAS = \frac{\sum_{i}^{n}(S_i - O_i)*100}{\sum_{i}^{n} O_i} \tag{2}$$

$$RMSE = \sqrt{\frac{\sum_{i}^{n}(S_i - O_i)^2}{n}} \tag{3}$$

$$NSE_C = 1 - \frac{\sum_{i}^{n}\left|O_i - S_i\right|}{\sum_{i}^{n}\left|O_i - \overline{O}\right|} \tag{4}$$

$$r^2 = \frac{\sum_{i}^{n}(O_i - \overline{O}) \times \sum_{i}^{n}(S_i - \overline{S})}{\sum_{i}^{n}(O_i - \overline{O})^2 \times \sum_{i}^{n}(S_i - \overline{S})^2} \tag{5}$$

$$\omega r^2 = \begin{cases} |b|^{-1}.r^2 & for\ b > 1 \\ |b|.r^2 & for\ b \le 1 \end{cases}$$

where O_i and S_i are the observed and simulated values, respectively. Also $\overline{O}$ and $\overline{S}$ are mean of those. In this study we prefer to compare GCMs outputs with using corrected Nash-Sutcliff (NSE_C) (see equation 4). Also determination coefficient is implemented with modified form, using of ωr^2 instead of r^2. More details are presented in a study of Krause et al, (2005). Best GCMs output may be appropriately selected through comparing of defined criteria.

3.5 Reliability assessment

Major components of rainwater harvesting systems are roof catchment area, conveyance system for conduct harvested water from roof area and storage tank capacity that store rainfall. Rainwater volume is evaluated based on algorithm which is recommended by Jenkins et al, (1978). This algorithm implements continuously in time for residential buildings and described in equation 6:

$$\begin{aligned} &for\ t = 2:b \\ &V_t = \{V_{t-1} + \min[(A.P_t.\varepsilon),(S - V_{t-1})] - O_t\} \\ &end \end{aligned} \tag{6}$$

where V_t and V_{t-1} are volume of captured rainwater for steps *'t'* and *'t-1'* respectively. b is number of time steps in operation priod, A is rooftop area (m^2), S is volume of storage tank (m^3), O_t is water demand in step *'t'* (m^3), P_t is mount of rainfall in step *'t'* and finally ε is conveyance efficiently. In this algorithm minimum of V_t considered zero. This algorithm can perform for each individual period and in last time step of operation ($t=b$) evaluate reliability of RWHS based on predetermined values of A and S. Reliability is defined proportion of time steps which RWHS met water demand.

In this study we achieved monthly rainfall time series from best GCM output and then reliability algorithm fulfilled at future period. Household water demand per capita assumed 30 *lit/day* (almost equal with 1 m^3*/capita.month*) and number of individuals at a house considered 5 persons. Roof

area and storage tank are sampled uniformly between 150 -500 m^2 and 5 -30 m^3 respectively. Also conveyance efficient set almost 0.8

4. RESULTS AND DISCUSSION

Comparison results of GCMs and observation monthly rainfall at historical period are provided in table 2. Four best models with high value in $NASH_C$ and R^2 mid low value for *RMSE* and *Pbias* have been selected and underlined and other remaining was refused.

Table 2. Performance assessment of GCMs

`ID	Model name	RMSE	R2	NASHC	Pbias
1	BCC-CSM1.1	19.403	0.068	0.280	-10.669
2	CCSM4	20.871	0.069	0.220	-14.692
3	CESM1(CAM5)	**18.078**	**0.143**	**0.352**	**-9.752**
4	CSIRO-MK3.6	19.425	0.123	0.275	3.481
5	GFDL-CM3	19.857	0.104	0.245	3.465
6	GFDL-ESM2G	20.074	0.086	0.232	0.907
7	GFDL-ESM2M	18.477	0.146	0.294	1.258
8	HadGEM2-ES	**18.196**	**0.242**	**0.337**	**10.845**
9	IPSL-CM5A-LR	21.629	0.060	0.222	-0.329
10	IPSL-CM5A-MR	18.685	0.158	0.293	-5.208
11	MIROC5	19.500	0.093	0.274	6.532
12	MIROC-ESM	**18.005**	**0.188**	**0.306**	**9.008**
13	MIROC-ESM-CHEM	**18.001**	**0.172**	**0.353**	**-7.584**
14	NorESM1-M	19.723	0.126	0.247	-5.977

Relying on value of used performances criteria, CESM1 (CAM5) was selected as top GCM. Reliability of RWHS as main objective of this study in historical period is evaluated. Figure 2 displays difference reliability levels of RWHS for Birjand city. This plot indicate that maximum of reliability of RWHS in birjand city is nearly 0.45 for historical monthly rainfall as well as lower bound is 0.05. Maximum reliability with upper limit of roof area and storage tank capacity may be accessible with 500 m^2 and 25 m^3. This point can likely satisfy nearly half of household water demand.

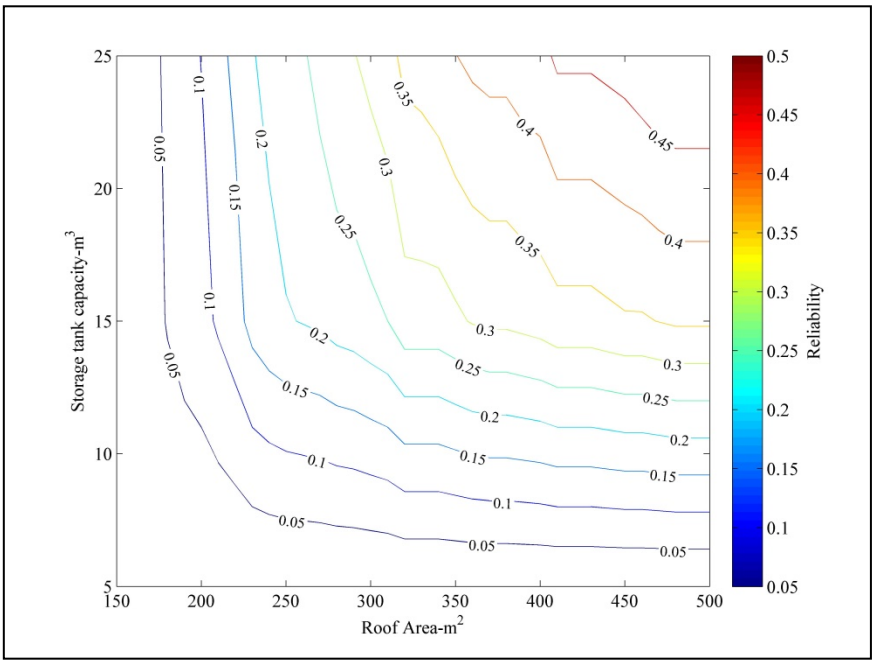

Figure 2. Reliability of RWHS in historical period

Curves of reliability levels future period (2017-2030) have achieved related to two scenarios and worst and best GCMs outputs.

Results of reliability levels for household water demand with 5 individuals for CESM1 (CAM5) under 2.6rcp and 8.6rcp have been presented in figure 3. Variation of reliability levels of RWHS between rcp8.5 and rcp2.6 is simply visible in CESM1 (CAM5). Therefore it can be pointed that reach to specific reliability level of RWHS in rcp2.6 is easier than rcp8.6 generally.

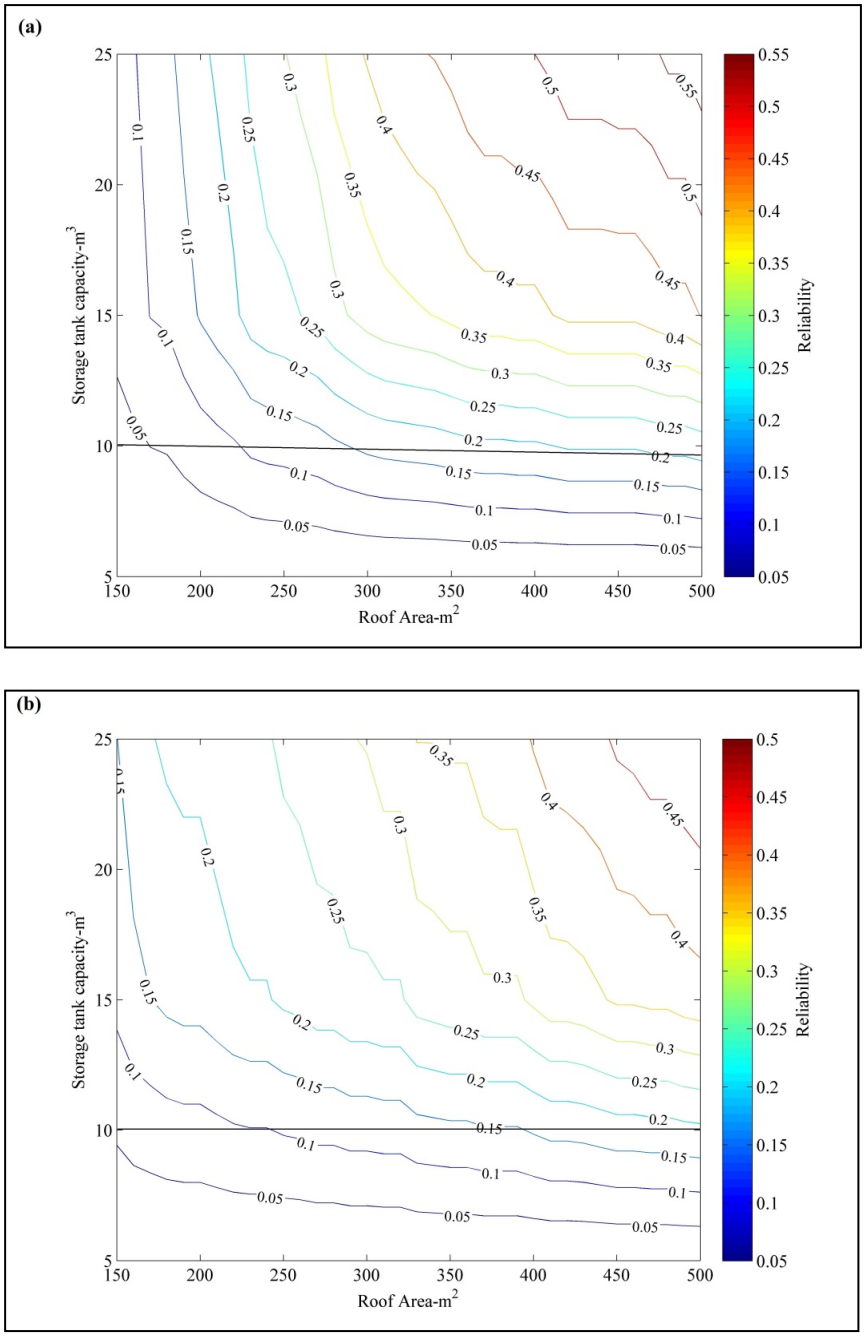

Figure 3. Reliability levels of RWHS based on CESM1 under 2.6rcp (a) and 8.6rcp (b)

According to the reliability of RWHS in historical and comparison with results of reliability related to best GCM it can demonstrated that reliability levels of RWHS in future period will increase specially relying on rainfall which forecast from 2.6rcp. In addition household water demand in nearly half of months at future period can be satisfied by relying on RWHS.

More precise analysis of reliability curves shows that distance between low levels is fewer than high levels of reliability. It means that high reliability levels are more dispersed. In other expression

reach to a higher reliability for low levels would be more achievable than high levels. This may be reasoned in dry regions such as birjand city major months are faced with low rainfall, so accessing to low reliability levels is more comfortable.

Also weighted mean of reliability relying on CESM1 (CAM5) calculated in historical and future period. Value of weighted mean of reliability in historical period evaluated 0.15 and this value for future period under 2.6rcp and 8.6rcp estimated 0.18 and 0.16 respectively.

5. CONCLUSION

In current study climate change effects on reliability of RWHS have investigated in future and historical periods. Reliability levels of RWHS were achieved by using future simulations of monthly rainfall which has projected by GCMs outputs downscaled by BCSD method and was interpolated through kriging automatically to Birjand rain-gauge location.

Results showed that reliability of RWHS based on monthly rainfall forecasted by acceptable GCMS under 2.6rcp is more than 8.6rcp. With regard to results of this investigation reliability levels of RWHS will increase at future period. Highest reliability level of RWHS is estimated to 0.5 relying on monthly rainfall projected by best GCMs. Also 20% increase of average of reliability level of RWHS in future period achieved proportion to historical.

REFERENCES

AbdelKhaleq, R. A., & Ahmed, I. A. 2007. Rainwater harvesting in ancient civilizations in Jordan. Water Science and Technology: Water Supply, 7(1), 85-93.

Afshar, A. A., Hasanzadeh, Y., Besalatpour, A. A., & Pourreza-Bilondi, M. 2016. Climate change forecasting in a mountainous data scarce watershed using CMIP5 models under representative concentration pathways. Theoretical and Applied Climatology, 1-17.

Aladenola, O., Cashman, A., & Brown, D. 2016. Impact of El Niño and Climate Change on Rainwater Harvesting in a Caribbean State. Water Resources Management, 30(10), 3459-3473.

Amin, M. T., Alazba, A. A., & ElNesr, M. N. 2013. Adaptation of climate variability/extreme in arid environment of the Arabian peninsula by rainwater harvesting and management. International journal of environmental science and technology, 10(1), 27-36.

Basinger, M., Montalto, F., & Lall, U. 2010. A rainwater harvesting system reliability model based on nonparametric stochastic rainfall generator. Journal of Hydrology, 392(3), 105-118.

Biau, G., Zorita, E., von Storch, H., & Wackernagel, H. 1999. Estimation of precipitation by kriging in the EOF space of thesea level pressure field. Journal of Climate, 12(4), 1070-1085.

Cressie, N. A., 1993, Statistics for spatial data. John Wiely.

Christensen, N. S., Wood, A. W., Voisin, N., Lettenmaier, D. P., & Palmer, R. N. 2004. The effects of climate change on the hydrology and water resources of the Colorado River basin. Climatic change, 62(1), 337-363.

Duan, K., andMei, Y. 2014.A comparison study of three statistical downscaling methods and their model-averaging ensemble for precipitation downscaling in China. Theoretical and Applied Climatology, 116: 707-719.

Farajzadeh, M., Oji, R., Cannon, A., Ghavidel, Y., Bavani, A.M. 2014.An evaluation of single-site statistical downscaling techniques in terms of indices of climate extremes for the Midwest of Iran. Theoretical and Applied Climatology, Pp: 1-14

Fowler, H. J., Kilsby, C. G., O'Connell, P. E. 2003. Modeling the impacts of climatic change and variability on the reliability, resilience, and vulnerability of a water resource system. Water Resources Research, 39(8).

Iranian Population and Housing Census, 2016.

Jenkins, D., & Pearson, F. 1978. Feasibility of rainwater collection systems in California. Contribution-California. University.

Krause, P., Boyle, D. P., & Bäse, F. 2005. Comparison of different efficiency criteria for hydrological model assessment. Advances in Geosciences, 5, 89-97.

124.

Ogungbenro, S. B., & Morakinyo, T. E. 2014. Rainfall distribution and change detection across climatic zones in Nigeria. Weather and Climate Extremes, 5, 1-6.

Pandey, D. N., Gupta, A. K., & Anderson, D. M. 2003. Rainwater harvesting as an adaptation to climate change. Current science, 85(1), 46-59.

Salas, J.C., König, K.W. & Lo, A., 2009. Rainwater harvesting providing adaptation opportunities to climate change. In: Barron, J. (Ed.), Rainwater Harvesting: A Lifeline for Human Well-being. A Report Prepared for UNEP by Stockholm Environment Institute York, UK/Stockholm Resilience Centre, Stockholm, Sweden. ISBN: 978-92-807-3019-7.

Tabari, H., & Talaee, P. H. 2011. Temporal variability of precipitation over Iran: 1966–2005. Journal of Hydrology, 396(3), 313-320.

Traboulsi, H., & Traboulsi, M. 2015. Rooftop level rainwater harvesting system. Applied Water Science, 1-7.

Wood AW, Maurer EP, Kumar A, Lettenmaier DP. 2002. Long range experimental hydrologic forecasting for the eastern U.S. J. Geophys. Res., 107 (D20): 4429.

Proceedings of the 10th World Congress of EWRA 'Panta Rhei', 5-9 July 2017, Athens, Greece
© 2017 *European Water Resources Association*

WSMN: An in-situ monitoring network for soil moisture monitoring in West Wales, UK

G.P. Petropoulos[1*] and J.P. McCalmont[2]
[1] *Department of Geography and Earth Sciences, University of Aberystwyth, SY23 2EJ, UK*
[2] *Institute of Biological Environmental and Rural Sciences, University of Aberystwyth, SY23 3EE, UK*
[*] *e-mail: petropoulos.george@gmail.com*

Abstract: Soil moisture (SM) is a significant component of climatological, hydrological and ecological systems. Thus, information on its variation over time and space domains is of key importance to both practitioners and researchers alike from a variety of disciplines. In view of the requirement for information on the spatial distribution of SM, ground-based observational networks have also been developed worldwide, providing soil moisture data operationally, and at no cost to the users' community globally. Such data are also pivotal in studies concerned with benchmarking related Earth Observation-based datasets, since ground measurements are often used as "reference" in validating satellite-derived products of SM. In this context, we present herein our recent progress towards the establishment of an autonomous in-situ network - named WSMN (Wales Soil Moisture Monitoring Network) - for obtaining, on a long term basis and in near real-time, measurements of SM and related parameters for west Wales, United Kingdom. The WSMN network currently consists of 9 stations based close to the Aberystwyth region and has been collecting data since 2011. The network is now fully deployed distributing all collected data via the International Soil Moisture Network (ISMN) platform. Herein, we present results on SM trends from a time series analysis conducted analysing the data collected until end of 2016. The availability of this new in-situ dataset is of very significant importance to the region as it is expected to help advance our understanding on the physical processes involved in water and energy exchanges at the local scale. At present, WSMN is also rapidly expanding thanks to funding obtained recently which allows more monitoring sites to be added to the network to the wider community interested in using its data.

Key words: soil moisture, in-situ measurement networks, operational networks, ISMN, WSMN

1. INTRODUCTION

Today, particularly so in the face of climate change and the need to meet global food and water security requirements, there is an urgent need for a better understanding of natural processes in the Earth System and of land surface interactions (LSIs) (Ireland et al., 2015). This is now widely recognised by the global scientific community as a matter urgently requiring further investigation. In this regard, information on the spatiotemporal variation of soil parameters, such as soil surface moisture (SSM), is of key significance due to the specific influence of these parameters on various physical processes of the Earth system, where they exert a strong control on the Earth's water cycle and ecosystem functioning in general (Shen et al., 2013; Petropoulos et al. 2016).

There are many options that can be considered for deriving estimates of SSM based on the use of ground instrumentation, each having distinct practical advantages and disadvantages (see recent reviews e.g. by Verstraeten et al., (2013)). Generally, the use of ground instrumentation has certain advantages, such as a relatively direct measurement, instrument portability, easy installation, operation and maintenance, the ability to provide measurement at different depths and also the relative maturity of the methods. In view of the importance of information on the spatial distribution of SSM in particular, various operational ground-based global observational networks have been developed over the last decade or so, freely distributing SSM (see in Petropoulos et al., 2013 for a review of existing networks). While there are now several long-term data sets of SSM available worldwide provided via platforms such as the International Soil Moisture Network (ISMN, Dorigo et al., 2011), to our knowledge, there are very few such sites set up in the United

Kingdom, particularly in Wales, despite the critical role its reservoirs, and its hillsides, plays in both domestic water provision and flood risk into its neighbouring populations. This paper provides a description of a +5 years (and ongoing) Wales Soil Moisture Network (WSMN) dataset produced from ground instrumentation installed in the vicinity of Aberystwyth, Wales, UK.

2. OVERVIEW

An operational in-situ monitoring network of soil moisture and temperature monitoring has been established in Wales, United Kingdom. WSMN has been functioning as a data collection network since 2011 and provides measurements, in near real time and on a long term basis, of SSM, soil temperature (ST), precipitation and incoming solar radiation (Rg) at regular intervals of either 30 minutes or an hour, varying by site. More information about WSMN can be found at the network web site as well (http://www.aber.ac.uk/wsmn). As well as two dedicated stations, this network currently incorporates monitoring stations installed as part of other, wider research projects (Carbo-Biocrop, ELUM, BSBEC and the Pwll Peiran Upland Research Platform). Briefly, WSMN currently consists of 9 stations spread across 5 sites (see Figure 1 & Table 1) situated in the Aberystwyth region, west Wales, United Kingdom.

Table 1: The implemented LULC Classes

Site	Coordinates	Elevation	Sensor Depth	Land Use
Site 1 – Comins Coch (Station 1)	52° 25′ 56.38″ N 4° 1 14.15″ W	30m	5cm	Agriculture/Grasslands
Site 2 – Comins Coch (Station 2)	52° 25′ 56.78″ N 4° 1′ 17.76″ W	28m	5cm	Agriculture/Grasslands
Site 3 – Penglais (Station 3)	52° 25′ 20.76″ N 4° 4′ 6.01″ W	114m	5cm	Ryegrass Pastureland transitions to Miscanthus x Giganteus Bioenergy Crop
Site 4 – Penglais (Station 4)	52° 25′ 17.24″ N 4° 4′ 14.15″ W	110m	5cm	Ryegrass Pastureland transitions to Miscanthus x Giganteus Bioenergy Crop
Site 5 – Cae Canol (Station 5)	52° 24′ 49.99″ N 4° 2′ 34.42″ W	128m	10cm	16 individual plots each of willow and Miscanthus and grass rows
Site 6 – Cae Canol (Station 6)	52° 24′ 49.67″ N 4° 2′ 35.18″ W	128m	10cm	16 individual plots each of willow and Miscanthus and grass rows
Site 7 – Pwllpeiran (Station 7)	52° 21′ 55.07″ W 3° 49′ 54.28″ W	375m	10cm	Semi-Improved U4 Grassland
Site 8 –Pwllpeiran (Station 8	52° 23′ 13.01″ N 3° 45′ 7.35″ W	500m	10cm	Peatland
Station 9 – PwllPeiran (Station 9)	52° 21′ 11.57″ N 3° 48′ 11.22″ W	260m	5cm	Semi-Improved grassland

3. SCIENTIFIC IMPORTANCE AND USE OF DATA

The data acquired from WSMN can be used for a wide range of purposes. First of all, the availability of this new in-situ dataset provides a unique contribution towards the development at different scales of long-term monitoring capability of land-surface interactions for Atlantic environments such as that of west Wales. Indeed, access to such data is of pivotal value to the region as it is expected to aid advancing our understanding of the physical processes involved in water and energy exchanges first of all at a local scale. Moreover, in larger scale studies such data can be incorporated into wider networks and used as forcing data in the development and validation of land surface process models (e.g. see Richter et al., 2004; North et al., 2015) or can be integrated with satellite data (e.g. via data assimilation schemes, (e.g. Petropoulos et al., 2011; Smith et al., 2012). WSMN is capable of providing data for studies focusing on spatio-temporal scaling of SSM & ST. Indeed, as both parameters can vary considerably in time as well as space, it is clear that the

high temporal resolution of the WSMN dataset can play a very useful role in understanding and developing methods to improve our understanding of this spatiotemporal variability. The WSMN data is also well-suited to be used in studies aimed at evaluating the capability of different EO-based algorithms and sensing systems in deriving SSM or ST (e.g. Petropoulos et al. 2014). Indeed, taking into account the increasing number of satellite missions being placed in orbit today capable of providing estimates of SSM and ST has made it indispensable to provide "reference" data across a wide range of environments and climates globally. In addition to the existing 9 stations (8 datasets currently available on the ISMN website with station 9 to be added), there are plans (and funding in place) to extend this to around 20 sites across a wider area of mid-Wales with the aim of providing a much wider picture of soil moisture and to extend the altitudinal gradient which is key to understanding hydrological dynamics, both in terms of flood risk and drought buffering.

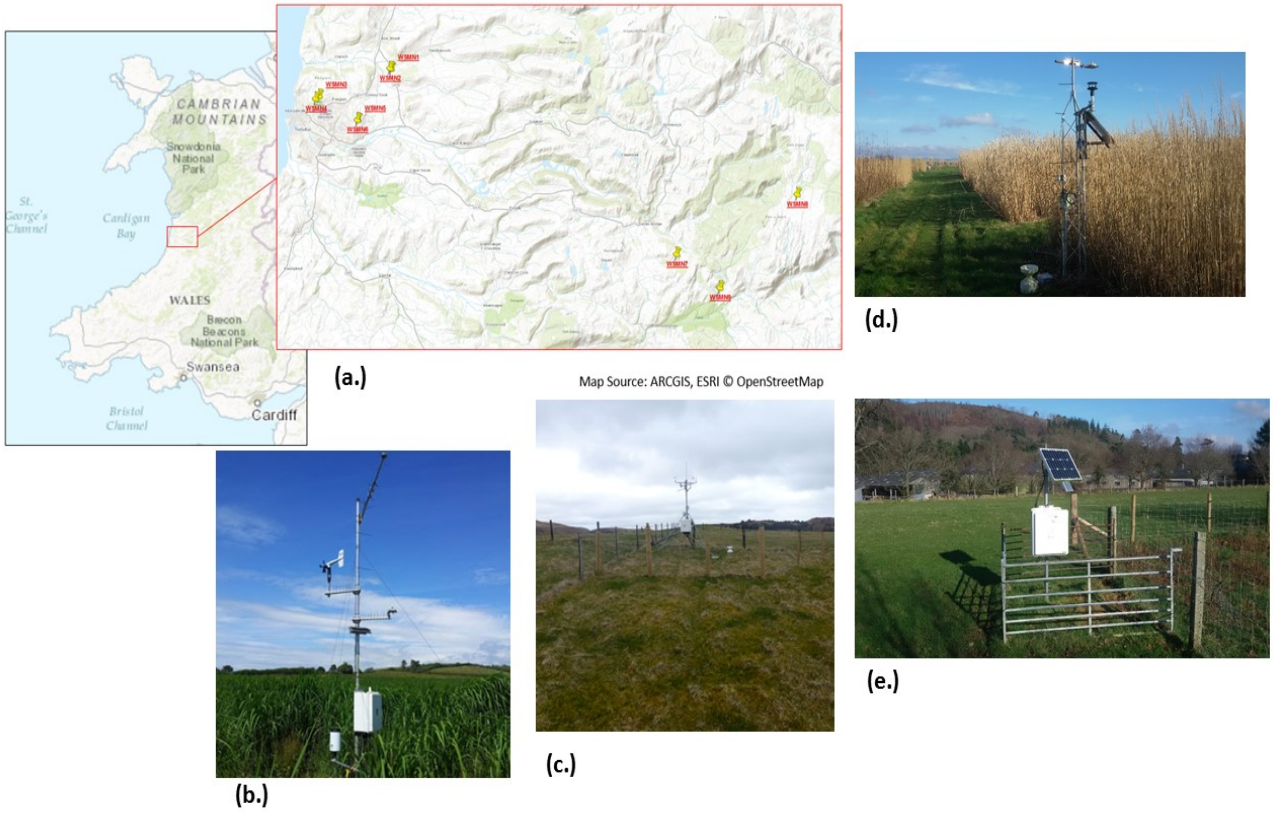

Figure 1: (a): Overview of the locations on which the WSMN experimental sites are installed to acquire SM, ST and ancillary data. Examples of images of the sites from: (b): Penglais, (c): Pwllpeiran, (d): Cae-Canol (e): Comins-Coch

4. DATA SUMMARY

Soil moisture measurements are acquired across the sites at a range of logged intervals (15, 30 and 60 minutes, see Table 1). For all sites, time domain reflectometry (TDR) instrumentation is used for the measurement of SSM. TDR is a method that uses propagation of a high-frequency transverse electromagnetic wave along a cable attached to a parallel conducting probe inserted into the soil. The signal is reflected from one probe to the other before being returned to a meter which measures the time elapsed between sending the pulse and receiving the reflected wave. Assuming that the cable and waveguide length are known, the propagation velocity, which is inversely proportional to the dielectric constant, can be directly related (through calibration) to SSM. This provides a measurement of the average volumetric water content in a soil volume along the length of the waveguide (Verstraeten et al., 2013). In the WSMN sites TDR probes have been permanently installed in each site in the ground horizontally at ~ 5-10cm depth from the soil surface layer. The recorded ST (see next section) is used to correct the soil moisture probes. All soil moisture data is

0.1% v/v resolution with a range of 0%–50% v/v at all sites.

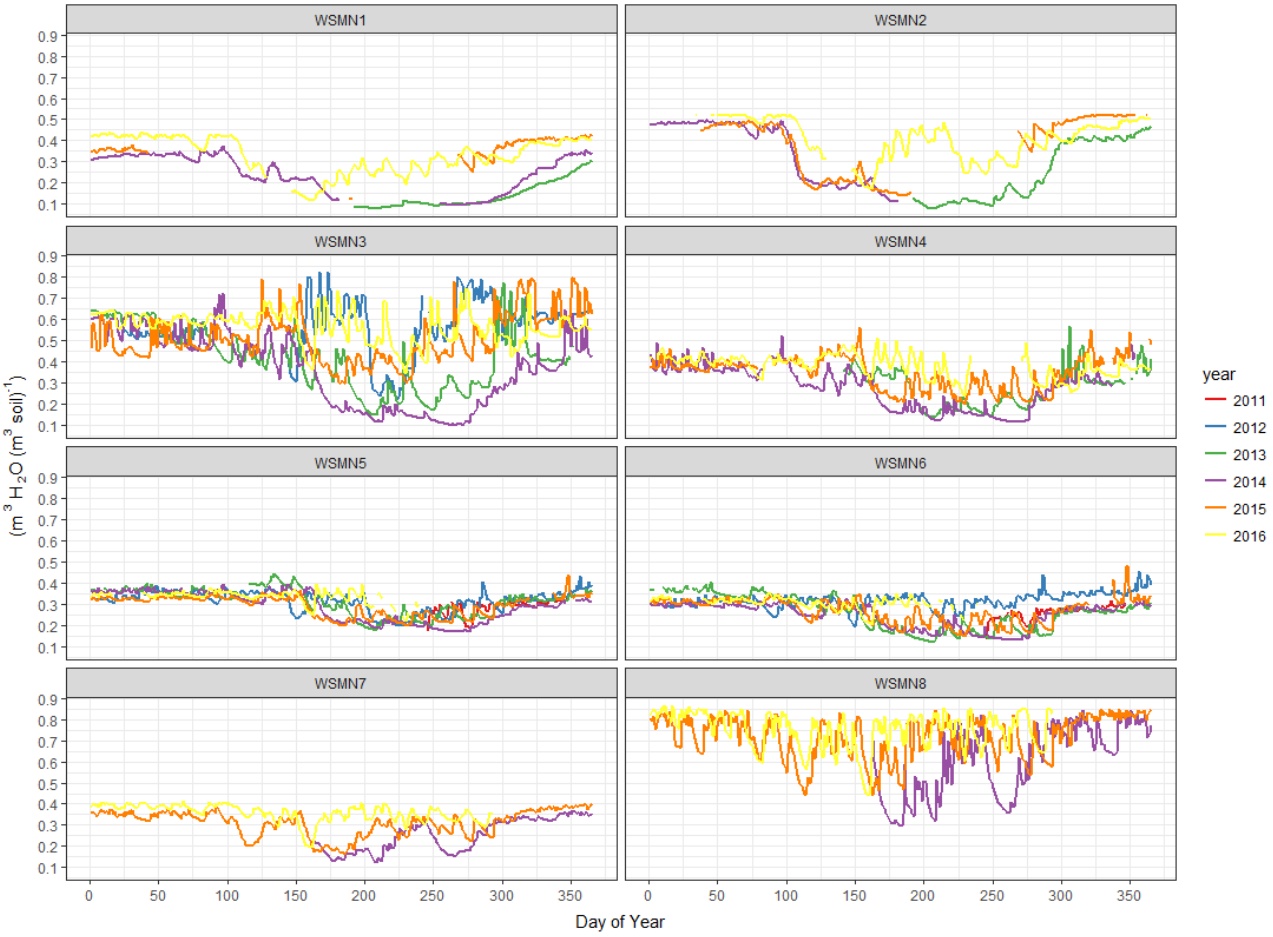

Figure 2: (a): Overview of the locations on which the WSMN experimental sites are installed to acquire SM, ST and ancillary data. Examples of images of the sites from: (b): Penglais, (c): Pwllpeiran, (d): Cae-Canol (e): Comins-Coch

5. DATA QUALITY AND AVAILABILITY

At present, WSMN data is collected on a weekly to monthly basis with collection carried out manually during routine research fieldwork being carried out at the sites. Following the data acquisition, collected data from the monitoring sites are visually inspected to identify any erroneous errors (e.g. anomalous and non-physical values). This step also includes comparisons between SSM with ST and compared to rainfall and incoming solar radiation where available. This checking is standard process done in other similar operational networks (e.g. Smith et al., 2012). All detected erroneous data are then removed from the database and flagged as missing. No gap filling of data has been undertaken, with all missing or poor quality data being flagged as 'N/A'. Within a process that is becoming at present fully automated, collected data will be harmonised in terms of measurement unit, sampling interval, and metadata, and after a basic quality check stored in a database. An operational algorithm developed in-house is used to generate a list of files that summarise the values, including hourly, daily mean, and monthly mean values for all of the measured variables of each station. The final dataset per site is saved in ascii and .csv (spreadsheet) formats and is then transferred to the ISMN team ready for distribution to the potential users' community for use in further experiments and applications.

Data is currently available via the International Soil Moisture Network (ISMN, Dorigo et al., 2011), https://ismn.geo.tuwien.ac.at/). On the ISMN web site, data viewing is possible without registration, however, to acquire the data one needs first to register, a process that is fast and straightforward. The website provides all of the information required for interpretation of these data

(including metadata), along with site photographs, maps, and descriptions. Due acknowledgment in any publication or presentation arising from use of these data is required. WSMN data collection is ongoing as of July 2011 for all WSMN sites, even though for a small number of sites data from year 2009 is available. The data base generated by WSMN is freely available for any research or scientific purpose or practical applications. An example of the WSMN data usage for the period July 1st 2016 - December 2016 is shown in Figure 3.

Country	Count	Country	Count
United States	23	Netherlands	3
Italy	13	Belgium	3
China	13	Brazil	2
United Kingdom	12	Sweden	2
France	9	Austria	2
Iran	8	Ghana	1
Japan	7	Switzerland	1
Germany	5	Russia	1
India	4	Spain	1

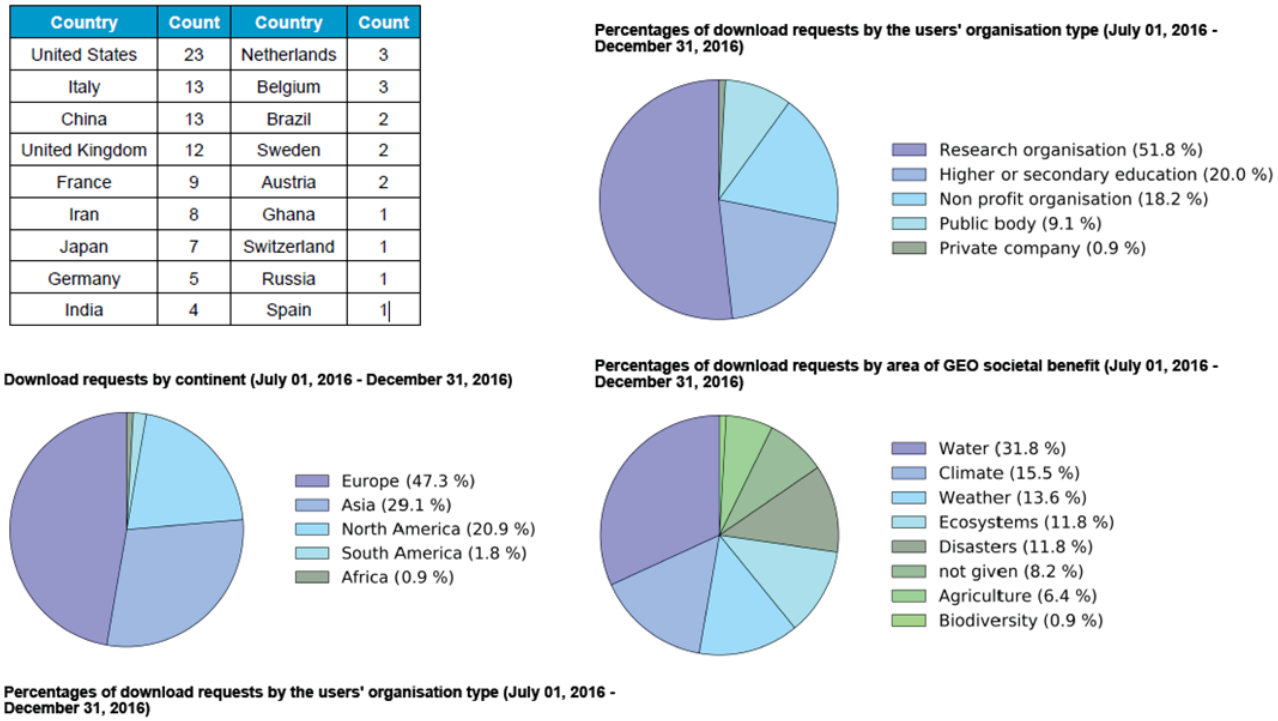

Figure 3: Summarised statistics of the WSMN data usage for the period July 1st 2016 to December 2016

6. SUMMARY

This paper presented an overview of an operational soil surface moisture (SSM) and soil temperature (ST) monitoring network which has been set up in west Wales, UK. The network, named as the "Wales Soil Moisture Network (WSMN)", has been acquiring and openly distributing data from +5 years from a total of 9 sites (with large scale expansion in process), representative of typical Welsh environments and land use/cover types. WSMN has been running operationally on a long-term basis and aims to support Earth Observation, land modelling, and Earth system process studies for oceanic climates such as those found in Wales. More data are expected to become available in the near future thanks to significant funding that was recently secured to facilitate this purpose. Users in Wales also systematically collecting SSM/ST are also welcomed to join WSMN and share their data publicly via the routes already established for this scope.

REFERENCES

Dorigo, W.A., W. Wagner, R. Hohensinn, S. Hahn, C. Paulik, M. Drusch, S. Mecklenburg, P. van Oevelen, A. Robock, T. Jackson (2011). The international soil moisture network: a data hosting facility for global in situ soil moisture measurements. Hydrol. Earth Syst. Discuss., 2011, 8, 1609-1663.

Ireland, G., G.P. Petropoulos, T.N. Carlson & S. Purdy. Addressing the ability of a land biosphere model to predict key biophysical vegetation characterisation parameters with Global Sensitivity Analysis Environmental Modelling & Software, 2015, 65, 94-107, doi.org/10.1016/j.envsoft.2014.11.010

North, M. R., Petropoulos, G.P., Rentall, D.V., Ireland, G.I. & J.P. McCalmont. Quantifying the prediction accuracy of a 1-D SVAT model at a range of ecosystems in the USA and Australia: evidence towards its use as a tool to study Earth's system interactions. Earth Surface Dynamics Discussions, 2015, 6, 217-265, DOI: doi:10.5194/esdd-6-217-2015

Petropoulos G., H. Griffiths and W. Dorigo. Surface Soil Moisture Estimation: Principles and Conventional Measurement Techniques, 23 pages. Accepted. To appear in "Remote Sensing of Land Surface Turbulent Fluxes & Soil Moisture". Edited by G.P. Petropoulos, Taylor & Francis, 2013, ISBN: 978-1-4665-0578-0.

Petropoulos G.P. & T.N., Carlson. Retrievals of turbulent heat fluxes and soil moisture content by Remote Sensing, pages 469-501, in "Advances in Environmental Remote Sensing: Sensors, Algorithms, and Applications", Ed. Taylor and Francis, 2011, pp. 556, ISBN: 978-1-4200-9175-5.

Petropoulos, G.P., G. Ireland, P.K. Srivastava & P. Ioannou-Katidis. An appraisal of soil moisture operational estimates accuracy from SMOS MIRAS using validated in-situ observations acquired at a Mediterranean environment. International Journal of Remote Sensing, 2014, 35 (13), 5239-5250, doi: 10.1080/2150704X.2014.933277.

Petropoulos, G.P., Ireland, G. & B. Barrett. Surface Soil Moisture Retrievals from Remote Sensing: Evolution, Current Status, Products & Future Trends. Physics and Chemistry of the Earth. 2015, DOI: 10.1016/j.pce.2015.02.009 [in press].

Richter, H., A. Western, and F. Chiew. The effect of soil and vegetation parameters in the ECMWF land surface scheme, J. Hydrometeor., 2004, 5, 1131–1146.

Shen, C., Niu, J., Phanikumar, M. S. Evaluating controls on coupled hydrologic and vegetation dynamics in a humid continental climate watershed using a subsurface-land surface processes model. Water Resources Research, 2013, 49(5), 2552-2572.

Smith, A.B., J.P. Walker, A.W. Western, R.I. Young et al. The Murrumbidgee soil moisture monitoring network data set. Water Resources Research, 2012, 48, 1-6, doi: 10.1029/2012WR011976.

Vereecken, H., Huisman, J. A., Pachepsky, Y., Montzka, C., van der Kruk, J., Bogena, H., Weihermüllera, L., Herbsta, M., Martinez, G., & Vanderborght, J. On the spatio-temporal dynamics of soil moisture at the field scale. Journal of Hydrology, 2013, 516, 76-96.

Verstraeten, W. W., F. Veroustraete, and J. Feyen. Assessment of evapotranspiration and soil moisture content across different scales of observation, Sensors, 2013, 8, 70–117.

Proceedings of the 10th World Congress of EWRA 'Panta Rhei', 5-9 July 2017, Athens, Greece
© 2017 *European Water Resources Association*

Uncertainty in estimated water cycle determined with atmospheric budget, water budget and total water storage

M. Birylo
University of Warmia and Mazury in Olsztyn, Oczapowski St. 1, 10-724 Olsztyn, Poland
* *e-mail: monika.sienkiewicz@uwm.edu.pl*

Abstract: An intensification of the global hydrological cycle is highly determined by a climate change. But an essential part of human being is fresh water availability. The availability can be computed as a difference between precipitation and evapotranspiration, which can be taken exactly from GLDAS (from Global Land Data Assimilation System) models. For the purpose of water cycle analysis, a water storage is needed, here, observations from GRACE (Gravity Recovery and Climate Experiment) were used. GLDAS (Global Land Data Assimilation System) is based on both, simulation and prediction models and observed data in a long-term period, which are merged. The data is in a form of gridded meteorological dataset at the global scale. The aim GLDAS is integration and a land information system preparation. The result is a set of parameters, consisting of water storage, energy storage and fluxes. Post processing is carried out to Limiting bias caused by an atmosphere and constraints that are resultant of the land surface states is obtained during postprocessing. The aim of the study is to estimate atmospheric budget on a basis of precipitation and evapotranspiration differentiate, considering Poland as a case study.

Key words: atmospheric budget, precipitation, evapotranspiration, GLDAS, GRACE

1. INTRODUCTION

Due to climatic changes, there is a need of water supply constant monitoring. Currently, in Poland components of the water and energy budgets in a large scale are very sparse. Estimation large-scale P-EV budget is provided by (Seneviratne et al, 2004); (Roads et al., 2003); (Swenson and Wahr, 2002), (Ropelewski and Yarosh, 1998).

In the paper I try to measure the flux of total water between the surface and the atmosphere. This can bring me information about the interaction of land and atmosphere. As a comparison, a water budget is presented, and total water storage from GRACE. Among all data, I chose GLDAS, and GRACE models.

2. COMPONENTS ANALYSES

For the purpose of the atmospheric budged computation, two parameters are considered: precipitation and evapotranspiration. Amount of rainfall/snowfall is the volume of rain/snow in an imaginary cubic container that collects rain/snow during some period. A very important part is to define the intensity of a rainfall/snowfall. It can be described as depth of water/snow received during fall, but divided into smaller periods of time (f.e. 24 hours divided into one hour periods). It is usually expressed in millimetres of water depth per hour. Among all factors that influenced an effectivity of the rainfall/snowfall we can distinguished: climate, soil texture, soil structure, depth of the rootzone, topography, initial soil moisture content, and irrigation methods.

It is important to be aware that some of water falls and stays on a soil, some is infiltrated into the soil (the amount is dependent on a soil type), and some run-off. The part of water that stagnates on a soil starts evaporating into the atmosphere. The second way of leaving water, but this time from by plant's leaves and stems is called transpiration.

Total amount of water transpired by the plants and water evaporated from a soil is called the

evapotranspiration. The unit of the evapotranspiration is millimetres per period of time. The biggest influence on the volume of the evapotranspiration has: climate, type of crop and soil moisture.

For the purpose of the water budget computation, a surface runoff component needs to be added. Surface run-off mainly is dependent on the neighbourhood of flows and basins.

Computed atmospheric and water budgets are then compared to the total water storage (TWS) values taken from GRACE model. The TWS change is the sum of water components, like water stored in land, rain and snow falls, infiltrated into the soil, evaporated, transpired and stored in the basins or steam flows. The TWS values are dependent on the chosen location.

All the parameters are described, presented in the graphical form and analysed in the paper.

3. METHODOLOGY

The main factor important for climate system is a stable atmospheric budget. Monitoring the process is especially important nowadays due to climate warms (Collins et al, 2013). Atmospheric balance calculated over land lets us observe the sum of surface and sub-surface run-off. The expected magnitude changes are much smaller over land than over large basins. As stated by (Byrne, O'Gorman, 2015), analysing P-EV changes gives positive result or about zero. It is caused by the fact that precipitation is always larger than evapotranspiration in the time mean over drained surface, as land (Byrne, O'Gorman, 2015).

Under climate change there are many uncertainties of rate of seasonal and annual precipitation and evapotranspiration, and thus atmospheric budget - measured as a difference between P-EV. The second analysis was comparison between water and atmospheric budget. The amount of water entering or recharging the system is the water budget. It is well known, that water stored in the water cycle is constant. But all fluxes depend on climatic conditions (Smith, Ummerow 2012). A water budget is computed as a difference between atmospheric budget and surface run-off.

For the purpose of water cycle understanding two sets of data are used: GLDAS (Global Land Assimilation System) and GRACE observations (Gravity Recovery and Climate Experiment). For the purpose of the research the following cells were taken into consideration:

- The cell including Olsztyn,
- The cell including Lublin, according to National Water Management Ministry Bulletin location with the highest values of the annual temperature considering a period 1951 – 2015; it is supposed to observe the highest values of the evapotranspiration.
- The cell including Jurgow, according to National Water Management Ministry Bulletin location with the highest values of the annual precipitation considering a period 1971 - 2015.

4. DATA

The GLDAS model is the kind of model globally consisting of 28 different fields, which are the geophysical parameters. GLDAS is published in a form of four sub-models (land surface models) – VIC (Variable Infiltration Capacity Model), NOAH (National Centers for Environmental Prediction/Oregon State University/Air Force/Hydrologic Research Lab Model), Mosaic Land Surface Model and CLM (Common Land Surface model. The aim of the GLDAS is to present land surface states and fluxes. The concept of the GLDAS is to distribute energy and water budget components (Rodell et al. 2004); (Zaitchik et al. 2010). GLDAS data was provided by: (Mocko, 2012), (Rodell and Beaudoing 2015). In the paper, the values recomputed into the total water storage (TWS) were derived from GRACE data, using CSR RL05a as source data. In the post-processing, the DDK5 filter was used and the degree of the GRACE gravity coefficients was set to 60. All measurements were prepared for the one-degree cells 1, for the period 2006.01-2010.12.

5. RESULTS

5.1 Atmospheric budget determination

The analyses aim at comparison of the values of P and EV given in the GLDAS NOAH sub-model, which is the closest to in-situ measurements among all GLDAS sub-models (Pennemann et al. 2016). Values of the precipitation P for the Olsztyn, Lublin and Jurgow cells are given in the Fig. 1. As it is seen, the values range from zero to 0.000000081 kg/m2/s. It can be also observed that values of the precipitation are growing over years 2006-2010. It needs to be also remembered that in 2010.05-2010.09 a tremendous and catastrophic flood occurred in Poland, especially in the southern part. The flood was the result of a huge rainfall in Poland and that is the reason of the chosen period of the research. As it was supposed, the biggest values of the precipitation are recognized in the Jurgow cell (it is convergent with the National Water Management Ministry Bulletin). Annually, the highest values of the precipitation are observed every August, but every August bigger in the tested period. Values near zero are at the beginning of the springs and the autumns. The shape of the graph in every tested cell is similar, but the amplitude is different. The smallest amplitude is observed in Olsztyn cell.

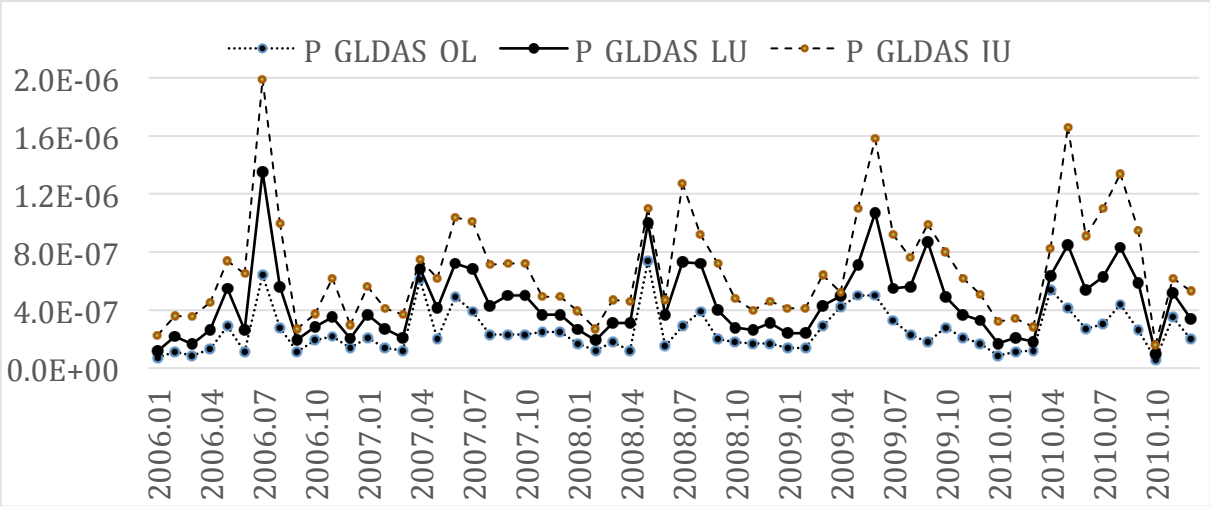

Figure 1. Precipitation values for the cell of Olsztyn, Lubin, Jurgow cells for the period 2006.01 – 2010.12. Unit: kg/m^2/s

Evapotranspiration values are presented in the Fig. 2. Samely, the highest values are observed in the Jurgow cell. Values are between 0 and 0,000034 kg/m^2/s. The highest values are in Julys. From Novembers and Marchs values achieve zero (winter, values zero or below zero Celsius degrees – almost no evapotranspiration).

Table 1 analysis let me assume and better percept that in the tested period values of the annual precipitation are growing; from 0.0001752kg/m^2/s up to 0.0003147kg/m^2/s in Olsztyn, from 0.0001495kg/m^2/s up to 0.0002456 kg/m2/s in Lubin, from 0.0002152 kg/m^2/s up to 0.000344 kg/m2/s in Jurgow cells. But, when final values are considered, surprisingly sums are similar. Analysing annual evapotranspiration let us conclude that there is no trend. The highest values of the evapotranspiration are in 2007, the smallest in 2006. Total sum for the five researched years are similar for every location.

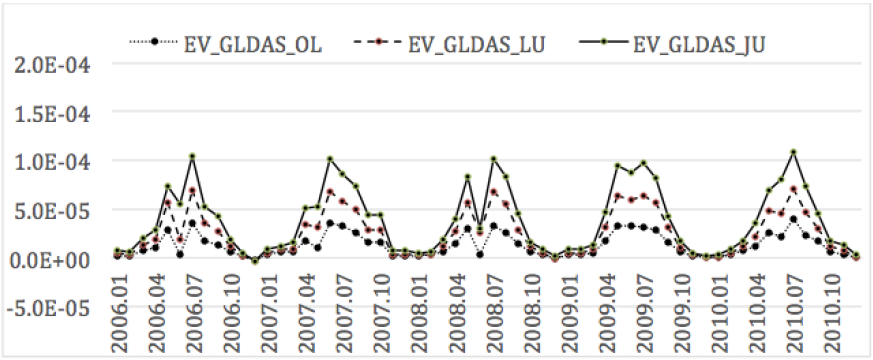

Figure 2. Evapotranspiration values for the cell of Olsztyn, Lubin, Jurgow cells for the period 2006.01 – 2010.12. Unit: kg/m^2/s

Table 1. Annual analysis of P and EV values.

	Sum P_GLDAS_ OL	Sum P_GLDAS_ LU	Sum P_GLDAS_ JU	Sum EV_GLDAS_ OL	Sum EV_GLDAS_ LU	Sum EV_GLDAS_ JU
2006	0.0001752	0.0001495	0.0002152	0.0001609	0.00014988	0.000164422
2007	0.0002801	0.0002165	0.000237	0.0001946	0.0001708	0.0001932
2008	0.0002214	0.0002264	0.0002272	0.00017755	0.000172241	0.0001767
2009	0.0002942	0.0002343	0.000291	0.0001809	0.00015828	0.0001746
2010	0.0003147	0.0002456	0.000344	0.000181421	0.00015006	0.0001783
Final sum	0.0012856	0.0010723	0.0013144	0.000895371	0.000801261	0.000887222

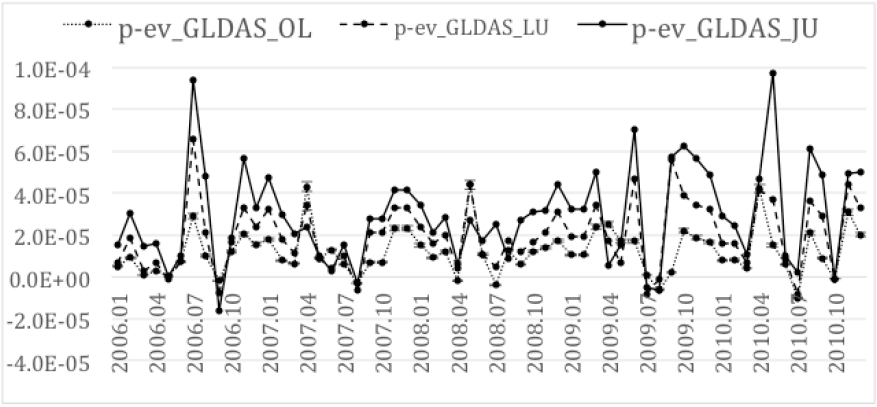

Figure 3. Atmospheric budget values for the cell of Olsztyn, Lubin, Jurgow cells for the period 2006.01 – 2010.12. Unit: kg/m^2/s

The aim of the research was to differentiate precipitation and evapotranspiration to achieve values of the atmospheric budget (Fig. 3). Values are between -0.000030 kg/m^2/s and 0.000060 kg/m^2/s. The shape of the graphs is similar for the three tested cells. The highest amplitudes are noticed are in Jurgow cell, while the smallest in Olsztyn cell. So, it can be concluded that in Jurgow cell precipitation values are much higher than evapotranspiration. It needs to be added that the highest month values of the atmospheric budget in Jurgow says that surface run-off values should be the highest. Other factors are not considered now. The highest values of surface run-off can be the effect of a bluff slopes and rocky soil which infiltrate small volumes of water. The smallest values of the atmospheric budget are noticed in Olsztyn cell. It can be stated that the highest values of the atmospheric budget can be observed in every tested cell in Novembers and Decembers, a little bit less in Januaries and Februaries. These are winter moths in Poland, characterized with temperatures about or below zero and with short days – low sun radiation. As it was supposed, these mentioned months can be distinguished with huge amount of precipitation (snow and rain, both)

and very little evapotranspiration. On the other hand, in Junes and Julies the smallest differences between P and EV are observed – summer in Poland, log sunny days. In the researched period, in the Olsztyn cell the same values of a low atmospheric budget are noticed in Marches and Aprils. In Lubin and Jurgow cells, low values of P-EV (but a bit higher than in Jan., Feb., Nov. and Dec.) are observed in Aprils and Mays.

5.2 Comparison to water budget

The results of the computed atmospheric budget were compared to computed water budget. The aim of the research was to check how important is surface run-off in the three locations. Results are presented in a Fig. 4 and 5. Firstly, surface run-off was analysed. In the years 2006-2008, from Julie to Januaries, values of the surface run-off are almost the same. Some peaks are observed about Mays, especially in Jurgow cell (from about zero up to 3.0 e-6 kg/m^2). From April 2009, many peaks are monitored, especially in May 2010 (the time of flood in Poland – a lot of rain, many water run-off).

Having three values: P, EV and SRO, I could compute the water budget for the period 2006.01-2010.12. The result is presented in the Fig. 5. Shapes of all three graphs are very like those presented in the Fig. 3. Values are the same when comparing atmospheric budget and water budget or values of water budget are a bit higher than atmospheric budget. Small differences are noticed about Mays up to 2009. From 2009.04 differences between atmospheric budget and water budget become bigger and bigger, grow up from 0.0 to 0.00005 kg/m^2/s.

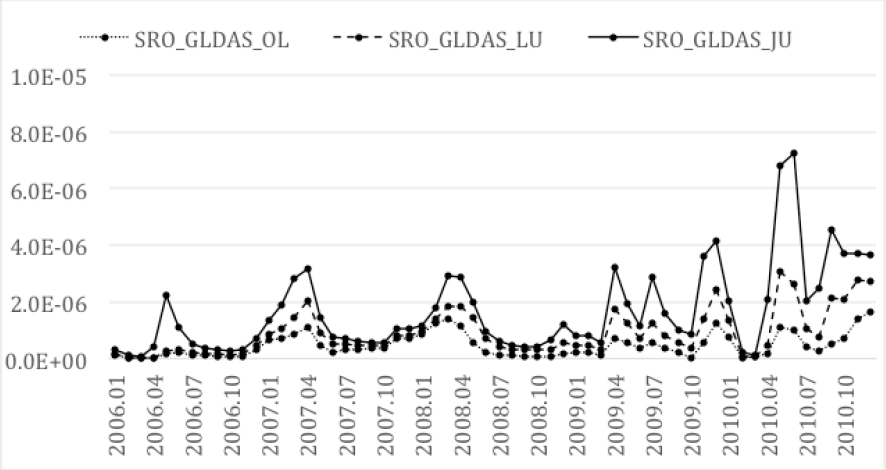

Figure 4. Surface run-off values for the cell of Olsztyn, Lubin, Jurgow cells for the period 2006.01 – 2010.12. Unit: kg/m^2/s

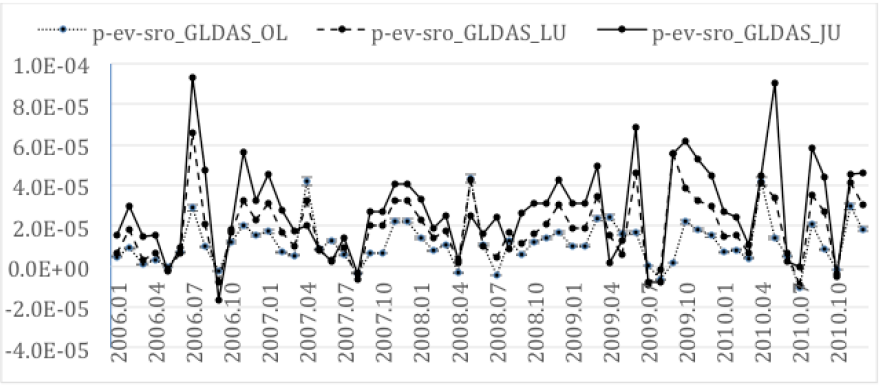

Figure 5. Water budget values for the cell of Olsztyn, Lubin, Jurgow cells for the period 2006.01 – 2010.12. Unit: kg/m^2/s

5.3 Comparison to GRACE

The last part of the paper was to compare atmospheric budget and water budget with the values of the total water storage from GRACE observations. Results are presented in the Fig. 6, 7 and 8. When analysing Olsztyn cell (Fig. 6) we can observe very small differences between the three presented observations. Values are from -0.16 to 0.12 m. It can be said that other factors (like water in canopies, groundwater, basins,) are not very important in Olsztyn cell and does not play a big role when comparing to atmospheric budget and water budget. It need to be added that in 2010 there were no flood in Olsztyn. This can be seen in the graph, situation id stable over five researched years. Lubin cell (Fig. 7) is stable till the end of 2008, values of the TWS are very like atmospheric budget and water budget. The range of the differences is -0.15 – 0.10. It becomes different at the beginning of 2009. Here, TWS is even two times bigger than water budget. It need to be concluded that in Lubin cell surface run-off from 2009.01 has bigger influence and the other factors are very important in this cell and need to be considered. The same situation is observed in the Jurgow cell (Fig. 8) – a stable situation till 2008.12, many peaks and differences between presented values from the beginning of 2009. But now, values of TWS are even three times bigger than water budget. Here, also other factors are important.

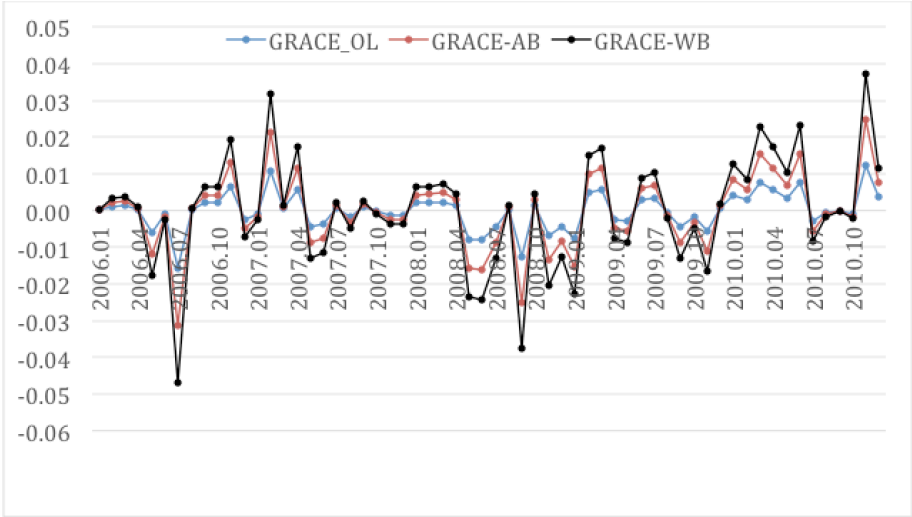

Figure 6. Total water storage derived from GRACE (unit: meter), difference between GRACE and atmospheric budget (unit: meter), difference between GRACE and water budget (unit: meter) for Olsztyn cell

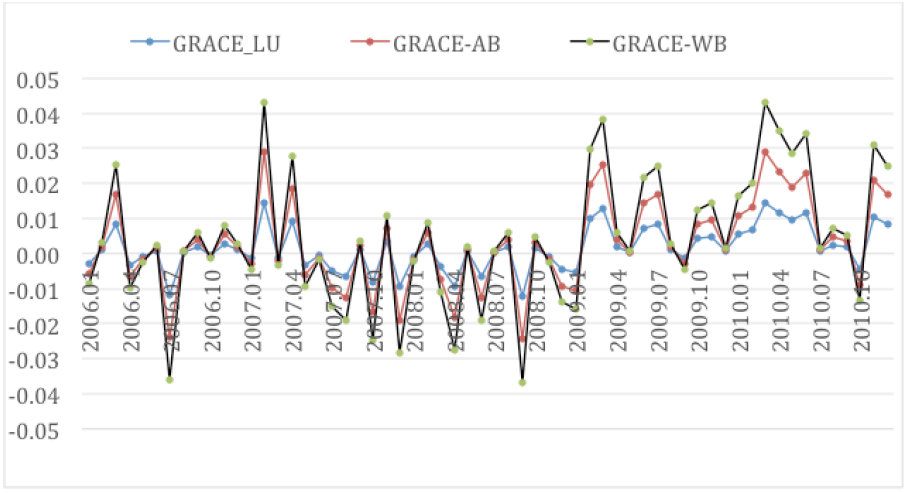

Figure 7. Total water storage derived from GRACE (unit: meter), difference between GRACE and atmospheric budget (unit: meter), difference between GRACE and water budget (unit: meter) for Lubin cell

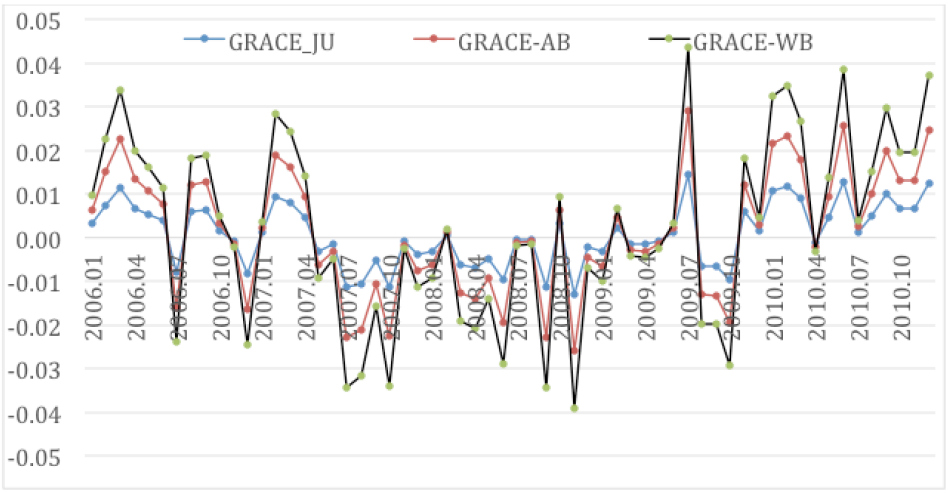

Figure 8. Total water storage derived from GRACE (unit: meter), difference between GRACE and atmospheric budget (unit: meter), difference between GRACE and water budget (unit: meter) for Jurgow cell

6. CONCLUSIONS

The research was performed relate to the area the three cells of Poland, located in Olsztyn cell, Lubin cell and Jurgow cell. The aim of the study was to determine the atmospheric budget in and analysing compatibility between atmospheric budget and water budget and total water storage. For the purpose of the research two models were used: GLDAS and GRACE. The aim of the paper was to examine three observations on this terrain, in the context of its data required for computation of variations.

It seems that the highest amplitudes of the atmospheric budget are noticed are in Jurgow cell (precipitation is bigger than evapotranspiration, while the smallest in Olsztyn cell). It can be concluded that the highest values of the atmospheric budget can be observed in Novembers and Decembers, a little bit less in Januaries and Februaries; in Junes and Julies the smallest values are observed.

Comparing atmospheric budget and water budget let me conclude that water budget values are a bit higher than atmospheric budget. Small differences are noticed about Mays up to 2009. From 2009.04 differences between atmospheric budget and water budget become bigger and bigger, grow up from 0.0 to 0.00005 $kg/m^2/s$.

When comparing water budget and atmospheric budget to the total water storage values I could state that another factor is very meaningful, especially from 2009. In Olsztyn cell situation of the three observations is stable during five analysed years. Lubin and Jurgow cells are stable till the end of 2008, values of the TWS are very like atmospheric budget and water budget. From 2009, in Lubin cell, TWS is two times bigger than water budget; in Jurgow cell three times bigger than water budget. Other factors are important.

ACKNOWLEDGEMENTS

The work was supported by the National Science Centre, Poland, agreement number UMO-2015/17/B/ST10/03927 from 16th March 2016

REFERENCES

Byrne M., O'Gorman P., 2015, The Response of Precipitation Minus Evapotranspiration to Climate Warming: Why the "Wet-Get-Wetter, Dry-Get-Drier" Scaling Does Not Hold over Land, Ametsoc, DOI: http://dx.doi.org/10.1175/JCLI-D-15-0369.1

Collins, M., R. Knutti, J. Arblaster, J.-L. Dufresne, T. Fichefet, P. Friedlingstein, X. Gao, W.J. Gutowski, T. Johns, G. Krinner, M. Shongwe, C. Tebaldi, A.J. Weaver, and M. Wehner, 2013, Long-term climate change: Projections, commitments and irreversibility. In Climate Change 2013: The Physical Science Basis. Contribution of Working Group I to the Fifth Assessment Report of the Intergovernmental Panel on Climate Change. T.F. Stocker, D. Qin, G.-K. Plattner, M. Tignor, S.K. Allen, J. Doschung, A. Nauels, Y. Xia, V. Bex, and P.M. Midgley, Eds. Cambridge University Press, 1029-1136, doi:10.1017/CBO9781107415324.024

National Water Management Ministry Bulletin, Water and Environment Programme, Appendix 3: Climate in Poland and analysis of the programs of actions due to climate changes up to 2015.2016

Mocko D., NASA/GSFC/HSL (2012), NLDAS Primary Forcing Data L4 Monthly 0.125 x 0.125 degree V002, Greenbelt, Maryland, USA, Goddard Earth Sciences Data and Information Services Center (GES DISC), DOI:10.5067/Z62LT6J96R4F

Pennemann P. C. S., Rivera J.A. R., Saulo A. C. E. & Penalba O. C. P., 2016, A Comparison of GLDAS Soil Moisture Anomalies against Standardized Precipitation Index and Multisatellite Estimations over South America, Journal of Hydrometeorology, vol. 16, doi:10.1175/JHM-D-13-0190.1.

Roads, J., et al., 2003, GCIP water and energy budget synthesis (WEBS). J. Geophys. Res, 108.8609, doi:10.1029/2002JD002583

Rodell M., Houser P. R., Jambor U., Gottschalck J., Mitchell K., Meng C.-J., Arsenault K., Cosgrove B., Radakovich J., Bosilovich M., Entin J. K., Walker J. P., Lohmann D. , Toll D., 2004, The Global Land Data Assimilation System, Bull. Amer.

Rodell M. and Beaudoing H. K., NASA/GSFC/HSL, 2015, GLDAS Noah Land Surface Model L4 monthly 1.0 x 1.0 degree V2.0, Greenbelt, Maryland, USA, Goddard Earth Sciences Data and Information Services Center (GES DISC), DOI:10.5067/QN80TO7ZHFJZ

Ropelewski, C. F., and E. S. Yarosh, 1998, The observed mean annual cycle of moisture budgets over the central United States. J. Climate, 11, 2180–2190Meteor. Soc., 85(3), 381-394.

Seneviratne, S. I., P. Viterbo, D. Luthi, and C. Schar, 2004, Inferring changes in terrestrial water storage using ERA-40 reanalysis data: The Mississippi River basin. J. Climate, 17, 2039–2057

Smith R., Ummerow Ch., 2012, A Comparison of in Situ, Reanalysis, and Satellite Water Budgets over the Upper Colorado River Basin, Journal of Hydrometeorology, Vol. 14, doi:10.1175/JHM-D-12-0119.1.

Swenson, S., and J. Wahr, 2002, Methods for inferring regional surface-mass anomalies from GRACE measurements of timevariable gravity. J. Geophys. Res, 107.2193, doi:10.1029/2001JB000576.

Zaitchik B.F., Rodell M. & Olivera F., 2010, Evaluation of the Global Land Data Assimilation System using global river discharge data and a source to sink routing scheme, Water Resour. Res., 46, W06507, doi:10.1029/2009WR007811.

Proceedings of the 10th World Congress of EWRA 'Panta Rhei', 5-9 July 2017, Athens, Greece
© 2017 *European Water Resources Association*

Seasonal mean Baltic Sea level change in coastal zone

K. Pajak and M. Birylo*
Faculty of Geodesy, Geospatial and Civil Engineering, University of Warmia and Mazury in Olsztyn, Oczapowskiego St. 2, Olsztyn, Poland
* *e-mail: monika.sienkiewicz@uwm.edu.pl*

Abstract: The mean Baltic sea level fluctuations are mainly due to long-term changes in the meteorological and hydrological phenomena, occurring within a few decades. In this paper, the analyses of mean Baltic sea level changes on the three locations in Baltic Sea, in the period of January 2003 – December 2015. We estimate seasonal mean Baltic sea level changes in the coastal zone using different data resources, including sea level anomalies, from satellite altimetry, time-variable gravity observations from the Gravity Recovery and Climate Experiment (GRACE) mission, and terrestrial water storage from the NASA global land data assimilation system (GLDAS). Sea level anomalies (SLA) and terrestrial water storage (TWS) data have been determined with a temporal resolution of approximately one month. The results from all estimates are consistent in amplitude and phase at the annual period. Sea level anomalies and total water storage time series in three locations are similar, the periods of upward trends and downward trends happen in similar time. The results provide a good measure of average annual sea level change and variation of water stored within in sea and over land. These results indicate that is important to consider estimating longer-term time series of sea level anomalies and water storage as a way of tracking climate change.

Key words: Sea level anomalies, GRACE, GLDAS, Seasonal

1. INTRODUCTION

Water level changes are not a phenomenon that equally occurs worldwide. Water level may significantly change not only on short terms, as a result of wind direction change, undulation, rising tides or changes in air pressure, but it can have long-term changes as well depending on the ocean currents or subsidence. In various regions, the trends may be different. Water level may rise for many years in one place and it may be low in the other (Church et al., 2010). The trend of the changes in the Baltic Sea level is about 2.15 m per year (Pajak and Birylo, 2016). The seasonality of sea level changes is an inequality which occurs in sea level anomalies (SLA) in relation to seasons, in which various phenomena that have an essential influence on the changes appear. Seasonal changeability of the sea is connected mainly with meteorological factors (atmospheric pressure, wind, evaporation and falls), water balance (rivers runoff), evaporation and changes in sea topography, or changes in water density (Chen et al., 2005). It is essential to constantly check and control seasonal fluctuations of sea level, both in one-year cycles and on longer terms.

The primary objective of this investigation was to clarify that what changes of sea level anomalies and total water storage occurred in the coastal zone during the test period. Moreover, the article presents the activities in sea level anomalies and total water storage within the time and it describes what time series occur. In order to achieve the aim, the authors tried to determine the occurrence of the cycles on the basis of monthly data of sea level anomalies and total water storage. To identify their length and force, the harmonic method was applied. The second objective of the research was to check the differences between GRACE-observed and GLDAS-derived terrestrial water storage (TWS), in the cell of 1 by 1 degree, and also to analyze the occurrence of seasonal fluctuations cycles. Moreover, the occurrence of the correlation between TWS data was researched. General results obtained within the study conducted and described in this paper, can help in the assessment of predictions of change sea level anomalies and total water storage variations in the coastal zone.

2. DATA SETS

The research involved three points of the Baltic Sea localized in Polish coastal zone (SWINOUJSCIE 53.917N, 14.233 E; KOLOBRZEG 54.183 N, 15.550 E; WLADYSLAWOWO 54.800N, 18).

The data used in the research on sea level changes are sea level anomalies (SLA) that were collected by satellite altimetry. The Ssalto/Duacs altimeter products were produced and distributed by the Copernicus Marine and Environment Monitoring Service (CMEMS) (http://www.marine.copernicus.eu). The details of standard processing applied to satellite altimetry data are available at www.aviso.oceanobs.com and www.marine.copernicus.eu. The TOPEX/Poseidon (T/P) and its successors Jason satellite radar altimeters have been measuring sea level change on a global basis. Highly accurate altimetry measurements from Topex/Poseidon and Jason made possible by the Doris system to give us the ability to observe sea surface height systematically (www.aviso.oceanobs.com).

For the purpose of the research, the mean total water storage determined from GRACE observations and terrestial water storage from GLDAS has been used.

The Gravity Recovery and Climate Experiment (GRACE) primary objective is to monitor gravity field variations (Tapley et al., 2004), moreover TWS variations can be derived (Kusche et al., 2009).

For the purpose of the test, RL05 product computed and processed by CSR center was used (http://www.thegraceplotter.com/). The chosen de-correlation filter was DDK5 with a low degree of smoothing radii. The GRACE land are available at http://grace.jpl.nasa.gov.

The goal of Global Land Data Assimilation System (GLDAS) is to estimate parameters relating land, like water storage, energy storage and fluxes (Rodell et al. 2004; Kumar et al., 2006). NOAH data, available for 2003-2014, has been used in this paper. The GLDAS data from "http://grace.jpl.nasa.gov", which used the "Goddard Earth Sciences Data and Information Services Center".

3. METHODOLOGY

The two most important aims of the time series analysis are recognizing the nature of the described phenomenon by the series of observations and forecasting future values. The realization of the aims is possible if particular time series elements are identified and described. It is assumed that in time series it is possible to distinguish the following elements, such as systematic component, which can be described as a trend (linear or not) and additionally by a seasonal component that is characterized by various lengths of fluctuations period; when the period is shorter than a year, one can treat it as seasonality, but when the period is longer, the economic cycle appears, and the random component called the noise. The identification is essential while using formalized forecasting method. To identify periodic phenomena, the harmonic analysis is a proper tool. In the analysis, one does not make a priori assumptions. The aim of the harmonic analysis is the decomposition of time series, which includes cyclical factors on sine and cosine function connected with given wave length.

The harmonic analysis concerns research on developing a phenomenon around the average level presented by a0 parameter. In the researched series, there is a trend so consequently, the oscillations should be researched around the developing tendency, i.e. by applying the following model (Pollock 2008):

$$y_t = \mathrm{f(t)} + \sum_{i=1}^{n/2} [\alpha_i \sin\left(\frac{2\pi}{n} it\right) + \beta_i \cos(\frac{2\pi}{n} it)] \tag{1}$$

where: - parameters estimated with the use of the method of least squares, f(t) – is a trend function, i

– harmonic's number.

For particular harmonics, the amplitudes and phase shift were calculated. The identification of cycle length was made with the use of the evaluation of particular harmonics share in explaining variance of the researched variable.

4. RESULTS

4.1 The harmonic analysis of SLA and TWS in the Baltic Sea

In order to analyze the dynamics of change in sea level, the linear trend estimation was made for SLA and TWS time series, which is presented in Figure 1. SLA and TWS trends show an increasing tendency.

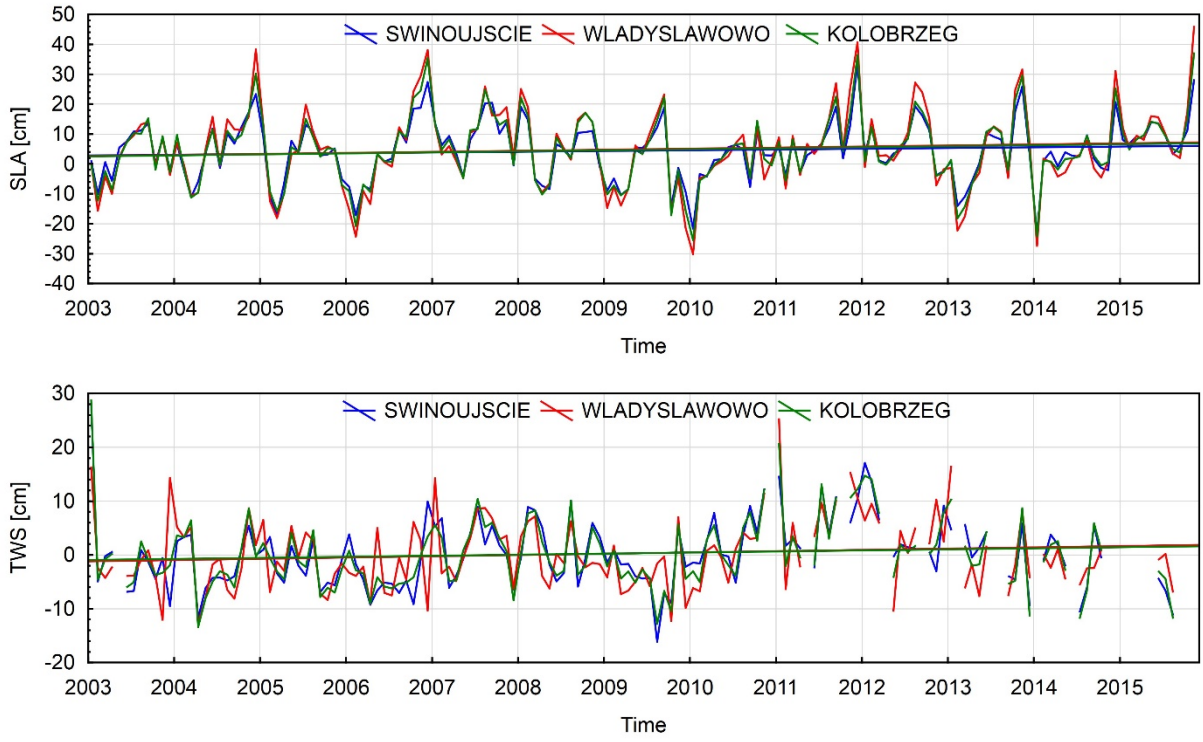

Figure 1. Values and trend for sea level anomalies (SWINOUJSCIE – trend 2.5 mm per year, WLADYSLAWOWO – trend 3.5 mm per year, KOLOBRZEG – trend 3.3 mm per year) and total water storage from GRACE (SWINOUJSCIE – trend 1.8 mm per year, WLADYSLAWOWO – trend 1.8 mm per year, KOLOBRZEG – trend 1.5 mm per year) between 2003-2015 for three points of the Baltic Sea

Time series of SLA and TWS in three locations are similar, the upward and downward periods appear in similar time. There are no vivid differences in SLA dynamics, the turning points are their common feature.

The length of the analyzed time series n=156 enabled the researchers to use 78 harmonics. Those that have the greatest shares in explaining the SLA and TWS changeability and the first and last harmonics were found. In the paper, 5 harmonics were used.

The result of the analysis showed the determination of the amplitude value of particular harmonics, phase shift and the share in explaining the variance in particular harmonics. Owing to the amplitudes, it was possible to determine how intensely the cycles deviate from particular harmonics. With the use of phase shift, it was noticed which variables undergo changes earlier

Table 1. The use of harmonic in time series for SLA and TWS in all analyzed points of the Baltic Sea

SLA			TWS		
Number of harmonics	Period		Number of harmonics	Period	
	months	years		months	years
1	156	13	1	156	13
3	52	4.3	3	52	4.3
13	12	1	13	12	1
16	9.75	0.8	20	7.8	0.65
78	2	0.17	78	2	0.17

For SLA in SWINOUJSCIE point, the most important aspect in explaining the variance of variable deviations from trends has harmonic 13, which corresponds to a one-year cycle, and harmonic 3, which is connected with a four-year cycle. They explain 20.75% and 8.39% of the variance respectively. Harmonic 16, which corresponds to 0.8 of a year, has over 5% share in explaining the variance. The greatest deviations of SLA value from the trend line are caused by fluctuations in a year cycle (harmonic 13). In October, SLA values deviate from trend line in plus, however, in April they deviate in minus by about 6.20 cm. Fluctuations in a four-year cycle (harmonic 3) cause the deviation of SLA values from trend line by 3.94 cm, the phase shift is 3.85, which means that the cycle takes the first extreme value in April. Fluctuations in the time of 0.8 of a year (harmonic 16) make the deviation of 3.29 cm. The first deviation in plus occurs in February. On the basis of the first harmonic representing fluctuations in a thirteen-year cycle, SLA value deviates from trend line by 1.42 cm maximally. Similarly, for SLA in WLADYSLAWOWO point, harmonic 13 (which relates to a one-year cycle) and harmonic 3 (which relates to a four-year cycle) have the greatest share in explaining the variance deviation from the trend line. They explain respectively 21.90% and 7.75% of the variance. Almost 5% of share in explaining the variance has harmonic 16, which relates to a 0.8 of a year cycle. The greatest deviation of SLA values from trend line are caused by fluctuations in a one-year cycle (harmonic 13). In October, SLA values deviate from trend line in plus, however, in April they deviate in minus by about 6.20 cm. The fluctuations in a four-year cycle (harmonic 3) cause the deviation from trend line by 5.14 cm, the value of phase shift is 4.94 cm, the first deviation in plus from trend line appears in May. Fluctuations in the period of 0.8 of a year (harmonic 16) cause deviations of 4.12 cm, the first deviation in plus from trend line occurs in February. On the basis of the first harmonic, which represents fluctuations in a 13-year cycle, SLA value deviates from trend line by 1.86 cm maximally.

In KOLOBRZEG point, similarly like in SWINOUJSCIE and WLADYSLAWOWO, the greatest amplitudes occur in a one-year cycle and a four-year cycle (they explain respectively 22.78% and 7.60% of the variance). The greatest SLA deviations from the trend line occur in a one-year cycle, the amplitude is 7.54 cm (the deviations in plus occur in October, in minus in April). In a four-year cycle, the fluctuation amplitude is 4.36 cm, the first in plus deviation from the trend line can be noticed in April. Fluctuations in the period of 0.8 of a year cause the deviations of 3.47 cm, the first deviation from the trend line in plus occurs in February. On the basis of the first harmonic, which represents the fluctuations in the period of 13 years, SLA value deviates from the trend line by 1.73 cm maximally.

For TWS time series in three points of the Baltic Sea, 5 harmonics were calculated. For TWS in SWINOUJSCIE point, the greatest share in explaining the variance of value deviation from the trend line have harmonic 13, which relates to a one-year cycle, and harmonic 3 connected with a four-year cycle. They explain respectively 10.36% and 9.08% of the variance. Precisely 5% share in explaining variance have also harmonic 20 (the period of 0.65 of a year) and harmonic 78 (0.17 of a year). The greatest TWS values deviations from the trend line are caused by fluctuations in a one-year cycle. In February, TWS value deviates from the trend line in plus, however, in August it deviates in minus by 2.69 cm. Fluctuations in a four-year cycle (harmonic 3) cause TWS deviations from the trend line by 2.52 cm, the cycle takes the first extreme value between May and June. Fluctuations in the period of 0.65 of a year (harmonic 20) make a deviation of 1.65 cm, the first deviation from the trend line in plus occurs in February. On the basis of the first harmonic that

represents the fluctuations in the period of 13 years, TWS value deviates from the trend line by 1.87 cm maximally.

In WLADYSLAWOWO point, the greatest share in explaining the variance of TWS values deviations from the trend line have harmonic 3**,** which relates to the four-year cycle, and harmonic 78, which relates to the period of 0.17 of a year, and harmonic 1 (connected with a one-year cycle). They explain respectively 10.40%, 6.15% and 6.11% of the variance. The greatest TWS values deviations from the trend line are caused by fluctuations in four-year cycles. Between May and June, TWS values deviate from the trend line in plus by 2.80 cm. Fluctuations in a one-year cycle (harmonic 13) and in the time of 0.17 of a year (harmonic 78) make TWS values deviate from trend line by 2.15 cm. In a one-year cycle, the first deviation in plus occurs between December and January. Fluctuations in 0.65 of a year (harmonic 20) cause the value deviate by 1 cm, the first deviation from trend line in plus occurs between January and December.

In KOLOBRZEG point, similarly like in WLADYSLAWOWO, the greatest amplitudes occur in a four-year cycle and a one-year cycle (they explain respectively 11.18% and 8.20% of variance). TWS deviations from the trend line are the greatest in a four-year cycle and the amplitude is 2.89cm (the first deviation in plus occurs between May and June). In a one-year cycle, the amplitude is 2.47 cm and the first deviation from the trend line in plus occurs between February and March. Fluctuations in the period of 0.17 of a year make deviations of 2.10 cm. On the basis of the first harmonic, which represents the fluctuations in the period of 13 years, TWS value deviates from the trend line by 1.70 cm maximally.

4.2 The harmonic analysis of TWS from GRACE and TWS from GLDAS over land

With the aim of analyzing the dynamics of change of TWS over land, one used the current surface mass change data based on the RL05 spherical harmonics from CSR, JPL and GFZ (maximum degree/order: n=60), and data from the NOAH 2.7.1 land hydrology model in the Global Land Data Assimilation System (GLDAS). The total water content from GLDAS is directly comparable to what GRACE measures over land. However, the GLDAS version used here does not include groundwater and separate surface water components (such as rivers and lakes). Deviations from GRACE Total Water Storage changes can thus be expected, in addition to any errors in the model or observations (https://grace.jpl.nasa.gov/data/get-data/land-water-content/). The linear tendency, i.e. linear trend function, was estimated for time series of dTWS from GRACE and dTWS from GLDAS in the cell of 1 by 1 degree with the center (the coordinates: 54.50N; 18.50E), which is presented in Figure 2.

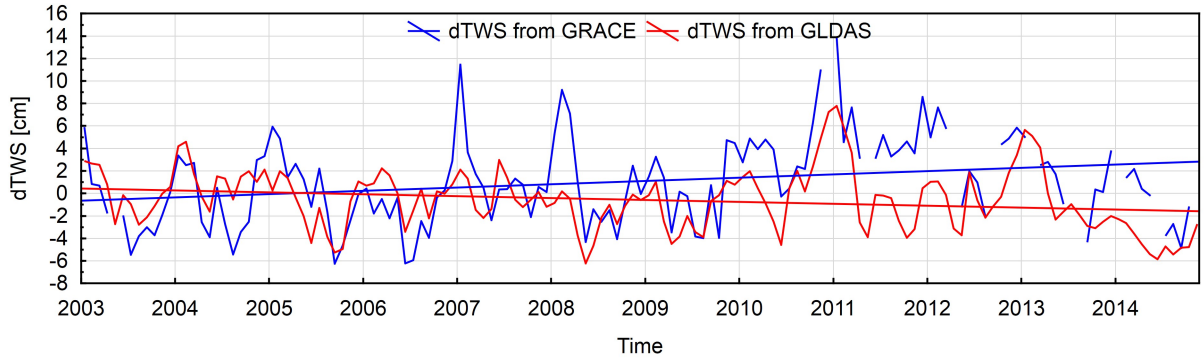

Figure 2. Value and trend of dTWS from GRACE and from GLDAS (trend 1.3 mm per year – from GRACE, trend -1.7 mm per year from GLDAS) in the period between January 2003 and December 2014 in the analyzed cell

Time series in dTWs are similar to each other, increase and decrease periods occur in similar time. The trend, which was marked on the dTWS from GRACE data diagram, shows an increasing value. However, the trend of dTWS from GLDAS has a decreasing tendency.

Figure 3 presents dTWS values deviations from the trend line. The deviations would be modelled with the use of the harmonic balance analysis.

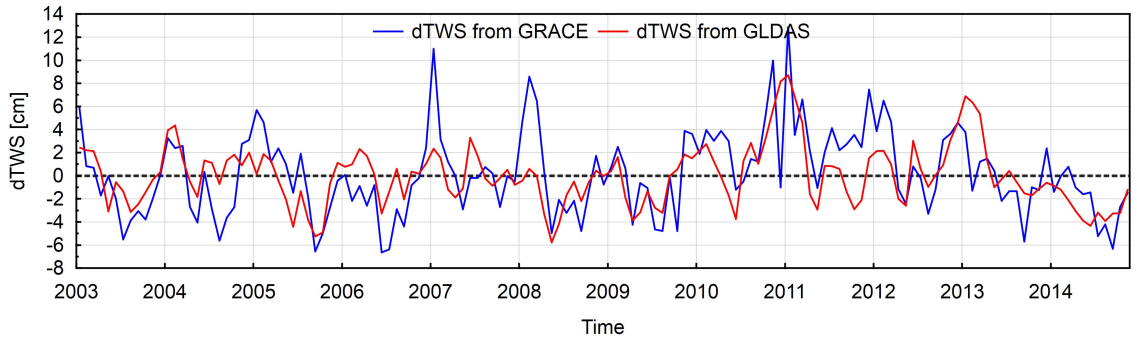

Figure. 3. Values deviations of dTWS from GRACE and dTWS from GLDAS from the trend line in the analyzed cell

The length of the analyzed dTWS from GRACE and dTWS from GLDAS time series n=144 permits the use of 72 harmonics. Five harmonics (with the same numbers as those presented in Table 2) were tested.

Table 2. The use of harmonic in time series for dTWS from GRACE and dTWS from GLDAS in the analyzed cell

dTWS from GRACE			**dTWS from GLDAS**		
Number of harmonics	Period		Number of harmonics	Period	
	months	years		months	years
1	144	12	1	144	12
2	72	6	2	72	6
4	36	3	4	36	3
12	12	1	12	12	1
72	2	0.17	72	2	0.17

For dTWS from GRACE and dTWS from GLDAS data, 5 harmonics, which correspond to particular periods (Table 2) were calculated. The determination of amplitudes for particular harmonics, phase shifts and variance share of variables in particular harmonics were the results of the analysis.

For dTWS from GRACE in the analyzed cell, the greatest share in explaining the variance of values deviation from the trend line have harmonic 12, which corresponds to a one-year period, and harmonic 1, which is connected with a twelve-year cycle. They explain respectively 33.57% and 10.61% of the variance. Over 5% share in explaining the variance has also harmonic 2, which relates to the period of 6 years. Harmonic 4 (period of 3 years) has also a great share in explaining the variance. The greatest deviation of dTWS from the trend line is caused by fluctuations in a one-year cycle. In March, the values deviate from the trend line in plus, however, in September they deviate in minus by 2.93 cm. The fluctuations in a twelve-year cycle (harmonic 1) make the maximal dTWS deviations from the trend line of 1.65 cm. Fluctuations in a six-year period (harmonic 2) make the deviation of 1.16 cm. For dTWS from GLDAS, the greatest amplitudes occur in a one-year cycle and a three-year cycle (they explain respectively 25.04% and 12.08% of the variance). dTWS deviations in a one-year cycle are 1.86 cm maximally. In a three-year cycle, the amplitude is 1.27 cm. Fluctuations in a six-year cycle (harmonic 2) make the deviation of 1.03 cm.

2.3 The correlations between the data sets dTWS from GRACE and dTWS from GLDAS over land

Another aspect of importance is the correlation between the data sets. As seen before, the trends in each data set have been established, but if they do not agree with one another, important

conclusions cannot be made. Therefore, the Pearson correlation coe□cient was computed between each time series at the cell.

The correlation coefficient between data dTWS from GRACE and dTWS from GLDAS is 0.59. Having analyzed the gravity of the correlation coefficient, it turned out that its value substantially differs from zero by $p<0.05$. Consequently, it was stated that there is a moderate positive dependence between dTWS from GRACE and dTWS from GLDAS.

Here, r is the correlation, X and Y are the mean values of each times series, and X and i Y are the time series values. With this statistic the closer the value is to 1, the more correlated the series are with each other. We also calculated the correlations between the data in each year. The results presented in Figure of 4. The highest correlation coefficient between the dTWS from GRACE and dTWS from GLDAS is 0.82 in 2005 and lowest in 2007 and 2011 is 0.46.

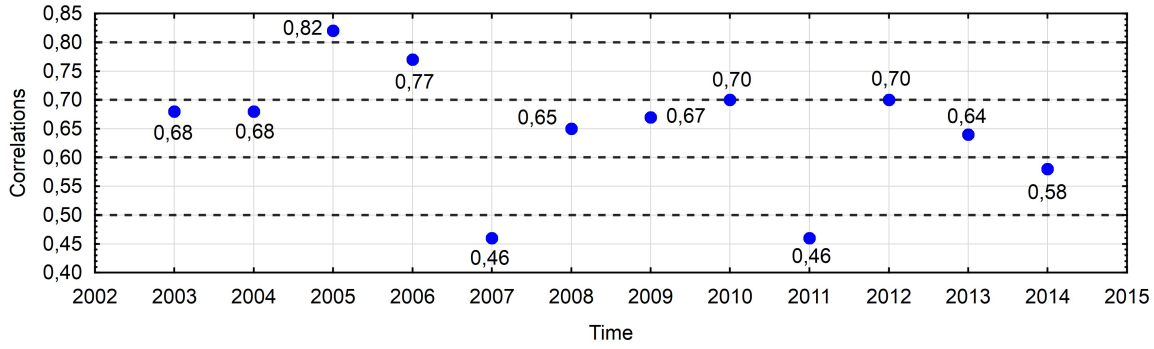

Figure 4. Coeffcients of correlation (r) of dTWS from GRACE and dTWS from GLDAS in the period January 2003 – December 2014 in the analyzed cell

4. CONCLUSIONS

The main research purpose of this article was to investigate whether and what changes of sea level anomalies (SLA) and total water storage (TWS) occurred in the coastal zone during the test period. Moreover, the article presents the activities of sea level changes and total water storage within time and what time cycles occur. In order to check the occurrence of fluctuation amplitudes, the harmonic balance analysis was used. The linear trend function for particular time series of SLA and TWS data shows the upward trend.

Sea level anomalies and total water storage time series in three locations are similar, the periods of upward trends and downward trends happen in similar time. On the basis of the analyses, it was stated that the greatest deviations from SLA trend line are caused by fluctuations in a one-year and four-year periods in all three analyzed points of the Baltic Sea. For TWS data from GRACE, one claimed that the greatest deviation from the trend line appears in a one-year and a four-year periods.

The second objective of the research was to check the differences between GRACE-observed over land and GLDAS-derived TWS , in the cell of 1 by 1 degree, by verifying the occurrence of correlations between TWS data. The analysis of the occurrence of seasonal fluctuations cycles was used. There is a moderate correlation between dTWS data from GRACE and GLDAS. The linear trend function for dTWS data from GRACE shows an increasing tendency, however, dTWS from GLDAS show a decreasing tendency. In the next research, the ground water levels will be considered in order to prove the results. On the basis of the harmonic balance analysis, it was stated that the greatest deviation of dTWS values from GRACE and dTWS from GLDAS from trend line are made by fluctuations in periods of one year, three years or within twelve years. Summing up, it can be stated that the rise in sea level can be precipitated by the process of a shoreline erosion caused by water. It is essential for investment areas. Even though water level of the Baltic Sea has changed within the dozen or so years, the trend has grown slightly.

ACKNOWLEDGEMENTS

We used SLA data from to the French Archiving, Validation and Interpretation of Satellite Oceanographic data (AVISO) (http://www.aviso.oceanobs.com/) and Copernicus Marine and Environment Monitoring Service (CMEMS) (http://www.marine.copernicus.eu)

We used the GLDAS data from "http://grace.jpl.nasa.gov", which used the "Goddard Earth Sciences Data and Information Services Center" and GRACE land data from http://grace.jpl.nasa.gov, supported by the NASA MEaSUREs Program.

REFERENCES

Bettadpur, S., 2012. Level-2 gravity field product user handbook, GRACE 327-734 (CSR-GR-03-01), Rev 3.0, May 29, 2012, University of Texas, Centre of Space Research.

Chambers, D.P., 2006. Evaluation of New GRACE Time-Variable Gravity Data over the Ocean. Geophys. Res. Lett., 33(17), LI7603.

Chen, J. L., C. R. Wilson, B. D. Tapley, J. S. Famiglietti, and M. Rodell, 2005. Seasonal global mean sea level change from satellite altimeter, GRACE, and geophysical models, Journal of Geodesy, 79(9), 532-539.

Church J.A., White N.J., 2006. A 20th century acceleration in global sea level rise, Geophys. Res. Lett., 33, L01602, doi: 10.1029/2005GL024826.

Church J.A., Woodworth P.L., Aarup T., Wilson W.S. (eds.), 2010. Understanding sea-level rise and variability, Wiley-Blackwell, Chichester, Oxford, Hoboken, 456 pp.

Donner R.V., EhrckeR., Barbosa S.M., Wagner J., Donges J.F., Kurths J., 2012. Spatial patterns of linear and nonparametric long-term trends in Baltic sea- level variability, NonlinearProc.Geoph., 19(1), 95–111,http://dx.doi.org/10. 5194/npg-19-95-2012.

Ekman M., 2009. The changing level of the Baltic Sea during 300 years: a clue to understanding the Earth, Summer Inst. Histor. Geophys., Aland Islands, 168 p.

Ekman M., Makinen J., 1996. Mean sea surface topography in the Baltic Sea and its transition area to the North Sea: a geodetic solution and comparisons with oceanographic models, J. Geophys. Res.-Oceans, 101(C5), 11993–11999.

Ekman M., Stigebrandt A., 1990. Secular change of the seasonal variation in sea level and of the pole tide in the Baltic Sea, J. Geophys. Res.-Oceans, 95(C5), 5379–5383.

Forste C., Schmidt R., Stubenvoll R., Flechtner F., Meyer U., Konig R., Neumayer H., Biancale R., Lemoine J.M., Briunsma S., Loyer S., Barthelmes F., Esselborn S., 2008. The GeoforschungsZentrum Postdam: EiGEN-GL04C, Journal of Geodesy, 82:331-346.

Földváry, L., 2007. Analysis of numerical differentiation methods applied for determination of kinematic velocities for LEOs, Periodica. Polytechnica Civil Engineering, 51/1, 17-24.

Horton R., Herweijer C., Rosenzweig C., Liu J., Gornitz V., Ruane A.C., 2008. Sea level rise projections for current generation CGCMs based on the semi- empirical method, Geophys. Res. Lett., 35(2), doi: 10.1029/ 2007GL032486.

Hunicke B., Zorita E., 2008. Trends in the amplitude of Baltic Sea level annual cycle, Tellus A, 60(1), 154–164.

Kowalczyk, K., 2006. New model of the vertical crustal movements in the area of Poland. Geodezija ir Kartografija, 32(4), 83-87.

Kumar, S. V., Peters-Lidardb, C.D., Tiana, Y., Houserb, P.R., Geigerb, J., Oldenb, S., Lightyb, L., Eastmana, J.L., Dotyc, B., Dirmeyerc, P., Adamsc, J., Mitchelld, K., Woode, E.F. and Sheffielde, J., 2006. Land information system: An interoperableframework for high resolution land surface modeling, Environ. Model. Softw., 21(10), 1402–1415.

Kusche, J., Schmidt, R., Petrovic, S., Rietbroek, R., 2009. Decorrelated GRACE time-variable gravity solutions by GFZ, and their validation using a hydrological model, Journal of Geodesy, doi:10.1007/s00190-009-0308-3.

Landerer F.W. and S. C. Swenson, 2012. Accuracy of scaled GRACE terrestrial water storage estimates. Water Resources Research, Vol 48, W04531, 11 PP, doi:10.1029/2011WR011453.

Pajak K., Birylo M., 2016. Evaluation of the Baltic Sea Basin using satellite altimetry data, 16th International Multidisciplinary Scientific GeoConference SGEM 2016, SGEM2016 Conference Proceedings, ISBN 978-619-7105-61-2 / ISSN 1314-2704, June 28 - July 6, 2016, Book3 Vol. 1, 297-304 pp.

Plag H.P., Tsimplis M.N., 1999. Temporal variability of the seasonal sea-level cycle in the North Sea and Baltic Sea in relation to climate variability, Global Planet.Change,20(2–3),173–203.

Pollock D.S.G., 2008. Statistical Fourier Analysis: Clarifications and Interpretations. Working Paper No. 08/36.

Poutanen M., Kakkuri J., 2000. The sea surface of the Baltic – a result from the Baltic Sea Level Project (IAG SSA 8.1). Geodesy Beyond 2000 – The Challenge of the First Decade, (ed) K.P. Schwarz, IAG General Assembly, Birmingham, 19-30 July 1999, IAG Symp. Vol. 121, Springer, pp. 289-294.

Rodell M, P. R. Houser, U. Jambor, J. Gottschalck, K. Mitchell, C.-J. Meng, K. Arsenault, B. Cosgrove, J. Radakovich, M. Bosilovich, J. K. Entin, J. P. Walker, D. Lohmann, and D. Toll, 2004. The Global Land Data Assimilation System. Bulletin of the American Meteorological Society, vol 85 (3), pp 381-394.

Statsoft Electronic Statistics Textbook, http://www.statsoft.pl/textbook/stathome.html.

Tapley BD, Bettadpur S, Watkins MM, Reigber C, 2004. The Gravity Recovery and Climate Experiment; Mission Overview and Early Results, Geophy. Res. Lett., Vol. 31, No. 9, L09607, 10.1029/2004GL019920.

Swenson, S. C. and J. Wahr, 2006. Post-processing removal of correlated errors in GRACE data, Geophys. Res. Lett., 33, L08402, doi:10.1029/2005GL025285.

Tapley B.D., Bettadpur S., Watkins M., Reigber C., 2004. The Gravity Recovery and Climate Experiment: Mission overview and early results, Geophys. Res. Lett., 31(9).V., Sorooshian, S., 1998. Multi – objective global optimisation for hydrologic models. Jurnal of Hydrol.; 204: 83-97.

Proceedings of the 10th World Congress of EWRA 'Panta Rhei', 5-9 July 2017, Athens, Greece
© 2017 *European Water Resources Association*

A simple scaling procedure to assess the impact of climate change on extreme precipitation

A. Forestieri, E. Arnone and L.V. Noto*
DICAM, Università degli Studi di Palermo, Italy
* *e-mail: leonardo.noto@unipa.it*

Abstract: In this study we used the products of the Regional Climate Models (RCMs) to evaluate the impact of climate alterations on extreme events across the Region of Sicily (Italy). Data have been retrieved from EURO-CORDEX simulations at 12 km of spatial resolution. Because of the low resolution, the RCMs products are likely unsuitable to reproduce consistently sub-daily heavy precipitations. For this reason, extreme events at daily scale were first checked out by comparing the quantiles estimated from raingauge observations and RCMs outputs. Secondly, we implemented a temporal downscaling approach to estimate rainfall for durations of 1, 3, 6, 12, 24 hours from the modeled daily precipitation. Lastly, future projections were analyzed at daily and sub-daily scale. Results indicated that estimated variations are not be homogeneous within the study area, with a general increase of extremes events proportional to the return period and inversely proportional to the duration.

Key words: Climate change, temporal downscaling, extreme precipitation, RCM

1. INTRODUCTION

The evaluation of the extreme precipitation is fundamental in the engineering applications since, for example, it allows for the estimation of the Depth-Duration-Frequency (DDF) curves. The awareness of the global warning has induced the scientific community to investigate how extreme precipitations have changed over the last decades (e.g. Arnone et al., 2013) and how they might change in the future. Global Climate Models (GCMs) represent a powerful tool for understanding the behavior of the global climate system. GCMs typically works at very large spatial scales (i.e. 50-150 km or greater), at which the characteristics of heavy precipitation are likely not capture. More precise information can be retrieved by means of Regional Climate Models (RCMs), which work at a finer temporal and spatial scale starting from boundary conditions provided by GCMs.

In this work, we used the products of the Coordinated Regional Climate Downscaling Experiment for Europe area (EURO-CORDEX) at 12 km of spatial resolution to (i) investigate the capability of the RCMs' products to reproduce the extreme precipitation in Sicily at daily scale (ii) estimate the possible climate evolution until the end of the 21th century, and (iii) to evaluate the impact of climate change on the projections of daily and sub-daily extremes. A procedure of bias correction was implemented to correct daily RCMs data whereas a temporal downscaling method was implemented in order to obtain sub-daily values of precipitation.

2. CLIMATE DATA

High-resolution RCMs are driven through nested regional climate modeling, i.e. a technique that consists of using initial conditions, time-dependent lateral meteorological conditions and surface boundary conditions from the global models. The climate projection framework within CORDEX framework is based on the set of new global model simulations planned in support of the IPCC Fifth Assessment Report (referred to as CMIP5). This set of simulations includes a large number of experiments ranging from new greenhouse-gas scenario simulations for the 21st century (Taylor et

al., 2012).

The EURO-CORDEX initiative provides regional climate projections for Europe at 50 km (EUR-44) and 12.5 km (EUR-11) resolutions, by downscaling the new CMIP5 global climate projections (Taylor et al., 2012) and considering the new representative concentration pathways (RCPs) Moss et al., (2010). Specifically for the Mediterranean area, the Med-CORDEX initiative has been proposed, which takes advantage of new very high-resolution RCMs (up to 10 km) and of new fully coupled Regional Climate System Models (RCSMs). Temporal resolution is daily.

The capability of such models in reproducing rainfall series depends also on the mechanism of rainfall generation and thus on the area of application. An ensemble of products is then generally adopted to evaluate the uncertainty. Table 1 shows the RCMs products used in this study in their control (i.e. past) and scenario (i.e. future) outputs.

Table 1. Regional climate models products used in this study. The available control period is also shown.

ID	Domain	Institute	RCM name	Resolution	Driving model	Driving experiment	Driving ensemble	Period
1	MED-CORDEX	ICTP	RegCM 4.3	0.11 deg		Hist/rcp45/rcp85	r1i1p1	1970-2005
2	EURO-CORDEX	KNMI	RACMO22E	0.11 deg	EC-EARTH	Hist/rcp45/rcp85	r1i1p1	1950-2005
3	EURO-CORDEX	CLMcom	CCLM4-8-17	0.11 deg	CNRM-CM5-LR	Hist/rcp45/rcp85	r1i1p1	1950-2005
4	EURO-CORDEX	CLMcom	CCLM4-8-17	0.11 deg	EC-EARTH	Hist/rcp45/rcp85	r12i1p1	1950-2005
5	EURO-CORDEX	CLMcom	CCLM4-8-17	0.11 deg	MPI-ESM-LR	Hist/rcp45/rcp85	r1i1p1	1950-2005
6	EURO-CORDEX	KNMI	RACMO22E	0.11 deg	EC-EARTH	Hist/rcp45/rcp85	r1i1p1	1950-2005
7	EURO-CORDEX	CLMcom	CCLM4-8-17	0.11 deg	HadGEM2-ES	Hist/rcp45/rcp85	r1i1p1	1950-2005
8	EURO-CORDEX	SMHI	RCA4	0.11 deg	CNRM-CM5	Hist/rcp45/rcp85	r1i1p1	1969-2005
9	EURO-CORDEX	SMHI	RCA4	0.11 deg	EC-EARTH	Hist/rcp45/rcp85	r12i1p1	1969-2005
10	EURO-CORDEX	SMHI	RCA4	0.11 deg	IPSL-CM5A-MR	Hist/rcp45/rcp85	r1i1p1	1969-2006
11	EURO-CORDEX	SMHI	RCA4	0.11 deg	HadGEM2-ES	Hist/rcp45/rcp85	r1i1p1	1969-2005
12	EURO-CORDEX	SMHI	RCA4	0.11 deg	MPI-ESM-LR	Hist/rcp45/rcp85	r1i1p1	1969-2005
13	EURO-CORDEX	DMI	HIRHAM5	0.11 deg	EC-EARTH	Hist/rcp45/rcp85	r3i1p1	1950-2005

Observed data from raingauges stations across Sicily have been retrieved in order to (i) correct the RCMs products and (ii) evaluate their capability in reproducing extreme precipitation ad daily scale (iii) implement the temporal downscaling. Specifically, the annual maxima at 1, 3, 6, 12, and 24 h (AMRd) of rainfall duration and the daily rainfall (DR) were selected from data provided by the local hydrological observatory (i.e., Osservatorio delle Acque-Agenzia Regionale per i Rifiuti e le Acque, OA-ARRA). The selected rainfall observations cover the period 1972-2003, whereas, with regard to the RCMs outputs, we considered simulations relative to the same control period and two future projections, i.e. 2006-2050 and 2051-2099, obtained from both the scenarios RCP 4.5 and RCP8.5.

3. BIAS CORRECTION METHOD

RCM outputs are typically affected by systematic and random model errors (Terink et al., 2009). A correction algorithm based on the comparison between RCM data and measurements can provide a bias correction method for RCM-simulated climate variables. A common assumption of most bias correction methods is stationary, or time invariance, of the model errors. This implies that the empirical relationships in the correction algorithm and its parameterization for current climate conditions do not change over time and are also valid for future conditions.

Statistical transformations attempt to find a function Ψ that maps a modeled variable RCM that has the same distribution of the observed variable. In order to correct the daily precipitation fields, we applied the Quantile-matching (QM) methodology (Déqué et al., 2007) to the RCM outputs. The QM approach is based on the assumption that a transformation Ψ exists to allow for “translation” of

the CDF of a RCM variable (e.g., precipitation). The transformation functions are based on the comparison between observations (gauge data) and simulations (RCM outputs).

Specifically, we extracted the daily precipitation time series from the RCMs cell outputs where at least a station is present. The QM method adjusts all the moments of the probability distribution function (PDF) of any variable of the model (Piani et al., 2010) using the CDFs to construct the transfer function.

Following Piani et al. (2010) the transformation can, in general, be formulated as:

$$obs = \Psi(RCM) \tag{1}$$

Such a statistical transformation is an application of the probability integral transform and, if the distribution of the variable of interest is known, the transformation is defined as:

$$obs = F_0^{-1}[F_m(RCM)] \tag{2}$$

Following the procedure proposed by Boè et al (2007), the empirical CDFs were approximated using tables of empirical percentiles thus obtaining the transfer functions (TF). The initial datasets for observed data and simulated RCM values can be characterized by the following equations:

$$X_{obs} = x_{obs}(\varphi,\theta,d,m,i) \tag{3}$$
$$X_{RCM} = x_{RCM}(\varphi,\theta,d,m,i) \tag{4}$$

where x_{obs} and x_{RCM} are observed and modelled precipitation respectively, for each grid point and sorted by depth precipitation; φ and θ are the longitude and latitude of the grid point, respectively, d and m are indexes of day and month respectively.

The bias correction was achieved considering different TFs derived for every month of the year. Therefore, data have been grouped according to calendar month. For fixed φ, θ, m, the emerging TF is defined for all i indexes as:

$$TF_{\varphi,\theta,m} = [x_{RCM}(\varphi,\theta,d,m,i)] = x_{obs}(\varphi,\theta,d,m,i) \tag{5}$$

Only the portion of TF with non-zero values, i.e.wet days, was fitted.

This method was applied to both control and future rainfall data extracted from each RCM.

4. TEMPORAL DOWNSCALING

In this study, a simple method of temporal downscaling was proposed starting from the idea developed by Srivastav et al. (2014) that have presented a methodology based on equidistance quantile matching (EQM) for updating the DDF curves under climate change. Specifically, it is based on the observed correlation between extreme rainfall at different subsequent durations, i.e. daily-24h, 24h-12h, 12h-6h, etc by assuming that this correlation remains invariant in the future.

The analysis of the correlation indicated the presence of high values of the coefficient of determination, confirming the hypothesis of a strong correlation between pairs of the subsequent durations. A non-parametric transfer function (TF) among the maxima daily and maxima sub-daily observed rainfall values using the data for the period 1972-2003 was estimated. The five TFs, obtained by a comparison among the empirical CDF for each station, were evaluated from the pairs of data relative to different durations, e.g. daily-24h, 24h-12h, etc. The process of temporal downscaling thus follows a "cascade method": the 24 hours maxima dataset is obtained from daily data through TF; 12 hours maxima dataset are generated from 24 hours maxima data previously obtained and so on until to the lowest duration of 1 hour.

As for the bias correction method, the procedure was applied to both control and future rainfall data extracted from each RCM.

5. RESULTS

The analysis of the extremes has been conducted following the Regional Frequency Analysis (RFA) described in Forestieri et al., 2016, according to which the region of Sicily can be divided in six statistically homogenous regions. Three probability distributions, i.e. Log-Normal with three parameters (LN3), General Extreme Value (GEV) and Two Component Extreme Value (TCEV), were adopted to estimate the quantiles at different return period.

A first insight on the capability of the RCMs outputs to reproduce the past observations is given in Fig. 1, which shows the comparison of the empirical quantiles obtained from the raingauges data and RCMs, for each regions (q-q plots). The black dots indicate the percentiles of observed dataset drew over the diagonal (obs vs obs), while the light and the dark shaded indicate the 5th and 95th of the quantiles of the ensemble dataset provided by RCMs, before and after bias correction respectively. In all cases, the q-q plots show that the spread increases quasi-linearly as quantile increases, denoting a lack of consistency of RCMs in correctly reproducing the extreme value of precipitation before the bias correction. Only in region 1, RCMs underestimate the observations for high quantile values. Moreover, the bias correction improves the estimation.

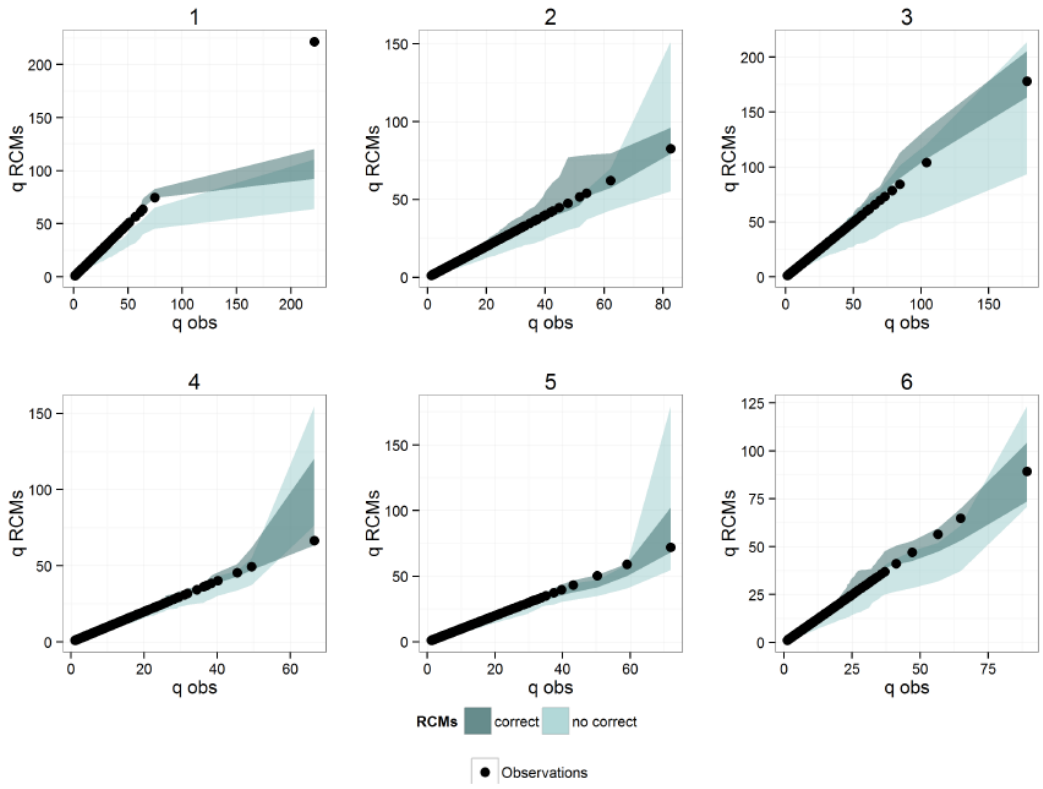

Fig. 1. Empirical quantiles (averaged in space) of observed vs RCMs daily rainfall for each of the six regions.

From the maximum sub-daily time series obtained from the temporal downscaling, we derived the quantiles of the median ensemble, provided by RCMs for both RCP4.5 and 8.5, by using the three distributions. For the six regions, figure 2a and figure2b show the results obtained with the LN3 distribution and for 24h duration obtained from the observations (blue), from RCMs outputs relative to the control period (black), and future scenario, RCP4.5 (green) and RCP8.5 (red) for the time intervals 2006-2050 (a) and 2051-2099 (b). The results show that the impact of climate change increases as the return period increases. A significant increase is observed for the region 4, period

2051-2099.

In order to provide a quantitative assessment of the future change of the quantiles obtained by the median of different RCMs, we evaluated the relative variation of the quantiles, Δ%, as:

$$\Delta\% = (Q_{RCP4.5/8.5} - Q_{hist})/Q_{hist} \quad (6)$$

where $Q_{RCP4.5/8.5}$ and Q_{hist} are the future and historical quantile, respectively.

Figure 2c and figure 2d report the values of Δ% as a function of duration for fixed distributions (points and hatchings) and return period (different colours) and for the two projection periods 2006-2050 (a) and 2051-2099 (b) obtained from the scenario RCP4.5. In particular, the central (region 6) and south-east area (region 1) of Sicily, for the scenario RCP4.5, do not show evident differences for distribution and return period. The Δ% for the south-east area for the period 2006-2050 are included between 25÷35% while, for the period 2051-2099, the Δ% ranges between 40 and 50%. These two regions have shown a weak dependence on return period.

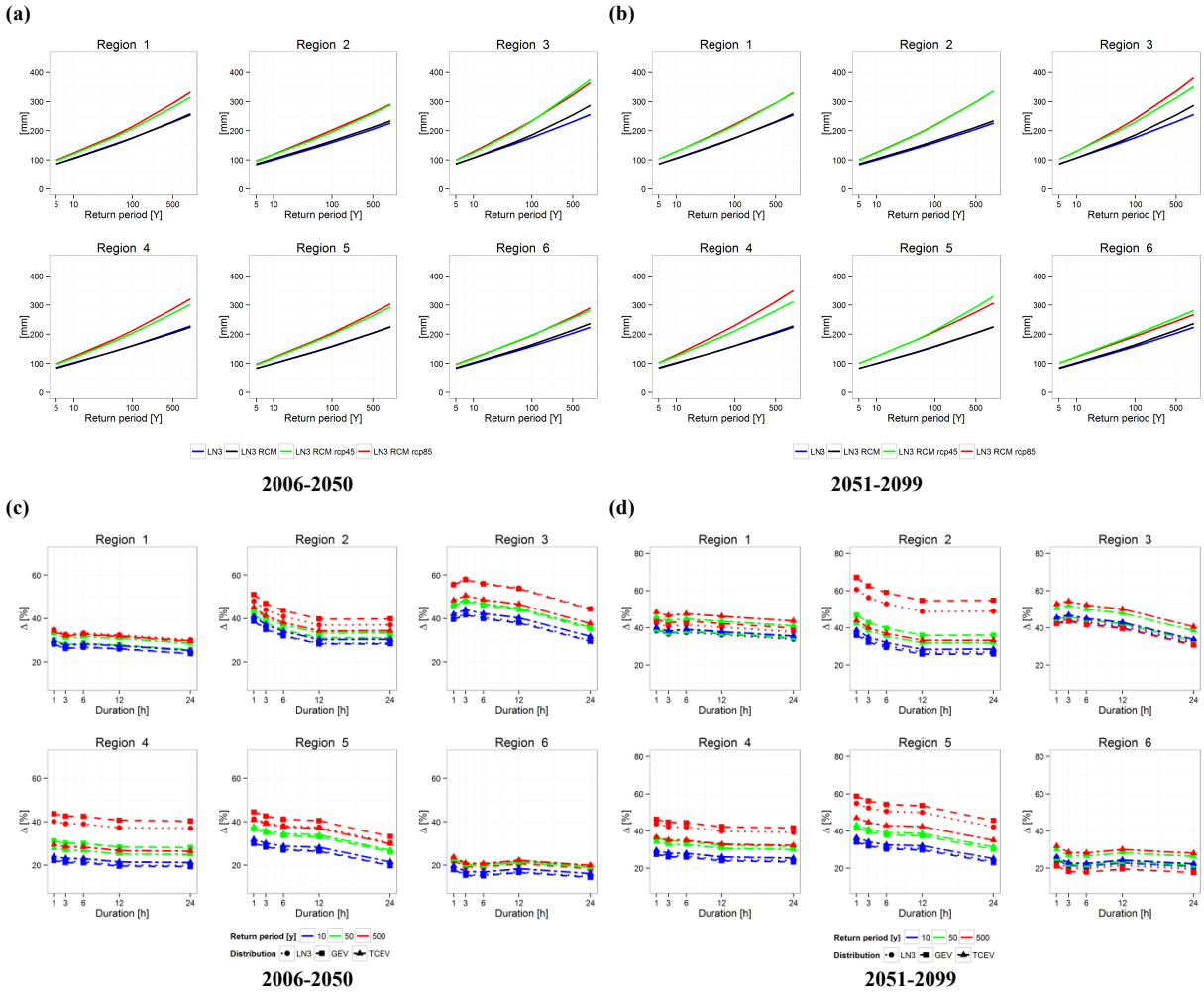

Fig. 2. Return levels curves for 2006-2050 (a) and 2051-2099 (b) obtained using the LN3 distribution starting from observations and RCM data. Δ(%) of quantile of precipitation, for the three distributions and at given return period, for the projections 2006-2050 (a) and 2051-2099 (b) obtained with the scenario RCP4.5.

The north-centre (region 2), north-east (region 3) and centre-west (region 5) area of Sicily show evident dependence on the duration and return period. For short durations, the Δ% reaches the highest values that tend to decrease for the longer durations. The value of Δ% increases regularly with the return period. The north-east area, does not show evident difference between the two different periods, wherein the maximum values of Δ% reach the 60% and decrease with the

duration until the value of about 50%.

The north-centre and north-east areas show a considerable increase of Δ% for both scenarios, between the first and second part of the century. For the north-centre area, relatively to period 2006-2050 and for both scenarios, the Δ% reaches the maximum of 50% with a minimum value equal to about 30%. For the same period in the centre-west area, the values range between 20% and 50%. When the period 2051-2099 is taken into account, these values oscillate between 30% and 65% for the north-centre. In the centre-west for the period 2051-2099, the values of Δ% range between the 30% and 60 %. Finally, in the west area (region 4), Δ% values do not show a strong dependence on the duration for both scenarios while they increase with the return period. For the scenario RCP4.5, the maximum value of Δ% is about equal to 45% while the minimum value is about equal to 20%.

5. CONCLUSIONS

A bias correction method and a temporal downscaling approach have been used in this study to evaluate the impacts of climate change on precipitation extremes staring from an ensemble of RCMs EURO-CORDEX simulations. The analysis of the changes in extreme precipitations showed an increase of the quantiles with simultaneous decrease of mean annual precipitation. These results provide an indication of a possible increment of the extreme rainfall. In particular, the relative variation Δ% of the quantiles of precipitation resulted to be almost always larger than 20%. In order to obtain the future projection of the quantiles could be useful to multiply the value of current quantiles of precipitation with a sort of future factor of safety, for fixed return period and selected distribution. In conclusion, these results could provide an indication for the use of the quantile of precipitation and the relative DDF curves for the hydrological analysis under climate change. For this reason, an increase of the attention on the management and planning of the future hydraulic infrastructures designed for high return periods must be indispensable. In the practical applications, in order to reduce the damage and loss of human lives in the future, a careful evaluation of the DDF curves taking into account effects of climate change could be essential.

REFERENCES

Arnone, E., Pumo, D., Viola, F., Noto, L. V., and La Loggia, G., 2013. Rainfall statistics changes in Sicily, Hydrol. Earth Syst. Sci., 17, 2449-2458.

Boé, J, L. Terray, F. Habets, and E. Martin. 2007. Statistical and dynamical downscaling of the Seine basin climate for hydro-meteorological studies. Int. J. Climatol., vol. 27, no. 12, pp. 1643–1656.

Déqué, M. , D. P. Rowell, D. Lüthi, F. Giorgi, J. H. Christensen, B. Rockel, D. Jacob, E. Kjellström, M. De Castro, and B. van den Hurk. 2007. An intercomparison of regional climate simulations for Europe: assessing uncertainties in model projections. Clim. Change, vol. 81, no. 1, pp. 53–70.

Forestieri, A., Blenkinsop, S., Fowler, H., Lo Conti, F., & Noto, L. (2016, April). Regional frequency analysis of extreme precipitation for Sicily (Italy). In EGU General Assembly Conference Abstracts (Vol. 18, p. 17928).

Moss, R. H., J. A. Edmonds, K. A. Hibbard, M. R. Manning, S. K. Rose, D. P. Van Vuuren, T. R. Carter, S. Emori, M. Kainuma, T. Kram, and others, 2010. The next generation of scenarios for climate change research and assessment. Nature, vol. 463, no. 7282, pp. 747–756.

Piani, C, J. O. Haerter, and E. Coppola. 2010. Statistical bias correction for daily precipitation in regional climate models over Europe. Theor. Appl. Climatol., vol. 99, no. 1–2, pp. 187–192.

Srivastav, R. K., A. Schardong, and S. P. Simonovic, 2014. Equidistance Quantile Matching Method for Updating IDFCurves under Climate Change. Water Resour. Manag., vol. 28, no. 9, pp. 2539–2562.

Taylor, K. E., R. J. Stouffer, and G. A. Meehl. 2012. An overview of CMIP5 and the experiment design. Bull. Am. Meteorol. Soc., vol. 93, no. 4, pp. 485–498.

Terink, W., R. Hurkmans, P. Torfs, and R. Uijlenhoet. 2009. Bias correction of temperature and precipitation data for regional climate model application to the Rhine basin. Hydrol. Earth Syst. Sci. Discuss., vol. 6, no. 4, pp. 5377–5413.

Proceedings of the 10th World Congress of EWRA 'Panta Rhei', 5-9 July 2017, Athens, Greece
© 2017 *European Water Resources Association*

Analysis of rainfall trend in southern Italy through the application of the ITA technique

T. Caloiero[1*], R. Coscarelli[2] and Ennio Ferrari[3]
[1] *Institute for Agricultural and Forest Systems in the Mediterranean, National Research Council of Italy, Rende (CS), Italy*
[2] *Research Institute for Geo-Hydrological Protection, National Research Council of Italy, Rende (CS), Italy*
[3] *Department of Computer Engineering, Modeling, Electronics, and Systems Science, University of Calabria, Rende (CS), Italy,*
[*] *e-mail: tommaso.caloiero@isafom.cnr.it*

Abstract: In the last decades, climate change has been the focus of considerable international attention due to the increase of phenomena such as flood, heat waves, forest fires and droughts. In this context, research on the patterns of precipitation trends, both at regional and local scale, has been paramount because these variations can negatively impact on ecosystems, agriculture, water supply and management, human welfare and regional political stability. In this paper, an investigation of the temporal rainfall variability has been carried out using a homogeneous monthly rainfall dataset of 559 rain gauges with more than 50 years of observation. The region under investigation is a large portion of the Italian peninsula, ranging from the Campania and the Apulia regions in the North, to Sicily in the South, and covering an area of about 85,000 km^2. Possible trends in monthly and seasonal rainfall values have been investigated by means of a new graphical methodology (Innovative Trend Analysis), which allows the trend identification of the low, medium and high values of a series. As a result, different values and tendencies of the highest and the lowest rainfall values have emerged among the five regions considered in the analysis. Especially at seasonal scale, a negative trend has been detected in winter and in autumn in the whole study area, whereas not well defined trend signals have been identified in summer and spring.

Key words: rainfall, trend, graphical techniques, southern Italy

1. INTRODUCTION

The latest Assessment Report (AR5) issued by the Intergovernmental Panel on Climate Change (IPCC 2013) has highlighted the global impact of human activities on climate and the effects that such activities produce. In Italy, numerous investigations carried out using long-term precipitation databases have detected a decreasing precipitation trend, even if rarely significant (e.g. Brunetti et al. 2006). The regions in which these trends were observed are principally located in southern Italy: Campania (Longobardi & Villani 2010), Basilicata (Piccarreta et al. 2004), Sicily (Liuzzo et al. 2016) and Calabria (Caloiero et al. 2015). These studies did not specify if low or high precipitation contributed to the detected trends. They were principally based on non-parametric tests, which are better suited than parametric ones to deal with non-normally distributed data in hydrometeorology (Onyutha 2016). However, as Kundzewicz and Robson (2000) showed, a powerful graphical technique for exploratory data analysis is required to avoid errors in identifying significant hidden (short-durational) sub-trends. For this reason, Şen (2012) proposed a new Innovative Trend Analysis (ITA) technique, which has found wide application in hydrology. Haktanir & Citakoglu (2014) applied the ITA method to 14 standard duration annual maximum rainfall series of Turkey. Kisi & Ay (2014) used ITA and MK to study the trends of some water quality parameters registered at five different Turkish stations. Temperature data recorded at the Marmara region in Turkey have been studied using ITA (Şen 2014); also, the monthly total precipitation trend of six different provinces in Turkey has been studied using MK and ITA methods (Ay & Kisi 2015). Further applications of ITA and Spearman's rho test include changes observed in temperature trends and heat waves in Northwestern Mexico (Martínez-Austria et al. 2015), and the trend analysis of monthly pan evaporations (Kisi 2015). In addition, a streamflow trend analysis in the northwest of

Iran has been carried out verifying the utility of ITA for these applications (Tabari & Willems 2015).

In this study, the monthly and seasonal high quality rainfall series recorded in southern Italy have been analysed and the temporal changes of the different series have been detected using the ITA technique. In particular, the investigation was carried out considering five different regions of the study area. The application of the ITA technique allowed to distinguish the trend of the low, medium and high precipitation monthly data at regional scale.

2. STUDY AREA AND DATA

The region under investigation is a large portion of the Italian peninsula, extending from the Campania and the Apulia regions in the North, to Sicily in the South, and covering an area of about 85,000 km^2 (Figure 1). The study area is located within the Mediterranean basin and is characterized by particular climatic conditions. The climate regime of the study area is typically a Mediterranean climate, which dominates in particular the islands and the coastal areas; the winter season is a rather mild and rainy period, whereas the summer season is very hot and dry.

The database used in this study was the one presented in Longobardi et al. (2016) in which available precipitation time series have been tested for time series homogeneity through the combined use of direct and indirect methods. The database consists of 559 monthly precipitation series, in the period 1917–2006, with an average density of 1 station per 138 km^2 (Figure 1).

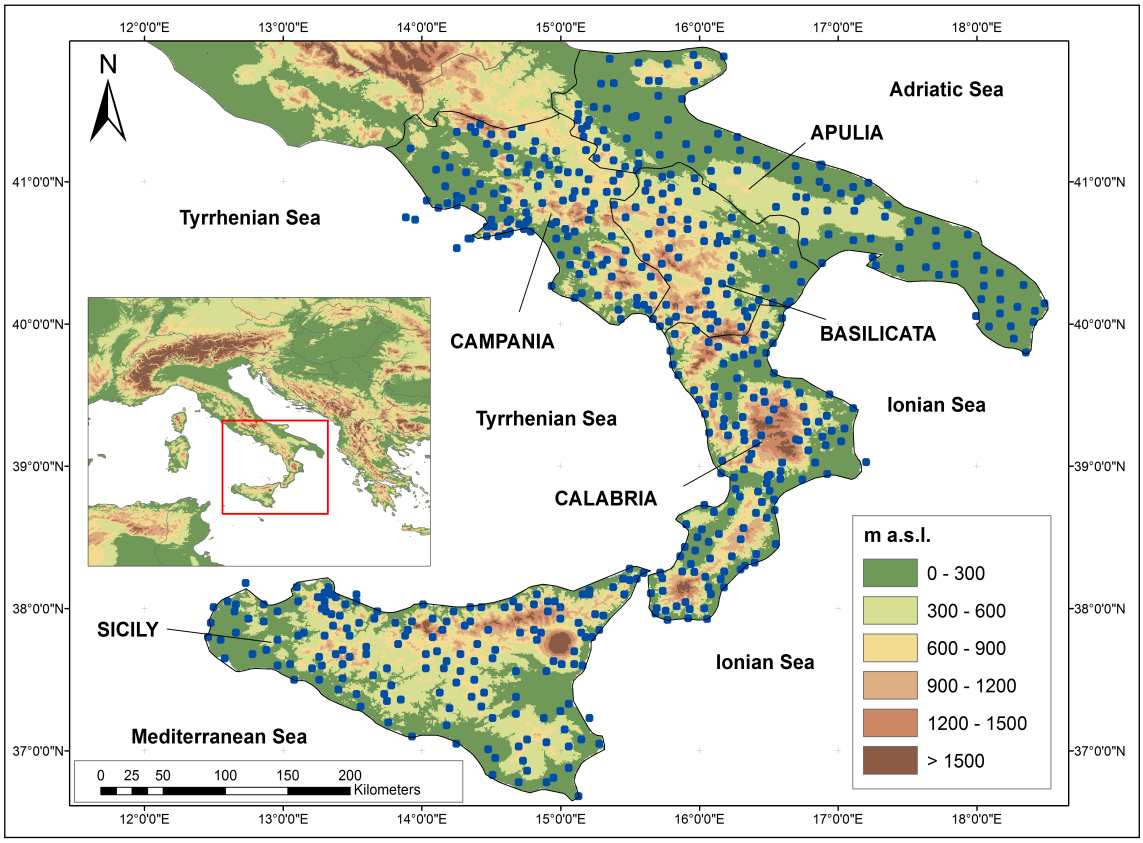

Figure 1. The study area with the localization of the 559 rain gauges

3. METHODOLOGY

The ITA method has been first proposed by Şen (2012) and presents the main advantage that it does not require any assumptions (e.g., serial correlation, non-normality, sample number etc.) as in

case of the non-parametric tests. First, the time series is divided into two equal parts, which are separately sorted in ascending order. Then, the first and the second half of the time series are located on the x-axis and on the y-axis, respectively. If the data are collected on the 1:1 ideal line (45° line), there is no trend in the time series. If data are located on the upper triangular area of the ideal line, an increasing trend in the time series exists. If data are accumulated in the lower triangular area of the 1:1 line, there is a decreasing trend in the time series (Şen, 2012, 2014). Thus, trends of low, medium and high values of any hydro-meteorological or hydro-climatic time series can be clearly identified through this method, even if it does not allow to evaluate the significance of the trends.

4. RESULTS AND DISCUSSION

The aim of this study was to analyse rainfall trend at regional scale in southern Italy. With this aim, for each region, an average rainfall series has been evaluated for every time-scale.

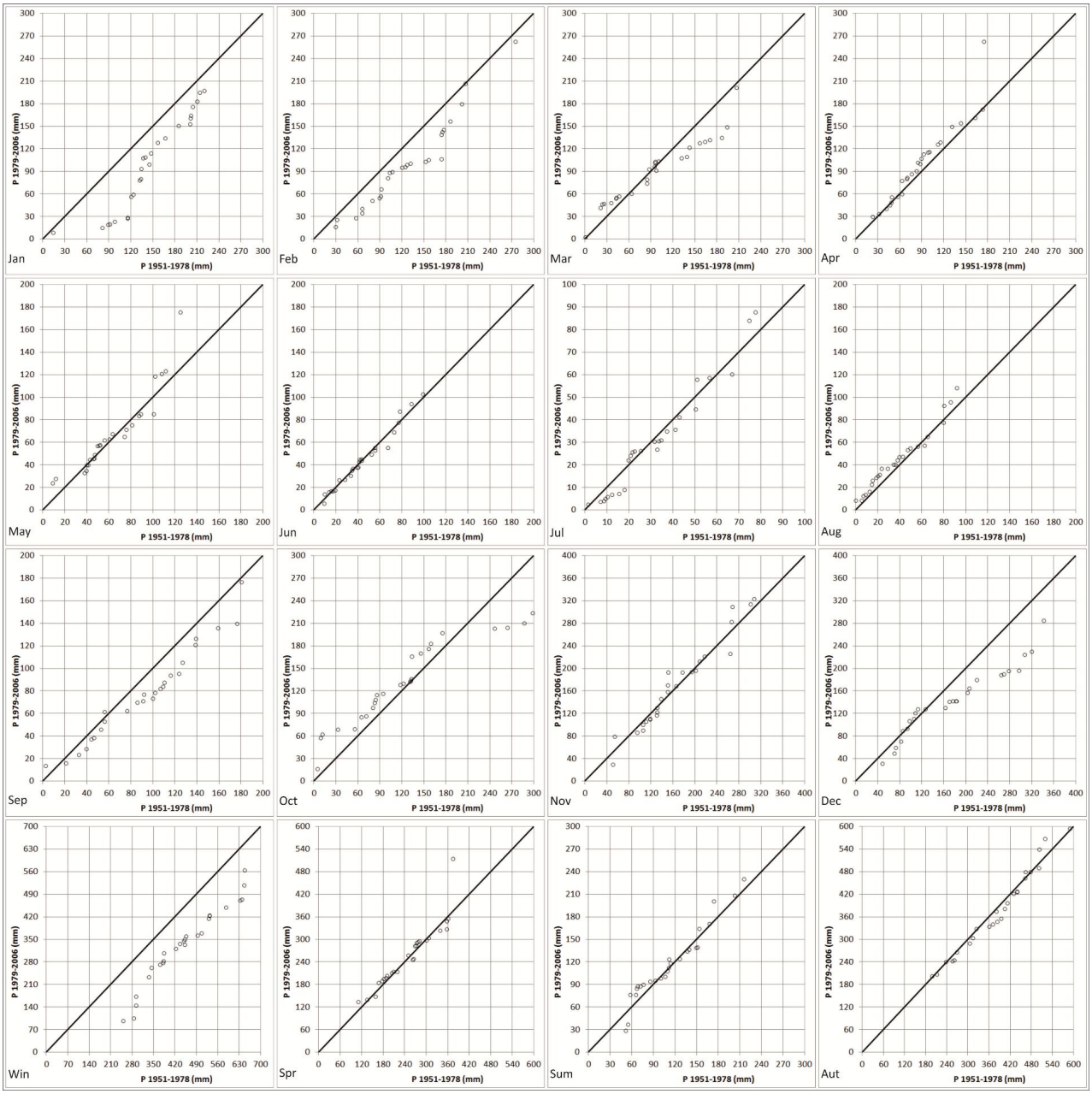

Figure 2. Results of the ITA method for the Campania region.

The results of the Campania region (Figure 2) showed a prevailing negative trend for all the rainfall values (low, medium and high) in January, February, September and in the winter season. A negative trend has also been observed in October and in December but only for the high and for the medium-high values, respectively. Some positive tendencies were detected in March (for the low values) and in October (for the low-medium values). The other months and seasons do not show clear tendencies.

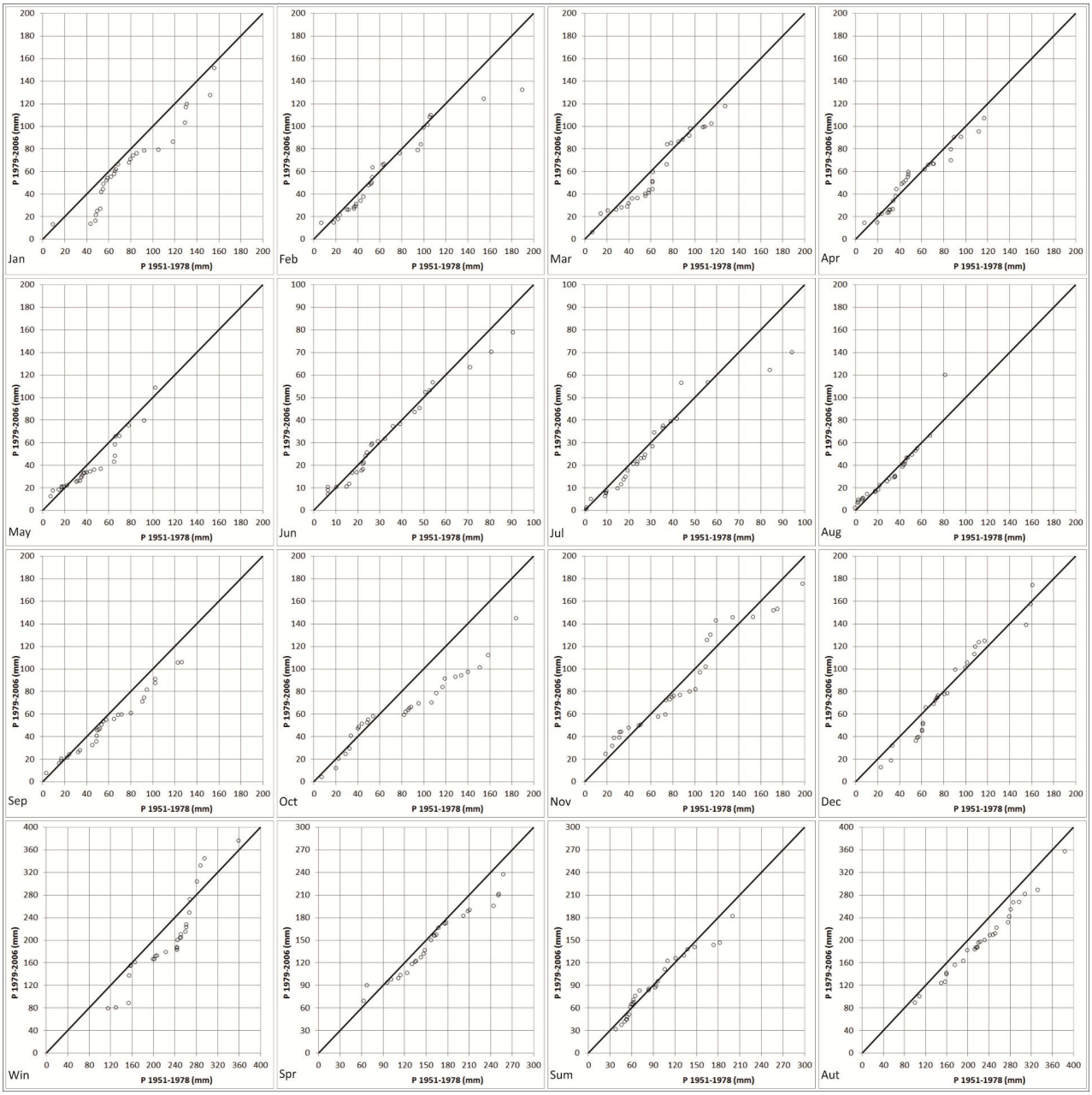

Figure 3. Results of the ITA method for the Apulia region.

Also in Apulia (Figure 3) January and September showed a clear negative trend for all the monthly values. Negative trends, but only for the medium-high values, also appear in February, in October and in the autumn season. Conversely, few positive trends have been evidenced in November (for the medium values) and in the winter season (for the high values).

In the Basilicata region (Figure 4) marked negative trends have been detected in January, in February and in autumn for all the values, in May, in spring and in summer for the medium values, in September and November for the medium-high values, and in October and in winter for the low-medium values. On the contrary, clear positive trends were also evidenced in March, July and in

summer for the medium values, in April and in May for the low values, and in August for all the values.

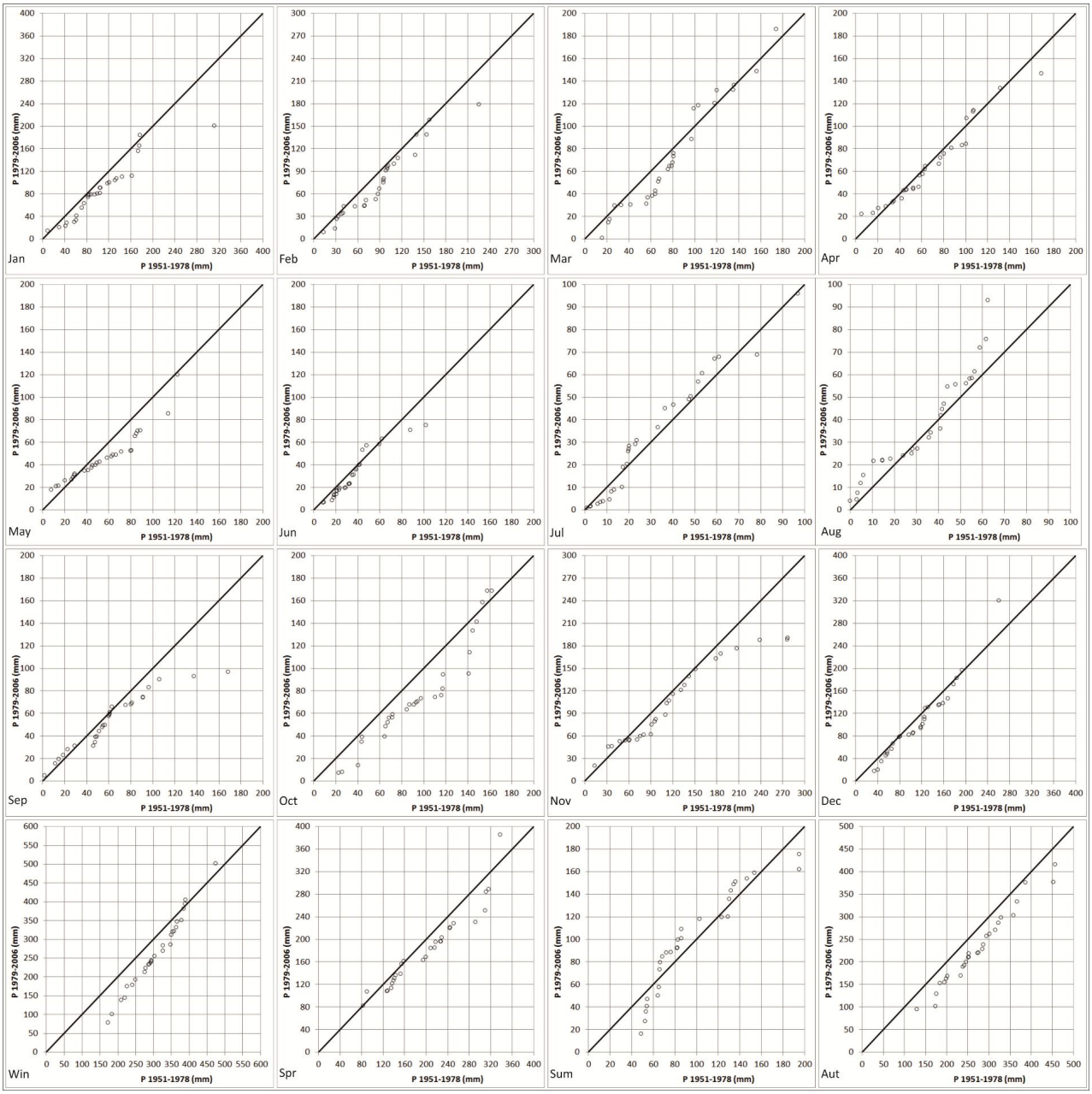

Figure 4. Results of the ITA method for the Basilicata region.

Figure 5 shows the results of the Calabria region, which presented a prevailing negative tendency. This trend behaviour has been evidenced especially in January and winter for the low-medium precipitation, in February, October and in autumn for all the precipitation classes, in May, June and November for the high values, in July only for the medium values. The few positive tendencies were detected in July for the low and high values, in August for the high values, in November for the low values.

Finally, the results for the Sicily region (Figure 6) showed a prevailing negative trend, more evident in February and October for all the values, in March for the low-medium values, in May, September, November, December, in summer and in autumn, especially for high values. Conversely, few positive tendencies were detected in April, August, September and November but only for the low values.

The results for the five regions, with some differences, show a general negative tendency of the

precipitation monthly data. These trends are particularly clear in some winter and autumn months, mostly for the medium and high values. Few positive trends have been evidenced only for the low data of the autumn months. At seasonal scale, a negative trend has been detected in winter and in autumn in the whole study area, whereas not well defined trend signals have been identified in summer and spring.

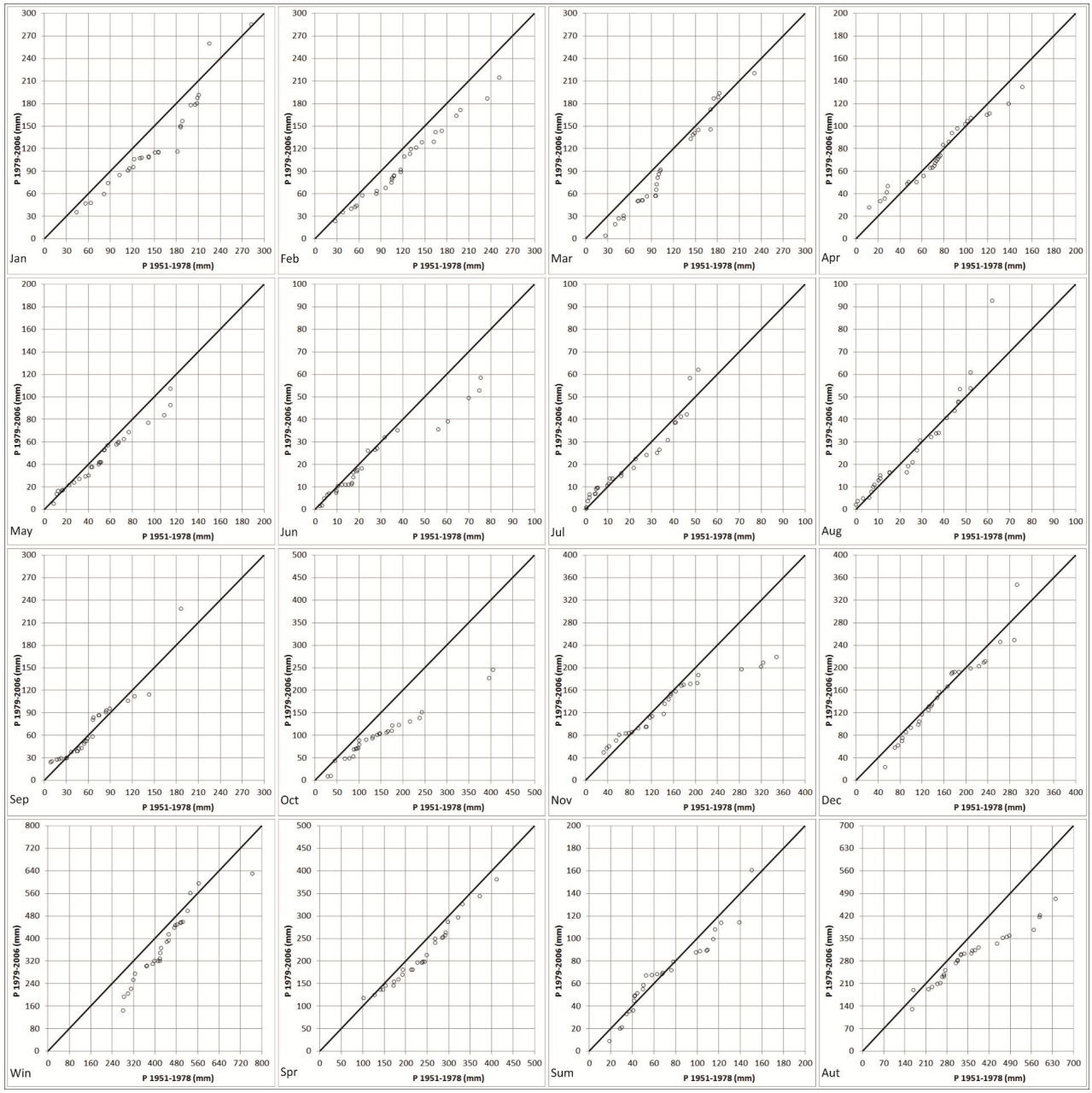

Figure 5. Results of the ITA method for the Calabria region.

5. CONCLUSIONS

This study analyses the temporal changes of the monthly and seasonal rainfall series, recorded in five regions of southern Italy, by means of the ITA technique. By applying this methodology, which allows to detect separately the trends of the low, medium and high precipitation data, it was possible to better explain the clear tendencies previously evidenced in past studies in some of the investigated regions. For example, for the Calabria region, the ITA technique allowed to state that the negative trends in January and in the autumn season, are mainly due to the medium-low values

and, conversely, that the high values contribute to the positive trends in summer. This feature of the ITA methodology is useful because low rainfall values trends are important for water management while high values ones are useful for investigating extreme phenomena, such as flood and soil erosion.

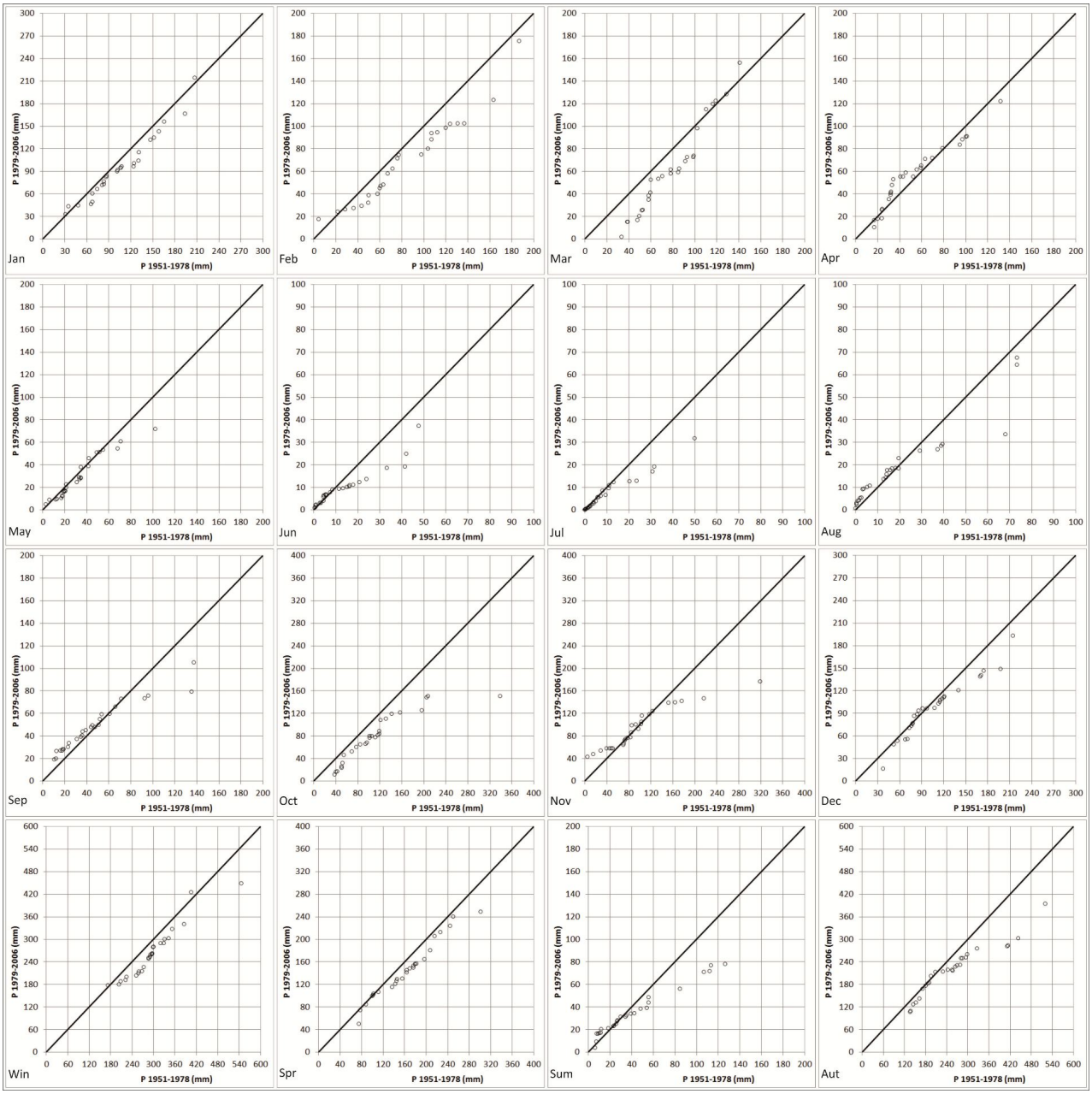

Figure 6. Results of the ITA method for the Sicily region.

REFERENCES

Ay, M. & Kisi, O. 2015 Investigation of trend analysis of monthly total precipitation by an innovative method. Theoretical and Applied Climatology, 120, 617–629.

Brunetti, M., Maugeri, M., Monti, F. & Nanni, T. 2006 Temperature and precipitation variability in Italy in the last two centuries from homogenised instrumental time series. International Journal of Climatology, 26, 345–381.

Caloiero, T., Buttafuoco, G., Coscarelli, R. & Ferrari, E. 2015 Spatial and temporal characterization of climate at regional scale using homogenous monthly precipitation and air temperature data: an application in southern Italy (Calabria Region). Hydrology Research, 46, 629–646.

Haktanir, T. & Citakoglu, H. 2014 Trend, independence, stationarity, and homogeneity tests on maximum rainfall series of standard durations recorded in Turkey. Journal of Hydrologic Engineering, 19, 9.

IPCC 2013 Summary for Policymakers. Fifth Assessment Report of the Intergovernmental Panel on Climate Change. Cambridge University Press, Cambridge

Kisi, O. & Ay, M. 2014 Comparison of Mann–Kendall and innovative trend method for water quality parameters of the Kizilirmak River, Turkey. Journal of Hydrology, 513, 362–375.

Kisi, O. 2015 An innovative method for trend analysis of monthly pan evaporations. Journal of Hydrology, 527, 1123–1129.

Kundzewicz, Z.W. & Robson, A. 2000 World climate program – water. Detecting trend and other changes in hydrological data. WMO/TD-No. 1013. Geneva, WMO.

Liuzzo L., Bono E., Sammartano V. & Freni, G. 2016 Analysis of spatial and temporal rainfall trends in Sicily during the 1921–2012 period. Theoretical and Applied Climatology, 126, 113–129.

Longobardi, A. & Villani, P. 2010 Trend analysis of annual and seasonal rainfall time series in the Mediterranean area. International Journal of Climatology, 30, 1538–1546.

Longobardi, A., Buttafuoco, G., Caloiero, T. & Coscarelli, R. 2016 Spatial and temporal distribution of precipitation in a Mediterranean area (southern Italy). Environmental Earth Sciences, 75, 189.

Martínez-Austria, P.F., Bandala, E.R. & Patiño-Gómez, C. 2015 Temperature and heat wave trends in northwest Mexico. Physics and Chemistry of the Earth, 91, 20–26.

Onyutha, C. 2016 Identification of sub-trends from hydro-meteorological series. Stochastic Environmental Research and Risk Assessment, 30, 189–205.

Piccarreta, M., Capolongo, D. & Boenzi, F. 2004 Trend analysis of precipitation and drought in Basilicata from 1923 to 2000 within a Southern Italy context. International Journal of Climatology, 24, 907–922.

Şen, Z. 2012 An innovative trend analysis methodology. Journal of Hydrologic Engineering, 17, 1042–1046.

Şen, Z. 2014 Trend identification simulation and application. Journal of Hydrologic Engineering, 19, 635–642.

Tabari, H. & Willems, P. 2015 Investigation of streamflow variation using an innovative trend analysis approach in northwest Iran. E-proceedings of the 36th IAHR World Congress, 28 June – 3 July, 2015. The Hague, the Netherlands.

Proceedings of the 10th World Congress of EWRA 'Panta Rhei', 5-9 July 2017, Athens, Greece
© 2017 *European Water Resources Association*

Climate change mitigation and adaptation plan for West Athens

V. Krommyda
Interdisciplinary Programme of Postgraduate Studies "Environment and Development", National Technical University of Athens, Greece
* *e-mail: vakrommyda@outlook.com*

Abstract: Climate change is considered part of the natural variability of Earth's conditions, but anthropogenic amplification of the phenomenon has accelerated the natural processes rapidly. This paper incorporates climate change policies in spatial planning, by developing mitigation and adaptation plan for Athens. The municipalities of West Athens are chosen as the field of focused spatial interventions after the analysis of the wider study area and the mapping of vulnerabilities. The aim of the article is to demonstrate the necessity of a strategic plan, specifically for Athens, which is the largest urban area of Greece. The implementation of that kind of a plan in Athens is highly important due to the large history of natural disasters with fatal results and strong socio-economic vulnerabilities. As it is known, "the best cure is prevention" hence the immediate and active participation of society is required. The main spatial interventions should be focused on creating suitable green and blue infrastructure, because the most likely and most dangerous impacts are related to heat waves and flood events. In conclusion, is regarded necessary to take measures in socioeconomic level in order to protect vulnerable groups as exacerbated inequalities lead to reduced social adaptability to external pressures such as climate change.

Key words: climate change, mitigation, adaptation, strategic plan, West Athens

1. INTRODUCTION

Climate change is considered part of the natural variability of Earth's conditions, but anthropogenic amplification of the phenomenon has accelerated the natural processes rapidly. IPCC defines this phenomenon as follows: "*Climate change refers to any change in climate over the years, either due to natural variability or as a result of human activities*" (IPCC 2007). The topics raised by the upcoming changes should be put on the table immediately as the effects of climate change will accompany the earth's evolutionary processes for hundreds of years (IPCC 2007). According to the multiple research reports by IPCC, climate change impacts are multidimensional and have as a reference space the whole planet, but they vary depending on the characteristics of each territorial entity. The impacts have effects on the natural and human systems (IPCC 2014) and they tend to worse the existing socio-economic disparities in various spatial units (Kyvelou 2010: 88). As a result climate change may disrupt the social strata greatly, especially in the cities through exacerbation of poverty (UN Habitat 2011: 19). Climate change, as a result of the production processes and people's lifestyle, composes a complex challenge that requires the planning process to encompass all the possible future scenarios in conjunction with all the possible impacts depending on the special characteristics of each area (UNDP 2010). Spatial planning is now required to be wider, holistic, participative and visionary and to respond quickly to the current and upcoming challenges (Davoudi 2009).

The Greek institutional framework for spatial planning seems to have a big gap on applicable policies and guidelines on climate change. Although there are theoretical guidelines on climate change, especially in General Framework for Spatial Planning and Sustainable Development (FEK 128 A/03.07.2008), the objectives of mitigation and adaptation are being approached indirectly through guidelines for sustainable development. The Greek legislation is characterized by its large quantity but the problem lies on the quality and the applicability. The use of vague terms such as sustainability (Hopwood 2005) probably creates more confusion on its practical application, while

the policies deriving from the top down result in the rejection of microscale's diversity. In 2015 an attempt conducted in order to change the situation through the National Adaptation Strategy (MEEN 2015). This strategy together with the regional climate change plans, which are being proposed, should be able to sustain the balance between the sectors and not consider only one sector, such as the economy.

2. STUDY AREA

2.1 Current situation in the wider area

The Attica basin constitutes the wider study area and is located in the Region of Attiki. The municipalities of Attica basin (including the municipalities of West Athens) exhibit multilevel inequalities. In demographic terms, the municipalities of Attica basin present a population decline between the years 2001 – 2011 (-6,49%) (Papagiannis, et al 2011: 3-1). Due to the economic crisis is provided that there will be a wave of migration, a declining birth rate (which is already the case for the whole country) and an increased mortality rate (Kalogirou, et al. 2011). At the same time, the declared income earnings reflect the intense disparities. The municipalities of north and south part of Attica basin demonstrate very high incomes while the spatial units of West Athens and Piraeus own the lowest incomes (Kalogirou, et al. 2011, Pantazis and Psycharis 2016). The Attica basin is surrounded by the mountains of Hymettus, Penteli, Parnitha and Aigaleo – Poikilo, while the coastline of the Saronic Gulf is the boundary in the south. These mountains are one of the most important natural resources of the basin, because they provide valuable ecosystems and flood protection; they form appropriate climatic conditions and contribute to the reduction of air pollution (Papagiannis, et al 2011: 3-80). However, they have lost their value as primary forest ecosystems through intensive human interventions. The major problems are related to the pressure from the building processes, fires, deforestation, tourism, soil erosion, intensive road network etc. (Papagiannis, et al 2011: 3-80, 3-81). *Figure 1* depicts the multidimensional vulnerabilities of each municipality in Attica basin by presenting social and biophysical vulnerabilities combined.

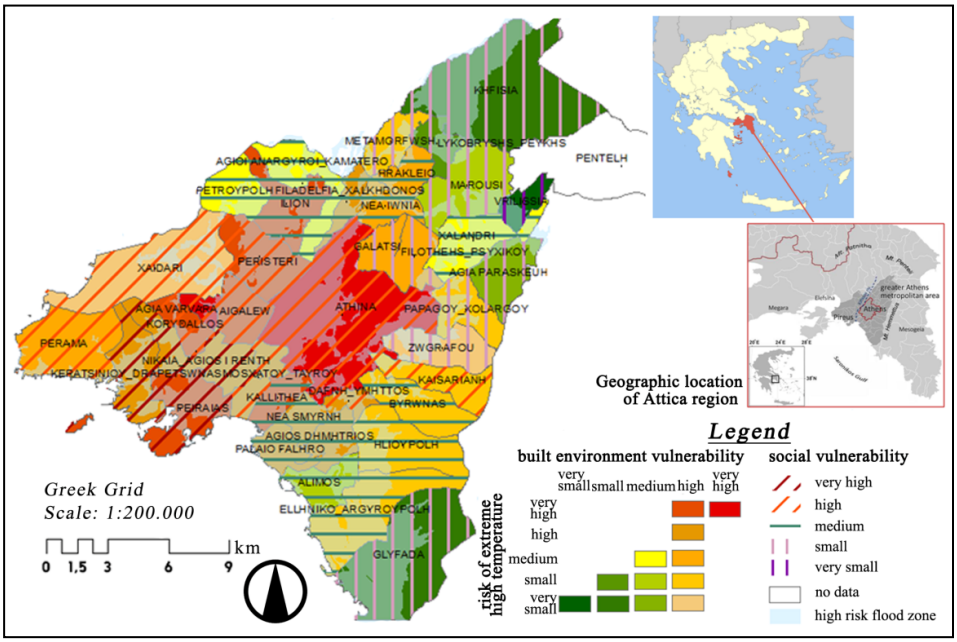

Figure 1. Built environment vulnerability in conjunction with the risk of extreme high temperatures, social vulnerability and high flood risk areas. Source: Krommyda (2015), EL.STAT. (2011), MEEN (2012) and Sapountzaki and Chalkias (2013), adaptation by the author.

Specifically the most economically vulnerable municipalities are located in the Regional Units of Piraeus and West Athens unlike the municipalities of the rest of the basin, which present a better condition. The three municipalities, which combine multilevel and high degree of vulnerability are Athens, Piraeus and Agia Varvara, where in times of heat waves and floods, is estimated that:

- The oldness of built environment will have unpredictable consequences in people's everyday life.
- Socio-economic vulnerabilities may get worse because of the unequal distribution of climate change impacts.
- Vulnerable environmental infrastructure will be further disrupted.

2.2 Focusing on West Athens

After identifying the most vulnerable spatial units (Figure 1), the municipalities of West Athens were chosen as focused study area. Table 1 gives a comprehensive inventory of the current situation in West Athens while Figure 2 shows the situation spatially.

Table 1. Current situation in West Athens.

Sector	Description
Geography	The Regional Unit of West Athens: - is located in the western part of Attica basin - is located nearby the mountains of Aigaleo and Poikilo - is penetrated by the river Kifissos and other streams (east side)
Demography	- Negative population change 2001-2011 [total: -2%, the largest decreases occurred in Agia Varvara:-15,3% and Aigaleo: -10,2%] - Strong emerging aging trend
Society / Economy	Bold socio-economic problems: - social segregation from the rest of Attica basin - unemployment (most of the municipalities have higher unemployment rate than the national average) - low average declared income (lower than the average reported income of Attiki) - increase of migrants
Regulation of space / Urban issues	- Intensely urbanized municipalities with high density and lack of public spaces: Agia Varvara, Aigaleo, Peristeri, Ilion, Agioi Anargiroi - Main land use: mixed - Degraded built environment - Total green spaces: available 1,3 m^2 of urban green space per inhabitant - Open spaces and green areas are as low as 4% of the total area of West Athens - Former quarries on the mountains of Aigaleo and Poikilo are required to be reforested
Risks / Vulnerabilities	- Eshatia's stream is the main recipient of rainwater - The parts that are traversed by Kifisos river are at risk from future floods - Most of the seven municipalities show high vulnerability of the build environment and increased risk of extreme high temperatures (in summer) combined with high social vulnerability (figure 1) - Major vulnerable social groups: elderly, poor families, homeless, children, patients, Roma, migrants

Source: Krommyda and Oikonomou (2016), ASDA (2014), EL.STAT. (2011), MEEN (2012), Lekkas et al. (2010) and Sapountzaki and Chalkias (2013), adaptation by the author.

Many municipalities of West Athens exhibit high vulnerability of the built environment, increased risk of high temperatures and future floods. Especially, the areas located in both sides of Kifissos River and Eshatia stream indicate very high flood risk. In socioeconomic level, problems like social segregation, high unemployment rates and low average declared income affect negatively the adaptive capacity of society. Moreover, high urbanized areas with high density, degraded built environment and lack of open spaces create unsustainable living conditions.

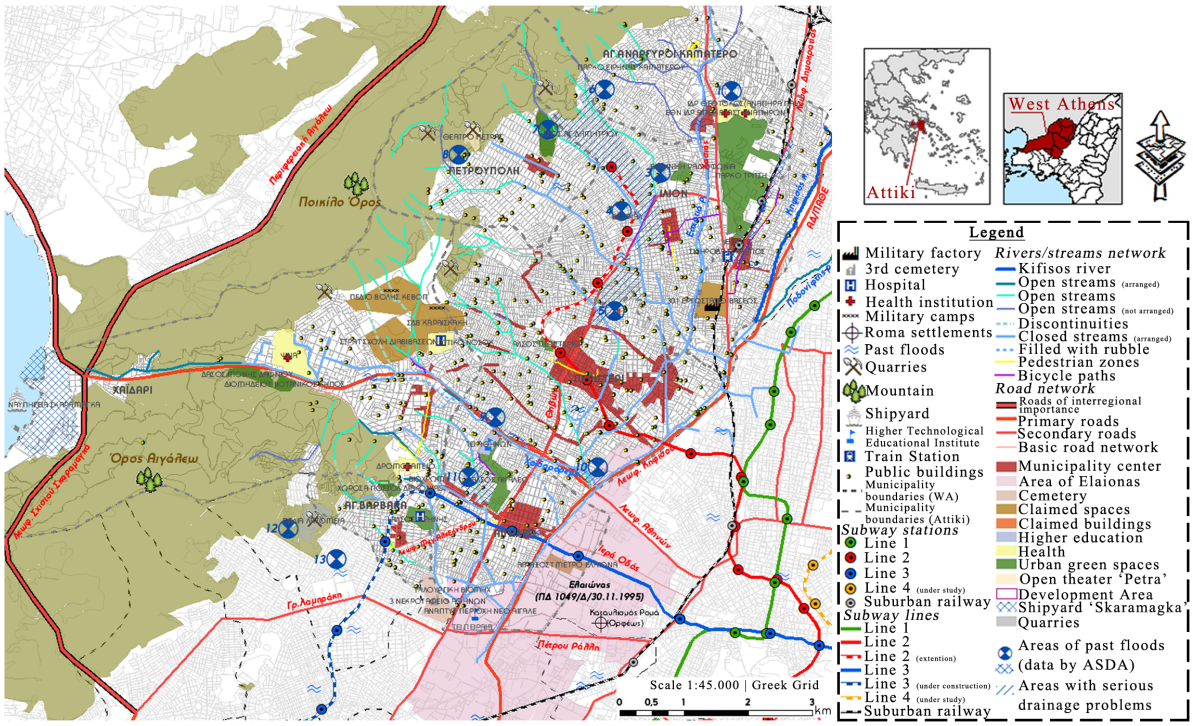

Figure 2. Current situation in West Athens. Source: Krommyda (2015), ASDA (2007), MEEN (2012), adaptation by the author.

3. PLANNING FOR CLIMATE CHANGE

3.1 The broader strategy

The tackling measures for climate change may apply to all governance levels (international, national, local), however empirical data show that mitigation acts mainly on the international and national scale, while adaptation has application on the local level (Wilson and Piper 2010: 95-96). This hierarchy of static scales is relatively unstable and may result in a complex process in which different levels of governance can use "climate change" as an argument in order to claim legitimacy on different governance scales (Wilson and Piper 2010: 100). Within this fuzzy and evolving framework, a 'Climate change mitigation and adaptation plan' is created in order to address the ongoing issue of climate change in Athens. It should be noted that the primary plan included 155 measures (spatial and intangible measures) for the whole of Attica basin, but this paper focuses on the spatial interventions particularly in the municipalities of West Athens.

The strategic direction for climate change mitigation defines Athens as "Climate Neutral City". According to UNEP (2009), climate neutrality means that there is no production of complex greenhouse gases and as a result the emissions are the minimum possible. A city can be considered climate neutral if its emissions do not have any effects on the threshold of 2°C (Reusswig et al 2014). In order to achieve this strategy, the following objectives are set:

M.1/ Energy supply and energy infrastructure
M.2/ Energy efficiency of buildings
M.3/ Social awareness and consumption
M.4/ Sustainable mobility and traffic congestion
M.5/ Urban Planning and Infrastructure
M.6/ Industry
M.7/ Economy and Innovation
M.8/ Waste Management

On the other hand, the adaptation will be based on the strategic direction which defines Athens as "Climate Resilient City". The specific objectives for this strategy are:

A.1/ Flood protection
A.2/ Protection from extreme high temperatures
A.3/ Network of green and blue infrastructure
A.4/ Informing citizens
A.5/ Special measures for vulnerable social groups

The goal of the both strategies is not to maintain the status quo, but to integrate the appropriate measures that will facilitate change. The form of such a plan is not foreseen by the Greek legislation, therefore is considered necessary to be an integral part of an overall strategic plan. This plan must be consistent with the guidance given by the 2nd National Climate Change Program (MEEN 2002), National Adaptation Strategy (MEEN 2015) and the Regulatory (Master) Plan for Athens. At the same time, coordination with the other sectoral plans and cooperation for the effective implementation of the cross-sectoral measures are necessary.

3.2 Action plan

The following inputs were used for the adequate composition of the action plan:

- 2nd National Climate Change Program (2002)
- Regulatory (Master) Plan for Athens
- Similar climate change plans of other countries' cities
- Relevant IPCC studies
- Studies by ICLEI
- UN studies

It should be noted that the greatest success of such a plan would become possible if citizens participate actively in every stage of the process (constant interaction, feedback process, participatory selection of objectives and implementation). The Action plan, which includes 15 spatial interventions, is attributed in Table 2*,* while Figure 3 shows the mapping of these measures.

Table 2. Action plan – spatial interventions for West Athens.

Objectives	Measures	Spatial interventions (description)
[M.4] Promoting public transport	Expansion of the subway network (**M1**)	Extension of subway network in Peristeri - Ilion, Ag. Varvara – Piraeus.
[M.4, M.5] Increase of pedestrians and bicycle use	Improving cycling infrastructure by increasing the number of cycle paths, while the existing cycle paths will be widened and upgraded (**M2**)	Combination with the measure AM8 and AM10. The aim is to link municipalities' centers and their recreational areas. The proposed bicycle network reaches 15.6 km. Bike rental stations and secure parking places are considered crucial. It is necessary to upgrade the pedestrian zones and sidewalks in order to create a better urban environment that will give impetus to cycling and hiking. [Areas of intervention: Agioi Anargiroi – Kamatero, Ilion, Petroupoli, Peristeri, Ag. Varvara, Haidari]
[A.1, A.2, A.3] Increasing the carbon storage capacity (sinks)	Retrieving woodlands through reforestation (**A1**)	Combination with the measure AM9. Quarries rehabilitation in Poikilo Mt. and conversion into green enclaves. Relocation and usage conversion of military camps in Haidari (SDV Karaiskaki A and firing range field KEVOP) and Agioi Anargiroi (301 military factory). [Areas of intervention: Agioi Anargiroi – Kamatero, Ilion, Petroupoli, Peristeri, Ag. Varvara, Haidari]
[M.2, A.3] Public buildings and facilities	Acquisition of former factories, use for cultural and leisure activities while the design of the buildings to be based on bioclimatic principles (**AM1**)	Acquisition of the former factories (which have no current use): BIOCHROM (located in Agia Varvara) and BIOFIAL (located in Ilion) - conversion into supralocal culture centers. The new buildings should serve as good examples of bioclimatic design (green surfaces and roofs).
[A.1, A.3, M.5] Flood protection	Continuous surface and underground network for rainwater collection (and storage) connected to underground pipelines. Connection between the surface transmission network and the streams (**AM2**)	Creation of additional rainwater network, especially in areas with drainage problems (*figure 2*): - Petroupoli: Ag. Triados St. - Ilion, Peristeri: Thivon St., Konstantinoupoleos St., Chiou St. - Andrea Papandreou St., Ag. Nikolaou – Elaion – Idomenos - Kamaterou St. - Peristeri: Athinon Av. – Sfakion St., junction of Kavala St. -Athinon Av. (Haidarorema), junction of Kyprou – Dionisiou Solomou St. - Aigaleo: Edessis St. – Koritsas St. - Agioi Anargiroi – Kamatero: central square and Bibiza St.

Objectives	Measures	Spatial interventions (description)
[A.1, A.2, A.3, M.5] Flood protection	Rehabilitation and reformation of the riverbed's open parts of Kifissos river and its tributaries (**AM3**)	Regeneration of Kifissos' uncovered riverside areas (from Attiki Odos to the military factory in Ag. Anargiroi - length 5.6 km). The same applies to the open section of the Eshatias' stream (Ag. Anargiroi– Kamatero).
[A.1, A.2, A.3, M.5] Flood protection	Design of linear parks in the uncovered riverside areas (**AM4**)	Directly related to the measure AM3. Design of linear parks in the uncovered riverside areas of Kifissos river and its tributaries (Ag. Anargiroi– Kamatero).
[A.1, A.3, M.5] Flood protection	Implementation of a sustainable urban drainage system with permeable pavement, green roofs on buildings, rainwater retention ponds, artificial wetlands and ditches (Sustainable Drainage Systems -SUDS) (**AM5**)	Adequate infrastructures in areas with drainage problems (the same areas that are mentioned in the description of measure AM2). [Areas of intervention: Agioi Anargiroi – Kamatero, Ilion, Petroupoli, Peristeri, Ag. Varvara, Haidari]
[A.1, A.3, M.5] Flood protection	Use of water reservoirs for the accumulation of water that comes from the mountains (**AM6**)	Water accumulation of the eastern slopes of Poikilo Mt. near the residential zone. [Areas of intervention: Agioi Anargiroi – Kamatero, Ilion, Petroupoli, Peristeri, Haidari]
[A.1, A.2, A.3, M.5] Flood protection	Integrated system for collection, storage and rainwater transfer (**AM7**)	Rainwater collection sites connected to the rainwater reservoirs network. [Areas of intervention: Agioi Anargiroi – Kamatero, Ilion, Petroupoli, Peristeri, Ag. Varvara, Haidari, Aigaleo]
[A.1, A.2, A.3, M.5] Increase of green spaces	Conversion of the roads into green corridors throughout the municipalities (**AM8**)	Networking green areas and public spaces - converting road expressways to green corridors: - Peristeri: Konstantinoupoleos Av. – Kyprou – Ethn. Makariou – tsaldari Av. – Anapafseos – Ag. Ierotheou –Ksenokratous – Ioanninon – Poikilo Mountain (theatre of 'Foinikas') - Haidari, Aigaleo: Iera Odos to Athinon Av. - Agioi Anargiroi – Kamatero, Ilion, Petroupoli: An. Papadreou Av. – Anatol. Romilias - Poikilo Mountain (theatre of 'Petra') - Agioi Anargiroi – Kamatero: Dimokratias Av.-Ir. Politechniou-Chasias-Eshatia stream-Filis - Agia Varvara: Meg. Alexandrou Av.-El. Venizelou Av. - Aigaleo, Peristeri: Thivon to Tsaldari Av. - Agioi Anargiroi – Kamatero, Peristeri: Har. Trikoupi-Solomou-Troon-Astrous to An. Papandreou Av. - Creation of pocket parks
[A.1, A.2, A.3, M.5] Increase of green spaces	Creation of metropolitan parks across the city (**AM9**)	- Regeneration of Elaionas' area and space acquisition for the creation of extensive green areas - Relocation and usage conversion of military camps in Haidari (SDV Karaiskaki A and firing range field KEVOP) and Agioi Anargiroi (301 military factory) - Quarries rehabilitation (Poikilo Mt.) and conversion into green enclaves - Aigaleo and Poikilo Mt. as supralocal green poles for recreation / culture /sports
[A.1, A.2, A.3, M.5] Increase of green spaces	Strengthening and planting of hedgerows along the sidewalks (**AM10**)	In combination with the measure AM8. [Areas of intervention: Agioi Anargiroi – Kamatero, Ilion, Petroupoli, Peristeri, Ag. Varvara, Haidari, Aigaleo]
[A.1, A.2, A.3, M.5] Increase of green spaces	Upgrading of the existing degraded green areas (**AM11**)	Upgrading of the Environmental Awareness Park 'Antonis Tritsis' (Agioi Anargiroi – Kamatero, Ilion)
[A.1, A.2, A.3, M.5] Increase of green spaces	Private and public urban gardens (**AM12**)	Creation of urban gardens in the Environmental Awareness Park 'Antonis Tritsis', on specific sites of Aigaleo and Poikilo Mt. and in Elaionas' area. Cultivation of 'pilot gardens' in public buildings' roofs. [Areas of intervention: Agioi Anargiroi – Kamatero, Ilion, Petroupoli, Peristeri, Ag. Varvara, Haidari, Aigaleo]

Source: Papagiannis, et al. (2011), Vlastos, et al. (2011), Reeve and Kingston (2014), Parmenidis et al. (2013), Rotterdam Office for Sustainability and Climate Change (2009 and 2010), British Graduates Society (2007), Lekkas et al. (2010), adaptation by the author.

4. FURTHER DISCUSSION

This article indicates that a plan for climate change must have a clear theoretical basis in order to identify sufficiently the guidelines and the action plan's measures. The main barrier lies on the "immaturity" and ambiguity of nodal terms such as resilience, adaptive capacity, vulnerability, etc. (Magnan 2010). At the same time, the relationship between local initiatives (microscale) and national or international strategies (macroscale) usually shows opposite results (Smit and Wandel

2006). This problem must be fully addressed as it leads to the strengthening of vulnerabilities and shifts the risks to the wider social strata (Sapoutzaki 2014). Additionally, the citizens' active involvement is crucial in the planning process as they are the ones who will be called upon to implement the measures.

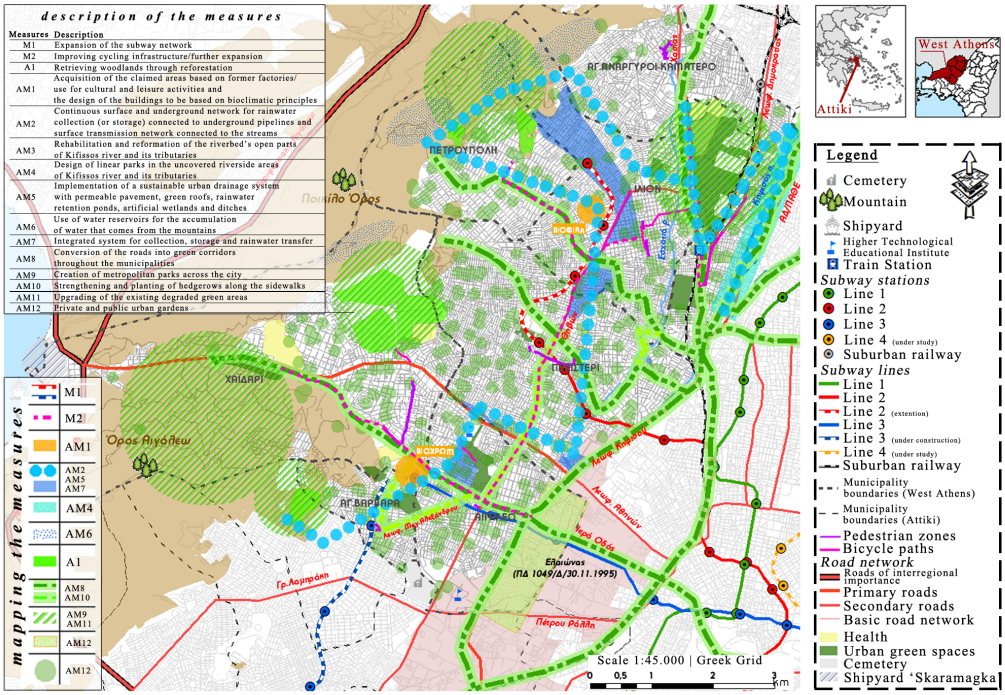

Figure 3. Spatial intervention proposals for climate neutrality and resiliency in West Athens. Source: Krommyda (2015), adaptation by the author.

As the Action Plan showed, the core idea of the spatial interventions is the proliferation and the upgrading of the green and blue infrastructure. This will lead to the enhancement of the absorption, collection and storage capacity of rainwater. In addition, the rational management of water will contribute to the prevention of catastrophic flooding, while the stored rainwater could be used for the irrigation needs. Furthermore, the urban green spaces and suburban green areas will function as enhanced "green ventilation systems" and as filters for retaining gaseous pollutants. These interventions are based on the principles of environmental planning and aim to improve the microclimate of the area, while the creation of "green routes" will increase the adaptive capacity of the urban systems and will form a better urban environment. Moreover, the Action Plan aims at providing the optimal interconnection between the municipalities, while the configuration of reachable and accessible neighbourhoods is attempted. The overall goal is to reinforce the resilience of society along with the other urban systems by not only territorial changes, but also changing the contemporary individualistic culture. This change is considered crucial and the first step for its achievement is regarded to be the active participation of citizens in public affairs.

REFERENCES

ASDA - Development Association of Western Athens. (2007). Map of rivers and streams in West Athens. Available at: http://home.asda.gr/LatestNews.aspx?ModuleID=688 (accessed 20.1.2017) (in Greek).

ASDA - Development Association of Western Athens. (2014). Preliminary Analysis Report and Strategy for the 'Integrated Urban Development Plan' of West Athens. Available at: http://home.asda.gr/soap/4part.pdf and http://home.asda.gr/soap/1part.pdf (accessed 20.1.2017) (in Greek).

British Graduates Society (2007). Environmental analysis and proposals towards a sustainable planning and development strategy - Kifissos…The Athens River. Available at: https://www.bgs.gr/lq-files/pdf/Kifissos%20Presentation_BGS-SITE-FINAL3.pdf (accessed 20.1.2017).

Davoudi, S. (2009). Framing the role of spatial planning in climate change. Electronic working paper N° 43, GURU. Available at: http://www.ncl.ac.uk/media/wwwnclacuk/globalurbanresearchunit/files/electronicworkingpapers/ewp43.pdf (accessed 20.1.2017).

EL.STAT. (2011). Population and Housing Census. Available at: http://www.statistics.gr/2011-census-pop-hous (accessed 20.1.2017).

General Framework for Spatial Planning and Sustainable Development. (2008). FEK 128 A/03.07.2008. Athens (in Greek).

Hopwood, B. et al. (2005). Sustainable Development: Mapping Different Approaches. Sust. Dev. 13, 38–52 (2005). John Wiley & Sons, Ltd and ERP Environment. DOI: 10.1002/sd.244.

IPCC. (2007). Fourth Assessment Report. Working Group I - The Physical Science Basis. Available at: https://www.ipcc.ch/publications_and_data/ar4/wg1/en/tssts-2-1.html (accessed 20.1.2017).

IPCC. (2014). Summary for policymakers, Climate Change 2014: Impacts, Adaptation, and Vulnerability. Part A: Global and Sectoral Aspects. Contribution of Working Group II to the Fifth Assessment Report of the IPCC [Field et al. (eds.)]. Cambridge, United Kingdom and New York, USA: Cambridge University Press.

Kalogirou, S., Tragaki, A., Tsibos, K., Moustaki, E. (2011). Final Report of the Study: "Spatial Income Inequalities, Growth and Poverty in Greece". Public Benefit Foundation Program J. S. Latsis: Scientific Studies 2011. Available at: http://gisc.gr/docs/FinalReport_GR_Skalogirou_et_al.pdf (accessed 20.1.2017) (in Greek).

Krommyda, V. (2015). Climate change and economic development in the regions of EU mediterranean countries. Case study: Planning for climate change in Attica. Bachelor's thesis. University of Thessaly. Volos (in Greek).

Krommyda, V. and Oikonomou, D. (2016). Planning for climate change in Attica. Mitigation and adaptation measures for West Athens. 9th Panhellenic conference of HellasGIs. 8-9 December 2016. Athens (in Greek).

Kyvelou, S. (2010). From spatial planning to spatial management - the concept of strategic spatial planning and territorial cohesion in Europe. Athens: Ekdoseis Kritiki (in Greek).

Lekkas, E. (scientific director), et al. (2010). Operational organization for civil protection and response to natural and environmental risks in municipalities of West Athens. Phase A: Flood Risk Reduction Projects. Applied research project by ASDA and the University of Athens. Athens. Available at:. https://home.asda.gr/PdfFiles/Publications/FysikoiKindynoi/01_Draseis_Meiosis_plimirikou_kindinou_2010.pdf (accessed 20.1.2017) (in Greek).

Magnan, A. (2010). For a better understanding of adaptive capacity to climate change: a research framework. Analyses No 02/10. IDDRI – Sciences Po.

Ministry of Environment and Energy - MEEN. (2002). National Programme for Reducing GHG Emissions 2000 – 2010. 2nd National Climate Change Program. Athens. Available at: http://www.env-edu.gr/Documents/Εθνικό Πρόγραμμα Μείωσης Αερίων Θερμοκηπίου 2000-2010.pdf (accessed 20.1.2017) (in Greek).

Ministry of Environment and Energy - MEEN. (2012). Identifying Areas with Potentially High Risk of Flood. Available at: http://www.ypeka.gr/Default.aspx?tabid=252 (accessed 20.1.2017) (in Greek).

Ministry of Environment and Energy – MEEN. (2015). National Adaptation Strategy. Law 4414/2016. Available at: http://www.ypeka.gr/LinkClick.aspx?fileticket=crbjkiIcLlA%3d&tabid=303&language=el-GR (accessed 20.1.2017) (in Greek).

Pantazis, P. and Psycharis, G. (2016). Residential segregation based on taxable income in the metropolitan area of Athens. Maloutas, Th. and Spyrellis, S. (eds). Athens Social Atlas. Electronic collection of documents and visual material. Available at: http://www.athenssocialatlas.gr/en/article/income-groups/ (accessed 20.1.2017).

Papagiannis, Th., et al. (2011). Strategic Environmental Assessment of Athens' Regulatory (Master) Plan for 2021. Planning Organization. Athens. Available at: courses.arch.ntua.gr/fsr/141464/SMPE%20-%20FINAL_RSA%202021-1.pdf (accessed 20.1.2017) (in Greek).

Parmenidis, G., et al. (2013). Investigation of strategies for networking urban interventions in the metropolitan center of Athens. Phase B: Specifications for nodal interventions. Administration of Attiki Region and NTUA. Athens. Available at: https://www.arch.ntua.gr/sites/default/files/resource/4540_/b_phase.pdf (accessed 20.1.2017) (in Greek).

Reeve, K. and Kingston, R. (2014). Green Works for Climate Resilience: A Guide to Community Planning for Climate Change. National Wildlife Federation, Washington, DC.

Reusswig, F., Hirschl, B. and LassSpecial, W. (2014). The Feasibility Study 'Climate-Neutral Berlin 2050'. Berlin: Senate Department for Urban Development and the Environment.

Rotterdam Office for Sustainability and Climate Change. (2009). Rotterdam Climate Proof – Adaptation Programme 2009. Available at: http://www.deltacities.com/cities/rotterdam/climate-change-adaptation (accessed 20.1.2017).

Rotterdam Office for Sustainability and Climate Change. (2010). Rotterdam Climate City – Mitigation Action Programme 2010. Available at: http://www.rotterdamclimateinitiative.nl/documents/ENG-mitigation-annual-plan2010.pdf (accessed 20.1.2017).

Sapountzaki, K. (2014). A conversation with Sapountzaki in search for a fair and sustainable city. Kafkalas, G. (editor). Available at: http://gkafkala.webpages.auth.gr/site/wp-content/uploads/2014/08/ΚΑΛΛΙΟΠΗ-ΣΑΠΟΥΝΤΖΑΚΗ-ΓΙΑ-ΤΗ-ΔΙΚΑΙΗ-ΚΑΙ-ΒΙΩΣΙΜΗ-ΠΟΛΗ1.pdf (accessed 20.1.2017) (in Greek).

Sapountzaki, K. and Chalkias, C. (2013). Urban geographies of vulnerability and resilience in the economic crisis era – the case of Athens. ITU A|Z. VOL: 11, NO:1, 36-58, 2014-1. Available at: http://www.az.itu.edu.tr/azvol11no1web/07-SapountzakiChalkias-1101.pdf (accessed 20.1.2017).

Smit, B. and Wandel, J. (2006). Adaptation, adaptive capacity and vulnerability. Global environmental change 16 282-292. Elsevier Ltd. DOI: 10.1016/j.gloenvcha.2006.03.008.

UN Habitat - United Nations Human Settlements Programme. (2011). Global report on human settlements – Cities and climate change: policy directions. London & Washington: Earthscan.

UNDP - United Nations Development Programme. (2010). Mapping Climate Change: Vulnerability and impact scenarios-A guidebook for sub-national planners. New York: United Nations Development Programme.

UNEP (2009). Hirsch, T. (writer). A Case for Climate Neutrality - Case Studies on Moving Towards a Low Carbon Economy. Nairobi.

Vlastos, Th., et al. (2011). Research for urban and traffic planning, specializing in cycling network design for long journeys (Part of the Regulatory Master Plan of Athens 2021). NTUA. Athens (in Greek).

Wilson E. and Piper J. (2010). Spatial Planning and Climate Change. Oxon & New York: Routledge.

Proceedings of the 10th World Congress of EWRA 'Panta Rhei', 5-9 July 2017, Athens, Greece
© 2017 *European Water Resources Association*

Spatiotemporal evaluation of reanalysis and in-situ surface air temperature over Ethiopia

T.W. Tesfaye*, C.T. Dhanya and A.K. Gosain
Department of Civil Engineering, Indian Institute of Technology Delhi, New Delhi-110016, India
* *e-mail: tewodros2002@gmail.com*

Abstract: Water resources management and modelling studies are often constrained by the scarcity of observed data, especially of the two major variables i.e., precipitation and temperature. Modellers, hence, rely on reanalysis datasets as a substitute; though its performance heavily vary depending on the data availability and regional characteristics. The present study aims at examining the ability of frequently used reanalysis datasets in capturing the spatiotemporal characteristics of maximum and minimum surface temperatures over Ethiopia and to highlight the biases, if any, in these over Ethiopian region. We considered ERA-Interim, NCEP 2, MERRA and CFSR reanalysis datasets and compared these with temperature observations from 15 synoptic stations spread over Ethiopia. In addition to the long term averages and annual cycle, a critical comparison of various extreme indices such as diurnal temperature range, warm days, warm nights, cool days, cool nights, summer days and tropical nights are also undertaken. Our results indicate that, the performance of CFSR followed by NCEP 2 is better in capturing majority of the aspects. ERA-Interim suffers a huge additive bias in the simulation of various aspects of minimum temperature in all the stations considered; while its performance is better for maximum temperature. The inferior performance of ERA-Interim is noted to be only because of the difficulty in simulating minimum temperature.

Key words: ERA Interim; NCEP Reanalysis; MERRA; CFSR; Diurnal temperature range; reanalysis performance

1. INTRODUCTION

The absence of representative climatic variable datasets for conducting extensive analyses in various hydrologic and climatic simulations, prompted the development of alternate data sources. Reanalysis is an approach that uses a widespread collection of observational data from various sources to appraise a modelling process to produce a temporally and spatially continuous global (or regional) best estimate of numerous atmospheric, terrestrial and oceanographic parameters. An advantage of reanalyses is that they provide data that cover the entire world or a region of interest (in the case of regional reanalysis). Reanalysis data are classified into three major phases corresponding to the advancements in the observing system: the 'early' period from 1940 to 1957, when the first upper air observations were established; the 'modern radiosonde network' era from 1958 to 1978; and the era of 'modern satellite' from 1979 to present (Kistler et al. 2001). Most frequently used reanalysis datasets are: European Centre for Medium-Range Weather Forecasts (ECMWF's) ERA-40 (Uppala et al. 2005) and ERA-interim (Dee et al. 2011), NASA's Modern-Era Retrospective Analysis for Research and Applications (MERRA) (Rienecker et al. 2011), Japanese Meteorological Agency's JRA-55 (Ebita et al. 2011; Kobayashi et al. 2015), NOAA National Center for Environmental Prediction's NCEP/NCAR Reanalysis I (Kalnay et al. 1996), NCEP-DOE Reanalysis 2 (Kanamitsu et al. 2002) and NCEP Climate Forecast System Reanalysis (CFSR) (Saha et al. 2010; Saha et al. 2014). Two variables of prime importance are precipitation and temperature. Our previous study on reanalysis precipitation had established the superiority of ERA-Interim and CFSR datasets in simulating the spatiotemporal characteristics of Ethiopian daily precipitation (Tewodros et al., unpublished manuscript, 2016). Usage of CFSR is also recommended by Dile and Srinivasan (2014) through hydrological modelling of data scarce upper Blue Nile basin. In this study, we focus on the performance of reanalysis datasets in simulating daily surface temperature over Ethiopia.

Studies have reported consistent warming trends in the maximum and minimum temperatures over Ethiopia, in the past decades. Minimum temperature has been increasing faster than the maximum temperature, which is an indication of warmer nights over this region (Mengistu and Lal 2014). This is consistent with the global increase of minimum and maximum temperatures (Easterling et al. 1997; Vose et al. 2005). While global minimum temperature increased around 0.01°- 0.02°C year^{-1}, global maximum temperature increased around 0.01 - 0.015°C year^{-1} over the last two decades. Gebrehiwot and Veen (2013) reported that the northern part of Ethiopia is warming faster than the national average of 0.02°C year^{-1}. At the same time, an increase of about 0.037°C year^{-1} over Ethiopia is also reported by McSweeney et al. (2010), considering the data over the period 1957-2005. Another aspect of temperature, the diurnal range, has decreased worldwide for the last four to five decades (Dai et al. 1999). Decrease in the diurnal temperature range (DTR) is approximately equal to the increase of mean temperature (Karl et al. 1993). In most of the regions, the decrement in DTR is due to the higher rate of increase in night time minimum temperature when compared that of maximum temperature (Easterling et al. 1997; Horton, 1995; IPCC, 2013). Spatially, high diurnal temperature variations are observed in arid areas and low diurnal temperature variations are characteristic of low lying humid areas. Contrary to other East Africa countries, Ethiopia experiences relatively cool temperatures due to the highland areas (Washington et al. 2012). Hence, elevation is an important element in determining the climate of Ethiopia, with temperature dropping about 6.5°C for every 1 km rise. In addition, favourable wind directions and cloud cover further lowers the temperatures in daytime, at higher elevations, even during dry season.

In addition, continent in compliance with the global average surface temperature rise in the range of 2°C to 4.5°C had reported an increase more than 3°C over African. This will result in an increase in frequency of hot days and decrease in frequency of cold days (IPCC, 2013). Global Climate Model historical projections over east Africa also replicated a warmer future (Washington et al. 2012). Future projected increase in surface temperature is found to be consistent irrespective of the emission scenarios considered.

In climatic research, examination of extreme temperature is far more important than the mean. East Africa is characterized by a diverse natural vegetation and varied topography. Temperature and rainfall, hence, widely vary from place to place within a short extent and with the temperature increasing and precipitation fluctuations, water availability and crop production are likely to decrease in the future (Khan, 2009). The extreme temperature fluctuations result in reduction in crop yields. The increase in temperature has an effect on physiology, biochemistry and gene regulation pathways of plants (Bita and Gerats, 2013). Crops able to resist to higher temperature will be favoured and those that resist cooler temperature will be affected. Under this context, it is worthwhile to note the recent reporting of increase in warm extremes and decrease in cold extremes (Omondi et al. 2014). It is further shown that the frequency of warm days and nights are increased, with a significant increase in the number of warm nights per year. As discussed above, while a few studies have investigated the climate change impact assessment and future temperature scenarios, the performance of reanalysis datasets in simulating different aspects of temperature and increasing trend of extremes have not been analysed over the region. Past studies over this region had either not focussed on the simulation of extremes as a performance criterion or had considered a short period of time (Mekasha et al. 2014).

Realizing the importance of availability of reliable climatic datasets which effectively simulates the extreme episodes, in the present study, it is aimed to investigate the performance of frequently used reanalysis datasets in simulating different aspects of daily minimum and maximum temperature over Ethiopia. Hence, the objective of the study is to identify the best reanalysis dataset that provides a realistic representation of observed in situ surface minimum and maximum temperatures. The efficacy of reanalysis datasets is examined by investigating its long term performance in simulating various aspects of minimum and maximum temperatures and also in capturing the spatiotemporal characteristics of extremes over Ethiopian region.

2. STUDY REGION AND DATA

2.1 Study region characteristics

Ethiopia is situated in East Africa, located between latitudes 2.9°N to 15.3°N and longitudes 32.7°E and 48.3°E. Ethiopia's topography is distinct with altitudes varying from as much as 116 m below m.s.l. in the Danakil depression to more than 4,600 m above mean sea level in the Ras Dashen. Country experiences highest mean maximum temperature in north-east regions, about 45°C in the months of April to September and around 40°C in the months of October to March. North-western lowlands also experience a mean maximum temperature of 40°C in June, while the western and south-eastern lowlands experience mean maximum temperatures of 35°C to 40°C during April. The lowest mean temperatures, of 4°C or lower, are recorded at night in highland areas in the months of November and February (National Meteorological Services Agency, 1989; Ethiopian Mapping Authority, 1988).

2.2 Observed and reanalysis datasets

2.2.1 Synoptic Data

Minimum and maximum daily temperature are obtained for 15 stations, namely, Debre Zeit, Awassa, Neghele, Mekele, Nekemte, Combolcha, Debre Markos, Gore, Arba Minch, Gondar, Bahir Dar, Gode, Dire Dawa, Jimma, and Addis Ababa. The stations are well-spread across the country and capture the spatial heterogeneity of the region. About 5% missing data in the observations are filled through climatological daily temperature (Henn et al. 2013).

2.2.2 Reanalysis Data

ERA-Interim; MERRA; NCEP/NCAR Reanalysis-II and CFSR Reanalysis data are used. Since, the four reanalyses datasets differ in their spatial resolution, an interpolation technique is employed to obtain the temperature values corresponding to the 15 station locations. Ideally an interpolation at regional/station scale may need any statistical and dynamical downscaling techniques, since the reanalysis data are of coarser resolution. However, considering the homogenous structure of temperature, in this study interpolation is done by adopting a simple procedure of regridding through a nearest neighbour method.

3. RESULTS AND DISCUSSION

Spatio-temporal characteristics of four reanalysis datasets are examined for its efficacy in reproducing minimum and maximum temperature values across Ethiopia. Various aspects of minimum and maximum temperature such as the diurnal temperature range, the frequency of 90th (10th) percentile of minimum and maximum temperature, number of cool nights, cool days, warm nights, warm days, summer days and tropical nights are compared for 15 locations. However, for the demonstration purpose, characteristics of only six stations, namely, Awassa, Mekele, Gore, Bahir Dar, Dire Dawa and Addis Ababa are shown in this section.

3.1 Performance of reanalysis data in simulating long term statistics

3.1.1 Minimum temperature

The comparison of ERA-Interim, MERRA, NCEP and CFSR datasets with the observational

data for 15 stations is carried out by estimating various moments and performance measures. While ERA fails in all the stations, the performance of NCEP 2, CFSR and MERRA is relatively better with minimum bias in standard deviation, correlation and root mean square error.

The long term behaviour of reanalysis datasets are further analysed by comparing annual mean and annual cycle variation. ERA, MERRA and NCEP 2 exhibit a hot bias in simulating the annual mean minimum temperature of most of the stations. An exception is CFSR, which either underestimates or lie very closely to the observed data. Similar behaviour is observed in annual cycle comparison, where the inferior performance of ERA is highlighted. While MERRA, NCEP 2 and CFSR simulates the annual seasonal fluctuations, the superiority of CFSR in capturing the long-term averages are distinguishable here. The significantly higher hot bias in ERA-Interim, hot bias in MERRA & NCEP 2 and cold bias in CFSR are also distinct over all stations. Further, the quality of reanalysis is analysed in simulating the overall distribution and various percentile values. While, the empirical cumulative density functions are distinctly different, ERA's overestimation of minimum temperature intensities are evident; whereas CFSR lies very close to the observed distribution in most of the stations.

3.1.2 Maximum temperature

Performance comparison was done by using a Taylor diagrams (Taylor, 2001) for six selected stations and the averaged maximum temperature over the region. The analysis shows that ERA and NCEP 2 are superior with maximum correlation, least RMSE and minimum bias in standard deviation of maximum temperature, for most of the stations and also for the area average. While CFSR closely follow NCEP 2, evidently, MERRA fails to simulate these statistics. While, ERA performs worse in simulating minimum temperature characteristics, it is seemingly superior in simulating maximum temperature relatively better.

The spread of annual mean maximum temperature reveal the inconsistency among the reanalysis datasets and the spatial heterogeneity displayed by them. None of the reanalysis can be pointed out as the best in capturing the long term statistics of maximum temperature. Nevertheless, the annual cycle and its seasonality is simulated by CFSR, ERA and to an extent NCEP 2 also. The contradictory behaviour of MERRA in simulating the climatological annual cycle averaged over the period 1981-2013 in few stations is noteworthy.

Further analysis of empirical cumulative density functions display a similar behaviour as that of annual mean, with no consistently accurate simulation from any reanalysis over all stations. On an average, CFSR and NCEP 2 perform relatively better in simulating the distribution of maximum temperature. Interestingly, quantile-quantile plots display strong relationship between the observed and the reanalysis datasets, though it also reveal consistent hot or cold bias in some stations. The biases towards the extremes are far less when compared to the Q-Q plots of minimum temperature.

3.2 Performance of reanalysis in simulating the extremes

European Climate Assessment Indices such as diurnal temperature range, warm days, warm nights, cool days, cool nights, summer days and tropical nights are used (Klein Tank et al. 2002; Zhang et al. 2011) for the analysis.

3.2.1 Minimum temperature

The 10th and 90th percentile of daily minimum temperature for all 15 stations shows that for both these extremes, CFSR closely follow the observed percentiles. All other reanalysis datasets are found to be overestimating both these percentiles. The frequency of observed cool nights is almost constant for all the stations. While ERA-Interim has null value for all the examined stations, confirming its inability in simulating various aspects of minimum temperature, MERRA and NCEP

2 underestimated the cool nights. CFSR, though was superior in simulating the 10th percentile, it overestimates the frequency of cool nights, indicating more dense left tailed distribution. A similar analysis of frequency of warm nights reveals that except CFSR, all other reanalysis overestimate the high minimum, with ERA being the worst. CFSR, either slightly underestimates or remain close to the observed warm night frequency. Another index, tropical nights with minimum temperature greater than 20 °C is demonstrated. All stations experience very few tropical nights, which is better captured by CFSR and overestimated by other reanalysis. ERA seems to have a definite additive bias in simulating minimum temperature over Ethiopian region.

3.2.2 Maximum temperature

The extreme indices related to maximum temperature are investigated. The performance of reanalysis in simulating 10th and 90th percentiles indicate that though CFSR can be pointed out as the better among the four datasets, its performance is not consistent for all stations. Similar performances can be noticed in the simulation of other extreme indices such as frequency of cool days, warm days and summer days. To conclude, in simulating the extreme characteristics of maximum temperature, though CFSR does perform well, all four reanalysis more or less exhibit same characteristics. It is worthwhile to note the absence of any definite additive bias in ERA simulations in the case of maximum temperature statistics.

3.2.3 Diurnal temperature range

The monthly average diurnal temperature range is computed. The superiority of CFSR, followed by MERRA and NCEP 2 is evident from the boxplots of diurnal range. Quite expectedly, ERA failed to capture the observed diurnal range (both mean and spread). Though the performance of ERA is satisfactory for maximum temperature, the underperformance can be attributed to the huge additive bias in ERA's minimum temperature.

4. CONCLUSIONS

Observed temperature datasets are often scarce, discontinuous and frequently contain discrepancies. Holistic spatial variability of temperature is not available over a data sparse country like Ethiopia. The topography of the country has also an effect in creating a non-uniform spatial distribution in temperature variables. Often, this compel the hydrological and climatological modelling studies to rely on proxy data, which frequently are reanalysis datasets. The performance of four reanalysis temperature data is evaluated and compared with observed station temperature data.

Various aspects of minimum and maximum temperature from reanalysis are compared with the 15 synoptic station data. The present study shows no single reanalysis datasets capture the spatio-temporal variation of temperature over the Ethiopian region. The bad performance of the reanalysis products could be due to the weak parameterization of the boundary layer, simulation of surface soil moisture, and coupling of the land to the atmosphere (Koster et al. 2004; Pitman and Perkins 2009). However, among the four reanalysis datasets considered, CFSR and NCEP 2 follow the observed variations closely, when compared with MERRA and ERA. It is worthwhile to point out the huge additive bias suffered by ERA, irrespective of the station, in simulating all the aspects of minimum temperature. However, its performance is reasonably good in the case of maximum temperature statistics. These results would be beneficial to various regional hydrological modellers and practitioners in selecting a suitable proxy dataset that better represent the region under consideration.

ACKNOWLEDGEMENT

We would like to acknowledge the following organizations for providing the datasets free of charge: National Metrologic Agency (NMA) of Ethiopia for synoptic station surface temperature data; ECMWF for ERA-Interim data; NASA for MERRA, NCEP/NCAR for Reanalysis II datasets and Climate Forecast System Reanalysis (CFSR).

REFERENCES

Bita C, Gerats T. 2013. Plant tolerance to high temperature in a changing environment: scientific fundamentals and production of heat stress-tolerant crops. Frontiers in plant science. Frontiers 4: 273.

Dai, A., K.E. Trenberth, and T.R. Karl, 1999: Effects of clouds, soil moisture, precipitation, and water vapor on diurnal temperature range, Journal of Climate, 12(8): 2451–2473.

Dee DP, Uppala SM, Simmons AJ, Berrisford P, Poli P, Kobayashi S, Andrae U, Balmaseda MA, Balsamo G, Bauer P. 2011. The ERA-Interim reanalysis: Configuration and performance of the data assimilation system. Quarterly Journal of the Royal Meteorological Society. 137(656): 553–597.

Dile, Y.T., and R. Srinivasan, 2014: Evaluation of CFSR climate data for hydrologic prediction in data-scarce watersheds: an application in the Blue Nile River Basin, JAWRA Journal of the American Water Resources Association, 50(5): 1226–1241.

Easterling, D.R., B. Horton, P.D. Jones, et al. 1997: Maximum and minimum temperature trends for the globe, Science, 277(5324): 364–367.

Ebita A, Kobayashi S, Ota Y, Moriya M, Kumabe R, Onogi K, Harada Y, Yasui S, Miyaoka K, Takahashi K. 2011. The Japanese 55-year Reanalysis "JRA-55": an interim report. Sola. Meteorological Society of Japan 7: 149–152.

Ethiopian Mapping Authority, 1988. "National atlas of Ethiopia." Addis Ababa.

Gebrehiwot T, and Veen A Van Der, 2013: Assessing the evidence of climate variability in the northern part of Ethiopia, Journal of Development and Agricultural Economics, 5, 104–119.

Horton, B., 1995: Geographical distribution of changes in maximum and minimum temperatures, Atmospheric Research., 37(1), 101–117.

Henn B, Raleigh MS, Fisher A, Lundquist JD. 2013. A comparison of methods for filling gaps in hourly near-surface air temperature data. Journal of Hydrometeorology 14(3): 929–945.

IPCC, 2013: Climate Change 2013: The Physical Science Basis. Contribution of Working Group I to the Fifth Assessment Report of the Intergovernmental Panel on Climate Change [Stocker, T.F., D. Qin, G.-K. Plattner, M. Tignor, S.K. Allen, J. Boschung, A. Nauels, Y. Xia, V. Bex and P.M. Midgley (eds.)]. Cambridge University Press, Cambridge, United Kingdom and New York, NY, USA, 1535 pp.

Kalnay E, Kanamitsu M, Kistler R, Collins W, Deaven D, Gandin L, Iredell M, Saha S, White G, Woollen J. 1996. The NCEP/NCAR 40-year reanalysis project. Bulletin of the American meteorological Society 77(3): 437–471.

Kanamitsu M, Ebisuzaki W, Woollen J, Yang S-K, Hnilo JJ, Fiorino M, Potter GL. 2002. Ncep–doe amip-ii reanalysis (r-2). Bulletin of the American Meteorological Society 83(11): 1631–1643.

Karl, T.R., R.W. Knight, K.P. Gallo, et al., 1993: A new perspective on recent global warming: asymmetric trends of daily maximum and minimum temperature, Bulletin of the American Meteorological Society, 74(6), 1007–1023.

Kennedy AD, Dong X, Xi B, Xie S, Zhang Y, Chen J. 2011. A comparison of MERRA and NARR reanalyses with the DOE ARM SGP data. Journal of Climate 24(17): 4541–4557.

Kistler R, Collins W, Saha S, White G, Woollen J, Kalnay E, Chelliah M, Ebisuzaki W, Kanamitsu M, Kousky V. 2001. The NCEP-NCAR 50-year reanalysis: Monthly means CD-ROM and documentation. Bulletin of the American Meteorological society 82(2): 247–267.

Klein Tank, A.M.G., J.B. Wijngaard, G.P. Können, et al., 2002: Daily dataset of 20th-century surface air temperature and precipitation series for the European Climate Assessment. International journal of climatology, 22(12), 1441–1453.

Khan S. 2009. Climate change impacts on crop yield, crop water productivity and food security-A review. Progress in Natural Science 12: 2.

Kobayashi S, Ota Y, Harada Y, Ebita A, Moriya M, Onoda H, Onogi K, Kamahori H, Kobayashi C, Endo H. 2015. The JRA-55 reanalysis: General specifications and basic characteristics. Journal of the Meteorological Society of Japan. Ser. II93(1): 5–48.

Koster RD, Dirmeyer PA, Guo Z, Bonan G, Chan E, Cox P, Gordon CT, Kanae S, Kowalczyk E, Lawrence D. 2004. Regions of strong coupling between soil moisture and precipitation. Science. American Association for the Advancement of Science 305(5687): 1138–1140.

McSweeney, C., M. New, and G. Lizcano, 2010: The UNDP Climate Change Country Profiles: improving the accessibility of observed and projected climate information for studies of climate change in developing countries, Bulletin of the American Meteorological Society, 91, 157–166.

Mekasha A, Tesfaye K, Duncan AJ. 2014. Trends in daily observed temperature and precipitation extremes over three Ethiopian eco-environments. International Journal of Climatology. Wiley Online Library 34(6): 1990–1999.

Mengistu, D., and R. Lal, 2014: Recent spatiotemporal temperature and rainfall variability and trends over the Upper Blue Nile River Basin , Ethiopia, Int. J. Climatol., 34, 2278–2292. doi:10.1002/joc.3837

National Meteorological Services Agency (NMSA). 1996. No Title. Climate and Agro climatic Resources of Ethiopia. Meteorological research report series 1(1).

Omondi, P.A., J.L. Awange, E. Forootan, et al., 2014: Changes in temperature and precipitation extremes over the Greater Horn of Africa region from 1961 to 2010. International Journal of Climatology, 34(4), 1262–1277.

Pitman AJ, Perkins SE. 2009. Global and regional comparison of daily 2-m and 1000-hPa maximum and minimum temperatures in three global reanalyses. Journal of Climate 22(17): 4667–4681.

Rienecker MM, Suarez MJ, Gelaro R, Todling R, Bacmeister J, Liu E, Bosilovich MG, Schubert SD, Takacs L, Kim G-K. 2011. MERRA: NASA’s modern-era retrospective analysis for research and applications. Journal of climate 24(14): 3624–3648.

Saha S, Moorthi S, Pan H-L, Wu X, Wang J, Nadiga S, Tripp P, Kistler R, Woollen J, Behringer D. 2010. The NCEP climate forecast system reanalysis. Bulletin of the American Meteorological Society. American Meteorological Society 91(8): 1015–1057.

Saha S, Moorthi S, Wu X, Wang J, Nadiga S, Tripp P, Behringer D, Hou Y-T, Chuang H, Iredell M. 2014. The NCEP climate forecast system version 2. Journal of Climate 27(6): 2185–2208.

Taylor, K.E., 2001: Summarizing multiple aspects of model performance in a single diagram. Journal of Geophysical Research: Atmospheres, 106(D7): 7183–7192.

Uppala SM, Kållberg PW, Simmons AJ, Andrae U, Bechtold V, Fiorino M, Gibson JK, Haseler J, Hernandez A, Kelly GA. 2005. The ERA-40 re-analysis. Quarterly Journal of the Royal Meteorological Society. 131(612): 2961–3012.

Vose, R.S., D.R. Easterling, and B. Gleason, 2005: Maximum and minimum temperature trends for the globe: An update through 2004. Geophysical Research Letters, 32, L23822, doi:10.1029/2005GL024379.

Washington, R., M. New, M. Hawcroft, H. Pearce, M. Rahiz, and J. Karnacharya, 2012: Testing climate models for agricultural impacts: recent trends, current projections, crop-climate suitability, and prospects for improved climate model information. CAFS project report. Copenhagen, Denmark: CGIAR Research Program on Climate Change, Agriculture and Food Security (CCAFS).

Zhang, X., L. Alexander, G.C. Hegerl, et al., 2011: Indices for monitoring changes in extremes based on daily temperature and precipitation data. Wiley Interdisciplinary Reviews: Climate Change, 2(6), 851–870.

Proceedings of the 10th World Congress of EWRA 'Panta Rhei', 5-9 July 2017, Athens, Greece
© 2017 *European Water Resources Association*

An investigation of the use of Sentinel-2 data for mapping wetlands: A case study from Greece

A. Chatziantoniou[1*], G.P. Petropoulos[2], E. Psomiadis[1]
[1] *Department of Natural Resources Management and Agricultural Engineering, Agricultural University of Athens, Greece*
[2] *Department of Geography and Earth Sciences, University of Aberystwyth, SY23 2EJ, UK*
[*] *e-mail: andromachi.chatz@gmail.com*

Abstract: This study aimed at evaluating the combined use of Sentinel-2 data with advanced machine learning image classification algorithms for mapping a typical wetland ecosystem in Greece. In addition, the potential added value of additional spectral information created from the initial bands and of elevation to the thematic information accuracy was also examined. As a case study the National Park of Koronia & Volvi lakes in Thessaloniki were selected due to its high environmental interest. A Sentinel-2 (S2) image acquired in August of 2016 and a Shuttle Radar Topography Mission digital elevation model (SRTM DEM) were the main datasets used in this study. The image was pre-processed using SNAP open source software. A Principal Component Analysis (PCA) and a Minimum Noise Fraction (MNF) transformation were applied to the original bands and the derivative bands were used to form two new multispectral images. The DEM was also stacked to the two images. The Support Vector Machines (SVMs) and Artificial Neural Network (ANN) classifiers were applied to the four images created. Accuracy assessment of the derived classification maps was conducted on the basis of the estimation of standard classification error statistics. Comparisons showed that for the particular dataset and study site the SVM algorithm outperformed ANN. Overall accuracy reached 91.32% (kappa: 0.9008) for SVMs and 82.07% (kappa: 0.7945) for ANN. Additionally, the inclusion of the DEM appeared to increase overall accuracies ~5% for SVMs and ~1% for ANN. In overall, results exemplified the appropriateness of the spatial and spectral resolution of the S2 imagery in obtaining a rapid and cost-effective wetlands mapping. This is of considerable scientific and practical value, as it provides additional evidence on the suitability of S2 data for improving our ability to understand better the physical processes embedded in wetland ecosystems.

Key words: wetlands, Koronia Lake, Sentinel, SRTM DEM, Greece, SVM, ANN, MNF, PCA

1. INTRODUCTION

Wetlands are complex and dynamic water – logged ecosystems, hosting a great amount of species of plant and animal communities, also supporting water regulation and peat related processes (Malak & Hilarides 2016). Thus, developing accurate and robust techniques for mapping and monitoring changes in such ecosystems is of crucial importance in water resources management. Earth Observation (EO) offers great advantages in this respect thanks to its capability of acquiring - often at no cost - spectral data over large areas and at regular time intervals. It is well established that the selection of the appropriate spectral band and the suitable classifier is essential for classification accuracies improvement when EO data is used (Erener 2012).

Sentinel-2 (S2) is a new land monitoring mission part of the Copernicus Program that provides high resolution optical imagery to perform terrestrial observations in support of land services. The mission provides a global coverage of the Earth's land surface every 5 days and at a spatial resolution of 10, 20 and 60 meters, making the data of great use in studies related to land use/cover mapping and quantification of its changes (Sentinel-2 User Handbook, 2015). Yet, to our knowledge, the use of contemporary classification algorithms (e.g. SVMs, ANN) combined with EO imagery acquired from S2 has not been adequately investigated so far.

In this context, this study aims at evaluating the use of S2 data combined with machine learning classification algorithms for mapping a typical wetland ecosystem in Greece. The study objectives were: (1) to compare the performance of the ANN and SVMs when each is used with S2 imagery,

(2) to evaluate the added value of information on elevation to the classification accuracy, and, (3) to assess the use of PCA and MNF transformations to the overall classification results.

2. STUDY SITE AND DATASETS

The National Park of Koronia and Volvi lakes is one of the most important Ramsar wetlands of Greece. The wetland is protected by numerous national and international conventions due to its high environmental interest. A large number of plants (aquatic and terrestrial), animals, birds and fish reproduce, nest, feed and rest in the wetland habitat. The wetland is also included in the European ecological network of protected sites "NATURA 2000". Lake Koronia is a very important ecosystem of Greece which is almost vanishing because of non sustainable water management practice in the region. It faces serious environmental issues, such as decreasing water levels, deterioration of water quality and water salinization. The ongoing unsystematic economic growth of the area has resulted to water depletion and environmental degradation with serious social and economic impacts (Perivolioti et al. 2016).

A single S2 – 2 MSI image acquired on 02|08|2016 was used in this study. S2 datasets are provided free of charge via ESA's Sentinels Scientific Data Hub (https://scihub.copernicus.eu/). The available products are in processing Level-1C. Level-1C processing includes radiometric and geometric corrections including ortho-rectification and spatial registration on a global reference system with sub-pixel accuracy. In addition, a digital elevation model of the area was obtained from the STRM sensor (spatial resolution of 90m). All images are in the WGS84 reference system and UTM projection, zone 34. The software used for data processing was SNAP 5.0.0 and ENVI 5.1.

3. METHODOLOGY

The S2 image was pre-processed using SNAP open source software. Pre-processing included atmospheric correction which was applied to convert the Top-of-Atmosphere reflectance values (TOA) to corrected Bottom-of-Atmosphere reflectance values (BOA). For the atmospheric correction ESA's Sen2Cor plugin was used. Subsequently, bands 1, 9 and 10 were removed from the dataset. Then, the image was resampled using a bilinear method and was also subset a smaller area surrounding the two lakes of interest.

3.1 Spectral transformations

Two transformation methods were implemented to the dataset, Principal Component Analysis (PCA) and Minimum Noise Fraction (MNF). PCA is a classical statistical method for transforming attributes of a dataset into a new set of uncorrelated attributes called principal components (PCs) and it is used to reduce the dimensionality of a dataset, while still retaining as much of the variability of the dataset as possible (Howley et al. 2006). The MNF transformation is used to determine the inherent dimensionality of image data, to segregate noise in the data and to reduce the computational requirements for subsequent processing (Boardman and Kruse, 1994). PCA components 1 to 3 and MNF components 1 to 5 were used in this study to compose the new image for classification. The used components contained over 98% of the original information.

3.2 SVM & ANN classification

The two algorithms that were tested (SVM, ANN) were applied to 4 images: "PCA", "MNF", "PCA + DEM" and "MNF + DEM". The same training sample of 14539 points was used for all the images and all methods. Our classification scheme consisted of the following information classes:

Crops, Water, Artificial Surfaces, Forest, Shrub, Sand, Soil, Marshes and Swamps. A set of training points were selected representative of each class.

Table 1: The implemented LULC Classes

LULC Classes	Class description
Crops	No - wetland class, healthy and high yield arable farming land
Water	Wetland class, exposed surface water
Artificial Surfaces	No - wetland class, impervious surfaces, urban fabric, roads, industrial facilities
Forest	No - wetland class, mixed forest with trees from medium to large size
Shrub	No-wetland class, long or short grass species, sparse trees and bushes
Sand	No - wetland class, exposed lake, river or estuarine bed, coarse sand
Soil	No - wetland class, bare land, very low or no vegetation
Marshes	Wetland class, aquatic plants that is either emerge, submerge or floating in water
Swamps	Wetland class, aquatic forest or shrubs

For the implementation of the Feed-Forward ANN classification the logistic activation function was used. The parameters kept as suggested: the training threshold contribution (0.9), the training rate (0.2), the training momentum (0.9), the training RMS exit criteria (0.1), one hidden layer and the number of training interactions (1000) (Srivastava et al., 2012, Kolios and Stylios, 2013). For the SVM classification, the RBF kernel function was used. The γ value was kept as suggested, *1/number of features*. After several tests, the optimum C value was found at 2000. From a C value of 1, overall accuracy was rapidly rose up to 500 before beginning to plateau off at 2000 (Fig. 1).

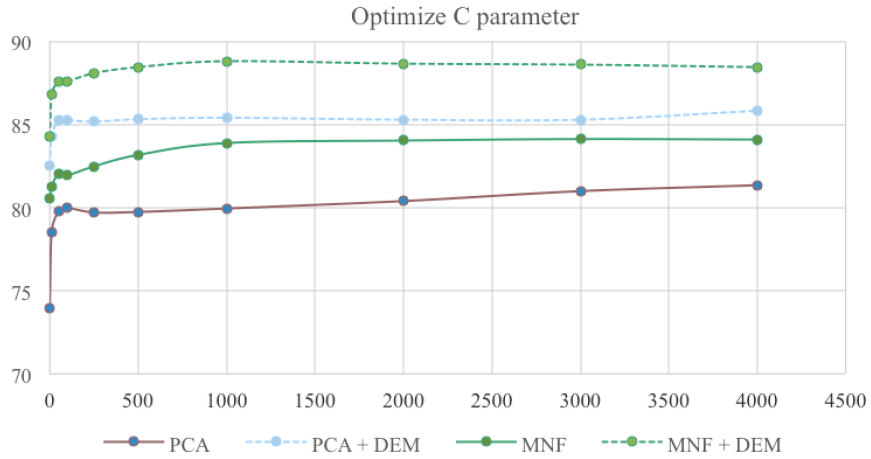

Figure 1: C parameter selection graph for SVM plotted against the overall accuracy

4. RESULTS - DISCUSSION

Accuracy assessment was carried out on the basis of the overall accuracy (OA) and kappa (K) statistics. In addition, each class accuracy was evaluated separately using User's and Producer's accuracy (UA, PA) and mapping accuracy (MA). The detailed error matrix was also computed for each of the classification images as it allowed evaluating the UA and PA accuracy for each of the information classes included in our classification scheme.

4.1 Overall accuracy

On the basis of the OA, SVM outperformed ANN with 91.32% and 82.02% respectively. Our findings also showed an improvement in the overall classification accuracy after information on elevation was included, particularly for the SVM classification. The elevation information appears to increase the OA by ~5% for SVM and ~1% for ANN. Additionally, the highest accuracies was

achieved using the MNF components in both classifiers (see Fig. 2). MNF transformation in both SVM and ANN is superior to PCA, with an increase in OA of ~10% in most cases.

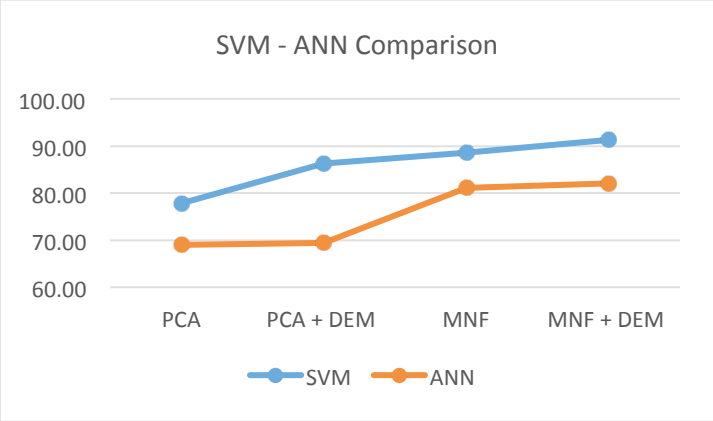

Figure 2: Comparison between SVM and ANN classifiers plotted against overall accuracy

4.2 Mapping accuracy

Individual accuracies for each class were assessed using the UA and PA accuracies. SVM exhibited highly accurate overall results; yet showed to be less effective in the separation of artificial, soil and sand classes. More than 70 soil and sand test pixels were misclassified in the artificial class. This was likely due to their low spectral separability. While the image was acquired in mid-summer, the presence of moisture is significantly low on the ground which can lead to high reflectance values and, thus, confusion between artificial surfaces and natural surfaces with no vegetation (soil, sand). A difficulty in distinguishing the aquatic and the inland vegetation was also observed. ANN performed slightly better distinguishing shrubs over forest, but it did a lot worse in classifying marshes and swamps which is the lead issue in this study.

Table 2: Mapping Accuracy for each class

Class	**SVM**		**ANN**	
Crops	92.37%	MNF	88.05%	MNF
water	94.23%	PCA + DEM	93.54%	PCA
artificial	69.73%	MNF + DEM	63.12%	MNF + DEM
forest	92.45%	PCA + DEM	85.69%	MNF + DEM
shrub	67.80%	PCA + DEM	70.88%	PCA
sand	83.62%	MNF + DEM	67.11%	MNF + DEM
soil	82.97%	MNF + DEM	78.27%	MNF + DEM
marshes	83.19%	PCA + DEM	75.24%	MNF + DEM
swamps	80.15%	MNF + DEM	32.13%	MNF

4.3 Discussion

Both algorithms achieved high classification accuracies but SVMs produced better results, especially in wetland classes. In a wetland area, the classes that prevail are water, aquatic vegetation and agriculture. In our case, water covers almost 15% of the area. Several studies using other types of multispectral satellite imagery have also indicated the superiority of SVMs against other methods and have evaluated their performance over different sites (Kavzoglu and Colkesen, 2009, Otukei and Blaschke, 2010, Vaglio Laurin et al., 2016). In terms of computational demands, SVM again outperformed ANN as the average runtime for the SVMs was almost half than the one for ANN.

It is also reasonable to some extend to expect that MNF will produce better results in comparison to PCA. This is because in comparison to PCA, MNF transform takes the noise information in the

spatial domain into consideration (Arslan et al., 2017). PCA channels achieved relatively low accuracy, even when compared with the initial bands. Although, when the same procedure was implemented on Landsat 7 ETM+, PCA improved the classification accuracy ~3%.

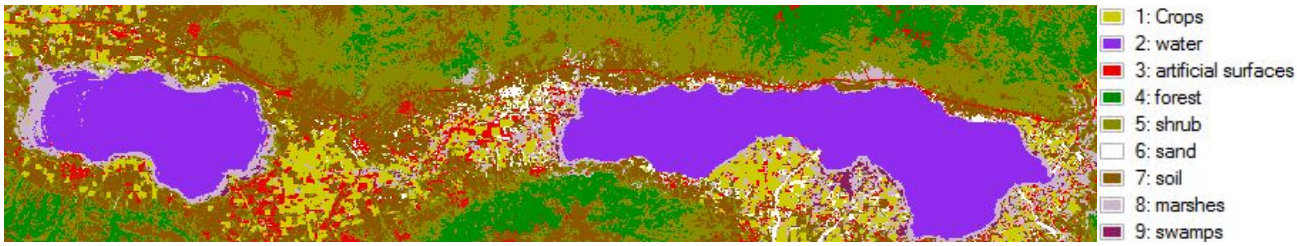

Figure 3: MNF + DEM classification result

5. CONCLUSIONS – FUTURE WORK

In this study, the combined use of Sentinel-2 (S2) imagery with the SVM and ANN advanced machine learning image classification algorithms for mapping a typical wetland ecosystem in Greece was explored. In addition, the added value of additional spectral information created from the initial bands and of elevation to the thematic information accuracy was also examined.

In overall, results showed that SVMs outperform ANN and that MNF is superior to PCA transformation for the specific dataset. Moreover, elevation information improves the classification accuracy for all cases. For the case of wetlands it seems that SVM algorithm is superior to ANN and the implementation of MNF over PCA transformation improves classification accuracy. Both SVM and ANN classifiers performed adequately in most scenarios, but ANN performed much worse in wetland classes. The high overall classification accuracy achieved by the SVM classifier in this study suggests that it is a promising algorithm which may be useful in conducting rapid and cost effective land cover analyses in wetland and coastal areas. Our findings also showed that MNF is superior to PCA when used with S2 data, at least this appeared to be the case in our study. Both transformations proved useful to reduce the size of the data and, thus, the time of the processing.

In overall, wetlands are complex systems with high presence of water and both natural and artificial surfaces. Thus, mapping and monitoring wetlands is a challenging procedure, especially when multispectral imagery is utilised for this purpose. S2 proved to be appropriate for mapping such complex areas, thanks to the high spectral and spatial resolution of the data. A synergistic approach examining the use of S2 and Sentinel – 1 (i.e. Synthetic Aperture Radar- SAR) data is potentially worthwhile to be investigated in the future to evaluate if mapping accuracy can be improved further. Besides this, in this context the use of other classifiers (e.g. decision trees, object-based) would be interesting to be investigated combined with multi-seasonal imagery, as could also potentially assist in improving thematic information extraction accuracy.

REFERENCES

Arslan, O., Akyurek, Ö. and Kaya, Ş. (2017). A comparative analysis of classification methods for hyperspectral images generated with conventional dimension reduction methods. Turkish Journal of Electrical Engineering & Computer Sciences, 25, pp.58-72.

Boardman, J. W., and Kruse, F. A. (1994), Automated spectral analysis: a geological example using AVIRIS data, north Grapevine Mountains, Nevada: in Proceedings, ERIM Tenth Thematic Conference on Geologic Remote Sensing, Environmental Research Institute of Michigan, Ann Arbor, MI, pp. I-407 - I-418.

Earth.esa.int. (2017). User Guides - Sentinel-2 MSI - Overview - Sentinel Online. [online] Available at: https://earth.esa.int/web/sentinel/user-guides/sentinel-2-msi/overview [Accessed 26 Jan. 2017].

Ec.europa.eu. (2017). Natura 2000 - Environment - European Commission. [online] Available at: http://ec.europa.eu/environment/nature/natura2000/index_en.htm [Accessed 26 Jan. 2017].

Ekby.gr. (2017). EKBY Web Site / Protected areas of Greece. [online] Available at: http://www.ekby.gr/ekby/en/EKBY_PA_en_.html [Accessed 26 Jan. 2017].

Erener, A., 2012. Classification method, spectral diversity, band combination and accuracy assessment evaluation for urban feature detection. International Journal of Applied Earth Observation and Geoinformation, 21(1), pp.397–408. Available at: http://dx.doi.org/10.1016/j.jag.2011.12.008.

Epa.gov. (2017). Why are wetlands important? | Wetlands Protection and Restoration | US EPA. [online] Available at: https://www.epa.gov/wetlands/why-are-wetlands-important [Accessed 26 Jan. 2017].

Howley, T., Madden, M., O'Connell, M. and Ryder, A. (2006). The effect of principal component analysis on machine learning accuracy with high-dimensional spectral data. Knowledge-Based Systems, 19(5), pp.363-370.

Islam, M., Thenkabail, P., Kulawardhana, R., Alankara, R., Gunasinghe, S., Edussriya, C. and Gunawardana, A. (2008). Semi-automated methods for mapping wetlands using Landsat ETM+ and SRTM data. International Journal of Remote Sensing, 29(24), pp.7077-7106.

Kavzoglu, T. and Colkesen, I. (2009). A kernel functions analysis for support vector machines for land cover classification. International Journal of Applied Earth Observation and Geoinformation, 11(5), pp.352-359.

Kolios, S. and Stylios, C. (2013). Identification of land cover/land use changes in the greater area of the Preveza peninsula in Greece using Landsat satellite data. *Applied Geography*, 40, pp.150-160.

Kulawardhana, R., Thenkabail, P., Vithanage, J., Biradar, C., Islam, M., Gunasinghe, S. and Alankara, R. (2007). Evaluation of the Wetland Mapping Methods using Landsat ETM+ and SRTM Data. Journal of Spatial Hydrology, 7(2).

Malak D. A., Hilarides L., (2016). 1st ed. [ebook] Available at: http://swos-service.eu/wp-content/uploads/2016/06/SWOS_Wetlands-delimitation-guidelines_FINAL_v1.1.pdf [Accessed 26 Jan. 2017].

Manandhar, R., Odeh, I. and Ancev, T. (2009). Improving the Accuracy of Land Use and Land Cover Classification of Landsat Data Using Post-Classification Enhancement. Remote Sensing, 1(3), pp.330-344.

Mountrakis, G., Im, J. and Ogole, C. (2011). Support vector machines in remote sensing: A review. ISPRS Journal of Photogrammetry and Remote Sensing, 66(3), pp.247-259.

Munyati, C. (2004). Use of Principal Component Analysis (PCA) of Remote Sensing Images in Wetland Change Detection on the Kafue Flats, Zambia. Geocarto International, 19(3), pp.11-22.

Otukei, J. and Blaschke, T. (2010). Land cover change assessment using decision trees, support vector machines and maximum likelihood classification algorithms. International Journal of Applied Earth Observation and Geoinformation, 12, pp.S27-S31.

Perivolioti T., Mouratidis A., Doxani G., Bobori D. (2016). Monitoring the water Quality of Lake Koroneia using long time – series of multispectral satellite images. ESA Living Planet Symposium 2016, Prague.

Roweis, S. (2000). Nonlinear Dimensionality Reduction by Locally Linear Embedding. Science, 290(5500), pp.2323-2326.

Srivastava, P., Han, D., Rico-Ramirez, M., Bray, M. and Islam, T. (2012). Selection of classification techniques for land use/land cover change investigation. *Advances in Space Research*, 50(9), pp.1250-1265.

Vaglio Laurin, G., Puletti, N., Hawthorne, W., Liesenberg, V., Corona, P., Papale, D., Chen, Q. and Valentini, R. (2016). Discrimination of tropical forest types, dominant species, and mapping of functional guilds by hyperspectral and simulated multispectral Sentinel-2 data. Remote Sensing of Environment, 176, pp.163-176.

Whyte, A. G. (2016). A Synergistic Approach to Monitoring Wetlands Using Sentinel 1 and 2 and Object Based Machine Learning Algorithms. Thesis. Wales / Aberystwyth University

Proceedings of the 10th World Congress of EWRA 'Panta Rhei', 5-9 July 2017, Athens, Greece
© 2017 *European Water Resources Association*

On the use of climate-flood links and CMIP5 projections to predict flood hazard under climate change scenarios

A.T. Silva[1*], M.M. Portela[1] and M. Naghettini[2]
[1] *CERIS, Instituto Superior Técnico, Universidade de Lisboa, Portugal*
[2] *Department of Hydraulics and Water Resources Engineering, Federal University of Minas Gerais, Belo Horizonte, Brazil*
[*] *e-mail: artur.tiago.silva@tecnico.ulisboa.pt*

Abstract: The Intergovernmental Panel on Climate Change (IPCC) assessed with medium confidence that there has been an anthropogenic influence in the intensification of heavy rainfall at the global scale. Nevertheless, when taking into account gauge-based evidence, no clear climate-driven global change in the magnitude or frequency of floods has been identified in recent decades. This work presents a study on the nonstationarity of floods in the Itajaí River, which is located in the Southeastern South America region, where the influence of El Niño-Southern Oscillation (ENSO) on hydrometeorological extremes has been reported. The analysis used a peaks-over-threshold (POT) approach and a Bayesian inferential framework, and revealed that occurrence rates and over-threshold peak magnitudes exhibit statistically significant and complex relationships with ENSO. The identified climate-flood link is further explored using sea surface temperature (SST) output from CMIP5 models under different representative concentration pathway (RCP) scenarios. Results are inconclusive as to whether it is possible to make a statement on scenario-forced climate change impacts on the flood regime of the Itajaí river basin. The overall outcome of the analysis is that, given that sample sizes are adequate, stationary models seem to be sufficiently robust for engineering design as they describe the variability of the hydrological processes over a large period, even if annual flood probabilities exhibit a strong year-to-year dependence on ENSO.

Key words: Nonstationarity, flood frequency analysis, climate change, design life level, CMIP5

1. INTRODUCTION

The Intergovernmental Panel on Climate Change (IPCC), through its Special Report on Managing the Risks of Extreme Events and Disasters to Advance Climate Change Adaptation (SREX, Field *et al.*, 2012) assessed that it is likely that there have been more statistically significant increases in extreme rainfall in more regions than there have been decreases. Furthermore, there is a medium confidence that there has been an anthropogenic influence in the intensification of heavy rainfall at the global scale. Nevertheless, when taking into account gauge-based evidence, no clear climate-driven global change in the magnitude or frequency of floods has been identified in recent decades. Regarding this issue, the SREX report states: 'overall, there is low confidence in projections of changes in fluvial floods. Confidence is low due to limited evidence and because the causes of regional changes are complex'.

In light of the conclusions of the IPCC SREX report, Kundzewicz *et al*. (2013) opt to take a cautionary stance and, rather than waiting for answers on the greenhouse-gas-forcing flood change issue, encourage 'the continuation of empirical and model-based science and a "no regrets" strategy for limiting flood losses'.

In the technical literature, the projection of flood hazard under climate change scenarios usually takes the following model chain approach: "emission scenario → general circulation model (GCM) → downscaling → catchment model → flood frequency analysis" (e.g., Dankers & Feyen, 2009). These model chains have a complex and difficult implementation and their results are associated with high uncertainty (Merz *et al.*, 2014). There are several sources of uncertainty in the model chain approach, one of the main ones being well-known shortcomings of all GCMs in simulating regional and local rainfall.

Delgado *et al.* (2014) argue that, if a strong climate-flood link is identified, it can be used to directly project future flood changes using GCM output, and propose the shortened climate change model chain "emission scenario → general circulation model (GCM) → nonstationary flood frequency analysis", thereby bypassing downscaling, rainfall, and catchment modeling. Merz *et al.* (2014) see great potential in this approach and single it out as one of the emerging perspectives of flood risk assessment and management.

In this paper, the shortened model chain approach proposed by Delgado *et al.* (2014) is applied to exploit a link between the flood regime in the Itajaí-açu river, in Southern Brazil, and ENSO using sea surface temperature, SST outputs from 34 atmosphere-ocean GCMs from the Coupled Model Intercomparison Project Phase 5 (CMIP5, Taylor *et al.*, 2012), which is used in the Fifth IPCC Assessment Report (AR5), for the hypothetical design life 2016-2065 (50 years). For CMIP5, instead of emission scenarios, the IPCC adopted Representative Concentration Pathway (RCP) scenarios (Moss *et al.*, 2010). This does not alter the above mentioned model chains except for changing their first element.

Notwithstanding the advantages of the selected shortened model chain for projecting flood hazard under climate change, it should be noted that GCM limitations go well beyond rainfall simulation errors. In fact, even the recent generation CMIP5 GCMs still need further development in order to realistically simulate the most basic ENSO characteristics and other fundamental atmospheric processes (Guilyardi *et al.*, 2012; Bellenger *et al.*, 2013). Given these limitations, we are not yet at the stage where GCM output is the answer to bridge the major impediment to full applicability of nonstationary flood frequency models to engineering design, as discussed in Silva *et al.* (2016, 2017): the nonexistence of climate covariate data long into the future. For that reason, the objective of this chapter is not an exploration of future dynamics of the flood regime in the study region. Rather, in agreement with suggestions of Serinaldi & Kilsby (2015) regarding the use of GCM experiments output in nonstationary flood frequency analysis, the objective here is to make a sensitivity analysis of a nonstationary flood frequency model under the understanding that GCM experiments output can provide a somewhat reasonable hypothetical evolution of a climate index under a certain scenario.

2. CASE STUDY AND METHODS

Silva et al. (2017) studied the influence of ENSO on the flood regime in the Itajaí-açu River, located in Southern Brazil, through nonstationary flood frequency analysis with Poisson-generalized Pareto (GP) models under a peaks-over-threshold approach and a Bayesian inferential paradigm. The analysis used data spanning from 1934 to 2014 at the gauging station Apiúna and, as a climate covariate, the Niño 3.4 December-to-February (DJF) mean SST anomaly, N34, calculated from the HadISST1 dataset by Rayner *et al.*, (2003). Poisson-GP models assume that the annual exceedance counts follow a Poisson distribution while the flood exceedance magnitudes follow a GP distribution. The CDF of the Poisson-GP model is given by:

$$F(x) = \exp\left\{-\lambda\left[1-\kappa\left(\frac{x-u_0}{\sigma}\right)\right]^{\frac{1}{\kappa}}\right\},\ \kappa \neq 0,\ x > u_0 \tag{1}$$

where λ, σ and κ are, respectively the Poisson, scale and shape parameters, and u_0 is the selected threshold (in this case, $u_0 = 650\,\mathrm{m^3/s}$, Silva *et al.*, 2016)

A detailed treatment of the analysis is provided in Silva *et al.* (2017). Using Bayesian model selection tools, such as Bayes factors and Deviance Information Criterion (DIC), it was found that the Poisson parameter follows a quadratic polynomial relationship with the N34 covariate, while the GP scale parameter follows a cubic polynomial relationship. Table 1 shows the dependence functions, posterior modes of the parameters and DIC score of the stationary (PD0 and GP0) and

nonstationary (PD2 and GP2) Poisson and GP models. The combination the pairs of components of the POT models into annual models forms the stationary (AM0) and nonstationary (AM2) models. Figure 1 shows the observed annual maxima and the quantile functions of both annual models, as well as sampling uncertainty estimated based on the posterior distribution (Silva *et al.*, 2017).

Table 1. POT models: dependence functions, posterior parameter modes and DIC.

Annual model	POT model	Dependence function	Parameter	Posterior mode	DIC
AM0	PD0	$\lambda = \lambda_0$	λ_0	3.513	344.021
	GP0	$\sigma = \sigma_0$	σ_0	445.751	4056.595
			κ	-0.086	
AM2	PD2	$\lambda = \lambda_0 + \lambda_1 N34 + \lambda_2 N34^2$	λ_0	2.933	334.581
			λ_1	0.253	
			λ_2	0.693	
	GP2	$\sigma = \sigma_0 + \sigma_1 N34 + \sigma_2 N34^2 + \sigma_3 N34^3$	σ_0	455.166	4052.697
			σ_1	-134.568	
			σ_2	-12.615	
			σ_3	59.041	
			κ	-0.035	

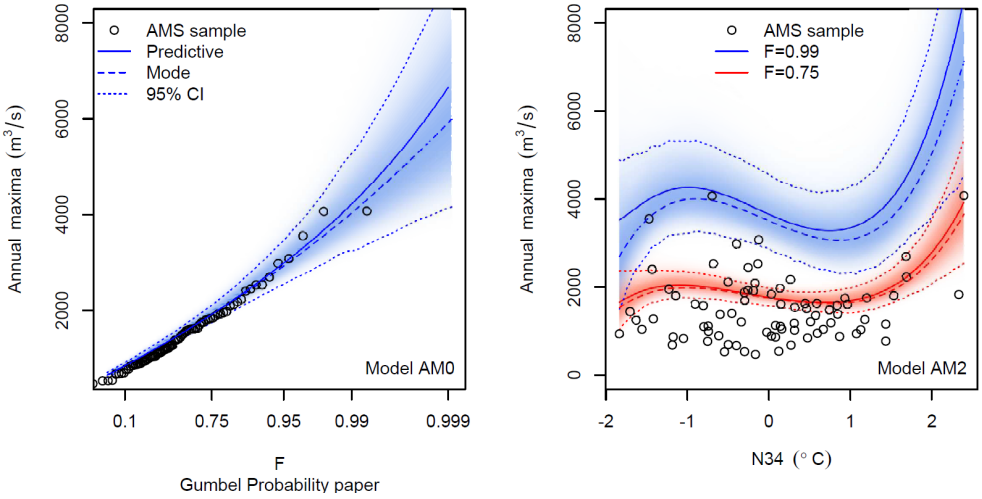

Figure 1. AM0 model (left): posterior predictive (continuous lines) and parameter mode distributions and 95% credibility intervals. AM2 model (right): posterior predictive (continuous lines), parameter mode (dashed lines) and 95% credibility intervals (dotted lines) for 2 nonexceedance probabilities as functions of N34. The darkness of the shadings is proportional to the pointwise posterior density of the corresponding quantiles.

3. ANALYSIS SETUP

The Bayesian posterior predictive distribution of future events, W, is integrated over all possible posterior realizations of the parameter vector, $\boldsymbol{\theta}$, thereby allowing the integration of the natural variability and sampling uncertainty in a single flood hazard estimation (Merz & Thieken, 2005). The predictive density is defined by:

$$g(w \mid \mathbf{x}) = \int_{\Theta} g(w \mid \boldsymbol{\theta}) \pi(\boldsymbol{\theta} \mid \mathbf{x}) d\boldsymbol{\theta} \tag{2}$$

where $\mathbf{x}$ is the sample and $\pi(\boldsymbol{\theta} \mid \mathbf{x})$ is the posterior parameter density.

Silva *et al.* (2017) combined this concept with that of the flood hazard measure proposed by Rootzén & Katz (2013) termed 'design life level' (DLL), which is defined as the flood level or flow

with a probability p of being exceeded over a design life period T_1:T_2. The approximation of the posterior predictive distribution of the DLL, using N_{sim} MCMC output simulations is (Silva *et al.*, 2017):

$$\hat{F}_{T_1:T_2}\left(w \mid \mathbf{x}\right) = \frac{1}{N_{sim}} \sum_{i=1}^{N_{sim}} \prod_{t=T_1}^{T_2} F_t\left(w \mid \theta_i\right) \tag{3}$$

where $F_t(x)$ is the CDF of annual maximum floods at year t. The application of this flood hazard measure under nonstationarity is dependent on the availability of covariate data during the design life period. In this work CMIP5 output is used to obtain several possible realizations of the climate covariate in the design life period of 2016:2065.

Projections of monthly SST averaged over the Niño 3.4 region under climate change scenarios were obtained from output data from CMIP5 experiments with models forced by RCP scenarios. CMIP5 experiment data were obtained from the KNMI Climate Explorer database (Trouet & van Oldenborgh, 2013, https://climexp.knmi.nl/). Four RCP scenarios were considered: RCP2.6, RCP4.5, RCP6 and RCP8.5. RCPs are labeled according to a rough estimate of the radiative forcing in the year 2100, relative to preindustrial conditions. van Vuuren *et al.* (2011) provide a detailed overview of the development and main characteristics of the RCP scenarios.

Table 2 lists the institutions and names of the CMIP5 experiments considered in this study, along with the number of realizations or runs by each experiment for each RCP scenario. Some experiments have more than one realization per scenario, in which case the distinction between realizations is due to initializing GCM runs from different, but equally realistic, starting conditions or they might be produced by different "perturbed physics" versions of the same model (Taylor *et al.*, 2011).

A preliminary analysis of the CMIP5 data under RCP forcing revealed an evident warming of Equatorial Pacific SSTs in the 21st century in all RCP scenarios. The warming is particularly evident after RCP forcing kicks in, in 2006. To deal with the upward trend in mean SST under RCP forcing, the data were detrended using the methodology described by Lindsey (2013), which is employed by the United States National Oceanic and Atmospheric Administration (NOAA) Climate Prediction Center: each 5-year period uses a 30-year average centered on the first year in the period. For example, the 2006-2010 period is compared to the 1991-2021 average, and so on.

After calculating the N34 covariate from CMIP5 data, a preliminary look into the resulting N34 time series revealed that some of the models did not adequately simulate the variance of the covariate: while some GCMs produced N34 time series with a very low variance, resulting in mostly ENSO-neutral years, others produced N34 realizations with a very high variance, characterized by an exaggerated proportion of strong El Niño/La Niña events, relative to the observed N34 regime from the HadISST1 dataset, particularly during the flood model estimation period (hydrologic years, starting on 1 October, from 1934/35 to 2013/14).

In light of the aforementioned limitations in preserving N34 variance from some GCMs, not all of the experiments listed in Table 2 were used in the analysis. A statistical test was employed to identify the experiments whose N34 variance was significantly different from the HadISST1 data, which were not considered. The utilized statistical test was the modified robust Brown-Forsythe Levene-type test based on absolute deviations from the median, which is implemented in the function levene.test() of the lawstat package (Hui *et al.*, 2008) in R (R Core Team, 2013). Given k random samples with variances σ_i^2, $i = 1,2,\ldots,k$, the null hypothesis of the Brown-Forsythe test considers that all variances are equal, $H_0 : \sigma_1^2 = \sigma_2^2 = \ldots = \sigma_k^2$, vs. the alternative hypothesis $H_1 : \sigma_i^2 \neq \sigma_j^2$ for at least one $i \neq j$ (Brown & Forsythe, 1974).

The samples used for the Brown-Forsythe test correspond to the subsets of the HadISST1 and CMIP5 model realizations spanning from 1970/71 to 2005/06, when the RCP forcing of the GCMs starts. In a similar approach to that of Delgado *et al.* (2014), the N34 time series were pooled so that for each pool there was a set of time series that were derived from the same experiment. Rejection

of the null hypothesis implied that the pool being tested was excluded from the analysis. This way, entire experiments were excluded instead of individual realizations, thereby preserving the variability of different runs within the same experiment. The significance level used was 5%. The experiments for which the null hypothesis was not rejected are marked with an asterisk in Table 2.

Table 2. CMIP5 experiments considered for analysis and corresponding number of realizations per RCP scenario. (*) Null hypothesis of the Brown-Forsythe test was not rejected. Number of remaining GCM runs after selection criteria were applied.

Institute	Experiment	Number of realizations per scenario			
		RCP2.6	RCP4.5	RCP6	RCP8.5
CSIRO-BOM	ACCESS1-0 *	0	1	0	1
	ACCESS1-3 *	0	1	0	1
BCC	BCC-CSM1-1	1	1	0	1
	BCC-CSM1-1-M	1	1	1	0
CCCMA	CanESM2	5	4	0	5
RSMAS	CCSM4	6	6	6	6
NSF-DOE-NCAR	CESM1-BGC	0	1	0	1
	CESM1-CAM5	3	3	3	2
CCMC	CMCC-CM *	0	1	0	1
	CMCC-CMS *	0	1	0	1
CNRM-CERFACS	CNRM-CM5 *	1	1	0	5
CSIRO-QCCCE	CSIRO-Mk3-6-0	10	10	10	10
EC-EARTH	EC-EARTH	1	6	0	6
FIO	FIO-ESM	3	3	3	3
NOAA GFDL	GFDL-CM3	1	3	1	1
	GFDL-ESM2G *	1	1	1	1
	GFDL-ESM2M	1	1	1	1
NASA GISS	GISS-E2-H	3	15	3	3
	GISS-E2-H-CC *	0	1	0	0
	GISS-E2-R	3	17	3	3
	GISS-E2-R-CC	0	1	0	0
MOHC	HadGEM2-AO *	1	0	1	0
	HadGEM2-CC *	0	1	0	1
	HadGEM2-ES *	4	4	3	3
INM	INMCM4	0	1	0	1
IPSL	IPSL-CM5A-LR	4	4	1	4
	IPSL-CM5A-MR *	1	1	0	1
	IPSL-CM5B-LR *	0	1	0	1
MIROC	MIROC5 *	3	3	3	3
MPI-M	MPI-ESM-LR *	3	3	0	3
	MPI-ESM-MR	1	3	0	1
MRI	MRI-CGCM3	0	1	1	1
NCC	NorESM1-M	0	1	1	1
	NorESM1-ME *	0	1	1	1
Total runs		57	103	43	73
Remaining runs	After Brown-Forsythe test	14	21	8	23
	After dismissing runs with N34 realizations exceeding the limits of the observed range plus 10 % on either side	8	13	4	14

Upon further analysis of the N34 time series produced by the GCMs which were not rejected by the test of equality of variances, it was found that many of them had N34 values well outside the range of the observed series in the period used for estimating the nonstationary model. Some model runs produced occurrences of N34 values larger than 3 and/or lower than -3, while the range of values used in estimation is [-1.835, 2.392]. While the plausibility of the occurrence of such anomalies is not disputed, the fact remains that, as with any regression model, using nonstationary models to predict flood probabilities outside the range of the observed covariate values bears careful consideration since it requires extrapolation beyond the observed data. N34 series produced by GCM runs with values outside of that range were dismissed from further analysis. Table 2 (bottom) shows the remaining number of runs after the two selection criteria were applied.

4. RESULTS

The predictive distributions of the design life level (DLL) were computed using GCM output data from the experiments selected in Section 2 and the nonstationary model posterior parameter MCMC samples obtained in Section 2, using the methodology described in Silva *et al.* (2017). A design life of 50 years was considered, starting on the hydrologic year 2016/17.

Figure 2 shows individual CMIP5 predictive DLL estimates organized by RCP scenario as well as the DLL of the stationary model for a design life of 50 years. For each scenario, the DLL curves show a range of results that both increase and decrease flood hazard estimates relative to the stationary model. However there is no consistent upward or downward shift according to increasing greenhouse gas pathway forcing via the RCP scenarios, i.e., apart from a single estimate that is a clear outlier (in RCP8.5), there is no clear difference between the range of results of scenarios RCP2.6 through RCP8.5.

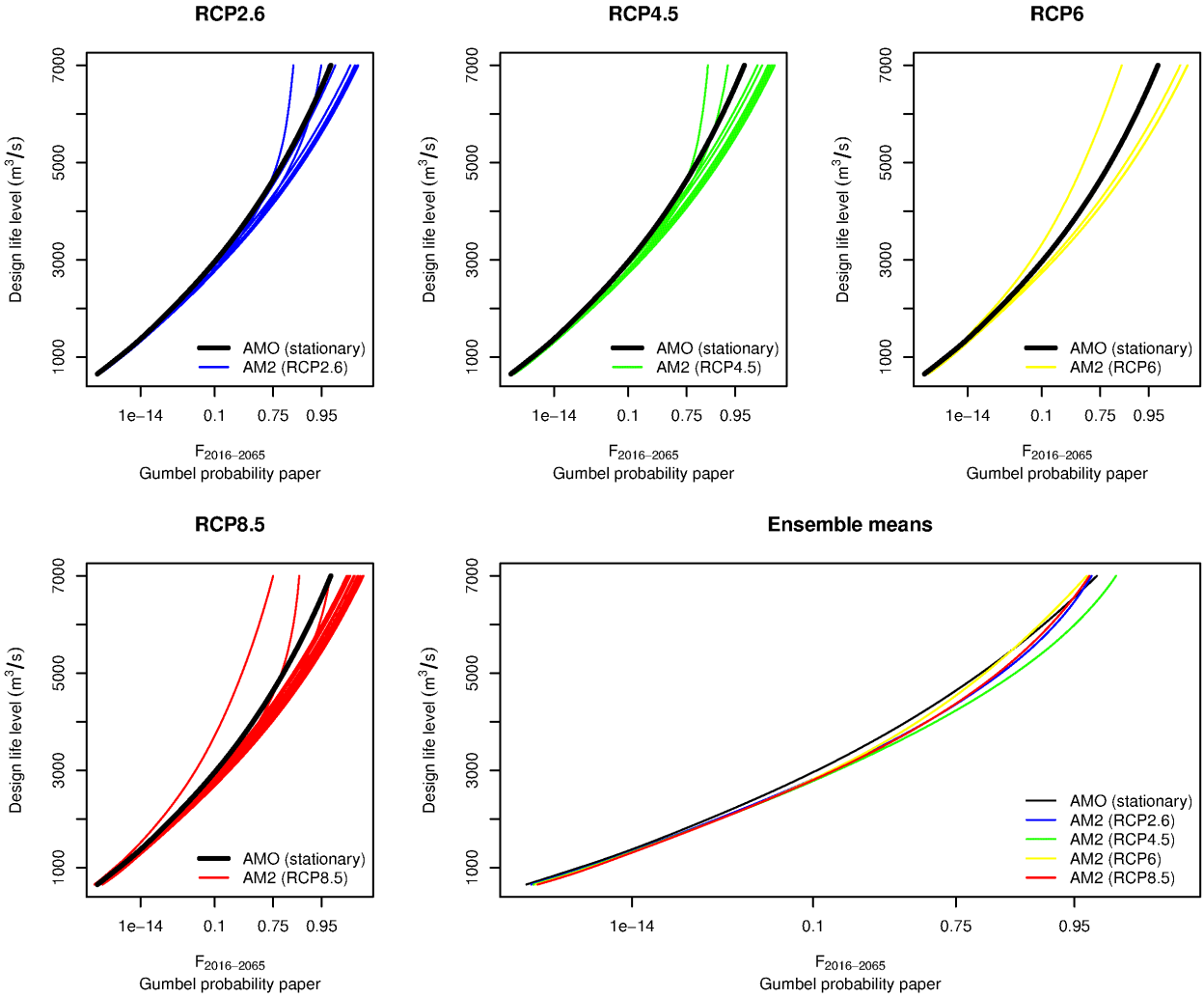

Figure 2. DLL for the life period 2016/17-2065/66 (50 years) for the AM0 and AM2 models with climate covariate calculated from CMIP5 model output under 4 RCP scenarios. Corresponding ensemble means.

Figure 2 also shows the CMIP5 ensemble mean DLL estimates for each RCP scenario, which are obtained by averaging the predictive DLL probabilities for each flood quantile, together with the DLL of the stationary model. It is apparent that, although the results of Figure 2 show both positive and negative changes in flood hazard estimate relative to the stationary model, the ensemble mean results under either scenario is not much different from the stationary results.

5. CONCLUSIONS

Given the practical results relevant to the case study at hand, we conclude that, to date, it remains impossible to make a statement on scenario-forced climate change impacts on the Itajaí river basin with any reliable statistical significance, since, for the 2016/17-2065/66 design life, the predictive DLL estimates of the nonstationary models do not differ greatly between different scenarios. Furthermore, the ensemble mean results are not clearly different from the results of the stationary model for a design life of 50 years. This suggests that, unless future climatic fluctuations are significantly different from those observed in recent decades and from the CMIP5 model outputs used in the analysis, the stationary model is sufficiently robust for engineering design as it describes the variability of the process over a large period, even if annual flood probabilities exhibit a strong year-to-year dependence on ENSO.

It is important to acknowledge the many drawbacks faced during the analysis briefly presented in this paper, from the reports in the technical literature of the ineptitude of CMIP5-generation GCMs in reproducing basic characteristics of the ENSO phenomenon, cited in Section 1, to the exclusion of the vast majority of GCM realizations of the N34 covariate by consideration of two reasonable and prudent selection criteria. This justifies interpreting the results with some degree of scepticism. Nevertheless, the CMIP5 models used here are the current state-of-the-art GCMs adopted by the IPCC and their results, despite the inherent uncertainties, are used by policy makers to develop adaptation options to climate change. Therefore, even under the assumption that the N34 series obtained from CMIP5 outputs do represent possible future realizations of the climate covariate, it is reasonable to conclude that the results presented here do not provide evidence supporting a clear advantage of nonstationary flood models, over stationary ones, for engineering design purposes.

To conclude, we stress that the analysis presented in this paper is inherently dependent upon the ability of current generation GCMs to simulate ENSO. In that regard, it is worthwhile to mention an assertion made by Bellenger *et al.* (2013) on CMIP5 and ENSO: many CMIP5 models are simulating more processes than they did in CMIP3 (the preceding generation of GCMs), which, by adding degrees of freedom to the models, makes simulating Earth's climate more challenging. Those authors comment that, since ENSO properties in CMIP5 are not degraded relative to CMIP3, there is added confidence for future improvements on the climate modeling enterprise. Therefore, it would be worthy to repeat this analysis when the next-generation GCMs are made available.

REFERENCES

Bellenger, H., Guilyardi, É., Leloup, J., Lengaigne, M., Vialard, J., 2014. ENSO representation in climate models: from CMIP3 to CMIP5. Climate Dynamics, 42(7-8): 1999-2018.

Brown, M.B., Forsythe, A.B., 1974. Robust tests for the equality of variances. Journal of the American Statistical Association, 69(346): 364-367.

Dankers, R. and Feyen, L., 2009. Flood hazard in Europe in an ensemble of regional climate scenarios. Journal of Geophysical Research: Atmospheres, 114(D16).

Delgado, J.M., Merz, B., Apel, H., 2014. Projecting flood hazard under climate change: an alternative approach to model chains. Natural Hazards and Earth System Sciences, 14(6): 1579-1589.

Field, C.B., Barros, V., Stocker, T.F., Dahe, Q., Dokken, D.J., 2012. Special Report on Managing the risks of Extreme Events and Disasters to Advance Climate Change Adaptation (SREX).

Guilyardi, E., Bellenger, H., Collins, M., Ferrett, S., Cai, W., Wittenberg, A., 2012. A first look at ENSO in CMIP5. Clivar Exchanges, 17(1): 29-32.

Hui, W., Gel, Y.R., Gastwirth, J.L., 2008. lawstat: an R package for law, public policy and biostatistics. J Stat Softw, 28, pp.1-26.

Kundzewicz, Z.W., Kanae, S., Seneviratne, S.I., Handmer, J., Nicholls, N., Peduzzi, P., Mechler, R., Bouwer, L.M., Arnell, N., Mach, K., Muir-Wood, R., 2013. Flood risk and climate change: global and regional perspectives. Hydrological Sciences Journal, 59(1): 1-28.

Lindsey, R., 2011. In Watching for El Niño and La Niña, NOAA Adapts to Global Warming. https://www.climate.gov/news-features/understanding-climate/watching-el-ni%C3%B1o-and-la-ni%C3%B1a-noaa-adapts-global-warming. Accessed on January 14th 2017.

Merz, B., Aerts, J.C.J.H., Arnbjerg-Nielsen, K., Baldi, M., Becker, A., Bichet, A., Blöschl, G., Bouwer, L.M., Brauer, A., Cioffi, F., Delgado, J.M., 2014. Floods and climate: emerging perspectives for flood risk assessment and management. Natural Hazards and Earth System Sciences, 14(7): 1921-1942.

Merz, B., Thieken, A.H., 2005. Separating natural and epistemic uncertainty in flood frequency analysis. Journal of Hydrology, 309(1): 114-132.

Moss, R.H., Edmonds, J.A., Hibbard, K.A., Manning, M.R., Rose, S.K., Van Vuuren, D.P., Carter, T.R., Emori, S., Kainuma, M., Kram, T., Meehl, G.A., 2010. The next generation of scenarios for climate change research and assessment. Nature, 463(7282): 747-756.

R Core Team, 2013. R: A language and environment for statistical computing.

Rayner, N.A., Parker, D.E., Horton, E.B., Folland, C.K., Alexander, L.V., Rowell, D.P., Kent, E.C., Kaplan, A., 2003. Global analyses of sea surface temperature, sea ice, and night marine air temperature since the late nineteenth century. Journal of Geophysical Research: Atmospheres, 108(D14).

Rootzén, H., Katz, R.W., 2013. Design life level: quantifying risk in a changing climate. Water Resources Research, 49(9): 5964-5972.

Serinaldi, F., Kilsby, C.G., 2015. Stationarity is undead: Uncertainty dominates the distribution of extremes. Advances in Water Resources, 77: 17-36.

Silva, A.T., Portela, M.M., Naghettini, M., Fernandes, W., 2017. A Bayesian peaks-over-threshold analysis of floods in the Itajaí-açu River under stationarity and nonstationarity. Stochastic Environmental Research and Risk Assessment, 31(1): 185-204.

Silva, A.T., Naghettini, M., Portela, M.M., 2016. On some aspects of peaks-over-threshold modeling of floods under nonstationarity using climate covariates. Stochastic Environmental Research and Risk Assessment, 30(1): 207-224.

Taylor, K.E., Balaji, V., Hankin, S., Juckes, M., Lawrence, B., Pascoe, S., 2011. CMIP5 Data Reference Syntax (DRS) and Controlled Vocabularies (Program for Climate Model Diagnosis and Intercomparison (PCMDI).

Taylor, K.E., Stouffer, R.J., Meehl, G.A., 2012. An overview of CMIP5 and the experiment design. Bulletin of the American Meteorological Society, 93(4): 485-498.

Trouet, V., Van Oldenborgh, G.J., 2013. KNMI Climate Explorer: a web-based research tool for high-resolution paleoclimatology. Tree-Ring Research, 69(1): 3-13.

van Vuuren, D.P., Edmonds, J., Kainuma, M., Riahi, K., Thomson, A., Hibbard, K., Hurtt, G.C., Kram, T., Krey, V., Lamarque, J.F., Masui, T., 2011. The representative concentration pathways: an overview. Climatic Change, 109: 5-31.

III. Water Resources Management

Proceedings of the 10th World Congress of EWRA 'Panta Rhei', 5-9 July 2017, Athens, Greece
© 2017 *European Water Resources Association*

On the barriers to adapt to less water under climate change in Mediterranean countries

Ana Iglesias[1*], Luis Garrote[2]
[1] *Department of Agricultural Economics and Social Sciences. Technical University of Madrid, Spain*
[2] *Department of Civil Engineering: Hydraulics, Energy and Environment. Technical University of Madrid, Spain*
[*] *e-mail: ana.iglesias@upm.es*

Abstract: This paper summarises barriers and constraints to adapting water resources management to climate change in the Mediterranean region. First, we synthesize and analyze the most promising strategies for adapting to less water in Mediterranean countries, expanding the application to other climatic regions. Theoretical measures include improved efficiency, optimisation of governance, enhancement of participation, development of risk-based choices, and economic instruments. Adjusting agricultural systems to water needs is a sound and feasible practice in both irrigated and rain-fed systems and presents a water saving potential up to 50% compared with a non-adjusted practice. Finally, the paper categorises the constraints to implement the measures, give specific examples about these issues and also quantify their impact. When considering constraints and opportunities to implement these water management practices, any environmental policy regulating their adoption should be based on recommending the use of extension and training to local actors on the application of the practices. While there is a continuing need to strengthen the climate change knowledge base (through research), improved understanding of climate change science will be insufficient on its own for adaptation policy development and to drive adaptation action. There is a complementary need to engage stakeholders, by developing suitable methodologies for assessment of impacts, vulnerabilities and planning as a pre-requisite for cost-effective adaptation. There may be many simple adaptation measures that could theoretically be introduced to address a particular risk or opportunity, these may only be practically possible under certain circumstances.

Key words: Water management, climate change adaptation, water availability, reservoir storage

1. INTRODUCTION

Agricultural growth in Mediterranean countries was achieved by consuming very large amounts of water and other inputs. Today, environmental and urban pressures challenge the use of water for food production. In Mediterranean countries, water scarcity has become so acute, that efforts should focus on water-saving priorities. Mediterranean countries have a long standing history of adapting to water scarcity. In many regions the achievements have been impressive, and there are new approaches for integrating all water users in a more coherent management scheme. However, the opportunities and limitations for implementing the solutions in all areas are diverse. And climate change will affect availability, access, stability, and utilization of water, making the challenge even greater (Iglesias et al., 2008).

Significant progress in reaching environmental and social targets on water use in the Mediterranean - particularly in areas with large ecosystem degradation - requires a collective effort across sectors. Increasing water use efficiency to meet agricultural demands is necessary, but is not sufficient. It is possible, however, to significantly improve water service to agriculture where it has been lagging behind, and thus improve current and future imbalances. This would slow the trend towards degradation of the environment and displacement of the rural population to urban areas, which is often driven by the low productivity and instability of dryland farming in Mediterranean countries. To achieve this, however, is important is to design and facilitate the transition towards local adaptation solutions. Adaptation will not happen by chance. This paper explores the regional barriers from the technical, social and economic points of view and discusses the scenarios for the future.

2. DIAGNOSIS: TWO OBJECTIVES OF WATER ADAPTATION MEASURES

Ensuring there is enough water for food, for people and for ecosystems implies visions about availability - being sufficient water -, accessibility - both physical and economic access -, and adequacy - being safe for ecosystems and human consumption. In this section we address the two main objectives of water adaptation measures.

2.1 Improve the ecosystem service of water

In areas exposed to water scarcity water is a limiting factor for development and is therefore considered a scarce resource. The adequate protection of aquatic ecosystems may further reduce water availability for consumptive uses. Competition for water will intensify with climate change. As an illustration, Figure 1 shows the projected changes in water availability in European countries for the short term (2040) and long term (2080) scenarios under emission scenarios RCP4 and RCP8, showing the strong reduction of water availability in the Mediterranean and implying limitations in many economic sectors. Current and future policy call for greater water allocation for ecosystem services. The scenarios that combine climate change with the social and environmental demands of water are essential for water policy formulation.

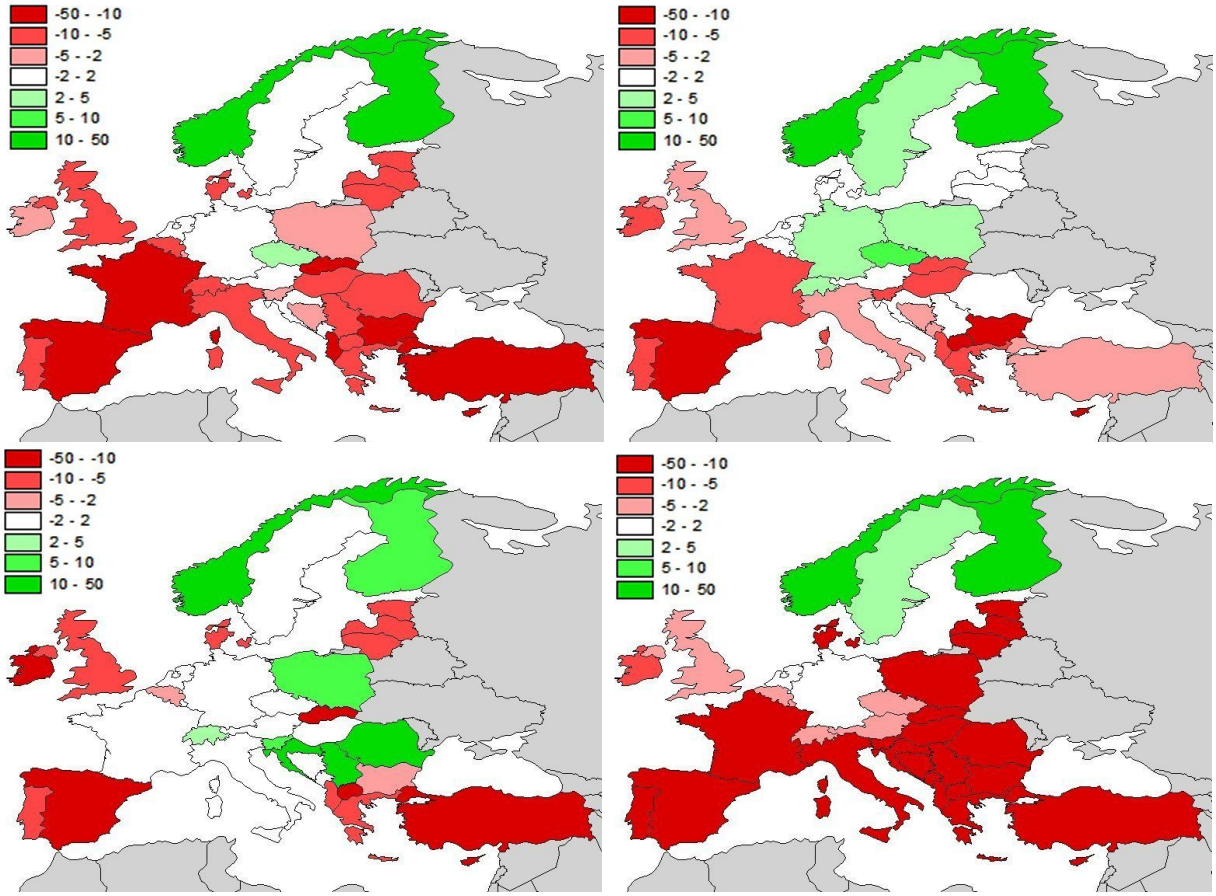

Figure 1. Average results by country of changes in surface water availability. Emission scenarios RCP4 (top) and RCP8 (bottom), in short term 2040 (left) and long term2080 (right) time slices.

2.2 Improve the social service of water

It has long been recognized that a stable and reliable supply of water for farmers reduces rural poverty. This was in fact the rationale behind the large irrigation projects developed during the past

century and continues to be one of the main objectives of water policy. By enhancing rural income, water for agriculture reduces farmers' reliance on external inputs and state subsidies. Indeed, rural areas with widespread irrigation, have more than double income than dryland areas.

The ability of societies to anticipate and face an external shock is often called their adaptive capacity. When the external shock is less water, this adaptive capacity is often linked to essential components of a country's development status and of the sustainability of its socio-economic model. The overarching importance of the water sector is best exemplified by its central role in two of the main development approaches – namely pro-poor growth and human capacity development.

The poor disproportionately bear the brunt of a weak water sector (UN 2010). Pro-poor growth policies seek to reduce overall poverty levels by enhancing the ability of poor people to participate in, contribute to, and benefit from growth (OECD 2006). Given the predominance of rural livelihoods in most low-income countries, problems in water availability, quality and management are likely to have a greater impact on poorer and more marginalized social sectors. For this reason water management has tangible pro-poor enhanced rights effects. Rights based policies are concerned with water accessibility. This involves the duties of providers and the rights of beneficiaries and their ability to supply and access water respectively. It also brings up issues of water quality and water conflicts all of which impinge upon a people's ability to access water.

An ineffective water sector reinforces inequalities and has negative economic impacts, a strong water sector can foster equality while creating opportunities for the disadvantaged. For instance, securing water rights and availability helps disadvantaged people move away from conditions of poor sanitation, high mortality rates or environmental degradation while creating opportunities for furthering education and employment. This, in turn, promotes people's capacity to achieve higher levels of education, health, and employment.

Efficiently dealing with climate change impacts will imply choosing between conflicting water needs in a way that maximizes adaptive capacity. Choosing between the preservation of valuable ecosystems and the reduction poverty, for instance, is not an easy choice, but successfully managing both needs is of paramount importance. To navigate these difficulties it is necessary to understand how society and water are interconnected, including the synergistic ties that exist between adaptive capacity and development status. Thinking and acting strategically is the only way forward - this implies taking a holistic approach towards water in order to minimize the negative effects of variability and uncertainty.

3. CHANGING ATTITUDES: HOW PEOPLE MAY MODIFY WATER AVAILABILITY

3.1 Strengthening social organisation by co-design of adaptation measures

The uncertainty associated with the definition of strategies for climate change adaptation poses a challenge that cannot be faced by science alone (De Stefano et al., 2016). Understanding stakeholders' perceptions towards solutions is crucial when defining adaptation strategies in order to identify barriers to necessary behavioral changes (Dessai and Sims, 2010), given the strong inter-linkages between problem perception and actions (Giordano and Vurro, 2010; Stoutenborough and Vedlitz, 2014; Urquijo and De Stefano, 2016).

Co-designing adaptation has led to demonstrate the value for public money and efficient use of resources (ref). A recent large-scale study points to the same conclusions in a complex socio-environmental system in southern Spain (Iglesias et al., 2016); the study highlighted that co-design led to burden-sharing arrangements and duties for cooperation and collaboration among stakeholders.

The recent past has demonstrated a high sensitivity of water resources to changes in climate and the resulting effects on the social system. Adaptation planning is inherently challenging and often, restricted by a number of factors, including limitations in the participatory processes with the

stakeholders that will have to adapt in the future. Uncertainties in climate change science and long planning horizons add to the complexity of adaptation decision-making. A further important complication is presented by the difficulties in identifying and linking adaptation and development policies in many areas in the Mediterranean where a large proportion of the population does not have access to clean water and sanitation. The uncertainty of the cost and benefits of the various policies suggested is also a barrier to implement solutions.

3.2 Investing in knowledge

Sometimes, seemingly minor innovations can provide high returns. This is the case of linking knowledge to farmers choices. For example, optimising crop-climate interactions is crucial to adjust the amount of water used to produce food. Possible adjustments include changes in planting dates, varieties, input application and water management in the field. But there are some technical and economic constraints associated with the year to year transformations that require an investment in knowledge.

Optimized crop management and irrigation techniques, not only save water, but also decrease greenhouse gas emissions in Mediterranean regions (Sanz-Cobeña et al., 2016) and reduce agronomic costs (e.g., for weed control or water applied) (Ayars et al., 2015).

Social constraints to change a management practice are largely associated to the limitations in governance or by the perception of the limited value of the management alternative. For example, conventional farmers can be reluctant to implement some of the practices because of strong traditions (e.g., planting always at the same time of year) or having a perception of decreased productivity due to the practice implementation (e.g., adjusting to deficit irrigation in periods of water scarcity to decrease the risk of crop failure), or by the negative perception of the practice by neighbouring farmers (Hussain et al. 2016). A lack of training for practices with high technical or maintenance requirements (e.g., irrigation technology) may cause management difficulties or the misuse and decline of yields, in turn encouraging the negative perception of the practice's effectiveness (Abalos et al., 2013; Cantero-Martínez et al., 2007). Knowledge transfer to water managers and users and to sectors linked to water use (technology, energy, health, agriculture, and tourism sectors) is essential to enable adaptive action.

3.3 Re-thinking reservoir management

Reservoir regulation has been one of the most important strategies for water resources management in Mediterranean countries and has generated significant impacts. A reservoir is a dynamic storage of water, which can be controlled, and is used to balance the irregularity of water resources. Existing reservoirs are being subjected to intense multi-objective demands on limited resources. Reservoir water uses include water supply, flood control, hydropower, navigation, fish and wild life conservation, and recreation. Water quality may also be considered a reservoir purpose when water is provided to assimilate waste effluents. Furthermore, reservoirs are components of complex water resources systems that may expand over a large territory. It is not surprising then that defining optimal reservoir operation for systems of reservoirs with multiple water uses is a challenge.

Reductions of water inflow and increased variability may result in significant decreases in the water availability. This clearly demands for adaptation measures with large impacts to society. In most Mediterranean basins the reductions in water availability will result in impositions of demand restrictions since regulation capacity is already at a maximum.

In a scenario of growing water scarcity, supply and demand will have tojointly managed in increasingly larger and more complex systems. Effective operation of complex systems optimize water availability. The combination of several sources of water supply with different characteristics increases the robustenss and resilience of ewater resources systems. Surface and groundwater

resources show differences in terms of variability and reliability. Even the same kind of resources, such as reservoir regulation, but from different locations, will show the logic differences in terms of hydrological conditions on each site and the characteristics of their hydraulic systems. The maximization of water availability will be obtained through the integration of a large number of water sources and reservoirs in a unique management unit that can best respond to situations of scarcity through optimal management, using every resource for the purposes that is more appropriate depending on its amount, regularity and reliability.

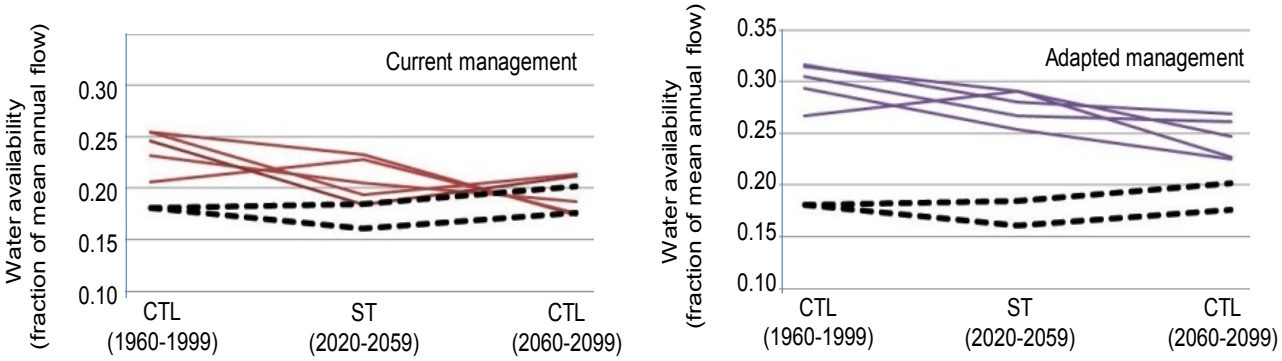

Figure 2. Evolution water availability in the Ebro basin as a fraction of current mean annual runoff. Left: Reference management. Right: Improved water management. The dashed black lines represent the range of estimated water abstractions.

An example of the effectiveness of this strategy is shown in Figure 2, where the projection of water availability in the Ebro basin is compared to the projection of the range of water abstractions in the basin. Water availability projections are computed from runoff estimates obtained with five different climate models under RCP4 emission scenario. The graphic on the left corresponds to reference water management and the graphic on the right correspondos to improved water management by joint optimization of all supply sources and demand nodes in the basin. The projected water scarcity for the long term time slice under reference management disappears as a consequence of the improvement in the management of water resources.

3.4 Transparent and accountable decision making

Other requirements include the need for transparent and accountable decision-making, informed through inclusive and participatory approaches, whereby the views of all stakeholders, including civil society, are considered. With so many competing pressures and drivers, and so many contributing factors to consider, not only in understanding the impacts of climate change, but also in developing adaptation options, it is likely that the decision making process is far from transparent.

It is important to consider whether adaptations are sustainable, or rendered irrelevant by other sectoral drivers. This holistic approach should also ensure that adaptation decisions and investments are both cost-effective and proportionate to the risks or benefits that may be incurred.

This is a particular challenge due to the need to balance and combine different policies to achieve a true integrated water resources management, which will require striking a balance between human resource use and ecosystem protection. This barrier is not a surprise, but has special relevance in the Mediterranean where water policies are often centuries old and socially embedded. Most analysts find reasons to be optimistic given the important role that science and technology will play in increasing adaptive capacity and improving water accessibility. There are however also reasons to be pessimistic. It remains to be seen whether the current inequalities that exist in the Mediterranean will be successfully redressed given the high costs associated with technology transfer for less advantaged regions and countries.

3.5 Adoption of voluntary measures despite disincentives

Citizens save water even in the absence of economic incentives (Iglesias et al., 2017). Most water management measures described in this review require the acquisition of a specific knowledge by the stakeholder that takes or promotes the action, and a more detailed planning in water management activities. However, farmers and water managers promote water saving practices even if they require an initial investment for the acquisition of specific equipment (e.g., irrigation technology for farmers), or if there is a regular cost to maintain the measure (i.e., to support advisory services to optimise crop climate interactions or early warning systems for drought management by the water basin authorities). Further, there are increasing innovative farmers and associations who are implementing adapted water management practices with positive results and are demonstrating their effectiveness and advising to other interested or neighboring farmers. For example the use of monitoring and remote sensing data to irrigate sonly the fields that are under water stress, is becoming clearly useful, economically feasible and with demonstrated water savings.

4. POLICY CHOICES TO OVERCOME THE BARRIERS

Adding the adaptive capacity evaluation to previous policy assessment we can formulate specific recommendations that respond to a range of water scarcity levels and address the weakest component of the adaptive capacity. The policy recommendations formulated in Table 1 vary according to the water scarcity level as described below and have a double aim: (1) to prioritise management strategies; (2) to evaluate synergies between environmental and development policies.

4.1 Low to medium water scarcity

In conditions of low to medium water scarcity where social and economic drivers of inequality prevail, policies should foment social and economic development policies that will improve policy formulation and implementation in the future, thus minimizing the risks of climate change impacts. In this case, basic needs such as education and health need to be taken care of. At the same time, in contexts of climate change, a longer term strategy that seeks to diversify a country's economy could also help mitigate the effects of climate change impacts.

Where water scarcity remains at low to medium levels and inequality is driven by technological eco-efficiency and natural capital, then environmental mitigation policies are recommended. Some policy options might include the development of more efficient technologies that would reduce water use in key economic activities.

When water scarcity is low or medium and climate drives inequality then current policies should be adjusted for adaptation. Policy options might include fostering greater flexibility in water storage options in order to choose those that will maximize sustainability and effectiveness. Other options could be building or improving physical infrastructure to prevent the risk of extreme events or developing safety net programmes to strengthen livelihood asset availability for vulnerable populations.

4.2 High water scarcity

If water scarcity levels are serious or very serious and social and economic drivers of inequality prevail, then pro-poor water management policies are recommended. Effective policies might include the development of micro-irrigation technologies, or the promotion of mechanisms that allow an integrated management of groundwater and surface water.

If water scarcity is serious or very serious and technological eco-efficiency or natural capital drive inequality then the most appropriate policies would be those that reform institutions for the

resolution of water conflicts. These reforms would imply developing a more holistic approach for the management of shared water resources that ensure that different user needs are taken care of. Increased cooperation and information-sharing at sub-national, national and even regional levels will be required in order to prevent water conflicts from aggravating.

Finally in conditions of serious to very serious water scarcity where climate drives inequalities than climate-driven policies that allow adaptation and a greater paradigm shift should be put in place. In this case, profound reforms aimed at transforming a country's economic activity should be emphasized. Particularly in agriculture-dependent countries the strengthening of other economic sectors such as industry or tourism would be in order.

The policies outlined above show that, for the water sector, planned interventions must consider both supply side and demand side solutions. On the supply side, adaptation options involve increases in storage capacity or abstraction from water courses; demand-side options, like increasing the allocative efficiency of water to ensure that economic and social benefit is maximised through use in higher-value sectors, aim to increase value per volume used and to ensure that quality is maintained. All in it becomes clear that the water sector's importance for numerous other productive and social arenas requires policies and management strategies to be well aware of water's widespread impacts.

Table 1. Proposal of potential policy interventions based on water scarcity and adaptive capacity

Water scarcity levels	Main barrier to adaptation	Policy Recommendations
Low to medium	Social and economic factors	Promote pro-poor management Promote health and education Improve access to water for production and sanitation
	Technological eco-efficiency & natural capital	Focus on environmental mitigation Promote more efficient technologies Reduce water use
	Climate	Promote flexible water storage options Invest in physical infrastructure Develop safety net programmes
Serious to very serious	Social and economic factors	Develop micro-irrigation technologies Integrate ground and surface water management
	Technological eco-efficiency & natural capital	Reform conflict prevention institutions. Promote information sharing and cooperative management
	Climate	Promote policies that help create a paradigm shift Design adaptation policies Develop new alternative sectors

5. CONCLUSIONS

Moving towards sustainability is vital for future water security and an essential component of climate change adaptation. There are a number of identified and well tested measure that could be adopted in order to make this transition. As the climate becomes more volatile, implementing adaptation to less water is now critical. The approach to impacts and adaptation presented in this study provides options for wide-ranging water scarcity problem.

Credible socio-economic scenarios are required to provide a framework for adaptation decision-making for practitioners and adaptation measures must include future climate and socio-economic scenarios. There may be many simple adaptation measures that could theoretically be introduced to address a particular risk or opportunity, these may only be practically possible under certain circumstances. For example, improving efficiency of irrigation or introducing water metering may only be options for societies that already have an understanding of alternative technologies, and who know how to encourage implementation.

A critical challenge for consideration is that of finance. Many potential adaptation options are low-cost and technically manageable by individual water managers. However there are also adaptations that require large scale and long-term effort, either water district management or in infrastructure development. In order for policy to be able to consider and take up such options, it

may be necessary for financial support mechanisms to be made available.

Finally, adaptation is unlikely to be facilitated through the introduction of new and separate policies, but rather by the revision of existing policies that currently undermine adaptation and the strengthening of policies that currently promote it. If adaptation is to become "mainstreamed", it will be necessary for relevant polices, such as the CAP and the Water Framework Directive to address the issue more directly.

ACKNOWLEDGEMENTS

We acknowledge the financial support of the European Commission BASE project (Grant agreement no: ENV-308337) of the 7th Framework Programme (http://base-adaptation.eu).

REFERENCES

Alexander, M., Priest, S. &Mees, H. (2016).A framework for evaluating flood-risk governance. Environmental Science & Policy, 64: 38–47. DOI: 10.1016/j.envsci.2016.06.004

Briguglio, M., Delaney, L. & Wood, A. (2016).Voluntary recycling despite disincentives. Journal of Environmental Planning and Management, 59: 10, 1751–1774. DOI: 10.1080/09640568.2015.1086323

García de Jalón S, Silvestri S, Granados A, Iglesias A (2015) Behavioural barriers in response to climate change in agricultural communities: An example from Kenya. Regional Environmental Change, 15, 851-865

Garrote L, Granados A, Iglesias A (2015) Strategies to reduce water stress in Mediterranean river basins. Science of the Total Environment (in press)

Garrote L, Iglesias A, Granados A, Mediero L, Martin-Carrasco F (2015) Quantitative Assessment of Climate Change Vulnerability of Irrigation Demands in Mediterranean Europe. Water Resources Management, 29 (2): 325-338. DOI 10.1007/s11269-014-0736-6

Granados A, Martín-Carrasco FJ, García de Jalón S, Iglesias A (2015) Adaptation of irrigation networks to climate change: Linking robust design and stakeholder contribution. Spanish Journal of Agricultural Research (in press)

Iglesias A, Garrote L (2015) Adaptation strategies for agricultural water management under climate change in Europe. Agricultural Water Management, 155 (2015) 113–124

Iglesias A, Sánchez B, Garrote L, López I (2015) Towards adaptation to climate change: water for rice in the coastal wetlands of Doñana, Southern Spain. Water Resources Management (in press)

Lampurlanes, J., D. Plaza-Bonilla, J. Álvaro-Fuentes, C. Cantero-Martínez (2016) Long-term analysis of soil water conservation and crop yield under different tillage systems in Mediterranean rainfed conditions

Proceedings of the 10th World Congress of EWRA 'Panta Rhei', 5-9 July 2017, Athens, Greece
© 2017 *European Water Resources Association*

Sensitivity analysis of a probabilistic flood inundation mapping framework for ungauged catchments

G. Papaioannou[1*], A. Loukas[1], L. Vasiliades[1] and G.T. Aronica[2]
[1] *Laboratory of Hydrology and Aquatic Systems Analysis, Department of Civil Engineering, University of Thessaly, Pedion Areos, 38334 Volos, Greece*
[2] *Department of Civil Engineering, Computer Science, Building, Environmental Science, and Applied Mathematics, University of Messina, Contrada Di Dio, 98166 Villaggio S. Agata - Messina, Italy*
[*] *e-mail: gpapaioa@uth.gr*

Abstract: A common natural disaster worldwide is flash-floods. Usually, the catchments affected by flash floods are ungauged. The absence of flood records leads to remarkable uncertainty in floodplain modeling and mapping estimation. In this study, a probabilistic framework for floodplain mapping has been developed to assess the uncertainty related to the roughness coefficient parameter used in hydraulic-hydrodynamic modeling. The popular hydraulic-hydrodynamic model HEC-RAS was implemented using a Visual Basic Monte Carlo code, to assess roughness coefficient uncertainty at ungauged catchments. A high-resolution DEM, created by Terrestrial Laser Scanner data has been used. Pebble count field surveys and empirical formulas have been used for the estimation of the initial Manning's n roughness coefficient value. Several probability distribution functions were fitted to the estimated roughness coefficient values and evaluated using various "goodness-of-fit" criteria. The Manning roughness coefficient values were sampled using Latin Hypercube sampling technique. Finally, flood inundation probability maps have been produced. The validation process is based on historical flood extent data, a binary wet-dry interpretation and the use of Median Absolute Percentage Error as an evaluation statistical measure. The proposed framework have been implemented at the ungauged Xerias stream watershed, Volos, Greece. The proposed floodplain mapping uncertainty framework justified through a detailed sensitivity analysis. The results indicate that the proposed framework enables probabilistic flood hazard mapping and may assist the decision-makers to devise better flood risk mitigation strategies for ungauged catchments.

Key words: probabilistic flood mapping; uncertainty analysis; Monte Carlo; ungauged streams

1. INTRODUCTION

Hydrologic hazards are an important category of natural hazards that preoccupy humans from ancient times. One of the most important hydrologic hazards is floods. The last decades have been observed a positive trend in the appearance of extreme flood inundation events (Hall et al., 2014). A typical category of extreme flood inundation events is flash floods for which the mortalities, structural damages, and economic losses are immense (Aronica et al., 2012). Usually, the areas affected by flash floods are small and medium sized ungauged catchments and appropriate flood data are not available due to the nature of the extreme event.

The use of gauged data, for calibration and validation of the hydraulic-hydrodynamic models, is the most common approach in floodplain modeling and mapping process (Bates et al., 2006). The flood inundation areas evaluation can be achieved using deterministic and/or probabilistic hydraulic approaches. However, in areas where sufficient data are not available, the typical deterministic hydraulic-hydrodynamic modeling approaches may result in erroneous outcomes due to the neglection of several sources of uncertainty (Alfonso et al., 2016). The prime uncertainty factor in floodplain modeling and mapping is the Digital Elevation Model (DEM) accuracy and it may be minimized with the use of DEM derived by new advanced topographical survey methods such as Airborne Laser Scanner (ALS), Terrestrial Laser Scanner (TLS), and Unmanned Aerial Vehicles (UAV). On another study of Papaioannou et al. (2016), it has been shown that the hydraulic-hydrodynamic modeling selection (1D, 2D, 1D/2D) may be insignificant when high-quality DEM

data are used. The usual hydraulic-hydrodynamic modeling choice when applying the probabilistic hydraulic approach using Monte Carlo analysis is 1D hydraulic models (Di Baldassarre et al., 2010).

Another source of uncertainty, especially for one-dimensional (1D) hydraulic-hydrodynamic models, is the uncertainty in the values of roughness coefficient. Many studies have investigated the effect of roughness coefficient in floodplain modeling and mapping using gauged data or adequate amount of data (Kiczko et al., 2013). However, there is a gap of knowledge in ungauged streams and a detailed investigation is needed. An uncertainty analysis framework of floodplain mapping due to roughness coefficient has been developed in this study. The hydraulic-hydrodynamic model HEC-RAS has been used in the modeling analysis. The framework has been implemented at the ungauged watershed of Xerias stream, Volos, Greece.

2. STUDY AREA

The location of the study area is the ungauged Xerias stream watershed, Thessaly region, Magnesia prefecture, Greece (Fig. 1). The extreme flood event of the October 9th, 2006 has been examined. A Clark Instantaneous Unit Hydrograph (CIUH) of the specific extreme event have been created and validated in a previous study (Papaioannou et al., 2016). The validation area (Fig. 1) have been set up using several sources such as newspaper reports, reports from local authorities, local residents' interviews and testimonies of flood victims (Papaioannou et al., 2016). The selection of the study stream reach of 2.2 km length was based on the major impacts of the flood event on that area and the stream geometry (Fig. 1). A detailed river and riverine area topography of the selected area created with the use of Terrestrial Laser Scanner (TLS) data (Papaioannou et al., 2013). Further details about the DEM creation, the watershed characteristics and the flood event of the October 9th, 2006 of the study area can be found on a number of previous publications (Papaioannou et al. 2013; 2015; 2016).

3. METHODOLOGY

A generic probabilistic framework for floodplain mapping for the assessment of the roughness coefficient uncertainty at ungauged streams has been developed and presented in this study. Figure 2 presents the flowchart of the proposed framework. The efficiency of the framework is evaluated using some prerequisite data, such as: 1) high-quality DEM, 2) bed material sampling 3) estimated hydrograph, 4) estimated flood validation area. The DEM creation, the hydrograph estimation and the estimated validation flooded area have been extensively presented in previous studies (Papaioannou et al. 2013; 2016). In this paper, the main parts of the framework presented are: the pebble count field survey, the estimation of Manning roughness value using several empirical formulas, the theoretical probability distribution fitting on the estimated Manning roughness values, the Manning roughness values generation using Latin Hypercube Sampling (LHS) and the hydraulic modeling (HEC-RAS 1-D model) using a Visual-Basic Monte Carlo code for the estimation of flood inundation probability maps (Fig. 2). It should be stated that all the steps of the proposed framework have been designed to minimize subjectivity and to generalize its applicability in other ungauged stream catchments with similar characteristics.

3.1 Hydraulic modeling

The selection of the 1D modeling approach is usually preferred because of the minimum input data requirements; it is not computationally expensive; there is a wide variety of freeware software and the modeling efficiency in flood inundation processes is established (Tsakiris, 2014). The acclaimed HEC-RAS one-dimensional (1D) hydraulic-hydrodynamic model has been selected and

used in the proposed framework. The river and riverine area geometry have been estimated using the HEC-GEORAS tool, and the TLS derived DEM. To benefit from the high-resolution DEM and avoid sensitivity of water surface profiles due to cross section spacing (Sarhadi et al., 2012) the cross-section spacing assigned to 1 m. The estimated CIUH have been used as input flow hydrograph. A Wolman pebble count field survey (Ward et al., 2016) conducted in Xerias stream by counting approximately 1000 samples from the river bed using a zig-zag pattern. According to pebble count analysis several standard size diameters, such us d_{50}, d_{65}, d_{75}, d_{84}, and d_{94}, have been estimated. Afterwards, the initial Manning's roughness coefficient (n) values were estimated using several empirical formulas. Finally, many theoretical probability distributions (e.g. Normal, Lognormal, Gamma, Logistic) were fitted to the initial roughness coefficient values and evaluated using several goodness-of-fit statistics and criteria for the optimum generation of roughness coefficient values with LHS. The optimum choice of theoretical probability distribution (i.e. Lognormal) was selected for the framework setup. Additionally, the theoretical probability distributions, Gamma, Weibull, Uniform, which have been successuly passed the statistical tests, have been used for sensitivity analysis.

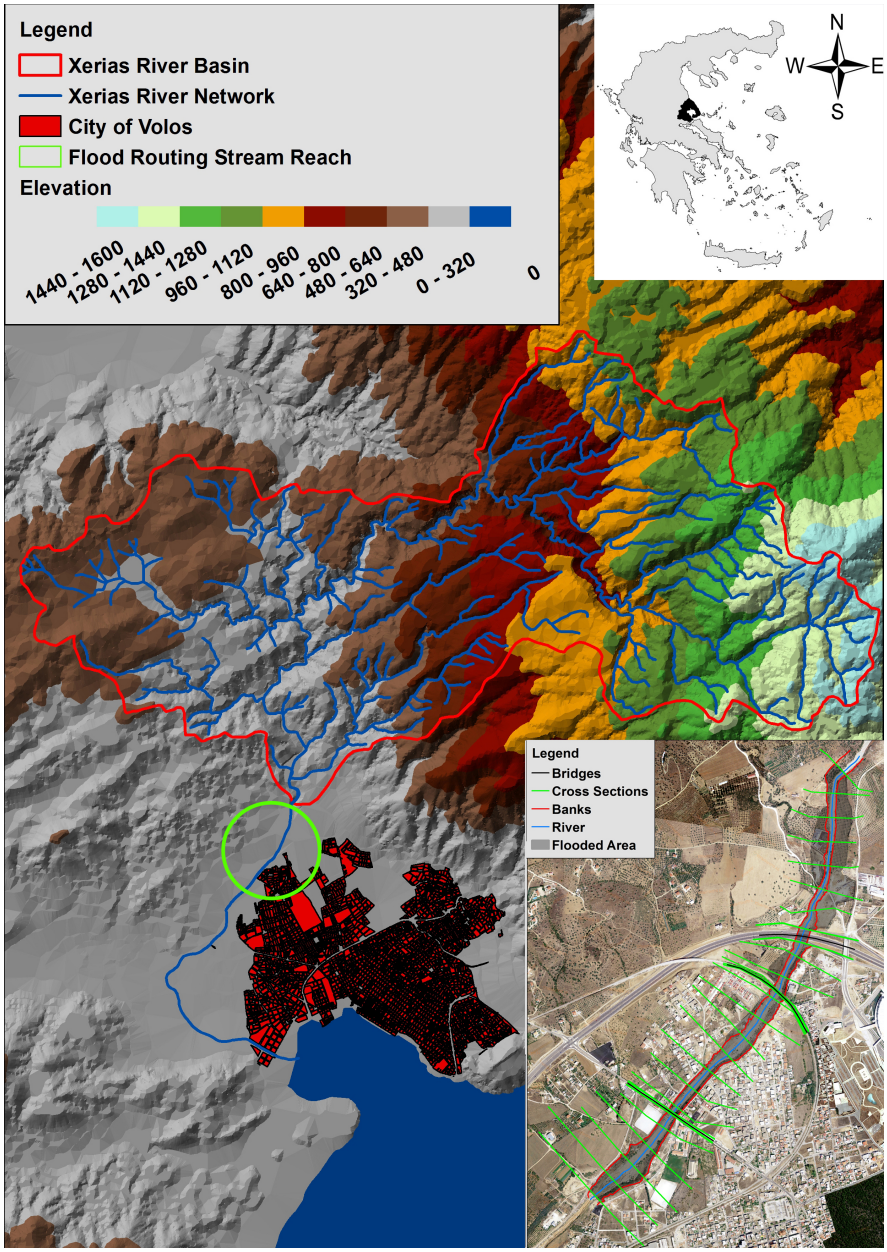

Figure 1: Study area and the selected stream reach with the observed flooded area.

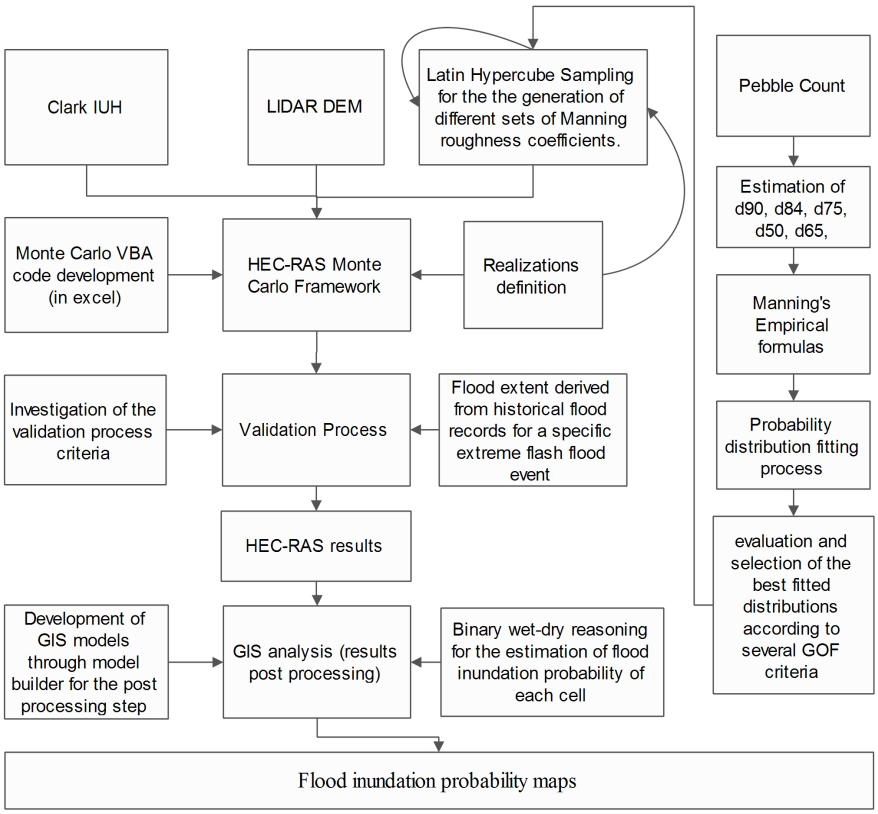

Figure 2: Flow diagram of the proposed framework.

3.2 HEC-RAS Monte-Carlo framework

The structure of the proposed framework is based on the manipulation of HEC-RAS software through Excel VBA routines and the linking of the outcomes with some geoprocessing tools in ArcGIS for the creation of the flood probability maps. The VBA routines have been created by the authors and some of them are based on the work of Goodell (2014). The operator of the framework should apply the following steps: a) adjust the number of desired acceptable solutions for probabilistic flood inundation mapping, b) import the desired Manning roughness coefficients data sets, and c) choose the statistical criteria based on the internal validation process for uncertainty analysis. For the estimation of Manning roughness coefficients data sets, the Latin Hypercube Sampling (LHS) is used. Several statistical quantitative metrics, such as the MSE, RMSE, MAE, Bias and MdAPE, have been tested for the selection of the acceptable runs by comparing the simulated flood inundation area with the respective observed area. The unbiased qualitative criterion of Median Absolute Percentage Error (MdAPE) (Hyndman and Koehler, 2006) have been selected for the validation of the framework. The selection of the validation criterion was based on several sensitivity analysis tests and the distribution resemblance of the qualitative criterion to the qualitative criterion of Critical Success Index (CSI) for the flood inundation area. The threshold of MdAPE for the acceptable runs was set to 20% (with a best fit to 16%) after preliminary sensitivity analysis of the employed statistical criteria. Finally, the acceptable realizations have been used for the creation of the flood inundation probability maps with a binary wet-dry reasoning in order to estimate the flood inundation probability of each cell. For computational purposes the probability maps were classified in 10 probability classes: 0-10%, 10-20%, 20-30%, 30-40%, 40-50%, 50-60%, 60-70%, 70-80%, 80-90%, 90-100%.

A brief description of the framework operation summarized in the following steps: 1) Import the input data to the framework, 2) In each simulation run the system assign a new roughness coefficient value is sampled from a probability distribution with the use of LHS, 3) In each

simulation run the system estimate the selected statistical criterion by comparing the simulated flood extent with the observed flood extent for all cross sections, 4) The framework approve or discard the simulation according to the MdAPE threshold, 5) A new simulation is assigned with a new Manning roughness coefficient value. The procedure continues until the pre-defined number of realizations of acceptable solutions is reached (e.g. 1000 realizations) and then, the entire process is terminated.

In order to examine the sensitivity of the proposed framework, the following different configuration sets have been employed: 1) Different realization sets applied using the best fitted probability distribution (i.e. Lognormal) for Manning's n sampling: 100, 200, 500, 1000, 2000, 5000 realizations, 2) Gamma, Weibull, and Uniform probability distributions for Manning's n sampling have also been examined for 1000 realizations, 3) Two extra validation threshold values of MdAPE, 22% and 18%, were examined, 4) Five river cross section spacings have been examined with distance varied from 2 m to 32 m (i.e. 2 m, 4 m, 8 m, 16 m and 32 m).

The flood inundation probability mapping of the above sensitivity analysis results have been compared with the respective results for the best configuration of the framework which is using 1000 relations, use of Lognormal probability distribution, a threshold 20% and river cross section spacing of 1m. The results are presented in the next paragraphs.

4. RESULTS

The proposed framework has been implemented at the ungauged Xerias stream reach, Volos, Greece (Fig. 1). The 1D HEC-RAS model has been used for probabilistic floodplain mapping that assesses the uncertainty related to the roughness coefficient. The framework applied for the extreme flash flood event of the October 9th, 2006. All the flood probability results were compared and examined based on their spatial distribution and the proposed probability classes categorization. Figure 3 presents the flood inundation probability map where each pixel express the probability of flooding incorporating the uncertainty introduced by the roughness values selection. The results have been acquired using the best simulation set up (i.e. using 1000 relations, use of Lognormal probability distribution for Manning's n sampling, a threshold of 20% value of MdAPE, and river cross section spacing of 1m). In the same figure, a high-resolution aerial orthophoto can been seen in order to emphasize the display of the inundated area (ten probabilistic classes) and the flood hazard (Fig. 3). Also, the optimum flood extent using a deterministic application of HEC-RAS is presented with a red line and the validation area with a black line for comparison (Fig. 3).

The first sensitivity test of the framework achieved using different realization sets and the best-fitted probability distribution (i.e. Lognormal). Thus, the methodology was run for 100, 200, 500, 1000, 2000 and 5000 realizations. These results indicated that the flood probability map is affected by the number of realizations for realizations less than 1000 realizations. For larger than 1000 realizations the system becomes almost insensitive (Fig. 4a). More specifically, the results of these analysis indicates that the flood inundation probability maps using 100, 200, 500, 1000 and 2000 realizations number differ from the 5000 realization number flood inundation probability map by 4.94%, 2.66%, 1.49%, 0.63% and 0.59% respectively. The effect of the number of realizations on simulation results has a consistent power pattern, as may be seen in Figure 4a.

The sensitivity of the method on the selection of probability distribution for the generation of the Manning roughness coefficient has been examined using three probability distributions (i.e. Gamma, Weibull and Uniform). The Gamma and Weibull probability distributions were two of the probability distributions which are satisfactorily fitted to the empirical values and they have passed the statistical goodness-of-fit criteria. The Uniform probability distribution has been used in the sensitivity analysis because is a common probability distribution used in similar studies (e.g. Dimitriadis et al., 2016). Figure 4b presents the results of the analysis and indicates that the flood

inundation probability maps using the Gamma, Weibull and Uniform probability distributions differ from the flood inundation probability map of the best-fitted Lognormal probability distribution by 1.53%, 4.48% and 19.22%, respectively. These results emphasize the importance of the appropriate probability distribution selection.

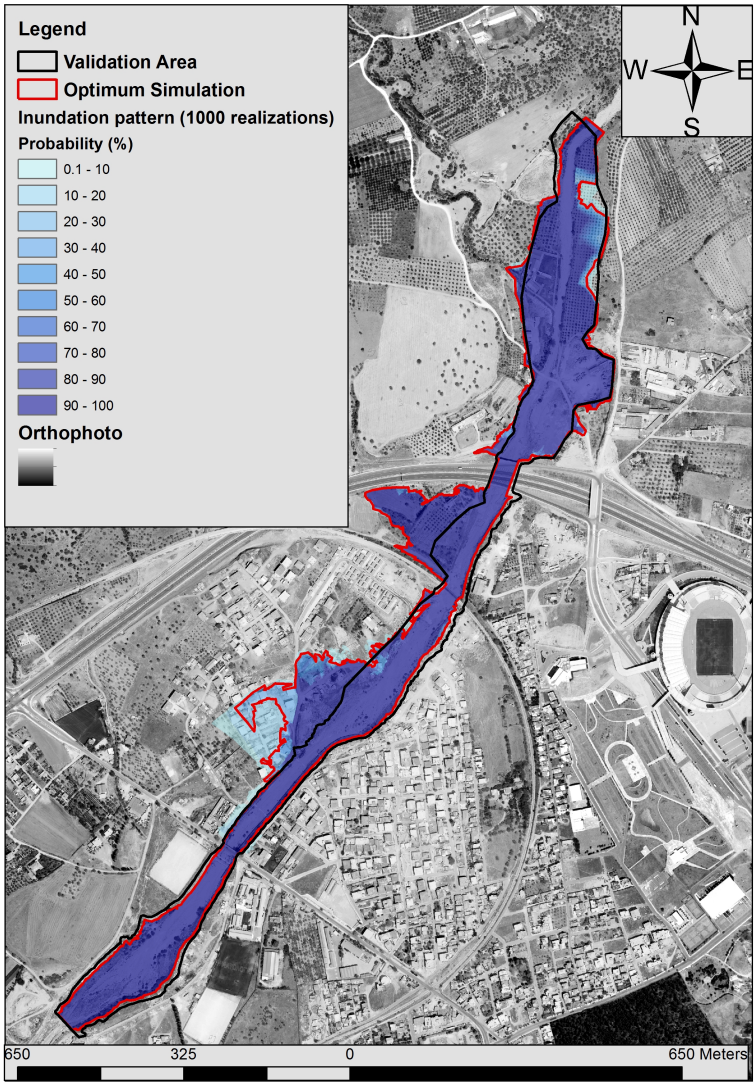

Figure 3: Flood inundation map for the best framework configuration (i.e. using 1000 realizations, lognormal probability distribution for roughness coefficient generation, MdAPE threshold 20% and 1 m cross section spacing).

The analysis of the threshold value selection showed that the flood probability map is sensitive to threshold changes (Fig. 4c). In particular, the results of flood inundation probability map using 18% and 22% of MdAPE threshold differ from the respective results using 20% MdAPE threshold by 11.73% and 10.69% , respectively (Fig. 4c).

The sensitivity on the cross section spacing used spacings of 2 m, 4 m, 8 m, 16 m, and 32 m. These results indicate that there is a significant effect of the river cross section spacing in the flood inundation probability mapping when the distance between the cross sections is equal and larger than 16 m. More specifically, the difference of the results for 2 m, 4 m, 8 m, 16 m, and 32 m cross section spacing result in differences of 2.07%, 3.69%, 3.20%, 8.43% and 13.29%, respectively, in the flood probability map (Fig. 4d). In Figure 4d can be seen that effect of the river cross section spacing has a consistent linear pattern.

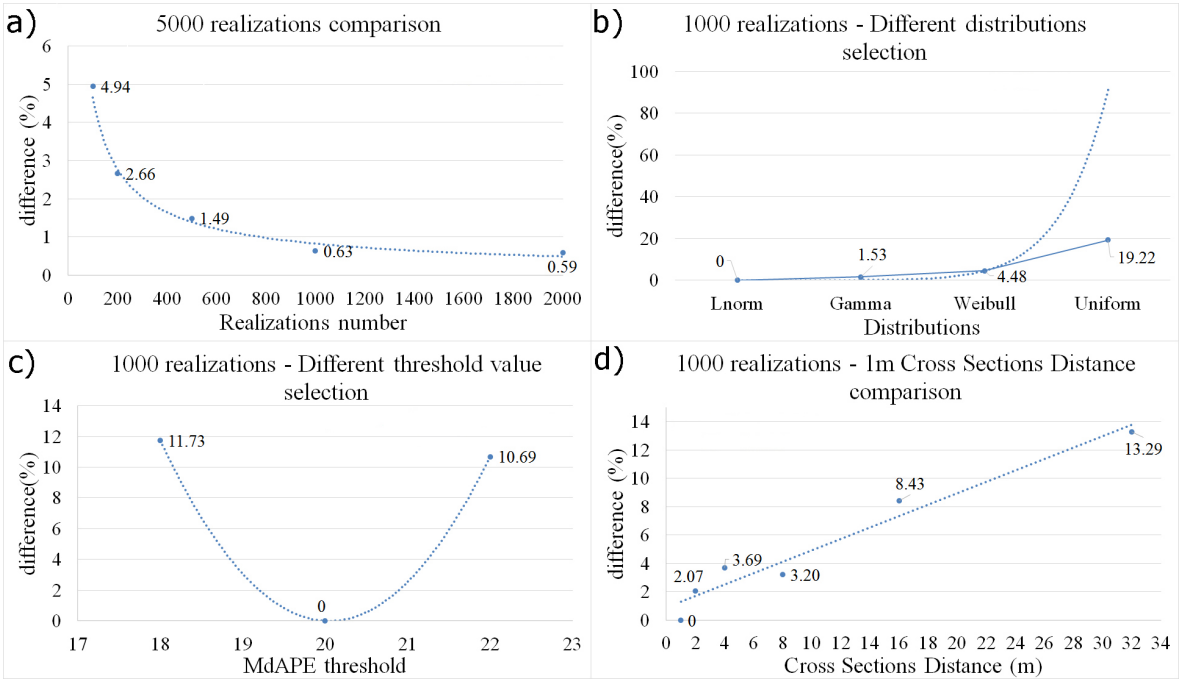

Figure 4: Framework sensitivity analysis using: a) Different realizations sets, b) Different distributions selection, c) Different threshold values, d) Different cross section distances selection

5. CONCLUSIONS

In this study, a floodplain mapping uncertainty framework for ungauged streams has been developed and implemented in complex riverine topography with cobble and gravel bed materials. The methodology is based on limited data using only flood extent data. Several sensitivity tests have justified the structure of the proposed floodplain mapping uncertainty framework using the following configurations: a) Lognormal probability distribution for Manning's n roughness coefficient sampling, b) 1000 realizations, c) MdAPE equal to 20% for the selection of the acceptable simulations, d) 1 m spacing of the cross sections. The results obtained from the application of the proposed framework compare well with the estimated data of flood extent for a historical flood event.

REFERENCES

Alfonso, L., Mukolwe, M. M., and Di Baldassarre, G., 2016. Probabilistic Flood Maps to support decision-making: Mapping the Value of Information, Water Resour. Res.: 52:1026-1043, doi:10.1002/2015WR017378.

Aronica, G. T., Brigandi, G., Morey, N., 2012. Flash floods and debris flow in the city area of Messina, north-east part of Sicily, Italy in October 2009: the case of the Giampilieri catchment. Nat Hazards Earth Syst Sci.: 12:1295-1309. doi:10.5194/nhess-12-1295-2012.

Bates, P. D., Wilson, M. D., Horritt, M. S., Mason, D. C., Holden, N., and Currie, A., 2006. Reach scale floodplain inundation dynamics observed using airborne synthetic aperture radar imagery: data analysis and modelling, J. Hydrol.: 328(1-2):306-318

Di Baldassarre, G., Schumann, G., Bates, P. D., Freer, J. E., Beven, K. J., 2010. Floodplain mapping: a critical discussion on deterministic and probabilistic approaches, Hydrolog. Sci. J.: 55:364-376.

Dimitriadis, P., Tegos, A., Oikonomou, A., Pagana, V., Koukouvinos, A., Mamassis, N., Koutsoyiannis, D., and Efstratiadis, A.: Comparative evaluation of 1D and quasi-2D hydraulic models based on benchmark and real-world applications for uncertainty assessment in flood mapping, J. Hydrol., 534, 478-492, 2016.

Goodell, C., 2014. Breaking the HEC-RAS code: A user's guide to automating HEC-RAS, h2ls, Portland, USA.

Hall, J., Arheimer, B., Borga, M., Brázdil, R., Claps, P., Kiss, A., Kjeldsen, T. R., Kriauciuniene, J., Kundzewicz, Z. W., Lang, M., Llasat, M. C., Macdonald, N., McIntyre, N., Mediero, L., Merz, B., Merz, R., Molnar, P., Montanari, A., Neuhold, C., Parajka, J., Perdigão, R. A. P., Plavcová1, L., Rogger, M., Salinas, J. L., Sauquet, E., Schär, C., Szolgay, J., Viglione, A., and Blöschl, G. 2014. Understanding flood regime changes in Europe: a state-of-the-art assessment. Hydrol Earth Syst Sci: 18:2735-2772. doi:10.5194/hess-18-2735-2014.

Hyndman, R. J. and Koehler, A. B., 2006. Another look at measures of forecast accuracy, Int. J. Forecasting: 22(4):679-688, doi:10.1016/j.ijforecast.2006.03.001.

Kiczko, A., Romanowicz, R. J., Osuch, M., Karamuz, E., 2013. Maximising the usefulness of flood risk assessment for the River Vistula in Warsaw. Nat. Hazards Earth Syst. Sci.: 13: 3443-3455, doi:10.5194/nhess-13-3443-2013.

Papaioannou, G., Loukas, A., Georgiadis, Ch., 2013. The effect of riverine terrain spatial resolution on flood modeling and mapping, Proc. SPIE 8795, First International Conference on Remote Sensing and Geoinformation of the Environment (RSCy2013), 87951H, doi:10.1117/12.2028218.

Papaioannou, G., Loukas, A., Vasiliades, L., and Aronica G. T., 2016. Flood inundation mapping sensitivity to riverine spatial resolution and modelling approach, Nat. Hazards.: 83:117-132, doi:10.1007/s11069-016-2382-1.

Papaioannou, G., Vasiliades, L., Loukas, A., 2015. Multi-criteria analysis framework for potential flood prone areas mapping, Water Resour. Manag.: 29(2):399-418, doi:10.1007/s11269-014-0817-6.

Sarhadi, A., Soltani, S., and Modarres, R., 2012. Probabilistic flood inundation mapping of ungauged rivers: Linking GIS techniques and frequency analysis, J. Hydrol.: 458-459:68-86. doi:10.1016/j.jhydrol.2012.06.039.

Tsakiris, G., 2014. Flood risk assessment: concepts, modelling, applications, Nat. Hazards Earth Syst. Sc.: 14:1361-1369, doi:10.5194/nhess-14-1361-2014.

Ward, A. D., Trimble, S. W., Burckhard, S. R., and Lyon, J. G.: Environmental Hydrology, 3rd Edition, CRC Press, 2016.

Proceedings of the 10th World Congress of EWRA 'Panta Rhei', 5-9 July 2017, Athens, Greece
© 2017 *European Water Resources Association*

Using cross-over analysis to support water user discussion about investments in water sources for irrigation

M.J. Nikkels[1,2,3*], J.H.A. Guillaume[4], P. Leith[2], N.J. Mendham[2], P.R. van Oel[1] and H. Meinke[2,5]
[1] *Water Resources Management (WRM) group, Wageningen University, Wageningen, Netherlands*
[2] *School of Land and Food, University of Tasmania, Hobart, Australia*
[3] *Aequator Groen & Ruimte, Harderwijk, Netherlands*
[4] *Water & Development Research group, Aalto University, Helsinki, Finland*
[5] *Centre for Crop Systems Analysis, Wageningen University, Wageningen, Netherlands*
[*] *e-mail: melle.nikkels@wur.nl*

Abstract: Regional long-term water management plans increasingly depend on investments by local water users such as farmers. However, local circumstances and individual situations vary and investment decisions are made under uncertainty. Therefore, the perceived values of costs and benefits may also vary considerably among water users, leading to non-uniform investment decisions. This variation can be explored by examining cross-over points, that is, points of equal preference when comparing alternatives. In a participatory context, cross-over analysis has the potential to structure and strengthen discussions among actors and enhance social learning. This paper presents a framework to use cross-over points in a group setting to support discussions among farmers about strategic investments in irrigation water. The framework is tested in a case study in the Coal River Valley in Tasmania, Australia, where various water sources are available. A discussion workshop is designed to learn from each other's perspectives and investment rationales. Instead of focusing on "what is best", participants engage in a dialogue about when and why a particular water resource is preferable over others for increasing on-farm water availability. These insights can provide valuable background information for investment decisions by other water users, irrigation scheme designers and water managers.

Key words: Cross-over analysis, Discussion support framework, Personal preference, Investment decisions, Irrigation water

1. INTRODUCTION

Changing and variable climatic and economic conditions call for strategic and adaptive decision making regarding strategies to increase sustainable on-farm water availability. Regional long-term water management plans increasingly depend on investments by local water users (Turral et al. 2010). When water user investments are expected to increase regional water availability, a good understanding of how and when investment decisions are made is essential. If multiple water sources are available to water users, comparison of alternatives may lead to a clear preference. However, personal preferences will vary with many variables, including: the heterogeneity of local circumstances and situations; real and perceived uncertainties; personal perceptions of the value irrigation might generate and individuals' tacit knowledge (Dampney et al. 2002). This means that preferences may differ based on the set of factors considered when making a decision, how those factors are integrated, and the values assumed for each of those factors. Farmers have individualised, personal decision rules when making investment decisions, whether implicit or explicit. Assuming that a group of water users would uniformly invest if a model indicates it is "worthwhile" might therefore not be accurate. A better understanding of the personal reasoning that determines water needs and preferences can provide valuable background information for investment decisions by other water users, irrigation scheme designers and water managers.

The concept of cross-over points, i.e. the point where two alternatives have the same preference, shifts the focus to two key questions; (1) *when* does an alternative out-favour another and (2) *what* drives the differences in various settings. Crossover analysis is a broadly applicable concept rather than a specific evaluation method. The concept of a crossover point has been applied in a wide

range of fields and variations, for example in agriculture (Dillon 1993), on farm water storage (Arshad et al. 2014), health care (Boles and Fleming 1996), energy systems Ekren et al. (2009), psychology of humans (Dixon et al. 2003) and birds (Mazur 2000). The concept has also been used to investigate modelled outcomes/recommendations by assessing sensitivity to assumed values for the factors that are taken into account (Guillaume et al. 2016, Hyde and Maier 2006, Ravalico et al. 2010). Crossover analysis has the potential to enhance learning and guide discussion between actors. However, this can only be done when the analytical power of crossover analysis is put in the hands of end users. So far, none of the crossover examples used the experience and expertise of stakeholders to influence the modelling process, as encouraged by Voinov et al. (2016). Further, the previous applications assumed an objective "optimal" outcome and a decision rule that can be captured in a model. This limits their applicability to the present case of interest, where preferences and decisions are at least partly personal or individual.

In this conference paper, we present a discussion support framework (Nelson et al. 2013) that extends the use of the concept of cross-over points to a group setting, aimed at guiding water user discussion about investments in irrigation water sources. To test applicability of the framework, we describe the set-up for a case study in the Coal River Valley in Tasmania, Australia, where multiple water sources are available. Outcomes of these discussions and the full evaluation of the workshop form the basis for continuing research in this field.

2. METHOD

In this section, we present a step-wise framework for using the concept of cross-over points to guide group discussion. Participants discuss 1) How factors under consideration would have to change to switch personal preference, i.e. for a cross-over point to occur and 2) Why and how this cross-over point differs from those of other participants. The framework is in the form of a checklist, to provide as general a definition as possible regarding its applicability in various settings and situations. The checklist defines the aims that the framework may achieve (2.1), the conditions that must be met for the framework to be applicable (2.2), and the steps required to achieve the aims given those conditions (2.3). The facilitator plays a significant role, discussed further in 2.4.

2.1 Aims

The proposed framework is considered suitable to achieve one or more of the following aims:

- Exploring the robustness of personal preferences. Cross-over points offer an alternative when specifying the uncertainty in inputs and parameters a priori may be difficult or undesirable (Guillaume et al. 2016). Understanding the conditions under which a preference changes gives an indication about the robustness of the preference. One can assess: How likely is it that these conditions occur?
- Eliciting personal reasoning. The proposed framework encourages participants to share the factors they consider, how they integrate them, and the values of each factor.
- Improving understanding of where differences in preference come from. When comparing with others, participants get the opportunity to reflect on their own personal reasoning and learn to understand why outcomes differ.
- Providing input to regional planning that depends on individual decision making. Sharing decision rules and preferences might help others to make investment decisions, reach consensus, or provide background information for planning.

2.2 Conditions

The framework is only suitable if ALL of the following conditions are met:

- Preferences are subjective; there is no objective optimum, with uncertainty in evaluation of alternatives and where reasoning is at least partly individual, unformalised, and non-explicit. In other words, what is "best" for me might not be "best" for you and we both have a personal decision rule based on explicit and tacit knowledge to decide what is "best".
- There are at least two discrete alternatives to compare, within which participants have a pre-existing preference, based one or more factors (which may be uncertain or incomplete).
- There is a dialogue situation, for example a group discussion, in which participants have experience with the alternatives and are willing and able to share their reasoning, with minimal reason to withhold information. For this dialogue to be enquiring and critical, participants need to be open to reflection. The participants must conceptualise the comparison of the alternatives as a "tame" problem (Rittel and Webber 1973) in that they can provide or explore the explanation for their personal preference.
- There are means to handle the range of experience/expertise. There is a facilitator that can provide a safe environment for the participants, and who can manage the process and "deepen" the discussion/dialogue.

2.3 Overview of steps

1. Define the aim of the application. Guiding questions are:
   - What is the choice to make?
   - Why is there a need to test for robustness of preferences?
   - Why is there a need for discussion/social learning?
2. Analyse the situation. Guiding steps are:
   - Identify alternatives,
   - Identify existing personal preferences,
   - Identify factors that influence personal preferences,
   - Check if all the crossover-over conditions are met (Go/No-go moment). Only if all the conditions are met, proceed to step 3.
3. Design a workshop, with guiding questions:
   - Who will participate?
   - Where does the workshop take place?
   - How long should the workshop last?
   - What are suitable techniques for facilitating dialogue for the group in question?
   - What is the role of the facilitator and participants? (see 2.4)
4. Define the needs for outputs of the workshop. The outputs depend on the aim but should contain:
   - Evaluating
   - Reporting

2.4 Role of facilitator

The main role of the facilitator is to improve the discussion by focussing on the "why?" Quickly pivoting from identifying a preference to the "why" is intended to increase depth of dialogue, drawing on the expertise, experience and reasoning of participants, related to both personal reasoning and definition/understanding of the factors discussed.

The facilitator informally guides discussion between participants, while looking for:

- Differences within the group and where the differences come from (reasoning);
- Agreements, which could be in the form of thresholds, after which none or all of the participants would change preference.

3. RESULTS

3.1 Aims of the application

The project has a theoretical and a practical component. The theoretical aim is to test whether the framework is applicable (yes/no), and worthwhile (tested by evaluating learning and perceived usefulness). The practical aim is to support discussion among experienced water users about irrigation water sources in the Coal River Valley in Tasmania, in order to provide valuable background information for investment decisions by other water users, irrigation scheme designers and water managers.

Farmers in the Coal River Valley in Tasmania have had experience with irrigation water since the construction of the Craigbourne dam in 1986. Since then, the valley has changed more than anyone expected as the benefits of irrigation water were hugely underestimated (Lejda et al. 2009). Water demand is still increasing, leading to development of other irrigation schemes and recently the use of recycled waste water from neighbouring communities.

Experienced water users are likely to have gathered skills and information that influenced their irrigation water demand and therefore preferred water source. What would be their preference if they would have to make an investment decision now? It could be beneficial for other farmers to learn from the insights of those with experience when having to make an investment decision or for other stakeholders when designing new irrigation schemes in comparable valleys.

3.2 Situation analysis

In October-November 2016, we conducted in-depth interviews, consisting of an accompanied survey and a semi-structured interview, lasting 1-2 hours, with 13 members of the executive committee of the Coal River Products Association. The elected members represent the range of enterprises in the valley. The members all know each other and have a history of knowledge sharing as they have organised monthly meetings to discuss a wide range of topics related to farming in the valley since 1967. The interview findings gave us sufficient confidence that all the conditions (2.2) were met to proceed and organise a workshop, with its set-up described in 3.3.

There are currently multiple, very distinct (Table 1) water sources in the valley, three of which we selected as the most relevant to discuss.

- Water from the Craigbourne dam, being the oldest and first source of irrigation water that farmers invested in. http://www.tasmanianirrigation.com.au/index.php/schemes/south-east-stage-1
- The use of treated waste water from nearby municipalities. Waste water from the nearby city of Hobart might provide a future extension of this water source. http://www.taswater.com.au/Customers/Recycled-Water
- Water from South East Stage 3 (SE3), coming from the river Derwent, the flow of which is mainly controlled by releases for hydroelectric power generation. The River Derwent has the potential to sustainably provide much more irrigation water than it currently does, however, the development of irrigation schemes is dependent on investment of both water users and the state. http://www.tasmanianirrigation.com.au/index.php/schemes/south-east-stage-3

All the participants mentioned cost, quality, reliability and manageability as being important for their water source preference. Manageability reflects tradability with neighbours, but also the flexibility for using the water (is the water available on demand or is it provided as a constant flow over the summer?). However, these factors, or “characteristics” as farmers called them, encompass different definitions that might also influence preferences. Depending on what farmers grow with the water, their preference and willingness to pay changes. In a sense, the non-monetary variables can bridge the gap between the cheapest and most expensive source, possibly making the latter worthwhile. One farmer said: “The two characteristics I find most important are high security and

high quality. For that, I pay whatever I need to pay to irrigate my orchard". Another farmer said: "I will deal with whatever reliability or quality but I am really focussed on cost. Cost is actually all I look at; if it gets higher than I want to pay, I will not grow a crop and will sell my stock."

Table 1. Water sources and range of values for the most relevant characteristics

	Craigbourne Dam	**Reuse**	**SE3**
Costs, including both capital and ongoing annual costs to get water at farm gate and costs to put it in the farm dam	Middle	Low	High
Quality	Variable but often too poor for sensitive crops	Comes with restrictions	Almost drinking water quality
Reliability	60-90%	80-100%	95% (according to Tasmanian Irrigation)

We divided the enterprises into three types: livestock, annual cropping and perennial cropping. As shown in Table 2, these enterprises have different demands for water.

Table 2. Demands for water, based on enterprise

	Livestock	**Annual cropping**	**Perennial cropping**
Cost (Willingness to pay)	Low	Middle	High
Quality demand	Low	Middle	High
Reliability demand	Low	Middle	High
Manageability	High	Middle	Low

We also learned that (valuation of) characteristics of both water sources and enterprises have changed in the past and are likely to change in the future. Over the years, the willingness to pay has changed; One farmer stated: "I remember when water from the Craigbourne costed 15 $/ML (1000 m^3) and it went to 20 $/ML and we all thought it was too dear. Sometimes you have got to pinch yourself and realise that I'm about to spend 250,000 dollars just to get access to 50 ML of water. If someone would have told me this 10 years ago, I would have thought he was living in fairyland but perceptions change in what you doing. If I tell other growers about the reality of irrigation water they often don't believe me. However, you really need a crop that generates the value that covers the costs".

3.3 Set-up of the workshop

The workshop was organised at the end of February 2017 in a meeting room at the University Farm. The participants were seated in a U-form, where they could see each other and the facilitator. The workshop was scheduled for an evening, lasting 2.5-3 hours, including introduction to the task, two discussion sessions separated by a tea break, and evaluation and wrap-up.

The facilitator, who also conducted the interviews, presented the outcomes of the interviews with the range of values for the characteristics listed in Table 2. This provided an overview of different perceptions, but does not answer "where these different perceptions come from" and "how these differences affect personal preferences". This is what was discussed during the rest of the workshop.

The discussion questions were focussed on how much one characteristic of the most preferred water source for a type of enterprise has to change before personal preference will shift to an alternative water source. The facilitator introduced discussion with a topic question of the form: "How (much) does a relevant characteristic have to change to switch from initial preference to second best?" Participants were asked to fill in their initial cross-over point via PowerPoint add-in for polling called TurningPoint and indicate how confident they were on a personal sheet. We displayed the range and took the average of the (anonymous) answers.

To begin the discussion, the facilitator asked for a volunteer or picked someone: Would this change lead to a personal change in preference? Why? Why not? How should it change to make it change your preference? From this initial personal reasoning, other participants added to the discussion why their cross-over point differed (or not). After 15 minutes, or when there was agreement among the participants, the facilitator ended the topic by asking the participants to fill in their final cross-over points on TurningPoint and their confidence, as well as whether (and why) their answer changed, on their personal sheet.

Example questions for perennial cropping, where the assumed preference is SE3 water:

- How much should the price of SE3 water go up before others become relevant? Why?
- How much does the reliability of SE3 have to change before others would become the preferred source? Why?
- How much value/ML do you have to create to still prefer SE3 above alternatives? Why?

3.4 Define needs for outcomes

To test applicability of the framework, we had a note taker to evaluate group dynamics, e.g. engagement, attitude, signs of problems. The note taker also looked for indicators of usefulness of the workshop and checked how (if) the concept of crossover contributed to the conversation.

We also want to provide valuable background information for investment decisions by other water users, irrigation scheme designers and water managers. Therefore, the note taker also made notes of the workshop regarding the usefulness of the discussion for generating transferable knowledge. Given the personal nature of preferences, the reasoning of participants is expected to be more transferrable and relevant for others.

We asked the participants to evaluate the framework and their learning by filling in an evaluation sheet with questions including change in reasoning and perceived usefulness of workshop for others.

4. DISCUSSION

We deliberately are specific about the conditions under which we expect the framework could be used. Yet, the restrictions still allow a broad range of topics to be discussed. Indeed, in informal settings, the authors discussed “What would have made you switch from chicken to vegetarian for lunch today?” and “Under which conditions would you quit your PhD?” The conditions may also be revised as a result of evaluation of the workshop.

The main strength of this framework is its ability to engage participants in a dialogue that explores their preference based on personal reasoning. During the workshop they receive input from others and have a discussion that provides valuable information/insights for both the participants and for outsiders.

A possible risk, anticipated for before the workshop, is that the conversation stays shallow. When reasoning is not sufficiently explicated or incomparable with other participants, the learning experience of participants and the development of transferable knowledge will be hampered. The facilitator has a significant role to play by encouraging participants to explain their “why”, while avoiding imposing their views. Another possible risk is that participants might have an incentive to not share their preference and reasoning as they might fear it can be used against them. Hence, the success of the approach strongly depends on the level of trust amongst all participants. The process must be legitimate and must be seen as legitimate for participants to gain.

During the workshop, the discussions started with focussing on one characteristic of the preferred water source for a particular enterprise. However, in real life, participants might have a combination of water sources, using water to irrigate various enterprises at their farm, which could allow mixing, risk spreading and opportunistic farming. Further, it could also be that characteristics are correlated, which makes it more intuitive to discuss water sources in a slightly different way.

For example by focussing on multiple characteristics at the same time or by discussing under which conditions participants would change enterprise, given a certain water source.

In our application we discussed personal preference within a homogenous group of stakeholders with the same aim: Improve water availability at their own farm. If social learning is "learning together to manage together" (Pahl-Wostl et al. 2007) it would be interesting to test the framework in a more heterogeneous group where preferred outcomes are based on different backgrounds, expertise and scope. An example discussion topic in the Coal River Valley would then be: Under which conditions is reuse water the most suitable water source to increase water availability in the valley?

The cross-over point framework presented in this paper shows promise to further support water user discussions. Follow-up research will focus on the outcomes of the discussions and on the evaluation of the framework. It will provide better insights into the conditions under which such discussions can take place (2.2) and evaluate the contribution of the framework to the aims (2.1). This allows us to explore applicability of the framework in different settings.

REFERENCES

Arshad, M., Guillaume, J.H.A. and Ross, A. (2014) Assessing the Feasibility of Managed Aquifer Recharge for Irrigation under Uncertainty. Water 6(9), 2748-2769.

Boles, K.E. and Fleming, S.T. (1996) Breakeven under capitation: pure and simple? Health Care Manage Rev 21(1), 38-47.

Dampney, K., Busch, P. and Richards, D. (2002) The Meaning of Tacit Knowledge. Australasian Journal of Information Systems 10(1).

Dillon, C.R. (1993) Advanced breakeven analysis of agricultural enterprise budgets. Agricultural Economics 9(2), 127-143.

Dixon, M.R., Marley, J. and Jacobs, E.A. (2003) Delay discounting by pathological gamblers. Journal of applied behavior analysis 36(4), 449-458.

Ekren, O., Ekren, B.Y. and Ozerdem, B. (2009) Break-even analysis and size optimization of a PV/wind hybrid energy conversion system with battery storage - A case study. Applied Energy 86(7-8), 1043-1054.

Guillaume, J.H.A., Arshad, M., Jakeman, A.J., Jalava, M. and Kummu, M. (2016) Robust discrimination between uncertain management alternatives by iterative reflection on crossover point scenarios: Principles, design and implementations. Environmental Modelling and Software 83, 326-343.

Hyde, K.M. and Maier, H.R. (2006) Distance-based and stochastic uncertainty analysis for multi-criteria decision analysis in Excel using Visual Basic for Applications. Environmental Modelling and Software 21(12), 1695-1710.

Lejda, A., West, J. and Nelle, S. (2009) Building regional innovation capability: The impact of irrigation in the Coal River Valley, Australian Innovation Research Centre, University of Tasmania, Hobart, Tasmania.

Mazur, J.E. (2000) Tradeoffs among delay, rate, and amount of reinforcement. Behavioural Processes 49(1), 1-10.

Nelson, R., Howden, M. and Hayman, P. (2013) Placing the power of real options analysis into the hands of natural resource managers – Taking the next step. Journal of Environmental Management 124, 128-136.

Pahl-Wostl, C., Craps, M., Dewulf, A., Mostert, E., Tabara, D. and Taillieu, T. (2007) Social learning and water resources management. Ecology and society 12(2).

Ravalico, J.K., Dandy, G.C. and Maier, H.R. (2010) Management Option Rank Equivalence (MORE) - A new method of sensitivity analysis for decision-making. Environmental Modelling and Software 25(2), 171-181.

Rittel, H.W.J. and Webber, M.M. (1973) Dilemmas in a general theory of planning. Policy Sciences 4(2), 155-169.

Turral, H., Svendsen, M. and Faures, J.M. (2010) Investing in irrigation: Reviewing the past and looking to the future. Agricultural Water Management 97(4), 551-560.

Voinov, A., Kolagani, N., McCall, M.K., Glynn, P.D., Kragt, M.E., Ostermann, F.O., Pierce, S.A. and Ramu, P. (2016) Modelling with stakeholders - Next generation. Environmental Modelling and Software 77, 196-220.

Proceedings of the 10th World Congress of EWRA 'Panta Rhei', 5-9 July 2017, Athens, Greece
© 2017 *European Water Resources Association*

Simulation and optimization of hydraulic-hydrologic complex system (case study in Iran)

Ramin Mansouri[1*], Hassan Torabi Pudeh[2], Mohammad Zounemat-Kermani[3], Ali Karbakhsh[1]
[1] *Civil Engineering Department, Islamic Azad University, Sirjan Branch*
[2] *Water Engineering Department, Lorestan University*
[3] *Water Engineering Department, Shahid Bahonar University of Kerman, Kerman, Iran*
[*] *e-mail: Ramin_Mansouri@yahoo.com*

Abstract: Water is one of the biggest challenges of this century in the very near future, which may be the source of many of the world's positive and negative developments. Increasing population and a shortage of water resources necessitates the need for proper management of reservoirs. On the other hand in the management of water resources in addition to the issues we face at the same time exploiting reservoirs with hydraulic and water resources were important and both hydraulic and hydrologic modeling flow conditions must be considered together. In this study, three dams and two water transfer tunnels were used for transferring water from Yalan dam to Gokan dam (Yalan-Pashandegan-Gokan Water Transfer (YPGWT) Project). For YPGWT Project simulating and optimizing, at first dynamic programming (forward-moving) was developed, and after solving it, the best diameter and dam height for optimization of water transfer system was determined. Since the water flow through the tunnel is under pressure, increasing dam height will cause the decrease of tunnel diameter for constant water conveyance efficiency. The purpose of this study is transferring 95% of water flow between two basins after supplying the agriculture consumption and environmental needs. The results showed that Yalan and Pashandegan dam with a height of 148.37 and 59.36 m, respectively, and Yalan-Pashandegan and Pashandegan -Gokan tunnel diameter with 2.8 and 2.95 m, respectively, were the most economically optimal combination for water transferring in YPGWT Project.

Key words: Water Resources Planning, Optimization, Simulation, Hydraulics, Reservoirs, Water Transfer Efficiency, Dynamic Programming

1. INTRODUCTION

In the management of water resources in addition to the issues we face at the same time exploiting reservoirs with hydraulic and water resources were important and both hydraulic and hydrologic modeling flow conditions must be considered together. Of these cases can be discussed inter-basin water transfer and noted the basin.

Inter-basin transfer of water or the basin to basin water transfer is: physical transfer of water from one basin to another river basin, in the movement of water one basin loses water and the other gains water.

White (1977) showed that the peak of the design and implementation of large projects for water in industrialized countries, dates back to the 1960s and 1970s. According to White, 1970 was a turning point in the management of water resources in the world. Transfer of water from one basin to another, in some countries, including the United States of America. The former Soviet Union and China is one of the common ways to increase water basins.

Other researches in the field of inter-basin water transfer and water resource management, such as Simpson (1995), Mutiga et al. (2010), Miller et al. (2013) and others.

Iran is located in the semi-arid areas and has uneven spatial and temporal distribution of rainfall and runoff, water transfer mechanisms have been considered.

Inter-basin water transfer projects and cross-basin water transfer tunnel to the upstream and downstream of the reservoir contain a combination of hydrology (reservoir level) and hydraulic (hydraulic pipe or tunnel) issues. The hydrology and hydraulic analysis to obtain the desired conditions must be simultaneously.

Many researches have been done on the field of optimization of inter-basin water transfer and water resource such as Tisdell and Harrison (1992), Luis (1999), Wang and et al. (2007, 2005), reed et al (2013), Condon and Maxwell (2013), Moslehi et al. (2015), Torabi et al. (2016) and etc.

In the previous studies, water transmission system were evaluated and optimized from the perspective of water allocation or the transfer volume, but in the inter-basin water transfers between bases. In addition to the discussion of hydrological and hydraulic transmission, which is a function of issues, the high cost of construction of the dam and tunnel is very important. Therefore, in this study, optimization and modeling of integrated hydraulic and water resources will be studied at the same time. So, by using a hydraulic balance equation with dynamic programming leading regard to the reform of inter-basin water transfer contains three dams and two tunnels have been optimized in Iran. These optimization issues should be such as providing and requiring water of the basin and also the whole water transfer system doesn't have any hydraulic problems.

2. MATERIAL AND METHODS

2.1 Case study

In this study, the target area is located in the west of Iran in longitudes 49º 42' to 50º 13' E and latitudes 25º 32' to 33º 00' N, which is part of Isfahan watershed of Iran. In this project, three dams (Yalan Dam, Pashandegan Dam and Gokan Dam) and two water transfer tunnels were used for transferring water from Yalan dam to Gokan dam (Yalan-Pashandegan tunnel and Pashandegan-Gokan tunnel) (Figure 1). The tunnels are under pressure condition and the elevation of tunnel at the beginning and the end are equal to the dead storage of upstream dam and normal elevation of downstream dam, respectively.

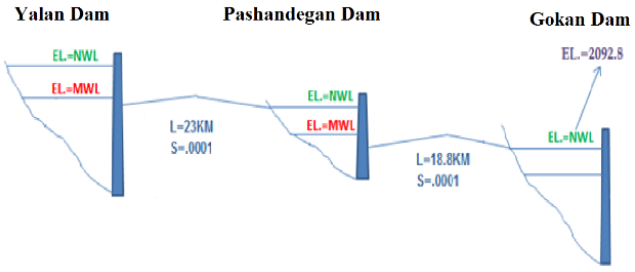

Figure 1. Schematic representation of YPGWT project

In Figure 1, the normal water level and dead elevation of water are specified at the Gokan dam and Yalan and Pashandegan reservoir, respectively. Tunnels is designed with two slope in YPGWT project. All of data in inflow to the reservoir, the volume elevation curve, precipitation and evaporation from the surface of the reservoir for the dams exist in a period of 40 years (1970-2010).

2.2 Methodology

In YPGWT project two conditions exist. Hydrological and hydraulic properties should be considered. The variables of water transfer are simulated by balance equation (hydrological condition), pipe hydraulic equation (hydraulic condition) and optimized by Dynamic Programing (DP) optimization model. So YPGWT project has divided to three parts, two parts are for simulating and one part is for optimizing. These three parts must be connected dynamically for optimizing and simulating YPGWT project.

For simulating hydrological conditions in every reservoirs is used the general water balance equation, as shown by the equation

$$S_{t+1}=S_t+Q_{in}-Q_{Tunnel}-Q_{Agri_t}-Q_{Envi_t}-LE_t+P_t-Sp_t \quad (1)$$

where S_{t+1} is reservoir storage volume at the beginning of period t+1 or end of period t; S_t is reservoir storage volume at the beginning of period t; Q_{in} is the volume of inflow to reservoir in period t; Q_{Tunnel} is transferred volume by the transmission tunnel in the period t; Q_{Agri_t} is the volume of water required for agriculture in period t; and Q_{Envi_t} is the required volume of environmental needs that must be released from the dam to downstream in period t; LE_t is volume of evaporation and infiltration losses in period t; Sp_t is the overflow discharge (spillway) from the reservoir in period t, and P_t is the volume of precipitation on reservoir surface in period t. The relation between precipitation and infiltration parameters is neglected due to their interactions. To simulate and compute the amount of transferred water from the reservoir by the tunnel from Yalan dam to Pashandegan dam and Pashandegan dam to Gokan Dam, Equation (1) must be solved.

Therefore, tunnel discharge is dependent on two characteristics, 1- hydrological characteristics such as reservoir water level, and 2- hydraulic characteristics or physical characteristics of the tunnel such as the tunnel diameter, wall roughness. In other side changes in reservoir level is affected by reservoir water balance.

As well as Sp_t is another unknown parameter in Equation (1). This parameter is dependent to volume of reservoir and difference between inflow and outflow. For calculated Sp_t is presented a model with a series of assumptions.

Considering that the Equation (1) has four unknown parameters (LE_t, Q_{Tunnel}, Sp_t and S_{t+1}). For solving this equation, should be identified a number of assumptions. These initial assumption are: $Sp_t=0$, LE_t is function of reservoir surface and calculated from S_t and also Q_{Tunnel} calculated at the beginning of period (S_t). Now there's an unknown parameter (S_{t+1}) in the equation (1). After specifying the S_{t+1}, three cases can happen that in Figure 2 can be seen reservoir simulation algorithm for a normal level and a diameter tunnel (It should be noted that discharge tunnel is achieved from Epanet software).

Case (1): $S_{t+1}>S_{Normal}$, in this situation Sp_t is not zero, so LE_t and Q_{Tunnel} calculate again in S_t and $S_{t+1}=S_{Normal}$ and the overflow of the dam (Sp_t) is determined.

Case (2): $S_{Minimum}<S_{t+1}<S_{Normal}$, in this case such as case 1, LE_t and Q_{Tunnel} calculate in S_t and S_{t+1}. Average values of LE_t and Q_{Tunnel} put in Equation (1) and calculations done again. This process continues until the new reservoir volume (S'_{t+1}) is almost equal to S_{t+1}.

Case (3): $S_{Minimum}>S_{t+1}$, in this condition tunnel discharge is equal zero ($Q_{Tunnel}=0$), so LE_t and Q_{Tunnel} calculate in S_t and $S_{t+1}=S_{Minimum}$.

These three cases run for 480 months (40 years) and this results use for optimizing and simulating YPGWT project. For calculating the flow discharge of the main tunnel by equations is not directly possible due to changes of discharge flow that depends to water level. Therefore, EPANET software was used to solve the hydraulic equation (1) and Q_{Tunnel} calculated.

2.3 Developed Dynamic Programming (DDP) model

In YPGWT project, dynamic programming cannot solve this optimize problem. Because the unknown variable in Equation (1) is very. So for solving the problem must be changed in dynamic programming. In this article Developed Dynamic Programming (DDP) was presented.

DDP model, which has been developed by the author of this article, is capable of simultaneous modeling of water balance equation and hydraulic analysis of water transfer tunnels for a single

reservoir system of water resource. This model has the capability of performing hydraulic calculations and could be linked to EPANET software for hydraulic calculations. In this study, in order to conduct hydraulic calculations, the model was linked to EPANET.

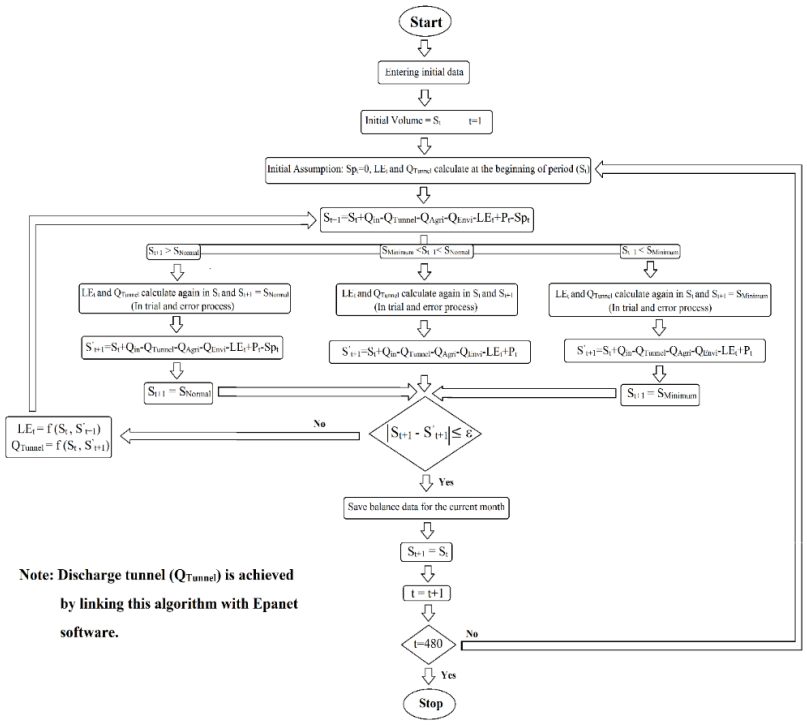

Figure 2. Reservoir simulation algorithm for a normal level and a diameter tunnel

Two parameters are crucial in any optimization problem, 1- objective function and 2- constraints; these parameters must be specified.

The purpose of this research is minimizing the economic costs of YPGWT project, while all administrative and technical constraints are considered. The cost of the project includes construction of Yalan and Pashandegan dam and tunnels to convey water to the reservoir in downstream dams.

In this study, tunnel and dam construction costs were calculated for different diameters and height by economic analysis, which are shown in Figure 3.

However, the maximum water velocity of the tunnel should not be more than 3m/s. In addition, due to the implementation problems, the tunnel diameter should not be less than 3m. Another limitation of the project was the water transfer efficiency, which considered equal to 95%. This efficiency should be determined after numerous simulation of system for a specific diameter of tunnel with different water height of reservoir.

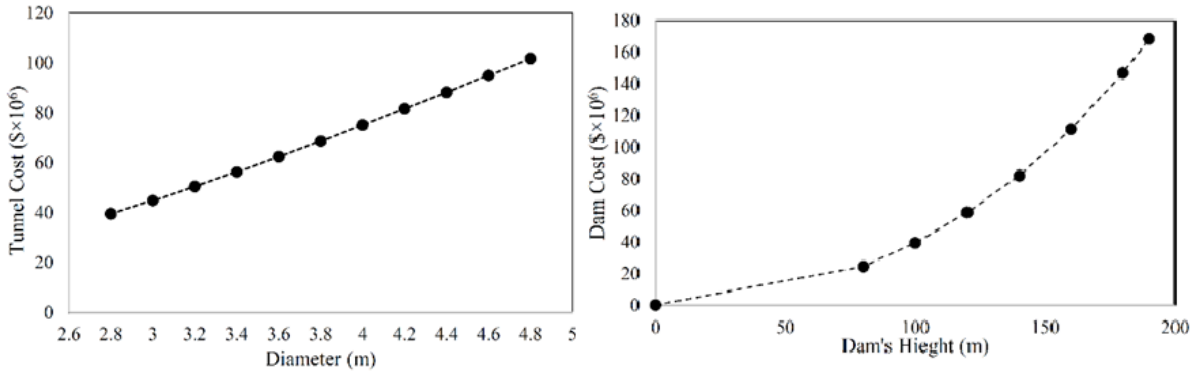

Figure 3. Tunnel and damconstruction costs

Changing the diameter of the tunnel and the dam height affects the entire system. In this case, the water level in Yalan, Pashandegan, Gokan reservoirs and the diameter of tunnels were considered as state variable and decision variable, respectively.

Water level in Gokan reservoir is specified. Because of the uncertainty of the time series inflow to Gokan reservoir, use DDP backward method for solving the problem is not possible. So must be used DDP forward method.

For solving the problem with use DDP forward method, must start from Yalan dam. DP model was developed by considering a number of assumptions and combining it with a process of trial and error. The algorithm (DDP Model) used in this study to solve governing hydraulic in Equation (1) has been depicted in Figure 4. Can be seen in this figure optimization and modeling process in YPGWT project.

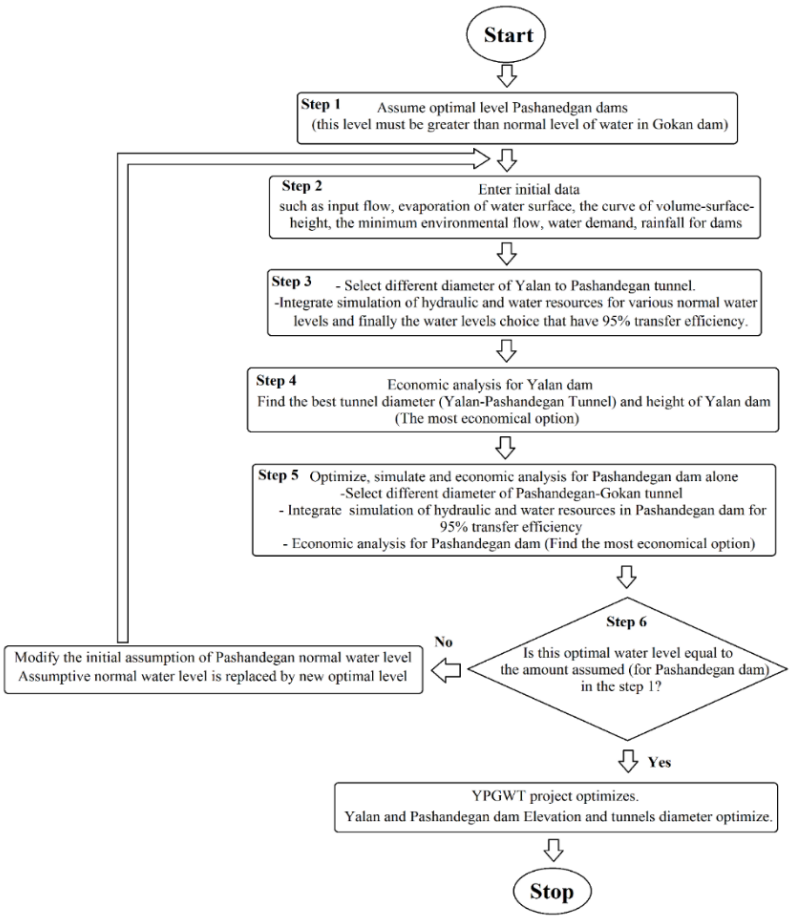

Figure 4. The DDP model of integrated modeling of water resources and hydraulics

3. RESULTS AND DISCUSSION

3.1 Dynamic programming method in combination with a trial and error process

According Figure 6, was derived optimum Yalan to Pashandegan tunnel diameter and volume of Yalan dam corresponding to water transfer efficiency equal 95%. So, is derived 95% water transfer efficiency curve, is shown in Figure 7.

By using the information in Figure 4 and 5 can be calculated the cost of dam and transfer tunnel. According to this result the best tunnel diameter and Yalan dam height that has optimum cost, is 2.8 m and 143.51 m, respectively. At this point Yalan dam and water transfer tunnel is optimum. Next step, Pashandegan dam and Pashandegan – Gokan tunnel must be simulation and optimization.

According to results, the optimal Pashandegan - Gokan tunnel diameter is 3 m and the optimal Pashandegan dam height is 59.55 that by adding 9m freeboard and alluvium, optimal Pashandegan crest elevation will be 2110.55 m.

In final step (Step 6), optimal Pashandegan crest elevation will be checked with Pashandegan elevation that is assumed in Step 1. The result from Step 5 shows optimal Pashandegan dam elevation (2110.55 m) is bigger than assumed value (2102 m). Due to these values, we find that our assumption quantity is not true. Hence, the new optimal Pashandegan elevation is replaced in assumed value and all of above step are repeated.

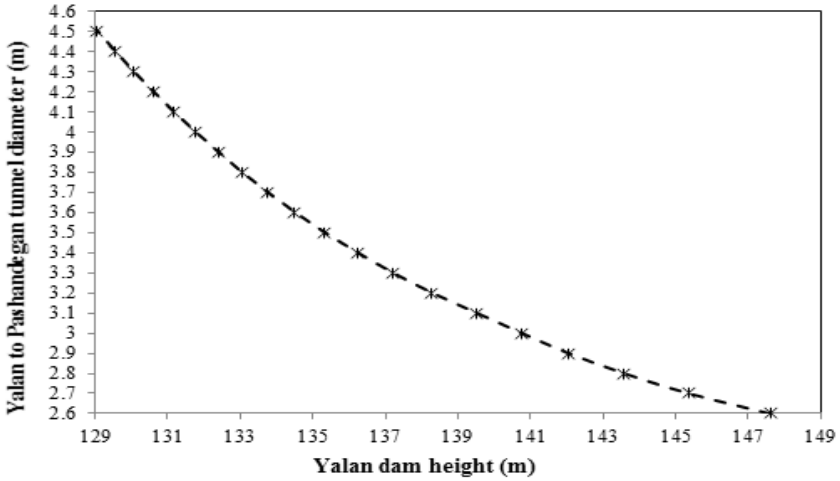

Figure 7. Yalan dam height at different diameter tunnel diameter for 95% water transfer efficiency.

With new Pashandegan dam level (2110.55), Yalan dam and Yalan – Pashandegan tunnel are simulated and optimized. The results for this optimize show Yalan dam level and Yalan – Pashandegan tunnel diameter is 148.37 m and 2.8 m, respectively (Table 1) for 95% water transfer efficiency.

Table 1. Calculation of the best combination of tunnel diameter and Yalan dam height in 95% water transfer efficiency (Pashandegan dam level = 2110.55 m).

Pashandegan Normal level (m)	Tunnel Diameter (m)	Pashandegan Dam Height (m)	Total Cost (Million $)
2119.158584	2.8	68.1586	54.704
2114.388201	2.9	63.3882	52.936
2110.551017	3	59.5510	51.879
2107.430636	3.1	56.4306	53.503
2104.882536	3.2	53.8825	54.915
2102.785584	3.3	51.7856	56.982
2101.065611	3.4	50.0656	58.718
2099.658812	3.5	48.6588	60.971
2098.503187	3.6	47.5032	62.926
2097.538437	3.7	46.5384	65.465
2096.610939	3.8	45.6109	67.548
2096.038191	3.9	45.0382	70.260
2095.458628	4.0	44.4586	72.437
2094.812337	4.1	43.8123	75.196
2094.388446	4.2	43.3884	77.515
2094.182994	4.3	43.1830	80.393
2093.979223	4.4	42.9792	82.771
2093.760361	4.5	42.7604	85.745
2093.521395	4.6	42.5214	88.147
2093.261212	4.7	42.2612	91.144
2092.984355	4.8	41.9844	93.536
2092.663296	4.9	41.6633	96.482
2092.288913	5.0	41.2889	98.781

Based on results, the best Pashandegan - Gokan tunnel diameter and height of Pashandegan dam are 2.95 m and 59.36 m for 95% water transfer efficiency (Table 2).

Pashandegan Dam elevation will be 2110.36 m by using above values. So, can be seen this value (2110.36 m) approximately equal to assumed Pashandegan dam level (2110.55 m). So the optimal combination will be obtained.

Finally, the best optimal combination of dams' height (Yalan and Pashandegan) and tunnels' diameter (Yalan to Pashandegan and Pashandegan to Gokan) was obtained that can be seen in Table 3.

Table 2. Calculation of the best combination of tunnel diameter and Pashandegan dam height in 95% water transfer efficiency (Yalan dam height = 148.37 m).

Pashandegan Normal level (m)	Tunnel Diameter (m)	Pashandegan Dam Height (m)	Total Cost (Million $)
2116.505349	2.8	65.5053	52.40
2114.228186	2.85	63.2282	51.60
2112.186432	2.9	61.1864	51.03
2110.36	2.95	59.3568	50.59
2108.710528	3.0	57.7105	51.38
2107.224454	3.05	56.2245	52.21
2105.881975	3.1	54.8820	53.08

Table 3. The best optimal combination of dams' height and tunnels' diameter and these cost

Dam name	Dam height (m)	Tunnel diameter (m)	Total cost (million $)	YPGWT project cost (million $)
Yalan	148.37	2.8	126.53	177.12
Pashandegan	59.36	2.95	50.59	

4. CONCLUSION

In this study, three dams and two water transfer tunnels were used for transferring water from Yalan dam to Gokan dam (YPGWT Project). For YPGWT Project simulating and optimizing, at first dynamic programming (forward-moving) was developed, and after solving it, the best diameter and dam height for optimization of water transfer system was determined. To solve the DDP (forward-moving), It was needed an integrated simulation of hydraulics and water resources for the various combinations of the water elevation and the tunnel diameter. The integrated solution of water balance and hydraulic equations were used to find both the optimal diameter of the tunnels and the optimal height of the dams. On condition that the existing softwares aren't capabilities integrated modeling hydraulic and water resources, the author developed a computer model in Visual Basic language, which could perform the integrated solution to find the optimal diameter of the tunnels and height of the dams. Our results showed that Yalan and Pashandegan dam with a height of 148.37 and 59.36 m, respectively, and Yalan – Pashandegan and Pashandegan -Gokan tunnel diameter with 2.8 and 2.95 m, respectively, were the most economically optimal combination for water transferring in YPGWT Project. This would easily provide the 95% of agricultural consumption and environmental needs and it concedes all constraints of target function. Furthermore, by increasing the roughness of the tunnel, is needed to reservoir volume and tunnel diameter be more.

RERERENCES

Condona, L.E., Maxwell, R.M., 2013. Implementation of a linear optimization water allocation algorithm into a fully integrated physical hydrology model, Advances in Water Resources; 60:135–147.

Luis, H., 1999. On equitable resource allocation problems: a lexicographic minimax approach. Oper Res.; 47(3):361–378.

Miller, C.T., Dawson, C.N., Farthing, M.W., Hou, T.Y., Huang, J., Kees, C.E., Kelley, C.T., Langtangen, H.P., 2013. Numerical simulation of water resources problems: Models, methods, and trends, Advances in Water Resources; 51:405–437.

Moslehia, M., Rajagopalb, R., Barros, F.P.J., 2015. Optimal allocation of computational resources in hydrogeological models under uncertainty, Advances in Water Resources; 83: 299–309.

Mutiga, J.K., Mavengano, S.T., Zhongbo, S., Woldai, T., Becht, R., 2010. Water allocation as a planning tool to minimise water use conflicts in the upper Ewaso Ng'iro North Basin, Kenya. Water Resour Manage.; 24:3939–3959

Reed, P.M., Hadka, D., Herman, J.D., Kasprzyk, J.R., Kollat, J.B., 2013. Evolutionary multiobjective optimization in water resources: The past, present, and future, Advances in Water Resources; 51:438–456.

Simpson, L.D., 1995. Transbasin diversion, the United States experience. Water Resources Management Consultant, World Bank

Tisdell, J.G., Harrison, S.R., 1992. Estimating an optimal distribution of water entitlements. Water Resour Res.; 28:3111–3117

Torabi, H., Mansouri, R., Haghiabi, A.H., Yonesi, H.A., 2016 Optimization of Hydraulic-Hydrologic complex system of reservoirs and connecting tunnel. Water Resource Management; 30:5177–5191. doi: 101007/s11269-016-1477-5

Wang, L., Fang, L., Hipel, K.W., 2007. Mathematical programming approaches formodeling water rights allocation. J. Water. Resour. Plan. Manage.; 133(1):50–59

Wang, L., Fang, L., Hipel, K.W., 2008. Basin-wide cooperative water resources allocation. Eur.J. Oper. Res.; 190(3):798–817

White, G., 1977. Comparative Analysis of Complex River Development. In Environmental Effect of Complex River Development, Gilbert White (Editor), West view Press, Boulder, Colorado.

Proceedings of the 10th World Congress of EWRA 'Panta Rhei', 5-9 July 2017, Athens, Greece
© 2017 *European Water Resources Association*

Evaluation and development of spatial decision support system

H. Alrayess[1*] and A. Ulke[2]
Department of Civil Engineering, Faculty of Engineering, Ondokuz Mayis University, Samsun,Turkey
[*] *e-mail: hesham.majed@hotmail.com*

Abstract: Studies have been expanded heavily at water networks sector especially at residential areas which including a high density of population. This paper discusses the use of a Geographic Information System (GIS) as a Decision Support System (DSS) generator to create Spatial Decision Support Systems (SDSS) to evaluate the hydraulic situation of the water network. A hydraulic model was used on the small zone of Gaza city (Case study the northern Nasser water network) to get a high accurately results. Calibration and SDSS used to identify the technical problems. The developed SDSS may be used at all zones of Gaza city to improve the network efficiency and effectiveness of operation. In addition, the results of this study will be the base of Supervisory Control and Data Acquisition (SCADA) system to make the system more automated and specify any sudden problem at the system and to give more accurate data. GIS software is recommended to be used in order to better utilize the developed water network database and make the operating and management more effectively. The results indicated that 82% of Zone 2, the water velocity ranged between 0-0.25 m/s while in Zone 1 the percentage is 59%. 70% of the water pressure at Zone 1 has 2 bars while in Zone 2 the percentage is 72% for 1 bar. The low values of the velocities may result from the leakage at the system.

Key words: Performance evaluation, Water distribution network, GIS, Water CAD, Gaza City

1. INTRODUCTION

Nowadays, water utilities of water supply systems (WSSs) in Gaza are facing a great challenge to save water. Like many large cities around the world, infrastructure has become very complex over time (Merchant, et al., 2014). At Gaza city, the water distribution networks (WDNs) suffers from many defects and a high percentage of losses which make the network works randomly at the hydraulic system without any development. Using Geographical Information System (GIS) makes operation, maintenance and planning of water supply more effective and economical. Decision-makers in Gaza municipality and non-technical water managers in water system management and more specifically in water network assessment usually face difficulties in dealing with sophisticated tools of information such as GIS through its adopted applications such as WaterCAD, ArcGIS, Geomedia Professional and other applications.

Studies on WDNs performance are a core issue as a tool for water management entities decision making. In order to achieve this goal, it is necessary to know both the WDN's infrastructure registration and the hydraulic operating conditions (flows and pressures) for simulation computation (Alves, et al., 2014). According to Walski et al. (2003) simulation is an emulating process where system's performance is computed using a mathematical representation of the real WDN in order to reproduce the responses of real systems for the same input conditions. This, so called model, must be calibrated. A network consists of pipes, nodespumps, valves and water supply. WaterCAD tracks the flow of water in each pipe, the pressure at each node, the height of water in each tank, and the concentration of a chemical species throughout the network during a simulation period comprised of multiple time steps. In addition to chemical species, water age and source tracing can also be simulated (Vuta & Piraianu, 2008). Custom open GIS applications could act as Decision Support System (DSS) and to some extent as a Spatial Decision Support System (SDSS). Typically, such a system will include spatial data relevant to the decision. The main aim of this Paper is to use (WaterCAD) modeling to develop SDSS for the water network in the Northern Nasser area as a

pilot small scale from the city. To be more specific assess the efficiency of the network (The Northern Nasser area) and Develop SDSS of The Northern Nasser water network as a pilot scale.

2. WATER DISTRIBUTION NETWORK

Continuous improvements on water loss management are being applied, based on the use of new available technologies. Nonetheless, the whole leakage localization process may still require long periods of time with an important volume of water wasted before the leak is found (Perez, et al., 2011). There are essentially two main types of performance evaluation tools available to water and wastewater utility managers (Cardoso, et al., 2004): systems of performance indicators and technical performance assessment tools.

2.1 GIS and ArcGIS

A GIS provides a powerful analytical tool that can be used to create and link spatial and descriptive data for problem-solving, spatial modeling and to present the results in tables or maps (Bice, et al., 2000). The most powerful feature of a GIS, from a planner's perspective, is probably the ability of GIS to integrate databases, through their spatial relationships, that would be difficult or impossible to do outside a GIS environment (Walski, et al., 2003). Physical configuration of WDNs such as coordinate, length, diameter and material of pipes, junctions, connections, elevations, etc. can be obtained from updated GIS (Geographical Information Systems) database systems in advanced WDNs (Kara, et al., 2016). Results of these GIS operations are stored in an ESRI personal geodatabase as a Microsoft Access database with sets of attribute tables designed for holding geodatabase metadata along with the feature geometry (Coelho, et al., 2012).

2.2 Decision Support System (DSS)

DSS may be considered to be a new generation of information systems, the goal of which is to try to discover what would happen if a series of decisions are taken or going even further, by automatically providing the decisions or suggestions that assist the manager (Adenso-Diaz, et al., 2005). DSSs are interactive programs, which embed traditional water resource simulation and optimization models, with adaptation of new approaches, to support users in semi-structural or ill-structural problem solving (Manoli, et al., 2001; Willuweit & O'Sullivan, 2013) Proposed a DSS focusing on urbanization in order to assess the performance of centralized and decentralized water management alternatives. DSS is also an integrated environment to share and manage data and to facilitate cooperation among different levels of users (Yingchun & Zhuotong, 2013). A DSS has been defined in many different ways, but it can be regarded in general as an interactive, flexible, and adaptable computer based information system especially developed for supporting the recognition and solution of a complex, poorly structured or unstructured, strategic management problem for improved decision-making (BFG, 2000).

3. OPERATING SYSTEM

Generally, Gaza operating system consists of two cycles for water distribution because the electricity crises which resulted from the Israeli siege at Gaza strip in Palestine since 2006 and according to supply areas, density of population and water sources. This operating system had become the standard operating system for the city to supply water for all population at Gaza city. This paper provides a base for WDN at Gaza city and the current system and the way of operation. The operating system was planned by elevation at zones. Cycle 1 was operated for the high elevation level and Cycle 2 was operated for the low elevation level. According to the operation cycles, the boundary of zones is determined and controlled by valves manually from technicians.

The distribution system depends mainly on direct pumping from the wells to the WDN. These pumping stations (Well Pumps) are managed manually through operators as three consecutive 8-hour shifts along the day. Decisions are made according to observations and feedback which is delivered through operators and SCADA system.

4. STUDY AREA

Palestine is one of the important places in the world, it's located at the middle part between Asia and Africa as shown in Figure 1. Gaza city is a Palestinian city in the Gaza Strip, its location in 31°31′N 34°27′E, it's considered one of highest overpopulation regions in the world. There are 588,033 capita in 45 km^2. It is considered one of the poorest regions of water resources. The existing supply of potable water in Gaza depends on well sources abstracted from the aquifer only and there are no other resources available for supplying people. As a prototype (Pilot scale) a small two zones were taken in this study as shown at Figure 2 with totally area 245814 m^2 (131084 m^2 for Zone 1 and 114730 m^2 for Zone 2) and totally population 12788 capita (4380 capita for Zone 1 and 8408 capita for Zone 2). These zones were supplied from one water well (Kamal Nasser) with total flow amount 65 m^3/hr for each zone. Zone 1 was suppling at operating system Cycle 2 on the other hand Zone 2 was suppling at operating system Cycle 1. Figure 3 shows that pump characteristic of Kamal Nasser well (Pump flow curve) located at Sheikh Radwan area in a good condition and work without any problems.



Figure 1. Palestine boundaries map.



Figure 2. Arial photo for Zone 1 and Zone 2 case study.

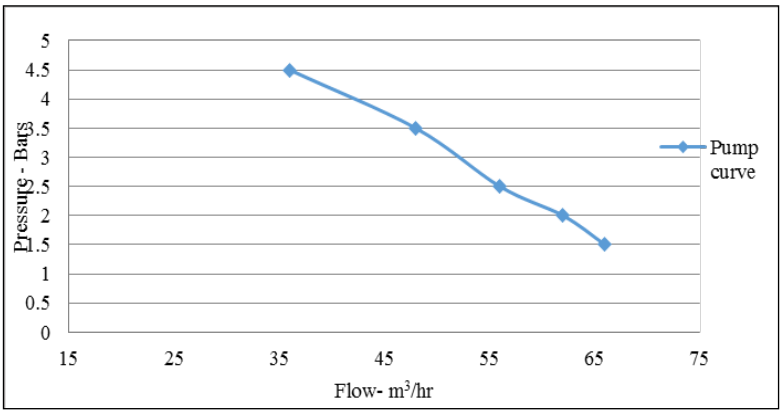

Figure 3. Pump characteristic curve at Kamal Nasser well.

Demand pattern is one of the critical component at the system, from which is identified how much inhabitants consume to describe in the graph. The distribution approach at each zone where the consumption is assumed equally at all supply interval (18 hours). The multiplier is constant at value equal one during all the eighteen operating hours. It means that all operating hours are critical not only in a specific interval.

5. SPATIAL DECISION MAKING

ArcGIS is operated this stage by export all elements at WaterCAD as shape files and import it at ArcGIS. Quires and statically analysis made indication for Decision support from many indicators: Pressure, demand, diameter, pipes material, flow and velocity. Pressure, flow and demand played a primary role of the critical components for decision support. SDSS components are consisted of: Pipes and junctions. Pipe indicators are divided to diameter, flow rate and velocity but for junctions, the indicators are divided to demand and pressure. Diameters vary according to pipes type's un-plasticized polyvinyl chloride (UPVC) and steel. Flow rates are transferred at pipes from the well to every junction. The velocity of flow is depended on the diameter. Demand is identified according to the population density. Performance criteria are used to evaluate the different perspectives of WDNs. In order to fully understand the hydraulic efficiency in water distribution systems (WDSs), the nodal pressure or water age parameters should be observed over a 24-h period of time.

6. APPLICATION

6.1 Model of the water distribution network

The water distribution network model consists of: 88 pipes (Divided to 32 pipes for Zone 1 and 56 pipes for Zone 2), one water well (Kamal Nasser well), 66 junctions (Divided to 24 junctions for Zone 1 and 42 junctions for Zone 2) and 4 gate valves. Originally, the pumping station was provided with an opened storage tank. The tank was supplied by the main water distribution network of the city. The general layout of the network, diameters and lengths of the pipes were introduced based on the information existing at the Water Distribution Company. In fact, obtaining a network model from an existing AutoCAD drawing (with attributes) or GIS is quite simple, by the use of additional software.

6.2 Components of SDSS in zone 1 and zone 2

A general layout of the water distribution network components of Zone 1 shows at Figure 4 for

the south part from Kamal Nasser well supplied at operation Cycle 2 which explained the pipe types and pressure values at junctions from 1 to 2 bar by ArcGIS. Another general layout to the components of Zone 2 for the north part from Kamal Nasser well supplied at operation Cycle 1 which explained the pipe types and pressure values at junctions from 1 to 3 bar by ArcGIS as shown at Figure 5.

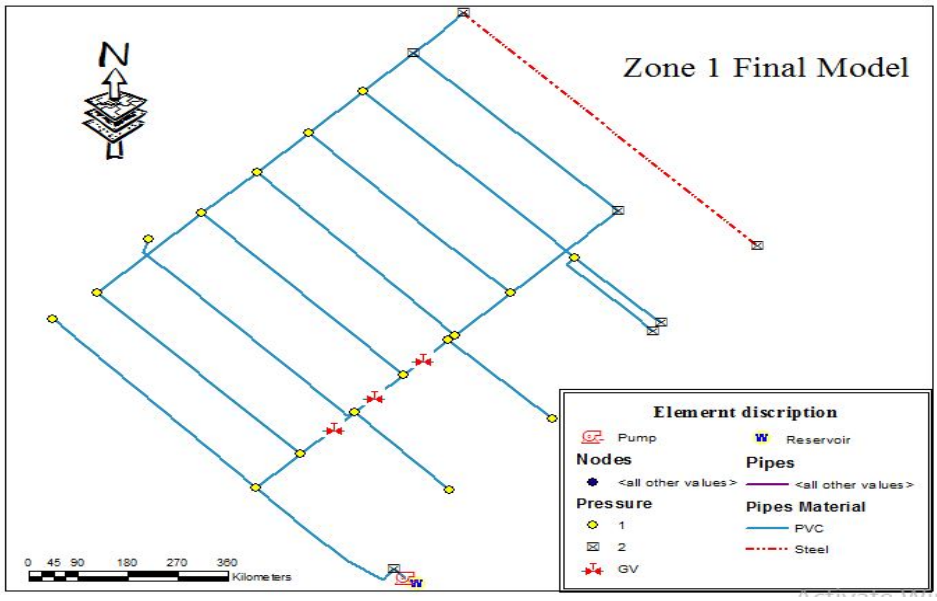

Figure 4. Water distribution network configuration (Zone 1).

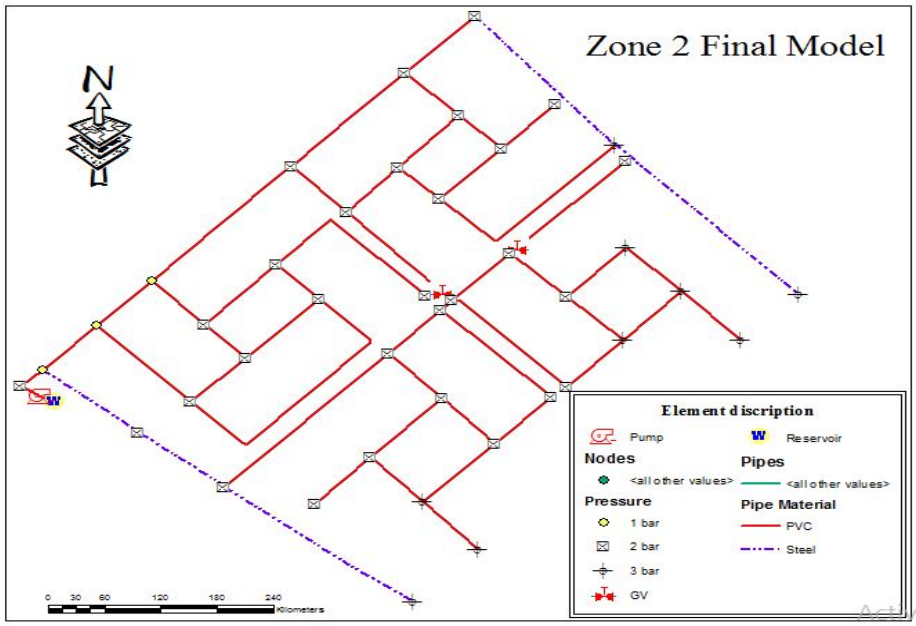

Figure 5. Water distribution network configuration (Zone 2).

SCADA system for Kamal Nasser well wasn't installed so it affected at well control and operated manually.

6.3 System results

By make the final analysis step the next table represents the results for two zones at the pilot area.

Table 1. Pilot scale study area results.

Zone No.	Flow Rate (m^3/hr)	Average daily consumption (L/day)	Total consumption (m^3/day)	Flow range (m^3/hr)	Pressure (Bar)	Operating hours (hr)
Zone 1	58	160	1401	1-58	1-2	18
Zone 2	63	90	1513	1-63	1-3	18

Table 1 shows a high accurately results of pilot study area after calibration stage with equal in operating hours 18 hr. Total population at Zone 1 equal 4380 capita but at Zone 2 equal 8408 capita, it means Concentration at Zone 2 is double Zone 1 because area for each zones near the same value. The Average daily consumption per capita was 90 L/day at Zone 2 but Zone 1 was got 160 L/day with review for total population is shown that Zone 1 have a clear leakage near 70 L/day for each capita, but model and calibration stages was defined the point of leakage with pressure head 13.78 m at the end of this point there was a valve normally close but from this study we discover all this valve fault of made a high percentage from leakage.

6.4 Junction's results

According to population distribution for each junction, a demand of Zone 1 is ranged between 27 – 134 m^3/day with a mean and standard deviation 58.46, 25.628, respectively. On the other hand, a demand of Zone 2 is changed between 14 – 60 m^3/day with a mean and standard deviation 36.024, 11.57, respectively.

Zone 1 pressure values, at 24 junctions were resulted between 1-2 bar near 70% at 1 bar with a mean of 1.29 bar as shown at Figure 6 and standard deviation 0.464 bar, but Figure 7 represented the pressure values for Zone 2, at 42 junctions between 1-3 bar near 72% at 2 bar with a mean of 2.14 bar and standard deviation 0.521.

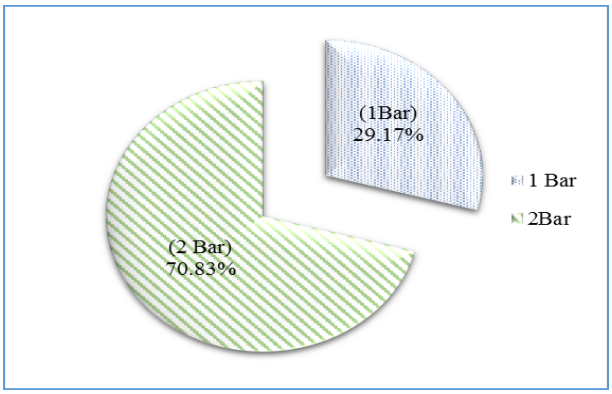

Figure 6. Zone 1 pressure percentage at junctions.

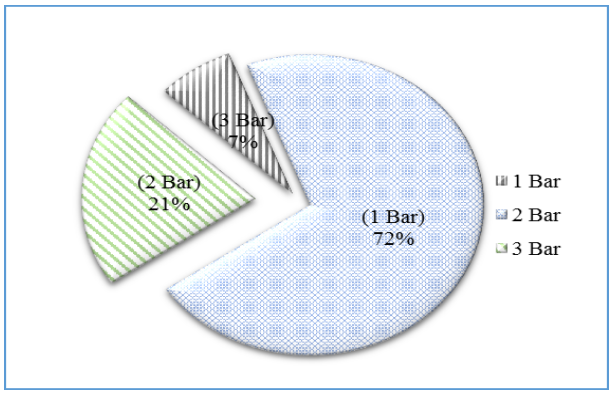

Figure 7. Zone 2 pressure percentage at junctions.

The critical problem at Zone 1 was resulted at the pressure values the highest percentage for 1bar (72%) and with some review for the differences at pressure head after calibration were resulted from fittings at zones and k coefficient. The results for Zone 2 was resulted more acceptable than Zone 1 but without 3 bar like Zone 1.

6.5 Pipe's results

32 Pipes of Zone 1 is changed between 101.5 mm (Steel), 110 mm UPVC and 160 mm UPVC. On the other hand, Zone 2 is consisted of 56 Pipes, it is recorded between 101.5 mm (Steel), 110 mm UPVC, 160 mm UPVC and 203.1 mm (Steel). But actually, the most used pipe diameter was 110 mm and UPVC material with percentage 59.38% and 76.79% for Zone 1 and Zone 2,

respectively.

Zone 1 has flow rate at the range from 0 to 1400 m^3/day which resulted from 18 hr of operating at Kamal Nasser well. Figure 8 shows Zone 1 flow rate percentage for pipes, distributed from 0 – 1400 m^3/day. Beside of this, Zone 2 had flow rate at the range from 7 to 1513 m^3/day, mean 213.45 m^3/day and standard deviation 364.83 m^3/day which resulted from 18 hr of operating at Kamal Nasser well and Figure 9 shows Zone 2 flow rate percentage for pipes, distributed from 0 – 1510 m^3/day.

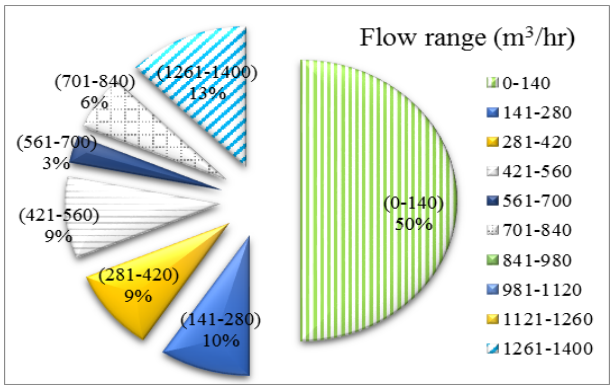

Figure 8. Zone 1 pipes flow rate percentage.

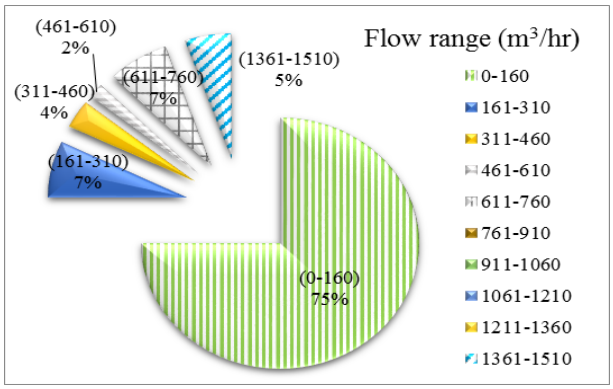

Figure 9. Zone 2 pipes flow rate percentage.

According to velocity results at Figure 10, the velocity percentage between pipes at Zone 1 divided into five intervals. The interval from 0 – 0.25 m/s takes the maximum value of 59% and the minimum percentage is for interval 1 – 1.5 m/s at operating hours. On the other hand, Figure 11 shows that Zone 2 velocity percentage between pipes divided into five intervals. The interval from 0 – 0.25 m/s take the maximum value of 82% and the minimum percentage is for interval 0.5– 1 m/s at operating hours.

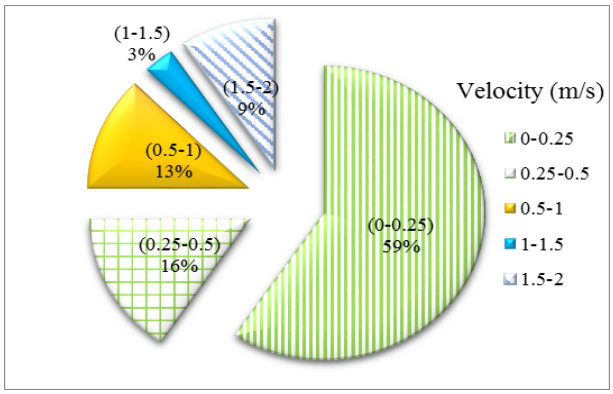

Figure 10. Zone 1 pipes velocity percentage.

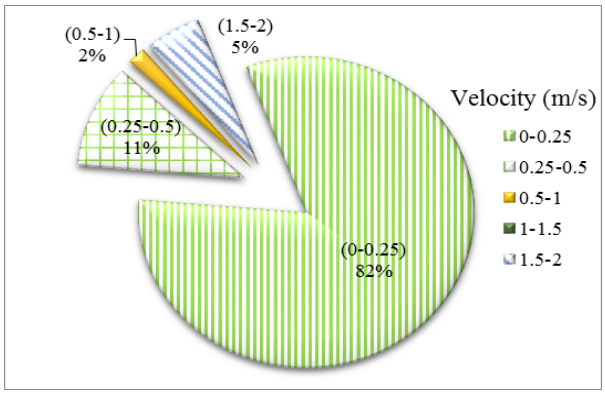

Figure 11. Zone 2 pipes velocity percentage.

The critical problem at pipes was resulted at the percentage of velocity, it describe the attitude of flow at pipes move slowly as shown at Figure10 and Figure 11 but as a temporary solution the system can be improved by change flow value to increase velocity value.

7. CONCLUSIONS AND RECOMMENDATIONS

A prototype spatial decision support system for the evaluation of WDN has been outlined. A pilot scale study provided a sample to apply at all zones of Gaza city to improve the network efficiency and effectiveness of operation. All outputs from this study about this pilot study zones (Zone 1 and 2) at Gaza city water network analysis:

On the first hand, the pressure values of Zone 1 were changed between 1 to 2 bar with

percentage 71% and 29% respectively. The pipe diameters were distributed for 101.5 mm with percentage 3.13%, 110 mm with percentage 59.38% and 160 mm with percentage 37.5%. Beside of that 59% of water velocity in Zone 1 ranged between 0-0.25 m/s. On the other hand, the pressure values of Zone 2 resulted 72% for 1 bar, 21% for 2 bar and 7% for 3 bar. The pipe diameters were distributed for 101.5 mm with percentage 3.57%, 110 mm with percentage 76.79%, 160 mm with percentage 14.29% and 8 inch with percentage 5.36%. However, 82% of water velocity in Zone 2 ranged between 0-0.25 m/s. This study must apply for Gaza city network by making an isolate zones to make control more easily especially at Zone 1 and identify the benefits from calibration and decision support system. The results have discovered enough values of operating hours for each zones to supply water. This study made explore problems and weakness points more easily, at Zone 1 demand high values (160 L/day/cap.) which reflect the high percentage of leakage at the whole network. Losses are one of many defects at the system it resulted from illegal connections, fittings and network situation. Calibration accuracy is reached to near 96%. Preventative maintenance for valves avoid the high percentage of losses. Automation approach for valves and well control through SCADA make two important points: historical data as a reference and future development planning. Pipes type was affected by the quality of zone operation so at this zone UPVC take the maximum percentage. The low values for velocity at Zone 1 and 2 need more solutions to avoid this problem because of the maximum percentage at 0 – 0.25 m/s velocity. Reduce valves as possible to avoid the high drop at pressure.

REFERENCES

Adenso-Diaz, B., Tuya, J., & Goitia, M., 2005. EDSS for the evaluation of alternatives in waste water collecting systems design. Environmental Modelling & Software; 20(5): 639-649.

Alves, Z., Muranho, J., Albuquerque, T., & Ferreira, A., 2014. Water distribution network's modeling and calibration. A case study based on scarce inventory data. Procedia Engineering; 70: 31-40.

BFG, 2000. Decision Support Systems (DSS) for River Basin Management. Bundesanstalt fur Gewa¨sserkunde (German Federal Institute of Hydrology), Koblenz, Germany, (Report No. 4/2000).

Bice, L., Van Remortel, R., Mata, N., & Ahmed, R., 2000. Source Water Assessment Using Geographic Information Systems. U.S. Environmental Protection Agency. USA: U.S. Environmental Protection Agency. 1-159.

Cardoso, M.A., Coelho, S.T., Matos, R., Alegre, H., 2004. Performance assessment of water supply and wastewater systems. Urban Water Journal; 1(1): 55-67.

Clark, A., 2012. Increasing Efficiency with Permanent Leakage Monitoring. In: Water Loss Reduction - Proceedings of the 7th IWA Specialist Conference; 26-29.

Coelho, A.C., Labadie, J.W., & Fontane, D.G., 2012. Multicriteria decision support system for regionalization of integrated water resources management. Water Resources Management; 26: 1325–1346.

Debiasi, S., Giorgio, C., Bosoni, A., Bertola, P., & Righetti, M., 2014. Influence of hourly water consumption in model calibration for leakage detection in a WDS. Procedia Engineering; 70: 467-476.

Hamilton, S., 2012. Technology-How far can we go? Pipelines. 523-530.

Kara, S., Karadirek, E. I., Muhammetoglu, A., & Muhammetoglu, H., 2016. Hydraulic modeling of a water distribution network in a tourism area with highly varying characteristics. Procedia Engineering; 162: 521-529.

Kiselychnyk, O., Bodson, M., & Werner, H., 2009. Overview of energy efficient control solutions for water supply system. Transactions of Kremenchuk State Polytechnic University; 3(56): 40-46.

Malczewski, J., 2004. GIS-based land-use suitability analysis: a critical overview. Progress in Planning; 62: 3-65.

Merchant, A, Mohan Kumar, M S., Ravindra, P N., Vyas, P., and Manohar, U., 2014. Analytics driven water management system for Bangalore City. 12th International Conference on Computing and Control for the Water Industry, CCWI2013. Procedia Engineering; 70: 1137-1146.

Perez, R., Puig, V., Pascual, J., Quevedo, J., Landeros, E., & Peralta, A., 2011. Methodology for leakage isolation using pressure sensitivity analysis in water distribution networks. Control Engineering Practice; 19(10): 1157-1167.

Vuta, L., & Piraianu, V., 2008. Infoworks WS and EPANET v2 - Modeling the water distribution networks. U.P.B. Sci. Bull., Series D; 70(4): 91-102.

Walski, T. M., Chase, D. V., Savic, D. A., Grayman, W., Beckwith, S., & Koelle, E., 2003. Advanced Water Distribution Modelling and Managment. USA: Heasted Press, Waterbury, CT, USA.

Willuweit, L., & O'Sullivan, J. J., 2013. A decision support tool for sustainable planning of urban water systems: presenting the dynamic urban water simulation model. Water research; 47(20): 7206-7220.

Yingchun, G., Li, X., Huang, Ch., and Zhuotong, N., 2013. A Decision Support System for irrigation water allocation along the middle reaches of the Heihe River Basin, Northwest China. Environmental Modelling & Software; 47: 182-192.

Proceedings of the 10th World Congress of EWRA 'Panta Rhei', 5-9 July 2017, Athens, Greece
© 2017 *European Water Resources Association*

Integrated water resources management in agro-economy using linear programming: The case of lake Karla basin, Greece

A. Alamanos[1*], S. Xenarios[2], N. Mylopoulos[1] and P. Stålnacke[3]
[1] *Laboratory of Hydrology and Aquatic Systems Analysis, Department of Civil Engineering, University of Thessaly, Pedion Areos, 38334 Volos, Greece*
[2] *Mountainous Societies Research Institute, University Central Asia (UCA), 138 Toktogul Str, 72001, Bishkek, Kyrgyzstan*
[3] *Norwegian Institute of Bioeconomy Research (NIBIO), Pb 115, NO-1431 Aas, Norway*
[*] *e-mail: alamanos@civ.uth.gr*

Abstract: Several hydrological factors that affect agricultural water use in the Mediterranean region have recently emerged. The financial crisis focuses on production, efficiency and profit, but all these should be achieved under environmental constraints. This requires a shift in policy towards more sustainable and efficient solutions. This research presents optimization problems related to the broader water resources management. The study area is Lake Karla basin (Central Greece). The problems aim to maximize production, productivity, water-use efficiency, net profit, and to minimize irrigation and production costs, by using linear programming in GAMS software. The final goal is to propose to the stakeholders the optimum crop distribution, suggesting different policy options. This approach can be used for further research (e.g. decision-making techniques) in order to combine the economic growth with the protection of the environment.

Key words: Optimization, Linear Programming, GAMS, Lake Karla Basin, Integrated Water Resources Management, Agro-economy, Policy-making, Data-scarce areas.

1. INTRODUCTION

In Greece, the lack of rational water management, especially of the irrigation sector, has led the research into finding solutions through technical optimization techniques. A typical example is the basin of Lake Karla, which faces serious problems of shortage of water and financial resources (Ministry of Environment, 2013). The above are creating constraints to the coverage of the water needs and the agricultural production. Therefore, the optimal use of water in the basin of Karla requires immediate priority, especially now that the reservoir's operation is expected, and the optimization is the most widely used method (Salvatici et al., 2000).

Optimization is a basic tool in the water resources management and has wide application in the rural economy (Hall and Dracup, 1970). In the study area there is no experience of such implementations, so an applied research case is performed on the optimization of agricultural water use which has not been yet scrutinized. In a previous work (Alamanos et al., 2016), a hydrological model of Lake Karla basin was developed evaluating the water balance and the irrigation water cost under several management and climatic scenarios. This paper focuses in finding the optimum solution to problems with multiple objectives under economic, environmental and production constraints, aiming to the investigation of alternatives and policies.

2. STUDY AREA

The basin of Lake Karla is located in the southeast of the Thessaly, between Volos and Larissa. It is an agricultural basin of 1660 km^2. An intensified irrigation was practiced for water demanding

crops for many years. The intensification was increased the pumping with devastating results to the local ecosystem (Sidiropoulos et al., 2013).

The water demand of the basin is covered by the surface network of Pinios Local Administration of Land Reclamation (LALR) and from the aquifer (the biggest supply source) of Karla basin. In particular, The future situation (and the suggested methodology) is referring to the operation of the reservoir and the new Karla network. At the time, the Karla's new network irrigation areas are served by the aquifer (with everything it entails for the ecosystem).

The basin is facing a lot of water resources management and policy problems. The current technical practices (losses, inefficient irrigation) deteriorate agricultural water use in the region. There is also an underpricing of the surface irrigation network, while the pricing is four times higher for groundwater irrigation. The last decades, through subsidies and high product prices, water demanding crops such as cotton were preferred over water resistant ones. With such policies and indirect subsidies, the actual productive abilities of the region are significantly reduced. Finally, regarding the area pricing system, it was revealed (Alamanos et al., 2016) that the water consumption was not correlated at all with the water consumption levels.

3. METHODOLOGY

3.1 Linear Programming on GAMS

The methodology is an optimization process with linear programming, where the objective function and constraints are linear functions of the decision variables:

$$maximize\ (or\ minimize)\ \ F(x_1,x_2,x_3,.....,x_n,\ e) \tag{1}$$

where (x_1, x_2, x_3,….,x_n), are the decision variables (data of the system), and the variable e is the error–risk, (uncertainty) which was tested in this way as a whole, due to insufficient data. In addition, it must satisfy a set of constraints (acceptable range of values):

$$u_i\ (x_1,x_2,x_3,....,x_n) \leq a_i \tag{2}$$

where a_i: known values. The optimum solution of the system has to meet all the constraints and the objective function. The problems were solved through a linear approach due to the straightforward and clear cut solutions that linearity functions can offer. Also, they lead to the solutions more quickly, without great demands of computational time. Another essential advantage of linear functions is the development of global optimum solutions through expanded modeling.

The software tool applied for our study was the General Algebraic Modeling Systems (GAMS), designed for linear programming, non-linear, integer and mixed optimization problems (Rosenthal, 1998).

The constraints used on each problem are all the factors that were available, while their exact number in each problem has been determined after tests, except of the cases that were deliberately chosen to study some specific parameters. Each function was examined separately because some were minimization problems, some were maximization problems, and without the same variables in all of them. The goal is to propose technically acceptable, economically sustainable and environmentally friendly solutions that result in issues of change of the following policy.

3.2 Materials and Methods

There are some data that were collected or calculated for the purposes of the study, and are characteristic for the current situation in the basin: Most of them have already been calculated (Alamanos et al., 2016) for the four main crops cultivated in the area which are alfalfa, corn, cotton and wheat. The rest of them were collected from databases of OPEKEPE (Greek Agency of Payments and Control).

For the calculations of requested on the optimization technique main variables were introduced. In principle, the net income (profit) for each crop was adopted which was considered to be the sum of the Gross Margin and the subsidy amount. Gross Margin is the revenue earned from the sale of the average estimated production based on the local market price. The total production cost of each crop was considered to be the sum of the expenditure incurred for producing one unit of product (Agrenda, 2014).

Furthermore, the efficiency of use of irrigation water (IWE) was calculated, as the ratio of the Actual Annual Water Requirements of each crop, by the Final Water Requirements, as they were calculated in Hydromentor (2015). Also, the Crop Water Productivity (CWP) was estimated, to combine the irrigation water with the efficiency to show the value of a "unit" of water. According to Faramarzi et al. (2010), with the appropriate modifications, it is the ratio of Crop Production to the Water Required.

The optimization analysis was formulated through the objective functions and constraints describe in Table 1.

Table 1. Description of the seven studied problems

OBJECTIVE	CONSTRAINTS
i. Optimum crop distribution for the following two objective functions: a) Irrigation cost (min) b) Irrigation water losses (min)	• maximum exploitation of the total available land • maximum possible net profit • maximum possible productivity in kg/km^2
ii. Production Cost (min) with the optimum crop distribution	• the maximum exploitation of the total available land • the maximum coverage of the water needs from surface water resources, • the maximum possible net profit + the maximum IWE + the maximum possible productivity in kg/km^2
iii. Farmer's Problem (max net profit+ max production) with the optimum crop distribution	• the total available arable land • the total available Units of Man Labor (UML) – labor hours • the total fertilizers required (total requirements of each crop in Nitrogen (N), Phosphorus (P_2O_5), Potassium (K_2O) and Zinc (Zn)) • the minimum possible total water requirements and its coverage from surface water resources + the minimum possible groundwater pumping, + the minimum possible irrigation water cost
iv. Productivity (max yield for the maximum production output). The variables are three crops (cotton, winter wheat and maize), because of the absence of more and more detailed data on the alfalfa crop in the basin.	• the total available arable land • the minimum UML • the minimum water requirements for these crops • the minimum possible production cost

4. RESULTS AND DISCUSSION

The solution gave the following results for the optimum crop distribution and the constraints of each problem:

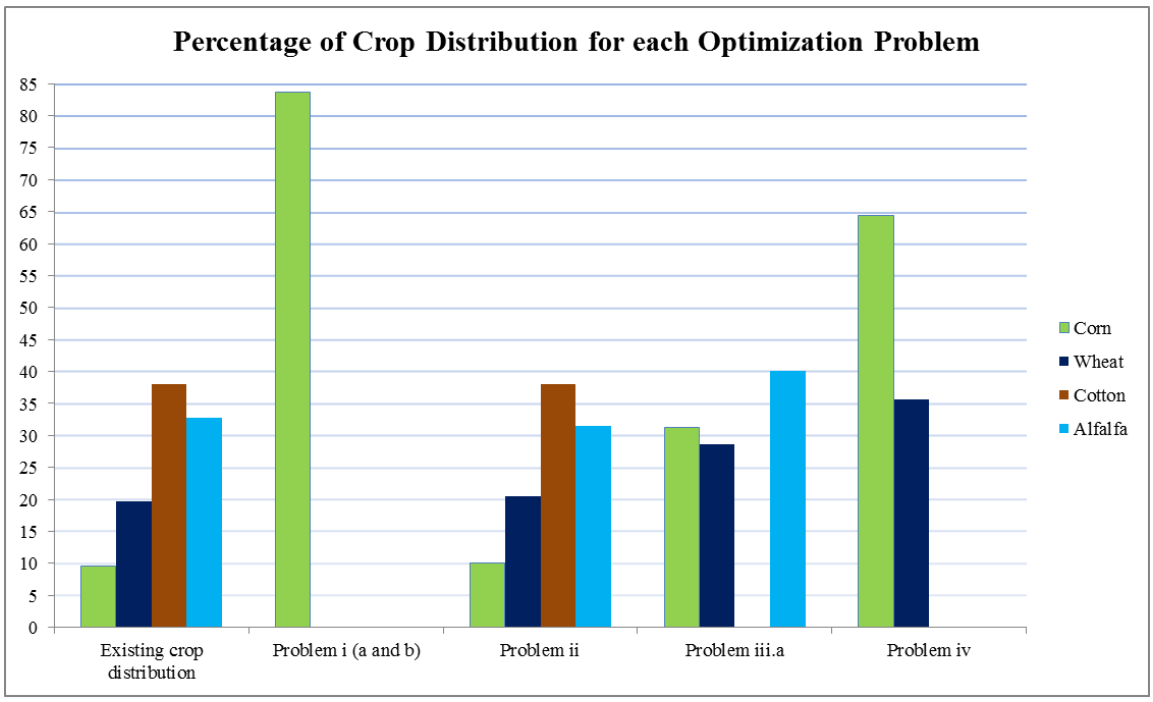

Figure 1. The results of crop distribution as percentages of the total area

Table 2. The constraints' values after each optimization. The highlighted values present the optimized objectives

Constraints	Existing values	Problem i.a	Problem i.b	Problem ii	Problem iii.a	Problem iii.b
Area (km^2)	399.62	399.62	399.62	399.62	399.62	170.92 of alfalfa
Production (tons)	277100	368147.2	368147.2	274600	-	**196561**
Irrigation Water Cost (10^3 €)	1934500.5	**673649.8**	-	-	-	-
Irrigation Water Losses (hm^3)	17101.4	-	**3558.9**	-	-	-
Labor Hours (10^3 h)	5014.5	-	-	-	3876.1	2102.3
Fertilizer (tons)	10977	-	-	-	10977	3931.2
Water Requirements (hm^3)	252.34	-	-	144332.9	252.34	-
Irrigation charge for groundwater (10^6€)	15.4	-	-	-	-	9.4
Production Cost (10^3 €)	81276	-	-	**80736**	-	-
Groundwater Requirements (hm^3)	70.16 (only for iii.b)	-	-	-	-	0
Net Profit (10^3 €)	8869	8869	8869	7963	**10875.3**	**4700.36**

In more detail:

i. a) Irrigation Water Cost

The production increased by 32.86% while the irrigation water cost decreased by 65.18%. The problem would be more complete and stable with more constraints and more competitive variables between the crops.

b) Minimization of irrigation water losses,

This example supports the above, and the importance of the constraints and the limits of the variables are shown.

The effect of the reduction of the losses by up to 79.19%, is in line with the results of previous work (Alamanos et al., 2016), and showing that the irrigation losses in the basin are immense.

ii. Production Cost

The areas of the crops that should be cultivated to satisfy these constraints and minimize production cost resulted almost the same with the existing crop distribution.

The total area and production values are within the constraints given in the linear functions, but the profit is 906.000€ less than the current level. The water needs can be hardly covered only by surface water sources. The production cost results almost equal to the existing values and it shows that with the available land and under these constraints, there cannot be lower production cost. These results illustrate the reality of Karla basin. The water needs are covered mostly by the aquifer and the production cost is already minimized under the given conditions. This crop distribution seems to be formed by farmers based on the minimum production cost, the factor that they eventually understand more directly.

At this point, another production cost minimization problem was developed with additional constraints of the maximum IWE and yield.

The optimum crops' areas under the additional constraints are 216.64 km^2 of wheat and 182.98 km^2 of corn. The total Crop Water Productivity is the same before and after this optimization, because the new total production and the final water requirements have not changed. However, a lower production cost is achieved (by 18 million€), and this is only due to the influence of the Water Efficiency in Irrigation. So, the production cost can be further reduced after all, if we consider some constraints that had not been examined or have not taken into account by stakeholders, so far.

iii. a) Farmer's Problem

The areas of these crops that should be cultivated to satisfy these constraints and maximize the net profit, as resulted, are more 'shared' now, because of the more competitive nature of the constraints.

This profit is increased by 22.62% for the entire basin in this scenario, but the larger scale introduces an uncertainty itself, in terms that the main variables used to find the net profit (objective function), such as production, production costs, etc., are records considered to be applicable in the basin, not controlled recordings by a farmer for his farm.

b)

The same problem was examined with two additional constraints (minimum irrigation cost and groundwater requirements) in order to maximize the Net Profit. The same problem was solved for a different objective function, the Production maximization. The results are shown in Table 2.

Regarding the Net Profit, the charges of using groundwater for irrigation is the same for all crops (according to the relevant departments-LALRs) and so there is no difference between the cost of most water consuming and less water consuming crops, such if there was a volumetric pricing policy.

Regarding the Production, the constraint's results are the same. Again, the solution does not exploit all the available arable land. According to these problems, if we cultivate more than 170.92 km^2, there will be no feasible solution due to the constraint of groundwater pumping limit (i.e. it requires more than 70.16 hm^3 and if so, then the constraint will not be satisfied). The net profit and the production do not exceed their current value, because it is impossible for the total area of 399.62 km^2 with the available of 70.16 hm^3 of water. Even if there were fewer constraints, the result would be exactly the same because the constraint of the water requirements reaches quickly its limit and the results practically are based on that. We can understand now more clearly how specialized are the results of each optimization, as a direct function of their constraints.

iv. Productivity

This problem is more 'stable' than the previous ones, as it uses four variables (one less than the others), but mainly because it has a large number of constraints, as a result of the division of the total production cost into components, something that was impossible in previous problems due to lack of data and recordings. The reduction rates of the constraints are shown in the graph:

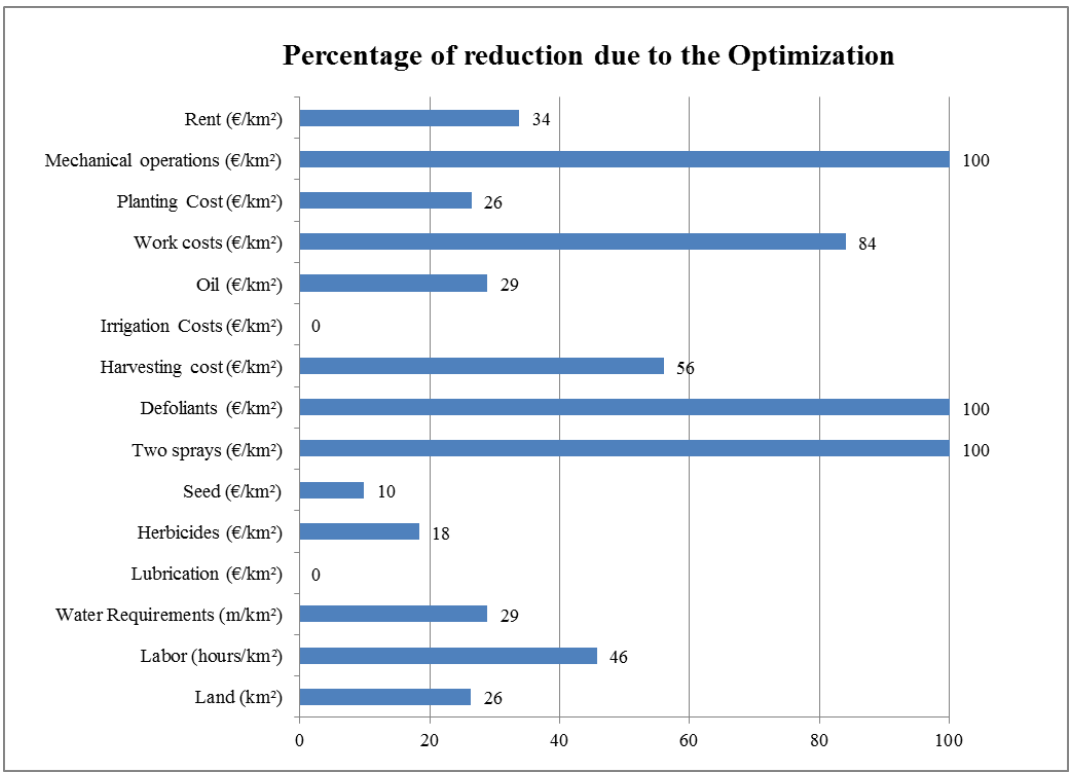

Figure 2. Percentage of the effects of the optimization of the productivity on the production costs

This total production which was resulted from this linear programming problem, under these constraints is much larger than the current one, which is estimated at 126.11 tons. Their difference is 164658.3 tons (i.e. 130566% increase!). Of course, the results are based mainly on the production, that is why there is no cotton in the solution and the maize crop is coming first, because its yield (in kg/km^2) is much more bigger and it has lower costs. For maybe more realistic results, there could have set an additional constraint – goal for the desired final annual producible quantity of each crop in the basin.

The inability to collect data and to simulate every farm of the basin, leads to the assumption that the basin operates as a single farm. This assumption introduces by its nature the uncertainties in the results and makes it difficult to be implemented, unless if there was a common plan-policy that would be followed by every farmer in the basin. Also, if someone wants to speak with certainty about the total agricultural income an exhaustive research on land property schemes should follow (e.g. land tenure and lease, co-sharing etc.)

All the results are referring to the basin's cultivated area by the studied crops. The study is based on a yearly data by confining the results to a more static than dynamic modeling approach. Also, the entire basin is considered as a single farm unit which cannot address many details and precise data on basin level.

5. CONCLUSIONS AND REMARKS

The current study has attempted to propose policy measures for agricultural water saving and cost-effectiveness in Lake Karla basin. Different scenarios focusing on the technical, agronomic and economic efficiency of the current irrigation and agricultural practices were tested.

An important stage in solving management mathematical models is the formation of the problem and the choice of the most appropriate expression of the management objectives. The difficulty of the simulation mainly lies in the fact of the involvement of many factors-parameters, which are not comparable to each other, without the same units and under conditions of incomplete or non-

existent data. It is recognized that the results are based only on selective constraints in a basin scale while mean values were calculated. Furthermore, all the cost variables refer to a specific year.

There is much room for improvement in research, which will attempt to be studied. This study was not intended to simulate the situation in the basin or to create a new methodology-approach based on optimization. The goal was to examine some policy scenarios through objective functions of maximization and minimization approaches.

ACKNOWLEDGEMENTS

This article was implemented through the project "Scholarships Greek State Scholarships Foundation in Integrated Marine and Inland Water Management" and co-funded by 85% of resources FM EEA 2009-2014 period and by 15% from the Public Investment Program. It was developed with the help of the members of the Laboratory of Hydrology and Aquatic Systems Analysis, the researcher of the Norwegian Department of Industrial Economics and Technology Management (NTNU), Per Ivar Helgesen, and elaborated under the hospitality of N.I.BIO.

REFERENCES

Alamanos A., Xenarios S., Mylopoulos N., Stalnacke P., 2016. Hydro-economic modeling and management with limited data: the case of Lake Karla Basin, Greece. European Water, 54: 3-18.

Dracup W.A., Hall J.A., 1970. Water Resources Systems Engineering. McGraw-Hill Series in Water Resources and Environmental Engineering.

Faramarzi M., Yanga H., Schulinc R., Abbaspoura K.C., 2010. Modeling wheat yield and crop water productivity in Iran: Implications of agricultural water management for wheat production. Agricultural Water Management, 97: 1861–1875.

GAMS Development Corporation, 2014. GAMS. A User´s Guide. GAMS Development Corporation, Washington, USA.

Hydromentor, 2011-2015. Development of an integrated monitoring system and management of quantity and quality of water resources in agricultural basins under climate change conditions. Application in the basin of Lake Karla.

Journal Agrenda, 2014. Weekly edition 20-21/09/2014 (p 32) and 27-28/09/2014, p 27. www.agronews.gr.

Ministry of Environment, 2013. Water Management Plan of Water District of Thessaly (GR08) in accordance with the requirements of Directive 2000/60/EC, under N.3199/2003 and P.D.51 / 2007.

OPEKEPE database, available at www.opekepe.gr

Rosenthal R.E., 1998. A Gams tutorial. GAMS Development Corporation, Washington, USA.

Salvatici L., Anania G., Arfini F., Conforti P., De Muro P., Londero P., Sckokai P., 2000. Recent developments in modelling the CAP: hype or hope? 65th EAAE Seminar "Agricultural Sector Modelling and Policy Information Systems", Bonn.

Sidiropoulos P., Mylopoulos N., Loukas A., 2013. Optimal Management of an Overexploited Aquifer under Climate Change: The Lake Karla Case. Water Resources Management, 27(6): 1635-1649.

Proceedings of the 10th World Congress of EWRA 'Panta Rhei', 5-9 July 2017, Athens, Greece
© 2017 *European Water Resources Association*

A land accounting system for integrated water resources management

G.E. Bariamis[1*], E.A. Baltas[1], V.A. Tsihrintzis[2] and M.A. Mimikou[1]
[1] *Department of Water Resources and Environmental Engineering, School of Civil Engineering, National Technical University of Athens*
[2] *Centre for the Assessment of Natural Hazards and Proactive Planning, School of Rural and Surveying Engineering, National Technical University of Athens*
[*] *e-mail: bariamis@mail.ntua.gr*

Abstract: Flood risk.

Key words: Urban model

1. INTRODUCTION

Land is an environmental asset that outlines all the space in which all the natural processes and human/economic activities are occurring. There are two main characteristics in which land could be classified: land cover (LC) and land use (LU). Due to the rapid industrialization and population growth, land resources are under pressures from physical, human and global causes such as soil erosion, desertification, pollution, food shortage, land conflicts, water shortages, and climate change. The urbanization of lands has also measurable impact on the quantity (Chen et al., 2015; Gyamfi et al., 2016; Kaplan et al., 2014; Ayala et al., 2016) and quality (McGrane, 2016; Wilson, 2015) of water resources.

All these complex and dynamic processes have been standardized in a coherent way under the System of Environmental and Economic Accounting Central Framework – SEEA (United Nations, 2014). The SEEA is a useful tool and has already been implemented throughout the world in the water (Bariamis et al., 2016; Dutta et al., 2017; Pedro-Monzonís et al., 2016) and land (EEA, 2006) domains. This study focuses on the changes of land cover under the SEEA proposed methodologies for the period 2001 to 2011 in a hydrologic sub-region in the USA, and explores the potential connection of land cover changes and indicators with primary hydrologic physical characteristics.

2. MATERIALS AND METHODS

2.1 Study area and data used

The study area selected to implement the land accounts concepts, is the Wabash River hydrologic sub-region as shown in Figure 1. The Wabash River is a tributary, covering 20% (~85,353 km^2) of the area of the Ohio River Region (421,960 km^2) (U.S. Geological Survey, b) . The river network stretches almost 765 km (State of Indiana Department of Natural Resources; U.S. Geological Survey, a) covering various counties in the States of Indiana and Illinois. The long term annual average (1940 - 2000) runoff of the sub-region is 852 m^3/s. The population of this area is estimated at 4.5 million people in 2011, presenting an 8% increase compared with the population of 2001. In order to elaborate the land accounts, the National Land Cover Database (NLCD) (Fry et al., 2011; Homer et al., 2007, 2015) has been used, covering the land cover status for 2001, 2006 and 2011, as well as, the land cover changes for the intermediate periods of 2001-2006 (Period A)

and 2006-2011 (Period B). The NLCD dataset is based on a two level classification system covering 20 land cover types in its full extent (Anderson et al., 1976).

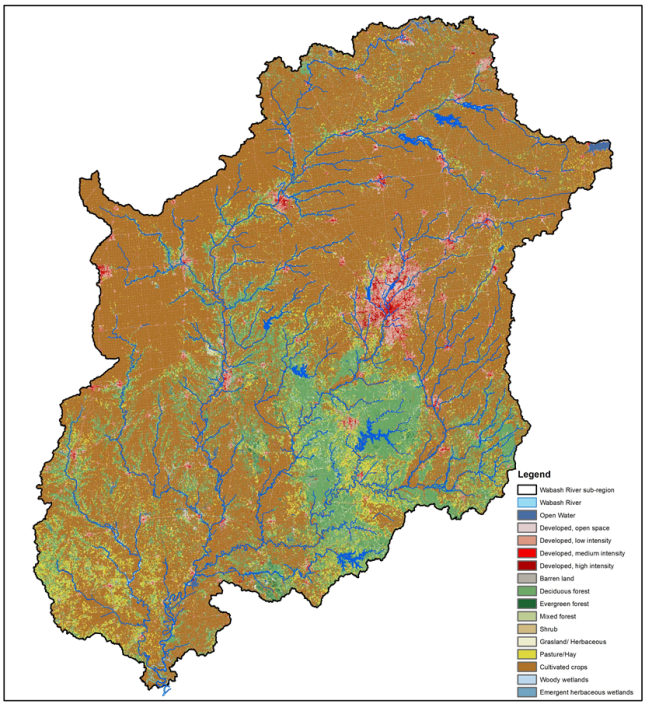

Figure 1. Wabash River sub-region's land cover status for 2011

2.2 Methods

The implementation of the land accounts, requires some steps to formulate and produce standardized tables which are quantifying parameters such as land "consumption", land "formation", physical "flows" from one category of land to another, and land cover stock changes among accounting periods. With this approach, indicators' development is also stimulated, such land intake per LC category. Total turnover, the absolute sum of formation and consumption of each of the land cover classes, could potentially reflect the ecosystems stability or the vulnerability of the land related assets.

3. RESULTS

The main results of the land accounting are presented in Tables 1 and 2. Analyzing the latest stocks of 2011 the 68% is planted areas, 19.5% forests and 9.5% developed areas cover almost the 97% of the Wabash river basin. The remaining 3% is shared among the rest five of the LC types; grasslands, open water, wetlands, shrubs and barren land. The approach is to quantify the LC stocks at the start of the accounting period, then measure the gains/losses of stock which will define the land type stock value at the end of the accounting period. Horizontal (total consumption) and vertical (total formation) evaluation of the land accounting tables reveal the main transformations occurring among the origin and destination of LC types. LC stocks of developed categories present an increase by 3.4% along with open water (3.5%) and wetlands (3%) areas from 2001 to 2011, while barren lands present the highest increase (+59.8%). An aggregation of the land stocks in natural (sum of water, barren lands, forest, grassland and wetlands) and manmade disturbed (sum of developed, barren and planted) areas, shows a 23% / 77% share, indicating high levels of human alteration in the Wabash River sub-region. The total turnover of land cover change (Table 1) in period A (2001-2006) was ~600 km^2 while in the period B (2006-2011) was ~460 km^2 representing

an increase in the ecosystems' stability as higher numbers of LC exchanges depict transactions between land formation and consumption. In both periods the 75% of total turnover is shared between medium/high developed density (43%) and planted areas (32%) making them the main contributors of change in the area.

3.1 Land cover consumption/formation analysis

In both periods the 65-70% of consumed areas are planted and forest lands, while the formation of developed land shares the 67-71% of total formation. This reveals the dynamics of urban and industrial areas expansion against the current agricultural planted areas and deciduous forests. Further analysis of period A indicates that the maximum LC category "consumption" of 158 km^2 occurred in the cultivated areas (LC code 82) in favor of urban expansion by 80%, while the maximum LC "formation" of 72 km^2 occurred in the open spaced developed areas (LC code 21). Land change indicator (area changed/year) presented highest gains in the developed LC (+31.9 km^2/y), while highest losses occurred in planted areas (-31.5 km^2/y). Forest loss was at -9.8 km^2/y. For the period B, the maximum LC category "consumption" of 103 km^2 occurred in the cultivated areas (LC code 82) in favor of urban expansion by 81%, while the maximum LC "formation" of 49 km^2 occurred in the medium intensity developed areas (LC code 23). This represents an internal redistribution of LC codes 21 and 22 by 55% and intake from planted areas by 40%. Land intake gains for the period B was +23.4 km^2/y for the developed LC codes while planted areas had highest losses (-21 km^2/y). Forest loss was at -8.5 km^2/y.

3.2 Land cover flows analysis

Land cover flows analysis is an important component that land accounts can provide by revealing the patterns of flows among different land cover types. The main contributors (alternatively origins) are the planted and forested areas while the main consumers (alternatively destinations) LC types are the developed areas. One particularity of the developed areas is that most of the flows cover internal exchanges. These areas present high stability and there is no significant sign of trend reversal or naturalization of them till now. The LC flows are presented more analytically in Figure 2, where no transitional land stocks are shown except developed, forest and planted areas, to make clearer the flows, as well as their relative significance.

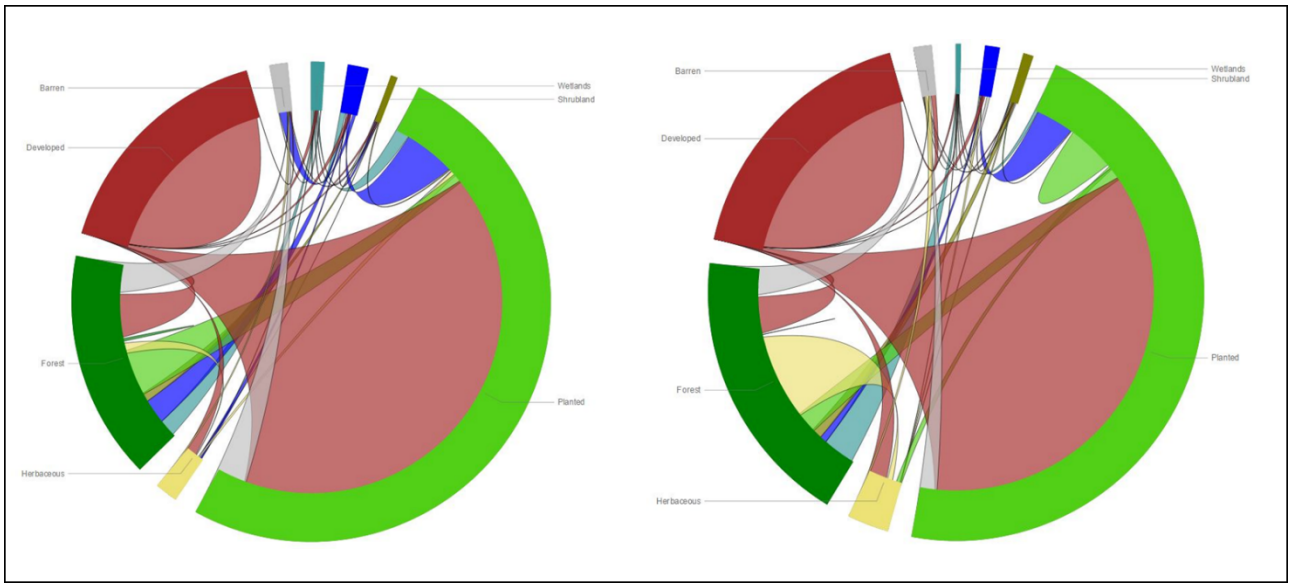

Figure 2. Land cover flows without transitional stocks for the Wabash River for the Periods A (left) and B (right)

3.3 Water resources and uses

An analysis of runoff and estimated water uses data from open sources (Hutson et al., 2004; Kenny et al., 2009; Maupin et al., 2010) for years 2001-2011 in the region has been conducted. Surface run off measured compared with the multi annual average of the period 1940-2000 (852 m^3/s) is increased by almost 30% to 1.115 m^3/s indicating an increase in the impervious surfaces which potentially could relate to the 3.5% increase in the developed areas and the parallel 1% decrease of forests. Further research is required in the topology of the changes to examine whether these changes are occurring in peri-urban areas affecting the hydrologic regime of the region.

Water uses linked with food production (irrigation, livestock and aquaculture) increased by 67%, while the planted areas have been slightly decreased (-0.45%) compared with the start of accounting period. Given that the areas of planted lands are quite stable, the increase in water volumes used in the agricultural and livestock sectors are an indication of water intensive yields produced. Further analysis of the status is required to define the types of agricultural and irrigation methods.

Table 1. Stock and change accounts for Wabash River region for the Periods A (2001-2006) and B (2006-2011)

	Land cover class (Level 1)	Water	Developed				Barren	Forest			Scrublands	Herbaceous	Planted		Wetlands		Total
	Land cover code (Level 2)	11	21	22	23	24	31	41	42	43	52	71	81	82	90	95	
Period A (2001-2006)	Land cover 2001 (km²)	881.4	5,003.7	2,101.3	581.3	238.9	37.7	16,463.7	223.5	6.1	140.7	951.3	5,422.2	52,775.8	409.3	116.6	85,353.5
	Consumption (C) of initial land cover (km²)	4.7	36.3	17.6	1.1	0.0	4.1	51.5	1.2	0.0	1.4	5.2	14.7	158.9	1.6	1.4	299.8
	Formation (F) of new land (km²)	27.1	72.2	49.0	66.0	27.0	18.8	1.7	1.2	0.8	2.9	5.5	0.8	15.3	0.7	10.7	299.8
	Net formation of land cover (km²)	22.4	36.0	31.4	64.9	27.0	14.8	-49.8	-0.1	0.8	1.5	0.3	-14.0	-143.6	-0.9	9.3	0.0
	Net formation as % of initial year	2.5%	0.7%	1.5%	11.2%	11.3%	39.2%	-0.3%	0.0%	13.5%	1.1%	0.0%	-0.3%	-0.3%	-0.2%	8.0%	
	Total turnover of land cover (C+F) (km²)	31.8	108.5	66.5	67.1	27.0	22.9	53.2	2.4	0.9	4.4	10.7	15.5	174.2	2.2	12.2	599.5
	Total turnover as % of initial year	3.6%	2.2%	3.2%	11.5%	11.3%	60.7%	0.3%	1.1%	14.0%	3.1%	1.1%	0.3%	0.3%	0.5%	10.4%	
	No land cover change (km²)	876.7	4967.4	2,083.7	580.2	238.9	33.7	16,412.2	222.3	6.1	139.2	946.1	5,407.5	52,616.9	407.7	115.2	85,053.7
	No land cover changes as % of initial year	99.5%	99.3%	99.2%	99.8%	100.0%	89.3%	99.7%	99.5%	99.8%	99.0%	99.5%	99.7%	99.7%	99.6%	98.8%	
	Land cover 2006 (km²)	903.8	5,039.7	2,132.7	646.2	265.9	52.5	16,413.9	223.4	7.0	142.1	951.6	5,408.3	52,632.1	408.4	126.0	85,353.5
	Land intake per year (km²/year) Period A	4.5	7.2	6.3	13	5.4	3.0	-10.0	0.0	0.2	0.3	0.1	-2.8	-28.7	-0.2	1.9	
	% change in stock Period A	2.5%	0.7%	1.5%	11.2%	11.3%	39.2%	-0.3%	0.0%	13.5%	1.1%	0.0%	-0.3%	-0.3%	-0.2%	8.0%	
Period B (2006-2011)	Land cover 2006 (km²)	903.8	5,039.7	2,132.7	646.2	265.9	52.5	16,413.9	223.4	7.0	142.1	951.6	5,408.3	52,632.1	408.4	126.0	85,353.5
	Consumption (C) of initial land cover (km²)	2.4	31.0	13.4	0.9	0.0	3.0	46.0	1.7	0.0	1.6	7.1	18.5	103.4	0.3	0.5	229.9
	Formation (F) of new land (km²)	10.5	42.5	40.3	49.5	22.3	10.8	4.8	0.3	0.0	2.4	21.4	5.7	11.4	7.3	0.7	229.9
	Net formation of land cover (km²)	8.0	11.5	26.9	48.6	22.3	7.8	-41.2	-1.4	0.0	0.8	14.3	-12.7	-92.0	7.0	0.2	0.0
	Net formation as % of initial year	0.9%	0.2%	1.3%	7.5%	8.4%	14.8%	-0.3%	-0.6%	-0.7%	0.6%	1.5%	-0.2%	-0.2%	1.7%	0.2%	
	Total turnover of land cover (C+F) (km²)	12.9	73.5	53.7	50.5	22.3	13.8	50.8	2.0	0.0	4.1	28.4	24.2	114.7	7.6	1.1	459.7
	Total turnover as % of initial year	1.4%	1.5%	2.5%	7.8%	8.4%	26.3%	0.3%	0.9%	0.7%	2.9%	3.0%	0.4%	0.2%	1.9%	0.9%	
	No land cover change (km²)	901.4	5,008.6	2,119.3	645.2	265.9	49.5	16,367.9	221.8	6.9	140.5	944.5	5,389.8	52,528.8	408.1	125.5	85,123.6
	No land cover changes as % of initial year	99.7%	99.4%	99.4%	99.9%	100.0%	94.2%	99.7%	99.2%	99.3%	98.8%	99.3%	99.7%	99.8%	99.9%	99.6%	
	Land cover 2011 (km²)	911.8	5,051.1	2,159.6	694.8	288.2	60.3	16,372.6	222.0	6.9	142.9	965.9	5,395.5	52,540.1	415.4	126.2	85,353.5
	Land intake per year (km²/year) Period B	1.6	2.3	5.4	9.7	4.5	1.6	-8.2	-0.3	0.0	0.2	2.9	-2.5	-18.4	1.4	0.0	
	% change in stock Period B	0.0	0.0	0.0	0.1	0.1	0.1	0.0	0.0	0.0	0.0	0.0	0.0	0.0	0.0	0.0	

Table 2. Land cover flows in the Wabash River region for Periods A (2001-2006) and B (2006-2011)

	Consumption→ / Formation ↓		Water	Developed				Barren	Forest			Scrublands	Herbaceous	Planted		Wetlands	
			11	21	22	23	24	31	41	42	43	52	71	81	82	90	95
Period A (2001-2006)	Water	11	876.7	0.5	0.2	0.2	0.1	0.9	-	-	0.0	0.0	0.2	0.0	1.2	0.0	1.5
	Developed	21	-	4,967.4	6.0	24.0	6.2	-	-	-	-	-	-	-	-	-	-
		22	-	-	2,083.7	8.9	8.6	-	-	-	-	-	-	-	-	-	-
		23	-	-	-	580.2	1.1	-	-	-	-	-	-	-	-	-	-
		24	-	-	-	-	238.9	-	-	-	-	-	-	-	-	-	-
	Barren	31	2.9	0.0	0.0	0.1	0.1	33.7	-	-	0.0	0.0	0.6	0.0	0.1	-	0.1
	Forest	41	7.0	7.5	2.9	1.4	0.5	8.1	16,412.2	0.1	0.7	2.6	2.8	0.6	12.5	0.4	4.5
		42	0.1	0.1	0.0	0.0	0.0	0.5	-	222.3	0.0	0.0	0.3	-	0.2	0.0	0.0
		43	0.0	-	-	-	-	0.0	-	-	6.1	-	-	-	0.0	-	-
	Scrublands	52	0.6	0.3	0.1	0.1	0.0	0.0	0.0	-	-	139.2	0.0	-	0.2	0.0	0.0
	Herbaceous	71	0.9	1.6	1.0	0.5	0.1	0.4	0.0	0.0	0.0	0.0	946.1	-	0.5	0.0	0.2
	Planted	81	0.6	7.4	3.2	1.6	0.4	0.5	0.6	0.1	0.0	0.0	0.1	5,407.5	0.0	0.0	0.2
		82	14.4	54.4	35.3	29.1	9.8	8.3	1.1	0.9	0.0	0.3	1.4	0.0	52,616.9	0.1	3.6
	Wetlands	90	0.3	0.2	0.1	0.0	0.0	0.0	-	0.1	-	0.0	0.1	0.0	0.2	407.7	0.6
		95	0.2	0.3	0.2	0.1	0.0	0.2	0.0	-	-	-	0.1	-	0.4	0.0	115.2
Period B (2006-2011)	Water	11	901.4	0.3	0.2	0.13	0.1	0.6	0.2	0	-	-	0.5	0.1	0.3	0.1	0
	Developed	21	-	5,008.6	5.4	20.1	5.5	-	-	-	-	-	-	-	-	-	-
		22	-	-	2,119.3	7.4	6.0	-	-	-	-	-	-	-	-	-	-
		23	-	-	-	645.2	0.9	-	-	-	-	-	-	-	-	-	-
		24	-	-	-	-	265.9	-	-	-	-	-	-	-	-	-	-
	Barren	31	0.6	0.2	0.2	0.2	0.3	49.5	0	-	-	-	1.2	0.2	0.1	-	-
	Forest	41	1.5	4.0	2.6	0.9	0.3	5.7	16,367.9	0	-	2.3	17.3	0.1	4.5	6.4	0.4
		42	0	0	0	0	-	0.3	0	221.8	-	0	1.3	-	0	0	-
		43	-	0	0	-	-	0	-	-	6.9	-	0	-	-	-	-
	Scrublands	52	0	0.1	0.1	0	0	0.2	0.7	-	-	140.5	0.2	0	0.2	0.1	0
	Herbaceous	71	0.	1.6	0.7	0.5	0.2	0.3	1.3	0	-	0.1	944.5	0.3	0.8	0	0
	Planted	81	0.3	5.7	4.2	1.5	0.4	0.3	0.3	0	-	-	0.3	5,389.8	5.4	0	0
		82	7.9	30.5	25.7	18.6	8.6	3.3	2.3	0.2	-	0.1	0.5	5	52,528.8	0.5	0.1
	Wetlands	90	0	0	0	0	0	0	-	-	-	-	0.1	-	0.1	408.1	0.1
		95	-	0.1	0.1	0	0	0	0	-	-	-	-	0	0.1	0.1	125.5

Note: Grey cells indicate the transitional stocks

4. CONCLUSIONS

Land is a finite and already overexploited natural resource which provides the necessary space for water resources, food and energy production services, as well as, climate regulation and carbon sequestration via organic and inorganic environmental assets such as water and forests.

Land accounting is a useful tool, offering a different perspective of analysis in the exchanges and dynamics of land resources of an area. The changes in land cover have been monitored for a long period in the highly human intervened Wabash River basin and trends have already been ascertained. Even though not significant changes have occurred in the major land cover categories from 2001-2011, the existing land cover stocks and flows indicate an accelerating urban sprawl against forested and planted areas. This is a signal of a probable future increase in water uses by the industrial sector and domestic/public water supply. New indicators such land intake, land use intensity coupled with water related parameters and even socio-economic input could potentially be used for integrated water resources management, identifying the main drivers that exert pressures on water resources and the ecosystems.

The interactions of land stocks with the water resources distribution and use, are the actual points in the common sphere of land and water accounting. Aggregated results of water use in the Wabash river indicate an increase in water volumes used in the food production sectors (agriculture, aquaculture and livestock) as well as an increase in the surface runoff measured. Additional measures to halt soil sealing as well as implement flood protection infrastructure projects could be the answer to ensure that water stocks will have the adequate quantity and quality required. The dynamics of the water cycle and land cover changes are differing in temporal resolution; however, there are ways to jointly assess the diverse layers of the land-water nexus. This analysis could offer the necessary input for revising existing environmental protection policies, increasing the water efficiency of the intensive activities and ensuring a sustainable use of water resources supporting water supply, food and energy production.

ACKNOWLEDGEMENTS

We would like to express our gratitude to the U.S. Geological Survey for the open access of the data under the NLCD, GAGES II, NHD and WBD programmes.

REFERENCES

Anderson, J. R., Hardy, E. E., Roach, J. T., & Witmer, R. E. (1976). A land use and land cover classification system for use with remote sensor data, 2001.

Bariamis, G., Zachos, A., Baltas, E., Zal, N., Panagos, D., Konstantinou, I., & Mimikou, M. (2016). Use of Freshwater Resources in Europe 2002 – 2012.

Chen, H., Tong, S. T. Y., Yang, H., & Yang, Y. J. (2015). Simulating the hydrologic impacts of land-cover and climate changes in a semi-arid watershed. Hydrological Sciences Journal, 60(10), 1739–1758. https://doi.org/10.1080/02626667.2014.948445

Dutta, D., Vaze, J., Kim, S., Hughes, J., Yang, A., Teng, J., & Lerat, J. (2017). Development and application of a large scale river system model for National Water Accounting in Australia. Journal of Hydrology, 547, 124–142.

EEA. (2006). Land accounts for Europe 1990–2000: Towards integrated land and ecosystem accounting. Europe (Vol. 11). Retrieved from http://scholar.google.com/scholar?hl=en&btnG=Search&q=intitle:Land+accounts+for+Europe+1990?2000#0

Fry, J., Xian, G., Jin., S., Dewitz, J., Homer, C., Yang, L., et al.. (2011). Completion of the 2006 National Land Cover Database for the Conterminous United States. Photogrammetric Engineering & Remote Sensing2, 77(9), 858–864.

Gyamfi, C., Ndambuki, J., & Salim, R. (2016). Hydrological Responses to Land Use/Cover Changes in the Olifants Basin, South Africa. Water, 8(12), 588. https://doi.org/10.3390/w8120588

Homer, C., Dewitz, J., Fry, J., Coan, M., Hossain, N., Larson, C., … Wickham, J. (2007). Completion of the 2001 National Land Cover Database for the Conterminous United States. Photogrammetric Engineering and Remote Sensing, 73(4), 337–341.

Homer, C., Dewitz, J., Yang, L., Jin, S., Danielson, P., Xian, G., … Megown, K. (2015). Completion of the 2011 National Land Cover Database for the Conterminous United States – Representing a Decade of Land Cover Change Information. Photogrammetric Engineering & Remote Sensing, 81(5), 345–354. https://doi.org/10.1016/S0099-1112(15)30100-2

Hutson, S. S., Barber, N. L., Kenny, J. F., Linsey, K. S., Lumia, D. S., & Maupin, M. A. (2004). Estimated Use of Water in the United States in 2000 Circular 1268 (Vol. 4).

Kaplan, S., Myint, S. W., Fan, C., & Brazel, A. J. (2014). Quantifying Outdoor Water Consumption of Urban Land Use/Land Cover: Sensitivity to Drought. Environmental Management, 53(4), 855–864. https://doi.org/10.1007/s00267-014-0245-7

Kenny, J. F., Barber, N. L., Hutson, S. S., Linsey, K. S., Lovelace, J. K., & Maupin, M. a. (2009). Estimated Use of Water in the United States in 2005 Circular 1344. Water. Retrieved from http://hbg.psu.edu/etc/Newsletter/doc/October2009.pdf

McGrane, S. J. (2016). Impacts of urbanisation on hydrological and water quality dynamics, and urban water management: a review. Hydrological Sciences Journal, 61(13), 2295–2311. https://doi.org/10.1080/02626667.2015.1128084

Miguel Ayala, L., van Eupen, M., Zhang, G., Pérez-Soba, M., Martorano, L. G., Lisboa, L. S., & Beltrao, N. E. (2016). Impact of agricultural expansion on water footprint in the Amazon under climate change scenarios. Science of The Total Environment, 569, 1159–1173. https://doi.org/10.1016/j.scitotenv.2016.06.191

Molly A. Maupin, Joan F. Kenny, Susan S. Hutson, John K. Lovelace, Nancy L. Barber, and K. S. L. (2010). Estimated Use of Water in the United States in 2010 Circular 1405. US Geological Survey. (Vol. 1405). https://doi.org/http://dx.doi.org/10.3133/cir1405

Pedro-Monzonís, M., Jiménez-Fernández, P., Solera, A., & Jiménez-Gavilán, P. (2016). The use of AQUATOOL DSS applied to the System of Environmental-Economic Accounting for Water (SEEAW). Journal of Hydrology, 533, 1–14. https://doi.org/10.1016/j.jhydrol.2015.11.034

State of Indiana Department of Natural Resources. (n.d.). Wabash River. Retrieved February 8, 2017, from http://www.in.gov/dnr/outdoor/4476.htm

U.S. Geological Survey. (n.d.-a). National Hydrography Dataset. Retrieved February 8, 2017, from https://nhd.usgs.gov/data.html

U.S. Geological Survey. (n.d.-b). Watershed Boundary Dataset. Retrieved February 8, 2017, from https://nhd.usgs.gov/wbd.html

United Nations. (2014). System of environmental-economic accounting: a central framework.

Wilson, C. O. (2015). Land use/land cover water quality nexus: quantifying anthropogenic influences on surface water quality. Environmental Monitoring and Assessment, 187(7), 424. https://doi.org/10.1007/s10661-015-4666-4

Proceedings of the 10th World Congress of EWRA 'Panta Rhei', 5-9 July 2017, Athens, Greece
© 2017 *European Water Resources Association*

Prospects for sustainable water resources management within the River Djetinja catchment

B.B. Matić* and Z. Simić
Jaroslav Černi Institute for the Development of Water Resources, Belgrade, Serbia
* *e-mail: branislava.matic@jcerni.co.rs*

Abstract: Water resources management that address various users' demand at the River Basin scale is the very important topic that involves comprehensive evaluation and consideration of catchment characteristics, and general professional and scientific postulates. Contemporary water management incorporates number of criteria merged in a way to target economic development, social equity, and environmental sustainability. However, the most vital subject is water supply for different users with sufficient amount of water that responds to quality standards. Integrated water resources management principles are incorporated in Republic of Serbia Water Act. Thus, at the river basin and sub basin level allocation among different users and sectors that is sustainable and provides enough water of required quality has to be attained. Due to water management complexity, the potential allocation has to consider natural conditions, water resources quantity, environmental protection, foreseen development, measures, etc. In addition to assessment of natural features (drainage area, topography, land cover, hydrogeology, erosion, etc.), existing water management issues this paper introduces the prospects for improvement of water resources management and allocation among different sectors (drinking water supply, hydropower, agriculture, tourism, etc.) based on planned development within Djetinja River drainage area. Brief overview of natural water retention measures benefits and role of hydrologic ecosystem services that are complementary with existing and foreseen technical measures indicate necessity for their incorporation in decision making process. Selection of measures results from comprehensive analyses and assessment given the complexity of domain. More frequent monitoring and additional data are prerequisite for multipurpose NWRM preference so it can contribute to sustainable and integrated water resources management.

Key words: Sustainable water resources management, integrated water resources management, water resources allocation, natural water retention measures

1. INTRODUCTION

Contemporary water resources management has to address development, social equity, and environmental sustainability. Since the Dublin Conference on water and environment (1992) the global community advocates for more comprehensive water resources management paradigm in order to accomplish sustainable development. This global shifts result in integrated water resources management (IWRM) doctrine incorporation in policy and legal framework at national, transboundary and global level. IWRM attempts to integrate prospects and processes of the hydrologic cycle, watershed features and economics, social interactions and policies (Mayfield et al., 2004) and to consider external impact (Climate Change, water allocation among different users, etc.). Serbia transposed (Water Act, Official Gazette of Republic of Serbia, 2010) but not fully implemented the integrated water management concept that includes harmonized water regime across Serbia's territory, water management that maximize economic and social benefits in an equitable and sustainable manner, while honoring international agreements, constitutes a long-term strategic goal that requires considerable time (more than two decades, with a proper approach) and enormous spending ,e.g., about one billion € annually (Water Management Strategy of the Republic of Serbia, 2016). As stated by Miloradov (1992) the multipurpose water use in all human activities and the intensive development and urbanization generated considerable increase in water demand and water pollution and the water resources management practice around the world is challenged by serious problems (Simonović, 2008). While implementation of IWRM advanced for large

transnational river basins (Danube, Mekong, Sava, etc.) the action is still pending for sub-basins and their sub catchments. Given that, this paper presents prospects for sustainable water resources management for the Djetinja River Basin (Figure 1) located inside the region with largest share of internal fresh water resources in Serbia, namely Western Morava River Basin. Several significant water management issues in catchment are pinpointed by previous studies, e.g., flooding, water pollution, and erosion (Urošev et al., 2009; Milijašević, 2010).

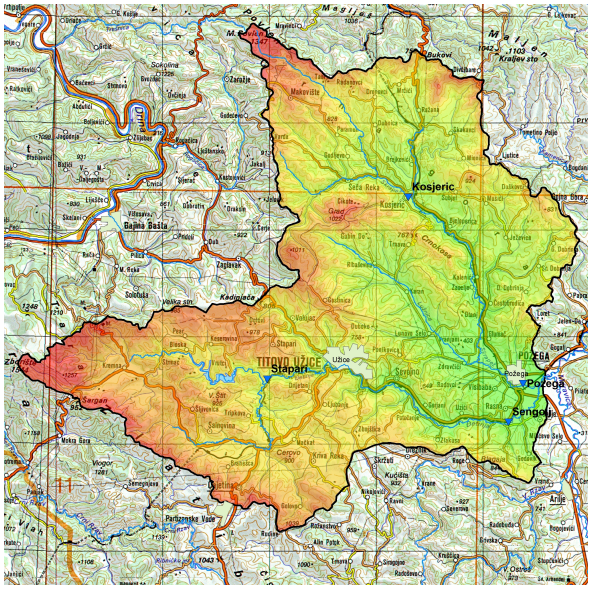

Figure 1. Djetinja River drainage area and existing hydrologic stations

The main goal of study is to illuminate potential issues and challenges for IWRM for catchment with no water stress given its natural features, hydrology, water use and planned future development with main idea to scratch the surface of natural water retention measures (NWRM) and resulting hydrologic ecosystems services (ESS) that are complementary with existing and planned technical measures at the catchment level. Detailed analyses and modelling are beyond the scope of this paper.

2. NATURAL FEATURES AND HYDROLOGY

The Djetinja basin Area is 1195 km^2 and main course length is 78 km. It originates in Kremna Basin as a joint of Bratišina and Konjska River, and Užički and Tomića streams. According to available data average catchment rainfall, unit runoff and slope are 807.16 mm, 9.4 l/s/km^2 and 12.47%, respectively. Figure 3 depicts their uneven spatial distribution.

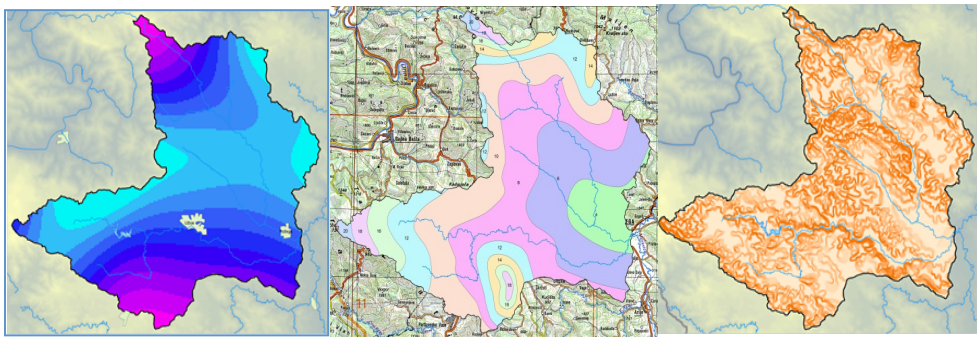

Figure 2. Djetinja River rainfall, unit runoff and slope spatial distribution

The most significant high flows are observed in March and April, while low flows conditions are typical for August and September (Figure 3). The normalized values refer to average monthly low flow magnitudes at hydrological stations used in analyses divided by their contributing drainage areas. As presented in Figure bellow the low flows condition are almost similar for Kosjerić and Požega stations.

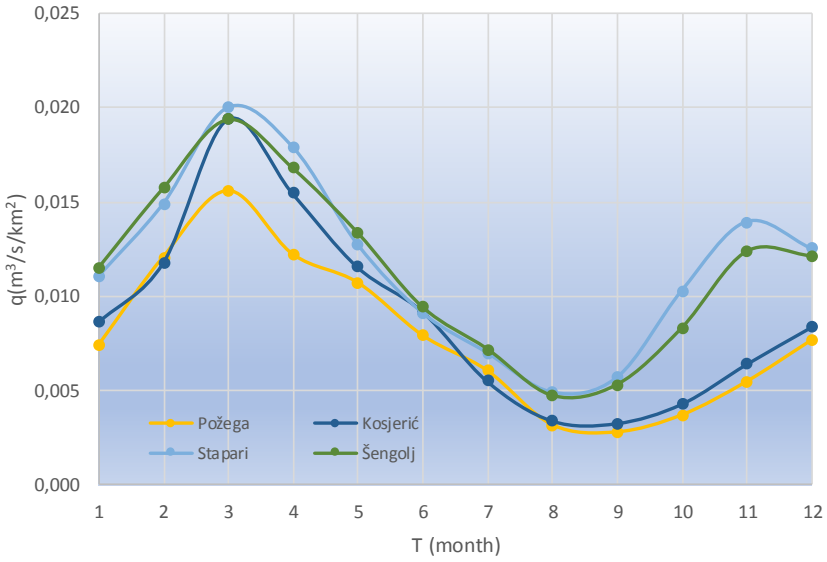

Figure 3. Djetinja River normalized average monthly low flow values

With runoff coefficient of 0.368 which is 50% higher than national average and 11.25 m^3/s discharge of almost pristine, mainly mountain fresh water, the study area is very significant as the water source for different users. Djetinja's catchment stretches across number of gorges with heterogeneous geological structure and has on average good permeability. Land use practices comprises of forests (43.14 %) followed by land principally occupied by agriculture, with significant areas of natural vegetation (27.45%), complex cultivation patterns (15.8%) with small share of discontinuous urban fabric (1.50), mineral extraction sites (0.09 %), Airports (0.09 %), Industrial or commercial units (0.08 %), Road and rail networks and associated land (0.03%). Erosion processes of different magnitude are presented due to natural features and hydrology. The summary for hydrogeology, erosion spatial distribution and land use practices, are exhibited in Figure 4.

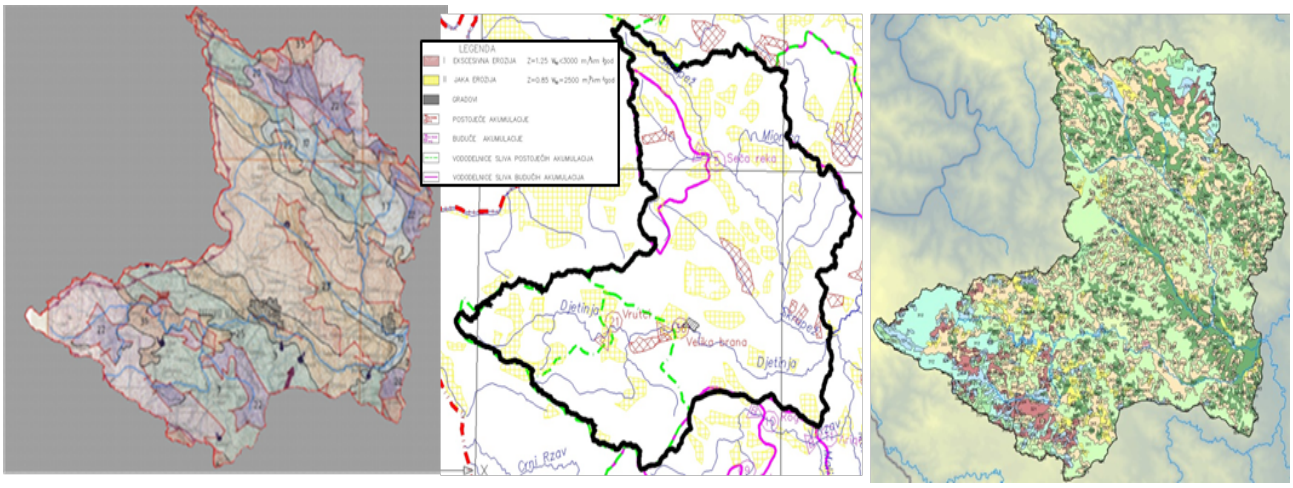

Figure 4. Djetinja River hydrogeology, erosion intensity and land use

3. EXISTING AND PLANED WATER RESOURCES MANAGEMENT

The first hydroelectric power plant in Serbia was started as early as in 1900 in Užice on the Djetinja River, using a Tesla's polyphase electric current system. After being out of operation for thirty years, today the facility is working well. The dam and reservoir Vrutci is developed in 1984 for water supply of Užice and other habitats, for flood protection, downstream low flow management and tourism. Few years ago the small hydropower plant (Q_{inst}=1m^3/s) that use water from Vrutci reservoirs become operational. There is also reservoir on Skrapež River. Based on Divac et al., (2001) planned development of large complex multipurpose hydro technical system Lim -West Morava includes connection of Vrutci system with Rzav system. The proposed development scheme includes water transfer from Drina River basin to West Morava Basin to provide stable water supply for population and industry and other water use (irrigation, tourism).

Several issues are significant from water resources management perspective. Despite the source water quality at the present, water quality issues exists in Vrutci reservoir. The largest polluters of the Djetinja basin are industries in the settlements of Užice, Sevojno and Požega. The water quality changes along the course. Although upstream of Užice, the water quality is high the catchment is being exposed to the pollution from agricultural activities, improper manure management, intensive pollution and partial self-purification from Užice to Požega. The degradation of the river ecosystems is noticeable through the town of Užice and downstream of it. Further use of the waters is in the close connection with the knowledge of water regime and protection from the pollution. In 2009 extreme rainfall resulted in flooding of Užice, and downstream localities and villages. The Mokra Gora, Kosjerić located in the upstream part of catchment were severe affects by flooding. Finaly, erosion and torrents are present within the river basin, due to natural features and hydrology. Erosion processes exist along the main river course from the headwaters to confluence with its tributary Skrapež. Yearly sediment production is approximately 117050.84 m^3 with suspended sediments accounts of 50.73 % and 49.27 % are chemically dissolved mineral matters.

4. OVERVIEW OF POSSIBLE NATURAL WATER RETENTION MEASURES

From the perspective of sustainable water management and IWRM Natural Water Retention Measures (NWRM) as the multi-functional approach have the potential to provide multiple benefits, including contribution to flood risk reduction, erosion management, water quality improvement, groundwater recharge, etc. The natural water retention capacity is the hydrologic ecosystem services (HYESS) that provides linkage among different sectors (water, agriculture, hydropower, environmental protection, etc) and is complementary with existing and foreseen technical measures.

As presented in Figure 5 ecosystems influence on hydrologic services are beneficial. Thus, HYESS incorporate the benefits to people produced by terrestrial ecosystem effects on freshwater. According to Brauman et al., (2007) these services can be grouped into five broad categories: improvement of extractive water supply, improvement of in-stream water supply, water damage mitigation, provision of water related cultural services, and water-associated, supporting services. Evidences of positive effects of HYESS and NWRM that enlarge river basin natural water retention capacity and contribute to sustainable water resources management and IWRM exist; however their implementation in planning process is still pending. Better knowledge base and exchange of good practices are required. More data and information on the effectiveness of NWRM under different conditions and their (potential) additional benefits in comparison to other measures will facilitate the identification of contexts and conditions where NRWM may provide multiple benefits and be cost-effective, and hence may promote more widespread implementation of NWRM (EU policy document on NWRM, 2014).

The establishment of connection of hydrology and ecosystem services is wicked problem given the complexity of each domain, and it becomes even more complicated when it comes to measures that are complementary with existing and planned technical measures. Given the natural features, water management practices existing issues (water quality, uneven flow distribution – temporal and

spatial, erosion, etc.) and planned development at the study area application of common decision making procedures will likely contribute to incorporation of NWRM that are multifunctional (e.g., buffer strips that decrease water pollution, trap sediments, etc.). Moreover, enhanced coordination between planning processes across different policy areas (e.g. River Basin and Flood Risk Management, nature protection, rural development and land use/spatial planning) is perceived as a pre-requisite for enhancing the chances of NWRM multiple benefits to be considered appropriately in management decisions.

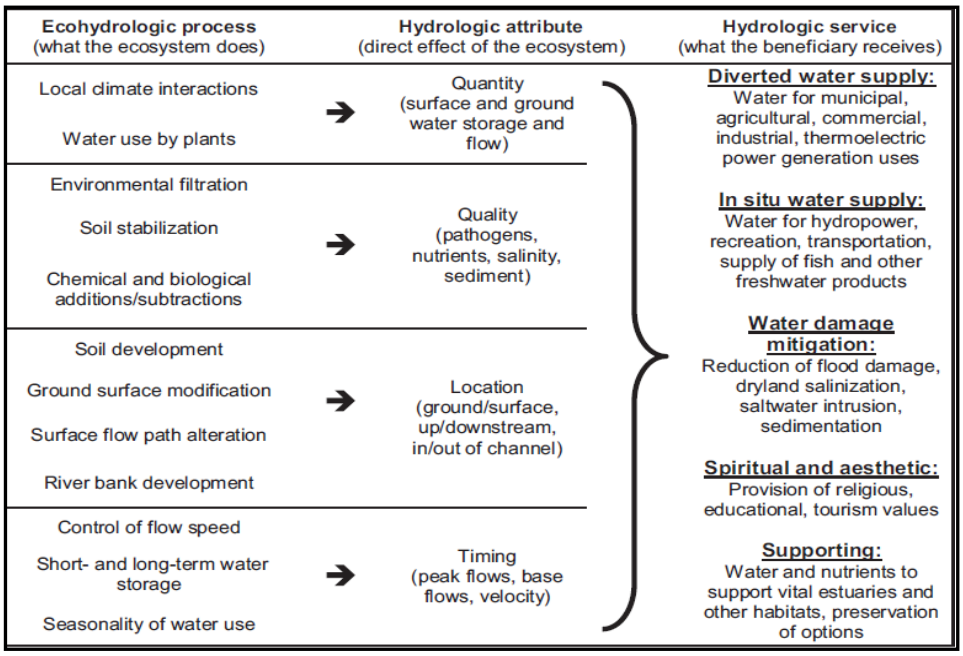

Figure 5. Relationship of hydrologic ecosystem processes to hydrologic services (Source: Brauman, et al., 2007)

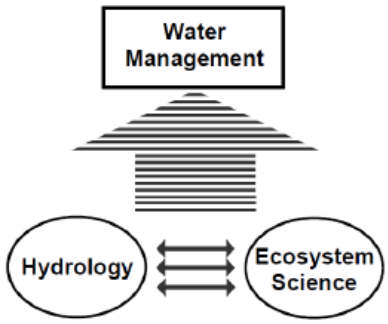

Figure 6. Schematic of hydrology and ecosystem since connection (Source: STELLA Consulting – NWRM Final Report)

5. CONCLUSIONS

River Djetinja catchment natural features, particularly hydrologic are not enough analysed. Thus more comprehensive and detailed research is needed within the study area. Additional data and information will significantly contribute to sustainable water management of almost pristine water resources within the study area. The development of new reservoirs will contribute to low flow management during the critical periods to maintain ecological requirements. The comprehensive evaluation NWRM that increase catchment natural water retention capacity is need. Application of available tools will contribute in decision making process. The more frequent monitoring with

respect to different adverse effects (floods, erosion, water quality, etc.) will contribute to Djetinja's catchment sustainable water resources management and nature protection.

REFERENCES

Brauman, A.K., Daily C.G.,T. Duarte, K.T,.and Mooney A.H., 2007. The Nature and Value of Ecosystem Services: An Overview Highlighting Hydrologic Services, The Annual Review of Environment and Resources, 32:67–98, doi:10.1146/annurev.energy.32.031306.102758

Divac D., Milovanović M., Arsić M., 2001. Hydro system Lim - West Morava, Management of Serbian Water Resources, The Jaroslav Černi Institute for the Development of Water Resources, Belgrade, Serbia

HidrositemLim – Zapadna Morava, Upravljanje vodnim resursima Srbije, Institut za vodoprivredu Jaroslav Černi, Beograd, Srbija

European Union (2014) EU policy document on Natural Water Retention Measures, ISBN 978-92-79-44497-5, doi: 10.2779/227173

Mayfield, C.I., Grover, V.I. and Daley, R.J., 2004. The United Nations Water Virtual Learning Centre: a flexible distance learning programme for integrated water resources management. Global Environmental Change – Part A, 13(4), pp.331-318

Milijašević D., 2010. Hydrogeographic study of the Đetinja River, Geographical Institute Jovan Cvijić - Serbian Academy of Sciences and Arts, Belgrade, Serbia, Special Issues no. 76, ISBN 978-86-80029-47-4, http://www.gi.sanu.ac.rs/rs/izdanja/posebna/pdf/gijc_pi_076_dragana_milijasevic_srp.pdf

Miloradov M., (1992) Planning and Management of Water-Resource Systems in Developing Countries. Journal of Water Resources Planning and Management,Volume 118, Issue 6, pp. 603 – 619

Simonović, S.P., 2008. Managing water resources: Methods and tools for a system approach, Proceedings of International Conference Planning and Management of water resource systems (September 25 – 27), Academy of Science and Arts of Vojvodina, ISBN: 978-86-85889-19-6, pp.37-47

STELLA Consulting (2012) NWRM Final Report, Costs, benefits and climate proofing of natural water retention measures (NWRM), European Commission, DG Environment, Contract 070307/2010/581332/SER/D1

United Nations, Report on the United Nations Conference on Environment and Development, Agenda 21, Rio de Janeiro, 1992

Urošev M., Milanović A., Milijašević D., 2009: Assessment of the river habitat quality in undeveloped areas of Serbia applying the RHS (River habitat survey) method. Proceedings book 59/2. Geographical Institute Jovan Cvijić - Serbian Academy of Sciences and Arts, Belgrade

Water Act, Official Gazette of Republic of Serbia, 30/2010

Water Management Strategy of the Republic of Serbia (2016), Republic of Serbia Ministry of Agriculture and Environmental protection - Water Directorate. URL: http://www.rdvode.gov.rs/doc/Strategija_FINAL.pdf

Proceedings of the 10th World Congress of EWRA 'Panta Rhei', 5-9 July 2017, Athens, Greece
© 2017 *European Water Resources Association*

Towards the optimization of water resource use in the Upper Blue Nile river basin

A.-T. Stamou* and P. Rutschmann
[1] *Technical University of Munich, Department of Civil, Geo and Envrionmental Engineering, Chair of Hydraulic and Water Resources Engineering*
* *e-mail: tatiana.stamou@tum.de*

Abstract: The Nile River is a source of water for millions of people. The continuously growing water demand in combination with the population growth and the lack of water resource management in the basin have led to enormous water scarcity. In order to provide water security, sufficient water resource management is required. For the integrated water resource management of one of the two main Nile sources, the Upper Blue Nile River basin in Ethiopia, the NIMA-NEX project is proposed. The goal is to develop a tool called NIMA-NEX (NIle MAnagement Nexus EXpert tool) to optimize the water resources within the basin. The optimization is achieved in terms of a nexus approach. Thus, water, food and energy are considered as three elements that interact with each other continuously. The present study deals with MA-NEX, the management and optimization module of NIMA-NEX. Within MA-NEX, the system of reservoirs and other projects, as well as the water allocation among the various uses in the Upper Blue Nile River basin are optimized. The study focuses on the maximization of ecological, economic and social benefits, and the political stability. For the simulation and optimization of the system, the model Hydronomeas is used. Various development and management scenarios are investigated and Pareto fronts are proposed for the Upper Blue Nile River basin.

Key words: water resources optimization, water resources management, water allocation, Pareto optimization, Hydronomeas

1. INTRODUCTION

The Nile River, the longest river in the world, is a source of water for millions of people. The continuously growing water demand in combination with the population growth, as well as the lack of water resource management, have led to enormous water scarcity in the basin. Among the countries that share the Nile River basin and compete for its resources is Ethiopia, in which one of the two Nile's main sources, the Upper Blue Nile River flows.

For the sustainable management of water resources in the Upper Blue Nile River (UBNR) basin, the NIMA-NEX project was proposed. This study deals with MA-NEX (part of NIMA-NEX) whose objectives are: (1) the management and optimization of the reservoirs and other projects in the UBNR, and (2) the optimization of water allocation among domestic, industrial, livestock, hydropower (energy) and irrigation (food) purposes. Both objectives focus on the maximization of ecological, economic and social benefits, as well as the political stability and the water resource optimization in the basin, using the nexus approach. According to nexus, water, food and energy are considered as three elements that interact with each other continuously. To achieve these objectives, a research procedure is applied that consists of the following 7 steps: (1) A literature review is conducted and a proper model is chosen. (2) Required data are collected and analyzed. (3) Development and management scenarios (policies) are defined. (4) The UBNR system is schematized in the selected model. (5) Model simulations are performed for all scenarios. (6) Objective functions are defined; model optimization is performed and Pareto solutions are developed for all scenarios. (7) Development and management scenarios are evaluated.

Five development scenarios are investigated (Table 1); these range from the natural state of the river (Scenario S0) to its full development (Scenario S4). Management scenarios are developed during the system simulation and optimization.

Table 1. Development Scenarios for the UBNR basin for implementation in Hydronomeas

Scenario Name	Type	Description
Scenario S0	Baseline Scenario	without any man-made changes
Scenario S1	Current Situation	in 2015 operating irrigation and hydropower projects, and water supply
Scenario S2	Medium-term Future Situation	until 2020 constructed and operating irrigation and hydropower projects, and increased water supply
Scenario S3	Long-term Future Situation	50 % of all irrigation and hydropower projects of the full developed river basin, and increased water supply
Scenario S4	Full Development	all planned irrigation and hydropower projects, and increased water supply

The scenarios were developed to study the downstream effect of future irrigation and hydropower projects, as well as the increase in water demand for domestic, industrial and livestock purposes (linked to population growth), and to draw conclusions for the feasibility, impacts and benefits of the projects and targets in the system in order to optimize it. In the present work, preliminary results for the current conditions (Scenario S1) are presented and discussed.

2. THE AREA OF STUDY: THE UPPER BLUE NILE RIVER BASIN

The UBNR basin, the so-called Abbay in Ethiopia, covers an area of approximately 199,812 km² (Yilma and Awulachew, 2009) and is of great importance for Ethiopia, since it supplies the country with water for hydropower, irrigation, domestic, industrial, livestock and touristic purposes. MA-NEX deals with the 14 sub-basins of the UBNR basin: Tana, Beshilo, Welaka, Jemma, North Gojam, Muger, Guder, Finchaa, South Gojam, Anger, Didessa, Wenbera, Dabus and Beles.

The basin topography has two significant features: the highlands in the center and eastern part of the basin, and the lowlands in the western part. There are several meteorological and hydrological stations in the basin. However, data availability is limited and records are sometimes incomplete. Furthermore, the coverage of improved water supply and sanitation facilities to the population within the basin is very low. The basin has great hydropower potential, from which however only a small percentage is exploited. Additionally, its irrigation potential accounts for a major share of the total irrigation potential in Ethiopia. Agriculture comprises the largest part of the Ethiopian economy, since it is contributing 50 percent of GDP and employing 85 percent of its population. The water use management in the basin is event driven and not subject to any sophisticated decision support system, a fact that shows the necessity of a management tool, like MA-NEX.

3. MATERIALS AND METHODS

3.1 The model HYDRONOMEAS

Throughout recent decades, different simulation-optimization models have been developed to enhance the management of water resource systems. A literature review was carried out to choose the most appropriate model for the simulation and optimization of the UBNR system. The investigated models share two main characteristics: they include the aspect of simulation and optimization, and are generalized models. The model Hydronomeas (Koutsoyiannis et al., 2001) was chosen, as the most appropriate for the study purposes.

Hydronomeas is a decision support tool for the planning and management of complex multi-reservoir multi-purpose systems, which was developed by the Department of Water Resources of the National Technical University of Athens (NTUA); it is capable of proposing management policies, which maximize the system yield as well as the overall operational benefit, and minimize

the operating cost as well as the risk of decision making. The mathematical framework of Hydronomeas is based on the parameterization-simulation-optimization scheme proposed by Nalbantis and Koutsoyiannis (1997).

3.2 Input data and analysis

Data collection was one of the most important, challenging and difficult tasks of the present work; data were collected by means of the international literature, but mainly during visits in Ethiopia and specifically to local authorities (Ministry of Water, Irrigation and Electricity, Abbay Basin Authorities), engineering offices (e.g. Eastern Nile Technical Regional Office), project sites, and via discussions with experts and researchers from the Addis Ababa University, Bahir Dar University, and the International Water Management Institute (IWMI). Collected data is categorized as: river discharges, water supply, irrigation and hydropower.

Most river discharge data were obtained from IWMI (Awulachew et al., 2012) and they refer to the flows in specific river locations, such as in tributaries' confluence with the main river. Water supply data were obtained from the Ministry of Water, Irrigation and Electricity and include domestic as well as livestock and industry demands and are categorized in urban and rural water supply. Although agriculture in the UBNR basin is mainly rain-fed, the basin has great irrigation potential. The irrigation projects are divided in three categories: small (<200 ha), medium (200-3,000 ha) and large scale (>3,000 ha). By considering various criteria (investment, operation and maintenance cost, distance and difference in attitude between source and destination, slope of irrigable land) the maximum irrigable area amounts to approximately 680,000 ha of gross irrigable land (medium and large projects); this is equivalent to approximately 578,000 ha of net area, whereas average water requirements are calculated at 4,895 Mm^3/year. Information on the main irrigation projects (gross and net potential area, water requirement and efficiency) was obtained from the Abbay River Master Plan Project (BCEOM, 1998). The Blue Nile's hydropower potential accounts for more than 70,000 GWh/year; hydropower data (head, discharge capacity, installed capacity, number and type of units, annual energy production) was obtained from the Abbay Basin Authority, reports collected from the Ministry of Water, Irrigation and Electricity, project site visits and the Abbay River Master Plan Project (BCEOM, 1998). Figure 1 shows the existing and potential irrigation and hydropower projects, as well as dam sites investigated in this study. Apart from these, the Abbay Basin Authority distinguishes possible hydropower development from already identified irrigation projects. This is considered in the full development scenario of the study.

4. CALCULATIONS AND DISCUSSION OF RESULTS

Figure 2 shows the schematization of the UBNR system in Hydronomeas for Scenario S1 (current situation) with its essential parameters that include topology, reservoirs, hydropower and irrigation projects, tributary inflows, targets and constrains. In the calculations, water is transported from the resources i.e. reservoirs and tributary inflows, to the water users for irrigation, hydropower and environmental preservation. In optimization mode Hydronomeas defines the optimum water allocation step by step, while considering the quantities in the system, the operating rules and the targets (Koutsoyiannis et al., 2001); the time step in all calculations was equal to one month.

In order to optimize the UBNR basin of Figure 2 in Hydronomeas, targets have to be assigned for the hydropower projects (HP) Tana Beles, Finchaa and Neshe with installed capacities of 420, 134 and 97 MW, respectively, and for the irrigation projects (IR) Koga, Finchaa and Neshe with gross irrigation areas of 6,000, 7,300 and 8,490 ha, respectively. Furthermore, constraints have to be set for the minimum-ecological/environmental outflow (EF) from Koga reservoir and Lake Tana (Tana Abbay Out) and for the reservoir outflow (Out) for hydropower production from Lake Tana (Tana Beles HP), Amerti, Finchaa and Neshe. A priority is assigned to each target and constraint,

with “priority 1” representing most important; by assigning priorities to targets and constraints, ecological, social and political factors can be taken into account directly or indirectly. Ecological factors are taken into account by setting minimum-ecological flows downstream of reservoirs aiming at river preservation and thus meeting the long-term needs of people; the minimum flow requirement serves also touristic purposes, e.g. Blue Nile Falls, and it is also linked to social factors. Social factors are also considered, by assigning different priorities to hydropower and irrigation projects, upstream and downstream projects, and projects close to and away from large cities. Furthermore, the political factor can be taken into account by setting a minimum flow at the border between Ethiopia and Sudan, i.e. to downstream countries that enhances political stability.

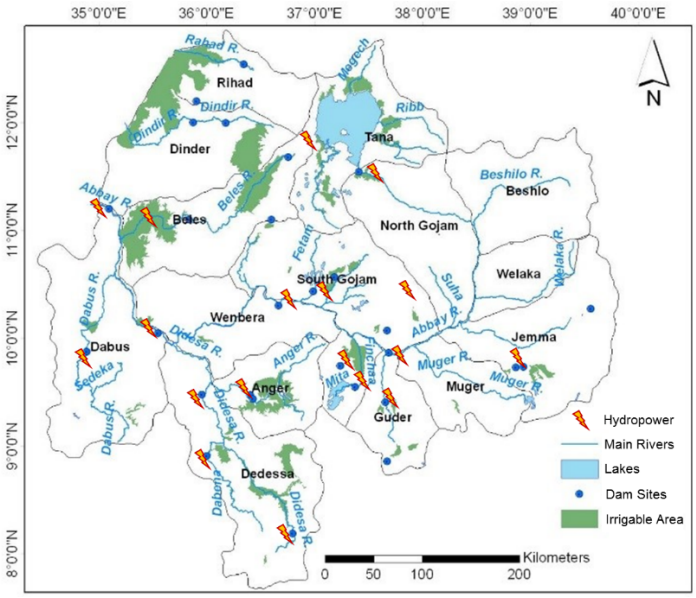

Figure 1. Existing and potential irrigation, hydropower and dam projects in UBNR, Yilma and Awulachew (2009)

Figure 2 shows that there are some main conflicting targets and constraints in the system (hydropower production, irrigation demand and minimum flow requirements). The aim is to optimize all targets and thus the optimization problem involves more than one objective function to be optimized. Since the targets and constraints are conflicting, there is no “one single solution” that optimizes all objectives simultaneously. In order to deal with that issue, the Pareto optimal solutions are introduced; these are solutions in which none of the objectives can be improved without degrading the others. By restricting attention to a set of choices, that forms the so-called Pareto front, the decision maker can make trade-offs within this set, rather than considering the full range of every parameter.

Figure 3 depicts the 2-D Pareto front of the UBNR system for two conflicting objectives that are the maximization of firm hydropower production (GWh) and the minimization of irrigation deficit (Mm^3). The Utopia point of Figure 3, represents the simultaneous maximization of firm hydropower production, i.e. 37.2 GWh and minimization of irrigation deficit, i.e. 12.1 Mm^3, a “solution” that can never exist. The remaining points represent feasible choices, with the two extremes representing the situation, in which only irrigation deficit is minimized, i.e. 12.1 Mm^3 while hydropower is not optimized, i.e. 16.6 GWh and the situation, in which only hydropower production is maximized, i.e. 37.2 GWh while irrigation deficit is not optimized, i.e. 13.9 Mm^3. Intermediate points represent the different weighting of the two objectives. Social factors are taken into account indirectly by weighting hydropower (and thus electricity) and irrigation (and thus food security).

It is worth mentioning that the two objectives of the Pareto front of Figure 3 are not conflicting in terms of water consumption, since hydropower is not consuming water, but due to the fact that water, which is consumed for irrigation purposes upstream, is then not available for hydropower production further downstream. The same procedure is performed for economic factors by

assigning monetary values e.g. to each kWh generated from hydropower and to each crop earned from irrigation practices.

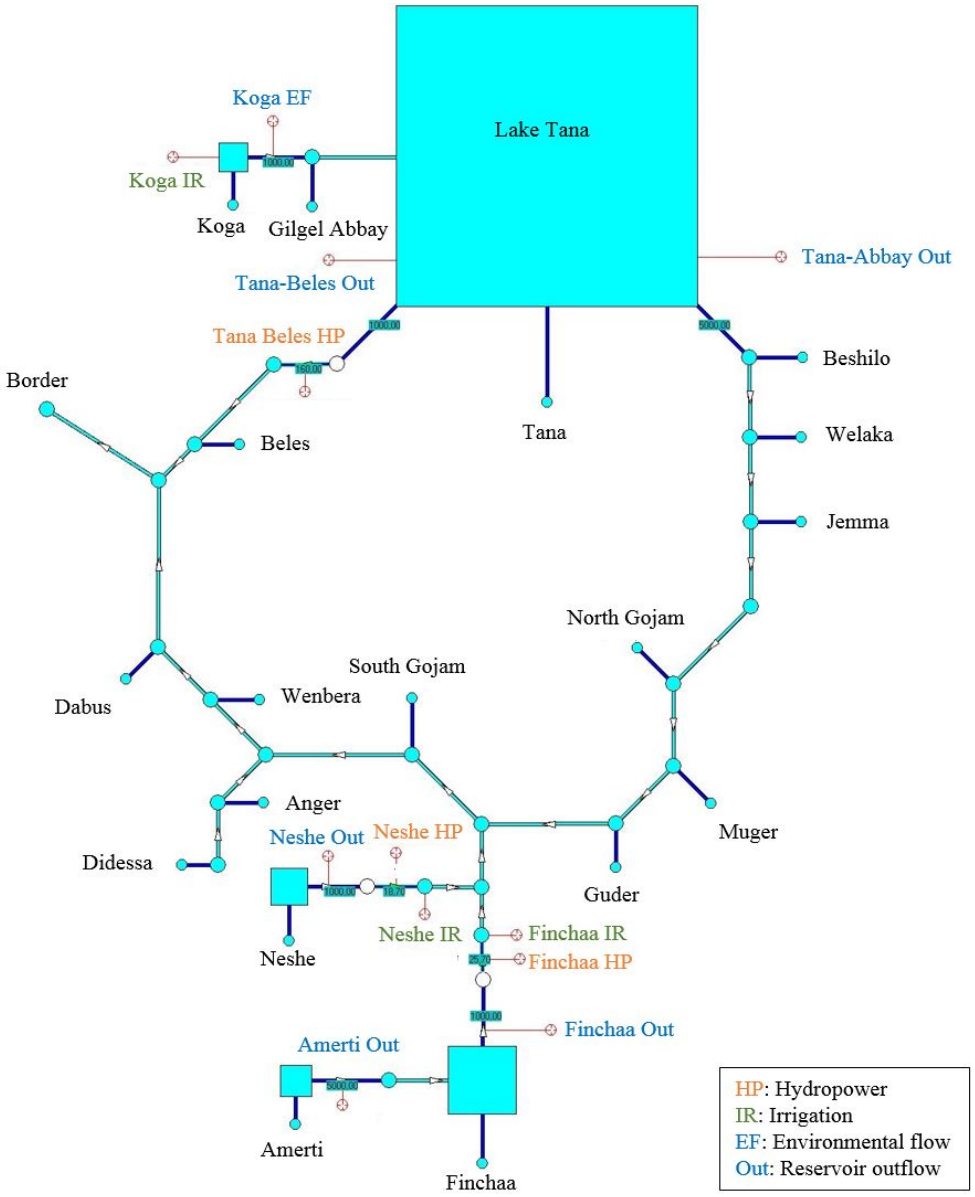

Figure 2. Schematization of the UBNR basin in Hydronomeas for Scenario S1

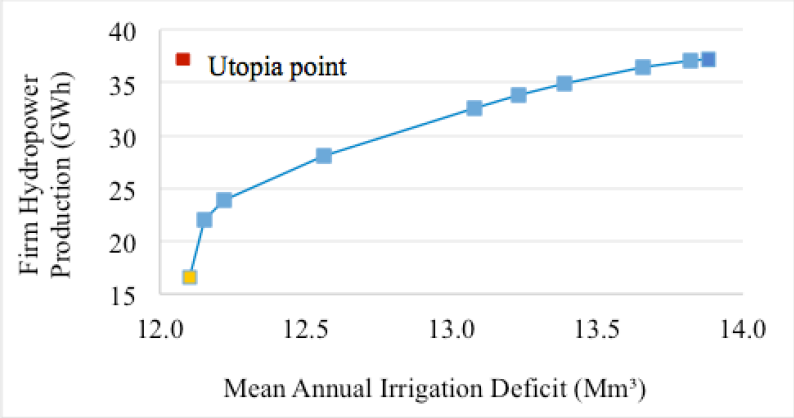

Figure 3. Example of a Pareto front of the UBNR for Scenario S1 (current situation)

5. CONCLUSIONS

From the preliminary results of the study, it is shown that only a few projects are currently operating in the UBNR basin, namely three irrigation and three hydropower projects. The basin has great irrigation and hydropower potential and since the resources allow it, it is worth implementing new projects, which will increase the life standards of the people in the region and help the development of the UBNR basin. The management and optimization of these projects is of great importance for the sustainable development of the basin, and to gain social, ecological and economic benefits and political stability in the region. The MA-NEX study is due to be completed at the end of 2017. After validating the model for Scenario S1, synthetic time series of 1,000 years are generated using the tool Castalia for the current and future development scenarios. The development scenarios are evaluated and management scenarios are developed, each with a new Pareto front. The tool Hydrognomon is used for the input data pre-processing and the results analysis.

AKNOWLEDGEMENTS

The NIMA-NEX project and MA-NEX module are supported by the TUM International Graduate School of Science and Engineering (IGSSE). The main NIMA-NEX partners are TUM, Germany (Prof. Peter Rutschmann and Prof. Markus Disse) and the University of Alberta, Canada (Prof. Thian Yew Gan).

REFERENCES

Awulachew, S. B., Smakhtin, V., Molden, D., Peden, D., 2012. The Nile River Basin. Water, Agriculture, Governance and Livelihoods. IWMI.

BCEOM, 1998. Abbay River Basin Integrated Development Master Plan Project. Report to Ministry of Water Resources. Federal Democratic Republic of Ethiopia.

Koutsoyiannis, D., Efstratiadis, A. Karavokiros, G., 2001. A decision support tool for the management of multi-reservoir systems, Proceedings of the Integrated Decision-Making for Watershed Management Symposium, Chevy Chase, Maryland, US Environmental Protection Agency, Duke Power, Virginia Tech.

Nalbantis, I., Koutsoyiannis, D., 1997. A parametric rule for planning and management of multiple reservoir system. Water Resour Res 33(9):2165–2177.

Yilma, A. D., Awulachew S. B., 2009. Characterization and Atlas of the Blue Nile Basin and its Sub basins. IWMI; https://cgspace.cgiar.org/handle/10568/38169.

Proceedings of the 10th World Congress of EWRA 'Panta Rhei', 5-9 July 2017, Athens, Greece
© 2017 *European Water Resources Association*

Indexing vulnerability of an embankment reach against breaching: A remote sensing and hydrodynamic based study

B. Talukdar*, A. Baid and R. Das
Civil Engineering Department, Assam Engineering College, Guwahati, Assam, India
* *e-mail: bipulaec@gmail.com*

Abstract: Floods of high magnitude are one of the major problems in the north-eastern region of India. Approximately 4464 km of embankments are being constructed in the Brahmaputra basin itself. The embankments are highly vulnerable to flood and flood disaster for embankment breaching is frequent in Assam. Remote Sensing data of a river system of highly unstable bank has been analyzed in GIS environment for identification of river bank erosion as well as reaches of embankment vulnerable to breaching. A case study was carried out in the Nona River, a tributary of river Brahmaputra, to identify reaches of embankment vulnerable to breaching during the flood time. Temporal dataset of satellite imagery for several years along with the topographical maps from Survey of India (SOI) were used for mapping the flow channel of river Nona. Based on the degree of convergence and narrowness between the flow channel and embankment observed from the digitized images of Nona River from 1999 to 2014, some reaches of embankment which are vulnerable to breaching were selected for the study. Hydrodynamic analysis by MIKE 21C – Curvilinear Flow Model was conducted on those vulnerable reaches in order to validate whether the embankment is going to breach due to change of flow pattern of the river observed from the digitized images of the river. Results obtained from remote sensing data and flow velocity profile from hydrodynamic analysis were split into different categories ranging from 0 to 10 which indicate the vulnerability of an specific embankment reach against breaching.

Key words: Vulnerability, Embankment, Breach, Hydrodynamic

1. INTRODUCTION

Floods of high magnitude are one of the major problems in the north-eastern region of India. Heavy flooding causes abrupt changes in the flow pattern of the rivers. The river Brahmaputra shows significant amount of erosion and deposition in the basin. The study area i.e. the *Nona River Basin* is a major tributary basin of the Baralia river catchment Brahmaputra basin in India.

Embankments are the structures constructed parallel to the river utilizing mostly the materials in situ. Due to the meandering nature of the river, the geometry between the flow channel of the river and the embankment does not remain parallel to each other. More the angle between these two more the thrust of water flow on the embankment resulting high probability of embankment breaching.

Integration of Geographic Information System (GIS) to RS, make it appropriate and ideal for studying and monitoring of river bank erosion, changes of channel configuration and the orientations between the river channel and its embankments. Various studies in this regard have been carried for some major rivers [Surian N. (1999), Yang X.et. al (1999), Fuller I. C. et. al (2003), L. Q. Li. X. X. Luand et. al (2007)]. Several investigators have been used RS data for mapping and ascertaining the channel changes of different rivers in the world [Bardhan M. (1993), Naik et. al (1999), Gogoi and Goswami (2014)].

2. METHODOLOGY

Resourcesat – 1- IRS-1D LISS III imagery obtained from North Eastern Space Application Centre, Shillong, Meghalaya have been used in this study. To study the changes in the flow pattern of the Nona River, five different year data over a span of seven years (1999 - 2006), six years

(2006-2012), one year (2012-2013-2014) have been considered so that short as well as long term flow pattern change in the Nona River can be seen.

First, geo- referencing of all the LISS III images were carried out with reference to the ground co-ordinates of Survey of India (SOI) Topographical maps 78-N-10 and 78-N-11 (Toposheet) in ERDAS Image Processing Software.

After geo-referencing, digitization of Nona River for each LISS III images was carried out using ArcGIS in scale of around 8000-10000 and considering standard RGB Composite as 3 2 1 and geographic coordinate system of WGS 1984. Using the Google Satellite Image, latest outline of embankment of Nona River has been digitized as shown in Figure 1.

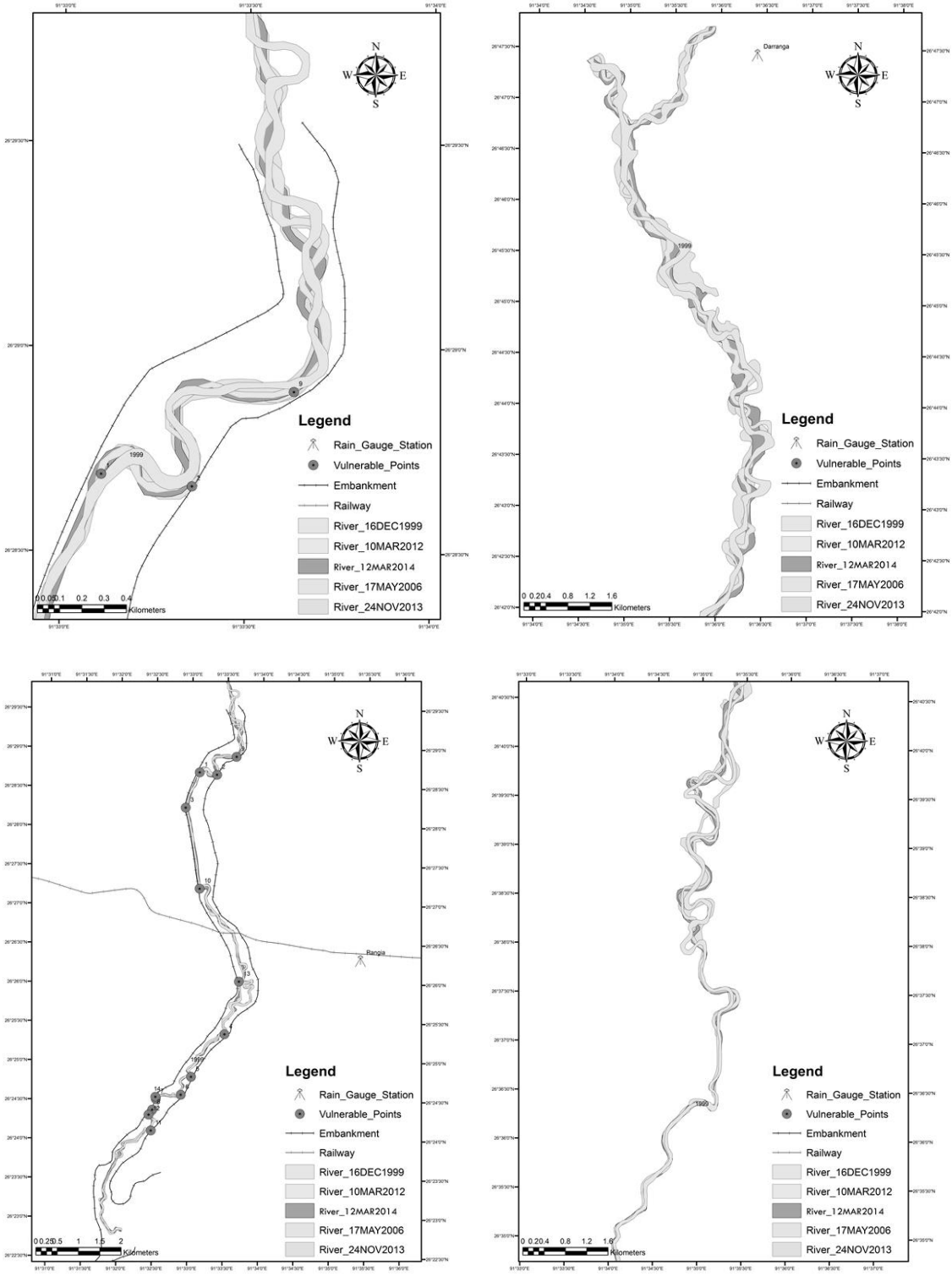

Figure 1. Digitized images of Nona river and vulnerable points.

3. IDENTIFICATION OF VULNERABLE EMBANKMENT REACHES

Identification of embankment reaches which are vulnerable to breaching due to bank erosion is carried out based upon the change of flow pattern of river towards the embankment observed from the digitized images of Nona River from 1999 to 2014 (Talukdar and Das, 2015)

From the digitized images of river, *fourteen vulnerable points* as shown in table number 1 were selected and from each points distance were measured from the bank line to the embankment for all selected years i.e. 1999, 2006, 2012, 2013 and 2014.

4. VALIDATION OF VULNERABLE POINTS USING DHI MIKE 21-C

From those vulnerable reaches, a part of river channel was selected for the simulation in MIKE 21C –Curvilinear Flow Model containing three vulnerable points i.e. 1, 2, and 9 as shown in figure number 2, in order to validate the remote sensing data observed from the digitized images of the river (DHI, 2014).

The effective area under consideration is 1100m x 650m. The individual cells and grid points (a cell being what is defined by four grid points in the corners of the cell) are addressed by indices j and k. The whole study area is covered by the grid, having 100 × 60 cells, so j = 0-98 and k = 0-58, j being used in the direction of the rivers and k is across the river. Thus each cell dimension being 10m x 12 m. A view of the generated grid in MIKE 21C is shown in figure number 3. For making bathymetry, depth value from bathymetric survey and corresponding contour map has been given at each cell as input (Deka, 2014 and Purkayastha, 2014).

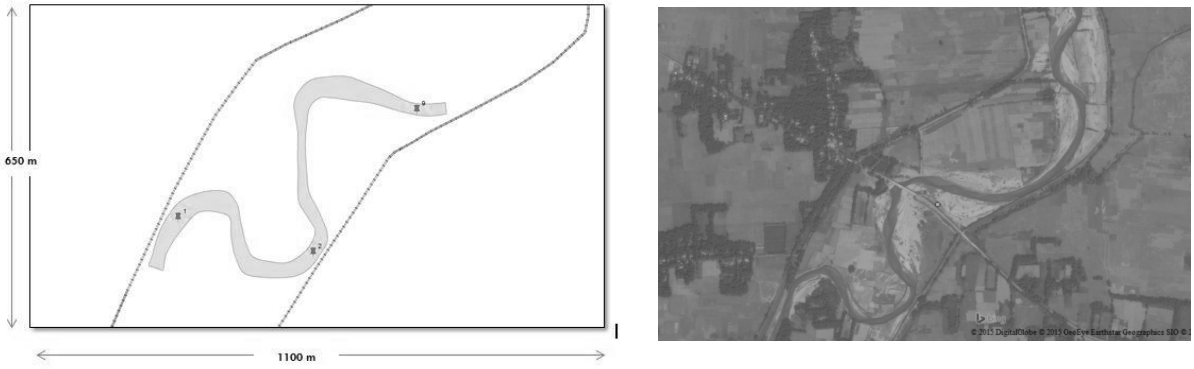

Figure 2. Vulnerable section used in MIKE 21 and satellite image of the site.

Hydrodynamic calibration and model validation is done by first simulating the present condition and then by comparing discharge values at upstream inlet section 1-1 and at downstream outlet section 2-2, which shows good agreement with each other. This indicates that the model is stable and continuity is maintained. Next the velocity profile around the vulnerable area near upstream side is observed and is found to be near the range of observed maximum velocity of 1.7 m/s at vulnerable points.

5. RESULTS AND DISCUSSION

The digitized images of multi date satellite images showed variation in the fluvial features. From this data it was very clear that both the banks have simultaneously undergone erosion and deposition which is clear from figure number 1.

From MIKE 21C it was observed that around point 1 and 2, the velocity of the river is around 1.5 to 2.0 m/s having a discharge of 160 m^3/s whereas at point 9 it is varies from 0.45-1.2 m/s.

Results obtain from remote sensing data and flow velocity profile from MIKE 21C, the

vulnerable points can be split into different categories ranging from 0 to 10 (table number 1) which will indicate the vulnerability of embankment breach based on the degree of convergence and narrowness between the flow channel and embankment observed from the digitized images of Nona River.

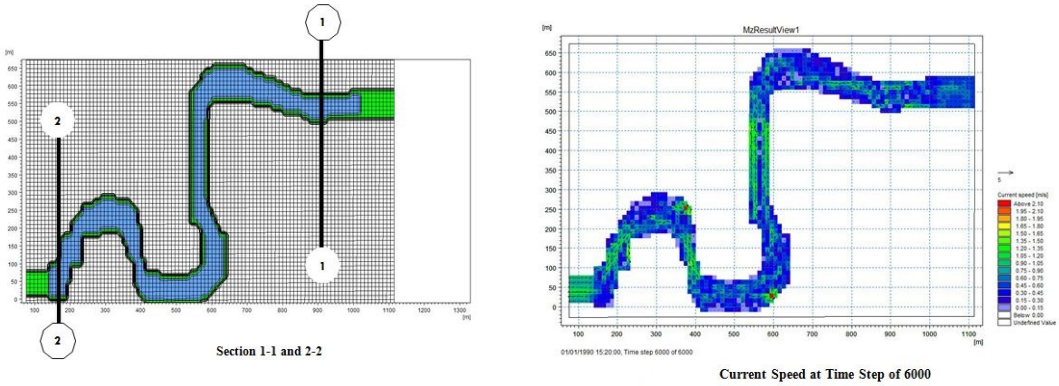

Figure 3. Simulation of vulnerable section in MIKE 21C.

Table 1. Vulnerability index of various points.

Vulnerable Points	Distance from the Embankment	Vulnerability	Range 0 to 10
2	10.3845	Very Highly Vulnerable*	10
3	10.6547	Very Highly Vulnerable	10
1	14.3141	Highly Vulnerable*	9.5
4	20.0563	Vulnerable	8
10	22.6116	Vulnerable	8
7	24.7652	Vulnerable	7.5
11	27.9931	Moderate Vulnerable	7
9	30.8302	Moderate Vulnerable*	7
5	39.8443	Low Vulnerable	6
8	42.4196	Low Vulnerable	5.5
14	46.8441	Low Vulnerable	5
6	55.4613	Low Vulnerable	4
13	56.0845	Low Vulnerable	4
12	59.7736	Low Vulnerable	3.5

Based on the degree of convergence and narrowness between the flow channel and embankment observed from the digitized images of Nona River, Point 1 and 2 are Highly Vulnerable as their distance from of bank line is less than 10m and if the velocity of the river is around 1.5 to 2.0 m/s during monsoon season based upon the simulation of MIKE 21-C, there is a chances that embankment near to the point 1 and 2 may get breached.

6. CONCLUSION

The method may be a good tool for predicting embankment vulnerability to breaching as well as understanding the problems caused by continuous change in the fluvial patterns of the river channels, amount of bank erosion, rate of sedimentation which can be implemented for planning of river bank protection work and preparedness in flood prone state like Assam.

REFERENCE

Bardhan, M., 1993. Channel stability of barak river and its tributaries between Manipur - Assam and Assm - Bangladesh borders as seen from satellite imagery. Proceeding of National Symposium on Remote Sensing application for Resource Management with Special emphasis on N. E. Region, Guwahati, 25-27 November 1993.

Deka M., 2014. Mathematical modeling of an erosion affected reach of river Beki. M.E. Dissertation, Assam Engineering College, Gauhati University, Assam.

DHI Group, 2014. User manual Mike 21C", hydrodynamic modeling part, Delhi

Fuller I. C., Large A. R. G., Milan D. J., 2003. Quantifying channel development and sediment transfer following cute-off in a wadering gravel-bed river. Geomorphology, 54(3-4): 307-323.

Gogoi, C., Goswami, D. C., 2014. A study on channel migration of the Subansiri river in Assam using remote sensing and GIS technology, Current Science,106(8).

L. Q. Li. X. X., Luand Z, Chen, 2007. River channel change during the last 50 years in the middle Yantze River: An example of Zianli Reach. Geomorphology, 85(3): 185-196.

Naik S. D., Chakravorty S. K., Bora T., Hussain I. 1999. Errosion at Kaziranga national park, Assam, A study based on multi temporal satellite data, Project Report. Space Application Centre (ISRO) Ahmadabad and Brahmaputra Board , Guwahati p. 70

Purkayastha P., 2014. “Mathematical modeling of an erosion affected reach of river Brahmaputra. M.E. Dissertation, Assam Engineering College, Gauhati University, Assam.

Surian N., 1999. Channel changes due to river regulation: The case of the Iave river. Italy, Earth Surface Processes and Landforms, 24(2): 1135-1151.

Talukdar B., Das R., 2015. Assessment of river bank erosion and vulnerability of embankment to breaching: A RS and GIS based study in Subansiri river in Assam, India” THA 2015 International conference on climate change and water & environment management in monsoon Asia, Bangkok, Thailand.

Yang X., Damen M.C. J., and Zuidam R. A. van., 1999. Satellite remote sensing and GIS for the analysis of channel migration changes in the active Yellow river delta, China. International Journal of Applied Earth observation and Geoinformation, 1(2): 145-157.

Proceedings of the 10th World Congress of EWRA 'Panta Rhei', 5-9 July 2017, Athens, Greece
© 2017 *European Water Resources Association*

Algiers water issue: Key indicators for a diagnosis of water resources carrying capacity

M. Naimi Ait-Aoudia[1,2*] and E. Berezowska-Azzag[2]
[1] *USDB, Université Saad Dahleb Blida, Route de Soumaa, BP 270, Blida, Algeria*
[2] *EPAU, Ecole Polytechnique d'Architecture et d'Urbanisme, Route de Beaulieu, El-Harrach, 16200, Algiers, Algeria*
[*] *e-mail:ce meriem.aitaoudia@gmail.com*

Abstract: In Algeria and especially in Algiers the capital city, ensuring inhabitants water requirements remains a critical issue despite huge investments made by the government to secure water supply over the past years. Indeed, in the face of erratic climate conditions with recurrent drought episodes and constantly increasing water demand, due to population growth and economic activity rise, the water supply system is subject to various problems of environmental, economic, technical and managerial nature. This could ultimately affect the water supply of Algiers city. A rigorous and effective management of water resources requires analysis of elements that affect in the long run water resources carrying capacity (WRCC). This latter can be defined as the level of human activity that can be withstood by the available water resources without major degradation of aquatic environments while maintaining an adequate standard of living for the population. Water resources carrying capacity depends mainly onto two major components that are water supply capacity and inhabitants' global water demand. This study aims at proposing key indicators and related thresholds for analysing Algiers water carrying capacity in order to provide a diagnosis tool for policy makers to lay down the foundations of a sustainable water strategy in Algiers city.

Key words: Algiers water supply, Key indicators, Water system diagnosis, Carrying Capacity

1. INTRODUCTION

Access to drinking water is a major concern as the survival of the human being depends entirely on it. Thus, the issue of securing water supply and sustainable management of this resource must be included in the priorities of any development strategy. This is all the more important in a country like Algeria, which have an average water availability less than 500 m^3 per inhabitant per year well below the scarcity threshold set at 1000 m^3 per inhabitant per year (Falkenmark, 1989), is clearly in water stress situation. Even worse, the situation will get more dramatic due to global warming, which could lead to an increased recurrence of drought episodes.

Among Algeria cities, Algiers, the political and economic capital, suffered from severe water scarcity due to several factors. The most important ones are recurrent droughts conditions and high pressure on resources, due to a fast population growth. In order to meet the growing demand for water, the Algerian authorities have favoured a policy of supply, investing heavily in new infrastructures. Transfer systems were implemented bringing water from dams located hundreds of kilometres from the capital. At the same time, desalination of seawater has been implemented to address the problem of the shortfall in natural water supply, in this region subjected to recurrent episodes of drought. It should be noted that this process is quite costly in terms of energy, and the long-term impact on aquatic ecosystems is unclear.

As a result of the efforts made, Algiers' citizens benefit now from water availability 24 hours a day. However, this relative comfort in terms of water supply remains questionable in many respects, because: groundwater, due to exploitation beyond its potential, is threatened with exhaustion and subject, as they are coastal, to the phenomenon of marine intrusion; about half the volume of water allocated to the capital comes from superficial resources located in neighboring departments, which are forced to concede part of their water resources to the detriment of their own development (Chikhr Saïdi, 1997); Recurrent droughts greatly affect the contribution of these surface resources,

while desalination of seawater cannot be a safe and sustainable solution as regards economical and environmental aspects (Cotruvo, 2011).

In view of these concerns, the objective of water policy is, on the one hand, to guarantee the sustainability of the resource and, on the other hand, to satisfy the demands of growing populations and different socio-economic activities, and allocating water amounts among different competitive uses taking into account local constraints (Kettab, 2001).

A rigorous and effective management of water resources requires analysis of elements that affect in the long run water resources carrying capacity (WRCC) (Shi and Qu, 1992; Zhongmin, 1999; Li et al., 2000; Liu and Chen, 2007; Feng et al., 2008; Li et al., 2010). This latter can be defined as the level of human activity that can be withstood by the available water resources without major degradation of aquatic environments while maintaining an adequate standard of living for the population (Naimi Ait-Aoudia and Berezowska-Azzag, 2016).

This study aims at proposing key indicators and related thresholds for analyzing Algiers water carrying capacity in order to provide a diagnosis tool for policy makers to lay down the foundations of a sustainable water strategy in Algiers city. This paper is organized as follows. Section 2 is devoted to Water carrying capacity key indicators. Thresholds of these indicators are detailed in section 3. The diagnosis of Algiers household water resources carrying capacity is given in section 4. Section 5 concludes the paper.

2. WATER CARRYING CAPACITY KEY INDICATORS

The study of the urban carrying capacity relative to water resources is based on two key concepts: supply capacity and the demand side. These two concepts will be fleshed out in a set of indicators.

2.1 Supply water indicators

To study the carrying capacity at the urban level, Oh et al. (2005) define four components that are: environmental capacity, infrastructure capacity, perceptual capacity and institutional capacity. These components focus on the description of supply capacity. In the area of water, the environmental component represents amounts of water provided by the annual average flow of rivers and the annual renewal of groundwater resources; The infrastructure component represents the infrastructure for water intake and transport, as well as facilities for the production of unconventional resources, namely desalination of seawater and waste water recycling; Integrated water resource management has several objectives as increasing water availability by preventing resources from depletion and by promoting reuse, limiting water withdrawals to sustainable levels by maximizing water use efficiency, minimizing wastewater production and optimizing the distribution of water between competing users (OCDE, 1998); Perceptual carrying capacity includes human attitudes and behaviors.

In this study we will focus on indicators related to the environmental, infrastructure and management components. The objectives of these indicators are diverse and varied. Indicators for the environmental component aim at describing the factors affecting the overall availability of water resources. Infrastructure component indicators aim at assessing the actual capacity and effectiveness of infrastructure. The indicators of the management component are intended to characterize the effectiveness of regulation, institutions, and water services.

Finally, 10 indicators were chosen to describe the supply capacity: 'exploitation rate of groundwater resources', 'surface water mobilization rate', 'desalination capacity', 'loss rate in adduction network', 'loss rate in the distribution network', 'Water reuse rate 'and' water structure', Quality of administration and water service (ordinal scale), Quality of regulation (ordinal scale), Law authority (ordinal scale).

2.2 Individual water consumption indicators

The domestic consumption component focuses on measures to reduce domestic demand for drinking water in order to reduce water withdrawals. The three axes that are favored to get people saving water, and which we propose to describe through indicators, are pricing, promotion of water-saving household equipment and rainwater harvesting.

Key indicators for individual water consumption are, 'water expenditure in household budget', 'percentage of households with water-saving devices' and 'percentage of homes using rainwater'.

3. INDICATORS THRESHOLDS

3.1 Measurement scale

The relevance of an indicator depends on its ability to depict the phenomenon being measured. In order for an indicator to be appreciable, it is important to compare it to a benchmark value on an ordinal scale (which makes possible to establish a hierarchy with respect to the measured indicator, e.g. good, fair, poor) or on a cardinal scale that allows quantification of the measurement with respect to a target value (Mayster, 1997; Spangenberg et al., 2002; Desthieux, 2005). This latter can be a standard proposed by international, national or even local bodies, resulting from a benchmark, or relating to the evaluation of the state of the phenomenon at different times (Von Stokar et al., 2001).

The three institutional indicators: Quality Index of Administration and Water Service, Quality of Regulation, Authority of Law, are qualitative indicators measured on an ordinal scale (good, fair, poor),

All the other selected indicators are cardinal, so their assessment is quantifiable and is done in relation to a benchmark value. All these quantitative indicators are expressed as a percentage and could take values between 0% and 100% called extreme thresholds, which after standardization take respectively the values 0 and 100. The significant thresholds in the range 0-100 represent benchmarks defining intervals of values that the indicator: could or should take (recommended) represented by the green color, could take with reserve (reserve) represented by the orange color, avoid taking (prohibited) represented by red color, and finally could take but its impact would be insignificant compared to the system studied (not significant), represented by the gray color. We adopted this color code, inspired by nutrition labeling in use in some countries for its obvious and easy apprehension by decision-makers.

3.2 Indicators significant thresholds

Significant thresholds for indicators as regards exploitation of superficial natural resources refer to United Nations standards (in the comprehensive inventory of world resources (E/CN.17/1997/9) which set a water withdrawal rate not exceeding 40% for a sustainable use of the resources respecting the minimum needs of the ecosystems. Beyond 70% the situation is called critical (PNUE, 2006) and reveals an intense shortage of water.

With regard to underground resources, water withdrawals should be made only from renewable water volume estimated 300 million cubic meter in order to avoid ground water lowering. In a study referred to as PAC on the coastal area of Algiers, a rate of withdrawals on the renewable water above 80 % is allowed, without exceeding the maximum threshold of 100% (Larid, 2003). For this indicator, the threshold of 100% means exploiting totally the renewed volume of water. Exceeding 100% means that the water table level will drop until a state of dangerous depletion.

Due to the absence of national standards about the loss rate in adduction network and the loss rate in the distribution network, we have referred to performances in developing and OECD

countries. Hence, the maximum threshold of lost in the distribution network is fixed at 10%, a performance achieved in several countries of the OECD (OCED, 1998). With regard to losses in adduction network, whose pipes are easier to fix, freed from the constraints of urbanization, a maximum threshold of 5% is adopted.

As well, a rate of 1% for the indicator 'water expenditure in household budget, constitutes the minimum threshold observed in several countries and local communities. Proper water pricing is necessary to cover the actual costs of water service but also to encourage the consumer to adopt a more sparing use of this scarce resource. The OECD estimates that it is possible to go up to a rate of 3%, if necessary. It is also worth noting that a rate of 10% or more can be a threat to the standard of living of low-income households.

Indicators related to wastewater reuse, rainwater recovery and the use of water-saving appliances reflect the success of the policy of promoting the rational use of water resources. The goal is to reuse 100% of the wastewater and to get 100% of the households installing rainwater recovery and water-saving appliances. However, below the threshold of 5%, the impact on water demand will not be significant.

As regards desalination of seawater, setting thresholds is not evident, since it is an expensive process for the production of drinking water (Thivet and Fernandez, 2012), and the knowledge surrounding this technique is still insufficient to assert that it is safe for the marine aquatic environment. In some countries the supply is only made through desalination but the use of this process is still subject to reservation. Therefore the whole field of value relating to this indicator will be set to reserve.

Table 1. Indicators and related thresholds.

Indicator	**Significant thresholds**		
Exploitation rate of renewable groundwater resource	≤80% Recommended	> 80% et <100% with reserve	>100% To avoid
Surface water mobilization rate	≤ 40% Recommended	> 40% et <70% with reserve	>70% To avoid
Desalination capacity		with reserve	
Loss rate in adduction network (%)	≤ 5% with reserve	> 5% To avoid	
Loss rate in the distribution network	≤ 10% with reserve	> 10% To avoid	
Water reuse rate	≤ 5% Not significant	> 5% Recommended	
Domestic water structure	<50% with reserve	≥50% Recommended	
Quality of administration and water service	Poor	Fair	Good
Quality of regulation	Poor	Fair	Good
Law authority	Poor	Fair	Good
Water expenditure in household budget	≥ 1% et ≤3% Recommended	<1%, >3% et ≤10% with reserve	>10% to avoid
Percentage of households with water-saving devices	< 5% Not significant	≥ 5% Recommended	
Percentage of homes using rainwater	< 5% Not significant	≥ 5% Recommended	

The same applies to the amount of water allocated to domestic households, which depends on socio-economic conditions, level of development, nature of the predominant activities in the region and also climatic hazard which, in some cases forces to privilege domestic consumption. The current amount of domestic use is about 51% but could be increased if measures are taken to promote more efficient use of water by other activities such as the generalization of economical irrigation techniques, wastewater reuse by industrial and agricultural activities.

4. ALGIERS HOUSEHOLD WATER RESOURCES CARRYING CAPACITY DIAGNOSIS

For an easy reading of the indicators values, we use a stacked bar chart. Every stacked bar, corresponding to one indicator, has colors according to defined significant thresholds. The diagram become, hence, a matrix for reading indicators values. Figure 1 shows color code for the indicators and the measured value of each indicator relative to the situation of Algiers.

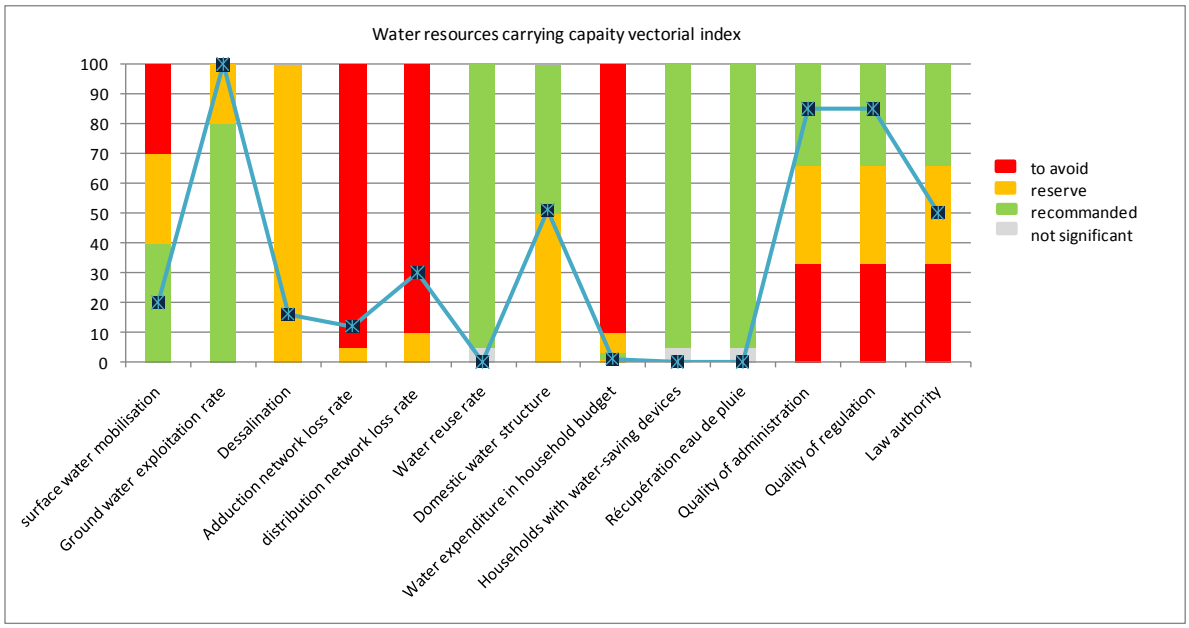

Figure 1. Vectorial stacked bar chart for the diagnosis of water policy.

The measurement of key indicators provides a global view of the main determinants of the carrying capacity of water resources in the capital city.

4.1 In terms of supply capacity

From a previous study, we know that the infrastructure in place allows us to mobilize about 20% of the water collected in the watersheds, that groundwater table is overexploited and that the desalination water constitutes 17% of the total amount of water allocated to the capital (Naimi-Ait-Aoudia and Berezowska-Azzag, 2014). In addition, the loss rates are around 12% in the supply networks (Benblidia, 2011) and 30% in distribution networks according to SEEAL the company in charge of water management in Algiers. Thus, apart from the exploitation of surface resources, which has a positive value and reflects the region's perspective in improving water supply capacity through the construction of new dams, the rest of the indicators of this category are in orange and red, which implies the need to take tangible measures to improve the availability of water and preserve the underground resources.

4.2 In terms of management capacity

The Algerian government seems to have succeeded in setting out a water management policy. The legislation adopted is clear (Benblidia and Thivet, 2010), covering all aspects related to the water sector, namely exploitation and concession of resources, pricing, combating water pollution and social policy. In addition, under a recent law, the concept of sustainability has become a guideline for water policy. The shift from sector management policy to sustainable and integrated

resource management was achieved through the establishment of river basin agencies (Benblidia and Thivet, 2010; Mozas and Ghosn, 2013) which take, among other things, responsibility to raise domestic, industrial and agricultural users awareness for rational use and protection of resources. It should be noted that the status of basin agencies provides for the participation of users in the preparation of master plans (BAfD/OCDE, 2007), a first in the annals of management in Algeria. However, river basin agencies face difficulties in becoming a mediator in integrated water resources management, due to duplication of work with central government departments and lack of financial resources. Despites this, the quality of the administration appears to be generally satisfactory. Mozas and Ghosn (2013) underline a better distribution of competences between the different agencies in the water sector compared to the past. Ultimately, it seems clear that the public authorities have the necessary institutional means to lead the management of a sensitive sector in the country, even if there some flouting in law enforcement.

4.3 In terms of demand regulation

While the Algerian government has made considerable efforts to increase supply capacity, efforts to make efficient use of this resource have been delayed or not undertaken at all.

From all the actions aiming at reducing water demand described by the key indicators selected, only that relating to pricing was implemented. Prices have been revised upwards in conjunction with gradual pricing in terms of volume consumption.

The incentive for water savings should be implemented through awareness of consumer about the importance of preserving this valuable resource and the advantages of adopting behaviors aimed at that goal both on environmental and economic aspects. Furthermore, the gain that might bring the reuse of water was unfortunately ignored for a long time by public authorities. But recently, the intention to exploit this water potential, especially in irrigation, was clearly stated in the preparation of the Metropolitan Land Use Plan.

5. CONCLUSION

The urban management aims at matching the objectives of urban development with urban ecosystem capacity to provide the necessary resources for human development. That is why the management of water demand as much as on supply is of critical importance especially in a country with limited fresh water resources like Algeria. In this respect, water carrying capacity assessment provides, policy makers, elements of appreciation to lay down the foundations of a sustainable urban development policy. Based on the characterisation of both supply and demand water components, we have proposed key indicators and related thresholds for analysing Algiers water carrying capacity in order to provide a diagnosis tool and a dialogue interface for policy makers to negotiate possibilities for improving the water service while maintaining water resource sustainability.

REFERENCES

BAfD/OCDE. (2007). Perspectives économiques en Afrique 2007. OCDE: Organisation de Coopération et de Développement Économiques.

Benblidia, M. (2011). L'efficience d'utilisation de l'eau et approche économique. Centre d'Activités Régionales PNUE/PAM. Plan Bleu.

Benblidia, M., & Thivet, G. (2010, Mai). Gestion des ressources en eau: les limites d'une politique de l'offre. (C: Méditerranéennes, Éd.) Les Notes d'analyse du CIHEAM (58), pp. 1-15.

Cotruvo, J. V. (2011). Desalination technology: health and environmental impacts. CRC Press.

Desthieux, G. (2005). Approche systémique et participative du diagnostic urbain. Processus de représentation cognitive du système urbain en vue de l'élaboration d'indicateurs géographiques. Thèse de doctorat, EPFL: Ecole Polytechnique Fédérale de Lausanne, Lausanne.

Falkenmark, M. (1989). The massive water scarcity now threatening Africa: why isn't it being addressed? Ambio , 18 (2), 112-118.

Feng, L.-H., Zhang, X.-C., & Luo, G.-Y. (2008). Application of system dynamics in analyzing the carrying capacity of water resources in Yiwu City, China. Mathematics and Computers in Simulation, 79 (3), 269–278.

Kettab, A. (2001). Les ressources en eau en Algérie: stratégies, enjeux et vision. Desalination, 136 (1), 25-33.

Larid, M. (2003). Analyse de durabilité dans le cadre du PAC « Zone côtière algéroise" (Algérie). Ministère de l’Aménagement du Territoire et de l’Environnement. PNUE, PLan Bleu.

Li, L., Guo, H., & Chen, B. (2000). Water resources supporting capacity of Chaidamu Basin. (20–23, Éd.) Environ. Sci., 21.

Li, X.-G., Wei, X., & Lu, Y.-D. (2010). Optimising the allocation of groundwater carrying capacity in a data-scarce region. Water SA, 36, 451-460.

Liu, S., & Chen, J. (2007). Water resources carrying capacity based on the theory of ANN. Resour. Sci., 29, 99–105.

Mayster, L. Y. (1997). Une démarche pour négocier les décisions relatives à l'aménagement des territoires et à la gestion de l'environnement. Biotechnol. Agron. Soc. Environ., 1 (4), 248-256.

Mozas, M., & Ghosn, A. (2013). État des lieux du secteur de l’eau en Algérie. IPEMED: Institut de Prospetive Economique du Monde Méditerranéen.

Naimi Ait-Aoudia, M., & Berezowska-Azzag, E. (2016). Water Resources Carrying Capacity Assessment: the case of Algeria’s Capital City. Habitat International, 58, 51-58.

Naimi-Ait-Aoudia, M., & Berezowska-Azzag, E. (2014). Algiers carrying capacity with respect to per capita domestic water use. Sustainable Cities and Society, 13, 1–11.

OCDE. (1998). La consommation de l'eau et la gestion durable des ressources en eau. OCED : Organisation de Coopération et de Développement Economique, Paris.

OCED. (1998). Gestion de l'eau. Performances et défis dans les pays de l'OCDE. OCED : Organisation de Coopération et de Développement Economique.

Oh, K., Jeong, Y., Lee, D., Lee, W., & Choi, J. (2005). Determining development density using the Urban Carrying Capacity Assessment System. Landscape and urban Planning , 73 (1), 1-15.

PNUE. (2006). Fiches méthodologiques des 34 indicateurs prioritaires pour le suivi de la Stratégie Méditerranéenne pour le Développement Durable. Plan Bleu. PNUE.

Shi, Y., & Qu, Y. (1992). Carrying Capacity ofWater Resources in Urumqi River Basin and its Rational Utilization. Science Press, Beijing , 128–139.

Spangenberg, J. H., Pfahl, S., & Deller, K. (2002). Towards indicators for institutional sustainability: lessons from an analysis of Agenda 21. Ecological Indicators , 2 (1), 61–77.

Thivet, G., & Fernandez, S. (2012). La gestion de la demande en eau : L'expérience méditerranéenne. Global Water Parnership. Plan Bleu.

Von Stokar, T., Frick, R., Schultz, B., Keiner, M., Rey, M., & Mettan, N. (2001). Planification directrice cantonale et développement durable. Berne: Office fédéral du développement territorial (ODT).

Zhongmin, X. (1999). Scenario-Based Framework for Multicriteria Decision Analysis in Water Carrying Capacity. J. Glaciology and Geocryology , 21, 100-106.

Proceedings of the 10th World Congress of EWRA 'Panta Rhei', 5-9 July 2017, Athens, Greece
© 2017 *European Water Resources Association*

The seismic risk of new and existing dams

P.N. Psarropoulos
School of Rural & Surveying Engineering, National Technical University of Athens, Greece
* *e-mail: prod@central.ntua.gr*

Abstract: The main issues of the design and construction of any dam are undoubtedly the safety and serviceability. It is evident that both of them depend mainly on the capability of the design group (a) to assess realistically all the local site conditions (hydrological, hydraulic, topographical, geological, geotechnical, etc.), (b) to decide the optimum dam shape and type (i.e. embankment dam, concrete gravity dam or arch dam), and (c) to design the dam accordingly in order to withstand all the potential hazards and/or loadings (e.g. gravity, hydrostatic pressure, differential settlements, etc.). Nevertheless, in areas characterized by moderate or high seismicity the design of a dam may be a more challenging and demanding task since both safety and serviceability are directly related to the earthquake-related geohazards and the seismic vulnerability of the dam under consideration. The term "earthquake-related geohazards" is used to describe various geological/geotechnical phenomena, such as strong ground motion, active-fault rupture propagation, earthquake-triggered slope instabilities and soil-liquefaction phenomena. Therefore, the main emphasis of this study is on the seismic risk of new or existing dams. The seismic risk may be estimated by the assessment of the earthquake-related geohazards and the realistic estimation of the seismic distress of a dam. The first part of the study is devoted on the qualitative and quantitative assessment of the main earthquake-related geohazards, while in the second part the main issues related to the seismic response and vulnerability of dams are presented.

Key words: dams, geohazards, earthquakes, seismic risk, safety, serviceability, seismic design

1. INTRODUCTION

The dams and all the related facilities are usually critical structures that must be designed and constructed to withstand all the potential loadings and hazards during their lifetime. One of the main types of hazards is the geohazards. The term "geohazard" is used to describe any hazard associated with geological features or processes in the vicinity of a dam that potentially pose a threat to the integrity or serviceability of the components of the dam. Apart from very compressive soils, karst phenomena and soil errosion, the main geohazards under static conditions are the potential ground movements from creep, slope intabilities and landslides. As shown in Figure 1, many dams have been damaged by geohazards in the past. In some case histories the damage has been related to the fact that the geohazard had not been identified by the geoscientists during the design phase. On the other hand, in some other cases the geoscientists had identified the problematic area, but their qualitative assessment was not followed by a quantitative assessment (with geotechnical surveys and realistic geotechnical analyses), being thus incapable to estimate the criticality of the area. Nevertheless, it should be emphasized that many failures especially of earth-fill dams have been related to poor design and/or construction.

In areas characterized by moderate or high seismicity the design against geohazards is a more demanding and chalenging task since, apart from the typical geohazards, various earthquake-related geohazards should be taken into consideration. The term "earthquake-related geohazards" is used to describe various geological/geotechnical phenomena that are related to the seismic activity. One of the main earthquake-related geohazard is the propagation of seismic waves and the consequent strong ground motion at the ground surface. Under these circumstances, during an earthquake the shaking at the ground surface will cause the vibration of a concrete or an earth-filled dam causing the development of horizontal and vertical inertial forces acting on its mass.

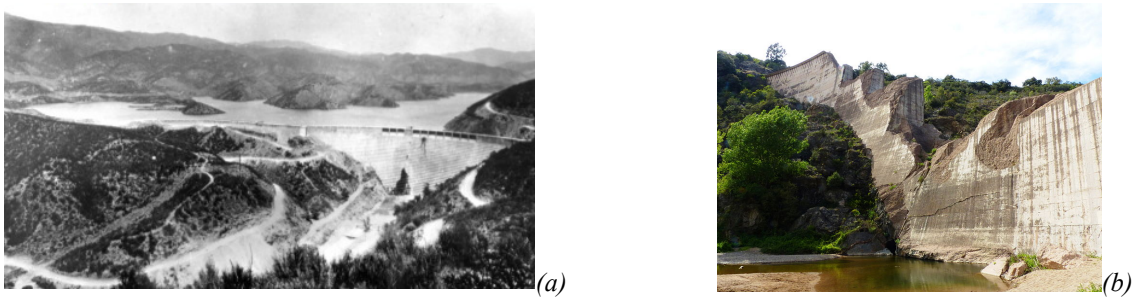

Figure 1. Geohazards and dam failures: (a) St. Francis Dam before the 1928 failure in Los Angeles County, California, in USA, (b) the 1959 failure of the Malpasset Dam in France. In both cases the failure have been attributed to poor geological and geotechnical conditions that had not been identified by the corresponding surveys and studies.

As shown in Figures 2 and 3, in the past dams have been damaged in areas that are characterized by moderate or high seismicity all over the world. Judging from Figures 2 and 3, it becomes evident that a serious failure or a collapse of a large dam may cause a disaster with exceptional risk to life and extreme economic and social consequences of failure.

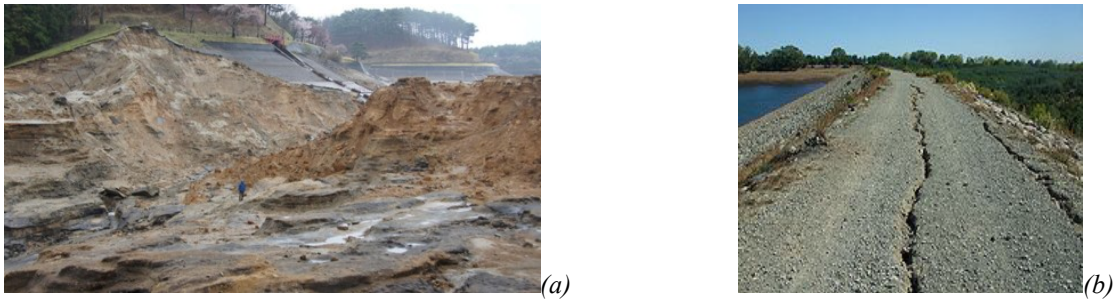

Figure 2. Earthquake-related geohazards and failure of dams: (a) collapse of the earth-filled Fujinuma Dam during the 2011 Tohoku earthquake in Japan, (b) damage to the Coihueco Dam during the 2010 Chile earthquake.



Figure 3. Earthquake-related geohazards and failure of dams: (a) collapse of the concrete Shih-Kan Dam during the 1999 Chi-Chi earthquake in Taiwan due to active fault rupture, (b) severe damage to the Lower Van Norman Dam during the 1971 San Fernando earthquake in USA.

Apart from the earthquake-related geohazard of strong ground motion (and the consequent inertial loading to the dam), there exist various earthquake-related geohazards that may induce permanent ground deformations (PGDs) to the dam and to any other related structure during (or just after) a moderate or strong earthquake. As shown in Figure 4, the main earthquake-related geohazards of this type are the active-fault ruptures, the soil-liquefaction phenomena (i.e. buoyancy, settlements or lateral spreading) and the earthquake-triggered slope instabilities and rockfalls. Note that in the case of a dam with a full reservoir the developed hydrodynamic pressures may be regarded as an additional earthquake-related geohazard. More details on the dynamic interaction of dams with the reservoir can be found in Papazafeiropoulos et al. (2010).

Note that strong ground motion and active fault rupture(s) are regarded as direct geohazards to any structure, while earthquake-triggered slope instabilities, soil liquefaction phenomena and the

hydrodynamic pressures are indirect geohazards that depend primarily on the characteristics of the strong ground motion. In addition, strong ground motion and hydrodynamic forces are dynamic loadings to a dam, while the rest are actually quasi-static loading to the examined structure as they cause induced PGDs.

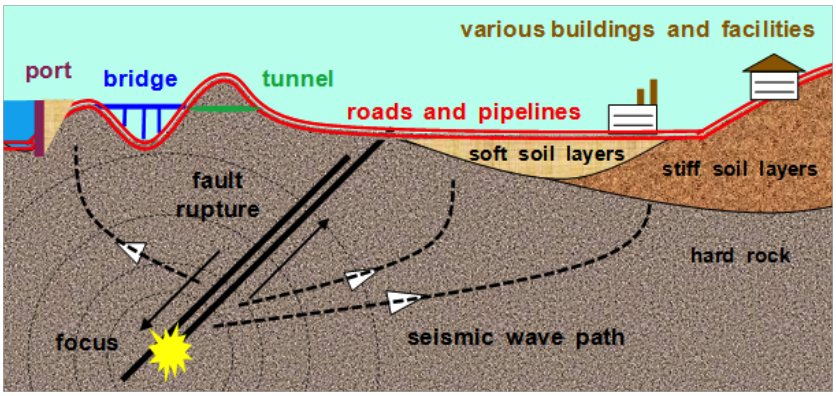

Figure 4. Sketch showing the main earthquake-related geohazards for various structures and infrastructures: (a) strong ground motion, (b) active fault rupture, (c) soil liquefaction phenomena (i.e. settlements and/or lateral spreading), (d) earthquake-triggered slope instabilities (i.e. landslides)

In contrast to long structures (such as highways, railways, pipelines), the dams are not very long structures, and therefore their installation is usually being performed in an area that is supposed to be without any geohazards. Nevertheless, the decision for the location of a dam is taken at a very preliminary phase of the project when the geological and mainly the geotechnical data are rather limited, and therefore the assessment is mainly qualitative (and not quantitative). On the other hand, apart from the observable geohazards (such as very compressive soils, karst phenomena, rockfalls, etc.), there exist some earthquake-related geohazards the intensity of which depends on the seismicity of the area under examination and the local site conditions (i.e. topographical, geomorphological, geological, geotechnical, etc.). For these geohazards there is a need for quantitative assessment in order to quantify both strong ground motion and potential induced PGDs.

The current paper is involved with (a) the quantitative assessment of the main earthquake-related geohazards and (b) the optimum seismic design of dams. Emphasis is given to the strong ground motion as usually the geohazards of landslide and fault rupture can be avoided during a preliminary phase of the design with the appropriate selection of the location of the dam. An exception may be the geohazard of soil liquefaction in liquefiable areas (i.e. areas with cohesionless soil materials and high groundwater table), since liquefaction potential is directly related to the strong ground motion (i.e. the acceleration levels at the ground surface).

It becomes evident that in many cases, the simplistic provisions of seismic norms cannot cover sufficiently all the issues of the seismic design. In these cases the geotechnical earthquake engineers and the structural engineers, with the help of seismologists and geologists, should perform special surveys and studies in order to assess quantitatively the earthquake-related geohazards and to verify that the dams (including their foundation) are capable to withstand the seismic distress (developed by the inertial forces and/or the induced PGDs). It is evident that in case that the seismic distress is excessive, the engineers should apply mitigation measures in order to reduce the geohazard(s) and/or increase the structural capacity depending on the circumstances. The final solution is directly related to various criteria such as risk, cost, environment issues, etc.

2. STRONG GROUND MOTION AT THE GROUND SURFACE

As it was mentioned, a dam comprises of various structures and facilities made of concrete or soil materials. The impact of strong ground motion on the structures and facilities of a dam is mainly the development of horizontal and vertical inertial forces. These forces depend on the mass

of each structure and the accelerations that will be developed at the center of this mass. These accelerations depend, not only on the geometrical and mechanical characteristics of the structure itself, but on the characteristics of the strong ground motion at the ground surface which is a function of (a) the strong ground motion at the seismic bedrock that have been defined by the seismological study and (b) the local site conditions (soil, geomorphology and topography) in two or three dimensions. Figure 5 depicts the main categories of local site conditions that usually coexist in nature.

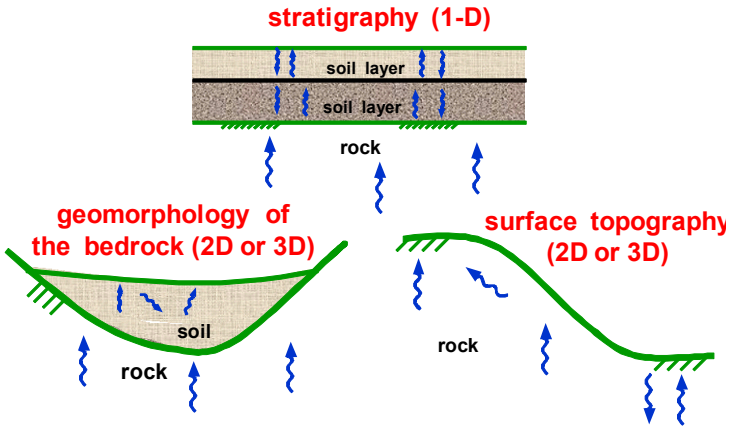

Figure 5. Sketch showing the three main categories of local site conditions: (a) soil stratigraphy, (b) geomorphology of the bedrock, and (c) surface topography

In general, the local site conditions tend to amplify the strong ground motion at the ground surface and modify its frequency content in comparison with the strong ground motion at the ground base. This phenomenon is taken into account in most of the modern seismic norms, such as EN1998 (i.e. Eurocode8) which introduces (a) a topographic amplification factor S_T, and (b) a soil amplification factor S. The topographic amplification factor S_T ranges between 1 and 1.4, while the soil amplification factor S with values ranges from 1 to 1.4 for high and moderate seismicity regions depending on the ground type (see Table 1). Note that ground type A corresponds to rock or rock-like geological formations, while on the other hand, ground types D and E correspond to soft and/or deep sediments.

Table 1. Soil amplification factor S for various ground types (according to EN1998) in the case of high and moderate seismicity regions (i.e. magnitude $M_S > 5.5$)

Ground type	S
A	1.00
B	1.20
C	1.15
D	1.35
E	1.40

However, it should be emphasized that most of the seismic norms worldwide ignore the potential impact of the geomorphology of the bedrock, and therefore, in the case of a valley or a basin, norms may underestimate substantially the amplitude and the spatial variability of the seismic motion at the ground surface. In addition, large dams are beyond the scope of many norms (such as EN1998), and therefore special geotechnical earthquake engineering studies are required.

It becomes evident that in these cases the design of a demanding project such as a dam with the simplistic and conservative norms may have a substantial cost for the project. For this reason, in the case of a dam (provided that a cost-effective solution is desired) there is need for reliable geophysical and geotechnical data and the consequent performance of one-dimensional or even two-dimensional ground response analyses (i.e. a soil amplification study) in order to assess realistically the acceleration levels at the ground surface. Note that these acceleration levels will

dominate (a) the structural design (i.e. the developed inertial forces) and the (b) the geotechnical design (e.g. induced PGDs from soil liquefaction phenomena and/or slope instabilities and selection of the optimum foundation system).

Finally, when the foundation of the dam is on soil layers (and not on rock) the common assumption of "fixed-based structures" cannot be regarded as realistic. Therefore, in the case of an earthquake there exists a dynamic interaction between the soil and the structure. The dynamic soil-structure interaction is a very important and complex phenomenon, since the presence of a structure makes the soil to deform under dynamic loading, while the underlying soil (a) reduces the structural stiffness leading to higher natural periods, and (b) increases the overall damping, since the material damping and the radiation damping of the soil layers are being developed as well.

Therefore, in many cases the analysis of the dynamic response of a structure requires the realistic simulation of the foundation and of the underlying soil as well. As a result of the presence of soil and local site conditions, the foundation compliance and other aspects should be carefully examined. Note that in current engineering practice, the dynamic soil-structure interaction is mainly considered via "soil springs", which in some cases may be an inadequate design simplification.

3. RUPTURE OF ACTIVE SEISMIC FAULTS

The rupture of an active fault may cause, apart from strong ground motion, substantial PGDs at the ground surface. Nevertheless, these deformations may be low in the case of areas characterized by soft and deep sediments. It is evident that the rupture of an outcropped fault is a direct threat to a crossing structure, such as a dam. However, in the case of a fault covered by soft and deep sediments the local ground conditions may alter the fault rupture propagation and the pattern of the PGDs at the ground surface. In other words, a possible fault rupture at the bedrock would propagate through the overlying soil(s) and alter the shape (i.e. the topography) of the surface.

The aforementioned alteration of the surface profile inevitably would cause differential settlements to the dam, which should be designed to sustain this fault-induced distress. Unfortunately, the assessment of the faulting hazard (dislocation and angle of emergence) is possible only within rock formations. Whereas the fault rupture at the bedrock is unambiguously defined by the dip angle and the magnitude of the expected dislocation (i.e. offset), as the rupture propagates through the softer soil layers, it usually deviates, bends and causes a rather smooth deformation of the surface, at least when compared with the abrupt dislocation at the rock (Figure 6).

The PGD pattern is a function of fault displacement and angle, soil deposit thickness and mechanical properties. To predict the deformation of the soil surface induced by the rupture propagation, a special analysis is required. Figure 7 shows some representative results of fault rupture propagation analysis with the finite-element code ABAQUS, where it becomes evident that the existence of a soft soil layer of 6m covering the hard bedrock leads to the following phenomenon: the applied fault offset Δf of 0.2m within a very narrow zone at the bedrock is transformed to a PGD of around 0.2m which is extended along a zone of around 5m at the ground surface. Despite the aforementioned capability of engineers to estimate realistically the pattern of PGDs at the ground surface in the case of a covered fault, and taking into account the limited capability of the dam to withstand differential settlements, it is recommended to avoid the construction of a dam in the vicinity of any active seismic fault (outcropped or covered).

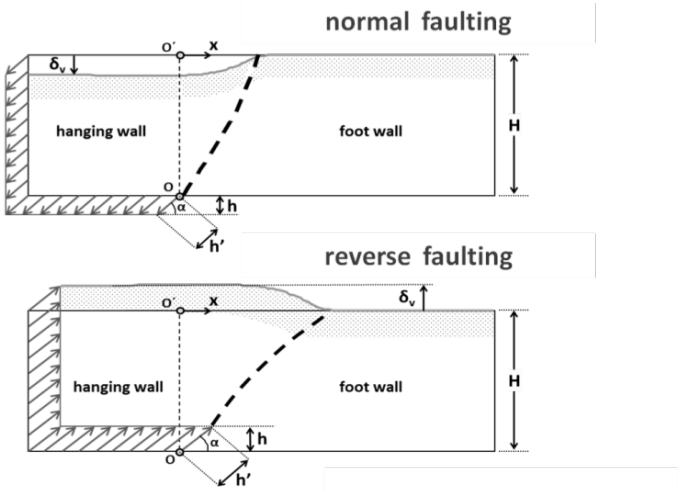

Figure 6. Schematic of the fault rupture propagation through soil, indicating the main parameters of the problem.

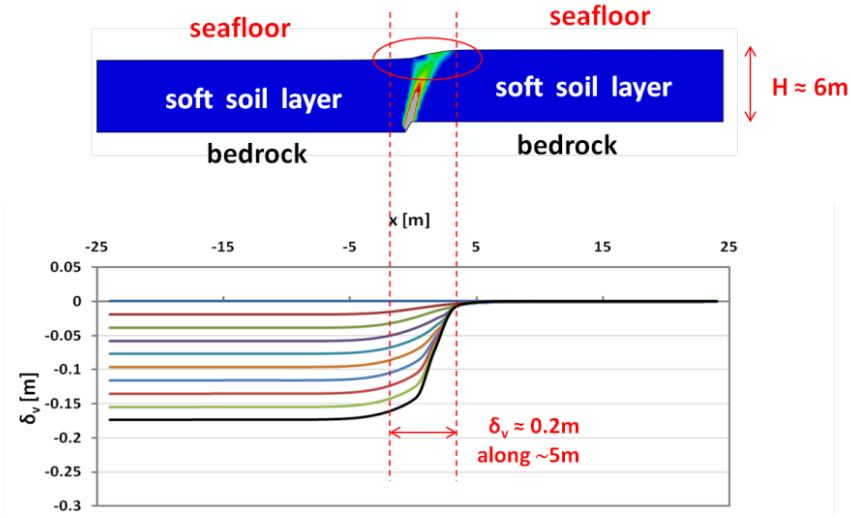

Figure 7. (a) Numerical simulation of the rupture propagation path of a covered normal fault with offset of 0.2m. (b) Pattern of the PGD at the ground surface. Note that the vertical scale of the graph is exaggerated.

4. SOIL LIQUEFACTION

Soil liquefaction is an extreme consequence of strong ground motion which leads to practically total loss of shear strength in relatively loose cohesionless soil formations below the ground water table. Soil liquefaction may cause either liquefaction-induced (differential) settlements (i.e. almost vertical PGDs) and/or lateral spreading (i.e. almost horizontal PGDs). In the presence of structures, foundation failure (i.e. excessive settlement or tilting) is possible. Soil liquefaction assessment is achieved through the estimation of soil liquefaction potential through simple design charts based on semi-analytical methods or advanced numerical modeling (Seed & Idriss, 1971). Finally, for silty and clayey sands, Andrews & Martin (2000) define a criterion based on liquid limit (LL) and clay content (%) for liquefaction susceptibility (Table 2).

Table 2. Liquefaction susceptibility of silty and clayey sands (Andrews & Martin, 2000)

	Liquid limit < 32	**Liquid limit > 32**
Clay content < 10%	susceptible	further studies required
Clay content ≥ 10%	further studies required	not susceptible

The following equation evaluates the liquefaction potential. Therefore, two primary seismic variables are required: (a) the level of cyclic stress induced by the earthquake on a sediment layer, expressed in terms of cyclic stress ratio (CSR), and (b) the capacity of a sediment layer to resist liquefaction, expressed in terms of cyclic resistance ratio (CRR).

Seed & Idriss (1971) formulated the following equation for calculating CSR:

$$CSR = \frac{\tau_{av}}{\sigma'_{v0}} \approx 0.65 \left(\frac{a_{max}}{g}\right)\left(\frac{\sigma_{v0}}{\sigma'_{v0}}\right) r_d \quad (1)$$

where

α_{max} : peak horizontal acceleration at the surface of the sediment deposit,
g : gravitational acceleration,
σ_{v0} and σ'_{v0} : total and effective overburden stress, respectively;
r_d : stress reduction factor.

Evaluation of the cyclic resistance ratio (CRR) has developed either using methods based on the results of laboratory tests, or methods based on in situ tests and field observations of liquefaction behavior in past earthquakes. In laboratory testing, the number of shear stress cycles to achieve liquefaction is the basis for expressing the resistance of sediment to the initiation of liquefaction. Liu et al. (2001) developed empirical regression equations that can be used to evaluate the number of uniform shear stress cycles of shaking as a function of magnitude, site-source distance, site condition, and near-fault rupture directivity effects, thus the cyclic resistance ratio of the sediment, CRR can be estimated. The potential for liquefaction can then be evaluated by comparing the earthquake loading (CSR) with the liquefaction resistance (CRR) in terms of factor of safety (FS) against liquefaction. Values of FS (= CRR/CSR) greater than one indicate that the liquefaction resistance exceeds the earthquake loading, and therefore, that liquefaction would not be expected.

If the potential for liquefaction is proven to be high, there exist various analytical and empirical methods in the literature for the realistic estimation of vertical (and horizontal) PGDs. If the latter are excessive for the integrity and serviceability of the dam, mitigation measures should be adopted. One option is to apply measures that aim to the reduction of the liquefaction-induced PGDs. This may be achieved by (a) dynamic compaction, (b) preloading, (c) increasing the dissipation of pore-water pressure (usually by gravel-columns), (d) grouting and deep soil mixing, and/or (e) lowering the groundwater level (if possible). An expensive alternative is to reduce the liquefaction risk by replacing liquefiable soils in the area of the dam with non-liquefiable materials. Note that in the case of extensive lateral spreading (i.e. horizontal PGDs), the relocation of the dam may be the wiser option since the cost of mitigation measures against lateral spreading is usually prohibitive.

5. EARTHQUAKE-TRIGGERED SLOPE INSTABILITIES AND ROCKFALLS

As it was mentioned before, the selection of the location of a dam is performed at a preliminary phase of the design with various criteria. Usually, this location is at an area where the risk of landsliding under static conditions is regarded low. Nevertheless, in some cases the area under examination may have a high inclination, while on the other hand a rather stable slope under static conditions may become unstable under certain seismic conditions (i.e. subjected to strong ground motion). Additionally, the existence of rock slopes around the dam may be characterized by rockfalls where great boulders of rock may be dispatched from their initial position (for various reasons) and travel for long distances (e.g. tens or even hundreds of meters), depending on the circumstances and the local site conditions (shape of the boulders, topography, geology, etc.). Therefore, although slope stability assessment is regarded as a secondary issue for the design of a dam (provided that the dam will be constructed in a flat area), a quantitative assessment may be required in cases of inclined areas with high acceleration levels.

6. SEISMIC RESPONSE OF A DAM

The seismic distress of a dam depends mainly on its geometry (i.e. height, inclinations) and its type (i.e. concrete or earth-filled), but many other parameters (such as local soil conditions, water level, etc.) may determine its dynamic/seismic response. In the case of concrete dam, the structural engineers should perform numerical dynamic simulations of the dam in order to estimate the horizontal and vertical inertial (and the hydrodynamic) forces that will develop on the dam mass in the case of the design earthquake. These forces (in addition to gravitational and hydrostatic forces) will lead to the total design stresses and strains that have to be assessed with the highest realism. It is evident that these forces will determine the reinforcement of the concrete. On the other hand, in the case of earth dams soil material nonlinearity and topographic aggravation are key parameters that will dominate the seismic slope stability. According to the modern seismic philosophy and the concept of "strain-based design", repairable damages to an earth dam are allowed, provided that the non-collapse requirement has been fulfilled. Therefore, apart from (the static and) the pseudostatic factors of safety, the permanent deformations of the dam should be estimated. The design should try to keep these deformations in low levels in order to achieve the integrity and the serviceability of the dam after the design earthquake. In any case, after a strong earthquake damages have to be identified and repaired as fast as possible since an aftershock may have a detrimental impact.

7. CONCLUSIONS

The dams usually comprise critical structures, and therefore they must be designed to withstand all the potential loadings and hazards. In areas characterized by moderate or high seismicity this design is more demanding and chalenging since, apart from the typical geohazards, various earthquake-related geohazards should be taken into consideration. The current paper is involved with (a) the quantitative assessment of the main earthquake-related geohazards (such as strong ground motion, earthquake-triggered landslides, soil liquefaction phenomena, and fault rupture) and (b) the optimum seismic design of dams. It becomes evident that in many cases, the simplistic provisions of seismic norms cannot cover sufficiently all the issues of the seismic design. In these cases the geotechnical engineers and the structural engineers, with the help of seismologists and geologists, should perform special surveys and studies to assess quantitatively the earthquake-related geohazards and to verify that all the structures and facilities of a dam (including their foundation) are capable to withstand the seismic distress (developed by the inertial forces and/or the induced PGDs). It is evident that in case that the seismic distress is excessive, the engineers should apply mitigation measures in order to reduce the geohazard(s) and/or increase the structural capacity.

REFERENCES

Andrews, D.C.A., Martin, G.R. (2000) Criteria for liquefaction of silty soils. 12th World Conference on Earthquake Engineering, Proceedings, Auckland, New Zealand.

Eurocode 8, Design of structures for earthquake resistance, CEN, European Committee for Standardization, Brussels, 2004.

IASPEI Handbook. Chapter 42. A List of Deadly Earthquakes in the World: 1500-2000. Tokuji Utsu, The University of Tokyo, Tokyo, Japan

Kramer S. (1995). Geotechnical Earthquake Engineering.

Liu, A.H., Stewart, J.P., Abrahamson, N.A., Moriwaki, Y. (2001) Journal of Geotechical and Geoenvironmental Engineering, 127 (12), 1017– 1026.

Papazafeiropoulos G., Tsompanakis Y. & Psarropoulos P. N., Dynamic interaction of concrete dams-reservoir-foundation: Analytical and numerical solutions, in M. Papadrakakis, N.D. Lagaros and M. Fragiadakis (Eds.), Computational Methods in Earthquake Engineering, ECCOMAS Series, Springer Publ., 2010.

Psarropoulos, P. N., Tazoh, T., Gazetas, G. Apostolou, M. (2007) Linear and non-linear valley amplification effects on seismic ground motion, Soils & Foundations, 47(5): 857-872.

Seed, H.B., Idriss, I.M. (1971) Simplified procedure for evaluating soil liquefaction potential. Journal of the Soil Mechanics and Foundations Division, ASCE 97 (SM9), 1249–1273.

Proceedings of the 10th World Congress of EWRA 'Panta Rhei', 5-9 July 2017, Athens, Greece
© 2017 *European Water Resources Association*

Water, energy and food nexus: The Q-Nexus model

A. Karnib
Lebanese University, Hadath Campus, Baabda, Lebanon
* *e-mail: karnib.ali@gmail.com*

Abstract: Water, energy and food (WEF) resources are interconnected systems that directly and indirectly affect one another. The water-energy-food nexus perspective as a conceptual framework is highly relevant to model and analyse WEF sectors holistically. Evaluating and analysing interactions across and between water, energy and food systems necessitates suitable methods to promote sustainable and efficient WEF resource use. The Q-Nexus Model is a practical and mathematically-based quantitative WEF nexus assessment framework that serves as platform to quantify, planning, simulate and optimize water, energy and food as an interconnected system of resources that directly and indirectly affect one another. It permits the evaluation of WEF planning scenarios and policy options based on changing demand, technology and resource allocation. This paper reviews the technical features of the Q-Nexus Model and presents method of evaluation of the direct and indirect effects resulted from WEF planning scenarios or policy options. Firstly, the methodological background of the Q-Nexus Model and its ability to simulate water, energy and food nexus systems in response to numerous key drivers is presented. Secondly, procedures of calculating direct and indirect intersectoral use quantities are introduced. At the practical level, a numerical experiment is presented and results are discussed. Lastly, the conclusions and further developments are presented.

Key words: Water, energy, food, nexus approach, sustainable development

1. INTRODUCTION

The substantial interactions among water, energy and food systems point out the importance of managing limited resources in the context of various competing interests (Karnib, 2017a; Hoff, 2011; DTU, 2016; Biggs EM et al., 2015; FAO, 2013, 2014a,b&c). WEF nexus framework can be used to guide policy makers where it is possible to simulate, quantify and optimize any objective representing the user own interest (Karnib, 2017a,b&c). Such models are necessary to support policy measures as well as technical actions that will ensure sustainable and efficient production and use of WEF resources (Karnib, 2017a&b; Bizikova et al., 2013; FAO, 2014c; Andrews-Speed et al., 2012; Waskom et al., 2014). A practical and mathematically-based quantitative assessment, simulation and optimization framework of the WEF nexus is proposed by Karnib (2017a,b&c). The methodological approach presented in Karnib (2017a) permits to perform simulation and evaluation of policy options and scenarios that respond to quantitative variations of the WEF resources. The simulation of policy options of adopting high efficient intersectoral use technologies is presented in Karnib (2017b). The applicability of coupling Q-Nexus Model simulator with optimization techniques to aid in WEF nexus decision making in terms of selection of best policy options is introduced in Karnib (2017c).

This paper presents a summary of the methodological aspects of the Q-Nexus Model and its associated quantification and simulation functions. Particularly, the evaluation of the direct and indirect intersectoral quantities resulted from projected WEF nexus scenarios will be introduced.

2. THE METHODOLOGY

The Q-Nexus Model is built on input-output theory and it is based on the quantitative balance of the WEF total quantities. The intersectoral use quantities (z), the end use quantities (y) and the sum

(x) of these two components are the main quantitative conceptual elements of the model (Karnib, 2017a, b).

A set of inflows are identified to represent the WEF sectors, for example, surface water, groundwater, desalination, wastewater and drainage water reuse inflows covering the water sector; petroleum and all types of electricity including renewable energy, covering the energy sector, and irrigated cereals, irrigated roots and other food production items covering the area of food. The organisation of these elements could change to take into account diversification related to local, national and regional particularities.

If we denote by:

n number of water resources inflows;

m number of energy resources inflows;

h number of food resources inflows;

$z_{ij}^{w\_e}$: the water use for energy production;

$z_{ij}^{w\_f}$: the water use for food production;

$z_{ij}^{e\_w}$: the energy use for water production;

$z_{ij}^{e\_e}$: the energy use for energy production;

$z_{ij}^{e\_f}$: the energy use for food production;

$z_{ij}^{f\_e}$: the food use for energy production;

$z_{ij}^{f\_f}$: the food use for food production.

The WEF quantitative balance equations are developed as follows (Karnib, 2017a):

$$\sum_{j=1}^{m} z_{ij}^{w\_e} + \sum_{j=1}^{h} z_{ij}^{w\_f} + y_i^w = x_i^w \qquad (i=1, 2, \ldots, n) \qquad (1)$$

$$\sum_{j=1}^{n} z_{ij}^{e\_w} + \sum_{j=1}^{m} z_{ij}^{e\_e} + \sum_{j=1}^{h} z_{ij}^{e\_f} + y_i^e = x_i^e \qquad (i=1, 2, \ldots, m) \qquad (2)$$

$$\sum_{j=1}^{m} z_{ij}^{f\_e} + \sum_{j=1}^{h} z_{ij}^{f\_f} + y_i^f = x_i^f \qquad (i=1, 2, \ldots, h) \qquad (3)$$

The water for water and food for water relations are considered quantitatively negligible and set equal to zero. The end use quantities (y) cover households, government and rest of the economy demands, losses, storage and exports.

To transform the above balance equations into active WEF nexus model of interconnected system of resources that directly and indirectly affect one another, the following intensity-based coefficients are introduced:

$$a_{ij}^{w\_e} = \frac{z_{ij}^{w\_e}}{x_j^e},\ a_{ij}^{w\_f} = \frac{z_{ij}^{w\_f}}{x_j^f},\ a_{ij}^{e\_w} = \frac{z_{ij}^{e\_w}}{x_j^w},\ a_{ij}^{e\_e} = \frac{z_{ij}^{e\_e}}{x_j^e},\ a_{ij}^{e\_f} = \frac{z_{ij}^{e\_f}}{x_j^f},\ a_{ij}^{f\_e} = \frac{z_{ij}^{f\_e}}{x_j^e} \text{ and } a_{ij}^{f\_f} = \frac{z_{ij}^{f\_f}}{x_j^f}$$

where x_j^w, x_j^e, x_j^f are the total use of the jth water resource inflow, total use of the jth energy resource inflow and total use of the jth food resource inflow, respectively.

These coefficients represents the extents of resource inflows use in the production of other resources.

By introducing the intensity-based coefficients into equations (2, 3 and 4), they become:

$$\sum_{j=1}^{m} a_{ij}^{w\_e}\, x_j^e + \sum_{j=1}^{h} a_{ij}^{w\_f}\, x_j^f + y_i^w = x_i^w \qquad (i=1, 2, \ldots, n) \qquad (4)$$

$$\sum_{j=1}^{n} a_{ij}^{e\_w} x_j^w + \sum_{j=1}^{m} a_{ij}^{e\_e}\, x_j^e + \sum_{j=1}^{h} a_{ij}^{e\_f}\, x_j^f + y_i^e = x_i^e \qquad (i=1, 2, \ldots, m) \qquad (5)$$

$$\sum_{j=1}^{m} a_{ij}^{f\_e}\, x_j^e + \sum_{j=1}^{h} a_{ij}^{f\_f}\, x_j^f + y_i^f = x_i^f \qquad (i=1, 2, \ldots, h) \qquad (6)$$

Equations (4, 5 and 6) can be written in simple form:

$$Ax + y = x \qquad (7)$$

Or in block matrix form (Karnib, 2017a):

$$\begin{bmatrix} 0 & A^{w\_e} & A^{w\_f} \\ A^{e\_w} & A^{e\_e} & A^{e\_f} \\ 0 & A^{f\_e} & A^{f\_f} \end{bmatrix} \begin{bmatrix} x^w \\ x^e \\ x^f \end{bmatrix} + \begin{bmatrix} y^w \\ y^e \\ y^f \end{bmatrix} = \begin{bmatrix} x^w \\ x^e \\ x^f \end{bmatrix} \qquad (8)$$

Finally, the total outputs (x) could be calculated for any end use quantities (y) using the following equation:

$$x = (I\text{-}A)^{-1} y \qquad (9)$$

where I is the identity matrix and $A = \begin{bmatrix} 0 & A^{w\_e} & A^{w\_f} \\ A^{e\_w} & A^{e\_e} & A^{e\_f} \\ 0 & A^{f\_e} & A^{f\_f} \end{bmatrix}$ is the WEF nexus technology matrix (Karnib, 2017a).

$(I\text{-}A)^{-1}$ matrix is known as the Leontief inverse or the total requirements matrix (Miller & Blair, 2009), it captures in each of its elements direct and indirect effects that the new technology options and/or the end use demands have on the outputs of the WEF sectors. The elements of this Leontief inverse matrix are often termed multipliers.

2.1 WEF nexus quantification

A set of indicators are identified based on the methodological approach of the Q-Nexus Model. These indicators are clustered into quantity-based indicators, intensity-based indicators and allocation-based indicators. Table 1 shows the descriptions and equations of the proposed indicators for the water use in energy production (water for energy). Similar type of indicators are used for the other intersectoral relationships between WEF resources, i.e., water for food; energy for water; energy for energy; energy for food; food for energy and food for food.

2.2 WEF nexus simulation

Three types of scenarios analysis could be performed using the Q-Nexus Model: i) the first type consists of analysing scenarios related to variation of end use demands or reducing end use losses; ii) the second type of simulation consists of analysing policy options and scenarios of adopting efficient intersectoral use technologies by considering "Best Practice" and "High Efficient" WEF production technological alternatives; and iii) thirdly the model permits to simulate different WEF

intersectoral allocation policies and evaluate the performance of the WEF nexus system. These three types of scenarios analysis will be presented in sequence:

i) Variation of end use demand: the developed model allows to simulate scenarios of change of end use demand and computing resulting change in intersectoral quantities. If the superscript "new" is used to represent the values of variables after the change in demand, assuming that technology of the WEF production (as represented in A matrix), do not change, the required total outputs (x^{new}) caused by new end use quantities (y^{new}) are then found (equation 9):

$$x^{new} = (I\text{-}A)^{-1} y^{new} \tag{10}$$

A detailed application of the variation of end use demand to evaluate the WEF nexus in Lebanon is presented in Karnib (2017a).

Table 1. WEF nexus water for energy indicators of the Q-Nexus Model

	Description	Equation
Quantity-based indicators	Water use in the production of the jth energy inflow	$z_j^{w\_e} = \sum_{i=1}^{n} z_{ij}^{w\_e}$
	Water use in the energy production	$z^{w\_e} = \sum_{j=1}^{m}\sum_{i=1}^{n} z_{ij}^{w\_e}$
Intensity-based indicators	Intensity of water use in the production of the jth energy inflow	$t_j^{w\_e} = \frac{z_j^{w\_e}}{x_j^{e}}$
	Intensity of water use in energy production	$s^{w\_e} = \frac{z^{w\_e}}{x^{e}}$
Allocation-based indicators	Proportion of water usage in the jth energy inflow to the total water use in energy	$d_j^{w\_e} = \frac{z_j^{w\_e}}{z^{w\_e}}$
	Proportion of water use in energy to the total water use	$g^{w\_e} = \frac{z^{w\_e}}{x^{w}}$

ii) Scenarios of adopting efficient intersectoral use technologies: the Q-Nexus Model allows analysing policy options of adopting high efficient or "Best Practice" technologies. "Best Practice" technology matrix alternatives could be proposed which reflect the WEF intersectoral use that are technologically most advanced at present. To illustrate this simulation innovation of the Q-Nexus Model, the following WEF intersectoral use intensities (t) intersectoral allocation coefficients (c) are introduced (Karnib, 2017b):

$$t_j^{w\_e} = \frac{z_j^{w\_e}}{x_j^{e}} \tag{11}$$

$$t_j^{w\_f} = \frac{z_j^{w\_f}}{x_j^{f}} \tag{12}$$

$$t_j^{e\_w} = \frac{z_j^{e\_w}}{x_j^{w}} \tag{13}$$

$$t_j^{e\_e} = \frac{z_j^{e\_e}}{x_j^{e}} \tag{14}$$

$$t_j^{e\_f} = \frac{z_j^{e\_f}}{x_j^{f}} \tag{15}$$

$$t_j^{f\_e} = \frac{z_j^{f\_e}}{x_j^e} \tag{16}$$

$$t_j^{f\_f} = \frac{z_j^{f\_f}}{x_j^f} \tag{17}$$

$$c_{ij}^{w\_e} = \frac{z_{ij}^{w\_e}}{z_j^{w\_e}} \tag{18}$$

$$c_{ij}^{w\_f} = \frac{z_{ij}^{w\_f}}{z_j^{w\_f}} \tag{19}$$

$$c_{ij}^{e\_w} = \frac{z_{ij}^{e\_w}}{z_j^{e\_w}} \tag{20}$$

$$c_{ij}^{e\_e} = \frac{z_{ij}^{e\_e}}{z_j^{e\_e}} \tag{21}$$

$$c_{ij}^{e\_f} = \frac{z_{ij}^{e\_f}}{z_j^{e\_f}} \tag{22}$$

$$c_{ij}^{f\_e} = \frac{z_{ij}^{f\_e}}{z_j^{f\_e}} \tag{23}$$

$$c_{ij}^{f\_f} = \frac{z_{ij}^{f\_f}}{z_j^{f\_f}} \tag{24}$$

The technology matrix A was demonstrated in Karnib (2017b) as function of t and c as follows:

$$A = \begin{bmatrix} 0 & C^{w\_e}\widehat{t^{w\_e}} & C^{w\_f}\widehat{t^{w\_f}} \\ C^{e\_w}\widehat{t^{e\_w}} & C^{e\_e}\widehat{t^{e\_e}} & C^{e\_f}\widehat{t^{e\_f}} \\ 0 & C^{f\_e}\widehat{t^{f\_e}} & C^{f\_f}\widehat{t^{f\_f}} \end{bmatrix} \tag{25}$$

where $(\hat{t})$ is the diagonal matrix with the elements of the (t) along the main diagonal.

A comprehensive application of the variation of intersectoral use technologies for the WEF nexus in Lebanon is presented in Karnib (2017b).

iii) Scenarios proposed based on change of WEF intersectoral allocation policies: In quantitative-based WEF nexus systems, several water and energy inflows are used in the production of the water, energy and food resources. For example, the total water use in the electricity and food production can be originated from different water sources (i.e. surface water, groundwater, desalination …). Moreover, the energy use to produce water differ according the type of water source, for example, the energy used to abstract surface water is usually less than the energy used to abstract groundwater or desalination. The Q-Nexus Model allows to consider finding the best water and energy allocations in WEF sectors that optimize the performance of the WEF nexus system by minimizing the total cost of resources required to produce additional food quantities. A detailed numerical experiment of analysing WEF intersectoral allocation policies could be found in Karnib (2017c).

Based on the three types of scenarios analysis mentioned above, Table 2 presents examples of WEF nexus policy options, potential related drivers and the corresponding input variables of the Q-Nexus Model.

Table 2. Examples of WEF nexus policy options, potential related drivers and the corresponding input variables of the Q-Nexus Model

Scenarios	Potential related drivers	Q-Nexus Model input variables		
		y	*t*	*c*
Increasing water demand	Population Growth, Urbanization	_		
Increasing energy demand	Population Growth, Urbanization	_		
Increasing food demand	Population Growth, Urbanization	_		
Reduction of cultivated lands	Urbanization	_		
Reducing Irrigated agriculture due to water scarcity	Climate Change (Precipitation)	_		
Increasing water recycling and reuse	Governance	_		_
Changing water allocation	Governance			_
Increasing use efficiency	Technology Change		_	
Change in cropping type/pattern	Governance, Climate Change	_	_	
Replacement of gravity irrigation with pressurized irrigation system	Governance, Technology Change		_	
Upgrade agricultural technologies	Governance, Technology Change		_	
Promote renewable and clean energy sources	Governance, Technology Change	_	_	_
Change in food crop productivity	Governance, Technology Change	_	_	
Technology change in energy production	Governance, Technology Change	_	_	_
Resources allocation policies	Governance			_
Reduce losses and wastes	Governance, Technology Change	_	_	

_: Applicable

3. THE DIRECT AND INDIRECT EFFECTS

The WEF nexus interactions are dynamic and they directly and indirectly affect one another and the term nexus is used to describe these interactions. The nexus quantitative assessment models can help in mitigating interactions effects and in identifying trade-offs. The key property that should categorize any WEF nexus quantitative model is its ability to calculate the direct and indirect intersectoral quantities emerging from projected change of the WEF nexus components. This property must be considered as a basic condition to distinguish between nexus systems and any other resources integrated system.

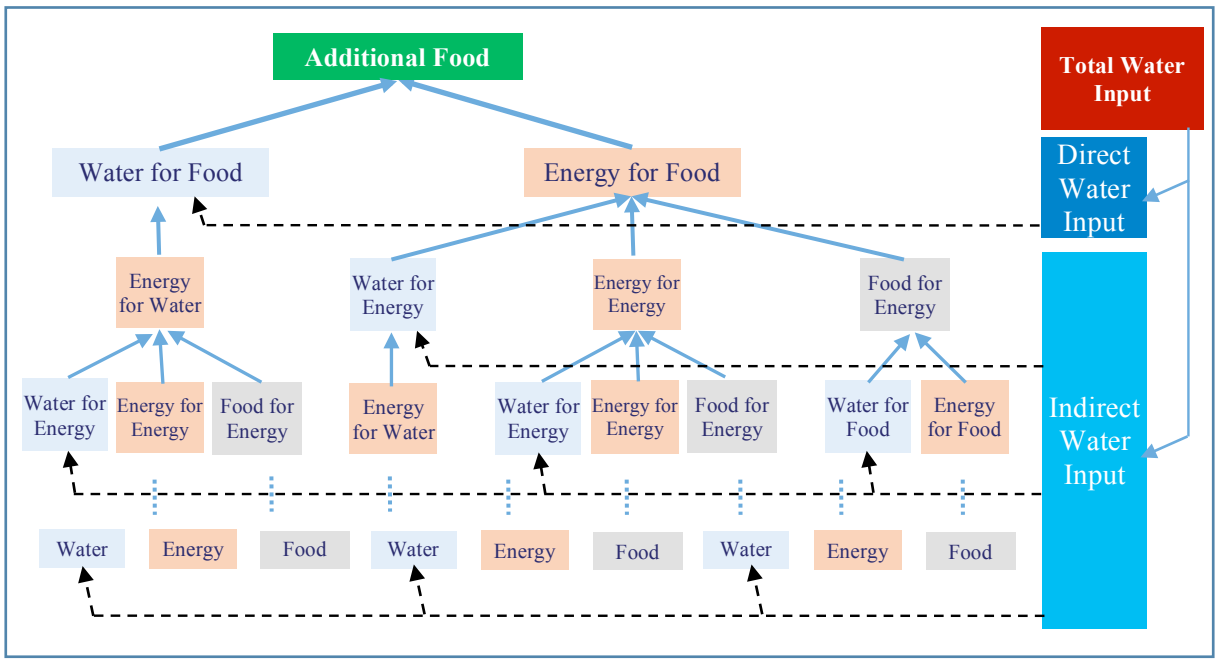

Figure 1. Direct and indirect water inputs for additional food demand

To better highlight the direct and indirect WEF interaction effects, Figure 1 shows an example of

the total water input (the sum of the direct and all indirect water inputs) required for new additional food demand.

As shown in Figure 1, the effect of new additional demand for food generates within the nexus a need for inputs from water and energy resources, this is the direct impacts. But these water and energy outputs themselves generate once again a need for additional resources, these are the first measures of the indirect impacts; and so forth.

The WEF quantitative nexus approaches derive their significance largely from the fact that outputs are quantifying the combined effects of the direct and indirect repercussions due to change in WEF production technology and/or change in end use demand.

Assuming that WEF technology is unchanged, the Q-Nexus Model allows to deal with changes in end use demands (Δy) and the resulting total (direct and indirect) changes in intersectoral quantities (ΔZ) and in total resources quantities (Δx) by using the following equations (Karnib, 2017a):

$$\Delta x = (I - A)^{-1}\Delta y \tag{26}$$

$$\Delta Z = A\widehat{(I - A)^{-1}}\Delta y \tag{27}$$

where $\widehat{(I - A)^{-1}}\Delta y$ is the diagonal matrix with the elements of the $(I - A)^{-1}\Delta y$ along the main diagonal.

The direct repercussions in intersectoral quantities (ΔZ_{direct}) resulted from change in WEF end use demand as revealed in Figure 1 above could be expressed as follows:

$$\Delta Z_{direct} = A\widehat{\Delta y} \tag{28}$$

The total changes in intersectoral quantities are the combined effects of the direct and indirect changes, which means:

$$\Delta Z = \Delta Z_{direct} + \Delta Z_{indirect} \tag{29}$$

and

$$\Delta Z_{indirect} = \Delta Z - \Delta Z_{direct} \tag{30}$$

Then by introducing equations 27 and 28 into equation 30, the indirect repercussions in intersectoral quantities could be expressed as follows:

$$\Delta Z_{indirect} = A(\widehat{\Delta x - \Delta y}) \tag{31}$$

Based on the concept of the quantitative balance of the WEF total quantities, we can write:

$$\Delta Z u = \Delta x - \Delta y \tag{32}$$

where u is a unit column vector, whose elements are 1 used to generate row sums of the matrix ΔZ.

Then equation (31) becomes:

$$\Delta Z_{indirect} = A\widehat{\Delta Z u} \tag{33}$$

where $\widehat{\Delta Z u}$ is the diagonal matrix with the elements of the $\Delta Z u$ along the main diagonal.

Evidently, the accurate analysis of WEF nexus systems necessitates evaluating the direct and indirect quantitative effects.

4. ILLUSTRATIVE EXAMPLE AND ANALYSIS OF RESULTS

A hypothetical case study of a WEF nexus system will be presented to illustrate the Q-Nexus Model features that capture the entire series of direct and indirect effects to overcome the limitations in many current WEF nexus systems. Consider a WEF nexus system where the following inflows are considered:

Water inflows (Mm^3/year): 1) surface water (*W1*); 2) groundwater (*W2*); 3) desalination (*W3*); 4) wastewater reuse (*W4*); 5) recycled water and agricultural drainage water reuse (*W5*). The values of energy use in these water inflows including extraction, treatment, conveyance and distribution.

Energy inflows (ktoe/year): 1) petroleum (*E1*); 2) electricity (petroleum) (*E2*); 3) electricity (hydro) (*E3*); 4) electricity (wind/solar) (*E4*); 5) biofuels (*E5*). These inflows are evaluated in terms of primary energy equivalent on a net calorific value basis.

Food inflows (kt/year): 1) irrigated cereals (*F1*); 2) irrigated roots and tubers (*F2*); 3) irrigated vegetables (*F3*); 4) irrigated fruits (*F4*); 5) Other Agriculture, Forestry and Food products (*F5*). These inflows are evaluated by including agriculture, food processing, transportation and storage.

Table 3 presents the WEF intersectoral use values ($z_{ij}^{w\_e}$, $z_{ij}^{w\_f}$, $z_{ij}^{e\_w}$, $z_{ij}^{e\_e}$, $z_{ij}^{e\_f}$, $z_{ij}^{f\_e}$, $z_{ij}^{f\_f}$) and the corresponding end use values (y_i^w , y_i^e , y_i^f). These values represent the Business As Usual (BAU) scenario.

Table 3. Intersectoral use of WEF inflows and the corresponding end use

	W1	***W2***	***W3***	***W4***	***W5***	***E1***	***E2***	***E3***	***E4***	***E5***	***F1***	***F2***	***F3***	***F4***	***F5***	**End Use**
W1	0.0	0.0	0.0	0.0	0.0	40.0	110.0	20.0	0.5	1.0	120.0	110.0	100.0	180.0	300.0	64.0
W2	0.0	0.0	0.0	0.0	0.0	20.0	30.0	0.0	0.5	1.0	65.0	55.0	60.0	90.0	150.0	320.0
W3	0.0	0.0	0.0	0.0	0.0	0.0	0.0	0.0	0.0	0.0	0.0	0.0	0.0	0.0	0.0	30.0
W4	0.0	0.0	0.0	0.0	0.0	0.0	1.0	0.0	0.0	0.0	5.0	5.0	5.0	5.0	5.0	0.0
W5	0.0	0.0	0.0	0.0	0.0	0.0	0.0	0.0	0.0	0.0	1.0	1.0	1.0	2.0	2.0	0.0
E1	10.0	12.0	10.0	5.0	5.0	0.0	0.0	0.0	0.0	0.0	100.0	60.0	70.0	80.0	150.0	1896.0
E2	80.0	110.0	25.0	2.0	1.0	0.0	0.0	0.0	0.0	0.0	40.0	20.0	30.0	30.0	70.0	3096.0
E3	1.0	1.0	2.0	0.0	0.0	0.0	0.0	0.0	0.0	0.0	5.0	5.0	5.0	5.0	5.0	100.0
E4	1.0	2.0	1.0	1.0	1.0	0.0	0.0	0.0	0.0	0.0	0.0	0.0	0.0	0.0	2.0	5.0
E5	0.0	0.0	0.0	0.0	0.0	0.0	0.0	0.0	0.0	0.0	0.0	0.0	0.0	0.0	0.0	60.0
F1	0.0	0.0	0.0	0.0	0.0	0.0	0.0	0.0	0.0	0.0	0.0	0.0	0.0	0.0	7.0	144.0
F2	0.0	0.0	0.0	0.0	0.0	0.0	0.0	0.0	0.0	0.0	0.0	0.0	0.0	0.0	0.0	352.0
F3	0.0	0.0	0.0	0.0	0.0	0.0	0.0	0.0	0.0	0.0	0.0	0.0	0.0	0.0	2.0	854.0
F4	0.0	0.0	0.0	0.0	0.0	0.0	0.0	0.0	0.0	0.0	0.0	0.0	0.0	0.0	0.0	508.0
F5	0.0	0.0	0.0	0.0	0.0	0.0	0.0	0.0	0.0	160.0	0.0	0.0	0.0	0.0	15.0	3449.0

The total intersectoral water, energy and food use (direct and indirect) are z^w = 1486.00 Mm^3 and z^e = 947.00 ktoe, respectively.

A scenario of increase of food end use demand of 20 % will be now considered. By assuming the intersectoral intensities and allocation coefficients are unchanged, the resulting changes in intersectoral quantities (ΔZ) caused by the changes in final demand quantities (Δy) are then evaluated using the Q-Nexus Model simulator. The results could be summarised as follows:

The water for food will have to increase its direct output by ΔZ_{direct}^{w} = 246.14 Mm^3, similarly, energy for food will have to increase its direct output by ΔZ_{direct}^{e} = 131.81 ktoe, but, these new direct intersectoral water and energy quantities necessitate to produce additional indirect intersectoral quantities. Water will ultimately have to increase its direct and indirect outputs by ΔZ^w = 253.71 Mm^3, similarly, the energy, in satisfying the new food demand, will have to increase its direct and indirect outputs by ΔZ^e = 162.41 ktoe. The indirect water quantity accounts for 3 % of

the total additional intersectoral water resources while the indirect energy quantity accounts for 18.84 % of the total additional intersectoral energy resources. So, to realize the above mentioned scenario, provision for the necessary additional direct and indirect water and energy resources could be now calculated.

5. CONCLUSIONS AND FURTHER DEVELOPMENTS

Water, energy and food nexus systems are developed to model and analyze interactions across and between WEF sectors. The accurate analysis when using nexus systems necessitates the evaluation of the direct and indirect quantitative effects. The capability of the Q-Nexus Model to quantify and simulate large set of WEF nexus response options to various drivers such as population growth, urbanization, climate change, governance and technology change is introduced. In addition, the methods of evaluating direct and indirect effects are formulated. This latter Q-Nexus Model feature permits the accurate analysis of WEF nexus systems, and demonstrates how intersectoral quantities are transmitted through the WEF sectors as direct and indirect effects.

The presented approach could be ultimately extended towards a sustainable development nexus framework for enhancing resource efficiency and for analyzing and informing sustainable development policies in effective way. This particular concern is still under development at our university.

REFERENCES

Andrews-Speed, P., Bleischwitz, R., Boersma, T., Johnson, C., Kemp, G., VanDeveer, S.D., 2012. The Global Resource Nexus: The Struggles for Land, Energy, Food, Water, and Minerals. Washington D.C., USA: Transatlantic Academy.

Biggs EM et al., 2015. Sustainable development and the water-energy-food nexus: A perspective on livelihoods. Environmental Science & Policy journal, 54: 389-397.

Bizikova, L., Roy, D., Swanson, D., Venema, H. D., & McCandless, M., 2013. The Water- Energy-Food Security Nexus: Towards a Practical Planning and Decision-Support Framework for Landscape Investment and Risk Management, IISD Report. Winnipeg, Canada: International Institute for Sustainable Development (IISD). Available at: http://www.iisd.org/pdf/2013/ wef_nexus_2013.pdf. Accessed September 2016.

FAO, 2013. An innovative accounting framework for the food-energy-water Nexus, Environment and Natural Resources Management. Working Paper No. 56, Rome: Food and Agriculture Organisation of the United Nations.

FAO, 2014a. The Water-Energy-Food Nexus at FAO, Concept Note. Rome: Food and Agriculture Organisation of the United Nations.

FAO, 2014b. Walking the Nexus Talk: Assessing the Water-Energy-Food Nexus in the Context of the Sustainable Energy for All Initiative. Rome: Food and Agriculture Organisation of the United Nations.

FAO, 2014c. The Water-Energy-Food Nexus - A new approach in support of food security and sustainable agriculture. Food and Agriculture Organization of the United Nations, Rome.

Hoff, H., 2011. Understanding the Nexus. Background Paper for the Bonn 2011 Conference: The Water, Energy and Food Security Nexus. Stockholm, Sweden: Stockholm Environment Institute (SEI).

Karnib, A., 2017a. Quantitative Assessment Framework for Water, Energy and Food Nexus. Computational Water, Energy, and Environmental Engineering Journal, 6: 11-23.

Karnib, A., 2017b. Evaluation of Technology Change Effects on Quantitative Assessment of Water, Energy and Food Nexus. Journal of Geoscience and Environment Protection, 5: 1-13.

Karnib, A., 2017c. Water-Energy-Food Nexus: A Coupled Simulation and Optimization Framework. Journal of Geoscience and Environment Protection, 5: 84-98.

Miller, R. E. and Blair, P. D., 2009. Input-output analysis. Foundations and extensions. Cambridge: Cambridge University Press. Second edition.

Technical University of Denmark (DTU), 2016. The Energy-Water-Food Nexus - from local to global aspects. International Energy Report 2016, DTU Web. http://www.natlab.dtu.dk/english/energy_reports/dier_2016. Accessed January 2017.

Waskom, R., Akhbari, M., and Grigg, N., 2014. U.S. Perspective on the Water-Energy-Food Nexus. Completion Report No.116, Colorado Water Institute.

Proceedings of the 10th World Congress of EWRA 'Panta Rhei', 5-9 July 2017, Athens, Greece
© 2017 *European Water Resources Association*

Small zoned earthfill dam simplified design with 3D solid modeling techniques

D. Myronidis
School of Forestry and Natural Environment, Aristotle University of Thessaloniki,University Campus 54124, P.O. Box 268, Thessaloniki, Greece
* *e-mail: myronid@gmail.com*

Abstract: The climate of the Mediterranean basin is characterized by an irregular hydrologic regime with low rainfalls during the dry season which necessitates the irrigation of crops. Climate change is expected to exacerbate water shortages in the region, which have intensified in recent years. Thus, is it important to improve water resource management in the area by exploiting surface water resources by constructing dams in river channels. These dams will enable the storage of water that can then be used to meet water deficits. Small earthfill zoned dams are ideal for Mediterranean conditions because of their low cost and fast and relatively easy construction. The objective of this article is to illustrate how the design of small earthfill zoned dams could be further simplified by introducing three-dimensional (3D) solid modeling operations. Additionally, the material quantities necessary for earthfill zoned dam construction are easily computed using the proposed techniques. Finally, these techniques could also be used in order to simplify the design of various hydraulic structures and in different computer aided design software's too.

Key words: Small zoned earthfill dam, computer aided design, 3D solid modeling, construction materials, AutoCAD

1. INTRODUCTION

Since the dawn of civilization, humankind has exerted control over water resources for its benefit through the construction of small dams. There is evidence that such hydraulic structures existed in India from the third century B.C. (Shaw et al., 2007), in Yemen no earlier than the beginning of the Christian era and no later than the end of the 3rd century (Francaviglia, 2000), and as part of the Maya civilization (Barrett and Guderjan, 2006). Moreover, the ancient Greeks developed technologies to capture, store, and convey water, and to simultaneously make agricultural areas productive while protecting them from flooding. Such technologies can be traced back to the Mycenaean period (1600–1100 BC) (Koutsoyiannis and Angelakis, 2007). In recent times, about 20,000 small earth dams were built on Californian farms between 1940 and 1965. Although these dams were built primarily as stock-watering ponds, farmers have also benefited from using the reservoirs for irrigation and even recreational purposes (Brown L. 1965).

Small earth dams are easier to design and simpler to construct than concrete and masonry dams (Water for the World 1D5, 1982). The principal advantages of small earth dams include the use of local natural materials, their straightforward design procedures, and the comparatively light equipment required. The main disadvantage of small earth dams is that they can be easily damaged or destroyed by water flowing on, over or against them (Stephens, 2010). Earth dams are considered suitable for the Greek arid and semi-arid conditions, in which the majority of streams are ephemeral type. In addition, their relatively low cost compared to concrete dams, and the simplicity of their construction makes them ideal for Greece, as well as other Mediterranean countries (Ministry of Agriculture, 2006).

The purpose of this paper is to illustrate the use of 3D solid modeling operations so as to simplify the design of small (up to 5 m high) earth dams. The dam designed here is mostly based on the guidelines of Kotoulas (1989 in conjunction with the computer aided design software AutoCAD 2006 for the dam's 3D design and the material quantities calculation. However, the proposed

techniques could be easily modified according to different regulations or any computer aided design software (e.g., Bricscad, Archicad, and AutoCAD Civil 3D) that facilitates the creation of complex geometric shapes by employing 3D solid modeling tools (Kirkpatrick, 1995).

2. STUDY AREA

The study area is a small agricultural catchment situated in the northern part of the Kassandra Peninsula in northern Greece within a range of approximately 68 km from Thessaloniki and encompasses about 1 km^2 (Fig. 1). It is a small tributary, which is located on a flat terrain that dominates the northern part of the Peninsula. Daily precipitation and temperature data covering the period 1974–2006, obtained from the nearby weather station (Fig. 1), demonstrated the fact that the mean annual precipitation and temperature were nearly 600 mm and 16.5°C, respectively (Myronidis, 2016). Geologically, the whole catchment is a homogenous area exclusively occupied by marls. The peninsula has a history of repeated wildland fires, with the most recent occurring on 21st August 2006, which burnt 22% of the Peninsula (Myronidis et al., 2010).

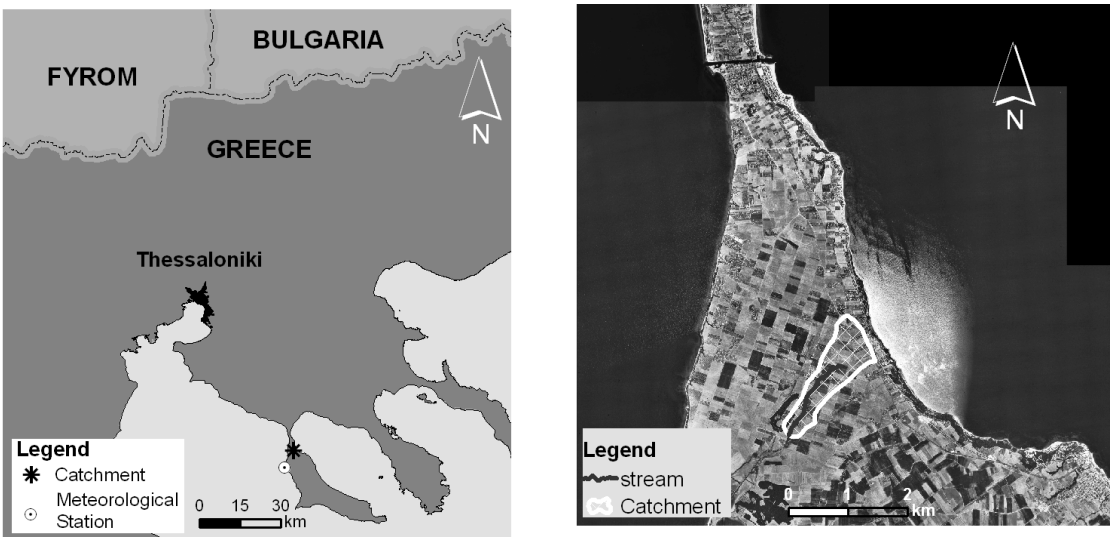

Figure 1. Maps of the study area

3. METHODOLOGY

3.1 Catchment Yield, Reservoir Storage Capacity, and Peak Discharge estimation

The annual runoff for the catchment is given by equation (1) (Tanko and Ankidawa, 2008, Stephens, 2010):

$$Y = Rr \times A \times 1000 \quad (1)$$

where Y is the catchment yield in an average year (m^3), Rr is 10% of the mean annual rainfall for the catchment area, and A is the catchment area (km^2).

Once the catchment's yield is computed, the volume of water to be stored in the reservoir could be determined. The latter is usually computed from the Digital Elevation Model (DEM) using a series of GIS techniques (Myronidis, 2017). However, when the DEM resolution is poor, the volume of water to be stored can also be estimated using equation (2) (Stephens, 2010):

$$C = H \cdot B / 3 \quad (2)$$

where C is the reservoirs storage capacity (m^3), H is the maximum depth (m), and B is the reservoir surface area (m^2).

The 50-year peak flow discharge is important for estimating the spillway dimensions. For small, poorly gauged catchments, such as many located in the Mediterranean region, the 50-year peak flow discharge can be estimated from the Rational Formula, taking into account the assumptions associated with the method and the runoff coefficient determination (Chow et al. 1998). Additionally, this method is most appropriate for catchments under 15 km^2 (Stephens, 2010) and is usually expressed by equation (3) (Chow et al., 1988):

$$Q = 0.278 \cdot C \cdot I \cdot A \tag{3}$$

where Q is the peak discharge (m^3/sec), C is a dimensionless runoff coefficient that ranges from 0 to 1, I is the intensity of rainfall (mm/h) of the return period T (years) and duration Tc, Tc is the time of concentration (hours) of the catchment, and A is the drainage area (km^2).

3.2 Front elevation view design

The height of the dam can be determined from the reservoir's storage capacity and the irrigation requirements. Equation (4) can be used to calculate the dimensions of a rectangular spillway to reduce the risks associated with an extreme rainfall event:

$$H_a = (Q_{max} / 1.9 \cdot b)^{2/3} \tag{4}$$

where H_a is the spillway height (m), Q_{max} is the 50-year peak flood discharge magnitude (m^3/sec), and b is the spillway length (m).

Once, the height and length of the rectangular spillway have been calculated it can be transformed to a trapezoid form, without altering its discharge capacity, so as to safely root the 50-year probable maximum flood over the dam.

The foundation depth in both the river bed and the banks depends on the cross section nature (rocky, earthy or mixed rocky-earthy type). The earth surface should be excavated until a more impermeable stratum is reached, which must then be backfilled (and compacted) with highly impermeable material to seal the earth dam against seepage (Stephens, 2010). Additionally, a 6-inch galvanized water pipe should be installed almost at the bottom of the earthfill dam in the case of a shallow reservoir. The use of such a waterpipe allows water to be drained from the reservoir for irrigation, watering stock, making repairs on the dam, locating leaks in the reservoir, disposing of floating debris, and removing undesirable fish or vegetative (Brown, 1965).

3.3 Cross-section design

The slopes of the dam sides depend on the stability of the material in the embankment. If the fill material is stable, the sides can be steeper than if the fill material was unstable, as suggested by Water for the World 1D5, (1982). Generally, homogeneous dams have relatively flat slopes (1:3 upstream and 1:2 downstream) as insurance against possible instability. Whereas the slopes of zoned embankments can be reduced to around 1:2 upstream and 1:1.75 downstream (or 1:2.25 upstream and 1:2 downstream) (Stephens, 2010).

The top width of the dam is calculated from equation (5) and must be a minimum of 2 m wide to ensure a stable embankment structure:

$$Dt = 1 + 1.1 \cdot (H_{Str})^{1/2} \tag{5}$$

where D_t is the top width of the dam (m), and H_{Strl} is the Dam's structural height (m).

The bottom width of the dam can be determined from Equation (6):

$$D_b = D_t + (n_u+n_d) \cdot H_{Str} \quad (6)$$

where D_b is the bottom width of the dam (m), D_t is the top width of the dam, n_u and n_d are the upstream and downstream slopes of the dam respectively, and H_{Str} is the structural height of the dam (m).

The core of this zoned dam is constructed of impermeable clay material so as to seal the embankment from seepage. The core has similar 1/6 upstream and downstream slopes and a top width equal to 1 m. The below ground section of the core is referred to as the cutoff (Kotoulas, 1989). Additionally, for the protection of the dam from wave action, the upstream above ground face of the dam must be pitched with stones, the spillway (which is continuous with the downstream face of the dam) must be concreted with 0.15 m cement, and the downstream above ground face of the dam must be seeded with grass.

3.4 Three-dimensional Earthfill Dam Design

a. Initially, the Dam's front elevation, the cross section, the core of the dam, and the stream cross-section outlines are formed individually as closed polylines. Also, in a distance equal to the height of the spillway, a parallel line to the downstream face and the spillway length must be created, which will serve as a path in order to subtract from the dam's body the spillway.

b. The closed polylines of the following elements of the dam can be extruded, so as to create 3D solids: The cylindrical water pipe is extruded with a height of extraction greater than the dam base width; the Dam's front elevation is extruded with a height of extraction equal to the dam base width; and the cross section of the dam and the core of the dam must be extruded with a height equal to the dam length. Additionally, the streams cross-section is extruded at a height equal to the dam base width. The latter extraction is only used to calculate the earth excavation volume.

c. The view of the solids must change to a 3D southwest perspective, and the cylindrical solid water pipe is subtracted from the Dam front elevation solid.

d. The dam cross section solid must be 3D rotated by -90°, and then all solids are 3D rotated again by 90°. Moreover, the stream cross-section solid must move in another layer.

e. The view is then changed to a southwest perspective in order to place the dam cross-section solid inside the dam front elevation solid body. These two solids are intersected together.

f. The spillway must be extruded to a 3D solid using the path line that was created in step *a*, and then should be subtracted from the downstream face of the dam. The latter produces a final the three-dimensional gravity dam representation.

3.5 Material quantities calculation

a. Since the earthfill dam is a 3D solid, its core volume can be determined with a simple inquiry.

b. The earthworks volume could be determined by subtracting the volume of the clay core from the total volume of the dam.

c. The ground excavation volume is computed by subtracting the above surface part of the dam from the dam volume.

d. The upstream face area, which must be pitched with stones, is calculated from a two-dimensional section of this face.

e. The downstream face area, which must be grassed, is computed from a two-dimensional section of this face.

f. The spillway sheathed area with cement is derived by changing the dam perspective to a top-down view and pointing on the spillway.

4. RESULTS AND DISCUSSION

4.1 Catchment Yield, Reservoir Storage Capacity, and Peak Discharge estimation

The catchments yield is an important factor in assessing the feasibility of a dam and in determining the required height of the embankment (Stephens, 2010). The catchment's yield was computed from Equation (1) as equal to 60,000 m^3. Moreover, at the outlet of the tributary, there is an appropriate cross section for the construction of an earth dam. This cross section is situated in a relative impervious terrain with steep riverbanks, 4/1 slope and 3/2 slopes for the left and the right bank respectively, while the length of the riverbed was 26 m. In this site, a zoned earthfill dam with 2.5 m maximum depth would flood 5,272 m^2 area and would enable, from Equation (2), the storage of almost 4,400 m^3 of water, which is considered sufficient for small-scale irrigation and for the extinction of wildland fires.

From the intensity–duration–frequency curves of the nearby meteorological station (Myronidis et al., 2016), the maximum average intensity for the rainfall duration interval equal to the concentration time, about 39 min as computed based on Kiprich formula (Chow 1988), was found approximately 64.21 mm/hr. The runoff coefficient for the flat cultivated land was 0.43 (Chow 1988) and the peak discharge with a 50-year return period was estimated as 8.17m^3/sec using Equation (3).

4.2 Front elevation view design

The maximum depth of the embankment from the previous section was set to 2.5 m, which results in a water storage capacity of nearly 4,400 m^3. To prevent water spilling over the top of the earth dam, a spillway length and Q_{50} peak discharge equal to 12 m and 8.17 m^3/sec respectively were calculated using Equation (4), and the height of the spillway was computed equal to 0.5 m. Once the rectangular spillway dimensions were determined, it was transformed into a trapezoid form (Fig. 2). Moreover, since the earthfill dam is situated in a relatively impervious terrain, the foundation depth in both the riverbed and the banks was set to 1.0 m, while a 6-inch cylindrical waterpipe was installed in the dam's body at the bottom of the earthfill dam. Finally, the front elevation view of the about 30 m length earthfill dam with a structural height of 4 m is shaped, as shown in Figure 2.

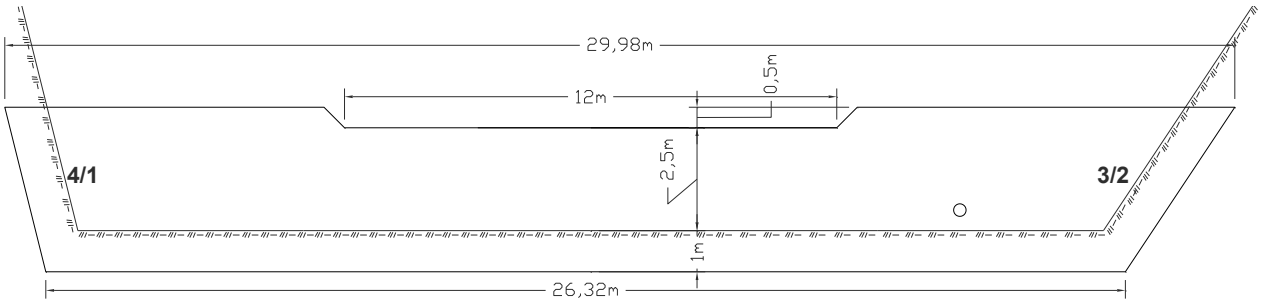

Figure 2. Earthfill dam front elevation view.

4.3 Cross-section design

Zoned embankments have the advantage that they generally control seepage much more efficient than homogeneous earthfill dams and have steeper slopes, which suggest that they require fewer earthworks in their construction. However, the decision of the type of the earthfill dam must also consider the availability of construction material, since otherwise, the cost of the dam will be

uneconomic, due to the high costs associated with transporting material to the site.

For a structural dam height of 4.0 m from Equation (5), the top width of the dam was calculated as 3.20 m, which is wider that the required 2.0 m minimum. The upstream and downstream slopes were set equal to 1:2.5 and 1:2.0 respectively, while the bottom width of the dam from Equation (6) was approximately 21.20 m. The results of all these actions are illustrated in Figure 3.

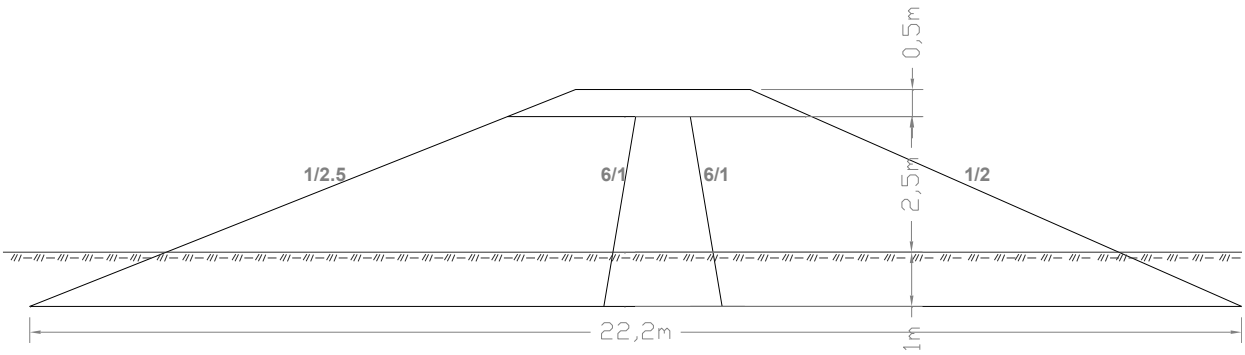

Figure 3. Earthfill dam cross-section.

4.4 Three-dimensional Earthfill Dam Design

a. The formation of the dam's front elevation, the cross section, the core of the dam, and the stream cross-section outlines from the individual closed polylines is achieved using the command *Polyline/join* from the *Modify/Object* menu, while a 0.5 m parallel line to the downstream face and the spillway length, equal to the spillway depth, is created using the *offset* command.

b. The command *extrude* is selected from the *Draw/Solids* menu in order to extrude: the cylindrical waterpipe with a height of extraction of 35.0 m and the dam's front elevation with an extraction height equal to 22.2 m. The cross section of the dam and the core of the dam were extruded by 26.3 m. Additionally, the stream cross section it is extruded to a height of 22.2 m.

c. The command *SW isometric* is selected from the *View/3D Views* menu so as to have a southwest isometric perspective of the solids. Then, the command *subtract* is selected from the *Modify/Solids editing* menu, and the cylindrical solid water pipe is subtracted from the dam front elevation solid by choosing first the dam front elevation solid and then the water pipe.

d. The employment of the *Rotate 3D* command from the *Modify/3D operations* menu provides the rotation of the dam cross section solid. This is achieved by: i) choosing the dam cross section; ii) defining two points on the upstream face of the solid as orientation axis; iii) setting the rotation angle equal to -90°. Moreover, the same command is used to select and rotate all solids by 90° by defining two points on the length of the dam as orientation axis. Furthermore, the stream cross-section solid is moved to another layer, and this layer is turned off.

e. The objects view is changed again to *SW isometric,* and then the command *move* is selected in order to move the dam cross-section solid inside to the dam front elevation solid, using as origin the upper right corner of the dam cross-section solid and as destination the upper right corner of the dam front elevation solid. Then, the command *intersect* is selected from the *Modify/Solids editing* menu, and the three-dimensional gravity dam representation is almost completed by pointing on the two solids, the dam front elevation, and the dam cross-section.

f. The spillway was *extruded* to a 3D solid using the path line that was created in step *a*. This solid is then subtracted from the dam's body by utilizing the *subtract* command from the *Modify/Solids editing.* The final three-dimensional illustration of the dam is shown in Figure 4.

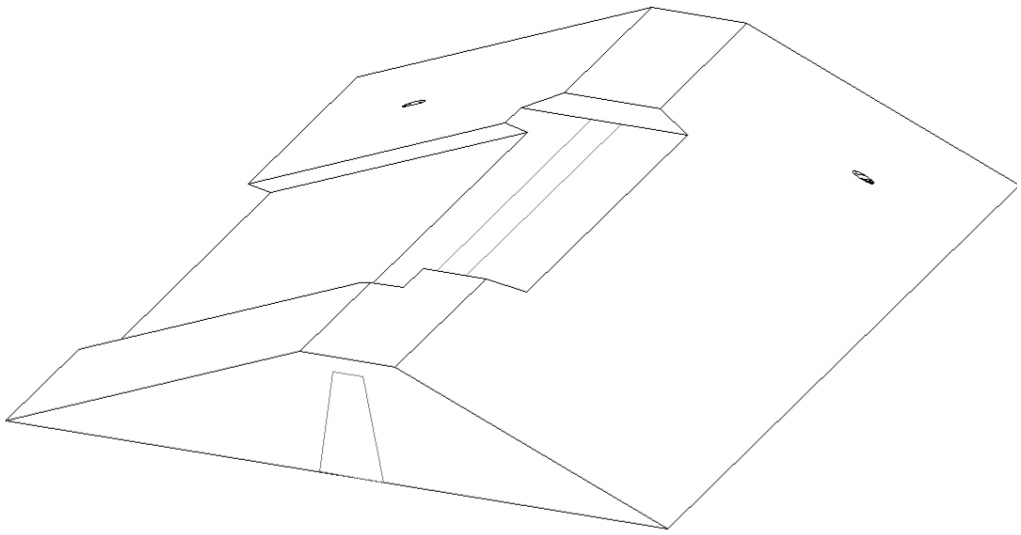

Figure 4. The southwest isometric view of the 4.0 m zoned earth-filled gravity dam.

4.5 Material quantities calculation

a. The earthfill clay core volume was calculated as 145.85 m^3 by selecting the command *region/mass properties* from the *Tools/inquiry* menu and by pointing on the dam.

b. By employing the same command as previous, the necessary earthworks for the construction of the dam are equal to the total dam volume (1,268.72 m^3) minus the clay core volume (145.85 m^3), which is 1,122.87 m^3.

c. The ground excavation volume is equal to 529.35 m^3 and is derived from the subtraction of the above surface part of the dam (739.37m^3) from the dam volume solid (1,268.72 m^3) by utilizing the command *subtract* from the *Modify/Solids* editing menu.

d. The upstream face area, which must be pitched with stones, is computed by i) changing the view to *SW isometric view*; ii) selecting the command *section* from the *Draw/Solids* menu; and iii) pointing three points in the upstream face so as to create a *section* of the dam's front elevation. Using the command *Area* from the *Tools/inquiry* menu, the area of this section is computed and found equal to 175.31 m^2.

e. The downstream face area, which must be grassed, is estimated using the same methods as in the previous step d) and is equal to 104.3 m^2.

f. The spillway-sheathed area with cement is equal to 179.88 m^3 and is estimated by first changing the solid perspective to *top view* and employing the command *Area* from the *Tools/inquiry* menu.

5. CONCLUSIONS

The simplified design and construction of small earth dams is necessary to enhance surface water development in rural communities (Tanko and Ankidawa, 2008). In this article initially the catchment yield, the reservoir storage capacity and the discharge are estimated for a small agricultural catchment. Then, the simplified design for an earthfill zoned dam (structural height of 4 m, length of 30 m) is illustrated using a series of innovating 3D solid modeling operations in AutoCAD 2006. For the aforementioned dam, the volume of its earthfill core, the total volume, the ground excavation volume, the upstream stone-pitched area, the downstream grassed area, and the cement-sheathed spillway area were computed quickly and accurately following the proposed methodology.

REFERENCES

Barrett, J.W., Guderjan, T.H (2006) An ancient Maya dock and dam at Blue Creek, Rio Hondo, Belize, Latin American Antiquity, 17(2): 227-239.

Brown L. (1965) Small Earth Dams. University of California, Circular 467: 1-24

Chow, V. T., Maidment, D. R., and Mays, L.W. (1988) Applied hydrology, McGraw-Hill, Singapore.

Francaviglia V.M. (2000) Dating the ancient dam of Mārib (Yemen), Journal of Archaeological Science, 27(7): 645-653.

Kirkpatrick, J. (1995) Engineering Drawings and Models Using Autocad Solid Modeling and Designer, 1–466, Prentice Hall College, New Jersey, USA.

Kotoulas D. (1989) The Small Dams, Published by the Geotechnical Chamber of Greece, 1-601 (In Greek).

Koutsoyiannis D., Angelakis A. N. (2007) Agricultural hydraulic works in ancient Greece, Encyclopedia of Water Science, Second Edition, edited by S. W. Trimble, 24–27, doi:10.13140/RG.2.1.2582.8084, CRC Press.

Ministry of Agriculture (2006) The Dams and the reservoirs of the Ministry of Agriculture, 1-105p (in Greek).

Myronidis D. (2017) Derivation of reservoir area-capacity curve and delimitation of the reservoir's conduit min elevation, Hydrotechnika, under publishing (in Greek).

Myronidis D., Emmanouloudis D., Mitsopoulos I., Riggos E. (2010) Soil erosion potential after fire and rehabilitation treatments in Greece, Environmental Modelling and Assessment, 15(4): 239-250.

Myronidis D., Stathis D., Sapountzis M. (2016) Post-Evaluation of Flood Hazards Induced by Former Artificial Interventions along a Coastal Mediterranean Settlement, Journal of Hydrologic Engineering, DOI: 10.1061/(ASCE)HE.1943-5584.0001413.

Shaw, J, Sutcliffe, J, Lloyd-Smith, L, Schwenniger, J.-L, Chauhan, M.S., Misra, O.P., Harvey, E. (2007) Ancient irrigation and Buddhist history in central India: Optically stimulated luminescence dates and pollen sequences from the Sanchi dams, Asian Perspectives, 46(1): 166-201.

Stephens T. (2010) Manual on small earth dams - A guide to siting, design and construction, FAO irrigation and drainage paper 64: 1-124.

Tanko A., Ankidawa B. (2008) Design and construction methods for small earth dams for small scale irrigation in developing countries, Global Jour, of Engg. & Tech, 1(4): 435-439.

Water for the World (1982) Designing Small Dams. Technical Note No. RWS. IC5, 1-7.

Proceedings of the 10th World Congress of EWRA 'Panta Rhei', 5-9 July 2017, Athens, Greece
© 2017 *European Water Resources Association*

Different design techniques in determining reservoir capacity

H. Alrayess[1], U. Zeybekoglu[2] and A. Ulke[1]
[1] *Department of Civil Engineering, Faculty of Engineering, Ondokuz Mayis University, Samsun,Turkey*
[2]*Department of Civil Engineering, Faculty of Engineering, Pamukkale University, Denizli, Turkey*
[*] *e-mail: hesham.majed@hotmail.com*

Abstract: Reservoirs are designed to provide the balance between the flow brought by the river which is high variable in time and volume of water required for some usage purposes of the flow. The storage required on a river to meet a specific demand depends basically on three factors; the magnitude and the variability of the river flows, the size of the demand and the degree of reliability of this demand being met. Several procedures have been proposed to estimate storage requirements. Critical period methods are those in which required reservoir capacity is equated to the difference between the water released from an initially full reservoir and the inflows for periods of low flow. In the presented study reservoir capacity-yield-reliability relationships are investigated for a single reservoir named Sami Soydam Sandalcık Dam. For this purpose, monthly and annual mean flow data observed for a period between 1962-2013, of EIE-811 Suçatı Flow Gauging Station on Dalaman River in West Mediterranean Basin in Turkey are used as case study. The required reservoir capacity is estimated required to meet a prescribed demand for a given model of annual inflows in this study by using mass curve, Dincer, Gould's Gama, McMahon.

Key words: Reservoir capacity, low flow hydrology, critical period, Dalaman River, Sami Soydam Sandalcık Dam, Turkey

1. INTRODUCTION

Reservoirs are constructed on rivers in order to respond to the water demand during periods where inflow is less than the demand. Determination of the required capacity, i.e. the operation study, for a river reservoir is done using a data set corresponding to a period of time (Linsley & Franzini, 1979). When the sequence of flow in a month becomes important, which is the case for small reservoirs, the time interval should be reduced to a week or a day.

The flow of a planned stream, such as energy production, storage and transportation, may show an irregular change in time. This may be different from the time needed for the amount of water required for such purposes. To correct this imbalance to some extent, it is being built storage reservoirs on rivers. Also it is necessary to determine the optimum volume of the storage reservoirs to meet the needs, according to the flow rate which change continuously over the time. The periods in which the natural flow of the river is greater than the demand are called wettest period, and vice versa is called dry period (Ağıralioğlu, 2004).

The critical period, defined as the scarcity according to the demand, is also of great importance in the determination of the volume of the reservoir (Aksoy, 2001; Oğuz & Bayazıt, 1991). If the reservoir is considered full at the beginning of the critical period, it will be completely empty at the end of the critical period. The accumulation volume capacity meets the requirements at the acceptable risk level (Rao, et al., 2001). The hydrological design of reservoirs is concerned with determining the storage capacity required to maintain a yield with a given probability of failure (Parks & Gustard, 1982).

In this study, monthly and annual mean flow data observed for a period between 1962-2013, of EIE-Suçatı (811) flow gauging station on Dalaman River are used. Three probabilities of failure (0%, 5% and 10%) are considered for reservoir estimation. The percentage of draft are taken 60% and 80% for the estimation of reservoir capacity and at the end of the study a comparison is made between the results.

2. METHODS

The volume of the reservoir that can meet the need of water depends on the size and variability of the stream, the amount of need, the level of reliability in meeting the need and the mode of operation (Bayazit, 1997). McMahon & Mein (1978) have classified the large number of different design procedures into three broad groups. The first group is termed "critical period techniques" which rely on analysing those events when the yield exceeds demand. Examples are provided by the methods proposed by Ripple (1883). This pattern is a common method used in the preliminary design stage, which is a commonly used method of adding water flows (Ripple diagram) as well as additional differences, minimum flows and successive peaks. However, it is not possible to define the risk that the reservoir volume predicted in these methods carries in the need. Methods such as Dinçer, and Gould Gamma where the appropriateness of a certain distribution is predicted and the risk can be expressed are found to be widespread application areas especially when risk is wanted to be defined (Mcmahon & Mein, 1986).

2.1 Critical period techniques

The critical period (CP) is defined as the period during which a reservoir goes from a full to an empty condition without spilling in the interim (Mcmahon & Mein, 1986). The CP represents a period of extreme low flows in the data record for which storage is required in the reservoir if the shortfall between the low inflow and the water demand placed on the reservoir system is to be met (Montaseri & Adeloye, 1999).

2.1.1 Mass curve method

Ripple (1883) determined the capacity of a reservoir by the mass curve method. This method is based solely on the historical inflow record. The reservoir mass curve has many useful applications in the design of a storage capacity, such as determination of reservoir capacity, operations procedure and flood routing (Bharali, 2015).

By using the mass curve method, the reservoir capacity is calculated as the next steps: 1- For the proposed dam site, construct a mass curve of the historical stream flows (annual or monthly data can be used for this method), 2- Determine the slope of the cumulative draft line for the graphical scales, 3- Superimpose on the mass curve the cumulative draft line for the reservoir, 4- Measure the largest intercept between the mass inflow curve and the cumulative draft line (Mcmahon & Mein, 1986).

2.1.2 Residual mass curve method

McMahon and Mein (1986), defined Residual mass curve is a slightly more complicated version of the mass curve, but with a much more appropriate graphical scale for the determination of the storage size. This method used by subtracting the mean flow from each flow value of the record, the results called residual values are plotted cumulatively and the cumulative draft line is superimposed such that the draft line is tangential to each hump of the residual curve, after that measuring the largest intercept between the mass inflow curve and the draft line.

2.1.3 Minimum flow approach

In a minimum flow approach, drought curves are constructed from the lowest sub-sequences of flows of varying durations from the historical record e.g. 5, 10, 20, 40, etc. consecutive months. Then a draft line is superimposed such that it passed through the origin, and the critical storage is

estimated by a mass curve procedure (Nagy, et al., 2002). The critical storage (C_{crit}) is a given by the maximum intercept between the draft line and the drought curve (Mcmahon & Mein, 1986).

2.1.4 Dincer's method

The Dincer procedure, developed by Dincer and reported in McMahon & Mein, in 1978, is a theoretical approach based on normally distributed annual flows to estimate the mean first passage time to emptiness for a given reservoir capacity, target and draft. Equations 1 and 2 show the calculation of the capacity.

$$CP= (Z_p^2/4(1-D)^2)* C_v^2 \quad (1)$$

$$\tau = C/ \mu = ((Z_p^2/4(1-D)^2)-d)* C_v^2 \quad (2)$$

In this method, CP: length of the critical drawdown period in years, C: reservoir capacity, C_v: annual coefficient of variation, z_p: standardized normal variate at p%, D: regulation rate and $\tau\tau_1$: maximum required storage expressed as a ratio of mean annual flow, d: correction factor.

2.1.5 Gould's gamma method

This method can be described as a combination of Alexander and Dincer methods. It uses the fact that, while parameters for the normal distribution are easy to calculate and probability tables for it are readily available, the gamma distribution is usually a better approximation to the distribution of annual flow data. Gould's procedure uses the normal distribution for the calculations, and then applies a correction to approximate the gamma distribution (Mcmahon & Mein, 1986). Table 1 shows Gould's correction factor d for various z_p.

$$\tau = C/ \mu = ((Z_p^2/4(1-D))-d)* C_v^2 \quad (3)$$

$$C =\tau \times \mu \quad (4)$$

Table 1. Gould's correction factor.

Lower p percentile value	z_p	d
0.5	3.30	d not constant
2.0	2.05	1.1
4.0	1.75	0.8
5.0	1.64	0.6
7.5	1.44	0.4
10.0	1.28	0.3

2.1.6 McMahon's empirical method

McMahon (1976) took 156 Australian rivers and used Gould's modified procedure to estimate the theoretical storage capacities for four draft conditions (90%, 70%, 50%, and 30% of mean annual flow) and three probabilities of failure values 2.5%, 5% and 10%).

$$\tau = C/ \mu = a*C_v^b \quad (5)$$

Where, τ: reservoir capacity divided by mean annual flow, μ: mean annual flow and a, b: empirically derived constants tabulated in Table 2.

Table 2. Reservoir capacity yield equation coefficients for McMahon's Empirical method.

Draft %	Parameter	Probability of Failure %		
		2.5	5	10
90	a	7.50	5.07	3.08
	b	1.86	1.81	1.82
70	a	2.51	1.81	1.21
	b	1.83	1.79	1.74
50	a	0.98	0.75	0.51
	b	1.91	1.93	1.83
30	a	0.28	0.22	0.15
	b	1.53	1.49	1.79

3. CASE STUDY

The Western Mediterranean basin which is shown in Figure 1, is one of the twenty-five basins in Turkey. There are Başöz, Eşen, Dalaman, Karacay and Kargıçay streams in the basin. The precipitation area of the basin is 20.953 km^2 and average annual flow is 8.93 km^3. Basin has seven flow gauging stations on rivers mentioned (Table 3). These stations are given in the next table (EIE, 2011).

Table 3. Number and names of stations at the Western Mediterranean basin.

Number	Stream	Name
808	Başgöz Çayı	Çatallar
809	Eşen Çayı	Kavaklıdere
811	Dalaman Çayı	Suçatı
812	Dalaman Çayı	Akköprü
815	Eşen Çayı	Kınık
818	Karaçay	Kayadibi
823	Kargı Çayı	Yanıklar

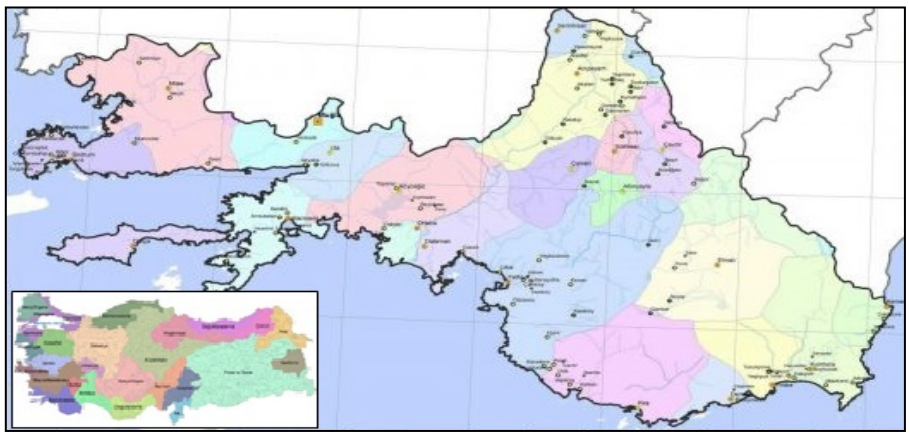

Figure 1. The study zone map at the southern west side of Turkey.

EIE-811 Suçatı Flow Gauging Station on the Dalaman stream in the western Mediterranean basin is located at (37° 05' 38'' N – 29° 06' 12'' E) coordinates and 595 m elevation. The precipitation area of the station is 3890.6 km^2. Sami Soydam Sandalcık Dam and Hepp is under construction in the downstream area of the current flow gauging station used in the study. It will be the biggest hydroelectric central of the Aegean Region. The type of soil is clay core rock fill. It's height from foundation is 115 m and its power capacity is 129 MW.

The flow values of station 1962-2013 are available. In the study, it is aimed to determine the necessary storage volume with different methods in the literature. Evaporation losses are not taken into consideration since the reservoir capacities to be obtained by different methods are intended to be compared.

4. APPLICATIONS

The preliminary design methods which used to determine the reservoir capacity at this study are critical period methods. Some critical period methods have been preferred in reservoir volume calculations as they are used more in practice. Three probabilities of failure (0%, 5% and 10%) are used for reservoir estimation. The percentage of draft didn't identified at the official reports because of that the percentage of draft at this paper were taken 60% and 80% for the estimation of reservoir capacity.

4.1 Mass curve method

At this paper the mass curve method was used for reservoir capacity estimation. The interval from 1962 to 2013 (52 years = 624 months) are used at calculations for this method to get the maximum available capacity to this reservoir as shown at Figures 2 and 3.

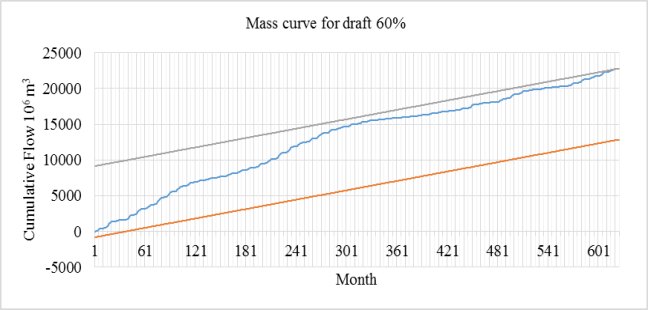

Figure 2. Reservoir capacity yield analysis by mass curve for draft equal 60%.

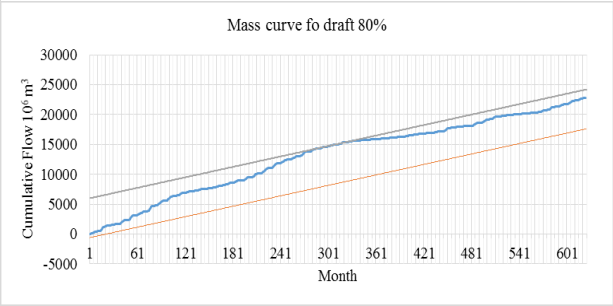

Figure 3. Reservoir capacity yield analysis by mass curve for draft equal 80%.

The monthly data is used for reservoir estimation. For draft 60%, the slope of the draft line is 21.87 x10^6 m^3/month, taken as 60% of the mean monthly flow 36.45 x10^6 m^3. The required storage was resulted 840.53 x10^6 m^3. On the other hand for draft 80%, the slope of the draft line is 29.16x10^6 m^3/month, taken as 80% of the mean monthly flow 36.45 x10^6 m^3. The required storage was resulted 2043.4 x10^6 m^3.

4.2 Residual mass curve

The reservoir storage capacity is calculated for monthly flow at the interval from 1962 to 2013. At Residual mass curve method, draft 60 and 80% were used to estimate reservoir capacity with monthly mean 36.45 x$10^6$$m^3$/month. The slope of the draft line is 21.87 x$10^6$$m^3$/month for draft 60% and for draft 80% is 29.16 x$10^6$$m^3$/month. Figure 4 and 5 show the storage capacity of a reservoir with draft 60% and draft 80%.

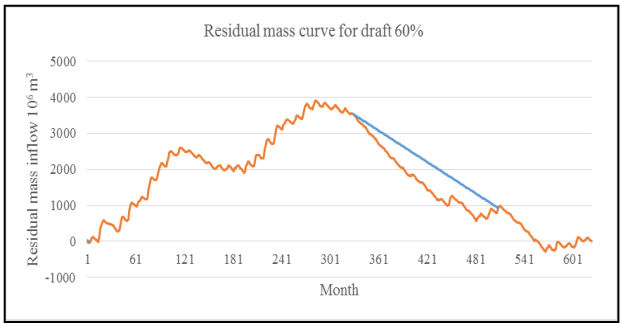

Figure 4. Residual mass curve method for determining the storage capacity of a reservoir with draft 60%.

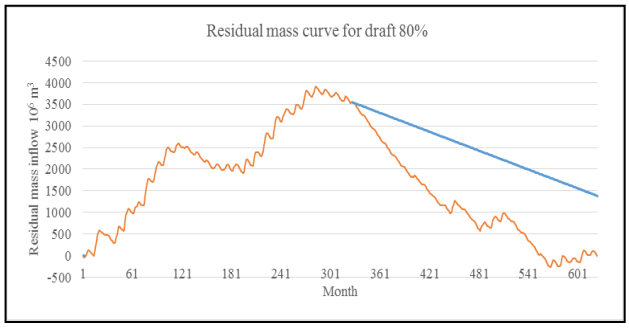

Figure 5. Residual mass curve method for determining the storage capacity of a reservoir with draft 80%.

The monthly data (624 months) is used for reservoir estimation. For draft 60%, the required storage was resulted 858.23 x10^6 m^3. On the other hand for draft 80%, the required storage was resulted 2071.92 x10^6 m^3.

4.3 Minimum flow approach

The reservoir storage capacity is calculated for monthly variation flow for 624 months with draft 60% and 80%, for 60% draft the mean was resulted 13646.9 x10^6 m^3/month and for 80% draft the mean was resulted 18195.872 x10^6 m^3/month. Reservoir capacity in draft 60% was resulted 814.22 x10^6 m^3 but for draft 80% was resulted 2145.74 x10^6 m^3 as shown in Table 4. Figure 6 shows both of the results for 60% draft and 80% draft.

Table 4. Minimum flow estimation table.

Duration (months)	Lowest Total Flow (10^6 m^3)	Draft 60% (10^6 m^3)	Reservoir Capacity (10^6 m^3)	Draft 80% (10^6 m^3)	Reservoir Capacity (10^6 m^3)
5	11.42	109.35	97.93	145.8	134.38
10	75.7	218.7	143	291.6	215.9
20	179.83	437.4	257.57	583.2	403.37
60	709.55	1312.2	602.65	1749.6	1040.05
80	1047.56	1749.6	702.04	2332.8	1285.24
110	1591.48	2405.7	**814.22**	3207.61	1616.13
120	1821.71	2624.4	802.69	3499.21	1677.5
140	2336.5	3061.8	725.3	4082.41	1745.91
200	3997.83	4374	376.17	5832.01	1834.18
260	5435.87	5686.2	250.33	7581.61	**2145.74**

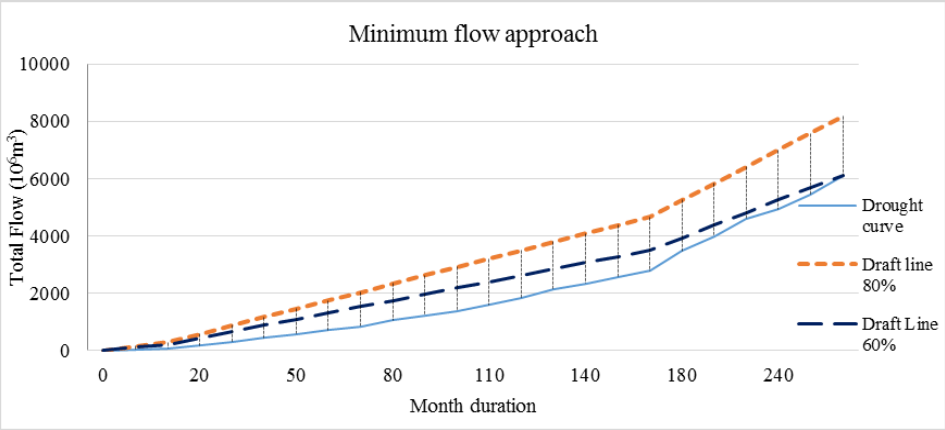

Figure 6. Minimum flow approach for determining the storage capacity of a reservoir with various drafts.

4.4 Dincer's method

Reservoir capacity was estimated for drafts 60% and 80% and probability of failure 5% and 10%. This capacity has to be adjusted to compensate for the annual auto correlation is obtained from appendix A (Fig. A-3) McMahon and Mein (1986), this capacity is represented at Table C_{adjust}.

Table 5. Storage capacity required by Dincer's method.

Draft	Probability of failure %	Z_p	d	C (10^6 m^3)	CP (yrs)	C adjust (10^6 m^3)
60%	5	1.64	0.6	218.39	1.2	633.32
	10	1.28	0.3	133.03	0.8	312.63
80%	5	1.64	0.6	436.78	5	1528.72
	10	1.28	0.3	266.07	3	824.81

According to the results at Table 5, the reservoir capacity for draft 60% probability of failure 5% was resulted 633.32 x10^6 m^3 and for probability of failure 10% was resulted 312.63 x10^6 m^3. On the other hand, for draft 80% probability of failure 5% was resulted 1528.72 x10^6 m^3 and for probability of failure 10% was resulted 824.81 x10^6 m^3.

4.5 Gould's gamma method

The results obtained with Gould's Gamma Method for the annual flow data of the stationary station are presented in Table 6.

Table 6. Storage capacity required by Gould's Gamma method.

Draft	Probability of failure %	Z_p	d	τ	C (10^6 m^3)	C adjust (10^6 m^3)
60%	5	1.64	0.6	0.321	140.44	323.01
	10	1.28	0.3	0.215	94.06	197.52
80%	5	1.64	0.6	0.8234	358.83	1220
	10	1.28	0.3	0.5192	227.09	635.86

The reservoir capacity for draft 60% probability of failure 5% was resulted 323.01 x10^6 m^3 and for probability of failure 10% was resulted 197.52 x10^6 m^3. On the other hand, for draft 80% probability of failure 5% was resulted 1220 x10^6 m^3 and for probability of failure 10% was resulted 635.86 x10^6 m^3.

4.6 McMahan's empirical method

Using the McMahon Method and annual flow data, the calculated values for reservoir capacity are presented in Table 7. This capacity has to be adjusted to compensate for the annual auto correlation is obtained from appendix A (Fig. A-5) McMahon and Mein (1986), this capacity is represented at table C_{adjust}.

Table 7. Storage capacity required by McMahon's method and probabilities of failure 5% and 10%.

Draft %	Probability of failure %	aC_v^b	C (10^6 m^3)	Probability of failure %	aC_v^b	C (10^6 m^3)
90	5	1.69	739.20	10	1.02	446.35
70		0.61	267.12		0.42	184.07
50		0.23	101.67		0.17	73.46
30		0.09	38.95		0.05	22.14

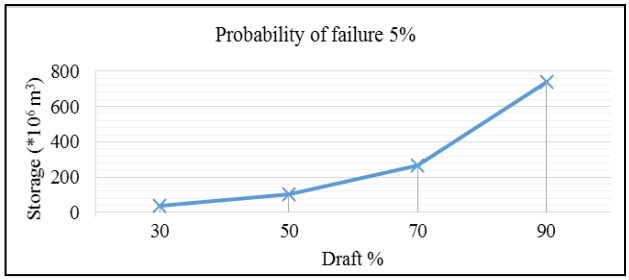

Figure 7. Interpolation on log-linear plot for McMahon's method with Probability of failure 5%.

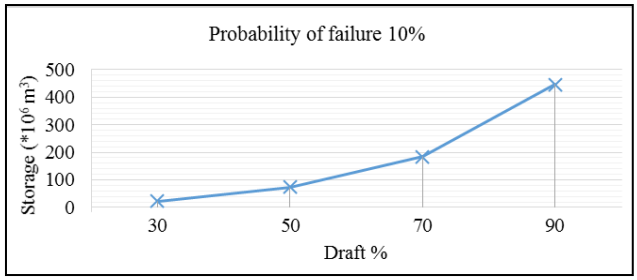

Figure 8. Interpolation on log-linear plot for McMahon's method with Probability of failure 10%.

The reservoir capacity for draft 60% probability of failure 5% was resulted 424.1 x10^6 m^3 and for probability of failure 10% was resulted 270.4 x10^6 m^3. On the other hand, for draft 80% probability of failure 5% was resulted 1459.16 x10^6 m^3 and for probability of failure 10% was resulted 819.54 x10^6 m^3.

Table 8. Storage capacity adjusted by McMahon's Empirical method.

Draft %	Probability of failure %	C (10^6 m^3)	C adjust (10^6 m^3)
60	5	184.395	424.1
	10	128.765	270.4
80	5	503.16	1459.16
	10	315.21	819.54

The final results by using Different Methods for EIE-811 Suçatı Flow Gauging Station data are represented at Table 9, which shows that the probabilities of failure and draft percentages which used at calculation procedures.

Table 9. Reservoir Volume by Different Methods for EIE-811 Suçatı Flow Gauging Station.

Method	Probability of failure	Storage estimate (10^6)	
		Draft 60%	Draft 80%
Mass Curve	0%	840.53	2043.4
Residual Mass Curve		858.23	2071.92
Minimum flow approach		814.22	2145.74
Dincer's method		633.32	1528.72
Gould's method	5%	323.01	1220
McMahan's method		424.1	1459.16
Dincer's method		312.63	824.81
Gould's method	10%	197.52	635.86
McMahan's method		270.4	819.54

5. CONCLUSION

The effect of the method selection on the reservoir volume to be determined is clearly visible, from Table 9, which shows the reservoir volumes obtained for different methods. As a result of the evaluation of the applied methods it is possible to make the following comments:

- There is no relationship between storage volume and risk in critical period approaches such as minimum flow method, which changes the volume of the reservoir over time. Large volumes are usually estimated by these methods.
- Six design techniques (Mass Curve, Residual Mass Curve, Dincer's method, Gould's method, McMahan's method and Minimum flow approach) are used in determining reservoir capacity, monthly and annual mean flow data observed for a period between 1962-2013, of EIE-811 Suçatı Flow Gauging Station on Dalaman River in West Mediterranean Basin in Turkey are used as case study.
- Three probabilities of failure (0%, 5% and 10%) and two percentage drafts (60% and 80%) are used for reservoir estimation. For 5% and 10% probability of failure three methods (Dincer's method, Gould's method and McMahan's method) are used to discover the range of difference between the two probabilities of failure. For 0% probability of failure the highest reservoir capacity was resulted for methods Mass Curve, Residual Mass Curve and Minimum flow approach at the range between 814.22 to 852.74 $*10^6$ m^3 for draft equal 60% and at the range between 2043.4 to 2145.74 $*10^6$ m^3 for draft equal 80%. On the other hand when high value of probability of failure (5% and 10%) are used for estimation, the reservoir capacity values were resulted lower than the other methods which estimated with probability of failure equal zero.
- When using other critical period methods (Dinçer and Gould's Gama methods) that predict a certain distribution suitability of low current sequences, it is possible to make more reliable estimates and to identify the risk relation with reservoir volume.
- It should be remembered that McMahon's empirical relationship, developed using Gould's probabilistic matrix method, is derived from streams in the Australian areas, although McMahon and Mein (1986) stated that it gives very good results in practice.
- Dinçer or Gould's Gamma Method seems to be the best method to be used in the preliminary

design phase for long-term critical periods (large storage). Choosing a method with acceptable assumptions for the distribution of the data array will increase the reliability of the results.

REFERENCES

Ağıralioğlu, N., 2004. Baraj Planlama ve Tasarımı. Su Vakfı Yayınları, Volume 1.

Aksoy, H., 2001. Storage Capacity for River Reservoirs by Wavelet-Based Generation of Sequent-Peak Algorithm. Water Resources Management, 15: 423-437.

Bayazit, M., 1997. Biriktirme Haznelerinin Tasarımı ve İşletilmesi. Istanbul: İTÜ Civil Engineering School Press.

Bharali, B., 2015. Estimation of Reservoir Storage Capacity by using Residual Mass Curve. Journal of Civil Engineering and Environmental Technology, 2(10): 15-18.

Elektrık Isleri Etut Idaresi Genel Mudurlugu, T.C., 2011. Su Akımları Yıllıgı.

Linsley, R. K. & Franzini, J. B., 1979. Water Resources Engineering. New York: McGraw-Hill Book Co.

McMahon, T. A., 1976. Preliminary estimation of reservoir storage for Australian streams. Civil Engineering, Transactions, 18(2): 55-59.

McMahon, T. A. & Mein, R. G., 1978. Reservoir Capacity and Yield. Amsterdam: Elsevier.

Mcmahon, T. A. & Mein, R. G., 1986. River and Reservoir Yield. Littleton, Colorado: Water Resources Publications.

Montaseri, M. & Adeloye, A. J., 1999. Critical period of reservoir systems for planning purposes. Journal of Hydrology, 224: 115-136.

Nagy, I. V., Asante-Duah, K. & Zsuffa, I., 2002. Hydrological Dimensioning and Operation of Reservoirs: Practical Design Concepts and Principles. 1 ed. Boston: Kluwer Academic Publishers.

Oğuz, B. & Bayazıt, M., 1991. Statistical properties of the critical period. Journal of Hydrology, 126: 183-194.

Parks, Y. P. & Gustard, A., 1982. A reservoir storage yield analysis for arid and semiarid climates. Optimal Allocation of Water Resources, July, 135: 49-57.

Rao, Z., Moore, I. N., O’Connell, P. E. & Jamieson, D. G., 2001. An Interactive Management System for Operational Control of Kirazdere Reservoir (Turkey). Water Resources Management, 15: 223-234.

Ripple, W., 1883. Capacity of storage reservoirs for water supply. Minutes of Proc., p. 71.

Proceedings of the 10th World Congress of EWRA 'Panta Rhei', 5-9 July 2017, Athens, Greece
© 2017 *European Water Resources Association*

Geo-Information analysis of the mini hydropower potential in the Liguria Region

A. Palla[1*], I. Gnecco[1], P. La Barbera[1], M. Ivaldi[2] and D. Caviglia[3]
[1] *Department of Civil, Chemical and Environmental Engineering, University of Genova, Genoa, Italy*
[2] *ITEC Engineering S.r.l., Genoa, Italy*
[3] *GIS&WEB S.r.l., Genoa, Italy*
[*] *e-mail: anna.palla@unige.it*

Abstract: The present paper deals with the implementation of a GIS-based tool for the definition and spatial evaluation of the mini hydropower potential. The investigation of the mini hydropower potential is performed at the catchment scale by integrating: catchment morphometric analysis; setting criteria for locating the weirs and powerhouses; hydrological modelling; engineering analysis; economic analysis and mapping. Hydropower potential results are synthetized through the synthetic index (MHP) resulting by the economic analysis based on the IRR dynamic method. A simplified understanding of MHP suggests that the investment is strongly recommended (MHP =1.0) when the initial cost equals the revenues occurring during a 10-years period. The integrated approach has been tested on a selected catchment of the Liguria Region (Italy): MHP map is plotted in order to provide an easily visualization of the results in selected catchments. Based on the preliminary results, the study proves that MHP analysis is a powerful tool in order to better support energy management strategies. The determination of MHP indexes in a simplified framework overcomes the typical problem due to the single prediction of hydropower potential for a specific plant configuration. Future perspectives of this research include the analysis of the spatial distribution of the water intakes on different reaches along the same river network in order to limit the aquatic ecosystem disturb and to enhance the sustainable water resource management.

Key words: Mini hydropower; flow duration curve; GIS-based tool; green energy; sustainable water resource management

1. INTRODUCTION

The environmental impact of small hydropower plants (SHP), though it is smaller than that produced by dams and large plants, is nowadays a debated issue among researcher (e.g. Lazzaro et al. 2013). Recently, policy strategies have been proposed to quantify the ecological stress caused by SHPs in a diverted river reach and consequently to support energy strategies that ensure the sustainable water resource management.

The main objective of the present research study is to propose a Geo-Information analysis to assess the mini hydropower potential based on engineering, economic and environmental criteria. The developed GIS-based tool allows investigating a larger number of potential sites in a given catchment than in a traditional hydropower preliminary study.

The proposed GIS-based tool has been tested on three selected catchments of the Liguria Region (Italy); in the present paper results for the Arroscia catchment are described.

2. METHODS

The mini hydropower potential mapping is obtained by using a dedicated GIS-based tool that allows integrating the available information (both spatial and non-spatial data) into a single organized and interactive system, computing new information and efficiently visualizing the computed information (Palla et al., 2016). The GIS-based tool provides a reliable estimation of the hydropower potential suitable for preliminary studies and/or large scale energy analysis. The analysis is focused on run-of-river hydropower plant equipped with a single turbine.

In this framework, the investigation of the mini hydropower potential is performed by integrating several modules as follows:

- Module 1: Catchment morphometric analysis;
- Module 2: Setting criteria for locating the weirs and powerhouses;
- Module 3: Hydrological modelling;
- Module 4: Engineering analysis;
- Module 5: Economic analysis and mapping.

Digital Elevation Model (DEM) is used to delineate the stream network and to calculate the area, mean slope, mean elevation and length of the main channel of a given catchment (Module 1).

Moving on the stream network, the weir locations are selected based on the following criteria: weir sites should be located downstream a confluence; the minimum required upstream area is equal to 3 km^2; an increase of at least 50% in catchment area or 30 km^2 is required to locate the downstream weir. Starting from each weir site, the powerhouse locations are selected based on the following criteria: powerhouse sites are located every 500 m and the distance between weir and powerhouse should not exceed 10 km (Module 2).

The hydrological model includes three components: the rainfall component is used to evaluate the mean precipitation over a given catchment; the rainfall-runoff component is based on a conceptual model using a cascade of linear reservoirs and the flow duration curve (FDC) component is implemented to determine flow statistics on a daily-basis (Module 3).

Using the FDC curves, the engineering analysis is performed to assess the plant capacity and the corresponding workable volume in order to design the run-of-river hydropower plant (Module 4).

The dynamic economic method is used to select the optimal power plant configuration with respect to the all possible alternatives. The resulting hydropower potential is illustrated on a readable and accessible map (Module 5).

The software packages used for the development of the GIS platform include: GRASS GIS for the morphometric analysis, engineering parametrization and mapping (Modules 1, 2 and 5); an ad-hoc hydrologic model developed for the FDC assessment (Module 3); an Excel workbook for the plant capacity assessment (Module 4) and Pentaho for the data integration and economic analysis of the mini hydropower potential (Module 5).

A synthetic description of the modules and the main evaluated variables is reported in Table 1.

Table 1. GIS-based tool structure: main evaluated variables, nomenclature, unit of measure and corresponding module.

	Symbol	Unit of measure	Module
Catchment area	A	km^2	Morphometric analysis
Hydraulic head	H	m	Morphometric analysis
Diversion channel length	L_{ch}	m	Morphometric analysis
Penstock length	L_p	m	Morphometric analysis
Flow duration curve	FDC	m^3/s Vs. d	Hydrologic analysis
Minimum flow discharge	MFD	m^3/s	Hydrologic analysis
Plant capacity	Q_d	m^3/s	Hydrol. and Eng. analysis
Rated power	P	kW	Engineering analysis
Annual revenue	R_1	€	Economic analysis
Internal rate of return	IRR	-	Economic analysis
Initial investment cost	C	€	Economic analysis
Mini Hydropower Potential	MHP	-	Economic and Mapping

2.1 The hydrologic module

In the Hydrologic module, the rainfall-runoff model is implemented to predict the daily flow rate using daily rainfall records as main input data. The Thiessen polygon method is used to estimate the average areal rainfall of a given sub-catchment.

The rainfall-runoff model predicts daily flow rate at a given river section. The different hydrologic components (evapotranspiration, vegetation interception, soil retention, runoff,

infiltration and groundwater flow) are simulated according to a conceptual approach by means of a cascade of three linear reservoirs. The first reservoir accounts for the interception/infiltration/runoff processes while the second and the third ones describe the groundwater flow processes. The actual evaporation is equal to the potential evaporation using the Thornthwaite equation. The model parameters consisting in the reservoir constants and threshold values are calibrated for the gauged sites. Subsequently, relationships between the calibrated model parameters and climatic, morphometric and land uses parameters for the gauged sites are derived using a multiple linear regression. The derived regression equations are then used to estimate model parameters for ungauged sites.

The procedure for deriving the FDC is based on the entire simulation period. The FDC is constructed by ordering the simulated daily flow data and computing the exceedance probability similarly to the period-of-record FDC. The construction method refers to a steady-state representation of FDC that measures the long-term streamflow regime and can be effectively used for assessing the long-term hydropower potential of a given site (Vogel and Fennessey, 1995).

Finally, the MFD estimation is defined according to the Water Authority prescriptions.

2.2 The engineering analysis

In the engineering analysis, the plant capacity is assessed in case of a run-of-river scheme according to the MFD rule: the flow which can be diverted from a river to the plant is equal to the difference between the upstream flow and the MFD (thus the plant can work only when such difference is positive). The actual range of diverted flow processed by the plant depends on the technical characteristics of the turbine, specifically the range between the maximum and minimum workable flows. The maximum workable flow corresponds to the design flow of the turbine while the minimum one corresponds to the cutoff flow which is generally expressed as a fraction of the design flow. In the present study the cutoff coefficient is assumed equal to 0.4.

The workable volume is then calculated using the flow duration curve according to the above mentioned MFD rule. In a first approach the plant capacity is estimated based on to the mean annual flow (Q_m). Secondly, the plant capacity that maximizes the energy production is obtained by computing the maximum workable volume (Q_{EN}). By evaluating the specific workable volume equal to the ratio between the workable volume and the corresponding plant capacity, the final design flow is selected between $0.8Q_m$ and Q_{EN} in order to maximize the specific workable volume. The state-of-the- art of the run-of river power plants supports the design choice given by the multiply factor equal to 0.8.

2.3 The economic analysis and mapping

In the economic analysis, the cost and revenue are analysed according to an economic dynamic method. The construction cost of the hydropower plant is assumed as the only cash outflow occurred; further any financing and the related interests are neglected. The cost occurring during the functioning of the plant are here neglected by considering that the small hydropower plants are characterized by initial investment cost much higher than the corresponding operational expenses (Aggidis et al. 2010). The construction cost is computed as the algebraic sum of the costs related to the following technical-engineering elements: the intake structure (including weir, intake and settling catchment), diversion channel, penstock, electro-mechanical equipment (including turbine, speed controls and generator) and powerhouse. According to the cost formulae documented in the literature (e.g. Ogayar and Vidal 2009), the construction cost is generally expressed as a power function of the main features of the plants. In the present study empirical cost formulae are derived using a simple regression analysis between the costs and the main features of SHPs installed in Italy. In particular, the costs relating to the intake structure, diversion channel and penstock are expressed as a function of the design flow while the cost relating to the electro-mechanical

equipment and powerhouse are expressed as a function of the rated power. Note that the cost formulae for the diversion channel and penstock are derived for length unit. In addition, a fixed amount equal to 60,000 € is considered to account the electric service connection expenses. Finally the total cost is incremented of 10% rate to account the cost related to the incidental expenses.

The annual revenue is calculated by multiplying the annual produced energy by the selling price of energy from renewable sources which is assumed to be constant. The energy selling price is estimated equal to 0.08 €/kWh according to the Italian Authority for Electric Energy and Gas deliberation for renewable energy from very small power plants producing not more than 1 MW.

The assessing of the mini hydropower potential (MHP) is based on the above mentioned economic analysis of the plant investment thorough the internal rate of return (IRR) method (Basso and Botter, 2012). The IRR is defined as the interest rate which makes the net present value of the investment equal to zero. The criterion for the selection between different plant alternatives is to choose the investment with the highest IRR that corresponds to the selection of the least risky choice. Note that the IRR values are computed by assuming a lifetime period of the hydropower plant equal to 30 years.

In order to easily quantify the IRR analysis results, a dedicated MHP indexes is here defined as follows:

$$MHP = \frac{C}{R_1} \cdot \frac{1}{10} \tag{1}$$

Therefore the project feasibility is classified according to the following MHP index values (i.e. to the corresponding IRR):

- if MHP $\leq$ 1.0 (i.e. IRR $\geq$ 0.09), the mini hydropower plant investment is strongly recommended when the initial cost equals the revenues occurring during a 10-years period;
- if 1.0 < MHP $\leq$ 1.5 (i.e. 0.05 $\leq$ IRR < 0.09) the mini hydropower plant investment is affordable;
- if MHP > 1.5 (i.e. IRR < 0.05), the mini hydropower plant investment is unaffordable.

3. CATCHMENT APPLICATIONS

The GIS-based tool to assess the mini hydropower potential of a specific catchment has been tested to three catchments of the Liguria Region (Italy) in the framework of the project “Preliminary study to assess mini hydropower potential in the regional territory”. In the present paper, the results obtained for the Arroscia catchment are described. The Arroscia catchment is located in the western Liguria Region and it has a drainage area of 273 km^2 with a mean annual discharge of about 4 m^3/s. The river network stretches along the west-easterly direction; the drainage system is dentritic and the main watercourse has a total length of 38 km. The Arogna and Giara di Rezzo streams are the main left-bank and right-bank tributaries respectively. Before entering into the River Centa, the Lerrone stream flows into Arroscia on the right-bank (see Figure 1). By considering the altimetry, vegetation and limited anthropogenic exploitation of the territory, the Arroscia is a mountain catchment characterized by steep slopes and high crest line.

The morphometric analysis of the Arroscia catchment is performed using the DEM from the Advanced Spaceborne Thermal Emission and Reflection Radiometer (ASTER) freely available at 30 meter resolution. By applying the criteria for locating the weir, 27 sub-catchments are picked out: 11 sub-catchments with a drainage area smaller than 10 km^2, 10 sub-catchments ranging between 10 and 50 km^2, 6 sub-catchments larger than 50 km^2. Starting from a reference weir, all the potential alternatives to locate the powerhouse are selected according to the setting criteria thus resulting from a morphometric analysis of the river network and slopes. For each alternative powerhouse, the gross hydraulic head is retrieved from DEM.

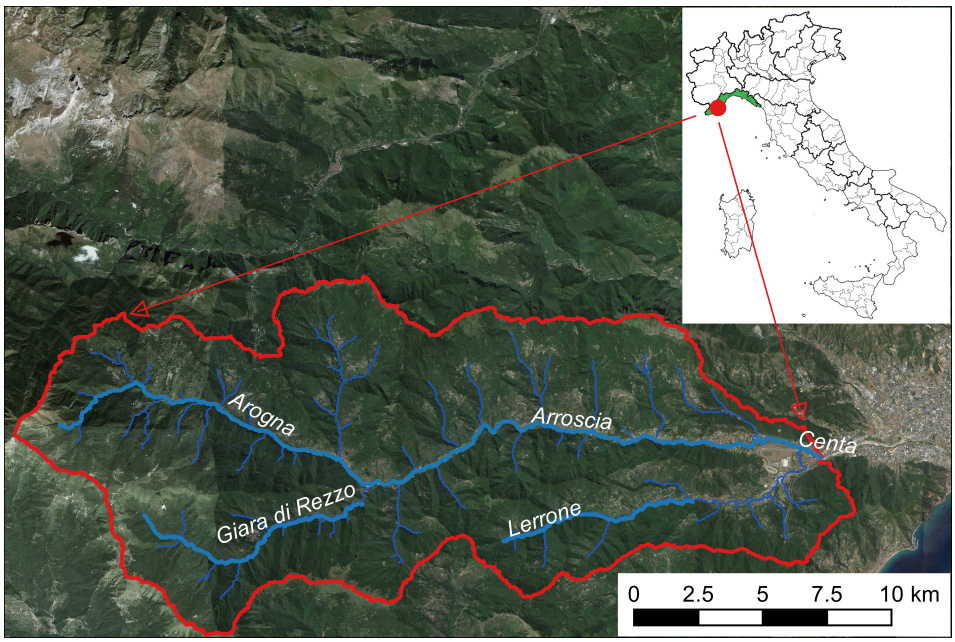

Figure 1. Overview of the Arroscia catchment in the Liguria region (Italy).

None streamflow measurements are available for the Arroscia catchment, therefore to estimate the flow statistic (FDC) at each weir section, the hydrologic model is implemented to predict the daily flow rate using observed daily rainfall records as main input data.

Finally, in order to estimate the flow rate which can be diverted from each river section the corresponding MFD is computed. The MFD estimation defined by the Water Authority of the Arroscia catchment is based on the following empirical expressions:

$$MFD = k \cdot q \cdot A \tag{2}$$

and

$$k = -2.39 \cdot 10^{-5} \cdot A + 0.058 \tag{3}$$

where k is an experimental parameter evaluated for each specific hydrographic area, q is the average specific flowrate on annual basis [l/(s·km^2)] and A is the drainage area [km^2].

Using the FDCs and adopting the MFD rule, the plant capacity is designed for each weir section by comparing the mean annual flow and the flow that maximizes the energy production according to the criteria implemented in Module 4.

By coupling the hydraulic characteristics of a specific weir site together with all the potential alternative powerhouse locations, the algorithm implemented in the engineering module evaluates the main features of the different mini hydropower plant alternatives. In particular, based on the morphometric analysis of the catchment, the gross hydraulic head and distance between the weir and the powerhouse are derived for each alternative. Further the economic assessment of the hydropower plant expressed in terms of the construction cost and annual revenue is performed.

The economic analysis (based on the IRR dynamic method) is finally synthetized through the MHP index evaluated for the 27 weir sections and the 640 mini hydropower plant alternatives. Results are mapped out in Figure 2 where a specific color is assigned to each weir based on the minimum MHP index corresponding to the optimal mini hydropower plant alternative for each weir section. In Figure 2, three different colors (green, yellow and red) are associated to the three corresponding classes of MHP index thus showing if a given catchment reveals suitable sites for installing a mini hydropower plant: the investment is strongly recommended in sites indicated as green dots while the investment is unaffordable in sites indicated as red dots. In 10 sub-catchments

over 27, the investment is affordable: for these sub-catchments it is possible to select at least a specific powerhouse location corresponding to a mini hydropower plant with MHP index ranging between 1.0 and 1.5 (yellow dots on Figure 2). On the other hands, in 13 sub-catchments over 27 the mini hydropower potential is no technically exploitable, namely the investment is unaffordable being characterized by MHP index values greater than 1.5. Looking at the data reported Figure 2, the implementation of mini hydropower plants is affordable mainly in the mountainous area (west side of the catchment).

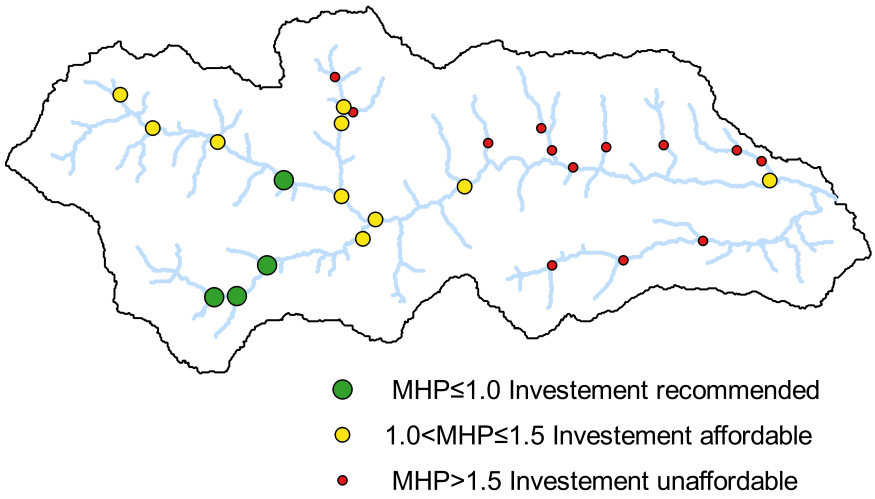

Figure 2. Map of the Mini Hydropower potential index for the Arroscia catchment (Italy).

4. CONCLUSIONS

The spatial evaluation of the hydropower potential for a given catchment has been analyzed by means of a dedicated GIS-based tool. The developed GIS-based tool involves the integrated analysis of environmental, technical and economic variables (based on spatially-distributed data).

All the potential plant alternatives (in terms of weir sections and the related powerhouses) are examined at the catchment scale in order to figure out the optimal solution corresponding to the minimum MHP index. Hydropower potential results are synthetized through the MHP map where a colored marker (from green to red) is associated to each investigated weir indicating the plant investment feasibility. Due to its readability and accessibility, the hydropower potential map can be easily used by practitioners as well as policymakers to support and promote the hydropower energy generation. Finally, the determination of MHP indexes in a simplified framework overcomes the typical problem due to the single prediction of hydropower potential for a specific plant configuration.

Future perspectives of this research include the analysis of the spatial distribution of the water intakes on different reaches along the same river network in order to limit the aquatic ecosystem disturb and to enhance the sustainable water resource management.

ACKNOWLEDGEMENT

The study was funded within the project “Preliminary study to assess mini hydropower potential in the regional territory” of the Regional Operational Program, co-financed by the European Regional Development Fund 2007-2013 (POR-FESR Liguria).

REFERENCES

Aggidis, G.A., Luchinskaya, E., Rothschild, R., Howard, D.C. 2010. The costs of small-scale hydro power production: Impact on the development of existing potential. Renew. Energy 35: 2632-2638.

Basso, S., Botter, G. 2012. Streamflow variability and optimal capacity of run-of-river hydropower plants. Water Resour. Res. 48: W10527.

Lazzaro, G., Basso, S., Schirmer, M., Botter, G. 2013. Water management strategies for run-of-river power plants: Profitability and hydrologic impact between the intake and the outflow. Water Resour. Res. 49: 8285–8298.

Ogayar, B., Vidal, P.G. 2009. Cost determination of the electro-mechanical equipment of a small hydro-power plant. Renew. Energy 34: 6-13.

Palla, A., Gnecco, I., La Barbera, P., Ivaldi, M., Caviglia, D. 2016. An integrated GIS approach to assess the mini hydropower potential. Water Resour. Manage. 30: 2979-2996.

Vogel, R.M., Fennessey, N.M. 1994. Flow-Duration Curves. I: New Interpretation and Confidence Intervals. J. Water Res. Pl-ASCE 120: 485–504.

Proceedings of the 10th World Congress of EWRA 'Panta Rhei', 5-9 July 2017, Athens, Greece
© 2017 *European Water Resources Association*

Trade-off between environmental flow policy and run-of-river hydropower generation in Mediterranean climate

A. Kuriqi[1*], A.N. Pinheiro[1], A. Sordo-Ward[2] and L. Garrote[2]
[1] *Civil Engineering Research and Innovation for Sustainability (CERIS), Instituto Superior Técnico, University of Lisbon, Lisbon 1049-001, Portugal*
[2] *Department of Civil Engineering: Hydraulics, Energy and Environment, Technical University of Madrid, Madrid 28040, Spain*
[*] *e-mail: alban.kuriqi@tecnico.ulisboa.pt*

Abstract: Run-of-River Hydropower plants are essential for the sustainable development of renewable energy resources. However, the increase in water demand for energy generation may conflict with the objectives of river conservation according to the Water Framework Directive (WFD). Therefore, the assessment of environmental flow requirements in river basins subjected to water abstractions is a crucial task for the integrity of aquatic ecosystems. The main objective of this study is to improve the assessment of interactions between energy generation and instream flow ecological indicators. In this study, we conducted an ecological and energy generation analysis for a run-of-river hydropower plant located in the Najerilla River, Ebro basin, Spain. The region under study is characterised by Mediterranean-Continental climate. The analysis was conducted considering 30 years' records of mean daily flow data, net head of the hydropower plant, turbine efficiency, and environmental flow constraints. We quantitatively estimated the instream flow alteration based on certain hydrological indicators by utilising seven hydrological methods for environmental flow definition. Subsequently, we compared their implication on hydropower generation and hydrological alteration of the instream flow regime. The results show that there are significant variations between the seven hydrological, environmental flow methods. We found that flow regime obtained by applying the *10% Daily* method shows similar pattern and magnitude to those of natural flow regime most of the time. We concluded that dynamic approaches (e.g., *10% Daily*) concerning the environmental flow definition are more reliable and feasible regarding energy generation and hydrological alteration-reduction.

Key words: run-of-river hydropower plants, flow regime alteration, environmental flow, hydrological alteration

1. INTRODUCTION

In this study, we analysed the implications of seven environmental flow methods (EFMs) on electricity generation and ecosystem integrity in a run-of-river (RoR) hydropower plant in the Iberian Peninsula. RoR is usually considered as an environmentally friendly electricity generation option because their alteration of natural flow is relatively low compared to the regulated hydropower plant (RHP), (Truffer *et al*., 2001). However, taking into account the increasing numbers of constructed and ongoing projects of RoR hydropower plants (Paish, 2002; Punys and Pelikan, 2007; Yüksel, 2007; Kelly-Richards *et al*., 2017), the cumulative impact on the ecosystem per unit generated electricity in some cases may be even higher than regulated hydropower plants (Fantin-Cruz *et al*., 2015). As stated by (Gilron, 2014; Godinho *et al*., 2014) water and electricity should be considered together not separately. Thus, it is critical to define the trade-off between the fraction of flow allocated as environmental flow (e-flow), and the fraction of flow allocated for electricity generation, which is a desirable renewable energy resource.

Numerous methods have been proposed to compute the e-flow that should be released at the diversion dam or weir. Tharme (2003) and Acreman and Dunbar (2004) classified EFMs into six categories: hydrological, hydraulic rating, habitat simulation, holistic, combined and other methodologies. Hydrological methods based only on flow data are the most used to determine the e-flow because of their sparse data requirements and their cost-effectiveness. Many authors recommended and used different hydrological EFMs to preserve the integrity in a river reach. Karimi *et al*. (2012) proposed that the e-flow should be *Q80%* of the Flow Duration Curve (FDC).

Mielach *et al.* (2012) compared four hydrological EFMs, which are widely applied in their countries: Austria, Italy, Slovenia, and Romania. They found that *Q95%* of FDC is even higher than legal, environmental flows established by each respective state law.

Penche (2004) recognised twenty-four EFMs based on an updated report prepared by the Thematic Network on Small Hydroelectric Plants (TNSHP) on behalf of the European Small Hydropower Association (ESHA). He classified the methods into four main groups based on hydrologic or statistic values, physiographic principles, velocity and depth of water and multi-objective planning taking into consideration ecological parameters. Considering the recommendations from ESHA and other literature, we analysed the implication of the choice of environmental flow methods on electricity generation and ecosystem integrity by applying seven hydrological EFMs. The selected case study is presented in section 2, the methodology is presented in section 3, the results and discussion are presented in section 4, and the conclusions are presented in section 5.

2. CASE STUDY

The RoR hydropower plant of Anguiano was selected as a case study in this paper. The power plant diverts water from the Najerilla River in the Ebro basin, near the Anguiano Municipality. The hydropower plant uses the head created by a diverting watercourse and the flow generated in a sub-basin with an area of approximately 541 km^2 (Figure 1).

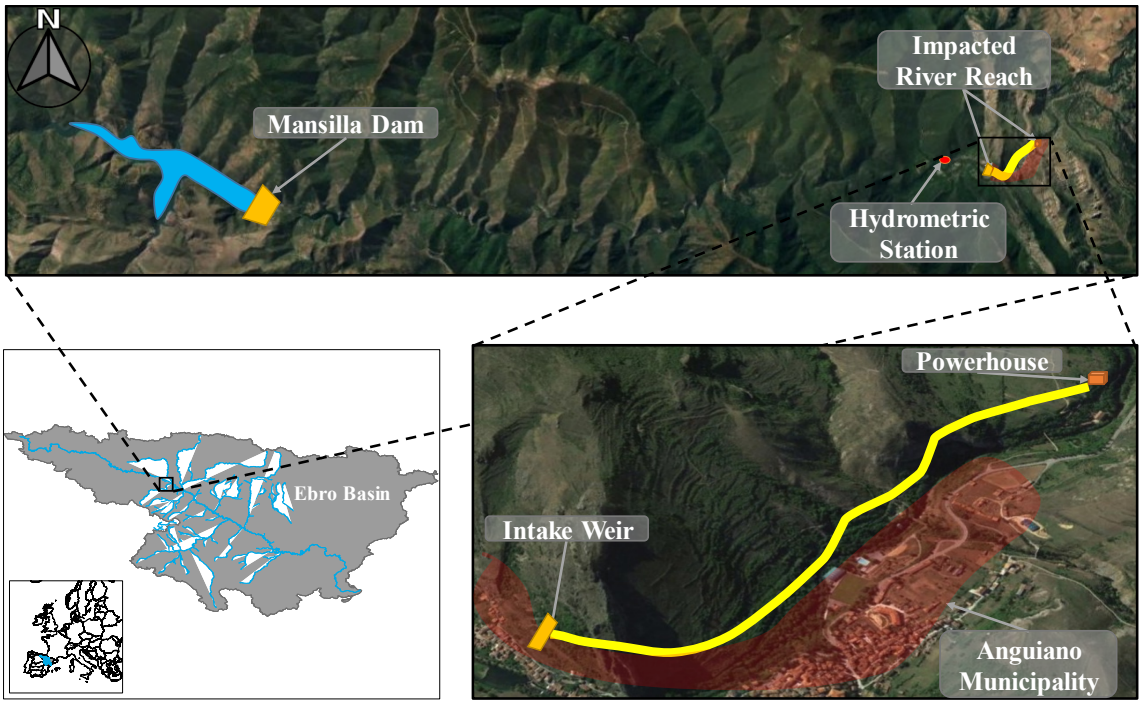

Figure 1. Najerilla River at Ebro Basin, the location of the hydrometric station 500 m upstream of the intake weir and Anguiano hydropower plant near to the Anguiano Municipality.

Topography. The basin topography is characterised by a significant diversity in altitude, varying from 610-2100 m a.s.l.

Climate and flow regime. The basin is located in a region of Mediterranean-Continental climate. Mean annual precipitation ranges between 400-2000 mm, with substantial variation along the basin because of its topography. At the highest altitude, the headwaters are covered by snow during the winter period, which results in relatively high runoff in spring and early summer. Since the main contribution to the Najerilla River is coming from runoff water, there is a significant variability in river flow. Mansilla dam located about 16 km upstream of the hydrometric station where the flow

data used in this study were obtained also alters the flow regime.

Flow data. In this study, we first identified a hydrometric station with an adequate flow data records and accuracy. We obtained daily mean flow data from the hydrometric station in Najerilla River provided by *Confederation Hidrográfica del Ebro* (CHE), the government agency that manages the water resources over the entire Ebro River basin. We analysed records of flow data between 01/01/1931 and 30/09/2009, resulting in 78 years of daily mean flow data. However, in our study, we did not consider the whole series, but only the last thirty years because we considered this period to be more reliable and with relatively fewer data gaps. These gaps were filled through an interpolation procedure, using linear trend regression.

3. METHODOLOGY

3.1 Description of environmental flow methods (EFMs)

The e-flow allocated to the ecosystem was defined based on seven EFMs selected after a review of international literature. Each EFM applied in this study represents a different category; the description of each method is given below.

Percentiles Q75 and Q95 - These are defined as the daily discharge values that have a probability of exceedance equal to 75% *(Q75)* and 95% *(Q95)*. *Q75* is considered as an adequate percentage of flow allocated to the ecosystem (Verma *et al*., 2016; Ates *et al*., 2016). *Q95* is a good indicator concerning low flows (Ates *et al*., 2016). Both methods are among the most common hydrological methods applied worldwide. The estimation of *Q75* and *Q95* was obtained from the FDC built with daily mean flow data.

Minimum Mean Flow in August (*NMQ_August)* - This approach recommends that e-flow should be at least between 7-100% of the minimum mean flow in August (Penche, 2004). We considered the most conservative scenario for the ecosystem and adopted 100% of *NMQ_August*. In our case study, 100% of *NMQ_August* corresponds to 4.3 m^3/s.

Linearised Matthey (L.M) – Environmental flow allocated to the ecosystem is determined by using the following linear relationship: $IF = 0.25 \times Q_{300} + 75$ (l/s) (Penche, 2004) where Q_{300} is the flow exceeded 300 days per year on average. In our case, the water amount allocated to the ecosystem by utilising this approach corresponds to a value of $IF = 1.2$ m^3/s, where $Q_{300} = 4.5$ m^3/s.

10% of Mean Annual Flow (10%MAF) - This method is widely used in many countries including Spain (Tharme, 2003). According to this approach, at least 10% of mean annual flow should be allocated to the ecosystem. In our case, the value obtained is 0.9 m^3/s.

Minimum Annual Flow (NNQ) - Minimum e-flow should be at least equal to the minimum flow recorded in the period considered in the analysis (Tharme, 2003). In the present study, the minimum flow recorded within the period of 30 years of mean daily flow data is 0.6 m^3/s.

10% of Daily Flow (10% Daily) – In our case, e-flow is defined as 10% of the natural mean daily flow, so e-flow is variable in time (Penche, 2004). In our study, the maximum daily flow allocated to the ecosystem by utilising *10% Daily*, is 20.8 m^3/s, occurring during the spring season, whiles the minimum flow takes place during the winter season, and is 0.06 m^3/s.

3.2 Energy model

The energy model was developed taking into account the environmental flow constraints imposed by the EFMs applied in this study. The essential parameters of run-of-river hydropower plants are the net head and the flow rate. The potential power was computed according to equation 1:

$$P = 9.81\ \rho\ Q\ H \tag{1}$$

where P is the power output, 9.81 the acceleration due to gravity (m/s^2), ρ is the density of water (1000 kg/m^3), Q is turbine flow in (m^3/s), H is net head in (m), and η is overall efficiency of the system. The energy production is computed by multiplying the generated power by the time duration when the flow is available. The nominal efficiency of the Francis turbine installed in the hydropower plant is 93%. However, the overall efficiency applied in this analysis was estimated to be 85% due to hydraulic, mechanical, and electrical equipment losses. We considered a design flow of 6.3 m^3/s, which corresponds to a time duration of 5260 h. The minimum operation flow of the Francis turbine is 1.9 m^3/s, which corresponds to 30% of the design flow. Thus, the effective range of flow used for power generation is from 6.3 to 1.9 m^3/s.

3.3 Indicators of hydrological alteration (IHA)

We calculated 33 Indicators of Hydrological Alteration (IHA) and 34 e-flow components (EFC's) to assess the degree of alteration induced as result of flow diversion for electricity generation. However, in this paper, we are presenting only the most relevant ones (Table 1). IHA were computed for the natural flow and the altered flow regime resulting from the application of the environmental flow constraints deriving from the seven EFMs applied in this study.

4. RESULTS AND DISCUSSION

4.1 Reliability analysis

As shown in (Figure 2), particular environmental flow constraints (methods) imply different flow regimes related electricity generation and e-flow. Figure 2, left, shows that taking into account design flow and minimum technical flow, *Q75%* is the method which allocates the least flow for electricity generation, the opposite occurs applying the *10% Daily* flow. While Figure 2 (right) shows that *Q75%* method allocates the highest fraction of the flow to the ecosystem.

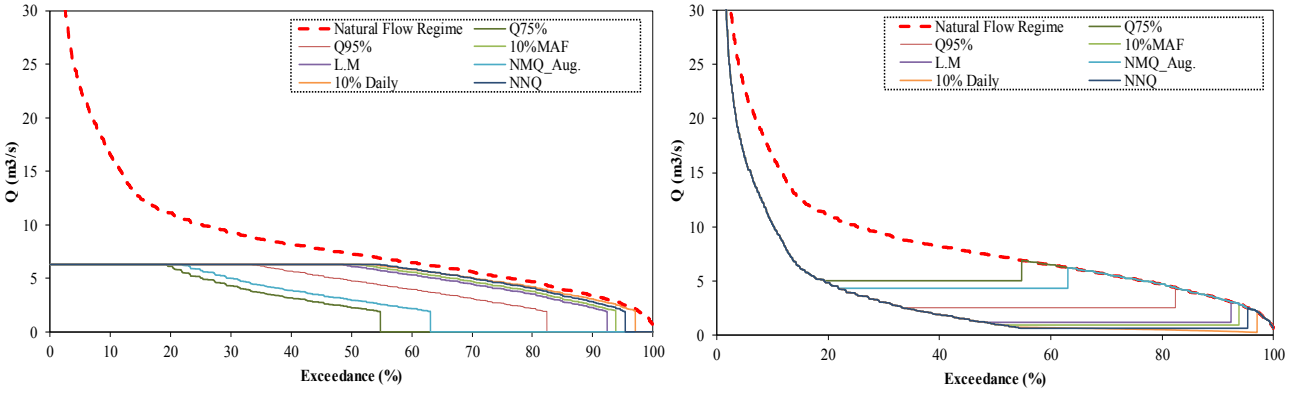

Figure 2. Flow duration curve allocated flow for hydropower production (left) and flow released as e-flow downstream (right) respecting applied EFMs

In some cases, e-flows obtained from EFMs applied in this study are higher than natural flow (this usually happens during low flow period). Therefore, we conducted a reliability analysis of the e-flow defined by the seven EFMs. The reliability index is computed as the fraction of time when the flow obtained by EFMs exceeds the natural flow, Equation 2.

$$RI = \left(T_{exceeds} T_{total}^{-1}\right) 100\% \quad (2)$$

where RI is reliability index, $T_{exceeds}$ is the time when e-flow obtained by EFMs exceeds natural

flow regime and T_{Total} is the total time span of mean daily flow data records.

We found that e-flow defined by *Q75%* has the least reliability; natural flow is below the e-flow specified by this method about 23.7% of the entire period of flow records used in this study. The second method, which is less reliable, is *NMQ_August*, which fails up to 17.3% of the time. *Q95%, L.M, 10%MAF, NNQ* and *10% Daily* demonstrate relatively low failure rates: 4.6%, 0.6%, 0.3%, 0% and 0%, respectively. Thus, we conclude that NNQ and *10% Daily* are the only fully reliable methods among the EFMs applied in this study.

4.2 Implications on energy generation and instream flow

Results indicate that *Q75%* and *NMQ_August* allocate the highest fraction of flow to the ecosystem (Figure 3), left the side, with a mean inter-annual flow about 7.2 and 6.5 m^3/s respectively. Compared with other methods, these methods also provide higher thresholds of minimum e-flow. Nevertheless, as it was shown in the reliability analysis, *Q75%* and *NMQ_August* are the methods with the highest uncertainty compared with other methods applied in this study. On the one hand, flow allocated to the ecosystem by applying *Q95%* has a mean value of 5.2 m^3/s with a little bit higher variability compared with the two first methods, as a result of the lower threshold of the minimum e-flow. On the other hand, flow provided to the ecosystem by applying the other four EFMs has approximately the same variability with slight changes between them. The mean flows obtained by applying *L.M, 10%MAF, NNQ,* and *10% Daily* are 4.3, 4.2, 4, and 3.9 m^3/s respectively. Concerning the mean inter-annual potential energy generation (Figure 3), right side, *Q75%* and *NMQ_August* allow the lowest mean potential energy production among the methods analysed. The mean inter-annual potential energy production that could be obtained is around 6 and 7.5 GWh respectively.

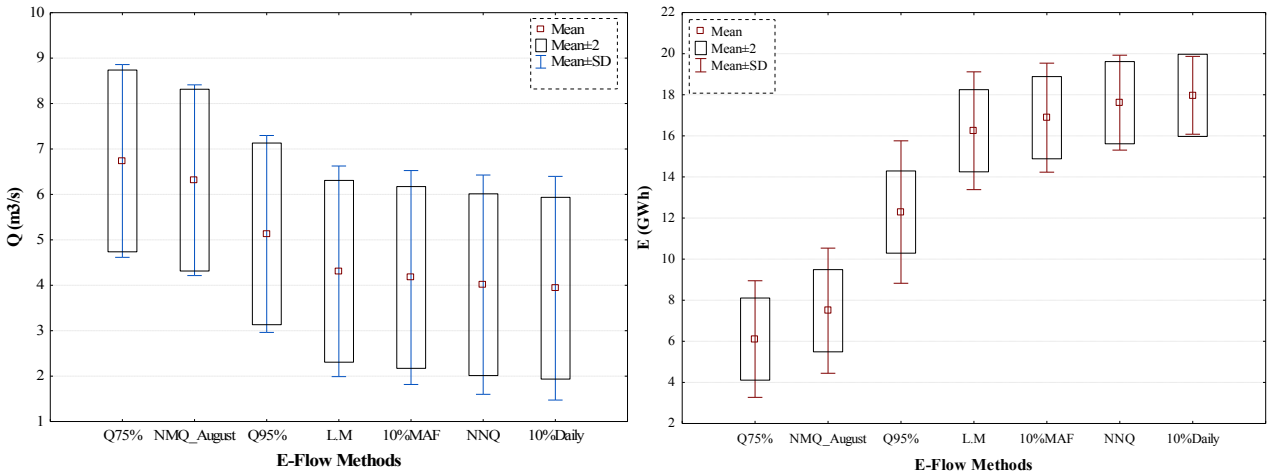

Figure 3. Mean values and dispersion of inter-annual altered flow regimes (left) and inter-annual potential energy generation (right) obtained by applying EFMs

Q75% and *NMQ_August* are characterised by significantly high variability concerning energy production. The mean inter-annual potential energy that could be obtained by applying *Q95%* is around 12.5 GWh, relatively greater than first two methods. Also, *Q95%* is characterised by relatively higher variability. *L.M* and *10%MAF* provide higher energy generation compared with the first three methods, with a mean of 16.7 and 17 GWh, respectively. They are characterised by lower variability compared to the first three methods. The potential energy productions that could be obtained by applying the last two methods, *NNQ,* and *10% Daily* are relatively higher than the other methods, in particular, compared with the first three methods. Mean inter-annual potential energies are 17.8 and 18 GWh, respectively. While *NNQ* and *10%Daily* are characterised by relatively lower variability.

We categorised the EFMs into three groups regarding flow allocated to the ecosystem and potential energy production. The first group contains the methods *Q75%* and *NMQ_August*, the second group consisting of *Q95%*, and the third group includes *L.M, 10%MAF*, *NNQ* and *10% Daily*.

4.3 Indicators of hydrological alteration (IHA)

To allow for a comprehensive interpretation of flow alteration, 33 IHA and 34 EFC's were computed for the altered flow regime obtained after application of seven EFMs. We chose the ten most relevant indicators among the 33 computing. These ten indicators are classified into three groups (Table 1). For each applied EFM, we computed the mean and coefficient of variation (CV) for both the natural and the altered flow regimes.

Table 1. Summary of ten indicators of hydrological alteration (IHA) originally proposed by (Richter et al., 1996), for the natural and altered flow regimes considering the applied EFMs

IHA Statistics	Means								Coefficient of Variation							
		Altered								Altered						
	Natural	Q 75%	NMQ August	Q 95%	L.M	MAF 10%	NNQ	Daily 10%	Natural	Q 75%	NMQ August	Q 95%	L.M	MAF 10%	NNQ	Daily 10%
#1																
Oct.	5.1	4.4	4.1	2.9	1.5	1.3	1	0.9	0.4	0.3	0.2	0.2	0.4	0.4	0.6	0.7
May	11.2	7.9	7.5	6.3	5.6	5.5	5.4	5.4	0.5	0.5	0.6	0.8	0.9	1	1	1
June	8.7	6	5.3	3.9	3.1	3	2.8	2.8	0.4	0.4	0.4	0.7	1	1.1	1.2	1.2
Aug.	8.1	5.3	4.7	3.1	2.3	2.2	2.1	2.1	0.2	0.1	0.1	0.3	0.6	0.7	0.8	0.8
#2																
7-day Min.	3.3	3.2	3.1	2.2	1.1	0.9	0.6	0.4	0.4	0.4	0.4	0.2	0.1	0.1	0	0.3
30-day Min.	3.9	3.6	3.4	2.3	1.2	0.9	0.6	0.5	0.4	0.3	0.3	0.2	0.1	0.1	0.1	0.4
7-day Max.	37.6	31.6	31.5	31.3	31.3	31.3	31.3	31.3	0.7	0.8	0.8	0.8	0.8	0.8	0.8	0.8
30-day Max.	23.3	17.8	17.7	17.3	17.1	17.1	17	17	0.5	0.6	0.7	0.7	0.7	0.7	0.7	0.7
#3																
Min. Date	324	323	315	255	261	261	268	325	0.2	0.2	0.2	0.2	0.2	0.2	0.1	0.2
Max. Date	137	131	138	137	137	137	137	137	0.3	0.3	0.3	0.3	0.3	0.3	0.3	0.3

The results (Table 1), show that the inter-annual mean (e.g., mean flow in October or 7-day Min) of the altered flow regime does not reveal a significant difference with the mean natural flow for some indicators, regarding particular EFMs (i.e., *Q75%, NMQ_August*). For the other five EFMs (i.e., *Q95 %, L.M, 10 % MAF, NNQ and 10 % Daily*), results do reveal a relatively high difference between the mean natural and altered flow. In this context, we computed a dimensionless aggregated alteration index (AAI) to estimate the degree of alteration implied by each EFM based on the IHA presented in (Table 1). AAI was calculated as follows: initially, we normalised the mean flow values by taking the difference (in absolute value) between the mean value of the indicator for the natural and the altered flow regime and dividing by the mean value for the natural flow regime. Afterwards, AAI was computed as the sum of all the normalised indicators. Thereby, *Q75%* and *NMQ_August* reveals the lowest AAI, 1.6 and 1.9 respectively. While *Q95%* demonstrate relatively higher AAI (3.4) than the first two methods. The other four EFMs (i.e., *L.M, 10% MAF, NNQ* and *10% Daily*) have slight differences between them, 4.5, 4.7, 5 and 4.9 respectively. So, *NNQ* has the highest AAI with 5 degrees of alteration. Nevertheless, the AAI takes into account only the flow

quantity allocated to the ecosystem regarding applied EFMs.

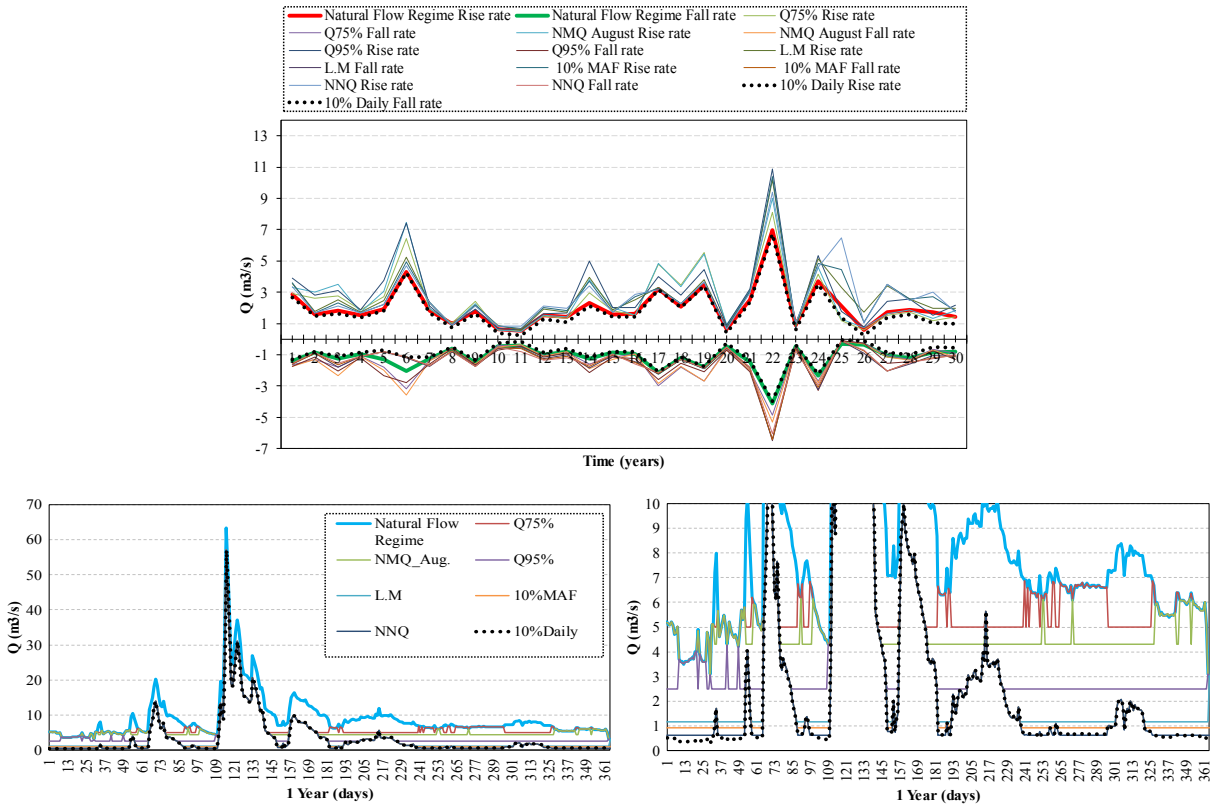

Figure 4. Intra-annual rise and fall rate for natural and altered flow regime (first up), natural and altered mean daily flow regime (left) for one-year records and higher resolution of natural and altered low flow regime (right) for one-year records considering applied EFMs

To maintain ecosystem integrity not only a particular water quantity is essential but also flow variability. This underlines the importance of a flow pattern closer to natural flow regime (Arthington *et al.*, 2006). Thus, considering another hydrologic indicator, the rise and fall rate (Figure 4), we conclude that *NNQ* and especially *10% Daily* provide a flow pattern very similar to the natural flow regime. These flow regimes do not only consider inter-annual flows but also daily flows. Daily hydrographs are presented in (Figure 4), down, left and right for one year of natural and altered flow regime regarding each applied EFMs. These daily hydrographs show that EFMs applied in this study do not affect high flows. Concerning low flows and high pulses, most of them cause a relatively higher alteration by completely modifying the natural flow regime.

5. CONCLUSION

We analysed the implications of seven hydrologic EFMs on energy production and ecosystem integrity. The analysis was performed considering a RoR hydropower plant as a case study. We conducted a reliability analysis to assess the degree of reliability/uncertainty of each applied EFMs. We found that five first EFMs are not entirely reliable. Concerning the energy generation and environmental protection, we found that *Q75%* provides more water to the ecosystem and less for energy generation, while *10% Daily* allows for higher energy generation but less water to the ecosystem in a short period during the year. Therefore, based on their implications for energy generation and ecosystem preservation, we categorised the applied EFMs into three groups. The first group includes *Q75%* and *NMQ_August*, the second group includes *Q95%*, and the third group includes *L.M, 10% MAF, NNQ,* and *10% Daily* methods. We computed a dimensionless Aggregated Alteration Index (AII), and we found that *NNQ and 10% Daily* have the highest AAI. However,

analysing the rise and fall rate, we found that *NNQ* and especially *10% Daily* produce flow regimes similar to the natural one and provide the highest energy generation. Thus, the flow regime obtained mainly by applying the *10% Daily* method has a low magnitude in a few periods of the year, although most of the time it presents a pattern and magnitudes similar to those of the natural flow regime. Therefore, it is possible to fulfil energy demands while preserving adequate flows for the environment and maintaining a dynamic e-flow (e.g., *10% Daily)* approaches which are more reliable and feasible concerning energy production and ecosystem integrity.

ACKNOWLEDGMENTS

The first author benefits from a PhD Scholarship funded by FCT (PD/BD/114558/2016) under the FLUVIO - River Restoration and Management PhD program.

REFERENCES

Acreman, M. C., & Dunbar, M. J. (2004). Defining environmental river flow requirements? A review. Hydrology and Earth System Sciences Discussions, 8(5), 861-876.

Ates, H., Dogan, S., & Berktay, A. (2016). The Effect of River Type Hydroelectric Power Plants on Aquatic Ecosystems: the Case Study of Göksu River-Eastern Mediterranean. European Journal of Engineering and Natural Sciences, 1(1), pp-39.

Arthington, A. H., Bunn, S. E., Poff, N. L., & Naiman, R. J. (2006). The challenge of providing environmental flow rules to sustain river ecosystems. Ecological Applications, 16(4), 1311-1318.

Fantin-Cruz, I., Pedrollo, O., Girard, P., Zeilhofer, P., & Hamilton, S. K. (2015). Effects of a diversion hydropower facility on the hydrological regime of the Correntes River, a tributary to the Pantanal floodplain, Brazil. Journal of Hydrology, 531, 810-820.

Gilron, J. (2014). Water-electricity nexus: matching sources and uses. Clean Technologies and Environmental Policy, 16(8), 1471-1479.

Godinho, F., Costa, S., Pinheiro, P., Reis, F., & Pinheiro, A. (2014). Integrated procedure for environmental flow assessment in rivers. Environmental Processes, 1(2), 137-147.

Karimi, S. S., Yasi, M., & Eslamian, S. (2012). Use of hydrological methods for assessment of environmental flow in a river reach. International Journal of Environmental Science and Technology, 9(3), 549-558.

Kelly-Richards, S., Silber-Coats, N., Crootof, A., Tecklin, D., & Bauer, C. (2017). Governing the transition to renewable electricity: A review of impacts and policy issues in the small hydropower boom. Electricity Policy, 101, 251-264.

Mielach, C., Schinegger, R., Schmutz, S., Zeiringer, B. (2012). See hydropower – clear water clean electricity: wp 4 - preserving water bodies' ecosystems – environmental flow comparison. 9th ISE, Viena (pp. 1-8).

Paish, O. (2002). Small hydro power: technology and current status. Renewable and sustainable electricity reviews, 6(6), 537-556.

Penche, C. (2004). Guide on how to develop a small hydropower plant. European Small Hydropower Association.

Punys, P., & Pelikan, B. (2007). Review of small hydropower in the new Member States and Candidate Countries in the context of the enlarged European Union. Renewable and Sustainable Electricity Reviews, 11(7), 1321-1360.

Richter, B. D., Baumgartner, J. V., Powell, J., & Braun, D. P. (1996). A method for assessing hydrologic alteration within ecosystems. Conservation biology, 10(4), 1163-1174.

Tharme, R. E. (2003). A global perspective on environmental flow assessment: emerging trends in the development and application of environmental flow methodologies for rivers. River research and applications, 19(5-6), 397-441.

Truffer, B., Markard, J., Bratrich, C., & Wehrli, B. (2001). Green electricity from Alpine hydropower plants. Mountain Research and Development, 21(1), 19-24.

Verma, R. K., Murthy, S., Verma, S., & Mishra, S. K. (2016). Design flow duration curves for environmental flows estimation in Damodar River Basin, India. Applied Water Science, 1-11.

Yüksel, I. (2007). Development of hydropower: a case study in developing countries. Electricity Sources, Part B, 2(2), 113-121.

Proceedings of the 10th World Congress of EWRA 'Panta Rhei', 5-9 July 2017, Athens, Greece
© 2017 *European Water Resources Association*

Effects of crop pattern changes on hydroelectric power generation in Gediz river basin

C.P. Çetinkaya[1] and M.C. Günaçtı[1]
Department of Civil Engineering, Dokuz Eylül University, Tinaztepe Campus, Buca 35160 Izmir, Turkey
[*] *e-mail: cem.cetinkaya@deu.edu.tr*

Abstract: Due to several socio-economic reasons, crop patterns of a basin may vary over the years. The primary reason generally tends to be on the economic aspect. Such a change has took place in Gediz Basin, Turkey; in between the years 1997-2012, a dramatic transition occurred in crop pattern due to economic pressures. Agricultural communities of Gediz Basin have shifted their main yearly crop from cotton to maize because of forcing benefit/cost ratios. Due to the total and monthly differences between two crops' water requirements, irrigation water demand has also altered throughout the years. The main reservoir Demirkopru has the primary purpose of providing water during the summer season for the lower basin embodying around 110 000 ha of irrigated area. The change in crop patterns has put the effectiveness of the produced energy now in question. Although the power generation contributes negligible amounts versus agricultural production to the gross income in the basin, its cost-effectiveness has become an important issue due to the privatization process of the power plant. In this study, over 20 years of recorded data of Demirkopru reservoir's inflows have been used for the synthetic data generation in order to examine the effects of on-going and future crop pattern changes and operational responses of Demirkopru reservoir. The results of operational studies of reservoir are evaluated in terms of power generation and its cost-effectiveness.

Key words: Crop pattern, Synthetic data generation, Cost-effectiveness, Electric power generation

1. INTRODUCTION

Gediz Basin in Western Anatolia (Figure 1), is a semi-arid region of Turkey. Generally, in semi-arid regions available water resources are the main limiting factor for agricultural production (Hiessl, 1987). Data shows that in Turkey, 96% of the agricultural areas do not get the precipitation they need in the growing season (Gurses, 2005). Also in Gediz Basin water scarcity is a significant problem. Water shortage is due basically to competition for water among various uses. Major consumer in the basin is irrigation with a total command area of 110 000 ha and competes with other sectors such domestic and fast growing industrial demands in the coastal zone. Main problem is environmental pollution however the basin experiences droughts from time to time which leads to allocation problems (Cetinkaya et.al., 2008). By the year of 2012 irrigated areas have shrunk half its potential amount due to maintenance and operation problems and lack of surface water in some areas (Duman, 2013).

These and other factors that can be counted seem to have affected the agricultural communities of the basin to change their habitual crop pattern to a new one. Observed crop pattern change over the years has indeed its consequences. As for the irrigational water demand perspective, it is obvious that with change in the crop pattern, amount and timing of the water demand will also differ in monthly scale. Demirkopru dam represents one of the main reservoirs of the basin. It has been built between 1954-1960 for the purpose of flood control, irrigation and energy generation. At first, it has been built to support the thermal power plants of the Aegean region but in time its goal has been shifted to irrigation. Correspondingly, the operational rules of installed power plant depend on water releases during irrigational season which is between May and October for Gediz Basin. Therefore, electricity generated through these releases related with agricultural water allocation from Demirkopru reservoir should be re-evaluated. As a consequence of the legislation for electricity market (No: 28603, Date: 30.03.2013), privatization of electricity production and

distribution has gained legal status. Like many other power plants, privatization process of electricity operation of Demirkopru came in to consideration. Therefore, the feasible cost of the privatization should be determined from both aspects of governmental bodies and private investors. In order to do so, one has to project the benefits and costs of the power plant regarding the operation of the reservoir under uncertainties of natural flows and socio-economic choices of community like crop pattern shifts due to economic and technological pressures during agricultural production. Thus the inflows, crop pattern changes, expected unit price for electricity, maintenance and operational costs of the power plant and interest rates are to be predicted. Within the context of this study, 25 years are selected for the economic analyses, as this time span corresponds to any privatization tender time. The observed natural inflows to Demirkopru reservoir are analysed and a seasonal first order auto-regressive model is built to generate synthetic inflows. These synthetic data is combined with future crop pattern change scenarios and annual electricity generation of the power plant is simulated. Thereafter, including energy market prices, theoretical operational and maintenance costs are calculated and used in economic analyses for different interest rates. Finally, a sensitivity analysis has been carried out in order to determine benefit cost ratios for each interest rate and crop pattern change scenario. The results are used to define minimum and maximum range of expected net benefit in order to obtain lower and upper limits of privatization bids to be expected. The obtained figures indicate that power plant is cost-efficient under certain circumstances.

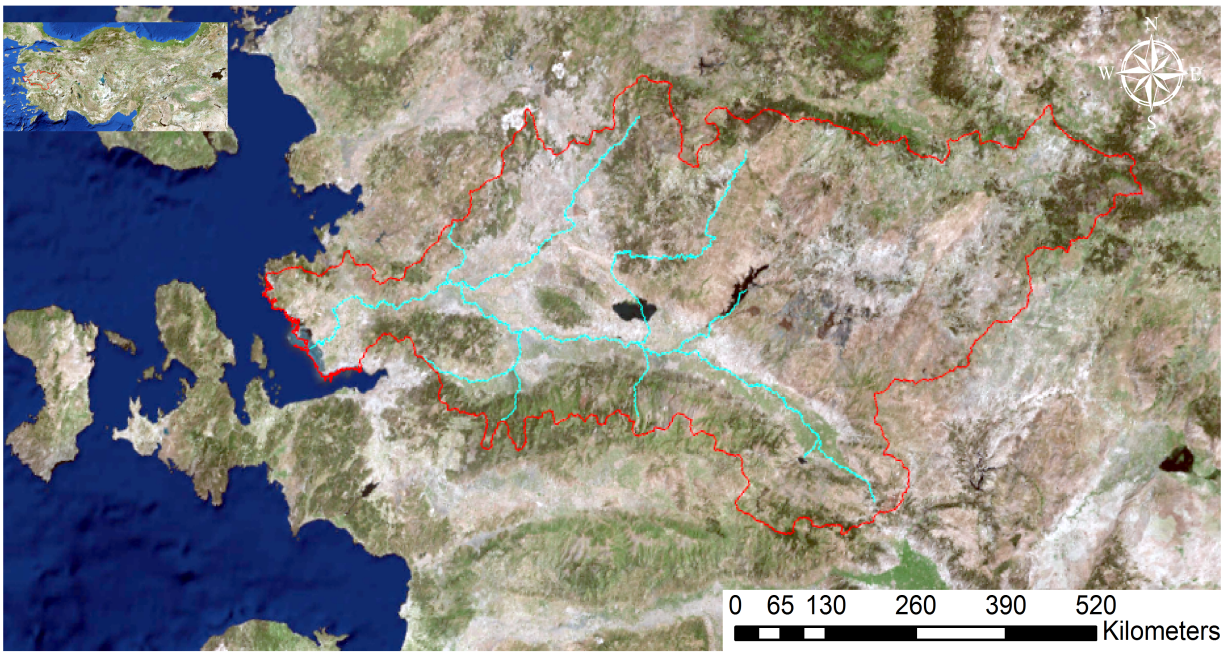

Figure 1. Gediz Basin

2. METHODOLOGY

2.1 Synthetic data generation

Historical monthly inflow data of Demirkopru for 27 years revealed that a seasonal AR1 model is significantly sufficient to represent natural inflows. Periodic components of the series have been determined by the "Parametric Fourier Series Approach" and one harmonic in the mean and two harmonics in standard deviation are sufficient to represent seasonality in natural flows. Main mathematical formulae utilized in synthetic data generation are given in equation 1, 2 and 3.

$$\widehat{\mu_\tau} = \sum_{j=1}^{m}\{a_j \times \cos(2\pi f_j \tau) + b_j \times \cos(2\pi f_j \tau)\} \quad (1)$$

where,
$\widehat{\mu_\tau}$= Periodic mean
a_j, b_j= Fourier coefficients
f_j = j/N
τ = Number of periods
N = Total number of periods
m = Number of harmonics

$$\widehat{\sigma_\tau} = \bar{S} + \sum_{j=1}^{m}\{a_j \times \cos(2\pi f_j \tau) + b_j \times \cos(2\pi f_j \tau)\} \quad (2)$$

where,
$\widehat{\sigma_\tau}$=Standard deviation of periods
$\bar{S}$= Average standard deviation of periods

Then, the weak stationary stochastic components, $\widehat{Z_{p,\tau}}$ obtained through,

$$\widehat{Z_{p,\tau}} = \frac{X_{p,\tau} - \widehat{\mu_\tau}}{\widehat{\sigma_\tau}} \quad (3)$$

where,
$\widehat{Z_{p,\tau}}$= Weak stationary stochastic components

Existing and generated monthly total inflow data throughout the years have been shown below (Figure 2):

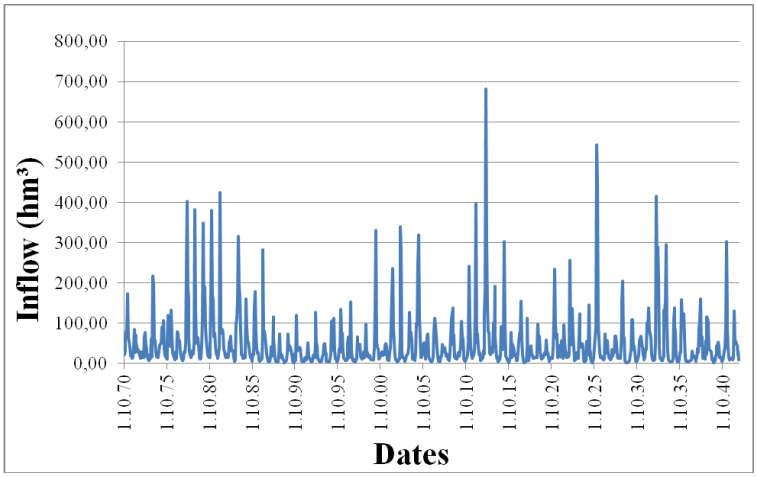

Figure 2. Monthly total inflows throughout the years

2.2 Crop pattern change

Gediz Basin generally has three types on main crop, which are cotton, maize and vineyard. Occurred crop pattern changes in the basin have been due to the economic reasons. Main costs of the cotton drove farmers to cultivate different types of crops. Cultivation of crop types and their irrigation water requirement changed, as in Figure 3.

2.3 Crop pattern scenarios

Crops cultivated in the basin have shown different types of trends (Figure 4). Cotton areas

decreased by 96%, maize and vineyard areas increased by 106% and 7% respectively. Maize has become the prior main crop and filled the gap which cotton left. This is a persistent trend however water availability affects the total area cultivated in the Gediz Basin. Therefore, three different crop pattern scenarios, that might occur in future, have been evaluated regarding the historical trends.

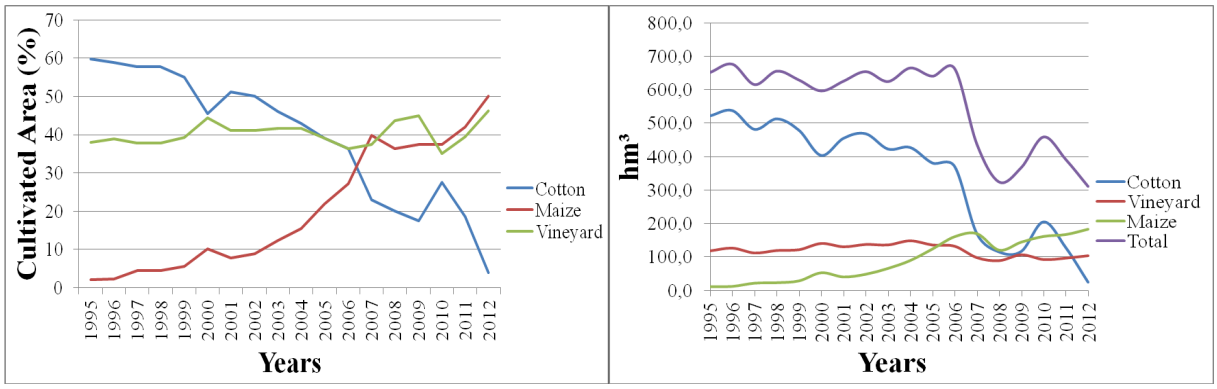

Figure 3. Annual crop cultivation percentage and annual irrigation water requirements

Scenarios meet on a common ground, where in all three, total area average increases from 55 000 ha to 70 000 ha in total of five years by investments. It is observed that in the long run the vineyard area average remains constant, therefore it is considered as constant in scenario development. Apart from other developed scenarios, in "Scenario A", cotton area average kept as constant and maize area average takes up the remaining areas. In "Scenario B" it is reverse and in "Scenario C" cotton and maize shares the rest of the areas equally.

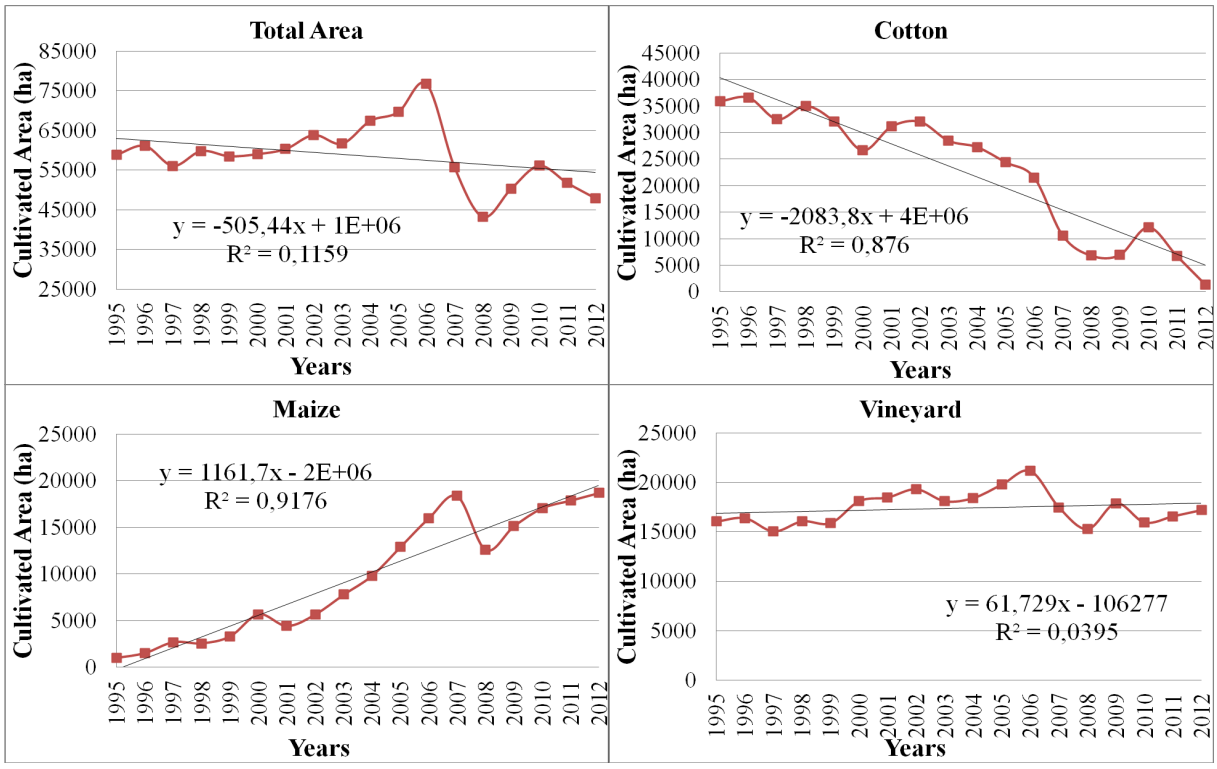

Figure 4. Change in cultivation areas throughout the years

2.3 Turbine operation and costs

Operational practices of hydroelectric plants are highly important due to their level of electricity

production. Failures and flaws in operation directly affects amount of power generated and this can be corrected by operational practices and an increase in the production can be obtained (Howitt and Sexton, 1998). Turbine operations due to inflows are represented below as the green, blue and red lines indicating first, second and the third turbine respectively. As the horizontal axis displays the total inflow, Vertical axis displays the each individual turbine's discharge. Second turbine does not become active until total inflow reaches 23 m³/s and for the third turbine it is 46 m³/s.

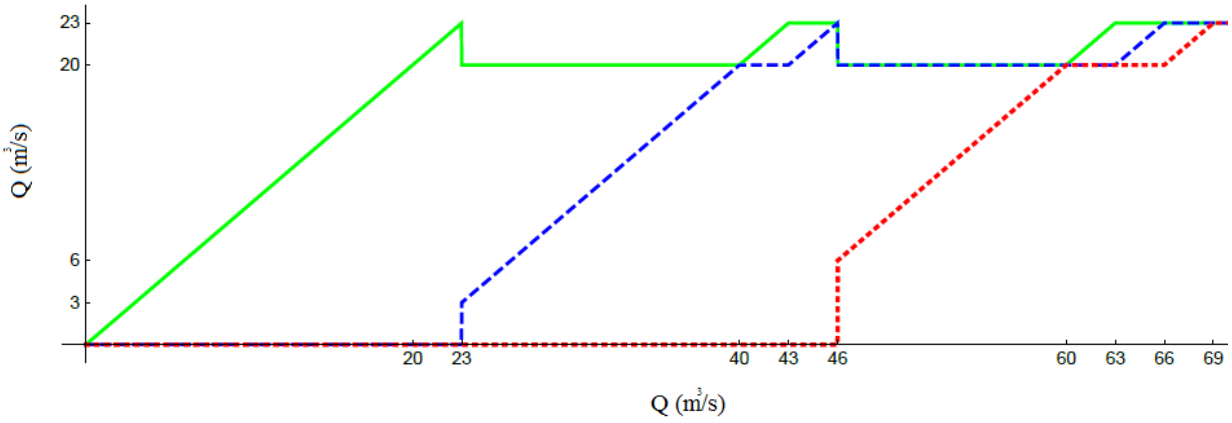

Figure 5. Operational constraints of the Demirkopru turbines

Operational practice functions only between 200 – 900 hm³ of stored volume of water; these limits also represent the lower and upper operation levels of the reservoir. Any value lower than 200 hm³ would be considered as inactive storage. Correspondingly any value higher than 900 hm³ would be considered as the volume which will be spilled away. However during the practice, no spills have been observed.

As for the hydroelectric plant's costs, there are two categories; a) equipment and maintenance costs and b) operational costs (Kaya and Koç, 2015). These costs have been determined according to the State Hydraulic Works (DSI) data (DSI, 2017), which are calculated depending on the installed capacity of the power plant (Table 1).

Table 1. Costs of hydroelectric plant

Cost Type	$/year
E/M	1,138,500.00
Operational	420,900.00
Total	1,559,400.00

3. RESULTS

Demirkopru has been operated according to the turbine constraints, forecasted inflows and irrigation water requirement scenarios projected to year of 2042. On the economic analysis, annual electricity production values have been taken into account, which are calculated by (Eq. 4) the up to date electricity purchase price as 0,09 $ /KWh (EPDK, 2017). Electricity purchase prices then projected to 2042 according to the U.S. Energy Information Administration (EIA, 2017). Present values of the annual future benefits and O&M costs determined (Figure 6) for different rates of interest are given below:

$$PV = \frac{FV}{(1+i)^n} \quad (4)$$

where,

P=Present value,

A= Annual Future value,
i= Interest rate,
n=year gap.

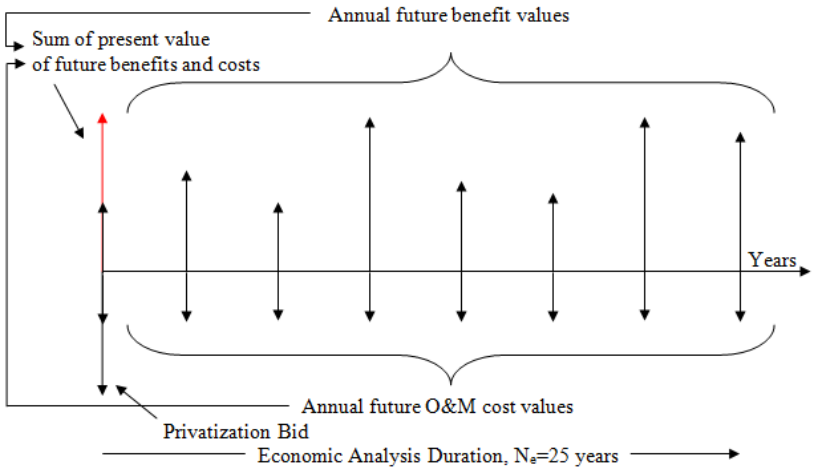

Figure 6. Determining the present values of future annual benefits and costs.

According to the interest rates and scenarios, benefit-cost ratios vary as in Table 2.

Table 2. Benefit-cost ratio values

Interest Rate	1%	3%	5%	7%	10%
Scenario A	2,115	2,092	2,068	2,043	2,005
Scenario B	2,335	2,311	2,284	2,257	2,217
Scenario C	2,285	2,261	2,234	2,208	2,170

Maximum and minimum privatization bids are capital present value costs for any investor. Therefore regarding their first investment maximum and minimum bids are calculated for internal rate of return (B/C=1) and feasible rate (B/C = 1,3) for different rates of interest (Table 3).

Table 3. Privatization bids

	Scenario	i= 1%	i= 3%	i= 5%	i= 7%	i= 10%
Maximum	A	$39.623.549,50	$30.454.316,82	$23.945.438,80	$19.233.829,08	$13.033.668,44
Privatization	B	$47.449.777,07	$36.537.750,65	$28.793.876,24	$23.186.176,36	$15.794.195,73
Bid	C	$45.689.940,48	$35.139.228,73	$27.673.074,21	$22.281.111,28	$15.197.927,43
Minimum	A	$22.276.536,40	$16.993.209,54	$13.246.492,01	$10.539.610,24	$6.993.916,32
Privatization	B	$28.296.711,46	$21.672.774,02	$16.976.059,27	$13.579.877,37	$9.117.398,85
Bid	C	$26.942.991,00	$20.596.987,93	$16.113.903,86	$12.883.673,46	$8.658.730,92

Finally, privatization bid ranges of the crop pattern scenarios vary as below (Figure 7).

CONCLUSIONS

In this study, sensitivity analysis of the privatization bid of Demirkopru hydroelectric power plant has been carried out regarding different kinds of crop pattern scenarios and interest rates. To achieve this, recorded inflows of the Demirkopru reservoir have been examined and synthetically extended over 25 years. Crop pattern change behaviors are considered based on previous tendencies in the basin which took place in between 1995-2012.

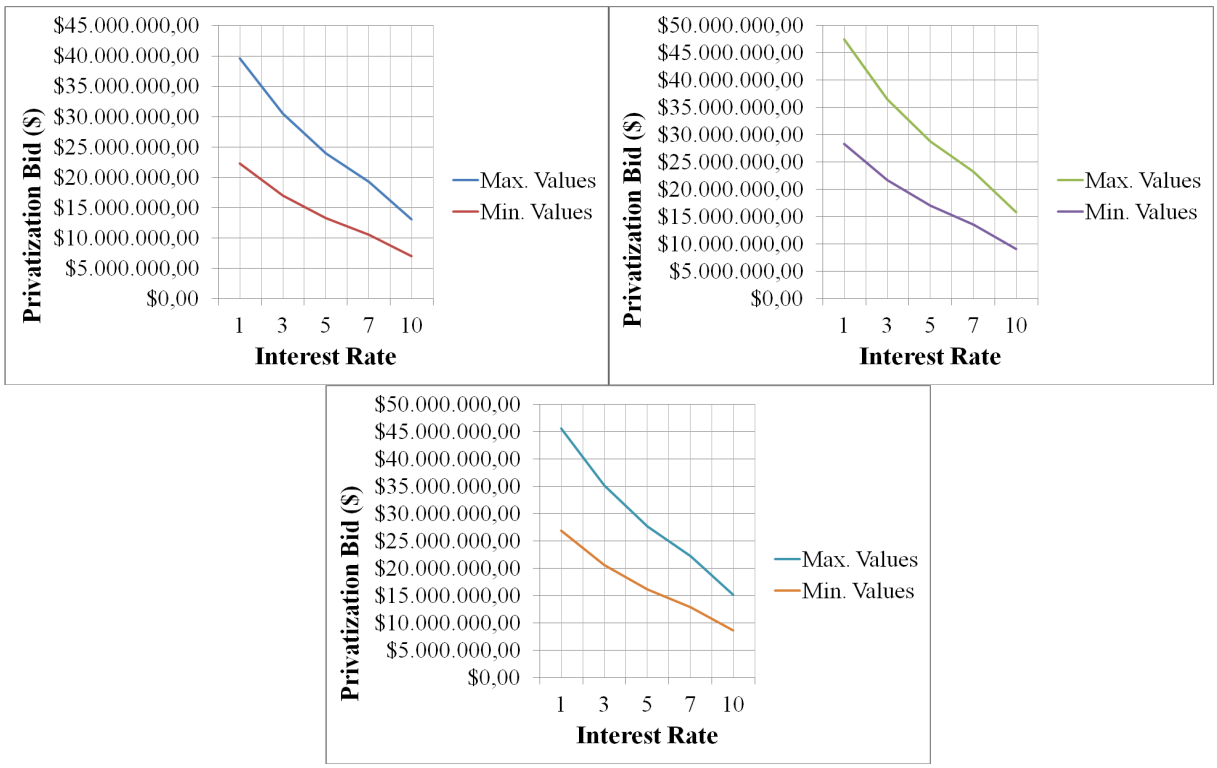

Figure 7. Privatization bid range of scenarios A, B and C respectively

B/C ratios, minimum and maximum privatization bids and privatization bid ranges have been determined. According to the results, maximum privatization bid is acquired by scenario B with the interest rate of 1% which is approximately 47,5 million $. This figure can be considered by governmental authorities as the maximum expected tender income from a privatization attempt. Minimum privatization bid achieved by scenario A with the interest rate of 10% which is approximately 7 million $. This figure indicates that any private company may make a bid for this investment as a capital investment cost as worst case regarding future natural and socio-economic uncertainties. Results suggest a profitable view both to the governmental authorities and the private companies, depending on their agreement on the privatization tender procedure. As a further step of this study, risk analysis can also be conducted regarding the expected probabilities of foreseen situations for future.

REFERENCES

Çetinkaya, C. P. Fistikoglu, O., Fedra, K., and Harmancioglu, N. B., 2008. Optimization methods applied for sustainable management of water-scarce basins. Journal of hydroinformatics;10.1 :69-95.

DSI, 2017. http://www.barajguvenligi.org/genel_barajonemi.htm

Duman, A. O., 2013. Aşağı Gediz sulamalarında bitki deseni ve alım fiyatları ilişkisi. Dokuz Eylül University, Bachelor Thesis, Izmir.

EIA, 2017. http://www.eia.gov/analysis/projection-data.cfm#annualproj

EPDK, 2017. http://www.epdk.org.tr/TR/Dokumanlar/TDB/Elektrik

Gürses, H., 2005. Gediz Havzası'nda sulanan alanlardaki ürün deseni ve ürün alım bedelleri arasındaki ilişkinin belirlenmesi. Dokuz Eylül University, Bachelor Thesis, Izmir.

Hiessl, H., 1987. Risk aspect in the determination of optimal cropping patterns. Engineering reliability and risk in water resources; 124: 485-498.

Howitt, R. E., Sexton, R. J., 1998. The optimal joint provision of water for irrigation and hydropower. Journal of environmental economics and management; 36: 295-313.

Kaya, K. and Koç, E., 2015. Enerji üretim santralleri maliyet analizi. Mühendis ve makina; 56: 61-68.

Proceedings of the 10th World Congress of EWRA 'Panta Rhei', 5-9 July 2017, Athens, Greece
© 2017 *European Water Resources Association*

GIS based analytic hierarchy process in determination of suitable site for water storage

I. Ahmad[1] and M.K. Verma[2]
[1] *Department of Civil Engineering, National Institute of Technology Raipur, G.E. Road, Raipur, Chhattisgarh - 492010, India*
[2] *Chhattisgarh Swami Vivekanand Technical University, Bhilai, Chhattisgarh - 490001, India*
[*] *e-mail: iahmad.ce@nitrr.ac.in*

Abstract: The need of the hour is to tap maximum possible water available in the river basin that can be utilized especially during the period of agricultural drought. This can be materialized by creating water storage structures, for this purpose the first task could to be the identification of suitable location for water storage sites. With the advent of remote sensing and GIS techniques, it becomes easier for water resources planner to identify the suitable location of water storage structure within the basin. In the present study an attempt has been made to identify the suitable locations in the upper basin of Sheonath River in Chhattisgarh State, India. Based on the various physical characteristics of the basin, GIS based Multi-Criteria Evaluation technique is being applied to determine the most suitable water storage sites. For this purpose runoff, hydrologic soil group, land use, lineament, slope, stream order and settlement data are used. Raster layers were formed based on the mentioned data; each layer has been given percentage importance. For determining the percentage importance, Analytic Hierarchy Process (AHP) is used. After determining the percentage importance all the layers are overlaid in GIS to produce suitable location for water storage. This mapping helps in selecting potential site for water storage structures.

Key words: GIS, remote sensing, water storage, runoff, hydrologic soil group, land use, stream order, multi-criteria evaluation, analytic hierarchy process

1. INTRODUCTION

Water availability for different purposes particularly for irrigation and domestic is of great concern in the near future. Hence, it becomes necessary to tap the maximum possible water within the river basin. Water harvesting technique is one of the techniques to tap the water by constructing storage structures like check dams, storage tanks, stop dams etc. Water storage serves like an insurance mechanism acting as a barrier to the variability of rainfall (Payen, Faures and Vallee, 2012). Water storage structures are one of the important components of watershed development which not only collects and stores water but can also be utilized to recharge the ground water (Ahmad and Verma, 2016). Storage structures require considerable investment and hence it is important to identify the suitable location of these structures before execution. Decision making and planning about the required number and type of water storage structures to be constructed using remote sensing and GIS techniques is extremely important to avoid huge investment (Singh et al., 2009). These techniques enable us to perform watershed analysis in shorter time and in a cost effective manner. A number of studies have been reported for site suitability using multi-criteria evaluation system and analytic hierarchy process (Ahmad and Verma, 2016; Ahmad and Masood, 2013; Bamne et al., 2014; Banai-Kashani and Reza, 1989; Bodin and Gass, 2004; Gavade et al., 2011; Hass and Meixner, 2005; Satty, 1980; Salih and Tarif, 2012; Teknomo, 2006; Triantaphyllou, and Mann, 1995). Analytic Hierarchy Process (AHP) is used as a decision-making tool to determine the percentage importance of various parameters used in the determination of suitable sites. The objective of the present paper is to identify suitable location for water storage site using Multi-criteria Evaluation technique under the guidelines of Integrated Mission for Sustainable Development (IMSD) (IMSD, 1995).

2. STUDY AREA DESCRIPTION

A portion of Upper Sheonath sub-basin was considered for this study. The study area extends between latitudes 20º25'00" N and 21º00'00" N, and longitudes 80º26'00" E and 80º55'00" E. The study area comprises of Durg (area= 93.52 sq.km.), Rajnandgaon (area= 991.83 sq.km.) Districts of Chhattisgarh state and Gondia (area= sq.km.), Garchirolli (area= sq.km.) districts of Maharashtra State. Total geographic area of the upper Sheonath basin considered is 1395.89 sq.km.. Study area was influenced by four rain gauge stations namely Amabagarh Chowki, Dongargaon, Doundi Lohara and Mohala. The study area map is shown in Figure 1. For achieving the objective several spatial and non-spatial dataset were used namely, Land use from NRSC Hyderabad, ASTER GDEM, Soil from NBSS&LUP, hydrological data from Chhattisgarh Water Resources Department & Central Water Commission, Bhubaneswar, India.

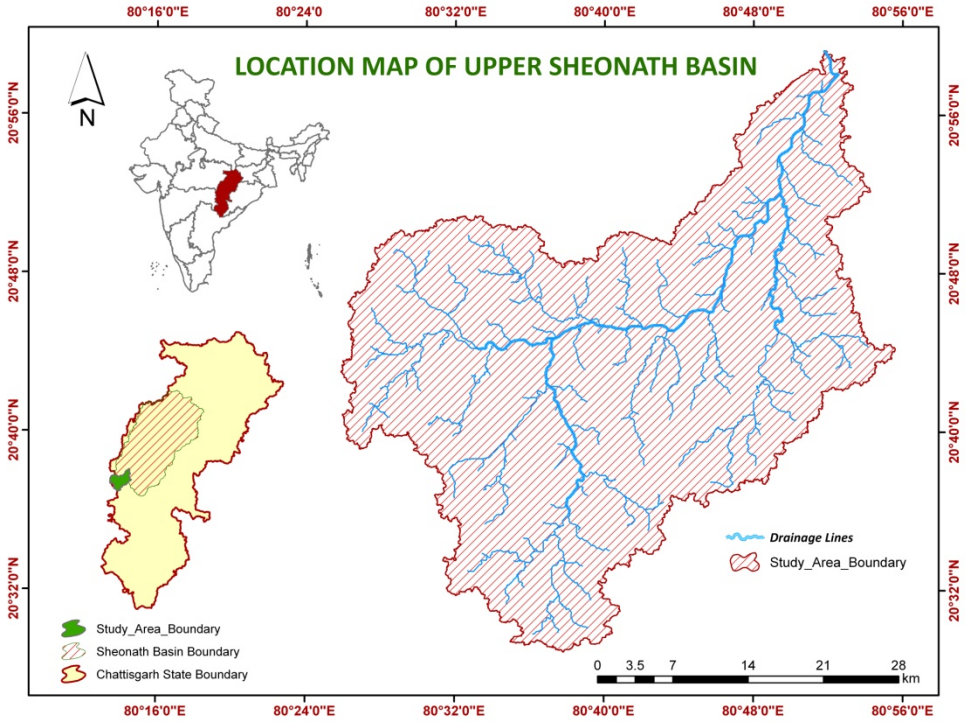

Figure 1. Location map of Upper Sheonath Basin

3. MATERIALS AND METHODS

To achieve the objectives of the study both spatial and non-spatial data are required which includes LULC from National Remote Sensing Agency, Hyderabad; Digital Elevation Model (DEM) from ASTER GDEM; Topographic Sheets from Survey of India (SOI); Soil Data from NBSS & LUP, Nagpur and Rainfall Data from Chhattisgarh WRD Raipur and CWC Bhubaneswar.

The data obtained were digitized and converted into digital format using in GIS for creating various criteria based layers. GIS based Multi-Criteria Evaluation is used to identify the most suitable sites for water storage. The input parametric criteria are runoff, hydrologic soil group, land use, lineament, slope, stream order and settlement data are used. AHP is applied to these parameters to determine the percentage importance. The methodology adopted t achieve the objective in shown with the help of flowchart in Figure 2

As per the Integrated Mission for Sustainable Development (IMSD) guidelines following criteria have been followed for selecting the suitable sites for water storage structures (IMSD, 1995; Padmavaty et al., 1993; Singh et al., 2009):

1. The slope should be less than 15%
2. The land use may be barren, shrub land and river bed.
3. The infiltration rate of the soil should be less.
4. The type of soil should be sandy clay loam.

The suitability of water storage structure is described with the help of Suitability Level Index. Gosschalk (2002) has described the suitability levels for regional dams scaled from 1 to 9. In this study suitability levels were in the range from 1 to 3. '1' for least suitable, '2' for moderate suitable and '3' for highly suitable. The Suitability Level Index adopted in the study is shown in Table 1. Suitability level factors includes Runoff, LULC, Slope, Soil type, Stream order, lineament.

The spatial data were used to prepare various thematic map's viz. drainage map, stream order map, land use map, slope map, settlement map, soil map and lineament map.

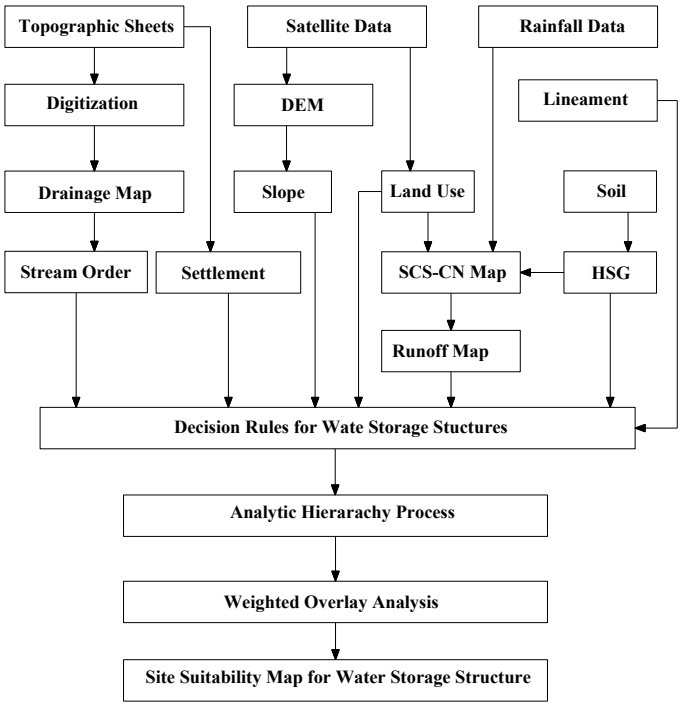

Figure 2. Flowchart showing the adopted methodology

Table 1. Suitability Level Index for different parameter for identifying potential water storage structures

Parameter	Suitability Level		
	1	2	3
Runoff Potential	Low	Moderate	High
LULC	Build Up, Plantation	Forest, Wasteland	Agriculture, Water bodies
Slope	High Slope, Moderate to High Slope	Moderate Slope	Gentle Slope, Level to Gentle Slope
Soil	HSG Group A & B	HSG Group C	HSG Group D
Stream Order	1st & 2nd Order	3rd & 4th Order	5th, 6th & 7th Order
Lineament	Fracture, Fault & Fold (100 m Buffer)	---	---
Settlement	500 m Buffer around the village and 1000 m Buffer around the towns	---	---

3.1 Analytic Hierarchy Process

Analytic Hierarchy Process (AHP) is one of Multi Criteria decision-making method that was originally developed by Prof. Thomas L. Saaty (1987). This method is used to determine the percentage importance of the parameters used in the identification of suitable sites for water storage in accordance with the guidelines laid by IMSD. The AHP procedure involves performing comparison of pairs of parameters within a set of reciprocal matrices. In comparing pairs of factors,

the AHP scale of relative importance is used in the scale 1 to 9. The AHP scale of paired comparison with its description is listed in Table 2 (Satty, 1987; Banai-Kashani, 1989).

Table 2. AHP Scale for pair wise comparison

Intensity of Importance	Description
1	Equal importance – two parameter contributes equally to the objective
3	Moderate importance – slightly favour one parameter over another
5	Strong importance – strongly favour one parameter over another
7	Very strong importance – very strongly favour one parameter over another
9	Extremely strong importance – highest possible order of importance of one parameter over another
2, 4, 6, 8	Intermediate values between the intensity of importance
Reciprocal of above numbers	If an activity has one of the above numbers assigned to it when compared with a second activity, then the second activity has the reciprocal value when compared to the first.

The number of comparison can be determined using

$$no.of\ comparison\ = n(n-1)/2 \tag{1}$$

where, n = number of parameter

After formation of pairwise comparison matrix, priority vector is computed (the normalized Eigen vector of the matrix). The pair-wise comparison matrix is normalized by dividing the values by the sum of each column. A new matrix is formed and the normalized principal Eigen vector (or the priority vector) can be obtained by averaging across the rows.

The relative importance given to the parameters one over another is acceptable if the consistency ratio (CR) is less than 10 %. If it increases 10%, a new value is assigned in the pair-wise comparison matrix. CR is computed as:

$$CR = CI/RI \tag{2}$$

where, CR = Consistency ratio
CI = Consistency index
$= (\lambda_{max} - n)/(n-1)$
λ_{max} = Principal Eigen value
= value obtained from the summation of products between each element of Eigen vector and sum of columns of reciprocal matrix.
RI = Randomness Index

RI which is derived from a sample of size 500 of a randomly generated reciprocal matrix using the scale 1/9, 1/8 . . . . . 1 . . . . . 8, 9, is given by the size of the matrix (or the number of parameters, n, in the comparison matrix) (Saaty, 1987; Banai-Kashani, 1989). When n is 1, 2, 3, 4, 5, 6, 7, 8, 9, 10 corresponding RI will be 0, 0, 0.58, 0.9, 1.12, 1.24, 1.24, 1.32, 1.41, 1.45, 1.49 respectively.

4. RESULTS

Spatial information on runoff, LULC, slope, soil, stream order, lineament and settlement plays a critical role in site selection for water storage structure. Information on these primary and secondary layers is given below.

4.1 Runoff Potential

Curve number (CN) map is prepared to determine the potential runoff in the study area. CN is basically a coefficient that reduces the rainfall to runoff. It depends upon two parameter land use and hydrologic soil group (HSG) (Ahmad et al., 2015). The CN ranges from 0 to 100, 0 implies no

runoff condition and 100 imply rainfall is equal to runoff. Land use map was procured from National Remote Sensing Agency (NRSC) Hyderabad in the scale of 1:250,000. As per NRSC (ISRO) the study area has been classified in buildup, plantation, forest, wasteland, agriculture (rabi, kharif, zaid, double/triple, current fallow) and water bodies. The same is shown in Figure 3 (f). Soil data has been procured from National Bureau of Soil Survey & Land Use Planning, Nagpur. The same is converted to digital format using ArcGIS. For the study purpose it is required to group the various soil. As per USDA Natural Resources Conservation Services (NRCS) (NRCS, 2001; Subramanya, 2013), depending upon the infiltration and runoff potential, soil is categorized into four groups A, B, C & D known as Hydrologic Soil Group [HSG]. Group A soil very low runoff potential, Group B low runoff potential, Group C soil moderate runoff potential and Group D soil is having high runoff potential. The spatial extent of these soil groups is shown with the help of Figure 3 (d). The extent of Group A soil (Entisol) is 6.27 sq. km., Group B (Inceptisol) soil 707.77 sq. km., Group C (Alfisol) soil 462.70 sq. km. and Group D (Vertisol) soil 217.98 sq.km. These two parametric layers are merged together to get the CN grid map. The runoff potential is based on the CN grid map, if CN ranges from 26-50 then low runoff, 50-75 moderate runoff and 75-100 high runoff.

4.2 Stream Order

Stream order map was prepared with the help of DEM analysis in ArcGIS. Spatial analyst tool is being applied for extracting the stream lines and stream order tool is utilized to derive the order of the stream lines. As per the GIS analysis, stream order ranges from 1st order to 6th order. The stream order map is shown in Figure 3 (d).

4.3 Lineament

Lineament involves fractures, faults and folds in identified in the study area. Lineament data is collected form Chhattisgarh Council of Science & Technology and the analyzed in GIS, creating a buffer of 100m around the lineaments. The lineaments are shown in Figure 3 (c).

4.4 Settlement

As per the 2001 census, there are 269 villages and 2 towns in the study area. The locations of these settlements were identified in terms of latitude and longitude. A buffer zone of 500m around the village location and 1000m around the towns were created. The settlement is shown in Figure 3 (c).

4.5 Slope

Slope is one of the important factor for deciding the location of storage structure. For deriving the slope layer ASTER GDEM (Property of METI and NASA) with 30m resolution DEM is used to determine the slope. The slope of the study area ranges from 0-80.69 %. The same is subdivided in sub-divided into 5 sub-groups; high slope (> 64 %), moderate to high slope (48-64 %), moderate slope (32-48 %), gentle slope (16-32 %) and level to gentle slope (0-16 %). The slope map of the study area has been shown in Figure 3 (e).

4.6 AHP Application

AHP is applied to determine the priority of each parameter over one another (i.e. relative importance) and is expressed in terms of relative weights (percentile). For all the seven parameters the relative importance is derived (Table 4). Thus, a common scale (0 % to 100 %) is obtained from AHP procedure. The runoff parameter emerges as the most important (relative weight 55%) followed by slope (11%), stream order (10%), HSG (10%), Land use (6%), settlement (4%) and lineament (4%). This judgement is checked for its consistency.

Principal Eigen vector = 7.75

Consistency Index (CI) $= (\lambda_{max} - n)/(n-1)$

= 0.13

For n = 7, RI = 1.32

Consistency Ratio (CI/RI) = 9.8 % (which is less than 10 %), hence the judgement is acceptable. This implies that the comparisons were performed in Step of Table 4 with good percentage importance (or weightage) judged for each parameter is suitable to for overlay.

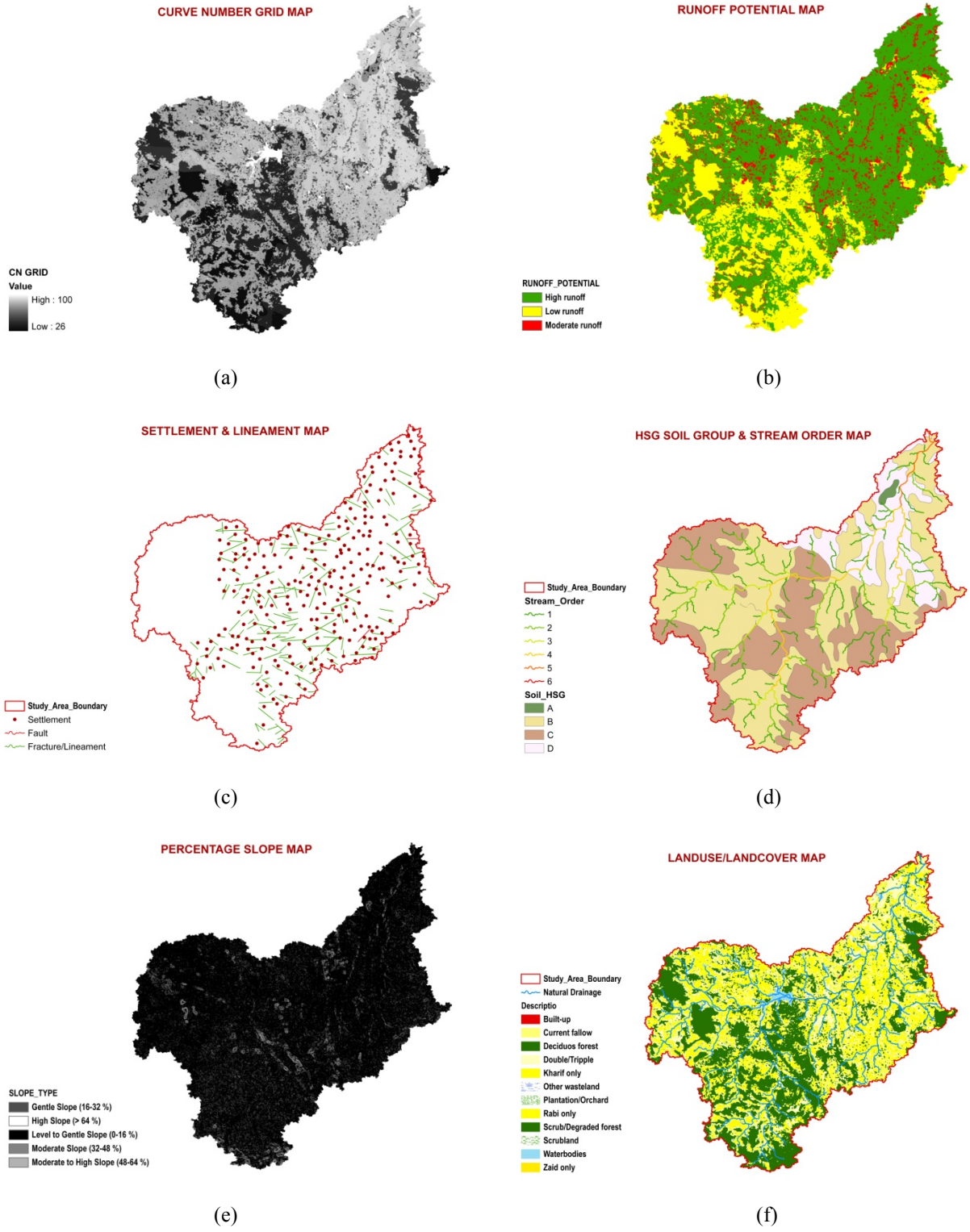

Figure 3. (a) Curve number (b) runoff potential (c) settlement & lineament (d) HSG & stream order (e) slope (f) LULC map of the study area

3.7 Weighted Overlay Analysis

To implement the rules laid down in Table 1 and the information layers prepared with their weightage are overlaid in GIS to identify the suitable water storage structure sites. The generated layers are in vector format, for Weighted Overlay Analysis the "Rasterization" of each layer is performed. The first step of data conversion is "Rasterization" for converting different lines and polygon coverage into raster data format. After this, reclassification of all the raster files is processed along with providing the scale value of each unit. A scale value in the range 1 to 3 is used in which '1' is for least suitable, '2' is for moderate suitable and '3' is for highly suitable. Based on this weighted overlay analysis a site suitability map is prepared and presented in Figure 4. It was found that there are 10 number of site under least suitable, 7 number moderate suitable and 3 number highly suitable.

Table 4. Determining the relative weight of parameters

Parameter	Step 1							Step 2							Step 3	
	R	LU	Sl	HSG	SO	L	S	R	LU	Sl	HSG	SO	L	S	Priority Vector	% of Priority
Runoff Potential (R)	1	9	9	9	9	9	9	0.58	0.44	0.68	0.67	0.67	0.36	0.43	0.55	55
LULC (LU)	1/9	1	1/3	1/3	1/3	3	1	0.07	0.04	0.03	0.03	0.03	0.12	0.05	0.05	5
Slope (Sl)	1/9	3	1	1	1	5	3	0.07	0.15	0.08	0.08	0.08	0.20	0.14	0.11	11
Soil (HSG)	1/9	3	1	1	1	3	3	0.07	0.15	0.08	0.08	0.08	0.12	0.14	0.10	10
Stream Order (SO)	1/9	3	1	1	1	3	3	0.07	0.15	0.08	0.08	0.08	0.12	0.14	0.10	10
Lineament (L)	1/9	1/3	1/5	1/3	1/3	1	1	0.07	0.02	0.02	0.03	0.03	0.04	0.05	0.04	4
Settlement (S)	1/9	1	1/3	1/3	1/3	1	1	0.07	0.05	0.03	0.03	0.03	0.04	0.05	0.04	4
Total	1.67	20.33	12.87	13.00	13.00	25.00	21.00	1.00	1.00	1.00	1.00	1.00	1.00	1.00	1.00	100 %

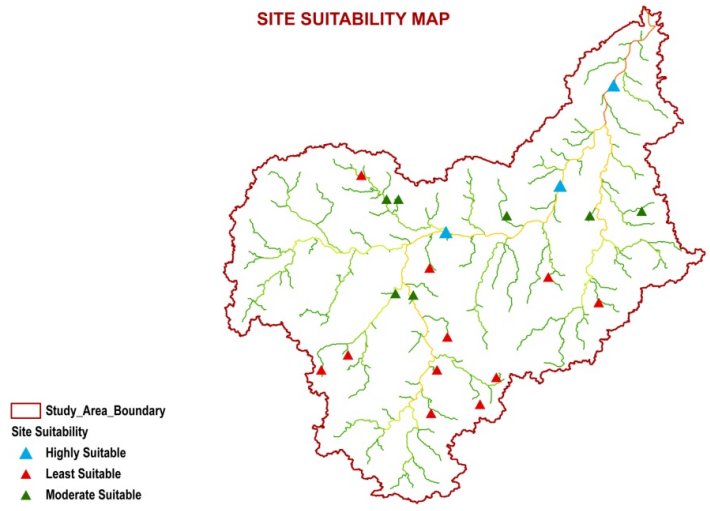

Figure 4. Site Suitability Map for Upper Sheonath River Sub-Basin

4. CONCLUSION

Water harvesting structures are extremely important to conserve precious natural resources like soil and water. The potential sites for Upper Sheonath basin were identified through GIS and AHP process. AHP process helps us in deciding the percentage importance of the parameters applied in determining the suitable location for water storage. With reference to the suitability level index presented in Table 1, the suitable locations identified are over the drainage lines only. Thus, it can be stated that either check dams or regional reservoirs along the drainage lines can be built for possible water storage. There may be other techniques which can be used for water harvesting in the

watershed. This can be achieved by increasing the number of parameters. Increasing the parameters involves more complexity and hence complexity in decision-making. AHP can be best utilized for decision-making in terms priority of parameter one over another. In the present study application of AHP has been demonstrated. AHP easily update suitability levels and weighted score of decision criteria on which the potential sites of water storage are based. The present study also demonstrates the capability of GIS in handling large data set and performing spatial as well as vector analysis.

To appraise the suitability of the selected site, the suitability map was superimposed over the LULC map of the study area and it was found that one of site under the category highly suitable is exactly located over the existing storage structure and in local language it is known as "Mahamara Anicut" in the Rajnadgaon District of Chhattisgarh State, India. This study demonstrated the integrated approach of remote sensing, GIS and AHP.

ACKNOWLEDGEMENT

The authors acknowledge the support provides by Chhattisgarh Council of Science & Technology Raipur, Chhattisgarh, India & State Data Centre, Water Resources Department Chhattisgarh Raipur, India, National Remote Sensing Centre (NRSC) Hyderabad, National Bureau of Soil Survey & Land Use Planning (NBSS&LUP) Nagpur.

REFERENCES

Ahmad I., Verma M. K., 2015. Application of RS & GIS in Estimation of Sub-Basin Runoff Potential using HEC-HMS. International Journal of Applied Engineering Research, 10(20): 41243-41248

Ahmad I., Verma V., Verma M. K., 2015. Application of Curve Number Method for Estimation of Runoff Potential in GIS Environment. International Proceedings of Chemical, Biological & Environmental Engineering, 80: 16-20

Ahmad I., Verma M. K., 2016. Site Suitability Mapping for Water Storage Structures using Remote Sensing & GIS for Sheonath Basin in Chhattisgarh State. International Journal of Applied Engineering Research, 11(6): 4155-4160

Ahmad S. R., Ahmad U., Masood A., 2013. Geo-Spatial Techniques in Selection of Potential Damsite. Pakistan Journal of Science, 65(1): 158-166

ASTER GDEM (NASA and METI) - jspacesystems.or.jp/ersdac/GDEM/E/4.html

Bamne Y., Patil K. A., Vikhe S. D., 2014. Selection of Appropriate Sites for Structures of Water Harvesting In a Watershed Using Remote Sensing and GIS. International Journal of Emerging Technology and Advance Engineering, 4(11): 270-275

Banai-Kashani R., 1989. A New Method for Site Suitability Analysis: The Analytic Hierarchy Process. Environmental Management, Springer, 13(6): 685-693

Bodin L., Gass S. I., 2004. Exercises for teaching the analytic hierarchy process. INFORMS Transactions on Education, 4(2), 1-13

Gavade V. V., Patil D. R., Palkar J. M., Kachare K. Y., 2011. Site Suitability Analysis for Surface Rainwater Harvesting of Madha Tahsil, Solapur, Maharashtra: A Geoinformatic Approach. 12th ESRI India User Conference, India

Gosschalk E. M., 2002. Reservoir Engineering: Guidelines for Practice. Thomas Telford, London

Haas R., Meixner O., 2005. An illustrated guide to the analytic hierarchy process. University of Natural Resources and Applied Life Sciences, Vienna

IMSD, 1995. Integrated Mission for Sustainable Development: Technical Guidelines. NRSA, Hyderabad, India, 1-27.

LULC, Bhuvan (ISRO) - bhuvan.nrsc.gov.in/gis/thematic/index.php

National Engineering Handbook, Part 630, Hydrology, 2001. USDA NRCS

Padmavathy A. S., Ganesha R. K., Yogarajan N., Thangavel P., 1993. Check Dam Site Selection Using GIS Approach. Advance Space Research, 13(11): 123-127

Payen J., Faures J. M., Vallee D., 2012. Small reservoirs and water storage for smallholder farming: The case for a new approach, Agriculture Water Management Business Proposal Document

Saaty T. L., 1980. The Analytic Hierarchy Process (AHP). McGraw-Hill, New York

Saaty R. W., 1987. The Analytic Hierarchy Process - What it s and How it is Used. Mathematical Modelling, 9(3): 161-176

Salih S. A., Al-Tarif A. S. M., 2012. Using of GIS Spatial Analyses to Study the Selected Location for Dam Reservoir on Wadi Al-Jirnaf, West of Shirqat Area, Iraq. Journal of Geographic Information System, 4: 117-127

Singh J. P., Singh D., Litoria P. K., 2009. Selection of Suitable Sites for Water Harvesting Structures in Soankhad Watershed, Punjab using Remote Sensing and Geographical Information System (RS & GIS) Approach – A case study. Journal of Indian Soc. Remote Sens. Springer, 37: 21-35

Subramanya K., 2013. Engineering Hydrology. Fourth Edition McGraw-Hill Education (India) Private Limited, New Delhi.

Teknomo K. , 2006. Analytic Hierarchy Process (AHP) Tutorial

Triantaphyllou E., Mann S. H., 1995. Using the Analytic Hierarchy Process for Decision Making in Engineering Applications: Some Challenges. International Journal of Industrial Engineering: Applications and Practice, 2(1): 35-44

Proceedings of the 10th World Congress of EWRA 'Panta Rhei', 5-9 July 2017, Athens, Greece
© 2017 *European Water Resources Association*

Water resources management and lack of water in the Zayandehroud river basin, Iran

A. Sharifi* and R. Mirabbasi
Department of Water Engineering, Faculty of Agriculture, Shahrekord University, Shahrekord, Iran
* *e-mail: areza_sharifi@yahoo.com*

Abstract: Iran is located in Middle East region and is facing a serious water crisis in recent decay, while in the past has been one of the leading countries in the field of water resources management. Zayandehroud river basin which is located in the center of Iran is experiencing different problems due to lack of available water in recent years. Some of the effective factors on the crisis are decreasing the amount of precipitation, changing in type and time of precipitation, declining the groundwater levels and increasing water demands due to population growth. In this study, we investigated the major reasons of the water crisis in Zayandehroud river basin. For this purpose, we create a conceptual model to unravel the effect of different factors on water shortage in this basin. Agriculture, drinking and industry are the main water consumer sectors in the basin, respectively. Although people and Iranian decision makers believe drought and climate change are the main reasons of the water crisis in this basin, the investigations shows that the mismanagement of water resources has more effect on deficiency of water. In addition, water supply is less than real demands. Therefore, it is necessary to follow long-term solutions in order to sustainable water resources management which lead to overcome this problem in the region with ancient civilization.

Key words: Water crisis, Water resources management, Zayandehroud River, Iran

1. INTRODUCTION

Zayandehroud River, as a crucial river in the center of Iran, has been the main reason of create big civilizations such as Isfahan city. In recent years, a lot of studies have been done on different aspects of the river such as drought and climate change (Gohari et al., 2014; Zareian et al., 2016; Khalili et al., 2016), water resources management and common crop pattern in the river basin (Gohari et al., 2013b), tourism (Khatun Abadi and Rast Ghalam, 2011), etc. But, this river has struggled with different problems especially drought during recent years. Generally speaking, can be divide river problem into three sections, including quantitative, qualitative, and physical issues. The quality of river decreases due to influx and leakage of wastewater and agricultural sewage containing fertilizers. On the other hand, the number of flood has increased due to reduce in soil humidity.

From the physical point of view, the active bed land of the river has been limited by the illegal seizures. In recent years, reduction the volume of the river and tourism attractions are worsen the situation. Because the center parts of Iran have the arid and semi-arid climate and the river has key role in this region, the discharge of the river is more important than other aspects. A number of water transfer projects have been implemented and designed for the basin and some researchers investigated the effects of these projects on different aspects in the basin (Gohari et al., 2013a; Safavi, 2014). Safavi (2014) announced that water transfer is a necessity for the Zayandehroud River not a choice. In addition, he proposed three solutions for solve the water crisis in the basin without water transfer including increase irrigation efficiency and save water in agriculture, optimal management of water in agriculture and water resources development through the watershed management operations. Ziaee (2014) investigated the situation of water resources in the Zayandehroud River basin and proposed five solutions to overcome the water problems, including management and save in water consumptions, cloud seeding, water transfer from Persian Gulf,

water transfer from adjacent basins and migrating people to other places with sufficient water resources.

Although each study has investigated the water crisis in the basin and proposed the solutions, some of the solutions need to more consideration. In this study, first we investigated the major reasons of water crisis in the basin and then try to propose some solutions for better water resources management.

2. STUDY AREA

Zayandehroud River is the most strategic river in the Iran central plateau (Madani and Mariano, 2009). Fig. 1 shows the river basin which covers an area of about 26917 km^2. The basin is located in four provinces of Iran, including Isfahan, Chaharmahal va Bakhtiari, Fars and Yazd. Although most of the basin is located in Isfahan province, 90 % of water in the river provides from Central Zagros Mountains locating in Chaharmahal va Bakhtiari province. This river starting from the mountains ends in Gavkhuni Marsh as one of the preserved marsh under the Ramsar convention (The Ramsar Convention of Wetlands, 1971). The annual precipitation in the basin is very variable and varies from 1500 mm in the mountains (west of the basin) to 50 mm near the Marsh (east of the basin). Table 1 shows some main characteristics of the basin.

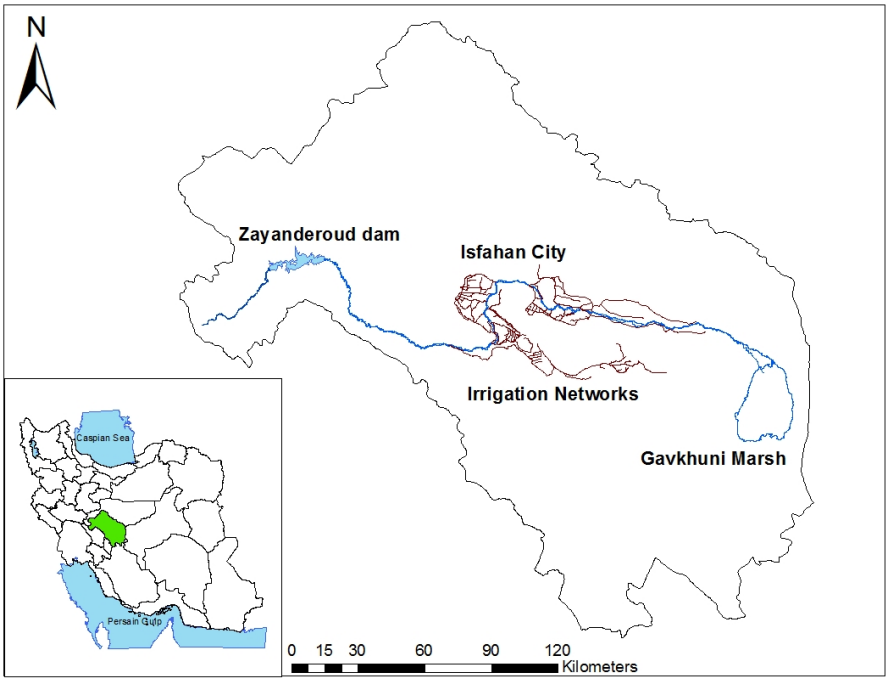

Figure 1: The Zayandehroud River basin

Agriculture is the biggest water consumer in the basin, as about 73 % of available water is used in this sector (Gohari et al., 2013a). On the other hand, the river is the main source of drinking water of Isfahan, Yazd and several cities around them. Industry is another water consumer sector in the basin as well.

Table 1: Some general characteristics of Zayandehroud River basin

Elevation range (m)	1470-3974
Annual average precipitation range (mm)	50-1500
Annual temperature range (°C)	3-30
Annual average humidity range (%)	24-57
River length (Km)	350

3. THE EFFECTIVE FACTORS ON DEFICITY OF AVAILABLE WATER

3.1 Agriculture development

As main occupation of people who lived in the region, agriculture in the basin has changed compared with the past. There was a specific structure and regime in order to divide water among the farmers which codified by Sheikh-e-Bahaei who lived in the late 16th and early 17th centuries. But, the situations of the regime changed after construction of Zayandehroud dam in 1970. In this time, there are 6 irrigation networks which are linked the river, including Abshar, Nekuabad, Mahyar, Borkhar, Rudasht and traditional networks. Table 2 shows some characteristics of the modern networks. Although some of the modern networks were built instead of traditional networks, most of them are developed as can be seen in Table 2 and irrigated farmland reach from 45000 ha to more than 130000 ha. In addition, pumping the water from the river caused most of rain fed land changed and became garden. The latest regime was for traditional networks while the situations were changed. In addition, drinking and industry sectors are added to the basin. As a results, it is necessary to codify new regime for the river.

Dinpashoh et al. (2011) showed the amount of ET_0 in Isfahan was decreased between 1964 and 2005. But, Zareian et al. (2016) stated in the best and worsen situations the annual mean temperature will increase 0.56 and 1.31 °C from 2015 to 2044, respectively. In addition, Sharifi and Dinpashoh (2014) showed 10 % increase in annual mean temperature causes 5 % increase in ET_0. Inasmuch as the amount of ET_0 has direct impact on actual evapotranspiration, the required water for irrigation will increase in the future.

Table 2: The main characteristics of modern irrigation networks in Zayandehroud river basin

Name of irrigation network		Length of Main channel (Km)	Discharge of main channel (m^3/s)	Cultivation area (ha)	
				Modification	Development
Nekuabad	Left	60	50	21300	17100
	Right	35.3	15		
Abshar	Left	36	15	4350	10650
	Right	32	15	4050	9950
Rudasht		89	50	16200	26000
Borkhar		86	12	0	3600
Mahyar		82	12	0	22000

3.2 Water transfer

Zayandehroud River is located in the arid and semi-arid area and has faced various droughts during the history. From about 400 years ago, water transfer was one the solutions in order to compensate deficiency of available water in the basin. The first water transfer project in the basin was operated in 1959. After that, several projects were operated for transfering water from Dez and Karun river basins to Zayandehroud basin. Table 3 shows the water transfer projects in the basin. Some of them are under study. Although water transfer projects were operated during the last decades, water shortage is very obvious in the basin and has affected all sectors especially agriculture. Gohari et al. (2013a) showed that the water transfer leads to water supply increase in the basin. Moreover, they stated the expectation due to operate water transfer projects is more than volume of water transferring by the projects. As can be seen in Fig. 2, the circle of water demand is bigger than water supply circle while these circle have to be equal.

3.3 Declining groundwater resources

Declining groundwater resources level is one of the reasons of available water crisis in the basin. There were a lot of springs in the river bed and it was the main reason for the river name. Because,

the level of groundwater was very high and it fed the river. In recent years, the situations have changed and the river loses its water along its path due to declining groundwater level. The main cause for this event is water extracting from aquifers by unauthorized wells.

There are about 1500 unauthorized wells around the river bed and most of them have been dug in last two decades (Isfahan Regional Water Authority, 2015). There are several separate aquifers in the basin. The River crosses trough some of them along its path, including Lenjanat, Najafabad, Isfahan-Borkhar and Kohpaieh-Segzi. The lack of volume of groundwater in the aquifers has shown in Fig. 3. It has been reduced about 90, 300, 3000 and 275 MCM in Lenjanat, Najafabad, Isfahan and Kohpaieh-Segzi plains from 1995 to 2014, respectively (Kolahdoozan et al., 2015).

Table 3: Water transfer projects in Zayandehroyd river basin

Name	Year of operation	Annual capacity (MCM)	Length (m)	Donor river basin
Kuhrang Tunnel No 1	1954	297	2800	Karun
Kuhrang Tunnel No 2	1985	246	2873	Karun
Kuhrang Tunnel No 3	2017 (expected)	268	23409	Karun
Cheshmeh-Langan Tunnel	2005	120	13700	Dez
Khadangestan Tunnel	Under study	80	11300	Dez
Yalan Tunnel	Under study	165	23000	Dez
Pashandegan Tunnel	Under study	245	18800	Dez
Goukan Tunnel	Under study	525	38000	Dez
Beheshtabad Tunnel	Under study	746	65000	Karun

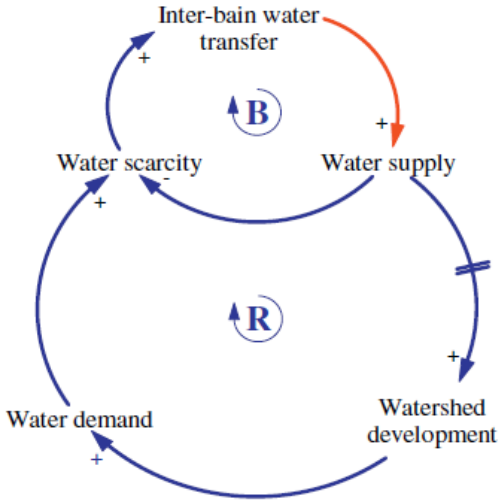

Figure 2: The main loops of the Zayandehroud river system (Gohari et al., 2013a)

3.4 Changes in the amount and type of precipitation

Generally speaking, the amount and type of precipitation in each region have varied in the time span. In Zayandehroud basin, the type of precipitation has changed and most precipitation is as rain in recent years. As a result, glaciers as regular source of steady flow in the river have declined with disturbing trend. On the other hand, the time of precipitation has changed and most precipitation fall in autumn instead of winter.

Zareian et al. (2016) showed that the annual precipitation in the basin under A2 and B1 emission scenarios in ideal situation will decrease about 13 and 6.5 % from 2015 to 2044. Table 4 shows the precipitation change under emission scenarios in different situations in the basin. For more information about emission scenario please refer to Solomon (2007).

The change in type, amount and time of precipitation cause input water to the Zayandehroud dam reservoir has decreased while some water transfer projects have operated in last two decades. Fig. 4 shows the amount of water entering to the reservoir in the time period. As can be seen in the

Fig. 4, the average of input water is about 1000 MCM in recent years, while it was about 1500 MCM from 1985 to 2005.

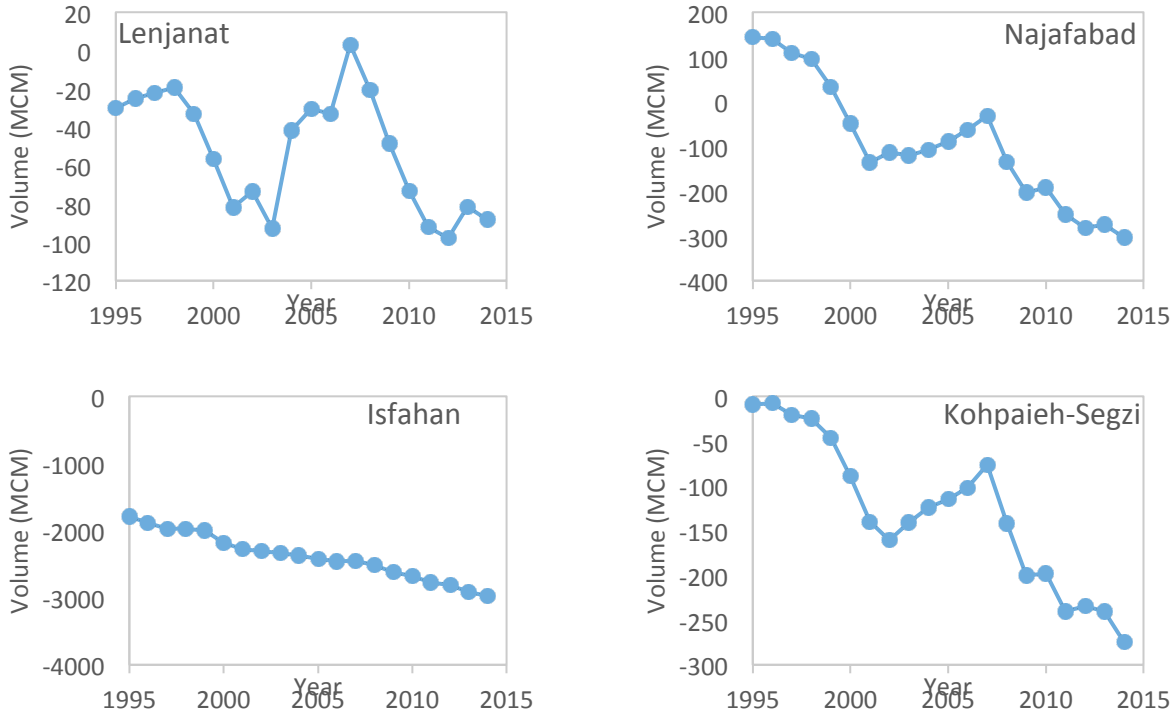

Figure 3: Lack of volume of groundwater in the aquifers from 1995 to 2014.

Table 4: Declining annual precipitation under the different emission scenarios between 2015 and 2044 (Zareian et al., 2016)

Ideal Pattern		Moderate Pattern		Critical Pattern	
A2	B1	A2	B1	A2	B1
-12.99	-6.56	-20.37	-13.14	-29.60	-21.41

4. DISCUSSION

Madani (2014) investigated the causes of Iran's water crisis and proposed several solutions in order to solve the problem. He stated that there are three main causes for the problem, including population growth and distribution, inefficient agriculture and mismanagement and thirst for development. Population distribution is not uniform in the basin. The river provides drinking water for more than 5 million people living in three provinces while about 2 million of them live in a city (Isfahan).

In recent years, people living in rural area have immigrated to urban area inasmuch as they did not have enough water for irrigate their farms.

On the other hand, most people and authorities do not believe most of the basin is located in arid and semi-arid area. For example thirst of development has been continued in different aspects, especially agriculture without any attention to the environment and limitation of water resources. Generally speaking, people living in the arid and semi-arid area in all over the world have been struggling with deficiency of available water. As a result, attention to the environment and water are very important in any project and program in the regions such as Zayandehroud basin. Drying Gavkhuni marsh and reduction of groundwater resources have caused people pay more attention and become vigilant to water crisis in recent years.

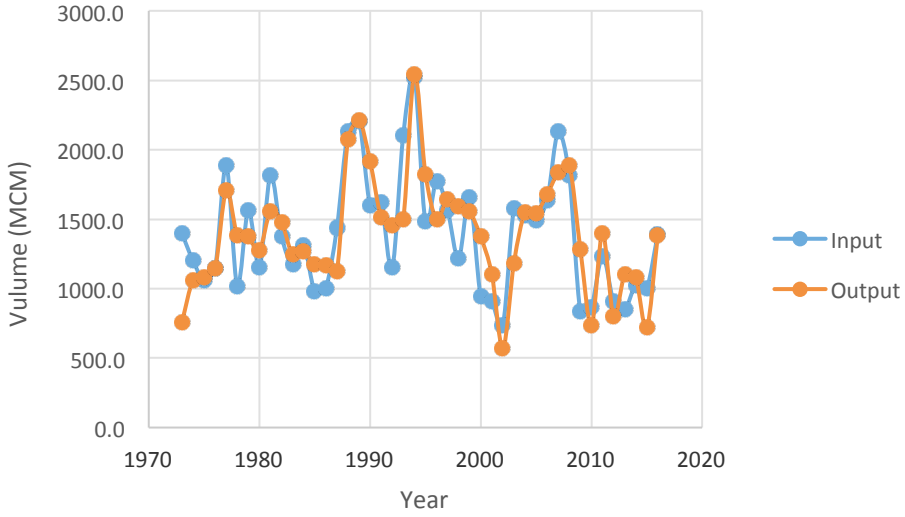

Figure 4: The volume of input and output water to Zayandehroud dam reservoir between 1973 and 2016.

In the basin, there is no balance between supply and demand, and the water demand is more than potential of the basin water supply. Water transfer projects are the sign of this reality. In recent years, water supply has been paid more attention compared with demand control. It led to groundwater extract increased inasmuch as all demand did not provide from the surface water resources, especially the river. Therefore, people living in Zayandehroud basin are facing water-bankruptcy situation. Madani et al (2016) stated Iran is suffering from a socio-economic drought (water-bankruptcy) because water demand is more than natural water supply.

Thirst of development led to illegal withdrawal from the river and groundwater resources increased in recent years. As a result, it had irreparable impacts to water resources.

Revising the crop pattern and increase water efficiency have to take into account as the first solution in order to overcome water crisis in the basin. Undoubtedly, crop pattern in the basin is not suitable to the basin climate. For example in 2016, more than 5000 hectares of rice was planted in the basin (according to the Ministry of Agriculture-Jahad statistics). From the water efficiency point of view, although changing irrigation method from traditional to under pressure increased the efficiency, rose the area under cultivation in recent years. For revising the crop pattern, it is necessary to educate and motivate farmers and compensate their possible financial losses.

Codification of new regime for the river is another way to overcome the river problems. As mentioned, the main principles of the last regime have changed and new consumers have added to the river; therefore, it is necessary to define new regime. For this purpose, first the demands in the basin have to determine with respect to new situations.

As third solution, integrated water resources and consumptions management can be very useful for the basin. About 10 years ago, hydrological boundaries were replaced by political boundaries. It created a competition among the people in the provinces in order to water withdrawal from the river and development and changed the natural situations. Integrated water resources management (IWRM) is a general concept and has different aspects.

German federal ministry of education and research (2015) which has worked on IWRM in several countries all over the world such as Jordan and Iran proposed four aspect for IWRM including capacity development, decision support, governance and participation. Some researchers investigated the IWRM in Zayandehroud basin such as Mohajeri et al. (2016).

Raising awareness about water crisis and diplomacy, as forth solution, can play key role in order to solve the conflicts among the people in the provinces and different sectors. It must be conceded that for sustainable water management, it is essential to do it; however, the political cost of it is very high (Madani, 2016).

5. CONCLUSION

Water shortage in Zayandehroud river basin is a complex problem and need to complex solutions. Therefore, it cannot be solved immediately. In recent decades, a lot of solutions have been proposed and most of them focus on structural ways, especially water transfer from other basins. These solutions solved the problem impermanent, but after some years the problem exacerbated. Investigation of the solutions showed that it did not compatible with the reality. In this study, after the consideration of the effective factors on water deficiency in Zayandehroud river basin, some solutions were proposed, including revising the crop pattern, increasing water efficiency, codification of new regime, IWRM, rising awareness and diplomacy.

In conclusion, for sustainable water management long-term solutions are needed. Zayandehroud decision makers have to realize the basin realities and try to focus on water resources management and demands control instead of structural methods.

REFERENCES

Dinpashoh, Y., Fakheri-fard, A., Moghaddam, M., Jahanbakhsh, S., Marina, M., 2004. Selection of variables for the purpose of regionalization of Iran's precipitation climate using multivariate methods. Journal of Hydrology; 197:109–123.

Khatuabadi, A., Rastghalam, M., 2011. Analysis of the development indices in the Chadegan (in the west of Isfahan).Quarterly Journal of Human Geography; 3(3): 43-55. (In Persian)

Isfahan Regional Water Authority, 2015. Sing life, pass on half a century of important construction activities. (In Persian)

German federal ministry of education and research, 2015. Integrated water resources management: from research to implementation. Helmholtz center for environmental research, Leipzig.

Gohari, A., Eslamian, S., Mirchi, A., Abedi-Koupaei, J., MasahBavani, A., Madani, K., 2013(a). Water transfer as a solution to water shortage: A fix that can backfire. Journal of Hydrology; 491 (2013) 23–39.

Gohari, A., Eslamian, S., Mirchi, A., Abedi-Koupaei, J., MasahBavani, A., Wang, D. Madani, K., 2013(b). Climate change impacts on crop production in Iran's Zayandeh-Rud River Basin; Science of the Total Environment 442: 405-415.

Gohari, A., Bozorgi, A., Madani, K., Elledgeand, J., Berndtsson, R., 2014. Adaptation of surface water supply to climate change central Iran. Journal of Water and Climate Change; 5(3): 391- 407.

Khalili, K., Nazeri Tahoudi, M., Mirabbasi, R., and Ahmadi, F., 2016. Investigation of spatial and temporal variability of precipitation in Iran over the last half century. Stochastic Environmental Research and Risk Assessment; 30(4): 1205-1221.

Kolahdoozan, A., Dinpashoh, Y., Mirabbasi, R., Asadi, E., Darbandi, S., 2015. Effect of Zayandehroud River Dry Becoming on Najafabad Aquifer Oscillations during Past Two Decades. Iranian Journal of Soil and Water Research, 46(1): 83-91. (In Persian).

Madani, K., 2014. Water management in Iran: what is causing the looming crisis? J. Environ. Stud. Sci.; 4:315-328.

Madani, K., AghaKouchak, A., Mirchi, A., 2016. Iran's Socio-economic Drought: Challenges of a Water-Bankrupt Nation, Iranian Studies; 49: 997-1016.

Mohajeri, Sh., Horlemann, L., Sklorz, S., Kaltofen, M., Ghanavizchian, Sh., Nuñez V. T., 2016. Integrated Water Resource Management in Isfahan: The ZayandehRud Catchment. Springer International Publishing, Switzerland.

Sharifi, A,. Dinpashoh, Y., 2014. Sensitivity Analysis of the Penman-Monteith reference Crop Evapotranspiration to Climatic Variables in Iran. Water Resources Management; 28:5465–5476.

Safavi, H. R., 2014. Water transfer to Zayanderoud Basin, a choice or a necessity. Technical-Professional Journal of Iranian organization for engineering order of building (Danesh-Nama); 23(3): 84-95. (In Persian).

Solomon, S., 2007. Climate change 2007-the physical science basis: Working group I contribution to the fourth assessment report of the IPCC. UK: Cambridge University Press.

Zareian, J., Eslamian, S. Safavi, H. R., 2016. Investigating the Effects of Sustainability of Climate Change on the Agriculture Water Consumption in the Zayandeh-Rud River Basin. Journal of science and Technological Agriculture, Natural Resources, Water and Soil Science; 20(75): 113-128 (in Persian)

Ziaee, L., 2014. Water crisis in Zayanderoud basin, components and solutions. Technical-Professional Journal of Iranian organization for engineering order of building (Danesh-Nama); 23(3): 8-21. (In Persian).

Proceedings of the 10th World Congress of EWRA 'Panta Rhei', 5-9 July 2017, Athens, Greece
© 2017 *European Water Resources Association*

Effect of land use change on flood extent in the inflow stream of lake Paralimni, Cyprus

C. Sophocleous and I. Nalbantis*
[1] *Centre for the Assessment of Natural Hazards and Proactive Planning and Laboratory of Reclamation Works and Water Resources Management; School of Rural and Surveying Engineering, National Technical University of Athens, Athens, Greece*
* *e-mail: nalbant@central.ntua.gr*

Abstract: Land use is a crucial factor that influences flood characteristics such as peak discharge, volume, peak water elevation and inundation extent. It is therefore logical that land use change entails changes in these characteristics, thus leading to increased potential harm. In this work the drainage basin of the Inflow Stream of Lake Paralimni, Cyprus (11.5 km^2) is investigated, which has undergone significant land use changes, primarily due to the conversion of agricultural land into urban space. At the methodological level, both hydrological and hydraulic modelling is used. Regarding hydrological modelling the SCS method is employed, combined with the synthetic Unit Hydrograph of the Institute of Hydrology of UK and the Muskingum method for river routing. Hydraulic modelling is based on the standard step method for solving the energy equation under 1D steady flow conditions. Software packages such as HEC-HMS, HEC-RAS, HEC-GeoHMS and HEC-GeoRAS are used together with a Geographical Information System. Regarding the input data, observed five-minute precipitation depths from three gauges are used for a historical storm event occurred in February 1988 which is known to have caused inundation. Also, a Digital Elevation Model at the resolution of 1 m is used which is based on Lidar data. Two periods with distinct land uses are examined (1983-2003 and 2006-2016), which allows the assessment of the impact of changes in curve numbers and Manning's roughness coefficients. Significant changes in peak flow rate, flood volume and inundation extent were found when passing from the old to the current land uses.

Key words: Land use change; flood mapping; Lake Paralimni, Cyprus; HEC-HMS; HEC-RAS

1. INTRODUCTION

As indicated in the title of the congress EWRA 2017 (Panta Rhei – Everything Flows), a critical issue in hydrological sciences is associated with the notion of "change". Additionally, the International Association of Hydrological Sciences (IAHS) has recently launched the "Panta Rhei" Initiative for the decade 2013-2022 (Montanari et al., 2013). As stated in that paper "Panta Rhei focuses on science for society" having set as its science question No 1 (SQ1) the following: "What are the key gaps in our understanding of hydrological change?". Within this broad question, the issue is raised regarding the hydrological effects of disasters in human societies (e.g., conflicts) and related changes in economy). Real-world examples of socioeconomic changes that impact hydrological processes are valuable for SQ1.

In this work the focus is on the effect on floods of the land use change that resulted from a rapid economic change. Land use changes may be due to various causes such as forest fires (Nalbantis and Lymperopoulos, 2012) or urbanisation (Efstratiadis et al., 2015). They may be hypothetical (Niehoff et al., 2002; Batelis and Nalbantis, 2014) or real such as the studied one.

The selected study area is the basin of the Inflow Stream of Lake Paralimni in Southeastern Cyprus. Before the events of 1974 the basin was mainly an agricultural area. Rapid changes in its economy and land uses in subsequent years transformed the agricultural land into a sparsely urbanised area with infrastructure that mainly serves tourism.

2. METHODOLOGY

2.1 General

The assessment of the flood extent and other flood characteristics is based on information on precipitation transformed into flood information using hydrological and hydraulic models. The output from a hydrological model is inserted as input to a hydraulic model, which, in turn, yields flood hydrographs for discharge and water elevation at selected river cross-sections. Peak water elevations are used to assess the inundation extent. The software packages of the Hydrologic Engineering Centre (HEC) of the U.S. Army Corps of Engineers are used for model implementation.

2.2 Hydrological modelling

The study basin is divided into sub-basins based on the hydrographic network and land uses for two periods. Historical hyetographs from a number of raingauges allow for the assessment of the hyetographs for each sub-basin, subsequently transformed into rainfall excess hyetographs using the SCS method (US Soil Conservation Service, 1986). The cumulative excess rainfall depth PE is

$$\mathrm{PE} = \begin{cases} \dfrac{(P - I_\mathrm{a})^2}{P + S - I_\mathrm{a}} & P > I_\mathrm{a} \\ 0 & P \le I_\mathrm{a} \end{cases} \tag{1}$$

where P is the cumulative rainfall depth from the beginning of the studied storm, S is the potential maximum retention, and I_a denotes the initial abstractions. The quantity S is related to the dimensionless curve number, CN, through

$$S = 254\left(\frac{100}{\mathrm{CN}} - 1\right) \tag{2}$$

where S is given in mm. Based on tabulated values of CN for combinations of soil and land use categories (Wanielista and Yousef, 1993) CN in each sub-basin is computed as a weighted spatial average.

Subsequently, a triangular Synthetic Unit Hydrograph (SUH) (NERC, 1975) for each sub-basin is constructed using the SCS formula for the basin lag time, t_L, i.e.

$$t_\mathrm{L} = \frac{L^{0.8}\left(2540 - 22.86\mathrm{CN}\right)^{0.7}}{1410\mathrm{CN}^{0.7} I_\mathrm{m}^{0.5}} \tag{3}$$

where t_L is in h, L is the maximum travel length (m), and I_m is the average ground slope (%).

The SUH allows for constructing the direct runoff hydrograph for each sub-basin, which is then routed downstream using the Muskingum method. Parameter K of the method is taken as the length of the studied river segment divided by flow velocity, whilst parameter x is set to 0.2, which is typical for the region.

The HEC-GeoHMS (Fleming and Doan, 2009) and HEC-HMS (Scharffenberg and Fleming, 2010) packages are used for calculations.

2.3 Hydraulic modelling

Hydraulic modelling in river reaches of the study basin is based on the following assumptions: (1) One-dimensional flow is considered; (2) steady flow conditions are adopted; (2) the energy equation is used, which is written and solved between successive river sections.

The energy equation is written as

$$z_2 + y_2 + a_2 \frac{V_2^2}{2g} = z_1 + y_1 + a_1 \frac{V_1^2}{2g} + h_e \tag{4}$$

where z_i, y_i, V_i, a_i are the bottom elevation (m), water depth (m), average water velocity (m/s), and kinetic energy correction factor respectively for cross-section i, where $i = 1$ for the upstream cross-section and $i = 2$ for the downstream one. Quantities h_e and g are respectively the total energy losses and the acceleration due to gravity. Details on calculations based on equation 4 are given by Brunner (2010).

The Manning's roughness coefficient, n, is calculated based on land use information and tabulated values found in Chow (1959). The HEC-GeoRAS and HEC-RAS (Brunner, 2010) packages are used for calculations.

3. STUDY BASIN AND DATA

3.1 The study basin

Paralimni is a village located at the southeastern part of the Island of Cyprus, close to the Lake of Paralimni. Up to 1974, its main economic activities were agriculture and fishing, whereas after 1974, the village was rapidly transformed into one of the most popular destinations for tourism in Eastern Mediterranean. Population rose from 5270 in 1976 to 14863 in 2011. Employment in the sectors of commerce and services showed a 100% increase within a decade, while for tourism the increase was 200%. Evidently, land uses in the study area followed its economic transformation.

The study basin is the basin of the Inflow Stream of Lake Paralimni whose area of 11.54 km^2 covers the entire area of the Paralimni municipality (Fig. 1). The length of the main watercourse is 5.884 km, while the maximum valley length is 9.237 km. The basin is considered as a flood-prone area according to the EU Flood Directive (European Council, 2007; Tsakiris et al., 2009).

3.2 Data used

Precipitation depths for the event that occurred in 15 February 1988 were collected for three recording raingauges (Aghia Napa, Paralimni, and Sotira) at the five-minute time step. The choice of this event was based on the knowledge that this has caused significant flooding. The Thiessen polygon method was used to estimate spatial averages of precipitation for each one of the sub-basins of the study basin (Sophocleous, 2016). Based on intensity-duration-frequency curves for point rainfall (Pasiardis, 2012) and by referring to the five-minute duration, the return period was found to be 87, 51, and 36 respectively for Aghia Napa, Paralimni and Sotira.

Land use information was provided in the form of two maps: a conventional map for the period 1983 – 2003 (Fig. 2) and the map for the period 2006-2016 from the project known as Corine 2000 (Fig. 3). The land uses are coded as follows: 242: Crops and dispersed houses; 112: Discontinuous urban surface; 121: Commercial and industrial areas; 211: Non-irrigated arable land; 212: Permanently irrigated areas; 122: Roads and Railway networks; 323: Sclerofyllous vegetation; 142: Sport and recreation facilities; 231: Pasture.

The Digital Elevation Model (Fig. 1) was provided by the Water Development Department of the

Republic of Cyprus and is based on Lidar measurements. The soil map of the Geological Survey Department of Cyprus was used for soil classification.

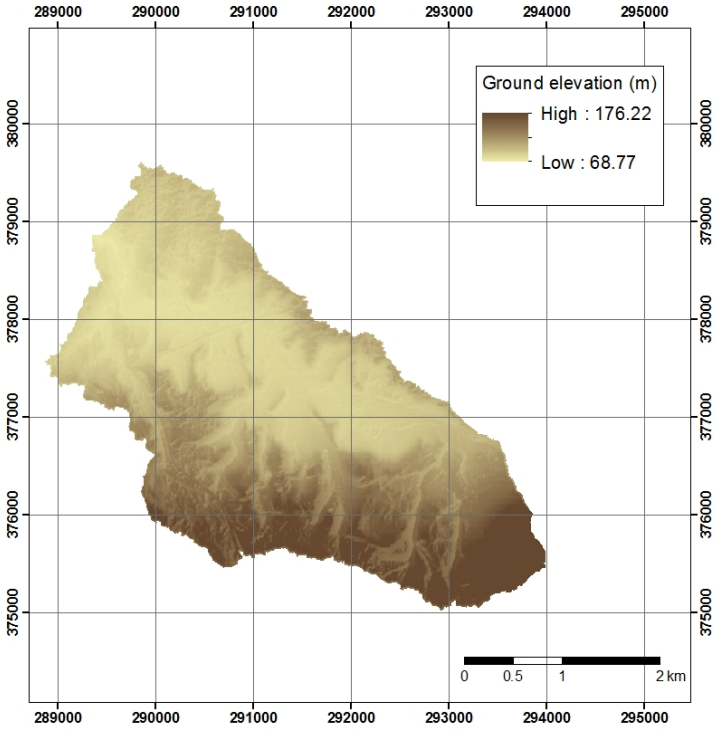

Figure 1. The basin of the Inflow Stream of Lake Paralimni.

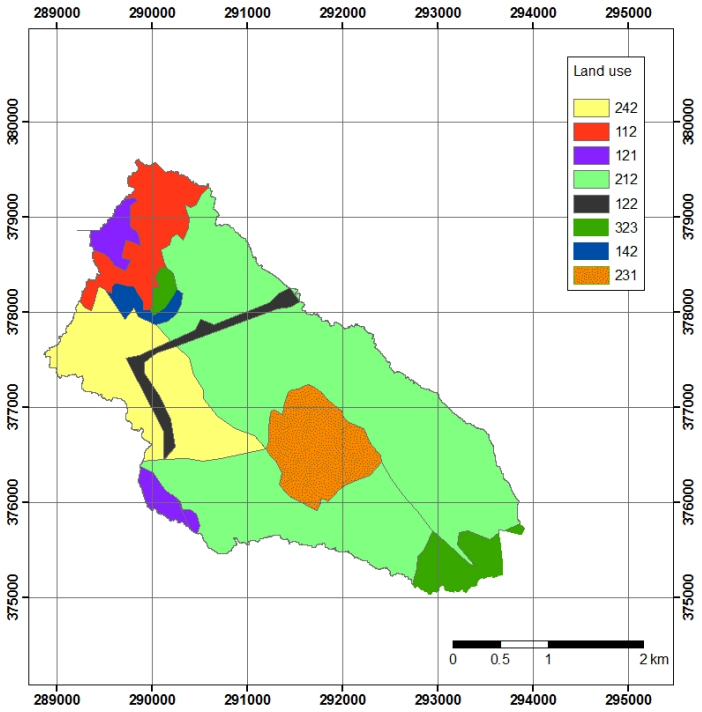

Figure 2. Land uses in the study basin for the period 1983-2003.

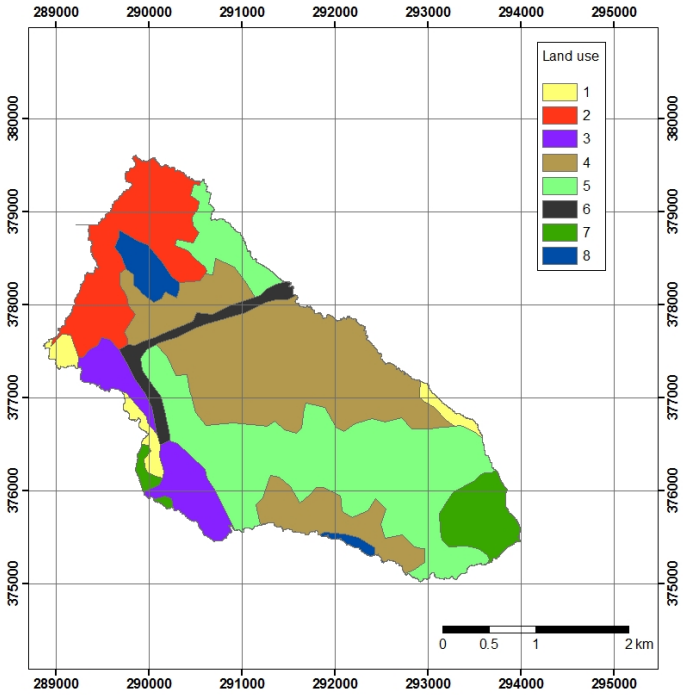

Figure 3. Land uses in the study basin for the period 2006-2016.

4. RESULTS

4.1 Land uses for the period 1983-2003

The study basin was subdivided into eleven sub-basins with the purpose to distinguish between homogeneous sub-areas with different land uses, while also capturing land use changes. The subdivision was kept constant from one land use case to another, which enables comparisons. Six river reaches were used for flood routing by adopting typical values for contraction and expansion coefficients and differentiating between main channel bed and right and left banks when selecting Manning's *n*.

The peak flow rate at the basin outlet was estimated at 38.9 m^3/s, while the flow volume was 621.5×10^3 m^3. The peak flow rate for each sub-basin is depicted in Fig. 4(a) (blue bars), while the variation of the flow volume from one sub-basin to another is shown in Fig. 4(b). The maximum inundation extent was 32.97 ha.

4.2 Land uses for the period 2006-2016

For the recent period 2006-2016 the land use change led to increased values of CN while also affecting roughness coefficients.

The peak flow rate at the basin outlet was estimated at 62.0 m^3/s, while the flow volume was 899.3×10^3 m^3. Again, the peak flow rate and flow volume for each sub-basin are depicted in Figs 4(a) and 4(b) respectively (red bars). The maximum inundation extent was 39.30 ha.

4.3 Comparison of results

Starting from the basin as a whole as the spatial level for comparison of the effect of land use change, results showed an increase of peak flow rate by 59.4 %. The flow volume was increased by

44.7 %. The examination of peak flow rates at the sub-basin level revealed that the median flow rate passed from 4.4 m^3/s to 5.5 m^3/s, which corresponds to a relative increase by 71.4 %. The maximum increase was found to be 233.3 %. As far as the flow volume per sub-basin is concerned, a median increase of 44.8 % was found, while the maximum increase was 162.5 %. The maximum inundation extent was found to have increased by 19.2 %.

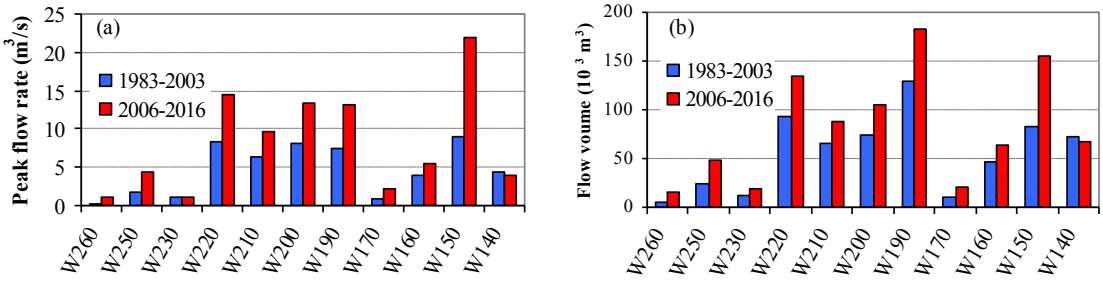

Figure 4. (a) Peak flow rate and (b) flow volume for each sub-basin and each one of the land use cases (1983-2003 and 2006-2016)

5. CONCLUSIONS

In this paper a typical approach was followed, which was aimed to assess the effect of land use change on flood characteristics in an ungauged basin in Cyprus. The basin of the Inflow Stream to Lake Paralimni was investigated, which is one of the flood-prone areas identified during the process of application of the EU Flood Directive in the Republic of Cyprus.

From the investigations we can draw the following conclusions:

1. The rapid changes in land uses in the studied area have, to a large extent, transformed it into an urbanised area, whereas the formerly extended cultivated areas have shrunk considerably after the events of 1974. Tourism being currently the dominant economic activity has replaced agriculture to a large extent.
2. The aforesaid land use changes have led to changes in soil permeability which, in this work, was reflected in significant changes in the curve number of the SCS method.
3. When considering the basin as a whole, the peak flow rate at the basin outlet was found to have been increased by 59.4 % with respect to the former situation, while the flow volume was increased by 44.7 %. The maximum inundation extent was found to have been increased by 19.2 %.
4. When focusing on the sub-basin level, the peak flow rate showed a maximum increase above 200 %. The maximum increase of flow volume was above 150 %, while the maximum change in inundation topwidth was 133.2 m.
5. The study basin is exposed to a flood hazard which is significantly higher than in previous periods. Given that the expected losses in tourism infrastructure are higher than those in cultivated areas, the risk of economic losses is now much higher than before and, thus, mitigation and protection measures are absolutely necessary.

ACKNOWLEDGEMENTS

The authors wish to thank the personnel of the Department of Town Planning and Housing, and the Geological Survey Department of the Republic of Cyprus, as well as the Cyprus Meteorological Service for providing the data. Also, K. Aristeidou of the Water Development Department Republic of Cyprus is warmly thanked for his support.

REFERENCES

Batelis, S.-C., Nalbantis, I., 2014. Potential effects of forest fires on streamflow in the Enipeas river basin, Thessaly, Greece. Environmental Processes; 1(1): 73-85.

Brunner, G. W., 2010. HEC-RAS, River Analysis System Hydraulic Reference Manual (version 4.1). US Army Corps of Engineers; Hydrologic Engineering Center.

Chow, V. T., 1959. Open Channel Hydraulics. McGraw-Hill, New York.

Efstratiadis, A., Nalbantis, I., Koutsoyiannis, D., 2015. Hydrological modelling of temporally-varying catchments: facets of change and the value of information. Hydrological Sciences Journal; 60(7-8): 1438-1461.

European Council, 2007. EU Directive of the European Parliament and of the European Council on the assessment and management of flood risks. 2007/60/EU.

Fleming, M. J., Doan, J. H., 2009. HEC-GeoHMS Geospatial Hydrologic Modeling Extension. US Army Corps of Engineers, Hydrologic Engineering Center.

Montanari, A., Young, G., Savenije, H. H. G., Hughes, D., Wagener, T., Ren, L.L., Koutsoyiannis, D., Cudennec, C., Toth, E., Grimaldi, S., Blöschl, G., 2013. “Panta Rhei—everything flows”: change in hydrology and society—the IAHS scientific decade 2013–2022. Hydrological Sciences Journal; 58(6): 1256-1275.

Nalbantis, I., Lymperopoulos, S., 2012. Assessment of flood frequency after forest fires in small ungauged basins based on uncertain measurements. Hydrological Sciences Journal; 57(1): 52-72.

NERC, 1975. Flood Studies Report, Volumes I-V. Natural Environment Research Council, London, UK.

Niehoff, D., Fritsch, U., Bronstert, A., 2002. Land-use impacts on storm-runoff generation: scenarios of land-use change and simulation of hydrological response in a meso-scale catchment in SW-Germany. Journal of Hydrology; 267(1): 80-93.

Pasiardis, S., 2012. Meteorological Note No 18. Cyprus Meteorological Service, Nicosia, Cyprus.

Scharffenberg, W. A., Fleming, M. J., 2010. Hydrologic Modeling System HEC-HMS User's Manual. US Army Corps of Enginners, Hydrologic Engineering Center.

Sophocleous, C., 2016. Impact of land use change on the assessment of inundation extent: The case of the drainage basin of the Inflow River of Lake Paralimni, Cyprus. Diploma Thesis, School of Rural and Surveying Engineering, National Technical University of Athens, 112 pages (in Greek).

Tsakiris, G., Nalbantis, I., Pistrika, A., 2009. Critical technical issues on the EU Flood Directive. European Water; 25/26: 39-51.

US Soil Conservation Service, 1986. Urban hydrology for small watersheds. US Soil Conservation Service Technical Release; 55, p.13.

Wanielista, M. P., Yousef, Y. A., 1993. Stormwater management. John Wiley and Sons.

Proceedings of the 10th World Congress of EWRA 'Panta Rhei', 5-9 July 2017, Athens, Greece
© 2017 *European Water Resources Association*

Robust prioritization for SEA with the missing data

D. Park
Department of Civil, Environmental and Plant Engineering, Konkuk University, Republic of Korea
e-mail: drpark@konkuk.ac.kr

Abstract: This study investigates how the priority analysis for dam construction sites vary with multi-criteria decision making techniques and generation approaches for incomplete information. Strategic environmental assessment (SEA) seeks to recommend sustainable dam construction sites based on their environmental and ecological impacts in a long-term plan for dam construction (LPDC) in South Korea. However, if specific information is missing, the SEA is less useful for choosing a dam construction site. In this study, we applied Analytical Hierarchy Process (AHP), ELimination Et Choice Translating REality (ELECTRE) III, Preference Ranking Organization Method for Enrichment Evaluation (PROMETHEE) II and Compromise Programming as multi-criteria decision making techniques, and used binomial and uniform distributions to generate missing information. We considered five dam site selection situations and compared the results as they depended on both multi-criteria decision making techniques and information generation methods. The binomial generation method showed the most obvious priorities. All multi-criteria decision making techniques showed similar priorities in the dam site selection results except for ELECTREE III. The results demonstrate that selecting an appropriate multi-criteria decision making technique is more important than the data generation method. However, using binomial distribution to generate missing information is more effective in providing a robust priority than uniform distribution, which is a commonly used technique.

Key words: AHP, ELECTRE III, Incomplete information, Multi-criteria decision making, Priority, PROMETHEE II, Strategic environmental assessment

1. INTRODUCTION

Water facilities such as dam, levee and river barrage have been contributed to Korean economic development for supplying water, preventing flooding damage and providing hydropower. However, the most government-lead water resources projects cause a social conflict since the late 1990s as paradigm of Korean economy moved from the government lead development to the free market economy and started to be interested in quality of life and environmental friendly landscape rather than economic growth. Since its introduction in 1970s, the Environmental Impact Assessment (EIA) has been introduced to many countries as an effective tool for harmony between development and conservation. The EIA has been implemented to estimate environmental effects and has served an awareness of the importance of environment-friendly development and conservation for engineers and planners (Song et al., 2006). However, the EIA is usually implemented after a number of strategic decisions have been made in the high-level plans. The inherent limitations, such as difficulties of projects which cause serious environmental damage, are exposed (Song et al. 2002). Therefore, it is necessary to have a strategic approach for an environmentally sound and sustainable development to consider environmental effects from the early stage of decision making including policy plan program and the Strategic Environmental Assessment (SEA) was suggested. The SEA is widely used to refer to systematic process of analyzing the environmental effects at the strategic level of decision-making process including policy, plan and program (Therivel et al., 1996; Sadler and Verheem, 1996). This study was to investigate the selecting probability of each dam candidate and choose the most appropriate dam sites among ten sites using the multi-criteria decision mthod (MCDM). Particularly, this study applied the MCDM to in case of not enough monitoring data. To consider no data in considerations, this study applied the uniform and the normal distributions of random sampling for the MCDM.

2. METHODS

2.1 Candidate sites selection

In Korea, the long term master plan for the dam construction is established every 10 years and modified or changed every 5 years and required to implement the SEA. Ten potential dam sites were considered for water resources planning in this study as shown in Figure 1. The most appropriate dam site was selected from the minimum effect of environmental issues. Among ten dam sites, four sites are located in the Han river, four sites are located in the Nakdong river and two sites are located in the Geum river as shown in Table 1. All dam candidate sites were generally located upstream of the river and distributed legal protection species from investigation results of these rivers. There are abandoned mines in upstream area and it needs the precise investigation of expected effects and reduction alternatives in the processing step of the future dam construction project. To evaluate environmental conditions of dam site candidates, environmental data is collected as topology and geology (landscape), animal and plant fauna (ecological worth), water quality, and environmental toxicity (abandoned mining).

Table 1 shows the grades of the evaluation in four criteria. Smaller numbers expect higher negative effects after the dam construction. This study specifies 1 to 9 to evaluate harmful dam construction effects. For example, 1 indicates the highest negative effect but 9 designates the lowest negative effect based on the dam construction.

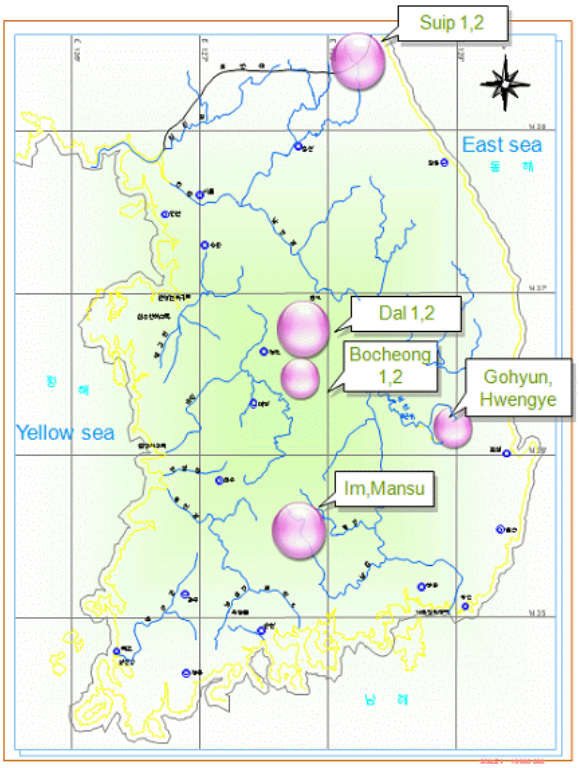

Figure 1. Location of candidate sites for dam planning in SEA.

Table 1. Assessment results of propriety based on environmental aspects in this study

CRITERIA	S1	S2	S3	S4	S5	S6	S7	S8	S9	S10
Natural Resources	1	1	7	1	1	1			7	7
Ecology	1	1	7	3	7	5	9	9	9	9
Water Quality	6.5	6.5	5.5	6	5.5	5	5	6	7	5
Environmental Toxicity	9	9	1	1	7	9				9

Note: grey color indicates missing information

2.2. Multi-criteria Decision-making Methods

The Elimination and Choice Translating Reality (ELECTRE) family and Preference Ranking Organization Method for Enrichment Evaluation (PROMETHEE) family of methods are the most prominent outranking methods. This study applied ELECTREE III and PROMTHEE II among the outranking methods. Four different multi-criteria decision-making methods—Analytical Hierarchy Process (AHP), ELECTRE III, PROMETHEE II, and Compromise Programming—were applied to estimate the uncertainty of priorities based on the incomplete information using standardized data. Decision strategies of PROMETHEE II and ELECTRE III are based on the concordance–discordance theory. On the other hand, AHP makes use of an eigenvector method to search for an optimal solution. Compromise Programming is a mathematical programming technique for use in a continuous context.

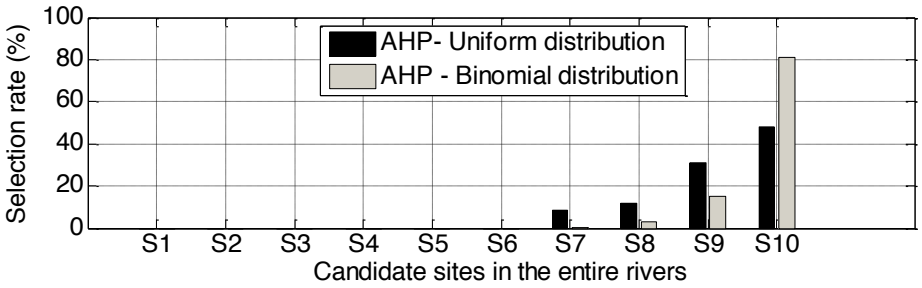

(a)

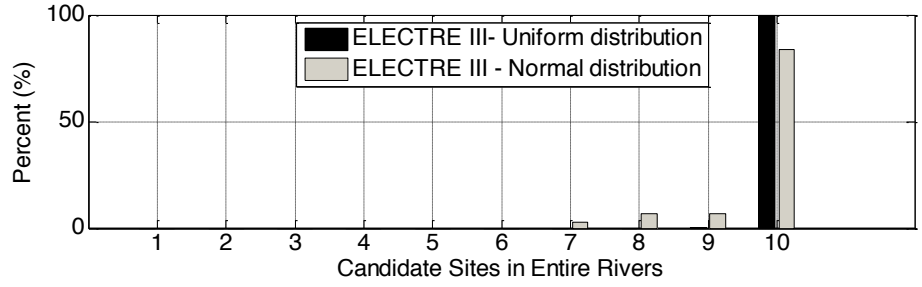

(b)

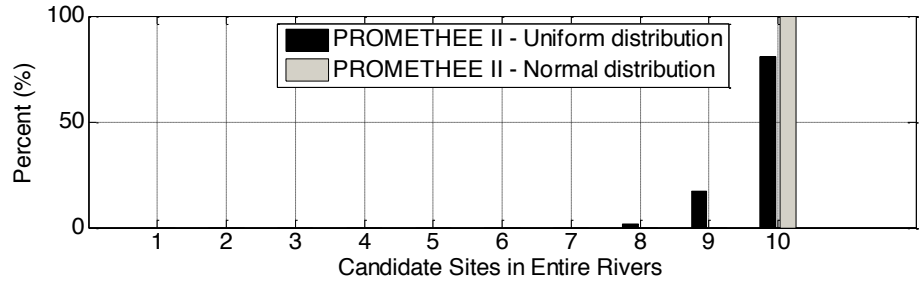

(c)

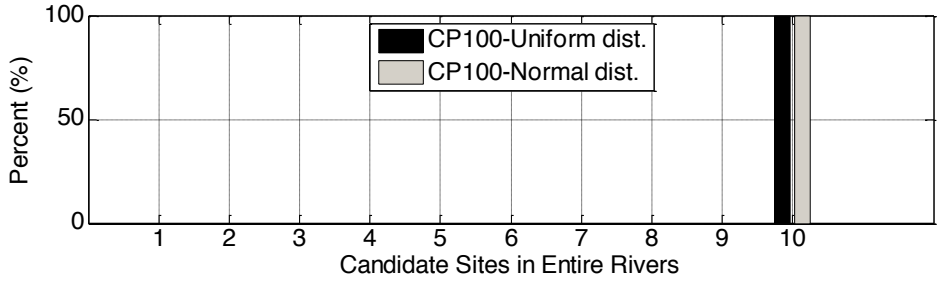

(d)

Figure 2. Priority of candidate sites depending on MCDM methods; (a) AHP; (b)ELECTRE III; (c) PROMETHEE II; (d) Compromise Programming

3. RESULTS AND DISCUSSION

As shown in Figure 2, all dam sites selected based on the rivers were consistent except dam selection in the Geumho River. Results for binomial distribution sampling in Figure 2 showed a more robust selection ratio rather than that of the uniform distribution sampling in all five dam selection scenarios. This indicates that binomial distribution sampling produces stronger results than uniform distribution to complete the incomplete information. Overall, all applied MCDM methods except ELECTRE III in this study did not significantly affect dam selection for the scenarios. However, the methods of incomplete information affected the selection and binomial distribution; similar normal distribution showed a more robust selection ratio than that of uniform distribution. Finally, the type of AHP, PROMETHEE II, or Compromise Programming with binomial distribution showed the most robustness and consistency in estimating priorities. ELETREE III with both binomial and uniform distributions produced the least robust results compared to the other combination approaches in this study.

ACKNOWLEDGMENTS

This research was supported by Basic Science Research Program through the National Research Foundation of Korea(NRF) funded by the Ministry of Science, ICT & Future Planning (2016R1C1B1013711) and by a grant (14AWMP-B082564-01) from Advanced Water Management Research Program funded by Ministry of Land, Infrastructure and Transport of Korean government.

REFERENCES

Sadler B., Verheem R., 1996. Strategic Environmental Assessment – Status, Challenges and Future Directions, Ministerie Van Volkshuisvesting, Ruimtelijke Ordering en Milieubeheer, Dan Haag. 188p.

Song, Young-Il et al., 2002. Improving Prior Environmental Review System," Korea Environment Institute, Korea Environmental Institute, Seoul, Korea.

Song, Young-Il et al, 2006. Study on the EIA after the Adoption of the Strategic Environmental Assessment, Final research report for MOE in Korea.

Therivel, R. et al., 1992. Strategic Environmental Assessment, Earthscan Publ. Ltd., London, UK.

Proceedings of the 10th World Congress of EWRA 'Panta Rhei', 5-9 July 2017, Athens, Greece
© 2017 *European Water Resources Association*

Research on conjunctive use of surface water and groundwater for managed aquifer recharge (MAR) at the River Nestos Delta, Greece

L. Avgeris, D. Karasogiannidis, I. Gkiougkis, F. Pliakas*, T. Tzevelekis, K. Bellos and I. Diamantis
Department of Civil Engineering, Democritus University of Thrace, 67100 Xanthi, Greece
* *e-mail: fpliakas@civil.duth.gr*

Abstract: In the framework of the rational water resources management at the eastern part of River Nestos Delta, NE Greece, this paper investigates the potential conjunctive use of surface water and groundwater in order to optimize the exploitation and utilization of the available water recourses from the River Nestos and to confront the continuous groundwater salinization at the coastal part of the study area. The present study targets: (i) to improve the flow conditions through the main water course of the irrigation network of the study area by applying proper technical implementation proposals, and (ii) to design a groundwater artificial recharge pilot project, while assessing the effectiveness of the recharge procedure. Several maps, figures and tables are compiled, indicating the positions and technical details of the proposed interventions based on a topographic survey and a numerical simulation, using the well-known one-dimensional software HEC-RAS. The proposed intersections, tested in the simulation, are distinguished in modifications into the watercourse bed and engineering works concerning the pipeline. Regarding the groundwater artificial recharge pilot project, a system of recharge basins is proposed, as well as the relevant design elements are calculated based on the hydrogeological and hydraulic characteristics of the underlying aquifer system.

Key words: Conjunctive use of surface water and groundwater, HEC-RAS, Managed aquifer recharge – MAR

1. INTRODUCTION

Conjunctive groundwater use with surface-water resources, in terms of practical water management, represents one of the most important responses to improving drought water-supply security and for long-term climate-change adaptation, and in terms of underpinning science, its design requires a refined understanding of resource interconnectivity (both naturally and perturbed by irrigation works or practices) and of aquifer salinization processes (Foster and van Steenbergen, 2011).

In the framework of the rational water resources management at the eastern part of River Nestos Delta, Greece, the present study targets: (i) to improve the flow conditions through the main watercourse K2 (Figure 1-[1]) of the irrigation network of the study area by applying proper technical implementation proposals, and (ii) to design an aquifer managed recharge (MAR) pilot project, while assessing the effectiveness of the recharge procedure. In particular, this paper investigates the potential conjunctive use of the main watercourse K2 and the underlying aquifer system in order to meet most effectively the irrigation and drainage needs of the wider Dekarcho - Maggana area (Figure 1-[1]), as well as to confront the continuous groundwater salinization at the coastal part of the investigated area. The whole research procedure aims at optimizing the exploitation and utilization of the available water recourses from the River Nestos.

2. DESCRIPTION OF THE STUDY AREA

Watercourse K2 (Figure 1-[1]) as a main part of the irrigation network of River Nestos East Delta, fails to transport adequately fresh water due to its incorrect design and the various erroneous interventions through its course. This defective flow function results in causing floods upstream and hardly meeting water demands at the coastal zone.

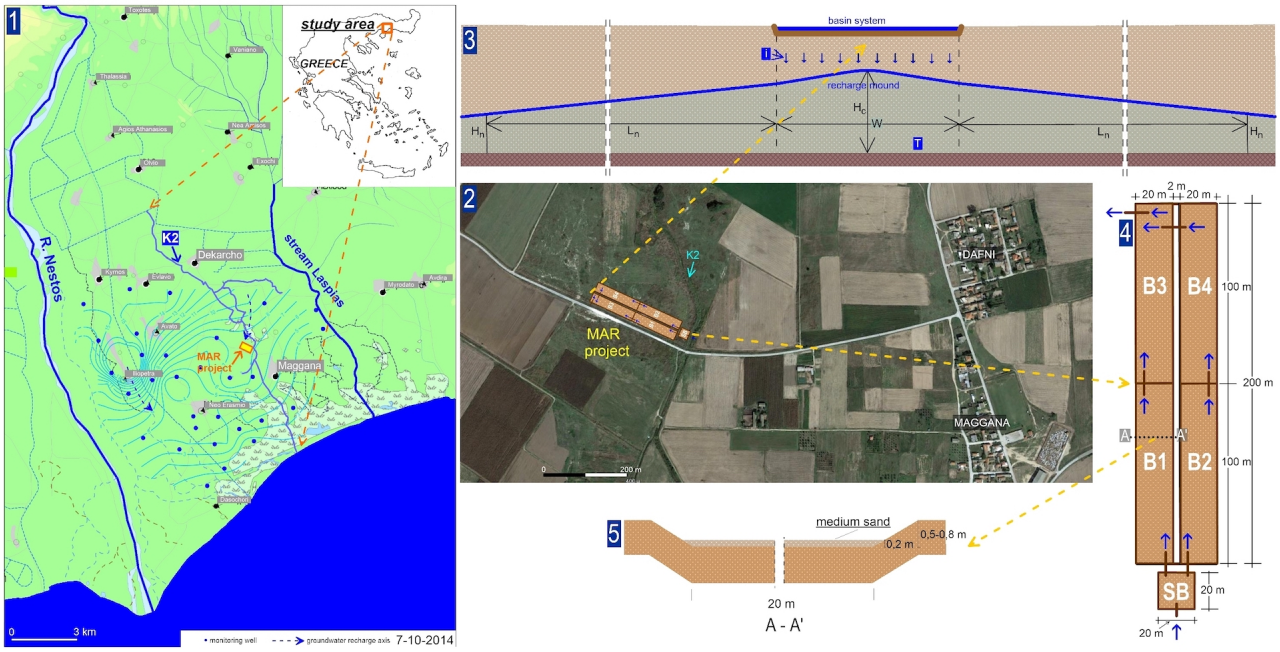

Figure 1. [1]: Study area. Location of the proposed pilot MAR project, piezometric map of the upper unconfined aquifer (7-10-2014). [2] Location of the proposed pilot MAR system (background: Google Earth 2015). [3] Cross section with the geometrical characteristics and relevant symbols regarding the recharge mount under the MAR basin system. [4] plan of the pilot MAR basin system. [5] Cross section of a representative recharge basin.

Furthermore, several hydrogeological researches in Eastern Delta of Nestos River (Sakkas et al., 1998; Pliakas et al., 2001; Gkiougkis et al., 2010; Gkiougkis et al., 2011; Pliakas et al., 2014a; Pliakas et al., 2014b; Gkiougkis et al., 2015; Pedreira et al., 2015; Pliakas et al., 2015) have pointed out the continuous quality degradation of the coastal aquifer system of the area due to groundwater and soil salinization.

The study area is located in a recent sedimentary deltaic environment with a thickness of some tens of meters deposited by Nestos River and consisting of alternating sand, clay and silt layering depositions (Gkiougkis et al., 2010). According to Gkiougkis et al. (2014), the east delta plain of R. Nestos extends to 176.4 km^2, from which the irrigated lands (mainly corn and cotton) extend to 89.90 km^2, while the 35 km^2 of them meet their irrigation needs from Nestos River. The rest of the area meets irrigation needs through groundwater exploitation. There are two hydrogeological systems formed within the alluvial deposits on the broader study area, a shallow one, consisting of phreatic and mostly of semi-confined aquifers extended down to a depth of about 30 m, and a deeper system, consisting of confined aquifers extended to a depth of at least 190 m. Evaluation of the relevant groundwater hydraulic parameters of the aquifer system resulted in values for (Pliakas et al., 2001, Sakkas et al., 1998): (1) transmissivity (T), ranging from 4.0×10^{-4} to 1.1×10^{-2} m^2/sec, (2) storage coefficient (S), ranging from very low values to 10^{-3}, characterizing the aquifers of the study area as confined mainly westward, and in some sites, as semiconfined. Figure 1-[1] shows the piezometric map of the upper unconfined aquifer in October 2014, after the irrigation period. The major groundwater flow direction is from northwest to south with minor flow from the N.E. and central parts of the study area to the south.

It is worth mentioning that the longest part of the K2 course is located above an underlying main groundwater recharge axis (Figure 1-[1]), which was confirmed by groundwater level measurements before and after the irrigation period of 2015 (13-5-2015 and 3-11-2015) in 18 monitoring wells located near to the K2 course bed. This ascertainment helps in identifying suitable groundwater artificial recharge sites. In addition, groundwater level fluctuation shows increased natural recharge due to high precipitation values during the time period of 2014-2015 (2009-2015 average annual value: 719.9 mm).

Regarding the groundwater quality in the study area, the conducted chemical analysis during July 2015, indicated groundwater salinization in the SE part of the study area, due to possible seawater intrusion and lateral groundwater inflow from Laspias stream. Some characteristic relevant values are shown below:

- Electrical conductivity (EC) values: 274 – 3080 μS/cm
- Chlorides (Cl^-) concertation values: 10.64 – 5319 mg/L
- Revelle coefficient values ($Cl^-/(CO_3^{2-}+HCO_3^-)$ in meq/L) (Revelle, 1941): 0.10 – 2.52.

3. HYDRAULIC MODELLING AND DESIGN OF WATER COURSE INTERVENTIONS

A detailed topographic mapping of the K2 watercourse was carried out in spring 2015 in 1:25000 scale. Specifically, recording positions were set every 100 m along the river, including both embankments and the main channel of the river. Furthermore, the existing technical structures and all points where abrupt flow changes occurred were noted. The hydraulic simulation of this watercourse was carried out with the aid of HEC-RAS for the investigation of two scenarios of interventions (Figure 2), which aim to increase the 0.50 m^3/s discharge capacity of the channel at the current state. The suggested modifications emanate from the inadequate water conveying capacity of the existing infrastructures and the necessity to provide water for irrigation.

1. Scenario 1 pertains to the alteration of the bed slope in specific parts of the watercourse in order to decrease the flow depth and increase the channel discharge capacity up to 0.75 m^3/s.
2. Scenario 2 includes bed slope alterations, such as those in Scenario 1, as well as improvement of the existing technical structures, leading to a discharge capacity of 1.00 m^3/s. These modifications could lead to increased discharge capacity, up to 1.50 m^3/s where water was observed to overflow at some specific points.

Figure 2-[2] shows the embankments details, which occurred from the topographic survey. The red and green dotted lines correspond to the left and right banks of the watercourse, respectively. The same figure presents the profile of the bed centerline, following the implementation of the suggested modifications in the second scenario, and the water depths between the cross-sections 41 to 1.

However, even after the suggested scenario implementations, there were still some problematic cross-sections where overflow was noted. In such cases backfilling was needed.

Based on the topographic survey and the results of the hydraulic simulation for the effective regulation of the watercourse operations, maps were designed (Figure 2-[3]) and tables were compiled indicating the positions and the technical details of the proposed interventions alongside the K2 watercourse, such as:

- excavation or backfilling of the watercourse bed
- interventions in structures, including the alternatives of: (i) deepening the bed, (ii) adding a second pipeline of the same diameter, (iii) pipeline replacement with a larger diameter pipeline, (iv) pipeline replacement with two larger diameter pipelines.

The number of cross-sections, tested and used in the simulation, was 223. The total amount of the proposed interventions was 76, which were distinguished in 61 interventions related to the watercourse bed and 15 interventions related to the technical structures.

4. PILOT MAR PROJECT

In the framework of investigating potential managerial interventions in the area of watercourse K2 for confronting the groundwater salinization in the coastal part of the study area, a MAR (managed aquifer recharge) pilot project is proposed in a position approximately 680 m west of village Dafni, near to the watercourse bed (Figure 1-[2]). The proposal is based on the following ascertainments that the MAR proposed location:

- is barren, so it appears that land property and expropriation issues may not occur,
- is above an underlying aquifer consisting of soil material suitable for groundwater recharge procedures (gravel-sand and sand layers alternating with interposing clay layers),
- is positioned above an underlying main groundwater recharge axis (Figure 1-[1]), which may contribute positively to the effectiveness of the MAR process,
- is in close proximity to the watercourse K2, from which the required fresh water for recharge, will be provided after a partial diversion into the K2 bed,
- is also located in close proximity to a small trench which extends parallel and immediately adjacent to the municipal road connecting Avato, Dafni and Maggana villages, whereby:
  - the access to the project is quite easy,
  - the trench seems to be the available recipient of the excess water after the recharge procedure.

Figure 2 presents all the design elements of the proposed MAR project. The following estimations of the required hydrogeological parameters are listed:

- Transmissivity: $T = Kb = 4\times10^{-4} \div 1.1\times10^{-2}$ m^2/sec = 34.56 ÷ 950 m^2/d → T_{mean} = 500 m^2/d
- Thickness of aquifer system: b ~ 40 m
- Hydraulic conductivity: $K = T/b = 12.5$ m/d = 1.45×10^{-4} m/sec (according to Cashman and Preene, (2001), the estimated average permeability is characterized as moderate to low)

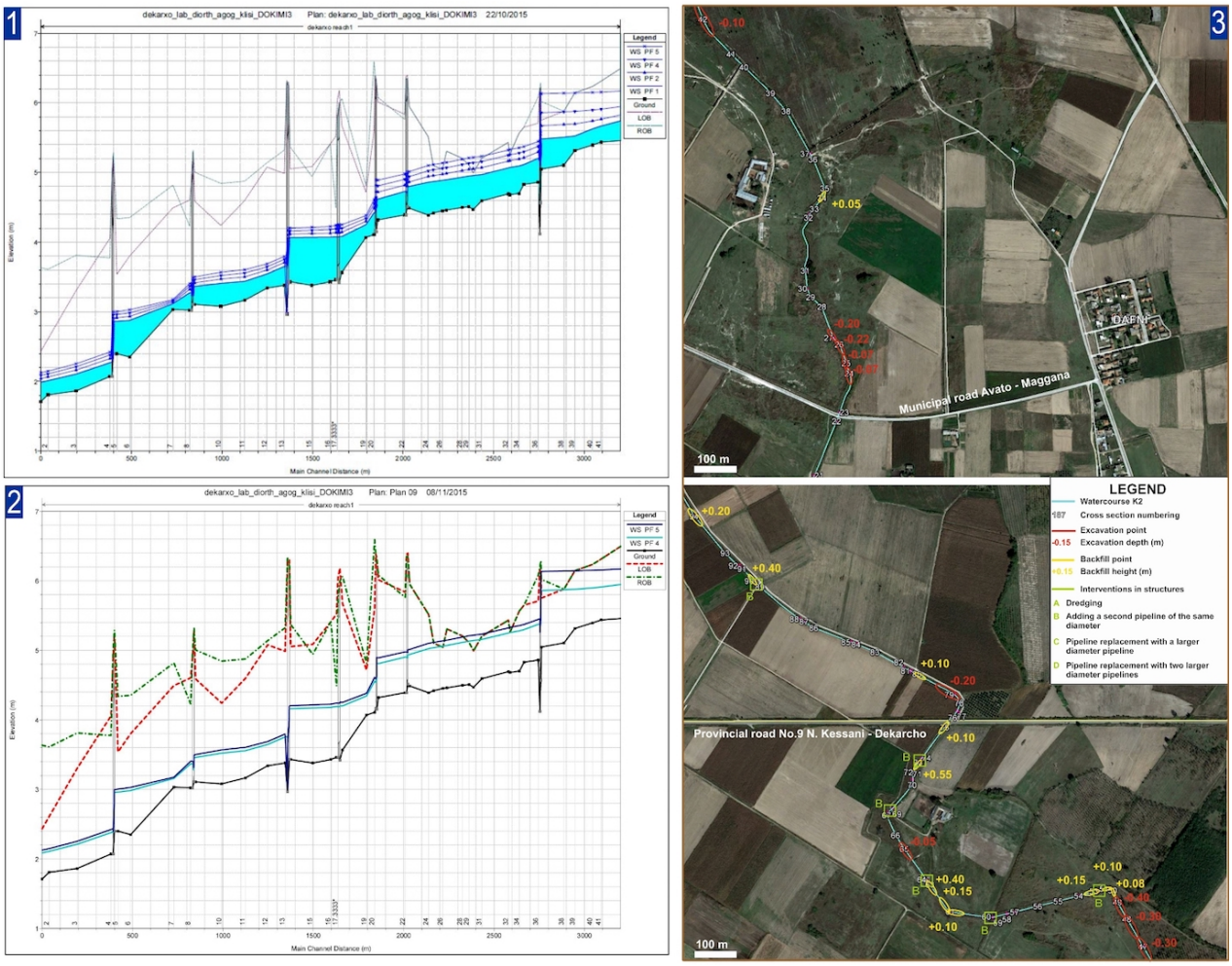

Figure 2. [1]: Longitudinal profile of the HEC-RAS software for the scenario 2 and flow rates Q=0.50 m^3/s, Q=0.75 m^3/s, Q=1.00 m^3/s, Q=1.25 m^3/s between the cross-sections 41 to 1. [2]: Embankments' altitude and longitudinal profile of the HEC-RAS software for the scenario 2 and flow rates Q=1.00 m^3/s, Q=1.25 m^3/s between the cross-sections 41 to 1. [3] Indicative maps with the proposed interventions along the watercourse K2: successive cross-sections: 94 -22 (background map: Google Earth 2013).

The proposed pilot MAR system should include the following (Figure 1-[2, 4, 5]):

- The construction of a sediment retention basin (SB), with estimated dimensions 20 m × 20 m in order to effectively receive the recharge surface water flowing from the K2 watercourse after a relevant hydraulic assessment for detailed dimensioning.
- The excavation and formation of 2 systems of shallow recharge basins, each system containing 2 recharge basins of individual dimensions: surface area 20 m × 100 m, depth 0.80 m - 1 m, in order to be filled with water not more than 20 cm – 30 cm in height so that the clogging of the basin bottom (and hence the effectiveness of the MAR system itself) will be minimized.
- Coating of the bottom of the recharge basins with the use of gravels or medium grained sand (0.10 – 0.20 cm)
- The installation of a monitoring network of groundwater wells and piezometers in order to inspect on a frequent basis the qualitative and quantitative effectiveness of the MAR system.

The basin system is considered as a long strip (L/W = 5). The ultimate rise of the groundwater mound below the center of the recharge basin system is calculated by the (1) (Bouwer et al., 1999; Bouwer, 2002; Todd and Mays, 2005):

$$H_c - H_n = \frac{iW}{2T}\left(\frac{W}{4} + L_n\right) \tag{1}$$

where H_c is the height of the groundwater mound in the centre of the recharge area, H_n is the height of the groundwater table at the control area, i is the average infiltration rate in the recharge area, W is the width of the recharge area, L_n is the distance between the edge of the recharge area and the control area and T is the transmissivity of the aquifer.

Thereby (Figure 1-[3]):

- mound rise $H_c - H_n$ = 2 m (estimated from relevant groundwater level measurements in adjacent monitoring wells for the 2014-2015 period)
- recharge rate Q = 50 m^3/h = 13.9 L/sec = 1200 m^3/d, W=40 m, L=200 m
- average infiltration rate i = 1200 / (40×200) = 0.15 m/d
- width of basin system W = 40 m
- Eq. (1) → L_n = 323.33 m

5. CONCLUSIONS AND MANAGERIAL PROPOSALS

This paper investigates the potential conjunctive use of surface water and groundwater in order to optimize the exploitation and utilization of the available water recourses of River Nestos and to confront the continuous groundwater salinization in the coastal part at the eastern part of River Nestos Delta, NE Greece. The research concludes to proposals for applying proper technical implementation in order to improve the flow conditions through the main water course of the irrigation network of the study area, and to design a suitable managed aquifer recharge pilot project (MAR).

It is worth mentioning that in the wider region of the study area, there are protected ecosystems intended to preserve the rich biodiversity of the existing environment system. Thus, any intervention must be in accordance with the relevant environmental protection regulations (Natura 2000, Ramsar Convention).

In the framework of this research and based on relevant experience of the Engineering Geology Laboratory of Department of Civil Engineering, Democritus University of Thrace, regarding the management of aquifers recharge and according to the relevant recommendations, specifications, propositions and guidelines of scientific organizations, committees and agencies in Greece and

worldwide (ASCE 1987, 2001; CMD, 2009; EU, 2006; US EPA, 1992; US NRC, 1994), the following research works and managerial proposals are concluded:

- detailed hydrological and hydraulic study of the hydrogeological regime of the aquifer system and feasibility study of MAR using recharge basins
- testing an experimental pilot recharge application and evaluation of the recharge effectiveness
- design of a network of wells monitoring the quality of the recovered water
- determination of the proper testing parameters
- confrontation of potential clogging problems
- cost study of the proposed interventions and MAR facilities
- environmental impact assessment for the broader region
- investigation of possible problems regarding public acceptance and indicative for communicating with the involved water users and stakeholders
- establishment of safety countermeasures in the designed recharge facilities.

ACKNOWLEDGEMENTS

The study was funded by the East Macedonia and Thrace Region, Regional Unit of Xanthi, Greece. Project title: "Study of the modification of the irrigation, drainage network axis of Dekarho, Avato, Maggana, facilitating irrigation, drainage and groundwater recharge needs", 2015.

REFERENCES

ASCE, 1987. Ground Water Management. Third Edition, ASCE Manuals and Reports on Engineering Practice No 40, New York.

ASCE, 2001. Standard Guidelines for Artificial Recharge of Ground Water. Environmental and Water Resources Institute, EWRI/ASCE 34-01, Virginia, USA.

Bouwer, H., 1999. Artificial recharge of groundwater: systems, design, and management. ln: Mays LW (ed) Hydraulic design handbook. McGraw-Hill, New York, 24.1-24.44.

Bouwer, H., 2002. Artificial recharge of groundwater: hydrogeology and engineering. Hydrogeology Journal, 10(1):121-142.

Cashman, P. M., Preene, M., 2001. Groundwater Lowering in Construction. A Practical Guide. Spon Press, New York.

Foster, S., van Steenbergen, F., 2011. Conjunctive groundwater use: a 'lost opportunity' for water management in the developing world? Hydrogeology Journal 19: 959-962.

Gkiougkis, I., Mwila, G., Pliakas, F., Kallioras, A., Diamantis, I., 2010. Hydrogeological assessment of groundwater degradation at the eastern Nestos River Delta, N.E. Greece. Proceedings of the 12th International Conference of the Geological Society of Greece, Patras, Greece, 19-22/5/2010, 4: 1697-1706.

Gkiougkis, I., Tzevelekis, T., Pliakas, F., Diamantis, I., Pechtelidis, A., 2011. Geophysical research of groundwater degradation at the eastern Nestos River Delta, NE Greece. Advances in the Research of Aquatic Environment, Environmental Earth Sciences, Springer, 1: 259-266.

Gkiougkis, I., Kallioras, A., Pliakas, F., Pechtelidis, A., Diamantis, V., Diamantis, I., Ziogas, A., Dafnis, I., 2015. Assessment of soil salinization at the eastern Nestos River Delta, N.E. Greece. Catena, Elsevier, 128: 238-251.

Glover, R. E., 1964. Ground water movement. US Bureau of Reclamation, Engineering Monography, 31, 67 pp.

Pedreira, R., Kallioras, A., Pliakas, F., Gkiougkis, I., Schuth, C., 2015. Groundwater vulnerability assessment of a coastal aquifer system at River Nestos eastern Delta, NE Greece, Environmental Earth Sciences, Springer, 73: 6387–6415.

Pliakas, F., Diamantis, I., Petalas, C., 2001. Saline water intrusion and groundwater artificial recharge in east delta of Nestos River. Proceedings of the 7th International Conference on Environmental Science and Technology, University of the Aegean, Dept. of Environmental Studies, and Global Nest, Ermoupolis, Syros, Greece, 3-6/9/2001, 2: 719-726.

Pliakas, F., Gkiougkis, I., Mimidis, K., Tzevelekis, T., Diamantis, I., 2014a. Hydrogeological approach in investigating a karst system, south-east of Nestos River, NE Greece. Proceedings of the 10th International Hydrogeological Congress of Greece, 8-10/10/2014, Thessaloniki, Greece, 653-661.

Pliakas, F., Diamantis, I., Gkiougkis, I., Mimidis, K., Tzevelekis, T., Bellos, K., 2014b. Surface water management of River Nestos Eastern Delta wider region for the optimal meet of irrigation needs and the improvement of groundwater quality. Technical report to the East Macedonia and Thrace Region, Regional Unit of Xanthi, 182 pp (in Greek).

Pliakas, F., Diamantis, I., Gkiougkis, I., Mimidis, K., Tzevelekis, T., Bellos, K., Avgeris, L., 2015. Study of the modification of irrigation and drainage network directing from Dekarcho and Avato up to Mangana to facilitate irrigation, drainage and groundwater recharge requirements. Technical report to the East Macedonia and Thrace Region, Regional Unit of Xanthi, 164 pp (in Greek).

Revelle, R., 1941. Criteria for recognition of sea water in ground-waters. Transactions of American Geophysical, Union, 22: 593-597.

Sakkas, I., Diamantis, I., Pliakas, F., et al., 1998. Groundwater artificial recharge study of Xanthi – Rhodope aquifers. Technical report to the former Ministry of Agriculture, 570 pp (in Greek).

Todd, D. K., Mays, L. W., 2005. Groundwater Hydrology (3rd edition). John Wiley & Sons, Inc., New York, USA.

U.S. Environmental Protection Agency – EPA, 1992. Guidelines for Water Reuse. Technology Transfer Manual EPA/625/R-92/004. U.S. EPA. Washington, D.C. 247 pp.

U.S. National Research Council, 1994. Ground Water Recharge Using Waters of Impaired Quality. National Academy Press, Washington, D.C., 283 pp.

Proceedings of the 10th World Congress of EWRA 'Panta Rhei', 5-9 July 2017, Athens, Greece
© 2017 *European Water Resources Association*

Land accounting perspective on water resources management

G.T. Paschos, G.E. Bariamis* and E.A. Baltas
Department of Water Resources and Environmental Engineering, School of Civil Engineering, National Technical University of Athens,Greece
* *e-mail: bariamis@mail.ntua.gr*

Abstract: Water availability and allocation are connected to various activities (e.g. irrigation, urbanisation, industrial production, recreation), which are taking place on the terrestrial surface. Considering the variation of the driving forces, it is necessary to examine possible patterns and trade-offs between land, water and social welfare. Land cover refers to a set of both natural features and anthropogenic establishments that mainly result from its use. Quantitative and descriptive attributes can be assigned to a land unit providing valuable information about the classification of land cover, the available stocks and flows among different types, the rate at which land cover types and their inherent socio-economic factors depend on water-related processes. Therefore, a total amount of changes that are related to water resources can be observed, recorded and analysed. This research focuses on the implementation of land accounting approach in Greece in order to identify the degree of pressures on water resources over time. Furthermore, the integration of diverse data sources, intends to emphasize the impacts of primary land use activities such as housing and cultivation that are prevalent within the Greek territory. Achieving these goals provides the opportunity to improve decision support tools towards sustainable development.

Key words: land cover, land accounting

1. INTRODUCTION

In 1992, Agenda 21 highlighted the need for the development of a systems approach in order to support sustainability and Green Economy policy. Among other initiatives, this systematic approach (United Nations, 2014) incorporates fundamental principles of economic accounting in an integrated statistical information pyramid. Its main purpose is the connection of basic (environmental, economic or socio-demographic) statistics with derived key aggregates and indicators that can be utilized in policy-planning and decision-making.

Land accounting, as an aspect of the conceptual framework, focuses on various natural and anthropogenic activities, which take place on the terrestrial surface and analyses their dimensions in terms of land cover and land use. Starting in 1985, the Coordination of Information on the Environment (CORINE) Land Cover program defines the partition of land by introducing a combination of these characteristics. The application of visual interpretation on satellite images led to the establishment of the Land Cover (CLC) and Land Cover Changes (CLC-C) inventories that consist of 44 total classes. Mapping, monitoring and quantifying data of these elements can be used as input to integrated land and water analysis (Serbina and Miller, 2014). The main challenge is to examine the permanent links between basic land use functions and water-demanding activities under the constraints that the first asset often underlies poor management and the latter is scarcely allocated. Over the last decade, it is alleged that the study of historical effects in land cover/use can be used in the understanding of the current situation and the prediction of future trends, factors and possible choices that will affect water resources in due course (Schilling et al., 2008).

2. METHODOLOGY

2.1 Classification, stocks and transitions

In 2006, European Environment Agency (EEA, 2006) published the results of a study based on the CORINE data. According to CORINE nomenclature, the classes of land cover can be grouped and arranged into three levels. In order to build the land accounts, EEA suggests a classification of eight broad types of land cover capable of giving a clear description on the main patterns of change upon the surface. This research complies with the context of the EEA methodology for land accounting and applies it to the country of Greece for the period 1990-2012.

As specified by the methodology, the reclassified data from the CLC_{1990} layer showed that the land resources status for Greece covered 27.4% semi-natural vegetation, 27.3% forested land, 22.9% arable land and permanent crops, 17.2% pastures, 1.9% artificial surfaces, 1.8% open spaces, 1.1% water bodies and 0.5% wetlands.

This broad classification method is particularly useful for the regulation of the CLC-C data. Thus, instead of managing a 44x44 pivot matrix, the analysis is widened to an 8x8 pivot matrix that facilitates focusing on specific cover types. The rows of the matrix refer to the initial characterization of land units, while the columns relate to the final land cover type assignment during a given time period. The basic functions used in this process are those of land consumption and land formation respectively. This interpretation represents a "from/to" procedure (Table 1) that constitutes the core of describing the observed conversions by means of both their quantitative and descriptive attributes.

Table 1. Broad land cover transitions (km^2) - The 'from/to' procedure, Greece 1990-2012

FROM/TO	**Artificial surfaces**	**Arable land**	**Pastures and mosaics**	**Forested Land**	**Semi-natural vegetation**	**Open spaces/bare soils**	**Wetlands**	**Water bodies**	**Total consumption (km^2)**
CORINE categories total (highest detail classification)	11 (111-142)	7 (211-223, 241)	4 (231, 242-244)	4 (311-313, 324)	3 (321-323)	5 (331-335)	5 (411-423)	5 (511-523)	
Artificial surfaces	126,85	1,47	14,04	25,73	6,94	0,49	0,00	10,99	**186,51**
Arable land	251,79	502,02	156,95	1,57	0,23	1,51	6,40	10,87	**931,34**
Pastures and mosaics	237,22	70,17	5,90	4,87	7,65	9,26	0,56	49,14	**384,76**
Forested Land	50,10	2,31	34,57	2007,80	119,40	272,91	0,00	12,59	**2499,67**
Semi-natural vegetation	165,48	27,98	72,34	199,28	182,03	268,60	0,00	14,34	**930,05**
Open spaces/bare soils	4,10	0,66	1,23	97,09	97,84	11,34	0,35	6,68	**219,30**
Wetlands	1,66	4,97	2,22	0,00	0,00	0,00	0,00	10,20	**19,04**
Water bodies	2,49	15,79	3,15	0,46	0,31	16,78	11,74	6,26	**56,98**
Total formation (km^2)	**839,67**	**625,37**	**290,41**	**2336,79**	**414,40**	**580,89**	**19,06**	**121,06**	

Eventually, consumption corresponds with the total amount of area distributed from a land cover category (initial year reference) to other classes, while formation explains the amount of area that originates from different cover classes and is unified in a single category (final year reference).

The determinant approach used for the assessment of transitions during 1990-2012 indicates that the land cover status of the final observation year derives from a stepwise aggregation of the initial CLC_{1990} layer data with the three CLC-C layers. The general consideration depends on consumption

and formation in order to produce additional functions such as net formation, total turnover and no change of land cover. In conjunction with the cover state of the initial observation year, these factors contribute to the formation of the stock and change account for Greece (Table 2). Given that, total land area (about 132.000 km^2) remains constant over time, the overview is restricted to gains and losses between different cover types. Indicators such as net formation and total turnover represent the amount of pressures that specific cover types are subjected to during the accounting season. Further analysis at the artificial surfaces category reveals that there was a significant increase in net formation (compared to the stock of the initial year) while the amount of land area that participated in the consumption-formation processes (total turnover) reached almost 42%. Other types, such as forested or bare land, are bounded to constant natural transitions (felling, afforestation) and instant threats (fires). This leads to elevation of their respective values especially in temporal resolution that exceeds two decades.

Table 2. Stock and change accounts, Greece 1990-2012

	Artificial surfaces	Arable land	Pastures and mosaics	Forested Land	Semi-natural vegetation	Open spaces/bare soils	Wetlands	Water bodies	Total km^2
Land Cover 1990	2469,83	30262,06	22711,73	36005,13	36101,21	2374,73	592,74	1476,28	131993,70
Consumption of initial land cover	186,51	931,34	384,76	2499,67	930,05	219,30	19,04	56,98	5227,66
Formation of new land cover	839,67	625,37	290,41	2336,79	414,40	580,89	19,06	121,06	5227,66
Net formation of land cover (Formation-Consumption)	653,16	-305,98	-94,35	-162,88	-515,65	361,59	0,02	64,09	0,00
Net formation as % of initial year	26,4%	-1,0%	-0,4%	-0,5%	-1,4%	15,2%	0,0%	4,3%	
Total turnover of land cover (Formation + Consumption)	1026,19	1556,71	675,17	4836,46	1344,45	800,18	38,11	178,04	10455,31
Total turnover as % of initial year	41,5%	5,1%	3,0%	13,4%	3,7%	33,7%	6,4%	12,1%	7,9%
No land cover change (Land Cover 1990-Consumption)	2283,32	29330,72	22326,97	33505,45	35171,16	2155,43	573,70	1419,30	126766,05
No land cover change as % of initial year	92,4%	96,9%	98,3%	93,1%	97,4%	90,8%	96,8%	96,1%	96,0%
Land Cover 2012	3122,99	29956,09	22617,37	35842,25	35585,56	2736,32	592,76	1540,37	131993,70

As mentioned above, land cover changes between different types are driven by human or natural activities. The classification of these one-to-one changes introduces the concept of land cover flows (LCF). Land units are either consumed or newly shaped with the transfers captured on net formation of each category. The "from/to" procedure can also be interpreted as flows of land that connect the initial with the final state. The EEA nomenclature proposes nine general types of land flows from which three are mentioned for the purposes of this study. The three land cover flows are in fact the drivers of change that cause the formation of artificial surfaces. Urban land management (LCF1) includes the internal land area transfers between the CORINE types that are characterized as artificial surfaces both in the initial and final state of the observation period. Urban residential sprawl (LCF2) refers to the extension of urban fabric (CORINE categories 111, 112) in expense of cover types that were initially classified as non-artificial. Likewise, sprawl of economic sites and infrastructure (LCF3) is the concentrated extension of transport sites, construction and similar facilities (CORINE categories 121-142) by consuming non-artificial land.

2.2 The CORINE limitations

Despite the significant effort in the design, updating and constant re-evaluation of the CORINE

database, there are some considerable limitations in land management applications. The minimum mapping unit is set at 25 hectares for the CLC layers and 5 hectares for the CLC-C layers. It is recommended that the users interested in changes during a period should rely on the CLC-C files instead of the difference between two CLC layers since the lower resolution of the status layers would lead to a more generalized product.

3. RESULTS

The valuation of Table 2, notes that the area occupied by artificial surfaces in Greece has increased about 26.4% over the accounting period of 23 years. An assessment of the respective land cover flows noted the area amount for LCF2 at 110,08 km^2 and higher values for LCF1 and LCF3 (115,99 km^2 and 613,61 km^2). The sum of the three LCF is equal to the formation of artificial surfaces. Moreover, LCF2 happens due to the consumption of pastures and arable land while LCF3 drains mainly from pastures, arable land and semi-natural vegetation. Although the classification method discerns the general direction regarding land transformations, at this point it is necessary to explore further the causes and consequences of these changes by focusing on thematic detail and the rate at which artificial sprawl unravels.

In this case, the implementation of the accounting approach is enhanced with the estimated net formation rate. Primarily, it is assumed that annual temporal resolution fits sufficiently enough in sequential procedures like extension of built-up areas or changes in cultivation patterns. This assumption is combined with the disaggregation of net formation in the three transitional periods (i.e. CLC-$C_{1990\text{-}2000}$, CLC-$C_{2000\text{-}2006}$ and CLC-$C_{2006\text{-}2012}$). Likewise, the rates of similar processes, such as urban residential sprawl, can be estimated.

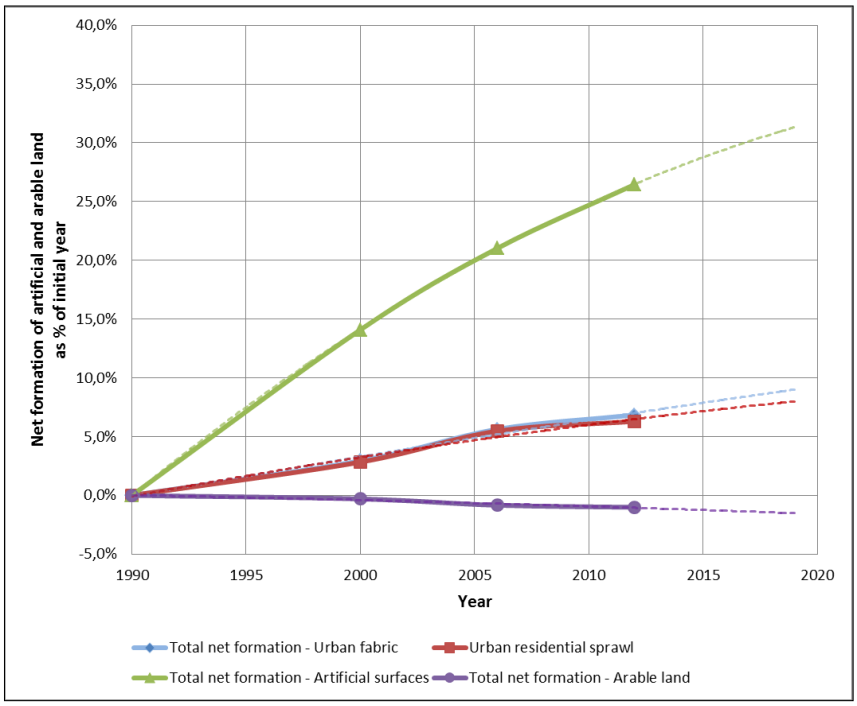

Figure 1. Net formation of land cover, Greece

Figure 1 illustrates the rates of net formation for key categories which are directly related to water resources. Urban fabric is a sub-category of artificial surfaces that includes housing and service activities. The net formation rate is quite similar to the urban residential sprawl rate which means that there is a proportionally small amount of land parcels that participate in urban internal conversions and thus most of the space occupied originates from other classes (mainly arable land and pastures). The artificial surfaces area was increased by 26%, which can be attributed to the

sprawl of economic sites and infrastructure in common with the extension of urban fabric (6.8 % increase). Last but not least, arable land area is reduced about 306 km^2 by 2012. The consumed amount estimated to contribute to LCF2 and LCF3 reached 252 km^2 over the years. The loss ratio of arable surfaces due to artificial sprawl is approximately 82 % resembling this category to a tank from which the majority of economy-driven land flows originates.

Water resources are subjected to constant pressure in this ever-changing reality. Via the operation of the information pyramid, it is possible to gain access to key details about the connection between land, socio-demographic and water statistics. As an example, Figure 2 illustrates an attempt to connect these characteristics in the urban regions of Greece. The database of Eurostat provided information regarding the average population of Greece for the period 2000-2007. The population density in urban regions was estimated in an annual basis from diversified data sources (CORINE and Eurostat). The primary axis refers to water use from public water supply for household activities for the same period (Eurostat). The decrease in the average density over the years indicates that the expansion of built-up areas benefits from the diffuse sprawl of the discontinuous urban fabric.

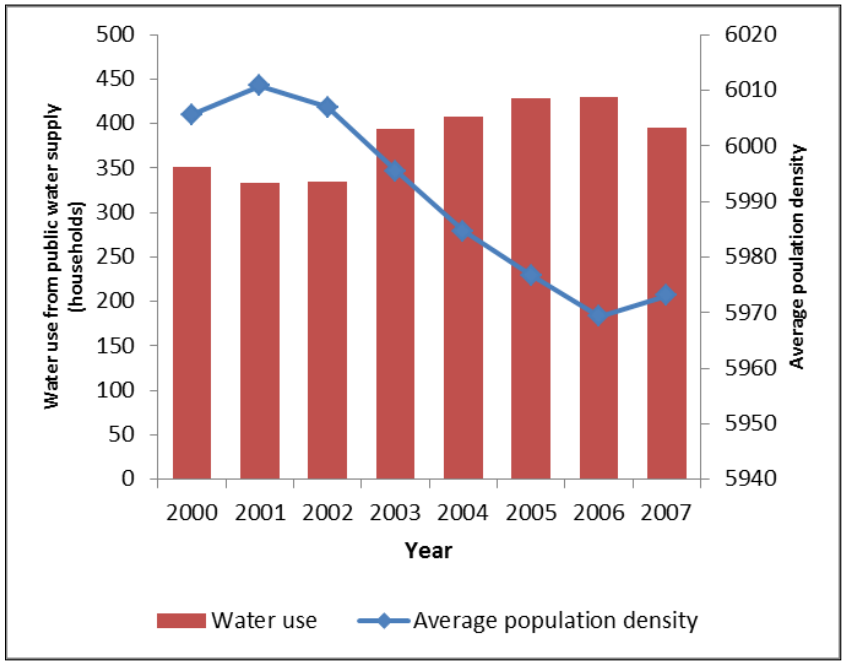

Figure 2. Water use (hm^3) for households and population density (inhabitants/km^2 of urban fabric), Greece

In cases where geographic or thematic detail is of prime importance, the adjustment of the approach depends on the scope of the task. In 1989, the Greek Government issued a Ministerial Decree about the limitations for rational water use in irrigation. Based on the Blaney-Criddle potential evapotranspiration method, the decree sets the estimated water demand requirements (in m^3 per 1000 m^2) for the reference crops of the water districts of Greece.

These limitations were applied to the water districts of Thessaly, Thrace and West Peloponnese. Four types of crops were selected from the broad category 'arable land' or in terms of CORINE nomenclature namely 'rice fields', 'vineyards', 'fruit trees and vegetables' and 'olive groves'. The land accounting approach was applied for the period 1990-2012 by calculating the annual net formation of the crops and subsequently used in the estimation of an average water amount according to the cover types and water district specifications. In Figure 3, the percent changes are presented comparatively. Water demand in Thessaly (approximately 138 hm^3 for a total area of 233 km^2 in 1990), decreases about 2 % by 2006 (total area 228 km^2). Also, in West Peloponnese (506 hm^3 for 924 km^2 in 1990) the requirements are gradually reduced until 2012. In Thrace (44 hm^3 for 86 km^2 in 1990), an increase is noted by the year 2000 followed by a gradual decrease until the estimated demand is balanced past 2006.

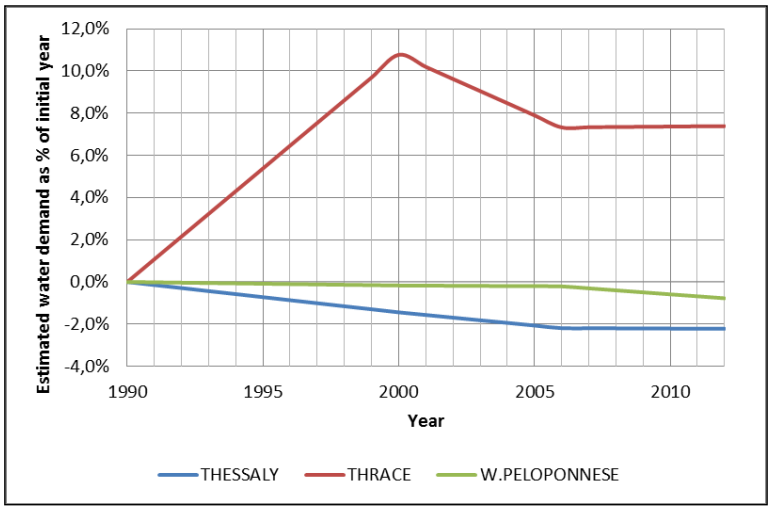

Figure 3. Estimated water demand changes for a total of four reference crops, Water districts of Thessaly (GR08), Thrace (GR12), West Peloponnese (GR01)

4. CONCLUSION

In Greece, urbanization is considered to be the dominant driver of land transitioning. As a consequence, the hydrological regime is affected due to natural vegetation or arable land consumption. Moreover, the variety of water use noticed in central and suburban regions is important, as inhabitants of the decentralized fabric tend to consume larger water amounts (horticulture, washing and cleaning activities, etc). In rural areas, an approximate 80 % of the exploitable water resources of Greece are used in irrigation. Monitoring cultivation activities is a crucial step to achieve both rational water usage and effective crop production. A better understanding of such patterns will aid in analyzing the reasons of human behavior against natural capital.

Land change impacts on water resources are often examined concurrently with various processes of the hydro-climatic cycle. However, the accounting approach clarifies to a certain extent their significance and can be used as a support tool in the development of mitigating measures and actions. At national level, a mutual collaboration between Administrative, Institutional and Public Sector should promote the goal of achieving water efficiency in urban and agricultural regions. A decisive step in this long-term process is the design and implementation of an integrated urban planning and water management strategy. As the expansion of built up areas appears to be the main driver that mobilizes the majority of human activities, preservation of the integrity of natural assets should be a matter of high priority.

REFERENCES

Copernicus Land Monitoring Service, 2012. The revised and supplemented CORINE land cover nomenclature; 2012 Technical library publication: 4-25.

Copernicus Land Monitoring Service, 2015. Pan European Component: CORINE land cover; October 2015 flyer publication:1-2.

European Commision, Eurostat Database. Water use by supply category and economical sector (Retrieved from http://ec.europa.eu/eurostat/tgm/refreshTableAction.do?tab=table&plugin=1&pcode=ten00013&language=en)

European Environment Agency, 2006. Land accounts for Europe 1990-2000; Report 11/2006: 6-29, 99-105.

Ministerial Decree 16/6631/89 of the Greek Gonverment on the limitations for rational water use in irrigation; Gonverment Gazette Issue, 428/B/2-6-1989: 4297-4304.

Schilling, K. E., M. K. Jha, Y.-K. Zhang, P. W. Gassman, and C. F. Wolter, 2008. Impact of land use and land cover change on the water balance of a large agricultural watershed: Historical effects and future directions; Water Resour. Res., July 2008, 44, W00A09: 1-12.

Serbina L., Miller H.M., 2014. Landsat uses and benefits-Case studies by application area; U.S. Geological Survey Open-File Report 2014–1108: 1-9.

United Nations, 2014. System of environmental-economic accounting 2012 – Central framework; United Nations Statistics Division: 173-183.

Proceedings of the 10th World Congress of EWRA 'Panta Rhei', 5-9 July 2017, Athens, Greece
© 2017 *European Water Resources Association*

Environmental flow assessment through integrated approaches

M. Tegos, I. Nalbantis and A. Tegos*
Centre for the Assessment of Natural Hazards and Proactive Planning and Laboratory of Reclamation Works and Water Resources Management; School of Rural and Surveying Engineering, National Technical University of Athens, Athens, Greece
** e-mail: tegosaris@yahoo.gr*

Abstract: The alteration of river flow regime downstream of artificial dams is known to negatively affect the health of the riparian ecosystems, the geomorphology of the riverbed and riparian zone as well as the quantity and quality of river waters. To avoid such impacts releases from dams are scheduled so as to sustain the so called environmental flow. This work aims at investigating the differences and complementarities of various methods used for the assessment of environmental flow. Firstly, we extended the historical daily flow time series through using a rainfall-runoff model so as to overcome the problem of inadequate length of it. Subsequently, different simple and advanced hydrological methods were applied (Tennant method; minimum monthly flow method; flow duration curve method; the method of basic maintenance flow; the Range of Variability Approach). Also, a hydraulic method (wetted perimeter-discharge technique) was applied using data from several river cross-sections. This method allowed the establishment of an empirical relationship between flow and wetted perimeter. Finally, crucial ecological criteria such as the fish survival requirements under different hydrological and hydraulic regimes were investigated in an effort to formulate an integrated framework for environmental flow assessment. The different approaches were tested on a human modified river with a water supply dam (Mornos), located in the Water District of West Sterea Hellas, Greece.

Key words: Environmental flow; dam operation; human modified river; Mornos river

1. INTRODUCTION

The continuing increase of water demand for irrigation abstractions, drinking water, and hydroelectric power production has led to the construction of large-scale water resources projects (Koutsoyiannis, 2011) that caused modifications to the biotic and abiotic environment of rivers. The constructed works often require scientific explanations regarding the alteration on the physical environment (Koutsoyiannis et al., 2007). The environmental flow (EF) as a key measure in water resources management has been intensively studied during the last five decades (Acreman et al., 2014). Usually, the sustainable use of water resources requires that conflicting water targets are met (Christofides et al., 2005) e.g., keeping water in storage and releasing it for various uses. The environmental flow depends on multiple factors, such as the size of river bed, flow seasonality at both coarse and fine time scales, flow duration characteristics, surface and subsurface water levels (Acreman and Dunbar, 2004), as well as the downstream ecological value and chemical status of the surface water bodies.

In this study, we focus on the assessment of environmental flow in Mornos river, where a water supply dam is operated without provision of environmental releases. We use several methods of wide applicability and discuss the practical use of different environmental flow policies for the maintenance of the riverine ecosystem, considering hydrological, hydraulic and ecological criteria.

2. METHODS FOR ASSESSING ENVIRONMENTAL FLOW

2.1 General

The first systematic attempt for the quantification of environmental flows started in the U.S.

around 1950 with the Tennant Method which was based on the correlation between fish sustainability and hydrological regime (Tennant, 1976). According to bibliography (Tharme, 2003), 207 methodologies have been applied to 44 different countries. These can be divided into four main categories depending on the type, size, quality and availability of the required data, data processing, assumptions time and cost. These categories are the following: (1) Hydrological methods (simplified or advanced); (2) Hydraulic rating methodologies; (3) Habitat simulation methodologies; (4) Holistic methodologies.

The first category of methods includes the most elementary approaches, in which EF is usually assessed as a constant percentage of a flow statistic at the annual or monthly scale. Recently, more sophisticated methods have been developed, suggesting a hydrological regime for the maintenance of the river system at acceptable levels. Examples of these advanced methods are the Range Variability Approach Method and the Basic Maintenance Flow method.

The second category evaluates a number of hydraulic, morphological and geometrical characteristics (wetted perimeter, depth, velocity, etc.). The key idea is to equate EF to a critical low flow based on the river cross section geometry (Gippel and Stewardson, 1998).

Methods of the third category, e.g., the Habitat Simulation method, assess EF on the basis of detailed analyses of the quantity and suitability of instream physical habitat, particularly target species or assemblages (mainly fish), observed under different flow regimes. These methods use hydrological, hydraulic and biological data within hydraulic simulation tools, thus allowing for the establishment of a direct link between habitat and discharge (Stalnaker et al., 1995).

The fourth category, referred to as Holistic Methods (Arthington et al., 1992) includes processes that allow aquatic scientists from many disciplines to integrate data and knowledge (King et al., 2003), thus which is a shift from prescriptive to interactive approaches (Tharme, 2003). Obviously, these are much more demanding than all other approaches, in terms of data and human resources. Details on the selected methods are given next.

2.2 Simple hydrological methods

The following methods were selected: (1) *Tennant method*: this method specifies percentages of mean flow that provide different river quality habitats, i.e. 10% for poor quality (survival), 30% for moderate habitat, and 60% for excellent habitat; (2) *Minimum Annual Flow (MAF)*: the discharge of the driest month over a long series of monthly flows is selected as EF; (3) *FDC method*: using the flow duration curve, typical flow quantiles are calculated such as Q_{60}, Q_{70} , Q_{80} and Q_{90}.

2.3 Basic maintenance flow (BMF) approach

The method studies the irregularities in the daily mean flow series using a moving average model (Palau and Alcázar, 2012; Efstratiadis et al., 2014). In this work, only two parameters were considered: the basic flow (Q_b) which represents the absolute minimum discharge that should flow in a river and the maintenance flow (Q_m) which represents the minimum instream flow requirements of the river throughout the year, usually calculated on a monthly basis (Peñas et al., 2014).

2.4 Range Variability Approach (RVA)

The method is based on the assumption that hydrological conditions of a river fully determine its ecological characteristics. It uses 32 hydrological parameters describing hydrological changes that influence the quality of ecosystems (Richter et al., 1996). The most important of them are: (1) the 25% and 75% quantiles of monthly discharge which specify the desirable range of monthly flows;

(2) indicators for extreme hydrological conditions, which are expressed as the mean and upper and lower limit for the annual maximum and minimum of *d*-day flow, where d = 1, 3, 7, 30, and 90 days.

2.5 Wetted perimeter - discharge method

The breakpoint of the wetted perimeter–discharge curve at characteristic cross-sections is typically used as an indicator of the corresponding critical flow. In this work, we employed the maximum curvature approach proposed by Gippel and Stewardson (1998) to define the lower breakpoint of each wetted perimeter–discharge curve; the latter was constructed using the Manning's equation.

2.6 Examination of the restrictions for the habitat growth

In an effort to exploit ideas of modern approaches such as the Habitat simulation and Holistic methods, we use survey data from a fish monitoring campaign downstream the studied dam. Then, we identified a number of fish species and some critical biological parameters related to flow (e.g., water depth, spawning seasonality).

3. STUDY AREA AND DATA

The Mornos dam (Figure 1, right) started its operation in 1981 as one of the largest clay core earthen dams in Europe. The dam embankment has a maximum height of 139 m from the foundation level, a crest width of 10 m, and a base length of 250 m. The altitude of the dam crest from the mean sea level stands at 446.5 m, while the highest flood level is 435 m. The related Mornos reservoir serves water supply of the Athens metropolitan area (Nalbantis et al., 1992).

Regarding the reservoir characteristics, the average annual water volume is 240×10^6 m^3 and 195×10^6 m^3 for inflows and releases respectively, while the total storage capacity is approximately 764×10^6 m^3. In this work the study area is the river basin at the dam site (Figure 1, left), as well as the river bed and floodplain downstream of the dam.

The geomorphological and hydrodynamic conditions of the estuary favoured the development of important wetlands, with significant biological diversity. Regarding fish fauna, seven species have been identified, including the five species presented in the results section and also Pseudophoxinus, and Valencia letourneuxi. Birds are the largest group of vertebrates (Aquila chrysaetos, Circaetus gallius, Buteo, Falco, Accipiter, Cachybaptus rufficollis, Alcedo atthis). Finally, there exist several species of reptiles and amphibians that are protected at the international level (e.g., Lutra- Lutra).

The daily streamflow time series is the main dataset for assessing EF. The absence of such series of significant length led us to resort to estimating streamflows using rainfall-runoff modelling. This included the following computational steps: (1) Preparation of the required geographical information; (2) collection of daily rainfall from eight stations for the period 1964-1980; (3) processing of rainfall data; (4) calibration of a lumped conceptual hydrological model for the period 29/1/1964-30/9/1966; the model used by Efstratiadis et al. (2015) was adapted using typical inputs such as rainfall and potential evapotranspiration (Tegos et al., 2013); the Nash-Sutcliffe Efficiency (NSE) was 0.82 in calibration; the agreement between the observed and simulated streamflows was satisfactory (Figure 2); (5) estimation of daily flow for the period 1964-1980 using the calibrated model.

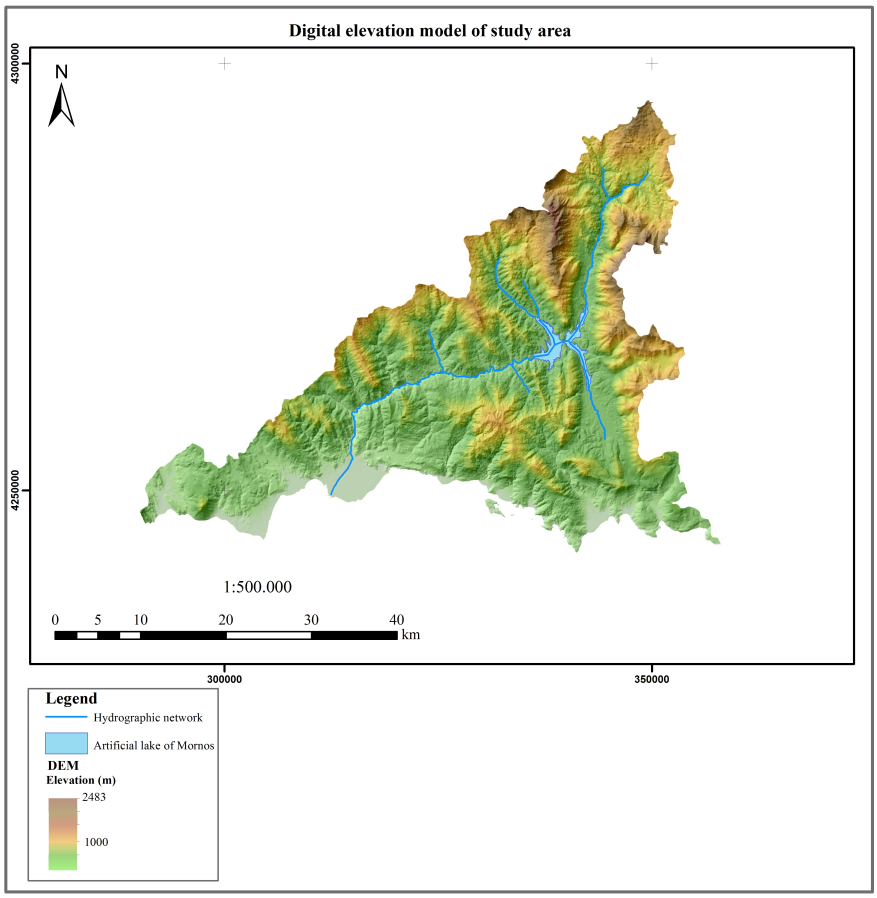

Figure 1. Digital Elevation Model of the Mornos river basin

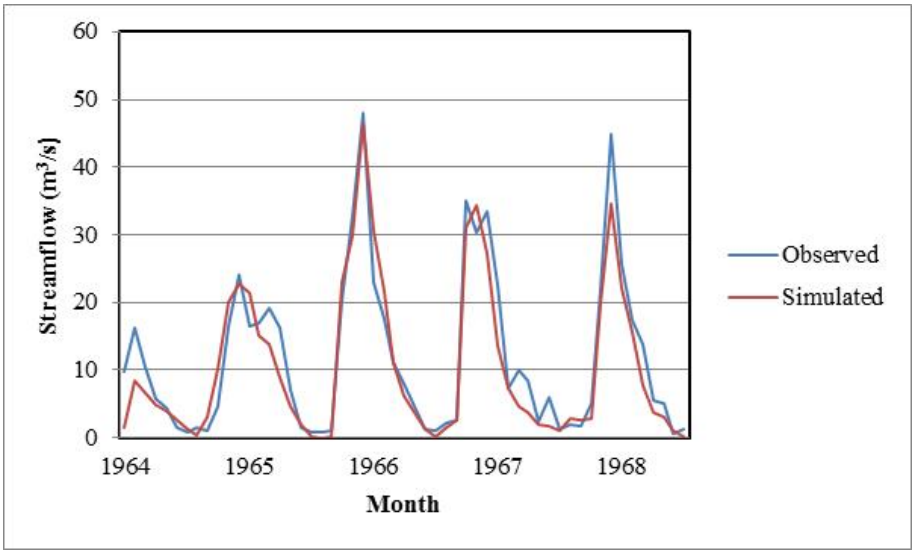

Figure 2. Monthly Simulated and Observed flows for both the calibration and validation periods

4. RESULTS

The simple hydrological methods provided the following results: (1) The Tennant method gave critical flow values for poor, moderate and excellent quality of habitat respectively 0.93, 2.80 and 5.60 m^3/s; (2) following the MAF method the driest month was August and its minimum flow over the period 1964-1980 equal to 0.85 m^3/s; (3) the FDC method yielded Q_{60} = 4.2 m^3/s, Q_{70} = 3.0

m^3/s, $Q_{80} = 2.0$ m^3/s and $Q_{90} = 0.9$ m^3/s).

The BMF method provided us with a basic flow estimated at 0.85 m^3/s and a monthly maintenance flow ranging between 1.06 and 5.33 m^3/s. The RVA method yielded the 25% and 75% flow quantiles shown in Table 1 as well as the indicators for extreme hydrological conditions given also in Table 1.

To apply the wetted perimeter–discharge method we selected eighteen representative river cross-sections along the lower course of Mornos river. Next, we constructed the wetted perimeter–discharge curve for each one of the selected cross-sections. The critical flow over the eighteen cross-sections was found to range from 2.36 to 9.75 m^3/s.

With regard to modern integrated approaches we collected fish survey data downstream the Mornos dam. Seven species were identified (Economou et al., 2014) and some critical biological parameters are related to flow variables which are given below. These constitute crucial restrictions for decisions regarding flow releases for Mornos reservoir.

1. *Salmo trutta macrostigma*, max height 40 cm, spawning period October- January.
2. *Knipowitschia Sp*, max height 40 cm, spawning period February- April
3. *Barbus peloponnesius*, max height 20 cm, spawning period May- June
4. *Barbus albanicus*, max height 30 cm, spawning period May.
5. *Leuciscus cephalus*, max height 22 cm, spawning period February

Additionally, the worldwide significant species of Lutra-lutra is susceptible to water quality and quantity changes and possible loss of the riparian vegetation (Koutsos et al., 2011).

Table 1. Monthly flow values and characteristic flows for Mornos river (m^3/s), calculated using the RVA method.

For flow in month	Mean (m^3/s)	Lower limit (m^3/s)	Upper limit (m^3/s)
January	21.38	10.41	32.36
February	19.64	12.55	26.72
March	13.46	8.62	18.29
April	9.56	6.17	12.96
May	5.39	3.05	7.73
June	3.03	1.80	4.26
July	1.55	0.67	2.42
August	0.85	0.39	1.29
September	1.36	0.36	2.36
October	4.38	0.41	8.35
November	13.32	5.97	20.67
December	21.49	12.46	30.52
Characteristic flow			
1-day minimum	0.15	0	0.50
3-day minimum	0.15	0	0.51
7-day minimum	0.18	0	0.57
30-day minimum	0.36	0	0.92
90-day minimum	0.92	0.24	1.60
1-day maximum	94.66	67.97	121.36
3-day maximum	70.21	49.85	90.57
7-day maximum	47.57	34.76	60.37
30-day maximum	29.60	21.55	37.66
90-day maximum	23.28	16.73	29.82

Table 2 summarizes the results of our analyses which showed the following: (1) The simplified hydrological methods (Tennant, MAF, FDC) propose a lower hydrological threshold which is compulsory; (2) the hydraulic method, even without streamflow data, constitutes a reliable alternative, but, in our case, the information on ground elevation in river bed and floodplain was inadequate and led to a significant overestimation of EF with respect to other methods; (3) the advanced hydrological methods (BFM, RVA) yield a seasonally varying EF regime which is physically consistent and hence more suitable.

Table 2. Summary of results

Category of method	Method	EF (m^3/s)	Flow regime
Hydrological	Tennant	0.93-5.60	Steady flow
	MAF	0.85	Steady flow
	BMF	1.06-5.33	Monthly seasonal flow
	FDC	0.9-4.2	Steady flow
	RVA	0.36-12.55	Monthly seasonal flow
Hydraulic	Wetted perimeter-discharge	2.36-9.75	Steady flow

5. CONCLUDING REMARKS

The assessment and selection of environmental flow is a complicated technical problem depending on the quantity and quality of the existing data (topographical, hydrological, hydraulic and biological) which, in turn, determines the type of the approach to be followed .The most representative hydrology-based approaches, as well as the wetted perimeter – discharge method were employed to assess the environmental flows for the Mornos dam in Western Sterea Hellas, Greece. The methods provided a wide range of values, in terms of critical flows or allowable range of them. We recommend a seasonally varying flow, which can better preserve the eco-hydrological regime of the river. The simplified hydrological methods fail to provide such seasonally varying regime which is known to exist in the Mediterranean region. Among two well-known methods accounting for seasonal flow variation, i.e., the Basic Maintenance Flow (BMF) and the Range of Variability Approach (RVA), the former is more suitable than the latter, which is quite complex, difficult to interpret and thus difficult to implement in practice. Finally, the use of data from biological surveys regarding biological parameters of the fish populations is necessary and useful for further optimization and validation of the EF releases.

REFERENCES

Acreman, M. C., Overton, I. C., King, J., Wood, P. J., Cowx, I. G., Dunbar, M. J., Young, W. J., 2014. The changing role of ecohydrological science in guiding environmental flows. Hydrological Sciences Journal; 59(3-4): 433-450.

Acreman, M. C., Dunbar, M. J., 2004. Defining environmental river flow requirements – a review. Hydrology and Earth System Sciences; 8: 861–876.

Arthington, A. H., King, J. M., O'Keefe, J. H., Bunn, S. E., Day, J. A., Pusey, B. J., Bluhdorn, D. R. Tharme, R., 1992. Development of a holistic approach for assessing environmental flow requirements of riverine ecosystems. In: Proceedings of an International Seminar and Workshop on Water Allocation for the Environment (eds. J. J. Pigram and B. P. Hooper). Armidale, USA, Centre for Water Policy Research, University of New England. pp. 69-76.

Christofides, A., Efstratiadis, A., Koutsoyiannis, D., Sargentis, G.-F. Hadjibiros, K. 2005. Resolving conflicting objectives in the management of the Plastiras Lake: can we quantify beauty? Hydrology and Earth System Sciences; 9(5): 507–515.

Eonomou, A. N., Barbieri, R., Zogaris, S., Gialcnumi, S., Dimitriou, E., 2004. Developing a database for a fish-based ecological quality assessment of the rivers of Greece.

Efstratiadis, A., Tegos, A., Varveris, A., Koutsoyiannis, D., 2014. Assessment of environmental flows under limited data availability: case study of the Acheloos River, Greece. Hydrological Sciences Journal; 59(3-4): 731-750.

Efstratiadis, A., Nalbantis, I., Koutsoyiannis, D., 2015. Hydrological modelling of temporally-varying catchments: facets of change and the value of information. Hydrological Sciences Journal; 60 (7–8). doi:10.1080/02626667.2014.982123

Gippel, C. J., Stewardson, M. J., 1998. Use of wetted perimeter in defining minimum environmental flows. Regulated rivers: research and\ management; 14(1): 53-67.

King, J., Brown, C., Sabet, H., 2003. A scenario-based holistic approach to environmental flow assessments for rivers. River Research and Applications; 19: 619–639.

Koutsoyiannis, D., 2011. Scale of water resources development and sustainability: Small is beautiful, large is great. Hydrological Sciences Journal; 56(4): 553–575.

Koutsoyiannis, D., Mamassis, N., Tegos, A., 2007. Logical and illogical exegeses of hydrometeorological phenomena in ancient Greece. Water science and technology: water supply; 7(1): 13-22.

Koutsos, T. M., Dimopoulos, G. C., Mamolos, A. P., 2011. Ecological impacts due to hydraulic technical projects to ecosystems near Natura 2000 network. In Advances in the Research of Aquatic Environment (pp. 29-37). Springer Berlin Heidelberg.

Nalbantis, I., Koutsoyiannis, D., Xanthopoulos, Th., 1992. Modelling the Athens water supply system, Water Resources Management; 6: 57-67, 1992.

Palau, A., Alcázar, J., 2012. The Basic Flow method for incorporating flow variability in environmental flows. River Research and Applications; 28: 93–102.

Peñas, F. J., Juanes, J. A., Álvarez Cabria, M., Álvarez, C., García, A., Puente, A., Barquín, J., 2014. Integration of hydrological and habitat simulation methods to define minimum environmental flows at the basin scale. Water and Environment Journal; 28(2): 252-260.

Richter, B. D., Baumgartner, J. V., Powell, J., Braun, D. P., 1996. A method for assessing hydrologic alteration within ecosystems. Conservation biology; 10(4): 1163-1174.

Stalnaker, C. B., Lamb, B. L., Henriksen, J., Bovee, K. Bartholow, J., 1995. The Instream Flow Incremental Methodology: A Primer for IFIM. Washington, DC: U.S. Geological Survey Biological Report 29. 45 p

Tegos, A., Efstratiadis, A., Koutsoyiannis, D., 2013. A parametric model for potential evapotranspiration estimation based on a simplified formulation of the Penman-Monteith equation. Evapotranspiration-an overview. InTech, Rijeka, Croatia: 143-165.

Tennant, D. L., 1976. Instream flow regimens for fish, wildlife, recreation and related environmental resources. Fisheries; 1(4): 6–10.

Tharme, R. E., 2003. A global perspective on environmental flow assessment: Emerging trends in the development and application of environmental flow methodologies for rivers. River Research and Applications; 19: 397–441.

Proceedings of the 10th World Congress of EWRA 'Panta Rhei', 5-9 July 2017, Athens, Greece
© 2017 *European Water Resources Association*

Sustainable management of water resources to safeguarding drinking water – The Water-Guard Project

S. Taskaris, I. Boskidis and P. Symeonidis*
Geospatial Enabling Technologies LTD, Athens, Greece
* *e-mail: psymeonidis@getmap.gr*

Abstract: The purpose of the WATERGUARD Project is the monitoring and protection of the quality of drinking water, as well as the overall qualitative characteristics of the aquifers in Ioannina Basin in Greece, in the Province of Taranto and in the municipality of Gallipoli in southern Italy, through the use of new processes, methodologies and technologies, which combine state-of-the-art integrated geographic information systems, decision support systems, telemetric technologies and knowledge management. This paper focuses on the development, the architecture and the functionalities of the WATERGUARD GIS Platform developed for the Water Association of Ioannina Basin, which is an integrated solution for the management of water supply networks and their infrastructures in a GIS environment. The software augments the functionalities of the existing SCADA system by offering a map centric, user friendly presentation of all the operational information in real time and place and by providing spatial analysis capabilities. The web-based architecture of the application makes it reachable for anyone from anywhere and, moreover, eliminates the need for additional licenses and installation for every user, thus allowing its utilisation by all the personnel with minimum costs. The software also includes an integrated Decision Support System (DSS) with ALERT capabilities, which consists of a set of rules applied in the database level to evaluate the water quality measurements from SCADA or other Operational Measuring Systems. The DSS rules can be easily configured to make possible the extension of the system in the future.

Key words: WATERGUARD Project, Water Supply Networks Management, GIS, SCADA

1. INTRODUCTION

The WATERGUARD project is implemented by Water association of Ioannina Basin, as Lead Partner and Decentralized Administration of Epirus and West Macedonia, Directorate of Water Management from Greece and Province of Taranto and Municipality of Gallipoli from Italy.

The purpose of the WATERGUARD Project is to monitor and ensure of the quality of drinking water and the qualitative characteristics of the aquifer in the Ioannina Basin in Greece, and in the other areas of the involved actors in Greece and Italy, using new processes, methodologies and technologies, which combine integrated geographic information systems (GIS), decision support systems (DSS), telemetric technologies and SCADA.

Several discrete and correlated actions were performed for the achievement of the Project's targets, including the determination and analysis of the present status regarding the water resources in the study areas, the suggestion of measures for the protection of the groundwater resources, Best Management Practises for the rational management of water supply networks, and the development of an integrated GIS operational monitoring software for the management of water supply networks.

The present study focuses on the development, the architecture and the functionalities of the WATERGUARD GIS Platform and its pilot implementation in the Water Association of Ioannina Basin. Such systems are used in different water utility agencies all over the world to improve their operational efficiency (Allen et.al., 2011; Allen et.al., 2013)

2. PLATFORM ARCHITECTURE

The software for operational monitoring of water supply is a complete GIS solution for management water supply, sewerage and any other related infrastructure. The software enhances the functions of SCADA systems that are installed in most Municipal Water and Sewerage Company, providing a friendly user interface that presents enterprise information (in real space and time) and other spatial analysis data. Thus, it provides an integrated environment for spatial sharing of information through an easy to use, web interface. The fact that the application is web based makes it accessible to everyone from anywhere. Moreover, it doesn't require additional licensing and installation for each user, and thus can be utilized by the entire staff of the Water Company without any extra financial burden.

The application leverages the modern features of an online geographic information system. Specifically, a spatial database is constructed using the technologies of ESRI ArcGIS Server and Microsoft SQL Server. The platform allows secure management of spatial information as well as the diffusion of internal and third party applications if required. Furthermore, it enables integrated spatial analysis using software of ESRI (ArcGIS) which include tools for processing networks or even for hydraulic modelling and solving. The web application is developed using the Microsoft Silverlight API.

The overall platform is developed under an n-tier, modular architecture which separates the system in the following modules: Presentation layer, Application layer, Database layer. The system architecture is shown in Figure 1, while the user interface is presented in Figure 2.

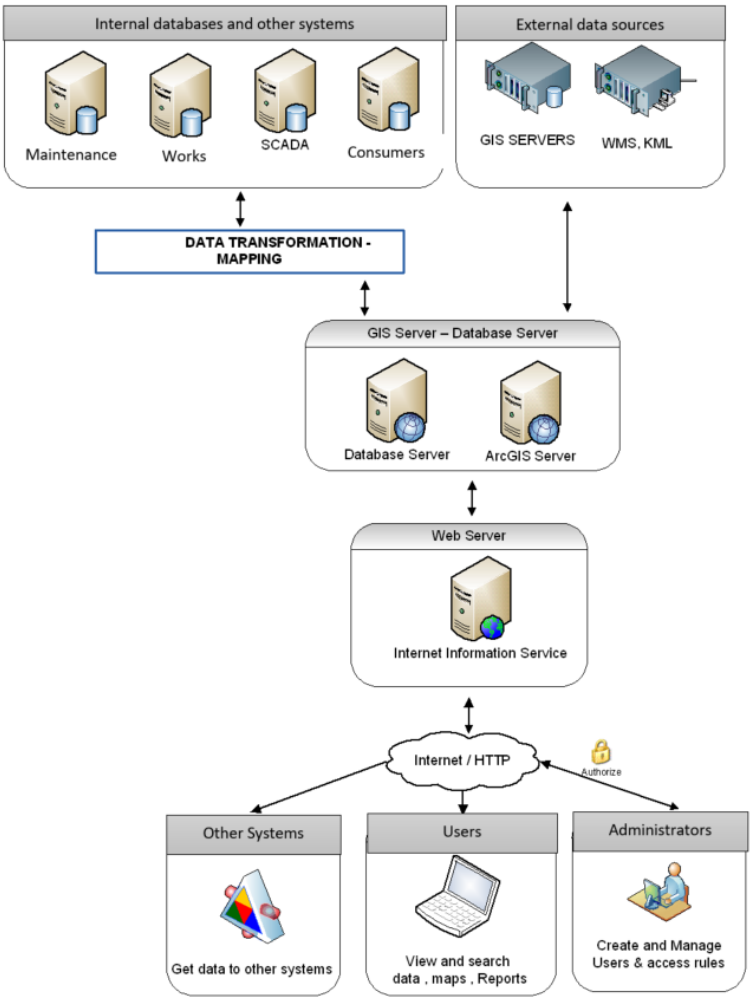

Figure 1. Platform architecture

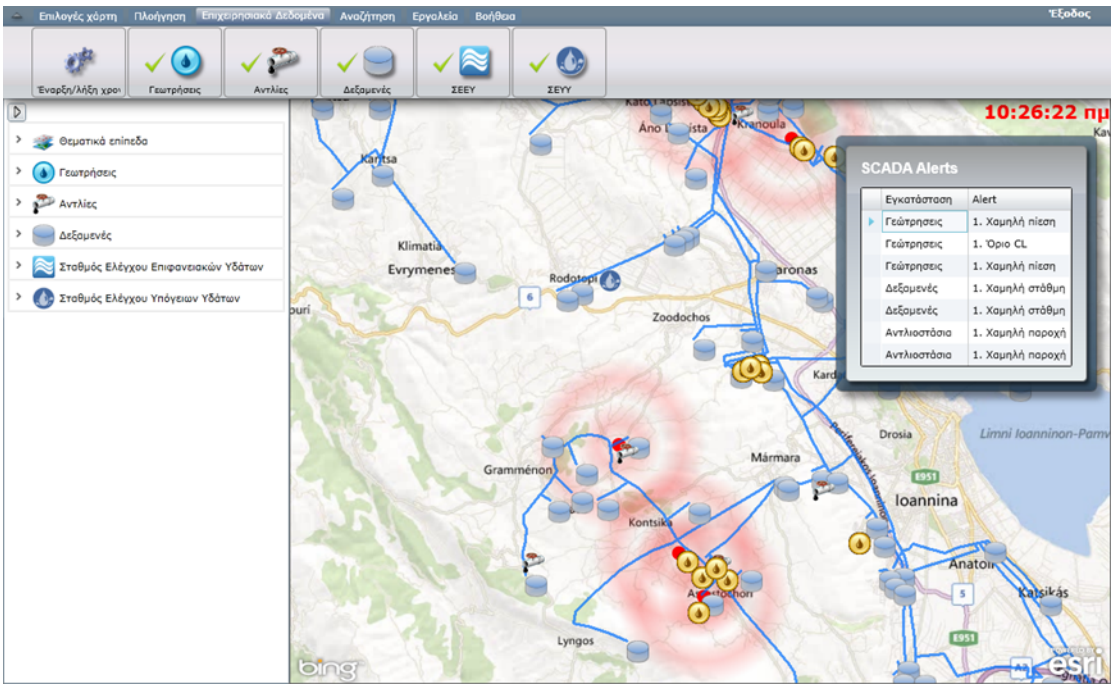

Figure 2. Web GIS interface

3. PLATFORM FUNTIONAL MODULES

The platform includes several functional modules for the integrated management of any water supply network. These modules include:

1. The core cartographic module. The WATERGUARD Platform is based in a state-of-the-art web-GIS system which provides cartographic functions to the end user through its web interface. Some indicative functions of the module are: different base maps, bookmarks, advanced search queries, annotation tools, distance/area measurements, address search.
2. The operation module. The specific module includes the operational data and the interaction with SCADA or other telemetric systems for the data presentation in the map in real time. The data are presented in the map and in a table format with direct connection between the two layers and with the capability of search queries based on specific measured values.
3. The incidents/works module. In this module, the end user can manage the various incidents and works that occurred in the water supply network. All the data are presented in the map layer and can be modified directly in the platform. Moreover, the network manager, through the module can manage the work efforts and send/receive notifications for the work progress.
4. The consumers' module. Through that module, the platform can communicate with the consumption database and augment the management/presentation capabilities of the system. The consumption data can be presented in the map and in a table format, while the module offers advanced search functions, with spatial or descriptive criteria.

4. DECISION SUPPORT SYSTEM

Another key component of the WATERGUARD Platform is its Decision Support System (DSS). The DSS is a set of rules that are applied in the database level in order to evaluate the operational measurements from SCADA or other Operational Measuring Systems. The DSS rules can be easily configured, allowing the extension of the system in the future. The DSS runs automatically each time the database is updated with new operational data. Each rule is validated with the latest data. In case of incompliance, an alert is generated for the specific measurement. The alert is related with a

specific feature like water tank, wells or water quality monitoring station so that it can be presented in a map.

The overall system architecture of the DSS is presented in the Figure 3.

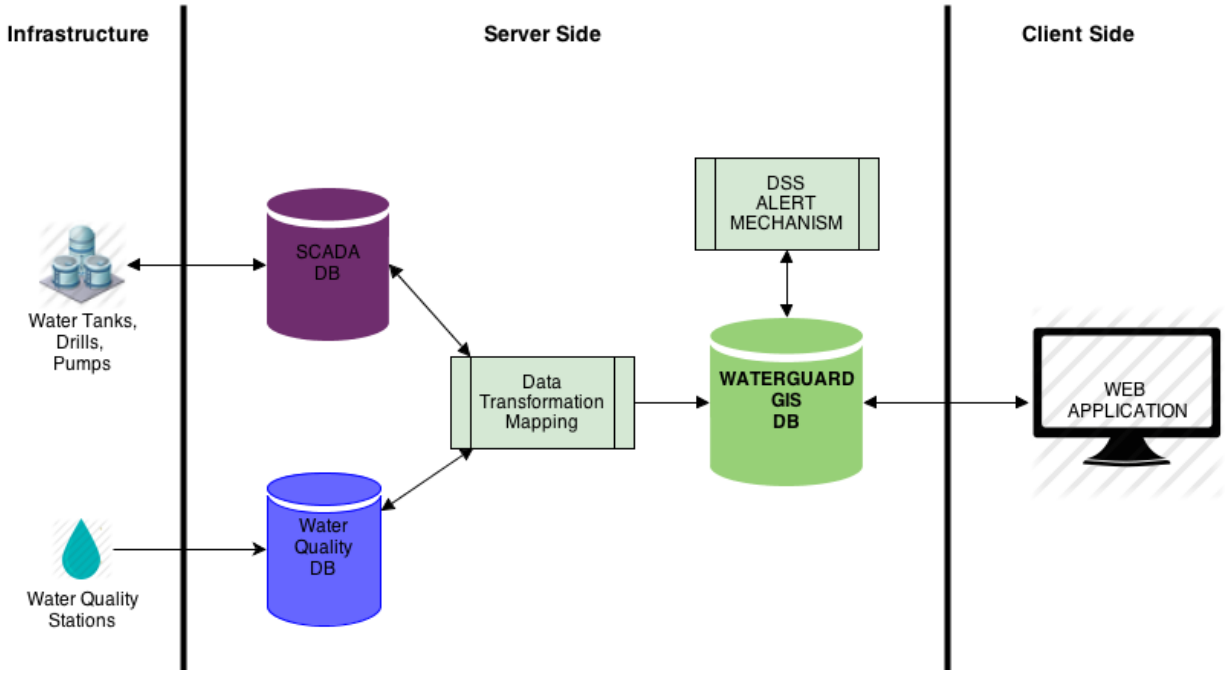

Figure 3. DSS architecture

The figure presents the three basic tiers that take part in the system. The first one is the Infrastructure which consists of the water infrastructures like water tanks, drills, pumps and water quality monitoring stations. These infrastructures are equipped with sensors that monitor different parameters of the water networks like water supply, water pressure, water level or water quality. The collected data can be stored locally in data loggers but are also transmitted to a central monitoring station where there are stored in a database. Different technologies can be used to ensure monitoring or / and control of the equipment's, like PLC / SCADA or data loggers.

The DSS is executed at the server side. There are two components responsible for the DSS execution.

- Data Transformation and Mapping
- DSS Alert Mechanism

The Data Transformation and Mapping is responsible to communicate with the other systems databases to update the internal GIS database. Data are validated (first level quality control), transformed and matched to the data structure of the GIS database. Actually, each monitored parameter is related to a feature class in the GIS database and specifically with a feature.

Communication with the SCADA server is based on Open Access Protocols like OLE for Process Control (OPC). The necessary parameters, like OPC server name, IP address, Port number etc. are provided in a configurable XML file that describes the OPC connectivity. Using this file, it is possible to access data from more than one OPC servers.

Communication with the SCADA databases is based on direct access to the database using the Open Database Connectivity (ODBC) API. For security reasons the application access only read only views of the original data.

The most important part of the DSS is the DSS Alert Mechanism. This subsystem is responsible for the generation of the Alerts. The system is running each time that the GIS database is updated from the execution of the Data Transformation and Mapping subsystem. Based on a set of rules (which are stored in an XML file) the data are evaluated at a feature level and one or more Alarms

are generated for each feature. The Alarm log stores the location (feature), the time and the description of the Alert.

In the Client side (presentation layer) the results of the DSS are presented. The basic User Interface is the Web Application which was developed in the framework of this project to monitor the Water Network Infrastructures. ALERTS are presented as points on the map as well as in a list (Figure 4).

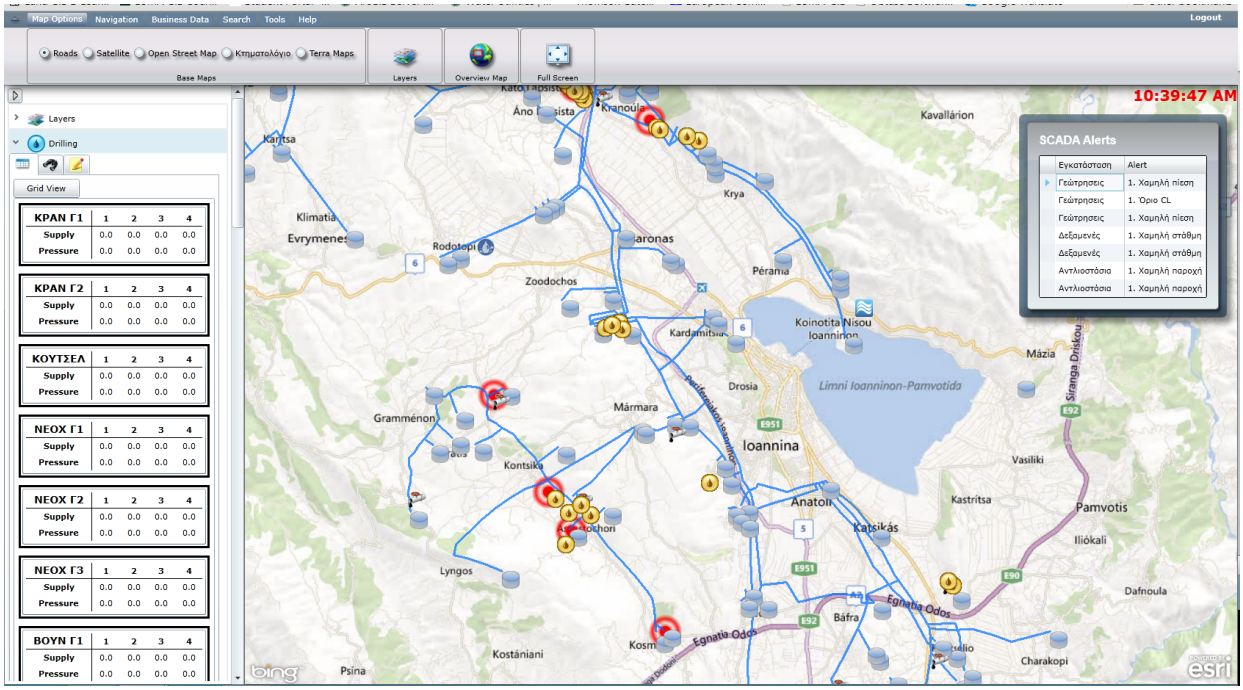

Figure 4. Alerts presentation

4. CONCLUSION – RESULTS

In the framework of the WATERGUARD Project a web-GIS Platform was developed for the Water Association of Ioannina Basin offering an integrated solution for the management of water supply networks and their infrastructures in a GIS environment. The software augments the functionalities of the existing SCADA system by offering a map centric, user friendly presentation of all the operational information in real time and place and by providing spatial analysis capabilities.

The Platform offers some distinct advantages for any water supply network, e.g.:

- Reducing the operational cost of the agencies
- Improving the response time in cases of emergencies
- Improving the offering services to the public
- Interconnecting all the information systems and databases (SCADA, consumption data, incidents logs, network maintenance data)
- Developing state of the art geographic information system infrastructures

In the future, the system could be extended to provide additional functionalities like maintenance (monitor and schedule), and operational performance monitoring according to IWA methodology (Alegre et.al., 2016)

AKNOWLEDGEMENTS

The WATERGUARD Project was financed by the cross-border European Territorial Cooperation Programme "Greece-Italy 2007-2013".

REFERENCES

Alegre, H., Baptista, J. M., Cabrera, E., Cubillo, F., Duarte, P., Hirner, W., Merkel, W., Parena, R., (2016). Performance Indicators for Water Supply Services: Third Edition. IWA Publications, ISBN13: 9781780406329

Allen, M., Preis, A., Iobal, M., Srirangarajan, S., Lim, H. B., et al., 2011. Real-time in-network distribution system monitoring to improve operational efficiency. American Water Works Association. Journal; Denver 103.7: 63-75,14

Allen, M., Preis, A., Iqbal M. and Whittle, A. J., (2013). Water Distribution System Monitoring and Decision Support Using a Wireless Sensor Network. 14th ACIS International Conference on Software Engineering, Artificial Intelligence, Networking and Parallel/Distributed Computing, Honolulu, HI, 2013, pp. 641-646. doi: 10.1109/SNPD.2013.97

IV. Droughts and Water Scarcity

Proceedings of the 10th World Congress of EWRA 'Panta Rhei', 5-9 July 2017, Athens, Greece
© 2017 *European Water Resources Association*

Drought management and policy: Changing the paradigm from crisis to risk management

D.A. Wilhite
School of Natural Resources, University of Nebraska-Lincoln, U.S.A
e-mail: dwilhite2@unl.edu

Abstract: There is increasing concern worldwide about the ineffectiveness of current drought management practices that are largely based on crisis management, i.e., managing disasters. These practices are reactive and, therefore, only treat the symptoms (impacts) of drought rather than the underlying causes for the vulnerabilities associated with impacts. Through the adoption of national drought policies that are focused on risk reduction and complemented by drought mitigation or preparedness plans at various levels of government, the coping capacity of nations to manage droughts can be improved. The time for adopting an approach that emphasizes drought risk reduction, i.e., managing risk, is now, given the spiraling impacts of drought in an ever-increasing number of sectors and the current and projected trends for the increased frequency, severity and duration of drought events in association with a changing climate. This presentation will discuss the principles and objectives of national drought policies and a template for the development of national drought policies for governments as a follow up to the High-level Meeting on National Drought Policies held in Geneva, Switzerland in March 2013. Other follow on activities including the launching of the Integrated Drought Management Programme by the World Meteorological Organization and the Global Water Partnership as well as a series of six regional capacity building workshops on national drought policies will illustrate the widespread adoption of a new paradigm for drought management.

Key words: drought policy; drought planning process; impacts of droughts; drought mitigation actions

1. INTRODUCTION

The implementation of a drought policy based on the philosophy of risk reduction can alter a nation's approach to drought management by reducing the associated impacts (risk). This concept helped motivate the World Meteorological Organization's (WMO) Congress, at its Sixteenth Session held in Geneva in 2011, to recommend the organization of a "High-level Meeting on National Drought Policy (HMNDP)." Accordingly, WMO, the Secretariat of the United Nations Convention to Combat Desertification (UNCCD), and the Food and Agriculture Organization of the United Nations (FAO), in collaboration with a number of UN agencies, international and regional organizations, and key national agencies, organized and held the HMNDP in Geneva from 11 to 15 March 2013. The theme of the HMNDP was "Reducing Societal Vulnerability – Helping Society (Communities and Sectors)."

Concerns about the spiraling impacts of drought on a growing number of sectors, the current and projected increase in the incidence of drought frequency and severity, and the outcomes and recommendations emanating from the HMNDP have drawn increased attention from governments, international and regional organizations, and non-governmental organizations. These impacts, regardless of the setting, can only be partially attributed to deficient or erratic rainfall. Drought is a complex natural hazard, and the impacts associated with it are the result of numerous climatic factors and a wide range of societal factors that define the level of societal resilience. Population growth and redistribution and changing consumption and production patterns are two of the factors that define the vulnerability of a region, economic sector, or population group. Some other factors include poverty and rural vulnerability; increasing water demand due to urbanization; poor soil and water management practices, climate variability and change; changes in land use; environmental degradation; and greater awareness of the need to preserve the integrity of ecosystems. Although

the development of drought policies and preparedness plans can be a challenging undertaking, the outcome of this process can significantly increase societal resilience to these climatic shocks.

2. NATIONAL DROUGHT POLICY: BACKGROUND

Simply stated, a national drought policy should establish a clear set of principles or operating guidelines to govern the management of drought and its impacts. The overriding principle of drought policy should be an emphasis on risk management through the application of preparedness and mitigation measures (HMNDP, 2013; Sivakumar et al., 2013; Wilhite et al, 2014). This policy should be directed toward reducing risk by developing better awareness and understanding of the drought hazard and the underlying causes of societal vulnerability along with developing a greater understanding of how being proactive and adopting a wide range of preparedness measures can increase societal resilience. Risk management can be promoted by encouraging the improvement and application of seasonal and shorter-term forecasts, developing integrated monitoring and drought early warning systems and associated information delivery systems, developing preparedness plans at various levels of government, adopting mitigation actions and programs, creating a safety net of emergency response programs that ensure timely and targeted relief, and providing an organizational structure that enhances coordination within and between levels of government and with stakeholders. The policy should be consistent and equitable for all regions, population groups, and economic sectors and consistent with the goals of sustainable development.

As vulnerability to and the incidence of drought has increased globally, greater attention has been directed to reducing risks associated with its occurrence through the introduction of planning to improve operational capabilities (i.e., climate and water supply monitoring, building institutional capacity) and mitigation measures that are aimed at reducing drought impacts. This change in emphasis is long overdue. Mitigating the effects of drought requires the use of all components of the cycle of disaster management, i.e. monitoring and prediction, disaster, impact assessment, response, recovery, mitigation, and planning, rather than only the crisis management portion of this cycle (impact assessment, response and recovery). Typically, when drought occurs, governments and donors have followed with impact assessment, response, recovery, and reconstruction activities to return the region or locality to a pre-disaster state. Historically, little attention has been given to preparedness, mitigation, and prediction/early warning actions (i.e., risk management) and the development of risk-based national drought management policies that could reduce future impacts and lessen the need for government and donor interventions in the future. Crisis management only addresses the symptoms of drought, as they manifest themselves in the impacts that occur as a direct or indirect consequence of drought. Risk management, on the other hand, is focused on identifying where vulnerabilities exist (particular sectors, regions, communities, or population groups) and addresses these risks through systematically implementing mitigation and adaptation measures that will lessen the risk to future drought events. Because societies have emphasized crisis management in past attempts at drought management, countries have generally moved from one drought event to another with little, if any, reduction in risk. In addition, in many drought-prone regions, another drought event is likely to occur before the region fully recovers from the last event. If the frequency of drought increases in the future, as projected for many regions, there will be less recovery time between these events.

Progress on drought preparedness and policy development has been slow for a number of reasons. It is certainly related to the slow-onset characteristics of drought and the lack of a universal definition. Drought shares the distinction of being a creeping phenomenon with climate change in terms of getting people to recognize changes that occur slowly over a long period of time. These characteristics of drought make early warning, impact assessment, and response difficult for scientists, natural resource managers, and policy makers. The lack of a universal definition often leads to confusion and inaction on the part of decision makers since scientists may disagree on the existence and severity of drought conditions (i.e., the onset and recovery time differences between meteorological, agricultural and hydrological drought). Severity is also difficult to characterize

since it is best evaluated on the basis of multiple indicators and indices, rather than on the basis of a single variable or index. The impacts of drought are also largely non-structural and spatially pervasive. These features make it difficult to assess the effects of drought and to respond in a timely and effective manner. Drought impacts are not as visual as the impacts of other natural hazards, making it difficult for the media to communicate the significance of the event and its impacts to the public. Public sentiment to respond is often lacking in comparison to other natural hazards that result in loss of life and property.

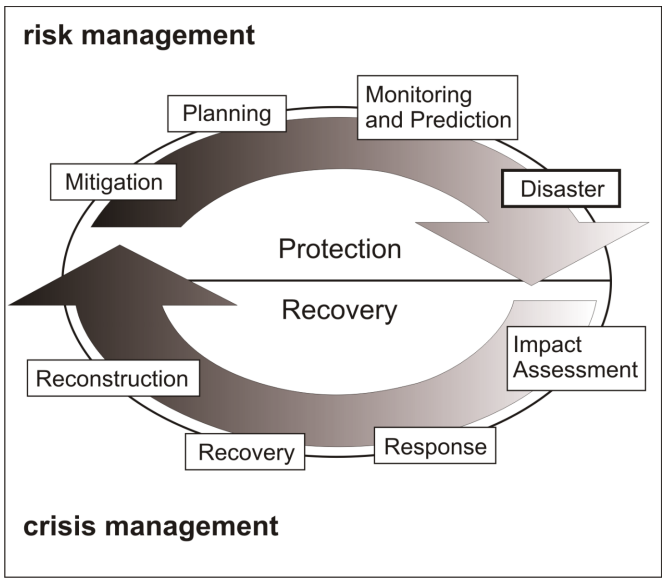

Figure 1. Cycle of Disaster Management. (Source: National Drought Mitigation Center)

Associated with the crisis management approach is the lack of recognition that drought is a normal part of the climate. Climate change and associated projected changes in climate variability will likely increase the frequency and severity of drought and other extreme climatic events. In the case of drought, the duration of these events may also increase and, thus, the period between severe drought episodes which leads to a reduction in recovery time. Therefore, it is imperative for all drought-prone nations to adopt a more risk-based approach to drought management in order to increase resilience to future episodes of drought.

It is important to note that each occurrence of drought provides a window of opportunity to move toward a more proactive risk management policy. Immediately following a severe drought episode, policy makers, resource managers, and all affected sectors are aware of the impacts that have occurred and the deficiencies that existed in the government's response. This is the appropriate time to approach policy makers with the concept of developing a national drought policy and preparedness plans in order to increase societal resilience.

2.1 Drought policy development: A template for action

To provide guidance on the preparation of national drought policies and planning techniques, it is important to define the key components of drought policy, its objectives, and steps in the implementation process. An important component of national drought policy is increased attention to drought preparedness in order to build institutional capacity to deal more effectively with this pervasive natural hazard.

A constraint to drought preparedness has been the dearth of methodologies available to policy makers and planners to guide them through the planning process. Drought differs in its characteristics between climate regimes, and impacts are locally defined by unique economic, social, and environmental characteristics. A methodology developed by Wilhite (1991) and revised to incorporate greater emphasis on risk management (Wilhite et al., 2000; Wilhite et al., 2005) has

provided a set of generic steps that can be adapted to any level of government (i.e., local, state or provincial, or national) or geographical setting for the development of a drought mitigation plan.

The Integrated Drought Management Program (IDMP) recognizes the urgent need to provide nations with guidelines for the development of national drought management policies (http://droughtinformation.org). To achieve this goal, the drought preparedness planning methodology referred to above has been modified to define a generic process by which governments can develop a national drought policy and drought preparedness plans at various levels of government that support the principles of that policy. A detailed version of this policy development process is provided in IDMP (2014) and, thus, is not described in this paper. The goal of this 10-step process is to provide a template for governments and organizations to follow to reduce societal vulnerability to drought. A national drought policy can be a stand-alone policy or a subset of a natural disaster risk reduction, sustainable development, integrated water resources or climate change adaptation plan that may already exist.

2.2 Drought policy: Characteristics and the way forward

As a beginning point in the discussion of drought policy, it is important to identify the various types of drought policies that are available and have been utilized for drought management. The most common approach followed by both developing and developed nations is post-impact government (or nongovernment) interventions. These interventions are normally relief measures in the form of emergency assistance programs aimed at providing money or other specific types of assistance (e.g., livestock feed, water, food) to the victims (or those experiencing the most severe impacts) of the drought. This reactive approach, characterized by the hydro-illogical cycle, Figure 2, is seriously flawed from the perspective of vulnerability reduction since the recipients of this assistance are not expected to change behaviors or resource management practices as a condition of the assistance. Although drought assistance provided through emergency response interventions may address a short-term need, it may in the longer term actually decrease the coping capacity of individuals and communities by fostering greater reliance on these interventions rather than increasing self-reliance. This reliance on the government for relief is contrary to the philosophy of encouraging self-reliance through an investment in appropriate mitigation actions that can improve drought coping capacity. Government assistance or incentives that encourage these investments would be a philosophical change in how governments respond and would promote a change in the expectations of livestock producers as to the role of government in these response efforts. The more traditional approach of providing relief is also flawed in terms of the timing of assistance being provided. It often takes weeks or months for assistance to be received, at times well beyond the window of when the relief would be of greatest value in addressing the impacts of drought. In addition, those livestock producers who previously employed appropriate risk reduction techniques are likely ineligible for assistance since the impacts they experienced were reduced and therefore do not meet the eligibility requirements. This approach rewards those that have not adopted appropriate resource management practices.

Although there is at times a need to provide emergency response to various sectors (i.e., post-impact assessment interventions), it is critically important for the purpose of moving toward a more proactive risk management approach that the two drought policy approaches described below become the cornerstone of the policy process.

The second type of drought policy approach is the development and implementation of policies and preparedness plans, which would include organizational frameworks and operational arrangements developed in advance of drought and maintained between drought episodes by government or other entities. This approach represents an attempt to create greater institutional capacity focused on improved coordination and collaboration within and between levels of government and with stakeholders in the primary impact sectors and with the plethora of private organizations with a vested interest in drought management (i.e., communities, natural resource or irrigation districts or managers, utilities, agribusiness, farm organizations, and others).

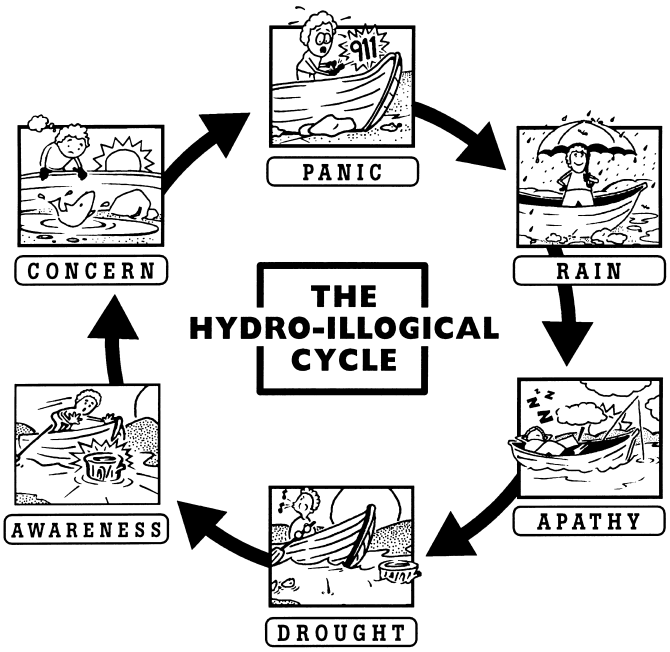

Figure 2. The Hydro-illogical Cycle expressing the typical crisis management approach to drought management. (Source: National Drought Mitigation Center)

The third type of policy approach emphasizes the development of pre-impact government programs or measures that are intended to reduce vulnerability and impacts. This approach could be considered a subset of the approach listed above. In the natural hazards field, these types of programs or measures are commonly referred to as mitigation measures. Mitigation in the context of natural hazards is different from mitigation in the context of climate change, where the focus is on reducing greenhouse gas (GHG) emissions. Mitigation in the context of natural hazards refers to actions taken in advance of drought to reduce impacts in the future. Drought mitigation measures are numerous, but they may be more confusing to the general public in comparison to mitigation measures for earthquakes, floods and other natural hazards where the impacts are largely structural. Impacts associated with drought are generally non-structural, and thus the impacts are less visible, more difficult to assess in a timely fashion (e.g., reductions in crop yield), and do not require reconstruction as part of the recovery process. Drought mitigation measures would include establishing comprehensive early warning and delivery systems, improved seasonal forecasts, increased emphasis on water conservation (demand reduction), increased or augmented water supplies through greater utilization of ground water resources, water reutilization and recycling, construction of reservoirs, interconnecting water supplies between neighboring communities, drought preparedness planning to build greater institutional capacity, and awareness building and education. In some cases, such water resource augmentation measures are best developed jointly with a neighboring state (or country), or at least such measures should be coordinated if they might have an impact on the other riparian state (or downstream use in general). Insurance programs, currently available in many countries, would also fall into this category of policy types.

2.3 Principal elements of a drought risk reduction policy framework

Drought policy should emphasize four principle components during the development process: (1) risk and early warning, including vulnerability analysis, impact assessment, and communication; (2) mitigation and preparedness, including the application of effective and affordable practices; (3) awareness and education, including a well-informed public and a participatory process; and (4) good governance and an effective policy framework, including political commitment and responsibilities (UNISDR, 2009). Another important component of this framework is the inclusion of policy options for emergency response and relief. In all cases, when severe drought occurs,

governments and other organizations must provide some form of emergency relief to those sectors most affected. However, it is crucial, as a part of a drought risk reduction policy, for this assistance to be provided in a form that does not run counter to the goals and objectives of the national drought policy, which would include a strong emphasis on the sustainability of the natural resource base.

3. NATIONAL DROUGHT MANAGEMENT POLICY: A PROCESS

The challenge that nations face in the development of a risk-based national drought management policy is complex. It requires political will at the highest level possible and a coordinated approach within and between levels of government and with the diversity of stakeholders that must be engaged in the policy development process. A national drought policy could be a stand-alone policy. Alternatively, as noted previously, it could contribute to or be a part of a national policy for disaster risk reduction with holistic and multi-hazard approaches that is centered on the principles of risk management.

The policy would provide a framework for shifting the paradigm from one traditionally focused on a reactive crisis management to one that is focused on a proactive risk-based approach that is intended to increase the coping capacity of the country and thus create greater resilience to future episodes of drought.

The formulation of a national drought policy, while providing the framework for a paradigm shift, is only the first step in vulnerability reduction. The development of a national drought policy must be intrinsically linked to the development and implementation of preparedness and mitigation plans at the sub-national level (provincial/state and local). These plans will be the instruments through which a national drought policy is executed.

The 10-step process that is provided below is intended to provide a template or roadmap that countries can follow in the development of a national drought management policy and drought preparedness/mitigation plans at the sub-national level. In other words, the process is not intended to be prescriptive, but rather to be adapted by countries to reflect their institutional infrastructure, legal framework, etc. This process has been modified from a 10-step drought planning process or methodology developed in the United States for application at the state level. Currently, 47 of the 50 U.S. states have developed drought plans, and the vast majority of these states have followed the guidelines provided by the 10-step process in the preparation or revision of drought plans (http://drought.unl.edu/Planning/PlanningInfobyState.aspx). This drought planning methodology has also been followed in other countries in the development of national drought strategies. The process, originally developed in the early 1990s, has been revised numerous times, placing greater emphasis on mitigation planning with each revision. Now, this original methodology has been modified once again to reflect an emphasis on capacity development for a national drought management policy, including the development of drought preparedness plans that are necessary in support of a national policy.

The 10 steps below provide an outline of the process for policy and preparedness planning. As indicated above, the process is intended to be generic, i.e., applying this methodology in each country setting would require adapting it to the current institutional capacity, political infrastructure, legal frameworks, and technical capacity. The reader is referred to a more complete description of this policy development process recently published by the IDMP (2014).

The 10 steps in the drought policy and preparedness process are:

Step 1: *Appoint* a national drought management policy commission

Step 2: *State* or *define* the goals and objectives of a risk-based national drought management policy

Step 3: *Seek* stakeholder participation; *define* and *resolve* conflicts between key water use sectors, considering also transboundary implications

Step 4: *Inventory* data and financial resources available and *identify* groups at risk

Step 5: *Prepare/write* the key tenets of a national drought management policy and preparedness plans, which would include the following elements:

- Monitoring, early warning and prediction
- Risk and impact assessment
- Mitigation and response

Step 6: *Identify* research needs and *fill* institutional gaps
Step 7: *Integrate* science and policy aspects of drought management
Step 8: *Publicize* the national drought management policy and preparedness plans and *build* public awareness
Step 9: *Develop* educational programs for all age and stakeholder groups
Step 10: *Evaluate* and *revise* national drought management policy and supporting preparedness plans

4. SUMMARY AND CONCLUSION

For the most part, previous responses to drought in all parts of the world have been reactive, reflecting what is commonly referred to as the crisis management approach. This approach has been ineffective (i.e., assistance poorly targeted to specific impacts or population groups), poorly coordinated, and untimely; more importantly, it has done little to reduce the risks associated with drought. In fact, the economic, social, and environmental impacts of drought have increased significantly in recent decades. A similar trend exists for all natural hazards.

The intent of the drought policy development and planning process included in this report and referenced (IDMP, 2014) is to provide a set of generic steps or guidelines that nations can use to develop the overarching principles of a national drought policy aimed at risk reduction through a national drought policy commission. This policy would be implemented at the sub-national (i.e., provincial, state or local) level through the development and implementation of drought mitigation and preparedness plans that follow the framework or principles of the national drought policy. Following these guidelines, a nation can significantly change the way they prepare for and respond to drought by placing greater emphasis on proactively addressing the risks associated with drought through the adoption of appropriate mitigation actions. These guidelines are generic in order to enable governments to choose those steps and components that are most applicable to their situation. The risk assessment methodology embedded in this process is designed to guide governments through the process of evaluating and prioritizing impacts and identifying mitigation actions and tools that can be used to reduce the impacts of future drought episodes. Both the policy development process and the planning process must be viewed as ongoing, continuously evaluating the nation's changing exposure and vulnerabilities and how governments and stakeholders can work in partnership to lessen risk.

REFERENCES

HMNDP (High-level Meeting on National Drought Policy) 2013. Final Declaration from the High-level Meeting on National Drought Policy. http://hmndp.org.

IDMP (Integrated Drought Management Programme) 2014. National Drought Management Policy Guidelines: A Template for Action. Prepared by D.A. Wilhite. Global Water Partnership and the World Meteorological Organization.

Sivakumar, M.V.K., D.A. Wilhite, R.S. Pulwarty and R. Stefanski. 2013. The Need for National Drought Policies: Summary of the High-level Meeting on National Drought Policy (HMNDP). Bulletin of the Amer. Meteorol. Soc.

UNISDR. 2009. Drought risk reduction framework and actions. United Nations International Strategy for Disaster Reduction. Geneva, Switzerland.

Wilhite, D.A. 1991. Drought planning: A process for state government. Water Resources Bulletin 27(1):29–38.

Wilhite, D.A., M.J. Hayes, C. Knutson, and K.H. Smith. 2000. Planning for drought: Moving from crisis to risk management. Journal of the American Water Resources Association 36:697-710.

Wilhite, D.A., M.J. Hayes, and C.L. Knutson. 2005. Drought preparedness planning: Building institutional capacity (Chapter 5). In: D.A. Wilhite (ed.), Drought and Water Crises: Science, Technology, and Management Issues, CRC Press, Boca Raton, Florida, pp. 93-136.

Wilhite, D.A., M.V.K. Sivakumar, R. Pulwarty. 2014. Managing Drought Risk in a Changing Climate: The Role of National Drought Policy. Weather and Climate Extremes, Elsevier Publishers.

Proceedings of the 10th World Congress of EWRA 'Panta Rhei', 5-9 July 2017, Athens, Greece
© 2017 *European Water Resources Association*

Near-real time hydrological drought monitoring in the European Drought Observatory

C. Cammalleri[1*], J. Vogt[2], and P. Salamon[3]
European Commission, Joint Research Centre (JRC), 21027 Ispra (VA), Italy
[*] *e-mail: carmelo.cammalleri@ec.europa.eu*

Abstract: A near-real time hydrological drought monitoring index, as recently implemented within the European Drought Observatory (EDO) is described. This index takes advantage of daily discharge data simulated by the Lisflood model to capture the dynamic nature of the drought phenomenon. Drought events are defined as prolonged periods in which the discharge values fall below a defined threshold, and the probability of occurrence of the total water deficit, compared to historical events, is used as measure of the severity of the drought. A daily-changing threshold is adopted for each modelling cell in order to account for the different hydrological regimes observed across the European domain. In this paper, the theoretical concept behind the indicator and its operational implementation in the EDO web portal are described. The proposed drought index demonstrated a good capability to capture the major drought events reported in the European Drought Reference (EDR) database since 1995, including the most recent drought that occurred during summer 2015 in Central Europe. In its current implementation, the index allows for a continuous monitoring of hydrological droughts of the major river basins (drainage area > 1,000 km2) in the pan-European domain.

Key words: Streamflow drought, Low-flow, Lisflood, EDO

1. INTRODUCTION

Hydrological drought is defined as a lack of water in the hydrological system, which may result in exceptionally low streamflow, lake level, reservoir and groundwater storage (Tallaksen and van Lanen, 2004). Anomalies in these hydrological variables are related to several vulnerable sectors, including drinking water supply, hydropower production and inland water transportation (van Loon, 2015). Tallaksen and van Lanen (2004) highlighted the rapid response of streamflow to meteorological drought, as compared, for example, to groundwater, and proved it to be a good descriptor for an operational monitoring of hydrological drought.

The aim of a streamflow-based hydrological drought monitoring system is to firstly identify the low-flow river regime and successively detect the occurrence of such low-flow periods and their magnitude as compared to the historical events. The first step is commonly achieved through the definition of a low-flow threshold in terms of a percentile of a historical record (usually between 70th and 95th percentiles, Corzo Perez et al., 2011); the second step is based on computing the main traits of the continuous periods during which the streamflow is below the low-flow threshold (e.g., duration, intensity, magnitude, severity).

In this paper, the low-flow index developed in the context of the European Drought Observatory (EDO, http://edo.jrc.ec.europa.eu) is described, including the hypotheses adopted to define the low-flow threshold and a suited drought severity metric, as well as the river discharge datasets used in the analysis.

The index has been operationally implemented within EDO by using the streamflow outputs provided by the Lisflood model at pan-European scale within the European Flood Awareness System (EFAS), which is part of the Copernicus Emergency Management Service (Smith et al., 2016), and examples of both data visualization and enquiring within the system are also reported.

2. MATERIALS AND METHODS

2.1 Low-flow index

The proposed low-flow index is based on the use of daily streamflow data (Q) as modelled by a hydrological model. The computation of the index can be divided into three phases: i) a preliminary phase where the low-flow regime for the specific river section is defined, ii) the analysis of the probability distribution of previous water deficit events, and iii) the computation of the low-flow index for the actual event compared to the low-flow historical condition.

The first phase is achieved by computing a daily-changing streamflow threshold value as the 95th percentile of a dataset constituted by 31×n daily discharge data (van Loon et al., 2010), with n equal to the number of years in the fitting dataset and a 31 days moving window centered on the specific date (t). This threshold time-series (namely $Q_{95,t}$) is used to discriminate between low-flow periods ($Q < Q_{95,t}$) and regular water regime.

Once $Q_{95,t}$ is defined, following the theory of runs (Yevjevich, 1967) an event can be defined by a period of consecutive days with $Q < Q_{95,t}$; as a synthetic measure of the magnitude of an event, the total deficit (D) is here adopted, represented by the integrated area of the discharge curve below the threshold. This quantity is usually considered more valuable than the simple duration (d) or the maximum intensity (maximum deviation from the threshold).

Due to the stochastic nature of this approach, separate events that are close in time may need to be pooled in order to account for their mutual dependence. In the proposed approach, the simple minimum inter-event time method proposed by Zelenhasić and Salvai (1987) is adopted, assuming that consecutive events should be merged if the inter-event time is < 10 days.

Additionally, in order to ensure a robust statistical analysis of the observed past events, the events shorter than 5 days are excluded by the successive analyses, following the minimum-duration approach suggested by Jakubowski and Radczuk (2004).

The full procedure is schematically described in Fig. 1, where five low-flow events are identified, but, actually, only two events are considered in the successive analyses, a fist one constituted by the sum of the first three events (pooling) and the fourth event, whereas the last event is ignored due to its small size.

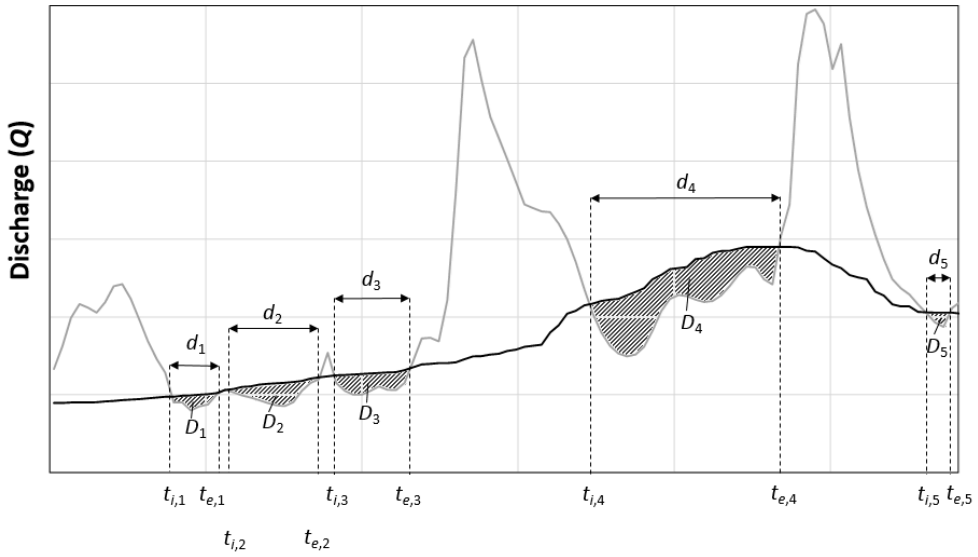

Figure 1. Schematic representation of a sequence of runs with examples of three mutual dependent events (1, 2, 3) and a minor event (5). Daily water discharge values (Q) are shown as a grey line, whereas the daily-changing low-flow threshold (Q_{95}) is represented as a black line.

The dataset constituted by past events observed in a baseline reference period is used to fit the inverse scale parameter, $\lambda > 0$, of an exponential distribution (equal to the inverse of the sample mean according to the maximum likelihood method) if at least 5 past events were observed.

The value assumed by the cumulative distribution function (cdf) for a specific value of *D*, computed as:

$$F(D_i) = 1\text{-}e^{-\lambda D_i} \quad \text{with} \quad D_i \geq 0 \tag{1}$$

is used as a measure of the severity of the hydrological drought event, ranging from 0 (no drought) to 1 (extreme drought).

In its operational implementation, the *F*(*D*) index is computed every day in a near-real time fashion with a delay of about two days, and maps are produced three times per month (corresponding to the dates 11, 21 and end-of-month); this approach allows accounting for the continuous nature of streamflow and it does not rely on a pre-defined accumulation period (i.e., month) unlikely other indicators (i.e., the Standardized Runoff Index, SRI; Shukla and Wood 2008), capturing also events that last more than a single accumulation period.

2.2 River discharge dataset

The daily river discharge data used in the operational computation of the low-flow index in EDO are derived from the Lisflood hydrological rainfall-runoff model (de Roo et al., 2000), a spatially distributed model developed by the water and floods research groups of the JRC (Joint Research Centre) of the European Commission, which is designed to reproduce the hydrology of large and trans-national European river catchments.

The version of the model used in this study is the one that operationally runs within EFAS on the pan-European domain on a regular grid with cell size of 5-km. In this setting, Lisflood adopts a number of static inputs (see van der Knijff et al., 2010, for more details), including the soil hydraulic properties derived from the European Soil Database (http://eusoils.jrc.ec.europa.eu/ESDB_Archive/ESDBv2/index.htm), land-use classes from the CORINE project (Batista e Silva et al., 2013) and monthly leaf area index maps from the MODIS (Moderate-Resolution Imaging Spectroradiometer) standard product (Myneni et al., 2003). The spatial structure of the river network and drainage areas have been derived from the JRC Catchment Characterisation and Modelling (CCM) project (http://ccm.jrc.ec.europa.eu, Vogt et al., 2007).

A daily meteorological forcing dataset is developed within the EFAS system by interpolating different point-scale data sources: the EU-FLOOD-GIS database, the JRC-MARS database (which integrates both national meteorological services and data acquired via the Global Telecommunication System, GTS), the World Meteorological Organization (WMO) synoptic observations, and the German Weather Service (Ntegeka et al., 2013).

3. RESULTS AND DISCUSSION

Calibration of the low-flow index, including the computation of the low-flow threshold and the fitting of the exponential distribution to past drought events was performed on a dataset constituted by 21 years (1995-2015) daily discharge data over Europe. The Lisflood simulations produce regular 5 × 5 km^2 gridded data, however, the low-flow index is computed only on the cells with at least a drainage area of 1,000 km^2. Additionally, as explained in the previous section, only cells where at least 5 past events and a statistical significant fitting (according to the Kolmogorov-Smirnov test at 0.05) were used, limiting the number of analysed cells to 20,217 (about 83% of the suitable river cells).

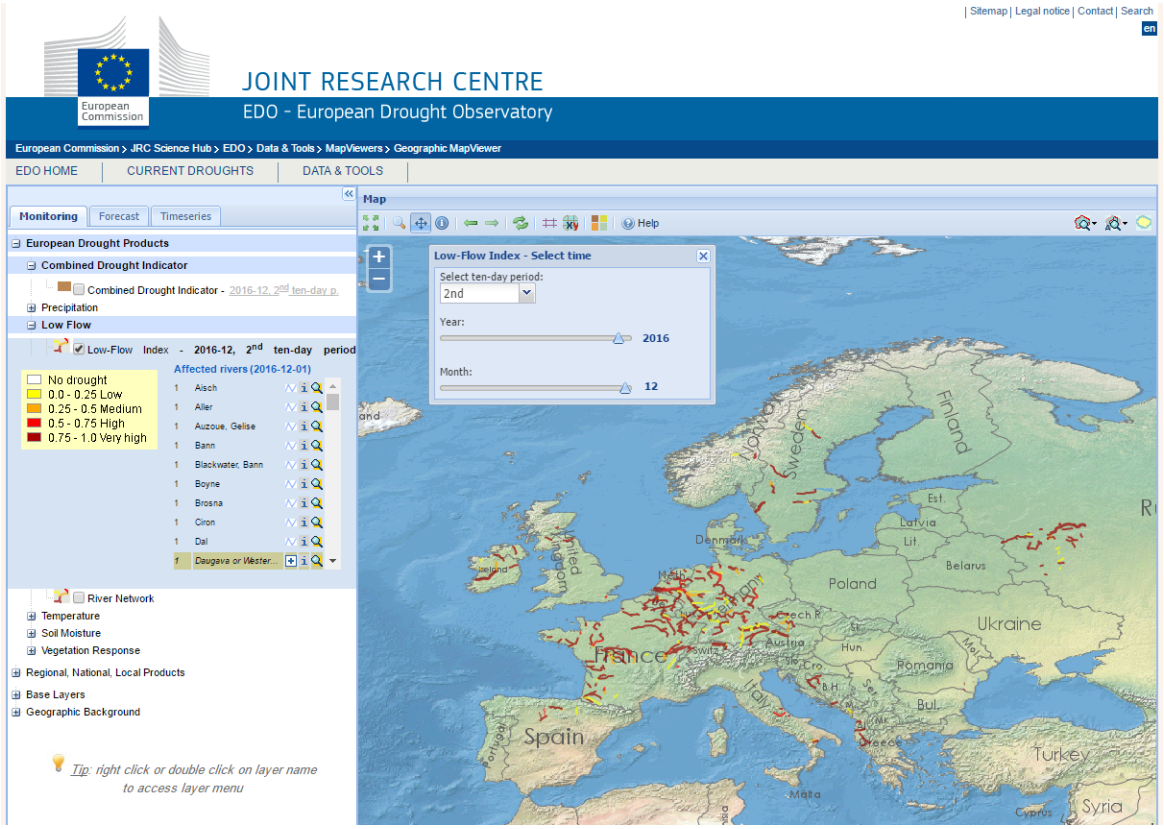

Figure 2. Example of the low-flow index map as shown in the EDO (http://edo.jrc.ec.europa.eu) system. The map displays the data for 21st December 2016 (i.e., 2nd 10-day period). The list of the affected rivers allows getting more information on each river segment, whereas the "select time" window allows easily changing the date to be visualized.

The low-flow threshold, pooling procedure and fitted distribution have been optimized to obtain a fair balance between operational constraints and scientific requirements, as described more in depth in Cammalleri et al. (2016); the same authors analysed the performance of the index on past drought events, including a comparison with previously available drought indicators. Following this analysis, daily low-flow threshold maps, as well as the exponential λ parameter map, are obtained and successively adopted for the near-real time computation of the low-flow index.

Low-flow index maps are uploaded in the EDO system about 2 days after the corresponding date (three times per month), and they can be visualized in the EDO system map viewer (Fig. 2). Even if the index is computed on 5-km cells, the data are visualized for river segments that match the CCM river network; the $F(D)$ value at the valley cell of each segment is represented in the map, even if all the cell values of the segment can be also visualized if the map are zoomed-in at higher scale (> 1:1,250,000). Only the river segments affected by drought ($F(D) > 0$) are displayed in a yellow-to-red colour scale, and the thickness of the river is displayed proportional to the corresponding river flow for the specific date. The entire river network can be displayed as well.

4. CONCLUSIONS

In this paper the implementation of a low-flow index for the monitoring of hydrological drought events within the European Drought Observatory (EDO) is fully described, including the theoretical framework at the basis of the development of the low-flow index, the river discharge dataset used for its operational near-real time implementation, and the web-based interface developed to visualize and inquire the data.

The proposed low-flow index exploits daily-scale streamflow long-term records (between 1995 and 2015) to define the upper boundary of the low-flow regime by means of 95th percentile threshold on a 31-day moving window. A drought event is defined as a persistent period of water

discharge below this threshold, and the severity of the event is evaluated accordingly to the cumulative distribution frequency following an exponential distribution. This approach allows avoiding the need of pre-defining an accumulation period (i.e., month), giving the possibility to capture the total severity of an event independently from its duration and occurring period.

The dataset used for the operational implementation of the index is based on modelled discharge as produced by the Lisflood model; this permits to have a near-real time update of the EDO web portal and to keep consistency with EFAS (as well as other products available in EDO, such as the soil moisture indices also based on Lisflood outputs).

An example of the map visualization tool is reported in this paper, showing how the EDO portal (http://edo.jrc.ec.europa.eu) allows a quick look at the spatial distribution of hydrological drought over Europe for a specific date, as well as to slide through the time-series of maps or zoom-in into a specific impacted area. The tactic to limit the approach to the major river segments only (discharge area > 1,000 km^2) aims at providing a general overview of the drought conditions at continental to national scale, whereas regional/watershed monitoring systems can detail those information at higher spatial scales.

ACKNOWLEDGMENTS

The authors would like to thank Alfred de Jager and Diego Magni for developing and managing the web component of the low-flow index in EDO, and EFAS, as part of the Copernicus Emergency Management Service, for providing the river discharge data.

REFERENCES

Batista e Silva, F., Lavalle, C., Koomen, E., 2013. A procedure to obtain a refined European land use/cover map. J. Land Use Sci.: 8(3): 255-283.

Cammalleri, C., Vogt, J., Salamon, P., 2016. Development of an operational low-flow index for hydrological drought monitoring over Europe. Hydrol. Sci. J.: doi: 10.1080/02626667.2016.1240869.

Corzo Perez, G.A., van Huijgevoort, M.H.J., Voβ, F., van Lanen, H.A.J., 2011. On the spatio-temporal analysis of hydrological droughts from global hydrological models. Hydrol. Earth Syst. Sci.: 15: 2963-2978.

de Roo, A., Wesseling, C., van Deusen, W., 2000. Physically based river basin modelling within a GIS: The LISFLOOD model. Hydrol. Process.: 14: 1981-1992.

Jakubowski, W., Radczuk, L., 2004. Estimation of hydrological drought characteristics NIZOWKA2003 – Software Manual. In: L.M. Tallaksen and H.A.J. van Lanen, eds. Hydrological Drought – Processes and estimation methods for Streamflow and groundwater. Amsterdam: Elsevier Sciences B.V. [CD-ROM].

Myneni, R., Knyazikhin, Y., Glassy, J., Votava, P., Shabanov, N., 2003. FPAR, LAI (ESDT: MOD15A2) 8-day Composite NASA MODIS Land Algorithm. User's Guide.

Ntegeka, V., Salamon, P., Gomes, G., Sint, H., Lorini, V., Zambrano-Bigiarini, M., Thielen, J., 2013. EFAS-Meteo: A European daily high-resolution gridded meteorological data set for 1990 – 2011. EUR - Scientific and Technical Research series.

Shukla, S., Wood, A.W., 2008. Use of a standardized runoff index for characterizing hydrologic drought. Geophys. Res. Lett.: 35: L02405.

Smith, P.J., Pappenberger, F., Wetterhall, F., Thielen Del Pozo, J., Krzeminski, B., Salamon, P., Muraro, D., Kalas, M., Baugh, C., 2016. On the Operational Implementation of the European Flood Awareness System (EFAS). In: Flood Forecasting: A Global Perspective, 313-348. doi: 10.1016/B978-0-12-801884-2.00011-6.

Tallaksen, L.M., van Lanen, H.A.J., 2004. Hydrological drought: processes and estimation methods for streamflow and groundwater. In: Developments in Water Science, vol. 48. Amsterdam, the Netherlands: Elsevier Science B.V.

van der Knijff, J.M., Younis, J., de Roo, A.P.J., 2010. LISFLOOD: A GIS-based distributed model for river basin scale water balance and flood simulation. Int. J. Geogr. Inf. Sci.: 24: 189-212.

van Loon, A.F., 2015. Hydrological drought explained. WIREs Water: 2: 359-392.

van Loon, A.F., van Lanen, H.A.J., Hisdal, H., Tallaksen, L.M., Fendeková, M., Oosterwijk, J., Horvát, O., Machilica, A., 2010. Understanding hydrological winter drought in Europe. In: Global Change: Facing risks and threats to water resources, Proc. of the Sixth World FRIEND Conference, October 2010 Fez. Wallingford: IAHS Publ.: 340: 189-197.

Vogt, J., Colombo, R., Bertolo, F., 2003. Deriving drainage networks and catchment boundaries: A new methodology combining digital elevation data and environmental characteristics. Geomorphology: 53(3-4): 281-298.

Yevjevich, V., 1967. An objective approach to definitions and investigations of continental hydrological droughts. Colorado State University, Fort Collins, Hydrology Paper 23.

Zelenhasić, E., Salvai, A., 1987. A method of streamflow drought analysis. Water Resour. Res.: 23(1): 156-168.

Proceedings of the 10th World Congress of EWRA 'Panta Rhei', 5-9 July 2017, Athens, Greece
© 2017 *European Water Resources Association*

Modification of the Palmer Drought Severity Index for Mediterranean environments: Model and application

A. Paulo[1], D.S. Martins[2, 3], P. Paredes[2], R.D. Rosa[2], L.S. Pereira[2*]
[1] *ESAS, Instituto Politécnico de Santarém, Portugal, ana.paulo@esa.ipsantarem.pt*
[2] *LEAF Linking Landscape, Environment, Agriculture and Food, Instituto Superior de Agronomia, Universidade de Lisboa, Portugal*
[3] *Instituto Dom Luiz, Faculdade de Ciências, DEGGE, Universidade de Lisboa, Lisboa, Portugal*
[*] *e-mail: lspereira@isa.ulisboa.pt*

Abstract: This article describes a modification of the Palmer Drought Severity Index (PDSI) as adapted to Mediterranean conditions, resulting in a new index, the MedPDSI. It differs from the original PDSI because the olives crop, a typical Mediterranean perennial resistant to water stress, is assumed as drought reference crop aiming at the application of the soil water balance. The adopted approach modifies the soil water balance computation, with the actual evapotranspiration computed with the FAO-PM reference ET_o and a crop coefficient obtained from the FAO dual K_c approach, $K_c = K_{cb} + K_e$. The basal crop coefficient K_{cb} refers to transpiration and is parameterized at the month scale for a typical rainfed olives grove. The soil evaporation coefficient K_e is estimated every month as a function of soil evaporation, thus depending on monthly precipitation, evaporative atmospheric demand and the soil evaporation characteristics following FAO56. The basic computations of PDSI are kept and self-calibration is adopted. MedPDSI was tested for various soil types and locations across Portugal. Comparing results of the water balance with MedPDSI and PDSI, it is apparent a larger actual ET during the rainy months and smaller in the dry months with MedPDSI; coherently, runoff and percolation decrease. It results, however, relatively similar identification of drought and wetness periods, with the MedPDSI responding quicker to changes in precipitation.

Key words: PDSI, MedPDSI drought index, soil water balance, rain-fed olives crop, actual evapotranspiration

1. INTRODUCTION

Drought is a climatic event characterized by a persistent lower than average precipitation with an uncertain frequency, duration and severity resulting in diminished water resources availability. Several drought indices have been developed with the purpose of drought monitoring and drought severity evaluation.

The Palmer Drought Severity Index (Palmer, 1965) is widely used for drought monitoring and in studies on climate change. Precipitation, temperature and soil water holding capacity are required to compute the PDSI. Main limitations of the PDSI refer to the adoption of the Thornthwaite's potential evapotranspiration and the soil water balance modelling (Alley, 1984).

Considering limitations of the method and developments in the ET and soil water balance domains, an adaptation of the PDSI to Mediterranean conditions, the Mediterranean Palmer Drought Severity Index (MedPDSI) was firstly proposed by Pereira et al. (2007). The MedPDSI has been already compared positively with the PDSI, SPEI and SPI in Portugal (Paulo et al., 2012). The backbone of MedPDSI is the soil water balance applied to an olive orchard, by estimating separately soil evaporation and transpiration of the olive crop adopting the dual crop coefficient approach (Allen et al., 1998) modified for a monthly time scale. The objective of this study is to model MedPDSI adopting a self-calibration procedure and to assess its performance for various locations in mainland Portugal comparatively to PDSI.

2. MODIFICATION OF PDSI AND DEVELOPMENT OF THE MedPDSI

2.1 Palmer's formulation

The computation of the PDSI begins with a soil water balance described by (Palmer, 1965)

$$P = ET + RO + (R - L) \tag{1}$$

where P is precipitation, ET is evapotranspiration, RO is runoff, R is soil water recharge and L is soil water loss. The soil is divided in two layers: the surface layer has an available water holding capacity of 25 mm, the water holding capacity of the underlying layer depends on the soil characteristics. The potential evapotranspiration (PET) is computed by the Thornthwaite equation. The ET from the surface layer takes place at its potential rate. ET rate from the underlying layer is a linear function of the ratio between available soil moisture in this layer to water holding capacity of both layers. The water extraction from the underlying layer begins after the total depletion of the surface layer. The recharge of the underlying layer takes place after the surface layer is replenished. Runoff occurs when both layers reach field capacity. The potential terms PRO, PR, PL express a hypothetical maximum of RO, R and L. The precipitation climatically appropriate for existing conditions represents the amount of precipitation expected to maintain normal soil moisture level in a single month i, here denoted by $\hat{P}_i$ as

$$\hat{P}_i = \alpha_j PET_i + \beta_j PR_i + \gamma_j PRO_i - \delta_j PL_i \tag{2}$$

where the coefficients α_j, $\beta_j, \gamma_j, \delta_j$ are calculated for each month j as the ratio between the average of estimated and potential terms over a calibration period.

The moisture anomaly index *z* is obtained by

$$z = k_j (P_i - \hat{P}_i) \tag{3}$$

where k_j is the climatic characteristic for the month j, obtained by an equation using central United States data. The PDSI for month i, X_i, is then derived from z_i, and the PDSI of month i-1, X_{i-1}:

$$X_i = p\,X_{i-1} + q\,z_i = 0.897 X_{i-1} + z_i / 3 \tag{4}$$

The p and q are called duration factors and express the sensitivity of the index to precipitation. The values p=0.897 and q=1/3 were obtained by Palmer using cumulated z during the driest periods of various lengths in two locations. The computation of the PDSI requires the computation of three intermediate indices, X_1, X_2 and X_3 using Eq. 4, X_1/X_2 representing the severity of a wet/dry spell that is becoming established, X_3 the severity index for any wet/dry spell that has become established. The selection of the PDSI from those indices relies on complex operating rules and a backtracking procedure.

The self-calibration of the PDSI replaces k_j and p and q by values computed in each location from the historical climatic data. The self-calibration procedure initiates after having calculated *d* and follows several sequential steps to obtain the self-calibrated PDSI, sc-PDSI (Wells et al., 2004). The methods for defining the wettest and driest periods and the choice of time lengths to obtaining the duration factors are analysed by Dai (2011). The adjustment of the climatic characteristic and the duration factors to local climate conditions allows a better spatial comparability and reduces PDSI range; however the sc-PDSI still does not have a symmetric distribution.

2.2 MedPDSI: the new soil water balance

The modifications base upon considering a rainfed olive crop as water balance reference crop because it is a perennial crop well adapted to water stress and to the Mediterranean environments. The current model to compute MedPDSI is modified from that proposed by Pereira et al. (2007).

The water balance may be performed for a variety of soils. Presently, the soil type may be chosen from nine different soil types, according to texture, the average soil water holding characteristics and soil evaporation parameters as for the dual K_c approach (Allen et al., 1998; Rosa et al., 2012). The soil water balance considers the rooting depth of a mature olive grove and the sensitivity of the olive tree to the water stress. The actual ET (ET_a) is computed through the soil water balance. The counterpart potential term is the maximum/standard crop evapotranspiration $ET_c=K_c\,ET_o$ where K_c is obtained using the FAO56 dual K_c approach. Other computational procedures follow Palmer´s rules (Section 2.1) and self-calibration is also adopted for MedPDSI.

The monthly weather input data are precipitation (P) and reference evapotranspiration (ET_o), computed by the FAO56 Penman-Monteith equation (Allen et al., 1998). The generic equation of the soil water balance is:

$$\Delta ASW = \left(P - ET_a - R_{off} - D_p\right) \tag{5}$$

where ΔASW is the variation of the available soil water stored (ASW) in the root zone, R_{off} is surface runoff due to non-infiltrated precipitation, ET_a is actual crop evapotranspiration and D_p is deep percolation through the bottom of the root zone. The deep percolation is computed assuming that drainage from the root zone occurs immediately after excess precipitation (Doorenbos and Pruitt, 1977). R_{off}=0 as daily data is required for its computation.

Water use and evapotranspiration of olive orchards has been often studied, recently adopting the dual K_c approach (e.g., Allen and Pereira, 2009; Cammallieri et al., 2014; Paço et al., 2015) thus partitioning ET into crop transpiration and evaporation from the soil. The crop coefficient is $K_c=K_{cb}+K_e$. The basal crop coefficient K_{cb} refers to transpiration and is parameterized at the month scale for a typical rain-fed olive grove with 30% ground cover based upon the referred studies. The resulting K_{cb} values are: 0.33 for the months of January to April and the autumn months of November and December, 0.28 for the summer months of June through September, and 0.30 for the transition months of May and October. For a rain-fed crop in a Mediterranean climate higher K_{cb} are expected when rain has refilled the soil and lower K_{cb} are observed during the dry summer months despite the atmospheric demand for evaporation is high. K_e is the soil evaporation coefficient, which was parameterized for every month based upon Paço et al. (2015) and simulations of the olive crop performed for various Portuguese locations using the SIMDualKc model (Rosa et al., 2012). It was therefore possible to establish the following equation

$$Ke_i = 0.2424 - 0.00131\,ETo_i + 0.002875\,P_i + 0.00126\,P_{i-1} \tag{6}$$

with K_e restricted to $0 \le K_e \le (1.2-K_{cb})$ and depending upon ET_o, the precipitation of the current and of the previous month, respectively P_i and P_{i-1}. K_e is further corrected for the evaporative characteristics of the surface soil layer. Fig. 1 shows that K_e generally decrease with the aridity of the station because more humid locations have larger and more frequent replenishment of the soil evaporation layer than semi-arid ones, i.e., larger P_i and P_{i-1} (eq. 6), particularly when $ET_{o\,i}$ change little in space as it is the case for the considered weather stations.

The computation of ET_a depends on the depletion of the soil water: when depletion is smaller than the soil water depletion for no stress, p (p=0.65 in this application), then no water stress occurs and actual crop ET equals the potential ET_c, i.e., $ET_a=ET_c$; differently, stress occurs when depletion exceeds p resulting $ET_a<ET_c$ (Allen *et al*., 1998; Rosa et al., 2012). These stress conditions relate with the concepts of total and readily available soil water (TAW, RAW). TAW is the total amount of water that can be extracted by the vegetation from the root zone when the soil is at field capacity

while RAW is the fraction of TAW that can be removed from the root zone without stress, i.e., RAW=p TAW. Therefore, adopting these concepts, droughts are differently identified for soils with large or small TAW and, consequently when also the rooting depth is larger or smaller. In this application, the root depth adopted for the olive trees is 1.5 m (Allen et al. 1998).

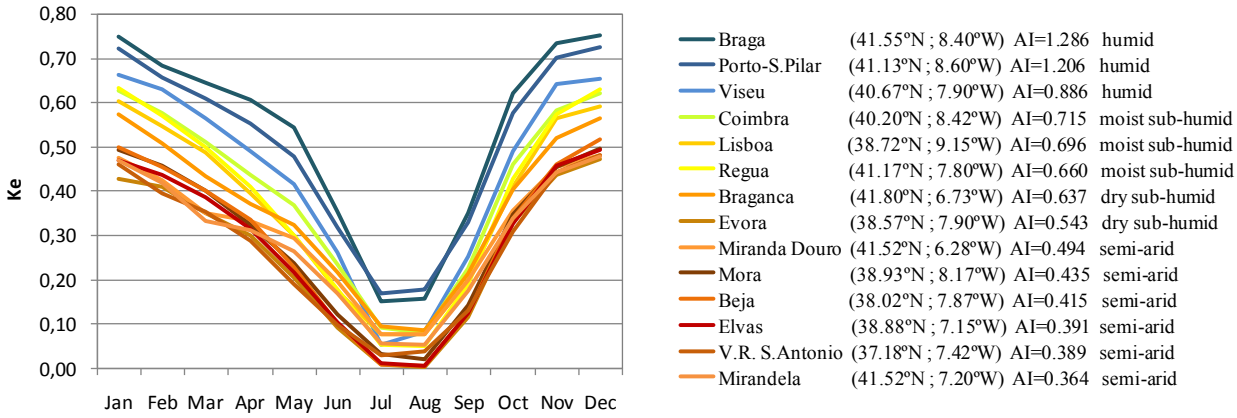

Figure 1. The monthly soil evaporation coefficient K_e averaged (1941-2006) at all locations

The computation of ET_a depends on the depletion of the soil water in the root zone: when depletion is smaller than the soil water depletion for no stress p (p=0.65 in this application) no water stress occurs and $ET_a=ET_c$; differently, when depletion exceeds p stress occurs and $ET_a<ET_c$ (Allen *et al*., 1998). These stress conditions relate with the concepts of total and readily available soil water, TAW and RAW=p TAW. Therefore droughts are differently identified for soils with large or small TAW and also for larger or smaller rooting depths. In this application, the root depth adopted for the olive trees was 1.5 m (Allen et al. 1998).

3. APPLICATION

3.1 Soil water balance: comparing MedPDSI with PDSI

The drought indices PDSI and MedPDSI were computed in 14 weather stations across Portugal in the period 1941-2006. The aridity index computed as per UNEP shows that locations cover a good range of climates, from humid to semi-arid. The latitude and longitude of the weather stations and respective aridity indices are shown in Fig 1.

The olives actual ET computed with MedPDSI and PDSI show non-negligible differences as depicted in Fig. 2a for three locations, Viseu having a humid climate, Bragança a dry sub-humid climate and Elvas a semi-arid climate. Adopting the Penman-Monteith ET_o and a simplified dual K_c approach, the soil water balance (SWB) used in MedPDSI leads to great changes in ET_a relative to the former Palmer's SWB. Results refer to a soil with TAW=180 mm. For all locations, ET_a computed with MedPDSI increases relative to PDSI computations during the rainy and spring months, January to May, as well November and December. Contrarily, ET_a decreases during the dry months (Fig 2c). This means that the SWB used in MedPDSI agrees with environmental conditions: actual ET is higher when more water is available in the soil, not only when the atmospheric demand is higher.

Changes in runoff and percolation (Fig. 2b) consistently indicate a decrease when computed with MedPDSI relative to PDSI. This may be explained by a likely better description of the soil and soil water dynamics with the approach used in MedPDSI, and to the fact that more soil water turns into ET_a. The ability of the model to perform in both humid and semi-arid conditions is demonstrated through the contrasting results relative to Viseu, Bragança and Elvas.

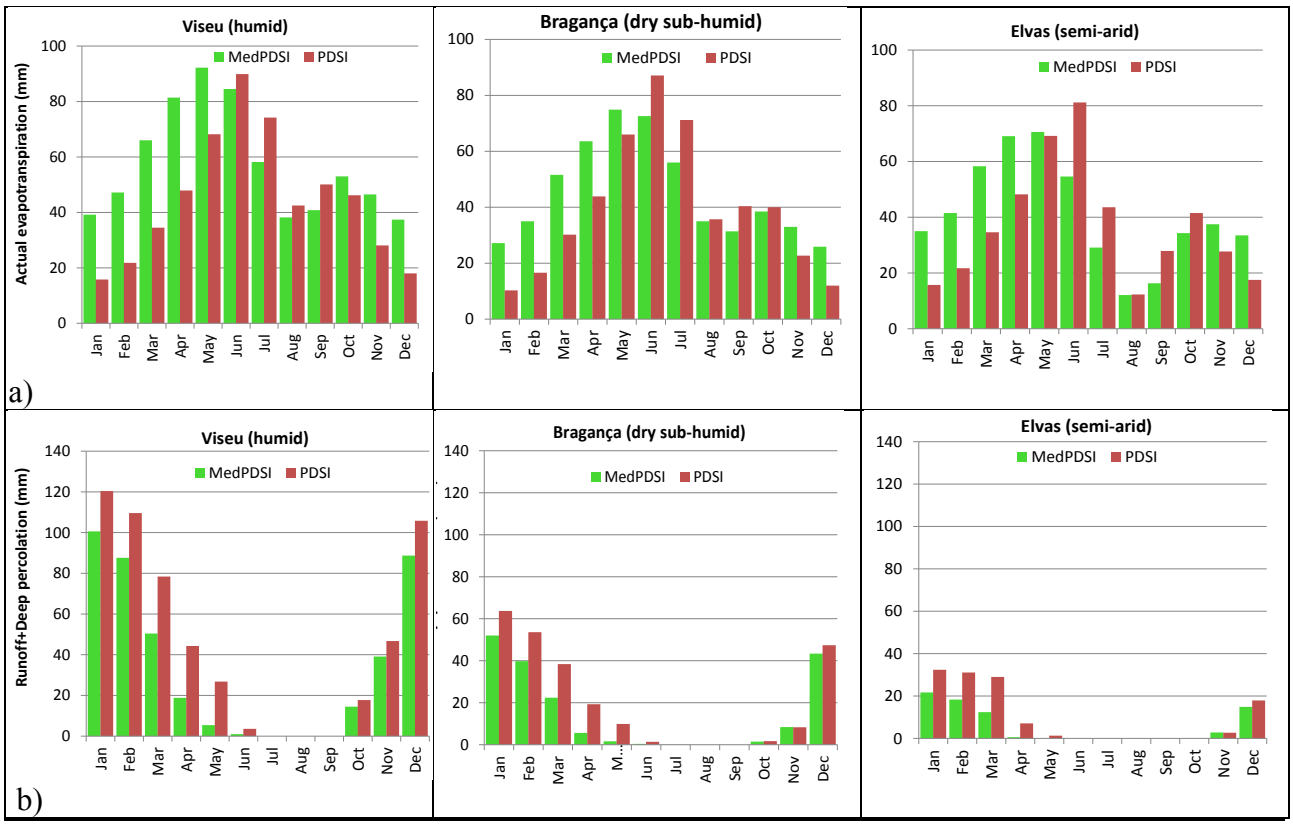

	Stations	MedPDSI ET_a Nov-May (mm)	PDSI ET_a Nov-May (mm)	Difference (%)	MedPDSI $R_{off}+D_P$ Jan-Dec (mm)	PDSI $R_{off}+D_P$ Jan-Dec (mm)	Difference (%)
	Braga	457.8	263.9	73%	664.9	844.2	-21%
	Porto-Serra do Pilar	411.4	274.7	50%	493.9	604.0	-18%
	Viseu	409.9	234.3	75%	390.6	532.0	-27%
	Coimbra/Bencanta	421.3	274.2	54%	228.8	335.4	-32%
	Lisboa (Geofisico)	341.4	286.9	19%	205.9	231.4	-11%
	Regua	405.2	256.6	58%	251.6	348.7	-28%
	Braganca	311.2	201.7	54%	173.2	240.6	-28%
	Evora	320.9	247.7	30%	136.5	170.9	-20%
	Miranda do Douro	283.5	195.3	45%	82.0	122.9	-33%
	Mora	340.1	243.2	40%	94.1	145.5	-35%
	Beja	348.7	245.1	42%	80.4	132.3	-39%
	Mirandela	286.4	208.2	38%	38.1	59.4	-36%
	Elvas	345.5	234.6	47%	70.7	121.5	-42%
c)	Vila Real de S. Antonio	323.2	256.6	26%	51.7	77.9	-34%

Figure 2. Comparing the monthly averages (1941-2006) of (a) actual evapotranspiration for Viseu, Bragança and Elvas with the MedPDSI and the PDSI; (b) runoff and percolation estimated for the same locations and using the same indices; (c) computed differences for ET_a and $R_{off}+D_p$ for all studied locations.

3.2 Drought identification by the PDSI and MedPDSI

The time variability of MedPDSI and PDSI is concordant for all locations. The time series of both indices and its calibrated variants (Fig. 3) are in agreement as shown for Viseu, Bragança and Elvas. The sc-MedPDSI in Viseu and Elvas reaches negative values before the sc-PDSI. For all stations (Table 1) the frequencies of the various drought and wetness classes show some discrepancies when comparing classic and self-calibrated MedPDSI with PDSI. The adoption of self-calibration tends to equilibrate the frequency of the various wet and dry classes, mainly in the case of sc-MedPDSI.

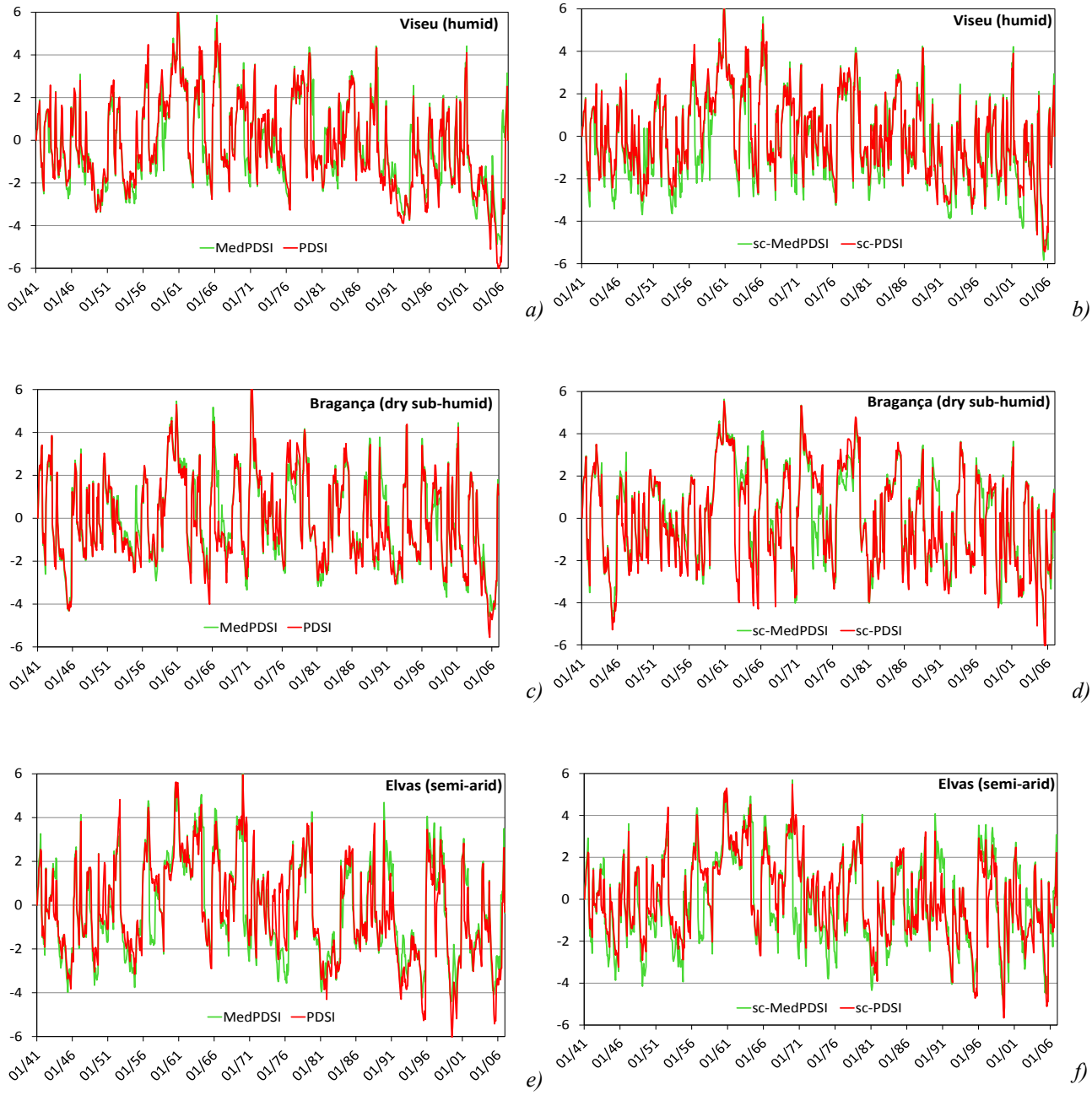

Figure 3. Time variability (1941-2006) of MedPDSI and PDSI (a, c, e) and self-calibrated MedPDSI and PDSI (b, d, f) in Viseu (a, b), Bragança (c, d) and Elvas (e, f)

4. CONCLUSIONS

The proposed drought index MedPDSI has been successfully developed considering the soil water balance of the olive crop and using an adaptation of the dual K_c approach. Monthly K_{cb} values were selected and K_e is determined for every month as a function of ET_o and precipitation of the current and past month. The soil characteristics are defined by the user, which determine both TAW and soil evaporative conditions. The adoption of the new SWB approach led to larger ET_a computed with MedPDSI than with PDSI during the rainy months, thus when more soil water is available. Contrarily, since with MedPDSI more water is used as ET_a, it results that the non-used precipitation, runoff and percolation, are smaller than for PDSI.

The self-calibration for dry and wet periods reduced the asymmetry and balanced the frequency

of mild/moderate dry and wet categories. Results from comparing MedPDSI and PDSI through the entire period of records led to conclude that both indices behave similarly in terms of time variability, but the sc-MedPDSI identified more frequently moderate, severe and extreme droughts than the sc-PDSI. This may indicate that the SWB performed with MedPDSI is well linked to the water supply-demand and is likely more realistic that PDSI.

Table 1. Average frequency (%) of drought/wet classes

Class		MedPDSI	PDSI	sc-MedPDSI	sc-PDSI
Average of all locations					
Dry	Extreme	1.5	2.8	2.0	2.2
	Severe	5.5	5.4	6.6	4.4
	Moderate	13.6	11.8	11.7	10.2
	Mild	37.9	37.2	29.6	33.5
Wet	Mild	22.8	23.1	29.7	29.2
	Moderate	10.7	11.2	11.6	11.7
	Severe	5.4	5.8	6.6	6.9
	Extreme	2.6	2.6	2.3	2.0
Average of the humid locations					
Dry	Extreme	0.5	0.8	1.9	3.3
	Severe	3.3	5.4	8.0	6.4
	Moderate	14.8	12.2	12.1	10.6
	Mild	41.6	40.0	27.6	30.3
Wet	Mild	24.5	24.6	31.9	31.8
	Moderate	8.5	10.2	10.8	10.4
	Severe	4.4	4.6	5.1	5.2
	Extreme	2.4	2.2	2.5	2.0
Average of the semi-arid locations					
Dry	Extreme	2.0	3.9	1.9	1.8
	Severe	7.0	6.3	6.3	3.1
	Moderate	13.7	11.1	10.8	9.3
	Mild	35.1	34.6	29.6	34.8
Wet	Mild	21.9	23.9	29.5	29.6
	Moderate	11.3	11.1	12.3	12.3
	Severe	5.9	6.1	7.2	7.0
	Extreme	3.1	3.0	2.4	2.0

ACKNOWLEDGEMENTS

Authors acknowledge the support of FCT, Lisbon, through the PhD grant SFRH/BD/92880/2013 to the second author, the post-doc grant SFRH/BPD/102478/2014 to the fourth author, and the grant attributed to research unit LEAF (UID/AGR/04129/2013).

REFERENCES

Allen, R. G., Pereira, L. S., 2009. Estimating crop coefficients from fraction of ground cover and height. Irrig. Sci., 28, 17-34.

Allen, R. G., Pereira, L. S., Raes, D., Smith, M., 1998. Crop Evapotranspiration. Guidelines for Computing Crop Water Requirements. FAO Irrig. Drain. Pap. 56, FAO, Rome, 300p.

Alley, W. M., 1984. The Palmer Drought Severity Index: limitations and assumptions. J. Climate Appl. Meteorol. 23:1100-1109.

Cammalleri, C., Rallo, G., Agnese, C., Ciraolo, G., Minacapilli, M., Provenzano, G., 2013. Combined use of eddy covariance and sap flow techniques for partition of ET fluxes and water stress assessment in an irrigated olive orchard. Agric. Water Manage., 120, 89– 97.

Dai, A., 2011. Characteristics and trends in various forms of the Palmer Drought Severity Index during 1900–2008. Journal of Geophysical Research, 116, D12115, doi:10.1029/2010JD015541, 2011

Doorenbos, J., Pruitt, W. O., 1977. Crop Water Requirements. Irrig. and Drainage Paper No. 24, FAO, Rome, Italy, 197p.

Paço, T. A., Pôças, I., Cunha, M., Silvestre, J. C., Santos, F. L., Paredes, P., Pereira, L. S., 2014. Evapotranspiration and crop coefficients for a super intensive olive orchard. An application of SIMDualKc and METRIC models using ground and satellite observations. J. Hydrol. 519, 2067–2080.

Palmer, W., 1965. Meteorological Drought. U.S. Weather Bureau, Res. Paper No 45, Washington.

Paulo, A. A., Rosa, R. D., Pereira, L. S., 2012. Climate trends and behaviour of drought indices based on precipitation and evapotranspiration in Portugal. Nat. Hazards Earth Syst. Sci., 12, 1481–1491.

Pereira, L. S., Rosa, R. D., Paulo, A. A., 2007. Testing a modification of the Palmer Drought Severity Index for Mediterranean environments. In: G. Rossi, T. Vega, B. Bonaccorso (eds.) Methods and Tools for Drought Analysis and Management. Springer, Dordrecht, pp. 149-167.

Rosa, R. D., Paredes, P., Rodrigues, G.C., Alves, I., Fernando, R. M., Pereira, L. S., Allen, R. G., 2012. Implementing the dual crop coefficient approach in interactive software. 1. Background and computational strategy. Agric. Water Manage. 103, 8–24.

Wells, W., Goddard, S., Hayes, M., 2004. A self-calibrating Palmer Drought Severity Index. J. Climate 17, 2335-2351.

Proceedings of the 10th World Congress of EWRA 'Panta Rhei', 5-9 July 2017, Athens, Greece
© 2017 *European Water Resources Association*

Climate change and water valuation in Souss-Massa region: Management and adaptive measures

L. Bouchaou[1*], R. Choukr-Allah[2,3], A. Hirich[3], M.S. Ennasr[1], M. Malki[1], H. Abahous[1], B. Bouaakaz[1,4] and A. Nghira[4]

[1] *Applied Geology and Geo-Environment Laboratory, Ibn Zohr University, Faculty of Science, Agadir, Morocco*
[2] *Hassan II Institute of Agronomy and Veterinary Medicine, Morocco*
[3] *International Center for Biosaline Agriculture, Dubai, UAE*
[4] *Souss-Massa-Drâa Hydraulic Basin Agency, Agadir, Morocco*
[*] *e-mail: l.bouchaou@uiz.ac.ma*

Abstract: Southern part of Morocco is characterized by a semi-arid climate with economy based mainly on tourism, fishery and agriculture. The population and quality life increase in these areas lead to an increase in the domestic and agricultural water demand. The groundwater constitutes the principal resource to satisfy the significant water demand. Water resources overexploitation combined with drought impacts during the last decades caused a depletion of water level in the main aquifers, reduction in water spring flow and deterioration of water and soil quality (increase in salinity, nitrates accumulation…). For a better management of this resource under changing conditions, several projects and studies were undertaken in Morocco and particularly in Souss-Massa basin focusing mainly in the renewal of groundwater, improvement of irrigation efficiency and crop adaptation. Since most of the IPCC climate models predict a significant decrease in precipitation in arid zones over the next few decades, water shortage and salinization induced by climate change and human pressure are expected to aggravate the already existing water crisis in these regions. Several studies conducted in Souss-Massa basin aimed to establish adequate management practices, and implement adaptive governance under water scarcity conditions. This report integrates a scientifically-based evaluation of water management scenarios coupled with analysis of institutional adaptation to achieve sustainable use of water resources under water shortage conditions and increasing salinity.

Key words: Water resources, arid climate, Scarcity, Management, Morocco

1. INTRODUCTION

In Morocco, climate change is already well documented in view of the climatic trends observed between 1960 and 2005. If the scarcity of water resources or their limitation is an intrinsic and structural characteristic of the climate in Souss Massa basin, this phenomenon experienced a certain accentuation during the last decades marked by longer and frequent droughts (Bouchaou et al., 2011; Ait Brahim et al., 2016) and consequently groundwater in the Souss-Massa region showed a continuous depletion in the last decades. The water deficit was equal to -58 Mm^3 for the Chtouka aquifer and -283 Mm^3 for the Souss aquifer in 2007 (ABHSMD, 2006, 2007). Several studies show that earth global climate is changing exhibited by a change in precipitation patterns and increase in extreme events frequency.

The water scarcity in Souss Massa basin coupled with growing demographic pressure, urban development, tourism and industrial sector development increase the demand of water in terms of volume and quality. The problem of water resources limitation requires the stakeholders to adopt a good management, preservation and governance of water within the context of climate change and groundwater overexploitation.

The objective of this study is to describe the current water resources situation in the Souss-Massa region and to summarize some relevant solutions for their management and sustainable development.

2. OVERVIEW OF CLIMATE CHANGE IMPACTS AND FUTURE FORECASTS FOR ADAPTATION

A recent study by Seif-ennasr et al. (2016), carried out in Chtouka Ait-Baha within the Souss-Massa basin, predicted under different models, that temperatures will increase up to 2°C during 2030-49 and up to 4°C during 2090-2100 under RCP8.5 scenario compared to the baseline (1986-2005). Precipitation will also decrease especially at high altitude areas, and the extreme change under RCP8.5 will concern the end of the 21st century attending -53%.

Obviously, these changes are meant to have several impacts on water balance (Fig.1). As a response to temperature and evapotranspiration increase, agricultural water demand will also increase. This phenomenon is accompanied by a significant depletion of groundwater reserves caused by several stressors including uncontrolled overexploitation of aquifers (Choukr-Allah et al., 2012; Hssaisoune et al., 2016).

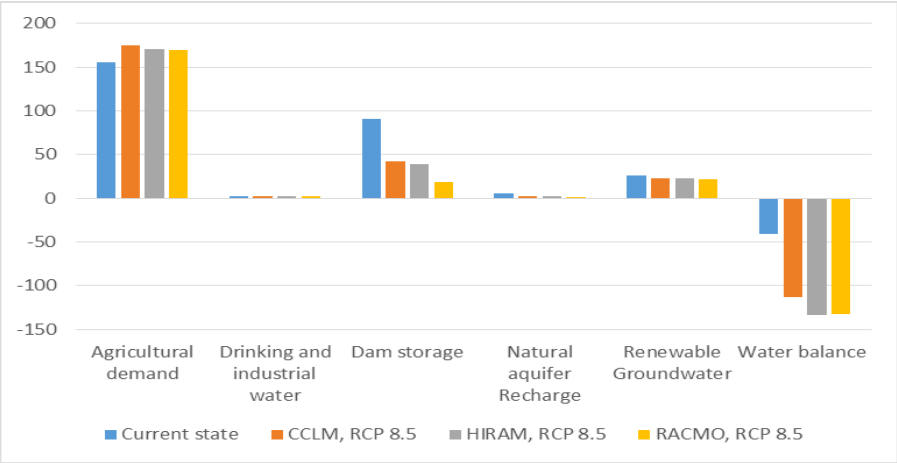

Figure 1. Climate change impacts on water resources in the Souss-Massa basin during 2030-2050 (Mm^3)

Souss-Massa river basins is located in semi-arid region and faced to important water scarcity challenges, which will be aggravated by climate change in the coming decades. Among other consequences, climate change will intensify the water cycle, altering water availability, timing, quality, and demand (Herrera-pantoja and Hiscock, 2015; Whitehead et al., 2017). As a result, actual problems such as drought, irrigation requirements increase and water quality deterioration will only be magnified by climate change (Bouchaou et al., 2008; Malki et al., 2016 a,b).

Thus, climate is related to many complex predicaments whose solutions are not always suitable to our conventional knowledge systems. For this reason, an improvement of resiliency and adaptive capacity is needed (Iglesias and Garrote, 2015; Seif-ennasr et al., 2016).

3. SOCIOECONOMIC PROFILE OF THE SOUSS-MASSA REGION

According to HCP (2014a), Souss-Massa population is equal to 2.6 million inhabitants (44.6% living in rural area) including 1.35 Million females. The total, rural and urban active population represents 44.3, 38.6 and 48.6% of the total population respectively. Most of active population is represented by male (73.8%) while female active population represents only 17% which indicates that gender issues still need to be addressed in the local development policies and programs. Souss-Massa contributes by 6.6% (61 Billion DH) of the national Gross Domestic Production (GDP). Agriculture and fishery contributes by 16.7% of the regional GDP of the region (HCP 2014b). The HCP 2014 report projects that Souss-Massa population will raise to 3.15 million by 2030 which clearly indicates a growing water and food demand. Agriculture is so far, the main economic activity of the Souss-Massa with 143,640 ha of irrigated lands of which about 60% is under modern

systems dedicated to fruit and vegetables 34%, citrus 25%, cereals 10%, and 28% livestock. The production of citrus and early vegetables contributes to over 50% of the national exports (Haddouch et al. 2016).

4. ECONOMIC VALUATION OF GROUNDWATER DEPENDENT ECOSYSTEM SERVICES

Groundwater plays an integral role in sustaining certain types of aquatic, terrestrial, and coastal ecosystems and associated landscapes, both in humid and arid climatic regions (Marre et al. 2016). It is thus a key factor in efforts to maintain the ecological integrity of some key ecosystems. In Souss-Massa region, all ecosystems including the agroecosystem, forest, wetlands, are depending on groundwater for their continuity (Fig.2). Hirich et al. (2016) reported that the agroecosystem in Souss-Massa region contributes by more than 74% in the Total Economic Value (TEV). This rate shows the important development of the agricultural sector making the region the most productive in Morocco. The forest who contributes by more than 13% in the TEV has more regulating services than provisioning services compared to agroecosystem where climate regulation, CO_2 sequestration, and erosion control services contribute by more than 43% to the TEV. Compared to agroecosystem where regulating services contribute only by 3% in the ecosystem TEV. Ecotourism represents about 6% of TEV in the whole Souss-Massa region ecosystem and reflects its importance in the ecological and socioeconomic development of the region. Aquifer ecosystem contributes by 5%; however, it is the most important ecosystem on which the whole ecosystem is depending for its sustainability.

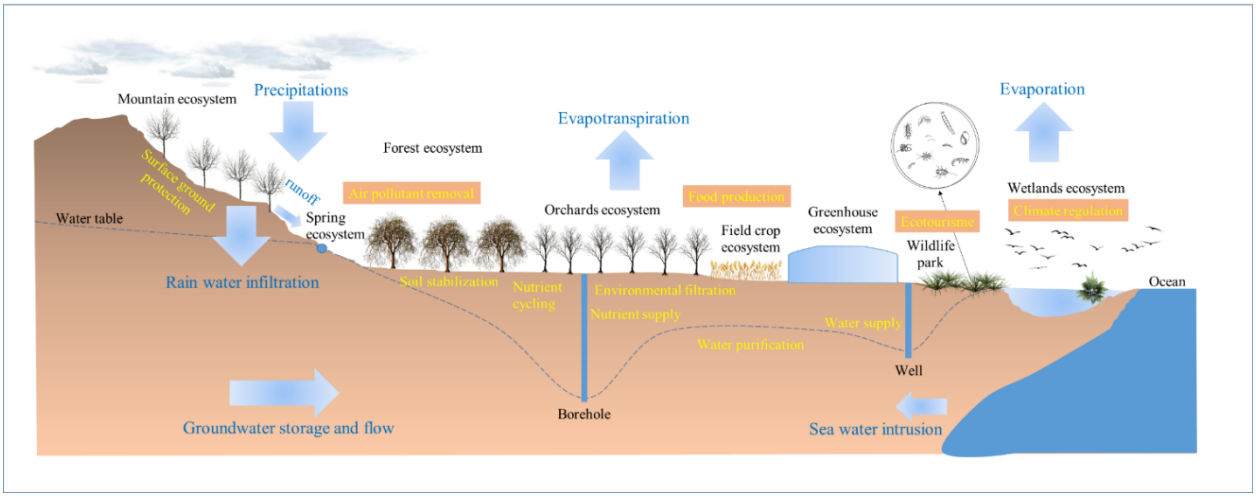

Figure 2. Groundwater dependent ecosystems in the Souss-Massa basin. The figure presents the water cycle in the watershed, blue words are related to water cycle, black present the different ecosystems and yellow show ecosystem services. The figure illustrates also the agricultural intensification exhibited by groundwater depletion caused by pumping, as result the sea water intrusion is occurred.

5. ECONOMIC AND CROP WATER PRODUCTIVITY OF IRRIGATION WATER

Productivity is a ratio between a unit of output and a unit of input. Here, the term water productivity is used exclusively to denote the amount or value of product over volume or value of water depleted or diverted. The value of the product might be expressed in different terms (biomass, grain, money) (Kijne 2003). Figure 3 shows the economic and crop water productivity for the main crops cultivated in the Souss-Massa region under two types of irrigation systems (drip and surface irrigation).

The presented data indicate that both crop and economic water productivity are lower for crops

cultivated under surface irrigation system, while drip irrigation system allows an important improvement of both crop and economic water productivity. For example, for field tomato crop and economic water productivity were increased by 2 and 10 times respectively. Production under greenhouse conditions is also a good practice to improve significantly crop and economic water productivity which were increased by 50 and 34,1% for tomato respectively and by 70 and 33,5% for pepper respectively (Elame et al. 2016). This finding indicates clearly that drip irrigation and greenhouse cropping system allow maximizing water use efficiency both at agronomic and economic level. Drip irrigation and greenhouse systems have been developed significantly during the last three decades and now most of farmers in the region adopt drip irrigation and greenhouse systems for better production and income improvement.

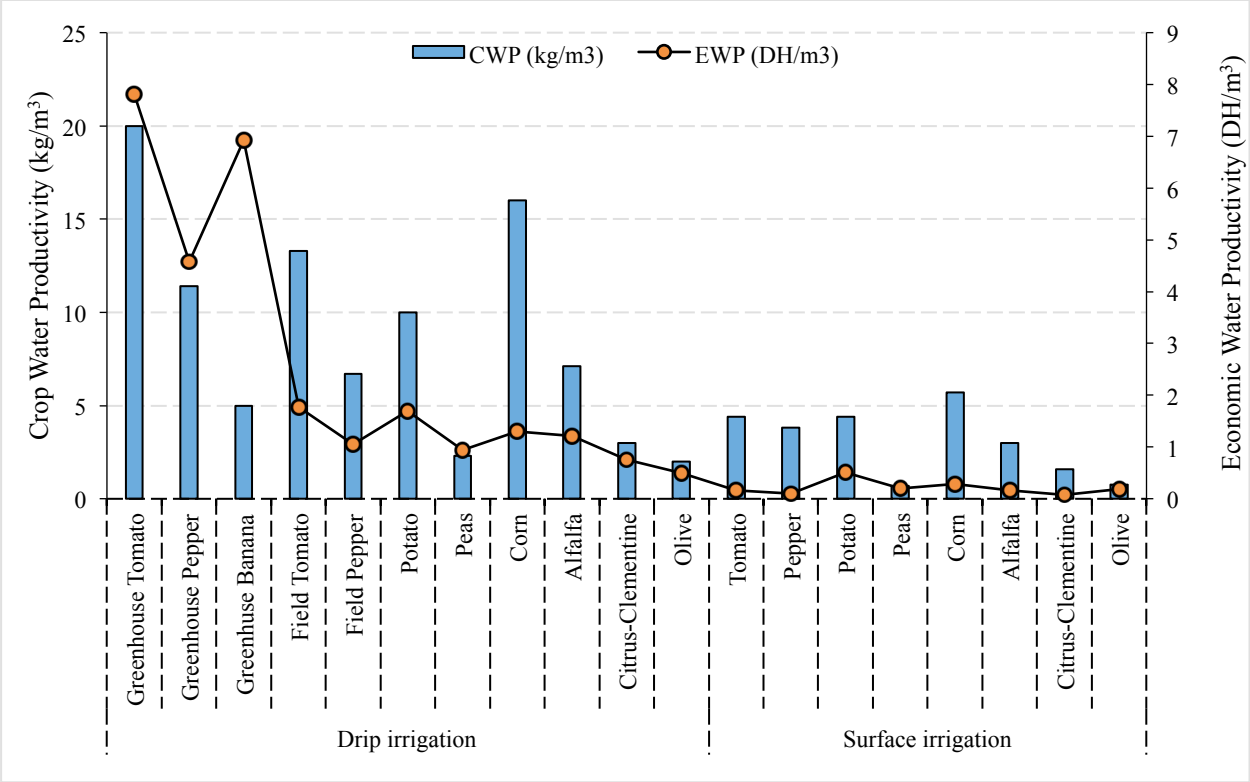

Figure 3. Economic and crop water productivity for the main crops cultivated in the region under two types of irrigation systems (drip and surface irrigation) in Souss-Massa region (Elame et al. 2016)

6. GROUNDWATER CONTRACT OF SOUSS-MASSA: OBJECTIVES, ADVANTAGES AND CHALLENGES

Since climate change significantly impacts the availability of water resources, Morocco has implemented its National Water Strategy, established in 2003 with main goals designed to overcome the negative impacts. The most important measure is regarding demand management and water efficiency through water saving irrigation program with incentives to use efficient practices. Then several options are supposed to improve water supply and increases water management flexibility at the local level including the construction of 60 large dams to mobilize 1.7 billion m^3/year and several small dams; water resources transfer from the North basin to the South (800 Mm^3/year); the mobilization of unconventional resources through the treated wastewater reuse, rainwater harvesting, seawater desalination and brackish water. Some of the above-mentioned strategies are already undertaken in the Souss-Massa region such as irrigation efficiency improvement through conversion from surface to drip irrigation (more than 90% of farmers are using drip irrigation), construction of seawater desalination plant for high cash crop irrigation. As well, water transfer from North to South is currently planned and the feasibility study was achieved.

The groundwater contract constitutes an innovative tool for local governance to meet sustainable management of water resources. Several participants and stakeholders are involved in this contract (Fig. 4).

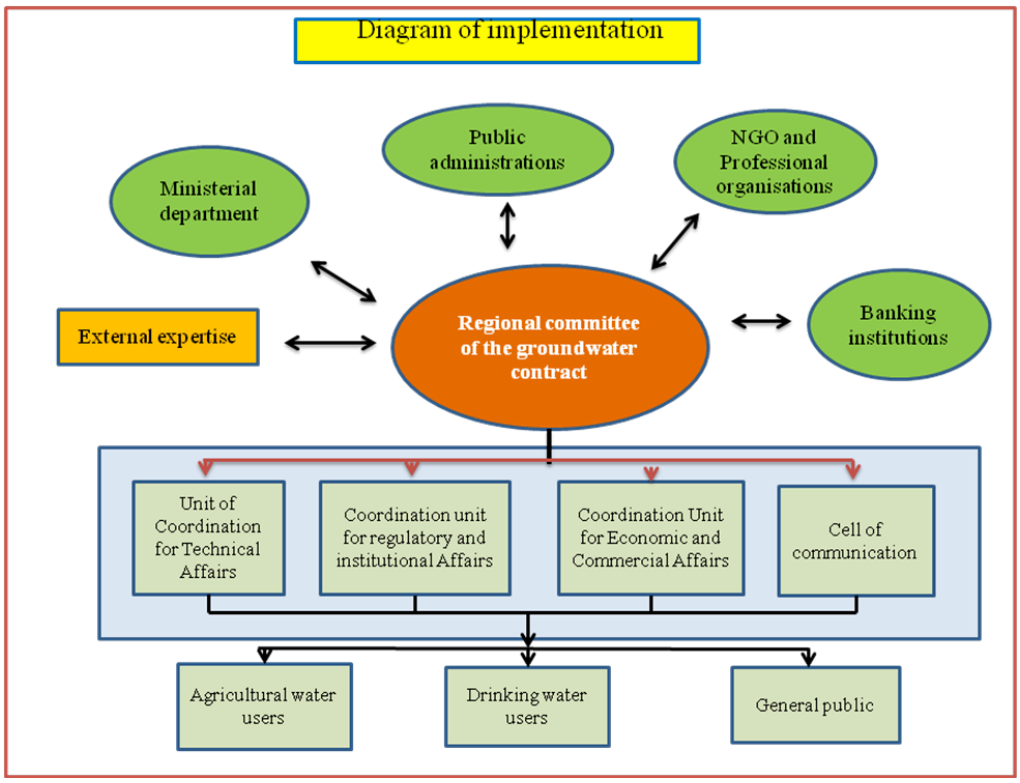

Figure 4. Scheme for implementing the Souss-Chtouka groundwater contract (ABHSMD, 2006)

The aquifer contract developed in the Souss-Massa region within public-private partnership for irrigation using groundwater constitutes a successful case. Saving groundwater is planned within a public service delegation to a private operator, which will be responsible for financing, designing, building and managing seawater desalination infrastructures and irrigation systems.

The objectives of the contract are:

- Contribution to the implementation of a participatory policy to protect groundwater in Souss-Massa;
- Completion of a negotiated and concerted participatory action plan in harmony with the recommendations and provisions of the water resources development plan for the protection and preservation of the groundwater in the area;
- Establish a (measurable) monitoring of the performance of groundwater management.
- Restore and maintain good water quality for user satisfaction;
- Concertedly manage water resources in the Souss-Massa and establish operational water governance through the development of an ambitious program of conversion from surface irrigation to drip irrigation.

To carry out water resources safeguarding, some action plans have been established: (i) desalination of sea water as a relay of conservation and safeguard of groundwater. Its objective is to meet an annual need of 58 Mm^3 of desalinated water with a rate of 167,000 m^3/day. This desalination plant will allow the region to compensate a deficit of 60 Mm^3 (Nakhil, 2015).

With this new resource, in addition to surface water from dams and groundwater, the Souss-Massa region will be rescued as well as water scarcity, climate change and salinization will be mitigated and mastered.

Moreover, relations are made between individual farmers and Hydraulic agency without intermediary mediation (AFD, 2012). This approach does not make it possible to ensure the

effective participation of users in the groundwater regulation groundwater.

It is important to note the rapid expansion of modern private areas, especially in the northern Chtouka, where the irrigated perimeter area has exceeded 7500 ha (ABHSMD, 2006)

Treated wastewater can be considered to cope with negative impacts of water scarcity and could be used for Agriculture and watering of green areas. Aquifer artificial recharge, forest irrigation and artificial wetlands are among other options being discussed for wastewater reuse in the region.

7. CONCLUSION AND RECOMMENDATIONS

The Souss-Massa is suffering from overexploitation and degradation of water resources aggravated by drought and climate change. The future of the region relies in the rational planning and integrated management based on water saving and quality protection to make the best use of the available water resources. To make water a factor in the sustainable development in the region, we must therefore adopt a new strategy based on three pillars:

- Larger and much more ambitious objectives;
- Improvement in population behavior;
- Strict long-term water management.

It is necessary to update the master plan for integrated water resources management, modeling groundwater with reliable models, and reducing vulnerability to water-related risks and adaptation to climate change. It is also important to identify and carry out a technical, economic and environmental assessment of the possibilities for water resources development, as well as actions to save these resources and develop non-conventional water resources.

ACKNOWLEDGEMENTS

This research was carried out within ERANET-MED, WASA and GLOBAQUA projects..

REFERENCES

AFD (French Development Agency) , 2012. water demand management in the Mediterranean basin - example from Morocco - case study of Souss Massa, final report, 214p

Ait Brahim Y., L. Bouchaou, A. Sifeddine, M. Khodri, B. Reichert, F.W. Cruz 2016. Elucidating the climate and topographic controls on stable isotope composition of meteoric waters in Morocco, using station-based and spatially-interpolated data. J.Hydrol., Vol. 543, Part B, pp 305–315

Bouchaou L., J.L. Michelot, A. Vengosh, Y. Hsissou, M. Qurtobi, C.B. Gaye, T.D. Bullen and G.M. Zuppi, 2008. Application of multiple isotopic and geochemical tracers for investigation of recharge, salinization, and residence time of water in the Souss-Massa aquifer, Southwest of Morocco. J. Hydrol. Vol. 352, 267-287.

Bouchaou L., Tagma T., Boutaleb S., Hssaisoune M.& El Morjani Z.. 2012. Climate change and its impacts on groundwater resources in Morocco: the case of the Souss- Massa basin. IAH Book series - International Contributions to Hydrogeology: Climate Change Effects on Groundwater Resources: A Global Synthesis of Findings and Recommendations. CHAPTER 8, pp 129-143,

Choukr-Allah R., Ragab R., Rodriguez-Clemente R., 2016. Integrated water resources management in the Mediterranean region: Dialogue towards new strategy. Springer Netherlands, 2012, pp. 356.

Elame F., Lionboui H., Choukr-Allah R. ,2016. Water Use Efficiency and Valuation in Agriculture in the Souss-Massa. In: Choukr-Allah R, Ragab R, Bouchaou L, Barceló D (eds) The Souss-Massa River Basin, Morocco. The Handbook of Environmental Chemistry. Springer Berlin Heidelberg, Berlin, Heidelberg, pp 1-9.

Haddouch M., Fouad E., Houria A., Choukr-AllahR.., 2016. Socio-Economics and Governance of Water Resources in the Souss-Massa River Basin. In: Choukr-Allah R, Ragab R, Bouchaou L, Barceló D (eds) The Souss-Massa River Basin, Morocco. The Handbook of Environmental Chemistry. Springer Berlin Heidelberg, Berlin, Heidelberg, pp 1-15.

HCP , 2014a. Annuaire statistique de la région de Souss Massa Drâa 2014. Haut commissariat au plan Rabat, Maroc

HCP,2014b. Note d'information relative aux comptes régionaux de l'année 2014. Haut commissariat au plan Rabat, Maroc

Herrera-pantoja, M., Hiscock, K.M., 2015. Environmental Science & Policy Projected impacts of climate change on water availability indicators in a semi-arid region of central Mexico. Environ. Sci. Policy 54, 81–89.

Hirich A., Choukr-Allah R., Nrhira A. , 2016. Groundwater-Dependent Ecosystems in the Souss-Massa River Region: An Economic Valuation of Ecosystem Services. In: Choukr-Allah R, Ragab R, Bouchaou L, Barceló D (eds) The Souss-Massa River Basin, Morocco. Springer Berlin Heidelberg, Berlin, Heidelberg, pp 1-34.

Hssaisoune M., Bouchaou L., N'da B., Malki M., Abahous H. & Fryar A., 2016. Isotopes to assess sustainability of overexploited groundwater in the Souss-Massa system (Morocco), Isotopes in Environmental and Health Studies Authors.

Iglesias, A., Garrote, L., 2015. Adaptation strategies for agricultural water management under climate change in Europe. Agric. Water Manag. 155, 113–124.

Kijne W (2003) Working towards unlocking the water potential of agriculture. FAO,

Malki M., Bouchaou L., Hirich A., Ait Brahim Y. and Choukr-Allah R.- 2016- Impact of agricultural practices on groundwater quality in intensive irrigated area of Chtouka-Massa, Morocco. STOTEN574:760-770

Malki M., Choukr-Allah R., Bouchaou L., Ait Brahim Y., Hirich A. and Barbara R.-2016- Evolution of groundwater quality in intensive agricultural zone: Case of Chtouka-Massa Aquifer, Morocco. Arab J Geosci (2016) 9:566

Marre J-B, Thébaud O, Pascoe S, Jennings S, Boncoeur J, Coglan L (2016) Is economic valuation of ecosystem services useful to decision-makers? Lessons learned from Australian coastal and marine management. Journal of Environmental Management 178:52-62.

Nakhil F., 2015. Water resources in the Souss A desalination station to compensate for the deficit. Journal of the Maghreb Economist, Edition N °: 4614, 23/09/2015.

Seif-ennasr, M., Zaaboul, R., Hirich, A., Nils, G., Bouchaou, L., El, Z., El, A., Hassane, E., Mcdonnell, R.A., Choukr-allah, R., 2016. Science of the Total Environment Climate change and adaptive water management measures in Chtouka Aït Baha region (Morocco). Sci. Total Environ. 573, 862–875.

Souss-Massa Hydraulic Basin Agency (2006). Review of the Master Plan for Integrated Water Resources Management Vol.3:, Final Report, 120 p

Souss-Massa Hydraulic Basin Agency (ABHSM), 2007. National Water Debate

Souss-Massa Hydraulic Basin Agency, 2006. Review of the Master Plan for Integrated Water Resources Management (PDAIRE) of the Souss Massa Basins, Mission I: Data collection, diagnosis and evaluation of water resources and Status of Use, Volume 4: Unconventional Water Resources, 37p

Whitehead, P.G., Wilby, R.L., Battarbee, R.W., Kernan, M., Wade, A.J., 2017. A review of the potential impacts of climate change on surface water quality A review of the potential impacts of climate change on surface water quality 6667.

Proceedings of the 10th World Congress of EWRA 'Panta Rhei', 5-9 July 2017, Athens, Greece
© 2017 *European Water Resources Association*

Analysis of drought severity in Seyhan river basin

G. Onusluel Gul* and A. Kuzucu
[1] *Dokuz Eylul University, Dept. of Civil Engineering,Tinaztepe Campus, 35160, Izmir, Turkey*
* *e-mail: gulay.onusluel@deu.edu.tr*

Abstract: Drought is one of the most common disasters in the world. Despite being a natural event, environmental changes combining climate and land-use changes increase its impacts. Seyhan river basin in the Mediterranean region of Turkey has great significance since agriculture has the biggest share and IPCC indicates the area among the regions subject to the highest levels of the climate change impacts. In the presented study, drought severity analysis was carried out in terms of both the standardized precipitation index (SPI) and the standardized precipitation evapotranspiration index (SPEI) at multiple time scales (3, 6 and 12 months). In order to quantify both temporal and spatial changes of drought phenomenon, monthly precipitation and temperature data covering the period 1970-2015 were evaluated at meteorological stations in the basin. Data pre-processing which includes missing value estimation and homogeneity analysis was carried out prior to the computation of drought severity indices. Missing data in the recorded series were completed using linear regressions with respective reference series. Standard normal homogeneity test, Buishand range test, Pettitt test and Von Neumann ratio test were used for homogeneity checks on the data set. Precipitation data were also analyzed for trends using the Mann-Kendall non-parametric test. The period 2011-2015 which was the warmest five-year period on record globally was specially analysed as well. Kriging method was additionally used in order to show the spatial distribution of droughts.

Key words: Drought, SPI, SPEI

1. INTRODUCTION

Drought is defined as the period of time that falls below the average precipitation in a given area, and is a natural disaster that causes long-term shortages in the water supply, atmospheric, surface waters or groundwater and needs combatting in some parts of the world. Drought as a slow-growing phenomenon also affects very large areas and populations, causing economic and environmental problems, which can lead to irreversible damages (Spinoni et al., 2015; Vogt et al., 2011; Vogt and Somma, 2000). Despite being a natural event, environmental changes combining climate and land-use changes increase its adverse impacts.

In recent years, Turkey experienced a very serious meteorological drought especially in 2013-2014, and this meteorological drought progressed towards agricultural and hydrological drought cases due to the significant decreases in winter precipitation (Kurnaz, 2014). According to the report on the effects of climate change (Krichak, 2014), the expected changes in Turkey and the Mediterranean basin are extremely worrisome. The most striking result is that the drought event experieced in the region is expected to continue (Kurnaz, 2014). According to the figures at the end of September 2015, the period 2011-2015 was the warmest five year period on the records for Asia, Europe, South America and Oceania, and North America (WMO, 2015). In January 2017, 2016 was assigned to be the recorded warmest year in the world by the relevant agencies around the world, e.g. NASA, NOAA, Met Office (NASA, 2017).

In this context, it is necessary to examine the studies related to drought in a multidirectional way. In the presented study, drought severity was analysed based on the standardized precipitation index (SPI) and the standardized precipitation evapotranspiration index (SPEI) in multiple time scales in Seyhan river basin in Turkey to assess drought conditions and related hydrological impacts.

2. MATERIALS AND METHODS

2.1 Study area

Seyhan river is one of the longest rivers in Turkey flowing into the Mediterranean Sea . The drainage area is about 21700 km² and is located in the south of Turkey (Figure 1) The main water source of the Seyhan river is from the Taurus Mountains. In the river basin, there are three different regional characterizations in terms of climate. While the northern part of the basin is influenced by the continental climate, the climate of the coastal plain is mostly dominated by the Mediterranean climate, known with hot and drought summers and mild winters with precipitation. For the middle part of the basin where Taurus Mountains extends in the northeast-southwest direction, the climate is more rainy and colder. The part of the basin associated with the highest rainfall is in the middle of the highland. In the basin, annual precipitation is about 700 mm in the coastal area. This increases to approximately 1000 mm at higher elevations, while decreasing to 400 mm in the northern part of the basin.

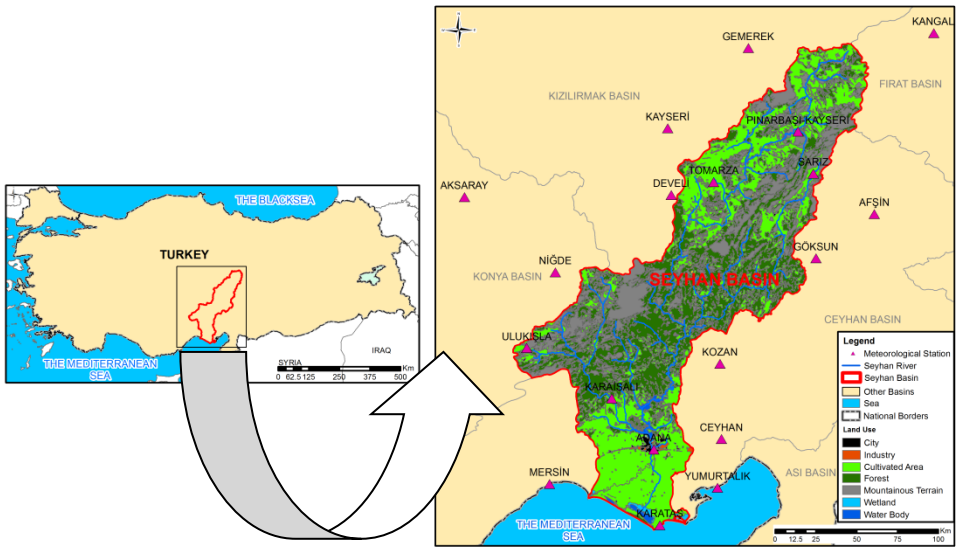

Figure 1. Location of Seyhan river basin.

Seyhan river basin has great significance from different aspects. Agriculture has the biggest share in the basin and IPCC indicates the area among the regions subject to the highest levels of the climate change impacts. The basin hosts the most fertile and productive agricultural land sections of Turkey and of Europe. In terms of geographical structure, Seyhan river basin consists of high steppes, mountainous areas, transition zones, low planes and the Çukurova Delta. The basin, which is one of the richest regions in the world also in terms of biodiversity, offers the people in the region various agricultural possibilities as dry farming, irrigated farming and livestock (Talu and Özüt, 2011).

2.2 Data

In order to calculate the SPI values, precipitation values are required. In addition to the rainfall measurements, temperature values should additionally be available to calculate the SPEI value. The World Meteorological Organization (WMO) recommends the use of at least 30 year precipitation totals as reference time line for rainfall statistics computation. Water Scarcity and Drought Expert Group at European Commission Joint Research Centre (JRC) strongly recommends the period from January 1971 to December 2010 for the reference period to calculate the SPI (JRC, 2011). In this research, the monthly precipitation and temperature data covering the period 1970-2015 were

provided by the Turkish State Meteorological Service and 19 meteorological stations in and near the basin were used. These are the stations associated with the common observation period 1970-2015. Figure 1 also shows the spatial distribution of the selected meteorological stations.

2.3 Data pre-processing

Data pre-processing which includes missing value estimation, homogeneity and trend analysis were carried out before computing the drought indices. Missing data in the recorded series were completed using linear regressions with respective reference series. Maximum missing data percentages in precipitation and temperature data are 3.2% and 1.6%, respectively. Homogeneity analysis was performed to ensure that the data used in the study have adequate quality. For this purpose, standard normal homogeneity test, Buishand range test, Pettitt test and Von Neumann ratio test were applied to monthly precipitation and temperature time series. The results of the homogeneity tests applied to both precipitation and temperature data confirm that both precipitation and temperature data at all stations are homogeneous. Finally, monthly precipitation and temperature time series were checked for trend by using Mann-Kendal non parametric test (Mann, 1945; Kendall, 1962).

2.4 Drought indices, temporal and spatial analysis

In this study, the SPI and the SPEI drought indices were used to characterize the droughts in Seyhan river basin. The SPI that was first introduced by McKee et al. (1993) to measure normalized anomalies in precipitation is the universal meteorological drought index recommended by the World Meteorological Organization (WMO, 2006) as described in the Lincoln Declaration on Drought Indices (WMO and GWP, 2016; Hayes et al., 2011). The SPI is defined as a statistical monthly drought indicator. It compares total precipitation values for an n-month duration with the long term precipitation distribution for the same period at a given location (Spinoni et al., 2015). First step to calculate SPI is fitting density function to frequency distribution of total precipitation values in a station for a given period. In this study, gamma probability density function was used since the software packages are generally based on the gamma distribution and because this distribution is used by Turkish State Meteorological Service and by the major research centres in the world (Wu, et al, 2007, JRC, 2011). In addition, the gamma distribution is suitable for use in arid regions where the average rainfall is low and the variability is high since it has a skewness in the positive direction. After the parameter estimation of the probability density function, the cumulative probability of the observed precipitation for the required time scale is calculated and then the SPI value is obtained by converting the standard normal distribution with a mean of zero and a variance of one. The drought event occurs when the SPI is constantly negative and ends when the SPI is positive.

SPEI, developed by Vicente-Serrano et al. (2010), is calculated using temperature data in addition to rainfall data used in the SPI calculation. The SPEI is expressed in terms of the differences between potential evaporation and precipitation data. Potential evapotranspiration is computed using the temperature data. SPEI is calculated similarly to SPI, except that the difference between the potential evapotranspiration and precipitation is used instead of the precipitation time series. In computation of the SPEI values, log-logistic distribution function was applied. The classification given by Mc Kee at al. (1993) was applied and the same classification was used for SPEI.

SPEI package of R statistical program (Beguería, S. and Vicente-Serrano, 2013) was used in estimating SPI and SPEI values. SPI and SPEI can be computed at any timescale (Tan et al., 2015). According to WMO and GWP (2016), SPI values for 3 months or less can be used for basic drought monitoring, while values for 6 months or less for monitoring agricultural impacts and values for 12 months or longer for hydrological impacts.

SPI and SPEI values were analysed for trends using the Mann-Kendall non-parametric test. In order to assess spatial variation of SPI and SPEI values, ordinary kriging method (Webster and Oliver, 2007) was applied. Among the several drought events, some of the most severe were selected and SPI and SPEI values were spatially predicted and mapped using ordinary kriging.

3. RESULTS AND DISCUSSION

Long-term (1970-2015) monthly trend analysis for precipitation and temperature data results indicates that while the long term monthly precipitation does not show significant trend, summer temperature values for all stations show increasing trend. SPI and SPEI values were computed for 3, 6 and 12 month-periods to assess drought conditions for each station. When the SPI values of these three different durationsare taken into account, the stations in the basin area with the most drought severity appear to be Karaisalı, Karataş and Tomarza, respectively. The Karaisalı station for 3 and 6-month SPEI values and the Tomarza station for 12-month SPEI values are the stations where the drought was detected to be the most intense. Figure 2 shows the temporal variations of computed SPI and SPEI values for Karaisalı station from 1970 to 2015. It can be seen that SPI and SPEI indices for multiple time scales over Seyhan river basin prove to indicate similar behavior especially in 12-month values, but show some differences especially in dry seasons (SPI/SPEI < 0) for 3 and 6-month drought severity and durations. However, when considering wet periods (SPI/SPEI < 0), SPI and SPEI values give similar results in all investigated time scales.

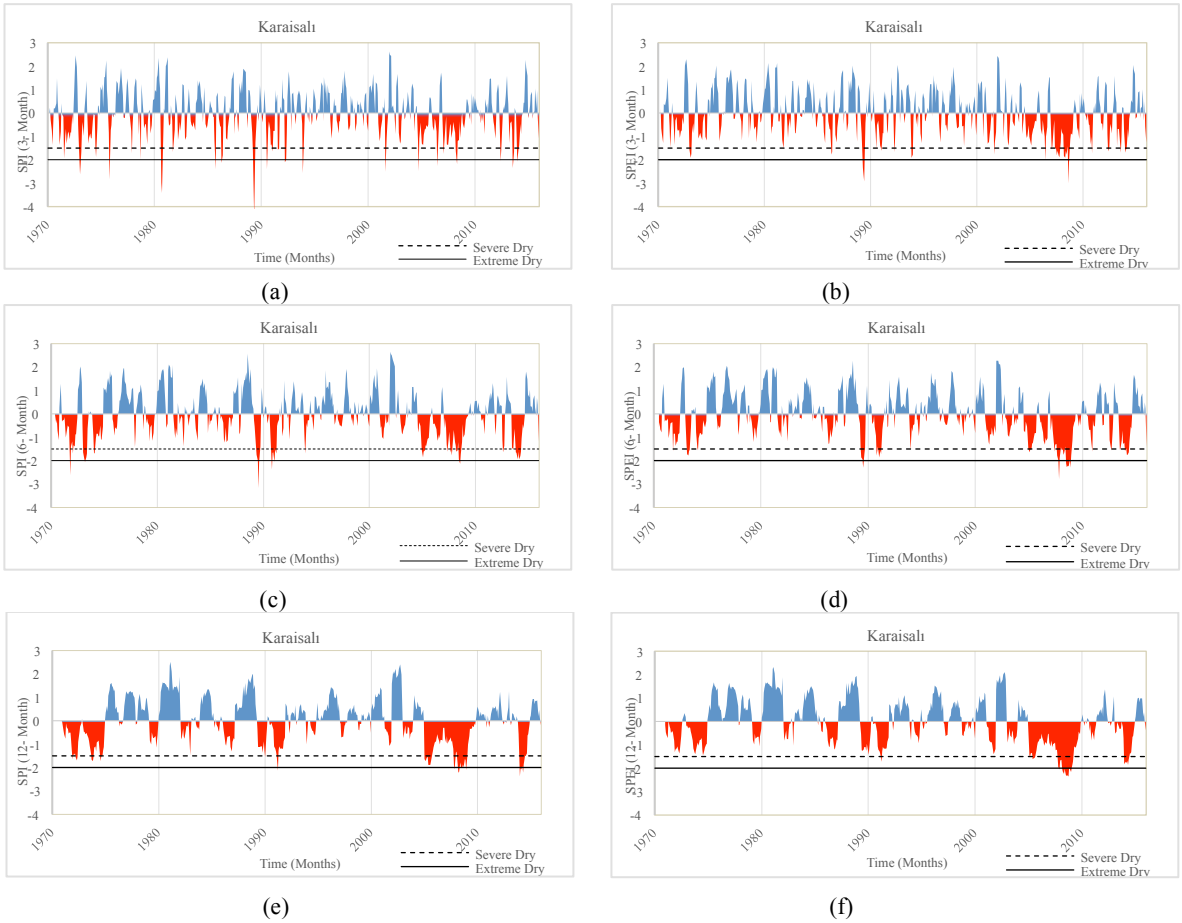

Figure 2. SPI and SPEI values calculated using the historical observed data (1970–2015) at Karaisalı station:(a) SPI 3 months (b) SPEI 3 months (c) SPI 6 months (d) SPEI 6 months (e) SPI 12 months (f) SPEI 12 months.

Figure 2 also shows the most severe drought periods. The first period is 1971-1975, the second one is 1989-1993, the third one is 2005-2009, and the last period is 2013-2014. For most of the

stations, the most severe drought years are 1973, 1989, 2013 and 2014.

Mann-Kendall test was applied to the computed SPI and SPEI values for detecting any possible trend. The trend analysis showed that there exist decrease tendencies in both SPI and SPEI for all stations. This result suggests that the drought is in an increasing trend.

In terms of showing the periodic changes in droughts, Table 2 was created for the period 1970-2015 organized in 10-year intervals and the remaining 6 years in the period 2010-2015.

Table 2. Drought events based on the SPI and SPEI.

Station No	Station Name	Period	Drought Events					
			SPI			SPEI		
			3-month	6-month	12-month	3-month	6-month	12-month
17351	Adana	1970-1979	5	4	1	3	1	1
		1980-1989	4	3	0	3	2	0
		1990-1999	3	3	1	4	3	1
		2000-2009	6	4	2	7	4	3
		2010-2015	4	2	1	3	3	1
		1970-2015	**22**	**16**	**5**	**20**	**13**	**6**
17802	Pınarbaşı Kayseri	1970-1979	3	1	0	2	0	0
		1980-1989	4	3	2	4	3	2
		1990-1999	3	1	1	4	1	2
		2000-2009	5	3	1	5	3	2
		2010-2015	3	2	2	5	3	3
		1970-2015	**18**	**10**	**6**	**20**	**10**	**8**
17837	Tomarza	1970-1979	6	3	1	5	2	0
		1980-1989	3	3	3	3	1	1
		1990-1999	6	2	1	5	2	1
		2000-2009	7	3	1	5	2	2
		2010-2015	2	2	2	3	3	2
		1970-2015	**24**	**13**	**8**	**21**	**10**	**6**
17840	Sarız	1970-1979	6	1	1	2	0	0
		1980-1989	5	3	1	4	3	1
		1990-1999	6	1	1	2	0	0
		2000-2009	4	3	2	5	3	2
		2010-2015	3	1	1	4	1	1
		1970-2015	**24**	**9**	**6**	**17**	**7**	**4**
17906	Ulukışla	1970-1979	4	3	2	4	4	0
		1980-1989	3	2	2	1	3	1
		1990-1999	4	3	2	3	3	2
		2000-2009	3	3	1	4	5	1
		2010-2015	1	2	1	3	2	2
		1970-2015	**15**	**13**	**8**	**15**	**16**	**5**
17936	Karaisalı	1970-1979	6	3	2	1	3	0
		1980-1989	5	1	1	2	1	0
		1990-1999	4	2	1	3	1	1
		2000-2009	4	2	1	3	2	1
		2010-2015	3	2	1	4	3	1
		1970-2015	**22**	**10**	**6**	**13**	**10**	**3**
17981	Karataş	1970-1979	4	3	1	2	1	1
		1980-1989	5	5	1	3	2	1
		1990-1999	3	2	2	3	2	1
		2000-2009	5	3	1	5	4	1
		2010-2015	2	3	1	4	4	1
		1970-2015	**19**	**16**	**6**	**17**	**13**	**4**

In the table only the stations within the basin are shown. The period 2010-2015 has a great importance as the period was the warmest 5-year recorded globally. When the drought events obtained by using the 3-month SPI values calculated for Karaisalı station are compared with the 10-year periods and the last 6 year period, three drought events were detected in the 6-year period between 2010 and 2015 and four drought events were experienced between 2000 and 2009. By using SPEI, there were four and three drought events detected for the period 2010-2015 and 2000-

2009, respectively. Table 2 shows that the occurrence of dry periods are more frequent. It can be said that the positive and high value index of NAO, which leads to the decrease of precipitation in the Mediterranean region (Visbeck et.al., 2001; Krichak et al., 2013), can be effective in these results.

Spatial distributions of drought severities were obtained by using the calculated SPI and SPEI values from the stations in and around the basin. Figure 3 shows the spatial distribution of 12-month SPI and SPEI values calculated for the year 2014 identified as one of the most severe drought years. The figure depicts that the drought indicated by the SPI values was more severe than the one indicated by the SPEI, and northern part of the basin seem to have been accompanied with comparably greater drought risks.

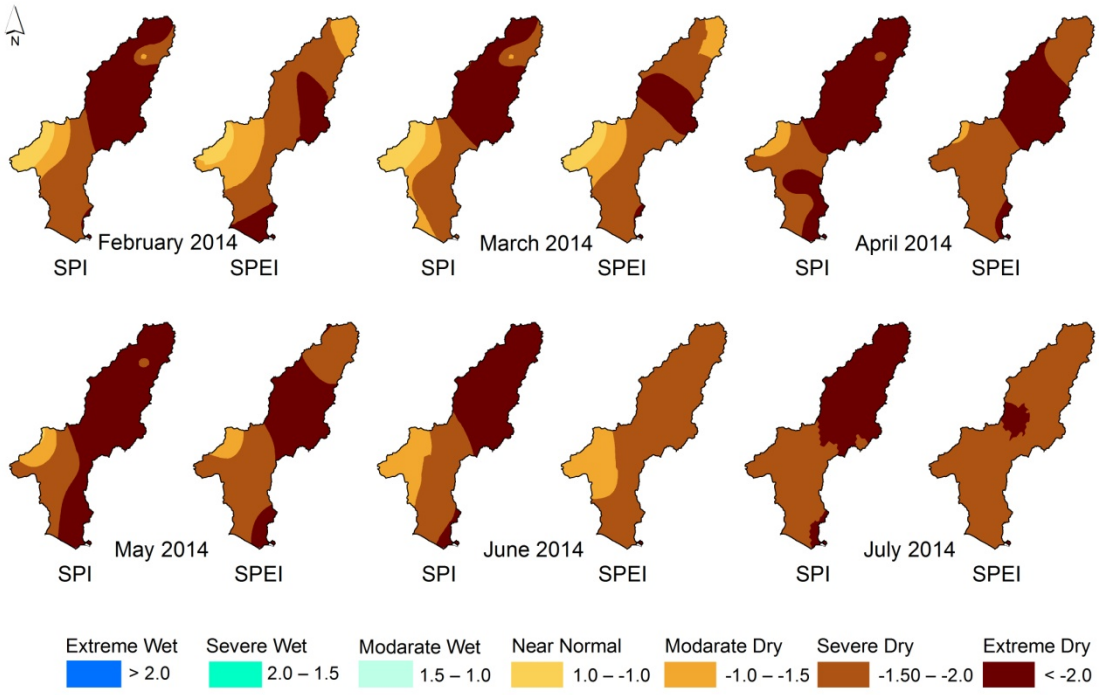

Figure 3. Spatial distribution of SPI and SPEI for selected months of 2014.

4. CONCLUSIONS

In the study presented, drought severity analysis was carried out based on the SPI and SPEI indices in Seyhan river basin and the most severe dry periods, drought durations and affected areas were identified. There were no significant trend in monthly precipitation but significant trend in temperature data for summer months. Trend analysis of SPI and SPEI reveals a clear decrease tendency which presents hardening drought conditions. The results of the analysis indicate that there is an increase in the drought frequency especially in recent years. Retrospective drought analysis using drought indices shows great importance as it provides substantial knowledge on drought severity, duration and frequency analysis. Although the Seyhan river basin has been shown to be among the regions that can be mostly affected by climate change as well as having significant agricultural areas, the basin drought management plan has not been established yet. In this study, some steps were taken including the evaluation of meteorological data, assessment of drought trends, temporal and spatial distribution of drought in the basin and identification of drought durations to prepare bases that could be used in the development of the drought management plan for the Seyhan river basin. As a next step, projections of climate change can be used on both precipitation and temperature, and the expected drought conditions can be analyzed and evaluated using the results of this study.

REFERENCES

Beguería, S. and Vicente-Serrano, S.M.,2013. SPEI: Calculation of the Standardised Precipitation-Evapotranspiration Index. R package version 1.6. http://CRAN.R-project.org/package=SPEI

Hayes, M., M. Svoboda, N. Wall and M. Widhalm, 2011. The Lincoln Declaration on Drought Indices: universal meteorological drought index recommended. Bulletin of the American Meteorological Society; 92:485–488.

JRC, Desert Action-LMNH Unit.,2011. SPI: Standardized Precipitation Index Factsheet-Europe, Version 1 September, 2011, Institute for environment and sustainability.

Kendall, M. G., 1962. Rank Correlation Methods. Hafner Publishing Company, New York.

Krichak, S. O., Breitgand, J. S., Gualdi, S. ve Feldstein, S. B.,2014. Teleconnection - extreme precipitation relationships over the Mediterranean region. Theor. Appl. Climatol. DOI 10.1007/s00704- 013-1036.

Kurnaz, L.,2014. Drought in Turkey, İstanbul Policy Center, Sabancı Üniversitesi-İstanbul.

Mann, H.B.,1945. Non-parametric tests against trend. Econometrica; 13:163-171.

McKee, T. B., Doeskin, N. J., and Kleist, J., 1993. The relationship of drought frequency and duration to time scales, in: Proceedings of the 8th Conference on Applied Climatology, American Meteorological Society, Boston, MA, 179–184.

NASA, 2017. NASA, NOAA Data Show 2016 Warmest Year on Record Globally, https://www.nasa.gov/pressrelease/nasa-noaa-data-show-2016-warmest-year-onrecord-globally.

Spinoni, J., Naumann, G., Vogt, J., 2015. Spatial patterns of European droughts under a moderate emission scenario. Adv. Sci. Res.; 12: 179–186.

Talu, N. and Özüt, H.,2011. Strategic Steps to Adapt to Climate Change in Seyhan River Basin. T.R. Ministry of Environment and Urbanization General Directorate of Environmental Management Department of Climate Change, Editor: Deniz Şilliler Tapan, BMS Matbaacılık, Ankara

Tan, C., Yang, J., Li, M., 2015. Temporal-Spatial Variation of Drought Indicated by SPI and SPEI in Ningxia Hui Autonomous Region, China. Atmosphere; 6: 1399-1421.

Vicente-Serrano S M, Begueria S, Lopez-Moreno J I. 2010. A multi-scalar drought index sensitive to global warming: The Standardised Precipitation Evapotranspiration Index. Journal of Climate; 23: 1696 – 1718.

Visbeck, M. H., Hurrell, J. W., Polvani, L. ve Cullen, H. M.,2001. The North Atlantic Oscillation: Past, present, and future. Proc. Natl. Acad. Sci.; 98: 12876-12877.

Vogt, J. V., Safriel, U., Von Maltitz, G., Sokona, Y., Zougmore,R., Bastin, G., and Hill, J., 2011. Monitoring and assessment of land degradation and desertification: Towards new conceptual and integrated approaches, Land Degrad. Dev.; 22: 150–165.

Vogt, J. and Somma, F. (Eds.), 2000. Drought and drought mitigation in Europe, Kluwer, Dordrecht, 325 pp.

Webster, R., Oliver, M.A., 2007. Geostatistics for environmental scientists. 2nd ed. Chichester, UK. John Wiley and Sons. ISBN 978-0-470-02858-2 pp. 330.

World Meteorological Organization, 2006: Drought Monitoring and Early Warning: Concepts, Progress and Future Challenges (WMO-No. 1006), Geneva.

World Meteorological Organization (WMO), 2015. https://public.wmo.int/en/media/press-release/wmo-2015-likely-be-warmest-record-2011-2015-warmest-five-year-period.

World Meteorological Organization (WMO) and Global Water Partnership (GWP), 2016. Handbook of Drought Indicators and Indices (M. Svoboda and B.A. Fuchs). Integrated Drought Management Programme (IDMP), Integrated Drought Management Tools and Guidelines Series 2. Geneva.

Wu, H., Svoboda, M. D., Hayes, M. J. Wilhite, D. A., and Wen, F., 2007 Appropriate application of the Standardized Precipitation Index in arid locations and dry seasons. Int. J. Climatol.; 27: 65–79.

Proceedings of the 10th World Congress of EWRA 'Panta Rhei', 5-9 July 2017, Athens, Greece
© 2017 *European Water Resources Association*

Coastal aquifer response to drought scenarios: The case of Rhodes island

H. Vangelis[1*], G. Kopsiaftis[2], D. Tigkas[1] and V. Christelis[2]
[1] *Centre for the Assessment of Natural Hazards and Proactive Planning, School of Rural and Surveying Engineering, National Technical University of Athens, Greece*
[2] *Lab. of Reclamation Works and Water Resources Management, School of Rural and Surveying Engineering, National Technical University of Athens, Greece*
[*] *e-mail: harrivag@central.ntua.gr*

Abstract: Considerable disagreement exists regarding the definition of drought. However, it is widely accepted that drought is a natural phenomenon caused mainly by a sustained below-average precipitation and high evapotranspiration over a large area. This prolonged water deficiency is propagated through the surface and groundwater systems. Since groundwater is the main reliable water resource in semi-arid areas, it is of interest to investigate the depletion of an aquifer under pumping, caused by the natural decrease in the recharge due to drought. In this study a large-scale groundwater model is developed in an aquifer of Rhodes Island (Greece) to examine its response to drought. The water table decrement and the seawater intrusion extend influence the fresh water volume, which is used as indicator for the coastal aquifer condition. This indicator is calculated based on a transient variable-density groundwater flow model, using SEAWAT numerical code. The pumping rates are selected to cover the actual consumption needs of the study area. The recharge volumes, which are used as input to the seawater intrusion model, are calculated by the Medbasin-M monthly hydrological model. The Reconnaissance Drought Index (RDI), which incorporates precipitation and potential evapotranspiration, both affecting the infiltration and recharge processes, is used to assess meteorological drought severity. The principal objective of the study is to relate the meteorological drought to the available water volumes at a temporal scale.

Key words: Drought, seawater intrusion, Reconnaissance Drought Index, semi-arid areas, Rhodes island

1. INTRODUCTION

The impact of meteorological drought on water resources has been increasingly studied, given the persistent/seasonal patterns of water scarcity in many parts of the world (Mishra and Singh, 2011). Therefore, the understanding of hydrological drought propagation constitutes a challenging topic, particularly for the groundwater component, which is globally less monitored and controlled than surface waters (Famiglieti, 2014). In general, groundwater hydrological variables are expected to exhibit a rather slow response to climatic driving forces such as those encountered during a drought event (Van Loon 2015). This 'silent' reception of meteorological droughts by subsurface water systems draw less attention in the past, but during the last decade, various researchers started to investigate spatial or temporal patterns of groundwater droughts based on hydrological variables, such as recharge/discharge, hydraulics heads and baseflow (Tsakiris et al. 2013).

Although groundwater systems are considered to be a resilient source of freshwater, the overexploitation of aquifers in several parts of the world has resulted in a persistent groundwater level decline (Konikow and Kendy, 2005). In addition, groundwater response to drought conditions is challenged by the abstraction schemes, which may either intensify or even initiate groundwater droughts (Mishra and Singh, 2010). This is particularly evident in the case of semi-arid and arid coastal areas where groundwater is typically the only available source of freshwater. Nevertheless, the contribution of groundwater abstraction on hydrological drought is poorly studied, despite that groundwater resources have been widely exploited around the world within a multipurpose demand framework of municipal, agricultural and industrial uses.

Recently, Kopsiaftis et al. (2017) proposed an approach linking meteorological drought with its effects on groundwater, which was evaluated for a coastal aquifer, with typical characteristics of a

semi-arid Mediterranean island. However, in the above application no pumping was considered and a hypothetical aquifer was used. In this study, a similar approach is evaluated in an aquifer of Rhodes Island (Greece), taking also into account the typical pumping rates of the region.

2. MATERIALS AND METHODS

2.1 Drought characterisation and hydrological models

The characterisation of meteorological drought is achieved through the Reconnaissance Drought Index (RDI). RDI incorporates precipitation and potential evapotranspiration, which both affect the infiltration and recharge processes, therefore is considered appropriate to be used as a link between meteorological drought and groundwater (Kopsiaftis et al., 2017).

The RDI is based on the ratio of the cumulative precipitation (P) to the cumulative potential evapotranspiration (PET) for a specified reference period of k months, which forms the alpha (α) value of the index (Tsakiris et al. 2007):

$$a_{e(k)} = \frac{\sum_{j=1}^{j=k} P_{ej}}{\sum_{j=1}^{j=k} PET_j} \tag{1}$$

The α value is then standardised using an appropriate statistical distribution, resulting at a region-independent index, for which positive values indicate wet periods, while negative values indicate dry periods (Tsakiris et al. 2008). DrinC software (Tigkas et al., 2015) is used for the calculation of RDI.

The hydrological processes and the surface water interactions are described in this study using the monthly-basis Medbasin-M rainfall-runoff model, included in Medbasin software (Tigkas and Tsakiris, 2004). Medbasin-M is a conceptual water balance model, based on the assumption that the water storage in the catchment takes place only into the upper soil zone. The main parameters of the model are the total soil storage capacity (S_{max}) and the deep percolation coefficient (K), while a third parameter (a) can be used for adjusting the monthly runoff distribution (Giakoumakis et al., 2015; Tigkas et al., 2012). The model is employed for the calculation of deep percolation, which is then used as the recharge value for the groundwater model.

The seawater intrusion is simulated using the variable density approach. Variable density (VD) models are based on the concept that two miscible fluids of different density (freshwater and seawater) are mixed due to dispersion mechanism. A transition zone of variable density is then formed between the two fluids. VD models describe seawater intrusion using a coupled differential equation system and specifically the mass balance equation and the solute transport equation. The first one could be expressed as (Guo and Langevin, 2002):

$$-\nabla \cdot (\rho \mathbf{q}) + \rho_s q_s = \rho S_f \frac{\partial h_f}{\partial t} + n \frac{\partial \rho}{\partial C} \frac{\partial C}{\partial t} \tag{2}$$

in which ρ is the fluid density $\mathbf{q}$ is the specific discharge vector, ρ_s is the density of water entering from a source or leaving through a sink, q_s is the volumetric flow rate per unit volume of porous medium representing sources and sinks, S_f is the specific storage, h_f is the freshwater head, n is porosity and C is the solute concentration.

The solute transport equation is expressed as follows:

$$\frac{\partial C}{\partial t} = \nabla \cdot \left(\mathbf{D} \cdot \nabla C \right) - \nabla \cdot \left(\mathbf{v} C \right) - \frac{q_s}{n} C_s \tag{3}$$

in which D is the hydrodynamic dispersion tensor, v is the fluid velocity vector and C_s is the solute concentration of water entering or leaving through sources and sinks respectively. It should be noted that no solute reactions are considered, while viscosity changes or thermal effects are considered negligible.

In order to solve the coupled differential equation system described above, the Darcy equations are required, which are formulated as follows:

$$q_x = -K_{fx}\left(\frac{\partial h_f}{\partial x}\right), \quad q_y = -K_{fy}\left(\frac{\partial h_f}{\partial y}\right), \quad q_z = -K_{fz}\left(\frac{\partial h_f}{\partial z} + \frac{\rho - \rho_f}{\rho}\right) \tag{4}$$

in which q_x, q_y, q_z are the specific discharge components in the principal directions, K_{fx}, K_{fy}, K_{fz} are the freshwater hydraulic conductivity components in the same directions, and ρ_f is the freshwater density.

The relation between water density and solute concentration is described by the following equation:

$$\rho = \rho_o \left(1 + \frac{\alpha}{(C_s - C_o)}\left(C - C_o\right)\right) \tag{5}$$

in which ρ_o is the freshwater density, α is the density difference ratio and C_o, C_s are reference and maximum concentration respectively. In the current study we consider $C_o = 0$.

The density difference ratio is expressed as:

$$\alpha = \frac{\rho_s - \rho_o}{\rho_o} \tag{6}$$

in which ρ_s is the maximum seawater density.

The SEAWAT numerical code is utilized to simulate seawater intrusion in the study area. SEAWAT code combines MODFLOW and MT3DMS (Guo and Langevin, 2002), to solve iteratively the flow and transport equations.

The impact of seawater intrusion on the aquifer is quantified using the temporal variability of freshwater volume, expressing the vulnerability of coastal aquifers (Werner et al., 2012; Morgan and Werner, 2014). A modification of this approach proposed by Kopsiaftis et al. (2017) introduces the FwV indicator aiming at being applicable to VD models. Freshwater volume is defined as the aquifer volume constrained by the water table, the aquifer boundaries and the 0.5 kg/m^3 isochlore surface, multiplied by the aquifer porosity. The FwV index is then calculated at each time step of the transient seawater intrusion simulation, as the difference of the values of freshwater volume between two consecutive years.

2.2 Study area and modelling approach

Rhodes Island is a relatively big island located at the eastern part of the Aegean Sea. Groundwater is the main water resource of the island, which is exploited through a dense network of private and public wells. The groundwater system of Rhodes Island is complex, consisting of a number of independent confined and unconfined aquifers. The simulated groundwater system is an alluvial unconfined aquifer located at the surrounding area of Gadouras stream valley, at the central east part of the island (Figure 1).

The lithology of the study area mainly consists of alluvial, river and coastal deposits: loose material, sands, soils, pebbles and gravel of various sizes. Secondarily, shallow marine massive limestones or locally coastal deltaic deposits are observed, as well as lacustrine to coastal clastic deposits of Upper Pliocene – Lower Pleistocene age. Based on the limited available point data from the borehole profiles, the mean thickness of the lithological formation is estimated to be approximately 50 m. Figure 1 presents a part of the geological map of Rhodes Island. The aquifer inland boundaries coincide with the geological boundaries and there is no significant evidence of hydraulic communication with the neighbouring geological formations, since they are impermeable, with the exception of a small area at the NE boundary, where an insignificant lateral inflow seems to take place. The aquifer has a total area of 23.19 km^2.

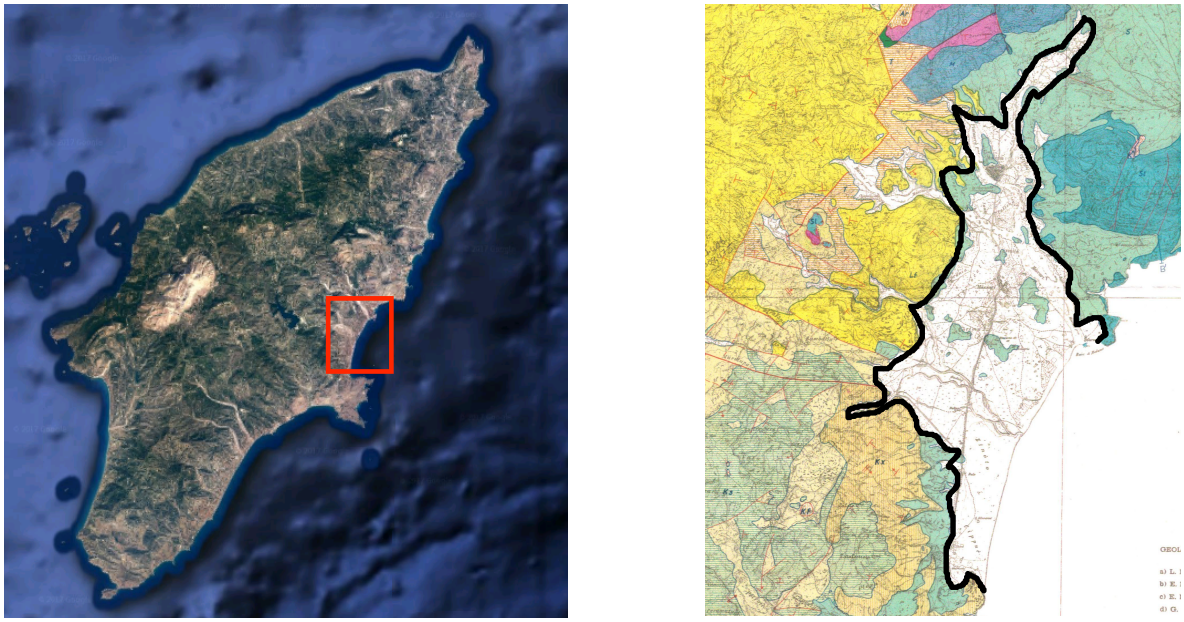

Figure 1. Location of the examined aquifer in Rhodes Island. The black thick line outlines the aquifer border (source of the geological map: Mutti et al., 1965).

Based on the aquifer data and information, a coastal aquifer model is developed. The aquifer is considered isotropic and homogeneous. The hydraulic conductivity value is set to 15 m/d, based on bibliographic data and an approximate trial and error calibration. Table 1 contains the basic model parameters.

The recharge timeseries is calculated using Medbasin-M model, based on the 34-year precipitation and potential evapotranspiration data. There are limited available field data regarding the pumping rates. The aquifer is pumped mainly during the summer months with a total pumping rate which amounts to 6000 m^3/d. The pumping is distributed to five wells and the highly productive inner wells are used to cover the water needs of smaller neighbouring islands (Gavalas, 2009).

Table 1: Basic model parameters

Parameter	Value
Hydraulic conductivity (Kx, Ky, Kz) (m/d)	(15,15,15)
Dispersivity (a_L,a_T,a_V) (m)	(20,2,0.2)
Porosity (%)	15
Seawater density ρ (kg/m^3)	1025
Freshwater density ρ_o (kg/m^3)	1000

4. RESULTS AND DISCUSSION

An initial steady state simulation is performed without pumping, using the mean precipitation values to obtain initial conditions regarding the hydraulic head and concentration. Then, the recharge time-series and the pumping rates are utilized to perform transient simulations. The FwV indicator is calculated from the final concentration and head results for each time step, i.e. on a monthly basis.

The values of RDI_{st} are calculated for several reference periods, from the available precipitation and temperature datasets and the results are presented in Figure 2. The calculated FwV values are also depicted in the same Figure in order to compare the evolution of the meteorological drought to the available water volumes.

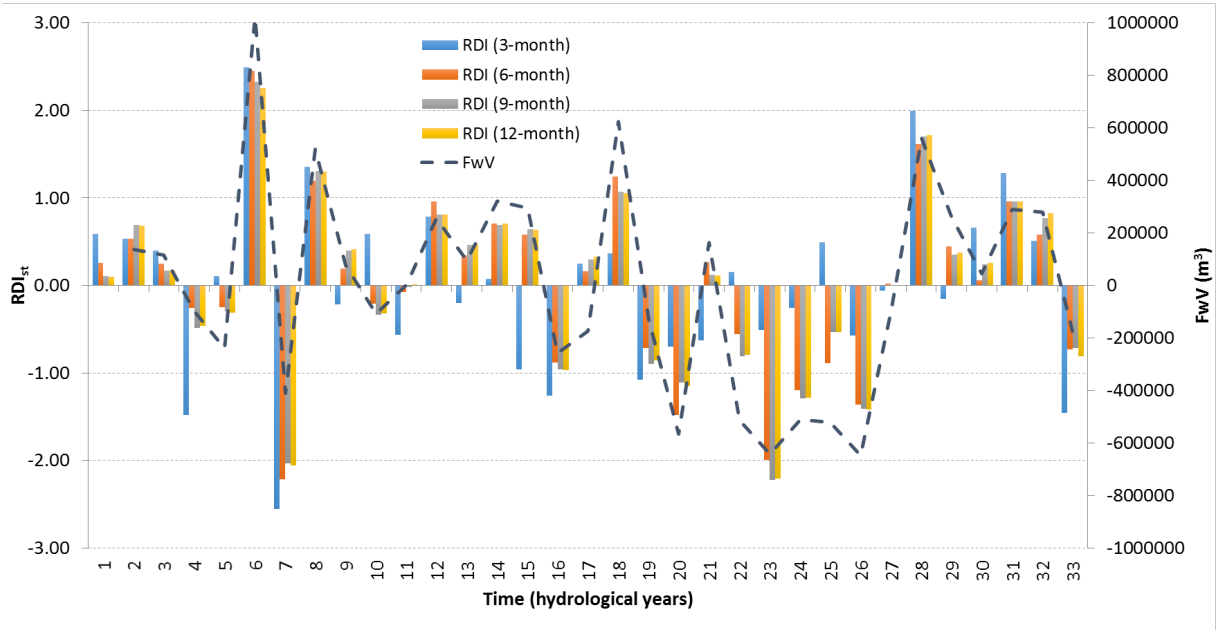

Figure 2. FwV values and RDIst values for 3-, 6-, 9- and 12-month reference periods (annual time step).

As observed from Figure 2, for the 6, 9 and 12 -month reference periods the FwV indicator seems to follow the drought occurrences. However, for the 3-month reference period a compatibility between FwV and RDI cannot be detected.

Further investigation on a monthly step could reveal interesting information regarding the correlation between the two indices. For this reason, in Figure 3 the RDI values for the 12-month reference period on a monthly step are plotted against the FwV at the end of each month. As shown, the FwV indicator responds adequately to the drought evolution, depicting, however, a slightly different variability.

The correlation between RDI and FwV indicator for a specific reference period could assist in achieving a forecast of the aquifer condition at the end of a specific period. Indicatively, the high correlation between the RDIst values for 12-month reference period and FwV on a monthly step is presented in Figure 4. Therefore, an estimate of the groundwater availability can be achieved using only meteorological data.

5. CONCLUDING REMARKS

The response of a coastal aquifer under pumping to meteorological drought is investigated in this paper. The examined aquifer is located in the Gadouras area in Rhodes island. The Reconnaissance Drought Index (RDI) is used to represent the meteorological drought conditions, while the aquifer response to drought is described through the Freshwater Volume (FwV) indicator.

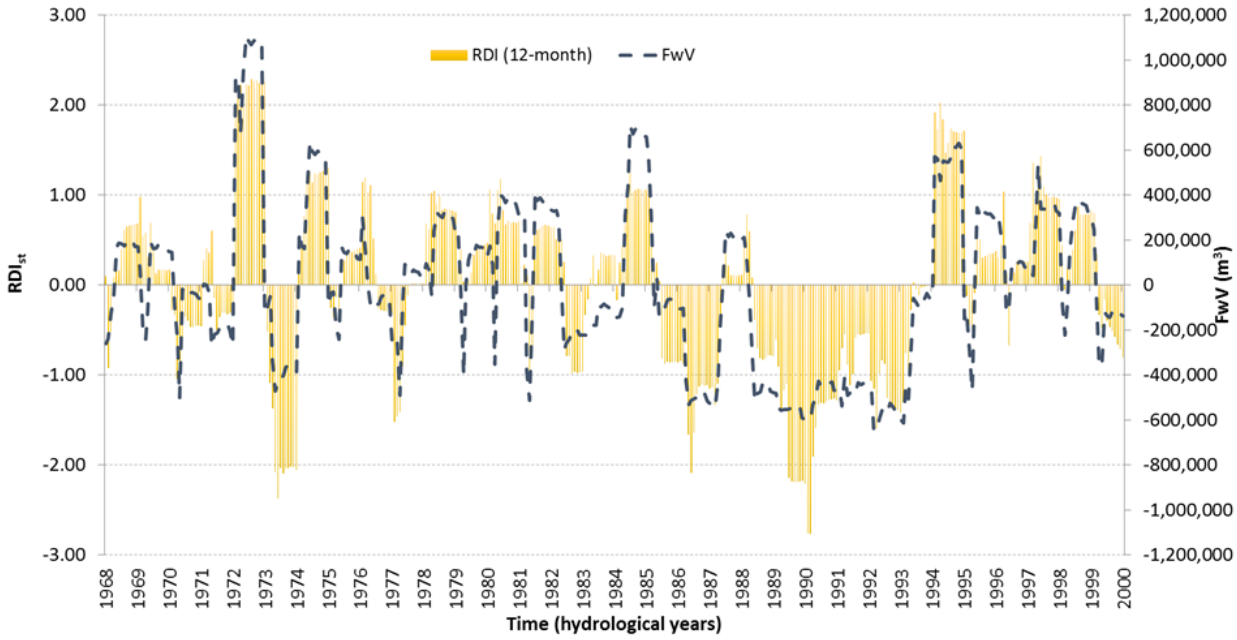

Figure 3. RDI$_{st}$ values for 12-month reference period plotted against monthly FwV values (monthly time step).

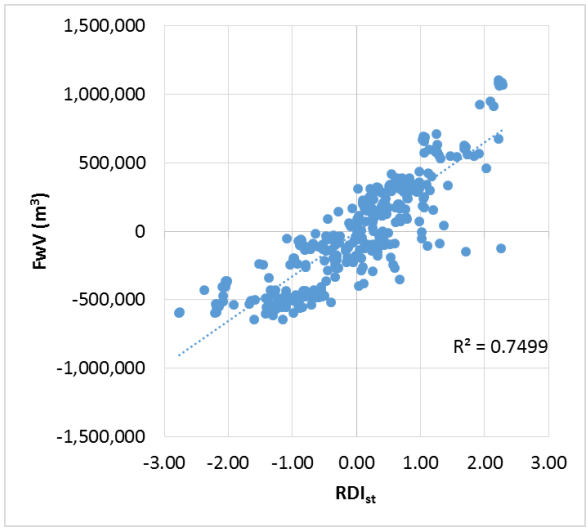

Figure 4. Correlation between RDI$_{st}$ values for 12-month reference period and FwV values (monthly time step).

The aquifer recharge was calculated through Medbasin-M model, using the available meteorological data of the area. Also, the pumping pattern used in the groundwater model, is based on real water demand of the area.

The average variation of the FwV seems to follow the drought occurrences for the 6, 9 and 12-month reference periods of drought, while the 3-month period presents a different behaviour. A detailed monthly step evaluation reveals that the FwV indicator responds adequately to the drought evolution. However, a slightly different variability of the RDI and FwV values is observed.

High correlation between RDI and FwV values is an evidence that groundwater availability could be estimated through RDI, using only meteorological data.

REFERENCES

Canters, F., Vanderhaegen, S., Engelen, G., Poelmans, L., Becker, P.De, Batelaan, O., 2013. A system-based paradigm of drought analysis for operational management. Water Resour Manage, 27:5281-5297.

Famiglieti, J.S., 2014. The global groundwater crisis. Nat. Clim. Change 4:945-948.

Gavalas, V., 2009. Estimation of the water balance and simulation of the coastal aquifer of the Gadouras watershed in Rhodes Island, Bachelor's thesis, National Technical University of Athens.

Giakoumakis S., Stamouli P., Tigkas D., 2015. Evaluating a modified simple rainfall-runoff model in Mediterranean river basins. European Water, 50: 35-42.

Guo, W., Langevin C. D., 2002. User's guide to SEWAT: A Computer Program for Simulation of Three – Dimentional Variable – Density Ground - Water Flow, BOOK 6, Chapter A7, Techniques of Water – Resources Investigations of the U. S. Geological Survey, 7-18.

Konikow, L.F., Kendy, E. 2005. Groundwater depletion: A global problem. Hydrogeol J, 13(1): 317-320.

Kopsiaftis, G., Tigkas, D., Christelis, V., Vangelis, H. 2017. Assessment of drought impacts on semi-arid coastal aquifers of the Mediterranean. Journal of Arid Environments, 137: 7-15.

Mishra, A.K., Singh, V.P., 2010. A review of drought concepts. . J Hydrol, 391:202-216.

Mishra, A.K., Singh, V.P., 2011. Drought modelling – A review. J Hydrol, 403:157-175.

Morgan, L. K., Werner, A. D., 2014. Seawater intrusion vulnerability indicators for freshwater lenses in strip islands. Journal of Hydrology, 508, 322-327.

Mutti, E., Orombelli, G., Pozzi, R., 1965. Geological Map of Rhodes Island (Greece), University of Milan (Italy), Institute of Geology, scale 1:50,000.

Tigkas D., Tsakiris G., 2004. Medbasin: a Mediterranean rainfall–runoff software package. European Water, 5/6: 3-11.

Tigkas D., Vangelis H., Tsakiris G., 2012. Drought and climatic change impact on streamflow in small watersheds. Science of the Total Environment, 440: 33-41.

Tigkas D., Vangelis H., Tsakiris G. 2015. DrinC: a software for drought analysis based on drought indices. Earth Science Informatics 8(3): 697-709.

Tsakiris G., Nalbantis I., Pangalou D., Tigkas D., Vangelis H. 2008. Drought meteorological monitoring network design for the reconnaissance drought index (RDI). In Franco Lopez A (ed) Proceedings of the 1st International Conference "Drought Management: scientific and technological innovations" Zaragoza, Spain, 12 - 14 June 2008, Option Méditerranéennes, Series A, No. 80, pp 57-62.

Tsakiris G., Nalbantis I., Vangelis H., Verbeiren B., Huysmans M., Tychon B., Jacquemin I., Canters F., Vanderhaegen S., Engelen G., Poelmans L., De Becker P., Batelaan O., 2013. A System-based Paradigm of Drought Analysis for Operational Management. Water Resources Management, 27(15): 5281-5297.

Tsakiris G., Pangalou D., Vangelis H. 2007. Regional Drought Assessment Based on the Reconnaissance Drought Index (RDI). Water Resources Management 21(5): 821-833.

Van Loon, A. F., 2015. Hydrological drought explained. Wiley Interdisciplinary Reviews: Water, 2(4): 359-392.

Werner, A. D., Ward, J. D., Morgan, L. K., Simmons, C. T., Robinson, N., I., Teubner, M. D., 2012. Vulnerability indicators of seawater intrusion, Ground Water, 50(1), 45-48.

Proceedings of the 10th World Congress of EWRA 'Panta Rhei', 5-9 July 2017, Athens, Greece
© 2017 *European Water Resources Association*

Comparison of hedging rule curves depending on available water and current storage in reservoir operation under droughts

S. Lee[1*], Y. Jin[1] and P. Jinhyeog[2]
[1] *Civil Engineering, Pukyong National Univ., Busan, Rep. of Korea*
[2] *Water Resources Research Center, K-water Institute, Daejeon, Rep. of Korea*
[*] *e-mail: peterlee@pknu.ac.kr*

Abstract: Hedging rule for water supply operation of a reservoir allows releases to be curtailed below target levels to avoid potentially more severe shortages later. This paper aims to derive two different hedging rule curves of a reservoir: one rule is based on available water that accompanies prediction of the current period inflow and the other rule is based on the beginning storage alone. The current period inflow was obtained by the ensemble streamflow prediction using historical precipitation data. A mixed integer programming algorithm was used to determine hedging rule curves for water supply operation of Hapcheon Dam, the Republic of Korea for the period from 1990 to 2005 that includes a drought period. Complying the derived hedging rules, reservoir simulation runs for the period from 2006 to 2010 were performed. The derived hedging rule curves based on the beginning storage were placed higher than the curves based on available water and induced earlier rationing of water supply. The rule based on available water included the current period inflow and its simulation resulted in faster recovery to the normal phase of water supply when the drought ended. The simulation results complying the rule based on available water were better in terms of the total water supply deficit. When, however, predicted inflow is not reliable, the hedging rule based on the beginning storage might be worth in practical reservoir operation to avoid more severe shortage resulted from the bad prediction of the inflow.

Key words: drought, reservoir, hedging, available water, beginning storage, mixed integer programming

1. INTRODUCTION

Water supply deficit may occur in drought periods and it may induce damage to societies. The hedging rule can be an effective method for water supply operation from a reservoir in critical drought periods. Hedging rule allows releases to be curtailed below target levels to avoid potentially more severe shortages later (U.S. Army Corps of Engineers, 1996). Shih and Revelle (1995) developed a discrete hedging rule that comprised two hedging phases. Neelakatan and Pundarikanthan (1999) applied a discrete hedging rule to reservoir systems. Taghian et al. (2014) developed a hybrid model of a genetic algorithm and a linear programming algorithm to optimize simultaneously both the conventional rule curve and the hedging rule.

The hedging rule in the previous studies (Shih and Revelle, 1995; Taghian et al., 2014) was formulated by relating the release with available water that is defined by the beginning storage plus inflow in the current period. The two articles did not include some methods to obtain inflow in the current period, and thus they did not cover some validation simulations on real- time status needing predicted inflow for the current period. Pointing out difficulties to predict the current period inflow, Neelakatan and Pundarikanthan (1999), on the other hand, formulated the hedging rule without the current period inflow, i.e., decided release based on the beginning storage alone.

When reliable inflow of the current period is predicted, the hedging rule formulated by the available water is useful in water supply operation of a reservoir. When, however, predicted inflow is not reliable, the hedging rule based on the beginning storage might be worth in practical reservoir operation to avoid more severe shortage resulted from the bad prediction of the inflow. The aim of this paper is twofold. One is to derive hedging rule curves of a reservoir based on available water that accompanies prediction of the current period inflow. The other is to derive hedging rule curves

based on the beginning storage alone and to compare the derived two kinds of hedging rule curves.

2. RESEARCH METHODS

2.1 Discrete hedging rule

2.1.1 Discrete hedging rule based on available water

The discrete hedging rule is a reservoir operation rule that combines the hedging rule and the zone-based operation rule. The zone-based operation rule divides single reservoir storage and each zone typically has a target release. The discrete hedging rule having four hedging phases is explained in Figure 1 (Jin, 2016). The discrete hedging rule uses the trigger volume, V, to ration the release of hedging phases. The horizontal axis of Figure 1 denotes two water volumes of available water or the beginning storage.

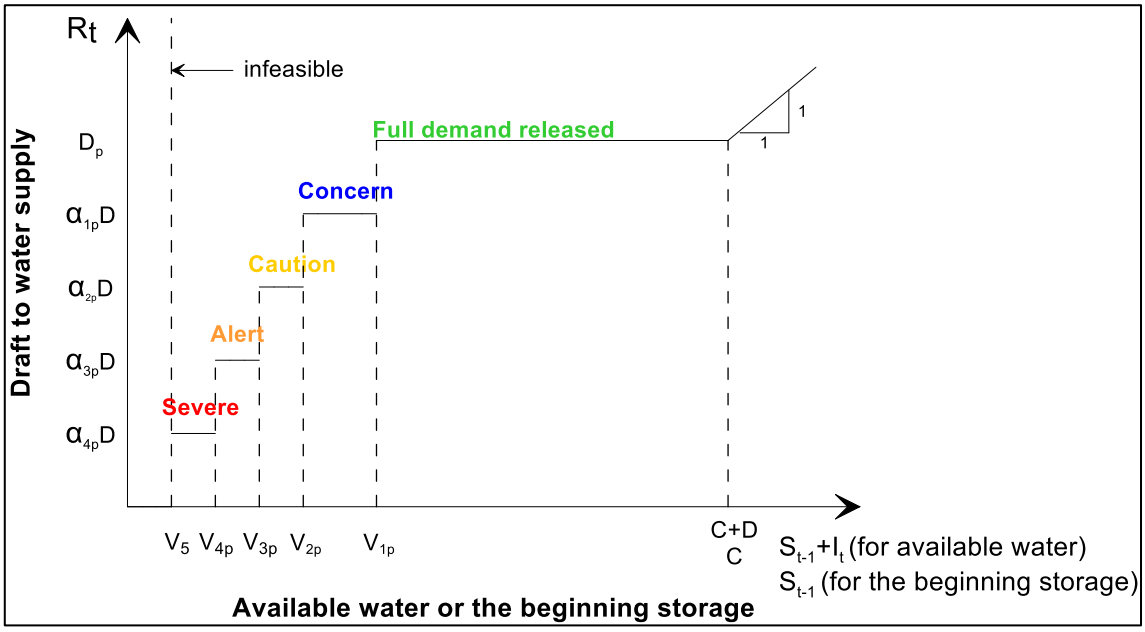

Figure 1. Schematic diagram of two discrete hedging rules with 4 phases.

The trigger volumes of available water to ration releases were decided by an optimization model. The objective function of the optimization model is expressed as equation (1):

$$Maximize \quad \sum_{t=1}^{T} y_{1t} - \omega \sum_{p=1}^{12} (V_{1p} + V_{2p} + V_{3p} + V_{4p} + V_5) \tag{1}$$

where y_{1t} = 1 if full demand is available during a period t or 0, otherwise; ω = a weight value; V_{1p} = the value of available water (= the beginning storage plus current period inflow) above which no restrictions on water use are placed; V_{2p} = the value of available water below which phase caution is implemented for month p; V_{3p} and V_{4p} = the values of available water below which alert or severe phases are implemented, respectively, for month p; V_5 = the lower bound storage plus current period inflow.

The optimization model includes twenty-five constraint equations. Typical and major constraints are written here and one can refer to Jin et al. (2016) for the other constraint equations. Constraint equation (2) in combination with integer requirements says that if the storage at the end of last

period, S_{t-1}, plus the current period inflow, $\hat{I}_t$, is greater than or equal to the trigger volume V_{1p}, then y_{1t} will be one; i.e. that no rationing is needed. Constraint equation (3) in combination with the integer requirements requires that y_{1t} be zero if available water is less than V_{1p}. If there were no ε in constraint equation (2), when '$S_{t-1} + \hat{I}_t = V_{1p}$,' the variable y_{1t} could be zero or one. To correct this, ε is incorporated into constraint (2) so that when '$S_{t-1} + \hat{I}_t = V_{1p}$,' the variable y_{1t} must be equal to 1.

$$y_{1t} \geq \frac{(S_{t-1}+\hat{I}_t)-(V_{1p}-\epsilon)}{M} \quad \forall t, p, \tag{2}$$

$$y_{1t} \leq 1 - \frac{V_{1p}-(S_{t-1}+\hat{I}_t)}{M} \quad \forall t, p, \tag{3}$$

The variables of y_{2t}, y_{3t}, and y_{4t} have a similar pair of constraint equations to (2) and (3), respectively.

Reservoir operation using a discrete hedging rule based on available water is affected by prediction of the current period inflow. When predicted inflow is not accurate enough, hedging rule based on available water might result in an increase of water supply deficit in drought periods. The following section proposes a discrete hedging rule based on current storage alone that cannot be affected by bad prediction of the current period inflow.

2.1.2 Discrete hedging rule based on the beginning storage

One can formulate the discrete hedging rule based on the beginning storage of a reservoir under which the current reservoir storage directly indicates corresponding rationing phases. The discrete hedging rule based on the beginning storage is conceptually explained in Figure 1.

The objective function of the optimization model deciding the discrete hedging rule based on the beginning storage is the same equation (1) as that of available water. Constraint equations of the two optimization models are slightly differently from each other. Equations (4) and (5) are major constraints of the optimization model formulated by the beginning storage and do not include the current period inflow, $\hat{I}_t$. One can refer to Jin (2017) on the other constraint equations.

$$y_{1t} \geq \frac{S_{t-1}-(V_{1p}-\epsilon)}{M} \quad \forall t, p, \tag{4}$$

$$y_{1t} \leq 1 - \frac{V_{1p}-S_{t-1}}{M} \quad \forall t, p, \tag{5}$$

2.2 Ensemble streamflow prediction

The discrete hedging rule described in section 2.1.1 is based on available water. The available water of a reservoir is defined by the beginning storage plus inflow in the current period. The current period inflow was computed by a simple ensemble streamflow prediction (ESP). The ESP procedures are explained in Figure 2, which use a watershed runoff model and historical weather condition scenarios. Before generation of ensemble streamflow, a calibrated watershed runoff model is run for several years to obtain the watershed initial condition. After that, the model is driven by resampled historical data sets to generate an ensemble of possible future streamflow in the basin. Each historical data is treated as a realization of the atmospheric forcing, which is used to simulate the streamflow trajectories (Najafi, 2015).

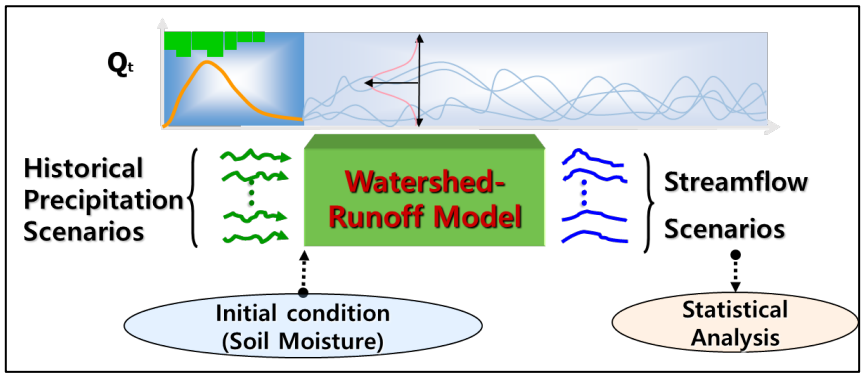

Figure 2. Schematic diagram of ensemble streamflow prediction.

3. RESULTS AND ANALYSIS

3.1 The study area

The optimization models to derive the two discrete hedging rules were applied to Hapcheon Dam. Hapcheon Dam was constructed in 1988 and is located in the upstream region of the Hwang River in the Republic of Korea. The watershed area is 925 km^2 and the effective storage capacity is 0.56 billion m^3. The inflow of the dam has been recorded since 1990. There have been three drought periods in that area after dam construction as follows: 1994-1996, 2000-2001, and 2008-2009.

3.2 Hedging rule curves

The hedging rule curves derived from the two optimization models are shown graphically in figure 3. Figure 3(a) shows the hedging rule curves based on available water drawn by the trigger volumes of available water. Figure 3(b) shows the hedging rule curves based on the beginning storage. The Box-Whisker plots in the figures were drawn by the historical data of available water volume or the beginning storage. The derived hedging rule curves based on the beginning storage are placed higher than the curves based on available water and may induce earlier rationing of water supply.

Compared with the other, the hedging reservoir operation based on available water has an additional water volume of the current period inflow. Hence, it does not need earlier rationing than that based on the beginning storage. That resulted in the relatively smaller trigger volumes of the hedging operation based on available water.

3.3 Results of reservoir simulations

To compare how the two hedging rule curves derived above mitigate water supply deficit, we performed reservoir simulations applying those rule curves. Both results of hedging reservoir simulations were better than historical data. Table 1 and figure 4 show the comparison results of the reservoir simulations. The hedging rule curves based on the beginning storage had relatively large trigger volumes, which induced early rationing of water supply in the reservoir simulation compared with the other. The reservoir simulation applying the hedging rule curves based on available water completely failed in water supply for a month because of the slower start of rationing. It utilized the predicted inflow using the ESP and resulted in rapid recovery to the normal status. In addition, the maximum water supply deficit from the results using available water was smaller than the results of the other hedging reservoir simulation by 28 million m^3/month. Its success periods of the planned water supply were two months longer than the other.

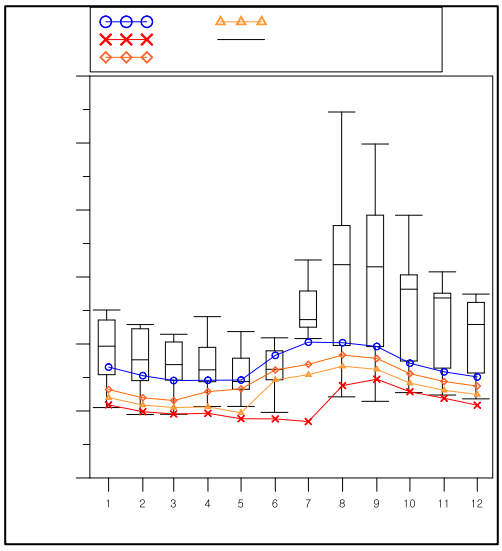

(a) Derived hedging rule curves based on available water.

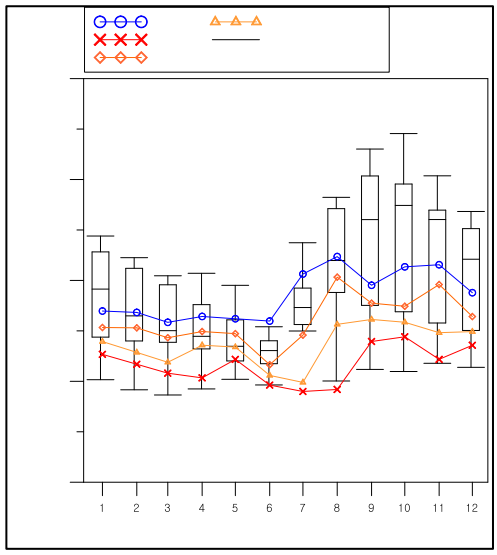

(b) Derived hedging rule curves based on the beginning storage.

Figure 3. Two types of derived hedging rule curves of Hapcheon Dam.

Table 1. Comparison of reservoir simulation results using the two hedging rule curves

Comparison item	**Historical data**	**Available water**	**The beginning storage**
The number of water supply deficit periods (month)	40	29	31
The number of no water supply periods (month)	0	1	0
Minimum water supply (10^6 m^3/month)	8	0	26
Maximum water supply deficit (10^6 m^3/month)	788	464	492
Occurrence of the minimum water supply	July 2009	May 2009	June 2009

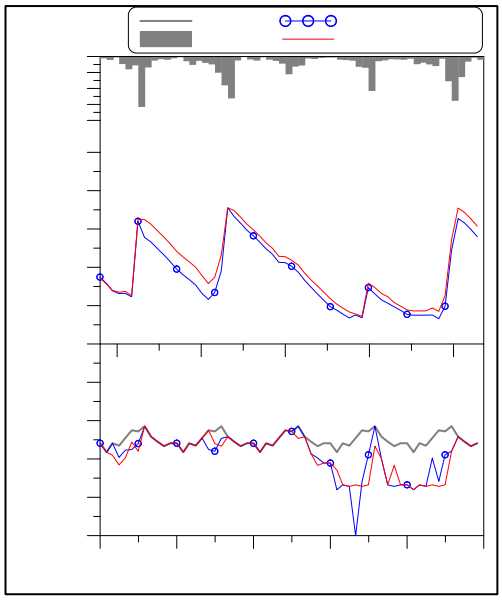

Figure 4. Comparison of water supply results using the two hedging rule curves.

4. CONCULUSIONS

The hedging rule can be an effective method for water supply operation from a reservoir in critical drought periods. The two kinds of hedging rule curves of a reservoir were derived by applying a mixed integer programming algorithm. The hedging rule curves based on the beginning

storage had relatively large trigger volumes, which induced early rationing of water supply. That rule might be excessive water saving method, but be worth practical reservoir operation. The hedging rule curves based on available water utilized the predicted inflow using the ESP and resulted in rapid recovery to the normal status. Overestimated prediction of inflow, however, may cause more severe water supply deficit later in drought periods. It is needed to use improved prediction methods of the current period inflow.

ACKNOWLEDGEMENT

This research was supported by a grant (14AWMP-B082564-01) from Advanced Water Management Research Program funded by Ministry of Land, Infrastructure and Transport of Korean Government.

REFERENCES

Jin, Y., Jung, T., Lee, S., and Kang, S. (2016) Reservoir operations of Hapcheon Dam applying a discrete hedging rule and ensemble streamflow prediction to cope with droughts. J Korean Soc Hazard Mitig, Vol. 16(1): 93-101.

Jin, Y., Lee, S., and Jung, T. (2017) Reservoir operations applying discrete hedging rule curves depending on current storage to cope with droughts. J Korean Soc Hazard Mitig, Vol. 17(1): 113-121.

Najafi, M.R. and Moradkhani, H. (2016) Ensemble combination of seasonal streamflow forecasts. J Hydrol Eng, 21(1): 04015043-1-13.

Neelakantan, T.R., and Pundarikanthan, N.V. (1999) Hedging rule optimization for water supply reservoirs system. Water Resour Manag, 13(6): 409-426.

Shih, J.S., and Revelle, C.S. (1995) Water supply operations during drought: a discrete hedging rule. J of Water Resour Plan and Manag, ASCE, 82: 163-175.

Taghian M, Rosbjerg D, Haghighi A, Madsen, H. (2014) Optimization of conventional rule curves coupled with hedging rules for reservoir operation. J Water Resour Plan Manag 140:693–698

U.S. Army Corps of Engineers. 1996. Developing seasonal and long-term reservoir system operation plans using HEC-PRM, Resources Development. Vol. 7, Hydrologic Engineering Center, Davis, CA.

Proceedings of the 10th World Congress of EWRA 'Panta Rhei', 5-9 July 2017, Athens, Greece
© 2017 *European Water Resources Association*

Monitoring drought in Shiraz, Iran, using Reconnaissance Drought Index (RDI) and Standardized Precipitation Index (SPI)

S. Ansarifard[1*] and S.A. Shamsnia[2]
[1] *Agricultural Engineering Department, Shiraz Branch, Islamic Azad University, Shiraz, Iran*
[2] *Shiraz Branch, Islamic Azad University, Shiraz, Iran*
[*] *e-mail: elmira.ansarifard@yahoo.com*

Abstract: Drought is a significant phenomenon affecting different economic, agricultural, social and environmental sectors. Therefore, monitoring drought in several areas is too important especially those with arid climates. In this study drought was monitored in Shiraz which located in southwest of Iran, between the years 1982 and 2017. Aimed to this purpose RDI and SPI indices was monitored and Due to the RDI annual values, there is near normal and moderately wet condition for all 35 years. According to the SPI values there is extreme dry condition in hydrological years (1983, 2008) and (1993) shows severely dry condition also very wet condition for the years (1992, 1995 and 2004). This research proposes a climatic index the Reconnaissance Drought Index, for drought monitoring particularly in arid and semi-arid area which precipitation amounts are low, evapotranspiration acts as a key factor for monitoring drought, because of using both precipitation and evapotranspiration. It is expected these documents be useful for future decisions and drought monitoring in another area.

Key words: drought monitoring, RDI, SPI, Iran, Shiraz

1. INTRODUCTION

Drought is precipitation shortage in long periods which leads to low humidity in the soil and reduction surface water and periodic natural phenomenon which is associated in deficiency available water resources in a vast geographical area and in a significant time period (Rossi, 2000). It could affects to the economic, environment, agriculture and community members (Asadi zarch et al., 2011; Tsakiris and Vangelis, 2005; Tsakiris, 2010). Based on this definition, drought is a regional phenomenon, characterized by three dimension: intensity, duration and extent, the most important of which is intensity. Though the drought intensity could be estimated based on the damage accrued to different economic, environmental and social sectors under influence, but using the drought indices has more supporters due to their higher accuracy. The drought indices are used extensively in the world because of easiness and both the scientists and specialists in water management suggest them (Tsakiris and Vangelis, 2005). The phenomenon of climate change is affected by change in the extent of energy exchange. Therefore, it has had an intensive influence on the hydrological cycle. Droughts are one of the usual variations that cover many of arid and semi-arid areas of the world with High intensities once per several years. There is a close relation between occurrence of droughts and change in the climate. Globe warming has led to increase in evaporation and water vapor density which as a result, the extent and pattern of precipitations (rain and snow) will change (Jaefari, 2007). It is considered as the most complex, but the least understandable phenomenon of all the natural hazards affecting more people than any other hazards (Mishra and Desai 2005).

Drought has been sorted into four types (Wilhite and Glantz 1985): meteorological, agricultural, hydrological and socio-economic (Asadi zarch et al., 2011; Tigkas et al., 2016). Meteorological drought is defined as the lack of precipitation over a region in a specific time period, lasting sufficiently to cause hydrological and agricultural hazards. It is determined in the form of deviation from normal precipitation. According to the meteorologists, a significant decrease in stream flow,

water level of lakes or a change in the ground water levels is the signal of an upcoming drought event. While according to hydrologists, drought prevails with the lack of soil moisture to sustain the crop growth. Agricultural scientists determine the drought as a famine condition, while economists monitor it in the form of short supply of tap water to the urbanite (Dracup et al., 1980; Asadi Zarch et al., 2011).

Droughts are common throughout the globe with a devastating damage potential on agriculture, economy, and society in many parts of the world. At the same time, due to the multi-discipline, character of this natural hazard, a single, unique definition of a drought does not exist, but is subject to the domain of interest of the observer (e.g. Niemeyer, 2008; Wilhite and Glantz, 1985; Maracchi, 2000; Tate and Gustard, 2000).

One half of the area of Iran is desert and two third of it is arid and semi-arid areas regarding to precipitation. The Iran's Weather is influenced by several systems, including: High pressure system, Mediterranean raining system which enters from the west and the low pressure system which in the Southern and Southwestern Iran leads to raining. The rate of precipitation in Iran is too variable. In the North it is more than 2113 millimeters, in desert areas it is about 15 millimeters, in Northwestern Areas it is about 500 millimeters and in other areas it is about 200 millimeters per year. Drought is one of the most important natural hazards in Iran and frequently affects a large number of people, causing tremendous economic losses, environmental damages and social hardships. Especially, it has a strong impact on water resources. This situation has made more considerations toward the study and management of drought. Also, in many years, the occurrence of drought is not recognized for some time Therefore, detection of drought is a valuable finding for management of Water Resources in some regions such as Iran which the major part of its constituted by arid and semi-arid areas (Hashemi and Shahmirzadi, 2011).

The Standardized Precipitation Index (SPI) is a widely used index to characterize meteorological drought on a range of timescales. On short timescales, the SPI is closely related to soil moisture, while at longer timescales, the SPI can be related to groundwater and reservoir storage. The SPI can be compared across regions with markedly different climates. It quantifies observed precipitation as a standardized departure from a selected probability distribution function that models the raw precipitation data.

Several studies have been conducted in different parts of Iran for determination of the drought, its intensity, endurance and extension. For instance, (Mohammad Amin Assadi Zarech et al.) used the RDI (Reconnaissance Drought Index) and SPI (Standardized Precipitation Index) to compare drought based on the two variables of evaporation and perspiration and precipitation. Findings of their study showed that since SPI uses precipitation as the unique factor for estimation of drought, it could not be a good criterion since the water deficiency could be estimated solely based on the input (such as precipitation) and the output (such as water consumption). Based on that argument, the newer index (RDI) was proposed since it uses the data of both factors affecting drought such as P and PET. Studies showed that RDI plays an important role in lowering the water resources of the watersheds. For that reason, it is regarded as an important index in relooking at drought in Iran (Asadi Zarch et al., 2011).

2. STUDY AREA

Fars Province is located in Southwest of Iran. Its climate in different points could be divided into three categories: mountainous, moderate and warm. The center of Fars Province is Shiraz city. The elevation is among 1480 and 1670 meters above the sea level in the mountainous region of Zagros which has a moderate weather. The extent of Shiraz is about 1268 km² which sets in the form of an east-west rectangle and located at 29°, 36' north and 52°, 33' east. Its average annual precipitation and temperature are about 337 millimeters and 18 centigrade (I.R. of Iran Meteorological Organization).

3. METHODS

The Reconnaissance Drought Index (RDI) proposed by Tsakiris et al. (2007). It is one of the most recent developments in the field of meteorological drought indices. Essentially, it relates precipitation to the potential evapotranspiration at a location, and can be considered as an extension of the SPI. However, Tsakiris et al. (2007) state that especially the characterization of drought severity could be improved in test areas of the Mediterranean region as compared to SPI (Niemeyer, 2008). Reconnaissance Drought Index (RDI) was characterized as a general meteorological index for the drought assessment. The RDI is expressed in three forms: the initial value (α_k) normalized and standardized RDI_{st}. The initial value (α_k) is presented in an aggregated form using a monthly time scale and may be calculated on a monthly, seasonal or annual basis.

The initial value (α_k) of RDI is calculated for the i-th year in time basis of k (months) as follow (Tigkas et al., 2016; Tsakiris et al., 2007):

$$\alpha_k^{(i)} = \frac{\Sigma_{j=1}^{k} P_{ij}}{\Sigma_{j=1}^{K} PET_{ij}}, \text{ i=1(1) N and j=1(1) k} \quad (1)$$

in which P_{ij} and PET_{ij} are the precipitation and potential evapotranspiration of the j-th month of the i-th year and N is the total number of years. The normalized form (RDI_n) is computed using the following equation:

$$RDI_n^{(i)} = \frac{\alpha_k^{(i)}}{\overline{\alpha_k^{(i)}}} - 1 \quad (2)$$

in which $\overline{\alpha_k^{(i)}}$ is the arithmetic mean of $\alpha_k^{(i)}$.

The values of α_k follow satisfactorily both the lognormal and the Gama distributions in a wide range of locations and different time scales, in which they were tested (Tigkas, 2008; Tsakiris et al., 2008). By assuming that the lognormal distribution is applied, the following equation can be used for the calculation of RDI_{st} (Tigkas et al., 2016; Tsakiris and Vangelis, 2005):

$$RDI_{st}^{(i)} = \frac{y^{(i)} - \overline{y}}{\hat{\sigma}_y} \quad (3)$$

in which y_i is the $\ln\left(\alpha_k^{(i)}\right)$, $\overline{y}$ is its arithmetic mean and $\hat{\sigma}_y$ is its standard deviation.

In case the gamma distribution is applied, the RDI can be calculated by fitting the gamma probability density function (pdf) to the given frequency distribution of (α_k) (Tigkas et al., 2013).

Drinc (Drought Indices Calculator) aims at providing a user-friendly tool for the calculation of several drought indices, with emphasis on two recently developed ones: the Reconnaissance Drought Index (RDI) and the Stream flow Drought Index (SDI). Also, the widely used Standardized Precipitation Index (SPI) and the Rainfall Declines can be calculated. The common characteristic of the selected indices is that they require relatively small number of data for their calculation and the results can be easily interpreted and used in strategic planning and operational applications. Drinc has full graphical user interface functionality (GUI) and runs on MS Windows operating systems (Tigkas et al., 2015, Tsakiris et al., 2007). In this study, computation and analysis of drought was made using Drinc software.

Table 1. RDI drought classifications

sr.No.	RDI Value	Category
1	2.0 and above	Extreme wet condition
2	1.5 to 1.99	Very wet condition
3	1.0 to 1.49	Moderately wet condition
4	-0.99 to 0.99	Near normal condition
5	-1.0 to -1.49	Moderately dry condition
6	-1.5 to -1.99	Severely dry condition
7	-2.0 and less	Extreme dry condition

4. RESULTS

Meteorological data (precipitation, minimum and maximum temperature and evapotranspiration) of Fars Meteorological Bureau for 35 years are used.

In figure 1, the values of the normalized and standard RDI also SPI in figure 2 are presented for three periods. The first one is annually period (October- September) which represents the entire hydrological year, the second period is (October- June), the first nine months of the hydrological year and the third is six months that corresponds to the first and the second half of the hydrological year.

RDI values in different periods of hydrological years (1982-2017), indicates bellow, according to the RDI_n annual values in the Figure 1; there is near normal and moderately wet condition for all 30 years.

The SPI index which surveys drought by precipitation, calculated for the years (1982- 2017) and presented in Figure 2.

The SPI and RDI have the same results for different values, so according to the table 1, there is extreme dry condition in hydrological years (1983-1984) and (2008-2009) also (1993-1994) shows severely dry condition. There are very wet condition for the years (1992-1993), (1995-1996) and (2004-2005). In spite of the SPI showed there were extreme and severely drought in the years of (1983-1984), (2008-2009) and (1993-1994), but due to lack of significant high evapotranspiration, extreme drought is not exactly correct condition for these years. As the RDI calculated, there were near normal condition in these years. The SPI has similar answer to RDI_{st} for drought, so in this paper the RDI_n considered to comparison with SPI. Drought observing in 3 or 6 months after October, gives the opportunity to adjust management plans for the late spring and summer during which demand is normally very high and no significant precipitation depths are expected to contribute towards the water balance of available quantities (Tsakiris and Vangelis, 2005).

5. CONCLUSION AND DISCUSSION

According to the research histories, aimed to determining the intensity and extension of drought, generally indices developed that, each of which has its own inputs and conditions. Review of the studies conducted on drought in Iran reveals the fact that due to changes in the physiographic and climatic characteristics in different areas of the country, the phenomenon of drought in Iran shows differences in positional extension, decrease in degree and intensities. Inconsistency of drought in different parts of the country is an important subject that effective factors must be identified. According to the existing theorizing and the history of the studies, probably the elevation from the sea level is one of those factors. Usually, droughts accompanies with high temperatures, resulting in higher evapotranspiration rates. Potential evapotranspiration (PET) represents the environmental

demand for evapotranspiration. It represents the evapotranspiration rate of a short green crop, completely shading the ground, with uniform height and adequate water status in the soil profile.

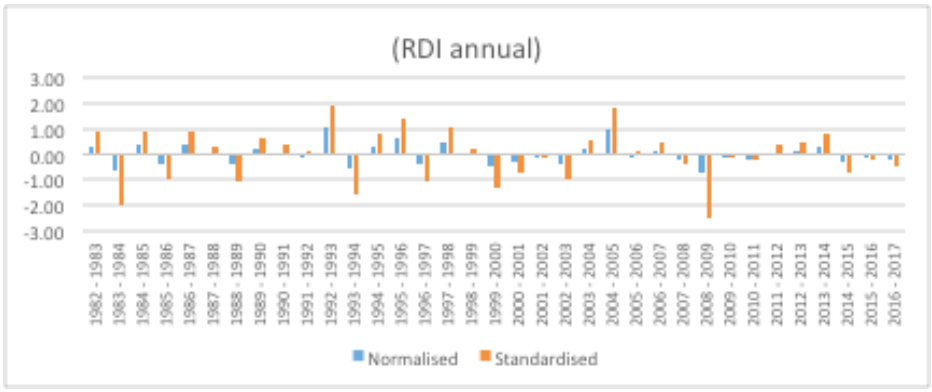

(a)

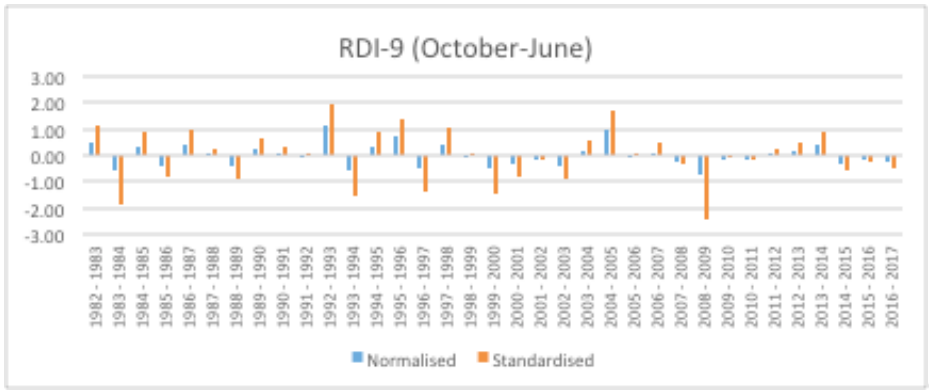

(b)

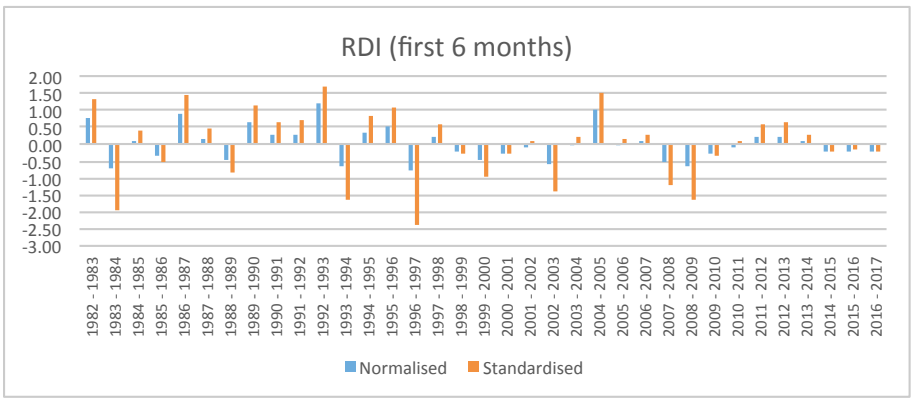

(c)

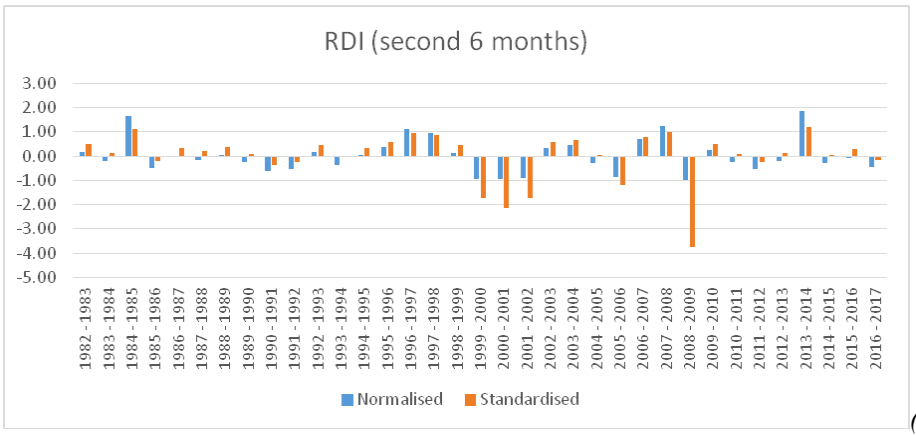

(d)

Figure 1. (a, b, c, d): values of the RDI, RDI-12 (October- September), RDI-9 (October- June), RDI-6 (October-March) and (March- September)

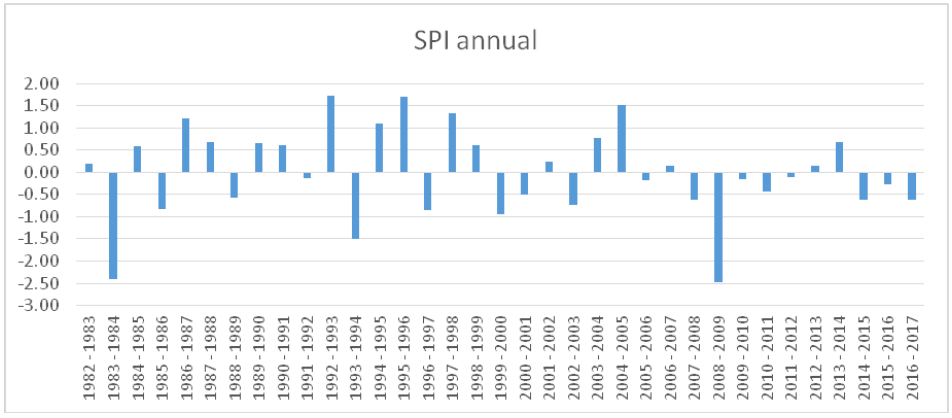

(a)

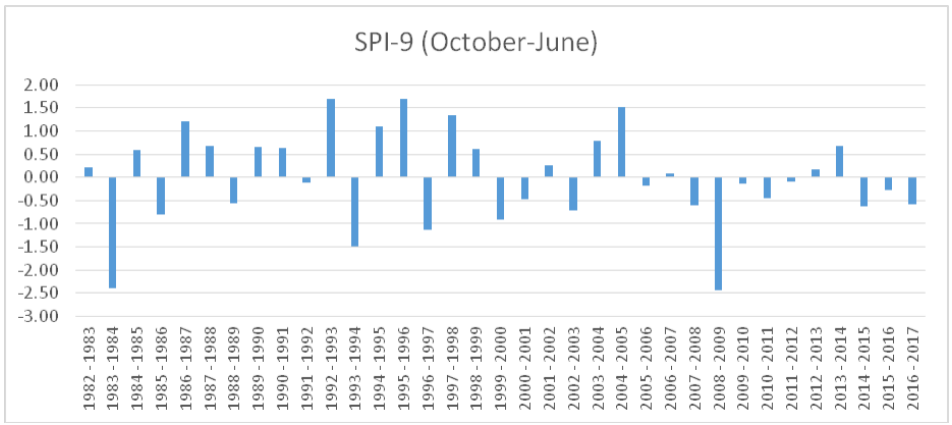

(b)

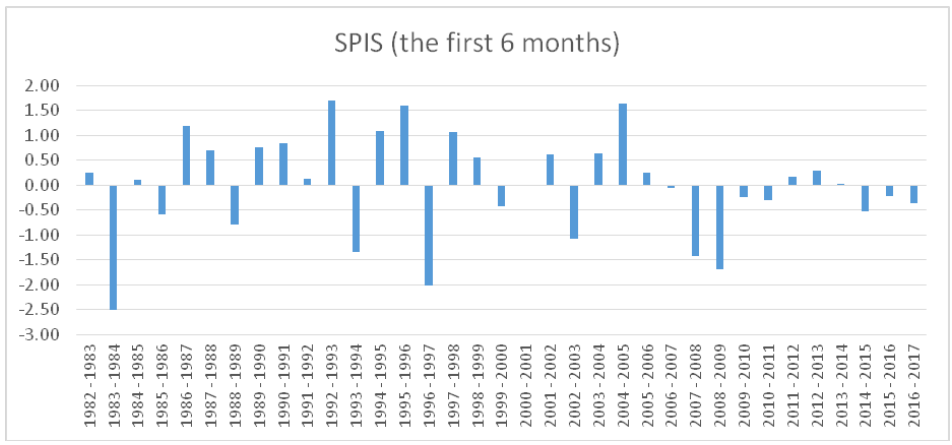

(c)

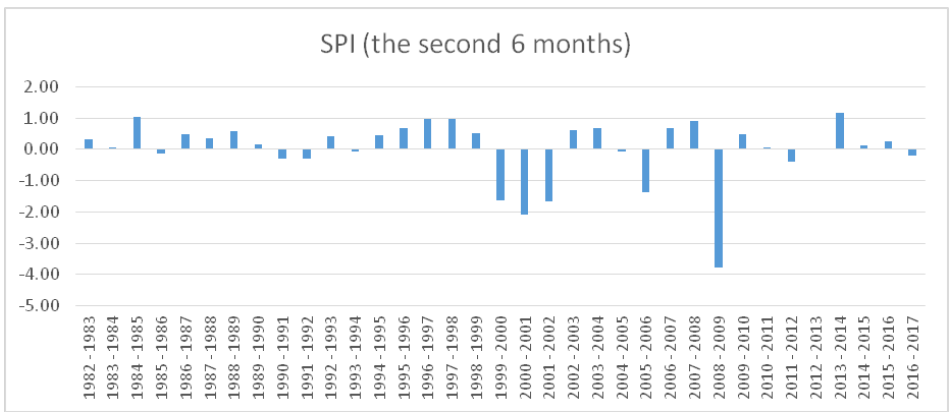

(d)

Figure 2. (a, b, c, d): values of the SPI, SPI-12 (October- September), SPI-9 (October- June), SPI-6 (October-March) and (March-September)

This index can used for every purpose in surveying drought especially agriculture sector. This study exhibits monitoring of drought during the hydrological years of 1982 to 2017, for surveying drought, SPI and RDI indices were used. This research proposes a climatic index the Reconnaissance Drought Index, for drought monitoring particularly in arid and semi-arid area which precipitation amounts are low, evapotranspiration acts as a key factor for monitoring drought, because of using both precipitation and evapotranspiration. It is expected these documents be useful for future decisions and drought monitoring in another area.

REFERENCES

Asadi Zarch, M.A., Malekinezhad, H., Mobin, M., Kousari, M.R. 2011. Drought Monitoring by Reconnaissance Drought Index (RDI) in Iran. Water Resources Management, 25: 3485-3504.

Dracup, J.A., Lee, K.S. and Paulson, E.G., 1980. On the definition of droughts. Water Resources Research, 16(2): 297-302.

Hashemi, Y., Shahmirzadi, S. 2011. Regulating Environmental Conditions. First edition, p. 6, 12, 13,102,105.

Jaefari, M. 2007. Project of Climate Change and Forest Ecosystem, Study of Effects on Khazar Forest Ecosystem.

Maracchi, G., 2000. Agricultural drought - a practical approach to definition, assessment and mitigation strategies. In Drought and drought mitigation in Europe, Springer Netherlands, pp. 63-75.

Mishra, A.K. and Desai, V.R., 2005. Drought forecasting using stochastic models. Stochastic Environmental Research and Risk Assessment, 19(5): 326-339.

Niemeyer, S., 2008. New drought indices. European Commission, DG Joint Research Center, Institute for environment and sustainability, T.P.261, JRC-IES, I21020 Ispra (VA), Italy. Series A, No 80.

Tate, E.L. and Gustard, A., 2000. Drought definition: a hydrological perspective. In Drought and drought mitigation in Europe Springer Netherlands, pp. 23-48.

Tigkas, D., 2008. Drought characterisation and monitoring in regions of Greece. European Water, 23-24: 29-39.

Tigkas, D., Vangelis H., Tsakiris, G. 2013. The RDI as a composite climatic index. European Water, 41: 17-22.

Tigkas, D., Vangelis, H., Tsakiris, G., 2015. DrinC: a software for drought analysis based on drought indices. Earth Science Informatics, 8(3): 697-709.

Tigkas, D., Vangelis, H., Tsakiris, G., 2016. Introducing a modified Reconnaissance Drought Index (RDIe) incorporating effective precipitation. Procedia Engineering, 162: 332-339.

Tsakiris, G., Nalbantis, I., Pangalou, D., Tigkas, D., Vangelis, H., 2008. Drought meteorological monitoring network design for the reconnaissance drought index (RDI). In Franco Lopez A (ed) Proceedings of the 1st International Conference "Drought Management: scientific and technological innovations" Zaragoza, Spain, 12 - 14 June 2008, Option Méditerranéennes, Series A, No. 80, pp. 57-62

Tsakiris, G. Vangelis, H. 2005. Establishing a Drought Index Incorporating Evapotranspiration, European Water, 9-10: 3-11.

Tsakiris, G., Loukas, A., Pangalou, D., Vangelis, H., Tigkas, D., Rossi, G., Cancelliere, A. 2007. Drought characterisation. In: A. Iglesias et al., (Eds.), Drought Management Guidelines Technical Annex, Options Mediterraneennes, Series B, No. 58, Zaragoza, Spain.

Tsakiris, G., Pangalou, D., Vangelis, H. 2007. Regional Drought Assessment Based on the Reconnaissance Drought Index (RDI), Water Resources Management, 21(5): 821-833.

Tsakiris, G., Vangelis, H. 2005. Establishing a Drought Index Incorporating Evapotranspiration, Lab. Of Reclamation Works and Water Resources Management. National Technical University of Athens. Eur. Water; 9-10.

Tsakiris, G., Vangelis, H., Tigkas, D. 2010. Drought impacts on yield potential in rainfed agriculture, Proceedings of 2nd International Conference On Drought Management 'Economics of Drought and Drought Preparedness in a Climate Change Context', Istanbul, Turkey. CIHEAM/ FAO/ ICARDA/ GDAR/ CEIGRAM/ MARM. n. 95: 191-197.

Wilhite, D.A. and Glantz, M.H., 1985. Understanding: the drought phenomenon: the role of definitions. Water International, 10(3): 111-120.

Proceedings of the 10th World Congress of EWRA 'Panta Rhei', 5-9 July 2017, Athens, Greece
© 2017 *European Water Resources Association*

Regional drought analysis for derivation the drought SAF curve using bivariate copula in the Lake Urmia basin, Iran

M. Montaseri, B. Amirataee* and H. Rezaie
Department of Water Engineering, Urmia University, Urmia, Iran
* *e-mail: babak.amirataee@gmail.com*

Abstract: Since droughts occur regionally in nature and given this fact that they often affect very large area, it may be concluded that this phenomenon should be studied in the context of regional analysis and a comprehensive assessment must be undertaken thereof. This study aimed to investigate the spatial variations of droughts in terms of monthly SPI using the copula functions so that the drought severity and percent of area under drought might be jointly modeled within the Lake Urmia basin, as one of the Iran's drought-prone basin. Besides, it was attempted to examine the relationships among the aforementioned variables and, consequently, the drought Severity-Area-Frequency (SAF) curve was developed in the region. Accordingly, seven families of copula functions, including Clayton, Gumbel, Frank, Joe, Galambos, Plackett and Normal, were used to model the joint dependence between the aforementioned two drought variables. Given the various assessment criteria, the Frank copula function was selected as the most appropriate copula for drought characteristics. Then, the conditional return periods were determined for the most appropriate copula and, then, the drought SAF curve was developed for the study area. It was indicated that the SAF curve could be of great importance in drought risk analysis in the region.

Key words: drought, copulas, SPI, SAF curves

1. INTRODUCTION

Drought is a long-term and natural phenomenon that affects large areas and it is characterized by less than expected rainfall. Since temporal and spatial characteristics of drought are considerably different from one region to another, they are considered as multivariate phenomena characterized by such variables as duration, severity, intensity and area under drought (areal extent). Although at-site drought analysis can provide useful information on a drought event in one limited region, it seems that these results will be embedded with high levels of uncertainty in drought management or drought risk assessment in a wide area (Hisdal et al., 2001). Usually, natural short/long-term droughts occur regionally and they often affect very large area. Thus, if droughts are studied in the context of regional analysis, it will be feasible to conduct more comprehensive assessment on this phenomenon in any given region. In fact this type of analysis is considered a crucial requirement of short-term and long-term strategic planning in water resources management (Mishra and Singh, 2011). Given such an analysis, drought duration and severity as well as the percent of area affected by drought should be evaluated thereof (Rossi et al., 1992; Bonaccorso et al., 2015).

Several studies have been conducted in order to understand the nature of spatial and temporal characteristics of droughts in the regional scale. Kim et al. (2002) analyzed the spatial and temporal characteristics of droughts using Palmer Drought Severity Index (PDSI) with developing the Severity-Area-Frequency curve in Conchos River basin, Mexico. Having derived the Severity-Area-Frequency curve, Hisdal and Tallksen (2003) attempted to model the monthly precipitation and streamflow time series in Denmark using the Empirical Orthogonal Functions (EOF). Mishra and Desai (2005) determine the Severity-Area-Frequency relations using SPI for the period 1965-2001 in Kansabati River basin, India. Santos et al. (2010) examined the meteorological drought in Portugal in the period 1910-2004 using SPI with 1-, 6- and 12-month time scales.

A brief look at the forenamed studies indicates that different methods are used to analyze two variables of drought severity and area under drought. However, these methods are embedded with serious limitations, such as limiting the analysis based on the impossibility of extracting the

predictions of future short-term and long-term drought events, failure to maintain a full correlation between two dependent variables and identical marginal probability distribution of dependent variables.

In recent years, the concept of copula has been widely used as a new advanced technique to model the bivariate or multivariate joint probability distributions in hydrology and water resources (De Michele and Salvadori, 2003; Zhang et al., 2012; Salvadori and De Michele, 2015; Liu et al., 2016). The copula functions are a flexible and highly efficient technique to model the characteristics of two or more dependent variables of natural phenomena such as drought duration and severity or severity and area under drought.

Shiau (2006) examined the bivariate joint probability distribution of drought duration and severity in the southern part of Taiwan using the SPI and theory of copula. Song and Singh (2010) modeled the joint probability distribution of duration, severity and inter-arrival time using the trivariate Plackett copula in China. Reddy and Ganguli (2012) made use of four different families of bivariate copula, including Archimedean, Extreme Values, Plackett and Elliptical families, to model the joint probability distribution of drought characteristics and, consequently, concluded that Gumbel–Hougaard copula was the best and most appropriate copula in that regard. In the end, they used Gumbel–Hougaard copula to derive the drought Severity-Duration-Frequency curve in Rajasthan, India. In another study, Reddy and Ganguli (2013) made use of gridded data and copula function in order to analyze the spatial and temporal characteristics of droughts in Kansabati, India, and develop the Intensity-Area-Frequency curve in the region.

All these studies stressed the capability and potency of copula function technique in modeling bivariate or multivariate dependent characteristics of any given drought. In addition, comprehensive reviews of the application of copula have been reported in the Genest and Favre (2007) and Salvadori et al. (2007).

Accordingly, this research attempted to regionally analyze the drought in Lake Urmia basin, as one of the most important basin with relatively high water potential in Iran. The main objectives of this study were as follow: 1) Modeling drought characteristics in the Lake Urmia basin, 2) Evaluating the performance of different families of copula in modeling the structure of drought characteristics in the study area, 3) Deriving the drought Severity-Area-Frequency curve on the basis of the selected appropriate copula in the study area.

2. MATERIAL AND METHODS

2.1 Drought characteristics

In this study, the one-month SPI index is used for drought mitigation. The SPI was the most appropriate and suitable meteorological drought index in reducing the uncertainty embedded with selecting the inappropriate drought index in analyzing the joint probabilities of droughts (Montaseri and Amirataee, 2016). The drought characteristics used in this study were as follows:

1) The percent of area under drought (A_t): it was equal to a specified percent of total area in a given time-step in which the value of SPI statistic was below a specified threshold (Reddy and Ganguli, 2013).

$$A_t = \frac{\sum_{i=1}^{N_p}\left(\mathrm{I}\left[SPI_{i,t} \le SPI_{thr}\right] \times A_i\right)}{\sum_{i=1}^{N_p} A_i} \tag{1}$$

where, I[.] represented the logical indicator function, $SPI_{i,t}$ represented the value of SPI in a given time-step (t), SPI_{thr} represented the SPI drought threshold, A_i represented the area affected by the drought in grid i, and N_p represented the total number of grids in the study area.

2) Drought severity (S_t): it was equal to sum of consecutive SPI values in each grid and time-step, which is located below the drought threshold, and is computed using the equation (2):

$$S_t = -\frac{1}{N_{p\_D}} \sum_{i=1}^{N_{p\_D}} \left(\mathrm{I}\left[SPI_{i,t} \le SPI_{thr} \right] \times SPI_{i,t} \right) \quad (2)$$

where, N_{p_D} represented the total number of grids affected by drought.

In this study, the drought thresholds of zero (SPI <0) is considered in order to regional drought modeling in the study area (Shiau, 2006).

2.2 Copula-based Joint distribution function

Copula is a stochastic and probability-based model. The copula-based multivariate distribution structure was developed by Sklar (1959), Joe (1997), Nelsen (2006), and Salvadori et al. (2007). According to Sklar's Theorem (Nelsen, 2006), if F_{xy} is a two-dimensional joint distribution function of dependent random variables of X and Y with marginal distribution functions F_x and F_y, then there exist a copula C such that:

$$P\left(X \le x, Y \le y\right) = F_{XY}\left(x, y\right) = C\left(F_X\left(x\right), F_Y\left(y\right)\right) \quad (3)$$

Conversely, for any distribution functions F_X and F_Y and any copula C, the function F_{XY} defined above is a two-dimensional function with marginal F_X and F_Y. Furthermore, if F_X and F_Y are continuous, C is unique. Copulas have been constituted from different families and the following seven types have been used in this study: Archimedean (Clayton, Frank, Gumbel and Joe), Extreme value (Gumbel, Galambos), Elliptical (Normal) and Others (Plackett) (Nelsen, 2006).

The identification and determination of the most appropriate marginal distribution for each of the dependent variables may play a key role in the joint probability analysis of drought characteristics using copula. Since the percent of area under drought variable (A) has a defined range and its range is between values of 0 to 100, therefore the use of bounded distribution is inevitable (Griffiths and Fenton, 2007). In this study, the Beta distribution as one of the bounded distribution was fitted on percent of area under drought variable. Also, seven probability distributions of Exponential, Gamma, Gumbel, Normal, two-parameter Log-normal, Logistic, and Weibull were directly used and examine to determine the most appropriate probability distribution of drought severity. The parameters of the probability distributions were estimated using the Maximum Likelihood Estimation (MLE). Also, the Akaike Information Criterion (AIC) was used to define the best probability distribution and goodness of fit test (Zhang and Singh, 2007; Shiau et al., 2010; Yusof et al., 2013; Liu et al., 2016).

In this study, the IFM method was employed for estimation of the parameters of copulas. Firstly, the parameters of the marginal probability distribution of drought variables were estimated using maximum likelihood estimation. Then, the copula dependence parameter (θ) was estimated through the maximization of the log-likelihood function of copula (Shiau, 2006). The Log-likelihood, AIC and RMSE criterion were used to evaluate the performance of fitted copula models. The model with the highest (lowest) Log-likelihood (AIC and RMSE) value represented the most suitable copula model (Shiau, 2006; Karmakar and Simonovic, 2009; Yusof et al., 2013).

2.3 Copula based conditional return periods

The conditional return period $T_{S|A}(s|a)$ of drought severity in return for area under drought A=a can be expressed as equation (4).

$$T_{S|A}(s|a) = \frac{\zeta}{1 - C_{S|A=a}} \quad (4)$$

where, $\zeta = N / n$, N represented the total length of SPI values (years), n represented the number of drought events during N years (years), $C_{S|A=a}$ represented the conditional cumulative distribution function of drought severity given percent of area under drought. The conditional distribution of joint copula functions can be calculated via equation (5), as follows:

$$C_{S|A=a} = \frac{\partial C(F_S(s), F_A(a))}{\partial F_A(a)} \tag{5}$$

In this study, it was tried to firstly determine the one-month SPI across all the selected stations. Then, the percent of area under drought in each station and finally in the entire region was determined in return for the concerned drought severity. Next, the extracted series were univariately fitted to different probability distributions and the best univariate marginal distribution was determined for variables of S and A, respectively. Then, different copula functions were fitted to values of cumulative distribution functions of variables. The most appropriate copula function was selected on the basis of various criteria. Finally, the Severity-Area-Frequency curve was extracted in return for the best copula function.

2.4 Study area and data

Lake Urmia is one of the largest salty lakes in the world located in the northwestern of Iran. Given the population growth, unsustainable agricultural development and occurrence of frequent droughts in Lake Urmia basin in recent decades, it seems that this natural habitat has faced a severe ecosystemic and environmental risk. Therefore, real analysis of the regional drought characteristics can be considered a very important tool in drought risk management in Lake Urmia basin. In this study, 24 rainfall gauge stations in Lake Urmia basin with 43-year (1971-2013) monthly rainfall records are selected. Topographical and geographical map of the study area is shown in Figure 1.

3. RESULTS

3.1. The drought characteristics

The SPI values in each selected station were calculated in order to determine the drought severity. Then, the entire area was subdivided into very small grids with a cell size of 2000×2000 m (Figure 1). With a programming code, it was attempted to determine the distances between the center of grids (13,400 grids) and all the selected stations. Given this fact that the SPI threshold was equal to zero, it was decided to apply the distance and weight of each of the stations (using Inverse Distance Weighting Method) in order to determine the SPI values. Finally, the area under drought in the region was determined via calculating the sum area of each of the grids in return for values less than the threshold. Actually, the latter was considered as the variable of the area under drought in the region. The scatter plot of two variables is depicted in Figure 2.

It is necessary that the dependency among variables should be evaluated prior to application of copula theory when analyzing the bivariate joint probability distribution of such random variables. The newly-developed graphical measures (Ranked scatter plot, Chi and Kendall plot) were used to determine the dependency between two variables of S and A (Genest and Favre, 2007) (Figure 3).

Given the Ranked scatter plot on the forenamed variables (Figure 3a), it was observed that there was a positive correlation between the two variables. Regarding the Chi plot (Figure 3b), it was indicated that most dots were located above the confidence interval. This fact indicated that there was a positive significant correlation between the two variables (Fisher and Switzer, 1985).

Regarding the Kendall plot, it was indicated that if the dots were located above the diagonal line, there would be a positive correlation between the variables (Genest and Boies, 2003). Figure 3d depicted the positive correlation between two variables. So that, pair data embedded with smaller

values (proximity to the diagonal line) would yield relatively less correlation compared to other dots.

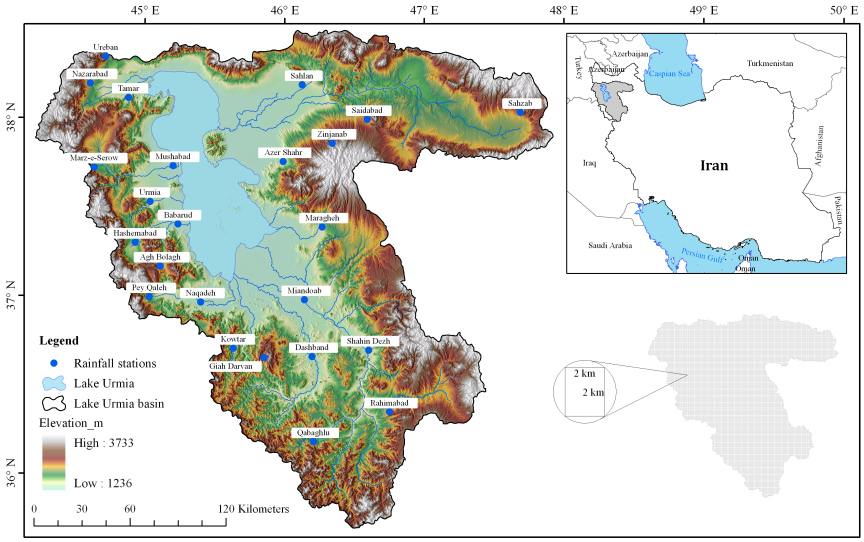

Figure 1. Location of study area and rainfall stations in Lake Urmia basin.

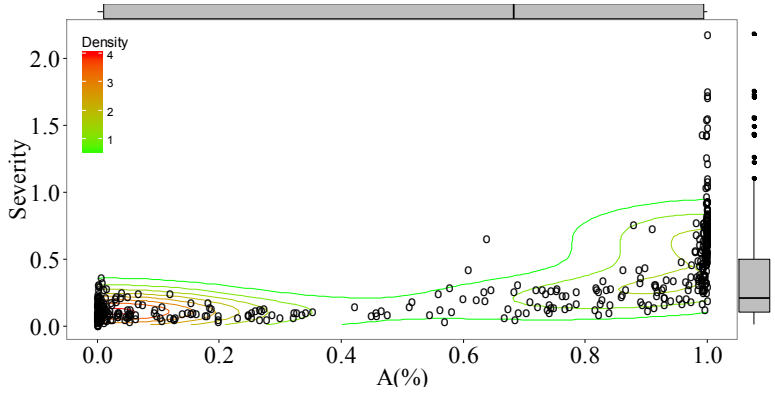

Figure 2. Scatter plot and boxplot of drought severity and percent of area under drought.

Regarding the Kendall plot, it was indicated that if the dots were located above the diagonal line, there would be a positive correlation between the variables (Genest and Boies, 2003). Figure 3d depicted the positive correlation between two variables. So that, pair data embedded with smaller values (proximity to the diagonal line) would yield relatively less correlation compared to other dots.

The results of the best distribution fitted to the two variables as well as parameters of fitted distributions were indicated that the two-parameter Lognormal represented the best performance in terms of drought severity based on AIC criteria. The probability density function (PDF), cumulative distribution function (CDF), P-P plot and Q-Q plot of fitted distributions have been depicted in Figure 4. Given the appropriate graphical fit of Beta distribution to observational data, it was determined that the Beta distribution was the appropriate marginal distribution of variables of *A*.

3.2 Joint dependence structure using copula

Having selected the marginal distribution, it was endeavored to model the joint distribution of drought characteristics using seven mentioned copula. The results of modeling the bivariate joint distribution of *S* and *A* in return for seven copulas have been summarized and represented in Table 1. It was deduced that three copula functions of Gumbel, Joe and Galambos represented weak performance and, thus, they were inappropriate to model the joint probability of *S* and *A* in the

study area. Besides, it was suggested that the application of these copula functions in other regions should be undertaken with much deliberation and caution. Conversely, Frank copula function yielded a very appropriate and satisfactory statistic in return for aforementioned evaluation measures.

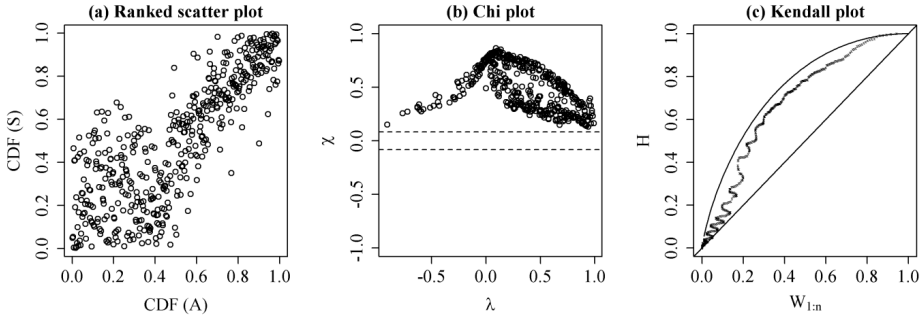

Figure 3. Graphical dependence a) Ranked scatter plot, b) Chi plot and c) Kendall plot.

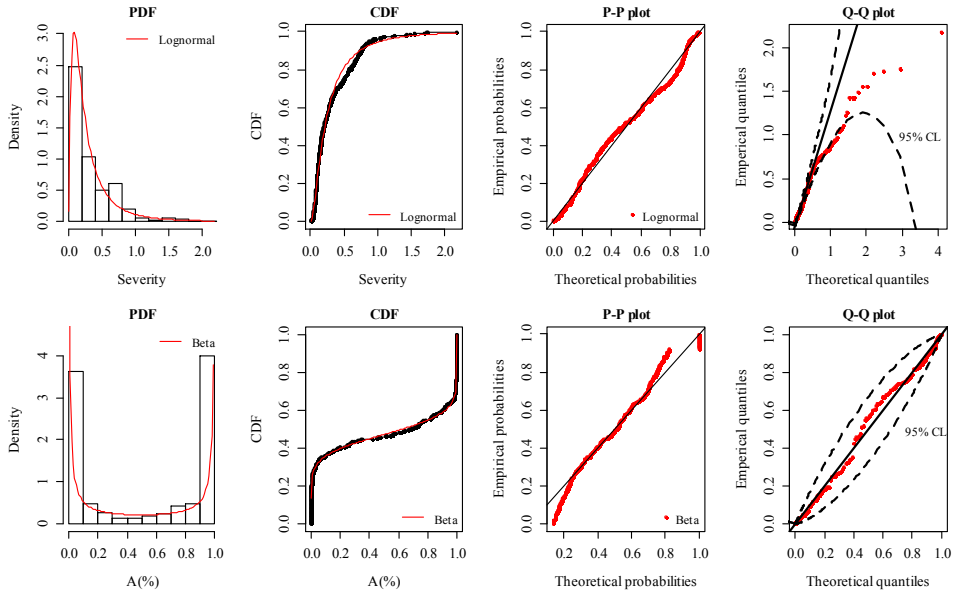

Figure 4. PDF, CDF, P-P and Q-Q plots of appropriate marginal distributions of drought severity and percent of area under drought.

Regarding the graphical performance of copula, 30,000 random marginal pairs from each copula were generated using the Monte Carlo simulation method and then transformed back into their original units using marginal distributions. The scatter plot of generated (gray dots) and observed (black dots) sample pairs in return for observed values has been depicted in Figure 5. As can be seen, the observed sample pairs represented more overlap in Frank copula than other copulas embedded with simulated sample pairs. Emphatically, the scatter plots show that the Frank copula function has represented an ideal performance in terms of explaining the observational data.

Table 1. The estimated parameters and their corresponding evaluation criteria for the fitted copulas

	Copula function						
	Clayton	Gumbel	Frank	Joe	Galambos	Plackett	Gaussian
Parameter	1.731	1.155	8.458	1.074	0.189	15.318	0.509
Log-likelihood	131.67	25.89	**235.04**	9.37	18.65	211.11	123.09
AIC	-261.34	-49.79	**-468.09**	-16.75	-35.31	-420.23	-244.19
RMSE	0.132	0.183	**0.109**	0.198	0.201	0.119	0.151

3.3 Drought Severity-Area-Frequency curve

The drought Severity-Area-Frequency (SAF) curve represented the relationship among spatial changes of drought severity and percent of area under drought in return for a return period. (Hisdal and Tallaksen 2003; Reddy and Ganguli 2013). Actually, this curve was derived on the basis of joint copula function and conditional distributions of drought variables. Given the specified return period $T_{S|A}(s|a)$,it was indicated that the drought severity related to the percent of area under drought might be calculated via numerical solution of Equation (5), in which in this study the value of ξ was calculated equal to 1.11. Besides, the value of $C_{S|A=a}$ in return for the best copula (Frank) could be determined via equation (6):

$$C_{S|A=a} = -\frac{e^{\theta}(e^{\theta v}-1)}{(e^{\theta v}-e^{\theta})e^{\theta u}-e^{\theta v+\theta}+e^{\theta}} \tag{6}$$

where, $u=F_A(a)$, $v=F_S(s)$, and θ represented Frank copula parameter.

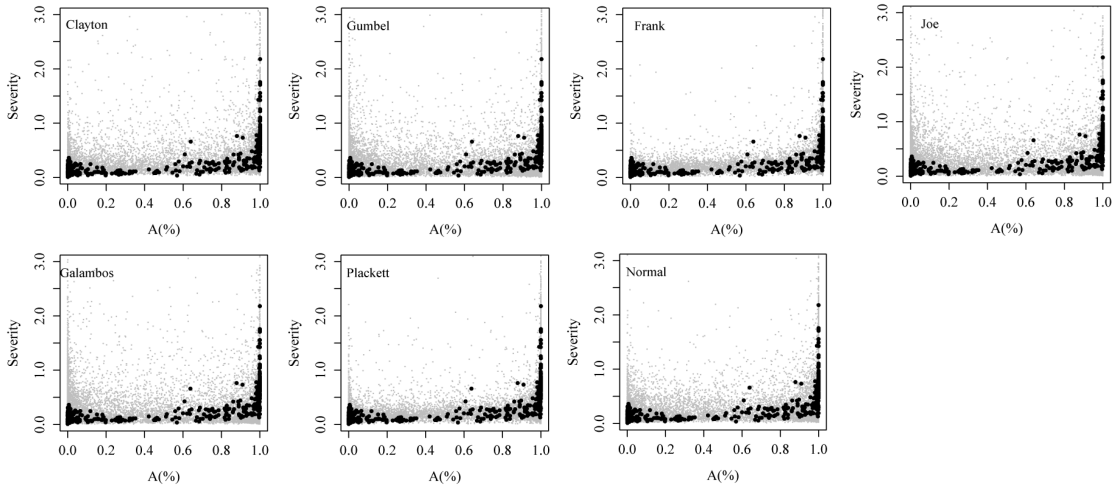

Figure 5. Scatterplots of generated and observed S and A, based on different copula functions.

The SAF curve in return for different return periods in the study area has been depicted in Figure 6. As seen, as the drought severity increased, the percent of area under drought increased as well. According to SAF Curve, it was possible to determine the drought severity for the percent of area under drought and the specified return period. For example, the drought severity with 20-year return period and 20% of area under drought in the study area was determined as 0.37. Such extraction curves can lead to a real understanding of the regional drought characteristics and related drought risk and is of great importance in the planning and management of drought.

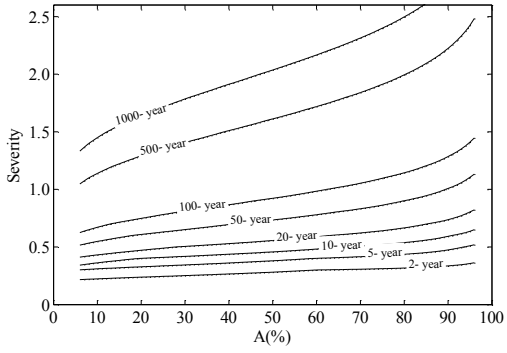

Figure 6. SAF curve based on different return periods in Lake Urmia basin.

4. CONCLUSIONS

Determining the probabilistic and regional characteristics of any given drought is considered as one of the most important steps in water resources planning and management. In this study, it was attempted to model the drought characteristics occurred in Lake Urmia basin, Iran, including drought severity and percent of area under drought, in return for one-month SPI and a 2000x2000 m spatial scale using the copula functions**.** To do this end, it was attempted to fit seven different families of copulas, including Clayton, Gumbel, Frank, Joe, Galambos, Plackett and Normal, in return for best marginal distributions of two-parameter Lognormal and Beta, as the marginal distributions fitted to drought variables. Given the statistical and graphical goodness of fit tests, it was concluded that the Frank copula was the most appropriate copula in modeling the drought severity and percent of area under drought in the region. Then, the relations between drought severity and percent of area under drought, entitled Severity-Area-Frequency curve, were determined in return for best copula and conditional distributions, which could be useful in planning and management of droughts. Drought risk assessment based on the results of this study can be a high priority in drought monitoring over large areas.

REFERENCES

Bonaccorso, B., Peres, D.J., Castano, A., Cancelliere, A., 2015. SPI-based probabilistic analysis of drought areal extent in Sicily. Water Resour. Manag. 29:459–470.

De Michele, C., Salvadori, G., 2003. A generalized Pareto intensity-duration model of storm rainfall exploiting 2-copulas. J Geophys. Res., doi:10.1029/2002JD 002534.

Fisher, N.I., Switzer, P., 1985. Chi-plots for assessing dependence. Biometrika, 72, 253-265.

Genest, C., Boies, J.C., 2003. Detecting dependence with Kendall plots. Am. Stat., 57:275–284.

Genest, C., Favre, A.C., 2007. Everything you always wanted to know about copula modeling but were afraid to ask. J. Hydrol. Eng., 12(4):347–368.

Griffiths, D.V., Fenton, G.A. 2007. Probabilistic Methods in Geotechnical Engineering. SpringerWien, New York.

Hisdal, H., Stahl, K., Tallaksen, L.M., Demuth, S. 2001. Have streamflow droughts in Europe become more severe or frequent?. Int. J. Climatol., 21:317–333.

Hisdal, H., Tallaksen, L.M., 2003. Estimation of regional meteorological and hydrological drought characteristics: a case study for Denmark. J. Hydrol., 281(3):230-247.

Joe, H. 1997. Multivariate models and dependence concepts, Chapman & Hall, London.

Karmakar, S., Simonovic, S.P., 2009. Bivariate flood frequency analysis. Part 2: a copula-based approach with mixed marginal distributions. J. Flood Risk. Manag., 2:32–44.

Kim, T.W., Valdes, J.B., Aparicio, J. 2002. Frequency and spatial characteristics of droughts in the Conchos River basin, Mexico. Water. Int., 27(3):420-430.

Liu, X., Wang, S., Zhou, Y., Wang, F., Yang, G., Liu, W., 2016. Spatial analysis of meteorological drought return periods in China using copulas. Nat. Hazards, 80(1):367–388.

Mirabbasi, R., Fakheri-Fard, A., Dinpashoh, Y., 2012. Bivariate drought frequency analysis using the copula method. Theor. Appl. Climatol., 108:191–206.

Mishra, A.K., Desai, V.R., 2005. Spatial and temporal drought analysis in the Kansabati river basin, India. Int. J. River Basin Management, 3(1):31–41.

Mishra, A.K., Singh, V.P., 2011. Drought modelling_a review. J. Hydrol., 403:157 175.

Montaseri, M., Amirataee, B., 2017. Comprehensive stochastic assessment of meteorological drought indices. Int. J. Climatol., 37(2): 998–1013.

Nelsen, R.B., 2006. An introduction to copulas, 2nd Ed., Springer, New York.

Reddy, M.J., Ganguli, P., 2012. Application of copulas for derivation of drought severity–duration–frequency curves. Hydrol. Process., 26(11):1672–1685.

Reddy, M.J., Ganguli, P., 2013. Spatio-temporal analysis and derivation of copula-based intensity-area-frequency curves for droughts in western Rajasthan (India). Stoch. Env. Res. Risk. A., 27:1975–1989.

Rossi, G., Benedini, M., Tsakiris, G., Giakoumakis, S., 1992. On regional drought estimation and analysis. Water Resour. Manag., 6:249-277.

Salvadori, G., De Michele, C., 2015. Multivariate real-time assessment of droughts via copula-based multi-site Hazard Trajectories and Fans. J. Hydrol., 526:101-115.

Salvadori, G., De Michele, C., Kottegoda, N.T., Rosso, R., 2007. Extremes in Nature: An Approach Using Copulas. Springer, Dordrecht.

Santos, J.F., Pulido-Calvo, I., Portela, M., 2010. Spatial and temporal variability of droughts in Portugal. Water Resour. Res., 46:W03503.

Shiau, J.T., 2006. Fitting drought duration and severity with two dimensional copulas. Water Resour. Manag., 20(5):795–815.

Shiau, J.T., Wang, H.Y., Tsai, C.T., 2010. Copula-based depth-duration-frequency analysis of typhoons in Taiwan. Hydrol. Res., 41(5):414-423.

Sklar, A., 1959. Fonctions de répartition à n dimensions et leurs marges, Publications de l'Institut de Statistique de L'Université, Paris, 8, 229–231.

Song, S., Singh, V.P., 2010. Frequency analysis of droughts using the Plackett copula and parameter estimation by genetic algorithm. Stoch. Env. Res. Risk. A., 24(5):783–805.

Yusof, F., Hui-Mean, F., Suhaila, J., Yusof, Z., 2013. Characterisation of drought properties with bivariate copula analysis. Water Resour. Manag., 27(12):4183–4207.

Zhang, L., Singh, V.P., 2007. Bivariate rainfall frequency distributions using Archimedean copulas. J. Hydrol., 332(1-2):93–109.

Zhang, Q., Singh, V.P., Li, J., Jiang, F., Bai, Y., 2012. Spatio-temporal variations of precipitation extremes in Xinjiang, China. J. Hydrol., 434:7-18.

Proceedings of the 10th World Congress of EWRA 'Panta Rhei', 5-9 July 2017, Athens, Greece
© 2017 *European Water Resources Association*

Assessing the use of SPI in detecting agricultural and hydrological droughts and their temporal cyclicity: Some Slovakian case studies

M.M. Portela[1*], A.T. Silva[1], J.F. Santos[2], M. Zeleňáková[3] and H. Hlavatá[4]
[1] *Instituto Superior Técnico, Universidade de Lisboa, CERIS, Portugal*
[2] *Instituto Politécnico de Beja, Beja, Portugal*
[3] *Technical University of Košice, Košice, Slovakia*
[4] *Slovak Hydrometeorological, Košice, Slovakia*
[*] *e-mail: maria.manuela.portela@tecnico.ulisboa.pt*

Abstract: One of the most common drought indices used to characterize the droughts is the Standardized Precipitation Index, SPI. This index that can be computed at different time scales uses only rainfall records and aims at detecting meteorological drought triggered by rainfall shortfall. If this deficit is combined with higher than normal evapotranspiration, an agricultural drought may occur. If the period with below average precipitation/above average evapotranspiration persists, the streamflows are affected resulting in a hydrological drought. This paper addresses the capability of the SPI to detect agricultural and hydrological droughts in Eastern Slovakia by comparing its values with those of other indices. Regarding agricultural drought, the comparison considered the Standardized Precipitation Evapotranspiration Index, SPEI. Results show that SPI and SPEI have almost identical performance in agricultural drought detection across the analysed rain gauges. Furthermore, to evaluate the capability of SPI to detect hydrological droughts, the Standardized Streamflow Index, SSI, developed using monthly streamflows and the methods of normalization within the computation of SPI, was applied to a small catchment and compared to the SPI at a rain gauge inside the catchment. This comparison revealed that SPI had a poor performance in detecting hydrological drought. Spectral analysis of the seasonal patterns of the SPI index, using the fast Fourier transform algorithm (FFT), showed that there is a generalized 5-6 year cycle in the agricultural pattern for Autumn and Spring.

Key words: Slovakia, droughts, SPI, SPEI, SSI, spectral analysis

1. INTRODUCTION

Previous works of the authors analysed the drought occurrences in Slovakia, including: (i) an extensive characterization of the events over the whole country; (ii) their spatial regionalization and (iii) temporal evolution; (iv) the analysis of the pattern of their annual rates of occurrence, as a way to look for links among those events and the climate change issue; and, finally, (v) the development of a very practical tool aiming at the early detection of the drought occurrences, based only on rainfall data, as synthesized in Portela *et al.* (2015).

Those studies utilized the Standardized Precipitation Index, SPI (McKee *et al.*, 1993), which is perhaps the most common drought index, due to its few data requirements, the simplicity of its computation when compared to other indices and its comparability because it is a dimensionless index (Santos *et al.*, 2010).

The SPI can be computed at different time scales and uses only rainfall data because. It aims at detecting meteorological drought triggered by rainfall shortfall. If this deficit is combined with higher than normal evapotranspiration, an agricultural drought may occur. If the period with below average precipitation/above average evapotranspiration persists, the streamflows are affected resulting in a hydrological drought.

The analysis of the droughts based on the SPI only requires the adjustment to monthly rainfall series or to cumulative rainfall series of a given statistical distribution. A drought event is considered to occur in a certain location/rain gauge when the SPI falls below a predetermined threshold level, defined according to the drought severity, from moderate to severe and to extreme drought.

Another multiscalar drought index is the Standardized Precipitation-Evapotranspiration Index SPEI. This index was designed to take into account both precipitation and potential evapotranspiration (PET) in identifying droughts, thus capturing the cumulated impact of increased temperature and low water availability. According to Vicente-Serrano *et al.* (2010), the method used to calculate the PET is not a critical issue when applying SPEI and the simpler method of Thornthwaite (1948), which only requires monthly temperature data, can be applied.

This paper addresses the capability of the SPI to detect agricultural and hydrological droughts in Eastern Slovakia by comparing its values with those of other indices. Regarding agricultural drought, the comparison considered the Standardized Precipitation Evapotranspiration Index, SPEI. Results show that SPI and SPEI have almost identical performance in agricultural drought detection across the analysed rain gauges. Furthermore, to evaluate the capability of SPI to detect hydrological droughts, the Standardized Streamflow Index, SSI, was applied to a small catchment and compared to the SPI at a rain gauge inside the catchment. The SSI uses only monthly streamflows or cumulative monthly and the same methods of normalization and computation as the SPI. This comparison revealed that SPI had a poor performance in detecting hydrological drought.

The study ends with a brief and simple example on the cyclicity of the SPI index based on spectral analysis.

2. STUDY AREA AND DATA

The comparison of drought indices in Eastern Slovakia utilized monthly precipitation and temperature data from 6 rain gauges, which were kindly provided by the Slovakian Meteorological Institute. Table 1 shows the code and name, period of records and coordinates of the rain gauges. Monthly streamflow data from the Medzev river gauge (January 1961 – December 2014, catchment area of *ca.* 90 km^2) was also utilized to compute SSI and to compare this index with the SPI. Figure 1 shows the schematic location of the 6 rain gauges, as well as that of the Medzev stream gauge and corresponding catchment drainage divides.

Table 1. Utilized rain gauges, period of records of monthly precipitation and temperature, and geographic coordinates.

Code	Name	Period of records	Latitude (º)	Longitude (º)
P1	Červený Kláštor	January 1961 – December 2014	49.387	20.424
P2	Štós	January 1961 – December 2014	48.718	20.798
P3	Skalnaté Pleso	January 1961 – December 2014	49.189	20.236
P4	Kamenica nad Cirochou	January 1951 – December 2014	48.939	22.006
P5	Bardejov	January 1961 – December 2014	49.289	21.274
P6	Tisinec	January 1963 – December 2014	49.216	21.650

3. METHODS

3.1 Drought indices

The SPI index was computed at a 3-month time scale in order to reflect short- and medium-term water deficit conditions whose awareness is important in primary agricultural regions such as Slovakia (Portela *et al.*, 2015). To be comparable, the same time scale was adopted for SPEI and SSI.

The computation of the SPI series followed the detailed formulation provided by Edwards & McKee (1997) and Vicente-Serrano (2005), among others. The Gamma distribution was applied to the series of cumulative precipitation in consecutive periods of 3 months (SPI3) in each rain gauge.

The SPEI uses the same formulation, but applied to cumulative climatic water balance, i.e., the difference between precipitation and potential evapotranspiration (P – PET) (Beguería *et al.*, 2014), in consecutive periods of 3 months (SPEI3). As suggested by Vicente-Serrano *et al.* (2010), the

monthly potential evapotranspiration was computed by applying the Thornthwaite method which has the advantage of only requiring monthly temperature series. The temperature data were acquired at the same monitoring stations as the rainfall data, as previously mentioned.

The SSI computation utilized exactly the same approach as for SPI but applied to monthly streamflows in consecutive periods of three months (SSI3).

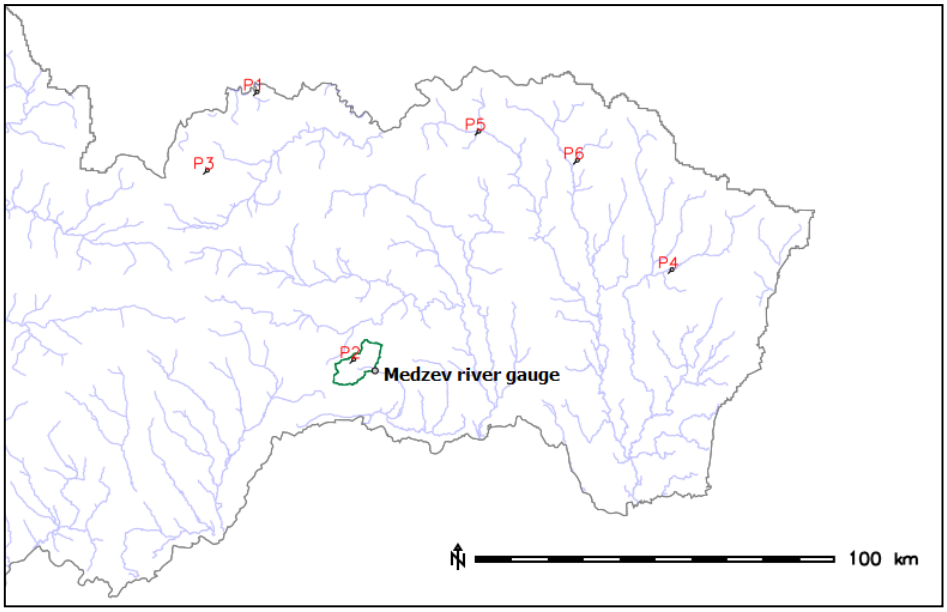

Figure 1. Map of Eastern Slovakia. Location of the 6 rain gauges and of the Medzev river gauge and corresponding catchment's drainage divide.

3.2 Spectral analysis

Spectral analysis methods were used to investigate structured temporal variations (periodicity) embedded in the drought indices in different time seasons. Spectral methods are also known as Fourier transform methods (Bloomfield, 2000) and have been widely used in the hydro-climatological field (e.g. Rajagopalan & Lall, 1998; Golyandina & Zhigljavsky, 2013; or more recently, Moreira *et al.*, 2015). The Fourier transform can describe a physical process either in time domain (function of time) or in the frequency domain were the physical process could be specified by giving its amplitude as a function of frequency, providing interesting features such as long memory, presence of high frequency variation and cyclical behaviour (e.g. McLeod & Hipel, 1995). The input data is generally a simple or multivariate time series, but some authors such as Hijmans (2013) or Golyandina & Usevich (2010), have been successfully testing the use of spectral analysis in multidimensional data like digital images.

The related periodogram, which is also a sample estimate of a population function called the spectral density, is a function that provides information about the periodic components of a time series, allowing identifying the dominant cyclical behaviour in a series.

Any time series can be expressed as a sum of cosine and sine waves oscillating at the fundamental (harmonic) frequencies. The periodogram gives information about the relative strengths of the various frequencies when explaining the variation in the time series. These strengths are also known as power spectrum, which can be defined as the distribution of variance across frequency (i.e. the spectrum is related to the Fourier transform of the autocorrelation function).

Mathematically, the spectral density is defined for both negative and positive frequencies. However, due to symmetry of the function and its repeating pattern for frequencies outside the range -1/2 to +1/2, we only need to be concerned with frequencies between 0 and +1/2.

The Spectral Analysis package was used in R (R Development Core Team, 2013) to estimate the spectral density of seasonal SPI and SSI time series for agricultural drought recognition by using a smoothed periodogram, which calculates the periodogram and smoothed the result with a series of modified Daniell smoothers to achieve consistency (Venables & Ripley, 2002).

4. RESULTS

4.1 Comparison between drought indices

The comparison between SPI3 (horizontal axes) and SPEI3 (vertical axes) in rain gauges P1 to P6 is shown in Figure 2. The results are very similar in all rain gauges: the scatter plot is slightly S-shaped, thus suggesting that the SPI index is more sensitive to water shortages and surpluses. These results are similar to those found in a humid region in Portugal by Paulo *et al.* (2012), who contend that the S shape of the relationship is related to the different behaviour of the variable of interest in SPEI (P – PET) from the variable of interest in SPI (P).

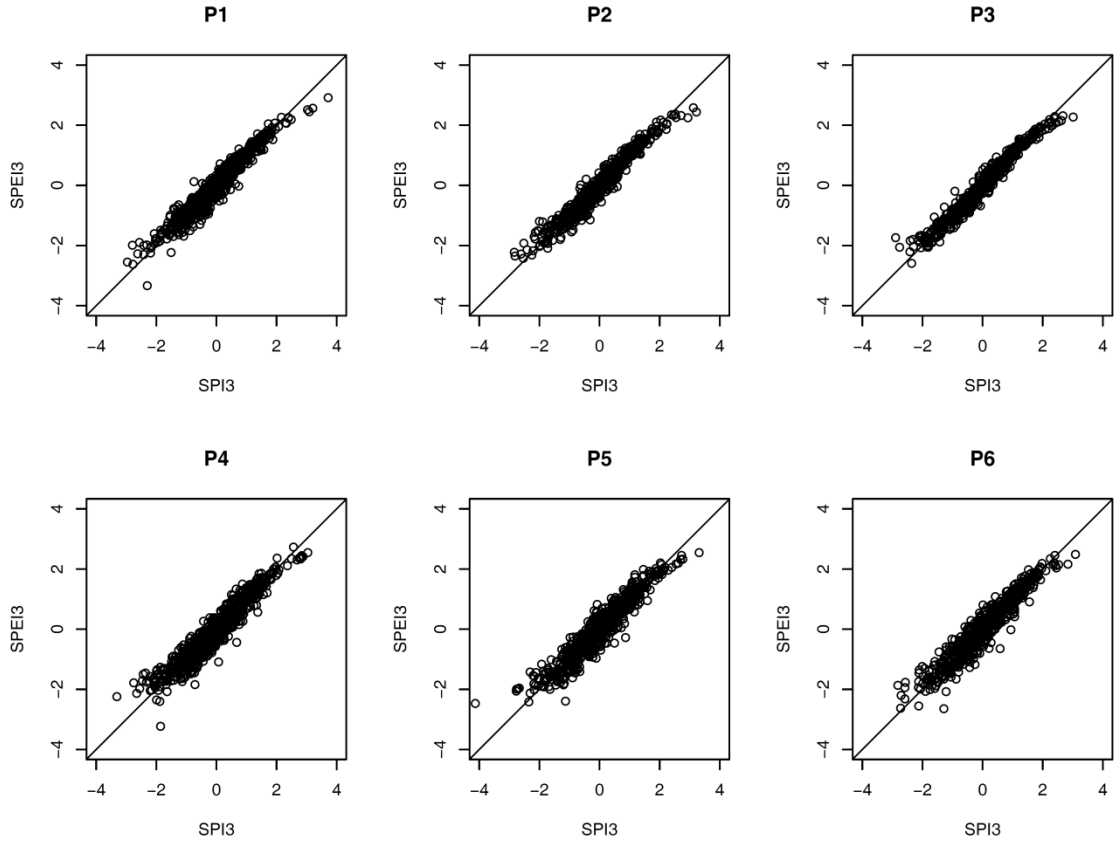

Figure 2. Comparison of SPI3 and SPEI3 values in the 6 analysed rain gauges (from P1 to P6).

Figure 3 shows the comparison between SPI3 at rain gauge P2 and SSI3 at the Medzev river gauge (Figure 1).

To account for the delay between precipitation and surface runoff, the SSI series were lagged comparatively to the SPI series from δ=1 to 3 months meaning that each SPI3 is compared to a SSI3 for a three month period starting δ months after, as proposed by Portela & Santos, 2010. Additionally, to account for the minor and mutually dependent droughts with little hydrological importance and that may disturb the analysis, some authors recommend combining those droughts into a single large event which allows capturing the true severity of the events (Moreno *et al.*, 2009). Among the various procedures proposed to do that (Tallaksen *et al.*, 1997), a low-pass filter,

namely, the moving average technique, was adopted to smooth the original drought index series. This procedure combines mutually dependent droughts into a single drought event; it also filters out the minor droughts, providing better results than other methods (Fleig et al., 2006). The time step adopted was n=10 as done before by Portela & Santos, 2010, exactly in the same scope and purpose.

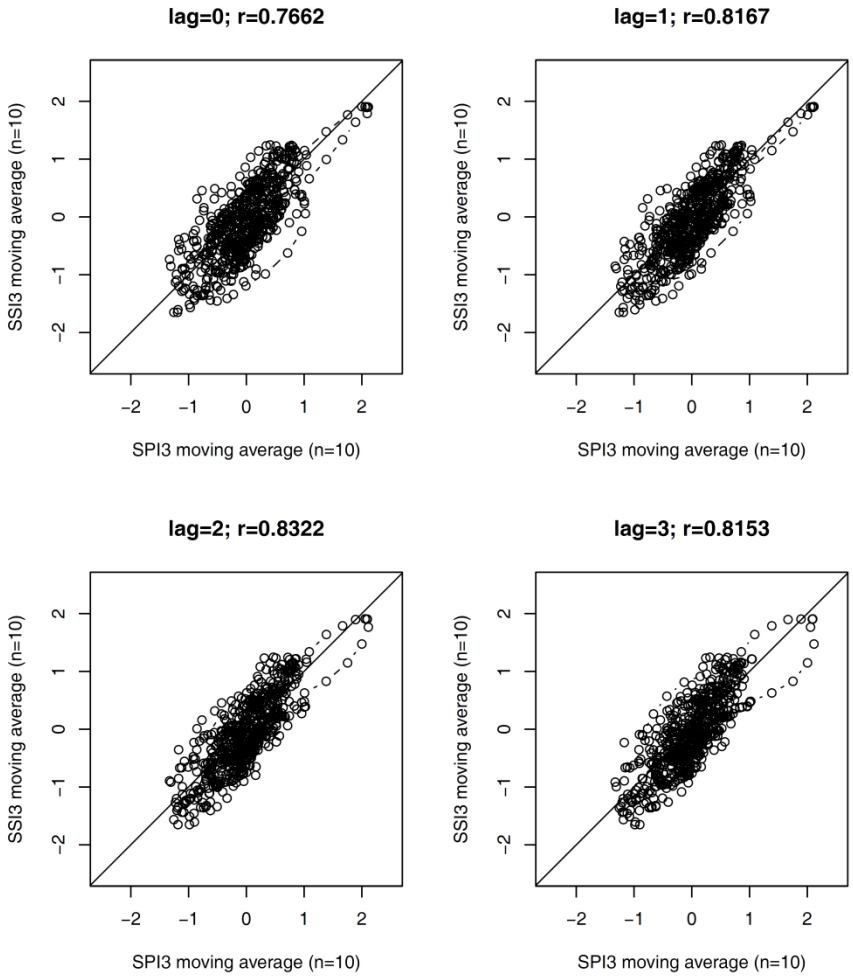

Figure 3. Comparison of moving averages (for n=10) of SPI3 at the Stós rain gauge and of SSI3 at the Medzev river gauge with different monthly lags between SPI3 series and SSI3 series and corresponding correlation coefficients.

Figure 3 shows that the relationship between SSI3 and SPI3 is not well-defined, even despite the applied smoothing of the moving average, which suggests that SPI is not a worthwhile descriptor of surface water availability. Furthermore, the correlation between the two indices improves when a 1- 2- or 3-month lag between precipitation and streamflow is introduces, thus suggesting that, given the small size of the catchment, groundwater may provide a significant contribution to surface flow.

3.2 Temporal cyclicity of the SPI3 series

The spectral analysis was applied to the SPI3 series at the 6 rain gages. The spectral density estimates obtained by the periodograms are shown in Figure 4. Representations as the one of this figure allow to detect the existence of relevant periodic components in the time series, as well as to conclude about their relative importance.

The main four seasonal SPI series (Winter – Jan to Mar; Spring – Apr to Jun; Summer – Jul to Sep and Autumn – Oct to Dec) were chosen for the spectral analysis as they reflect the main weather periods in Slovakia. The method was applied only to SPI3 since the SPEI3 and the SPI3 time series have a similar temporal behaviour.

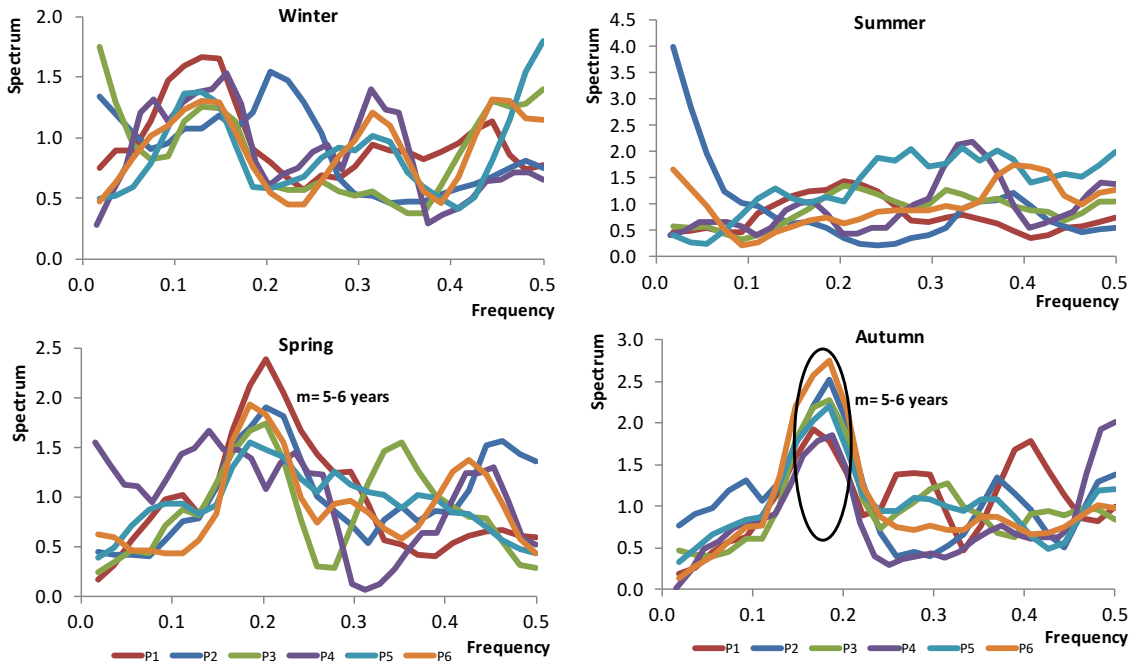

Figure 4. Spectral density for SPI3 in the 6 analysed rain gauges (from P1 to P6), where m is the period in years.

The raw periodogram is a rough sample estimate of the population spectral density, since normally it uses only the discrete fundamental harmonic frequencies for the periodogram whereas the spectral density is defined over a continuum of frequencies. In order to deal with this problem and to provide more consistency to the results the periodograms have been smoothed. Bloomfield (2000) recommends the Daniell window (Daniell, 1946) as a smoothing filter for generating an estimated spectrum from the periodogram (moving averages giving half weight to the end values). The periodograms obtained used coef [-2, -1, 0, 1, 2] = [0.125, 0.250. 0.250, 0.250, 0.125].

Since each value of the SPI3 is computed in an annual basis, the results obtained by the periodogram plots (spectral density) for the agricultural drought temporal patterns manifest a clear peak of m = 5-6 years in Spring and Autumn (Figure 4), where n is the period in years such that m=1/Frequency. Winter and Summer seasons show several high peaks which indicates the existence of several periodic components with different periods, without any clear individualized strong peak. In general, few of those peaks represent a strong periodical signal that cannot be assigned to statistical fluctuations, nevertheless the peaks obtained by the smoothed periodograms were not tested for statistical significance in this paper.

5. CONCLUSIONS

Regarding the drought assessment, namely in a region prone to agricultural droughts as Slovakia, the results achieved showed that the Standardized Precipitation Index, SPI, is as good an indicator as the Standardized Precipitation Evapotranspiration Index, SPEI, since it provides almost the same information. Besides allowing identifying the same occurrences, SPI has the advantage of being more sensitive to water shortages and surpluses.

In what concerns the hydrological droughts that affect the river streamflows, SPI proved not to be able to detect those identified by the SSI3 index. Because this conclusion was based on a single case study it cannot be generalized. It should be mentioned that other authors find a relationship between SPI and SSI although in a different hydrological framework (Portela & Santos, 2010).

In respect to spectral analysis, only a few rain gages in a very small region were analysed which also points towards the need for further research. Despite its preliminary nature, the results showed that the cyclicity of the indices can provide some information about the temporal variability of the agricultural droughts in Slovakia.

Other authors such as Halmova *et. al.* (2015) have also found wet and dry periods in multiannual precipitation series in a southwestern station in Slovakia. From several significant cycles the authors found one that had a duration of 5 years, which statistical relationship with the cycles of Figure 4 derived from SPI3 series should be further investigated.

The multi-year fluctuations here obtained by spectral analysis could also be linked to the energy bands that characterize some climate indices affecting the European climate, such as the North Atlantic Oscillation (NAO), a teleconnection pattern which is recognized as a major climatic factor on the European hydrological variables as seen in Rimbu *et al.* (2004) and Trigo *et al.* (2004).

REFERENCES

Beguería, S., Vicente□Serrano, S.M., Reig, F. and Latorre, B., 2014. Standardized precipitation evapotranspiration index (SPEI) revisited: parameter fitting, evapotranspiration models, tools, datasets and drought monitoring. *International Journal of Climatology*, 34(10):3001-3023.

Bloomfield, P., 2000. *Fourier analysis of time series: an introduction*, 2nd edition. New York, John Wiley & Sons, Inc., 261 p.

Daniell, P.J., 1946. Discussion on the symposium on autocorrelation in time series. Journal of the Royal Statistical Society (Suppl.), 8:88-90.

Edwards, D.C., & McKee, T.B., 1997. Characteristics of 20th century drought in the United States at multiple time scales. *Climatology Report* 97–2, Department of Atmospheric Science, Colorado State University, Fort Collins, Colorado.

Fleig, A. K., Tallaksen, M., Hisdal, H., Demuth, S., 2006. A global evaluation of streamflow drought characteristics, *Hydrology and Earth System Sciences*, 10, 532–552.

Golyandina. N., & Usevich, K., 2010. 2D-extension of Singular Spectrum Analysis: algorithm and elements of theory. In: *Matrix methods: theory, algorithms and applications* (Eds. V.Olshevsky and E.Tyrtyshnikov). World Scientific Publishing, pp.449-473.

Golyandina, N., & Zhigljavsky, A., 2013. *Singular spectrum analysis for time series*, Springer, available at: http://www.springer.com/statistics/statistical+theory+and+ methods/book/978- 3- 642- 34912- 6 (last access: 19 September 2013).

Halmova D., Pekarova P., Olbrimek J., Miklanek P. and Pekar J., 2015. Precipitation Regime and Temporal Changes in the Central Danubian Lowland Region. *Advances in Meteorology*. Volume 2015, Article ID 715830, 12 pages.

Hijmans, R.J., 2013. raster: Geographic Data Analysis and Modeling. R package version 2.1- 49, URL http://CRAN.R-project.org/package=raster.

McKee, T.B., Doesken, N.J. and Kleist, J., 1993, January. The relationship of drought frequency and duration to time scales. In *Proceedings of the 8th Conference on Applied Climatology*, 17(22):179-183. Boston, MA: American Meteorological Society.

McLeod, A.I., & Hipel, K.W., 1995. Exploratory spectral analysis of hydrological times series. *Stochastic Hydrology and Hydraulics*, 9:171-205.

Moreira, E.E., Martins, D.S., Pereira, L.S., 2015. Assessing drought cycles in SPI time series using a Fourier analysis. Natural Hazards and Earth System Sciences, 15:571–585.

López-Moreno, J.I.; Vicente-Serrano, S.M.; Beguería, S.; García-Ruiz, J.M.; Portela, M.M.; Almeida, A.B., 2009, Dam effects on droughts magnitude and duration in a transboundary basin: The Lower River Tagus, Spain and Portugal, *Water Resources Research*, 45, Article Number: W02405, ISSN=0043-1397, WOS:000263180500003, doi:10.1029/2008WR007198

Paulo, A.A., Rosa, R.D. and Pereira, L.S., 2012. Climate trends and behaviour of drought indices based on precipitation and evapotranspiration in Portugal. *Natural Hazards and Earth System Sciences*, 12:1481-1491.

Portela, M.M., Zelenáková, M., Santos, J.F., Purcz, P., Silva, A.T., Hlavatá, H., 2015, A comprehensive drought analysis in Slovakia using SPI. European Water, 51:15-31.

Portela, M.M., & Santos, J.F., 2010. Caracterização de secas por aplicação do índice de precipitação padronizada, SPI, a séries de precipitação e de escoamento: casos de estudo em Portugal Continental, *XXIV Congresso LatinoAmericano de Hidráulica*, Punta del Este, Uruguay (in Portuguese).

R Development Core Team (2013). R: A Language and Environment for Statistical Computing, R Foundation for Statistical Computing, Vienna, Austria, available at: http://www.R-project.org.

Rajagopalan, B., & Lall, U., 1998. Interannual variability in Western US precipitation. *Journal of Hydrology*, 210: 51-67.

Rimbu, N., Dima, M., Lohmann, G. and Stefan, S. 2004. Impacts on the North Atlantic Oscillation and the El Niño-Southern Oscillation on Danube river flow variability. *Geophys. Res. Lett*., 31, L23203, doi:10.1029/2004GL020559.

Santos, J.F., Pulido-Calvo, I., Portela, M.M., 2010. Spatial and temporal variability of droughts in Portugal, *Water Resources Research*, 46, W03503, doi:10.1029/2009WR008071.

Thornthwaite, C.W., 1948. An approach toward a rational classification of climate. Geographical review, 38(1):55-94.

Tallaksen, L.M.; Madsen, H.; Clausen, B., 1997. On the definition and modelling of streamflow drought duration and deficit volume, *Hydrological Sciences Journal*, 42:15–33.

Trigo, R.M., D. Pozo-Vázquez, T.J. Osborn, Y. Castro-Diez, S. Gamiz-Fortis, and M.J. Esteban- Parra, 2004. North Atlantic Oscillation influence on precipitation, river flow and water resources in the Iberian Peninsula. *Int. J. Climatol*., 24, 925–944.

Venables, W.N. & Ripley, B.D., 2002. *Modern Applied Statistics with S.* Fourth edition. Springer.

Vicente-Serrano, S.M., 2005. *Las sequías climáticas en el calle medio del Ebro: factores atmosféricos, evolución temporal y variabilidad espacial*, Ser. Invest., vol. 49, Publ. Cons. de Prot. de la Nat. de Aragón, Zaragoza, Spain (in Spanish).

Vicente-Serrano, S.M., Beguería, S. and López-Moreno, J.I., 2010. A multiscalar drought index sensitive to global warming: the standardized precipitation evapotranspiration index. *Journal of climate*, 23(7):1696-1718.

Proceedings of the 10th World Congress of EWRA 'Panta Rhei', 5-9 July 2017, Athens, Greece
© 2017 *European Water Resources Association*

Peak drought severity time analysis of Cheongmicheon watershed using meteorological and hydrological drought index

S.H. Kim and E.-S. Chung*
Department of Civil Engineering, Seoul National University of Science & Technology, Seoul, Korea
* *e-mail: eschung@seoultech.ac.kr*

Abstract: This study analyzed the peak drought severity time of the Cheongmicheon watershed according to evaluation period based on 1) Past (period from 1985 to 2015) and 2) Future Climate Change scenarios (RCP 4.5 & 8.5 period from 2011 to 2100) . In order to assess the peak drought severity of lag time and relationships between various drought indices, we used meteorological and hydrological drought index. Standardized Precipitation Index (SPI) was based on precipitation and Standardized Precipitation Evapotranspiration Index(SPEI) was based on precipitation and evapotranspiration, were applied as meteorological drought index. Stream Drought Index (SDI) based on Runoff data was applied as hydrological drought index. In the case of SDI, we use Soil and Water Assessment Tool (SWAT) model for simulation of daily runoff data and SWAT Calibration and Uncertainty Procedures (SWAT-CUP) for optimization of SWAT parameters. In order to analyze the relationship between meteorological drought index and hydrological drought index, SDI was selected in the case of less than -1.5. We compare SPI, SPEI and SDI's peak drought severity time. As a result, in case of RCP 4.5, the difference of peak drought point between SDI and SPI was 0.8 months and SPEI was 0.54 months. In case of RCP 8.5, the difference of peak drought point between SDI and SPI was 0.89 months and SPEI was 0.99 months. And, when duration was increased, the frequency of drought was decreased. This confirmed that, SPEI gives a significant impact on SDI more than SPI.

Key words: Peak drought severity time, Meteorological drought index, hydrological drought index, SWAT

1. INTRODUCTION

Due to global warming, temperature is rising and precipitation is greatly changed, leading to an increase in evapotranspiration. As a result, areas of drought occurrence are widening, and drought severity and frequency are becoming serious. Various drought indices have been developed in order to minimize the damage of increasing drought areas and studies are being conducted to quantify the severity of drought (Du Pisani et al., 1998; Sung and Chung, 2014). Generally, drought is classified as agricultural, meteorological, hydrological, and socioeconomic droughts (Wilhite and Glantz, 1985; Correia et al., 1991).

Among the drought indices used to evaluate drought, Standardized Precipitation Index (SPI; Mckee et al., 1993) is easy to calculate and is most actively used because it can quantify the drought severity by the lack of precipitation. In recent years, Standardized Precipitation Evapotranspiration Index (SPEI; Vincente-Serrano et al., 2010) have been actively used to evaluate drought more physically by considering both precipitation and evapotranspiration (Lee et al., 2015). Furthermore, Nalbantis (2008) proposed a Streamflow Drought Index (SDI), a river water drought index, also proposed a method to distinguish severity and duration of drought with monthly flow.

Therefore, this study compares the difference between meteorological and hydrological drought indices at the time of peak drought severity, one of the characteristics of drought index. The study area is Chungmicheon watershed and the considered drought durations ranged from 60days to 270days in units of 30days, and the time of occurrence time of peak drought severity were analyzed using past and future scenarios. The past scenario is from 1985 to 2015 and the future scenario is analyzed from 2016 to 2100 using RCP 4.5/8.5. SPI and SPEI, which are meteorological drought indices, and SDI, a hydrological drought index were used as the drought index. The SWAT model was applied to the study watershed to simulate the runoff for calculating the hydrological drought

index.

2. MATERIALS AND METHODS

2.1 Study watershed

The Cheongmichun watershed, which is the target area of this study, includes all or a part of Yeongju, Yeongju, Icheon, Anseong, Yongin in Gyeonggi Province and Eumseong in Chungcheongbukdo. When it is divided into water unit map, it is divided into the Han River basin and the south Han River middle basin. The total area of the watershed is 596.13km^2. The weather data for the study were obtained from the Icheon observatory. The precipitation from 1985 to 2015 was collected and used. The annual average precipitation for 31 years was 1,372.8 mm, which is the lowest annual average precipitation of 791.5 mm, which is 57.5% of the average annual precipitation in 2014.

2.2 Meteorological and hydrological drought indices

The drought index is an important factor in this study. SPI and SPEI which are meteorological drought indices, and SDI, which is hydrological drought index, were used in this study.

The meteorological drought index, SPI, is calculated as creation of a precipitation time series by time unit, Parameter estimation using Pearson Type-Ⅲ (PT-Ⅲ) distribution, Estimation of the cumulative distribution function and calculation of the drought index applied to the standard normal distribution. Finally, SPI is divided into seven stages.

SPEI is calculated by the difference between precipitation and potential evapotranspiration (PET). Thornthwaite (Thornthwaite, 1948) method, which is easy to collect data, was applied to obtain PET. SPEI's drought classification standard is the same as SPI.

SDI is calculated using cumulative stream flow volume from different time period. According to Nalbantis and Tsakiris (2009), hydrologic droughts defined by SDI, is extreme drought if the value is below -2, severe drought below -1.5, moderate drought below -1, mild drought below 0 and value is more than 0, it is classified as not drought.

2.3 RCP scenarios

To project water quantity, we used the projected precipitation and temperature of RCP4.5 and RCP8.5 to build SWAT program which has already been calibrated. RCP8.5 assumes that the increase of greenhouse gas in the future will cause direct effect of 8.5 W/㎡ on the global climate system by 2100 and so is regarded as a scenario of extreme case which assumes that there will be no specific reduction policy, and the highest amount of greenhouse gases will be emitted, compared with RCP4.5.

2.4 SWAT formulation

The Soil and Water Assessment Tool (SWAT) model has been used effectively to estimate the runoff of a watershed considering soil characteristics, land use and various climatic conditions. The SWAT model is a semi - distributed long - run runoff simulation model that can be simulated daily for each watershed. It is divided into four kinds of parent types: hydrological, nutrient, soil loss, and river tracing.

Among these, the hydrologic parent type calculates the water balance on a daily basis by the continuous equation. The composition of the water balance includes water loss, runoff, groundwater

flow, evapotranspiration, surface, interception, and penetration. In this way, the runoff is calculated independently for each Hydrological Response Unit (HRU) and the runoff at the exit point of the watershed is calculated through the runoff trace.

For the observed flow in 2013, the simulated flow was optimized using the SUFI-2 algorithm. A total of 19 parameters were used to optimize parameters related to flow simulations. Monthly and seasonal volatility is well reproduced, and the corresponding monthly flow rates are similar. In order to make a more quantitative comparison, the Nash-Sutcliffe Efficiency (NSE) and correlation coefficient were compared together. NSE was 0.88 and correlation coefficient was 0.90.

3. RESULTS

3.1 Comparison of peak drought time occurring in the past

This study assessed the timing of meteorological and hydrological drought at the peak of drought severity based on hydrological drought by duration. For evaluation, drought was quantified, when the severity of SDI is less than -1.5, the difference of the peak occurrence time and duration of drought period are shown in Figure 1.

The 60–day duration of drought confirmed that SDI had a total of 9 severe droughts. The drought period of each drought index was 3.22 months for SDI, 2.44 months for SPI, 2.22months for SPEI. The difference between SDI, SPI and SPEI at the peak drought point is 1 month. The 90-day duration drought confirmed that, SDI had a total of 6 severe droughts. The drought period of each drought index was 4.83 months for SDI, 3.83 months for SPI, 4 months for SPEI. The differences in SDI at the peak drought point are 0.68 month for SPI and 1 month for SPEI, respectively. Also 120-day duration of drought confirmed that, SDI had a total of 5 severe droughts. The drought period of each drought index was 4.4 months for SDI, 4.2 months for SPI and SPEI. The difference between SDI, SPI and SPEI at the peak drought point is 0.8 month. The 150-day duration of drought confirmed that SDI had a total of 4 severe droughts. The drought period of each drought index was 4.5 months for SDI, 4.75 months for SPI, 5 months for SPEI. The difference between SDI, SPI and SPEI at the peak drought point is 0.5 month. Droughts from 180-day to 270-day duration were observed, and SDI had 2 severe droughts. At 180-day duration, the drought period was 7 months for SDI, 6.5 months for SPI and 7 months for SPEI. In 210-day duration, the drought period was 8 months for SDI, 7 months for SPI and SPEI. In 240-day duration, the drought period were 8.5 months for SDI, 7 months for SPI, 8 months SPEI and 270-day duration, the drought period were 7.5 months for SDI, 7 months for SPI, 7.5 months for SPEI, respectively. According to the difference in the point of peak occurrence, the 180 days SPI was 0.5 months, SPEI 1.5 months, the 210 days, SPI and SPEI were 0 month, the 240 days, SPI was 0.5 months, SPEI 1.5 months, and the 270 days, SPI was -1 months, SPEI -2 months. When compared to the overall average of duration, SDI and SPI differ by 0.51 month and SPEI differs by 0.72 month.

3.2 Comparison of peak drought time occurring in the RCP scenarios

This study selected RCP 4.5 and RCP 8.5 scenarios among future climate change scenarios to predict future drought. According to the drought assessment using the RCP4.5 scenario, SDI had a total of 29 drought events for a 60-day duration. The mean period drought in SPI, SPEI and SDI was 0.78, 0.78 and 1.17 months. Respectively, the mean difference of the SDI and peak drought occurrence point was 0.7 months for SPI and SPEI. SDI had a total of 30 drought events for a 90-day duration. The mean period drought in SPI, SPEI and SDI was 1.37, 1.6 and 1.57 months. The mean difference of the SDI and peak drought occurrence point was 0.67 months for SPI and 0.7 months for SPEI. SDI had a total of 21 drought events for a 120-day duration. The mean period drought in SPI, SPEI and SDI was 1.85, 2.13 and 2.48 months. The mean difference of the SDI and

peak drought occurrence point was 1 month for SPI and 0.27 months for SPEI. SDI had a total of 19 drought events for a 150-day duration. The mean period drought in SPI, SPEI and SDI was 2.33, 3.23 and 3.05 months. The mean difference of the SDI and peak drought occurrence point was 0.83 months for SPI and 0.23 months for SPEI. SDI had a total of 17 drought events for a 180-day duration. The mean period drought in SPI, SPEI and SDI was 3.47, 3.83 and 3.53 months. The mean difference of the SDI and peak drought occurrence point was 1.07 months for SPI and 0.42 months for SPEI. SDI had a total of 18 drought events for a 210-day duration. The mean period drought in SPI, SPEI and SDI was -3.94, 3.43 and 3.78 months. The mean difference of the SDI and peak drought occurrence point was 0.88 months for SPI and 0.86 months for SPEI. SDI had a total of 15 drought events for a 240-day duration. The mean period drought in SPI, SPEI and SDI was 4, 4.33 and 4 months. The mean difference of the SDI and peak drought occurrence point was 1 month for SPI and 0.92 months for SPEI. SDI had a total of 13 drought events for a 270-day duration. The mean period drought in SPI, SPEI and SDI was 4.33, 4 and 3.46 months. The mean difference of the SDI and peak drought occurrence point was 0.25 months for SPI and 0.18 months for SPEI. The result of the RCP 4.5 drought evaluation are shown in the following Figure 2.

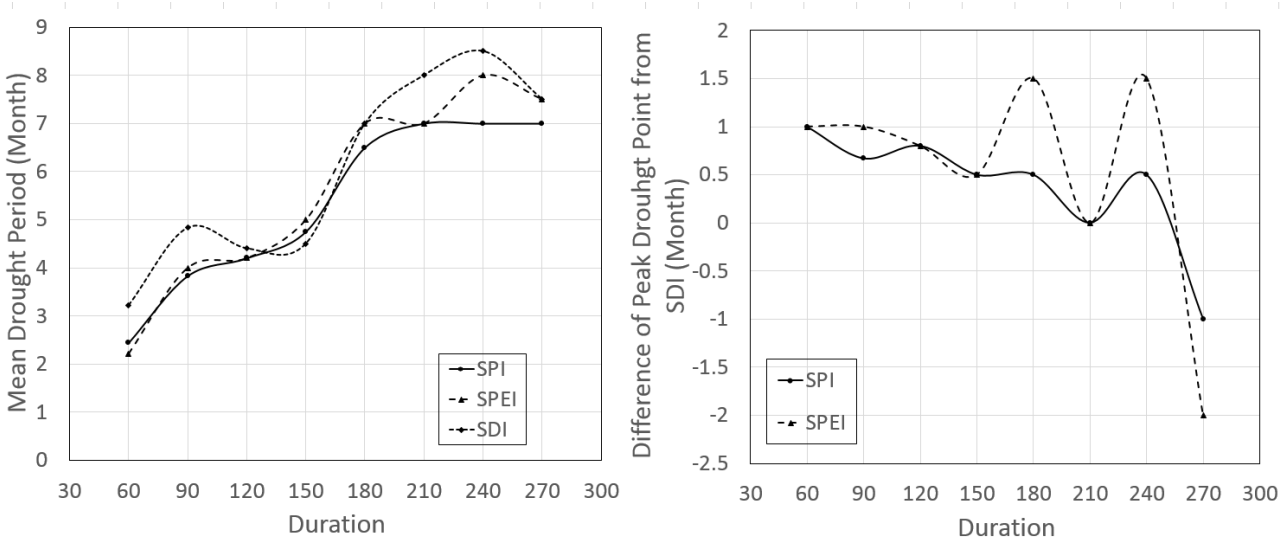

Figure 1. Results of mean drought period and difference peak occurred time in the past

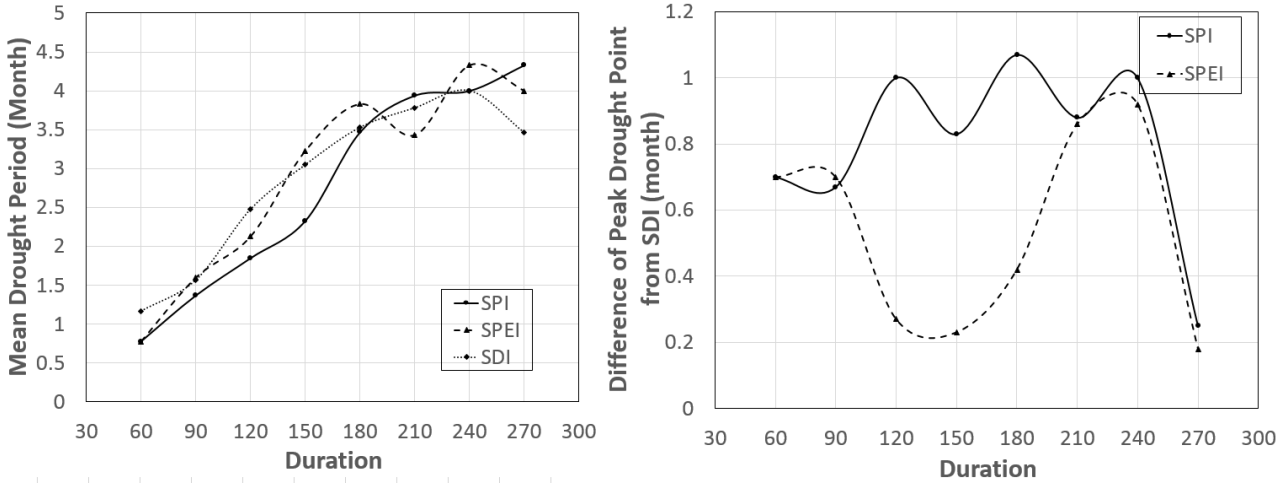

Figure 2. Results of mean drought period and difference peak occurred time in the RCP 4.5

According to the drought assessment using the RCP8.5 scenario, SDI had a total of 27 drought events for a 60-day duration. The mean period drought in SPI, SPEI and SDI was 0.44, 0.56 and 1.33 months. The mean difference of the SDI and peak drought occurrence point was 1.56 months

for SPI and 1.2 months for SPEI. SDI had a total of 25 drought events for a 90-day duration. The mean period drought in SPI, SPEI and SDI was 1.61, 1.58 and 1.48 months. The mean difference of the SDI and peak drought occurrence point was 0.83 months for SPI and 0.89 months for SPEI. SDI had a total of 22 drought events for a 120-day duration. The mean period drought in SPI, SPEI and SDI was 1.71, 1.94 and 1.64 months. The mean difference of the SDI and peak drought occurrence point was 0.95 months for SPI and 0.94 months for SPEI. SDI had a total of 22 drought events for a 150-day duration. The mean period drought in SPI, SPEI and SDI was 2, 1.75 and 1.86 months. The mean difference of the SDI and peak drought occurrence point was 0.6 months for SPI and 0.94 months for SPEI. SDI had a total of 19 drought events for a 180-day duration. The mean period drought in SPI, SPEI and SDI was 2.06, 2.85 and 2.37 months. The mean difference of the SDI and peak drought occurrence point was 0.94 months for SPI and 0.92 months for SPEI. SDI had a total of 18 drought events for a 210-day duration. The mean period drought in SPI, SPEI and SDI was 2.18, 2.85 and 2.89 months. The mean difference of the SDI and peak drought occurrence point was 0.53 months for SPI and 0.85 months for SPEI. SDI had a total of 16 drought events for a 240-day duration. The mean period drought in SPI, SPEI and SDI was 2.71, 2.9 and 2.94 months. The mean difference of the SDI and peak drought occurrence point was 0.93 months for SPI and 1.1 months for SPEI. SDI had a total of 15 drought events for a 270-day duration. The mean period drought in SPI, SPEI and SDI was 3.14, 4 and 3.13 months. The mean difference of the SDI and peak drought occurrence point was 0.79 months for SPI and 1.09 months for SPEI. The result of the RCP 4.5 drought evaluation are shown in the following Figure 3.

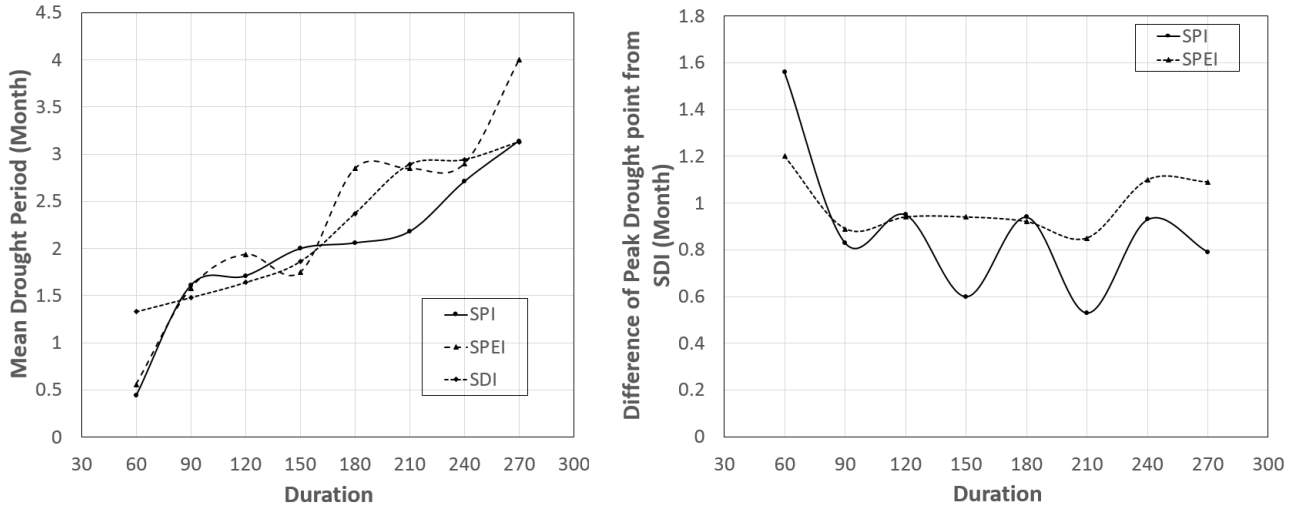

Figure 3. Results of mean drought period and difference peak occurred time in the RCP 8.5

4. CONCLUSION

This study assessed and predicted past drought (from 1985 to 2015) and future drought (form 2016 to 2100) using two meteorological drought indices and one hydrological drought index. In order to evaluate the future drought, the RCP scenarios were applied. Study area is Chungmicheon watershed located in Korea

At this time, the daily flow rate data used in SDI was calculated using SWAT model, and the weather data obtained from the Icheon Observatory. For effective comparison, only the drought severity of SDI was evaluated to be -1.5 or less. The past droughts from 1985 to 2015 were assessed by durations. Based on the SDI, the difference in peak drought occurrence point was 0.59 months for SPI and 0.72 months for SPEI, and Maximum difference was 2 months for both of SPI and SPEI.

As a result of evaluating the future drought from 2016 to 2100 using the RCP scenarios are follows. For RCP 4.5, mean period of drought by SPI was 2.76 months, SPEI was 2.92 months and

SDI was 2.88 months. The mean difference in peak drought occurrence point was 0.8 months for SPI and 0.54 months for SPEI, and mean maximum difference was 9 months for SPI and 7 months for SPEI. And in the case of RCP 8.5, mean period of drought by SPI was 1.98 months, SPEI was 2.3 months and SDI was 2.21 months. The mean difference in peak drought occurrence point was 0.89 months for SPI and 0.99 months for SPEI, and mean maximum difference was 5 months for both of SPI and SPEI.

It was confirmed that the meteorological drought affects the hydrological drought as the peak drought occurrence point was confirmed. However, in addition to the SPI, SPEI and SDI used in this study, various drought indices are considered to be necessary. Therefore, the follow-up study will be applied to various watershed evaluation and evaluation using various drought index, and sill study drought according to watershed size.

ACKNOWLEDGMENTS

This research was supported by a grant (14AWMP-B82564-01) from Advanced Water Management Research Program funded by Ministry of Land, Infrastructure and Transport of Korean government and also supported by the funding from the Basic Science Research Program of the National Research Foundation of Korea (NRF), which is funded by the Ministry of Education (NRF-2016R1D1A1B04931844).

REFERENCES

Ministry of Land, Infrastructure and Transport. 2012. Report of Cheongmicheon river master plan.

Beven, K. 1989. Changing ideas in hydrology-the case of physically-based models. Journal of. Hydrology, Vol. 105, 157–172.

Beven, K. 2002. Towards an alternative blueprint for a physically based digitally simulated hydrologic response modelling system. Hydrological Processes, Vol. 16, 189–206.

Correia, F.N., Santos, M.A., and Rodrigues, R.P. 1991. Reliability in regional drought studies. Water Resources Engineering Risk Assessment, 63-72.

Du Pisani, C.G., Fouché, H.J., and Venter, J.C. 1998. Assessing rangeland drought in South Africa. Agricultural Systems, Vol. 57, No. 3, 367-380.

Lee, B.R., Sung, J.H., and Chung, E.S. 2015 Comparison of meteorological drought and hydrological drought index. Journal of Korea Water Resources Association, Vol. 48, No. 1, 69-78.

McKee, T.B., Doeskin, N.J., and Kleist, J. 1993. Drought monitoring with multiple time scales. Proceeding of 9th Conference on Alied Climatology, American Meteorological Society, 233-236.

Nalbantis, I. 2008. Evaluation of a hydrological drought index. European Water, Vol. 23, No. 24, 67-77.

Sorooshian, S., and Gupta, V. 1995. Chapter 2: Model calibration. Computer Models of Watershed Hydrology, Singh VP, Publications, LLC, Highlands Ranch, CO, 23–68.

Sung, J., and Chung, E.S. 2014. Development of stream drought severity-duration-frequency curves using the threshold level method. Hydrology and Earth System Science. Vol. 18, 3341-3351

Vicente-Serrano, S.M., Begueria, S., and Lopez-Moreno, J.I. 2010. A multiscalar drought index sensitive to global warming: the standardized precipitation evapotranspiration index. Journal of Climate, Vol. 23, No.7, 1696-1718.

Wilhite, D.A., and Glantz, M.H. 1985. Understanding: the drought phenomenon: The role of definitions. Water International, Vol. 10, No. 3, . 111-120.

Won, K.J., Sung, J.H., and Chung, E.S. 2015. Parametric assessment of water use vulnerability of South Korea using SWAT model and TOPSIS. Journal of Korea Water Resources Association, Vol. 488, 657-657.

Won, K.J., Chung, E.S. 2016. Drought analysis of Cheongmicheon watershed using meteorological, agricultural, and hydrological drought indices. Journal of Korea Water Resources Association, Vol. 496, 509-518.

Proceedings of the 10th World Congress of EWRA 'Panta Rhei', 5-9 July 2017, Athens, Greece
© 2017 *European Water Resources Association*

Wavelet transform based trend analysis for drought variability over 566 stations in India

M.K. Goyal* and A. Sharma
Department of Civil Engineering, Indian Institute of Technology Guwahati, India
* *e-mail: vipmkgoyal@gmail.com*

Abstract: Drought, which occurs in all climate zones, is the most complex hydro-meteorological hazard. This paper presents an analysis of the spatial pattern of trends in drought variables carried out at 566 stations spread all across India over 102 years (1901 to 2002). As a measure of drought intensity, standardized precipitation index (SPI) was computed at all stations. Six drought variables namely annual SPI, monsoon SPI, non-monsoon SPI, annual drought severity (ADS), annual drought duration (ADD) and annual drought peak (ADP) were computed at station level. Mann-Kendall (MK) test and Sen's slope were used for trend analysis of drought variables. Discrete wavelet transform (DWT) along with MK test was used to identify the dominant periodic components in trends. Further, continuous wavelet transform (CWT) based global wavelet spectrum (GWS) was used to examine the significant periodic components. The results of the study show an increasing trend in drought for eastern, north-eastern and extreme southern regions, and a decreasing trend for northern and southern regions. Trends were influenced by 2-4 year periodic component in southern India, 4-8 years periodic component in western, eastern and north-eastern India, 8-64 year periodic components in middle India and 32-128 years periodic components in northern India. CWT based GWS shows that most of the periodic components were not significant.

Key words: Drought trend analysis, Discrete wavelet transform, Continuous wavelet transform, Mann-Kendall test

1. INTRODUCTION

Drought is a well-known natural phenomenon, which occurs frequently in different parts of the world. It is defined by the persistent shortage of water in meteorological, hydrological, agricultural, socioeconomic or groundwater systems for a longer period such as a season or year. The phenomenon is not limited to the arid regions (i.e. the regions with less rainfall) but occurs in all climate zones (i.e. in regions of high as well as low rainfall) (Mishra and Singh 2010). Rapid growth in population and the expansion of industrialization and agriculture have resulted in a rise in water demand in various parts of the world, especially in developing countries like India. Hence, in order to fulfill the demands, the available water resources have been exploited above the sustainable limits, which are leading to anthropogenic droughts. Further, global warming and climate change are believed to aggravate the drought patterns around the globe (IPCC 2007; Dai 2011; Trenberth et al. 2014).

India is a developing country, which relies mainly on the agricultural sector for its economic growth. The rain-fed agriculture is predominant in India, which makes agriculture dependent on climatic conditions, primarily on rainfall. Droughts or long-term deficient rainfall are a serious threat to the national food security. Indian sub-continent had around 27 drought years between 1875 and 2005 (Shewale and Kumar 2005), some of which had created a deficit in food production (Mishra and Singh 2010). The spatiotemporal assessment of drought occurrence is vital for the better understanding of drought patterns, forecasting, and preparedness. Many studies have examined the spatiotemporal patterns of droughts in India (Shewale and Kumar 2005; Pai et al. 2011; Jain et al. 2015; Joshi et al. 2016). Most of these studies were focused on the traditional methods of trend analysis. However, it has been reported that these methods are not efficient for non-stationary hydro-climatologic variables (Adamowski et al. 2009). Hence, the wavelet methods have emerged as an effective tool for the analysis of hydro-climatological variables (Torrence and

Compo 1998). Adamowski et al. (2009) reported that the wavelet based methods offer an effective tool for detection and estimation of complicated signals present in hydrological time series. Araghi et al. (2015) used the discrete wavelet transform (DWT) along with Mann-Kendall (MK) trend test for find out the long term temperature trends and dominant periodicities in Iran. The continuous wavelet transform (CWT) is also found effective in trend detection and finding the dominant periodic components (Adamowski et al. 2009; Joshi et al. 2016).

This study presents a long-term trend analysis of six drought variables at 566 stations in India over 102 years (1901 to 2002). The drought variables were computed based on standardized precipitation index (SPI). Drought variables include annual drought severity, annual drought duration, annual drought peak, annual SPI, monsoon SPI and non-monsoon SPI. DWT along with the Mann-Kendall Test was used for trend analysis and identification of periodic component at station level. CWT was used for finding the significant periods of variability.

2. STUDY AREA AND DATA

We took 566 districts of India for this study. In general, the northeastern region of the country receives high rainfall, whereas the western regions receive less rainfall. In the southern parts of the country, Western Ghats receive high rainfall. Mean monthly precipitation data for 102 years (from 1901 to 2002) was used for this study. The source for data was India water portal. Complete rainfall time series of rainfall was available at all stations and hence no preprocessing was done on the data.

3. METHODOLOGY

3.1 Standardized Precipitation Index (SPI)

SPI is one of many drought indices present in literature. It was proposed by McKee et al. (1993) and, thereafter, has been used in many drought studies. It offers some advantages such as: 1) it requires only rainfall data; 2) it can be used for different timescales; 3) it is not adversely affected by the topography; and 4) it can be used to compare stations in different climate zones due to the use of standard normal distribution. The negative values represent the dry conditions, whereas the positive values represent the wet conditions. For more details about SPI, its computation and applications, the reader is referred to McKee et al. (1993); Mishra and Desai (2005) and Goyal and Sharma (2016).

3.2 Wavelet Transform (WT)

Wavelet analysis, introduced by Grossmann and Morlet (1984), is an advanced mathematical tool that is capable of providing the time-frequency representation of a signal or time series. WT splits the signal into wavelets of finite duration and zero mean (Torrence and Compo 1998). These wavelets are localized in both frequency and time domains. There are two forms of WT, discrete wavelet transform (DWT) and continuous wavelet transform (CWT). In the case of DWT, the WT is applied using a discrete set of the wavelet scaling and shifting, whereas, in the case of CWT, the WT is applied for a continuous scaling and shifting. DWT decomposes the signal into high and low-frequency components called detail (D) and approximation (A) components respectively. The A component provides information about important characteristics of the signal and is important for the trend analysis. A number of studies have used DWT for trend analysis and identification of dominant periodic components in the data (Araghi et al. 2015; Joshi et al. 2016). A wide range of literature is available on wavelet transform and its application in hydrology; hence, it is not discussed in detail here. For more details about the basic concepts of WT, the reader is referred to

Grossmann and Morlet (1984); Mallat (1989) and Daubechies (1990). Further information regarding the applications of wavelet transform in hydrology and meteorology can be found in Nason and von Sachs (1999); Adamowski et al. (2009); Belayneh and Adamowski (2013); Nourani et al. (2014) and Araghi et al. (2015).

3.3 Procedure

Based on the methods discussed above, following procedure was adopted to carry out this study:

1. First, 6-month SPI (SPI6) was computed at 566 stations using the mean monthly rainfall data. SPI6 was used to identify the beginning and ending of drought events. The annual drought duration (ADD), annual drought peak (ADP) and annual drought severity (ADS) were computed at all stations. Further, annual SPI (A-SPI), monsoon SPI (M-SPI) and non-monsoon SPI (N-SPI) series were also computed at all stations.
2. MK (Mann 1945; Kendall 1975) test and Sen's slope (Sen 1968) test were performed on six drought variables at all stations. To examine the statistical significance of the trend, a significance level of 0.05 (i.e. p-value $\leq$ 0.05) was used.
3. The series of drought variables was decomposed using DWT to get the A and D components. MK test was used to analyze the presence of a trend in A, D, and the combinations of A and D components.
4. Dominant periodic components were identified based on the comparison of MK test Z-statistics of original series and A + D components.
5. Further, significant periods of variability was found using CWT based global wavelet spectrum (GWS).

4. RESULTS AND DISCUSSION

Figure 1 shows the results of the trend analysis of drought variables at 566 stations. Figure 1(a) shows that many stations had a non-significant trend for A-SPI. Significant increasing trends were found for north-western and southern parts, whereas significant decreasing trends were found for northern and central parts. It should be noted that decreasing trend in SPI implies an increase in drought events, whereas the reverse is true of ADS, ADS, and ADP. Table 1 presents the number of stations with increasing or decreasing trends for different variables. Stations having a decreasing trend (294) were more compared to those having an increasing trend (272). However, stations with the significant increasing trend (84) were more than those with the significant decreasing trend. In the case of M-SPI (Figure 1b), significant increasing trends were found for north-western regions and significant decreasing trends were found for northern regions. The southern part of the country showed increasing trend, however, only a few stations had significant trends. Stations with the significant decreasing trend (90) were more than the stations with significant increasing trends (39). This shows that overall there was a decreasing trend in M-SPI, which signifies an increase in monsoon droughts, especially in northern, eastern and north-eastern regions. Figure 1(c) and Table 1(d) shows that there is no station with the significant decreasing trend for N-SPI. However, many stations (74) in north-central and northern regions had a significant decreasing trend in N-SPI. Figure 1(d) shows increasing trends in ADS for most of the stations in eastern and north-eastern regions. A cluster of stations with significant increasing trend can be seen in northern regions of the Bihar state. The significant decreasing trend can be seen for north-western and southern regions. Out of 566 stations, 90 stations had a significant decreasing trend in drought severity, whereas only 50 stations had a significant increasing trend. Figure 1(e) shows a similar pattern of trends for ADD. Figure 1(f) shows significant increasing trends in ADP for northeastern, eastern and extreme southern parts; whereas station is northwestern regions and mid-southern regions showed significant decreasing trends. The number of stations with significant decreasing and increasing trend were 107 and 25 respectively. Overall, it can be summarized that increasing trend in droughts

was found for eastern and north-eastern regions, whereas a decreasing trend was found for north-western and mid-southern parts. No significant trends were found in western and central India.

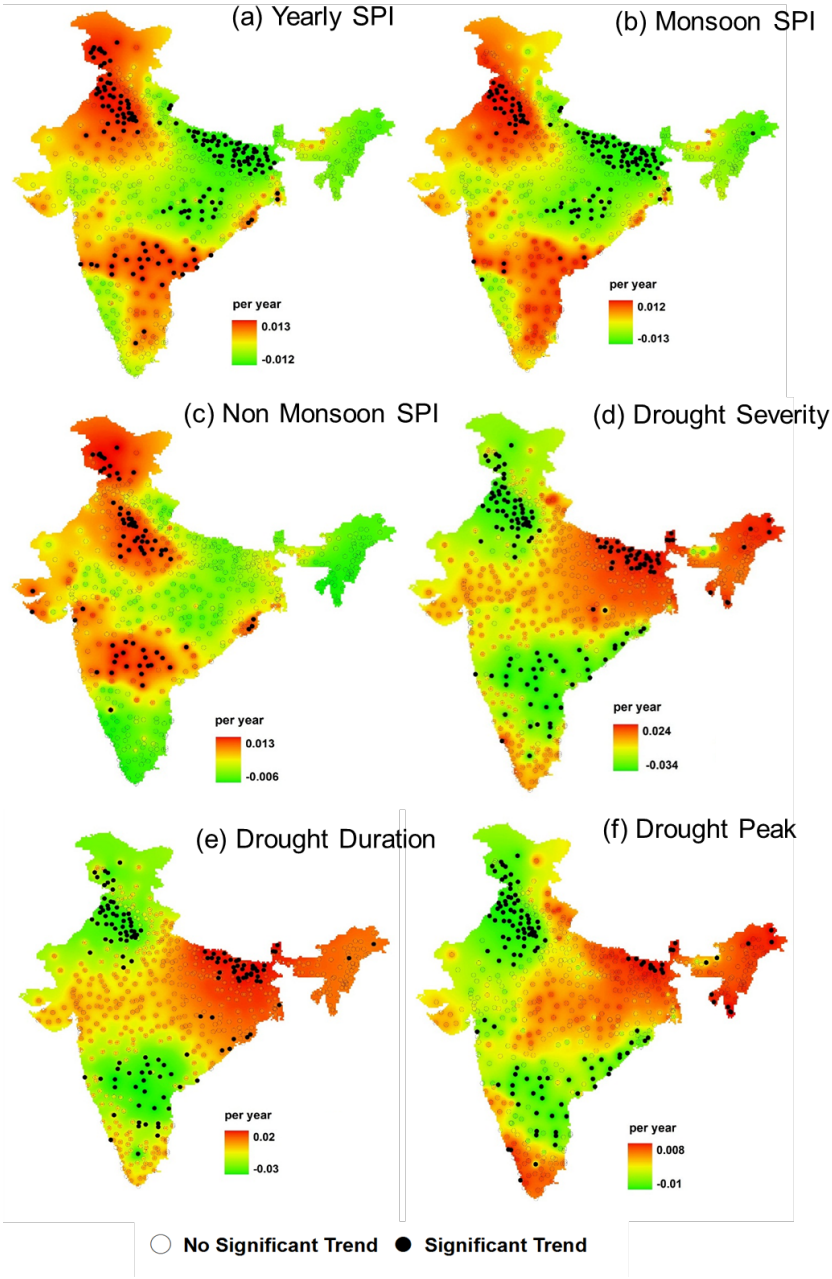

Figure 1. Trend analysis for different drought variables at 566 stations in India

The drought variables were decomposed using DWT as mentioned in the methodology section. After getting the decomposed A and D components at all stations, A+D components were calculated for six drought variables. Trend analysis was carried out for A, D and A+D components. Studies have shown that A + D combination is useful in determining the dominant periodicity components (Araghi et al. 2015; Joshi et al. 2016) Due to the space limitation, we are not presenting the complete results for trend analysis of A, D, and A+D components; instead, only results for dominant periodicity are discussed. The dominant periodic components were identified by comparing the MK-Z statistics of A + D component with the Z statistics for original series (Joshi et al. 2016). Figure 2 shows the results for dominant periodic components of trend for different drought variables. Figure 2(a) shows the spatial distribution of dominant periodic component for A-SPI. It is seen that most of the stations were influenced by a dominant periodicity of 2 to 8 years, however, some parts of northern and northeastern India were influenced by higher periodic

components (low frequency). From Figure 2(b), M-SPI was also influenced mainly by low periodic components (2-8 years). For N-SPI (Figure 2c), although, most of the stations were influenced by low periodic components, but trends at few stations in northern and extreme southern regions were dominated by 32-64 years periodic components. Figure 2(d) shows that 2-4 year periodic components were dominant for trends in ADS in most parts of the country except for some parts of central and northern India. The 32-64 year periodic components were found dominating in these regions. Figure 2(e) shows that the number of stations with a dominant periodic component of 2-4 years have reduced for ADD. More stations had 8-32 year dominant periodic component compared to other drought variables. The trend in northern regions and some parts of central regions were again dominated by 32-64 year periodic components. For ADP (Figure 2f), there was a wide range of periodic components influencing the trends. In eastern, western and southern regions, 2-4 year periodic components were dominating the trend. In northeastern and middle regions 8-16 year periodic components were more dominating, whereas in some parts of northern India 32-128 year periodic component was found dominating.

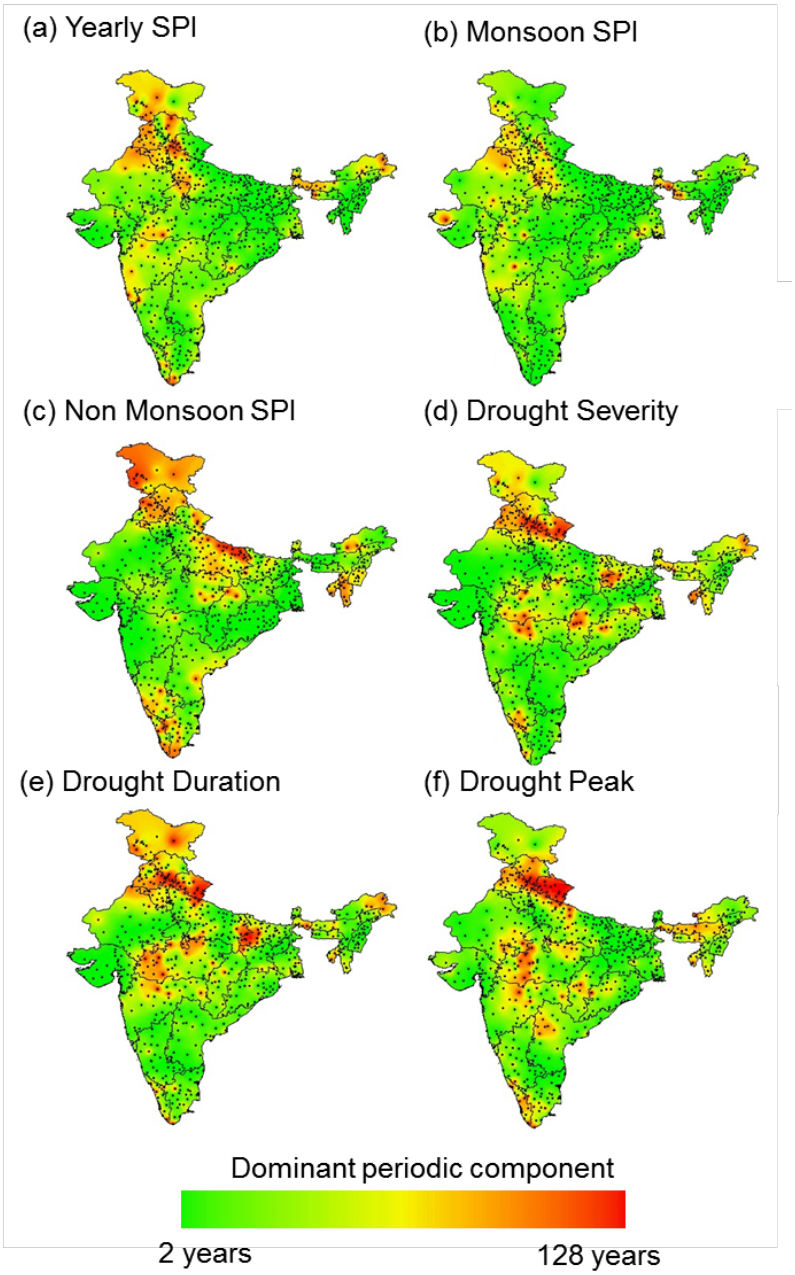

Figure 2. Dominant period component for different drought variables at 566 stations in India

Overall, it can be summarized that the trends in drought variables were influenced by 2-4 year periodic component in southern region, 4-8 years periodic component in the western, eastern and northeastern region, and 8-64 periodic components in the middle region and 32-128 years periodic components in the northern region. To investigate whether the periodic components found using DWT and MK test, CWT based GWS was used to identify the significant periodic component in the series. Results are not discussed in details here. The number stations with a significant periodic component for different drought variables are shown in Table 1(e). It can be seen that for most of the stations there was no significant periodic component influencing the trend. Maximum (117) and minimum (27) number of stations with significant periodic components were obtained for M-SPI and N-SPI respectively.

Table 1. Number of stations having increasing, decreasing, significant-increasing and significant decreasing trends for different drought variables.

Drought variable	Number of stations having				
	Increasing trend (a)	Decreasing trend (b)	Significant increasing trend (c)	Significant decreasing trends (d)	Significant period of variability (e)
Annual SPI	272	294	84	79	100
Monsoon SPI	253	312	39	90	117
Non monsoon SPI	400	164	74	0	27
Annual drought severity	240	326	50	98	83
Annual drought duration	254	310	44	90	97
Annual drought peak	231	335	25	107	54

5. CONCLUSIONS

Trend analysis of six drought variables was carried out at 566 stations in India. Based on Mann-Kendall (MK test), increasing trend in droughts in eastern, northeastern and extreme southern region was found, whereas decreasing trend was found for the stations in northern and southern regions. It should be noted that trends at most of the stations were non-significant. Discrete wavelet transform (DWT) along with MK test was used to find out the dominant periodic components in trend for different drought variables for all stations. It is found that trends in drought variables are influenced by 2-4 year periodic component in southern India, 4-8 years periodic component in western, eastern and northeastern India, and 8-64 periodic components in middle India and 32-128 years periodic components in northern India. In order to identify the significant periodic components, global wavelet spectrum (GWS) obtained using continuous wavelet transform (CWT) was used. It was found that trends at most of the stations were not influenced by any significant periodic component.

REFERENCES

Adamowski K, Prokoph A, Adamowski J (2009) Development of a new method of wavelet aided trend detection and estimation. Hydrol Process 23:2686–2696.

Araghi A, Mousavi Baygi M, Adamowski J, et al (2015) Using wavelet transforms to estimate surface temperature trends and dominant periodicities in Iran based on gridded reanalysis data. Atmos Res 155:52–72.

Belayneh A, Adamowski J (2013) Drought forecasting using new machine learning methods. J Water L Dev 18:3–12.

Dai A (2011) Drought under global warming: A review. Wiley Interdiscip Rev Clim Chang 2:45–65.

Daubechies I (1990) The wavelet transform, time-frequency localization and signal analysis. IEEE Trans Inf Theory 36:961–1005.

Goyal MK, Sharma A (2016) A fuzzy c-means approach regionalization for analysis of meteorological drought homogeneous regions in western India. Nat Hazards 84:1831:1847.

Grossmann A, Morlet J (1984) Decomposition of hardy functions into square integrable wavelets of constant shape. SIAM J Math Anal 15:723–736.

IPCC (2007) Climate Change 2007: Synthesis report. Contribution of working group I, II and III to the fourth assessment report of the Intergovernmental Panel on Climate Change. Geneva, Switzerland

Jain VK, Pandey RP, Jain MK (2015) Spatio-temporal assessment of vulnerability to drought. Nat Hazards 76:443–469.

Joshi N, Gupta D, Suryavanshi S, et al (2016) Analysis of trends and dominant periodicities in drought variables in India: A wavelet transform based approach. Atmos Res 182:200–220.

Kendall MG (1975) Rank Correlation Methods. Griffin, London.

Mallat SG (1989) A Theory for Multiresolution Signal Decomposition: The Wavelet Representation. IEEE Trans Pattern Anal Mach Intell 11:674–693.

Mann HB (1945) Nonparametric Tests Against Trend. Econometrica 13:245–259.

McKee TB, Doesken NJ, Kleist J (1993) The relationship of drought frequency and duration to time scales. In: AMS 8th Conference on Applied Climatology. Anaheim, California, pp 179–184.

Mishra AK, Desai VR (2005) Drought forecasting using stochastic models. Stoch Environ Res Risk Assess 19:326–339.

Mishra AK, Singh VP (2010) A review of drought concepts. J Hydrol 391:202–216.

Nason GP, von Sachs R (1999) Wavelets in time-series analysis. Philos Trans R Soc London Ser A- Math Phys Eng Sci 357:2511–2526.

Nourani V, Hosseini Baghanam A, Adamowski J, Kisi O (2014) Applications of hybrid wavelet-Artificial Intelligence models in hydrology: A review. J Hydrol 514:358–377.

Pai DS, Sridhar L, Guhathakurta P, Hatwar HR (2011) District-wide drought climatology of the southwest monsoon season over India based on standardized precipitation index (SPI). Nat Hazards 59:1797–1813.

Sen PK (1968) Estimates of the regression coefficient based on Kendall’s Tau. J Am Stat Assoc 63:1379–1389.

Shewale MP, Kumar S (2005) Climatological features of drought incidences in India. Report: 21/2005, Indian Meteorological Department, Pune.

Torrence C, Compo GP (1998) A practical guide to wavelet analysis. Bull Am Meteorol Soc 79:61–78.

Trenberth KE, Dai A, van der Schrier G, et al (2014) Global warming and changes in drought. Nat Clim Chang 4:17–22.

Proceedings of the 10th World Congress of EWRA 'Panta Rhei', 5-9 July 2017, Athens, Greece
© 2017 *European Water Resources Association*

Frequency and severity of dry spell phenomenon in Ghezala Dam reservoir (Tunisia)

M. Mathlouthi[1*] and F. Lebdi[2]
[1] *Research Laboratory in Sciences and Technology of Water in National Agronomic Institute of Tunisia, 43 Avenue Charles Nicolle, 1082 Tunis, Tunisisa*
[2] *National Agronomic Institute of Tunisia (INAT), University of Carthage, 43 Avenue Charles Nicolle, 1082 Tunis, Tunisia*
[*] *e-mail: majid_mathlouthi@yahoo.fr*

Abstract: An analysis by event of dry event, according to a predetermined threshold, from series of observations of the daily rainfall was carried out. The approach has been illustrated on a case study of the Ghézala dam localized Northern Tunisia where the average rainfall is 680 mm. The dry events are constituted of a series of dry days framed by the rainfall event. Rainfall events are defined themselves in the form a uninterrupted series of rainfall days understanding at least a day having received a precipitation superior to a threshold of 3.6 mm. The rainfall events are defined by depth and duration, which are found to be correlated. An analysis of the depth per event conditioned on the event duration has been undertaken. The negative binomial distribution appears the best overall fit for the depth per event. The duration of the rainfall event follows a geometric distribution while that the dry event follows the negative binomial distribution. The length of the climatically cycle adjusts to the Incomplete Gamma. This analysis is used to generate a synthetic sequence of rainfall and dry events with correspondent lengths of rainy season for study the water resources management and the impact of climate change.

Key words: event-based analysis, dry event, rainfall event, severity

1. INTRODUCTION

Proper simulation of precipitation is important. Precipitation is a very important climatological element of climate that affects both the natural environment and human society. Events ranging from prolonged droughts to short-term, high intensity floods are often associated with devastating impacts both to society and the environment (Hui and al., 2005). An alternative to the Markov chain process which is typically used to simulate the occurrence of precipitation, is to use a wet-dry spell or alternating renewal model based on the alternate extraction of wet and dry spell durations from their known probability distributions. Earlier studies using the wet-dry spell approach are, for example, Bogardi and Duckstein (1993), Semenov and Barrow (1997), Wilks (1999), Mathlouthi and Lebdi (2007, 2008, 2015), Mathlouthi (2009). As said before this study focuses on the modelling of rainfall occurrences under a Mediterranean climate by a wet-dry spell approach. An event-based concept of analysis is favoured over continuous type data generations methods. Synthetically produced rainfall data can be used, for example, for reservoir simulation studies, estimation of irrigation water demand and the study of the effects of climate change. The paper concentrates solely on the characterization of the events of the dry spell in a basin in Northern Tunisia.

2. DATA

The daily precipitation records have been collected by the Ghézala-dam rain gauge, located in the basin of Ichkeul in Northern Tunisia (lat. 37°02'75"N, long. 9°32'07"E) (Fig. 1). The rainy season starts in September and lasts until the beginning of May. The mean annual rainfall amounts 680 mm; the coefficient of variation is 0.25. The climate of the Ichkeul basin is classified as sub-

humid; average annual rainfall is below 40 percent of the total annual potential evaporation. Except in wet years, most precipitation is restricted to the winter months in this basin. The dry season lasts from May to August. Daily values of precipitation are quite variable. There is also considerable variation from year to year. A complete time serie of daily precipitation exists for the period from 1968 to 2007. In this 40-year period the highest annual amount was recorded in 1982, with 1037.8 mm, and the lowest amount in 1977, with 394.8 mm. Of the 480 months that constitutes this sample, 13% of the months had less than 1.0 mm of rainfall. On average, the wettest month was December, with 105.5 mm of rainfall, and the driest months were July and August, with less than 3 mm of rainfall each.

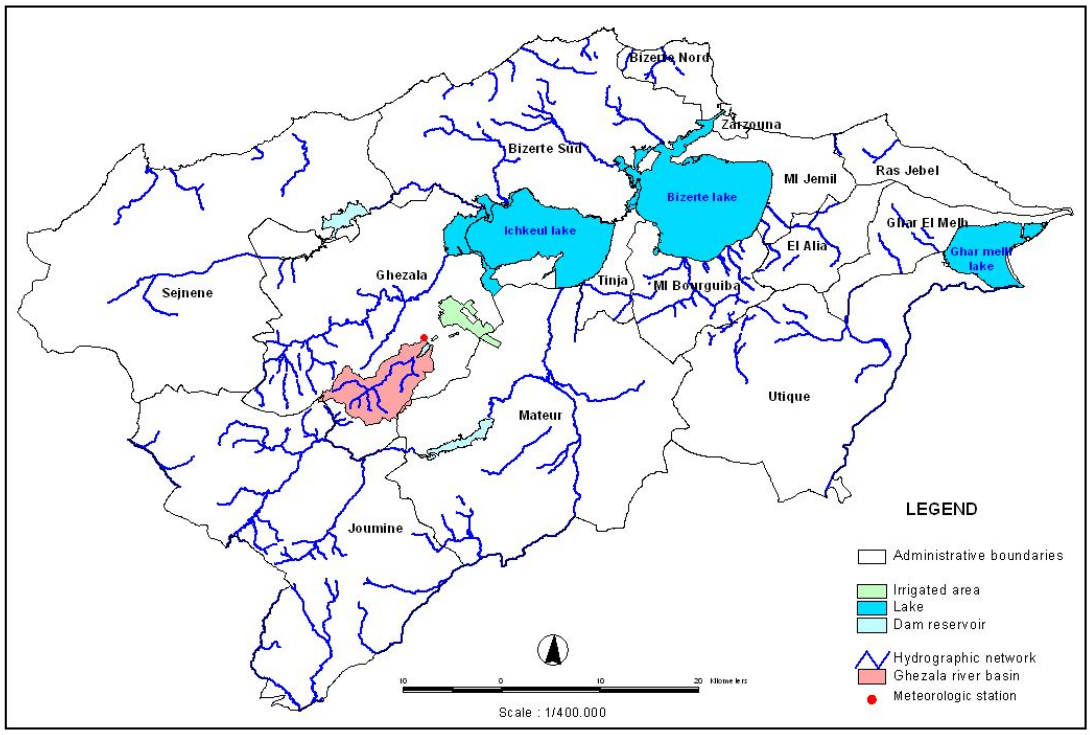

Figure 1. Case study: Ghézala dam (Tunisia)

3. METHODOLOGY

In a *wet-dry spell* approach, the time-axis is split up into intervals called *wet periods* and *dry periods*. A rainfall *event* is an uninterrupted sequence of wet days. The definition of an event is associated with a daily rainfall threshold value of 4 mm d^{-1} which defines a *wet day*. The choice of this threshold corresponds to the expected daily evapotranspiration rate, marking the lowest physical limit for considering rainfall that may produce utilizable surface water resources. In this approach, the process of rainfall occurrences is specified by the statistical distributions of the length of the wet periods (storm duration), and of the length of the dry periods (time between storms or inter-event time).

The rainfall event m in a given rainy season n will be characterized by its duration $D_{n,m}$, the temporal position within the rainy season, the dry event or inter-event time $S_{n,m}$ and by the cumulative rainfall amounts of $H_{n,m}$ of $D_{n,m}$ rainy days in mm:

$$H_{n,m} = \sum_{i=1}^{Dn,m} h_i \tag{1}$$

where h_i is positive and represent the daily precipitation totals in mm. Note that for at least one $h_i>4\ mm$.

The varying duration of events requires that the cumulative rainfall amounts of each event should be conditioned by the duration of the event. The identification and fitting of conditional probability distributions to rainfall amounts may be a problem especially in the case of short records and for events with extreme (long) durations (Foufoula-Georgiou and Georgakakos, 1991).

In this paper a rainy season, of random duration, starts and ends with a rainfall event. Its length L_n is defined as the time span between the start of the first and the end of the last rain event and is the sum of all durations of wet and dry events. Thus, if the number of wet events per rainy season is N_n, then the number of dry events is N_n *-1*. The climatic cycle C_n is determined by the time lapse between the onset of two subsequent rainy seasons.

4. RESULTS

A regression analyses have been conducted in order to detect the interrelationship between the parameters extracted from the analysis by events. Table 1 summarizes, for some selected parameters, the maximum value of coefficients of determination. The relationship between event duration $D_{n,m}$ and the cumulative rainfall amounts $H_{n,m}$ is medium, while no significant pairwise correlation could be detected (Table 1) between $S_{n,m}$ and the duration $D_{n,m}$ and cumulative rainfall amounts $H_{n,m}$. Thus, the assumption that rainfall events in a rainy season are elements of an independent random process seems to be justified. Table 1 shows that the number of events per season, N_n, is roughly independent of the other parameters except, as might be expected, of the total event-based rainfall depth $H_{t,n}$ (sum of cumulative rainfall amounts $H_{n,m}$). The length of the climatic cycle C_n is independent of the number of events per season N_n, however it shows a dependence of the length of the rainy season L_n.

Table 1. Coefficients of determination for the parameters of the analysis by events

Seasonal characteristics	N_n	$S_{n,m}$ max (day)	C_n (day)
$H_{t,n}$ (mm)	0.49	0.50	0,02
L_n (day)	0.33	0.21	0.62
C_n (day)	0.22	0.23	1
Event-related characteristics	$H_{n,m}$ (mm	$D_{n,m}$ (day)	
$D_{n,m}$ (day)	0.64	1	
$S_{n,m}$ (day)	0.02	0.02	

$S_{n,m}$ max : *Longest dry event of the rainy season (day)*

4.1 Number of events per rainy season

By taking account of the assumption of the sequential independence of the rainfall events, as formulated above, the Poisson density function should adequately describe the distribution of the number of events per season:

$$f\left(N,\lambda\right)=\frac{e^{-\lambda}\lambda^{N}}{N!}\ ,N\ =\ 0,1,2,... \tag{2}$$

where N describes the number of events during a rainy season. The parameter λ is the average number of events per rainy season.

Fig. 2 shows the fitted Poisson probability density function. The arithmetic mean is 22.54 and the standard deviation 4.67. The goodness-of-fit has been assessed by the Kolmogorov-Smirnov test at the 95% significance level. The arithmetic mean appears to provide a stable estimate of the parameter λ of the Poisson pdf, in preference to the sample variance, which shows more substantial fluctuations (Bogardi and al., 1988).

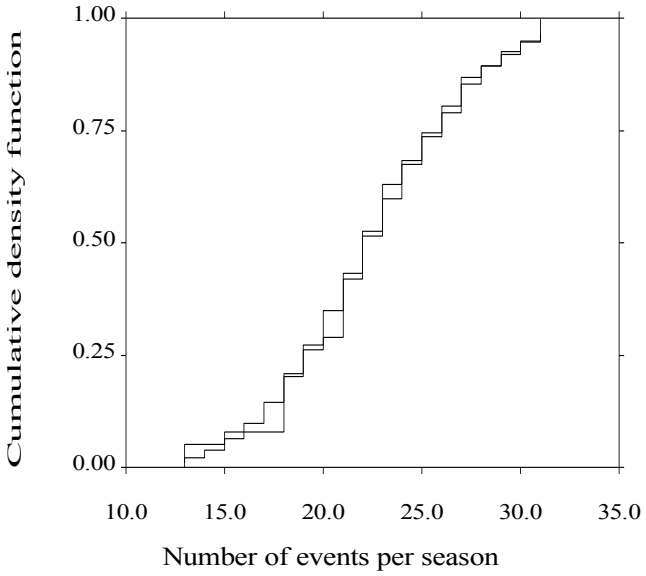

Figure 2. Distribution of the number of wet events per season

4.2 Duration of wet events

Approximately 33% of the events last one day (Fig. 3). The persistence of uninterrupted sequences of rainy days sometimes lasts more than a week (the maximum observed duration is 13 days). However, the frequency of long-duration events decreases rapidly with increasing duration. An arithmetic mean of 2.79 days and a standard deviation of 1.87 were obtained. The geometric pdf appears most adequate for fitting the observations:

$$f(m) = p q^{m-1} \tag{3}$$

where m is the duration of a wet event in days; $p = 1/\bar{m}$, being the reciprocal value of the mean event duration; and $q = 1 - p$.

The moment's method is used for the estimate of the parameters of the fitting.

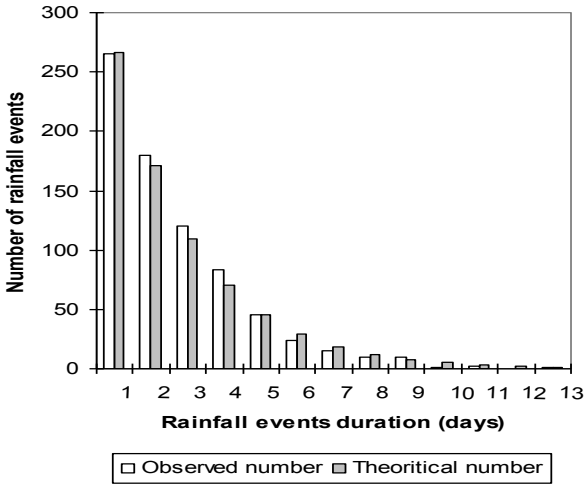

Figure 3. Distribution of wet event duration

4.3 Rainfall depth per event

Table 1 indicates the existence of a relationship between rainfall depth $H_{n,m}$ and duration. Therefore it is necessary to distinguish between pdf's of rainfall depth for different values of wet event duration. Here this is done by estimating six conditional pdf's for durations of 1 to 5 days and > 5 days. The $H_{n,m}$-values are grouped into 4 mm wide classes, starting with the (4-8 mm) class. As an example, for the class of wet events lasting > 5 days the Gamma distribution provides the best fit (Fig. 4). Again, the goodness-of-fit has been assessed by the Kolmogorov-Smirnov test. For this class the arithmetic mean and the standard deviation are respectively 69.81 mm and 38.02 mm.

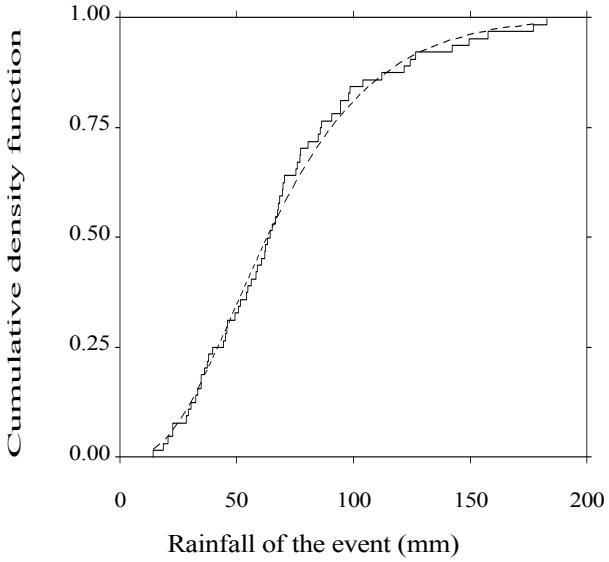

Figure 4. Fitting Gamma distribution for the rainfall depth of the > 5-day long wet events

4.4 Duration of dry events

The regression analysis (Table 1) displays that the lengths of dry events can be assumed to be independent from the lengths of wet events and the rainfall depth per event. Thus the statistical distribution of dry events (inter-event time), which can only assume integer values, follows a single

probability density function. The negative binomial pdf gives the best fit to describe the distribution of the dry events (Fig. 5). As Fig. 5 reveals, the shortest interruption (one day) is the most frequent one. Almost 20 percent of the observed dry events are only one day long. Dry periods up to 30 or even more days may be recorded (a 56 days maximum is recorded). The arithmetic mean and the standard deviation of dry events are respectively 7.3 days and 7.9. For the sample of values of the longest dry event per rainy season, the arithmetic mean and the standard deviation are respectively 30.2 days and 3.6.

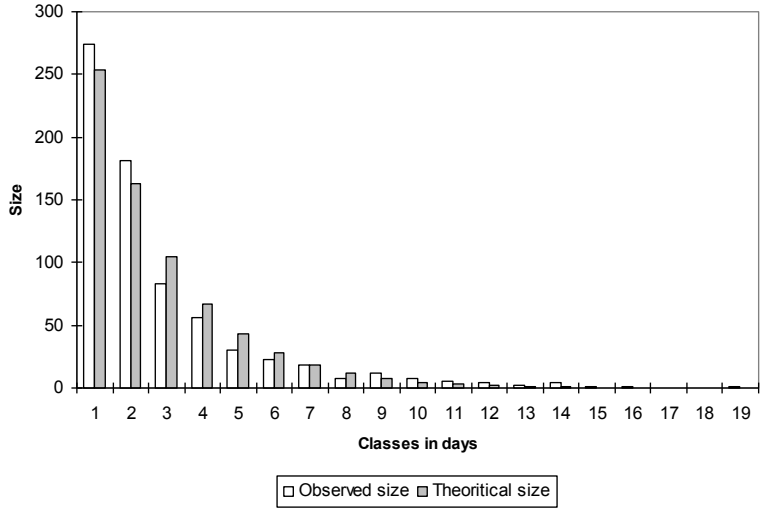

Figure 5. Distribution of the time lapse between wet events or the distribution of dry event durations.

4.5 Advent of the rainy season

The 40 dates characterizing the beginning of the first wet event in the climatic cycle were statistically analyzed. The best fit of this random variable is acquired by the so called 'loi des Fuites' (Fig. 6), using HYFRAN software (INRS-Eau, 2002). It shows that on average the first rainfall event occurs in the mid-September whereas the probability of surpassing this value is 0.52 for a biennial return period. In the extreme case, the climatic cycle starts in the first decade of October.

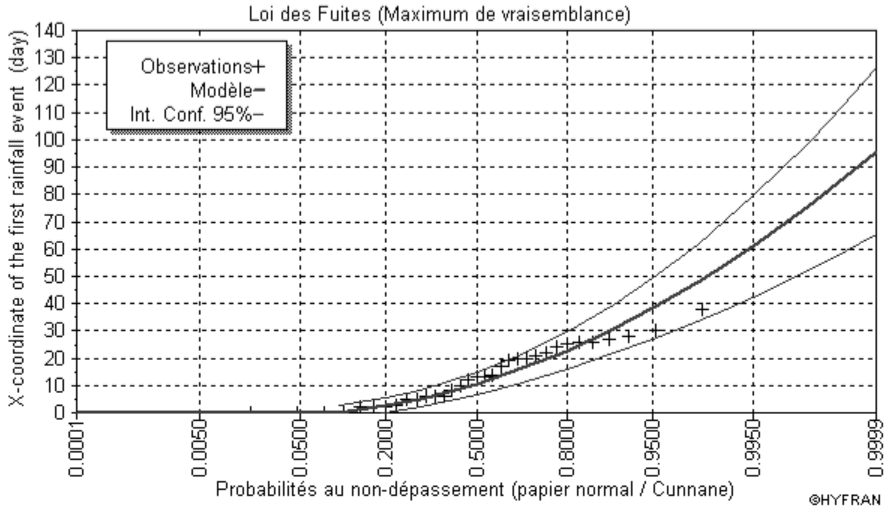

Figure 6. Fit of the 'Loi des Fuites" for the chronological position of the first rainfall event in rainy season, starting from the first of September.

5. CONCLUSIONS

This case study, using rainfall records of the Ichkeul basin, illustrates the independency between the durations of wet and dry events. In this region dry spells can well be described by the negative binomial pdf.

The procedure defines the inter-event time as being the dry event period. For the wet event duration, the theoretical requirement of the fitted geometric pdf are satisfied (Fig. 3).

Event-based analysis can now be used to generate synthetic rainfall event time series (Bogardi and al., 1988). By coupling this with a rainfall-runoff model, one can obtain synthetic streamflow series for reservoir simulation studies and for deriving design floods or for estimating water demand irrigation.

REFERENCES

Bogardi, J.J., Duckstein, L. and Rumambo, OH. (1988). Practical generation of synthetic rainfall event time series in semi-arid climatic zone. Journal of Hydrology, 103: 357-373.

Bogardi, J.J. and Duckstein, L. (1993). Evénements de période sèche en pays semi-aride. Revue des Sciences de l'Eau, 6(1), pp. 23-44.

Foufoula-Georgiou, E. and Georgakakos, K.P. (1991). Hydrologic advances in space-time precipitation modeling and forecasting. In: Bowles, D.S., and P.E. O'Connell (eds.), Recent advances in the modeling of hydrologic systems. NATO ASI Series, Serie C: mathematical and physical sciences, vol. 345. Kluwer Academic Publishers, Dordrecht, The Netherlands, 47-65.

Hui, W., Xuebin, Z. and Elaine, M.B. (2005). Stochastic Modelling of Daily Precipitation for Canada. ATMOSPHERE-OCEAN, 43 (1): 23–32.

INRS-EAU, 2002. Chaire en Hydrologie Statistique Hydro-Québec. Logiciel HYFRAN 1.1. Québec.

Mathlouthi, M. et Lebdi, F. (2007). Analyse des périodes sèches pour la gestion d'un barrage au Nord de la Tunisie. In. Proc. Quantification and Reduction of Predictive Uncertainty for Sustainable Water Resources Management, Symposium at IUGG2007, Perugia, 2007. IAHS Publ. no. 313, pp, 487-496.

Mathlouthi, M. & Lebdi, F. (2008) Event in the case of a single reservoir: the Ghèzala dam in Northern Tunisia. Stochastic Environ. Res. and Risk Assessment 22, 513–528.

Mathlouthi, M. (2009) Optimisation des règles de gestion des barrages réservoirs pour des évènements extrêmes de sècheresse. Thèse de Doctorat, Institut National Agronomique de Tunisie, Tunis, Tunisie.

Mathlouthi, M. & Lebdi, F. (2015) Identification hydrologique des événements secs extrêmes dans le bassin d'Ichkeul (Tunisie). In Hydrological Sciences and Water Security: Past, Present and Future (Proceedings of the 11th Kovacs Colloquium, Paris, France, June 2014). (ed. by C. Cudennec, S. Demuth, A. Mishra, and G. Young), 153- 154. IAHS Publ. 366, 2015.

Semenov, M.A. and Barrow. E.M. (1997). Use of a stochastic weather generator in the development of climate change scenarios. Clim. Change, 35: 397–414.

Wilks, D.S. (1999). Interannual variability and extreme-value characteristics of several stochastic daily precipitation modes. Agric. Meteorol. 93: 153–169.

Proceedings of the 10th World Congress of EWRA 'Panta Rhei', 5-9 July 2017, Athens, Greece
© 2017 *European Water Resources Association*

Drought analysis with SPI index and entropy

T. Baran[1], U. Guner Bacanli[2*] and F. Dikbas[1]
[1] *Dokuz Eylul University, Civil Engineering Department, İzmir, Turkey*
[2] *Pamukkale University, Civil Engineering Department, Denizli, Turkey*
[*] *e-mail: ugbacanli@pau.edu.tr*

Abstract: Drought is a natural disaster adversely affecting the survival and economy of the living organisms. Drought is related with many factors including climate and regional properties. Many different measures are used to determine drought. The goal of this study is the investigation of the Meteorological drought in Central Anatolian Region in Turkey. In the presented study, the Standard Precipitation Index and the Apportionment Entropy (AE) method are investigated and compared. For this purpose, observations of 13 meteorological stations located in Central Anatolia Region by The Turkish State Meteorological Service (DMİ) are evaluated. The results of the study contributed to the identification of drought parameters and consequently the missing information and data on this subject were completed. The entropy method provided similar results to the results obtained by other methods widely used in the literature regarding the data for the Central Anatolia Region. The entropy method was determined to yield similar results to that of the SPI method as indicated by the comparison of the relative frequencies of the severity of drought in the regional stations. Therefore, the method can be proposed as a method to be used in long-term drought calculations and regional drought calculations. The results of the present study showed that entropy method can be an alternative to be used in the analysis of drought.

Key words: Drought, Drought parameters, Entropy, SPI index

1. INTRODUCTION

Drought is a persistence period of water deficit and adversely affects the survival and economy of the living organisms. It is initiated by a significantly reduced precipitation at a local region within a definite time period and is intensified by the effect of other climatic factors such as high temperatures, high wind speed and low moisture content (Sırdaş, Şen; 2003, Chen et al. 2009, (Fontaine and Steinemann, 2009). The severity and intensity of drought is expected to increase with deteriorating climate conditions, increasing population and water demand, destruction of the natural vegetation and desertification and reaches such a magnitude as to threaten human kind (Kallis, 2008). Drought adversely influences the ecosystem, agriculture and the environment.

Prevention of drought requires carrying out a detailed basin specific analysis and monitoring of the area closely. Different drought severity parameters based on single or multiple variables were proposed by researchers in order to define drought as well as to identify the interactions between drought and hydrological/meteorological events (e.g. Palmer, Erinc, Standard Precipitation Index or De Martonne, Thornthwaite methods). Methods such as trend analysis or statistical/stochastic evaluations and entropy were also used as alternative approaches for defining and investigating drought in addition to the previously mentioned indices.

Developing an accurate index for drought is difficult due to the complexity of the relationships between hydro climatic variables and drought. The indices that were proposed for the analysis of drought are mainly based on water budget calculations and they consider one type of drought, meteorological, hydrological or agricultural.

The Standard Precipitation Index (SPI) is a measure of precipitation deficit and it has found widespread use because it is based on the probability of precipitation at different time scales (Mckee et al., 1993; 1999). SPI is computationally simple to calculate and on-going research focuses on the improvement of the application of both SPI and PDSI (Keyantash and Dracup, 2002;

Wu et al., 2001; 2005). SPI has been widely used for monitoring drought in many regions (Vicente-Seriano et.al (2004), Cancelliere et al. (2007); Raziei et al. (2009), Liu et al. (2012); Zhang et al. (2012), Mallya et al. (2016)).

Entropy (Shannon, 1949) is a measure of dispersion, uncertainty, disorder and diversification. Therefore, an entropy-based approach becomes useful for evaluating variability patterns of spatial and temporal precipitation (Mishra *et al.* 2009). This study investigates the applicability of entropy as a novel measure of drought based on long-term precipitation data collected from a number of stations in the Central Anatolian Region. For this purpose, the drought parameters determined based on the apportionment entropy values for Central Anatolia were compared with the Standard Precipitation Index.

2. THE STUDY AREA AND AVAILABLE DATA

Turkey has been separated into seven major geographic regions. The Central Anatolian Region occupies 19% of the total area of Turkey with its 151.000 square kilometers of land, it's the second largest region of Turkey after Eastern Anatolia. The Central Anatolian Region is divided into four sections, Upper Kızılırmak Basin, Middle Kızılırmak Basin Upper Sakarya Basin and Konya Basin. The climate of the Central Anatolian region is a steppe climate, with a great temperature difference between day and night. Rainfall is low and there is more snow in the winter. The average temperature is about 23°C in summer and -2°C in winter. Annual mean temperature is 10.8°C. Mean annual precipitation is 413.8 mm and most of the precipitation is in winter and spring seasons. Seasonal distribution of rainfall is as follows: Spring %36, winter %28, autumn %19, summer %17 (DMI, 2009; Bacanlı et al., 2011).

In this study, the meteorological stations are evaluated to define meteorological drought. The meteorological stations which are managed by DMI (State Meteorological Service) and DSI (State Hydraulic Works) are pre-evaluated for available long term precipitation and temperature data. The drought analyses have been performed on Aksaray, Ankara, Çankırı, Eskişehir, Karaman, Kayseri, Konya, Kırıkkale, Kırşehir, Nevşehir, Niğde, Sivas and Yozgat meteorological stations. The evaluated records are observed in the 1965 - 20014 period.

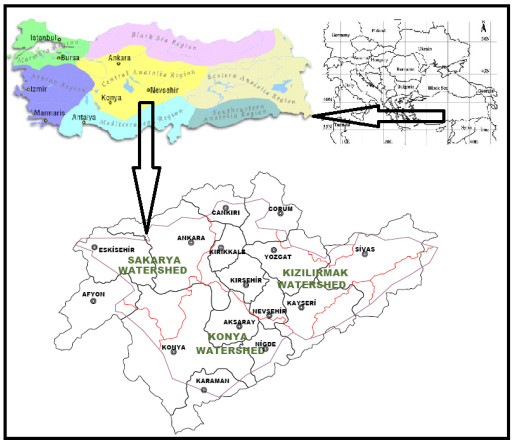

Figure 1. Central Anatolian Region

3. IDENTIFICATION OF THE SEVERITY OF DROUGHT

3.1 Entropy method

The concept of entropy is derived from classical thermodynamics and probability. The word "Entropy" was derived from "transinformation" by Classius. Boltzmann later characterized it as the

"number of microscopic states of the particles making up a portion of the material" and stated that "all these portions appeared similar to the main macroscopic body" (Wehrl 1978; Schrader 2000).

Shannon showed that the concept of entropy could be used to describe the extent of disorder in a system following the notion established by Boltzmann. (Shannon and Weaver, 1949).

Entropy finds itself an extensive area of application in water resources engineering and in many other subjects. Entropy is defined as the measure of the uncertainty that the hydrologic processes of random character embody and described as the information gained by observations = overcome uncertainty in water resources engineering applications. Owing to this attribute, the concept of entropy is used as an indirect measure of information content. The concept of entropy has application areas in many different aspects of hydrology and water resource studies including the identification of uncertainty in hydrological processes, information transfer between hydrological processes, planning of the measurement network, optimization and decision making theory. The concept of statistical entropy is used in these applications to overcome and account for the uncertainty in the systems or in the data content. The versatile application areas of entropy in hydrology and water resource problems were discussed extensively by Singh (1997 and 2003).

Random variable entropy is a measure of the attained information or the overcome uncertainty. Information content, joint information, conditional information and transferred information concepts were described as marginal entropy H(X), joint entropy H(X,Y), conditional entropy H(X/Y) and transinformation T(X,Y), respectively (Karmeshu and Pal, 2003):

$$H(X) = -\sum_{i=1}^{n} p(x_i) \log p(x_i) \tag{1}$$

$$H(X,Y) = -\sum_{i=1}^{n}\sum_{j=1}^{m} p(x_i, y_j) \log p(x_i, y_j) \tag{2}$$

$$H(X|Y) = -\sum_{i=1}^{n}\sum_{j=1}^{m} p(x_i, y_j) \log p(x_i|y_j) \tag{3}$$

$$T(X,Y) = -\sum_{i=1}^{n}\sum_{j=1}^{m} p(x_i, y_j) \log\left(\frac{p(x_i, y_j)}{p(x_i)p(y_j)}\right) \tag{4}$$

where x and y in the statements are stated as two independent variables defined in the same probability space as that of x_i *(i*= 1, 2,…,*n* and y_j *j*= 1,2, …, *m)* while $p(x_i)$, $p(x_i,y_j)$ and $p(x_i|y_j)$ are defined as the discrete, point and conditional probabilities, respectively (Baran and Bacanlı, 2007).

3.2 Apportionment Entropy (AE)

Because the concept of entropy could be defined as the overcome uncertainty = attained information, this concept is thought to be a measure of determining how much information can be gained from a measured parameter. The apportionment entropy values for daily precipitation that were described by Kawachi *et al*. (2001) were also used by Maruyama *et al*. (2005) in a study regarding monthly precipitation.

The initial step in the calculation of apportionment entropy (AE) is the computation of the R value by consecutively adding the daily/monthly precipitation values (r_i):

$$R = \sum_{i=1}^{12} r_i \tag{5}$$

R value can only be determined through the use of annual monthly mean precipitation or temperature data and can be represented as the sum of r_i where I = 1 to i = 12. r_i is the sum of the monthly mean precipitation or temperature values on the ith month of the year.

Finally, the apportionment entropy (AE) could be described as below by defining the probability of the occurrence of (r_i/R) as described in Equation 5:

$$AE = -\sum_{i=1}^{12} (r_i / R) \ \log_2 (r_i / R) \quad \text{(bit)} \tag{6}$$

The entropy values are independent of the order of r in the series. Therefore, AE could be used to measure the change in precipitation and/or temperature. Unless a frequency is defined for precipitation, the entropy value (AE) could be zero. A uniform (equal) distribution of entropy across months would maximize the entropy value (AE).

Using the values from the same station for m years, a mean entropy ($\overline{AE}$) can be predicted using the annual total precipitation and monthly mean temperature data.

$$\overline{AE} = (1/m) \sum^{m} AE \quad \text{(bit)} \tag{7}$$

where $\overline{AE}$ is the mean entropy.

The previous works of Bacanlı et al. (2009, 2011, 2012) on AE produced similar results with other drought indices showing that AE can be used as a drought index. AE indicates the process of drought when it is used as a drought index. AE might perform cyclic behaviour at station scale when it is used on all existing observations. In the present study, the AE values are standardized and classified as shown in Table 1.

Table 1. Classification of the drought index of apportionment entropy

Apportionment Entropy - AE	Classification
≥ 1.1	Extremely Wet (W3)
1.1>Z ≥ 1.05	Wet (W2)
1.05>Z ≥ 1.03	Moderately Wet (W1)
1.03>Z ≥ 1.0	Normal (N)
1.0>Z ≥ 0.98	Moderate Drought (D1)
0.98>Z ≥ 0.95	Drought (D2)
0.95>Z ≥ 0.9	Extreme Drought (D3)
0.9>Z	Maximum Extreme Drought (D4)

3.3 Standard Precipitation Index (SPI)

SPI method is used commonly to monitor the drought. The SPI was developed by (McKee et al 1993). Seasonal (3, 6-month time scale) or long period (9, 12, 24, 48-month time scale) drought can be analyzed. Underground water, rivers and reservoirs do not respond rapidly to swift precipitation changes. Therefore, 12-month or long period time scale (24, 48, 72-month) monitoring is chosen. There are lots of studies about Standardized Precipitation Index for monitoring drought all around the world like (McKee et al 1993; Edwards & McKee 1997; Guttman 1999; Türkes 1999; Kömüscü

2001; Lloyd-Hughes & Saunders 2002; Tonkaz 2006; Li et al 2008; Abolverdi & Khalili 2010; Keskin & Sorman 2010).

The SPI is the non-dimensional drought index. This index is computed for long time precipitation series for the preferred time scales. The SPI calculated by Equation 8.

$$SPI = \frac{x_i - \mu}{\sigma} \tag{8}$$

where: SPI, standardized precipitation index; X_i, data point; μ , mean; σ , standard deviation of the data.

The gamma distribution is convenient for precipitation series and the distribution parameters can be calculated by maximum likelihood approximation of Thom (1958). If precipitation data has zero values, mixed distribution by Thom (1951) can be used for incorporation of zero probability and non-zero probabilities (Equation 9).

$$H(x) = q + (1-q)\, G(x) \tag{9}$$

where: q, the probability of zero precipitation; G(x), the gamma cumulative probability function. Probabilities calculated by Equation 2 are transformed into the standard normal distribution for calculation of the SPI values (Guttman 1998; Abolverdi and Khalili 2010).

SPI method shows the drought category corresponds to output values (Table 2). If the SPI gives negative values, it means there is drought and lack of precipitation; if the SPI gives positive values, it means there is no drought and enough precipitation. Yet, the negative values are getting lower, the degree of the drought shifts from no drought to extremely drought and then catastrophe bursts. And same for the positive values, if the positive values are getting higher.

Table 2. Standardized precipitation index categories (McKee et al.,1999).

SPI index values	Drought Category
≥ 2	Extreme Wet
1.50 ~ 1.99	Severe Wet
1.00 ~ 1.49	Moderate Wet
0.99 ~ 0	Normal
0 ~ -0.99	Mild Drought
-1.00 ~ -1.49	Moderate Drought
-1.50 ~ -1.99	Severe Drought
≤ - 2	Extreme Drought

4. APPLICATION

In the present study, the Standard Precipitation Index and the Entropy method were used on the data collected from all of the precipitation stations in the Central Anatolian Region. Monthly precipitation observations were used. A tendency of decrease in precipitation data was determined throughout the region for the months November, December, February, March and April.

Time periods of 1, 3, 6, 9, 12 and 24 months in the calculation of the Standard Precipitation Index (SPI) were taken into consideration. These time periods were selected subjectively. They would roughly represent the time until the effect of a decrease in precipitation could be observable on the usable water resources.

In this study, every station in the Central Anatolian Region was evaluated based on these SPI and Entropy classifications. Relative frequencies were also calculated. Results from selected stations are displayed in Table 3 and 4. Evaluation of the SPI and Entropy classifications calculated for different time periods in the region did not indicate the presence of any significant change in terms of the stations with regards to the ratio of the dry and wet periods.

Table 3. The drought (DR) ratios (%) of the SPI and Entropy values of several stations in the Central Anatolian Region for time periods of 3, 6, 9, 12 and 24 months

	Entropy	1 Month	3 Month	6 Month	9 Month	12 Month	24 Month
Eskişehir	35	43	47	44	44	41	44
Ankara	18	46	50	51	50	51	52
Çankırı	16	49	50	48	49	50	51
Konya	45	47	45	46	48	50	46
Aksaray	27	47	48	50	53	52	53
Karaman	51	48	49	46	46	48	54
Sivas	20	47	45	48	51	50	20
Kayseri	16	48	50	50	50	50	55
Nevşehir	29	48	46	50	47	46	51
Niğde	31	48	45	44	46	48	47
Kırşehir	31	48	46	48	49	52	47
Kırıkkale	31	48	49	49	54	55	52
Yozgat	20	49	48	46	48	48	20

The results of the Standard Precipitation Index (SPI) analysis indicated that a significant change could not be observed in terms of the ratios of the dry, normal or wet periods of a single station. However, near-normal or mild droughts were more frequently encountered in short-term periods (3-6 months) whereas severe and very severe drought was observed during longer-term time periods (12-24 months). The drought ratios of the stations under investigation in the Central Anatolian Region were determined to vary drought ratios between 55% and 15%, the wetness ratios between 63% and 13% based on their SPI and Entropy indices.

Table 4. The wetness (WR) ratios (%) of the SPI and Entropy values of several stations in the Central Anatolian Region for time periods of 3, 6, 9, 12 and 24 months

	Entropy	1 Month	3 Month	6 Month	9 Month	12 Month	24 Month
Eskişehir	55	15	16	18	16	15	16
Ankara	63	16	17	16	16	16	15
Çankırı	59	16	18	16	16	14	16
Konya	31	16	15	14	16	14	13
Aksaray	45	16	16	17	18	17	16
Karaman	27	16	17	16	16	15	16
Sivas	61	15	16	16	18	17	18
Kayseri	53	16	16	17	16	16	18
Nevşehir	53	16	16	16	16	16	16
Niğde	47	16	17	15	16	15	14
Kırşehir	37	16	17	16	18	18	19
Kırıkkale	37	16	17	15	17	17	18
Yozgat	55	15	15	17	16	15	16

The relative frequency of SPI and Entropy in 3, 6, 9, 12 and 24 month time periods for Konya Station in the Central Anatolian Region are given in Figures 2.

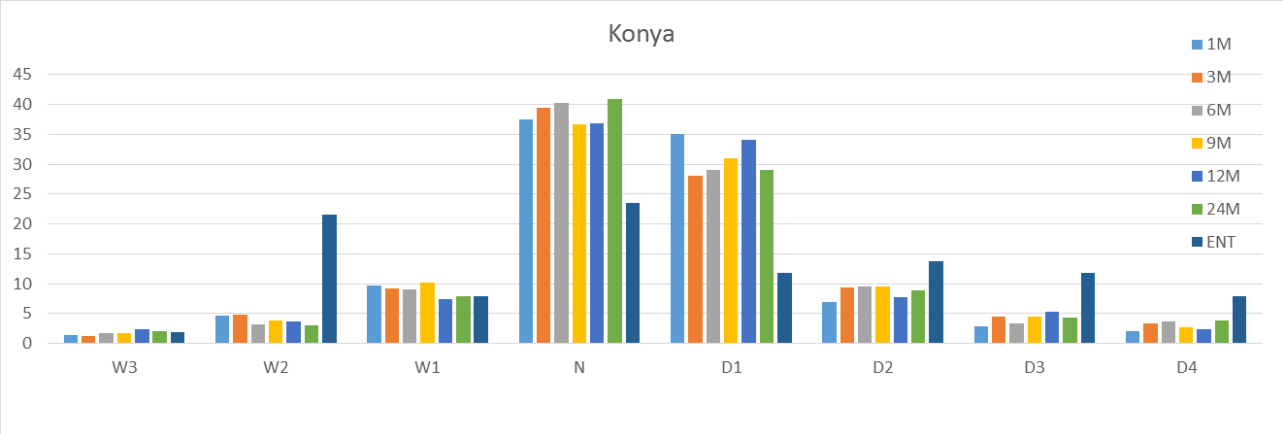

Figure 2. Relative frequency of SPI and Entropy for the Konya

Although the plots of precipitation and precipitation entropy displayed similar trends, the apportionment entropy values could specifically reflect the effect of the precipitation received especially during periods of drought. Similarly, the adverse distribution of precipitation, despite the sufficient total amount of precipitation, could be followed via the trends of the entropy values. The comparative precipitation and precipitation entropy values for the Konya station is given in Figure 3.

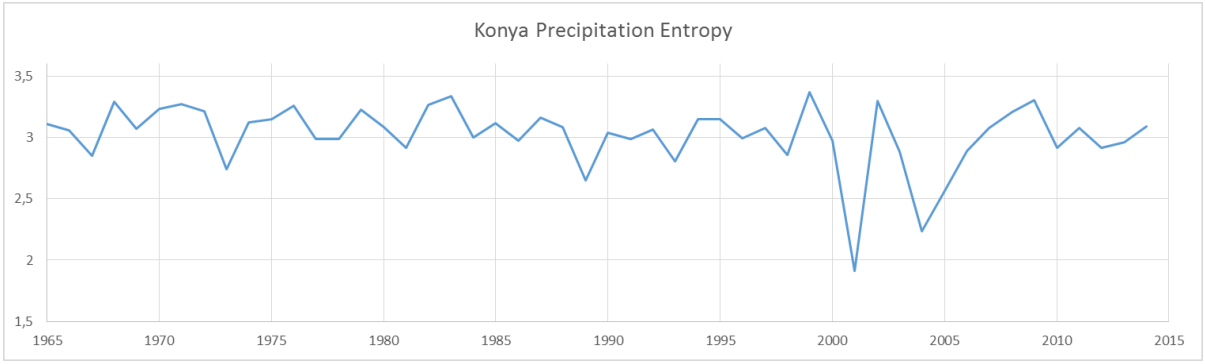

Figure 3. Drought Index Plot for the Konya Meteorology Station as calculated by the Entropy Method

5. RESULTS

Monitoring drought conditions with the use of reliable drought indices can help decision makers. In this study, SPI and AE was calculated from monthly precipitation values. Central Anatolian Region have shown a decreasing trend precipitation in winter, and spring seasons. The drought periods have shown a cyclic behavior in Central Anatolian Region as indicated by the long term observation data.

The AE method produced results similar to that of the SPI method as observed when the proportional frequencies of the drought severities in the stations of the region are compared. As shown in Figure 4, the SPI and the standardized entropy values are close to each other in Konya and Karaman stations, but, the ratio between SPI and the standardized entropy values are 1.4 in Eskisehir; 1.6 in Kırıkkale, Kırsehir, Nevsehir and Niğde stations; 1.9 in Aksaray; 2.5 in Yozgat and Sivas and it is 2.7 in Çankırı, Kayseri and Ankara.

The calculation of entropy by considering the monthly variation of precipitation provides a significant advantage to entropy in the determination of annual drought tendencies. It was observed from the series of precipitation and apportionment entropy that the relationship between the annual total precipitation values and entropy decreases. The apportionment entropy values are independent from the annual total precipitation values.

The assessment of drought plays an important role in the planning, design and determination of construction properties of water structures. Therefore, use of the entropy concept in drought assessment might be regarded as an alternative to the existing methods.

REFERENCES

Abolverdi J, Khalili D, 2010. Development of regional rainfall annual maxima for southeastern Iran by L-moments. Water Resour. Manage, 24, 2501–2526.Bacanlı UG, Dikbas F, Baran T, 2009. Entropi Yöntemini Kullanarak Kuraklık Parametrelerinin Belirlenmesi, Kuzey Ege Örneği. TÜBİTAK ÇAYDAG 107Y348, 1-174, Turkey.

Bacanlı UG, 2012. Entropy based assessment and palmer drought severity index of drought analysis. Scientific Research and Essays 7(44), 3823-3833.

Baran T, Bacanlı UG, 2007. An entropy approach for diagnostic checking in time series analysis. Water SA 33(4), 487-496.

Bacanlı UG, Dikbas F, Baran T, 2008. Meterological Drought Analysis Case Study, Central Anatolia. ULE2009 International Workshop on Urbanisation, Land Use, Land Degradation, and Environment 28 September-01 October 2009, Denizli; TURKEY.

Bacanlı UG, Dikbas F, Baran T, 2011. Meteorological Drought Analysis Case Study, Central Anatolia. Desalination and Water Treatment 26, 1-10.

Cancelliere A, Di Mauro G, Bonaccorso B, Rossi G, 2007. Drought forecasting using the Standardized Precipitation Index. Water Resour Managent. 21, 801–819.

Chen ST, Kuo CC, Yu PS. 2009. Historical trends and variability of meteorological droughts in Taiwan/Tendances historiques et variabilité des sécheresses météorologiques à Taiwan. Hydrological sciences journal 54, 430-441

DMI (State Meteorological Service), 2009. http, //www.dmi.gov.tr/fi les/en-US/climateof turkey.pdf, Last Access, November, 2009.

Fontaine, M.M., Steinemann, A.C., 2009. Assessing vulnerability to natural hazards, impact-based method and application to drought in Washington state. Nat. Hazard. Rev. 10 (1), 11–18.

Guttman 1999. Accepting the standardized precipitation index: A calculation algorithm. Journal of the American Water Resources Association, 35, 311-322.

Kallis G. 2008. Droughts Annual Review of Environment and Resources 33, 85.

Karmeshu and Pal N.R., 2003. Uncertainty, entropy and maximum entropy principal- An overwiew. In Entropy Measures, Maximum Entropy Principle and Emerging Applications, Karmeshu (Eds) Springer-Verlag, Berlin, 1-53.

Kawachi T, Maruyama T, Singh VP, 2001. Rainfall entropy for delineation of water resources zones in Japan. Journal of Hydrology 246, 36–44.

Keyantash J, Dracup J, 2002. The quantification of drought, An evaluation of drought indices. Bulletin of the American Meteorological Society 83, 1167–1180.

Keskin F, Sorman A, 2010. Assessment of the dry and wet period severity with hydro meteorological index. International Journal of Water Resources and Environmental Engineering 2 (2), 029-039.

Komuscu AÜ, 2001. An analysis of recent drought conditions in Turkey in relation to circulation patterns. Drought Network News, 13(2-3): 5-6.

Li YJ, Zheng XD, Lu F, Ma J, 2012. Analysis of drought evolvement characteristics based on Standardized Precipitation Index in the Huaihe River Basin. Proced. Eng. 28, 434–437.

Liu L, Hong Y, Bednarczyk NC, Yong B, Shafer AM, Riley R, Hocker EJ, 2012. Hydro-Climatological Drought Analyses and Projections Using Meteorological and Hydrological Drought Indices, A Case Study in Blue River Basin, Oklahoma. Water Resource Managent. 26, 2761–2779.

Mallya G, Mishra V, Niyogi D, Tripathi S, Govindraju RS, 2016. Trends and variability of droughts over the Indian monsoon region. Weather Clim Extremes. doi, 10.1016/j.wace.2016.01.002.

Maruyama T, Kawachi T, Singh VP, 2005. Entropy-based assessment and clustering of potential water resources availability. Journal of Hydrology 309, 104–113.

Mckee TB, Doesken NJ, Kleist J, 1993. The Relationship of Drought Frequency and Duration to Time Scales. 8th Conference on Applied Climatology, 17-22 January, Anaheim, CA, 179-184.

Mckee TB, Doesken NJ, Kleist J, 1999. Drought monitoring of climate. Geographical Reviews, 38, 55–94.

Raziei T, Saghafian B, Paulo AA, Pereira LS, Bordi I, 2009. Spatial Patterns and Temporal Variability of Drought in Western Iran. Water Resour Managent. 23, 439–455.

Schrader R, 2000. On a quantum version of Shannon's conditional entropy. Fortschr. Physics 48, 747 -762.

Shannon C, Weaver W, 1949. The Mathematical Theory of Communication. The University of Illinois Press, Urbana, Illinois.

Sırdaş S, Şen Z, 2003. Meteorolojik kuraklık modellemesi ve Türkiye uygulaması, İTÜ Mühendislik Dergisi, 2(2), 95-103.

Singh VP,(1997. The use of entropy in hydrology and water resources. Hydrological Process, 11, 587-626.

Singh VP, 2003. The Entropy Theory as a Decision Making Tool in Environmental and Water Resources. In Entropy Measures, Maximum Entropy Principle and Emerging Applications, Karmeshu (Eds) Springer-Verlag, Berlin, 261-297.

Türkeş, M. 1999. Vulnerability of Turkey to desertification with respect to precipitation and aridity conditions. Turkish Journal of Engineering and Environmental Science, 23, 363-380.

Thom HCS, 1958. A Note on the Gamma Distribution, Monthly Weather Review, 86 (4): 117-122.

Vicente-Serrano SM, González-Hidalgo JC, De Luis M, Raventós J, 2004. Drought patterns in the Mediterranean area, the Valencia region (eastern Spain). Clim Res 26, 5–15.

Zhang Q, Xiao M, Singh VP, Li J, 2012. Regionalization and spatial changing properties of droughts across the Pearl River basin, China. J. Hydrol. 472-473, 355–356.

Wu H, Hayes MJ, Welss A, Hu Q, 2001. An evaluation the standardized precipitation index, the China-Z index and the statistical Z-score. International Journal of Climatology 21, 745–758.

Wu H, Hayes MJ, Wilhite DA, Svoboda MD, 2005. The effect of the length of record on the standardized precipitation index calculation. International Journal of Climatology 25, 505–520.

Wehrl A, 1978. General properties of entropy. Reviews of Modern Physics. 50, 221 -260.

Proceedings of the 10th World Congress of EWRA 'Panta Rhei', 5-9 July 2017, Athens, Greece
© 2017 *European Water Resources Association*

Long-term variation of PDSI and SPI computed with reanalysis products

D.S. Martins[1], A.A. Paulo[2,3], C. Pires[1] and L.S. Pereira[3*]
[1] *Instituto Dom Luiz, Faculdade de Ciências, DEGGE, Universidade de Lisboa, Lisboa, Portugal*
[2] *Escola Superior Agrária de Santarém, Instituto Politécnico de Santarém*
[3] *LEAF Linking Landscape, Environment, Agriculture and Food, Instituto Superior de Agronomia, Universidade de Lisboa, Portugal*
[*] *e-mail: lspereira@isa.ulisboa.pt*

Abstract: Long-term temporal variation of droughts in Portugal was assessed using the Palmer Drought Severity Index (PDSI) and the Standardized Drought Index (SPI) with a 9 month time scale. Weather data from the NOAA-CIRES Twentieth Century Reanalysis Project version 2c, which spans from 1851 to 2014 with a spatial coverage of 2.0º latitude x 2.0º longitude were used. For PDSI, monthly evapotranspiration was computed using the FAO PM-ET_o method. Monthly data from reanalysis products consisted of maximum and minimum air temperature, net radiation, wind speed and relative humidity. Precipitation data was obtained from the same source. To assess how the long-term climate variability influences the identification of dry events in the drought indices, five different calibration periods were selected to estimate, respectively the potential values of evapotranspiration, runoff, soil moisture recharge and percolation loss of the PDSI water balance and the distribution function parameters of the SPI. Results show that the adopted calibration period have a significant impact of the frequency of extreme events detected in both drought indices. A Fourier analysis was applied to PDSI and SPI time series to search for significant cycles that could relate to return periods of droughts, with North Atlantic Oscillation cycles previously identified for Portugal.

Key words: PDSI; SPI; long-term variability; 20th century reanalysis

1. INTRODUCTION

Drought indices (DI) are the most usual tools to assess drought characteristics (severity, duration and magnitude). Most used are the Palmer Drought Severity Index (PDSI; Palmer, 1965) and the Standardized Precipitation Index (SPI; McKee et al., 1993). PDSI combines precipitation and evapotranspiration in a simple soil water balance to define a deviation from normal conditions, while SPI requires precipitation data only and it is obtained by adjusting a probability distribution function (pdf) to the precipitation cumulated over a defined number of months. Thus, the SPI depends on the time scale and calibration period (CP) considered to estimate the pdf parameters. Paulo et al. (2016), using long-term time series of precipitation in Portugal, from 1863 to 2007, showed that long-term precipitation variability influences SPI and highlighted the importance of the reference period considered to estimate pdf parameters, especially for non-stationary precipitation time series.

Such long-term variability of climate may also have an influence on PDSI. Thus, herein PDSI and SPI, the latter computed at 9 month time scale (SPI-9) because it compares better with PDSI (Paulo et al., 2012), were computed using long records of monthly precipitation, and reference evapotranspiration (PM-ET_o; Allen et al. 1998). Data were obtained from the NOAA-CIRES Twentieth Century Reanalysis Project, (20th-century reanalysis, Compo et al., 2011), which spans from 1851 to 2014 with a spatial resolution of 2.0º latitude x 2.0º longitude. In this study, both PDSI and SPI-9 were computed with the reanalysis data for Portugal considering 5 CP to assess the impacts that different CP have on the PDSI and SPI-9 time series. To assess the quality of those computations, the SPI and PDSI obtained from reanalysis were compared with PDSI and SPI-9 time series computed with long records of observed precipitation and PM-ET_o data retrieved from the Climate Research Unit (CRU) project (Harris et al., 2014). The aim of this study is (1) to assess the

accuracy of the reanalysis data to estimate the PDSI and SPI; (2) assessing the impact of the CP used on both DI; (3) searching for significant cycles of drought occurrence, using spectral analysis applied to the 164 years of data of 20th-century reanalysis.

2. DATA AND METHODS

To study the impacts of long-term variability of precipitation and ET_o on drought assessment by the SPI and PDSI, monthly records of precipitation rate (kg m^{-2} s^{-1}), maximum and minimum temperature (K) , downwards shortwave radiation (W m^{-2}), meridional (v) and zonal (u) wind components, both at 10 m height (m s^{-1}), specific humidity (kg kg^{-1}) and surface level pressure (kPa) from NOAA-CIRES 20th-century reanalysis were retrieved for the period 1851-2014.

ET_o, used in the water balance of the PDSI was computed using the PM-ET_o equation because it is preferable than using temperature methods to describe climate variability (Ren et al. 2016a, b). Results from Martins et al. (2016) showed that, overall, reanalysis data are suitable for PM-ET_o estimation in a monthly time-scale for the Iberian Peninsula. To calculate ET_o, wind speed was computed using zonal u and meridional v components at 10 meter height converted to 2 m. Relative humidity (%) was obtained from the temperature data, specific humidity and surface level pressure.

To assess the accuracy of the reanalysis based PDSI and SPI, both indices were also computed with long records (1911-2007) of precipitation from weather stations and PM-ET_o from the CRU TS3.21 (Harris et al., 2014) with data of the same period. Those data were previously used to assess long-term variability of droughts in Portugal (Moreira et al. 2012; Paulo et al. 2016). Fig.1 depicts the spatial distribution of the three groups of data. Precipitation and ET_o values from the CRU grid were interpolated to the coarser grid mesh of the reanalysis in order to obtain comparable datasets. The observed PDSI and SPI were computed for the common period of 1911-2007.

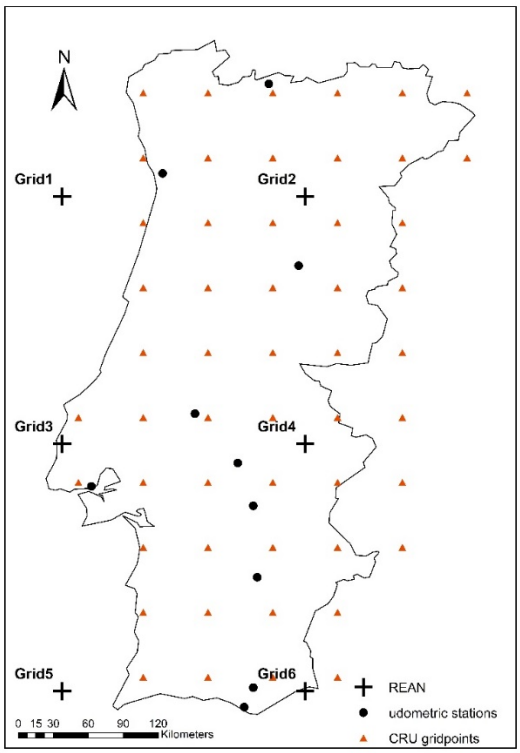

Figure 1. Distribution of the 20th-century reanalysis (REAN) grid-points, weather stations and CRU grid-points.

The SPI-9 was computed following the procedure proposed by Edwards (2000) with the Gamma pdf parameters being estimated with unbiased probability weighted moments.

The PDSI is based on a supply-and-demand concept of the soil water balance applied to a two-

layer soil (Palmer, 1965). The index computes a moisture departure, i.e., the difference between actual precipitation and the precipitation expected to occur for the average conditions of the climate through the computation of a monthly water balance and the calibration of local monthly coefficients for the various terms of the soil water balance. Thus, four values related to the water balance - evapotranspiration (ET), recharge (R), runoff (RO) and loss (L) - and the respective multiplier parameters (α, β, γ and δ) used to obtain the potential values are computed for each month of the year. These potential values of the water balance are, thus, the ones which are 'climatically appropriate for existing conditions' (CAFEC). The selection of the period to estimate the CAFEC potential may impact the PDSI index. In this study the water balance was computed considering a soil water holding capacity of 150 mm, with 25 and 125 mm, respectively in the first and the second layer.

PDSI and SPI-9 were computed with the 20th-century reanalysis time series for the period 1851-2014, using five different CP of 40 years' length each: 1851-2014, 1851-1891, 1892-1932, 1933-1973 and 1974-2014. This approach aimed at assessing the impact of the CP used to estimate the Gamma pdf parameters of the SPI-9 and the potential values of the PDSI.

Additionally, drought cyclicity was analyzed for PDSI and SPI-9, using spectral analysis, and results were compared to those obtained by Moreira et al. (2015) who used Fourier analysis applied to time series of SPI-12 of 66 years.

3. RESULTS

3.1 Time variability of precipitation and ET_O

To search for changes in the long-term variability of time series of precipitation and ET_o in the six grid-points (P_{REAN} and $ET_{o\text{-}REAN}$) used in this study, the mean value and the standard deviation were computed for the entire period of data (1851-2014) and to each period of 40 years (Table 1). Results in Table 1 show that the variability of P_{REAN} is enormous, with a variance close to the mean, while the variability of $ET_{o\text{-}REAN}$ is smaller. In the 164 years analyzed, the lowest values of both of the mean and variance of the precipitation were observed in the latest period (1974-2015) in all the grid-points, which is consistent with the negative precipitation trend over Iberian Peninsula related to more frequent North-Atlantic Oscillation (NAO) positive phases (Puebla and Nieto, 2010). The periods 1892-1932 and 1933-1973 were the wettest periods, both in terms of mean and variance of precipitation. ET_o variability changes little throughout the period with a slow increase in both mean value and variability over the years.

Table 1. Comparison of mean (μ) and standard deviation (σ^2) of reanalysis precipitation and ET_o in each grid-point for the five calibration periods.

	1851-2014		1851-1891		1892-1932		1933-1973		1974-2014	
	μ	σ^2	μ	σ^2	μ	σ^2	μ	σ^2	μ	σ^2
Precipitation (mm month^{-1})										
Grid1	70.8	70.5	70.8	71.2	74.2	68.6	74.7	73.9	63.3	67.6
Grid2	78.3	73.4	77.0	74.7	80.5	70.0	83.6	77.9	71.9	70.5
Grid3	60.4	68.3	60.4	70.2	62.3	67.1	64.5	69.7	54.5	65.8
Grid4	65.0	72.6	63.5	74.9	65.6	69.7	70.6	75.5	60.2	69.7
Grid5	45.7	57.2	45.8	59.7	46.8	55.1	49.0	57.3	41.2	56.3
Grid6	43.5	56.5	42.0	58.2	43.9	53.6	48.1	59.6	40.2	54.2
ET_o (mm d^{-1})										
Grid1	2.8	1.3	2.7	1.3	2.7	1.2	2.8	1.3	2.8	1.2
Grid2	2.9	1.3	2.8	1.4	2.8	1.3	2.9	1.3	2.9	1.3
Grid3	3.2	1.3	3.2	1.4	3.2	1.3	3.3	1.3	3.3	1.3
Grid4	3.3	1.3	3.2	1.4	3.2	1.3	3.3	1.3	3.3	1.3
Grid5	3.6	1.3	3.6	1.4	3.6	1.3	3.7	1.3	3.7	1.3
Grid6	3.6	1.3	3.6	1.4	3.6	1.3	3.7	1.3	3.7	1.3

3.2 Comparing the 20th-century reanalysis with observations

P_{REAN} and $ET_{o\text{-}REAN}$ were compared with the respective grid-points obtained from the average of the observed precipitation and ET_o (P_{OBS} and $ET_{o\text{-}OBS}$) in the grid area of the 20th-century reanalysis, for the common period between 1911-2007 (Table 2) using a set of statistical diagnostics. These indicators were previously applied to compare monthly ET_o estimated from reanalysis data with ET_o estimated from observations (Martins et al. 2016) and are defined by these authors.

P_{REAN} was largely underestimated in 4 out of 6 grid-points with negative percent bias (PBIAS) reaching 40% (Table 2). However, P_{REAN} in Grid4 overestimates considerably those of observations. Only for Grid3 a fairly good fit was observed between P_{REAN} and P_{OBS}, but still having considerable large estimation errors (30.22 mm/month). $ET_{o\text{-}REAN}$ overestimates $ET_{o\text{-}OBS}$ but are closer, in mean, to the observed values with smaller bias (Table 2). Results for the modelling efficiency EF relative to both P_{REAN} and $ET_{o\text{-}REAN}$ show that the approach used is adequate since EF exceed 0.55, thus indicating that the mean square errors of estimates are much higher than the variance of observations.

Table 2. Performance indicators relative to the comparison between P_{REAN} and $ET_{O\text{-}REAN}$ against P_{OBS} and $ET_{O\text{-}OBS}$.

	b	*a**	*b_0*	*R^2*	*RMSE**	*EF*	*PBIAS*
P_{OBS} vs P_{REAN} (mm/month)							
Grid1	0.71	-0.51	0.71	0.82	49.30	0.70	-29.20
Grid2	0.52	11.73	0.56	0.82	87.48	0.55	-39.50
Grid3	0.94	3.48	0.97	0.80	30.22	0.78	0.10
Grid4	1.20	1.40	1.21	0.83	33.78	0.62	22.60
Grid5	0.72	6.49	0.76	0.76	34.64	0.74	-16.30
Grid6	0.80	2.55	0.82	0.74	31.67	0.72	-14.70
$ET_{o\ OBS}$ vs $ET_{o\ REAN}$ (mm/day)							
Grid1	0.93	0.41	1.07	0.72	0.70	0.62	9.30
Grid2	0.73	0.84	0.96	0.76	0.77	0.75	2.90
Grid3	0.83	0.94	1.09	0.77	0.81	0.66	16.00
Grid4	0.65	1.13	0.92	0.80	0.87	0.77	-0.60
Grid5	0.80	1.26	1.14	0.78	0.96	0.57	22.00
Grid6	0.68	1.38	1.00	0.79	0.87	0.75	8.30

*b is the regression coefficient of a linear regression, a is the intercept of the linear regression, b_0 is the regression coefficient of a linear regression forced to the origin, R^2 is the coefficient of determination, RMSE is the Root Mean Square Error, EF is the efficiency of modelling, PBIAS is the Percent Bias. * indicates the same units as the variables.*

3.3 Comparing PDSI and SPI when computed from reanalysis products or observations

Fig. 2 shows the comparison between PDSI and SPI-9 obtained from the reanalysis data ($PDSI_{REAN}$, $SPI\text{-}9_{REAN}$) and the respective PDSI and SPI-9 computed with the observed data ($PDSI_{OBS}$, $SPI\text{-}9_{OBS}$) by comparing the frequency of each drought class. The different drought classifications relative to both indices were adopted. Results show that the frequency of extreme and severe drought events are much larger when PDSI was computed from reanalysis data. Only for Grid4 the frequency of severe events of $PDSI_{REAN}$ is lower. However, the frequency of drought events detected by $SPI\text{-}9_{REAN}$ is closer to $SPI\text{-}9_{OBS}$. Extreme wet events are more frequent through the $SPI\text{-}9_{OBS}$, and extreme and severe events are more frequent through $SPI\text{-}9_{REAN}$ although the difference is smaller than when comparing $PDSI_{REAN}$ with $PDSI_{OBS}$.

Considering the nature of the DI, the underestimation of precipitation and the overestimation of ET_o, results in Fig.3 are acceptable to analyze how PDSI and SPI changed with time and with the CP. Since PDSI combines precipitation and ET_o through a water balance, if precipitation is greatly underestimated and ET_o is overestimated, then drier, more frequent, events are expected. Differently, as the SPI is a probabilistic index that computes the deviation from average precipitation conditions, the underestimation of P_{REAN} should not affect the frequency of dry events

detected as long as the reanalysis time series are able to describe the variability of observed precipitation, which was the case for precipitation (Table 1).

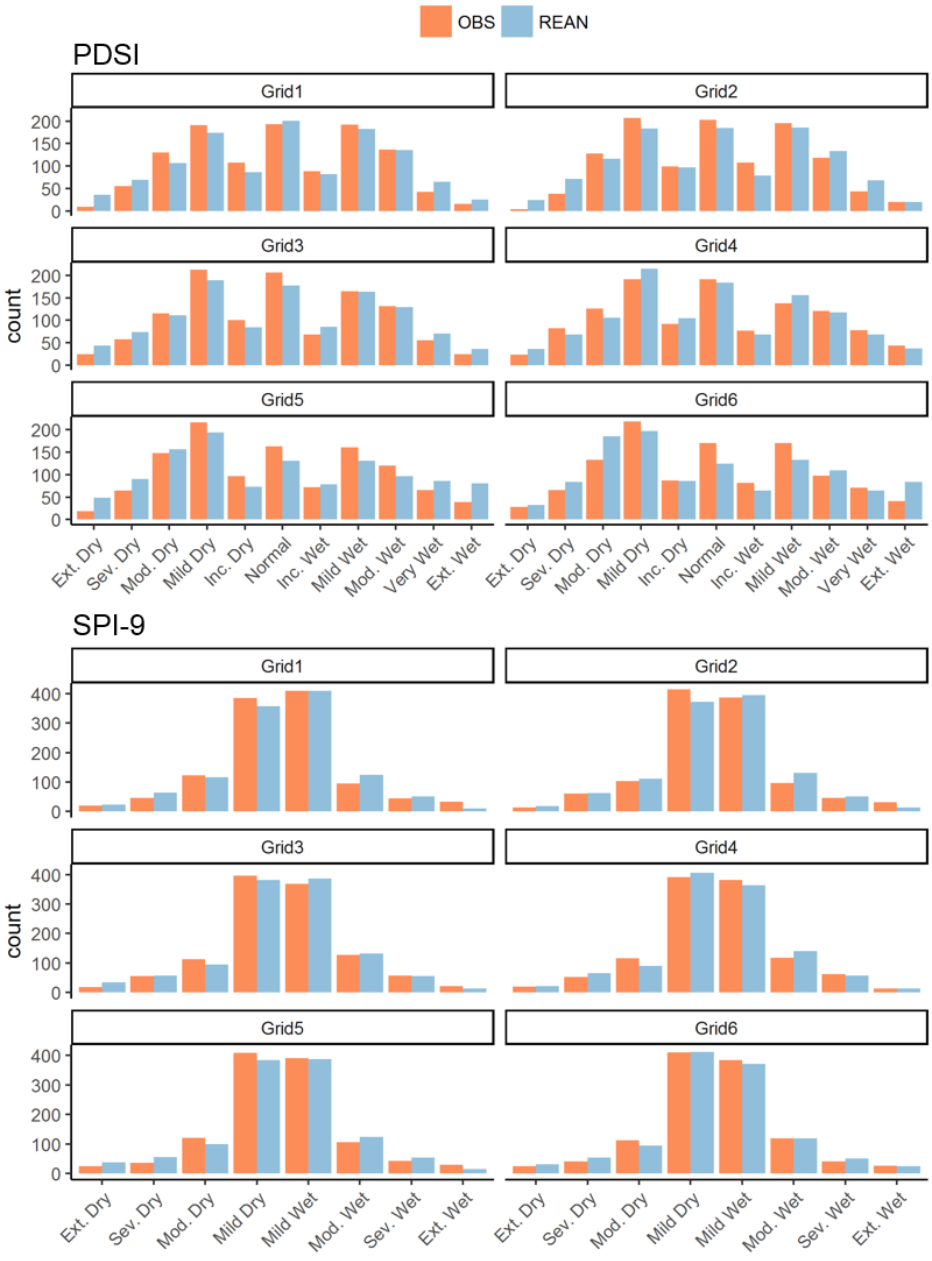

Figure 2. Comparison of the count of occurrences in each class of PDSI and SPI-9 computed reanalysis and observations (Ext. Dry: Extreme droughts; Sev. Dry: Severe droughts; Mod. Dry: Moderate droughts; Mild Dry: Mild droughts; Incip. Dry: Incipient drought; Incip. Wet: Incipiently wet; Mild Wet: Mildly wet; Mod. Wet: Moderately wet; Very Wet: Very wet; Ext. Wet: Extremely wet).

3.4 Analyzing the long-term variability of PDSI and SPI-9 and effects of the calibration period

To assess how the climate variability affect both PDSI and SPI-9, different CP periods were used to estimate the Gamma pdf parameters, for SPI-9, and the potential values of the water balance of the PDSI, using the 20th-century reanalysis data for the period 1851-2014.

Results show that despite no major changes occurred in the time variability of precipitation and ET_o in the entire period, the selection of the reference period is important. Results are coherent for all grid-points and to both PDSI and SPI; however in Table 3 only examples for Grid2 and Grid3 are shown. Focusing the analysis on the occurrence of extreme and severe events, there are clear

differences between the PDSI time series calibrated for the five reference periods. The PDSI calibrated using the complete period (1851-2014) identified more extreme and severe drought events relative to calibration for the periods 1851-1891 and 1974-2014, and lesser number of extreme and severe wetness events than those identified when the PDSI was calibrated for those periods. In fact, the PDSI calibrated for 1974-2014 is the most different when compared to the other CP. Only 4 or 5 extreme dry events were identified in 164 years in Grid2 and Grid3, respectively, and 30 severe drought events were identified, which are much less than those identified for all other periods. The number of severe and extreme wet events increased significantly in this period in all grid-points when compared to the PDSI calibrated for the other periods. Similar results were found for SPI-9 for all grid-points. Lower occurrence of extreme and severe events were identified when the SPI-9 was calibrated for the period 1974-2014 and with the highest occurrence of extreme and severe wet events being identified for this CP as well. The highest occurrence of severe and extreme dry events occurred when both DI were calibrated using the wet periods 1892-1932 and 1933-1973 (Table 3) Although not fully comparable, these results agree with those reported by Paulo et al. (2016), highlighting the importance of the reference period selected for calibration.

Table 3. Count of occurrences in each class of PDSI and SPI-9 using different calibration periods for Grid2 and Grid3

Index	Calibration Period	Ext. Dry	Sev. Dry	Mod. Dry	Mild Dry	Inc. Dry	Normal	Inc. Wet	Mild Wet	Mod. Wet	Very W.	Ext. W.
PDSI												
Grid2	1851-2014	35	137	200	323	150	304	149	322	209	98	41
	1851-91	22	93	191	313	165	308	168	303	225	124	56
	1892-32	100	167	246	320	173	297	141	285	160	56	23
	1933-73	74	175	240	354	167	325	140	260	155	53	25
	1974-14	4	30	161	256	136	305	135	353	263	197	128
Grid3	1851-2014	68	137	207	324	143	270	137	281	218	127	56
	1851-1891	62	134	220	320	150	266	151	265	223	123	54
	1892-1932	124	165	236	328	126	287	131	239	205	86	41
	1933-1973	128	163	261	345	150	290	115	266	162	56	32
	1974-2014	5	45	143	261	97	255	137	305	293	207	220
		Ext. Dry	Sev Dry	Mod Dry	Mild Dry	Mild Wet	Mod. Wet	Very Wet	Ext. Wet			
SPI-9												
Grid2	1851-2014	35	104	203	593	703	207	90	25			
	1851-1891	21	62	179	617	757	212	87	25			
	1892-1932	150	147	233	491	610	173	99	57			
	1933-1973	93	154	232	615	637	149	61	19			
	1974-2014	13	35	119	561	779	264	128	61			
Grid3	1851-2014	44	100	173	638	688	205	75	37			
	1851-1891	23	72	177	659	741	196	62	30			
	1892-1932	134	119	231	590	540	191	101	54			
	1933-1973	91	144	220	628	617	157	63	40			
	1974-2014	12	35	112	564	759	283	124	71			

The time variability of PDSI and SPI-9 was further studied by identifying the main cycles for drought occurrence. A spectral analysis was applied to the time series of the September values of both SPI-9 and PDSI for all grid-points. The analysis was done using the September values because it is the last month of the hydrological year and with the SPI-9 the index value of September included all the precipitation that occurred that year. For PDSI the most relevant cycles identified for all grid-points were the 6.21 and 7.83 year cycles. Other cycles of 12 and 90 years were also present in all grid-points for PDSI. Results for SPI, show in general, shorter cycles of drought occurrence with cycles of 2.02, 3.91 and 6.21 years present in all grid-points. These results agree with previous studies (Moreira et al., 2015) in which the most frequency cycles found with SPI-12 were of 9.4 and 6.0 years, although cycles of 2.0 and 4.7 years were also identified. Like discussed in Moreira et al. (2015) the 6 year and 7.83 year cycle are likely influenced by the North Atlantic Oscillation (NAO) that influence winter precipitation in Portugal.

4. CONCLUSIONS

In the present study, the long-term variability of droughts was assessed with the PDSI and the SPI-9 using data derived from the 20th-century reanalysis products, with data from 1851 to 2014. The accuracy of reanalysis precipitation and PM-ET_o were compared against observations. The resulting drought indices computed using those variables were also compared with those computed from observations. Results showed that SPI-9_{REAN} relates well with SPI-9_{OBS} for all grid-points; in all cases the frequency of events in each class of the SPI-9_{REAN} is very close to those of SPI-9_{OBS}. $PDSI_{REAN}$ relates worst with $PDSI_{OBS}$ than referred for both SPI-9 because the frequency of extremely dry (wet) events identified with $PDSI_{REAN}$ is considerably larger (lower) then that identified by $PDSI_{OBS}$. This may be explained by the underestimation of P_{REAN} and the overestimation of $ET_{o\ REAN}$ resulting in less water availability when the water balance is performed, which leads to drier $PDSI_{REAN}$. With SPI-9, due to its probabilistic feature, the consistent underestimation of precipitation does not significantly affect its standardized values. Statistical downscaling techniques should be studied to correct the biases in precipitation and ET_o to improve the accuracy of the PDSI from reanalysis.

To study how the long-term variability precipitation and ET_o affect the DI, both indices were calibrated for 5 different periods. Results showed very distinct index values depending on the CP used. With the same patterns for all grid-points, when the DI were calibrated with the most recent period (1974-2014) the amount of severe or extreme droughts were the lowest when compared to the $PDSI_{REAN}$ and SPI-9_{REAN} computed for other CP; also, with this CP, the number of severe and extreme wet events were the highest. In contrast, if the CP selected was the period 1892-1932, the opposite occurred with a larger amount of dry events and fewer wet events detected. In general wetter (dryer) CP lead to an SPI biased towards drier (wetter) classes. These results showed the importance that the selection of the CP has to both PDSI and SPI-9. However, further studies are required to understand if the changes observed with $PDSI_{REAN}$ and SPI-9_{REAN} represent the reality, particularly after using an appropriate bias correction for P_{REAN} and $ET_{o\ REAN,}$ and which CP should be used for drought monitoring.

ACKNOWLEDGMENTS

Authors acknowledge FCT for the PhD research grant SFRH/BD/92880/2013 attributed to the first author and the grants attributed to the research units IDL (RECI/GEO-MET/0380/2012 and UID/GEO/50019/2013) and LEAF (UID/AGR/04129/2013).

REFERENCES

Allen, R.G., Pereira, L.S., Raes, D., Smith, M., 1998. Crop Evapotranspiration. Guidelines for Computing Crop Water Requirements. FAO Irrig. Drain. Pap. 56. Rome, 300 p.

Compo, G.P., J.S. Whitaker, P.D. Sardeshmukh, N. Matsui, et al., 2011. The Twentieth Century Reanalysis Project. Quarterly J. Roy. Meteorol. Soc., 137, 1-28.

Edwards, D., 2000. SPI defined, in: http://ulysses.atmos.colostate.edu/SPI.html, Colorado.

Martins, D.S., Paredes, P., Raziei, T., Pires, C., Cadima, J. and Pereira, L.S., 2016. Assessing reference evapotranspiration estimation from reanalysis weather products. An application to the Iberian Peninsula. Int. J. Climatology. DOI: 10.1002/joc.4852.

McKee, T.B., Doesken, N.J., Kleist, J., 1993. The relationship of drought frequency and duration to time scales. In: Proc. 8th Conference on Applied Climatology (Vol. 17, No. 22, pp. 179-183). Boston, MA: American Meteorological Society.

Moreira, E.E., Martins, D.S. and Pereira, L.S., 2015. Assessing drought cycles in SPI time series using a Fourier analysis. Nat Hazards Earth Syst Sci , 15(3), pp.571-585.

Moreira, E.E., Mexia, J.T. and Pereira, L.S., 2012. Are drought occurrence and severity aggravating? A study on SPI drought class transitions using log-linear models and ANOVA-like inference. Hydrol Earth Syst Sc, 16, pp.3011-3028.

Palmer, W.C., 1965. Meteorological Drought, Research Paper 45, U.S. Department of Commerce Weather Bureau, Washington, D.C.

Paulo A.A., Rosa R.D., Pereira L.S., 2012. Climate trends and behaviour of drought indices based on precipitation and evapotranspiration in Portugal. Nat. Hazards Earth Syst. Sci.; 12:1481–149.

Paulo, A., Martins, D., Pereira, L.S. 2016. Influence of precipitation changes on the SPI and related drought severity. An analysis using long-term data series. Water Resour. Manag., 1-21.

Ren, X., Martins, D.S., Qu, Z., Paredes, P. and Pereira, L.S., 2016. Daily Reference Evapotranspiration for Hyper-Arid to Moist Sub-Humid Climates in Inner Mongolia, China: II. Trends of ETo and Weather Variables and Related Spatial Patterns. Water Resour Manag, 30(11), pp.3793-3814.

Rodríguez-Puebla, C. and Nieto, S., 2010. Trends of precipitation over the Iberian Peninsula and the North Atlantic Oscillation under climate change conditions. Int. J. Climatology, 30(12), pp.1807-1815.

Proceedings of the 10th World Congress of EWRA 'Panta Rhei', 5-9 July 2017, Athens, Greece
© 2017 *European Water Resources Association*

Water shortage characterisation for surface water systems with storage

I. Nalbantis
Centre for the Assessment of Natural Hazards and Proactive Planning and Laboratory of Reclamation Works and Water Resources Management; School of Rural and Surveying Engineering, National Technical University of Athens, Athens, Greece
e-mail: nalbant@central.ntua.gr

Abstract: From all forms of water appearing in the Earth's hydrological cycle, surface water is known to constitute the largest resource that provides water to human societies and ecosystems. Droughts affecting surface water can considerably reduce water availability for various water uses, which, in turn, may lead to water shortage, depending on water demand. Therefore, information on the balance between water availability and water demand is of vital importance in water resources management. Various indices expressing this balance have been proposed, including the Demand Sensitive Drought Index (DSDI). In this paper we propose a modified form of DSDI, termed 'Surface Water Shortage Index' (SWSI). This can be applied to any spatial unit ranging from a large geographical area to an isolated hydraulic work. Focusing on a single drainage basin with a storage reservoir at its outlet, the variables involved in SWSI are selected to be water volumes for streamflow, demand, withdrawal, storage and spill. The water balance equation for the reservoir is used for formulating the index, which reflects the water demand deficit with respect to water availability by also taking into account a finite water storage capacity. The index is calculated for three-month intervals. An application is presented based on data from the Evinos river basin, Greece. Results are compared to those of a simplified version of SWSI resembling to DSDI and termed 'adjusted DSDI' (DSDIa).

Key words: Surface water; water shortage characterisation; water demand; water availability; Demand Sensitive Drought Index

1. INTRODUCTION

Drought is a recurring natural phenomenon that reduces water availability for various water uses. The surface water percentage of global withdrawals for irrigation during the period 1998-2002 was 52%, whereas, when all uses were considered, this grew to 65% (Döll et al., 2012). Hence, this is undoubtedly the largest water resource. Tsakiris et al. (2013) defined the water system in terms of its components (e.g., watersheds and water consumption centres) while also describing various subsystems along with their basic variables. Concentrating on the surface water subsystem, precipitation and water transfer are the input variables, while state variables include surface water storage in various forms. Output variables are surface runoff, actual evapotranspiration, soil infiltration and water withdrawals for various uses. From the three attributes of drought (severity, duration and spatial extent), the authors proposed assessing only drought severity using various drought indices while fixing the other two attributes. For the spatial dimension of the system, they proposed using a fixed geographical area, e.g., a river basin, or a river basin district according to the Water Framework Directive (European Council, 2000). Drought indices use variables that are related to natural processes, whereas they ignore variables that represent human intervention (e.g., water withdrawals). However, a complete knowledge of the water volume that is available in the studied system requires that water withdrawals be also considered. A recently proposed index, termed 'Demand Sensitive Drought Index' (DSDI) (Etienne et al., 2016) constitutes an effort towards this direction. In this study, we propose a modified form of DSDI, which explicitly takes into account the available capacity for surface water storage in the study area. The proposed index is tested on data from a river basin in Greece.

2. METHODOLOGY

2.1 The Demand Sensitive Drought Index

Etienne et al. (2016) formulated the Demand Sensitive Drought Index (DSDI), which can be applied for any water use or category of water use. The index is based on the well-known sequent peak algorithm (Thomas and Burden, 1963) and has been applied in India (Devineni et al., 2013), China (Chen et al., 2013) and the United States (Devineni et al., 2015). The index employs a daily time series of water supply, WS_t, and water demand D_t, where t denotes time in days. The cumulative water deficit is obtained as

$$\text{deficit}_t = \max\left(\text{deficit}_{t-1} + D_t - \text{WS}_t, 0\right) \tag{1}$$

Then, the Drought Index Cumulated (DIC) is calculated as the maximum accumulated deficit over the whole time series, i.e.

$$\text{DIC} = \max\left(\text{deficit}_t\right) \quad t = 1, 2, 3, n \tag{2}$$

where n is the total number of days.

The value of DSDI is obtained as

$$\text{DSDI} = \frac{\text{DIC}}{\text{AP}} \tag{3}$$

where AP is the average annual precipitation volume.

2.2 The proposed index

We intended to construct an index that fulfils three requirements: (i) It characterises a surface water system with regard to the satisfaction of water demand and not the magnitude of its water storage; (ii) it uses fixed time intervals within each hydrological year (e.g., 1st, 2nd, 3rd, and 4th trimester); (iii) it takes into account the storage capacity for surface water in the studied system. Observing that DSDI fails to fulfil the last two requirements, we propose a modified version of the index following the syllogisms described next.

The maximum water volume that is available for withdrawal in time interval t is the sum of the storage in the end of the previous interval S_{t-1}, and the streamflow in the current interval Q_t. The actual withdrawal W_t is equal to water demand D_t provided that the available water exceeds D_t, i.e.

$$W_t = \min\left(S_{t-1} + Q_t, D_t\right) \tag{4}$$

The unused water is held in storage, unless it exceeds the total storage capacity SC, in which case the excess water becomes the spill SP_t, given as

$$\text{SP}_t = \max\left(S_{t-1} + Q_t - W_t - \text{SC}, 0\right) \tag{5}$$

The water balance in the studied system is expressed as

$$S_t = S_{t-1} + Q_t - W_t - \text{SP}_t \tag{6}$$

The relative deficit RD_t, expressed as the fraction of the unsatisfied water demand, is

$$\mathrm{RD}_t = 1 - \frac{W_t}{D_t} \tag{7}$$

The beta distribution function is selected as the marginal distribution of relative deficit time series. This distribution is fitted to data using the method of moments. The relative deficit of equation 7 is proposed as an index of water shortage, termed 'Surface Water Shortage Index', or SWSI. A zero value of it classifies the examined time interval as a "No shortage" one, while a value equal to unity corresponds to the "Total shortage" class. For non-zero values of SWSI in the interval (0, 1) the classes of Table 1 are defined by adopting probability masses used for drought indices such as the Reconnaissance Drought Index (Tsakiris and Vangelis, 2005; Tsakiris et al., 2007), or the Streamflow Drought Index (Nalbantis and Tsakiris, 2009). For convenience, a number is assigned to each one of the shortage classes of Table 1. It is worth noting that, for accuracy reasons, all calculations that precede equation 7 are carried out using a monthly time step, whereas subsequent computations are made at the three-month time step. Also, due to strong seasonality in both streamflow and water demand, the series of each trimester is analysed separately.

By examining equations implementing DSDI and SWSI it is understood that no direct comparison of the two indices is possible. For this reason, in this work, we removed from SWSI the restriction of finite storage capacity, which led to an index similar to DSDI. This is referred to as the 'adjusted DSDI' (DSDIa) in the results section.

Table 1. Definition of water shortage classes according to the Surface Water Shortage Index (SWSI)

Value of SWSI	Non-exceedance probability p or probability mass p'	Water shortage class	Water shortage class notation
SWSI = 0	$p' = p_0$	No shortage	0
0 < SWSI < 1	$0 < p \leq 0.3829$	Low shortage	1
0 < SWSI < 1	$0.3829 < p \leq 0.6827$	Moderate shortage	2
0 < SWSI < 1	$0.6827 < p \leq 0.8664$	High shortage	3
0 < SWSI < 1	$0.8664 < p < 1$	Extremely high shortage	4
SWSI = 1	$p' = p_1$	Total shortage	5

3. STUDY AREA AND DATA

The proposed methodology is applied to data from a basin with a reservoir at its outlet. The Evinos river basin is chosen, which is located in the West Sterea Hellas Water District, western Greece. The dam at the basin outlet was built at the site of Aghios Demetrios and serves to divert stored water to the adjacent reservoir on Mornos river. Reservoirs of the two basins are part of the reservoir system for water supply of the Athens Metropolitan area. For more details readers may refer to Nalbantis et al. (1992).

The Evinos river basin at the dam site has an area of 351.9 km^2. Streamflow data at the dam site were estimated based on measurements at the Poros Reganiou hydrometric station (870 km^2) for the period 1970-71 to 1999-2000, while, for the period 2001-2010, i.e., after the start of the dam operation in September 2001, streamflow estimates have been obtained using the reservoir water balance. In this work, a synthetic series of monthly streamflow of length equal to 2000 hydrological years is used, obtained using the stochastic modelling scheme proposed by Koutsoyiannis (1992). This has already been applied to hydrological variables related to the Athens water supply system (Nalbantis and Koutsoyiannis, 1997).

4. RESULTS

The methodology described in section 2 was applied to the synthetic time series of monthly streamflow mentioned in section 3. This allowed the assessment of the frequency of appearance of

each water shortage class for each one of the four trimesters of the hydrological year. As for the water demand, a constant annual value of it was used, which was distributed to the months using known monthly water demand distribution coefficients. We selected to use two values for the annual water demand; (i) 262.5×10^6 m^3, which is equal to the mean annual streamflow; (ii) 400.0×10^6 m^3, which reflects an unsustainable state of the studied system. The results in terms of water shortage frequency are presented in tables 2 and 3 respectively for the cases with annual demand equal to 262.5×10^6 m^3 and 400.0×10^6 m^3. Both SWSI and DSDIa are employed so as to enable comparison. Also, results of Table 2 are depicted in Fig. 1 so as to better perceive the variation of shortage frequency across different shortage classes.

Table 2. Frequency of water shortage for the case with annual water demand equal to 262.5×10^6 m^3

Shortage class	Frequency (%) for trimester							
	1st		2nd		3rd		4th	
	SWSI	DSDIa	SWSI	DSDIa	SWSI	DSDIa	SWSI	DSDIa
0	34.05	95.85	90.30	99.15	92.30	99.40	61.10	96.70
1	21.60	1.80	3.55	0.35	2.90	0.15	15.75	1.50
2	26.95	1.25	3.20	0.20	2.75	0.30	10.00	0.70
3	9.10	0.50	1.10	0.10	1.10	0.05	7.85	0.80
4	7.95	0.60	1.20	0.15	0.95	0.10	5.30	0.30
5	0.35	0.00	0.65	0.05	0.00	0.00	0.00	0.00

Table 3. Frequency of water shortage for the case with annual water demand equal to 400.0×10^6 m^3

Shortage class	Frequency (%) for trimester							
	1st		2nd		3rd		4th	
	SWSI	DSDIa	SWSI	DSDIa	SWSI	DSDIa	SWSI	DSDIa
0	0.25	4.35	76.15	76.20	61.85	62.00	0.00	8.95
1	47.25	44.35	8.65	8.60	13.65	13.55	39.20	31.55
2	26.20	25.75	7.45	7.45	12.00	12.00	18.80	26.65
3	13.35	13.15	4.20	4.20	8.10	8.05	39.70	32.60
4	12.55	12.00	2.90	2.90	4.40	4.40	2.30	0.25
5	0.40	0.40	0.65	0.65	0.00	0.00	0.00	0.00

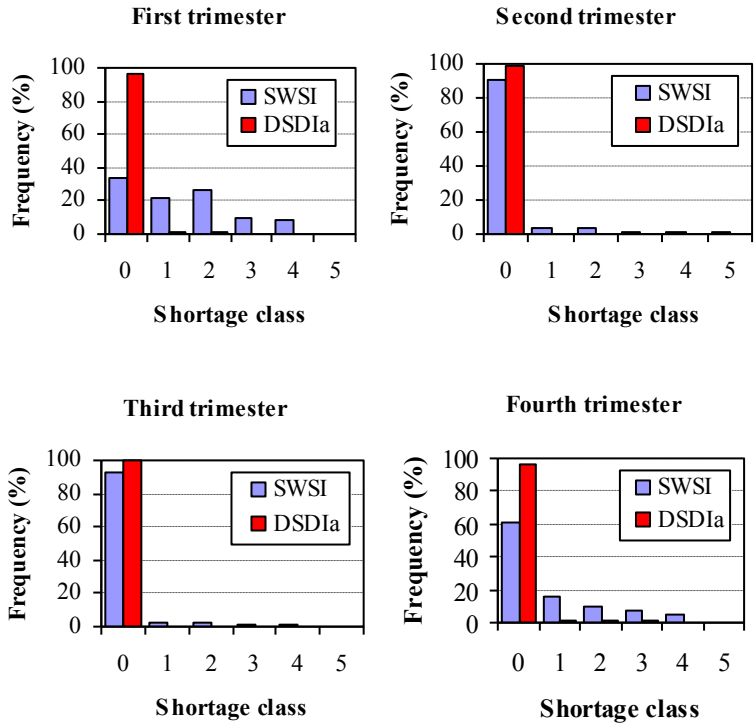

Figure 1. Frequency of water shortage for the case with annual water demand equal to 262.5×10^6 m^3

5. CONCLUSIONS

In this paper the focus was on the characterisation of surface water systems with regard to their state of water shortage. Starting from a known index, namely the Demand Sensitive Drought Index (DSDI), a modified form of it, the Surface Water Shortage Index (SWSI), was formulated with the aim to consider the finite storage capacity available in the system. Tests on data from a real-world river basin revealed the following:

1. For all trimesters and levels of annual water demand, the shortage frequency based on the adjusted DSDI (DSDIa) (explained in sub-section 2.2) is lower than that of the cases based on SWSI; hence, DSDIa tends to provide optimistic estimates of shortage frequency.
2. In the case with the proposed index and the annual water demand taken equal to the mean annual streamflow, the frequency of the 'No shortage' class is about 60% for the fourth trimester, while, starting from about 16% for the 'Low shortage' class, it is progressively decreased to 0.0% for the 'Total shortage' class; for the first trimester, the picture is less favourable: the frequency of the 'No shortage' class is rather low (34%), while, for all other classes, it remains above 7%, with the exception of the 'Total shortage' class for which it is very low (0.35%). For the remaining trimesters (second and third) the frequency of the 'No shortage' class exceeds 90%, which results in very low values for all other classes (below 4%).
3. Using DSDIa with the same water demand as in item 2 revealed that the frequency of the 'No shortage' class is very high (above 95%) in all cases, whereas it takes very low values for all the remaining classes.
4. In the case with the proposed index and an unsustainable water demand, the frequency of the 'No shortage' class drops to very low values, namely 0.25% and 0.0% for the first and fourth trimester respectively; for these two trimesters the 'Low shortage' class is the most frequent (47% and 39% respectively), while frequencies of the next three shortage classes remain significant, before dropping to practically zero for the 'Total shortage' class; for the second and third trimester, the frequency is concentrated on the 'No shortage' class, showing rather high values (76% and 62% respectively) while it progressively drops to low values thereafter.
5. Using DSDIa with the same water demand as in item 4 reveals that, for all classes, the frequency is close to that of the case of using SWSI with a tendency to a slightly more favourable distribution, i.e., with less frequent shortage; this is especially noticeable for the 'No shortage' class.
6. The proposed index is suitable for characterising the state of a surface water system for coarse and fixed time intervals within each hydrological year.

REFERENCES

Chen, X., Devineni, N., Lall, U., Zenchun, H., Leihua, D., Qin, J., Jiahu, W., Shicheng, W., 2013. China's water sustainability in the 21st century: a climate informed water risk assessment covering multi-sector water demands. Hydrology and Earth System Sciences Discussion; 10: 11129–11150.

Devineni, N., Perveen, S., Lall, U., 2013. Assessing chronic and climate-induced water risk through spatially distributed cumulative deficit measures: A new picture of water sustainability in India. Water Resources Research; 49(4): 2135-2145.

Devineni, N., Lall, U., Etienne, E., Shi, D., Xi, C., 2015. America's water risk: current demand and climate variability. Geophysical Research Letters; 42(7): 2285–2293.

Döll, P., Hoffmann-Dobrev, H., Portmann, F. T., Siebert, S., Eicker, A., Rodell, M., Strassberg, G., Scanlon, B. R., 2012. Impact of water withdrawals from groundwater and surface water on continental water storage variations. Journal of Geodynamics; 59: 143-156.

Etienne, E., Devineni, N., Khanbilvardi, R., Lall, U., 2016. Development of a Demand Sensitive Drought Index and its application for agriculture over the conterminous United States. Journal of Hydrology; 534: 219-229.

European Council, 2000. Directive of the European Parliament and of the Council of 23 October 2000 establishing a framework for Community action in the field of water policy (2000/60/EC). Official Journal L 327 , 22/12/2000 P. 0001 – 0073.

Koutsoyiannis, D., 1992. A nonlinear disaggregation method with a reduced parameter set for simulation of hydrologic series. Water Resources Research; 28(12): 3175–3191.

Nalbantis, I., Koutsoyiannis, D., 1997. A parametric rule for planning and management of multiple reservoir systems. Water Resources Research; 33(9): 2165–2177.

Nalbantis, I., Tsakiris, G., 2009. Assessment of hydrological drought revisited. Water Resources Management; 23(5): 881-897.

Nalbantis, I., Koutsoyiannis, D., Xanthopoulos, T., 1992. Modeling the Athens water supply system. Water Resources Management; 6(1): 57-67.

Thomas Jr, H. A., Burden, R. P., 1963. Operations research in water quality management. Harvard University, Cambridge Massachussets, Division of Engineering and Applied Physics.

Tsakiris, G., Vangelis, H., 2005. Establishing a drought index incorporating evapotranspiration. European Water; 9/10: 3-11.

Tsakiris, G., Pangalou, D., Vangelis, H., 2007. Regional drought assessment based on the Reconnaissance Drought Index (RDI). Water Resources Management; 21(5): 821-833.

Tsakiris, G., Nalbantis, I., Vangelis, H., Verbeiren, B., Huysmans, M., Tychon, B., Jacquemin, I., Canters, F., Vanderhaegen, S., Engelen, G., Poelmans, L., De Becker, P., Batelaan, O., 2013. A system-based paradigm of drought analysis for operational management. Water Resources Management; 27(15): 5281-5297.

Proceedings of the 10th World Congress of EWRA 'Panta Rhei', 5-9 July 2017, Athens, Greece
© 2017 *European Water Resources Association*

Sustainable management of rainwater harvesting systems: A case study of semi-arid area

M. Nanekely[1*] and M. Scholz[1,2]
[1] *Civil Engineering Research Group, School of Computing Science and Engineering, University of Salford,UK*
[2] *Division of Water Resources Engineering, Faculty of Engineering, Lund University, P.O. Box 118, Lund 221 00, Sweden*
[*] *e-mail: m.a.a.nanekely@edu.salford.ac.uk*

Abstract: In this paper, Erbil province in Iraqi Kurdistan has been chosen as a representative case study for a large number of provinces in semi-arid areas, lacking imbalance between water demands and supply. Climate change is expected to bring higher average temperatures and lower precipitation, which would intensify the pressure on water resources and increase the environmental concerns. A set of fifty-five detention ponds in Erbil were investigated, with storage capacities ranging from nearly 49,000 m^3 to 250,000 m^3. These ponds were constructed to mainly supply smallholder farms, watering livestock, and for groundwater recharge. The paper seeks to examine the function and necessity of retention ponds, as a sustainable drainage system measure in semi-arid areas, to mitigate the growing combined impacts of a water shortage and inter-annual climate variability. A set of indicators was adopted: (a) the cost of construction; (b) harvested water volume; (c) irrigated farms; (d) the number of beneficiaries; (e) the number of livestock kept; (f) groundwater recharge; (g) recreation activity; and (h) biodiversity, in addition to checking its materialising by concerned authorities and residents. A detention pond application plan has been developed to support the sustainable functioning of Rain Water Harvesting System (RWHS).

Key words: Detention pond; climate change; supportive strategy; water shortage; integrated water resources management

1. INTRODUCTION

In the World Economic Forum 2017, it has been pointed out that Environment-related risks also stand out in this year's global risk landscape. The most frequently cited of these being the pairing of "water crises" as well as "failures to climate change mitigation and adaptation". Furthermore, The World Bank expects that water stress could cause extreme societal overstrain in regions like the Middle East, where the economic effects of water scarcity could reach at risk 6% of Gross Domestic Product (GDP) by 2050 (Van Der Heijden, 2015).

Water shortages problem can affect the daily life needs in its various forms, agricultural, industrial and then to varying degrees the economic activities. In large cities, rainwater storage tanks can be used to save rainwater, but in peri-urban development and suburb areas, different rainwater means such as tanks or ponds are used as a unique water supply for many households and families to support agricultural livelihoods, mitigate water insecurity, and enable ecosystem services.

(Amin, Alazba, & ElNesr, 2012) have pointed out that an increasing maximum rainfall with decreasing annual rainfall has been observed for the cities signifying the more extreme rainfall events and resulting floods for short durations. The assessments of any systematic changes in view of the increased rain intensities and extreme climate events are viewed to demonstrate the harvested rainwater value and management as a local adaptation to the climate variability and extreme. In Iraq, the semiarid Kurdistan region is suffering from water shortages problem. Erbil province has been chosen as a representative case study for a large number of provinces that suffers from water shortage, climate variability and the consequences associated with drought problem (Figure 1).

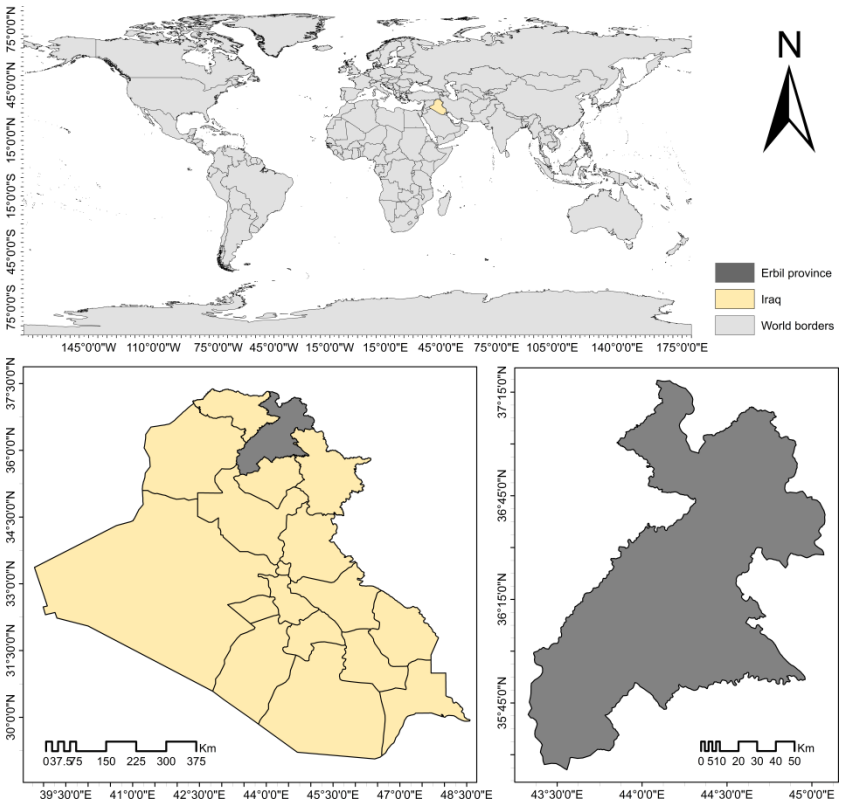

Figure 1. The location of Erbil province with respect to Iraq and the world

Studies have shown that the application of Macro RWH will provide good provision for water-scarcity (Zakaria, Al-Ansari, Mustafa, Knutsson, Ahmad, & Ghafour, 2013), thereby helps to minimize the water crises. RWHS technique encourages harvesting rainwater for the last two decades and has given hopeful results in semi-arid region (Al-Ansari, Knutsson, Zakaria, & Ezzeldin, 2015). This had been conducted based on variables of: harvested water volume, water surface area, catchment areas, and the minimum cost of small dams. (Bitterman, Tate, Meter, & Basu, 2016) have explored that there are a number of components that are basic components which govern water security, the components are; Land use/land cover, Hydrology, groundwater, socio-economic, social equity, ponds functionality as ponds capacity and management, and agriculture productivity. Therefore, taking into account further variables such as livestock's watering, area of ponds, biodiversity value, bio-retention consideration, recreation aspects, groundwater recharge, and beneficiaries support, those additional variables would give more comprehensible outcomes for the same studied period.

2. MATERIALS AND METHOD

2.1 RWHS data analysis

Microsoft Excel (2010) was used to manage the data set, to categorise it into sub-sets and further to make analysis associated with the application of Mathematical functions. The process of analysing the data follows the following steps: (a) the minimum value of each indicator has been subtracted from the maximum value then the result divided by four to make the weighting judgment more precise by differentiating the data into intervals; (b) every subset of data for every single indicator has been selected and given a relative (proportional) weight values, either 25% = 0.25, 50% = 0.5, 75% = 0.75, or 100% = 1.00, there has been sorted out into four intervals; (c) the relative weights have been ordered as 25%, 50%, 75%, and 100%. Functions that have been used for this purpose were (INDEX) and (SUMPRODUCT): (e) the formula that has been used to pick

out the corresponding values for every interval is illustrated in Equation 1 as a sample for irrigated area. The least subset has been given relative weight of % 25 as it has little impact compared with the data within its set, i.e., the data which have the less values the least percentage 0.25 were given. On the other hand, the data, which have the more values the most percentage 1.00, were given.

There were exceptions, two indicators that are; construction cost and ponds area, their percentages have been taken inversely, these exceptions attribute to; whenever the cost increases the economic cost-effectiveness decrease, as for the ponds area; whenever the basin inundation area increased, legal issues will excite and raises property ownership issues, in addition to the reduction in size of agricultural lands.

Selected relative weight = INDEX (range from 0.25 to 1.00, SUMPRODUCT (--(all selected data under irrigated area column ≤ maximum ranges from 1000 to 4000),--(selected data under irrigated area column ≥ minimum ranges from 0 to 1000), ROW (number of rows to be analysed))) (1)

This process has been repeated for all indicators, and hence, all were resulted relative weights for every nominated pond inserted into corresponding table cells. Thereafter, Equation 2 has been used to find out the weighted score for every detention pond, i.e. each scaled weight is then multiplied by the appropriate relative weight, giving a weighted score, and i.e. all results are out of 37. Giving scaled weights for every indicator can be differing from points of view and the aims of the study; this is true even the set of indicators is the same. Therefore, the scaling is chosen based on the essentiality and the importance of each indicator for our purpose.

2.2 RWHS ponds data

A set of fifty-five detention ponds in Erbil province has been investigated. These detention ponds form a RWHS as one of the commonly used sustainable drainage systems (SuDS) in the arid and semi-arid areas (Harb, 2015) & (Ziller & Ertl, 2010). Ten indicators have been investigated and examined. These indicators are: (a) the cost of construction; (b) the size of inundated area; (c) the harvested water volume; (d) proposed livestock's watering; (e) irrigation area; (f) groundwater replenishment; (g) flood risk mitigation; (h) the number of beneficiaries and socio-economic development; (i) the appropriateness for recreation; and (j) biodiversity. A weighted scale approach has been used in which a weighted scale factor (WSF: 1 to 5) was given to each indicator. The weights are (1: very low impact; 2: low impact; 3: medium impact; 4: high impact; and 5: very high impact). The (Ministry of Agriculture and Water Resources, 2016) Kurdistan Regional Government-Iraq (KRG) has facilitates the access of available data and gathering it from a number of departments. Site visits have been undertaken to a number of detention ponds in order to better understanding the current situation and to meet with the local communities.

Since the data were collected, they consist of figures (numbers) for every indicator, and each indicator represents as an indicator of the effectiveness of the system, moreover, how the indicators data can be inducted, therefore, the approach of Multiple-criteria decision analysis (MCDA) have been chosen. (MCDA) is deemed as a sub-discipline of research methods, which distinctly evaluates multiple conflicting and non-conflicting indicators for evaluation or decision-making. One of the methods that widely have considered as a sort of (MCDA) techniques is Weighted Sum Model (WSM), (Zardari, Ahmed, Shirazi, & Yusop, 2015); (Herath & Prato, 2006). In decision theory, the (WSM) is well known and simplest (MCDA) for evaluating a number of indicators in terms of a number of criteria (Ben-Ariehand & Triantaphyllou, 2002); (Marler & Arora, 2010); (Alanazi, Abdullah, & Larbani, 2013). The common formula for obtaining the weighted score (Odu & Charles-Owaba, 2013); is shown in Equation 2:

$$Ii^{WSM}\text{-score} = \sum_{j=1}^{n} Sw * Rw, \quad \text{for } n = 1, 2, 3, \ldots \tag{2}$$

where: Ii ^{WSM} is Indicator score weight, Sw is Scaled weight, and Rw is Relative weight (Proportional weight).

2.3 Data derived from concerned people

In 2016, 57 individuals, representing villagers, farmers and towns Notables' and 42 water professionals have been interviewed. Face-to-face and telephone structured interviews have been adopted and carried out (Opdenakker, 2006). Ethical approval from the Ministry of Agricultural and Water Resources (KRG) were obtained including the consents from all participants.

3. RESULTS AND DISCUSSION

3.1 Results obtained from the RWHS

The highest scaled weight of "5" has been associated with four indicators: harvested water volume; irrigated area; livestock's watering; beneficiaries and socio-economic, this has been based on the perspective of water shortages in semiarid regions, the harvested rainwater volume plays the pivot role to grow livestock's numbers and widen the irrigated area, as a result, this would be beneficial for socio-economic prosperity.

The potentiality of groundwater recharge in such area cannot be marginalised, it is considered as an assurance of water provision for the next generations;; that has been facing depression since last decade (Werner & Gleeson, 2012); (Everard, 2016); (Ebrahimi, Ghazavi, & Karimi, 2016). Therefore, it led to consider that the groundwater issue has to be given a scaled weight of "4".

A scaled weight "3" was given to the construction cost and flood risk management indicators, as these two indicators have not been considered among the major objectives for the application of RWHS in the studied area. Despite there is still limited proofs on the effectiveness of these systems and a need to quantify their admitted benefits, i.e. in terms of flood protection and water quality among others (Perales-Momparlera, et al., 2016), but also we cannot be given lowest rates of scaled weights. This has been seeing in terms of the essentially of financial supports, cost-benefit considerations, in addition for tackling disasters that following flood events in semi-arid regions.

Ponds provide aesthetic worth to areas that construct in. Origin birds, migratory birds, attract hovering around ponds as well as wild animals. Studies (Bogaski, 2012); (Barron, 2009) show aesthetic beauty, recreational values and biodiversity conservation are almost equal, and come to following the utilization for irrigation purposes and economy costs, therefore have given scaled weights "2" and "1".

Economic benefits from the ponds show that benefit cost ratio in almost crops are nearly double that assert the high value in financial returns the alternate land use by cultivating grasses that have a great desire in dairy farms (Shrivastava, Kumar, & Singh, 2015).

Findings show that economically this system in this area was effectively and benefit cost. In other words, 48 out of 55 ponds have cost in a higher range of relative weight, i.e. less cost, which is a good indicator that can be inferred from the results, as this system of (SuDS) would be feasible for applying in such region,. It is worth mentioning, that this result not necessarily be generalised, there are many factors are involving; for instance, the economic situation of the country, pond site selection, availability of raw materials, high quality of construction techniques, and many other interrelated factors.

Two other indicators; the pond basin area and flood risk reduction, were counted 48 and 55 ponds out of 55, both are within the higher ranges of relative weights respectively, which is also considered as a significant evidence for relative use of SuDS techniques for this region.

Turning to the other four indicators; harvested water volume; irrigated areas; livestock's watering; and number of beneficiaries, it can be noticed that most ponds were got less weights,

here, it can be noticed; that there are many other factors lie behind this; (a) The survey or the assumption of the designers on feasibility study might be inaccurate. (b) A number of ponds have situated in non-arable areas. (c) The number of villagers and farmers were not counted as it is. (d) Or can be attributed to the political situation that most of villagers had migrated to urban areas in the past decades due to political conflicts, and still most of them are living there, this will reduce the number of beneficiaries and livestock's watering.

It has been noted that the ponds which are located within the steppe areas are most likely supporting water shortages in dry-spell seasons for the areas known as rain-fed lands. Therefore, those ponds are considered the most feasible than others pertaining to the use for agricultural exploitation. Obviously, villagers are gathering around areas in which water are available, a larger number of farmers and villagers are living in the plateau, this indicates that in addition to the availability of rains, the topography has the role for gathering people and get benefit from this technique.

These ponds have been supporting livestock's watering; big portions of livestock flocks are secured watering after the run of these ponds. It is worth mentioning, based on the availability of rainfall and suitable topography; the (RWHS) performances are differed to varying degrees in terms of irrigation, watering livestock's, ground water recharge, socio-economic development, and biodiversity.

There are only 3 ponds out of 55 (approximately 5.5%) has thoroughly been contributing for recharging groundwater. This suggests that further site investigations and hydro-geological studies are needed to properly improve groundwater recharge.

Regarding to recreation and bio-diversity, as weights; it looks likely as same level for all ponds, these two indicators were also governed by many other factors, to clarify more; the data were collected by official departments might be gathered at early period of ponds construction, or the observations were not taken in suitable seasons and so on.

The frequency distribution of results have been categorised into 4 groups, almost half of ponds got scores between 17.8 and 20.3 out of 37 as (group 1 and 2), whereas, the rest of 6 ponds i.e. one tenth were laid in high score weights as group 3 and 4. This attributed to what have been previously clarified besides the other influential factor that is; setting the scaled weights that pointed out the importance of each indicator, which governs the total weighted scores.

3.2 Results derived from stakeholders

The transcripts were re-reviewed for many times, key points has been selected through the review that was focused on by most of the respondents, based on the highlighted significant key points, those were classified under categories as a number of themes, that can be inferred as strategies:

Strategy 1: Identifying the function of stormwater systems

Most of residents' responses indicated that they either "do not know how the detained water goes through evaporation and ground percolation" or "do not know the socio-economic benefits are".

Strategy 2: Identify related indices to education

Terminology and their accompanying notions such as stormwater runoff, watershed and sustainability specifically may be too strange and complex for people who casually pay attention to SuDS. Choosing a physical, visible indicator can help effectively communicate and introduce somewhat abstract concepts. Rationalisation of water consumption, maintain water quality are intangible concepts needs to be understood.

Strategy 3: The necessity for municipal ordinances issue pertaining RWHS

Another strategy for increasing the adoption of SuDS is to take external opportunities or link recommended SuDS to recent rule changes. For example, the municipalities' councils and the department of Environmental Protection should implement restrictive ordinances and develop a regional model ordinance for harvesting rainwater that is appropriate to the interests of both urban

and suburb communities. For example, land owners' rights and water sharing quotas between breeders and farmers.

Strategy 4: Capacity Building for Green Industry Professionals

Provide guidelines for landlords and green industry professionals on the use of fertilisers, herbicides, and pesticides.

Strategy 5: Raise the awareness of residents, farmers and villagers to Increase Adoption of Ponds and Plants

Education about plantings nearby ponds can be divided into different types and delivered to groups depending on how likely they are to adopt plantings as a way to exploit harvested water to sustain crop production and pave the way for bio-diversities environments.

Strategy 6: Action plans

Solid plans are needed to improve the socio-economic situation for farmers and villagers. Practical steps are needed to adopt disease prevention program due to increase of harmful insects.

4. CONCLUSIONS

The semi-arid regions have been encountering to water crisis since subjected to climate alterations, therefore, joint effect alleviation is needed for both water scarcity and climate variability. Thus, the interests to RWHS are essential to avoid most of the environmental, economic and social ramifications.

In the economic perspective, this system is costly effective. Results reveal that RWHS has a significant role in flood risk reduction. Due to climatic alteration, these regions have been experiencing both long drought period and combined with extreme rainfall events, the detained rainwater mostly cannot be sufficient a long drought seasons for the purposes of livestock watering and farm irrigation, it can be regarded as a mitigation measure, despite that and as long as the system has been operated, water needs were rather securely. Recreation issue can be utilised a long certain seasons where the climate are moderate. As for bio-diversity; despite there were not a satisfactory results, but joint actions are needed to involve Tourism Board, Environment Agency with Water resources management. More hydro-geological studies are needed to properly manage groundwater recharge.

Actions are required as attempts to successfully apply RWHS in a sustainable manner based on developed strategies that should be considered. In semiarid areas, a comprehensive database of all the components that can be incorporated into SuDS and water resources management is needed. On the other hand, a strategic planning is also needed to better understand the philosophy of SuDS supported by a solid action plan.

5. REFERENCES

Alanazi, Hamdan O., Abdul Hanan Abdullah, and Moussa Larbani. “Dynamic Weighted Sum Multi-Criteria Decision Making Mathematical Model.” International Journal of Mathematics and Statistics Invention (IJMSI) 1, no. 2 (2013): 16-18.

Al-Ansari, N., S. Knutsson, S. Zakaria, and M. Ezzeldin. “Feasibility of using small dams in water harvesting, Northern Iraq.” Hydropower'15. Stavanger, Norway, 2015. 1-8.

Amin, M. T., A. A. Alazba, and M. N. ElNesr. “Adaptation of climate variability/extreme in arid environment of the Arabian peninsula by rainwater harvesting and management.” International Journal of Environmental Science and Technology, 2012: 27-36.

Barron, Jennie. Rainwater harvesting: a lifeline for human well-being. UNEP/Earthprint. Stockholm: UNEP/Earthprint, 2009.

Ben-Ariehand, D., and E. Triantaphyllou. Multi-Criteria Decision Making Methods: A Comparative Study. Boston: Springer, 2002.

Bitterman, Patrick, Eric Tate, Kimberly J. Van Meter, and Nandita B. Basu. “Water security and rainwater harvesting: A conceptual framework and.” Applied Geography, 2016: 75-84.

Bogaski, Kathleen. Strategies for Sustainable Surface Water Management in Master Planned Communities in Semi-Arid to Arid Environments. Doctoral Dissertation, University of Mashigan, 2012.

Ebrahimi, Hydar, Reza Ghazavi, and Haji Karimi. “Estimation of groundwater recharge from the rainfall and irrigation in an arid environment using inverse modeling approach and RS.” Water Resources Management 30, no. 6 (2016): 1939-1951.

Everard, M. "Community-based groundwater and ecosystem restoration in semi-arid north Rajasthan (1): Socio-economic progress and lessons for groundwater-dependent areas." Ecosystem Services 16 (2016): 125-135.

Harb, Rayyan. "Assessing the potential of rainwater harvesting system at the Middle East Technical University–Northern Cyprus campus." Middle East Technical University Library Web site. 2015. http://etd.lib.metu.edu.tr/upload/12619225/index.pdf (accessed November 10, 2016).

Herath, Gamini, and Tony Prato. Using multi-criteria decision analysis in natural resource management. Ashgate Publishing, Ltd., 2006.

Marler, R. Timothy, and Jasbir S. Arora. "The weighted sum method for multi-objective optimization: new insights." Structural and Multidisciplinary Optimization 41, no. 6 (2010): 853–862.

Ministry of Agriculture and Water Resources, KRG. Feasibility Study And Design Of Detention Ponds-Erbil Governorate. Annual report, Erbil, Iraq, Erbil: Ministry bulletins, 2016.

Odu, G. O., and O. E. Charles-Owaba. "Review of Multi-criteria Optimization Methods – Theory and Applications." IOSR Journal of Engineering (IOSRJEN) 3, no. 10 (2013): 1-14.

Opdenakker, Raymond. "Advantages and disadvantages of four interview techniques in qualitative research." Qualitative Social Research 7, no. 4 (August 2006): 1-13.

Perales-Momparlera, Sara, et al. "The role of monitoring sustainable drainage systems for promoting transition towards regenerative urban built environments: a case study in the Valencian region, Spain." Journal of Cleaner Production, 2016.

Shrivastava, P. K., S. Kumar, and N. Singh. "Evaluation of benefits from harvested rain water in farm ponds." Indian Journal of Soil Conservation 43, no. 3 (2015): 471-276.

Van Der Heijden, K., B. Otto, and A. Maddocks. Beyond conflict, water stress contributed to Europe's migration crisis. 3 November 2015. http://www.wri.org/blog/2015/11/beyond-conflict-water-stress contributedeurope% (accessed February 10, 2017).

Werner, Aeschbach-Hertig, and Tom Gleeson. "Regional strategies for the accelerating global problem of groundwater depletion." Nature Geoscience 5, no. 12 (2012): 853-861.

Zakaria, Saleh, N. A. Al-Ansari, Y. Mustafa, Sven Knutsson, Payman Suhbat Ahmad, and Bahra Dhahir Ghafour. "Rainwater Harvesting at Koysinjaq (Koya), Kurdistan Region, Iraq." Journal of Earth Sciences and Geotechnical Engineering, 2013: 25-46.

Zardari, Noorul Hassan, Kamal Ahmed, Sharif Moniruzzaman Shirazi, and Zulkifli Bin Yusop. Weighting Methods and their Effects on Multi-Criteria Decision Making modell Outcomes in Water Resourceses Management. Springer, 2015.

Ziller, Annette, and Thomas Ertl. "Assessment of structural stormwater measures in Tehran through indicators of sustainable development." 2010: 1-9.

Proceedings of the 10th World Congress of EWRA 'Panta Rhei', 5-9 July 2017, Athens, Greece
© 2017 *European Water Resources Association*

The effect of reservoir networks on drought propagation

P.R. van Oel[1*], E.S.P.R. Martins[2] and A.C. Costa[3]
[1] *Water Resources Management group, Wageningen University, The Netherlands*
[2] *Fundação Cearense de Meteorologia e Recursos Hídricos, Fortaleza, Brazil*
[3] *University of International Integration of the Afro-Brazilian Lusophony, Redenção, Brazil*
[*] *e-mail: pieter.vanoel@wur.nl*

Abstract: Human interventions in response to drought can both alleviate and enhance drought. Developments of infrastructure for freshwater storage, groundwater abstraction and irrigation have proved to be effective in overcoming meteorological and agricultural drought in many locations worldwide. At the same time such developments may exacerbate hydrological drought, especially during and following extended periods of (meteorological) drought. In order to effectively manage drought, there is an urgent need to better understand and evaluate the drivers of such events. This means that we need to separate between human and natural factors that affect hydrological processes in basins. In this paper, we demonstrate how the Downstreamness concept can be used for Drought Diagnosis. This is done for a subcatchment of the Jaguaribe basin in Northeast Brazil. Our diagnosis focuses on the propagation of three severe multi-year droughts that have developed during the period 1979-2016. Our study shows how a network of surface water storage reservoirs has affected the propagation of drought. Applying the proposed approach is helpful for the spatiotemporally-explicit assessments of droughts and their propagation. Strategic and operational water (and drought-risk) management relies on valuations of trade-offs between commitments of upstream and downstream uses and technical implementations of upstream and downstream measures. Our study offers valuable insights through the inclusion of sub-basin points of view as an integral part of a river basin perspective. In this way, the effects of anthropogenic processes affecting drought propagation can be better understood.

Key words: Drought propagation, Downstreamness, Jaguaribe basin, Brazil

1. INTRODUCTION

Drought refers to a below-average anomaly of selected variables and occurs when a deficiency of precipitation over some period of time results in a water shortage for human and natural purposes. Determining the magnitude and duration (from onset to demise) of droughts is not straightforward. Different types of drought include meteorological, soil moisture, hydrological, socioeconomic and ecological drought (NDMC, 2017). Hydrological drought may materialize by low levels of streamflow and stored volumes. Hydrological drought typically follows meteorological drought, and there can be a time-lag between them (NDMC, 2017). Water can be stored in surface water storage reservoirs, ranging from large public dams (WCD, 2000) to a multitude of small privately owned dams, often designed to overcome periods of water deficit. The use of reservoirs may lead to smoothed hydrographs, with lower peak flows and higher low flows. Thus, to some extent, the effect of increased water use can be compensated by river regulation using reservoirs (Wanders & Wada, 2015). To improve our understanding of the effects of human activities on the development and propagation of drought (either positively or negatively) new statistical and modelling tools are needed (Van Loon et al., 2016).

In this paper we assess the influence of a network of surface water storage reservoirs on the propagation from meteorological to hydrological drought for a subcatchment of the Jaguaribe basin in Brazil. This is done by using the Downstreamness concept (Van Oel et al., 2011).

2. METHODS

A common indicator of meteorological drought is the Standardized Precipitation Index (SPI;

McKee et al., 1993). For analysing hydrological drought the Standardized Streamflow Index (SSFI) can be used. For the definition drought we have adopted the definition proposed by McKee et al. (1993) for both SPI and SSFI. This means that a period in which the SPI (or SSFI) is continuously negative and the SPI reaches below a value of -1. The drought begins when the SPI first falls below zero and ends with the positive value following a value of -1 or less (McKee et al., 1993). Drought magnitude (DM) is defined as the negative summation of SPI (or SSFI) for all months of the drought (McKee et al., 1993). To account for the effect of seasonal variations a 'running' 12-month SPI and SSFI values are used.

Our approach comprises three steps, as described below. The case study that is used to illustrate our approach is first introduced.

2.1 Case study description

The semi-arid Northeast of Brazil has a history of recurrent water stress (Gaiser et al., 2003; Guerra & Guerra, 1980), which is related to both rainfall variability and human intervention. Annual precipitation is characterized by high levels of temporal and spatial variability (FUNCEME) and is concentrated from January to June. In the area reservoirs of various sizes are so numerous (thousands), that their effect on basin hydrology is significant (de Araújo & Piedra, 2009; Van Oel et al., 2008). High reservoir densities (exceeding three times average annual runoff) in the area have led to reduced hydrologic sustainability (Malveira et al., 2011; Mamede et al., 2012). The largest reservoirs are monitored by Water Agencies, such that changes in volumes over time can be analysed. For this study the catchment of the streamflow gauging station in Morada Nova (sub-catchment of the Jaguaribe basin in Ceará) was selected (Figure 1). For this study all data (precipitation, streamflow and reservoir storage) were obtained from FUNCEME, the Organization for Meteorology and Water Resources for the State of Ceará (Fundação Cearense de Meteorologia e Recursos Hídricos).

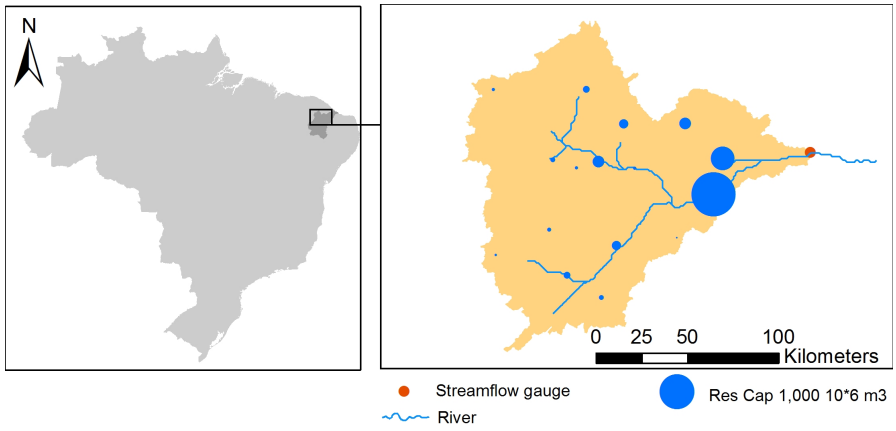

Figure 1. The sub-catchment of the streamflow gauging station Morada Nova, located inside of the Jaguaribe basin in Ceará, Northeast Brazil. Also reservoirs which are monitored by Water Agencies have been indicated.

2.2 Step 1: Calculation of the running 12-month SPI and SSFI.

For showing meteorological drought in the catchment area of a streamflow gauging station the 'running'12-month SPI is determined from a time series of precipitation data at the level of the entire catchment area. Thiessen polygons are used for interpolation monthly values of multiple stations for a representative period. To determine the SPI a downloadable program was used (NDMC, 2017). For showing hydrological drought in the catchment of the same streamflow gauging station the 'running'12-month Standardized Streamflow Index (SSFI) was determined using the same program as for SPI (NDMC, 2017).

2.3 Step 2: Evaluation of drought propagation in time

To show how drought propagation behaves over time 12-month SPI and 12-month SSFI for the end of the wet season (the month of June in our case) were compared for selected periods of drought. In this way it was explored how meteorological drought compares to hydrological drought for selected periods of time.

2.4 Step 3: Explanation of drought propagation using information on storage

For the catchment area (upstream of the Morada Nova streamflow gauging station) it is determined how the Downstreamness (Van Oel et al., 2011) of upstream stored volumes and storage capacity have developed over time. The findings of this analysis have been used to explain the propagation of drought. Every location x in a catchment can be characterized by the size of its upstream area. To indicate the relative positioning in the context of the entire catchment area, the upstream area, $A_{up;x}$, is divided by the total catchment area of the river basin, A_{tot}. The fraction determined is called Downstreamness (Van Oel et al., 2011), D_x:

$$D_x = \frac{A_{up,x}}{A_{tot}} \times 100\% \quad (1)$$

The Downstreamness of a function on the basin is defined as the Downstreamness-weighted integral of that function divided by the regular integral of that function. For a function defined on a discrete set of locations in the basin, the Downstreamness is similarly defined as the Downstreamness-weighted sum of the function divided by the regular sum (e.g., Eqs. 2, 3).

In this study, the Downstreamness of storage capacity (D_{SC}) and stored volume (D_{SV}) are defined as in equations 2 and 3, respectively. By comparing the Downstreamness of storage capacity to the Downstreamness of actual stored volumes, one can evaluate how stored volumes are allocated over the storage facilities included in the analysis.

$$D_{SC} = \frac{\sum_{x=1}^{n} SC_x D_x}{\sum_{x=1}^{n} SC_x} \quad (2)$$

$$D_{SV} = \frac{\sum_{x=1}^{n} SV_x D_x}{\sum_{x=1}^{n} SV_x} \quad (3)$$

3. RESULTS

3.1 Meteorological and hydrological drought

Figure 2 shows the development of meteorological drought (running 12-month SPI for the catchment) and hydrological drought (running 12-month SSFI at the Morada Nova streamflow gauging station) for the period December 1979 – June 2016. From Figure 2 it can be seen that SPI and SSFI do not coincide for this area. For certain periods of (meteorological) drought the hydrological drought is mitigated (or even avoided). However, following periods of meteorological drought, extended periods of hydrological drought take place. This is clearly seen for the (meteorological) droughts starting in 1992, 1998 and 2012.

3.2 Propagation of drought in time

One way of representing human-modified drought is to compare the values of SPI and SSFI for periods of drought directly (Figure 3). It is clear that for the first two periods shown, years with low

SPI values and low SSFI values are followed by years of above-average SPI and low SSFI. The periods of 1990-1996 and 1997-2003 show similar patterns. For the drought period that started around 2010 one would expect to observe a similar pattern, unless a flood event would take place such as happened in 2004.

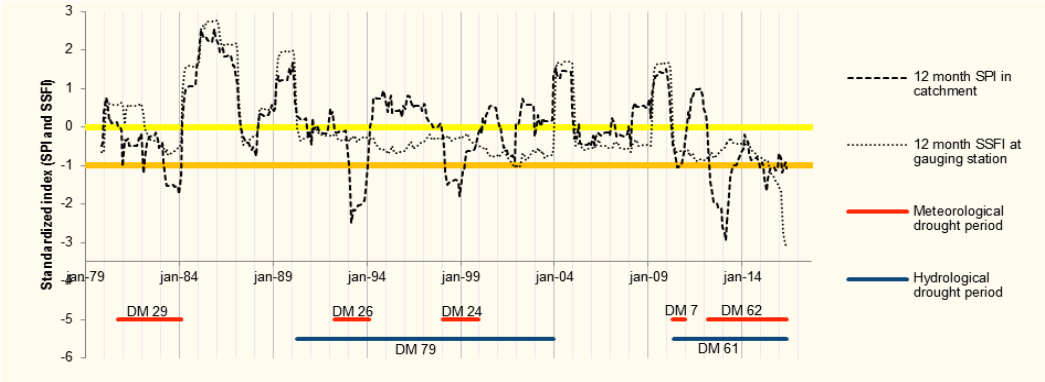

Figure 2. Drought profile for the catchment upstream of the Morada Nova Streamflow gauging station: SPI based on a Thiessen-interpolated time-series of monthly rainfall values for the catchment area; SSFI based on a time-series of streamflow values for monthly values at the Morada Nova Streamflow gauging station; Stored volumes in surface water reservoirs upstream of the gauging station. For periods of hydrological and meteorological drought the Drought Magnitude (DM) is been indicated

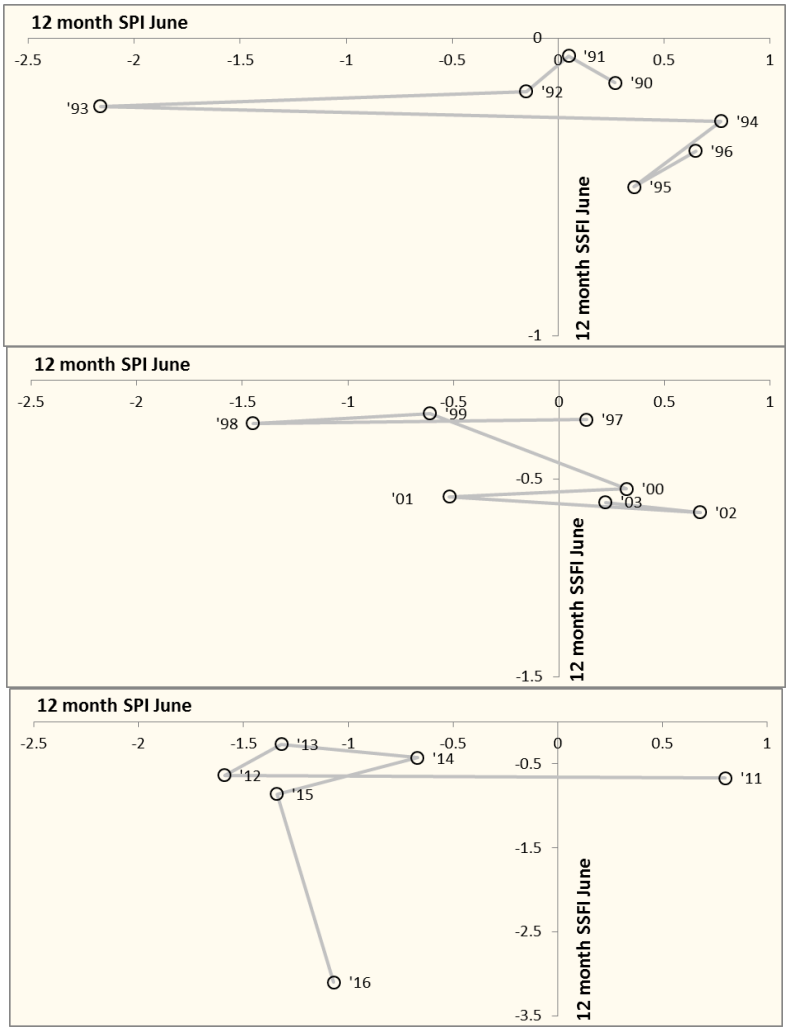

Figure 3. Morada Nova human-modified drought diagram. Periods with low values for both SPI (12 month SPI for June) and SSFI (12 Month SSFI for the month of June) are followed by periods with higher SPI and low SSFI.

3.3 Downstreamness of storage capacity and stored volume

For the catchment of the Morada Nova streamflow gauging station meteorological drought (e.g. 1998-1999) led to a drop in reservoir volumes. Then, when it started raining (moderately) again (2000, 2001) a stabilization of reservoir volumes took place. However, this situation coincided with a drop in the Downstreamness of stored volumes (Figure 4). This means that the water that was stored in the basin was mostly stored in reservoirs located in relatively upstream locations. In fact, the largest reservoir located furthest downstream almost ran empty. The effect of this imbalance was the human-modified drought (or extended hydrological drought), continuing until 2003. During this period it was not possible to generate streamflow of the same level as during the meteorological drought (1998-1999) because of the relatively low volumes in the reservoir located furthest downstream. In fact, a flood (2004) was required to restore the balance. Between 2004 and 2014 a situation existed in which the Downstreamness of stored volumes and storage capacity were around the same level (Figure 4). However, from 2014 onwards a drop in Downstreamness of stored volume is observed again. This time, even more articulated than the previous one. This makes it very well possible that an extended period of hydrological drought will follow, unless a significant flood event occurs, such as the one in 2004.

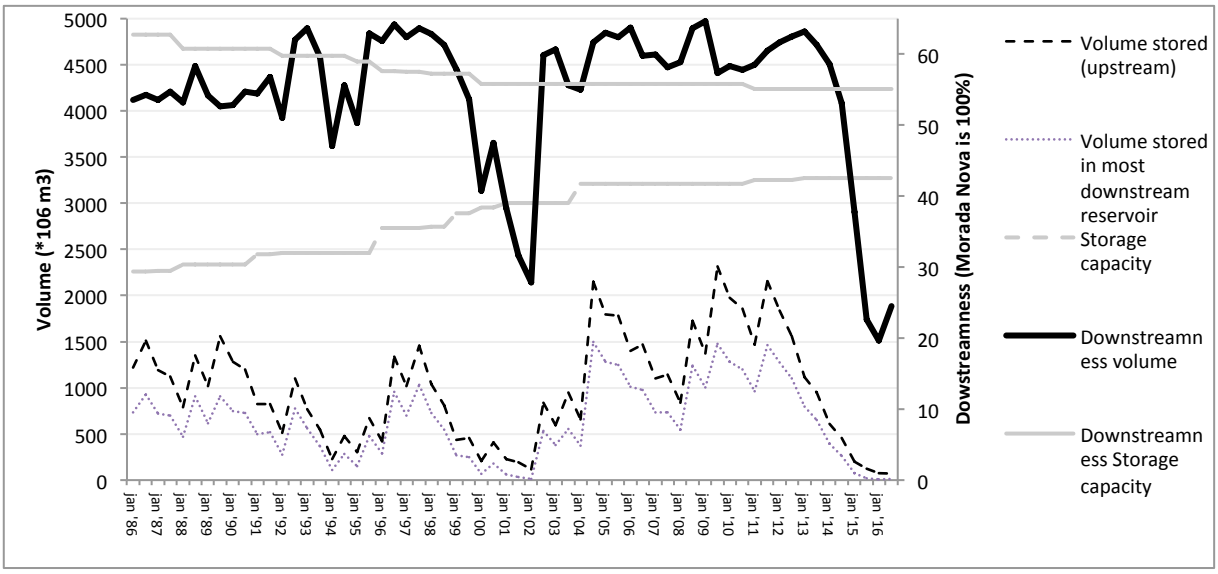

Figure 4. Downstreamness of the surface water storage capacity (solid grey line), stored volume (solid black line) in the catchment of the Morada Nova gauging station as it developed over the period 1986-2016.

4. DISCUSSION

This study provides an approach to investigate the effect of a reservoir network on drought propagation. In human-modified systems there can be enlarged differences between meteorological and hydrological, as shown in this paper. Additional information can be obtained from using the Downstreamness concept. Our results show clear indications that the present ongoing drought could be extended for many years to come. That is, unless a substantial flood will restore the balance in storage and thus ends the hydrological drought.

The datasets used to determine SPI and SSFI do not take into account changes in the anthropogenic influence over time. This can lead to a skewed distribution in which hydrological drought in early years remains undetected because of the severity of the later droughts.

The process of overbuilding basins, that is to increase reservoir density well-beyond average annual runoff is associated with basin closure (Molle et al., 2010). This process of overbuilding is only for a limited part initiated by organizations involved in planning and management of large-scale infrastructure. In this study we only took into account such large-scale infrastructure (large

dams). So our view is limited. In reality the situation could even be much more skewed to upstream, since a huge amount of small reservoirs is installed and managed by farmers acting according to local irrigation needs, particularly during droughts (Mamede et al., 2012), which can be considered to be less sustainable under drought conditions (Krol et al., 2011). A long-term period of human-induced hydrological drought may persist which may only be overcome by extreme anomalies in terms of flooding. Next to physical factors (ground water deficits, dry soils), also perverse incentives may play a role. During periods of scarcity at the basin level, water use may increase (Van Oel et al., 2008) and investments in additional storage capacity may be done. Also investments in modern irrigation technologies often prove to be less effective at a basin scale than on a local scale (Berbel et al., 2014).

5. CONCLUSION

By analysing data on precipitation, streamflow, surface water storage capacity and stored volumes, using the Downstreamness concept the effect of a network of reservoirs on drought propagation was assessed. For our case study area it was found that hydrological drought can continue well beyond meteorological drought due to a skewed distribution pattern of stored volumes towards upstream locations. Explaining the occurrence of this process can be used to inform decision-makers in predicting the severity of an ongoing drought. In this way meteorological predictions can be better interpreted and become more useful for drought risk management and strategic water resources management.

REFERENCES

Berbel, J., Gutiérrez-Martín, C., Rodríguez-Díaz, J. A., Camacho, E., & Montesinos, P. (2014). Literature Review on Rebound Effect of Water Saving Measures and Analysis of a Spanish Case Study. Water Resources Management, 29(3), 663-678

de Araújo, J. C., & Piedra, J. I. G. (2009). Comparative hydrology: Analysis of a semiarid and a humid tropical watershed. Hydrological Processes, 23(8), 1169-1178

Gaiser, T., Krol, M., Frischkorn, H., & Araújo, J. C. (Eds.). (2003). Global change and regional impacts: water availability and vulnerability of ecosystems and society in the semi-arid northeast of Brazil. Berlin, Germany: Springer.

Guerra, P., & Guerra, T. (1980). Seccas contra as seccas (Vol. 29). Mossoro, Brazil

Krol, M. S., De Vries, M. J., Van Oel, P. R., & De Araújo, J. C. (2011). Sustainability of Small Reservoirs and Large Scale Water Availability Under Current Conditions and Climate Change. Water Resources Management, 25(12), 3017-3026

Malveira, V. T. C., Araújo, J. C. D., & Güntner, A. (2011). Hydrological Impact of a High-Density Reservoir Network in Semiarid Northeastern Brazil. Journal of Hydrologic Engineering, 17(1), 109-117

Mamede, G. L., Araújo, N. A. M., Schneider, C. M., De Araújo, J. C., & Herrmann, H. J. (2012). Overspill avalanching in a dense reservoir network. Proceedings of the National Academy of Sciences of the United States of America, 109(19), 7191-7195

McKee, T. B., Doesken, N. J., & Kleist, J. (1993). The Relationship of Drought Frequency and Duration to Time Scales 8th Conference on Applied Climatology. Boston, USA: American Meteorological Society.

Molle, F., Wester, P., & Hirsch, P. (2010). River basin closure: Processes, implications and responses. Agricultural Water Management, 97(4), 569-577

NDMC. (2017). National Drought Mitigation Center. Retrieved from http://drought.unl.edu/Home.aspx

Van Loon, A. F., Gleeson, T., Clark, J., Van Dijk, A. I. J. M., Stahl, K., Hannaford, J., . . . Van Lanen, H. A. J. (2016). Drought in the Anthropocene. Nature Geoscience, 9(2), 89-91

Van Oel, P. R., Krol, M. S., & Hoekstra, A. Y. (2011). Downstreamness: A Concept to Analyze Basin Closure. Journal of Water Resources Planning and Management, 137(5), 404-411

Van Oel, P. R., Krol, M. S., Hoekstra, A. Y., & de Araujo, J. C. (2008). The impact of upstream water abstractions on reservoir yield: the case of the Oros Reservoir in Brazil. Hydrological Sciences Journal-Journal Des Sciences Hydrologiques, 53(4), 857-867

Wanders, N., & Wada, Y. (2015). Human and climate impacts on the 21st century hydrological drought. Journal of Hydrology, 526, 208-220

WCD. (2000). Dams and development: A new framework for decision making. London, UK: Earthscan.

Proceedings of the 10th World Congress of EWRA 'Panta Rhei', 5-9 July 2017, Athens, Greece
© 2017 *European Water Resources Association*

Low flow conditions evaluation within the western Morava river basin

Z. Simić* and B.B. Matić
Jaroslav Černi Institute for the Development of Water Resources, Belgrade, 11226, Serbia
** e-mail: zoran.simic@jcerni.co.rs*

Abstract: The largest share of renewable internal fresh water resources in Serbia is located within the Western Morava River basin in central part of Serbia. Despite of the favourable natural conditions and water resources abundance, in last few years noticeable shortage in drinking water supply is detected in some regional water supply systems within the river basin, in particularly during the peak seasons, namely summer and autumn. Thus, like in many other parts of the world, consequences of observed changes in low flow accompanied with significant seasonal fluctuations in precipitation and runoff, emphases necessity for trough evaluation and analyses of the observed precipitation regime, runoff and low flows seasonal fluctuations within the drainage area. Moreover, evaluation of land use, hydrogeology and soil type provides better insight into natural retention capacity of significance for ground and surface water sources. Established correlation among precipitation, runoff, and natural retention capacity as a result of land use practices indicated significant differences of season low flow conditions. The results presented in this paper manifest necessity of comprehensive regional hydrological low flow investigation for future drinking water supply infrastructure and other water management facilities to sustain sustainable water resources management at the watershed level.

Key words: Low flow conditions, drinking water sources, natural retention capacity, seasonal fluctuations

1. INTRODUCTION

The Western Morava River basin (15,796 km^2) is mainly located within the Serbian territory with small share (446 km^2) located in Montenegro. Moreover, it has the largest share of renewable internal fresh water resources in Serbia and presents the most immense drinking water source reserves in the country that results in development of several large drinking water supply systems, e.g., Rzav water supply system, Gazivode water supply system, Rasina water supply system, Djetinja water supply system, Kragujevac water supply system (Republic of Serbia Water Management Master Plan, 2001; Water for 21st Century, 1999. Thus, assessment of low flows and natural retention capacity are of great interests given the noticeable shortage in existing drinking water supply systems located within the river basin.

The Western Morava drainage area stretches south – north direction with well-developed hydrographic network (Figure 1). The river originates in Požeška ravine at the 300 m a.s.l. as the confluence of Moravica (1,513 km^2), Djetinja (1,210 km^2) and Skrapež (630 km^2) rivers. Ibar River is the main Western Morava tributary with drainage area of 7,925 km^2, followed by Rasina (990 km^2), Čemernica (629 km^2), Gruža (617 km^2), etc.

Despite the abundance good quality of fresh water the water shortage during the low flow conditions is detected, very likely due to competition among different users (water supply, hydropower, agriculture, industry). In addition, possible alteration in hydrological cycle (Houghton et al., 1996) and water resources (will have adverse effects on sustainable water resources management. Multipurpose dams that serve many of the typical water management functions (Lindström et al., 2012) together with natural retention capacity as one the hydrological ecosystem service (Addressing Environmental Aspects and Ecosystem Issues in Integrated Water Resources Management - UNEP, 2008; Water security and ecosystem services: The critical connection – WWAP, 2009; Burkhard et.al., 2014) advance water resources resilience to diverse pressures and changes.

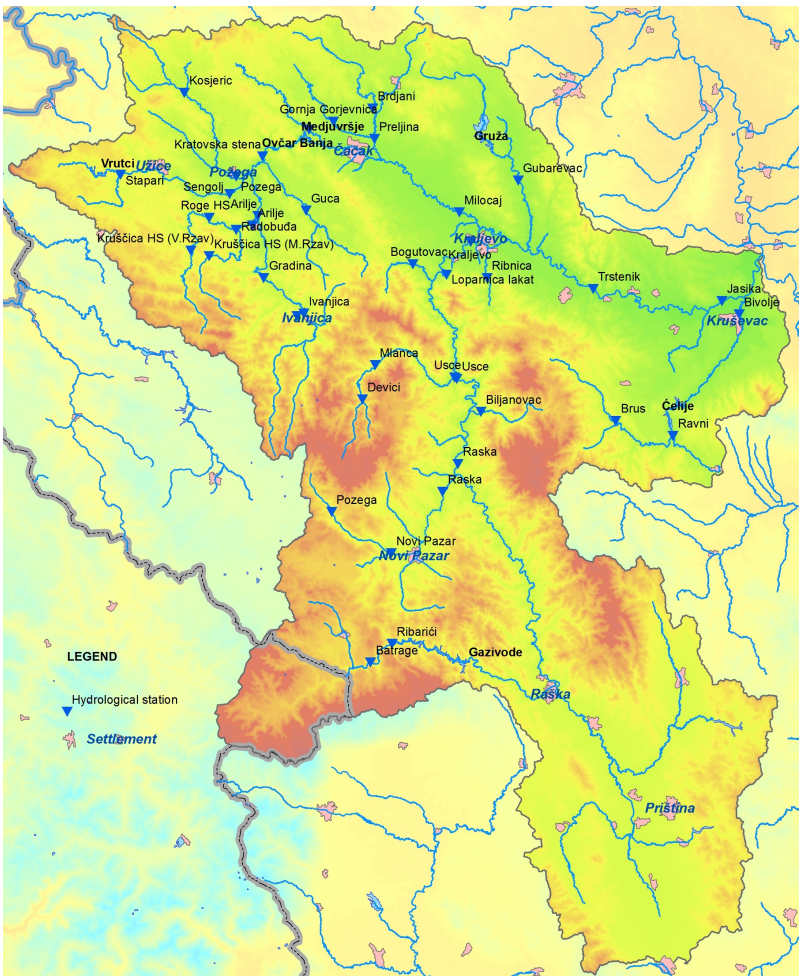

Figure 1. The Western Morava drainage area with main tributaries and evaluated hydrological stations

At the present, there are several multipurpose dams within the drainage area. Reservoir Gazivode (average flow 13.5m^3/s) on river Ibar that serve for water supply, irrigation, hydropower. Ćelije reservoir results from damming of river Rasina and is utilized for water supply, flood control and sediment management. It has average flow of 5.9 m^3/s and uniform environmental flow of approximately 0.56 m^3/s. Vrutci reservoir located on Djetinja river main goal is city of Užice drinking water supply combined with flood control and environmental flow regulation for downstream locations. With respect to different users' water supply there are few large reservoirs, e.g., Ovčar Banja, Medjuvršje, and Gruža for Kragujevac and Kraljevo drinking water supply. Finally, the regional drinking water supply system Rzav is located within the studied drainage area.

2. LOW FLOW FREQUENCY ANALYSES

At the present, 45 hydrological stations exist within the river basin. There is rationale to evaluate average monthly low flow data for selected 30 hydrological stations (Figure 1) that fully portray Western Morava drainage area hydrological regime. For selected localities observed data are fitted with theoretical distributions (Pearson, log Pearson, log Normal and Gumbel) to generate best fit curves for low flow probabilities. The low flow assessment is based on criteria that 95% of average minimum flows have to be maintained with purpose to set permit discharge limits downstream (Matić and Simić, 2016) of evaluated stations. To provide more uniform approach low flow probabilities at each hydrological station are normalized by equation:

$$NQLF_{(1\text{-}30)} = Qlf_{(1\text{-}30)} / A_{(1\text{-}30)} \quad (1)$$

where NQlf is the normalized low flow probability, QLF is low flow probability derived from the observed data and A is hydrological station contributing drainage area. The summary results for all evaluated hydrological stations are exhibited in Figure 2.

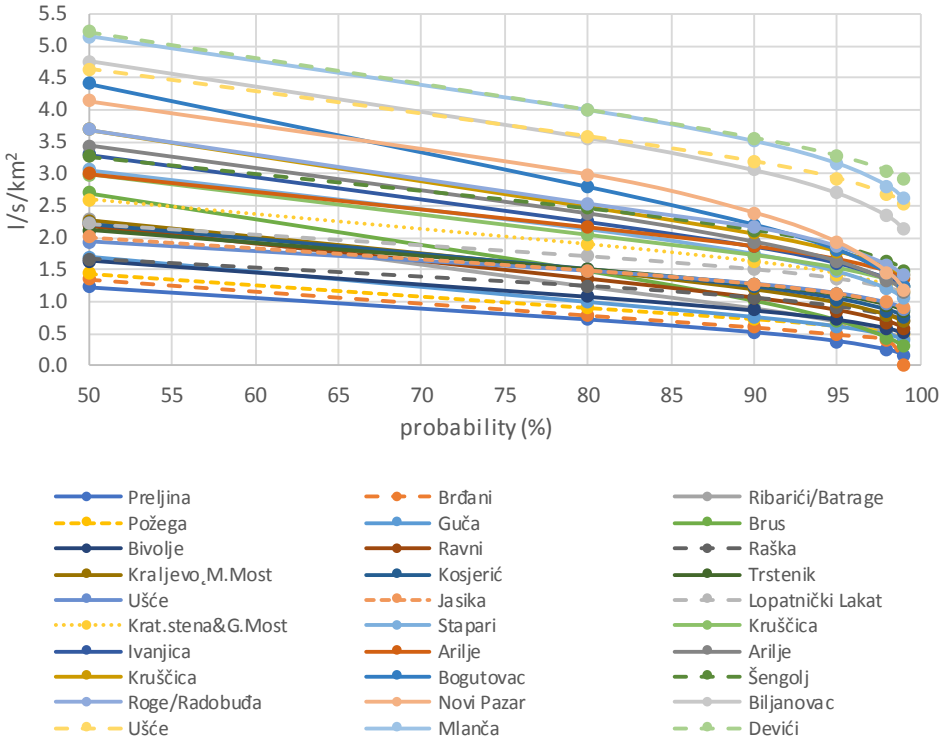

Figure 2. Normalized average monthly low flow probability values for evaluated hydrological stations

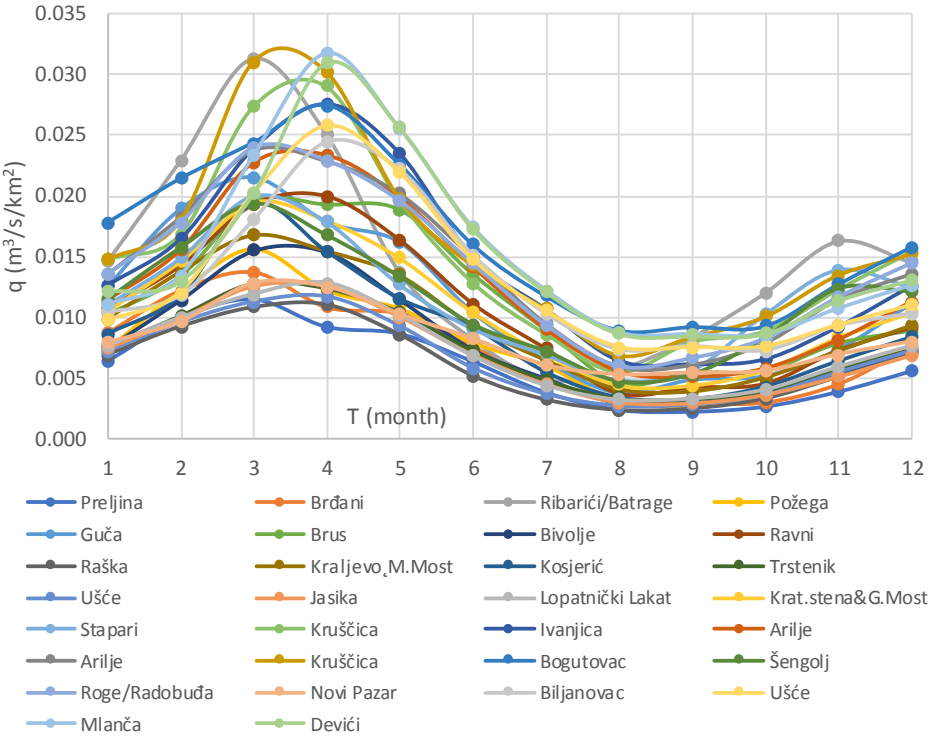

Figure 3. Normalized average monthly low flow values within the Western Morava River Basin for hydrological stations

Based on Figure 3 that exhibits results for average monthly low flows analyses at each location it is evident that highest low flows are observed from August to October on River Lopatnica followed

by upper part of River Ibar, etc.

Since the scope of study is low flow evaluation within the whole river basin, the results presented above are grouped in four categories and the Western Morava river basin in divided in 4 zones with respect to that:

- Zone 1: with NQLF, >2.5 l/s/km^2
- Zone 2: 2.5 l/s/km2> NQLF>1.5 l/s/km^2
- Zone 3: 1.5 l/s/km2>NQLF>1.0 l/s/km^2
- Zone 4: NQLF < 1.0 l/s/km^2

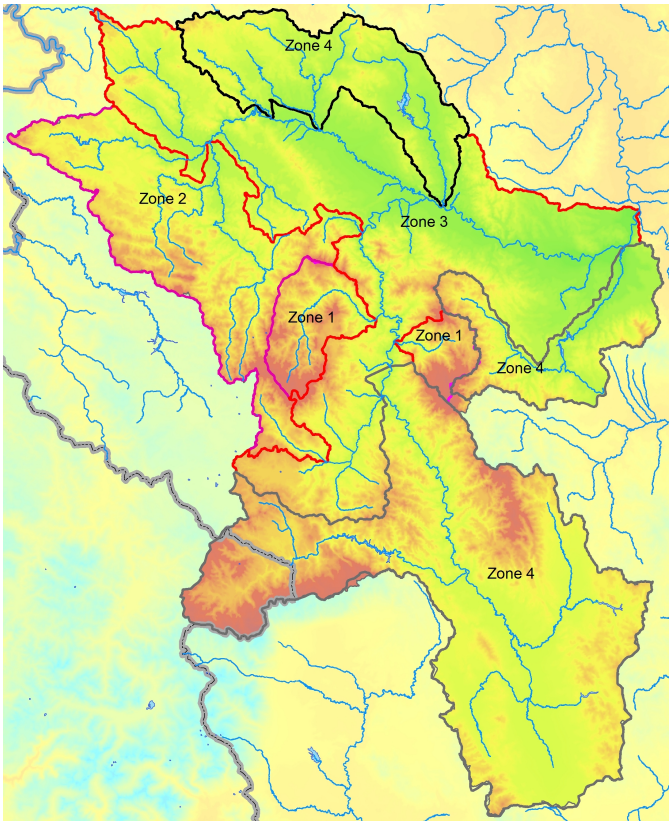

Figure 4. Delineation of the Western Morava River basin

Spatial presentation on Figure 3 indicates that Zone 1 is located in the middle part of the Western Morava basin which is quite surprising it was expected that the largest reserves are located along the basins' perimeter. Zone 2 is located within the Rzav catchment in western part. Zone 4 is comprised of smaller rivers catchments located on the north part and main share of Ibar River on the south. The remaining part of Western Morava basin is within the Zone 3. Given that based on available data and methodology the Zone 1 has the largest water yield during the low flow conditions.

3. NATURAL CONDITIONS EVALUATION WITHIN THE DEFINED NORMALIZED LOW FLOW ZONES

Introduction of the natural retention capacity is simplified by evaluation of main natural features within the four defined NQLF Zones e.g. precipitation, land cover, etc., with no intention to go in detailed assessment of it, since it is the beyond the scope of this paper. The four Zones natural characteristics located in Western Morava Basin are summarized in Table 1 and Figures 3 and 4 exhibits graphically natural features, elevation, hydrogeology, slope and land use practices, in a given order.

Table 1. Natural characteristics of evaluated zones within the Western Morava River Basin

	Zone 1	Zone 2	Zone 3	Zone 4
Area (km^2)	809	2351.7	4962.27	7673.05
Precipitation (mm/god)	912.1	841.7	768.6	820.6
Average basin elevation (m.a.s.l)	1123.16	839.59	545.48	754.79
Average slope (%)	24.48	19.66	13.29	13.76
Forest (311+312+313)	65.69%	53.68%	40.63%	44.31%
Pedology	distric	distric	distric kam.	mix
Broad-leaved forest (311)	34.86%	44.27%	35.42%	41.15%
Land principally occupied by	11.91%	23.64%	20.23%	14.33%
Complex cultivation patterns (242)	4.72%	7.58%	20.42%	12.91%
Transitional woodland-shrub (324)	12.05%	7.75%	6.29%	7.22%
Non-irrigated arable land (211)	0.25%	0.32%	5.73%	10.65%
Mixed forest (313)	16.93%	5.34%	2.85%	1.58%
Coniferous forest (312)	13.91%	4.07%	2.35%	1.58%
Natural grasslands (321)	2.86%	4.01%	1.47%	3.43%
Discontinuous urban fabric (112)	0.00%	0.77%	2.12%	2.36%
Pastures (231)	2.00%	1.77%	1.38%	2.22%

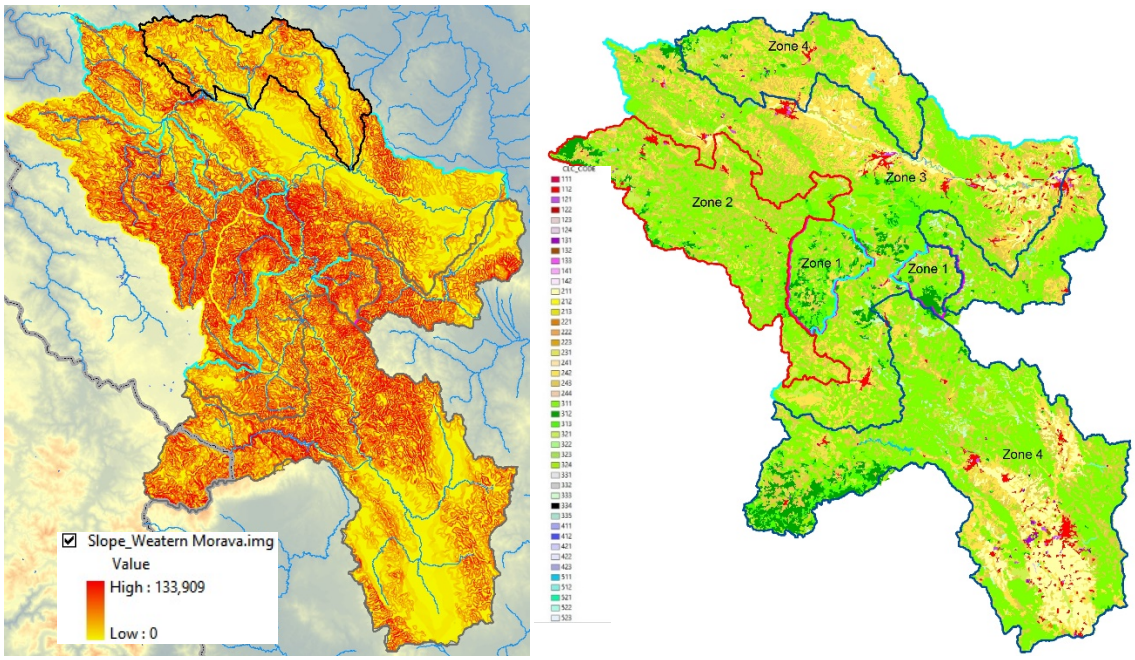

Figure 5. Slope (%) and CLC Corine 2012

Based on overview of data and information presented above the Zone 1 has the highest NQLF and natural retention capacity given the average precipitation, during the low flow conditions given the average precipitation of 912 mm, 66 % land covered by forest and low urbanization. Although the Zone 2 have favourable values with respect to NQLF and natural conditions (54 % land covered by forest) the shortage in water supply is observed there during the peak seasons (summer and autumn) likely due to highest percentage of agricultural activities (24 %). Zone 3 is more urbanized in comparison to Zone 1 and 2 and has less than 50 % of forests in addition to lowest average precipitation. The outputs for Zone 4 are quite interesting since the average precipitation, percentage of land covered by forest are higher than in Zone 3.

4. CONCLUSIONS

The study of low flows within the Western Morava River Basin emphasizes existence of four normalized low flow (NQLF) zones. The findings indicated that the highest NQLF is observed in central part of the drainage area where in addition to precipitation other features relevant for natural

retention capacity (land cover, low urbanization, the highest elevation). The quite interesting findings refer to Zone 2 in which water shortage exists during the peak seasons (summer and autumn). The general overview of potential natural retention capacity based on available data and information underlined necessity for its more comprehensive evaluation as a part of contemporary water resources management. It is of particular interest for drinking water supply, since it requires enough quantity of water that corresponds to high quality standards. The new drinking water supply systems within Western Morava River should be located in the Zone 1 at the First place, followed by Zone 2, 3 and 4. Moreover, the environmental protection criteria should be the most inflexible in the Zone with highest NQLF and natural retention capacity.

The methodology developed in this study that comprises of low flow analyses and natural retention capacity general overview is suitable for any large river basin. The more comprehensive and detailed analyses and evaluation are more applicable at the sub basins level and smaller river basins. Outcomes presented here are useful for strategical planning and delineation of the most significant locations for drinking water supply.

ACKNOWLEDGMENTS

Hydrological data presented in this study are based on available data and Jaroslav Černi Institute for Water Resources Development research, studies, and reports are supported by Ministry of Education, Science, and Technological Development of Serbia projects TR 37013 (Development of decision support system for large dam maintenance in Serbia) and TR 37005 (Assessment of climate change impacts on water resources in Serbia).

REFERENCES

Burkhard, B, Kandziora, M, Hou, Y, Muller, F, (2014) Ecosystem Services Potentials, Flows and Demands – Concepts for Spatial Localisation, Indication and Quantification, Landscape Online 34:1-32;

Houghton, J. J., L. G. Meiro Fihlo, B. A. Callander. N. Harris, A. Kattenberg, and K. Maskell (Editors), 1996. Climate Change (1995): The Science of Climate Change. Contribution of Working Group I to the Second Assessment Report of the Intergovernmental Panel on Climate Chang (IPCC). Cambridge University Press, Port Chester, New York;

http://www.hidmet.gov.rs/ciril/hidrologija/povrsinske_godisnjaci.php

http://www.activeremedy.org/wp-content/uploads/2014/10/achim_steiner_executive_director_of_unep_water_security_and_ecosystem_services_the_critical_connection.pdf

Lindström, Andreas; Granit, Jakob (2012) Large-Scale water storage in the water, energy and food nexus Perspectives on benefits, risks and best Practices. Retrieved from: http://www.siwi.org/documents/Resources/Papers/Water_Storage_Paper_21.pdf;

Matić B., Simić Z. (2016) Comparison of Pre and Post Development Low Flow Conditions for Drina River, Procedia Engineering, ISSN 1877-7058, Publisher: Elsevier, vol. 169, pp. 284-292;

Republic of Serbia Water Management Master Plan, The Jaroslav Černi Institute for the Development of Water Resources (2001)

UNEP (2008) Addressing Environmental Aspects and Ecosystem Issues in Integrated Water Resources Management;

UNEP (2009) Water security and ecosystem services: The critical connection, A Contribution to the United Nations World Water Assessment Programme. Retrieved from:

Water for 21st Century, Belgrade, Serbia (1999) Proceedings published by Serbian Association for Water Technology and Sanitary Engineering, Belgrade, Serbia.

Proceedings of the 10th World Congress of EWRA 'Panta Rhei', 5-9 July 2017, Athens, Greece
© 2017 *European Water Resources Association*

Stochastic generation of low stream flow data of Perigiali Stream, Kavala city, NE Greece

T. Papalaskaris[1] and T. Panagiotidis[2]
[1] *Department of Civil Engineering, Democritus University of Thrace, Kimmeria Campus, 67100 Xanthi, Greece*
[2] *Department of Mechanical Engineering, Eastern Macedonia & Thrace Institute of Technology, 65404 Kavala, Greece*
[*] *e-mail: tpapalas@civil.duth.gr*

Abstract: The present study generates synthetic low stream flow time series of an entire calendar year considering the stream flow data recorded during two certain interval periods of the years 2016 and 2017. We examined the goodness of fit tests of six theoretical probability distributions to low stream flow data acquired at the exit of the Perigiali stream, Kavala city, NE Greece watershed, during part of May, June, July, part of August, part of December 2016 and part of January 2017, using either a combination of a 3-inches U.S.G.S. modified portable Parshall flume in conjunction with a 3-inches Montana portable flume and a combination of a 3-inches conventional portable Parshall flume in conjunction with a 3-inches Montana portable flume and calculated the corresponding probability distributions parameters. The six specific probability distributions used in this study were the following: (1) Gumbel min (Minimum Extreme Value Type 1) distribution, (2) 3-Parameter Log-Normal distribution, (3) Pearson Type 5 distribution, (4) Pearson Type 6 distribution, (5) Two-Parameter Weibull distribution and (6) Wakeby distribution. The Kolmogorov-Smirnov, Anderson-Darling and Chi-Squared, GOF tests were employed to show how well the probability distributions fitted the recorded data and the results were demonstrated through interactive tables providing us the ability to effectively decide which model best fits the observed data.

Key words: artificial time series, discrepancy ratio, goodness-of-fit tests low flow data, conventional and modified Parshall flumes

1. INTRODUCTION

Artificial stream flow time series generation is a means of paramount importance in hydrology and water resources management in order to handle efficiently precarious or doubtful situations, pertinent to a natural watercourse's flow regime, associated particularly to a short period of stream flow rate data acquisition. The increasing water demands worldwide, caused primarily by the global population increase and exacerbated by the water scarcity due to the climate change, especially in North-Eastern Europe, gives significant prominence to the wise use of the available water resources, showcasing stream flow rate monitoring as a factor of paramount importance with the view to design water storage reservoirs and other water resources management infrastructure works. Therefore, the necessity to minimize dubiety and ambivalence in estimating the flow regime of a natural watercourse constitutes a challenging task in the sector of hydrology and water resources management. This difficulty can only be adequately worked out employing artificial stream flow time series generation procedures and techniques, as a common process.

2. LITERATURE REVIEW

Numerous studies and reviews have been carried out in the field of low flows, handling different subjects such as the fit of theoretical probability distribution functions on observed low stream flow rate data, surface runoff and groundwater exchange relationships, watershed drought management, hydrological low-flow and drought indices estimation, watershed water budget and balance compilation, evapotranspiration estimation, daily stream flow variation computations, in-stream environmental stream flows calculation etc. (Matalas, 1963; Beard, 1968; Singh and Stall, 1973;

Singh, 1987; Vogel and Kroll, 1989; Ming-Ko and Kai, 1989; Vogel and Kroll, 1990; Vogel and Wilson, 1996; Wang, 1997; Smakhtin and Toulouse, 1998; Young et al., 2000; Smakhtin, 2001; Stahl, 2001; Spangler, 2001; Zaidman et al., 2002; Acreman and Dunbar, 2004; Laaha and Blöschl, 2005; Yongqin et al., 2006; Černohous and Šach, 2008; Tallaksen and Hewa, 2008; Gribovszki et al., 2008; Nalbantis, 2008; Gribovszki et al., 2010; Sen and Niedzielski 2010; Demirel et al., 2013; Orlowski et al., 2014; Wittenberg, 2015; Yürekli et al., 2005; Büyükkaraciğan, 2014; Papalaskaris and Panagiotidis, 2016).

3. MATERIALS AND METHODS

3.1 Study area

The stream flow rate gauging station, which was established in Kavala city area, a coastal city, located at the north of the Aegean Sea, across the Thassos Island, and surrounded by the Lekani mountain series branches to the North and East and the Paggaion Mountain ramifications to the West, (established in the proximity of the city urban web center and at the eastern exit of the city as well), located at the specific co-ordinates 40°56'727" N and 24°25'929" E, Perigiali city area, and operated continuously, spanning two individual between each other time interval period from 14.05.2016 to 30.08.2016 and 24.12.2016 to 05.01.2017, as illustrated in Figure 1.



Figure 1. 3-inches U.S.G.S. modified portable Parshall flume gauging station, Perigiali area, Kavala city, Greece (Source: Google Earth).

3.2 Sample collection and data used in this study

A total number of 203 individual stream flow rate (discharge) measurements were performed within 109 consecutive days, between 14.05.2016 and 30.08.2016 and a total number of 13 individual stream flow rate (discharge) measurements were performed within 13 consecutive days, 24.12.2016 to 05.01.2017, during which a thorough presentation of the methodology and procedure

followed up was analytically supplied, whereas, all of them were recorded and uploaded on the first author's personal Youtube platform web-site, namely, "Thomas Papalaskaris". The first stream flow rate (discharge) measurement (14.05.2016) lasted 1 hour sharp and the last one (30.08.2016), respectively, 48':01", as far as the first stream flow rate measurements set time interval is concerned. The first stream flow rate (discharge) measurement (24.12.2016) lasted 1 hour sharp and the last one (05.01.2017), respectively, 48':01", as far as the first stream flow rate measurements set time interval is concerned.

In accordance with the recorded observations of the only available private meteorological station located at Dexameni area, Kavala city, Greece, Kavala city received total monthly rainfalls as following: 56.80 during May 2016, 14.00 mm during June 2016, 1.60 mm during July 2016 and 10.40 mm during August 2016 (82.80 mm in total respecting the four months) respectively. The recorded stream flow rate (discharge) (denoted by the blue-colored continuous line) and the observed rainfall (denoted by the red-colored vertical bars) during the time period 14.05.2016 and 29.08.2016 are simultaneously illustrated within Figure 2.

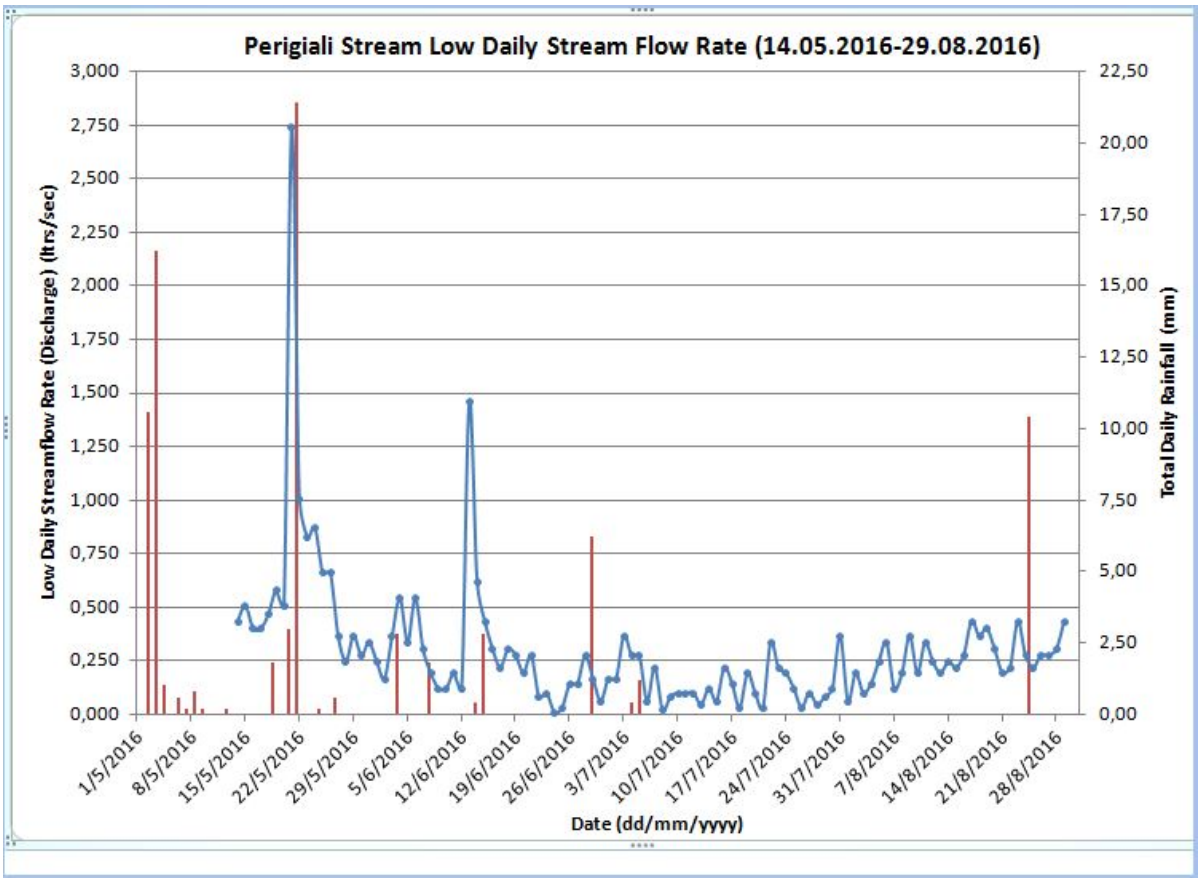

Figure 2. Recorded stream flow rate at Perigiali area, 3-inches U.S.G.S. modified Parshall flume, gaging station vs. observed rainfall at Dexameni area station, Kavala city, Greece (Source: First author's personal archive and https://www.meteokav.gr).

3.3 Sample analysis and checking the goodness of fit

Mathwave EasyFit and StatAssist software packages was employed to estimate the best probability distribution (based on the Anderson-Darling, Chi-Squared and Kolmogorov-Smirnov goodness-of-fit criteria tests), together with the associated parameters, fitting the daily lowest stream flow data, as well as the goodness-of-fit of all the other candidate probability distributions. Moreover, after having calculated the parameters of the examined probability distributions, we generated a sequence of high quality random numbers for each individual candidate probability distribution with the same parameter values to the origina calculated ones. The Kolmogorov-

Smirnov test (KS-test) tries to determine if two datasets differ significantly, whilst, it has the advantage of making no assumption about the distribution of the data (technically speaking it is non-parametric and distribution free). MS Excel software is employed in order to plot the real observed (recorded) against the artificial (generated, forecasted) low stream flow rate (discharge) data. The calculation of six examined candidate probability distribution estimates are of paramount importance as they enable us, by assigning different specified scores, according to their goodness of fit performance, to evaluate which is the most appropriate one simulating the recorded stream flow rate values. The goodness of fit tests are performed in order to evaluate which distribution fits to the low stream flow rate (discharge) data series in the best possible way. The values of Anderson-Darling statistics, Chi-square (χ^2), Kolmogorov-Smirnov (D) respectively are computed and illustrated within Table 2, for the entire low stream flow rate (discharge) time series data. It should be underlined that, employing an improvised scoring system, the superscript number makes reference to the order ranking of the probability distribution which best fits the low-flow time series data, ranging from 1 (the best one) to 3 (the worst one). Further, the ranking score values of numbers 3, 2, and 1, are, inversely assigned to the already given, (as above mentioned followed procedure), ranking scores 1, 2, and 3 correspondingly, in order to assess the highest final goodness of fit score obtained for each candidate individual probability distribution, determining, as an outcome, the best one which best fits the observed low stream flow rate (discharge) time series data.

Table 1. Goodness of fit tests results for the 3-inches U.S.G.S. modified portable Parshall flume, Perigiali area, Kavala city Greece, gauging station, data series,(Source: EasyFit, Goodness of Fit).

Probability distribution	**Perigiali Gauging Station (Goodness of fit types)**			
	Anderson - Darling	**Chi - Squared**	**Kolmogorov - Smirnov**	**Highest final goodness of fit score obtained**
Gumbel min (2P)	18.08300	N/A	0.272100	-
Log-Normal (3P)	0.560700^{2}	9.692300	0.089250	2
Pearson type 5 (3P)	0.471140^{1}	3.233500^{2}	0.085580^{3}	6
Pearson type 6 (3P)	0.619000^{3}	9.641300^{3}	0.093730	2
Weibull (2P)	0.764610	3.204500^{1}	0.064910^{2}	5
Wakeby (5P)	4.119200	N/A	0.050610^{1}	3

It can be identified from Table 1, that all the examined probability distributions can be accepted to fit to the low stream flow rate (discharge) time series data at the significant level α of 0.05, except Gumbel min. (2P) and Wakeby (5P) probability distributions, based on the Chi-squared goodness of fit test, whilst, at the same time, based on all three individual goodness of fit tests, Pearson type 5 (3P) obtained the highest score of six. Still, the probability density function of Wakeby (5P) probability distribution (which obtained the highest score based on the Kolmogorov - Smirnov goodness of fit test) is finally chosen in order to produce artificial low flow time series data.

Visually inspecting the Figure 3, where the real observed (recorded) low stream flow rate (discharge) time series data are plotted against the artificial ones, for the same time period (14.05.2016-29.08.2016) we can identify that both, by first sight, coincide (for the most of the paired values) remarkably well.

3.4 Hydrodynamic methods and equipment for sample data collection and analysis

Due to the extremely shallow waters, in conjunction with the extremely low water stream flow velocity prevailing at the gauging station, it is impossible to implement the area-velocity method in order to assess the stream flow rate (discharge), using a current meter mounted on a wading rod,

owing to the fact that there isn't available depth to submerge the current meter as well as the extremely low water stream flow velocity is not sufficient enough to trigger the operation of a current meter; Under those particular circumstances the only alternatives are the use of either a small-sized portable weir plate or a small-sized flume which, eventually, was our final selected option, more specifically, a "3-inch U.S.G.S. Modified Portable Parshall Flume", constructed by means of sea plywood, covered with a sprayed thin smooth polyester coating similar. to that the industry usually covers the outside surface of high developing speed sea vessels, in order to reduce the friction between the outside area of those sea vessels and the sea water, thus ensuring that the friction developed between the bottom as well as the walls of the Flume are minimized to a minimum (Johnson, 1963; Rantz, 1982).

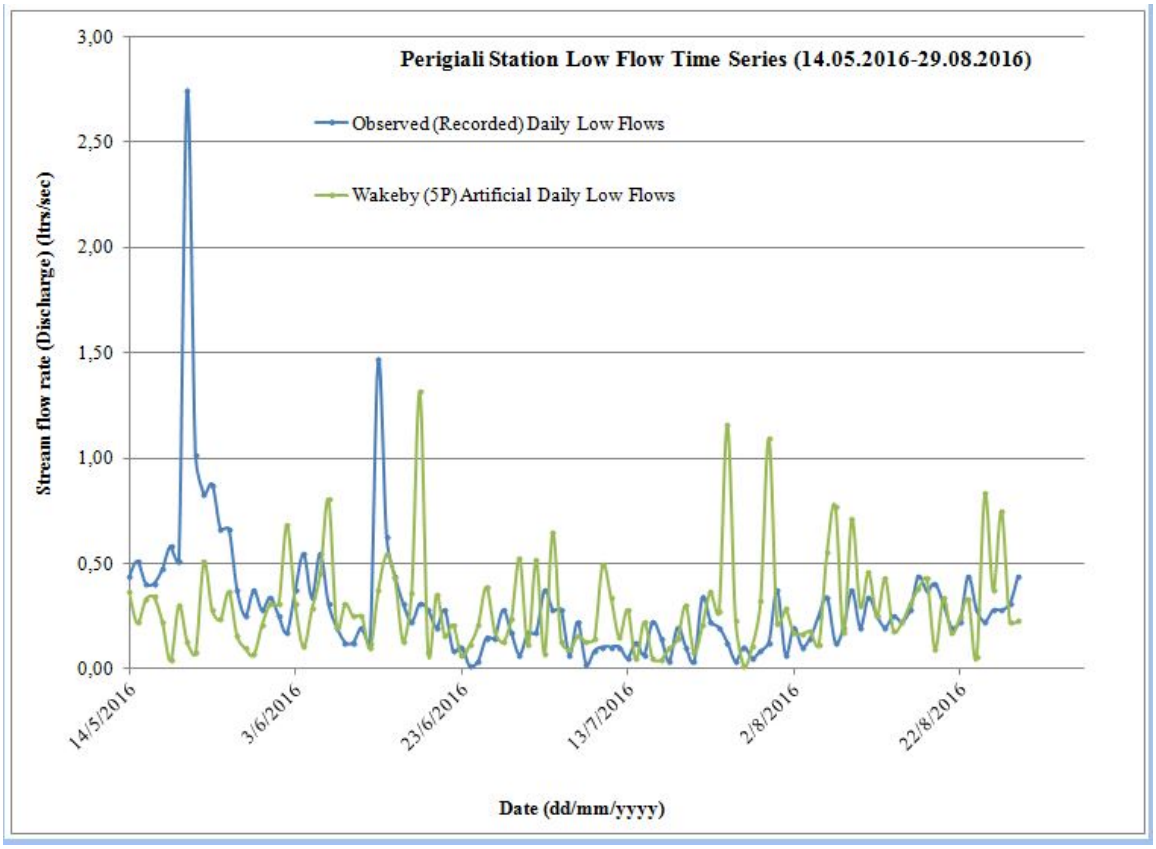

Figure 3. Plot of observed against artificial low stream flow rate time series data for 3-inches modified ortable Parshall flume gauging station, Perigiali area, Kavala city, Greece (Source: Author's plot compilation).

5. COMPARISON BETWEEN CALCULATED AND SITE-MEASURED LOW STREAM FLOW RATE (DISCHARGE) VALUES

The comparison between calculated and site-measured values of low stream flow rates (discharges) is made on the basis of several statistical criteria such as, root mean squared error (R.M.S.E.), relative error (R.E.), efficiency coefficient (E.C.), linear correlation coefficient (r), determination coefficient (r^2) and discrepancy ratio (D.C.) (Nash and Sutcliffe, 1970; Krause et al., 2005), as depicted within Table 2. The plot depicted within Figure 4 represents the discrepancy ratio concerning Perigiali Stream, Kavala city, North-Eastern Greece, during the time period between 14.05.2016 and 29.08.2016. At this point, it should be noted that both coordinate axes are in logarithmic scale; therefore, the equations y=x, y=0.5x and y=2.0x are represented graphically by parallel straight lines.

In general, the obtained values of the statistical criteria R.M.S.E., R.E., E.C. for Perigiali Stream 3-inches U.S.G.S. modified portable Parshall flume can be considered fairly satisfactory

considering the low stream flow rate numerical values. Additionally, the degree of linear dependence between calculated and measured bed load transport rate is very weak, implying that more iterations should be carried out until an artificial low stream flow rate time series data which best fits (by the perspective of the overall achieved statistical efficiency criteria) the observed low stream flow rate time series data is generated.

Table 2. Statistical criteria values of 3-inches U.S.G.S. modified portable Parshall flume gauging station Perigiali Stream, Kavala city, Greece, (14.05.2016-29.08.2017) (Source: Authors' plot compilation archive)

Number of paired values	RMSE [kg/(m s)]	RE (%)	EC	r	r^2	Discrepancy ratio
108	0.3983	-0.8155	-0.5490	-0.0133	0.0002	0.5000

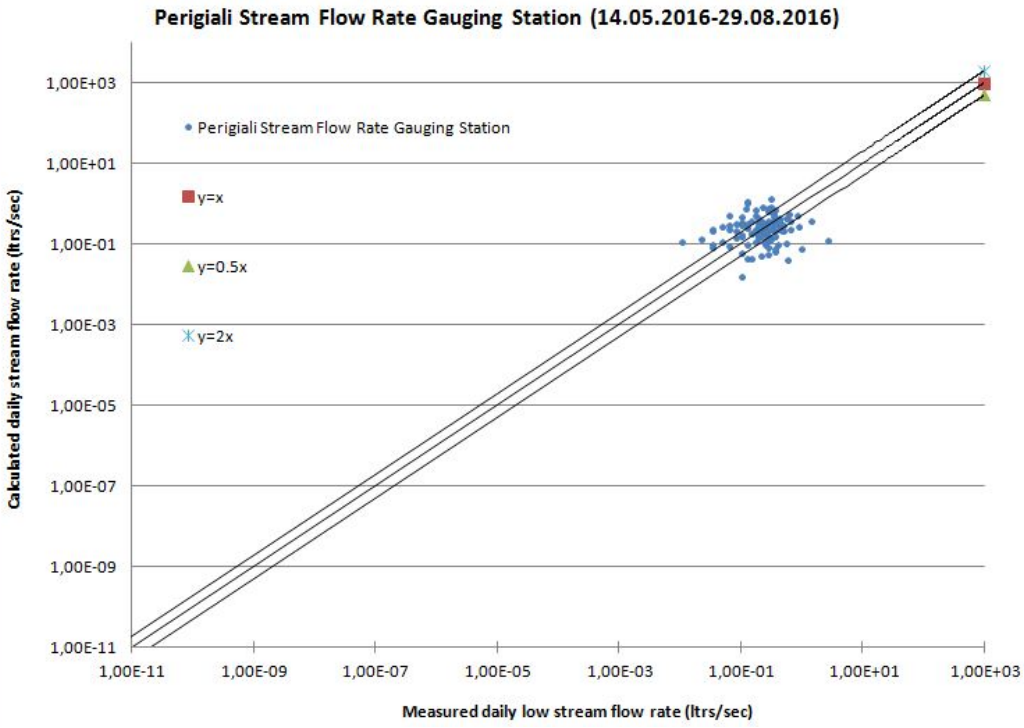

Figure 4. Discrepancy ratio plot of observed against artificial low stream flow rate time series data for Parshall flume gauging station, Perigiali area, Kavala city, Greece (14.05.2016-29.08.2016) (Source: Authors' plot compilation).

The above mentioned statistical criteria values concerning Perigiali Stream, Kavala city, North-Eastern Greece, are listed within Table 4. It is noted that the relative error value depicted within Table 4 represents the average value of the relative errors calculated for each pair of calculated and measured bed load values.

5. RESULTS AND DISCUSSION

A total number of 203 individual stream flow rate (discharge) measurements were performed within 109 consecutive days, between 14.05.2016 and 29.08.2016, at the Perigiali area, Kavala city, north eastern Greece, at the exit of the homonymous watershed and main stream channel by means of a "3-inch U.S.G.S. Modified Portable Parshall Flume". The daily lowest flows were undergone a probability distribution analysis and six candidate probability distributions were fitted to the low stream flow rate time series data proving that the Pearson type 5 (3P) probability distribution best fitted the data based on three different goodness of fit tests. As normally anticipated the stream flow rate (discharge) observed early in the morning, late in the evening and during the night patrols were (due to decreased evapotranspiration rate, stemming from the relatively lower temperature, solar

radiation and dry wind intensity values hitting, in turn, the entire Perigiali area watershed) relatively higher that those performed around mid-day hours and early in the evening.

6. CONCLUSIONS - FUTURE RESEARCH

Perigiali watershed and main stream channel can sustain extremely low flow conditions which are essential for low flow studies in order to compile an as much consistent watershed and drought management plan and bridge the research and knowledge pertinent to the south eastern part of Europe were, as generally admitted, only a few stream flow rate (discharge) measurement gauging stations exist and transfer the acquired knowledge to ungauged watersheds as well, in accordance to the suggestions of the Braunschweig Declaration. Furthermore, Perigiali Mediterranean watershed could be proposed to be incorporated within the global network of long-term small hydrological scientific research basins network the importance of which has been worldwide acknowledged.

More future stream flow measurements would contribute to the production of extended stream flow rate (discharge) time series data which are of paramount importance in hydrology in order to compile accurate, consistent and sustainable watershed balance and budget computation and drought management plans compilation.

REFERENCES

Acreman M., and Dunbar M.J. (2004). Defining environmental river flow requirements – a review. Hydrology and Earth System Sciences, 8 (5), 861-876.

Beard L. (1968). Simulation of Daily Streamlow, United States Corps of Engineers (Institute of Water Resources - Hydrologic Engineering Centre) Technical Paper 6 (TP-6), Davis, pp. 1-13.

Büyükkaraciğan N. (2014). Determining the best fitting distributions for minimum flows of streams in Gediz Basin. International Journal of Environmental, Chemical, Ecological, Geological and Geophysical Engineering, 8 (6), 417-422.

Černohous V., and Šach F. (2008). Daily baseflow variations and forest evapotranspiration. Ekológia (Bratislava), 27 (2), 189-195.

Demirel M.C., Booij M.J. and. Hoekstra A.Y. (2013). Impacts of climate change on the seasonality of low flows in 134 catchments in the River Rhine basin using an ensemble of bias-corrected regional climate simulations. Hydrology and Earth System Sciences, 17 (10), 4241-4257.

Gribovszki Z., Kalicz P., Kucsara M., Szilágyi J. and Vig P. (2008). Evapotranspiration calculation on the basis of the riparian zone water balance. Acta Silvatica & Lignaria Hungarica, 4, 95-106.

Gribovszki Z., Szilágyi J. and Kalicz P. (2010). Diurnal fluctuations in shallow groundwater levels and streamflow rates and their interpretation – A review. Journal of Hydrology, 385 (1-4), 371-383.

Johnson A. (1963). Modified Parshall flume, United States Geological Survey (USGS) Open-File Report - United States Department of the Interior Geological Survey, Denver, U.S.A., pp. 1-8 (in English).

Krause P., Boyle D.P. and Bäse F. (2005). Comparison of different efficiency criteria for hydrological model assessment. Advances in Geosciences, 5, 89-97.

Laaha A.K. and Blöschl G. (2005). Low flow estimates from short stream flow records – a comparison of methods. Journal of Hydrology, 306 (1-4), 264-286.

Matalas N. (1963). Probability Distribution of Low Flows, United States Geological Survey Professional Paper 434-A (Statistical Studies in Hydrology), United States Government Printing Office, Washington, pp. A1-A27.

Ming-Ko W. and Kai W. (1989). Fitting Annual Floods with Zero-Flows, Canadian Water Rresources Journal, 14 (2), 10-16.

Nalbantis I. (2008). Evaluation of a hydrological drought index. European Water, 23/24. (6), 67-77.

Nash J.E. and Sutcliffe J.V. (1970). River flow forecasting through conceptual models, Part I - A discussion of principles. Journal of Hydrology, 10, 282-290.

Orlowski N., Lauer F., Kraft P., Frede H.G. and Breuer L. (2014). Llinking spatial patterns of groundwater table dynamics and streamflow generation processes in a small developed catchment. Water, 6 (10), 3085-3117.

Papalaskaris T. and Panagiotidis T. (2016). Artificial low stream flow time series generation of Perigiali stream, Kavala city, NE Greece. Proceedings 6th International Symposium on Environmental and Material Flow Management ("6th E.M.F.M. 2016") (eds. Ž. Živković, I. Mihailović and P. Dordević), Bor, Serbia, 2016, pp. 20-38.

Rantz S.E. and others (1982). Measurement of Discharge by Miscellaneous Methods - Portable Parshall Flume, Chapter 8, Measurement and Computation of Streamflow: Volume 1. Measurement of Stage and Discharge, Superintendent of Documents, U.S. Government Printing Office, Washington, pp. 275-577.

Sen A.K. and Niedzielski T. (2010). Statistical characteristics of riverflow variability in the Odra River Basin, Southwestern Poland. Polish Journal of Environmental Studies, 19 (2), 387-397.

Singh K.P. and Stall J.B. (1973). The 7-Dday 10-Years Low Flows of Illinois Streams, State of Illinos-Ch. 127, IRS, Par. 58.29 (12-73-2000), Urbana, pp. 1-24.

Singh V.P. (1987). On derivation of the extreme value (EV) type III distribution for low flows using entropy. Hydrological Sciences Journal, 32 (4), 521-533.

Smakhtin V.U. (2001). Low flow hydrology: a review. Journal of Hydrology, 240 (3-4), 147-186.

Smakhtin V.Y. and Toulouse M. (1998). Relationships between low-flow characteristics of South African streams. Water SA, 24 (2), 107-112.

Spangler L.E. (2001). Delineation of Recharge Areas for Karst Springs in Logan Kanyon, Bear River Range, Northern Utah, U.S. Geological Survey Karst Interest Group Proceedings, Water Resources Investigation Report 01-4011, edited by E.L. Kumansky, Salt Lake City, Utah, pp. 186-193.

Stahl K. (2001). Hydrological Drought – A Study across Europe. Dissertation zur Vergabe des Doktorgrabes der Geowissenschaftlichen Fakultät der Albert-Ludwigs-Universität Freiburg im Breisgau, University of Freiburg, Freiburg, Germany (in German/English).

Tallaksen L. and Hewa G. (2008). Extreme value analysis, Chapter 7, Manual on low flow estimation and prediction, edited by A. Gustard and S. Demuth, Chairperson Publications Board – World Meteorological Organization (WMO), Geneva, Switzerland, pp. 57-70 (in English).

Vogel R.M. and Kroll C.N., (1989). Low-flow frequency analysis using probability-plot correlation coefficients. Journal of Water Resources Planning and Management, 115 (3), 338-357.

Vogel R.M. and Kroll C.N., (1990). Generalized Low-Flow Frequency Relationships for Ungaged Sites in Massachusetts. Water Resources Bulletin (American Water Resources Association), 26 (2), 241-253.

Vogel R.M. and Wilson I., (1996). Probability Distribution of Annual Maximum, Mean, and Minimum Streamflows in the United States. Journal of Hydrologic Engineering, 1 (2), 69-76.

Wang Q.J. (1997). LH moments for statistical analysis of extreme events. Water Resources Research, 33 (12), 2841-2848.

Wittenberg H. (2015). Groundwater abstraction for irrigation and its impacts on low flows in a watershed in Norhwest Germany. Resources, 4 (3), 566-576.

Yongqin D.C., Guoru H., and Chong-Yu X. (2006). Spatial and temporal variations in the occurrence of low flow events in the UK. Hydrology and Earth System Sciences, 51 (6), 1051-1064.

Young A.R., Round C.E. and. Gustard A. (2000). Spatial and temporal variations in the occurrence of low flow events in the UK. Hydrology and Earth System Sciences, 4 (1), 35-45.

Yürekli K., Kurunç A. and. Gül S. (2005). Frequency analysis of low flow series from Çekerek stream basin. Journal of Agricultural Sciences, 11 (1), 72-77.

Zaidman M.D., Keller V. and Young A.R. (2002). Low Flow Frequency Analysis – Guidelines for Best Practice (R & D Technical Report W6-064/TR1), edited by A. Wall and D. Cadman, Environment Agency, Rio House, Waterside Drive, Aztec West, Bristol, pp. 1-24.

Proceedings of the 10th World Congress of EWRA 'Panta Rhei', 5-9 July 2017, Athens, Greece
© 2017 *European Water Resources Association*

Crop pattern modification for long term mitigation planning against persisting droughts

V. Tsakiris[1], D. Tigkas[2*] and H. Vangelis[2]
[1] *Department of Civil and Environmental Engineering, Imperial College London, United Kingdom*
[2] *Centre for the Assessment of Natural Hazards and Proactive Planning, Laboratory of Reclamation Works and Water Resources Management, School of Rural and Surveying Engineering, National Technical University of Athens, Greece*
[*] *e-mail: ditigas@mail.ntua.gr*

Abstract: Droughts are hazardous phenomena affecting practically all the sectors of the economy. Generally, agriculture is the most vulnerable sector, dependent on both the characteristics of the drought episode and the sensitivity of the crops of the existing crop pattern. Sensitive crops to water deficit (rainfed or irrigated) may lose significant part of their yield in case of an intense and long-lasting phenomenon. To face the drought phenomena and their consequences the responsible authorities devise preparedness plans including strategic long-term and short-term measures. Among the most important long-term mitigation measures is the modification of the crop pattern of the agricultural area which is vulnerable to droughts. The paper evaluates this option using the approach of the annualised drought risk assessment. Drought risk is a metric representing the average annual loss in revenue due to the detrimental activity of the drought hazard. To implement this approach, a long series of drought events should be analysed and the sensitivity of the crops to water deficit should be known. For the demonstration of the proposed procedure a numerical example is presented involving rainfed crops.

Key words: Crop pattern, agricultural drought, persisting droughts, drought indices, preparedness planning, crop yield modelling, annualised drought risk

1. INTRODUCTION

Droughts are hazardous phenomena affecting practically all the sectors of the economy. Municipalities, industry and agriculture suffer from each intense and persisting drought episode. The agricultural sector seems to suffer more than the others due to its partially direct influence on rainfall (green water) and the huge amounts needed for irrigation (blue water). During severe drought events, the sensitive crops to water deficit may lose significant part of their yield and their economic revenue. For comprehensive information on drought identification and characterization the reader should consult specialized books (e.g., Rossi et al. 2003; Iglesias et al. 2009; Pereira et al. 2009)

To face drought hazards and their acute consequences, the responsible authorities have to devise and implement Drought Preparedness and Mitigation Plans in order to limit the negative consequences to manageable levels. For the successful implementation of these plans all important stakeholders (farmer unions, representatives from industry, NGOs etc.) have to be involved with the formulation of the plans.

The Preparedness Plans for a territorial unit or a system (e.g. a river basin) generally include a module for the assessment and monitoring of drought events, a module for the estimation of the anticipated losses and damages, and a module of measures which should be implemented in short and long term (Rossi et al 2007; IDMP 2014; Tsakiris et al. 2015).

This paper focuses on the estimation of impacts of droughts on the loss in yield and revenue of rainfed crops using the approach of the annualised drought risk. Based on the same approach, one of the most important long-term series of measures, the "crop pattern modification" is analysed and assessed.

2. THE METHOD

2.1 Water deficit and crop yield reduction

As known, the water deficit in agriculture can be characterised as the most negative factor for the crop production process. The impact is more profound if the deficit occurs during the period of growth with high sensitivity for the crop. It is therefore important for the calculation of the total yield loss to know the level of water deficit caused and when it occurs. We can then model the production process and estimate the anticipated crop yield and revenue reduction due to deficient water supplied to the crops. The modelling of the crop production process is a very cubersome task with several uncertainties introduced by the variability of the parameters involved in the production process. Simplifying assumptions can lead to a wide range of crop models from those highly detailed models to simple dated crop production functions.

Among the most popular dated crop production functions are those presented by FAO (Doorenbos and Kassam, 1979) and the production functions of Jensen (Jensen, 1968; Tsakiris, 1982). The latter functions are either additive or multiplicative.

As known, the actual yield depends on various factors, such as soil characteristics, cultivation techniques, plant diseases, etc., crop modelling would be more appropriate. Since the purpose of this study is to assess the effects of drought on yield, which is determined by the climatic conditions, the AquaCrop model is the most appropriate tool to use for the simulation of crop yield. This way, all other influencing factors can be set to have a neutral role in crop growth, without affecting the interpretation of the results.

AquaCrop is a water-driven simulation model that was developed by FAO. The model uses the water production function approach (Doorenbos and Kassam 1979) as a starting point, and evolves from it by calculating the crop biomass based on the amount of water transpired, and the crop yield as the proportion of biomass that goes into the harvestable parts. The model requires a relatively small number of parameters and input data to simulate the yield response to water for most crops. AquaCrop has been used in several applications around the world (e.g., Andarzian et al. 2011; Abedinpour et al. 2012; Kumar et al 2014), and its simulation results appear to be satisfactory, despite of the simplifications introduced in the model.

2.2 Drought severity modelling

Drought severity is conventionally estimated by drought indices. A large variety of indices have been proposed and used all over the world. For detailed presentation of various popular indices (e.g., SPI, RDI, PDSI etc.) the reader can consult the specific or review publications (Mishra and Singh 2010; Tsakiris et al. 2007, 2013; Tsakiris 2017). For the easy calculation of drought indices a software package has been developed (Tigkas et al. 2015). The criterion for the selection of the appropriate drought index in our study is its ability to be associated with the crop production.

Recently, modified versions of two popular drought indices, the SPI (Mckee et al. 1993) and RDI (Tsakiris and Vangelis 2005; Tsakiris 2007), have been used successfully in crop production studies. The new versions of the above indices are similar to the originals apart from the precipitation, which is replaced by the effective precipitation (Tigkas et al. 2017). Tigkas et al. recently concluded that for the evaluation of drought impacts, the eRDI can enhance the link between drought severity and the reduction of the agricultural production. Further, the same authors concluded that the entire development period of each crop is sufficient for characterizing the drought severity.

2.3 Drought risk assessment

As known from various publications in the literature, the concept of drought risk in agriculture of a certain drought episode is a metric of losses in revenue due to the drought event which is

associated with a certain probability of occurrence. Needless to say, that the magnitude of risk, apart from the level of severity, duration and timing of the drought episode, is highly dependent on the sensitivity of the crop to water shortage (in general named "vulnerability" in the glossary of natural hazards).

Since the drought hazard is in fact described by a long time-series of drought events, it is wise to assess all these activities of concurrent events and their impact on the agricultural sector by calculating the average (annualised) drought risk, using the following equation: The average (annualised) risk of each parcel of land in which a certain crop is grown (R_{jk}) can be calculated using the following equation considering 3 crops (Tsakiris 2009):

$$R_{ij} = \sum_{1}^{3} x_{ijk} \cdot V_{ijk} \cdot f_k \tag{1}$$

in which x_{ijk} is the potential consequences/losses of the parcel of land (element) ij in quantitative terms (e.g. monetary units), V_{ijk} is the vulnerability of the element ij under the drought pressure of class k and f_k is the relative frequency of drought pressure of class k.

It is to note that R_{ij} is expressed in quantitative terms such as monetary units as the consequences.

The expected total annualised drought risk of the entire agricultural system, R_{total}, can be calculated as the sum of annualised risks of all the crop parcels.

$$R_{total} = \sum_{i=1}^{n} \sum_{j=1}^{m} R_{ij} \tag{2}$$

The total annualised risk represents the average (annual) level of losses of the entire system (in monetary units) due to drought hazard (that is the sequence of drought events in a historical timeseries). It is therefore a very powerful tool to test possible changes in the crop pattern in the direction of minimizing revenue losses due to recurrent drought events in the area under study.

3. APPLICATION

The application of the proposed methodology is demonstrated through a synthesized example with rainfed crops. The three main rainfed crops of an agricultural area (1200 ha) and the corresponding land parcels (acreage) of each crop can be found in Table 1.

Table 1 The data of the three main rainfed crops of the selected agricultural area

	Acreage (ha)	max marketable yield (kg/ha)	unit price (euros/kg)
Crop 1	700	10000	0.1
Crop 2	300	5000	0.2
Crop 3	200	12000	0.3

The analysis of drought events through the 7-month eRDI drought index corresponding to the total duration of growth of the crops, is calculated for large number of years, indicated that the frequency of moderate drought is 0.30 whereas the frequency of severe and extreme droughts is 0.10 and 0.05, respectively.

The calculation of R_{total} is presented in Table 2. In this example, the three crops grown in the area specified in Table 1, are used to demonstrate the proposed methodology. The vulnerabilities which appear in Table 2 represent the expected percentage of loss in yield and consequently the loss in revenue from the corresponding agricultural activity.

Table 2. The calculation of R_{total} in a simplified example with three crops

Severity level	Relative frequency	Vulnerability		
		Crop 1	Crop 2	Crop 3
1 (moderate)	0.30	0.10	0.50	0.33
2 (severe)	0.10	0.33	0.75	0.66
3 (extreme)	0.05	0.66	1.00	0.90
Potential losses (monetary units)		700x10000x0.1	300x5000x0.2	200x12000x0.3

R_{total} = 0.30 (0.10x700x10000x0.1 + 0.50x300x5000x0.2+ 0.33 x200x 12000x0.3)
+0.10 (0.33x700x10000x0.1 + 0.75x300x5000x0.2+ 0.66 x200x12000x0.3)
+0.05 (0.66x700x10000x0.1 + 1.00 x300x5000x0.2+ 0.90 x200x12000x0.3) = 300900 EUR/yr

It should be emphasized that the estimation of damages/losses for any level of pressure class (severity level) and therefore the vulnerability of each element/crop is a rather complex task. In most cases droughts create water shortages and the water shortages losses. In other cases, such as the rainfed agriculture, droughts affect directly the soil moisture and the crop yield production. In the former case, we deal with blue water problems, whereas for the latter with green water problems. In both cases, however, the consequences can be direct or indirect, tangible or intangible.

Using the procedure described above, we are able to estimate the loss in yield and revenue for each drought year associated with a certain probability of occurrence.

Finally, using the annualized risk estimation (Eq. 1 and Eq. 2), the total annualised revenue reduction due to drought is produced for the area under study for this crop pattern (base line scenario) is 300900 EUR/yr. For this crop pattern, the max annual revenue without the effect of droughts is 1720000 EUR/yr.

Then, a number of viable changes in the crop pattern can be analysed through the above procedure. The selected scenarios of crop pattern changes proposed by the stakeholders are presented in Table 3. The total annualised drought risk of each of these new crop patterns is calculated and compared with the baseline scenario of Table 2. Needless to say, that only the scenarios which are proposed or accepted by the stakeholders are processed further.

Table 3. Three alternative crop patterns proposed by the stakeholders

	Acreage (ha)		
	CP1	CP2	CP3
Crop 1	600	800	600
Crop 2	400	200	300
Crop 3	200	200	300

From the results obtained, the total annualised drought risk of CP1 is 318800, CP2 is 283000 and CP3 is 366900 EUR/yr. The max revenue from these crop patterns is 1720000 for CP1 and CP2 and 1980000 for CP3. Therefore, ranking the crop patterns based on the anticipated annualised revenue results, Table 4 is produced. As seen the crop pattern CP3 can be selected because it results in the highest anticipated annualised revenue after the subtraction of the drought risk.

Table 4. Ranking of crop patterns with respect to the best possible revenue

Crop Pattern	Anticipated annualised revenue (EUR/yr)
CP3	1613100
CP2	1437000
CP0	1419100
CP1	1401200

4. CONCLUDING REMARKS

The paper presented a methodology for the rational modification of the crop pattern to face intense and persistent droughts. The methodology is based on the anticipated annualized revenue from the entire agricultural area after the subtraction of the total annualised drought risk. All viable

and acceptable by the stakeholders' crop pattern modifications are tested versus the historical drought episode probabilities of occurrence. The crop pattern leading to the highest annualised revenue can be selected.

Since the proposed methodology is a rather mathematical methodology, it is of outmost importance to be guided by the stakeholders' opinion and preferences.

REFERENCES

Abedinpour M, Sarangi A, Rajput TBS, Singh M, Pathak H, Ahmad T (2012) Performance evaluation of AquaCrop model for maize crop in a semi-arid environment. Agricultural Water Management 110:55-66

Andarzian B, Bannayan M, Steduto P, Mazraeh H, Barati ME, Barati MA, Rahnam A (2011) Validation and testing of the AquaCrop model under full and deficit irrigated wheat production in Iran. Agricultural Water Management 100:1-8

Doorenbos J, Kassam AH (1979) Yield response to water. FAO Irrigation and Drainage Paper No 33, Rome

Iglesias A., Garrote L., Cancelliere A., Cubilo F., Wilhite D. (eds) (2009) Coping with Drought Risk in Agriculture and Water Supply Systems. Springer

IDMP (2014) National Drought Management Policy Guidelines: A Template for Action. Global Water Partnership and World Meteorological Organisation

Jensen M. E. (1968). Water consumption by agricultural plants. In T.T. Kozlowski (editor) Water Deficits and Plant Growth, Vol. II, Academic Press, NY, pp. 1-22.

Kumar P, Sarangi A, Singh DK, Parihar SS (2014) Evaluation of AquaCrop model in predicting wheat yield and water productivity under irrigated saline regimes. Irrigation and Drainage 63:474–487 doi: 10.1002/ird.1841

McKee T.B., Doeskin N.J., Kleist J. (1993) The relationship of drought frequency and duration to time scales. In: Proceedings of the Eighth Conference on Applied Climatology. Anaheim, CA, January 17-23, 1993. American Meteorological Society. Boston, MA. pp 179-184

Mishra A. K., Singh V. P. (2010) A review of drought concepts. Journal of Hydrology 391(1):202-216

Pereira L. S., Cordely I., Iacovides I. (2009) Coping with Water Scarcity. Springer

Rossi G., Canceliere A., Pereira L, Oweis T., Shatanawi M., Zairi A. (2003) Tools for Drought Mitigation in Mediterranean Regions. Kluwer Academic Publishers

Rossi G., Castiglione L., Bonaccorso B. (2007) Guidelines for planning and implementing drought mitigation measures. In: Rossi G., Vega T. and Bonnaccorso B. (Eds) "Methods and Tools for Drought Analysis and Management. Springer, pp 335-347

Tigkas D, Vangelis H, Tsakiris G, 2015. DrinC: a software for drought analysis based on drought indices. Earth Science Informatics 8(3):697-709

Tigkas D., Vangelis H. and Tsakiris G. (2017) An enhanced effective reconnaissance drought index for the characterisation of agricultural drought. Environmental Processes, doi:10.1007/s40710-017-0219-x

Tsakiris G (1982) a method for applying crop sensitivity factors in irrigation scheduling. Agricultural Water Management, 5:335-343

Tsakiris G. (2009) A Paradigm for applying risk and hazard concepts in proactive planning. In: Iglesias et al. (eds) Coping with Drought Risk in Agriculture in Water Supply Systems. Springer, pp. 81-91

Tsakiris G (2017) Drought risk assessment and management. Water Resources Management 31(10): 3083-3095

Tsakiris G. Nalbantis I., Vangelis H., Verbeiren B., Huysmans M., Tychon B., Jacquemin I., Canters F., Vandehaegen S., Engelen G., Poelmans L., De Backer P., Batalaan O. (2013) A system-based paradigm of drought analysis for operational management. Water Resources Management, 27: 5281-5297

Tsakiris G., Pangalou D., Vangelis H. (2007) Regional drought assessment based on the Reconnaissance Drought Index (RDI). Water Resources Management 21(5):821-833

Tsakiris G., Spiliotis M., Vangelis H., Tsakiris P. (2015) Evaluation of measures for combating water shortage based on beneficial and constraining criteria. Water Resources Management, 29: 505-520

Tsakiris G., Vangelis H. (2005) Establishing a Drought Index incorporating evapotranspiration. European Water, 9-10:1-9

Proceedings of the 10th World Congress of EWRA 'Panta Rhei', 5-9 July 2017, Athens, Greece
© 2017 *European Water Resources Association*

Characterization of drought in Italy applying the Reconnaissance Drought Index

R. Zucaro, C. Antinoro* and G. Giannerini
Council for Agricultural Research and Economics Research - Center for Policies and Bioeconomy, Rome
** e-mail: chiara.antinoro@crea.gov.it*

Abstract: The mitigation of drought impacts is one of the most important challenges in the management of water resources and can only be properly realized through integrated management of this phenomenon. Regional drought analysis is conventionally based on drought indices for the identification of drought intensity, duration and areal extent. The aim of this study is to characterize the impact of the drought phenomena in Italy through the application of the Reconnaissance Drought Index (RDI). The basic form of the index is the ratio of the cumulative precipitation to potential evapotranspiration, for a specified reference period; it represents the intensity of water consumption in a given system, which varies in time and space but is entirely independent of the crops and soil characteristics and is also easily determinable. The Reconnaissance Drought Index (RDI) was considered more appropriate to the case-study examined. The run method is used to determine the characteristics of the drought phenomenon and to identify drought periods. As expected the RDI index shows more frequent events of drought in the Northern regions than in the South of Italy where the droughts is a structural condition. In the South the agricultural system has a more robust coping capacity and is more prepared to deal with water scarcity. This information is extremely useful for the evaluation of drought risk through mitigation measures with the appropriate management of water resources.

Key words: agricultural drought, drought indices, Reconnaissance Drought Index (RDI), drought assessment, mediterranean crops, drought mitigation measures

1. INTRODUCTION

The mitigation of drought impacts is one of the most important challenges in the management of water resources and can only be properly realized through an integrated management of this phenomenon. The term drought indicates "a natural, temporary and casual situation of strong reduction in water availability compared to normal values for a significant period of time and over a wide area" (Yevjevich, 1967).

This phenomenon is generally due to a series of natural causes such as high pressure, the localized subsidence, the lack of precipitation, the absence of the moist air flows. The causes of water scarcity can also be attributed to anthropogenic factors such as population growth, climate change and the resulting global warming, degradation of soil resources, pollution of water resources, which reduces the availability (Pickup, 1998).

As it is widely known, drought can be classified into four different types (Dracup, 1980; Wilhite and Glantz, 1985): meteorological, agricultural, hydrological and socio-economic.

Particularly the phenomenon of drought is basically of meteorological nature and it is identified as a precipitation deficit. The soil moisture deficit (agricultural drought), and the runoff deficit in surface and groundwater bodies (hydrological drought) are determined as a result of meteorological drought. The phenomenon is serious and complex. The consequences that it produces can give rise to multiple types of impacts on environment, economic and social sector (Yevjevich, 1967). According Tzakiris (2016) the methodology DPSIR (Driver-Pressure-State-Impacts-Response) can be applied to analyze the drought phenomenon in its complexity.

Applying this scheme, in this study the drought phenomenon is analyzed, providing an overview at national level. The meteorological drought [Driver] creates the hydrological and agricultural droughts [Pressure]. The drought phenomena produce water scarcity [State], this presents

unavoidable negative consequences on various sectors (economic, social and environmental) [Impacts]. The last step of this analysis involves identifying measures to prevent and monitor the negative consequences of the drought [Response] by applying appropriate water policies at National level.

Many Authors have proposed indices for assessing the drought phenomena. However, taking into account the drought as a water deficit, the Reconnaissance Drought Index (RDI) was considered more appropriate to assess the drought phenomenon throughout Italy (Tsakiris and Vangelis, 2005; Tsakiris et al., 2007).

This index is based on the relationship between the precipitation (P) and potential evapotranspiration (PET), it represents the intensity of water consumption in a given system, which varies in time and space but is entirely independent by crops, by the characteristics of the soil and also easily determined (only climatic parameters). For this reason the index is more suitable to monitor the agricultural drought (Rossi, 2007). The aim of this study is the agricultural drought characterization through RDI implementation at regional scale. The proposed methodology could be used by the Italian Government of Water to develop measures and strategies finalized to combat drought in the agricultural sector especially.

2. METERIALS AND METHODS

The meteorological data considered in this investigation were taken from Agro-climatic Observatory of the Ministry of Agriculture. The weather and climate statistics published are estimated with data of daily time series of meteorological stations of the National Agro-meteorological network (RAN). The estimate of weather and climate statistics of the areas of interest or geographic domain names is performed with a non-stationary geostatistical model that takes into account the location of the stations of both the trend and the geographical correlation of climatic factors.

For each Italian region, the annual rainfall and potential evapotranspiration data were used from 2006 to 2015 and their long-term climatic averages for each station.

An initial value of the Reconnaissance Drought Index (RDI, hereinafter) (Tsakiris and Vangelis 2005; Tsakiris et al., 2006; Tsakiris et al., 2007) was calculated for each year of the period considered:

$$RDI = \alpha_y = \frac{Pi}{PETi}, i = 1\ to\ N \quad (1)$$

where P_i e PET_i are the precipitation and potential evapotraspiration of the *ith* year and N is the total number of years of the available data.

A second expression, the Normalized RDI (RDI_{norm}) was calculated for each year, using the following equation:

$$RDI_{norm} = \frac{\alpha_y}{\alpha_{avg}} - 1 \quad (2)$$

where the parameter α_y is the annual average value and $\bar{\alpha}_{avg}$ is the average value calculated for all N years of data. The RDI_{norm} was used to determine the critical value below which define the drought "severe", so the negative values below the average were used to identify drought events.

The Run Method (Yevjevich, 1967; Rossi, 2007) was applied directly on RDI_{norm} for identifying drought periods and average intensity.

Therefore a drought period was identified by the number of consecutive years in which RDI_{norm} assumed negative values. While for each drought period, the average intensity (severity) was calculated from the relationship between cumulative RDI_{norm} and the number of years of drought.

3. RESULTS OF RDI APPLICATION

This application tested the scenario of drought events of the past decade. The Run Method was applied to identify droughts periods for each Italian Region. For the sake of brevity, the results for three Italian Regions are presented in Figure 1 (a northern region, Lombardy, a central region, Lazio, and a southern region, Sicily).

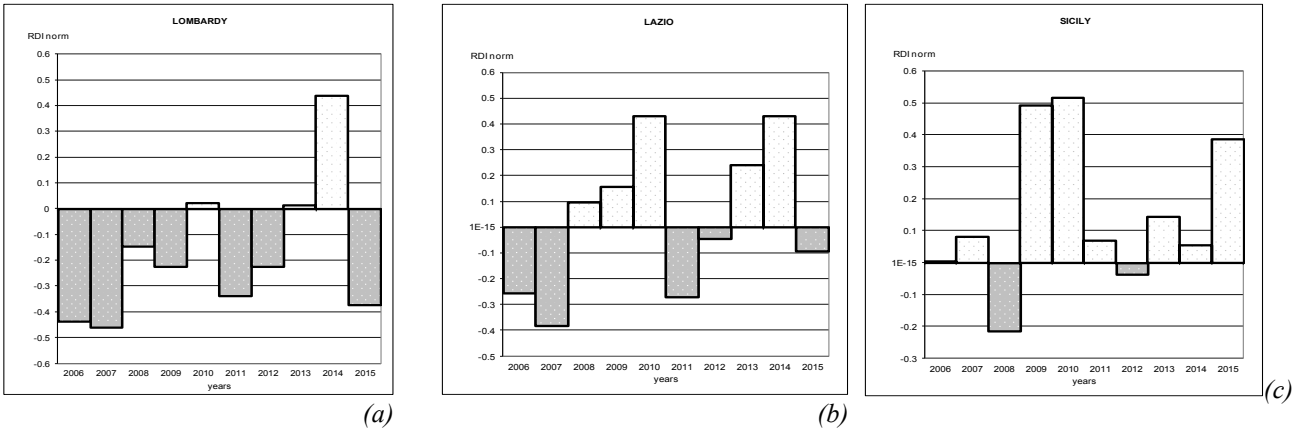

Figure 1. Application of the Run Method for three Italian Region: Lombardy(a), Lazio (b) and Sicily (c).

As expected, the RDI_{norm} shows more frequent drought events in the Northern region, Lombardy. As illustrated in figure 1(a), the negative values show the dry years and, as a result, four dry periods are identified: the first long 4 years, the second two years and the third one year only (even if it is the upper limit of the analyzed time series) and all of four present a certain severity. A different situation was found in the southern Region, in Sicily, as the dry periods are only two (one year each one), as well as presenting a lower severity (Fig. 1(c)). The central region, Lazio, presents intermediate results (Fig. 1(b)).

The total number of drought years were obtained for each Italian Region that correspond to negative values of calculated RDI_{norm} (Fig. 2a). For each drought period the corresponding severity (average intensity) was calculated (Fig. 2b).

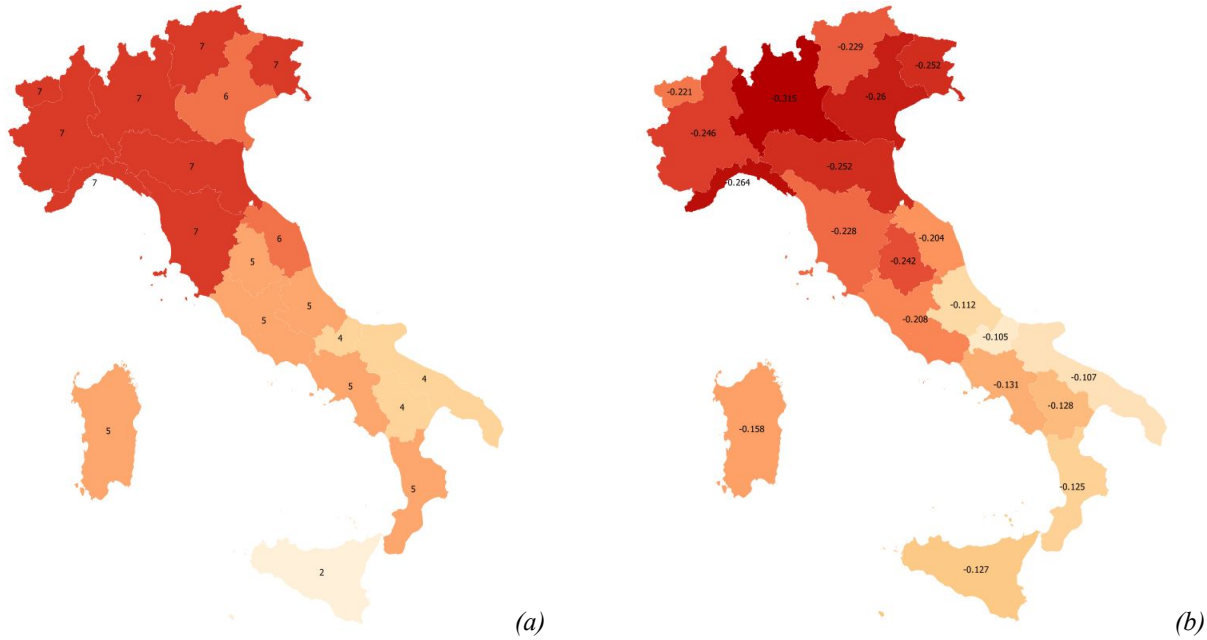

Figure 2. The total number of drought years for each Italian Region (a) and the corresponding average severity (b).

As illustrated in Figure 2 the longest drought events occur in the North of Italy showing also a greater severity while in the south of Italy a less worrisome condition occurs.

This is due to the fact that, over the past decade, the Mediterranean climate showed a significant trend toward the so-called phenomenon of climate extremes showing more and more frequent and sensitive deviations from historical trends of climate parameters. In fact deviations from the climate average are more evident in the North. This analysis demonstrates that rainfall is the primary factor that controls the drought whereas other climatic factors such as high temperatures and relative humidity may amplify its intensity.

4. THE RESPONSE: PROACTIVE STRATEGIES AGAINST DROUGHT IN ITALY

The impacts caused by the drought are well known. The consequences that it produces may give rise to a multiple types of impacts, in particular on the environment, economic and social sector. The magnitude of the impact depends on the vulnerability of the different sectors affected.

Particularly at the level of water supply systems, the risk of water scarcity is also connected to the structural measures, management, administrative actions, economic support, which are adopted both proactive measures and emergency reactive measures, that is, when the phenomenon has already manifested. During 2016, the Italian Government of Water identified measures to prevent and monitor the negative consequences of drought. According Water Framework Directive (WFD), the National Observatories of Water Uses (OWU) were established. The OWUs were included among the measures provided in the River Basin Management Plans for each Italian River Basin Districts (Fig. 3). Members of the OWU are the public water authorities:

- Water district authorities;
- Ministry of Agriculture (MIPAAF);
- Ministry of Environment (MATTM);
- Civil Protection Agency;
- Regional Administrations;
- Italian National Institute for Environmental Protection and Research (ISPRA);
- Council for Agricultural Research and Economics (CREA);
- Italian National Institute of Statistics (ISTAT).



Figure 3. Extent of the River Basin Districts in Italy.

The observatories are operating bodies in charge of monitoring the water uses and coordinating the management responses in case of drought events. For the identification of different levels of severity of the drought phenomenon, The World Meteorological Organization (WMO) defines the specific indexes related to some of the cumulative effects of a prolonged and abnormal moisture deficiency. Identifying appropriate indices and triggers (specific values that can define a level of a drought plan and associated management responses) based upon the local climate and data availability is a critical aspect of drought management. The WMO defines three levels of severity as well as the resulting measures to implement for each of these levels. In Table 1. the aspects involving the irrigation sector are outlined.

Table 1. Relations between levels of drought and measures for risk management

Drought severity level	Definition	Measures for irrigation
Normal situation	No drought	• Monitoring water usage/volumes in the water district
Mild drought	water demand is fulfilled but drought indices and weather forecasts show a clear worsening	• definition of impact scenarios for agricultural sector • evaluation of drought mitigation strategies/measures • monitoring • notices on climatic situation, its evolution and related risks • ex-post analysis of the drought events • ex-post evaluation of strategies/measures adopted
Moderate drought	water demand is not fulfilled, river flows and reservoirs are lower than the average. Economic losses are foreseen	Same of the mild drought but having a higher intensity and a higher frequency
Severe drought	Crops are suffering damages. State of calamity	Support the civil protection in the event management

The drought indices which mark the severity levels are defined by a Technical Committee (TC) at national level. TC has been established last October and is currently working on the indices definition and a common format for the notices provided by the OWU during the drought events.

5. CONCLUDING REMARKS

At the present study, the drought occurrences have been identified in Italy during the decade 2006-2015. For this purpose the RDI index (Tsakiris and Vangelis 2005; Tsakiris et al., 2006;Tsakiris et al., 2007) was implemented at regional scale. The proposed methodology provide an overview of drought phenomena at national level. As expected, this application shows more frequent events of drought in the Northern regions than in the South of Italy where the droughts is a consolidated condition. The results have shown that the drought has a more severe impact on the regions of northern Italy.

The management of drought impacts is one of the major challenges in water management. An important element to implement an effective drought management strategy is to identify in advance the measures to be taken to prevent the adverse effects on the water supply system, the productive sectors and the environment. These strategies must be based on a preventive approach. Moreover, the planning tools for risk management must be identified and the combination of better short- and long-term measures should be selected.

The Italian Government of Water identified measures to prevent and monitoring the negative consequences of drought. During 2016, the National Observatories of Water Uses (OWU) were established. At this moment the observers are in operation and are implementing the risk management policies with a proactive approach for effectively dealing the consequences of the drought in Italy.

It has been shown that The Reconnaissance Drought Index is a useful tool to improve the management of water resources. It can also be used by OWUs for drought monitoring. In fact this

analysis is the starting point of further investigation.

REFERENCES

Agro-climatic Observatory of the Ministry of Agriculture: https://www.politicheagricole.it/flex/FixedPages/Common/miepfy700_riferimentiAgro.php/L/IT

Dracup JA, Lee KS, Paulson EG (1980) On the statistical characteristics of drought events. Water Resour Res 16:289–296

Pickup G (1998) Desertification and climate change—the Australian perspective. Clim Res 11:51–63

Rossi, G. (2007). Monitoraggio del fenomeno (Risk monitoring). Siccità: analisi, monitoraggio e mitigazione. Applicazioni in Sicilia (Drought: analysis, monitoring and mitigation. Applications in region Sicily). Nuova Bios, Cosenza, 15-48.

Tsakiris G, Rossi G, Iglesias A, Tsiourtis N, Garrote L, Cancelliere A (2006) Drought Indicators Report. Report made for the needs of the European Research Program MEDROPLAN (Mediterranean Drought Preparedness and Mitigation Planning)

Tsakiris G, Vangelis H (2005) Establishing a drought index incorporating evapotranspiration. Eur Water 9–10:1–9

Tsakiris, G. (2016). Proactive Planning Against Droughts. Procedia Engineering, 162, 15-24.

Tsakiris, G., Pangalou, D. and Vangelis, H., 2007. Regional drought assessment based on the Reconnaissance Drought Index (RDI). Water resources management, 21(5), pp.821-833.

UNEP. (1992). WorldAdas ofDeserdficarion. London. Edward Arnold. ix+ 69pp.

UNESCO (1977) Map of the world distribution of arid regions. MAB Technical Notes 7.

Wilhite DA, Glantz MH (1985) Understanding the drought phenomenon: the role of definations. Water Int 10:111–120

Yevjevich, V. M. (1967). An objective approach to definitions and investigations of continental hydrologic droughts. Hydrology papers (Colorado State University); no. 23.

Proceedings of the 10th World Congress of EWRA 'Panta Rhei', 5-9 July 2017, Athens, Greece
© 2017 *European Water Resources Association*

SPI analysis over Greece using high resolution precipitation gridded datasets

E.G. Feloni[1*], K.G. Kotsifakis[1], P.T. Nastos[2] and E.A. Baltas[1]
[1] *Department of Water Resources and Environmental Engineering, School of Civil Engineering, National Technical University of Athens, 5 Iroon Polytechniou, 157 80, Zofrafou, Attiki, Greece*
[2] *Laboratory of Climatology and Atmospheric Environment, Faculty of Geology and Geoenvironment, University of Athens, University Campus 157 84, Athens, Greece*
[*] *e-mail: feloni@chi.civil.ntua.gr*

Abstract: This research work focuses on the analysis of the Standardized Precipitation Index (SPI) over Greece for three time scales; three, six and 12 months (SPI_3, SPI_6, SPI_{12}; respectively). The SPI_i timeseries were calculated using the DrinC open-access software.. The estimation of the index, as well as, its mean values and trends were based on the E-OBS gridded precipitation data v.11.0 for the period 1950 - 2014 with 0.25°x0.25° spatial resolution. Moreover, an analysis concerning the moving average fluctuation within the same period was performed, providing the corresponding patterns. Additionally, five elevation zones were created with the aim of investigating any particular relation between the altitude of a location and the means and trends of SPI_i. In order to determine the most severe drought events that have occurred in Greece, the SPI_i anomalies were also estimated. It was found that the means of seasonal index present distinct spatial pattern over Greece, while the SPI_i trends patters also differ. A systematically high SPI_i in the zone of 200-500m is observed, while the maximum negative trends are presented in the zone of the lowest altitudes (0-200m), where the large amount of agricultural activities is located.

Key words: SPI, means, trends, elevation patterns, Greece

1. INTRODUCTION

Drought is a natural phenomenon which is characterized by extended periods of precipitation shortage, normally for a season or more, resulting in water deficiency for some human activities, such as farming, irrigation or domestic use. In the last decades, many drought indices were formulated into a single number by integrating meteorological parameters, such as, rainfall, evapotranspiration and temperature (Patel et al., 2007). One of the most common indices is the SPI, which McKee et al. (1993) proposed as an indicator that may be served as a versatile tool in drought alert, monitoring and analysis. It is a valuable tool for the estimation of the intensity and duration of drought events and its vantage was highlighted in 2010, when World Meteorological Organization (WMO) selected SPI as a key meteorological drought indicator to be produced operationally by meteorological services. Later studies proved that the SPI is in good agreement with the corresponding values of the Palmer Drought Severity Index (PDSI) (Keyantash and Dracup, 2002), which is traditionally the most common drought index used in the United States. SPI's asset is that identifies emerging droughts months sooner than the Palmer Index (Hayes et al., 1999). Despite the fact that the majority of drought indices have a fixed time-scale, SPI is designed in such a way that it can detect drought over different periods at multiple time scales. As SPI is based on precipitation alone, it is easy to use, taking into account its fundamental strength; that it can be calculated for a variety of timescales. The applicability of SPI varies with the time scale because the 1-month SPI reflects short-term conditions and its application can be related closely to soil moisture; the 3-month SPI provides a seasonal estimation of precipitation; 6- and 9-month SPI indicates medium term trends in precipitation patterns (Ji and Peters, 2003). The SPI has several limitations and unique characteristics of its own that must be considered when it is used. For example, the SPI is only as good as the data used in calculating it (Hayes et al., 1999). Important factors are the timeliness of

the station data, especially in an operational use of the index, and the spatial distribution and density of the stations. Guttman (1999) reports that at least a fifty years long dataset is necessary for the definition of the SPI on time scales smaller than 12-months, while longer datasets are required on 24-, 36- or 48-month periods. Hayes et al. (1999) considered that for small time scales, thirty years long datasets may be used.

In Greece, Livada and Assimakopoulos (2007) studied the spatial and temporal variations of monthly precipitations over Greece, using 51 years (1950–2000) of monthly rainfall data from the available meteorological monitoring network, by applying the Standardized Precipitation Index (SPI), to detect on a regional basis, drought frequency, drought intensity and drought duration. From the estimation of the SPI on 3- , 6- and 12-month time scales, they found that the frequency of mild and moderate drought conditions is approximately of the same order of magnitude over the whole Greek territory. However, frequencies present a small reduction moving from north to south and from west to east. They illustrate the persistence of severe or more drought conditions during 1988–1990 and 1999–2000, which in turn was caused by the immanent anticyclonic systems over the eastern part of the Mediterranean basin (Rossi and Somma, 1995). Given the enormous potential of the SPI to detect and characterize drought episodes, this research work focuses on the analysis of the Standardized Precipitation Index (SPI) over Greece for three time scales; three, six and 12 months ($SPI_{3,i}$, $SPI_{6,i}$, SPI_{12}; respectively). The main findings are concentrated in the spatial and temporal variability of the index in Greece using the EOBS gridded precipitation dataset (v.11). The EOBS dataset (Haylock et al., 2008) is the first publicly available daily gridded dataset covering the whole land of Europe at a high spatial resolution and it is continuously updated, making it one of the most widely used datasets and a useful tool for the scientific community (Turco et al., 2013). This dataset provides daily timeseries for a long period; from 1950 until today (v.14). For the SPI_i calculations, all the precipitation data were converted to monthly values. Subsequently, the calculation of the index was made using the DrinC open-access software, which has been developed at the National Technical University of Athens (also see Tigkas et al., 2015). For all the SPI_i values, the patterns of the means and trends are provided, as well as, an analysis concerning the moving average fluctuation of the index. These results are presented in the first and second part of the results, respectively. Moreover, the SPI anomalies for the most severe drought events in Greece are displayed, enabling any comparisons and, for this reason, a series of maps is presented to demonstrate the versatility of the SPI in monitoring the dynamics of the drought nationally, in part three. Finally, this work intends to illustrate the different characteristics of the SPI means and trends in individual elevation zones, providing the corresponding plots in part four.

2. DATASETS AND METHODS

2.1 Description of the data used

Monthly precipitation data were used as input for the SPI calculations, which are based on the EOBS gridded precipitation dataset (v.11.0).The EOBS dataset covers the whole land of the European continent and it is the result of the European research project ENSEMBLES (http://ensembles-eu.metoffice.com) and ECA&D (http://www.ecad.eu/). EOBS dataset was created using a large number of meteorological stations in Europe (including Greece, using the HNMS station data), after a process that involves spatial integration. This data provide the daily information of the rainfall intensity, the surface temperature, as well as, the atmospheric pressure at sea level, in a grid of 0.25° x 0.25° spatial resolution. The algorithms used to create the dataset are updating continuously, in order to encounter errors and inconsistencies of the product, comparing to the grounded data. The latest version of the algorithm (v.14.0) was issued in October 2016 and the access of the data is freely available through the website of the program (http://www.ecad.eu/download/ensembles/ensembles.php). EOBS data considered at the moment as the most reliable for calculating the precipitation intensity and surface temperature in places where no measurements are

available or incomplete, in Europe. Additionally, they have an advantage in comparison with other similar products, because of their high spatial resolution, as well as, the time series length; data cover the period from 1950 to present.

Moreover, a dataset of 24 rain gauge stations well distributed over Greece (Figure 1), which belong to the Hellenic National Meteorological Society, was also used in order to crosscheck the individual results of SPI calculations. Furthermore, a digital elevation model of 30m spatial resolution has been used, for the distinction of the elevation zones and the match with the SPI_i values (in section 3.4).

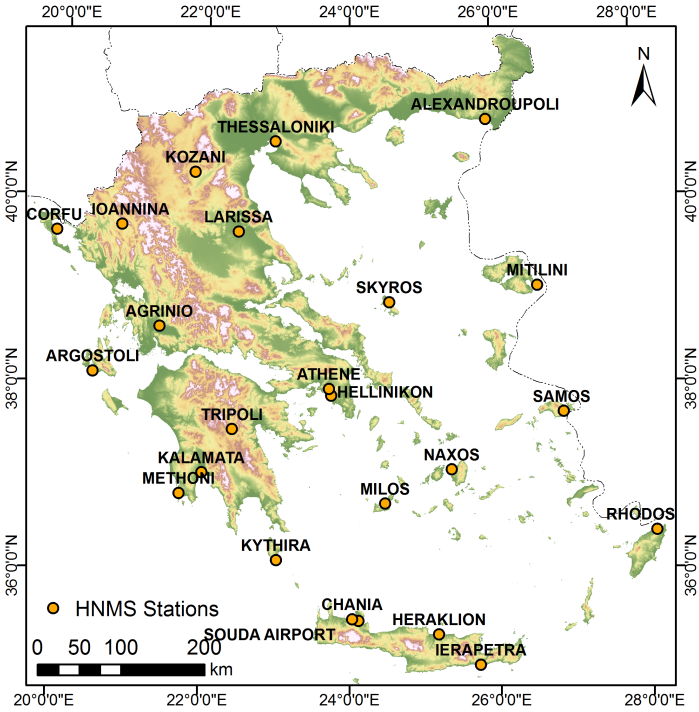

Figure 1. Meteorological stations and topography of Greece

2.2 Methods

The DrinC open access software was used for the calculation of the Standardized Precipitation Index. This software can also estimate the Reconnaissance Drought Index (RDI), the Streamflow Drought Index (SDI) and the Precipitation Deciles (PD), so this tool is useful for the estimation of the agricultural, meteorological or hydrological drought. Apart from the originally proposed methods of calculation for each index, DrinC incorporates alternative methods that allow the comparison of the results among the indices (Tigkas, et al., 2015). Concerning the SPI calculations, it requires a long-term precipitation record, in which it fits a probability distribution, usually gamma (Thom, 1958), which is then transformed into a normal distribution so that the mean SPI for the location and desired period is zero (McKee et al. 1993; Edwards and McKee 2015). Since the SPI is normalized, the positive values represent dry conditions while the negative values wet (see Table 1). In this context, SPI is the number of standard deviations that the observed value would deviate from the long-term mean, for a normally distributed random variable (Tigkas, et al., 2015).

Table 1. Classification scale for SPI values.

SPI values	≥ 2.00	1.99 - 1.50	1.49 - 1.00	0.99 - -0.99	-1.00 - -1.49	-1.50 - -1.99	≤ -2.00
Category	Extremely wet	Very wet	Moderately wet	Near normal	Moderately dry	Severely dry	Extremely dry

Concerning the input data, DrinC calculations are based on the hydrological year (October – September). The main time scales are 1-month, 3-months, 6-months and annual SPI. However, it is flexible software, so the user can define other calculation steps and starting months. In this research work, the SPI_3 means and slopes were estimated, in order to illustrate the particular seasonal characteristics. SPI_6 also calculated, which depicts the wet ($SPI_{6,1}$) and dry ($SPI_{6,2}$) period. Finally, SPI_{12} was taken into account as an annual index which is also useful for the moving average depiction and for the detection of the greatest anomalies for the period 1950-2014. After the aforementioned computations, an analysis concerning the moving average fluctuation as well as the computation of the most significant anomalies, in terms of severe drought events, was held. Because of the large number of the outputs, only selected results are displayed. For instance, SPI_{12} moving average is presented spatially distributed, as a snapshot of the 30-year mean index per decade. So, through four different maps (1950-1980, 1960-1990, 1970-2000, and 1980-2014) one can see the variability of the index.

The calculation of the SPI anomalies was focused on the driest and hottest years within the examined period (1950-2014). According to Kostopoulou et al. (2017), who have studied the temporal and spatial trends of the SPI using RCM outputs, the most severe drought episodes occurred in Greece, were found in 1977, 1989–90, 1992–93 and 2000. Also, summer of 2007 and 2010 were particularly hot, and led to extensive fires. For these years, selected maps with the spatiotemporal distribution of the index are provided. Finally, an investigation of any relation of SPI to elevation was done, using GIS technics. For this purpose, the digital elevation model (DEM; 30 m spatial resolution) was divided into five elevation zones (Table 2.i) after taking into account the guidelines of SOil and TErrain Digital Database, SOTER (Dobos et al., 2005). In section 3.4, the mean values and mean slopes of SPI per elevation zone are illustrated. Due to the negative trends of the index in the lowest zones, a more detail investigation was done, using a second classification with nine elevation zones (Table 2.ii), with smaller classes in low levels.

Table 2. Elevation classification: i. Dobos et al., 2005, ii. Nine classes.

i. Zone	Elevation (m)	ii. Zone	Elevation (m)
A	0-200	A	0-20
B	200-500	B	20-50
C	500-800	C	50-100
D	800-1200	D	100-200
E	>1200	E	200-500
		F	500-800
		G	800-1000
		H	1000-1500
		I	>1500

3. RESULTS AND DISCUSSION

3.1 SPI means and trends

The analysis of SPI means demonstrates that SPI for all time scales is within its normal values for Greece. As Figure 2 displays, Southern Greece displays positive values, especially the Eastern Peloponnese and Crete. The wider range in values is shown in $SPI_{3,4}$, i.e., the summer quarter (Figure 2, right map, upper panel). This pattern is similar for all time scales; however, a comparison with the spatial distribution of the SPI trends leads to special features per region. For instance, although there is a positive value of SPI mean in Eastern Peloponnese, this area has negative SPI values for both summer months ($SPI_{3,4}$) and dry period ($SPI_{6,2}$). In contrast, Attica region presents negative mean values of SPI for all time scales and positive trends even in summer months, and this trend is close to the maximum observed in Greece. The combination of negative mean values and slightly decreasing trends is illustrated in Northeastern Greece.

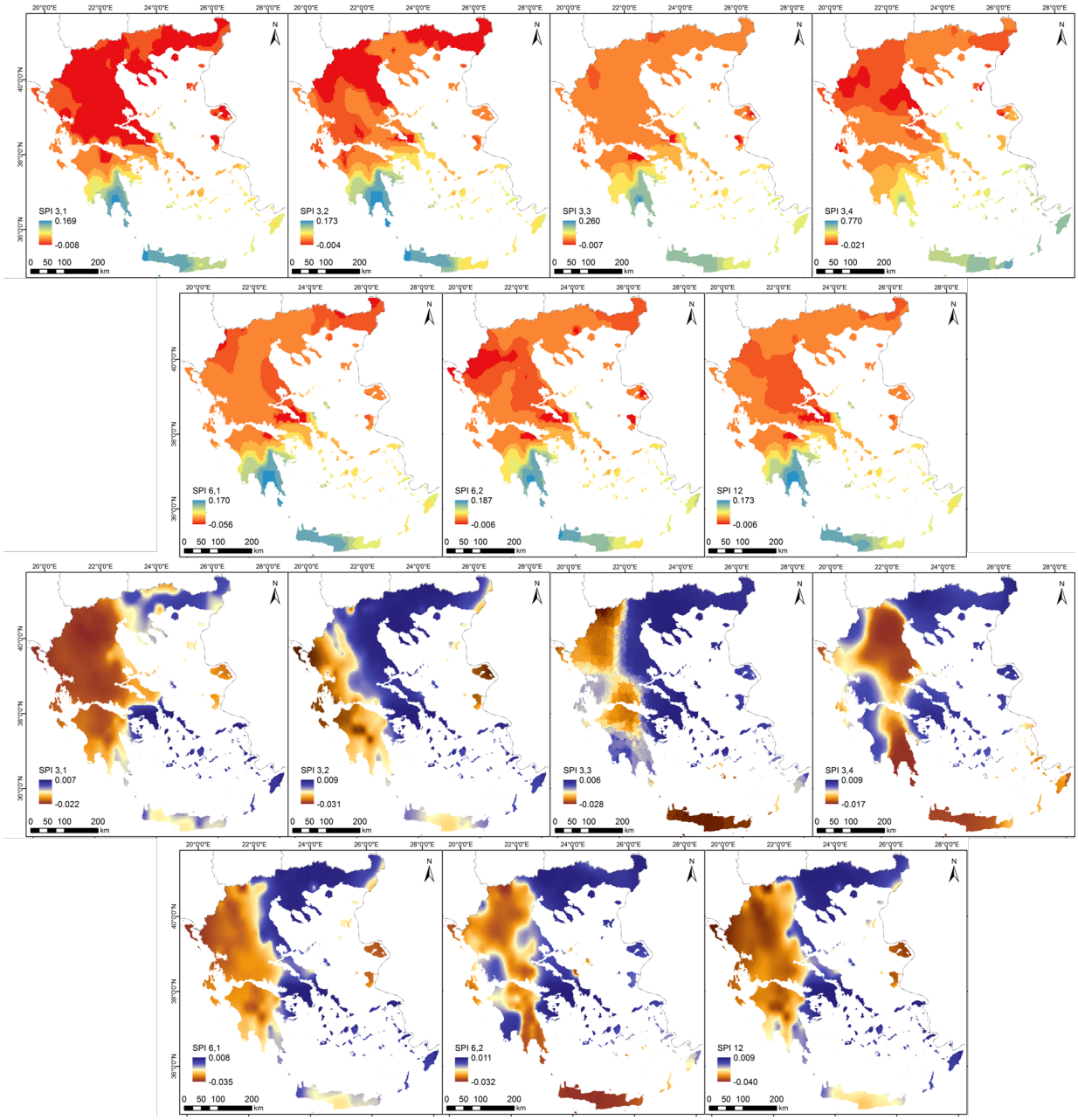

Figure 2. SPI means (upper maps) and trends (lower maps). Each index presents different spatial patterns. From left to right: $SPI_{3,1(Oct\text{-}Nov\text{-}Dec)}$, $SPI_{3,2(Jan\text{-}Feb\text{-}Mar)}$, $SPI_{3,3(Apr\text{-}May\text{-}Jun)}$, $SPI_{3,4(Jul\text{-}Aug\text{-}Sep)}$, $SPI_{6,1(wet\ period)}$, $SPI_{6,2(dry\ period)}$, $SPI_{12(annual)}$.

3.2 SPI moving average

In this section, the results concerning the moving average fluctuation are presented, based on the 30-year SPI_i means. Only spatial patterns of SPI_{12} per consecutive 30-years are displayed, and one can observe the differences in patterns of mean values (Figure 3). A similar image is given through the SPI means of the other time scales. A relative analysis of SPI_i using the 24 stations precipitation data argues the finding that the fluctuation presents a significant spatial differentiation within the examined period. The 30-year SPI_i means are close to the normal values of the index, however, the highest negative values are systematically presented in the period between1970-2000, which is the period that encloses the majority of drought events. Comparing these patterns with the temporal average, the second displays a smaller range in mean values, as expected. SPI_6 patterns also reveal the spatiotemporal fluctuation of the index. From the view of spatial distribution, $SPI_{3,4}$ is the most stable index; negative values are systematically observed in the North, while positive in the South, - a pattern that is in agreement with that of the temporal mean.

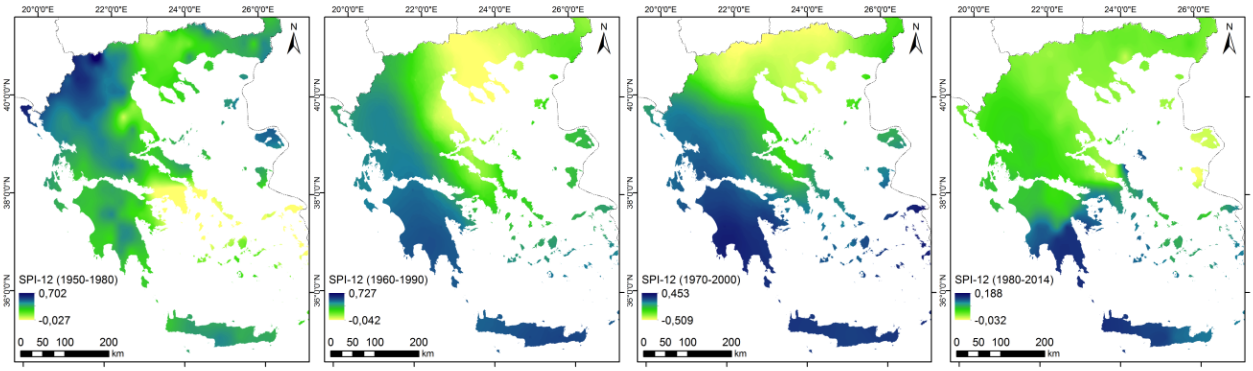

Figure 3. SPI_{12} means per consecutive 30-years.

3.3 SPI anomalies

Anomalies are a useful tool in meteorological applications, as they denote the departure of an element (SPI_i, in our case) from the long-term average value (1961-1990 average, according to the international standard). As a general result in this analysis, anomalies range in space and time, while they are higher in Southern Greece. Its highest absolute value was calculated in the drought event of 1989-1990, which corresponds to extremely dry conditions (SPI_i<2). According to the results, the most representative index seems to be the $SPI_{6,1}$, which depicts the conditions of the autumn afterwards the dry period, as well as, the SPI_{12} of the hydrologic year which encloses the drought event(s). The anomalies for these indices are displayed in Figure 4. The values of the anomalies in combination with the average values reveal the severity of these drought events. The SPI patterns for the other time scales, delimit a region of significant negative anomalies from the South up to the Central Greece. Any exceptions of high negative anomalies in Northern Greece are located in lowlands; however this allegation needs further investigation.

3.4 SPI elevation patterns

The calculation of the mean SPI_i and the mean trend of SPI_i for different elevation zones showed that there is a systematically negative trend in the lowest altitudes, up to the elevation of 200 m (Table 3). However, the analysis reveals that this general pattern varies spatially (e.g., the standard deviations of the means per zone are smaller in the South). All things considered, subjectivity in the elevation zones classification is another factor that influences these results. The unequal distribution of the area per zone also affects the results, comparing the values of the two selected classifications.

Table 2. SPIi means and trends for different elevation zones (red dots indicate SPI values over the specific zones).

Patterns for:	**$SPI_{3,1}$ mean**	**$SPI_{3,2}$ mean**	**$SPI_{3,3}$ mean**	**$SPI_{3,4}$ mean**	**$SPI_{6,1}$ mean**	**$SPI_{6,2}$ mean**	**SPI_{12} mean**	**$SPI_{3,1}$ trend**	**$SPI_{3,2}$ trend**	**$SPI_{3,3}$ trend**	**$SPI_{3,4}$ trend**	**$SPI_{6,1}$ trend**	**$SPI_{6,2}$ trend**	**SPI_{12} trend**
Elevation Zone														
A	0.002	0.004	0.001	0.000	0.001	0.001	0.000	-0.015	-0.014	-0.012	-0.003	-0.019	-0.010	-0.020
B	0.001	0.004	0.001	0.003	0.001	0.001	0.000	-0.015	-0.011	-0.011	-0.003	-0.017	-0.010	-0.018
C	0.022	0.026	0.024	0.069	0.022	0.023	0.022	-0.013	-0.012	-0.011	-0.003	-0.015	-0.010	-0.016
D	0.025	0.030	0.025	0.051	0.027	0.025	0.026	-0.014	-0.009	-0.010	-0.005	-0.014	-0.009	-0.015
E	0.033	0.040	0.039	0.087	0.036	0.036	0.036	-0.010	-0.006	-0.007	-0.004	-0.009	-0.007	-0.011
F	0.019	0.027	0.021	0.062	0.021	0.020	0.021	-0.005	0.000	-0.002	0.002	-0.003	0.000	-0.003
G	0.006	0.009	0.005	0.045	0.005	0.005	0.005	-0.007	-0.013	-0.006	0.004	-0.014	-0.002	-0.013
H	0.013	0.016	0.012	0.092	0.012	0.013	0.011	-0.007	-0.014	-0.007	0.003	-0.014	-0.003	-0.015
I	0.002	0.006	0.000	0.016	0.001	0.001	0.001	-0.011	-0.019	-0.008	0.006	-0.020	-0.002	-0.020
Elevation Zone														
A	0.012	0.016	0.013	0.029	0.013	0.012	0.013	-0.014	-0.012	-0.011	-0.003	-0.016	-0.010	-0.017
B	0.033	0.040	0.039	0.087	0.036	0.036	0.036	-0.010	-0.006	-0.007	-0.004	-0.009	-0.007	-0.011
C	0.019	0.027	0.021	0.062	0.021	0.020	0.021	-0.005	0.000	-0.002	0.002	-0.003	0.000	-0.003
D	0.020	0.020	0.021	0.086	0.019	0.019	0.019	-0.006	-0.006	-0.007	0.000	-0.007	-0.005	-0.008
E	0.007	0.011	0.006	0.055	0.006	0.007	0.006	-0.008	-0.016	-0.007	0.004	-0.016	-0.002	-0.016

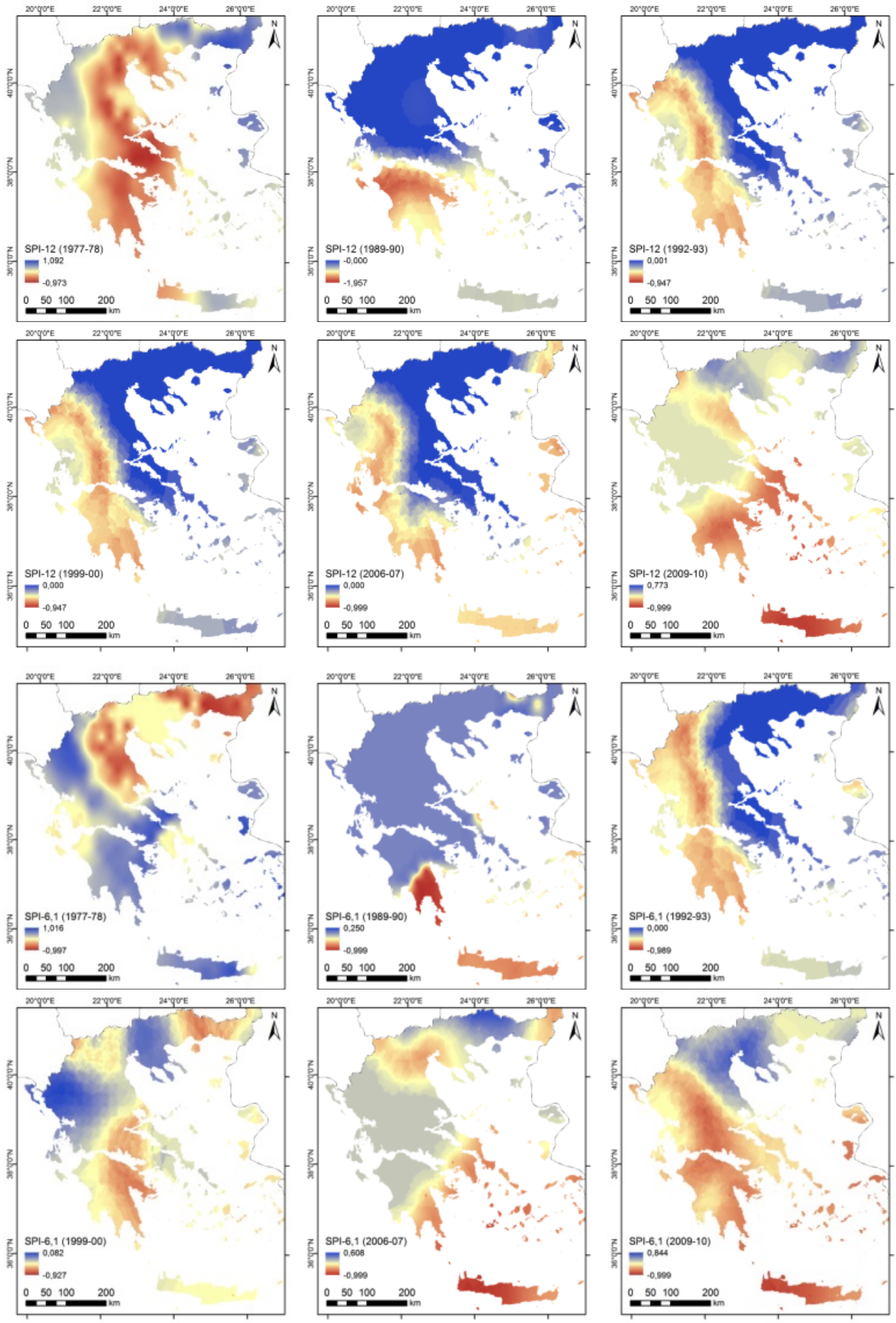

Figure 4. SPI_{12} and $SPI_{6,1}$ anomalies for selected drought events.

4. CONCLUSIONS

This research work focuses on the analysis of SPI_i means, trends, selected anomalies and elevation patterns, using the high resolution EOBS gridded precipitation data for the period 1950 - 2014. The main findings are concentrated as follows:

- SPI_i means and 30-year moving average values are near the normal, with the lowest mean negative values in the period 1970-2000, while a large number of drought events were occurred.
- SPI_i trends show that there is a slight positive trend in the Eastern Greece, and a systematically negative trend in the Northwestern part; a feature that is also illustrated through the computation of the moving average, which passes from positive to negative values for this region.
- The estimation of the SPI_i anomalies overall confirmed the severe drought events of the past, and the most representative index for the detection of a severe drought of a year *t* is the $SPI_{12,(t)}$ and $SPI_{6,1,(t+1)}$.
- Results in relation to the means and trends patterns for different elevation zones showed that further investigation is needed. However, negative trends of SPI_i are in accordance with the spatial patterns in all time scales of SPI_i.

REFERENCES

Dobos, E., Daroussin, J. and Montanarella, L., 2005. An SRTM-based procedure to delineate SOTER Terrain Units on 1: 1 and 1: 5 million scales. European Communities.

Edwards, D.C. and McKee, T.B., 2015. Characteristics of 20th century drought in the United States at multiple time scales. Atmospheric science paper; no. 634.

Guttman NB (1999) Accepting the Standardized Precipitation Index. A calculation algorithm. J AmerWater Resour Assoc 35: 311–322

Hayes, M.J., Svoboda, M.D., Wilhite, D.A. and Vanyarkho, O.V., 1999. Monitoring the 1996 drought using the standardized precipitation index. Bulletin of the American Meteorological Society, 80(3), pp.429-438.

Haylock, M.R., Hofstra, N., Klein Tank, A.M.G., Klok, E.J., Jones, P.D. and New, M., 2008. A European daily high□resolution gridded data set of surface temperature and precipitation for 1950–2006. Journal of Geophysical Research: Atmospheres, 113(D20).

Ji, L. and Peters, A.J., 2003. Assessing vegetation response to drought in the northern Great Plains using vegetation and drought indices. Remote Sensing of Environment, 87(1), pp.85-98.

Keyantash, J. and Dracup, J.A., 2002. The quantification of drought: an evaluation of drought indices. Bulletin of the American Meteorological Society, 83(8), pp.1167-1180.

Kostopoulou, E., Giannakopoulos, C., Krapsiti, D. and Karali, A., 2017. Temporal and Spatial Trends of the Standardized Precipitation Index (SPI) in Greece Using Observations and Output from Regional Climate Models. In Perspectives on Atmospheric Sciences (pp. 475-481). Springer International Publishing.

Livada, I. and Assimakopoulos, V.D., 2007. Spatial and temporal analysis of drought in Greece using the Standardized Precipitation Index (SPI). Theoretical and applied climatology, 89(3), pp.143-153.

McKee, T.B., Doesken, N.J. and Kleist, J., 1993, January. The relationship of drought frequency and duration to time scales. In Proceedings of the 8th Conference on Applied Climatology (Vol. 17, No. 22, pp. 179-183). Boston, MA: American Meteorological Society.

Patel, N.R., Chopra, P. and Dadhwal, V.K., 2007. Analyzing spatial patterns of meteorological drought using standardized precipitation index. Meteorological Applications, 14(4), pp.329-336.

Rossi, G. and Somma, F., 1995. Severe drought in Italy: Characteristics, impacts, and mitigation strategies. Drought Network News (1994-2001), p.75.

Thom, H.C., 1958. A note on the gamma distribution. Monthly Weather Review, 86(4), pp.117-122.

Tigkas, D., Vangelis, H. and Tsakiris, G., 2015. DrinC: a software for drought analysis based on drought indices. Earth Science Informatics, 8(3), pp.697-709.

Turco, M., Zollo, A.L., Ronchi, C., Luigi, C.D. and Mercogliano, P., 2013. Assessing gridded observations for daily precipitation extremes in the Alps with a focus on northwest Italy. Natural Hazards and Earth System Sciences, 13(6), pp.1457-1468.

Proceedings of the 10th World Congress of EWRA 'Panta Rhei', 5-9 July 2017, Athens, Greece
© 2017 *European Water Resources Association*

System based multivariate drought characterisation for surface water

I. Nalbantis* and G. Tsakiris
Centre for the Assessment of Natural Hazards and Proactive Planning and Laboratory of Reclamation Works and Water Resources Management; School of Rural and Surveying Engineering, National Technical University of Athens, Athens, Greece
* *e-mail: nalbant@central.ntua.gr*

Abstract: By adopting the systemic approach for drought analysis, the surface water subsystem turns out to be the most critical element of the studied water system due to the fact that the largest part of water abstractions worldwide originates from surface water. Ideally, to characterise drought conditions in this subsystem, all variables involved in its water balance should be conjunctively analysed. In an effort towards this direction, multiple variables are used which are accessible through measurement or are easily estimated. These include precipitation, potential evapotranspiration and streamflow. All three variables are jointly employed in a multivariate drought index constructed using copulas. The univariate normal, Gamma and log-normal distributions serve as the candidate marginal distributions, while elliptical copulas are selected to represent the dependence structure of the three variables. Fitting of marginal distributions and copulas is performed using the maximum likelihood method. Values of the proposed index are compared to those of known indices which are the Streamflow Drought Index (SDI), the Reconnaissance Drought Index (RDI), and the Standardized Precipitation Evapotranspiration Index (SPEI). Time series of annual values are used, while the area is fixed at the surface of a river basin. The analysis is carried out on data from two river basins in western Greece (Mornos and Evinos). Results indicated that the proposed index is a reasonable compromise of existing indices tested.

Key words: Drought characterisation; copulas; systemic approach; SDI, RDI, SPEI

1. INTRODUCTION

As reported by Döll et al. (2012), 35% of total water withdrawals at the global scale during the period 1998-2002 originate from groundwater. When concentrating on consumptive use, which covers 33% of total water withdrawals, this fraction becomes 40%. It is therefore evident that the largest part of water withdrawn for various uses stems from surface water. Drought is known to affect surface water availability and, consequently, water withdrawals. According to Tsakiris et al. (2013) using a system based approach is the only viable alternative for operational drought management. In that paper, the authors defined the water system as "the entity expanding over a geographical area which includes all watersheds and groundwater recharge areas together with all water consumption centres and ecosystems associated with the processes occurring in the natural (abiotic or biotic) and human subsystems.". They then presented the various subsystems along with their basic variables or determinants. Focusing on the surface water subsystem, precipitation and water transfer are the typical input determinants, while state variables involve surface water storage and snow pack water equivalent. Output variables are diverse: surface runoff, actual evapotranspiration, soil infiltration and water abstraction. The systemic approach adopts a fixed area which is the drainage basin, and fixed time intervals within each hydrological year (e.g., one year or two semesters). The only free variable being drought severity this is typically modelled using drought indices based on hydrological variables whose measurements or estimates are readily available. These variables include streamflow (Q), precipitation (P) and potential evapotranspiration (PET). The employed indices are based on either one of the above variables such as the Streamflow Drought Index (SDI) (Nalbantis and Tsakiris, 2009), which uses Q, or are pre-decided functions of P and PET such as the Reconnaissance Drought Index (RDI) (Tsakiris and Vangelis, 2005; Tsakiris et al., 2007) and the Standardized Precipitation Evapotranspiration Index (SPEI) (Vicente-Serrano et al., 2010).

In this study, the focus is on characterising the drought state of a surface water subsystem using a new index that is based on all three hydrological variables mentioned above. In an effort to avoid using pre-decided functions relating the variables, we select using the joint probability distribution as the most convenient approach. This leads us to using copulas, an approach which has been used extensively in drought analysis by various researchers (e.g., Shiau, 2006; Shiau et al., 2007; Serinaldi et al., 2009; Song and Singh, 2010; Tsakiris et al., 2016). The proposed index is compared to the drought indices SDI, RDI and SPEI using data from two river basins in western Greece (Mornos and Evinos).

2. METHODOLOGY

2.1 The copula approach

The most popular method for constructing joint probability distributions of random variables is the use of copulas. As stated in Sklar's theorem (Sklar, 1959), for any n-dimensional joint probability cumulative distribution function $H(x_1, x_2, x_3, ..., x_n)$ of random variables $\mathbf{X} = (X_1, X_2, X_3, ..., X_n)$ with marginals $F_1, F_2, F_3, \ldots, F_n$ and any point $\mathbf{x} = (x_1, x_2, x_3, ..., x_n)$ in the n-dimensional space, there exists a copula $C(.)$ such that

$$H\left(x_1, x_2, x_3, \ldots, x_n\right) = C\left(u_1, u_2, u_3, \ldots, u_n\right) \tag{1}$$

where $u_i = F_i(x_i)$ with $i = 1, 2, 3, ..., n$, and $C(.)$ is unique if marginals are continuous.

In this study, we use elliptical copulas such as the Gaussian copula and the Student's t copula (Frahm et al., 2003). The Gaussian copula is given by

$$C\left(u_1, u_2, u_3, \ldots, u_n\right) = \Phi_R\left(\Phi^{-1}\left(u_1\right), \Phi^{-1}\left(u_2\right), \Phi^{-1}\left(u_3\right), \ldots, \Phi^{-1}\left(u_n\right)\right) \tag{2}$$

where $\Phi_R(.)$ is the multivariate standard normal cumulative distribution function (cdf) with covariance matrix equal to the correlation matrix R, and $\Phi^{-1}(.)$ is the inverse univariate standard normal cumulative distribution function. The cdf $\Phi_R(.)$ has a probability density function (pdf) $\varphi_R(.)$ as follows:

$$\varphi_R\left(\mathbf{u}\right) = \frac{1}{\left(2\pi\right)^{\frac{n}{2}} \sqrt{\det R}} \exp\left(-\frac{1}{2}\mathbf{u}^T R^{-1}\mathbf{u}\right) \tag{2}$$

where $\mathbf{u} = (u_1, u_2, u_3, ..., u_n)^{\mathrm{T}}$, det$R$ is the determinant of R. and the superscripts T and -1 mean the transpose and the inverse of the matrix R, respectively.

The Student's t copula is

$$C\left(u_1, u_2, u_3, \ldots, u_n\right) = t_{\nu,R}\left(t_\nu^{-1}\left(u_1\right), t_\nu^{-1}\left(u_2\right), t_\nu^{-1}\left(u_3\right), \ldots, t_\nu^{-1}\left(u_n\right)\right) \tag{3}$$

where $t_{\nu,R}(.)$ is the multivariate Student's t cdf with covariance matrix equal to the correlation matrix R and ν degrees of freedom, while $t_\nu^{-1}(.)$ is the inverse univariate Student's t cdf with ν degrees of freedom. The multivariate Student's t pdf is

$$f_{\nu,P}\left(\mathbf{u}\right) = \frac{\Gamma\left(\frac{\nu+n}{2}\right)}{\Gamma\left(\frac{\nu}{2}\right)\left(\pi\nu\right)^{\frac{n}{2}} \sqrt{\det R}} \left(\frac{\nu+1}{\nu}\mathbf{u}^T R^{-1}\mathbf{u}\right)^{-\frac{\nu+n}{2}} \tag{4}$$

The elements of matrix R are the copula parameters, while the number of degrees of freedom v is usually predefined.

2.2 Statistical analysis

As mentioned in the introduction, three hydrological variables, namely streamflow, Q, precipitation, P, and potential evapotranspiration, PET, are analysed statistically. The analysis includes the steps described next. In the first step marginal distributions are fitted to available data series for each one of the variables tested; the normal, Gamma and log-normal distributions are used as candidates, while the maximum likelihood method is employed for the parameter estimation; Q-Q plots are also employed to visually locate the best distribution; the Kolmogorov-Smirnov (K-S) test (Wang et al., 2003) is employed to explore the goodness-of-fit of the tested cdfs; from the distributions that are not rejected by the K-S test the one with the lowest value of the Akaike Information Criterion (AIC) (Akaike, 2011) is selected as the final marginal distribution for each one of the tested variables. Thus, the cdfs $F_Q(q)$, $F_P(p)$, and $F_{\mathrm{PET}}(\mathrm{pet})$ are obtained for variables Q, P and PET respectively, where q, p, and pet are respective values for the three variables.

In the second step, a number of candidate copulas are constructed using the best marginal distributions identified in the first step; copulas involve the Gaussian copula of Equation 2, and five Student's t copulas with v = 2, 3, 4, 5, 6 (Equation 4). The Cramér-von Mises test (Kojadinovic and Yan, 2011) is used to explore the goodness of fit for the tested copulas; from copulas that are not rejected by this test, the best one is selected, again using the Akaike Information Criterion. The maximum likelihood method is used for fitting copulas.

In the third step the drought severity for each time interval in the available data series is assessed using a new index called Surface Water Drought Index (SWDI). This is based on the probability that a drought state worse than the observed one appears. We assume that the studied surface water system is complex in the sense that it involves components (in the form of water uses and related hydraulic works) that directly depend on precipitation (e.g., rain-fed agriculture, rainwater harvesting), while other components rely on water storage originating from streamflow. We accept that the system is in a state of drought if both kinds of components are water deficient, which means that the joint probability $\Pr(Q \le q, P \le p)$ is a measure of the drought state of the system, where all quantities were defined above and Pr(.) denotes probability. However, actual evapotranspiration among other quantities, leads to reducing water availability. Frequently, potential evapotranspiration is used to represent this loss. It is therefore legitimate to consider PET also in drought characterization, as done with RDI and SPEI. Yet, PET cannot induce drought by itself, but it acts on the available water, i.e., Q and P; moreover, it accentuates drought when increased. With this in mind, one could propose $\Pr(Q \le q, P \le p, \mathrm{PET} \ge \mathrm{pet})$ as a measure for drought state. This would however lead to a rare event and, in this work, we propose using the event $(Q \le q, P \le p)$ under the condition in which we know that PET is at least equal to pet. This, in turn, leads to defining the probability of drought as the conditional probability $\Pr(Q \le q, P \le p \mid \mathrm{PET} \ge \mathrm{pet})$ which is calculated as

$$\Pr\left(Q \le q, P \le p \mid PET \ge pet\right) = \frac{\Pr\left(Q \le q, P \le p, PET \ge pet\right)}{\Pr\left(PET \ge pet\right)} \tag{5}$$

The new index, SWDI, is estimated as the standard normal variate for the above probability.

The last two steps of our methodology involve calculating the existing indices SDI, RDI and SPEI, and, then, comparing these indices to SWDI. The corresponding return periods for all indices are also assessed and compared.

3. TEST RIVER BASINS

To illustrate the proposed methodology the neighbouring basins of Mornos and Evinos rivers are chosen. Both of them are located in the West Sterea Hellas Water District, mainland Greece. Dams on both rivers serve mainly the water supply of the Athens Metropolitan area. Details are given by Nalbantis et al. (1992).

The Mornos river basin at the dam site has an area of 588.1 km^2 and its mean annual flow is 235×10^6 m^3. Streamflow data are available for the period 1980-81 to 2000-01, while data on average precipitation for the period 1967-68 to 1992-93 was obtained based on eight meteorological stations in the basin. Potential evapotranspiration was computed based on minimum and maximum air temperatures at the meteorological station of Lidoriki using the Hargreaves method (Tsakiris et al., 2007).

The Evinos river basin at the dam site has an area of 351.9 km^2 and its mean annual flow is 285 $\times10^6$ m^3. Streamflow data are available for the period 1970-71 to 1999-2000, while data on average precipitation for the period 1963-64 to 1996-97 was obtained based on eight meteorological stations in the basin. As far as the potential evapotranspiration is concerned, the data from the Lidoriki station are also employed.

In this study, all analyses refer to annual values of the examined variables in mm. It goes without saying that similar methodological analysis for shorter period (e.g., 3-month) may lead to different results concerning the marginal distributions and copulas from those derived in this study.

4. RESULTS

The application of the methodology described in section 2 revealed that the univariate normal distribution is the most suitable marginal distribution to describe the three variables in both basins. Whereas none of the three distributions (normal, Gamma, log-normal) is rejected according to the K-S test, the values of AIC indicate a slightly better fit for the normal distribution. An example of Q-Q plots for the three variables and the three probability distributions is given in Figure 1 for the Mornos river basin.

Fitting of 3-copulas of section 2 to data showed that, in the case of Mornos river basin, only the Gaussian copula was not rejected by the Cramér-von Mises statistical test, whereas for Evinos river basin, none of the six copulas of section 2 could be rejected. Values of AIC indicated that the Student's t copula with $\nu = 2$ is the best for Evinos basin.

The time series of annual values for all indices, including the proposed one, are depicted in Figures 2 and 3 for the Mornos and Evinos river basins respectively. Also, values of the return period corresponding to all indices are presented in Table 1 for each year of the dry period 1989-1993.

5. CONCLUSIONS

In this paper a novel drought index is proposed with the aim to characterise the drought state of surface water systems. This is based on multivariate statistical analysis of annual values of three variables (streamflow, precipitation and potential evapotranspiration), using elliptical copulas. Tests on data from two river basins revealed the following:

1. The normal distribution is, in both selected river basins, the best marginal distribution for all three variables involved.

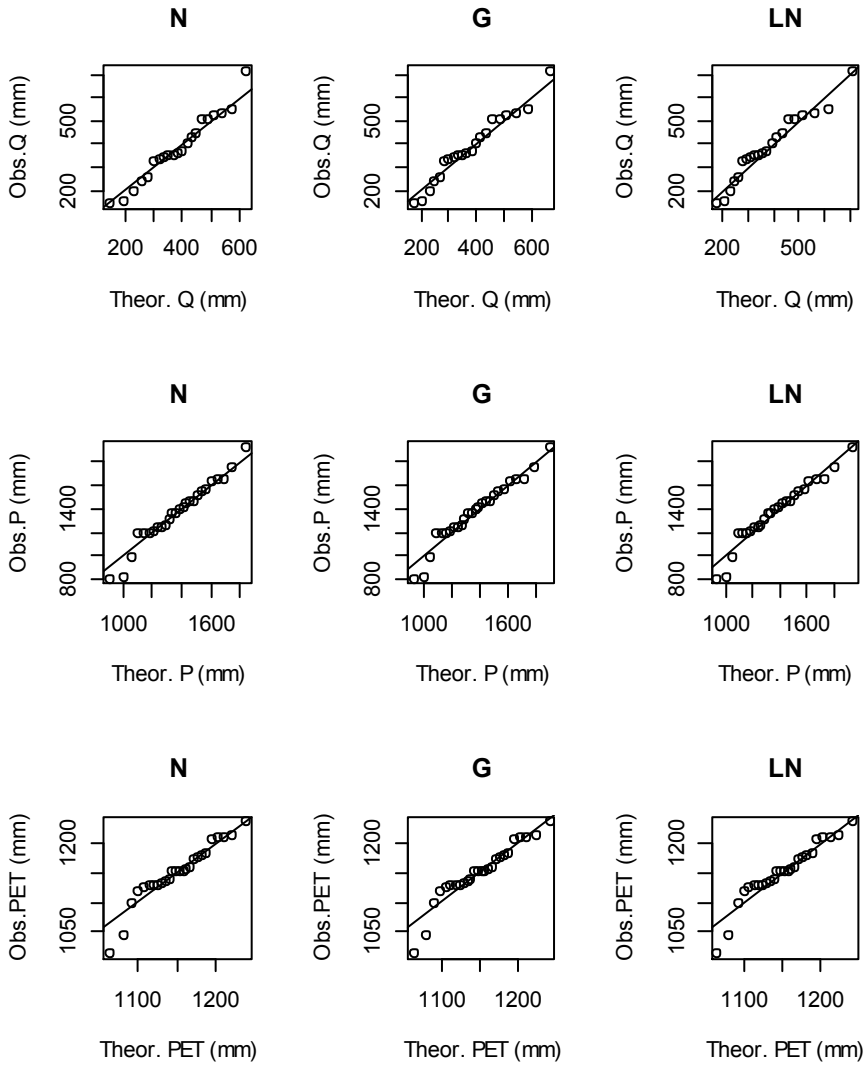

Figure 1. The Q-Q plots for streamflow (Q), precipitation (P), and potential evapotranspiration (PET) for Mornos river basin and various distributions (N = normal, G = Gamma, LN = log-normal)

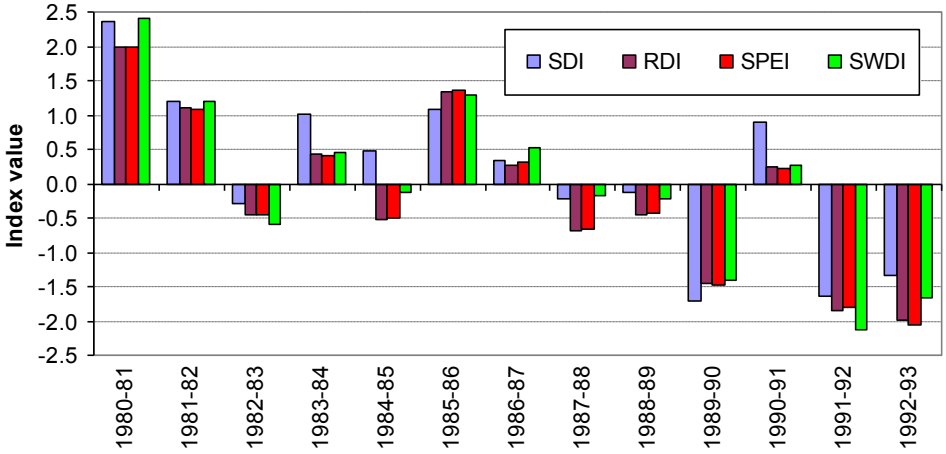

Figure 2. Values of drought indices for Mornos river basin and the common period of data availability

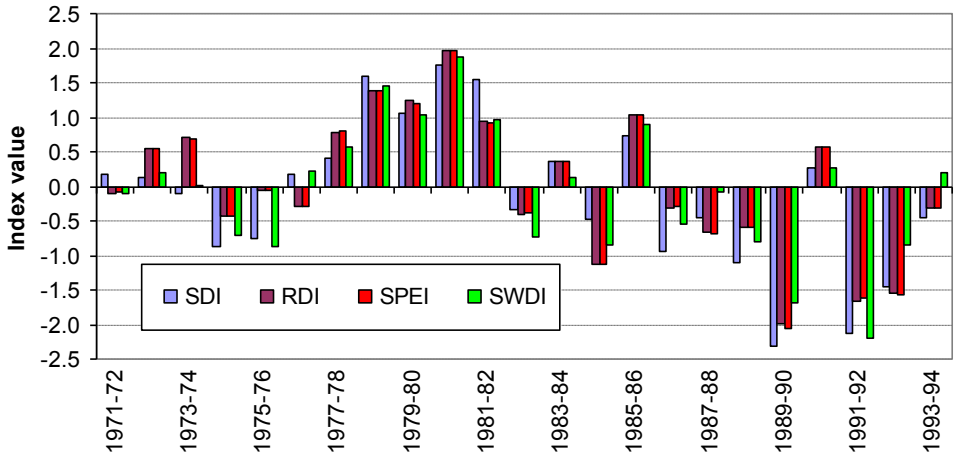

Figure 3. Values of drought indices for Evinos river basin and the common period of data availability

Table 1. Return period of drought, based on the related drought indices for the dry years 1989-90 to 1992-93

Hydrological Year	Return period for			
	SDI	RDI	SPEI	SWDI
	Mornos river			
1989-90	22.5	13.5	14.1	12.8
1990-91	1.2	1.7	1.7	1.7
1991-92	19.6	30.7	28.3	60.8
1992-93	11.2	43.6	49.7	20.9
	Evinos river			-
1989-90	97.9	43.6	50.0	22.2
1990-91	1.6	1.4	1.4	1.6
1991-92	61.0	20.9	18.6	72.8
1992-93	14.0	16.1	17.6	5.0

2. From the family of elliptical copulas, the Gaussian copula proved to be the most suitable for Mornos river basin, whereas for Evinos river basin, the Student's *t* copula with two degrees of freedom proved superior to all others.
3. The new index takes values that are more or less close to the existing indices tested, without showing systematic preference to resemble to one of them.
4. Differences between the new index and the existing indices are reflected to differences in return period, which, as does the index itself, does not show systematic agreement with the return period of one of the existing indices.
5. The new index is, by construction, less subjective than the existing indices, because the latter enable only a partial view of the drought impact on surface water systems.

REFERENCES

Akaike, H., 2011. Akaike's information criterion. In International Encyclopedia of Statistical Science, Springer Berlin Heidelberg, pp. 25-25.

Döll, P., Hoffmann-Dobrev, H., Portmann, F. T., Siebert, S., Eicker, A., Rodell, M., Strassberg, G., Scanlon, B. R., 2012. Impact of water withdrawals from groundwater and surface water on continental water storage variations. Journal of Geodynamics; 59: 143-156.

Frahm, G., Junker, M., Szimayer, A., 2003. Elliptical copulas: applicability and limitations. Statistics & Probability Letters; 63(3): 275-286.

Kojadinovic, I., Yan, J., 2011. A goodness-of-fit test for multivariate multiparameter copulas based on multiplier central limit theorems. Statistics and Computing; 21(1): 17-30.

Nalbantis, I., Koutsoyiannis, D., Xanthopoulos, T., 1992. Modeling the Athens water supply system. Water Resources Management; 6(1): 57-67.

Nalbantis, I., Tsakiris, G., 2009. Assessment of hydrological drought revisited. Water Resources Management; 23(5): 881-897.

Serinaldi, F., Bonaccorso, B., Cancelliere, A., Grimaldi, S., 2009. Probabilistic characterization of drought properties through copulas. Physics and Chemistry of the Earth; Parts A/B/C, 34(10): 596-605.

Shiau, J. T., 2006. Fitting drought duration and severity with two-dimensional copulas. Water Resources Management; 20(5): 795-815.

Shiau, J. T., Feng, S., Nadarajah, S., 2007. Assessment of hydrological droughts for the Yellow River, China, using copulas. Hydrological Processes; 21(16): 2157-2163.

Sklar, M., 1959. Fonctions de répartition à n dimensions et leurs marges. Université Paris 8.

Song, S., Singh, V. P., 2010. Meta-elliptical copulas for drought frequency analysis of periodic hydrologic data. Stochastic Environmental Research and Risk Assessment; 24(3): 425-444.

Tsakiris, G., Vangelis, H., 2005. Establishing a drought index incorporating evapotranspiration. European Water; 9/10: 3-11.

Tsakiris, G., Pangalou, D., Vangelis, H., 2007. Regional drought assessment based on the Reconnaissance Drought Index (RDI). Water Resources Management; 21(5): 821-833.

Tsakiris, G., Nalbantis, I., Vangelis, H., Verbeiren, B., Huysmans, M., Tychon, B., Jacquemin, I., Canters, F., Vanderhaegen, S., Engelen, G., Poelmans, L., De Becker, P., Batelaan, O., 2013. A system-based paradigm of drought analysis for operational management. Water Resources Management; 27(15): 5281-5297.

Tsakiris, G., Kordalis, N., Tigkas, D., Tsakiris, V., Vangelis, H., 2016. Analysing drought severity and areal extent by 2D Archimedean copulas. Water Resources Management; 30(15): 5723-5735.

Vicente-Serrano, S. M., Beguería, S., López-Moreno, J. I., 2010. A multiscalar drought index sensitive to global warming: the standardized precipitation evapotranspiration index. Journal of Climate; 23(7): 1696-1718.

Wang, J., Tsang, W. W., Marsaglia, G., 2003. Evaluating Kolmogorov's distribution. Journal of Statistical Software; 8(18).

Proceedings of the 10th World Congress of EWRA 'Panta Rhei', 5-9 July 2017, Athens, Greece
© 2017 *European Water Resources Association*

Drought Identification and Trend Analysis in Peloponnese, Greece

K. Saita, I. Papageorgaki* and H. Vangelis
Lab. of Reclamation Works and Water Resources Management, School of Rural and Surveying Engineering, National Technical University of Athens, Greece
* *e-mail: ino@central.ntua.gr*

Abstract: Drought is one of the worst natural disasters. According to the Emergency Event Database, drought incidents affect more than 25% of all people affected by all types of weather related disasters, even though they represent only 5% of natural disasters worldwide. Identifying drought is, therefore, of major interest, since it is the basis towards assessing the impacts of drought and defining appropriate measures to mitigate their effects. In this paper drought is assessed in the three River Basin Districts of Peloponnese, Greece. Identification is achieved using two well known drought indices, the Standardized Precipitation Index (SPI) and the Reconnaissance Drought Index (RDI). Precipitation data utilised by both indices and temperature data used in RDI calculations through the estimation of potential evapotranspiration, were obtained from a number of stations in the area. Data processing is performed in Geographic Information Systems (GIS). Spatial and geostatistical functions are applied in a model builder tool. Also, mapping tools are employed to create map layouts. Descriptive statistics for each Water Basin are presented using Box and Whisker Plots. Finally, drought trends are detected and their statistical significance is evaluated using the Spearman and Mann-Kendal non-parametric tests. Sen's slope is calculated to present a more accurate estimate of drought trends. Based on the meteorological time series used and the analysis of trends, Peloponnese cannot be considered a drought prone area for the recent past (period 1968 – 2008).

Key words: Standardized Precipitation Index (SPI), Reconnaissance Drought Index (RDI), Spearman test, Mann-Kendall test

1. INTRODUCTION

According to the Emergency Event Database, in the period 1995-2015, even though drought accounted for less than 5% of all natural hazards, more than one billion people were affected by droughts, that is more than a quarter of all people affected by all types of weather related disasters worldwide (CRED and UNISDR, 2015). In this regard, drought identification is essential, since it is the basis towards assessing the impacts of drought and defining appropriate measures to mitigate their effects.

The present paper deals with the characterization of drought and the detection of trends, in Peloponnese. Two well-known drought indices are employed to characterize drought, while widely used non-parametric trend tests are applied in order to test the significance of trend in drought severity and consequently the magnitude of drought impacts. The Sen's slope is also evaluated to determine the accuracy of trends. Graphs with timeseries of drought indices and thematic maps are used to illustrate the temporal and spatial distribution of drought in Peloponnese.

2. MATERIALS AND METHODS

2.1 Study area

In this study, drought is assessed for the area of Peloponnese in Greece. According to Water framework Directive 2000/60/EC the study area is divided in three River Basin Districts. A subdivision of these River Basin Districts into seven Water Basins is proposed by the Greek Special Secretariat for Water of the Ministry of Environment and Energy, as documented in the River Basin

Management Plans. The area is covered by a network of meteorological stations, spatially distributed as shown in Figure 1. The set of 25 meteorological stations which were used in this study are also presented in Figure 1, along with the water basins of the area. The climate of the area is typical Mediterranean with a mean annual precipitation from about 750 mm to 1600 mm.

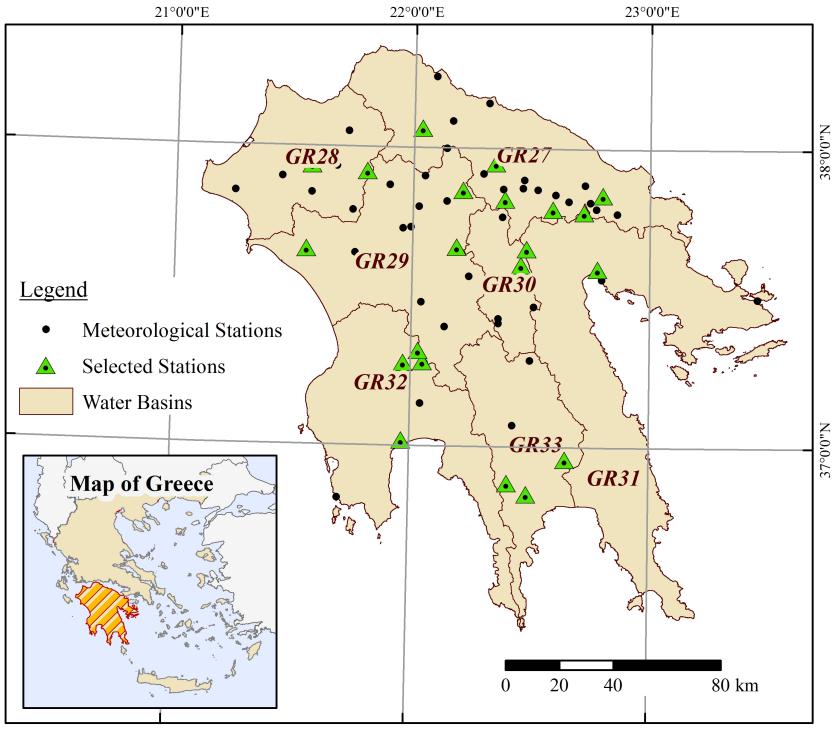

Figure 1. The meteorological station distribution in water basins in Peloponnese

2.2 Data collection and analysis

Since not all the stations have full timeseries of data, a selection was made based on several criteria, in order to use timeseries of adequate length with less possible missing data. The criteria used to select data are correlation coefficient, homogeneity between the stations, the range of years of each timeseries, and the number of missing data. The timeseries length finally used is forty years (1968 – 2008) and the meteorological data from the stations are monthly precipitation and monthly air temperature.

Data timeseries were processed for the computation of the average precipitation and temperature over each basin. The weighted average precipitation was calculated according to the Thiessen polygons and then corrected for the deviation in the altitude, as precipitation is never uniform over the entire area of the basin. The same interpolation technique is followed also to compute average basin temperature. The interpolation technique was performed in a GIS-based software. Spatial and geostatistical functions are applied in a model builder tool for all needed iterations, for all the water basins and all the reference periods (as defined in drought indices section).

2.3 Drought indices

Drought severity is conventionally assessed through drought indices. In this study, the Standardised Precipitation Index (SPI) and the Reconnaissance Drought Index (RDI) were used. SPI (McKee et al, 1993) requires only precipitation data. RDI (Tsakiris and Vangelis, 2005), on the other hand, uses cumulative precipitation and potential evapotranspiration. Calculation of RDI is typically performed based on reference periods (3, 6, 9, 12-months) of the hydrological year (Tsakiris et al, 2007). Potential evapotranspiration is calculated using Hargreaves method as

proposed by Vangelis et al. (2012). Gamma distribution is applied in both indices for the specific study. According to these indices, drought severity can be categorized in mild, moderate, severe and extreme classes, with corresponding boundary values (-0.5 to -1.0), (-1.0 to -1.5), (-1.5 to -2.0) and (< -2.0), respectively.

2.4 Statistical trend tests

In order to detect the significance of trends in the RDI and SPI timeseries, trend analysis is carried out using non-parametric Mann-Kendall and Spearman's Rho tests. The Mann-Kendall and the Spearman's Rho tests (Yue et al., 2002) are appropriate for this analysis, since they are distribution-free, and can accommodate outliers, the first meaning that the underlying distribution may be unknown (Ferrari and Terranova, 2004). Moreover, Sen's slope (Sen, 1968) was calculated to determine a more accurate slope of the trends (Gocic and Trajkovic, 2013). The tests were performed for four timescales according to the reference periods used in the calculation of drought indices. Linear regression trend was also calculated for reconnaissance assessment.

3. RESULTS AND DISCUSSION

The values of the indices are calculated for all water basins and reference periods. Results are visualised through graphs for temporal variations and through thematic maps for spatial distribution of drought. Indicatively, in Figure 3 the values of both indices are presented for the annual reference period for the years under study. Linear regression trends are also presented. As derived from Figure 3, small deviations appear among the two indices in temporal terms.

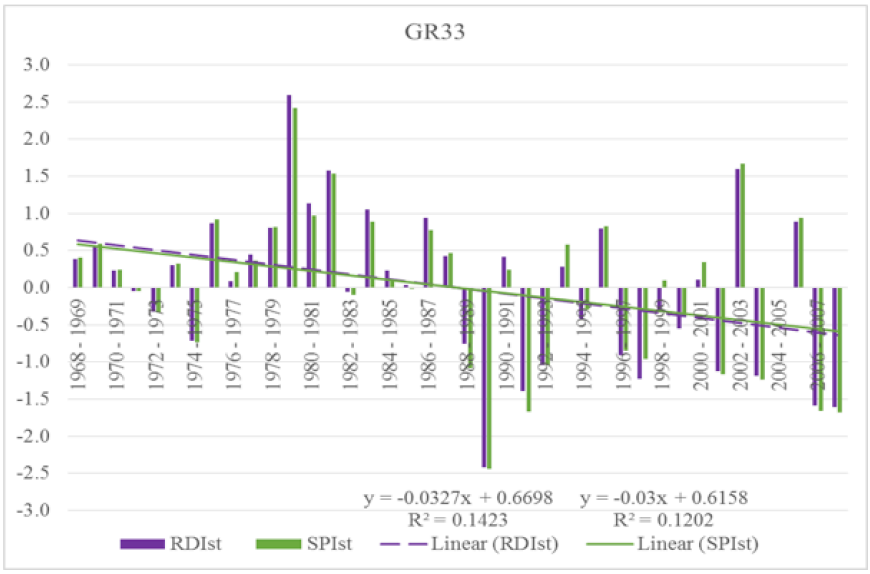

Figure 3. Values of SPI and RDI in annual timescale for water basin GR33

Regarding spatial analysis of the RDI patterns, thematic maps for every year illustrate the drought severity level (category) in each water basin. The map layouts created in a GIS-based software by applying projection. An example is presented in Figure 4 of the RDI index, for the hydrological year of 2007-2008.

Drought years were categorized according to the severity level of drought for each water basin. Indicatively, for the GR33 water basin presented in Figure 5, 12 drought years are detected, corresponding to a 30% of the entire period. However, only 4 drought years falls within the extreme and severe drought categories, representing 10% of the entire period. Therefore it cannot be

concluded that Peloponnese is a drought prone area.

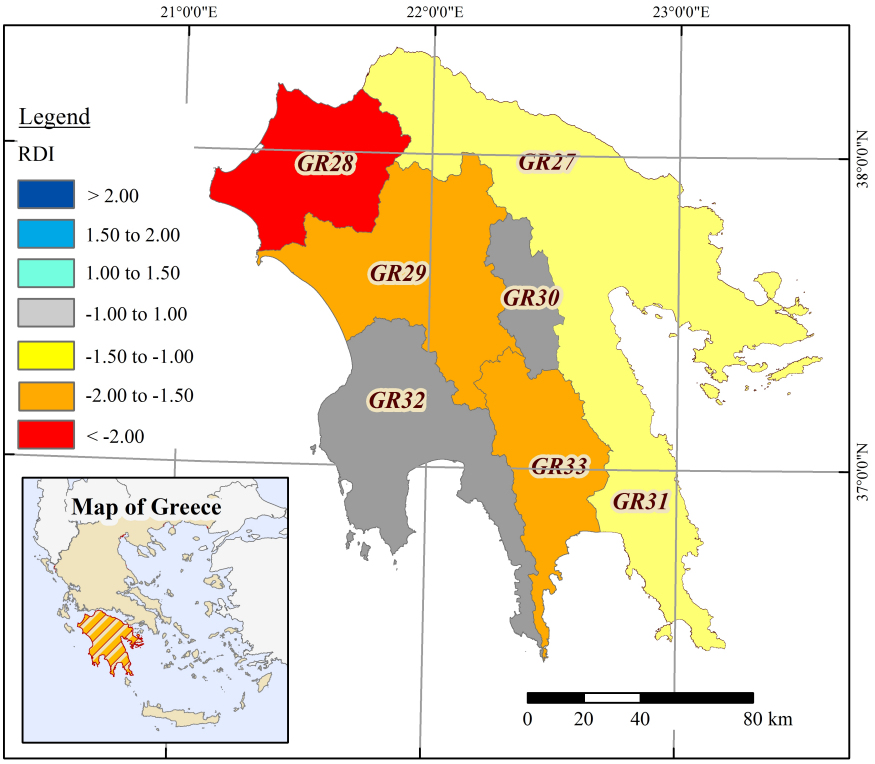

Figure 4. Thematic map presents drought/humidity categories, for the year 2007-08

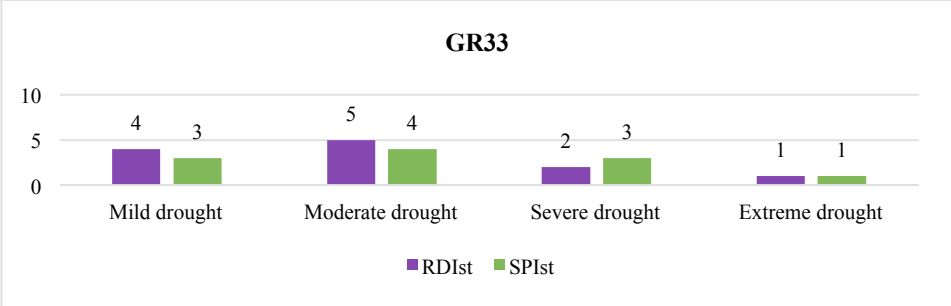

Figure 5. Number of years for each drought category of both indices, for water basin GR33

Multi-year droughts are also investigated (Tsakiris et al., 2010). The analysis showed that only few multi-year droughts exist in all water basins comprising mainly two consecutive years. A three-year drought was identified in the case of two of the basins only once in the entire timeseries.

Finally, Box and Whisker Plots are used in order to examine the existence of seasonality. According to Kundzewicz and Robson (2000), seasonal variation can be detected with Box and Whisker Plots by combining a line-plot of the underlying average seasonal pattern. Specifically, if the boxes between each season have similar median and upper and lower quartiles then no seasonality exists. As derived from Figure 6, no seasonality exists in the values of RDI for the three months reference period. The same applies to all the water basins for all the calculated reference periods.

The results of the non parametric trend tests are presented in Table 1 for the annual timescale. The values were compared with the value, z, of the standard normal distribution for the significance level of 0.05 (z = 1.96). Both tests lead to the same conclusions, since their z values are simultaneously above or below the threshold. Only two of the water basins seem to have significant trends (GR29 and GR33).

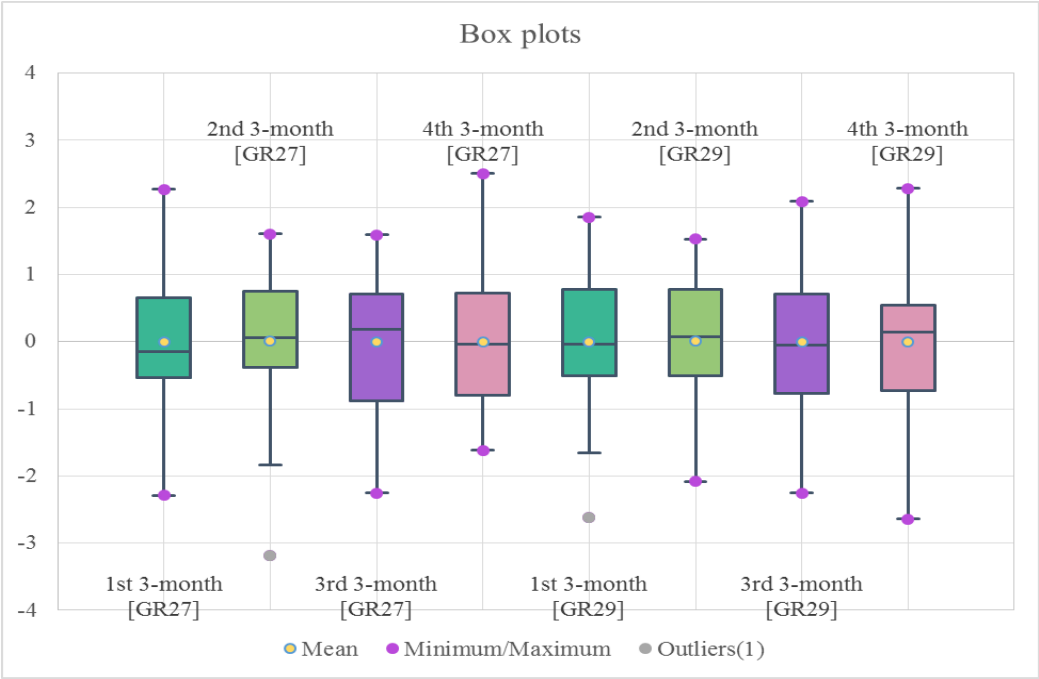

Figure 6. Box-and-Whisker Plots of RDI for each water basins GR27 and GR29, on a 3-month basis

In Table 1 results, '+' corresponds to the existence of significant trend while '-' corresponds to the absence of significant trend.

Table 1. Results of MK and SR tests,for the annual timescale and significance level 0.05

Water Basins	Kendall's tau	Spearman's rs	Z	Z_{SR} (Spearman)	Results of MK test /SR test	Sen's slope
GR27	-0.187	-0.258	-1.689	-1.649	- / -	-0.028
GR28	-0.197	-0.303	-1.783	-1.959	- / -	-0.019
GR29	-0.326	-0.469	-2.948	-3.277	+ / +	-0.041
GR30	0.036	0.027	0.315	0.169	- / -	0.004
GR31	-0.033	-0.059	-0.291	-0.366	- / -	-0.006
GR32	-0.085	-0.122	-0.757	-0.760	- / -	-0.014
GR33	-0.267	-0.384	-2.412	-2.564	+ / +	-0.032

4. CONCLUSIONS

Drought analysis is performed in the area of Peloponnese, Greece. Two well-known drought indices are used, the SPI and the RDI. The main conclusions are summarized as follows:

- The analysis revealed that no significant diferrences exists among the two indices in the temporal scale, whereas small deviations appear in the spatial scale. Significant diferences among the basins appear.
- The area does not appear to be drought prone, especially in terms of severe and extreme drought, since less than 10% of the years used in the analysis are in these categories.
- The non-parametric trend tests do not uncover significant trend in most of the basins. Only two out of seven basins show a significant negative trend.
- No apparent seasonality is detected.
- Very few multi-year droughts were detected comprising mainly two consecutive years. A three-year drought was identified in the case of two of the basins only once in the entire timeseries.

REFERENCES

CRED and UNISDR, 2015. The human cost of weather related disasters: 1995-2015. Centre for Research on the Epidemiology of Disasters, Brussels, 30p.

Ferrari, E., Terranova, O., 2004. Non-parametric detection of trends and change point years in monthly and annual rainfalls. In Proceedings of 1st Italian-Russian Workshop New Trends in Hydrology, CNR Publ,Vol. 2823: 177-188.

Gocic, M., Trajkovic, S., 2013. Analysis of changes in meteorological variables using Mann-Kendall and Sen's slope estimator statistical tests in Serbia. Global and Planetary Change.; 100: 172-182.

Kundzewicz, Z. W., Robson, A., 2000. Detecting trend and other changes in hydrological data. World Meteorological Organization (WMO/TD No. 1013). Geneva: 157.

McKee, T. B., Doesken, N. J., Kleist, J., 1993. The relationship of drought frequency and duration to time scales. In Proceedings of the 8th Conference on Applied Climatology (Vol. 17, No. 22). Boston, MA: American Meteorological Society. 179-183.

Sen, P.K., 1968. Estimates of the regression coefficient based on Kendall's tau. Journal of the American Statistical Association 63, 1379–1389

Tigkas, D., Vangelis, H., Tsakiris, G., 2012. Drought and climatic change impact on streamflow in small watersheds. Science of the Total Environment, 440: 33-41.

Tsakiris, G., Vangelis, H., 2005. Establishing a drought index incorporating evapotranspiration. European Water; 9(10): 3-11.

Tsakiris, G., Loukas, A., Pangalou, D., Vangelis, H., Tigkas, D., Rossi G., Cancelliere, A., 2007. Drought characterization [Part 1. Components of drought planning. 1.3. Methological component]. In : Iglesias A. (ed.), Moneo M. (ed.), López-Francos A. (ed.). Drought management guidelines technical annex. Zaragoza : CIHEAM / EC MEDA Water, (Options Méditerranéennes: Série B. Etudes et Recherches; n. 58): 85-102.

Tsakiris, G., Vangelis, H., Tigkas, D., 2010. Assessing water systems vulnerability to multi-year droughts. European Water 29, 21-29.

Yue, S., Pilon, P., Cavadias, G., 2002. Power of the Mann–Kendall and Spearman's rho tests for detecting monotonic trends in hydrological series. Vol. 259: (issue ?1–4): 254–27.

V. Water Quality and Environmental Processes

Proceedings of the 10th World Congress of EWRA 'Panta Rhei', 5-9 July 2017, Athens, Greece
© 2017 *European Water Resources Association*

Unusual river turbidity and water quality hysteresis in the most urbanised catchment in the UK

D.M. Lawler
Centre for Agroecology, Water and Resilience, Coventry University, CV1 5FB, UK
e-mail: Damian.Lawler@coventry.ac.uk

Abstract: Over 50% of the world's population is now urbanised, and this proportion will rise to 60% by 2020. It is vital, therefore, that we develop understanding of how urban processes and related hydrological changes impact on water resources, water quality and water pollution dynamics. However, little is known of the dynamics of storm-event sediment and pollutant transport in urban rivers. In many catchments, it is often assumed that polluting fine sediment fluxes are delivered early in the storm, peaking before the flow maximum, i.e. the 'First-Flush' Model (FFM). This paper tests the validity of this First-Flush Model in the most urbanised catchment in the UK: the River Tame, Birmingham, which is 42% urbanised. The paper presents high-resolution hysteresis analyses of key turbidity and water quality datasets, using very high frequency 15-minute data. Determinands include storm-event river flow, rainfall intensity, turbidity, electrical conductivity and Ammonia. Crucially, in 90% of storm events, turbidity peaks occurred, unusually, after river flow peaks. This generated anticlockwise hysteresis - contrary to classic 'First-Flush' model predictions. Of 10 explanatory hypotheses tested, three are of special interest, including (a) the impact of Combined Sewer Overflow ingress, (b) delayed bed sediment destabilization effects (with a new BASS model - Biofilm Adhesion of Sediment Supplies); (c) road-derived particulates generated by some of the heaviest traffic loads in Europe. This unusual storm behaviour suggests that urban impacts on water resources are much more significant and complex than thought, as discussed in a 'Senile Cities' model.

Key words: 'First Flush' model; turbidity; suspended sediment; hysteresis; urban river

1. INTRODUCTION

Sediment inputs and dynamics in rural basins are well understood. However, significant research gaps remain for urban catchments, and rates of global urbanisation are increasing. Research is essential because fine sediment river pollution and water turbidity issues are increasingly problematic, including in estuaries (e.g. Chon et al., 2012; Jonas and Millward, 2010; Murdoch et al. (2010)). Key issues include: light penetration problems in the water column, sediment-associated contaminant transport, habitat impacts (Lawler and Wilkes, 2015; Conroy et al., 2016), biological oxygen demand (BOD) implications and water abstraction and treatment problems. Many of these problems increase as urbanization progresses.

Therefore, an improved understanding of sediment pollution dynamics in heavily modified urban systems is needed to improve modelling and management of sediment issues. But this is a challenge, partly because sediment sources and delivery routes and can be modified hydrologically, geomorphologically and anthropogenically (including by direct engineering).

The pioneering work from the 1970s to 1990s by D.E. Walling on fluvial fine sediment transport rates and their differences between seasons, and between rising and falling hydrograph limbs, for a given flow during storm-events (e.g. Walling, 1977; 2008). Such work has been associated with the First Flush Model (FFM) to explain the dynamics of storm-event fluvial suspended sediment concentrations and loads. The First-Flush Model predicts that in-channel suspended sediment concentrations (SSC) will rise sharply early in a storm event and peak *earlier* than maximum discharge. Sediment concentrations will then fall rapidly, as sediment sources become exhausted, even as discharge continues to increase. This generates a positive, clockwise hysteresis loop when discharge is plotted against suspended sediment concentration or turbidity.

However, although the FFM has been shown to apply to a large range of basins, its applicability has been questioned for some urbanised catchments. For example, Lawler *et al. (*2006a, 2006b) and Lawler and Wilkes (2015) found that turbidity levels in many storm events were *higher* for a given discharge on the *falling* limb, which generated an anticlockwise, rather than a clockwise, hysteretic response. This is inconsistent with the FFM.

2. OBJECTIVES

The research reported here builds on these urban river analyses, in which the appropriateness of the First Flush model in the highly urbanised catchment of the River Tame, Birmingham, UK (42% urbanised) is tested for an important spring storm period. High resolution, multivariate water quality datasets at 15-minute time-step are used to define turbidity hysteresis dynamics during a typical storm event.

3. STUDY AREA

The River Tame basin is the most urbanised catchment in the UK (~42% urban). It is located in central England, in the West Midlands region of the country (Fig. 1). The river system drains part of industrial Wolverhampton, Walsall and Birmingham, before flowing into the River Trent, which then discharges into the North Sea via the Humber Estuary (Fig. 1).

The upper catchment has been heavily impacted by disused mine shafts, industrial workings, motorway and highway drainage, contaminated land and waste water treatment works (WWTWs). The catchment contains two monitoring stations, operated by the UK Environment Agency (EA). The main focus here is the James Bridge upstream station with latitude and longitude of 52° 34' 40.5" North and 02° 00' 58.9" West. The Water Orton monitoring station lies approximately 28 km river distance downstream of James Bridge station (Fig. 1).

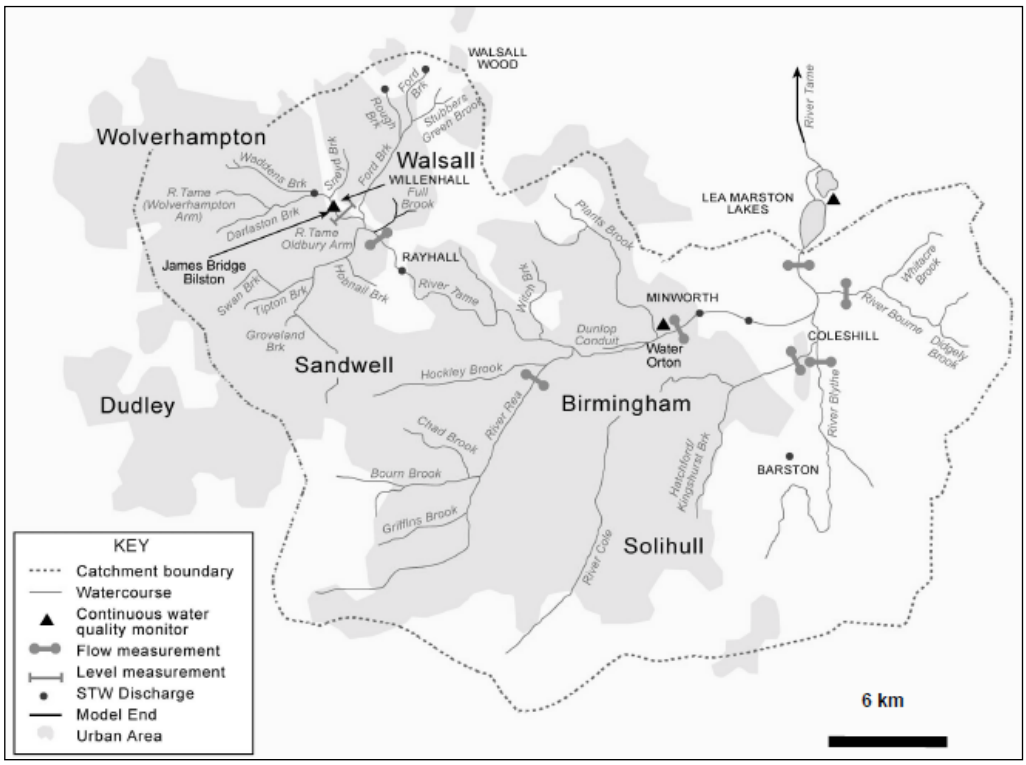

Figure 1. The Tame catchment, Birmingham, central UK, with monitoring stations at James Bridge in Bilston, Walsall (upstream), and at Water Orton (downstream).

4. METHODS

The automatic gauging and water quality monitoring station at James Bridge (Fig. 1) generated 15-minute data on river flow, turbidity, electrical conductivity (EC), water temperature, pH, dissolved oxygen (DO) and ammonia ($NH_3(N)$) (see Lawler et al., 2006a for further details). River water samples were also pumped up automatically from a near-bank intake to a measurement facility housing the detectors for some events. The instrumentation system was cleaned at weekly intervals. Turbidity was monitored in-line with a pHOX 750M absorptiometric turbidity head (Lawler, 2016). Turbidity was measured using a red LED, and optics were automatically wiped clean five times per hour. Monthly end-point calibrations were performed with deionized water and a liquid turbidity standard of 500 FTU (Formazin Turbidity Units; Lawler, 2016). Good correlations were obtained between turbidity and suspended sediment concentrations. Catchment precipitation data at 15-min resolution were available from Willenhall rainfall station (Fig. 1), upstream of James Bridge (Lawler and Wilkes, 2015).

5. RESULTS

An early example of a storm event is shown in Figure 2.

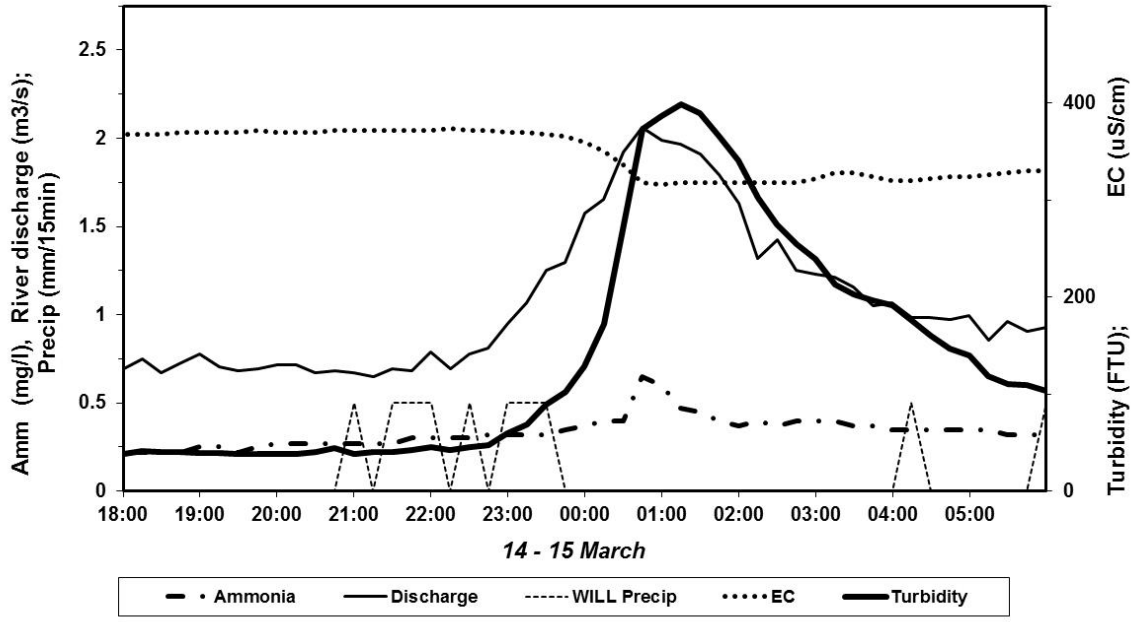

Figure 2. An early example of turbidity peaks following the flow peak for the River Tame at James Bridge, Birmingham, UK. Water quality time series are also shown for this 14-15 March 2002 rainstorm event. 'WILL Precip' is 15-minute frequency precipitation data for Willenhall, in northwest Birmingham. EC is Electrical Conductivity of river water in $\mu S\ cm^{-1}$.

Figure 2 shows a dynamic response of urban river flow to precipitation recorded at Willenhall (Fig. 1). River flow rates begin to rise within 90 minutes of rainfall falling, and the flow rate peaks 4.5 hours after rainfall onset.

Importantly, Figure 2 shows that fine sediment transport response is contrary to normal First-Flush Model (FFM) assumptions. First-Flush Models predict, for a given flow, greater sediment transport on the rising limb of the flow hydrography compared to the falling limb (e.g. Gellis and Walling; Walling, 2008; Lawler et al. 2017). A number of causes have been hypothesised

worldwide. One oft-cited driver is the greater sediment availability from pre-weathered exposed soil surfaces and weakened river banks, sediment which become available for erosion and routing to river channels early in a storm (e.g. Walling, 2008). Once this readily-available supply of loosened sediment has been eroded, however, suspended sediment concentrations decline, relative to river discharge.

However, in the River Tame here, the opposite is the case. Most turbid waters come through *after* the discharge peak in the Tame, rather than *before* the flow maximum. Lawler (2006a; 2006b) named these turbid flushes which come through late in the hydrograph as 'Falling-LImb Turbidity Extensions' (FLITEs), as they occur on the recessional limb of the hydrograph. These features also partly relate to limited natural soil and sediment surfaces in urban areas to produce particulate material available for transport to the river channel.

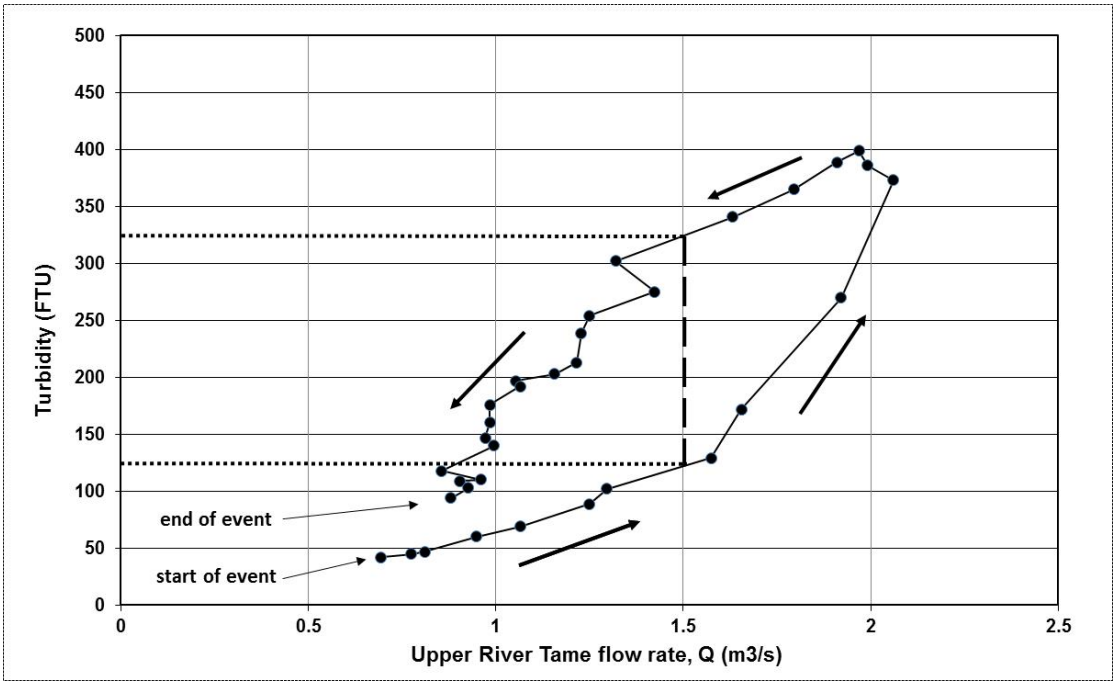

Figure 3. Clear anticlockwise turbidity hysteresis monitored at James Bridge gauging station, west Birmingham, for the storm event in Fig. 2 (14-15 March 2002). Automated observations were made at 15-minute intervals throughout the event.

It is clear from the example event in Figure 3 that the delay in the turbidity pulse results in strong *anticlockwise* hysteresis**.** Indeed, at an intermediate flow rate of 1.5 m^3 s^{-1}, for example, the turbidity value on the *recessional* limb is almost three times higher than the turbidity on the *rising* limb at the same discharge of 1.5 m^3 s^{-1}.

Preliminary work suggests that many other storm events analysed to date follow this pattern, with clear *anticlockwise* hysteresis (e.g. Lawler et al., 2006a).

Fig. 3 supports the idea that river flow rate (or any other flow index such as shear stress or stream power), is not necessarily a strong explanatory variable or a predictor of *fine* sediment transport in fluvial systems. Stronger relationships can generally be defined between *coarse* gravel transport and river flow variables.

6. DISCUSSION AND CONCLUSIONS

Typical turbidity responses in the Tame can be seen in Figures 2 and 3. These show turbidity peaks clearly lagging discharge (Q) peaks. The resultant anti-clockwise hysteresis patterns here are contrary to First Flush Model assumptions, which predict hysteresis loops with a strong clockwise

direction.

Work is ongoing to define the key variables which drive these anticlockwise hysteresis loops and late turbidity waves on the recessional limb of the hydrograph. Amongst others, key drivers are the roles of (a) Waste water discharges from Waste Water Treatment Works (WwTW) and (b) sewage which enters the River Tame from Combined Sewer Overflows (CSOs). These contaminants are likely to enter river systems during and after rainstorms, when Waste Water Treatment infrastructure is eventually overwhelmed during or after intense rainfall events. Indeed, Figure 2 shows a clear peak in Ammonia as the turbidity wave passes, and Ammonia is an indicator of sewage contamination of stream water here.

The First Flush model appears to have less application in the heavily urbanised Tame catchment, and further research is required to establish any additional multiple causes. Further work aims to develop analyses of longer-term records, and comparisons with downstream locations. It would be interesting to test, collaboratively, the First-Flush model in other urban or urbanising catchments worldwide, and this work would help to assess the generality of the findings here.

This result challenges the traditional First Flush Model. The FFM predicts that suspended sediment and/or turbidity peaks will occur *prior to* discharge peaks, before falling sharply. Much of the turbid water ingress appears to be derived from Waste Water Treatment Works or Combined Sewer Overflows (CSOs). These contributions are likely to be routed into the river at the end of a storm, when storages provided by holding tanks at sewage plants are breached.

This departure from the First Flush model requires further investigation to establish fully the controls, fluxes and processes in the River Tame - and if these are identifiable in other European and global world river systems. The next stage is to test for, and model, the controls on these anticlockwise turbidity and fine sediment transport dynamics.

Significant research gaps exist in the study of fine sediment fluxes and pollution dynamics in urbanised catchments more generally. Internationally, it would help to develop more general conclusions from compiling, modelling and interpreting worldwide hysteretic tendencies across many urban or rural catchments worldwide. One objective would be to assess the prevalence of negative hysteresis behaviour in urbanising river basins globally. An additional aim is to establish and compile a global inventory and database of fluvial fine sediment transport dynamics and patterns and datasets, including urban catchments: this will be called 'SEDISTORE'.

ACKNOWLEDGEMENTS

I would like to thank the UK Natural Environment Research Council (NERC) URGENT programme for funding this research initially, the Environment Agency for raw datasets for the James Bridge station, and from Severn Trent Water. Support from research assistants, research students and technical staff is greatly appreciated, including Dr Johannes Steiger, Richard Johnson, Andrew Best, Ben Hansford, Jon Weller, Ian Morrissey and Paul Frost. I would also like to acknowledge The University of Birmingham, UK (School of Geography, Earth and Environmental Sciences), where this work started, and ongoing support from the Centre for Agroecology, Water and Resilience at Coventry University, UK.

REFERENCES

Chon, H.S., Ohandja, D.G. and Voulvoulis, N. (2012) The role of sediments as a source of metals in river catchments. Chemosphere, 88: 1250–1256**.**

Conroy, E., Turner, J.N., Rymszewicz, A., Bruen, M., O'Sullivan, J.J., Lawler, D.M., Lally, L., Kelly-Quinn, M. (2016). Evaluating the relationship between biotic and sediment metrics using mesocosms and field studies, Science of the Total Environment**,** 547, 17–29.

Jonas, P.J.C. and Millward, G.E. (2010) Metals and nutrients in the Severn Estuary and Bristol Channel: Contemporary inputs and distributions. Marine Pollution Bulletin, 61: 52-67.

Lawler D.M. 2016. Turbidity, Turbidimetry, and Nephelometry. In: Reedijk, J. (Ed.) Elsevier, Reference Module in Chemistry, Molecular Sciences and Chemical Engineering. Waltham, MA: Elsevier, London, UK. 15-July-2016; doi: 10.1016/B978-0-12-409547-2.11006-6, 13pp.

Lawler, D.M. and Wilkes, M. 2015. Improved Fluvial Sediment Impact Assessment (FSIA) approaches within Environmental Impact Assessments, Croatian Geographical Journal; 77 (2): 7-31.

Lawler, D.M., Petts, GE, Foster, IDL and Harper, S. 2006a. Turbidity dynamics and hysteresis patterns during spring storm events in an urban headwater system: the Upper Tame, West Midlands, UK, Science of the Total Environment, 360: 109-126.

Lawler, D.M., Foster, I.D.L., Petts, G.E., Harper, S. and Morrissey, I.P. 2006b. Suspended sediment dynamics for June storm events in the urbanized River Tame, UK, In: Rowan, J.S., Duck, R.W. & Werritty, A. (Eds), Sediment Dynamics and the Hydromorphology of Fluvial Systems (Proceedings of a Symposium held in Dundee, UK, July 2006). International Association of Hydrological Sciences Publ. 306: 96-103.

Lawler, D.M., A. Rymszewicz, L. Conroy, J. O'Sullivan, M. Bruen, J. Turner, M. Kelly-Quinn. 2017. SILTFLUX Literature Review, Ireland Environmental Protection Agency Report, EPA Research Report 2010-W-LS-4., 93pp.

Murdoch, N., Jonas, P.J.C., Falconer, R.A. and Lin, B. (2010) A modelling assessment of contaminant distributions in the Severn Estuary. Marine Pollution Bulletin, 61: 124-131.

Walling, D.E. 1977. Assessing the accuracy of suspended sediment rating curves for a small basin, Water Resources Research, 13(3), 531 – 538.

Walling, D.E. 2008. The Changing Sediment Load of the Mekong River, Ambio: A Journal of the Human Environment, 37(3): 150-157.

Proceedings of the 10th World Congress of EWRA 'Panta Rhei', 5-9 July 2017, Athens, Greece
© 2017 *European Water Resources Association*

Pyrosequencing analysis of ammonia oxidizing bacteria in municipal activated sludge system

O.O. Awolusi*, S. Kumari and F. Bux
Institute for Water and Wastewater Technology, Durban University of Technology, P. O. Box 1334, Durban 4000, South Africa
* *e-mail: oluyemiawolusi@gmail.com*

Abstract: Nitrification is a critical step that depends on the physiology and function of nitrifying microbial diversity in the activated sludge treatment systems. Optimum and efficient nitrification hinges on in-depth understanding of the structure and dynamics of the nitrifying community structure within the wastewater treatment systems. In this study, high-throughput pyrosequencing was employed in profiling ammonia-oxidizing bacteria (AOB) in activated sludge system treating municipal waste. During the investigation, the average temperature was 16.5 ± 2.1°C and 22.8 ± 2.7°C during winter and summer respectively. During this study, the dissolved oxygen level in the plant was constantly lower than the optimum (0.6 ± 0.3 and 0.6 ± 0.1 mg/l winter and summer respectively). The plant treated wastewater with influent ammonia concentration between 24.4 and 31.6 mg/l. The average influent flow rate (ML/Day) was 96.81 during this period. The diversity of AOB, the nitrifiers involved in the first and the rate-limiting step of ammonia removal had correlation with nitrification efficiency and temperature. Pyrosequencing revealed significant differences in the AOB population, which was 6 times higher during summer compared to winter. The AOB sequences related to uncultured bacterium and uncultured AOB showed an increase of 133% and 360% respectively when the season changed from winter to summer. This study suggests that vast population of novel, ecologically significant AOB species that remain unexploited, still inhabit the complex activated sludge communities.

Key words: 454-pyrosequencing; AOB; WWTP; Nitrification

1. INTRODUCTION

Understanding the complex microbial community in wastewater treatment plants (WWTPs) is important in designing functionally stable and effective treatment systems. The advent of molecular techniques has revealed the inadequacies of traditional microbiological methods of identifying and quantifying microbes in wastewater (Xia et al., 2010). The different Sanger-sequencing based molecular approaches including; polymerase chain reaction – denaturing gradient gel electrophoresis (PCR-DGGE), terminal restriction fragment length polymorphism (T-RFLP), temperature-gradient gel electrophoresis (TGGE) and cloning have been used in profiling the microbial diversity harboured in WWTPs (McMahon et al., 2009, Gomez-Silvan et al., 2010). Fluorescent in situ hybridization among others have also been used in microbial diversity profiling of engineered wastewater treatment environments with some degrees of success (Awolusi et al., 2015). More recently, it has been shown that the traditional Sanger sequencing is yet, grossly underestimating the communities of the complex environmental samples due to the hundreds or thousands of important sequences that go unnoticed when employing this method (Shokralla et al., 2012). A major shortcoming of this technique is that it requires in vivo amplification of DNA fragments in bacterial hosts (cloning) prior to sequencing. Cloning is labour-intensive, tediously long and subject to bacterial host bias (Morozova and Marra, 2008).

Due to the thousands of template DNA usually present in wastewater samples there is need for technique that is capable of simultaneous reading from different DNA templates (Shokralla et al., 2012). The Next generation sequencing (NGS) approach offers a speedy, and extensive data production with the opportunity of investigating the microbial ecology on a larger scale and with more details (Ju and Zhang, 2015). Next generation sequencing offers the advantage of direct sequencing from environmental samples without prior cloning into a bacterial host before

sequencing, as obtained in the traditional Sanger approach. The NGS has revolutionized the genomic and metagenomic research with different platforms being commercially available. In this study, variation in community structure of the aerobic nitrifying activated sludge over the winter and summer was evaluated using the pyrosequencing techniques.

2. MATERIALS AND METHODS

2.1 Wastewater treatment plant operation

The full-scale WWTP selected for this study is situated in the midlands of KwaZulu-Natal province, South Africa. The plant receives a discharge of 82880 ± 20832 m^3/d (average dry weather flow), including 90% domestic and 10% industrial wastewaters. The plant was designed based on the criteria of a modified Johannesburg (JHB) configuration, which offered anaerobic, anoxic, and aerobic biological processes (Daims and Wagner, 2010). As shown in Fig. 1, the effluent from primary settling tank is distributed to the pre-anoxic and anaerobic tanks. The pre-anoxic basin is enriched with return activated sludge from the bottom of a final settler, whilst effluent from anaerobic tank is discharged into the anoxic unit. An internal recycle is pumped from the last part of aerobic units to the anoxic zone. The mixed liquor, containing activated sludge, flows from the aerobic zone to a secondary settler, where it is separated under a quiescent condition into treated wastewater and return activated sludge. Wastewater characteristics and operational parameters for the plant are shown in Table 1.

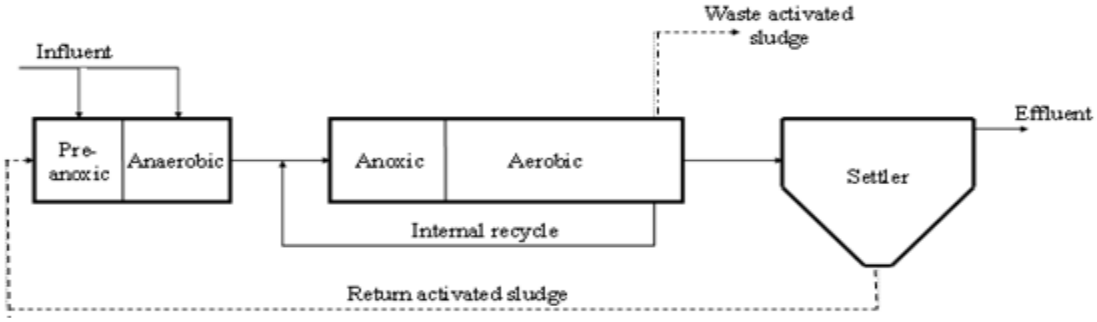

Figure 1. Schematic representation of the wastewater treatment plant.

Table 1. Average (winter and summer) wastewater characteristics and operational parameters of the selected plant as observed during the study period

Parameter	Phase-1	Phase-2
	Winter	Summer
Rainfall (mm)	26.0 ± 18.6	116.8 ± 32.0
Temperature	16.5 ± 2.1	22.8 ± 2.7
pH	7.3 ± 0.2	7.2 ± 0.1
DO (mg/l)	0.6 ± 0.3	0.6 ± 0.1
MLSS (mg/l)	6157 ± 783.3	4728 ± 1282.0
Chemical oxygen demand (mg/l)	1156 ± 976.1	684.7 ± 258.9
Ammonia (mg/l)	31.6 ± 6.0	24.4 ± 4.5
Flow Rate (ML/Day)	62.0 ± 2.2	96.8 ± 14.5
HRT (h)	6.3 ± 0.2	4.3 ± 1.0
OLR (kg-COD/m^3.d)	4.0 ± 1.1	4.5 ± 1.8
ALR (g-NH_4/m^3.d)	121 ± 22.0	144 ± 29.0
F/M (g-COD/g-MLSS.d)	0.6 ± 0.1	0.9 ± 0.3
COD removal (%)	97.5 ± 1.3	94.1 ± 2.6
Ammonia Removal (%)	60.0 ± 18.0	83.0 ± 13.0

COD: chemical oxygen demand; HRT: hydraulic retention time; OLR: organic loading rate; ALR: ammonia loading rate; F/M: food to micro-organisms ratio

Composite sludge samples (from the aeration tank), influent and effluent water samples were collected fortnightly for a period of 237 days (May - July 2012 and November 2012 - March 2013). Sterile sampling bottles were used in collecting the samples and all samples were maintained at 4°C while in transit to the lab. Temperature, dissolved oxygen (DO) concentrations and pH measurements were done using a portable YSI meter (YSI 556 Multiprobe System). The plant operational parameters were obtained from the plant operators.

2.2 Sample preparation and DNA extraction for seasonal community structure analysis in the activated sludge

The diversity of ammonia oxidizing bacteria was assessed using high-throughput pyrosequencing approach. Samples taken between the 1st and 78th day represented the winter period (May - July 2012) whilst the samples from 79th through 237th day (November 2012 - March 2013) represented summer. The extracted DNA samples for the winter months were pooled together in equimolar quantities to make up the winter template DNA sample, whilst the same was done for the summer months. These resulted in two separate template DNA samples that used for pyrosequencing analysis. The freeze-thaw DNA extraction was according to modified Briese (2002) protocol.

2.3 Sequencing and Analysis

The amoA locus of the AOB in the activated sludge was amplified using the primer set: amoA-1F/amoA-2R. The PCR was performed in a total reaction volume of 50 µl containing 10 ng of DNA template. The final concentrations of the different components in the reaction mix (200 µM of DNTPs, 1.5 mM of MgCl [Taq buffer with initial MgCl concentration of 20 mM], 2.5 U of Taq DNA polymerase [Thermo Scientific, Lithuania] and 0.5 µM of each primer) were according to modified protocols from Degrange and Bardin (1995). The PCR products were purified and end-repaired. The amoA amplicons generated from the PCR were sent to Inqaba Biotechnical Industries (Pty), South Africa, where the composition of the amplicon of amoA targeted locus was then determined by pyrosequencing. The barcodes for multiplexing were incorporated between the forward primers (amoA-1F) and the 454-adpter sequence for pyrosequencing using Roche 454 FLX Titanium sequencing platform (Roche, USA) (Schloss et al., 2009). After sequencing, the unique tags obtained were aligned with the 16S rRNA database with the aid of the BLASTN programme (Sekar et al., 2014). The tag redundancy was eliminated and sequences were assigned into OTU based on similarities of greater than 90%. With the aid of MEGA6 software, representative sequences were aligned using the ClustalW programme. The neighbour-joining method was employed for the phylogenetic analysis (Tamura et al., 2013). The raw pyrosequencing .sff file has been deposited into the NCBI sequence Read Archive.

2.4 Short-read archive accession numbers

The raw reads for the pyrosequencing have been deposited into NCBI Sequence Read Archive under the accession numbers SRP053412.

3. RESULTS AND DISCUSSION

3.1 Ammonia oxidizing bacteria profiling based on amoA gene using high throughput pyrosequencing

Ammonia oxidation has been identified as the rate-limiting step in nitrification hence, the diversity of the AOB in this system was examined to understand their role in nitrification

efficiency. The AOB diversity for the different seasons was revealed by 454-pyrosequencing using the amoA-1F and amoA-2R primer sets (with multiplex barcodes inserted between the forward primers and the 454 adapter sequence). With the aid of MEGA6 software, representative sequences were aligned using the ClustalW programme and the neighbour-joining method was employed for the phylogenetic analysis (Figs. 2-3). A total record of 212 and 1192 effective sequences were obtained from the winter and summer samples respectively. After comparing them with the NCBI database, substantial percentages of the read from the two samples (72 % in winter and 78 % in summer samples) returned no hits and could not be assigned to any phylum. (Fig. 4).

The identified AOB populations during the study were related to uncultured ammonia oxidizing bacteria, uncultured bacterium, *Nitrosomonas oligotropha,* and Uncultured *Nitrosospira sp.* (Figs. 2-4). Among these identified AOB populations, the uncultured ammonia oxidizing bacteria was the most dominant throughout the study with 97% and 95% during summer and winter seasons respectively, whilst the uncultured bacterium was 2% and 5% during the summer and winter respectively. The *Nitrosomonas oligotropha* was about 1% of the AOB population during the summer season, however, it was not detected during the winter (Fig. 4). Figs 2-3 indicated that the AOB diversity during winter were not related to that detected in summer. Moreover, Uncultured *Nitrosospira sp.* were only detected during the summer (Fig. 2). The AOB diversity was 6 times higher during summer than winter (Fig. 4) when a higher NH_3 removal rate and temperature were recorded (Table 1). The AOB sequences related to uncultured bacterium and uncultured AOB showed increase of 133% and 360% respectively when the season changed from winter to summer (Fig. 4).

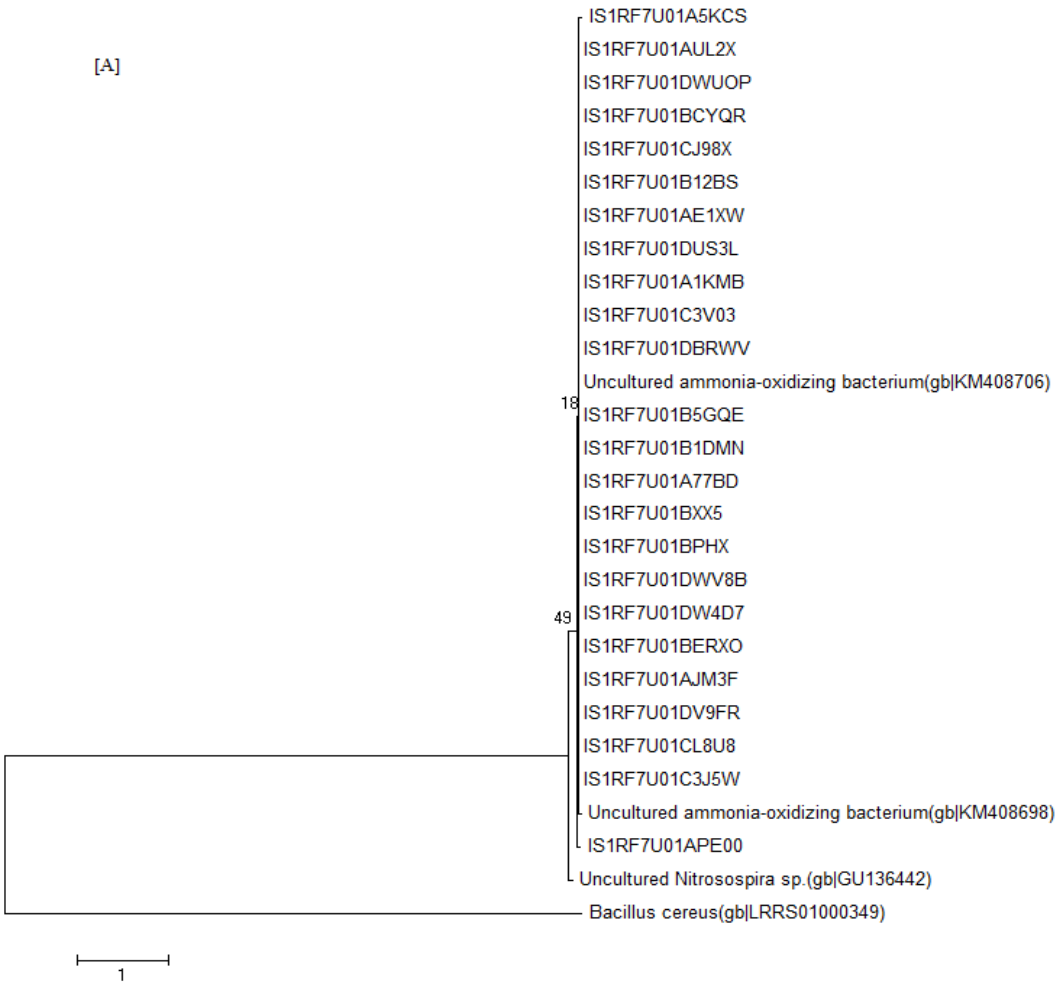

Figure 2. Phylogenetic tree of some selected ammonia oxidizing bacteria OTUs based on amoA gene locus pyrosequencing reads using BLASTN and MEGAN for samples collected during summer.

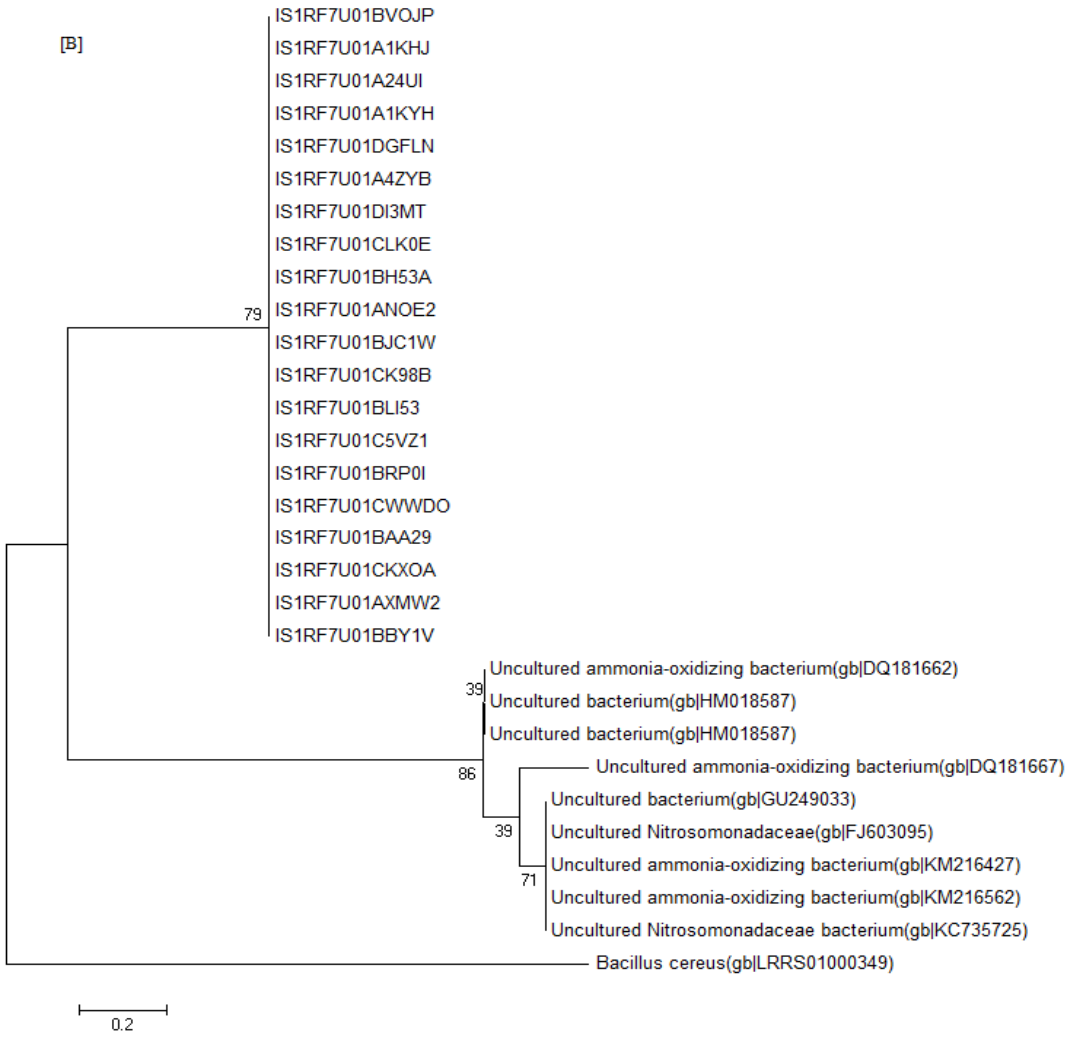

Figure 3. Phylogenetic tree of some selected ammonia oxidizing bacteria OTUs based on amoA gene locus pyrosequencing reads using BLASTN and MEGAN for samples collected during winter.

The plant had significant variation in the influent wastewater compositions, prevailing operational and environmental parameter (Table 1) which correlated with variations in the microbial community structure of the reactor. This variation in microbial diversity affects the planted seasonal nitrification performance as earlier reported (Rowan et al., 2003, Miura et al., 2007). The highest percentage ammonia removal efficiency was recorded during summer when the greatest AOB diversity was found in the reactor (Table 1). It indicates that AOB diversity could be a contributory factor to efficient ammonia removal in activated sludge.

Based on the pyrosequencing analysis, the higher AOB diversity was observed in summer when there was a comparatively higher ammonia removal efficiency (Table 1). The *Nitrosomonas oligotropha* was only detected in the summer sample which indicated a possible higher diversity during summer compared to the winter period (Fig 4). Furthermore, the AOB diversity was 6 times higher during summer than winter when a higher NH_3 removal rate and temperature were recorded. Using pyrosequencing, Zhang et al. (2015) also observed higher AOB diversity in summer compared to winter when monitoring three different WWTP. Niu et al. (2016) also reported a significant decrease in bacterial amoA genes copy numbers during winter, in a water purification plant. In this study, the AOB sequences related to uncultured bacterium and uncultured AOB showed increase of 133% and 360% respectively when the season changed from winter to summer. *Nitrosomonas oligotropha*-like sequence that were detected from summer samples (1%) were absent in winter samples (Fig 4). Earlier research efforts have documented similar trend in different environment. Temperature has a major influence on AOB diversity and population structure with lower species richness correlating to lower temperatures (Urakawa et al., 2008). Similarly, Ju et al.

(2014) observed a higher abundance of *Nitrosomonas* in activated sludge during summer. Faulwetter et al. (2013) also reported seasonal impact on AOB community structure in constructed wetland with higher diversity during summer compared to winter. A higher diversity of amoA gene was also recorded during summer in the tidal wetland investigated by Zheng et al. (2013).

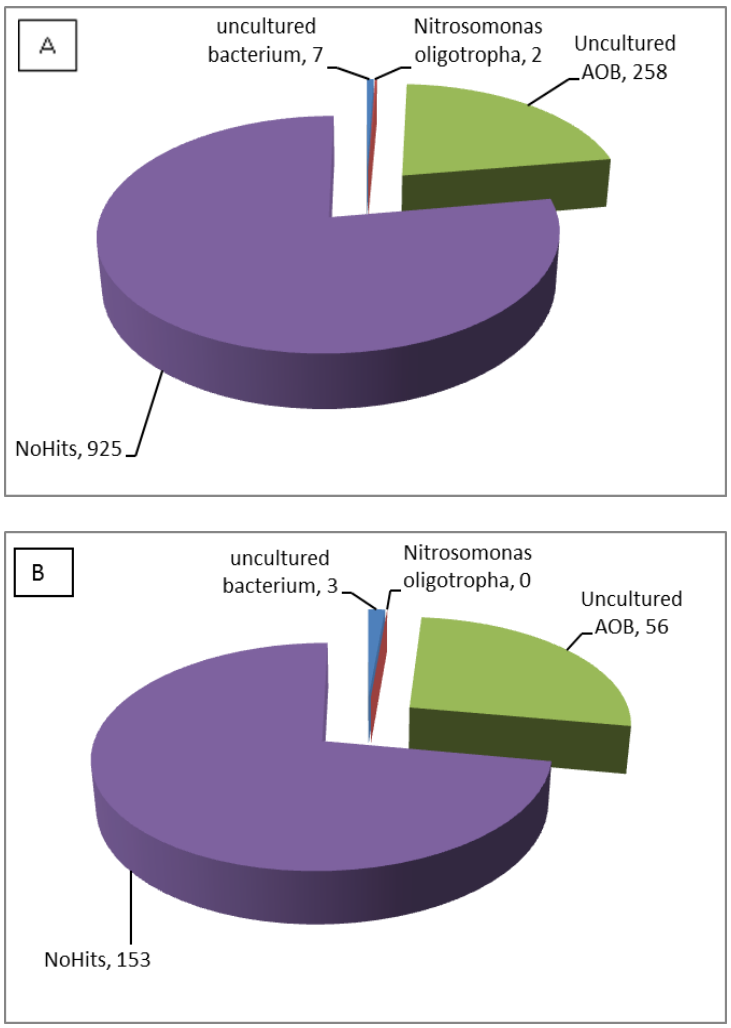

Figure 4. (a) AOB diversity as revealed by pyrosequencing during summer, (b) AOB diversity as revealed by pyrosequencing during winter.

Overall, the summer period harboured larger AOB diversity compared to winter as revealed in this study. A significant proportion of the effective sequences (72 % in winter and 78 % in summer sample) termed "no hits" could not be successfully classified into any known bacterial 16S rRNA sequences since they showed no similarity to the available sequences in NCBI database. This suggests yet unidentified populations and vast unexploited AOB diversity. This corroborates a recent report (Abe et al., 2017) in which phylogenetic analysis of the pure strains isolated from a domestic WWTP revealed a deeply branching, previously unknown lineage and diversity within the genus *Nitrosomonas*. Yang et al. (2011) earlier on had reported that unassigned or unclassified bacteria usually consists higher proportion in activated sludge compared to other environments such as soil, because activated sludge have a more complex microbial communities. In a study by Shi et al. (2013) the occurrence of unclassified bacteria sequences in chlorination and clear water tanks were detected. They noted that these unclassified OTUs from the different samples were closely clustered in the phylogenetic tree. Therefore, there is need for more study in order to identify these ecologically significant diversity of novel AOB species which makes up the complex activated sludge communities.

4. CONCLUSIONS

Pyrosequencing reveals higher diversity of AOB in the reactor during summer that was characterized by higher temperature. Furthermore, *N. oligotropha* and Uncultured *Nitrosospira sp.* were only identified during summer. This indicates that higher temperature elicited increased AOB diversity.

The AOB diversity was 6 times higher during summer than winter when a higher NH_3 removal rate and temperature were recorded. The AOB sequences related to uncultured bacterium and uncultured AOB showed increase of 133% and 360% respectively when the season changed from winter to summer. This suggests that higher AOB diversity resulted in increased nitrification in activated sludge.

The finding suggests that vast diversity of novel, ecologically significant AOB species, which remain unexploited still inhabit the complex activated sludge communities

Future research should target characterization of the nitrifying populations in wastewater as pyrosequencing revealed a large percentage of the microbial community that did not match any of the know sequences on the existing database.

REFERENCES

Abe , T., Ushiki, N., Fujitani, H. & Tsuneda, S. 2017. A rapid collection of yet unknown ammonia oxidizers in pure culture from activated sludge. Water Research, 108**,** 169-178.

Awolusi, O. O., Kumari, S. K. S. & Bux, F. 2015. Ecophysiology of nitrifying communities in membrane bioreactors. Int J Environ Sci Technol, 12**,** 747-762.

Briese, V. 2002. DNA precipitation [Online]. Available: http://www.protocol-online.org/cgi-bin/prot/view_cache.cgi?ID=2744 [Accessed 9/15/ 2012].

Daims, H. & Wagner, M. 2010. The Microbiology of Nitrogen Removal. In: SEVIOUR, R. J. & NIELSEN, P. H. (eds.) Microbial ecology of activated sludge. London: IWA.

Degrange, V. & Bardin, R. 1995. Detection and counting of Nitrobacter populations in soil by PCR. Appl Environ Microbiol, 61**,** 2093-2098.

Faulwetter, J. L., Burr, M. D., Parker, A. E., Stein, O. R. & Camper, A. K. 2013. Influence of season and plant species on the abundance and diversity of sulfate reducing bacteria and ammonia oxidizing bacteria in constructed wetland microcosms. Microb Ecol, 65**,** 111-127.

Gomez-Silvan, C., Molina-Munoz, M., Poyatos, J. M., Ramos, A., Hontoria, E., Rodelas, B. & Gonzalez-Lopez, J. 2010. Structure of archaeal communities in membrane-bioreactor and submerged-biofilter wastewater treatment plants. Bioresour Technol, 101**,** 2096-105.

Ju, F., Guo, F., Ye, L., Xia, Y. & Zhang, T. 2014. Metagenomic analysis on seasonal microbial variations of activated sludge from a full-scale wastewater treatment plant over 4 years. Environ Microbiol, 6**,** 80-89.

Ju, F. & Zhang, T. 2015. 16S rRNA gene high-throughput sequencing data mining of microbial diversity and interactions. Appl Microbiol Biotechnol, 99**,** 4119-4129.

Mcmahon, K. D., Gu, A. Z., Nerenberg, R. & Sturm, B. M. 2009. Molecular methods in biological systems. Water Environ Res, 81**,** 986-1002.

Miura, Y., Hiraiwa, M. N., Ito, T., Itonaga, T., Watanabe, Y. & Okabe, S. 2007. Bacterial community structures in MBRs treating municipal wastewater: relationship between community stability and reactor performance. Water Res, 41**,** 627-37.

Morozova, O. & Marra, M. A. 2008. Applications of next-generation sequencing technologies in functional genomics. Genomics, 92**,** 255-264.

Niu, J., Kasuga, I., Kurisu, F., Furumai, H., Shigeeda, T. & Takahashi, K. 2016. Abundance and diversity of ammonia-oxidizing archaea and bacteria on granular activated carbon and their fates during drinking water purification process. Appl Microbiol Biotechnol, 100**,** 729-42.

Rowan, A. K., Snape, J. R., Fearnside, D., Barer, M. R., Curtis, T. P. & Head, I. M. 2003. Composition and diversity of ammonia-oxidising bacterial communities in wastewater treatment reactors of different design treating identical wastewater. FEMS Microbiol Ecol, 43**,** 195-206.

Schloss, P. D., Westcott, S. L., Ryabin, T., Hall, J. R., Hartmann, M., Hollister, E. B., Lesniewski, R. A., Oakley, B. B., Parks, D. H., Robinson, C. J. & Sahl, J. W. 2009. Introducing mothur: open-source, platform-independent, community-supported software for describing and comparing microbial communities. Applied and Environmental Microbiology, 75**,** 7537-7541.

Sekar, S., Zintchem, A. a. E. A., Keshri, J., Kamika, I. & Momba, M. N. B. 2014. Bacterial profiling in brine samples of the Emalahleni Water Reclamation Plant, South Africa, using 454-pyrosequencing method. FEMS Microbiol Lett**,** 1-9.

Shi, P., Jia, S., Zhang, X. X., Zhang, T., Cheng, S. & Li, A. 2013. Metagenomic insights into chlorination effects on microbial antibiotic resistance in drinking water. Water Res, 47**,** 111-20.

Shokralla, S., Spall, J. L., Gibson, J. F. & Hajibabaei, M. 2012. Next-generation sequencing technologies for environmental DNA research. Mol Ecol, 21**,** 1794-805.

Tamura, K., Stecher, G., Peterson, D., Filipski, A. & Kumar, S. 2013. MEGA6: molecular evolutionary genetics analysis version 6.0. Mol Biol Evol, 30**,** 2725-2729.

Urakawa, H., Tajima, Y., Numata, Y. & Tsuneda, S. 2008. Low temperature decreases the phylogenetic diversity of ammonia-oxidizing archaea and bacteria in aquarium biofiltration systems. Appl Environ Microbiol, 74 894–900.

Xia, S., Duan, L., Song, Y., Li, J., Piceno, Y. M., Andersen, G. L., Alvarez-Cohen, L., Moreno-Andrade, I., Huang, C. L. & Hermanowicz, S. W. 2010. Bacterial community structure in geographically distributed biological wastewater treatment reactors. Environ Sci Technol, 44**,** 7391-7396.

Yang, C., Zhang, W., Liu, R., Li, Q., Li, B., Wang, S., Song, C., Qiao, C. & Mulchandani, A. 2011. Phylogenetic diversity and metabolic potential of activated sludge microbial communities in full-scale wastewater treatment plants. Environ Sci Technol, 45**,** 7408-15.

Zhang, Y., Chen, L., Sun, R., Dai, T., Tian, J. & Wen, D. 2015. Ammonia-oxidizing bacteria and archaea in wastewater treatment plant sludge and nearby coastal sediment in an industrial area in China. Appl Microbiol Biotechnol, 99**,** 4495-507.

Zheng, Y., Hou, L., Liu, M., Lu, M., Zhao, H., Yin, G. & Zhou, J. 2013. Diversity, abundance, and activity of ammonia-oxidizing bacteria and archaea in Chongming eastern intertidal sediments. Appl Microbiol Biotechnol 97**,** 8351–8363.

Proceedings of the 10th World Congress of EWRA 'Panta Rhei', 5-9 July 2017, Athens, Greece
© 2017 *European Water Resources Association*

Evaluation of membranes as promising technique for reclamation and reuse of wastewater

B. Maryam*, S. Ustun and H. Buyukgungor
Engineering Faculty, Environmental Engineering Department, Ondokuz Mayis University, 55200 Atakum, Samsun, Turkey
** e-mail: bareera.mses147@iiu.edu.pk*

Abstract: In 21st century water is a precious resource and after the emphasis on the water sustainability, its proved to be a challenge for water treatment systems to treat wastewater good enough to make it reusable for different purposes. Studies around the world reported the presence of many organic micropollutants like pharmaceuticals and pesticides in the water treated with conventional treatment processes. These micropollutants pose a serious threat towards the aquatic environment especially in case of antibiotic resistances bacteria. Advance treatment processes are one of the most discussed methods to minimize this treat. But rapid expansion of the population in developing countries caused the existing conventional wastewater treatments plants overloaded and there will be no space available for expansion of the existing treatment plants. This leads towards an attractive option of membrane technology. Plenty of membrane designs and operational setups are available in the market. Efficiencies of membrane technology differs with the types of targeted pollutants presents in wastewater and type of membrane being used. The scope of present study covers the types, mechanisms and constraints of the membrane systems to treat wastewaters for pharmaceuticals. A short review has been presented in which reliability on Nanofiltration is discussed with respect to pharmaceutical removals. It was noticed that drugs can be successfully treated by using NF coupled with other advance treatment methods.

Key words: Membrane Technology, wastewater reuse, Nanofiltration, pharmaceuticals, micropollutants

1. INTRODUCTION

Wastewater treatment with membrane technology is not a new concept. Different types of membranes are used for the rejection of pollutants around the word. However, efficiency of membranes is strictly dependent on type of membrane and the nature of pollutant (Alturki et al., 2010). Therefore, selection of membrane according to the properties of pollutant is very crucial to avoid membrane fouling and to secure economic losses. Pharmaceuticals are chemical compounds of concern in recent year because of their regular appearances in fresh water resources and drinking water. Although detected pharmaceuticals are in the range of µg/L – ng/L but their impacts are many folds for both aquatic life and humans (Mompelat et al., 2009). Membranes are an attractive technique because of their selective selection property. They restrict the passage of pollutants and make reclaimed water reusable.

Membrane processes are becoming prominent in wastewater reclamation/reuse and drinking water treatments due to their effectiveness in removing both organic macro, micro and micropollutants. Membranes are divided in MF (Microfiltration), UF (Ultrafiltration), NF (Nanofiltration) and RO (Reverse Osmosis) based on pore size. Pharmaceuticals are treated by membrane technology and in this attempt, studies have published very diversified results regarding efficiency. All of membranes are not effective for all the pharmaceuticals. Membrane rejection is strictly dependent upon water chemistry, drug chemistry and membrane characteristics (Alygizakis et al., 2016).

1.1 Nanofiltration

Nanofiltration (NF) is covered by many studies, particularly for the removal of micropollutants

(Verliefde 2009; Yangali Quintanilla 2010). However, these studies were conducted mainly with target compounds spiked in synthetic model water or directly in demineralized water.

NF (0.001µm pore size) and RO are considered to be in same group due to similar characteristics of membrane material, solute removal and transport (Yoon Y. and Lueptow R.M. 2005) but NF has advantage of low operating pressure compared to RO and has high rejection of organic compounds rather than UF. Although only Nanofiltration/Reverse Osmosis (NF/RO) has been reported to be efficient for removal of Pharmaceutically active compounds (PhACs) and other dissolved contaminants from wastewater because the size and molecular weight (MW) of most PhACs are smaller than the molecular weight cutoff (MWCO) of most microfiltration (MF) and ultra-filtration (UF) membranes but RO is still not applicable in every country and in every situation because of its high economic values (Comerton et al., 2009).

Both charge and size are important in NF rejection as at a neutral pH most NF membranes are negatively charged at lower pH it is positively charged. Physical sieving is the dominant rejection mechanism for the colloids and large molecules, however for ions and lower MW organics, chemical interactions between the solutes and membrane can play an important role in rejection mechanism. Characteristics of Nanofiltration along with advantages and disadvantages are given in Table 1.

Table 1. Characteristics of Nanofiltration and advantages and disadvantages

NF Characteristics	Advantages	Disadvantages
Membrane Finely porous/asymmetric composite	Very compact system low liquid holdup	Can be fouled with particulates
Transfer mechanism Sieving, electrostatic hydration/diffusive	Low capital cost	Not good for viscous material
Law governing transfer Fick's law	Back flushable	Limited range of products
Typical solution treatments Ions, small molecules	High packing density	Higher fouling tendency
Typical pure water flux (L/m_2h) 20-200	Lower investment cost	-
Pressure requirement (atm) 7-30	Lower operating cost	-

The aim of this study was to investigate evaluate and demonstrate the effective treatment of pharmaceuticals with Nanofiltration because of it property of multiple treatment mechanism, a low-pressure and relatively low fouling makes NF membrane a promising technique.

2. MATERIAL AND METHODS

For the present study three drugs has been selected i.e. Ibuprofen, Diclofenac and Paracetamol from the group of non-steroidal anti-inflammatory drugs on the bases of their frequent detection from waters, high consumption, low biodegradability, polarity and their adverse impacts on the environments. Among the most consumed non-steroidal anti-inflammatory drugs frequently found in aquatic environments are aspirin, ibuprofen, naproxen and diclofenac and Paracetamol (Fent et al., 2006). Physicochemical and other properties of selected pharmaceuticals are given in table 2. A short review was performed in order to get a close idea about the efficiency of Nanofiltration regarding the treatment of these selected pharmaceuticals.

3. RESULTS AND DISCUSSIONS

In the literature, there are very few NF studies on PhAC removal from drinking water and surface water (Radjenović et al., 2008) because of Nanofiltration mechanism is still not completely studied for pharmaceuticals. But in some cases, high and broad pharmaceutical removal efficiencies

are reported with zero by-products formation and without farther disinfection units (Joss et al., 2008) but cost and energy requirements are still an important issue. A short review of selected drugs of concern regarding their rejection by Nanofiltration is given in table 3 to understand the relationship between chemistry of drug and method.

Table 2. Properties and occurrence of selected pharmaceuticals (Nonsteroidal anti-inflammatory drug (NSAID)) in waters. (Padhye et al. 2011; Feng et al 2013; Albero et al 2014; Ding et al 2011)

Compound	**Diclofenac**	**Ibuprofen**	**Paracetamol (Acetaminophen)**
Class	Analgesic/ Nonsteroidal anti-inflammatory drug (NSAID)	Analgesic/ Nonsteroidal anti-inflammatory drug (NSAID)	Analgesics/ Nonsteroidal anti-inflammatory drug (NSAID)
Formula	$C_{14}H_{11}Cl_2NO_2$	$C_{13}H_{18}O_2$	C_8H_9NO
Molecular weight [g/mol]	296.15	206.29	151.16
Solubility (mg/L	2/2.37	21	1.40×10^4
Log *K*ow (octanol-water coefficient)	4.26/4.51	3.84/3.97	0.46-0.49
pKa (acid dissociation coefficient)	4.15	4.52/4.91	9.86/9.38
Nature	Hydrophobic ionic	Hydrophobic ionic	Hydrophilic nonionic
Structure	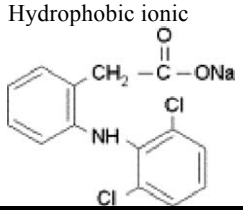	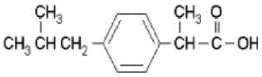	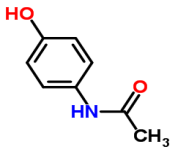

Table 3. Rejection of pharmaceuticals by Nanofiltration

Diclofenac		**Ibuprofen**		**Paracetamol (Acetaminophen)**	
% Rejection	**Reference**	**% Rejection**	**Reference**	**% Rejection**	**Reference**
≤10	Yoon et al., 2007	55-61	Vergili, 2013	22-78	Yangali-Quintanilla et al., 2010
60	Vergili, 2013	85 - 97	Yangali-Quintanilla et al., 2010	≤10	Yoon et al., 2007
60	Yangali-Quintanilla, et al., 2011	15	Yoon et al., 2007	100	Alturki et al., 2010
85	Alturki et al., 2010	≥95	Alturki et al., 2010	43	Radjenović et al., 2008
100	Radjenović et al., 2008	100	Bellona & Drewes, 2007	*BDL	Bellona & Drewes (2007).
53	Bellona & Drewes, 2007	88	Verliefde, et al., 2009		
*BDL	Kimura et al., 2003				
89	Verliefde et al., 2009				

**BDL=Below Detection Limit*

3.1 Mechanism of Nanofiltration

It is to be noted while performing experiments with NF different mechanisms of solute rejection occur, and each of those mechanisms is influenced by solute, as well as membrane parameters (Asano et al 2007). Also, feed water composition and operating parameters have an influence on rejection. Three different interaction types are differentiated: size exclusion by steric hindrance, electrostatic interactions and adsorptive interactions (Yangali Quintanilla, V. 2010)

3.1.1 The molecular weight cut-off (MWCO)

The molar mass above which more than 90% of the compounds are rejected by Nanofiltration

membranes is situated in the range of 200-500 g/mol, which corresponds to the molar mass of the organic micropollutants in the source waters for drinking water (mostly surface water, groundwater or riverbank filtrate). Rejection of uncharged or neutral solutes in Nanofiltration often increases with increasing solute molar mass. If the molar mass of an uncharged compound is higher than the MWCO of the membrane, rejection of the compound will usually be high. Molecular size of a compound can be compared to theoretical values for the membrane pore size (Verliefde. 2009)

3.1.2 Polarity Charge on the PhACs

Polarity is also an important parameter to describe rejection in Nanofiltration. Uncharged compounds with a molecular size larger than the pore size of the membrane will be well rejected due to the sieving effect of the membrane polymer network. Polarity can be defined in two ways; Van der Bruggen et al. (1999) described the effect of the permanent dipole moment on rejection. Solutes with a high dipole moment are assumed to be aligned in the direction of the pores of the membrane, due to electrostatic interactions with the membrane charge, which causes the solutes to permeate more easily and thus have a lower rejection (Yangali Quintanilla. 2010). Rejection of charged solutes is dependent on charge repulsions/attractions between the solute and the charged membrane surface. For a negatively charged membrane, charge attractions cause an increase of solute concentration at the membrane surface for positively charged solutes and a decrease of solute concentration at the membrane surface for negatively charged solutes. Rejection of uncharged solutes is mainly dependent on solute size and hydrophobicity (Verliefde. 2009).

3.1.3 Hydrophobicity

Hydrophobic interactions between solute and membrane can cause adsorption of the solute on the membrane surface and in the membrane pores. The higher the hydrophobicity of a compound (expressed by the octanol water partitioning coefficient (log Kow)), the higher the expected adsorption on the membrane. Rejection of hydrophobic solutes is lower compared with hydrophilic solutes of similar size: solute transport increases due to hydrophobic interactions between the solute and the membrane. The more hydrophobic the solute, the larger the influence of hydrophobic interactions on solute rejection. Rejection of hydrophilic solutes is mainly dependent on size exclusion between the solute and the membrane matrix (Verliefde. 2009).

3.1.4 Adsorption

Adsorption on the membrane causes a high initial rejection of the solute. Solution of a solute in the membrane (partitioning) and diffusion through the membrane are important transport mechanisms in membrane filtration processes. It can be expected theoretically, that the more a compound adsorbs on the membrane, the easier it will dissolve into the membrane and thus be transported to the permeate side. A higher log Kow-value (i.e. a higher hydrophobicity) should thus lead to a higher transport of solute and a lower rejection. Initial adsorption of hydrophobic molecules will be high, which causes a high initial rejection, which eventually will drop to an equilibrium concentration when breakthrough is observed (Braghetta et al., 1997).

4. CONCLUSION

A very limited set of publications are available that reported rejection of pharmaceuticals with the help of Nanofiltration. Cost benefit analysis should be conducted regarding pharmaceuticals removal and membrane application in normal wastewater treatment plants.

It was reported that hydrophilic trace organic compounds are effectively removed by NF Membranes but in the case of acetaminophen the retention was observed to be low (i.e., 0, 23,44 %), probably due to its small molecular size (i.e., MW < MWCO). The highest rejections in NF

processes were recorded for negatively charged pharmaceuticals diclofenac (95%) and Ibuprofen (≥95). In some literature, negatively charged pharmaceuticals also showed poor removal for which no explanation was found. That means there is still a huge gap in research. Finally, positively charged pharmaceuticals are assumed to have good removal above 90% according to NF mechanism but further research is required. The study proved NF membranes to be very efficient in removing nearly all the pharmaceutical residues. However, after carefully reviewing literature it was observed that sometimes process combinations (membrane-hybrid process) give more than 95% removal of selected drugs. Nano membrane filtration with other technique can achieve an enhanced removal efficiency of a wide range of trace organic contaminants that they alone can't achieve in case of some drugs.

REFERENCES

Albero, B., Sánchez-Brunete, C., Miguel, E., Aznar, R., & Tadeo, J. L., 2014. Determination of selected pharmaceutical compounds in biosolids by supported liquid extraction and gas chromatography–tandem mass spectrometry. Jurnal of Chromatography A.; 1336: 52-58.

Alturki, A. A., Tadkaew, N., McDonald, J. A., Khan, S. J., Price, W. E., & Nghiem, L. D., 2010. Combining MBR and NF/RO membrane filtration for the removal of trace organics in indirect potable water reuse applications. Jurnal of Memb Sci.; 365(1): 206-215.

Alygizakis, N. A., Gago-Ferrero, P., Borova, V. L., Pavlidou, A., Hatzianestis, I., & Thomaidis, N. S., 2016. Occurrence and spatial distribution of 158 pharmaceuticals, drugs of abuse and related metabolites in offshore seawater. Sci of the Total Envment.; 541: 1097-1105.

Bellona, C., & Drewes, J. E., 2007. Viability of a low-pressure nanofilter in treating recycled water for water reuse applications: a pilot-scale study. Water research; 41(17): 3948-3958.

Braghetta, A., DiGiano, F. A., & Ball, W. P., 1997. Nanofiltration of natural organic matter: pH and ionic strength effects. Jornal of envnmtal engg,; 123(7): 628-641.

Comerton, A. M., Andrews R. C., and D. M. Bagley. 2009. Practical overview of analytical methods for endocrine-disrupting compounds, pharmaceuticals and personal care products in water and wastewater. Philosophical Transactions of the Royal Society A: Mathematical, Physical and Engg Sci.; 367 (1904): 3923-3939.

Ding, Y., Zhang, W., Gu, C., Xagoraraki, I., & Li, H., 2011. Determination of pharmaceuticals in biosolids using accelerated solvent extraction and liquid chromatography/tandem mass spectrometry. Jornal of Chromatography A,; 1218(1): 10-16.

Feng, L., van Hullebusch, E. D., Rodrigo, M. A., Esposito, G., & Oturan, M. A., 2013. Removal of residual anti-inflammatory and analgesic pharmaceuticals from aqueous systems by electrochemical advanced oxidation processes. A review. Chemcl Engg Jornal,; 228: 944-964.

Fent, K., Weston, A. A., & Caminada, D. (2006). Ecotoxicology of human pharmaceuticals. Aquatic toxicology, 76(2), 122-159.

Joss, A., Siegrist, H., & Ternes, T. A., 2008. Are we about to upgrade wastewater treatment for removing organic micropollutants? Water Sci and Tech.; 57(2): 251-255.

Kimura, K., Amy, G., Drewes, J. E., Heberer, T., Kim, T. U., & Watanabe, Y., 2003. Rejection of organic micropollutants (disinfection by-products, endocrine disrupting compounds, and pharmaceutically active compounds) by NF/RO membranes. Jornal of Memb Sci.; 227(1): 113-121.

Mompelat, S., Le Bot, B., & Thomas, O., 2009. Occurrence and fate of pharmaceutical products and by-products, from resource to drinking water. Envt internl.; 35(5): 803-814.

Padhye, L. P., Yao, H., Kung'u, F. T., & Huang, C. H., 2014. Year-long evaluation on the occurrence and fate of pharmaceuticals, personal care products, and endocrine disrupting chemicals in an urban drinking water treatment plant. Water research; 51: 266-276.

Radjenović, J., Petrović, M., Ventura, F., & Barceló, D., 2008. Rejection of pharmaceuticals in nanofiltration and reverse osmosis membrane drinking water treatment. Water Research; 42(14): 3601-3610.

Van der Bruggen, B., Schaep, J., Wilms, D., & Vandecasteele, C., 1999. Influence of molecular size, polarity and charge on the retention of organic molecules by nanofiltration. Jornal of Memb Sci.; 156(1); 29-41.

Vergili, I., 2013. Application of nanofiltration for the removal of carbamazepine, diclofenac and ibuprofen from drinking water sources. Jornal of envntl managt.; 127: 177-187.

Verliefde, A. R., Cornelissen, E. R., Heijman, S. G. J., Petrinic, I., Luxbacher, T., Amy, G. L., ... & Van Dijk, J. C., 2009. Influence of membrane fouling by (pretreated) surface water on rejection of pharmaceutically active compounds (PhACs) by nanofiltration membranes. Jornal of Memb Sci.; 330(1): 90-103.

Yangali Quintanilla, V., 2010. Rejection of Emerging Organic Contaminants by Nanofiltration and Reverse Osmosis Membranes: Effects of Fouling, Modelling and Water Reuse. PhD thesis, UNESCO-IHE, Delft, CRC Press/Balkema, Leiden, NL

Yangali-Quintanilla, V., Maeng, S. K., Fujioka, T., Kennedy, M., & Amy, G., 2011. Proposing nanofiltration as acceptable barrier for organic contaminants in water reuse. Jornal of Memb Sci.; 362(1): 334-345.

Yoon, Y., Westerhoff, P., Snyder, S. A., Wert, E. C., & Yoon, J., 2007. Removal of endocrine disrupting compounds and pharmaceuticals by nanofiltration and ultrafiltration membranes. Desalination; 202(1): 16-23.

Proceedings of the 10th World Congress of EWRA 'Panta Rhei', 5-9 July 2017, Athens, Greece
© 2017 *European Water Resources Association*

The effect of polymer concentration on electrospun PVDF membranes for desalination by direct contact membrane distillation

S.B. Armand[1], A. Fouladitajar[2*], F.Z. Ashtiani[1] and M. Karimi[3]
[1] *Department of Chemical Engineering, Amirkabir University of Technology, No. 424, Hafez Ave., Tehran, Iran*
[2] *Power generation deputy, Monenco Iran Consulting Engineering Company, No.12, Attar St., Vanak Sq., Valiasr Ave., Tehran 1994643511, Iran*
[3] *Department of Textile Engineering, Amirkabir University of Technology, No. 424, Hafez Ave., Tehran, Iran*
[*] *e-mail: fouladi.amir@monenco.com*

Abstract: Membrane separation technology holds great potential in advancing desalination and water/wastewater treatment to improve the efficiency of impurities removal as well as to augment water supply. Various membrane based technologies are currently being applied for these purposes. Among the current membrane-based technologies, the MD process presents many attractive features compared to others. MD is a low pressure, non-isothermal membrane separation process with a hydrophobic microporous membrane which offers a solution for the treatment of concentrated solutions that are not viable for reverse osmosis. An increasing array of research is being conducted to fabricate novel membranes in order to optimize the performance of the MD process. Different parameters such as pore size, porosity and thickness affect membrane performance during the MD process. Electrospining method for fabrication of membranes allows for controlling of mentioned properties. In this study, by taking into consideration that the polymer concentration has the significant effect on the resultant nanofiber diameter and electrospun nanofibrous membrane (ENM) structure, different Polyvinylidene fluoride (PVDF) membranes with different fiber diameters and physical properties were obtained by varying polymer concentration from 20 to 24.5 wt%. Fabricated membranes were tested for desalination by direct contact membrane distillation (DCMD). The bead-free nanofiber with diameter of 240nm obtained at 20 wt% concentration of polymer solution and increasing PVDF concentration lead to an increase of fiber diameter to 464nm. Results of DCMD operation show that by increasing concentration of polymer solution, the permeate flux decreases. For all membranes the salt rejection ratio was more than 99.9%.

Key words: PVDF Concentration, Electrospun nano-fiberous membranes, Desalination, Membrane distillation

1. INTRODUCTION

Increase in demand for fresh water has become one of the most significant challenges nowadays. Swift growth of population alongside with industrial and agricultural activities has caused the need for water. Predictions demonstrate that the demand continues to rise up to 40% of today's need in 2030 (Shirazi et al. 2016).

As regards that saline water is very abundant, considerable amount of research has been done in order to supply fresh or agricultural water from these resources. Technologies based on membranes have played a significant role in desalination and purification of water and wastewater. Among these technologies, Membrane Distillation compared to other approaches has showed some substantial aspects (Khawaji et al. 2008). This process is appropriate for desalination of saline water that is impossible to purify by other membrane methods such as reverse osmosis. Membrane distillation (MD) is a non-thermal membrane technology which has been introduced for over 50 years and still requires development for industrial application. Driving force for membrane distillation is vapor pressure which is cause by temperature difference alongside the membrane (Tijing et al. 2014).

Membrane used for MD should be hydrophobic and porous so that it prevents pore wetting by aqueous feed. Furthermore, membrane should also have high porosity, appropriate pore size with narrow distribution and high thermal and chemical resistance. These specifications can be met by proper material and fabrication method (Essalhi & Khayet 2014).

Electrospinning process has been used to produce nano-fibers for over 20 years now. Newly, some membranes applied for MD processes have been made of nano-fibrous membranes (ENMs), which have some proper aspects for application in membranes distillation process such as high hydrophobicity, high void volume fraction (i.e. very large surface area to volume ratio), high surface roughness and low thermal conductivity (low thermal conductivity due to elctrospun nano-fibrous causes high efficiency for the MD process), interconnected inner structure and good mechanical resistance (Liao et al. 2013).

In this paper, with regards of the fact that polymer concentration has a significant effect on the final diameter of nano-fiber, performance of fabricated nano-fibrous membranes with various fibers' diameters in direct contact membrane distillation for saline water desalination has been investigated. In fact, the main objective of this article is to inquire the effects of fibers' diameter on the permeation rate of nano-fibrous membranes. At the beginning, various concentrations of polyvinylidenefluoride (PVDF) were electrospun in efficient conditions. The concentration in which we achieved the bead-free nano-fiber with smallest diameter was opted as the suited concentration for fabrication. Afterwards, to investigate diameter alterations, four solutions with different concentrations in the range of 20%wt to 24.5%wt were electrospun. Conclusions of the stated alterations will be thoroughly discussed in conclusion part.

2. MATERIALS AND METHODS

2.1 Materials

Polyvinylidene fluoride (PVDF) with average molecular weight of 146000 grams per mole and granule shape was used as polymer. N,N-dimethylacetamide(DMAC) and acetone purchased from merck, were used to form the polymer solution which have density of 0.94 and 0.791 grams per cubic centimeter respectively. Lithium chloride (LiCl) purchased from merck was used as an additive to increase the conductivity of the polymer solution.

2.2 Preparation of polymer solution

Preparation of solution was done by adding different weights of PVDF polymer to the mixture of dimethylacetamide and acetone by the weight ratio of 6 to 4. Amount of 0.004 wt% of Lithium chloride results in increase of conductivity and improves dope electro-spin ability. Afterwards, the solution was placed on stirrer for 6 hours to become completely homogenous and transparent.

2.3 Electrospining of PVDF membranes

Firstly, the solution is inserted in a glass syringe. Then, by applying the most efficient condition, feed rate of 1 ml/hr, voltage 2 kV, 21 cm distance between the needle and collector, electrospining process was began. After the fabrication, membranes were dried in oven at 80 °C for 30 min.

2.4 Direct contact membrane distillation (DCMD)

Performance of the membrane with an effective area of 50 cm^2 was tested by the DCMD apparatus. DCMD apparatus has two containers. In this work, distilled water and a solution containing salt and water with the concentration of 42 g/l (approximately concentration of The Persian Gulf seawater) were used as permeate and feed respectively. During experiment concentration of salt in both solutions was measured by a conductivity meter. Then, the membrane is placed in module between two hot and cold chambers. Temperatures of the feed and permeate are held at 60 and 20 °C respectively. Volumetric flows of both streams are 1.4 l/min and the pressure of the both sides is controlled at 0.2 bar. Both containers are placed upon balance to record the mass

difference in a computer connected to them.

3. CHARACTERIZATION OF ELECTROSPUN MEMBRANE

To examine the surface of the nano-fibrous membrane, field emission scanning electron microscope was used. At first, samples were sprayed with gold vapor for 80 seconds to form a thin layer of gold on the surface of the membrane. To analyze the fiber diameter imagej software was used. To obtain the average diameter of the nano-fibers, 100 different fibers are measured and their average is reported.

To calculate the thickness of the nano-fibrous layers ACCUD IP54 digital micrometer was used.

4. RESULTS AND DISCUSSIONS

4.1 SEM images of the ENMs and effects of the PVDF polymer concentration

Firstly to determine the proper concentration, different polymer concentrations have been (18 wt%, 19 wt%, 20wt%, 21 wt%, 22 wt%) electrospun. In the first and second columns of the figure 1 field emission scanning electron microscopic images of nano-fibrous surface of PVDF in two different sizes are shown. According to images, a mixture of nano-fibers and beads form the structure of electrospun layer from the solutions which had the polymer concentrations of 18wt% and 19wt% in the same conditions. Formation of beads is in conjunction with surface tension, polymer concentration, solution viscosity, net charge density and electrical conductivity. Solutions with low viscosity turn into droplets more easily while exiting the jet and they are more likely to from beads. As can be seen in the figure 1 despite beads presence, electrospun nano-fibers in low concentrations also are discontinuous. Therefore, with gradually increasing the polymer concentration, beads density decreases and finally bead-free and continuous electrospun nano-fibers achieved from higher concentrations than 20wt%. This phenomenon is related to the entanglement of polymer chains which are controlled by average polymer molecule weight, distribution of molecular weight, polymer concentration and solution viscosity. In a low polymer concentration solution chain overlap does not exist, but when the concentration is increased the polymeric chains begin to overlap and entangle each other. Hence, for stability of the jet and nano-fiber formation proper entanglement of polymeric chains is necessary. According to results, when the polymer concentration is higher than 20wt%, solution density and overlapping of the polymeric chains/polymer is increased dramatically. As a result, 20wt% concentration was selected as the appropriate concentration for electrospinning of the first membrane. Other membranes were elecrospun with the step of 1.5wt%; other membranes' concentrations for electrospinning were 21.5wt%, 23wt% and 24.5wt%.

4.2 Characteristics of the ENMs

FESEM images of PVDF nano-fibers' surface with two different scales are shown in figure 2. Results from measuring average diameter of nano-fibers are reported in table1. It was illustrated that with altering concentration from 20wt% to 24.5wt% average diameter of nano-fibers is increased. Higher polymer concentration in electrospinning process causes stronger viscoelastic force compared to electrostatic force. Therefore, it brings about higher resistance of solution to bending and stretching of jet's fluid when it flows from needle to collector. Because nano-fibers are formed by evaporation and solidification of polymer fluid, their diameter mostly is related to the amount of polymer in jet and its size. Generally, the higher the polymer solution concentration is used, the thicker nano-fibers are formed.

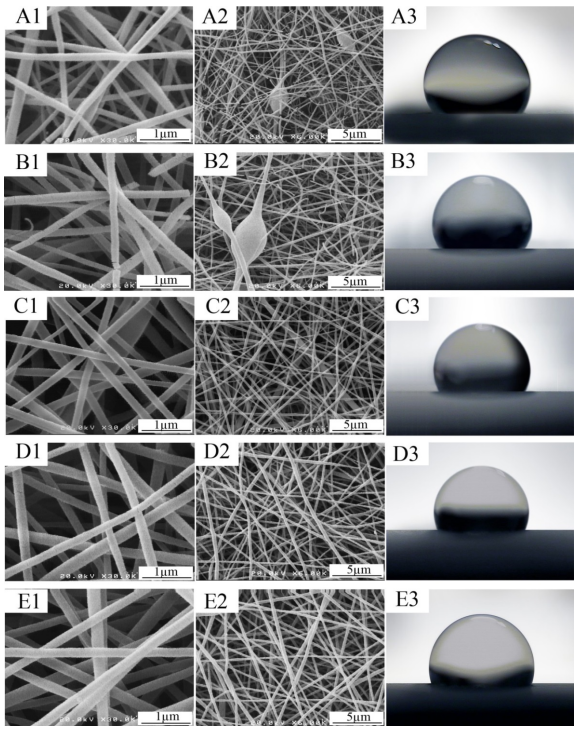

Figure 1. FESEM images and water angle contact of nano-fibrous layer of PVDF were provided from different solution concentrations (A1, A2, A3: solution 18wt%, B1, B2, B3: solution 19wt%, C1, C2, C3: solution 30wt%, D1, D2, D3: solution 21wt%, E1, E2, E3: solution 22wt%)

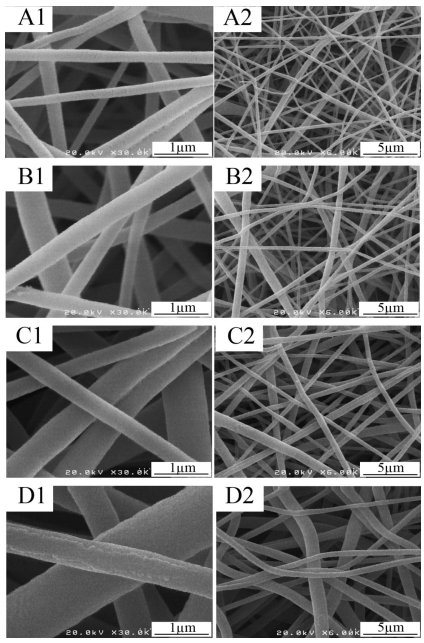

Figure 2. FESEM images and water angle contact of nano-fibrous layer of PVDF were provided from different solution concentrations (A1, A2: solution 20wt%, B1, B2: solution 21.5wt%, C1, C2: solution 23wt%, D1, D2: solution 24.5wt%)

To compare the performance of the membranes, they must have the same thickness. However with the increase of PVDF concentration in the polymer solution an increase in the thickness of the membranes was observed. According to table1, the thickness of the M24-5 is considerably different from other membranes. When the fiber diameter is small, it is more prone to dissipate the electric charges to metallic collector and the repulsion among fibers will be reduced favoring a tightly packed ENM structure with thin thickness. To investigate the effect of nano-fiber diameter on the flux of the different membranes, effect of thickness should be eliminated. So, real flux is divided by

the membrane thickness in order to obtain the normalized flux according to thickness. This topic is discussed in more details further.

Table 1. Nano-fibers' diameters and Membranes' Thickness

Concentration of the solution (wt%)	Membrane code	Diameter of nano-fiber (nm)	Thickness (µm)
20	M20	198±50	150±12
21.5	M21-5	221±75	215±14
23	M23	327±112	280±8
24.5	M24-5	465±145	348±16

4.3 Performance evaluation of the nano-fibrous PVDF in DCMD

As stated before, to eliminate the effect of the membrane's thickness when measuring flux, transmitted and real flux is divided by the membrane's thickness for each sample. This allows us to investigate the effect of normalized flux only with respect to concentration alterations for membrane fabrication. Figure 3 illustrates the amount of normalized flux divided by the thickness for nano-fibrous fabricated membranes by PVDF solution against different concentrations. As can be seen, with the increase of the solution concentration used for fabrication, the amount of the flux is reduced. As stated before, diameter of the nano-fibers is ranged from 197 nm (sample M20) to 465 nm (sample M24-5). Presence of thicker nano-fibers causes pores with smaller diameters and finally leads to the reduction in flux. Besides, with the increase of the nano-fibers' diameter, porosity is decreased. Structure of thicker fibers allows less empty space between them. As a result, the porosity is decreased. In general, this can be stated that with the increase of the PVDF concentration of the solution and forming thicker nano-fibers, pore diameters and porosity are decreased because of the reasons stated and as a result the amount of the transmitted flux is decreased.

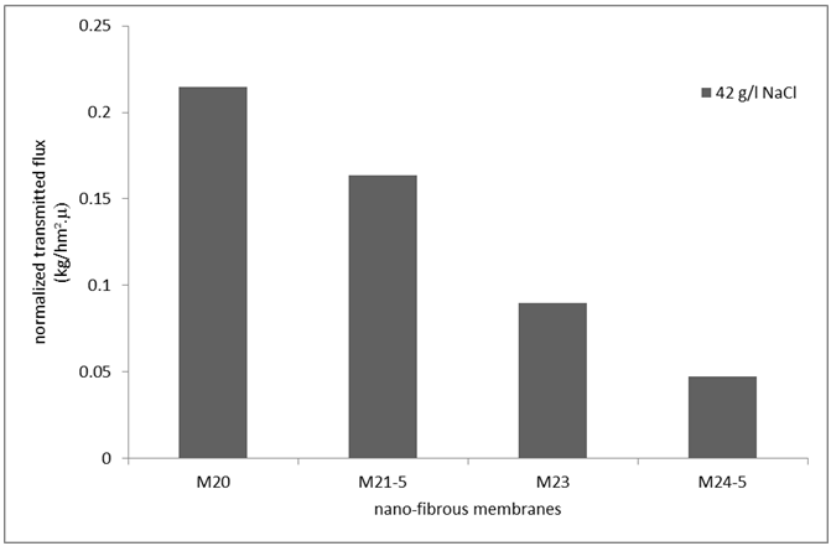

Figure 3. Transmitted flux of the PVDF fabricated electrospun membranes with different solution concentrations in DCMD

Figure 4 shows the amount of the salt rejection of the membranes. This parameter is determined by the equation:

$$\alpha=(1-C_p/C_f)*100 \quad (1)$$

in which **α** shows the salt rejection, C_p is salt concentration in the permeate side and C_f is the salt

concentration in the feed side. As we can see, this parameter is obtained 99.9 percent for all membranes which shows the independence from polymer concentration and as a result nano-fibers' diameter.

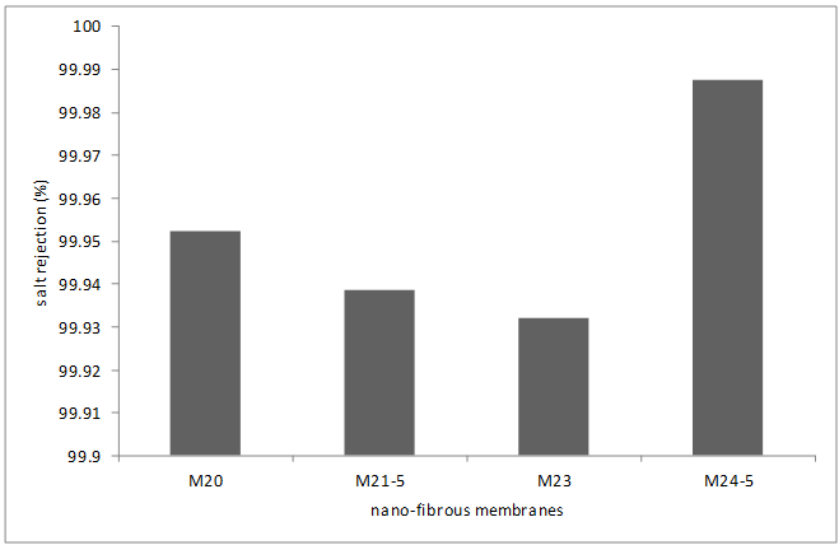

Figure 4. Comparison of desalination parameter of PVDF membranes fabricated by different solution concentrations

5. CONCLUSION

At first, different concentrations of the PVDF polymer solution with dimethyl acetamide and aceton is provided and they are electrospun in the most efficient conditions. Then, properties of the nano-fibrous layers such as nano-fibers' diameter in order to use them in DCMD are investigated. Among 5 different PVDF concentrations provided (18wt%, 19wt%, 20wt%, 21wt%, 22wt%), nano-fibrous resulted from 20wt% concentration has continuous fibers and bead-free with thinnest diameters possible. Therefore, this amount is considered the most appropriate concentration for electrospinning the first membrane. Afterwards, structures of electrospun membranes with different concentrations (20wt%, 21.5wt%, 23wt%, 24.5wt%) were examined. Performance of membranes with different nano-fibers' diameters were compared with each other. Results from DCMD test showed that with altering the concentration and consequently changes in nano-fibers' diameter, caused by the decrease in porosity and also decrease of pore diameter, leads to reduction in flux. On the other hand, increase in the pores' diameter results in increase of the overall thickness and mechanical and thermal resistance.

REFERENCES

Essalhi, M. & Khayet, M., 2014. Self-sustained webs of polyvinylidene fluoride electrospun nano-fibers: Effects of polymer concentration and desalination by direct contact membrane distillation. Journal of Membrane Science, 454, pp.133–143.

Khawaji, A.D., Kutubkhanah, I.K. & Wie, J.M., 2008. Advances in seawater desalination technologies. Desalination, 221(1–3), pp.47–69.

Liao, Y. et al., 2013. Fabrication of polyvinylidene fluoride (PVDF) nanofiber membranes by electro-spinning for direct contact membrane distillation. Journal of Membrane Science, 425–426, pp.30–39.

Shirazi, M.M.A. et al., 2016. Computational Fluid Dynamic (CFD) opportunities applied to the membrane distillation process: State-of-the-art and perspectives. Desalination, 377, pp.73–90.

Tijing, L. et al., 2014. Recent progress of membrane distillation using electrospun nanofibrous membrane. Journal of Membrane Science, 453, pp.435-462

Proceedings of the 10th World Congress of EWRA 'Panta Rhei', 5-9 July 2017, Athens, Greece
© 2017 *European Water Resources Association*

High performance functionalized MWCNT/PES membrane for oil-in-water treatment

S.M. Abedan Dehkordi[1], F. Zokaee Ashtiani[1] and A. Fouladitajar[2]
[1] *Department of Chemical Engineering, Amirkabir University of Technology, Tehran, Iran*
[2] *Research Branch, Islamic Azad University, Tehran, Iran*
[*] *e-mail: smehdi.abedan@gmail.com*

Abstract: Membrane filtration is a promising technology for oily wastewater treatments considering its high separation efficiency along with simplicity and fairly short process time. However, the application of this technology has been limited by severe fouling caused by oil droplets in the oil-in-water separation resulted in less performance. In this study, pure polyethersulfone membrane was modified by two different functionalized multi-walled carbon nanotube, Carboxylated MWCN and Hydroxylated MWCNT, to increase its hydrophilicity and oil resistant. Carboxylated and Hydroxylated MWCNT/PES mixed matrix membranes were manufactured via NIPS method. Nanocomposite / polymer solutions for membrane formation were prepared in DMF with 16 wt% PES and 1 wt% PVP. The functionalized MWCNTs were added to the casting solution in different concentrations (based on the polymer constituents) and dispersed by sonication stirrer. The effect of these functionalized MWCNTs on the performance of PES membranes permeability was investigated in terms of oil water flux via cross-flow flat sheet module. The results indicated that the performance of the membrane was enhanced by blending functionalized MWCNT to the casting solution. Carboxylated MWCNT increased the oil/water flux by 80 percent, however, the hydroxylated MWCNT increased the flux by only 50 percent. Comparison of the flux in different concentrations of MWCNT also showed that membrane has the best permeability at 0.1% of Carboxylated MWCNT and 0.15% of Hydroxylated MWCNT. Higher concentration of MWCNT showed a reverse effect on the permeability and decreased the flux due to the aggregation of the nanoparticles in the membrane matrix.

Key words: PES membrane, Carboxylated MWCNT, Hydroxylated MWCNT, Membrane performance, Permeate flux

1. INTRODUCTION

Membrane technologies have gained an important place in separation techniques, specially their remarkable performance in removing oil from wastewater produced from industries (Pagidi et al., 2014). Although membranes have superior advantages because of their low energy consumption, high quality water produced, simpler process design and low amount of chemicals used compared to other treatment techniques, they are not without difficulties. Fouling is a serious problem in membrane filtration caused either by oil droplets, blocking membrane pores or accumulation of an oil layer on the membrane surface, decreasing the performance of the membrane and a significant flux decline (Celik et al., 2011).

Non-solvent induced phase separation (NIPS) is a technique mostly used for preparation of polymeric membranes in which, the solution is cast onto a glass support using a casting knife, and then is immersed into a coagulation bath. At the interface, the solvent diffuses out to coagulation bath, while the non-solvent transfers into the casting solution. Subsequently, phase inversion occurs between casting solution and coagulation bath resulting in formation of membrane film (Yin et al., 2013).

Polyethersulfone (PES) is a well-known polymer with characteristics such as excellent toughness, good thermal stability and approved for being used in food, water and medical applications. High hydrophobicity is the main disadvantage of PES membrane resulting in fouling and extremely lower flux decreasing the membrane lifetime and increasing the operation cost (Daraei et al., 2014).

Many studies have been done to increase the antifouling capacity of prepared membranes by

improving the membrane hydrophilicity, however, it has been still remained challenging. Substantial effects of nanoparticles, added in the casting solution, have been reported by many researchers. It is well accepted that interactions between the polymeric chains and nanoparticle surface during the membrane fabrication process result in more hydrophilic membrane and increase of the membrane performance. According to the superior properties such as high hydrophilicity nature, high flexibility and low mass density, multi-wall carbon nanotube is an excellent modifying additive for PES membranes (Vatanpour et al., 2014).

Fabrication of hydrophilic modified membrane using these additives for membrane preparation faces two problems. Firstly, MWCNTs have unsuitable dispersion and dissolution in various organic solvents. Secondly, there is a weak interaction of the interface between the MWCNTs and the polymer matrix. Hence, to obtain uniform dispersion of nanoparticles in the polymeric solution and amplify stability of nanoparticles in polymer matrix, hydrophilic functional groups are introduced into the surface of the MWCNTs via functionalization by chemical agents and attaching polar groups to MWCNT sidewalls. Hydroxyl and carboxyl groups are two approved functional agents widely used to overcome the undesirable dispersion of MWCNTs into the polymer matrix (Vatanpour et al., 2011).

This work is a comparative study on the effects of embedding two different functionalized MWCNTs on PES membrane performance in order to find the optimum amount of nanoparticles that profoundly enhance the performance of fabricated membranes. Carboxylated-MWCNTs and hydroxylated-MWCNTs were added into the casting solution in a selected number of concentrations to obtain optimum level and avoid aggregation of nanoparticles. The trends of changes in performance of modified membranes are obtained via oil-water flux runs through cross flow flat sheet module.

2. EXPERIMENTAL

2.1 Materials

Functionalized multi-wall carbon nanotube (95% of purity) with 10–30 nm in outer diameter and 3 wt% of OH and COOH content was obtained from Neutrino Corporation (Iran). Polyethersulfone (PES, E6020p) was purchased from BASF. Dimethylformamide (DMF) were provided from MERCK. Polyvinylpyrrolidone (PVP) of k25 grade (MW ~ 25,000 g/gmol) was kindly obtained from Rahavard Tamin Pharmaceutical Company (Iran). Distillated water was used as the non-solvent in the coagulation bath and also in all flux runs.

2.2 Preparation of functionalized MWCNT/PES mixed matrix membranes

Nonsolvent-induced phase separation (NIPS) was used to fabricate functionalized MWCNT/PES mixed matrix membranes using casting solutions containing PES (16 wt%) as the base polymer, polyvinyl pyrrolidone (PVP, 1 wt%) and measured amount of functionalized MWCNT in DMF as solvent in order to increase the hydrophilicity of PES membranes. Exact amount of functionalized MWCNT (0, 0.05, 0.1, 0.15 and 0. 2 wt% with respect to PES concentration) were ultrasonicated in DMF for 20 min until uniform MWCNT solution was obtained. After preparation of well dispersed MWCNTs in the solvent, PES and PVP, were dissolved in the dope solution by continuous stirring and heating at 45 °C to obtain homogenous casting solution. 5 min of ultrasonication was again used to remove the air bubbles produced during stirring. The solution then was casted on a glass plate using a casting knife with 180 μm thickness, and the glass plate was immediately immersed in the non-solvent bath (distilled water at 25 ±1 °C). A thin polymeric film was separated from the glass within a few minutes. Eventually, the formed membranes were washed with and stored in distillated water for 24 h to attain full leach out of residual solvent and additives.

2.3 Membrane Performance

A flat sheet module in a lab scale experimental setup with 50 cm^2 of effective area at ambient temperature was used to examine the performance of prepared membranes. This setup was employed in previous works of this research team (Fouladitajar et al., 2013: De Lannoy et al., 2013). The flow pattern on this module is cross flow with feed flow rate, trans membrane pressure (TMP) and the oil concentration of 2 L/min, 2 bar, and 2000 mg/L, respectively. All fabricated membranes were applied under the cross flow pattern process at the same operating conditions.

2.4 Feed preparation

The oil-in-water emulsion was prepared by mixing gasoil (Tehran Refinery) and surfactant for 20 min at a mixing rate of 10,000 rpm. Polyoxyethylene (80) sorbitanmonooleate (Tween 80, Merck) was used as the surfactant at concentration of 100 mg/L (Ghandashtani et al., 2015). COD test was used to measure the amount of oil rejection in each experiment which is an important parameter for analysis of membrane separation performance. For all modified cases, oil rejection was higher than 95%.

3. RESULT AND DISCUSSION

Permeate flux was used to investigate effects of hydroxyl and carboxyl groups on modification properties of MWCNTs along with percentage of functionalized MWCNTs in the dope solution on the performance of fabricated membranes.

3.1 Permeate flux reduction

Fig. 1 shows the permeate flux of feed, after 20 minutes of distilled water circulation in flat sheet module. A sharp initial decline of permeation flux at the beginning of separation process was observed which is due to deposition of organic particles and formation of fouling layer on the membrane surface as well as internal fouling caused by deformation of oil droplets during migration to the bulk of membranes (Sun et al., 2010)**.** After this rapid reduction, decline of flux was gradually slowed down until a relatively constant value was achieved. Note that obtained permeate flux of pristine PES membrane was 63 $L/m^2.h$.

3.2 MWCNTs concentration

The trends of permeate fluxes shown in Fig. 1 indicates that addition of nanoparticles has increased the permeate flux of membranes up to the optimum concentration of functionalized MWCNTs which was observed at 0.1% and 0.15% for COOH-MWCNTs and OH-MWCNTs, respectively. Permeate flux of membranes is reduced with further increase of nanoparticles in the solution due to the pore blockage caused by aggregation of nanoparticles in the membrane structure, despite the increased hydrophilicity.

The cross-sectional FESEM images of the membranes in different concentration of nanoparticles exhibited in Fig. 2 are used to explain this phenomenon. A typical characteristic of a dense skin top-layer along with asymmetric porous structure with finger-like macro-pores was observed for all membranes. Smallest pores in the top-layer appeared in the pristine PES membrane (Fig. 2a). Macro finger-like structure started to appear by addition of low amounts of nanoparticles due to hydrophilic nature of functionalized MWCNTs increasing the mass transfer rate between solvent and non-solvent during phase inversion. The finger-like pores were promoted in membrane structure till addition of 0.1 wt% nanoparticles (Fig. 2b-c). Irregular positioning of MWCNTs in the

membrane structure appeared by exceeding this optimum concentration due to aggregation of nanoparticles. The tendency of MWCNTs to migrate to lean-polymer phase of solution and their aggregation in the membrane structure demolishes the uniform dispersion of nanoparticles in the polymeric solution and consequently blocks the pores in bulk of membrane matrix which results in smaller pores and thus a flux decline. A better look of aggregation in the bulk of membrane matrix is shown in Fig. 3. As shown, pores blockage is occurred by aggregated nanoparticles which obstruct the feed from passing easily through the film.

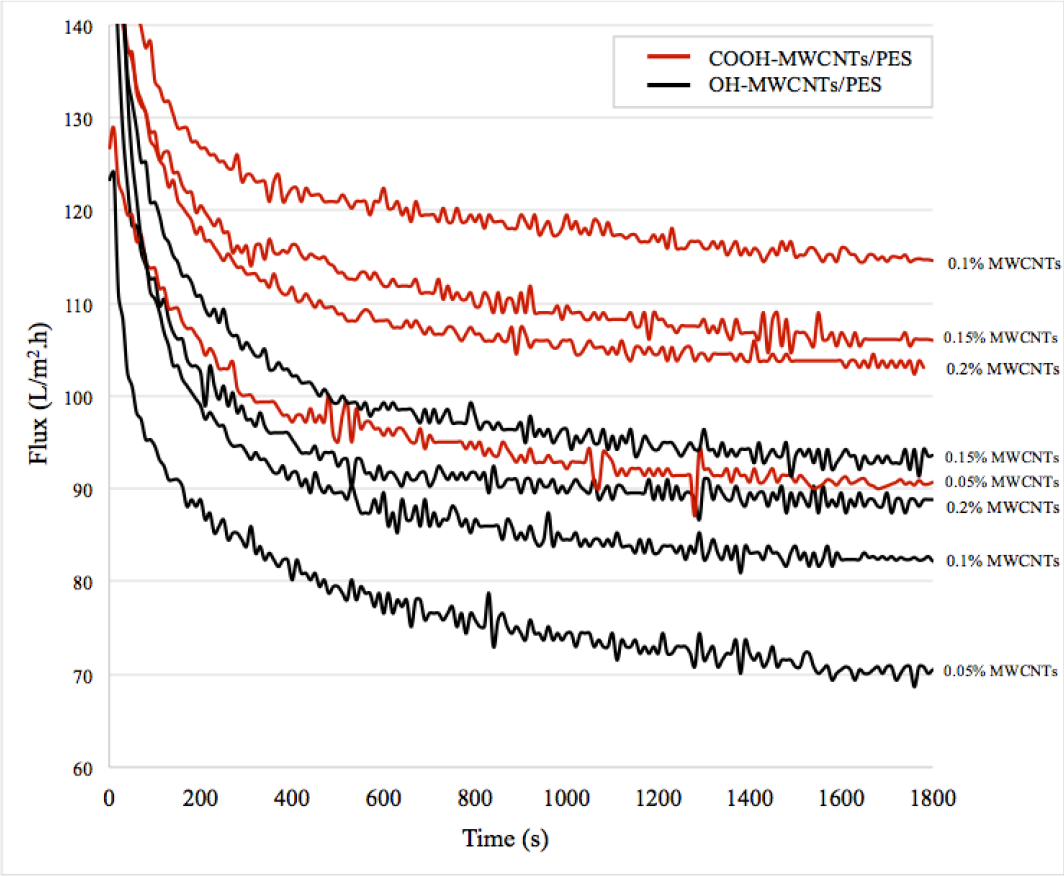

Figure 1. Permeate flux of functionalized-MWCNT/PES membranes.

3.3 Comparison of different functionalized MWCNTs

As illustrated in Fig. 1, at equal amount of nanoparticle, all COOH-MWCNTs/PES membranes exhibited better permeate flux, therefore better performance compared to OH-MWCNTs/PES membranes. Two reason could describe the preferable effects of the former than latter. On one hand, carboxylated functional group have better ability to form hydrogen bond with water molecules during the phase inversion process which reduces the interface energy between solvent and non-solvent. As a result, an increase in membrane porosity thus a higher flux is obtained. On the other hand, compared to linear spatial geometry of hydroxylated functional group, more empty spaces are formed between polymeric chains of PES due to V-shape spatial geometry of carboxylated functional group in which solvent gets trapped. Solvent leaves these spaces during phase inversion causing more porous structure in the bulk of the membrane. The authors believe that this reason, neglected in other studies, is of a great importance to appearance of the porosity in fabricated membranes. As a result, mentioned increase in the porosity of membrane matrix leads to a higher permeate flux. This argument goes in good agreement with the trend of porosity variation of the prepared membranes.

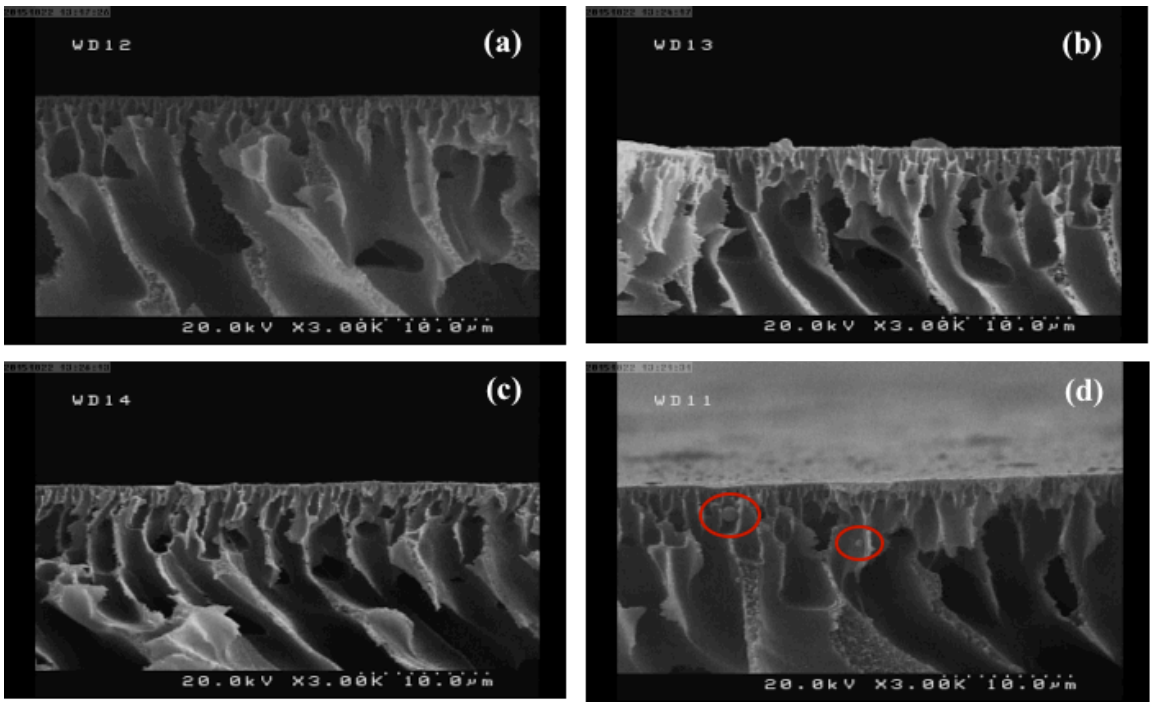

Figure 2. Cross-sectional FESEM images of membranes with different blend compositions of MWCNTs. (a) Pristine PES, (b) 0.05 wt% COOH-MWCNTs/PES (c) 0.1 wt% COOH-MWCNTs/PES (d) 0.15 wt% COOH-MWCNTs/PES

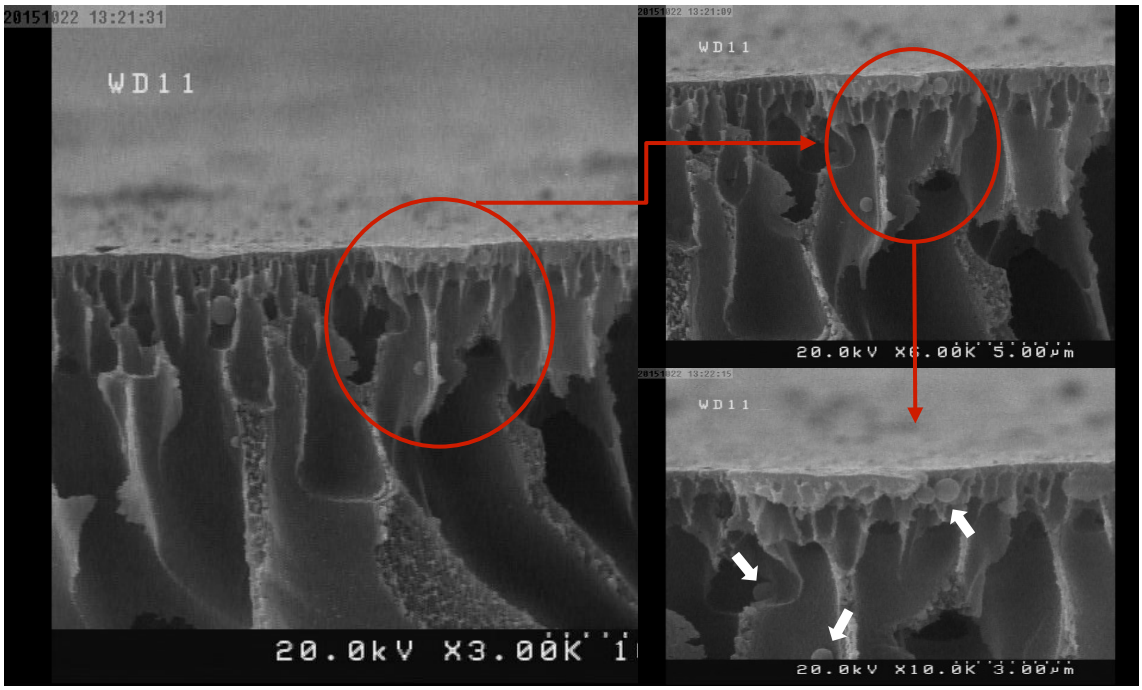

Figure 3. Cross-sectional FESEM images of membrane with aggregation in the bulk.

Table 1 compares the flux of COOH and OH functionalized MWCNTs/PES membranes with their porosity at different content of nanoparticles. As shown in Table 1, all carboxylated-MWCNTs/PES membranes showed more porosity than membranes modified with hydroxylated-MWCNTs which resulted in higher flux of the former which confirms the favourable effects of COOH functional group compared to less desirable effect of OH functional group on the performance of the prepared membranes. Although, as explained before, lower porosity of the fabricated membranes is observed at nanoparticle content higher than optimum concentration due to the aggregation of functionalized nanoparticles which adversely influenced the uniform dispersion of MWCNTs.

Table 1. Comparison of porosity of different functionalized MWCNTs/PES membranes

Carboxylated-MWCNTs/PES			Hydroxylated-MWCNTs/PES		
Nanoparticle (%)	Flux (L/m2.h)	Porosity (%)	Nanoparticle (%)	Flux (L/m2.h)	Porosity (%)
0.5%	90.6	70.16	0.5%	70	66.57
0.1%	115	73.84	0.1%	82.3	67.8
0.15%	105.9	72.05	0.15%	93.8	70.04
0.2%	102.5	69.51	0.2%	88	68.21

4. CONCLUSIONS

In this paper, the effect of hydroxylated and carboxylated multi-walled carbon nanotubes on the performance of PES membrane permeability in oily water separation was investigated in term of permeate flux via cross-flow flat sheet module. The results indicated that the performance of the membrane was increased by embedding functionalized MWCNTs to the casting solution, however, carboxylated MWCNT showed a better modifying effect on the membrane permeability and increased the oil/water flux by 80 percent, where hydroxylated MWCN increased the flux by only 50 percent. Comparison of the flux in different concentration of MWCN also showed that the optimum concentration for hydroxylated and carboxylated MWCN in polymeric solution were 0.15% and 0.1%, respectively. Flux reduction was observed at higher concentration of MWCNT due to the aggregation of the nanoparticles in the membrane matrix.

REFERENCES

Celik, E., Park, H., Choi, H., 2011. Carbon nanotube blended polyethersulfone membranes for fouling control in water treatment. Water Research; 45: 274-282.

Daraei, P., Madaeni, S. S., Ghaemi, N., Khadivi, M., Astinchap, B., 2013. Enhancing antifouling capability of PES membrane via mixing with various types of polymer modified multi-walled carbon nanotube. Journal of Membrane Science; 444: 184–191.

De Lannoy, C., Soyer, E., Wiesner, M. R., 2013. Optimizing carbon nanotube-reinforced polysulfone ultrafiltration membranes through carboxylic acid functionalization. Journal of Membrane Science; 447: 395–402.

Fouladitajar, A., Zokaee Ashtiani, F., Okhovat, A., Dabir, B., 2013. Membrane fouling in microfiltration of oil-in-water emulsions; a comparison between constant pressure blocking laws and genetic programming (GP) model. Desalination; 329: 41–49.

Ghandashtani, M. B., Zokaee Ashtiani, F., Karimi, M., Fouladitajar, A., 2015. A novel approach to fabricate high performance nano-SiO2 embedded PES membranes for microfiltration of oil-in-water emulsion. Applied Surface Science; 349: 393–402.

Pagidi, A., Saranya, R., Arthanareeswaran, G., Ismail, A. F., Matsuura, T., 2014. Enhanced oil–water separation using polysulfone membranes modified with polymeric additives. Desalination; 344: 280–288.

Sun, M., Su, Y., Mu, C., Jiang, Z., 2010. Improved antifouling property of PES ultrafiltration membranes using additive of silica-PVP nanocomposite. Ind. Eng. Chem. Res; 49: 790–796.

Vatanpour, V., Esmaeili, M., Davood Abadi Farahani, M. H., 2014. Fouling reduction and retention increment of polyethersulfone nanofiltration membranes embedded by amine functionalized multi-walled carbon nanotubes. Journal of Membrane Science; 466: 70–81.

Vatanpour, V., Madaeni, S. S., Moradian, R., Zinadini, S., Astinchap, B., 2011. Fabrication and characterization of novel antifouling nanofiltration membrane prepared from oxidized multiwalled carbon nanotube/polyethersulfone nanocomposite. Journal of Membrane Science; 375; 284–294.

Yin, J., Zhu, G., Deng, B., 2013. Multi-walled carbon nanotubes (MWNTs)/polysulfone (PSU) mixed matrix hollow fiber membranes for enhanced water treatment. Journal of Membrane Science; 437: 237–248.

Proceedings of the 10th World Congress of EWRA 'Panta Rhei', 5-9 July 2017, Athens, Greece
© 2017 *European Water Resources Association*

Purification of Humic acids contained simulated wastewater using membrane ultrafiltration

S. Saha and C. Das*
Department of Chemical Engineering, Indian Institute of Technology Guwahati, Assam, Pin 781039, India
* *e-mail: cdas@iitg.ac.in*

Abstract: Treatment of water from any industrial effluent can provide valuable profits towards the living environment. The resolution of the treatment of effluent is the minimization of water pollution and reuse of water. Several researches have already been performed to remove natural organic matters from wastewater. In our present work, simulated wastewater was treated using membrane batch ultrafiltration with polyethersulfone membrane. Commercial Humic acids was used as a common natural organic matter present in industrial wastewater. The effects of different transmembrane pressure drops (207, 276 and 345 kPa) on permeate flux and permeate quality were explored using 50 kDa molecular weight cut off membrane. The concentration of Humic acids in water was maintained at 50 mgL^{-1}. In order to overcome compaction effect of the membrane, the module was pressurized with deionized (DI) water for 2 hours at 345 kPa applied transmembrane pressure (TMP) drop. Maximum permeate flux was obtained at 345 kPa TPM drop. The percentage removal of pollutant was 93.8%. Flux decline was analysed using Hermia's pore blocking mechanism and artificial neural network. Apart from this, module performance was characterized by calculating total resistance during purification of synthetic wastewater.

Key words: Humic acids (HAs), natural organic matters, membrane ultrafiltration, wastewater

1. INTRODUCTION

Water pollution causing by natural organic matters has seemed to be a severe issue in recent times (Bhatnagar et al., 2017). The effective treatment and utilization of wastewater are the main objectives for the growing countries to control water pollution (Liu et al., 2017). The minimization of harmful organic components like, Humic substances present in the industrial effluent is a major concern in the recent years. The leaching of Humic substances and other organic matters from the untreated effluents into the fresh water is a critical problem towards the living environment (Jia et al., 2016). The natural substances are the mixture of a complicated matrix of heterogeneous organic components. Due to these substances, the test of drinking water becomes deteriorate (Bhatnagar et al., 2017). It causes severe problems including generation of toxic and disinfected by-products. The amount of dissolved oxygen in the water is also becoming decrease (Fu et al., 2017). Activated sludge process or any biological technology are not suitable to remove the natural organic materials from the industrial effluent totally (Andrews et al., 2014). However, researches have already been performed using chlorine disinfection process (Wang et al., 2017), the formation of toxic components like, dichloro and trichloroacetic acid, chloroform and other toxic chlorinated products trihalomethanes is the main demerit for this process (Lyon et al., 2014). Few studies were done to treat Humic substances or other materials using advanced oxidation, most of which was the changing of the structure of organic components (Choi et al., 2010, Wang et al., 2017). Apart from adsorption, liquid extraction, coagulation or previously said techniques; membrane ultrafiltration is an effective, time consuming, low cost alternative operation to treat wastewater contained natural organic maters (Galambos et al., 2004) because of its efficient operating system, very less chemical consumption, and non-polluting concept (Manttari et al., 2006).

In our current study, commercial Humic acids powder was used as a model natural organic matters present in many industrial effluents. A robust treatment technology, membrane

ultrafiltration was carried out to remove the model organic matters from simulated wastewater varying different TMP drop from 207 to 345 kPa. The main aim of this project work was to analyze the flux decline behavior using artificial neural network (ANN) system. Cake filtration and intermediate pore blocking law were applied to identify the fouling mechanism with respect to ultrafiltration time.

2. MATERIALS AND METHODS

2.1 Materials

The ultrafiltration study was performed using lab grade Humic acids (HAs) powder obtained from Loba Chemie, India. Without further treatment commercial Humic acids (Has) powder was used during preparation of feed sample.

2.2 Membrane

A commercial flat sheet asymmetric polyethersulfone membrane (MWCO of 50 kDa), purchased from Permionics Membranes Pvt. Ltd., Vadodara, Gujarat, India was used to treat the HAs simulated wastewater. The active membrane surface area was 33.4×10^{-4} m^2. The water permeability (L_p, m Pa^{-1} s^{-1}) and fresh membrane resistance (R_{fresh}, m^{-1}) were found about 4×10^{-11} and 1.3×10^{13}, respectively.

2.3 Experimental design and procedure for batch ultrafiltration

An unstirred batch cell module was used to purify HAs contained simulated wastewater. The batch cell set up was made of stainless steel with the capacity of 0.35 L. A cylindrical vessel (77.5×10^{-3} m, inner diameter) was attached with flanges. To maintain the mechanical support on flat sheet membrane, a circular grid made of aluminum was used as a base. Two matching rubber gaskets were used to prevent the leakage during ultrafiltration. To maintain the transmembrane pressure drop (TMP) during separation, an air compressor was used. Figure 1 represents the schematic diagram of the batch cell module. At first, membrane was compacted with DI water for 2h in order to control the compaction effect on the membrane active surface area. The applied pressure was 345 kPa. To observe the permeate flux behavior at different TMP drops, the pressure was varying from 207 (30 psi) to 345 kPa (50 psi). The HAs concentration was 50 mg L^{-1}. The feed concentration was constant throughout the experiment.

2.4 Sample analysis

The concentration of HAs solution was measured at 254 nm λ_{max} using UV-vis spectroscopy (Thermofisher Scientific, India). The auto-ranging ion meter (VSI Electronics Pvt. Ltd., Punjab, India) was used to analyze the electrical conductivities (S m^{-1}) and total dissolved solids (TDS, mg L^{-1}) (Das et al., 2006). The pH meter (Jenway, Bibby Scientific UK) was used to check the pH of HAs solution.

2.5 Theoretical study for ultrafiltration and fouling characteristics

Theoretical analysis of batch cell ultrafiltration was performed using Darcy's law of permeation which is represented in the Eq. (1). Water flux (J_w) was calculated before starting the experiment.

$$J_w = L_p\Delta P = dV/A_m dt \quad (1)$$

A_m was the active membrane surface area (m^2). Hydraulic permeability was L_p ($mPa^{-1}s^{-1}$).

Variation of solute rejection (R_s, %) was studied using Eq. (2)

$$R_s\ (\%) = [1-(C_{pHumic}/C_{0Humic})]\times 100 \quad (2)$$

C_{pHumic} was the solute concentration in the permeate side (mg L^{-1})

C_{0Humic} was the solute concentration in the prepared feed solution (mg L^{-1})

In the present study, the formation of cake layer was analyzed using Hermia's cake filtration model. Eq. (3) signifies the Hermia's pore clogging model for any dead end filtration (Das et al., 2015).

$$d^2t/dV^2 = K\,(dt/dV)^n \quad (3)$$

The four different fouling models such as, complete pore blocking model (CPBM, *n=2*), standard pore blocking model (SPBM, *n=1.5*), intermediate pore blocking model (IPBM, *n=1*) and cake filtration model (CFM, *n=0*) have already been discussed in the previous work (Saha et al., 2015). Based on the regression coefficient (R^2) value, IPBM and CFM have been chosen for further discussion. In the present study, the stage wise analysis of IPBM followed by CFM has been discussed with respect to process contact time. In the Eq. (3), when *n=1*, it analyses irreversible pore blocking (IPBM) characteristics. The simplified form is as follows:

$$1/J_{ps} = (1/J_0) + k_{ii}t \quad (4)$$

where, k_{ii} ($k_{ii}=k_{Am}$) is model constant for IPBM (m^{-1}).

When *n=0*, it signifies the formation of cake layer (CFM) on the membrane surface

$$1/J_{ps}^2 = (1/J_0^2) + k_{clHumic}\,t \quad (5)$$

where, $k_{clHumic}$ ($k_{clHumic} = 2R_{cake}k_{DC}/J_0R_{fresh}$) is model constant for CFM ($m^{-2}s^{-2}$).

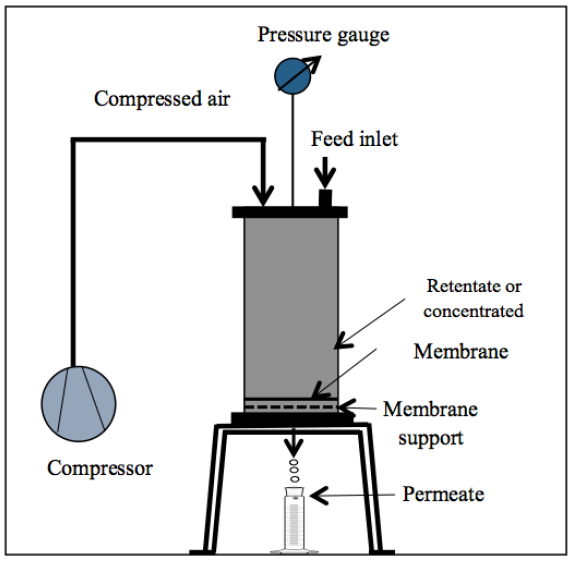

Figure 1. Schematic diagram of unstirred membrane batch ultrafiltration module

2.6 Artificial neural network (ANN)

An artificial neural network (ANN) is a theoretical model made by a computational approach based on the real function of human brain neurons. This computing process is prepared by a number of interconnected signalling elements. These process elements release the valuable information by

the help of their own dynamic state response to the external objects. ANN are made of multiple nodes and they interact with each other to perform operations on the given data. The result is passed to the output node, called activation through the other internal nodes (Baguena et al., 2016). To predict the relationship between experimental and theoretical data, a two layered feed-forward Levenberg-Marquardt algorithm was applied during ANN analysis. The number of hidden neuron was 10. The total experimental points were circulated in the following stages: training: 19, validation: 9 and testing: 9 points. Root mean square error (RMSE) were performed to identify the highest regression coefficient (R^2) using MATLABR2015b neural network toolbox.

3. RESULTS AND DISCUSSIONS

3.1 Experimental and theoretical analysis of permeate flux decline with respect to time and transmembrane pressure drop (ΔP, kPa)

The deviation of permeate flux for the three different TMP drops has been represented in Figure 2. The theoretical study of the flux decline using ANN analysis with respect to time has also been shown here. The permeate flux deviates from its initial point with the process time for each case. The deviation of permeate flux is higher for low TMP drop of 207 kPa due to the pore blocking phenomena. At the high TMP drop of 345 kPa, the slower deviation has been noticed due to the gradual increasing of gel layer formed by retained solute particles. The detailed experimentation of the variation of transient flux decline with different parametric conditions has already been discussed in our previous research (Saha et al., 2015). The comparative study between theoretical and experimental flux deviation has been performed here. To identify the best fitting prediction using ANN model, a statistical analysis has been performed with the experimental data for all the TMP drops. Table 1 represents the statistical analysis of variance (ANOVA) for theoretical flux decline behavior during batch ultrafiltration of Humic acids contained simulated wastewater. The statistical analysis describes the error calculation and significant difference between the experimental and theoretical flux decline behavior. From the Table 1, it is clear that the comparative study is significant with 0.99 regression (R^2) for all the TMP drops. Figures 3(a)-(c) represent the prediction of theoretical and experimental flux decline analysis using ANN for different TMP drops condition. It is found that all the data points are very close to the diagonal line with perfect regression for all the TMP drops. The high F-value and low p-value remark the good model prediction during theoretical analysis of permeate flux decline. However, at low TMP drop of 207 kPa, a minimum mean square error of 0.71 is obtained than other TMP drops.

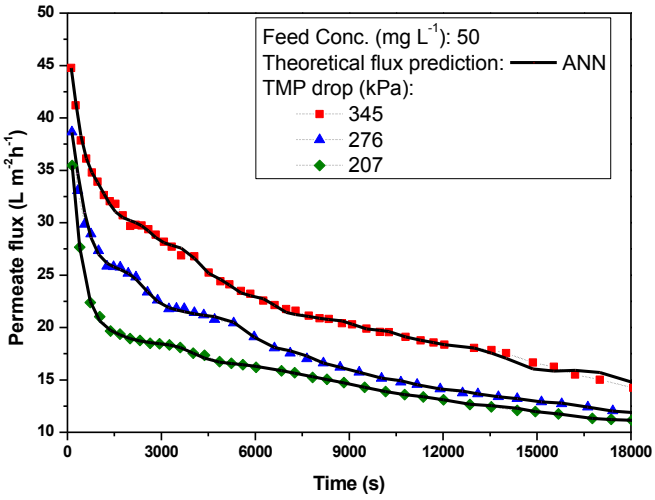

Figure 2. Experimental and ANN predicted transient flux decline behavior with respect to process time for different TMP drop (ΔP , kPa)

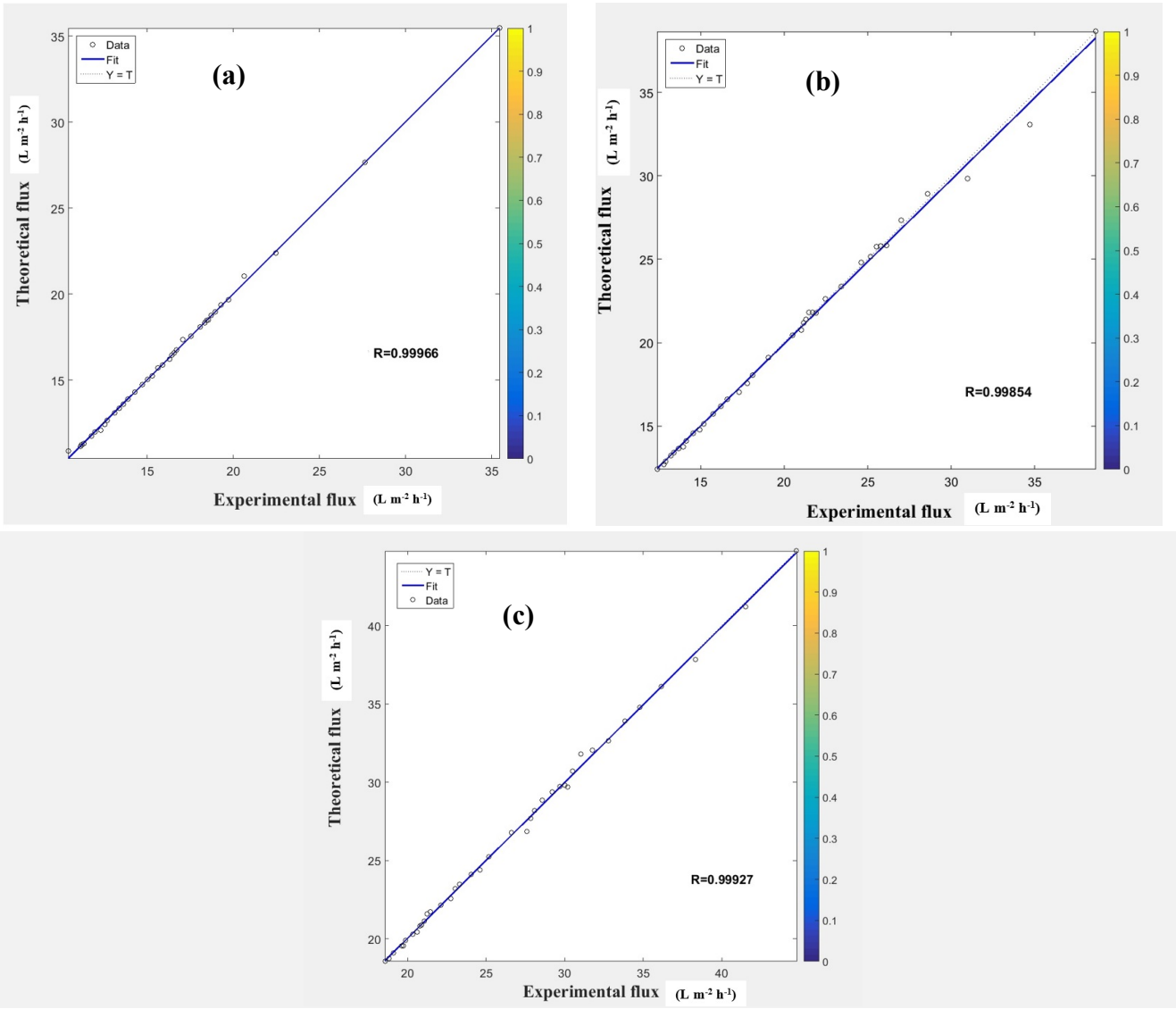

Figure 3. The prediction of theoretical and experimental flux values using ANN analysis at different TMP drops (a) 207, (b) 276 and (c) 345 kPa

Table 1. Analysis of variance (ANOVA) for theoretical permeate flux at different ΔP, (kPa)

Source ΔP,(kPa)	Sum of square	Degrees of freedom	Mean square error	F-value	p-value	Total error	Regression R^2
207	36.65	52	0.71	4.41	0.0001	8.47	0.99
276	506.63	52	9.74	375.38	0.0001	1.38	0.99
345	1091.34	52	20.98	216	0.0001	5.13	0.99

3.2 Analysis of permeate quality in terms of removal of TDS and conductivity

The analysis of permeate quality at different operating TMP drop (207 to 345 kPa) has been represented in Figure 4. The rate of decreasing of conductivity and TDS is linear with increasing TMP drop. The ionic conductivity has been decreased up to 0.0103 S m^{-1} from its initial state of 0.274 S m^{-1}. With the increasing of TMP drop from 207 to 345 kPa, the rejection rate of solute particles has been increased thus, the ionic conductivity is also decreased from the solution. The same trend has been found for the removal of TDS from the collected permeate. The initial TDS content was 45 mg L^{-1}. Whereas, with the increasing of operating pressure, dissolved solids has been removed from the permeate which has been shown in the following Figure. It is very clear that with the increment of TMP drop the permeate quality in terms of removal of TDS and ionic

conductivity has been improved. On the other side, the maximum Humic acids (HAs) rejection (R_s, %) was found around 93.8% at high TMP drop of 345 kPa. With increasing TMP drop, the formation of gel layer on the active membrane surface has been increased. The gel layer provides an extra mass transfer resistance which increases the rejection rate at high TMP drop. Near about 90% reduction of Humic substance from water was reported using ferrate (IV) oxidization at pH 7.1 to 7.8 (Qu et al., 2003). This comparison reveals that membrane filtration has better rejection efficiency than other processes.

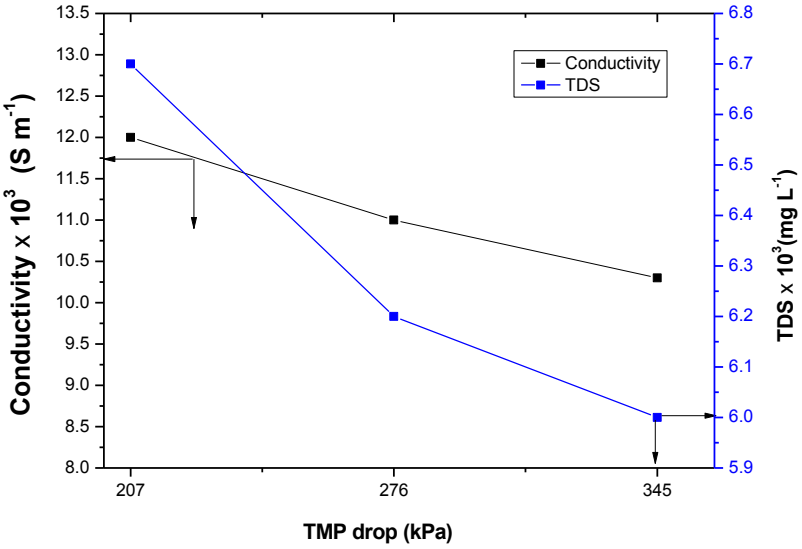

Figure 4. Variation of permeate quality in terms of TDS and conductivity at different operating pressure (TMP drop, kPa)

3.3 Prediction of cake layer formation with respect to time based on Hermia's pore blocking method

The formation of cake layer with respect to process contact time has been characterized using Hermia's power law model. The overall analysis of pore clogging characteristics of HAs ultrafiltration has already been discussed in our previous work (Saha et al., 2015). It was discussed that intermediate pore blocking mechanism (IPBM) revealed the good agreement with experimental data points. In the present study, the close observation of pore blocking mechanism with cake layer formation has been performed with the filtration time. The fitness of the two models is shown in Figure 5. A gradual change in slope decline has been observed in Figure 5(a). This criterion reveals that intermediate pore clogging occurs at the very beginning of the filtration. Whereas, a sharp slope decline is found in Figure 5(b). The change in slope decline reveals that the formation of cake layer happens after 50 min of process filtration. According to the predicted values, the cake layer model (n=0) fits the experimental data after 50 min of filtration, whereas IPBM (n=1) reveals the decline of permeate flux at the initial stage of filtration. The predicted regressions (R^2) and residuals for both the cases are enlisted in Table 2.

Table 2. Summary of the Hermia's model prediction of IPBM and CFM

	IPBM (n=1)				CFM (n=0)			
	Initial stage		Final stage		Initial stage		Final stage	
ΔP(kPa)	R^2	Residual sum of square	R^2	Residual sum of square	R^2	Residual sum of square	R^2	Residual sum of square
207	0.99	1.4×10^{-5}	0.99	1.7×10^{-6}	0.84	5.1×10^{-7}	0.99	4.7×10^{-7}
276	0.98	1.8×10^{-6}	0.98	7.1×10^{-7}	0.85	2.1×10^{-7}	0.99	1.1×10^{-7}
345	0.98	3.5×10^{-6}	0.98	8.9×10^{-6}	0.85	4.1×10^{-7}	0.99	5×10^{-7}

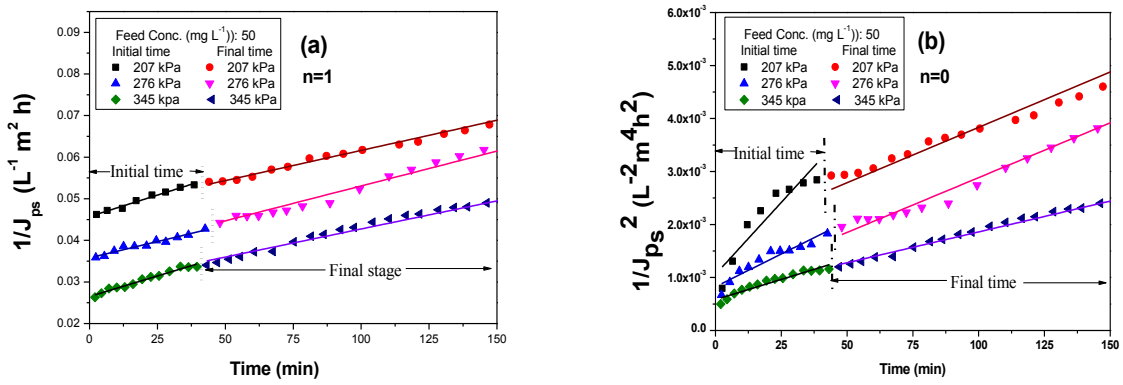

Figure 5. Fitness graph for (a) IPBM and (b) CFM during ultrafiltration

4. CONCLUSIONS

Treatment of HAs containing synthetic wastewater was performed using membrane batch ultrafiltration. The TMP drop was an important parameter to explore the permeate flux decline nature. Transient flux decline behavior was analyzed and compared with the theoretical approach using artificial neural network (ANN) system. According to ANOVA analysis, 0.71 mean square error at a low TMP drop of 207 kPa reveals the good theoretical prediction during membrane filtration. The permeate quality in terms of removal of ionic conductivity and TDS was also verified at different TMP drops. Moreover, 93.8% rejection of HAs was achieved at 345kPa TMP drop. Pore blocking law reveals that the pores were clogged with solute particles internally at the very beginning of the filtration than cake layer formation on the membrane surface.

LIST OF SYMBOLS

A_m	Active membrane surface area (m^2)
C_{pHumic}	Solute concentration in the permeate side (mg L^{-1})
C_{0Humic}	Solute concentration in the prepared feed solution (mg L^{-1})
J_{ps}	Permeate flux (L m^{-2} h^{-1})
J_w	Pure water flux (L m^{-2} h^{-1})
J_0	Initial flux (L m^{-2} h^{-1})
k_{ii}	IPBM constant (m^{-1})
k_{Am}	Membrane surface blocked per unit of total volume permeated (m^{-1})
$k_{clHumic}$	CFM constant ($m^{-2}s^{-2}$)
k_{DC}	Cake layer area per unit of membrane filtration (m^{-1})
L_p	Water permeability (m Pa^{-1} s^{-1})
n	Hermia's pore blocking exponent
R_{cake}	Cake layer resistance (m^{-1})
R_{fresh}	Fresh membrane resistance (m^{-1})
R_s	Percentage of rejection coefficient (%)
R^2	Regression coefficient
ΔP	Transmembrane pressure drop (kPa)

REFERENCES

Andrews, J., Smit, A. M., Wijeyekoon, S., Mcdonald, B., Baroutian, S., Gapes, D., 2014. Application of hydrothermal treatment to

affect the fermentability of Pinus radiata pulp mill effluent sludge. Bioresour. Technol.; 170: 100-107.

Bhatnagar, A., Sillanpaa, M., 2017. Removal of natural organic matter (NOM) and its constituents from water by adsorption-A review. Chemosphere.; 166: 497-510.

Baguena, M. J. C., Vela, M. C. V., Zafrilla, J. M. G., Blanco, S. A., Garcia, J. L., Martinez, D. C., 2016. Comparison between artificial neural networks and Hermia's models to assess ultrafiltration performance. Sep. Purif. Technol.; 170: 434-444.

Choi, Y., Choi, Y. J., 2010. The effects of UV disinfection on drinking water quality in distribution systems. Water. Res.; 44: 115-122.

Das, A., Paul, D., Golder, A. K., Das, C., 2015. Separation of Rebaudioside-A from stevia extract: Membrane selection, assessment of permeate quality and fouling behavior in laminar flow regime. Sep. Purif. Technol.; 144: 8-15.

Das, C., Patel, P., De, S., Gupta, S. D., 2006. Treatment of tanning effluent using nanofiltration followed by reverse osmosis. Sep. Purif. Technol.; 50: 291-299.

Fu, J., Lee, W. N., Coleman, C., Meyer, M., Carter, J., Nowack, K., Huang, C. H., 2017. Pilot investigation of two stage biofiltration for removal of natural organic matter in drinking water treatment. Chemoshere.; 166: 311-322.

Galambos, I., Vatari, G., Molnar, E. B., 2004. Membrane screening for humic substance removal. Desalination.; 162: 111-116.

Jia, S., Yang, Z., Ren, K., Tian, Z., Dong, C., Ma, R., Yu, G., 2016. Removal of antibiotics from water in the coexistance of suspended paricles and natural organic matters using amino-acid-modified-chitosan flocculants: A combined experimental and theoretical study. J. Hazard. Mat.; 317: 593-601.

Liu, Y., Liu, Jing., Zhang, A., Liu, Z., 2017. Treatment effects of genotoxicity of the toxic organic pollutants in semi-coking wastewater by combined treatment process. Environ. Pol.; 220: 13-19.

Lyon, B. A., Cory, R. M., Weinberg, H. S., 2014. Changes in dissolved organic matter fluoresence and disinfection byproduct formation from UV and subsequent chlorination/ chloramination. J. Hazard. Mat.; 264: 411-419.

Manttari, M., Viitikko, K., Nystrom, M., 2006. Nanofiltration of biologically treated effluents from pulp and paper industry. J. Membr. Sci.; 272: 152-160.

Qu, J. H., Liu, H. J., Liu, S. X., Lei, P. J., 2003. Reduction of fulvic acidin drinking water by ferrate. J. Environ. Eng. ASCE.; 129: 17-24.

Saha, S., Das, C., 2015. Analysis of fouling characteristics and flux decline during Humic acids batch ultrafiltration. J. Chem. Eng. Process Technol.; 6: 252-258.

Singh, V.,Jain, P. K., Das, C., 2013. Performance of spiral wound ultrafiltration membrane module for with and without permeate recycle: Experimental and theoretical consideration. Desalination.; 322: 94-103.

Wang, H., Zhu, Y., Hu, C., 2017. Impacts of bacteria and corrosion on removal of natural organic matter and disinfection byproducts in different drinking water distribution systems. Inter. Biodeter. Biodeg.; 117: 52-59.

Proceedings of the 10th World Congress of EWRA 'Panta Rhei', 5-9 July 2017, Athens, Greece
© 2017 *European Water Resources Association*

Removal of diclofenac in drinking water with fenton process

S. Ustun Odabasi* and H. Buyukgungor
Ondokuz Mayis University, Environmental Engineering Department, Atakum, Samsun 55200, Turkey
* *e-mail: sevde.ustun@omu.edu.tr*

Abstract: Pharmaceutical residues are found in low concentrations (µg/L-ng/L) in aquatic environment. Pharmaceuticals are used to treat human and animal diseases. These drugs and their metabolites are excreted unchanged and they are continuously mixed in wastewaters. The residues of these compounds can be involved in environment in different ways: for example, expired drugs, hospital wastewater, human and animal excretion, pharmaceutical industry. Diclofenac sodium salt is a non-steroidal anti-inflammatory drug (NSAID) and is used commonly in worldwide. Conventional wastewater treatment plants are not sufficient to remove micropollutants, therefore advanced oxidation process have become an emerging solution. Fenton process is a branch of advanced oxidation process. Therefore, fenton process is used to clear out the effectiveness of diclofenac degradation in drinking water. In the present study, under laboratory conditions, coagulation and advance oxidation, with H_2O_2 and $FeSO_4$ (Fenton process) are used to degrade the concentrations of diclofenac from water conducted. To find out, biodegradability of the treated solutions the COD and TOC values of the background constituents in the water matrix are planned to measure. For this purpose, we used 10 mg/l diclofenac sodium salt synthetic solution with selected different parameters as, pH (2-6), $FeSO_4$ and H_2O_2 concentration (30-75-150 mg/l), stirring time (10, 20, 30 minutes), residence time (30, 60, 90 minutes) all in room temperature. These selected parameter are the determined optimal values. After processing, 150 ml of sample is taken out from the upper layers of the solutions to make COD and TOC tests.

Key words: Diclofenac, Fenton Process, Pharmaceuticals, Water, Wastewater

1. INTRODUCTION

Diclofenac (DFC) is a non-steroidal anti-inflammatory drug (NSAID) mostly used to treat inflammatory and painful diseases (Basavaraju, 2012, Vogna et al. 2004). This pharmaceutical is excreted about %15 unchanged after human consumption (Basavaraju, 2012). Diclofenac, other name is [2-[(2,6-Dichlorophenyl)amino]phenyl]acetic acid, is shown in Table 1. Pharmaceutical residues are transported to water body. DFC leaves the body in the shape of metabolized and non-metabolized after excretion (Lishman et al. 2006). To say more clearly, after using DFC by patients, the disused parts are removed out of body by urine. In this way, the residue of DFC goes through canalization and reaches the treatment plant. It is a way to survive not only for contamination but also cumulating in sediments. The water from treatment plant and sediment can be used for agriculture which has access to reach soil and ground water (Kummerer, 2001, Heberer, 2002). The wastewater treatment plants are not capable to remove of micropollutant. Furthermore, micropollutants can be introduced to drinking water. For example, DFC was detected at less than 10 ng/L in drinking water sample taken from a private water tap in Berlin (Heberer, 2002). Therefore, it is recommended to use advanced oxidation processes in micropollutant removal. The studies show that classic fenton, fenton like process, ozonation, ultraviolet system are good for micropollutant removal. Fenton process is suitable for the degradation of diclofenac because of cheap, efficient and fast. The classic fenton process to degrade and mineralize diclofenac in synthetic solution is investigated (Jianlong et al. 2016).

In this paper, DFC is chosen as the target contaminant to investigate the oxidation performance with different parameters including the oxidant dosage, pH, stirring time and waiting time (Fenton process).

Table 1. Physico-chemical and pharmacological properties of DFC (Zhang et al. 2008)

Chemical structure	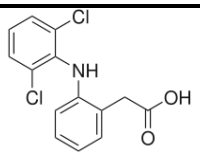
Molecular formula	$C_{14}H_{11}C_{12}NO_2$
Molecular weight	269,16 g mol−1
Water solubility	23,73 mg L−1 (25 °C)
Octanol-water partitioning	-
pKa	4,15
Usage	Analgesic, anti-inflammatory
Excretion	Biliary excretion: 65 % of oral dosage excreted in urine.

2. MATERIAL AND METHODS

In the present study, under laboratory conditions, coagulation and advance oxidation, using H_2O_2 and $FeSO_4$ (Fenton process) is used to degrade the concentrations of diclofenac from water are conducted. In the experiments, Tablet is used to obtain diclofenac content. We used 10 mg/l diclofenac synthetic solution. To find out, biodegradability of the treated solutions the COD and TOC values of the background constituents in the water matrix are planned to measure. In the end of the experiments, to determine the efficiency of Fenton process, optimum pH, $FeSO_4$, H_2O_2, stirring time and waiting time is measured. Before starting our experiments we checked initial values of COD, TOC and amount of diclofenac in untreated samples. Later, we used 10 mg/l diclofenac sodium salt synthetic solution with selected different parameters as, pH (2-6), $FeSO_4$ and H_2O_2 concentration (30-75-150 mg/l), stirring time (10, 20, 30 minutes), residence time (30, 60, 90 minutes) all in room temperature. After processing, 150 ml of sample is taken out from the upper layers of the solutions to make COD and TOC tests.

Chemicals used were 35% pure grade Hydrogen Peroxide (Merck); 99.5% pure grade Iron Sulphate (Sigma Aldrich); 98% pure grade Sulfuric Acid (Merck); >99 % Sodium Hydroxide (Merck) for Fenton processes. Potassium Dicromate >99.9 (Merck); Iron Ammonium Sulphate (Carlo Erba) 99% pure grade; 1.10-phenanthroline and monohydrate (Sigma Aldich) >99.9%; Mercury Sulphate (Sigma Aldrich) >98%; Silver Sulphate (Sigma Aldrich) >99% for COD analysis. All chemicals are used as received without further purification. All aqueous solutions are prepared with distilled water. Total organic carbon (TOC) are measured using Apollo 9000 combustion TOC analyzer. The COD tests are analyzed according to standard method (Methods: 5220 C. Closed Reflux Titrimetric Method). The pH of all the samples are measured using pH meter (Ohasus).

3. RESULTS AND DISCUSSION

Before starting the analysis, initial physicochemical properties of synthetic wastewater prepared from tap water are recorded and are given in Table 2.

Table 2. Physicochemical properties of synthetic wastewater

Parameters	Units	Results
pH	pH birimi	6,92
TDS	µS/cm	403
Turbidity	NTU	1,4
Temperature	ºC	21,9
Dissolved oxygen	mg/L	6,98

Firstly, all experiment with different pH like 2, 3, 4 and 6 is performed with concentrations: 75 mg/l, $FeSO_4$; 75 mg/l, H_2O_2; stirring time, 20 minutes and waiting time, 60 minutes, at room

temperature. After measuring COD and TOC, pH < 3,5 is decided as also optimum as discussed in different studies (Sonmez, 2016; Ustun Odabasi et al. 2016). Results of TOC are described in Figure 1.

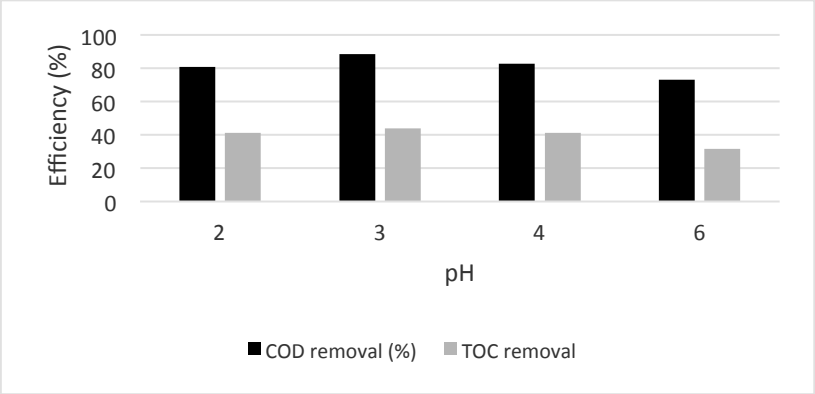

Figure 1. DFC removal with Fenton process (pH<3,5 effect)

In the second step, optimum concentration of $FeSO_4$ for the degradation of drug is determined. For this purpose with optimum pH of <3.5, 75 mg/l, H_2O_2; stirring time, 20 minute; waiting time, 60 minute, different concentrations of $FeSO_4$ like, 30-75-150 mg/L are applied. For every observed results of COD and TOC, the best value of $FeSO_4$ is found to be 75 mg/L. Results of TOC and COD are provided in Figure 2.

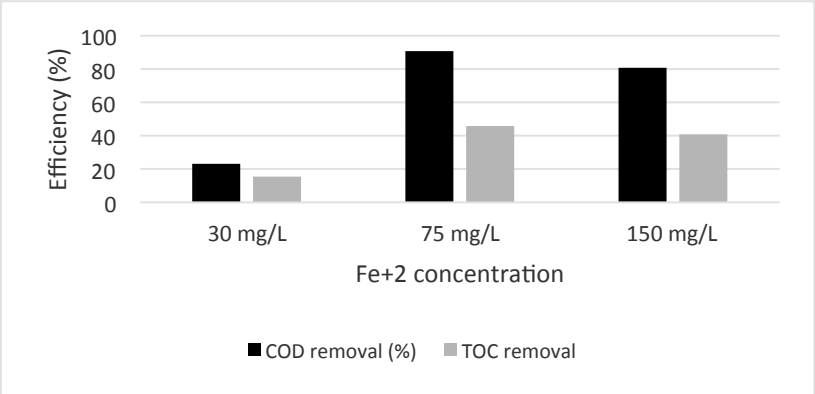

Figure 2. DFC removal with Fenton process (Fe^{+2} effect)

The purpose of third step was selection of optimum value of H_2O_2. In this step different concentrations of H_2O_2 like 30-75-150 mg/l are selected with optimum pH<3.5, optimum value of $FeSO_4$ 75 mg/L along with stirring time, 20 minute and waiting time, 60 minute. According to the observed values of COD and TOC, optimum value of H_2O_2 is selected as 75 mg/l. Published literature has shown that degradation of drugs increases with the increase amount of H_2O_2, hence increased amount of H_2O_2 means good degradation (Kang et al. 2000; Ustun Odabasi and Buyukgungor, 2016). H_2O_2 is not a sustainable chemical because of its harmful impact on environment. For this reason, it should not be used in large quantities. 150 mg/l and 75 mg/l H_2O_2 of dosage results were close to each other. Therefore, 75 mg/l of H_2O_2 dosage is chosen in this study. Observed TOC and COD results are shown in Figure 3.

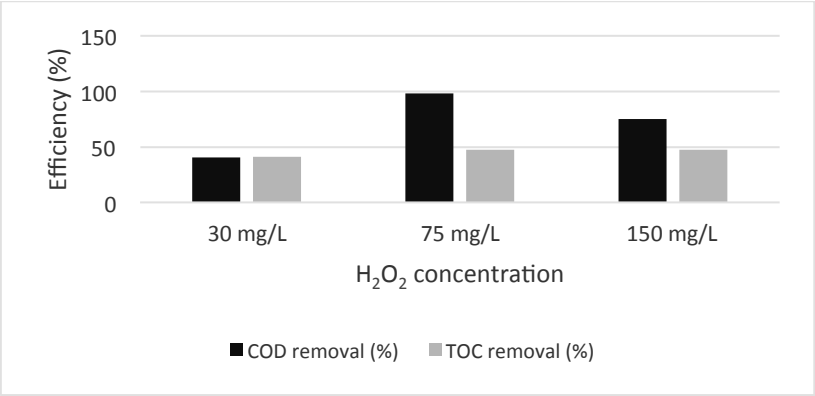

Figure 3. DFC removal with Fenton process (H_2O_2 effect)

In the fourth step, the optimum stirring time is figured out by applying different stirring times of 10-20-30 minutes with selected optimum pH<3.5, optimum value of $FeSO_4$ 75 mg/L, H_2O_2 75 mg/l along with waiting time; 60 minute. COD and TOC results showed that 20 minute is the best optimum stirring time. Values of TOC and COD are showed in Figure 4.

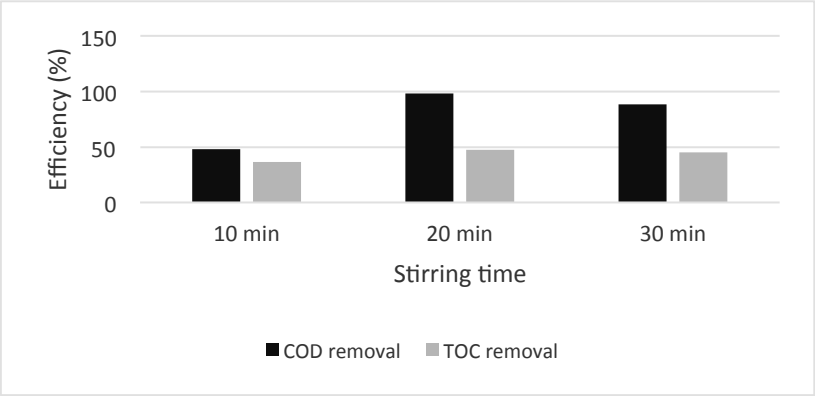

Figure 4. DFC removal with Fenton process (stirring time)

In the fifth step, the waiting time is figured out by applying different waiting times of 30-60-90 minutes to the solution under optimized parameters: pH<3.5, optimum value of $FeSO_4$ 75 mg/L, H_2O_2 75 mg/l, 20 minute stirring time. COD and TOC results showed that 90 minute is the best optimum waiting time. Values of COD and TOC are showed in Figure 5.

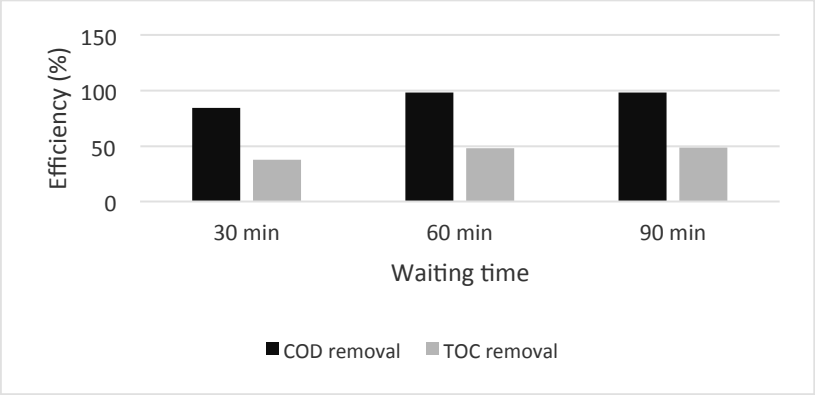

Figure 5. DFC removal with Fenton process (waiting time)

Total results are shown in Table 3.

Table 3. Results of total analysis

		COD results (mg/l)	COD removal (%)	TOC results (mg/l)	TOC removal (%)
pH	**2**	32	80,76	36,56	41,25
	3	19,2	88,46	34,83	44,03
	3,5	15	90,98	33,70	45,85
	4	28,8	82,69	36,68	41,06
	6	44,8	73,08	42,61	31,53
Fe^{+2} (mg/l)	**30**	128	23	52,68	15,35
	75	15	90,98	33,70	45,85
	150	32	80,76	36,92	40,68
H_2O_2 (ml)	**30**	99,2	40,38	36,52	41,32
	75	3,2	98,07	32,60	47,62
	150	41,6	75	32,81	47,28
Stirring Time (min)	**10**	86,4	48,07	39,39	36,71
	20	3,2	98,07	32,60	47,62
	30	19,2	88,46	34,18	45,08
Waiting Time (min)	**30**	25,6	86,41	38,84	37,59
	60	3,2	98,07	32,40	47,94
	90	3,1	98,13	32,08	48,45

*(Initial pH; 6,92, COD value; 166,4 mg/l, TOC value; 62,24 mg/l)

4. CONCULSION

There is a limited number of studies to determine the presence of micropollutant in drinking water. Most of the studies, report very low concentration or below detection concentration in drinking water treatment plants (Yunlong et al. 2014). Diclofenac is widely present in wastewaters and ultimately in water bodies. Therefore, it is necessary to evaluate and address their impact on the ecosystems by applying degradation techniques.

In the present study, all the results and best working conditions for the degradation of DFC are precisely described as: pH<3,5, $FeSO_4$; 75 mg/l, H_2O_2; 75 mg/l, stirring time; 20 minutes and waiting time; 90 minutes. According to these results, highest removal efficiencies for COD and TOC are 98,13 and 48,45% respectively at room temperature. Results suggested that DFC degradation enhanced as the H_2O_2 dosage increased. But, excessive usage of H_2O_2 should be avoided because of its harmful impacts. Although DFC degradation is difficult with conventional and biological treatments but still fenton process is a compromising technique. We suggest further experiments at different conditions.

REFERENCES

Basavaraju M. M., 2012. Degradation kinetics of diclofenac in water by Fenton's oxidaiton. Journal of Sustainable Energy & Environment, 3, 173-176.

Heberer T., 2002. Occurance, fate and removal of pharmaceutical residues in the aquatic environment; a review of recent research data. Toxicol. Lett., 131, 5-17.

Jialong W., Wang S., 2016. Removal of pharmaceuticals and personal care products (PPCPs) from wastewater: A review, J. Environ. Manage., 182, 620-640.

Kang, Y.W., Hwang K., 2000. Effect of reaction conditions on the oxidation efficiency in the Fenton process, Water Res., 10, 2786-2790.

Kummerer K., 2001. Drugs in the environment-. Emissions of drugs, diagnostic acids and disinfectants into wastewater by hospitals in relation to other sources-a review, Chemosphere, 45, 957-969.

Lishman L., Smyth S. A., Sarafin K., Kleywegt S., Toito J., Peart T., Lee B., Servas M., Beland M., Seto P., 2006. Occurrence and reductions of pharmaceuticals and personal care products and estrogens by municipal wastewater treatment plants in Ontario, Canada, Sci. Total Environ., 367, 544-558.

Sonmez G., 2015. Removal of some pharmaceutical residues by advanced chemical oxidation process, Aksaray University, Science Enstitue, November.

Ustun Odabasi S., Maryam B., Buyukgungor H., 2016. Assessment and investigation of paracetamol from wastewater by using oxidation process and TOC, 3rd International Conference on Recycling and Reuse, Istanbul, Turkey, 28-30 September, 161-166.

Ustun Odabasi S., Buyukgungor H., 2016. Investigation of degradability of ibuprofen from wastewater by using advanced oxidation process, ICOEST International conference on environmental science and technology, Belgrade, Serbia, 28 September- 2 October, 162-167.

Vogna D., Marotta R., Napolitano A., Andreozzi R., d'Ischia M., 2004. Advanced oxidation of the pharmaceutical drug diclofenac with UV/H_2O_2 and ozone, Water Res., 38, 414-422.

Yunlong L., Wenshan G., Huu H. N., Long D. N., Faisal I. H., Jian Z. Shuang L., Xiaochang C. W., 2014. A review on the occurrence of micropollutants in the aquatic environment and their fate and removal during wastewater treatment, Sci. Total Environ., 473–474, 619–641.

Zhang Y, Geißen S. U., Gal C. 2008.Carbamazepine and diclofenac: Removal in wastewater treatment plants and occurrence in water bodies. Chemosphere, 73:1151–1161.

Proceedings of the 10th World Congress of EWRA 'Panta Rhei', 5-9 July 2017, Athens, Greece
© 2017 *European Water Resources Association*

CFD-aided modelling for hydrodynamic analysis of biological reactor

S. Manenti*, S. Todeschini, M.C. Collivignarelli and A. Abbà
Dipartimento di Ingegneria Civile e Architettura, Università di Pavia, Pavia, Italy
* *e-mail: sauro.manenti@unipv.it*

Abstract: The performance testing of treatment plants is of great concern in the field of environmental engineering, especially regarding the management of wastewater plants devoted to treatment and reuse. The efficiency of the treatment process is strictly related to both biological kinetics and hydrodynamics, influencing each other. In fact, the actual hydrodynamic behaviour of a biological reactor can deviate significantly from the design hypotheses, leading to hydraulic defects such as formation of dead volume and bypass. These problems exert a strong influence on the biological process and therefore affect the treatment efficiency of the plant. The Residence Time Distribution (RTD) analysis is commonly adopted for quantifying the type and amount of the functioning deficiencies affecting the process. However, to address the corrective intervention, these deficiencies should be localized by integrating RTD method with Computational Fluid Dynamics (CFD). This paper shows the early studies of a wider research project aiming at developing a standardized method combining RTD and CFD techniques for mitigating or eliminating functioning defects in biological reactors. An application of CFD-aided modelling for assessing hydrodynamic behaviour of an activated sludge (AS) pilot plant is illustrated. The obtained results are compared with experimental results from RTD analysis, showing how the CFD model can help supporting design of new facilities and the optimization or retrofitting of existing facilities for wastewater treatment.

Key words: finite volume modelling, RTD analysis, biological reactor, pilot plant, experimental verification, hydrodynamic analysis, functioning defects, dead volume

1. INTRODUCTION

Biological processes represent the central step in the urban wastewater treatment, as well as in the treatment process of several industrial wastewater. Their management has been significantly improved in the last century on the basis of both scientific and technical experiences thus meeting the specific requirements imposed by discharge permits (Hreiz et al. 2015).

Anyway the cost-effective management of these plants to match high treatment efficiency with suitable quality standard of the effluent is still an open challenge (Karpinska & Bridgeman, 2016).

As well known, the treatment efficiency is equally determined by biological kinetics and the hydrodynamic behaviour; thus similar treatment efficiencies can be obtained with reactors of quite different volume depending on their hydrodynamics and possible related defects (most frequently, bypass and dead volume).

The experimental verification of the hydrodynamic behaviour of a reaction tank can be carried out through the retention time distribution (RTD) analysis (Nauman, 2007); it derives from the well-established knowledge in the field of chemical engineering (Levenspiel, 1998) that has been successfully applied to pilot plants for biological nutrient removal with the aim of evaluating volume utilization through the identification of both short circuiting and dead volumes (Newell et al. 1998).

The experimental stimulus-response test can be carried out by injecting a tracer at the reactor's inflow and measuring over time its concentration at the outflow. The obtained experimental RTD curve can be interpolated through tank-in-series analytical models that mimic the reactor's hydrodynamic response by accounting for possible bypass and dead volume.

This diagnostic phase of the RTD analysis provides "global" information about the presence of possible hydrodynamic defects and their extent. In order to address proper remedial interventions, a

corrective phase is necessary in which the "local" flow conditions should be evaluated; such a goal can be achieved, for example, with the adoption of computational fluid dynamics (CFD) techniques (Le Moullec et al. 2010).

The numerical modelling allows evaluating, at each elementary volume inside the reactor, the local mean residence time of the occupying fluid particle, that is the average time to reach that volume since this particle entered the inlet's reactor. This calculation is of major concern in order to characterize the process (Baléo et al. 2000) and to detect possible hydrodynamic defects.

This work presents the early results of a wider study that integrates the RTD analysis with finite volume modelling applied to the AS reactor in a pilot plant for wastewater treatment with the aim of assessing and localize possible hydrodynamic defects. It is assumed that the pilot plant operates with a steady state flowrate.

In the following sections, the basic features of the numerical model of the reactor are illustrated. Subsequently, the relevant results are commented, concerning the spatial distribution of the mean residence time that helps to localize the hydrodynamic defects in the worse functioning condition. The numerical results are compared with the experimental results from the RTD analysis carried out in the pilot plant to assess the reliability of the finite volume modelling.

2. NUMERICAL MODELLING

The stationary hydrodynamic analysis of the biological reactor has been carried out with a finite volume commercial software (CD-adapco, STAR-CCM+).

To reduce computational effort, the symmetry of the tank has been taken into account; the simulated half geometry of the reactor is shown in Fig 1. An upstream compartment is devoted to nitrogen removal, while the downstream compartment combines substrate oxidation and nitrification.

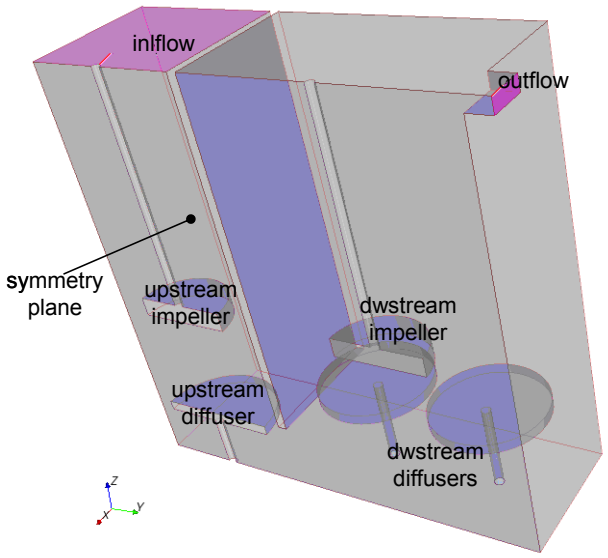

Figure 1. Geometry of the half reactor.

Since the study is focused on the hydrodynamics, the pilot plant operates with clear water; furthermore, all the diffusers at the bottom of the reactor are turned off because the organic matter is absent. These conditions allow simplifying the numerical model by carrying out single-phase stationary analysis of a Newtonian-fluid.

The inflow and outflow rate are equal to about Q = 0.02 L/s, while the total volume of the half reactor is roughly V = 0.22 m^3. Therefore, the average hydraulic retention time of the reactor is approximately $\bar{t} = V/Q = 3$ h.

The steady turbulent incompressible isothermal flow is obtained through numerical solution of RANS model that, in general, assumes the following form:

$$\nabla \cdot \mathbf{v} = 0$$
$$\frac{\partial \mathbf{v}}{\partial t} + \mathbf{v} \cdot \nabla \mathbf{v} = -\frac{1}{\rho} \nabla p + (\nu + \nu_T) \nabla^2 \mathbf{v} + \mathbf{g} \tag{1}$$

The symbols in Eqs. (1) are: **v** ensemble average velocity vector, ρ = 1000 kg/m^3 fluid density, p pressure, ν = 1.0e-6 m^2/s kinematic viscosity, ν_T eddy viscosity, **g** gravity acceleration.

The Eqs. (1) are coupled with standard k-ε model to obtain closure of the mathematical problem. The following balance differential equations of the specific turbulent kinetic energy k (TKE) and its specific dissipation rate ε are considered:

$$\frac{\partial k}{\partial t} + v_j \frac{\partial k}{\partial x_j} = \frac{\partial}{\partial x_j} \left[\left(\frac{\nu_T}{\sigma_k} + \nu \right) \frac{\partial k}{\partial x_j} \right] + \nu_T \left(\frac{\partial v_i}{\partial x_j} + \frac{\partial v_j}{\partial x_i} \right) \frac{\partial v_i}{\partial x_j} - \varepsilon$$
$$\frac{\partial \varepsilon}{\partial t} + v_j \frac{\partial \varepsilon}{\partial x_j} = \frac{\partial}{\partial x_j} \left[\left(\frac{\nu_T}{\sigma_\varepsilon} + \nu \right) \frac{\partial \varepsilon}{\partial x_j} \right] + C_{1\varepsilon} \frac{\varepsilon}{k} \nu_T \left(\frac{\partial v_i}{\partial x_j} + \frac{\partial v_j}{\partial x_i} \right) - C_{2\varepsilon} \frac{\varepsilon^2}{k} \tag{2}$$

The symbol v_i denotes the Cartesian components of the average velocity **v** in the coordinate system x_i (i = 1, 2, 3); summation convention is assumed for repeated indices. The symbols $C_1\varepsilon$ =1.44, $C_2\varepsilon$ =1.9, σ_ε = 1.3, σ_k = 1.0 in the transport Eqs. (2) are empirical coefficients; the turbulent coefficient ν_T is related to the empirical coefficient C_μ = 0.09 by the following relation:

$$\nu_T = C_\mu \frac{k^2}{\varepsilon} \tag{3}$$

Once the stationary flow field has been calculated through the solution of the balance Eqs. (1) coupled with the turbulence quantity transport Eqs. (2), the local mean residence time T_{res} of a fluid particle at any elementary volume within the reactor is evaluated by solving a transport equation for the passive scalar field Θ:

$$\frac{\partial \Theta}{\partial t} + \mathbf{v} \cdot \nabla \Theta = \left(\frac{\mu}{\sigma} + \frac{\mu_T}{\sigma_T} \right) \nabla^2 \Theta \tag{4}$$

In Eq. (4) σ and σ_T are, respectively, the laminar and turbulent Schmidt numbers.

The three dimensional computational domain has been discretized by means of polyhedral meshes resulting in a total number of about 316000 elementary volumes.

The constant flow rate Q has been assigned at the inflow boundary, while constant pressure of 0.0 Pa is assumed at the outflow section (Fig. 1). The obtained solution is identical to the one that would be obtained by mirroring the mesh about the symmetry plane outside the computational domain. All the solid surfaces delimiting the tank are treated as impermeable wall boundaries.

3. RESULTS, DISCUSSION AND CONCLUSIONS

Two functioning conditions of interest have been investigated: *a*) only upstream impeller turned on, and *b*) upstream and downstream impellers turned off (no-mixing).

In both cases the numerical results confirm the experimental results obtained from RTD analysis of the pilot plant through pulse injection of non-reactive tracer at the inflow.

No bypass occurs in both operating conditions *a*) and *b*); this is due to the peculiar geometry of the reactor that avoids hydraulic short-circuiting. Therefore the inflowing fluid crosses the whole reactor's volume before reaching the outflow section (see also Fig 3).

Concerning the operating condition *b*) with absence of mechanical mixing, the numerical model confirms the results of the RTD analysis that has detected an overall dead volume of about 5%.

This is visible in Fig. 2 where is plotted the cumulative distribution of the residence time as percentage of the reactor's volume (blue curve). The *y*-parallel dashed black line is traced at T_{res} = 30 h, that is ten times the average hydraulic retention time $\bar{t}$, which can be assumed as a limit of the retention time to detect a dead volume (Collivignarelli et al. 1995).

The ordinate of the intersection point between the black line and blue curve is equal to about 0.95 meaning that approximately 5% of the total reactor's volume is characterized by a residence time that exceed 30 hours.

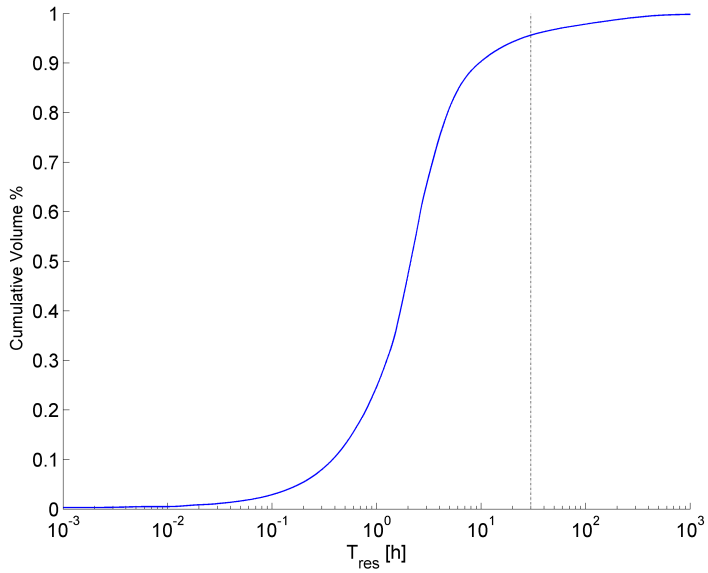

Figure 2. Cumulative distribution of the residence time (no-mixing).

From Fig. 3 it can be seen that the major part of the detected dead volume is located in the upper left-hand portion of the downstream compartment: in this zone the calculated local mean residence time exceeds the above mentioned limit of 30 hours.

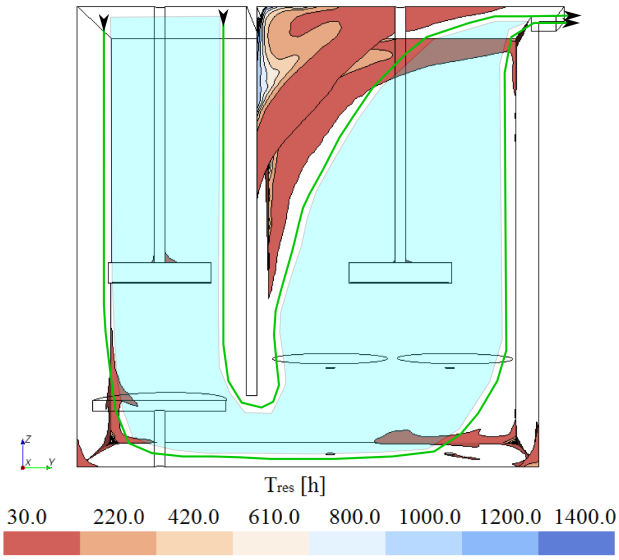

Figure 3. Dead volume distribution with both impellers turned off (no-mixing).

The pale-blue area between the two green streamlines shows, in a qualitative manner, the average hydrodynamic path of the fluid inside the reactor and points out those zones outside the path where recirculating flow occurs. Among these zones, those ones located at the bottom left-hand corner of the upstream compartment and at the bottom right-hand corner of the downstream compartment are almost negligible.

In conclusion, CFD modelling proved to be effective for quantifying and localizing dead volume in the investigated reactor. This is also confirmed by the comparison with the RTD experimental analysis of the pilot plant.

Further studies will be carried out to evaluate the effects of possible remedial measures for reducing the amount of dead volume, such as changing the position of the outflow section or modifying the tank geometry near the outflow.

This numerical tool seems therefore reliable to support the design of new facilities and optimization or retrofitting of existing plants by helping to address proper corrective interventions for mitigating hydrodynamic defects.

REFERENCES

Baléo J.N. & Le Cloirec P. 2000 Validating a Prediction Method of Mean Residence Time Spatial Distributions. AIChE Journal Vol. 46, No. 4.

Collivignarelli C., Bertanza G., Bina S. 1995 La verifica idrodinamica nel trattamento delle acque. Basi teoriche - procedure di applicazione - esempi. Collana Ambiente V.8 ISSN 1121-8215 (in Italian).

Hreiz R., Latifi M.A., Roche N. 2015 Optimal design and operation of activated sludge processes: State-of-the-art. Chemical Engineering Journal V. 281 pp. 900–920.

Karpinska A.M., Bridgeman J. 2016 CFD-aided modelling of activated sludge systems. A critical review. Water Research 88 861-879.

Le Moullec Y, Gentric C., Potier O, Leclerc J.P 2010 CFD simulation of the hydrodynamics and reactions in an activated sludge channel reactor of wastewater treatment. Chemical Engineering Science V. 65(1), pp. 492-498.

Levenspiel O. 1998 Chemical Reaction Engineering, 2nd Edition, John Wiley & Sons, New York.

Nauman E.B. 2007 Residence Time Distributions. John Wiley & Sons, Inc., New Jersey, NJ, USA.

Newell B., Bailey J., Islam A., Hopkins L., Lant P. 1998 Characterising bioreactor mixing with residence time distribution (RTD) tests. W. Science and Technology, V. 37 (12), pp. 43-47.

Proceedings of the 10th World Congress of EWRA 'Panta Rhei', 5-9 July 2017, Athens, Greece
© 2017 *European Water Resources Association*

Bimetal doping on TiO_2 for photocatalytic water treatment: A green route

V. Rao and A.K. Golder*
Department of Chemical Engineering, Indian Institute of Technology Guwahati, Assam, Pin 781039, India
* *e-mail: animes@iitg.ernet.in*

Abstract: Herein, we propose a new and green technique of bio-mediated bimetal doping on TiO_2 ($Zn/Cu/TiO_2$) using the aqueous leaf extract of Chayote plant which is rich in ascorbic acid (354 mg/kg leafs). The proposed method was successful to bring down the band gap of TiO_2 to 2.3 eV for $Zn/Cu/TiO_2$ at 1:1:98. The crystallite size of TiO_2 at higher dopants loading was increased significantly (16.3 to 38.4 nm) because of Cu^{2+} and Zn^{2+} induction into the Ti^{4+} lattice and, there was as high as 12% transformation of the anatase phase to the rutile phase of TiO_2. The increase in the absolute value of zeta-potentials of $Cu/Zn/TiO_2$ was notably faster (5 mV per unit pH increase) at $pH>pH_{zpc}$ which was resulted from the rise in oxygen vacancies and, $Cu/Zn/TiO_2$ were mostly present as a separated non-aggregated unit in water with a polydispersity index of 0.201. $Zn/Cu/TiO_2$ exhibited 98% Congo red dye decolourization compared to 59.3 and 68.7% with Zn/TiO_2 and Cu/TiO_2 under the visible light illumination (17700 Lux). COD reduction was 80.6, 71.2, and 75.9% with $Zn/Cu/TiO_2$, Zn/TiO_2, and Cu/TiO_2 with the quantum efficiency of 23.4, 30.8 and 41.5%, respectively. It was found that $O_2^{\bullet-}$ radicals were mostly caused the dye decomposition as evidenced from the electron spin resonance spectroscopy.

Key words: Bimetal doped photocatalyst; Band gap reduction; Visible light absorption; Dye degradation

1. INTRODUCTION

The heterogeneous photocatalysis using TiO_2 is one of the most preferred advanced oxidation processes for the treatment of such effluents (Riaz et al., 2013). The catalyst is easily available, cheap, non-toxic and enough chemical stability (Behera et al., 2016). However, bare TiO_2 is only active in UV region. Therefore, to make it active in the visible region, doping with the transition metals is a common technique (Riaz et al., 2013).

Bi-metal doped photocatalyst shows a better photocatalytic activity than the mono-metal doping or bare systems in many times (Malika et al., 2016; Riaz et al., 2013; Tobaldi et al., 2016). The doping techniques and dopant metal composition could considerably differ the activity of photocatalysts (Malika et al., 2016). Ag and Au doped TiO_2 shows around 3-fold rise in the phenol decomposition rate for bi-metal doped photocatalyst compared to mono-metal doping [8]. Cu and Zn bimetal-doped TiO_2 synthesized by sol–gel method increases the visible light aided photocatalytic activity by a factor 1.5-2 times compared to pristine TiO_2 for decomposition of methyl orange dye (Zhang and Zeng, 2011). Tobaldi et al. synthesized $Cu/Ni/TiO_2$ photocatalyst by thermal induced sol-gel process and reported bi-metal doped TiO_2 is more effective than and mono-metal doping in degradation of gas-solid phase nitrous oxides and isopropanol than decolorization of orange II (Tobaldi et al., 2016).

The visible light absorption could enhance with bi-metal doping and stimulate faster photo-generated electron (e^-) transfer to dopant metal from TiO_2 owing to increase the separation of e^- and hole (h^+) (Malika et al., 2016). The recombination of e^-/h^+ and its separation, plays a key role on the photocatalytic activity. Cu and Zn are low-cost and easily available than many transition metals.

The conventional techniques for metals doping on semiconductor supports are employed by hazardous chemical intensive (Harraz et al., 2013), high thermal energy intensive (Wen et al., 2007) and UV photo-reduction (Bokare et al., 2013). The preferred size and morphology can be attained by these techniques but they are expensive, complex as well as harmful for the environment.

Here we use a bio-inspired method of metal doping on the semiconductor supports mediated by

plant extract as the reserve of the analytes (reducing agent). This work focus on Cu/Zn bimetal-doping on TiO_2 support using the analytes such ascorbic acid (Chelli and Golder, 2016; Ordonez et al., 2006; Rao and Golder, 2016) present in *S. edule* leaf-extract. Thus, the aim of this study was the bio-mediated doping of Cu and Zn on TiO_2 in a bimetallic system for the determination of its impact on dye degradation efficiency. The photocatalysts were characterized in terms of XRD patterns, DR-UV–vis spectroscopy, FTIR spectroscopy and zeta-potentials. The catalytic activity of Cu/TiO_2, Zn/TiO_2, and $Cu/Zn/TiO_2$ was studied for degradation of Congo red (CR) dye and determination of quantum yield (QY).

2. MATERIALS AND METHODS

2.1 Reagents

Deionized water (dH_2O) was prepared using Millipore water synthesis system (Elix-3, USA) for reagent and dye solution preparations. $Zn(NO_3)_2{,}6H_2O$ (99% w/w purity), $CuSO_4.5H_2O$ (99% w/w purity), $K_2Cr_2O_7$ (99.9 % purities w/w), $AgSO_4$ (98.5 % purities w/w), $HgSO_4$ (99 % purities w/w), NaOH (98% w/w purity), H_2SO_4 (98% v/v purity), and KBr (99.5% w/w purity) were obtained from Merck, Mumbai. TiO_2 (99% w/w purity) containing 80% anatase and 20% rutile by weight was procured from Sigma Aldrich, India. Congo Red (CR) dye (696.6 g/mol, 96% w/w purity) was supplied by Loba Chemie, Mumbai. All chemicals were used as received without further purification.

2.2 Preparation of bio-extract extract

Fresh 20 g *Sechium edule* leaves were collected from the nearby locality, and were washed with dH_2O. They were shredded into small pieces, 100ml dH_2O was added and the mixture was stirred for 30 minutes at 80 ^oC. Then the solution was filtered and chayote leaves extract was collected in an amber glass container and stored at 4 ^oC for further use.

2.3 Bio-mediated doping method

Metal precursors $CuSO_4$ and $ZnNO_3$ were used respectively to prepare Cu and Zn mono and bi-metal nanoparticles. TiO_2 powder (2 g) was added in 200 mL of $CuSO_4$ solution corresponding to Cu-concentration 2 g per 100 g catalyst. The obtained mixture was stirred for 60 min to facilitate adsorption of Cu^{2+} on TiO_2. Then it was centrifuged at 4000 rpm for 30 min, and the supernatant was analysed for the residual Cu^{2+} concentration. The Cu^{2+}/TiO_2 residue was further dispersed in 180 mL dH_2O, and a 20 mL *S. edule* extract was added with stirring at 300 rpm on a magnetic stirrer for 24 h. The brown colour Cu doped TiO_2 (Cu/TiO_2) residue was filtered out and rinsed 4 times with ethanol and dH_2O. Cu/TiO_2 was dried at 100 ^oC in a hot-air oven (N-101, Navyug, India) for 12 h and ground in a mortar and pestle. The synthesized Cu/TiO_2 particles were stored in an airtight container in dark. Similar procedure was employed for the preparation of Zn/TiO_2 (2:98 % w/w) as well as bimetal doped $Cu/Zn/TiO_2$ (1:1:98 % w/w).

2.4 Analytical techniques

FTIR spectra were recorded within the wavenumber ranging from 400 to 4000 cm^{-1} (IR affinity-1, Shimadzu, Japan). KBr was first dried for 2 h at 110 °C to remove water and mixed with the sample at 99:1 ratio before pelletization. The diffuse reflectance of synthesized photocatalyst was acquired in the range of 250 to 1200 nm using UV-vis Spectroscopy of

Shimadzu, Japan (Solid Spec 3700/3700DUV). The X-ray diffraction (XRD) (model: D8 11 Adavnce, bruker, Germany) pattern were obtained at 2 angle from 20 to 80° with a step of 0.05^o and integration time of 0.5 s. Zeta-potential was measured at different pH solution (Delsa nano analyser, Beckman Coulter, Switzerland). pH measurement was performed using a precision pH meter of Eutech Instruments (pH/ion 510, Malaysia). The dye concentration was monitored by UV-vis Spectroscopy (UV 2300, M/s Thermo Fisher India).

2.5 Photocatalytic activity test using bio-mediated Cu/Zn-doped TiO_2

Photocatalytic degradation of 100 ppm CR dye was conducted with visible light irradiation at different initial pH (3-11). The catalyst was added to the solution and then the suspension was stirred in dark for 30 minutes to equilibrate on the catalyst surface before illumination. A visible lamp of 200 W/250 V (17 K Lux, M/s Bajaj Electricals Ltd., India) was then irradiated for 2 h at different catalyst loadings with continuous stirring. The collected samples were analysed for residual dye concentration by using UV-vis spectrophotometer.

3. RESULTS AND DISCUSSION

3.1 Determination of Cu and Zn loading onto TiO_2

Cu^{2+} and Zn^{2+} uptake efficieny of TiO_2 with the equilibrium (after 1 h of adsorption) Cu^{2+} and Zn^{2+} concentration is illustrated in Table 1. The initial concentration of Cu^{2+} and Zn^{2+} was maintained 2 % (w/w) each and for bimetal 1:1 % (w/w) per 10 g TiO_2. The time of doping test was set to 24 h. It was selected from a trial run of only Cu^{2+} and Zn^{2+} precursor and bio-extract without TiO_2 and, the formation of Cu and Zn-nanoparticle were complete in 24 h. The efficiency of Cu and Zn-doping was found to be 80.7 and 74.2 % with 2 % (w/w) each which were obtained in the pre-immobilization (adsorption) study. It implies that the true loading of Cu and Zn onto TiO_2 was about 1.61 and 1.48 (w/w w.r.t. Cu/TiO_2 and Zn/TiO_2). There was insignificant amount of Cu^{2+} and Zn^{2+} ions leached out in the solution during the doping test.

Ascorbic acid (AA) was found to be the most abundant compound (176.92 m/z) (Rao and Golder, 2016) in *S. edule* which was consisting of 354 mg AA/kg leafs. AA is an ideal e^- donor which can reduce metal ions into zero valence leading to nucleation onto the TiO_2.

Table 1. Quantitative retention of Cu^{2+} and Zn^{2+} ions onto TiO_2.

Catalyst	Ionic matter	Initial loading, % (w/w)	True loading, % (w/w) on TiO_2	% Residual concentration	
				After 1 h adsorption	After 48 h reaction
Cu/TiO_2	Cu^{2+}	2	1.614	19.3	1.43
Zn/TiO_2	Zn^{2+}	2	1.484	25.8	1.76
$Cu/Zn/TiO_2$	Cu^{2+}	1	0.938	6.2	0.5
	Zn^{2+}	1	0.792	20.8	0.9

3.2 Characteristics of $Cu/Zn/TiO_2$

3.2.1 X-ray diffractogram

The XRD patterns of pristine, mono- and bi-metal doped $Cu/Zn/TiO_2$ are shown in Figure 1. It exhibited the major characteristic peaks of highly crystalline TiO_2. The intense peaks at 2θ = 25.34, 37.85 and 48.15º confirm the crystalline planes of anatase phase. Whereas 2θ = 27.45, 35.98, 41.42 and 54.21º attribute to the rutile phase. Three additional characteristic peaks

appeared at 41.8, 50.1 and 73.9◦ were corresponding to the (1 1 1), (2 0 0) and (2 2 0) crystalline planes of face-centered cubic structured Cu nanoparticles (JCPDS No. 04-0836, a = 3.609 Å) and, a small peak observed at 61.1º associated to (2 2 0) plane of Cu_2O (Cuya Huaman et al., 2011). Similarly two more peaks at 31.6 and 67.9º corresponding to (1 0 0) and (1 1 2) planes of ZnO nanoparticles (JCPDS No. 361451) (Bala et al., 2015). The existence of Cu/Zn species also conformed by the EDX image mapping (Figure 2). It displays that assembles of numerous nanoparticles by the structural functionalization comprising of Ti, O, Cu and Zn elements. The crystallite size was determined by using the Scherrer's equation (Rao and Golder, 2016). The crystallite size for the intense peak of anatase phase at (1 1 1) plane was found to be 16.66, 22.38, 38.2 and 24.84 nm nm for TiO_2, Cu/TiO_2, Zn/TiO_2, $Cu/Zn/TiO_2$, respectively. The same for the rutile phase at (1 1 0) plane was calculated as 28.21, 29.46, 32.75 and 65.68 nm, respectively. The change in the size of crystal lattice is dependent with the variation in the ionic radius of the metal dopants (Malika et al., 2016). The induction of larger ionic radius metal dopants into the Ti^{4+} lattice was resulted in higher crystallite size. The anatase phase was found as 80.06, 81.38, 70.47 and 76.54% for TiO_2, Cu/TiO_2, Zn/TiO_2, $Cu/Zn/TiO_2$, respectively, from the integrated peak intensities at (1 0 1) and (1 1 0) planes(Rao and Golder, 2016). It indicates a maximum of 12% phase transmission from anatase to rutile. A similar trend of crystallite size increment was reported by Behnajady and Eskandarloo (Behnajady and Eskandarloo, 2013) in the case of bi-metal doped TiO_2.

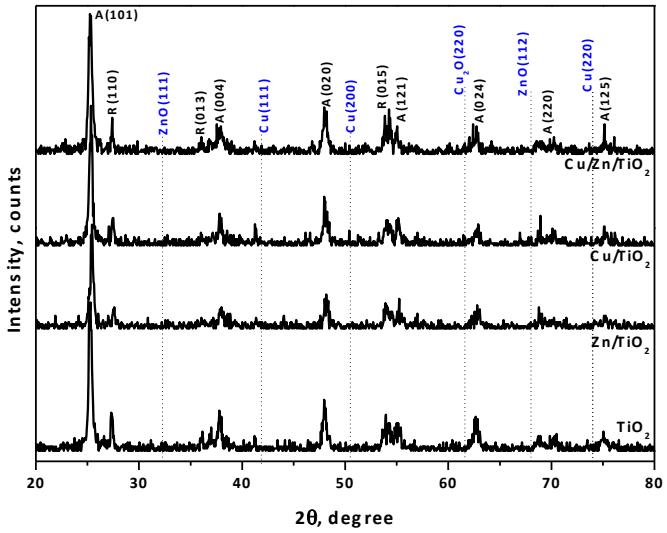

Figure 1. XRD patterns of bare, mono and Cu/Zn bimetal doped TiO_2 nanostructures.

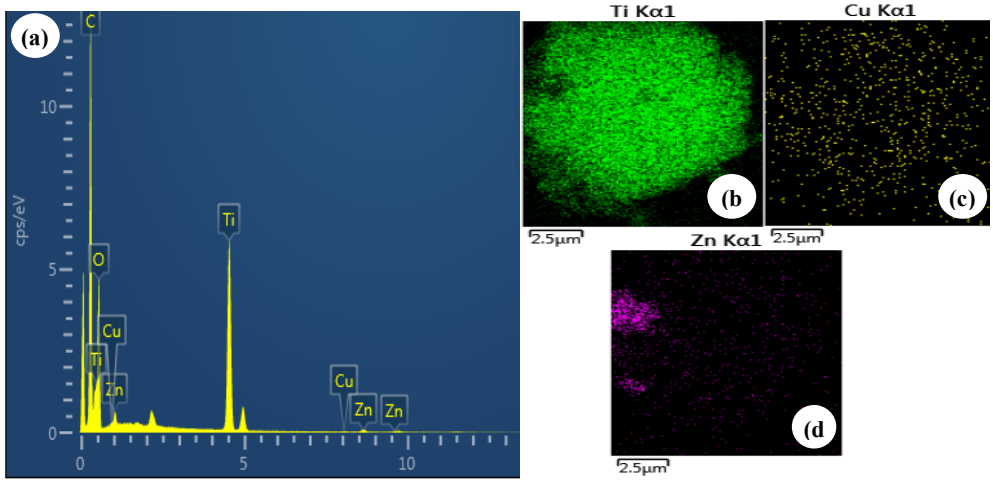

Figure 2. (a): Relative dispersity of Ti, O, Cu and Zn elements, (b-d): Dispersity of individual element Ti, Cu and Zn.

3.2.2 Spectral absorbance of bio-mediated doped Cu/Ni/TiO_2

An intense absorption peak in the UV domain (Figure 3) can be noticed for pristine TiO_2, which is assigned to the band-to-band transition (Malika et al., 2016). A maximum absorption band around 315 nm in the TiO_2 spectrum related to the route of charge transferring from O^{2-} (2p) to Ti^{4+} (3d) (Paulino et al., 2016). Cu doping displayed an important absorption tail in the visible domain from 400 to 800 nm. The band at 250–310 nm is assigned to the ligand-to-dopant charge transfer formation of Cu^{2+}(3d) from O^{2-}(2p), happening in separated Cu^{2+} locates. In addition, the band at 340 nm is evidence that the existence as well as large distribution of $(Cu–O–Cu)^{2+}$ assembles. In the case of Zn-doping, the energy absorption spectrum poses a maximum wavelength near to 400 nm little above to TiO_2. Cu/Zn/TiO_2 absorption spectrum exhibited a broader band than the other photocatalysts spectra, indicating greater photocatalytic activity.

The band gap energy (*E*) of doped catalysts was determined using the indirect transition model also called Touc plot (Rao and Golder, 2016) (Figure 3 (Inset)). TiO_2 showed *E* of 3.05 eV whereas Zn doping (2%, w/w) alone did not reduce much. However, Cu-doping showed a superior performance in band gap reduction with 2.397 eV. The change in *E* suggests that the induction of Cu changes the material functionalization, owing a reallocation of its electrical charge. Cu acts as a h^+ scavenger leading to a lengthier isolation between the e^-/h^+ pairs produced by enhancing material photoefficiency. As it was expected, Zn-doping did not stimulate a reduction in *E* for Cu/Ni/TiO_2 since its *E* value (2.79 eV) is small raise to that of TiO_2. Paulino et al. also reported the band gap results of 3.17, 2.95 and 3.02 eV with TiO_2, Cu/TiO_2, Cu/Zn/TiO_2, respectively (Paulino et al., 2016).

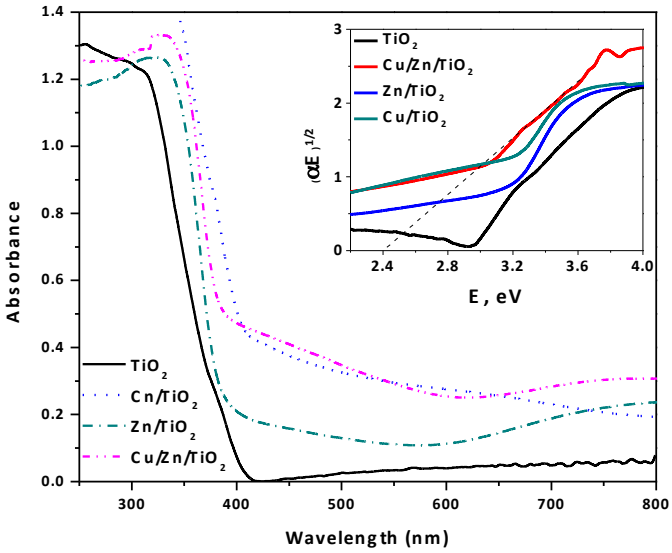

Figure 3. UV–vis DR spectra of pristine, mono and bimetal-doped TiO_2. Inset: Optical direct band gaps (Tauc plot).

3.2.3 FTIR spectra of Cu/Zn/TiO_2

FTIR spectra of pristine, mono and bimetal doped TiO_2 particles are shown in Figure 4(a). The bands at 3460 and 1600 cm^{-1} attributed to the OH–stretching and OH–bending modes, respectively of physically absorbed moisture. A small band observed at 2891 cm^{-1} can be assigned to dimer –OH (Behera et al., 2016). The metal-doped TiO_2 enhanced the surface adsorption of –OH and water groups. Ti^{4+} in TiO_2 lattice substituted by Cu^{2+} and Zn^{2+} ions and formed Cu–O or Zn–O. It enhances the oxygen vacancies that are equilibrated by the adsorption of more H_2O or –OH groups (Malika et al., 2016). The peaks detected at 472, 523, and 482 cm^{-1} are for the stretching mode of Ti–O, Cu–O, and Zn–O, respectively (Malika et al., 2016; Tobaldi et al., 2016). A wide peak observed at 1184 cm^{-1} can be attributed to scissoring mode of H_2O molecule. A band at 783 cm^{-1}

corresponding to Ti-O was shifted to 727 and 732 cm^{-1} after doping because of Cu–O–Ti and Zn–O–Ti stretching asymmetric vibrations. These changes were detected due to the defects raised by the induction of metal dopants into TiO_2 lattice (Behera et al., 2016).

3.2.4 Colloidal stability of TiO_2 and Cu/Zn/TiO_2

The polydispersity index was found to be 0.201 for Cu/Zn/TiO_2 which is a measure of the size distribution of particles in an aqueous colloidal sample. The zeta-potentials (ξ) of bare TiO_2 and doped Cu-Zn/TiO_2 are presented in Figure 4(b). ξ were measured for different pH (from 3 to 10) to understand the behaviour of surface charge of modified TiO_2 in its aqueous solution. The zero point charge (pH_{zpc}) was dropped from 6.42 to 5.91 after doping of TiO_2. The pH_{zpc} is potentially affect the adsorption behaviour of organic compounds on the photocatalyst surface during a photocatalytic reaction (Malika et al., 2016). The surface of the photocatalyst is positively charged below pH_{zpc} and carries a negative charge above it. A low pH_{zpc} indicates a higher concentration of OH^- ions on the surface of catalyst. The raise in the induced oxygen vacancies enhances the surface adsorbed –OH groups that leads to an increase in the surface charge due to the metal doping (Rao and Golder, 2016). At higher pH, more negative charged particles were observed due to higher electrostatic repulsion which prevents the formation of agglomerates as well as enhances the colloidal stability with raise in ξ towards more negative (Behera et al., 2016). It shows that Cu-Zn/TiO_2 particles are comparatively greater stable at higher pH.

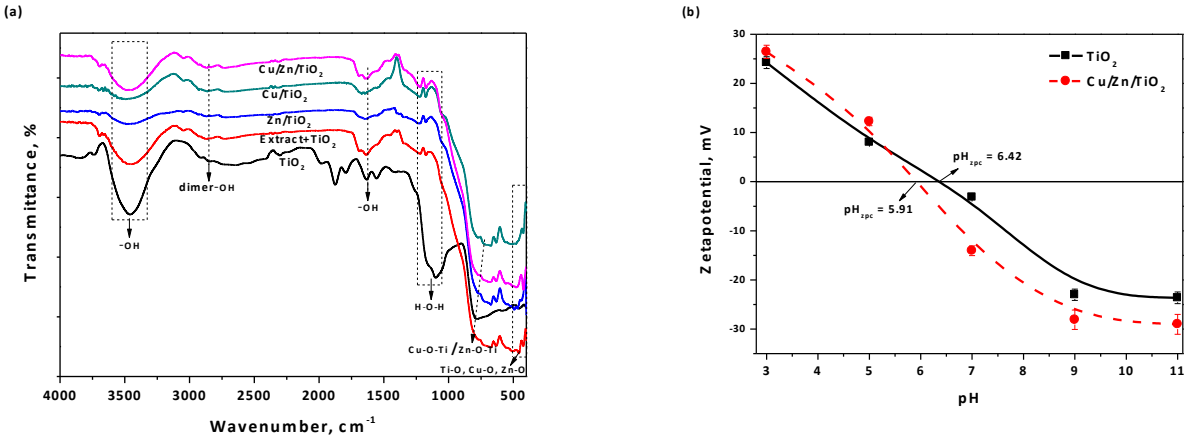

Figure 4. (a) FTIR Spectra for different catalysts (b) Effect of pH on the Zeta-potential for bare and doped TiO_2.

3.3 Cu/Zn/TiO_2 photocatalytic performance under visible light

It was found that there was about 98 % CR decomposition at pH 5 with Cu/Zn/TiO_2 upto irradiation time of 120 min (Figure 5). It was 14.1, 68.7 and 59.3 % in the case of TiO_2, Cu/TiO_2 and Zn/TiO_2 with the similar experimental condition which is line with the optical response of photocatalysts in the visible region (Figure 3). The results indicate that the bimetal doped TiO_2 was more efficient than mono-metal doping under the visible light irradiation. The activity of Cu/TiO_2 was also better than Zn/TiO_2 indicating that the Cu doping could enhance the charge separation effectively with a low recombination rate.

It was observed that bi-metal doped catalyst showed the maximum COD (chemical oxygen demand) removal of 80.6 % as compared to mono-metal doped as well as bare TiO_2 (Figure 5). The COD removal was found to be 10.5, 75.9 and 71.2 % for TiO_2, Cu/TiO_2 and Zn/TiO_2, respectively, which is following the similar trend of CR dye colour removal.

The quantum yield (QY) for the degradation of CR dye was also determined (Shidpour, 2015) (Figure 5). The maximum QY was found to be 41.5 % in 120 min of reaction time for

Cu/Ni/TiO_2. The QY of bio-mediated Cu/Zn-doped TiO_2 was more than many earlier reports (Kusiak-Nejman et al., 2011, Li et al., 2012). The $O_2^{\bullet-}$ radicals were mostly responsible for the degradation of CR dye as evidenced from the electron spin resonance spectra (results not shown here).

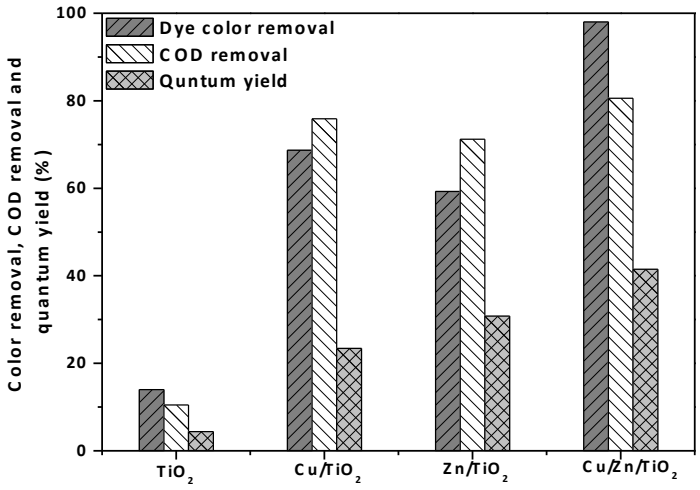

Figure 5. Congo red dye color, COD removal, and quantum yield for bare and doped catalysts.

4. CONCLUSIONS

The bio-mediated co-metal doping of Cu and Zn onto TiO_2 showed a significant decrease in the band gap energy than the mono-metal doping at the same weight loading. This technique increased the crystallite size in bimetal doping for both anatase and rutile phases. The absolute zeta potential value was more with bimetal doping which is indicative of a better tendency to oppose the destabilization. The visible light aided degradation of CR dye with Cu/Zn/TiO_2 was significantly higher, and could cause almost complete decolourization in 2 h. The quantum yield of bimetal doped TiO_2 catalyst in the current study exhibited a clear superiority over many existing studies using conventional doping methods.

REFERENCES

Bala, N., Saha, S., Chakraborty, M., Maiti, M., Das, S., Basu, R., Nandy, P., 2015. Green synthesis of zinc oxide nanoparticles using Hibiscus subdariffa leaf extract: effect of temperature on synthesis, anti-bacterial activity and anti-diabetic activity. RSC Adv. 5, 4993–5003. doi:10.1039/C4RA12784F

Behera, A.K., Rao, C.V., Das, R.K., Giri, A.S., Golder, A.K., 2016. Fabrication and characterization of Ag-doped titania: impact of dye-sensitization, phenol decomposition kinetics and biodegradability index. Desalin. Water Treat. 57, 9488–9497.

Behnajady, M.A., Eskandarloo, H., 2013. Silver and copper co-impregnated onto TiO2-P25 nanoparticles and its photocatalytic activity. Chem. Eng. J. 228, 1207–1213.

Bokare, A., Pai, M., Athawale, A.A., 2013. Surface modified Nd doped TiO2 nanoparticles as photocatalysts in UV and solar light irradiation. Sol. Energy 91, 111–119.

Chelli, V.R., Golder, A.K., 2016. pH dependent size control, formation mechanism and antimicrobial functionality of bio-inspired AgNPs. RSC Adv. 6, 95483–95493. doi:10.1039/C6RA16475G

Cuya Huaman, J.L., Sato, K., Kurita, S., Matsumoto, T., Jeyadevan, B., 2011. Copper nanoparticles synthesized by hydroxyl ion assisted alcohol reduction for conducting ink. J. Mater. Chem. 21, 7062–7069. doi:10.1039/c0jm04470a

Harraz, F.A., Abdel-Salam, O.E., Mostafa, A.A., Mohamed, R.M., Hanafy, M., 2013. Rapid synthesis of titania-silica nanoparticles photocatalyst by a modified sol-gel method for cyanide degradation and heavy metals removal. J. Alloys Compd. 551, 1–7.

Kusiak-Nejman, E., Janus, M., Grzmil, B., Morawski, A.W., 2011. Methylene Blue decomposition under visible light irradiation in the presence of carbon-modified TiO2 photocatalysts. J. Photochem. Photobiol. A Chem. 226, 68–72. doi:10.1016/j.jphotochem.2011.10.018

Li, B., Liu, T., Wang, Y., Wang, Z., 2012. ZnO/graphene-oxide nanocomposite with remarkably enhanced visible-light-driven photocatalytic performance. J. Colloid Interface Sci. 377, 114–121. doi:10.1016/j.jcis.2012.03.060

Malika, M., Rao, C.V., Das, R.K., Giri, A.S., Golder, A.K., 2016. Evaluation of bimetal doped TiO2 in dye fragmentation and its comparison to mono-metal doped and bare catalysts. Appl. Surf. Sci. 368, 316–324.

Ordonez, A.A.L., Gomez, J.D., Vattuone, M.A., Isla, M.I., 2006. Antioxidant activities of Sechium edule (Jacq.) Swartz extracts. Food Chem. 97, 452–458. doi:10.1016/j.foodchem.2005.05.024

Paulino, P.N., Salim, V.M.M., Resende, N.S., 2016. Zn-Cu promoted TiO2 photocatalyst for CO2 reduction with H2O under UV light. Appl. Catal. B Environ. 185, 362–370. doi:10.1016/j.apcatb.2015.12.037

Rao, C.V., Golder, A.K., 2016. Development of a bio-mediated technique of silver-doping on titania. Colloids Surfaces A Physicochem. Eng. Asp. 506, 557–565.

Riaz, N., Chong, F.K., Man, Z.B., Khan, M.S., Dutta, B.K., 2013. Photodegradation of Orange II under visible light using Cu–Ni/TiO_2: Effect of calcination temperature. Ind. Eng. Chem. Res. 52, 4491–4503.

Shidpour, R., 2015. A Power-law relationship between characteristics of light source and quantum yield in photocatalytic systems. J. Phys. Chem. C 119, 22425–22431. doi:10.1021/acs.jpcc.5b02318

Tobaldi, D.M., Piccirillo, C., Rozman, N., Pullar, R.C., Seabra, M.P., Skapin, A.S., Castro, P.M.L., Labrincha, J.A., 2016. Effects of Cu, Zn and Cu-Zn addition on the microstructure and antibacterial and photocatalytic functional properties of Cu-Zn modified TiO_2 nano-heterostructures. J. Photochem. Photobiol. A Chem. 330, 44–54. doi:10.1016/j.jphotochem.2016.07.016

Wen, Z., Wang, G., Lu, W., Wang, Q., Zhang, Q., Li, J., 2007. Enhanced photocatalytic properties of mesoporous SnO2 induced by low concentration ZnO doping. Cryst. Growth Des. 7, 1722–1725.

Zhang, D., Zeng, F., 2011. Photocatalytic oxidation of organic dyes with nanostructured zinc dioxide modified with silver metals. Russ. J. Phys. Chem. A 85, 1077–1083. doi:10.1134/S0036024411080073.

Proceedings of the 10th World Congress of EWRA 'Panta Rhei', 5-9 July 2017, Athens, Greece
© 2017 *European Water Resources Association*

CFD modelling of wind effect on rectangular settling tanks of water treatment plants

A. Gkesouli* and A. Stamou
Laboratory of Applied Hydraulics, School of Civil Engineering, National Technical University of Athens, 5 Heroon Polytechniou Str., 15780 Athens, Greece
* *e-mail: anthi.gkesouli@gmail.com*

Abstract: Sedimentation is a simple physical process which is widely applied on conventional water treatment plants; however, the tanks' efficiency depends on numerous factors including the wind action. In the present study, calculations are performed with a VOF model and one-phase model, which uses as an input the location of free surface and the surface velocity which are determined by the VOF model, to investigate the effect of a strong co-current wind (11 m/s) on a rectangular settling tank of a conventional water treatment plant. The results show that: (1) The flow field is highly affected by wind action, i.e. under windy conditions the tank is coved by an extended wind-generated eddy, while the suspended solids' concentration fields are influenced by the corresponding flow fields. (2) Without wind, the tank's removal efficiency is calculated equal to 85.4%, by the VOF model, and equal to 85.3%, by the one-phase model; these values are in satisfactory agreement with the experimentally determined value (86.0±1%). (3) For a co-current wind of 11 m/s, the tank's efficiency decreases to 83.4% (VOF) and 83.6% (one-phase model), which is also in satisfactory agreement with the experimentally determined value (84.0%); however, the wind effect is slight (≈2%). (4) Both the VOF and the one–phase model can predict satisfactorily the tank's removal efficiency; so the one-phase model can be used to assess wind effect on all types of settling tanks, according to the proposed methodology, since it is a significantly less time consuming model compared to the VOF model.

Key words: wind effect; settling tank; tank's performance; water treatment plant; CFD

1. INTRODUCTION

Conventional water treatment plants are still widely used for the production of potable water. The first stage of treatment in these units is performed in settling tanks where the "heavy" solids are removed from the flow, through the hoppers at the tanks' bottom, after undergoing the effect of sedimentation, also known as settling by gravity. Although the settling is a simple physical process, the efficiency of settling tanks depends on numerous factors since settling can be affected by both the complex hydraulics of the tanks and the characteristics of the solids. Wind action is one of the factors which are considered to affect the tank's efficiency (Asgharzadeh *et al.*, 2012); however, the studies that can be found in the literature regarding the wind effect are limited (Gkesouli *et al*., 2016; Stamou and Gkesouli, 2015; Khezri *et al.* 2012; Sivakumar and Lowe, 1990).

In the present study we perform calculations using two different approaches to investigate the effect of a strong co-current wind on the flow field and the removal efficiency of a rectangular settling tank of a conventional Water Treatment Plant (WTP), i.e. a tank with low inlet concentrations of suspended solids. Firstly, we formulate and apply a 2D two–phase CFD model (VOF) and, then, we carry out calculations with a 2D one-phase CFD model which "uses" as an input (a) the location of the free surface and (b) the surface velocity which are determined by the two-phase calculations; the results of the present study are also compared with previous studies (Gkesouli *et al*., 2016, Stamou and Gkesouli, 2015). The proposed methodology can be used to assess the wind effect on all types of settling tanks, including rectangular and circular tanks, used for water and wastewater treatment.

2. THE MATHEMATICAL MODEL

The calculations are performed with the CFD model ANSYS-CFX 16.1. In the present section the basic equations of the model are briefly presented (ANSYS-CFX, 2017).

2.1 Flow field equations and turbulence modelling

A homogenous multiphase Eulerian – Eulerian fluid approach is used to determine the location of free surface, i.e. air and water share the same quantities (e.g. velocity and turbulence) and they are separated by a distinct resolvable interface. In this approach, the continuity (Eq. 1) and the momentum equations (Eq. 2), which involve the bulk density, ρ_m, (Eq. 4) and the bulk viscosity, μ_m, (Eq. 5) of air – water mixture, are solved to determine the 2D flow field in the tanks.

Bulk continuity equation

$$\frac{\partial \rho_m}{\partial t} + \frac{\partial \rho_m U_i}{\partial x_i} = 0 \tag{1}$$

Bulk momentum equations

$$\frac{\partial \rho_m U_i}{\partial t} + \frac{\partial \rho_m U_j U_i}{\partial x_j} = -\frac{\partial P}{\partial x_i} + \frac{\partial}{\partial x_j}\left[\mu_m\left(\frac{\partial U_i}{\partial x_j} + \frac{\partial U_j}{\partial x_i}\right) + RTS\right] + g_i \rho_m \tag{2}$$

Reynolds Turbulent Stresses (RTS)

$$RTS = \mu_{tm}\left(\frac{\partial U_i}{\partial x_j} + \frac{\partial U_j}{\partial x_i}\right) - \frac{2}{3}\delta_{ij}\rho_m k \tag{3}$$

$$\rho_m = r_w \rho_w + r_a \rho_a \tag{4}$$

$$\mu_m = r_w \mu_w + r_a \mu_a \tag{5}$$

where t is the time, x_i is the Cartesian coordinate in the i-direction, U_i is the common velocity, P is the pressure, g_i is the gravitational acceleration and r is the volume fraction; the subscripts ‘m’, ‘w’ and ‘a’ denote air - water mixture, water and air, respectively.

For turbulence modeling the SST k - ω model is applied; in the k-ω transport equations (Eq. 6 and Eq.7) of the model, k is the turbulent kinetic energy, ω is the turbulence frequency, μ_{mt} is the eddy viscosity and P_k is the production term of k.

k - ω transport equations

$$\frac{\partial(\rho_m k)}{\partial t} + \frac{\partial(\rho_m U_i k)}{\partial x_i} = \frac{\partial}{\partial x_i}\left[\left(\mu_m + \sigma_k \mu_{t_m}\right)\frac{\partial k}{\partial x_i}\right] + P_k - 0.09\rho_m k\omega \tag{6}$$

$$\frac{\partial(\rho_m \omega)}{\partial t} + \frac{\partial(\rho_m U_i \omega)}{\partial x_i} = \frac{\partial}{\partial x_i}\left[\left(\mu_m + \sigma_\omega \mu_{t_m}\right)\frac{\partial \omega}{\partial x_i}\right] + \alpha\frac{\omega}{k}P_k - \beta\rho_m\omega^2 + (1-F_1)2\rho_m\sigma_{\omega 2}\frac{1}{\omega}\frac{\partial k}{\partial x_i}\frac{\partial \omega}{\partial x_i} \tag{7}$$

F_1 and F_2 are blending functions; F_1 switches between 1 near the wall and 0 outside the boundary layer. All constants are computed by a blend from the corresponding constants of k-ε and k-ω

models via a linear combination e.g. $\alpha=\alpha_1 F_1+\alpha_2(1-F_1)$. The values of the constants are the following $\alpha_1=5/9$, $\beta_1=3/40$, $\sigma_{k1}=0.85$, $\sigma_{\omega 1}=0.5$, $\alpha_2=0.44$, $\beta_2=0.0828$, $\sigma_{k2}=1$, $\sigma_{\omega 2}=0.856$ (Menter *et al*., 2003).

2.2 VOF model

As aforementioned, the location of free surface is determined via an interface-capturing method i.e. the homogeneous model, also known as Volume of Fraction (VOF) model. The VOF model determines the volume fractions of air and water in the tank (Eq. 8, Eq. 9) which vary from 0 (empty cells) to 1 (fully filled cells) while a volume conservation equation is also solved (Eq. 10).

Continuity equations

$$\frac{\partial r_w \rho_w}{\partial t} + \frac{\partial r_w \rho_w U_i}{\partial x_i} = 0 \tag{8}$$

$$\frac{\partial r_a \rho_a}{\partial t} + \frac{\partial r_a \rho_a U_i}{\partial x_i} = 0 \tag{9}$$

Volume conservation equation

$$r_w + r_a = 1 \tag{10}$$

2.3 The Suspended Solids equation

For calculating the suspended solids' concentration field in the tank the Algebraic Slip Model is used. The 'dirty' water (dw) which enters into the settling tank from the upstream coagulation–flocculation unit consists of 'pure' water and suspended solids of varying diameters that can be classified based on their characteristic diameter. For each class (c_i) with mass fraction, Y_{ci}, the concentration field in the tank is calculated by a mass balance equation (Eq. 11), where the slip velocity (Uc_i) is equal to the settling velocity of the class. More details can be found in Stamou and Gkesouli (2015).

$$\frac{\partial(\rho_{dw} Y_{c_i})}{\partial t} + \frac{\partial\left(\rho_{dw} Y_{c_i}\left(U_j + U_{c_i j}\right)\right)}{\partial x_j} = \frac{\partial}{\partial x_j}\left(\mu_{dw}\frac{\partial Y_{c_i}}{\partial x_j} + \frac{\mu_{t\,dw}}{0.9}\frac{\partial Y_{c_i}}{\partial x_j}\right) \tag{11}$$

Since the 'dirty' water is a mixture of 'pure' water and suspended solids, its density, viscosity and eddy viscosity are bulk quantities which are calculated by equations similar to Eq. 4 and Eq. 5. In the present study, all quantities of water included in Eq.1 to Eq. 10 refer to dirty water.

3. TANK'S GEOMETRY AND CALCULATION DETAILS

3.1 Geometry of the settling tank

The settling tank is rectangular with length equal to 73.2 m, width equal to 14.4 m and average water depth equal to 3.5 m. The 'dirty' water enters into the tank via 4 rectangular openings (0.5 m x 0.5 m), which are placed at y=0.35 m above the tank's bottom, and overflows via 3 outlet channels, with length equal to 10 m, which are installed at x=63.2 m. The sludge, which is collected at the bottom of the tank, is removed every day via 2 hoppers. In the present study the tank is

modeled 2 dimensionally considering that the 'dirty' water enters into the tank via a slot opening equal to 0.15 m and overflows via a rectangular outlet weir which is placed at x=63.2 m, i.e. at the beginning of the outlet channels.

3.2 Field measurements

Hourly measurements of wind direction and wind velocity near the tank were performed with an anemometer for a total period of 2 years; these measurements showed that the strongest co-current winds in the study area have velocities equal to W≈11.0 m/s (at y≈10 m above the water surface). During these "strong wind periods" turbidity at the tank's inlet and outlet was measured by on-line turbidimeters while the tank's inlet flow rate was also recorded. The removal efficiency of the tank during the strongest recorded co-current wind (W≈11 m/s) was estimated equal to ≈84.0%, for steady state flow conditions, based on the above mentioned measurements.

3.3 Methodology of calculations

Firstly, we performed two-phase calculations with the VOF model in order to determine the flow field, the suspended solids' concentration field and the removal efficiency of the tank and, consequently, to assess the wind effect on tank's performance; based on these calculations we also derived (a) the location of free surface and (b) the surface velocity caused by wind action. Then, we used these data as an 'input' in a significantly less time consuming one-phase model and we performed the same kind of calculations (velocity and solids' field, removal efficiency); the calculated removal efficiencies by the VOF model and the one-phase model were then compared. The proposed methodology can be used to assess the wind effect on all types of settling tanks.

3.4 Computational domains

In the case of two-phase calculations, the computational domain had length equal to 63.2 m, i.e. equal to tank's length, and height equal to 13.5 m, i.e. equal to tank's expected average water depth plus 10 m (representing the air domain). At the borders of the domain the following boundary conditions were applied: (i) inlet of the tank: horizontal velocity equal to 0.115 m/s deduced by the measured inlet flow rate of the tank (0.25 m^3/s) divided by the inlet area, (ii) outlet of the tank: pressure and direction of the flow, (iii) walls and bottom of the tank: no slip walls, (iv) side walls: symmetry, (v) inlet of air domain: log law theoretical wind velocity profile and (vi) outlet of air domain: pressure and direction of the flow. The location of free surface was calculated by the VOF model.

In the case of one-phase calculations, the computational domain consisted exclusively of the tank, i.e. we did not take into account the air domain; its length was equal to 63.2 m and the water depth was equal to ≈3.46 m (determined by the VOF model). At the free surface we applied the wind-caused surface velocity which was also calculated by the VOF model; the rest of the boundary conditions were the same as in two-phase calculations.

Both grids were selected after a series of grid independency tests and they were structured and refined at tank's inlet, outlet and bottom and near the free surface.

3.5 Scenarios of calculations

In order to investigate the wind effect on tank's performance and removal efficiency, we carried out calculations (a) for no wind conditions (W=0 m/s) and (b) for the strongest co-current wind which was recorded at the area of study (W=11 m/s). It is noted that the number of the classes at the tank's inlet, their inlet concentrations and their settling velocities were taken from a previous study

(Gkesouli *et al*., 2016).

4. RESULTS AND DISCUSSION

In Figure 1 the calculated flow field in the tank is presented for (a) W=0 m/s, based on the one-phase calculations, (b) W=11 m/s, based on the VOF model, and (c) W=11 m/s, based on the one-phase calculations using the surface velocity predicted by VOF. The corresponding calculated suspended solids' concentration fields are presented in Figure 2. The tank's calculated removal efficiencies by the VOF and one-phase model are shown in Table 1 together with the experimentally determined values and the removal efficiencies calculated by a 3D model and a 2D model applied in previous studies.

Figure 1 shows that under no wind conditions the inlet jet creates an anticlockwise eddy that covers the first ≈20 m of the tank while at the rest of the tank the water flow is practically parallel to axis x. The presence of the strong co-current wind 'suppresses' the anticlockwise eddy to approximately 12 m and at the rest of the tank an extended clockwise eddy is created due to wind action; the structure of the flow field predicted by the VOF and one-phase model is practically the same while VOF predicts relatively higher velocities. Therefore, it is obvious that the presence of wind highly affects the hydraulic regime in the tank since it leads to the creation of a massive dead zone. Figure 2 depicts that the suspended solids' concentration fields are highly affected by the respective flow fields e.g. for W=0 m/s a 'sludge' layer is created in the region of the anticlockwise eddy while for W=11 m/s the suspended solids' concentration field in the wind-generated eddy is more uniform. As expected in the case of the co-current wind, the iso-concentration contours are shifted upwards, towards the free surface, after undergoing the effect of the wind–generated eddy; thus, the outlet concentration increases and the efficiency of the tank is reduced. The suspended solids' concentration fields predicted by the VOF (Fig. 2b) and one-phase model (Fig. 2c) are similar.

Table 1 shows that without wind the tank's removal efficiency is calculated equal to 85.4%, by the VOF model, and equal to 85.3%, by the one-phase model; these values are practically equal and are also in satisfactory agreement with (a) the experimentally determined value (86.0±1%) and (b) the values determined by a 3D model (85.7%) and a different 2D model (83.1%). For W=11 m/s, the calculated removal efficiencies decrease to 83.4% (VOF model) and 83.6% (one-phase model). It is obvious that the wind has a detrimental effect on tank's settling performance; however, this reduction is low (≈2%). These values are also in satisfactory agreement with previously performed calculations with a 3D model (84.2%) and a different 2D model (82.4%) and with the experimental value (84.0%) which was determined using the turbidity measurements at the tank's inlet and outlet during a strong wind event in the tank in May 2015. These results show that both the VOF model and the one-phase model can satisfactorily predict the removal efficiency of the tank; however, it is noticed that the VOF model is significantly more time consuming compared to the one-phase model. For the performance of the present calculations we used an Intel Core i7 - 3.33 GHz desktop and the CPU time/Real time was equal to 0.007 in the case of the one-phase model and equal to 1.8 in the case of the VOF model. Therefore, the proposed methodology (see also section 3.3) can be applied to assess the wind effect on tank's efficiency and decrease significantly the required computational time.

Table 1. Removal efficiencies (%) of the tank

Wind velocity	**W=0 m/s**	**W=11 m/s**
Experimentally determined value	**86.0 ± 1.0[b]**	**84.0**
2D model - VOF model	85.4	83.4
2D model - One-phase model / Surface velocity	85.3	83.6
3D model	85.7[b]	84.2[a]
2D model - FLOW 3D	83.1[b]	82.4[b]

[a] *Obtained from Stamou and Gkesouli (2015)*
[b] *Obtained from Gkesouli et al. (2016)*

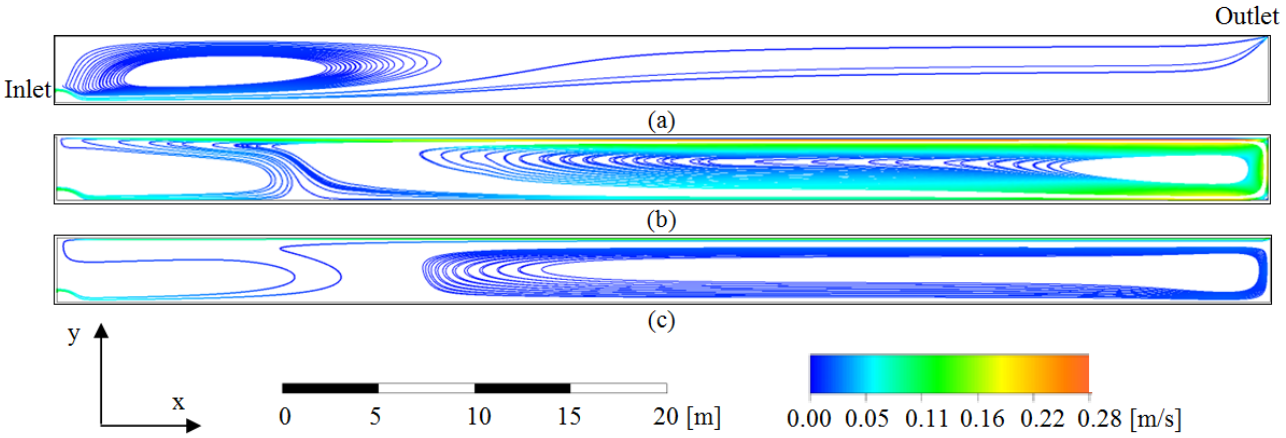

Figure 1. Calculated flow field for (a) W=0 m/s, (b) W=11 m/s (VOF model) and (c) W=11 m/s (one-phase model).

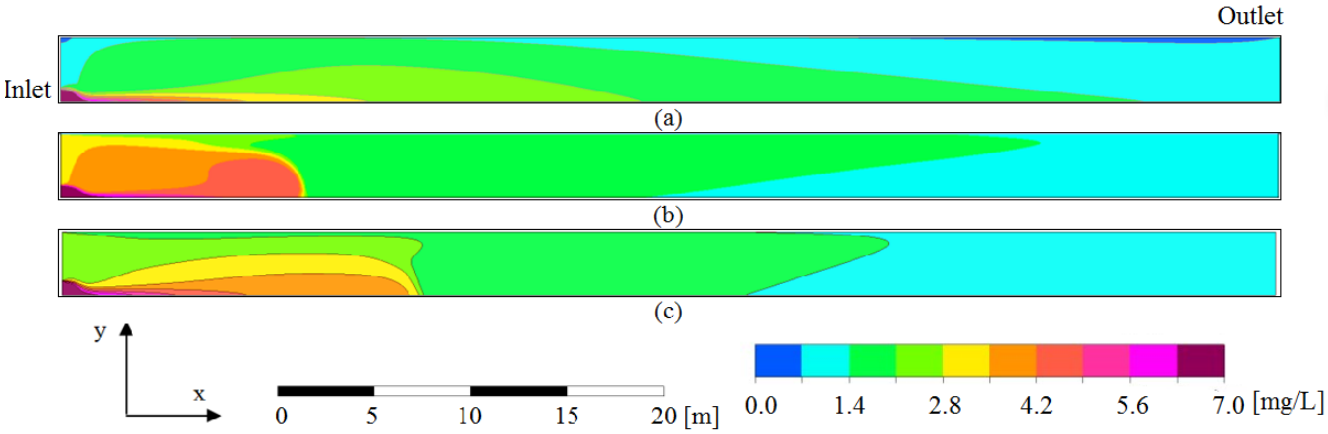

Figure 2. Suspended solids' concentration field for (a) W=0 m/s, (b) W=11 m/s (VOF model) and (c) W=11 m/s (one-phase model).

5. CONCLUSIONS

Calculations were performed to assess the wind effect on a rectangular settling tank of a conventional WTP with two approaches: we performed (a) two-phase calculations with a VOF model and (b) calculations with one-phase model in which we used as an input the location of free surface and the surface velocity which were determined by the VOF model. The results of these calculations showed that: (1) The flow field in the tank is highly affected by the wind action; under windy conditions the tank is coved by an extended wind-generated eddy. The suspended solids' concentration fields are influenced by the corresponding flow fields. (2) The tank's removal efficiency without wind is calculated equal to 85.4%, by the VOF model, and equal to 85.3%, by the one-phase model; these values are in satisfactory agreement with the experimentally determined value (86.0±1%) and previous studies (85.7% - VOF, 83.1% - one phase model). (3) Under windy conditions (W=11 m/s), the tank's efficiency decreases (83.4% - VOF, 83.6% - one-phase model); however, the effect is slight (≈2%). (4) The removal efficiencies predicted by the VOF and the one –phase model are practically the same; so the proposed methodology i.e. performing calculations with one-phase model which uses as an input the location of free surface and the surface velocity predicted by the VOF model can reduce significantly the required computational time. The proposed methodology can be used to assess the wind effect on all types of settling tanks.

REFERENCES

Asgharzadeh, H., Firoozabadi, B. and Afshin, H. 2012 Experimental and numerical simulation of the effect of particles on flow structures in secondary sedimentation tanks. Journal of Applied Fluid Mechanics 5 (2), 15–23.

Gkesouli, A., Nitsa, M., Stamou, A., Rutschmann, P. and Bui, M. D. 2016 Modeling the effect of wind in rectangular settling tanks for water supply. Desalination and Water Treatment 57 (54), 26345-26354.

Khezri, S. M., Biati, A. and Erfani, Z. 2012 Determination of the effect of wind velocity and direction changes on turbidity removal in rectangular sedimentation tanks. Water Science and Technology 66 (12), 2814–2820.

Menter, F. R., Kuntz, M. and Langtry, R. 2003. Ten Years of Industrial Experience with the SST Turbulence Model. Turbulence, Heat and Mass Transfer 4, 625-632.

Stamou, A. and Gkesouli, A. 2015 Modeling settling tanks for water treatment using computational fluid dynamics. Journal of Hydroinformatics 17 (5), 745-762.

Sivakumar, M. and Lowe, S. A. 1990 Simulation of the effect of wind on rectangular sedimentation tanks. In: Conference on Hydraulics in Civil Engineering, Sydney, Australia, 74–78.

ANSYS-CFX, Release 16.1. Available at: http://www.ANSYS.com (accessed 14/02/2017).

Proceedings of the 10th World Congress of EWRA 'Panta Rhei', 5-9 July 2017, Athens, Greece
© 2017 *European Water Resources Association*

Investigation of preparation conditions of Nano-SiO_2 embedded PES membranes for producing clean water from wastewater

A. Fouladitajar[1*], M.B. Ghandashtani[2] and F.Z. Ashtiani[2]
[1] *Department of Chemical Engineering, College of food science and technology, Science and research branch, Islamic Azad University, Tehran Iran*
[2] *Department of Chemical Engineering, Amirkabir University of Technology, No. 424, Hafez Ave., Tehran, Iran*
[*] *e-mail: fouladi@srbiau.ac.ir*

Abstract: The goal of this study was to determine the desired preparation conditions of Polyethersulfone (PES) membrane for producing clean water. Membranes were fabricated via a combination of vapor induced phase separation (VIPS) and non-solvent induced phase separation (NIPS) methods. SiO_2 nanoparticle were used as the hydrophilicity modification agent in the casting solutions which led to a negative impacts on the permeate flux in high concentrations due to aggregation. Nowadays one of the biggest problems of most of industries, especially petroleum and petrochemical industries is water pollution with oil materials, hence study of such systems is highly applicable. VIPS and NIPS are two methods for porous membrane fabrication each of which needs some modifications for formation of the membrane with regular pore size distribution and regular structure, so the combination of these two methods is such beneficial that VIPS can help to produce a neat surface pores and NIPS can generalize this surface structure to the whole membrane and then form a membrane with suitable morphology for highly water production. In this study, oil-water separation process has been accomplished for fabricated membranes under the same operating conditions and effects of each preparation factor on permeate flux investigated and amount of rejection has been calculated by COD test and finally the best membrane for this separation was selected.

Key words: membrane formation; water purification; vapor induced phase separation; non-solvent induced phase separation; PES membrane

1. INTRODUCTION

Nowadays one of the biggest problems in most industries is water pollution with oil, so finding an economical way with high efficiency is necessary. In recent years, the use of the membrane technology has been beneficial while the type of membrane and its properties determine the performance of oil-water separation process. Experience has shown that PES is an appropriate material for wastewater treatment but the type of materials which are used in polymeric casting solution (such as solvent, non-solvent and additives) and preparation method are very important in membrane structure (M. Takht Ravanchi et al., 2009; M. Cheryan et al., 1998; K. Jsarakulski et al., 1998). Polyethersulfone (PES) was selected as a membrane material because of its commercial availability, processing ease, favorable selectivity, permeability characteristics, and good mechanical and thermal properties. PES is an amorphous glassy and hydrophilic polymer containing sulfone groups (G. Wu et al., 2008).

There are two very common methods for preparation of porous membranes. in Nonsolvent induce phase separation (NIPS) method, there are three important and separable species (polymer, solvent and non-solvent) which have different interactions on each other based on thermodynamic concepts, so selection of solvent and non-solvent in this system have vital effect on membrane morphology and consequently on membrane performance (H. Susanto et al., 2009). The other method is vapor induced phase separation (VIPS) which is the most common method for the formation of ordered micro-porous thin films and has received much attention (J. Huang et al., 2012). Combination of these two mentioned methods is feasible and effective in fabrication of suitable membrane for waste water treatment as observed in previous research (V. Vatanpour et al.,

2012). In fact control of this suggested method is difficult because there are several effective parameters such as, selected solvent, selected non-solvent, amount of relative humidity, exposure time in humid condition, coagulation bath temperature and etc. which directly influence on the structure of the produced membrane (A. Fouladitajar et al., 2013; A. Fouladitajar et al., 2014).

PES which is used in this study has desired properties for oily wastewater treatment membranes as previously mentioned, but its hydrophobic properties causes deposition of organic particles in membrane surface and pores which consequently limits the permeate flux and sometimes results in irreversible fouling that leads to shorten the membrane life and increase in the costs. So using nanoparticles in polymeric casting solution has attracted much interest because it causes significant change in composition and solution properties by interaction between the nanoparticle surface and polymeric chains or solvent during the membrane fabrication process. Also the wetting properties of nanoparticles can prevent and control the fouling phenomenon.

The objective of this study was preparation a proper membrane for oily waste water treatment. In order to reach this aim we investigated the effect of preparation condition parameters including exposure time in humid condition and SiO_2 nanoparticle concentration on membrane performance, which occurs in high flux as well as high rejection.

2. EXPERIMENTAL

2.1 Materials

Polyethersulfone (PES) with molecular weight of 400,000 g/mol was purchased from BASF, the solvent DMF (Dimethylformamide) was supplied from MERCK Company as polymer solvent, SiO2 nanoparticles (average particle size of 10 nm, specific surface area of 380 m2/g, containing hydrophilic groups) were obtained from MERCK Company and Deionized water was used as a non-solvent in coagulation bath.

2.2 Membrane preparation

For preparation method (combination of VIPS and NIPS) at first the different amounts (0%, 0.2%, 0.7%, 1.2% and 1.4% based on the polymer weight) of dry SiO2 particles were added into DMF, the solution was ultrasonicated for 20 min to ensure good dispersion of the particles. PES was dried at 110 ^{o}C under vacuum for 12 hours, after that polymer (14 wt%) was dissolved in the solution and subjected to magnetic stirrer for 5 hours to obtain a homogenous solution.

While the solutions were forming due to vigorous stirring, many air bubbles were generated so to remove these bubbles they were kept in room condition without stirring overnight for complete degassing. In NIPS method The casting solution was cast with 180 μm casting knife onto a glass plate at room temperature and immediately was immersed in coagulation water bath but in combined technique the nascent membrane was put in humid chamber with 70% relative humidity at 25 ^{o}C temperature for specific time, then was immersed in coagulation water bath (25 ^{o}C), where an exchange of solvent and non-solvent occurred and membrane sheets were formed. After a few minutes, PES membrane film was detached from the glass plate. After primary phase separation, the membrane was transferred to fresh distilled water for 24 h to leach out the remaining solvent from the membrane structure. The list of fabrication parameters which considered in this study are as below, Table 1.

Table 1. Values of variables

Variables	**Values**				
Nano particle concentration (wt. %); C_{SiO2}	0	0.2	0.7	1.2	1.4
Exposure time (s); t	6	10	20	30	34

2.3 Membrane performance

The membrane performance was investigated with respect to microfiltration. The performance of the prepared membranes was examined by a flat sheet module, which was used in previous studies of this research team (10, 11), with an effective membrane area of 50 cm2 at ambient temperature. All prepared membranes were processed at same operating conditions, TMP (trans-membrane pressure) and feed flow rate are 3 bar and 3 L/min, respectively. The oil-in-water stable emulsion was made using gasoil (Tehran Refinery) with the dispersed oil prepared by mixing gasoil and surfactant at a mixing rate of 12,000 rpm for 30 min. The surfactant used was polyoxyethylene (80) sorbitanmonooleate (Tween 80, Merck) at concentration of 100 ppm. For analysis of membrane performance, the amount of oil rejection which is an important parameter was measured by COD test that presented the permeate oil content.

3. RESULTS AND DISCUSSION

The main purpose of this study is investigation of performance of different fabricated membrane which can be affected by the preparation method along with nanoparticle concentration and exposure time in humid box. The effect of these probed as below.

3.1 Effect of Nano concentration

For investigation the effect of Nano concentration, different membrane were fabricated in five different level of Nano concentration as mentioned in Table 1 with considering only 20 s as exposure time in 70% humidity of humid box. Fabricated membrane evaluated in main process for oil-water separation and the result of them for permeate flux in same operation condition show as Figure 1.

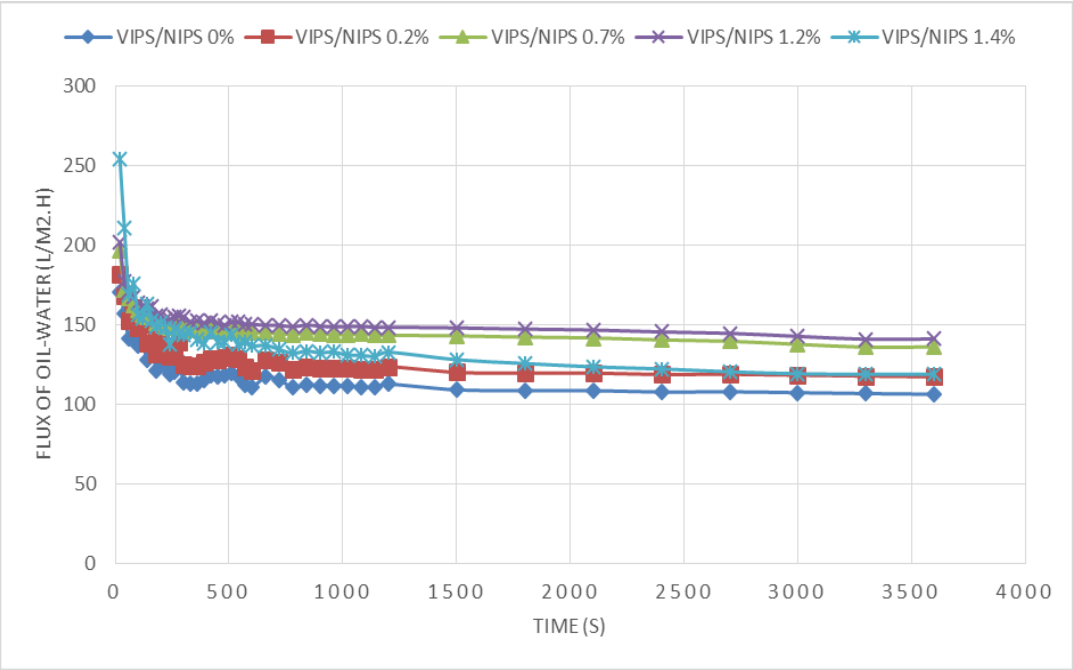

Figure 1. Flux of oil-water for membrane with different nanoparticle concentration

The results show that the permeate flux of different cases increased by increasing nanoparticle concentration until a specific value (1.2 Wt. %) and after this value presence of a higher SiO2 concentration caused a negative effect on the permeate flux. The incorporation of SiO2 nanoparticle

enhanced the hydrophilicity of membrane which improved the permeation. But further increasing in concentration results in permeate flux reduction which might be attributed to the agglomeration of particles in the membrane.

3.2 Effect of exposure time

Water vapor can be easily absorbed into a polymer solution which cause a primary phase inversion and form the surface pores. The exposure time in this process is an essential factor which can improve the membrane structure while in some cases lead to an adverse effect on the membrane performance (Huang et al., 2012). As indicated in Figure 2, at the condition in which humidity is 70% with Nano concentration of 0.7%, increasing the time exposure has positive effect on permeate flux.

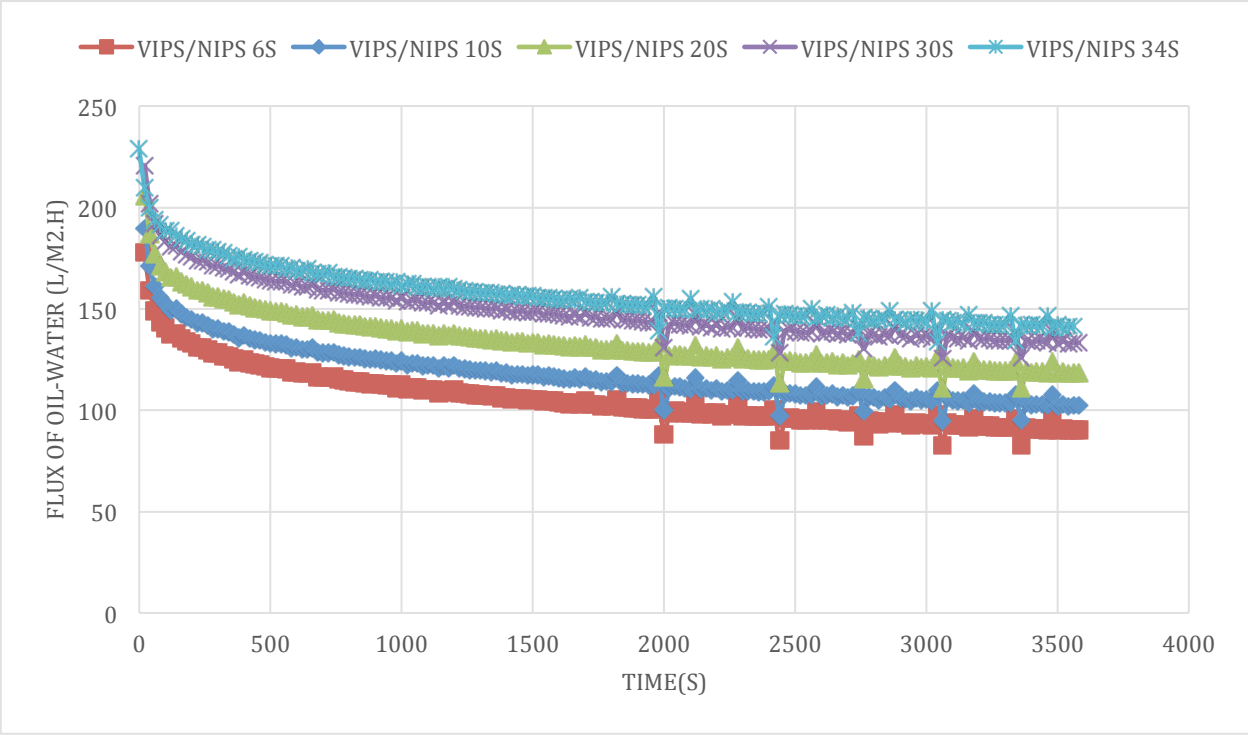

Figure 2. Flux of oil-water for membrane with exposure time

In this preparation method when humidity is applied, although the top surface of polymeric film adsorbs water droplets, the bulk remains unchanged. But after precipitation in coagulation non-solvent bath, those changes on the surface generalized to the whole of the final obtained membrane. Thus, one of the most important factors in the first step of phase separation in the humid chamber is to adjust the effective conditions that not only influence on the surface structure but also can change the bulk morphology.

The plasticity nature of the cast film let vapor drops leave their footprint on the surface in contrast to solid surface and intensity of these traces can produce different morphologies based on considered conditions. Immediately after inserting the cast film to the humid chamber the water vapor droplets intended to cover the film surface due to the high affinity between DMF and water. In fact the physical properties of solvent which are evaporation rate and solvent-non-solvent interaction caused a competition between water vapor condensation on the surface and evaporation of solvent from the polymeric film which inhere based on figure 2 the higher time exposure the water vapor condensation, in the other word in 70% humidity and 0.7% Nano concentration increasing the time will help vapor droplet to make more pores on the surface of casing film which finally effect on membrane performance.

3.3 Rejection measurement

After examinations of each fabricated membrane the obtained permeate water was provided for COD test which reveals the oil content. The performance of each membrane in separation process was determined by using this parameter. For all fabricated membranes, the rejection was more than 98%. This amount of separation for oil-water feed showed the pore size is not very large to let the oil through but changing of preparation conditions could improve the permeate flux significantly with the same amount of rejection.

4. CONCLUSION

A novel approach was applied to fabricate high performance Nano-SiO_2 embedded PES membranes by combination of VIPS and NIPS methods for microfiltration of oil-in-water emulsion. SiO_2 nanoparticles were used as the hydrophilicity modification agents which resulted in more adsorption of water vapor droplets onto the film surface in VIPS step, while made larger pores on the membrane surface during rapid phase separation in NIPS step. All membranes were examined in constant operating conditions and the results showed a regular trend for permeate flux in case of 70% humidity and 0.7% Nano concentration with increasing the exposure time in which the best performance of membrane obtained in the higher exposure time. But the behavior of fabricated membrane with high SiO_2 content in fabrication process implies vice versa effect on performance, high addition of nanoparticles caused a reduction in permeate flux which is due to the aggregation of particles in the membrane surface and the bulk of membrane resulting to the pore blockage. The COD test have been done for all experiments. Results showed about more than 98% rejection for each fabricated membrane which indicates that with maintaining the high rejection, permeate flux has increased by increasing the SiO_2 concentration until 1.2% in 70% and 34s exposure time.

REFERENCES

Cheryan M. and N. Rajagopalan, 1998, "Membrane processing of oily streams. Wastewater treatment and waste reduction," Journal of Membrane Science, 151, 13–28.

Fouladitajar A., F. Zokaee Ashtiani, A. Okhovat, and B. Dabir, 2013, "Membrane fouling in microfiltration of oil-in-water emulsions; a comparison between constant pressure blocking laws and genetic programming (GP) model," Desalination, 329, 41–49.

Fouladitajar A., F. Zokaee Ashtiani, H. Rezaei, A. Haghmoradi, and A. Kargari, 2014, "Gas sparging to enhance permeate flux and reduce fouling resistances in cross flow microfiltration," Journal of Industrial and Engineering Chemistry, 20, 624–632.

Huang J., K. Zhang, K. Wang, Z. Xie, B. Ladewig, and H. Wang, 2012, "Fabrication of polyethersulfone-mesoporous silica nanocomposite ultrafiltration membranes with antifouling properties," Journal of Membrane Science, 423. 362–370.

Jsarakulski K., A. Kozfowskib, and A. W. Morawskia, 1995, "Purification of oily wastewater by ultrafiltration," 5, 197–205.

Susanto H., N. Stahra, and M. Ulbricht, 2009, "High performance polyethersulfone microfiltration membranes having high flux and stable hydrophilic property," Journal of Membrane Science, 342, 153–164.

Takht Ravanchi M., T. Kaghazchi, and A. Kargari, 2009, "Application of membrane separation processes in petrochemical industry: a review," Desalination, 235, 199–244.

Vatanpour V., S. S. Madaeni, A. R. Khataee, E. Salehi, S. Zinadini, and H. A. Monfared, 2012, "TiO2 embedded mixed matrix PES nanocomposite membranes: Influence of different sizes and types of nanoparticles on antifouling and performance," Desalination, 292, 19–29.

Wu G., S. Gan, L. Cui, and Y. Xu, 2008 "Preparation and characterization of PES/TiO2 composite membranes," Applied Surface Science, 254, 7080–7086.

Proceedings of the 10th World Congress of EWRA 'Panta Rhei', 5-9 July 2017, Athens, Greece
© 2017 *European Water Resources Association*

Understanding the anaerobic fluidized membrane bioreactor for wastewater treatment

J. Wang[1,2], A.G. Fane[2] and J.W. Chew[1,2*]
[1] *School of Chemical and Biomedical Engineering, Nanyang Technological University, 637459, Singapore*
[2] *Singapore Membrane Technology Center, Nanyang Environment and Water Research Institute, Nanyang Technological University, 637141, Singapore*
[*] *e-mail: JChew@ntu.edu.sg*

Abstract: The fluidization of Granular Activated Carbon (GAC) particles has received much attention in recent years as a promising method for mitigating membrane fouling particularly in membrane bioreactors (MBRs). In particular, the fluidized GAC particles are acknowledged to be beneficial in terms of adsorption of organic foulants, and mechanical scouring and surface shear of the membrane surface. Both lab-scale and pilot-scale studies have affirmed the efficacy of GAC fluidization in maintaining a depressed extent of membrane fouling in anaerobic fluidized bed - membrane bioreactors (AnFMBRs). More in-depth studies have also correlated the hydrodynamics of fluidized GAC particles with the effectiveness of membrane fouling mitigation. This study aimed at understanding the improvement of fine (micron-sized) particle critical flux in the presence of fluidized GAC via the Direct Observation Through the Membrane (DOTM) technique. The model foulant was a suspension of polystyrene particles (5 mm sized), and the parameters investigated included GAC particle diameter (d_p), superficial liquid velocity (U_l) and thereby power requirement (P_r), and height along the vertically aligned membrane. Results indicate that: (i) fluidized GAC increased the critical flux by an order-of-magnitude relative to that with tangential liquid shear alone; (ii) the overall critical flux ($J_{critical,overall}$) expectedly increased with power input (P_r), but the relationship between local critical flux ($J_{critical}$) and power input (P_r) depended on the position along the membrane height; (iii) at the same P_r, although the larger GAC particles were more effective locally (i.e., higher $J_{critical}$) due to greater particle inertia, the smaller GAC particles were more effective overall (i.e., higher $J_{critical,overall}$) due to greater bed expansion enabling scouring of more membrane heights; and (iv) a higher power input (P_r) was required for sufficient bed expansion to enable more consistent critical flux ($J_{critical}$) values over the whole membrane height.

Key words: membrane fouling mitigation; liquid-solid fluidization; critical flux; direct observation; energy input

1. INTRODUCTION

Membrane bioreactors (MBRs) are becoming increasingly popular for wastewater treatment, because of the significant advantages of high efficiency, small footprint and high quality of effluent. The major obstacle for more widespread use of MBRs is the severe membrane fouling, which significantly increases the maintenance and operation cost (Le-Clech et al., 2006). The introduction of unsteady-state tangential shear on the membrane surface as an energy-efficient means of fouling mitigation holds much promise (Jaffrin, 2011; Zamani et al., 2015). The fluidization of powdered activated carbon (PAC, whose particle diameter is about 100 μm) has been presented as a viable alternative to bubbling (Park et al., 1999), and more recently the fluidization of the larger millimetre-sized granular activated carbon (GAC) has been reported to confer membrane-fouling mitigation with energy requirements at least an order-of-magnitude lower than that of bubbling (Kim et al., 2011). Reports on the efficacy of fluidized millimeter-sized GAC particles have since flourished (Bae et al., 2014; Bae et al., 2013; Gao et al., 2014a; Gao et al., 2014b; Hu and Stuckey, 2007; Kim et al., 2011; Li et al., 2014; Ren et al., 2014; Shin et al., 2014; Yoo et al., 2014; Yoo et al., 2012). Other than the capability to adsorb organic contaminants, our previous studies have confirmed that the hydrodynamics of the fluidized GAC is directly relatable to the effectiveness of fouling mitigation even for inorganic foulants (e.g., bentonite) (Wang et al., 2016a; Wang et al., 2016b). The current study aims to investigate this further, and represents the first systematic study

of the effect of millimetre-sized GAC particle fluidization on critical flux ($J_{critical}$) in the microfiltration of fine (micron-sized) particulate foulants.

2. MATERIALS AND METHODS

2.1 Experimental setup

The Direct Observation Through the Membrane (DOTM) technique, first reported in 1998 (Li et al., 1998), was used in this study for characterizing the critical flux in a liquid-solid fluidization membrane filtration cell. The key component is the Zeiss microscope coupled with a camera (Axiocam 105 Color), which allowed for the visual observation of the deposition of the foulant on the feed-membrane interface. Two pumps allowed for cross-flow of the feed and permeate, while another was used for the permeate flux across the membrane.

The membrane used was an Anopore disk (Whatman, Germany), which was transparent when wetted, with a diameter of 47 mm and nominal pore size of 0.2 μm. Polystyrene (also known as latex) particles (Sigma Aldrich, Singapore) with particle diameter of 5 μm were used as the model foulant. The GAC particles (FILTRASORB 300, Calgon Carbon Corporation) obtained were first sieved using Cole-Parmer U.S. Standard Brass Test Sieves and the Ro-Tap sieve-shaker in order to investigate specific sizes with a narrower particle size distribution (PSD).

2.2 Determination of critical flux

Critical flux is defined as the flux above which fouling occurs significantly and below which negligible fouling occurs (Field et al., 1995). In the current study, the flux-stepping method was adopted to characterize critical flux. Specifically, each flux was held constant for 10 minutes, at the end of which the flux was increased by 5 L/(m^2 h), and two DOTM images were captured for each flux at the end of the 1st and 10th minute. The percentage change in the number of deposited polystyrene particles was calculated as follows:

$$\frac{dN}{dt} = \frac{N_{10th\ minute} - N_{1st\ minute}}{9\ \text{min}} \quad (1)$$

A plot of *dN/dt* versus flux identified the critical flux as the flux at which *dN/dt* started to rapidly increase.

3. RESULTS AND DISCUSSION

3.1 Critical flux

Figure 1 shows that polystyrene particles started to deposit discernibly at critical flux, while many polystyrene particles deposited above critical flux. Critical flux was determined as the onset of a significant change in the rate of the number of deposited polystyrene particles (*dN/dt*), as presented in Eq. (1).

Figure 2 shows a plot of *dN/dt* versus flux at a superficial liquid velocity (U_l) of 0.032 m/s and dimensionless height (*h/H*) of 0.46 for conditions with and without GAC. The critical fluxes were 45.8 L/(m^2 h) and below 5 L/(m^2 h) for the cases of fluidized GAC with d_p = 1.85 mm and when GAC was absent, respectively. This underscores the significant effect of 'large particle' (i.e., millimeter-sized) fluidization on the polarization of 'fine particles' (i.e., micron-sized).

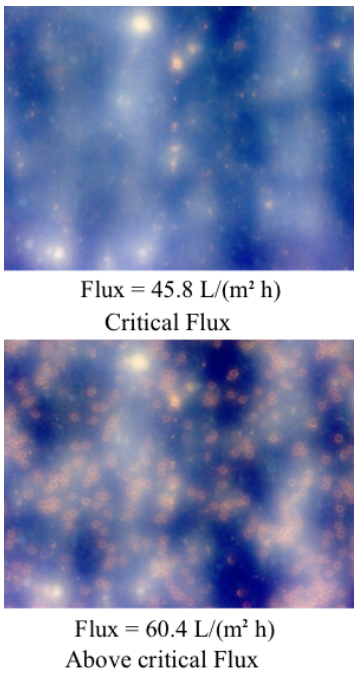

Figure 1. DOTM images at U_l = 0.032 m/s (3.5 times U_{mf}) and h/H = 0.46 for the fluidized GAC particles with d_p = 1.85 mm at the 10th minute of the flux of (a) 15.7 L/(m^2 h) (i.e., below critical flux), (b) 45.8 L/(m^2 h) (i.e., at critical flux), and (c) 60.4 L/(m^2 h) (i.e., above critical flux).

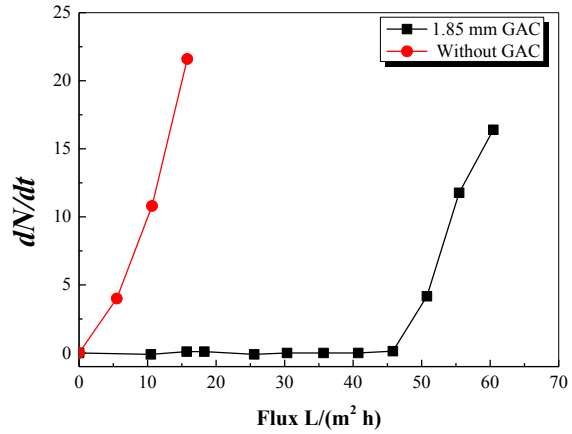

Figure 2. Rate of change of the number of deposited polystyrene particles (dN/dt) versus flux at U_l = 0.032 m/s and h/H = 0.46. Critical fluxes were determined as 45.8 L/(m^2 h) and 5 L/(m^2 h) for the cases of fluidized GAC with d_p = 1.85 mm and when GAC was absent, respectively.

3.2 Power Requirement

The power required for fluidizing the GAC particles (P_r; unit of kW) can be calculated by:

$$P_r = \Delta P_{bed} Q \tag{2}$$

where ΔP_{bed} is the pressure drop across the liquid-solid fluidized bed (kPa) and Q is the volumetric flow rate (m^3/s). The volumetric flow rate (Q) has to high enough to enable the particles to be fluidized.

Figure 3 depcits the overall critical flux ($J_{critical,overall}$) as a function of power requirement (P_r) for the three GAC particle diameters (d_p) investigated. For each particle diameter (d_p), a higher power input (P_r) expectedly gave a higher $J_{critical,overall}$ value. Notably, at the same power input (P_r), the smaller particles gave higher $J_{critical,overall}$ values, which agreed with our previous study on the effect

of $U_l - U_{mf}$(Wang et al., 2016a). The largest particle required at least 50% more power (P_r) than the smallest particle to confer the same $J_{critical,overall}$.

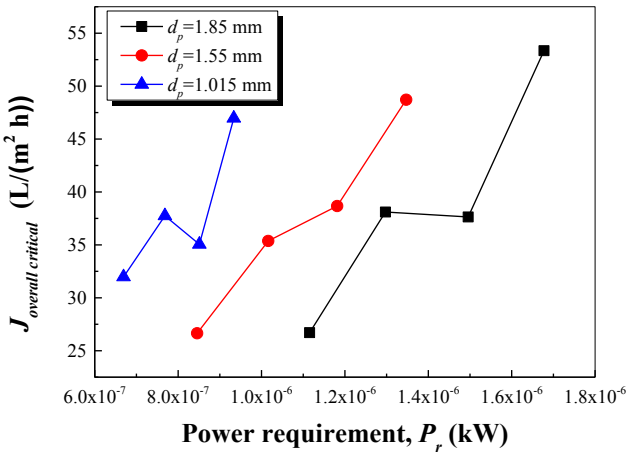

Figure 3. Overall critical flux ($J_{critical,overall}$) versus power requirement with GAC particle diameters of 1.85 mm, 1.55mm, and 1.015 mm.

REFERENCES

Bae, J., Shin, C., Lee, E., Kim, J., McCarty, P.L., 2014. Anaerobic treatment of low-strength wastewater: A comparison between single and staged anaerobic fluidized bed membrane bioreactors. Bioresource Technology 165, 75-80.

Bae, J., Yoo, R., Lee, E., McCarty, P., 2013. Two-stage anaerobic fluidized-bed membrane bioreactor treatment of settled domestic wastewater. Water Sci. Technol 68, 394-399.

Field, R.W., Wu, D., Howell, J.A., Gupta, B.B., 1995. Critical flux concept for microfiltration fouling. Journal of Membrane Science 100, 259-272.

Gao, D.W., Hu, Q., Yao, C., Ren, N.Q., 2014a. Treatment of domestic wastewater by an integrated anaerobic fluidized-bed membrane bioreactor under moderate to low temperature conditions. Bioresource Technology 159, 193-198.

Gao, D.W., Hu, Q., Yao, C., Ren, N.Q., Wu, W.M., 2014b. Integrated anaerobic fluidized-bed membrane bioreactor for domestic wastewater treatment. Chemical Engineering Journal 240, 362-368.

Hu, A.Y., Stuckey, D.C., 2007. Activated carbon addition to a submerged anaerobic membrane bioreactor: Effect on performance, transmembrane pressure, and flux. Journal of Environmental Engineering-Asce 133, 73-80.

Jaffrin, M.Y., 2011. Hydrodynamic Techniques to Enhance Membrane Filtration. Annual Review of Fluid Mechanics 44, 77-96.

Kim, J., Kim, K., Ye, H., Lee, E., Shin, C., McCarty, P.L., Bae, J., 2011. Anaerobic fluidized bed membrane bioreactor for wastewater treatment. Environmental Science & Technology 45, 576-581.

Le-Clech, P., Chen, V., Fane, T.A.G., 2006. Fouling in membrane bioreactors used in wastewater treatment. Journal of Membrane Science 284, 17-53.

Li, H., Fane, A.G., Coster, H.G.L., Vigneswaran, S., 1998. Direct observation of particle deposition on the membrane surface during crossflow microfiltration. Journal of Membrane Science 149, 83-97.

Li, J., Ge, Z., He, Z., 2014. A fluidized bed membrane bioelectrochemical reactor for energy-efficient wastewater treatment. Bioresource technology 167, 310-315.

Park, H., Choo, K.H., Lee, C.H., 1999. Flux enhancement with powdered activated carbon addition in the membrane anaerobic bioreactor. Separation Science and Technology 34, 2781-2792.

Ren, L.J., Ahn, Y., Logan, B.E., 2014. A two-stage microbial fuel cell and anaerobic fluidized bed membrane bioreactor (MFC-AFMBR) system for effective domestic wastewater treatment. Environmental Science & Technology 48, 4199-4206.

Shin, C., McCarty, P.L., Kim, J., Bae, J., 2014. Pilot-scale temperate-climate treatment of domestic wastewater with a staged anaerobic fluidized membrane bioreactor (SAF-MBR). Bioresource Technology 159, 95-103.

Wang, J., Wu, B., Yang, S., Liu, Y., Fane, A.G., Chew, J.W., 2016a. Characterizing the scouring efficiency of Granular Activated Carbon (GAC) particles in membrane fouling mitigation via wavelet decomposition of accelerometer signals. Journal of Membrane Science 498, 105-115.

Wang, J., Zamani, F., Cahyadi, A., Toh, J.Y., Yang, S., Wu, B., Liu, Y., Fane, A.G., Chew, J.W., 2016b. Correlating the hydrodynamics of fluidized granular activated carbon (GAC) with membrane-fouling mitigation. Journal of Membrane Science 510, 38-49.

Yoo, R., Kim, J., McCarty, P., Bae, J., 2014. Effect of temperature on the treatment of domestic wastewater with a staged anaerobic fluidized membrane bioreactor. Water Science & Technology 69, 1145-1150.

Yoo, R., Kim, J., McCarty, P.L., Bae, J., 2012. Anaerobic treatment of municipal wastewater with a staged anaerobic fluidized membrane bioreactor (SAF-MBR) system. Bioresource technology 120, 133-139.

Zamani, F., Chew, J.W., Akhondi, E., Krantz, W.B., Fane, A.G., 2015. Unsteady-state shear strategies to enhance mass-transfer for the implementation of ultrapermeable membranes in reverse osmosis: A review. Desalination 356, 328-348.

Proceedings of the 10th World Congress of EWRA 'Panta Rhei', 5-9 July 2017, Athens, Greece
© 2017 *European Water Resources Association*

Moving towards a water-sustainable chemical industry: Novel water recovery processes

G. Kolliopoulos*, E. Shum, J. Marial and V.G. Papangelakis
Department of Chemical Engineering and Applied Chemistry, University of Toronto
* *e-mail: g.kolliopoulos@mail.utoronto.ca*

Abstract: A key factor to consider when thinking of a sustainable chemical industry that is using water in its operations (such as the metals and mining industry) is the energy footprint of the applied water recovery technologies. Forward Osmosis (FO) and Freeze Crystallization (FC) are two innovative processes promising to minimize fresh water intakes in the chemical industry at a significantly lower energy input compared to conventional processes, such as Reverse Osmosis (RO), evaporation, or crystallization. FO is a membrane process able to recover water from dilute feed solutions (i.e., industrial process water, high salinity streams), into a concentrated draw solution (CDS). The flow of water into the CDS occurs spontaneously, due to the osmotic pressure gradient generated between the two solutions, diluting the CDS. The draw solutes must then be separated from the resulting dilute draw solution (DDS) to regenerate and recycle the CDS in the process, leaving behind clean water. This step is the main source of energy consumption in the overall FO process, which only requires moderate heating. On the other hand, FC involves processes in which water is removed from an aqueous solution by freezing or freeze-thaw cycling, while the solutes remain in a concentrated aqueous phase from which they can be recovered or contained. The energy advantage is due to the fact that the latent heat of freezing is about 7 times lower than its evaporation analogue. Research advancements in the aforementioned processes are reported.

Key words: Water recovery, forward osmosis, natural freezing, freeze crystallization

1. INTRODUCTION

Currently in Ontario, Canada, around 2 million m^3 of hazardous effluent streams are disposed off at an average cost of CAD$ 115/m^3. Recovering water from these streams by an energy efficient process presents several advantages: clean water production, which can be recycled in industrial operations, and reduced volumes of concentrated effluents that require disposal.

Desalination technologies such as membrane processes, (RO: Reverse Osmosis), and evaporative processes are energy intensive, and often limited to effluent streams with less than sea-like water concentration (Hancock, 2013). RO is more energy efficient at recovering water from low salinity streams, up to 35,000 ppm total dissolved solids (TDS). However, Forward Osmosis (FO) is more attractive compared to distillation or crystallization processes in recovering water from effluent streams of higher salinity, i.e., 60,000-240,000 ppm TDS, as the overall cost is significantly decreased(Kolliopoulos et al., 2016b). The FO process treatment window can be seen in Figure 1.

In FO, water molecules flow from a feed solution, i.e., an effluent stream, into an engineered concentrated draw solution (CDS) across the pores of a semi-permeable membrane that selectively allows this passage. This flow occurs spontaneously, due to the osmotic pressure gradient generated between the two solutions, and results in the recovery of water into the CDS. The latter gets diluted and must be treated to separate and recover the draw solutes from the product water. Energy requirements in FO arise from the separation and regeneration of the draw solution. Therefore, the draw solution selection impacts on the effectiveness of FO; an ideal draw solution must have high osmotic pressure and high volatility relative to water. Thermolytic salts present such properties and have been thoroughly studied as draw solutions in FO (Boo et al., 2015; Ge et al., 2013; Kolliopoulos et al., 2017; Kolliopoulos et al., 2015; Kolliopoulos et al., 2016b; McCutcheon et al.,

2005; McCutcheon et al., 2006; McGinnis et al., 2007). Among these is aqueous carbonated trimethylamine (TMA), which was found to be superior in FO applications (Boo et al., 2015; Kolliopoulos et al., 2017; Kolliopoulos et al., 2016a; Kolliopoulos et al., 2015; Kolliopoulos et al., 2016b). The focus of this study is to determine the effectiveness and optimal operating conditions of the separation and regeneration of an aqueous carbonated TMA draw solution. The performance specifications selected for this study were: maximum of 200 ppm residual TMA in the recovered water, maximum energy consumption of 0.20 kWh per kg of H_2O produced, and 95% recovery of draw solutes.

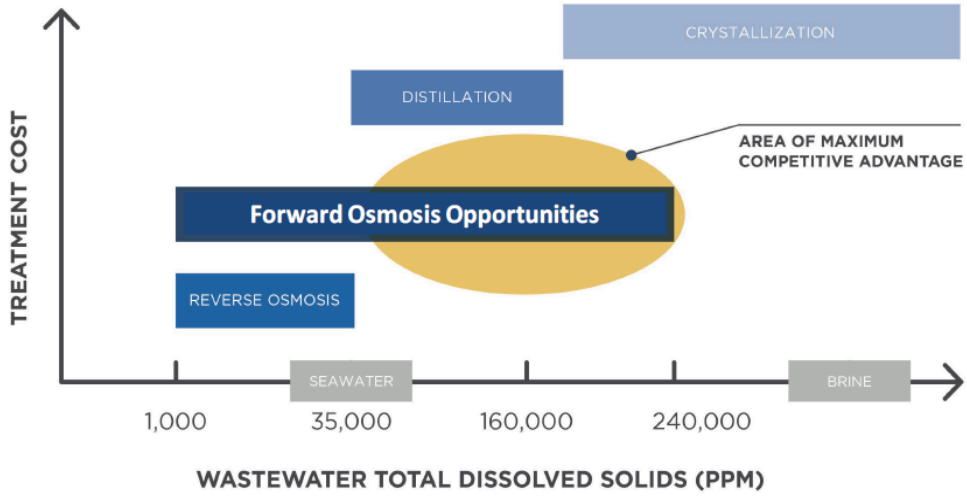

Figure 1. FO process treatment window (Kolliopoulos et al., 2016b)

Another promising technology to recover water from contaminated sources at a low energy footprint is "Freeze Crystallization" (FC). Advances in refrigeration technology have made low-temperature separation processes increasingly appealing to an energy-conscious society. The latent heat of water freezing is about seven times smaller that the latent heat of evaporation providing freezing with a strong thermodynamic advantage. The result is the development of a wide variety of processes called FC techniques, in which an aqueous solution is concentrated by the creation and subsequent removal of ice (Williams et al., 2015). FC processes exploit the freezing behaviour of aqueous solutions as dictated by the water-salt phase diagram. When, for example, a solution of magnesium sulfate is cooled to a temperature below its freezing point but above its eutectic temperature of – 4.1 °C then, if the concentration of $MgSO_4$ is less than the eutectic concentration (about 1.7 molal), ice will form until the solution concentration reaches its equilibrium concentration at the given temperature on its phase diagram. If the concentration is greater than the eutectic concentration, $MgSO_4$ solid will precipitate until the concentration reaches equilibrium. Therefore, ice can be selectively produced in FC processes (Randall and Nathoo, 2015). Attempts to reduce energy requirements further resulted in the development of climate-induced techniques, i.e., "Natural Freezing", to freeze and purify aqueous solutions. The principle is based on that of frozen lakes: a container filled with aqueous solution is left with its surface exposed to a sub-zero atmosphere. An ice layer forms on the surface, much like it would in nature, and grows in the direction of gravity (Hasan and Louhi-Kultanen, 2016). Although the objective of FC is to produce concentrated solution and pure ice, the presence of impurities trapped within the ice necessitates further processing to obtain pure water. It is believed that the thawing of ice crystals also releases solutes trapped between their grain boundaries (Mandri et al., 2011; Yee et al., 2004). Dendritic crystals beyond a given fineness -the result of high solute concentrations during ice growth requiring greater heat transfer- are too small to form channels, and instead melt away along with the trapped solution (Yee et al., 2003).

2. MATERIALS AND METHODS

2.1 Forward osmosis

The main source of energy consumption in the overall FO process arises from the separation and the regeneration of the draw solution. It has been shown that an FO process that uses stripping to separate the draw solution from the water recovered is the most economically efficient, with regards to the overall energy requirements of the process (Kolliopoulos et al., 2016a). Also, aqueous carbonated TMA has been identified as a very effective draw solution for both desalination and process water recovery via FO. Response Surface Methodology (RSM) was implemented as an optimization technique to identify the optimum operating conditions of the overall FO process; Aspen Plus (www.aspentech.com) and Minitab (www.minitab.com) were used in this computational study. There are two phases to the simulation work: the first one is the identification of the parameters that impact the stripping and regeneration steps, while the second involves the optimization of those parameters.

In the first phase, fractional factorial experiments were designed in Minitab. The experiments were then simulated in Aspen Plus using the model presented in Figure 2. An aqueous carbonated TMA draw solution is sent through an FO cell. The resulting dilute draw solution (DDS) is then sent to a stripping column, where TMA and CO_2 are stripped upon slight heating. Clean water is recovered and sent back into the process. The gaseous TMA and CO_2 go to an absorption column to regenerate the CDS.

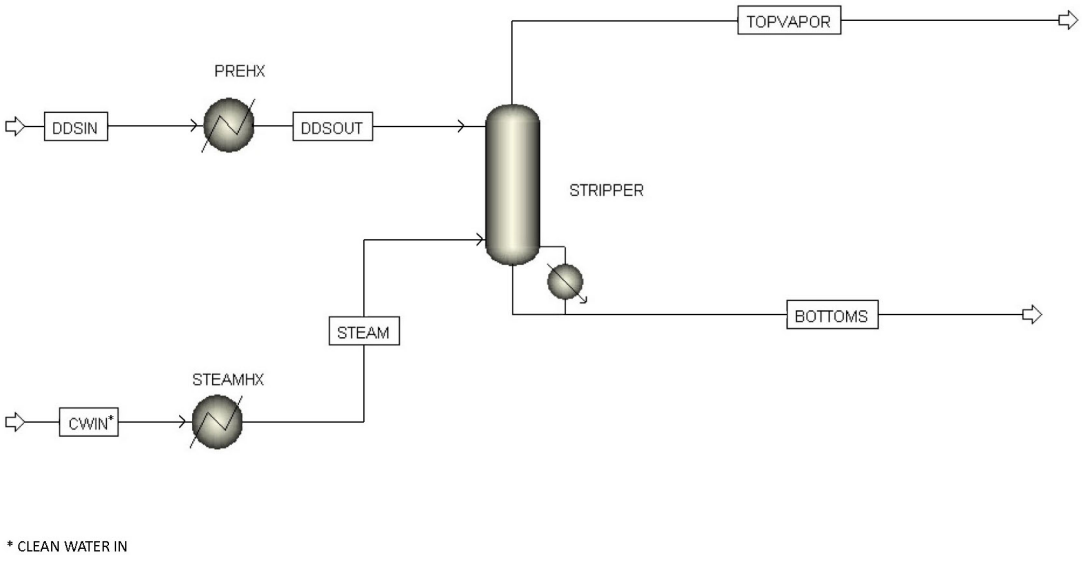

Figure 2. FO Process Aspen Model

The response data collected from Aspen was then imported into Minitab to identify the most important parameters at a confidence level of 95%. The parameters investigated include the number of stages (NS), feed to steam ratio (mass/mass) (FSR), column pressure (CP), feed temperature (FT), feed dilution factor (FDF) and steam temperature (ST).

In the second phase, the optimization experiments were designed in Minitab using the RSM package; Central Composite Design (CCD) was used. The experimental design from Minitab was used to obtain the response data in Aspen Plus. The latter was then imported back into Minitab for the regression analysis, which was completed by considering each adjustable variable at time. The optimization goals were entered into Minitab, to locate the best setting of the important parameters. Finally, a simulation at the optimal conditions was carried out in Aspen Plus to obtain the results when operating at the optimum set of conditions.

2.2 Natural freezing

Natural freezing was simulated by placing heat exchangers and a fan in a Styrofoam box. Coolant from a refrigerating circulator passed through the heat exchangers, and the temperature in the box was regulated by means of a Pt100 temperature probe connected to the refrigerating circulator. A 500 mL of 0.5 molal $MgSO_4$ solution was placed in a silicone container insulated on the sides and bottom with Styrofoam to present only the surface of the solution to the cold air. The temperatures tested ranged from -1 °C to -6 °C, and the solution was frozen for four days. After freezing the ice was removed and washed with 100 mL of chilled deionised water (Hasan and Louhi-Kultanen, 2016). The ice was then either left to melt at room temperature or placed right-side-up on a metal plate heated to 50 °C, which caused the solid that grew last to melt first. The run-off from melting was periodically collected. All liquid collected was then diluted to fixed volumes. Analysis was performed via ICP-OES on the molten ice, the concentrated solution left behind in the container, and the rinse water in order to measure the magnesium content.

3. RESULTS AND DISCUSSION

3.1 Forward osmosis

The main optimization objectives were: maximum of 200 ppm of TMA in the recovered water, at most 0.20 kWh/kg of H_2O produced, and 95% recovery of draw solutes. Important Parameters that impact the effectiveness of the stripping step were identified: FSR, FT, ST, and FDF. It was found that the number of stages and column pressure did not have a significant impact on the separation of TMA and CO_2. The latter can be explained by the big difference between the boiling points of TMA and CO_2. Therefore, NS=2, and CP=1 atm, since this is the minimum value requirement by a Radfrac Model in Aspen Plus, and the most economical operation setting for a column, respectively. The Radfrac model is the main separation block in Aspen Plus, used to simulate column separation. The important parameters were then optimized with respect to the recovery of draw solutes and the total process energy consumption; their optimal settings and the corresponding values for the response parameters are summarized in Table 1a-b.

Table 1. Optimization results

a. Optimal settings for the most important parameters			
Parameter	**Value**		
FSR (g/g)	4.13		
FT (°C)	20		
ST (°C)	110		
FDF	2.75 (13.8 wt.% TMA, 9.2 wt.% CO_2, balance: H_2O)		
b. Comparison of Aspen Plus and Minitab models for the response variables at the optimal conditions			
Variable	**Aspen Values**	**Minitab Values**	**Target Values**
TMA Concentration in Recovered Water (wt.%)	0.77	0.047	0.07
TMA Concentration in Top Vapor Stream (wt.%)	49.54	42.99	35
CO_2 Concentration in Top Vapor stream (wt.%)	33.28	26.44	23
% Recovery of TMA	93.93	99.36	100
Energy Consumption (kWh/kg)	0.29	0.24	0.20

Generally, there is good agreement between the data obtained from Aspen Plus and Minitab. The only major discrepancy is observed in the TMA level in the bottoms stream of the stripping column, where the values obtained differ by one order of magnitude. This discrepancy was attributed to the optimization process being done in Minitab, and not directly in Aspen Plus, which has thermochemical property models and is able to calculate mass balances with a considerable degree of accuracy.

3.2 Natural freezing

From the raw data collected, the amount of water frozen and magnesium sulfate solution entrapped in the ice was measured. Furthermore, the cumulative effect of freezing was calculated by measuring discrete volumes of solid melt. From this data the cumulative molality of the remaining un-melted ice was plotted against the percentage of the initial water remaining in the ice.

From an initial concentration of ~0.5 molal $MgSO_4$ it was possible to produce ice nearly fifteen times purer (from 0.5 molal to virtually no magnesium sulfate). It was found that experiments where the ice was melted by means of a heated plate resulted in increased magnesium concentration vs. water recovery, while experiments where the ice was allowed to melt at room temperature (labelled SM on Figure 3) had significantly lower magnesium concentrations. The trade-off was that while it took roughly 1 h to melt the ice produced using a heated place, it took roughly 3 h to melt a similar mass of ice at room temperature. Furthermore, high rates of water recovery inevitably resulted in increasingly impure ice. The water recovery percentage for the -1 °C heated plate experiment ends at ~30% because a much lower amount of solution was frozen after four days compared to the other experimental runs.

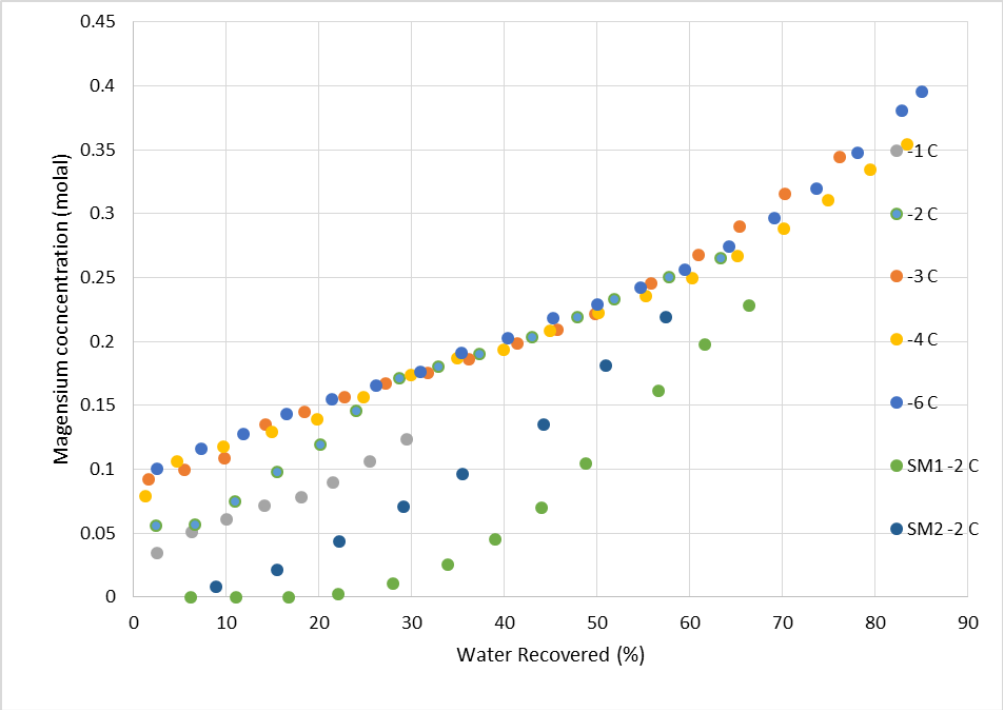

Figure 3. Magnesium concentration of solid plotted against water recovered as ice

Although it was expected that lower temperatures would result in the production of ice with more impurities as increased speed of ice growth would result in greater entrapment of magnesium sulfate solution, it was found that an air temperature of -3, -4, and -6 °C resulted in concentration/ice production profiles that were virtually identical in appearance (Figure 3). However, for air temperatures of -1 and -2 °C it was found that warmer temperatures (close to the solution liquidus temperature of ~ -0.8 °C) resulted in lower concentrations of solid.

The slow melting of ice at room temperature dramatically decreased the magnesium concentration at higher water recovery rates, with ~25% water recovery at a magnesium concentration of nearly zero molal in one experimental run. It is believed that this is due to the fact that slower melting allows for the entrapped solute to drain from between the grain boundaries of ice crystals, leaving behind purer ice. This effect is lost at higher temperatures when the ice crystals melt at rates similar to the draining of entrapped solute.

4. CONCLUSIONS

The most important parameters were identified to be FSR, FT, ST, and FDF; NS and CP were identified to have insignificant impact on the degree of separation. The optimal conditions were identified as a FSF=4.13, FT=20 °C, ST=110 °C, and FDF=2.75. The current set up in Aspen Plus makes a strong case for low capital cost, due to the low number of required stages and the near ambient operating pressure. It is apparent that the required energy input is somewhat higher (0.29 kWh/kg than the targeted one (0.20 kWh/kg). However, in this setup no waste heat integration was considered; in another setup that would incorporate waste heat integration, the energy requirements of the FO process are expected to decrease significantly.

The application of freezing technology towards the recovery of water is still in its relative infancy. However, it is evident that the process of applying natural freezing towards the recovery of water by freeze concentration does result in the production of ice that is purer than the original solution. This effect is further enhanced by the thawing at room temperature of ice produced by natural freezing which allows entrapped solute to drain away. Current experiments can recover nearly 25% of the original water at very low magnesium sulfate concentrations, leaving behind a more concentrated solution. As the extent of pure water recovery appears to be linked to the thawing temperature, further experiments are to be conducted to increase water recovery, thereby increasing the concentration of the remaining solution to the point where it can be treated using conventional processes.

ACKNOWLEDGMENTS

The authors would like to acknowledge the University of Toronto, NSERC, Ontario Centres of Excellence and Southern Ontario Water Consortium (SOWC) for the financial support in this project, and Forward Water Technologies Inc. for their technical advice.

REFERENCES

Boo, C., Khalil, Y.F. and Elimelech, M., 2015. Performance evaluation of trimethylamine–carbon dioxide thermolytic draw solution for engineered osmosis. Journal of Membrane Science, 473(0): 302-309.

Ge, Q., Ling, M. and Chung, T.-S., 2013. Draw solutions for forward osmosis processes: Developments, challenges, and prospects for the future. Journal of Membrane Science, 442(0): 225-237.

Hancock, N., 2013. Engineered Osmosis for Energy Efficient Separations: Optimizing Waste Heat Utilization Final Scientific Report DOE F 241.3. DOE/EE003467-1 United States 10.2172/1067379 GFO English, ; Oasys Water Inc, Boston, MA.

Hasan, M. and Louhi-Kultanen, M., 2016. Water purification of aqueous nickel sulfate solutions by air cooled natural freezing. Chemical Engineering Journal, 294: 176-184.

Kolliopoulos, G., Carlos, M., Clark, T.J., Holland, A.M., Peng, D.-Y., Papangelakis, V.G., 2017. Chemical Modeling of the TMA–CO_2–H_2O System: A Draw Solution in Forward Osmosis for Process Water Recovery. Journal of Chemical & Engineering Data, 62(4), 1214-1222

Kolliopoulos, G., Carlos, M., Holland, A.M., Clark, T.J. and Papangelakis, V.G., 2016a. Forward Osmosis for Process Water Purification Using Carbonated Trimethylamine as the Draw Solution, Water in Mining 2016, 5th International Congress on Water Management in Mining, Proceedings of the 5th International Congress on Water Management in Mining. Editors: Jacques Wiertz, Neil McIntyre. Paper No. 71. Santiago, Chile. May 18-20, 2016.

Kolliopoulos, G., Clark, T. and Papangelakis, V.G., 2015. Forward Osmosis for Industrial Process Water Recovery: The Case of TMA-CO_2-H_2O as Draw Solution, COM 2015 | The Conference of Metallurgists hosting AMCAA | America's Conference on Aluminum Alloys. Publisher: Canadian Institute of Mining, Metallurgy and Petroleum (CIM), ISBN: 978-1-926872-32-2. Paper No. 8991. Toronto, ON, Canada. August 23-26, 2015.

Kolliopoulos, G., Karlov, A., Holland, A.M., Clark, T.J. and Papangelakis, V.G., 2016b. Forward Osmosis: A Promising Process for Industrial Process Water Recovery, 77th Annual International Water Conference (IWC) 2016, Publisher: Engineers' Society of Western Pennsylvania (ESWP). Paper No. IWC 16-29. San Antonio, Texas, USA. November 6-10 2016.

Mandri, Y. et al., 2011. Parametric study of the sweating step in the seawater desalination process by indirect freezing. Desalination, 269(1–3): 142-147.

McCutcheon, J.R., McGinnis, R.L. and Elimelech, M., 2005. A novel ammonia—carbon dioxide forward (direct) osmosis desalination process. Desalination, 174(1): 1-11.

McCutcheon, J.R., McGinnis, R.L. and Elimelech, M., 2006. Desalination by ammonia–carbon dioxide forward osmosis: Influence of draw and feed solution concentrations on process performance. Journal of Membrane Science, 278(1–2): 114-123.

McGinnis, R.L., McCutcheon, J.R. and Elimelech, M., 2007. A novel ammonia–carbon dioxide osmotic heat engine for power generation. Journal of Membrane Science, 305(1–2): 13-19.

Randall, D.G. and Nathoo, J., 2015. A succinct review of the treatment of Reverse Osmosis brines using Freeze Crystallization. Journal of Water Process Engineering, 8: 186-194.

Williams, P.M., Ahmad, M., Connolly, B.S. and Oatley-Radcliffe, D.L., 2015. Technology for freeze concentration in the desalination industry. Desalination, 356: 314-327.

Yee, P.L., Wakisaka, M., Shirai, Y. and Hassan, M.A., 2003. Effects of Single Food Components on Freeze Concentration by Freezing and Thawing Technique. Nihon Shokuhin Kougakukaishi (Japan Journal of Food Engineering), 4(3): 77-83.

Yee, P.L., Wakisaka, M., Shirai, Y. and Hassan, M.A., 2004. Effect of Sodium Chloride on Freeze Concentration of Food Components by Freezing and Thawing Technique. Nihon Shokuhin Kougakukaishi (Japan Journal of Food Engineering), 5(2): 97-103.

Proceedings of the 10th World Congress of EWRA 'Panta Rhei', 5-9 July 2017, Athens, Greece
© 2017 *European Water Resources Association*

Biological treatment of a low strength domestic wastewater in a membrane bioreactor

A. Bezirgiannidis, N. Marinakis, S. Ntougias and P. Melidis*
Laboratory of Wastewater Management and Treatment Technologies, Department of Environmental Engineering, Democritus University of Thrace, Vas. Sofias 12, 67100 Xanthi, Greece
* *e-mail: pmelidis@env.duth.gr*

Abstract: Apart from facing eutrophication, wastewater treatment is a major environmental issue, due to the exhaustion of human resources and the enforcement of stricter legislation limits. Limited economic resources and land availability as well as the high cost of conventional wastewater treatment plants led us to find alternative sustainable methods to treat wastewater, such as membrane bioreactor technology. In this work, we evaluated the depuration of a low strength domestic wastewater derived from a coagulation-flocculation process. An MBR system was operated under alternating aeration and periodic feed, where membrane cleaning was achieved by periodic pumping. MBR performance was examined with and without external carbon source addition, whereas either raw urban wastewater or glycerol from the biodiesel production served as the external carbon source. In all cases, BOD_5, COD, TKN and NH_4^+-N removal rates were greater than 86% and their effluent values were below the legislation limits. However, denitrification efficiency was low in the absence of external carbon source or during addition of the raw effluent (<16.9% and 25.6%, respectively) and only glycerol addition as the external carbon source resulted in complete denitrification. In particular, TN removal efficiency was above 85%, with effluent NH_4^+-N and TN concentrations being below 1.7 and 11.7 mg/L, respectively. Indeed, glycerol addition improved system performance, fulfilling the disposal limits set by the law.

Key words: Domestic wastewater, low strength, MBR

1. INTRODUCTION

Due to the constantly increasing population and to the fact that modern societies become more consuming than ever, there is a need to expand wastewater treatment plants capabilities. Activated sludge systems, which are commonly used, are costly to construct and most important, have high carbon footprint demands. Many alternative methods to treat wastewater have been developed, one of which is membrane bioreactor technology. The advantages of these configurations in comparison to activated sludge systems are their excellent flow quality, the smaller carbon footprint and the operation flexibility (Visvanathan et al., 2000; Melina et al., 2006). Submerged MBRs need half land area than activated sludge systems and sludge production is half amount (Gander et al., 2000).

A MBR system includes a bioreactor, where all biological processes for nutrients removal are taken place. Inside the bioreactor, the separation of activated sludge from the treated water is achieved through membrane filtration, without the need for sedimentation tank, which is required in conventional activated sludge systems (Judd et al., 2006). The membrane acts as a barrier, permitting passed through the pores some components of mixed liquor and retaining the others (Tchobanoglous et al., 1998).

In order to protect the environment and subsequently the human health, every country enforces criteria for the quality of the treated wastewater. Regulations on wastewater reclamation and reuse are essential, because they protect public health, increase water availability by saving water resources, prevent coastal pollution and deal with water drought problems (Angelakis et al., 1999). Reuse of wastewater in Greece complies with the disposal limits set by the Joint Ministerial Decree 145116/2011.

The aim of current work is to investigate the removal efficiency of a lab-scale MBR system,

treating a low strength wastewater. Wastewater was derived from a chemically enhanced primary treatment pilot-scale unit, located in the wastewater treatment plant of the city of Xanthi. The main factor to classify a wastewater as high, medium or low strength is the C/N or the COD/TKN ratio (Carrera et al., 2004; Ryu and Lee, 2009). Microbial growth in wastewater treatment plants relies on various nutrient requirements and operating conditions, with organic content being a major growth factor (Ma et al., 2009). Therefore, an efficient sewage treatment process should be applied in order to achieve high nutrient removal efficiencies from a wastewater with low C/N ratio (Wang et al., 2015).

2. MATERIALS AND METHODS

A membrane bioreactor system, shown in Figure 1, was set up and operated under alternating aeration and periodic feed. The unit consisted of a storage tank containing the low strength wastewater, which was derived from the chemical treatment of a domestic wastewater. A pump was supplying wastewater inside a buffer tank in order to feed system at once. The bioreactor comprised of a 25 L tank and a submerged microfiltration membrane of 0.1 μm pore size and 1.5 m^2 area. A blower was placed inside the tank for supplying air, while a submersible mixer was used to avoid solid particles sedimentation. The filtrate was pumping through the membrane and stored in a tank for chemical analysis. A second tank was also included for providing external carbon source (glycerol from biodiesel production) to improve denitrification.

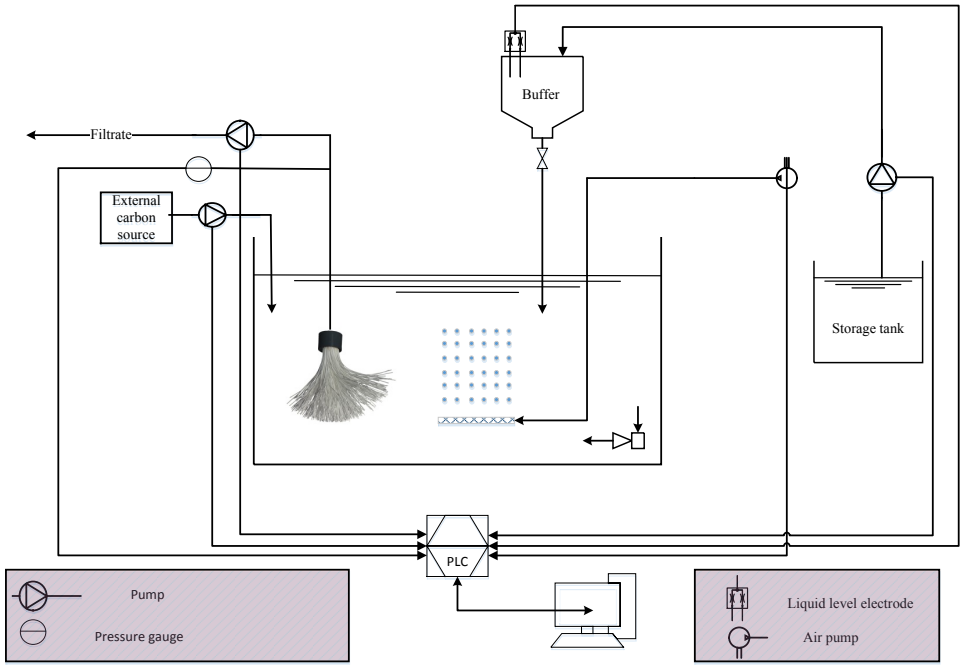

Figure 1. MBR system chart flow

A Programmable Logic Controller (PLC) was used for unit control and operation. Every operating cycle consisted of two phases, an aerobic and an anoxic, which were successively changing during the whole experimental period to achieve denitrification. At the beginning of each cycle, i.e. at the beginning of the anoxic phase, wastewater was entering inside the bioreactor tank. Aerobic and anoxic phase duration, filtration period, wastewater and external carbon source pumping were controlled by the PLC system.

Each operating cycle consisted of a 30 min aerobic and 30 min anoxic phase duration. The influent and permeate flow was equal to 0.5 L/h, which corresponded to an HRT of 1.25 d and an working volume at 15 L. Samples were withdrawn from the influent, the effluent and the storage tank in order to evaluate system performance.

3. RESULTS AND DISCUSSION

Organic carbon removal rates were sufficient during unit operation. BOD_5 and COD removal efficiency was over 96% and 93%, respectively. Similar results were concluded in another MBR system, reporting overall BOD and COD removal efficiencies of 96% and 95%, respectively (Lim et al., 2007). Effluent quality was also comparable with that of Melin et al. (2006), who achieved 97% BOD removal efficiency during wastewater treatment. In any case, effluent was characterized by a low organic content, with BOD and COD concentrations being equal to 4 and 25 mg/L, respectively. Such values were much lower than the legislation limits set in Greece for wastewater reuse.

Nitrification was also efficient, resulting in high ammonia nitrogen and total Kjeldahl nitrogen removal efficiencies of 95% and 87%, respectively. Similar performance showed a MBR unit, operating under the alternating aeration mode (Chaize and Huyard, 1991), measuring effluent TKN concentrations less than 10 mg/L, which corresponded to an average TKN removal efficiency of 85%. In a pilot-scale MBR treating municipal wastewater (Monclus et al., 2010), TKN removal efficacy was 81.3%, with effluent TKN concentration being equal to 10 mg/L. The ammonia nitrogen removal efficiency in an MBR equipped with a submerged microfiltration membrane was 80-83%, with effluent NH_4^+-N concentration being equal to 5.6 mg/L (Rosenberger et al., 2002), which is higher than the respective value determined in this study (effluent NH_4^+-N was below 3 mg/L).

During the first experimental period (without external source addition), a high NO_3^--N concentration was determined in the effluent, indicating an insufficient denitrification process, due to the limited organic carbon availability. Thus, external carbon addition was needed to improve system denitrification process. In the next experimental period, raw wastewater was added to increase the COD/TKN ratio from 4.1 to 5. Although nitrate reduction was slightly improved, total nitrogen concentration in the effluent was still above the legislation limits. In the last experimental period, glycerol was added as external carbon source, resulting in an average COD/TKN ratio of 8.7. As shown in Figure 2, NO_3^--N and total nitrogen concentrations in the effluent were equal to 3.6 and 11.7 mg/L, which are below the legislation limits.

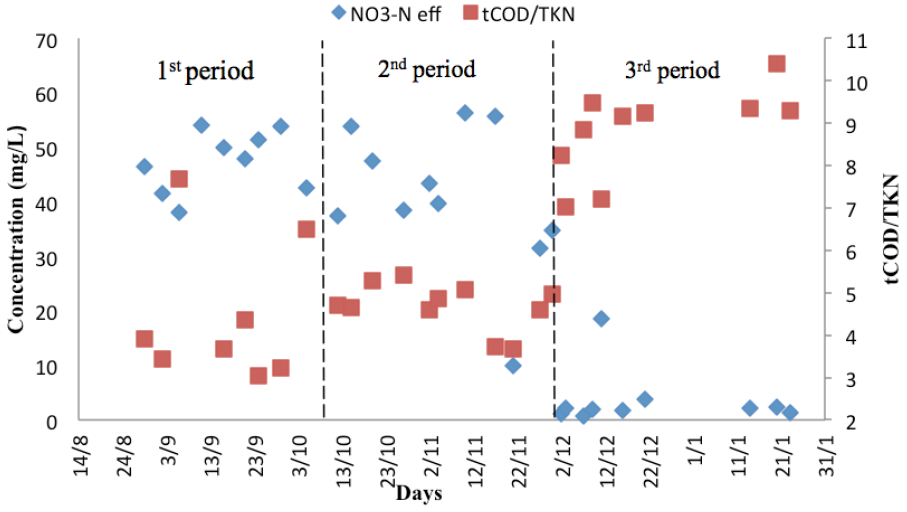

Figure 2. NO_3^--N effluent concentrations under different COD/TKN ratios

Total suspended solids were not detected in the effluent during the whole experimental period, as a result of microfiltration membrane. Phosphorus removal efficiency almost reached 100%, especially during glycerol addition. Nutrients' concentrations in the effluent and the respective Greek legislation limits, according to the Joint Ministerial Degree (JMD) 145116/2011 for wastewater reuse, are presented in Table 1. Considering the Greek legislation, a low effluent BOD_5 concentration was achieved, which met the legislative limits for unrestricted irrigation and urban

use. The effluent TN and ammonia nitrogen concentrations met the legislative limits for unrestricted irrigation, industrial use, urban and suburban green applications, and groundwater recharge. The suspended solids concentration complied with the required limits for unrestricted use.

Table 2. MBR effluent characteristics and the respective Greek legislation limits

Parameter (mg/L)	**BOD**	**COD**	**TKN**	**NH_4^+-N**	**NO_3^--N**	**TN**	**PO_4^{-3}-P**	**TSS**
MBR effluent	3	13	7.9	1.7	3.6	11.7	0.1	0
Legislation limit	25	125	-	2	-	15	2	35

4. CONCLUSIONS

MBR unit resulted in high BOD, COD, TKN and NH_4^+-N removal efficiencies (96, 93, 86 and 95%, respectively) during treatment of a low strength wastewater. Partial addition of high strength wastewater, to enhance denitrification, did not affect the overall unit performance, determining BOD, COD, TKN and NH_4^+-N removal efficiencies of 97, 92, 87.5 and 95%, respectively. In the abovementioned experimental periods, total nitrogen removal was restricted and denitrification efficiency was low. Addition of glycerol increased C/N ratio over 8 and BOD, COD, TKN, NH_4-N and TN removal efficiencies were greater than 99.4, 97, 89 and 97%, respectively. Indeed, nitrate reduction highly improved and total nitrogen concentration in the effluent was equal to 11.7 mg/L. Addition of external carbon source also resulted in MLSS increase, without affecting system operation. MBR effluent characteristics fulfill with the disposal limits set by the Greek Joint Ministerial Decree, not only for wastewater discharge, but also for wastewater reuse for limited irrigation, industrial use and aquifer enrichment.

REFERENCES

Angelakis, A. N., Marecos Do Monte, M. H. F., Bontoux, L., Asano, T., 1999. The status of wastewater reuse practice in the Mediterranean basin: Need for guidelines. Water Res.; 33(10): 2201-2217.

Carrera, J., Vicent, T., Lafuente, J., 2004. Effect of influent COD/N ratio on biological nitrogen removal (BNR) from high-strength ammonium industrial wastewater. Process Biochem.; 39: 2035-2041.

Chaize, S., Huyard, A., 1991. Membrane bioreactor on domestic wastewater treatment sludge production and modeling approach. Water Sci. Technol.; 23(7-9): 1591-1600.

Gander, M., Jefferson, B., Judd, S., 2000. Aerobic MBRs for domestic wastewater treatment: a review with cost considerations. Sep. Purif. Technol.; 18: 119-130.

JMD 145116/2011 (OJ B 354/8.3.2011) "On the determination of measures, conditions and procedures for the reuse of treated liquid waste and other provisions"

Judd, S., Judd, C., 2006. The MBR book. Elsevier Ltd.

Lim, B., Choi, B., Yu, S., Lee, C. 2007. Effects of operational parameters on aeration on/off time in an intermittent aeration membrane bioreactor. Desalination; 202(5): 77-82.

Ma, Y., Peng, Y., Wang, X., 2009. Improving nutrient removal of the AAO process by an influent bypass flow by denitrifying phosphorus removal. Desalination; 246(1-3): 534-544.

Melin, T., Jefferson, B., Bixio, D., Thoeye, C., De Wilde, W., De Koning, J., van der Graaf, J., Wintgens, T., 2006. Membrane bioreactor technology for wastewater treatment and reuse. Desalination; 187: 271-282.

Monclús, H., Sipma, J., Ferrero, G., Rodriguez-Roda, I., Comas, J., 2010. Biological nutrient removal in an MBR treating municipal wastewater with special focus on biological phosphorus removal. Bioresour. Technol.; 101(11): 3984-3991.

Rosenberger, S., Krüger, U., Witzig, R., Manz, W., Szewzyk, U., Kraume, M., 2002. Performance of a bioreactor with submerged membranes for aerobic treatment of municipal waste water. Water Res.; 36(2): 413-420.

Ryu, H., Lee, S., 2009. Comparison of 4-stage biological aerated filter (BAF) with MLE process in nitrogen removal from low carbon-to-nitrogen wastewater. Environ. Eng. Sci.; 26(1): 163-170.

Tchobanoglous, G., Darby, J., Bourgeous, K., McArdle, J., Genest, P., Tylla, M., 1998. Ultrafiltration as an advanced tertiary treatment process for municipal wastewater. Desalination; 119(1-3): 315-322.

Visvanathan, C., Aim, R.B., Parameshwaran, K., 2000. Membrane separation bioreactors for wastewater treatment. Crit. Rev. Environ. Sci. Technol.; 30(1): 1-48.

Wang, X., Wang, S., Xue, T., Li, B., Dai, X., Peng, Y., 2015. Treating low carbon/nitrogen (C/N) wastewater in simultaneous nitrification-endogenous denitrification and phosphorous removal (SNDPR) systems by strengthening anaerobic intracellular carbon storage. Water Res.; 77: 191-200.

Proceedings of the 10th World Congress of EWRA 'Panta Rhei', 5-9 July 2017, Athens, Greece
© 2017 *European Water Resources Association*

Influence of clay lens on contaminant transport in unconfined coastal aquifers

B. Sharma*, D.S. Rishi, B.K. Mudai and R.K. Bhattacharjya
Department of Civil Engineering, Indian Institute of Technology Guwahati, Guwahati 781039, Assam, India
* *e-mail: bhrigumanisharma@yahoo.com*

Abstract: Groundwater serves as the most reliable source of freshwater for domestic, industrial and agricultural purposes in most of the coastal areas of the world. However, the freshwater aquifers hydraulically connected with the sea or ocean has been deteriorating day by day due to different anthropogenic activities. Therefore, a better understanding of contaminant transport processes in coastal aquifers is highly important to prepare and implement proper water resources planning and management policies for coastal environment. The coastal groundwater flow is very complex due to the occurrence of a freshwater-saltwater diffusion zone and the tidal variation of sea level at the seaward end also contributes to the complexity of coastal groundwater flow. In this study, an experimental investigation has been carried out to understand the behavior of contaminant plume in unconfined coastal aquifers under the influence of horizontal clay lens. The laboratory experiment is conducted in a rectangular flow tank filled with glass beads as the porous medium. A constant head was maintained on the freshwater and saltwater boundary using respective chambers during the experiment. A colored dye with the salt solution was used to differentiate the saltwater from the freshwater. This also helps in visualization of the contaminant. The experimental results show that there are two saltwater wedges developed, one at the base of the aquifer and the other one is above the clay lens. Experimental results also show that the contaminant travels slightly along the saltwater wedge towards the seaward boundary. This experimental study helped us to better understanding of contaminant transport processes occurring in coastal aquifers.

Key words: Contaminant Transport, Unconfined Coastal Aquifer, Laboratory Experiments, Saltwater Interface, Clay Lens

1. INTRODUCTION

Coastal groundwater contamination is a very serious environmental problem throughout the world that threatens the human health and the integrity of aquatic ecosystems in coastal areas. The interest in understanding the mechanism of contaminant transport in coastal groundwater systems is garnering increased attention worldwide with the growing population and rapid development of coastal areas since about 70% of the world's population lives in coastal zones (Bear et al., 1999). However, coastal aquifers play a vital role all over the world due to the availability as well as high quality of groundwater resources they provide. The freshwater aquifers hydraulically connected with the sea or ocean have been deteriorating day by day due to different anthropogenic activities and natural events such as climate change and sea level rise. Once it is highly contaminated, it is very challenging and expensive to remediate contaminated aquifers. Therefore, a quantitative understanding of contaminant transport dynamics in coastal aquifer systems is indispensable with regard to water resources planning, development and management in coastal and island environments.

In the past, numerous scientific investigations related to contaminant transport in coastal aquifers have been conducted. Various approaches, including numerical and experimental studies have been carried out to investigate the contaminant transport patterns in coastal aquifers. For example, Zhang et al. (2002) who experimentally investigated the migration of a contaminant plume of different densities in a coastal aquifer system. They performed a series of laboratory experiments in a rectangular flow tank filled with glass beads as the homogeneous porous medium. Based on the experimental results, they hypothesized that the less dense contaminant plume had less diffusive front than the dense contaminant plume in the seaward direction towards the coastline. As pointed

out by them, the contaminant plume became more diffusive when it approached the saltwater-freshwater interface. A numerical study was conducted by Volker et al. (2002) using a two-dimensional variable-density flow and transport model, 2DFEMFAT to investigate the movement of a dense contaminant plume in an unconfined coastal aquifer. They concluded that neglect of seawater density results in the underestimation of solute mass rate exiting around the shoreline. More recently, Chang and Clement (2013) conducted both experimental and numerical studies to quantify the contaminant plume migration processes occurring within and above the saltwater wedge. Their experimental datasets were numerically simulated by SEAWAT model and they found that numerical prediction matches well with the experimental results. They reported that the contaminant transport dynamics occurring above the saltwater-freshwater interface are much faster than the contaminant migration processes occurring within the interface.

However, as per the author's knowledge, this is the first time an experimental study has been conducted to investigate the contaminant transport dynamics in presence of a horizontal clay lens in an unconfined coastal aquifer system. In this effort, we have successfully completed a laboratory experiment to investigate the influence of a horizontal clay lens on the behavior of contaminant plume patterns in an unconfined coastal aquifer. The experiment was carried out in a laboratory-scale flow tank model with constant head boundary conditions.

2. LABORATORY METHODS

2.1 Experimental setup and measurements

The laboratory experiment was conducted in a rectangular flow tank made of 6 mm thick glass, simulating a two-dimensional flow system in a homogenous and unconfined coastal aquifer (Figure 1). The internal dimensions of the flow tank used was 55.6 cm (length) × 40 cm (height) × 6.8 cm (width).

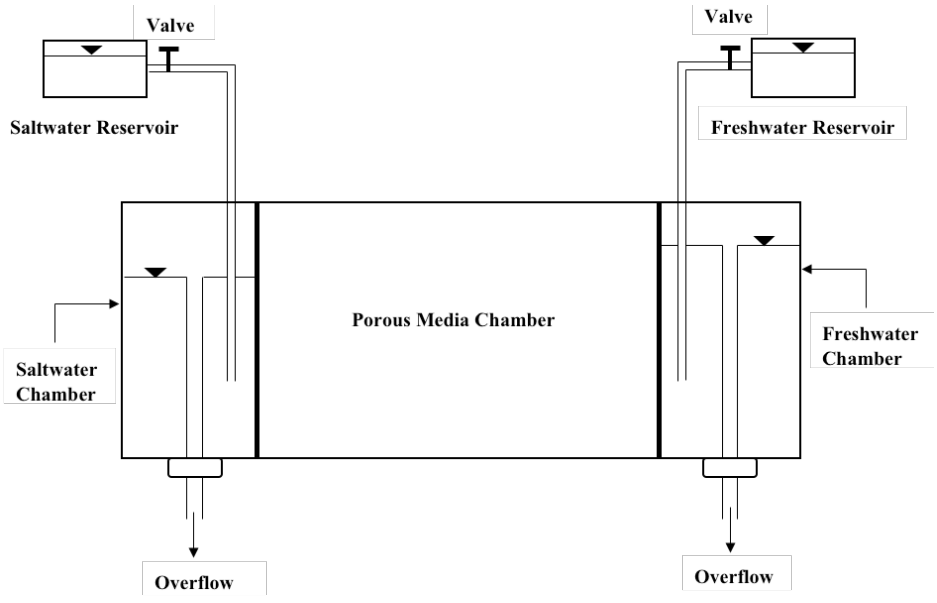

Figure 1. Schematic diagram of experimental setup.

As shown in Figure 1, the flow tank was divided into three distinct chambers and the central flow chamber contains the porous medium (the aquifer). The other two side chambers were used for maintaining constant water heads at the boundary. The left hand and the right hand side constant-head chambers represent the seaward and landward boundary respectively. The constant-head chambers are of length 5.3 cm each and are separated from the central porous media chamber by 7 mm thick Plexiglas plate, which contains 120 holes of 0.7 cm diameter each. The holes are provided

to allow the flow through the chamber into the porous media. These two Plexiglas plates were then wrapped by 500-micron stainless steel meshes in order to prevent the passage of granular material from the central chamber to the side ones. Moreover, thin strips of foam were attached to seal the sides of the wrapped Plexiglas plate to prevent any kind of leakage. In this study, we have used glass beads as a porous media as used by many researchers in their study (Volker et al., 2002; Zhang et al., 2002; Goswami and Clement, 2007; Abarca and Clement, 2009; Chang and Clement, 2013 etc.). The central porous media chamber (45 cm × 40 cm ×6.8 cm) was filled with uniform glass beads of an average diameter of 0.57 mm to a height of 31.5 cm. Both freshwater and saltwater were supplied at constant flow rates to the respective chambers from two overhead chambers whose outlets were attached by PVC pipe with adjustable valve for adjusting the discharge. The overflow from both the freshwater and saltwater chambers were released by PVC pipes diameter of 2.5 cm. Printable rulers were attached on the sides and at the bottom of the flow tank to allow quick measurements.

In this study, tap water was used as freshwater and saltwater was prepared by dissolving 35 g of commercial salt (NaCl) in 1L of deionized water, yielding an effective concentration of 35 g/L. A red color dye was mixed at a ratio of 100 ml per 32 liters of saltwater to differentiate the saltwater from freshwater. The density of the dyed saltwater was measured by using the G8030@JAPSINR specific gravity hydrometer and its value was estimated to be as 1.025 g/cm3. We also measured the density of freshwater as 0.9943 g/cm3 using the aforementioned hydrometer. The saturated hydraulic conductivity (K) of the flow tank was measured using the in-situ method described by Goswami and Clement, 2007 and the average value was estimated as 0.251 cm/s. The main geometrical and hydraulic properties of the porous medium are listed in Table 1.

Table 1. Properties of the Porous Medium

Parameter	Value
Average grain size, mm	0.57
Average bulk density, g/cm^3	1.443
Specific gravity	2.49
Average saturated hydraulic conductivity, cm/s	0.251
Porosity	0.43

2.2 Experimental procedures

Prior to the experiment, the flow tank was packed with glass beads in layers of about 5 cm under fully saturated condition to prevent entrapment of air bubbles inside the flow tank. The glass beads were prudently compressed by hand pressure after each layer was completed. To replicate a horizontal clay lens, we placed an approximately 3 cm thick layer of bentonite clay at a certain height inside the flow tank. It was covered the entire width of the flow tank.

Before starting the contaminant transport experiment, the flow tank was initially flushed with freshwater towards the left side from the right side through a fixed gradient condition until it reaches steady state flow. After establishing steady state flow, the left side chamber was fed quickly with dyed saltwater and when the saltwater in the left side chamber attained a constant level, the saltwater began to intrude the porous media. After a certain duration of time, a steady state saltwater wedge was achieved. After achieving a steady state saltwater wedge position, the contaminant was injected at a specific location of the porous media through a pipette of length 43.8 cm diameter of 1.4 cm. A constant rate of injection of the contaminant into the porous medium was maintained. The pipette was buried in the main flow tank when the porous media was wet packed and contaminant was poured into the pipette using a syringe. A yellow color dye was used as the contaminant in this study to visualize the behavior of the contaminant plume. The left bottom corner of the central flow chamber was considered as the origin to record experimental observations. A Nikon digital camera was used to record images of the behavior of contaminant plume during the experiment. The recorded images were cropped and presented at a suitable scale to provide better visualization.

2.3 Laboratory-scale experiment

This experiment was performed to study the influence of a horizontal clay lens on the behavior of contaminant plume patterns in an unconfined coastal aquifer system. The height of the freshwater level and saltwater level at the respective chambers were fixed at 28.5 cm and 27.5 cm respectively. The clay lens was prolonged horizontally from the left side of the flow tank to a distance of about 28 cm and at a height of 20 cm from the bottom of the tank. After developing a steady state saltwater wedge, the contaminant about 5 ml in volume was injected and the location of the injection point was: x = 20 cm, y = 0.7 cm and z = 13.5 cm. The contaminant plume was allowed to migrate with the freshwater flow and the images were taken at different times. The time of injection of the contaminant was recorded as 35 minutes from starting the experiment.

3. EXPERIMENTAL RESULTS AND DISCUSSIONS

The experimental data of the contaminant transport patterns under the influence of a clay lens are shown in Figure 2. The digital images were recorded to examine the contaminant migration patterns and photographs were taken at 0, 10, 17, 25 and 37 min after injecting the contaminant.

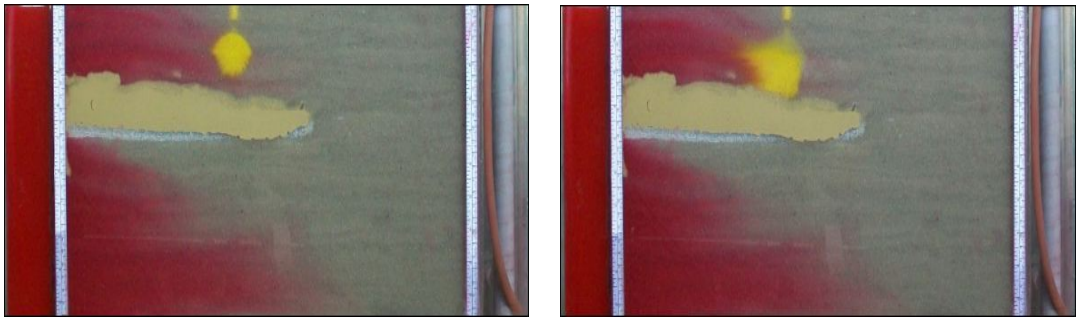

(a) 0 min *(b) 10 min*

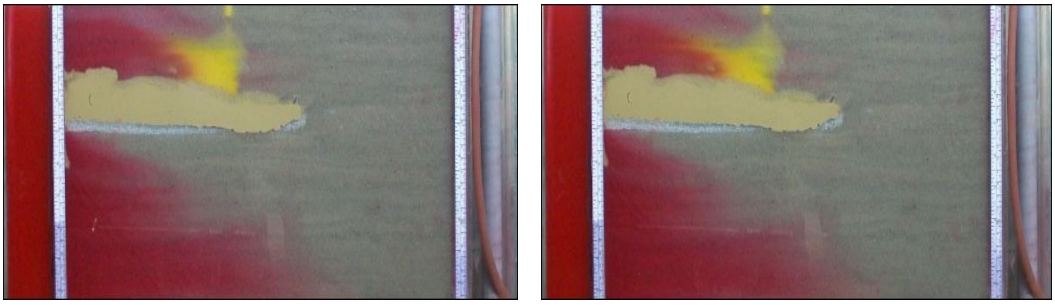

(c) 17 min *(d) 25 min*



(e) 37 min

Figure 2. Contaminant transport experimental results.

Figure 2 shows photographs of the contaminant plume as it moved from the injection point towards the saltwater boundary. From the experimental results, we observed that there are two saltwater wedges developed, one below and the other above the clay lens. Because of the presence of a horizontal stratified layer, it was observed that in addition to the formation of the usual saltwater wedge, there was an additional wedge formed on top of the clay lens. Figure 2(a) was recorded instantly after injection and it indicates that the initial shape of the injected contaminant plume was nearly circular. As time advanced, the plume transported in downward direction towards the saltwater wedge and eventually attained an elongated shape when it came closer to the saltwater wedge. Due to higher level of mixing occurring near the interface, the plume formed an elongated shape as it approached the freshwater-saltwater interface. The shape of the migrating plume was elongated as shown in Figures 2(b), 2(c), 2(d), and 2(e). It was also observed that the contaminant plume moved along the top surface of the saltwater wedge and eventually discharged at the saltwater boundary.

4. CONCLUSIONS

Groundwater contamination in coastal aquifers has been an ongoing and most challenging environmental management problem faced by water resources planners worldwide. Therefore, understanding of contaminant transport patterns in coastal aquifers is an important subject of research work in the field of contaminant hydrology. In this effort, an experimental study was conducted in a laboratory-scale flow tank model to investigate the contaminant plume patterns under the influence of a horizontal clay lens in an unconfined coastal aquifer. The experimental results indicate that there are two saltwater wedges developed, one at the base of the aquifer and the other one is above the clay lens. Experimental data also indicate that the contaminant plume moves along the top surface of the saltwater-freshwater interface towards the seaward boundary and then exits around the shoreline. Due to dispersion effects, the contaminant plume attains an elongated shape as it approaches the interface. Higher velocities occurring near the interface creates a rapid transport of contaminant plume mass along the mixing zone forming this elongated shape. This experimental study helps us to better understanding of contaminant transport dynamics occurring in an unconfined coastal aquifer system.

REFERENCES

Abarca, E., Clement, T. P., 2009. A novel approach for characterizing the mixing zone of a saltwater wedge. Geophysical Research Letters; 36 (6), L06402.

Bear, J., 1972. Dynamics of Fluids in Porous Media. American Elsevier Publishing Company, Inc., New York; 764.

Bear, J., 1979. Hydraulics of Groundwater. McGraw-Hill Publishing Company, Inc., New York; 569.

Bear, J., Cheng, A. H., Sorek, S., Quazar, D., Herrera, I., 1999. Seawater intrusion in coastal aquifers, concepts, methods and practices, Kluwer Academic publisher, Dordrecht, The Netherlands.

Brovelli, A., Mao, X., Barry, D. A., 2007. Numerical modeling of tidal influence on density-dependent contaminant transport. Water Resources Research; 43 (10), W10426.

Chang, S. W., Clement, T. P., 2012. Experimental and numerical investigation of saltwater intrusion dynamics in flux-controlled groundwater systems. Water Resources Research; 48 (9), W09527.

Chang, S. W., Clement, T. P., 2013. Laboratory and numerical investigation of transport processes occurring above and within a saltwater wedge. Journal of Contaminant Hydrology; 147, 14-24.

Goswami, R. R., Clement, T. P., 2007. Laboratory-scale investigation of saltwater intrusion dynamics. Water Resources Research; 43 (4), W04418.

Goswami, R. R., Clement, T. P., Hayworth, J. H., 2012. Comparison of numerical techniques used for simulating variable-density flow and transport experiments. Journal of Hydrologic Engineering; 17 (2), 272-282.

Kuan, W. K., Jin, G., Xin, P., Robinson, C., Gibbes, B., Li, L., 2012. Tidal influence on seawater intrusion in unconfined coastal aquifers. Water Resources Research; 48 (2), W02502.

Lu, C., Chen, Y., Zhang, C., Luo, J., 2013. Steady-state freshwater-seawater mixing zone in stratified coastal aquifers. Journal of Hydrology; 505, 24-34.

Todd, D. K., 1980. Ground-Water Hydrology. John Wiley and Sons, New York; 535.

Volker, R. E., Zhang, Q., Lockington, D. A., 1999. Simulation of contaminant transport in unconfined coastal aquifers, In: Oxley, L., Scrimgeour, F. (Eds.), MODSIM'99, Proceedings of International Congress on Modelling and Simulation, Hamilton, New Zealand, 6th-9th Dec. 1999; 1, 13-18.

Volker, R. E., Zhang, Q., Lockington, D. A., 2002. Numerical modelling of contaminant transport in coastal aquifers. Mathematics and Computers in Simulation; 59, 35-44.

Zhang, Q., Volker, R. E., Lockington, D. A., 2001. Influence of seaward boundary condition on contaminant transport in unconfined coastal aquifers. Journal of Contaminant Hydrology; 49, 201-215.

Zhang, Q., Volker, R. E., Lockington, D. A., 2002. Experimental investigation of contaminant transport in coastal groundwater. Advances in Environmental Research; 6 (3), 229-237.

Proceedings of the 10th World Congress of EWRA 'Panta Rhei', 5-9 July 2017, Athens, Greece
© 2017 *European Water Resources Association*

Application of nanostructured materials in fluoride removal from contaminated groundwater

S. Bhattacharya
School of Ecology and Environment Studies, Nalanda University, Bihar, India
e-mail: sbhattacharya@nalandauniv.edu.in

Abstract: Fluoride is a water pollutant of great environmental concern due to its wide abundance and devastating effects on human health. Defluoridation of drinking water is one of the effective solutions for mitigating fluoride pollution. Extensive research has been done so far on various methods for removal of fluoride from water and wastewater. Precipitation processes involve the addition of chemicals and formation of fluoride precipitates. Strong base exchange resins remove fluorides either on hydroxyl cycle or chloride cycle along with anions. Researchers had paid their attention on adsorption technology since last two decades for fluoride removal. Adsorption processes are generally more popular because of their efficiency, convenience, simplicity of design and for their eco-friendly nature. Adsorbents used in fluoride removal are bone charcoal, tricalcium phosphate, florex, activated carbon, magnesia, activated alumina, plant materials, limestone, special soils and clay, fly ash etc. Nanomaterials have gained attention recently and have been widely used as sorbents due to properties such as high surface-to-volume ratio and short diffusion route. Hydrous titanium dioxide (TiO2), Aluminum–cerium (Al–Ce) hybrid adsorbent, Aluminium hydroxide impregnated limestone, sulfate-doped Fe_3O_4/Al_2O_3 nanoparticles, Fe_3O_4 nanoparticles were used for fluoride removal. Micro/nano-hierarchal web consisting of activated carbon fibres and carbon nano fibres impregnated with Al used as an adsorbent for fluoride removal from wastewater. The future research should be focused on evaluating the efficiency of adsorbents in terms of cost and feasibility for removal of fluoride.

Key words: Fluoride, Adsorption, Nanomaterials, Remediation, Groundwater

1. INTRODUCTION

Fluoride is a water pollutant of great environmental concern due to its wide abundance and devastating effects on human health. Fluoride releases into the environment naturally through the weathering and dissolution of minerals, in emissions from volcanoes and in marine aerosols, via coal combustion and from industrial wastes (Ayoob and Gupta, 2006). WHO has prescribed the range of fluoride from 0.6 to 1.5mg/l in drinking water as suitable for human consumption (WHO, 1984; WHO 2002). WHO estimated that more than 260 million people living all over the world consume water with fluoride concentration above 1mg/l.

High fluoride contents in the groundwater have been found in many parts of the developing countries and fluorosis is endemic in around 25 countries of the world. The affected zones include arid parts of northern China, India, Srilanka, African countries, Northern Mexico and central Argentina. Out of 85 million tons of fluoride deposits on the earth's crust, 12 million are found in India (Teotia and Teotia, 1994). In India, about 62 million people in 17 states are affected with dental, skeletal and or non-skeletal fluorosis (Susheela, 1999). Out of 6 lakh villages in India, atleast 50% have fluoride content in groundwater with a concentration more than 1.0 ppm (Gupta, 1995). Many rivers flowing through different states of India are reported to have fluoride contents varying from 0.1 to 12.0 ppm (Bulusu et al., 1979).

Very low doses of fluoride (<0.6 mg/l) in water can induce tooth decay. However, higher doses (>1.5 mg/l), can lead to dental fluorosis or mottled enamel and excessively high concentration (>3.0 mg/l) of fluoride may cause skeletal fluorosis (Yadav and Khan, 2010). General clinical symptoms includes severe pain in the backbone and joints, muscle weakness, increased density of bones, arthritis, brittle bones, paralysis, cancer, infertility, brain damage, thyroid disorder etc. During later

stages, calcification of the bones takes place, osteoporosis in long bones and symptoms of osteosclerosis can be seen where the bones become denser and develop abnormal crystalline structure. (Ibrahim et al., 2011).

2. FLUORIDE REMOVAL TECHNOLOGIES: NANOMATERIAL APPLICATION

Fluoride poisoning can be prevented or minimized by using alternative water sources (surface water, rainwater, and low-fluoride groundwater), by improving the nutritional status of populations at risk and by removing excessive fluoride from drinking water. Defluoridation of groundwater is one of the feasible options to overcome the problem of excessive fluoride in drinking water. The methods developed for this purpose are divided as follows depending upon the mode of action.

2.1 Based on precipitation–coagulation (Nalgonda Technique)

Precipitation processes involve the addition of chemicals and formation of fluoride precipitates. Among these, one of the effective methods are precipitations with calcium and aluminium salts. Precipitation chemicals must be added daily in batches and precipitation techniques produce a certain amount of sludge every day**.** Lime and alum are the most commonly used coagulants (John, 1996; Parker and Fong, 1975). Nalgonda Technique is an economical and simple method for fluoride removal which involves addition of aluminium salts, lime and bleaching powder followed by rapid mixing, flocculation, sedimentation, filtration and disinfection (Nawalakhe et al., 1975). Aluminium salt is only responsible for removal of fluoride from water. Lime facilitates the formation of dense floc for rapid settling.

However, the process removes only a smaller portion of fluoride (18–33%) in the form of precipitates and converts a greater portion of ionic fluoride (67–82%) into soluble aluminium fluoride complex ion, which is a neurotoxin. Hence adoption of Nalgonda technique for defluoridation of water is not desirable. The residual aluminium in excess of 0.2 $mg.L^{-1}$ in treated water can cause pathophysiological, neurobehavioral, structural and biochemical changes (Nayak, 2002). The maintenance cost of the plant is very high, and the process is not automatic and large space is required for the drying of sludge (Meenakshi and Maheshwari, 2006).

2.2 Based on electrochemical method

A technology of defluoridation through electrochemical route has been developed**.** The process utilizes 0.3 to 0.6 $kw.h^{-1}$ of electricity per 1000 L of water containing 5- 10 $mg.L^{-1}$ of fluoride. The anode is continuously consumed and needs to be replenished. The process generates sludge at the rate of 80- 100 gm per 1000 L (on dry basis). However, high cost of electricity in third world countries like India makes the use of this method unsuitable (Feng et al., 2003).

2.3 Based on Ion exchange mechanism

Strong Base Exchange resins remove fluorides either on hydroxyl cycle or chloride cycle along with anions (Runaska et al., 1951). Some inorganic ion exchangers, eg. complex metal chloride silicates, formed from barium or ferric chloride with silicic acid, also exchanged fluoride for chloride. Polystyrene anion exchange resins and strongly basic quaternary ammonium type resins are known to remove fluorides from water along with other anions.

Cation exchange resins impregnable with alum solution have been found to act as defluoridating agents. “Avaram bark” based cation exchange resin works effectively in removing fluoride from water (Meenakshi and Maheshwari, 2006). Few examples of ion exchange resins are given in Table 1.

Table 1. Fluoride removing ion exchange resins

Anion exchange resins	Cation exchange resins
Tulsion, A-27	Carbion
Deaceodite, FF-1P	Wasoresin-14
Lewatit, MIH-59	Polysteren resin
Amberlite, IRA-400	Sulphonated saw dust carbon

However, the process has some limitations like the efficiency is reduced in presence of sulphate, carbonate, phosphate and alkalinity; regeneration of resin is a problem because it leads to fluoride rich waste, which has to be treated separately before final disposal; the technique is expensive because of the high cost of resin; pre-treatment required to maintain the pH, regeneration and waste disposal; treated water has a very low pH and high levels of chloride; the process can make the water totally demineralised and hence is not hygienic.

2.4 Based on membrane process

In spite of various conventional techniques of defluoridation described earlier, the reverse osmosis (RO) membrane process has emerged as a preferred alternative to provide safe drinking water without posing the problems associated with other conventional methods (Pervov et al., 2000). Applications of reverse osmosis to purification of water are discussed by several researchers (Schneiter and Middlebrooks, 1983). Nanofiltration makes use of the same overall phenomenon as reverse osmosis. For nanofiltration, the membranes have slightly larger pores than those used for reverse osmosis and offer less resistance to passage both of solvent and of solutes. As a consequence, pressures required are much lower, energy requirements are less, removal of solutes is much less exhaustive, and flows are faster. Dialysis separates solutes by transport of the solutes through a membrane rather than using a membrane to retain the solutes while water passes through it as in reverse osmosis and nanofiltration. The membrane pores are much less restrictive than those for nanofiltration, and the solute can be driven through by either the Donnan effect (Donnan, 1911) or an applied electric field.

The process has some limitations like it removes all the ions present in water, hence, some essential minerals are also removed and remineralisation is required after treatment. The process is also comparatively expensive; the water can become acidic and needs pH correction; huge amount of water gets wasted as brine which has disposal issues.

2.5 Based on adsorption process

Many researchers are being focused on adsorption technology since last two decades for contaminated ground and surface water treatment. Adsorption appears to be an effective method for fluoride removal because it is eco-friendly, simple and cost effective option for the common people using groundwater as a main source. Activated alumina, activated carbon, activated alumina coated silica gel, calcite, activated saw dust, activated coconut shell carbon and activated fly ash, groundnut shell, coffee husk, rice husk, magnesia, serpentine, tricalcium phosphate, bone charcoal, activated soil sorbent, carbion, defluoron- 1, defluoron-2, etc. are different kinds of adsorbents reported in the previous research works (Min et al., 1999; Wang and Reardon, 2001; Nava et al., 2003). Several bone formulations, synthetic tricalcium phosphate and hydroxy apatite etc. were investigated for their fluoride removal efficiency.

Biosorption is an emerging technique for water treatment utilizing abundantly available biomaterials. Various biosorbents have been developed for fluoride removal. Chitin and chitosan are attractive adsorbents because of their unique properties like biodegradability, biocompatibility and low cost, in addition to their particular physical and mechanical properties, resulting from the presence of chemical reactive groups (hydroxyl, acetamido or amino functions) in polymer chains (Yao et al., 2009).

Sujana et al. (2013) synthesized new biopolymer beads, composite of hydrous ferric oxide (HFO) and alginate, characterized and examined it, with aim of fluoride removal from water. The authors concluded that pH had significant effect on fluoride adsorption efficiency of the beads. The biomass of the natural plant *Tinospora cordifolia* demonstrated a good capacity of fluoride biosorption, highlighting its potential for the drinking water treatment process (Pandey et al., 2012). Fungal biosorbent prepared from *Fusarium moniliforme* for removal of fluoride was investigated by Merugu et al. (2012). A new type of adsorbent was prepared from orange waste by a simple method of saponification reaction with lime water and used for the removal of some metal ions and, after that, for fluoride removal from water (Paudyal et al., 2012). Gopal et al. (2004) and Yadav *et al.* (2013) studied the removal of fluoride from water using sawdust, groundnut husk and sand. The obtained results indicate that these chemically treated natural adsorbents can remove fluoride effectively. Conducting the experiments on water defluoridation with bauxite, Sajidu *et al.* (2008) reported that up to 93.8% fluoride was removed from fluoride solution with initial concentration of 8 mg/L when adsorbent dose of 2.5 g/200 mL were used. Sivasankar et al. (2010) showed the defluoridation capacities of activated tamarind fruit shell (ATFS) and MnO_2 coated tamarind fruit shell (MTFS). Alagumuthu and Rajan (2010) studied zirconium-impregnated cashew nut shell carbon (ZICNSC) to assess its capacity for the adsorption of fluoride from aqueous solutions. The method is simple and has shown great potential for the removal of fluoride ions.

2.6 Use of nanostructured materials

Nanomaterials are fast emerging as potent candidates for water treatment in place of conventional technologies because of their low cost and high efficiency. This would be beneficial for developing nations like India and Bangladesh. Nanoparticles can be used as potent sorbents as separation media, as catalysts for photochemical destruction of contaminants; nano-size zerovalent iron used for the removal of metals and organic compounds from water and nanofiltration membranes (Savage and Diallo, 2005).

Adsorption of fluoride on to solid adsorbent usually occurs through three phases (Mohapatra et al., 2009; Fan et al., 2003):

1. Diffusion or transport of fluoride ions to the external surface of the adsorbent from bulk solution across the boundary layer surrounding the adsorbent particle, called external mass transfer;
2. Adsorption of fluoride ions on to particle surfaces;
3. The adsorbed fluoride ions probably exchange with the structural elements inside adsorbent particles depending on the chemistry of solids, or the adsorbed fluoride ions are transferred to the internal surfaces for porous materials (intra particle diffusion).

Many researchers reported successfully fluoride remediation using different metal oxides and hydroxides characterized by high surface area and numerous of them have used iron oxide as an adsorbent to treat heavy metals, anions, and hazardous elements in wastewater (Huang et al., 2011). Hydrous titanium dioxide (TiO2) has been found to be a potential selective adsorbent for fluoride ions, as well as halogens and arsenic compounds. Chen *et al.* (2012) investigated the possibility of fluoride removal using a nano-adsorbent bimetallic oxide adsorbent synthesized by co-precipitation of Fe(II) and Ti(IV) sulfate solution using ammonia titration at room temperature. Goswami and Purkait (2012) applied acidic alumina for adsorbing fluoride from water and found it to be highly pH dependent with 94% fluoride removal efficiency at pH value of 4.4. The defluoridation capacity of alumina with alkoxide origin varied from 3.14 to 0.59 mg/ g for dosage varying from 0.5 to 8 g/L (Kamble et al., 2010). A modified immobilized activated alumina (MIAA) using alum through the sol gel process was prepared, which gave a performance 1.35 times better than unmodified immobilized alumina and the removal rate was also comparatively faster (Rafique et al., 2012). Other modified forms of AA used for fluoride removal include modification by using different metals such as magnesia, manganese oxide, manganese dioxide, cerium and titanium. Aluminum–

cerium (Al–Ce) hybrid adsorbent was synthesized through the co-precipitation method, which had high sorption capacity up to 27.5 mg/g for fluoride at equilibrium fluoride concentration of 1 mg/L (Liu et al. 2010). Since, aluminium has the highest affinity for fluoride ions; calcium based adsorbents impregnated or doped with aluminium, aluminum oxide or aluminate is being developed to increase the defluoridation capacity. Aluminium hydroxide impregnated limestone (AILS) was prepared and defluoridation experiments were performed (Jain and Jayaram, 2009). The highest adsorption capacity shown by limestone was 43.10 mg/g; while in case of AlLS sorbent it increased to 84.03 mg/g.

Iron and aluminum binary oxide (FeAlO*x*H*y*), aluminum oxyhydroxide (AlO*x*H*y*) and iron oxyhydroxide (FeO*x*H*y*) were investigated with the aim to evaluate their removal efficacy towards arsenate and fluoride, to determine the effects of pH and the ratios of iron to aluminum on the removal of arsenate and fluoride, and finally, to investigate the competitive adsorption between arsenate and fluoride onto FeAlO*x*H*y* (Liu et al., 2012). Magnesium-doped nano ferrihydrite was used for fluoride removal by Mohapatra et al. (2012). The preliminary test showed that increase of Mg content on nano ferrihydrite from 0.39% to 0.98% increased fluoride removal from 66% to 91%.Poursaberi et al. (2012) synthesized adsorbent for fluoride removal using Fe_3O_4 nanoparticles, obtained by co-precipitation of ferrous and ferric ions in a 3-aminopropyl triethoxysilane and additionally functionalized them using a zirconium(IV) porphyrin complex. A granular zirconium-iron oxide composed of amorphous and nano-scale oxide particles were prepared and their adsorption characteristics in fluoride removal were investigated by Dou et al. (2011). Due to the results of batch tests, the authors reported a high adsorption capacity of 9.80 mg/g under an equilibrium concentration of 10 mg/L and at pH = 7.0, and efficient fluoride removal over a wide pH range (3.5–8.0), especially between pH 6.0 and 8.0. Fluoride removal efficiency of CeO_2-ZrO_2 nanocages prepared by Kirkendall effect and a study of its structure was conducted by Wang et al. (2013). Due to results of batch adsorption study, the porous CeO_2-ZrO_2 nanocages showed the maximum capacity was calculated to be 175 mg/g at pH = 4.0 and isotherm are described well by the Langmuir model. The synthesized Fe–Al–Ce trimetal hydroxide adsorbent (Fe–Al–Ce) obtained by spraying of a Fe–Al–Ce nano-adsorbent suspension onto glass beads with acrylic-styrene copolymer latex used as a binder was used for fluoride removal from drinking water by Chen et al. (2011).

Few carbon based sorbents have also been explored for fluoride removal by some researchers. Carbon nanotubes (CNTs) have huge potential since their discovery. Their small sizes, large surface area, high mechanical strength and remarkable electrical conductivity properties make them useful materials for water remediation. Gupta et al. (2009) developed a micronanohierarchal web (MiNaHiWe) consisting of activated carbon fibers (ACF) and carbon nanofibers (CNF), impregnated with Al for the removal of fluoride from wastewater. Various grades of graphite have also been used as adsorbents and tested for the removal of fluoride from aqueous solution (Karthikeyan and Elango, 2008). Adsorbent exhibited commendable fluoride sorption in wide pH range.

Graphene is a single flat atomic sheet of carbon with the atoms arranged in a two-dimensional (2D) honeycomb configuration (Romero et al., 2009). Graphene has drawn much scientific attention since its discovery and exhibits great promise for potential applications in developing field-effect transistors, solar cells, sensors, and adsorbent for heavy metal removal. The adsorption capacities and rates of fluoride onto graphene at different initial pH, contact time, and temperature were evaluated by Li et al. (2011). The experimental results showed that graphene is an excellent fluoride adsorbent with an adsorption capacity of up to 17.65 mg/g at initial fluoride concentration of 25 mg/L and temperature of 25 °C.

3. CONCLUSIONS

Various technologies are currently applied for fluoride removal from groundwater, however, adsorption processes are generally more popular because of their efficiency, convenience,

simplicity of design and for their eco-friendly nature. Performance comparison of different adsorbents is difficult because of the inconsistent data due to different experimental conditions.

The reuse and recycling perspectives are essential in case of developing an efficient adsorbent for defluoridation of drinking water. However, very few researchers have considered these perspectives in their research works. Many natural adsorbents are considered to be inexpensive, but it is difficult to regenerate most of these adsorbents due to complexity in their structures. Presence of residual ions from metal adsorbents used for water treatment is a major area of concern. A particular sorbent which can show high adsorption of fluoride in the laboratory may fail to do so in field conditions. Hence, the selection of the appropriate technology/sorbent media would be essential for remediation purpose.

Adopting a particular method of fluoride remediation depends on the initial fluoride concentration, source and cost effectiveness in an area. Communities should be educated and encouraged to actively participate in the technical and management systems of fluoride remediation. Development of community based defluoridation unit is needed for rural areas with an adsorbent which is cost effective, technologically simple in operation while is able to keep the fluoride level in permissible limit.

REFERENCES

Alagumuthu, G., Rajan, M., 2010. Equilibrium and kinetics of adsorption of fluoride onto zirconium impregnated cashew nut shell carbon. J.Chem. Eng.; 158: 451–457.

Arora, M., Maheshwari, R.C., Jain, S.K., Gupta, A., 2004. Use of membrane technology for potable water production. Desalination.; 170: 105–112.

Ayoob, S., Gupta, A.K., 2006. Fluoride in Drinking Water: A Review on the Status and Stress Effects. Crit. Rev. Environ. Sci. Technol.; 36: 433–487.

Bulusu, K.R., Sundaresan, B.B., Pathak, B.N., Nawlakhe, W.G., Kulkarni, D.N., Thergaonkar, V. P., 1979. Fluorides in water, Defluoridation Methods and their limitations (I) Jl.,.60, 1-25.

Chen, L., He, B.Y., He, S., Wang, T.J., Su, C.L., Jin, Y., 2012. Fe–Ti oxide nano-adsorbent synthesized by co-precipitation for fluoride removal from drinking water and its adsorption mechanism. Powder Technol.; 227: 3–8.

Chen, L., Wang, T.J., Wu, H.X., Jin, Y., Zhang, Y., Dou, X.M., 2011. Optimization of a Fe–Al–Ce nano-adsorbent granulation process that used spray coating in a fluidized bed for fluoride removal from drinking water. Powder Technol.; 206: 291–296.

Donnan, F.G., 1911. Z. Elektrochem., 572–581, cited by Loeb, J., 1921. Donnan equilibrium and the physical properties of proteins. J. Gen. Physiol.; 667–690.

Dou, X., Zhang, Y., Wang, H., Wang, T., Wang, Y., 2011. Performance of granular zirconium-iron oxide in the removal of fluoride from drinking water. Water Res.; 45: 3571–3578.

Fan, X., Parker, D.J., Smith, M.D., 2003. Adsorption kinetics of fluoride on low cost materials. Water Res.; 37: 4929–4937.

Feng, S., Xueming, C., Ping, G., Guohua, C., 2003. Electrochemical removal of fluoride ions from industrial wastewater. Chem. Eng. Sci.; 58: 987– 989.

Gopal, K., Srivastava, S.B., Shukla, S., Bersillon, J.L., 2004. Contaminants in drinking water and its mitigation using suitable adsorbents: An overview. J. Environ. Biol.; 25: 469–475.

Goswami, A., Purkait, M.K., 2012. The defluoridation of water by acidic alumina. Chem. Eng. Res. Des. 90(12): 2316–2324.

Gupta, I., 1995. Drinking water and fluoride in Doda. National seminar on water for life, Jammu, India.

Gupta, A.K., Deva, D., Sharma, A., Verma, N., 2009. Adsorptive removal of fluoride by micro-nanohierarchal web of activated carbon fibers. Ind. Eng. Chem. Res.; 48: 9697–9707.

Huang, Y.H., Shih, Y.J., Chang, C.C., 2011. Adsorption of fluoride by waste iron oxide: The effects of solution pH, major coexisting anions, and adsorbent calcination temperature. J. Hazard. Mater.; 186: 1355–1359.

Ibrahim, M., Asimrasheed, M., Sumalatha, M., Prabhakar, P., 2011. Effects of fluoride content in groundwater: A review. Int. J. Pharma. Appl.; 2(2): 128-134.

Jain, S., Jayaram, R.V., 2009. Removal of fluoride from contaminated drinking water using unmodified and aluminium hydroxide impregnated blue lime stone waste. Sep. Sci. Technol.; 44(6):1436–1451.

John, D.J., 1996. Water treatment, Handbook of Drinking Water Quality Standards and Controls. Van Nostrand Reinhold, NewYork: 407–490.

Karthikeyan, M., Elango, K.P., 2008. Removal of fluoride from aqueous solution using graphite: A kinetic and thermodynamic study. Indian J. Chem. Technol.; 15: 525–532.

Li, Y., Zhang, P., Du, Q., Peng, X., Liu, T., Wang, Z., Xia, Y., Zhang, W., Wang, K., Zhu, H., 2011. Adsorption of fluoride from aqueous solution by graphene. J. Colloid. Interface. Sci.; 363: 348–354.

Liu, H., Deng, S., Li, Z., Yu, G., Huang, J., 2010. Preparation of Al–Ce hybrid adsorbent and its application for defluoridation of drinking water. J. Hazard. Mater.; 179(1): 424–430.

Liu, R., Gong, W., Lan, H., Yang, T., Liu, H., Qu, J., 2012. Simultaneous removal of arsenate and fluoride by iron and aluminum binary oxide: Competitive adsorption effects. Sep. Purif. Technol.; 92: 100–105.

Meenakshi, Maheshwari, R.C., 2006. Fluoride in drinking water and its removal. J. Hazard. Mater.; 137: 456–463.
Merugu, R., Domala, R., Rao Kudle, K., Pratap Rudra, M.P., 2012. Factors influencing the removal of fluoride from water using a fungal biosorbent prepared from Fusarium moniliforme. Int. J. Chem. Tech. Res.; 4: 1094–1098.
Min, Y., Hashimoto, T., Hoshi, N., Myoga, H., 1999. Fluoride removal in a fixed bed packed with granular calcite. Water. Res.; 33(16): 3395–3402.
Mohapatra, M., Anand, S., Mishra, B.K., Giles, D.E., Singh, P., 2009. Review of fluoride removal from drinking water. J. Environ. Manage.; 91: 67–77.
Mohapatra, M., Hariprasad, D., Mohapatra, L., Anand, S., Mishra, B.K., 2012. Mg-doped nano ferrihydrite—A new adsorbent for fluoride removal from aqueous solutions. Appl. Surf. Sci.; 258: 4228–4236.
Nava, C.D., Rios, M.S., Olguin, M.T., 2003. Sorption of fluoride ions from aqueous solutions and well drinking water by thermally heated hydrocalcite. Sep. Sci. Technol.; 38(1): 131–147.
Nawalakhe, W.G., Kulkarni, D.N., Pathak, B.N., Bulusu, K.R., 1975. Defluoridation of water by Nalgonda technique. Ind. J. Environ. Health.; 17: 26-65.
Nayak, P., 2002. Review aluminium: impacts and disease. Environ. Res. Sec. A89: 101–115.
Pandey, P.K., Pandey, M., Sharma, R., 2012. Defluoridation of water by a biomass: Tinospora cordifolia. J. Environ. Prot.; 3: 610–616.
Parker, C.L., Fong, C.C., 1975. Fluoride removal technology and cost estimates. Ind. Wastes.; 21: 23–25.
Paudyal, H., Pangeni, B., Ghimire, K.N., Inoue, K., Ohto, K., Kawakita, H., Alam, S., 2012. Adsorption behavior of orange waste gel for some rare earth ions and its application to the removal of fluoride from water. Chem. Eng. J.; 195–196: 289–296.
Pervov, A.G., Dudkin, E.V., Sidorenko, O.A., Antipov, V.V., Khakhnov, S.A., Makarov, R.I., 2000. RO and NF membrane systems for drinking water production and their maintenance techniques. Desalination.; 132: 315-321.
Poursaberi, T., Hassanisadi, M., Torkestani, K., Zare, M., 2012. Development of zirconium (IV)-metalloporphyrin grafted Fe3O4 nanoparticles for efficient fluoride removal. Chem. Eng. J.; 189–190: 117–125.
Rafique, A., Awan, M.A., Wasti, A., Qazi, I.A., Arshad, M., 2012. Removal of fluoride from drinking water using modified immobilized activated alumina. J Chem. 2013: 1-7. doi:10.1155/2013/386476
Romero, H.E., Joshi, P., Gupta, A.K., Gutierrez, H.R., Cole, M.W., Tadigadapa, S.A., Eklund, P.C., 2009. Adsorption of ammonia on graphene. Nanotechnology; 20(24): 245501.
Runaska, W., Kawane, M., Kajima, T., 1951. Removal of Fluoride Ion by Anion Exchange Resin, Chemical Abstracts, 45 5033 and 7725.
Sajidu, S.M.I., Masamba, W.R.L., Thole, B., Mwatseteza, J.F., 2008. Groundwater fluoride levels in villages of Southern Malawi and removal studies using bauxite. Int. J. Phys. Sci.; 3: 1–11.
Savage, N., Diallo, M.S., 2005. Nanomaterials and water purification: Opportunities and challenges. J. Nanopart. Res.; 7: 331–342.
Schneiter, R.W., Middlebrooks, E.J., 1983. Arsenic and fluoride removal from groundwater by reverse osmosis. Environ. Int.; 9: 289–291.
Sivasankara V., Ramachandramoorthy T., Chandramohan, A., 2010. Fluoride removal from water using activated and MnO2-coated Tamarind Fruit (Tamarindus indica) shell: batch and column studies. J. Hazard. Mater.; 177: 719–729.
Sujana, M.G., Mishra, A., Acharya, B.C., 2013. Hydrous ferric oxide doped alginate beads for fluoride removal: Adsorption kinetics and equilibrium studies. Appl. Surf. Sci.; 270: 767–776.
Susheela, A.K., 1999. Fluorosis Management Programme in India. Current Sci.; 77: 1250-1256.
Teotia, S.P., Teotia, M., 1984. Endemic fluorosis in India: A challenging national health problem. J. Asso. Physicians. India.; 32: 347-352.
Wang, J., Xu, W., Chen, L., Jia, Y., Wang, L., Huang, X.J., Liu, J., 2013. Excellent fluoride removal performance by CeO2–ZrO2 nanocages in water environment. Chem. Eng. J.; 231: 198–205.
WHO, 2002. Fluorides, Environmental Health Criteria: 227, First Draft. Geneva.
WHO, 1984. Guidelines for Drinking Water Quality. In: Health Criteria and Other Supporting Information (2nd edition), World Health Organization, Geneva.
Yadav, A.K, Khan, P., 2010. Fluoride and Fluorosis Status in Groundwater of Todaraisingh Area of District Tonk (Rajasthan, India): A Case Study. Int. J. Chem. Environ. Pharma. Res.; 1(1): 6-11.
Yadav, A.K., Abbassi, R., Gupta, A., Dadashzadeh, M., 2013. Removal of fluoride from aqueous solution and groundwater by wheat straw, sawdust and activated bagasse carbon of sugarcane. Ecol. Eng.; 52: 211–218.
Yao, R., Meng, F., Zhang, L., Ma, D., Wang, M., 2009. Defluoridation of water using neodymium-modified chitosan. J. Hazard. Mater.; 165: 454–460.

Proceedings of the 10th World Congress of EWRA 'Panta Rhei', 5-9 July 2017, Athens, Greece
© 2017 *European Water Resources Association*

Distribution and assessment of heavy metals and physicochemical parameters in riverine basin

M. Khalilzadeh Poshtegal[1*], S.A. Mirbagheri[1] and M. Noury[2]
[1] *Faculty of Civil Engineering, K. N. Toosi University of Technology, Tehran, Iran*
[2] *Iran Water Resources Management Company*
[*] *e-mail: maryam.khalilzadeh61@gmail.com*

Abstract: Water is the most precious resource to sustain the life on earth. Rapid industrialization and urban development results in inclusion of variety of pollutants into rivers. In the present study, a comparison of characteristics of water quality with respect to heavy metal (Fe, Al, Mn and Se) and their interrelationships with some physiological parameters during different seasons of year 2015 has been investigated flowing through the two geographical regions, namely Kurdistan region (Chamsaghez, Chamkhorkhoreh, Jaghatoo Rivers) and West Azarbaijan Region (Sarough River) , in Zarrineh river basin one of the most important and longest rivers in the Lake Urmia basin in Iran which branches from the mountains of Chehelcheshmeh at the being of Kurdistan province. All observed values of Se in spring, observation of Al in 14 stations, observation of Fe in 11 stations and observation of Mn in 9 stations exceed WHO standard for drinking water. However, all of the observation of Se in winter are found with the standard limit. In the present study, the metals Fe, Al and Mn show negative correlation with pH and also the Mn and Se, show negative correlation with DO. Metals Al and Fe found to have strong positive correlation with each other. Distribution of Al and Se in river Chamsaghez and Al, Se and Mn in river Sarough systems, Al in Jaghatoo river and Fe in Chamkhorkhoreh river during entire study period shows significant difference at 95 % level of significance. Spatially all the metals in different river systems do not show any significant spatial difference in their distribution among different river systems.

Key words: Pollution, Dissolved heavy metals, spatial distribution, physicochemical parameters

1. INTRODUCTION

River water is often used for domestic needs and also supplied as potable water by municipal corporations which contamination of drinking water resources with hazardous chemicals like nitrate, nitrite, ammonium and heavy metals has become an increasing concern in developing countries. Regular monitoring of drinking water at the source of supply and at consumer end is of prime importance for generating the database on overall feature and chemical characteristics of water that can help minimize the health hazards to a large extent (Shah and Singh 2016). Physicochemical parameters play an important role to determine the water quality.(Kouamé et al. 2014). The physical and chemical characteristics of water are important parameters as they may directly or indirectly affect its quality(Nevoh et al. 2015). During the last decades, there has been an increasing demand for monitoring water quality of many rivers by regular measurements of various water quality parameters(Khalilzadeh Poshtegal et al. 2016a; Khalilzadeh Poshtegal et al. 2011). Quality of water is generally refers to component of water, which is to be present at the optimum level suitable for growth of aquatic plants and animals. Various factors like water temperature, turbidity, nutrient, hardness, alkalinity, dissolved oxygen (DO) play an important role for the growth of plants and animals in the water. The contamination of water with heavy metals is another major environmental problem. Anthropogenic activities continuously increase the amount of heavy metals in the environment, especially in aquatic ecosystem. Community development and growth of industrial and agricultural activities have led to increase in aquatic contamination such as heavy metals and nutrients (Shoaei et al. 2014). Pollution of heavy metals in aquatic system is growing at an alarming rate and has become an important worldwide problem (Malik et al. 2010; Shanur et al. 2015). Heavy metals have an adverse effect on riverine ecosystem that point sources of heavy metals in the water and sediments should be closely monitored;(Mir Mohammad et al. 2016). Heavy metal and agricultural toxics in Garasou river for water quality assessment was investigated in Iran

to show the distribution of pollution in the river basin (Fatehi et al. 2010). Transport of heavy metals through the soils may lead to the groundwater contamination and their accumulation in soils and crops.(Khalilzadeh Poshtegal et al. 2016b) The use of wastewater in agricultural lands enriched soils with heavy metals to concentrations that may pose potential environmental and health risks in the long-term (Islam et al. 2014; Mirbagheri et al. 2014; S.A.Mirbagheri 2008; Yi et al. 2011). Assessment of the spatial and temporal variability of the heavy metal concentration can help determine the sources of these pollutants, and then provide better water quality management in the upper basins.

Table 1. Sampling locations and site characteristics

Sampling point	Location	Altitude (m)	Geographical position
CH-1	Chamsaqez after the Tamugheh village	1526	$N: 36^o12'03'', E: 46^o07'14''$
CH -2	Ghamsaghez, before Kileshin village	1717	$N: 36^o05'52'', E: 46^o00'20''$
CH -3	Ghamsaghez, before the Veis dam workplace	1540	$N: 36^o11'09.3'', E: 46^o06'34.1''$
CH -4	Ghamsaghez before entering the Saqez	1475	$N: 36^o13'35'', E: 46^o15'52.7''$
CH -5	Ghamsaghez exiting the Saqez	1458	$N: 36^o15'18.3'', E: 46^o18'10''$
CH -6	Ghamsaghez entering the Shahid Kazemi dam	1441	$N: 36^o18'25.05'', E: 46^o23'05.8''$
J -1	Jaghatooo after the Bastam village	1730	$N: 35^o48'02'', E: 46^o24'20''$
J -2	Jaghatooo , Talejar village	1540	$N: 36^o00'53.3'', E: 46^o18'38.1''$
J -3	Jaghatooo , Polgeshlagh village	1475	$N: 36^o05'59.7'', E: 46^o20'50.5''$
J -4	Jaghatooo entering the Bookan dam	1435	$N: 36^o12'31.5'', E: 46^o25'53.4''$
Kh-1	Chamkhorkhoreh, Mahidar Olia village	1600	$N: 35^o59'27.8'', E: 46^o28''38.5''$
Kh-2	Chamkhorkhoreh, Gataloo village	1530	$N: 36^o05'22.1'', E: 46^o29'47.6''$
Kh-3	Chamkhorkhoreh entering the Bookan Dam	1438	$N: 36^o17'28'', E: 46^o35'48.7''$
Sa-1	Entering Tekab city	1834	$N: 36^o22'24.7'', E: 47^o08'00.3''$
Sa-2	Downstream of Tekab city	1757	$N: 36^o26'18.4'', E: 47^o05'25.2''$
Sa-3	Madanchai, upstream of Zarnikh mine	2260	$N: 36^o43'21.3'', E: 47^o07'27.8''$
Sa-4	Aqh-Darreh, upstream of Pooyazarkan factory	1867	$N: 36^o36'53.8, E: 47^o05'29.6''$
Sa-5	Balacholeh, Shirmard village	1837	$N: 36^o35'54.9'', E: 47^o05'32.7''$
Sa-6	Balacholeh, Tekab Road	1716	$N: 36^o28'13.3'', E: 47^o01'38.1''$
Sa-7	Gugerdchi hydrometric station (right branch Alasaggal)	1725	$N: 36^o23'59.7, E: 47^o06'13.6''$
Sa-8	Sarough river before entering Bukan Dam	1442	$N: 36^o24'00.9'', E: 46^o39'18.7''$

2. MATERIALS AND METHODS

2.1 Study area and site description

Zarrineh river is one of the most important and longest rivers of the basin in the Lake Urmia which branches from the mountains of Chehelcheshmeh at the being of Kurdistan. The main branches of the river are as Chamghoreh, Chamkhorkhoreh and Sarough River. Zarrineh river basin area from its branches to the entrance of the Urmia Lake is about 11780 Km^2 which is located between the longitudes 45° 45′ to 45° 15′ and the latitudes 35° 45′ to 37° 20′. All the rivers of the study area are grouped into four sectors: (a) River Chamsaghez System having 6 sampling/monitoring stations, (b) river Chamkhorkhoreh system having 3 monitoring/sampling stations (c) river Jaghatooo system having 4 sampling/monitoring stations and (d) Sarough river system having 8 sampling/monitoring stations which making a total of 21 sites. Sampling locations and site characteristics are given in Table 1 and Fig. 1. The locations are selected on upstream of Bukan Dam. Samples were collected during all different seasons of 2015.

2.1.1 Sample collection protection and analysis

1.5 liter water bottles for water sampling were used (samples later covered by a sheet of aluminum in disposable plastic containers were placed with a tight lid)**.** At each station according to the calculated flow cross-section of the river and water in multi-axis average speed was estimated and evaluated. Water samples, if necessary, by special stabilizers (such as sulfuric acid and nitric

acid) in fixed or hand-held and glaciers in sterile containers at temperatures below 4 ° C (without freezing), maintenance and within 4 to 6 hours were sent to the laboratory**.** Heavy metals samples also stabilized in sterile containers and refrigerate within 2 days of manually maintained and were sent to the laboratory.

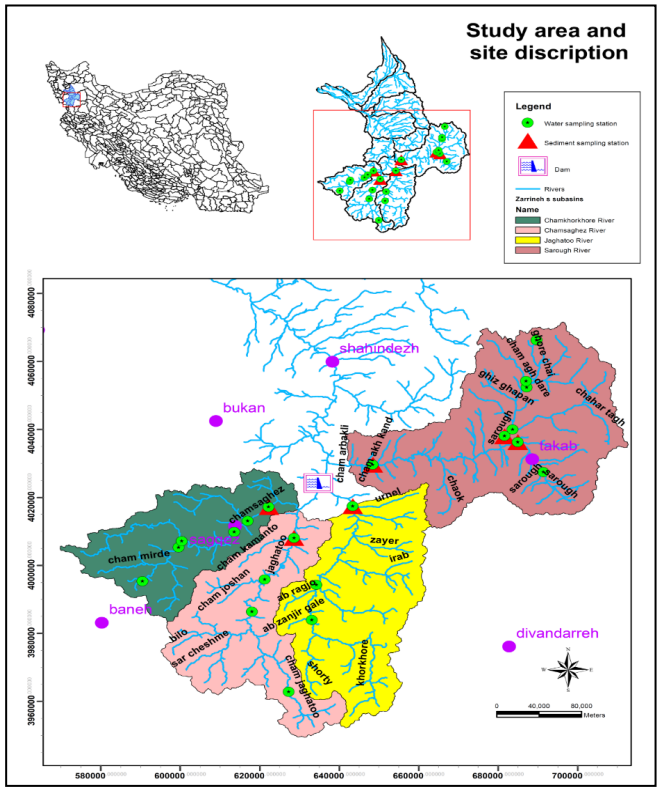

Figure 1. Site location map

2.2.2 Sample transfer device

A number of water samples after the packaged ice in glaciers were transferred to the laboratory, with the assurance of receipt by the director of the lab. Water samples after fixation of heavy metals and minerals were delivered to the laboratory to perform the needed analysis. Water samples were preserved at pH <2 in separate 300-ml plastic bottle by adding concentrated HNO_3 for heavy metal analysis.

Table 2. Mean, standard deviation, range of the analyzed data for heavy metals in different seasons in two geographical regions of the study area

Statistics	Al (mg/l)	Fe (mg/l)	Mn (mg/l)	Se (mg/l)
Kurdistan region (Chamsaghez, Chamkhorkhoreh, Jaghatoo Rivers)				
Mean	0.31	0.39	0.07	0.05
SD	0.34	0.25	0.06	0.04
Min	0.01	0.12	0.02	0.008
Max	1.18	1.28	0.23	0.10
West Azarbaijan Region (Sarough River)				
Mean	0.08	0.18	0.14	0.05
SD	0.10	0.10	0.17	0.04
Min	0.01	0.01	0.02	0.01
Max	0.30	0.41	0.60	0.10
WHO Standard 2008 for drinking water	0.1	0.3	0.4	0.01
Institute of Standards and Industrial Research of Iran, ISIRI,1053, 5th.Revision	0.1	0.3	0.1	0.01

Due to the primary analyzes between all the 14 measured metals, only four heavy metals were

analyzed and mention in the research as their role was important. Observed values for various parameters were statically analyzed by using correlation study on MS Excel and SPSS software.. All instruments used for analysis are calibrated with standard solutions to check their precision and accuracy. A blank sample had been run for each parameter, and necessary corrections have been made to achieve accurate results. At least three readings for each parameter had taken for getting precise information**.**

3. RESULTS AND DISCUSSION

Average concentration, range, and standard deviation along with values of different standards are given in Table 2. Temporal and spatial variations of studied heavy metals, namely Al, Fe, Mn and Se are presented at Figs. 2, 3, 4 and 5, respectively. However, mean concentration and standard deviation of Al, Fe, Mn and Se in the Chamsaghez, Chamkhorkhoreh, Jaghatoo and sarough rivers systems in winter and spring are presented in Figs. 6, 7, 8, and 9, respectively.

Mean value of (a) Al is found 0.17, 0.30, 0.62 and 0.08 mg/l; (b) Fe is found 0.33, 0.36, 0.53 and 0.18 mg/l; (c) Mn is found 0.06, 0.08, 0.10 and 0.14 mg/l; (d) Se is found 0.05 mg/l in Chamsaghez, Jaghatoo , Chamkhorkhoreh, and Sarough rivers respectively. However, concentration of Al and Fe varied spatially with higher levels in Jaghatoo and Chamkhorkhoreh river system and the concentration of Mn varied spatially with higher level in Sarough river system. Al is detected in 42 samples with mean value of 0.31 and 0.08 mg/l in Kurdistan and West Azarbaijan region respectively. The highest value of 1.18 mg/l of observed in river Chamkhorkhoreh of Kurdistan region. Iron is detected in all samples with mean value of 0.39 and 0.18 mg/l, respectively, in Kurdistan and West Azarbaijan regions, respectively. The highest value of 1.28 mg/l of observed in river Chamkhorkhoreh of Kurdistan region. Manganese is detected in 42 samples and the mean values are 0.07 and 0.14 mg/l in Kurdistan and West Azarbaijan regions, respectively. The highest value of 0.60 mg/l of observed in river Sarough of West Azarbaijan region. Selenium is detected in all samples and the mean value is 0.05 mg/l for both Kurdistan and West Azarbaijan regions. The highest value of 0.10 mg/l observed in mostly all stations in four rivers in spring. Selenium did not show much variation in winter in all stations and regions of study area. 14 observation of the Al, 11 observations of Fe, 9 observations of Mn and all observed values of Selenium only in spring were exceeded with the WHO standard for drinking water (WHO 2009).

Two observations of Mn in Sarough river in West Azarbaijan regions, found to be exceeded with the Institute of Standards and Industrial Research of Iran ISIRI ,1053; 5th Revision. As compared with the standards for fresh water as prescribed under Environment Protection Rules some rivers are found not suitable for drinking; Locations where Fe exceeded with 0.5 mg/l , Al exceeded with 0.1 mg/l in Chamkhorkhoreh, Jaghatoo rivers in Kurdistan region and for Mn which exceeded with 0.1 mg/l in Sarough River in West Azarbaijan Region , are also not suitable for drinking.

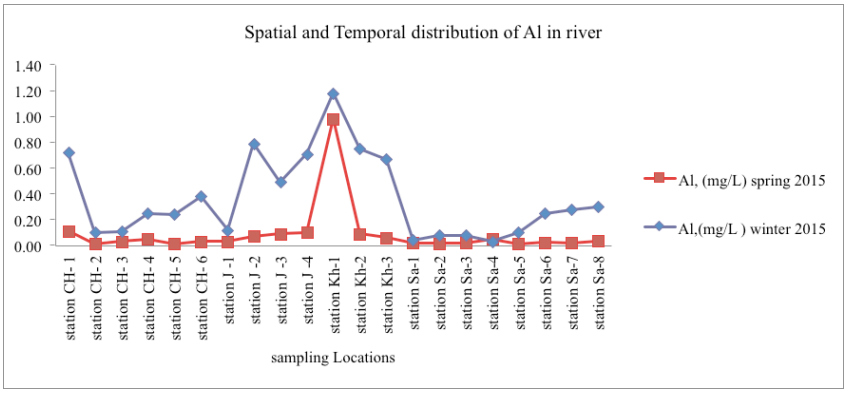

Figure 2. Temporal and spatial distribution of Al

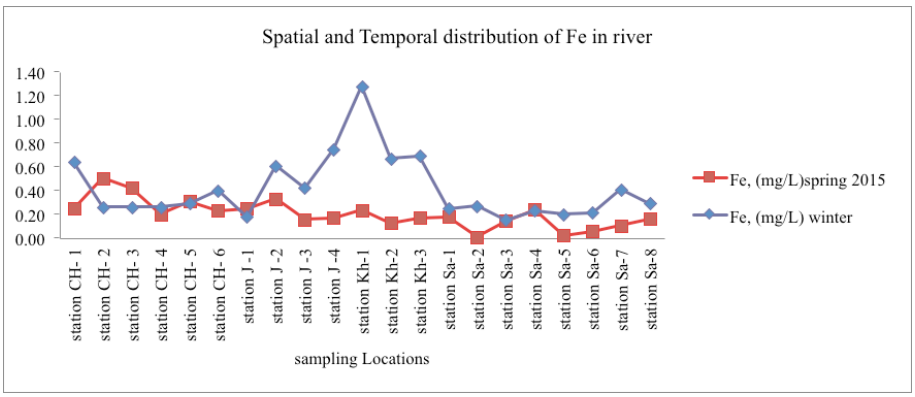

Figure 3. Temporal and spatial distribution of Fe

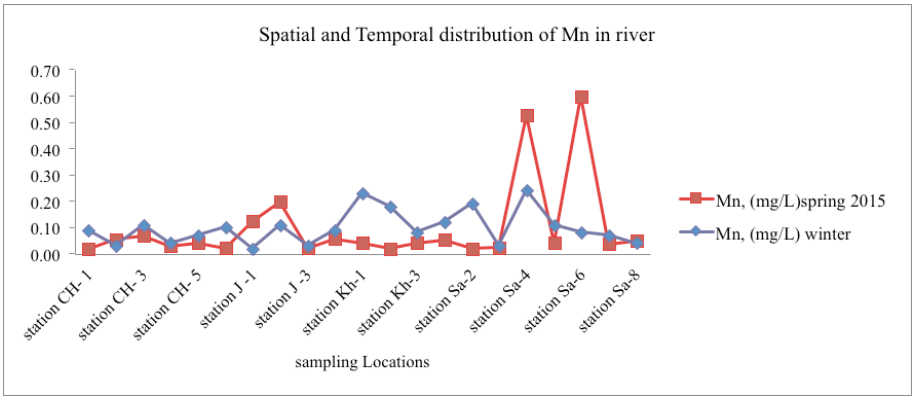

Figure 4. Temporal and spatial distribution of Mn

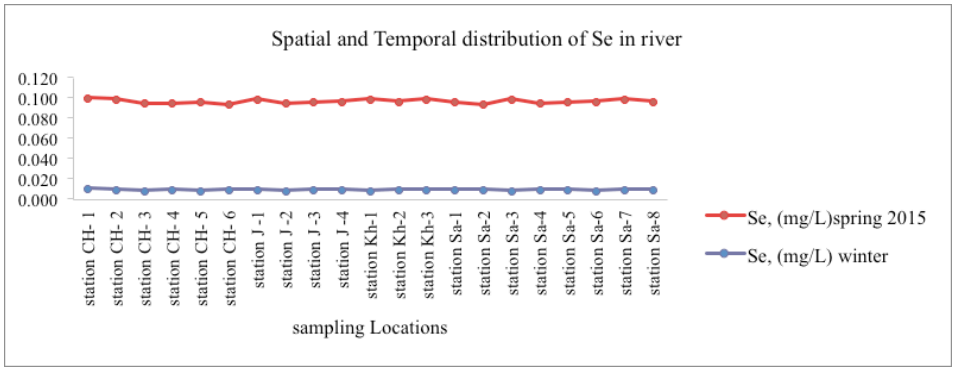

Figure 5. Temporal and spatial distribution of Se

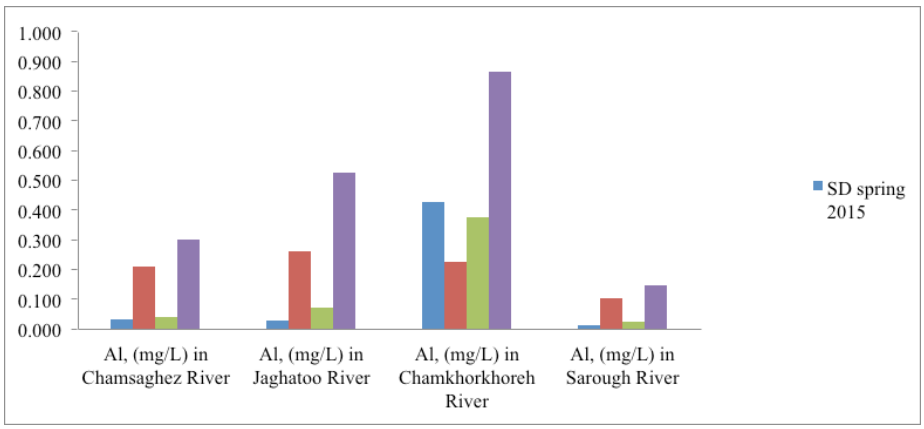

Figure 6. Mean and standard deviation of Al

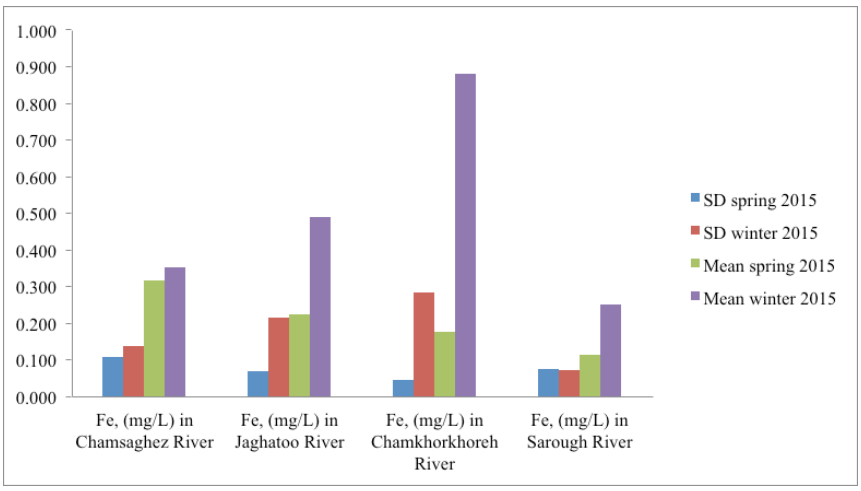

Figure 7. Mean and standard deviation of Fe

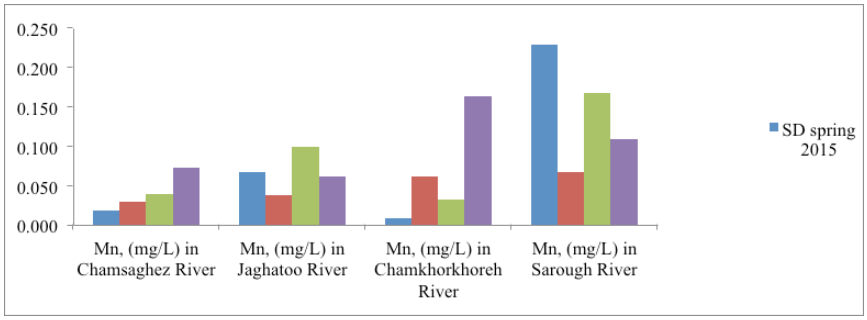

Figure 8. Mean and standard deviation of Mn

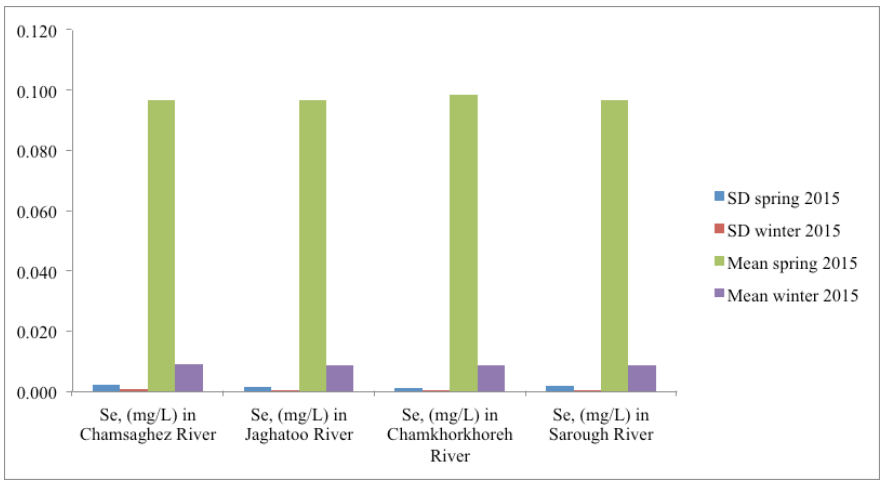

Figure 9. Mean and standard deviation of Se

Average concentration of dissolved oxygen, pH, and electrical conductivity and their correlation are presented in Tables 3 and 4, respectively. In the present study, the metals Fe, Al and Mn show negative correlation with pH and also the Mn and Se, show negative correlation with DO which indicates that the more organic load in the water bodies, the more will be the concentration of heavy metals because organic matter provides surface for lechation of metals in acidic conditions; While in the other hand Se shows positive correlation with pH ; Al and Fe also show positive correlation with DO. Metals Al and Fe showed negative correlation with electrical conductivity that Mn and Se show positive correlation with electrical conductivity which may be the result of rock–bed interaction with flowing water (Kansal et al. 2013).Metals Al and Fe found to have strong positive correlation with each other in the present study.

Table 3. Mean concentration and standard deviation DO (milligrams per liter), pH, PO_4 and EC (micromhos per centimeter)

Rivers	pH		DO		EC		PO_4	
	Mean	SD	Mean	SD	Mean	SD	Mean	SD
Chamsaghez	7.38	0.63	7.66	2.05	551.54	278.37	1.01	1.68
Jaghatoo	7.41	0.56	8.81	1.71	412.69	191.54	0.45	0.76
Chamkhorkhoreh	7.29	0.545	8.952	1.269	377	136.2	0.26	0.178
Sarough	7.34	0.53	8.31	2.03	1058.44	612.64	0.21	0.27

Table 4. Correlation of physicochemical parameters with heavy metals

	Fe	Mn	Se	pH	DO	EC	PO_4
Al	0.797**	0.029	-0.462**	-0.410**	0.443**	-0.405**	-0.185
Fe		0.110	-0.459**	-0.406**	0.375*	-0.317*	0.012
Mn			0.002	-0.093	-0.085	0.007	-0.037
Se				0.680**	-0.770**	0.225	0.351*
pH					-0.361*	0.348*	0.250
DO						-0.134	-0.367*
EC							-0.002

**Correlation is significant at the 0.05 level, **Correlation is significant at the 0.01 level*

Data are also analyzed statistically for analysis of variance (ANOVA) on SPSS. ANOVA is a measure to test the data statistically for its significant difference with the compared values at different levels of significance. In its simplest form, ANOVA provides a statistical test of whether or not the means of several groups are all equal and therefore generalize t test to more than two groups. In the present study, ANOVA is used to find the significant variation of data while analyzing in different seasons and at different sites, i.e., temporal and spatial variation; such data are presented in Table 5, 6 and 7 respectively.

Table 5. T test for heavy metals in different river systems

Parameter	Temporal variation							
	Chamsaghez river		Jaghatoo river		Chamkhorkhoreh river		Sarough river	
	t	Sig.	t	Sig.	t	Sig.	t	Sig.
Al	5.818	0.037	6.621	0.042	2.780	0.171	44.025	0.000
Fe	0.172	0.688	4.749	0.072	10.971	0.030	0.283	0.603
Mn	1.875	0.201	1.429	0.277	5.362	0.082	9.476	0.008
Se	9.657	0.011	3.419	0.114	3.200	0.148	7.860	0.014

Table 6. Spatial ANOVA for heavy metals in different river systems

	Spatial variation							
	Chamsaghez river		Jaghatoo river		Chamkhorkhoreh river		Sarough river	
Parameter	F	Sig.	F	Sig.	F	Sig.	F	Sig.
Al	0.693	0.648	0.396	0.764	2.241	0.254	0.470	0.832
Fe	0.480	0.781	0.543	0.678	0.282	0.772	0.410	0.871
Mn	0.562	0.728	2.449	0.204	0.267	0.782	1.600	0.262
Se	0.001	1.000	0.001	1.000	0.000	1.000	0.000	1.000

Table 7. Spatial ANOVA for heavy metals in river systems

Parameter	Spatial variation	
	All river system	
	F	Sig.
Al	7.182	0.001
Fe	4.255	0.011
Mn	1.158	0.339
Se	0.001	1.000

From the ANOVA, it is found that distribution of Al and Se in river Chamsaghez and Al, Se and Mn in river Sarough systems, Alminium in Jaghatoo river and Fe in Chamkhorkhoreh river during

entire study period shows significant difference at 95 % level of significance. Spatially all the metals in different river systems do not show any significant spatial difference in their distribution among different river systems. It can conclude that the region of three Chamsaghez, Chamkhorkhoreh and Jaghatoo Rivers are located in Kurdistan province and due to few industrial activities along these river, concentration of pollutants in this river system is found less as compared to other river systems in the basin. Comparing the ANOVA test for all the rivers system, it can be also, concluded that among all the metals only the Al and Fe show significant spatial difference among all the river systems. Scope of further research Present study is limited to quarterly analysis of water quality of major water bodies. It may extend up to monthly and even daily monitoring. Apart from that, only four heavy metals have been analysed among almost the 14 metals which be available and cause problem in water quality. Future work in this area may be expanded in analysis of more trace metals, covering more monitoring points in another water bodies. Ground water deterioration cannot be denied due to discharge of industrial effluent and direct injection of effluent into ground water strata. Further scope of work may be elaborated to monitoring of groundwater quality in the Zarrineh river basin.

REFERENCES

Fatehi E, MONAVARI SM, HASANI AH, KARBASI AR, MIRBAGHERI SA (2010) Heavy Metal and Agricultural Toxics Monitoring in Garasou River in Iran for Water Quality Assessment Asian J Chem 22:2991-3000

Islam M, Ahmed M, Habibullah-Al-Mamun M, Islam K, Ibrahim M, Masunaga S (2014) Arsenic and lead in foods: a potential threat to humanhealth in Bangladesh Food Addit Contam Part A 31:1982–1992

Kansal A, N A S, Gautam A (2013) Assessment of heavy metals and their interrelationships with some physicochemical parameters in eco-efficient rivers of Himalayan region Environ Monit Assess 185:2553–2563 doi:DOI 10.1007/s10661-012-2730-x

Khalilzadeh Poshtegal M, Jafari a, Noury m (2016a) River Quality and Quantity Modeling Using Neural Wavelet Network Technical Journal of Engineering and Applied Sciences

Khalilzadeh Poshtegal M, noury m, mirbagheri sa, Nikoo s (2016b) Investigation of heavy metal and susepended sediment in river. Paper presented at the The 8th National Conference on Environmental Engineering, Iran,

Khalilzadeh Poshtegal M, University of the Aegean LIDoES, Lekkas T Investigation the relationship between the land use and the rainfall, run off and sediment by GIS and RS(case study: Shaharchai River, Orumieh, Iran). In: Proceedings of the International Conference on Environmental Science and Technology, 2011. University of the Aegean, Rhodes Island(Greece),

Kouamé MK, Safiatou C, Boua CA, Essetchi PK (2014) SURVEY OF HEAVY METALS CONCENTRATIONS IN WATER AND SEDIMENTS OF THE ESTUARY BIETRI BAY, EBRIE LAGOON, COTE D'IVOIRE International Journal of Research In Earth & Environmental Sciences 1

Malik N, Biswas A, Qureshi T, Borana K, Virha R (2010) Bioaccumulation of heavy metals in fish tissues of a freshwater lake of Bhopal Environ Monit Assess 160:267-267

Mir Mohammad A, Mohammad Lokman A, Md SI, Md ZR (2016) Preliminary assessment of heavy metals in water and sediment of Karnaphuli River, Bangladesh Environmental Nanotechnology, Monitoring & Management 5:27–35

Mirbagheri S, Biglarijoo N, keyhanezghad M (2014) Pilot plant studies for the removal of heavy metals from industrial wastewater using adsorbents Turkish J Eng Env Sci 38:159-166

Nevoh GO, Akhionbare SMO, Uzoma HC (2015) Water Quality Aspects of River Okpoka in Relation to Watershed Activities Resources and Environment 5:124-133 doi:10.5923/j.re.20150504.03

S.A.Mirbagheri AB, and A. H. Javid (2008) Heavy Metals Transport in the Soil Profiles under the Application of Sludge and Wastewater International Journal of Civil, Environmental, Structural, Construction and Architectural Engineering 2

Shah AB, Singh RP (2016) Monitoring of Hazardous Inorganic Pollutants and Heavy Metals in Potable Water at the Source of Supply and Consumers end of a Tropical Urban Municipality Int J Environ Res:149-158

Shanur JH, Mohosena BT, Md.Istiaque Haidar, Tayfa A, AKM SAR (2015) Physico-chemical characteristics and accumulation of heavy metals in water and sediments of the river Dakatia, Bangladesh International Journal of Fisheries and Aquatic Studies 2:300-304

Shoaei SM, Mirbagheri SA, Zamani A, Bazargan J (2014) Dissolved Heavy Metals in the Reservoir of Shahid Rajaei Dam, Sari, Iran Int J Environ Res 8:997-1004

WHO (2009) Global health risks: mortality and burden of disease attributable to selected major risks. In.

Yi Y, Yang Z, Zhang S (2011) Ecological risk assessment of heavy metals insediment and human health risk assessment of heavy metals in fishes in themiddle and lower reaches of the Yangtze river basin Environ Pollut 159:2575–2585

Proceedings of the 10th World Congress of EWRA 'Panta Rhei', 5-9 July 2017, Athens, Greece
© 2017 *European Water Resources Association*

Desalination and alternative water resources

N.X. Tsiourtis
Water and Desalination Consultant, Cyprus
* *e-mail: tsiourti@gmail.com*

Abstract: With water demand increasing due to population growth, life style change, more water for irrigation to feed the increasing population and increasing environmental needs, and water availability remaining the same or reducing due to pollution or droughts and in some parts of the world decreasing because of climate change, the need for additional water in many countries is increasing. With almost all the conventional water resources developed and exploited, the desalination seems to be an alternative water supply. Desalination is now becoming relatively cheaper when compared to the increased cost of developing conventional water resources. This report examines the subject of Desalination, as an Alternative water supply, outlining in general the basic principles that a water entity and engineer must be aware when embarking on the subject. It also outlines the step that a water entity must make for establishing a desalination plant.

Key words: Desalination, membranes processes, thermal processes, seawater, brackish water, environment, marine works, on land works, product water quality.

1. INTRODUCTION

Water, a limited finite resource, vital for the very existence of life on earth and a necessity for economic and social development and for the environmental sustainability, is becoming a scarce commodity, caused by the population growth, the change of life style, water pollution caused by the human intervention, the inefficient use of water, droughts that are more frequently occurring and the climatic change. Where the water availability cannot be increased by using conventional resources or by recycling or cannot be made safeguarded by water demand management and integrated water resources management methods, the desalination of sea or brackish water offers an alternative solution. The desalination of water has been practiced since ancient times but was not widely used due to technological limitations, the prohibitive high capital cost, the high-energy consumption and finally very high unit cost when compared to conventional water. New technological advances, in the last fifty years, reduced tremendously the capital cost and the energy consumption so that desalination projects can be considered economically affordable as alternative solutions to water development. Today many countries in the Mediterranean basin, the Gulf Area, Australia, Asia, and Western USA and all over the world, use desalinated water for domestic water supply, for industry to satisfy their increasing or special quality needs and even for irrigation. However, desalination projects are still not very cheap to be easily accommodated by the economies of many countries, energy consumption is still comparatively high, and acceptance of such projects is questioned by environmentalist, politicians, engineers and other groups of the population on economic, social and environmental issues. The present paper shall highlight the desalination technologies, the growth of desalination, the energy requirements, the advantages and disadvantages, the desalination projects capital cost and desalinated water unit cost, the options for financing of desalination projects and the environmental impacts and considerations. The paper also outlines the steps that are necessary to establish a desalination project.

2. DESALINATION TECHNOLOGIES

Desalination was first used by Greek sailors in the 4th century BC to evaporate seawater and create drinking water. The same method was used later by Caesar in his invasion of Egypt to secure potable water for his soldiers. Today there are two commercially available desalination technologies used extensively for desalinating water, the membranes technology (Reverse Osmosis and Electrodialysis) and the thermal (MED, MVC and MSF) process desalination (Burros. O. K. 2000).

2.1 Membrane processes

This technology uses membranes which have the ability to differentiate and selectively separate salts and water. There are two important commercially available membrane desalting processes, depending on the form of the driving force, the Reverse Osmosis and the Electrodialysis, as follow:

a) *Reverse Osmosis:* This was initially developed in the late 1950s, with successful commercialization occurring in 1970 after efficient effective membranes development which now is the leading desalination technology globally, offering the most cost effective process to desalinate seawater. In this process, membranes are used where the saline solution is pressurized to go through, which have the ability to separate the solutes from the water. The energy required for this process is for pressurizing the feed water through high pressure pumps to overcome the osmotic pressure. The salty water is pumped against the membranes, with a portion passing through the membranes after desalination where the rejected salt becoming brine is discharged back to the sea or to special rejection points. Depending on the quality of the product water the reverse osmosis process may have one or two passes. A Reverse Osmosis plant is made of the following systems (a) Intake system, (b) Pre-treatment system, (c), High Pressure pumps, (d) Energy recovery system (f) Pass 1 and Pass 2 membranes systems (g) Post treatment, (h) Brine discharge system and (i) Effluent Treatment Plant (Wilf, M., 2007).

b) *Electrodialysis:* This was commercially introduced in the early 1960's and provided a cost effective way to desalinate brackish water. This technology uses, membranes which permit selective passage of anion or cation ions, and electrons connected to an outside source. Anions and Cations selective membranes and positive and negative electrodes are placed in a container of saline water and when electrical current is carried through the solution the ions migrate to the electrode with the opposite charge, thus desalting the saline water. By this arrangement and operation, concentrated and diluted solutions are created in the spaces between the alternating membranes (Burros. O. K. 2000).

2.2 Thermal processes

In this process saline water is heated, producing water vapor that in turn is condensed to form fresh water. Most applied methods are the Multi-Stage Flash Distillation process, the Multi-Effect Distillation process and the Vapor Compression Distillation. Thermal desalination uses heat, often waste heat from power plants or refineries, to evaporate and condense water to purify it. In the most advanced desalination plants, water is pretreated in order to improve the efficiency of the plants.

3. GROWTH OF DESALINATION

Desalination of brackish and seawater is expanding rapidly, primarily to support urban and industrial developments in arid and semi-arid areas and in remote areas where, water is not available or it is too costly to transfer or develop. The market is driven by the water scarcity created by the limited water supply, the population growth, the improvement of the life style, which

increases water demand, the climatic changes and droughts and human intervention that reduce water availability. The market is driven also by the falling costs of the desalination, which are due to the technological advances in the desalination process.

Figure 1 shows the Global Yearly contracted desalination capacity and the Cumulative Contracted and the Commissioned Quantities (IDA, 2009-2016). From the Graph the following is observed.

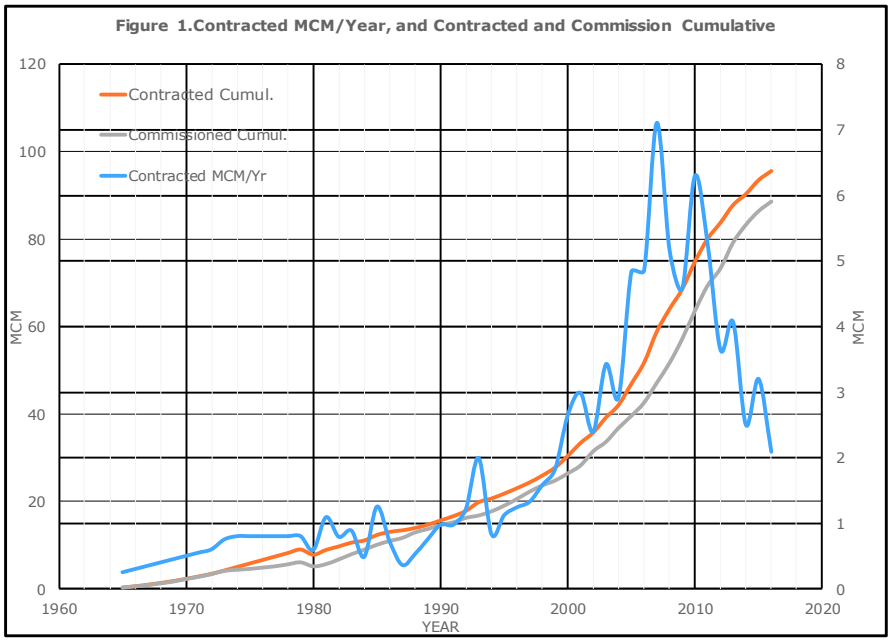

Figure 1. Contracted MCM/Year, and Contracted and Commission Cumulative.

- The Global cumulative desalination capacity contracted is 95.6 MCM/day.
- The Global annual contracted desalination capacity has reached a maximum of 7 MCM/day in 2007 and since then is reduced to 2.1 MCM/day in 2016.

Table 1 shows the evolution of Membranes versus Thermal Technology, Globally, in the MENA region and the GCC (IDA, 2009-2016).

Table 1. Evolution of membranes vs thermal technologies

YEAR	GLOBAL		MENA		GCC	
	Membranes	Thermal	Membranes	Thermal	Membranes	Thermal
2000-2009	75%	25%	55%	45%	40%	60%
2010-2014	88%	12%	76%	24%	61%	39%
2015-2016	93%	7%	86%	14%	82%	18%

There are so far 18,486 desalination Plants in more than 150 countries serving around 300 million people and many industries.

Since 2006 the additional desalination capacity commissioned is 48.4MCM out of which 60.1% are for potable water and the rests 39.9% for industry.

4. WATER AND POWER EQUIREMENTS AND SUPPLY

The desalination process requires raw water and power energy. The water for desalination may be abstracted from underground brackish water or from wastes and/or from the sea, depending on the selected site. It also requires a brine discharge point which is better served by the sea. So at the present large scale desalination plants must be located next to sea. For the desalination process,

depending on the technology, energy in the form of electricity from oil or natural gas, or from renewable resources (hydraulic, solar, wind etc.) for membranes technology or steam preferable from power stations for thermal technology (Burros. O. K. 2000). For the reverse osmosis process the energy required ranges from 2.5-3.0 Kwh/m^3 of desalinated water, plus 0.5-1.0 KWH/m^3 for the pumping of water other than desalination process. The energy for the membranes systems may come from the national Grid, from an Independent Power Production Plant, or solar energy or wind energy. The solar energy and wind energy desalinations are at present confined to small plants. Today's thermal MED/TVC plants use about 1 KWH/m3 in addition to the steam input required which ranges from 8-15 GOR (Gained Output Ratio), approaching equivalent to 5-8 KWh/m^3 and these are best suited to take advantage of co-production of energy and water. GOR is defined as follows. How many kilograms of distilled water are produced per kilogram of steam consumed and it varies from 1 to 15 Kg/Kg (IDA, 2011). For Renewable Energy Desalination Projects the readers are referred to World Bank publication "MENA Development Report Renewable Energy Desalination" (The World Bank, 2012).

5. ADVANTAGES AND DISADVANTAGES OF DESALINATION WATER SUPPLY PROJECTS

Advantages:

- It is an alternative water supply not dependent on the rainfall,
- It provides the design production rate with a relatively high security.
- The water quality may be chosen to meet the consumers' requirements (potable or industrial)
- It can be installed in remote areas where conventional water supply is not available.
- The time required for its development is comparatively small compared to other alternatives.

Disadvantages:

- High capital cost and high energy demand
- High production costs because of high energy consumption.
- It may cause Environmental problems on the marine, land, underground and air environment including noise pollution.
- It may face the rejection by the owners of the neighboring land because the plants look like industrial buildings reducing the price of the neighboring land.

6. CAPITAL COST OF PROJECTS AND UNIT COST OF DESALINATED WATER

6.1 Capital cost of desalination projects

This cost depends mainly on the plant location, the quality of the raw water, the quality of the product water, the site environmental sensitivity, the intake and brine discharge systems, the intake pumping system, the on land raw and brine discharge systems, the Pre-treatment system, the High pressure Pump and energy recovery systems, the desalination process system (SWRO and/or BWRO, or the thermal desalination unit, the Post Treatment, the Pretreatment Effluent Plant, the Power supply system (Grid or IPP or else) and the energy supply and the energy unit cost. Also added are the insurances and guarantees during the construction phase.

6.2 Production unit Cost

The Unit cost of desalinated water depends on the Capital cost, the financing costs, the years of depreciation of the Plant (10, 15, 20 or 25 years), the energy consumption, the energy price, the

chemicals costs, the operation and maintenance team costs, the plant size, the insurances and guarantees during operation (Tsiourtis, 2004).

7. FINANCING OF DESALINATION PROJECTS

With the desalination projects having a very high cost, big utility projects may be financed by one of the following methods.

a) *Turn Key Method*: By the Government issuing a Turn Key Project tender for the execution of the proposed desalination project, undertaking to construct and commission a project all in accordance with the tender specification and either operate the project by itself or by hiring a special entity to operate the project. This method is not preferred by most of the Governments because it creates a financial problem to the Governments who do not want to have deficits in their budgets.
b) *Public Private Partnership method*: By issuing a Tender by the Government for a Build, Operate and transfer (BOT) project or other forms, under which the successful Tenderer will undertake to design, build, commission and operate the specified project with the undertaking by the Government that it will buy the conforming quantities of water for a fixed period of time with an agreed price updated to compensate for fiscal changes. By this method the Government will not have to pay for the capital cost. The cost of the water (capital and variable) are directly transferred to the water consumers.

In all cases the Projects must be economically viable (Tsiourtis, 2011; Tsiourtis, 2016; Latterman and Hopner, 2003; Sommariva, 2004).

8. ENVIRONMENTAL AND OTHER IMPACTS

In all cases, the environmental and economic impacts of the project on the site and in the lands lying in the vicinity of the site must be carefully considered. An environmental study must be carried out to evaluate the projects impact and mitigation measures must be proposed to reduce or minimize the impacts during construction and during operation of the project Just to summarize the possible impacts, which are mostly mitigated with a proper project design and execution and during the construction and operation phases are the following (Tsiourtis, 2001a).

- Impacts by the intake and brine discharge systems on the marine environment. The adverse impact may affect the marine life in the vicinity of the intake heads and at the brine discharge points during the operation and during the construction phase (Tsiourtis, 2001a; Latterman and Hopner, 2003; Tsiourtis, 2008a).
- Impacts on the on-shore area, near the Intake pumping Station on the onshore land corridors and the plant area and underground aquifers, during construction and during the operation phase due to seawater and or brine spillage (Tsiourtis, 2001a).
- Noise impact during construction and operation because of big pumps and machinery.
- Air pollution during construction and gas emissions during the operation of the plant for the production of the energy.

All the above impacts are manageable by adopting the required designs which shall secure the environment. Concerning the emissions to the atmosphere for the energy production the following can be said. With a specific energy consumption for the production of one cubic meter around 3 KWH, the energy required for the production of 200 liters per day for the daily needs of one person, is only 0.6 KWH. It is the responsibility of all of us to make a saving of 0.6 KWH per day for securing the water quantity necessary to satisfy our daily demand. This is a very small quantity of energy, compared to the average daily consumption of around 10KWH/Day per person in a household and compared to our car consumption estimated at 1 KWH per kilometer.

9. EXPERIENCE IN VARIOUS COUNTRIES IN THE MEDITERRANEAN

Desalination is now in use in many countries of the world. I shall concentrate on the experience of countries in the Mediterranean. Such countries are Cyprus (Tsiourtis, 2001b), Israel, Malta, Spain, Algeria, Morocco, Egypt and Greece. Israel has developed desalination in the last 15 years and it has now five plants of reverse osmosis with an annual production of 575 MCM and Cyprus has four plants of reverse osmosis with an annual capacity of 70 MCM, Malta has three plants of reverse osmosis, with an annual capacity around 30 MCM. Algeria and Spain have embarked on a large scale desalination in the last decade. The rest of the countries have less desalination capacity except the Gulf countries which have very big hybrid plants (thermal and SWRO Plant).

10. STEPS TO ESTABLISH A DESALINATION PROJECT

For the establishment of the Desalination Project the water authority must organize a team consisting of various disciplines to carry out the various steps as follow.

Step 1: Carry out a diagnostic study to establish the real extra needs of water for short and long term and if a desalination project is justified (Tsiourtis, 2008b).

Step 2: If Step 1 shows that there is a need for more water resources, and desalination is justified decide on the technology of desalination, the power supply and raw water supply etc.

Step 3: Locate 2-3 potential sites and carry out preliminary environmental studies for each of them and select the most suitable site (Tsiourtis, 2008a; Tsiourtis, 2008b).

Step 4: For the selected site prepare the possible draft P&I diagrams and the layout for all the systems and draft the technical specifications.

Step 5: Prepare the Contract conditions (including risk allocation) and the material specification which shall constitute the Tender Documents, for a Turnkey or a Public Private Partnership (PPP) project (Tsiourtis, 2016). The specifications and the Contract documents shall provide for a Bankable project.

Step 6: Issue Tenders and accept offers from qualified Contractors.

Step 7: Evaluate the Tenders received and award the Contract to a qualified Contractor who shall meet the tender requirements criteria.

Step 8: After signature of the Contract in the event of a PPP project carry out the Due Diligence Study for securing the project's financing.

Step 9: Proceed with the construction of the project in accordance with the approve Time Schedule.

Step 10: Upon Construction Completion carry out the machinery and the systems complete test to secure that the Plant attains the guaranteed performance criteria and the Permit to Operate and start the Commercial Operation Phase.

11. CONCLUSIONS

With the water demand increasing because of population increase, life style change, etc. while the conventional water resources shall not be able to close the gap between supply and demand, many countries will face water shortages. Some countries, possibly will be able to close the gap between supply and demand with better management of their conventional resources where others have to secure additional non-conventional water coming from further treatment of wastewater, seawater or brackish water. Under such conditions the desalination may be an alternative water supply source. The desalination project must prove to be bankable so that the incomes secure the capital cost (studies, machinery constriction erection test etc.) the production costs during commercial operation phase, the management costs, the loan repayment installments with the interest any overflow costs and secure a logical profit for the project owners.

REFERENCES

Buros O. K. 2000. The ABCs of Desalting. Published by the International Desalination Association, Topsfield, Massachusetts, USA.

IDA Desalination Yearbooks 2009-2016.

IDA, 2011. Desalination at a glance

Latterman, S. and Hopner, T., 2003. Sea water desalination Impacts of Brine and Chemical Discharge on the Marine Environment.

Sommariva, C. 2004. Desalination Management and Economics. Sponsored by Mott MacDonald. Published by Faversham House Group.

The World Bank, 2012. MENA Development Report Renewable Energy Desalination. The World Bank Washington D.C.2012.

Tsiourtis, N. X., 2001a. Desalination and the Environment. Keynote Speech. Contribution to the European Desalination Society European Conference on Desalination. Limassol Cyprus, May.

Tsiourtis, N. X., 2001b. Sea water desalination Projects. The Cyprus Experience. Desalination; 139: 139-147.

Tsiourtis, N. X., 2004. Desalination Water Costing the Financiers View: Conference organized in Lemesos by the Middle East Desalination Research Centre, December.

Tsiourtis, N. X., 2008a. Criteria and Procedure for selecting a site for a desalination project. Desalination; 221: 115-125.

Tsiourtis, N. X., 2008b. Diagnostic of the Situation. Published in the Options Mediterrannennes Series B, No 58, Technical Annex of the Drought Management Guidelines.

Tsiourtis, N. X., 2011. Bankability of Desalination Projects. 12th Annual Conference of Israel Desalination Society, Technion Haifa 14-15 Dec 2011.

Tsiourtis, N. X., 2016. Specifying and Keeping bankable desalination projects. EDS Conference on Desalination and the Environment, Clean Water and Energy, Rome, 22-26 May.

Wilf, M., 2007. The Guidebook to Membrane Desalination Technology. Balaban Desalination Publications.

Proceedings of the 10th World Congress of EWRA 'Panta Rhei', 5-9 July 2017, Athens, Greece
© 2017 *European Water Resources Association*

Source separation technologies, opportunities for sustainable wastewater management

T. Zinati Shoa*, M. Barjenbruch and A. Wriege-Bechtold
Department of Urban Water Management, Technical University of Berlin, Gustav-Meyer Allee 25, 13355 Berlin
* *e-mail: t.zinati@campus.tu-berlin.de*

Abstract: Recent challenges regarding urban sanitation system require innovative ideas to ensure high quality wastewater management in future. The drive towards sustainable wastewater management is challenging the conventional wastewater treatment method. Source separation sanitation method could be a new approach to minimize the pressure of population and help to improve the sustainability indicators. It is required the information about new ideas; systems and technologies become more readily accessible for addressing wastewater problems in order to reach solutions for environmental, economic and social balance. This comprehensive review focuses on the statues of current source separation sanitation techniques and summarize the efficiency of each type of technology. The method would be in modular descriptions of component and description of alternative wastewater systems, and facilitates evaluating how well each design satisfies the given context. The review shows clearly that a wide range of technique options is available to treat each type of wastewater, but none of these options can meet all the requirements of treatment in one specific technique and a combination of technique is required to treat separated water to reach optimized nutrient recovery and treated water.

Key words: Source separation sanitation system, greywater, blackwater, yellow water, conventional sanitation system, removal efficiency

1. INTRODUCTION

Even though conventional wastewater treatment resolve acute hygiene and aquatic environment related problems, it doesn't have control on generated wastewater at the source and does not consider resource recycling (Otterpohl, 2002). The conventional sanitation system usually involves enormous amounts of potable water for collection, complex treatment processes due to mixing of several types of wastewater flow of residential area and have a limited potential regarding recycling of wastewater components.

As alternatives to conventional wastewater treatment systems, many approaches based on source separation sanitation system has been introduced. Most of source separation sanitation system can be found in small scale and proposed projects in many various configuration of separating wastewater from source (Otterpohl, 2002; Peter-Fröhlich, et al., 2007; Zeeman et al., 2008; Augustin et al., 2013). Based on the proposed goal of each study, source separation of wastewater is including greywater (bathroom, kitchen and laundry water), blackwater (urine, faeces and flush water) and yellow water (only urine). In many system configurations, the greywater is collected by a gravity system and treated in natural ponds or in a technical process. The blackwater is collected by a vacuum system and then treated in an anaerobic digester together with organic waste from house (Thibodeau et al., 2014).

A Comparison of different aspects of source sanitation systems has been done by many different assessment frameworks. One of the usual method is Life Cycle assessment which it can assess the potential environmental impacts of the entire value of a chain (a product system from cradle to grave) (Remy, 2009; Hellweg and Mila i Canals, 2014). Other quantitative tools such as Material Intensity Per Service unit (MIPS), exergy analysis have been used to draw material and energy balances of different source separation sanitation system and conventional treatment system (Benetton et al., 2009). These studies present data on energy consumption, production, material

intensity, and emission of source separated faeces, urine, and greywater treatment and conventional wastewater treatment. However, these methods need a lot of information that is time-consuming and complicated.

Hence, from a system developer's point of view, there is still lack, which source separation sanitation system would be the most promising one to develop further in order to minimize both environmental impact and cost. With regards to the source separation sanitation systems, key processes have been identified, but the level of efficiency they must achieve in terms of source sanitation systems performance equals that of conventional for environmental and economic indicators have not been clearly determined. The previous studies presented the environmental or the economic performance of source separation sanitation system which they are specified in each study to some limited methods and mostly in the lab scale where is not still enough comparable with well-structured of conventional treatment system. Present study aims to compare the efficiency of possible source separation treatment technology that it has been used in at least pilot scale and to review their performance.

This study aims to compare various source separation sanitations systems based on the pollutant removal efficiency to determine which one has better functionality compare to conventional system.

This review report is primarily concerned with systems and technologies directly related to separated wastewater and only those sanitation technologies which have been applied in the scale of lager than lab experiments.

2. METHODOLOGY DESCRIPTION

The goal of this study is to compare different developments of source separation systems more feasible than conventional treatment of wastewater considering sustainability criteria. This study focuses on innovative systems and leading edge technologies that are commercially available and have the potential to be implemented in a real housing project in the short or mid-term. As the results are meant to guide the development of source separation sanitation system entailing better environmental performance, the study is intended for use by sanitation system designers, sanitation system providers, urban planners and decision makers dealing towards sustainable sanitation system in urban areas. The scope of the study entails the treatment of sanitation systems under analysis. The model of source separation sanitation systems was developed by the authors based on a literature review, brainstorming and expert advice. The data for analysing is gained from the facilities of different source separated projects in mostly Germany (WWTP Stahnsdorf in Berlin which was owned and operated by the Berliner Wasserbetriebe, SCST, 2006 and Lübeck-Flinterbreute housing development) and the Netherlands (Sneek and Groningen) and Sweden.

Based on the proposed goals of the study, different technologies for separated wastewater treatment is investigated. Technologies are defined as the specific infrastructure or method to treat wastewater. A wide variety of sanitation technologies are either currently under development or are not yet fully mature and available. 57 technologies have been introduced in the compendium of sanitation systems and technologies (Tilley et al., 2014). However, the quantitative data of this technologies are not available. A comparison model in Excel was developed based on literature data to investigate existing various treatment technologies of source separation system based on the type of separated wastewater. The concentration of this study is just only on liquid fraction of wastewater and the domestic bio-waste is not considered.

For better comparison between various technologies, the pollutant loading in the wastewater influent was considered to originate only from the domestic wastewater streams of urine, faeces and greywater including COD (Chemical Oxygen Demand), TN (Total Nitrogen), TP (Total Phosphorus) and the effluent of each sanitation technology is considered based on the percentage of pollutant removal efficiency. Description of the technologies is done based on dividing to the type of separated wastewater since these are used as the basis for comparison.

3. RESULTS

3.1 Greywater treatment processes

Commonly treatment systems are used to remove organic material and nutrients from greywater including sequencing batch reactor (SBR) (Hernandez, et al., 2010) and constructed wetlands (CW) (Avery, et al., 2007). Greywater flows through a gravity sewer network and collected in a lager pipe systems or stored for a long period that need for pre-treatment and then to a constructed wetland. In pre-treatment, suspended solids are removed mechanically by gravity, screens, filters or other possible method. The need for this removal depends on how the water will be treated and used.

Due to the considerably high land area requirement, the use of CW is not suitable for densely populated urban areas (Brix and Arias, 2005). One alternative could be implement CW as a green roof (Avery et al., 2007). To utilize the organic material present in greywater, excess sludge from the greywater treatment system can be potentially co-digested in the UASB reactor instead of using energy-intensive sludge transport and disposal (Hernandez et al., 2010). To avoid extensive mineralization of greywater sludge, a bio-flocculation unit, such as a high loaded membrane bioreactor (MBR) or A-trap from the AB-process (Böhnke, 1981) can be used to concentrate greywater at short hydraulic and sludge retention times (HRT and SRT). A post-treatment system (such as TF) can be applied to remove the remaining organic material from greywater effluent prior to reuse. (Tervahauta et al. 2013)

Other technical components such as, soil filtration systems (Wissing and Hofmann, 2002, Geller and Hoener, 2003) septic tank, sand filters (Ridderstolpe, 2004) are used to remove particles and purified the greywater in different steps of the treatment process.

The selected treatment process of greywater is presented in Table 1 shows the basic removal efficiency of the different treatment processes of greywater.

Table 1. Pollutant removal efficiency of various technologies for greywater treatment (%)

Parameter\system	SBR (1)	Atrap (2)	MBR (3)	septic tank (4)	constructed wetland (4)
COD	90	45	75	33	94
BOD5	90	42	75	70	90
TSS	76	42	95	19	-
TN	35	36	81	54	63
TP	28	40	65	9	88

1. Zeeman et al., 2008, 2. Kujawa, 2005, 3. Vlaeminck et al., 2009, 4. Peter-Frohlich et al., 2007

The greywater treatment in a soil filter system needs less energy than a technical process. The natural process of appropriate for the purification of the nutrient-depleted greywater. The treatment of faeces filtrate together with the greywater can increase the nutrient loads considerably. In general, the natural process can reach sufficient results in greywater treatment if the required area for soil filter is available (Remy et al, 2006). Otherwise, the greywater is proposed to be treated in a compact system, a subsequent UASB/SBR or AS (activated sludge), instead of a constructed wetland preceded by a septic tank. By applying a UASB instead of a septic tank for greywater treatment, a substantial lower reactor volume can be installed and moreover produced biogas (Elmitwalli & Otterpohl 2007; Zeeman et al., 2008)

According to different studies, the efficiency of pollutant removal and effluent quality is affected by SRT (Sludge Retention Time) Wilsenach and van Loosdrecht (2006) showed higher effluent quality of A-trap by SRT 0.8 day compare to A-trap with SRT 0.6 day (DeSaH, 2010). However due to limited experimental data and the different composition of greywater, more research is required to confirm the relation between the SRT of the A-trap and the pollutant removal efficiencies. Consequently, if the SRT of the A-trap for greywater treatment is increased to 0.8 day, the pollutant removal efficiency could be increased, resulting in higher effluent quality (Tervahauta et al., 2013)

3.2 Yellow water source separation

Urine contains most of the soluble nutrients in very high concentrations. Separation and direct use of urine as a fertilizer can be used to increase nutrient recovery, improve wastewater effluent quality and to decrease operational energy consumption, due to lower nutrient concentration in wastewater (Maurer et al., 2003). Urine separation and use as a secondary fertilizer are as an essential part of the source separation approach in terms of efficiency use of valuable nutrients. Most important target in urine treatment are volume reduction, improved handling, and inactivation of micro pollutants.

The collection and direct application of urine as a fertilizer has been surveyed in pilot projects in Sweden (Johansson et al., 2001) and in smaller scale in Germany (Otterpohl et al., 2002) and in addition, Maurer et al. (2003, 2006) reviewed possible urine treatment and related process to volume reduction and the elimination of micro-pollutants in a lab scale. Pilot scale experiments of urine treatment process has been done in Sweden (Ganrot, 2005) and Germany (Peter- Fröhlich et al., 2007). Most of urine treatment option found in the literature are: hygienisation (storage), volume reduction (freeze-thaw, reverse osmosis), stabilisation (acidification), P-recovery (struvite formation), N-recovery (ion-exchange, ammonia stripping), nutrient removal (annamox) and handling of micropollutant (electrodialysis) (Maurer et al., 2006). Since a single unit process cannot provide all the treatment process, a combination of technique is required. In the present study, different process combination for yellow water treatment are compared based on the efficiency of nutrient recovery and result has been shown in Table 2. In the accessible of the yellow water studies, the result has been shown based on the recovery of material.

Table 2. Efficiency of nutrient recovery of various technologies for yellow water treatment (%)

Parameter\system	Storage (1)	Struvite precipitation+ Ion exchange (2)	Steam stripping+ Ozone+ Evaporation (3,4)	Struvite precipitation+ Steam stripping (2,3,4)
N recovery %	99	90	96	95
P recovery %	100	99	100	90
K recovery %	-	30	100	30

1. Johansson et al., 2001, 2. Ganrot,2005, 3. Maurer et al., 2006, 4. SCST, TUHH, 2007

Source separation of urine not only increase the effluent quality in terms of nutrient concentration and the overall pollutant loading, but also improves the energy balance and nutrient recovery (Tervahauta et al., 2013). Social acceptance of stored urine may be difficult due to strong smell and some may find it offensive to work with or to have it nearby (Tilley et al., 2014). The transport of a large volume of yellow water over long distance can consume considerable amount of truck fuel and cause respective emission of CO_2. A further consideration of yellow water to reduce transport volume and inactivate potentially harmful micro-pollutant is possible; however, energy intensive process like steam stripping and evaporation should be ecologically optimized (Remy et al., 2006)

3.3 Blackwater source separation

The blackwater source separation system is investigated on the sanitation facilities in Lübeck-Flinterbreute housing development in Germany (Otterpohl et al., 2002) Using a vacuum and pumping system, blackwater is collected and directed to a centralized treatment station. Processes that are specific to blackwater treatment based

Anaerobic treatment is a key technology of blackwater in an up-flow anaerobic sludge blanket (UASB) reactor (Zeeman et al., 2008; Kujawa, 2005). These technologies can be specified based on the digested mass reduction goal with reverse osmosis and acidification or digestate treatment by

means of phosphorus precipitation and nitritation -anammox reactors (Thibodeau et al., 2014). Nutrient recovery and pollutant removal from the UASB reactor effluent can be established by struvite precipitation, autotrophic nitrogen removal using oxygen limited anaerobic nitrification denitrification (OLAND) reactor and a post-treatment, such as a trickling filter (TF), to remove remaining organic material (Zeeman et al., 2008).

As shown in Table 3 from different studies, nitrogen removal during struvite precipitation is negligible, introduction of an additional treatment step is needed. Nitrogen removal based on the autotrophic conversion of ammonium to nitrogen like CANON (Sliekers et al., 2003) and OLAND (Windey et al., 2005) are promising in combination with anaerobic processes. The biorotor system as presented by Windey et al. (2005) could be a simple post treatment process for removal of nitrogen from anaerobically pre-treatment blackwater.

Table 3. Pollutant removal efficiency of various technologies for blackwater treatment (%)

Parameter\system	UASB (1)	OLAND (1)	Struvite (2)	TF (3)	Septic tank (4)	Constructed wetland (4)
COD	83	53	-	85	14	93
BOD5	83	53	-	85	7	98
TSS	83	-	-	85	21	-
TN	1	73	9	-	19	41
TP	33	-	96	-	10	76

1. Kujawa, 2005, 2. Wilsenach et al., 2006, 3. Tervahauta et al., 2013, 4. Peter-Frohlich et al., 2007

3.4 Brown water source separation

In the source separation sanitation concept, brown water produced from faeces where with flush water are either drained off by gravity drainage and composted together with bio-waste or collected by a vacuum system and co-digested with bio-waste to gain biogas for energy production and then is pumped to solid-liquid separators. The filtrate from the faeces dewatering is treated together with the remaining household wastewater from kitchen, washing machine, and personal hygiene (greywater) and in this study, has been analyse in the blackwater section. The solid fraction is further thickened and transported by truck to a composting plant. Although composting of faeces to produce organic fertilizer is a well-known treatment for small scale sanitation units or dry toilet, most of the studies for brown water is in lab scale and it has not been investigated and tested within the dimension of a larger settlement. Therefore, analysing of this kind of flow was not possible.

4. CONCLUSIONS

In this paper, the number of unit processes for treating separated wastewater have been studied in respect of their removal efficiency. The review of different processes of source separated sanitation made clear that a very large number of technical options are available with different strengths and weaknesses. We are aware that much more literature is available and regret not being able to refer to all of it.

However, all the processes cannot be archived with a single unit process. Whether the aim is to concentrate on a specific purpose such a nutrient removal or to combine different process unit to achieve a more comprehensive goal depends on the circumstances and is not discussed in this paper.

The choice of technique treatment system depends on many factors such as climate, density, type of habitation, land-use patterns, existing drainage systems, degree of pollution and sensitivity of the recipient. Therefore, the best solution suit to the local conditions and consider the potential risks the different techniques bring about.

A general assessment of source separation sanitation system is not possible only based on process engineering technology. Although other aspects connected to source separation system may be more difficult to solve. However, it is important to carefully evaluate the new approaches in

terms of their sustainability, including environmental, economic and social impacts.

Source separating technologies are still considered immature and risky by most wastewater professionals. This turns into a self-fulfilling prophecy. The present centralized system was developed over decades by uncountable researchers and practitioners; therefore, more research is required in source separating technologies to identify more realistic picture of new approaches.

ACKNOWLEDGEMENTS

Erasmus Mundus Lot 3 and UWI (Urban Water Interface) are acknowledged for the financial support of this project.

REFERENCES

Augustin K, Skambraks A K, Li Z, Giese T, Rakelmann U, Meinzinger F, et al., 2013. Towards sustainable sanitation—the HAMBURG WATER cycle in the settlement Jenfelder Au. Water Sci Technol: Water Supply, http://dx.doi.org/10.2166/ws.2013.158 (In press, Uncorrected proof).

Avery, L.M.; Frazer-Williams, R.A.D.; Winward, G.; Shirley-Smith, C.; Liu, S.; Memon, F.A.; Jefferson, B., 2007. Constructed wetlands for greywater treatment. Ecohydrol. Hydrobiol. 7, 191–200.

Balkema AJ, Preisig HA, Otterpohl R, Lambert FJD., 2002. Indicators for the sustainability assessment of wastewater treatment systems. Urban Water;4(2):153–61.

Benetto E, Nguyen D, Lohmann T, Schmitt B, Schosseler P., 2009. Life cycle assessment of ecological sanitation system for small-scale wastewater treatment. Sci Total Environ;407(5):1506–16.

Böhnke, B., 1981. Energieminimierung durch das Adsorptions-Belebungsverfahren; Gewässerschutz Wasser Abwasser No. 49; Instituts für Siedlungswasserwirtschaft der RWTH: Aachen, Germany,

Brix, H.; Arias, C.A., 2005.The use of vertical flow constructed wetlands for on-site treatment of domestic wastewater: New Danish guidelines. Ecol. Eng., 25, 491–500.

Elmitwalli, T. A. & Otterpohl, R., 2007. Anaerobic biodegradability and treatment of greywater in upflow anaerobic sludge blanket (UASB) reactor. Water Res. 41(6), 1379.

Eriksson, E., Auffarth, K., Henze, M. & Ledin, A., 2002. Characteristics of grey wastewater. Urban Water 4(1), 85.

Hellweg S, Milà i Canals L., 2014. Emerging approaches, challenges and opportunities in life cycle assessment. Science;344(6188):1109–13, http://dx.doi.org/10.1126/science.1248361.

Hern´andez Leal, L.; Temmink, H.; Zeeman, G.; Buisman, C.J., 2010. Comparison of three systems for biological greywater treatment. Water, 2, 155–169.

Johansson, M., Jönsson, H., Höglund, C., Stintzing, A., and Rodhe, L., 2001. Urine separation - closing the nutrient cycle, Stockholm Vatten, Stockholm, Sweden.

Jönsson, H., Stenström, T.-A., Svensson, J. & Sundin, A., 1997. Source separated urine-nutrient and heavy metal content, water saving and faecal contamination. Water Sci. Technol. 35(9), 145–152.

Geller, G., and Höner, G., 2003. Anwenderhandbuch Pflanzenkläranlagen (User guide for constructed wetlands). Springer. Berlin, Germany.

Ganrot, Z., 2005. Urine processing for efficient nutrient recovery and reuse in agriculture. Department of Environmental Science and Conservation, Göteborg University

Sliekers, A. O., Third, K. A., Abma, W., Kuenen, J. G. & Jetten, M. S. M. 2003. CANON and Anammox in a gas-lift reactor. FEMS Microbiol. Lett. 218(2), 339.

Kujawa-Roeleveld, K., Fernandes, T., Wiryawan, Y., Tawfik, A., Visser, M. & Zeeman, G., 2005. Performance of UASB septic tank for treatment of concentrated blackwater within DESAR concept. Water Sci. Technol. 52(1-2), 307–313.

Maurer M, Schwegler P, Larsen TA., 2003. Nutrients in urine: energetic aspects of removal and recovery. London, UK: IWA Publishing;

Maurer, M.; Pronk, W.; Larsen, T., 2006. Treatment processes for source-separated urine. Water Res., 40, 3151–3166.

Otterpohl, R., Albold, A. & Oldenburg, M., 1999. Source control in urban sanitation and waste management: ten systems with reuse of resources. Water Sci. Technol. 39(5), 53–160.

Otterpohl R., 2002. Options for alternative types of sewerage and treatment systems directed to improvement of the overall performance. Water Sci Technol;45(3):149–58.

Peter-Fröhlich A, Pawlowski L, Bonhomme A, Oldenburg M., 2007. EU demonstration project for separate discharge and treatment of urine, faeces and greywater—part I: results. Water Sci Technol;56(5):239–49.

DeSaH, Reactor Performance of AB-Process at the DeSaH Demonstration Site., 2010. DeSaH: Sneek, the Netherlands.

Remy, D.I.C.; Ruhland, I.A., 2006. Ecological Assessment of Alternative Sanitation Concepts with Life Cycle Assessment. Technical University Berlin, Berlin, Germany, Volume 55.

Remy C., 2009. Life cycle assessment of conventional and source-separation systems for urban wastewater management. Berlin, Germany: Department of Water Quality Control, Technische Universität Berlin; (Ph.D. thesis; Available from: http://opus.kobv.de/tuberlin/volltexte/2010/2543/pdf/remy christian.pdf [accessed 27.05.11]).

Ridderstolpe, P., 2004. Introduction to greywater management, EcoSanRes Programme, Stockholm Environment InstituteISBN 91 88714 96 9

Thibodeau C, Monette F, Bulle C, Glaus M., 2014. Comparison of blackwater source separation and conventional sanitation systems using life cycle assessment. J Clean Prod 2014;67:45–57.

Wilsenach, J.A.; van Loosdrecht, M.C.M., 2006. Integration of processes to treat wastewater and source-separated urine. J. Environ. Eng., 132, 331–341

Windey, K., De Bo, I. & Verstraete, W., 2005. Oxygen-limited autotrophic nitrification-denitrification (OLAND) in a rotating biological contactor treating high-salinity wastewater. Water Res. 39(18), 4512.

Wissing F, Hoffmann K.F., 2002. Wasserreinigung mit Pflanzen (Water treatment with plants).2nd edition, Verlag Eugen Ulmer, Stuttgart.

Tervahauta T, Hoang T, Hern´andez L, Zeeman G, Buisman C., 2013. Prospects of source-separation-based sanitation concepts: A model-based study, Water 2013, 5, 1006-1035; doi:10.3390/w5031006

Zeeman G, Kujawa K, de Mes T, Hernandez L, de Graaf M, Abu-Ghunmi L, et al., 2008. Anaerobic treatment as a core technology for energy, nutrients and water recovery from source-separated domestic waste(water). Water Sci Technol;57(8):1207–12.

Vlaeminck, S.E.; Terada, A.; Smets, B.F.; Linden, D.V.D.; Boon, N.; Verstraete, W.; Carballa, M., 2009. Nitrogen removal from digested blackwater by one-stage partial nitritation and anammox. Environ. Sci. Technol., 43, 5035–5041.

Tilley, E., Ulrich, L., Lüthi, C., Reymond, Ph. and Zurbrügg, C., 2014. Compendium of Sanitation Systems and Technologies. 2nd Revised Edition. Swiss Federal Institute of Aquatic Science and Technology (Eawag). Dübendorf, Switzerland.

Proceedings of the 10th World Congress of EWRA 'Panta Rhei', 5-9 July 2017, Athens, Greece
© 2017 *European Water Resources Association*

Assessing ecological flow conditions for wetlands fed from ungauged stream reaches

A. Gül*, K. Ayyıldız, F. Barbaros and T. Baran
Department of Civil Engineering, Faculty of Engineering, Dokuz Eylul University, Buca, 35160 Izmir, Turkey
* *e-mail: ali.gul@deu.edu.tr*

Abstract: Wetlands, which are greatly associated with intensive ecological services and high rates of biological diversity and ecological reserve, depend very much on prevailing flow conditions and hydrologic alterations in river systems that supply water to the wetland area. Alterations in flow regimes due to changing climatic conditions and/or anthropogenic impacts (e.g., damming, regulated water release, changing land uses, etc.) make diverse and considerable impacts on ecosystem sustainability for wetlands, thus need to be quantified for unfolding the observed (or predicted) degrees of connected changes in ecological flow conditions. This quantification is, however, problematic for stream reaches with inadequate or no records of measured flows. The presented study implements a holistic approach for comparing ecological flow conditions and detecting alterations between subsequent time periods for a number of wetlands along the Mediterranean transect of Turkey, which primarily lack flow measurements in associated stream reaches. In the approach, time series data of monthly flows for ungauged locations, which are selected at stream entrance points for different wetlands, are first generated by employing the logic that is behind the Massachusetts Sustainable-Yield Estimator (MA-SYE) tool and is based on a number of regression relationships with a defined set of catchment characteristics and also between different flow quantiles. Synthetic time series for monthly flows are later used in computing monthly series of environmental flows through a desktop estimation approach. Inter-periodic comparisons for environmental flow series between subsequent and equi-length time periods help display observed alterations in ecological states of the investigated set of Mediterranean wetlands.

Key words: Stream flow prediction, ungauged sites, wetlands, environmental flows

1. INTRODUCTION

Wetlands in regards to their ecological functioning accommodate significant rates of ecological biodiversity and involve intensive ecological services. This normally makes these areas substantially dependent on hydrologic/hydraulic conditions in the catchments and alterations in the hydrology of rivers feeding these wetland systems. Major changes in the river hydrology may result normally from a changing regional climate or be the consequence of anthropogenic interventions over the river system. They are greatly associated with substantial impacts on ecosystem sustainability. In this respect, there are strong needs toward the identification and quantification of such variations from on-going hydrologic conditions also with the aims of estimating the connected changes in ecological conditions.

This quantification is, however, not straightforward for many rivers due to inadequacy or lack of flow measurements. The presented study implements a holistic approach first for generating synthetic time series of river flows at ungauged locations and then assessing ecological flow conditions through estimations of environmental flows for the wetland systems investigated. The process of generating synthetic flow series depends on the similarities of catchment characteristics in the region and the representativeness of the flows recorded in the reference stations, which are distinguished from a wider set of stream flow monitoring locations marked with sufficiently long gauge records.

2. CASE-STUDY, SOFTWARE AND DATA SOURCES

The study for assessing ecological conditions of wetland systems in terms of environmental flow quantities received by these systems was conducted on the case-study sites selected from the Mediterranean region in Turkey, including the river basin systems in West Mediterranean, Antalya and East Mediterranean Basins (Figure 1). The significance of the Mediterranean wetlands originates from the foresights involved in climate change related assessments that describe the Mediterranean transect of Turkey with high concerns in relation to the expected negative impacts under the changing climate conditions.



Figure 1. Case-study basins (West-, East-Mediterranean and Antalya) in the Mediterranean region of Turkey.

Monthly discharge data on river flows for 28 monitoring stations (6 in West Mediterranean, 9 in Antalya and 13 in East Mediterranean basin systems) (see Figure 2) were acquired from the data yearbooks previously published by the Electric Power Resources Survey and Development Administration (EIE, partly assigned under the State Hydraulic Works as of the year 2011). Land cover data for computing stocks of different land cover types inside drainage basins were obtained from the Corine Land Cover (CLC) dataset produced by the Turkish Ministry of Environment and Urbanization. Software tools which were employed for performing the intended study mainly included the Global Environmental Flow Calculator (GEFC) software, which was developed in collaboration of the International Water Management Institute (IWMI) and the University of New Hampshire, ArcGIS software by ESRI and the Excel software of the Microsoft Corporation.

3. METHODOLOGICAL FRAMEWORK AND APPLICATION

3.1 Estimation of monthly stream flow for ungauged stream locations

For generating estimates of monthly flow time series, the methodological rationale and the analytical approach described for/embedded in the Massachusetts Sustainable-Yield Estimator (MA-SYE) tool was utilized (Archfield et al., 2009). First, a number of physical and meteorological basin characteristics, which included, among few others, the sizes of drainage areas upstream of the monitoring stations with gauged flow information, the maximum, minimum and mean elevations inside these areas, slope averages, geospatial coordinates for the stations, drainage area centroids, outlets, the relative shares of forested and open water land covers, average annual precipitation, average maximum temperature, etc. (Figure 2), were calculated through convenient spatial operations (Table 1). Stream flow quantiles associated with the 0.000062, 0.01, 0.05, 0.2, 0.4, and 0.8 probabilities of exceedance in the flow duration curves of the gauged stream flow monitoring locations were regressed against this set of basin characteristics. As described in the MA-SYE

approach, natural-log transformations of the stream flow quantiles (each obtained separately from the 28 gauged stations) as dependent variables and physical/meteorological basin characteristics (grouped sets for the gauged stations) as independent explanatory variables were employed for definitions of multivariate linear regression relationships between the variables. Table 2 indicates the sets of independent variables and the associated regression coefficients defined separately in equations for each of the stream flow quantiles that were investigated in the first round.

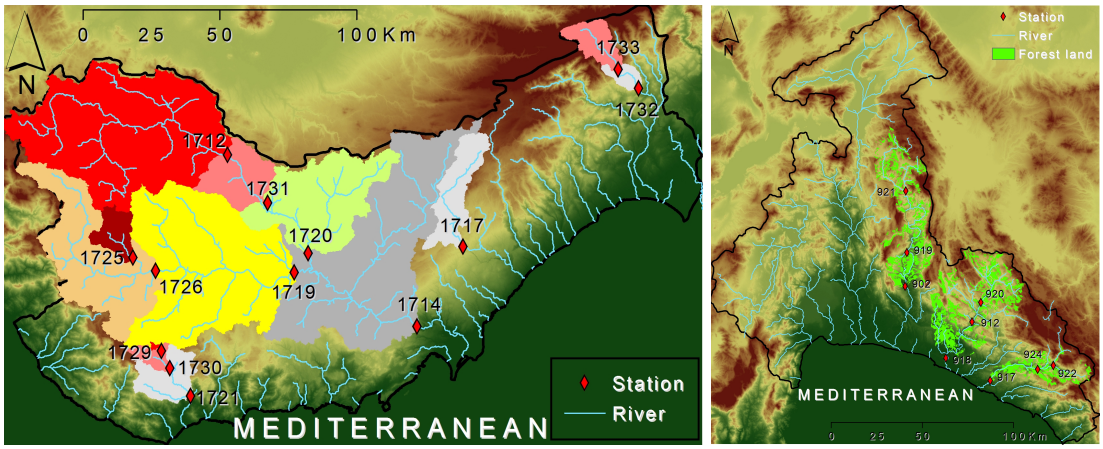

(a) *(b)*

Figure 2. (a) River systems and drainage areas associated with the flow monitoring stations selected in the East-Mediterranean Basin and (b) forested areas isolated for the drainage areas in Antalya Basin.

After the six quantiles for stream flows were regressed against physical and climate basin characteristics (Figure 3a), eleven additional quantiles on corresponding flow duration curves were estimated for providing physical consistency and increasing the graphic precision by including intermediate data points for the quantile estimates (Figure 3b). This process was implemented by generating regression relationships in a recursive manner, by relating one quantile to another between two values which are assumed to be mostly relevant. For example, the stream flow quantile at the 80-percent exceedance probability was initially obtained by solving a quantile-based regression equation that is a function of basin characteristics. Then, the stream flow quantile at the 85-percent exceedance probability was obtained by using the relation between the stream flow quantiles at the 80- and 85-percent exceedance probabilities. The total set of equations that allowed estimations for the additional data points on the flow duration curves are listed below:

$$\ln(Q15) = 0.16345 + 0.99465 * \ln(Q20) \quad (1)$$

$$\ln(Q10) = 0.27214 + 0.97449 * \ln(Q15) \quad (2)$$

$$\ln(Q30) = 0.30510 + 0.98962 * \ln(Q40) \quad (3)$$

$$\ln(Q50) = -0.28431 + 0.99944 * \ln(Q40) \quad (4)$$

$$\ln(Q60) = -0.29922 + 1.00662 * \ln(Q50) \quad (5)$$

$$\ln(Q70) = -0.43962 + 1.04648 * \ln(Q60) \quad (6)$$

$$\ln(Q85) = -0.15462 + 1.01351 * \ln(Q80) \quad (7)$$

$$\ln(Q90) = -0.19844 + 1.02271 * \ln(Q85) \quad (8)$$

$$\ln(Q95) = -0.16981 + 1.00446 * \ln(Q90) \quad (9)$$

$$\ln(Q99) = -0.54721 + 1.12050 * \ln(Q95) \quad (10)$$

$$\ln(Q100) = -0.24125 + 1.06296 * \ln(Q99) \quad (11)$$

Table 1. Physical and meteorological drainage area characteristics computed for the gauged stream flow stations

Parameter / Station	**808**	**809**	**811**	**812**	**815**	**818**	**902 ...**
Drainage area, in square kilometers	2,175.50	551.48	3,852.72	5,004.22	2,477.45	285.55	1,948.14
Mean basin elevation, in meters	1,559.78	1,537.44	1,291.40	1,260.91	1,082.54	1,232.71	1,315.84
Maximum basin elevation, in meters	3,070	2,707	2,576	2,576	2,982	2,982	2,988
Minimum basin elevation, in meters	362	1,129	668	148	19	68	134
Percent of basin with highlands	100	100	100	100	91	98	100
Elevation at the outlet of the station, in meters	362	1,129	668	148	19	68	134
Slope, in percent rise	25.96	21.73	20.58	23.54	27.79	28.91	35.16
X-coordinate at the station, in meters	647,316	602,702	562,621	547,264	577,953	581,733	749,491
Y-coordinate at the station, in meters	4,454,928	4,494,710	4,527,808	4,508,148	4,443,682	4,453,831	4,523,718
X-coordinate at the center of the basin, in meters	632,133	613,683	599,794	591,312	593,325	594,432	749,986
Percent of basin that is forested	6.96	2.40	19.75	25.76	28.55	50.14	28.42
...							

Table 2. Coefficients of the regression relationships between quantile estimates and drainage area characteristics

Basin Independent Variables	Exceedance Probability					
	0.00062	0.01	0.05	0.2	0.4	0.8
Constant term	-849.619	-529.790	-705.079	-898.909	-951.449	-1397.27
Drainage area (km^2)	0.524	0.854	0.650	0.542	0.534	-
Maximum basin elevation (m)	-	-6.416	-	-	-	-
Minimum basin elevation (m)	-	-	-	-0.367	-0.440	-
Slope (%)	-	-	-	-	-	-3.864
X-coord. at the station (m)	-	-	2.066	1.532	1.355	-
X-coord. at the center of the basin (m)	2.017	-	-	-	-	2.343
Y-coord. at the center of the basin (m)	51.635	34.986	41.729	55.706	59.245	85.732
Average annual precipitation (mm)	4.093	6.735	5.709	3.967	4.043	6.440
Average min. temperature (^oC)	-	-0.850	-	-	-	-0.469
Average max. temperature (^oC)	1.984	-	-	-	-	9.215
Percent of basin that is open water	-	-	-	-0.180	-0.220	-

The starting point of the intended study was to allow environmental flow assessments for the wetlands receiving water from the ungauged river systems. The rationale behind this approach was to generate synthetic flow time series for a number of virtual monitoring locations identified in the upstream to the wetlands of interest through certain defined relationships, with a set of reference monitoring stations available with flow records, based on geographic representativeness and similar basin characteristics. For this purpose, a selection of a number of candidate locations for positioning the virtual stations was performed (Figure 4) and the corresponding physical and meteorological basin characteristics were obtained from the spatial analyses conducted in the drainage catchments. This allowed computing the first six quantile points on the flow duration curve for each individual virtual location. The additional quantiles were then recursively generated by using the inter-quantile regression equations as defined in Figure 3b.

In the next step before translating flow duration curves of the virtual stations into the time series by the use of reference monitoring stations which relate most to the virtual locations, Pearson correlation coefficients were computed mutually between all possible pairs of the gauged stations to obtain point correlations in each layer that indicate correlation values of any selected gauged monitoring point to the rest. These point layers for each individual gauged station were then spatially interpolated into correlation surfaces. The values in a virtual station were then queried in all computed correlation surface layers for assigning a gauge station that is mostly correlated to the virtual location to each of the virtual stations. In Figure 5, the point location of the virtual station 1, for example, received the highest correlation value from the correlation surface valid for the station 809 (computed r value as 0.926). In this manner, all virtual locations were paired with a gauged

station that proved to be mostly correlated.

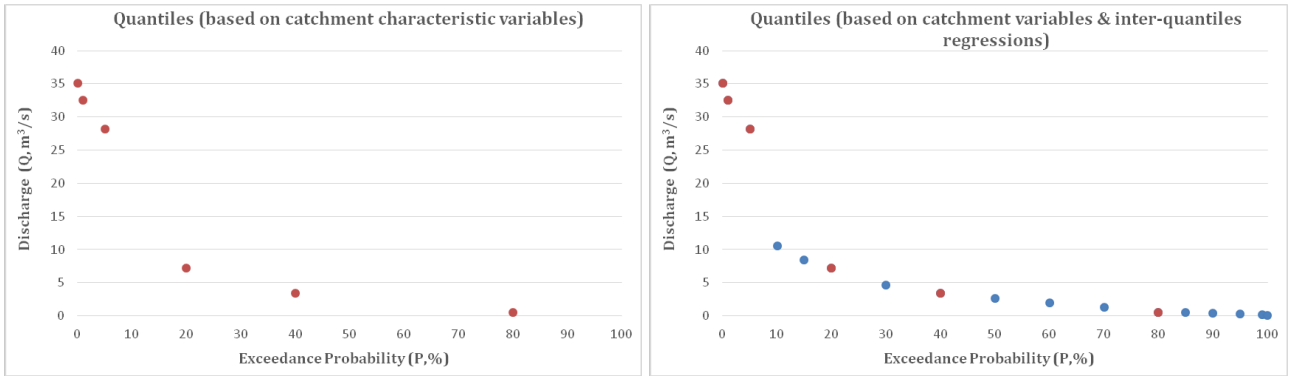

(a) *(b)*

Figure 3. (a) Quantile data points regressed against basin characteristics, and (b) the points densified through inter-quantile regressions.

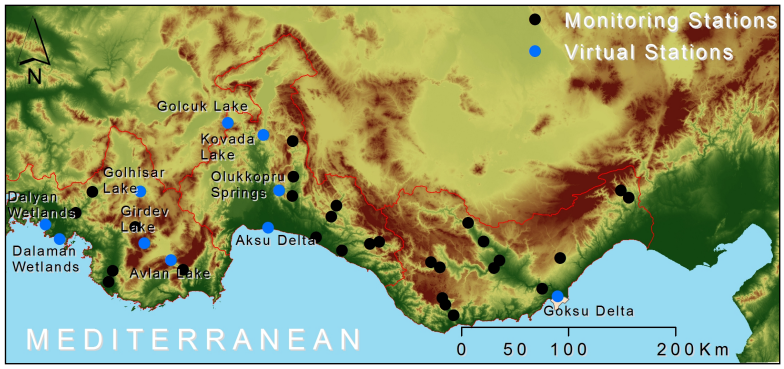

Figure 4. Locations of the selected virtual stations with respect to the actual gauged stations.

Following these designations, monthly virtual time series of the virtual stations were generated by using the QPPQ method (Fennessey, 1994; Hughes and Smakhtin, 1996; Smakhtin, 1999; Smakhtin and Masse, 2000; Mohamoud, 2008). In implementing the method, each individual data value on the graph of monthly discharges for the gauged reference station was considered for computing the corresponding probability of exceedance from the flow duration curve for the reference station. From the curve previously estimated for the virtual station, the discharge value associated with the same exceedance probability were extracted and placed as a new data point over the time series generated for the virtual location. The process was repeated until each monthly value is placed in the time series (Figure 6).

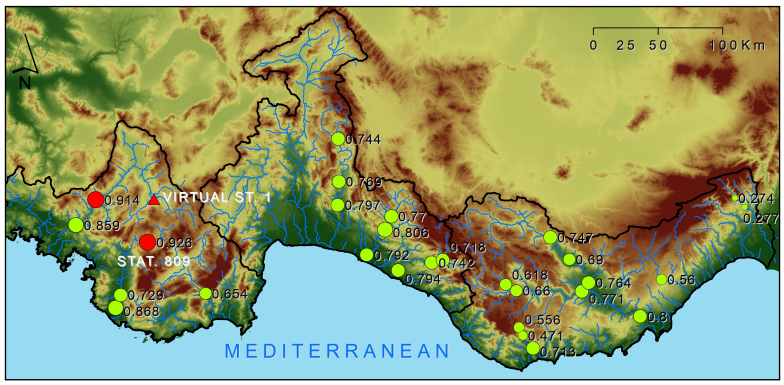

Figure 5. An example for the mutual correlation degrees computed for the virtual station 1 assigned for the Golhisar lake wetland.

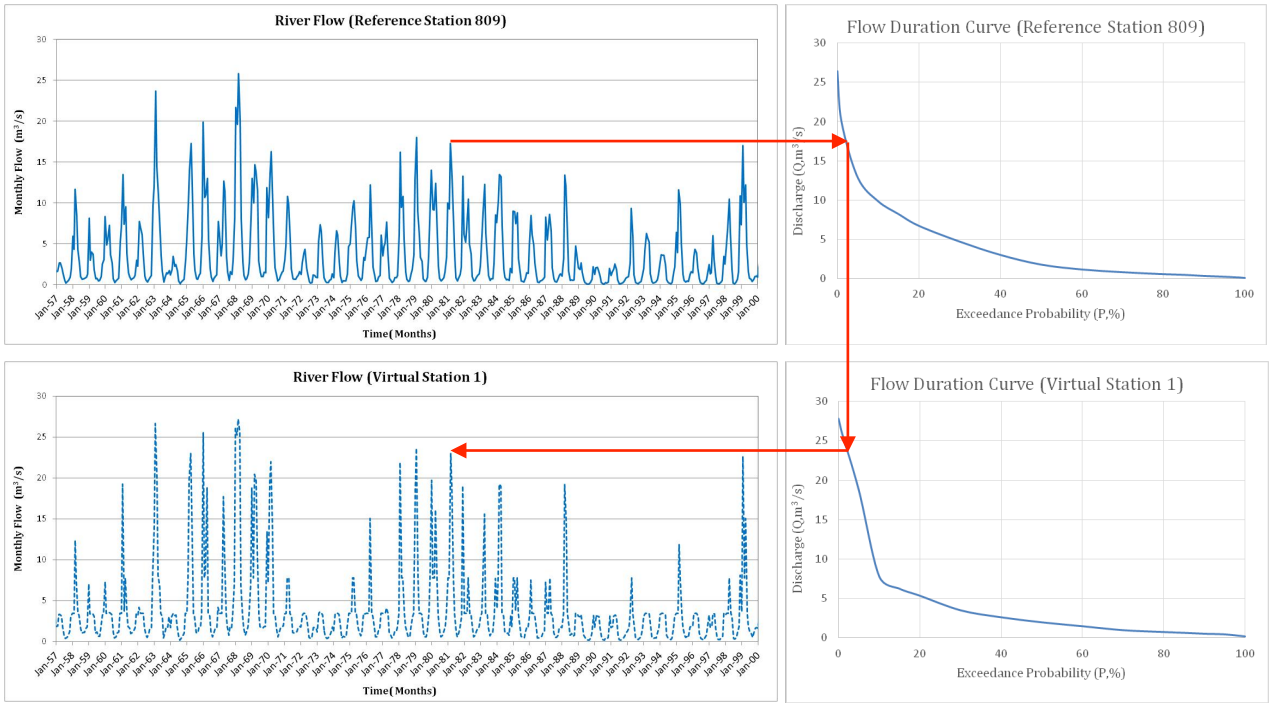

Figure 6. Implementation of the QPPQ approach for generating monthly discharges of the virtual station for Golhisar lake wetland by using the discharges recorded at the selected reference station 809.

3.2 Estimating environmental flow capacities for ungauged stream locations

Virtual time series for monthly discharges at ungauged locations are useful for investigating environmental flow capacities which are necessary for preserving biodiversity and sustaining ecosystem functioning of the wetlands systems analyzed. These assessments were implemented with the so-called desktop approach through the use of the GEFC software. In GEFC, it is possible to define targeted or predicted degree of environmental management in forms of environmental management classes (EMCs). EMCs can be explained as prescribed or negotiated conditions in which wetland ecosystems are desired to be maintained or upgraded to (Acreman and Dunbar, 2004). EMCs differ in six classes ranging from class A to represent pristine conditions or minor modifications in habitat to class F to indicate critical modifications in the ecosystem with almost total loss or natural habitat and biota. In the presented study, capacities of environmental flows for the investigated wetland systems were estimated in forms of environmental flow monthly time series, considering all six EMC classes to provide assessments in a wide range of environmental conditions. Figure 7 shows the monthly river flow series, which were estimated for the virtual station 4 close to Dalyan wetlands based on the gauge records of the river station 812, as well as the environmental flow series that consider different management strategies for the wetland area. Although the figure displays the conditions only for two EMCs, the same analysis was implemented for all six different strategies of environmental management and for all wetland systems studied in the paper. It is apparent in the case of the Dalyan wetlands that there are decreases in environmental flow potentials in accordance with the decreasing river discharges between the subsequent periods.

The analyses were extended to assess alterations in environmental flow potentials estimated for different periods through changes in long-term averages for the months of a year. Figure 8 shows the changes in long-term monthly averages computed for the three wetland systems in the Mediterranean region. In parallel to the change indications over the periodic mean flows for Dalyan wetlands system as in Figure 7, a distinguishable decrease pattern is also visible in Figure 8 where more considerable changes associate with the months of greater flow potentials estimated for the within-year period from December to May. A similar decrease pattern is visible for the Golhisar lake, but with a comparably bigger decrease after the period 1961-1970. Some of the wetlands like

the Avlan lake shows rather ambiguous change patterns between the subsequent periods but again indicating the most limited potentials in the most recent period 1991-2000 analyzed.

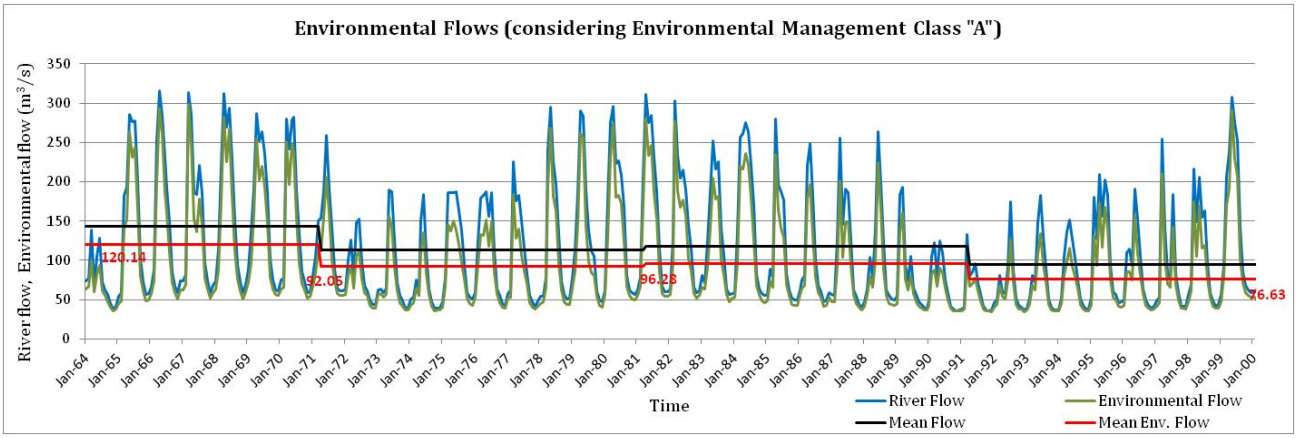

(a)

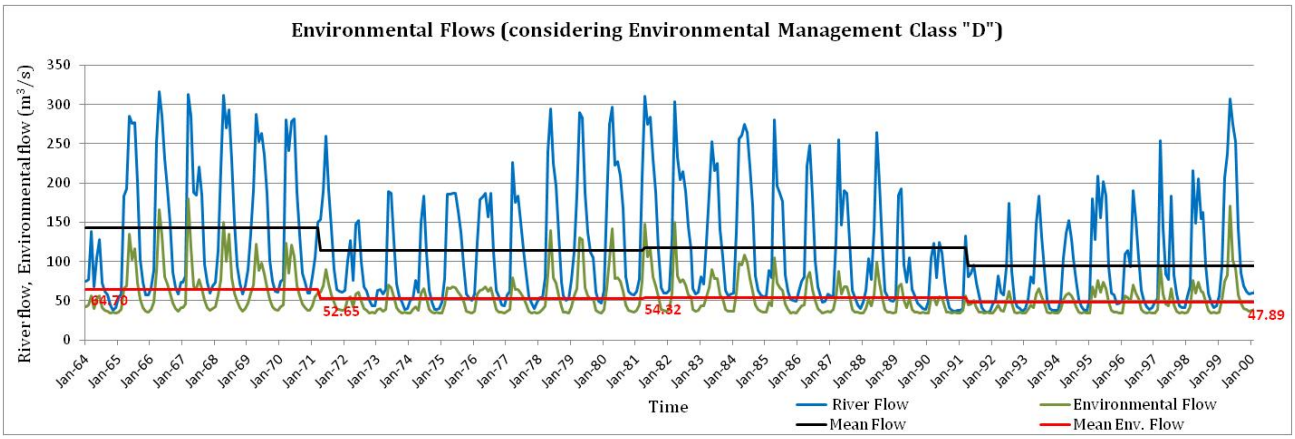

(b)

Figure 7. (a) Monthly series of environmental flow, considering (a) EMC-A and (b) EMC-B for Dalyan wetlands, displayed against the river flow monthly discharges .

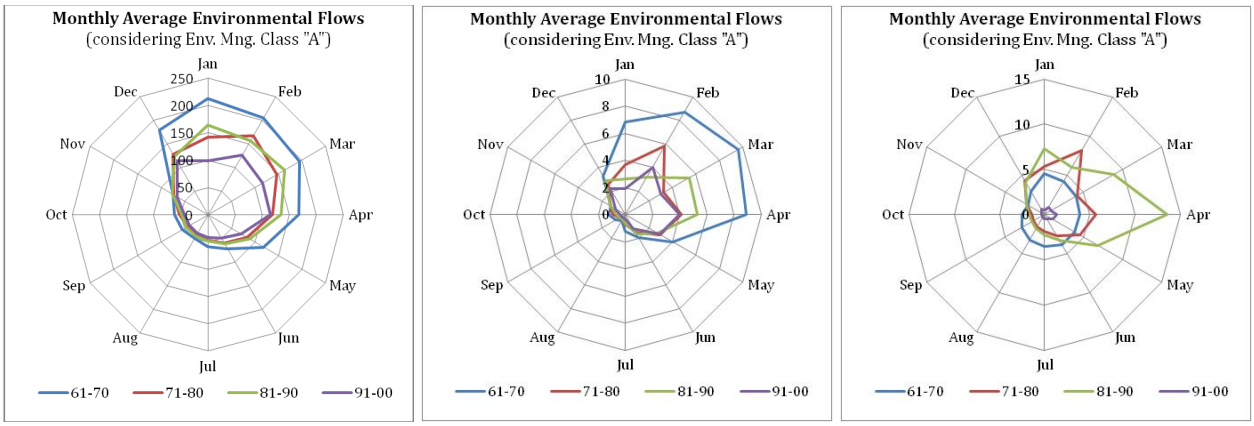

(a) *(b)* *(c)*

Figure 8. Graphic displays of monthly mean environmental flows computed in the 10-year periods 1961-1970, 1971-1980, 1981-1990 and 1991-2000 for the case-study wetlands: (a) Dalyan, (b) Golhisar lake, and (c) Avlan lake.

4. CONCLUSIONS

Turkey's wetlands are in general subject to substantial risks in terms of environmental flow

supplies due to climatic and anthropogenic impacts. Assessments for risk identification and reduction depend very much, however, on the availability of gauge records collected from the monitoring stations that sufficiently help to unfold wetland hydrology and ecosystem sustainability. Since the data needs are not fully satisfied for all wetland systems, or environmentally-protected areas in a much general sense, there are strong needs for making estimations in ungauged locations for providing a complete picture while performing assessments. The presented study employed a hydro-spatial methodology, which originated from the MA-SYE approach, for generating estimated series of river flows in such locations, and then the assessments were extended also to address ecosystem sustainability from the hydrologic point of view while providing inter-periodic comparisons for revealing the changes experienced.

REFERENCES

Acreman, M., Dunbar, M. J., 2004. Defining environmental river flow requirements - a review. Hydrol. Earth Syst. Sc., 8, 861–876.

Archfield, S. A., Vogel, R. M., Steeves, P. A., Brandt, S. L., Weiskel, P. K., Garabedian, S. P., 2009. The Massachusetts Sustainable-Yield Estimator: A decision-support tool to assess water availability at ungaged stream locations in Massachusetts. U.S. Geological Survey Scientific Investigations Report 2009–5227, 41 p.

Fennessey, N. M., 1994. A hydro-climatological model of daily streamflow for the northeast United States. Medford, MA, Tufts University, Ph.D. dissertation.

Gul, A., 2015. Comparing Past and Present Hydrologic Aspects of a Mediterranean Wetland from a Sustainable Management Perspective. Water Resour Manag., 29 (8), 2771–2787.

Gul, A., Onusluel Gül, G., Dikmen, A. C., Kuzucu, A., 2014. Investigating hydrologic alterations for wetland systems in terms of river environmental flows. Water Environ. J., 28 (3), 329–339.

Hughes, D. A., Smakhtin, V. U., 1996. Daily flow time series patching or extension: a spatial interpolation approach based on flow duration curves. Hydrolog Sci. J., 41 (6), 851–871.

Mohamoud, Y. M., 2008. Prediction of daily flow duration curves and streamflow for ungauged catchments using regional flow duration curves. Hydrolog Sci. J., 53 (4), 706–724.

Smakhtin, V. U., 1999. Generation of natural daily flow time series in regulated rivers using a non-linear spatial interpolation technique. Regulated Rivers: Research and Management, 15, 311–323.

Smakhtin, V. U., Masse, B., 2000. Continuous daily hydrograph simulation using duration curves of a precipitation index. Hydrol. Process., 14, 1083–1100.

Proceedings of the 10th World Congress of EWRA 'Panta Rhei', 5-9 July 2017, Athens, Greece
© 2017 *European Water Resources Association*

Evaluation of streamflow habitat relationships using habitat suitability curves and HEC-RAS

Christina Papadaki[1], Vasilis Bellos[2,3], Maria Stoumboudi[1], George Kopsiaftis[2] and Elias Dimitriou[1*]
[1] *Hellenic Centre for Marine Research, Institute of Marine Biological Resources and Inland Waters, Greece*
[2] *Laboratory of Reclamation Works and Water Resources Management, School of Rural and Surveying Engineering, National Technical University of Athens, Greece*
[3] *CH2M, UK*
[*] *e-mail: elias@hcmr.gr*

Abstract: Habitat Suitability Curves (HSCs) were developed for two freshwater fish species, namely *Salmo pelagonicus* and *Barbus balcanicus,* using microhabitat data obtained at a mountainous stream, in upper Axios River, Greece, for habitat evaluation on the micro scale. Twelve riverine HSCs associating two size classes with three microhabitat parameters (water depth, velocity and substrate) were developed and used. For the hydraulic simulation of the stream, the well-known, one-dimensional HEC-RAS software was implemented. The Weighted Usable Area (WUA) was estimated by combining habitat suitability indices with the output of the hydraulic model, to evaluate the relationship between streamflow and fish habitat availability. For the calibration of the model, water depth and flow velocity measurements were performed on April 2016. In the framework of the calibration phase, an algorithm was developed, to automate this process and to implement a sophisticated optimisation method. For the upstream and the downstream boundary conditions, water velocity and depth measurements were used as well, to reduce the uncertainty propagation due to the model's parameters. The presented approach may provide a better understanding of how flow variability affects fish microhabitats, while it can contribute considerably to the sustainable water management of hydrologically altered rivers and the concomitant conservation of riverine biota.

Key words: Habitat suitability curves (HSCs), HEC-RAS software, automation, WUA

1. INTRODUCTION

The habitat requirements of freshwater fish, normally expressed as Habitat Suitability Curves (HSCs), may provide valuable information regarding the physical structure and the flow regime of a stream channel (Terrell 1984; Bovee 1986; Brown et al. 2000). Electrofishing is a common technique for fish sampling, defining at the same time fish microhabitats and consecutively collecting microhabitat use data in rivers (Copp and Garner 1995) for the development of the HSCs. However, in Greece, little relevant work has been carried out that could assist the estimation of environmental flows, as well as the identification of priority habitats for conservation and restoration purposes (Vardakas et al 2017).

Minimum environmental flows estimated using the relationship between WUA and discharge are recommended for having a river alive and conserving its ecosystem when found in critical condition for a short time period (Nikghalb 2016). WUA estimations for habitat indexing requires estimates of depth and velocity, which can be obtained using a computational hydraulic model. One dimensional river models are far more abundant and commonly used, among others, for such hydraulic simulations. However, the spatial distribution of the habitat suitability indices (SI), require more detailed hydraulic data to determine the spatial distribution of depth and velocity throughout the reach (Bovee et al. 1998). Moreover, the geomorphology of the river is a very important factor for the output of hydrodynamic models (Boyraz & Kazezyılmaz-Alhan 2014; Benjankar et al. 2015; Greco 2015), which also influences the output of the habitat models (Papadaki et al. 2016).

The shape of the WUA curves is a function of the species/size habitat preferences and reflects

the interaction between hydraulic variables and channel structure with increasing discharge. In that context, habitat simulation models for fish and other species are important tools for evaluating the present state of a river, the effects of altered morphology or altered hydrology on habitat suitability, and to predict the ecological consequences of certain restoration measures or management strategies (Alcaraz-Hernández et al. 2011). In this study, an adaptation of the Physical Habitat Simulation (PHABSIM) technique, covering the Greek conditions (Papadaki et al. 2014) for the estimation of minimum environmental flows, was used. Moreover, summer habitat use of two freshwater fish species, namely the Pelagonian trout, *Salmo pelagonicus* Karaman, 1938 and the large spot barbel, *Barbus balcanicus* Kotlík, Tsigenopoulos, Ráb and Berrebi, 2002*,* was examined, using microhabitat data in terms of water velocity, depth, and substrate, obtained at a mountainous stream, the Drosopigi stream located in the upper part of Axios River drainage in Greece. Differences in habitat use were explored, to obtain species-specific HSCs, and to estimate minimum environmental flows according to the habitat requirements of these two fish species.

2. MATERIALS AND METHODS

2.1 Study area

Microhabitat data were collected from the Drosopigi stream, a perennial mountainous stream located 14 km southern of the city of Florina, in northern Greece. Habitat mapping was performed in a segment of 1.5 km length to select a representative study reach of 200 m, in the beginning of August 2015, in low flow conditions. The survey involved identification of several types of hydromorphological units (i.e. pools, runs, riffles, cascades and rapids) and measurement of their physical attributes (width, mean depth). The channel and floodplain were surveyed to create a digital elevation model (DEM) of the stream. A detailed topographic survey with a GPS/GNSS Geomax - Zenith 20 was performed, using reference stations at geodetic control points for highest accuracy. In Figure 1, the location of the case study is shown.

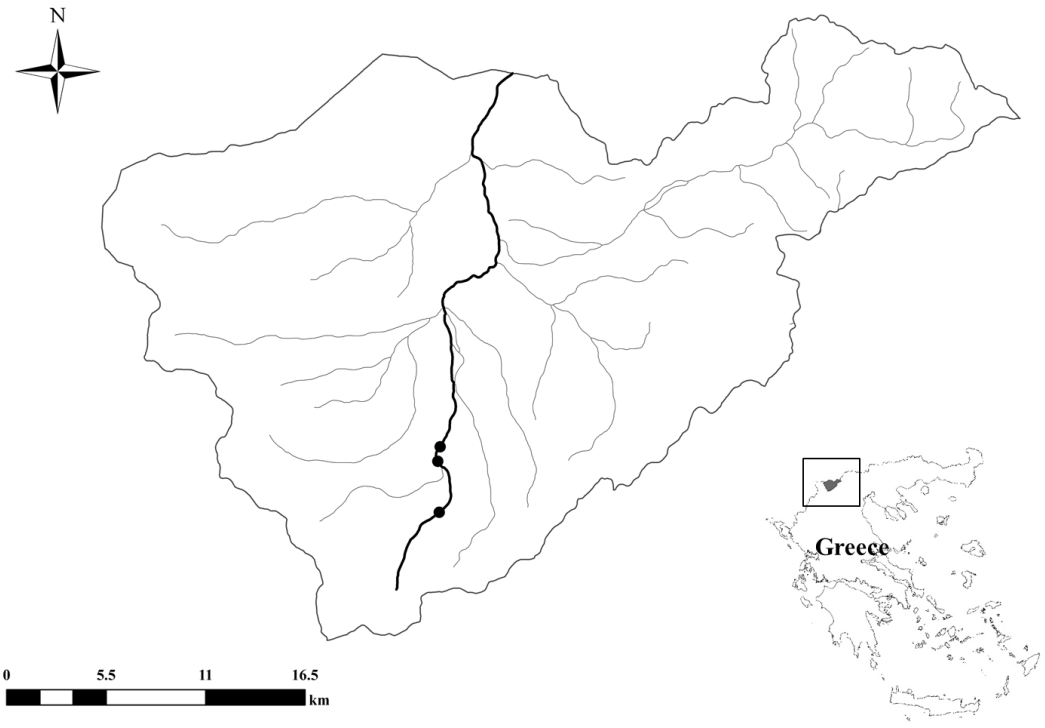

Figure 1. Drosopigi stream and its main tributaries; the location of the surveys for fish microhabitat use is marked with dots.

2.2 Fish and microhabitat data

Salmo pelagonicus and *Barbus balcanicus* are the most abundant or the only fish species, in the upper section of the Drosopigi stream where the survey took place, and for this reason, they were selected as the HSCs target species. For both species, two size-classes were recorded: small sized fish 5–15 cm, Total Length (TL) and large sized >15 cm TL. Fish data were collected using point-abundance sampling during daylight hours, using a Hans-Grassl GmbH battery-powered backpack electrofishing device (Model IG200-2, DC pulsed, 1.5 KW output power, 35-100 Hz, max. 850). Starting at the downstream point of the reach, sampling proceeded with the electrofishing crew that consisted of one operator and two netters moving in a zigzag pattern upstream, to sample all types of available fish habitats. To minimize disturbance, sampling locations were spaced about 4-5 m apart, so that the fish would not be disturbed by the previous electrofishing operation. Stunned fish were identified to species level, measured for TL and then, they were returned alive to the stream. A total of 135 observations (61 small and 74 large specimens) were recorded for *Salmo pelagonicus* and 451 observations for *Barbus balcanicus* (237 small and 214 large specimens) along the study reach. At each microhabitat, three variables were recorded: water velocity, water depth, and substrate type (Simonson, 1993). Water velocity (V, m/s) and depth (D, cm) were measured using an OTT C20 flow meter. At each point the spatial coordinates and the dominant substrate type were recorded in the river channel and floodplain.

2.3 Hydraulic modelling

For the derivation of the required water depth and flow velocity variables, HEC-RAS software was used, assuming steady inflow into the computational domain. The upstream boundary of the model was derived solving the Manning equation, using as input the value of the desired steady flow. The required parameter in this case was the energy slope. The energy slope was calculated by the following equation (Chaudhry, 2008):

$$S_f = S_0 - S_L(1 - Fr^2) \quad (1)$$

where S_f is the energy slope, S_0 the bottom slope, S_L the gradient of the water surface and Fr the Froude number. Since the case study is a mountain stream, the flow was expected to be supercritical with high Froude numbers. The energy slope was calculated from field observations, for a steady flow equal to 0.02 m^3/s, using the observed data obtained in the first two upstream cross-sections. For this purpose, the bottom slope, the gradient of the water surface and the flow velocity were measured, while the Froude number was calculated. Following this approach, the energy slope was calculated equal to S_f=0.0231, whereas the bottom slope was equal to S_0=0.0426. For the downstream boundary condition, the critical depth was selected, since the downstream boundary of the computational domain was the outlet of a small pool. Therefore, the flow was considered as critical. The required parameters of the software which had to be defined, was the Manning coefficient of the computational domain.

The computational domain was classified in 10 friction zones. The classification was made depending on whether each hypothetical zone could be characterised as a small pool or a cascade. It is noticed that in real-world applications Manning coefficient values gained from the relative literature probably underestimate the energy losses, due to turbulence phenomena that often occur in a river (Jarrett, 1985). Therefore, they should be calibrated (Christelis et al. 2016) if relevant measurements exist, which is the case in the present study.

For the calibration of the Manning coefficients for each friction zone, a generic algorithm was selected (Goldberg, 1989). The objective function adopted was the Root Mean Square Error between the simulated water depth and flow velocity using the HEC-RAS software and observed data from five cross-sections. Since both water depth and flow velocity were measured, a normalisation process followed by transforming the simulated water depths and flow velocities in a

normalised [0,1] variable *NV*, with the following equation:

$$NV_i = \frac{S_{max} - S_{sim}}{S_{max} - S_{min}} \quad (2)$$

where *S* can be either the water depth or the flow velocity, the subscript *max* and *min* indicates the maximum or the minimum value of this variable in the *i*-th cross-section, whereas the subscript *sim* indicates the value of the variable derived by the simulation. Following the above procedure, the calibrated Manning coefficient values are provided in Table 1.

Table 1. Manning coefficient values for each friction zone

Friction zone	n (s/m$^{1/3}$)
1	0.2500
2	0.2500
3	0.2489
4	0.0204
5	0.0203
6	0.1155
7	0.2219
8	0.0203
9	0.0345
10	0.2045

2.4 Habitat suitability curves development and habitat assessment

The HSCs were developed following the relevant methodology suggested by Bovee (1986). These curves relate the hydraulic to the habitat variables with a suitability index (SI), ranging from 0 (unsuitable for the aquatic species) to 1 (excellent). Each variable (water depth, flow velocity, substrate) was divided into classes, and frequencies of each class utilization by fishes were estimated. Once the histograms for the continuous variables were developed, a smooth curve was adjusted to them by using 3rd order polynomials, in R (R Development Core Team, 2014). These individuals' suitability indices were then combined to form a composite SI for every cell of the hydraulic model, using the product mathematical operation (Vadas & Orth 2001). At the cell scale, Cell Suitability Index (CSI) indicates whether the physical parameters (depth, velocity and substrate) are within those required by individual species and particular life stages (Bovee 1978). Integration of biological data by using the HSCs, with the HEC-RAS outputs (depth, velocity and substrate maps) were made, to calculate the Weighted Usable Area (WUA). Nineteen different discharge scenarios were selected between 0.02 and 4.5 m^3/s (Figure 5) to estimate the WUA. WUA was calculated by multiplying the CSI for a given cell of the hydraulic model, by the area assigned to that specific cell and then aggregate all the values in a single figure per discharge scenario. The whole procedure was carried out in R software (R Development Core Team, 2014).

2.5 Minimum environmental flow assessment

Optimisation matrices were developed depicting nineteen flows relative to summer conditions for two size classes (small sized: 5–15 cm and large sized: >15 cm) of the *Salmo pelagonicus* and the *Barbus balcanicus*, according to the optimization criterion of Bovee (1982). These flow values were arrayed across the top of the matrix and the WUA values for the aforementioned species were recorded accordingly (Table 2). Then, the minimum WUA value was identified for each flow. Finally, the minimum environmental flow was estimated based on the flow with the highest WUA value among all size classes and species (Bovee et al. 1998). This value corresponds to the flow that maximizes the habitat area for the particular fish species during the dry period in the study site.

3. RESULTS

For the calibration phase of the hydraulic model, constraints for the range of the Manning coefficient values were adopted. Specifically, the Manning coefficient values were ranging from 0.02 to 0.25 s/m$^{1/3}$. In Figure 2 the simulated water surface elevation and the flow velocities against the corresponding observed data are shown, for five cross-sections. The performance of the model was quite better for the water depths than for the flow velocities. This was expected, since it is generally accepted that flow velocity is more difficult to be simulated than the water depths (Guinot and Cappelaere 2009).

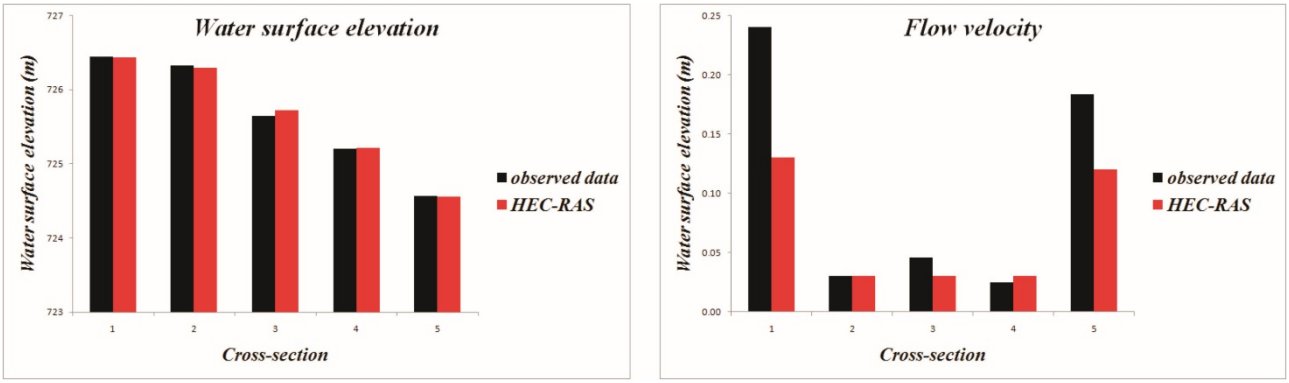

Figure 2. Performance of HEC-RAS model against observed data in five cross-sections

Water depth and current velocity ranged from 0 to 1.2 m and from 0 to 1.4 m/sec, respectively, in the study reach (Figure 3 a, b). Substrate resulted to be mainly composed of boulders (>264 mm) and cobbles (64–264 mm). Regarding size differences in depth use (Figure 3.a), depths most frequently used by both size classes of *Salmo pelagonicus* were between 0.4 to 0.9 m. *Barbus balcanicus* individuals smaller than 15 cm in TL occurred at depths between 0.1 m and 0.6 m, while the larger sized individuals of the same species were mostly found at depths ranging from 0.3 to 0.8 m. Water velocity HSCs (Figure 3.b) calculated for the small sized *Salmo pelagonicus* showed optimum velocity values at 0.25 m/s. As expected, the large sized trout individuals occupied positions with higher velocities (0.45 m/sec). Regarding *Barbus balcanicus*, small sized fish were found in positions with relatively lower velocities (0.05 to 0.6 m/sec) than the large sized ones (0.2 to 0.8 m/sec).

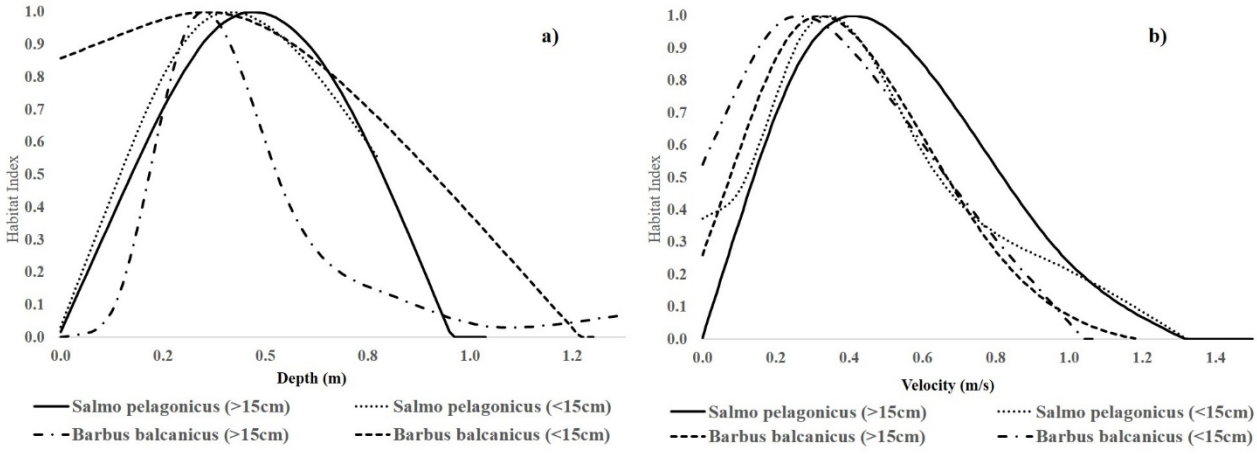

Figure 3. Habitat use curves for depth (a) and velocity (b) for two size classes of Salmo pelagonicus and Barbus balcanicus.

Typical habitat types are mainly riffles, runs and small pools. Substrate types are mainly cobbles,

boulders and gravel. Substrate data are shown in Figure 4. Both fish species displayed a strong association to boulders and bedrocks, which are coarse enough to provide shelter.

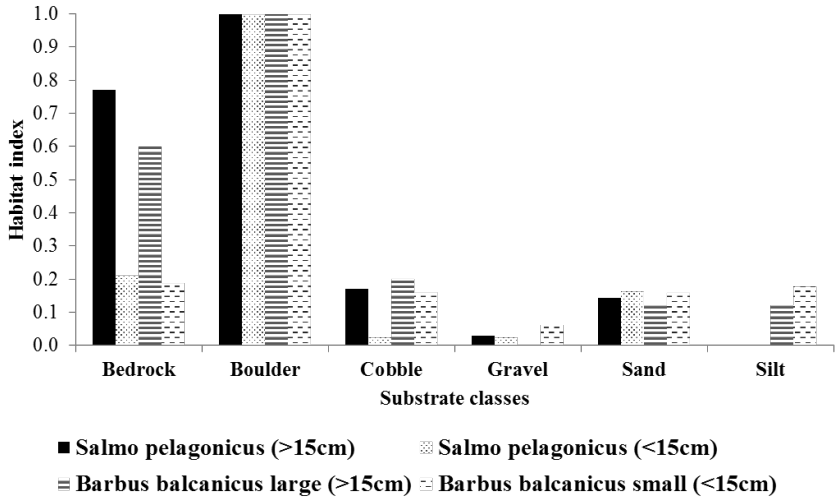

Figure 4. Small and large sized Salmo pelagonicus and Barbus balcanicus habitat index for substrate.

Discharge values ranging from 0.2 to 1.9 m^3/sec provided the most suitable habitat for both species and both size classes. WUA increases rapidly over a specific point (0.4 m^3/sec, threshold), and slowly becomes moderate, especially for the small sized fish. This variation shows that a small decrement in discharge, results to a noticeable decrement in the WUA also, which will affect the suitable habitat for the selected species. In Table 2 the habitat assessment results are expressed as WUA values.

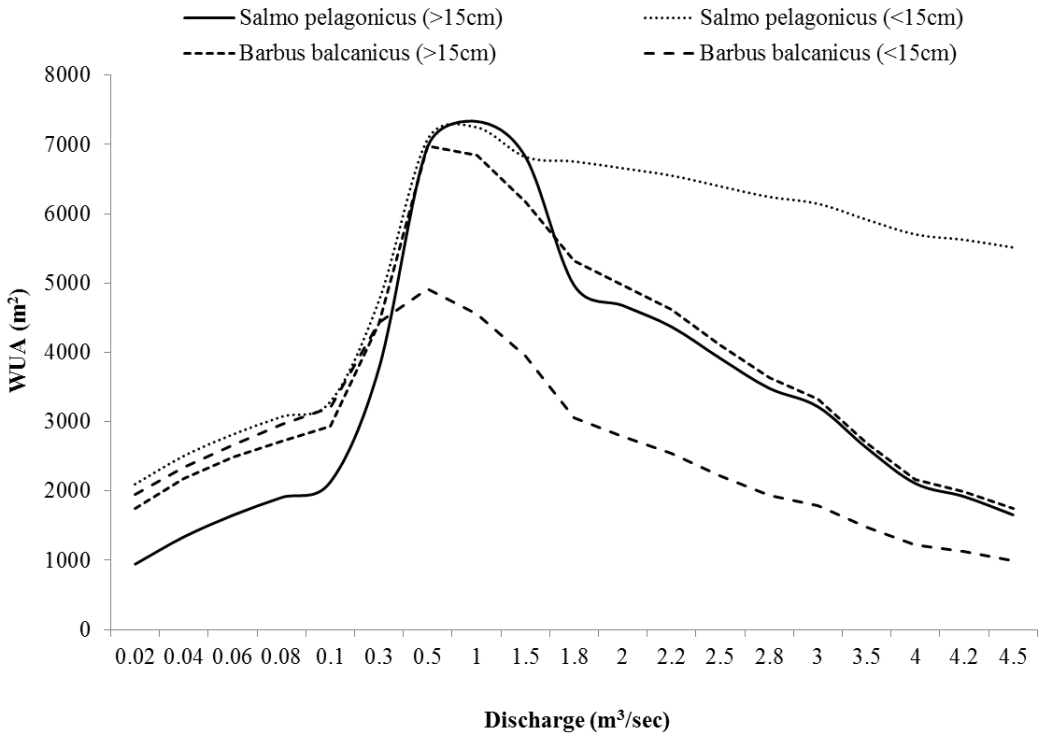

Figure 5. WUA-discharge relationship

The minimum environmental flow that minimise habitat losses for dry period conditions, was estimated according to Table 2 (0.5 m^3/sec).

Table 2. WUA values for two size classes of Salmo pelagonicus and Barbus balcanicus over a range of possible flows under summer conditions for the specific study site.

	Discharge (m^3/sec)																		
WUA	**0.02**	**0.04**	**0.06**	**0.08**	**0.1**	**0.3**	**0.5**	**1**	**1.5**	**1.8**	**2**	**2.2**	**2.5**	**2.8**	**3**	**3.5**	**4**	**4.2**	**4.5**
Salmo pelagonicus (>15cm)	945	1340	1651	1907	2130	3779	**6976**	7334	6825	4968	4677	4369	3914	3483	3217	2622	2110	1920	1657
Salmo pelagonicus (<15cm)	1746	2182	2486	2721	2931	4416	**6980**	6849	6171	5320	4973	4620	4112	3629	3332	2693	2173	1990	1744
Barbus balcanicus (>15cm)	2095	2503	2812	3069	3285	4749	**7082**	7248	6820	6755	6657	6550	6395	6243	6145	5913	5700	5624	5513
Barbus balcanicus (<15cm)	1955	2341	2663	2960	3207	4428	**4923**	4553	3950	3061	2793	2548	2221	1943	1787	1474	1224	1128	992
minimun WUA	945	1340	1651	1907	2130	3779	**4923**	4553	3950	3061	2793	2548	2221	1943	1787	1474	1224	1128	992

4. CONCLUSIONS

The present study indicated that the two investigated fish species have different habitat preferences, i.e. large sized *Salmo pelagonicus* abundances peaked at higher velocities and water depths than the small sized. The small sized *Barbus balcanicus* were spatially and temporally more dynamic, occupying habitats within relatively wider ranges of depth conditions than the large ones.

Fish habitat simulation methods can set operational benchmarks for flow and water level conditions during the most stressful seasonal period in Mediterranean Mountain Rivers. In this study, a minimum flow criterion could be set based on a threshold point, which in this case is the discharge value of 0.5 m^3/sec, under which the WUA decreases rapidly. Nevertheless, aquatic species have variable preferences at their life stages, and to set a constant minimum environmental flow for the whole year may lead to degradation of their habitats. Therefore minimum environmental flows should be used in conjunction with other techniques, which together produce a recommended environmental flow regime.

REFERENCES

Alcaraz-Hernández, J.D., Martínez-Capel, F., Peredo-Parada, M. and Hernández-Mascarell, A.B., 2011. Mesohabitat heterogeneity in four mediterranean streams of the Jucar river basin Eastern Spain. Limnetica, 30, 363–378.Copp, G.H., Garner, P., 1995. Evaluating the microhabitat use of fresh-water fish larvae and juveniles with point abundance sampling by electrofishing. Folia Zool. 44, 145–158.

Benjankar, R., Tonina, D. & Mckean, J., 2015. One-dimensional and two-dimensional hydrodynamic modeling derived flow properties: Impacts on aquatic habitat quality predictions. Earth Surface Processes and Landforms 40 (3): 340–356 doi: 10.1002/esp.3637.

Bisson, P.A., Nielsen, J.L., Palmason, R.A. & Grove, L.E., 1982. A system of naming habitat types in small streams, with examples of habitat utilisation by salmonids during low stream flow. Acquisition and Utilisation of Aquatic Habitat Information, 62-73. Western Division of the American Fisheries Society, Portland, OR.

Bovee, K. D., 1978. The incremental method of assessing habitat potential for coolwater species, with management implications. American Fisheries Society Special Publication. 11: 340-3. Report 85(6):1–393.

Bovee, K. D., 1982. A guide to stream habitat analysis using the Instream Flow Incremental Methodology. Instream Flow Information Paper 12. U.S.D.I. Fish and Wildlife Service, Office of Biological Services. FWS/OBS-82/26. 248 pp.

Bovee, K. D., 1986. Development and evaluation of habitat suitability criteria for use in the instream flow incremental methodology. Instream Flow Information Paper 21, U.S. Fish and Wildlife Service Biological Report 86(7):1–235.

Bovee, K.D., Lamb B.L., Bartholow J.M., Stalnaker, C.B., Taylor, J., Henriksen, J., 1998. Stream Habitat Analysis Using the Instream Flow Incremental Methodology. U. S. Geological Survey, Biological Resources Division Information and Technology Report USGS/BRD-1998-0004. VIII. Fort Collins, CO.

Boyraz, U. & Kazezyılmaz-Alhan, C.M., 2014. An investigation on the effect of geometric shape of streams on stream/ground water interactions and ground water flow. Hydrology Research 45 (4-5): 575 doi: 10.2166/nh.2013.057

Brown, S. K., K. R. Buja, S. H. Jury, M. E. Monaco, and A. Banner. 2000. Habitat suitability index models for eight fish and invertebrate species in Casco and Sheepscot bays, Maine. N AM J FISH MANAGE; 20:408–435.

Chaudhry, M. H., 2008. Open Channel Flow, 2nd edition, Springer.

Christelis, V., Bellos, V., Tsakiris, G., 2016. Employing surrogate modelling for the calibration of a 2D flood simulation model. Proceedings of 4th IAHR Congress, 'Sustainable Hydraulics in the Era of Global Change', edited by S. Erpicum, B. Dewals, P.

Archambeau, M. Pirotton, Liege, Belgium: 727-732.
Copp, G. H. and Garner, P., 1995. Evaluating microhabitat use of fish larvae and juveniles with Point Abundance Sampling. Folia Zool. 44: 145-158
Goldberg, D. E., 1989. Genetic Algorithms in Search, Optimization & Machine Learning, Addison-Wesley.
Greco, M., 2015. Effect of bed roughness on grain-size distribution in an open channel flow. Hydrol. Res.; 46 (1): 1–10; doi: 10.2166/nh.2013.122
Guinot, V., and Cappelaere, B., 2009. Sensitivity analysis of 2D steady-state shallow water flow. Application to free surface model calibration. Advances in Water Resources, 32(4), 540-560.
Jarrett, R., 1985. Determination of roughness coefficients for streams in Colorado; Water Resources Investigation Report; 85-4004, US Geological Survey.
Nikghalb, S., Shokoohi, A., Singh, V.P., Yu, R., 2016. Ecological Regime versus Minimum Environmental Flow:Comparison of Results for a River in a Semi Mediterranean Region. Water Resour. Manag. 30, 4969–4984. doi:10.1007/s11269-016-1488-2
Papadaki, Ch., Ntoanidis, L., Zogaris, S., Martinez-Capel, F., Mũnoz-Mas, R., Evelpidou, N., Dimitriou, E., 2014. Habitat hydraulic modelling forenvironmental flow restoration in upland streams in Greece. In: 12thInternational Conference on Protection and Restoration of the Environment;,Skiathos island, (Greece).
Papadaki, Ch., Bellos, V., Ntoanidis, L., Dimitriou, E., 2016. Comparison of West Balkan adult trout habitat predictions using a Pseudo-2D and a 2D hydrodynamic model; Hydrol. Res.; 1–13. doi:10.2166/nh.2016.352
Terrell, J. W., 1984. Proceedings of a workshop on fish habitat suitability index models. U.S. Fish and Wildlife Service Biological
Vadas, R.L., Orth, D. J., 2001. Formulation of Habitat Suitability Models for Stream Fish Guilds: Do the Standard Methods Work? T Am Fish Soc; 130 (2): 217–235; doi: 10.1577/1548-8659(2001)130<0217:FOHSMF>2.0.CO;2
Vardakas, L., Kalogianni, E., Papadaki, C., Vavalidis, T., Mentzafou, A., Koutsoubas, D., Skoulikidis Th., N., 2017. Defining critical habitat conditions for the conservation of three endemic and endangered cyprinids in a Mediterranean intermittent river before the onset of drought. Aquat. Conserv. Mar. Freshw. Ecosyst. 1–11. doi:10.1002/aqc.2735

Proceedings of the 10th World Congress of EWRA 'Panta Rhei', 5-9 July 2017, Athens, Greece
© 2017 *European Water Resources Association*

Simulation of organics and nitrogen removal from wastewater in constructed wetland

M. Taheriyoun[1] and M. Rad[2]
Department of Civil Enigineering, Isfahan University of Technology, Iran
[*] *e-mail: m.taheriyoun@gmail.com*

Abstract: Modelling wastewater treatment processes is an effective tool for prediction and analysis of treatment system performance. In this study, removal of organics and nitrogen compounds of municipal wastewater is simulated in a constructed wetland based on system dynamic approach using Stella software. In the developed model, organics are represented by BOD and nitrogen compounds including nitrate, ammonia and organic nitrogen. Removal mechanisms for BOD include microbial degradation, plant absorption, and sedimentation. The mechanisms for nitrogen removal are denitrification, sedimentation and plant absorption. The model was calibrated and validated for a horizontal subsurface flow wetland in Arundel mills, Maryland based on 24 data gathered biweekly during one year. An acceptable R2 and Nash– Sutcliffe coefficient of efficiency between the simulated and observed concentration values were obtained which provides a reliable tool in operation and management of the specified wetland in this case study. Based on the results of the model, overall BOD removal consists of 43% for the share of microbial degradation, 27% plant absorption and 30% for sedimentation. Also from the overall nitrogen removal, the share of sedimentation for organic nitrogen is 22%, plant absorption 14% and denitrification is 45%. According to the results, the developed model can be efficiently used in prediction, design and operation of constructed wetland.

Key words: Constructed wetland, wastewater treatment, System dynamic model, organics, nitrogen

1. INTRODUCTION

Constructed wetlands (CWs) are artificial wastewater treatment systems designed to remove pollutants from contaminated water using natural processes. These systems have developed rapidly over the past decades, and CWs are now recognized as an alternative to conventional mechanical treatment systems in small communities. They offer low operation and maintenance costs since no mechanical components or external energy supply is required. (Vymazal, 2011).

Modeling the treatment process is an effective tool in design and operation of these systems rather than spending a lot of time and cost to gather and analyze the experimental data. The models used for CWs are categorized in two groups: black box model and process models. Black box models are called as data driven model that can be trained and tested for a set of data, but process models consider the cause and effect analysis in the processes that occur in a treatment unit.

System dynamics (SD) is an object-oriented simulation method based on feedback. In addition to its ability to discuss the complex systems, it offers the user with the possibility of intervention in model development which provides the user confidence. The simplicity in model change and the ability of sensitivity analysis are the advantages of this method in comparison with the other methods.

CWs are complex systems that function according to a set of interrelated removal mechanisms such as absorption, biodegradation and sedimentation. One of the main functions of CWs is the removal of organics and nitrogen compounds from wastewater. SD has great abilities in prediction of dynamic behavior of a system and survey the share of each effective process in total removal of pollutants. Thus, in this study, this approach is used to simulate the removal process of organics and nitrogen in a horizontal subsurface CW. SD has been applied to model wetland systems by a number of researchers.

Pimpan & Jindal (2008) developed a mathematical model for the cadmium removal process in

the free water surface (FWS) CWs using STELLA software as SD model tool. The concluded that the developed model could be used to explain the cadmium removal process in the FWS constructed wetland.

Wynn & Liehr (2001) modeled a subsurface-flow constructed wetland. The model consists of six submodels, including the nitrogen and carbon cycles, both autotrophic and heterotrophic bacteria growth and metabolism, and water and oxygen balances. The main problem in this work was that too many processes and components were considered in the model with very little data.

Wang et al. (2012) applied a system dynamic simulation model for free-water surface constructed wetlands , the major parameters that affect the simulation output was obtained via sensitivity analysis by using generalized likelihood uncertainty estimation (GLUE). The model was able to simulate the variations of DO, BOD5, and TSS, TN and TP.

Galanopoulos and Lyberatos (2016) used Activated Sludge Model (ASM) methodology to model free water surface CW. The model predicts plant mass and water uptake rate, BOD5 and TN removal on a year round basis. They demonstrated that given inflow, climatic and effluent data, the required surface area to achieve adequate treatment could be determined.

Xuan et al. (2010) applied STELLA software to model nitrogen removal in a subsurface upflow wetland system. The model was calibrated for nitrate, ammonia and organic nitrogen using parameters such as ammonification constant, plant growth rate, plant N content, nitrosomonas growth rate and yield coefficient and denitrification rate.

In this study, SD approach was used to model BOD and nitrogen removal in a horizontal subsurface CW. The modeling approach used in this study is based on the available data and the most possible simple model structure.

2. CASE STUDY

The case study is a horizontal subsurface flow wetland constructed in Arundel mills, Maryland. The data for nitrogen and organics was available from June 1991 to June 1992 including 24 data gathered biweekly during one year. The outflow from a septic tank enters the wetland system for further treatment. The specification of wetland and influent wastewater are indicated in Tables 1 and 2 (Thompson & Liehr, 2001).

Table 1. The case study CW characteristics

Length	Width	Depth	Water depth	Porosity	Mean detention time
70.1m	45.7m	0.8m	0.75m	40%	2days

Table 2. Influent wastewater characteristics

Parameter	Unit	Mean	Standard deviation	Maximum	Minimum
Flow	m^3/d	510	169.5	1000	380
BOD	mg/L$\frac{gr}{m^3}$	17.1	12.6	38.0	2.2
Nitrate	mg/L$\frac{gr}{m^3}$	5.84	1.05	7.94	4.52
Ammonium	mg/L$\frac{gr}{m^3}$	3.76	2.708	9.75	0.00
Organic Nitrogen	mg/L$\frac{gr}{m^3}$	4.44	2.281	8.98	2.27

3. METHODOLOGY

3.1 Simulation of BOD removal process

A conceptual model for BOD removal in the wetland is illustrated in Figure 1. This model

consists of two stocks for dissolved and particulate organic carbon, which are related with hydrolysis process. Other processes consist of carbon removal, microbial degradation, plant absorption and sedimentation.

The assumptions considered in the model are as, the wetland system reacts as a complete mixed reactor, all processes of BOD removal are first order and the processes mostly effective in BOD removal include bacterial degradation, plant absorption and physical process of sedimentation (DeBusk, 1999).

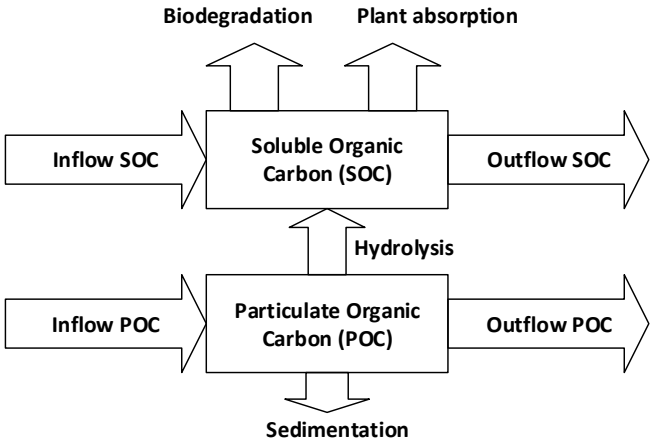

Figure 1. Conceptual model of organic carbon removal

3.2 Simulation of Nitrogen removal process

To develop the model for nitrogen removal, firstly the conceptual model is illustrated in Figure 2. The assumptions used in this model are, wetland reacting as a complete mixed reactor, the only processes that are effective in nitrogen removal include plant absorption and bacterial degradation. Processes such as sedimentation is ignored due to little effect on N removal (Mayo & Bigambo, 2005), all processes follow first order reaction kinetics. As seen in Figure 2 three stocks of organic nitrogen, nitrate and ammonia nitrogen are considered and interrelation between the stock are presented. The models are developed in STELLA software and 12-month data of the case study are input in the model.

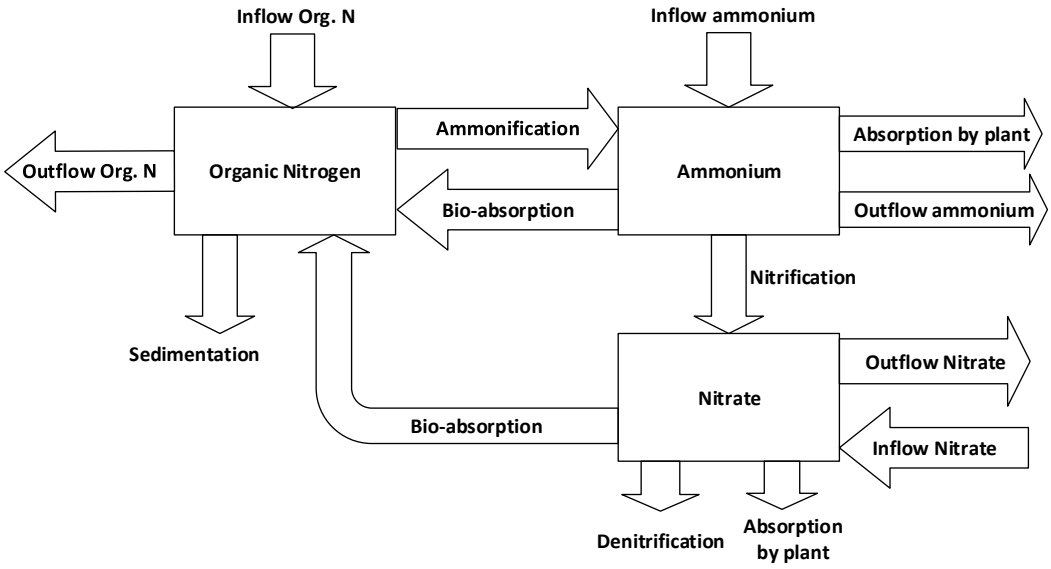

Figure 2. Conceptual model of nitrogen

The performance of each simulation is evaluated by the Nash–Sutcliffe coefficient of efficiency, (Nash and Sutcliffe, 1970), computed as follows:

$$E = 1 - \frac{\sum_{i=1}^{n}(S_i - O_i)^2}{\sum_{i=1}^{n}(O_i - O_{avg})^2} \quad (1)$$

where O_{avg} represents the mean of the observed values, *Si* and *Oi* are the simulated and observed values respectively, and n is the number of values considered. In addition, correlation coefficient R^2 is between simulated and observed data are calculated for further assessment.

To calculate the share of each effective process in BOD and Nitrogen removal in the wetland, the average removal efficiency due to each process is divided by the total average removal of BOD and Nitrogen according to the Eq. (1).

$$S_i = \frac{R_i}{R_T} \times 100 \quad (2)$$

where S_i is the share of process i, R_i average removal efficiency of the process i and R_T is total average annual biweekly removal.

One of the main objectives of modeling is the scenario analysis, which is the process of analyzing possible future events in the system by considering alternative possible outcomes. Scenario building is designed to improve system operation by analyzing the future results from the specified scenarios. In this study, scenarios of different input organic and nitrogen loading into the wetland is considered and the results of their simulation is analyzed.

4. RESULTS

Calibration and validation of models were done for all 24 biweekly data during one-year period. Data are divided into two sets including the first 16 data for calibration and the second 8 data for validation.

Figure 3 illustrates the observed and simulated BOD and nitrogen data for calibration and validation periods. Nash–Sutcliffe (Eq. 1) and correlation coefficients (R^2) are shown in the figures. They demonstrates acceptable agreement between observed and simulated data in both calibration and validation periods.

The share of each effective process in BOD and Nitrogen removal is shown in Figures 4 and 5 according to Eq. 2. Figure 4 indicates that the most effective process in organic removal in the wetland is the microbial degradation. In the removal of total nitrogen, denitrification is the dominant process, which is about 45%, and the absorption by plant has the minimum effect on total N removal in the wetland.

For the scenario analysis, four scenarios are defined based on fluctuation of input load of the wetland. These scenarios include the change of input load in the base scenario (existing condition) multiplied by the factors 0.5, 0.75 as lower level and 1.5 and 2 as upper level. Figure 6 shows the results of scenarios for BOD and TN removal by the wetland system. The graphs show time series of effluent concentration due to base scenario and other four scenarios indicated by the load factors (alpha).

Generally, it can be concluded that the sensitivity of the wetland performance to the change of input load is increased in higher loads, i.e. the sensitivity is maximum in peak concentration and it is minimum after a decline in concentration.

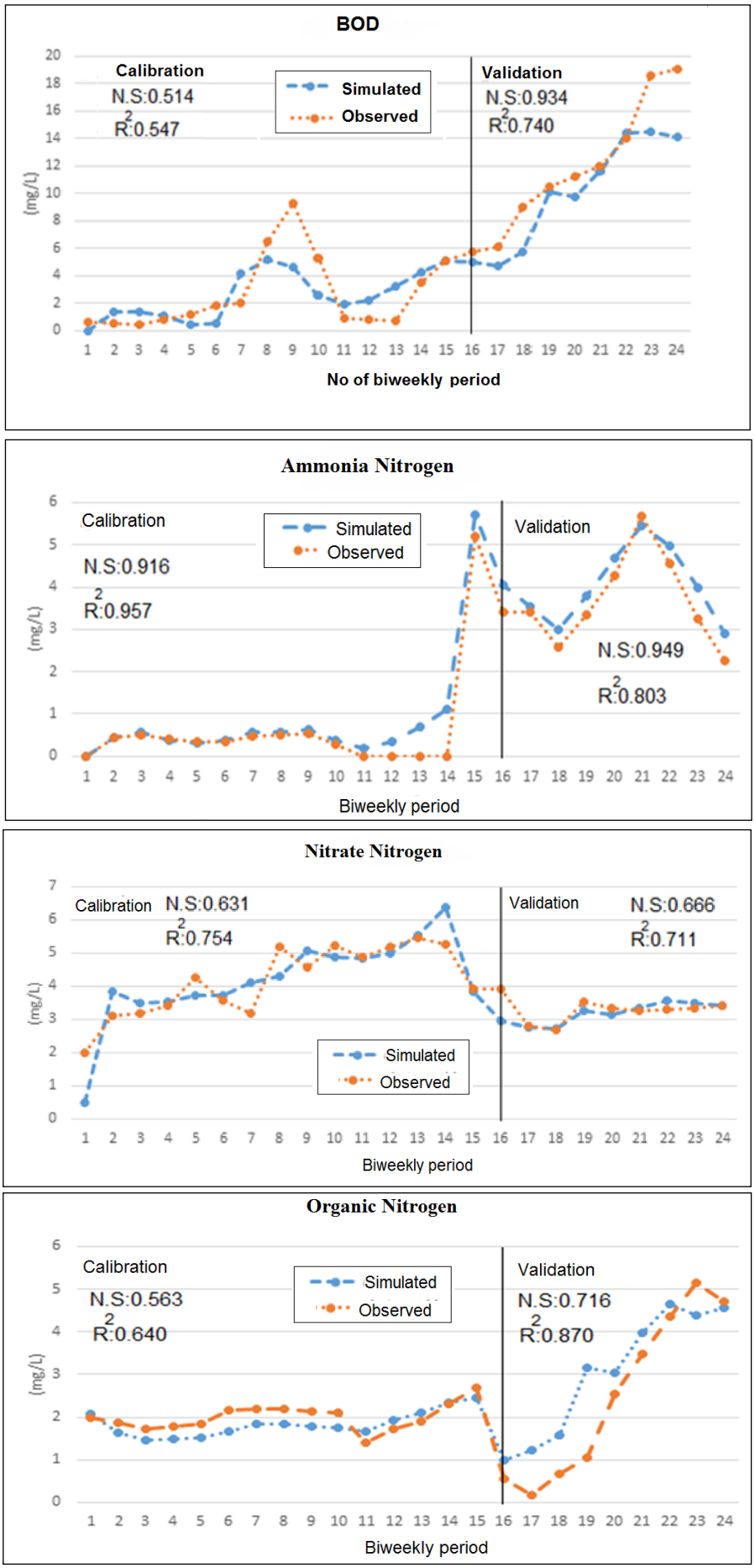

Figure 3. Results of calibration and validation of BOD, Ammonia, Nitrate, Organic Nitrogen

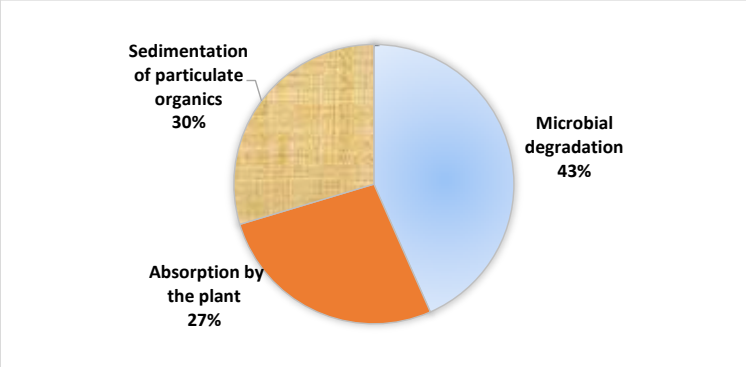

Figure 4. The share of effective processes in BOD reduction

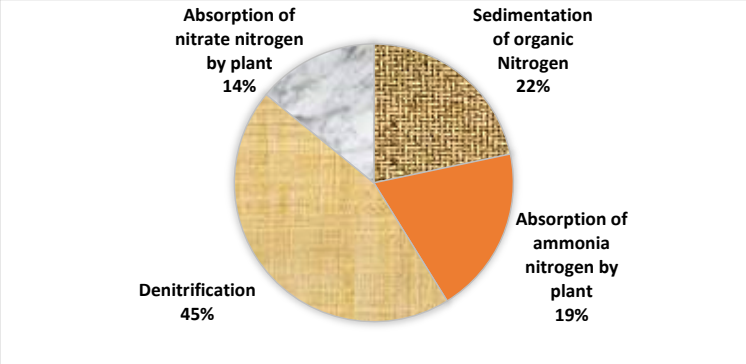

Figure 5. The share of effective processes in total Nitrogen reduction

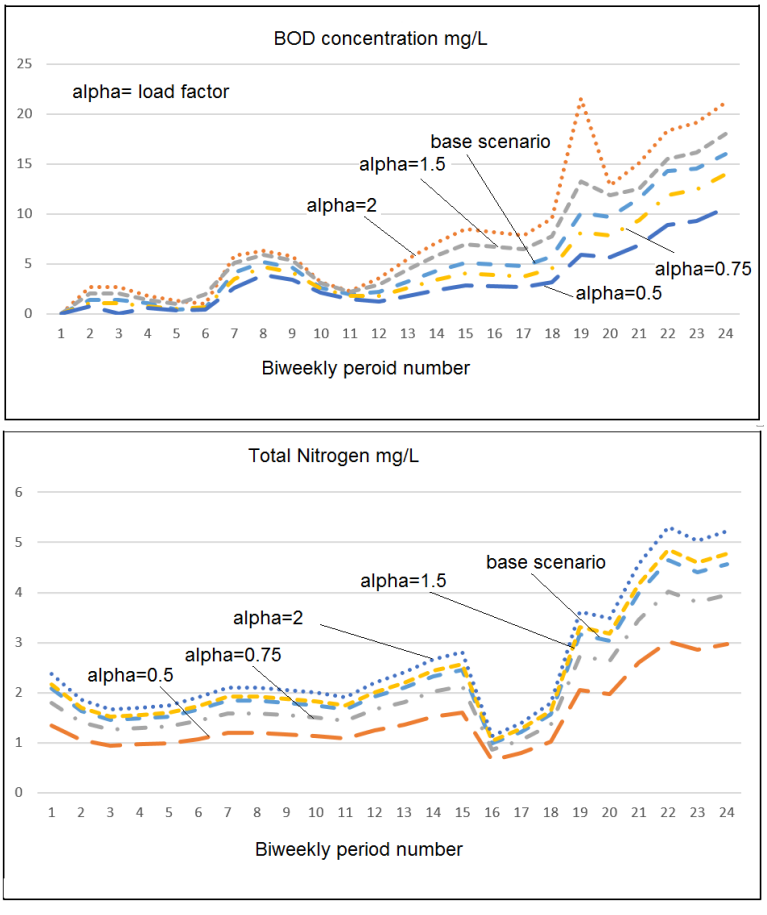

Figure 6. Scenario analysis of different BOD and Nitrogen load input to the wetland

5. CONCLUSION

A system dynamic approach was used to simulate the BOD and nitrogen removal processes in a constructed wetland. Bacterial degradation, plant absorption and physical process of sedimentation were considered as the most effective mechanism in BOD removal. For Nitrogen removal, plant absorption and bacterial degradation were the substantial processes. The model was calibrated and validated for one year biweekly data of a constructed wetland in Maryland, US. To demonstrate the application of the model in the wetland operational analysis, the apportionment of each effective process in organic and nitrogen removal is calculated. The results showed that the most effective process in organic removal is the microbial degradation and in nitrogen removal is denitrification. Scenario analysis showed that the sensitivity of effluent concentration due to the change of input load is maximum in peak concentration and it is minimum after a decline in concentration. Totally, results showed that the developed model is an effective tool in process analysis, prediction, design and operation of constructed wetlands.

REFERENCES

DeBusk William F. (1999). Wastewater Treatment Wetlands Contaminant Removal Processes. University of Florida Cooperative Extension Service, Institute of Food and Agriculture Sciences, EDIS.

Galanopoulos C. and Lyberatos G. (2016), Dynamic modelling and design of free water surface constructed wetland systems, Global NEST Journal, 18(2), 321-328.

Mayo, A. W., and T. Bigambo. (2005). Nitrogen Transformation in Horizontal Subsurface Flow Constructed Wetlands I: Model Development. Physics and Chemistry of the Earth, 658-667.

Pimpan, P., and R. Jindal. (2009). Mathematical Modeling of Cadmium Removal in Free Water Surface Constructed Wetlands. Journal of Hazardous Materials, 163, 1322-1331.

Thompson Wynn, Liehr Sarah (2001). Development of a Constructed Subsurface-flow Wetland Simulation Model. Ecological Engineering, 16(4): 519-536.

Vymazal, J., 2011. Constructed wetlands for wastewater treatment: five decades of experience. Environ. Sci. Technol. 45 (1), 61e69.

Vymazal J, Kropfelova L. (2008) .Wastewater Treatment in Constructed Wetlands with Horizontal Sub-Surface Flow.Springer, Berlin.

Wang Y.-C., Lin Yu-Pin, Huang C. W., Chiang L. C., Chu Hone-Jay, Ou W. S., 2012, A System Dynamic Model and Sensitivity Analysis for Simulating Domestic Pollution Removal in a Free-Water Surface Constructed Wetland, Water Air Soil Pollut 223:2719–2742

Xuan Z., Chang N., Daranpob A. Wanielista M., 2010, Modeling subsurface upflow wetlands systems for wastewater effluent treatment, Environmental engineering Science, 27(10)

Proceedings of the 10th World Congress of EWRA 'Panta Rhei', 5-9 July 2017, Athens, Greece
© 2017 *European Water Resources Association*

Assessing the source of nitrate and heavy metals in groundwater resources of Abarkooh plain, central Iran

M. Meraat[1,2*], H. Jafari[1] and A. Qishlaqi[1]
[1] *School of Geosciences, Shahrood University of Technology, Shahrood, Iran*
[2] *Yazd Science & Technology Park (YSTP), Yazd, Iran*
[*] *e-mail: mmeraat@yahoo.com*

Abstract: Abarkooh alluvial aquifer is located in southwest of Yazd city at the center of Iran. Groundwater is the main source for irrigation and domestic uses, considered as the potential causes of groundwater contamination in this plain. The study was carried out to assess hydrogeochemical properties of groundwater with the aim to find probable sources of major contaminants including nitrate and heavy metals. In this regard 37 water samples were collected and analyzed for major ions (Ca, Mg, Na, K, Cl, HCO_3 and SO_4), nitrate and heavy metals with environmental priority including arsenic (As), lead (Pb) and cadmium (Cd). Values of electrical conductivity (EC) increase from recharge area at the west to the eastern discharging parts where the playa is present. The abundance of cations and anions vary in the order of $Na^+>>Mg^{2+}>Ca^{2+}>Ka^+$ and $Cl^->>SO_4^{2-}>HCO_3^-$, respectively. The highest values of Na and Cl are observed at the east where the saline water intrusion is probable due to the intensive abstraction of groundwater which reverses the flow direction. Pb and Cd is highly correlated with Na, Cl and EC, confirm their geogenic source due to saline water intrusion. Nitrate is high at the west where the un-managed application of fertilizers in agricultural lands is so dominant. A geogenic source for As was proposed based on the results of principal component analysis (PCA). The study confirms the main role of anthropogenic processes in contamination of Abarkooh aquifer generally resulted from over-exploitation of the aquifer and agricultural activities.

Key words: nitrate, heavy metal, geogenic, anthropogenic, Abarkooh, Iran

1. INTRODUCTION

The water is the major key in sustainable development, so it is necessary to be managed and conserved (UNESCO, IHP 2014). In this regard the groundwater resources need more attention especially in arid areas, where the surface waters are not generally available. Chemical composition of groundwater is mainly controlled by natural or geogenic factors (Fig. 1) including chemistry of recharge water, soil processes, aquifer mineralogy, as well as the man-made contaminant (Davidson and Wilson 2011).

Geology of the groundwater basin and the materials in contact with the water, as well as the process and reactions that occur from recharge to discharge points affect the quality of groundwater (Gannon et al. 2011). The chemical quality of groundwater is evolved as the residence time of groundwater in contact with geological materials is increased (Environment Southland, 2010). Agricultural, industrial and mining activities are the main man-made causes threatening or degrading the quality of the aquifers. Irrigation is the main use of water in arid region, known as the major diffuse source of groundwater pollution, as well (Todd and Mays 2005).

Abarkooh plain, located in south west of Yazd province at central Iran, is important for agriculture and industry development. The main activity is agriculture as the irrigated lands cover about 11000 hectare of the plain area. The Alluvial aquifer of Abarkooh is being discharged by 730 wells, 30 qanats and 1 spring with the total discharge annual rate of 178 million cubic meters (Pourab consulting engineers, 2012). The plain groundwater hydrograph shows decrease in water table with an average rate of 0.6 m/year, which is mainly due to reduction in rainfall recharge, as well as, over-exploitation of the aquifer. The mean annual precipitation is 59 mm (Pourab consulting engineers, 2012). Low rate of aquifer recharge and over-drafting the aquifer for

agricultural uses increase the potentials for aquifer contamination. Therefore, this study was aimed to assess the chemical quality of the aquifer and to find probable sources of the contaminant in the groundwater, especially those important from environmental viewpoint such as nitrate and heavy metals.

2. STUDY AREA DESCRIPTION

The study area is located in central Iran, 140 km far from Yazd city (Fig. 2). The alluvial aquifer of the Abarkooh plain is unconfined, which is recharged from the western boundaries. The general groundwater flow direction is from west to the east. The aquifer is surrounded by carbonate rocks in the west and north and evaporate sediments in a playa at the east (Fig. 3).

Exploitation of groundwater mainly for agricultural use changes the flow direction and creates a depression in water table. Concentration of groundwater flow lines toward the depression reverses the flow direction, enhancing the contamination of the aquifer by saline water intrusion.

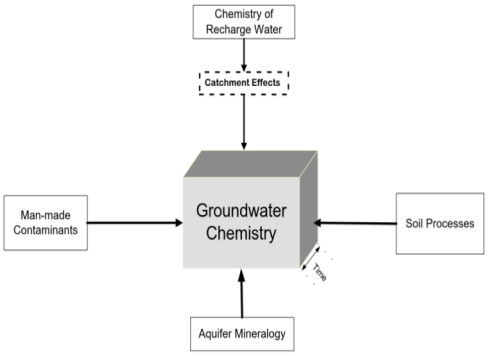

Figure 1. Influences on groundwater chemistry (Davidson and Wilson 2011).



Figure 2. Location of Abarkooh aquifer in Yazd province, central Iran.

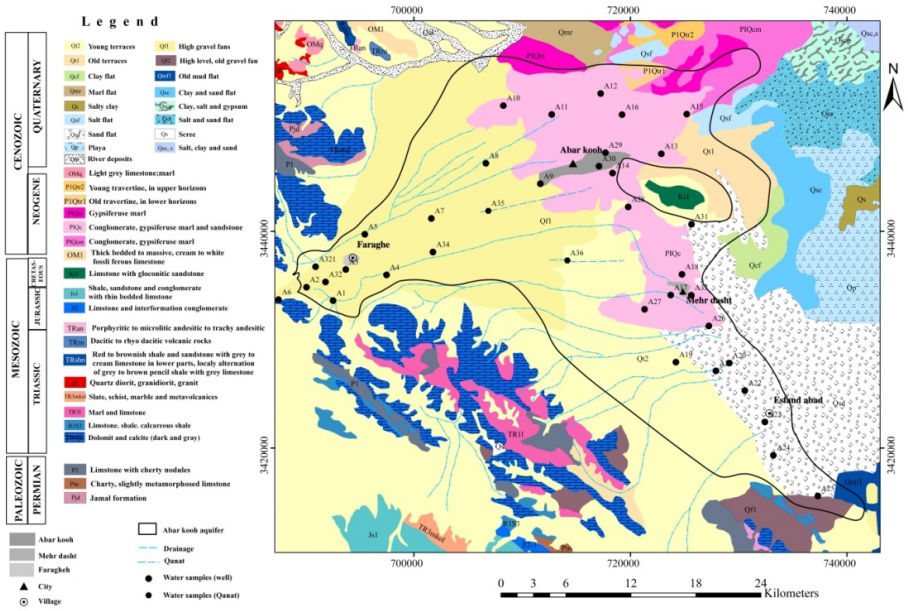

Figure 3. Geological map of the study area representing groundwater sampling locations.

3. MATERIALS AND METHODS

A total of 37 groundwater samples were collected in a systematic random way in April 2016.

Figure 3 shows the location of the sampling points in Abarkooh aquifer. Electrical conductivity (EC) and pH were measured in the field. Two polyethylene bottles were field in each location after they were rinsed with water twice before sampling. The samples for measuring heavy metals were filtered (0.45 µm cellulose filter) and acidified by nitric acid to a pH lower than 2. Sampling and chemical analysis were performed based on APHA (2005). Calcium, magnesium, chloride and bicarbonate were determined by titration, sodium and potassium by flame photometer and sulfate and nitrate by spectrophotometer. Environmental high priority heavy metals including Cd and Pb measured by GF-AAS* and As by HG-AAS†. The accuracy of the chemical analysis was checked by the ion balance approach. The error was less than 5% for most of the samples (80%). In some samples with EC greater than 6000 µs/cm, the calculated error was less than 10%, confirming the accuracy of the analysis (Hounslow 1995; Montcoudiol et al. 2014).

4. RESULTS AND DISCUSSION

4.1 Descriptive analyses and correlation coefficients

A summary of descriptive statistics of the chemical parameters including major ions, nitrate and selected heavy metals is presented in Table 1. Except for pH and nitrate with a normal distribution, the other parameters with skewness greater 1, having abnormal distribution (Montcoudio et al. 2014). So, the correlation coefficients (Table 2) were calculated based on spearman method (Thilagavathi et al. 2012). The highest correlation coefficient was found between Cl, Na and EC, which is significant at the 0.01 level. The lowest one is related to As showing no-dependent on the other parameters.

Table 2. The statistical summary of the hydrochemical parameters in Abarkooh aquifer.

Parameter	Max	Min	Mean	Std. Deviation	Skewness
pH	7.76	6.86	7.32	0.21	0.00
EC µs/cm	15330.00	1192.00	3667.35	3631.78	1.81
TH mg/l	2300.00	325.00	839.05	612.24	1.24
TDS mg/l	7262.60	667.40	1776.56	1637.44	1.83
Cl mg/l	6423.00	199.93	1070.53	1456.14	2.13
SO_4 mg/l	624.01	124.52	249.29	103.61	1.64
HCO_3 mg/l	460.00	84.00	172.65	78.24	2.18
NO_3 mg/l	49.90	5.57	21.69	12.62	0.82
Na mg/l	2990.00	101.20	445.64	619.87	2.58
K mg/l	29.00	3.00	8.31	6.50	2.00
Mg mg/l	488.00	39.04	113.97	101.21	1.96
Ca mg/l	408.81	30.06	140.11	104.99	1.31
As µg/l	12.72	0.38	2.53	2.98	2.46
Cd µg/l	7.20	0.06	0.80	1.65	2.75
Pb µg/l	16.43	0.88	2.56	3.81	2.29

n= 37 samples, TH: as $CaCO_3$

Table 2. Correlation matrix between various parameters in Abarkooh aquifer.

Correlations

			EC	pH	Na	Ca	Mg	K	Cl	SO4	HCO3	NO3	As	Cd	Pb
Spearman's rho	EC	Correlation Coefficient	1.000	-.391*	.848**	.700**	.777**	.729**	.922**	.417*	-.179	.015	-.006	.780**	.681**
		Sig. (2-tailed)	.	.017	.000	.000	.000	.000	.000	.010	.289	.931	.973	.000	.000
		N	37	37	37	37	37	37	37	37	37	37	37	37	37
	pH	Correlation Coefficient	-.391*	1.000	-.300	-.528**	-.331*	-.519**	-.345*	-.385*	-.527**	-.003	-.046	-.532**	-.341*
		Sig. (2-tailed)	.017	.	.071	.001	.045	.001	.036	.019	.001	.985	.788	.001	.039
		N	37	37	37	37	37	37	37	37	37	37	37	37	37
	Na	Correlation Coefficient	.848**	-.300	1.000	.554**	.570**	.678**	.862**	.235	-.137	-.147	.089	.768**	.676**
		Sig. (2-tailed)	.000	.071	.	.000	.000	.000	.000	.162	.420	.385	.598	.000	.000
		N	37	37	37	37	37	37	37	37	37	37	37	37	37
	Ca	Correlation Coefficient	.700**	-.528**	.554**	1.000	.394*	.439**	.507**	.722**	.124	.543**	.125	.719**	.660**
		Sig. (2-tailed)	.000	.001	.000	.	.016	.007	.001	.000	.465	.001	.461	.000	.000
		N	37	37	37	37	37	37	37	37	37	37	37	37	37
	Mg	Correlation Coefficient	.777**	-.331*	.570**	.394*	1.000	.701**	.810**	.224	-.276	-.220	-.060	.651**	.495**
		Sig. (2-tailed)	.000	.045	.000	.016	.	.000	.000	.182	.098	.191	.726	.000	.002
		N	37	37	37	37	37	37	37	37	37	37	37	37	37
	K	Correlation Coefficient	.729**	-.519**	.678**	.439**	.701**	1.000	.764**	.167	-.061	-.313	-.125	.754**	.644**
		Sig. (2-tailed)	.000	.001	.000	.007	.000	.	.000	.324	.721	.059	.462	.000	.000
		N	37	37	37	37	37	37	37	37	37	37	37	37	37
	Cl	Correlation Coefficient	.922**	-.345*	.862**	.507**	.810**	.764**	1.000	.173	-.227	-.264	-.097	.779**	.673**
		Sig. (2-tailed)	.000	.036	.000	.001	.000	.000	.	.306	.176	.114	.568	.000	.000
		N	37	37	37	37	37	37	37	37	37	37	37	37	37
	SO4	Correlation Coefficient	.417*	-.385*	.235	.722**	.224	.167	.173	1.000	.301	.663**	.432**	.287	.216
		Sig. (2-tailed)	.010	.019	.162	.000	.182	.324	.306	.	.070	.000	.008	.085	.199
		N	37	37	37	37	37	37	37	37	37	37	37	37	37
	HCO3	Correlation Coefficient	-.179	-.527**	-.137	.124	-.276	-.061	-.227	.301	1.000	.149	.274	-.073	-.106
		Sig. (2-tailed)	.289	.001	.420	.465	.098	.721	.176	.070	.	.378	.101	.666	.531
		N	37	37	37	37	37	37	37	37	37	37	37	37	37
	NO3	Correlation Coefficient	.015	-.003	-.147	.543**	-.220	-.313	-.264	.663**	.149	1.000	.265	-.083	-.038
		Sig. (2-tailed)	.931	.985	.385	.001	.191	.059	.114	.000	.378	.	.113	.625	.823
		N	37	37	37	37	37	37	37	37	37	37	37	37	37
	As	Correlation Coefficient	-.006	-.046	.089	.125	-.060	-.125	-.097	.432**	.274	.265	1.000	-.062	-.166
		Sig. (2-tailed)	.973	.788	.598	.461	.726	.462	.568	.008	.101	.113	.	.715	.327
		N	37	37	37	37	37	37	37	37	37	37	37	37	37
	Cd	Correlation Coefficient	.780**	-.532**	.768**	.719**	.651**	.754**	.779**	.287	-.073	-.083	-.062	1.000	.872**
		Sig. (2-tailed)	.000	.001	.000	.000	.000	.000	.000	.085	.666	.625	.715	.	.000
		N	37	37	37	37	37	37	37	37	37	37	37	37	37
	Pb	Correlation Coefficient	.681**	-.341*	.676**	.660**	.495**	.644**	.673**	.216	-.106	-.038	-.166	.872**	1.000
		Sig. (2-tailed)	.000	.039	.000	.000	.002	.000	.000	.199	.531	.823	.327	.000	.
		N	37	37	37	37	37	37	37	37	37	37	37	37	37

*. Correlation is significant at the 0.05 level (2-tailed).

**. Correlation is significant at the 0.01 level (2-tailed).

4.2 Splatial variations of pH and EC

The pH of the groundwater samples varies from 6.9 to 7.8, which is in the range (6.5-8.5) for the

* Graphite Furnace-Atomic Absorption Spectrometry
† Hydride Generation-Atomic Absorption Spectrometry

natural waters (Stumm and Morgan 1996; WHO 2011; EPA 2012). Spatial variations of pH in Abarkooh aquifer (Fig. 4) shows the pH values are generally more than 7, due to buffering effects as a result of the high salinity of the groundwater (Isa et al. 2013).

The variations of EC in the Abarkooh aquifer are presented in Figure 4. It ranges from 1000 to 15000 µs/cm with an increasing trend from recharge area at the west to the east where the playa is existed. Iso-potential map of the aquifer (Fig. 8) shows the general groundwater flow direction is from west to the east. A depression in water-table is observed at the east where the discharging wells are concentrated. So, the saline water intrusion is probably occurred at this part of aquifer.

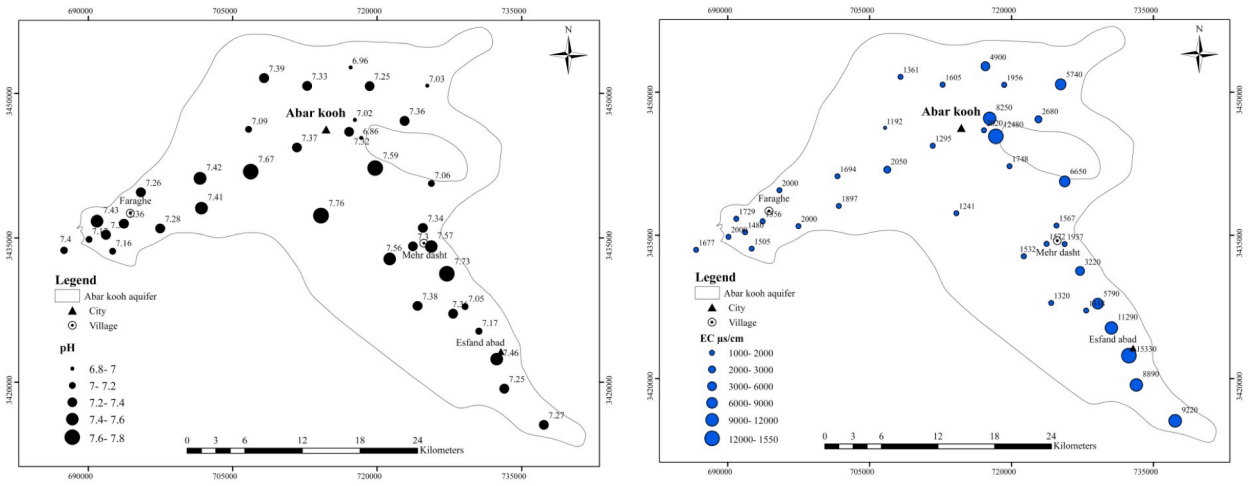

Figure 4. Spatial variations of pH and EC in Abarkooh aquifer.

4.3 Spatial variations of major ions and hydrochemical facies

Figure 5 shows the statistics for major ions analysis. The highest coefficient of variation and standard deviation is observed for Cl^- and Na^+. Concentrations of the major ions follow are ordered as the following sequence: $Cl^- >> SO_4^{2-} > HCO_3^-$, $Na^+ >> Mg^{2+} > Ca^{2+} > Ka^+$.

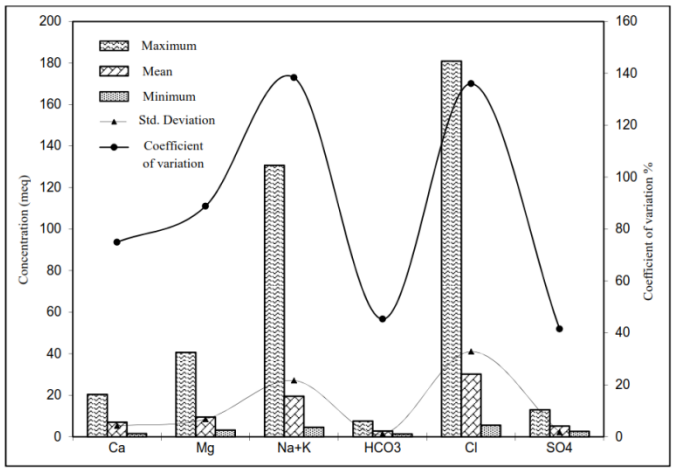

Figure 5. Statistical graph of the major ions analyses in Abarkooh aquifer.

Spatial variations of the dominant ions of Na^+ and Cl^- are displayed in Figure 6. The highest concentrations are observed at the east, where the probable saline water intrusion is occurred. This is in coincidence with the increase in EC, as it was mentioned before.

Plotting chemical analysis on Piper diagram (Fig. 7) confirms the dominant water type is Na-Cl (67% of the water samples). Other water types such as Mg-Cl (22%), Ca-Cl (8%) and Ca-So_4 (3%) are also observed. Distribution of water types in Abarkooh aquifer (Fig. 8) shows change in type of

water as the groundwater flows in the aquifer. The dominant water type at the recharge area at the west is Ca-Cl where the limestone and dolomite rocks are presented (Fig. 3).

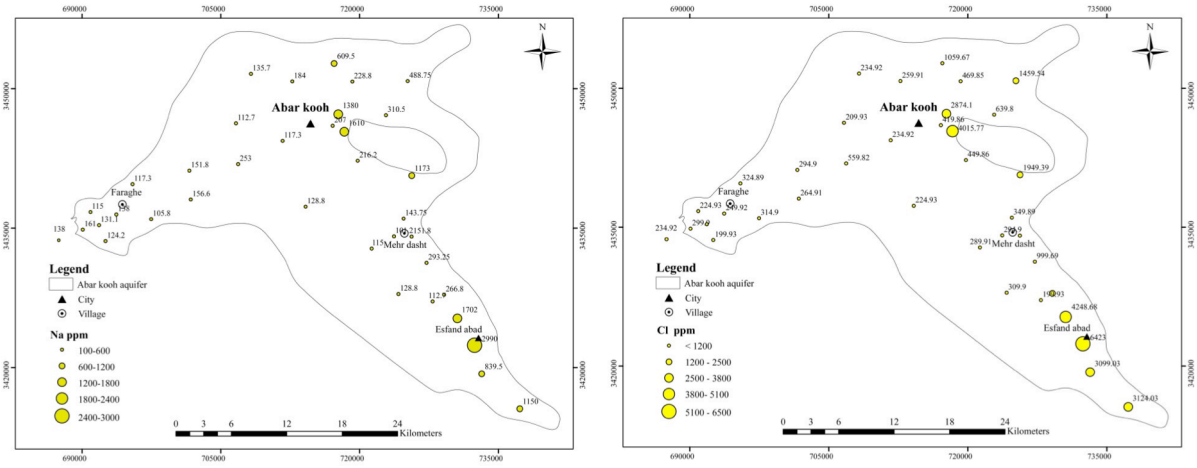

Figure 6. Spatial variations of Na and Cl in Abarkooh aquifer.

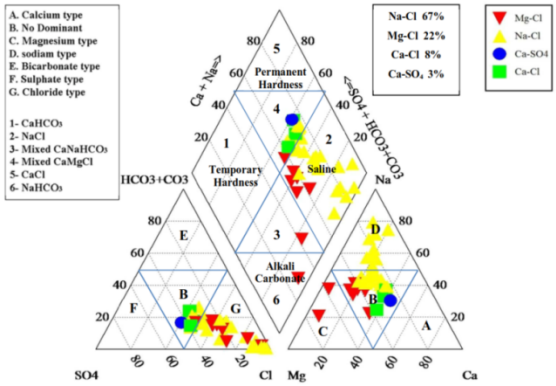

Figure 7. Piper diagram and water type of the groundwater samples from Abarkooh aquifer.

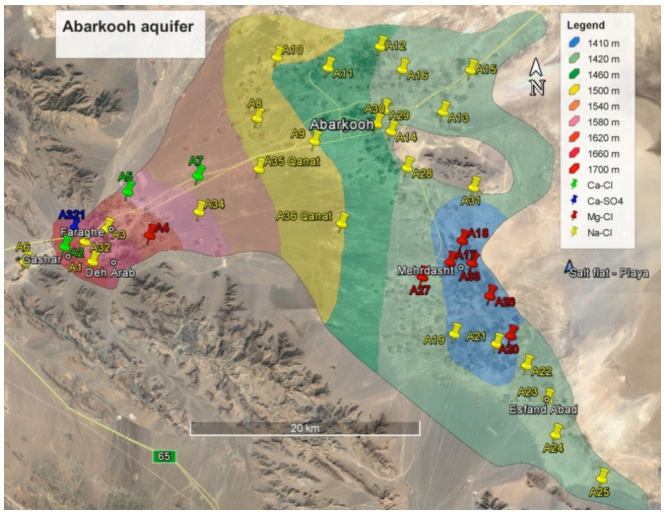

Figure 8. Spatial distribution of water types in Abarkooh aquifer.

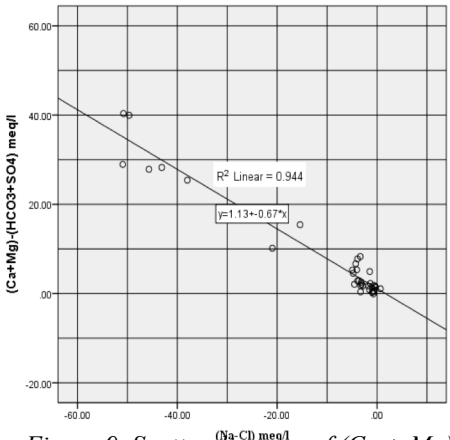

Figure 9. Scatter diagram of (Ca + Mg) – (SO4 + HCO_3) versus (Na – Cl)

The water types change to Na-Cl at the east. The Mg-Cl water types are also presented locally at the east near the Mehrdasht village. This is probably related to ion-exchange process. The scatter diagram Na-Cl versus (Ca+Mg)-(HCO_3+SO_4) in Figure 9 shows most of the samples (about 80%) locate near the zero, confirming the congruent dissolution of calcite, dolomite and gypsum as the likely processes in the Abarkooh aquifer. The other samples are scattered along the line with the

slope of -1, stating occurrence of the ion exchange process in the aquifer (Marie et al. 2001; Tlili-Zrelli et al. 2012).

4.4 Spatial variations of the nitrate ion

Changes in the nitrate concentrations in Abarkooh aquifer are displayed in Figure 10. The nitrate concentrations range from 5.6 to 50 mg/l. The average concentration is about 22 mg/l which is lower than the drinking standard of 50 mg/l (WHO 2011). The natural limit for nitrate is lower than 10 to 15 mg/l (CDPH[‡], 2010) and the values greater suggest the anthropogenic contamination of the groundwater (Multer 1995). More than 85% of groundwater samples from Abarkooh aquifer have nitrate concentrations greater than 10 mg/l as most of them locate at the western part of the aquifer. Lowest depths to water table, coarse grained sediments of the aquifer and development of orchards enhance the potentials for agricultural contaminations in this area. Correlations between nitrate and other ions (Table 2) show the highest coefficient with Ca and SO_4, as these ions are also concentrated in western part of the aquifer.

4.5 Spatial variations of heavy metals

In this study, environmental high priority heavy metals consisting As, Cd and Pb were measured and analyzed. Spatial changes of As in Abarkooh aquifer are illustrated in Figure 11. Arsenic is relatively high at the north-east of the aquifer, where the concentrations exceeding standard limits of 10 ppb (WHO, 2011) in two samples. The concentration of As in fresh non-contaminated waters is usually less than 1 ppb. Increase in water salinity enhances the concentration to about 2-3 ppb. Arsenic concentrations more than 10 to 30 ppb are found in polluted waters by pesticides and fertilizers used in agriculture (Moore and Ramamoorthy 1984).

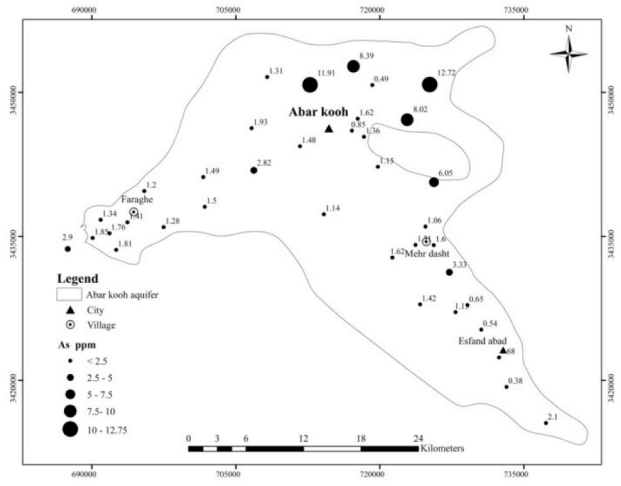

Figure 11. Spatial variations of As in Abarkooh aquifer.

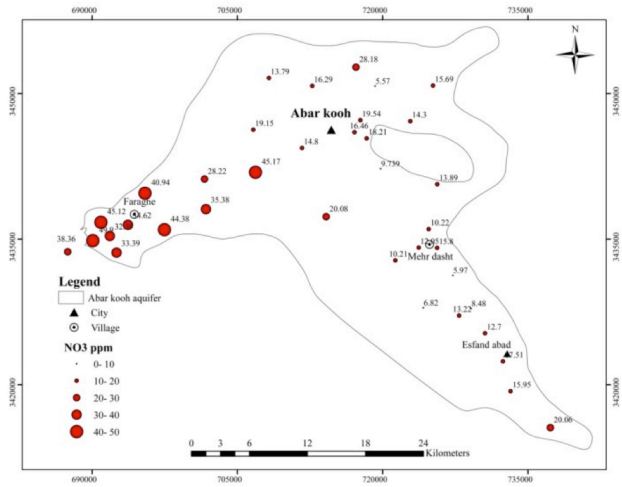

Figure 10. Spatial variations of nitrate in Abarkooh aquifer.

The concentrations of Pb and Cd are more than detection limit of 1 and 0.1 ppb, respectively, in 10 groundwater samples. The spatial changes in concentration of Pb and Cd are presented in Figure 12. A good correlation is found between these two heavy metals, as well as the EC (Fig. 13). The concentrations of Pb and Cd increase more than 5-16 ppb and 1-7 ppb, respectively, at the east and southeast of the aquifer. The concentrations are exceeding MCL of WHO, which is 10 ppb for Pb and 3 ppb for Cd. The increase in concentration of Pb and Cd in this part of the aquifer is probably related to saline water intrusion which is more expectable in this area where the groundwater flow direction is reversed due to the concentrated discharge of the aquifer by the wells.

[‡] The California Department of Public Health (CDPH) regulates nitrate as a drinking water contaminant.

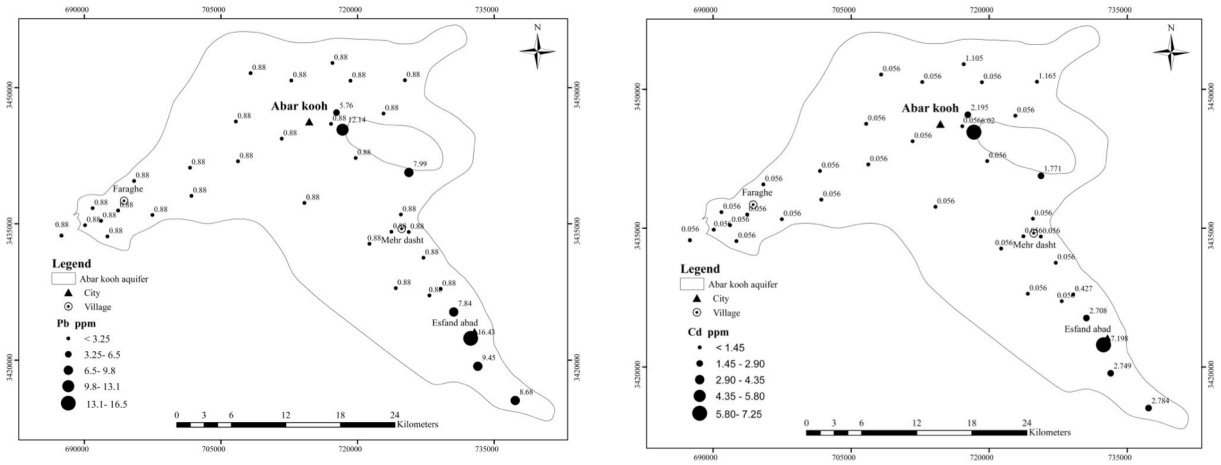

Figure 12. Spatial variations of Pb (left) and Cd (right) in Abarkooh aquifer.

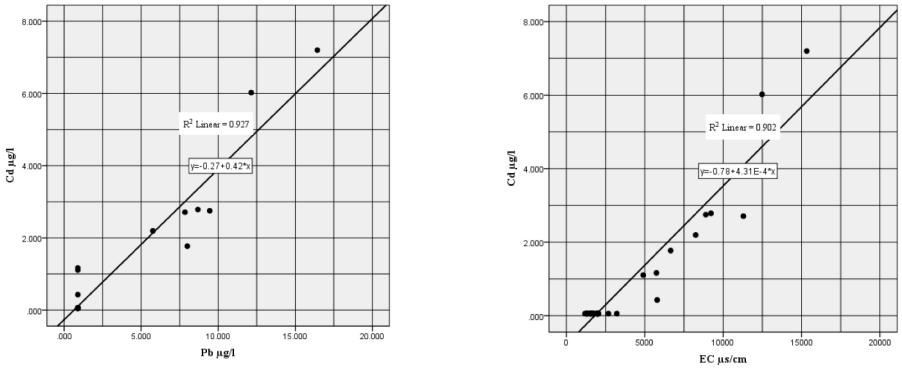

Figure 13. Scatter diagram of Cd versus Pb (left) and EC (right).

4.6. Source of nitrate and heavy metals

In this research principle component analysis (PCA) was performed to identify origin of the elements in groundwater from Abarkooh aquifer. The rotated component matrix by Varimax method (Table 3) shows the parameters classified in 3 main groups (Fig. 14). In each component the parameters with loading rate more than 0.5 are considered (Miller and Miller 2000). The first component with the highest variance is composed of Cl, EC, Na, Ca, Mg, Cd and Pb. This is the main factor enhancing the salinity of the Abarkooh aquifer. As it was mentioned before it is mainly resulted from saline water intrusion which increases the major ions as well as the heavy metals (Pb, Cd) at the east and the southeast of the aquifer. The second component composed of As, HCO_3, SO_4 and pH probably identifies a geogenic source such as dissolution or weathering of pyrite. The process increases the concentration of As, HCO_3 and SO_4 simultaneously. It decreases the pH which is confirmed by the negative loading rate of pH. The third component is only comprised of NO_3 which confirms its anthropogenic source from agricultural activities. The SO_4 with the high loading rate in this component in accordance with the high correlation coefficient between NO_3 and SO_4 (Table 2) confirm the impact of agriculture on enhancement of the contaminants in the groundwater resources.

5. CONCLUSION

Hydrochemical characteristics of Abarkooh aquifer in central Iran show the major role of human impacts on contamination of the groundwater resources. The EC, major ions and heavy metals including Pb and Cd are increased at the east and the southeast where the saline water intrusion is

occurred in response to the over-exploitation of groundwater by deep wells. It reverses the groundwater flow direction, causing intrusion of saline groundwater from playa located outside the aquifer boundary. Based on the results the source of As in the northeast of the aquifer is probably related to the geology. The nitrate ion with highest concentrations at the west of the aquifer is mainly resulted from agricultural activities. The spatial variations of the element which approved by PCA fairly confirm the ideas.

Table 3. Rotated component matrix[a].

parameter	Component		
	1	2	3
EC	.985	.124	-.071
Cl	.986	.003	-.110
SO4	.170	.712	.488
NO3	-.146	.017	.946
HCO3	.041	.731	.031
Na	.951	.037	-.040
Mg	.645	.131	-.312
Ca	.837	.357	.270
As	-.140	.758	-.106
Cd	.964	.072	-.006
Pb	.966	-.029	-.004
pH	-.355	-.721	.012

Extraction method: Principal component analysis.
Rotation method: Varimax with kaiser normalization.[a]
a. Rotation converged in 4 iterations.

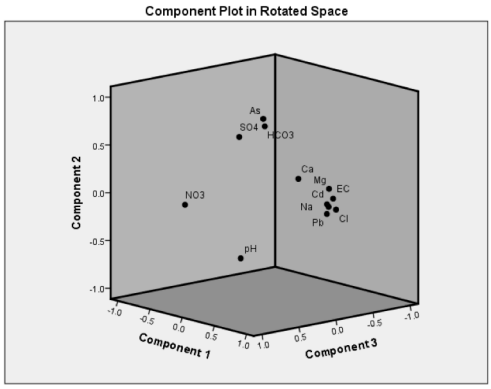

Figure 14. Component plot in rotated space.

ACKNOWLEDGMENTS

This research was financially supported by Shahrood University of Technology and Yazd Science and Technology Park. Their corporations are highly acknowledged.

REFERENCES

Davidson, P., Wilson, S., 2011. Groundwaters of Marlborough. The Caxton Press, Christchurch, New Zealand, Chapter 11, p 94.

Environment Southland, State of the environment: Groundwater quality technical report., 2010. Liquid Earth.

Gannon, John P., Burbey Thomas J., Bodnar Robert J., Aylor Joseph., 2011. Geophysical and geochemical characterization of the groundwater system and the role of chatham fault in groundwater movement at the Coles Hill uranium deposit, Virginia, USA.; Hydrogeology Journal., 2012.

Hounslow, A. W., 1995. Water quality data: analysis and interpretation. Lewis, Boca Raton, FL.

Isa, N. M., Aris. A. Z., Lim, Sulaiman, W. N. A. W., Praveena, S. M., 2013. Evaluation of heavy metal contamination in groundwater samples from Kapas Island, Terengganu, Malaysia. Arab J Geosci.; DOI 10.1007/s12517-012-0818-9.

Marie, A., Vengosh, A., 2001. Sources of salinity in ground water from Jericho area, Jordan Valley. Ground Water.; 39: 240-248.

Miller, N. J., Miller, J.C., 2000. Statistics and chemometrics for analytical chemistry (4th. ed.). Pearson Education: 288.

Mohamed, M. A. Mohamed., Hassane Aissata B., 2016. Hydrochemistry assessment of groundwater quality in Al-Ain city, UAE. Environ Earth Sci, 75:353.

Montcoudiol, N., Molson, J., 2014. Groundwater geochemistry of the Outaouais Region (Québec, Canada): a regional-scale study. Hydrogeology Journal.; DOI 10.1007/s10040-014-1190-5.

Moore, J. W., Ramamoorthy, S., 1984. Heavy metals in natural waters. Applied monitoring and impact assessment. Springer-Verlag New York Berlin Heidelberg Tokyo.; ISBN-13: 978-1-4612-9739-0

Mueller, David K., Hamilton, Pixie A., Helsel, Dennis R., Hitt, KerieJ., and Barbara C Ruddy., 1995. Nutrients in ground water and surface water of the United States—An Analysis of Data Through 1992. U.S. Geological Survey Water Resources Investigations Report 95-4031.

Pourab Consulting Engineers., 2012. Quality and quantity of groundwater models in study area of Abarkooh. Geological and hydrogeological reports, Yazd Regional Water Authority, Yazd, Iran.

Stumm, W., Morgan, J. J., 1996. Aquatic chemistry: chemical equilibria and rates in natural waters. 3rd edn. Willey, New York.

Thilagavathi, R., Chidambaram, S., Prasanna, M. V., Thivya, C., Singaraja, C., 2012. A study on groundwater geochemistry and water quality in layered aquifers system of Pondicherry region, southeast India. Appl Water Sci.; 2:253–269.

Tlili-Zrelli, B., Hamzaoui-Azaza, F., Gueddari, M., Bouhlila, R., 2012. Geochemistry and quality assessment of groundwater using graphical and multivariate statistical methods. A case study: Grombalia phreatic aquifer (Northeastern Tunisia). Arab J Geosci.; 6:3545–3561, DOI 10.1007/s12517-012-0617-3.

Todd, D. K., Mays, L. W., 2005. Groundwater hydrology. Third edition, Wiley.; IBSN 0-471-45254-8 (WIE).

WHO (World Health Organization)., 2011. Guidelines for Drinking water Quality.; 1:4rd edition.

Zandaryaa, S., 2014. Water in the post-2015 development agenda and sustainable development goals. International Hydrological Programme (IHP), UNESCO.

Proceedings of the 10th World Congress of EWRA 'Panta Rhei', 5-9 July 2017, Athens, Greece
© 2017 *European Water Resources Association*

Case studies investigating hydraulic parameters in full-scale constructed wetlands

V.G. Ioannidou* and J.M. Pearson
School of Engineering, University of Warwick, Coventry, CV4 7AL, UK
* *e-mail: v.ioannidou@warwick.ac.uk*

Abstract: Constructed wetlands and ponds are increasingly used worldwide for purifying various types of water effluents. The lack of current knowledge on how efficient they are hydraulically and how to maximise their efficiency is still a challenge. As water movement plays key role in the pollutants mitigation, understanding of the hydrodynamic processes and factors related to pollutants removal would improve the estimation of mixing coefficients, influence of vegetation, and system design. The majority of previous research investigating the effects of wetlands' hydrodynamics on mixing and pollutants removal rates, has been conducted either in pilot-scale units under controlled conditions or via computer simulations, which might introduce uncertainties in the establishment of rules, the prediction of coefficients, and in modelling. Empirical data obtained from full-scale studies are required to quantify the effects of hydrodynamic factors on mixing processes and hydraulic performance during a season. This paper presents results from tracer tests conducted during 2015-2016 in six full-scale systems in the UK under different flow regimes, water depths, and in-/outlet conditions. The aim is to quantify their hydraulic performance and mixing characteristics, trying to open the black box. Results indicate that deeper systems controlled from downstream allow for longer residence times and provide greater treatment efficiency, and that retrofitting using baffles in the system significantly improves the hydraulic performance.

Key words: Constructed Wetlands; Full-Scale; Longitudinal Mixing; Residence Time; Fluorescent Tests

1. INTRODUCTION – LITERATURE REVIEW

Within the best management practices (BMP) context, constructed wetlands (CWs) and constructed ponds are increasingly utilized for the treatment of a variety of contaminants, including agricultural, urban and highway runoff, wastewater, mine and other industrial water effluent types. They aim to moderate and control the impact of source and non-point source water pollution, affording environmentally friendly and promising infrastructure (Vymazal & Březinová, 2015). Beyond purification properties, CWs and ponds offer a variety of services, including flood moderation, ecological and recreational use.

The success of CWs in removing a diversity of pollutants is registered and ratified by numerous published studies internationally (most recently, including Diaz et al, 2012; Fia et al, 2013; Lee et al, 2015; Pappalardo et al, 2016; Rossmann et al, 2013; Selvamurugan et al, 2010; Tournebize et al, 2015). Nevertheless, a great deal of research in CWs and ponds has been directed towards treatment processes, i.e. biological and chemical, comparing in-/outgoing concentrations of pollutants. However, this approach treats the systems as black boxes, overlooking the hydraulics and the fact that water flow is the key factor of the overall system performance (Polprasert & Bhattarai, 1985; Kadlec, 1994; Min & Wise, 2009). As such, there has been less research dedicated to the hydraulic performance of systems, to the investigation of vegetation related to hydraulic processes, and to the interdependence between hydraulic and water quality processes, which is intended to be covered in this literature review.

Factors that importantly determine the performance of CWs involve hydrological and meteorological elements (Persson & Wittgren, 2003), and actual system shape (Persson, 2000). It is generally agreed that the hydraulic residence time (HRT) dictates the removal efficacy, and is principally connected to hydrological conditions (Dierberg et al, 2002). Furthermore, Lee et al

(2015) highlighted that rainfall intensity, rainfall depth, and antecedent dry days are critical components in the diffused pollutants removal. The overall hydrodynamics of CWs are highly dependent upon the aspect ratio (A_R), the in-/outlet arrangement, and obstructions appointment and determination, i.e. vegetation, isles etc. (Persson et al, 1999). Importantly, Johannesson et al (2015) noted high dependence between pollutants' retention and CW A_R, recommending higher aspect ratios. Therefore, it is apparent that the hydraulic design of a CW should not be ignored.

Several studies have investigated factors that influence hydraulic performance of CWs and ponds, and have tried to optimise the systems and to provide general design guidelines (Aguwamba, 2006; Bodin et al, 2012; Diaz et al, 2012; German et al, 2005; Holland et al, 2004; Jadhav & Buchberger 1995; Koskiaho, 2003; Persson et al, 1999; Persson, 2000; Somes et al, 1999; Su et al, 2009; Wörman & Kronnäs, 2005). Nevertheless, the majority of the studies was either conducted via simulations, or has neglected vegetation. In order to add further knowledge and rigour on the CW hydrodynamics, studies have been undertaken using empirical data (lab or field), and vegetation (synthetic, dowel, or real) (Chyan et al, 2014; Nepf et al, 1997; Nepf, 1999; Nepf, 2012; Shucksmith, 2008; West, 2016).

This paper presents empirical data obtained in full-scale cells of free-water surface (FWS) CWs and lagoons across the UK, and aims to assemble, contrast and assess results from several case studies. The ultimate objective is to contribute to the current knowledge regarding various hydraulic performance parameters, vegetation, and longitudinal mixing, obtained in full-scale units through the application of tracer tests.

2. METHODOLOGY – EXPERIMENTAL SETUP

2.1 The cases studied

The six full-size studied sites included four CWs and two ponds/lagoons. The topographic map and details of each system are provided in this section. The geometric characteristics, influent type, and location of the systems are summarised in Table 1.

Table 1. Geometric characteristics of the investigated systems, influent type, and location.

	SW1	**SW2**	**NW**	**A-WMTS**	**Control Lagoon** *(Clough Foot)*	**Baffled Lagoon** *(Clough Foot)*
General shape	Trapezium	Trapezium	Trapezium	Rectangular	Rectangular	Rectangular
Length (m)	35	32	30	105	64.5	64.5
Width (m)	10	7	6	40	23.5	23.5
A_R	3.5	4.6	5	2.63	2.74	2.74
Mean water depth (m)	0.2	0.2	0.4	0.5	3.8	3.8
Surface area (m^2)	175	169	121	4,200	1,516	1,516
V_{tot} (m^3)	22.7	21.3	57.0	2,100	5,760	5,760
Vegetation	Phragmites	Phragmites	Phragmites	Phragmites	-	-
Other obstacles	-	-	-	-	-	Baffle Curtains
Influent type	Agricultural Runoff	Agricultural Runoff	Agricultural Runoff	Mine Water	Mine Water	Mine Water
Location	Cambridge	Cambridge	Cambridge	Derbyshire	Yorkshire	Yorkshire

2.2.1 South wetlands, RSPB farm

Two CWs are located in the RSPB farm, Cambridgeshire, and are in-series and connected via a 115m open channel,, with South Wetland 1 (SW1) upstream, and South Wetland 2 (SW2) downstream , as illustrated in Figure 1. Both units are shallow and unbunded, with fully emergent vegetation, Phragmites australis. Flow depends on precipitation.

2.2.2 North wetland, RSPB farm

North Wetland (NW) is located at the north part of the RSPB farm, Cambridgeshire. This is

deep, bunded downstream, with water discharged via a closed pipe (see Figure 2). Flow depends on the seasonal rainfall, and is intermittent. Phragmites australis is the main plant species.

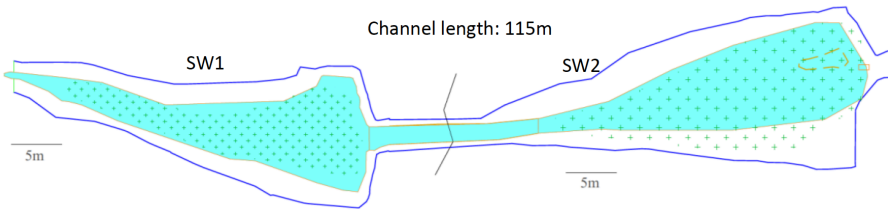

Figure 1. Schematic plan view for the in-series SW1 and SW2.

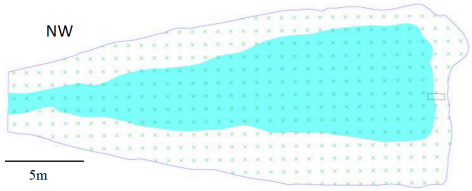

Figure 2. Schematic plan view for NW.

2.2.3 A-WMTS reedbed, Derbyshire

The A-Winning Minewater Treatment Scheme (A-WMTS) is a CW planted with Phragmites, in Derbyshire. It has two inlets, each of which receives water from an upstream lagoon, and two outlets, depicted in Figure 3. Water is pumped at a constant rate, and distributed along the inlet.

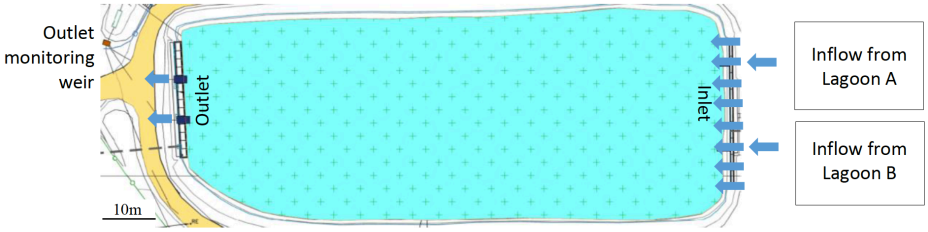

Figure 3. Schematic plan map for A-WMTS.

2.2.4 Clough Foot Lagoons, Yorkshire

Clough Foot minewater treatment scheme (Yorkshire), consists of two identically sized lagoons, operating in parallel arrangement. There is a control, and a baffled system, with the latter having been retrofitted by curtains to enhance lagoon hydraulics. The schematic of the baffled system is shown in Figure 4.

2.3 Hydraulic Tracer Tests

In order to derive residence time distribution (RTD), Rhodamine WT (RWT) was used as tracer, injecting an impulse at the inlet of each system. Fluorescent tracer concentrations were determined at the outlet using Cyclops-7 fluorometers.

2.4 Background on wetland hydraulic theory

Hydrodynamic transport parameters derived from the RTDs analysis are listed in Table 2.

In plug flow theory, it is customary to adopt the theoretical or nominal residence time, t_n. This is denoted as the fraction of wetland volume, V_{tot}, over discharge, Q. However, this basic standard rule

might not fit well in actual wetland conditions, due to: variations in flow velocity, heterogeneous mixing processes (i.e. bed topography and spatial vegetation distribution), and wind interference, all of which create a distribution of residence times in each water particle entering the system, ultimately leading to a distribution of travel times. Such deviations from the ideal pattern cause some water particles to depart earlier or later from the system resulting either in short-circuiting or dead zones (Thackston et al, 1987). The RTD function *E(t)* is defined in:

$$E(t) = \frac{Q(t)C(t)}{\int_0^\infty Q(t)C(t)dt} = \frac{Q(t)C(t)}{\sum_{i=1}^{n} Q(t)C(t)dt} \quad (1)$$

where *E(t)*=RTD function (s^{-1}); *Q(t)*=outlet flow rate at time t (m^3 s^{-1}); *C(t)*=outlet tracer concentration at time t (ppb); *t*=sampling time (s); *dt*=sampling time interval (s).

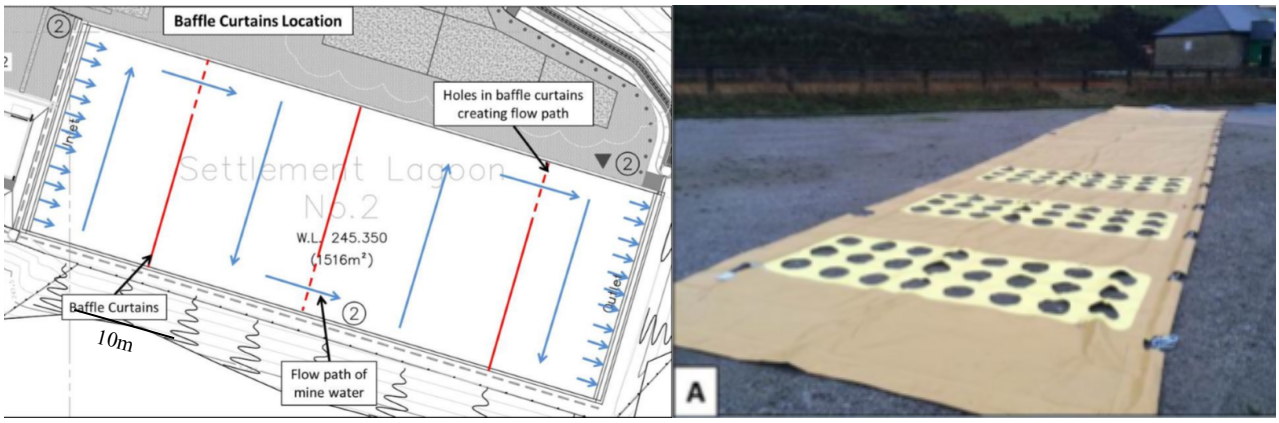

Figure 4. (Left) Clough Foot Baffled Lagoon, indicating curtain locations, orientations and flow path through the lagoon. (Right) Baffle curtains (Taken from Chamberlain & Moorhouse, 2016).

Table 2. Hydrodynamic transport parameters obtained from RTD analyses.

	SW1	**SW2**	**NW**	**A-WMTS**	**Control Lagoon** *(Clough Foot)*	**Baffled Lagoon** *(Clough Foot)*
Q (l/s)	20	20	12	70	25	25
Vegetation configuration	F. EM. (Dec)	F. EM. (Dec)	F. EM. (Dec)	F. EM. (Dec)	No Veg	No Veg
t_1'	7.0 min	8.5 min	39 min	1.97 h	1.4 h	4.2 h
t_{10}	8.7 min	10.3 min	49.4 min	3.3 h	3.0 h	21.1 h
t_1'/t_m	0.60	0.68	0.56	0.31	0.084	0.078
t_{50}/t_n	0.52	0.70	0.79	0.66	0.20	0.75
t_p	10 min	12.0 min	55 min	3.7 h	2.1 h	34.6 h
t_n	34 min	35 min	79 min	8.3 h	64 h	64 h
t_m	11.7 min	12.6 min	70.1 min	6.36 h	16.9 h	53.6 h
u_{mean}	0.047	0.044	0.010	0.0066	0.0011	0.0003
u_{max} (m/s)	0.079	0.065	0.017	0.021	0.013	0.004
σ^2 (h^2)	0.0036	0.0014	0.139	19.4	203.9	835.1
D_x (m^2/s)	0.073	0.023	0.019	0.236	0.025	0.003
$M_o=t_{90}/t_{10}$	1.69	1.40	2.00	5.09	12.45	4.42
Pe	21.2	63.3	19.61	4.17	2.79	6.88
N	10.6	31.64	9.80	2.08	1.40	3.44
V_{eff} (m^3)	17.4	15.4	50.5	1,604	2,258	3,439
e	0.58	0.74	0.89	0.76	0.26	0.84
λ	0.85	0.95	0.78	0.58	0.12	0.64

F. EM = Fully Emergent; No Veg = Unplanted

The mean residence time, t_m, is the average time that a tracer particle stays in the system, defined as the first moment of the RTD, given in:

$$t_m = \int_0^\infty tE(t)dt = \sum_{i=1}^{n} tE(t)dt \quad (2)$$

Variance, σ^2 (s^2), is a measure of the RTD spread and corresponds to the second moment, computed by:

$$\sigma^2 = \int_0^\infty (t_m - t)^2 E(t) dt = \sum_{i=1}^n (t_m - t)^2 E(t) dt \quad (3)$$

The hydraulic efficiency, λ, is a measure of the system's capacity to distribute the flow evenly within the occupying water volume, and also to achieve adequate mixing or recirculation. Persson et al (1999) have classified λ into bands of good (λ>0.75), satisfactory (0.5<λ≤0.75), and poor (λ≤0.50). The λ in this paper was calculated by (Bodin et al, 2012; Chyan et al, 2014):

$$\lambda = \frac{t_p}{t_m} = e \cdot \left(1 - \frac{1}{N}\right) \quad (4)$$

in which t_p=peak concentration time (s) of RTD.

The shortest travel time, t_1', from the inlet to the outlet identifies a common index for short-circuiting. This refers to the quickest flow path in the system and corresponds to the first arrival time of the tracer at the outlet. Another commonly used index is t_{10}, which is the 10th percentile of the tracer having exited the outlet. Two further short-circuiting indices examined were t_{50}/t_n and t_1'/t_m.

3. RESULTS AND DISCUSSION

In this study, four CWs and two lagoons were assessed for their hydrodynamic properties through application of RWT. RTD curves are firstly analysed qualitatively to define the general hydrodynamic trends. Secondly, transport parameters obtained from the RTD analyses are compared (see Table 2). Lastly, discussion and general conclusions and rules are drawn from the empirical data, to add rigour and knowledge in the current operational and design CW/ponds considerations.

3.1 RTD curves

The obtained RTDs from the monitoredtracer concentrations at the outlet of the systems are presented from Figure 5 to Figure 7, allowing assessment of the global flow trends. In particular, there is a strong correlation between the left Figures 5 - 7, suffering from strong short-circuiting. This type of RTD combines *plug flow*, with some *longitudinal mixing* for the long trailing edge according to Danckwerts (1953) . The high short-circuiting in the control lagoon is attributed to the buoyancy effect from water temperature (stratification), where most of the dye was stuck at upper part of the water column, eventually preventing full mixing. The right Figures 5 - 7 indicate lower short-circuiting, higher *e* and greater dispersion, either due to more complete mixing, or due to prolonged tails.

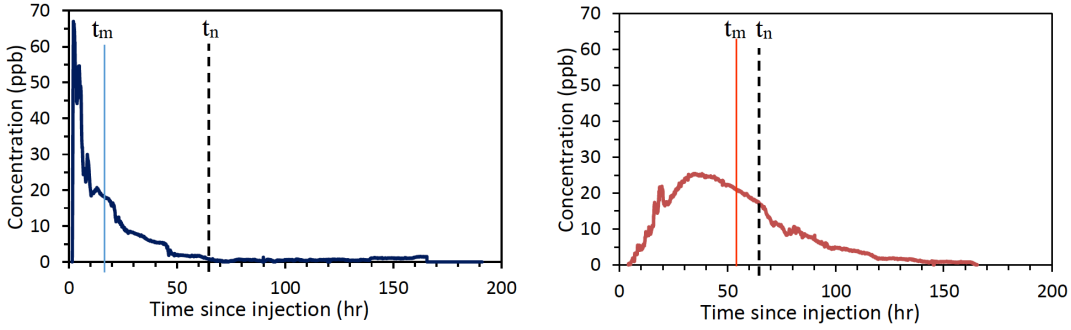

Figure 5. (Left) RTD in control Clough Foot Lagoon; (Right) RTD in baffled Clough Foot Lagoon.

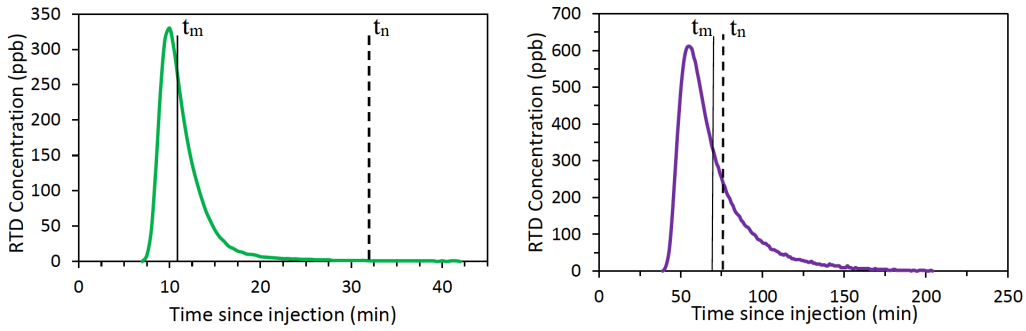

Figure 6. (Left) RTD in SW1; (Right) RTD in NW.

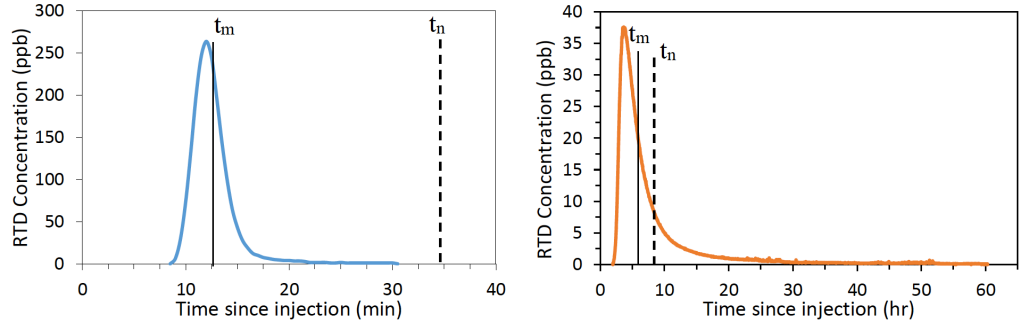

Figure 7. (Left) RTD in SW2; (Right) RTD in A-WMTS.

3.2 HRT, effective volume, hydraulic efficiency

HRT is an indication of the hydraulic performance, where longer HRT entails greater treatment (Dierberg et al, 2002; Lee et al, 2015; Stern et al, 2001; Pappalardo et al, 2016; Tournebize et al, 2016). HRT is dependent on the hydrology (i.e. water depth, flow rate), and hydraulics (i.e. obstructions, i.e. vegetation, and aspect ratio (system shape)) (Johannesson et al, 2015; Kadlec, 1990; Jadhav & Buchberger, 1995).

It is observed that for the same A_R the baffles retrofitting increased λ by 5 times, e by 3 times, and HRT by 7 times. Likewise, Su et al (2009) recommended application of obstructions to enhance λ, if it is poor by construction. The authors furthermore found that the number of obstructions is not so important, as is their width, to enhance λ and reduce internal recirculations. It is recommended that A_R be at least larger than 1.88 to allow for λ>0.7, which despite fulfilling this criterion for all the studied cases, it does not necessarily entail high λ. Furthermore, Su et al (2009) recommend A_R>5 to achieve λ>0.9, case that is observed to apply merely for the NW. The divergence of Su et al's (2009) design recommendations should be dealt only as indicators, mainly because those results were produced through numerical simulations using ideal shapes, and because in reality this is rarely the case.

Good λ is noticed in the baffled lagoon, NW, SW1-SW2. However, by λ definition (Eq. 4, the high λ values obtained for SW1-SW2 are superficial, as the t_p and t_m values are very close to each other (Figure 6, left and right), inducing an erroneous outcome. To avoid seeming information, it would be advisable to consider additionally either e or V_{eff} values, which provide insights into the amount of volume actively used in the system.

3.3 Short-circuiting index

The short-circuiting indices used in this study included t_1', t_{10}, t_1'/t_m and t_{50}/t_n. Greatest short-circuiting was observed in SW1-2 and in the control lagoon. This is instantly observed in left Figures 5 – 7, where the t_n is substantially far from t_m, demonstrating advective flow as dominant pattern. However, NW, of similar shape and dimensions with SW1-2, retains the tracer 6 times

longer, dissipates maximum and mean velocities at least by 5 times, while t_1' is 4-fold. This is particularly attributed to the deeper outlet layout conditions, providing a good reference for design construction.

Investigating the short-circuiting in the two identical lagoons, results suggest that the baffle curtains retrofitting attenuates the short-circuiting at least by 50%. Therefore, it is attested that simple system modifications using berms or baffles of long width can improve radically the short-circuiting.

Comparing between the four estimated indices, it is inferred that t_1'/t_m and t_{50}/t_n do not always represent the actual short-circuit conditions. To the contrary, t_1', t_{10}, showed more consistency and reliability. This is because the values of t_{50} and t_n, and t_1' and t_m are very close to each other in the cases of SW1-2, thus producing erroneously high ratios of t_{50}/t_n and t_1'/t_m respectively. t_{50} is not a pure indicator of preferential paths, as it indicates the 50% percentile of the tracer removed at the outlet and also involves other physical phenomena, such as recirculations and dead regions. Therefore, both ratios do not find universal application to assess short-circuiting.

3.4 Comparative evaluation of the six investigated cases

Considering the highest t_m, the baffled lagoon probably affords the best removal efficiency. However, as its depth is 3.8m, it cannot be regarded suitable for CWs, because by design CWs' operational depth is up to 1m. Nonetheless, the curtains installation is an option that can be implemented in any system to improve internal hydraulics. NW would be deemed the best suited in terms of λ, where the impact of dead zones on removal mechanisms is minimised. This is attributed to the bunded outlet layout. Greater dispersion occurs in the A-WMTS and control lagoon, while advective flow is pronounced in SW2 mainly due the irregular bed topography creating preferential path.

The differences in longitudinal mixing between the systems are further confirmed by the D_x, Pe and mixing index (M_0) values (see Table 2). There is a distinct alteration of flow regime after the baffles installation, with substantial increase of the HRT, effective volume utilisation, and λ.

4. CONCLUSIONS

The present study investigated full-scale case studies of different hydrodynamic properties and design considerations. Although the aspect ratio was similar or larger than what the literature recommends, the hydraulic efficiency and effective volume did not necessarily matched the expected results. Therefore, those design guidelines should yet be used as indicators, as they might not fully apply in reality. Furthermore, some studied cases demonstrated strong correlation in their RTDs and hydraulic performance, behaving like this due to high short-circuiting.

The various sizes and shapes radically influence hydrodynamic features of the systems and thus their removal capacities. Hence, the design of new systems should aim at the optimisation of shape, outlet conditions, and vegetation cover, as they all impact on the flow regime and dispersion levels. This could include for example: inlet and outlet layout optimisation, where entering water would be distributed evenly across to allow spread of the polluted inflow, and outlet would be bunded/controlled to secure longer HRTs and greater hydraulic efficiency. For existing systems, retrofitting using obstacles would be an approved option to enhance hydraulic performance.

ACKNOWLEDGEMENTS

The work has been financially supported by the School of Engineering, University of Warwick, through a PhD scholarship for V. Ioannidou. The authors gratefully acknowledge the RSPB Hope Farm staff invaluable support, kind collaboration, and permission to access their wetlands; The Coal Authority staff for their productive collaboration, and access to their facilities in Derbyshire and Yorkshire; the technical support from Ian Baylis in the School of Engineering; the kind

collaboration and Venturi flumes supply from Dr Whelan, Leicester University.

REFERENCES

Agunwamba, J.C. (2006). Effect of the location of the inlet and outlet structures on short-circuiting: Experimental investigation. Water environment research, 78(6), 580-589.

Bodin, H., Mietto, A., Ehde, P.M., Persson, J. & Weisner, S.E.B. (2012). Tracer behaviour and analysis of hydraulics in experimental free water surface wetlands. Ecological Engineering, 49, 201-211.

Chyan, J. M., Tan, F. J., Chen, I. M., Lin, C. J., Senoro, D. B., & Luna, M. P. C. (2014). Effects of porosity on flow of free water surface constructed wetland in a physical model. Desalination and Water Treatment, 52(4-6), 1077-1085.

Danckwerts, P.V. (1953). Continuous flow systems: Distribution of residence times. Chemical Engineering Science, 2(1), 1-13.

Diaz, F.J., O'Geen, A.T., Dahlgren, R.A. (2012). Agricultural pollutant removal by constructed wetlands: Implications for water management and design. Agricultural Water Management, 104, 171-183.

Dierberg, F. E., DeBusk, T. A., Jackson, S. D., Chimney, M. J., & Pietro, K. (2002). Submerged aquatic vegetation-based treatment wetlands for removing phosphorus from agricultural runoff: response to hydraulic and nutrient loading. Water research, 36(6), 1409-1422.

Fia, R., de Matos, A. T., & Fia, F. R. L. (2013). Biological systems combined for the treatment of coffee processing wastewater: II-Removal of nutrients and phenolic compounds. Acta Scientiarum. Technology, 35(3), 451-456.

German, J., Jansons, K., Svensson, G., Karlsson, D. & Gustafsson, L. G. (2005). Modelling of different measures for improving removal in a stormwater pond. Water Science & Technology, 52(5), 105-112.

Holland, J.F., Martin, J.F., Granata, T., Bouchard, V., Quigley, M. & Brown, L. (2004). Effects of wetland depth and flow on residence time distribution characteristics. Ecological Engineering, 23, 189-203.

Jadhav, R.S., Buchberger, S.G., 1995. Effects of vegetation on flow through free water surface wetlands. Ecol. Eng. 5, 481–496.

Johannesson, K. M., Kynkäänniemi, P., Ulén, B., Weisner, S. E. B., & Tonderski, K. S. (2015). Phosphorus and particle retention in constructed wetlands - A catchment comparison. Ecological Engineering, 80, 20-31.

Kadlec, R. H. (1990). Overland flow in wetlands: vegetation resistance. Journal of Hydraulic Engineering, 116(5), 691-706.

Kadlec, R.H. (1994). Detention and mixing in free water wetlands. Ecological Engineering, 3, 345-380.

Koskiaho, J. (2003). Flow velocity retardation and sediment retention in two constructed wetland-ponds. Ecol. Eng., 19, 325-337.

Lee, S. H., Cha, S. M., Lee, J. C., & Lee, J. Y. (2015). Performance Evaluation of the Free Water Surface Constructed Wetland Treating Nonpoint Source Pollutants in the Agricultural Area. Journal of Environmental & Analytical Toxicology, 5(4), 1.

Min, J. H. & Wise, R. W., (2009). Simulating short-circuiting flow in a constructed wetland: the implications of bathymetry and vegetation effects. Hydrological Processes, 23, 830-841.

Nepf, H.M., Mugnier, C.G. & Zavistoski, R.A. (1997). The effects of vegetation on longitudinal dispersion. Estuarine, Coastal and Shelf Science, 44, 675-684.

Nepf, H.M. (1999). Drag, turbulence, and diffusion in flow through emergent vegetation. Water Resources Research, 35(2), 479-489.

Nepf, H. M. (2012 a). Hydrodynamics of vegetated channels. Journal of Hydraulic Research, 50(3), 262-279.

Pappalardo, S. E., Otto, S., Gasparini, V., Zanin, G., & Borin, M. (2016). Mitigation of herbicide runoff as an ecosystem service from a constructed surface flow wetland. Hydrobiologia, 774(1), 193-202.

Persson, J., Somes, N.L.G. & Wong, T.H.F. (1999). Hydraulics efficiency of constructed wetlands and ponds. Water Science and Technology, 40(3), 291-300.

Persson, J. (2000). The Hydraulic Performance of Ponds of Various Layouts. Urban Water, 2, 243-250.

Persson, J., & Wittgren, H. B. (2003). How hydrological and hydraulic conditions affect performance of ponds. Ecological Engineering, 21(4), 259-269.

Polprasert, C. & Bhattarai, K.K. (1985). Dispersion model for waste stabilization ponds. Environmental Engineering, 111(1), 45-59.

Rossmann, M., Matos, A. T., Abreu, E. C, Silva, F. F. & Borges, A. C. (2013). Effect of influent aeration on removal of organic matter from coffee processing wastewater in constructed wetlands. Journal of Environmental Management, 128, 912-919.

Rutherford, J.C. (1994). River mixing. Chapter 4, Longitudinal Dispersion. John Wiley & Sons, Inc., Chichester, U.K.

Selvamurugan, M., Doraisamy, P., & Maheswari, M. (2010). An integrated treatment system for coffee processing wastewater using anaerobic and aerobic process. Ecological Engineering, 36(12), 1686-1690.

Shucksmith, J. D. (2008). Impact of vegetation in open channels on flow resistance and solute mixing (Doctoral dissertation, Sheffield).

Somes, N. L. G., Persson, J., & Wong, T. H. F. (1998). Influence of wetland design parameters on the hydrodynamics of stormwater wetlands. Hydrastorm, Adelaide, 27(30), 123-128.

Stern, D.A., Khanbilvardi, R., Alair, J.C. & Richardson, W. (2001). Description of flow through a natural wetland using dye tracer tests. Ecological Engineering, 18, 173-184.

Su, T.M., Yang, S.C., Shih, S.S. & Lee, H.Y. (2009). Optimal design for hydraulic efficiency on free-water-surface constructed wetlands. Ecological Engineering, 35, 1200-1207.

Thackston, E.L., Shields, D. & Schroeder, P.R. (1987). Residence time distributions of shallow basins. Journal of Environmental Engineering, 113(6), 1319-1332.

Tournebize, J., Chaumont, C., Fesneau, C., Guenne, A., Vincent, B., Garnier, J., & Mander, Ü. (2015). Long-term nitrate removal in a buffering pond-reservoir system receiving water from an agricultural drained catchment. Ecological Engineering, 80, 32-45.

Tournebize, J., Chaumont, C., & Mander, Ü. (2016). Implications for constructed wetlands to mitigate nitrate and pesticide pollution in agricultural drained watersheds. Ecological Engineering. In press.

Vymazal, J., & Březinová, T. (2015). The use of constructed wetlands for removal of pesticides from agricultural runoff and drainage: a review. Environment international, 75, 11-20.

West, P. O. (2016). Quantifying solute mixing across low velocity emergent real vegetation shear layers (Doctoral dissertation, University of Warwick).

Wörman, A. & Kronnäs, V. 2005. Effect of pond shape and vegetation heterogeneity on flow and treatment performance of constructed wetlands. Journal of Hydrology, 301, 123–128.

Proceedings of the 10th World Congress of EWRA 'Panta Rhei', 5-9 July 2017, Athens, Greece
© 2017 *European Water Resources Association*

Modelling of nickel dynamics in vertical subsurface flow constructed wetlands using a System Thinking Environment

C. Defo[1*] and R. Kaur[2]
[1] *University of Dschang, Ebolowa Campus, School of Wood, Water and Natural Resources, Ebolowa, Cameroon*
[2] *Indian Agricultural Research Institute, Water Technology Centre, New Delhi, India*
[*] *e-mail: defo1.celestin@yahoo.fr*

Abstract: The application of modelling approaches for simulating and designing of constructed wetlands is still a challenge in environmental science. A mathematical model was developed in STELLA software to simulate Ni dynamics (adsorption, plant uptake and effluent concentrations) from synthetic wastewaters loaded with Ni 0.5 ppm and treated in vertical subsurface flow constructed wetlands vegetated with *Phragmites Karka* on gravel beds. Plant and water samples were collected, pre-treated in the laboratory, digested with diacid and their Ni concentrations were determined using atomic absorption spectrophotometer (AAS), after filtrating the samples on Whatman paper No. 42. A graphical model was developed in STELLA and the data recorded from the experiment were used to calibrate and validate the related mathematical model in the software. Results showed a good agreement between experimental and simulated data indicated by the Wilcoxon Signed Ranks Test p values > 0.05 for Ni adsorbed in gravel, uptake in plant and Ni effluent concentrations. The overall removal analysis showed the following distribution pattern: Experimental data (Total Removal Percentage (%): 84.2; adsorption percentage (%):50.6; plant uptake percentage (%): 33.6). Simulated data (Total Removal Percentage (%): 83.5; adsorption percentage (%): 52.8; plant uptake percentage (%): 30.6). Thus the adsorption played a major role the removal of Ni from wastewater compare to plant uptake and the overall constructed wetland showed its high removal performance in eliminating Ni from wastewater.

Key words: Process-based models, STELLA software, Wilcoxon Signed Ranks Test, Model validation

1. INTRODUCTION

In recent decades, constructed wetland models were developed for predicting their behaviour over extended period of time in wastewater treatment processes. Available constructed wetland models are primarily of two types: black box types and process based models (Kumar and Zhao 2011). Instead of developing relationship between input and output of constructed wetlands as considered in "black-box" approach modelling, process-based models show up the increased understanding of the processes involved in the pollutants transfer in constructed wetlands (Langergraber, 2007, Garcia *et al.,* 2010, Meyer *et al.,* 2015). Kumar and Zhao (2011) further stated that these models can provide insight into the "black-box" and give indulgent information which helps highly for the design purpose. Among the existing models, very few models (in numbers, not in quality) were developed for simulating pollutant dynamics in vertical subsurface flow constructed wetlands. Additionally, most of these models were developed for only assessing nutrient and organic pollutant removal in constructed wetlands. Thus very limited modelling efforts were devoted for the simulation of metal removal dynamics in vertical subsurface flow constructed wetlands. The purpose of this study is to develop a mathematical model in STELLA software to simulate Ni dynamics (adsorption, plant uptake and effluent concentrations) from synthetic wastewaters loaded with Ni 0.5 ppm and treated in vertical subsurface flow constructed wetlands vegetated with *Phragmites Karka* on gravel beds.

2. MATERIALS AND METHODS

In this study, STELLA software was used to simulate nickel removal from artificial wastewater.

STELLA is an object-oriented, graphical modelling environment developed by High Performance Systems, Inc. (HPS) (Bullen et al., 2011) and is specifically functional for highly dynamic and independent systems.

2.1 Experimental set up and data collection

The experimental setup consisted of vertical subsurface flow constructed wetlands (VSSF CW) in form of wetland microcosm (50 litres plastic container) at Indian Agricultural Research Institute, in New Delhi, India. Each wetland microcosms had a cylindrical shape, a diameter of 35 cm and a height equal to 50 cm. The wetland microcosms were filled with gravel (size ranging from 1 to 3 mm for fine gravel and from 5 mm to 25 mm for coarse gravel and a total weight of 60.1 kg per wetland) to a depth of 35 cm and planted with *Phragmites Karka*. These plant species had similar age and height at a spacing of 2-5 cm. The experiment was replicated thrice. To find the relative contribution of vegetation, the unvegetated wetland microcosm (containing only gravel) was also used for each treatment (this time without replication).These microcosms were irrigated with Ni, at one strength (0.5 ppm). The levels of concentrations (low) were designed to mimic their current concentration levels (low) found in sewage water. Solutions containing different concentration levels of Ni were prepared using salts of Ni $(NO_3)_2 \cdot 6H_2O$. The use of nitrates was justified by the fact that these ions do not form ion pair with metal ions. A total of 4 wetland microcosms were used for the whole experiment. Plant and wastewater samples were analysed in the laboratory to determine their Ni content according to standard procedures (digestion with diacid and Ni determination using atomic absorption spectrophotometer after filtration) (Houba et al., 1989).

2.2. Model development

For simulation, the data collected (experimental data on Ni adsorption, plant uptake and effluent) were used to perform linear models which the coefficients (Table 1) were applied as inputs in the STELLA graphical model (Figure 1) to calibrate the developed mathematical model and to produced simulated outputs. Figure 1 illustrates the components of the models (building blocks), connections and influences between stocks, flows and convertors.

The models were run repetitively by adjusting its parameters using trial and error until the simulated and experimental values showed good agreement.

3. RESULTS AND DISCUSSION

3.1 Determination of adsorption and plant uptake coefficients using linear models

3.1.1 Testing of normality of data

To ensure the normality of data trend before development of regression equations, the Shapiro-Wilk test (Razali and Wah, 2011) was performed using the data acquired from experiment. It was observed that the parameter W and p-value obtained from Shapiro-Wilk normality test were 0.957 0.0672, which were close to one and greater than 0.05, respectively. These parameters were well within the adjudged range and corroborated that all datasets followed the normal distribution.

3.1.2 Plant Uptake and gravel adsorption coefficients for Ni in VSSF CWs

It was observed that the p values of different models were < 0.001, for the regression analysis performed (plant uptake and gravel adsorption). The coefficient of determination value (R^2) of the linear model was 0.91. Therefore, these high values of R^2, coupled with positive values of regression coefficients (RC) indicated that there existed a linear relationships between Ni uptake in plant and the Ni influent concentrations. The regression equations developed between the amount of Ni (mg/kg) adsorbed in gravel (predicted variable) and the Ni influent concentration (mg/L) (regressor) showed a good fit between these variables, indicated by $R^2 = 0.72$ for Ni 0.5 ppm.

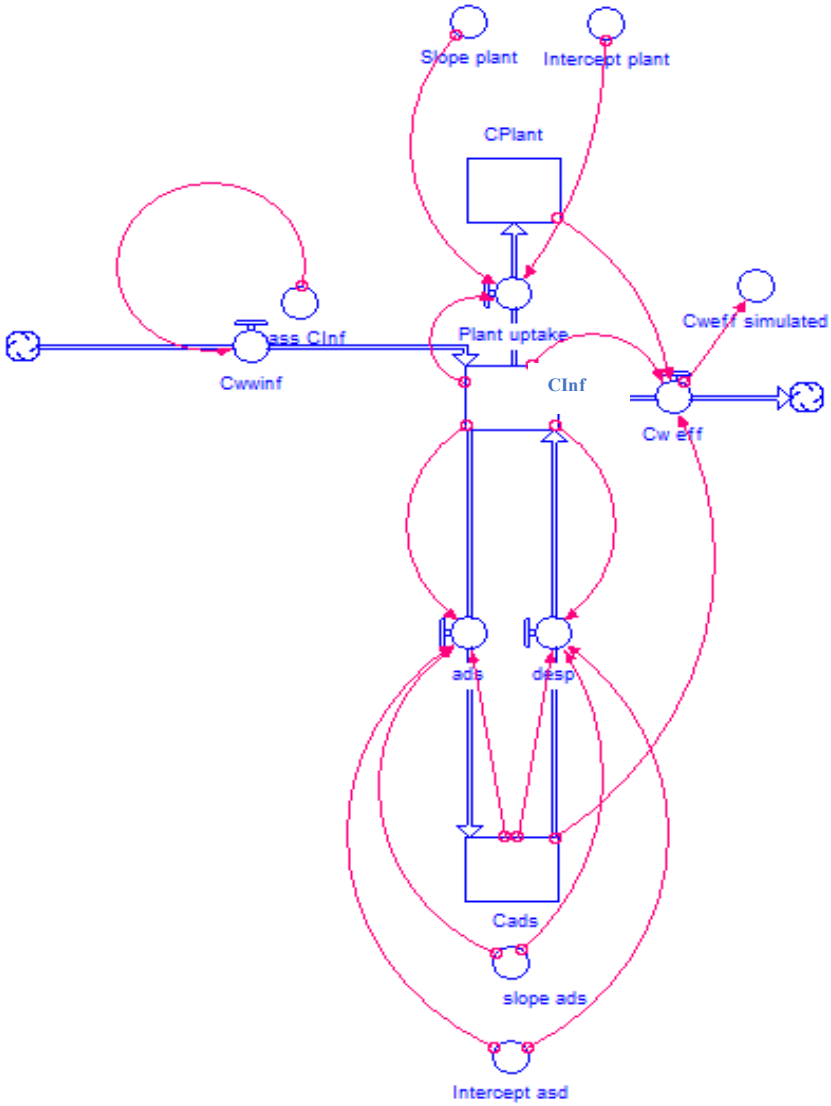

Figure 1. Graphical model of heavy metal dynamics in subsurface flow constructed wetland [ads = adsorption, desp = desorption, Cads = Ni concentration adsorbed on the substrate (mg), Cw effluent = mass (mg) of Ni in the effluent water, CInf = amount of Ni in the influent (mg); Cplant = mass of Ni uptake in the dry weight of plant tissues (mg)]

Table 1. Plant uptake and gravel adsorption coefficients and intercepts for Ni linear models

Ni (ppm)	Variables	Phragmites	Gravel adsorption
0.5	P value	5.92E-08	1.06E-05
	Intercept	0.003	0.10
	Coefficient	0.779 ***	0.69 ***
	R^2	0.913	0.72

3.2 Ni adsorption/desorption models on gravel

The results of model calibration for Ni accumulation in the gravel medium using the concentration of 0.8 mg/L of Ni, hence 19.58 mg of Ni in influent over a period of 15 months are presented below.

The adsorption and desorption equations performed in the Stella model is shown in the following equation:

$$\text{Adsorption} = \text{IF } (\text{Cads} < 1.30*\text{CInf} - 6.09) \text{ THEN } (1.30*\text{CInf-} (6.09+ \text{ads})) \text{ ELSE } (0);\ R^2 = 0.79. \quad (1)$$

While the desorption equation is:

$$\text{Desorption} = \text{IF } (\text{Cads}>1.30*\text{CInf } -6.09)\text{THEN}((\text{Cads}-(-6.09)/1.30-\text{CInf})\text{ELSE}(0) \quad (2)$$

The instantaneous values of Ni adsorbed are given by a mathematical model as follows:

$$\text{Cads } (t) = \text{Cads } (t - dt) + (\text{adsorption - desorption}) * dt \quad (3)$$

$$\text{INITIAL Cads} = 0 \text{ mg} \quad (4)$$

3.3 Ni plant uptake model

The plant uptake equation performed in the Stella model is shown in the following equation:

$$\text{Plant\_uptake} = (0.067295*\text{CInf}+0.502241),\ R^2=0.72 \quad (5)$$

The values of Ni in effluent are given by the linear model computed in STELLA program.

$$\text{Cw\_effluent} = (\text{CInf-CPlant-Cads}) \quad (6)$$

3.4 Model validation and mass balance

A relative comparison between experimental and simulated data of Ni in gravel, plant, influent and effluent during experimental period are shown in figure 2. The Ni from wastewater was accumulated in gravel by the adsorption process. A fraction of Ni adsorbed was released in pore water through the desorption process. Ni accumulated in plant (plant uptake) constituted an important part in the removal process, despite the fact that the decomposed plant mass could return in the reactor and release the metal previously removed. To minimize this impact in the system, the dead plants were regularly harvested.

The simulated and experimental Ni 0.5 ppm removal efficiencies in the VSSF CWs during the study are presented in Table 2 for relative comparison.

Table 2. Mass balance (%) comparing simulated and experimental data for Ni

Ni 0.5 ppm	Designation	Efficiency %	*Phragmites Karka*
	Simulated	RE	83.5
		Ads	52.8
		Plant	30.6
	Experimental	RE	84.2
		Ads	50.6
		Plant	33.6

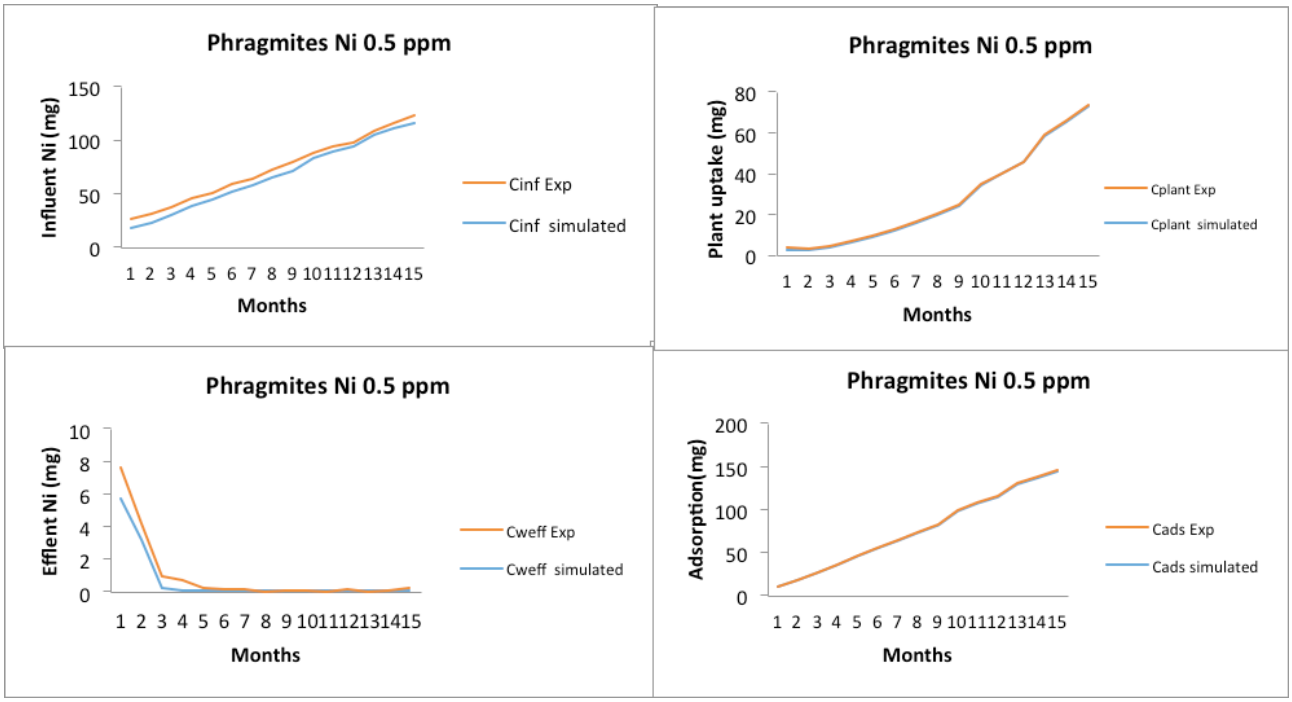

Figure 2. Graphical model of heavy metal dynamics in subsurface flow constructed wetland

The overall removal efficiencies (RE in %) of Ni in VSSF CWs were ranged between 83.5 % for simulated data and between 84.0 % for observed data, indicating a good performance of the system. Amongst them, 52.8 % of Ni were adsorbed in gravel regarding simulated data while there was 50.6 % of adsorption for observed data. For plant uptake, simulated removal efficiencies were 30.6 % for simulated data while it 33.6 % for experimental data. Therefore, it appeared that the adsorption efficiencies were higher than plant uptake in the overall system for the level of concentration Ni 0.5 ppm. Gravel played a major role in the removal of Ni 0.5 ppm in VSSF CWs, while plant species played secondary role.

For the removal of Ni concentrations studied, a good agreement was observed between experimental and simulated data indicated by large values of Asymp Sig. (p values > 0.156) that were recorded from Wilcoxon Signed Ranks Tests. Therefore, there was no significant difference between experimental and simulated data. The validation of the model showed that there is no significant difference between experimental and simulated data (p value > 0.05) for adsorption, plant uptake, influent and effluent values of Ni studied. Additionally, the Pearson coefficient confirmed the good fit between simulated and experimental values: $R^2 > 0.7$ regardless of the component of the model studied. Similar results were obtained by Bullen et al. (2011) who simulated the removal of cadmium from wastewater in free water surface constructed wetlands. But, the substrate used in constructed wetlands was a soil material.

The mathematical model developed in this paper is a new facility to simulate the behaviour of metal in subsurface flow constructed wetland including, inflow and outflow, adsorption/desorption and plant uptake removal processes.

4. CONCLUSIONS

Constructed Wetlands in recent decades are pointed out by several authors as the effective alternative to conventional system for the treatment of agricultural, industrial and municipal wastewater. Numerous models have been developed to simulating and predicting the behaviour of CWs over extended period of time. These are categorized as black-box and process-based models. In black-box category the first order model is still widely used to design CWs but has numerous inadequacies to predict the outlet contaminant concentrations. Despite the fact that mechanistic

models highlight the comprehension of internal processes involving in pollutant dynamics in CWs, is still unable to take in account all the processes and interactions that exist in CWs. Besides this more efforts should be devoted for modelling heavy metal dynamics in CWs and especially more modelling studies should be extended to SSF CWs and hybrid systems for improving their performances in effective wastewater treatment processes in a better way. The application of STELLA Software for developing a mathematical model (STELLA model) to simulate Ni dynamics in subsurface flow constructed showed a good fit (p value > 0.05) between experimental and simulated data (Pearson coefficient R^2 > 0.70). The model developed showed a very high performance in the removal of Ni from artificial wastewater, indicated by a removal efficiency of 83.0 %, in agreement with the real system which showed a removal efficiency (RE = 84.0 %). Hence, keeping in view the fact that most modelling approaches developed have concentrated only on hydrodynamics and nutrient cycling and very less efforts devoted for heavy metals dynamics, the developed mathematical model is a significant contribution that is useful to describe the Ni dynamics in different component of a vertical subsurface flow constructed wetland and to simulate and understand its behaviour over an extended period of time.

ACKNOWLEDGEMENT

The fellowship received from India-Africa programme is duly acknowledged.

REFERENCES

Bullen, P. G., Jindal, R. and Tantrakarnapa, K. 2011. Modeling of cadmium removal from domestic wastewater in constructed wetlands using Stella Simulation Program. Journal of Hazardous, Toxic, and Radioactive Waste*;* Doi: 10.1061/AsceHz.1944-8376.0000083.

Garcia, J., Rousseau, D. P. L., Morató, J., Lesage, M., Els, V., Bayona, J. M. 2010. Contaminant Removal Processes in Subsurface-Flow Constructed Wetlands: A Review, Critical Reviews in Environmental Science and Technology; 40, 561- 661.

Houba, V.J.G., Van Der Lee, J.J., Novozamski, I. and Walinga, I. 1989. Soil and Plant Analysis. A series of Syllabi. Part 5: soil analysis procedures. Fifth edition. Agricultural University of Wagningen. Department of Soil Science and Plant Nutrition.

Kumar, J. L. G., Zhao, Y. Q. 2011. A review of numerous modelling approaches for effective, economic and ecological treatment wetlands. Journal of Environmental Management*;* 92, 400-406.

Langergraber, G. 2007. Simulation of the treatment performance of outdoor subsurface flow constructed wetlands in temperate climate. Science of the Total Environment*;* 380, 210-219.

Meyer, D., Chazarenc, F., Claveau-Mallet, D., Dittmer, U., Forquet, N., Molle, P., Morvannou, A., Palfy, T., Petitjean, A., Rizzo, A., Samso, C. R., Scholz, M., Soric, A., Langergraber, G. 2015. Modelling constructed wetlands: Scopes and aims – a comparative review. Ecological Engineering*;* 80, 205–213.

Razali, N. and Wah, Y.B. 2011. Power comparisons of Shapiro–Wilk, Kolmogorov–Smirnov, Lilliefors and Anderson–Darling tests. Journal of Statistical Modelling and Analytics; 2 : 21–33.

Proceedings of the 10th World Congress of EWRA 'Panta Rhei', 5-9 July 2017, Athens, Greece
© 2017 *European Water Resources Association*

Multi-criteria evaluation of wastewater treatment technologies in constructed wetlands

B. Srdjevic[1*], Z. Srdjevic[1] and K. Suvocarev[2]
[1] *University of Novi Sad, Faculty of Agriculture, Department of Water Management, Trg D. Obradovica 8, 21000 Novi Sad, Serbia*
[2] *University of Arkansas, Biological & Agricultural Engineering, Fayetteville AR 72701, USA*
[*] *e-mail: bojans@polj.uns.ac.rs*

Abstract: Segmenting constructed wetland for natural wastewater treatment can be considered as multi-criteria decision-making problem because there are conflicts between criteria while assessing alternative orderings of treatment technologies among segments. Criteria such as: size of wetland area, possible economic effects, technical effectiveness, hydraulic conductivity of soil, and plant coverage and growing conditions, are by nature qualitative, quantitative and 'grey'. Alternatives' performance across criteria is difficult to measure because of incommensurate units and inter-dependence between criteria. In this paper the results obtained with different decision-making tools are presented for the problem of selecting best ordering of treatment technologies in wetland segmentation. Methods used are: analytic hierarchy process (AHP), simple additive weighting (SAW), simple product weighting (SPW), technique for order preference by similarity to ideal solution (TOPSIS) and compromise programming (CP). Horizontal flows, vertical flows and shallow gravel ditches are evaluated across criteria in different orderings considering differences in effects that their ordering produce during purification of incoming wastewaters. A decision-making problem is hierarchically structured and the AHP-based pair wise comparisons are used to derive the weights of criteria and local weights of orderings regarding each criterion. With the decision matrix created in this way, the weighting and distance methods are used along with the AHP to declare the best ordering of technologies by segments. The results obtained for a typical wetland in Serbia are presented to illustrate an approach and the results of sensitivity analysis are discussed, indicating advantages and possible drawbacks of combining or parallel using the results from more multi-criteria methods.

Key words: Wetland segmentation, wastewater treatment technologies, AHP, TOPSIS, CP

1. INTRODUCTION

Real life problems in water resources management are commonly observed in atmosphere of abundance of impacts and multiplicity of choices. Making decisions is a complex procedure, especially in cases when multiple contrasted or extremely conflict criteria must be used to evaluate different alternative solutions to the problem in hand. As a process, decision making requires deep understanding of the problem and assumes competency and responsibility of human(s) for the final decision and its consequences in either individual or group context. To validate possible solutions and choose an optimal one (in multi-criteria sense) means that the decision maker's preferences about alternatives will be elicited in some way, e.g. by direct rating or face-to-face comparison of alternatives versus each criterion, preceded by the same procedure applied to criteria versus the goal.

Eliciting decision maker's preferences can be achieved in different ways. In most cases, it depends on the selected multi-criteria decision-making (MCDM) methodology. There is a plenty of approaches, methodologies and tools that can support the whole process, within both individual and group decision-making frameworks in water management. In all cases, a key issue is: (a) how to provide consistent procedure in deriving solution; (b) why to use specific scientifically proven decision-making model to attain and that outcomes (consequences of decision made) will be monitored and additionally evaluated with assumed criticism. trustful decisions; and (c) to be aware that audit trial will eventually follow.

Based on earlier research and published papers (e.g., Suvocarev and Srdjevic, 2007; Srdjevic et

al., 2008; Srdjevic et al., 2013), in this paper we describe how various multi-criteria decision-making methods are used to select best segmentation of one constructed wetland in Serbia. Created decision-making framework included selection of methodology for decision-making, enabling judgment process in which five experts from academia, engineering and management evaluated six alternative segmentations against six selected criteria. In Chapter 2 methodological approach is briefly described. Chapter 3 contains the main results and discussion, and Chapter 4 concludes the paper.

2. METHODOLOGICAL APPROACH

2.1 Decision-making problems and multi-criteria solving methods

In certain phase of the decision-making process the decision matrix is commonly created. For instance, for given set of n alternatives ($A_1, A_2, ..., A_n$), and set of m criteria ($C_1, C_2, ..., C_m$), this matrix is of dimension nxm with rows corresponding to alternatives and columns to criteria, Eq. (1). Entries of the matrix (r_{ij}) represent scores (ratings) of alternatives with respect to criteria. Values $(w_1,w_2,...,w_m)$ written above the matrix are the importance weights of criteria defined by the decision maker (DM), or derived in another way; they usually (but not necessarily) sum up to 1.

$$R = \begin{array}{c} \begin{array}{cccccc} (w_1 & w_2 & . & . & w_m) \\ C_1 & C_2 & . & . & C_m \end{array} \\ \begin{array}{c} A_1 \\ A_2 \\ . \\ . \\ A_n \end{array} \begin{bmatrix} r_{11} & r_{12} & . & . & r_{1m} \\ r_{21} & r_{22} & & & r_{2m} \\ . & & & & . \\ . & & & & . \\ r_{n1} & r_{n2} & . & . & r_{nm} \end{bmatrix} \end{array} \tag{1}$$

Decision problems can be divided in two categories, i.e. selection and allocation. The first category is characterised by preferential ordering of alternatives, e.g. ranking of candidate development plans for given catchment or selecting the best supplier of irrigation equipment. Allocation of resources on the other hand means that exact values are needed to determine on how to divide certain commodity or any measurable resource. For instance, allocation problems can be how to divide available agricultural land for application of different cropping schemes, or how to allocate reservoir storage to water uses such as flood protection, urban supply, irrigation, hydroelectric power generation, navigation, fishing and other outdoor activities. The solution of the problem that belong to the selection category is of ordinal type, which means that ordering of alternatives commonly does not provide any additional information to the user, e.g. how big is the difference between any two ranked alternatives. If allocation decision problem is solved, the output information is the set of weights of alternatives (usually normalized to sum to 1). This is cardinal information which implies ordinal information after alternatives are ranked by ascending or descending order.

Different multi-criteria decision methods (MCDM) do not yield the same best outcome (see, for instance, Tavana and Hatami-Marbini, 2011). Majority of well-established MCDM methods generate ordinal information, that is provide ranking of alternatives. Only few known methods produce cardinal information (weights) of alternatives. In our research of the constructed wetland segmentation we selected five MCDM methods: analytic hierarchy process (AHP), simple additive weighting (SAW), simple product weighting (SPW), TOPSIS and compromise programming (CP).

The first method, the AHP, served as a base in this research. The method relies on structured decision problem represented by the hierarchy with goal on the top, criteria at level bellow and alternatives at the third, bottom, level. The roadmap of the method consists of three main steps. Decision maker firstly performs pair wise comparisons of criteria versus goal, and then alternatives

versus criteria by using certain ratio scale (e.g. Saaty, 1980; Ma et al, 1999). A set of comparison matrices is the result of this step. The method then applies selected mathematical procedure (matrix calculus or optimization) and prioritize decision elements and compute local weights of criteria vs. goal, and alternatives vs. criteria. The final step is the synthesis of local weights and obtaining the global weights of alternatives with respect to the goal. In turn, AHP 'controls' consistency of the decision maker while making pair wise comparisons and indicates if there are violations in preferential judgements and computed local and final weights.

The next two methods SAW and SPW are simple and they are based on additive and geometrical aggregation of alternatives' ratings with respect to criteria, assuming that normalization or scalarization of the decision problem is performed to make data consistent. Although the methods are simple and intuitively correct, they are nevertheless good decision making methods, in that their results are usually very close to more sophisticated methods. To apply these two methods, weights of criteria must be known.

The methods TOPSIS and CP belong to a class of similarity-to-ideal-solution methods. For their application, it is required that decision matrix with alternatives ratings exist and that weights of criteria are known. Both methods are well described in pertinent literature (e.g., Hwang and Yoon, 1981; Zeleny, 1982).

2.2 Methodology

The solving methodology is organized in four steps:

2.2.1 Step #1: Problem formulation and its hierarchy

The overall goal is set as to identify the best option for constructed wetland segmentation assuming that the constructed wetland will have three segments, and that the internal ordering of the possible three wastewater natural treatment technologies will anticipate preferences from a group of decision makers coming from academia, engineering and water management.

By reaching full consensus, five decision makers (DMs) specified six evaluation criteria and six technologically justified options for wetland segmentation. They created hierarchy with three levels in top down direction goal-criteria-alternatives. DMs also decided to work in a best will to reach agreement in each judgment they will make while performing AHP pair wise comparisons. For comparisons of decision elements, it was decided to use well known 9-point rating scale presented in Table 1.

Table 1. Saaty's scale for pair wise comparisons in AHP

Judgment term	Numeric value of judgment*
Absolute preference (element *i* over element *j*)	9
Very strong preference (*i* over *j*)	7
Strong preference (*i* over *j*)	5
Weak preference (*i* over *j*)	3
Indifference of *i* and *j*	1
Weak preference (*j* over *i*)	1/3
Strong preference (*j* over *i*)	1/5
Very strong preference (*j* over *i*)	1/7
Absolute preference (*j* over *i*)	1/9

**Intermediate numerical values are used in both scales to model hesitations between two adjacent judgments*

The decision elements are contained in the set of six criteria and the set of six alternatives. In the decision-making process five experts took place.

Criteria set (6). AREA – size of wetland area needed; (2) COST – cost of constructing the wetland; (3) EFFECT – effectiveness of the wetland segmentation alternative; (4) COND –

hydraulic conductivity of soil; (5) COVER – planned/available plant coverage; and (6) LOAD – amount of collected water in the future. Criterions are given in Fig. 1 as second level of the hierarchy and they were mutually compared in pairs versus stated goal.

Alternatives (6). Alternatives are defined based on the idea that both horizontal and vertical water flows should be present for a better purifying effect, especially in the secondary segment where the main purification process takes place. To achieve better purification, solutions that combine vertical flows and flows in shallow gravel ditches are also considered as alternatives. Alternative abbreviations in the bottom level of the hierarchy shown in Fig. 1 are given according to the combination of segmentation flows. For example, H-T-V means that the primary purification is within a segment with horizontal groundwater flow (H), the secondary is within a segment with shallow gravel ditches (T), and the tertiary occurs in the final segment where vertical water flow (V) is dominant.

Decision Makers (5). The group of five decision makers (DMs) participated in assessing mutual importance of criteria against goal, and then alternatives against each criterion. DMs are all with specific experience gained during planning and implementation of several constructed wetlands in Serbia, mainly for purification of wastewaters in small rural municipalities in the Vojvodina Province. Three DMs came from academia, one is experienced professional and one is a consultant.

2.2.2 Step #2: Judgment elicitation (pair wise comparisons)

Based on pair wise comparisons of decision elements in pairs with respect to adjacent elements in upper hierarchical level, a set of 7 matrices is created for further computation within the AHP methodology, Table 2. Note that all judgments are elicited in a consensus manner differently from several other cases presented in earlier papers (e.g., Suvocarev and Srdjevic, 2007).

2.2.3 Step #3: Prioritization by eigenvector method

Local weights of criteria and alternatives are obtained after prioritization process took place. The eigenvector method proposed in (Saaty, 1980) is used to compute all local vectors containing weights of decision element.

2.2.4 Step #4: Application of other multi-criteria methods to check the AHP results

The AHP prioritization in the previous step enabled creation of standard decision matrix for direct use of another four multi-criteria methods: SAW, SPW, TOPSI and CP. Differently from AHP, these methods use decision matrix given by Eq.1 with known weights of criteria. The AHP prioritization at the top two levels (goal-criteria) produces these weights, while prioritizations at the second and third level (criteria-alternatives) produce local weights of alternatives for each criterion which can be understood as ratings of alternatives for criteria (Cf. Eq.1).

3. RESULTS AND DISCUSSION

Recall that the hierarchy of the decision making came out from a real-life application of AHP in supporting the segmentation of a specific wetland for water purification under the sanitation plan developed for a small rural area in the Vojvodina Province of Serbia (Srdjevic et al., 2008). Results presented hereafter are obtained by the original software DECIDE, developed by the authors.

Based on results of prioritization performed with the eigenvector method (applied on matrices in Table 2), the criteria weights and local weights of alternatives with respect to criteria are summarized in Table 3.

Table 2. Pairwise comparisons of crteria and alternatives

	AREA	COST	EFFECT	COND	COVER	LOAD
AREA	1	2	1/5	2	2	1/5
COST		1	1/7	1/2	1/4	1/5
EFFECT			1	5	7	2
COND				1	1/2	1/2
COVER					1	1/2
LOAD						1

AREA

	A_1	A_2	A_3	A_4	A_5	A_6
A_1	1	2	1/3	1/4	5	3
A_2		1	1/2	1/4	3	4
A_3			1	1/4	7	5
A4				1	8	9
A_5					1	1/3
A_6						1

COST

	A_1	A_2	A_3	A_4	A_5	A_6
A_1	1	3	1/5	1/7	7	2
A_2		1	1/5	1/6	4	1/2
A_3			1	1/3	8	7
A_4				1	9	8
A_5					1	1/5
A_6						1

EFFECT

	A_1	A_2	A_3	A_4	A_5	A_6
A_1	1	1/2	3	5	1/7	1/2
A_2		1	5	6	1/3	2
A_3			1	2	1/8	1/4
A_4				1	1/9	1/5
A_5					1	6
A_6						1

COND

	A_1	A_2	A_3	A_4	A_5	A_6
A_1	1	1/4	1/3	1/2	3	3
A_2		1	6	1/3	3	5
A_3			1	1/3	4	2
A_4				1	7	5
A_5					1	2
A_6						1

COVER

	A_1	A_2	A_3	A_4	A_5	A_6
A_1	1	3	1/2	1/3	1)2	1/3
A_2		1	1/5	!/2	1/2	1/5
A_3			1	3	2	1/2
A_4				1	1	3
A_5					1	2
A_6						1

LOAD

	A_1	A_2	A_3	A_4	A_5	A_6
A_1	1	1/2	3	2	2	3
A_2		1	5	1	3	5
A_3			1	1/5	1	3
A_4				1	7	5
A_5					1	4
A_6						1

Table 3. Weights of criteria and local weights of alternatives versus criteria

		AREA	COST	EFFECT	COND	COVER	LOAD
		0.105	0.042	0.439	0.073	0.101	0.241
		$*CR_{CRIT}$=0.066					
A_1	**H-T-V**	0.130	0.103	0.097	0.103	0.088	0.224
A_2	**H-T-T**	0.107	0.053	0.193	0.299	0.054	0.285
A_3	**H-V-V**	0.219	0.284	0.043	0.135	0.262	0.073
A_4	**H-V-H**	0.465	0.471	0.030	0.364	0.213	0.287
A_5	**T-T-T**	0.031	0.023	0.505	0.054	0.177	0.089
A_6	**V-T-V**	0.048	0.067	0.132	0.045	0.206	0.042
$*CR_{ALTER}$		*0.062*	*0.095*	*0.043*	*0.128*	*0.144*	*0.088*

**CR values represent inconsistency of decision makers.*
Suggested tolerant values are 0.100

Structure of Table 3 completely corresponds to the decision matrix represented by Eq. 1. Local weights of alternatives in columns under criteria are local weights of alternatives derived by AHP from comparison matrices in Table 2.

Note that consistency coefficients (CRs) computed in AHP for the group of decision makers was acceptable in 5 of 7 cases (comparison matrices in Table 2). What is especially important, criteria weights are derived in very consistent way (CR is equal to 0.066, well below tolerant value 0.100). Consistency of decision making at upmost level of the hierarchy is essential because derived weights of criteria drive the rest of AHP synthesis.

Referring to CR values in Table 3, one may see that in two cases (for criteria COND and

COVER), consistency values CR are slightly higher (0.128 and 0.144, respectively). This may be considered as acceptable as well because it simply may happen. Finally, the overall consistency of a hierarchy reached the value HCR = 0.070 which is very good.

The global weights and ranking of alternative segmentations of constructed wetland presented in Table 4 show that the best segmentation is to use shallow gravel ditches in all three segments (T-T-T). The second-best solution(H-V-H) is to use horizontal groundwater flow in border segments and vertical water flow in medium in in-between segment. The third top ranked solution is (H-T-T), that is horizontal groundwater flow in the first segment, and shallow gravel ditches in the remaining two, etc.

Table 4. Final AHP weights and ranking of alternatives

Alternative	**A1**	**A2**	**A3**	**A4**	**A5**	**A6**
Order of segments	H-T-V	H-T-T	H-V-V	H-V-H	T-T-T	V-T-V
Weight	0.131	0.194	0.108	0.199	0.269	0.100
Rank	(4)	(3)	(5)	(2)	(1)	(6)

The decision matrix represented by Table 2 is directly used to prioritize alternatives by methods SAW, SPW, TOPSIS and CP (p=2). The rankings are presented in Table 5, and Borda Count method from Social Choice Theory is applied to identify best alternative across all methods. Obviously, the best option is segmentation T-T-T (A5). This alternative significantly outperforms the others. The second-best option is segmentation H-T-T (A2), and the third-best is H-T-V (A1).

Table 5. Ranking of alternatives derived by different MCDM methods

Methods / Alternatives	**A1**	**A2**	**A3**	**A4**	**A5**	**A6**
AHP	4	3	5	2	1	6
SAW	3	2	4	5	1	6
SPW	3	2	6	4	1	5
TOPSIS	3	2	4	5	1	6
CP	3	2	6	4	1	5
Sum of ranks (Borda Count)	16	11	25	20	5	28
Final ranking	**(3)**	**(2)**	**(5)**	**(4)**	**(1)**	**(6)**

Note that the second-best alternative H-V-H (A4) identified by the AHP is ranked at the forth place if other MCDM are used for cross-checking the results of AHP. This once more suggest that different MCDM methods may produce different final results and that one must be aware of the importance which method to use, or how to combine the results from different methods even the judgment process of decision makers is performed in unique way.

4. CONCLUSIONS

Constructed wetlands are sometimes useful to locate near small cities or villages to enable natural wastewater treatment, once solid wastes are removed and just waste water is transferred from urbanized area into the wetland area. Segmenting the wetland usually means that three to four consecutive fields are constructed with different purification technologies applied. The purpose of wetland will be fulfilled if its segments will efficiently purify waste water, i.e. preserve that water discharged from the field into recipient (usually canal or river) is of acceptable quality.

During the planning phase, i.e. before construction takes place, segmenting the wetland field and application of available technologies in segments, more options of combining technologies in segments should be assessed and select the one which best satisfies standards related to water quality, but also assure that most of objectives are satisfied. To enable this, segmenting wetland is good to treat as the multi-criteria decision-making problem because there are conflicts between criteria while assessing alternative orderings of treatment technologies among segments.

In several installations of constructed wetlands in Serbia experts, project engineers and managers

concluded that for any particular wetland there could be many contrasted and/or conflicted criteria to be respected in order to achieve community or management goals related to handling of urban wastewaters. This paper presents results of one completed application of multi-criteria decision making methodology to evaluate 6 possible segmentations of three commonly used natural purification technologies. For three segments and six criteria, five decision-makers participated in evaluating six alternative combinations of technologies. They used well known analytic hierarchy method (AHP) as a decision-making tool and in completely consensual manner prioritized alternative segmentations. In addition, four other multi-criteria methods are used to assess the results of AHP, i.e. the weighting methods SAW and SPW, and distance methods TOPSIS and CP. All methods identified the same segmentation as the best option for constructing the wetland in hand. It was also concluded that at lower ranking positions the ordering of alternatives may differ from method to method and that analysts must be aware how to combine methods or share their results. The results obtained for typical wetland in Serbia indicate that aside of advantages of different methods, there are possible drawbacks of their combining or parallel using their results, especially in cases if analysis should continue by using several top ranked alternatives. Major drawback in combining multi-criteria methods can be reordering of alternatives and selection of the wrong one. This can happen in reality if methodological approach is not carefully selected and sensitivity analyses are not undertaken.

ACKNOWLEDGMENTS

This work was supported in part by Ministry of Education, Science and Technological Development of Serbia under the grant 174003 (2011-2016) - Theory and application of Analytic hierarchy process (AHP) in multi-criteria decision making under conditions of risk and uncertainty (individual and group context).

REFERENCES

Hwang C.L., Yoon K.S. 1981. Multiple attribute decision making: methods and applications. Springer.

Ma J., Fan Z-P., Huang L-H. 1999. A subjective and objective integrated approach to determine attribute weights. European Journal of Operations Research 112: 397-404.

Saaty T.L. 1980.The Analytic hierarchy process. McGraw-Hill.

Srdjevic B., Suvocarev K., Srdjevic Z. 2008. AHP group decision-making without consensus: an example application in planning of wetland segmentation. Vodoprivreda 40: 51-58.

Srdjevic B., Srdjevic Z., Blagojevic B., Suvocarev K. 2013: A two-phase algorithm for consensus building in AHP-group decision making. Applied Mathematical Modeling 37: 6670-6682.

Suvocarev K., Srđević B., 2007. AHP assessment of technical solutions in segmentation of the constructed wetland. Annals of Scientific Work 31 (1): 106-113.

Tavana M., Hatami-Marbini A. 2011. A group AHP-TOPSIS framework for human spaceflight mission planning at NASA. Expert Systems with Applications 38: 13588-13603.

Zeleny M. 1982.: Multiple criteria decision making. McGraw-Hill.

Proceedings of the 10th World Congress of EWRA 'Panta Rhei', 5-9 July 2017, Athens, Greece
© 2017 *European Water Resources Association*

Assessment at mid-Black Sea coast of Turkey for recovery valuable heavy metals from sediments

A.Şimşek* and G. Bakan
Department of Environmental Engineering, Ondokuz Mayıs University, 55139 Samsun, Turkey
** e-mail: arife.simsek@omu.edu.tr*

Abstract: Rapid industrialization and urbanization has led to the contamination of sediments with heavy metals and organic contaminants and created a pervasive problem worldwide. Major sources of contamination include agricultural and urban lands, industrial activities, spills, and accidents. Arsenic (As), cadmium (Cd), cobalt (Co), copper (Cu), mercury (Hg), nickel (Ni), lead (Pb), and zinc (Zn) are often found in sediments and other areas affected by anthropogenic activities. Sediments containing these contaminants act as secondary sources of contamination, posing significant direct and indirect environmental risks through bioaccumulation in aquatic organisms and incorporation into aquatic food webs that may lead to human exposure. Heavy metal accumulation, bioavailability, and toxicity to sediment-dwelling organisms are largely influenced by the physicochemical conditions and geochemical properties of sediments. Ongoing assessment at mid-Black Sea coast of sediment samples was digested using the 1 ml $HCIO_4$ % 65, 6 ml HNO_3 % 65, 1 ml H_2O_2 % 30 for metal analysis. Digested samples were analyzed at Perkin Elmer Optima 4300DV Inductively Coupled Plasma Optical Emission Spectrometer (ICP-OES). Samples were taken from the four stations; S1, S2, S3, S4. The results show us that all metals have the highest value in the sample number S4. These values found for Cr 7.65 mg/l, Cu 3.05 mg/l , Zn 6.40 mg/l, Cd 11 mg/l ,Pb 1.32 mg/l and Al 2120 mg/l . According to these results, valuable heavy metals may also be treated and extracted from for recovery.

Key words: Heavy metals, Sediments, Recovery, Black Sea, SEF

1. INTRODUCTION

The pollution of the marine ecosystem by heavy metals is a worldwide problem. The ecosystem of the Black Sea has been damaged as a result of chemical pollution. Much of the pollutants come from major rivers and from smaller sources in all Black Sea coastal countries. Additionally, the Black Sea coastal waters are heavily impacted by sewage, a situation exacerbated by the weak economies of coastal states. Black Sea waters remain heavily impacted by a number of pollutants originating from different sources such as the direct and indirect discharge of land-based pollutants, sewage etc. The Black Sea environment is highly contaminated in many urban and industrialized areas of the many countries, resulting in severe ecotoxicological impacts. Heavy metals are toxic substances that accumulate in food chains with the increasing concentrations.

The Black Sea, a semi-enclosed sea, is situated between 40°55' to 46°32' N and 27°27' to 41°32' E. The Black Sea is surrounded by six countries located in Europe and Asia: Bulgaria, Georgia, and Romania; Russia, Turkey, and Ukraine. In fact, the Black Sea is influenced by seventeen countries, thirteen capital cities and some 160 million people (Bakan and Büyükgüngör, 2000).

Sediments have proved to be excellent indicators of environmental pollution, as they accumulate pollutants to the levels that can be measured reliably by a variety of analytical techniques (Ariman and Bakan, 2008). This phenomenon makes sediment as an effective sink for most heavy metals from both crustal and anthropogenic sources. The Black Sea environment has suffered a catastrophic degradation from the waterborne waste from 17 countries. The objectives of this study were determined concentrations of six heavy metals (Cu, Pb, Cd, Al, Cr, Zn,) in sediments of the mid-Black Sea coast of Turkey. The effects of the accumulation of heavy metals in sediments of the mid-Black Sea coast of Turkey were examined in this study.

2. MATERIALS AND METHODS

2.1 Collection of sediment samples

Marine offshore water samples were collected from 4 stations at 3 miles and 20 miles distance from the coast during the spring season at 2014. The area is bound by the latitude 40° 59'30 N and 42° 22' 12 N and longitude 35° 11' 23 E and 37° 54' 15 E. The coordinates of the samples collected at four points shown in Table 1.

Table 1. The coordinates of the sediment samples taken from the Mid-Black Sea coast of Turkey

Sampling Points	Station	Coordinates (N-E)
Terme	S1	41.13.397 37.07.776
Fenerköy	S2	41.23.768 36.48.130
Canik	S3	41.23.104 36.17.294
Dereköy	S4	41.34.467 36.12.547

Wet sediments were dried at 103 ^{o}C. After drying to below 63 μm remaining marine sediment samples were digested by adding 1 ml $HCIO_4$ % 65, 6 ml HNO_3 % 65, 1 ml H_2O_2 % 30 at the Milestone Start D Digestion System.

2.2 Determination of sediment enrichment factor (SEF)

Digested samples were analyzed at Perkin Elmer Optima 4300DV Inductively Coupled Plasma Optical Emission Spectrometer (ICP-OES) for concentrations of the metals Cr, Cd, Cu, Al, Zn, and Pb.

The extent of metal contamination compared to the background area was assessed using the enrichment factor, EF (Selvaraj et al., 2004; Woitke et al., 2003).The concentration of each metal measured in the Mid-Black Sea coast sediments is normalized to aluminum data and to the aluminum crystal value. Aluminum, being a conservative element, is generally assumed to have a uniform flux to the sediments over the past century from crustal rock sources. The sediment enrichment factor (SEF) for metal concentration in sediments at all stations were calculated from:

$$\text{SEF} = \frac{\text{X /Al (sediment)}}{\text{X/Al (Earth's crust)}} \quad (1)$$

where X is the metal studied and X/Al is the ratio of the concentration of element X to aluminum. Aluminum was chosen as the element of normalization also because of natural sources (98%)vastly dominates its input (Kamau, 2002).

2.3 Determination of geo-accumulation index

A first quantitative check of metal pollution in aquatic sediments has been proposed by Müller and Suess (1979) in an equation and it is called the " Index of Geoaccumulation", that is, the enrichment on the geological substrate:

$$I_{geo} = \ln (C_n / 1.5 * B_n) \quad (2)$$

where:

Cn: measured concentration,

Bn: geochemical background value

1.5: a factor for lithologic variations of the heavy metals.

The sediment pollution was investigated by following the concentration of 5 studied heavy metals such as Zn, Cr, Pb, Cu, and Cd. The factor 1.5 was introduced to minimize the effect of possible variations in the background values which might be attributed to lithologic variations in the sediments (Al-Haidarey et al., 2010). According to the crustal abundance data of Krauskopf and Bird (1995) the reference samples were Zn:70, Cr:100, Pb:13, Al:81300 Cu:55 and Cd:0.2 mg/kg.

3. RESULTS AND DISCUSSIONS

This study investigated the effects of heavy metals pollutants in the mid-Black Sea coastline. heavy metal concentrations measured at four different stations are given in Table 2.

Table 2. Heavy metal concentrations in sediments collected from the mid-Black Sea coast of Turkey

Station	Cr(mg/kg)	Cu (mg/kg)	Zn(mg/kg)	Cd(mg/kg)	Pb (mg/kg)	Al(mg/kg)
S1	2.052	0.56	1.148	2.72	0.092	380
S2	1.764	0.648	1.176	2.56	0.1	420
S3	2.292	0.516	1.288	3.28	0.076	372
S4	3.06	1.22	2.56	4.615	0.528	848

The results are given figure 1, all heavy metal concentrations are high at S4 station.

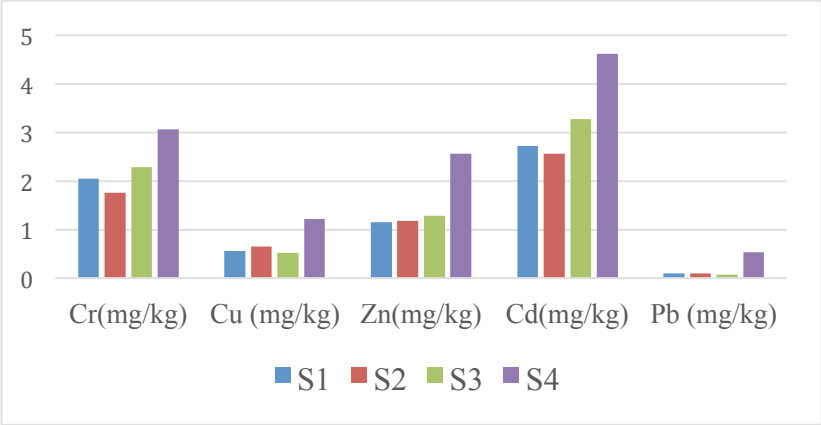

Figure 1. Schematic representation of the heavy metal concentrations in sediments collected from the mid-Black Sea coast of Turkey

3.1 Sediment enrichment factor

The sediment enrichment factor (SEF) is a convenient measure of geochemical trends and is used for making comparisons between areas (Sinex and Helz, 1981). A value of unity denotes neither enrichment nor depletion relative to the Earth's crust.

With the support of the classification of Taylor, 1964 (Table 3) the sediment enrichment factor (SEF) values were interpreted (Table 4).

Table 3. The degree of metal pollution based on seven sediment enrichment factor classes (Taylor, 1964).

SEF value	Designation of sediment quality
50	Extremely severe enrichment
25-<50	Very severe enrichment
10-<25	Severe enrichment
5-<10	Moderately severe enrichment
3-<5	Moderate enrichment
1-<3	Minor enrichment
<1	No enrichment

Table 4. The results of enrichment factor of some heavy metals of sediment samples from the mid-Black Sea coast of Turkey.

Station	S1	S2	S3	S4	Sediment quality
Cr	1.756	1.36	2.00	1.17	Minor enrichment
Cu	0.87	0.91	0.82	0.85	No enrichment
Zn	1.40	1.30	1.60	1.40	Minor enrichment
Cd	1164	991	1434	885	Extremely severe enrichment
Pb	0.6	0.59	0.51	1.55	Minor enrichment

The sediment enrichment factor for 5 studied heavy metals for each station was listed in Table 4. According to Taylor (1964) classification, the EF value of some heavy metals as Cr, Cu, Zn, and Pb was < 1 and 1-<3, indicated that there was no enrichment or minor enrichment by these metals in the sediments of the mid-Black Sea coast. But heavy metal Cd is greater than 50, so sediment extremely severe enrichment.

3.2 The geo-accumulation index

The geo-accumulation index (I_{geo}) values were interpreted (Table 5) with support of the classification of Abrahim and Parker (2008). Generally, the I_{geo} consists of 7 grades or classes.

Table 5. The degree of metal pollution in terms of seven enrichment classes (Abrahim and Parker,2008).

I_{geo}	Value I_{geo}	Class designation of sediment quality
>5	6	Extremely contaminated
4-5	5	Strongly to extremely contaminated
3-4	4	Strongly contaminated
2-3	3	Moderately to strongly contaminated
1-2	2	Moderately contaminated
0-1	1	Uncontaminated to moderately contaminated
<0	0	Uncontaminated

The I_{geo} classes for 5 studied heavy metals for each station are listed in Table 6. The I_{geo} values revealed that the value of Cr, Cu, Zn and Pb in all stations fell into class 0. But also Cd value is 2 at S1 station and ın all other stations, the value is 3. According to this sediment was moderately to strongly contaminated.

Table 6. The results of geo-accumulation index classes of some heavy metals of the mid-Black Sea coast of Turkey.

Station	S1	S2	S3	S4	Sediment quality
Cr	0	0	0	0	uncontaminated
Cu	0	0	0	0	uncontaminated
Zn	0	0	0	0	uncontaminated
Cd	2	3	3	3	moderately to strongly contaminated
Pb	0	0	0	0	uncontaminated

So, this analysis revealed that the sediments of the mid-Black Sea coast were suffering from slight contamination to moderately to strongly contamination with the studied heavy metals according to I_{geo} values. All station were suffering moderately from Cd metal.

4. CONCLUSIONS

Heavy metal pollution in the Black Sea has attracted considerable research attention since last 20 years. Sources of heavy metals in the Black Sea environment can be mainly attributed to terrestrially derived wastewater discharges, agricultural and industrial run-off, river run-off atmospheric deposition of combustion residues, and shipping activities. It is clear from many studies conducted that the heavy metal pollution should be taken into account in the Black Sea.

Additionally, the sediment enrichment factor and geo-accumulation index results show that Cd metal was created moderate pollution in the mid-Black Sea coast of Turkey. Therefore heavy metal recovery will be provided to using suitable treatment techniques of one of these: the sequential extraction, thermal extraction, bioremediation, chemical oxidation, solidification, vitrification methods.

REFERENCES

Abrahim, G.M.S., Parker, R.J., 2008. Assessment of heavy metal enrichment factors and the degree of contamination in marine sediments from Tamaki Estuary, Auckland, New Zealand. Environmental Monitoring and Assessment 136, 227–238.

Al-haidarey, M.J.S., Hassan, F.M., Al-kubaisey, A.R.A., Douabul, A.A.Z., 2010. The Geoaccumulation İndex Of Some Heavy Metals İn Al-Hawizeh Marsh, Iraq. E-Journal of Chemistry 7, 157–162.

Ariman, S., Bakan, G., 2008. Sequential Extraction of Heavy Metal in Sediments at River and Marine of Mid-Black Sea Coast, Turkey. 22-26 Jun 2008, 35 th International Symposium on Environmental Analytical Chemistry, ISEAC 35, Gdansk-Poland.

Bakan, G., and Buyukgungor, H., 2000. The Black Sea. Marine Pollution Bulletin 41, 24–43.

Kamau, J.N., 2002. Heavy Metal Distribution And Enrichment at Port-Reitz Creek, Mombasa.

Krauskopf, K.B., Bird, D.K., 1995. Introduction to Geochemistry, 3rd edition. McGraw- Hill, Inc., New York. (647 pp.).

Müller, P.J., and Suess, E.,1979. "Productivity, Sedimentation Rate, and Sedimentary Organic Matter in the Oceans.I.-Organic Carbon Preservation", Deep Sea Research, Vol.26,pp.1347-1356.

Sinex, S.A., Helz, G.R., 1981. Regional geochemistry of trace elements in Chesapeake Bay sediments. Environmental Geology 3, 315–323.

Taylor, S.R., 1964. Abundance of chemical elements in the continental crust: a new table. Geochimica et Cosmochimica Acta 28, 1273–1285.Western Indian Ocean Journal of Marine Science 1, 65–70.

Proceedings of the 10th World Congress of EWRA 'Panta Rhei', 5-9 July 2017, Athens, Greece
© 2017 *European Water Resources Association*

Evaluation of clogging in HSF pilot-scale CWs using tracer experiments

G.D. Gikas[1*], V.A. Papaevangelou[1], K. Moutsopoulos[1] and V.A. Tsihrintzis[2]
[1] *Laboratory of Ecological Engineering and Technology, Department of Environmental Engineering, School of Engineering, Democritus University of Thrace, 67100 Xanthi, Greece*
[2] *Centre for the Assessment of Natural Hazards and Proactive Planning & Laboratory of Reclamation Works and Water Resources Management, School of Rural and Surveying Engineering, National Technical University of Athens, Athens, Greece*
[*] *e-mail: ggkikas@env.duth.gr*

Abstract: The worst operational problem that may occur during the operation of horizontal subsurface flow (HSF) constructed wetlands (CWs) is the clogging of the porous media. Clogging phenomena cause hydraulic malfunction, and therefore, may lead to inadequate performance of HSF-CWs, and finally, to the reduction of their lifetime expectancy. The main objective of the study was the investigation of clogging in HSF-CWs pilot-scale systems, and its influence on the hydraulics of these systems. Additionally, the study also aims at the evaluation of the sustainable operation of HSF-CWs after their long-term use. One HSF pilot-scale CW was used. The experiment was conducted using an impulse tracer test using KBr, which provided residence time distribution (RTD) curves, and generally, information regarding the effect of clogging on flow dynamics (possible short-circuiting, dead volumes, uneven distribution). For the conduction of the experiment, the conservative tracer was introduced at the inlet through the influent distribution system and the monitoring was performed at various points along the wetland bed (i.e., 1/3 and 2/3 of the length, and the outlet). Equations are used to compute, based on the tracer test data, the mean actual HRT, the tracer mass recovery, the normalized variance and the hydraulic efficiency. The results indicate that the unit operated smoothly without serious clogging phenomena. Generally, this system has shown a sustainable and successful long-term operation. The presented method is an effective method to evaluate performance of horizontal subsurface flow constructed wetlands in terms of clogging.

Key words: Constructed wetlands, Horizontal subsurface flow, Hydraulics, Clogging, Impulse tracer test, Potassium bromide

1. INTRODUCTION

Constructed wetlands (CWs) are vastly being used over the last decades throughout the world for the treatment of several wastewaters and the removal of various pollutants, such as nutrients, heavy metals, pesticides, organic substances etc. (Wu et al., 2015; Papaevangelou et al., 2016a, 2017a, 2017b). This green technology offers many advantages against conventional treatment systems, such as easy and trouble-free operation, low maintenance and operational cost, tolerance to high flow and load variability, and use of natural energy sources (Kadlec and Wallace, 2009; Gkika et al., 2014). Horizontal subsurface flow (HSF) represent one of the most common types of CWs employed throughout the world. In HSF CWs, wastewater flows beneath the surface of the porous media in a fully saturated flow pattern (Kadlec and Wallace, 2009).

The worst operational problem that may occur during the operation of HSF-CWs is the clogging of the porous media (Pedescoll et al., 2011; de la Varga et al., 2013). As wastewater passes through the system, the removal of the pollutants occurs through several interactions between sediments, substrate, micro-organisms, litter, plants, atmosphere and the wastewater (Nivala et al., 2012; Gikas and Tsihrintzis, 2010; Kadlec and Wallace, 2009; Tsihrintzis and Gikas, 2010); Several mechanisms, including biological, physical and chemical develop and eventually lead to the saturation and the gradual clogging of the porous media (Pedescoll et al., 2011; Nivala et al., 2012; Pozo-Morales et al., 2013). Clogging phenomena cause hydraulic malfunction, and therefore, may lead to inadequate performance of HSF CWs and to the reduction of their lifetime expectancy (Caselles-Osorio et al., 2007; Pedescoll et al., 2011; Nivala et al., 2012; de la Varga et al., 2013).

There are several ways of evaluating the extent and severity of clogging in a wetland environment, including: hydraulic conductivity measurement and tracer studies (Nivala et al., 2012). The main objective of the study was the investigation of clogging in HSF-CWs pilot-scale systems and the eventual influence on the hydraulics of these systems with the use of an inert impulse tracer. Additionally, the study also aims at the evaluation of the sustainable operation of HSF-CWs after their long-term use.

2. MATERIALS AND METHODS

2.1 System configuration

The research was conducted at the outdoor facilities of the Laboratory of Ecological Engineering and Technology, Department of Environmental Engineering, Democritus University of Thrace (location 41°08'47"N, 24°55'09"E). Specifically, the experimental area included a horizontal subsurface flow pilot-scale constructed wetland, which has been described in detail by Akratos and Tsihrintzis (2007). The HSF CW (unit code name: MG-C) was a rectangular tank with dimensions 3 m long, 0.75 m wide and 1 m deep, filled with medium gravel (MG; D_{50} = 15.0 mm, range 4–25 mm) as porous media at a thickness of 45 cm, and planted with *Typha latifolia* (Figure 1). The unit was constructed in 2003 and has been in operation since then in the conduction of several experiments (e.g., see Akratos and Tsihrintzis, 2007; Stefanakis et al., 2009a; Stefanakis and Tsihrintzis, 2009b; Stefanakis et al., 2011; Papaevangelou et al., 2012; Papaevangelou et al., 2016b; Papaevangelou et al., 2017a). Therefore, this study attempts to assess the hydraulic conditions and efficiency in this pilot-scale HSF CW after its long-term use, and observe the extent of clogging over time.

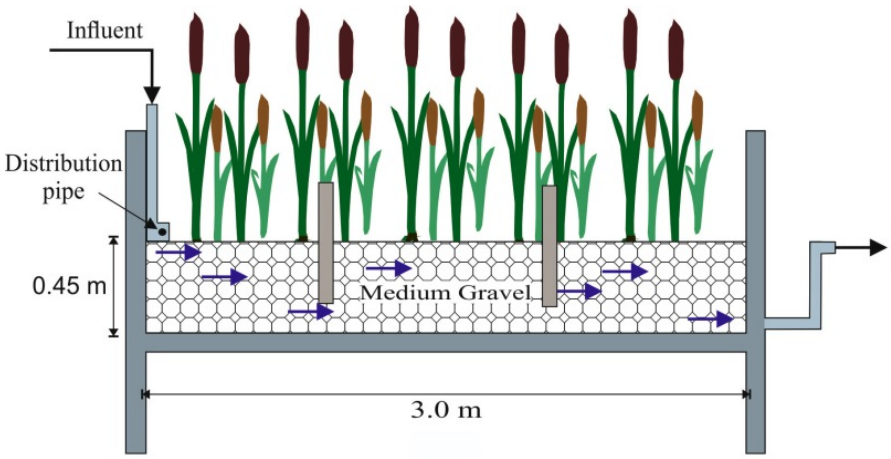

Figure 1. Schematic layout of the HSF-CW unit

2.2 Impulse tracer test

Hydraulic tracer tests are very useful not only in order to gain information regarding the hydraulic characteristics, but also to monitor the hydraulic regime and hydraulic efficiency. Any preferential flows or dead zones within the wetland environment can be identified through the introduction and the monitoring of a tracer throughout the wetland (Headley and Kadlec, 2007; Nivala et al., 2012). Two are the most common approaches of conducting a tracer experiment: either a single injection (impulse input) or a step injection (step input) (Headley and Kadlec, 2007). For the current study, the impulse technique was applied, because it requires both less quantity of tracer and less human labor.

There is a wide range of substances that can be used as tracers but three are the most popular choices; lithium cation, bromide anion and fluorescent dyes. Bromide and lithium are the most preferred choices due to their low cost and ease of analysis (Headley and Kadlec, 2007; Avila et al., 2016). In the current study, bromide was chosen, because it has a very low natural background and negligible sorption, it is highly soluble, and it is not susceptible to degradation (Lange et al., 2011; Avila et al., 2016).

The tracer test was conducted in July 2014 by a single injection of bromide and the whole experiment lasted 8.5 days. The applied hydraulic loading rate (HLR) was 90 L per day, and the nominal HRT (nHRT) was 4 days. The daily feeding regime included 3 loadings (30 L each). The tracer solution was prepared by diluting approximately 2.26 g of potassium bromide (KBr) in 30 L of water (Table 1), which was completely dissolved, and was then introduced to the unit using a pump with a volume counter. The monitoring (sampling) started the same day 8 h after the tracer injection. Samples were collected every 8 hours from the effluent of the pilot-scale unit (Figure 1; Table 1). Bromide concentration was determined with the use of Ion Chromatography (IC 3000, Dionex). Before the beginning of the tracer experiment, the porosity of the substrate material was determined and was found to be 0.32.

Table 1. Data of the tracer experiment

Parameter	Value or Type
Type of tracer	Potassium Bromide, KBr
Type of injection	Impulse
Duration of the experiment, d	8.5
Time of injection of tracer	1st day (morning)
Amount of tracer (injected mass), g	2.26
Hydraulic loading rate (HLR), L/d	90
Nominal HRT, nHRT, d	4
Sampling points	Effluent of the CW
Sampling interval, h	8

2.3 Processing of data and calculation of statistical parameters

The nominal or theoretical HRT is calculated as follows:

$$\tau_n = \frac{V}{Q} = \frac{\varepsilon h A}{Q} \quad (1)$$

where: τ_n [d] is the nominal HRT; V [m^3] is the wetland water volume; Q [m^3/d] is the volumetric flow rate; ε [-] is the porosity of the substrate material; h [m] is the average water depth; and A [m^2] is the wetland surface area.

In order to evaluate the reliability of the tracer test, the recovery percentage Rr (tracer mass recovery) was calculated, using the following equation (Garcia et al., 2004). This parameter is an indicator of the lost mass:

$$Rr = \frac{\int_0^{\infty} Q(t)C(t)dt}{M_t} x100 \quad (2)$$

where: Q(t) [m^3/h] is the time-dependent flowrate function; C(t) [g/m^3] is the time-dependent exit tracer concentration function; and M_t [g] is the added tracer mass.

The average time (τ) the tracer particle or the water remains in the HSF wetland is referred as "mean actual HRT" or "tracer HRT" or "tracer detention time". The variance (σ^2) describes the

spread of tracer response curve about the mean actual HRT. τ and σ^2 are calculated by Eqs. (3) and (4), respectively (Headle and Kadlec, 2007; Kadlec and Wallace, 2009):

$$\tau = \frac{\int_0^\infty tC(t)dt}{\int_0^\infty C(t)dt} \tag{3}$$

$$\sigma^2 = \frac{\int_0^\infty (t-\tau)^2 C(t)dt}{\int_0^\infty C(t)dt} \tag{4}$$

and the normalized variance [-] is calculated by Eq. (5):

$$\sigma^2_\theta = \frac{\sigma^2}{\tau^2} \tag{5}$$

where: t [h] is the time; and the other parameters as defined above.

Persson et al. (1999) proposed the hydraulic efficiency λ parameter, which evaluates not only the effective volume utilization but also the tracer response curve. This parameter is calculated by Eq. (6):

$$\lambda = \frac{t_p}{\tau_n} \tag{6}$$

where: t_p is the time to the peak tracer concentration; and τ_n is the nominal HRT.

3. RESULTS AND DISCUSSION

The monitoring of the bromide concentration at the effluent of the pilot-scale CW unit provides the residence time distribution (RTD) response curve which is presented in Figure 2. The tracer (i.e., bromide) was detected at the outlet of the MG-C, after a delay time of 0.8 days (Figure 2). After a time of about 8.2 days, the tracer was not detected (Figure 2), and therefore, a time period of 8.2 days was enough to complete the experiment of the bromide injection. The values of statistical parameters, which were calculated as described before, i.e., using Eqs. (1) to (6), were 91%, 4.56 d, 2.18 d^2, 0.10, 3.5 d and 0.87 for Rr, τ, σ^2, σ^2_θ, t_p and λ, respectively. These parameters define the hydraulic behavior of the pilot-scale CW.

The tracer mass recovery rate Rr, as mentioned before, is an index which can evaluate the reliability of the tracer test, and it is considered acceptable if the values fluctuate between 80 and 120 % (Kadlec and Wallace, 2009). In tracer recovery rate calculation, the mean daily evapotranspiration (ET) rate in the MG-C was estimated at 13.8 (mm/d) based on Papaevangelou et al. (2012) method. The value of recovery rate was high and acceptable, as its value was 0.91, indicating that the experiment was carried out in a proper way.

The mean actual HRT (i.e., 4.56 days) in MG-C unit was greater than nHRT, which was 4.0 days. According to Hedley and Kadlec (2007), the actual HRT in the CW may be shorter than nHRT due to the existence of dead zones or, in other cases, longer due to incorrect measurement of flow rate and wetland volume. US EPA (2000) also reported that the mean actual HRT in many horizontal subsurface flow CWs was found to be from 40 to 80% less than the nHRT due to loss of

pore volume. In the present study, the flow rate, the surface area and the porosity of the substrate material were directly measured, and therefore, the errors in the estimation of actual HRT were negligible. The results of the present study (i.e., value of mean actual HRT > nHRT) reveal that the loss of pore volume is negligible.

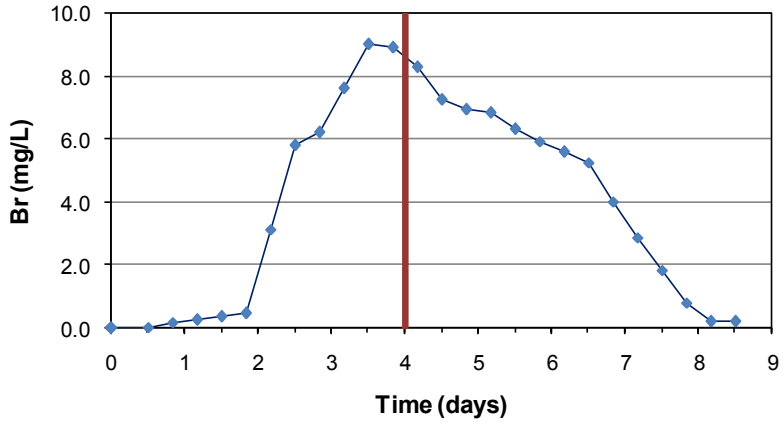

Figure 2. Tracer concentration in the effluent of the pilot-scale HSF CW. The vertical bar represents the nominal HRT (nHRT=4 days)

The variance (σ^2) of the RTD of the MG-C unit was 2.18 d^2 and the dimensionless variance of it was 0.10. Garcia et al. (2004), who investigated the effect of aspect ratio on hydrodynamics of horizontal subsurface flow CWs, reported that the shape of the RTD is affected by the aspect ratio. Also, according to US EPA (2000), the dispersion decreases with the increase of the aspect ratio. These statements explain the low values of dimensionless variance of the pilot-scale unit in the present study, since it has a high aspect ratio of 4.

According to Persson et al. (1999), the hydraulic efficiency parameter (λ), as mentioned before, indicates the existence of dead zones and short-circuiting in the wetland. The hydraulic behavior is categorized, depending on the λ value, into three groups, as follows: (1) for $\lambda > 0.75$, good hydraulic efficiency; (2) for $0.5 < \lambda \leq 0.75$, satisfactory efficiency; and (3) for $\lambda \leq 0.5$ poor efficiency. Based on these ranges, and taking into account the λ value for the pilot-scale unit which is 0.87, it can be concluded that the unit had a good hydraulic efficiency. The results indicated that the unit operated smoothly without important clogging phenomena.

4. CONCLUSIONS

A procedure was developed and applied, based on impulse tracer test, to evaluate clogging in a horizontal subsurface flow constructed wetland. Potassium bromide was used as a conservative tracer, which proved to be a good option, showing low mass loss along the experimental CW. Equations have been presented to compute, based on the tracer test data, the mean actual HRT, the tracer mass recovery, the normalized variance and the hydraulic efficiency. Based on these, the evaluation of clogging is possible.

REFERENCES

Akratos, C.S., Tsihrintzis, V.A., 2007. Effect of temperature, HRT, vegetation and porous media on removal efficiency of HSF CWs. Ecol. Eng., 29: 173-191.

Avila, C., García, J., Garfí, M., 2016. Influence of hydraulic loading rate, simulated storm events and seasonality on the treatment performance of an experimental three-stage hybrid constructed wetland system. Ecol. Eng., 87: 324–332.

Caselles -Osorio, A., Puigagut, J., Segú, E., Vaello, N., Granés, F., García, D., García, J., 2007. Solids accumulation in six full-scale subsurface flow constructed wetlands. Water Res., 41(6): 1388–1398.

de la Varga, D., Diaz, M.A., Ruiz, I., Soto, M., 2013. Avoiding clogging in constructed wetlands by using anaerobic digesters as pre-treatment. Ecol. Eng., 52: 262– 269.

Garcia, J., Chiva, J., Aguirre, P., Alvarez, E., Sierra, J.P., Mujeriego, R., 2004. Hydraulic behavior of horizontal subsurface flow constructed wetlands with different aspect ratio and granular medium size. Ecol. Eng., 23: 177-187.

Gikas, G.D., Tsihrintzis, V.A., 2010. On-site treatment of domestic wastewater using a small-scale horizontal subsurface flow constructed wetland. Water Sci. Technol., 62(3): 603–614.

Gkika, D., Gikas, G.D., Tsihrintzis, V.A., 2014. Construction and operation costs of constructed wetlands treating wastewater. Water Sci. Technol., 70(5): 803–810.

Headley, T.R., Kadlec, R.H., 2007. Conducting hydraulic tracer studies of constructed wetlands: a practical guide. Ecohydrol. Hydrobiol., 7(3-4): 269-282.

Kadlec, R.H., Wallace, S.D., 2009. Treatment Wetlands. CRC Press, Boca Raton, Florida.

Lange, J., Schuetz, T., Gregoire, C., Elsasser, D., Schulz, R., Passeport, E., Tournebize, J., 2011. Multi-tracer experiments to characterise contaminant mitigation capacities for different types of artificial wetlands. Int. J. Environ. Anal. Chem., 91: 768-785.

Nivala, J., Knowles, P., Dotro, G., Garcia, J., Wallace, S., 2012. Clogging in subsurface-flow treatment wetlands: Measurement, modeling and management. Water Res., 46: 1625-1640.

Papaevangelou, V.A., Gikas, G.D., Tsihrintzis, V.A., 2012. Evaluation of evapotranspiration in small on-site HSF constructed wetlands. J. Environ. Sci. Health A, 47(5): 766–785.

Papaevangelou, V.A., Gikas, G.D., Tsihrintzis, V.A., 2016a. Effect of operational and design parameters on performance of pilot-scale horizontal subsurface flow constructed wetlands treating university campus wastewater. Environ. Sci. Pollut. Res., 23: 19504-19519.

Papaevangelou, V.A., Gikas, G.D., Tsihrintzis, V.A., 2017a. Chromium removal from wastewater using HSF and VF pilot-scale constructed wetlands: Overall performance, and fate and distribution of this element within the wetland environment. Chemosphere, 168: 716-730.

Papaevangelou, V.A., Gikas, G.D., Tsihrintzis, V.A., Antonopoulou, M., Konstantinou, I.K., 2016b. Removal of endocrine disrupting chemicals in HSF and VF pilot-scale constructed wetlands. Chem. Eng. J., 294: 146–156.

Papaevangelou, V.A., Gikas, G.D., Vryzas, Z., Tsihrintzis, V.A., 2017b. Treatment of agricultural equipment rinsing water containing a fungicide in pilot-scale horizontal subsurface flow constructed wetlands. Ecol. Eng., 101: 193-200.

Pedescoll, A., Corzo, A., Alvarez, E., Garcva, J., Puigagut, J., 2011. The effect of primary treatment and flow regime on clogging development in horizontal subsurface flow constructed wetlands: an experimental evaluation. Water Res., 45: 3579–3589.

Persson, J., Somes, N.L.G., Wong, T.H.F., 1999. Hydraulic efficiency of constructed wetlands and ponds. Water Sci.Tech., 40(3): 291–300.

Pozo-Morales, L., Franco, M., Garvi, D., Lebrato, J., 2013. Influence of the stone organization to avoid clogging in horizontal subsurface-flow treatment wetlands. Ecol. Eng., 54: 136– 144

Stefanakis, A.I., Akratos, C.S., Gikas, G.D., Tsihrintzis, V.A., 2009a. Effluent quality improvement of two pilot-scale, horizontal subsurface flow constructed wetlands using natural zeolite (clinoptilolite). Microporous Mesoporous Mater., 124(1–3): 131–143.

Stefanakis, A.I., Akratos, C.S., Tsihrintzis, V.A., 2011. Effect of wastewater step-feeding on removal efficiency of pilot-scale horizontal subsurface flow constructed wetlands. Ecol. Eng., 37(3):, 431–443.

Stefanakis, A.I., Tsihrintzis, V.A., 2009b. Effect of outlet water level raising and effluent recirculation on removal efficiency of pilot-scale, horizontal subsurface flow constructed wetlands. Desalination, 248(3): 61–976.

Tsihrintzis, V.A., Gikas, G.D., 2010. Constructed wetlands for wastewater and activated sludge treatment in north Greece: a review. Water Sci. Technol., 61(10): 2653–2672.

US EPA, 2000. Constructed Wetlands Treatment of Municipal Wastewaters. EPA/625/R-99/010. United States Environmental Protection Agency, Office of Research and Development, Cincinnati, OH, pp. 165.

Wu, H., Zhang, J., Ngo, H.H., Guo, W., Hu, Z., Liang, S., Fan, J., Liu, H., 2015. A review on the sustainability of constructed wetlands for wastewater treatment: design and operation. Bioresource Technol., 175: 594–601.

Proceedings of the 10th World Congress of EWRA 'Panta Rhei', 5-9 July 2017, Athens, Greece
© 2017 *European Water Resources Association*

Earth Observation based monitoring in Natura-2000 sites, providing ecosystem services for their adaptive management

A. Zouboulis[1*], A. Tsirika[2], E. Terzopoulou[3], G. Skoufas[4], I.-D. Adamakis[3], S. Kyriakidis[3], V. Liakopoulos[3], N. Tziolas[2] and G. Zalidis[2]

[1] *Aristotle University of Thessaloniki, Department of Chemistry, Laboratory of Chemical & Environmental Technology, 54124 Thessaloniki, Greece*

[2] *Aristotle University of Thessaloniki, School of Agriculture, Laboratory of Remote Sensing, Spectroscopy and GIS, 54124 Thessaloniki, Greece*

[3] *Interbalkan Environment Center, Loutron 18, 57200, Lagadas, Greece*

[4] *Alexander Technological Educational Institute of Thessaloniki, Department of Civil Engineering, 57400, Sindos, Greece*

[*] *e-mail: zoubouli@chem.auth.gr*

Abstract: Epanomi and Aggelochori lagoons and their wider coastal-marine zone are situated in the eastern part of Thermaikos Gulf (N. Greece, near to Thessaloniki) and are considered as very important natural sites, because they include priority marine habitat types, according to 92/43/EEC Directive, i.e. 1120* (*Posidonia beds*) and 1150* (*Coastal lagoons*). The implementation of Water Framework Directive requires both lagoons to achieve good ecological Status in these coastal water bodies and to conserve their habitats. The objectives of this work were to develop an innovative monitoring system in order to provide ecosystem services, in almost real time, for the adaptive management and enhancement of conservation status of coastal habitats. The monitoring of water quality included the assessment of biotic and abiotic factors and it was implemented via the combination of destructive (active and passive sampling based on an early warning system, followed by laboratory analysis) and non-destructive methods (earth *in situ* monitoring, using an Autonomous Water Telemetry Sensing System (AWTSS), employing spectra sensors and space-born remote sensing data). The main objectives of monitoring, in addition to develop an efficient operational monitoring protocol, based on integrated Earth Observation (Earth *in situ* and space-borne) data, include the evaluation of management effectiveness and the establishment of a feedback mechanism, used to provide ecosystem services for the effective adaptive management. In addition, the performed monitoring was able to provide the ecosystem services needed for the adaptive management, proposed for these habitat types, and to serve the relevant stakeholders.

Key words: coastal water bodies-habitats; ecosystem services through Earth observation; innovative integrated monitoring system

1. INTRODUCTION

The increased urbanisation and industrialisation in several Mediterranean coastal areas, especially during the last decades, has generally led to the degradation of water quality and of marine habitat types (Claudet & Fraschetti, 2010). The main issues include water and sediment eutrophication, pollution, disruption of the sedimentation/erosion balance along the coast, direct destruction imposed by human modifications of the coastline, degradation by boat trawling and anchoring, etc. (UNEP/MAP, 2005; EEA, 2006; Airoldi and Beck, 2007). Epanomi lagoon (including its wider coastal-marine zone) and Aggelochori lagoon (including a saltpan, salt marshes and the marine zone) constitute areas of NATURA 2000 network with SCI codes GR1220012 and GR1220005, respectively. Both sites are characterized by high ecological importance and they host priority marine habitat types and species. Specific actions for the conservation of coastal habitats and significant avifauna species in those two NATURA 2000 network sites were implemented under the frame of ACCOLAGOONS project (LIFE+ NATURE AND BIODIVERSITY).

The sustainable water resource management supports multiple water-dependant economic activities, and conserves aquatic resources, while protecting public health. However, the required environmental health decisions need to be supported by real-time sophisticated water monitoring

systems, noting that monitoring constitutes an essential tool towards the conservation of species, habitats, ecological and developmental processes it is strongly related to the sustainable management (Borja et al., 2009). Monitoring is crucial for the assessment of conservation status, regarding the structural and operational characteristics of a natural system, for the evaluation of efficiency, regarding the management measures implemented in the affected area, for the early diagnosis and prediction of degradation problems, etc. Regarding water quality, the application of traditional methods for monitoring biotic and abiotic factors have been performed during the past decades mainly by the *in situ* measurements and/or data collection, as well as sampling and transfer to appropriate chemical or biological laboratories for further analysis and evaluation of collected samples. However, the recent advances in communication and sensor technologies have accelerated the progress of remote monitoring capabilities, applied for water quality (Bonin–Font et al., 2016). In several cases the recent monitoring programs have been directed towards the inclusion of continuous data collection, by using appropriate *in situ* detectors. These data may be accessed either through on-site downloading, or even remotely. The application of Autonomous Surface Vehicles (ASVs) is rapidly becoming popular and rather common place within the marine and aquatic science community (Caccia, 2006; Dunbabin et al., 2009).

The main aim of this research is the contribution to environmental protection and sustainable use of marine resources, through the planning and development of tools, for implementing actions in the framework of Integrated Coastal Zone Management (ICZM). The current study presents a novel robotic exploration system, equipped with a set of advanced technological capabilities. The system enables a range of application cases in a variety of operational environments and in almost real-time, providing added-value services for knowledge-based applications, such as adaptive management and enhancement of conservation status, regarding coastal habitats, as well as tracking the enhancement of conservation status of common marine habitat types, resulting from the implementation of management actions under the frame of «LIFE + Nature and Biodiversity 2009» ACCOLAGOONS project.

2. MATERIALS AND METHODS

The development of the respective Monitoring Program included the determination of parameters to be measured, the methodology and the frequency of monitoring, as well as the location of appropriate sampling points. In order to estimate the success of implemented management measures, the monitoring protocol of "ACCOLAGOONS LIFE + Nature & Biodiversity" project was considered. The monitoring of water quality included the assessment of biotic and abiotic factors and it was implemented through the combination of destructive and non-destructive methods. Sampling, preservation and analytical protocols are conducted according to the respective Standard Methods for the Examination of Water and Wastewater (22nd Ed.). The samples were collected every month from nine sampling sites (Figure 1a.).

The importance of non-destructive monitoring is well known, as it can tackle several limitations that can occur with the application of destructive *in-situ* methods, most importantly the high cost and the low spatial and temporal resolution of such campaigns. In this context, the ATWSS was utilized, enabling the "clever" capturing of a wealth of information from the water systems and hence, facilitating the smart water management.

The biotic factors, which were monitored, were the coastal and marine benthic biocommunities, emphasizing in *Posidonia oceanica* meadows, and the phytoplankton communities. The main abiotic factors which were monitored *in situ* were: pH, temperature, salinity, specific conductivity, Dissolved Oxygen and turbidity. Furthermore, specific samples were collected in order to perform supplementary water analysis at the Laboratory (*in vitro* measurements). The main parameters which were measured in this case were nutrients (nitrate, phosphate, nitrite, silicate and ammonium ions), heavy metals (cadmium, lead, arsenic, nickel, iron and chromium), pesticides (over 100 pesticides), organic content (TOC) and biological indicators (chlorophyll a).

2.1 Technical description of the autonomous water telemetry sensing system

ATWSS prototype consists of mechanical and electrical hardware components and a remote sensing platform, as illustrated in Figure 1b. ATWSS has designed in order to be easily maneuvered in various water bodies and can carry different types of sensors and processing data systems. In the lower part of this system all the electronic equipment, the sensors, the motor and the hardware automation are situated, while in the upper part two Wi-Fi antennas, four solar panels, an anemometer and a IP camera were placed. The two parts are firmly sealed to each other, offering full isolation to water securing all-weather functionality. At the front of the vessel an electric Minn Kota motor can keep the vessel "anchored" within 3 meters of a specific control or sampling point. The motor can store up to 6 pre-defined paths, a feature that is very useful for systematic and targeted water monitoring missions.

The ATWSS was developed using a "plug and play" architecture, hence all sensors, power supplies and communications can be adjusted (even by a non-expert user) to the current needs. The vessel is powered by 2 rechargeable batteries, which can be charged during the mission via the 4 solar panels, located on the top part of the vessel. As a result, the AWTSS can operate continuously for at least 4 h, enabling the mapping of large areas within the time framework of a single mission.

Additionally, it is equipped with an electrical winch, with a 30 m stainless wire rope, which can be used in conjunction with a multi-parameter probe, or with an active sampler for water profiling applications. Furthermore, the prototype can carry a variety of passive samplers for water quality monitoring, as well as depth sonar in order to perform bathymetric sounding surveys.



Figure 1. a. Epanomi and Aggelochori sites and the sampling points, b. Autonomous Telemetry Water Sensing System (ATWSS).

The collection of measurements requires an accurate and robust protocol at the highest level of standards to facilitate the subsequent data processing step. Considering this, the main rationale is to offer certified *in-situ* observation data through the application of telemetry, adhering to the same principles and standards, as the working Group on Earth Observation System of Systems and Open

Geospatial Consortium, standard information models related to Water (WaterML). Therefore, the AWTSS is continuously connected to a base station (platform) for data transferring and handling. The operator has full control of the vessel navigation and of the sampling procedure. For this reason, custom software with a Graphical User Interface was specifically developed. In addition, the operator has optical contact with the environment around, as well as inside the platform, by using the two IP cameras that are installed; one located externally at the top part, and one located internally at the bottom part.

In order to connect with the base station (platform), the AWTSS can employ 3 different telecommunication modes: (1) Local Wireless LAN connection, (2) Remote operation by using the cellular network (telemetry), and (3) RC operation by using a remote control programmed with the basic functions of the vessel, such as speed, direction and spot-lock, with effective range up to 20 km. In addition to these communication modes, the vessel can be activated and deactivated remotely and notify the operator in case of low battery level, or even theft protection, via SMS.

3. RESULTS AND DISCUSSION

Under the frame of the current survey, the following marine habitat types (included in the Annex I of the Directive 92/43/EC, or not) were identified in both sites: 1110 – Sandbanks, which are slightly covered by sea water all the time, *1120 - *Posidonia beds (*Posidonion oceanicae*), *1150 - *Lagoons, 1170–Reefs, 119A-Soft substrata without vegetation, and 119B-Soft substrata with vegetation.

The range of selected measured parameters (from *in situ*, as well as from laboratory data, including the measurements taken by AWTSS) in the nine sampling sites of the two examined lagoon cases during April-November 2016 are presented in Table 1. Furthermore, the concentrations of selected heavy metals (cadmium and lead) are presented in Figures 2a & b. The observed toxic phytoplankton taxa are shown in Figure 3.

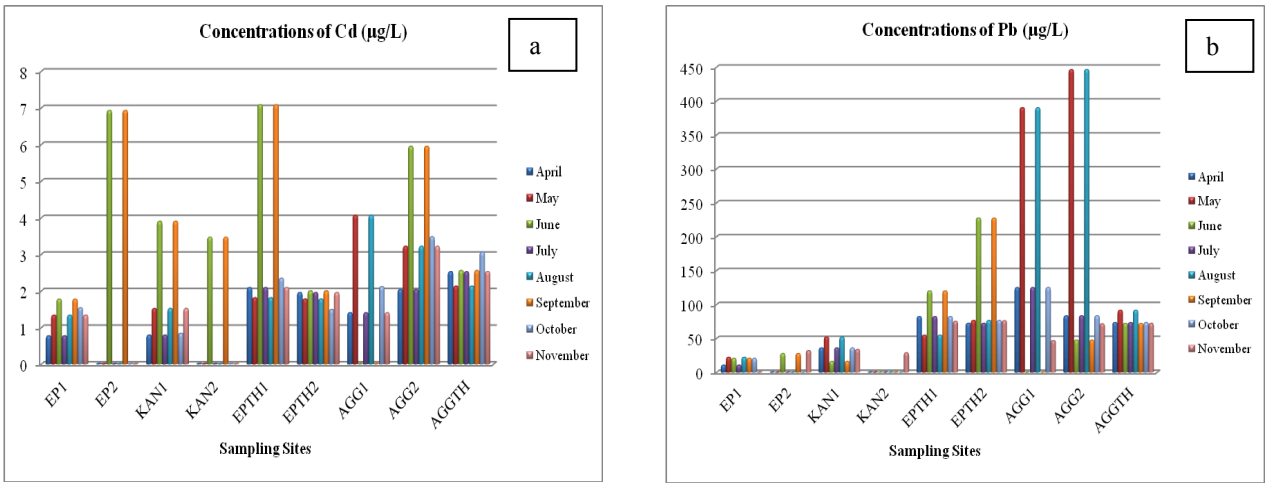

Figure 2. (a) Concentrations of Cd and, (b) concentrations of Pb, during the period April-November 2016.

An evaluation of ATWSS operation has been performed under real conditions at 25th of Nov. 2016. For the performance evaluation several laboratory measurements were also obtained and compared, highlighting a significant agreement with the relevant values, obtained from AWTSS. The testing and validation of measurements' protocol has been carried out, resulting approximately up to 80 measurements/h. Moreover, the findings and testing activities will allow the refinement of prototype sub-systems to meet the targeted application needs. Another development strand concerns the ATWSS ability to support aerial data calibration. Besides the vicarious calibration of the air-spaceborne sensors, these data can be also used for the development of prescription maps.

Generally the environmental situation differs, depending on the monitored water bodies, as well as on the period/season of monitoring (winter-spring-summer-autumn). E.g. during the summer

period the water level decreases, as expected, which leads to an increase of pollutants' concentration. On the other hand, during the winter period high rainfall incidents are usually observed and as a result, the whole region of Epanomi wetland is covered with water, increasing significantly also the volume of water in *Epanomi lagoon*. This situation leads to a reduction of all pollutants' concentrations, due to dilution effect; noting also that the organic content is high, especially in Epanomi lagoon. This is a common fact in most lagoons, as well in wetlands, due to the presence of generally shallow waters. pH, temperature, salinity, specific conductivity, Dissolved Oxygen, total dissolved and suspended solids and turbidity values are considered to be at normal (expected) levels. The concentration of nutrients is highly depending to the respective monitoring period and to the non-treated effluents that are disposed in the monitoring areas, indicated as point- or diffuse pollution, whose origin however, cannot be easily determined.

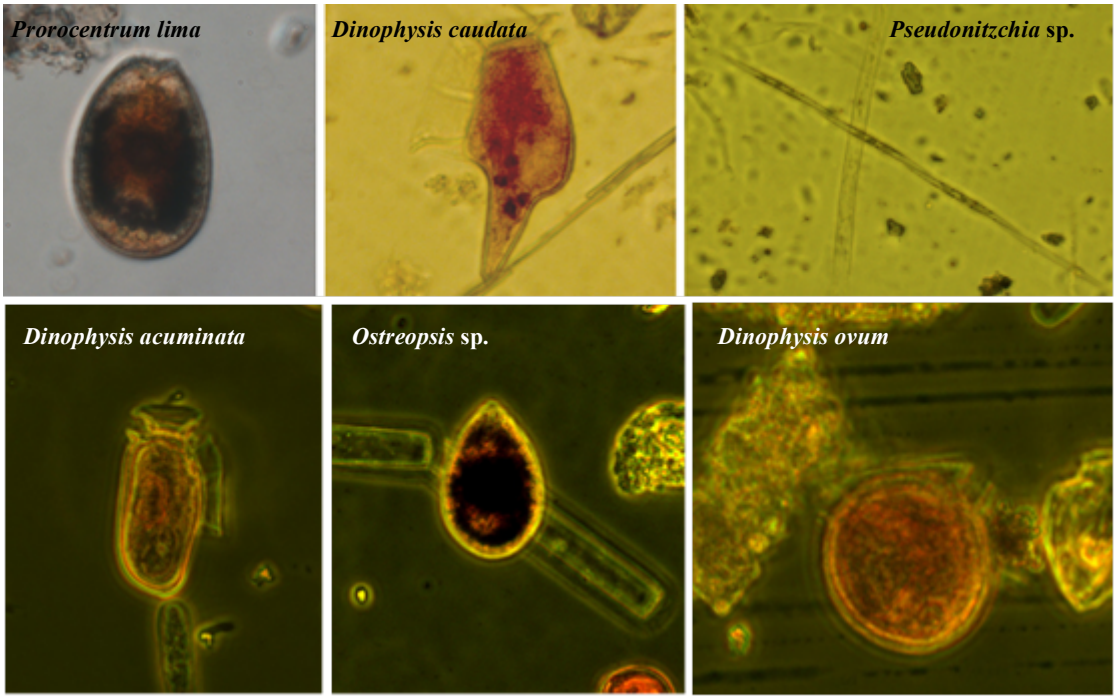

Figure 3. Photos (received by optical microscope) of potentially toxic phytoplankton species.

Table 1. Range of selected measured parameters.

Parameters		EP1	EP2	KAN1	KAN2	EPTH1	EPTH2	AGG1	AGG2	AGGTH
Temperature	°C	.	8.7-31.7	10.3-32	9.3-29.3	10.8-28.5	13.5-27.3	8.2-35.6	8.5-35	13.1-30.3
pH		7.9-8.68	6.5-9.3	5.67-9.5	7.1-8.75	7.7-9.01	6.69-8.24	6.46-8.78	6.62-8.14	6.82-9.5
EC	mS/cm	21.19-68.49	35.5-941.7	26.07-855.2	20.3-548.8	40.6-172.7	41.4-170.6	38.59-739.9	34.12-726.7	35.63-165.3
Salinity	ppt	12.72-45.39	22.4-60	21.29-68.9	13.63-68.19	30.4-64.67	41-68.53	24.7-58.2	20.88-48.4	28.8-67.84
TDS	g/L	13.79-44.7	23.1-153.3	23-298.9	14.69-409	20.45-112.4	21.14-111.3	25.18-941.6	22.01-979.3	28.29-107.4
Turbidity	NTU	117-2170	103-622	25.7-1950	85.5-590	17-292	28-136.8	47.5-2200	25.3-2500	35.5-157.6
DO	mg/L	8.3-12.1	2-11.4	0.98-10.4	0.123-10.5	5.6-10.73	5.7-10.1	2.92-11.4	3.92-11.1	6.72-10.56
TN	mg/L	0.73-1.11	n.d.	0.446-0.45	n.d.	n.d.-0.02	0.02-0.1	n.d.	n.d.	n.d.
TOC	mg/L	56.82-85.23	n.d.-51.3	19.45-22.6	n.d.-23.1	2.05-2.36	2.51-4.57	12.15-17.36	14.26-21.2	2.04-2.68
TSS	mg/L	122.4-2386	64-204.4	41-668	60-113.6	35.52-90.8	38.4-92.4	56.64-202.4	64.9-316	33.9-110.4
Total Phosphorous	mg/L	0.02-5.33	0.01-0.07	0.01-0.91	0.01-0.91	0.01-0.05	0.01-0.03	0.03-0.06	0.02-0.26	0.01-0.18
PO_4^{-3}	mg/L	n.d.-16.34	n.d.-0.22	0.18-2.79	0.12-2.79	0.03-0.15	0.09-0.49	0.09-0.18	0.06-0.8	0.12-0.55
NO_3^-	mg/L	7.53-25.87	0.5-12.4	0.8-14.17	0.6-14.17	0.3-10.63	0.4-16.39	0.6-12.84	0.4-21.7	0.4-14.2
NO_2^-	mg/L	n.d.-0.07	n.d.-0.07	0.03-0.16	0.01-0.07	0.03-0.06	0.03-0.07	n.d.-0.07	0.03-0.1	0.03-0.07
NH_4^+	mg/L	n.d.-0.78	0.08-0.6	0.03-0.36	0.08-0.89	0.04-0.53	0.05-0.53	0.09-0.66	0.08-0.54	0.04-1.21
SiO_2	mg/L	1.18-17.69	0.73-11.25	1-6.27	1.63-17.05	0.49-1.35	0.38-7.42	0.45-7.66	0.36-8.3	0.36-2.87

The same situation is prevailing in the Aggelochori area. During the summer period the water level decreases, which leads to an increase of pollutants' concentration, mainly at the two sampling points of *Aggelochori lagoon*. pH, temperature, salinity, specific conductivity, Dissolved Oxygen, total dissolved and suspended solids and turbidity values are considered to be at normal levels,

despite the fluctuation in the concentration of nutrients, which are mostly depending on the respective monitoring period, as well as to the non-treated effluents that are being disposed in the monitoring area, most of measured parameters remain at normal levels.

In terms of biological species composition, phytoplankton in lagoons is poorer, than the neritic phytoplankton. It is frequently enriched by benthic diatoms, which, due to the small depth of lagoons, can be suspended by the wind. In addition, neritic species enter passively from the sea and remain in the lagoon for a period of time. In particular, the diatoms are rather few, restricted mostly to the marine channels, while dinoflagellates (*Oxyrrhis marina, Goiniodoma sphaericum, Peridinium depressum* and *Gymnodinium heterostriatum*) are quite well represented, especially in the innermost part of the lagoon. Moreover, the potential toxic species of *Dinophysis sp.* and *Ostreopsis sp., Pseudonitzchia sp.* and *Prorocentrum lima* were also observed (Figure 3).

The increase of human activities in the coastal area of Epanomi and Aggelochori directly reflected on water quality and indirectly to the conservation of habitats and species. The existence of pollutants in the project area comes mainly from the diffused untreated effluents of the surrounding area's seasonal cultivation and from the point throwing wastes.

Due to the relatively short time of monitoring period after the completion of recently applied restoration works for the improvement of lagoons' environment, the overall assessment of environmental impact is still a difficult task and as a result, it is difficult to determine the appropriate management improvement decisions, regarding this area. It is considered as necessary for the studied ecosystem to reach equilibrium, so that to launch an objective assessment of obtain results. For this reason, the project should be strengthened by continued monitoring and all the obtained data should be used to support the respective management decisions, concerning the protection and rehabilitation of this important natural (and protected) area.

4. CONCLUSIONS

This monitoring program constitutes a demonstrative action, applied in two coastal lagoons and it is going to act as an attempt for the future establishment of an Environmental Observatory in Thermaikos Gulf, especially regarding water quality issues. The developed monitoring protocol resulted to the production of necessary geospatial layers of Earth observation data, which in combination with the developed fusion algorithms, was able to generate (in almost real-time) an improved picture, regarding the ecological status of these ecosystems. In addition, the effective monitoring can provide the appropriate ecosystem services, which needed for the adaptive management, proposed for these habitat types, serving the relevant stakeholders. The developed technology (a fully Autonomous Water Telemetry Sensing System**)** constitutes an innovative approach of environmental monitoring, as any deviation from the control (base) level is mentioned, recorded and the incidents of pollution are detected in time, giving the respective alarm signal. Moreover, ATWSS aims to support with high confidence the validation and calibration procedures for all the air- and space-borne sensors, due to the meticulously recording of a vast quantity of detailed hyperspectral and spatio-temporal data.

REFERENCES

Airoldi L., Beck M.W., 2007. Loss, status and trends for coastal marine habitats of Europe. Oceanography and Marine Biology, 45: 345–405.

Bonin-Font F., Miquel Massot C., Codina G.O., 2016. Towards Visual Detection, Mapping and Quantification of Posidonia Oceanica using a Lightweight AUV. IFAC-Papers On Line 49-23 (2016) 500–505

Borja. A., Ranasinghe A., Weisberg S., 2009. Assessing ecological integrity in marine waters, using multiple indices and ecosystem components: challenges for the future. Marine Pollution Bulletin, 59: 1–4.

Caccia. M., 2006. Autonomous surface craft: prototypes and basic research issues. In Proc. 14th Mediterranean Conference on Control and Automation: 1–6.

Claudet J., Fraschetti S., 2010. Human –driven impacts on marine habitats: a regional meta-analysis in the Mediterranean Sea. Biological Conservation, Issue 9. Volume 143: 2195–2206.

Dunbabin M., Grinham A., Udy J., 2009. An Autonomous Surface Vehicle for Water Quality Monitoring. Australasian Conference on Robotics and Automation (ACRA).

EEA, 2006. Priority Issues in the Mediterranean Environment. European Environment Agency, Copenhagen. Denmark.

Glasgow H.B., Burkholder J.A.M., Reed R.E., Lewitus A.J., Kleinman J.E., 2004. Real-time remote monitoring of water quality: a review of current applications, and advancements in sensor, telemetry, and computing technologies. Journal of Experimental Marine Biology and Ecology: 300: 409– 448.

UNEP/MAP, 2005. Review and Assessment of National Strategies for Sustainable Development in the Mediterranean Region. United Nations Environment Programme/Mediterranean Action Plan, Athens, Greece.

Proceedings of the 10th World Congress of EWRA 'Panta Rhei', 5-9 July 2017, Athens, Greece
© 2017 *European Water Resources Association*

Water quality estimation in Greek lakes from Landsat 8 multispectral satellite data

E. Kontopoulou*, P. Kolokoussis and K. Karantzalos
Remote Sensing Laboratory, National Technical University of Athens, Greece
* *e-mail: evi.kontopoulou@gmail.com*

Abstract: The European Water Framework Directive (WFD) requires that a Good Environmental Status is retained for all water bodies along their constant monitoring. However, the frequent (e.g., weekly, monthly) monitoring of numerous and extensive inland water bodies places several logistic and economic challenges. Remote sensing is considered one of the most cost-effective methods for providing the spatial and temporal environmental data that are necessary for the effective monitoring and implementation of the WFD. In this study the goal was to establish concrete relations between satellite observations and key quality parameters over several permanent lake monitoring stations in Greece. In particular, water quality indicators such as Chlorophyll-a and turbidity through Secchi disk depth were estimated through the analysis of Landsat 8 satellite and in-situ data. The employed multispectral images and in-situ measurements were selected to have a maximum temporal offset of 15 days, while relations were established based on regression models. The experimental validation indicated correlations with R^2 values of up to 0.75 for Chl-a (n>160) and 0.70 for turbidity (n>190). These promising results along with a further multi-temporal validation can be employed for the development of operational, remote sensing monitoring systems for the accurate and timely estimation of key water quality indicators.

Key words: Remote sensing, Water Framework Directive, Earth observation, regression, chlorophyll, turbidity

1. INTRODUCTION

Water is a natural resource of utmost importance and a precondition for human, animal and plant life cycles. The adoption of the Water Framework Directive (WFD) in 2000, establishes a legal framework to guarantee sufficient quantities of good quality waters across Europe. In order to obtain a coherent and comprehensive overview of water status, frequent surveillance and a well organised monitoring program is required.

The rife methodology to examine the quality of water consists of in-situ sampling and the consequent chemical analysis, method that leads to accurate estimations for several water quality parameters. However, the results correspond to the exact location/region from which the sample was taken but not to the total extend of the water body. Moreover, it is an expensive method due to the equipment used and the frequent sampling required for monitoring crucial phenomena.

In this study the possibility of estimating key monitoring indicators for lakes, using Remote Sensing and specifically Landsat 8 high resolution satellite data has been examined. More precisely, this study has tried to evaluate water quality indicators documented in relevant literature as well as to determine new indicators, capable of providing significant correlations between high resolution satellite data and in-situ ground truth data, for two key monitoring indicators, Chlorophyll-a and Secchi disk depth. The literature is particularly focused on these parameters, since they are the main indicators of eutrophication.

Satellite remote sensing is already internationally used for water quality estimation. However, because of the optical complexity of natural inland waters, the creation of a widely used algorithm is difficult and an ongoing research is necessary (Bukata et al., 1985; Carder et al., 1989; Theologou et al., 2016).

The most widespread Chlorophyll-a retrieval algorithms used for the estimation of Chlorophyll-a concentration employ the blue, the green, the yellow, the red and the infrared spectral regions. The

selection of the most appropriate bands to be used depends on the water body category. For inland water bodies the preferred band ratios for Chlorophyll-a concentration include blue and green bands (440-550 nm), because chlorophyll absorption is maximum at this spectral region. For coastal waters the above ratios are not sensitive enough and the use of the red (620-700nm) and infrared spectral bands (>700nm) are also required (Le et al., 2013; Theologou et al., 2016).

For the turbidity estimation in relevance to the Secchi disk depth measurements the use of ratios that include red reflectance are widely used. For multispectral sensors like Landsat 8, there are promising results for Secchi disk depth correlation even with the red band itself (Hellweger et al., 2007). The reflection at this bandwidth increases when the turbidity and Secchi disk depth decrease. Additionally, the red to blue band ratio provides good results when used for a lake (Kloiber et al., 2002).

2. MATERIALS AND METHODS

The methodological steps (Figure 1) followed for establishing correlations between high resolution satellite data and in-situ ground truth data were the following:

- Collection of in-situ measurements
- Acquisition of high resolution Landsat 8 satellite data
- Correlation of high resolution satellite data and in-situ ground truth data
- Determination of adequate water quality indicators via regression analysis
- Production of water quality maps showing Chl-a and Turbidity spatial distribution

Since up to now a single open database with all in-situ measurements per inland monitoring station does not exist, in-situ data from 11 representative lakes in Greece have been gathered. In particular, Chlorophyll-a and Secchi disk depth measurements were collected from the Greek Biotope/Wetland Centre and the Management Body of Ecodevelopment Area of Karla-Mavrovouni-Kefalovriso-Velestino for the years 2013, 2014 and 2015 (Table 1).

Atmospherically corrected satellite data were downloaded via the 'United States Geological Survey' website. From the available Landsat 8 images, those that included the 11 lakes of the study area and had a maximum 15 days time-offset between the in-situ sampling date and the acquisition of the satellite image (Table 2), were used.

Methodology	
Study Area	**11 Greek Lakes** • 6 natural: Amvrakia, Vegoritida, Volvi, etc • 5 artificial: Polifitou, Tauropos, etc
In-situ Data	• **Chl-a** & • **Secchi disk depth** (Table 1)
Satellite Data	Multispectral **Landsat 8** data • Atmospherically corrected • Maximum 15 days offset (Table 2)
Established Correlations	Linear Regression: • 155 indeces for Chl-a • 105 for Secchi disk (Table 3)
Model Selection	Selection of the regression models with the highest correlations rates
Produce Geospatial Maps	Production of water quality estimation maps (Figure 2)

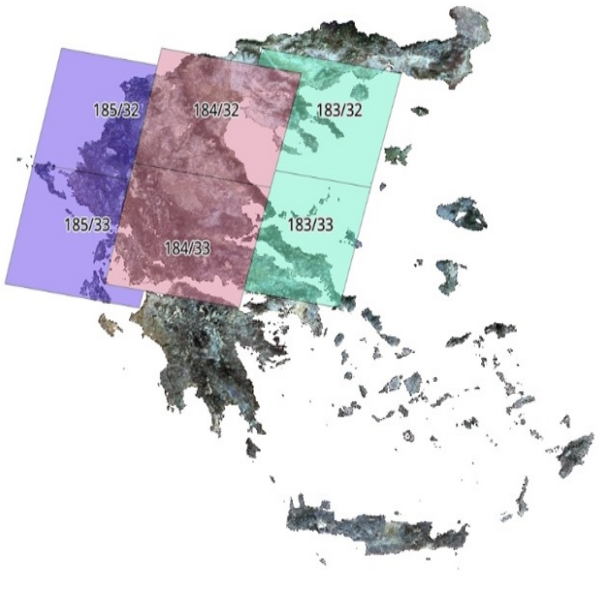

Figure 1. Methodological steps followed and Path/Row Map for Landsat 8 images used.

Table 1. Number of in-situ measurements for the quality parameters / lake

Measurements / Quality Parameter	Chl-a	Secchi Disk Depth	Total Measurements
Amvrakia	8	8	24
Vegoritida	8	8	23
Volvi	8	7	23
Megali Prespa	16	16	47
Trichonida	8	8	24
Yliki	5	5	15
Polifitou	8	8	23
Tauropos	8	8	24
Kastraki	7	7	21
Kremasta	8	8	23
Karla	16	33	49
Total	**100**	**124**	**304**

In order to extract the reflectance values from the selected images at the sampling coordinates, a Python script has been employed. Outliers due to extensive cloud cover and certain inaccurate reflectance calculations during atmospheric correction were excluded.

The possible consistent relationships between the water quality parameters and the satellite reflectance values of Landsat 8 images were examined via regression techniques, and more specifically via simple linear regression. This method was selected in accordance with the empirical models of the literature. Additionally, the correlation between the Chl-a concentration logarithms and the satellite reflectance values was also examined via linear regression equations. Finally, the best regression models were selected and water quality estimation maps were produced for Chl-a and Secchi disk depth spatial distribution.

Due to the large volume of the data, the automation of the process was essential and has been achieved with the implementation of regression analysis through Matlab scripts. The methodological steps mentioned above as well as a path/row map of the Landsat 8 images used are presented in Figure 1.

Table 2. Path, Row, Number of Landsat 8 Surface Reflectance images used / lake

Quality Parameters	Landsat Data		
	WRS Path	WRS Row	Number of images
Amvrakia	184/185	33	29
Vegoritida	184/185	32	26
Volvi	183/184	32	26
Megali Prespa	185	32	15
Trichonida	184	33	12
Yliki	183	33	8
Polifitou	184	32	13
Tauropos	184	33	16
Kastraki	184/185	33	25
Kremasta	184/185	33	31
Karla 1	184	32/33	55
Karla 2	183	33	

3. EXPERIMENTAL RESULTS AND VALIDATION

From the 155 satellite image indices used for Chl-a and ln(Chl-a) and the 105 indices used for Secchi disk depth, the best fitting indices between the water quality in-situ measurements and the high resolution Landsat 8 data are presented in Table 3.

It is worth mentioning that by employing more complex models through for example neural networks higher regression rates may be achieved. However, simple linear, exponential and logarithmic models have been employed in this work, similar to relevant models of the literature, in order to mainly examine the degree of correlation between in-situ observations and high resolution Landsat 8 data for different time windows, number of observations, water quality parameter ranges

and satellite image indices.

Table 3. Regression results for various time windows (dt), number of observations (n), water quality parameter ranges and satellite data indices (b1 to b7 are the atmospherically corrected Landsat 8 bands).

Parameter	**R^2**	**R^2**	**R^2**
Chl-a	**dt = 0-15**	**dt = 0-5**	**dt = 0-3**
	n =168	**n = 54**	**n = 39**
	0.45-118.88 μg/l	**0.45-118.88 μg/l**	**0.45-72.00 μg/l**
b4-b7	0.74	0.77	0.60
exp(b4÷b2)	0.66	0.71	0.77
b3+b4-b5	0.64	0.62	0.52
exp(b4÷(b2+b7))	0.59	0.72	0.77
exp(b4÷(b2+b5))	0.59	0.63	0.80
Chl-a	**dt = 0-15**	**dt=0-3**	
	n=54	**n=13**	
	9.00-118.88 μg/l	**12.52-72.00 μg/l**	
b4-b7	0.63	0.69	-
b3+b4-b6	0.60	0.55	-
b3-b7	0.59	0.63	-
b3-b6	0.57	0.65	-
b2-b6	0.46	0.67	-
Ln (Chl-a)	**dt = 0-15**	**dt = 0-5**	**dt = 0-3**
	n =168	**n = 54**	**n = 39**
	0.45-118.88 μg/l	**0.45-118.88 μg/l**	**0.45-72.00 μg/l**
(b2-b4)÷(b3-b6)	0.78	0.77	0.80
b2-b4	0.76	0.72	0.71
b4÷b2	0.75	0.77	0.79
Secchi disk depth	**dt = 0-15**	**dt = 0-5**	
	n =193	**n =65**	
	0.01-14.00 m	**0.01-1.40m**	
b2÷(b1+b2+b3)	0.70	0.70	-
log(b2÷b3)	0.63	0.63	-
ln((b2-b7)÷(b3-b6))	0.46	0.65	
log(b2÷b3)	0.63	0.63	-
b2÷b3	0.63	0.63	-
b3÷b2	0.60	0.60	

4. DISCUSSION

The experimental results demonstrated quite promising results and were generally in accordance with the literature. In particular, high R^2 values (up to 0.74) have been achieved for the estimation of Chl-a concentration for a concentration range between 0.45 to 118.88 μg/l and 168 observations. A better relation has been achieved with a linear regression of the Chl-a concentration logarithms and the satellite reflectance values (max R^2=0.78, n=168).

Moreover, for a narrower three day time offset between the in-situ sampling date and the acquisition of the satellite image, the correlation rate of Chl-a and ln(Chl-a) with the satellite reflectance values exceeded 0.80 for 39 observations.

The regression models which have been suggested by the relevant literature for Chl-a estimation (Zhang & Han, 2015; Kabbara et al., 2008; Han and Jordan, 2005; Giardino et al., 2007; Hellweger et al., 2004; Theologou et al., 2015; Theologou et al., 2016) have achieved correlations with R^2 ranging from 0.67 to 0.93. However, these results were based on less number of observations and with a relatively narrower time window between the sampling date and the acquisition of the satellite images. It is worth mentioning that in most relevant studies as well as in this work, the models that presented the higher correlation rates for Chl-a always included the red spectral band. Most of the relevant studies did find good relation between Chl-a and a combination of the red with the blue and/or green spectral bands, while in this work relatively high correlations were also established between the red spectral band and the infrared.

Concerning the turbidity, as measured with Secchi disk depth, the experimental results demonstrated a correlation of 0.70 for 193 observations with a depth range from 0.01 to 14 m and

for a 15 day time window. In another experiment, similar R^2 rates were established for 65 observations and a 3 day time offset between the sampling date and the acquisition of the satellite image, but for smaller depth range (0.01-1.40 m). In the relevant literature (Kabbara et al., 2008; Kratzer et al., 2008; Zhang, 2005; Hellweger et al., 2004) the suggested models accomplished correlations with R^2 values ranging from 0.54 to 0.85 but for less observations and relatively narrower time windows. The models with the highest correlation rates, both in this study and the literature, used indices which included the blue, green and red spectral bands and sometimes bands from the infrared spectral region. It is worth mentioning that the best correlation in this study for Secchi disk depth has been achieved by combining the reflectance values of the coastal band of Landsat 8 with the reflectance values of the blue and green spectral bands: b2/(b1+b2+b3).

Overall, the experimental results of this study indicate that high resolution, multispectral satellite data can be operationally employed for remotely monitoring key water quality parameters. Such remote sensing techniques have the advantage of being cost-effective, and have the ability to monitor consistently large areas even over not easily accessible water bodies. In addition, the high resolution remote sensing data can densely map the spatial distribution of the phenomena and provide information for the quality throughout the water body and not only at the sampling points (Figure 2).

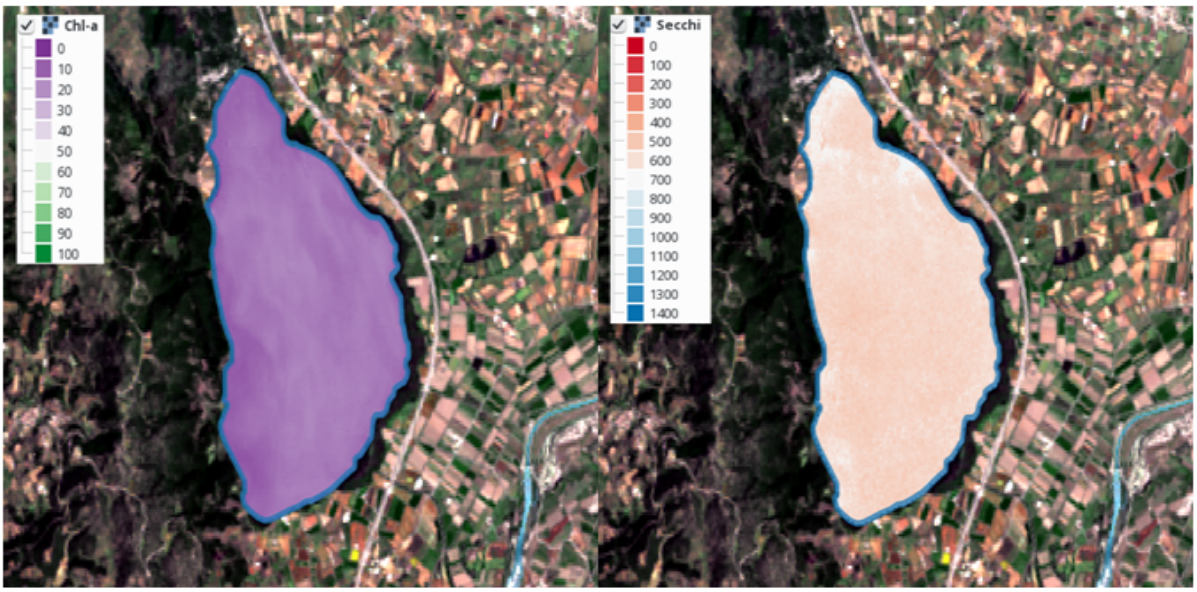

Figure 2. Water quality maps for the lake Amvrakia based on the established Chl-a (b4-b7) and turbidity (b2/(b1+b2+b3)) models.

5. CONCLUSIONS

In this study correlations were established between satellite and in-situ data for 11 representative lakes of Greece. The quite promising results regarding the estimation of Chl-a and turbidity indicate that operational earth observation systems can be developed through frequent satellite image acquisitions and thorough validation with dense spatially and temporarily in-situ data. The provision of the responsible authorities to carry out in-situ sampling as close as possible to the satellite image acquisition could make the evaluation more effective. Improving the calibration of the satellite sensors would also be a new asset for the accomplishment of better water quality parameter estimations. New perspectives for remote sensing technology arise from the upgrade of the satellites' spatial and spectral resolution, as the European Space Agency (ESA) has launched the new earth observation satellites Sentinel II and Sentinel III, and have already broadened the horizons in this field.

REFERENCES

Bukata, P., Bruton, E., & Jerome, H., 1985. Application of direct measurements to the estimation of lake water quality indicators. Environment Canada Inland Waters Directorate.;140:35.

Carder, L., Steward, G., Harvey, G., Ortner. P.,1989. Marine humic and fulvic acids: their effects on remote sensing of ocean chlorophyll. Jurnal of Limnology and Oceanography.; 34: 68-81.

Giardino, C., Brando, V., Dekker, A., Strömbeck, N., Candiani, G., 2007. Assessment of water quality in Lake Garda (Italy) using Hyperion. Remote Sensing of Environment.; 109(2): 183-195.

Han, L., Jordan, K., 2005. Estimating and mapping chlorophyll a concentration in Pensacola Bay, Florida using Landsat ETM data. International Journal of Remote Sensing,; 26 (23): 5245–5254.

Hellweger, Schlosser, L., Lall, U. and Weissel, K., 2004. Use of satellite imagery for water quality studies in New York Harbor. Estuarine, Coastal and Shelf Science.; 61(3): 437-448.

Kabbara, N., Benkheil, J., Awad, M., Barale, V., 2008. Monitoring water quality in the coastal area of Tripoli (Lebanon) using high-resolution satellite data. ISPRS Journal of Photogrammetry & Remote Sensing.; 63, 488–495.

Kloiber, M. S., Brezonik, L. P., Olmanson, G. L., Bauer, E. M., 2002. A procedure for regional lake water clarity assessment using Landsat multispectral data. Journal of Remote Sensing of Environment.;82: 38-47.

Kratzer, S., Brockmann, C., Moore, G., 2008. Using MERIS full resolution data to monitor coastal waters — A case study from Himmerfjärden, a fjord-like bay in the northwestern Baltic Sea, Remote Sensing of Environment.;112(5): 2284–2300.

Le, C., Hu, C., Cannizzaro, .J, Lee, Z., 2013. Evaluation of chlorophyll-a remote sensing algorithms for an optically complex estuary. Remote Sensing of Environment.;Vol. 129: 75-89.

Theologou I., Kagalou I., Papadopoulou M., Karantzalos K., 2016. Multitemporal Mapping of Chlorophyll–α in Lake Karla from High Resolution Multispectral Satellite data, Environmental Processes, Vol. 3(3), pp.681-691.

Theologou, I., Patelaki, M. & Karantzalos K., 2015. Can single empirical algorithms accurately predict inland shallow water quality status from high resolution, multi-sensor, multi-temporal satellite data? ISPRS Archives, Editors: G. Schreier, P. E. Skrovseth, and H. Staudenrausch, International Symposium on Remote Sensing of Environment.; Volume XL-7/W3: pp.1511-1516

Zhang Y., 2005. Surface water quality estimation using remote sensing in the Gulf of Finland and the Finnish Archipelago Sea, Ph.D. thesis, Lab. Space Phys., Helsinki Univ. Technol.;55: 82 p.

Proceedings of the 10th World Congress of EWRA 'Panta Rhei', 5-9 July 2017, Athens, Greece
© 2017 *European Water Resources Association*

Assessment of the environmentally minimum lake level based on morphological features

C. Doulgeris[1*], P. Georgiou[2], A. Apostolakis[1], D. Papadimos[1], Di. Zervas[1], O. Petriki[3], D. Bobori[3], D. Papamichail[2], V. Antonopoulos[2], C. Farcas[4] and P. Stålnacke[4]

[1] *The Goulandris Natural History Museum, Greek Biotope/Wetland Centre, 14th km Thessaloniki-Mihaniona, 57001 Thermi, Greece*

[2] *School of Agriculture, Faculty of Agriculture, Forestry and Natural Environment, Aristotle University of Thessaloniki, 54124 Thessaloniki, Greece*

[3] *Laboratory of Ichthyology, Department of Zoology, School of Biology, Aristotle University of Thessaloniki, 54006 Thessaloniki, Greece*

[4] *Norwegian Institute of Bioeconomy Research, Ås, NO-1431, Norway*

[*] *e-mail: haris@ekby.gr*

Abstract: The determination of environmentally minimum water level in lakes is essential for the protection of their ecosystems. The assessment of minimum water level depends on a number of biotic and abiotic factors of the lake ecosystem; however, in many cases these factors are not easy to collect and assess in their entirety. At the same time, the lakes in many cases consist an important water reserve to meet the requirements arising from economic activities, e.g. industry, agriculture. In this paper, the morphological features in four lakes – Vegoritida, Petron, Cheimaditida and Zazari – of Northern Greece are analysed in order to assess their environmentally minimum water level. The morphological analysis is based on the relationship of the lake surface area and volume with the water level. An optimization method is applied taking into account that the biodiversity is favoured as the surface area covered by the lake is increased and the human water requirements are satisfied to the greatest possible extent by the available water volume of the lake. The environmentally minimum water level determined by the morphological analysis in the four lakes is compared with the minimum water level based on the analysis of the requirements of fish fauna and macrophytes.

Key words: minimum ecological lake level, lake morphological analysis, Vegoritida-Petron-Cheimaditida-Zazari

1. INTRODUCTION

Hydromorphological pressures in aquatic ecosystems are usually associated to the need to control the water level in lakes and the flow in rives for the supply of water to economic sectors, such as industry, hydropower, domestic and agriculture. Also, the lake water volume, which depends on water level, is an easily available source of water to meet the human needs. Thus, the determination of the environmentally minimum water level in lakes is a key for the sustainable management of their ecosystems, as the minimum water level is the critical level below which there should be no further withdrawal to decrease the water level, and hence, ensuring the protection of lake ecosystems.

Many methods exist for the assessment of the environmentally minimum flow in rivers (Tharme, 2003; Jain, 2012); however, only few assessment methods exist to define a minimum water level in lakes and wetlands, probably due to partial understanding of the relationship between lake level and lake ecosystem. Furthermore, minimum water level assessment methods have not been used widely in lake management since they usually consider only part of the factors influencing the lake ecosystem. In general, minimum water level assessment methods include the historical lake level method (Xu et al., 2004; Leeper and Ellison, 2015), lake morphology analysis method (Li et al., 2007; Shang, 2013), habitat analysis method and species-environment models (Cui et al., 2005; Abbaspour and Nazaridoust, 2007; Mjelde et al., 2013). The historical lake level method integrates statistics in historical records, without including a direct connection between historical lake level

and lake ecosystem. The lake morphology analysis method examines the existence of the inflection point in water level-area-volume curves of lakes to determine the minimum water level. On the other side, habitat analysis and species–environment models require intensive and detailed in situ survey.

In this paper, a lake morphological analysis based on the lake surface area-volume relationship is evaluated to assess the environmentally minimum water level of Lakes Vegoritida, Petron, Cheimaditida and Zazari in Greece. The minimum lake level determined by the morphological analysis method is compared with the seasonal minimum lake level based on the analysis of the requirements of fish fauna and macrophytes.

2. MATERIAL AND METHODS

2.1 Case study and data sets

Lakes Vegoritida, Petron, Cheimaditida and Zazari are located in the water district of Western Macedonia in Northern Greece (Fig. 1). The hydrological catchment of the lakes covers an area of 2,145 km^2 and is drained mainly by the streams Sklithro, Amyntas and Pentavryso (or Soulou). The four lakes are connected through the hydrographic network of the catchment and the excess of surface water is transferred from one lake to the other. Specifically, the water level in Lake Zazari is controlled by a weir and above the altitude of 599.7 m a.m.s.l., the excess of water overflows into Lake Cheimaditida via a canal. Similarly, the excess of water in Lake Cheimaditida overflows above 592.0 m into a drainage canal, which is joined downstream to the Amyntas stream, which ends up to Lake Petron. The latter overflows above 573.1 m and the water is driven through a tunnel into Lake Vegoritida.

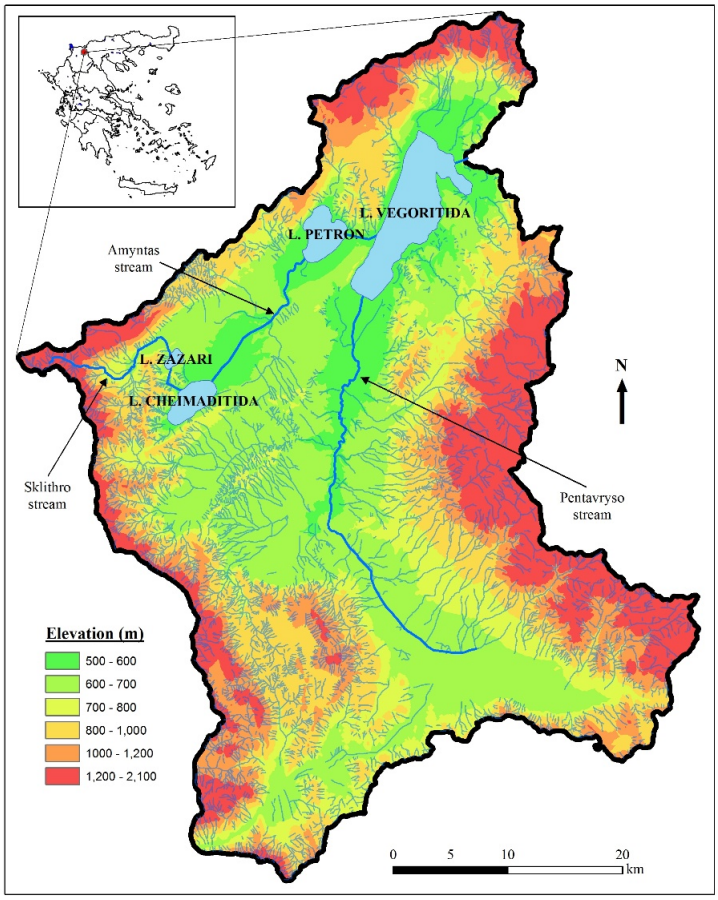

Figure 1. The hydrological catchment of Lakes Vegoritida, Petron, Cheimaditida and Zazari

The economic activities in the catchment that exert pressures in the lakes ecosystems are related mainly with industry and agriculture. Several steam-electric power plants exploit the lignite deposits in the region, consume water and augment the pollution load. Agricultural activity consume water for irrigation and produce non-point pollution; the main crops are wheat, corn, alfalfa and vineyard. Most populated urban areas in the catchment are Ptolemaida and Amyntaio, and the sewage treatment plant of the latter outflows into Lake Petron.

Lake Vegoritida has undergone great changes on its natural environment in the last decades as a result of its water level alteration. Based on water level recordings from the 1980s and afterwards, the water level dropped from 525 m to 510 m a.m.s.l. circa in the early 2000s, mainly due to water abstraction by the Public Power Corporation. During this period the lake has lost 45% of its volume and 29% of its surface area. Ever since the abstraction ceased, the water level is rising and nowadays varies around to 518.5 m.

The morphology of the shallow lakes Cheimaditida and Petron as well as the deeper lakes Zazari and Vegoritida has been studied recently by the Greek Biotope/Wetland Centre, in the context of the National Water Monitoring Network (http://nmwn.ypeka.gr/en). Specifically, the bottom elevation of the lakes Vegoritida, Zazari and Cheimaditida has been recorded by using a portable shallow water echo sounder equipped with GPS and dual frequency capabilities. Elevation data from in situ measurements were enriched by data available in maps from the Hellenic Military Geographical Service and processed by using GIS tools to create the bathymetric Digital Elevation Model (DEM) of each lake. The bathymetric DEMs were used to extract a high accuracy hypsographic curve and water level-volume curve for each lake. In Table 1 are given the hydromorphological features of the lakes at the maximum/overflow water level.

Table 1. Hydromorphological features in Lakes Vegoritida, Petron, Cheimaditida and Zazari

	Vegoritida	**Petron**	**Cheimaditida**	**Zazari**
Surface area (km^2)	47.2	12.6	10.1	2.0
Stored volume (10^6 m^3)	1,206.2	40.8	14.7	9.7
Average depth (m)	26	3.5	1.5	5
Maximum depth (m)	52.6	5.5	4.8	7.6

2.2 Methodology

The morphological features of a lake ecosystem play an important role to the determination of the environmentally minimum water level. In most cases, the morphology of a lake is described adequately by a hypsographic curve, i.e. a relationship of lake's water level-surface area, and a water level-volume curve. Lake surface area is an appropriate index for the habitat protection of lake ecosystems, assuming that the biodiversity in lakes increases with the surface area (Browne, 1981). On the other hand, the water volume stored in a lake could be taken as an index for available water to meet the water requirements for industry, agriculture etc. Based on the above, the lake surface area method has been proposed by Shang (2013) to define the minimum ecological lake level by considering both to protect lake ecosystems and to meet water requirements of economic activities.

Lake surface area increases with the lake volume, but the rate of increase or the slope of surface area-volume (S-V) relationship may increase or decrease with the volume depending on lake morphology, and thus, a critical lake storage at which the lake surface area does not change significantly may exist. The critical storage corresponding to the breakpoint of the lake surface area-volume curve can be used to define the minimum water level in lakes, similarly to the wetted perimeter method for determining the minimum environmental flow in rivers (Gippel and Stewardson, 1998). Specifically, the minimum water level could be calculated from the multi-objective optimization model (Shang, 2008; 2013):

$$\max z_1=s(v)=S(V)/V_{max} \quad (1)$$

$$\min z_2=v=V/V_{max} \quad (2)$$

where z is the water level, and s and v are the dimensionless lake surface area and volume, respectively. The first objective (eq. 1) represents the maximization of lake surface area taking into account that the biodiversity of lake is favoured as the lake surface area increases. The second objective (eq. 2) represents the minimization of lake storage in order to meet the water requirements of economic activities to the greatest possible extent. The solution of the optimization problem results in:

$$\min \{w_1v+w_2[1-s(v)]\} \quad (3)$$

where w_1, w_2 are non-negative weights. Weight w_1 expresses the minimization of lake volume to meet water requirements and w_2 expresses the maximization of lake surface area to protect as much as possible habitats in the lake ecosystem. If the weights have the same value, i.e. $w_1=w_2=50\%$, the two objectives of the optimization model are expressed equally.

3. RESULTS AND DISCUSSION

In Table 2 is given the minimum water level in Lakes Vegoritida, Petron, Cheimaditida and Zazari by applying the analysis of their morphological features. The assessed minimum water level is strongly depended by the values of the weighted factors w_1 and w_2. In Lake Vegoritida for the case of *envScenario* ($w_1=30\%$, $w_2=70\%$), the minimum water level is 1.8 m below the maximum level resulting to a decrease of lake surface area by 3% and to an exploitation of available water volume by 7%. In the cases of *eqScenario* ($w_1=w_2=50\%$) and *wuScenario* ($w_1=70\%$, $w_2=30\%$), the minimum water level is assessed around 27 m and 40 m below the maximum level, respectively; these non-realistic minimum water levels corresponds to a decrease of the lake surface area by 51% and 77%, respectively, compared to the maximum lake surface area. Furthermore, if the *eqScenario* is assumed for example, the lake water volume will be decreased by 933.4 million m^3 (i.e. 77% decrease compared to the maximum water volume) and, based on the lake catchment runoff, several years will be required to the rise of the water level up to its maximum level.

Table 2. Maximum water level and proposed minimum water level according to the morphological analysis in Lakes Vegoritida, Petron, Cheimaditida and Zazari

Water Level (WL), m a.m.s.l.	**Vegoritida**	**Petron**	**Cheimaditida**	**Zazari**
Maximum WL	518.0	573.1	592.0	599.7
Minimum WL, *envScenario*: ($w_1=30\%$, $w_2=70\%$)	516.2	571.1	591.3	596.0
Minimum WL, *eqScenario*: ($w_1=w_2=50\%$)	490.9	570.3	591.2	594.9
Minimum WL, *wuScenario*: ($w_1=70\%$, $w_2=30\%$)	477.9	569.1	589.2	594.0

In Lake Petron, the minimum water level is assessed 2.0 m below the maximum level for the *envScenario*. In this case, the lake surface area and water volume is decreased by 18% and 56%, respectively. According to the *eqScenario*, the minimum water level is 2.8 m below the maximum level resulting to a decrease of lake surface area and water volume by 31% and 75%, respectively.

In Lake Cheimaditida, the minimum water level is assessed 0.7 m below the maximum level for the *envScenario* resulting to a decrease of lake surface area by 17% and water volume by 46%. In the *eqScenario* the assessed minimum water level is similar to the minimum level of the *envScenario*.

In Lake Zazari, the minimum water level is 3.7 m below the maximum level for the *envScenario*

resulting to a decrease of lake surface area by 26% and water volume by 66%. In the case of *eqScenario*, the minimum level is 4.8 m below the maximum level resulting to a decrease of lake surface area and water volume by 37% and 82%, respectively.

It is mentioned that for the *wuScenario* (w_1=70%, w_2=30%), the assessed minimum water level in the four lakes corresponds to an exploitation of the available water volume above 90% and a decrease of the lake surface area among 50 to 90%, which practically leads to a severe disorder of the aquatic ecosystems if not in their disappearance.

Figure 2 shows the monthly minimum water level assessed by the analysis of fish fauna requirements (Petriki and Bobori, 2016) and the analysis of macrophytes requirements (Zervas, 2016) in comparison to the minimum water level assessed by the analysis of lakes' morphological features and according to the *envScenario* (w_1=30%, w_2=70%). In Lake Vegoritida, the minimum level assessed by the morphological analysis is 40 to 90 cm below the water level assessed by the macrophytes analysis and 1.6 m above the water level assessed by the fish fauna analysis. In Lake Cheimaditida, the morphological analysis suggests a minimum water level quite close to the minimum water level proposed by the analysis of fish fauna and macrophytes requirements. In Lake Petron and Lake Zazari, the minimum water level assessed by the morphological analysis is below the minimum level proposed by the species requirements, especially in Lake Zazari.

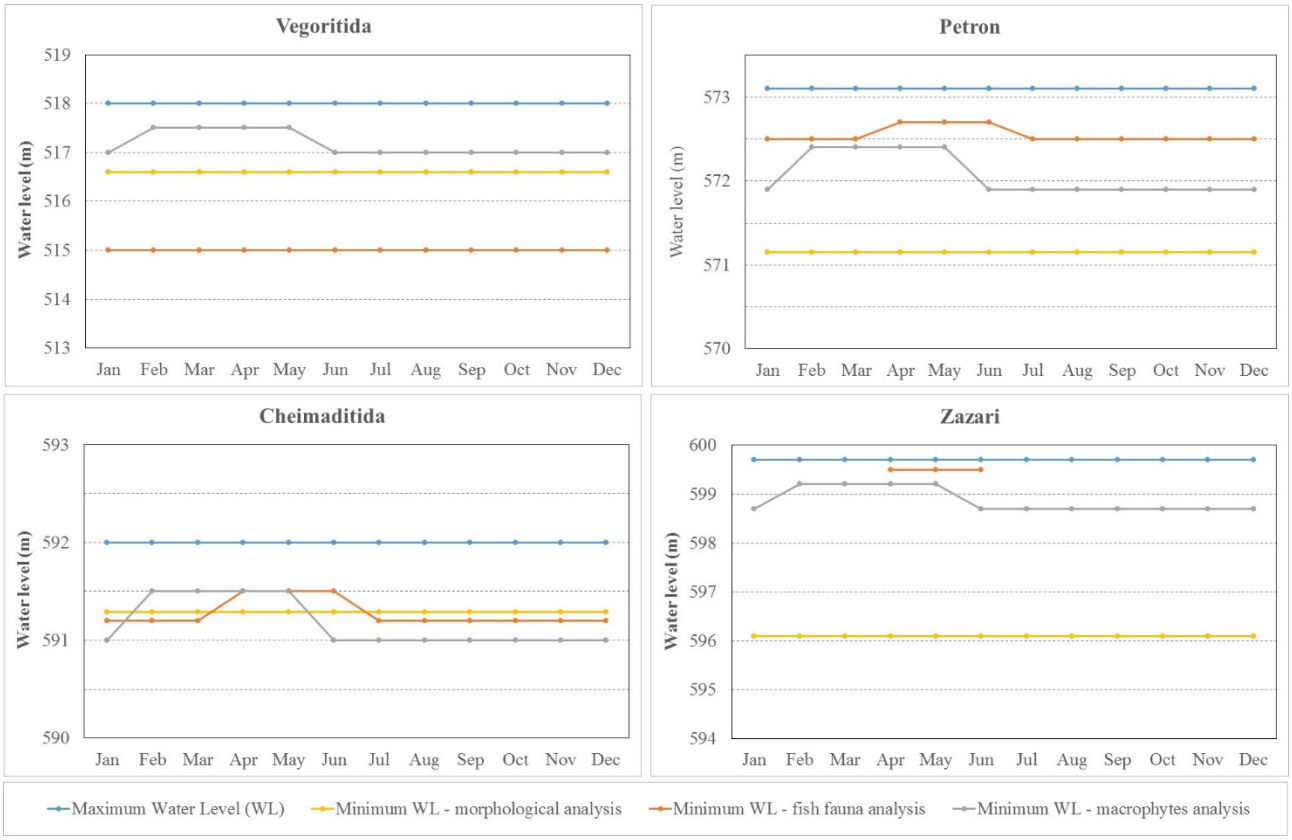

Figure 2. Environmentally minimum water level based on the analysis of species requirements and morphological features in Lakes Vegoritida, Petron, Cheimaditida and Zazari

4. CONCLUSIONS

A lake morphology analysis method based on the hypsographic curve and the water level-volume curve was proven useful to assist a quick decision for a reliable assessment of the environmentally minimum water level in four lakes of Northern Greece. The method propose a balance to protect biodiversity and to meet human water requirements. The application of the method showed clearly that among the three scenarios, only the *envScenario* (w_1=30%, w_2=70%) –

in which the protection of biodiversity is favoured against the fulfillment of human water requirements to the greatest possible extent – may lead to safe assessments of the environmentally minimum water level. Regarding the minimum water level based on the analysis of biological species requirements, the morphological analysis estimates comparable minimum water level in Lakes Vegoritida and Cheimaditida and lower minimum water level in Lake Perton and, especially, in Lake Zazari.

The morphological features of a lake are important data that should be taken into account to the determination of the environmentally minimum water level. The method applied in this paper reconciles the protection of lake ecosystems and the availability of water volume to meet the economic activities.

ACKNOWLEDGEMENTS

This work is part of the project «Improving the knowledge in determining the minimum water level and flow of water bodies» (http://eordaia-nestos.gr/en), which is financed by the European Economic Area Financial Mechanism 2009-2014 and the Public Investment Program.

REFERENCES

Abbaspour, M., Nazaridoust, A., 2007. Determination of environmental water requirements of Lake Urmia, Iran: an ecological approach. International Journal of Environmental Studies, 64(2): 161–169.

Browne, R. A., 1981. Lakes as islands: biogeographic distribution, turnover rates, and species composition in the lakes of central New York. Journal of Biogeography, 8(1): 75–83.

Cui, B. S., Zhao, X., Yang, Z. F., 2005. Eco-hydrology-based calculation of the minimum ecological water requirement for lakes. Acta Ecologica Sinica, 25(7): 1788–1795.

Gippel, C. J., Stewardson, M. J., 1998. Use of wetted perimeter in defining minimum environmental flows. Regulated Rivers: Research & Management; 14(1): 53–67.

Jain, S. K., 2012. Assessment of environmental flow requirements. Hydrological Processes, 26(22): 3472–3476.

Leeper, D. A., and Ellison, D.L., 2015. Proposed Minimum and Guidance Levels for Lake Hancock in Polk County, Florida. Southwest Florida Water Management District. Brooksville, Florida.

Li, X. H., Song, Y. D., Li, Y. T., et al. 2007. Calculation methods of lowest ecological water level of lake. Arid Land Geography, 30(4): 526–530.

Mjelde, M., Hellsten, S., Ecke, F., 2013. A water level drawdown index for aquatic macrophytes in Nordic lakes. Hydrobiologia; 704:141–151

Petriki, O., Bobori, D., 2016. Analysis of fish fauna requirements on minimum seasonal water level and water quality in Lakes Zazari, Cheimaditida, Petron and Vegoritida (D.A1.1). Fisheries Research Institute (INALE). N. Peramos, Greece. 67 p.

Shang, S. H., 2008. A multiple criteria decision-making approach to estimate minimum environmental flows based on wetted perimeter. River Research and Applications, 24(1): 54–67.

Shang, S. H., 2013. Lake surface area method to define minimum ecological lake level from level–area–storage curves. J Arid Land; 5(2): 133−142.

Tharme, R. E., 2003. A global perspective on environmental flow assessment: Emerging trends in the development and application of environmental flow methodologies for rivers. River Research and Applications, 19(5–6): 397–441.

Xu, Z. X., Chen, M. J., Dong, Z. C., 2004. Researches on the calculation methods of the lowest ecological water level of lake. Acta Ecologica Sinica, 24(10): 2324–2328.

Zervas, D., 2016. Analysis of aquatic macrophytes requirements on minimum seasonal water level and water quality in Lakes Zazari, Cheimaditida, Petron and Vegoritida (D.A1.2). Greek Biotope/Wetland Centre (EKBY). Thermi, Greece. 63 p.

Proceedings of the 10th World Congress of EWRA 'Panta Rhei', 5-9 July 2017, Athens, Greece
© 2017 *European Water Resources Association*

Critical review of adaptation strategies for the restoration of Lake Koronia

D. Malamataris[1*], E. Kolokytha[1], I. Mylopoulos[1] and A. Loukas[2]
[1] *Laboratory of Water Resources Management, Department of Civil Engineering, University of Thessaloniki, University Campus, 54124 Thessaloniki, Greece*
[2] *Laboratory of Hydrology and Aquatic Systems Analysis, Department of Civil Engineering, University of Thessaly, Pedion Areos, 38334 Volos, Greece*
[*] *e-mail: dmalamat@civil.auth.gr*

Abstract: Lake Koronia water basin, located in Northern Greece, depicts a characteristic example of non-sustainable water management case in Greece. The irrational pumping for irrigation in the catchment resulted in the overexploitation of groundwater resources and a serious decrease in the runoff to lake Koronia. Furthermore, the reduction of the mean annual precipitation and the increase of the mean annual temperature, and, therefore, the evaporation that were being observed in the area, due to climate change, are expected to further deteriorate the already distributed water balance of the lake. UTHBAL model along with MIKE SHE and MIKE HYDRO BASIN models are utilized in the present study for the calculation of the historical (1970-1999) and future (2020-2049, 2070-2099) water balances of lake Koronia. The water balance of the lake for the long-term time period was found to be negative even after the implementation of the adaptation measures that have been proposed in the most recent revised Master Plan for the restoration of the lake. An assessment of the efficiency of the most important measures that have already been implemented, in terms of decreasing the future water deficit of the lake, is carried out. The paper concludes that even after the implementation of the measures the water balance of lake Koronia still remains negative for the long-term future period and so complementary adaptation measures should be implemented in order to restore the negative water balance of the lake.

Key words: Lake Koronia, water balance, adaptation measures, climate change, Master plan

1. INTRODUCTION

Lake Koronia case study is a complex problem that needs an integrated approach taking into consideration social, technical, environmental, political and economic aspects in order to be efficiently resolved. In terms of water quality, many studies have been carried out (e.g. Perivolioti, T.M. et al., 2016; Moustaka-Gouni, M., et al., 2012) about ecological changes that have been occurred in lake Koronia during the last decades threatening its ecosystem.

In terms of water quantity, the number of studies regarding the water balance problem of the lake are limited. In their studies, Manakou et. al. (2013) developed a mathematical programming approach to restore the water balance of the hydrological basin of lake Koronia and they concluded that investment options including the water transfer from larger water sources, the creation of irrigation networks and canals and provision of subsidies to promote alternative land use for agriculture need to be taken. Kolokytha (2010) examined the contribution of Water Framework Directive and EU Common Agricultural Policy application in Lake Koronia towards the rehabilitation of its water balance in the future and she concluded that both European Policies can help to reduce the water problem of the lake but cannot solve it themselves. Mylopoulos et al. (2007) developed a groundwater model to simulate the lake Koronia-aquifer interaction and they suggested that a combination of a project recharging the lake with groundwater and water saving measures in the agricultural sector must be implemented to confront the water depletion of the lake.

2. STUDY AREA

Mygdonia water basin is located in Northern Greece and it belongs to the Water District of

Central Macedonia. The water basin covers an area of 2.061,48 km^2 and the mean elevation is 338 m. Lakes Koronia and Volvi are located at the lowest part of the basin at about 10 km and 35 km eastern of the city of Thessaloniki. Both lakes compose a wetland that affects and, also is being affected by the current economic activities in the whole catchment. The wetland is protected by several international and national laws. In particular, it constitutes a "Wetland of International Importance" (Ramsar site), a "Special Protection Area" (Directive 79/409/EEC), a "Site of Community Importance" (Directive 92/43/EEC) and a "National Wetland Park of Lakes Koronia – Volvi and Macedonian Tempi".

Mygdonia catchment (figure 1) was divided into the Koronia subcatchment (768.11 km^2) and the Volvi subcatchment (1.293,37 km^2). Afterwards, each one of them was further divided into six and thirteen subcatchments respectively in order for the surface water bodies to be more efficiently studied.

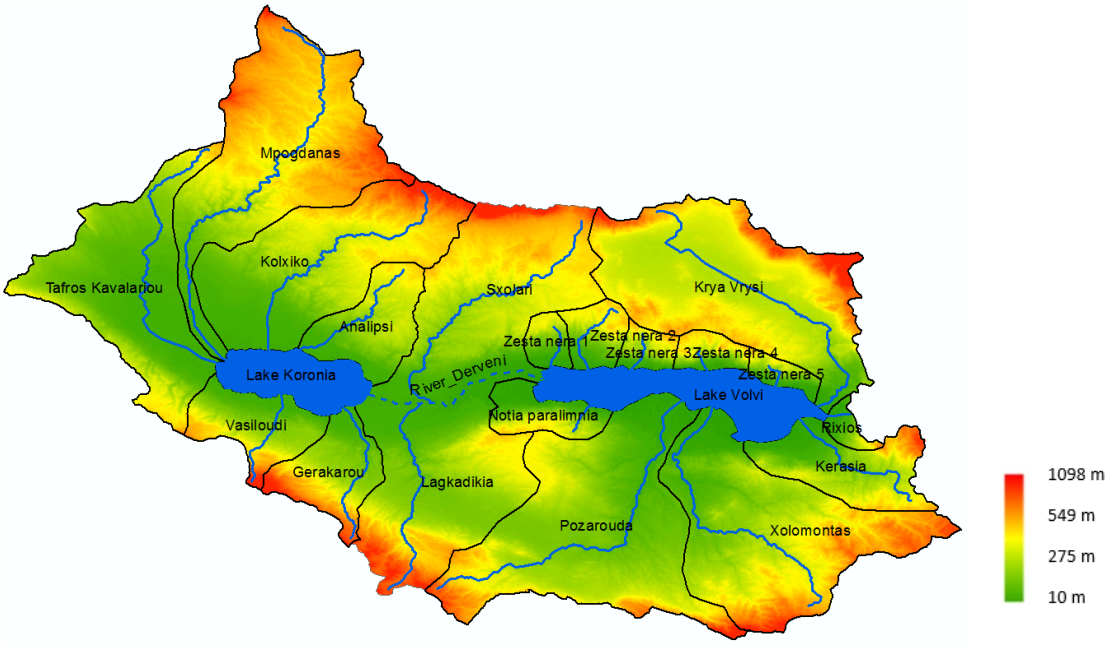

Figure 1. The nineteen subcatchments of the Mygdonia catchment

3. CALCULATION OF THE WATER BALANCE OF LAKE KORONIA

An integrated hydrological study has been carried out for the simulation of water inflows and outflows to lake Koronia. In particular, three different models have been applied: the UTHBAL hydrological model for the simulation of the surface hydrological processes, the MIKE SHE model for the simulation of the hydraulic interaction between lake Koronia and groundwater, and finally, the MIKE HYDRO BASIN model for the simulation of the water balance of the lake.

3.1 Simulation of surface hydrological processes

The conceptual hydrological model UTHBAL (University of Thessaly water BALance model) (Loukas et al., 2007) has been used for the calculation of the hydrological parameters for the historical period 1970-1999.

UTHBAL model has six parameters to be optimised in order to estimate the hydrological cycle parameters. The model uses monthly time-series of areal precipitation, mean areal temperature, mean areal potential evapotranspiration and observed monthly discharge values as inputs. Mean areal surface precipitation and temperature for the whole Mygdonia catchment were calculated

equal to 518.69 mm/year and 13.27 ^{O}C using the Thiessen method along with the precipitation gradient method, and the temperature gradient method respectively. Mean areal potential evapotranspiration was calculated using the Thornthwaite method, and, finally observed monthly discharges of Mpogdanas, Analipsi, Lagkadikia, Sxolari, Gerakarou and Vasiloudi streams as measured at the outfall points for the period 1995-1999 (Veranis and Katirtzoglou, 2001) were also imported to the model.

The model was calibrated and validated with the observed monthly discharges of the six streams and the monthly hydrological cycle components for each one of the six subcatchments were calculated. The six hydrological parameters of the UTHBAL model were then transferred to the other thirteen subcatchments based on land use, slope and geological criteria in order to estimate the hydrological parameters of these subcatchments too.

The main outputs of the model are monthly time series of actual evapotranspiration, surface runoff and groundwater recharge. Mean annual runoff to lake Koronia was calculated equal to 7.49 hm^3/year. It must be noted that only limited water amounts (about 6 hm^3/year) flow into lake Koronia after the year 1985 due to the extensive pumping in the surrounding area that has resulted in the increase of recharge to groundwater and decrease of the surface runoff (Veranis and Katirtzoglou, 2001).

3.2 Simulation of groundwater resources

Mygdonia catchment is an endorheic basin in hydrogeological terms (Mpallas, 2007). The groundwater flow follows the longitudinal axis of the catchment; in normal conditions groundwater flows from Koronia subcatchment to Volvi subcatchment, and then a part of this discharge outflows to a neighbouring subcatchment at the eastern part of the Mygdonia catchment.

Mygdonia groundwater simulation was performed using the MIKE SHE model. At first, the catchment was divided into six groundwater subcatchments (Koronia, Volvi, Mavrouda, Kroussion-Kerdyllion, Nteve Koran and Xolomonta-Oraiokastrou) for the analytical study of groundwater resources. Geometrical and hydraulic parameters, namely upper level, lower level, horizontal hydraulic conductivity, vertical hydraulic conductivity, specific yield and storage coefficient were imported to the groundwater model for each layer of each one of the above six groundwater subcatchments. Also, daily time-series of recharge to groundwater and pumping for agricultural, livestock, tourist and household water needs were also imported to the model.

The whole catchment of Mygdonia was divided into 8,244 grid cells (500x500 m the area of each grid cell) and the simulation was carried out from 01 October 1970 until 30 September 2000 with a daily time step. It was found that there is no hydraulic interaction between groundwater and lake Koronia.

3.3 Simulation of lake Koronia

Lake Koronia covers a maximum area of 46.03 km^2, its bed elevation is 66.50 m above the sea level and it has a maximum depth of 6.50 m. Lake Volvi is located at 11 km eastern of lake Koronia and its bed elevation is 52.50 m lower than the one of lake Koronia. The overflow of lake Koronia flows by gravity through an artificial drainage ditch called River Derveni and it outflows to lake Volvi (figure 1). Nowadays, the physical interaction between the two lakes has been interrupted because of the tremendous decline of the water depth of lake Koronia.

Mean annual precipitation and evaporation for the lake Koronia were calculated equal to 20.61 hm^3/year and 29.51 hm^3/year respectively from 1970 until 1999. As for the pumped water from the lake, according to the article 4, paragraph 2 of the Joint Minesterial Decision 6919/2004, pumping from lake Koronia is prohibited.

Simulation of inflows and outflows to lake Koronia was performed using the MIKE HYDRO BASIN model at a daily time step for the historical period 1970-1999. It was found that lake

Koronia had an average negative water balance of -1.41 hm^3/year. The water level variation of lake Koronia for the period 1970-1999 is presented in Figure 2. The continuously decreasing trend of the water level of the lake is a result of the decreasing trends of precipitation and runoff to lake, and the increasing trend of evaporation from the lake.

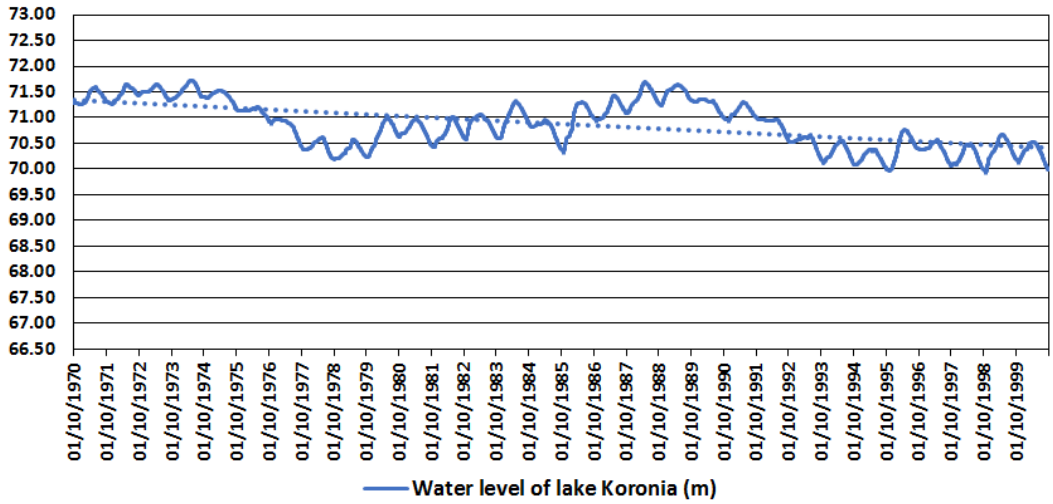

Figure 2. Water level of lake Koronia for the period 1970-1999

4. LAKE KORONIA WATER BALANCE REHABILITATION STRATEGIES

4.1 Revised Plan for the restoration of lake Koronia

In 1998, Knight Piesold Ltd. & Karavokyris and Partners conducted a "Master Plan" for the restoration of lake Koronia proposing a number of alternative measures to confront its water deficit. In 2004, a "Revised plan for the restoration of lake Koronia in the Prefecture of Thessaloniki" was carried out revising the Master Plan and proposing several scenarios to fulfil the Master Plan goals. Both the Master Plan and the Revised Plan have focused on lake Koronia considering it within the broader context of the Koronia subcatchment. In this study, a more integrated analysis considering the surface-groundwater interaction for the whole Mygdonia catchment has been carried out for the calculation of input and output water amounts to lake Koronia.

The Revised Plan proposes three scenarios for the quantitative and two others for the qualitative rehabilitation of lake Koronia. The three scenarios regarding the quantitative rehabilitation of lake Koronia are presented below: (a) *Ecosystem connectivity and exports from lake Koronia*: Under normal conditions water and nutrient exports from lake Koronia drain into lake Volvi and so they are considered as important driving factors for the structure and ecosystem operation of both lakes. Lake Koronia is in danger of becoming a permanently closed basin because of its significant water level decrease. Therefore, the maximum level of lake Koronia was proposed to be declined from 73 m to 72 m. Also, embankments were constructed at the Western part of the lake resulting to the decrease of the maximum surface area and volume of the lake at about 2.59 km^2 and 41.72 hm^3 respectively. (b) *Streams diversion:* Sxolari and Lagkadikia streams drain a wide area in the northern and southern part of the Mygdonia catchment respectively and they outflow to the artificial ditch. It was proposed two spillways to be constructed before their outflow to the ditch in order the 15% of the Sxolari stream discharge and the total discharge of Lagkadikia stream to outflow to lake Koronia. (c) *Rehabilitation of the groundwater aquifer:* The irrational pumping for irrigation has resulted in a very significant pressure on the water resources of the area and the continuously decline of the groundwater table. The wells surrounding the Mpogdanas stream are proposed to be removed and a public irrigation network to be established.

4.2 Review of the lake Koronia water balance rehabilitation strategies

The proposed measures in the "Revised plan for the restoration of lake Koronia in the Prefecture of Thessaloniki" do not take into account climate change effects. In this paper, their suitability, in terms of confronting the water deficit of the lake for the future time periods, is tested.

At first, monthly precipitation and temperature data were calculated for a mid-term (2020-2049) and a long-term (2070-2099) time period. Raw monthly precipitation and temperature data of the KNMI-RACMO2 GCM-RCM (Global Climate Model – Regional Climate Model) under the SRES A1B (IPCC, 2007) were collected from the EU ENSEMBLES project database for the periods 1970-1999, 2020-2049 and 2070-2099 at a 25-km resolution. Because of the significant bias in the raw model projections, the Bias Correction Quantile Mapping (BCQM) method was selected to be performed in order to reduce the bias in the GCM-RCM projections for both precipitation and temperature. The BCQM method has been successfully used in many studies to correct RCM outputs over Europe (e.g. Sunyer et al., 2015; Gudmundsson et al., 2012). In this study, BCQM was implemented in *R* programming language using the *qmap* package. After the implementation of the BCQM, it was found that the mean annual surface precipitation and the mean monthly temperature for the whole Mygdonia catchment will be equal to 499.50 mm and 486.67 mm, and 13.65 ^{O}C and 14.57 ^{O}C for the mid-term (2020-2049) and the long-term (2070-2099) periods respectively.

The first two of the quantitative measures described in the previous section, namely the "Ecosystem connectivity and exports from lake Koronia" and the "Streams diversion" were taken into account in this study since they have already been implemented. The third measure has not been further described in the Revised Plan since the exact number and location of the agricultural wells were unknown until the end of the year 2016 when all the illegal wells have been recorded. However, these data have not been provided for public use yet.

The mean water balance of lake Koronia was calculated equal to 0.04 hm^3/year and -3.42 hm^3/year for the mid-term (2020-2049) and long-term (2070-2099) periods respectively. Hydrological inputs and outputs to lake Koronia for the historical and future periods are presented in Table 1. It was found that the already implemented infrastructure works in lake Koronia cannot confront its negative water balance which will be further deteriorated until 2100 due to climate change.

Table 1. Historical and future water balance of lake Koronia

	1970-1999	**2020-2049**	**2070-2099**
Inflows to lake (hm^3/year)			
Precipitation	20.61	19.76	19.10
Runoff	7.49	11.24	10.48
Outflow from groundwater to lake	0.00	0.00	0.00
Outflows from lake (hm^3/year)			
Evaporation	29.51	30.14	32.39
Recharge to groundwater	0.00	0.00	0.00
Outflow from lake to River Derveni	0.00	0.82	0.61
Water balance (hm^3/year)	**-1.41**	**0.04**	**-3.42**

5. CONCLUSIONS AND DISCUSSION

The negative water balance of lake Koronia for the long-term future period reveals the deficiency of the proposed technical measures of the Revised Plan to confront the problem of the negative water balance on their own. Additional measures need to be taken for the restoration of the water balance of the lake. Those measures should be both structural and non-structural. A possible option is the development of a structural model providing farmers and policymakers with an understanding of how to improve adaptation in order to reduce climate-driven compensations to agriculture, since agriculture is the main water consumer in the area. Reforms in the agricultural sector, may require a change towards more heat-tolerant and less water intensive crops. Technical interventions, in terms of irrigation technique improvements would also provide valuable water

conservation.

As the development model in the area is mainly based on agricultural activities, the restoration of the lake would need a brave shift towards new development activities that are based on the carrying capacity of the whole ecosystem. Solutions should be built taking advantage of the main strengths of the area such as the natural landscape, human resources and crops compatible with the climate and the soil.

This work is part of a PhD thesis which is currently investigating potential land use changes and other structural and non-structural measures in providing a new sustainable development model for the area.

ACKNOWLEDGEMENTS

This research was funded by the Greek State Scholarships Foundation (IKY) – SIEMENS Programme under the conciliation agreement between the Greek Republic and SIEMENS. Special thanks to DHI for the kind provision of the software MIKE SHE and MIKE HYDRO BASIN licence that was used for the modelling tasks of this paper and their support throughout the modelling process.

REFERENCES

Gudmundsson, L., Bremnes, J. B., Haugen, J. E., and Engen-Skaugen, T., 2012. Technical Note: Downscaling RCM precipitation to the station scale using statistical transformations – a comparison of methods, Hydrol. Earth Syst. Sci., 16, 3383–3390.

IPCC, 2007. Summary for Policymakers. In: Climate Change 2007: The Physical Science Basis. Contribution of Working Group I to the Fourth Assessment Report of the Intergovernmental Panel on Climate Change [Solomon, S., D. Qin, M. Manning, Z. Chen, M. Marquis, K.B. Averyt, M.Tignor and H.L. Miller (eds.)]. Cambridge University Press, Cambridge, United Kingdom and New York, NY, USA.

Kolokytha, E., 2010. European policies for confronting the challenges of climate change in water resources. Current Science, 98(8).

Loukas, A., N. Mylopoulos, and L. Vasiliades, 2007. A modeling system for the evaluation of water resources management strategies in Thessaly, Greece. Water Resources Management, 21(10), 1673-1702.

Manakou, V., Tsiakis, P., & Kungolos, A., 2013. A mathematical programming approach to restore the water balance of the hydrological basin of Lake Koronia. Desalination and Water Treatment, 51(13-15), 2955-2976.

Moustaka-Gouni, M., Michaloudi, E., Kormas, K.A., Katsipai, M., Vardaka, E., & Genitsaris, S., 2012. Plankton changes as critical processes for restoration plans of lakes Kastoria and Koronia. European Water, 40, 43-51.

Mpallas, L., 2007. Implementation of fuzzy rules in the water resources management – Case study of the Volvi catchment. Phd thesis submitted in School of Rural and Surveying Engineering, Aristotle University of Thessaloniki, Thessaloniki, Greece.

Mylopoulos, N., Mylopoulos, I., Kolokytha, E., & Tolikas, D., 2007. Integrated water management plans for the restoration of Lake Koronia, Greece. Water International, 32(S1), 720-738.

Perivolioti, T.M., Mouratidis, A., Doxani, G., & Bobori, D., 2016. Monitoring the Water Quality of Lake Koronia Using Long Time-Series of Multispectral Satellite Images. In Lining Planet Symposium, 740, 249.

Sunyer, M. A., Hundecha, Y., Lawrence, D., Madsen, H., Willems, P., Martinkova, M., Vormoor, K., Burger, G., Hanel, M., Kriauciunien, J., Loukas, A., Osuch, M. and Yucel., I., 2015. Inter-comparison of statistical downscaling methods for projection of extreme precipitation in Europe. Hydrology and Earth System Sciences, 19(4), 1827-1847.

Veranis, N. And Katirtzoglou, K., 2001. Study of the potential of the deep aquifer of the lake Koronia subcatchment. Calculation of the water balance of the Koronia subcatchment. Greek Institute of Geology and Mineral Exploration.

Proceedings of the 10th World Congress of EWRA 'Panta Rhei', 5-9 July 2017, Athens, Greece
© 2017 *European Water Resources Association*

Evaluating the ecological restoration of a Mediterranean reservoir

P. Sidiropoulos[1,2], M. Chamoglou[1] and I. Kagalou[1,3*]
[1] *Management Body of Ecodevelopment Area of Karla - Mavrovouni – Kefalovriso – Velestino, Stefanovikio, Greece*
[2] *University of Thessaly, School of Engineering, Department of Civil Engineering, Laboratory of Hydrology and Aquatic Systems Analysis, Volos, Greece*
[3] *Democritus University of Thrace, School of Engineering, Department of Civil Engineering, Sector of Hydraulics, Xanthi, Greece*
[*] *e-mail: ifikagalou@gmail.com*

Abstract: The restoration of Lake's Karla environment and ecosystem is studied through the evaluation of its current status. Its drainage, in 1962, created a series of environmental problems and led to the local economy contraction. The Lake Karla reconstruction project has begun since 2000. The construction of a reservoir at the lowest part of Lake Karla watershed is among the parts of this project, which will be supplied from Pinios River and the runoff of the surrounding mountains. This newly re-established water body is considered a vital aquatic ecosystem as it is listed in the network of Natura 2000 and has been characterized as a Permanent Wildlife Refuge by Greek Law. The results indicate that the delay of implementation of Lake Karla reconstruction project, the violation of Environmental Terms and the lack of environmental policy are the most important cause of pressures.

Key words: ecosystem restoration, eco-technology, anthropogenic pressures, biodiversity

1. INTRODUCTION

Lake Karla (Thessaly, Greece) was considered one of the most important shallow lakes in Greece until 1962, where complete drying of the lake took place - creating more agricultural land - and is now being re-constructed, establishing a 'new' reservoir offering multi services (i.e social, economic and ecological sustainable development of the region). Prior to 1960's Lake Karla was considered one of the most important hydro-ecosystems in the region as it served as a natural reservoir providing water storage and recharge to groundwater. Accordingly the importance of restoring this water body and reversing the environmental conditions caused by manmade activities was considered of high importance by the European Union. The concept of the Lake Karla' restoration project is, probably, the first European project towards nature conservation following the eco- technological approach. The Karla's project has been recognized as an important opportunity for addressing the complex challenges in the hydro-ecological management in the main agricultural region of Greece with growing demand of freshwater, providing also the traditional and new services to the people.

In this paper we discuss the restoration approach of Karla Lake as well as the pressures and their causes that negatively affect the restoration process. This is achieved by evaluating the results of the monitoring and fieldwork programs that Management Body of Ecodevelopment Area of Karla – Mavrovouni – Kefalovriso - Velestino performs the years 2012-2013 funded by the European Union.

2. THE STUDIED SITE-DATA DESCRIPTION

2.1 The biogeographical context

Former Lake Karla occupied the lowest part of its natural basin and was considered as one of the

most important wetlands in Greece until 1962. Surface runoff from the watershed and floodwaters of the Pinios River (discharging via the Asmaki ditch) supplied the lake with large quantities of freshwaterThe river occasionally overflowed, and floodwaters rich in oxygen and nutrients drained into Karla. Much of the surrounding farmland was inundated when floodwaters were held in the lake, but today, the river is levelled to prevent flood damage. The climate of the area is typical continental with cold and wet winters and hot and dry summers. Mean annual precipitation in the lake's watershed is about 560 mm and is distributed unevenly in space and time. Mean annual potential evapotranspiration is about 775 mm and the mean annual temperature is 14.3^{o}C (Vasiliades et al. 2009). The geological structure consists mainly of recent grains of various sizes originating from the lake's deposits. The decision for the complete drying of the lake in 1960s took place in order to create more land for agriculture and to avoid the flooding of the low elevation lands because of its surface area fluctuations.

2.2 The project design

Technical studies, recommended draining the lake via the Karla Tunnel and building a smaller reservoir instead of the natural lake for flood protection and for the revelation of agricultural fields. The re-constructed Lake Karla occupies the lowest part of the former Lake Karla. It lies between latitude 39°26′49′′S to 39°32′03′′N and longitude 22o46′47′′W to 23o51′50′′E and has a surface of 38 km2. It is characterized by its shallow depth with a maximum water depth of 4.5 m and a mean depth of 2 m.

Among the targeted measures were: the establishment of riparian zones to control the diffuse agricultural pollution sources, the operation of a peripheral buffer zone for the elimination of the nutrients input, the establishment of habitats corridors to avoid the ecosystem fragmentation and to improve the re-habilitation, the re-operation of a controlled outlet to improve flushing effect minimizing the water retention time, the construction and operation of artificial wetland for the improving of water quality, the construction of fish ladders at Pinios pumping station, the re-organization and the modification of the agricultural strategy in the whole region according to agri-environmental friendly practices.

Finally, the restoration plan included the designation of the area as a protected Eco development area under the Natura 2000 network because of its biodiversity and the establishment of a Management Body which is responsible for the implementation of the restoration plan, the monitoring program, and the application of management principles taking into consideration the local socio-economic needs.

2.3 The post-monitoring program

A monthly monitoring programme of water quality took place from January 2012 to July 2013 in three sampling stations (Fig. 1). The European Directives (i.e the Water Framework Directive and the Habitat Directive) were used as guidelines for the applied methodology, with respect to the characterization of the water body and for the assessment of its status. More details about the sampling and monitoring methodology concerning nutrients (Dissolved Inorganic Nitrogen, DIN, Total Phosphorus, TP), turbidity (Secchi depth), Chlorophyll-a as a proxy of algal biomass have been described in detail and published by Sidiropoulos et al. (2012) and Chamoglou et al. (2014). Also, monthly lake level was recorded throughout the years 2012, 2013. In the present paper the hydrological regime and the eutrophication trends are discussed under the light of the pressures and the undertaken measures.

3. RESULTS

The design of the restoration project and the establishment of the protected area have been addressed the increase of the provisional services as well as the promotion of regulating services and yet, the re-establishment of the cultural services delivered in the wide area named: Eco development Area of Karla-Kefalovriso-Mavrovounio-Velestino (Fig. 1).

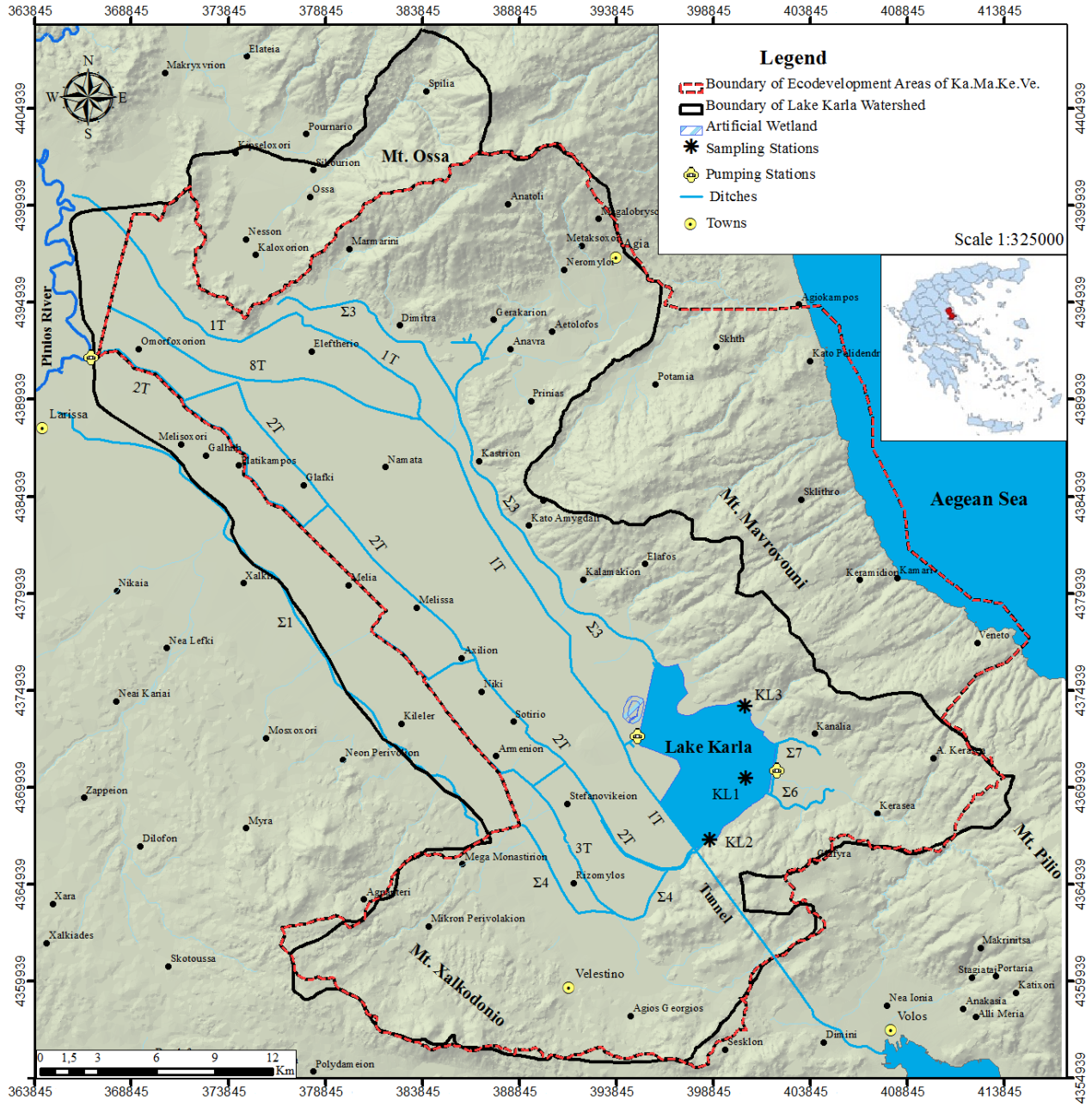

Figure 1. Map of Eastern Thessaly showing the boundaries of Lake Karla Watershed and Ecodevelopment Area. The monitoring stations (water quality) are also depicted.

In the former Lake Karla, there was no a natural surface outlet of the aquatic system Pinios River-Lake Karla, while it is thought that discharge took place through a system of karstic sinkholes of Mavronouni Mountain to Pagasitikos Gulf (Fig. 1). Nowadays, this discharge has been avoided with the creation of a non flow embankment, where the new reservoir meets the kartsic structures of Mavrovouni Mountain. So, the new Lake Karla is supposed to be drained artificially, by means of a tunnel (Fig. 1) to the Pagasitikos Gulf, which – at present - is closed and operates only in

emergency situations. Thus, water losses from Lake Karla are through evaporation, withdrawals for irrigation and recharge to the aquifer.

Figure 2 demonstrates the water level fluctuation in Lake Karla during the years 2012 and 2013. It comes clear that the water level in the new reservoir was always lower than lowest ecological limit (+46.4 m), except once, on the 11/06/2012. This happens because the reservoir receives less water inputs since 2012 both from its basin because of unfinished works, and from Pinios River due to an interruption in their connection but also due to the withdraws before the river inflows the reservoir. During the winter period, precipitation feeds the lake while, at the moment, the Karla reservoir experiences intra-annual water level fluctuations due to the bad and unsustainable management of the inflows from Pinios river.

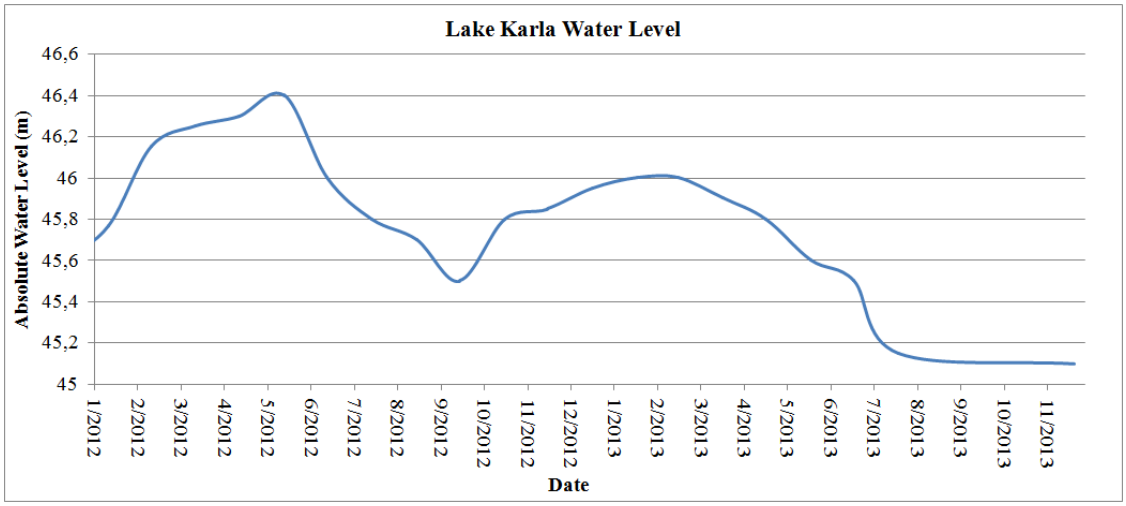

Figure 2. Water lever fluctuation of Lake Karla for the years 2012 and 2013.

3.1 Water quality/eutrophication

In Figure 3, the monthly variation of the key- eutrophication parameters (Nitrate-N, Ammonia-N, Total Phosphorous) along with the Secchi depth (SD) and Chlorophyll-a are presented. The water quality variables and the nutrients dynamics, are thought to be strong predictors of the trophic status. With regard to nutrient concentrations, Nitrate-N was always the most important form, in terms of percentage contribution, in the Dissolved Inorganic Nitrogen pool, exhibiting higher values during the summer months while Ammonium-N ranged from 0.009 mg/lt (June 2012) to 0.511 mg/lt (June 2013). Also, mainly the first year of sampling period, Ammonia-N concentrations were found a lot times above the value of 0.2 mg/lt, which is the limiting value for fish intoxication, according to the European Directive (2006/44). Total Phosphorus (TP) fluctuated between 0.004 mg/lt (March 2013) and 0.461 mg/lt (April 2012) appearing also high values during the warm months. The peak value of TP coincides with high inflows by the drainage channel located at the southeast part of the lake (Management Body Report 2012). Chlorophyll- α ranged between 6.19 mg/cm^3 (January 2012) and 403.58 mg/cm^3 (August 2012), with higher values recorded during the warmer months indicating a strong hypertrophication. The new reservoir did not appear any clear phase during the monitoring period as the Secchi depth ranged between 0.19 and 0.5 m reflecting its turbid character.

3.2 Pressures and mitigation measures

In Table 1 the main pressures affecting the new reservoir are presented along with the relevant measures undertaken, the ecosystem's state and the associated impacts on its goods and services. Pressures were separated in five categories while some of the relevant measures were implemented

to a percentage up to 50% while the implementation of other did not started at all. Restoration measures in order to avoid flooding, to cover irrigation needs and to establish the hydrological regime make up the 50% of all implementations measures and they are purely mechanical measures. The eco-engineering, "green" measures (Table 1, in bold) mainly addressing the habitat conservation and the nutrient's retention did not yet implemented.

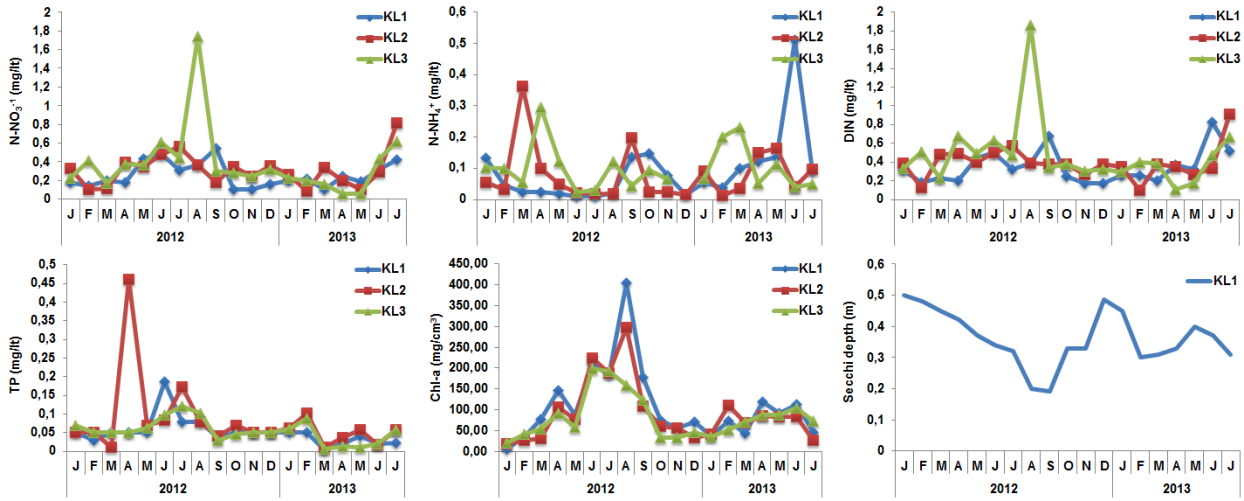

Figure 3. Monthly variation of Nitrate-N, Ammonia-N, Dissolved Inorganic Nitrogen, Total Phosphorus, Chl-α, Secchi Depth during the sampling period (January 2012 - July 2013).

Table 1. Main pressures, mitigation measures, implementation level during the restoration project on Lake Karla

Pressure	Restoration measure	Implementation status	Impacts
Flooding	Implementation of flood protection and mountainous water projects and of collectors /Diversion of flooded water into the reservoir with the pumping stations operation	**60%** *Constructed*: Reservoir and pumping stations *Non constructed:* Collectors and mountainous water projects	Damage to agricultural crops and infrastructures, removal of soil making the land barren
Point & Diffuse pollution sources	Treatment of inflow water to the reservoir, improvement of water quality/ **Establishment of riparian zones, operation of a peripheral buffer zone, construction and operation of artificial wetland**	**0%** No project or tool has been implemented.	Deterioration of water quality, eutrophication, pressure on biota, changes in the structure and function of the water body, sedimentation, elimination of ecosystem services.
Habitat fragmentation	**Tree planting project, creation of land corridors, buffer zones.**	**10%** Failure on planting growth, incomplete establishment of corridors.	Habitat loss due to ineffective implementation, habitats isolation, impacts on flow energy, impacts on ecosystem services.
Hydromorphological alterations	Restoration of hydrological balance, rehabilitation of groundwater. Creation of a 38 km^2 water body and supplement channels.	**50%** *Constructed*: Reservoir *Non constructed:* Water distribution projects	Negative hydrological balance of Lake Karla Watershed, continuous degradation of water resources, soil salinization, desertification, land subsidence.
Human needs (irrigation)	Creation of the main reservoir and distributing irrigation channels	**50%** Incomplete construction of irrigation channels	Not implementation of social needs, no withdrawals.

4. DISCUSSION AND CONCLUSIONS

Lake Karla, in terms of typology (according the WFD) is considered as an artificial lake, and furthermore, as a highly modified water body. Based on the available dataset, historical data and expert judgment we could argue that the lake Karla experiences a long eutrophication period with signals of hypertrophication.

The environmental conditions of the new reservoir have not improved in spite of the undertaken measures. The new reservoir is characterized as eutrophic with the frequent occurrence of algal blooms dominated by cyanobacteria (Chamoglou et al. 2014). A reduced water transparency due to organic material and plankton, along with the presence of frequent algal blooms (*Anabaena* sp., *Aphanizomenon* sp.) reported by Ananiadis (1956), suggests that the lake has been eutrophic since at least the 1950s. Nutrient pollution and associated eutrophication of the new reservoir threaten the ecological integrity and the services provided to the local community.

At present, Lake Karla has an extremely high water retention time since there is no outflow (Chamoglou et al. 2014) thus shaping the biological communities (Stabouli et al. 2012), while the phosphorous in- lake concentrations are very far to maintaining even the mesotrophic conditions in a Mediterranean water body (Meerhof et al. 2012).

Regarding Lake Karla, restoration measures addressing the balancing of the hydrological regime are not yet finalized.

With increasing warming in the whole area (Loukas et al. 2014) it may be more difficult to fulfil the suggested ecological state targets of the lake, without undertaking additional efforts to reduce nutrient loading to levels lower than the present-day expectations. Although nutrient loading is, generally, expected to decline in warm Mediterranean area because of the low precipitation and lower runoff, however much higher concentrations are currently observed due to increased evapotranspiration leading to high concentrations in the remaining water (Jeppesen et al. 2011).

To conclude, the "alarming" current status of Lake Karla ecosystem is a synergy of three factors:

1. Decline of Environmental Terms of the project (Ministry of Environment, Planning and Public Works 2000) and failures in the planning of the project. According to the Environmental Terms the scheduled wetland, (in the west part of the reservoir,) ought to be constructed firstly thus filtering the inflows. Yet, the water level of reservoir has never been over the lowest ecological stage (+46.4 m.) that the Environmental Terms commands. The artificial wetland which will upgrade the water quality has not been operated yet thus there is a nutrient rich inflow into reservoir.
2. The great delay of the Lake Karla project implementation leading to a hysteresis of the ecological restoration of the site. That was revealed from the two year monitoring of physicochemical parameters which indicated the eutrophic character of the reservoir aided by the fact that is still under the filling process. The only work that has been completed is the construction of the reservoir, the pumping stations and the water transfer project from the Pinios river. The collectors, who will supply the reservoir with flushing water from the surrounding mountainous area, have not been constructed yet. Irrigation work, which will act as an “outflow” thus enhancing flushing, is still uncompleted. Therefore there is no doubt that the new lake is far from an equilibrium stage which could be support its function.
3. Lack of environmental policy due to fragmentation of responsibilities, and further due to competent authorities dealing with water management where in some cases their responsibilities overlap. Moreover, due to the fact that the active involvement of the local communities is very weak, the increased participation in the whole basin management decisions by a wide range of stakeholders has been widely advocated by the Management Body of Lake Karla.

The re-constructed Lake Karla will success to regain its multiple functional role only if we respect the characteristics of the former Lake Karla in relation to present environmental and socioeconomic needs. An integrated watershed management approach should be developed rather

than focusing only on the lake itself. Conservation of the "new"lake requires protection of watershed at ecosystem basis.

ACKNOWLEDGEMENTS

This research has been co-financed by the European Union (ERDF: European Regional Development Fund- ERDF) and Greek Nation in the framework of the Operational Program "Environment and Sustainable Development" 2007-2013 - Priority Axis "Protecting Nature and Biodiversity".

REFERENCES

Ananiadis, C.I., 1956. Limnological study of lake Karla. Bull. Inst. Oceanologr.; 1083:1-19.

Bellos, D. and Savvidis ,T. 2005. Chemical pollution monitoring of River Pinios (Thessalia, Greece). J. of Environ. Manage.; 76(4): 282-292.

Chamoglou, M., Papadimitriou, Th., Kagalou, I. 2014. Keys-Descriptors for the Functioning of a Mediterranean Reservoir: The Case of a New Lake Karla-Greece. Environ. process.; 1:127-135

European Commission, 1992. Directive 92/43/EEC, Conservation of natural habitats and of wild fauna and flora. Official Journal of the European Communities No L 206/7/1992.

European Commission, 2000. Directive 2000/60/EC of the European Parliament and the Council of the 23 October 2000 establishing a framework for Community action in the field of water policy. Official Journal of the European Communities. L 327:1-73.

Jeppesen, E., Meerhoff, M., Davidson, A.T., Trolle, D., Sondergaard, M., Lauridsen, L.T., Bekioglu, M., Brucet, S., Volta, P., Gonzalez-Bergonzoni, I., Nielsen, A., 2011. Climate change impacts on lakes: an intergrated ecological perspective based on a multi-faceted approach, with special focus on shallow lakes. J. Limnolo.,2014; 73(s1):88-111. doi: 10.4081/jlimnol.2014.844.

Joint Ministerial Decision, 2000. Re-flooding of former Lake Karla at Perfectures of Larissa and Magnisia, Athens: Greece (in Greek).

Katsiapi, M., Michaloudi, E., Moustaka-Gouni, M., Pahissa López, J. 2012. First ecological evaluation of the ancient Balkan Lake Megali Prespa based on plankton. J. Biol. Res.; 17:51-56.

Kottelat, M., Freyhof, J. 2007. Handbook of European freshwater fish. Kottelat,Cornol and Freyhof, Berlin.

Loukas, A., Kagalou, I., Laspidou, Ch., Vasiliades, L., Papadimitriou, Th., Sidiropoulos, P. 2014. Evaluation of restored lake Karla status and operation under climate change scenarios. 10th International hydrogeological congress of Greece, 8-10 October, Thessaloniki, Greece. (in Greek).

Meerhoff, M., Teixeira-de Mello, F., Kruk, C., Alonso, C., Gonzalez-Bergonzoni, I., Pacheco, J.P., Lacerot, G., Arim, M., Bekliog lu, M., Brucet, S., Goyenola, G., Iglesias, C., Mazzeo, N., Kosten, S., Jeppesen, E., 2012. Environmental warming in shallow lakes: a review of potential changes in community structure as evidenced from spacefor-time substitution approaches. Adv. Ecol. Res.; 46:259–350

Ministry of Environment, Planning and Public Works, 2000. Joint Ministerial Decision 112839/18-12-2000: Modification – Supplementation – Codification of the Environmental Terms for the construction and operation of former lake Karla re-flooding project at Prefectures of Larisa and Magnesia, Athens: Greece (In Greek).

Papadimitriou, Th., Katsiapi, M., Kormas, K., Moustaka-Gouni, M., Kagalou, I., 2013. Artificially-born "killer" lake: phytoplankton based water quality and microcystin affected fish in a reconstructed lake. Sci. Total Environ.; 452-453:116-124.

Sidiropoulos, P., Papadimitriou, Th., Stabouli, Z., Loukas, A., Mylopoulos, N., Kagalou, I., 2012. Past, present and future concepts for conservation of the re-constructed lake Karla (Thessaly- Greece). Fresen. Environ. Bull.; 21(10a.2012):3027-3034.

Stabouli, Z., Papadimitriou, Th., Kagalou, I. 2012. Assessment of the ecological status of Lake Karla, using populations of zooplankton. Congress of E.E.B.E., Trikala: Greece.

Vasiliades, L., Loukas, A., Patsonas, G., 2009. Evaluation of a statistical downscaling procedure for the estimation of climate change impacts on droughts. Nat. Hazard. Earth SyS.; 9:879–894.

World Health Organization, 1998. Cyanobacterial toxins: microcystin-LR. In Guidelines for drinking water quality. 2nd Edition, Addendum to vol.2. Health criteria and other supporting information: 95-110. Geneva: Switzerland.

Proceedings of the 10th World Congress of EWRA 'Panta Rhei', 5-9 July 2017, Athens, Greece
© 2017 *European Water Resources Association*

Adaptive management of Koronia ecosystem based on external-internal dynamics

E. Ntonou[1,2*], C. Mitraki[2], V.A. Tsihrintzis[3], T.L. Crisman[4] and G.C. Zalidis[1,2]
[1] *Aristotle University of Thessaloniki, School of Agriculture, Laboratory of Remote Sensing, Spectroscopy and GIS, 54124 Thessaloniki, Greece*
[2] *Interbalkan Environment Center, 57200, Lagadas, Greece*
[3] *National Technical University of Athens, School of Rural and Surveying Engineering, Department of Infrastructure and Rural Development, Laboratory of Reclamation Works and Water Resources Management, 15780, Athens, Greece*
[4] *University of South Florida, Department of Integrative Biology, 4202 E.Fowler Ave. SCA 110, Tampa, FL 33620-8100, USA*
[*] *e-mail: ntonou@agro.auth.gr*

Abstract: Lake Koronia, a Ramsar and Natura site has a prolonged history of degradation to wetland status due to intensive groundwater use. In 2015 Lake Koronia water-level increased due to restoration works and a favorable hydrologic year. Consequently, Lake Koronia has progressed considerably towards autotrophy and distinct open water and littoral ecosystems and is expected to oscillate around autotrophy-heterotrophy and wetland-lake transitions depending on annual water budget. Lake Koronia, as it has been configured following water volume increase, presents ecological status assessment and management challenges. The purpose of this paper is to develop an integrated management approach combining internal and external system dynamics and an indicator detecting spatial and temporal changes. Internal factor management centers around dissolved oxygen, as it reflects primary production based on nutrient concentrations in water and sediment, exchanges at the sediment-water interface and littoral-open water interactions. The development of a dynamic aeration scheme, based on spatial and temporal ecosystem variability and real time earth insitu monitoring is proposed. External factor management focuses on agriculture, as it contributes greatly to nutrient loading and water budget determination. The eco-hydrological model SWAT assesses the impact of spatial and temporal fertilization and irrigation water application using space born geodata. Proposed agricultural practices effectiveness is evaluated. Adaptive management and ecological status assessment is based on the proposed indicator, which integrates near real time monitoring, developed protocol, and appropriate layers of Earth observation geodata. This indicator addresses water column, littoral zone, sediment and watershed loading, while complimenting the European Water Framework Directive 2000/60/EC.

Key words: ecosystem management, watershed interactions, ecosystem functions, integrated indicators, earth observation, WFD

1. INTRODUCTION

Lake Koronia, a Ramsar and Natura 2000 site is located in Northern Greece at approximately 75 m a.s.l. The watershed is drained by five creeks, extents to about 350 km2, is inhabited by 45,000 people. Lake Koronia had maximum depth >5 m and was eutrophic in 1970s prior to the intensification of irrigation and fertilization agricultural practices. Industrialization in the 1980s and 1990s accelerated groundwater use and wastewater addition to the lake. Consequently, water-level declined progressively from about 4 m in mid-1980s to <1 m in 1995 (Mitraki et al. 2004). Concomitant water quality deterioration led to hypertrophy, aquatic trophic web collapse and massive fish and waterfowl deaths.

Despite gradual loss of industry in the watershed after 2000, water-level in Lake Koronia fluctuated from 0-1 m with periodic complete desiccation. During this low water-level period of approximately twenty years, the flocculent sediments of the lake were either permanently or periodically exposed and subjected to progressive dessication, oxidation and compaction. Ultimately wetland soils were established. Phragmites littoral vegetation expanded lakeward displacing open water areas by dense stands (Crisman et al. 2014), while communities of both wetland and upland plants were established on permanently exposed areas, and opportunistic plants invaded periodically exposed sediments (Alexandridis et al. 2014). Thus, Lake Koronia developed

all three characteristics of wetland ecosystems: minimal water-level fluctuating hydroperiod, intermittently saturated soils and hydric vegetation. Overall ecosystem metabolism shifted to heterotrophy, a characteristic of wetlands and hypertrophic lakes, at a lake depth of 1.5-2.5m (Mitraki et al. 2004). Wetland characteristics, however, supported avian fauna diversity and abundance increase. The deterioration of Lake Koronia led to a comprehensive restoration plan (Zalidis et al. 2004) that has been partially implemented.

In spring 2015, water-level increased in Lake Koronia, as a result of restoration actions and a wet hydrologic year. Since then, maximum depth has been consistently maintained >2.5 m resulting in the formation of an open water area. Water quality improved, and trophic state declined considerably, while the deepest part of the lake shifted to increased autotrophy. However, a considerable part of the lake has remained below the autotrophy threshold water-level of 1.5 m and has been experiencing prolonged diel anoxia especially during summer. Lake Koronia is predicted to oscillate between autotropy-hetrotrophy and wetland-lake transitions, as a function of annual water budget, which reflects both fluctuations in annual precipitation and groundwater use in the watershed.

The purpose of the Water Framework Directive 2000/60/EC (WFD) is to establish a framework for the protection of inland surface waters, transitional waters, coastal waters, and groundwater. Emphasis is placed on prevention of further deterioration, protection, and enhancement of the status of aquatic ecosystems; promotion of sustainable water use; reduction of priority substances discharges; reduction of groundwater pollution; and mitigation of flood and drought events. This Directive dictates integrated river basin management purposed to achieve "good water status" for both surface water bodies and groundwater. Ecological status is assessed based on biological, hydromorphological, and physicochemical elements. No wetland definition is provided by WFD, but their functionality is recognized both at the level of water body - adjacent wetland interaction and as a part of the hydrological cycle of a river basin.

The WFD dictates protection and enhancement of status, both ecological and chemical, of inland surface waters. Although ecological status is defined in article 2 as "an expression of the quality of the structure and functioning of aquatic ecosystems associated with surface waters", quantification of this expression is based largely on taxonomy and ecosystem structure metrics. Contemporary freshwater and terrestrial ecosystem research, however, concludes that anthropogenic stressors influence both structure and function, or either one (Sandin and Solimini 2009, Crisman et al. 2004). Consequently, effective ecosystem management considers both structure and function. However, this approach is only applied to wetlands. The expansion of the functional indicator concept to rivers and lakes led to the conclusion that ecosystem functions serve the purpose and objectives of the European Framework Directive (Barker et al. 2009). Such an approach is particularly appropriate in shallow lakes, where interactions with littoral and adjacent wetlands are prevalent compared to stratifying lakes.

Traditional lake management approaches focus on water column and water-sediment processes. This is usually sufficient in deep stratifying lakes, where the hypolimnion functions as nutrient sink and predator refugium. In shallow non-stratifying lakes, however, hypolimnion is functionally replaced by the littoral zone, which is usually managed for structure. Crisman et al. (2004) recognized that ecosystem structure does not imply function and proposed that traditional vertical water column-sediment management approaches be integrated with horizontal management plans based on plant-sediment and littoral-open water interactions to enhance functions performed by shallow lakes. To separate littoral function and structure, vegetated littoral areas were divided into lakeward littoral wetlands and landward adjacent, core wetlands. The core wetland receives runoff and outflow water from the watershed, functions as a sediment and nutrient sink, is heterotrophic and predominantly anoxic, and interacts with open water only during extreme weather phenomena. The littoral wetland interacts intensively with open water, receiving dissolved oxygen by wave action, while functioning as a source of carbon and faunal predation refugium. The littoral wetland is mostly well oxygenated and autotrophic (Crisman et al. 2004). This functional optimization management approach is integrated with external dynamics, as the watershed functions as a source

of nutrients and suspended solids to the lake ecosystem. Different land uses have distinct impacts on the export of nutrients, chemicals, and sediment to the lake. Thus, integrated management for ecosystem function can be expanded to watershed and the land-core wetland interface.

The purpose of this article is to develop: a) an integrated long-term management approach for Lake Koronia combining internal (ecosystem) and external (watershed) system dynamics; and b) a system of indicators for management and ecological status assessment addressing both ecosystem structure and functions. Indicators are based on in-situ and satellite borne earth observation. These purposes support Social Benefit Areas (SBA) of the Group of Earth Observations (GEO). Focus is placed on the SBAs of biodiversity and ecosystem sustainability, food security and sustainable agriculture, and water resources management. Moreover, this project supports the GEO-Glows Initiative, which is intended to facilitate the use of Earth observation assets to contribute to mitigating water shortages, excesses and degraded quality arising from population growth, climate change, and industrial development.

2. METHODS

Data collection for proposed indicators follow protocols developed by the Global Earth Observation System of Systems (GEOSS) and the Open Geospatial Consortium (OGS). Thus data are of identified quality and provenance, interoperable supporting tool development, and readily accessible to multiple public and private users. Proposed indicators are based on both in-situ measurements and spaceborne images analysis. Indicator estimation at the watershed level is performed by the ecohydrological model SWAT using both in-situ and spaceborne data.

Frequency of data collection and analyses frequency varies. Telemetric stations record values hourly, water sample collection is monthly, and sediment sampling occurs approximately at five year intervals. Satellite images analyses, and watershed contribution estimations and predictions by ecological monitoring is performed annually.

3. LAKE KORONIA MANAGEMENT

Lake Koronia management objectives are determined in the restoration plan: habitat diversity, food-web support, water quality and trophic state improvement, and increased water retention capacity (Zalidis et al. 2004). This approach includes structural, and mostly functional components. It calls for a shallow lake with littoral and open water phases and sustainable land uses and agricultural practices in the watershed.

Reflooding and subsequent formation of open water phase re-introduced vertical management challenges in Lake Koronia. Overall system metabolism shifted towards autotrophy, as sediment decomposition impact to dissolved oxygen concentration was reduced. Additionally, sediment became more inorganic through repeated cycles of atmospheric exposure and flocculent material consolidation to the deepest part of the lake basin (Crisman et al. 2004). However, the extent of the well oxygenated open water areas varies seasonally with water-level. Moreover, extensive littoral wetlands rely on open water for oxygen input, while remaining below the autotrophy water-level threshold. Consequently, oxygen regime within the open water-littoral wetland areas periodically reach hypoxia and even anoxia. Anoxic periods are more likely to occur or be more pronounced during summer, because oxygen solubility is a function of water temperature; and nighttime, if nocturnal respiration surpasses daytime oxygen input in the water column. Thus, anoxic conditions posing threats to the survival of fish communities may occur either occasionally during periods of increased autotrophy (water-level >2.5 m) or daily at times of heterotrophy (water-level <2.5m). Mechanical aeration is proposed for preventing dissolved oxygen depletion in the water column, while maintaining heterotrophic metabolism in core wetlands. The mechanical aeration scheme needs to be based on a predictive oxygen regime model based on water-level, water temperature and biotic community needs.

Littoral areas are a substantial part of an integrated management plan. Prior to degradation, Lake Koronia had a minimal littoral zone with negligible contribution to lake metabolism (Crisman et al. 2004). However, gradual water-level decline allowed aggressive aerial expansion of dense Phragmites stands at the rate of 29% annually. Phragmites habitats followed slowly water-level contours, but lakeward margin progression was far greater than landward margin retreat (Crisman et al. 2014). Despite being native in Europe, Phragmites is a invasive nuisance species in many North-European lakes displacing indigenous plant communities. The effect of Lake Koronia reflooding on Phragmites cover is not yet fully measured and understood due to delayed Phragmites response to water-level changes. Although Phragmites habitats might be structurally similar throughout, functionally stands are divided into core and littoral wetlands (Crisman et al. 2004). Unruly expansion of either wetland habitat may compromise functionality of remaining habitats, especially open water ones. Consequently, ecosystem maintenance requires sufficient water-level and suitable littoral:open water area ratio. Such a ratio can be maintained with Phragmites harvesting, which also contributes to nutrient removal from water and sediment. The harvesting scheme needs to include proper biomass disposal, especially if Phragmites analyses indicate heavy metal uptake from sediments.

Lake Koronia restoration and management plans were designed at the watershed level, where ecosystem degradation causes lie. Proposed actions in the restoration Masterplan were introduction of sustainable agriculture practices and groundwater recharge enhancement (Zalidis et al. 2004). Ecohydrological model SWAT applications in Koronia watershed showed that if low input sustainable agriculture practices, providing water and fertilizer to plants only where and when needed, replaced conventional practices at watershed level, annual nutrient input to Lake Koronia would be reduced by 3.5%. However, saved water would contribute to groundwater recharge instead of stream flow, which would increase several years later. Additionally, production increase with crop redistribution according to soil quality characteristics would result to reduced nutrient input to the lake, only if combined with low input sustainable agriculture practices. Besides being the prevalent land use in the watershed, agriculture is the economic activity of greatest groundwater demand. It also adds considerable nutrient load to Lake Koronia. Proposed management practices are low input sustainable agriculture and crop redistribution according to soil quality characteristics.

4. ECOLOGICAL STATUS INDICATORS

In accordance with the WFD the indicator system proposed for Lake Koronia addresses both adaptive management and ecological status assessment and integrates ecosystem structure, function, and watershed interactions (Table 1). These three components were considered in the determination of Lake Koronia ideotype, restoration plan, and ongoing management (Management Body of Lakes Koronia and Volvi, 2009, Zalidis et al. 2004).

Proposed indicators of biological elements compatible with WFD describe littoral and open water aquatic communities. Indicators chosen are littoral extent, littoral:open water areas ratio, and planktonic community abundance and diversity (Table 1). Littoral extent corresponds to the function of floodwater detention, because intermittently inundated mostly core wetlands provide space for water storage, absorb water in unsaturated parts of the sediment and reduce incoming water velocity by means of hydrophyte resistance to flow. Littoral extent is also an indicator of groundwater recharge/discharge, as groundwater exchange between lakes and aquifers occurs predominantly in littoral areas. These areas are also critical for nutrient retention, because nutrients are commonly immobilized and/or metabolized in wetland plants and soil. Littoral:open water area ratio addresses conservation of open water habitats, which are threatened by water-level reduction and/or lakeward littoral zone expansion. Consequently, this ratio pertains to the ecological functions of ecosystem maintenance ensuring multiple habitat existence, and food-web support providing multiple primary producers growth (vegetation and phytoplankton) and thus supporting consumers diversity. Additionally, littoral:open water ratio describes in-situ carbon retention, as long-term carbon storage occurs in highly organic sediments in both littoral and open water areas,

accumulated dead littoral plants, and woody littoral vegetation. Both above mentioned indicators are monitored with satellite image analyses at the peak of littoral vegetation growth in late summer (Alexandridis et al. 2014). Additional analyses during the wet season (spring) is also informative. The biological indicator of planktonic community corresponds to food-web support, as a major determinant of energy and carbon flow in open water communities.

Hydromorphological WFD elements monitored are hydrology and sediment characteristics. Hydrology is described by water-level (Table 1), which is of upmost importance in Lake Koronia. Water-level describes the hydrological functions of floodwater detention, as it is directly connected to water storing ability; groundwater/discharge, as it is a determining factor of inflow/outflow equilibrium; and ecosystem maintenance, because it controls open water aerial extent. Water-level is monitored telemetrically and best interpreted in conjunction with meteorological parameters particularly precipitation.

Table 1. Proposed indicators integrating WFD elements, wetland functions, and watershed processes in Lake Koronia

Wetland functions	**WFD elements**				**Watershed**
	Biological	**Hydromorfological**		**Physicochemical**	
	Aquatic Communities	**Hydrology**	**Sediment**	**Water Quality**	**Land Use**
Hydrological					
Floodwater Retention/Water storage	Littoral Extent	Water-Level			Land Use/Agricultural Practices Changes
Groundwater Recharge/Discharge	Littoral Extent	Water-Level			Groundwater Budget, Water table
Sediment Retention	Littoral Extent		TOC, TC:TN	Transparency, Conductance, TOC, TSS	Suspended Solids Inflow
Biogeochemical					
Nutrient Retention	Littoral Extent		TN, TP	TN, TP	TN, TP Lake Input
Nutrient Export			TN , TP	TN, TP	
In-situ Carbon Retention	Littoral: Open Water Ratio		TOC		
Trace Element Storage			Priority Substances	Priority Substances	Land Use/Agricultural Practices Changes
Ecological					
Ecosystem Maintenance	Littoral: Open Water Ratio	Water-Level	TOC, TC:TN, Substrate Structure	Transparency, Conductance, pH	Land Use Changes
Food-Web Support	Littoral: Open Water Ratio, Planktonic Community		TOC, Substrate Structure	Dissolved Oxygen Regime, TN, TP, TOC	

Open water sediment characteristics pertain to total organic carbon (TOC), total nitrogen (TN), total phosphorus (TP), priority substances and sediment substrate (Table 1). Although some functions can be assessed by a single chemical variable, multiple sediment attribute synthesis enhances functional ecosystem assessment. Sediment TOC, TN, TP, and TC:TN integrates both external (watershed) and internal (littoral, water column) processes and overall ecosystem metabolism, although calculating contributions of individual processes may not be possible. Allochthonous material not retained in the littoral zone carry both inorganic and organic particles, thus reducing TOC content and changing TC:TN in comparison to sediments of water column origin. Littoral debris contributes also carbon reach plant material, while phytoplankton decomposition contributes low TC:TN organic matter to the sediment. Also, nutrient recycling processes in both water and sediment are reflected in sediment chemistry. Consequently, TOC, TN and TP relate to the functions of sediment and nutrient retention, nutrient export (to the atmosphere and harvested plants), in-situ carbon retention, ecosystem maintenance and food-web support. The last two functions also depend on substrate structure, because the latter creates habitat for benthic

invertebrates, which are in turn primary and secondary consumers passing energy to higher foodweb levels. Trace element storage is monitored with priority substances sampling, which in the case of Koronia are mostly heavy metals of possible industrial origin. Sediment attributes change very slowly depending on sedimentation rates and sediment-water interactions, so sampling frequency should be about five years and adjusted according to results. Most sediment biotic and abiotic processes happen in the top 10 cm, but deeper layers are needed for reference. Total phosphorus fractionation provides additional information about water and sediment procedures. Substrate structure is inferred from gravimetric analyses; and secondarily by visual core inspection of surface flocculent material.

Water quality indicators follow closely physicochemical properties described in WFD (Table 1). The hydrological function of sediment retention occurs primarily in the littoral zone. Low retention efficiency is reflected in the water quality indicators of transparency (Secchi disk depth, and turbidity), electric conductance, TOC and total suspended solids (TSS). TN and TP concentrations are anticipated to increase, when the functions of nutrient retention and export are not performed sufficiently in littoral areas and open water sediments. Priority substances concentrations in the water column are directly related to trace element storage and metabolism in sediments, and woody or accumulated dead littoral vegetation. However, metabolism of some toxic organic substances also occurs in the water column. All above mentioned water quality indicators are integrated in the functions of ecosystem maintenance and foodweb support. Transparency, conductance, and pH determine habitat suitability for organisms and correspond to the function of ecosystem maintenance. TN and TP determine autotrophic production and TOC provides food to heterotrophic organisms, thus supporting foodwebs. Dissolved oxygen regime is an important physicochemical component in all lakes. It determines ecosystem ability to support both producers and consumers, and shapes habitats especially at the water-sediment interface and in hypolimnia. However, dissolved oxygen regime is of critical consequence in Lake Koronia, where autotrophy/heterotrophy gradients vary both spatially (littoral vs. water), daily (daytime vs. nighttime), annually (winter vs. summer), and interannually, as a function of annual water budget. Consequently, dissolved oxygen needs to be monitored telemetrically, so mechanical aeration can be designed and applied effectively. Conductance, pH, and turbidity are also measured telemetrically, while water sampling for remaining variables is proposed to be monthly.

Direct interactions among natural and anthropogenic processes in the watershed, wetland functions, and elements determining ecological status according to the WFD are widely recognized. However, proposing indicators for watershed procedures and practices supporting ecosystem functions is a novel approach (Table 1). Land use changes and cultivation practices affect greatly ecosystem floodwater retention, as they determine water flow velocity, temporary floodwater storage and infiltration rate to groundwater. Industrial and residential uses increase impervious surfaces, while irrigation, tillage, and soil cover determine soil porosity and water infiltration rates. Land uses and practices also affect indirectly priority substances storage in the ecosystem, as industrial operations may contribute heavy metals, and agricultural practices may add pesticides to the ecosystem. Additionally, agricultural land has been expanding in littoral areas impacting ecosystem maintenance. Groundwater management is a priority in the watershed of Koronia. However, the functions of groundwater recharge and discharge both at the ecosystem and watershed levels can only be assessed by groundwater modeling and water budget calculations based on water table measurements. Suspended solids inflow is determined by agriculture and forestry practices in the watershed. Practices reducing erosion enhance the function of sediment retention in littoral wetlands. Nutrient (TN, TP) input to the lake is directly related to nutrients applied in agricultural lands and wastewater from residential areas and animal raising facilities in the watershed. Fertilizer use reduction and wastewater treatment support nutrient retention in Lake Koronia. Most watershed indicators (land use/agricultural practices changes, sediment inflow, TN, TP inputs) derive from hydrological models, such as SWAT, which use data from statistical surveys and satellite image analyses. However, these models need to be calibrated with actual nutrient and suspended solids inflow measurements. The importance of water-level in ecosystem maintenance dictates the need

for groundwater modeling for accurate estimation of irrigation effects to lake water volume especially during dry years.

5. CONCLUSIONS

Ecological status assessment in the context of the WFD and adaptive water body management purposed to protect, conserve, and enhance ecosystem status need to be based on ecosystem properties and processes quantification. Measurements of structural ecosystem components can rely on readily available biological and chemical protocols that provide accurate, and reliable data, comparable among different water bodies. Data with these characteristics are greatly appreciated by aquatic scientists and managers. However, ecosystem structure does not necessarily imply function, as exemplified by littoral and core wetlands adjacent to lakes. Although they both are structurally similar, the former functions as a nutrient and carbon source, while the latter as a nutrient and carbon sink. Integrated ecosystem assessment addressing both functional and structural aspects enhances ecosystem status description and management plan efficiency, while serving the purposes of the WFD.

The WFD places water body management at the river basin level recognizing the importance of interactions between aquatic systems and their watersheds. Integration of these interactions in indicators enables adaptive management based on feedback provided by the indicators. Integrated indicators also need to address water body uniqueness. Shallow lakes present intensive interactions between open water and littoral zone compared to deep stratifying lakes. Lake Koronia is a shallow lake, where water-level and groundwater properties define aquatic structure and function. A system of indicators for ecological status assessment and adaptive management integrates structural and functional ecosystem aspects, interactions between water body and watershed and interactions among aquatic ecosystem components. These integrated indicators combine in-situ (telemetry and field sampling) and spaceborne earth observation, and ecohydrological modeling.

REFERENCES

Alexandridis, T.K., Dimitrakos, A., Gitas, I.Z., Tompoulidou, M., Mitraki, C., Crisman, T.L., Zalidis, G., 2014. Identification of successive zones in an evolving lake to wetland ecosystem using object based classification. South-Eastern European Journal of earth Observation and Geomatics.; 3: 617-620.

Barker, T., Maltby, E., Hering, D., 2009. Deliverable No. 281. Manuscript on how to transfer the functional indicator concept on rivers nd lakes, including deliverable 387 (Functional indicators of climate change impacts) (WP7, Task 3). Project No. GOCE-CT-2003-505540. European Commission.

Crisman, T.L., Alexandridis, T.K., Zalidis, G.C., Takavakoglou, V., 2014. Phragmites distribution relative to progressive water level decline in Lake Koronia, Greece. Ecohydrology.; 7: 1403-1411.

Management Body of Lakes Koronia and Volvi, 2009. Management Plan of the National Park of Lakes Koronia, Volvi and the Macedonian Tempe. In Greek.

Mitraki, C., Crisman, T.L., Zalidis, G., 2004. Lake Koronia, Greece: Shift from autotrophy to heterotrophy with cultural eutrophication and progressive water-level reduction. Limnologica.; 34: 110-116.

Sandin, L., Solimini, A.G., 2009. Freshwater ecosystem structure-function relationships: from theory to application. Freshwater Biology.; 57: 2017-2024.

Zalidis, G.C., Takavakoglou, V. and Alexandridis, T., 2004. Revised Restoration Plan of Lake Koronia. Aristotle University of Thessaloniki, Department of Agronomy, Laboratory of Applied Soil Science. In Greek, English Summary.

Proceedings of the 10th World Congress of EWRA 'Panta Rhei', 5-9 July 2017, Athens, Greece
© 2017 *European Water Resources Association*

A comparative study of water quality in a highly frequented seacoast in Albania

E. Hamzaraj*, P. Lazo, A. Paparisto and R. Bami
Faculty of Natural Sciences, University of Tirana, Tirana, Albania
* *e-mail: etleva.hamzaraj@fshn.edu.al*

Abstract: The control and monitoring of environment is done not only to guarantee healthy ecosystems but also to put in evidence if they present any risk for humans. The new demographic changes in our country, especially in seacost regions, have increased the interes concerning their negative effects from environmental point of view in these areas. The objective of this study was to evaluate dynamics of water quality in a highly frequented seacoast in Albania in a ten years period. For this reason, a bacteriological and chemical study was carried out from July 2015 to June 2016 on seacoast of Durrës, and the data collected were compared with those of a similar study during 2005 and 2006. Seawater samples were taken monthly from six stations evenly distributed on this coast line. Total coliforms, faecal coliforms and intestinal enterococci were estimated using MPN method, while chemical parameters like pH, ammonia, phosphate, nitrite and nitrate where estimated using standard methods. Our data show that after ten years, in general, bacterial indicators were increased, but at least in one station, where a new system of waste water pipes is built, bacterial parameters are decreased. High concentrations of faecal bacteria were associated with high concentration of nitrite and nitrate. The results of this study indicate that there is no improvement in the quality of seawater in Durres, and there is still much work to be done in order that water in this area becomes safe for bathing.

Key words: water quality, faecal coliforms, intestinal enterococci, MPN method

1. INTRODUCTION

Human activity exerts a significant impact on coastal ecosystems. The pressures exerted are diverse and result from many activities such as coastal engineering, sediment dredging, pollution, fishing, aquaculture, urban development, maritime transport, tourism, oil extraction, transport, agricultural and industrial activities, etc. Sewage and untreated industrial effluents are being discharged from decades into the sea which leads to increase in pollution level (Chrost, R., 1990).

Contamination of water is a serious environmental problem as it adversely affects the human health and the biodiversity in the aquatic ecosystem. Among many pollutants, faecal waste presents the most acute risk to human health. Faecal waste generally harbors enteric pathogens in addition to agents that cause skin, eye, ear, and respiratory illnesses. Enteric pathogens are typically responsible for waterborne diseases (Stewart, J.R., et. al., 2008, Halpern et al., 2007, 2008).

Current guidelines in the three water-related areas (drinking water, wastewater and recreational water) assess quality, in microbiological terms, by measuring indicator organisms. Faecal coliforms and intestinal enterococci are widely used for assessment of water pollution and possible water quality deterioration in fresh water sources (Foden, J., 2008). Coliforms are Gram-negative, no spore-forming, oxidase-negative, rod-shaped facultative anaerobic bacteria that ferment lactose (with β-galactosidase) to acid and gas within 24–48h at 36±2°C. Not specific indicators of faecal pollution. Thermotolerant coliforms are coliforms that produce acid and gas from lactose at 44.5±0.2°C within 24±2h, also known as faecal coliforms due to their role as faecal indicators. *Escherichia coli* is part of thermophilic coliforms that produce indole from tryptophan, but also defined now as coliforms able to produce β-glucuronidase (although taxonomically up to 10% of environmental *E. coli* may not). This is the most appropriate group of coliforms to indicate faecal pollution from warm-blooded animals (Karaboze, I., 2003). Intestinal enterococci are Gram-

positive, catalase-negative cocci from selective media (e.g. azide dextrose broth or m Enterococcus agar) that grow on bile aesculin agar and at 45°C, belonging to the genera *Enterococcus* and *Streptococcus* possessing the Lancefield group D antigen. The presence of these bacteria in water could be from human origin or animal origin (Prescott, L.M., 2002, Nogales, B., 2007).

We focused our study in seacost line of Durrës as one of the most frequented areas during summertime. Swimming in seawater with faecal contamination increases the possibility of getting a disease like gastro-intestinal ones, or different infections. For this reason estimation of microbiological water quality is very important for public health (Borrego, 1991). Normally beaches where swimming is allowed should be tested for water quality before the swimming season begins, to get a baseline of contamination due to natural wildlife or run-off and each week thereafter until the area closes (UNEP, 1990).

The objective of this study was to monitor the quality of seawater in Durrës coastline and to compare it with a similar study done ten years ago.

2. MATERIALS AND METHODS

We carried out a bacteriological and chemical study from July 2015 to June 2016 along the seacoast of Durres. Seawater samples were taken monthly from 6 stations evenly distributed: Aragosta (St. 1), Porti (St. 2), Ura e Dajlanit (St. 3), Hekurudha (St. 4), Shkembi i Kavajes (St. 5), Perroi i Agait (St. 6).

Total coliforms, faecal coliforms and faecal streptococci were measured using the most probable number (MPN) method, while chemical parameters like pH, ammonia, phosphate, nitrite and nitrate where measured using standard methods (APHA, 1998, Elmir SM, 2007). MPN for total coliforms and faecal coliforms was determined by fermentation test on lactose broth for preliminary test, and on brilliant green bile confirmatory test. The concentration of intestinal enterococci was determined using, also, MPN method but the media used were azide dextrose broth for preliminary test, and TTC agar for confirmatory test.

3. RESULTS AND DISCUSSION

As previously mentioned, the region under study was seacoast of Durrës as one of the most frequented beaches in Albania. The objective of our study was not only to monitor the quality of coastal water during a one year period, but also to compare it with the data obtained by a similar study done during 2005-2006.

Indicators of faecal pollution comprises the bacteria which are normally taken as indicators of the degree of purity of water. In our study we used three parameters for fecal contamination: concentration of total coliform bacteria, *E. coli* and *Streptococcus faecalis*. Mean values of bacteriological and chemical indicators in all sampling sites during the investigation period are presented in Table 1. The highest values of microbiological parameters registered are at: total coliforms concentration 2075 CFU/100ml at sampling station No. 5 (Shkëmbi i Kavajës), and *E. coli* 1187 CFU/100ml and intestinal enterococci 1147 CFU/100ml at sampling station No. 6, Përroi i Agait (Table 1). We think that these high values of microbial load in this area are due to many visitors that frequent this area especially during summertime and due to a channel that spill sewage into the sea. The minimum concentration of same parameters are registered at sampling station No. 2, Porti: total coliforms concentration 798 CFU/100ml, *E. coli* 532 CFU/100ml and intestinal enterococci 407 CFU/100ml. Comparison of the data obtained from both studies put in evidence the decrease of faecal indicator organisms concentration only in one sampling site that is “Porti” (Table 5). For the last years a new system of waste water pipes is built in Durres and this could be the reason why the bacterial load in this sampling site is decreased.

Table 1. Mean values of bacteriological and physico-chemical indicators in all sampling sites during the investigation period

	St. 1	St. 2	St. 3	St. 4	St. 5	St. 6
Coliform total	1493	798	1243	1360	2075	1447
E. coli	1047	532	1048	898	1063	1187
Intestinal enterococci	638	407	695	712	668	1147
Nitrites NO_2^- mg/l	0.011	0.017	0.031	0.067	0.061	0.075
Nitrates NO_3^{2-} mg/l	0.905	0.513	0.903	0.45	0.787	0.461
Phosphates PO_4^{3-} mg/l	1.81	1.285	1.325	1.185	1.37	2.23
Ammonia NH_3 mg/l	2.2	1.595	1.825	1.475	1.71	1.97
pH	6.8	7.4	7.5	7.2	7.45	7.43

According to Directive 2006/7/EC of the European Parliament concerning the management of bathing water quality, the quality of coastal waters in the bay of Durrës during the period of investigation falls in the category "Poor". The 90th percentile for intestinal enterococci is 1015 CFU/100ml (which is higher than 185 CFU/100ml), while for *E. coli* is 1500 CFU/100ml (which is higher than 500 CFU/100ml). As mentioned above, a similar study was conducted in 2005-2006. By comparing the data it appears that there is an increase of 90th percentile values of *E. coli* concentration at each sampling site, except for the site "Porti" where impairment is significant (Table 3). However, even according to the study conducted in 2005-2006 coastal water quality was under the category "Poor", based on Directive 2006/7/EC. (The 90th percentile for intestinal enterococci was 742 CFU/100ml, while for *E. coli* was 1300 CFU/100ml). This means that in all these years although efforts were made to minimize the causes of pollution of the sea water, we are far from bathing coastal waters of good quality.

Table 2. Directive 2006/7/EC of the European Parliament concerning the management of bathing water quality

	A	B	C	D	E
	Parameter	Excellent quality	Good quality	Sufficient	Reference methods of analysis
1	Intestinal enterococci (cfu/100 ml)	100 (*)	200 (*)	185 (**)	ISO 7899-1 or ISO 7899-2
2	Escherichia coli (cfu/100 ml)	250 (*)	500(*)	500 (**)	ISO 9308-3 or ISO 9308-1

(*) Based upon a 95-percentile evaluation
(**) Based upon a 90-percentile evaluation

Table 3. 90th percentile values for E. coli in all sampling sites in two periods of investigation

	2005	2015
Aragosta	1100	1750
Porti	2400	930
Ura e Dajlanit	1240	1450
Hekurudha	1100	1100
Shk. i Kavajës	1100	1300
Përroi i Agait	1100	1750

Besides microbiological parameters we measured some chemical parameters that help determine water quality, such as nitrates, nitrites, phosphates, ammonia and pH. Correlation coefficients between the three microbiological indicators of water quality and chemical parameters measured during the study are presented in Table 4. From these data it appears that there is a strong positive correlation between *E. coli* and total coliform (r = 0.7) and between *E. coli* and intestinal Enterococci (r=0.78) (Aulicino, 1980).

These correlations suggest that there is one source of pollution. Our data show also that there is strong to medium positive correlation between faecal indicators and some nutrients as nitrite, phosphate and ammonia. This is an expected result because these affect directly microbial growth. The presented data confirm the known ecological phenomena consisting in the cooperation of biotic and abiotic factors of the environment influencing the life, dynamics and distribution of microorganisms in the waters.

Table 4. Pearson's correlation coefficient between different parameters

	Total coliforms	***E. coli***	**Intestinal enterococci**
Coliform total	1		
E. coli	0.7	1	
Intestinal enterococci	0.34	0.78	1
Nitrites NO_2^- mg/l	0.48	0.47	0.71
Nitrates NO_3^{2-} mg/l	0.35	0.34	-0.26
Phosphates PO_4^{3-} mg/l	0.17	0.59	0.76
Ammonia NH_3 mg/l	0.21	0.58	0.35
pH	-0.05	-0.06	0.17

Table 5. Mean values of microbial and chemical parameters measured during 2005-2006 and 2015-2016 in six sampling stations along the seacoast of Durrës

Parameters		**St. 1**	**St. 2**	**St. 3**	**St. 4**	**St. 5**	**St. 6**
Coliform faecal	2005-6	125	657	665	291	382	613
	2015-16	1047	531	1048	898	1063	1187
Coliform total	2005-6	521	997	451	610	690	325
	2015-16	1493	798	1243	1360	2075	1446
Ammonia	2005-6	0.36	0.46	0.42	0.37	0.43	0.51
	2015-16	2.2	1.39	1.83	1.48	1.71	1.97
Nitrite	2005-6	0.02	1.44	0.74	8.43	8.44	0.01
	2015-16	0.014	0.017	0.031	0.066	0.061	0.075
pH	2005-6	7.98	7.97	7.99	8	8	8.05
	2015-16	7.2	7.5	7.7	7.2	7.6	7.4

The graph below (Figure 1) shows cleraly the growing trend of bacterial concentration in a ten years period, which confirms a deterioration in the quality of coastal seawater in bay of Durres.

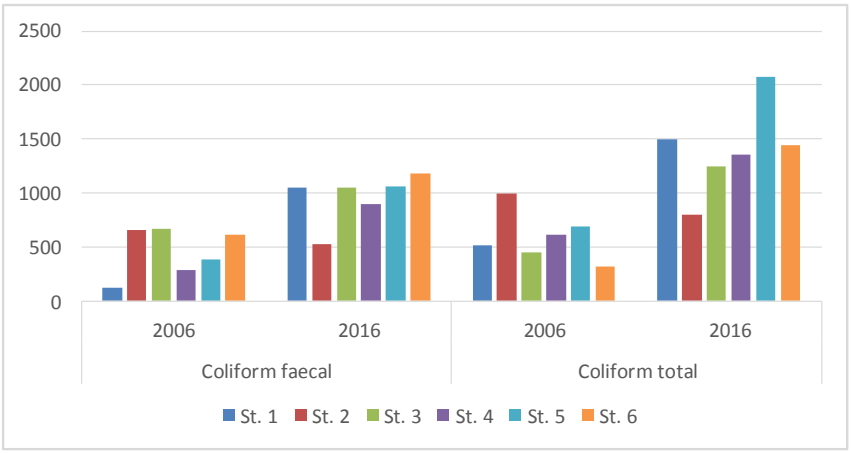

Figure 1. Dynamics of microbial indicators

Results, received during this study indicate that seawater along the seacoast of Durres is under high anthropogenic impact. Waste water from the settlements located in the watershed, especially on the shore, have distinct human impact to the water quality. It is more than evident that there is still much work to be done in order that water in this area become safe for bathing.

REFERENCES

APHA: Standard methods for the examination of water and waste water. American Public Health Association, Washington D.C. (20th edition), (1998).

Aulicino, F.A. et.al., 1980. Rilevamento microbiologico dell'inquinamento marino del golfo di Napoli; Raporto di Attivita Anni, Edizione di Instituto Superiore di Sanita, Istisan, Roma, Nr.33: 6-27.

Borrego, J. J., et al., 1991. Epidemiological study on bathers from selected beaches in Malaga. Mediterranean Action Plan (MAP), Technical Reports Series Nr53, UNEP, Athens, 1-3, 25 – 26.

Chrost, R. J., Overbeck, J., 1990. Introduction: Aims, Problems, and Solutions in Aquatic Microbial Ecology. In: Aquatic Microbial Ecology, Overbeck, J. Chrost, J. R., (eds). Springer-Verlag. New York.

Elmir, S.M., Wright, M.E., Abdelzaher, A. et al., 2007. Quantitative evaluation of bacteria released by bathers in a marine water; Water Res 41: 3–10.

Elmir, S.M., Shibata, T., Solo-Gabriele, H.M., Sinigalliano, C.D., Gidley, M.L., Plano, L.R.W., Kish, J., Withum, K., Fleming, L.E., 2009. Quantitative evaluation of enterococci and Bacteroidales released by adults and toddlers in marine water; Water Res 43: 4610–4616.

Environmental European Agency (EEA), 2006. Priority issues in the Mediterranean environment; EEA Report No. 4. Office for Official Publications of the European Communities, Luxembourg.

Foden, J., Roger, S.I., Jones, A.P., 2008. A critical review of approaches to aquatic environmental assessment; Mar Pollut Bull 56: 1825–1833.

Halpern , B.S.,Walbridge, S., Selkoem, K.A., et al., 2008. A global map of human impact on marine ecosystems; Science 319: 948–952.

Howarth, R.W., 2008. Coastal nitrogen pollution: a review of sources and trends globally and regionally; Harmful Algae 8: 14–20.

Karaboze, I., Ucar, F., Eltem, R., Ozdmir, G., Ates, M., 2003. Determination of existence and count of pathogenic microorganisms in Izmir Bay; JES 26: 1-18.

Nogales, B., Aguilo-Ferretjans, M.M., Martin-Cardona, C., Lalucat, J., Bosch, R., 2007 Bacterial diversity, composition and dynamics in and around recreational coastal areas; Environ Microbiol 9: 1913–1929.

Prescott, L.M., Harley, J.P., Klein, D.A., 2002. General Microbiology (5th Edn) MacGram hill inc Publishing company.

Stewart, J.R., Gast, R.J., Fujioka, R.S. et al., 2008. The coastal environment and human health: microbial indicators, pathogens, sentinels and reservoirs; Environ Health 7 (suppl 2): S3.

UNEP, 1988. Guidelines for monitoring the quality of coastal recreation and shellfish growing areas; Reference methods for Marine Pollution Studies, Nr.1 Rev 1, 1-33.

UNEP, 1990. Interin Environmental quality criteria for bathing waters; MAP Technical Reports Series Nr.38.

WHO , 2003. Guidelines for Safe Recreational Water Environmental. Volume 1. Coastal and Fresh Waters.

Proceedings of the 10th World Congress of EWRA 'Panta Rhei', 5-9 July 2017, Athens, Greece
© 2017 *European Water Resources Association*

Performance of direct contact membrane distillation for simulated dyeing wastewater treatment

M. Lou[1], L. Ding[1], F. Zhao[1], F. Li[1,2*], C. Ma[1], Q. Tian[1] and Y. Liu[1,2]
[1] *School of Environmental Science and Engineering, Donghua University, Shanghai 201620, China*
[2] *Textile pollution controlling Engineering Ccenter of Ministry of Environmental Protection, Shanghai 201620, China*
[*] *e-mail: lifang@dhu.edu.cn*

Abstract: It is highly desirable to develop effective technologies to address the serious environmental issues caused by dyeing wastewater. Herein, a promising direct contact membrane distillation (DCMD) process was developed for the treatment of simulated dyeing wastewater. Commercial polytetrafluoroethylene (PTFE) and polyvinylidene fluoride (PVDF) membranes were comparatively studied with phenol, aniline and sulfanilic acid served as the model foulants of simulated dyeing wastewater. The influence of several important operation parameters including feed temperature, feed flow rate, feed concentration on flux and rejection was systematically investigated. The result indicated that increasing working temperature of feed and cross flow velocity contribute positivelyto flux of DCMD process. Limited rejection for phenol and aniline was achieved due to the effumability of these compounds. Sulfanilic acid at lower concentration presented higher rejection performance at all operating conditions. Furthermore, the PTFE membranes presented higher rejection than that of PVDF membranes, which can be due to the strong negatively charged surface of the PTFE membranes. These promising results suggest that DCMD process could be served as an effective process to recover high purity water from dyeing wastewater in practice.

Key words: Dyeing wastewater; direct contact membrane distillation; hydrophobic membrane; model foulant

1. INTRODUCTION

Textile industry in China plays an important role in national economy development because of the increasing demand in both international and domestic markets. With the rapid development of textile industry, huge amounts of dyeing wastewater have been discharged into water bodies and causing serious environmental problems we are currently facing (Gao, 2014). It is, therefore, highly desirable to develop effective technologies to address such issue (Ntuli et al., 2009, Dasgupta et al., 2015, Ozturk et al., 2016). A number of effective water treatment technologies, such as biotechnology and physicochemical methods, have been recently developed (Chen et al., 2007), Chhabra et al., 2015). The biotechnology treatment could achieve efficient BOD removal at lower cost in comparison with physicochemical methods, realizing remarkable improvement in treating textile wastewater (Basava Rao and Ram Mohan Rao, 2006). Nevertheless, the bio-treatment processes are ineffective to deal with dissolved ions from textile effluent. Other effective treatment methods combined with biotechnology and membrane separation are rather limited in industrial applications due to high cost (Liu et al., 2011, Ong et al., 2012). Alternatively, membrane distillation (MD), a thermally driven separation process, allows only water vapor to pass through the pores of a hydrophobic membrane at relatively low temperature and pressure, has been considered as a potential candidate for treating dyeing wastewater (Lawson and Lloyd, 1997, Song et al., 2007, Volkov et al., 2016). Previous studies have proven that MD is a promising process for the treatment of dyeing wastewater using hydrophobic membranes (An et al., 2016, Molehtar et al., 2016).

In this work, direct contact membrane distillation (DCMD) process was developed to treat simulated dyeing wastewater containing several model intermediate products. Commercial PTFE and PVDF membranes with similar pore size were comparatively studied. Meanwhile, the effect of other important operational parameters on foulant rejection and water vapor flux during DCMD process were also systematically investigated.

2. EXPERIMENT

2.1 Materials

Commercial hydrophobic PTFE and PVDF membranes were employed without further modification and their specific structural parameters were presented in Table 1. Phenol, aniline and sulfanilic acid were purchased from Sinopharm Chemical Reagent Co., Ltd and used as model intermediate products of dyeing wastewater.

Table 1. Parameters of the membranes in DCMD system

Membrane	PTFE	PVDF
Mean pore size (mm)	0.22	0.22
Porosity (%)	85.12	70.35
Contact angle (°)	128.5	110.1
LEP of water (kPa)	271	203

2.2 DCMD experiment

The working temperature of feed solution (*e.g.,* 30, 40, 50 and 60 °C) and permeate solution (*e.g.,* 20 °C) were controlled *via* a thermostat water bath. The (hot) feed with initial volume of l.0 L and the (cold) permeate with an initial volume of 0.2 L was circulated continuously in opposite directions across the membrane with effective area of 6.0 cm^2. Different feed flow rate of 0.25, 0.34 and 0.43 L/min were comparatively studied, while the cross flow rate of permeate was maintained at 0.25 L/min during the whole process. The mass change of permeate was recorded using an electronic balance connected with a computer. Each test was repeated three times to guarantee reliable results.

2.3 Permeate flux and rejection efficiency

The permeate flux *J*, in units of LMH can be expressed as follows:

$$\mathrm{J} = \frac{\Delta W}{\Delta t \times A} \tag{1}$$

where ΔW was the change in the mass of permeate collected (kg), Δt was the distillation time (h), A was the effective area of membrane (m^2).

During the DCMD test, the concentration of model foulant in the permeate was determined by an UltiMate 3000 high-performance liquid chromatography (HPLC). The foulant rejection efficiency R (%) was determined by the following equation (Lu et al., 2016):

$$\mathrm{R} = (1 - \frac{C_P}{C_f}) \tag{2}$$

where C_p was the final foulant concentration (mg/L) on the permeate side and C_f was the initial foulant concentration (mg/L) on the feed side. The dilution factor was taken into consideration.

3. RESULTS AND DISCUSSION

3.1 Influence of the feed temperature

In order to investigate the influence of temperature on the performance of DCMD process, short-

term distillation test was conducted. As shown in Figure 1, the permeate flux increased with the increasing of feed temperature, both for PTFE and PVDF membranes. As expected, higher temperature produced higher saturated vapor pressure, leading more vapor across the pores of the membranes (Wiklund and Davis). It was noteworthy that the permeate flux of PTFE membranes was higher than that of PVDF regardless of the temperatures. This phenomenon can be explained by the strong negatively charged surface of PTFE membrane (Abd Jalil et al., 2017).The model foulants block the pores of the MD membranes due to the association and dissociation of the functional groups on the membrane surface. However, the negatively charged PTFE membranes generated stronger repulsion to these negative model foulants in comparison with PVDF counterparts. The rejection result was shown in Figure 1 (b) and (d). DCMD test for sulfanilic acid presented higher rejection than others. Moreover, phenol and aniline could hardly achieve desirable rejection with the increasing temperature, which can be due to different volatility of these compounds. Non-volatile chemicals kept liquid in the feed solution, hardly occurred trans-membrane motion at low temperature.

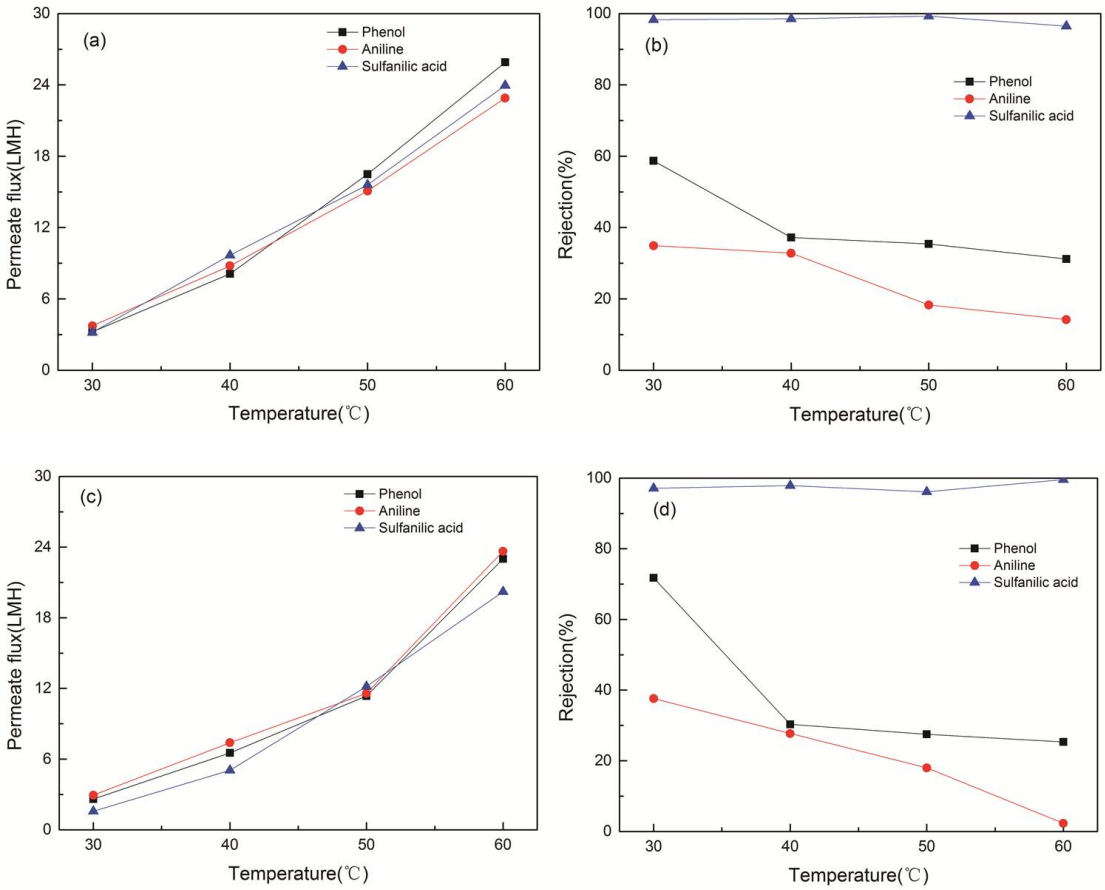

Figure 1. Permeate flux and rejection for three chemicals using PTFE membranes (a), (b) and PVEF membranes (c), (d).

3.2 Influence of cross flow rate

To investigate the effect of cross flow rate and working temperature on the DCMD process, sulfanilic acid was selected as a model intermediate of dyeing wastewater. As displayed in Figure 2, higher flow rate led to higher permeate flux. The formation of a laminar flow on the membrane surface in lower cross flow rate may impede heat transfer between feed stream and membrane surface. Generally, higher velocity leads to higher turbulence which results in reduced boundary layer effects and temperature polarization, hence increasing the driving force across the membrane (Sundar et al., 2017). One key point was that a higher flow rate accelerated the process referred to

water vapor and non-condensable gas through the membrane pores. As for the rejection, with increasing the flow rate and temperature, irregular results were obtained as a precondition to experimental deviations. Lower feed concentration may not achieve desirable result for DCMD. Nevertheless, sulfanilic acid at low concentration presented higher rejection at all given operating conditions.

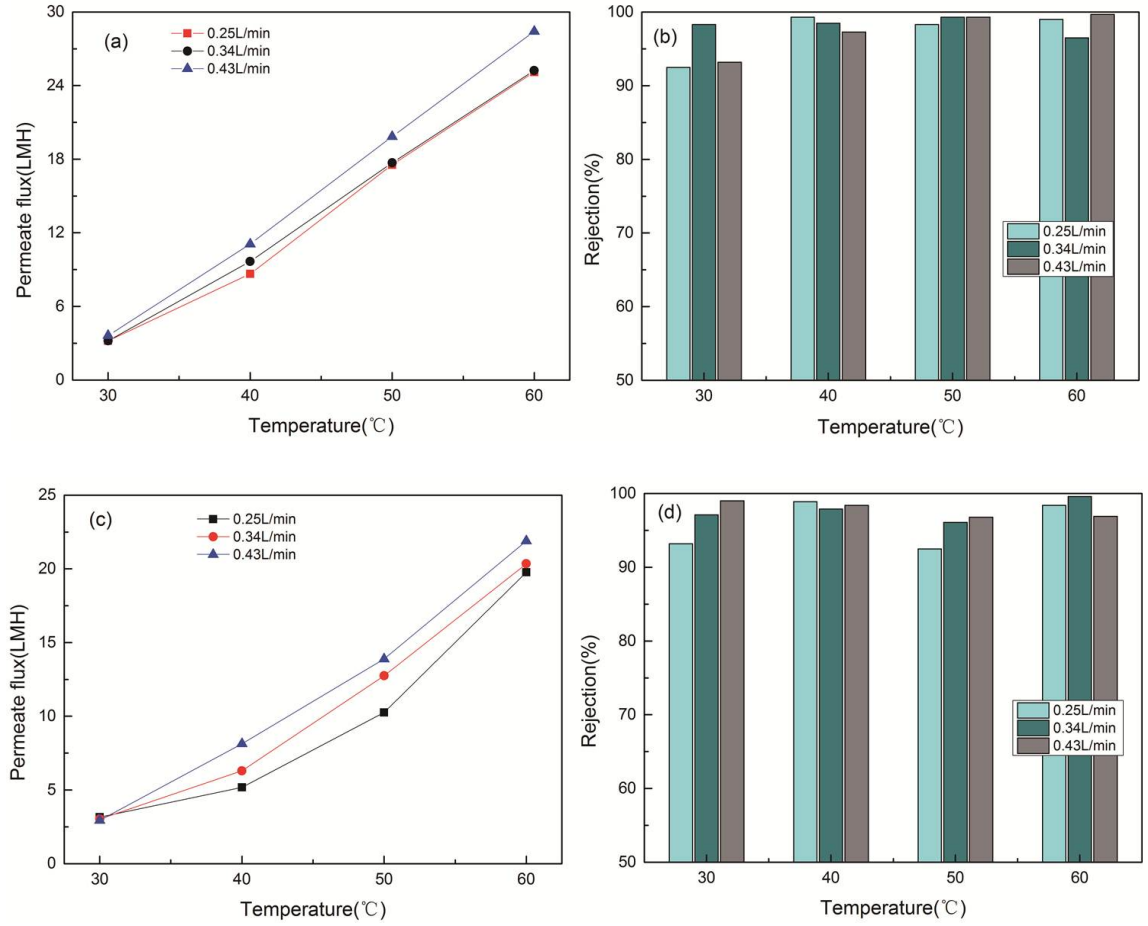

Figure 2. Permeate flux and rejection for chemicals using PTFE membranes (a), (b) and PVDF membranes (c), (d) at various temperatures and cross flow rates.

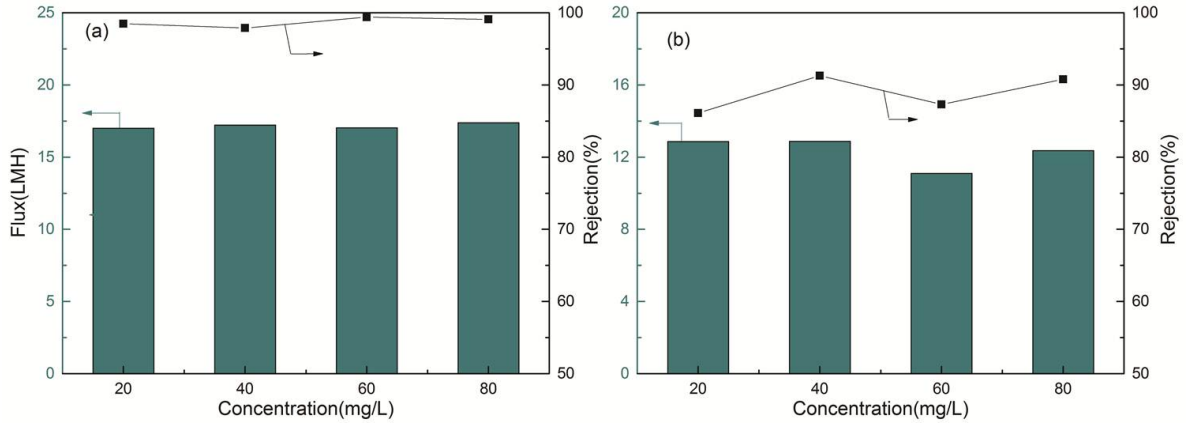

Figure 3. Permeate flux and rejection for chemicals were measured by using (a) PTFE membranes and (b) PVDF membranes at a function of feed concentrations.

3.3 Influence of the feed concentrate

The feed concentration was an important parameter impacting the performance of the DCMD process. As shown in Figure 3, the rejection had no obvious correlation with the feed concentration using sulfanilic acid as a model compound, both for PTFE and PVDF membranes. However, the PTFE membrane presented higher rejection compared with that of PVDF membrane, which may be due to the relatively higher hydrophobicity of PTFE membranes preventing the feed stream into membrane pores (Figoli et al., 2017). In other words, PVDF membranes may suffer from potential wetting during the process of DCMD test.

4. CONCLUSIONS

An effective direct contact membrane distillation (DCMD) system was developed to treat simulated dyeing wastewater. The impact of various important parameters, includes feed temperature, cross flow rate and feed concentration, on the DCMD performance were systematically investigated. Additionally, high feed temperature and fast feed flow facilitated water vapor passing through the membranes and improved the permeate flux. It was noticeable that the PTFE membranes obtained the better performance, *i.e*., higher permeate flux and longer stability during the experiment, due to its improved porosity and hydrophobicity. In summary, although only limited rejection for phenol and aniline was achieved by the DCMD process, DCMD technique still can be considered as a potential candidate way in reclaiming dyeing wastewater because of its energy-efficient and simplicity.

ACKNOWLEDGMENTS

This work is supported by the National Natural Science Foundation of China (Grant No. 51478099, 51508082, 51508082), the Fundamental Research Funding for the Central Universities (Grant No. 2232015A3-04), the National Key Research and Development Program of China (Grant No. 2016YFC0400501) and the Start-up Grant of Donghua University (Grant No. 113-07-005710).

REFERENCES

Abd, Jalil. S. N., Wang, D. K., Yacou, C., Motuzas, J., Smart, S., Diniz, Da. Costa. J. C., 2017. Vacuum-assisted tailoring of pore structures of phenolic resin derived carbon membranes. Journal of Membrane Science.; 525: 240-248.

An, A. K., Guo, J., Jeong, S., Lee, E-J., Tabatabai, S. a. A., Leiknes, T., 2016. High flux and antifouling properties of negatively charged membrane for dyeing wastewater treatment by membrane distillation. Water Research .;103: 362-371.

Basava, Rao. V. V., Ram, Mohan. Rao. S., 2006. Adsorption studies on treatment of textile dyeing industrial effluent by flyash. Chemical Engineering Journal .; 116: 77-84.

Chen, J., Wang, Q., Hua, Z., Du, G., 2007. Research and application of biotechnology in textile industries in China. Enzyme and Microbial Technology .; 40: 1651-1655.

Chhabra, M., Mishra, S., Sreekrishnan, T. R., 2015. Combination of chemical and enzymatic treatment for efficient decolorization/degradation of textile effluent: High operational stability of the continuous process. Biochemical Engineering Journal .; 93: 17-24.

Dasgupta, J., Sikder, J., Chakraborty, S., Curcio, S., Drioli, E., 2015. Remediation of textile effluents by membrane based treatment techniques: A state of the art review. Journal of Environmental Management.; 147: 55-72.

Figoli, A., Ursino, C., Galiano, F., Di, Nicolò. E., Campanelli, P., Carnevale, M. C., Criscuoli, A., 2017. Innovative hydrophobic coating of perfluoropolyether (PFPE) on commercial hydrophilic membranes for DCMD application. Journal of Membrane Science.; 522: 192-201.

Gao, S., 2014. Study on contributions of China's textile industry to national economic development. Journal of Textile Research .; 35: 145-151.

Gullinkala, T., Digman, B., Gorey, C., Hausman, R., Escobar, I. C., 2010. Chapter 4 Desalination: Reverse Osmosis and Membrane Distillation . Sustainability Science and Engineering.; Elsevier: 65-93

Lawson, K. W., Lloyd, D. R., 1997. Membrane distillation. Journal of Membrane Science .; 124: 1-25.

Liu, M., Lu, Z., Chen, Z., Yu, S., Gao, C., 2011. Comparison of reverse osmosis and nanofiltration membranes in the treatment of biologically treated textile effluent for water reuse. Desalination.; 281: 372-378.

Lu, K-J., Zuo, J., Chung, T-S., 2016. Tri-bore PVDF hollow fibers with a super-hydrophobic coating for membrane distillation. Journal of Membrane Science.; 514: 165-175.

Molehtar, N. M., Lau, W. J., Ismail, A .F., Kartohardjono, S., Lai, S. O., Teoh, H. C., 2016. The potential of direct contact membrane distillation for industrial textile wastewater treatment using PVDF-Cloisite 15A nanocomposite membrane. Chemical Engineering Research & Design.; 111: 284-293.

Ntuli, F., Ikhu-Omoregbe, D., Kuipa, P. K., Muzenda, E., Belaid, M., 2009. Characterization of Effluent from Textile Wet Finishing Operations.

Ong, C. S., Lau, W. J., Ismail, A. F., 2012. Treatment of dyeing solution by NF membrane for decolorization and salt reduction. Desalination and Water Treatment.; 50: 245-253.

Ozturk, E., Koseoglu, H., Karaboyaci, M., Yigit, N. O., Yetis, U., Kitis, M., 2016. Sustainable textile production: cleaner production assessment/eco-efficiency analysis study in a textile mill. Journal of Cleaner Production.; 138: 248-263.

Song, L., Li, B., Sirkar, K. K., Gilron, J. L., 2007. Direct contact membrane distillation-based desalination: Novel membranes, devices, larger-scale studies, and a model. Industrial & Engineering Chemistry Research.; 46: 2307-2323.

Sundar, L. S., Sharma, K. V., Singh, M. K., Sousa, A. C. M., 2017. Hybrid nanofluids preparation, thermal properties, heat transfer and friction factor – A review. Renewable and Sustainable Energy Reviews.; 68: 185-198.

Volkov, A. V., Novitsky, E. G., Borisov, I. L., Vasilevsky, V. P., Volkov, V. V., 2016. Porous condenser for thermally driven membrane processes: Gravity-independent operation. Separation and Purification Technology.; 171: 191-196.

Wiklund, D. E., Davis, D. S., System for correcting flow measurements of e.g. methane, containing saturated water vapor in pipe of natural gas industry, has measurement circuitry for determining flow of gas compensated for saturated water vapor in gas.; Rosemount Inc.

Proceedings of the 10th World Congress of EWRA 'Panta Rhei', 5-9 July 2017, Athens, Greece
© 2017 *European Water Resources Association*

Stable isotopes (dD & $d^{18}O$) and major ion chemistry of surface waters in Tajikistan, arid Central Asia

Q. Li[1,2], J. Wu[1*] and H. Zeng[1]
[1] *State Key Laboratory of Lake and Environmental Sciences, Nanjing Institute of Geography and Limnology, Chinese Academy of Sciences, Nanjing 210008, China*
[2] *University of Chinese Academy of Sciences, Beijing 100049, China*
[*] *e-mail: w.jinglu@niglas.ac.cn*

Abstract: Major ions and isotopes of hydrogen and oxygen were measured in lake, river and spring water samples collected in Tajikistan from September to October 2011. Stable isotopic values and ion concentrations in waters reflect the environmental conditions in different areas of Tajikistan. Ca^{2+} and HCO_3^- are the dominant ions of river and spring waters, and come mainly from calcite and dolomite weathering. Several water samples are of the Ca-SO_4^{2-} and Na-HCO_3^- type and reflect strong evaporation and silicate weathering. Most lakes of Tajikistan are located in the eastern, mountainous area and are of the Mg-SO_4^{2-} and Na-Cl^- type, reflecting persistent, long-term evaporation under an arid climate. The hydrogen and oxygen isotope values of river and spring water in Tajikistan range from -129 to -65‰ and -17 to -9.3‰, respectively, and display larger values in the west, indicating that river and spring waters in the east are supplied mainly by glaciers, and waters in the west come mainly from precipitation. Relations between hydrogen and oxygen isotopes in waters from the eastern ($\delta D=9.2\times\delta^{18}O+28.0$) and western ($\delta D=5.5\times\delta^{18}O-10.7$) rivers differ as a consequence of different water sources in the two areas. Correlations between hydrochemical and isotope values in lake water mainly reflect the intensity of evaporation.

Key words: Tajikistan; hydrogen and oxygen isotopes; hydrochemical types; environmental characteristics

1. INTRODUCTION

Asia is now experiencing some of the most serious environmental degradation in the world. This is especially evident in Central Asia where the environment is particularly vulnerable and the distribution of water resources is quite uneven (Becker and Li 1990; Zhou et al. 2007). Environmental problems and water crises have restricted social and economic development in the countries of Central Asia and are therefore of particular interest to researchers (Josef et al.1997; Wu et al. 2009). Tajikistan is located in Central Asia and has an arid to semi-arid temperate, continental climate. The topography is characterized by a pronounced contrast in altitude, from the low-lying plains in the southwest to the high Pamir Mountains in the east. The highest peak, Somoni, has an altitude of 7495 m asl and lies in the central Pamir (Liu et al. 2015). A large number of glaciers surround the high mountains of Pamir (Aizen et al., 1996) and meltwater from these glaciers is Tajikistan's main water resource. Most precipitation in the region falls in winter and spring, a consequence of westerly circulation and the North Atlantic Oscillation (Aizen et al. 2001; Chen et al. 2011). Total annual precipitation in Tajikistan varies from approximately 100 mm in the east to 500 mm in the west (Zhao et al. 2017). Tajikistan accounts for more than half of the total available water in all of Central Asia, and it is thus important to understand the hydrological cycle of this region. We collected river, spring and lake waters along a west-east transect in Tajikistan to measure ion concentrations and stable isotopic composition, which can be used to evaluate the condition of the surface waters in Tajikistan. We used the data to investigate the influence of geographic factors on the hydrochemical character of surface waters and provide vital information about water resources in this arid region.

2. MATERIALS AND METHODS

2.1 Sampling

Major ions and stable isotopes (δD and $\delta^{18}O$) were measured in surface water samples collected in Tajikistan from September to October 2011 (Fig. 1). Samples for isotope analysis were collected in 20-mL bottles. The bottles were filled completely to prevent contact with air until they were opened for analysis in the laboratory.

2.2 Laboratory analysis

The pH of water samples was measured using a pH meter (pHS-2C; Lida Instruments, Shanghai, China). Total dissolved solids (TDS) and major ions were described in Ma et al. (2016). Stable isotopes (δD and $\delta^{18}O$) were analyzed using an LGR DT-100 Liquid Water Isotope Laser Analyzer (Los Gatos Research Inc., Mountain View, California, USA) calibrated using Vienna Standard Mean Oceanic Water 2 (VSMOW2; IAEA). All hydrogen and oxygen isotope analyses are expressed in conventional δ notation (δ‰) referenced to VSMOW. Reproducibility was better than 1.0‰ for δD and 0.15‰ for $\delta^{18}O$.

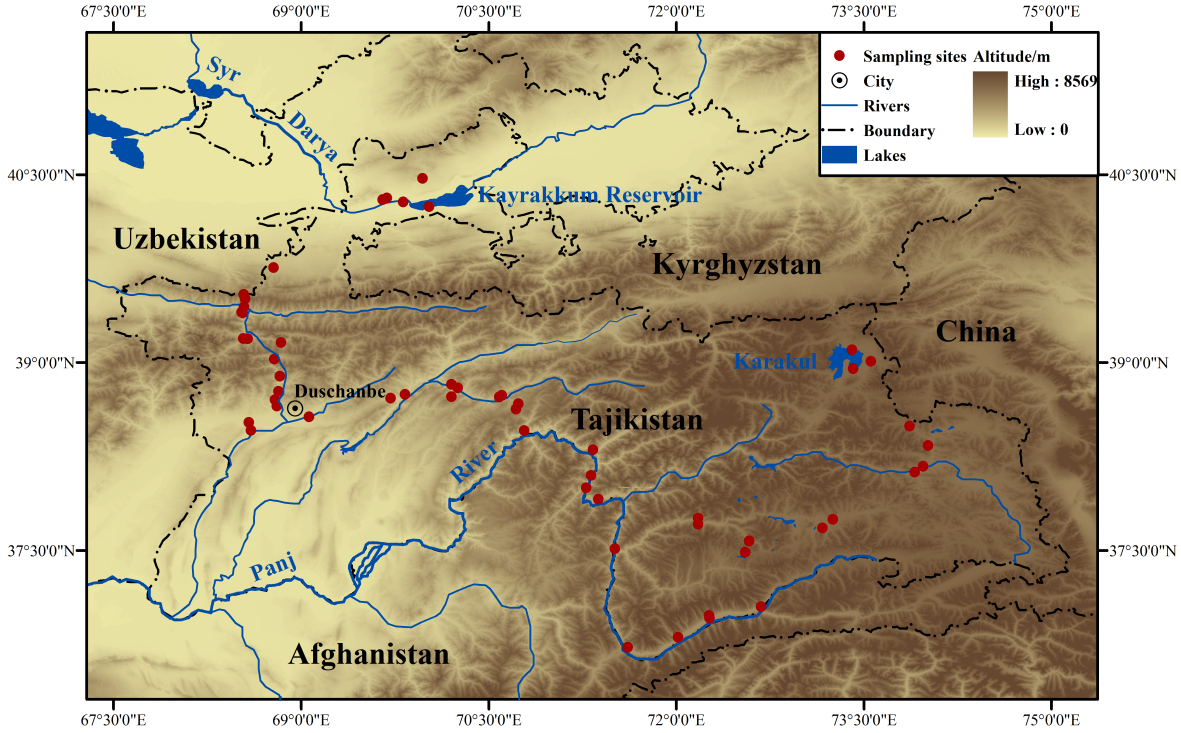

Figure 1. Location of sampling sites in Tajikistan.

3. RESULTS AND DISSCUSSION

3.1 Statistical variables for different water types

We collected 38 water samples from rivers, 12 samples from springs, and six samples from lakes in Tajikistan. Basic statistics for pH, stable isotopes, TDS, and major ion concentrations in waters samples are shown in Table 1. Values of deuterium (δD) and oxygen ($\delta^{18}O$) in river waters ranged

from -127‰ to -66‰ (-92±21‰) and from -17 to -9.3‰ (-13±2.2‰), respectively. For the spring waters, δD and $\delta^{18}O$ values varied from -129‰ to -65‰ (-96±25‰) and from -17‰ to -10‰ (-13±2.7‰), respectively. For the lake waters, δD and $\delta^{18}O$ values ranged from -79‰ to about -38‰ (-63±16‰) and -11‰ to about -1.8‰ (-7.1±4.0‰), respectively.

In river water, TDS varied from 0.06 to 1.4 g/L, with a mean value of 0.28±0.25 g/L. Among the major cations, Ca^{2+} predominated, accounting for an average of 64±11% of the total cation meq, followed by Mg^{2+} and Na^{+}, which both represented an average of 16% of cation meq. Among the major anions, HCO_3^- dominated with on average 70±19% of the total anion meq. Samples from springs had slightly higher TDS values (0.51±0.61 g/L) than those from rivers, whereas the pH was not significantly different between the two water sources. Among the major cations, Ca^{2+} was also the most abundant cation (meq) in spring water, accounting for, on average, 57±21%. Na^{2+} and Mg^{2+} represented an average 24±27% and 17±8%, of the cation meq, respectively. Among the major anions, HCO_3^- dominated (68±27% of the total anion meq), whereas SO_4^{2-} and Cl^- represented, on average, 29±26% and 3±3%, respectively. In general, the hydrochemical characteristics of water were similar in samples from rivers and springs. There was, however, a significant difference in lake waters, which had greater TDS values than river and spring waters, ranging from 1.1 to 91 g/L (19±36 g/L). Among the major cations, Na^+ predominated, accounting for, on average, 42±28% of the total cation meq, followed by Mg^{2+} and Ca^+, which both represented an average of 27%. Among the major anions, SO_4^{2-} was the main anion, representing 67±13% meq.

Table 1 Statistical variables for surface waters in Tajikistan

Sample type	Item	pH	δD	$\delta^{18}O$	Ca^{2+}	K^+	Mg^{2+}	Na^+	Sr^{2+}	Cl^-	SO_4^{2-}	HCO_3^-	TDS
			‰	‰	mg/L	mg/L	mg/L	mg/L	mg/L	mg/L	mg/L	mg/L	g L^{-1}
Rivers (n=38)	Min[1]	7.4	-127	-17	10	0.31	0.78	2.0	0.04	0.38	1.81	35	0.06
	Max[2]	9.0	-66	-9.3	202	6.3	68	177	2.9	107	731	306	1.4
	Mean[3]	8.2	-92	-13	48	1.9	13	17	0.41	11	80	142	0.28
	SD[4]	0.39	-21	-2.2	34	1.2	14	33	0.61	25	139	64	0.25
Springs (n=12)	Min	7.4	-129	-17	2.0	0.21	0.04	2.3	0.04	0.46	7.29	96	0.15
	Max	9.3	-65	-10	545	3.4	80	151	11	87	1444	292	2.3
	Mean	8.2	-96	-13	86	1.8	20	33	1.4	17	199	166	0.51
	SD	0.59	-25	-2.7	147	1.1	22	45	3.0	27	406	59	0.61
Lakes (n=6)	Min	7.8	-79	-11	4.0	2.5	16	66	0.13	80	527	184	1.1
	Max	9.8	-38	-1.8	335	1622	1216	33067	8.0	31214	22830	854	91
	Mean	8.5	-63	-7.1	120	326	441	5894	2.5	5743	5795	355	19
	SD	0.76	-16	-4.0	128	640	585	13320	3.1	12497	8578	252	36

[1] *minimum value*; [2] *maximum value*; [3] *average value*; [4] *standard deviation*

3.2 Spatial variation of δD and δ18O in different water types

There were differences in δD and $\delta^{18}O$ among water samples (river, spring and lake water) from different parts of Tajikistan (Fig. 2). To assess this spatial variation, we separated the samples into two groups based upon the topography of the sampling sites. To the west of ~70.5º E, an area characterized by plains and low mountain topography, the elevation was < 2000 m asl. To the east of ~70.5º E are the high-mountain and glacier regions, and sampling sites were generally between 2000 and 4000 masl. In low-lying western Tajikistan, the δD and $\delta^{18}O$ of river and spring waters (-75±7.9‰ and -11±1.0‰ for river water, and -75±11‰ and -11±1.3‰ for spring water, respectively) were greater than in samples from eastern Tajikistan (-115±7.8‰ and -15±0.8‰ for river samples, and -117±11‰ and -16±1.3‰ for spring samples, respectively). For lake waters, however, the δD and $\delta^{18}O$ values displayed the opposite trend, with δD and $\delta^{18}O$ in the eastern lakes (-49±9.3‰ and -3.6±1.6‰, respectively) slightly greater than values in the western lakes (-76±4.2‰ and -11±0.2‰, respectively). In general, δD and $\delta^{18}O$ values in river and spring water gradually increased from east to west, perhaps related to different water supply. The slight decline in δD and $\delta^{18}O$ in lake waters from east to west reflects mainly the intensity of evaporation.

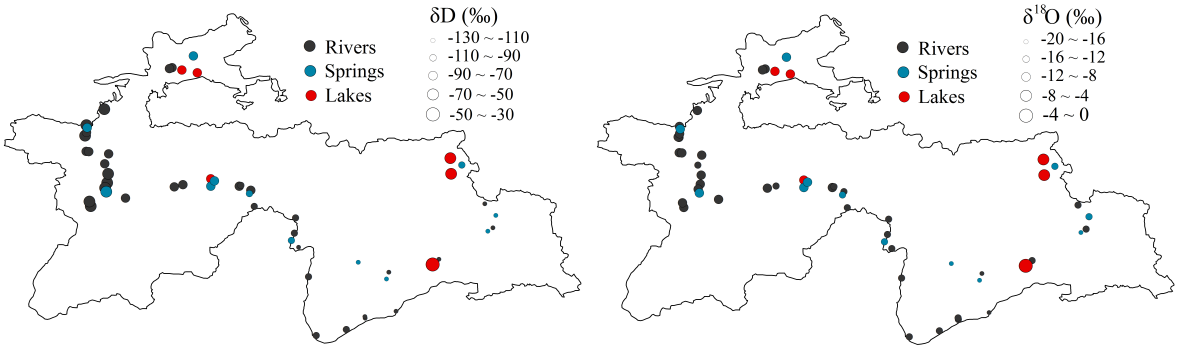

Figure 2. Distribution of hydrogen and oxygen isotope values in different surface waters from Tajikistan

Regression lines between δD and $\delta^{18}O$ for both river and spring waters in Tajikistan deviated slightly from the global meteoric water line (GMWL). In western Tajikistan, most values for river and spring waters were scattered above the GMWL ($\delta D = 5.5\delta^{18}O-10.7$), whereas the scatter points were mostly on or below the GMWL in eastern Tajikistan ($\delta D = 9.2\delta^{18}O+28.0$). Local evaporation can change the relation between δD and $\delta^{18}O$ in residual water and can result in a linear relation between δD and $\delta^{18}O$ values that falls below the GMWL. This, however, was not the case in western Tajikistan, as the distribution of δD and $\delta^{18}O$ values was well above the GMWL (Fig. 3), implying that the river and spring water in western Tajikistan is not strongly influenced by local evaporation. In fact, there is an abundance of winter and spring precipitation in western Tajikistan, influenced by westerly circulation and the North Atlantic Oscillation, and precipitation is thus the main water supply in the region (Chen et al. 2011). In eastern Tajikistan, the linear relation between $\delta^{18}O$ and δD values in river and spring waters fell slightly below the GMWL. This probably reflects higher land surface evaporation in that region, and the fact that river and spring waters in the east are supplied mainly by glacier meltwater. Three lake samples from eastern Tajikistan fell below the GMWL, but above the evaporation line of Lake Karakul ($\delta D = 5.0\delta^{18}O-35.2$) reported by Mischke et al. (2010), revealing that the hydrologically closed lakes in the Pamir Mountains are dominated by long-term evaporation under arid climate conditions.

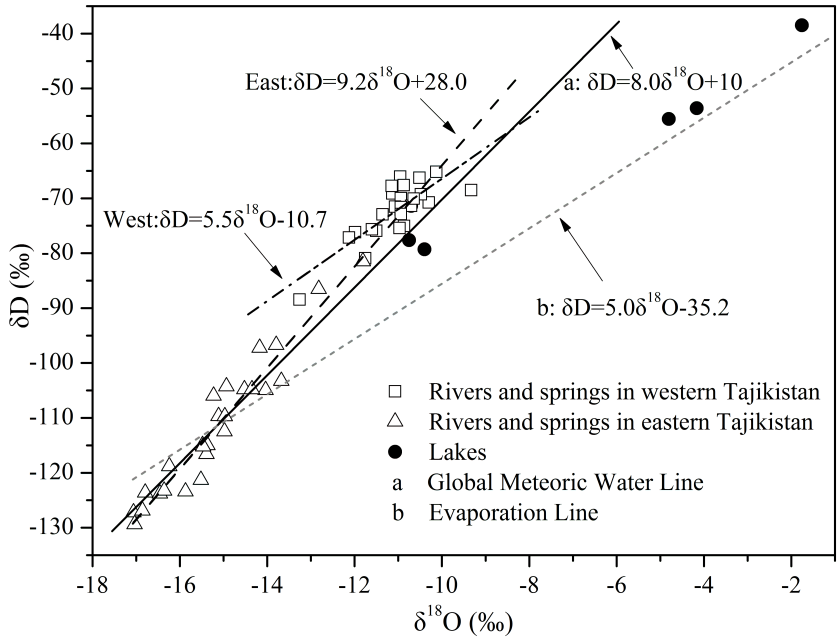

Figure 3. Linear relation between δD and δ18O in different surface water types in Tajikistan, compared with the Global Meteoric Water Line (GMWL) and evaporation line of Lake Karakul. The solid line (a) indicates the GMWL; the small dashed line (b) indicates the evaporation line of Lake Karakul.

3.3 Hydrochemical facies of different surface water types in Tajikistan

Most river water from Tajikistan plots in the field of the Ca^{2+}-Mg^{2+}-HCO_3^- hydrochemical facies type, accounting for 74.4% of the river samples (Fig. 4) and suggesting that the dissolved ions in the water originated mainly from calcite and dolomite weathering. The other 25.6% of river waters in eastern and southwestern Tajikistan were in the field of the Ca^{2+}-Mg^{2+}-Cl^- -SO_4^{2-} hydrochemical facies, and only one sample was categorized as dominated by Na^+-HCO_3^-. The hydrochemical facies of spring waters were similar to river samples, which were mainly in the field of the Ca^{2+}-Mg^{2+}-HCO_3^- type (Fig. 4). This is interpreted as the result of water-rock interactions (Dindane et al. 2003; Belkhiri et al. 2010) and reflects the abundance of carbonate lithology in this region. Lake waters, however, displayed significant differences (Fig. 4). Eastern lakes in the Pamir Mountains are virtually closed hydrologically, and are subject to intense evaporation under arid climate conditions. They possess Na^+-dominant Cl^--SO_4^{2-} type waters. These lake samples had high salinity that may be the result of halite (NaCl) and thenardite (Na_2SO_4) dissolution or cation exchange. The southwest outlet lake water of the Kayrakkum Reservoir was in the field of the Ca^{2+}-Mg^{2+}-Cl^- -SO_4^{2-} hydrochemical facies, the same as river water in southwestern Tajikistan.

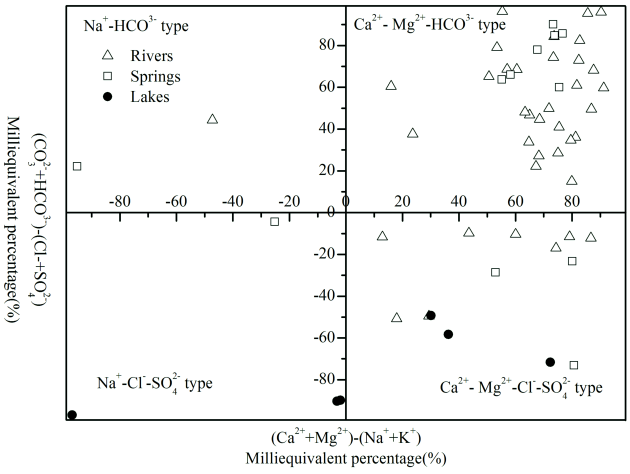

Figure 4. Hydrochemical facies of different water types in Tajikistan

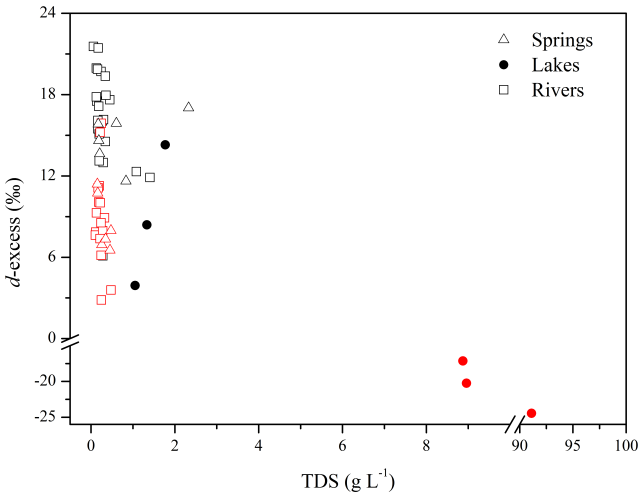

Figure 5. TDS concentrations vs. d-excess of different water types in Tajikistan. The red color indicates the water samples from eastern Tajikistan; the black color indicates water samples from western Tajikistan.

3.4 Relationship between hydrochemical and isotopic characters of different water types

The deuterium excess parameter (*d*-excess; $d=\delta D-8\times\delta^{18}O$) is an important index in the study of surface water (Dansgaard 1964), having an average value of about 10‰ in global precipitation. In this study, *d* of river and spring water was in the range from 11.6‰ to 21.5‰ (16.0±3.4‰) in the west and between 2.8‰ and 15.8‰ (8.8±3.1‰) in the east (Fig. 5), implying a spatial difference in moisture sources. The higher *d* in river and spring water in western Tajikistan reflects the influence of moisture from long-distant transport, such as from the Mediterranean, Caspian and Aral Seas (Liu et al. 2015). The lower *d* in river and spring water of east Tajikistan is consistent with moisture transport from local evaporation. Moreover, dissolved ions and TDS are enriched, along with heavy isotopes, during evaporation (Ma et al. 2016). This phenomenon was especially evident in eastern lake waters (Fig. 5), in which *d* (-20.6±3.7‰) was much lower than in global average precipitation and TDS concentrations were higher, indicating the significant long-term evaporation under arid climate conditions. Correlations between hydrochemistry and isotope values of different water types in Tajikistan are shown in Table 2. There is no strong correlation between hydrogen or oxygen

isotopes and major ions in river water, suggesting rivers are influenced mainly by recharge water sources. The hydrogen and oxygen isotopes of spring water, however, had a positive correlation with HCO_3^-, interpreted as a consequence of water-rock interactions when atmospheric precipitation enters the below-ground aquifer. A significant correlation between hydrogen and oxygen isotopes and Ca^{2+}, Na^+, Cl^-, SO_4^{2-}, HCO_3^- was found in lake waters because in such closed-basin lakes intense evaporation causes isotopic fractionation, enriching the lake water in the heavier isotopes, and leads to greater ion concentrations (Wang et al. 2013).

Table. 2 Correlations between stable isotopes and dissolved ions in different water types from Tajikistan

Water types		K^+	Na^+	Ca^{2+}	Mg^{2+}	Sr^{2+}	Cl^-	SO_4^{2-}	HCO_3^-	TDLs
Rivers (n=38)	δD	0.14	-0.20	0.14	0.20	0.20	0.18	0.09	0.15	0.36
	$\delta^{18}O$	0.21	-0.15	0.18	0.26	0.29	0.23	0.15	0.17	0.42
	d	-0.12	-0.30	-0.04	-0.07	-0.13	-0.06	-0.13	0.25	0.23
Springs (n=12)	δD	-0.15	0.26	0.39	0.48	0.39	0.50	0.38	0.58*	0.38
	$\delta^{18}O$	-0.13	0.29	0.36	0.46	0.36	0.49	0.36	0.62*	0.36
	d	-0.25	0.03	0.47	0.52	0.49	0.48	0.45	0.28	0.39
Lakes (n=6)	δD	0.807	0.757	-0.732	0.353	-0.680	0.771	0.870*	0.865	0.801
	$\delta^{18}O$	0.738	0.680	-0.852	0.471	-0.821	0.696	0.811	0.816*	0.730
	d	-0.638	-0.574	0.937**	-0.562	0.918**	-0.591	-0.716	-0.731	-0.627

** Significant correlation at p<0.05 level; ** Significant correlation at p<0.01 level*

4. CONCLUSIONS

Relations among stable isotopes and major ion concentrations indicate that river and spring waters in Tajikistan are related, with precipitation having the greatest influence on river and spring waters in western Tajikistan, and glacier/snow meltwater contributing most water to rivers and springs in the east. Ca^{2+}-Mg^{2+}-HCO_3^- is the dominant hydrochemical facies type for both rivers and springs, suggesting that carbonate rocks in the basins control the hydrochemistry. Hydrogen and oxygen isotope values, and their correlation with hydrochemical variables of lake water reflect the intensity of evaporation. Negative deuterium excess values and higher TDS in east lake waters reveal stronger evaporation under arid climate conditions, with a Na^+-Cl^--SO_4^{2-} hydrochemical facies type dominating, along with high salinity that reflects possible dissolution of halite (NaCl) and thenardite (Na_2SO_4).

ACKNOWLEDGEMENTS

We thank the CAS Research Center for Ecology and Environment of Central Asia for assistance with field work. Thanks are also due to Mark Brenner for his valuable suggestions and revision of the text. This paper was supported by the National Natural Science Foundation of China (41671200; U1603242).

REFERENCES

Aizen, V. B., Aizen, E. M., Melack, J.M., Martma, T., 1996. Isotope measurements of precipitation on central Asian glaciers (southeastern Tibet, northern Himalayas, central Tien Shan). J. Geophys. Res. 101, 9185-9196.

Aizen, E. M., Aizen, V. B., Melack, J. M., Nakamura, T., Ohta, T., 2001. Precipitation and atmospheric circulation patterns at mid-latitudes of Asia. Int J Climatol. 21: 535-556.

Becker, F., Li, Z. L., 1990. Towards a local split window method over land surface. Int J Remote Sens. 11: 369-393.

Belkhiri, L., A. Boudoukha, L. Mouni, and T. Baouz. 2010: Application of multivariate statistical methods and inverse geochemical modeling for characterization of groundwater-A case study: Ain Azel plain (Algeria). Geoderma. 159: 390-98.

Chen F. H., Huang, W., Jin, L. Y., Chen J. H., Wang, J. S., 2011. Spatiotemporal precipitation variations in the arid Central Asia in the context of global warming. Science China: Earth Sciences. 41: 1647-1657 (in Chinese).

Dansgaard, W. 1964. Stable isotopes in precipitation. Tellus 16: 436-68.

Dindane, K., L. Bouchaou, Y. Hsissou, and M. Krimissa. 2003. Hydrochemical and isotopic characteristics of groundwater in the Souss Upstream Basin, southwestern Morocco. Journal of African Earth Sciences 36: 315-27.

Josef, C., Hung, L. Y., Li, Z. L., 1997. Multi-temporal, multi-channel AVHRR data sets for land biosphere studies-Artifacts and corrections. Remote Sens Environ. 60: 35-57.

Liu, Q., Tian, L.D., Wang, J.L., Wen, R., Weng, Y.B., Shen, Y.P., Vladislav, M., Kanaev, E., 2015. A study of longitudinal and altitudinal variations in surface water stable isotopes inWest Pamir, Tajikistan. Atmospheric Research. 153:10-18.

Ma, L., Wu, J. L., Abuduwailia, J. L. L., 2016. Hydrochemical and isotopic characters of surface water in agricultural oases of the Tianshan Mountains, Northwest China. Arid Land Research and Management.1: 37-48.

Mischke, S., Rajabov, I., Mustaeve, N., Zhang, C. J., Herzschuh, U., Boomer, I., Brown, E. T., Andersen, N., Myrbo, A., Ito, E., Schudack, M. E., 2010. Modern hydrology and late Holocene history of Lake Karakul, eastern Pamirs (Tajikistan): A reconnaissance study. Palaeogeography, Palaeoclimatology, Palaeoecology. 289: 10-24□

Wang, J. Z., Wu, J. L., Zeng, H. A., Bai, R. D., 2013. Characteristics of water isotope and hydrochemistry in Hetao plain of Inner Mongolia. Journal of Earth Sciences and Environment. 35:104-112 (in Chinese).

Wu, J. L., Ma L. Jilili, A., 2009. Lake surface change of the Aral Sea and its environmental effects in the arid region of the central asia Arid Land Geography. 32: 418-422 (in Chinese).

Zhao, Z. H., Zeng, H. A., Wu, J. L., Zhang, L. 2017. Concentrations, sources and potential ecological risks of polycyclic aromatic hydrocarbons in soils from Tajikistan. International Journal of Environment and Pollution. 61:13-18.

Zhou, K. F., Zheng, Q., Chen, X., Sun, L., 2007. Features and trends of the environmental change in the arid areas in Central Asia. Science in China Series D: Earth Sciences, 50 (Supp. l): 142-148.

Proceedings of the 10th World Congress of EWRA 'Panta Rhei', 5-9 July 2017, Athens, Greece
© 2017 *European Water Resources Association*

New, energy saving, cleaning procedures in MBR systems

L. Lintzos[1], K. Chatzikonstantinou[1], N. Tzamtzis[1*] and S. Malamis[2]
[1] *School of Chemical Engineering, Department of Chemical Science, National Technical University of Athens, 15780, Greece*
[2] *School of Civil Engineering, Department of Water Resources and Environmental Engineering, National Technical University of Athens, 15780, Greece*
[*] *e-mail: nipitz@central.ntua.gr*

Abstract: Global climate changes result in serious consequences to ecosystems. Worldwide governments are taking steps to address the challenge in order to find measures to tackle the problem. The UNFCCC in 1992 in Rio de Janeiro and the Kyoto Protocol, were formed the international framework for combating climate change. One of the measures endorsed this protocol was about a sensible use of limited water resources and reuse them. Nowadays, Membrane Bioreactor systems (MBR) are introduced as an appropriate wastewater treatment method, having the advantage to produce effluent at high quality, suitable for reuse. Unfortunately the MBR systems seem to over consume energy due to aeration needs for membrane cleaning. In this study, new membrane cleaning approaches of an MBR pilot plant for a synthetic urban wastewater treatment are examined. These are based on membrane backwashing procedures, using water at increased temperature (up to 28°C), or/and in combination with high frequency powerful vibration (HFPV) on the membrane's module. Using the above procedures fewer backwash cleaning steps are required using higher backwash water temperatures in a certain backwashing period, contributing in energy savings of the backwash system of about 50%. This rate becomes even higher in combination of HFPV with backwash procedures and it reaches a profit in energy consumption of around 90% of the backwash system. In addition the influence of HFPV in combination with backwash procedure on the cleaning efficiency of membrane's module has a result the increase even more the effluent flow, giving an extra profit of the overall system performance.

Key words: Backwash, vibration, HFPV, wastewater treatment

1. INTRODUCTION

Membrane Bioreactor (MBR) technology for waste water treatment has been a credible alternative to the conventional one (CAS – conventional activated sludge) with many advantages (Le-Clech et al, 2006).The importance of membrane technology is growing in the field of environmental protection. The global Membrane Bioreactor market was worth $838.2 million in 2011 and is expected to witness positive growth and revenue sales through 2018 (The MBR site) .The global MBR operation is expected to grow from 3,879 thousand cubic meters/day in 2011 to 12,344 thousand cubic meters/day by 2017, at an estimated Compound Annual Growth Rate (CAGR) of 20.8% for the period 2012 to 2017. As of year 2011, Asia-Pacific leads MBR market with a share of 41.2% in terms of value, followed by Europe and N. America (SBWire site). Membrane fouling has been the most severe problem and barrier to the increased use of MF (micro filtration) and UF (ultrafiltration) membrane technologies (Güell and Davis, 1996, Chellam et al, 1998). The degree of fouling in submerged membrane systems is a complex function of feed characteristics, membrane properties and operating conditions (Raffin, et al, 2012, Aimar, 2010, Tang et al, 2011). Membrane fouling results a biofilm formation all around the membranes, which gradually increases the permeate flow resistance and reduces the permeate flow (flux). It affects operating cost, due to the frequent membrane cleaning and the continuous high aeration demands of the system (Zhang et al, 2006). Several necessary strategies are employed in order to reduce membrane fouling nowadays, such as the pre-treatment of feed waste water, chemical or physical membrane cleaning procedures applied at shorter intervals, flux reduction and other methods which, either leads to increased operating and maintenance costs and produces chemical wastes, or rising

up the installation size. It has been found that backwash cleaning procedures successfully remove the majority of reversible contamination and partly dislodge loosely adherent aggregates sludge from the membrane surface, returning the membrane in good operating condition (Bouhabila et al, 2001, Psoch and Schiewer, 2005, Psoch and Schiewer, 2006). Backwash cleaning procedures are used in both UF and MF types, mainly in HF (hollow fiber) and in some appropriate FS (flat sheet) membranes. The above procedures are performed in MBR systems, without interrupting the system's operation. The frequency, the duration and their value ratio in the backwashing process, are the key for the design the backwashing programs which have proven more effective in several studies (EUROMBRA, 2006). In the current literature there is a lack of experimental data for backwash cleaning procedures using water at elevated temperatures or/and in combination with membrane module vibration. In addition at most previous studies the same permeate flow (or aqueous solutions of various chemicals) at ambient temperatures was used for backwash cleaning (Katsoufidou et al., 2005, Yigit et al., 2009). Also, in many studies, several kinds of vibration are referred but none in combination with backwash cleaning (Chatzikonstantinou et al., 2015, Beier et al 2016, Genkina and Waiteb, 2016). This study introduces a new energy saving, cleaning membrane procedure which is based on membrane backwashing with pure water at increased temperature, or/and in combination with high frequency powerful vibration (HFPV) on the membrane's module via pneumatic vibrators. This HFPV technique uses high frequency oscillatory vibration to create high shear forces at the surface of the filter membrane.

2. MATERIALS AND METHODS

Two modules of three identical HF type membranes (at each module) were used in this study in two parallel lines in an MBR tank. The membrane characteristics and the experimental conditions used in this study are presented in Table 1 and Table 2 correspondingly.

Table 1. HF membrane characteristics

Membrane Type	Filtration Type	Membrane Material	Pore Size (μm)	Membrane Area (m^2)	Frame Dimensions (mm)	Critical Flux (l/m^2H)
HF	UF	R-PVDF	0.1	0.05	24x22	25

Table 2. MBR/Backwash experimental conditions

Working Time/Cycle (min)	Relaxing Time/ Cycle (min)	pH	Bubble type	Max TMP (mbar)	MLSS (mg/lt)	Backwash Period/ frequency	Backwash recommended flow (L/hm^2)	Max Backwash Pressure (mbar)	Backwash Water Temp. (^oC)
8	2	7-8	Coarse	180	7,000-12,000	see exp. proced.	30	<50	18, 28

It was chosen to apply the backwashing procedure every time the membranes presented significant clogging in terms of TMP recorded values (not above 180mbar) and the flux limited lower value (not below 10 l/ m^2h).

The pilot plant which was used is presented in Figure 1 and a brief description is followed.

In each module a vacuum suction line is attached through a peristaltic, suction pump. Each HF membrane module is controlled by an independent suction line. At the exit of each effluent line a glycerin pressure indicator is installed (-1 ÷ 0 bar) and also an analog vacuum pressure transducer (-1 ÷ 0 bar) in series with an analogue flow meter (FM). The working and relaxing time of the suction pump as well as the operating pressure of each suction line were adjusted according to the manufacturer for the protection of HF membrane elements. In the backwash line there are in series: a flow control solenoid valve, a glycerin pressure indicator and an analog pressure transducer (0 ÷ 1 bar). The backwash pump was connected to a volume calibrated water container which it was

supplied with a regulated thermostat and an immersed heater. The backwash pump was calibrated manually to provide the recommended volume of backwash cleaning water. It should be noticed that the MBR pilot unit treats continuously and for a long period a synthetic urban wastewater under limited aeration conditions for a faster simulated membrane fouling. The analytical description of the MBR unit is given elsewhere (Chatzikonstantinou et al., 2015).

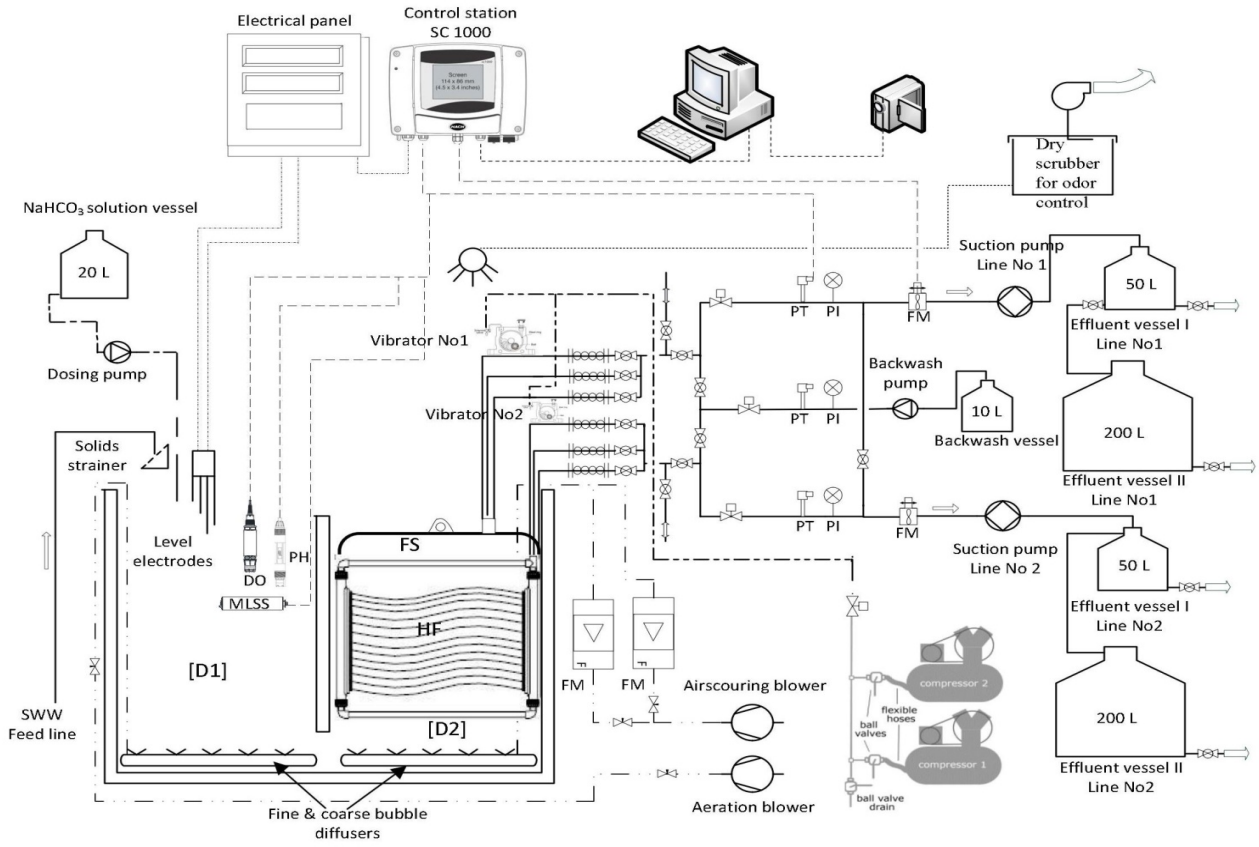

Figure 1. MBR pilot plant and backwashing layout.

HFPV applied in each module of three membranes with a pneumatic ball vibrator. The vibrator was a V8 industrial type with a frequency of 233Hz at 4 bar. The vibrator is fastened properly in order to provide shear forces through powerful vibration in all over the membrane. The system consists of the vibration header, air compressor, feed air pipes, regulation/control valves and pressure measurement/control apparatus. Prior to isolation valve each suction line is equipped with an anti-vibration flex connector for limiting the transmission of vibration to the rest of the system. In all experimental cycles the pressure of compressed air remains constant in order to keep the frequency and the produced centrifugal force almost stable .Each time vibration implementation took place, it lasted for three minutes in combination with backwash scheme. In Table 3 presented the type and characteristics of the used vibrator.

Table 3. Vibrator type and characteristics

Vibrator Type	Vibrator's supply air pressure (bar)	Vibration frequency (Hz)	Vibration velocity RMS (mm/s)	Vibration acceleration RMS (g)	Vibration Displacement p-p (mm)
V8	4	223	142	20	0.3

3. EXPERIMENTAL PROCEDURE

In this study four experimental cycles were performed under almost the same working

parameters (MLSS, SRT, pH, DO) and operational parameters (starting TMP and flux). In the first experimental cycle, backwash was performed in a module of three HF membranes using water at 18°C for three minutes time period. In the second cycle, backwash performed in another module, using water at 28°C for the same as above time period. At the following two experimental cycles the backwash procedures were the same as the previous ones but these were combined with HFPV. First and second experimental cycle took place at parallel lines at the same time. Similarly the third and the fourth experimental cycle were performed. Each experimental cycle lasted ten days. In this period of ten days, a lot of cleaning procedures were performed on modules depending on the monitored TMP and flux upper and lower values accordingly. The backwash procedure was conducted manually and at the end of the process the system returns to the operating automation (8 min. working/2 min. relax). All the presented TMP and flux values are normalized to a standard temperature of 20°C.

4. RESULTS AND DISCUSSION

Figure 2 presents the monitored TMP values during all the experimental cycles in a ten days (240 hours) working period of the MBR unit. It is observed that the membrane module which was cleaned using backwash water at 18°C returned to its upper (before backwash) TMP value in a short period, about 24 hours. By increasing the backwash water temperature from 18°C to 28°C, the rate of increase (after cleaning procedure) of TMP was lower. As a result, the number of cleaning steps reduced to the half with respect to the previous for the same time period (from 10 to 5 steps in 240 working hours). In the last two experimental cycles where HFPV was performed in combination with backwash the increasing rates (after cleaning procedure) of TMP was even lower. Specifically, in the case of backwash using water at 18°C in combination with HFPV only 3 cleaning procedures steps during 240 hours working period were needed. On the contrary only 1 cleaning procedure in the case of combination HFPV with backwash using water at 28°C was needed for the same working period.

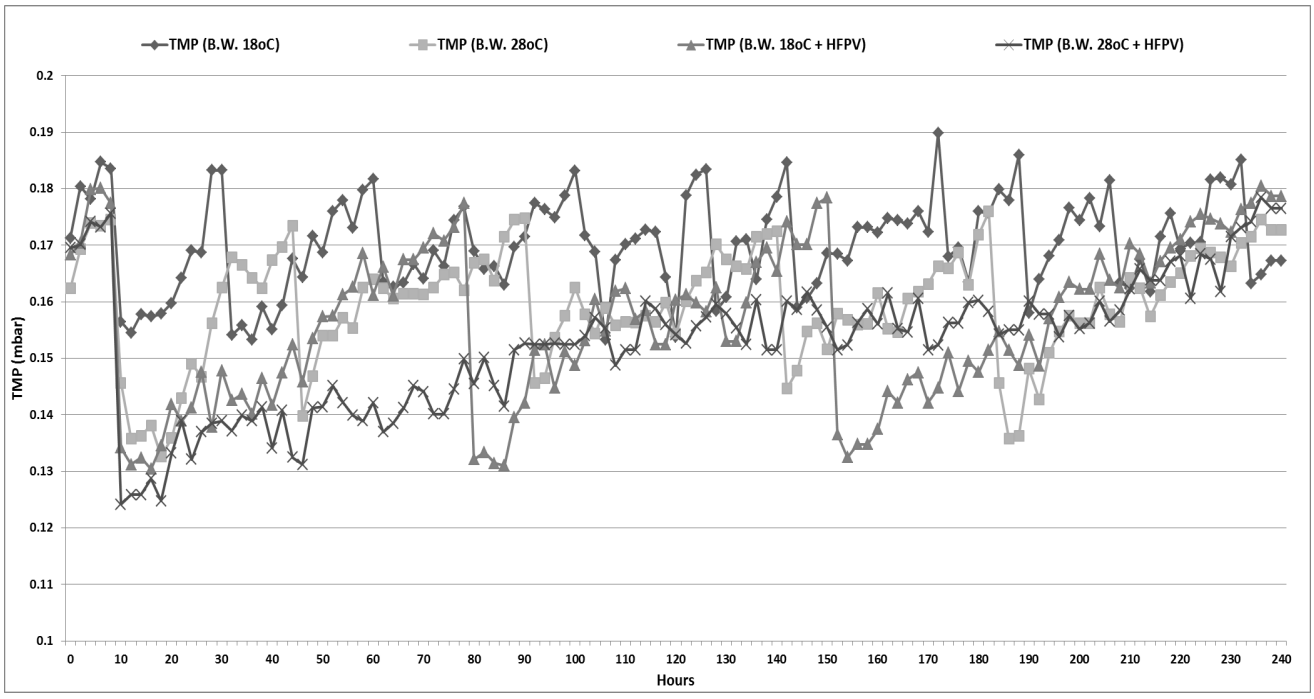

Figure 2. TMP monitored values during a period of 240 working hours for the examined membrane cleaning procedures.

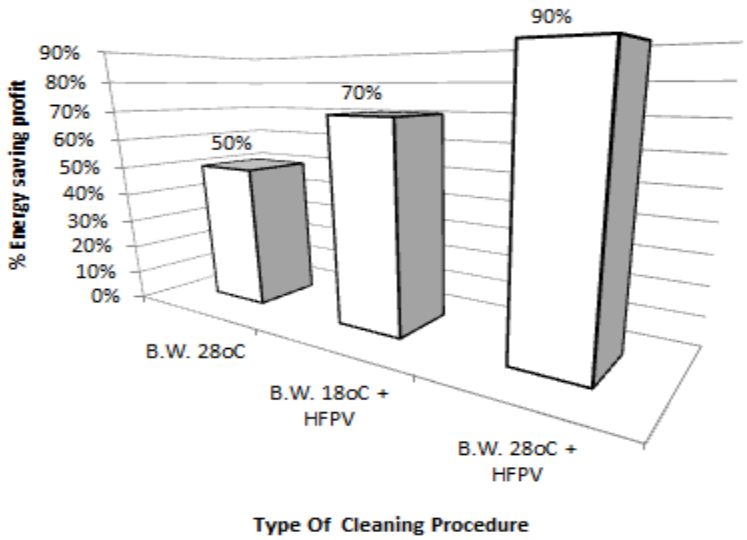

Figure 3. Energy consumption of backwash system depending on the type of membrane's cleaning in respect to backwash at 18°C.

Figure 3 shows the % energy saving profits, with respect to backwash at 18°C, referring to the backwash system, based on the different backwash cleaning procedures. It is shown that as the temperature increases from 18°C to 28°C it is achieved 50% energy saving. The combination of vibration and backwash offer 70% and 90% energy savings using backwash water in 18 and 28°C accordingly. The energy consumed by vibration is negligible so it not considered in the above rates.

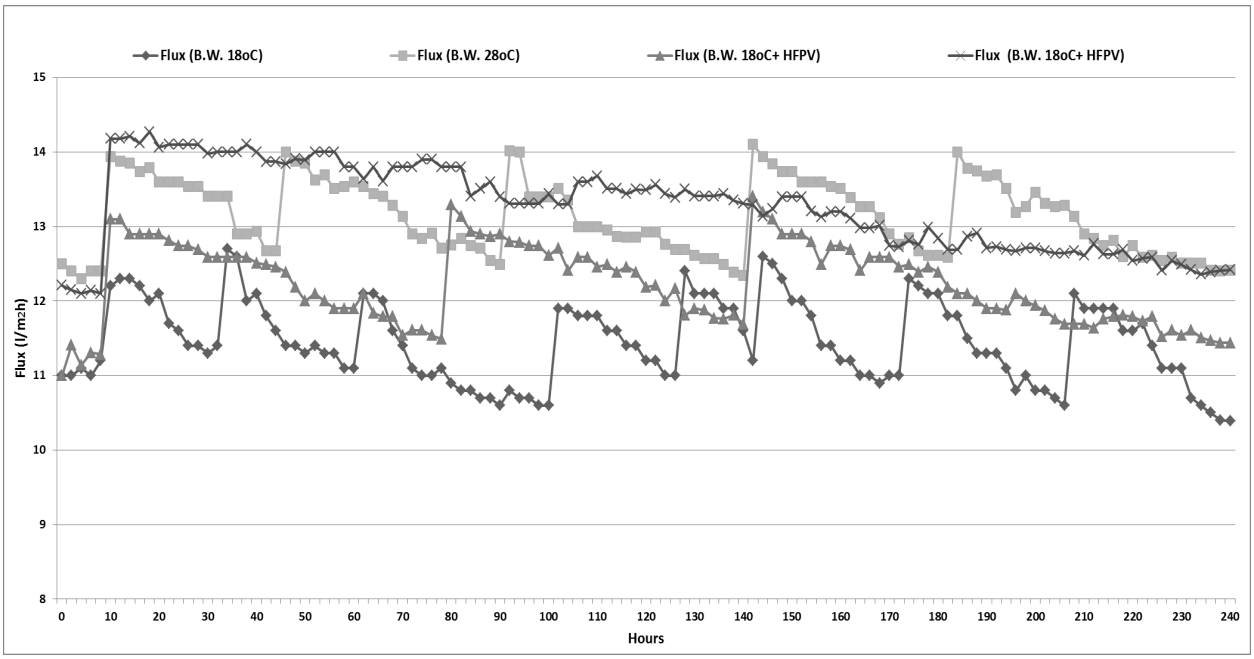

Figure 4. Flux monitored values during a period of 240 working hours for the examined membrane cleaning procedures.

Figure 4 presents the flux monitored values with respect to the type of cleaning procedure during all the experimental cycles in 240 hours working period of the MBR unit. It is shown that the rate that the flux decreases, after each cleaning procedure, in the case of combination of backwash using water at 28°C and HFPV presents less TMP fluctuations than the other cleaning procedures. It should be noted that the flux in all experiments decreases time proceeding, since the unit automation does not allow the flux stability.

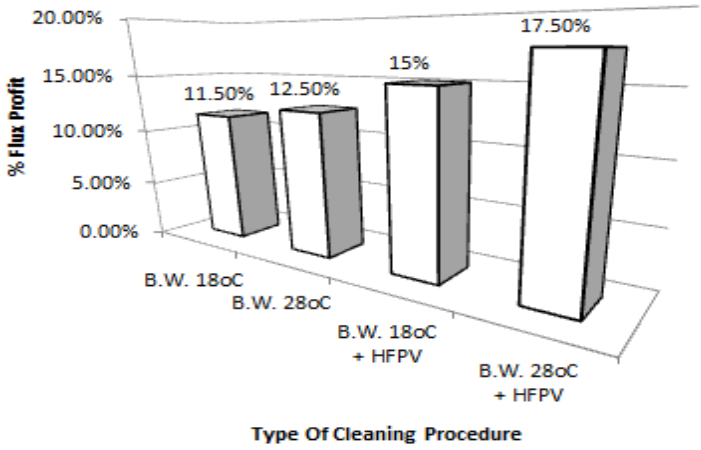

Figure 5. Mean values of flux profit for the examined membrane cleaning procedures in period of 240 working hours.

In Figure 5 it is shown the % flux profits after each cleaning procedure with respect to the corresponding flux just before the first cleaning procedure of each experimental cycle. Specifically, the greater flux profit is 17.50% achieved with the combination of HFPV and backwash using water at 28°C. It follows flux profit of 15% which refers to the combination of HFPV with backwash water at 18°C. These % profits were less when HFPV was not performed. Specifically the % flux profit of backwash cleaning using water at 18°C and 28°C was found to be 11.5% and 12.5% accordingly.

5. CONCLUSIONS

The results from all types of cleaning procedures which examined in this study were positive. It was found that membranes presented better operating performance as the backwash temperature of water was increased. Particularly, by increasing the backwash water temperature from 18 to 28oC both greater flux profits and energy consumption were achieved. Also it was found that the cleaning procedure using backwash water in combination with HFPV increases even more the % flux profit and offers energy saving which reaches 90% with respect to the conditional backwash using water of 18°C. In addition, just after the cleaning procedure the rate of increase of TMP was lower where HFPV was combined, giving the advantage for less number of membrane cleaning steps in a certain operating time. Specifically during first experimental cycle (backwash using 18°C water) 10 cleaning steps were required which were reduced to the half during second cycle (backwash using 28°C water). In the case of backwash using water at 18°C in combination with HFPV only 3 cleaning procedures steps were required and only 1 in the case of combination HFPV with backwash using water at 28°C.Finally, in all examined cases it was found, using analytical methods that the effluent quality is not affected using the above cleaning procedure.

REFERENCES

Aimar P.,2010. Slow colloidal aggregation and membrane fouling. Journal of Membrane Science.; 360:70–76.

Bouhabila E.H., Ben Aim R., Buisson H.,2001. Fouling characterization in membrane bioreactors. Separation and Purification Technology.;22:123-132.

Chatzikonstantinou K., Tzamtzis N., Pappa A., Liodakis S., 2015. Membrane fouling control using high-frequency power vibration, in an SMBR pilot system—preliminary studies. Desalination and Water Treatment.;57:11550-11560

Chellam S., Jacangelo J.G., Bonacquisti T.P., 1998. Modeling and Experimental Verification of Pilot-Scale Hollow Fiber, Direct Flow Microfiltration with Periodic Backwashing. Environmental Science Technology.; 32:75–81.

EUROMBRA, 2006.Membrane bioreactor technology (MBR) with an EU perspective for advanced municipal wastewater treatment strategies for the 21st century, Sixth Framework Programme, Contract No. 018480, Deliverable Report – D5

Genkina G., Waiteb T.D., 2016. The effect of vibration and coagulant addition on the filtration performance of submerged hollow fibre membranes. Journal of Membrane Science.; 281:726-734

Güell C., Davis R.H., 1996. Membrane fouling during microfiltration of protein mixtures. Journal of Membrane Science.; 119:269–284.

Katsoufidou K., Yiantsios S.G., Karabelas A.J., 2005. A study of ultrafiltration membrane fouling by humic acids and flux recovery by backwashing: Experiments and modeling. Journal of Membrane Science.; 266:40-50

Le-Clech P., Chen V., Fane T. A.G., 2006. Fouling in membrane bioreactors used in wastewater treatment. Journal of Membrane Science.; 284:17–53.

Prip Beier S., Guerra M., Garde A., Jonsson G., 2016. Dynamic microfiltration with a vibrating hollow fiber membrane module: Filtration of yeast suspensions.Journal of Membrane Science.; 281:281-287

Psoch C., Schiewer S. ,2005.Critical flux aspect of air sparging and backflushing on membrane bioreactors. Desalination and Water Treatment.;175:61-71.

Psoch C., Schiewer S., 2006. Resistance analysis for enhanced wastewater membrane filtration. Journal of Membrane Science.;280:284-297.

Raffin M., Germain E., Judd S.J., 2012. Influence of backwashing, flux and temperature on microfiltration for wastewater reuse.Separation and Purification Technology.; 96:147–153.

SBWire - The Small Business Newswire, http://www.sbwire.com/press-releases/global-membrane-bioreactor-mbr-systems-market-worth-2052-million-by-2017-187069.htm

Tang C.Y., Chong T.H., Fane A.G., 2011.Colloidal interactions and fouling of NFand RO membranes: a review. Advances in Colloid and Interface Science.; 164:126–143.

The MBR site, http://www.thembrsite.com/about-mbrs/what-are-mbrs/mbr-market

Yigit N.O., Civelekoglu G., Harman I., Koseoglu H., Kitis M., 2009. Effects of various backwash scenarios on membrane fouling in a membrane bioreactor.Desalination.; 237:346-356

Zhang J.S., Chuan C.H., Zhou J.T., Fane AG., 2006. Effect of sludge retention time on membrane bio-fouling intensity in a submerged membrane bioreactor. Separation Science and Technology.; 41, 7:1313 – 1329

Proceedings of the 10th World Congress of EWRA 'Panta Rhei', 5-9 July 2017, Athens, Greece
© 2017 *European Water Resources Association*

Comparative study of the environmental state of Ohrid and Prespa Lakes, Albania

A. Shehu*, M. Vasjari, S. Duka, L. Vallja and N. Broli
Department of Chemistry, Faculty of Natural Sciences, University of Tirana, Tirana, Albania
* *e-mail: alma.shehu@fshn.edu.al*

Abstract: The present study was undertaken to evaluate the environmental situation of Ohrid and Prespa Lakes with regard to heavy metals present in water in relation to different factors controlling metals occurrence in these environments. A total of 15 water samples, collected at different stations and depths were selected to monitor Ohrid Lake whilst 4 samples were collected at Prespa Lake. Content of heavy metals such as Cr, Ni, Fe, Pb, Cd, Cu was determined in the filtered fraction of water, using the GF-AAS technique whilst chlorophyll "a" content was used as algal content estimation in both lakes. The relative abundance of heavy metals in Ohrid Lake followed the order: Fe>Cr>Ni>Pb>Cu>Cd while in Prespa Lake the metals order changed to Fe>Ni>Cr>Pb>Cu>Cd. Total mean concentration of Fe, Ni and Cr varied significantly (α=0.05) between the lakes whilst the mean concentration of Cu, Pb and Cd exhibited no significant variation. Variation of metals concentration with regard to different depths was more evident for Fe, assuming that the content of the dissolved fraction of this element was closely related to water parameters such as pH, water oxygenation, redox potential, etc. Cluster analyses confirm that positive correlation existed between stations S1-S3 and S4-S6 as well as between Fe-Cr-Ni, assuming that metals content was closely related to station location. Estimation of the quality state of the lakes was evaluated based on the European Directives of fresh surface waters such as [78/659/EEC] and (EU, 1989). Given the results, it can be concluded that waters of Ohrid and Prespa Lakes fall in Class A1 of waters quality regarding the heavy metals content, whilst low levels of dissolved oxygen, followed by higher levels of chlorophyll "a" classify deep waters of Prespa Lake in Class A2 of surface waters quality.

Key words: Heavy metals, water column, Ohrid and Prespa Lake, GFAAS

1. INTRODUCTION

Heavy metals contamination of surface water is a worldwide environmental problem because trace amounts of heavy metals are always present in fresh waters from the weathering of rocks and soils and a variety of anthropogenic activities (Achterberg et al., 1995; Loring et al., 1992).

Albania is rich in water resources, including rivers, groundwater, lakes, lagoons and seas. Although its resources exceed by far its consumption, locally water shortage and conflicts among users may occur in the dry season (Selenica et al., 2011).

Ohrid and Prespa Lakes lie in the south-eastern part of Albania. Lake Ohrid straddles the mountainous border between eastern Albania and southwestern Macedonia. It is one of Europe's deepest and oldest lakes, preserving a unique aquatic ecosystem that is of worldwide importance, with more than 200 endemic species. Lake Ohrid is the deepest lake of the Balkans peninsula, with a maximum depth of 288 m and a mean depth of 155 m (Merolli et al., 2003). Population growth and development of industry have impacted the lake ecosystem in many ways.

Prespa Lakes are a high altitude basin (850 masl) with two interconnected lakes: Micro Prespa (shared between Albania and Greece) and Macro Prespa (shared between Albania, Greece and Macedonia) (Talevski et al., 2009). The lake has suffered many pressures in the last forty years, with harmful effects on the health of the water, such as the rapid growth of biomass deriving from farming practices, erosion, untreated wastes and wastewaters.

Previous studies on Ohrid and Prespa lakes have mainly been focused on physical-chemical parameters while there are no reliable studies regarding heavy metals (Merolli, 2003; Adhami et al., 2015). The present study was undertaken to evaluate the environmental situation of Ohrid and

Prespa Lakes with regard to heavy metals present in water in relation to different factors controlling metals occurrence in these environments.

Evaluation of the contamination status of lakes waters was carried out based on two important Directives which determine the criteria for heavy metals content in fresh surface waters such as the EU Directive, 1989 and [78/659/EEC] (EPA, 2001).

2. MATERIALS AND METHODS

Estimation of the environmental situation of Ohrid and Prespa Lakes with regard to heavy metals was accomplished by determining the metals content in the filterable fraction of water samples. The field cruise was conducted during October, 2014. Sampling stations selected at each lake are illustrated in Figure 1.



Figure 1. Map of sampling stations of Ohrid and Prespa Lake

2.1 Sampling procedure of water samples

A Ruthner (Hydro – bios, Kiel, Germany) bottle was used for samples collection whilst polyethylene bottles were used for storage and transport of samples for further analyses. Sampling was conducted according to the standard method No. 105, described in APHA/AWWA, 1995. Physic-chemical parameters were measured in situ, while the chlorophyll content was determined in the suspended material after the filtration of samples, as soon as their arrival to the laboratory.

The analyzed metals were Iron, Chromium, Copper, Cadmium, Lead, Nickel and their content in water samples was determined according to the standard method No. 304 of the "Standard Methods for the Examination of Water and Waste Water" (APHA/AWWA, 1995). NOVAA 400, Atomic Absorption Spectrometer, equipped with a graphite furnace from Analytic Jena was used to carry out water analyses.

2.2 Sampling sites description

The water quality of Ohrid and Prespa Lakes was monitored in four stations in Ohrid Lake and in two stations in Prespa Lake, respectively:

Station S 1 - 4 km in the N-E part of Pogradeci City. (Max depth: 166m). Samples were collected in six different depths of S1.

Station S 2 – 2 km far from Tushemishti city, in the north part of Ohrid Lake (Max depth: 60 m). Samples were collected in three different depths of S2.

Station S 3 - In front of Fe-Ni mine damp, Lake Ohrid, (Max depth 53m). Samples were collected in three different depths of S3.

Station S 4 - 2 km in the East part of Lini village, Ohrid-Lake, (Max depth 72 m). Samples were collected in three different depths of S4.

Station S 5 - Prespa Lake (Gorica). 4 km in the East part, having a maximum depth of 14 m. Samples were collected in two different depths of S5.

Station S 6- Prespa Lake. 5 km far from Gorica, in the East part, with a maximum depth of 15 m. Samples were collected in two different depths of S6.

3. RESULTS AND DISCUSSION

3.1 Analysis of physic-chemical parameters

Results of physic-chemical parameters as well as the content of chlorophyll "a" in waters of Ohrid and Prespa Lakes are presented in Table 1. Descriptive statistics was used aiming to evaluate water quality of both lakes with regard to physic-chemical parameters.

3.1.1 Temperature

In great lakes studies, variation of temperature in water column is the main indicator of lake stratification, a process occurring mainly during summer and winter (Burns et al., 1999). Based on temperature variation that existed in different depths of Ohrid Lake, from 20.8 ^{o}C at 20 m depth to 7.5^{o}C below this layer, it can be concluded that Ohrid Lake was stratified during the period of field cruise. Such situation was not observed for Prespa Lake, were the interval of temperature variation was not significant. Temperature of water in both lakes followed the normal expected values, recommended by the EU [1989] and [78/659/EEC] Directives, ranging from 7.5 – 25°C. Higher water temperature can reduce the dissolved oxygen concentrations in water and may thus affect the aquatic organism's life.

3.1.2 DO

Dissolved oxygen in water samples of both lakes varied significantly with regard to sampling stations depths (α=0.05). Results obtained for Ohrid Lake demonstrated that stratification occurs at 20 m depth, where the values of dissolved oxygen decrease from about 105% to about 88%, as depth increased.

The lowest concentration of dissolved oxygen (5.48mg.L^{-1}) was recorded in station S5, belonging to Prespa Lake, at 10 m depth. This value was closer to the lower accepted limit (>5 mg/l) of no risk for the support of aquatic life, [78/659/EEC]. Intensive growth of aquatic vegetation in this station has led to severe de-oxygenation of the water.

The DO levels in the other stations resulted higher than this limit, ranging from 8.36-10.48 mg.L^{-1}, falling consequently within the recommended levels for the support of fisheries and aquatic life (≥60%), EU [1989].

3.1.3 pH

The pH of the samples varied from 7.0 – 8.68. Observed variations of pH values were not significant and the pH ranges obtained fall within the surface water quality regulation, being respectively 5.5-8.5 according to the EU [1989] Directive, and ≥6 and ≤ 9 according to the Freshwater Fish Directive, [78/659/EEC].

3.1.4 Chlorophyll a

There is a strong relationship between chlorophyll, phosphorus and trophic state of lakes around the world. It was observed that the content of Chl "a" in waters of Prespa Lake resulted to be four times higher compared to its content in Ohrid Lake, ranging from 4.00 - 4.20 μgL^{-1} and from 0.6-1.40 μgL^{-1}, respectively. These values correspond to trophic state indexes, TSI, being respectively 44.19-44.68 and 25.58-33.90, according to Carlson & Simpson formula: TSI(Chl) = 9.81 ln Chl a ($\mu g.L^{-1}$) + 30.6, (Carlson & Simpson, 1996). TSI values confirm the oligotrophic state of Ohrid Lake, while waters of Prespa Lake were found to be in mesotrophic state.

Table 1. Statistical parameters for physic chemical parameters in each station of Ohrid and Prespa Lakes

Stations	Coordinates	Sample	Temp. °C	pH	DO (%)	Cond. ($\mu s.cm^{-1}$)	Chlorophyll "a" ($\mu g.L^{-1}$)
		Mean	14.4	8.2	98.92	238.8	0.90
S 1	N:40°55'441",	Min.	7.5	7.89	83.7	227.0	0.74
	E:20°41'449"	Max.	21.9	8.68	109.0	263.0	1.14
		Mean	16.7	8.10	101.3	234.7	1.40
S 2	N:40° 54'821",	Min.	8.6	7.77	94.5	229.0	0.98
	E:20° 42'319"	Max.	21.6	8.30	106.0	243.0	1.92
		Mean	14.8	7.80	100.4	235.0	0.70
S 3	N:40°05'713",	Min.	8.0	7.00	90.9	227.0	0.01
	E:20° 38'826".	Max.	20.3	7.30	104.7	246.0	1.20
		Mean	14.8	8.30	100.1	236.0	0.60
S 4	N:41° 04'343",	Min.	8.0	8.03	83.4	229.0	0.26
	E:20° 38'904"	Max.	20.0	8.40	115.4	247.0	0.93
		Mean	17.5	8.20	88.5	242.0	4.00
S 5	N:40° 52'291",	Min.	17.0	7.88	70.7	217.0	2.99
	E:20° 58'182"	Max.	18.0	8.47	106.3	267.0	4.97
		Mean	19.4	8.40	98.1	245.0	4.20
S 6	N:40°52'917",	Min.	18.0	8.28	88.9	217.0	3.33
	E:20° 58'642"	Max.	20.7	8.57	107.2	273.0	4.98
Recommended			A1 25	A1 5.5-8.5	≥60	1000	0.95-2.6 [O]
Value (EU, 1989)			A2 25	A2 5.5-9.0	≥50	1000	2.6-7.3 [M]
			A3 25	A3 5.5-9.0	≥30	1000	7.3-20 [E]
[78/659/EEC]				≥6 and ≤9	≥50	na	na

3.2 Distribution of heavy metals in waters of ohrid and prespa lakes

Results on heavy metals distribution in waters of Ohrid and Prespa Lakes are presented in Figures 2, 3 and 4. Boxplot graphs were used to evaluate spatial variation of each element concentration in all sampling points (Figure 2). Distribution of metals content in different depth of each station is presented in Figure 3. Mean concentrations of Fe, Ni, Cr and Cd varied significantly (α=0.05) between Ohrid and Prespa Lakes, resulting to be higher in waters of Ohrid Lake (Fig.2), while no significant changes were observed between Cu and Pb concentration in both lakes (α=0.05). According to the obtained results, the relative abundance of heavy metals in Ohrid Lake followed the order: Fe>Cr>Ni>Pb>Cu>Cd while in Prespa Lake mean concentrations of metals followed e different order, respectively: Fe>Ni>Cr>Pb>Cu>Cd.

More specifically:

3.2.1 Iron

Among the studied metals, Fe resulted to have the highest concentration in waters of both lakes, ranging from 9.34 - 54.63 $\mu g.L^{-1}$ in waters of Ohrid Lake and from 1.63-16.92 $\mu g.L^{-1}$ in waters of Prespa Lake. Mean concentration of Fe in Ohrid Lake was approximately 3.4 times higher than its concentration in Prespa Lake. Former mining activities of nickel, chromium, iron and coal

production may contribute to the higher levels of iron in waters of Ohrid Lake compared to Prespa Lake. Concentration of Fe varied significantly in samples collected at different depths, being more evident for Ohrid Lake, reaching the maximum value at the deepest point of (S1, 150 m depth), (Figure 3). Concentration of dissolved Fe in bottom waters of deep lakes increases as the dissolved oxygen and redox potential lowers (Davidson et al., 1984; Morel et al., 1985). The shapes of the dissolved metal profiles indicate that dissolved Fe is supplied to the deeper layer during stratification by diffusion of Fe (II) from the sediments into the overlying anoxic water as well as reduction of Fe oxide particles settling through the anoxic water column (Balisteri et al., 1992; Murray, 1987).

It was observed that mean concentration of Fe in different stations of both lakes did not exceeded the recommended values for Fe content in surface waters (being respectively 0.1 mg.L^{-1}), according to the Directives [78/659/EEC] and EU, 1978.

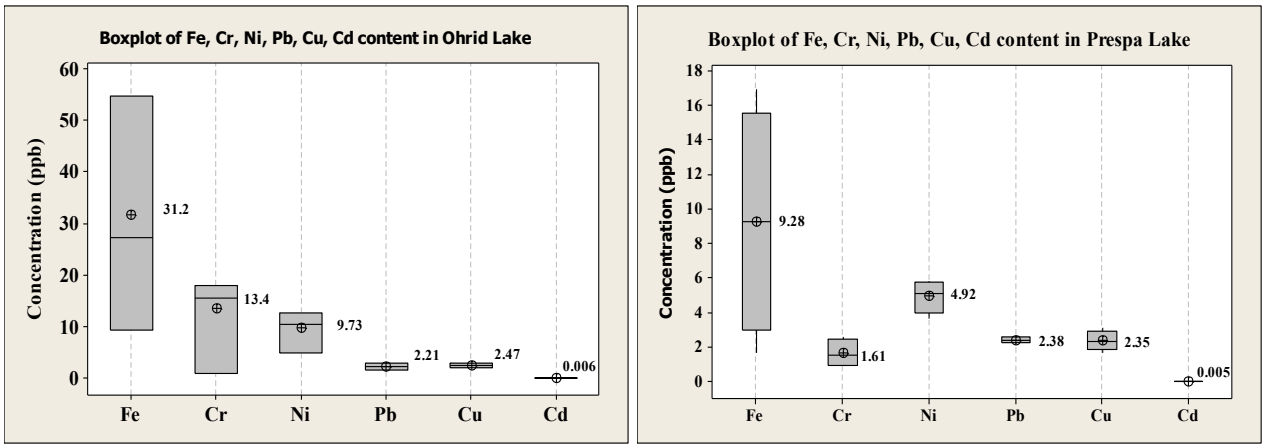

Figure 2. Variation of metals concentration in Ohrid and Prespa Lakes.

3.2.2 Chromium

Chromium content varied from 0.98-17.93 μg.L^{-1} in samples of Ohrid Lake and from 0.9-2.6 μg.L^{-1} in waters of Prespa Lake. Mean concentration of Cr in Ohrid Lake resulted to be about 8 times higher compared to its content in waters of Prespa Lake (Figure 2). Intensive former and actual mining activities can contribute to the levels of chromium in Ohrid Lake. Stations S1-S3 of Ohrid Lake were characterized by higher levels of Cr compared to stations S4-S6. Station S4 is regarded as the reference point for Ohrid Lake. Situated at the northern part of the lake, it is more isolated from the other stations which suffer more the effects of anthropogenic contamination. It is evident that the content of chromium in waters of Prespa Lake, represented by stations S5 & S6, was more related to natural factors such as the geology of the area. Higher concentrations were recorded at samples collected at 20 m depth, while its concentration decreased as the depth increased. Sedimentation and precipitation processes followed by reductive conditions of water such as low oxygen levels and redox potential contribute to lower chromium levels in bottom waters (Murray, 1987). Obtained results show that concentration of this metal falls below the recommended value (0.05 mg.L^{-1}) of chromium content in surface waters, according to the [78/659/EEC] EU Directive.

3.2.3 Nickel

Similar situation was concluded for nickel, where the mean concentration resulted to be approximately two times higher in waters of Ohrid Lake, varying from 4.93 to 12.26 μg.L^{-1}, whilst in Prespa Lake its content varied from 3.64 to 5.81 μg.L^{-1}. Even for this element, the main

contributors are the wastes derived from mining activity. Stations S1-S3 were characterized by higher levels of Ni compared to stations S5 & S6 which belong to Prespa Lake. Variation of Ni content in different depths of each station resulted to be low, assuming that its content was not related to water depth. Values of nickel concentration in waters of Ohrid and Prespa Lakes fall below the value 0.1 mg.L^{-1}, which is the upper limit recommended by the surface fresh waters Directive [78/659/EEC].

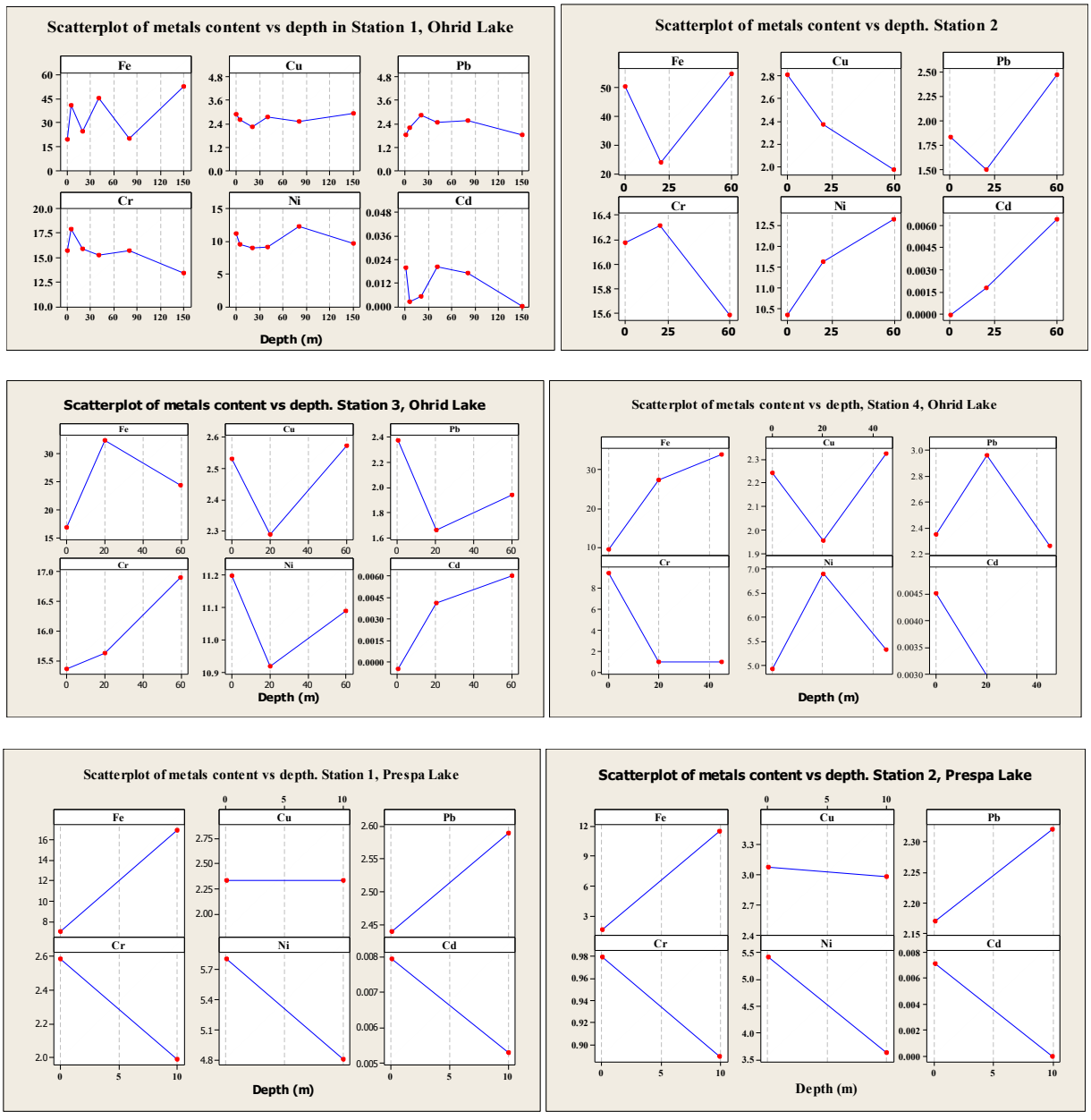

Figure 3. Distribution of heavy metals in different depths of each station (μg.L^{-1})

3.2.4 Copper and Lead

There were no significant differences between the mean concentrations of these metals in waters of both lakes. Copper content varied from 1.97-2.96 μg.L^{-1} in Ohrid Lake and from 2.99-3.08 in Prespa Lake waters, having very close mean values of its content. Lead concentration exhibited small variation in both lakes, being respectively 1.50-2.96 μg.L^{-1} and 2.17-2.59 μg.L^{-1}.

3.2.5 Cadmium

Mean concentration of cadmium in both lakes didn't exhibit significant differences, but the concentration of this metal resulted to be higher in some points of station S1. Cadmium content in Ohrid Lake varied between values below the detection limit of the AAS/ETA method to 0.020 $\mu g.L^{-1}$, while in Prespa Lake the maximum concentration observed was 0.008 $\mu g.L^{-1}$.

Concentration of cadmium in waters of Ohrid and Prespa Lake did not exceed the recommended value of its content in surface waters, being respectively 5 $\mu g.L^{-1}$, according to the European Council Directive, EEC, 1989.

4. CONCLUSIONS

Comparative study conducted on heavy metals concentration as well as on physic-chemical parameters of Ohrid and Prespa Lakes assumes that the quality of lakes water is threatened by both human and anthropogenic activities. Heavy metals resulted to be of great concern for Ohrid Lake due to higher levels of Fe, Cr, Ni, Cu, and Cd compared to Prespa Lake. The comparison of our results with former reported values was rather difficult because of the lack of existing data.

Considering the geology of the zone, large areas of central Albania are covered by serpentine soils which are highly enriched in heavy metals such as Cr, Cu, Ni, Fe, and Zn (Miho et al., 2005; Cullaj et al., 2007). On the other hand, some known anthropogenic sources of nickel, chromium and iron deriving from former mining activities, contribute to the levels of these metals in waters of Ohrid Lake. To the east of Pogradeci, a number of old mines that used to produce chromium, nickel, iron and coal are situated. Of these, only one remains in operation, but the mining sites still have many large piles of waste material that is exposed to the rain, which washes the pollutants from the piles into the lake.

Results on parameters such as oxygen saturation as well as content of Chl "a" give important information regarding the trophic state of the lake. In large and deep lakes such as Ohrid Lake, chances of water deterioration are very low compared to small and shallow lakes like Prespa. Levels of dissolved oxygen as well as the content of Chl "a" classify waters of Ohrid Lake in A1 class of waters quality, according to EU Directive [78/659/EEC] while low levels of dissolved oxygen, reaching the minimum value 5.83 $mg.L^{-1}$ (70.7%) at station S5, as well as high levels of Chl "a" suggest that nutrient loadings are deteriorating the quality of Prespa Lake waters.

Based on the obtained results as well as on EU Directives regarding the quality of surface waters, it can be concluded that waters of Ohrid and Prespa Lakes fall in Class A1 of waters quality regarding the heavy metals content, whilst low levels of dissolved oxygen, followed by higher levels of chlorophyll "a" classify deep waters of Prespa Lake in Class A2 of surface waters quality.

REFERENCES

Achterberg, E.P., van den Berg, C.M.G., Boussemart, M.; Davison, W., (1995). Speciation and cycling of trace metals in Esthwaite Water: A productive English lake with seasonal deep-water anoxia. *Geochimica et Cosmochimica Acta 61*: 5233–5253.

Adhami E., Bacu A., Beqiraj S., 2015. Initial characterization of Lakes Prespa, Ohrid and Shkodra/Skadar. Implementing the EU Water Framework Directive in South-Eastern Europe. Published by Deutsche Gesellschaft fur Internationale Zusammenarbeit (GIZ) GmbH.

APHA/AWWA, 1995. Standard Methods for the Examination of Water and Waste Water.

Balistrieri, L. S., Murray, J. W., Paul, B., (1992). The cycling of iron and manganese in the water column of Lake Sammamish, Washington. Limnology and Oceanography, 37: 510 – 528

Burns, N.M., Rutherford, J.C., Clayton, J.S., (1999). A monitoring and classification system for New Zealand lakes and reservoirs. Lake and Reservoir Management. 15:255-271.

Carlson, R.E. and Simpson, J. (1996) A Coordinator's Guide to Volunteer Lake Monitoring Methods. North American Lake Management Society, 96 p.

Council Directive of 18 July 1978 on the quality of fresh waters Freshwater Fish needing protection or improvement in order to support fish life. Official Journal of the European Communities No L 222, pp 1-10.

Çullaj A., Baraj B. 2007 "Assessment of the environmental situation of Albanian rivers based on physico-chemical analyses", http://siba-ese.unisalento.it/

Davison, W., and E, Tipping., (1984). Treading in Mortimer's footsteps: The geochemical cycling of iron and manganese in Esthwaite Water. Freshwater Biol. Assoc. Annu. Ren 52. D. 9 l-101.

Environmental Protection Agency, 2001. Parameters of water quality. Interpretation and Standards.

Loring, H.D. and Rantala, R. (1992) Manual for the Geochemical Analyses of Marine Sediments and Suspended Particulate Matter. Earth-Science Review, 32, 235-283.

Merrolli, A., Watzin, M. C., 2003. State of Environmental Report. Project Implementation Unit of the Lake Ohrid Conservation Project

Miho A., Çullaj A., Hasko A., Lazo P., Kupe L., Bachofen R., Brandl H., Schanz F., Baraj B., 2005. "Environmental state of some rivers of Albanian adriatic lowland", Evaluation Report/ Joint research project 7ALJ065583(SCOPES).

Morel, F. M. M., and R. J. M. Hudson., (1985). The geo-biological cycle of trace elements in aquatic systems: Redfield revisited, p. 25 l-28 1. In W. Stumm [ed.], Chemical processes in lakes. Wiley.

Murray, J. W., (1987). Mechanisms controlling the distribution of trace elements in oceans and lakes, p. 153-184. Zn R. A. Hites and S. J. Eisenreich [eds.], Sources and fates of aquatic pollutants. Am. Chem. Sot.

Salminen R., 2006. Geological Atlas of Europe, Part1, ISBN 951-690-913 2 (electronic version). http://weppi.gtk.fi/publ/foregsatlas/index.php.

Selenica A., Ardicioglu M.,Kuriqi A. Risk assessment from floodings in the rivers of Albania. International Balkans Conference on Challenges of Civil Engineering, BCCCE, 19-21 May 2011, EPOKA University, Tirana, ALBANIA.

Talevski, Milosevic, Maric, Petrovic, Talevska and Talevska (2009). Biodiversity of Ichtyofauna from Lake Prespa, Lake Ohrid and Lake Skadar. Biotechnology & Biotechnological Equipment 23(2). ISSN 1310-2818

Watzin, M.C., 2003. Lake Ohrid and its watershed: Our lake, our future. A State of the Environment Report. Project Implementation Unit of the Lake Ohrid Conservation Project.

Proceedings of the 10th World Congress of EWRA 'Panta Rhei', 5-9 July 2017, Athens, Greece
© 2017 *European Water Resources Association*

Water quality in Osumi, Devolli and Shkumbini rivers, using benthic invertebrates

B. Pepa[1*], A. Paparisto[2], E. Keci[3] and E. Halimi[2]
[1] *Faculty of Technical Sciences, "Ismail Qemali" University, Vlore, Albania*
[2] *Faculty of Natural Sciences, Tirana University, Albania*
[3] *Faculty of Professional Studies, "Aleksander Moisi" University, Durres, Albania*
[*] *e-mail: bled_pepa@hotmail.com*

Abstract: Anthropogenic activities have increased recently affecting among others, the ecological integrity within the aquatic ecosystems in the river waters in Albania. This paper promotes the biological monitoring of water quality, using macro invertebrates as bio indicators and definition of biological indices as a useful method of evaluating the ecological health status of rivers. Water Frame Directive (2000) implementation requires the use of benthic macro invertebrates as biological indicators for monitoring of water quality. The study presents the relation between benthic macro-invertebrate quantity, and the water quality status in Osumi, Devolli and Shkumbini Rivers, south Albania, during the Summer of 2011 through the Spring of 2013. The results obtained from the study refer to a total number of individuals of 4845 (42 families) in Osumi River, 3469 individuals (31 families) in Devolli River and 5991 individuals (34 families) in Shkumbini River. Based on the SWRC-Biotic Index calculations the following results have been obtained: Osumi River; St.1 (4.31; 5.39; 4.20; 4.61; 4.37; 4.26; 4.23; 4.15): St.2 (4.77; 5.52; 3.85; 4.12; 4.76; 4.04; 4.03; 4.07): St.3 (5.57; 5.15; 3.85; 3.99; 5.42; 5.29; 5.09; 4.91). Water quality bio classification has been carried out as well during the study. Based on the results of this study the two first sampling stations at Osumi River are classified as "good" water quality, while the third sampling station is qualified as "fair" water quality. Generally we can conclude that the water quality of the three Rivers in Albania is still good and slightly impacted..

Key words: Macro-invertebrates, WFD, bio classification, SWRC-Biotic Index

1. INTRODUCTION

Along with the physical-chemical approaches, currently the biological monitoring is recognized as one of the most valuable tools in the assessment of water quality (Bode, 2002).

Many years ago, in 1972 the NY State undertook bio-monitoring as an alternative method of monitoring and assessing its streams and rivers. For this reason, in 1977 CLEAN WATER ACT was committed to observe and save the chemical, physical and biological parameters of many rivers. After this, many countries developed different monitoring methods, to assess the water quality (Arscott et al., 2006); (EEA, 200696-107. 2007). Water Frame Directive implementation also requires the use of benthic macro invertebrates as part of biological monitoring of surface waters as biological indicators for monitoring of water quality (Directive, 2000/60/EC).

Benthic macro-invertebrate species are differentially sensitive to many biotic and abiotic factors in their environment.The presence of numerous families of highly tolerant organisms usually indicates poor water quality Some river's organisms have a high variety, or they can be under the threat of water quality conditions (Lenz. B. N., and Rheaume. S. J., 1995).

A high number of macro-invertebrates are very sensitive to the pollution (0-10). The short circle of life and the fast change of the species' number can ensure us a clear evidence of the returning of favorable water quality after water pollution state (Mc.Gonigle, 2000); (Bouchard, 2004); (S.W.R.C, 2007).

2. MATERIALS AND METHODS

Material has been collected based on method proposed by Campaioli et al. (1994); Bode et al. (1997); Bailey et al. (2001).

The macro invertebrates were sampled from the bottom of the river at the depth 30-50 cm, using a kick-net. This net was put vertically in the river's bed, while from a one meter distance we stirred up the river bed with our feet for 30 seconds (Herbst & Silldorff, 2009).

The sampled macro-invertebrates were stored and preserved with an alcohol solution (95 %) (Beatty et al., 2006).

In the laboratory the samples were poured into a large watch glass. Approximately one teaspoon of materials was removed from the sample and processed in a white enamel pan. Macro-invertebrates were placed in a smaller watch glass for identification under a dissecting microscope. Organisms in order EPT were identified at least at family level (Tachet et al., 1980; Campaioli et al., 1994; Taxonomic Key to Macro-invertebrates Families of Maryland Streams, 2004).

The results were used to determine parameter S.W.R.C. - BI (Stround Water Research Center – Biotic Index, 2007). Biotic index calculations coming from this study were taken into consideration to determine the water quality of each river for two years from summer 2011 to spring 2013.

2.1 The study area

Osumi River: The Osumi river is a main branch of *Semani* River that originates from the Vithkuqi Mountain located in the South Western Part of Albania. Some of the morphmetric parameters of *Osumi* River are: length 161 km, watershed surfaces 2150 km^2, average altitude 828 m. At the both sides of *Osumi* River there are located three urban area regions, Çorovode city, Berati city, Ura Vaj-Gurore city. Most of the waste of the urban areas is released in this river.

Devolli River: The Devolli river originates from Gramozi Mountains located also in the Western Part of Albania. Its length is 196 km. This river is also a branch of *Semani* River with the following morphometric parameters: a watershed surfaces of 3139 km^2 and an average altitude of 960 m. Part of its watershed are three urban area regions including Gramshi, Cerrik, Kuçova cities which were used as well as sampling sites for this study.

Shkumbini River: The Shkumbini river has a length of 181, 4 km. Its average flow is 61 m^3/sec, with a flowing module from 25, 21l sec/km^2 to 27, 3l sec/km^2. At the both sides of *Shkumbini* River there are located three urban regions including Librazhd, Peqini cities and Elbasani industrial zone (Pano, 1984).

Sampling stations are situated in representative areas of the three rivers; within one sampling station samples were taken randomly (Beatty *et al*. 2006). The sampling stations and their respective codes are indicated in the following (Figure 1): *Osumi* River: Os.1 - Poliçan; Os.2 - Gorica bridge (Berat); Os.3 - Ura Vajgurore. *Devolli* River: D.1 - Gramsh; D.2 - Gostime bridge (Cerrik); D.3 - Kucovë. *Shkumbini* River: S.1 - Librazhd; S.2 - Paper bridge (Elbasan); S.3 - Peqini bridge (Peqin).

3. RESULTS AND DISCUSSION

Results obtained from the study refer to a total number of 4845 (42 families) individuals in Osumi River, 3469 individuals (31 families) in Devolli River and 5991 individuals (34 families) in Shkumbini River. Water quality bio-classification of *Osumi, Devolli* and *Shkumbini* Rivers was carried out based in biological parameter SWRC - Biotic Index. The relation between water quality and the value of the SWRC – Biotic Index is described and documented by McGonigle (2000), S.W.R.C (2007). Values of SWRC – Biotic Index are: {(0-3.75) - *Exellent*; (3.76-5.0) - *Good*; (5.10-6.50) - *Fair*; (6.60-10.0) - *Poor*}.

SWRC - Biotic Index is calculated for all the sampling stations for the 3 rivers, *Osumi, Devolli*

and *Shkumbini* River (Table 2) by the following formula (1), (SWRC, 2003) (McGonigle 2000),

$$[SWRC - Biotic\ Index\ ] = \frac{\sum (TV)*d}{D} \quad (1)$$

where TV is given tolerance values for all the families found during our study, (McGonigle 2000), *d* is the density of each family and *D*, the total amount of densities. Bio-classification was based on the data of the following tables (Table 1, 2,) where are presented Biotic Index Parameter, Stroud Water Research Centre, of organic water pollution and its quality for all the sampling stations of *Osumi, Devolli* and *Shkumbin* Rivers.

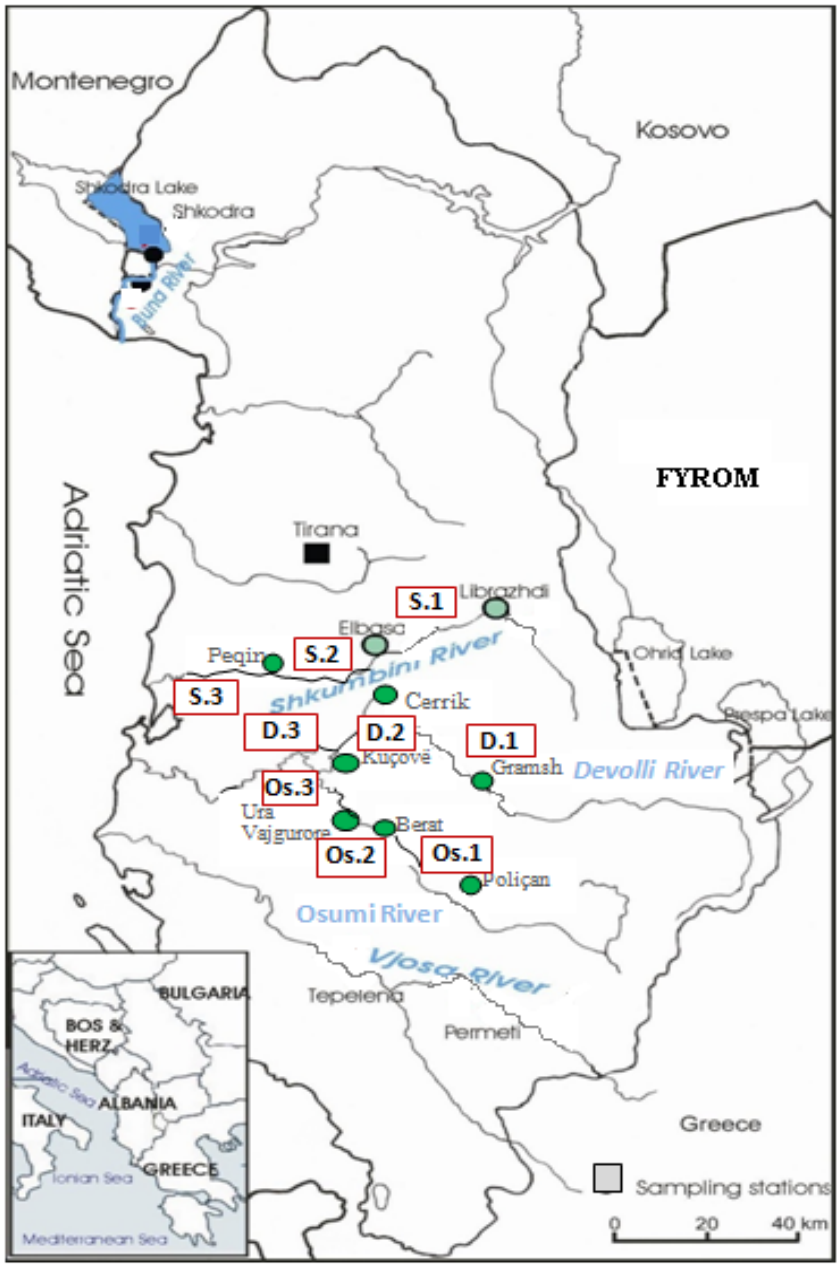

Figure 1. The stations and their codes: Osumi River, Os.1 - Poliçan; Os.2 - Gorica bridge (Berat); Os.3 - Ura Vajgurore. Devolli River, D.1 - Gramsh; D.2- Gostime bridge (Cerrik); D.3 - Kucovë. Shkumbini River, S.1 - Librazhd; S.2 - Paper bridge (Elbasan); S.3 - Peqini bridge (Peqin).

Herewith we are giving water quality bio-classification of each river, based on S.W.R.C - Biotic Index:

3.1 Osumi River

Based on the results of SWRC-Biotic Index shown on Table 1 the water quality in the first station (Poliçan - Os.1) and the second station (Berat - Os.2) of the *Osumi* River where most of sampling too place, is "*Good"* as the index is within (3.75 – 5.00). While in the third station (Ura Vajgurore - Os.3), bio classification of water quality is "*Fair"* the index is within (5.10 - 6.50) throughout five sampling sessions. The worst water quality in the third station (Ura Vajgurore - Os.3), is during the summer and the autumn (2011, 2012). This station is located in downstream part of the *Osumi* River nearby the urban area, thus it's affected continuously by the presence of non pointed resources of organic pollution.

3.2 Devolli River

The results of Table 1 based on SWRC-Biotic Index for *Devolli* River show a better water quality in the two first stations (Gramsh – D.1 and Gostima bridge/Cerrik – D.2). The water quality is remaining in the bio-classification class "*Good*" with the index of (3.75 – 5.00), during the study period except the session of autumn 2011, where the water quality on those stations belong to the bio-classification class "*Fair"with index of* (5.10 - 6.50). Meanwhile in the third station of this river (Kuçovë - D.3) the bio-classification of water quality shows alternation values between "*Fair"* in summer and "*Good"* in all other sessions, due to the summer income of waste. Based on the values of the biotic index it is obvious shown a tendency of water quality improving in the last period of this study.

3.3 Shkumbini River

Based on the S.W.R.C - Index values (Table 1) in the first and third monitoring station (Librazhd – S.1, Peqin – S.3) of *Shkumbini* River the water quality for all sampling sessions was "*Good*" (3.75-5.00). Only during autumn 2011 the water quality was "Fair" (5.10 - 6.50).

The second station (Elbasan – S.2) shows considerable differences in its bio-classification values compared to the station S.1 (Librazhd) and station S.3 (Peqin). The water quality of the station (S.2 -Elbasan) during all the study period except winter 2011, belongs to the bio- class "*Fair*". The station (S.2-Elbasan) is impacted directly by pollution of sewage and other discharges from the industrial area (Miho et al., 2005).

Based on the results of this study, the first station (Librazhd S.1) and the third station (Peqin S.3) show a better water quality with a slight impact, while station (Elbasan S.2) shows poorer water quality with a moderate impact.

3. CONCLUSIONS

This study presents biological monitoring data based on macro-invertebrate compositions collected during the summer of 2011 through the spring of 2013 from three principal Rivers of the South Central Albania (*Osumi*, *Devolli* and *Shkumbini*). Data analyzing shows that only the second station of *Shkumbini* River (S.2 -Elbasan) and third station of *Osumi* River (Os.3 - Ura Vajgurore) have a moderate pollution impact. This situation can be explained with the position of both stations in the downstream part of the rivers, nearby urban and industrial areas where the level of point and nonpoint organic pollution is higher. All other stations analyzed on those rivers during this period represent a bio-classification of "*Good",* indicating a slight impact in water quality. Differences between values of bio-indexes in different periods of the year can be explained by the presence of changes in sensitive macro-invertebrate populations and level of flow. Those changes are reflected directly in the water quality.

Based on the values of S.W.R.C. – Biotic Index calculated on this study, we can say that for the

three Albanian rivers the situation of water quality is still good with a slight impact.

Table 1. Bioclassification of water quality of Osumi, Devolli and Shkumbini River according to the SWRC - Biotic Index

River	Station \ Session		Summer 2011	Autumn 2011	Winter 2011	Spring 2012	Summer 2012	Autumn 2012	Winter 2012	Spring 2013
Osumi river	St. 1	SWRC- Index	4.31	5.39	4.20	4.61	4.37	4.26	4.23	4.15
		Bio-classification	*(good)*	*(fair)*	*(good)*	*(good)*	*(good)*	*(good)*	*(good)*	*(good)*
	St. 2	SWRC- Index	4.77	5.52	3.85	4.12	4.76	4.04	4.03	4.07
		Bio- classification	*(good)*	*(fair)*	*(good)*	*(good)*	*(good)*	*(good)*	*(good)*	*(good)*
	St .3	SWRC- Index	5.57	5.15	3.85	3.99	5.42	5.29	5.09	4.91
		Bio- classification	*(fair)*	*(fair)*	*(good)*	*(good)*	*(fair)*	*(fair)*	*(fair)*	*(good)*
Devolli river	St. 1	SWRC- Index	5.0	5.76	4.57	4.50	4.92	4.61	4.25	4.32
		Bio-classification	*(good)*	*(fair)*	*(good)*	*(good)*	*(good)*	*(good)*	*(good)*	*(good)*
	St. 2	SWRC- Index	4.90	5.56	4.74	4.73	4.82	4.69	4.72	4.45
		Bio-classification	*(good)*	*(fair)*	*(good)*	*(good)*	*(good)*	*(good)*	*(good)*	*(good)*
	St. 3	SWRC- Index	5.25	4.68	4.27	4.70	5.32	4.44	3.96	4.16
		Bio-classification	*(fair)*	*(good)*	*(good)*	*(good)*	*(fair)*	*(good)*	*(good)*	*(good)*
Shkumbini river	St. 1	SWRC- Index	4.37	5.18	4.22	4.85	4.31	5.0	4.98	4.84
		Bio classification	*(good)*	*(fair)*	*(good)*	*(good)*	*(good)*	*(good)*	*(good)*	*(good)*
	St. 2	SWRC- Index	5.95	5.50	4.58	5.26	5.88	5.55	5.28	5.44
		Bio classification	(fair)	*(fair)*	*(good)*	*(fair)*	*(fair)*	*(fair)*	*(fair)*	*(fair)*
	St. 3	SWRC- Index	4.91	5.50	3.78	4.71	4.88	4.35	4.59	4.36
		Bio classification	*(good)*	*(fair)*	*(good)*	*(good)*	*(good)*	*(good)*	*(good)*	*(good)*

Table 2. S.W.R.C. - Biotic Index calculated for all the sampling stations on Spring, 2013

Spring 2013			Osumi River							Devolli River						Shkumbini River					
Nr	Taxon	TV	St. 1	St. 2	St. 3	St. 1	St. 2	St. 3	St. 1	St. 2	St. 3	St. 1	St. 2	St. 3	St. 1	St. 2	St. 3	St. 1	St. 2	St. 3
			D			TV*D			D			TV*D			D			TV*D		
1	Ephemeroptera	**3.6**	205	87	79	738	313.2	284.4	54	41	19	194.4	147.6	68.4	60	97	92	216	349.2	331.2
	Plecoptera	**1**	12		6	12	0	6	2	1		2	1	0	2	1	13	2	1	13
3	Trich/ Hydropsychidae	**5**	175	28	31	875	140	155	34	56	7	170	280	35	18	5	85	90	25	425
4	Trichoptera (others)	**2.8**	4		1	11.2	0	2.8				0	0	0	1	0	0	2.8	0	0
5	Odonata/ Anisoptera	**4**			1	0	0	4	0	0	1	0	0	4	0	0	1	0	0	4
6	Odonata/ Zigoptera	**7**				0	0	0				0	0	0				0	0	0
7	Megaloptera/ Corydalidae	**3**				0	0	0				0	0	0				0	0	0
8	Megaloptera/ Sialidae	**4**				0	0	0				0	0	0				0	0	0
9	Diptera					0	0	0				0	0	0				0	0	0
10	Diptera/ Athericidae	**2**				0	0	0				0	0	0				0	0	0
11	Diptera/ Chironomidae	**6**	2	2	87	12	12	522	5	2	1	30	12	6	55	262	21	330	1572	126
12	Diptera/ Simliidae	**6**		2		0	12	0	2	3	1	12	18	6				0	0	0
13	Diptera / Tipulidae	**3**				0	0	0				0	0	0	2	0	0	6	0	0
14	Diptera (others)	**6**	1	4	27	6	24	162	6	0	0	36	0	0	18	70	15	108	420	90
15	Coleoptera	**4.6**				0	0	0	0	1	3	0	4.6	13.8	0	5	0	0	23	0
16	Oligochaeta	**8**			1	0	0	8				0	0	0	0	1	0	0	8	0
17	Hirudinea	**8**				0	0	0				0	0	0				0	0	0
18	Gastropoda	**8**				0	0	0				0	0	0				0	0	0
19	Amphipoda	**6**				0	0	0				0	0	0				0	0	0
20	Isopoda	**8**				0	0	0				0	0	0				0	0	0
21	Decapoda	**5**				0	0	0				0	0	0				0	0	0
22	Turbellaria	**8**				0	0	0				0	0	0				0	0	0
Total			**399**	**123**	**233**	**1654**	**501.2**	**1144**	**103**	**104**	**32**	**444.4**	**463.2**	**133.2**	**156**	**441**	**227**	**754.8**	**2398**	**989.2**
SWRC - Biotic Index = [Σ (TV*d)]: D						**4.15**	**4.07**	**4.91**				**4.32**	**4.45**	**4.16**				**4.84**	**5.44**	**4.36**

REFERENCES

Arscott, D. B., Jackson, J. K., Kratzer, E. B., 2006. Role of rarity and taxonomic resolution in a regional and spatial analysis of stream macro invertebrates. In: *Journal of the North American Benthological Society*, Vol. 25; 977–997. Bio One

Bailey, R. C., Norris, R. H., Reynoldson, T. B., 2001. Taxonomic resolution of benthic macro- invertebrate communities in bioassessments. In: *Journal of the North American Benthological Society*, Vol. 20. (2); 280-286.

Beatty, M. J., McDonald, L. E., Westcott, F. M., Chris, J., Perrin, J. CH., 2006. Guidelines for sampling benthic invertebrates in British Columbia streams; Ministry of Environment Kootenay Region, British Columbia; 15.

Bode, R.W., Novak, M. A., Abele, L. A., Heintzman, D. L., Smith, A.J., 2002. *Quality assurance work plan for biological stream monitoring in New York State*. New York State Department of Environmental Conservation, Albany, New York. (Available from: New York State Department of Environmental Conservation, 625 Broadway St., Albany, New York, 12233).

Bode, R.W., Novak, M. A., Abele, L. A., 1997. *Biological stream testing*. NYS Department of Environmental Protection; Division of Water; Bureau of Monitoring and Assessment; Stream Monitoring Unit; Albany, USA

Bouchard, R. W., 2004. *Guide to aquatic macroinvertebrates of the Upper Midwest*. Water resources center, University of Minesota, St.Paul, and MN; 208.

Campaioli, S., Gheti, P. F., Minelli, A., Ruffo, S., 1994. *Manuale per riconoscimento dei Macroinvertebrati delle acque dolci italiane*. Vol.1. Provincia Autonoma di Trento; 9-14. 27-190.

Directive 2000/60/EC, EU., 2000. Directive 2000/60/EC of the European Parliament and of the council of 23 October 2000 establishing a framework for community action in the field of water policy. Off. J. Eur .Commun.; 327:372.

EEA, 200696-107, 2007. European Environment Agency, Technical report No. 11/2007, Halting The Loss of Biodiversity by 2010; Proposal for the first set of indicators to monitor progress in Europepp/ 17-22, 33-48; 130-136.

Herbst, D. B., Silldorff, E. L., 2009. Development of a Benthic Macroinvertebrate Index of Biological Integrity (IBI) for Stream Assessments in the Eastern Sierra Nevada of California; Report: Sierra Nevada Aquatic Research Lab., University of California; 8.

Lenz, N. B., Rheaume, J. S., 1993-1995. Benthic invertebrates of fixed sites in Western Lake Michigan Drainages, Wisconsin and Michigan

McGonigle J., 2000. Education: Education: Leaf Packs and Beyond, Spring 2000. Stround Water Research Center

Miho, A., Cullaj, A., Hasko, A., Lazo, P., Kupe, L., Brandl, H., Schanz, F., Baraj, B., 2005. Environmental State of some rivers of Albanian Adriatic Lowland. Evaluation report; 215.

Pano, N., 1984. Hidrologjia e Shqipërisë. Akademia e Shkencave të Shqipërisë. I.H.Tiranë; 170-220.

SWRC, (Stroud Water Research Center)., 2003. Water quality monitoring in the source water areas for New York City: An integrative approach. A report on the first phase of monitoring Stroud Water Research Center, Avondale, Pennsylvania. (Available from: http://www.stroudcenter.org/research/nyproject.htm)

SWRC, Stroud Water Research Center 2007. Leaf Pack Network: Watersheds. (Available from: www.stroudcenter.org/ lpn/more/data)

Tachet, H., Bournaud, M., Richoux, P., 1980. Introduction á l'étude des macroinvertebres des eaux douces. C. R.D.P. Lion; 130-150.

Proceedings of the 10th World Congress of EWRA 'Panta Rhei', 5-9 July 2017, Athens, Greece
© 2017 *European Water Resources Association*

Assessment of pollution pressure over water bodies in Thessaly region

D. Dinouli[1*], P.T. Nastos [2] and A. Papaioannou [3]
[1] *Chemical and microbiological laboratory, Faculty of Municipal Enterprice of Drinking and Sewage, Larissa, Greece*
[2] *Laboratory of Climatology and Atmospheric Environment, Faculty of Geology and Geoenvironment, University of Athens, Athens, Greece*
[3] *Technological Educational Institute of Thessaly, Department of Medical Laboratories, 41110, Larissa, Greece*
[*] *e-mail: dimi.din@hotmail.com*

Abstract: Water, as an irreplaceable resource for the survival of all living organisms ,health and economic development, has an outstanding role to biodiversity, to vulnerable ecosystems and bio-geological cycles preservation. Especially in the Mediterranean region, on one hand, the observed and the future projected precipitation decreases due to climate changes and on the other hand, the contamination of water bodies due to anthropogenic activities, set in danger water systems balance. The scope of this study is to quantify the effect of pollution pressure, so that to contribute in the environmental protection on the water bodies of Thessaly region. Microbiological, biological and physio-chemical parameters are studied and defined in order to estimate the pollution of Thessaly's water resources, focusing on surface waters of rivers and lakes, underground and rain waters predestined for drinking water. Furthermore, the meteorological conditions along with the back trajectories of air masses during rain events over the wider area of Thessaly are also investigated. As the interest in protection and exploitation of water bodies is increased, the knowledge of the contaminants and the quality changes is important. The results of this research can contribute to the design and taking of appropriate measures to confront the impacts on water bodies.

Key words: Pinios River, pollution pressure, basin of River, ecological and chemical balance

1. INTRODUCTION

The worldwide tendency to restore the river ecosystems and to properly use the rivers that results from the Framework Directive 2000/60/EK, inflicts the evolvent of complete administration plans for every Basin of River, in order to achieve ecological and chemical balance. There are two primary classes of distinction of waters, surface water and underground water. Surface water located at the ground level, are related to the surface runoff. In contrary, the underground waters are related to infiltration, and sit in large underground surfaces (Papaioannou A. et al, 2010). Even though there is not a clear distinction among the surface and underground waters, as, commonly, there is hydraulic communication as well as qualitative and quantitative interaction between the both, their distinction serves the elaboration as well as the usage of the waters. Therefore, the underground waters quality has an immediate effect on the surface waters quality, as well as on the correlated aquatic ecosystems (Papaioannou A. et al, 2016). Nevertheless, according to the Directive, an ecological and chemical balance is pursued for the surface waters, while a quantitative and chemical balance for the underground waters.

Contamination, as a human intervention, relates to the direct or indirect intake of substances or heat to the waters that may be really harmful either for human beings or for the aquatic and aquatic-dependent land ecosystems quality. Contamination may be organic, thermal, or pesticide, metal and nutrient originated.

The current paper deals with:

i. A big and representative river in Greece, Pinios river
ii. An aggregation of grilling's in Greece both for water supply and irrigation in order to answer or even set the grounds to deal with a series of issues like:

- The designation of the characteristics of river basin, and the chronicle of the current condition of Pinios River.
- The consideration of the results of pollution pressure both to the aquatic particles (surface waters), or to the aquatic system (underground waters) in Thessally region, as long as their reclamation at the river basin.

2. STUDY AREA

The aquatic compartment of Thessaly includes the Basin of Pinios River, as well as Basin of Almyros - Pelion, with the Pinios rivers' basin to be the main one in Thessally region, and the biggest one in Greece, as it extends up to 11.062 km^2.

The Basin of Pinios River has simple geo-morphological features, as its mountainous regions are located perimetrical and the lowlands centrally. Pinios River is 262 km long and is formed by the juncture of Kastaniotis River that springs from Katara, the Malakasiotis River that springs from Lakmos Mountain and the Mourgani stream that springs from Antihasia. The main Pinios' tributaries are: *Enipeas, Sofaditis, Kalentzis, Pamisos, Portaikos, Farsaliotis, Litheos, Neoxoritis, and Titarisios.*

The average annual flow of all Thessaly Rivers is 3.540 million m^3, 3.325 millions of which corresponds to Pinios River. Pinios basin and its tributaries are stained into Thermaikos bay, via the straits of Tembi alley.

The rivers' oufall forms a delta. The main exploitation of the river is for irrigation. The rivers' surface waters are mainly reclaimed by the Plastiras and Smokovos banks of water. The recreation of Karlas Lake is a construction of big importance.

Pinios river is loaded by spotted, or not, originations of pollution. This loadings are of great importance regarding the waters' quality, owing to increasingly urbanization, to the large amount of drugs and fertilizers used in farming and pressure pollution caused by industrial centers (Bellos et. al, 2004, Loukas A, 2007, Mahleras et al., 2006).

The collected data on the spotted originations of pollution at the Pinios River basin indicates that pollution pressure is increased due to a variety of activities that takes place in Trikala, Karditsa and Larisa cities (Loukas, et al., 2007).

The non-spotted originations of pollution, that affects the surface waters, are related to runoff waste, such as loadings of nutrients accumulating by agricultural activity, stockraising and sewage coming from regions that lacks draining facilities, as well as sewage treatment facilities (Papaioannou A.et.al,). It worth mentioning that the main load of organic cargo is exclusively originated by stockraising, the total nitrogen is derived from both stockraing and farming, (Peña-Haro et al., 2009; Papaioannou A.et.al, 2007). Whereas the load of phosphorous is derived mainly from farming. 10mg BOD/L, 10mg N/l and 1mg P/l are the ceiling values used as indicators of high pollution pressure. These values correspond to tertiary sewage treatment, suitable for unlimited treatment. (Directive 2000/60EC).

There is a major exploitation of the underground waters, at the whole reach of Pinios river basin, that results to their excessive pumping. The exploitation occurs mainly by drillings in this area (Papaioannou A.et.al, 2010) (about 30.000-33.000 drillings).

3. METHODOLOGY

3.1 Sampling

Sampling from surface waters, occurs in significant geographical sites, allocated around Thessally s water basin. In these sites, surface water runoffs, atmosphere precipitation as well as phreatic aquifers, can easily be exploited. There are five topographical sites for sampling long wise

Pinios River, five on main confluent and two on lakes. The topographical sites are ten (10) in total, and they are mentioned: Pinios 1 (FOTADA), Pinios 2 (PINIADA), Pinios 3 (KOULOURI), Pinios 4 (PIRGETOS), Pinios 5 (MOURGANI), Enipeas 1 (YPEREIA), Litheos1 (KARIES), Titarisios 1 (RODIA), Titarisios 2 (ELASSONA), Kalentzis 1 (MAKRYGORI).

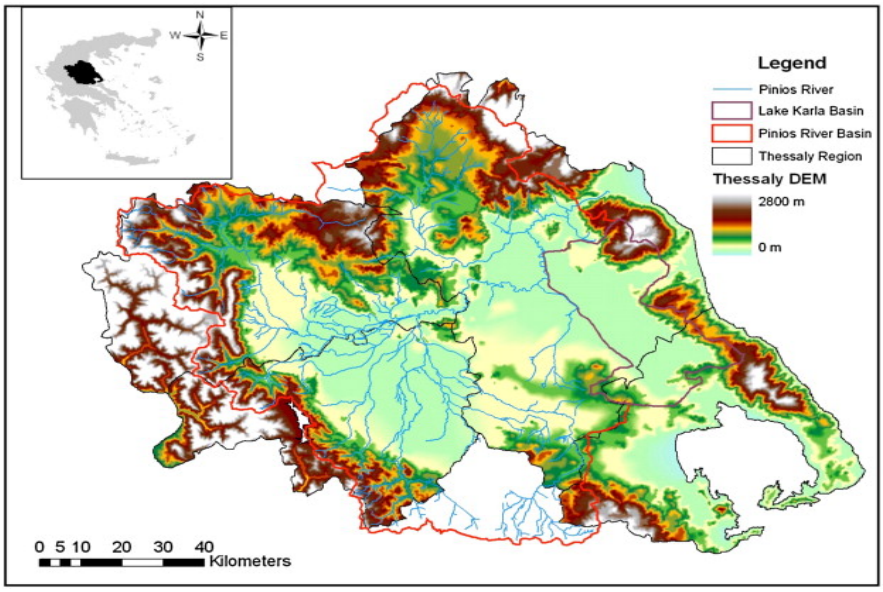

Figure 1. Thessaly region

3.1.1 Sampling from river flows

The sampler should get as close to the sampling site in the river flow as possible, carefully not to damage the vegetation or any sediments around. When in position, the container should be upstream and down the surface of the river flow, at least 25cm deep, so that its nozzle is submerged (ISO 5667-6:2006).

3.1.2 Sampling from riversides

Sampling from riversides will be done in the center of the riverside flow. The process is the following: We wash out the container at least three times, with the river water. Afterwards, we fill up the container so that it will not be agitated and the diluted substances can be analyzed. In order to take a sample, the container should be submerged at least 25cm down the surface, avoiding to scraping the river ground or to receive any water from the surface membrane (ISO 5667-6:2006).

3.2 Materials and methods

The main parameters analyzed are:

Physicochemical parameters: Temperature, color, conductance, turbidity, pH, sulfate ions, chlorides, nitrates, nitrites, iron, manganese, lead, chrome, mercury, arsenic and cadmium, as well as BOD, TDS, DO and SS measurement for the surface waters.

On the spot analysis

Electrical conductivity was measured on the spot with a portable conductivity instrument HANNA HI 98360. a rapid increase to the water conductance is a clue of water pollution.

pH measurement is conducted with a pHmeter WTW, diluted oxygen is measured with a portable oximetry WTW and the results are recorded on the sampling brochure.

Spectrophotometric analysis

The parameters that were measured in the laboratory with a spectrophotometer HACH-LANGE DR 2800 are the following: *Ammonium, Nitrates, Nitrites, Phosphates, Sulphates*, *Chlorides, Iron*, *Manganese.*

B.O.D$_5$ measurement

B.O.D$_5$ measurement (biochemical oxygen demand) for five days is completed in mostly six hours. B.O.D$_5$ is the main indicator of the extensive organic pollution.

Atomic absorption spectrophotometric analysis.

Measurements of metals like Nickel, (Ni), Chromium (Cr), Cadmium (Cd), Lead (Pb), Aluminum (Al), in samples of underground or surface waters was accomplished by atomic absorption spectrophotometric analysis in a graphite oven. Measurements of other metals like Arsenic (As) or Mercury (Hg) were accomplished both with atomic absorption and usage of hydrides device.

3.3 Classification

By measuring the particularities of surface waters, we are able to define their chemical substance. In order to do that tree years results (2014-2016) were evaluated, by calculating the average of every quarter of every year. In table 1 are recorded values that presents the limit of well-mediocre condition, which sets the opportunity for a water system to fall under the well condition to the mediocre condition, based on its ecological status as well.

Table 1. Limits of parameters who contribute to the classification of good/medium situation

Reverberations	Parameter	Limit of well-mediocre condition
Oxygenation	Diluted oxygen	70%
	Ammonia	0,01mg/l NH_3
	B.O.D.$_5$	4 mg/l
Acidification	pH	6-9
Trophic status	Total phosphorus	200 μg/l P
Nutrient status	Ammonium	1mg/l NH_4^+
	Nitrate	25mg/l NO_3
	Nitrite	0,05 mg/l NO_2^-

4. RESULTS AND DISCUSSION

The results for the measurements of the main elements that consist Pinios water ecosystem are presented on the following figures.

B.O.D$_5$ is the total amount of oxygen that is consumed by the microorganisms during the first five days of bio-degradation. According to figure 2 there seems to be a variance both longwise the river and throughout the year, whereas there is an increase of the values during the third quarter of the year.

The concentration of nitrates in Pinios waters, which is presented on figure 3, together with those in Litheos river, seem to be outside the limit of 15mg/l for the surface waters, given by the U.E. Based on the measurements, the values for nitrates displays seasonal changes, where the maximum value is measured during winter and springtide months and the minimum ones during the summer and autumnal months due to the decreased use age of fertilizers as well as less rainfalls that can wash out farming ranges.

Respectively about nitrites (NO_2) (Figure 4) concentration seems to change proportional to the season changes, and it varies between 0 and 1,5 mg/l NO_2.

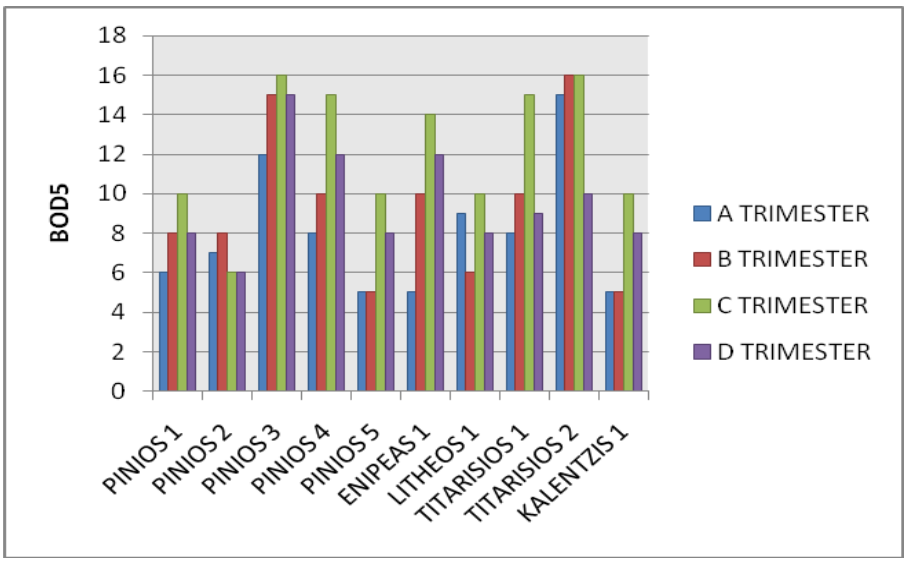

Figure 2. Concentration of BOD5 to the runoff in the basin of the Pinios river

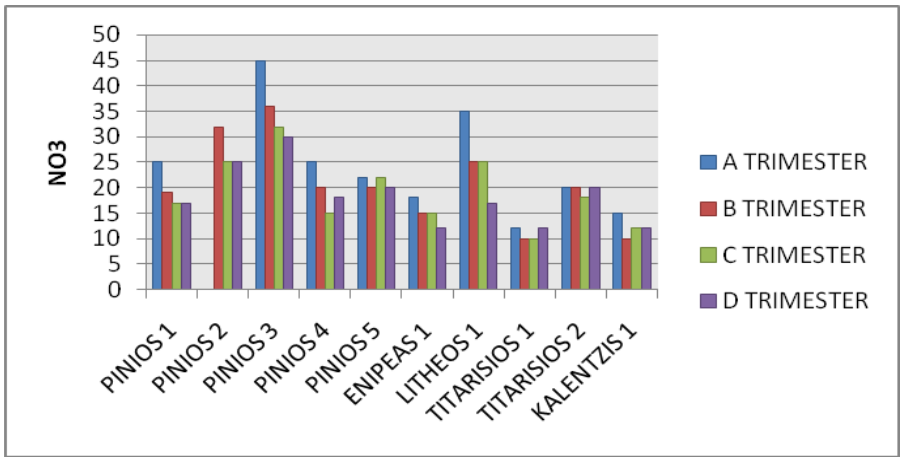

Figure 3. Concentration of NO3 to the runoff in the basin of the Pinios river

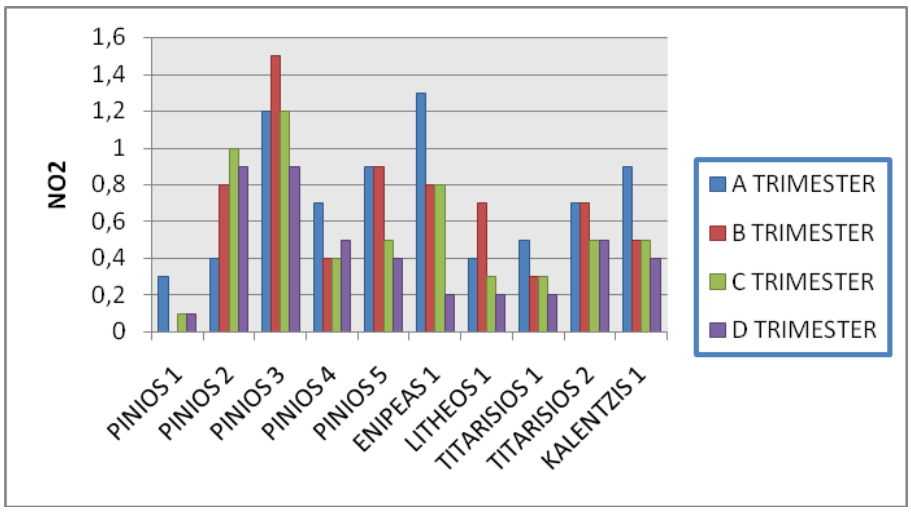

Figure 4. Concentration of NO_2 to the runoff in the basin of the Pinios River

Ammonium ions (NH_4) originated by ammonium fertilizers runoffs from farming, but mainly by wasting sewage in the rivers. The average value of ammonium ions of Pinios river is between 0 and 1,5 mg/l. Although higher values have been measured in Koulouri and lower ones in Fotada.

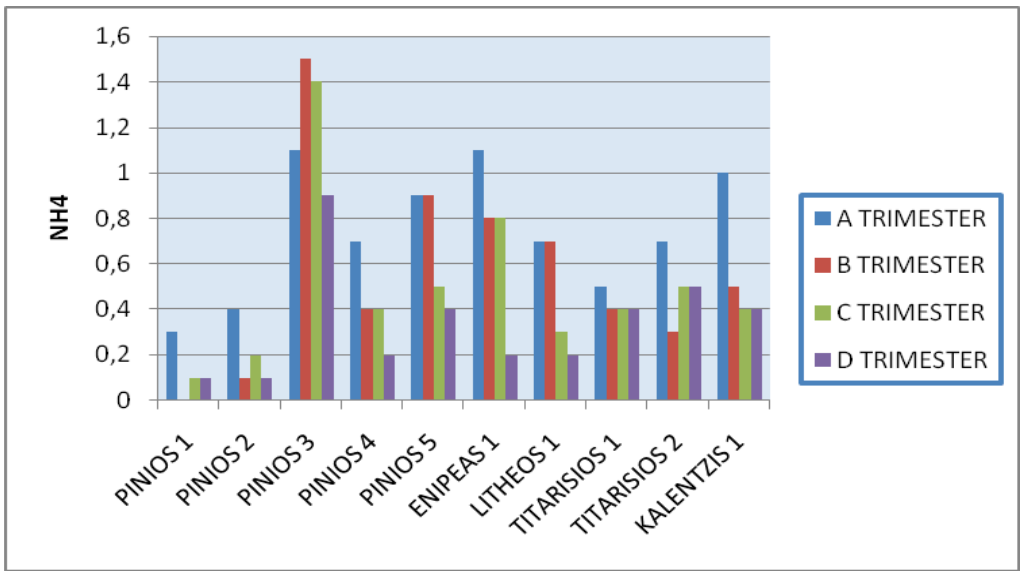

Figure 5. Concentration of NH4 to the runoff in the basin of the Pinios River

Phosphates existence in the surface waters is caused both by the washout of phosphate fertilizers and the existence of urban and industrial sources of pollution. Notable higher values were measured near Larisa city and Koulouri, ought to wasting processed sewage deriving from Larisa city,(figure 6) as well as a variety of industrial waste. Although the values seem to decrease for the area of Tempi.

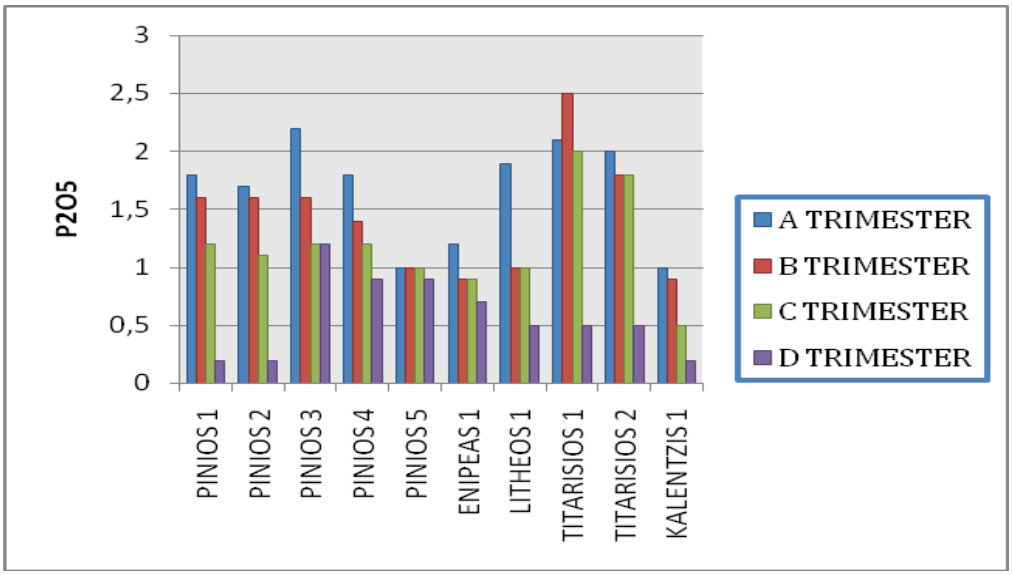

Figure 6. Concentration of P2O5 to the runoff in the basin of the Pinios River

5. CONCLUSIONS

For every surface water system, characterization of the chemical status (Good, Inferior good), depends on the annual average concentrations, which must not exceed the statutory limits (Dovriki et al., 2010). The price exceeded at any position of a system implies the designation as the Inferior Good (1st Review on directive 2000/60EC).

Furthermore, for the classification into high or good status is required to examine and physicochemical parameters other than biological, while the assessment of the status of water bodies to moderate, poor or bad can be based solely on the examination of biological parameters,

because you default and physicochemical parameters are consistent with the predicted values for this situation Good(1st Review on directive 2000/60EC) (Figure 7).

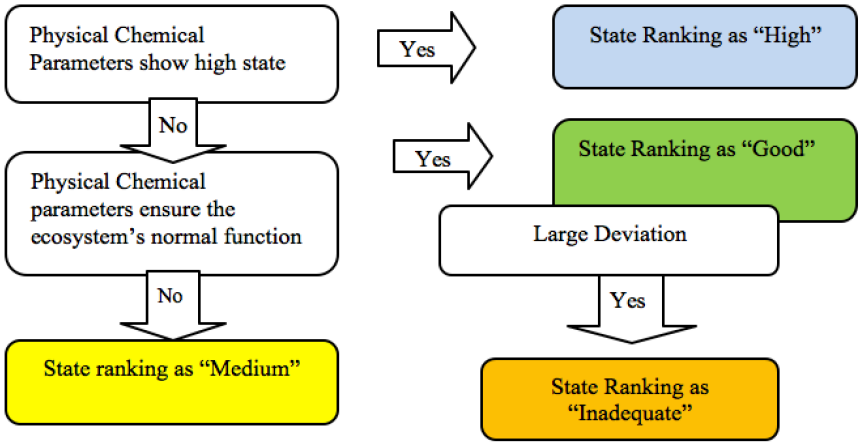

Figure 7. Evaluation Aquatic System

Generally to the study of biological and physico-chemical parameters in a Basin assessed an aquatic luteum. The study of the data used and the results leads to the source of most problems the basin faces: policy and management issues.

REFERENCES

1st Review on directive 2000/60EC (EL08 Thessaly), Classification of the status of surface water systems

Bellos D., Sawidis T., Tsekos I. 2003, Nutrient chemistry of river Pinios (Thessalia,Greece) Environment International30(2004) 105 -115 Elsevier

Dovriki E., Kokkora M., Gourgoulianis K., Hadjichristodoulou Ch., Petinaki E., Gerogianni I., Rigas G., Dinouli D., Papaioannou A. "Assessment and Modelling River Quality Data by Environmetric Methods". X International Conference Protection and Restoration of the Environment, Corfu Greece 5-9 July 2010.

European Directive 2000/60 council of E.E. for Water Resources Management in 2000.10.23

ISO 5667-6:2006. Water quality- Sampling- Part 6: Guidance on sampling of rivers and streams

Loukas A., Surface water quantity and quality assessment in Pinios River, Thessaly, Greece, 1st Conference on Environmental Management, Engineering, Planning and Economics (CEMEPE), Skiathos, Greece, 24–28 June, 2007.

Loukas, A., Mylopoulos N., Vasiliades L., 2007. A modeling system for the evaluation of water resources management scenarios in Thessaly, Greece. Water Resource. Management., 21(10): 1673-1702

Mahleras A., Kontogianni A., Skourtos M. (2006), *Title Report: Pinios river Basin Greece*, Subtitle report: Status report, EU.

Papaioannou A., Rigas G., Kella S., Lokkas F., Dinouli, D., Papakonstantinou A., Spiliotis X., Plageras P., Assessment of Groundwater Quality by Chemometrics. Water Environment Research 2016, 88(7), 631-643.

Papaioannou A., Dovriki E., Rigas N., Plageras P., Rigas I., kokkora M., Papastergiou P.. «Assessment and Modelling of Groundwater Quality Data by Environmetric Methods in the Context of Public Health». Water Resources Management, 2010, 124, 3257-3278.

Papaioannou A., Kakavas K., Dovriki E., Plageras P., Noulas A., Minas A., KrikelisV. And A. G. Paliatsos."Quality Control of Groundwater of Region Thessaly (Greece)". Fresenius Environmental Bulletin, 2006, 15, 1015-1022.

Papaioannou A., Mavridou A., Hadjichristodoulou Ch., Papastergiou P., Pappa O., Dovriki E., Rigas I.. "Application of Multivariate Statistical Methods for Groundwater Physicochemical and Biological Quality Assessment in the Context of Public Health". Environmental Monitoring Assessment 2010.

Papaioannou A., Plageras P., Dovriki E., Kakavas K., Nastos P.TH.and A.G. Paliatsos."Quality Control of Drinking Water and Public Health". WSEAS Transactions On Environment and Development, 2006.

Papaioannou A., Plageras P., Dovriki E., Minas A., Krikelis V., Nastos P.Th., K. Kakavas and A.G. Paliatsos. "Groundwater's quality and location of productive activities in the region of Thessaly (Greece)". Desalination, 2007, 213, 209-217.

Papaioannou A., Plageras P., P. TH. Nastos, Grigoriadis D., Dovriki E., Spanos TH., Koutseris S. and A.G. Paliatsos. "Assessment of Soil and Groundwater Quality and Hydro geological Profile of Drama's Prefecture, North Greece". WSEAS Transactions On Environment and Development, 2006.

Peña Haro S., 2009. A Hydro-Economic Modeling Framework for Optimal Management of Groundwater Nitrate Pollution from Agriculture, PhD Thesis, Instituto de Ingeniería del Agua y Media Ambiente, Universidad Politécnica De Valencia

Peña-Haro S., Pulido-Velazquez M., Sahuquillo A., 2009. A Hydro-Economic Modeling Framework for Optimal Management of Groundwater Nitrate Pollution from Agriculture, J. Hydrol., doi:10.1016/J.Jhydrol.2009.04.024

Proceedings of the 10th World Congress of EWRA 'Panta Rhei', 5-9 July 2017, Athens, Greece
© 2017 *European Water Resources Association*

Study of contamination of the transboundary river Kura in Georgia

E. Bakradze[1], G. Kuchava[1] and L. Shavliashvili[2]
[1] *LEPL National Environmental Agency, Georgia*
[2] *Georgian Technical University, Georgia*
[*] *e-mail:ce@pimi.t*

Abstract: In the article is presented pollution study on the River Kura and its surrounding area at background and anthropogenic points - dynamics of the last year. The study covers the Kura river basin with its tributaries from the Turkish border up to the Azerbaijan border in the article is presented the assessment of the pollution distribution from the upstream to downstream taking into account transboundary issues. River Kura environmental assessment on the territory of Georgia was based on physical-chemical and chemical parameters, which are characteristic for the basin. physical-chemical (water temperature, pH, BOD5, biogenic elements, main anions and cations, total petroleum hydrocarbons (TPH), heavy metals and other parameters were measured depending the EU Water Framework Directive. The sampling of the water, conservation, labelling, storage and transportation were produced in the accordance with the International Standard Organization (ISO) methodology. The study was conducted in the accredited laboratory by the ISO 17025 standard. Analyzes were carried out by the atmospheric air, water and soil analyses laboratory of the National Environmental Agency of the Ministry of environment and natural resources protection of Georgia in the following technical and instrumental support: plasma –emission spectrometer (ICP-OES) on the ISO 11885: 2007; Ion chromatography ICP_OES; spectrometers; GC_MS; IC; conductivity meter; pH meter; turbidity meter; DO meter.

Key words: anthropogenic impact, pollution transboundary Georgia, Turkey, Azerbaijan, Kura, water quality, pollutants, EU directives

1. INTRODUCTION

The basin of the river Kura cover the territory of the five countries of Armenia, Azerbaijan, Georgia, Iran, and Turkey. The total area of the Kura basin is approximately 188,400 km^2, occupying the greater part of the South Caucasus (Egorov 1951) (Figure 1).

The ecosystems of the Kura basin, similar to the entire Caucasus Eco region, are highly diverse and include a broad range of landscapes, from semi-deserts and arid shrub lands to mesophyll relic broadleaf forests and alpine grasslands (https://en.wikipedia.org/wiki/Kura_River).

Human activities in the second half of the twentieth century have had its effects on the quality and quantity of the water in the rivers (Shiklomanov1979). Ranges of factors, including industrial pollution, domestic waste, agricultural pesticides, large-scale irrigation, flood control, hydropower schemes and watershed degradation have affected the basin.

2. MAIN PART

The Kura river basin is an internationally significant river system, which is seriously degraded and continues to be degraded. The basin covers almost all of Armenia and Azerbaijan, and a sizeable part of the populated and urbanized parts of Georgia. Kura river system is a source of water for all sectors and users: industry, agriculture, energy and residential uses (Trapaidze 2012).

Deterioration of water quality in the Kura river basin has significant transboundary consequences in the downstream countries (http://www.fao.org/nr/water/aquastat/basins/kura-araks/index.stm). This can be confirmed by the presence of chemical compounds of anthropogenic origin in the transboundary sections of the basin as well as in bottom sediments of the Kura Delta in the Caspian Sea. Water pollution in the Kura basin comes from a number of land based sources including

industrial and mining sites, agricultural lands, households in rural areas and municipalities. Wastewater treatment facilities are absent in many municipalities and enterprises, and are available only in some locations in the Aras basin in Iran. Most of the wastewater treatment facilities were built 20- 30 years ago and are currently non-operational (National Environmental Agency).

The largest source of pollution for the Kura River is municipal wastewater, which specifically affects the river Kura downstream of large cities. Hence, water pollution in the Georgian part of the Kura River and its tributaries is mainly linked to human activities stemming from point and non-point pollution sources. The key drivers for these sources and the related pressures on water resources are the following.

Point sources:

1. Municipal sewage from cities and settlements.
2. Industrial wastewater.
3. Wastewater from hospitals, recreation and etc.

Non-point sources:

1. Surface run-off from agricultural fields.
2. Storm runoff from cities and landfills.

Key pressures from point sources:

Municipal sewage from cities and settlements pollute water with organic matters, nitrogen and phosphorus compounds.

Industrial wastewater impacts the rivers in the basin causing the pollution with heavy metals, in particular cases, rivers: Mashavera and Kazretula flows near the vicinity of the "RMG Copper", (formerly JSC Madneuli) it is a mining company Established in 1975, RMG Copper is currently involved in ore, copper, and gold mining and smelting.

2.1 Transboundary water cooperation

Transboundary water basins of the Caucasus include: The basin of the Kura River, Chorokhi River, Psou River, the Terek River, the Alazani River, the Debed (Debet) River, and lakes of Kartsakhi, Djandara, and others.

The extent of two longest Rivers in the Caucasus – the Kura and Araks (Araz) constitutes more than 1000 kilometers. Average volume of the river flow of Caucasus rivers fluctuates sharply, reaching its maximum in the regions of the Great Caucasus and Adjara (Adjara-Trialeti ridge), where these levels reach 1000 mm, in the lowland of Kura-Araks (Araz) they constitute 50 mm.

When it comes to transboundary monitoring it can be said that no joint monitoring activities on the river Kura between Georgia and Azerbaijan are undertaken as part of the regular monitoring programme. However, transboundary monitoring activities have been undertaken as part of the EU funded EPI project: Transboundary River Management for the Kura River basin Phase II and III – Armenia, Georgia, Azerbaijan to help Georgia, Armenia and Azerbaijan to understand and practice a common approach to surface water quality monitoring and assessment based on the EU WFD methodology. In 2012 three rounds of field surveys in pilot basins using WFD methodology were made: Khrami and Alazani basins (Georgia); Ganikh basin (Azerbaijan) (Matthews 2011-2013).

River Kura environmental assessment on the territory of Georgia was based on physical-chemical and chemical parameters, which are characteristic for the basin.

The Major transboundary problems are: the reduction of water flow and changes, deterioration of water quality, ecosystem degradation and flooding.

Therefore, the issue is very relevant and needed transboundary ecological situation assessment depending the European Union Water Framework Directive (EU WFD).

Physical-chemical (water temperature, pH, BOD_5, biogenic elements, main anions and kations, total petroleum hydrocarbons (TPH), (Nauka, 1986) heavy metals and other parameters were measured depending on the international standard organization (ISO) standards in compliance with the EU WFD methodologies implementation of the environmental quality standards, introduction of intercalibration were in place. In addition, it is important to mention that human activity impacts on

the river objects were assessed (Turkey build HPP on the river Kura; municipal and food industry waste water discharges into the river; irrigation etc) which is necessary for characterization and identification of the water bodies at risk to define environmental goals.

2.2 Research methods

The following parameters were measured in the laboratory: cations, anions, nutrients, BOD5, heavy metals.

- Sampling and transportation were implemented according to ISO 5667-4:1987; ISO 5667-3;
- Field analysis of physical-chemical (dissolved oxygen, pH, temperature, salinity) parameters were determined on the sampling site with the mobile devices;
- Laboratory analysis of samples in particular, cations, anions, nutrients were made in accordance with (ISO 10304-1: 2007, ISO 7150-1, ISO 9964, ISO 6059), BOD5 (ISO 5815-1: 2010);
- Heavy metals in water samples were determined using inductively coupled plasma optical emission spectrometry (ICP-OES) on the basis of ISO 11885: 2007 standard.

2.3 Results

According to the obtained data from 32 points on 36 measured ingredients on the river Kura and its tributaries, water belongs to the hydrocarbonate class, calcium group. The highest concentration of ions in this basin has been observed in summer and autumn, the lowest– in winter and spring. The latter is caused by the factor of water dilution during floods. The above specified dynamics have been adhered to at all sites of water quality control. The river Kura is a polluted river according to some ingredients in lower course due to anthropogenic activities (Khashuri, Gori, Tbilisi and Rustavi cities); also polluted are the tributaries of the river Kura Suramula and Lekhura, Debed, Mashavera (Figure 1).

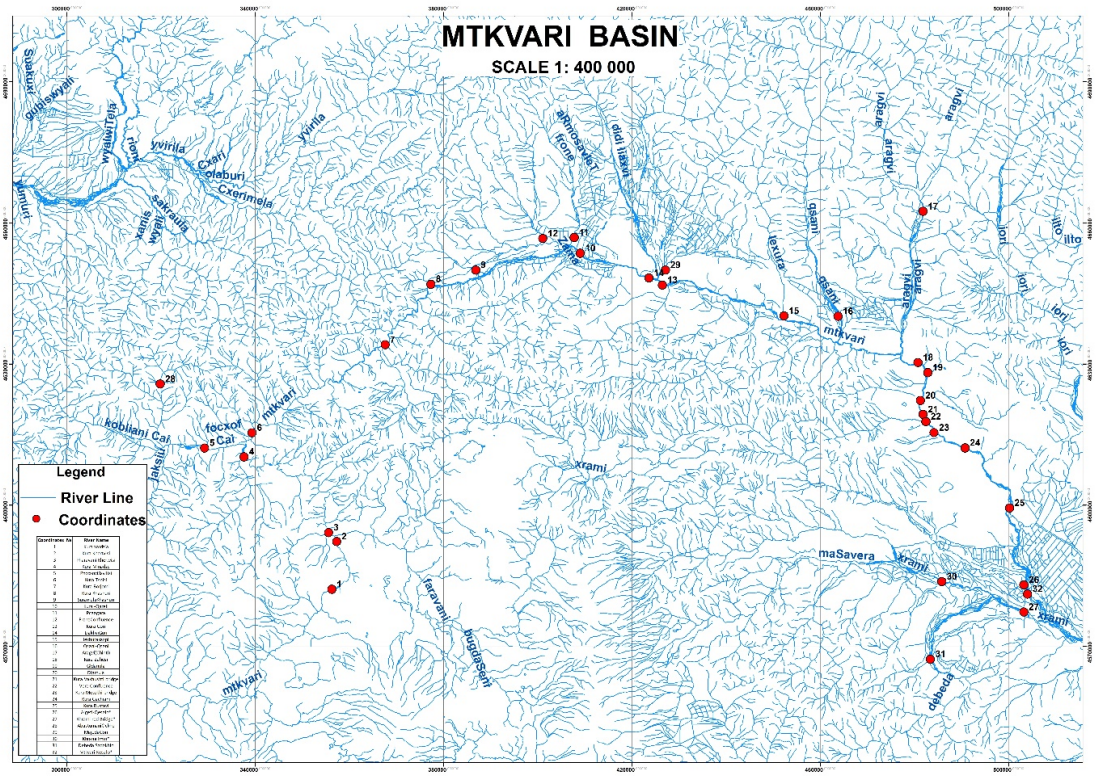

Figure 1. Map of the monitoring stations on Kura River and its tributaries of NEA 2016 year

The observed pH values were normal and typical for mountainous rivers, especially in the upper reaches of the basin in Georgia.

Dissolved Oxygen (DO) refers to the amount of oxygen dissolved in river water, and is the most important indicator of the health of a water body and its capacity to support a balanced aquatic ecosystem of plants and animals. Depending the obtained data dissolved oxygen is always satisfied. Conditioned by the rather natural hydro-morphological conditions and hydrological regime of the river. The higher the flow rate, the higher the DO concentration.

Ammonium (NH_4^+) is the ionized form of ammonia (NH_3), which occurs when the water is acidic. The degree to which NH_3 forms NH_4^+ depends on the pH of the river water. If the pH is low, more NH_3 molecules are converted into NH_4^+ ions, while when the pH is high the hydroxide ion abstracts a proton from the NH_4^+ ion, generating NH_3. When NH_4^+ nitrogen levels in surface waters are too high, they can be toxic to some aquatic organisms. On the other hand, if the levels are only moderately high, plant and algal growth will usually increase, due to the abundance of nitrogen available as a nutrient. Accordingly, this will impact on other water quality attributes, such as increasing the BOD_5 and lowering DO levels. DO levels can also be lowered when NH_4^+ nitrogen is high due to the increased occurrence of nitrification See figure 2. Average annual concentrations of ammonium.

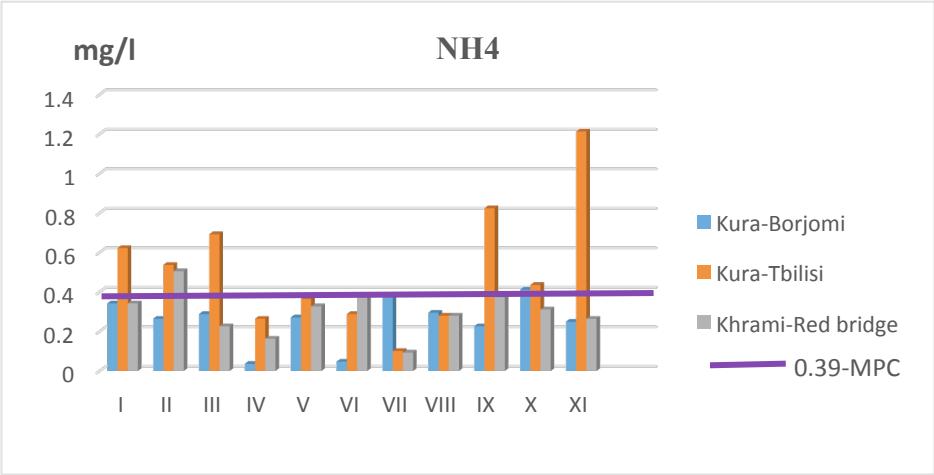

Figure 2. Average annual concentrations of ammonium.

Figure 2 is showing that Ammonium concentrations in different monitoring stations in Georgia has increasing trend in downstream direction from Khertvisi near the Turkey-Georgia border towards Rustavi upstream of Georgia-Azerbaijan border. This trend is typical for river water impacted by municipal waste water and agricultural drainage water, causing an increasing organic pollution load from upstream to the downstream section of the river. Meanwhile, even at the Tbilisi monitoring location the observed NH_4^+ concentration is still below the MPC (maximum permissible concentration) in various periods of the year (0.39 mg/l).

Figure 3 shows the dynamic of changes of BOD_5 concentration for the year 2016.

According to the overall data, the concentrations of BOD_5 and NH_4^+ indicate a limited impact of human activities on water quality in the Kura river basin, as most measured concentrations did not exceed the established MPC limits. Exemptions were observed for certain months during the low flow seasons. Although the impact on river water quality appears to be and there is an urgent need for the riparian countries to develop a long-term integrated regional environmental compliance action plan aiming at reducing the pollution loads from different sources, with special focus on municipal waste water from main cities and villages located in the river basin. Meanwhile there is a lack of information on the biological river water quality.

The heavy metals with a high relative atomic mass, including arsenic, copper, cadmium, chromium, lead, manganese, mercury, nickel, and selenium, persisting in nature and potentially causing damage or death in animals, humans, and plants, even at concentrations as low as 1-2

micrograms. Heavy metals used in industrial processes can be carried by air and water when discharged in the environment. Since heavy metals have a propensity to accumulate in selective body organs (such as brain and liver) the average safety levels in food or water is often misleadingly. Figure 4 shows the dynamic of changes of heavy metals concentration for the year 2016.

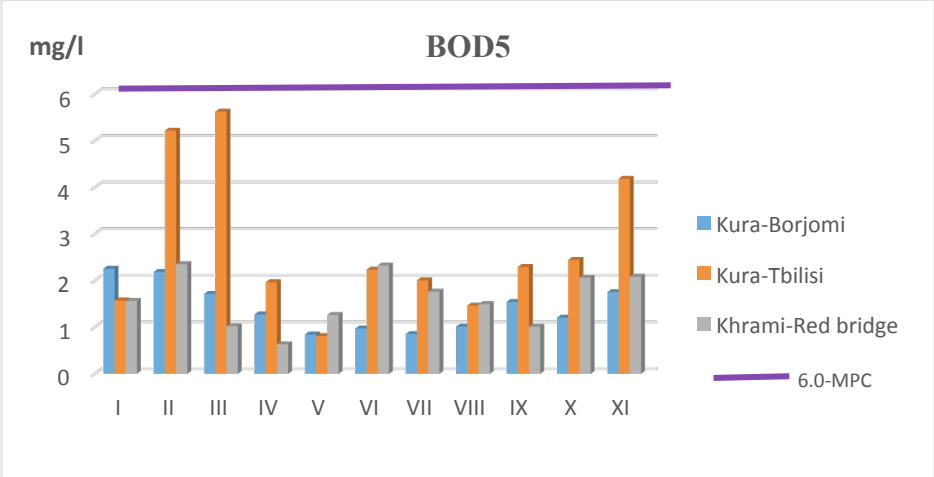

Figure 3. BOD_5- concentration for 2016 years in Kura River

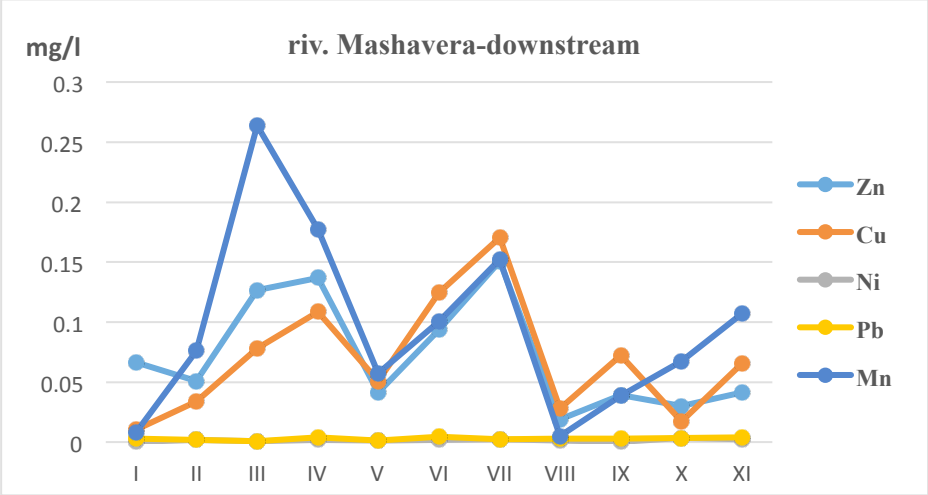

Figure 4. Heavy metal- concentration for 2016 years in the river Mashavera a right tributary of the Kura River

Industrial wastewater impacts the rivers in the basin causing the pollution with heavy metals, in particular cases, rivers: Mashavera and Kazretula flows near the vicinity of the "RMG Copper", (formerly JSC Madneuli) it is a mining company established in 1975, RMG Copper is currently involved in ore, copper, and gold mining and smelting. In the countries of the Kura river basin increased attention is paid to the problem of heavy metal pollution of the aquatic environment. Mining activities, metallurgical, chemical and leather industries, as well as natural geochemical and hydro-chemical processes all pose a threat to surface water contamination with heavy metals. Depending the Figure 4. Mn concentrations exceeds the MPC (0.1mg/l) in various periods of the year.

3. CONCLUSIONS

The research can be considered as scientific-technological and innovative that means that up-to-

date newest technologies and innovative methodologies were used in the scientific study. Tasks were accomplished at proper level. Modern procedures of QA/QC, standards elaborated by ISO and US Environmental Protection Agency (EPA) were used for result verification.

- Were implemented Kura River water environmental assessment depending the improved monitoring program in accordance with the EU Water Framework Directive;
- Were identified sensitive areas on the Kura basin in direction of pollution;
- Were identified point and diffuse sources of pollution.

Water quality standards harmonization between the states of Georgia, Azerbaijan and Turkey is needed for sustainable use of natural resources and ecosystems for this purposes measures should be undertaken such as public awareness rising about the sustainable use of water in that way transoundary countries can benefit each other in scientific, technological and economical way.

REFERENCES

Egorov VV, 1951. Problems of Physical Geography. Formation History, Natural Features, and the Perspectives of Economic Development of Kura Delta.

Matthews MM, 2011-2013 Shared Waters Shared Challenges: A summary of the Transboundary Diagnostic Analysis for the Kura Ara(k)s River Basin. http://kura-aras.iwlearn.org/Welcome_files/TDA_FINAL_GEO_EN_SCREEN.pdf;

Nauka, 1986. Kaspiiskoe More: Gidrologiya i Gidrokhimiya (The Caspian Sea: Hydrology and Hydrochemistry), Moscow

Shiklomanov IA, 1979. Antropogennye izmeneniya vodnosti rek (Anthropogenic Changes in the Flow of Rivers) - Leningrad: Gidrometeoizdat.

Trapaidze Vaja 2012. Water resources.

Proceedings of the 10th World Congress of EWRA 'Panta Rhei', 5-9 July 2017, Athens, Greece
© 2017 *European Water Resources Association*

Biodiversity indices and nutrient load assessment in Ishmi River, Albania, during 2012-2013

E. Keçi[1*], B. Pepa[2], A. Paparisto[3] and S. Duka[3]
[1] *Faculty of Professional Studies, Aleksander Moisiu University, Durres, Albania*
[2] *Faculty of Technical Sciences, Vlora University, Albania*
[3] *Faculty of Natural Sciences, Tirana University, Albania*
[*] *e-mail: erjolakeci@yahoo.it*

Abstract: Ishmi River basin is located in the central part of Albania crossing inhabited, industrial and agriculture areas. These activities have a direct impact on the aquatic ecosystem and water quality. The catchment area of Ishmi River consists of several tributaries, including the Lana, Tirana, and Tërkuza Rivers which join to create the Gjola Tributary; close to the River Delta, Zezë and Gjola Rivers together with Droja spring join into Ishmi River which flows into Adriatic Sea (Eftimi, 1989). Taking into consideration the River catchment area, its hydrological characteristics and recent rural and urban development's and industrial activities, we have monitored and analysed the water quality by assessing the biodiversity indices of benthic bio indicators and nutrient load in three monitoring stations along the River during 2012 – 2013. Benthic macro invertebrates are sampled seasonally according to Water Framework Directive (WFD) requirements and the Shannon and Simpson Indices were calculated; while nutrient load for each of the water samples was assessed according to Standard Methods for Examination of Water and Wastewater, APHA, 1998. The study' results indicate that the nutrients content as $P\text{-}PO_4^{3-}$, $N\text{-}NO_3^-$, $N\text{-}NH_4^-$, $N\text{-}NO_2^-$, increases due to the high organic pollution load and it causes the decrease of benthic invertebrate taxa and variation of Biodiversity Indices.

Key words: Shannon Index, Simpson Index, nutrient load, water quality

1. INTRODUCTION

Being a candidate to EU membership and a costal country Albania has to handle important issues related to water quality and management. The implementation of the Water Framework Directive (WFD) in Albania is an opportunity to improve water quality according to European Standards and Practices. In the present study we have assessed the water quality of Ishmi River, by analysing nutrient load and benthic invertebrates' biodiversity variances at three monitoring stations along the River. The relation between benthic invertebrates' number of individuals and their relative abundance and nutrient load is presented as well. A variable macro benthic community, being able to adapt better to climate changes and water quality, is a good indicator of the environmental status.

2. METHODS AND MATERIALS

2.1 Sampling

Sampling was undertaken seasonally, on daily expeditions, in order to sample at each of the monitoring stations within the same day and weather conditions during 2012-2013. At each monitoring station three samples are taken randomly. Benthic invertebrates were collected from the river bottom (40 – 60 cm) with a kick – net (500μ) in order to gain sufficient samples from larger depths of water. The net is held upright on the stream bed by one individual, while the stream bottom upstream of the net is physically disrupted by a second individual. Kicking and turning over rocks and logs with the feet and hands dislodges organisms which are washed into the net by the

current (Barbour et al, 1999; Bode et al, 1995; Bode et al, 1997; Cardoso et al, 2005; Downing & Rigler, 1984; Voeiz et al, 2001; Pollard, 1981). The samples were collected from areas of differing current speed. All benthic macro invertebrates are kept in 95% ETOH. Before mailing to the Laboratory, the jars are completely filled with alcohol to reduce damage to the specimen and labelled. Each label consists on name of the station, no. of the sample and date of sampling.

2.2 Sorting

Sorting consists on disaggregating the invertebrate taxa from the substrate, assessing the abundance of each groups found in the respective samples (Braukman, 2000; Peter Haase et al, 2004). Sorting has been carried out at using a stereomicroscope (OPTIKA zoom stereo microscopes SZM – Led 2).

Each of the invertebrate present in the sample is counted and stored in alcohol 95% in separate plastic tubes, which are labelled with the data on the period, site or monitoring station. Each of the above phases is exercised for each replicate separately, for respective sampling sites and monitoring stations. The substrate disaggregation is realised carefully using the stereo microscope.

2.3 Species identification

For the identification of benthic invertebrates different publications are used: Wallace and Wallace (2003), Edington & Hildrew (2005), Hickin (1967), Macan (1994), Hynes H.B.N (1993), Tachet et al. (1980) Cao et al. (1997), Parker and Salansky, (1998), Campaioli et al. (1994).

2.4 Biodiversity Indices Calculation

Shannon & Simpson Indices are diversity indices that provide important information on the commonness and rarity of species within the community. The diversity quantifying is an important tool for understanding the community structure (Magurran, 2004):

2.4.1 Shannon Index Calculation

$$H = -\sum_{i=1}^{S} p_i \ln p_i \tag{1}$$

H = Shannon Index

P_i = proportion of *S* made up of the ith species

S = total number of species in the community/ richness

$\sum$ = Sum from 1st individual to S individual

Equitability (evenness) (E_H) can be calculated by dividing H by H_{max} (here: $H_{max} = \ln S$). Equitability assumes a value between 0 and 1 with 1 being complete evenness.

2.4.2 Simpson Index Calculation

Simpson Index calculation comprises a simple mathematical measure that characterizes species diversity in a community. Simpson's index is based on the probability of any two individuals drawn at random from an infinitely large community belonging to the same species: $D = \Sigma\, p_i^2$ where pi is the proportion of individuals found in species i.

Simpson Index calculation for a finite community:

$$D = \Sigma [n_i (n_i - 1)/N (N - 1)] \quad (2)$$

2.6 Chemical analyses

Nutrient load assessment of the water samples has been carried out at the Laboratory of Analytical Chemistry, Faculty of Natural Sciences, Tirana, Albania. The water samples are taken seasonally during 2013, using 0,5L sterilized bottles, closed hermetically. Each bottle has been labelled with the date and monitoring station name. The bottle is opened and closed within water, in order to avoid air presence. Measurement of nitrites and nitrates have been carried out using UV-VIS Spectrophotometer; while for the assessment of total phosphorus has been used the Spectrophotometer UV-VIS Pay-Unicam SP-5 (for the measurements at 880nm wave length). Water samples storage, pre-treatment and chemical analyses have been executed according to Standard Methods for Examination of Water and Wastewater (APHA, 1998).

3. RESULTS AND DISCUSSION

3.1 Biodiversity Indicess assessment in Ishmi River

Increase of Shannon Index and Equitability values show the increase of the heterogeneity or richness of macroinvertebrates' community; decrease of Shannon Index value reflects the poorness and homogeneity of benthic invertebrates' community (Magurran, 2004).

D - Simpson Index is considered as measure of dominance, so increase of its value (in equitability basis) is an indicator of species diversity decrease (Magurran, 2004).

Table 1. Shannon & Simpson Indices in Ishmi River, Albania, per each monitoring station during 2012 – 2013; Water quality classification per each monitoring station in Ishmi River based on P-PO_4^{3-} and N-NH_4^+ according to UNECE classification

Monitoring stations	H – Shannon Index	E (Shannon Equitability)	D – Simpson Index	P-PO_4^{3-} µg/L	UNECE	N-NH_4^+ mg/L	UNECE
Lanës/Rinas Bridge	1.928232236	0.838361842	0.181606901	333.4	V	4.94	IV
Zezë/Fushë-Krujë	0.899912379	0.391266252	0.59602767	114.7	IV	2.84	IV
Gjuricaj/Sukth	1.001172789	0.526933047	0.532999376	360.3	V	7.22	V

Biodiversity Indices have slight differences from one monitoring station to another along the River (Table 1); H decreases from the first monitoring station to the second reflecting poorness of the community diversity. The decrease of taxa is a consequence of water pollution at the monitoring stations; the increase of H value at the 3rd monitoring stations shows an increase of identified taxa. However the identified taxa are of a higher tolerance toward pollution compared to the 2nd monitoring station, while the density per taxa is lower than at 2nd monitoring station. Water pollution increases from the first monitoring station to the River delta, where the pollution concentration is higher compared to the upper parts of the river basin/catchment area. Monitoring stations are located at different sites along the river basin: at Lana/Rinas Bridge and Zezë/Fushë-Krujë i.e. in the medium section of River basin, while the 3rd monitoring station Gjurica/Sukth is close to the River Delta. The location of the monitoring sites justifies the obtained results, i.e. the dominance of *Olighocheta* taxa (with a tolerance value toward pollution 8; Mandaville, 2002; Lenat, 1998) at the 3rd monitoring station; while in the samples of 2nd monitoring station the dominant taxa is *Chironomidae* (with a tolerance value toward pollution 6; Mandaville, 2002).

Simpson Index value increases from the 1st to the 2nd monitoring station and decreases from the 2nd to the 3rd monitoring station reflecting the same result as Shannon Index.

3.2 Nutrient load and water quality in Ishmi River

The nutrient load in Ishmi River/ selected monitoring stations is been assessed and is as follows:

The nutrient load in the water samples of each of the monitoring stations reflects an overview of eutrophic waters, which are characterized by low levels of dissolved oxygen and decrease of benthic invertebrates and other living species in the ecosystem (Cullaj *et al.,* 2004; Minnesota Pollution Control Agency, 2005). Based on the mean values of P-$PO_4^{3-}$and N-NH_4^+ in all monitoring stations the water is classified as highly polluted belonging to the IV and V water quality class; the aforementioned classification indicates a bad quality of water and high pollution level (Table 1).

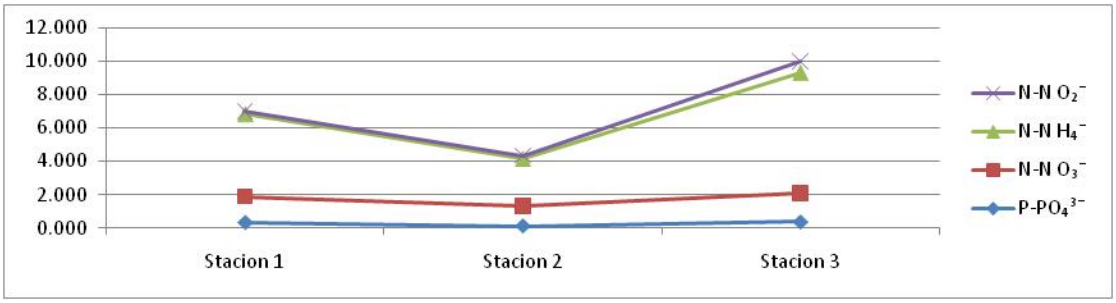

Figure 1. Nutrient load variances in three monitoring stations of Ishmi River, Albania during 2012 – 2013

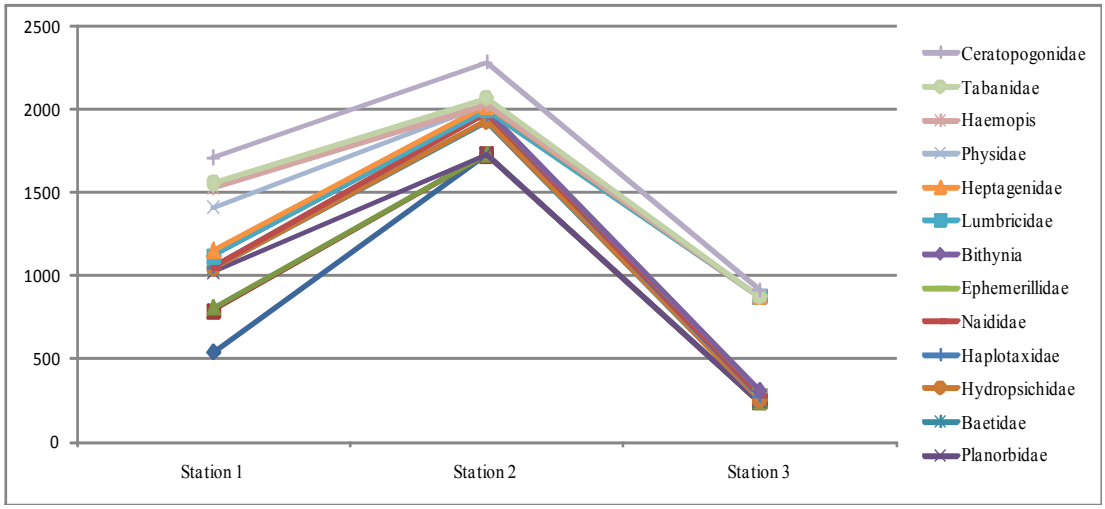

Figure 2. Benthic invertebrate individuals' variances per each monitoring station in Ishmi River, Albania during 2012 – 2013

Figures 1 and 2 present the decrease of the benthic invertebrates according to the considerable increase of the nutrient load into the water. It is noted that in the 2nd monitoring station (Zezë/Fushë-Krujë) the mean value of the nutrients decreases slightly, showing a slight improvement of water quality compared to the other monitoring stations. The slight decrease of nutrient load at the 2nd monitoring station has been accompanied by the increase of mean number of macro invertebrate individuals in this monitoring station. High level of nutrient load and high density of benthos tolerant invertebrates in the monitoring stations reflect a high level of water pollution of Ishmi River, (Table1; UNCE; EPA-USA; Miho *et al*, 2005; Cullaj *et al*, 2004).

4. CONCLUSIONS

1. H decreases from the first monitoring station to the second reflecting the poorness of the community diversity. The decrease of taxa is a consequence of water pollution within the

monitoring stations;
2. Taxa identified in the 3rd monitoring station are of higher tolerance toward water pollution compared to the 2nd monitoring station, while the density per taxa is lower than the 2nd monitoring station.
3. Invertebrate taxa density increase in the 3rd monitoring station justifies the slight increase of H value from the 2nd to the 3rd monitoring station.
4. Simpson Index value increases from the 1st to the 2nd monitoring station and decreases from the 2nd to the 3rd monitoring station reflecting the same result as Shannon Index.
5. High level of nutrient load (fig 1) and high density of benthos tolerant invertebrates in the monitoring stations (fig 2) reflect a high level of water pollution in Ishmi River, (Table 1; UNCE; EPA-USA; Miho *et al*, 2005; Cullaj *et al*, 2004).

REFERENCES

Barbour M. T., Stribling J. B. and Carr J. R., 1995. The multimetric approach for establishing bio criteria and measuring biological condition - Biological Assessment and Criteria: Tools for Water Resource Planning and Decision Making. Lewis Publishers, Boca Raton, FL; 415: 63-80

Barbour, M. T., J. Gerritsen, Snyder B. D. and Stribling J. B., 1999. Rapid Bio-assessment Protocols for Use in Streams and Rivers: Periphyton, Benthic Macro invertebrates, and Fish. Second Edition. EPA 841-B-99-002. Office of Water, US Environmental Protection Agency, Washington, DC. 151 p. + appendices

Bode R. W. Novak M., A., Abele L., A., 1997. Biological stream testing. NYS Department of Environmental Protection ; Division of Water ; Bureau of Monitoring and Assessment ; Stream monitoring unit ; USA.

Bode R.W., Novak M. A., Abele L. A., 1995. Quality assurance Work plan for biological stream monitoring in New York State. Department of Environmental protection; Division of water; Bureau of Monitoring and assessment ; Stream Bio-monitoring Unit ; Albany , NY.

Braukmann, U., 2000. Hydrochemische und biologische Merkrnale regionaler Bachtypen in Baden-Wtirttemberg. Oberirdische Gew~isser, Gew~isser6kologie; 56:1-501.

Campaioli S., Gheti P. F., Minelli A., Ruffo S., 1994. Manuale per riconoscimento dei Macroinvertebrati delle acque dolci italiane. Vol.1. Provincia Autonoma di Trento; 9-14: 27-190.

Cao Y., Barl A. W., Williams P., 1997. A comparison of clustering methods for benthic community analysis. Hydrobiologia; 347: 25-40.

Cardoso C. A., Solimini G .A. Premazzi G., 2005. Report on Harmonisation of Freshwaters biological methods; 61-95.

Cullaj A., Hasko A., Miho A., Schanz F., Brandl H., Bachofen R., 2004. The quality of Albanian natural waters and the human impact; Elsevier, Environment International 31: 133– 146.

Downing J.A., Rigler F. H. 1984. A manual on methods for the Assessment of secondary productivity in fresh waters. 2ndedn. IBP Handbook No.17, Blackwell scientific Publications, Oxford; 19-58.

Edington, J .M. Hildrew, A. G., 2005. A revised key to the caseless caddis larvae of the British Isles. Freshwater Biological Association. The Ferry House; 133.

EEA, 200696 - 107. 2007. European Environment Agency, Technical report No. 11/2007, Halting the Loss of Biodiversity by 2010; Proposal for the first set of indicators to monitor progress in Europepp; 17-22, 33-48, 130-136.

Eftimi R., 1989. "Rajonizimi hidrogjeologjik i Shqiperise", Buletini i Shkencave gjeologjike Nr 4.

Environmental Protection Agency - USA.

Giuseppe Sansoni, 1998. Atlante per il riconoscimento dei macroinvertebrati dei corsi d'acqua Italiani; Agenzia Provinciale per la Protezione dell'Ambiente-Provincia Autonoma di Trento; 3a edizione, Italy.

Hickin, N. E., 1967. Caddis larvae of the British Trichoptera. Hutchinson of London; 499.

Horning C.E., Pollard J. E., 1978. Macro invertebrate sampling techniques for streams in semi – arid areas. Comparison of the Surber method with a unit effort travelling kick method. U.S. Environmental Protection Agency-EPA-600 / 4-78—040.

Hutchinson, G.E., 1967. A treatise on limnology. Vol. 2, Introduction to lake biology and the limnoplankton. Wiley New York

Hynes H.B.N., 1993. The ecology of running waters. The Blackburn Press; 112-271

Lampert W and Sommer U., 1997. Limno-ecology; the ecology of Lakes and Streams. 2nd edition, Oxford University Press. ISBN: 0195095928.

Lee N. Rudd H., 2003. Conserving Biodiversity in Greater Vancouver; Indicator Species and Habitat Quality. Douglas College, Institute of urban ecology, 2nd Edition.

Lenat D. R., 1998. Water quality assessment of streams using Qualitative collection methods for benthic macro invertebrates. Journal of the North American Benthological Society; 7: .222-233.

Lenat. D.R., 1993. A biotic index for the south-eastern United States: derivation and list of tolerance values, with criteria for assigning water quality ratings. Journal of the North American Benthological Society 12: 279-290.

Macan, T.T., 1994. A key to the British fresh – and brackish- water gastropods. Freshwater Biological Association. The Ferry house. Scientific Publication; 11: 46.

Mandaville S.M., 2002. Benthic Macro invertebrates in Freshwaters - Taxa Tolerance Values, Metrics, and Protocols; (Professional Lake Manage.) (Project H-1); Soil & Water Conservation Society of Metro Halifax (http://chebucto.ca/Science/ SWCS/SWCS.html)

Magurran, A.E., 2004. Measuring Biological Diversity. Blackwell.

Markert, B., Wappelhorst, O., Weckert, V., Herpin, U., Siewers, U. and Friese, K.., 1999. The use of bio indicators for monitoring the heavy-metal status of the environment. Journal of Radio analytical Nuclear Chemistry; 240(2): 425-429.

Miho A., Cullaj A., Hasko A., Lazo P., Kupe L., Brandl H., Schanz F ., Baraj B., 2005. Environmental State of some rivers of Albanian Adriatic Lowland. Evaluation report; 215. http://www.unitir.edu.al/doc/fshn

Minnesota Pollution Control Agency, 2005. Lake Data assessment workbook; a citizen guide to analyse data to better understand lake conditions.

Parker R. Ch, Salansky K .G., 1998. Benthic Macroinvertebrate Protocol Manual; 16.

Peter Haase, Steffen Pauls, Andrea Sundermann, Armin Zenker, 2004. Testing different sorting techniques in macroinvertebrate samples from running waters; Elsevier-Limnologica; 34: 366-378.

Pollard J.E., 1981. Investigator differences Associated with a kicking method for sampling macro invertebrates. Journal of Freshwater Ecology; 1: 215-224.

Rađa B. and Puljas S., 2010. Do Karst Rivers “deserve” their own biotic index? A ten years study on macro zoo benthos in Croatia; International Journal of Speleology, Bologna, Italy; 39(2): 137-147. www.ijs.speleo.it.

Rosenberg, D. M., Danks H. V. and Lehmkuhl D. M., 1986. Importance of insects in environmental impact assessment. Environmental Management; 10: 773-783.

Rosenberg D.M. and Resh V.H., 1993. Freshwater bio monitoring and benthic macro invertebrates. Chapman and Hall, New York.

Rundle S S. D., Robertson A.L., Schmid-araya J. M., 2002. Freshwater meiofauna. Biology and ecology. Blackhuys Publishers. Leiden; 217-321.

Schmiedt K., Jones R. L., Brill I., Pikalw., 1998. EPT Family richness modified biotic index.

Simboura N., Zenetos A., 2002. Benthic indicators to use in ecological quality classification of Mediterranean soft bottom marine ecosystems, including a new biotic index. Mediterranean Marine Sciences; 3/2: 77 – 111.

Standard Methods for Examination of Water and Wastewater - APHA, 1998. American Public Health Association, American Water Works Association, Water Environment Federation.

Tachet, H., Bournaud, M., Richoux, P., 1980. Introduction á l’étude des macro invertebres des eaux douces. C. R.D.P. Lion; 130-150.

UNECE - The United Nations Economic Commission for Europe.

Voeiz N.J., Shieh S., Ward J.V., 2001. Long-term monitoring of benthic macro invertebrate community structure. Aquatic ecology; 34/3: 261-278.

Wallace, I. D., Wallace, B., 2003. Keys to the case bearing larvae of Britain and Ireland. Freshwater Biological Association. The Ferry House. Scientific Publication; 61: 249.

Wallace J.B., Grubaugh J.W., and Whiles M. R., 1996. Biotic indices and stream ecosystem processes. Results from an experimental study. Ecological Applications; 6(1): 140-151.

Proceedings of the 10th World Congress of EWRA 'Panta Rhei', 5-9 July 2017, Athens, Greece
© 2017 *European Water Resources Association*

Possibility of artificial beach nourishment using crushed limestone aggregate

S. Juradin*, M. Rajkovic and M. Vranjes
University of Split Faculty of Civil Engineering, Architecture and Geodesy, Matice hrvatske 15, Split, Croatia
* *e-mail: sandra.juradin@gradst.hr*

Abstract: Beach feeding has become one of the most popular approaches to coastal engineering over the past decade and many see it as the ultimate saviour, both for increased coastal defence and for tourism. There are two aims of this research: to analyze the change of particle size distribution and grains shape after nourishment and to analyze how shape of crushed limestone aggregate can be improved before beach nourishment to become more comfortable. For this purpose, 13 samples from different parts of an artificial hotel's beach located at Split (Adriatic Sea) were taken and analyzed almost two years after filling the beach with the crushed limestone with coarser grains (16 – 31.5 mm) mixed with the same size river pebbles. The particle size distribution and shape index were analysed for all samples. Also, a few samples of the crushed limestone were taken from the quarry, where the material was taken for beach nourishment. In order to improve grains shape, these samples were subjected to abrasion, by mixing in a laboratory pan mixers or in a ball mill. The particle size distribution and shape index were then analyzed and compared with results obtained on samples from the beach. Shape of crushed aggregate can be improved by the methods of abrasion. For the purpose of beach nourishment this could be too expensive, but the power of the waves to create shape of aggregate before beach filling can be useful for this goal.

Key words: beach renourishment, crushed limestone, shape index, Faury coefficient

1. INTRODUCTION

The term of beach renourishment means that sediment will be placed on the existing beach material and adapt its shape to the changing wave, tidal conditions and other natural conditions. Renourishment is often applied to eroded beaches but it may be useful for the purposes of tourism, so it is important to know reason for renourishment. "Beach renourishment is costly, but may be economically justifiable on sectors of the coastline, such as seaside resorts, where the emplaced beaches will be much used, or where the beach will protect property or infrastructure that is at risk from erosion or flooding" (Bird and Lewis, 2015). The beaches are popular for summer tourism, especially if they are suitable for sunbathing and swimming. Sediment used for renourishment should have similar grain size characteristics to the natural beach and rounded particles are more comfortable and preferable than flat or elongated particles. Badly shaped natural sand usually comes from glacially formed pit deposits and rounded particles like pebbles come from rivers or beaches. Good sources of sediment for beach renourishment are sometimes too far from the beach. In order to minimise transportation costs, suitable material should be sought as close as possible to the beach (Bird and Lewis, 2015; Day et al., 2014; Evangelista et al., 1992).

An artificial hotel's beach located at Split on Adriatic Sea is observed. In the earlier period this part of the coast was quite unsightly with a very narrow walking trail and unattractive beach, Figure 1 (left). In the last 15 years, the beach has been built into the shape as shown in Figure 1 (right). During this time, the beach was several times nourished mainly with crushed limestone coarse gravel. In the experimental part of the work, 13 samples from different part of beach were taken and analysed after 1.5 year of renourishment.



Figure 1. An artificial hotel's beach at 1966. (left) and 2010. (right)

2. EXPERIMENTAL PART

2.1 Testing on the samples taken from beach after renourishment

The artificial hotel's beach was renourished in the summer 2010. with crushed limestone from the nearby quarry mixed with the river pebbles, which were added to improve roundness of borrow material. The marks and location of the taken samples are shown in Figure 2.

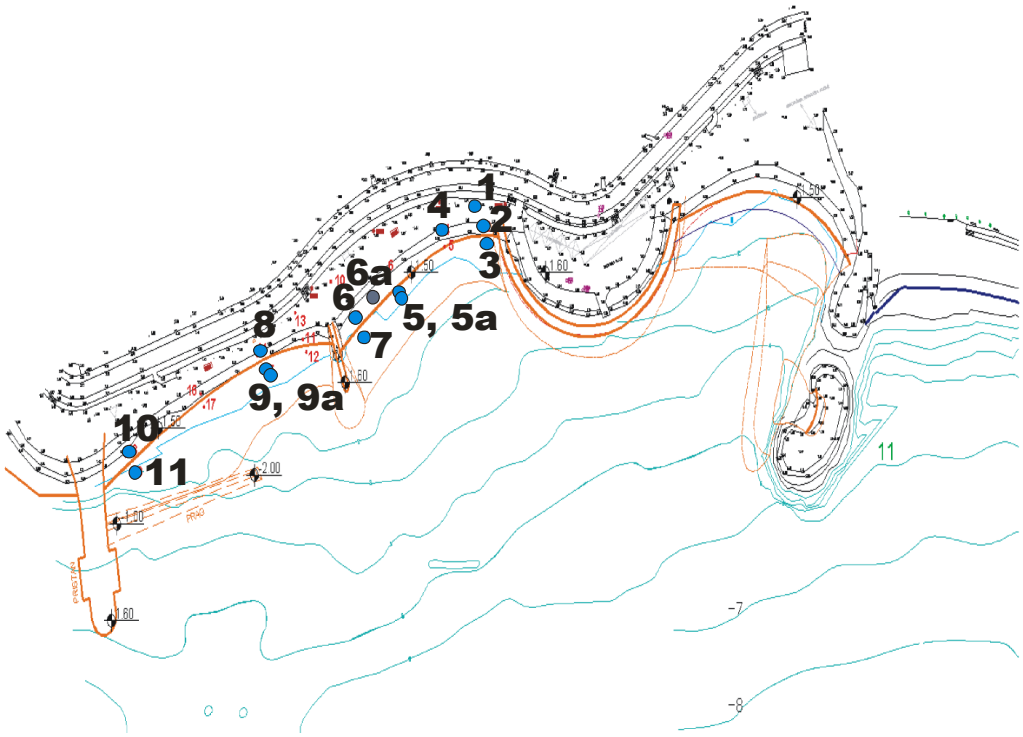

Figure 2. The marks and location of the taken samples

All samples, except 6a, were taken in October or November 2011. and sample marked with 6a was taken in the spring 2013. The purpose of sample 6a was to notice potential changes in the sample 6 through the period of 18 months. Some samples were taken from the beach and some from the shoreline, like samples marked with 5 and 5a. The particle size distribution for all samples is shown in Figure 3.

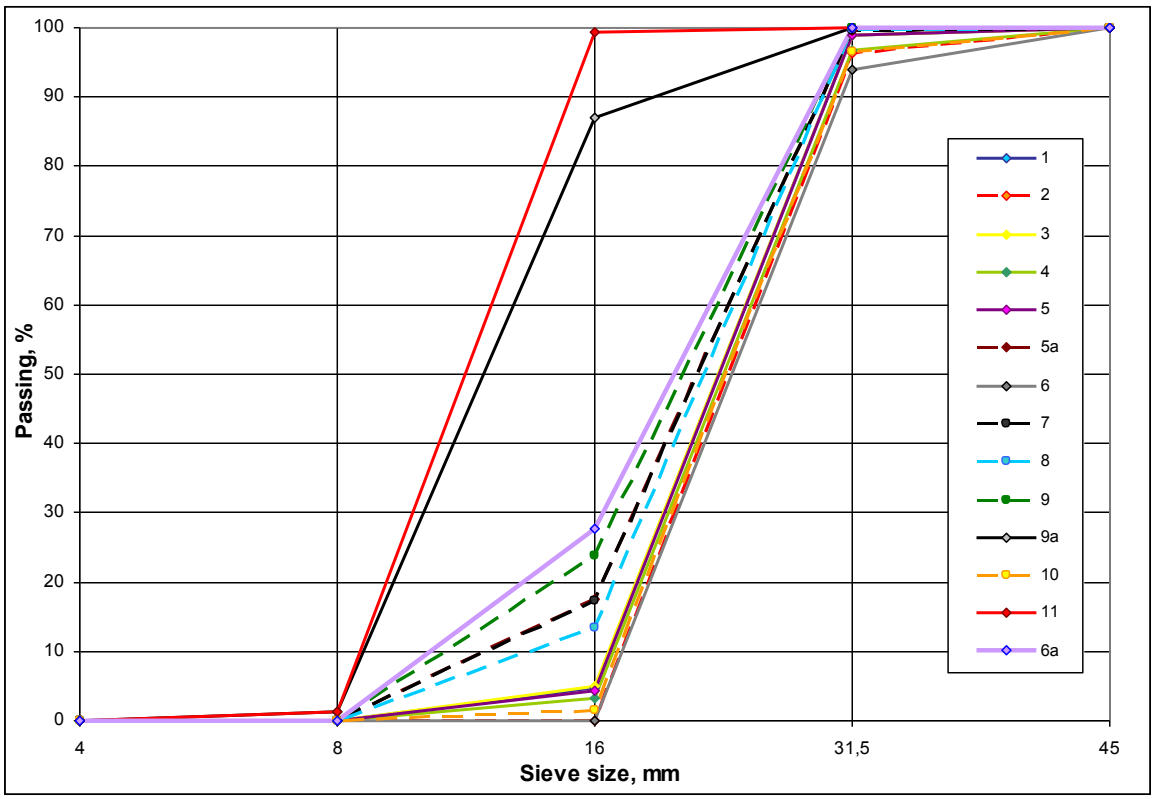

Figure 3. Grading curves of all samples

According to Figure 3, for the samples 9a and 11 the percentage of aggregate passing through 16 mm sieve were 87.1 and 99.3 %, while the samples marked 2 and 6 had no grains smaller than 16 mm. The samples 5a and 7 had the same grading curves and both were taken from the shoreline. The grading curve of the sample labels 6a in regard to the grading curve of the 6 was different. It is obvious that, through a period of 18 months, parts of the grains were crushed.

Volumetric coefficient by Faury and shape index were analyzed for 8-16 and 16-31.5 mm fractions. These methods are based on measurement of the aggregate dimensions giving several shape characteristics as degree of sphericity and elongation.

Volumetric coefficient by Faury is ratio between the total volume of aggregate grains to the volume of spheres with diameter equal to the longest axis of the each grains. This method sets down the amount of measured grains to minimum 100 grains from each size of the coarse aggregate.

The shape index (Uthus et al., 2005; HRN EN 933-4:1999) is a method for determining the elongation of coarse aggregate grains. The length L is defined as the longest axis of the grain and the thickness E is the shortest axis. Shape index SI is defined as a ratio between the weight of particles with L/E > 3 and weight of all measured particles in percents. The obtained results are shown in Table 1.

According to Table 1, the grains from the sample 1 had the highest roundness. This sample had a high percentage of river pebbles in its composition, Figure 4 (left). The sample 9a had a lowest value of the volumetric coefficient, Figure 4 (right). The grains from the 6a were more round than grains from the sample 6 and there weren't elongated grains in 8-16 mm fraction (SI = 0). According to SI index, the samples 4 and 8 had a large number of elongated and broken grains.

2.2 Laboratory testing

The purpose of this part of the experimental work is to test abrasion of the crushed aggregate and possibility to improve the roundness of grains. Two samples of crushed limestone with coarser gravel (16 – 31.5 mm) were subjected to abrasion, one by mixing in a laboratory pan mixer and

other in a ball mill. The crushed limestone was from the same quarry and the same size as the material for renourishment.

Table 1. Faury coefficient and shape index for grain size 16-31.5 and 8-16mm

Sample	Number of grains in the sample	Faury coefficient C	Shape index SI	Number of grains in the sample	Faury coefficient C	Shape index SI
	16-31.5 mm			8-16 mm		
1	105	0.305	7.02	100	0.255	*
2	103	0.255	13.54	-	-	-
3	105	0.272	13.97	105	0.193	21.70
4	104	0.243	20.65	61**	0.166	45.95
5	106	0.281	6.98	108	0.212	23.08
5a	105	0.279	11.92	104	0.226	19.40
6	105	0.244	10.15	-	-	-
7	105	0.279	11.92	105	0.279	16.37
8	104	0.230	25.73	102	0.180	75.38
9	104	0.256	14.21	102	0.219	22.29
9a	105	0.269	19.17	105	0.143	13.25
10	104	0.273	8.63	-	-	-
11	103	0.285	7.92	-	-	-
6a	102	0.311	12.20	103	0.260	0.00
CLA	105	0.179	24.02			
CLPan	104	0.260	7.90			
CLMill	104	0.242	15.70			

* - *grains were too small and inconvenient*
** - *insufficiently number of grains in the sample*



Figure 4. The sample 1 with C=0.305 (left) and the sample 9a with C=0.143 (right)

Testing in a pan mixer: The 15 kg of crushed aggregate and 4.5 kg of quartz sand (0.5 - 1 mm) were placed in the pan mixer. Water was added after 3 minutes of dry mixing. The amount of water was determined by visual observation to form dense-graded mix of water and particles of quartz, without water separation. After wet abrasion through 195 minute, aggregate was dried and sieved. Size distribution of the sample taken from the quarry (CLA) and the sample from the pan (CLPan) are shown in the Figure 5. In CLPan grading curve, particles smaller than 1 mm include particles of quartz, but the increase in the passage of particles through the sieve 1- 16 mm is obvious.

The obtained values for Faury coefficient and shape index are shown in Table 1. According to Table 1, Faury coefficient for CLPan is increased from 0.179 for CLA to 0.260 and became almost equal to average value for the beach (0.267). It should be noted that rounded river pebbles contribute to this average value.

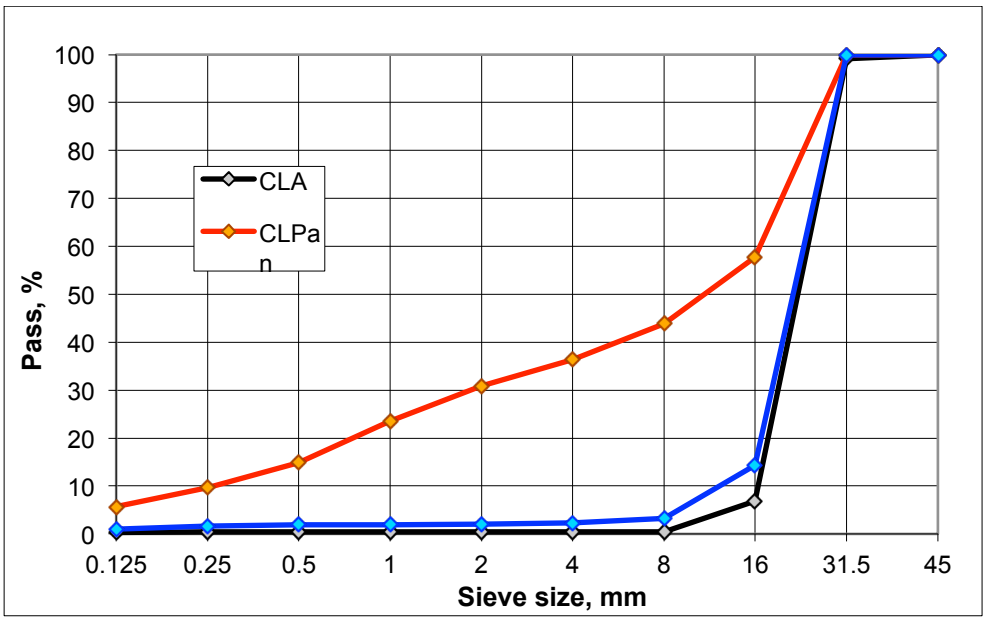

Figure 5. Grading curves of CLA, CLPan and CLMill samples

SI is decreased from 24.02 to 7.90, which means that there are less elongated grains. The difference between the CLA and CLPan grains are shown on the left picture in the Figure 6.



Figure 6. Grains: left - CLA vs CLPan and right - CLA vs CLMill

Testing in a ball mill: The 7 kg of crushed aggregate and 3 kg of steal balls with diameter of 20 mm were placed into a ball mill and put into work as long as pan mixer - 195 minutes. The material was sieved and the grading curve was shown in Figure 5. There was no significant difference between grading curves CLA and CLMill, but Faury coefficient was increased to 0.242 and SI was decreased to 15.70. The grains are shown on the right picture in the Figure 6. The CLMill grading curve is the most similar to the grading curves from the samples 7 and 8. This method provides a satisfy grain shape without additional crushing aggregate.

3. CONCLUSION

The hotel's beach is an artificial beach, which was brought into the present situation with series of activities. In the final phase of the project, the beach was renourishment with crushed limestone from the nearby quarry. The fraction was 16 – 31.5 mm with badly shaped grains, so the river pebbles were added to improve a shape.

- Analysis of the samples taken from the beach after 1.5 year of renourishment showed that crushed aggregate changed grains shape and reduced the grain size in places with a stronger action of the waves.
- Shape of crushed limestone aggregate can be improved by the methods of abrasion by mixing in a laboratory pan mixers or in a ball mill. The method in a ball mill provides a satisfy grain shape without additional crushing aggregate.
- Abrasion of aggregate for beach nourishment would maybe be too expensive, but coastal engineering experts can try to use the power of the waves, tidal conditions and other natural conditions to create shape of aggregate before beach filling.

REFERENCES

Bird, E., Lewis, N., 2015. Beach Renourishment

Day, K. W., Aldred, J., Hudson, B., 2014. Concrete Mix Design,Quality Control and Specification, Fourth Edition

Evangelista, S., La Monica, G. B., Landini, B., 1992. Artificial beach nourishment using fine crushed limestone gravel at Terracina (Latium, Italy). Bollettino di Oceanologica Teorica ed Applicata 10:273–278

HRN EN 933-4:1999: Tests for geometrical properties of aggregates. Part 4: Determination of particle shape, Shape Index.

Uthus, L., Hoff, I., Horvli, I., 2005. Evaluation of grain shape characterization methods for unbound aggregates. In Proceedings of the 7th International Conference on the Bearing Capacity of Roads, Railways and Airfields, Trondheim Norway https://www.sintef.no/globalassets/upload/154.pdf

Proceedings of the 10th World Congress of EWRA 'Panta Rhei', 5-9 July 2017, Athens, Greece
© 2017 *European Water Resources Association*

The impact of drinking water on the prevalence of *H. Pylori* in humans in Elbasan, Albania

S. Mali[1], L. Vrushi[2] and N. Hila[1]
[1] *Faculty of Natural Sciences, "Aleksander Xhuvani",University, Elbasan, Albania*
[2] *"Luis Pasteur" Laboratory, Elbasan, Albania*
[*] *e-mail: sotirmali@hotmail.com*

Abstract: Many studies are carried out about the *Helicobacter pylori* in different countries these three last decades, but this is the first one in Albania. In some of them the authors are focused on its biology and in some others on the impact of environmental conditions in the persons affected by it. The aim of this paper is to present the impact of drinking water consumed by humans on the prevalence of Helicobacter pylori in the district of Elbasan in Albania. The study concerns the period from January 2011 to May 2014. In order to find out the presence of this bacteria in these persons, some analyzes based on the "Sandwich Elisa Test "are carried out. During this period of time are analyzed 886 blood samples taken from 886 persons and resulted that 74 % of them were affected by Helicobacter pylori. The data show that there is different number of persons affected by this bacteria based on the different type of drinking water consumed by them. Some other data about the prevalence of *Helicobacter pylori* regarding the age and their dwelling-place are presented too. In conclusion, some very important recommendations in order to decrease the value of this prevalence are given.

Key words: Helicobacter pylori, drinking water, dwelling-place, Elbasan

1. INTRODUCTION

The contaminated drinking water has the greatest impact on human health worldwide, especially in developing countries, (WHO/UNICEF, 2000; 2004; WHO, 2003). The World Health Organization (WHO) reported that 80% of diseases and one-third of deaths in developing countries are due to consumption of contaminated water (WHO, 1996). It is estimated that 538 species of bacteria are human pathogens (Woolhouse, 2006). *Helicobacter pylori*, is one of many bacterial agents on the U.S.EPA drinking water contaminant list. This *bacterium* was found in the majority of surface water and shallow groundwater and although *it can't* grow up in the environment, it can survive for 3 weeks in biofilms and up to 20–30 days in surface waters (Hegarty et al., 1999). More than 50 % of the world population is infected by *Helicobacter pylori* and 80 % of them are asymptomatic (Pounder, 1995). It causes peptic ulcers, stomach cancer, lymphoma and adenocarcinoma (Cardenas et al., 2006; Muhsen and Cohen, 2013). Some studies show the presence of *Helicobacter pylori* in feces, saliva, dental plaque and gastric juice.

According to some others studies *Helicobacter pylori* is transmitted mostly via person-to person route, and potentially via the waterborne and food borne routes and it may infect both humans and animals, especially domestic cats (Brown, 2000). Consumption of contaminated drinking-water has been suggested as a potential source of infection, but further investigation is required to establish any link with waterborne transmission (Hulten et al., 1996).

2. MATERIALS AND METHODS

In this study 886 blood samples of persons aged from 20 to over 60 years old are carried out. All these persons went by chance to see the physician after some general symptoms such as nausea, cough, septum, sore throat, mouth bad smell and larynx's edema, but the majority didn't have

stomach pain. The period of study concerns from January 2011 to May 2014. Beside the blood test all these persons filled up a questionnaire with some questions about the dwelling-place, type of drinking water, wastewater treatment, water disinfection and distance of septic tanks from the water well. The technique for the *Helicobacter pylori* detection in the blood based on the serological method named "*Sandwich Elisa Test* ". Based on this method the presence of *IgG* and *IgM* in the blood samples are carried out (Frank, 2005).

3. RESULTS AND DISCUSSIONS

The data in Table 1 show that 53 % is the highest percentage value of persons infected by *H.pylori* which belongs to the persons who have used the well water, not only as drinking water, but for other needs as well. All these persons live in rural areas. During the interview they declared that the majority of the septic tanks are so close to the water well. Also they use the farm and domestic manure without any preliminary treatment. Furthermore, for many years they didn't use the chlorination for the water well disinfection. According to some authors, water, wastewater, food, or soils can also harbor infectious agents and serve as reservoirs (Berger and Oshiro, 2002; Woolhouse, 2006). The lower percentage value of infected persons, 17 % is as a result of the continuous tap water chlorination. In this case, some other sources of *H. pylori* infection need to take into account.

Table 1. The number of infected persons by H. Pylori, based on the type of drinking water

Drinking water type	Persons infected by H. Pylori	% of infected persons
Tap water	117	17 %
Plastic bottled water	204	30 %
Well water	341	53 %
Total	**662**	**100 %**

Table 2. Some data about spreading infection of H. pylori based on the dwelling-place

Dwelling-place	Persons infected by *H. Pylori*	% of infected persons
Rural area	372	56 %
Urban area	290	44 %
Total	**662**	**100 %**

Based on the data shown in Table 2 the prevalence of *Helicobacter pylori* is higher in the rural area than in the urban area. This is as a result of absence of preliminary treatment of well water. According to some authors the untreated municipal water was considered as a main source of the increased *H. pylori* prevalence (Goodman et al., 1996); Lu Y et al., 2002). Also a recent study from Japan supports the idea of river water-associated incidence (Fujimura et al., 2008).

In addition, Azevedo (2005) strongly argues that drinking water can pose a substantial threat of *H. pylori* infection based on the ability of *H. pylori* to adhere to different materials and to co-aggregate with other bacteria and form complex structures on pipes or other surfaces in contact with water. In these circumstances this bacterium can't survive alone in running water, but it can develop a symbiotic relationship and form complex structures on contact surfaces. Based on that groundwater is a reservoir for *H. pylori* due to its stagnant nature (Azevedo et al., 2006).

Table 3. Some data about spreading infection based on the age group

Aged-group (years) Number of persons infected by *H. Pylori*		% of infected persons
20-40	84	12 %
40-60	234	35 %
>60	344	53 %
Total	**662**	**100 %**

Among 886 persons analyzed in our study 662 or 74 % of them are infected by *H. Pylori*. The IgG was present in 371 infected persons, while IgM in 291 ones. Based on the data in table 3 is shown that, 53 % of infected persons by this bacterium belongs to the age group older then 60, meantime the less one is 12 % and belongs to the aged group 20-40. Both two last values are approximatelywith those in the developed countries, where 50 % of infected persons belongs to those older than 60 and 10 % to those from 10 to 30 years old (Goodman et al., 2005). According to Brown, (2000), there is a correlation between the *H. pylori* infection prevalence and the socioeconomic status, human races in different countries. In the USA the probability≥ 50 % of being infected belongs to > 50 years old, for African American minorities 40-50%, for the Latino American emigrants from the developing countries is > 60 %, and for the emigrants from the East Europe this probability is > 50 %.

4. CONCLUSIONS

a) The value 74 % of infected persons by *Helicobacter pylori* in the district of Elbasan of Albania is higher then average values of infected persons in developed and developing countries presented by the other authors.
b) Based on the data of this study the higher prevalence of *Helicobacter pylori* in humans belongs to the persons who use the water of the well.
c) The data of this study support the hypothesis, supported by many other authors that the polluted drinking water is one of the main routes of *Helicobacter pylori* human infection, but more studies need to carry out in the future.

4.1 Recommendations

a) A good management of wastewater, manureand a continuous disinfection of well water, especially in rural area is a necessity.
b) The improvement of hygienic conditions of the population, especially in rural area.
c) More deep studies regarding the drinking water as a main source of *Helicobacter pylori* human infection, especially in the rural area in Albania need to be carried out in the future.

REFERENCES

Azevedo, NF., 2005 Survival of Helicobacter pylori in drinking water and associated biofilms. University of Minho and University of Southhampton; 137

Azevedo, NF., Pinto, AR., Reis, NM., Vieira, MJ., Keevil, CW., 2006. Shear stress, temperature, and inoculation concentration influence the adhesion of water-stressed Helicobacter pylori to stainless steel 304 and polypropylene. Appl Environ Microbiol; 72:2936–41.

Berger, S.B. and Oshiro R.K., 2002. Source water protection: microbiology of source water. In Encyclopedia of Environmental Microbiology, G. Bitton (Editor-in-Chief). Wiley-Interscience, New York, ; 2967–2978.

Brown, L.M., 2000. "Helicobacter pylori: epidemiology and routes of transmission". Epidemiol.Rev. 22:283–297.

Cardenas, V.M., Mulla, Z.D., Ortiz, M. and Graham, D.Y., 2006. Iron deficiency and Helicobacter pyloriinfection in the United States. Am. J. Epidemiol. 163:127–134.

Frank, J. T., Griffin, J. F. T., 2005. Evelyn Spittle, Christie R. Rodgers, Simon Liggett, Marc Cooper, Douwe Bakker, and John P. Bannantine. "Immunoglobulin G1 Enzyme-Linked Immunosorbent Assay for Diagnosis of Johne's Disease in Red Deer (Cervuselaphus)". Clin. Diagn. Lab. Immunol.

Fujimura, S., Kato, S., Watanabe, A., 2008. Water source as a Helicobacter pylori transmission route: a 3-year follow-up study of Japanese children living in a unique district. J Med Microbiol. ; 57:909–10.

Goodman, KJ., Correa, P., Tengana,´ Aux, HJ., Ramirez, H., DeLany, JP., Guerrero Pepinosa, O., 1996. Helicobacter pylori infection in the Colombian Andes: a population-based study of transmission pathways. Am J Epidemiol ; 144:290–9.

Goodman, KJ., O'Rourke, K., Day RS et al. 2005. "Dynamics of Helicobacter pylori infection in a US-Mexico cohort during the first two years of life". Int J Epidemiol.

Hegarty, JP., Dowd, MT., Baker, KH., 1999. Occurrence of Helicobacter pylori in surfacewater in the United States. Journal of Applied Microbiology, 87; 697–701.

Hulten, K., et al. 1996. Helicobacter pylori in drinking-water in Peru. Gastroenterology, 110:1031–1035.

Lu, Y., Redlinger, TE., Avitia, R., Galindo, A., Goodman, K., 2002. Isolation and genotyping of Helicobacter pylori from untreated municipal wastewater. Appl Environ Microbiol. ; 68:1436–9.

Muhsen, K,. and Cohen, D., 2013. Letter to the editor: Helicobacter pylori infection and anemia. Am. J. Trop. Med. Hyg., 89:398.

Pounder, RE, Ng, D., 1995. "The prevalence of Helicobacter pylori infection in different countries".World Health Organization (WHO). Guidelines for Drinking Water Quality, Vol. 2: Recommendations, WHO, Geneva, Switzerland.

WHO/UNICEF. 2000. Global Water Supply and Sanitation Assessment 2000. http://www.who.int/water_sanitation_health (accessed May 5, 2014).

WHO/UNICEF. 2004. Meeting the MDG Drinking Water and Sanitation Target: A Mid-Term. Assessment of Progress. WHO, Geneva.

Woolhouse, M.E.J., 2006. Where do emerging pathogens come from? Microbe 1(11): 511– 515.

World Health Organization, (WHO). 2003. The Right to Water, WHO, Geneva, Switzerland.

Proceedings of the 10th World Congress of EWRA 'Panta Rhei', 5-9 July 2017, Athens, Greece
© 2017 *European Water Resources Association*

Groundwater contamination from uninsulated sewage tanks in an eastern Hungarian settlement

T. Mester*, G. Szabó, G. Karancsi and D. Balla
University of Debrecen, Department of Landscape Protection and Environmental Geography, H-4010, Debrecen, Egyetem tér 1. Pbox. 9. Hungary
* *e-mail: mester.tamas@science.unideb.hu*

Abstract: In settlements without sewage systems the uninsulated sewage tanks are the most important sources of groundwater contamination. In our specific eastern Hungarian case study, we attempted to demonstrate the effects of wastewater effluent on the groundwater level and the spatial distribution of the organic matter (OM) and Na^+ in the autumn of 2013. In 2012 we established 3 metre deep monitoring wells within a 25 metre radius of a sewage tank, which were sampled, and the level of groundwater was recorded. The results show that the outflow wastewater formed a groundwater dome. The difference between the groundwater levels measured in the monitoring wells was 49 cm. In the immediate environment of the sewage tank we measured a chemical oxygen demand (COD) of more than 24 mg/l. Moving away from the sewage tank the values decreased rapidly; in the farthest monitoring wells we detected COD values of between 4 and 7 mg/l. The high Na^+ content of domestic wastewaters significantly increases the Na^+ content of the groundwater. In the vicinity of the sewage tank, we detected very high concentrations above 450 mg/l, which continuously decreased when moving away from the sewage tank. In the farthest monitoring wells west and southeast from the sewage tank we measured concentrations of Na^+ of 270 mg/l and 159 mg/l.

Key words: Groundwater salinity, contamination, wastewater, sewage tank, chemical oxygen demand, modelling

1. INTRODUCTION

Domestic wastewater is one of the most important sources of contamination of shallow and deep groundwater supplies, both in the less-developed and the developed areas of the world (Jumma et al. 2012, Jilali et al. 2015, Machiwal & Jha 2015; Smoroń 2016). Salinization and the decrease in the chemical parameters of the groundwater in settlements without sewage system is a common problem (Kang & Jackson 2016, Szabó et al. 2016). As evidenced by several studies, the groundwater salinity is not only governed by mineral weathering and dissolution, but also significantly influenced by anthropogenic inputs (Cary et al. 2013, Chaudhuri & Ale 2014, and Yan et al. 2016). Marie and Vengosh (2001) concluded, on the basis of their investigation carried out in the Jordan Valley, that the salinity in the shallow aquifer system could be derived from natural and anthropogenic sources such as the agricultural return-flow and local wastewater of the city of Jericho.

In the rural areas of Hungary, the collection of wastewater remains an unsolved problem in many places (Mester & Szabó 2013; Szabó et al., 2016). Because of the expensive transportation costs, in many cases local inhabitants have chosen to build sewage storage sites in a permeable way, so that the wastewater is able to seep into the soil, resulting in the contamination of groundwater (Mester et al., 2016). In 1990, 43% of households in the public water supply system were not connected to the sewage system, with this rate decreasing to 17.7% in 2014 (KSH 2014). In our case study, we attempt to demonstrate the effects of sewage tanks on the groundwater, carrying out investigations in the immediate environment of a sewage tank. In this study we investigated the amount of organic matter (OM) and the Na^+ content of the groundwater. Since Na^+ has a negligible retardation factor (Sayyed & Bhosle 2011) it is suitable to model the contaminant transport. The aims of this study were the following: 1) to demonstrate the spatial distribution of Na^+ and organic matter (OM) in the

immediate environment of the sewage tank, and 2) based on the results, to draw conclusions regarding the level of groundwater contamination caused by the sewage tank.

2. MATERIAL AND METHODS

The settlement is located in the eastern part of the Great Hungarian Plain, in the Nagy-Sárrét region (Fig. 1), and has a population of 2631 (KSH 2015). The Nagy-Sárrét region is an alluvial plain, with a moderately warm and dry climate (Dövényi 2010). Due to the low altitude (85-89 m) compared to neighboring regions the groundwater level can be found close to the surface, at a depth of 1-2 metres. In the sample area the most frequent soil types (WRB) were Solonetz, Vertisol, Kastenozem and Chernozem, while in the built-up area Technosol soils modified as a result of anthropogenic effects could also be identified (Novák & Tóth 2016).

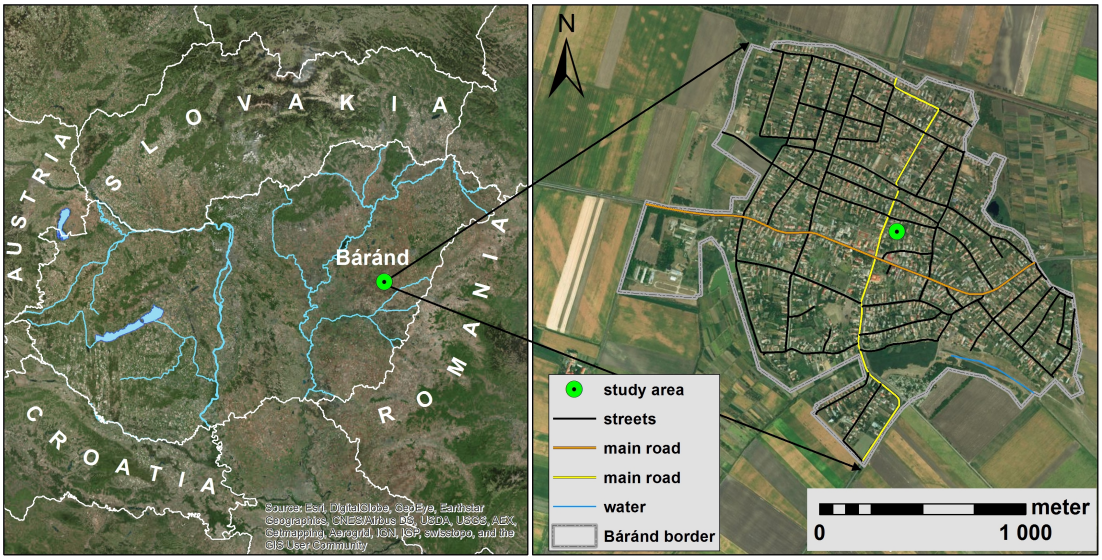

Figure 1. Location of the study area.

In order to analyze the effect on the groundwater of sewage tanks located in the settlement, we selected a sewage tank located in the centre of the settlement (Fig. 1, Fig. 2).

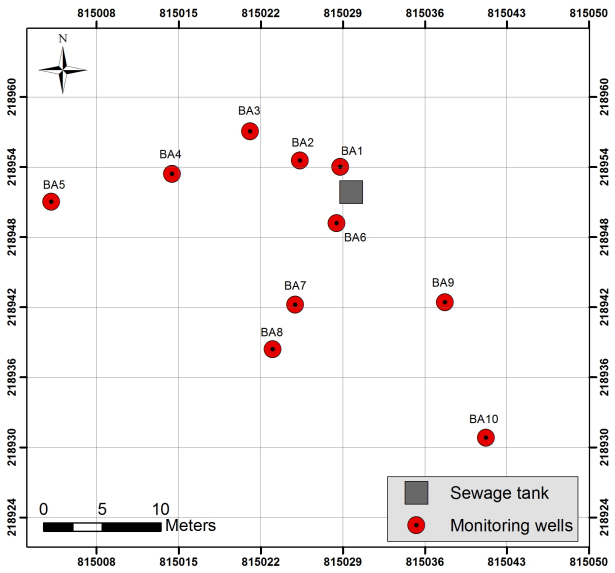

Figure 2. Location of the monitoring wells in the study area.

We established monitoring wells with a depth of 3 metres in the immediate environment of the sewage tank (Fig. 2). The total depth of the monitoring wells was at least one metre deeper than the groundwater level in every case.

The water samples were collected in the autumn of 2013, in accordance with the MSZ 21464 standard. The water chemistry investigations were carried out in the geographical laboratory of the University of Debrecen. The OM content of the groundwater was determined by applying indirect determination methods used for quantitative measurements of the chemical oxygen demand (COD). The Na^+ concentration was measured by using a PerkinElmer 3110 AAS. Soil samples were collected from the BA5 monitoring wells at every 20 cm interval and their granulometric composition was determined by the Köhn-pipette method [Müller et al. 2009].

To identify the exact altitude of the groundwater levels, we used the results of our on-site measurements performed by two Trimble S9 dual-frequency, high precision geodesic GPS systems (accuracy 2 cm). The interpolation of the surface was completed with a free triangular mesh.

The 3D models of the spatial distribution of the OM and Na^+ have been developed with RockWorks 14 modelling software, using kriging interpolation. Based on the solid models created with RockWorks, we have identified the volume of the water bodies contaminated with OM and Na^+ in terms of the given concentrations. Since the soil texture in the investigated area is loam, we calculated on the basis of a pore space of 45%.

3. RESULTS

The values of the COD and Na^+ concentrations and the groundwater levels are summarized in Table 1. The Na^+ concentrations measured in the sewage tank are characteristic of wastewaters (Table 1).

Table 1. Groundwater level, Na+ and COD concentrations in the monitoring wells

Wells	Sewage tank	BA1	BA2	BA3	BA4	BA5	BA6	BA7	BA8	BA9	BA10
mBf	88.92	88.23	87.94	88.01	88.05	87.99	88.32	87.98	87.92	87.93	87.70
COD (mg/l)	300*	24.25	6.32	5.68	6.55	4.12	27.14	6.22	6.13	5.69	6.44
Na^+ (mg/l)	469.1	452.6	323.8	344.1	277.8	272.3	458.7	417.7	288.9	159.6	163.3

**Value characteristic of wastewaters based on Barótfi I. (2003).*

Based on the 3D model created from the groundwater level (Fig. 3), it can be concluded that the outflow wastewater formed a groundwater dome. The difference between the groundwater levels measured in the monitoring wells was 49 cm (Table 1). Because of the wastewater effluent, the COD values measured in the groundwater exceeded the contamination limit of 3.5 mg/l characteristic of groundwaters (201/2001 Government Decree) (Fig. 3/I).

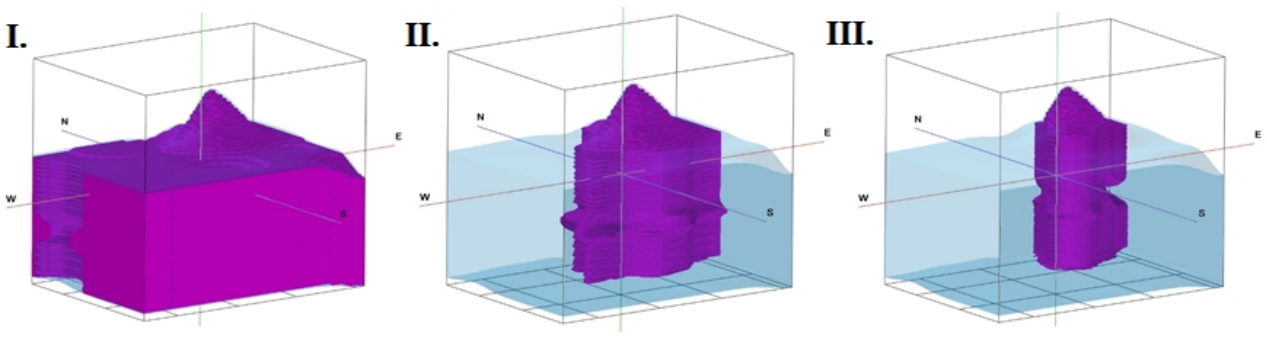

Figure 3. Spatial distribution of COD. I. higher than 3.5 mg/l, II. higher than 10 mg/l, III. higher than 20 mg/l

In the study we modelled the contamination of the groundwater down to a depth of 3 meters

from the surface. Based on our calculations, in the case of OM the total water volume of 801 m^3 can be considered contaminated (Table 2, Fig. 3/I). The volume of the more contaminated water body characterized by a value of at least 10 mg/l is 215 m^3 (Fig. 3/II). The volume of the groundwater body characterized by at least 20 mg/l was 101 m^3, which could evidently be measured directly near the sewage tank (Fig. 3/III). By investigating the spatial distribution of COD values it can be concluded that moving away from the sewage tank, the organic material content of the groundwater decreased constantly. This was caused by the dilution of the pollution and the decomposition of OM. Whereas in the BA1 monitoring well located 1 meter from the sewage tank, we detected a concentration of 24.25 mg/l, in the BA5 monitoring well located 25 metres from the sewage tank we detected a concentration of only 4.12 mg/l.

Table 2. The volume of water bodies with different levels of contamination

COD	Volume of water body (m^3)	concentration Na^+	Volume of water body (m^3)
20 mg/l <	101.3	**400 mg/l <**	126.4
10 mg/l <	215.4	**300 mg/l <**	352.9
3.5 mg/l <	801,7	**200 mg/l <**	718.9
total	801.7	**total**	801.7

Based on the spatial distribution of the Na^+ concentration we can also conclude that the effluent wastewater resulted in a groundwater characterized by a concentration which exceeded the contamination limit of 200 mg/l in the majority of the sample area, which affected 90% of the investigated water body (Table 2, Fig. 4/I). A concentration above 300 mg/l was measured in 44% of the investigated water body (Table 2, Fig. 4/II), while a Na^+ concentration above 400 mg/l could be detected only in the vicinity of the sewage tank in a water body with a volume of 126 m^3, which made up only 16% of the investigated water body (Table 2, Fig. 4/III).

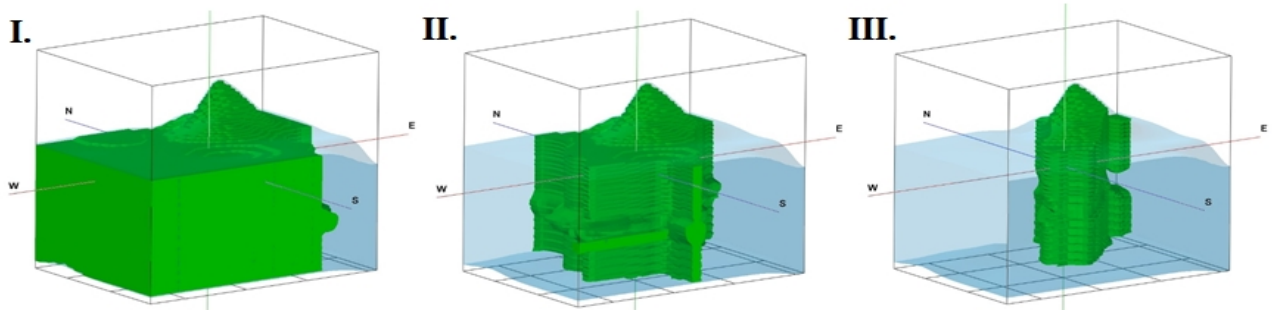

Figure 4. Spatial distribution of Na^+. I. higher than 200 mg/l, II. higher than 300 mg/l, III. higher than 400 mg/l

In the vicinity of the sewage tank, we detected very high concentrations above 450 mg/l, which decreased continuously by dilution as we moved away from the sewage tank. In the farthest monitoring wells west and southeast from the sewage tank we measured 272 mg/l and 159 mg/l.

4. CONCLUSIONS

The results of our investigation clearly show that in settlements without a sewage system, the water effluent from the uninsulated sewage tanks significantly modifies the level and the chemical characteristics of the groundwater. The wastewater effluent from the sewage tank forms a groundwater dome, the height of which was 49 cm at the time of measurement. In the immediate environment of the sewage tank we measured high Na^+ and COD values, which decreased as we moved away from the tank. Using the 3D model we were able to precisely determine the volume of water bodies with different levels of contamination. The Na^+ content of the groundwater exceeded the contamination limit of 200 mg/l in 90% of the sample area. The high salinity of the groundwater is clearly the consequence of the effluent wastewater, evidenced by the fact that the Na^+

concentration rapidly decreased when moving away from the sewage tank, but at the same time, lithological factors can also play a role in the Na^+ concentration since saline soils can also be found in the vicinity of the sample area. The COD values exceeded the contamination limit of 3.5 mg/l at every measurement point; therefore the groundwater can be considered 100% contaminated in the sample area. Therefore, regarding the two water quality parameters investigated (COD, Na^+) it can be concluded that the contaminating effect of an uninsulated sewage tank could be clearly detected within a circle with a radius of 25 metres. However, the extent of the contamination decreased to the level of the contamination limit at a distance of 25 metres from the sewage tank.

Despite the fact that the subject of our investigations was the effect of a specific sewage tank on groundwater, we can assume that similar processes could occur in other households in the settlement, which should be considered during the groundwater quality investigations in the settlement. The experience of this case study could be useful for the investigations of groundwater in settlements with similar characteristics.

REFERENCES

201/2001. (X. 25.) Korm. rendelet az ivóvíz minőségi követelményeiről és az ellenőrzés rendjéről.

Barótfi I. 2003. Környezettechnika, Mezőgazda Kiadó, Budapest 982 p.

Cary, L., Casanova, J., Gaaloul, N., & Guerrot, C. (2013). Combining boron isotopes and carbamazepine to trace sewage in salinized groundwater: a case study in Cap Bon, Tunisia. Applied geochemistry, 34, 126-139.

Chaudhuri, S., & Ale, S. (2014). Long term (1960–2010) trends in groundwater contamination and salinization in the Ogallala aquifer in Texas. Journal of Hydrology, 513, 376-390.

Hungarian Standards Institution (MSZT). MSZ-21464:1998. Sampling of groundwaters.

Jilali, A., Abbas, M., Amar, M., & Zarhloule, Y. (2015). Groundwater contamination by wastewater in Figuig Oasis (eastern High Atlas, Morocco). Nature Environment and Pollution Technology, 14(2), 275.

Jumma, A. J., Mohd, E. T. & Noorazuan, M. H. 2012. Groundwater pollution and wastewater management in Derna City, Libya. International Environmental Research Journal, 6(1): 50-54.

Kang, M., & Jackson, R. B. (2016). Salinity of deep groundwater in California: Water quantity, quality, and protection. Proceedings of the National Academy of Sciences, 201600400.

KSH. 2014. Hungarian Central Statistical Office https://www.ksh.hu/docs/hun/xstadat/xstadat_eves/i_zrk006.html

KSH. 2015. Hungarian Central Statistical Office https://www.ksh.hu/docs/hun/hnk/hnk_2015.pdf

Machiwal, D. & Jha, M. K. 2015. Identifying sources of groundwater contamination in a hard-rock aquifer system using multivariate statistical analyses and GIS-based geostatistical modeling techniques. Journal of Hydrology: Regional Studies Volume 4, Part A, September 2015, p. 80–110

Marie A, Vengosh A (2001) Sources of Salinity in Ground Water from Jericho Area,. Jordan Valley; Ground Water V. 39, No2 pp. 240-248.

Mester, T., Szabó, Gy., Balla, D., Karancsi, G., Szabó, G. & Tóth, C. 2016. The investigation of the effects of an open sewage tank on the groundwater level. Egy nem zárt rendszerű szennyvízakna talajvízszintre gyakorolt hatásának vizsgálata (in Hungarian). Theory meets practice in GIS VII. pp. 311-317.

Mester, T. & Szabó, Gy. 2013. Nitrate contamination in the groundwater wells of an Eastern Hungarian settlement. In: International Conference on Environmental Science and Technology - Conference CD. Digital Proceeding Of THE ICOEST'2013 / ed. Cappadocia C. Ozdemir, S. Şahinkaya, E. Kalıpcı, M. K. Oden, pp. 1-16.

Müller, H. W., Dohrmann, R., Klosa, D., Rehder, S., & Wolf Eckelmann, W. 2009. Comparison of two procedures for particle-size analysis: Köhn pipette and X-ray granulometry. J. Plant Nutr. Soil Sci, 172, 172–179.

Novák, T. J. & Tóth, Cs. A. 2016. Development of erosional microforms and soils on semi-natural and anthropogenic influenced solonetzic grasslands. Geomorphology 254: 121-129.

Sayyed, A. J., & Bhosle, B. A. (2011). Analysis of chloride, sodium and potassium in groundwater samples of Nanded City in Mahabharata, India. European Journal of Experimental Biology, 1(1), 74–82.

Shirazi S.M., Adham M.I., Zardari N.H., Ismail Z., Imran H.M., Mangrio M.A. 2015. Groundwater quality and hydrogeological characteristics of Malacca state in Malaysia. Journal of Water and Land Development. No. 24 p. 11-19

Smoroń S. 2016. Quality of shallow groundwater and manure effluents in a livestock farm. Journal of Water and Land Development. No. 29 p. 59-66.

Szabó, Gy., Bessenyei, É., Hajnal, A., Csige, I., Szabó, G., Tóth, Cs., Posta, J. & Mester, T. 2016. The Use of Sodium to Calibrate the Transport Modeling of Water Pollution in Sandy Formations Around an Uninsulated Sewage Disposal Site. Water Air Soil Pollut 227 (2), 1-13.

Yan, M., Wang, Q., Tian, Y., Wang, J., Nie, Z., & Zhang, G. (2016). The dynamics and origin of groundwater salinity in the northeast Hufu Plain. Environmental Earth Sciences, 75(16), 1154.

Proceedings of the 10th World Congress of EWRA 'Panta Rhei', 5-9 July 2017, Athens, Greece
© 2017 *European Water Resources Association*

Linkages between physicochemical status and hydromorphology in Greek lakes under WFD policy

E. Mavromati[1], I. Kagalou[2], D. Kemitzoglou[1], A. Apostolakis[1] and V. Tsiaoussi[1]
[1] *The Goulandris Natural History Museum – Greek Biotope Wetland Centre (EKBY), 14th km Thessaloniki - Mihaniona, 57001 Thermi, Greece*
[2] *Department of Civil Engineering, School of Engineering, Democritus University of Thrace, University Campus, Kimmeria, 67100, Xanthi, Greece*
[*] *e-mail: emavromati@ekby.gr*

Abstract: The national monitoring network of waters in Greece, in the context of Water Framework Directive, has been operational since 2012. It comprises 50 lake water bodies, both natural and artificial (24 and 26 respectively). The aims of the study are i) to present the main features of Greek lakes; ii) to position them according to hydromorphological and physicochemical data from the first period of monitoring and iii) to investigate how the hydromorphological features influence water quality. Greek lakes are discerned in relation to hydromorphological aspects such as mean depth, volume, surface area, catchment area. Impacted and unimpacted lakes are separated when positioned along physical and chemical attributes, such as Secchi depth, TP and ion concentrations. The dataset covers a gradient of eutrophication, which seems to be the main anthropogenic pressure on lakes in Greece and probably one of the most widespread anthropogenic pressures on lakes across Europe. Catchment areas of the Greek lakes have undergone substantial agricultural, industrial, and urban development over recent years, leading to eutrophication and hydromorphological alterations. Management measures at a catchment scale aiming to control land uses would be needed in order to maintain and/or improve water quality in Greek lakes, supplemented by site-specific measures when appropriate. The monitoring network provides baseline data that will allow the assessment of status and trends of Greek lakes.

Key words: WFD, Greek lakes, hydromorphology, water quality

1. INTRODUCTION

The Water Framework Directive (WFD) foresees the operation of monitoring programmes for surface waters and groundwater in order to assess their ecological and chemical status (article 8). Comparable pan-European datasets, with hydromorphological, physicochemical and biological information are used to assess ecological status of surface waters and improve our knowledge on the structure and function of these ecosystems (Hering et al. 2010, Moe et al. 2013).

The complex geomorphology of Greece, the uneven distribution of precipitation and different regional demands for irrigation and drinking water are some of the characteristics that affect the hydromorphological features of Greek lakes (Zacharias 2002); this in turn strongly governs various ecosystem functions (Schindler and Scheurell 2002). According to Nõges (2009), nutrient inputs are profoundly affected by catchment and lake area through surface and groundwater drainage while nutrient retention, a fundamental property of every aquatic ecosystem, is linked to its geomorphological, hydrological, edaphic and biotic characteristics (Hansson et al. 2005). Furthermore, intensive agriculture activities, domestic and industrial inflows have changed the surface water distribution and use (Skoulikidis et al. 1998).

In line with WFD, Greece had to establish a national monitoring network (JMD 140384/2011); EKBY now operates the monitoring network for lakes in Greece, establishing baseline data to assess their ecological status and trends. The aims of the study are i) to present the main features of Greek lakes, ii) to position them according to morphological and physicochemical data from the first period of monitoring and iii) to investigate how the hydromorphological features influence water quality.

2. MATERIALS AND METHODS

2.1 Study area and data sets

The Greek National Water Monitoring Network for lakes comprises 50 water bodies, both natural and reservoirs. The heterogeneity of Greek geology, climate and topography has resulted in a lake dataset with a broad range of morphological, physical and chemical characteristics. Fifty-three stations have been established, 27 of which are subject to surveillance monitoring and 26 to operational. Most water bodies have one sampling station each, except transboundary lakes Megali Prespa, Mikri Prespa and Doirani, which have two sampling stations each (Figure 1).

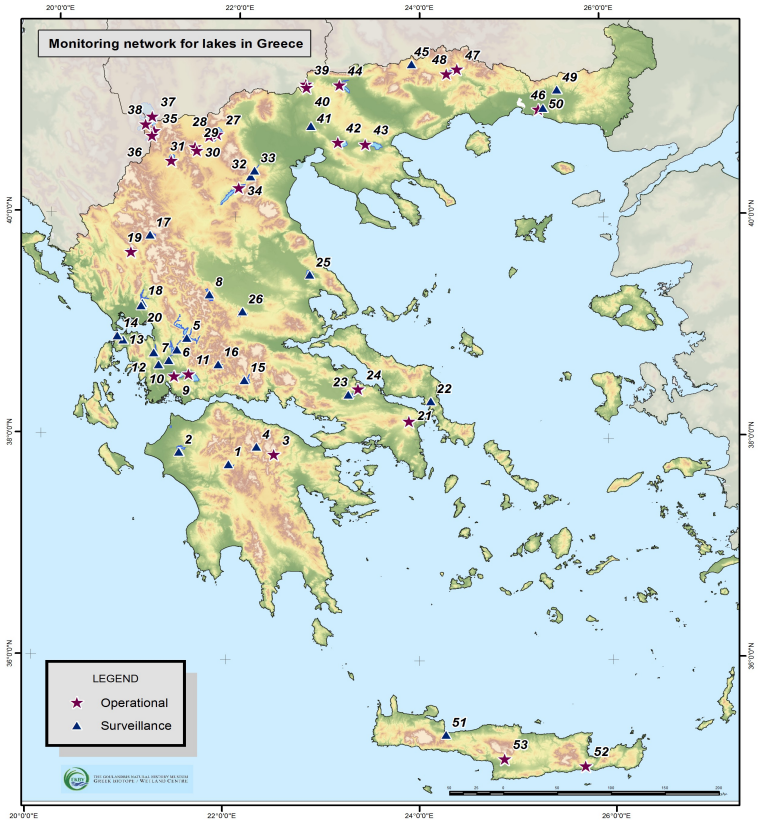

Figure 1. Monitoring network for lakes in Greece.

Physicochemical features were measured seasonally and each month during growing season (May to October). Samples were taken from euphotic zone [2,5xSecchi Depth (SD)]. In particular: Transparency was measured with a Secchi disc. Temperature, pH, oxygen, conductivity and Total Dissolved Solids were measured with portable meters from ThermoScientific instruments. Filtrations for Chlorophyll *a* measurements were carried out through Whatman GF/F glass-fiber filters and Chlorophyll *a* was estimated using standard methods (APHA 2012). Analyses for Na^+, K^+, Cl^- and $SO4^-$ were carried out with the use of Ion Chromatography (ISO 14911 1999, ISO 10304-01 2009). Analyses of Total Phosphorus (TP) were carried out in unfiltered water using ascorbic method following persulfate digestion (APHA 2012). Data used for this study were taken from samplings carried out in 2015. To estimate the catchment area impact on water bodies, the Schindler's ratio was calculated as the ratio between the catchment and the surface area to lake volume (Stefanidis and Papastergiadou 2012). Intensive agriculture was measured as the sum of the Corine Land Cover categories corresponding to a high potential impact from agricultural activities, such as arable land (including irrigated land), permanent crops (with associated annual crops), vineyards, orchards, olive groves and complex cultivation patterns. Morphological parameters of transboundary lakes were estimated including data from sharing countries.

2.2 Statistical Analysis

All statistical analysis, including Boxplots, Pearson's Correlations and Principal Component Analysis (PCA), was conducted using R Statistical Software (R Core Team 2014).

Data analysis was performed only in stations sampled for at least two months over growing season. Very shallow natural lakes Koroneia, Saltini, Pikrolimni, Stymfalia and Dystos were excluded from analysis, due to either outlier values or lack of data caused by drought. Values below the quantification limit were replaced with the value of quantification. Variables were tested for skewness and log transformed when needed. Correlation Analysis was conducted in order to elucidate possible relationships between parameters. PCA was used to interpret the major patterns of variation within the data and ordinate the lakes with respect to selected hydromorphological and physicochemical variables.

3. RESULTS

Correlation analysis between TP and Schindler's Ratio revealed a significant relationship ($p<0.05$), as the two variables were positively correlated in both reservoirs and natural lakes ($r=0.45$ and $r=0.41$, respectively) (Table 1). The relationship between TP and Mean depth was statistically significant in both cases ($p<0.01$) and the r values confirmed the strong negative correlation between the two variables.

Table 1. Pearson correlation between TP, Schindler's Ratio and Mean Depth

	Natural Lakes (n=20) LogTP	**Reservoirs (n=23)** LogTP
LogSchindler's Ratio	0.41*	0.45*
LogMeanDepth	-0.60**	-0.79**

** significant at p<0.05, ** significant at p<0.01*

Boxplots in Figure 2 show TP and Chlorophyll a data (growing season mean) plotted against Intensive Agriculture and Population Density groups. Intensive agriculture activities affirmed their high impact on TP loading in water bodies, both reservoirs and natural lakes. Population density showed the same positive relationship with TP, as expected.

PCA revealed the ordination of Greek natural lakes in two PCs, with eigenvalues above one ($\lambda_1=3.11$ and $\lambda_2=1.42$, respectively), which captured 91.51% of total variance (Figure 3). All variables had high scores on the major PCA axis I, with lake volume standing out and negatively correlated with the axis. The second axis was positively associated with Schindler's ratio and catchment area. In reservoirs, the two first axes captured 81.94% of total variance, with lake volume and catchment area, being strongly correlated with PC1 whereas PC2 was only affected by Schindler's ratio.

With regard to the physicochemical aspects, the two principal components of the PCA explained 84.04% of the data variance, in natural lakes (Figure 4). The first axis ($\lambda_1=2.13$) was driven mainly by electrical conductivity and sodium and less by calcium ions. The second axis was associated with Secchi depth and TP, revealing a clear gradient from deep, clear water bodies to shallow more impacted ones. The same gradient was evident in reservoirs, as TP and Secchi depth were the principal drivers of the second axis, with the former being now the strongest one. Electrical conductivity, sulphate and sodium ions were the most influential parameters of axis 1, separating the two reservoirs from Crete, T.L. Faneromenis and T.L. Bramianon. One reservoir, T.L Pournariou is separated from the others, as it is highly associated with calcium ions.

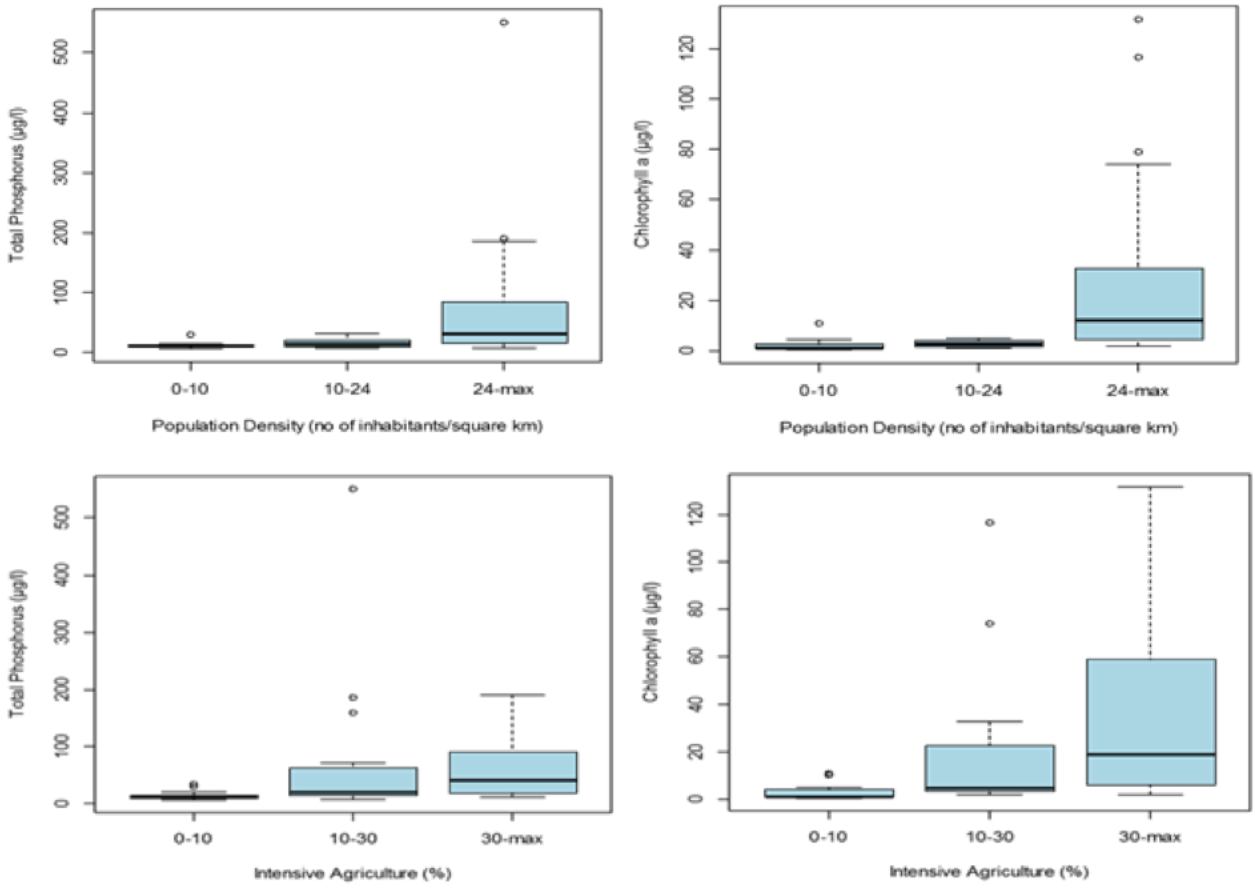

Figure 2. Boxplots of Intensive Agriculture and Population Density groups in relation to TP and Chorophyll a.

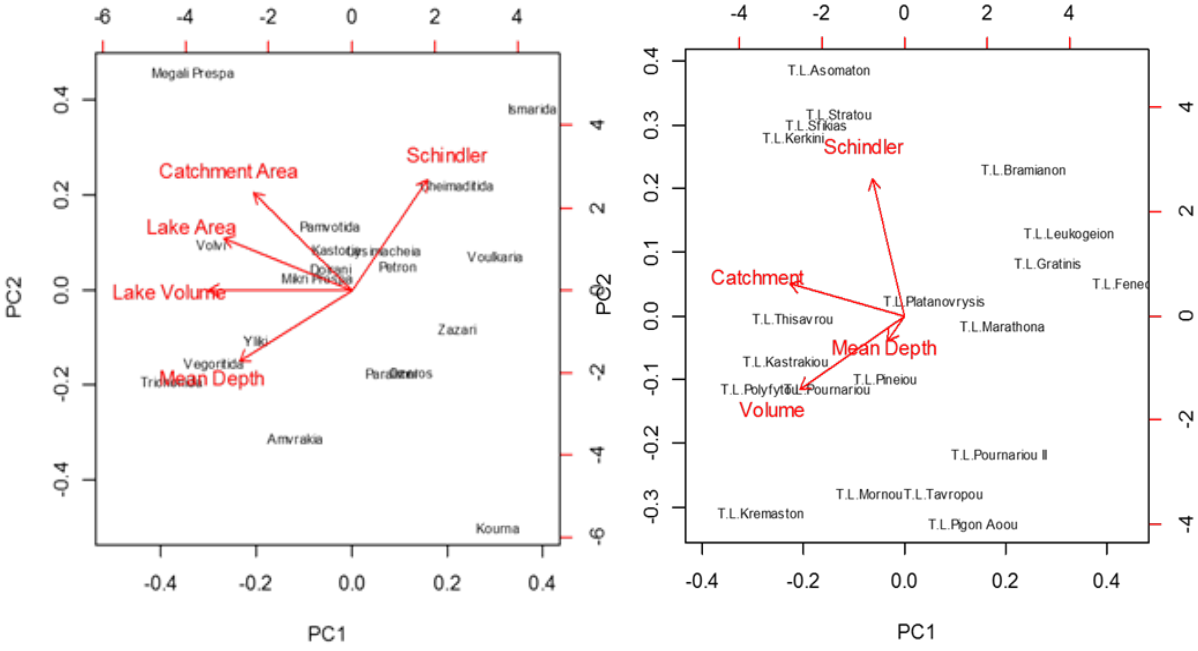

Figure 3. PCA biplots of selected morphological variables in Greek lakes dataset.

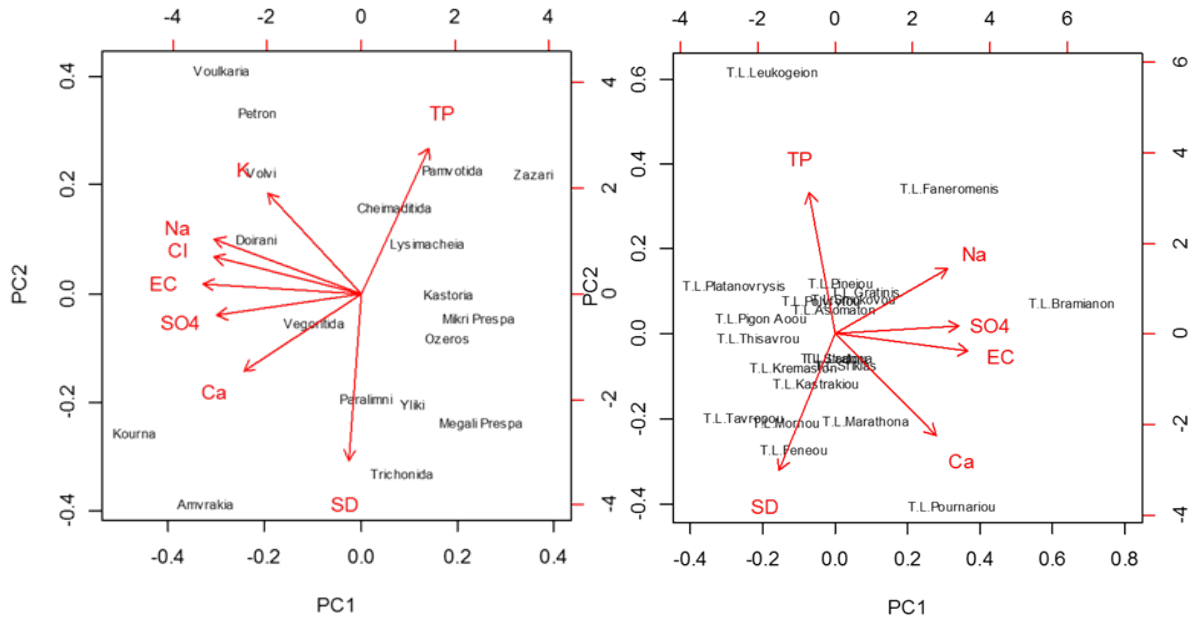

Figure 4. PCA biplots of selected physicochemical variables in Greek lakes dataset.

4. DISCUSSION

Totally non-impacted lakes are scarce in Europe (Poikane et al. 2010); the main pressures include nutrient inputs from point and non-point sources, water abstraction and morphological changes (EEA 2012). The majority of Greek lakes have been modified to some degree by the same pressures, as described in the River Basin Management Plans (http://wfd.ypeka.gr/).

The strong relationship between Schindler's ratio and mean depth with TP reflects the influence of catchment area's size and lake morphological parameters to lake water quality and further to eutrophication. Lake morphometry parameters (e.g. mean depth) indicate the buffer capacity to nutrient inputs (Nõges 2009). Furthermore, as Kolada et al. (2005) suggested, lakes with large catchment area are more susceptible to degradation. In such cases, we suggest that efficient restoration and mitigation strategies could focus rather at catchment level than in lake itself. Land uses and population density in the catchment, further influence water quality, as boxplots revealed a pattern of high population densities and intensive agriculture related to high TP and chlorophyll a values. The impacts of land use changes are complex. They may lead to a gradual conversion (e.g. habitat alterations, invasion of alien species) or total modifications (e.g. turbid conditions, food web changes) (Moss 1998, Zogaris et al. 2009). Similarly, the catchment areas of the Greek lakes have undergone substantial agricultural, industrial, and urban development over recent years, leading to eutrophication and hydromorphological alterations.

With regard to hydromorphology of Greek natural lakes, lake volume and mean depth stand out and highlight three large deep lakes, Yliki, Vegoritida, Trichonida. Schindler's ratio and catchment area reveal a gradient of increasing catchment area impact along the second axis of PCA. Lakes Trichonida, Vegoritida and Amvrakia have by far the lowest Schindler's ratio, whereas Ismarida has the highest value. Urban lakes Kastoria and Pamvotida along with Cheimaditida, Lysimacheia and Petron are clustered on the top right of the plot and distinguished by high values of Schindler's ratio. Using the reservoirs' dataset, the mountainous ones with low Schindler ratio impact, such as Aoou and Tavropou, are discriminated from lowland reservoirs with high catchment area impact. Furthermore, lake volume grouped large lakes Thisavrou, Kastrakiou, Kremaston, Polyfytou and Pournariou.

The physicochemical variables in PCA plots revealed a similar pattern in both reservoirs and

natural lakes. A gradient of increasing TP along the second component, separate clear reservoirs and deep natural lakes with high Secchi depth from shallow, impacted lakes with low Secchi depth. This describes the sensitivity of shallow lakes to resuspension process and further to nutrient loading. Urban lake Pamvotida, along with lakes Zazari, Cheimaditida and Lysimacheia are clustered on the top left quadrat of the plot, highly associated with TP. Nutrient loading is the result of household wastewater inputs and intense agriculture activities (Skoulikidis et al. 1998). Specifically, regarding the urban lakes, as lakes Pamvotida and Kastoria, it is well documented that they tend to receive high nutrient loads and show higher trophic status than non-urban ones (Naseli-Flores 2008); thus site-specific mitigation measures should be implemented. Water bodies, Kourna and Amvrakia, are positioned together on the bottom left of the plot, as they are highly associated with calcium, with the latter also related with sulphates. In Amvrakia, a hard water lake, several studies have been reported high concentrations of these ions, mainly due the presence of gypsum of the surroundings (Danielidis et al. 1995, Skoulikidis et al. 1998).

Findings suggest that intervention at a catchment scale aiming to control land uses would be needed in order to maintain and/or improve water quality in Greek lakes, supplemented by site-specific mitigation measures when appropriate. The sustainable and cost-effective management of Greek lakes requires a proper understanding of the relationships between morphometry and physicochemical variables. Continuous surveys would be useful in providing long-series data to be able to link hydromorphology and physicochemical conditions to ecological processes and biological responses.

ACKNOWLEDGEMENTS

This study has been prepared in the framework of the National Water Monitoring Network for lakes, according to the Joint Ministerial Decision 140384/2011. The acquisition of data was financed by ERDF - Operational Program Environment and Sustainable Development and national funds.

REFERENCES

APHA, 2012. Standard methods for the examination of water and wastewater. American Public Health Association, American Water Works Association, Water Environment Federation. 22nd Ed.

Danielidis D.B., M. Spartinou and A. Economou-Amilli, 1995. Limnological survey of Lake Amvrakia, western Greece. Hydrobiologia, 318: 207-218.

European Commission, 2000. Directive 2000/60/EC of the European Parliament and of the Council of 23 October 2000 establishing a framework for Communities in the field of water policy, Official Journal of the European Communities, L 327/1, 22.12.2000.

European Environment Agency, 2012. European Waters – Assessment of Status and Pressures. European Environment Agency, Copenhagen.

Hansson, L., C. Brönmark, N. P. Andersm and K. Åbjörnsson, 2005. Conflicting demands on wetland ecosystem services: nutrient retention, biodiversity or both? Freshwater Biology, 50(4): 705–714.

Hering, D., A. Borja, J. Carstensen, L. Carvalho, M. Elliott, C. K. Feld, A.S. Heiskanen, R.K. Johnson, J. Moe, D. Pont, A.L. Solheim, W. van de Bund, 2010. The European Water Framework Directive at the age of 10: A critical review of the achievements with recommendations for the future. Science of the Total Environment, 408: 4007-4019.

ISO 14911, 1999. Water quality - Determination of dissolved Li^+, Na^+, K^+, $NH4^+$, Mg^{2+}, Ca^{2+}, Mn^{2+}, Sr^{2+} and Ba^{2+} using ion chromatography – Method for water and waste water. pp. 18

ISO 10304-01, 2009. Water Quality - Determination of dissolved anions by liquid chromatography of ions-Part 1: Determination of bromide, chroride, fluoride, nitrate, nitrite, phosphate and sulfate. pp. 15

Joint Ministerial Decision No 140384/2011 (Official Gazette 2017 II 09.09.2011) establishing the "National Monitoring Network for the quality and the quantity of waters".

Kagalou, I. and I. Leonardos, 2009. Typology, classification and management issues of Greek lakes: Implication of the water framework directive (2000/60/EC). Environmental Monitoring and Assessment, 150: 469-484.

Kolada A., H. Soszka, D. Sydzik and M. Golub, 2005. Abiotic typology of Polish lakes. Limnologica, 35: 145-150.

Ministry of Environment, Special Secretariat for Waters. Approved River Basin Management Plans (http://wfd.ypeka.gr/index.php?option=com_content&task=view&id=113&Itemid=19)

Moe, S. J., A. Schmidt-Kloiber, B. J. Dudley and D. Hering, 2013. The WISER way of organising ecological data from European rivers, lakes, transitional and coastal waters. Hydrobiologia, 704: 11-28.

Moss B., 1998. Ecology of freshwaters: Man and Medium, Past to Future. 3rd Ed , Blackwell Publishing, pp. 14–35.

Nõges, 2009. Relationships between morphometry, geographic location and water quality parameters of European lakes. Hydrobiologia, 633: 33-43.

Naselli-Flores L., 2008. Urban Lakes: Ecosystem at risk, worthy of the best care. Proceedings Taal2007: The 12th World Lake Conference, pp. 1333:1337.

Poikane S., M.H. Alves, C. Argillier, M. van den Berg, F. Buzzi, E. Hoehn, C. de Hoyos, I. Karottki, C. Laplace-Treyture, A.L. Solheim, J. Ortiz-Casas, I. Ott, G. Phillips, A. Pilke, J. Pádua, S. Remec-Rekar, U. Riedmüller, J. Schaumburg, M. L. Serrano, H. Soszka, D. Tierney, G. Urbanič, and G. Wolfram. 2010. Defining Chlorophyll – a reference conditions in European lakes. Environmental Management, 45 (6): 1286–1298.

R Core Team, 2014. R: A language and environment for statistical computing. R Foundation for Statistical Computing, Vienna, Austria.

Schindler D.E. and M.D. Scheuerell, 2002. Habitat coupling in lake ecosystems. Oikos 98: 177–189.

Skoulikidis, N., Bertachas I. and T. Koussouris, 1998. The environmental state of fresh water resources in Greece (rivers and lakes). Environmental Geology, 36: 1–17.

Stephanidis, K. and E. Papastergiadou, 2012. Relationships between lake morphology, water quality and aquatic macrophytes in lakes of Western Greece. Fresenius Environmental Bulletin 21: 3018-3026.

Zacharias, I., I. Bertachas, N. Skoulikidis and T. Koussouris, 2002. Greek Lakes: Limnological overview. Lakes & Reservoirs: Research and Management, 7: 55-62.

Zogaris S., A. Economou and P. Dimopoulos, 2009. Ecoregions in the Southern Balkans: should their boundaries be revised? Environmental Management, 43: 682–697.

Proceedings of the 10th World Congress of EWRA 'Panta Rhei', 5-9 July 2017, Athens, Greece
© 2017 *European Water Resources Association*

Relationship between water yield and water quality in broadleaf forested watersheds

F. Gokbulak*, Y. Serengil, I. Yurtseven, B.U. Erdogan, M.S. Ozcelik, S. Ozhan and K. Sengonul
Istanbul University, Faculty of Forestry, Department of Watershed Management, Bahcekoy 34473, Istanbul, Turkey
* *e-mail: fgokbulak@istanbul.edu.tr*

Abstract: Forest ecosystems provide fresh water with best quality in sustainable manner but they consume huge amount of water. Researchers apply different forestry practices to increase water yield by minimizing water loss through evapotranspiration and maximizing amount of rainwater reaching soil surface in the watersheds. Studies showed that water yield and nutrient losses increase after clear cutting. High nutrient concentrations in the streamwater cause deterioration in the water quality. Therefore, objectives of this study were to investigate relationship between amount of annual streamflow and nutrient outflux and quantify nutrient losses in three oak-beech mixed forest covered watersheds. The experimental watersheds were located in Istanbul with sizes of 77.4 ha, 71.9 ha, and 17.5 ha. Water samples were collected from the streams of the watersheds on weekly basis and analyzed for pH, electrical conductivity (EC), total suspended sediment (TSS), chloride (Cl^-), calcium (Ca^{2+}), magnesium (Mg^{2+}), total nitrogen (TN), sodium (Na^+), potassium (K^+), iron (Fe^{3+}), aluminum (Al^{3+}), ammonium nitrogen (NH_4^+ - N), and sulfate $(SO_4)^{2-}$. Regression equations were developed between annual water yields and nutrient outfluxes. Results showed that there were significant relationships between annual water yield and nutrient outflux except for pH and EC and these parameters showed increase with the increase in the streamflow discharge. This means that if the water yield increases after timber harvest then water quality can be deteriorated in the watersheds.

Key words: Water yield, water quality, forestry activities, nutrient flux

1. INTRODUCTION

Water has a vital importance in human life and there is also an increasing demand for the water resources worldwide due to population growth and industrial developments. On the other hand, forest covered watersheds provide fresh water with the best quality compared to other land use types (Neary et al., 2009). Forest cover in the watersheds also cause decreases in the streamflow (Zhang et al. 2014) because of great interception and transpiration capacities (Özhan et al., 2010). Water quality and quantity in a forested watershed are influenced by watershed characteristics, climate, and forest cover. Among these factors, forest cover is the only factor that can be modified to increase water yield in the watersheds due to their enormous transpiration and interception losses. Therefore, a number of studies have been carried out around the world to investigate the effects of forest harvest on water yield (Swank et al., 2001; Özyuvacı et al., 2004; Dung et al., 2012). In general, these studies showed that forest harvest can increase water yield depending on harvest intensity. For instance, Bosch and Hewlett (1982) and Stednick (1996) stated that at least 20 % of the forest cover in a watershed must be harvested in order to perceive an increase in the water yield whereas Sahin and Hall (1996) claimed that a minimum of 10 % forest cover removal would be sufficient to significantly increase the water yield in their review papers. On the other hand, there is also a potential increase in nutrient losses from the watersheds together with streamflow after timber harvest. In fact, Reuss et al. (1997) found significant increases in both streamflow and nutrient export from the watershed after the treatment in Colorado. Stednick (2000) reviewed the studies about effects of forest harvest on water yield and quality and reported that nutrient discharges from the forest cover harvested watersheds were significantly greater than those from the forest cover untouched ones. Similar results were also reported in other studies (Bäumler and Zech, 1999; Wang et al., 2006). In general, it can be concluded from all these studies that forest harvest

can increase water yield and nutrient losses from the watersheds depending on the harvest intensity and amount of precipitation. In the long run, high nutrient loads in the streamflow due to tree removal can result in poor water quality and productivity losses in the soils of watersheds.

In Turkey, forest-water relations have been received attention since late 1970s (Özyuvacı, 1976; Özhan, 1977) but studies investigating impacts of forest harvest on streamflow quantity and quality are limited (Balcı et al., 1986; Özyuvacı et al., 2004; Serengil et al., 2007a; Serengil et al., 2007b; Gökbulak et al., 2008a; Gökbulak et al., 2008b). Therefore, objectives of this study were to examine the relationship between streamflow discharge and nutrient outflux and quantify amount of nutrient export in three forested watersheds.

2. MATERIAL AND METHODS

2.1 Study area

Three experimental watersheds with similar elevation, slope, drainage density, and ecological conditions in Belgrad Forest of Istanbul were selected for this study (41°13′00″– 41°14′13″ N, 28°54′25″-28°56′37″ E) (Table 1). The sizes of the watersheds are 71.9 ha for W-I, 77.5 ha for W-IV, and 17.5 ha for W-V. All watersheds have second-order streams that flow into a dam supplying drinking water for Istanbul city. Thickness of the forest floor and crown closure were similar among the watersheds and varied from 4 to 6 cm and from 74% to 100 %, respectively. Dominant parent materials in the area are carboniferous clay schists and Neogene loamy, gravelly deposits. The soil type is Vertic Xerochrept (USDA, 1994) and soil texture is sandy clay loam and sandy loam. Average annual precipitation is around 1129 mm and mostly falls between October and April. Mean annual temperature is about 12.3 °C and changes from 4.2 °C in February to 21.7 °C in August (Özhan et al., 2008). The study area has a subhumid Mediterranean climate with mild-rainy winter and hot-dry summer months. Dominant trees are mostly oak [*Quercus petraea* (Mattuschka) Liebl. and *Q. frainetto* Ten.] and beech (*Fagus orientalis* Lipsky) species with low proportions of other tree species such as *Q. cerris* L., *Alnus glutinosa* L., *Carpinus betulus* L., *Acer trautvetteri* Med., *Acer campestre* L., *Castanea sativa* Mill., and *Ulmus campestris* L.

Table 1. Some characteristics of experimental watersheds.

Watershed characteristics	Watershed - I	Watershed - IV	Watershed - V
Area (ha)	71.9	77.5	17.5
Mean elevation (m)	140.3	123.5	128.7
Mean slope (%)	10	14	13
Form factor	1	0.7	0.6
Drainage density (km/km^2)	3.60	3.80	3.60
Stream density (number of streams / km^2)	0.14	0.13	0.18
Road density (m/ha)	12.93	12.36	0.00
Slope of main stream channel (%)	3	5	6
Elevation range (m)	99-170	97-190	98-170

2.2 Data collection and analysis

Three neighboring watersheds were selected with similar vegetation, soil, topography, elevation, slope, geology, and aspect and monitored for streamflow and nutrient outflow since late 1979.

Stream stages were recorded in 90° and 120° concrete sharp-crested V-notch weirs instrumented with automatic water stage height recording systems at the outlets of the watersheds. Stream discharge was estimated by using the following formula:

$$Q = C \times H^n \quad (1)$$

where Q = the runoff (m^3/s), H = the depth of the water column above the bottom of the V-notch in meter, n = a coefficient taken as 2.48, and C= a constant and changes in relation to the angle of the notch and unit of the measurement (Özhan et al., 2010). Precipitation was measured with an automatic tipping-bucket type rain gauge installed near the watersheds. Streamwater grab samples were collected from the watersheds on weekly basis and analyzed usually at the same day of collection for pH, EC, TSS, Cl^-, Fe^{3+}, Al^{3+}, TN, NH_4^+-N, Ca^{2+}, Mg^{2+}, K^+, Na^+, and SO_4^{2-}according to the standard methods of APHA–AWWA–WEF (1998). The pH and EC measurements were made according to the methods 4500-HB and 2510 B, respectively with the WTW Multiline P4 Universal Meter (WTW, Weilheim, Germany). Concentration of TSS was determined by evaporation procedure performed on 500 ml stream water samples. Concentrations of Fe^{3+}, Al^{3+}, and $(SO_4)^{2-}$ were measured by using UV visible spectrophotometer. TN, Ca^{2+}, and Mg^{2+} were determined with titration method, and NH_4^+-N, K^+, and Na^+ were measured with ion selective electrode method. Average annual export for each chemical parameter was estimated by multiplying mean annual concentration of each nutrient with the mean annual streamflow. Simple linear regression equations were developed between mean annual streamflow and water characteristics to determine relationship between streamflow and water quality parameters and results were evaluated at α level of 0.05 (Zar, 1996).

3. RESULTS

All experimental watersheds had similar trends for mean annual outflow of ions, pH, EC and TSS. Average annual exports of chemical parameters, along with pH, EC, and TSS were also given in Tables 2 and 3. pH and EC were only the parameters differed significantly among the watersheds ($P < 0.05$) (Table 2). Mean annual pH value was 7.31 and varied between 7.14 and 7.48. Mean annual EC of the streamwater was 262 µS/cm and varied from 205 to 332 µS/cm (Tables 2 and 3). The watersheds had similar TSS discharge and changed between 5024.4 and 6253.8 kg/ha/yr. The watersheds had statistically similar ion fluxes with the same order and the trend (Table 2). The order of ion flux was in descending order of $Cl^- > (SO_4)^{2-} > Ca^{2+} > Na^+ > Mg^{2+} > K^+ > TN > Fe^{3+} > NH_4^+$-N $> Al^{3+}$. Cl^- (1146.4 kg/ha/yr) and $(SO_4)^{2-}$ (743.6 kg/ha/yr) were dominant ions in the streamwater and mean annual losses of the cations were lower than the anions. On the other hand, Cl^- had the highest mean annual outflow (1146.4 kg/ha) whereas Al^{3+} had the lowest outflow (3.6 kg/ha) from the watersheds (Table 3). Among the cations, streamwater had a higher calcium load compared to other cations (Table 3) and showed changes from 486.2 to 741.4 kg/ha (Table 2).

Table 2. Annual losses (mean ± SEM) of streamwater quality parameters.

Parameters	W-I	W-IV	W-V	Significance level
pH	$7.42^{ab} \pm 0.06$	$7.14^{a} \pm 0.09$	$7.48^{b} \pm 0.07$	$P < 0.05$
EC (µS/cm)	$298^{a} \pm 8.44$	$205^{b} \pm 6.59$	$332^{c} \pm 12.70$	$P < 0.05$
TSS (kg/ha/yr)	6253.8 ± 870.6	5482.3 ± 711.0	5024.4 ± 1063.4	$P > 0.05$
Cl^- (kg/ha/yr)	1104.0±156.3	1180.4±154.3	1173.0 ± 244.8	$P > 0.05$
Ca^{2+} (kg/ha/yr)	741.4±105.7	530.0±60.4	486.2 ± 96.9	$P > 0.05$
Mg^{2+} (kg/ha/yr)	309.3±50.9	271.4 ± 42.4	282.6 ±57.2	$P > 0.05$
TN (kg/ha/yr)	133.2 ± 49.1	$40.7^{a} \pm 17.7$	$22.0^{a} \pm 12.9$	$P > 0.05$
Na^+ (kg/ha/yr)	328.5 ± 56.0	$378.1^{a} \pm 56.5$	$311.4^{a} \pm 89.2$	$P > 0.05$
K^+ (kg/ha/yr)	163.4 ± 67.6	47.0 ± 7.0	28.7 ± 5.2	$P > 0.05$
Fe^{3+} (kg/ha/yr)	28.9 ± 6.9	23.9 ± 5.0	20.8 ± 4.8	$P > 0.05$
Al^{3+} (kg/ha/yr)	4.0 ± 1.6	4.0 ± 1.4	2.7 ± 2.0	$P > 0.05$
NH_4^+-N (kg/ha/yr)	8.1 ± 1.9	7.0 ±1.8	4.9 ± 0.8	$P > 0.05$
$(SO_4)^{2-}$ (kg/ha/yr)	893.0 ± 186.0	684.4 ± 120.2	630.8 ± 119.2	$P > 0.05$

Simple linear regression equations showed that there was a statistically significant relationship between mean annual streamflow and mean annual outflow of the parameters except for pH and Al^{3+}. Streamwater had almost a neutral character with a pH value of 7.3 and it did not have a significant relation with amount of annual streamflow (Table 3). Al^{3+} load in the streamwater was the lowest compared to those of other chemicals and it did not have a significant relationship with streamflow. Among the water quality parameters, significantly high correlation coefficients greater than 80 % were found between streamflow and TSS, Cl^-, Ca^{2+}, NH_4^+-N, and Fe^{3+} while low correlation coefficients smaller than 80 % were determined between streamflow and EC, Mg^{2+}, TN, Na^+, K^+, and $(SO_4)^{2-}$ (Table 3).

Table 3. Regression equations and correlation coefficients for the relationship between mean annual streamflow (m^3/ha/yr) and streamwater quality parameters.

Parameters	Regression equations	Correlation coefficient (*r*)	Mean values (mean ± SEM)
pH	Y = 7.24 + 3E-05*X	r = 0.12^{ns}	7.31 ± 0.05 (n = 67)
EC (µS/cm)	Y = 289.61 - 0.01*X	r = 0.31*	262 ± 7.95 (n = 67)
TSS (kg/ha/yr)	Y = 387.92 + 2.24*X	r = 0.94***	5754.8 ± 503.6 (n = 67)
Cl^- (kg/ha/yr)	Y = 108.46 + 0.44*X	r = 0.96***	1146.4 ± 99.1 (n = 65)
Ca^{2+} (kg/ha/yr)	Y = 103.57 + 0.21*X	r = 0.82***	616.9 ± 55.7 (n = 66)
Mg^{2+} (kg/ha/yr)	Y = 39.51 + 0.10*X	r = 0.75***	289.6 ± 29.4 (n = 66)
TN (kg/ha/yr)	Y = 8.42 + 0.03*X	r = 0.26*	78.9 ± 23.4 (n = 64)
Na^+ (kg/ha/yr)	Y = 32.95 + 0.13*X	r = 0.80***	347.7 ± 36.1 (n = 60)
K^+ (kg/ha/yr)	Y = - 63.33 + 0.06*X	r = 0.48***	95.0 ± 30.2 (n = 60)
Fe^{3+} (kg/ha/yr)	Y = - 2.37 + 0.01*X	r = 0.93***	25.0 ± 3.4 (n = 35)
Al^{3+} (kg/ha/yr)	Y = 2.14 + 0.001*X	r = 0.19^{ns}	3.6 ± 0.9 (n = 31)
NH_4^+ - N (kg/ha/yr)	Y = - 0.144 + 0.003*X	r = 0.85***	6.8 ± 1.0 (n = 28)
$(SO_4)^{2-}$ (kg/ha/yr)	Y = 176.80 + 0.23*X	r = 0.79***	743.6 ± 85.8 (n = 28)

** Significant at α level of 0.05, ** 0.001, and *** 0.0001*
^{ns} Nonsignificant

4. DISCUSSION

Significantly high correlation coefficients were found between annual stream discharge and mean annual nutrient and sediment losses (Table 3). Thus, annual streamflow affected nutrient outflux and hence water quality as found in other studies (Balcı et al., 1986; Lewis, 1998; Serengil et al., 2007b). High correlation coefficients between stream discharge and nutrient losses can be considered as an indication of how forestry practices can influence water quality in the forested watersheds. In general, nutrient concentrations in the waters coming from forested watersheds are lower than those coming from other land use types (Ryan, 2000; Gravelle et al., 2009) but nutrient loads of waters from forest covered watersheds can be increased after timber harvest. In fact, several studies already have shown that intensive timber harvest practices can increase runoff in the watersheds and result in nutrient losses from the forest soil and deterioration in water quality. For example, Bäumler and Zech (1999), Swank et al. (2001), and Wang et al. (2006) found that nutrient

export increased in relation to increases in the stream discharge after timber harvest. All these studies showed that forest harvest practices can be used as a tool to increase water yield but they can also have an adverse impact on water quality due to nutrient and sediment losses, and leaching. Thus, nutrient and sediment losses can be detrimental to quality of potable streamwater. For instance, Burns and Murdoch (2005) found that NO_3^- concentration increased more than 1400 μmol/L after clearcut and its concentration can deteriorate water quality in the streams and cause mortality of aquatic lives like brook trout (Baldigo et al., 2005). Similarly, increased concentration of chemicals in the streamflows can create problems such as eutrophication. In some places around the world like in Portland, streamwater from forested watersheds can be used without filtering (Neary et al., 2009) but the waters from forest areas can be polluted by excessive phosphorus and nitrogen concentrations as a result of intensive timber harvest (Gravelle et al., 2009; Tremblay et al., 2009). Therefore, impact of timber harvest must be evaluated before harvest activities are applied in watersheds because water is a valuable commodity without alternative.

5. CONCLUSION

The study examined the relationship between mean annual streamflow and outflow of some chemical water quality parameters showed that there were high correlations between streamflow and nutrient losses in the watersheds. This means that application of forest harvest to increase water yield is also detrimental to water quality and hence aquatic lives in forested watersheds. Purification of polluted water resources can affect sustainability of domestic water supply and increase cost of treatment and then water consumption. Additionally, leaching of nutrients from forest soils after timber harvest can affect productivity of forest soils and influence sustainability of forest ecosystems in the long term. Therefore, timber harvest programs and water management policies should be well developed and pros and cons of timber harvest especially in fresh water producing watersheds should be taken into account before actions.

REFERENCES

APHA–AWWA–WEF, 1998. Standard Methods for the Examination of Water and Wastewater. 20th ed. American Public Health Association, 1015 Fifteenth Street, NW, Washington DC (USA), 20005-2605.

Balcı A.N., Özyuvacı N., Özhan S., 1986. Sediment and nutrient discharge through stream water from two experimental watersheds in mature oak-beech forest ecosystems near Istanbul, Turkey. J. Hydrol., 85:31–47.

Baldigo B.P., Murdoch P.S., Burns D.A., 2005. Stream acidification and mortality of brook trout (Salvelinus fontinalis) in response to timber harvest in Catskill Mountain watersheds. New York. USA. Can. J. Fish. Aquat. Sci., 62: 1168–1183.

Bäumler R., Zech W., 1999. Effects of forest thinning on the streamwater chemistry of two forest watersheds in the Bavarian Alps. Forest Ecol. Manag., 116:119–128.

Bosch J.M., Hewlett J.D., 1982. A review of catchment experiments to determine the effect of vegetation change on water yield and evapotranspiration. J. Hydrol., 55(1/4):3–23.

Burns D.A., Murdoch P.S., 2005. Effects of a clearcut on the net rates of nitrification and N mineralization in a northern hardwood forest. Catskill Mountains. New York. US. Biogeochemistry, 72:123–146.

Dung B.X., Gomi T., Miyata S., Sidle R.C., Kosugi K., Onda Y., 2012. Runoff responses to forest thinning at plot and catchment scales in a headwater catchment draining Japanese cypress forest. J. Hydrol., 444-445:51-62.

Gökbulak F, Serengil Y, Özhan S, Özyuvacı N, Balcı A.N., 2008a. Effect of timber harvest on physical water quality characteristics. Water Resour Manag., 22:635-649.

Gökbulak F., Serengil Y., Ozhan S., Ozyuvacı N., Balcı A.N., 2008b. Relationship between streamflow and nutrient and sediment losses from an oak–beech forest watershed during an 18-year long monitoring study in Turkey. Eur. J. Forest Res., 127: 203–212.

Gravelle J.A., Ice G., Link T.E., Cook D.L., 2009. Nutrient concentration dynamics in an inland Pacific Northwest watershed before and after timber harvest. Forest Ecol Manag., 259: 1663–1675.

Lewis J., 1998. Evaluating the impacts of logging activities on erosion and suspended sediment transport in the Caspar Creek watersheds. In: Proceedings of the conference on the coastal watersheds. The Caspar Creek story. May 6, Ukiah, California, 55-69. USDA Forest Service, Pacific Southwest research station. General technical report, PSW-GTR-168.

Neary D.G., Ice G.G., Jackson C.R., 2009. Linkages between forest soils and water quality and quantity. Forest Ecol. Manag., 258: 2269-2281.

Özhan S., 1977. Variation in Some Hydrologic Properties of Forest Floor as Related to Certain Environmental Factors in Ortadere Watershed of Belgrad Forest. Istanbul University, Faculty of Forestry Publication Number: 235, Istanbul (in Turkish).

Özhan S., Hızal A., Şengönül K., Gökbulak F., Serengil Y., Özcan M., 2008. Hydrological and hydrochemical modeling of watershed systems in Belgrad Forest. Unpublished research project report (supported by the Scientific and Technological Research Council of Turkey (TUBITAK) with a grant number of TOVAG - 105 0 182).

Özhan S., Gökbulak F., Serengil Y., Özcan M., 2010. Evapotranspiration from a mixed deciduous forest ecosystem. Water Resour. Manag., 24 (10): 2353-2363.

Özyuvacı N., 1976. Hydrologic Characteristics of the Arnavutköy Creek Watershed as Influenced by Some Plant-Soil-Water Relations. Ph.D. Thesis. Istanbul University, Faculty of Forestry, Istanbul-Turkey.

Özyuvacı N., Özhan S., Gökbulak F., Serengil Y., Balcı A.N., 2004. Effect of selective cutting on streamwater in an oak-beech forest ecosystem. Water Resour. Manag., 18: 249–262.

Reuss J.O., Stottlemyer R., Troendle C.A., 1997. Effect of clear cutting on nutrient fluxes in a subalpine forest at Fraser, Colorado. Hydrol. Earth Syst. Sci., 1(2):333–344.

Ryan D.F., 2000. Synthesis. In: Proceedings of drinking water from forests and grasslands. A synthesis of the scientific literature. 202-206, Editor: G.E. Dissmeyer. US Forest Service, Southern Research station, General technical report SRS-39.

Sahin V., Hall M.J., 1996. The effects of afforestation and deforestation on water yields. J. Hydrol., 178: 293–309.

Serengil Y., Gökbulak F., Özhan S., Hızal A., Şengönül K., Balcı A.N., Özyuvacı N., 2007a. Hydrological impacts of a slight thinning treatment in a deciduous forest ecosystem in Turkey. J. Hydrol., 333:569–577.

Serengil Y., Gökbulak F., Özhan S., Hızal A., Şengönül K., 2007b. Alteration of stream nutrient discharge with increased sedimentation due to thinning of a deciduous forest in Istanbul. Forest Ecol. Manag., 246(2): 264-272.

Stednick J.D., 1996. Monitoring the effects of timber harvest on annual water yield. J. Hydrol., 176: 79–95.

Stednick J.D., 2000. Timber management. In: Proceedings of drinking water from forests and grasslands. A synthesis of the scientific literature. US Forest Service, Southern Research station, General technical report SRS-39.

Swank W.T., Vose J.M., Elliot K.J., 2001. Long term hydrologic and water quality responses following commercial clearcutting of mixed hardwoods on a southern Appalachian catchment. Forest Ecol. Manag., 143: 163–178.

Tremblay Y., Rousseau A.N., Plamondon A.P., Lévesque D., Prévost M., 2009. Changes in stream water quality due to logging of the boreal forest in the Montmorency forest, Québec. Hydrol. Process., 23:764-776.

USDA, 1994. Keys to Soil Taxonomy. Soil Survey Staff, sixth ed. US Department of Agriculture, Soil Conservation Service. Pocahontas Press, Inc. Blacksburg, Virginia, USA.

Wang X., Burns D.A., Yanai R.D., Briggs R.D., Germain R.H., 2006. Changes in stream chemistry and nutrient export following a partial harvest in the Catskill Mountains, New York, USA. Forest Ecol. Manag., 223:103–112.

Zar J.H., 1996. Biostatistical Analysis. 3rd ed. Prentice-Hall, Upper Saddle River.

Zhang X., Yu G.Q., Li Z.B., Li P., 2014. Experimental study on slope runoff, erosion and sediment under different vegetation types. Water Resour. Manag., 28:2415–2433.

Proceedings of the 10th World Congress of EWRA 'Panta Rhei', 5-9 July 2017, Athens, Greece
© 2017 *European Water Resources Association*

Water quality model of Alibeykoy watershed and LID implementation

S. Gulbaz and C.M. Kazezyılmaz-Alhan*
Department of Civil Engineering, Istanbul University, Avcılar, Istanbul, Turkey
* *e-mail: meleka@istanbul.edu.tr*

Abstract: Uncontrolled urbanization causes flood and poor water quality which results in an increase in peak flow rate and in Total Suspended Solid (TSS) concentration. Low Impact Development (LID) is a Best Management Practice (BMP) and land planning method which may be used to manage storm water runoff to reduce flooding as well as simultaneously improve water quality. Preserving and recreating natural landscape features, minimizing effective imperviousness to create functional and appealing site drainage, which treats storm water as a resource rather than as a waste product, are intended by implementing LID. There are several LID type of storm water BMPs such as bioretention, vegetated rooftops, rain barrels, vegetative swales and permeable pavements. In this study, the impact of LID implementation on TSS are investigated by developing a water quality model for Alibeyköy Watershed located in Istanbul, Turkey. For this purpose, the calibrated hydrologic model of Alibeyköy Watershed developed by using Environmental Protection Agency Storm Water Management Model (EPA SWMM) is employed. The water quality model is integrated into the hydrological model using EPA SWMM. Then, several LID types such as retention basins, vegetative swales and permeable pavement are incorporated into the water quality model and their impacts on TSS in Alibeyköy Watershed are observed.

Key words: Storm water treatment; Low Impact Development; Watershed Model; Total Suspended Solid (TSS) concentration

1. INTRODUCTION

High peak flow rates and huge amount of TSS yield problems such as flooding and poor water quality. These problems are observed more frequently due to high urbanization on watersheds. Implementing Low Impact Development (LID) type of storm water Best Management Practices (BMPs) has recently been recognized as a useful solution. LID BMPs is an approach of land re-development in order to manage storm water runoff and quality. LID implementation mitigates some of the negative effects of urbanized watersheds by decreasing surface peak flow rate, increasing evapotranspiration, infiltration, and ground water recharge, reducing the pollutants in surface and ground water and protecting animal habitats (Zhang and Guo 2014; Gülbaz and Kazezyılmaz-Alhan 2014; Brown and Hunt 2011; Trowsdale and Simcock 2011; Li and Davis 2009; Li et al. 2009; Davis 2008; Dietz 2007; Hunt et al. 2006; US EPA 2000). The importance of LID BMP implementation has been recognized recently in the literature (Ahiablame et. al., 2012; Fassman, 2012; Alfredo et. al., 2010; Elliott et. al., 2010; Lucas, 2010; Gilroy and McCuen, 2009; Bedan and Clausen, 2009; Gülbaz et al. 2015; Gülbaz and Kazezyılmaz-Alhan, 2017). There are several LID type of storm water BMPs such as bioretention, vegetated rooftops, rain barrels, vegetative swales and permeable pavements (US EPA, 2000; Davis et al. 2009; US EPA 1999).

The aim of this study is to investigate the effects of LID implementation on TSS concentration during different storm events by developing a water quality model for Alibeyköy Watershed. For this purpose, EPA SWMM is employed for watershed modelling. The water quality model is integrated into the calibrated hydrological model. Then, by using the hydrologic and water quality model, the TSS concentration in surface runoff developed over the watershed are simulated using measured rainfall data. Finally, retention basins, vegetative swales and permeable pavement types of LID BMPs are tested and their influence on reduction of TSS concentration is obtained. Consequently, the possible effects of LID BMPs on TSS in Alibeyköy Watershed are observed.

2. MATERIAL AND METHODS

2.1 EPA SWMM

EPA SWMM is a watershed hydrological and water quality model among several other software programs. In the literature, there are many studies related to water quantity and quality modeling by using EPA SWMM (Huber and Dickinson 1988). Furthermore, some LID types such as bioretention, rain garden, green roof, infiltration trench, permeable pavement, rain barrel, and vegetative swale can be modelled in EPA SWMM to simulate the effects of LID. In the literature, there are many studies related to water quantity and quality modeling by using EPA SWMM (Huber and Dickinson 1988; Rossman 2010); however, studies on LID implementation using EPA SWMM are quite rare. In order to model water quality, EPA SWMM includes buildup and wasoff functions described as follows.

Pollutant accumulation (Pollutant Buildup) in EPA SWMM is calculated as proportional to time raised to some power, until a maximum limit is achieved by using Power Function. For Exponential Function, pollutant buildup follows an exponential growth curve. Finally, for Saturation Function, pollutant buildup begins at a linear rate. Furthermore, the amount of pollutant accumulation is a function of number of preceding dry days. In this study, power function is used for pollutant buildup and is given as follows (Rossman, 2010):

$$B = Min\left(C_{1p}, C_{2p}\, t^{C_{3p}}\right) \tag{1}$$

where B is the pollutant buildup (M/L^2), C_{1p} is the possible maximum buildup (M/L^2), C_{2p} is the buildup rate constant (M/TL^2), C_{3p} is the time exponent for the buildup parameter (*dimensionless*) and t is the time (T).

Pollutant washoff in EPA SWMM is calculated as proportional to the product of runoff raised to some power and to the amount of buildup remaining by using Exponential Function. For Rating Curve Function, pollutant washoff is calculated as proportional to the runoff rate raised to some power. And finally, Event Mean Concentration is a special case of Rating Curve Washoff where the Rating Curve exponent is 1. Rating Curve washoff function is used in this study and is given as follows (Rossman, 2010):

$$W_{rc} = C_{3rc}\, Q^{C_{4rc}} \tag{2}$$

where W_{rc} is the amount of washoff pollutant (M/T), C_{3rc} is the washoff coefficient (M/L^3), C_{4rc} is the washoff exponent (*dimensionless*) and Q is the runoff rate (L^3/T).

2.2 Alibeyköy watershed

Alibeyköy Watershed is located on the European Continental side of Istanbul in Turkey (Figure 1). It has a drainage area of 161 km^2 and supplies an important portion of Istanbul's drinking water. There are 10 streams which gather overland flow generated over the basin. These streams are Cebeci stream, Boğazköy stream, Bolluca stream, Kocaman stream, Çıplak stream, Ayvalı stream, Elmalı stream, Gülgen stream, Malkoç stream, Çiftepınar stream. The land morphology of the great part of the watershed is in the form of sandy clay loam. The altitude of the watershed is between 30-170 m in the topographic boundaries. Alibeyköy Watershed area is composed of 23% of agricultural and pasture land, 15% of residential and industrial areas, 60% of forest and 2% of dam area. However, there is a great potential of population growth due to the new developments of infrastructures in the basin. These new infrastructures include third Bhosphorus Bridge, third airport of Istanbul and finally Canal Istanbul project. Therefore, high urbanization is expected in the next

10 years and these changes will have negative effects on the ecosystem in the future, if no action is taken. In Fig. 1, the boundary of Alibeyköy Watershed and Alibeyköy Dam are shown.

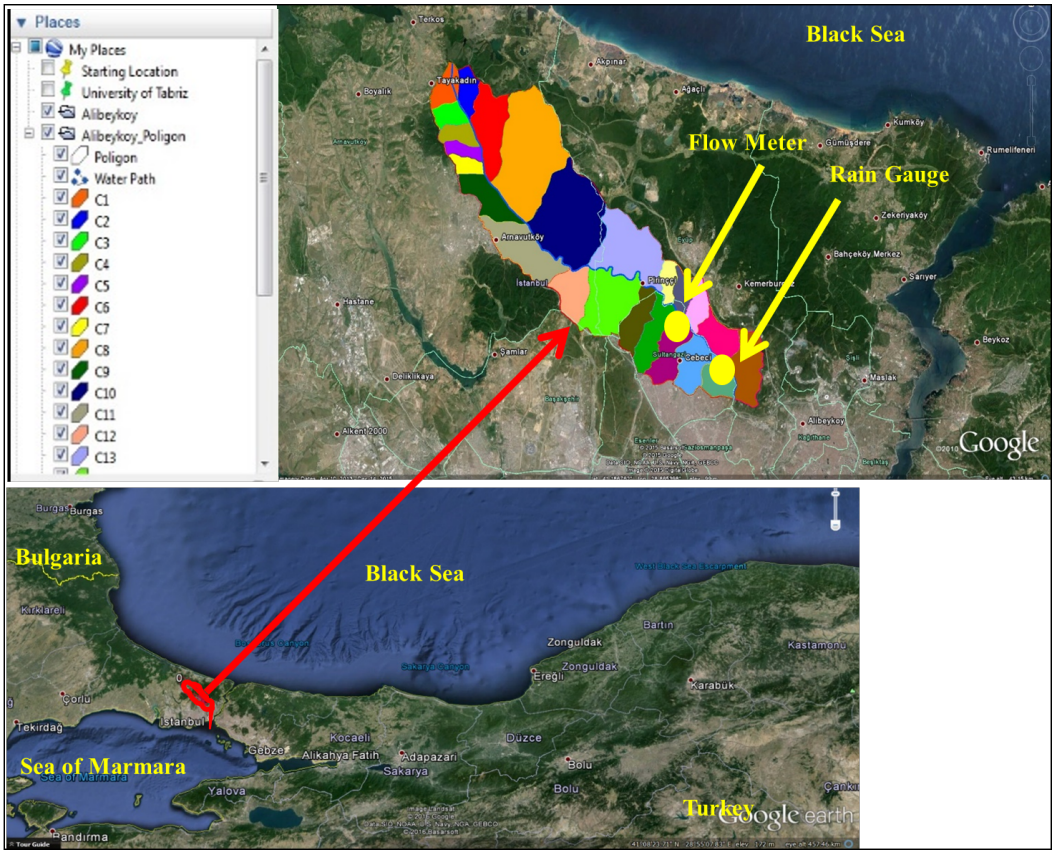

Figure 1. General view of Alibeyköy Watershed and subcatchments (Retrieved from Google Earth and Istanbul Metropolitan Municipality).

2.3 Model development

The water quality model of the watershed is based on the calibrated hydrological model. In the hydrological model, the area consists of 24 subcatchments which are defined by using slope, area, and width. Main channels, which collect the surface runoff generated over the watershed, are defined using the conduits with parameters of length, cross sectional area, roughness, and start-end points. Each link is connected with junctions which are described by invert elevation and maximum depth. The measured flow rate and rainfall data are used for calibration of the hydrological model. The water quality model is formed by defining the buildup and washoff functions of TSS. For this purpose, Power function for build-up of TSS and Rating Curve function for washoff TSS are defined on low-density residential, high-density residential, highway and commercial land use. In order to determine water quality input parameters, which belong to these functions, buildup rate constant, time exponent for the buildup parameter, washoff coefficient and washoff exponent are calculated based on the formula given by Tsihrintzis and Hamid (1998). These calculated parameters are defined into the water quality model. Then, some LID types, which are retention basins, vegetative swales, infiltration trench and permeable pavement, are introduced into the model. In order to implement these four types of LID into the model, the LID parameters are defined in the water quality model. These parameters depend on the surface, pavement, soil, and storage layers for each LID type. The values for these parameters are selected by using EPA SWMM manual (Rossman, 2010) and are given in Table 1. LID BMPs are performed about 2% of the modelled watershed. The hydrologic and water quality model of Alibeyköy Watershed is shown in Figure 2.

Table 1. Properties of surface, pavement, soil and storage layers for LID implementation (Rossman, 2010).

Layer	Parameters	Bioretention	Vegetative Swale	Infiltration Trench	Permeable Pavement
Surface Layer	Bern Height (mm)	500	500	500	500
	Storage Depth *(mm)*	NA	NA	NA	NA
	Vegetation Volume *(Fraction)*	0.2	0.2	0.2	0.2
	Surface Roughness *(Manning's N)*	0.1	0.1	0.1	0.1
	Surface Slope *(Percent)*	1.0	1.0	1.0	1.0
	Swale Side Slope *(Run/Rise)*	NA	5.0	NA	NA
Pavement Layer	Thickness *(mm)*	NA	NA	NA	150
	Void Ratio *(voids/solids)*	NA	NA	NA	0.15
	Impervious Surface Fraction	NA	NA	NA	0
	Permeability *(mm/hr)*	NA	NA	NA	100
	Clogging Factor	NA	NA	NA	0
Soil Layer	Thickness *(mm)*	1000	NA	NA	1000
	Porosity *(volume fraction)*	0.5	NA	NA	0.5
	Field Capacity *(volume fraction)*	0.2	NA	NA	0.2
	Wilting Point *(volume fraction)*	0.1	NA	NA	0.1
	Conductivity *(mm/hr)*	380	NA	NA	380
	Conductivity Slope	10	NA	NA	10
	Suction Head *(mm)*	19	NA	NA	19
Storage Layer	Thickness *(mm)*	500	NA	500	250
	Void Ratio *(voids/solids)*	0.75	NA	0.75	0.75
	Seepage Rate *(mm /hr)*	0.5	NA	0.5	0.5
	Clogging Factor	0.0	NA	0.0	0
Drain Layer	Flow Coefficient	0	NA	0	0
	Flow Exponent	0.5	NA	0.5	0.5
	Offset Height (mm)	6	NA	6	6

NA= Not Applicable

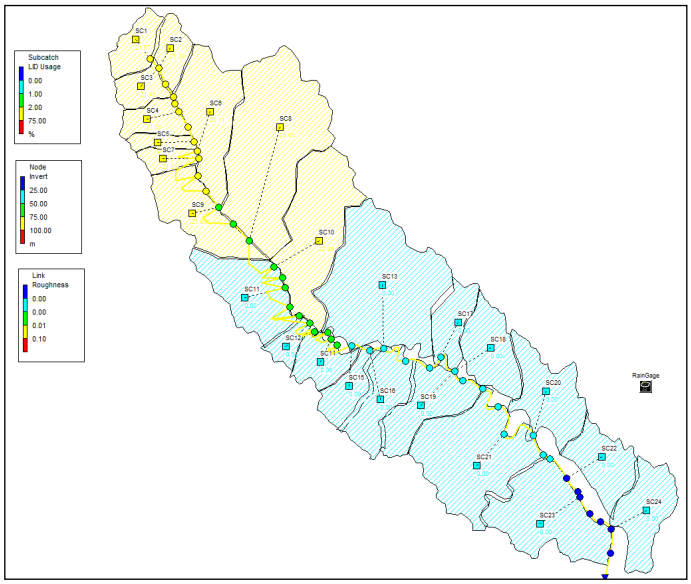

Figure 2. Hydrologic and water quality model of Alibeyköy Watershed in EPA SWMM

3. RESULTS AND DISCUSSION

The simulation results are presented for the storm events observed during March 06-09, 2010 and September 07-09, 2009 to model low and high (extreme) rainfall intensity impacts, respectively. The change in TSS concentration with and without LID BMP implementations are observed and compared. Figure 3 shows the predicted TSS concentration versus time at the outfall of the Alibeyköy Watershed with LID BMP implementation and with no LID BMP implementation. As it can be seen from this figure, for the case with LID BMPs, the peak of the pollutograph decreases from 191 mg/L to 175 mg/L. Moreover, the peaks of the polllutograph at 60th and 80th hours diminish as shown in Figure 3. Furthermore, the total amount of TSS washoff over the watershed decreases from 182,130 kg to 67,298 kg. The simulations are repeated for the storm event occurred on March 06-09, 2010 and the result is presented in Figure 4. As it can be seen from this figure, for the case with LID BMPs, peak of the pollutograph decreases from 64 mg/L to 61 mg/L. Furthermore, the total amount of TSS washoff over the watershed decreases from 11,382 kg to 11,094 kg. In addition, we observe that LID implementation is more effective during severe storms when the results of Figure 3 are compared with the results of Figure 4.

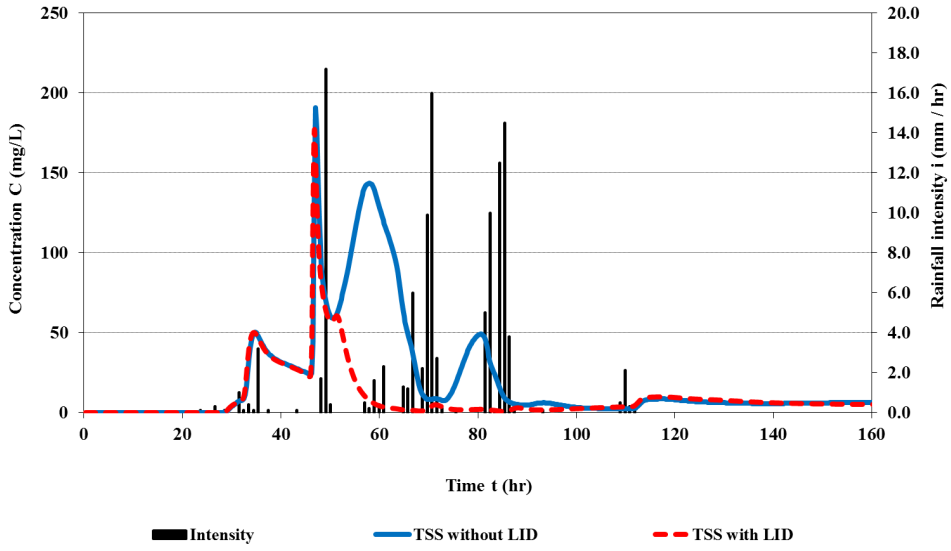

Figure 3. Predicted TSS concentration versus time at the outfall of the Alibeyköy Watershed with LID BMPs and with no LID BMPs during storm event observed between September 07-09, 2009.

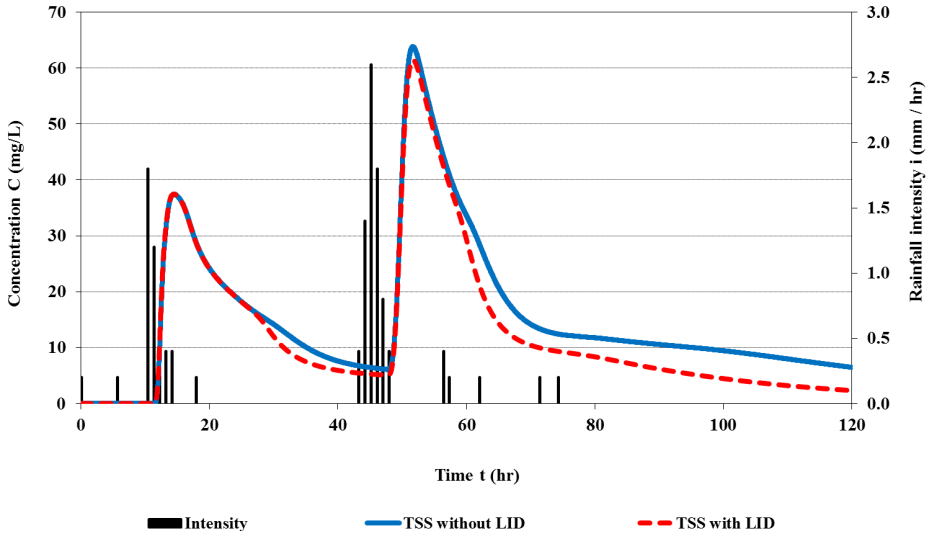

Figure 4. Predicted TSS concentration versus time at the outfall of the Alibeyköy Watershed with LID BMPs and with no LID BMPs during storm event observed between March 06-09, 2010.

4. CONCLUSIONS

The effect of LID implementation on water quality are investigated in this study. For this purpose, a water quality model is developed for Alibeyköy Watershed in Istanbul, Turkey by using EPA SWMM and integrated into the calibrated hydrological model. TSS is introduced into the model by using build up and wash off functions. Then, several types of LID are employed into the model. The TSS concentration for current urbanization with and without LID implementation are simulated under typical and extreme rainfall events using the hydrologic and water quality model. It is observed that LID implementation in the Alibeyköy Watershed results in a considerable decrease in the TSS concentration after implementing LID type of storm water BMPs.

ACKNOWLEDGMENTS

This work was supported by Scientific Research Projects Coordination Unit of Istanbul University, Project number 49485 and 23914. The writers would like to thank Scientific Research Projects Coordination Unit of Istanbul University, Turkish State Meteorological Service (DMI), and Istanbul Water and Sewerage Administration (ISKI) for their data support and valuable discussions in undertaking this work.

REFERENCES

Ahiablame L. M., Engel B. A. and Chaubey I., 2012. Effectiveness of Low Impact Development Practices: Literature Review and Suggestions for Future Research. Water Air Soil Pollutution; 223 (7): 4253–4273.

Alfredo K., Montalto F. and Goldstein A., 2010. Observed and Modeled Performances of Prototype Green Roof Test Plots Subjected to Simulated Low- and High-Intensity Precipitations in a Laboratory Experiment. Journal of Hydrologic Engineering; 15 (6): 444-457.

Bedan E. S. and Clausen J. C., 2009. Stormwater Runoff Quality and Quantity From Traditional and Low Impact Development Watersheds. Journal of the American Water Resources Association (JAWRA); 45 (4): 998-1008.

Brown, R.A., Hunt, W.F., 2011. Underdrain configuration to enhance Bioretention exfiltration to reduce pollutant loads. Journal Environmental Engineering; 137: 1082–1091.

Davis, A.P., 2008. Field performance of bioretention: Hydrology impacts. Journal of Hydrologic Engineering; 13: 90–95.

Davis, A.P., Hunt, W., Traver, R., Clarn, M., 2009. Bioretention technology: Overview of current practice and future needs. J. Environ. Eng.; 135: 109–117.

Dietz, M., 2007. Low impact development practices: A review of current research and recommendations for future directions. Water Air Soil Pollution; 186: 351–363.

Elliott A.H., Spigel R.H., Jowett I.G., Shankar S.U. and Ibbitt R.P., 2010. Model application to assess effects of urbanisation and distributed flow controls on erosion potential and baseflow hydraulic habitat. Urban Water Journal; 7 (2): 91–107.

Fassman E., 2012. Stormwater BMP treatment performance variability for sediment and heavy metals. Separation and Purification Technology; 84 (SI): 95–103.

Gilroy K.L. and McCuen R.H., 2009. Spatio-temporal effects of low impact development practices. J. of Hydrology; 367 (3-4): 228–236.

Gülbaz, S., Kazezyılmaz-Alhan, C.M., 2014. Investigating Effects of Low Impact Development on Surface Runoff and TSS with a Calibrated Hydrodynamic Model. Houille Blanche-Revue Internationale De L Eau; 3 : 77–84.

Gülbaz, S., Kazezyılmaz-Alhan, C.M., Copty, N.K., 2015. Evaluation of Heavy Metal Removal Capacity of Bioretention Systems. Water Air and Soil Pollution; 226 (11): 376.

Gülbaz, S., Kazezyılmaz-Alhan, C.M., 2017. Experimental Investigation on Hydrologic Performance of LID with Rainfall-Watershed-Bioretention System. Journal of Hydrologic Engineering; 22(1), D4016003.

Huber, W.C., and Dickinson, R.E., 1988. "Storm Water Management Model, Version 4, User's Manual." Athens, GA. Environmental Research Laboratory, Office of Research and Development, U.S. Environmental Protection Agency (EPA).

Hunt, W., Jarrett, A., Smith, J., Sharkey, L., 2006. Evaluating Bioretention hydrology and nutrient removal at three field sites in North Carolina. J. Irrig. Drain. Eng.; 132: 600–608.

Li, H., Davis, A.P., 2009. Water quality improvement through reductions of pollutant loads using bioretention. J. Environ. Eng.; 135: 567–576.

Li, H., Sharkey, L.J., Hunt, W.F., Davis, A.P., 2009. Mitigation of impervious surface hydrology using bioretention in North Carolina and Maryland. Journal of Hydrologic Engineering; 14: 407–415.

Lucas W.C., 2010. Design of Integrated Bioinfiltration-Detention Urban Retrofits with Design Storm and Continuous Simulation Methods. Journal of Hydrologic Engineering; 15 (6): 486-498.

Rossman, L.A., 2010. "Storm Water Management Model, User's Manual, Version 5." Water Supply and Water Resources Division National Risk Management Research Laboratory, Cincinnati, Ohio, U.S. Environmental Protection Agency, EPA/600/R-05/040.

Trowsdale, S.A., Simcock, R., 2011. Urban stormwater treatment using bioretention. Journal of Hydrology; 397 (3-4): 167–174.

United States Environmental Protection Agency (USEPA). 2000. Low Impact Development (LID), A Literature Review. EPA-841-B-00-005. USEPA Office of Water: Washington, D.C.

United States Environmental Protection Agency (US EPA). 1999. Storm water technology fact sheet: Bioretention. EPA 832-F-99-012, USEPA Office of Water: Washington, D.C.

Zhang, S., Guo, Y., 2014. Stormwater Capture Efficiency of Bioretention Systems Water Resources Management; 28 (1): 149–168.

Proceedings of the 10th World Congress of EWRA 'Panta Rhei', 5-9 July 2017, Athens, Greece
© 2017 *European Water Resources Association*

Change of land use and soil coverage in the area of influence of natural national park Los Nevados

D.A. Patino Rincon[1], S.A. Camargo[2], D. Rey[3], J.J. Velez[4] and J. Zambrano[5]
[1] *Universidad Nacional de Colombia-sede Manizales, Colombia*
[2] *Universidad de Manizales, Colombia*
[*] *e-mail: jjvelezu@unal.edu.co*

Abstract: The Nevados National Natural Park (NNNP) and its glaciers El Ruiz and Santa Isabel have been affected by different changes during last decades as land use changes, climate change and changes in extreme events, reason why it has been prioritized to understand its impacts in order to counteract these effects or to delay them. The paper focuses on the recent state of glaciers, moorlands and tropical forests and their changes occurred in the area of influence of NNNP during last decades. This project use remote sensing (Landsat Images) and application of geophysics (Mission Grace) to obtain results. The evaluation carried out from the analysis of satellite images show a notorious retreat of the glacier layer and the geophysical approach has been indicating a reduction of its thickness, keeping in mind that land use and soil covers in the area of influence of NNNP are changing. The reduction of moorlands in favour of livestock and potato crop with its impact on social and environmental aspects is a relevant conclusion. All these changes in general comprise the area of influence of NNNP and have affected its initial dynamics. This analysis serves as a tool for decision makers in the water resources planning and land management in their hydric and social part, based on information of free access as remote sensors images.

Key words: Land use changes, soil cover changes, Remote sensing, glacier retreat

1. INTRODUCTION

The area of influence of the Nevados National Natural Park (NNNP), located in central Andes of Colombia has been affected by different changes during last decades as land use changes, climate change and changes in extreme events including social and agricultural alterations among many others. This paper seeks to understand the temporal evolution of these changes through the use of remote sensing (Landsat imagery) and the application of geophysics (Mission Grace). The paper focuses on the recent state of glaciers, moorlands and tropical forests and their changes occurred in the area of influence of the NNNP during last decades. It has been demonstrated by some researchers that Tropical Andes glaciers are retreating (Poveda and Pineda, 2006; Marulanda et al. 2016), the analysis was performed using satellite images. This paper presents a geophysical approach to estimate the glacier thickness.

The area of influence of the NNNP has been affected noticeably during last decades and its initial dynamic has changed. Therefore, this study allow us to understand the dynamic of moorlands, glaciers and tropical forests. In general, the glacier retreat is inevitable and the moorlands have been reduced by land change use, especially due to potato crop and livestock, which modifies the water resources availability in the area of influence of the NNNP. The water supplied by the NNNP serves to several communities in the Andean region jeopardizing their future sustainability.

Colombia has currently 6 snowy peaks, 4 are located on the Central Mountain Range of the Andes and are monitored constantly by Institute of Hydrology, Meteorology and Environmental Studies of Colombia (IDEAM) and the Colombian Geological Service (SGC), being these glaciers of special interest because they belong to a chain of active volcanoes which has hindered in some way the acquisition of information. The values of thickness of the glacier layer show a high uncertainty due to variable climatic conditions in the tropical Andes.

The first studies from a point of view of flora and fauna were carried out in glacial zones in Colombia by Friedlader (1926-1927) and Kruger (1918). From a geophysical - geological point of view was Van der Hammen and Krauss (1934) who implemented seismic refraction to evaluate the internal structure of the glaciers associated with volcanoes. During 1986 the Agustín Codazzi Geographic Institute of Colombia (IGAC) through the use of photointerpretation began a series of studies to determine surface changes at glacial zones, a first characterization was obtained in 1994. The IDEAM carried out a technical studies to measure the surface changes in glaciers IDEAM (1993), those study still remains valid. Recently, Euscátegui-Ceballos and Ceballos Liévano (2012) shows the effect of climate changes on glaciers near the equator, evidenced by a clear change in glacier dynamics.

The area of influence of the NNNP presents the same typology to the glaciers studied by Baranowski (1977), who defined these from their geography, temperature and water content, being the Colombian glaciers contained in a group. This characterization highlights the presence of humidity in the ablation zones caused by the atmospheric interaction that melts the glacier and it is one of the main reasons why these studies should be generated in terms of remote sensing information.

The issue of calculating the exact volume of the glacier layer in the country is clear, since gravimetry has only been used in order to measure variations in gravity and indicate changes or contrasts of density, these measurements are carried out by SGC in the El Ruiz Volcano glacier in order to identify alterations inside the Volcano.

The first measurements of thickness of glacier layer in South America were made in Chile using gravimetry in the year of 1986, where thicknesses above 1400 m were estimated considering a subglacial topography inferior to the average level of the sea in the field of North Ice (Casassa, 1987). In Colombia, some studies have been carried out in order to know the thickness of the Earth's crust, such as Camargo (2011) who applied a methodology based on the spectral analysis of the gravitational field. In order to complement this function with the Airy Isostasy Hypothesis (based on the variation of the thickness of the crust considering a distribution of masses along the surface) an expansion of Bouguer Total Anomaly and Topographic Height is obtained a function with a mean square error tendency to zero, that is, it generates the best fit by minimizing the error (Parker, 1981).

Based on the information obtained from the GRACE Satellite for satellite gravimetry. A grid or gravimetric profile was obtained from the area of influence of the NNNP. The data used in the study are applied in order to obtain values of Bouguer Total Anomaly throughout the area then apply Parker's methodology and thus determine thickness values in the earth's crust (Parker, 1981), but especially calculate the thickness in El Ruiz glacier. The estimation of glacier layer thickness is performed using the geostatistical technique of Kriging, which allows to determine the structure of autocorrelation existing among the data.

2. CASE STUDY

The area of influence of NNNP is located in the Western Center of the Andean region, covering a surface of 625 km^2 as shown in Figure 1. The climate is normally intertropical and is characterized by small fluctuations in interannual temperatures but large daily temperature fluctuations. The rainfall displays a bimodal distribution during the year, due to the influence of the intertropical convergence zone (ITCZ) and the mountainous terrain of the region (Jaramillo, 2005). The temperature is largely a function of the elevation.

3. METHODOLOGY

This study will estimate the retreat of the three glaciers located in the NNNP, and its land use and land cover changes, which could affect the water supply of some municipalities in the area of

influence. The process consists in relating the geospatial information to the different hydroclimatic variables reported by the stations belonging to the subdivision of ecosystems of IDEAM, present in the area of influence of the NNNP for the period 2000-2010-2015. The Figure 2 shows an outline of the applied methodology for relating geospatial data and hydroclimatic information.

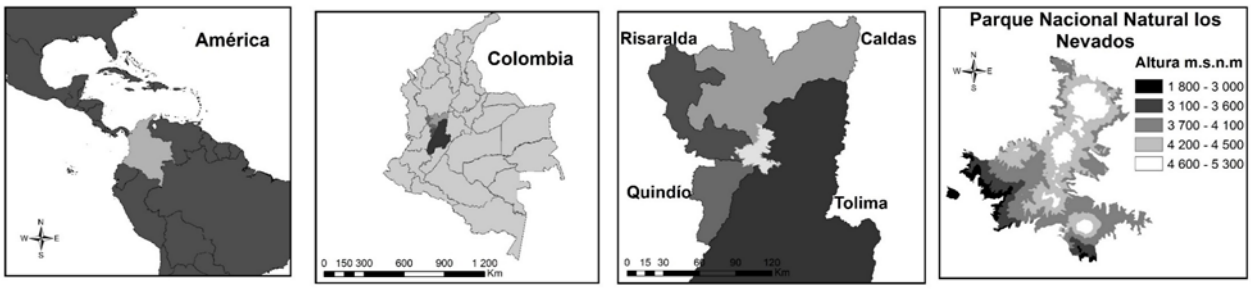

Figure 1. Location of the area of influence of the Nevados National Natural Park (NNNP).

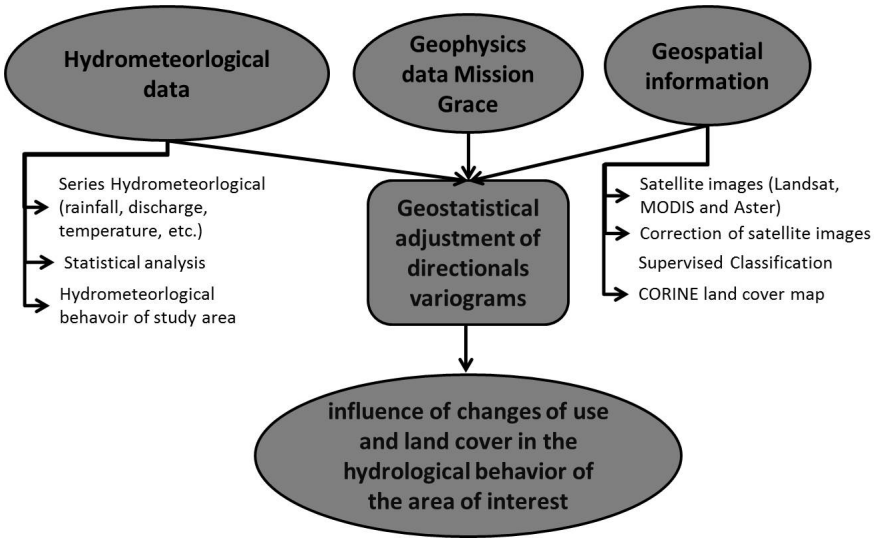

Figure 2. Methodology analysis of the influence of changes of use and land cover in the hydrological behaviour of the area of interest.

3.1 Geospatial information

The spatial analysis and the behaviour of the Bouguer anomaly in the El Ruiz glacier are shown through the data of Radar Altimetry and the Satellite GRACE for October of the year 2015. These data are distributed evenly in a grid space of 0.0331 degrees in latitude and 0.0334 degrees in longitude. The database contains a total of 84 records.

3.2 Selecting imagery type

For the construction of land cover and land use maps and subsequent analysis of holdings, it is important to consider the type of sensor, which offers a spatial resolution given by the smallest object captured in the study area, (Chuvieco, 1995).

3.3 Obtaining the images

The images are obtained free of charge through the University of Maryland's GLOBAL FOREST CHANGE platform (http://earthenginepartners.appspot.com/science-2013-global-forest).

The images of the Landsat 5 and Landsat 7 were downloaded for the years 2000 and 2010.

3.4 Spatial filtering

For the case study, the spatial filtering was applied from an inspection mask of size 3 x 3, whose function is to contain the components of low spatial frequency of the image (Aldalur & Santamaria, 2002). It was used to improve the contrast between vegetation cover and exposed soil present in the area of influence of the NNNP.

3.5 Radiometric correction

The radiometric correction factor was applied as a function of the values of wavelength captured by the Landsat sensor, which favoured the identification of the covers. It is performed for each band separately as shown below:

$$L = a_1 + a_0 * DN \quad (1)$$

where, L is the radiance that reaches the instrument, a_0 is the slope or gain number of counts per radiance change unit, a_1 is a constant, offset or bias. Counting value corresponding to the instrument response when the radiance is zero, and DN is the Digital Counting.

3.6 Convert radiance to reflectance

To convert radiance to reflectance the following equation is used:

$$\rho(\lambda) = (L * \pi * d^2)/(Ei(\lambda) * \cos(\theta)) \quad (2)$$

where, $\rho(\lambda)$ is the reflectance at the top of the atmosphere, L is the radiance, d is the ground-sun distance, $Ei(\lambda)$ is the solar irradiance and θ is the solar zenith angle. The values used to convert the Digital Numbers to Radiance and Reflectance of the ETM Sensor of the Landsat satellite is shown in the Table 1.

Table 1. Conversion Factors for Radiometric Correction

Band	Bias	Gain	Irradiance [W/m_2*µm]
1	-6.2	0.7757	1969.0
2	-6.4	0.7957	1840.0
3	-5.0	0.6192	1551.0
4	-5.1	0.9655	1044.0
5	-1.0	0.1257	225.7
7	-0.35	0.043	1368.0

3.7 Atmospheric correction

Atmospheric distortions are characterized by spatial and temporal variations, that is, the dispersions are not constant throughout the image, but certain zones may have been more affected than others (Chuvieco, 1995). For this purpose, the FLAASH model was applied in satellite imagery analysis software, using parameters such as orbit height, geographic coordinates of the image center, type of study area (rural or urban), and date and time of the picture.

3.8 Geometric correction

It corrects any change of position that the pixels occupy over the physical space that encompasses the image, which modifies only the geographical coordinates of each pixel. The Figure 3 shows the corrected images for the years 2000 and 2010, where the location of the glacier and the retreat suffered in the period of interest is clearly observed.

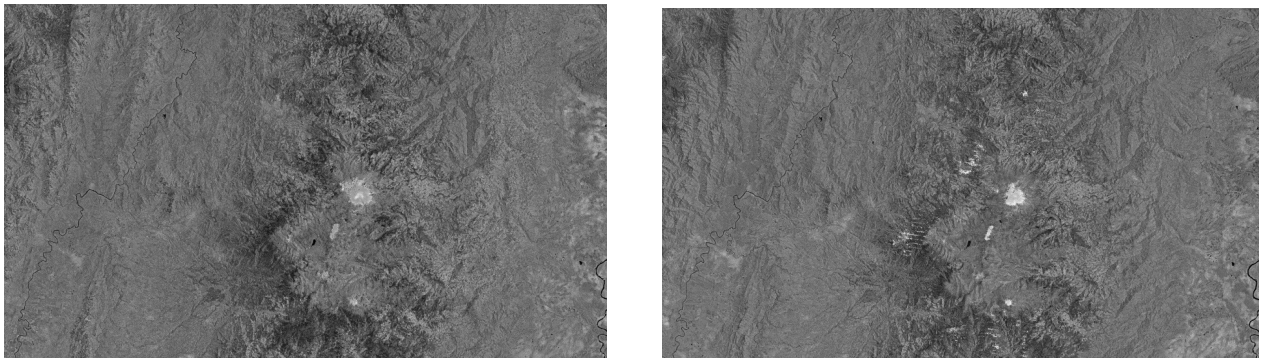

Figure 3. Corrected images of the years 2000 (upper) and 2010 (lower) RGB combination: 543.

3.9 Supervised classification

The process consists in defining the polygons from the combinations of bands that best highlight the coverage of interest, save the spectral values of the image corresponding to the digitized polygon, and then classification process can be carried out for all polygons. Figure 4 shows the allocation of training polygons for cloud cover and glacier cover.

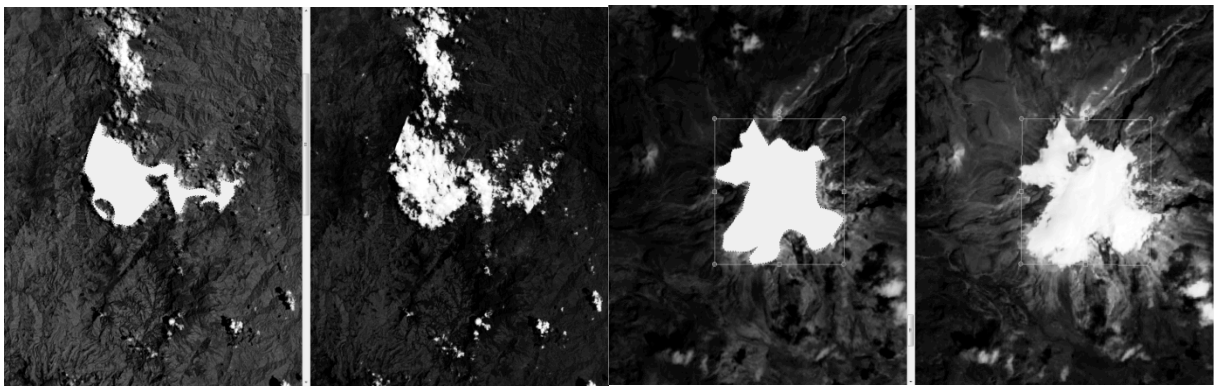

Figure 4. Assignment of polygons for the clouds cover (Left) and glacier cover (Right).

3.10 Neighbourhood (salt and pepper effect)

It is a matrix interpolation process that allows redefining the contours of the previously identified covers. Figure 5 shows the reduction of the salt and pepper effect in a portion of the image.

3.11 Adjustment of the legend according to the national legend

The land covers identified in the area of influence of the NNNP must be adjusted to the standardized cartographic units according to the methodology of the CORINE Land Cover National Legend. The standard suggested by IDEAM proposes three levels of classification composed by 5 covers in Class, 15 for Subclass and 57 in Covers (IDEAM, 2010). The classification level reached

according to the Landsat images used and the area of interest was 4 types of covers for class and 8 for the Subclass (See Figure 6).

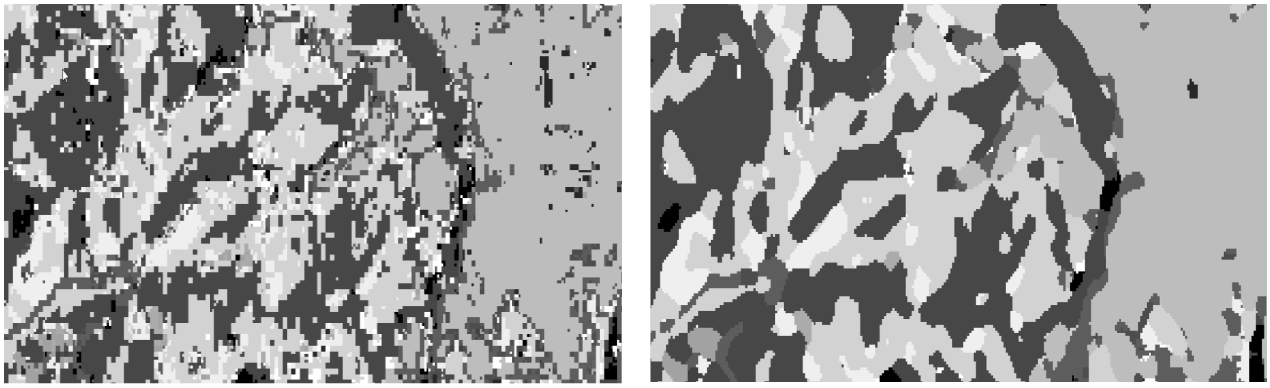

Figure 5. Image Assigned (Left), Processed Image Neighbourhood (Right).

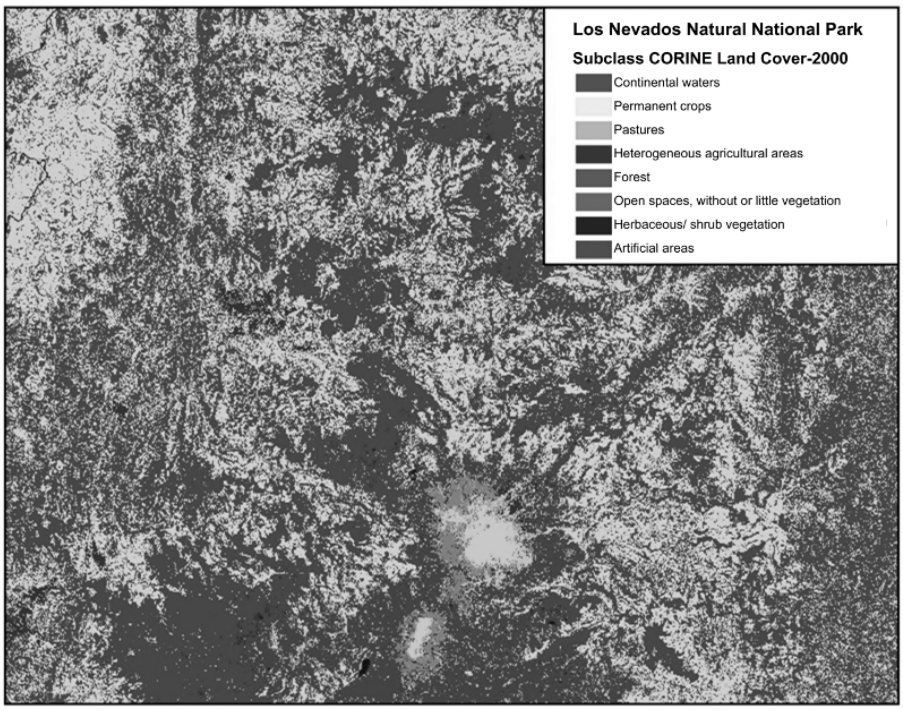

Figure 6. Subclasses map of land use and coverage in the area of influence of NNNP.

4. RESULTS

Different land use map were obtained and compared according to the methodology of the CORINE Land Cover National Legend, indicating the relevance of land use changes in the NNNP since 2000.

From the Structural Analysis of gravity data (Bouguer Anomaly), used to obtain the thickness of the glacier layer, it was concluded that a trend removal of order two at a global level (100%) has to be carried out, in order to obtain the interpolation map of the prediction values and finally compare the models.

From the geostatistical analysis, the best fit for the semivariogram is the spherical model. The values of this one, as the scatter plot allows to determine the surface and to generate the map of Bouguer Total Anomaly predictions, with the following characteristics: Highest Rank: 0.18699 degrees, Lesser Rank: 0.09574 degrees, Anisotropy: Address 54 (North-East), Sill: 1464.7 and

Nugget Effect: 203.03

The spherical model with Ordinary Kriging method shows the mean error close to zero (0.1201), the mean square error (24.46), the mean of the standardized error is very close to zero (0.004935) Standardized EMC root (0.8533) close to 1. Meanwhile for the spherical model with the Simple Kriging method the corresponding values are: -0.7044, 18.78, -0.01791 and 0.6251 (See Figure 8).

If we compare the values of each model, we can conclude that the best model is the Spherical Kriging Ordinary Model whose equation is:

1464,7*Spherical*(0.18699,0.095742,54.0)+203,03*Nugget (3)

The scatter plots shown in Figure 7, indicate the Error Scatter, Standard Error, and QQPlot for each model, allowing to visually check the differences between each model.

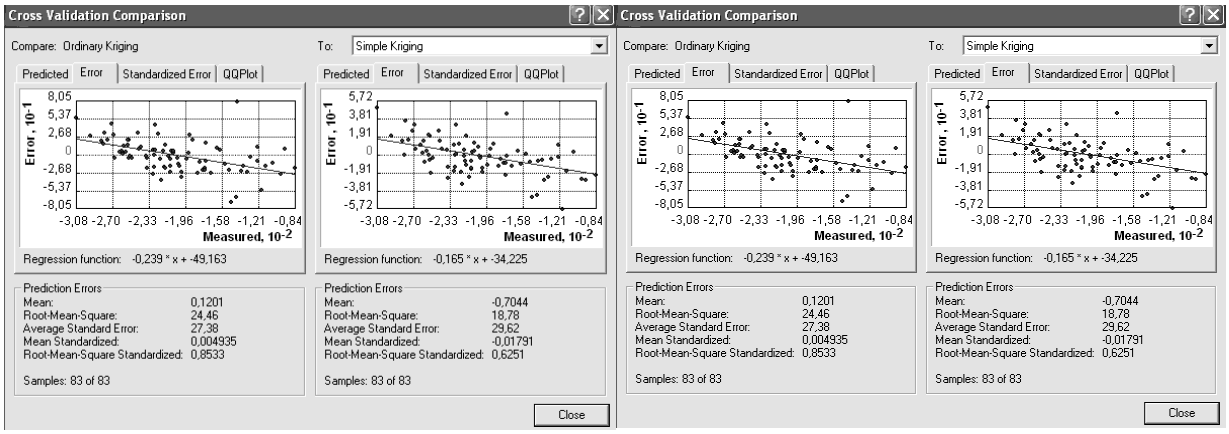

Figure 7. Comparison Prediction of Ordinary Kriging and Simple Kriging Models (left) and Comparison of Errors of the Ordinary Kriging and Simple Kriging Model (right)

Taking into account the above and using the Demenickaja (Equation 4), which takes into account the average thickness of a glacier layer (50 m) with volcanic structures similar to those of El Ruiz in Colombia, and using the density contrast values between Ice (0.92 g / cm3) and rock (2.67 g / cm3), we obtain the general preliminary model of the thickness of the glacier layer, where the expected thickness has higher values, and a lower thickness layer is identified in the Northeast area with values around 5 meters (see Figure 8).

0,05*(1-TANH(0.0034*bouguer)) (4)

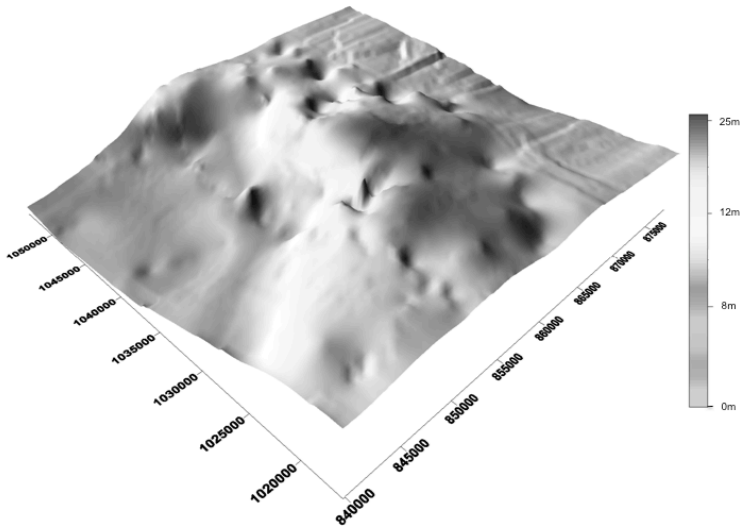

Figure 8. Preliminary model of the glacier thickness layer at El Ruiz glacier

5. CONCLUSIONS

The Radar Altimetry analysis obtained from GRACE images for 2015 allowed to estimate the glacier layer thickness, with values up 25 meters depth of ice.

The multi-temporal analysis (2000 and 2010) of land use and soil cover changes in the area of influence of the NNNP was obtained satisfactorily. From this analysis was detected a reduction of the Forest and an increment of the Agricultural territory, it also showed the retraction of El Ruiz and Santa Isabel glaciers. The reduction of moorlands in favour of livestock and potato crop with its impact on social and environmental aspects, like the reduction of the hydrologic response and the increase of pollution. This analysis serves as a tool for decision makers in the water resources planning and land management in their hydric and social part, based on remote sensors information of free access.

ACKNOWLEDGEMENTS

Authors want to thank the Joint Project University of Caldas and UNAL "Multitemporal analysis of change of land use and land cover in the area of influence of the Los Nevados National Natural Park, a social perspective", the Institute of Hydrology, Meteorology and Environmental Studies of Colombia (IDEAM) for supply information, and CORPOCALDAS.

REFERENCES

Aldalur, B., & Santamaria, M. 2002. Realce de imágenes : filtrado espacial. Revista de Teledetección, 17, 31–42.

Baranowski, S. 1977. The subpolar glaciers of Spitsbergen seen against the climate of this region. Acta University Wratisl.

Camargo, S. 2011. Determinación del Espesor de Corteza para el Noreste de Suramérica por Gravedad y PseudoGravedad, Universidad Distrital Francisco José de Caldas, Bogotá.

Camargo Vargas S.A. 2011. Determinación del espesor de la corteza terrestre para el Noreste de Suramerica por Gravedad. Universidad Distrital. Bogotá

Casassa, G. 1987. Ice Thickness deduced from gravity anomalies on Soler Glacier, Nef Glacier and the Northern Patagonia Icefield. Bulletin of Glacier Research, 4: 43-57.

Ceballos J. & Euscategui C. 1999. El Cambio Climático sobre los Glaciares Colombianos. V Congreso de Meteorología. Bogotá.

Ceballos, J. & Euscátegui, C. 2002. Clima y deglaciación en el Nevado de Santa Isabel. Bogota, IDEAM, 10 p.

Chander, G., Markham, B. L., & Helder, D. L. 2009. Summary of current radiometric calibration coefficients for Landsat MSS, TM, ETM+, and EO-1 ALI sensors. Remote Sensing of Environment, 113(5), 893–903. http://doi.org/10.1016/j.rse.2009.01.007

Chuvieco, E. 1995. Fundamentos De Teledeteccion Espacial (Segunda). Madrid: EDICIONES RIALP, SA.

Chuvieco, E. 2005 Teledetección ambiental citado por CASTILLO, Martha y Pinta, Juan..Análisis multitemporal del cambio de uso del suelo con relación a la cobertura vegetal protectora. Trabajo de grado (Geógrafo). Página 34, 35.

Euscategui, C. 2002. Incidencias de las variaciones del Brillo Solar en la Dinámica Glaciar del Volcán Nevado de Santa Isabel, Revista Meteorología Colombiana.

Fonseca, J. J. 2003. Análisis Multitemporal Mediante Imágenes Landsat Caso De Estudio: Cambio De Área Laderas De La Ciénaga De Tumaradó Parque Natural Los Katíos. Universidad Militar Nueva Granada.

Flórez, A., 1992. Los Nevados de Colombia, Glaciales y Glaciaciones. Análisis Geográficos. Vol. 22. Instituto Geográfico Agustín Codazzi. Bogotá. Colombia. 95 pp.

Hasan, K. F. 2006. A Digital Approach of Satellite Image Processing for Retrieving Surface Parameters. International, 1(3), 1242-1246.

IDEAM. 1997. Los Glaciares Colombianos, expresión del cambio climático. Bogota.

IDEAM. 2010. Leyenda nacional de coberturas de la tierra. Metodología CORINE Land Cover adaptada para Colombia, escala 1:100.000. Area, TH-62-04-1(257), 16.

INGEOMINAS. 1984. Compilación sobre glaciares en Colombia. Bogotá, Oficina de Planeación, Instituto Nacional de Investigaciones Geológico-Mineras.

Jaramillo A. 2005. Clima andino y café en Colombia [Andean climate and coffee in Colombia]. Cenicafé Chinchiná Caldas 2005.

Marulanda A., Fonseca O.A., Vélez J.,J., and Cardona, O.D. 2016. Hydrological study of the potential effects of the melting of Nevado del Ruiz glacier on urban growth zones in Manizales, Colombia. Hydrological Sciences Journal 61(12)

Maryland, U. (2016). Global Forest Change. http://earthenginepartners.appspot.com/science-2013-global-forest

Parker L.R. 1994, Geophysical Inverse Theory, Princeton University Press, New Jersey, 380-389 pág.

Poveda, G. and Pineda, K., 2009. Reassessment of Colombia's tropical glacier retreat rates: are they bound to disappear during the RamaKrishnan, R., Manthira Moorthi, S., Prabu, S., & Swarnalatha, P. (2013). Comparative analysis of various methods for preprocessing of satellite imagery. International Journal of Engineering and Technology, 5(1), 431-437.

Rodríguez, N., Pabón, J., Bernal, R., & Martinez, J. 2010. Cambio climático y su relación con el uso del suelo en los Andes colombianos (p. 84). Instituto de Investigación de Recursos Biológicos Alexander von Humboldt, Universidad Nacional de Colombia y Departamento Administrativo de Ciencia, Tecnología e Innovación, 2010.

Proceedings of the 10th World Congress of EWRA 'Panta Rhei', 5-9 July 2017, Athens, Greece
© 2017 *European Water Resources Association*

Comparison of two habitat modeling approaches for the determination of the ecological flow

G. Papadonikolaki[1*], A. Stamou[1], E. Dimitriou[2], M.-D. Bui[3] and P. Rutschmann[3]
[1] *Department of Water Resources and Environmental Engineering, School of Civil Engineering, National Technical University of Athens (NTUA), Athens, Greece*
[2] *Hellenic Centre for Marine Research (HCMR), Anavyssos, Greece*
[3] *Institute of Hydraulic and Water Resources Engineering, Technical University of Munich, Munich, Germany*
[*] *e-mail: georgia.papadon@gmail.com*

Abstract: Over the past decades, severe environmental problems have been caused by the inefficient water resources management by humans; in rivers, diversions, dam constructions and water abstractions mainly for irrigation purposes lead to flow-regime alterations and threat river ecosystems mainly during the dry period when the flow is dramatically reduced. To prevent fish extinction and ensure the good ecological status of aquatic ecosystems, the EU Water Framework Directive proposes the definition of a minimum flow rate, commonly called "Ecological Flow", in rivers. In this study, we compare two different approaches for the determination of the Ecological Flow in Sperchios river, Central Greece, for the case of Squalius vardarensis which is the most important species inhabiting this river. The first approach is the habitat model PHABSIM which is an easy-to-use engineering tool utilizing one-dimensional calculations both for hydraulic and habitat modeling. We define Ecological Flow via the calculation of the Weighted Usable Area of the river as a function of discharge. The second approach is an integrated two-dimensional habitat model which was developed in the National Technical University of Athens in cooperation with the Technical University of Munich and the Hellenic Centre for Marine Research; this model is a combination of the hydrodynamic model TELEMAC-2D and a habitat model. The results of the two methods are in reasonable agreement; however, the two-dimensional calculations offer higher accuracy and reliability but require much more detailed input data and computational time compared to the one-dimensional method.

Key words: Ecological flow, Habitat Modeling, PHABSIM, Telemac-2D, Sperchios river

1. INTRODUCTION

Severe environmental issues have arisen over the past decades due to over-exploitation and inefficient management of water resources. In rivers, diversions, dam constructions and water abstractions lead to flow-regime alterations threatening river ecosystems, mainly during the dry period when the flow is dramatically reduced. To prevent fish extinction and ensure the good ecological status of aquatic ecosystems, the EU Water Framework Directive proposes the definition of a minimum flow rate, commonly called "Ecological Flow". Several methodologies for the definition of Ecological Flow exist; these can be divided into (1) Hydrological, (2) Hydraulic-Habitat and (3) Holistic (Tharme, 2003; Petts, 2009; Linnansaari et al., 2012). Hydraulic-Habitat simulation is one the most accurate and easy to apply methodologies combining hydraulic calculations with biological models.

In this work, we apply the Hydraulic-Habitat simulation by employing the one-dimensional (1D) model PHABSIM to calculate the Ecological flow for Sperchios River, Greece. The results are compared against the calculations of Stamou et al. (2017) who applied a two-dimensional (2D) Hydraulic-Habitat model which was a combination of the hydrodynamic model TELEMAC-2D and a habitat model which they developed in the National Technical University of Athens in cooperation with the Technical University of Munich and the Hellenic Centre for Marine Research.

2. CALCULATIONS

2.1 Study area and data

The Sperchios River is located in Central Greece and is characterized by a Mediterranean climate with low flows in the summer and high flows in late autumn, winter and spring. It flows through an area of former wetlands which have been reclaimed for agricultural uses and finally discharges into Maliakos Gulf. Subsequently, its water is used primarily for irrigation purposes via local water abstractions; these abstractions lead to severe reduction of its flow, especially during the summer, and thus cause detrimental effects on river ecosystem. For this reason the definition of Ecological flow for this river is considered to be critical.

For the calculation of Ecological flow for Sperchios River we exploited the data from Stamou et al. (2017) who selected a 200 m long river reach at location Loutra Ypatis (see Figure 1) based on the intense upstream water abstractions for irrigation. They initially conducted a detailed topographic survey to obtain the geomorphology of the reach and the flood plain. In this reach, they selected 5 cross-sections in order to take water depth and flow velocity measurements using a propeller current meter. Moreover, they characterized the bed material, which was predominantly pebbles and cobbles, to divide the reach into two segments; the 75 m long upstream part was characterized by the presence of clay accumulated at the banks of the river, while in the downstream segment the slope was steeper, silt was washed out and heavier cobbles were distributed evenly throughout the bottom of the river. Manning coefficient (n) was estimated next; for the upstream and downstream parts n was taken equal to 0.028 and 0.032 respectively. Stamou et al. (2017) used these data in the first part of their model, i.e. in the calibration, verification and application of the hydrodynamic model TELEMAC-2D.

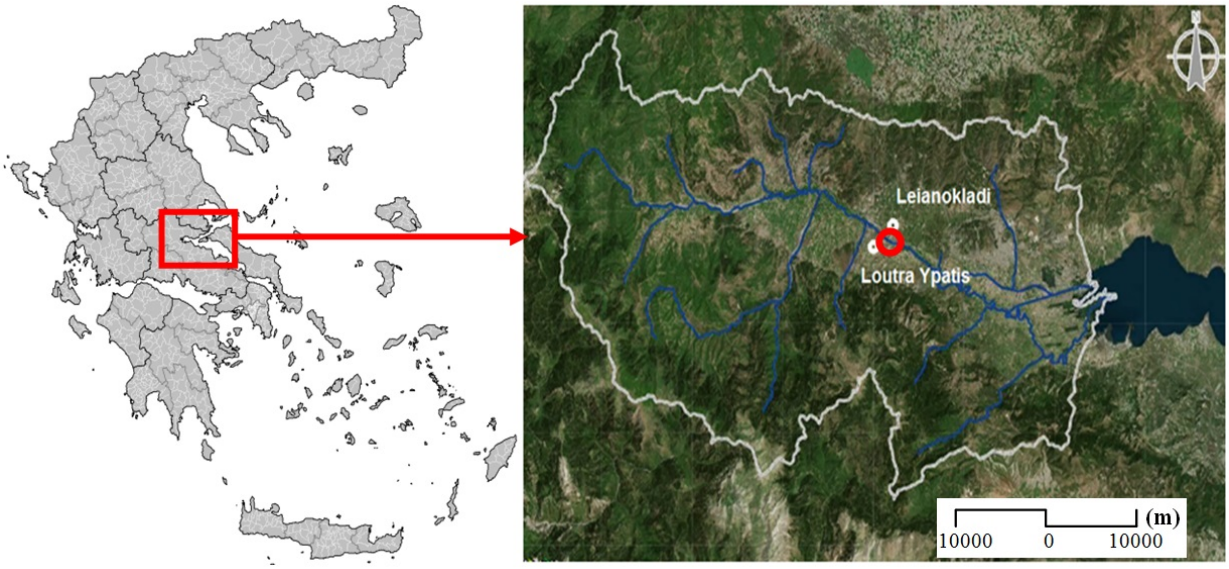

Figure 1. The study area

For the application of their habitat model Stamou et al. (2017) detected the most important fish species in Sperchios river, i.e. *Squalius vardarensis* or commonly called Chub. Two size classes were examined, i.e. the small sized (<10 cm) and large sized Chub (>10 cm). They developed the Habitat Suitability Curves (HSCs) for water depth (D) and mean velocity (V), which are shown in Figure 2, based on international standards (Heggenes and Saltveit, 1990; Martínez-Capel et al., 2009) and literature (Bovee et al., 1986; Brosse and Lek, 2000; Fukuda et al., 2011).

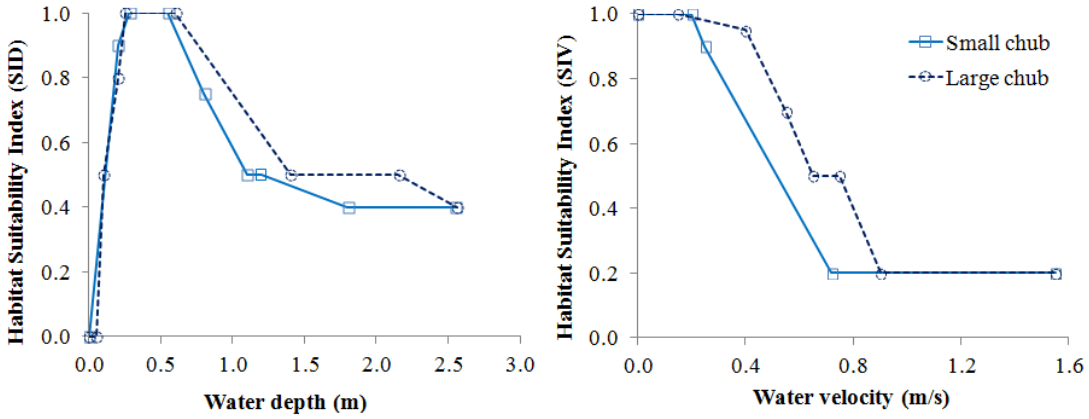

Figure 2. Habitat Suitability Curves for water depth and mean velocity

2.2 Application and results of the Hydraulic-Habitat Models

PHABSIM, which is applied in the present study, is a 1D Physical Habitat Simulation that includes two sub-models: a hydraulic model and a habitat model. In this model the study area is divided into a number of cross sections, for which the available data field is large enough, whereas each cross section is divided into a number of smaller cells; each cell is characterised by its index (i) and area (Ai). For each cell the Velocity (V_i), Water Depth (D_i), Channel Index (CI_i) and bed profile data are defined as inputs (Stamou, 2015). Thus, for the application of PHABSIM we divided the chosen river reach into 5 cross sections exploiting the geometric and hydraulic data available by Stamou et al. (2017); these cross sections were CS0 (x=0.0 m), CS50 (x=50.0 m), CS154 (x=154.0 m), CS163 (x=163.0 m) and CS197 (x=197.0 m), where CS0 is the most upstream cross section.

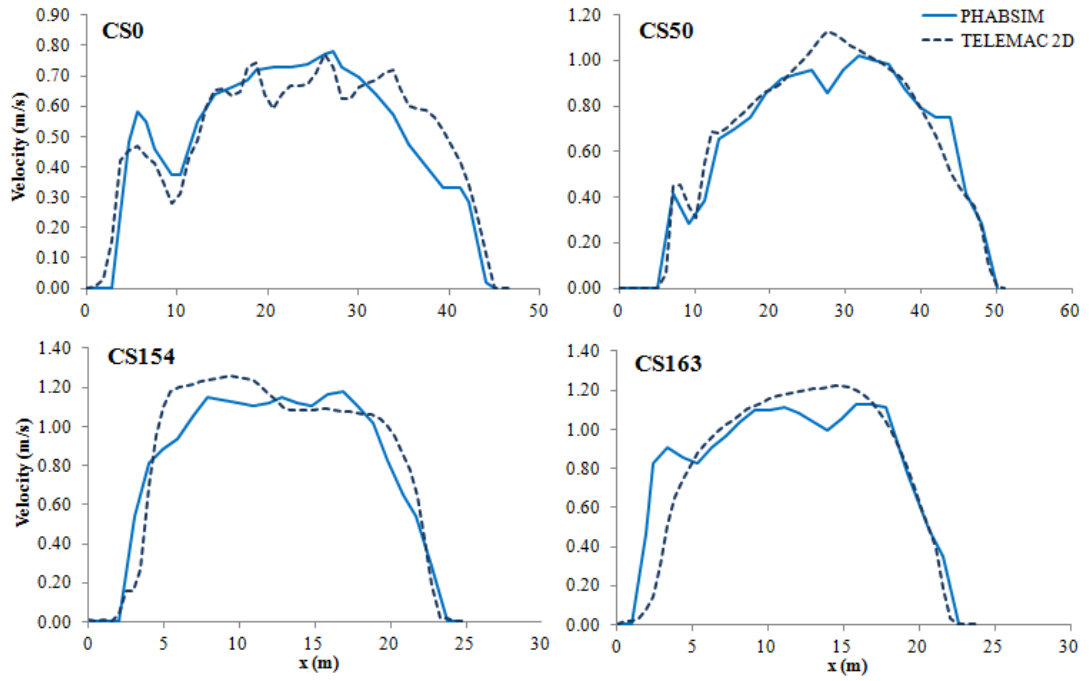

Figure 3. Velocity calculations by PHABSIM and TELEMAC-2D (Stamou et al., 2017) for Q=8.10 m^3/s

Based on the study of Stamou et al. (2017), we initially calibrated the hydraulic model for a discharge equal to Q=8.10 m^3/s to define the Stage-Discharge Curves that would be used next for the calculation of Water Depth for each cross section. Hydraulic calculations were performed for the discharge scenarios used by Stamou et al. (2017), i.e. for Q=0.3, 0.5, 0.9, 1.8, 6.3, 8.1 and 10.0

m^3/s. Velocity profiles for each cross section were calculated using Manning equation; the comparison between the results by the 1D model PHABSIM and TELEMAC-2D (Stamou et al., 2017) shows very good agreement, as shown in Figure 3. It is noted that Stamou et al. (2017) constructed a 2D computational grid based on the spatial coordinates and elevations from 1255 points of the river reach and the flood plain, which they obtained during their topographic survey; the same grid was used in the application of the hydrodynamic and the habitat model.

After conducting the hydraulic calculations, we applied the habitat modeling part for the two size classes of Chub, using the HSCs shown in Figure 2; in order to estimate the Ecological flow, we calculated the so-called Weighted Usable Area (WUA) for each class and discharge scenario, which expresses amount of in-stream habitat. Based on similar studies (Jowett and Davey, 2007, Lambert and Hanson, 1989) and the study of Stamou et al. (2017), for the calculation of WUA we neglected the effect of substrate and took the effect of water depth and mean velocity into account. Moreover, since in PHABSIM for the calculation of WUA along the examined river reach a weight is assigned to each chosen cross section, we performed a sensitivity analysis on its effect on the results; this weight is called Upstream WF (Upstream Weighting Factor). Figures 4 and 5 show the results of WUA by PHABSIM for various Upstream WF scenarios, compared against the results of Stamou et al. (2017).

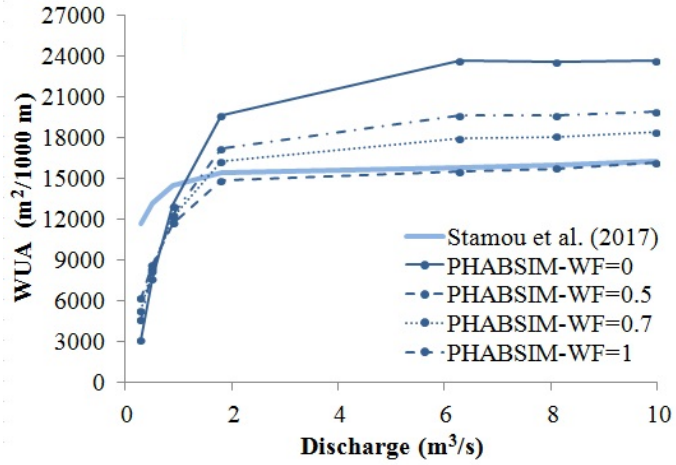

Figure 4. Variation of WUA with discharge and the Upstream WF for the Small Chub

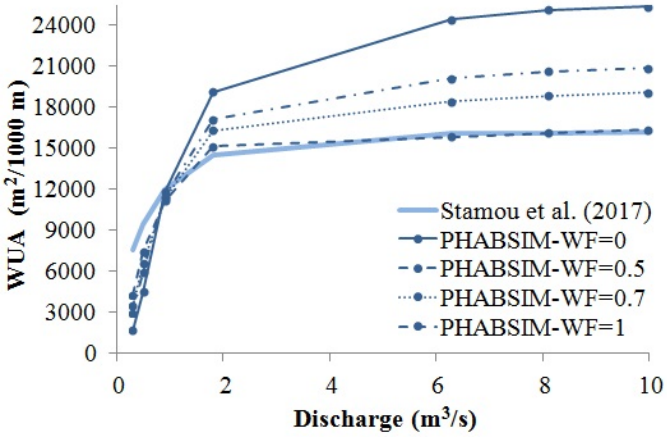

Figure 5. Variation of WUA with discharge and the Upstream WF for the Large Chub

3. DISCUSSION AND CONCLUSIONS

PHABSIM is a useful and easy to use engineering tool, demanding limited input data and

offering very small computational times whereas the application of a 2D Hydraulic-Habitat model, like the one developed by Stamou et al. (2017), requires much more detailed inputs and computational time. 2D calculations offer much more accuracy since the study area is thoroughly examined being divided into a large number of cells whereas in the 1D model it is divided into a discrete number of cross sections which are examined independently; a weight chosen by the Hydraulic Engineer is assigned to each cross section to calculate the WUA along the study area. However, based on the results of Figures 4 and 5, we conclude that the results of WUA by PHABSIM are very sensitive to the effect of this weight, i.e. the Upstream WF, taken into account. Only for Upstream WF=1 we notice very good agreement with the 2D calculations of Stamou et al. (2017). Finally, we conclude that the minimum flow rate that needs to be ensured, i.e. the Ecological Flow, for Sperchios river is the 2 m^3/s both for the Small and the Large Chub; this is in accordance with the calculations of Stamou et al. (2017).

REFERENCES

Bovee, K.D., 1986. Development and evaluation of habitat suitability criteria for use in the instream flow incremental methodology. Instream flow information paper no. 21, US Fish and Wildlife Service. Biological Report; 86 (7), Washington, DC.

Brosse, S., Lek, S., 2000. Modelling roach (Rutilus rutilus) microhabitat using linear and nonlinear techniques. Freshwater Biol.; 44 (3): 441-452. http://dx.doi.org/10.1046/j.1365-2427.2000.00580.x.

Fukuda, S., Mouton, A.M. and De Baets, B., 2011. Abundance versus presence/absence data for modelling fish habitat preference with a genetic Takagi-Sugeno fuzzy system. Environ. Monit. Assess.; 184 (10): 6159– 6171. http://dx.doi.org/10.1007/s10661-011-2410-2.

Heggenes, J., Saltveit, S.J., 1990. Seasonal and spatial microhabitat selection and segregation in young Atlantic salmon, Salmo salar L., and brown trout, Salmo trutta L., in a Norwegian river. J. Fish Biol.; 36: 707–720.

Jowett, I.G., Davey, A.J.H., 2007. A comparison of composite habitat suitability indices and generalized additive models of invertebrate abundance and fish presence-habitat availability. Trans. Am. Fish. Soc.; 136 (2): 428-444. http://dx.doi.org/10.1577/t06-104.1.

Lambert, T.R., Hanson, D.F., 1989. Development of habitat suitability criteria for trout in small streams. Regul. River.; 3 (1): 291-303. http://dx.doi.org/10.1002/rrr.3450030128.

Linnansaari, T., Monk, W.A., Baird, D.J. and Curry, R.A. 2012. Review of approaches and methods to assess Environmental Flows across Canada and internationally. DFO Can. Sci. Advis. Sec. Res. Doc. 2012/039. viii + 74 p.

Martínez-Capel, F., García De Jalón, D., Werenitzky, D., Baeza, D., Rodilla-Alamá, M., 2009. Microhabitat use by three endemic Iberian cyprinids in Mediterranean rivers (Tagus River Basin, Spain). Fish. Manag. Ecol.; 16: 52–60.

Petts G.E. 2009. Instream Flow Science For Sustainable River Management. JAWRA Journal of the American Water Resources Association; 45:1071–1086. doi: 10.1111/j.1752-1688.2009.00360.x.

Stamou, A., 2015. Ecological modeling of surface waters. Notes, Technical University of Munich, Munich.

Stamou, A., Polydera, A., Papadonikolaki, G., Dimitriou E., Bui, M-D, Rutschmann,P., (2017). Determination of Ecological Flow in rivers using an Integrated Hydrodynamic-Habitat Modeling Approach. (submitted in the international journal Ecological Modelling)

Tharme, R.E., 2003. A global perspective on environmental flow assessment: emerging trends in the development and application of environmental flow methodologies for rivers. River Res. Appl.; 19 (5–6): 397–441.

Proceedings of the 10th World Congress of EWRA 'Panta Rhei', 5-9 July 2017, Athens, Greece
© 2017 *European Water Resources Association*

Annual sediment yield prediction by means of three soil erosion models at the basin scale

K. Kaffas*, V. Hrissanthou
Department of Civil Engineering, Democritus University of Thrace, Kimmeria Campus, 67100 Xanthi, Greece
* *e-mail: kostaskaffas@gmail.com*

Abstract: The objective of this study is the estimate of annual sediment yields deriving from soil and streambed erosion, at the outlet of a basin. Continuous simulations of soil and streambed erosion processes are performed in Nestos River basin, on an hourly time basis, for a five-year period. Three different soil erosion models are applied, as part of three Composite Mathematical Models. The first and third Composite Mathematical Models consist of three submodels: a rainfall-runoff submodel, a soil erosion submodel and a sediment transport submodel for streams, whilst the second one does not include a rainfall-runoff submodel and only consists of the soil erosion submodel and of several empirical sediment delivery ratio methods, for the estimation of the final sediment yield at the basin outlet. The rainfall-runoff submodel that is used for the computation of the surface runoff and the streamflow in the sub-basins, is the hydrologic model HEC-HMS 4.2. The first soil erosion submodel, utilized for the estimate of soil erosion in a sub-basin, is based on the relationships of Poesen (1985), the second is the widely known Universal Soil Loss Equation (USLE), while the third is the Modified version of USLE (MUSLE). The sediment routing for the first and third Composite Mathematical Models is achieved by means of the stream sediment transport model of Yang and Stall (1976). The three models are compared as to their ability to realistically predict annual sediment yields at the basin scale.

Key words: annual sediment yields, soil erosion, sediment transport, USLE, MUSLE

1. INTRODUCTION

The impacts of sediment yield in the form of concentrated sediment in the inlet of receptors, such as lakes, coastal zones, dams etc., is mainly limited in the receptor' morphological changes (sedimentation in lakes and dams, decline of coastal zones) and their potential contamination in the case that sediments are carriers of polluting factors. Hence, a more comprehensive evaluation results by assessing sediment yield in its preceding forms of soil erosion and sediment discharge. According to Collins et al. (2001), reliable information on soil erosion rates is an essential prerequisite for the design of targeted erosion and sediment control strategies. Despite the fact that sediments constitute the foundation stone for the balance and survival of - not only - the various aquatic and riparian ecosystems, but the very riverine systems themselves, they are - in the same time - negatively associated with a variety of complications. Erosion and deposition chisel and reshape the wet cross-sectional area, raising the risk of flooding in the case of excessive deposition. Soil erosion is directly connected to a series of environmental issues such as problems with the vegetation growth, increase of soil acidity levels, muddy floods etc. Excessive sedimentation is also associated to an increase of turbidity in streams, increase of water temperatures, decline of the dissolved oxygen's levels and destruction of the natural habitats of the aquatic and riparian life. Furthermore, sediments are potential carriers of contaminant factors. This is more evident in agricultural basins, where fertilizers and pesticides are in use.

The development of models that can reliably simulate soil erosion and sediment transport and predict sediment yields at a basin's outlet is indispensable. A large number of complex methodologies have been introduced for predicting the stream sediment discharge and sediment yield, during the last century, none of which, however, enjoys a broad acceptance so far. Thus, the estimation of sediment discharge endures as one of the utmost elusive goals in the field of sediment

dynamics. This study presents the application of three different soil erosion models as a part of three Composite Mathematical Models (hereafter referred to as CMMs), aiming at the calculation of annual sediment yields at the outlet of Nestos River basin.

2. DESCRIPTION OF THE STUDY AREA

The under study part of Nestos River basin concerns the Greek mountainous part downstream of Platanovrysi dam (Figure 1). The basin extends to an area of 838.63 km^2, the altitude varies between 38 m and 1747 m, the average land slope of the basin is 37% and the length of the part of Nestos River that runs the basin, is approximately 63 km.

The characteristic of the basin is the presence of a dam at its upper boundary, which greatly affects the discharge, as well as the sediment transport in Nestos River. Along with this, two irrigation canals slightly upstream of the basin outlet (Egnatia bridge of Nestos River) are culpable of a recession of water, during the irrigation period, disrupting the final discharge at the basin outlet.

The four main soil types of the basin are: sandy clay loam, silty loam, loamy sand and silty clay loam. The basin is covered in its greatest part by forested and bushy areas and secondarily by crops, while a small fraction corresponds to urban areas and areas with no significant vegetation.

There are four meteorological stations in the area of study: “Mesochori”, “Prasinada”, “Oraio” and “SWAT” (Figure 1). The distribution of the meteorological stations to areas of influence was achieved with Thiessen polygons (Thiessen, 1911) (Figure 1).

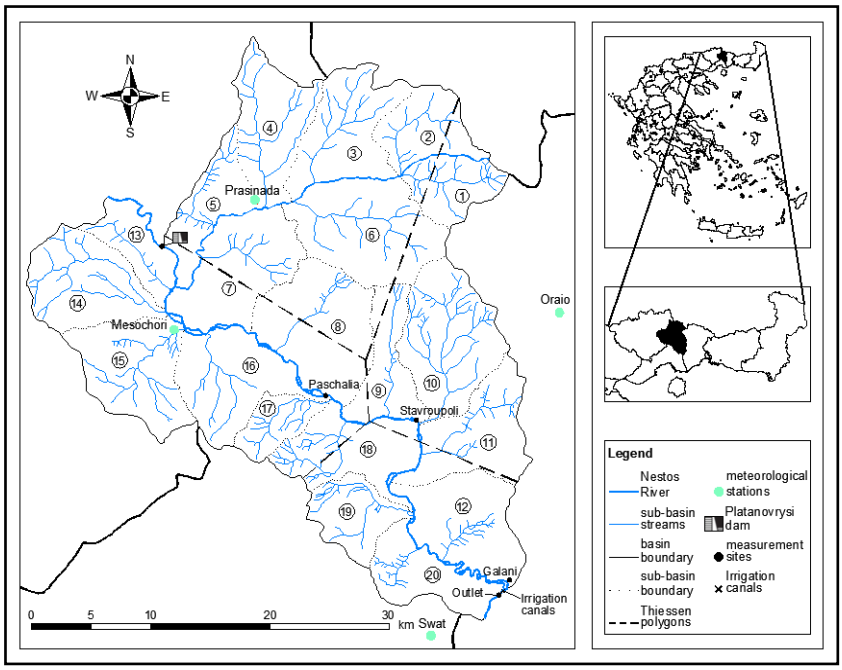

Figure 1. Nestos River basin

3. THEORETICAL DESCRIPTION OF THE MODELS

3.1 Rainfall-runoff submodel

A combination of known methods composes the rainfall-runoff submodel, which was built and simulated by the deterministic, semi-distributed hydrologic model HEC-HMS 4.2. More specifically, the Soil Conservation Service - Curve Number method (SCS, 1972) was used for the estimation of the hydrologic losses (mm) into the ground, as well as the amount of rainfall excess

(mm), the FAO-56 Penman-Monteith method (Allen et al., 1998) was used for the estimation of hydrologic losses due to evapotranspiration, whilst the transformation of rainfall excess to runoff hydrograph was achieved by means of the Soil Conservation Service dimensionless synthetic unit hydrograph (SCS, 1971). The Pasini's formula (Pasini, 1914) was applied for the estimation of the concentration time, while lag time was calculated by means of the - most commonly used - empirical equation of Soil Conservation Service (SCS, 1972). The model also comprises an exponential recession model to represent the time variation of baseflow (Barnes, 1939). Finally, the routing of the total discharge (direct runoff + baseflow) hydrograph from the outlet of a sub-basin to the outlet of the whole basin is enabled by means of Muskingum-Cunge model, which is based on the well known hydrologic routing Muskingum model (Cunge, 1969).

A much more thorough outline of the rainfall-runoff submodel can be found in Kaffas and Hrissanthou (2014) and Kaffas and Hrissanthou (2017).

3.2 Soil erosion submodels

3.2.1 First soil erosion submodel - Relationships of Poesen (1985)

The amount of soil loss in a basin is due to soil erosion caused by rainfall (detachment by raindrop impact) and soil erosion caused by runoff (shearing force of flowing water).

The estimation of soil erosion due to rainfall was achieved by the relationships of Poesen (1985):

$$q_{rs} = C\left(KE\right)r_s^{-1}\cos a \tag{1}$$

$$q_r = q_{rs}\left[0.301\sin a + 0.019D_{50}^{-0.22}\left(1-e^{2.42\sin a}\right)\right] \tag{2}$$

where q_{rs} is the mass of detached particles per unit area (kg/m^2); C is the soil cover factor; KE is the rainfall kinetic energy (J/m^2); r_s is the soil resistance to drop detachment (J/kg); a is the slope gradient (°); q_r is the downslope splash transport per unit width (kg/m); and D_{50} is the median particle diameter (m).

The soil erosion due to runoff is calculated by means of Nielsen's equation (Nielsen et al., 1986), whilst the sediment transport capacity by runoff is computed by the modified formula of Engelund and Hansen (1967). The sediment yield that reaches the stream, is calculated by means of a comparison between the available sediment and the sediment transport capacity by runoff. A detailed version of the first soil erosion submodel can be found in Kaffas and Hrissanthou (2015).

3.2.2 Second soil erosion submodel - Universal Soil Loss Equation

The widely known Universal Soil Loss Equation (USLE) (Wischmeier and Smith, 1965) quantifies soil erosion caused by rainfall as a function of six factors, according to Equation (3):

$$A = R_{rainfall}\cdot K\cdot L\cdot S\cdot C\cdot \mathrm{P} \tag{3}$$

where A is the soil loss per unit area [t/(ha yr)]; $R_{rainfall}$ is the rainfall erosivity factor [MJ mm/(ha h yr)]; K is the soil erodibility factor [t h/(MJ mm)]; L is the slope length factor; S is the slope steepness factor; C is the cover and management factor; and P is the support practice factor.

The calculation of the rainfall erosivity factor, $R_{rainfall}$, requires the intensity and duration of erosive rainfalls (İvrem et al., 2007). This would result to the derivation of individual unique values of $R_{rainfall}$ factor for each rainfall event. At this point, it has to be stated that the rainfall erosivity

factor, alone, anchors the USLE at the estimation of soil erosion by single rainfall events, making it an event-based erosion model. This study, however, aims at the estimation of annual sediment yields at the basin outlet. For this reason, an average annual value of rainfall erosivity factor was estimated by means of six empirical models, using mean monthly and annual rainfall depths.

Arnoldus (1977) modified Fournier's index to:

$$F = \sum_{i=1}^{12} \frac{p_i^2}{P} \tag{4}$$

where F is the modified index value; p_i is the average monthly rainfall depth (mm); and P is the average annual rainfall depth (mm).

The formulas of the six empirical models, used for the estimation of $R_{rainfall}$, are given in Equations (5) - (10), below:

Arnoldus (1977):

$$R_{rainfall} = 0.302 \cdot F^{1.93} \tag{5}$$

Arnoldus (1980):

$$R_{rainfall} = \left[\left(4.17 \cdot F\right) - 152\right] \cdot 17.02 \tag{6}$$

Lo et al. (1985):

$$R_{rainfall} = 38.46 + 3.48 \cdot P \tag{7}$$

Renard and Freimund (1994):

$$R_{rainfall} = 0.739 \cdot F^{1.847} \tag{8}$$

Renard and Freimund (1994):

$$R_{rainfall} = 0.0483 \cdot P^{1.61} \tag{9}$$

Yu and Rosewell (1996):

$$R_{rainfall} = 3.82 \cdot F^{1.41} \tag{10}$$

Williams (1995) proposed the following equation for the soil erodibility factor:

$$K = f_{csand} \cdot f_{cl-si} \cdot f_{orgc} \cdot f_{hisand} \tag{11}$$

where f_{csand} is a factor that reduces the K in soils with high coarse-sand contents and increases it in soils with little sand; f_{cl-si} is a factor that reduces the K in soils with high clay to silt ratios; f_{orgc} is a factor that reduces the K in soils with high organic carbon content; and f_{hisand} is a factor that reduces the K in soils with extremely high sand contents.

The cover and management factor, C, is estimated as a cover factor, due to the fact that the basin is mountainous and the lack of management practices, as a function of the various cover types

of the basin.

The slope length factor, L, and the slope steepness factor, S, are calculated as a combined topographic factor, LS, by Equation (12):

$$LS = \left(\frac{L_s}{22.1}\right)^m \cdot \left[65.41 \cdot \sin^2(a) + 4.56 \cdot \sin a + 0.065\right] \quad (12)$$

$$m = 0.6 \cdot \left[1 - \exp\left(-35.835 \cdot s\right)\right] \quad (13)$$

where L_s is the slope length (m); m is the exponential term; a is the angle of the slope; and s is the average slope of the sub-basin (m/m).

The support practice factor, P, expresses the impact of support and conservation practices on the average annual soil loss. The closer to unity the P factor, the less the support practices and conservations plans. An average value of 0.9502 was considered, for the area of study, from Panagos et al. (2015).

3.2.3 Third soil erosion submodel - Modified Universal Soil Loss Equation

The key difference between the Universal Soil Loss Equation (USLE) and its Modified version (MUSLE) (Williams, 1975) is that MUSLE, in contrast to USLE, estimates sediment yield due to runoff erosion instead of rainfall erosion. Thus, the rainfall erosivity factor, $R_{rainfall}$, in USLE, is replaced in MUSLE by a runoff erosivity factor, R_{runoff}. The R_{runoff} factor allows MUSLE to be applied for both event and continuous (long-term) erosion modeling, in contrast to the $R_{rainfall}$ factor which anchors USLE to the estimation of soil loss on an event basis. However, rainfall is also taken into account in MUSLE, in the sense that the runoff factor is a function of antecedent moisture condition, as well as of rainfall energy. Another critical difference between USLE and MUSLE that needs to be taken under consideration, in relevant studies, is that the USLE estimates the amount of eroded soil per unit area and time, whilst the MUSLE estimates the sediment yield - due to soil erosion - that reaches the main streams per unit of time. The rest of the MUSLE factors (*K, L, S, C, P*) are computed in the same way as in the USLE.

The Modified Universal Soil Loss Equation (MUSLE) is given below:

$$sed = 11.8 \cdot \left(Q_{surf} \cdot q_{peak} \cdot area_{sub}\right)^{0.56} \cdot K \cdot L \cdot S \cdot C \cdot P \quad (14)$$

where sed is the sediment yield, in t, per unit of time; Q_{surf} is the surface runoff volume (mm/km^2); q_{peak} is the peak runoff rate (m^3/s); $area_{sub}$ is the area of the sub-basin (km^2).

3.3 Models for the calculation of the final sediment yield at the basin outlet

3.3.1 Stream sediment transport model of Yang and Stall (1976)

Sediment transport capacity by streamflow is estimated from the sediment concentration in the stream, which is computed by the relationships of Yang and Stall (1976):

$$\begin{aligned} \log c_{ts} = {} & 5.435 - 0.286 \log \frac{wD_{50}}{v} - 0.457 \log \frac{u_*}{w} \\ & + \left(1.799 - 0.409 \log \frac{wD_{50}}{v} - 0.314 \log \frac{u_*}{w}\right) \log\left(\frac{us}{w} - \frac{u_{cr}s}{w}\right) \end{aligned} \quad (15)$$

where c_{ts} is the total sediment (sand) concentration by weight (ppm); w is the terminal fall velocity of sediment particles (m/s); D_{50} is the median particle diameter (m); ν is the kinematic viscosity of the water (m^2/s); s is the energy slope; u is the mean flow velocity (m/s); u_{cr} is the critical mean flow velocity (m/s); and u_* is the shear velocity (m/s).

A more thorough outline of the stream sediment transport submodel can be found in Kaffas and Hrissanthou (2015).

3.3.2 Sediment delivery ratio

As it has already been mentioned, the USLE estimates the amount of eroded soil per unit area and time. This indicates that a method for the estimation of the amount of eroded soil that gets deposited in the basin, and does not reach the main stream, has to be included. Four different empirical models estimating the sediment delivery ratio - namely the percentage of the total erosion amount that reaches the outlet of the basin - were used in this study. However, as with all empirical models, these formulas have been developed for certain conditions and limitations and they do not guarantee efficient application in an environment that differs from the one they were primarily created for. The following formulas [Equations (16) - (19)] were developed for certain sites in the USA.

Maner (1958):

$$\log\left(DR\right) = 2.94259 - 0.82362 \cdot \log\left(\frac{\ell}{RL}\right) \tag{16}$$

where DR is the delivery ratio (%); l is the length of the main stream (ft); and RL is the difference between the altitude of the two ends of the main stream (ft).

Maner (1962):

$$\log\left(DR\right) = 1.8768 - 0.14191 \cdot \log\left(10 \cdot FL\right) \tag{17}$$

where DR is the delivery ratio (%); and FL is the basin area (mi^2).

Williams and Berndt (1972):

$$DR = 0.627 \cdot s^{0.403} \tag{18}$$

where DR is the delivery ratio (decimal); and s is the mean bed slope of the main stream.

Williams (1977):

$$DR = 1.366 \cdot 10^{-11} \cdot FL^{-0.0998} \cdot \left(\frac{RL}{\ell}\right)^{0.3629} \cdot CN^{5.444} \tag{19}$$

where DR is the delivery ratio (decimal); FL is the basin area (km^2); RL is the difference between the altitude of the two ends of the main stream (m); l is the length of the main stream (km); and CN is the average value of the Curve Number for the entire basin.

The aforementioned models were applied to the total erosion amount (soil erosion and streambed erosion). The USLE estimates an overall mean annual amount of soil erosion, and the soil erosion products cannot be routed through a stream sediment transport model, as the one presented in Subsection 3.3.1. Hence, the erosion of the streambed and banks was estimated empirically as a fraction (20%) of soil erosion by bibliographic suggestions (Roehl, 1962).

4. APPLICATION OF THE MODELS

HEC-HMS ran continuously for a five year period, from 2009 to 2013, resulting in runoff, baseflow and total stream discharges (surface runoff + baseflow) at an hourly time step. The rainfall depths and runoff hydrographs constitute the decisive input data to the first soil erosion submodel (Poesen), whilst only the runoff hydrographs were used as input to the third soil erosion submodel (MUSLE). The outcome of the two models is the sediment yield that reaches the main streams of the sub-basins. All the simulations were carried out at the sub-basin scale and for this reason the basin was divided into twenty natural sub-basins (Figure 1). The application of the first and third CMMs results to hourly sediment yields, which are summed to provide the annual sediment yields at the basin outlet.

Rainfall data for an eleven-year period, from 2003 to 2013, were used to define the $R_{rainfall}$ factor, which was calculated separately for each of the twenty sub-basins. Each of the Equations (5) - (10) provided a different value for $R_{rainfall}$ factor and, finally, an average value was obtained for each sub-basin. The $R_{rainfall}$ factor varies between 1413.37 MJ mm/(ha h yr) and 2291.96 MJ mm/(ha h yr). The result from the USLE is the total soil erosion amounts of the sub-basins which were summed to provide the amount of soil erosion for the entire basin. This was multiplied by 1.2 to reckon in the streambed and bank erosion. Finally, the sediment delivery ratio, DR, was computed by each of the Equation (16) - (19) which provided an average value of 10.24%. This means that 10.24% of the total erosion amount (soil erosion + erosion from the main streams) reaches the outlet of the basin.

5. RESULTS

Table 1 displays the annual sediment yield values as they resulted from the application of the first and third CMMs. The sediment yields are provided in t/yr, while these values are divided by the area of the basin to provide sediment yields in t/km^2/yr.

Table 1. Annual sediment yields at the basin outlet

Year	Annual sediment yield (10^6 t/yr)		Annual sediment yield (t/km^2/yr)	
	First Composite Mathematical Model (Poesen)	Third Composite Mathematical Model (MUSLE)	First Composite Mathematical Model (Poesen)	Third Composite Mathematical Model (MUSLE)
2009	1.05	1.23	1250	1470
2010	1.09	1.35	1303	1611
2011	0.41	0.62	482	734
2012	1.31	1.12	1567	1334
2013	0.98	1.10	1166	1311

In Table 2, the average annual sediment yield values of all the three CMMs are given for the period 2009-2013, in t/yr and t/km^2/yr.

Table 2. Average annual sediment yields at the basin outlet for the period 2009-2013

Model	Average annual sediment yield (10^6 t/yr) for the time period 2009-2013	Average annual sediment yield (t/km^2/yr) for the time period 2009-2013
First Composite Mathematical Model (Poesen)	0.97	1154
Second Composite Mathematical Model (USLE)	1.58	1888
Third Composite Mathematical Model (MUSLE)	1.08	1292

6. CONCLUSIONS

It is concluded that there is a very good approximation between the results of the first (Poesen) and the third (MUSLE) CMMs. The sediment yield values of the second CMM (USLE) are also nigh to those of the other two models, but slightly higher. This can be attributed to the various empirical methods included in the second CMM, as well as to the fact that the annual sediment

yields in the first and third CMMs resulted as a sum of hourly sediment yields. This high level of disaggregation (hourly time steps) imparts to these models a very high degree of precision. It could be stated that the connection of the submodels, in the CMM, through the input-output data ensures the almost parallel running of the models, which approximates the natural reality.

Knowledge of the sediment yield at the outlet of a basin or at another point of interest, as well as the study of its preceding processes (soil and streambed erosion) constitutes the most vital information when it comes to the hydromorphological study at the basin scale and the study of riverine systems.

Given the fact that the process of measuring the sediment yield is a difficult and laborious task, yet of great significance for a variety of reasons, the CMMs presented here, can be used in both the Greek and the Mediterranean mountainous terrain to successfully estimate soil erosion, sediment discharges and sediment yields at the basin scale.

REFERENCES

Allen, R. G., Pereira, L. S., Raes, D., Smith, M., 1998. Crop Evapotranspiration: Guidelines for Computing Crop Requirements. FAO Irrigation and Drainage Paper No. 56, FAO, Rome, Italy.

Arnoldus, H. M. J., 1977. Methodology used to determine the maximum potential average annual soil loss due to sheet and rill erosion in Morocco. FAO Soils Bulletins (FAO).

Arnoldous, H. M. J., 1980. An approximation of the rainfall factor in the USLE in assessment of erosion. England: Wiley Chichester; pp. 127-132.

Barnes, B. S., 1939. The structure of discharge recession curves. Transactions of the American Geophysical Union; 20(4): 721-725.

Collins, A. L., Walling, D. E., Sichingabula, H. M., Leeks G. J. L., 2001. Using 137 Cs measurements to quantify soil erosion and redistribution rates for areas under different land use in the Upper Kaleya River basin, southern Zambia. Geoderma; 104(3): 299-323.

Cunge, J. A., 1969. On the Subject of a Flood Propagation Computatronal Method (Muskingum Method). J. of Hydraulic Research; 7(2): 205-230.

Engelund, F., Hansen, E., 1967. A monograph on sediment transport in alluvial streams. Teknisk Forlag, Copenhagen, Denmark.

İrvem, A., Topaloğlu, F., Uygur, V., 2007. Estimating spatial distribution of soil loss over Seyhan River Basin in Turkey. Journal of Hydrology; 336(1), 30-37.

Kaffas, K., Hrissanthou, V., 2014. Application of a continuous rainfall-runoff model to the basin of Kosynthos river using the hydrologic software HEC-HMS. Global NEST Journal; 16(1): 188-203.

Kaffas, K., Hrissanthou, V., 2015. Estimate of Continuous Sediment Graphs in a Basin, Using a Composite Mathematical Model, Environmental Processes; 2(2): 361-378.

Kaffas, K., Hrissanthou, V., 2017. Computation of hydro-geomorphologic changes in two basins of northeastern Greece. Geomorphology, INTECH Open Access Publisher, ed. Shukla D.P. (forthcoming).

Lo, A., El-Swaify, S. A., Dangler, E. W., Shinshiro, L., 1985. Effectiveness of EI30 as an erosivity index in Hawaii. In: S.A. El-Swaify, W.C. Moldenhauer and A. Lo (Editors), Soil Erosion and Conservation. Soil Conservation Society of America, Ankeny; pp. 384-392

Maner, S. B., 1958. Factors affecting sediment delivery rates in the Red Hills physiographic area. Transactions American Geophysical Union; 39(4), 669-675.

Maner, S. B., 1962. Factors influencing sediment delivery ratios in the Blackland Prairie land resource area. USDA, Soil Conservation Service, Fort Worth, Texas, USA.

Nielsen, S. A., Storm, B., Styczen, M., 1986. Development of distributed soil erosion component for the SHE hydrological modelling system. Proceedings of the International Conference on Water Quality Modelling in the Inland Natural Environment, BHRA, Bournemouth, UK; pp. 1-13.

Panagos, P., Borrelli, P., Meusburger, K., van der Zanden, E. H., Poesen, J., Alewell, C., 2015. Modelling the effect of support practices (P-factor) on the reduction of soil erosion by water at European Scale. Environmental Science & Policy; 51: 23-34.

Pasini, F., 1914. Report on the renana recovery plan, Bologna, Italy (in Italian).

Poesen, J., 1985. An improved splash transport model. Zeitschrift für Geomorphologie; 29: 193-211.

Renard, K. G., Freimund, J. R., 1994. Using monthly precipitation data to estimate the R-factor in the revised USLE. J. of Hydrol. 157: 287-306.

Roehl, J. W., 1962. Sediment source areas, delivery ratios and influencing morphological factors. International Association of Scientific Hydrology; 59: 202-213.

Soil Conservation Service (SCS), 1971. National Engineering Handbook, Section 4: Hydrology. USDA, Springfield V.A., USA.

Soil Conservation Service (SCS), 1972. National Engineering Handbook, Section 4: Hydrology. USDA, Washington D.C., USA.

Thiessen, A. H., 1911. Precipitation averages for large areas. Monthly Weather Review; 39(7): 1082-1089.

Williams, J. R., Berndt, H. D., 1972. Sediment yield computed with universal equation. Journal of the Hydraulics Division; 98(Hy 12).

Williams, J. R., 1975. Sediment-Yield Prediction with Universal Soil Loss Equation Using Runoff Energy Factor. In Present and Prospective Technology for Predicting Sediment Yields and Sources. Proc. of the Sediment Yield Workshop, Oxford, MS; 244-252.

Williams, J. R., 1977. Sediment delivery ratios determined with sediment and runoff models. IAHS Publ; 122: 168-179.

Williams J.R., 1995. In: Computer models of watershed hydrology. Water Resources Publications, Chapter 25, the EPIC Model; 909-1000.

Wischmeier, W. H., Smith, D. D., 1965. Predicting rainfall-erosion losses from cropland east of the Rocky Mountains. Agriculture Handbook 282, USDA-ARS.

Yang, C. T., Stall, J. B., 1976. Applicability of unit stream power equation. Journal of the Hydraulics Division, ASCE; 102(5): 559-568.

Yu, B., Rosewell, C. J., 1996. A robust estimator of the R-factor for the universal soil loss equation. Trans. Am. Soc. Agric. Eng; 39: 559-561.

Proceedings of the 10th World Congress of EWRA 'Panta Rhei', 5-9 July 2017, Athens, Greece
© 2017 *European Water Resources Association*

Bioavailability of metals in soils irrigated by synthetic wastewater: Metal speciation

S.I. Korfali* and H. Karaki
Natural Science Department, Lebanese American University, P.O.Box 1305053, Chouran Beirut 1102 2801,Beirut, Lebanon
** e-mail: skorfali@lau.edu.lb*

Abstract: In Lebanon, Bekaa valley is an agricultural zone; during the dry season, water is withdrawn from Litani River for irrigation which is mostly domestic and industrial waste water. Metal mobility, bioavailability, or potential risks can be anticipated by metal speciation in soil and water. The objective of this study was to investigate the speciation of metals in soil and water of upper Litani basin. Soils samples were subjected to a modified BCR sequential extraction technique that operationally extracts metals as acid soluble, reducible, oxidizing, and residual fraction. Metal content in each fraction and total metal in water were determined by AAS and ICP-MS techniques. Sediment pH, Eh and TOC and macro water parameter were determined. Speciation of metals in water was predicted PHREEQC geochemical computer model. Results indicated in non-residual fraction respectively highest average % of total metal are in reducible and acid soluble (Mn: 27 %, 18; Zn: 18 %; Cr: 27%, 34%; As: 28% , 20%); in oxidizing and acid soluble (Cu: 25%, 10%; Ni: 24%, 33%; Cd: 16%, 23%, Hg: 23;%, 12%). Metal speciation variations among sites were related to the levels of TOC and Eh and water BOD. The ICF values indicate a considerable contamination for As, Cd, Cr, Ni; and GCF indicated 50 % of sites of considerable contamination. Speciation in water predicted existence of the toxic free aqua ion (Mn: 6-97%; Zn: 35-89%; Ni: 60-90%; Cd: 35-82%). These and soil GCF values reflect the high degree of metal bioavailability, toxicity, and potential risk.

Key words: wastewater, soil, metal speciation, bioavailability, Upper Litani basin, Lebanon

1. INTRODUCTION

In Lebanon, the Bekaa is an agricultural zone and best known as the food reservoir of the country (Ammar, 2014). Its soils are mostly irrigated by the Litani River and/or ground water. However, the Litani River watershed receives different pollutant sources such as industrial and domestic waste water (Wazne and Korfali, 2016). During the dry season, water is withdrawn from Litani River for irrigation which is mostly wastewater. Irrigation with wastewater is known to contribute significantly to the heavy metal concentrations of soils (Deshmukh et al., 2015, Farahat and Linderholm, 2015). These metals can bio-accumulate in plants and animals, and eventually passing to humans through the food chain (Gu et al., 2016). Thus the soils of the ULB are potentially subjected to heavy metal disposal resulting from previously mentioned reasons. Nonetheless, the behavior of metals in the environment cannot be reliably predicted on the basis of their total concentration. Whereas, the chemical fractionation, speciation of metals in soils can provide information on metal mobility, bioavailability, or potential risks that it poses to the environment and to human health (Sadee et al., 2016). Sequential extraction methods have been widely applied to characterize the chemical forms of metal elements present in soils. Metals bound in the different geochemical fractions in soils are extracted by different reagents, where several chemicals are used consecutively to extract operationally defined phases from the soil in a set of sequence from the most labile to the most resistant. One of these is the modified BCR sequential extraction technique by Rauret et al. (1999) that extracts metals from different soil fractions, operationally defined as: acid-extractable, reducible, oxidizable, and residual (Wali et al. , 2014) . The first three fractions are the labile ones affected by environmental conditions, such as pH, redox potential, organic content and can be easily mobilized and be bioavailable. Moreover, the degree of soil contamination can be assessed by the individual contamination factor (ICF) and global

contamination factor (GCF) and these would reflect the overall potential risk caused by the toxic metal to the environment (Naser et al., 2015). In parallel to these the forms of chemical metal species in the water column, the organic and inorganic metal complexes and the free solvated metal ions (toxic metal specie), could be used as a predictor of bioavailability (Korfali and Jurdi, 2011, Ahmad et al., 2014, Magu et al., 2016). The free ion activity model (Morel 1983) states that there is a correlation between the toxicity of a metal to an organism and the thermodynamic activity of the free aqua-metal ion. Few studies have been conducted in Lebanon on metal speciation of bed load river sediments, but no citation to present on metals speciation in Lebanese soils. Previous study tackled total metal content in soils of Upper Litani Basin (Korfali et al., 2014). Hence the objective of this study is to investigate the speciation of metals in soil and water of the upper Litani basin so as to establish the metal potential mobility, bioavailability and predict their potential risks.

2. MATERIAL AND METHODS

2.1 Study area, sampling sites and sampling

The Litani basin is the largest hydrographic basin in Lebanon flowing longitudinally from the NE to SW, draining over 20% of the countries area. It is in Bekaa valley between two mountainous chains, 170 km in length with 60 km of tributaries, it springs from Nabeh Al Oleik and drains into the Mediterranean Sea (Ammar, 2014). The details of the rocks outcropping in the ULB basin and soil characteristics were discussed in previous work (Korfali et. al, 2014). Basically the soils are red Mediterranean rich in iron oxides and high clay content (Darwish and Zurayk, 1997).

The sampling sites for soils (24 sites) paralleled the sites of earlier work of total metal levels in ULB basin (Korfali et al, 2014). It was observed that most industries and domestic wastewater dispose directly effluents into the river flow and soils irrigated by this river water.

Soil sample were collected during the dry season in accordance to method given by EPA, (2014). In parallel water samples were collected from river channel adjacent to soil collection and in accordance with APHA, AWWA, WPCF (2012) standard methods.

2.2 Field methods

Temperature, electrical conductivity (ECw), total dissolved solids (TDS), pH, and Eh for water were measured at site using (Hach Model 44600 Conductivity/TDS meter), and DO by membrane electrode.

2.3 Water treatment and analysis

The collected water samples were immediately filtered through 0.45-µm pore cellulose filters into two polyethylene bottles. One bottle was acidified with nitric acid to pH < 2 and stored at 4°C for metal analysis (Fe, Mn, Zn, Cu, Cr, Ni, Cr, Pb and Cd) using AAS ("Shimadzu" AA-6300). The concentrations of As and Hg determined by ICP-MS (Agilent ICP-MS 7500-Ce).

The other bottle was used for immediate analysis using: titration for alkalinity, Ca^{2+} and Mg^{2+}; spectrophotometry for NO_3^- SO_4^{2-} and PO_4^{3-} and procedures followed standard method of analysis of water and waste water; Cl^- was determined by ion chromatography (Ion Chromatograph, "Shimadzu" PIA-100).

2.4 Soil treatment and analysis

Soil samples were air dried, homogenized, plastic sieved and the <75 µm fraction was retained for metal analysis.

A modified BCR sequential extraction technique by Rauret et al. (1999) was used on one gram of each soil sample and the four (operationally defined) fractions were derived:

F1: Exchangeable, water and acid soluble (carbonate) by CH_3COOH (0.11 mol/L), pH=2.85

F2: Reducible (Fe and Mn oxides/hydroxides) by 0.1 mol L^{-1} $NH_2OH.HCl$, pH=2.

F3: Oxidizable (organic substances) by 0.02 mol L^{-1} HNO_3/ 30% H_2O_2 and heat; followed by: CH_3COONH_4 (1.0 mol L^{-1}) at pH=2

F4: Residual (native metals) by 10 ml combination (ratio of 4:1) of concentrated HNO_3 and $HClO_4$

(Details of procedure is given by Naji et al. (2010) and Tokalioğlu, S. (2012).

Metals in solution of each derived fraction on three replicates were determined using AAS and ICP-MS techniques. Analytical quality control was monitored by analysis of certified reference material of NIST (National Institute of Standards and Technology 2586). Eight replicates of SRM 2704 were analyzed; the percentage relative standard deviation (% RSD) was < 10%. The organic carbon content was determined by carbon analyzer ("Shimadzu" V_{CPN}).

2.4 Software used in analysis

Statistical analyses were performed using SigmaStat (version 3). The speciation of each metal in water was predicted using AQUACHEM (™) software applications interfaced with the geochemical modeling program (PHREEQC). The input data to the modeling program were water measured parameter (Table 1), metals as total content, and modeling was done for each site, not as mean values.

Table 1. Average values of measured water parameters

	Average	Min	Max	SD	%CV
pH	7.83	7.3	8.6	0.34	4.3
Temperature (oC)	22	15	29	3.4	15
Eh (mV)	10.5	-80	120	50	480
Cond. (µS/cm)	987	336	2520	707	72
DO (mg/L)	3.6	0.4	8.5	2.7	74
BOD (mg/L)	790	28	2530	697	88
HCO3(mmol/L)	3.4	3.0	3.6	0.23	6.8
Cl (mmol/L)	2.7	0.24	9.2	2.5	93
NO- (mmol/L)	5.8	0.44	21.7	5.97	103
NH3 (mmol/L	28.3	0.73	83.2	29	103
PO43(mmol/L)	0.170	0.002	1.03	0.31	180
SO4(mmol/L)	0.168	0.008	0.700	0.150	90
Ca (mmol/L)	43	16	98	23	54
Mg(mmol/L)	4.3	0.00	13	3.2	74
Fe (µmol/L)	55	0.72	269	83	150
Mn(µmol/L)	4.2	0.18	18	5	119
Zn(µmol/L)	0.75	0.05	3.06	0.9	120
Cu(µmol/L)	0.51	0.06	1.58	0.45	87
Cr(µmol/L)	0.47	0.02	1.92	0.56	119
Ni(µmol/L)	0.63	0.03	2.55	0.70	111
Pb(µmol/L)	0.04	0.005	0.145	0.035	97
Cd(µmol/L)	0.042	0.009	0.134	0.032	76
As(µmol/L)	0.176	0.014	0.667	0.217	117
Hg(µmol/L)	0.036	nd	0.250	0.048	135
pH (sediment)	8.0	7.1	8.8	0.4	5
Eh(sediment)	71	-70	160	71	288
% TC(sediment)	40.7	6.1	79	18	45
% OC (sediment)	17.7	1,0	41.8	11.4	65

3. RESULTS AND DISCUSSION

3.1 Speciation of Metals in Soils

Table 2 presents the speciation scheme (metals in the four operationally defined fractions). The

results of the studied ten sites were combined for each element, and the data is presented as mean fraction metal content (mg metal kg^{-1}). Figure 1 and Figure 2 present the mean percentage of the metal from total in the different soil fractions.

Table 2. Mean metal content in the different soil fraction

Metal Content (mg kg^{-1})	F1	F2	F3	F4
Fe	2058	8286	3488	18527
Mn	133	167	51	246
Zn	20	16	11	47
Cu	6.0	3.8	12.0	25.0
Cr	54	41	8.0	40
N	35	8.0	24	31
Pb	3.5	2.0	4.3	9.5
Cd	1.67	0.43	0.98	1.62
As	4.12	4.99	1.35	6.90
Hg	0.87	0.31	1.42	2.69

The speciation of Fe and Pb were mainly in the native residual soil fraction. The mean percentage speciation of Fe in residual fraction was 46%, which most probably are due to red Mediterranean soils, rich in iron oxides. While, the mean percentage speciation of Pb in residual fraction was 67%, and low percent (27) at site 13, that exhibited high percentages in F1 (33 %) and a high total Pb content 164 ppm. This indicates a site receiving pollutant from the solid waste dump of the asphalt industry at this site (Korfali et al., 2014).

3.2 Speciation of Mn, Zn, Cr, As

Speciation results (mean values) of Mn, Zn, Cr, and As indicated the highest percentages of these metals were in Mn and Fe oxide hydroxide fraction (reducible, F2), and acid soluble (F1) Figure 1. High percentages in these fractions indicate pollutant inputs and metal bioavailability by environmental changes. The mean percentage of Mn in F2 and F1 were respectively 27% and 18%, with a range between 15% and 35%, and 5% and 40%. The association of Mn in Fe oxides/hydroxide has been reported in literature (Jackson, 2015). For Zn, the mean percentage in F2 and F1 were approximately 18%, with a range between 9% and 31%, and 5% and 35% respectively. High percentages in F1 were at sites with low sediment Eh values (site S1 and S17). Similarly As speciation, with higher percentages in F2 than F1.The mean percentage of As in F2 was 27% , with a range between 6% and 40% ; F1 it was 21% , with a range between 3% and 40%. The association between Zn and As with Fe and Mn oxide hydroxide fraction arises from the strong binding of Zn and As to Fe oxides that cannot be released except the matrix subjected to reducing conditions (Suda and Makino, 2016). Whereas Cr speciation were higher in F1 than those in F2. The mean percentage of Cr in F2 and in F1 were respectively 27%, and 35 % , with a range between 17% and 34% , with a wide range in F1 between 5% and 49% (sites 6 and 8). These sites are in the vicinity of tanneries that discharge their wastes in river and/or on adjacent soils; which may justify the high levels in F1. Our results were in line with Reijonen and Hartikainen (2016) that indicate Cr speciation in Fe and Mn oxides/hydroxides soil fraction. The speciation of Cr in the reducible fraction is mainly influenced by the oxidizing environment of soil that enhance the formation of the insoluble oxides/ hydroxides of Fe and Mn. Whereas, under reducing conditions, these oxides and hydroxides forms are reduced to soluble Fe and Mn types, leaching Cr metals and decreasing the levels of Cr in F2 fraction. This is justified by the lower percentage of Cr at site 17 (17% and Eh = -70 mV).

Hence, the high speciation of Zn, Cr, As in F1 resulted probably either from direct waste discharge into soil and/or to the reducing media of many sites that released these metals from the reducible fraction and consequent association with the most labile fraction F1.

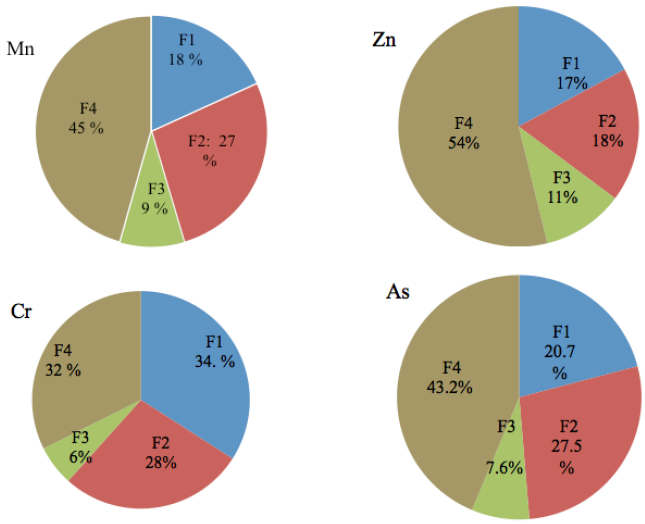

Figure 1. Mean percentage speciation of Mn, Zn, Cr, As in the different soil fractions

3.3 Speciation of Cu, Hg, Ni, Cd

The soil labile fractions, the acid soluble (F1) and organic (F3) were of significance to Cu, Ni, Cd, and Hg speciation (Figure 2). Copper and Hg showed higher speciation in F3 than F1. The mean percentage speciation in F3 were for Cu 25%, and Hg 23%, and respectively with range between 18% and 34%; and between 8% and 36%. Association of Cu and Hg with organic fraction results from the stability of Cu and Hg organic complexes and ease of complexation with humic and fulvic acids (Bavec and Gosar, 2016). While, the mean percentage of Cu in F1 was 10%, with a range between 5% and 15% at site 19 that showed lowest speciation in organic fraction. This site also had very low DO levels in water (DO = 1.06 mg/L), high levels of BOD (1625 mg/L) and low OC % in sediment (0.95 %) as indicated in Table 1. Hence the high discharge of waste water at this site, high in organic material was probably accountable to the high oxidation of organic substances releasing metals from organic sediment fraction and association with the most labile fraction F1. Likewise for Hg , the mean % of Hg in F1 was 13%, with a range between 1% and 26% at site 11, that had low speciation in organic fraction (13%) , very low levels DO in water (0.38 mg/L) , very high levels of BOD (2530mg/L) and lower organic soil content (Table 1). However, the percentage speciation of Ni and Cd in soil fraction F1 was higher than fraction F3. The mean percentage in F1 were 22% for Cd, and 33 % for Ni, with a range between 7% and 40%; and between 6% and 48%. Previous studies indicated the high speciation of Cd in carbonate fraction (F1) of Lebanese sediments, the Nahr-Ibrahim River and Qarraoun Reservoir. The strong high association of Cd to carbonate fraction is most probably due to the similarity of the ionic radii of Cd (0.97 Å) and Ca (0.99 Å), where Cd will enter the calcite crystal as a camouflaged element and precipitate with carbonates (Korfali and Davies, 2004, Korfali and Jurdi, 2011). Furthermore, earlier studies exposed the organic fraction (F3) not to be of significance to Cd speciation, explained by Cd smaller organic stability coefficient than other metals (Forghani et al., 2015). The mean percentage of Cd in F3 was 16%, with a range between 3% and 30%. The high association of Cd to organic soil fraction is most probably due to the high %OC in soils, which is reflected at site 10 (% OC was 32, and Cd in F3 was 30%). In regard to Ni, previous studies designated high association of Ni with reducible sediment fraction (Korfali and Jurdi 2011). Whereas, this study revealed a higher association with acid soluble (F1), mainly carbonate, mostly due to the higher reducing media and alkaline pH values that dissolved Ni and consequent precipitation with carbonate (Zhu et al., 2016). Furthermore, the higher association of Ni with organic fraction (F3), mean percentage 25%, with a range between 7% and 38% than F2 could have resulted from an increase in % OC in soil. This is indicated at site 16 (% OC was 41.8, and Ni in F3 highest 38 %).

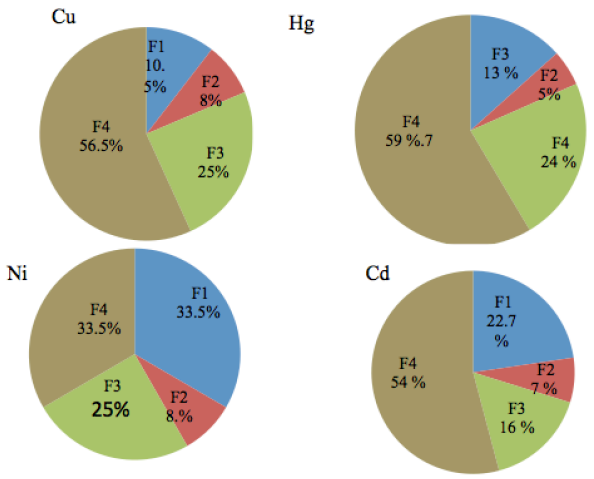

Figure 2 Mean percentage speciation of Cu, Hg, Ni, Cd in the different soil fractions

Hence, what affected speciation of Cu, and Hg is water dissolved oxygen and BOD expelling these from organic fraction and association with acid soluble. For Cd and Ni, the reducing media and % organic carbon in sediment affected the speciation.

3.4 Individual and global contamination factor

The individual and global contamination factors were calculated to evaluate the metal contamination and their bioavailability in soils of ULB. The ICF for the various sampling sites were calculated from the result of the speciation study by dividing the sum of the first three extractions (acid-reducible, oxidisable and organic forms) by the residual fraction for each sampling station. The GCF for each sampling station was computed by summing the ICF. The ICF and GCF classifications are: ICF < 1 & GCF < 6 –indicates low, 1 < ICF < 3 & 6 < GCF < 12– moderate, 3 < ICF < 6 & 12 < GC < 24 –considerable and ICF > 6 & GCF > 24 –high contamination (Benson et al., 2016),

Results indicated considerable contamination for the metals Cr, Ni, Cd and As, their ICF values were between 3 < ICF < 6; with metal order Cr ≻ Ni ≻ Cd ≈ As. While moderate contamination (1 < ICF < 3) for metals in corresponding order Mn ≻ Zn ≻ Hg ≻ Cu. These indicate the mobility and bioavailability and risks to plant uptake specially Cr, Ni, Cd, and As. Whereas, the GCF that elucidate the overall contamination among sites is presented in Figure 3, and it is explicit that 50% of sites were of moderate contamination (6 < GCF < 12) and 50 % of considerable contamination (12 < GC < 24). These sites receive excessive domestic and industrial waste, beside agricultural runoffs.

3.5 Speciation of metals in water

The speciation of metal in water is critical to understand metal behavior in aquatic system as that of metal speciation in soil. The forms of the chemical species of toxic metals in water column: the organic and inorganic metal complexes and the free solvated metal ion could be used as a predictor of bioavailability to particular aquatic organism. The free ion activity model states that there is a correlation between the toxicity of a metal to an organism and the thermodynamic activity of the free aqua metal ion in solution (Morel 1983). The speciation of each metal in Litani River was predicted using computational approach, the geochemical modeling program PHREEQC. The application computes and reports the speciation of metals in terms of their free aqua ion and inorganic complexes. The organic metal species were not tackled based on the assumption that the organic metal complexes would be reduced in basic aqueous media with high alkalinity content

(Korfali and Jurdi, 2011). The measured values (Table 1) were the input data for the metal speciation calculation. Table 3 presents percentage range within the sampling sites of the speciated forms of studied metals in water.

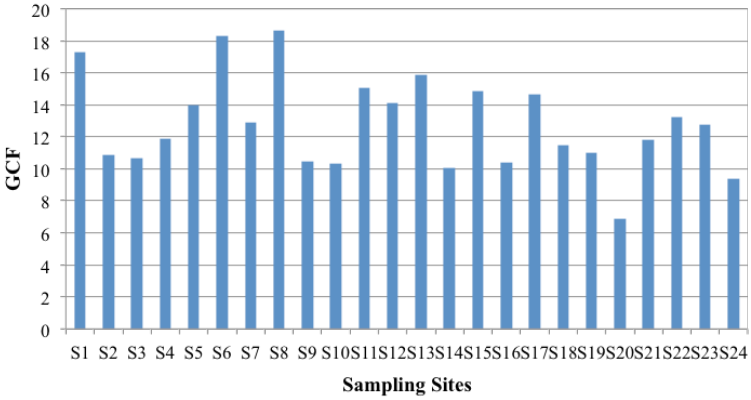

Figure 2. Variation of GCF among sampling sites

Table 3. Range of Highest % of speciated metal forms in Litani River water

Element	Speciated forms	% Range
Mn	Mn^{2+}	60-97
	$MnCO_3^o$	2-25
Zn	Zn^{2+}	35-89
	$ZnCO_3^o$	4-50
	ZnOH+	1-12
Cu	$CuCO_3^o$	50-79
	$Cu(OH_2)_2^o$	20-49
	Cu^{2+}	<1
Cr	CrO_4^{2-}	20-94
	$HCrO_4$-	1-18
	$CrOH^{2+}$	1-10
Ni	Ni^{2+}	60-90
	$NiCO_3^o$	8-35
	NiOH+	2-5
Pb	$PbCO_3^o$	70-96
	Pb^{2+}	3-26
	PbOH+	1-4
Cd	Cd^{2+}	35-82
	$CdCO_3^o$	10-40
	CdCl+	6-18
	$CdSO_4^o$	2-7
AS	$HAsO_4^{2-}$	40-98
	$HASO_4$-	2-50
	$HAsO_3^o$	2-15

Speciation as free aqua ion were high for Mn, Zn, Ni and Cd. Manganese occurred as free ion due to the low stability of Mn complexes (Stum and Morgan, 1996), and Mn speciation were in accordance with other works for wastewater (Magu et al., 2016). Whereas, Zn, Ni and Cd speciated to a lower extent as carbonate ion pair complexes ($ZnCO_3^o$, $NiCO_3^o$, CdCO3o) and higher as free ion when compared to previous works on Lebanese water resources (Korfali and Davies, 2004, Korfali and Jurdi, 2011). But in previous studies, the water media had high levels of dissolved oxygen, high Eh values and organic content was low. While speciation of Cu was highly as the ion pair carbonate complex $CuCO3^o$ and nil occurrence as free toxic ion. These were in accordance with previous work of Cu association with carbonate due to the high formation constant (Korfali and Davies, 2004). Cr and As existed as anion oxygen forms (CrO_4^{2-} and $HAsO_4^{2-}$) when media was oxidizing and limited occurrence as reduced species in reduced condition ($Cr(OH)^{2+}$, $H_3AsO_3^0$); and these coincide with other reported speciation works (Magu et. al, 2016).

4. CONCLUSION

This study has assessed the mobility, bioavailability, and toxicity of heavy metals through determining the metal speciation in the different soil fraction irrigated by contaminated wastewater, and metal speciation in water. Results indicated due to high organic content, reducing environmental media, high levels of BOD in water, metals in soils existed highly in labile bioavailable soil fractions. High percentages of free toxic metal ion also prevailed in water. These results imply an immediate action plan for the construction of excessive wastewater treatment plant and prohibiting discharges of waterwater into rivers that are used for irrigation.

REFERENCES

Ahmed, I.A.M., Taylor, J.H., Bieroza, M., Zhang, H., William Davison, W., 2014. Improving and testing geochemical speciation predictions of metal ions in natural waters. Water Research; 67: 276- 291.

Ammar, R., (2014). Geochemical and isotopic study of urban and rural watersheds: assessment of water resources and soil pollution in Lebanon. Dissertation, L'Universite Liber de Bruxelles et L'Ecole Doctorale des Sciences et Technologie - Université Libanaise.

APHA, AWWA, WPCF (2012). Standard methods for the examination of water and wastewater (22 ed.).Washington, D.C

Bavec, Ŝ, Gosar, M., 2016. Speciation, mobility and bioaccessibility of Hg in the polluted urban soil of Idrija (Slovenia). Geoderma; 273: 115-130.

Benson, N.U, Asuquo, F.E., Williams, A.B., et al., 2016. Source evaluation and trace metal contamination in benthic sediments from equatorial ecosystems using multivariate statistical techniques. DOI:10.1371/journal.pone.0156485, -19.

Darwish, T., Zurayk, R. R., 1997. Distribution and Nature of Red Mediterranean Soils in Lebanon along an Altitudinal Sequence. Catena; 28: 191-202.

Deshmukh, S.K., Singh, A.K, Datta, S.P., 2015. Impact of wastewater irrigation on the dynamics of metal concentrations in the vadose zone: monitoring: part I. Environmental Monitoring and Assessment; 187: 695 DOI 10.1007/s10661-015-4898-3.

Farahat, E., Linderholmb, H.W., 2015. The effect of long-term wastewater irrigation on accumulation and transfer of heavy metals in Cupressus sempervirens leaves and adjacent soils adjacent soils. Science of the Total Environment; 512–513: 1–7.

Forghani, G. , Mokhtari, A.R., Kazemi, G.A., M.D., 2015. Total concentration, speciation and mobility of potentially toxicelements in soils around a mining area in central Iran. Chemie der Erde; 75: 323-334

EPA, 2014. SESDPROC-300-R3, Soil Sampling. Accessed December 2, 2015 https://www.epa.gov/sites/production/files/2015-06/documents/Soil-Sampling.pdf

Gu, Y-G, Gao, Y-P, Lin, Q., 2016. Contamination, bio accessibility and human health risk of heavy metals in exposed-lawn soils from 28 urban parks in southern China's largest city, Guangzhou. Applied Geochemistry; 67: 52 – 58.

Jackson, A., 2015. Variations in the abundance of photosynthetic oxygen through Precambrian and Paleozoic time in relation to biotic evolution and mass extinctions: evidence from Mn/Fe ratios Togwell. Precambrian Research; 264: 30–35

Korfali, S. I., Davies, B. E, 2004. Speciation of metals in sediment and water in a river underlain by limestone: Role of carbonate species for purification capacity of Rivers. Advances in Environmental Research; 8: 599–612.

Korfali S. I., Jurdi, M., 2011. Speciation of metals in bed sediments and water of Qaraaoun Reservoir, Lebanon. Environmental Monitoring and Assessment; 178(1–4): 563–579.

Korfali, S.I., Jurdi, M., Amacha, N., 2014. Sources and Levels of Metals in the Upper Litani Basin Soils: Lebanon. Journal of Environmental Science and Engineering; A 3: 55-71

Magu, M.M. , Govender, P.P., Ngila, J.J. , 2016 . Geochemical modelling and speciation studies of metal pollutants present in selected water systems in South Africa/ Physics and Chemistry of the Earth; 92: 44-51.

Morel, F. M. M., 1983. Principles of Aquatic Chemistry. New York: Wiley.

Naji, A.,Ismail,a., Ismail, A.R., 2010. Chemical speciation and contamination assessment of Zn and Cd by sequential extraction in surface sediment of Klang River, Malaysia.Microchemical Journal; 95: 285–292

Nase r, S.M.,,Okbah , M.A., El Haddad, H., S., Soliman, N.F., 2015. Fractionation profile and mobility pattern of metals in sediments from the Mediterranean Coast, Libya. Environmental Monitoring and Assessment; 187: 430-438.

Rauret, G., Lopez-Sanchez, J.F., Sahuquillo, A., Rubio, R., at al., 1999. Improvement of the BCR three step sequential extraction procedure prior to the certification of new sediment and soil reference materials. J. of Environ. Monit.; 1: 57-61.

Reijonen, I., Hartikainen, H., 2016. Oxidation mechanisms and chemical bioavailability of chromium in agricultural soil-pH as the master variable. Applied Geochemistry; 74: 84-93

Sadee, B.A., Foulkes, M.E., Hill, S.J., 2016. A study of arsenic speciation in soil, irrigation water and plant tissue: A case study of the broad bean plant, Vicia faba. Food Chemistry; 210: 362–370. Geoderma; 270: 68-75.

Stumm, W., Morgan, J.J., 1996. Aquatic chemistry, chemical equilibria and rates in natural waters. Trace Metals: Cycling, Regulation, and Biological Role. 3rd ed. John Wiley and Sons, Inc, USA.

Suda, A., Makino, T. 2016.. Functional effects ofmanganese and iron oxides on the dynamics of trace elements in soils with a special focus on arsenic and cadmium: A review.

Tokalioğlu, S. 2012. Determination of Trace Elements in Commonly Consumed Medicinal Herbs by ICP-MS and Multivariate Analysis. Food Chemistry; 134: 2504-08.

Wali, A., Colinet, G., Ksibi, M., 2014. Speciation of heavy metals by modified BCR sequential extraction in soils contaminated by Phosphogypsum in Sfax, Tunisia. Environmental Research, Engineering and Management; 4(70): 14–26

Wazne, M., Korfali, S.I., 2016. Spatial and temporal assessment of metal pollution in the sediments of the Qaraoun reservoir, Lebanon. Environmental Science and Pollution Research; 23:7603–7614

Zhu, X., Li, W., Zhan, L., Huang, M., Zhang, Q., Achal, V., 2016. The large-scale process of microbial carbonate precipitation for nickel remediation from an industrial soil. Environmental Pollution; 219: 149-155.

Proceedings of the 10th World Congress of EWRA 'Panta Rhei', 5-9 July 2017, Athens, Greece
© 2017 *European Water Resources Association*

Finding a sustainable balance in the water food nexus – Socio-economic transformation in an agricultural catchment

M. Roobavannan[1], J. Kandasamy[1*], S. Pande[2], S. Vigneswaran[1] and M. Sivapalan[3]
[1] *School of Civil and Environmental Engineering, University of Technology Sydney, Sydney, NSW, Australia*
[2] *Department of Water Management, Faculty of Civil Engineering and Geosciences, Delft University of Technology, Delft, the Netherlands*
[3] *Department of Civil and Environmental Engineering and Department of Geography and Geographic Information Science, University of Illinois at Urbana-Champaign, Urbana IL 61801, USA*
[*] *e-mail: jaya.kandasamy@uts.edu.au*

Abstract: Increasingly the competition for water between food production and the environment threatens the viability of agricultural communities. This paper focused on this water-food-environment nexus in the Murrumbidgee River Basin, Australia, and how it contributed to the evolution of the regional economy and changing demographic patterns. Paradoxically, against expectations, changes in water management favouring the environment coincided with falling unemployment and increase in average regional income, despite a decline in agriculture. To understand this, and to explore how the competition for water played out in the Murrumbidgee Basin, we develop and use a socio-hydrologic model that explicitly considers bi-directional feedbacks between human and water systems. The modelling shows that in response to widespread ecosystem degradation, community sentiment forced new water management policies that favoured ecosystems which inevitably led to reductions in agriculture production. In response, the basin economy reorganized through sectoral transformation to the manufacturing and service sectors, improved agricultural practices, and out-migration of basin residents. The sectoral transformation was facilitated by capital available for investment in manufacturing and service sectors with knock-on impacts on population dynamics and unemployment. Collectively these contributed to a sustainable transformation of the basin economy. The study shows how transformation of the basin economy and demographics mitigated potentially adverse economic outcomes and enabled society to cope with water management decisions that favoured the environment. The dynamics outlined here highlight the adaptive capacity of people and movement of capital in a free economy, supported by appropriate strategies and funding, to cope with water stress.

Key words: socio-hydrology, irrigation, ecosystems, water management, employment, sectoral transformation

1. INTRODUCTION

Water plays a key role in economic development, particularly in agricultural economies. Rising human population has heavily impacted the hydrological cycle and in many places, water resources are being adversely affected in terms of both quantity and quality and fresh water resources have depleted. In addition, climate change further exacerbates both water supply and demand. Increasingly this issue is becoming further compounded as awareness of water scarcity and food security rise with increasing population (Gleick and Palaniappan, 2010) and with climate change (Jiménez Cisneros et al., 2014). Increasing water use in agriculture inevitably reduces the share available for ecosystems, leading to its degradation, and in places where ecosystem services are valued by humans, community sentiment turns adverse. Water management decisions made that favour ecosystem sustainability can, however, impact a region's economy, employment, and population, especially in agriculture centred economies. The potential for conflict is self-evident as different users of water attempt to maximize their benefits at the expense of others. Kandasamy et al. (2014) depicted this tension in the form of a pendulum that swung from a situation that favoured agricultural water consumption to one that favoured environmental water use.

In this paper, we hypothesize that even though water restrictions did in fact impact agriculture, various sectors of the wider basin economy also adapted, leading to sustainable economic

transformation of the region even as tangible environment protection was implemented. This study attempts to discover the complexities which resulted in these observations and how the catchment adapted to cope with water stress. We carry out data analysis and detailed socio-hydrologic modelling to mimic and explain how the complex interactions and feedbacks between various subsystems of the human-water system within the Murrumbidgee basin that may have given rise to the observed phenomena, considered here as emergent dynamics, and to facilitate scenario testing to further our understanding. We examine the co-evolutionary mechanisms through which humans responded to the reallocation of water and the changing norms and values that inspired this, how theses impacts translated to the remainder of the basin economy and society, how they reorganised to cope and to explain the changes in terms of detailed process insights of the system.

2. MODEL AND PARAMETERIZATION

In this study the human-water dynamics is explored using a conceptual model that explicitly utilizes a socio-hydrology framework. This model (Figure 1) consists of the following sub-models: water availability (labelled a in Figure 1); agriculture (b); environment health (c); manufacturing and services (d); technology (e); and human population (g). Each of these sub-systems was coupled to mimic their co-evolution over time and in order to facilitate this coupling, two link-models are employed. The operation of the model and model equations was explained in Roobavannan (2017a,b).

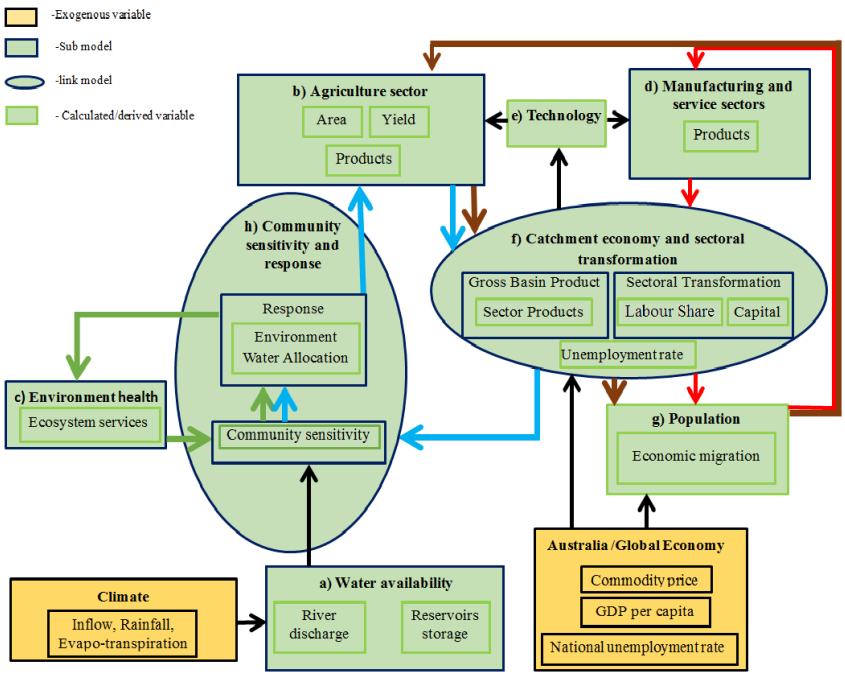

Figure 1. Socio-hydrology conceptual framework for Murrumbidgee.

3. MODEL INPUT DATA

3.1 External drivers

Two groups of data are input to the model as external drivers and they are related to the climate and to the Australian or global economy (Figure 1). The input data used in the model is summarized in Table 1. Hydro-climatic drivers of the model are inflows from the Snowy Mountains hydro-

scheme that flow into the Blowering Dam and into Burrinjuck Dam, and rainfall and evapotranspiration data. Gross domestic product per capita of Australia (GDP_t), national unemployment rate (Ua_t), the rate of return to capital (r), and price of crops (cp_{it}) cultivated in the basin, are the economic drivers of system.

3.2 Parameters, initial data and variables

Parameters are constant values that are used in equations in the various sub-models (Figure 1). Initial data are the values at the first time-step and are used to initiate the model computations. Values at subsequent time steps are updated based on model calculations. The values of variables are model calculated even at the first time-step. Some variables are compared against available observed data to gauge the fit of the model (see results and discussion).

3.3 Simulation period and time-steps

Model simulates the coupled dynamics from 1976 to 2012 where coupled dynamics and thresholds are apparent. The availability of detailed data for external drivers and for calibration of the model limited the simulation to the 1976-2012 period. The model was run on time-steps of one year. Data to calibrate the model was available on an annual basis. The storage in dams in catchment are calculated daily based on daily rainfall and inflows. Water allocation (Wa_t) was calculated on a monthly basis to account for seasonal cropping patterns.

4. MODEL SIMULATION RESULTS

The CEST link-model (Figure 1 link-model f) translates the impact of community inspired cuts to agricultural water allocation and the contraction of agriculture across to the rest of the basin economy. Central to the operation of the CEST link-model is the accumulation and growth of capital (Eqn. 19-20, S1). The capital creates employment in the economic sectors of the basin and subsequently production is created from this. Unemployment is calculated based on the size of the labour force.

4.1 Basin sectoral transformation

During the period of cuts to agriculture water (1995-2010) sectoral transformation occurred from the agriculture sector to the manufacturing and service sectors (Figure 2a, b). Here the sectoral transformation is demonstrated by the growth in employment in manufacturing and service sectors and the post-1995 decline in the agriculture. Figure 2a shows the number of employees in the agricultural sector, and the manufacturing sector and service sector. Figure 2b shows the employment share in agricultural sector (Na_t), manufacturing sector (Nm_t) and service sector (Ns_t). The correlation with observed data in Figure 2a were $r^2 = 0.99$ (manufacturing and services) and 0.75 (agriculture) and in Figure 2b were $r^2 = 0.83$ (Nm_t), 0.83 (Ns_t) and 0.79 (Na_t).

The employment share of agriculture was strongly influenced by land under cultivation, which is determined from water allocation and allows calculation of Na_t. The employment share of the manufacturing and services sector depends on capital (K_t) (Figure 2c) and consumption (C_t) in these sectors. Figure 2c shows the capital (K_t) accumulated from the difference between the production (discussed in the next section) and consumption. The employment share of services and of manufacturing are then determined.

Sectoral transformation was occurring even before 1995. Figure 2a shows that employment growth in manufacturing and services was faster than agriculture (Figure 2a). The growth of the manufacturing and service sectors compounded the accumulated capital (K_t) and enhanced growth

of employment in these sectors. Meanwhile the diminishing availability in land and water resources constrained growth in employment in the agriculture sector. Employment was further impacted by improved agricultural practices (mechanisation, technology improvements, corporate farming practices, etc.).

Post-1995, the sectoral transformation was more rapid as employment growth in manufacturing and services grew while agriculture employment declined, (Figure 2a, 2b). Figure 2c shows the capital growth continued to rise post-1995 from the continued growth in production in manufacturing and services. Employment demand in manufacturing and services (Dm_t) continued to grow. A lower demand for agriculture employment (Da_t) meant lower competitive demand for labour, a growing employment share in manufacturing and services (N_t). The growth of employment in the manufacturing and service sectors supported the viability of the basin economy during a period of agriculture contraction. Later, after 2010, the breaking of the drought, and the availability of more water resulted in a rise in agriculture employment.

4.2 Basin economy and production

Figure 3a shows the gross basin product per capita ($GBPc_t$) which is based on the sum of the production in the three economic sectors. The production in the three sectors is shown in Figure 2c. Data on $GBPC_t$ for the Murrumbidgee is not available and in its absence the median household income (MHI) is shown. In developed countries MHI is generally higher than $GBPc_t$ as it includes contributions not in the later (e.g. superannuation, workers' compensation, child support, etc.).

Initially, $GBPc_t$ grew steadily. The introduction of the government water reform in 1995 and the subsequent drought saw the $GBPc_t$ decline which fell annually till 2002 and the Murrumbidgee was in recession for 7 consecutive years. The $GBPc_t$ did not recover pre-1995 levels until 2004. While the drought did not break till 2010 and while irrigation water allocation declined during this period the $GBPc_t$ did not similarly decline. The $GBPc_t$ reached a low in 2000, and except for the period of 2008-10 when the drought was extreme, generally increased. It was in 2009 that Australia felt the economic impact of the global financial crisis. The increase in the basin economic production may be attributed to sectoral transformation from agriculture to manufacturing and service sectors and to diversification in agriculture.

4.3 Population dynamics and human migration:

The population changes by natural means (births, deaths) and by migration into/out of the basin. Figure 3b shows a continuous increase in population between 1976-1995 before slowing till the late 2000s. The fit with recorded population data was $r^2 = 0.96$.

In/out migration is explained by considering the operation of the attractiveness state variable (Figure 2, sub-model g). Attractiveness is a human behaviour state variable similar to community sensitivity which captures human preference to stay in the basin or migrate to the outside considering economic ($GBPc_t$, unemployment) and resource (land and water) gradients. The attractiveness of migration (Figure 3c) to the basin was positive up to 1997, albeit generally declining. The composite effect of unemployment, gross production, the availability of land and water resources was still conducive to net migration.

After 1995, the attractiveness of the basin to in-migration (Figure 3c) dramatically fell and was predominantly negative due to economic recession and resource constraints leading to out-migration. Out-migration countered natural population growth giving a slower population growth.

4.4 Unemployment

Figure 3d shows the unemployment in the Murrumbidgee. Pre-1995, attractiveness to the basin

was positive (Figure 3c), driven by agricultural potential and expansion of manufacturing and service sectors. While cumulative in-migration and basin population rose, so did unemployment (Figure 3d). In effect, the addition to the basin labour force through natural growth and in-migration exceeded labour demand. This observation parallels the Todaro paradox (Todaro, 1976) where job creation in a region leads to increased unemployment due to factors such as in-migration. This rise in unemployment could also in part be explained by technological advances and improved practices which increased productivity and reduced the need for workers. Nonetheless, humans motivated to migrate by attractiveness signals (in herd-like behaviour) were always more likely to do so in a manner that overshot the potential that existed (Bikhchandani et al., 1992; Todaro, 1976).

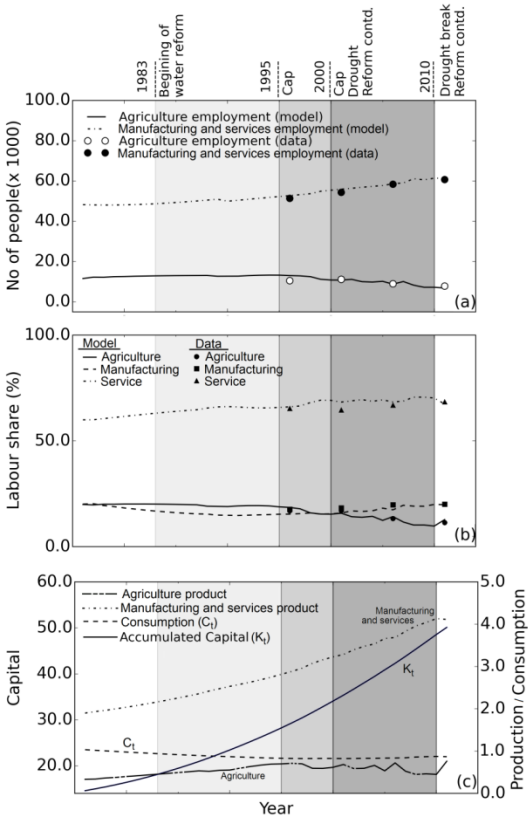

Figure 2 (a) basin employment, (b) labour share, and (c) accumulated capital (K_t), consumption (C_t) and production in Murrumbidgee

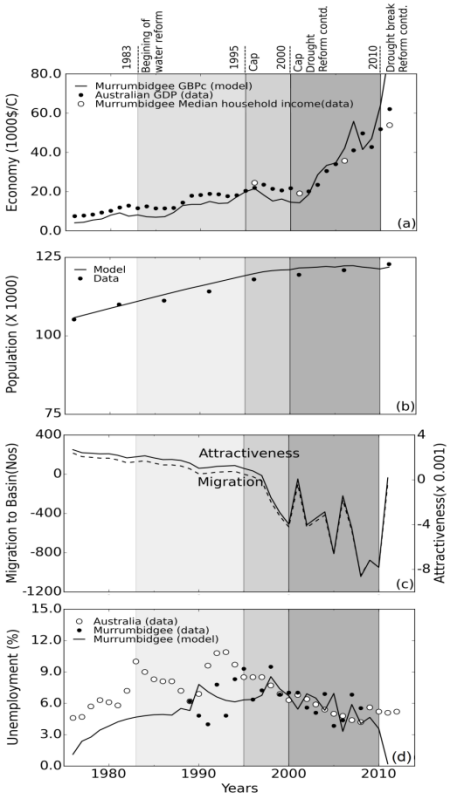

Figure 3 (a) Australian GDP_t and Murrumbidgee $GBPc_t$ (b) basin population, and (c) attractiveness of migration, and basin migration (d) unemployment rate in the basin and in Australia.

Paradoxically post-1995, unemployment actually fell (Figure 3d). The peak in unemployment (in 1997) lagged the cuts to water allocation (in 1995) by 2 years, in part reflecting the inertia of enterprises to immediately retrench workers in a period of transition from a temporary cap in water allocation in 1995 and to a permanent cap in 1997 (not foreshadowed in 1995). After 1995, the economic wellbeing and future potential of agriculture was bleak. Between 1995-2002, the Murrumbidgee was in recession (Figure 3a). At this time Australia's GDP was rising and from 2003 rose sharply largely in response to Australia's mining boom. Unemployment in the rest of Australia was falling (generally since 1993) and was lower than in the Murrumbidgee for many years after 1997 (Figure 3d). Basin attractiveness was negative (Figure 3c), and to enhance their economic wellbeing, some people moved to the manufacturing and service sectors (Figure 2a, b) while others migrated to regions outside the basin where prospects were better (Figure 3c). Unemployment declined even as net basin population was stagnant (Figure 3b) contributed to by out-migration. In Australia, the mining boom attracted many workers from regional areas, including the Murrumbidgee. Moreover in the Murrumbidgee, youth unemployment is reasonably low, with most leaving to find work elsewhere (Wilkinson and Montoya, 2012). Out-migration and sectoral transformation helped the basin to cope with water stress.

These population dynamics that contributed to a fall in the basin's unemployment appear counter-intuitive and not self-evident without the benefit of the socio-hydrologic analysis presented here. The unemployment rate and the preceding discussion on population dynamics and basin economy leading to it frames the discussion and illustrates the complex dynamics in terms of composite changes in the economic sectors and their relative production, workforce within the basin and population migration, and natural population growth. The CEST link-model was able to translate the impact of community inspired cuts to agriculture water allocation and the resulting contraction in agriculture across to the basin economy, employment, and population dynamics in a manner consistent with what historically happened in the Murrumbidgee Basin. It tracked the dynamics and feedback between the various variables, captured the co-evolution of the complex system and allowed an understanding of what occurred.

5. CONCLUSIONS

This paper has focused on the water-food-environment nexus being played out in the Murrumbidgee River Basin located in south-eastern Australia and which contributed to the evolution of the regional economy and changing demographic patterns. It used a coupled socio-hydrologic system model, which considers the bi-directional feedbacks between human and water systems, with explicit consideration of increased wealth, technological changes, and community sensitivity to environmental degradation, sectoral transformation, and population movements, and used it to explore how the competition for water between humans and the environment impacted on the catchment economy and demography. The model captures the feedbacks, internal dynamics and thresholds resulting from the changes in water management, which was well correlated with what actually occurred in the Murrumbidgee. The dynamics was arbitrated by the 2 link-models.

In the Murrumbidgee agriculture first expanded with abundant land and water resources. The growth in prosperity and the corresponding accumulation of capital naturally led to growth in manufacturing and services. Expansion of agriculture with the harnessing of more water inevitably degraded the environment. Community's sensitivity to the environment increased. In this instance, the CSR link-model determined the impetus for action towards more environment-centric measures and water reallocation for the environment as community sensitivity passed through critical sensitivity threshold. The model captured the initial community sensitivity to agriculture expansion, subsequent reversal in sensitivity with depleting water resources, the decline in agriculture and collectively simulated the pendulum swing in this complex system.

The dynamics triggered by the change in community sensitivity and the impact on water allocation and agriculture production were translated across the basin economy by the CEST link-model. The link-model simulated the accumulation of capital, the employment generated from this and the production in each of the three economic sectors of the basin. The model showed that the basin adapted to the economic stress through sectoral transformation to the manufacturing and service sectors, increased production in these sectors, changes in employment, including the paradoxical observation in the unemployment rate, and the out-migration of residents to regions outside the basin where prospects were better. Diversification of agricultural cropping and improved water use efficiency slowed the decline of agriculture production. These changes enabled the basin economy to cope and transform without collapse. The water reforms made to mediate the competition between humans and the environment impacted agriculture therefore did not translate to economic contraction and high unemployment as was feared earlier. The model showed how such contraction was averted, leading to a sustainable transformation of the region's economy even while tangible environment protection measures were implemented. These changes are counter-intuitive and not self-evident without the benefit of the socio-hydrologic analysis presented here.

This type of socio-hydrological model is a useful tool that can assist in the debate of the future of the agriculture industry in the Murrumbidgee. It can also contribute to more sophisticated water management. The information and insights that the socio-hydrologic model provides can be beneficially inform how communities could transform in response to water reallocation, and to open

up different adaptation pathways.

Around the world, fresh water crisis is imminent due to growing human populations, exacerbated by climate change. The present modelling study can guide other water stressed regions where competition for water between different users is taking place. Further, more comparative studies can further understanding of why water management in some basins fail (e.g., Aral Sea, Lake Urmia), and can help define the role of economic transformation in water management decisions and help a region’s economy to transform itself.

The structure of the socio-hydrologic model used here has been tailored to the Murrumbidgee in terms of the type of economy, role of government, type of administration and level of support, the role of the community and it’s valuing of the environment. For example in the Murrumbidgee, crop diversification leading to better returns and lower water requirements was enabled by water trading. This may not be possible elsewhere without the kind of reforms that the government instituted. More such models need to be developed for other coupled human-water systems in different localities and jurisdictions to learn and identify what is unique and what is generally applicable and to determine relationships between variables that may be valid more universally. In this way more generic coupled human-water system models could be developed for universal applications. This is left for further research.

REFERENCES

AghaKouchak, A., Norouzi, H., Madani, K., Mirchi, A., Azarderakhsh, M., Nazemi, A., Nasrollahi, N., Farahmand, A., Mehran, A., Hasanzadeh, E., 2015. Aral Sea syndrome desiccates Lake Urmia: Call for action. J. Great Lakes Res., 41, 307–311. doi:10.1016/j.jglr.2014.12.007

Gleick, P.H., Palaniappan, M., 2010. Peak water limits to freshwater withdrawal and use. Proc. Natl. Acad. Sci., 107, 11155–11162. doi:10.1073/pnas.1004812107

Jiménez Cisneros, B.E., Oki, T., Arnell, N.W., Benito, G., Cogley, J.G., Döll, P., Jiang, T., Mwakalila, S.S., 2014. Freshwater resources, in: Field, C.B., Barros, V.R., Dokken, D.J., Mach, K.J., Mastrandrea, M.D., Bilir, T.E., Chatterjee, M., Ebi, K.L., Estrada, Y.O., Genova, R.C., Girma, B., Kissel, E.S., Levy, A.N., MacCracken, S., Mastrandrea, P.R., White, L.L. (Eds.), Climate Change 2014: Impacts, Adaptation, and Vulnerability. Part A: Global and Sectoral Aspects. Contribution of Working Group II to the Fifth Assessment Report of the Inter-governmental Panel of Climate Change. Cambridge University Press, Cambridge, United Kingdom and New York, USA, 229–269.

Mahendran Roobavannan, Jaya Kandasamy, Saket Pande, Saravanamuthu Vigneswaran, Murugesu Sivapalan, 2017a. Understanding the co-evolution of socio-economy and water management in the Murrumbidgee basin, Australia. Ecological Economics, (paper reviewed, revision submitted to Journal)

Mahendran Roobavannan, 2017b. Socio-hydrology in the Murrumbidgee basin, PhD thesis, University of Technology Sydney, 2017

Todaro, M.P., 1976. Urban job expansion, induced migration and rising unemployment. J. Dev. Econ., 3, 211–225. doi:10.1016/0304-3878(76)90049-3

Todaro, M.P, 1969. A model of labor migration and urban unemployment in less developed countries. Am. Econ. Rev., 59, 138–148.

Proceedings of the 10th World Congress of EWRA 'Panta Rhei', 5-9 July 2017, Athens, Greece
© 2017 *European Water Resources Association*

Assessing the quality of bottled water brands using a new water quality index

V. Tsakiris*, D. Alexakis and V.A. Tsihrintzis
Laboratory of Reclamation Works and Water Resources Management, School of Rural and Surveying Engineering, National Technical University of Athens, 15780 Zografou, Greece
* *e-mail: vasileios-kaisar.tsakiris16@imperial.ac.uk*

Abstract: The aim of the paper is to present a newly derived water quality index, specifically developed for assessing the quality of bottled water. Several requirements have been set by the European Union through legislation which all the member states are obliged to fulfil for the bottled waters available in their markets. So, the question arises how good these waters are, if the values of the various parameters shown on the labels are close to reality, and how the consumer can easily and quickly evaluate bottled water brands. A total of 79 different bottled water brands available in the Greek market were evaluated and compared using a specially designed bottled water quality index (BWQI). The index combines one microbiological and six physicochemical parameters. The assessment is based on both laboratory analysis results and values on bottle labels. The index calculator was installed at a specially designed webpage which is easily accessible via personal computers or smart phones. According to the results obtained, it is concluded that the majority of the bottled water samples examined were of excellent or very good quality, a small number was characterised as of good quality, and very few samples failed to attain the good quality status. The new water quality index proved to be a quick, sensitive and powerful tool to assess and compare the quality of bottled waters.

Key words: Bottled waters, water quality, laboratory tests, bottled water quality index (BWQI), multiplicative model

1. INTRODUCTION

Water intended for human consumption should be of high quality so that public health is protected (Tsakiris and Tsakiris, 2012). Water quality is recognized as the most important issue, not only related to consumers and their requirements, but also to the protection of the water resources and the environment (Benedini and Tsakiris, 2013).

The assessment of water quality is a difficult task due to the many parameters involved in its characterization. This difficulty was recognized and led to proposals for adopting simplified approaches, such as the water quality indices. A water quality index is a unique score which combines information based on a number of important water quality parameters.

The first modern water quality index was set by Horton (1965). Several water quality indices have been developed and used by researchers and institutions for rating water of various origins (e.g., Brown et al., 1970; Bhargava, 1983; CCME, 2001; Boyacioglu, 2007; Cude, 2001; Dunnette, 1980; Liou et al., 2004). The application of water quality indices in evaluating water bodies has a main advantage, which is the presentation of water quality state into a single digit score (Alexakis et al., 2016; Nuanchan, 2017). Moreover, many computer–automated tools and mathematical formulations have been developed in order to generate and introduce water quality indices (Sarkar and Abbasi, 2006; Swammee and Tyagi, 2000, 2007).

In the case of bottled water quality, no significant work has been done for developing water quality indices. This is most probably due to the fact that bottled water is generally considered as water of high quality (Toma et al., 2013). Toma et al. (2013) applied a water quality index in evaluating water quality in several bottled water brands of Iraq. Recently, a new index, suitable for the assessment of bottled water quality was developed (Tsakiris, 2016a, b). In this study, this index is used to assess the various brands of bottled water which are available in the Greek market.

2. THE BOTTLED WATER QUALITY INDEX

The Bottled Water Quality Index (BWQI) is a two-stage index. The first stage is an ON/OFF process testing the bottled water sample on fulfilling two requirements: (a) absence of population of the bacteria *Escherichia coli*; and (b) pH values lying between 6.5 and 9.5. If these two requirements are fulfilled, the evaluation procedure continues from the first stage to the second stage, which is based on a multiplicative model using five sub-indices with their corresponding exponents (Tsakiris, 2016a, b). The five sub-indices represent the following five physicochemical parameters: nitrate (NO_3^-), nitrite (NO_2^-), chloride (Cl^-), sulphate (SO_4^{2-}) and specific electrical conductivity (SPC). This multiplicative process is presented by Eq. (1):

$$\boldsymbol{BWQI} = \prod_{\boldsymbol{i=1}}^{\boldsymbol{N}} \boldsymbol{SI}^{\lambda_i} \tag{1}$$

In this equation, the exponents λ_i are the sensitivity coefficients and represent the sensitivity of each sub-index (SI) in the final index, while N represents the total number of sub-indices which take part in this multiplicative model. The determination of sensitivity coefficients is presented by Tsakiris (2016a, b). It is important to note that due to the multiplicative character of the index, the BWQI is very sensitive to each of the selected parameters. Further, in order to increase the impact of each sub-index on the final index, each coefficient of sensitivity is increased by 20 percent. Therefore, the coefficients of sensitivity for the multiplicative model of BWQI are $\lambda_1=\lambda_2=0.30$, $\lambda_3=\lambda_4=0.20$, $\lambda_5=0.20$ (Tsakiris, 2016a, b).

3. QUALITY PARAMETERS AND SUB-INDICES

The most critical issue in the development of the BWQI is obviously the selection of the parameters and the transformation process of the absolute values of the quality parameters into sub-indices.

As in the development of any water quality index, it is not possible to avoid the subjectivity when selecting the parameters of the proposed index. To decide which parameters to include and their severity of impact, several experts were consulted together with a thorough bibliographic analysis on the subject.

In regard to the transformation of the absolute values of the parameters to standardised values in the same scale 0-1, the membership function method, used in the fuzzy sets, was adopted. According to this method, the absolute values covering a range within the allowable boundaries are transformed by the membership function into values between 0 and 1. Triangular or trapezoidal types of membership functions are used for the parameters of *E.coli*, pH, nitrates, nitrites, chloride, sulphates and electrical conductivity (20°C), respectively. Graphically these membership functions are given by Tsakiris (2016a, b). It should be mentioned that the maximum absolute allowable values of the selected parameters are adopted by the values proposed in the European directive 98/83/EU. It is easily observed that if the absolute value is out of the permissible interval, the standardised value becomes zero. Due to the ON/OFF process (first stage) or the multiplicative model (second stage), if only one sub-index is zero, then the final BWQI becomes also zero.

In order to facilitate the easy and quick calculation of BWQI, an online application is built. The user is asked to fill a specially developed form including all the necessary water quality parameters in absolute values (concentration of *E.coli*, pH, nitrates, nitrites, chloride, sulphates and specific electrical conductivity). The final BWQI is calculated automatically after the submission of the inserted values.

The basic assumptions for the development of the BWQI are:

a) The bottled water is consumed by different people irrespectively of their age, gender, health status etc. It is also assumed that it is consumed continuously for long time. Based on these assumptions the proposed index has to be relatively general and fulfil the requirements of potable water (EC directives, WHO standards etc). These legislative documents were used

for determining the boundaries of values above which the water is not appropriate for human consumption. Based on these thoughts the maximum allowable concentrations for the selected parameters of the BWQI are given in Table 1.

Table 1. Maximum allowable concentrations of BWQI parameters

Parameter	Unit	Allowable concentrations
Escherichia Coli	Number/250 mL	0
Nitrate (NO_3^-)	mg/L	0-50
Nitrite (NO_2^-)	mg/L	0-5
Chloride (Cl^-)	mg/L	0-250
Sulphate (SO_4^{2-})	mg/L	0-250
pH	pH scale	6.5-9.5
Electrical Conductivity (20°C)	μS/cm	0-2500

b) The bottled water is generally of good or excellent quality and there is no need to test it towards indicators which represent severe pollutants (e.g., test on BOD). However, for security reasons one microbiological parameter (concentration of bacteria *E. coli*) was included in the first stage process of the BWQI. The same applies to pH for which the bottled water has to fulfil the criteria $6.5 \leq pH \leq 9.5$.
c) The selected parameters involved in the multiplicative model belong to three categories with respect to their severity. It is assumed that the nitrates and nitrites belong to the first severity class (3). In the second class of severity (2) are chloride and sulphates and in the third class of severity (1) several salts (e.g., Ca^{++}, Na^+, K^+, etc.) represented by the electrical conductivity. It is also assumed that the first (highest) severity class has a triple impact on the final index in comparison with the third (lowest) severity class. Also, the second (medium) severity class has a double impact on the final index in comparison to the third (lowest) severity class. Finally, it is assumed that the sub-indices of the same severity class have the same coefficient of sensitivity.

4. ASSESSMENT OF BOTTLED WATER BRANDS USING THE BWQI

Using the Bottled Water Index, 79 brands of bottled water available in the Greek market have been assessed based on their labels. In general, most of the brands performed successfully with only 6 (that is 8%) being characterized as unacceptable according to the BWQI rating. Thirty seven brands (47%) reached scores above 0.85 and were characterized as excellent. Nine achieved scores between 0.70 and 0.85 and were assessed as good. Finally, 27 brands (34%) were not assessed due to missing information.

The assessment and rating of the various brands based on the laboratory tests showed slightly different results. The tests were performed in the Laboratory of Reclamation Works and Water Resources Management of the National Technical University of Athens through a number of Diploma theses (Tzima, 2012; Paloglou, 2012; Tsakiris, 2016a, b). From the 57 samples tested, 43 brands (75%) were rated as excellent (score above 0.85), 6 (11%) as good (scores between 0.70 and 0.85) and 8 (14%) were characterized as unacceptable according to the BWQI assumptions. The brands with their scores set in descending rating order appear in Table 2. The brands which failed in attaining successful scores appear with zero score in Table 2.

5. CONCLUDING REMARKS

In this paper, several brands of bottled water available in the Greek market have been assessed using the Bottled Water Quality index (BWQI). The BWQI consists of two stages. The first is a ON/OFF process for testing each bottled water sample against the *E. coli* concentration and the

permissible range of pH. The second stage is a multiplicative model, which includes three types of the most representative quality parameters for bottled water assessment. According to the results obtained (using the information in the labels on the bottles and from laboratory tests), it is concluded that the majority of the bottled water samples examined are of excellent quality, a small number is of good quality, and very few failed to attain the good quality status. It can also be concluded that the new bottled water quality index proved to be a quick, sensitive and powerful tool to assess and compare the quality of bottled waters.

Table 2. The bottled water brand ratings based on laboratory tests and the BWQI

Brand code number	BWQI rating	Brand code number	BWQI rating
32	0.978	26	0.914
56	0.975	51	0.914
22	0.962	40	0.911
20	0.958	38	0.908
25	0.955	30	0.905
10	0.954	14	0.898
21	0.954	8	0.882
9	0.948	11	0.879
43	0.945	24	0.878
28	0.941	31	0.869
48	0.936	45	0.865
7	0.934	29	0.860
1	0.934	37	0.860
4	0.933	39	0.853
35	0.933	2	0.845
34	0.933	36	0.834
42	0.933	33	0.825
6	0.932	54	0.825
41	0.931	16	0.822
18	0.931	5	0.809
13	0.931	46	0.000
27	0.925	47	0.000
44	0.924	49	0.000
17	0.924	50	0.000
3	0.923	52	0.000
12	0.921	53	0.000
15	0.921	55	0.000
19	0.918	57	0.000
23	0.918		

REFERENCES

Alexakis, D., Tsihrintzis, V.A., Tsakiris, G., Gikas, G.D., 2016. Suitability of water quality indices for application in lakes in the Mediterranean. Water Resources Management. 30(5), 1621-1633.

Benedini, M. and Tsakiris, G., 2013. Water Quality Modelling in Rivers and Streams. Springer.

Boyacioglu, H., 2007. Development of a water quality index based on a European classification scheme. Water SA 33 (1), 101-106.

Bhargava, D.S., 1983. Use of water quality index for river classification and zoning of Ganga river. Environmental Pollution Series B: Chemical and Physical 6(1),51-67.

Brown, R.M., McClelland, N.I., Deininger, R.A., Tozer, R.G., 1970. A water quality index - do we dare? Water Sewage Works 117, 339-343.

Canadian Council of Ministers of the Environment (CCME), 2001. Canadian water quality guidelines for the protection of aquatic life. CCME water quality index 1.2, User's Manual, Winnipeg.

Cude, C.G., 2001. Oregon water quality index: A tool for evaluating water quality management effectiveness. Journal of the American Water Resources Association 37 (1), 125-137.

Dunnette, D.A., 1980. Oregon Water Quality Index Staff Manual. Oregon Department of Environmental Quality, Portland, Oregon.

Horton, R.K., 1965. An index number system for rating water quality. Journal of Water Pollution Control Federation 37 (3), 300-306.

Liou, S.M., Lo, S.L., Wang, S.H., 2004. A generalized water quality index for Taiwan. Environmental Monitoring and Assessment 96 (1-3), 35-52.

Nuanchan, S., 2017. Determining overall water quality related to anthropogenic influences across freshwater systems of Thailand. International Journal of Water Resources Development, 33:132-151.

Paloglou, C., 2012. Investigation of quality characteristics of bottled water. Diploma thesis, School of Rural and Surveying Engineering, National Technical University of Athens (in Greek).

Sarkar, C., Abbasi, S.A., 2006. Qualidex - A new software for generating water quality indices. Environmental Monitoring and Assessment 119, 201-231.

Swamee, P.K., Tyagi, A., 2000. Describing water quality with aggregate index. ASCE Journal of Environmental Engineering 126 (5), 451-455.

Swamee, P.K., Tyagi, A., 2007. Improved method for aggregation of water quality sub-indices. Journal of Environmental Engineering 133 (2), 220-225.

Toma, J., Ahmed, R., Abdulla, Z., 2013. Application of water quality index for assessment water quality in some bottled water Erbil City, Kurdistan Region, Iraq. Journal of Advanced Laboratory Research in Biology 4 (4), 118-124.

Tzima, M., 2012. Assessement of bottled waters. Diploma thesis, School of Rural and Surveying Engineering, National Technical University of Athens (in Greek).

Tsakiris, G and Tsakiris, V., 2012. Pipe technologies for urban water conveyance and distribution systems. Water Utility Journal 3, 29-36.

Tsakiris, V., 2016a. Assessment and rating of bottled waters based on a specific index of water quality. Diploma thesis, School of Rural and Surveying Engineering, National Technical University of Athens (in Greek).

Tsakiris, V., 2016b. A new water quality index for bottled water assessment. European Water 54:19-26

Proceedings of the 10th World Congress of EWRA 'Panta Rhei', 5-9 July 2017, Athens, Greece
© 2017 *European Water Resources Association*

GIS-based spatial decision support system for the optimum siting of offshore windfarms

E. Sourianos[1*], K. Kyriakou[1] and G.A. Hatiris[2,3]
[1] *Department of Civil Engineering, Aristotle University of Thessaloniki, 54006, Thessaloniki, Greece*
[2] *Institute of Oceanography, Hellenic Center for Marine Research, 19013, Anavissos, Greece*
[3] *Department of Geography, Harokopio University, 17671. Athens, Greece*
[*] *e-mail: esouriano@gmail.com*

Abstract: The development of Renewable Energy Sources (RES) as an alternative to fossil fuels has gained significant ground in the last years with the EU aiming at 27% energy production from RES until 2030. However, the lack of suitable land based RES sites due to various constrains (aesthetic nuisance, environmental impacts etc.) has led to the development of offshore windfarms sites. Currently available software packages for wind farms siting take into consideration only wind power, cost and potential energy production but they do not give to the users the capability to simultaneously evaluate various candidate sites; instead, the users have to pre-select a site and then analyze the data. Nevertheless, this procedure is complex and crucial factors must be considered (environmental, socio-economic, spatial planning) and a software that would analyze critical data and compare the candidate sites would contribute remarkably to the evolution of offshore windfarms siting. The current study is aiming to the development of a holistic methodology for the optimum siting of offshore windfarms that will be implemented through a web-based GIS software. The whole process could be briefly depicted by the following steps: exclude sites that do not fulfil the criteria, asses the candidate sites through an analytical hierarchical process, form energy scenarios for every candidate site and then select the optimum. This software will be a precious decision support system for the stakeholders.

Key words: GIS-based software, Offshore Wind Farms, Siting, Analytic Hierarchical Process, Public Participation

1. INTRODUCTION

Raise of green energy (tidal, wind and solar) and implementation of renewable energy technologies is a way towards independency from fossil fuel oils. Each form of renewable energy is characterized by advantages, drawbacks and different impacts on natural and anthropogenic environment. Wind energy is a rapidly evolving RES and also the most exploited because humans have been gathering endless amounts of energy for hundreds of years with different types of windmills. Nowadays, there is a trend towards offshore wind farms (OWF) due to their various advantages comparing to onshore wind farms. As there are no geographical obstacles at the open sea OWFs can be extended spatially causing only slight acoustic and optical disturbance. OWF's construction and maintenance costs are high and their affection on the marine environment certain but as they exploit the moving air above the oceans their operating speed is higher and this means higher efficiency and electricity production (Miller & Spoolman, 2009).

Greece's wind potential is rich and classified among the most promising in Europe, with onshore air velocities exceeding 8 m/sec. To site an OWF involves a series of different factors such as financial, social, ecological and technological constraints and many methods for applying multi-criteria analysis at coastal areas have been proposed, targeting at finding suitable RES for best siting and energy production. However, none of them focuses on an approach that ensures the compatibility and complementarity of regional planning and marine spatial planning for sustainable development (Wimmler, et al., 2015). The combination of RES in inland and maritime areas has not been studied sufficiently and especially in Greece where most of the researches until now concerns the inland.

Also, through a literature investigation there is a major failure regarding participatory planning

in Greece. Specifically, a few researches include the perspective of local residents and stakeholder engagement in a comprehensive sustainable energy-planning project. Siting RES without the public acceptance and institutions can lead to severe reactions and finally to the cancellation of the project. Therefore, the acceptance of the proposed project by local residents and operators should be one of the most important criteria for any type of RES siting.

The core idea of this study is the development of a GIS-based software tool that will implement the proposed methodology. A similar tool is the Geospatial toolkit of National Renewable Energy Laboratory (NREL), USA and is distributed totally free. It is a GIS-based software with graphic user interface and constitutes a tool for searching the ideal site of wind and solar farms. The user has the ability to select from a list of criteria. This tool can be used in many countries?? but not?? in Greece. Another tool is Energy Zones Mapping Tool (EZMT), which is online and identify potential areas for siting various RES, including marine areas. The user can choose between various RES, select the criteria and get the final map with the eligible areas. This tool is feasible to be implemented by any user without requiring a subscription, but can be applied only within the US.

As it was noted, there is only one software for offshore and onshore RES siting and its use is restricted to United States only. Therefore, the proposed software is highly innovative because it is generic and so it can be used without geographical restrictions, it implements a holistic methodology including several criteria (social, economic, environmental and technical, etc.) in the framework of marine Spatial Planning and it incorporates the participatory planning and stakeholder engagement aiming at sustainable development.

2. THEORETICAL FRAMEWORK

2.1 Offshore wind farm trend

According to EWEA, there are 1371 offshore wind turbines installed in Europe seas with a total capacity of 3812.6 MW approximately. These wind turbines are located in 53 OWF in 10 European countries producing 14 TWh covering the 0.4% of the total consumption in European Union.

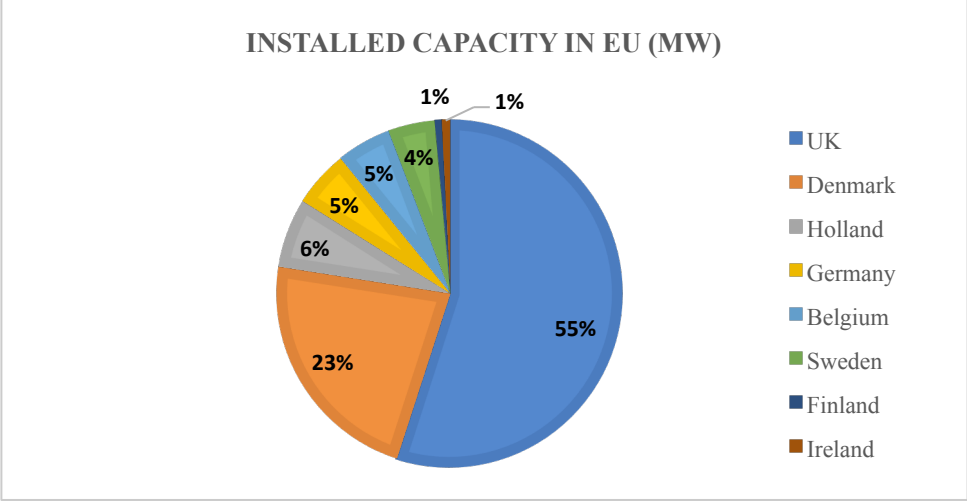

Figure 1. Installed capacity in EU (EWEA, 2013)

Southern countries of EU have not installed so many wind turbines (Figure 1) as the sea depth constitutes a limiting factor for offshore wind farms development. Until today, wind turbines in OWF are installed on the seabed with 4 different type of foundation: gravity (20%), monopile (75%), tripod and jacket that are ideal for seas with depth more than 40 meters.

As a result of technology evolution, the distance of OWF from shore and their installation depth

are both increasing: in 2011, the average depth of installation was about 23 meters and the average distance from shore was about 23 km while for current projects the average depth is 25 m and the average distance is 33 km. A large number of wind turbines constructors (41) have announced their will to develop new models for offshore projects and that means that the offshore wind energy will be one of the most significant sectors for development and investment globally. New models will have capacity more than 5 MW. The aim of two companies, Vestas and Alstom, are turbines of 7 MW and 6 MW capacity, respectively while Siemens has already test a new model with 6 MW capacity in Denmark (EWEA, 2013).

The development of OWF further from shore and in deeper seas seems to be a cost-effective solution if it is combined with high capacity wind turbines and for this reason, development of offshore wind turbines constitutes a basic of European energy policy.

Although there are not any installed offshore wind turbines in the Greek seas due to the complexity of their geomorphological characteristics (Xaviaropoulos, 2012) the significant offshore wind velocity could contribute to the development of RES in Greece. Moreover, given the current market trend of installing bigger turbines into deeper waters it is concluded that to install offshore wind turbines in Greece it may be now feasible. According to National Renewable Energy Action Plan (NREAP) the offshore renewable energy target for Greece for 2020 is 1500 MW (EWEA, 2013).

2.2 Siting criteria

The siting of an OWF may provoke potential spatial conflicts with other resources exploitation sites. So, the optimum siting of offshore wind farms should take into consideration technological, ecological and social parameters because the limitation of their negative effects will maximize the overall value of the wind farm development. Based on this concept, evaluation of candidate areas have been successfully used in wind farm macro-siting analysis, considering the best wind farm location within a region, through marine spatial planning analysis (MSP). MSP has been shown to substantially increase the overall value of the area with little to no cost for the wind farm developers (O'Reilly, et al., 2012).

The siting criteria that must be taken into account have been selected through a bibliography and legislation research and are presented in the following Table 1. (Vagiona, et al., 2012), (Vasileiou, et al., 2017), (Ministry of Environment & Energy, 2011), (O'Reilly, et al., 2012).

Table 1. Siting criteria

Field of interest	Factors	Exclusionary	Mitigable	Constraint
Environment	National parks, NATURA2000, Marine Protected Areas, RAMSAR etc.	x		yes / no
Military	Fire zone, submarine zone, training zone, airport, etc.	x		yes / no
Navigation	Cables, signalization, channels		x	yes / no
Radars	Harbors, safety navigation, military		x	yes / no
Economics	Fisheries		x	yes / no
	Economic Exclusion Zones	x		yes / no
Technical	Wind velocity	x		> 6 m/s
	Water depth	x		< 500 m
	Distance from shore	x		> 3 km
	Proximity to a local electrical grid with high voltage capacity		x	220-400 kV / 220 kV / 150kV / 66kV
Tourism	Saturated		x	yes / no
Other	Distance from shore	x		> 6 km
	Shipping route density		x	low / high traffic
	Licensed areas for exploration and exploitation of Hydrocarbons	x		yes / no

2.3 Decision making through Analytical Hierarchical Process

Decision analysis using the Analytical Hierarchical Process (AHP) has three concepts: a) structuring the complex decision problem as a hierarchy of goal, criteria and alternatives, b) pair-wise comparison of elements at each level of the hierarchy with respect to each criterion on the preceding level and c) vertically synthesizing the judgments over the different levels of the hierarchy (Vagiona, et al., 2012). AHP is selected for a multi-criteria analysis, as it uses a ratio scale, which, contrary to methods using interval scales (Kainulainen et al., 2007), requires no units in the comparison (Ishizaka and Labib, 2009). At each node of the hierarchy, a matrix collects the pairwise comparisons, performed according to information generated from the corresponding maps (Karanikolas, et al., 2011).

2.4 Stakeholder engagement and public participation

Stakeholder engagement and public participation are a means of achieving:

- Participatory democracy
- Transparency in decision-making process
- Community empowerment and support
- Reduced conflict over decisions between decision-makers and public groups, and between the groups.

If the public participation is to be effective it requires that citizens be informed and aware of the topic or issue of concern. They must also be willing and able to be involved in the process, which typically involves investing significant personal time (Yee, 2010).

Spatial planning should be based on a participatory, synthetic and comprehensive series of negotiations, but also needs to be a flexible process which is possible to be modified depending on each areas' needs, requirements and characteristics. Public participation in spatial planning usually is leading in exchanging personal views on certain topics. Stakeholders involved are often able to bring different levels of knowledge to the table, an approach very useful due to the fact that planning activities require different areas of expertise and knowledge. Local society is also regarded to be a valuable source of information to evaluate the priorities on which planning policies should be based on (Lazoglou, et al., 2015).

3. SOFTWARE ARCHITECTURE

The aim for this software is to create a support decision system for OWF siting that will be possible to be used by someone not necessarily an expert. It is GIS-based and all the results are presented on thematic maps at GIS environment permitting the user to navigate on the map as well as to export the map to a shapefile. The interface was tried to be user friendly without requesting too many inputs but the user is also given the possibility to parameterize the factors or add more of them. The methodology that is implemented through the software is divided into two phases: exclusion and assessment. It should be noted that stakeholders' engagement and public participation are included in the exclusion phase and at assessment phase, respectively.

First of all, there is a database with two categories of criteria: exclusion criteria and assessment criteria. The user is asked to decide if he will use the criteria with the defined parameters. In case that user does not agree with the parameters or the legislation is different from Greece's, it is feasible to edit the database of criteria. The user also can edit the impact factor of each criteria. The criteria have already defined impact factors that have been provided by implementing an AHP at Greek stakeholders. If user agrees with theses impact factors continues to the next step. Otherwise, it is suggested to implement a new AHP and insert his impact factors. Thus, each criterion has an

Impact Factor (IF). At the next step, it is asked to load the needed data in shapefile format. The needed data are the following: wind velocity, bathymetry, land uses, protected areas, special uses and other data. The output is a thematic map in GIS environment and the shapefile overlapping provides with a new map in which unsuitable areas have been excluded. So, there are "n" eligible areas. Each eligible area has an index indicating the satisfaction of each exclusion criterion (EC). There is a process at the background that scores (SC) the fulfilment of each criterion. The index is calculated by the following equation for each eligible area:

$$EPSI_n=SCEC_1*IFEC_1+SCEC_2*IFEC_2+SCEC_3*IFEC_3+SCEC_4*IFEC_4+SCEC_5*IFEC_5+SCEC_6*IFEC_6 \quad (1)$$

The best value for the index is 1. Then, the eligible areas are evaluated using the assessment criteria. At this phase, it is suggested to implement a crowdsourcing process to investigate the public acceptance for each eligible area. An index of satisfaction is also produced

$$APSI_n=SCAC_1*IFAC_1+SCAC_2*IFAC_2+SCAC_3*IFAC_3+SCAC_4*IFAC_4+SCAC_5*IF\ AC_5+SCAC_6*IFAC_6 \quad (2)$$

A total satisfaction index is also calculated for each area. This process reveals out the most suitable area based on all the criteria, exclusion and assessment.

$$TSI_n = APSI_n + EPSI_n \quad (3)$$

Then, a type of Offshore Wind Turbine (monopile, gravity, tripod et-c) is selected for each suitable area and energy scenarios are produced and for each one of them critical values such as the available area (m^2), the satisfaction of each criterion through TSI and the potential energy that can be produced are calculated. Then An index is also considered, a median installed cost (€/MW). These scenarios are the final output and the user has acquired valuable knowledge on some suitable areas, the cost and the potential energy. It should be noted that it is possible that for one area two energy scenarios to be produced because at deeper waters more than one Offshore Wind Turbine (OWT) type can be installed. At this case, the cost may be a crucial factor. The software's architecture is briefly depicted at the following figures.

4. CONCLUSIONS

The present paper is depicting a holistic methodology that can be implemented through an open architecture software and can be used as a precious tool for supporting decision process. The methodological framework is based on GIS and AHP combination, incorporating public acceptance and stakeholders' expertise, for the identification of the most appropriate marine areas for OWF siting. Many approaches concerning this topic have been presented in the past but the implementation of the proposed methodology through a software is really innovative as there in not similar software. Another pioneering component of this approach. Additional innovative elements is the integration of public participation, the fact that the software is open so any user, expert or not, can parametrized it by adding or editing the criteria and their parameters. This generic character of the software permits its implementation worldwide. Last but not least, the software is based on GIS and its outputs are in "shapefile" format so it is possible to be used with every GIS software for further analysis. It should be noted that it is not a tool that provides the final decision but it significantly helps to the investigation for an OWF potential use. It is obvious that a further analysis even in a micro-scale analysis is needed should a stakeholder or an investor aims at finding the final area of siting an OWF.

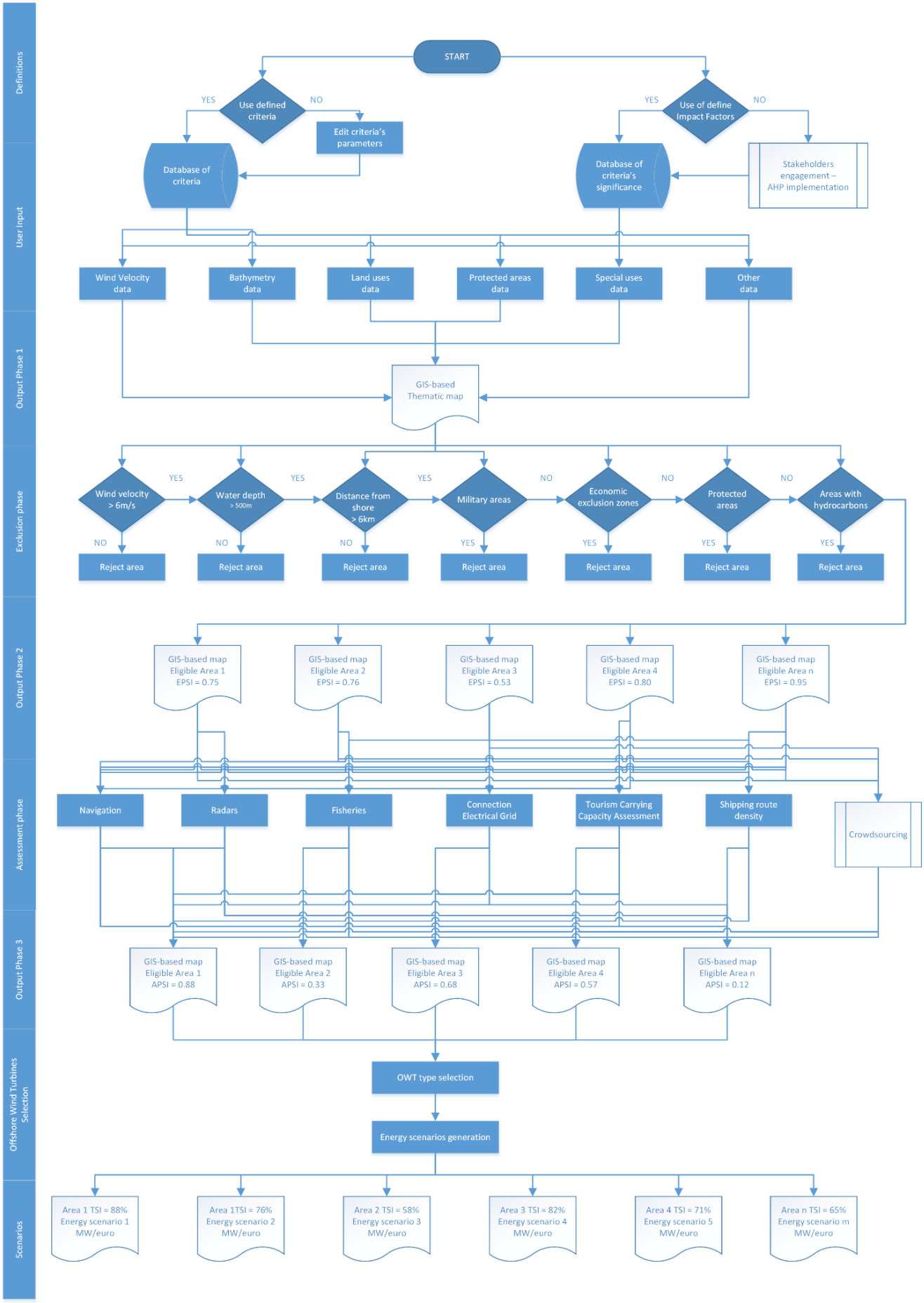

Figure 2. Workflow of software

REFERENCES

European Wind Energy Association, 2011. Offhsore Renewable Energy and Maritime Spatial Planning. Seanergy 2020. [Online] http://www.seanergy2020.eu/wp-content/uploads/2011/11/111020_Seanergy2020_Deliverable3.2_Final.pdf.

EWEA, 2013. Deep Water. EWEA. [Online] http://www.ewea.org/fileadmin/files/library/publications/reports/Deep_Water.pdf. 978-2-930670-04-1.

Karanikolas N., et al. 2011. Offshore wind power in europe: perspectives of development in Greece. Cest2011, Rhodes, Greece.

Lazoglou M., Sourianos E. and Kyriakou K. 2015. Creating a system for supporting integrated spatial planning in island areas. 10th International Geographical Congress, Thessaloniki, pp. 1024-1040.

Miller, A. and Spoolman, S. 2009. Living in the environment, Cengage Learning. Canada

Ministry of Environment & Energy. 2011. Tendering procedure for the construction and operation of offshore wind farms. Athens

O’Reilly, Christopher M., Grilli R. Annette and Potty R. Gopu. 2012. Offshore wind farm siting using a genetic algorithm. Trivandrum, Kerala, India. University of Rhode Island, International Conference on Green Technology (ICGT 2012).

Vagiona, D. G. and Karanikolas, N. M. 2012. A multicriteria approach to evaluate offshore wind farms. Global NEST Journal. 2012, Vol. 14, 2, pp. 235-243.

Vasileiou M., Loukogeorgaki E. and Vagiona D.G. 2017. GIS-based multi-criteria decision analysis for site selection of hybrid. Renewable and Sustainable Energy Reviews. 2017, Vol. 73.

Wimmler, C., et al. 2015. Assessing offshore renewable energy technologies based on natural conditions and site characteristics. Renewable Energies Offshore. 2015.

Xaviaropoulos, P. K. 2012. Offshore Wind Farms, European ecolutions and Greek perspectives. okeanos-dspace. [Online]

Yee, S. 2010. Stakeholder engagement and public participation in environmental flows and river health assessment. WaterCentre.

Proceedings of the 10th World Congress of EWRA 'Panta Rhei', 5-9 July 2017, Athens, Greece
© 2017 *European Water Resources Association*

Development of an updated water quality index based on legislation and experts' opinion

F. Iakovidou*, E. Trikoilidou, G. Samiotis, A. Stamos, L. Tsikritzis and E. Amanatidou
Environmental Chemistry and Wastewater Treatment Laboratory, Department of Environmental Engineering and Pollution Control, Western Macedonia University of Applied Sciences, 50100, Kozani, Greece
* *e-mail: waterlab4@teiwm.gr*

Abstract: Water quality assessment is based on measurements of physical, chemical and biological parameters according to enforced legislation, while water quality characterization is achieved by using water quality indices (WQI) developed during the past decades. These indices transform a plethora of measurement data into a single characterization value. Nevertheless, the results obtained from the application of various water quality indices are not easily comparable because of their different calculation methodologies. Additionally, many water quality monitoring parameters that are prioritized by legislation (pesticides, halogenated hydrocarbons, heavy metals, pathogens, etc) are excluded from the indices´ calculation. This work presents the effort to update the water quality indices, by taking into account additional monitoring parameters that are considered important, and to redefine their weight coefficients. For this purpose, over 1000 questionnaires were send to researchers, institutions, universities, national, European and international organizations, water management authorities, relevant ministries, water supply companies and non-governmental organizations worldwide. From the questionnaires' interpretation a new water quality index, named "ΥΔΩΡ WQI", was created. "ΥΔΩΡ WQI" characterizes water quality in relation to monitoring parameters included in the latest guidelines of European Union, United States Environmental Protection Agency and World Health Organization. The new water quality index was validated using over three years' data from surface water and groundwater of Western Macedonia Region, Greece, and by comparing its results to those obtained from other indices (NSF, Canadian etc.).

Key words: Water Quality Indices; water quality classification; water quality assessment

1. INTRODUCTION

Water quality assessment and water characterization is a complex process, requiring a plethora of measurements of physicochemical and biological parameters, with a specified frequency, according to complex legislation. Water Quality Indices (Water Quality Index, WQI) are used as an easy, short and simplified characterization tool and are widely applicable. WQI convert complex numerical data resulting from the analysis of water quality parameters into a single value that refers to a characterization of the water body quality.

The characterization of water quality based on WQI was developed by Brown (1970) and was globally accepted. Brown formulated a water quality index for the National Sanitation Foundation (NSFWQI) of the United States of America. He put particular emphasis on developing a single water quality characterization scale, on the methodology for choosing the adequate water quality parameters and on assigning weight coefficients to them (Abbasi and Abbasi 2012).

From 1970 many other WQI (Dinius 1987; Smith 1990; Said et al. 2004; Debels et al. 2005; Bhargava et al. 1998) where formed, which differentiate according to their calculation methodology (Advanced Statistical Analysis, Fuzzy Logic and Other Methods of Artificial Intelligence, etc.), to the parameters that take into account (based on bibliography or literature or current legislation) or to the use of weight coefficients for each control parameter.

The use of WQI presents some shortcomings; one of the most important is that in order to make it a flexible and easily applicable tool, uses a limited number of water quality control parameters; thus significant data may be omitted, with high probability to overshadow dangerous parameters, leading to erroneous conclusions and inconsistent characterization. Since 1970 the control

parameters proposed from legislation have changed significantly. Directive 2000/60/EC defines control parameters of surface water and groundwater most of which are not included in the present WQI.

The consistency of a WQI is examined by verifying its results and comparing them with other indices (Johnson et al. 2013). This procedure is difficult to be achieved as WQI take into account different type of information (water quality parameters). Furthermore in most cases small changes in the analysis results of the measured control parameters, is not apparent to the final water quality characterization.

Scope of this work is the creation of a new WQI from the Environmental Chemistry and Wastewater Treatment Laboratory, which is named "YDOR" (pronunciation húdōr) word deriving from the ancient Greek "ΥΔΩΡ" that means water. "YDOR" includes a sufficient number of monitoring parameters from different categories (bacteria, pesticides, heavy metals, nutrients, organic substances, etc) based on experts' opinion and latest guidelines of National, European and International legislation, while maintains its sensitivity and consistency. The study also introduces the use of additional parameters in calculating a WQI and redefines the weight coefficients of the previous according to the needs of time. All these data will assist everyone involved in water quality management to modify "YDOR" based on their needs and specificities of their area.

2. MATERIALS AND METHODS

Literature review of Water Quality Indices, from the first one created (1965) until our days (Smith 1990, Bharti et al. 2011, Tyagi et al. 2013; Alexakis et al. 2016; Tsakiris 2016), was conducted for choosing the basic calculating equation for "YDOR". The selected equation is additive (Equation 1); control parameters, weight coefficients and characterization limits of water quality are changeable, and make the proposed WQI not only flexible to use but also comparable to other indices.

$$WQI = \frac{\sum_{i=1}^{n}(q_i \times RW_i)}{\sum_{i=1}^{n} RW_i} \quad (1)$$

where, q_i = Sub-index of "*i*" water quality parameter; RW_i weight coefficient of *i* parameter.

The *sub-index* (Equation 2) is calculated according to measured physicochemical and microbiological water quality parameter values, standard values deriving from legislation limits, and desired or ideal values.

$$q_i = \frac{100 \times |C_i - V_{i0}|}{|S_i - V_{i0}|} \quad (2)$$

where, q_i = Sub-index of "*i*" water quality parameter; C_i = measured value of the "*i*" water quality parameter; S_i = permitted "*i*" water quality parameter value obtained from legislation; V_{io} = the ideal value of "*i*" water quality parameter.

Permitted values of control parameters arose from limit values of European Directives and National legislation, relating to the quality of inland surface water and groundwater (Directive 75/440/EOK, Directive 98/83/EE, Greek Legislation189/B/68, Directive 78/659/EOK)

Ideal values can be selected either by using guide values from legislation (Zaidi et al. 2016; Wanda et al. 2016) or by using zero values for pollutants (Chauhan et al. 2010; Chowdhury et al. 2010; Balan et al. 2012) or by using reference values from an undisturbed site within the study area (2000/60/EC) or by using the Lower Detection Limit (LDL) of determination method of parameter (REFCOND 2003). In this study detection limits were selected as defined by Directive 98/83/EC.

For selecting the control parameters that should be included into the calculation of WQI and for defining the weight coefficients, the Delphi method was applied. Three appropriate questionnaires were compiled; the first one was sent to 1000 Water Management Agencies, Water Supply Companies, Relevant Ministries, Research Institutes and Universities, National, European and

International Organizations and to Non-Governmental Organizations, globally. The respondents were asked to choose among 70 parameters (Table 1) to be included in "YDOR" having the following options "mandatory", "optional", "should not be included" and "not sure". The parameters were selected from the Environmental Quality Standards (EQS) and from the priority substances as defined in Directive 2000/60/EC. The respondents had the option to propose and other parameters, considered important by them that had been excluded from the research.

After processing the responses to the first questionnaire, a second questionnaire, was compiled; survey respondents were asked to rate the significance of each parameter by assigning a Weight Score (AWS). The questionnaire included all parameters, even those whose inclusion in WQI was considered as "optional". The AWS ranged from "1" (low significance) to "5" (high significance).

The AWS of each parameter is calculated based on the results of the questionnaires and using Equation 3.

$$\mathrm{AW_i} = \frac{\Sigma\, AWSij}{n} \tag{3}$$

where, AWS_{ij} = assigned weight score of *"i"* parameter from the *"j"* respondent; n= the number of respondents.

The Relative Weight (RW) of the included parameters in the index, is calculated by using Equation 4

$$RW_i = \frac{AW_i}{\sum_{i=1}^{n} AW_i} \tag{4}$$

where, RW_i = the relative weight of *"i"* parameter; AW_i = the assigned weight of of *"i"* parameter.

At the second questionnaire respondents were also requested to specify three pollutants that are often found in their region and require systematic monitoring.

The final choice of the control parameters included in the "YDOR", was based on the AW of each parameter, on the statistical results from the questionnaires regarding which parameters must be included "mandatory" or "optionally" in a WQI and the proposed pollutants from the respondents.

The third questionnaire informed the respondents about the results that emerged from analyzing their answers, while at the same time the new WQI was presented. The respondents were asked to intervene with observations and comments regarding the final defining of the index.

The new water quality index was validated by using physicochemical analysis data from surface water and groundwater of Western Macedonia Region, Greece. Specifically, qualitative data of Vegoritida Lake (Ministry of Agriculture 2012) and of groundwater from Vegoritida Basin were used (Municipality of Amyntaio 2012). The water quality data of Vegoritida Lake concern the period 1999-2000, before the enforcement of protection measurements of the Lake (waste water treatment plants, good agronomic practices, etc) while the groundwater database is relatively recent, 2010-2011.

Water quality according to "YDOR" is characterized as Excellent: (0-25) Good: (26-50) – Fair: (51-75)- Marginal:(76-100)- Poor: (> 100).

The results of "YDOR YΔΩP" were compared with those from other indices such as modified NSFWQI (Kumar et al. 2009), and Canadian Council of Ministers of the Environment Water Quality Index (CCMEWQI), for the same databases. NSFWQI was chosen because it uses predefined parameters, previous weight coefficients (assigned in 1970), and it does not compare parameters' values to legislation. CCMEWQI was chosen because it can be applied for the same parameters and permitted values as "YDOR", without the use of weight coefficients.

3. RESULTS AND DISCUSSION

From the 1000 questionnaires send to different specialists, 134 responses were received, while

the latest survey was based on 102 answers (Brown, 1970). The panelists indicated that all of the 76 parameters should be included in the "YDOR" calculation, "mandatory" or "optionally". More than 30% of the panelists indicated that 29 parameters (Table 1, those in grey background) should be included "optionally".

Table 1. Significance values obtained by the study in order of decreasing importance

		RESULTS				ASSIGNED WEIGHT SCORES					ASSIGNED WEIGHTS
A/A	Parameter	Optional	Mandatory	Do not include	Not Sure	1	2	3	4	5	M.O
1.	Chromium (VI)	3	167	0	10	0	0	0	39	141	4,78
2.	E-coli	11	161	0	8	0	0	0	41	139	4,78
3.	Arsenic	4	165	3	8	0	0	21	9	150	4,72
4.	Lead	19	159	1	1	0	0	18	12	150	4,72
5.	Cadmium	17	154	6	3	0	0	18	17	145	4,67
6.	Fecal Coliforms	39	133	1	7	0	0	0	60		4,50
7.	Mercury	4	168	0	8	0	0	29	19	132	4,56
8.	Ammonium	20	155	0	5	0	0	30	42	108	4,44
9.	Salmonella	75	65	26	14	8	12	17	13	130	4,33
10.	COD	23	151	1	5	0	0	26	60	94	4,40
11.	Nitrite Ions	14	158	5	3	0	10	20	47	103	4,40
12.	Nitrate Ions	20	155	0	5	0	0	8	102	70	4,33
13.	Phenols	12	115	0	5	0	10	38	47	85	4,11
14.	Heptachlor	40	95	0	45	0	11	39	50	80	4,11
15.	Epoxi - Heptachlor	59	76	2	43	0	1	35	67	77	4,11
16.	PCB's - PCT's	45	130	0	5	0	17	20	56	87	4,06
17.	Mineral Oil	75	100	0	5	0	20	33	49	72	4,06
18.	Dieldrine	49	91	2	38	0	9	44	58	69	4,06
19.	Total Phosphorus	16	159	0	5	0	0	20	89	71	4,34
20.	Residual Chlorine	65	107	0	8	10	0	30	70	70	4,06
21.	PAH's	47	128	1	4	0	30	10	60	80	4,05
22.	Aldrine	41	94	5	40	0	22	28	61	69	4
23.	Total Coliforms	20	154	0	6	0	10	40	70	60	4
24.	BOD	21	155	0	4	0	11	49	50	70	4
25.	TOC	85	87	0	8	0	9	61	29	81	4
26.	Benzene	70	105	0	5	0	40	11	49	80	3,94
27.	Nickel	40	136	0	4	1	9	70	22	78	3,94
28.	Chromium (III)	30	135	0	11	10	31	19	20	100	3,94
29.	Ps.Aeraginosa	90	75	0	15	10	10	33	57	70	3,94
30.	pH	83	55	40	2	0	8	52	60	60	3,94
31.	Surfactants	90	80	0	10	0	9	51	69	51	3,89
32.	Manganese	19	146	11	4	1	19	49	38	73	3,89
33.	Copper	38	132	1	9	0	30	54	16	80	3,83
34.	Selenium	59	103	2	16	11	20	39	39	71	3,83
35.	Antimony	55	110	0	15	10	20	42	42	66	3,78
36.	Conductivity	30	115	30	5	2	18	61	40	59	3,78
37.	Dissolved Oxygen	39	136	0	5	0	20	60	40	60	3.77
38.	Zinc	55	115	0	10	20	11	29	45	75	3,77
39.	Total Tri-alomethanes	60	95	0	25	11	31	31	40	67	3,72
40.	TKN	34	126	2	18	10	10	53	54	53	3,72
41.	TSS	50	120	0	10	0	19	61	61	39	3,67
42.	Radon	112	44	16	8	12	33	40	33	62	3,67
43.	Fat, Oil and Grease	62	108	0	10	0	29	60	42	49	3,61
44.	Sulfates	23	147	0	10	1	31	64	42	42	3,61
45.	Ferrous	58	114	0	18						3,56
46.	Gamma Radion.	72	103	4	1	20	20	40	40	60	3,56
47.	Radium	79	97	1	3	10	30	53	31	56	3,56
48.	Uranium	94	80	2	4	9	39	39	23	70	3,56
49.	Vinyl Chloride	77	93	5	5	21	31	31	42	55	3,50
50.	Aluminium	65	100	5	10	10	11	82	39	38	3,50
51.	Phosphates	30	145	0	5	10	0	10	110	50	3,50
52.	Gross Alpha & Beta	83	86	8	3	19	10	60	40	51	3,50
53.	Acrylamide	102	67	6	5	21	23	39	58	39	3,44
54.	Chlorides	29	146	4	1	0	40	70	20	50	3,44
55.	Radioactive Cesium	65	105	5	5	21	22	53	42	42	3,44
56.	Hardness	41	134	2	3	20	30	42	41	47	3,39
57.	Turbidity	37	142	0	1	8	53	32	74	13	3,28
58.	TDS	72	103	0	5	0	30	90	22	38	3,39
59.	Sodium	44	133	1	2	3	43	65	39	30	3,33
60.	Color	26	149	0	5	0	50	60	30	40	3,33
61.	Radioac. Iodine	112	66	1	1	33	10	70	9	58	3,33
62.	Tritium	83	46	3	38	18	32	54	36	40	3,33
63.	Silver	74	98	6	2	11	40	62	31	36	3,28
64.	Potassium	69	111	0	1	0	40	78	31	31	3,27
65.	Magnesium	70	105	5	0	20	40	60	30	30	3,06
66.	Alkalinity	34	136	0	10	19	61	42	28	30	2,94
67.	Calcium	77	101	0	2	30	60	49	11	30	2,72
68.	Temperature	55	45	74	6	39	50	60	20	11	2,57
69.	Total Pesticides	74	86	0	20	0	0	0	60	120	4,5
70.	Clostridium Perfringens	70	75	10	25	0	10	40	60	70	*

The participants' comments highlighted the importance of adjusting the WQI depending on water use and the needs of each area. For this reason, the second questionnaire included all the control parameters (as the first questionnaire) with the difference that Herbicides, Fungicides, Nematicides, Acaricides, Rodenticides, Slimicides consolidated into Total Pesticides.

The second questionnaire was send to 134 experts, who responded to the first questionnaire. The AWS assigned by experts for each parameter and the calculation of AW (equation 1), are given in Table 1. The parameters were arranged in decreasing order of AW (Table 1).

By processing the 134 responses of the second questionnaire, it was found that some control parameters, which are considered "mandatory" in calculating the WQI, have a low Assigned Weight (AW <4) (Table 1). The panellists believe that these parameters should be included in the calculation of the index but should not affect significantly the final result. Therefore, the choice of the parameters which must be included in "YDOR" WQI was made by excluding initially the parameters that had AW <4, afterwards the parameters that were considered by the 30% of the panelists as "optional" and from the final list of 18 (Graph 1) parameters those that affected insignificantly the "YDOR WQI" result. From Graph 1 it is obvious that "YDOR WQI" result deviates until the parameters of TP is inserted in the calculation. After TP the results stabilize and values even over the permitted limits do not affect them. The calculations were made on real surface water data for "YDOR" parameters and for marginal values for the excluded parameters.

Consequently, the following parameters 12 parameters were initially selected sto be included in "YΔΩP" WQI calculation: hexavalent chromium (Cr(VI)), Arsenic (As), Mercury (Hg), Cadmium (Cd), Lead (Pd), e–coli, Faecal Coliforms, Total Pesticides, Ammonium, COD, Nitrites, Nitrates and total Phosphorus.

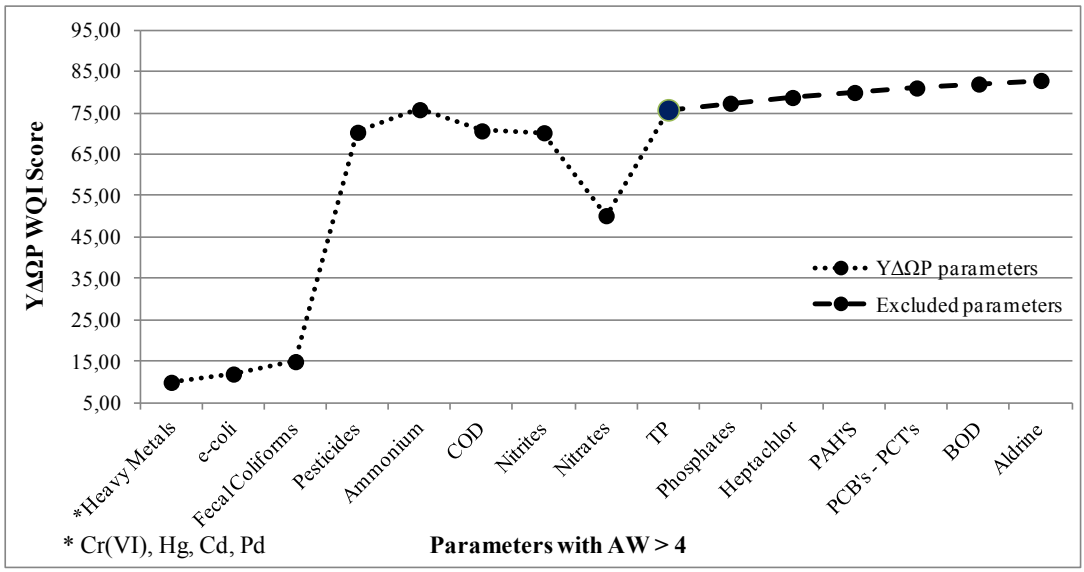

Figure 1. YDOR WQI results in relation to parameters.

This study has many differences in comparison to the one conducted by Brown et al. in 1970 mainly to the parameters that should be included in the calculation of WQI as well as and to their significance. Since 1970, new parameters have been introduced to the monitoring programmes of water quality such as mercury, lead, cadmium, chromium (VI), arsenic, and nickel, heavy metals mainly used in agricultural and industrial activities. These parameters have high Assigned Weight (Table 1) while in 1970 only copper was included and its AW was low (AW=3.40). pH and dissolved oxygen are not considered, in this study, as significant parameters for calculating a WQI and are not included in the calculation of "YDOR", in contradiction to Brown's study where had high AW (AW=4.9 & AW=4.38 respectively) and were chosen for the calculation of NSF WQI. Nowadays, COD analysis is preferable from that of BOD5 (Brown's study) probably because COD method needs less time to be completed and is safer (less toxic reagents) than it was in 1970.

Additionally, the pollutants that were proposed as the most frequently encountered in Greece and require systematic monitoring are chlorides (41%). Specifically, the coastal areas face pollution problems with chlorides, mainly due to salinization phenomena. Also, the parameter of Hexavalent Chromium occurs at high rates in regions which associate with intense industrial activity or geological formations which upon dissolution release Chromium VI. Nitrogen compounds are found in agricultural regions. It was considered necessary to include the parameter of Chlorides in the final calculation parameters of «YDOR » WQI, as the problem of salinization is intense both in Greece and other countries. In conclusion the final parameters thet were included in the calculation of "YDOR" WQI are given in Table 2.

After the determination of the water quality parameters the RW for each one of them was calculated according to equation 4 and "YDOR" was applied on the available water quality data. In Table 2 the calculated RW, the permitted (Si) and the ideal (Vio) values used for calculating "YDOR" are given.

Table 2. Final parameters Relative Weight Values (RW), permitted (Si) and ideal values (Vio) used for the calculation of "YDOR" WQI.

A/A	Parameter	RW	Permitted Values (mg/l)	Ideal Values (mg/l)
1.	Chromium Hexavalent (Cr(VI))	0,077	0,05[1]	0,005
2.	E – Coli	0,076	20[3]	0
3.	Arsenic (As)	0,076	0,01[3,2]	0,001
4.	Lead (Pb)	0,076	0,01[2]	0,001
5.	Cadmium (Cd)	0,075	0,005[3,2]	0,0005
6.	Fecal Coliforms	0,075	20[3]	0
7.	Mercury (Hg)	0,073	0,001[3,2]	0,0002
8.	Total Pesticides	0,072	0,0001[3,2]	0,000025
9.	Ammonium	0,072	0,05[4]	0,005
10.	Nitrites	0,070	0,03[4]	0,003
11.	Nitrates	0,070	50[3,2]	5
12.	COD	0,064	30[3]	0,005
13.	Total Phosphorus (TP)	0,069	0,4[4]	0,04
14.	Chlorides	0,055	0,05	0,005

[1]Directive 75/440/EOK, [2]Directive 98/83/EE, [3]Greek Legislation 189/B/68, [4]Directive 78/659/EOK,

The groundwater is characterized by "YDOR" as "High" and the surface as "Marginal" according to their physicochemical and microbiological characteristics (Table 3). It should be noted that the database for the surface water is before the enforcement of protective measurements of the area and the characterization will be improved if a most recent database is used.

The values of "YDOR" are comparable to those of CCMEWQI which characterizes the quality of groundwater as "High" and of surface water as "Medium". The calculation of CCMEWQI is based on the percentage of control parameters that present deviations from the permitted values, on the percentage of the individual tests that do not meet the permitted values and on the amount by which failed test values do not meet the permitted values.

Table 3. Water characterization as calculated for the three indices

	NSFWQI	CCMEWQI	ΥΔΩΡ WQI
Surface water	84 Excellent	67,80 Fair	75,80 Marginal
Groundwater	95 Excellent	95,40 Excellent	19,50 Excellent

Water quality is ranked as Excellent: (95-100) Good: (80-94) – Fair: (65-79)- Marginal:(45-64)-

Poor: (0-44). The CCMEWQI was calculated for the same water quality parameters and the same permitted values with "YDOR". The small differentiations between them are likely because "YDOR" inserts in its calculation and the ideal value. When the value of an parameter diverges from the ideal and gets closer to permitted, the water characterization changes (degrades), making "YDOR" more sensitive to marginal conditions in contrast to CCMEWQI which is based only to deviations from permitted values.

"YDOR" had significant deviations from NSF at the characterization of surface water. NSF characterized the both the groundwater and surface water as "Excellent". The calculation of NSF is based on pre-determined water quality parameters (dissolved oxygen, BOD, TSS, nitrates, pH, turbidity, total coli forms, total phosphates, and temperature) and uses weight coefficients determined in 1970, while it does not compare the parameter values with any permitted values. The NSF characterizes water quality as Excellent: (90-100) Good: (90-70) – Medium: (70-50)- Bad:(50-25)- Very bad: (25-0). The majority of the NSF included parameters, according to the responds to the questionnaires of this study belong to those that 30% of the respondents believe that should be included in a WQI calculation "optionally" and have a AW <4.

The differences of the characterization among the two WQI that have similar results, "YDOR" and CCMEWQI, and NSF is probably due to the parameters of pesticides and E-Coli. These two parameters affected significantly the results of CCMEWQI and "YDOR", as they exceed the permitted limit values, while they are not included in the calculation of NSF.

4. CONCLUSIONS

Water quality indices are useful tools for the assessment of water quality and water management. Since 1970, when the last similar study has been conducted, water quality control parameters and their permitted values changed significantly. In order to avoid erroneous conclusions and inconsistent characterization of water quality, "YDOR" a new WQI was created. "YDOR" includes prioritized monitoring parameters, redefined weight coefficients and inserts in its calculation the ideal value. "YDOR" can more accurately characterize a water body's quality by taking into consideration both legislation and experts' opinion and is more sensitive to marginal conditions, in contrast to other indices (CCMEWQI and NSF). "YDOR" introduces monitoring parameters from different categories (bacteria, pesticides, heavy metals, nutrients, organic substances) that were not used previously. "YDOR" can easily be modified to cover the needs and specificities of every area.

REFERENCES

Abbasi, T., Abbasi, S. A., 2012. Water quality indices. Elsevier, B. V.

Alexakis, D., Tsihrintzis, V.A., Tsakiris, G., Gikas, G.D., 2016. Suitability of Water Quality Indices for Application in Lakes in the Mediterranean, Water Resour Manag; 30: 1621-1633

Balan, I.N., Shivakumar, M., Kumar, P.D.M., 2012. An assessment of ground water quality using water quality index in Chennai, Tamil Nadu, India. Chronicles Young Scient; 3(2): 146-150

Bhargava, D. S., Use of a Water Quality Index for River Classification and Zoning of Ganga River. Environmental Pollution; 6: 51-67

Brown, R.M., McClelland, N.I., Deininger, R.A., Tozer, R.G., 1970. Water quality index-do we dare? Water Sewage Works.; 117(10): 339-343.

Chauhan, A., Singh, S., 2010. Evaluation of Ganga water for drinking purpose by water quality index at Rishikesh, Uttarakhand, India. Report Opinion; 2(9): 53-61

Chowdhury, R.M., Muntasir, S.Y., Hossain, M.M. 2012. Water quality index of water bodies along Faridpur-Barisal road in Bangladesh. Glob. Eng. Tech. Rev.; 2(3): 1-8

Debels, P., Figueroa, R., Urrutia, R., Barra, R., Niell, X., 2005. Evaluation of water quality in the Chilla' N River (Central Chile) using physicochemical parameters and a modified water quality. Environmental Monitoring and Assessment; 110: 301–322

Dinius, S. H., 1987. Design of an index of water quality. American water resources association.; 23(5).

Bharty, N., Katyal, D., 2011. Water quality indices used for surface waters vulnerability assesment. International journal of environamental sciences.; 2(1): 154-173

Johnson, R.K., Lindegarth, M., Carstensen, J. 2013. Establishing reference conditions and setting class boundaries Deliverable 2.1-2, WATERS Report no. 2013:2. Havsmiljöinstitutet, Sweden

Kumar, D., Alappat, B. J., 2009. NSF-Water quality index : Does it represent the experts' opinion?. Pract.Period. Hazard. Toxic Radioact. Waste Manage.; 13:75-79

Miistry of Agricultural Development and Food Safety (Greek), 2012. Irrigation chemical water quality monitoring on river basin scale of Macedonia-Thrace and Thessaly. “Alexandros Mpaltarzis” Greek Agricultural Developemnt Project 2007-2013.

Municipality of Amyntaio, 2012. Ground water monitoring programme. Technical services.

REFCOND 2003, Guidance Document No 10: Rivers and Lakes – Typology, Reference Conditions and Classification Systems, Common Implementation Strategy for the Water Framework Directive (2000/60/EC), European Commission.

Said, A., Stevens, D. K., Sehlke, G., 2004. An Innovative Index for Evaluating Water Quality in Streams. Environmental Management; 34(3): 406–414

Smith, D. G., 1990. A better water quality indexing system for rivers and streams. Wat. Res.; 24(10): 1237-1244.

Tsakiris, V., 2016. A new water quality index for bottled water assessment. European Water,; 54: 19-26

Tyagi, S., Sharma, B., Singh, P., Dobhal, R., 2013. Water Quality Assessment in Terms of Water Quality Index. American Journal of Water Resources; 1(3): 34-38

Wanda, E., Mamba, B.B., Msagati, T., 2016. Determination of the water quality index ratings of water in the Mpumalanga and North West provinces, South Africa. Phys Chem Earth.; 92: 70-78

Zaidi, F.K., Mogren, S., Mukhopadhyay, M., Ibrahim, E., 2016. Evaluation of groundwater chemistry and its impact on drinking and irrigation water quality in the eastern part of the Central Arabian graben and trough system, Saudi Arabia. J Afr Earth Sci; 120: 208-219

Proceedings of the 10th World Congress of EWRA 'Panta Rhei', 5-9 July 2017, Athens, Greece
© 2017 *European Water Resources Association*

Water management in nuclear power plant using advanced low-temperature systems

G. Zakrzewska - Kołtuniewicz
Institute of Nuclear Chemistry and Technology (INCT), ul. Dorodna 16, 03-158 Warsaw, Poland
e-mail: g.zakrzewska@ichtj.waw.pl

Abstract: Nuclear power plants (NPPs) consume large quantity of water, more than coal-burning plants. Water is used for every-day plant operation, for dissipation of large amount of heat produced in nuclear reactors. Big volumes of clean water are needed in emergency situations for decontamination of contaminated buildings, equipment and apparatus. On the other hand, the need for cleaning large amounts of contaminated water in such cases requires appropriate purification systems. Moreover, during regular operation the NPPs produce also some amounts of contaminated liquid effluents that need treatment. Appropriate water management in nuclear power plants reduces water consumption and decreases emission of radioactive pollutants to the environment. In the paper the possibility of using membrane methods for water desalination, which could be coupled with nuclear reactor supplying heat and electricity for operation of membrane installations, is reported. Such processes like reverse osmosis and membrane distillation are low-temperature desalination methods that could be driven using heat from the condenser or from the vapour generator. The main aims to construct the membrane installation in the NPP will be production of large amount of clean water for power plant purposes, as well as wastewater decontamination. The use of nuclear energy for desalination provides number of benefits; such an approach is economic and environment-friendly. Shared facilities, low operational costs and the possibility of optimisation make nuclear desalination competitive and profitable method for production of pure water, as well as rational for low-level waste management in the future NPPs.

Key words: nuclear desalination, reverse osmosis, membrane distillation, water management

1. INTRODUCTION

Desalination is high-energy consuming process; it uses much of electricity, most often drawn from conventional power plants burning fossil fuels which emit gaseous pollutants. However, it was proved that desalination can also utilize low-temperature heat sources like solar, geothermal energy or waste heat.

Last years, growing interest in using nuclear reactors to supply heat for production of fresh water has arisen. The twin production system which combines generation of energy by nuclear reactors and turning the seawater into potable water known in the literature as "nuclear desalination" seems economically viable in many water shortage regions (*Introduction of nuclear desalination*, 2000). It has been revealed that small and medium-size nuclear reactors are convenient for that purpose; they can be used for desalination, often with cogeneration of electricity using low-pressure steam from the turbine or hot seawater feed from the final cooling system. Desalination can be the next to district heating low temperature, non-electric application of nuclear energy.

The methods used for desalination typically run with phase change; they are energy intensive and costly. Searching for new technologies that could replace the distillation methods, and their more economical varieties, such as multi-stage flash, multiple effect distillation or distillation with vapour compression, is necessary. Great expectations are associated with membrane techniques, such as reverse osmosis, electrodialysis, or hybrid systems combining two or more processes acting in synergy.

The common technologies applied for desalination are the multi-stage flash (MSF), an evaporation process using steam, and reverse osmosis (RO), which is driven by high-pressure

electric pumps. Less often in desalination plants multi-effect distillation (MED) or vapour compression (VC) are used. The hybrid plants coupling two different processes were also considered for industrial applications. The hybrid processes like combination of MSF-RO allow obtaining products of different quality, depending on actual, local needs.

Many activities are undertaken concerning application of nuclear reactors in technologies of water desalination in many countries around the world (Khamis, 2016). Most systems developed use thermal processes, which usually require the use of high temperatures and large amount of energy.

In the present paper application of such processes like membrane distillation (MD) and reverse osmosis, separately or in combined systems, is proposed for nuclear desalination. Membrane distillation (MD), thermally driven process, advantageous beacuse of use of low-temperature heat sources seems reasonable for water desalination (Hogan *et al.* 1997, Quist-Jensen *et al*. 2016, Drioli *et al.* 2015). RO, pressure-driven process, however it is intensified when works at elevated temperatures. Both processes can be considered as components of low-temperature desalination systems employed in nuclear desalination.

The objective of the work currently undertaken in the INCT is to develop a desalination system that consumes heat from low-temperature sources and is useful within a nuclear power plant in the management of water and wastewater. These works are connected with the plans to build the first nuclear power plant in Poland.

2. MEMBRANE PROECESSES FOR WATER DESALINATION

2.1 Reverse osmosis

Reverse osmosis (RO) became a common method for water desalination (Bindra *et al.* 2001, Wade 2001, and Avlontis *et al.* 2003). There are examples of researches on use of reverse osmosis in nuclear desalination (Uchiyama *et al.* 2003, Hanra 2000, Nuclear desalination of sea water 1997, Epimakhov *et al.* 2004, Nisan 2003) using heat from PWRs. The concept to use fusion reactors for this purpose was also evaluated (Borisov *et al.* 2001). The first commercial nuclear desalination plant based on MED and MSF was built in Kazakhstan, at Aktau (*Introduction of nuclear desalination* 2000, I. Khamis 2016). The BN-350 fast breeder reactor produced up to 135 MWe of electricity and 120 000 m^3/day of potable water over some 27 years. Ten MED units produced drinking quality water (TDS up to 200 mg/L) and high quality water for boiler feed water (TDS 2-10 mg/L). Several installations were operated in Japan for production of drinking water. Initially MSF process was applied there, however more effective appeared MED and RO.

The idea of coupling the RO plant with nuclear reactor is based on the possibility of use hot water from the main condensers of the PWR type of plants. The viscosity of water is inversely proportional to its temperature. Therefore, as temperature increases, water viscosity decreases and RO membrane becomes more permeable, with a consequent increase in productivity. It was revealed that reverse osmosis with pre-heating (ROph) can lead to a desalination cost reduction of about 14% as compared to the desalination cost of a conventional RO system. The ROph process was initially applied to the economic assessment of nuclear desalination systems in the EURODESAL project carried out under the aegis of the European Commission's 5th Framework Programme (Nisan et al. 2003, 2005). Later, the CEA studied a new method for the mathematical description of the process, extending its application to all power producing plants. The mathematical tool developed took into account performance parameters like the recovery ratio, the total production, and the product salinity of the system as functions of operating variables such as temperature, feed salinity and feed flow. The method was then applied to the specific site study for la Skhira, Tunisia (*Status of Nuclear Desalination in IAEA Member States* 2007).

2.1 Membrane distillation

Membrane distillation is a reltively novel separation process proposed for water desalination and wastewater treatment. It can be also applied for concentration of acids, bases or salt solutions.

The driving force of MD is temperature gradient across the membrane that generates vapour pressure difference. The temperature of the feed solution is below its boiling point. Because of that MD can use low-enthalpy sources of heat, e.g. waste heat or solar energy (Hogan *et al.* 1997, Alkhudhiri *et al.* 2012). Moreover, it does not involve high pressures at all. The process seems to be a cost effective method anywhere, where sources of waste heat are available, e.g. in convential or nuclear power plants.

Membrane distillation for water desalination and waste water treatment was studied at the Institute of Nuclear Chemistry and Technology (Zakrzewska-Trznadel *et al.* 1999, 2001) with the laaboratory plant, 0.05 m^3/h of capacity, equipped with the PTFE membrane module, working surface area of 4 m^2. The experiments conducted with NaCl solutions at initial feed concentration up to ca. 50 g/L confirmed the feasibility of the process. During 120 hours of the experiments carried out with recycling of the excess of the distillate to the vessel with the concentrate, there was no change of the salt concentration in both streams. At the same time purification of the distillate occurred and the obtained product had the parameters of distilled water. However, longer expriments at the concentration higher than 50 g/L resulted in decrease of membrane hydrophobicity and in some cases membrane breakthrough took place. Moreover, distillate flow rate significanly declined and the process efficiency decreased, especially at low inlet temperatures applied.

Wetting the hydrophobic membrane due to crystallization of salts inside the pores is a serious drawback of membrane distillation process. Operation at higher temperatures may reduce the risk of crystallization and may avoid hydrophilization of the membranes; it can also be economic, as previous experience showed. At elevated temperatures energy consumption per unit of the product was lower, especially when part of the heat supplied to the system was recovered by appropriate installation design (Zakrzewska-Trznadel et al. 1999).

Membrane distillation is promising technology; however it still needs more attention and studies on influence of high salt concentration, membrane hydrophobic character and process economy. Most of conducted MD investigations are based on laboratory-scale experiments; large-scale studies and industrial applications are still scarce. Although some pilot plant and full-scale testes are reported in literature (Jansen *et al.* 2013, Guillen-Buriezza *et al.* 2012, and Raluy *et al.* 2012).

The combination of MD with nuclear reactor supplying heat or working in cogeneration seems to be reasonable solution (Zakrzewska-Koltuniewicz, 2016). MD plant can be used for production of pure water for NPP and cleaning radioactive effluents; it could be essential element of water management system across the whole nuclear power plant helpful also in emerging situations. MD installation can operate alone or in combination with other techniques. It can replace other distillation processes in hybrid desalination plants.

2.1 Hybrid processes

The hybrid MD-RO system combines the advantages of the desalting performance of membrane distillation and lower energy requirements of RO process. It allows a better match between power and water requirements. Hypothetic hybrid MD/RO system was shown in Figure 1.

The coupling enables better utilization of the heat from MD plant to RO unit. RO plant can be fed by the sea water heated up by the brine from the MD unit. Higher feed temperature is advantageous because it results in higher productivity of RO modules (reduction of the water viscosity, higher diffusion rate of water through the membrane). However, lower salt rejection takes place in case of RO.

The hybrid system aims in reducing operational costs. Both plants have common seawater intake facilities and post-treatment facilities. Blending the product water is possible. Other advantages are

higher overall availability and flexibility, lower power demand, and improved water quality. RO can use the electricity from the power plant and can operate during periods of reduced power demand (off-peak), thus optimizing the overall efficiency of the entire operation. RO plant can be designed to produce water with higher level of total dissolved salts and thus it lowers its production costs. In hybrid systems, it is also possible to use the cooling seawater return stream from the thermal desalination component as feed to the RO component.

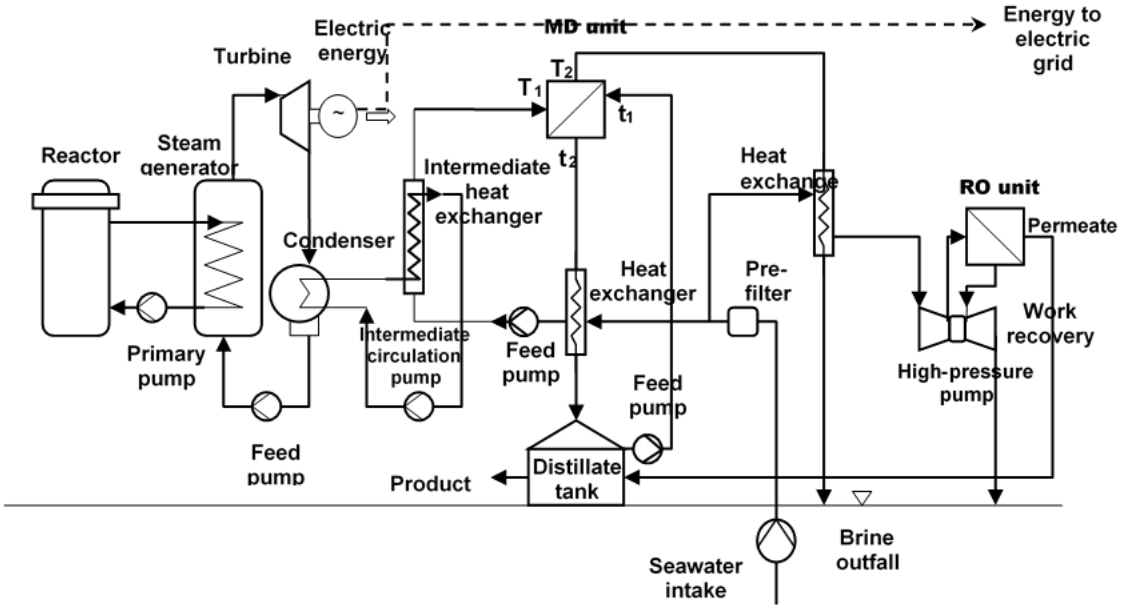

Figure 1. The concept of hybrid MD/RO system with energy recovery device (ERD).

To optimize the hybrid system with minimization of energy consumed it is possible to use energy recovery devices, e.g. energy recovery turbine and motor on the same drive shaft. Booster pump with e.g. HPB^{TM} provides brine energy recovery in reverse osmosis. The HPB^{TM} uses the high pressure brine to energize the turbine which drives the single-stage feed booster pump. The feed pressure boost generated by HPB^{TM} reduces the required feed pump discharge pressure resulting in significant energy savings and a reduction in size of the feed pump and motor (*Fluid Equipment Development Company, LLC* 2013).

Speaking about nuclear desalination one should mention the safety aspects which are very important for the society. The safety of coupled nuclear desalination plants depends mainly on the safety of nuclear reactor itself, and the interface between desalination plant and nuclear system. Potential for release of radioactive materials into the product water is avoided by multiple barriers and pressure differentials to block the transport of radioactive materials to the desalination plant (Khamis and Kavvadias 2013).

The use of two different forms of energy; electricity for the RO plant and heat for the MD plant provides much flexibility and independence of particular desalination technology. Moreover, the thermal efficiency of the power plant improves as a greater part of the installed power capacity can be beneficially utilized.

3. MEMBRANE PROECESSES FOR RADIOACTIVE WASTEWATER TREATMENT

In addition to desalination of sea water for household and industry purposes, membrane systems driven by heat from nuclear power plants could perform numerous other functions. They might be used for:

- Production of water for NPP's purposes, cleaning the coolant, recycling of water with

recovery of boric acid, preparation of water for decontamination actions;
- Treatment of low-level radioactivity effluents during regular, every-day operation (waste from laboratories, floor drains, boron recycling water, wastes contaminated with transuranic elements, waste from decontamination);
- Decontamination of wastewater in case of accident.

The work performed in INCT proved that such processes like RO and MD are effective methods for treatment of liquid radioactive waste. On the basis of research and development works done the reverse osmosis plant for the treatment of radioactive waste generated from application of radioisotopes was designed by INCT and built in Radioactive Waste Management Plant in Swierk, the organization responsible for processing the radioactive waste from all of Poland (Chmielewski et al. 2001).

The experiments performed in the laboratory confirmed applicability of membrane distillation for removal of radioactive compounds from wastewater (Zakrzewska-Trznadel, et al. 1999, Khayet et al. 2006). Hydrophobic membrane used in MD process is enable to reject all dissolved species as well as macromolecular compounds. The experimental results of MD filtration of water solution with radioactive cesium 137Cs was shown in Figure 2. 8-fold volume reduction of the waste caused almost 3-fold reduction of radioactivity in the retentate, while distillate remained pure and did not contain radioactive cesium.

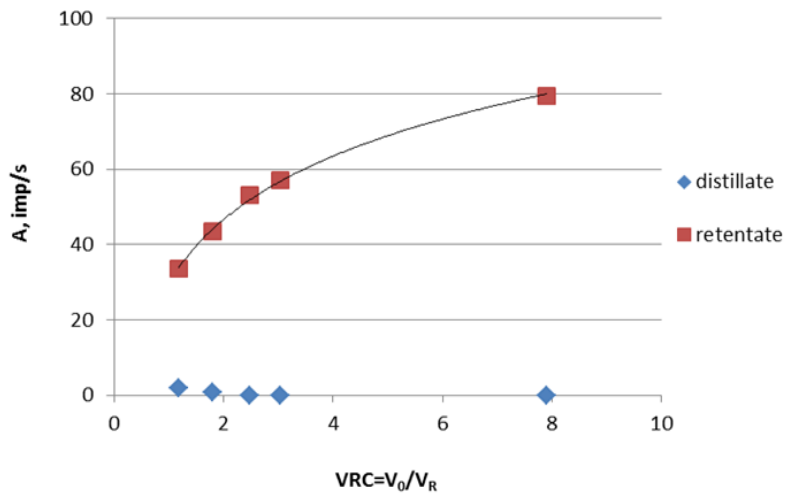

Figure 2. Concentration of ^{137}Cs water solution by membrane distillation

Membrane instllations based on RO and MD built in the NPPs are reasonable soultion for proper management of water and for decontamination of radioactive streams. The presence of adequatly designed systems that can produce large amount of water, and in case of emergency can treat great amounts of contamined streams, would increase the safety of nuclear power plants.

4. CONCLUSIONS

Nuclear desalination is an attractive technology since desalination is energy intensive process that can utilize the waste heat from the nuclear reactor and/or the electricity produced by the plant. Membrane processes are effective desalination methods operating alone, as well as a part of hybrid distillation-membrane systems. The use of membrane desalination is advantageous because of the lowest ratio of energy input to the amount of produced water, a high salt retention, and easiness of the process and equipment servicing. RO is a mature technology; it needs only process intensification by development of more advanced membranes and membrane systems, as well as energy recovery devices. The operation at elevated temperatures brings many benefits, therefore

coupling RO plant with nuclear reactor seems to be economically justified.

MD uses low-temperature heat sources and is reasonable for non-electric applications of nuclear energy. The combination with other membrane techniques like RO is very advantageous creating very efficient and flexible system for water treatment. The process needs more studies concerning feasibility of long operation, membrane wettability and economy.

ACKNOWLEDGMENTS

The research described in this paper was financially supported by the IAEA Coordinated Research Project No 18539/R2 "Application of Advanced Low Temperature Desalination Systems to Support NPPs and Non-electric Applications" and MNiSW research project „Application of advanced membrane systems for nuclear desalination".

REFERENCES

Alkhudhiri A., Darwish N., Hilal N., 2012. Membrane distillation: A comprehensive review. Desalination; 287; 2-18.

Avlonitis S.A., Kouroumbas K., Vlachakis N. , 2003. Energy consumption and membrane replacement cost for seawater RO desalination plants. Desalination; 157; 151-158.

Bindra S.P., Abosh Walid, 2001. Recent developments in water desalination. Desalination; 136; 49-56.

Borisov A.A., Desjatov A.V., Izvolsky I.M., Serikov A.G., Smirnov V.P., Smirnov Yu.N., Shatalov G.E., Sheludjakov S.V., Vasiliev N.N., Velikhov E.P., 2001. Fusion power plant for water desalination and reuse. Fusion Eng. Des.; 58-59; 1109-115.

Chmielewski, A. G., Harasimowicz, M., Tymiński, B., Zakrzewska Trznadel, G., 2001. Concentration of Low- and Medium-Level Radioactive Wastes with 3-stage Reverse Osmosis Pilot Plant. Sep. Sci. Technol.; 36, 5&6; 1117-1129.

Drioli E., Ali A., Macedonio F., 2015. Membrane distillation: recent developments and perspectives. Desalination; 356; 56-84.

Epimakhov V. N., Oleinik M. S., Moskvin L. N., 2004. Reverse Osmosis Filtration Based Water Treatment and Special Water Purification for Nuclear Power Systems. Atomic Energy. 96; 4; 234-240.

Guillen-Buriezza E., Zaragoza G., Miralles-Cuevas S., Blanco J., 2012. Experimental evaluation of two pilot-scale membrane distillation modules used for solar desalination. J. Membr. Sci. 409-410; 264-275.

Hanra M.S., 2000. Desalination of sea water using nuclear heat. Desalination; 132; 1-3; 263-268.

Hogan P. A., Sudjito, Fane A. G., Morrison G. L., 1997. Desalination by solar heated membrane distillation. Desalination; 81; 81-90.

Introduction of nuclear desalination. A guidebook. Vienna 2000. IAEA Technical Reports Series No. 400.

Jansen A.E., Assink, J.W. Hanemaaijer J.H., van Medevoort J., van Sonsbeek E., Development and pilot testing of full-scale membrane distillation modules for deployment of waste heat. Desalination; 323; 55–65.

Khamis I., 2016. Non-Electric Applications of Nuclear Energy. Technical Meeting on Operating Experience with, and Project Feasibility of, Process Heat Applications; Budapest, Hungary, 23-25 May 2016..

Khamis I., Kavvadias K.C., 2013. Nuclear desalination: Practical measures to prevent pathways of decontamination. Desalination; 321; 55-59.

Khayet M., Mengual J.I, Zakrzewska-Trznadel G., 2006. Direct contact membrane distillation for nuclear desalination:, Part II-Experiments with radioactive solutions. J.Nucl. Desalination; 2; 1; p. 56-73.

Nisan S., Caruso G., Humphries J.-R., Mini G., Navigilio A., Bielak B., Asuar Alonso O., Martins N., Volpi L., 2003. Seawater desalination with nuclear and other energy sources, Nuclear Engineering & Design; 221; 251–275.

Nisan S., Commercon B., Dardour S., 2005. A new method for the treatment of a reverse osmosis process with preheating of the feed water. Desalination; 182; 485–495.

Quist-Jensen C. A., Macedonio F., Drioli E., 2016. Integrated Membrane Desalination Systems with Membrane Crystallization Units for Resource Recovery: A New Approach for Mining from the Sea. Crystals; 6, 36, www.mdpi.com/journal/crystals.

Raluy R.G., Schwantes R., Subiela V. J., Peñate B., Melián G., Betancort J.R., Operational experience of a solar membrane distillation demonstration plant in Pozo Izquierdo-Gran Canaria Island (Spain). Desalination; 290; 1-13.

Status of Nuclear Desalination in IAEA Member States, 2007. IAEA-TECDOC-1524, IAEA, Vienna.

Uchiyama Y., Minato A., Shimamura K., 2003. Seawater desalination using reusable type small PWR. Int. J. Nucl. Desalination; 1;1; 81-94.

Wade N.M., 2001. Distillation plant development and cost update. Desalination; 136; 3-12.

Zakrzewska-Trznadel G., Harasimowicz M., Chmielewski A.G., 1999. Concentration of radioactive components in liquid low-level radioactive waste by membrane distillation. J. Membr. Sci.; 163; 257-264.

Zakrzewska-Trznadel G., Harasimowicz M., Chmielewski A.G., 2001. Membrane processes in nuclear technology – application for liquid radioactive waste treatment. Sep. Purif. Technol.; 22-23; 617-625.

Zakrzewska-Koltuniewicz G., 2016. The possibility of nuclear cogeneration in the future NPPs in Poland. Technical Meeting on Operating Experience with, and Project Feasibility of, Process Heat Applications, Budapest, Hungary, 23-25 May 2016.

Proceedings of the 10th World Congress of EWRA 'Panta Rhei', 5-9 July 2017, Athens, Greece
© 2017 *European Water Resources Association*

Productivity analysis based on fuzzy logic on paddy area irrigated by varied water sources

B. Aydin and Y. Ahi*
Department of Biosystem Engineering, Faculty of Agriculture, Namık Kemal University, 59030 Tekirdağ, Turkey
** e-mail: yesimahi@nku.edu.tr*

Abstract: This study aims to determine the quality of water resources used in four paddy areas selected in Meriç-Ergene Basin of Turkey and find out the effects of these waters on soil productivity using Fuzzy Logic which have recently been used both in Turkey and in the world. Primarily, quality parameters of different water resources which are the water from River Ergene, ground water, the water from River Meriç and dam lake water were determined and analyzed in the running of the model. Changes in the properties of water resources are modeled and interpreted in terms of soil productivity with Fuzzy logic. Chemical analysis of samples obtained from water resources examined in the study is done according to standard methods. In the analysis of water samples saltiness (EC, pH, Na), trace element (Mn, Zn, Fe, Cu), and heavy metal (Pb, As, Cd, Ni, Cr, Co) parameters were examined. In the model, these parameters which directly effects soil productivity are considered as input variables, and productivity is considered as output variable. Soil productivity profiles (%) of the region consisting different soil types have been determined by obtaining the fuzzy values related to these parameters. Soil productivity values differ between 40-60%. According to the obtained results; it can be said that Fuzzy Logic model which is used in many sciences should be useful in agricultural field studies.

Key words: Fuzzy logic, water quality, macro and micro elements, modelling

1. INTRODUCTION

In many parts of the world, factors such as rapid population growth and migration (approximately 400,000 people every year), misuse of land, disorganized structuring within drainage basins, industrial consumption (ground water consumption, transferring of untreated waste water to water sources), excessive use of fertilizers and pesticides in agriculture as well as climatic changes are threatening water sources. In Thrace region, especially the Meriç-Ergene basin which covers 14,657 km^2 of land, water and therefore soil sources are getting increasingly poorer in terms of both quality and quantity. The quality of soil, depending also on the type of plant production, is changing day by day.

It is necessary that we, first of all, ensure water and soil and therefore food production in sufficient quality and amount. Within this scope, it is a must that we define, protect and improve the conditions of the region we inhabit. The most important surface water sources of Meriç-Ergene basin, one of the 25 basins in Turkey, are River Meriç and River Ergene and their arms. Basin area consists of 11,000 km^2 and total water potantial is 1.71 billion m^3/year. Total ground water reserve in the Ergene basin is 0.376 billion m^3/year (Anonymous, 2015). The basin contains approximately 1.24 million hectares of cultivable agricultural land and 1.05 million hectares of this area is irrigable. The terrain in this basin provides approximately 50% of the country's rice production. Using up most of agricultural water, the rice plant is cultivated under water throughout the season or under saturated conditions. Under constant water load conditions, the quality of water being used causes an additional burden on soil and produce quality.

In this study; it is aimed that the quality of different water sources used on 4 different rice production fields within the Meriç-Ergene basin is determined and that the complex conclusions arrived at in explaining their effects on soil productivity, are cleared by way of using any one of the fuzzy logic models. To this end, it is aimed that a fuzzy logic model that has been used in many

recent agricultural studies carried out both within and outside of our country (McBratney and Odeh, 1997; Mitra et al., 1998; Chang et al., 2001; Altunkaynak et al., 2005; Lermontov et al., 2009; Duru et al., 2010; Karadavut and Akkaptan, 2012; Gharibi et al., 2012; Ambuel et al., 2013; Dökmen and Aslan, 2013) be used.

The notion of fuzzy logic was first suggested by Lotfi A. Zadeh (1965), by way of expressing some ambigous expressions mathematically. It is based on the Fuzzy Set Theory by which the true and false values are determined. There is again the values of (1) and (0) here, as in traditional logic. However, fuzzy logic goes beyond these values and by making use of intermediate values, tells us, for example, not only if a certain distance is far or near, but also how far or near it is (Odabaş et al., 2009). In this context, with the use of Fuzzy Logic model, complex conclusions derived of various parameters were evaluated all together.

2. MATERIAL AND METHODS

2.1 Material

The research was carried out throughout the 2015-2016 cultivation season, on four different rice plant fields within the Meriç-Ergene basin, which are Uzunköprü-Merkez, Aslıhan, Eskiköy and Delibedir, and with 4 different water sources which are respectively the water from River Ergene, ground water, the water from River Meriç and dam lake water.

The soil in Aslıhan and Eskiköy research area is in general sandy, whereas the soil in Eskiköy and Delibedir research area is generally clay; organic matter content is poor, non-calcareous and there are no such problems as saltiness or excessive sodium in ground water.

In all research areas, the technique of agriculture, the type and amount of seeds, timing and amounts of fertilization and spraying as well as all other inputs were studied and recorded, making sure the data is homogenized.

In the research, Fuzzy Logic and Matlab R2015a modules were used in order to perform fuzzy logic applications. Throughout the research, the irrigation water to be applied to borders has been chemically examined and additionally, heavy metal analyses were made both for the soil and for the water.

2.2 Methods

2.2.1 Determining the physical and chemical properties of soil samples

In each research area, field treatment plots of 5 da were selected as sampling areas. In each plot, all sampling and measuring applications were performed with at least 3 repetitions.

At the beginning and the end of the cultivation season, disturbed soil samples were taken from a depth of 0-30, 30-60 and 60-90 cm from each field treatment plot. The samples taken were dried in the shade, sifted through a 2 mm filter and so prepared for analysis. Soil texture was measured with a hydrometer as explained in Bouyoucos (1962).

2.2.2 Determining the physical and chemical properties of water sources

Irrigation water samples were taken at the source point, or at the plot entrance to put it differently, twice a month, with 3 repetitions and the samples were brought to the lab. In the water samples brought to the lab, anions, cations, organic and inorganic pollutant parameters were determined and then, their limitedness was determined according to the Quality Criteria Based on Intra-Continental Water Source Classifications, Irrigation Water Quality Criteria for the Classification of Irrigation Waters that are found in the Technical Procedure Communication (Anonymous, 1991) and the quality criteria prescribed in the food legislation.

Water samples brought to the lab were analysed with the methods below:

Chloride (Cl^-), sulfate (SO_4^{-2}), nitrate (NO_3^-), nitrite (NO_2^-) were determined according to the Standard Method-4500 Ion Chromatographic Method; carbonate (CO_3) and (HCO_3) were determined according to the fundamentals indicated in Tüzüner (1990), with titration; Cations (Na+, Ca++, Mg++, K+) and total phosphorus (P) were determined according to the Standard Method-3500, on an ICP-OES device.

Inorganic Pollutant Parameters; Cadmium (Cd), lead (Pb), copper (Cu), chrome (Cr), cobalt (Co), nickel (Ni), zinc (Zn), iron (Fe), manganese (Mn), boron (B), selenium (Se), aluminium (Al); were determined on the ICP-OES device according to the Standard Method-3500.

Organic Matter was determined with the Potassium Permanganate Method, according to Eltan (1998). In addition, pH and saltiness levels (EC) were measured respectively with a pHmeter and electrical conductometer (Ayyıldız M, 1983). Analyses were verified with certified standard water samples.

2.2.3 Application of fuzzy logic model

An effort was made to evaluate all analysis results by taking into account average values, based on Fuzzy Logic System.

After the membership functions and rules were established of the system whose input and output variables were identified, values of pH, saltiness, thrace elements etc. that were measured in each water source were fed to the system as input values and fuzzy values were acquired in return.

Fuzzy Logic system was built by making use of MATLAB R2015a. The steps taken in this stage can be expressed as below:

1. It was identified what the input and output variables of the system will be. pH, saltiness, lime and organic matter, etc. values were taken as input variables as they are factors which directly effect the soil productivity and productivity was taken as an output variable in return.
2. Membership functions and threshold values were determined concerning the input and output variables.
3. In this step, in line with the interactions of input variables with each other, an effort was made for setting rules concerning the possible outcome.

By bringing together as related groups the input variables, 4 different sets of input variable parameter groups were formed for water. These groups are; salinity parameter group (Sodium (Na), electrical conductivity (EC) and pH); Trace element parameter group (Manganese (Mn), Zinc (Zn), Iron (Fe) and Copper (Cu)) and also Heavy metal parameter group (By half-life; first one is Lead (Pb), Arcenic (As), Cadmium (Cd) and second one is Nickel (Ni), Crom (Cr), Cobalt (Co)).

3. RESULTS

By making use of Fuzzy Logic model program, with the purpose of determining the effects of the quality of the water source used in the selected farming lands on soil productivity and of observing the collective effects of multiple elements within the framework of fuzzy logic, firstly the input and output variables for each parameter group were established. The model stages that were attained for saltiness parameters have been provided in the paper so that they serve as a model. Also, the conclusions for all parameter groups are summarized.

3.1 Productivity analysis results of the parameters determined in irrigation waters

3.1.1 Results of the irrigation water saltiness parameters

Input and output variables, membership functions and threshold values of the saltiness parameters that were determined by making use of MATLAB R2015a are shown in Figures 1, 2, 3

and 4. Of the membership functions, two were decided to be trapezoids and others to be triangles.

After the establishment of membership functions and rules of the system whose input and output variables were identified, pH, EC and Na values that were measured in different water sources were fed to the system as input values and productivity was taken as the output varible in return.

In line with membership functions, the rules were established. A total of 48 rules were written for this parameter group. In line with the interactions of input variables with each other, some of the rules that were written concerning what the output could be are shown in Figure 5.

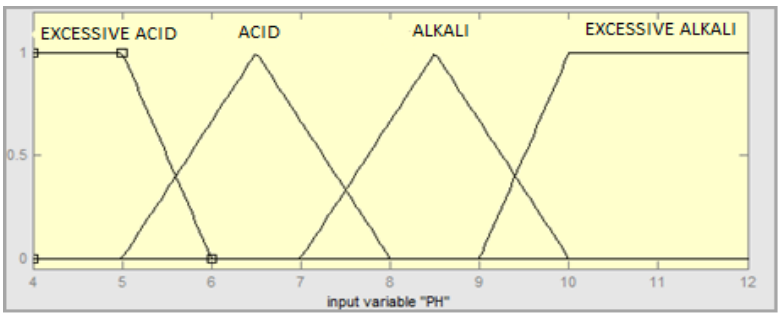

Figure 1. The membership function of pH variable

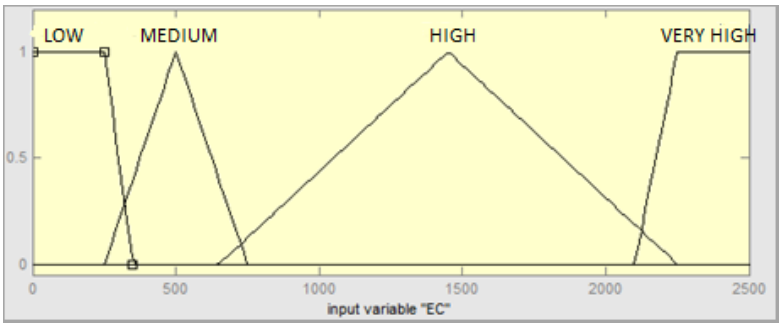

Figure 2. The membership function of EC variable

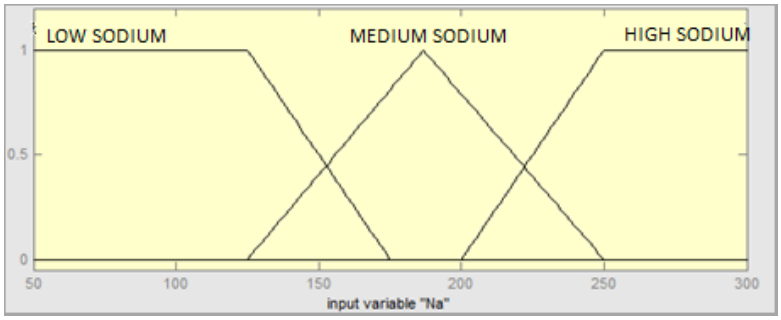

Figure 3. The membership function of Na variable

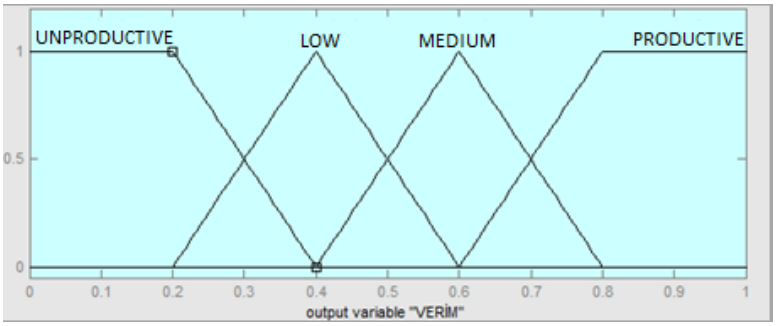

Figure 4. The membership function of productivity

3D demonstrations for the selected parameters that set up the rules are on Figure 6a,b,c. On Figure 6a are productivity, the changes seen in EC and pH in relation to each other; and on Figure 6b are productivity and 3D demonstrations of the rules that show the changes in pH and Na in relation to each other. The system evaluates four different input and output variables together, but only the rules concerning three selected variables can be seen on the 3D demonstration.

1. If (pH is ACID) and (EC is LOW) and (Na is LOW-SODIUM) then (PRODUCTIVITY is PRODUCTIVE)
2. If (pH is ACID) and (EC is LOW) and (Na is MEDIUM SODIUM) then (PRODUCTIVITY is PRODUCTIVE)
3. If (pH is ACID) and (EC is LOW) and (Na is HIGH SODIUM) then (PRODUCTIVITY is MEDIUM)
4. If (pH is ACID) and (EC is MEDIUM) and (Na is LOW SODIUM) then (PRODUCTIVITY is PRODUCTIVE)
5. If (pH is ACID) and (EC is MEDIUM) and (Na is MEDIUM SODIUM) then (PRODUCTIVITY is PRODUCTIVE)

.....

45. If (pH is EXCESSIVE-ALKALI) and (EC is HIGH) and (Na is HIGH SODIUM) then (PRODUCTIVITY is LOW)
46. If (pH is EXCESSIVE-ALKALI) and (EC is VERY HIGH) and (Na is LOW SODIUM) then (PRODUCTIVITY is LOW)
47. If (pH is EXCESSIVE-ALKALI) and (EC is VERY HIGH) and (Na is MEDIUM SODIUM) then (PRODUCTIVITY is LOW)
48. If (pH is EXCESSIVE-ALKALI) and (EC is VERY HIGH) and (Na is HIGH SODIUM) then (PRODUCTIVITY is UNPRODUCTIVE)

Figure 5. A part of the rules of the salinity parameter group in irrigation water

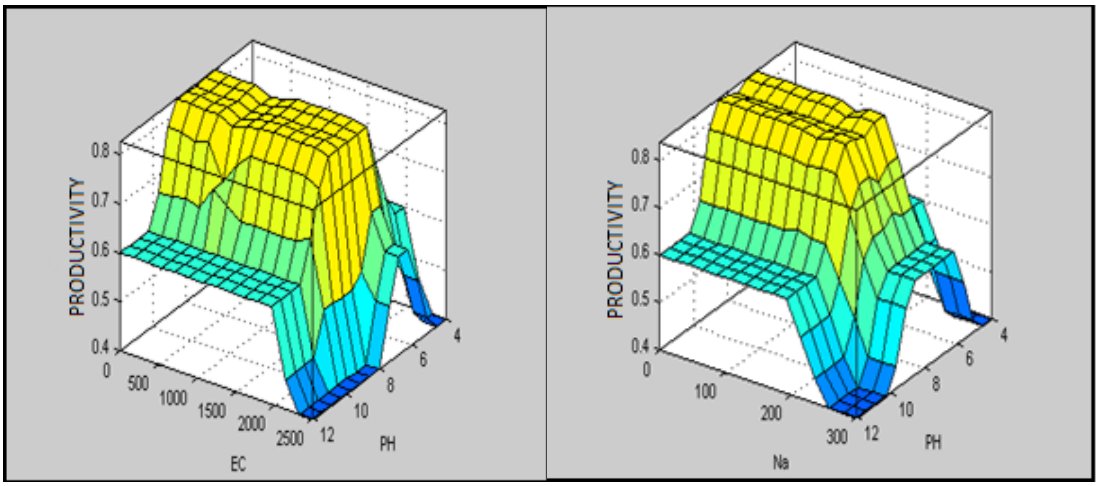

(a) *(b)*

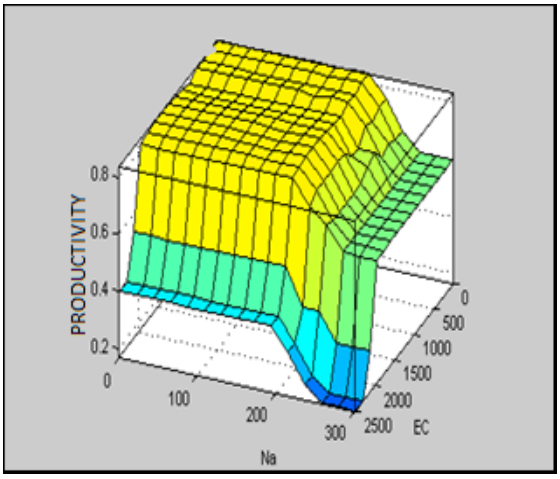

(c)

Figure 6. Three-dimensional presentation of the rules relating to the selected three variables (a), (b), (c).

The saltiness parameters whose average values are given on Table 1 (EC, pH, Na) were fed into the system as input variables and soil productivity values for each region were obtained (Table 2). As can be tracked on the table, the variance in productivity levels based on water quality is very obvious. The highest productivity (82%) was seen in the region Aslıhan where the water source used was ground water, whereas the lowest productivity (26%) was seen in the region Uzunköprü where the levels of pollution and saltiness were quite high. In Eskiköy terrains where the water from River Meriç was used, the soil productivity was 59% and in Delibedir where the dam water was used, it was 71%.

Table 1. Results of analysis as mean of salinity parameters by regions

Parameter	Months	Region			
		Aslıhan	Eskiköy	Uzunköprü	Delibedir
pH	May	6.80	7.20	7.68	7.09
	June	6.97	8.08	7.90	8.02
	July	8.07	7.39	7.42	7.74
	August	7.56	7.03	7.38	7.48
	September	7.05	-	-	-
	Average	6.80	58	7.60	7.58
EC (µS/cm)	May	945	1069	3610	998
	June	767	3020	8690	2398
	July	1261	2846	7510	2072
	August	1808	2462	2921	1925
	September	1614	-	-	-
	Average	945	2349	5683	1848
Na (ppm)	May	26.37	43.48	408.15	50.40
	June	26.35	62.23	459.56	59.04
	July	21.69	57.93	415.59	50.65
	August	25.53	52.72	398.97	54.32
	September	25.26	-	-	-
	Average	26.37	54.09	420.57	53.60

The results obtained in the study from all parameter groups are shown on Table 3. When Table 1 is reviewed, it is seen that pH values have varied between 6.5-8.5 in all of the sources and that they are water sources of good quality based on the standards. EC values of irrigation water vary between 750-2000 µS/cm for the village of Aslıhan and it is a water source of utilizable quality that will not impose any limitations on rice plant agriculture. As explained in Meral and Temizel (2006), no yield loss is experienced up to 2.0 dS/m for the rice plant. For the water source in Eskiköy, it is seen that the EC values are moderately utilizable in the month of May while it is of bad quality in other months. EC values of the water source in Uzunköprü are above 2000 µS/cm and the Na value is above 250 ppm and it is IVth grade water of inutilizable quality which could decrease the yield of the rice plant and the soil quality. The relative highness of these amounts can be due to the fact that the source is River Ergene and that it is subject to quite a high dose of waste water discharge. In parallel with these results, the soil productivity values reached by the model have remained low in these areas. And in the water source in Delibedir, EC values are around 2000 µS/cm and of mid-quality according to the classification. With respect to other parameters it exhibits a quality of Ist grade water that is utilizable, according to the standards.

As can be tracked on Table 3, depending on the trace element change, the variation in the productivity levels has shown parallels with respect to different regions. Productivity was seen to be around 84% in Aslıhan, Eskiköy and Delibedir regions and 74% in the Uzunköprü region.

Based on the changes in heavy metals, the levels of productivity were found to be close to each other in average with approximately 70%. But as can be clearly seen on the table, the productivity levels have greatly varied in different months. The lowest productivity was found to be 50%, whereas the highest was 85%. This situation seems likely for Uzunköprü and Eskiköy with respect to the fact that industrial and domestic waste water is occasionally mixed with the water sources there. But it was found not to be very meaningful for the other water sources.

When the possible productivity levels based on the model results from measured parameters of water sources are examined; in the region Uzunköprü which is the region with the poorest water quality, the overall expected soil productivity level was seen to be quite low. Soil productivity levels have also varied in parallel with the variance in the quality parameters.

Table 2. Values of productivity of different water supply for salinity parameters

Region	Months	pH	Na (ppm)	EC(mμhos/cm)	Productivity
Aslıhan	*May*	6.80	26.371	945	0.820
	June	6.97	26.346	767	0.810
	July	8.07	21.693	1261	0.836
	August	7.56	25.526	1808	0.821
	September	7.05	25.260	1614	0.832
Eskiköy	*May*	7.20	43.479	1069	0.827
	June	8.08	62.227	3020	0.400
	July	7.39	57.930	2846	0.522
	August	7.03	52.722	2462	0.593
Uzunköprü	*May*	7.68	408.152	3610	0.239
	June	7.90	459.558	8690	0.189
	July	7.42	415.589	7510	0.301
	August	7.38	398.972	2921	0.311
Delibedir	*May*	7.09	50.403	998	0.823
	June	8.02	59.036	2398	0.400
	July	7.74	50.655	2072	0.814
	August	7.48	54.324	1925	0.819

Table 3. Values of productivity(%) of all parameter groups by regions

Parameter Group	Months	Region			
		Aslıhan	Eskiköy	Uzunköprü	Delibedir
Salinity	May	82	83	24	82
	June	81	40	20	40
	July	84	52	30	81
	August	82	60	31	82
	Average	82	58	26	71
Thrace Elements	May	85	83	40	85
	June	85	84	85	85
	July	85	84	85	85
	August	83	85	85	84
	Average	84	84	74	85
Heavy Metal	May	85	85	85	85
	June	85	60	60	60
	July	60	84	83	83
	August	83	57	54	51
	Average	78	72	71	70

4. CONCLUSIONS

In the light of the results attained, it was seen that Fuzzy Logic model which is made use of in many fields of science can also be used in studies performed in the field of agriculture.

Determining the relations of model parameters with each other soundly and establishing the relevant rules, in environments where various variable impact factors are present is of great importance for ensuring that the model arrives at correct conclusions.

The values obtained from the triangles that are formed in fuzzy logic constitute an additional alternative application range in comparison to standard quality criteria tables. This situation brings forth fuzzy logic as an advantage in the field of agriculture. And the application ranges are seen as tolerable levels which will not effect the productivity of the rice plant negatively.

This study will constitute the basis for many future researches as it proves that fuzzy logic systems which allow the evaluation of the collective effects of many parameters in the field of agriculture yield utilizable results.

ACKNOWLEDGMENT

The authors would like to thank the Namık Kemal University Scientific Research Projects Unit (NKUBAP) for its financial support to the project of NKUBAP.00.24.YL.15.08.

REFERENCES

Altunkaynak, A., Özger, M., Çakmakçı, M., 2005. Water consumption prediction of Istanbul City by using Fuzzy Logic approach. Water Res. Manage. 19: 641-654.

Ambuel, J.R., Colvin, T.S., Karlen, D.L., 2013. A fuzzy logic yield simulator for prescription farming. Transactions of the ASAE. 37(6): 1999-2009.

Anonymous, 2015. DSI, the General Directorate of State Hydraulic Works. www. http://en.dsi.gov.tr/ (Acc. date, 27.06.2016).

Anonymous, 1991. The Official Journal of the Republic of Turkey, 01.07.1991, Issue: 20748. Available: http://www.resmigazete.gov.tr/default.aspx [Accessed 08 February 2017]

Ayyıldız, M., 1983. Sulama Suyu Kalitesi ve Tuzluluk Problemleri. Ankara Üniv. Ziraat Fakültesi Yayınları. No:897, 282s. Ankara.

Bouyoucos, G. J., 1962. Hydrometer method improved for making particle-size analysis of soils. Agron. J. 53: 464 – 465.

Chang, N., Chen, H.W., Ning, S.K., 2001. Identification of river water quality using the fuzzy synthetic evaluation approach. J. of Environ. Manage. 63: 293-305.

Duru, N., Canbay, M.M., Kurtuluş, C., Dökmen, F., 2010. Soil productivity analysis based on a fuzzy logic system. J. Sci. Food Agric. 90: 2220-2227.

Eltan, E., 1998. İçme ve Sulama Suyu Analiz Yöntemleri. Köy Hizmetleri Gn. Müdürlüğü Yayınları

Gharibi, H., Mahvi, A.H., Nabizadeh, R., Arabalibeik, H., Yunesian, M., Sowlat, M.H., 2012. A novel approach in water quality assessment based on fuzzy logic J. of Env. Manage. 112: 87-95.

Karadavut, U., Akkaptan, A., 2012. Bitkisel üretimde bulanık mantık uygulamaları. Türk Bilimsel Derlemeler Dergisi. 5(2): 77-82.

Lermontov, A., Yokoyama, L., Lermontov, M., Machado, M.A.S., 2009. River quality analysis using fuzzy water quality index: Ribeira de Iguape River watershed, Brazil. Ecological Indicators 9: 1188-1197.

McBratney, A.B., Odeh, I.O.A., 1997. Application of fuzzy sets in soil science: fuzzy logic, fuzzy measurements and fuzzy decisions. Geoderma. 77: 85-113.

Meral, R., Temizel, K.E., 2006. Çeltik tarımında sulama uygulamaları ve etkin su kullanımı. KSÜ Fen ve Mühendislik Dergisi, 9 (2): 104-109.

Mitra, B., Scott, H.D., Dixon, J.C., McKimmey, J.M., 1998. Applications of fuzzy logic to the prediction of soil erosion in a large water shed. Geoderma 86: 183-209.

Odabaş, C., Pehlivan, İ., Cinal, D.M., 2009. Bulanık mantık ile güneş enerjisi uygulaması. 5. Uluslararası İleri Teknolojiler Sempozyumu. (IATS'09). Karabük, Türkiye.

Tüzüner, A., 1990. Toprak ve Su Analiz Laboratuarı El Kitabı. KHGM Yayınları, Tarım Orman ve Köy İşleri Bakanlığı, Ankara.

Zadeh, L.A., 1965. Fuzzy sets. Information and Control. 8: 338-353.

Proceedings of the 10th World Congress of EWRA 'Panta Rhei', 5-9 July 2017, Athens, Greece
© 2017 *European Water Resources Association*

Wastewater treatment by solar air gap multi-stage membrane distillation

I.J. Siddique, R. Bahar, S. Ibrahim and M.H.F. Al Hazza
[1] *Department of Manufacturing and Materials Engineering, International Islamic University Malaysia, Jalan Gombak, 50728 Kuala Lumpur, Malaysia*
[2] *Department of Civil Engineering, University of Malaya, 50603 Kuala Lumpur, Malaysia*
[*] *e-mail: rbahar@iium.edu.my*

Abstract: Scarcity of fresh water and availability of solar irradiation constitute the perfect condition for developing small-scale solar waste water treatment plants. One of the suitable low energy process applicable is Membrane Distillation (MD). MD is a relatively lower temperature process which does not need to operate under high pressure like Reverse Osmosis (RO). A hydrophobic membrane maintains a barrier between hot feed water and coolant flowing outside. The vapour generated due to partial pressure difference crosses the pores of this hydrophobic membrane and travels toward the cooler side to condense and produce distillate. In this paper, performance of a solar assisted multi-stage MD system has been analysed. Our previous experimental multi-stage MD setup gave a hike of 5.6 times in production per kWh of energy input compared to a single stage. In this study, an average annual solar radiation of 1571 kWh/m^2 has been incorporated in the multi-stage MD system with a narrow air gap between the coolant and feed. It has been observed that using smaller sized multiple chambers in the process can enhance the production of fresh water compared to a bigger sized chamber with a single large membrane. Association of solar heat into the MD module can contribute to further energy savings and producing up to 220 l/day of freshwater in hot tropical climate.

Key words: Air Gap Membrane Distillation, Multi-stage Membrane Distillation, Solar Energy, Wastewater Treatment

1. INTRODUCTION

The demand of alternate water distillation methods has been ever rising with the world tending to lean on renewable energy sources rather than land & energy extensive methods. Among these alternate methods membrane distillation (MD) has shown a great potential. Since MD requires least amount of space and energy, has ability to use renewable energy and can produce pure distillate from high concentration of wastewater (Raluy et al., 2012), thus MD has the option to be used as household water treatment facility as well as industrial wastewater treatment plant (Gryta, Tomaszewska, & Karakulski, 2006).

MD is a thermally driven separation process in which only vapour molecules pass through a microporous hydrophobic membrane due to the vapour pressure difference between the two sides of the membrane by flowing hot and cold solution on each side of the membrane (Lawson & Lloyd, 1997). The nature of the membrane restricts the aqueous solution in the pore openings. The vapour transferring through the membrane is then cooled by different methods to get the pure distillate. Depending on this cooling method MD can be classified to Direct Contact Membrane Distillation (DCMD), Air Gap Membrane Distillation (AGMD), Sweep Gas Membrane Distillation (SGMD) and Vacuum Membrane Distillation (VMD). In AGMD instead of directly letting the pure water mix with the distillate an air gap is used to separate them. The permeate vapour is cooled by the coolant plate which is in direct contact with the circulating cold solution. Figure 1 shows how AGMD works.

One of the main drawbacks of MD is lower flux compared to RO processes, thus optimization and improvement is needed in MD to make it competitive with RO. Over the time many modification is made to MD technology (Zhani et al., 2015) and it has been observed that with optimum design MD can produce fluxes more than conventional systems. (Chafidz et al., 2016) has reviewed some of the major solar powered membrane distillation (SPMD) systems. It can be seen

that either the distillate production rate or the quality is low, and if both of the parameters are satisfactory the energy consumption is higher due to complex machinery. With the recent trends of green technology, people have shown a tendency to use multi-staging in MD process as well to extract more available energy (Bahar, Hawlader, Nga, & Haw, 2014), as introducing multistaging helps better mixing of the working fluid in successive stages and improves flux production. In this paper we have presented the performance of a solar assisted multi stage AGMD and compared with the performance of a single stage MD module.

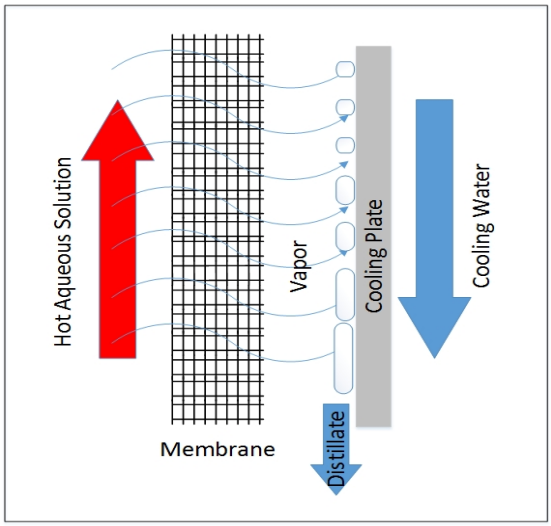

Figure 1. Working method of AGMD.

2. EXPERIMENTAL SETUP AND PROCEDURE

The designed module was made out of grade 'A' polycarbonate sheets having thickness 5 mm and the hot and cold chamber had these dimensions 162.4 x 162.4 x 106.6 mm. It consisted of six parts: 1) Hot solution Chamber, 2) Membrane, 3) Membrane Ramp, 4) Air gap frame with hole on the bottom surface to collect distillate, 5) Coolant plate, 6) Cold solution chamber. The overall 3-D design of the module can be seen in figure 2. The three modules were connected in series and the schematic diagram is shown in figure 3. Instead of directly feeding the salty water from solar heater to the hot chamber a heat exchanger has been used to protect the solar heater from corrosion. Module performance parameters like permeate flux, gained output ratio (GOR), rejection factor and specific energy consumption for feed heating were evaluated using equation (1) – (5) respectively,

Permeate flux, J (L/m^2h):

$$J = \frac{V}{At} \tag{1}$$

Gained output ratio (dimensionless):

$$GOR = \frac{\Delta h_{evap} * m_d}{Q_{input}} \tag{2}$$

$$Q_{input} = m_f * C_{pf} * (T_f - T_o) \tag{3}$$

Module separation efficiency:

$$\% \text{ Separation} = \frac{C_f - C_p}{C_f} \tag{4}$$

$$\text{Specific energy consumption} = \frac{m_f C_{pf}(T_f - T_o)}{m_d} \quad (5)$$

Here V (L) is the volume of the permeate collected, A (m^2) area of the membrane used, Δh_{evap} is the latent heat required to evaporate the water produced and the Q_{input} is input energy supplied to the system. C_f and C_p are the feed and permeate concentrations respectively, m_f and m_d (Kg/s) are the mass flow rates of the feed and permeate waters, T_f and T_o are the temperature of the feed entering the feed channel and leaving the feed channel for each stage and C_{pf} (4.1 KJ/Kg℃) is the specific heat capacity of water. The reason behind taking the feed inlet and exit temperature at each stage as a parameter in GOR and specific energy consumption calculation is that the feed chambers were not insulated, so much of the heat has been lost to the environment.

The system presents the following main characteristics:

- Permeate flux 6 - 13 L/m^2h
- Membrane material polytetrafluroethylene (PTFE), 0.45μm pore size
- Membrane effective area 0.013 m^2/stage
- Air gap thickness 11 mm
- Feed temperature at inlet 40-70 ℃
- Coolant water temperature 20-30 ℃
- Solar field area 2 m^2, tank capacity 180 L, with efficiency 85%
- Location Selangor, Malaysia
- Pump energy requirement 10 W
- Feed and coolant flow rate 1 L/min
- Feed concentration 14.625 g/L of NaCl
- Permeate quality 9-12 $\mu S/cm$
- Operational hours 8h
- GOR 0.5-7.88
- % Separation 99.96%
- Specific energy consumption was 0.0794 – 0.819 kWh/kg

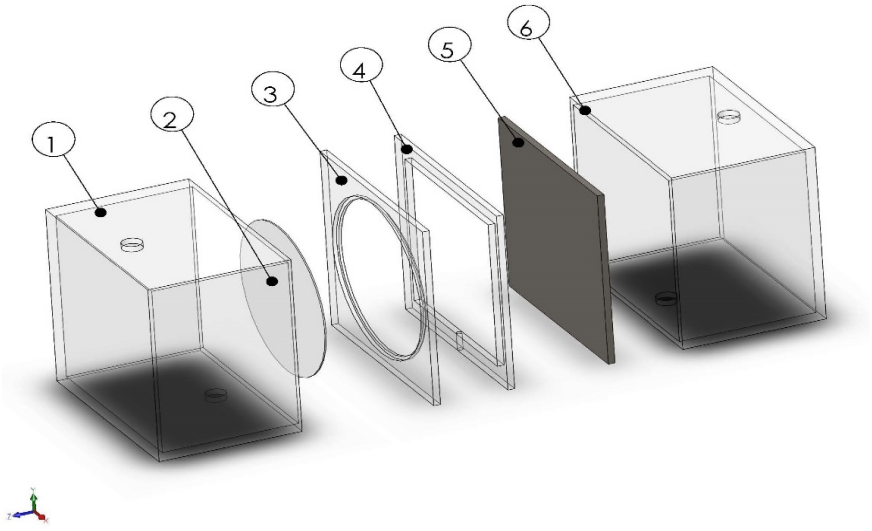

Figure 2. 3D image of the MD module.

3. RESULTS AND DISCUSSION

The system was operational during the daytime and was shut down at night, but it remained operational even during the rainy days. The solar heater used had a water storage tank which helped during these hours. The permeate flux obtained was tested by a conductivity meter to check the

distillate quality. Also food colour was mixed with the feed solution to check if there is any serious leak in the MD module.

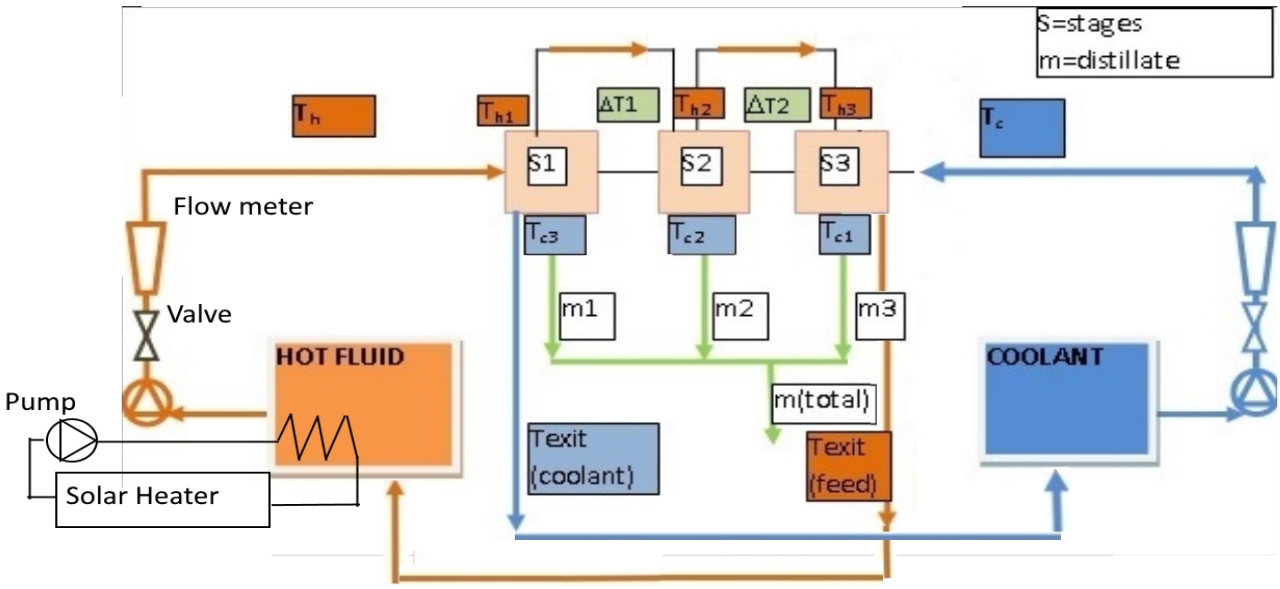

Figure 3. Schematic of the Multi Stage MD module.

3.1 Effect of Temperature

Before coupling the MD system with the solar heater it was tested experimentally to obtain the performance parameters. The feed temperature was varied from 40 ℃ to 70 ℃ and the corresponding flux was plotted. The result is shown in figure 4. The flux increases almost linearly. From the figure we can see that permeate flux for multi stage becomes almost double than single stage at 70 ℃. The data for single stage was obtained from a theoretical model developed by (Alsaadi, Francis, Maab, Amy, & Ghaffour, 2015). Their result matched with our laboratory experiment and thus helped in scaling up the membrane area.

Figure 5 represents the relationship between flux and cold solution temperature. Flux gradually decreases with the increase of cold solution temperature, this is well established from the literature and it can be seen that flux doesn't change as steeply as it does when feed temperature is changed meaning that flux has less sensitivity to cold solution temperature.

3.2 Water Production using the solar heater

The solar heater was used to obtain the average temperature during the day time and was coupled with MD system. The results were used to obtain the water production during the day (8 hours runtime) if the membrane area was 2 m^2 which is equivalent to a small scale plant. Figure 6 shows the water production during the month of February, 2017. It is clear that with this system pure water production of 220L per day is achievable. And even in the cloudy seasons producing 90L of water is possible.

4. CONCLUSION

The permeate flux achieved is quite high compared to some of the previous experiment running similar parameters mainly because of using simple string support instead of net like support (Guillén-Burrieza et al., 2011) which reduces the flux heavily. But at the same time experiments on multi-effect membrane distillation shows even more improved flux (Pangarkar, Deshmukh, &

Thorat, 2016). Thus both of these systems need to be compared with the same specification to achieve an optimized MD system. The system tested in this paper could have been improved more if air gap thickness and pressure (Alsaadi et al., 2015) were reduced, also adding internal heat recovery and spacers/baffles to reduce polarization in the feed chamber would greatly increase the distillate production rate.

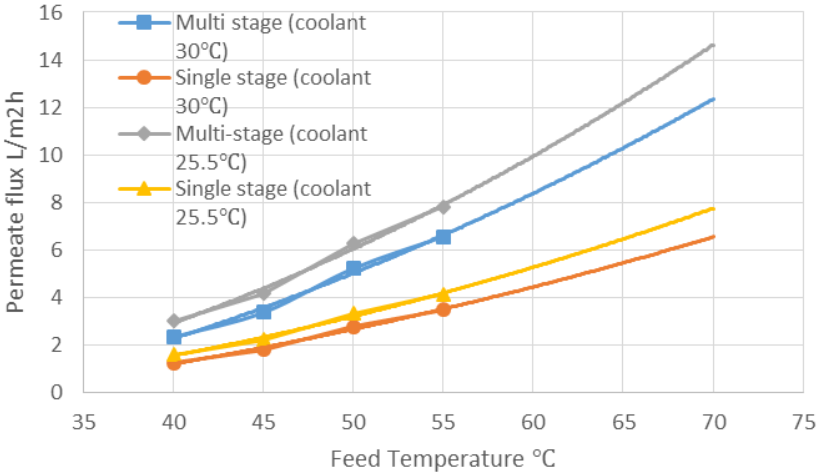

Figure 4. Relationship with permeate flux with feed temperature.

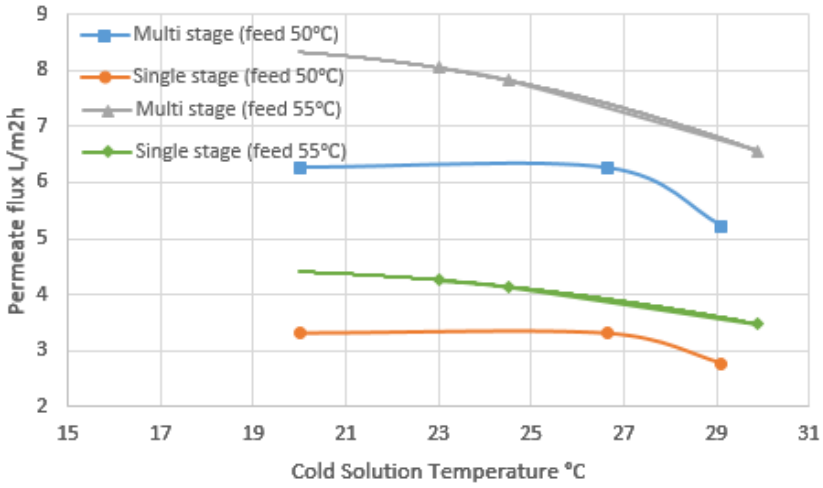

Figure 5. Relationship with permeate flux with cold solution temperature.

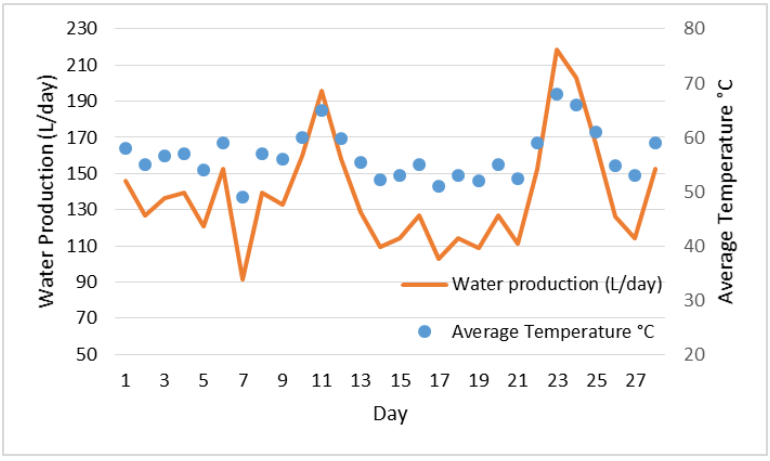

Figure 6. Expected water production during the month of February, 2017.

ACKNOWLEDGEMENT

The work is jointly supported by Fundamental Research Grant Scheme (FRGS-14-118-0359) and IIUM-UM joint grant (CG015-2014) by providing necessary financial and technical assistance.

REFERENCES

Alsaadi, A. S., Francis, L., Maab, H., Amy, G. L., & Ghaffour, N. (2015). Evaluation of air gap membrane distillation process running under sub-atmospheric conditions: Experimental and simulation studies. Journal of Membrane Science, 489, 73–80. https://doi.org/10.1016/j.memsci.2015.04.008

Bahar, R., Hawlader, M. N. A., Nga, K. C., & Haw, Y. J. (2014). Experimental study on a multi-stage air gap membrane distillation (AGMD) unit. Jurnal Teknologi (Sciences and Engineering), 69(9), 89–92.

Chafidz, A., Kerme, E. D., Wazeer, I., Khalid, Y., Ajbar, A., & Al-zahrani, S. M. (2016). Design and fabrication of a Portable and Hybrid Solar-Powered Membrane Distillation System. Journal of Cleaner Production. Elsevier Ltd. https://doi.org/10.1016/j.jclepro.2016.05.127

Gryta, M., Tomaszewska, M., & Karakulski, K. (2006). Wastewater treatment by membrane distillation. Desalination, 198(1–3), 67–73. https://doi.org/10.1016/j.desal.2006.09.010

Guillén-Burrieza, E., Blanco, J., Zaragoza, G., Alarcón, D.-C., Palenzuela, P., Ibarra, M., & Gernjak, W. (2011). Experimental analysis of an air gap membrane distillation solar desalination pilot system. Journal of Membrane Science, 379(1–2), 386–396. https://doi.org/10.1016/j.memsci.2011.06.009

Lawson, K. W., & Lloyd, D. R. (1997). Membrane distillation. Journal of Membrane Science,124(1), 1–25. https://doi.org/10.1007/s00216-011-4733-9

Pangarkar, B. L., Deshmukh, S. K., & Thorat, P. V. (2016). Experimental study of multi-effect membrane distillation (MEMD) for treatment of water containing inorganic salts, 11(4), 765–773. https://doi.org/10.2166/wpt.2016.077

Raluy, R. G., Schwantes, R., Subiela, V. J., Peñate, B., Melián, G., & Rosa, J. (2012). Operational experience of a solar membrane distillation demonstration plant in Pozo Izquierdo-Gran Canaria Island (Spain). DES, 290, 1–13. https://doi.org/10.1016/j.desal.2012.01.003

Zhani, K., Zarzoum, K., Bacha, H. Ben, Koschikowski, J., Pfeifle, D., Zarzoum, K., Pfeifle, D. (2015). Autonomous solar powered membrane distillation systems : state of the art, 3994(December). https://doi.org/10.1080/19443994.2015.1117821

VI. Urban Water Networks

Proceedings of the 10th World Congress of EWRA 'Panta Rhei', 5-9 July 2017, Athens, Greece
© 2017 *European Water Resources Association*

Efficient parallel evolutionary optimization algorithm applied to a water distribution system

T.T. Tanyimboh[1,2] and A.G. Seyoum[1,3]
[1] *Department of Civil and Environmental Engineering, University of Strathclyde, Glasgow, UK*
[2] *School of Civil and Environmental Engineering, University of the Witwatersrand, Johannesburg, South Africa*
[3] *SWS Consultancy, Addis Ababa, Ethiopia*
[*] *e-mail: tikutanyimboh@hotmail.co.uk*

Abstract: Water distribution systems are key components of public infrastructure and it is essential to design, manage and rehabilitate them economically without compromising the required performance and regulatory standards. Evolutionary optimization algorithms such as genetic algorithms have become popular in providing optimal and near optimal solutions to various optimisation problems on water distribution systems. However, one of the main challenges associated with genetic algorithms in the optimization of water distribution systems is that they are time consuming when applied to problems on real-world water distribution networks with large numbers of pipes and multiple operating conditions. For example, in the optimisation of large water distribution systems, a single optimisation run may involve millions of hydraulic and water quality simulations that may take many days on modern powerful computers such as workstations. One way to address this difficulty is by utilising parallel computing methods. The aim of the research was to investigate the potential improvement in computational efficiency achievable through parallel computing by optimizing a design based on a real-world water distribution network with a large number of decision variables, large solution space and complex response surface. The results showed that the parallel algorithm developed was practical and found optimal and near-optimal solutions reliably and efficiently, and the solutions achieved were consistently competitive. The average speedup achieved on an eight-core workstation was 15, based on an optimization problem with hundreds of decision variables for a real-world water distribution network with extended period simulation.

Key words: Water distribution network, penalty-free multiobjective evolutionary optimization, pressure-driven analysis, discrete optimization, demand satisfaction ratio, controller-worker model

1. INTRODUCTION

Water distribution systems (WDSs) are key components of public infrastructure and it is essential to design and rehabilitate them in a cost effective manner without compromising the required performance and regulatory standards. Evolutionary algorithms (EAs) such as genetic algorithms (GAs) have become popular in providing optimal and near optimal solutions to WDS optimisation problems.

One of the main issues with genetic algorithms is that the algorithms are time consuming when applied to optimisation problems on real-world networks with large numbers of pipes and multiple operating conditions (Van Zyl *et al.* 2004). For example, in the optimisation of large water distribution systems, a single optimisation run may involve millions of hydraulic and water quality simulations (Rossman 2000, Ghebremichael *et al.* 2008, Spiliotis and Tsakiris 2011, Todini and Rossman 2013) that may take many days on modern computers such as workstations.

One way to improve the computational efficiency of evolutionary optimization algorithms is by adopting parallel computing. Indeed, parallel computing has the added benefit that it can be used together with other strategies. In the context of water distribution systems, some of the other strategies for improving efficiency include: (a) the use of supercomputers (Barlow and Tanyimboh 2014); (b) regression models to estimate the hydraulic properties rapidly (Vairavamoorthy and Ali 2000); (c) surrogate measures of system performance, such as flow entropy, that are relatively easy to calculate (Tanyimboh and Setiadi 2008, Moosavian and Lence 2016); (d) techniques for reducing

the solution space of the optimization problem (Kadu *et al.* 2008, Kang and Lansey 2012); and (e) local search and hybrid methods (Haghighi *et al.* 2011).

Evolutionary algorithms for water distribution systems often use penalties to evaluate the merits of infeasible solutions when solving optimization problems that have constraints. By contrast, the penalty-free multi-objective evolutionary algorithm (PF-MOEA) proposed by Siew and Tanyimboh (2012b) uses pressure-dependent analysis that accounts for the pressure dependency of the nodal flows and thus avoids the need for penalties to address any violations of the minimum nodal pressure constraints. The hydraulic simulator used was a pressure-driven extension of EPANET 2 called EPANET-PDX (Seyoum and Tanyimboh 2014, 2016, Siew and Tanyimboh 2012a, Tsakiris and Spiliotis 2014, Sivakumar and Prasad 2015).

Given that fitness evaluation is often the most computationally expensive step in evolutionary optimization algorithms (Alba and Tomassini 2002, Schutte *et al.* 2004), the aim of this research was to investigate the improvement in the computational efficiency achievable through parallel computing. A design problem on a real-world water distribution network with a large number of decision variables and large solution space was investigated using extended period simulation.

2. OPTIMIZATION PROBLEM FORMULATION AND SOLUTION

Evolutionary algorithms (EAs) by nature start with a randomly generated set of candidate solutions that may include both feasible and infeasible solutions. To address the node pressure constraints, penalty methods have been applied widely (Broad *et al.* 2005, Ostfeld and Tubaltzev 2008). The major drawback of the penalty-based approach is that additional case-specific parameters are required whose calibration is generally challenging (Prasad and Park 2004).

In an attempt to alleviate the difficulties associated with the minimum node pressure constraints, Siew and Tanyimboh (2012b) proposed a penalty-free multi-objective evolutionary algorithm (PF-MOEA) based on NSGA II (Deb *et al.* 2002). The PF-MOEA algorithm uses pressure-driven analysis to assess each individual in the population of solutions. In this way, the pressure-driven analysis addresses the node pressure constraints as an integral part of the hydraulic simulations. PF-MOEA employs the pressure-driven extension of EPANET 2 that is known as EPANET-PDX (Siew and Tanyimboh 2012a) and carries out pressure-driven analysis seamlessly. Hence, when comparing infeasible solutions, PF-MOEA does not employ the constraint dominance approach used in NSGA II.

The PF-MOEA formulation has been applied previously to various aspects of WDS optimization that included design, operation and long-term rehabilitation and upgrading (Siew and Tanyimboh 2012b, Siew *et al.* 2014, 2016). Overall, PF-MOEA generated superior results for the optimization problems solved in terms of the cost, hydraulic performance and computational efficiency, compared to all other results in the literature.

The PF-MOEA approach is practical and straightforward to implement as it utilises the most basic operators such as single-point crossover and single-bit mutation. The algorithm was selected in this research to investigate the relative merits of parallel computing due to the above-mentioned advantages. The decision variables in PF-MOEA are represented using binary coding. Single-point crossover, single-bit mutation and binary tournament selection for crossover are the genetic operators used in the algorithm.

Minimising the total network cost (capital and operation) and maximising the network hydraulic performance were the two conflicting objectives adopted, subject to the constraints of conservation of mass and energy and the minimum nodal pressures, as follows.

$$\text{Minimise: } f_1 = (CR)^2 \tag{1}$$

$$\text{Maximise: } f_2 = (DSR)^4 \tag{2}$$

where f_1 and f_2 represent the first and second objective functions, respectively. *CR* is the cost ratio i.e. the ratio of the cost of a particular solution to the cost of the most expensive solution in the whole population within a single generation. *DSR* is the demand satisfaction ratio i.e. the ratio of the available flow to the required flow and measures the feasibility of a solution. Feasible solutions have a *DSR* value of unity; solutions with *DSR* values below unity are infeasible.

Large problems can be divided often into smaller ones that can be solved simultaneously on parallel processors in a shorter time (Trobec *et al.* 2009). A controller-worker approach was applied to parallelise the penalty-free optimization algorithm employed. The controller-worker approach, with a potential to improve the computational performances of algorithms significantly, is relatively straightforward (Cantú-Paz and Goldberg 2000).

The fitness evaluation of the child population was parallelized, as fitness evaluation is often the most computationally expensive step in evolutionary algorithms (Alba and Tomassini 2002, Schutte *et al.* 2004). The fitness evaluations were divided equally among all the processors including the controller processor. The controller processor performed the rest of the operations of the evolutionary algorithm including selection, crossover and mutation, and all the other procedures of the optimization. The authors wrote the parallel algorithm program in C++ with Message Passing Interface (MPI) routines. Microsoft HPC pack 2008 was used to run the program in Microsoft Visual Studio (version 2010). A detailed description of the parallel evolutionary algorithm is available in Seyoum (2015).

3. RESULTS AND DISCUSSION

The example considered was one of the water supply zones of a network in the UK (Seyoum and Tanyimboh 2014, 2016). The network and pipe cost data were obtained from the water utility. The system comprised 251 pipes, 199 demand nodes, 29 fire hydrants, 5 variable-head supply nodes and three water demand categories including leakage (Kanakoudis and Gonelas 2016, Tabesh *et al.* 2009). The minimum residual pressure required at the demand nodes was 20 m. The minimum residual pressure required at the fire hydrants for a flow rate of 8 litres per second was 3 m. A fire demand was operational in each hour, except for the first and last hours. Extended period simulation for a period of operation of 31 hours with a hydraulic time step of one hour was used. The Darcy–Weisbach formula for the head loss due to friction in the pipes was used (Rossman 2000). Figure 1 shows the network topology and pipe diameter options.

The network was optimised as a new design. Ten commercially available pipe diameters were selected based on the existing network's pipe diameters that range from 32 mm to 400 mm. The 10 candidate pipe diameters correspond to 10^{251} feasible and infeasible solutions in total. The crossover and mutation probabilities were 1.0 and 0.005, respectively. The maximum number of function evaluations allowed per optimization run was 1,000,000. Ten optimization runs with different initial populations of 1000 were carried out. A workstation that comprised dual Intel Xeon 2.4 GHz CPU (four cores each) and 16 GB RAM running the Windows operating system was used. The workstation had eight cores in total and all were utilized for the parallel computing.

The least expensive solution achieved by the parallel algorithm had a cost of £418,685 within 975,000 function evaluations. This is the best solution obtained for the network to date. The solution is 0.2% cheaper than the best solution reported in Tanyimboh and Seyoum (2016), i.e. £419,514 within 985,000 function evaluations. Figure 2 shows the pipe diameters of the solutions from the parallel and serial algorithms and existing network. The solution for the serial algorithm was obtained from Tanyimboh and Seyoum (2016). All the solutions shown are fully feasible, i.e. the minimum residual pressure requirements for all the operating conditions were satisfied. Figure 3 illustrates the progress of the algorithm in terms of the least expensive feasible solution in successive generations.

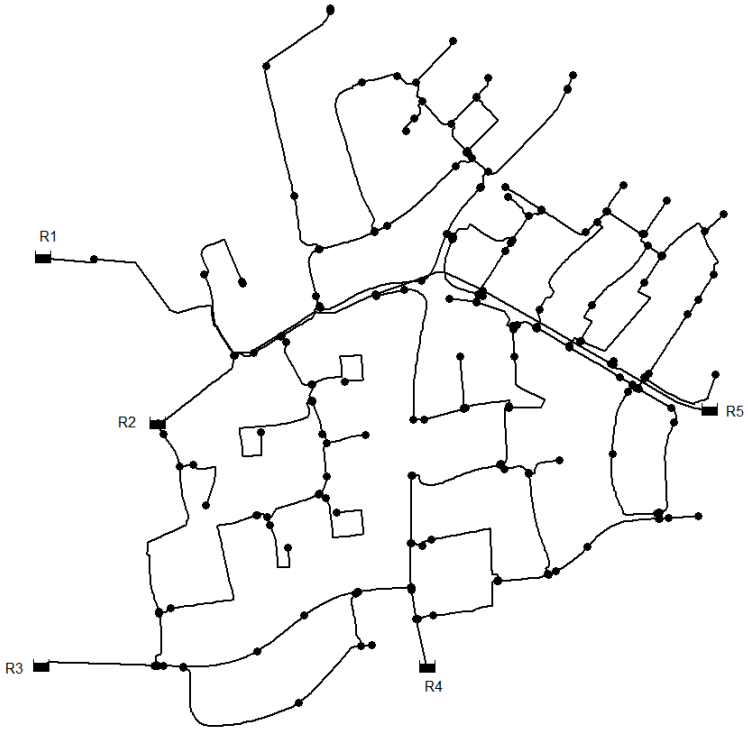

(a) Topology

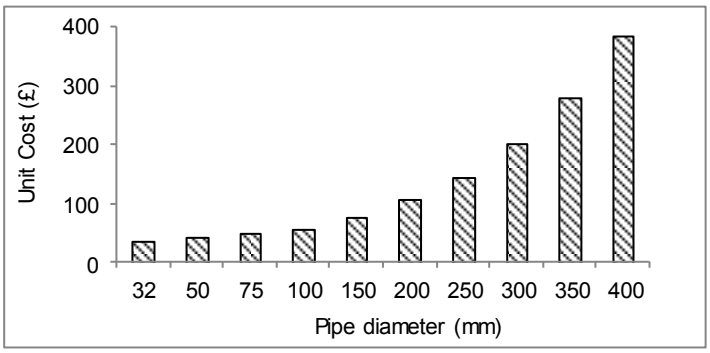

(b) Pipe diameters selected for the optimization

Figure 1. Network topology and pipe diameter options. R1-R5 represent the supply nodes.

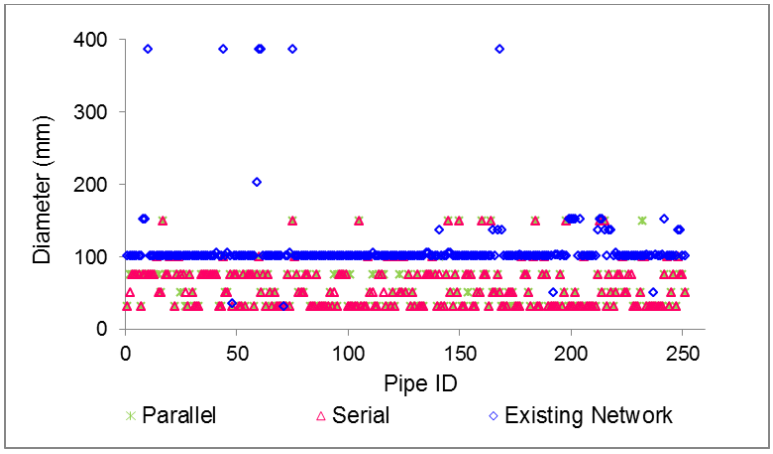

Figure 2. Comparison of the existing and optimised pipe diameters

A single optimization run with 1,000,000 function evaluations using the serial algorithm required an average CPU time of 30 days while the parallel algorithm required only two days on average. Thus, the parallel algorithm achieved a considerable improvement in the execution time. The speedup achieved by the parallel algorithm ranged from 10.96 to 17.15 as shown in Figure 4. On average, the parallel algorithm achieved a speedup of 15; in other words, the CPU time for the parallel algorithm was approximately 6.7 % of the CPU time for the serial algorithm.

4. CONCLUSIONS

The results showed that the parallel algorithm developed found optimal and near-optimal solutions reliably and efficiently; the solutions were consistently competitive and a new best solution was achieved. The number of solutions analysed before finding the Pareto-optimal solutions was extremely small in comparison to the total number of solutions available.

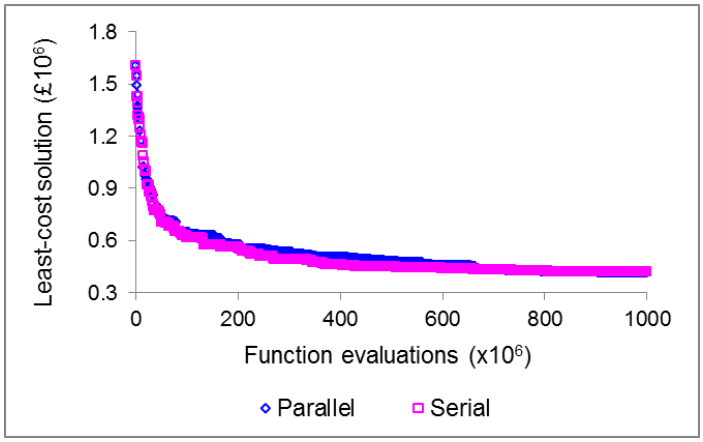

Figure 3. Illustration of the progress of the least expensive feasible solution in successive generations. The graphs show the least-cost feasible solutions for the serial and parallel algorithms, using the same initial population.

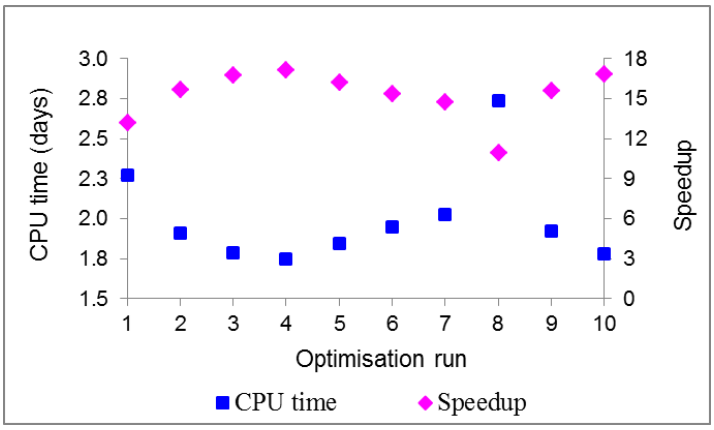

Figure 4. The CPU times and speedup achieved by the parallel algorithm

The average speedup achieved on an eight-core workstation was 15, based on an optimization problem with hundreds of decision variables for a real-world water distribution system. In other words, the average execution time for the parallel algorithm was approximately 6.7 % of the execution time for the serial algorithm. Though highly effective, the improvement achieved previously by search space reduction was smaller (Kadu *et al.* 2008, Siew *et al.* 2014). Thus, the results reinforce previous evidence in the literature that fitness evaluation is often the most computationally expensive step in evolutionary optimization algorithms (Alba and Tomassini 2002, Schutte *et al.* 2004). Hence, the results seem encouraging and further studies with more advanced

approaches (e.g. the island model) may be worth considering as parallel computing has the added benefit that it can be used together with other strategies that can improve the computational efficiency further. The network considered comprised one water supply zone of a water distribution system in the UK. Therefore, additional investigations regarding the speed and other properties of the proposed parallel algorithm in the context of optimization problems with significantly more decision variables may be worth considering.

ACKNOWLEDGMENT

This project was funded in part by the UK Engineering and Physical Sciences Research Council (EPSRC Grant Reference EP/G055564/1), the British Government (Overseas Research Students Awards Scheme) and the University of Strathclyde. The authors wish to thank Veolia Water UK (now Affinity Water) for their invaluable contribution and support.

REFERENCES

Alba, E., Tomassini, M., 2002. Parallelism and evolutionary algorithms. IEEE Transactions on Evolutionary Computation; 6(5): 443-462.

Barlow, E., Tanyimboh, T. T., 2014. Multi-objective memetic algorithm applied to the optimisation of water distribution systems. Water Resources Management; 28(8): 2229-2242.

Broad, D. R., Dandy, G. C., Maier, H. R., 2005. Water distribution system optimization using metamodels. Journal of Water Resources Planning and Management; 131(3): 172-180.

Cantu-Paz, E., Goldberg, D. E., 2000. Efficient parallel genetic algorithms: theory and practice. Computer Methods in Applied Mechanics and Engineering; 186(2): 221-238.

Deb, K., Pratap, A., Agarwal, S., Meyarivan, T., 2002. A fast and elitist multi-objective genetic algorithm: NSGA II. IEEE Transactions on Evolutionary Computation; 6(2): 182-197.

Ghebremichael, K., Gebremeskel, A., Trifunovic, N., Amy, G., 2008. Modelling disinfection by-products: coupling hydraulic and chemical models. Water Science and Technology: Water Supply; 8(3): 289-295.

Haghighi, A., Samani, H. M., Samani, Z. M., 2011. GA-ILP method for optimization of water distribution networks. Water Resources Management; 25(7): 1791-1808.

Kadu, M. S., Gupta, R., Bhave, P. R., 2008. Optimal design of water networks using a modified genetic algorithm with reduction in search space. Journal of Water Resources Planning and Management; 134(2): 147-160.

Kang, D., Lansey, K., 2012. Revisiting optimal water-distribution system design: issues and a heuristic hierarchical approach. J. Water Resour. Plann. Manage; 138(3): 208-217.

Kanakoudis, V., Gonelas, K., 2016. Analysis and calculation of the short and long run economic leakage level in a water distribution system. Water Utility Journal; 12:57-66.

Moosavian, N., Lence, B. J., 2016. Nondominated sorting differential evolution algorithms for multiobjective optimization of water distribution systems. J. Water Resources Planning and Management; 10.1061/(ASCE)WR.1943-5452.0000741.

Ostfeld, A., Tubaltzev, A., 2008. Ant colony optimization for least-cost design and operation of pumping water distribution systems. J. Water Resour. Plann. Manage.; 134(2): 107-118.

Prasad, T. D., Park, N. S., 2004. Multiobjective genetic algorithms for design of water distribution networks. Journal of Water Resources Planning and Management; 130(1): 73-82.

Rossman, L. A., 2000. EPANET 2 users manual. Water Supply and Water Resources Division. National Risk Management Research Laboratory, US EPA, Cincinnati.

Schutte, J. F., Reinbolt, J. A., Fregly, B. J., Haftka, R. T., George, A. D., 2004. Parallel global optimization with the particle swarm algorithm. International J. Numerical Methods in Engineering; 61(13): 2296-2315.

Seyoum, A. G., 2015. Head-dependent modelling and optimisation of water distribution systems. PhD thesis, University of Strathclyde, UK.

Seyoum, A. G., Tanyimboh, T. T., 2014. Pressure dependent network water quality modelling. Proceedings of ICE: Water Management; 167(6): 342-355.

Seyoum, A. G., Tanyimboh, T. T., 2016. Investigation into the pressure-driven extension of the EPANET hydraulic simulation model for water distribution systems. Water Resources Management; DOI:10.1007/s11269-016-1492-6.

Siew, C., Tanyimboh, T. T., 2012a. Pressure-dependent EPANET extension. Water Resour Manag; 26(6): 1477-1498.

Siew, C., Tanyimboh, T. T., 2012b. Penalty-free feasibility boundary convergent multi-objective evolutionary algorithm for the optimization of water distribution systems. Water Resour Manag; 26(15): 4485-4507.

Siew, C., Tanyimboh, T. T., Seyoum, A. G., 2014. Assessment of penalty-free multi-objective evolutionary optimization approach for the design and rehabilitation of water distribution systems. Water Resour Manag; 28(2): 373389.

Siew, C., Tanyimboh, T. T., Seyoum, A. G., 2016. Penalty-free multi-objective evolutionary approach to optimization of Anytown water distribution network. Water Resour Manag; 30(11): 3671-3688.

Sivakumar, P., Prasad, R. K., 2015. Extended period simulation of pressure-deficient networks using pressure reducing valves. Water Resour Manag; 29(5): 1713-1730.

Spiliotis, M., Tsakiris, G., 2011. Water distribution system analysis: Newton-Raphson method revisited. J. Hydraul. Eng. ASCE; 137(8): 852-85.

Tabesh, M., Yekta, A. H. A., Burrows, R., 2009. An integrated model to evaluate losses in water distribution systems. Water Resour Manage; 23(3): 477-492.

Tanyimboh, T. T., Setiadi, Y., 2008. Sensitivity analysis of entropy-constrained designs of water distribution systems. Engineering Optimization; 40(5): 439-457.

Tanyimboh, T. T., Seyoum, A. G., 2016. Multiobjective evolutionary optimization of water distribution systems: Exploiting diversity with infeasible solutions. J. Environ Manag; 183:133-141, DOI:10.1016/j.jenvman.2016. 08.048.

Todini, E., Rossman, L., 2013. Unified framework for deriving simultaneous equation algorithms for water distribution networks. J. Hydraulic Engineering; 10.1061/(ASCE)HY.1943-7900.0000703, 139(5): 511-526.

Trobec, R., Vajtersic, M., Zinterhof, P., 2009. Parallel computing: numerics, applications, and trends. Springer Science & Business Media.

Tsakiris, G., Spiliotis, M., 2014. A Newton-Raphson analysis of urban water systems based on nodal head-driven outflow. European J. Environmental and Civil Eng.; 18(8): 882-896.

Vairavamoorthy, K., Ali, M., 2000. Optimal design of water distribution systems using genetic algorithms. Computer-Aided Civil and Infrastructure Engineering; 15(5): 374-382.

Van Zyl, J. E., Savic, D. A., Walters, G. A., 2004. Operational optimization of water distribution systems using a hybrid genetic algorithm. J. Water Resour. Plann. Manage; 130(2): 160-170.

Proceedings of the 10th World Congress of EWRA 'Panta Rhei', 5-9 July 2017, Athens, Greece
© 2017 *European Water Resources Association*

Modeling and optimization control of a hybrid water system

H. Mu[1*], T. Rauschenbach[2], D. Karamanzia[2] and N. Cai[1]
[1] *Fraunhofer Beijing Representative Office, Landmark Tower II 0611, Chaoyang, Beijing, PR. China*
[2] *Advanced System Technology (AST) Branch of Fraunhofer IOSB, Am Vogelherd 50, 98693 Ilmenau, Germany*
[*] *e-mail: muh@fraunhofer.com.cn*

Abstract: In most deltas, rivers and channels compose to a water network system. Different water conservancy projects, such as pumping stations, sluices, and barriers are constructed in the water system. These water conservancy projects change the natural water flows, i.e. the direction of a water flow is no longer controlled by the natural terrain, but by the difference in the state of the water heads between sluice gates. Even the flow of the rivers is not clear anymore. The water system influenced by a discrete state control has evolved into a complex hybrid water system. The conventional way to manage such a water system is to monitor water level changes and to control different sluice gates based on experience. However, such management is challenging and causes a serious loss of energy and resources. Therefore, a model-based optimal scheduling process is expected in practice. Unfortunately traditional hydrological models are unable to model hybrid water systems totally. Interdisciplinary research is needed, especially inheriting some approaches from the field of automation technology. This paper models a complex hybrid water system with a scheduling optimization approach. The definition "virtual tank" is introduced to solve the bi-directional flow problem of the hybrid water system. Scheduling processes in short or midterm periods are optimized with the Model Predictive Control Method (MPC). The modeling and optimization approaches are demonstrated in a case study – Smart flood control in the hybrid water network area of Jiangyin, PR China.

Key words: Bi-directional flow, Hybrid water system, MPC-MLD optimisation, Water network modelling

1. INTRODUCTION

Artificial water conservancy projects, such as pumping stations, sluices, and barriers, densely cover a plain river network area. They change the natural hydrologic dynamic flow and form a hybrid water system (Definition of Hybrid Water System see chapter 2). The water flow in the river is no longer caused by the natural terrain, but by the difference in the water level of sluices on the ends of the river. Changing the state of a sluice causes a change in the water flow situation. Therefore, for the management of water resource scheduling, not only the dynamic change of the continuous variable should be considered, but also the discrete event caused by opening and closing the sluices should be analyzed. In order to solve such complex hybrid water systems, two concepts are developed and implemented in this work:

1. With the introduction of an innovated concept, the "virtual tank", the modeling process for the dynamic flow changes based on state changes (sluice gate open or closed) in hybrid water systems can be solved. The modeling not only provides a visual simulation, which makes it easy for decision makers to understand the water situation, but also provides a basement for optimal scheduling.
2. Model Predictive Control (MPC) Method based on Mixed Logical Dynamic (MLD), is applied to solve the optimization scheduling in short and midterm periods. The system can calculate and deliver suggestions for control strategies in time, based on the weather forecast and scenario definition.

The goal of this study is to set up scenarios with short-term regional hydrological changes, i.e. heavy precipitation in a short timeframe. The hybrid water system is then modelled to forecast the water situation. According to the limiting conditions of engineering projects (dams, gates, sluices,

barriers) and optimization objectives for scheduling, the management strategies are then determined by the MPC-MLD approach. This paper refers to some research results of Delft University of Technology in Netherlands(van Ekeren, 2011), but the models have been redefined in this work with the innovated concept called the "virtual tank", and was implemented as a large scale research in a dense river network area of Yangzi delta in Jiangyin (987.5km^2), Jiangsu Province, PR China.

2. METHODOLOGY

2.1 Modelling

First of all, we must define the term "hybrid system". The term "hybrid system" originates from Cybernetic science. In this system, not only do dynamic continuous variables exist, but also discrete state events. A hybrid water system is a special reflection in water resources management. Figure 1 shows a typical hybrid water system with natural river flow, sluices, etc.

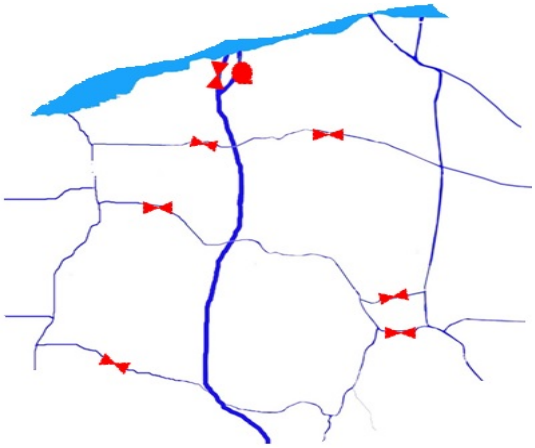

Figure 1. A typical hybrid water system

In Figure 1, only the big river in the north is still flowing relatively natural in the entire river system. Sluice gates are densely constructed on other rivers. Due to the opening and closing of these sluice gates, the water level, the flow activity, and the direction of water are changed actively. Therefore, in order to simulate the actual interactions of the hydrological dynamic variables, i.e. the river flow, and the discrete state variables caused by opening and closing pump stations and sluice gates, this paper introduces an innovated concept of the virtual tank. A virtual tank can be applied at two different application levels:

1. The intersection of two or more channels is assumed to be a virtual tank. Neighboring virtual tanks are connected by channel between them. For the flow calculation the Chézy model is introduced as follows:

$$f_{chézy}\left(x_i(k), x_j(k)\right) = A_{c,ij}\left(x_i(k), x_j(k)\right) C_{ij} Sign\left(x_j - x_i\right) \times \sqrt{\frac{R_{ij}\left(x_i(k), x_j(k)\right)\left|\left(x_j - x_i\right)\right|}{l_{ij}}} \qquad (1)$$

x_i and x_j are the water level of two virtual tanks i and j, $A_{c,ij}\left(x_i(k), x_j(k)\right)$ is the minimum section area of flow $q_{ij}\left(x_i(k), x_j(k)\right)$, C_{ij} is roughness coefficient, $R_{ij}\left(x_i(k), x_j(k)\right)$ is hydraulic radius of flow $q_{ij}\left(x_i(k), x_j(k)\right)$, l_{ij} is the length of the connection between i and j. $Sign\left(x_j - x_i\right)$ express the flow direction.

The model calculates the flow direction in each time interval. When the calculated value is positive the flow is the same as the initial direction of flow; when it is negative the flow is in the opposite direction. Figure 2 shows the structure of the first concept of the virtual tank.

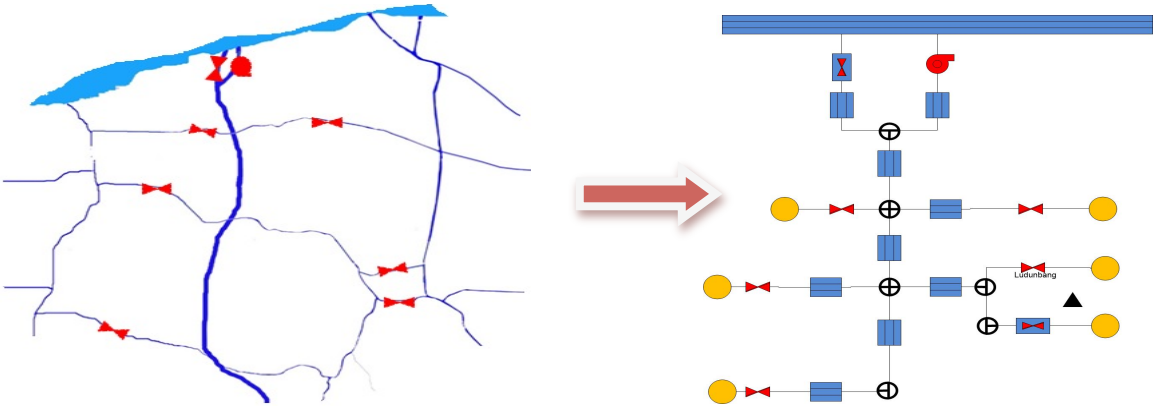

Figure 2. Structure of the first description of the model based on the virtual tank

This application is good for modeling of river networks considering the time discrete state changes. This enables a clear expression of the water situation. It can be used for testing the control strategies, river flood control, and water diversion management.

2. The second application of the virtual tank concept is at a higher level in considering the catchment area, the administrative area, and the river channel characteristics. The study area is divided into a set of submodel areas, each partition is assumed to be a virtual tank. Both neighboring partitions, i.e. virtual tanks, are connected by a main channel in between. Figure 3 shows an expression of the second application of the concept of a virtual tank:

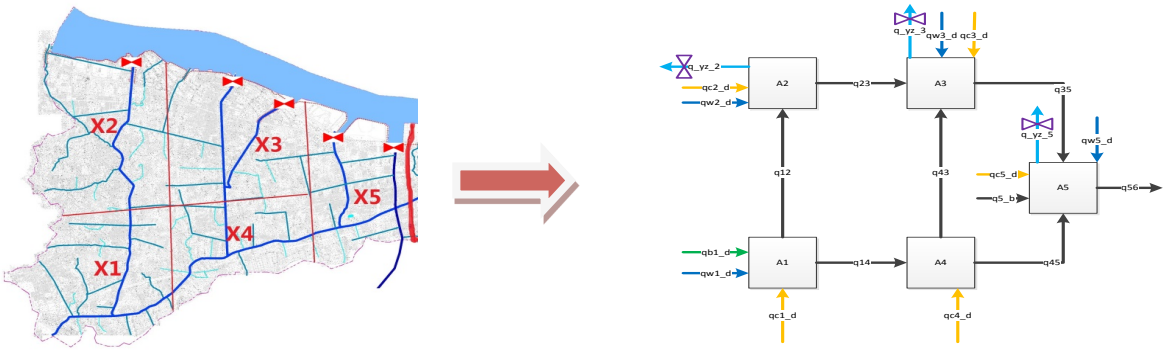

Figure 3. Higher level of the application of a virtual tank

This application is suitable for modelling of large regions. The region is divided into different sub-regions (virtual tanks). All tanks were modelled at lower level and their behaviours were analysed. This method can express the impact on each model area caused by the rainfall and runoff. It has a profound significance for flood control in the whole region.

Based on the concept of the virtual tank, a hybrid water system can be modeled. Take Figure 3 for example. This water system consists of 3 sluices and 5 virtual tanks, which are connected by main channels in between. Some additional inflows to the virtual tanks are also considered respectively. The state of each tank is represented by the water level. According to the mass balance principle, the change of the water level in the discretized time step k+1 is described as follows:

Virtual Tank A1:

$$X_1(k+1) = \frac{Ts}{A_{s1}}\left[q_{b1\_d}(k) + q_{w1\_d}(k) + q_{c1\_d}(k) - q_{12}\left(X_1(k), X_2(k)\right)\right] + X_1(k) \quad (2)$$

Virtual Tank A2:

$$X_2(k+1) = \frac{Ts}{A_{s2}}\left[-q_{yz\_2}\left(X_2(k), Yz\_L_2(k), u_2(k)\right) + q_{w2\_d}(k) + q_{c2\_d}(k) + q_{12}\left(X_1(k), X_2(k)\right) - q_{23}\left(X_2(k), X_3(k)\right)\right] + X_2(k) \quad (3)$$

The Virtual Tank A3 to A5 expressed in the same way, where k is the discrete time step, Ts is the sample time; A_{si} (i=1,2,….,5) is the surface area of the water surface in each tank; $X_i(k)$ (i=1,2,…,5) is the water level of each corresponding virtual tank at k time step; $q_{ci\_d}(k)$ (i=1,2,3,4,5) is the disturbance inflow due to the precipitation and transpiration; $q_{w1\_d}(k)$, $q_{w2\_d}(k)$, $q_{w3\_d}(k)$, $q_{w5\_d}(k)$ are the inflows due to the water supply from the external river; $q_{b1\_d}(k)$, $q_{5\_b}(k)$ are the disturbance inflows from the boundaries; $q_{yz\_2}\left(X_2(k), Yz\_L_2(k), u_2(k)\right)$, $q_{yz\_3}\left(X_3(k), Yz\_L_3(k), u_3(k)\right)$, $q_{yz\_5}\left(X_5(k), Yz\_L_5(k), u_5(k)\right)$ are flows between the large north river and the local channels, which controlled by the sluices; and $q_{12}\left(X_1(k), X_2(k)\right)$, $q_{23}\left(X_2(k), X_3(k)\right)$, $q_{43}\left(X_4(k), X_3(k)\right)$, $q_{35}\left(X_3(k), X_5(k)\right)$, $q_{14}\left(X_1(k), X_4(k)\right)$, $q_{45}\left(X_4(k), X_5(k)\right)$ *and* $q_{56}\left(X_5(k), X_6(k)\right)$ are the flows between two connected tanks, this is equivalent to $q_{ij}\left(X_i(k), X_j(k)\right)$ in the Chézy formula(van Ekeren, 2010), and can be expressed as:

$$q_{ij}\left(x_i(k), x_j(k)\right) = f_{chézy}\left(x_i(k), x_j(k)\right) \quad (4)$$

$$f_{chézy}\left(x_i(k), x_j(k)\right) = A_{c,ij}\left(x_i(k), x_j(k)\right) C_{ij} Sign\left(x_j - x_i\right) \times \sqrt{\frac{R_{ij}\left(x_i(k), x_j(k)\right)\left|\left(x_j - x_i\right)\right|}{l_{ij}}} \quad (5)$$

The section area variable $A_{c,ij}\left(x_i(k), x_j(k)\right)$ and the hydraulic radius $R_{ij}\left(x_i(k), x_j(k)\right)$ are the functions of the water level. Their values are inflected according to the change in water level between the two tanks in each time step. The section area variable h_{mean} is approximated with the average value of x_i, x_j. Under this kind of approximation, the area of the cross section and the hydraulic radius are only related to the channel parameters (b the width of the channel and m the slope):

$$A_{c,ij}\left(x_i(k), x_j(k)\right) = (b + m \times h_{mean}) \times h_{mean} \quad (6)$$

wetted perimeter calculation formula:

$$P_{c,ij}\left(x_i(k), x_j(k)\right) = b + 2 \times h_{mean}\sqrt{1 + m^2} \quad (7)$$

It follows that the hydraulic radius can be calculated as:

$$R_{ij}\left(x_i(k), x_j(k)\right) = \frac{A_{c,ij}\left(x_i(k), x_j(k)\right)}{P_{c,ij}\left(x_i(k), x_j(k)\right)} = \frac{A_{c,ij}\left(x_i(k), x_j(k)\right)}{b + 2 \times h_{mean}\sqrt{1+m^2}} \quad (8)$$

The flows $q_{yz\_2}\left(X_2(k), Yz\_L_2(k), u_2(k)\right)$, $q_{yz\_3}\left(X_3(k), Yz\_L_3(k), u_3(k)\right)$, $q_{yz\_5}\left(X_5(k), Yz\_L_5(k), u_5(k)\right)$ are described by the formula of Chézy, the difference here is that a key variable $u_i(k)$ is added, which represents the state of corresponding sluices, therefore the formula can be rewritten as:

$$q_{yz\_i}\left(X_i(k), Yz\_L_i(k), u_i(k)\right) = u_i(k)\, f_{chézy}\left(x_i(k), Yz\_L_i(k)\right) \quad (9)$$

where, $Yz\_L_i(k)$ is the water level of the north river (see Figure 2), and the state of the sluice is given by:

$$u_i(k) = \begin{cases} 0 & if\ the\ sluice\ closed\ at\ the\ time\ k \\ 1 & otherwise \end{cases} \quad (10)$$

Now, all the variables are defined. Through the time series of the input data (the disturbance inflows) and static state data, the water level output data can be calculated under the conditions of the initial data. Then virtual tank model parameters ($A_{c,ij}\left(x_i(k), x_j(k)\right), l_{ij}$) can be inferred backwards by comparing the actual levels of output data.

2.2 Optimization using MPC based on MLD

MPC (Model Predictive Control) originates from the process industry, but nowadays MPC is used in many different fields. In water resources management, especially in dealing with water hybrid systems, MPC is quite new. MPC as a technology of Advanced Process Control (APC) is based on a prediction model. Several models could be selected for the hybrid system, such as Hybrid Automata, Petri Net, Piece Wise Affine, and MLD (mixed logical dynamical). Because the virtual tank model can be easily extended to the MLD model, the MLD model is selected here. (Zhang, 2007).

An MLD system has these well-known expressions:

$$\boldsymbol{X}(k+1) = \boldsymbol{A}(k)\boldsymbol{X}(k) + \boldsymbol{B}_1(k)\boldsymbol{U}(k) + \boldsymbol{B}_2(k)\boldsymbol{\delta}(k) + \boldsymbol{B}_3(k)\boldsymbol{Z}(k) + \boldsymbol{B}_4(k)\boldsymbol{D}(k) \quad (11)$$

$$\boldsymbol{Y}(k) = \boldsymbol{C}(k)\boldsymbol{X}(k) + \boldsymbol{D}_1(k)\boldsymbol{U}(k) + \boldsymbol{D}_2(k)\boldsymbol{\delta}(k) + \boldsymbol{D}_3(k)\boldsymbol{Z}(k) + \boldsymbol{D}_4(k)\boldsymbol{D}(k) \quad (12)$$

$$\boldsymbol{E}_1(k)\boldsymbol{X}(k) + \boldsymbol{E}_2(k)\boldsymbol{U}(k) + \boldsymbol{E}_3(k)\boldsymbol{\delta}(k) + \boldsymbol{E}_4(k)\boldsymbol{Z}(k) + \boldsymbol{E}_5(k)\boldsymbol{D}(k) \le \boldsymbol{G} \quad (13)$$

The expression shows a MLD system which is defined as a linear relation consisting of continuous variables and binary variables, where, X is the state of the system, Y is the output variable of the system, U is defined as input vector and is a control variable of the system, Y and U have the same structure like X. δ is the logical statement of the system: $\delta \in \{0,1\}^{r_l}$; Z is the auxiliary continuous statement: $z(k) = x(k) * \delta(k)$, $z(k) \in \Re^{r_c}$; D represents disturbance variables. $z(k)$ Equation is nonlinear, therefore some inequality constraints have to be defined (van Ekeren, 2010):

$$z(k) \le M\delta(k) \quad (14)$$

$$z(k) \ge m\delta(k) \quad (15)$$

$$z(k) \le x(k) - m\left[1 - \delta(k)\right] \quad (16)$$

$$z(k) \ge x(k) - M\left[1 - \delta(k)\right] \quad (17)$$

In the case study, M is defined as the maximum possible value of the state of virtual tank, and m is the minimum possible value of the virtual tank. The relation (2), (3) are multiple expressions, and the part of the nonlinear flow functions are piecewise smooth. In practice, it is impossible to get an analytic solution, which requires the use of multiple linear regression algorithms. Therefore, linearization operations have to be conducted. For example, the part $q_{12}(X_1(k), X_2(k))$ after linear regression can be written as $a_{12}X_1(k) + b_{12}X_2(k)$, where a_{12} and b_{12} as regression coefficients can be obtained by the unconstrained nonlinear multivariable optimization method (in this work fminunc function in Matlab was used to obtain the coefficients). The approximated linear functions used for MLD are presented in the following:

$$X_1(k+1) = \frac{Ts}{A_{s1}}\left[q_{b1\_d}(k) + q_{w1\_d}(k) + q_{c1\_d}(k) - a_{12}X_1(k) - b_{12}X_2(k)\right] + X_1(k) \quad (18)$$

$$X_2(k+1) = \frac{Ts}{A_{s2}}\left[-a_{yz_2}z_2(k) - b_{yz_2}Yz_{L_2}(k)\delta_2(k) + q_{w2_d}(k) + q_{c2_d}(k) + a_{12}X_1(k) + b_{12}X_2(k) - a_{23}X_2(k) - b_{23}X_3(k)\right] + X_2(k) \quad (19)$$

2.3 Optimization

For the optimization, the objective function and some constraints have to be defined. There are two kinds of objectives, $J_i(\tilde{x}_i(k))$ and $\mathrm{J_k}\left(\tilde{\delta}_\mathrm{k}(\mathrm{k})\right)$. $J_i(\tilde{x}_i(k))$is the objective function for water level of each virtual tank, the water level have to stay in the safety region, r_{i1} is the unsafe level, $\mathrm{r_{i2}}$ is the dangerous level, which can cause flood disaster. λ_{i1}, λ_{i2}, λ_{i3} are cost factors, $\mathrm{e_{max,i1}(k)}$ and $\mathrm{e_{max,i2}(k)}$ are the exceedances of reference water level $\mathrm{r_{i1}}$ and $\mathrm{r_{i2}}$ respectively; $\mathrm{e_{i3}(k)}$ is a binary auxiliary variable, which shows whether or not the water level has been exceeded.

$$J(k) = J_1(\tilde{x}_1(k)) + J_2(\tilde{x}_2(k)) + J_3(\tilde{x}_3(k)) + J_4(\tilde{x}_4(k)) + J_5(\tilde{x}_5(k)) \quad (20)$$

$$J_i(\tilde{x}_i(k)) = \lambda_{i1}e_{max,i1}(k) + \lambda_{i2}e_{max,i2}(k) + \lambda_{i3}e_{i3}(k) \text{ (i=1,2,3,4,5)} \quad (21)$$

$$e_{max,i1}(k) = \max(\max(\tilde{x}_i(k)) - r_{i1}, 0) \quad (22)$$

$$e_{max,i2}(k) = \max(\max(\tilde{x}_i(k)) - r_{i2}, 0) \quad (23)$$

$$e_{i3}(k) = \begin{Bmatrix} 1\ if\ e_{max,i2}(k) > r_{i2} \\ 0\ if\ e_{max,i2}(k) \le r_{i2} \end{Bmatrix} \quad (24)$$

The minimization of this cost function is reformulated into the following equivalent form:

$$\min J_i(\tilde{x}_i(k)) = \min\left(\lambda_{i1}e_{max,i1}(k) + \lambda_{i2}e_{max,i2}(k) + \lambda_{i3}\delta_{i3}(k)\right) \quad (25)$$

$\mathrm{J_k}\left(\tilde{\delta}_\mathrm{k}(\mathrm{k})\right)$ represents the objective function for sluices. The first term denotes the cost of closing the sluices, the second term stand for the cost of changing the state.

$$J_k\left(\tilde{\delta}_k(k)\right) = \lambda_{k1}\sum_{j=1}^{N}[1 - \delta_k(k+j-1)] + \lambda_{k2}\sum_{j=1}^{N}|\delta_k(k+j-1) - \delta_k(k+j-2)| \quad (26)$$

The minimization of the first part is rewritten as follows:

$$\min \lambda_{91}\sum_{j=1}^{N}[1 - \delta_9(k+j-1)] = \min -\lambda_{91}\sum_{j=1}^{N}\delta_9(k+j-1) \quad (27)$$

The minimization of the second part is :

$$\min \lambda_{92}\sum_{j=1}^{N}|\delta_9(k+j-1) - \delta_9(k+j-2)| = \min \lambda_{92}\sum_{j=1}^{N}p_j \quad (28)$$

$\boldsymbol{\lambda}$ is a weighting factor, $\mathrm{p_j}$ are continuous auxiliary variables. Considering the objective functions and constraints, the optimization problem can be solved by the MILP (linear programming mixed-integer) method.

$$\min \mathbf{c}^{\mathrm{T}}\boldsymbol{\theta} \quad (29)$$

$$\boldsymbol{G\theta} \le \mathbf{h} \quad (30)$$

where C is a matrix of the weight coefficients; $\boldsymbol{\theta}$ is the matrix of the optimal target factors.

3. CASE STUDY

The area of the case study is located in the Yangtze River Delta in Middle East of china. The area has a flat terrain, with dense river network, and each river (Channel) has more than one water conservancy project. North of the area is the Yangtze River. The water level of Yangtze River is affected by the upstream runoff and tide factors of the downstream. Therefore, along the Yangtze River not only dams were built for the flood protection, but also in the crossing between local rivers and the Yangtze River a set of gates were constructed for the management of navigation and controlling of the river water level, and exchanging the water between local rivers and the Yangtze. In some special positions two-way water pump stations were constructed for flood and drought control. Within the local river network, different kinds of sluices were constructed for the easy management of wateruse. Because of the artificial structure, the natural water system has evolved into a complex hybrid water system. In this case study, the model region is divided into 19 virtual tanks, and contains six Yangtze River gates, eight river control sluices and a pumping station (consist of five 20m^3/s two-way pumps).

3.1 Scenario description

The rainfall forecast for the next three days from 09:00 on 10.Aug.2016 to 15:00 on 13.Aug.2016 shows a lot of rain (especially, there is a heavy rainfall with 210mm on 10.Aug.). Figure 4 give the overview of the rainfall situation.

The control goals are shown in Table 1.

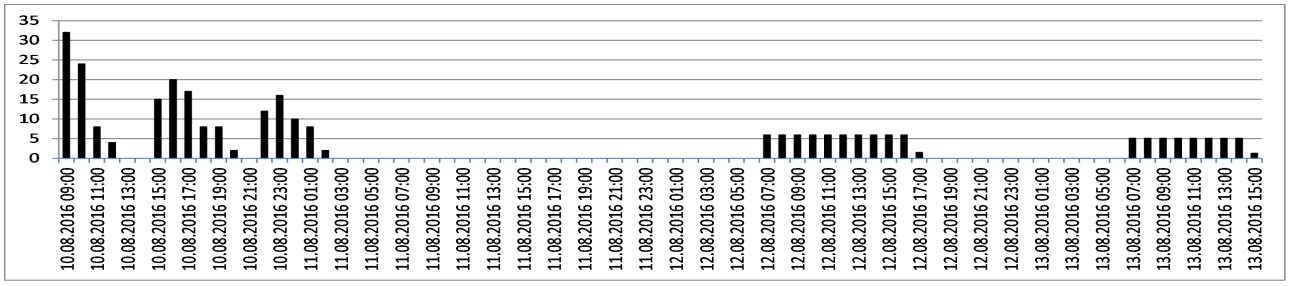

Figure 4. Precipitation forecast

Table 1. The control goals

Submodel	Risk water level	Flood water level
Virtual Tank 03	3,4m	4,0m
Virtual Tank 04	3,3m	4,2m
Virtual Tank 05	3,4m	4,1m

The whole system was compiled and run under the MATLAB environment. The simulation model shows you how the water level changed through the control from experience (see Figure 5, the dotted line). It shows very clearly that after one day of the heavy rainfall the water level can cause a flood, the operation plan is not suitable for this heavy rain event, it has to be optimized.

The solid line in Figure 5 shows the new operation plan for Gate(YZ-03) using the optimization model. There are two significances in this figure: on one hand, it is very clear that the water situation using the optimization control is be much better than from the expert experience, the risk of flood would be belayed about 8 hours (look the quadrangle), in this time humans can take a lot of counter measures and actions against the flood; and on the other hand, the optimization calculate within a defined time period, in this time period the water level could be also reached the risk level

of flood, therefore, the optimization process should be renewed by the actual water situation, so that the modified optimized control plan would be suggested.

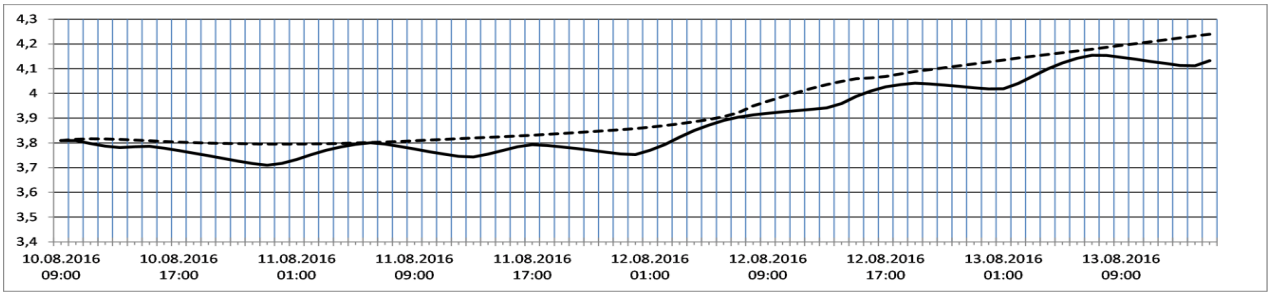

Figure 5. Water level on A03 with empirical operation and optimization

4. CONCLUSIONS

In this study, the model of a hybrid water system based on Visual Tank concept is established. The theory of the solution for bi-directional flow in hybrid water system is discussed. A water resources scheduling optimization system for hybrid water system was developed based on MPC-MLD optimization method. MPC-MLD is a well-known approach from cybernetics area, but very fresh application in hybrid water systems. This method can support the target of flood control, drought or environmental diversion in complex river networks for in short-term period. This work provides a new method to solve the optimization scheduling problem. In the future research, the special water policy of water resources protection will be implemented in MPC-MLD method. The optimization will be made more efficient und fit for the practical applications.

REFERENCES

Karimanzira D., H. Mu, H. Linke, and T. Rauschenbach. 2011. Water resources and environmental management of Cities in the Beijiang river basin: A pilot project. The 8th international conference on urban watershed management.

Mu H., T. Rauschenbach, D. Karimanzia. 2013. Modeling and Control of Bi-Directional Water Flow with Application to the Taihu Lake Basin. Global Perspective on Engineering Management.

Pfuetzenreuter T., and Th. Rauschenbach. 2007. A Simulation Library for an Integrated Water Resources Management.

van Ekeren H., 2010. Master of Science Thesis - Hybrid Model Predictive Control of the Rhine-Meuse delta. Delft University of Technology

van Ekeren H., R.R. Negenborn, P.J. van Overloop, and B. De Schutter, 2011. Hybrid model predictive control using time-instant optimization for the Rhine-Meuse Delta. IEEE International Conference on Networking.; 15(2):215-220

Zhang P., 2007. Mater of Engineer Thesis - Model Predictive Control for Hybrid Systems Based on Mixed Logic Dynamical Model. Jilin University

Proceedings of the 10th World Congress of EWRA 'Panta Rhei', 5-9 July 2017, Athens, Greece
© 2017 *European Water Resources Association*

Using bayesian networks for risk assessment of real losses in water distribution systems

M. Tabesh[1*], N.R. Faghihi[2], A. Roozbahani[3], R. Heidarzadeh[2] and B. Roghani[2]
[1] *Center of Excellent for Engineering and Management of Civil Infrastructure, School of Civil Engineering, College of Engineering, University of Tehran, Tehran, Iran*
[2] *School of Civil Engineering, College of Engineering, University of Tehran, Tehran, Iran*
[3] *Department of Irrigation and Drainage Engineering, College of Abouraihan, University of Tehran, Tehran, Iran*
[*] *e-mail: mtabesh@ut.ac.ir*

Abstract: Severe restrictions on water resources and rapidly increasing water demands as well as the threats arising from the design and the operation of water distribution networks (WDN) are unavoidable. Deciding on which alternative to choose amidst conflicting multiple criteria and different interests of stakeholders is a rather challenging task. Therefore, the recognition of major drivers of Non-Revenue Water (NRW) and its components in WDNs is an effective strategy that addresses water scarcity. Real losses are challenging components of NRW and lead to loss of about 10 percent of water inflow; hence it is crucial to identify and reduce the effective factors on them. This paper aims to identify effective factors on real losses and score their level of presence in the pilot through questionnaires. Then it presents a Bayesian Network (BN) to demonstrate the probability relationships between factors influencing real losses. To the authors' knowledge, this is the first attempt to model factors influencing real losses in WDN using BN. The methodology properly handles the unavoidable uncertainties in available information and lack of data. To demonstrate the application of the proposed model, District 4 of Tehran Water and Wastewater Company has been studied. Results indicate that "wrong and non-standard installation of pipes and other devices" and "poor training for workers and experts" have the most influence on real losses, respectively.

Key words: Bayesian network, questionnaire, real losses, water distribution networks

1. INTRODUCTION

One of the major challenges facing water utilities is the high level of water losses (Mutikanga et al., 2010). Water loss reduction is more cost effective than developing new water sources, which not only requires large amounts of financial resources, but also poses high costs and threats to the environment (Adams and LutzLey, 2012). Non-Revenue Water (NRW) is defined as the difference between total inflow and measured consumptions that has two components, apparent and real losses. Apparent losses are caused by unauthorized consumption, personnel errors, management and operational errors, data-handling errors, and unbilled authorized consumptions. Real losses comprise leakage from system parts and overflows of storage tanks. Losses are also caused by poor operations and maintenance, lack of active leakage control, and poor quality of underground assets and so on. Real losses contain visible leakage and invisible leakage.

Although it is widely acknowledged that NRW levels in developing countries are very high, in fact, very few data are available in the literature regarding the actual figures (Kingdom et al., 2006). This is largely because most water utilities in developing regions do not have adequate monitoring systems for assessing water losses and there is a great deal of uncertainty about data available (Kingdom et al., 2006). In the absence of adequate data and a proper methodology, most developing countries use default values. For instance, unauthorized consumption is computed as 0.5% of the total system input for NRW components (District 4 of Tehran Water and Wastewater Company, 2015). Moreover, since lack of accurate data regarding NRW and its components leads to data uncertainties, it is crucial to use appropriate probabilistic tools for modelling. In the context of a probabilistic framework, the Bayesian Network (BN) is naturally suited to handle such data cases

and update the description with new information (Nannapaneni et al., 2016).

According to National Water and Wastewater Engineering Company of Iran reports, the level of average NRW is in the range of 25-30 percent of total inflow. Moreover, according to these reports around 40-60 percent of NRW is lost through pipelines and other parts of the urban water systems in Iran; so, consumers do not receive that amount. As a matter of fact, in order to preserve the water resources and prevent financial losses, it is crucial to gain a better understanding of all of the reasons and factors influencing real losses by clearly identifying design and performance parameters affecting the emergence of visible and invisible leakage.

Tabesh et al. (2009) focused mainly on leakage and proposed a methodology for assessment of NRW and water losses in WDN. In this research they applied some approaches and methodologies to estimate the nodal and pipe leakage as the main components of NRW. A methodology was presented by Mutikanga et al. (2011) for assessment of different components of apparent losses. They tried to determine the most significant components of apparent losses. In a separate research, Van den Berg (2015) assessed the major drivers of NRW. He proposed a water loss function that describes the relationship between NRW and physical characteristics of the water infrastructure, management characteristics of the utility, country effects and area in which the utility is located. Zyoud et al. (2016) applied MCDA* in order to prioritize a set of water loss management strategies. They introduced the integration of fuzzy AHP† and Fuzzy TOPSIS‡ to assign the importance of different options considering several stakeholder groups' preferences. Abu-Mahfouz et al. (2016) proposed a real-time DHM§ connected to near real-time sensing and actuation capability on the WDN. This model addresses the limitation of current design and operation of most WDNs which are based on steady-state hydraulic models.

This paper mainly focuses on the evaluation and assessment of all of the factors influencing real losses and its components. The methodology is applied for District 4 of Tehran Water and Wastewater Company (DTWWC). The proposed methodology is a combination of designing a questionnaire to gather information and using BN to evaluate the probabilistic relationships between the factors. In the aggregate, influencing parameters will be ranked based on their extent of impact.

This paper is organized as follows. Section 2 outlines the concepts and frameworks of designing questionnaires and BN. Section 3 demonstrates the application of the proposed methodology in a case study. Finally the conclusions and discussion are drawn in section 4.

2. METHODOLOGY

2.1 Assessment of Factors

The initial objective of this research is gaining a profound perception of factors influencing components of real losses. Therefore, the first step is bound to identify the threats and factors which increase the level of real losses. Using the concepts and information in global standard IWA** and taking advantage of the experiences of researchers and experts, all of the factors are collected for both visible and invisible leakage.

2.2 Preparing Questionnaire

Owing to the qualitative nature of the specified factors and lack of quantitative data, it is

* Multi Criteria Decision Analysis
† Analytic Hierarchy Process
‡ Technique for Order of Preference by Similarity to Ideal Solution
§ Dynamic Hydraulic Model
** International Water Association

necessary to find an approach to gather the required information of the factors. Quantifying real losses and its components using various computing methods mostly presented by IWA is insufficient to address the drivers of real losses. Therefore, a questionnaire was designed to collect qualitative data regarding the level of presence of all factors. In the questionnaire for each of the effective factors three states of "high", "low" and "not available" were designed. On the one hand, this category makes the questionnaire convenient to understand and answer. On the other hand, the impact of each factor on its child factor would be clearly demonstrated.

2.3 Bayesian Network

Bayesian belief network is a graphical model that permits a probabilistic relationship among a set of variables (Pearl, 1988). In the BN, there are two types of nodes: parent nodes and child nodes. One of the favourable characteristic of this network is the potential to transform qualitative data into equivalent quantitative measures. In other words, BN has the capability to combine the knowledge of expertise and available data.

For illustration, consider the BN shown in Fig. 1, which presents the joint probability distribution of three random variables A, B, C (B and C are parent nodes and A is child node). All three variables have two possible values, T (for true) F (for false). The joint probability function is (Nannapaneni et al., 2016):

$$P(A,B,C) = P(A).P(B|A).P(C|A,B) \quad (1)$$

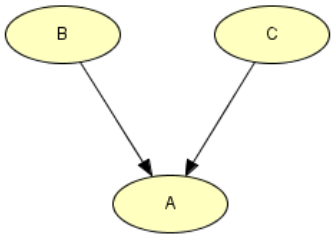

Figure 1. An example of a Bayesian Network

The first task in the development of BN is structure learning; but this step has been skipped owing to the fact that the cause-effect network of BN is fixed and defined in this article. The next step is the development of the conditional probability table (CPT) which determines the probability distribution of the value of a variable starting from the probability distribution of the parent variables (Pagano et al., 2014). In this article the Bayesian model was developed by aggregating the experts' knowledge from questionnaires as input data.

2.4 Sensitivity Analysis

In order to use the probability distribution of variables in BN model, sensitivity analysis is carried out. In this regards, for each parameter, the Sensitivity Index (SI) is computed as:

$$SI = (\Delta C_i / \Delta P_i) \times 100 \quad (2)$$

where ΔPi: is the variation of parent node and ΔCi: is the variation of child node. To apply this approach, one specific state of all of the parameters increases to the same level. Considering the variation of the parent node, for all of the influencing factors on real losses, the SI would be computed. It is worth mentioning that the higher the SI, the higher the priority of a factor for real losses risk management.

3. CASE STUDY

The proposed methodology is applied on the (DTWWC), the area covered by tank no.2. Special features of this area distinguishes it from other areas; for instance, its old water network, the high level of groundwater that contributes to decay of pipes and repair and maintenance problems of urban design. Based on the reports from DTWWC, NRW was 22% and real losses account for about 9.5% of the total NRW in 2015 (District 4 of Tehran Water and Wastewater Company, 2015).

3.1 Data Collection

Following the collecting all of the probable factors affecting real losses in the case study, their level of presence are asked through questionnaires. The designed questionnaire is shown in Table 1.

Table 1. A questionnaire on factors influencing real losses

	Factors	State		
		High	Low	Not available
Visible leakage	Inappropriate quality selection for pipe and other devices			
	Wrong and non-standard installation			
	Failure to collect and complete details of events			
	Low speed and quality of repair			
	Lack of regular inspection and navigation of networks			
	Poor movement of pipes and other devices			
	Poor construction of pipes and other devices			
	Wrong design of network			
	Lack of timely replacement of devices			
	Lack of pressure management			
	Lack of investigating the cause of fractures			
	Poor management of overflow of tanks			
	Lack of modern leakage management technologies (telemetry-SCADA)			
	Lack of prevention maintenance (PM)			
	Financial shortage in w/w companies			
	Poor training for workers and experts			
	Poor management (lack of updated maps and GIS)			
Invisible Leakage	Lack of step testing			
	Lack of District Metering Areas (DMA)			
	Lack of trying to find the cause of leakage in the network			
	Poor management (lack of updated maps and GIS)			
	Failure to purchase and use of precise measurement and calibration tool			
	Failure to purchase and use of leakage detection tools and modern technologies in leakage management			
	Inappropriate quality selection for pipes and other devices			
	Incorrect and non-standard installation			
	Lack of prevention maintenance (PM)			
	No justification for leakage detection because of the low price of water			
	Poor movement of pipes and other devices			
	Poor construction of pipes and other devices			
	Incorrect design of network			
	Lack of timely replacement of devices			
	Lack of pressure management			
	Lack of timely and continuous leakage detection			
	Financial shortage in w/w companies			
	Poor training for workers and experts			
	Poor operational procedures and contracts			

3.2 Summary Questionnaire Data

In order to decrease the uncertainty of responses, knowledgeable and experienced personnel in Tehran Water and Wastewater Company and university professors were asked to fill out the questionnaires based on their area of expertise. In the aggregate, 36 questionnaires were returned completed. Analysing questionnaires data leads to identifying the final factors in BN modelling. In

addition, the personnel's response to each factor is considered as Bayesian model input.

3.3 Application of Bayesian Network

Base on the questionnaires data, some of the factors which have similar states combine as a single factor. Therefore, the final list of factors influencing real losses comprise of 23 parameters that affect visible leakage or invisible leakage or both. The next step is defining the probability relationship of these parameters using BN. In this article an available software has been used; Hugin Lite 8.4, for constructing the BN graphical model (Fig. 2). In this network all of the nodes have two possible states which are determined as H (High) and L (Low). Besides, selected labels for each node are shown in Table 2.

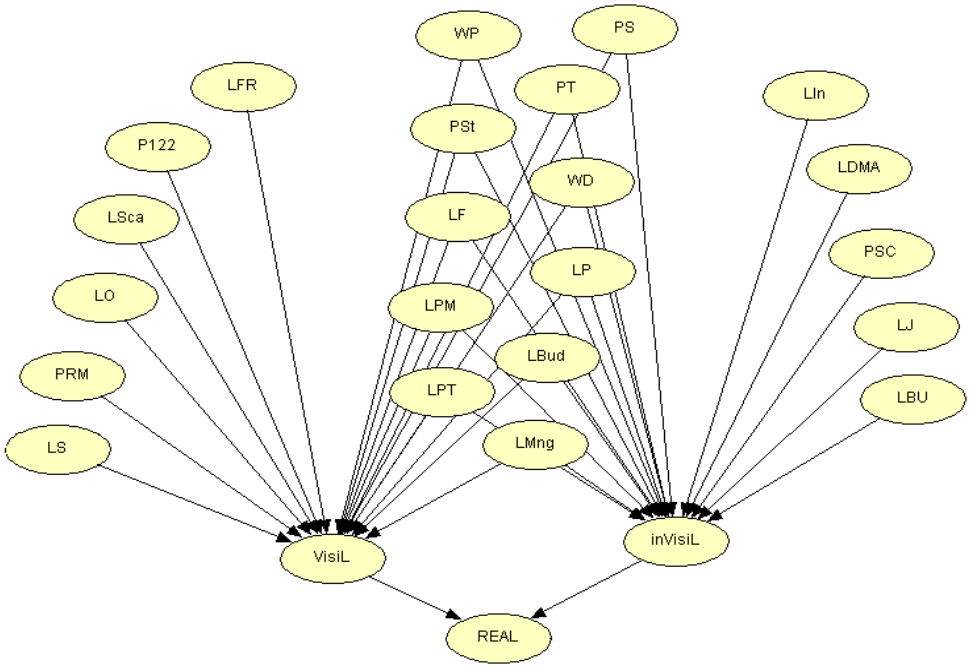

Figure 2. Bayesian Network

The next important step is parameter learning. In this article, expectation-maximization algorithm (EM) has been used for parameter learning. EM algorithm is particularly useful when probability distributions of the variables in a BN are unknown (HUGIN EXPERT A/S, 2016).

Since the prepared questionnaires merely asks about the state of the identified factors, information relative to the state of real "visible leakage", "invisible leakage" and "real losses" were required. Therefore, for each parameter, the weighting approach was applied by assigning 7 to "high" state, 5 to "low" state and 1 to "N/A" state. As a result the percentage of visible and invisible leakage in each questionnaire is determined. In order to consider real condition of the WD in the pilot, the percentage of real losses was derived from annual water balance reports of DTWWC from 2011 to 2015. Using the percentage of visible and invisible leakage of these reports indicates that visible and invisible leakage account for 70% and 30% of real losses, respectively. Finally, for each questionnaire, the state of real "visible leakage", "invisible leakage" and "real losses" were defined. Eventually, the BN runs and the probabilities of a node in a certain state are shown in Fig. 3.

According to sensitivity analysis, a specific state of all of the nodes is changed to a certain extent and the changes in child nodes will be evaluated. Generally, the more parent nodes change, the more accurate sensitivity analysis is done. Nevertheless, the node "LBud" is restrictive and the factors have to be increased up to 25%. To do so in the software, the "high" and "low" states in Conditional Probability Table (CPT) have been altered for each node manually. Then, the

sensitivity index is calculated for all of the nodes. For instance; for lack of investigating the cause of fractures (LFR) node, the “high” state is 57.58% and it would change into 71.98%. This alteration contributes to the modification of its child nodes; real losses, from 35.04% to 35.07%. So, the SI for the LFR node is computed as:

$$SI = (71.98-57.58)/(35.04-35.07) = 0.002084 \quad (3)$$

Table 2. Labels of each factor in Bayesian Network

Labels	Factors
VisiL	visible leakage
inVisiL	invisible leakage
LS	low speed and quality of repair
PRM	poor management of overflow of tanks
LO	lack of regular inspection and navigation of networks
LSca	lack of modern leakage management technologies
P122	failure to collect and complete details of events
LFR	lack of investigating the cause of fractures
WP	incorrect and non-standard installation
PS	inappropriate quality selection
PT	poor movement
PSt	poor construction
WD	incorrect design of network
LF	lack of timely replacement of devices
LP	lack of pressure management
LPM	lack of prevention maintenance
LBud	financial shortage in w/w companies
LPT	poor training for workers and experts
LMng	poor management
LIn	lack of trying to find the cause of leakage in the network
LDMA	lack of step testing and district metering areas
PSC	poor operational procedures and contracts
LJ	no justification for leakage detection because of the low price of water
LBU	failure to purchase and use of precise measurement and calibration tool, modern technologies in leakage management failure to purchase and use of leakage detection tools and

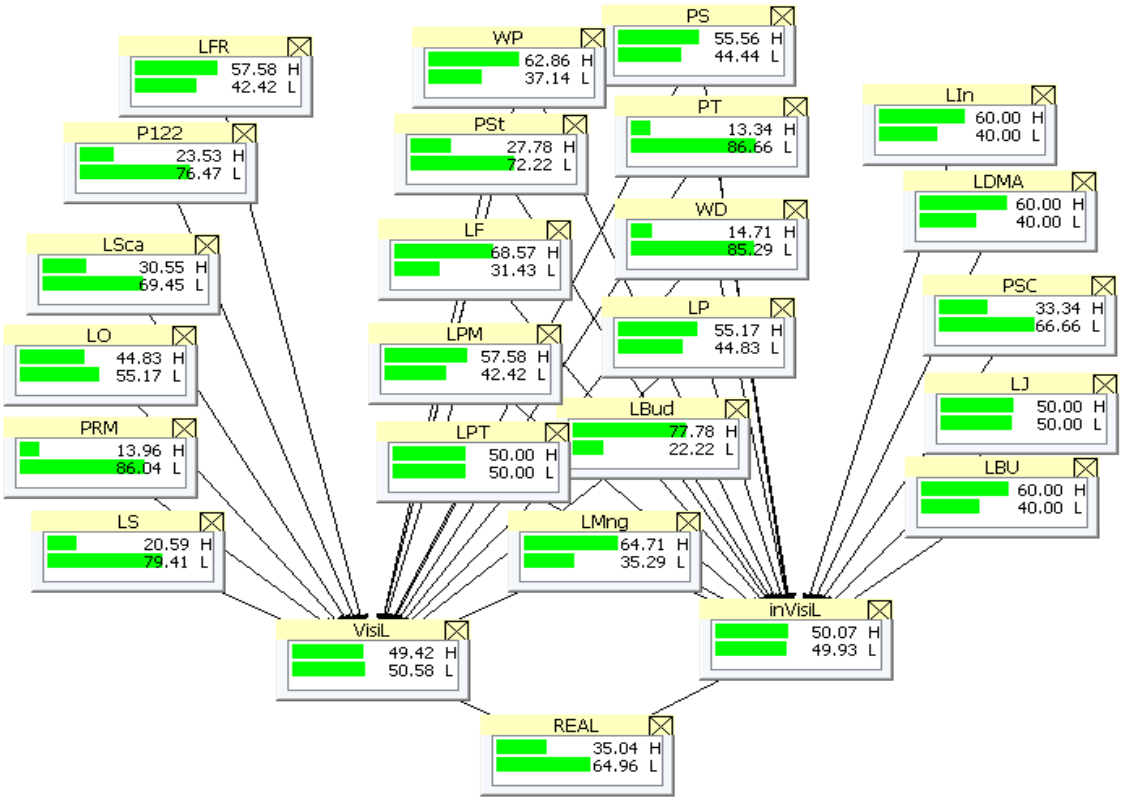

Figure 3. Trained Bayesian Network

Table 3. Ranking factors influencing real losses

Rank	Factors influencing real losses	Sensitivity Index (%)
1	Incorrect and non-standard installation	0.891
2	Poor training for workers and experts	0.88
3	Lack of timely replacement of devices	0. 875
4	Inappropriate quality selection	0.864
5	Poor management	0.433
6	Poor construction	0.43
7	Failure to collect and complete details of events	0.34
8	Poor movement	0.3
9	Lack of prevention maintenance	0.278
10	Incorrect design of network	0.272
11	Lack of regular inspection and navigation of network	0.267
12	Lack of pressure management	0.218
13	Lack of investigating the cause of fractures	0.208
14	Low speed and quality of repair	0.194
15	Financial shortage in w/w companies	0.103
16	Lack of trying to find the cause of leakage in the network Lack of step testing and District Metering Areas Failure to purchase and use of precise measurement and calibration tool and Failure to purchase and use of leakage detection tools and modern technologies in leakage management	0.067
17	Poor management of overflow of tanks Lack of modern leakage management technologies Poor operational procedures and contracts No justification for leakage detection because of the low price of water	0

4. CONCLUSION

Since authorities in water companies seek to find an optimal solution to achieve an economic balance between the costs of physical water losses control and the benefits that accrue, it is important to prioritize the most effective factors of real losses components. In this study, initially, effective factors on real losses were identified and a questionnaire was designed to ask the state of these factors (high or low) in the case study, DTWWC. Then, BN, a graphical model, was constructed to evaluate the conditional probabilities of the factors. After that, by sensitivity analysis of the model output, effective factors were prioritized in order to find out which of them have the most impact on NRW. The results showed that among all of the factors influencing real losses, "incorrect and non-standard installation of pipes and other devices", "poor training for workers and experts" and "lack of timely replacement of devices" were respectively the significant components of real losses in this case study. It is worth mentioning that the results of the BN and sensitivity analysis particularly depend on the questionnaire data and their accuracy; hence, if respondents change their answers, the priority of strategies for reducing real losses will definitely be altered. The result of this research/article will be a valuable reference for senior managers and decision makers, who may require an overview of the principles and procedures for controlling real losses.

REFERENCES

Abu-Mahfouz, A. M., Hamam, Y., Page, P. R., Djouani, K., & Kurien, A., (2016), "Real-time dynamic hydraulic model for potable water loss reduction", Procedia Engineering, 154, 99-106.

Adams, A. S., & LutzLey, A. N., (2012), "An empirical study of factors affecting water loss in Mexican cities", Journal of Water Sustainability, 2(3), 167-178.

District 4 of Tehran Water and Wastewater Company, (2015), "Annual Water Balance reports from 2012 to 2015", Tehran, Iran.

HUGIN EXPERT A/S, (2016), "Hugin Researcher Userguide, version 7.8", HUGIN EXPERT A/S, Denmark.

Kingdom, B., Liemberger, R., & Marin, P., (2006), "The challenge of reducing non-revenue water (NRW) in developing countries. How the Private Sector Can Help: A Look at Performance-based Service Contracting", Water Supply and Sanitation Board Discussion Paper Series, Paper No. 8, The World Bank Group, Washington DC, USA.

Mutikanga, H. E., Sharma, S. K., & Vairavamoorthy, K., (2011), "Assessment of apparent losses in urban water systems", Water and Environment Journal, 25(3), 327-335.

Mutikanga, H. E., Sharma, S. K., & Vairavamoorthy, K., (2011), "Multi-criteria decision analysis: a strategic planning tool for water loss management", Water Resources Management, 25(14), 3947-3969.

Nannapaneni, S., Mahadevan, S., & Rachuri, S., (2016), “Performance evaluation of a manufacturing process under uncertainty using Bayesian networks” Journal of Cleaner Production, 113, 947-959.

National Water and Wastewater Engineering Company of Iran, (2015),

National Water and Wastewater Engineering Company of Iran, (2015), “Water and wastewater industryat a glance report”, Tehran, Iran.

Pagano, A., Giordano, R., Portoghese, I., Fratino, U., & Vurro, M., (2014), “A Bayesian vulnerability assessment tool for drinking water mains under extreme events” Natural Hazards, 74(3), 2193-2227.

Pearl, J., (1988), “Probabilistic reasoning in intelligent systems: Networks of plausible inference”, San Francisco: Morgan Kaufmann Publishers, Inc.

Tabesh, M., Yekta, A. A., & Burrows, R., (2009), "An integrated model to evaluate losses in water distribution systems", Water Resources Management, 23(3), 477-492.

van den Berg, C., (2015), “Drivers of non-revenue water: A cross-national analysis”, Utilities Policy, 36, 71-78.

Zyoud, S. H., Kaufmann, L. G., Shaheen, H., Samhan, S., & Fuchs-Hanusch, D., (2016), "A framework for water loss management in developing countries under fuzzy environment: Integration of Fuzzy AHP with Fuzzy TOPSIS", Expert Systems with Applications, 61, 86-105.

Proceedings of the 10th World Congress of EWRA 'Panta Rhei', 5-9 July 2017, Athens, Greece
© 2017 *European Water Resources Association*

Diagnosis of water pipeline systems by frequency domain analysis

M. Ferrante* and C. Capponi
Dipartimento di Ingegneria Civile ed Ambientale, University of Perugia, Via G. Duranti, 93, 061125 Perugia, Italy
** e-mail: marco.ferrante@unipg.it*

Abstract: Inverse transient analysis is a tool for the diagnosis of water distribution systems based on the comparison of the results of analytical or numerical models with pressure signals acquired during transients. The needed numerical models can be derived in the time domain or in the frequency domain. The time domain approach is the most followed and lead to the method of characteristics. The traditional models derived in the frequency domain as solutions to the linearized water hammer equations, namely the impulse response and the transfer matrix methods, are efficient in the simulation but are not suited for complex arbitrarily configured networks. An alternative frequency domain formulation is the network admittance matrix method, where the equations are reorganized into a matrix form using graph-theoretic concepts. In this paper the network admittance matrix method is applied to assess its reliability in the diagnosis of water distribution systems. The unsteady-friction term is introduced in the formulation and a numerical case study is used to detect a pipe replacement in a simple system of metallic pipes. The length, the diameter and the position of the pipe replacement are considered as unknowns and estimated by means of a calibration procedure.

Key words: transients; frequency domain; unsteady-friction; admittance; diagnosis; water pipe systems

1. INTRODUCTION

The interest for transients in pressurised pipe systems date back to the beginning of the past century and was motivated by the needs of the design and the safe operation of penstocks in hydropower systems. Hence, for these historical reasons, for a long time transients have been considered as dangerous and their effects as destructive (the term "water hammer" is evocative). Starting from the pioneering works of the 90's (Brunone, 1989; Jonsson et al., 1992; Liggett and Chen, 1994; Liou and Tian, 1995), the interest for the unsteady-state conditions was also motivated by the ability of controlled transients to reveal information about the system. Since then, transients have been extensively investigated to this aim and numerical models of transients are now considered as diagnostic tools to detect leaks, blockages, valve opening degree, and the general conditions of the pipe.

For the purposes of hydraulic transient simulation, the 1-D water hammer equations can be solved in the time-domain or in the frequency-domain. The method of characteristic (MOC) is the most used method in the time domain (Ghidaoui et al., 2005) while classical solutions in the frequency-domain are the impedance method or the transfer matrix method (Chaudhry, 2014; Wylie and Streeter, 1993).

Compared to the time-domain approaches, the frequency-domain description of pipeline systems requires the linearization of the steady-friction term but enable the direct determination of the relationship between system responses and system properties, which is particularly useful in solving inverse problems and hence in the diagnosis. As an example, pipe lengths are introduced as parameters without the need a space discretization, avoiding the constrains introduced by the compatibility with the time discretization and the Courant condition (Kim, 2008). The required linearization affects only the steady-friction term. Both viscoelasticity and unsteady-friction terms, which can be expressed as convolutions in time (Weinerowska-Bords, 2015), can be efficiently implemented in the frequency-domain models.

The application of the traditional impedance and transfer matrix to arbitrarily configured

networks is challenging. To simplify the frequency domain analysis of complex systems, (Zecchin, 2010; Zecchin et al., 2009) introduced the network admittance matrix method (NAMM), combining admittance forms of the link equations in the frequency domain with graph-theoretic matrices. In previous papers the viscoelasticity terms have been introduced in the NAMM, to simulate the transient response of polymeric pipes. In this paper the unsteady-friction term is introduced to simulate transients in metallic pipes.

In the following sections, the theory of the NAMM is briefly reviewed and the equations presented in (Zecchin et al., 2009) are modified to take into account the effects of the unsteady-friction. Numerical tests are then used to verify the capabilities of the model for the diagnosis of a water pipe system by means of transients.

2. THE ADMITTANCE MATRIX FORMULATION

In the usual schematization of water pipeline system as an oriented network of links and nodes, the graph theory provides a simple formalization of the governing continuity and momentum equations. The same link-node incidence matrix, or simply incidence matrix, **A**, expressed as

$$a_{ij} = \begin{cases} -1 \text{ if } \lambda_j \in \Lambda_{U,i} \\ 1 \text{ if } \lambda_j \in \Lambda_{D,i} \\ 0 \text{ otherwise} \end{cases} \tag{1}$$

which defines the topology of a network $\mathcal{G}(\mathcal{N},\Lambda)$, with node set $\mathcal{N} = \{1,2,...,n_{n_n}\}$ and link set $\Lambda = \{\lambda_1,\lambda_2,...,\lambda_{n_l}\}$, is also the cornerstone of the coefficient matrix in the steady-state model formulation (Todini and Pilati, 1988). In Eq. **Error! Reference source not found.**, Λ_U (Λ_D) represent the subset of links for which node *i* is the upstream (downstream) node. The left multiplication of the incidence matrix for the link state variable, i.e. the flows, provides the compact expression of the flow continuity equations for the pipe network

$$AQ=q_0 \tag{2}$$

where Q is the column vector of the n_l flows in each link and q_0 is the column vector of the demands at junctions, defined as the outflows from the systems toward the environment. The left multiplication of the transpose of the incidence matrix, or node-link incidence matrix, for the node state variable, i.e. the pressure heads, provides the gradients used in the momentum equations

$$DQ+A^TH=0 \tag{3}$$

where D is the diagonal matrix of the resistances, H is the column vector of the n_n heads at each node, and the superscript ^{T} denotes the matrix transpose. Extensions and modification to the equations **Error! Reference source not found.** and **Error! Reference source not found.** can be introduced considering interior nodes, where the head is unknown and exterior nodes, where the head is specified. Pressure dependent demands to model leaks and user connections can be also introduced. Several algorithms based on Eqs. **Error! Reference source not found.** and **Error! Reference source not found.**, and the Global Gradient Algorithm proposed by (Todini and Pilati, 1988) have been implemented and widely used in the water pipeline system management.

For several reasons, the algorithms used for water hammer unsteady-state analysis in complex networks did not evolve analogously, as a simple extension of the steady-state analysis. The historical and technical motivations behind this evolution cannot be discussed here in details. Recently, (Zecchin et al., 2009) have shown that a matrix formulation, similar to those obtained for

the steady-state, can be obtained when the governing equations are linearized and integrated in the frequency domain. The main difference is in the need for four variables, defined as the Fourier or Laplace transform of pressure heads and flows at the upstream (h_U and q_U) and downstream (h_D and q_D) nodes, to define the pipe behaviour of each link. Starting from the well known unsteady-flow governing equations (Chaudhry, 2014; Ghidaoui et al., 2005; Wylie et al., 1993), the Laplace transform of the linearized expressions leads to a system of equations for each link.

$$\begin{bmatrix} q_{Uj} \\ q_{Dj} \end{bmatrix} = \begin{bmatrix} \dfrac{Z_{C1j}\, e^{\Gamma_{1j}} + Z_{C2j}\, e^{-\Gamma_{2j}}}{Z_{C1j}\, Z_{C2j}\left(e^{\Gamma_{1j}} - e^{-\Gamma_{2j}}\right)} & -\dfrac{\left(Z_{C1j} + Z_{C2j}\right)}{Z_{C1j}\, Z_{C2j}\left(e^{\Gamma_{1j}} - e^{-\Gamma_{2j}}\right)} \\ \dfrac{\left(Z_{C1j} + Z_{C2j}\right) e^{\Gamma_{1j}}\, e^{-\Gamma_{2j}}}{Z_{C1j}\, Z_{C2j}\left(e^{\Gamma_{1j}} - e^{-\Gamma_{2j}}\right)} & -\dfrac{Z_{C2j}\, e^{\Gamma_{1j}} + Z_{C1j}\, e^{-\Gamma_{2j}}}{Z_{C1j}\, Z_{C2j}\left(e^{\Gamma_{1j}} - e^{-\Gamma_{2j}}\right)} \end{bmatrix} \begin{bmatrix} h_{Uj} \\ h_{Dj} \end{bmatrix} \tag{4}$$

To define the dependence of the j-th link propagation operators, $\Gamma_{1,2\,j}$, and characteristic impedances, $Z_{C1,C2\,j}$, on the Laplace variable, s, and on the properties of the pipe, the three auxiliary variables are introduced.

$$\begin{aligned} \alpha_j &= C_j s \\ \beta_j &= L_j s + R_j \\ B_{Rj} &= \frac{a k_{Bj}}{2 g A_j} \end{aligned} \tag{5}$$

where $C_j=A_j g/a_j^2$, $L_j=(1+ k_{Bj} /2)/(gA_j)$, $R_j = f_{Cj}\, f_{Fj}\, q_{0j}/(gD_j A_j^2)$, f_{Fj} is the Darcy-Weisbach friction factor, q_{0j} is the initial steady state flow in the pipe, l_j, a_j, and A_j are the length, the wave speed, and the cross-sectional area of the j-th pipe respectively, and g is the acceleration of gravity. k_{Bj} is the unsteady-friction parameter proposed by (Brunone et al., 1995) while f_{Fj} is an equivalence factor that can be used to balance the linearization effect in the steady-friction term. If the Fourier transform is considered instead of the Laplace transform, as here, it is $s = i\omega = \sqrt{-1}\,\omega$, where ω is the angular frequency.
By means of the terms introduced in Eqs. **Error! Reference source not found.**, it is

$$\begin{aligned} \gamma_{1,2\,j} &= \frac{\mp \alpha B_R + \sqrt{\alpha_j^2 B_{Rj}^2 + 4\alpha_j \beta_j}}{2} \\ \Gamma_{1,2\,j} &= \gamma_{1,2\,j} l_j;\ Z_{C1,C2\,j} = \gamma_{1,2\,j} / \alpha_j \end{aligned} \tag{6}$$

When only the steady-friction is considered, it is $\Gamma_{1j} = \Gamma_{2j} = \Gamma_j$, $Z_{C1j} = Z_{C2j} = Z_{Cj}$ and Eq. **Error! Reference source not found.** simplifies in

$$\begin{bmatrix} q_{Uj} \\ q_{Dj} \end{bmatrix} = Z_{Cj}^{-1} \begin{bmatrix} \coth\Gamma_j & -\operatorname{csch}\Gamma_j \\ \operatorname{csch}\Gamma_j & -\coth\Gamma_j \end{bmatrix} \begin{bmatrix} h_{Uj} \\ h_{Dj} \end{bmatrix} \tag{7}$$

As a consequence of the presented formalization of the unsteady-state problem, the flows in each link, q_{Uj} and q_{Dj}, are not defined by a single value as for the steady-state but are different at the two link ends. Hence, the continuity equations at the nodes cannot be directly expressed by Eq. **Error! Reference source not found.** since the contribution of upstream and downstream link flow should be separately considered. In other words, the vector **q** has to be split in two vectors, $\mathbf{q_U}$ and $\mathbf{q_D}$, containing the q_{Uj} and q_{Dj} elements, respectively. The momentum equations show the same

increase in complexity with respect to **Error! Reference source not found.**, since **h** has to be split to consider upstream and downstream link piezometric head, giving raise to the vectors $\mathbf{h_U}$ and $\mathbf{h_D}$.

An elegant and simple solution has been provided by (Zecchin et al., 2009), where a double incidence matrix ($\mathbf{N_U}$ $\mathbf{N_D}$) is defined as a matrix of two upstream and downstream incidence matrices, $\mathbf{N_U}$ and $\mathbf{N_D}$, respectively, with

$$\begin{aligned} n_{Ui,j} &= \begin{cases} 1 \text{ if } \lambda_j \in \Lambda_{U,i} \\ 0 \text{ otherwise} \end{cases} \\ n_{Di,j} &= \begin{cases} 1 \text{ if } \lambda_j \in \Lambda_{D,i} \\ 0 \text{ otherwise} \end{cases} \end{aligned} \tag{8}$$

The relationship between the steady-state and the unsteady-state double incidence matrices is given by $\mathbf{A}= -\mathbf{N_U}+\mathbf{N_D}$. The left multiplication of the double incidence matrix for the unsteady-state link state variables, upstream and downstream link flows, provides the imbalance of the continuity equations at nodes, to be balanced by the Laplace transform of the demands at nodes, Θ ,

$$\begin{bmatrix} -\mathbf{N_U} & \mathbf{N_D} \end{bmatrix} \begin{bmatrix} \mathbf{q_U} \\ \mathbf{q_D} \end{bmatrix} = \Theta \tag{9}$$

Similarly, the left multiplication of the transpose of the double incidence matrix with the Laplace transform of the pressure head at nodes, Ψ , define the upstream and downstream pressure head column vectors $\mathbf{h_U}$, $\mathbf{h_D}$

$$\begin{bmatrix} \mathbf{h_U} \\ \mathbf{h_D} \end{bmatrix} = \begin{bmatrix} \mathbf{N_U^T} \\ \mathbf{N_D^T} \end{bmatrix} \Psi \tag{10}$$

Introducing the diagonal matrices $E^{\mathbf{\Gamma}_{1,2}} = \text{diag}\left\{e^{\Gamma_{1,2j}}\right\}$ and $\mathbf{Z_{C1,2}} = \text{diag}\left\{Z_{C1,2j}\right\}$, Eq. **Error! Reference source not found.** can be extended to the whole system and not to a single link

$$\begin{bmatrix} \mathbf{q_U} \\ \mathbf{q_D} \end{bmatrix} = \begin{bmatrix} \dfrac{\mathbf{Z_{C1}}\, E^{\Gamma_1} + \mathbf{Z_{C2j}}\, E^{-\Gamma_2}}{\mathbf{Z_{C1}}\, \mathbf{Z_{C2}} \left(E^{\Gamma_{1j}} - E^{-\Gamma_{2j}}\right)} & -\dfrac{\left(\mathbf{Z_{C1}} + \mathbf{Z_{C2}}\right)}{\mathbf{Z_{C1}}\, \mathbf{Z_{C2}} \left(E^{\Gamma_1} - E^{-\Gamma_2}\right)} \\ \dfrac{\left(\mathbf{Z_{C1}} + \mathbf{Z_{C2}}\right) e^{\Gamma_1}\, e^{-\Gamma_2}}{\mathbf{Z_{C1}}\, \mathbf{Z_{C2}} \left(E^{\Gamma_1} - E^{-\Gamma_2}\right)} & -\dfrac{\mathbf{Z_{C2}}\, e^{\Gamma_1} + \mathbf{Z_{C1}}\, e^{-\Gamma_2}}{\mathbf{Z_{C1}}\, \mathbf{Z_{C2}} \left(E^{\Gamma_1} - E^{-\Gamma_2}\right)} \end{bmatrix} \begin{bmatrix} \mathbf{h_U} \\ \mathbf{h_D} \end{bmatrix} \tag{11}$$

Combining Eqs. **Error! Reference source not found.**, **Error! Reference source not found.** and **Error! Reference source not found.**, the admittance formulation is obtained, relating the Fourier transform of the pressure head at nodes with the Fourier transform of the demands

$$\Theta = \begin{bmatrix} \mathbf{N_U} & \mathbf{N_D} \end{bmatrix} \begin{bmatrix} \mathbf{t_1} & -\mathbf{c_1} \\ \mathbf{t_2} & -\mathbf{c_2} \end{bmatrix} \begin{bmatrix} \mathbf{N_U^T} \\ \mathbf{N_D^T} \end{bmatrix} \Psi = \mathbf{Y}\Psi \tag{12}$$

Since the admittance matrix **Y** is the sum of four terms

$$\mathbf{Y} = -\mathbf{N_U t_1 N_U^T} + \mathbf{N_D c_2 N_D^T} + \mathbf{N_U c_1 N_D^T} - \mathbf{N_D t_2 N_D^T} \tag{13}$$

the construction of the matrix is easy considering that, after (Zecchin et al., 2009), it is

$$\mathbf{N_D c_2 N_U^T} = \begin{cases} c_{2j} \text{ if } \lambda_j = (k,i) \in \Lambda_{D,i} \\ 0 \text{ otherwise} \end{cases} \tag{14}$$

$$\mathbf{N_U c_1 N_D^T} = \begin{cases} c_{1j} \text{ if } \lambda_j = (i,k) \in \Lambda_{D,i} \\ 0 \text{ otherwise} \end{cases} \tag{15}$$

$$\mathbf{N_D t_2 N_D^T} = \begin{cases} \sum_{\lambda_j \in \Lambda_{D,i}} t_{2j} \text{ if } k = i \\ 0 \text{ otherwise} \end{cases} \tag{16}$$

$$\mathbf{N_U t_1 N_U^T} = \begin{cases} \sum_{\lambda_j \in \Lambda_{U,i}} t_{1j} \text{ if } k = i \\ 0 \text{ otherwise} \end{cases} \tag{17}$$

It is worth of noticing that the admittance matrix is essentially a generalised form of the Laplacian matrix of a weighted directed graph, and it is the analogous of the product $\mathbf{ADA^T}$ used in the GGA (Todini and Pilati, 1988).

To speed up the solution algorithm, Ψ and Θ are partitioned distinguishing between demand- and pressure-control nodes. At the demand-control nodes, denoted by the subscript "*d*", the demand is known but the pressure is unknown. At pressure-control nodes, similar to the previously defined exterior nodes and denoted by the subscript "*p*", the demand is unknown and the pressure known. Junctions are typically demand nodes whereas reservoirs are pressure nodes.

Since the transformed nodal pressures, Ψ, represent the perturbation around a mean value, a boundary condition of prescribed pressure head at a node, such as at a constant head reservoir, corresponds to $\Psi_p = 0$. Similarly, the transformed values of the flows, Θ, represent the variation of the demand outflowing at a node and hence for junctions without demands it is also $\Theta_d = 0$.

The partition of $\Psi = [\Psi_d^T \quad \Psi_p^T]^T$ and $\Theta = [\Theta_d^T \quad \Theta_p^T]^T$ allows the uncoupling of the unknowns Ψ_d from the unknowns Θ_p, so that it is possible to calculate them separately, after a consistent partition and a reorganization of the admittance matrix (Zecchin et al., 2009), as in the following

$$\left[\begin{array}{c} \Psi_d \\ \hline \Theta_p \end{array}\right] = \left[\begin{array}{c|c} \mathrm{Y}_d^{-1} & -\mathrm{Y}_d^{-1}\mathrm{Y}_{d-p} \\ \hline \mathrm{Y}_{p-d}\mathrm{Y}_d^{-1} & \mathrm{Y}_p - \mathrm{Y}_{p-d}\mathrm{Y}_d^{-1}\mathrm{Y}_{d-p} \end{array}\right] \left[\begin{array}{c} \Theta_d \\ \hline \Psi_p \end{array}\right] \tag{18}$$

where Ψ_p and Θ_d are known at the boundaries (e.g., at a valve) or are zero ($\Theta_d = 0$ at junctions and $\Psi_p = 0$ at reservoirs). If the unknown of interest are the pressure heads and only junctions are considered, Eq. **Error! Reference source not found.** simplifies in

$$\Psi_d = \mathrm{Y}_d^{-1}\Theta_d \tag{19}$$

The inverse of the partitioned admittance matrix allows the evaluation of the unknown pressures in the frequency domain while the inverse Fourier transform can be used to represent the solutions in the time domain.

In the following an implementation of the described admittance matrix algorithm is shown with reference to a numerical case study.

2. THE NUMERICAL CASE STUDY

A system of three pipes in series is considered (Fig. 1) with D_1=D_3=80 mm and D_2=100 mm. The total length of the pipe L_T= 938 m is the sum of the lengths of three pipes, L_1=546 m, L_2=70 m and L_3=322 m. In the initial steady-state conditions, the discharge of 0.47 l/s is delivered from the upstream reservoir, R_U, to downstream reservoir, R_D. The water level in the downstream reservoir is used as datum. The transient is introduced in the system by means of the complete closure of the valve V, located between R_U and the upstream and of the pipe (node 1). To simulate the transient in the system, the effects of the maneuver are introduced in a numerical model based on the MOC as the flow variation at the node 1 (Fig. 2).

The results of the simulation in terms of the variation in time of the piezometric head at the node 1, or pressure signal H_1, are given in Fig. 3. The numerical signal generated by the MOC is then used as a measured signal to calibrate the parameters of the NAMM model and diagnose the system. Assuming that the second pipe is a replacement of a damaged trunk of a pipeline, three unknowns are introduced in the calibration: the length, L_2, the diameter D_2 and the position of the replacement, defined by L_1. The unknowns are calibrated by means of an optimization procedure based on the minimization of the sum of squared residuals, RSS, between the signals simulated by MOC and NAMM at node 1. Two algorithms are used in series. A Genetic Algorithm (GA) is used to explore a large range of variation of the parameters. The solution obtained by the GA is then used as a starting point of a Nelder-Mead algorithm (NM), to find the solution with the required tolerances.

Two calibrations are considered. In Calibration 1 the position is considered as known and hence only L_2 and D_2 are estimated. In Calibration 2 the three parameters, L_1, L_2, and D_2 are considered as unknown. The parameter values estimated by the calibrations are given in Table 1. The numerical signal obtained by the NAMM model with the results of Calibration 2 (Synth) is compared with the MOC signal (Num.) in Fig. 1. The RSS is evaluated on the duration of 10 s and on n= 1044 samples, with RSS/n=0.015 m^2 for both GA and NM. In fact, in Calibration 2 the solution provided by GA almost coincides with the solution found by NM.

If the model calibrated on 10 s in Calibration 2 is validated with the MOC signal on 55 s and 5737 samples, such as in Fig. 3, the ratio RSS/n changes from 0.015 to 0.036 m^2. Hence, the calibrated NAMM model is able to reproduce accurately the MOC signal on longer durations, compared to that used for the calibration.

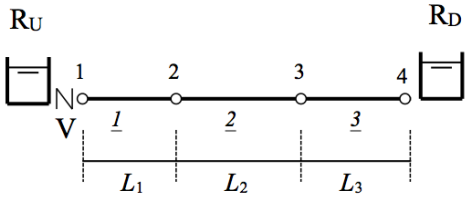

Figure 1. Layout of the system used for the numerical case study.

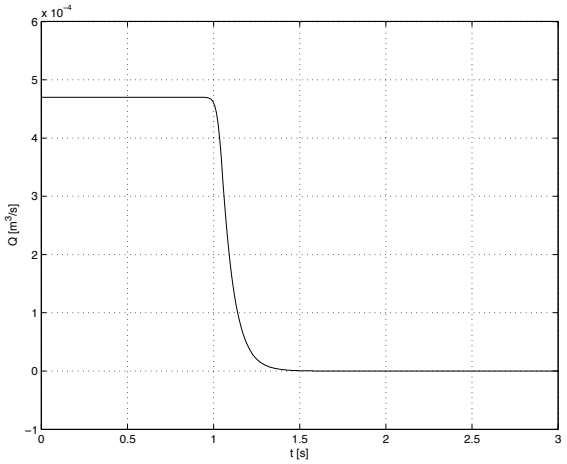

Figure 2. Flow variation at node 1 *due to the closure of the upstream end valve* V.

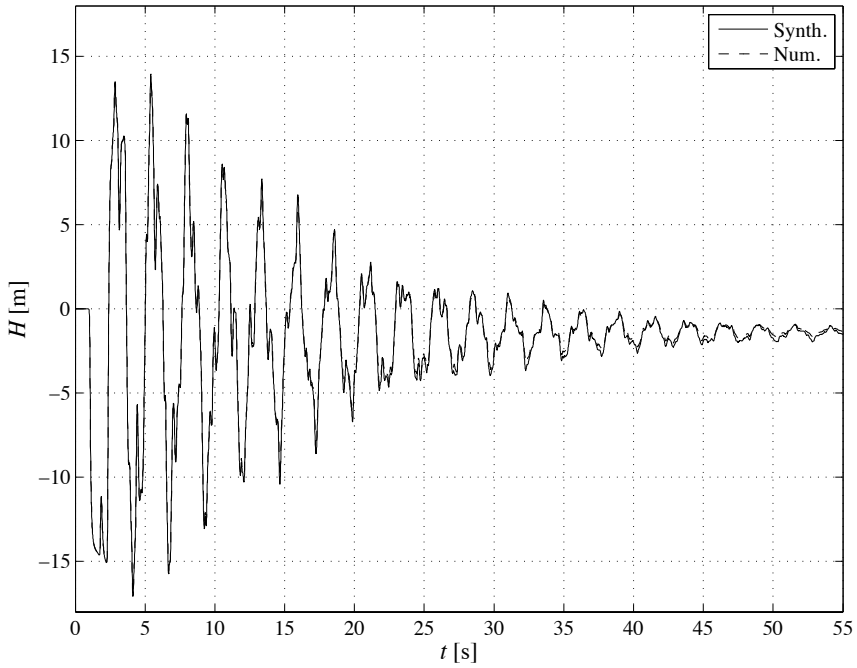

Figure 3. Piezometric head variation at node 1, H_1, simulated by MOC (Num.) and estimated by Calibration 1 (Synth.).

Table 1. Results of the calibration (data in bold are considered as known)

		Calibration 1		Calibration 2	MOC
Algorithm		GA	NM	GA = NM	
RSS/n	(m^2)	10.336	.004	.015	
L_1	(m)	**546.0**	**546.0**	542.8	**546.0**
L_2	(m)	2.62	69.0	75.5	**70.0**
D_2	(m)	0.565	0.100	0.099	**0.100**

3. CONCLUSIONS

In this paper the network admittance matrix method has been extended, introducing the Brunone's unsteady-friction formula, to improve its capabilities in the diagnosis of pressurised pipe networks by means of transients. A numerical case study has hen considered to estimate the length, the diameter, and the position of a pipe with a different diameter in a trunk main between two reservoirs. The preliminary results confirm that the diagnosis can be successful in the given

conditions. Further work is needed to verify the effects of the unsteady-friction and the sensitivity to the parameters involved in the calibration. Besides the shown preliminary results, a test on field data is needed to confirm the capabilities of NAMM to diagnose functioning systems.

ACKNOWLEDGMENTS

This research has been supported by the University of Perugia and by the Italian Ministry of Education, University and Research (MIUR), under the Project of Relevant National Interest "Tools and procedures for an advanced and sustainable management of water distribution systems".

REFERENCES

Brunone, B., 1989. A technique for leak detection in wastewater outfalls. Numerical experiments (in Italian), Proceedings of the Congress on "Wastewater outfalls," Ischia, Italy.

Brunone, B., Golia, U.M., Greco, M., 1995. Effects of two-dimensionality on pipe transients modeling. J Hydraul Eng-Asce 121, 906–912.

Chaudhry, M.H., 2014. Applied Hydraulic Transients, Third. ed. Springer New York, New York, NY. doi:10.1007/978-1-4614-8538-4

Ghidaoui, M.S., Zhao, M., McInnis, D.A., Axworthy, D.H., 2005. A Review of Water Hammer Theory and Practice. Appl. Mech. Rev. 58, 49–28. doi:10.1115/1.1828050

Jonsson, L., Larson, M., Coulbeck, B., Evans, E., 1992. Leak detection through hydraulic transient analysis, International conference on Pipeline Systems, Manchester, U.K.

Kim, S.H., 2008. Address-oriented impedance matrix method for generic calibration of heterogeneous pipe network systems. J Hydraul Eng-ASCE 134, 66–75. doi:10.1061/(ASCE)0733-9429(2008)134:1(66)

Liggett, J.A., Chen, L.-C., 1994. Inverse transient analysis in pipe networks. J Hydraul Eng-Asce 120, 934–955.

Liou, J., Tian, J., 1995. Leak detection - Transient flow simulation approaches. Journal of Energy Resources Technology-Transactions of the Asme 117, 243–248.

Todini, E., Pilati, S., 1988. A Gradient Algorithm for the Analysis of Pipe Networks, in: Computer Applications in Water Supply. pp. 1–20.

Weinerowska-Bords, K., 2015. Alternative Approach to Convolution Term of Viscoelasticity in Equations of Unsteady Pipe Flow. J. Fluids Eng. 137, 054501–9. doi:10.1115/1.4029573

Wylie, E.B., Streeter, V., 1993. Fluid transients in systems. Prentice-Hall, Inc., Eaglewood Cliffs, New Jersey, USA.

Zecchin, A.C., 2010. Laplace-domain analysis of fluid line networks with applications to time-domain simulation and system parameter identification.

Zecchin, A.C., Simpson, A.R., Lambert, M.F., White, L.B., Vítkovský, J.P., 2009. Transient Modeling of Arbitrary Pipe Networks by a Laplace-Domain Admittance Matrix. J. Eng. Mech. 135, 538–547. doi:10.1061/(ASCE)0733-9399(2009)135:6(538)

Proceedings of the 10th World Congress of EWRA 'Panta Rhei', 5-9 July 2017, Athens, Greece
© 2017 *European Water Resources Association*

Reliability-based design of water distribution networks considering mechanical failures

S. Sirsant* and M.J. Reddy
Department of Civil Engineering, Indian Institute of Technology Bombay, Mumbai – 400076, India
* *e-mail: swatisirsant@gmail.com*

Abstract: For effective design of Water Distribution Networks (WDNs), it is necessary to consider the reliability of the system subject to mechanical and hydraulic failures. In this paper, a reliability based framework is presented for design of WDNs using self-adaptive differential evolution (SaDE) algorithm. The framework includes three main components: a simulation model, a reliability assessment model and an optimization model. Simulation model uses EPANET toolkit for simulation of flows and pressure distribution in pipe network, and its outputs are used in reliability assessment model to determine the minimum cut sets. Reliability assessment model consists of determination of system and nodal reliabilities based on minimum cut sets. The reliability is estimated in terms of demand satisfaction subject to the mechanical failure of components. The optimization model finds optimal pipe diameters considering minimization of network cost as objective subject to a minimum level of reliability and other constraints, and the model is solved by using SaDE algorithm. The application of model is illustrated by applying it to a hypothetical WDN consisting of 17 pipes, 13 nodes, a supply source and a pump. On comparison of the results of study with previous studies, it is found that the present framework yields in better solutions and saves significant amount of computational time.

Key words: Water Distribution Network, Reliability based design, Self-Adaptive Differential Evolution Algorithm

1. INTRODUCTION

Any water supply system (WSS) consists of the WDN, which is meant to receive the treated water and supply it to the consumers. WDN consists of a supply source (such as a reservoir or a tank), pipes, junctions or nodes, and other components such as valves or pumps. The problem of design of WDNs consists of determining the diameter of the pipes such that the cost is minimum subject to the minimum head requirements and conservation of mass and energy constraints. In order to ensure demand satisfaction, it is necessary to access the reliability of the network, for two types of failures: mechanical and hydraulic (Bao and Mays, 1990). Mechanical failure consists of the failure or unavailability of components such as pipes, pumps, valves etc.; whereas hydraulic failure consists of changed pressure and flow conditions in the network due to uncertainty in parameters such as nodal demands and pipe roughness coefficients. Mechanical failure of any component leads to changed flow and pressure conditions inside the network, which may lead to reduced supply at certain nodes. The level of demand satisfaction in such cases is represented as the reliability of the WDN.

Mechanical failure of the pipes can occur due to various factors such as excessive internal pressure, corrosion, sudden failure of pump, external loadings etc. Various factors can be attributed to the rate of failure of pipes such as pipe diameter, age, length, material and previous breakage data. Pipe age and diameter have been found to be the most influential parameters affecting future failure rates of pipes (Kettler and Goulter 1985). Various models have been developed for assessing the future failure rates of the components, such as neural networks (Achim *et al*. 2007), Bayesian Belief Network (Kabir *et al.* 2015). However, the relationships developed will vary with the study area and hence requires a detailed analysis based on previous breakage records (Asnaashari *et al* 2013). The developed relationship will be useful in assessing the mechanical reliability of the network.

Reliability has been assessed in various ways in the past. Shamir and Howard (1981), Su *et al.* (1987) and Fujiwara and Silva (1990) measured reliability as the shortfall due to failure of links. Bao and Mays (1990) considered the uncertainties in demand and roughness coefficients for estimating the reliability of the system. Shibu and Reddy (2014) considered fuzzy random demands for assessment of the reliability of the WDNs. Reliability has been found to be an important consideration for the design of WDNs.

Initially the problem of design of WDNs was considered as a single objective problem considering only minimization of cost. In recent past, the WDN problems were solved using different meta-heuristic methods such as Genetic Algorithm (GA, Kadu *et al*. 2008), Ant Colony Optimization (ACO, Maier *et al.* 2003), Particle swarm optimization (PSO, Montalvo *et al.* 2008), Differential Evolution (DE, Suribabu 2010) etc. Also, in few studies, the concept of reliability was introduced and reliability based design was performed using single objective as well as multi objective techniques (Fu and Kapelan, 2011; Shibu and Reddy, 2014).

In the field of optimal design of WDNs, the use of Evolutionary Algorithms (EAs) has increased tremendously due to the various inherent advantages they possess, such as fast convergence, ability to avoid local optima, obtaining a set of non-dominated solutions etc. Two EAs namely GA and DE are the most widely used algorithms in the field of optimal design of WDNs. It has been seen that DE converges faster than GA (Suribabu 2010). However, use of DE requires sensitivity analysis in order to determine the optimal values of mutation and cross over factors. In order to overcome this difficulty, many self-adaptive DE algorithms have been developed, such as fuzzy adaptive DE (FADE, Liu and Lampinen 2005), Self-Adaptive DE (SaDE, Qin and Suganthan 2005), DE with Self-Adaptive Population (DESAP, Teo 2006), jDE (Brest et al. 2006) and Adaptive DE with optional external archive (JADE, Zhang and Sanderson 2009). Out of these algorithms, SaDE is the first self-adaptive algorithm, which has been found to perform better compared to the previously existing algorithms, in terms of obtaining optimal solutions and convergence speed (Zhang and Sanderson 2009). The present study thus implements SaDE for the purpose of WDN design problem.

The objective of the present study is to perform reliability based design of WDNs using self-adaptive DE algorithm, through application to a hypothetical WDN and evaluate its performance by comparing with previous studies.

2. METHODOLOGY

The overall methodology consists of three components: a simulation model, a reliability assessment model and an optimization model. The simulations have been performed by using EPANET 2 toolkit. Reliability has been estimated using minimum cut set method (Su *et al* 1987). Optimization has been performed using SaDE algorithm (Qin and Suganthan 2005).

2.1 Problem formulation

The problem is formulated as an optimization problem for determining the size of the pipes, such that the cost would be minimum with a minimum level of reliability and following the constraints of minimum head requirement and conservation of mass and energy. Mathematically the problem can be stated as

$$\text{Minimize Cost} = \sum_{i=1}^{n_p} f(D_i) L_i \tag{1}$$

subject to:

$H \geq H_{min}$ (for all nodes) (2)

$$\sum HL_i - \sum E_p = 0 \quad \text{(for all loops)} \tag{3}$$

$$\sum Q_{in} - \sum Q_{out} = 0 \quad \text{(for all nodes)} \tag{4}$$

$$R \geq R_{\min} \quad \text{(for both system and individual demand nodes)} \tag{5}$$

where $HL_i = \dfrac{10.68\ Q^{1.85}\ L_i}{C_{HW}^{1.85}\ D_i^{4.87}}$ and $Q = \dfrac{\pi}{4}\ D^2 V$

Here D_i, L_i = diameter and length of pipe i, H is the head, H_{min} is the minimum required head at any node, HL is the head loss for a pipe, E_p is the energy added by the pump, R is the reliability and R_{min} is the minimum required reliability value, Q_{in} and Q_{out} are the discharges flowing towards and away from a node respectively, C_{HW} is the Hazen William's roughness coefficient and V is the velocity of flow for any particular pipe.

2.2 Simulation model

Simulations have been performed by using EPANET 2 toolkit, in order to generate the pressure and flow conditions in the network. EPANET is a hydraulic simulation tool useful for design of water piping system and it was developed in 1993 by the United States Environmental Protection Agency (EPA) Water Supply and Water Resources Division (Rossman 2000). It is a computer program that performs extended period simulation of hydraulic and water quality behavior within pressurized pipe networks.

EPANET simulates the water distribution network using the Gradient Algorithm, and the solutions of flows and heads at a particular time step is obtained by solving a set of equations which mainly involves: (a) Conservation of mass equation at a junction (b) Head loss equation for a loop (Todini and Pilati 1987). In this study, the pipe failure conditions have been simulated by setting the status of the pipe as close, using the EPANET DLL files, through matlab coding.

2.3 Reliability assessment model

Reliability is estimated using the minimum cut set method. A minimum cut set consists of the minimum number of components which when fail together causes system failure, however if any of the components is in working state, then the system failure does not occur. In order to calculate the reliability of the network using this method, first the minimum cut sets are found, which can be done by simulating failure of different pipes (i) individually (ii) combinations of pipes which do not form minimum cut sets for single pipe failure case. The probability of failure of each cut set is calculated as multiplication of failure probabilities of all the members forming that cut set.

Thus, if there are k components in a minimum cut set, then the failure probability of that cut set can be calculated as

$$P(MC_i) = \prod_{j=1}^{k} P_j = P_1 \text{ x } P_2 \text{ x } .....P_k \tag{6}$$

If there are m minimum cut sets, then the failure probability of the system will be equal to the sum of failure probabilities of all the cut sets, i.e.

$$P_s = \sum_{i=1}^{m} P(MC_i) = P(MC_1) + P(MC_2) + ... + P(MC_m) \tag{7}$$

Reliability can be calculated as

$$R = 1 - P_s \tag{8}$$

2.4 SaDE algorithm

Optimization is performed by using Self Adaptive Differential Evolution (SaDE) algorithm (Qin and Suganthan, 2005). The basic steps involved in SaDE are as follows:

1. Initialise the population with some random values.
2. Set initial values of the means of mutation and cross over factors as 0.5 each and standard deviation as 0.3 and 0.1 respectively.
3. Generate initial random values of mutation and cross over factors for each individual from a normal distribution with the specified mean and standard deviation values.
4. Now calculate the cost and reliability values for each individual.
5. Perform mutation for each individual using the relation

$$V_{i,G} = X_{r_1,G} + F_i(X_{r_2,G} - X_{r_3,G}) \tag{9}$$

   where Vi,G = mutant vector associated with population i and generation G
   Xr1,G, Xr2,G and Xr3,G are three randomly chosen population vectors from the present generation and Fi is the mutation factor for population vector i.
6. The next step is to perform cross over, which is nothing but to select certain features from the original vector and rest from the mutant vector, to generate a trial vector. Cross over can be performed using the equation

$$u_{j,i,G} = \begin{cases} v_{j,i,G} \text{ if } (rand_j[0,1] \le CR \text{ or } (j = j_{rand}) \\ x_{j,i,G}, \text{ otherwise} \end{cases} \tag{10}$$

   where, $u_{j,i,G}$ is the trial vector, $rand_j$ is a random value between 0 to 1 for each dimension of the vector and j_{rand} is a random number from 1 to D, the dimension of each vector.
7. Now, for the trial vector generated, compute the cost and reliability values. The fitness function can be calculated as cost plus penalty, where penalty is computed using the rule

$$Penalty = \begin{cases} (R_{\min} - R) \text{ x } 10^6 & \text{if } R < R_{\min} \\ 0 & \text{otherwise} \end{cases} \tag{11}$$

8. Generate the new population by applying the selection process. Here, the selection is kept simple by comparing the fitness function of the trial vector with the corresponding original population vector. The one with better fitness function is forwarded to the next generation.
9. The process is continued till the convergence criteria is fulfilled. Here convergence criteria is that either a maximum number of iterations are achieved or there is no improvement in the fitness function value for a certain number of iterations (say 20).

In order to update the values of mutation and cross over factors, the values of these factors leading to successful trial vectors are noted for a certain number of iterations, say 10. After the required number of iterations are over, the mean of mutation and crossover factors are updated as equal to the mean of the successful values of these factors respectively. New set of mutation and crossover factors are then generated from normal distributions with the updated mean values.

The overall working procedure for the model has been depicted in Figure 1.

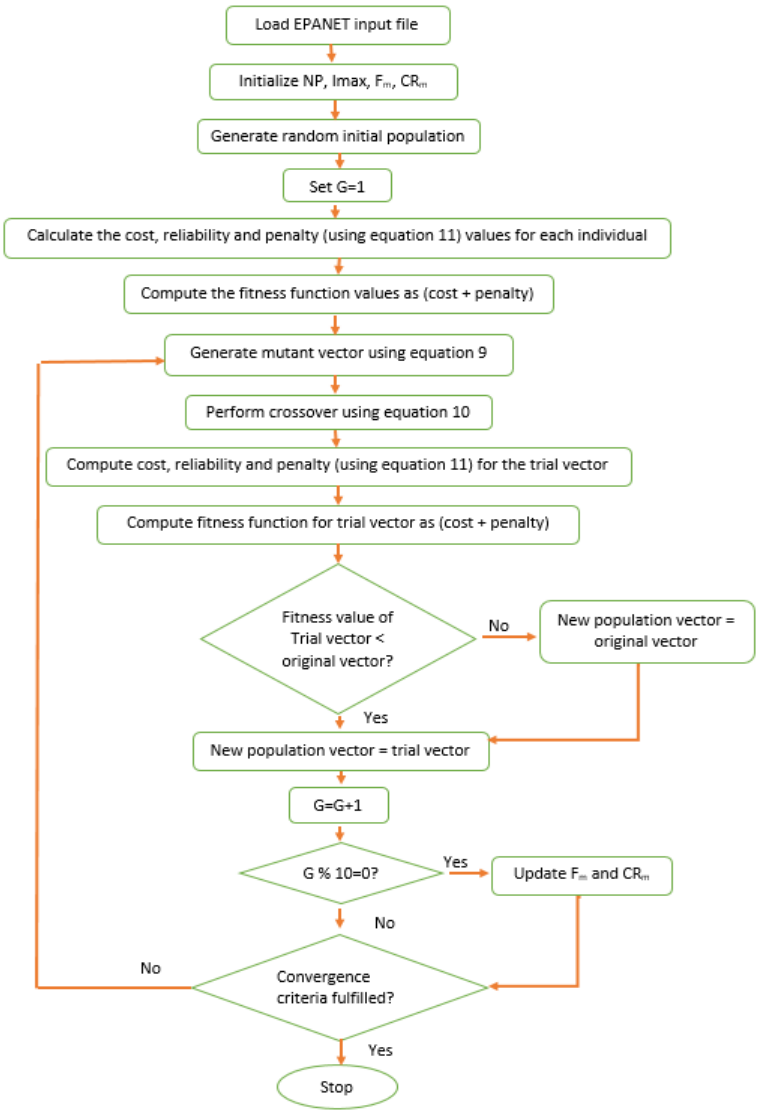

Figure 1. Overall Model Framework

3. RESULTS AND DISCUSSION

The model is applied on a hypothetical WDN (Su *et al*., 1987), as shown in Figure 2. Complete data set for the network can be found in Su *et al.* (1987).

The probability of failure of pipes was modelled using Poisson's distribution as follows:

$$P_j = 1 - e^{-\beta_j} \tag{11}$$

where P_j is the probability of failure of jth pipe and β_j is the expected number of failures per year for pipe j and is given by

$$\beta_j = r_j L_j \tag{12}$$

where r_j = expected number of failures per year per unit length of pipe j and can be calculated as

$$r_j = \frac{0.6858}{D_j^{3.26}} + \frac{2.7158}{D_j^{1.3131}} + \frac{2.7685}{D_j^{3.5792}} + 0.042 \tag{13}$$

The minimum required head at all the nodes for full supply is taken as 28 m. The minimum system reliability is set as 0.8, whereas the minimum nodal reliability is taken as 0.95 for all the nodes.

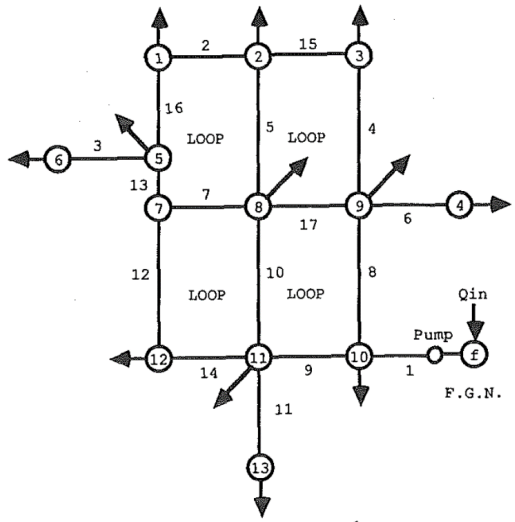

Figure 2. Hypothetical Network (Su et al., 1987)

The model is run for different population sizes for 10 trial runs each. It was found that for population sizes of 100, 150, 200 and 250, the average minimum cost was found as 4.3125 x 10^5, 3.4638 x 10^5, 3.4384 x 10^5 and 4.1733 x 10^5 $ respectively, and requiring minimum number of function evaluations for obtaining optimal solution as 28800, 32100, 31500 and 48750 respectively. Thus, population size of 200 performs best in terms of average minimum cost and number of function evaluations needed to obtain the optimal solution. The corresponding F_m and CR_m values are obtained as 0.3 and 0.9 respectively. The algorithm converges to optimal solution at around 150 iterations.

Table 1. Comparison of optimal solutions obtained in the present study with previous study of Su et al. (1987).

Pipe id	Optimal diameter value (inches)	
	Present Study	**Su et al. (1987)**
1	20	34.55
2	6	14.93
3	12	16.96
4	6	9.71
5	6	15.83
6	10	16.98
7	12	26.38
8	20	21.53
9	20	19.01
10	12	6.94
11	12	13.63
12	12	22.37
13	12	16.20
14	12	5.13
15	6	11.12
16	6	11.53
17	15	9.30
Cost ($)	3.4204 x 10^5	6.1626 x 10^5
Reliability	0.8463	0.83797

The obtained optimal values of pipe diameters are listed in Table 1. The optimal cost is obtained as 3.4204 x 10^5 $ with a reliability value of 0.8463. The average computational time needed is 70 minutes. The results as obtained by Su *et al*. (1987), led to a cost of 6.1626 x 10^5 $ with reliability of 0.8379 requiring 200.5 minutes of computational time. Thus, the SaDE algorithm is able to find

better solution in terms of optimality and is efficient in terms of computational time needed. Also, in the algorithm used by Su *et al.* (1987), the diameter values have been assumed as continuous, which is not the case in real WDNs. This drawback has been eliminated in the present study, by incorporating discretization of the decision variables to the practically available pipe sizes.

4. CONCLUSIONS

This paper presented self-adaptive differential evolution (SaDE) algorithm for reliability based design of WDNs considering mechanical failure of pipes. The methodology can also be used in optimizing the extension of an existing WDN, by keeping the diameters of existing pipes as constant values and optimizing the diameters of extensions. The model is found to be efficient in terms of the obtained optimal solution. The solutions obtained are more accurate and practically feasible since it considers discrete value for the decision variables. Moreover, the solutions can be obtained in reasonable amount of computational time. The self-adaptive nature of the algorithm eliminates the need of initializing the mutation and crossover factors, which is basically problem dependent and requires proper sensitivity analysis to determine the optimal values of these parameters. The need for such analysis is eliminated in the present study. The algorithm can be suitably modified to incorporate other factors such as failure of pumps, location of valves and hydraulic failures.

REFERENCES

Achim D., Ghotb F., and McManus K. (2007). Prediction of Water Pipe Asset Life Using Neural Networks. Journal of Infrastructure Systems, 13(1), 26-30.

Asnaashari A., Mcb E. A., Gharabaghi B., and Tutt D. (2013). Forecasting water main failure using artificial neural network modelling. Canadian Water Resources Journal, 38(1), 24-33.

Bao Y., and Mays L. W. (1990). Model for Water Distribution System Reliability. Journal of Hydraulic Engineering, 116(9), 1119-1137.

Brest J., Greiner S., Borkovic B., and Mernik M. (2006). Self-Adapting Control Parameters in Differential Evolution: A Comparative Study on Numerical Benchmark Problems. IEEE Transactions on Evolutionary Computation, 10(6), 646-657.

Eiger G., Shamir U., and Ben-Tal A. (1994). Optimal Design of Water Distribution Networks. Water Resources Research, 30(9), 2637-2646.

Fu G., and Kapelan Z. (2011). Fuzzy Probabilistic Design of Water Distribution Networks. Water Resources Research, 47(W05538), 1-12. doi:doi:10.1029/2010WR009739

Fujiwara O., and Silva A. U. (1990). Algorithm for Reliability-Based Optimal Design of Water Networks. Journal of Environmental Engineering, 116(3), 575-587.

Kabir G., Tesfamariam S., Francisque A., and Sadiq R. (2015). Evaluating Risk of Water Mains Failure Using a Bayesian Belief Network Model. European Journal of Operational Research, 240(1), 220-234.

Kadu M. S., Gupta R., and Bhave P. R. (2008). Optimal Design of Water Networks Using a Modified Genetic Algorithm with Reduction in Search Space. Journal of Water Resources Planning and Management, 134(2), 147-160.

Kettler A. J., and Goulter I. (1985). An Analysis of Pipe Breakage in Urban Water Distribution Networks. Canadian Journal of Civil Engineering, 12(2), 285-293.

Liu J., and Lampinen J. (2005). A Fuzzy Adaptive Differential Evolution Algorithm. Soft Computing, 9(6), 448-462.

Qin A., and Suganthan P. (2005). Self-adaptive Differential Evolution Algorithm for Numerical Optimization. IEEE Congress on Evolutionary Computation, 2, pp. 1785-1791.

Shamir U., and Howard C. D. (1981). Water Supply Reliability Theory. American Water Works Association, 73(7), 379-384.

Shibu A., and Reddy M. J. (2014). Optimal Design of Water Distribution Networks Considering Fuzzy Randomness of Demands Using Cross Entropy Optimization. Water Resources Management, 28(12), 4075–4094.

Su Y. C., Mays L. W., Duan N., and E. Lansay K. (1987). Reliability-Based Optimization Model For Water Distribution Systems. Journal of Hydraulic Engineering, 113(12), 1539-1556.

Suribabu C. (2010). Differential Evolution Algorithm for Optimal Design of Water Distribution Networks. Journal of Hydroinformatics, 12(1), 66-82.

Teo J. (2006). Exploring Dynamic Self-Adaptive Populations in Differential Evolution. Soft Computing, 10(8), 673-686.

Todini E., and Pilati S. (1987). A Gradient Method for the Analysis of Pipe Networks. International conference on computer applications for water supply and distribution. Leicester Polytechnic, UK.

Zhang J., and Sanderson A. C. (2009). JADE: Adaptive Differential Evolution with Optional External Archive. IEEE Transactions on Evolutionary Computation, 13(5), 945-958.

Proceedings of the 10th World Congress of EWRA 'Panta Rhei', 5-9 July 2017, Athens, Greece
© 2017 *European Water Resources Association*

Stochastic gradient methods for the optimization of water supply systems

A.A. Gaivoronki[1], J. Napolitano[2*] and G.M. Sechi[3]
[1] *Department of Industrial Economics and Technology Management, Norwegian University of Science and Technology, Norway*
[2] *Department of Civil and Environmental Engineering and Architecture, University of Cagliari, Italy*
[*] *e-mail: jacopo.napolitano@unica.it*

Abstract: Reductions of water deficits for users and energy savings are frequently conflicting issues when optimizing large-scale multi-reservoir and multi-user water supply systems. Undoubtedly, a high level of uncertainty due to hydrologic input variability and water demand behaviour characterizes these problems. The aim of this paper is to provide a decision support for the water system authority, in order to realize a robust decision policy, minimizing the risk of wrong future decisions. This has been done through the optimization of emergency and costly water transfer activation. Hence, a cost–risk balancing problem has been modelled to manage this problem, balancing the damages in terms of occurrences of water shortages and energy and cost requirements for emergency transfers. In Napolitano et al. (2016), we dealt with this problem using a scenario analysis approach. The obtained results were appreciable considering a limited amount of scenarios and a short time horizon. Nevertheless, if we have to increase the number of considered scenarios, taking into account the effect of climate and hydrological changes, computational problems arise. Therefore, to solve this kind of problem, it is necessary to apply a specialized approach for optimization under uncertainty. We develop herein a simulation-optimization model using the stochastic gradient methods. The study case is a multi-reservoir and multi-user water supply system in a specific area in south Sardinia (Italy), characterized by Mediterranean climate.

Key words: Stochastic gradient methods, water schedules optimization, cost–risk balancing problem

1. INTRODUCTION

The optimization of water supply systems under a high uncertainty level due to hydrologic input variability and water demand behaviour has been a subject of substantial interest in the research literature (Cunha and Sousa, 2010; Kang and Lansey, 2014; Yuan et al. 2016). In this context, pumping plants' activation schedules are a relevant topic recently treated in Napolitano et al. (2016), considering complex water resource systems management. The successful approaches to solve this kind of problems should be able to incorporate the uncertainties in the management of water systems by searching for a robust decision policy. The main aim is to provide the water system's authority with a decision support system, in order to realize a decision policy that minimizes the risk of making wrong future decisions. Through the optimization, we manage to provide the water system authority with optimal rules considering both historical and generated synthetic scenarios of hydrologic inputs to reservoirs. Using synthetic series, we analyse the climate change impacts and balance the rules while also considering future behaviour under the risk of the occurrence of shortages and the cost of early warning procedures to avoid water scarcity, mainly related to activation of emergency water transfers.

Among the considered methodologies, the scenario analysis approach (Pallottino et al., 2004; Kang and Lansey, 2014) has been proposed as an efficient optimization tool. However, it frequently needs a substantial, sometimes huge, set of hydrological scenarios to avoid the risk of system failure under a significant change of conditions over time. Despite the reasonable quality of the obtained results for standard test cases reported in Napolitano et al. (2016), this methodology encounters considerable problems in managing large-size real cases due to the high number of data and variables in scenarios. Therefore, in this study, we treat this problem with an efficient optimization model based on the stochastic gradient methods (Gaivoronski, 2005), which allows us to solve

substantially larger models and to provide optimal solutions under high uncertainty.

2. OPTIMIZATION UNDER UNCERTAINTY AND THE STOCHASTIC GRADIENT METHODS

The main aim of this paper is to define the optimal thresholds for the activation of the pumping stations. When the reservoirs' storage volumes cross these thresholds, the activation of pumping is triggered. In order to optimize the activation rules, we must define a critical stored volume in reservoirs that may supply the downstream demand centres. To compose the multi-period model, we need to define the multi-period network starting from a basic graph given by a single-period static design of the water system. The multi-period network is constructed by repeating this single period model for every period using multi-period rules, as defined in Sechi and Zuddas (2008).

The climate change effects result in an increment of the different hydrological scenarios to consider their time horizon dimensions and, consequently, the level of uncertainties. In such situations, the dimensions of the multi-period model become sizable and it is very difficult to manage this stochastic problem. Therefore, to solve it efficiently we need special algorithms, designed for optimization under uncertainty. In Napolitano et al. (2016), we showed the limits of the classical scenario analysis approach (Rockafellar and Wets, 1991) caused by the high number of linear and nonlinear variables and parameters involved. We highlighted the requirements for this problem through a nonlinear variables parametrization. To solve this class of problems, the stochastic gradient methods (Birge and Louveraux, 2001; Gaivoronski, 2005) can be used as an efficient tool.

The stochastic gradient approach belongs to a class of methods specifically designed for problems with continuous distributions of random parameters and nonlinear optimization problems. These methods are suited for optimization and simulation models, where an analytical relationship between the objective function and parameters is difficult to obtain. Supply chain management, energy generation, and financial applications are some areas of research where these approaches have been successfully used (Gaivoronski, 2005).

The stochastic gradient could be described as the statistical estimate of the gradient of the objective function, which provides an optimal direction for iterative updating of the current approximation to the solution of the optimization problem. The stochastic gradient has its roots in the stochastic approximation and in the mathematical programming algorithms with gradient techniques.

These methods solve the stochastic optimization problems of the following type:

$$\text{Minimize}_{\ x \in X}\ \mathbb{E}_{\omega} f_0(x, \omega) \tag{1}$$

where $\omega \in \mathbb{R}^k$ is a vector of random parameters and $x \in X \subseteq \mathbb{R}^n$ is a vector of decision variables; X represents the set of feasible solutions.

The problem statement describes a large set of dynamic and static stochastic optimization problems. Usually, these methods can be divided into two categories: *deterministic equivalents* and *iterative sampling algorithms*.

The deterministic equivalents start by approximating the problem (1) with a problem where the original probability distribution of the random parameters ω is substituted by a discrete distribution concentrated in a finite number of values ω^i, which describe different scenarios. Therefore, the original problem could be substituted by a deterministic optimization problem with a particular structure, where the expectations in (1) are replaced by weighed sums.

Iterative sampling algorithms require statistical estimates of functions $F_i(x)$ and their gradients and Hessians. These estimates are obtained through the generation of the different observations of random parameters ω^i. The generation process supports the solution process; herein the estimates are used as substitutes for the exact values in the iterative algorithms, which are adopted from linear

and nonlinear programming. Stochastic quasi-gradient (SQG) methods belong to this class of problems.

The optimization algorithm starts from an initial point x^0 and moves forward to the current approximation x^s of the optimal solution of the original problem (1) according to the following rule:

$$x^{s+1} = \pi_X(x^s - \rho_s \xi^s) \tag{2}$$

where ρ_s represents the size of the step in the direction opposite to the current estimate ξ^s of the gradient $F_0(x)$ at the point x^s .The resulting point is projected onto the set X. The projection operator π_X transforms an arbitrary point $z \in \mathbb{R}^n$ into the point $\pi_X(z) \in X$ such that:

$$\|z - \pi_X(z)\| = \min_{x \in X} \|z - x\| \tag{3}$$

the structure of the set X should allow a fast solution of the problem (3); indeed, it should be solved many times during the optimization. This means that the set X should be defined by linear constraints in order to guarantee an efficient solution process.

The crucial part of the SQG implementation consists in the evaluation of statistical estimates ξ^s of the gradient of the objective function $F_0(x) = \mathbb{E}_\omega f_0(x, \omega)$ in (1). This estimate is characterized by considerable flexibility since it is sufficient that the following condition is satisfied:

$$\mathbb{E}(\xi^s | \mathbb{B}_s) = F_{0x}(x^s) + a_s \tag{4}$$

here, $\mathbb{B}_s$ is the σ-field, defined by the history of the process, while $F_{0x}(x^s)$ represents the gradient of the function $F_0(x)$ at the point x^s. The vector ξ^s, which satisfies the property (4), is called the *stochastic gradient*.

For example, in the simplest case, the stochastic gradient ξ^s can be obtained as follows:

$$\xi^s = f_{0x}(\omega^s, x^s) \tag{5}$$

where ω^s is a single observation of a random vector ω. When the classical gradient does not exist, such as with convex but non-smooth functions, ξ^s can be estimated through a generalization of the gradient called the *stochastic quasi-gradient*.

The step-size definition is another fundamental aspect when using the SQG algorithm. Indeed, the convergence to the optimal solution depends on the selection of the correct step ρ_s, which should satisfy the following property:

$$\rho_s \geq 0, \quad \rho_s \to 0 \quad \sum_{s=0}^{\infty} \rho_s = \infty \tag{6}$$

The required condition in (6) that the step-size tends to zero is not necessary if the precision of the stochastic gradient ξ^s increases with iterations. On the other hand, ρ_s tends to zero faster if the variance of the stochastic gradient grows with the number of iterations.

A recursive simulation and optimization process can efficiently optimize the simulation models by applying the SQG algorithm iteratively. This methodology is suited for optimization problems characterized by a large number of decision variables, described by a simulation model for each single problem. The novelty of this paper lies in the application of SQG to a real problem of water resource management that is characterized by several decision variables and an extended time horizon needed in the optimization.

3. SQG FOR A WATER RESOURCE MANAGEMENT PROBLEM

A recursive simulation and optimization algorithm based on the stochastic gradient methods has

been developed for solving a water resource management problem. This is the first application of the SQG approach to such problems.

In these problems, the level of uncertainty is high, and to implement decision-making solutions it is necessary to develop correct future system management tools and to improve the security level in the decision-making process. Specifically, we can define a *cost–risk balancing process* (Gaivoronski et al., 2012a; Gaivoronski et al., 2012b; Napolitano et al., 2016) considering the pumping energy and management costs (cost elements) needed in order to avoid water deficits for users (representing the risk elements). The optimization approach tries to obtain a robust decision policy, minimizing the risk of taking wrong and harmful decisions for the future. In this way, the water system's authority is able to define a water resource "target value" to deliver to the centres of consumption in order to minimize the costs and to reduce the hardships for system users. We assume that the resource in question is scarce and that, for this reason, the demand cannot be satisfied in many scenarios. In such scarcity situations, managers should develop an emergency policy to alleviate the effect of shortages. In order to do so, each user should know in advance the reduced target level of demand satisfaction that the system manager is willing to deliver to him. This target value has to be "barycentric" relative to future uncertain hydrological scenarios. In this way, we can also manage the activation of some emergency measures, such as decreasing the water distributed to the users or activating emergency transfers.

Specifically, we consider finding the optimal set of parameters q that describe the activation pumping rules while minimizing the average monthly costs, which are the sums of all costs supported in the water system management. The network state v^t (water volumes in reservoirs) evolves in discrete time $t = 1, \dots, T$ (months). At each t, water demand d^t and inflow r^t arrives. Therefore, the pumping schedules are defined by pumping rules with parameters q, and at each t; the network flows x^t are obtained by minimization of costs (7):

$$C^T(q, v^t, d^t, r^t) = \min_{x \in X} C(x, q, v^t, d^t, r^t) \tag{7}$$

subject to constraints (8) (flow continuity, bounds, etc.).

$$\Phi(x, q, v^t, d^t, r^t) = 0 \tag{8}$$

The state v^{t+1} at the beginning of period $t + 1$ is obtained from the state equation (9):

$$v^{t+1} = \Psi(x^t, q, v^t, d^t, r^t) \tag{9}$$

where the functions $C(\cdot), \Phi(\cdot),$ and $\Psi(\cdot)$ are linear with respect to (x, v).

The objective is to find the set of parameters $q = (q_1, \dots, q_n)$ that minimizes the average steady state costs, thus solving the optimization problem with an infinite time horizon (10).

$$\text{Minimize}_{q \in Q} F(Q), F(q) = \lim_{t \to \infty} \frac{1}{t} C^t(q, v^t, d^t, t^t) \tag{10}$$

where Q is some feasible set for parameters q.

This problem can be solved using SQG methods as described in the previous section. In relation to water resources, these methods have been applied to the optimization of general simulation models of discrete event dynamic systems in Dupačová et al. (1991) and Gaivoronski (2005).

The solution approach resorts to a concurrent interrelation between simulation, optimization, and evaluation steps. In the following, we give a description of the concurrent interaction between them:

– *Simulation step for all threads with LP searching for optimal flows*: the simulation process is referred to each single period t of the time horizon and is characterized by n-processes simultaneously. Each process has different sets of pumping activation threshold parameters q according to (11):

$$q^t + \delta e_k \tag{11}$$

where $\delta > 0$ is a small positive value and e_k is a vector of zeros with value 1 in the k-th position.

Here the objective function of costs referred to the single period t (7) is minimized in order to obtain an optimal configuration of the network water flows x^t.

– *Optimization step searching for stochastic gradients*: the optimization process will be applied between two consecutive periods and the new parameter configuration will be evaluated according to Equation (12):

$$q^{t+1} = \prod_Q (q^t - \rho_t \xi^t) \tag{12}$$

where $\rho_t > 0$ is the step size and $\prod_Q(\cdot) = (\xi_1^t, \dots, \xi_n^t)$ will be estimated by (13):

$$\xi_k^t = \frac{C_k^t - C_0^t}{\delta} \tag{13}$$

– *Evaluation step*: simultaneously, there is an estimation step based on a moving average.

$$C_0^{t+1} = (1 - \alpha_t)\bar{C}_0^t + \alpha_t C_0^t \tag{14}$$

The estimated costs C_0^{t+1} are dependent on the average costs $\bar{C}_0^t$, referred to all periods, and the costs evaluated in the previous step C_0^t. The relationship between these terms is regulated by an averaging parameter α_t.

4. CASE STUDY: SOUTHERN SARDINIA WATER SUPPLY SYSTEM

The SQG approach has been applied to the case of the water supply system of southern Sardinia (Italy), which is shown in Figure 1 considering the pumping energy needed in order to avoid the water deficits documented by different hydrological series.

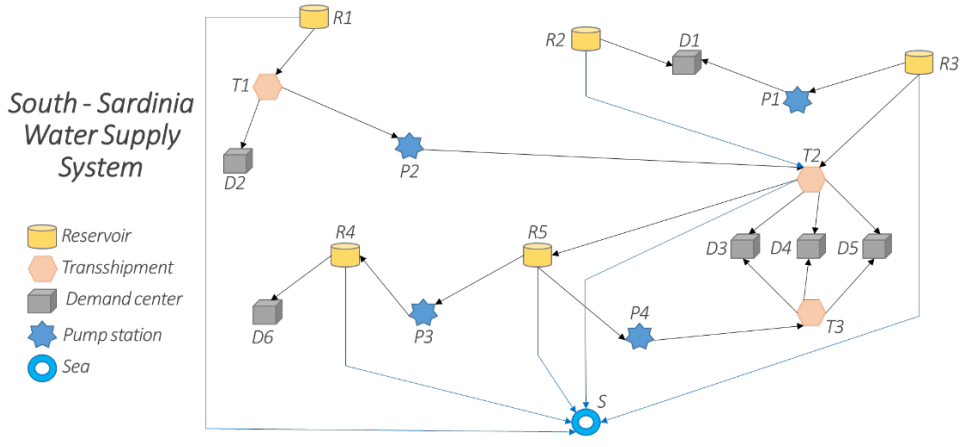

Figure 1: The south Sardinia water supply system

Water sources are given by five artificial reservoirs, while the water demands have been grouped in six centres according to three different uses: civil, irrigation, and industrial. Pump stations allow demand centres to be supplied with increased economic burden, namely by incurring pumping costs in addition to the ordinary management costs. Figure 1 simplifies the real configuration complexity of the system, but can adequately represent the system, analysing the flow configuration for values driven by the pumping stations. All the main features of this system have been extensively described in Napolitano et al. (2016). Defining the lifting rules, we assume that thresholds levels for

pump activation are referred to stored volume in reservoirs that supply the downstream demand node. This could be related in some cases to a single reservoir or to two of them; in the second case the threshold value is derived from the storage volumes in both reservoirs.

4.1 SQG simulation process

In a first stage of analysis, the SQG has been implemented, adopting the activation thresholds values evaluated on historical water inputs, as described in Napolitano et al. (2016) using the scenario analysis approach; they are expressed in units of 10^6 m^3 and are equal to: S1 = 1.624, S2 = 35.451, S3 = 5.07, and S4 = 37.558.

In this paper, starting from the observed data for 53 historical years reported in the Sardinia Region Water Plan (RAS 2006), synthetic hydrological inflows to reservoirs have been evaluated by a Monte Carlo generation. In this way, the optimization time horizon has been expanded to 6360 monthly periods.

The simulation process using SQG has been developed for the synthetically generated series in order to compare the threshold values obtained in reservoirs for the activation of pumping stations. According to this, in a first stage, the thresholds are equal to the values obtained in the scenario analysis approach and running the SQG simulation these threshold values are given as parameters. The aim of this stage is to validate the pump station activation threshold results along the available database using the SQG method. SQG give us the possibility to evaluate all supported costs and the objective function value along the extended time horizon. The final objective function has been obtained as the sum of different cost elements, as shown in the left side of Table 1, under the caption “simulation process”.

The total cost function has been split into three main elements: spilling, shortage (deficit costs), and pumping. The main contributions are given by shortage and pumping costs, which have higher values.

4.2 SQG recursive simulation and optimization process

In the second phase, the SQG optimization approach has been applied to the extended time horizon, expanded to 6360 monthly periods, in order to obtain the optimized threshold values.

A relevant aspect has to be highlighted: SQG succeeds in managing this extended time horizon, which was impossible with the scenario analysis due to excessive computational requirements, as reported in Napolitano et al. (2016). The results obtained using SQG and the extended hydrology define a new set of activation thresholds for pumping transfer activation: new values are always evaluated in units of 10^6 m^3 and are equal to S1 = 0.271, S2 = 72.480, S3 = 2.775 and S4 = 21.316.

Table 1. Objective function results

Simulation Process			**Simulation and Optimization Process**		
Mean costs	10^6 € /month	10^6 € /year	Mean costs	10^6 € /month	10^6 € /year
Spilling	0.005	0.065	Spilling	0.005	0.064
Shortage	0.259	3.106	Shortage	0.231	2.767
Pumping	0.211	2.535	Pumping	0.215	2.578
Total	0.475	5.641	Total	0.451	5.345

The new values for the objective function have been obtained as shown on the right side of **Error! Reference source not found.**, under the heading “simulation and optimization process”. The total value is smaller than the result obtained in the previous stage (**Error! Reference source not found.**) due to a significant decrease of the deficit and a small increment of the pumping contributions.

5. CONCLUSIONS

5. CONCLUSIONS

The cost–risk balancing approach aims to contextually restrict deficit risks for users and to minimize the costs of managing the system in shortage conditions. The potential of the recursive simulation and optimization process based on the stochastic gradient methods is confirmed when it is applied to water resource system management, especially compared to the scenario analysis approach. Indeed, this methodology allowed us to consider substantially larger models and to provide an enhancement for the optimal solutions under large uncertainty with the need to extend the analysis to a significant number of synthetic scenarios. The results highlight an improvement in the objective function and lower computational time compared with the scenario optimization approach developed in Napolitano et al. (2016) for the same type of problem.

REFERENCES

Birge, J.R. and Louveaux, F. (2001). Introduction to Stochastic Programming. New York: Springer-Verlag.

Cunha M.C. and Sousa J.J.O. (2010). Robust design of water distribution networks for a proactive risk management. Journal of Water Resources Planning and Management, 136 (2), 227–236.

Dupačová, J., Gaivoronski, A., Kos, Z., and Szántai, T. (1991). Stochastic programming in water management: A case study and a comparison of solution techniques. European Journal of Operational Research, 52, 28–44.

Gaivoronski, A. (2005). SQG: Stochastic programming software environment. In S.W. Wallace and W.T. Ziemba, editors, Applications of Stochastic Programming. SIAM & MPS.

Gaivoronski, A., Sechi, G.M., and Zuddas, P. (2012a). Cost/risk balanced management of scarce resources using stochastic programming. European Journal of Operational Research, 216, 214–224.

Gaivoronski, A., Sechi, G.M., and Zuddas, P. (2012b). Balancing cost-risk in management optimization of water resource systems under uncertainty. Physics and Chemistry of the Earth, 42–44, 98–107.

Kang, D. and Lansey, K. (2014). Multiperiod planning of water supply infrastructure based on scenario analysis. Journal of Water Resources Planning and Management, 140 (1), 40-54.

Napolitano, J., Sechi, G. M., and Zuddas, P. (2016). Scenario optimization of pumping schedules in a complex water supply system considering a cost-risk balancing approach. Water Resource Management, 30, 5231-5246.

Pallottino, S., Sechi, G.M., & Zuddas, P. (2004). A DSS for water resources management under uncertainty by scenario analysis. Environmental Modelling & Software, 20, 1031–1042.

RAS (2006). Piano Stralcio di Bacino Regionale per l'Utilizzo delle Risorse Idriche. Regione Autonoma della Sardegna, Italy.

Rockafellar, R.T. and Wets, R.J.B. (1991). Scenarios and policy aggregation in optimization under uncertainty. Mathematics of Operation Research, 16, 119–147.

Sechi, G. M. and Zuddas, P. (2008). Multiperiod hypergraph models for water systems optimization. Water Resource Management, 22, 307–320.

Yuan, L., Zhou, J., Li, C., Xie, M., and Mo, L. (2016). Benefit and risk balance optimization for stochastic hydropower scheduling. Water Resource Management, 30, 3347–3361.

Proceedings of the 10th World Congress of EWRA 'Panta Rhei', 5-9 July 2017, Athens, Greece
© 2017 *European Water Resources Association*

Spectral analysis and topological and energy metrics for water network partitioning of Skiathos island

A. Di Nardo[1,2*], M. Di Natale[1,2], C. Giudicianni[2], C. Laspidou [1,4], F. Morlando[3], G.F. Santonastaso[1,2] and D. Kofinas[4]

[1] *Action Group CTRL+SWAN of European Innovative Partnership on Water, EU*

[2] *Department of Civil Engineering, Design, Building and Environment, University of Campania Luigi Vanvitelli,, Aversa (CE), 81031, Italy*

[3] *Department of Civil, Architectural and Environmental Engineering., Federico II University, via Claudio 21, 80125 Napoli, Italy*

[4] *Department of Civil Engineering, University of Thessaly, Pedion Areos, 38334 Volos, Greece*

[*] *e-mail: armando.dinardo@unina2.it*

Abstract: Water network partitioning (WNP) into supply clusters aims at improving management of the whole system and subsequent definition of District Meter Areas (DMAs), simplifying water budget and pressure management as well as the identification and reduction of water losses. This solution is a strategic option used by water utilities to control and operate their Water Distribution Networks (WDNs). Thus, it is important to design DMAs in optimal way, inserting flow meters and gate valves in boundary pipes. This is a demanding task, since closure of some network links can worsen network performance in terms of hydraulic and topologic redundancy. This paper presents the application of a novel optimization approach, based on network theory and Graph Partitioning (GP), coupled with heuristic optimization techniques. The methodology uses SWANP software to cluster the network and proceeds with a novel approach for the partitioning phase, based on the minimization of a multi-objective function including both energy and spectral metrics. The methodology is tested on Skiathos Island, Greece WDN. We present interesting preliminary results based on the analysis of several performance indices that measure resilience and robustness of the partitioned network. Overall, an adequate solution to the optimal definition of hydraulic districts through DMAs is presented.

Key words: water network partitioning, spectrum, topological metrics, optimization, multi-objective function

1. INTRODUCTION

The paradigm of "divide and conquer" applies fruitfully on clustering data, objects or other sets into smaller subsets. Clustering allows identifying sub-groups in a way that objects within are closely related (Hastie et al., 2001), showing similarity expressed in different ways according to the purpose of the problem (Herrera et al., 2012). The division in groups allows management improvement and analysis simplification. In this regard, the application of "divide and conquer" to WDNs, by the insertion of gate valves and flow meters, allows improvements in the WDN management, such as water balance (AWWA, 2003) and pressure control (Alonso et al., 2000), facilitating detection and reduction of water losses (Xia and Guo-Jin, 2010) and obstructing accidental or intentional water contamination (Grayman et al. 2009; Di Nardo et al., 2015).

Although this strategy is generally used to improve WDNs operation, WNP in permanent DMAs, achieved by closure of some pipes through gate valves, reduces topologic and energy redundancies (Mays, 2000). Additionally, this may significantly decrease hydraulic performance and network robustness (Di Nardo et al., 2013a). Traditionally, defining DMAs has been strongly empirical without a proper methodology. In the last decades, studies that have allowded to overcome empirical approaches (review by Perelman et al., 2015) generally suggest two main phases: a) clustering, for the network subsets shaping and dimensioning through minimization of edge-cuts and balance of nodes number for each district, by means of graph theory algorithms (Tzatchkov et al., 2006; Alvisi and Franchini, 2014), spectral approach (Herrera et al., 2010; Di Nardo et al, 2017), multi-agent approach (Izquierdo et al., 2011), community structure (Diao et al., 2013, Di

Nardo et al., 2015); and b) dividing, for the selection of pipes where the insertion of flowmeters or gate valves is needed to minimize both the economic investment and the hydraulic performance deterioration, based on iterative (Ferrari et al., 2014; Diao et al., 2013) or Genetic Algorithms (GA) (Di Nardo et al., 2016). To achieve efficient network division, geometrical, topological and hydraulic characteristics need to be considered, guaranteeing correct layout and function of hydraulic districts, as well as satisfying minimum service level at all demand nodes.

This paper aims to contribute to the arduous problem of WDN partitioning by proposing a technique that efficiently and automatically defines optimal DMAs, based on the minimization of a novel multi-objective function that considers simultaneously both topological and hydraulic aspects. In particular two basic metrics from Complex Networks Theory (Boccaletti et al., 2006) were selected: a) average path length L (Watts and Strogatz, 1998), fundamental for the characterization of different network models, and b) algebraic connectivity λ_2 (Fiedler, 1973) on which spectral theory is mainly based (Von Luxburg, 2007). After the first clustering phase, in which the sub-regions are defined through a GP method, the selection of pipes in which gate-valves or flowmeters have to be alternatively inserted is obtained by minimizing hydraulic deterioration, while preserving communication (low value of average path length) and connectivity (high value of algebraic connectivity λ_2) through a heuristic optimization criterion.

The procedure is tested on the WDN of Skiathos Island, Greece, through the analysis of dimensional and robustness indices (Yazdani and Jeffrey, 2010) that measure the performance of the partitioned network.

2. METHODOLOGY

The partitioning procedure used consists of: Phase 1, Water network clustering and Phase 2, Water network physical dividing.

Regarding *Phase 1*, considering a simple graph $G=(V,E)$ $G = (V, E)$, $G = (V, E)$ where V is the set of n vertices v_i (or nodes) and E is the set of m edges e_l (or links), a k-way graph clustering problem consists of partitioning V vertices of G into k subsets, $P_1, P_2, \ldots, P_k$ (Di Nardo et al., 2017).

Graph clustering can be achieved by optimizing an objective function related to one of the clustering aims (i.e. clusters balancing, minimization of boundary pipes) (Boccaletti et al., 2006; Fortunato, 2010). In this paper, for the clustering phase, a GP algorithm was implemented in SWANP 3.0 software (Di Nardo et al., 2013a).

GP is a computer science technique developed to solve problems that requiringe huge computational power, such as finite element based simulations that require the distribution of a finite element mesh among different processors. Therefore, GP techniques were developed in computer science for optimal allocation of a computational mesh in parallel or distributed computing architectures (Di Nardo et al., 2013a).

Specifically, *Phase 1* was achieved with SWANP 3.0, through a Multi-Level Recursive Bisection (MLRB) algorithm, a highly effective method for the k-way graph clustering (Karypis and Kumar 1998a, b). MLRB techniques are based on the following principal phases: a) *coarsening*, which simplifies the original graph $G_0=(V_0, E_0)$, through a node aggregation that generates a sequence of smaller graphs $G_i=(V_i, E_i)$, namely the coarser graphs, each with fewer vertices so that $|V_i|<|V_i-1|$. This phase is essential for reducing the dimensions of a graph and, consequently, the complexity of finding a k-way clustering. b) *Clustering*, through which a k-way clustering is found by recursive bisection, performing a sequence of 2-way clustering. In this phase, through an optimization procedure, a clustering is obtained with the minimum number of edges N_{ec} and with a balanced number of vertices n_p belonging to each subset, with the optimal limit condition of n_p=n/k. c) *Uncoarsening* (also with refinement), a projection from the coarser graph G_m back to the original graph G_0 by going through the graphs $G_{m-1}, G_{m-2}, \ldots, G_1$ (uncoarsening), with a local optimization of the partition (refinement) using heuristic algorithms (Hendrickson and Leland,

1993), thus decreasing the edge-cuts by moving a vertex from one partition to another. This was implemented in the SWANP 3.0 software (Di Nardo et al., 2013a).

After defining the set N_{ec} of the edge-cuts, *Phase 2* aims to establish the pipes in which, gate-valves N_{gv} and flow meters N_{fm}=(N_{ec}-N_{gv}) need to be inserted. This can be assimilated to a WDNs valve placement problem, an NP-hard problem (Bodlaender et al., 2010) that requires heuristic algorithms to find optimal solutions in the following space of combinations N_c computed by the binomial coefficient:

$$N_C = \binom{N_{ec}}{N_{fm}} \tag{1}$$

To achieve the goal of *Phase 2*, a GA was designed (Di Nardo et al., 2013a). In this paper, once the number of flow meters N_{fm} is fixed, to define optimal location of gate valves and flow meters, five Objective Functions (OFs), combining energy, topological, and spectral metrics, were tested:

$$OF_1 = \frac{P_N}{P_N^*} \tag{2}$$

where $P_N = \gamma \sum_{i=1}^{n} Q_i H_i$ is the total nodal power of the partitioned layout, γ is the water specific weight, Q_i and H_i are respectively the water demand and the hydraulic head at each node, while P^*_N is the total nodal power of the original network layout;

$$OF_2 = \frac{APL^*}{APL} \tag{3}$$

where $APL = \sum_{\forall s \neq t} \sigma(s,t)/0.5n(n-1)$ is the average path length (Watts and Strogatz, 1998) of the partitioned layout, n is the total number of the network vertex, $\sigma(s, t)$ is the shortest path between two nodes s and t, computed as the number of edges or the sum of the weights of the edges respectively for unweighted/weighted network, APL^* is the average path length of original network layout;

$$OF_3 = \frac{\lambda_2}{\lambda_2^*} \tag{4}$$

where λ_2 is the second smallest eigen-value of Laplacian matrix (Fiedler, 1973) of the partitioned layout, defined as L=D-A, in which D=diag(d_i) is the diagonal matrix of the node-degrees, A=(a_{ij}) is the adjacency matrix of graph G in which the element $a_{ij}\neq 0$ if the nodes i and j are connected, for an unweighted network a_{ij}=1, while for weighted network a_{ij}=w_{ij} with w_{ij} equal to the weight associated to the link ij; λ^*_2 is the corresponding value of original network layout;

$$OF_4 = \frac{P_N}{P_N^*} + \frac{APL^*}{APL} \tag{5}$$

$$OF_5 = \frac{P_N}{P_N^*} + \frac{\lambda_2}{\lambda_2^*} \tag{6}$$

The last two multi-objective functions consider the effect of hydraulic energy coupled with network topology (OF4) and spectral metric (OF5). This multi-objective optimization approach is known as the "weighted-sum" or "scalarization" method (Caramia and Dell'Olmo, 2008) that represents a new optimization problem with a unique objective function composed by two functions.

3. SIMULATION RESULTS

The proposed procedure was tested on the real medium size WDN of Skiathos, a Greek touristic Aegean Sea island of 6,000 inhabitants. The network (Figure 1) was modeled in EPANET2

(Rossman, 2000). with m=282 pipes, n=184 nodes, one source and a total pipe length L_{tot}=18.25 km.

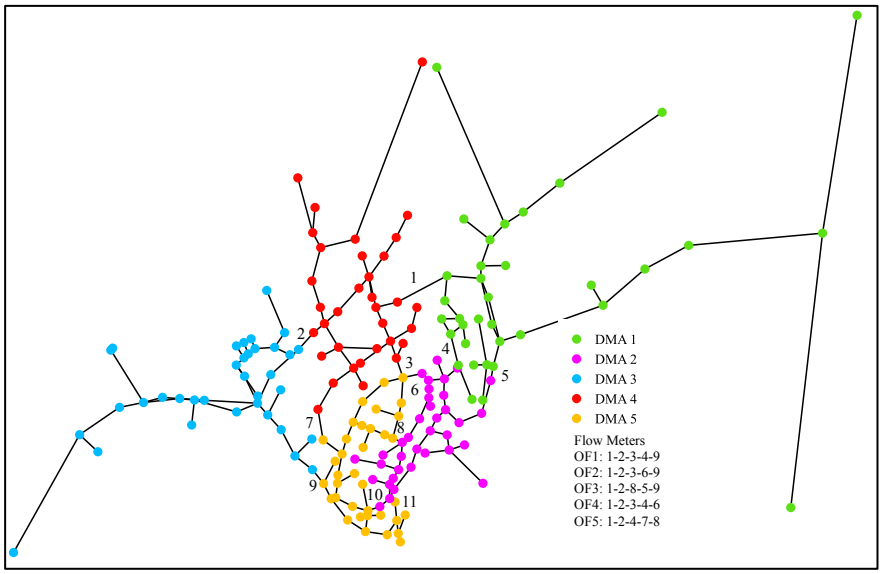

Figure 1. Skiathos WDN with representation of DMAs and boundary pipes.

Firstly, the WDN was clustered (*Phase 1*) by SWANP 3.0 software in 5 DMAs of approximately equal nodes as confirmed by the balancing index I_B=1.02 and with N_{ec}=11 boundary pipes (or edge-cuts). Then, starting from the same clustering layout, the number of flow meters was fixed to N_{fm}=5 (consequently, N_{gv}=6) and the dividing phase (*Phase 2*) was carried out for each previously defined OFs (equations 2, 3, 4, 5 and 6). For comparing simulation results, two categories of Performance Indices (PIs) were involved:

a) *resilience performance indices*: mean node pressure h_{MEAN}, maximum node pressure h_{MAX}, minimum node pressure h_{MIN}, standard node pressure deviation $h_{SD,}$ resilience index I_R (Todini, 2000) and resilience deviation index I_{RD};

b) *robustness performance indices*: index of robustness deviation, R_D, obtained as a modification of the Piraveenan et al (2013) robustness coefficient R (7), that evaluates the network ability to avoid malfunctioning when a fraction of its elements, links or nodes, is damaged:

$$R = \frac{0.5 \cdot S_0 + \sum_{j=1}^{m-1} S_j + 0.5 \cdot S_m}{0.5 \cdot S_0^* + \sum_{j=1}^{m-1} S_j^* + 0.5 \cdot S_m^*} \tag{7}$$

where S_j represents the largest size of connected component of water partitioned network after the removal of j links and S^*_j the corresponding value for the original network. The large size of connected component S will become S=1 only when all links are removed.

Values of OFs and energy and topological performance indices are reported, respectively, in Tables 1 and 2 for all WNP layouts obtained with different OFs (WNP_{OF}) and for the original network layout (ONL).

The impact of a multi-objective approach on the positioning of flow meters and gate valves in the boundary pipes can be observed in Table 1, which depicts different values when energy, topological or spectral metric, or their combinations, were used in the OF. As expected, P_N is higher with WNP_{OF1} while the lowest increase of *APL* corresponds to the partitioned layout obtained with WNP_{OF2} and the best λ_2 value is obtained with WNP_{OF3}. Nevertheless, the optimization of WNP_{OF4} and WNP_{OF5} provided interesting results. The values of P_N of WNP_{OF4} and WNP_{OF5} are substantially equal to the partitioned layout obtained with *OF1* (computed only with energy consideration) and better than the WNP carried out by optimization of WNP_{OF2} and WNP_{OF3} (computed without energy considerations). Furthermore, the solutions obtained with *OF4* and *OF5*

improve significantly the values of *APL* and λ_2 of WNP_{OF1}, although they obviously worsen the corresponding values of WNP_{OF2} and WNP_{OF3} (computed only with topological and spectral considerations, respectively).

Table 1. Simulation results obtained with GA using different OFs vs ONL

	ONL	**WNP_{OF1}**	**WNP_{OF2}**	**WNP_{OF3}**	**WNP_{OF4}**	**WNP_{OF5}**
P_N (kW)	104.846	104.588	102.431	102.615	104.266	104.005
APL (m)	981.63	1135.72	1022.62	1098.03	1044.74	1097.22
λ_2	0.4815	0.1315	0.2646	0.3206	0.2279	0.2670
OF	-	0.998	0.960	0.666	1.934	1.546

Table 2. Resilience and robustness performances indices of all WNP layouts vs ONL

	ONL	**WNP_{OF1}**	**WNP_{OF2}**	**WNP_{OF3}**	**WNP_{OF4}**	**WNP_{OF5}**
h_{MIN} (m)	7.06	7.10	7.28	7.09	6.99	6.97
h_{MEAN} (m)	47.98	47.91	47.17	47.16	47.77	47.68
h_{MAX} (m)	61.54	61.54	61.54	61.54	61.54	61.54
h_{SD}(m)	10.29	10.30	10.27	10.35	10.30	10.32
I_R	0.961	0.957	0.921	0.924	0.951	0.947
I_{RD} (%)	-	0.42	4.16	3.85	1.04	1.46
R_D (%)	-	69.85	77.34	72.52	69.09	64.03

The result analysis in terms of performance indices (Table 2) shows that maximum and mean nodal pressure of the original WDN, h_{MAX}=61.54 m and h_{MEAN}=47.98m, are both significantly higher than the design pressure of h^*=15 m required to satisfy water demand at all nodes. However, minimum pressure h_{MIN}=7.06 m is lower than h^*, which means that there are nodes (particularly only one node) for which the design pressure limit is not fulfilled. This also determines a high value of standard deviation h_{SD}=10.29 m. Moreover, the system shows high energy resilience I_R=0.961 and, consequently, "good availability" to be partitioned without a decrease in hydraulic performance (Greco et al, 2012).

All WNP layouts show satisfying energy performance with deviation of resilience index I_{RD}<5.00%. Indeed, values of minimum, mean and maximum pressure are practically equal to the value of original network (Table 2) with best results for WNP_{OF1}, WNP_{OF4} and WNP_{OF5} with an I_{RD}<1.5%. In terms of robustness, instead, the best results are by far those associated to the network layouts WNP_{OF2} (R_D=77.34) and WNP_{OF3} (R_D=72.52).The simulation results confirm the effectiveness of the proposed optimization approach with significant and coherent changes of objective functions as reported in Table 1. Therefore, evidently, the choice of the best partitioning layout depends on the operator objectives. Anyway, for this case study, the layout WNP_{OF1} shows a good compromise between energy (I_{RD}=0.42) and robustness (R_D=69.85). Furthermore, although WNP_{OF4} and WNP_{OF5} provide better values of *APL* and λ_2 metrics than layout WNP_{OF1}, the robustness deviation of WNP_{OF1} layout (R_D=69.85) is better.

In Figure 1, to show all layout solutions, the boundary pipes N_{ec} are highlighted using a numerated label and, for each WNP, the index of pipes where flowmeters were inserted are reported.

4. CONCLUSIONS

The proposed multi-objective optimization approach based on energy, topological and spectral metrics represents an effective methodology to define the optimal positioning of flowmeters and gate valves on boundary pipes. Despite the small size of the WDN tested, results show a remarkable sensibility of energy, topological and spectral metrics to describe alterations of the network.

Therefore, the proposed approach, that will be applied in future studies on larger WDNs, provide water utilities with a novel tool to define optimal water network partitioning by evaluating, simultaneously, network resilience and robustness.

REFERENCES

Alonso, J. M., Alvarruiz, F., Guerrero, D., Hernàndez, V., Ruiz, P.A., Vidal, A.M., Martìnez, F., Vercher, J, Ulanicki, B., 2000. Parallel computing in water network analysis and leakage minimization. J. Hydr. Engineering; 126:251-260.

Alvisi, S., Franchini, M., 2014. A Procedure for the Design of District Metered Areas in Water Distribution Systems. Procedia Engineering; 70: 41-50.

AWWA Research Foundation, 2003. Water loss control committee. Applying wordwide BMPs in water loss control. J Am Water Works Assoc 95(8):65–79.

Boccaletti, S., Latora, V., Moreno, Y., Chavez, M., Hwanga, D-U., 2006. Complex networks. Structure and dynamics. Physics Reports; 424:175-308.

Bodlaender, H. L., Hendriks, A., Grigoriev, A., Grigorieva, N.V. 2010. The valve location problem in simple network topologies. *INFORMS Journal on Computing*, vol. 22, n. 3, pp 433-442.

Caramia, M., Dell'Olmo, P. 2008. Multi-objective Management in Freight Logistic. Springer-Verlag.

Di Nardo, A., Di Natale, M., Giudicianni, C., Greco, R., Santonastaso, G.F., 2017. Water supply network partitioning based on weighted spectral clustering. Complex Networks & Their Applications V, Studies in Computational Intelligence; 693: 797-807.

Di Nardo, A., Di Natale, M., Giudicianni, C., Santonastaso, G. F., Tzatchkov, V.G., Varela, J. M. R., Yamanaka, V.H.A., 2016. Water Supply Network Partitioning Based on Simultaneous Cost and Energy Optimization. Procedia Engineering; 162: 238-245.

Di Nardo, A., Di Natale, M., Musmarra, D., Santonastaso, G. F., Tzatchkov, V., Alcocer-Yamanaka, V. H., 2015. Dual-use value of network partitioning for water system management and protection from malicious contamination. Journal of Hydroinformatics; 17:361-376.

Di Nardo, A., Di Natale, M., Santonastaso, G. F., Venticinque, S., 2013a. An Automated Tool for Smart Water Network Partitioning. Water Resources Management; 27: 4493-4508.

Diao, K., Zhou, Y., Rauch, W., 2013. Automated creation of district metered area boundaries in water distribution systems. Journal of Water Resources Planning and Management; 139:184-190.

Ferrari, G., Savic, D., Becciu, G., 2014. A graph theoretic approach and sound engineering principles for design of district metered areas. J. Water Resour. Plan. Manag.; 140: 04014036.

Fiedler, M., 1973. Algebraic connectivity of graphs. Czech. Math. J.; 23:298.

Fortunato, S., 2010. Community detection in graphs. Physics reports; 486:75-174.

Grayman, W. M., Murray, R., Savic, D. A., 2009. Effects of redesign of water systems for security and water quality actors. In: Starrett S (eds) Proc of the World Environmental and Water Resources Congress; 342:504-514.

Greco, R., Di Nardo, A., Santonastaso, G. F., 2012. Resilience and entropy as indices of robustness of water distribution networks. Journal of Hydroinformatics; 14:761-771.

Hastie, T., Tibshirani, R., Friedman, J., 2001. Elements of statistical learning: data mining, inference and prediction. Springer-Verlag; 2001.

Hendrickson, B., Leland, R., 1993. A multilevel algorithm for partitioning graphs, tech. report SAND93-1301. Sandia National Laboratories, Albuquerque.

Herrera, M., Canub, S., Karatzogloub, A., Perez-Garcıa, R., Izquierdo, J., 2010. An approach to water supply clusters by semi-supervised learning. International Congress on Environmental Modelling and Software Modelling for Environment's Sake, Fifth Biennial Meeting, Ottawa, Canada.

Herrera, M., Izquierdo, J., Pérez-García, R., Montalvo, I., 2012. Multi-agent adaptive boosting on semi-supervised water supply clusters. Advances in Engineering Software; 50: 131-136.

Izquierdo, J., Herrera, M., Montalvo, I., Pérez-García, R., 2011. Division of water distribution systems into district metered areas using a multi-agent based approach. Communications in Computer and Information Science; 50:167-180.

Karypis, G., Kumar, V., 1998a. A fast and high quality multilevel scheme for partitioning irregular graphs. SIAM J Sci Comput 1; 20:359-392.

Karypis, G., Kumar, V., 1998b. MeTis: a software package for partitioning unstructured graphs, partitioning meshes and computing fill-reducing orderings of sparse matrices. Version 4.0. University of Minnesota, Minnesota.

Mays, W., 2000. Water distribution systems handbook. McGraw-Hill, New York.

Perelman, L. S., Allen, M., Preis, A., Iqbal, M., Whittle, A.J., 2015. Automated sub-zoning of water distribution systems. Environ. Model. Softw.; 65:1-14.

Rossman, L. A., 2000. EPANET2 Users Manual. US EPA, Cincinnati, Ohio.

Todini, E., 2000. Looped water distribution networks design using a resilience index based heuristic approach. Urban Water 2; 2:115-122.

Tzatchkov, V., Alcocer-Yamanaka, V., Bourguett-Ortíz, V., 2006. Graph theory based algorithms for water distribution network sectorization projects. In Proc. of the 8th Annual Water Distribution Systems Analysis Symposium WDSA, Cincinnati, Ohio, USA.

Von Luxburg, U., 2007. A Tutorial on Spectral Clustering. Statistics and Computing; 17:395-416.

Watts, D. J., Strogatz, S. H., 1998. Collective dynamics of 'small-world' networks. Nature; 393; 440-442.

Xia, l., Guo-Jin, L., 2010. Leak Detection of Municipal Water Supply Network Based on the Cluster-analysis and Fuzzy Pattern Recognition. International Conference on E-Product E-Service and E-Entertainment (ICEEE); 1:7-9.

Yazdani, A., Jeffrey, P., 2010. Robustness and vulnerability analysis of water distribution networks using graph theoretic and complex network principles. Proceeding of Water Distribution System Analysis, Tucson, Arizona, September 12-15.

Proceedings of the 10th World Congress of EWRA 'Panta Rhei', 5-9 July 2017, Athens, Greece
© 2017 *European Water Resources Association*

Waterloss detection in streaming water flow timeseries using change-point anomaly methods

S.E. Christodoulou[1,2], E. Kourti[1] and A. Agathokleous[1]
[1] *Nireas International Water Research Center, University of Cyprus, 1 Panepistimiou Avenue, Aglantzia, Cyprus*
[2] *Department of Civil and Environmental Engineering, University of Cyprus, 1 Panepistimiou Avenue, Aglantzia, Cyprus*
[*] *e-mail: schristo@ucy.ac.cy*

Abstract: The work described herein evaluates the utilization of a change-point method for the detection of anomalies in water consumption time series, and its applicability to waterloss detection in water distribution networks. The change-point detection method is based on the Relative unconstrained Least-Squares Importance Fitting (RuLSIF) algorithm and was implemented on a three-month-long hourly water consumption signal, successfully detecting unusual reductions and increases in the water consumption patterns, and classifying them as anomalies. The first water consumption anomaly type related to a discontinuity in the signal (a break in the consumer's water consumption patterns), whereas the second type related to an unusual increase in the signal (two waterloss incidents). Unlike traditional approaches that monitor the average current periodic consumption and compare this average to the one from a corresponding past period, the RuLSIF change-point detection approach is dynamic and sensitive to any change in the time series in study. Even though the proposed analysis does not predict future anomalies, it is suitable for past and near-real-time anomaly detection; an attribute that is sufficient for waterloss management as it allows for a timely detection of anomalies is streaming water flow data. Further, the method dynamically assigns anomaly scores to the detected changes in the signal, thus easing waterloss detection and appraising the severity of each detected incident. The change-point detection method is able to extract knowledge from past consumption patterns (the water flow signal over time) to detect anomalies in the signal, both in the past and in near-real-time, and for both physical and apparent water losses.

Key words: Waterloss detection; Water-flow anomaly detection; Real-time time-series analysis

1. INTRODUCTION

As water distribution networks (WDNs) worldwide are rapidly degrading and damages in them are increasing, the need for efficient assessment and real-time monitoring is increasingly becoming pressing. The damages in WDNs are most often manifested as pipe-failure incidents and are leading to significant levels of non-revenue water (typically in the range 20%-30%). While data on pipe-failures can, post-event, be analyzed and provide useful knowledge on the causalities of the failures, records of these incidents are usually hard to produce, are inconsistent and poorly recorded, and most often only span over short periods of time. Thus, the need for timely detection of any anomalies in the WDNs and the correlation of such anomalies to waterloss, has become of outmost importance to the efficient operations of WDNs.

Anomalies in WDN operations usually manifest themselves in the form of pipe-failure incidents (pipe breaks) and in the form of water loss. While pipe-failures are not a perfect indicator of WDNs, they are amongst the primary symptoms of network degradation and one of the few sources of information on the condition of WDNs. However, recording pipe-failure incidents is a relatively recent practice. Furthermore, knowledge of the type of pipes and their condition over an area is often unknown prior to a pipe-failure incident which requires repair.

Past efforts had led to the identification of several risk factors influencing the fragility of WDNs and devising decision support systems for sustainably managing them. For example, Christodoulou & Deligianni (2009) used data mining techniques and neurofuzzy systems in order to identify pipe-failure data clusters and convert these into decision support rules for waterloss management. Subsequently, Christodoulou & Agathokleous (2012) studied the effects of intermittent water

supply on the vulnerability of WDNs, reporting that intermittent water supply policies resulted in increased stresses in the network they were applied to that eventually lead to an abnormally high number of pipe-failure incidents and higher volumes of water losses. The spatial distribution of pipe-failure incidents was studied by Gagatsis et al. (2012) who, first used spatial analysis techniques and a spatial clustering method to study the extend of pipe-failure clustering in the Limassol WDN and, then, transformed the deduced knowledge into a decision support system.

To date, pipe-failure incident records are usually the result of customer complaints (e.g. low pressure, no water, high bills, etc.) which are then investigated by Water Board technicians. However, all of these sources of information often require a certain amount of time before the source of a leak is discovered thus resulting in significant water losses until the damage is repaired. In order to resolve this problem, the use of automatic meter reading (AMR) is being advocated and is currently implemented widely.

Automatic meter readers are devices embedded in house connection meters which can provide readings in frequent intervals. These readings are transferred to a monitoring server. By examining unusual rises or drops in water consumption, water board technicians can be made aware of potential leaks and investigate them, thus resulting in a faster, more efficient leak detection method. Furthermore, the use of AMR can provide near real-time information on the water consumption within a district metered area (DMA) and compare it with the total water input in that DMA. A DMA is an area of the WDN where water originates and is distributed to the network from a single point of entry and where the network's water pressure is approximately uniform. Large differences between periodic readings indicate large leaks within the network.

In principle, the use of AMR devices permits Water Boards to detect water leaks before they are reported by customers. This is particularly useful in cases when customers are away on vacation or in cases when the leak is not detectable by the customers. The AMR devices send consumption information in frequent intervals to the central database. This data is then analyzed for detecting abnormal increases in water consumption readings sent from the AMR units. When such an abnormal increase is detected an alert is sent to the WDN operators of possible WDN malfunction, and then the WDN operators are tasked with linking the event with a possible water leakage.

This process is in many aspects subjective (in terms of how the anomaly thresholds are set) and manual (thus time consuming) with regards to the analysis of indicators (outliers) of water consumption anomalies. Further, the architecture shown in Figure 1 relies heavily on the wide use of AMR devices in the WDN (one for each house connection) and thus it is not cost-efficient.

A solution could be the selective location of AMR devices (or sensors) within the WDN, for which several sensor placement optimization techniques exist (Ostfeld et al. 2008, Christodoulou et al. 2013, Christodoulou 2015). The problem, though, of analyzing the sensed operational data of a WDN still remains, in terms of processing time-related data and sifting through this data for possible anomalies in the WDN's behavior.

A recent work on the dynamic analysis of time series related to water consumption was recently reported upon by Christodoulou et al. (2016), in which wavelet change-point detection classifiers were utilized for identifying anomalies in the consumption patterns. The wavelet change-point method utilizes the continuous wavelet transform (CWT) of time-series (signals) to analyze how the frequency content of a signal changes over time. In the case of water distribution networks the time-series relates to streaming water consumption data from automatic meter reading (AMR) devices, at either the individual consumers' level or at an aggregated district meter area (DMA) level. The wavelet change-point detection method analyzes the provided time-series to acquire inherent knowledge on water consumption under normal conditions at household or area-wide levels, to then make inferences about water consumption under abnormal conditions.

The paper proposes an approach to the timely identification of anomalies in WDN by use of a change-point anomaly detection algorithm and of streaming water consumption data from consumers and from district meter areas (DMA), in the form of 'automatic meter reading' devices (AMR). The anomaly detection approach is then coupled with spatio-temporal analysis to arrive at spatial decision support systems (DSS) that automate the process of waterloss detection, reduce

water loss and increase the efficiency in the management WDN, and eventually positively contribute to the sustainability of such networks.

2. CHANGE-POINT DETECTION

Change-point detection refers to the identification of both whether or not a change (or several changes) has occurred in a time series (signal), and of the times of any such changes. Common change-point detection methods relate to changes in the mean, variance, correlation, density, or slope of the signal in study.

Among the several change-point detection methods found in literature, notable is the approach proposed by Yamada et al. (2013) and Liu et al. (2013), who presented a statistical change-point detection algorithm based on non-parametric divergence estimation between time-series samples from two retrospective segments. The algorithm uses the relative Pearson (PE) divergence as a divergence measure and a method of direct density-ratio estimation. Mathematically, the PE divergence from *p(x)* to *p'(x)* is defined as

$$PE[p(x), p'(x)] \coloneqq \frac{1}{2}\int \left(\frac{p(x)}{p'(x)} - 1\right)^2 p'(x)dx \tag{1}$$

and, in their work, Yamada et al. (2013) and Liu et al. (2013) proposed an approach to distribution comparison called α-relative divergence estimation, by which they estimated the α-relative divergence (defined as the divergence from *p(x)* to the α-mixture density $\alpha p(x) + [1 - \alpha p'(x)]$ for $0 \leq \alpha < 1$. By use of Eq. 1, the α-relative Pearson (PE) divergence is given by

$$PE_a[p(x), p'(x)] \coloneqq \frac{1}{2}\int \left(\frac{p(x)}{\alpha p(x)+(1-\alpha)p'(x)} - 1\right)^2 [\alpha p(x) + (1-\alpha)p'(x)]dx \tag{2}$$

and the α-relative divergence was estimated by the researchers by direct approximation of the α-relative density ratio given by

$$r_\alpha(x) \coloneqq \frac{p(x)}{\alpha p(x)+(1-\alpha)p'(x)} \tag{3}$$

Yamada et al. (2013) also showed that using an estimator of the α-relative density-ratio $r_\alpha(x)$, we can construct several estimators of the α-relative PE divergence, of which the following one is easy to compute:

$$\widehat{PE}_\alpha \coloneqq \frac{1}{2n}\sum_{i=1}^{n} \hat{r}\,(x_i) - \frac{1}{2} \tag{4}$$

In its final form, and by using an estimator $\hat{g}(Y)$ of the α-relative density ratio, the RuLSIF method approximates the α-relative PE divergence by use of the following equation (Yamada et al., 2013):

$$\widehat{PE}_\alpha \coloneqq -\frac{\alpha}{2n}\sum_{i=1}^{n} \hat{g}\,(Y_i)^2 - \frac{1-\alpha}{2n}\sum_{i=1}^{n} \hat{g}\left(Y'_j\right)^2 + \frac{1}{n}\sum_{i=1}^{n} \hat{g}\left(Y'_j\right) - \frac{1}{2} \tag{5}$$

where, *y(t)* is the time-series sample at time *t*, *Y(t)* is the subsequence of *k* timeseries samples at time *t*, and *n* is the number of points in the analysis window.

3. CASE-STUDY IMPLEMENTATION, ANALYSIS AND DISCUSSION

The RuLSIF change-point detection method is tested on a three-month-long hourly timeseries of a water flow signal (approximately 2,200 hours), depicting the water consumption of a 3-person

household, with an average total daily water consumption of about 419 L (based on records from a local Water Board), distributed hourly across the day as per Figure 1. Water consumption starts in the early morning hours (around 06:00), increases peaking up at around 10:00, then drops until the early afternoon hours (16:00), peaking up again in the late afternoon and early evening hours (18:00 - 21:00), before dying down at night (21:00 - 06:00). It should be also noted that the household's daily water consumption does not, at any point in time, zero out. This is in agreement with the 'minimum night flow (MNF)' concept, commonly used in WDN operations. MNF is a common method used to evaluate water loss in a water network, and refers to the water volume flowing through the network even when all true water demand is zero (typically in the time band of 02:00 - 04:30).

Further to the profiled daily water consumption, three induced anomalies in the household's consumption are recorded (as shown in Figure 1): (1) a three-day-long drop in consumption (t ∈[680, 720] hours); (2) a 1-L/hour water loss for a duration of 48 hours (t ∈[510, 558] hours); and (3) a 2-L/hour water loss for a duration of 48 hours (t ∈[990, 1038] hours). The water consumption's time series (Figure 1) is first processed macroscopically to identify the time periods of concern, and then microscopically to zoom in on possible consumption anomalies.

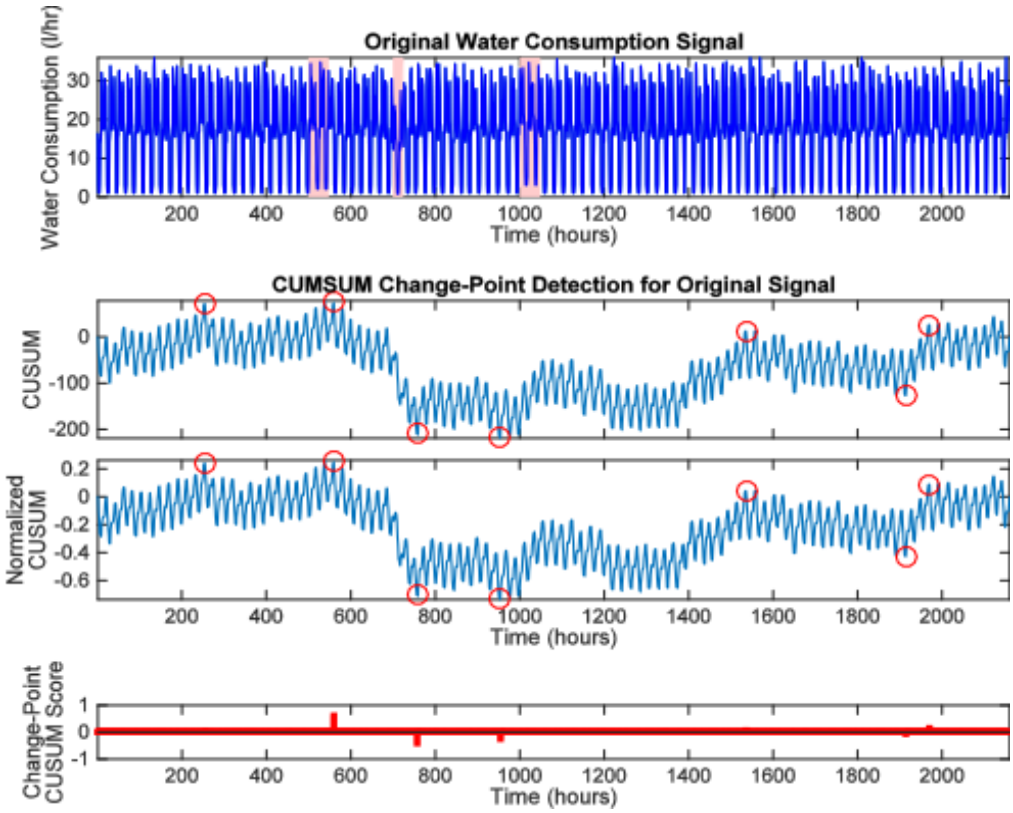

Figure 1. Water consumption signal for the period in study (approximately 2200 hours) and the CUSUM-based anomaly detection.

As a point of reference and subsequent assessment of the RuLSIF approach, the water consumption signal is first analyzed for anomalies by use of the cumulative sum (CUSUM) method, which is a well-known anomaly detection method. CUSUM is a statistical control chart used to track the variation of a process, able to detect small shifts in the process' mean. The CUSUM anomaly detection method is a statistical method for anomaly detection in univariate time series, using the out of control signals of the CUSUM charts to locate anomalous points. In effect, CUSUM works by tracking the individual cumulative sums of the negative and positive deviations from the mean (the high and low sums respectively), and by thresholding them against a predefined level of tolerance.

The water consumption signal with the three induced anomalies highlighted and the CUSUM-

based anomaly detection for this signal are as depicted in Figure 1. As shown, the CUSUM method correctly identifies the time periods of anomalies in the signal, but it also gives several false-positive alarms.

We then turn our attention to the RuLSIF method and its suitability to water-flow anomaly detection, first investigating the abnormal drop (Figure 2) and then the abnormal increase in water flow (Figures 3 and 4).

Figure 2 shows the signal for the period in vicinity to the observed water-flow drop ($t \in [680, 720]$ hours), and the corresponding RuLSIF-based anomaly detection. As depicted, the observed drop in water flow is correctly identified by the RuLSIF change-point detection method (with a slight time-shift in the detection as a result of the parameters used in the computation), and high anomaly scores are assigned to the approximate start and end points of the corresponding period.

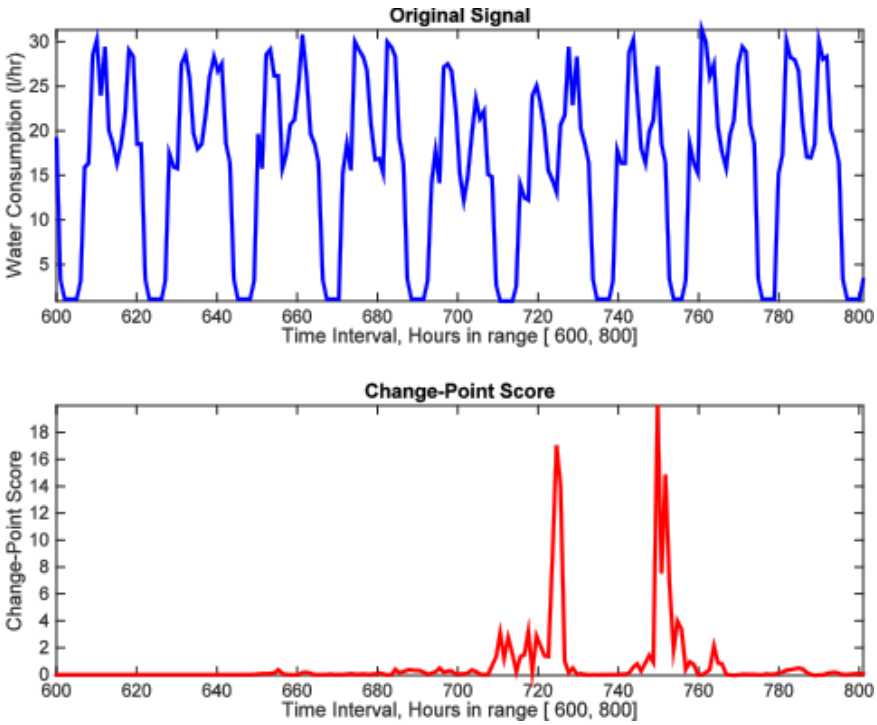

Figure 2. Water consumption signal for the period $t \in [600, 800]$ hours, and the RuLSIF-based change-point detection of a drop in water consumption.

The method performs equally well in detecting the sudden increase in water flow values (case of water loss), for both the 1-L/hour and the 2-L/hour anomalies (Figures 3a and 3b, respectively). Further, the computed anomaly scores can be used as a measure of the extent of the observed anomalies. In our case study, the change-point score for the 1-L/hour water loss is lower than the corresponding score for the 2-L/hour water loss (~0.75 vs. ~3.2, respectively).

4. CONCLUSION

The work described herein evaluates the utilization of the relative unconstrained least-squares importance fitting (RuLSIF) change-point method for the detection of anomalies in water consumption time series, and its applicability to water-loss detection in water distribution networks. The RuLSIF change-point detection method was implemented on an hourly water consumption signal of about 2200 hours duration, successfully detecting unusual reductions and increases in the water consumption patterns, and classifying them as anomalies. The first water consumption anomaly type related to a discontinuity in the signal (a break in the consumer's water consumption patterns), whereas the second type related to an unusual increase in the signal (two water-loss incidents).

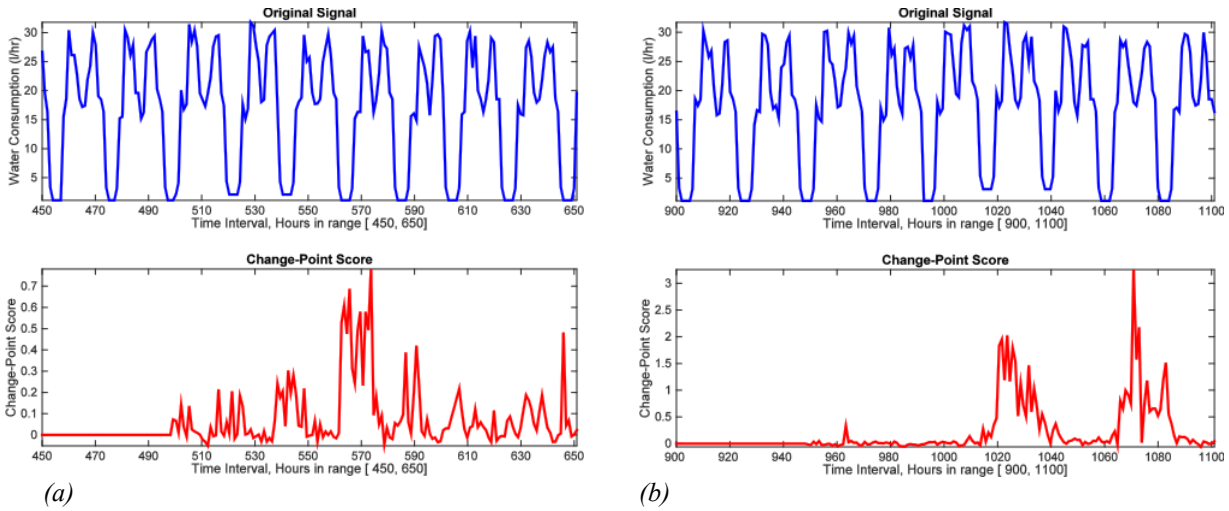

Figure 3. Water consumption signal for the periods $t \in [450, 650]$ and $t \in [900, 1100]$hours, and the RuLSIF-based change-point detection of an increase in water consumption; Case of (a) 1-L/hour water loss and (b) 2-L/hour water loss.

Unlike traditional approaches that monitor the average current periodic consumption and compare this average to the one from a corresponding past period, the RuLSIF change-point detection approach is dynamic and sensitive to any change in the time series in study. Even though the proposed analysis does not predict future anomalies, it is suitable for past and near-real-time anomaly detection; an attribute that is sufficient for water-loss management as it allows for a timely detection of anomalies is streaming water flow data. Further, the method dynamically assigns anomaly scores to the detected changes in the signal, thus easing water-loss detection and appraising the severity of each detected incident.

Ongoing research work on wavelet change-point detection will address spatial mapping and heat-map generation for the identification of areas of concern in a distribution network, as well as the blending of automatic meter reading (AMR) technologies and water auditing at a district meter area (DMA) level, for the dynamic (and near-real-time) detection of water leaks in an urban water distribution network.

REFERENCES

Christodoulou, S., 2015. Smarting up water distribution networks with an entropy-based optimal sensor placement strategy. Journal of Smart Cities; 1(1): 47-58.

Christodoulou, S., Agathokleous, A., 2012. A study on the effects of intermittent water supply on the vulnerability of urban water distribution networks. Journal of Water Science and Technology; 12(4): 523-530

Christodoulou, S., Deligianni, A., 2009. A neurofuzzy decision framework for the management of water distribution networks. Water Resources and Management; 24(1): 139-156.

Christodoulou, S., Gagatsis, A., Xanthos, S., Kranioti, S., Agathokleous, A., Fragiadakis, M., 2013. Entropy-based sensor placement optimization for waterloss detection in water distribution networks. Water Resources Management; 27(13), 4443-4468.

Christodoulou, S.E., Kourti, E., Agathokleous, A., 2016. Water Resources Management; doi:10.1007/s11269-016-1558-5.

Gagatsis, A., Kranioti, S., Christodoulou, S., Agathokleous, A., Xanthos, S., 2012. An integrated software solution for identifying, monitoring and visualizing water leak incidents in Water Distribution Networks. Proc., IWA's intern. conf. on new developments in IT & water, Amsterdam, Netherlands, 4-6 November 2012.

Liu, S., Yamada, M., Collier, N., Sugiyama, M., 2013. Change-point detection in time-series data by relative density-ratio estimation. Neural Networks; 43, 72-83.

Ostfeld, A., Uber, J.G., Salomons, E., Berry, J.W., Hart, W.E., Phillips, C.A., et al. 2008. The battle of the water sensor networks (BWSN): A design challenge for engineers and algorithms. Water Resources Planning and Management; 134:556-569.

Yamada, M., Suzuki, T., Kanamori, T., Hachiya, H., Sugiyama, M., 2013. Relative density-ratio estimation for robust distribution comparison. Neural computation; 25 (5), 1324–1370.

Proceedings of the 10th World Congress of EWRA 'Panta Rhei', 5-9 July 2017, Athens, Greece
© 2017 *European Water Resources Association*

Towards resilient water networks by using resilience key performance indicators

D. Ayala-Cabrera[1], O. Piller[1], J. Deuerlein[2] and M. Herrera[3]
[1] *Irstea, UR ETBX, Dept of Water, F-33612 Cestas, France*
[2] *3S Consult GmbH, D 76137 Karlsruhe, Germany*
[3] *EDEn-ACE Dept., University of Bath, Claverton Down, BA2 7AY Bath, UK*
[*] *e-mail: david.ayala@irstea.fr*

Abstract: The main objective of a water distribution network (WDN) is to deliver the required amount of water to the customer under a certain threshold of the desired pressure and quality. These networks are critical infrastructures that should face multiple and continuous changes and even abnormal events that alter their normal service provision. Water utility managers require modelling tools to be able to predict how the WDN will perform during disruptive events and understand how the system can better absorb them. Assessing and enhancing resilience in water infrastructures is a crucial step towards more sustainable urban water management. Several resilience key performance indicators (RKPIs) have been suggested to quantify and assessing WDNs resilience. This work proposes a structured classification for measuring and understanding the supply system by means of RKPIs. The proposed classification is based on a three-stage resilience concept which includes absorptive, adaptive, and restorative stages. This classification attempts to provide engineers, modellers, and managers with structured tools which allow a comprehensive analysis of crisis management case studies in order to enhance the WDN resilience. As the resources in supply are usually limited, recovery phases have a crucial role in resilience enhancing, while under sufficient availability of resources, deploying redundancy, making critical components stronger and ensuring a rapid recovery are all effective responses of the system.

Key words: resilience, key performance indicators, water distribution networks, critical infrastructures

1. INTRODUCTION

Water distribution networks (WDNs) provide the cities with an essential service for the life. In this sense, the main objective of a WDN is to deliver the required amount of water to the customer under a certain threshold of the desired pressure and quality (Jung, 2013). These networks are critical infrastructures that should face multiple changes and eventually abnormal events that alter their normal service. Water network security refers to the water supply guarantees under safety conditions for consumers, being necessary to count on assessing all kind of potential vulnerabilities. In addition, a WDN need to guarantee the availability of required quantity of water for sensitive customers, such as hospital, etc. (NIPP, 2013). In general context, resilience refers to the strength of the network and its behaviour under different anomalous events. The latter, in order to provide the network managers with measures that allow the implementation of actions and for supporting the decision-making process (NIPP, 2013). Resilience may also be perceived as a more general concept that is relied on three-capabilities of the system: 1) absorptive, 2) adaptive, and 3) restorative and may be characterized by four properties/attributes: 1) robustness, 2) redundancy, 3) resourcefulness and 4) rapidity (Francis & Bekera, 2014).

Water network resilience refers to design maintenance, and operations of water supply infrastructure that limit the effects of disruptions and enable rapid return to normal delivery of safe water to customers. The framework of the study is based on the Franco-German ResiWater Project (ResiWater, 2017), where the notion of resilience attempts to develop tools in order to prepare water utilities for crisis. Nowadays, water utility managers require modelling tools to predict how the WDN performs during disruptive events and to understand how the system can best absorb,

successfully adapt, and recover from them. Simulation and analysis tools help WDN managers to explore how their networks respond to unexpected events. So, demand-driven modelling (DDM) for normal operating conditions, and pressure-driven modelling (PDM) for failure conditions, help to simulate WDNs performance under failure event conditions.

This paper focuses on water quantity, and for the sake of simplicity we will work with a hypothetical benchmark network. This benchmarking network allows to: derive network resilience results, use resilience indicators under two different modelling approaches (DDM and PDM), and quantify the three resilience stages. Ultimately, this work proposes a structured classification by means of resilience key performance indicators (RKPIs). The classification is based on the conceptual definition proposed by the ResiWater Project. This attempts to provide engineers, modellers, and managers with structured tools which allow a comprehensive analysis of crisis management case studies with the aim of enhancing the WDN resilience.

2. MATERIAL AND METHODS

2.1 Three resilience stages

The proposed resilience paradigm might be implemented via the set of resilience capacities outlined above: absorptive, adaptive, and restorative capacity. Where absorptive capacity refers to the capacity of the system to absorb the impact of system perturbation and to minimize consequences with little effort. Adaptive capacity is the ability of the system to adjust undesirable situations by undergoing some changes if absorptive capacity has been exceeded. Restorative capacity refers to the ability of the system to implement long-term solutions so that the system performance reaches a stable or better level than the initial.

Three different states of WDN performance, P, are defined: normal, degraded, and failed. The three states for P, are determined by two thresholds: $\mathrm{P_{normal}}$ and $\mathrm{P_{failure}}$ corresponding to minimum P level for the network working in normal mode, and P level when the system is considered in failure mode, respectively.

The absorptive stage is measured since the event starts ($\mathrm{t_{event}}$) and goes until the water utility starts taking appropriate actions, which is denoted as palliative time ($\mathrm{t_{pall}}$). Additionally, two additional times, the degradation time ($\mathrm{t_{deg}}$) and the failure time ($\mathrm{t_{fail}}$), are defined. These correspond to the time at which the first consumer is affected by the event at different states of network performance. Thus, if the $\mathrm{t_{deg}}$ is greater than $\mathrm{t_{pall}}$, the state for absorptive stage corresponds to the normal state. For quantifying the resilience for this stage (R_{abs}), there are proposed three values for resilience $\mathrm{R_{abs}} = \{3, 2, 1\}$ that correspond to the three states at $\mathrm{t_{pall}}$ {NORMAL, DEGRADED, FAILED}. At this point, the internal vulnerability of the system ($\mathrm{V_{sys}}$) is a mirror of the absorptive capacity of the system, and may be assessed as $\mathrm{V_{sys}} = 4 - \mathrm{R_{abs}}$.

The adaptive stage begins before the absorptive stage ends and with the anomaly detection. It is characterized by a stabilization time, $\mathrm{t_{stab}}$, which is the time when all emergency measures are in place for maintaining the system performance.

To qualify the degree of severity, the acceptable time ($\mathrm{t_{acc}}$) is defined that corresponds to the maximum stipulated time in which the network can be in failure conditions. The quantification of the resilience in this stage (R_{adap}) will depend on the state of performance at $t = \min(t_{stab}, t_{acc})$. If $t_{stab} \leq t_{acc}$ then $R_{adap} = \{3, 2, 1\}$ but if $t_{acc} < t_{stab}$ then $R_{adap} = \{2, 1, 1\}$ with the state {NORMAL, DEGRADED, FAILED}.

The restorative stage begins when the $\mathrm{t_{stab}}$ ends, and when long-term solutions begin to be implemented (for instance, repairing or replace affected component). The last two stages end when the system performance reaches a stable level of performance equal or better than the initial one in nominal way ($\mathrm{P} \geq \mathrm{P_{normal}}$). Finally, the resilience for restorative stage will be determined whether the system succeeds in finding a new NORMAL state, then $R_{rest} = 3$ else it is less.

2.2 Selecting suitable indicators

The selection of the appropriate measure of resilience depends on the characteristic of the system in order to provide a specific service (IRGC, 2016). In this sense, for resilience studies it is crucial to specify what system state is being considered (resilience of what) and what perturbations are of interest (resilience to what). In this sense, several studies have been proposed in order to quantify the resilience of water distribution networks (Herrera et al., 2016).

In the group of indicators based on system power, the most popular is the resilience index by Todini (2000). The index is a ratio of the power arriving to the users, to the maximum power that can be dissipated in the network to meet the consumers' demand. In order to obtain a better representation of the network reliability other authors have proposed other definitions for the Todini's resilience index such as: minimum surplus head and Network resilience index by Prasad & Park (2004) and modified resilience index by Jayaram & Srinivasan (2008), among others.

Additional modifications for this index, which attempts to include different pressure-dependent modelling, are Saldarriaga et al. (2010). The most recent modification of Todini's resilience index was proposed by Creaco et al. (2016). The authors attempt to include in the indicator two different pressure-dependent modeling cases (leakage and consumption).

2.3 Model and Equations

The hydraulic conditions of the networks have generally been evaluated using DDM models as a function of demand under normal operating conditions and additional PDM implementations which have shown better response to approach WDN analysis under failure conditions. Thus, the operation of water distribution networks can be assessed by using hydraulic computer models, such as PORTEAU and EPANET. On the one hand, in the application for systems with inadequate capacity or pipe failure, the classical DDM approach is stretched to its limits (Braun et al., 2016). On the other hand, a consumption model that doesn't consider the available pressure is especially damaging in abnormal situations, such as low pressures resulting from hydraulic and mechanical failures. This is the reason why PDMs have been introduced (Piller et al., 2003).

Topological characteristics of the Network. In hydraulic modelling the simplified topological structure of a WDN is described by a directed graph. This graph represents pipe sections as links and pipe junctions as nodes. The mathematical description of this graph is given by the incidence matrix $A^{N}_{i,j}$ (see, Equation 1).

$$A^{N}_{i,j} = \begin{cases} -1, & \text{if node } i \text{ is terminal point of pipe } j \\ 0, & \text{if node } i \text{ is not connected to pipe } j \\ 1, & \text{if node } i \text{ is the initial point of pipe } j \end{cases} \quad (1)$$

DDM. Matrix A^N can be partitioned into two submatrices, A_f and A; that represent nodes with fixed head (reservoirs or tanks) and nodes with unknown head (demand or junction nodes), respectively. The equations that describe the steady-state of the system by the potential at the nodes (head) and the current links flows (Piller et al., 2003) are given by Equation 2.

$$\begin{cases} Aq + d = 0; & \text{mass balance at every node} \\ \Delta h(r,q) - A^{T}h - A_f^{T}h_f = 0; & \text{energy balance} \end{cases} \quad (2)$$

where; q and h are vectors of flow rates in the links and the heads at junction nodes, respectively; d is the vector of demand; h_f is the head at fixed head nodes; r is the pipe friction coefficient; and $\Delta h(r,q)$ describes the head losses in the links.

PDM. In DDM, nodal demands are always satisfied at all nodes, independent of the available pressure head values at the corresponding demand nodes. In DDM analysis, available flow at node i, c_i (available outflow at node i) is always equal to the required design d_i (demand at node i);

hence, $c_i = d_i$ (Sivakumar & Prasad, 2014). In contrast, in PDM the outflow is determined by a relationship between the available pressure head and the outflow. This relation, is denoted Pressure –Outflow Relationship (POR). The PORs are able to show how the system has the ability to regulate itself in terms of the available outflow and reordering the supply head pressure if it is under failure conditions. In this way, it can be supplied a remainder of delivered flow. Wagner et al. (1988) formulation (Equation 3) is the most accepted POR to evaluate networks operation under failure conditions.

$$c(h) = d \times \begin{cases} 1 & \text{, if } h_s \leq h \\ \left(\frac{h-h_m}{h_s-h_m}\right)^{0.5} & \text{, if } h_m < h < h_s \\ 0 & \text{, if } h \leq h_m \end{cases} , \quad (3)$$

where: h_s is the service head necessary to fully satisfy the required demand; h_m is the head below which no water can be supplied. The latter is the minimum head which is usually defined as nodal elevation.

The DDM system (Equation 2) and its PDM counterpart can be solved efficiently by a damped Newton method (Elhay et al., 2015). Moreover, explicit formulae exist for calculating the DDM and PDM sensitivities with respect to the demand parameter (Piller et al., 2017). These local sensitivities bring important information about the influence of the parameter on the hydraulic state: for example, where to place sensors or confidence intervals for the hydraulic predictions.

3. RESULTS AND COMMENTS

3.1 Definition of the network and performance analysis

The study of the resilience that is applied in this section is based on the three stages of resilience. For demonstration, a hypothetical network, originally proposed by Islam et al. (2011) is used. The network is composed of two reservoirs, twenty–five water demand nodes and forty pipes (Figure 1.a). The total length of all pipes is 19.5 km. The water is supplied by gravity from the elevated reservoirs with the total heads of 90 m and 85 m, respectively. Pipe length varies from 100 m to 680 m and the diameters vary from 200 mm to 700 mm. The basic demand is in the range of 33.33 L/s to 133.33 L/s and the demand pattern is defined for 24 hours (Figure 1.c).

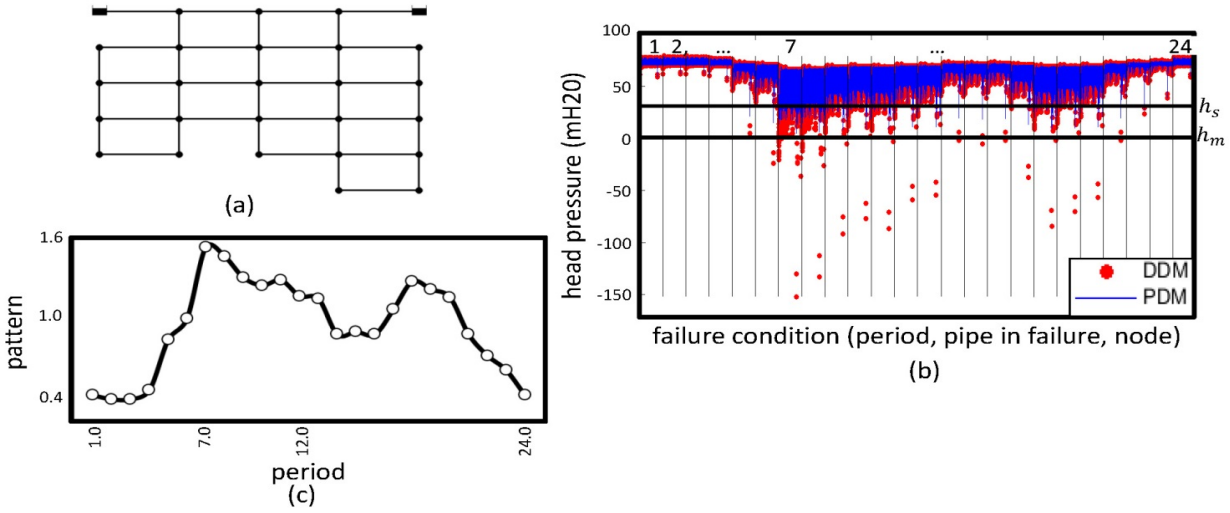

Figure 1. Pipe characteristics and pressure results. (a) Network layout; (b) single pipe failure condition for all periods; (c) demand pattern.

The analysis was developed for all the periods under study, and consists in isolating one by one every pipe of the system in each period and analysing the performance response at every node. The following analysis will be carried out based on the differences obtained by comparing the failure conditions using a DDM and PDM approach. We have analysed the available pressures at the nodes for each proposed period (Figure 1.b). The Figure 1.b shows for all tested periods how the head pressure at each node is increases under PDM (blue area), in opposite to DDM approach. This shows that the system regulates itself because of the failure, and this self-regulation is not reflected in the DDM approach.

In Figure 1.b shows that the maximum effect of failure at any individual system component, namely pipe (isolation) or tank (minimum level), is in the absorptive stage. The issue increase its impact for periods of high demand (periods 7 and 8). Similarly, Figure 1.b shows that, under PDM, the network can self-regulate its pressures by supplying the system with additional energy enough to provide user's demands.

3.2 Example of application

In this study, we applied the resilience index (IrT, Equation 4) by Todini (2000) and its generalization (IrC, Equation 5) by Creaco et al. (2016). The interest of the application of these two indicators in this study is due to the fact that the first one operates under a DDM and the second one under a PDM. And both let us to quantify the resilience in terms of the available power of the system.

$$IrT = \frac{max[d^T h - d^T h_s,\ 0]}{h_f{}^T A_f q - d^T h_s} \tag{4}$$

$$IrC = \frac{max[c^T h - d^T h_s,\ 0]}{h_f{}^T A_f q - d^T h_s} \tag{5}$$

As example of application, the three-stage resilience study was applied to a random pipe (Figure 2.b) of the network. The sequence of the scenario is: pipe burst, isolation of the pipes, repairing then flushing.

Pipe Burst Leak. It is assumed in this study that a leak starts at the beginning of the period 6, and ends at the end of this period (once the leaky pipe is isolated). Duration 1 hour. Simulated using the orifice equation.

Isolation of the pipe/repairing. Starts at the beginning of period 7 and ends at the end of the period 9. Duration 3 hours.

Flushing of the isolated pipe. This action seeks to operate the repaired or replaced pipe in optimal conditions, consider here cleaning of the pipe and air extraction (not simulated in this work).

An initial analysis of the pressures for the systems for the stipulated performance conditions $P_{normal} = h_s = 30$ mH20 and $P_{failure} = h_m = 0$, shows that under no mechanical failure in the network, this network is already deficient in pressure head, at hour 7 (demand peak). Although the selection of the period, in case of the pipe isolation, was analyzed in the period 7. So, it operates in degraded state at nodes (J24, J25), see Figure 2.b, with a head pressure of (29.31, 29.58) and (29.51, 29.76) mH20 in DDM and PDM predictions, respectively. In this sense, the network already starts with hydraulic failure given its inability to supply water under requirements for these consumers.

Based on this information, t_{event}=6 period (pipe burst leak); the event is assumed detected within this period; t_{pall}=7 period (isolation of the affected pipe); t_{stab}=8 period (repairing actions). In addition, we assumed that t_{acc}=3 hours, criteria: time that the street can be closed, so t_{acc}=9 period.

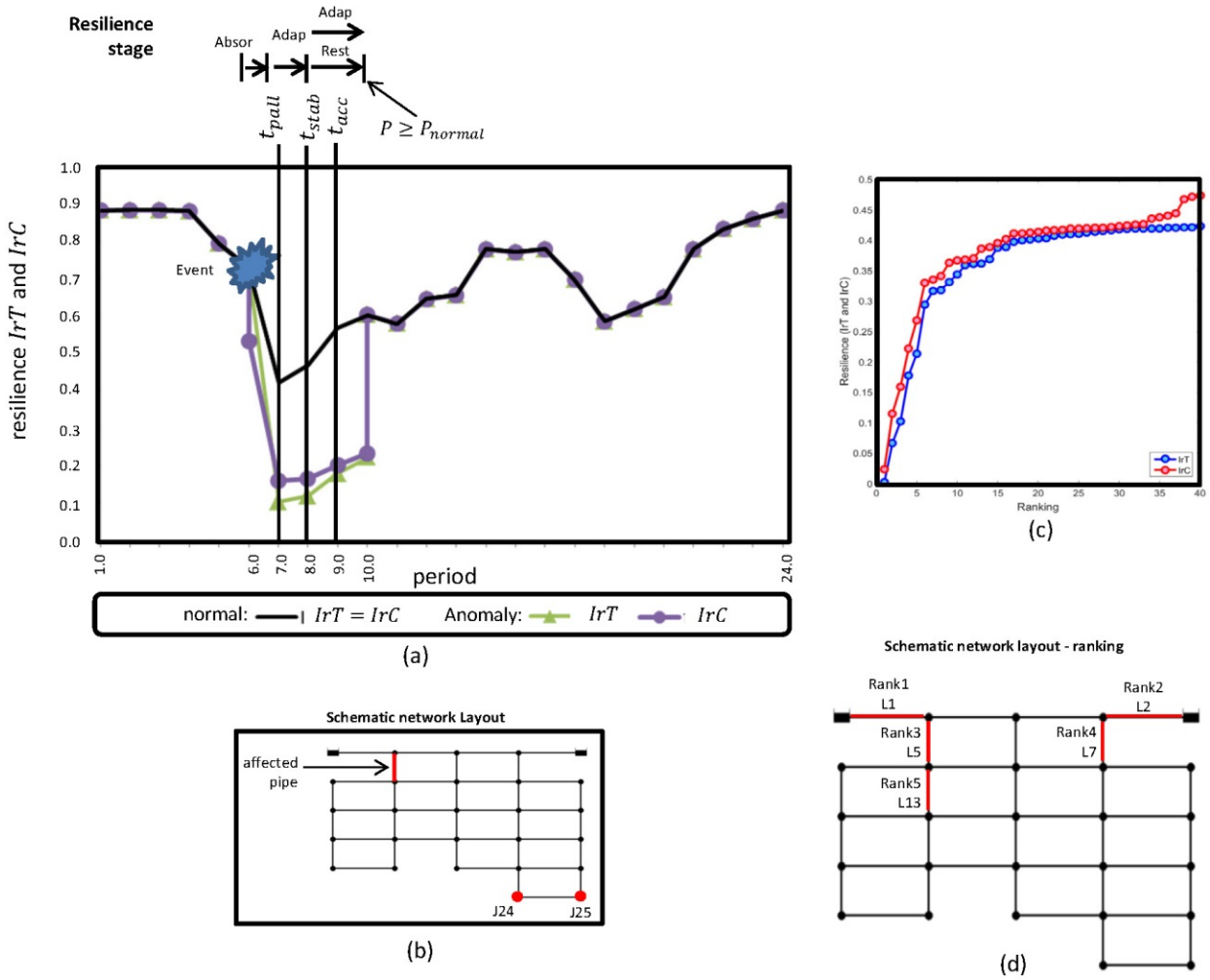

Figure 2. Resilience indicators. (a) Resilience stages; (b) network layout – stages; (c) ranking of pipe – peak demand period; (d) network layout.

In both cases, we can observe a favourable enhancement of the value of the index for IrC in comparison with IrT. Those are the consequences of the performance results used for the index IrC, which provide more realistic condition of the behaviour of the system under the failure condition evaluated. The a priori analysis performed for the system based on the resilience metrics, allows us to know the ranking of the relative importance of the components. Thus, this allows us to observe the plausible maximum impact in the network (event placed on maximum demand peak). This shows that any damage in pipes connected with the reservoirs can have a high unfavourable impact on the network operation conditions. Likewise, this shows that any change in the tank levels, where the levels of the tanks are below to the minimum level (for the maximum peak demand), can provide to the system with a high unfavourable effect on the system resilience.

4. CONCLUSIONS

This paper presents an application example of the resilience key performance indicators, based on three system capacities and its application into the three stages of the event. The results have shown the importance of applying different measures that enable to quantify network changes under stress conditions. The study highlights using tools that allows better understanding of the network's performance facing different disruptive events. This is the case of the application of hydraulic models under PDM approaches, in comparison with DDM approaches. Providing this information to WDN managers allow them to implement actions to prevent catastrophic effects on water networks.

ACKNOWLEDGEMENTS

The work presented in the paper is part of the French-German collaborative research project ResiWater that is funded by the French National Research Agency (ANR; project: ANR-14-PICS-0003) and the German Federal Ministry of Education and Research (BMBF; project: BMBF-13N13690).

REFERENCES

Braun, M., Piller, O., Deuerlein, J. Mortazavi, I., 2016. Limitations of demand- and pressure-driven modeling for large deficient networks. In: 14th International Computing and Control for the Water Industry Conference, Amsterdam, The Netherlands.

Creaco, E., Franchini, M., Todini, E., 2016. Generalized resilience and failure indices for use with pressure-driven modeling and leakage. Water Resour. Plann. Manage. 142, 1-10.

Elhay, S., Piller, O., Deuerlein, J. Simpson, A., 2016. A robust, rapidly convergent method that solves the water distribution equations for pressure-dependent models. J. Water Resour. Plann. Manage. 142, 1-12.

Francis R., and Bekera, B., 2014. A metric and frameworks for resilience analysis of engineered and infrastructure systems. Reliability Engineering and System Safety. 121, 90–103.

Herrera, M., Abraham, E., Stoianov, I., 2016. A graph-theoretic framework for assessing the resilience of sectorised water distribution networks. Water Resour. Manag. 30(5), 1685-1699.

IRGC, 2016. Engineering Resilience in Critical Infrastructures. http://www.dhs.gov/xlibrary/assets/niac/niac_critical_infrastructure_resilience.pdf (last accessed: Aug. 2016).

Islam, M.S., Sadiq, R., Rodriguez, M.J., Francisque, A., Najjaran, H., Hoorfar, M., 2011. Leakage detection and location in water distribution system using a fuzzy-based methodology. Urban Water Journal, 8(6), 351-365.

Jayaram, N., Srinivasan, K., 2008. Performance-based optimal design and rehabilitation of water distribution networks using life cycle costing. Water Resour. Res., 44(1), 1-15.

Jung, D., 2013. Robust and resilient water distribution systems. PhD. Thesis, University of Arizona, Tucson, Arizona (USA).

NIPP, 2013. Partnering for critical infrastructure security and resilience. https://www.dhs.gov/sites/default/files/publications/National-Infrastructure-Protection-Plan-2013-508.pdf (last accessed: Aug. 2016).

Piller, O., Brémond B., Poulton, M., 2003. Least action principles appropriate to pressure driven models of pipe networks. In: Conference on World Water and Environmental Resources Congress, Philadelphia, Pennsylvania, United states.

Piller, O., Elhay, S., Deuerlein, J., Simpson, A., 2017. Local sensitivity of pressure-driven modeling and demand-driven modeling steady-state to variations in parameters. J. Water. Resour. Plann. Manage. 143(2), 1-12.

Prasad, T.D., Park N.S., 2004. Multi-objective genetic algorithms for design of water distribution networks. J. Water. Resour. Plann. Manage. 130(1), 73-82.

ResiWater, 2017. URL: http://www.resiwater.eu/, (last accessed: Jan. 2017).

Saldarriaga, J.G., Ochoa, S., Moreno, M.E., Romero, N., Cortés, O.J., 2010. Prioritised rehabilitation of water distribution networks using dissipated power concept to reduce non-revenue water. Urban Water Journal. 7(2), 121-140.

Sivakumar, P., Prasad, R.K., 2014. Simulation of water distribution network under pressure-deficient condition. Water Resour. Manag. 28(10), 3271-3290.

Todini, E., 2000. Looped water distribution networks design using a resilience index based heuristic approach. Urban Water. 2(2), 115-122.

Wagner, J.M., Shamir, U., Marks, D.H., 1988. Water distribution reliability: simulation methods. J. Water. Resour. Plann. Manage. 114(3), 276–294.

Proceedings of the 10th World Congress of EWRA 'Panta Rhei', 5-9 July 2017, Athens, Greece
© 2017 *European Water Resources Association*

Data mining for household water consumption analysis using self-organizing maps

A.E. Ioannou, D. Kofinas, A. Spyropoulou and C. Laspidou*
Department of Civil Engineering, University of Thessaly, Pedion Areos, Volos 38334, Greece
** e-mail: laspidou@uth.gr*

Abstract: Household water consumption is a part of the human related water cycle that can get into the core of water resources management. Analysis of water consumption data can reveal great potentials of individualized water services planning. Data mining is the process of identifying and extracting potentially useful information from data sets. Self-Organizing Maps (SOMs) is a data mining technique that involves an unsupervised learning method to analyze, cluster, and model various types of large data sets. In this paper, it is presented how the daily water consumption of a household in Sosnowiec can be clustered into days of week, through some features. The features used to discretize the days of water consumption are statistic metrics and time zone consumption metrics. The time zoning is realized in two ways, the first being the typical morning, noon, afternoon, evening and night and the second considering the local working hour time zones of three main working sectors, banks, offices and shops. We use the SOM algorithm in three approaches. In each approach we use some of the selected features. We have managed to get some clusters with specific features that divide the days of this household in weekdays and weekends.

Key words: Data mining, self-organizing maps, water consumption analysis

1. INTRODUCTION

Smart Cities have been defined in many ways. Special focus is given on Information and Communication Technologies (ICTs) as a key driver. Other important aspects of instrumenting the landscape of a smart city would be society, economy, and policies driven by participatory processes. The concept of Smart Cities sets, in the core of urban planning, monitoring, recording, analyzing and transferring in real time all data relative to social activity; thus, enabling social and governmental awareness of all significant design variables. The monitored variables are linked to basic networks and environments such as city services, transport, water and energy (Manville et al., 2014).

Subsequently, the need of collecting and managing great amounts of temporal and spatial high-granularity data becomes of conclusive importance. Great progress in ICTs, social network, and Data Mining (DM) enable new paths of urban planning, empowering the resilience of urban infrastructure and the adequacy of resources and systems (Laspidou, 2014).

DM is an ongoing research area, responding to the presence of large databases in commerce, industry and research (Bishop, 1995). It is a very useful technique in research; because, not only can someone extract meaningful information from certain databases, but can also predict changes, discover patterns and relations hidden among the data (Fayyad et al., 1996). In addition, DM is an interactive process that requires the intuition, background knowledge and the computational efficiency of modern computer technology. Clustering techniques can reveal patterns and identify similar trends and components linked to similar behaviors. Clustering visualization is a very important part of DM and can be successfully accomplished, by the use of self-organizing maps (Kaski, 1997).

One of the fundamental urban activities, firmly related to all human well-being aspects, such as public health, is the urban water consumption. The Water Distribution Networks (WDNs) are to be thoroughly monitored in different scales, from an aggregated urban water resources view, down to a

household water consumption view, so as to gather all useful data that will enable the improvement of water resources management, through all the available data analysis techniques. The aforementioned DM techniques can realize water consumption forecasting at small scales, by clustering householders in different consumption patterns; thus, enabling water utilities to get more efficient by heading towards more individualized customer services (Beckel et al., 2012, Laspidou et al., 2015). Parallel to increasing resolution at individualized scale, analysis can also enable temporal clustering resolution, identifying different daily consumption patterns. Past research (Arampatzis et al., 2014) has already indicated weekdays/weekends water use particularities at urban level, revealing the potential to further investigate daily patterns at household level.

The aim of the present study is to investigate how specific daily household patterns can be inferred from household water consumption profiles. We make an effort to cluster days of similar water consumption profiles. The automatic classification of days into clusters is accomplished with the application of the SOM methodology.

2. MATERIALS AND METHODS

In this paper we develop a methodology for the detection of daily patterns in household water consumption, through a detailed patterns analysis using SOM (Kohonen, 1995). The methodology is a popular neural network algorithm based on unsupervised learning. SOM uses specifically chosen features of a population; then it calculates the Euclidean distances of each unit of the population considering the features as dimensions or components of the input vectors. Lastly, it converts the multidimensional positions of the units into 2-dimensional and maps them. These maps depict all units in a sense that neighboring units correspond to similar features; thus making clustering of similar units possible. The SOM has proven to be a valuable tool in DM with applications in financial data analysis (Deboeck et al, 1998), in engineering applications, pattern recognition (Kohonen et al., 1996), image analysis, process monitoring and fault diagnosis (Simula et al., 1995). SOM method is widely used to cluster a variety of attributes such as fine-grained electricity consumption, water consumption, etc. (Beckel et al., 2012, Laspidou et al., 2015, Räsänen et al., 2008).

Water consumption is recorded by sensors installed in individual households. Input vectors are produced from water consumption data from a household in Sosnowiec, an industrial city in southern Poland. In this household, sensors were installed in seven different faucets, so we summed all our data in order to have time-series of the total consumption of the house. Water consumption values are recorded every 30 sec and a 445-days sample is used for the analysis. Each day is considered to be a unit of a population of 445 and the analysis aims at clustering days that are linked to similar profiles by mapping them closely.

We use 13 features to describe the daily consumption behavior, listed in *Table 1*. The features refer to total daily consumption (feature 1), daily standard deviation (σ) of daily water consumption (feature 6) and partitioning of daily consumption into specifically chosen time-zones (features 2-5 & 7-13). Our data are divided in the following time zones: morning (feature 2), noon (feature 3), afternoon (feature 4), evening (feature 5) and night (feature 7). Another time zone division considers the working hours and rest hours of offices (feature 8 & 10, respectively), banks (features 9 & 11, respectively) and shops (features 12 & 13, respectively). The features are chosen in the sense that total consumption, σ and time zones consumption are suspected to possibly characterize different days' patters. Specifically the working hours' features are taken into account, because the household is located in an urban environment and most probably its water consumption is directly affected by the working routines. The aforementioned features are combined to create three different dimension sets for the three approaches of our investigation. The features regarded for each approach are listed in *Table 1*.

After the preparation of the data and estimation of the feature table of its single day of consumption, a matlab SOM-toolbox and its scripts are used to preprocess data, initialize, normalize and train SOM and construct the maps (Vesanto et al., 1999). The normalization of data is of great

importance for a very specific reason: The estimated features and components of the input vectors of a SOM, due to their different nature, exhibit values of very different magnitude. The feature with the greater magnitude would affect the Euclidean distance unequally to the features with smaller magnitude. With the normalization we achieve, equal partitioning of the features.

Another very significant pre-process is that of labeling each feature table after its corresponding day. The purpose of this process is that the maps created are legible and comprehensible and the clusters, possibly created, are easily visualized. This means, that we expect Saturdays, for example, to gather around the same area of a SOM map and this way construct a cluster of similar consumption profile corresponding to that of a typical Saturday.

Table 1. Features of daily consumptions used for the 3 different SOM approaches

approach 1	**approach 2**	**approach 3**
1. total daily consumption	7. night consumption *(12am-8am)*	8. consumption at offices working hours *(8am-4pm)*
2. morning consumption *(6am-10am)*	8. consumption at offices working hours *(8am-4pm)*	9. consumption at bank working hours *(8am-6pm)*
3. noon consumption *(10am-2pm)*	9. consumption at bank working hours *(8am-6pm)*	12. consumption at shops working hours *(11am-7pm)*
4. afternoon consumption *(2pm-6pm)*	10. consumption at office rest hours *(4pm-10pm)*	
5. evening consumption *(6pm-10am)*	11. consumption at bank rest hours *(6pm-10pm)*	
6. standard deviation of water consumption (σ)	12. consumption at shops working hours *(11am-7pm)*	
	13. consumption at shops rest hours *(7pm-10pm)*	

3. RESULTS AND DISCUSSION

The results of the runs are depicted with use of three kinds of SOM maps (*Figures 1, 2 &3*). The U-matrix is the 2-dimensional depiction of the multi-dimensional Euclidean distances of all the daily consumption profiles. As we see from top to bottom there is gradation from dark blue, small distances to light yellow, big distances. This means that two units in neighboring cells are closer if the cells are in the blue area than if they were in the yellow area. In the labels map, the location of each unit is presented according to its characterization as a day of the week. This way it can be revealed if same days of the week tend to cluster in neighboring cells; thus prove to have similar water consumption profiles. At the right side of the figures, the feature matrixes are presented. These maps depict the behavior of each feature separately.

In approach 1 (*Figure 1*), we use features 1 to 6, namely, total daily, morning, noon; afternoon, and evening consumptions and σ. Two main cluster areas, area 1 and area 2, are formed. In the first one, weekends are more frequent, while as, in the second one, weekdays seem to dominate. This clustering of weekdays separately than weekends proves that in the household depicts different water use profiles in working days than in non-working. Moreover, weekend cluster cells are much closer one another than weekday cells. That means that weekend profiles are more uniform than the weekdays. In area 2, three sub-clusters 2a, 2b, and 2c seem to be formed. Sub-cluster 2a includes only Tuesdays, sub-cluster 2b includes only Wednesdays and finally sub-cluster 2c includes only Mondays. The sub-clustering of cluster 2 justifies its looseness, as it seems that throughout the working days, some more specific daily consumption prototypes are formed with some differences. Observing the feature matrixes, we can see that total daily consumption and σ are similar. These two show that weekends in the upper are firmly located, in contrast to weekdays which are more loosely located. This pattern is almost followed by the afternoon consumption feature. On the other hand, morning, noon, and evening consumption features are more uniform in an extended area, with some yellow "gorges" low at the weekdays' area. Subsequently the U-matrix is formed as a combination of the six features degrading top to bottom from blue to yellow.

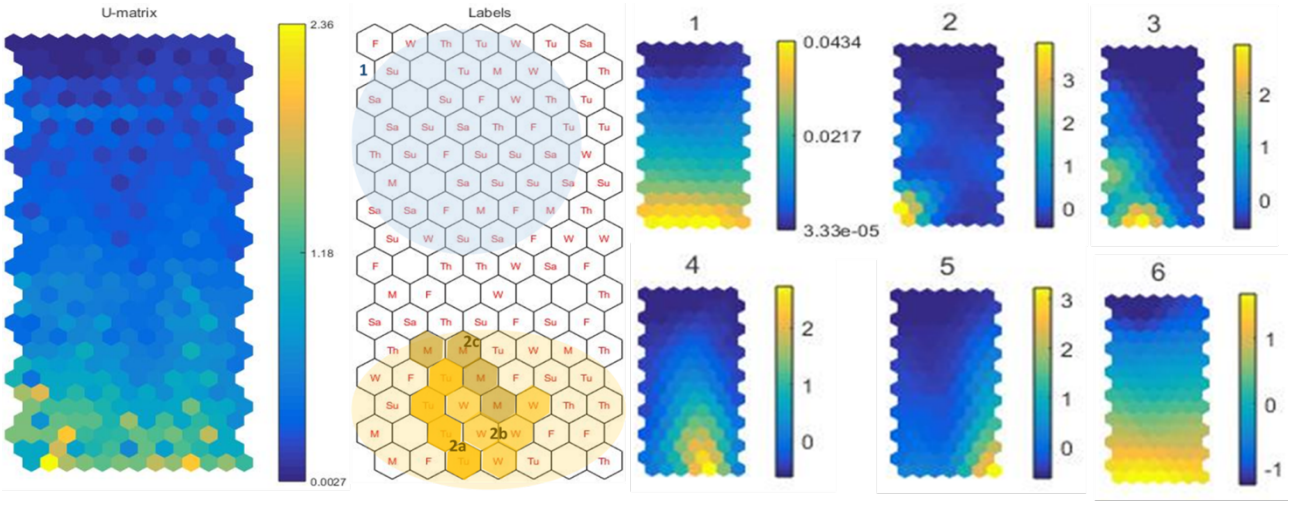

Figure 1. It is depicted the SOM map results: U-matrix, Labels, feature 1 total daily consumption, feature 2 morning consumption, feature 3 noon consumption, feature 4 afternoon consumption, feature 5 evening consumption, and feature 6 σ (Approach 1).

In Approach 2 (*Figure 2*), we use features 7 to 13, which refer to the working and resting hours consumptions as well as the night consumption. With this approach, we see that clusters are formed in the same way (weekends upper and weekdays down). However, the clusters appear more discretized and more extended than those of approach 1. This proves that the working and resting hours features are more proper than the typical time zoning of morning, noon, afternoon, and evening features. This could be an indicator that the case study household members follow the prevailing working routine of Sosnowiec. In contrary to approach 1, two sub clusters, 1a and 1b, are formed in cluster area 1 rather than in area 2. The cluster 1 mostly contains weekends, while its sub clusters 1a and 1b contain exclusively Saturdays and Sundays. The weekdays in this approach don't seem to further sub-cluster discretized. In Approach 3 (*Figure 3*), only three features are used, the working hours consumptions. This improves clustering, since in the weekend area, Saturdays and Sundays rise up to 3 out of 4. In the weekday area, 86 % of the cells are occupied by weekdays. In all approaches, we can see that Fridays are equally distributed in both areas. This indicates that Fridays water consumption profiles are somewhere in between and have characteristics of both weekday and weekend profiles.

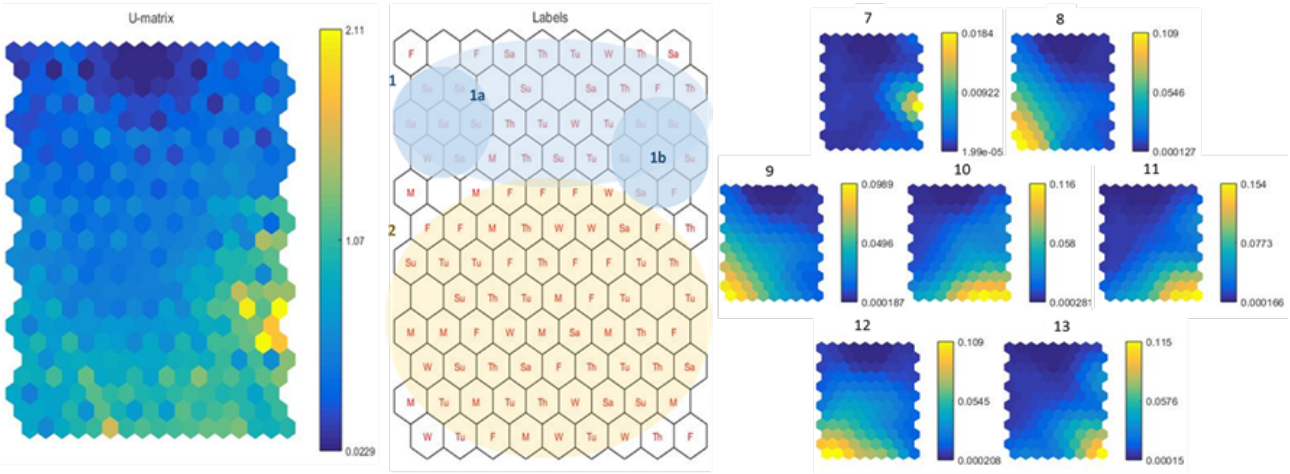

Figure 2. It is depicted the SOM map results: U-matrix, Labels, feature 7 night consumption, feature 8 consumption at offices working hours, feature 9 consumption at banks working hours, feature 10 consumption at offices rest hours, feature 11 consumption at banks rest hours, feature 12 consumption at shops working hours, and feature 13 consumption at shops rest hours (Approach 2).

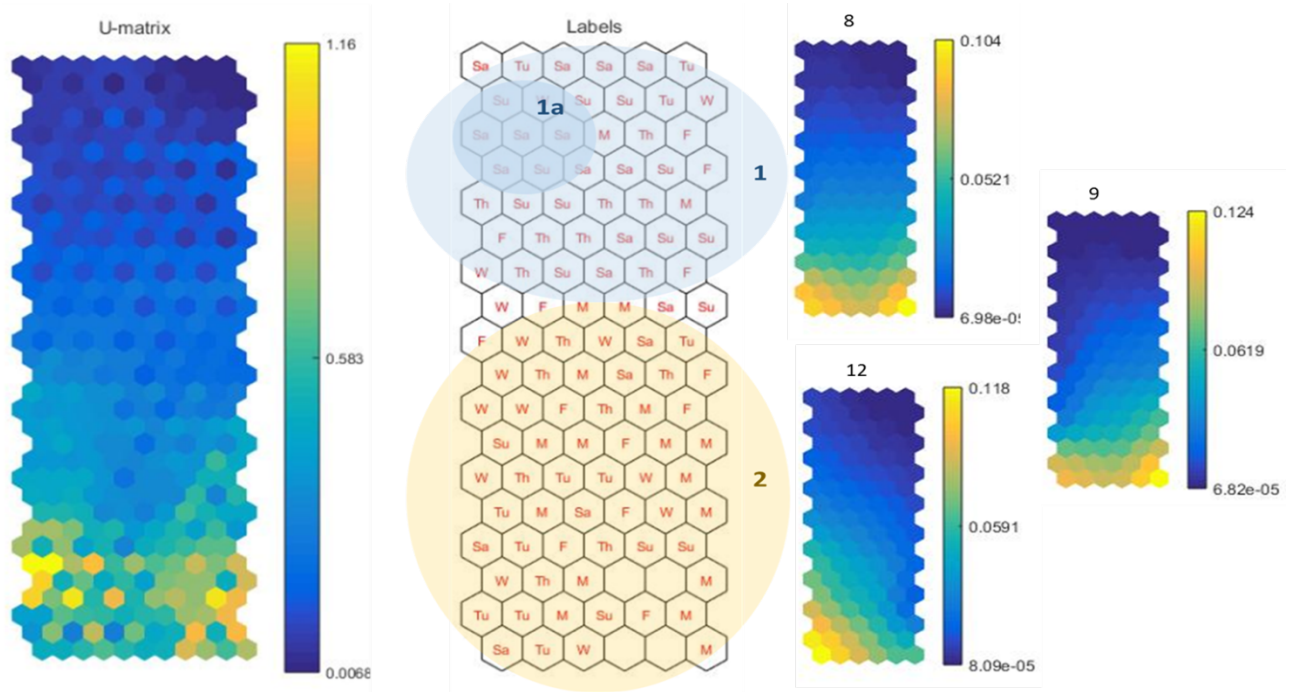

Figure 3. It is depicted the SOM map results: U-matrix, Labels, feature 8 consumption at offices working hours, feature 9 consumption at banks working hours, and feature 12 consumption at shops working hours (Approach 3).

4. CONCLUSIONS

In this paper, we perform automatic classification of daily water consumption patterns for a household in Sosnowiec, using data collected by sensors. Our investigation is built upon three approaches accomplished with use of the SOM algorithm. Thirteen descriptive features of daily consumption patterns are used for the classification. Approaches 1 and 2, distinguishes two water consumption profiles dividing days of consumption into two main clusters, weekdays and weekends. In approach 3, with use of features partitioning daily water consumption into the time-zones of Sosnowiec working hours, the two clusters get more solid and the methodology gets more efficient. In all approaches, the clustering of days of consumption into weekdays and weekends implies that the household is affected by the urban working routine.

In future scenarios, this investigation could be expanded to more households in order to achieve a further classification, even manage to identify each day of the week. Investigation among households in working areas, or leisure places might indicate different water consumption daily patterns. In all cases the choice of good descriptive features seems to be important. The features have to be customized to better describe daily routines of different types of household.

ACKNOWLEDGMENTS

This work was supported by the project Water4Cities—Holistic Surface Water and Groundwater Management for Sustainable Cities—which is implemented in the framework of the EU Horizon2020 Program, Grant Agreement Number 734409.

REFERENCES

Arampatzis, G., Perdikeas, N., Kampragou, E., Scaloubakas, P., and Assimacopoulos, D., 2014. A water demand forecasting methodology for supporting day-to-day management of water distribution systems. In 12th International Conference "Protection and Restoration of the Environment", Skiathos, Thessaloniki, Greece.

Beckel, C., Sadamori, L., and Santini, S. 2012. Towards automatic classification of private households using electricity consumption data. In Proceedings of the Fourth ACM Workshop on Embedded Sensing Systems for Energy-Efficiency in Buildings (pp. 169-176). ACM.

Bishop, C.M. 1995. Neural Networks for Pattern Recognition, Oxford University Press, Oxford.

Deboeck, G and Kohonen T. 1998. Visual Explorations in Finance using self-organizing Maps, Springer, London.

Fayyad, U.M., Piatetsky-Shapiro, G., Smyth, P., and Uthurusamy R. 1996. Advances in knowledge Discovery and Data Mining, AAAI Press/The MIT Press, California.

Kaski, S. 1997. Data Exploration Using Self-Organizing Maps, Ph.D. thesis, Helsinki University of Technology.

Kohonen, T. 1995. Self-Organizing Maps, Springer, Berlin.

Kohonen, T., Oja, E., Simula, O., Visa, A. and Kangas, J. 1996. Engineering applications of the self-organizing map. Proceedings of the IEEE, 84(10), 1358-1384.

Laspidou, C. 2014. ICT and stakeholder participation for improved urban water management in the cities of the future. *Water Util. J*, *8*, 79-85.

Laspidou, C., Papageorgiou, E., Kokkinos, K., Sahu, S., Gupta, A. and Tassiulas, L. 2015. Exploring patterns in water consumption by clustering. Procedia Engineering,119, 1439-1446.Räsänen, T., Ruuskanen, J., and Kolehmainen, M. 2008 Reducing energy consumption by using self-organizing maps to create more personalized electricity use information. Applied Energy, 85(9), 830-840.

Manville, C., Cochrane, G., Cave, J., Millard, J., Pederson, J. K., Thaarup, R. K., and Kotterinkf, B., 2014. Mapping smart cities in the EU.

Simula, O. and Kangas, J. 1995. Process monitoring and visualization using self-organizing maps, in: Neural Networks for Chemical Engineers, Computer-Aided Chemical Engineering, vol 6, Elsevier, Amsterdam.

Vesanto, J., Himberg, J., Alhoniemi, E. Parhankangas, J. 1999, November. Self-organizing map in Matlab: the SOM Toolbox. In Proceedings of the Matlab DSP conference (Vol. 99, pp. 16-17).

Proceedings of the 10th World Congress of EWRA 'Panta Rhei', 5-9 July 2017, Athens, Greece
© 2017 *European Water Resources Association*

Incorporating uncertainty in the design of water distribution systems

M. Spiliotis[1*] and G. Tsakiris[2]
[1] *Division of Hydraulic Engineering, Department of Civil Engineering, Democritus University of Thrace, Kimmeria Campus, Xanthi 67100, Greece*
[2] *Centre for the Assessment of Natural Hazards and Proactive Planning, School of Rural and Surveying Engineering, National Technical University of Athens, Athens, Greece*
[*] *e-mail: mspiliot@civil.duth.gr*

Abstract: During the design stage of urban water supply and distribution systems several assumptions and projections to future horizons are made. The analysis and design is then based on a deterministic basis in which all the involved parameters have crisp values. In reality however, most of the parameters exhibit significant variability over the life span of the system. The resistance to flow is among the most important parameters exhibiting variability. This is caused by the variability of the friction coefficient of pipes and the variability of internal diameters of the pipes. This study attempts to incorporate these uncertainties in the analysis and design of urban water supply and distribution systems, following a copula approach. Because of the low data availability, fuzzy membership functions are assigned to describe both variability of friction coefficients and variability of internal pipe diameters. Instead of the min intersection, the use of copulas is proposed in order to combine the uncertainties and calculate the fuzziness of the pipe resistance to flow. Thus, the input variables are fuzzy numbers and the problem is to find the output of the system which will consists also of fuzzy quantities. The system itself is described by the set of precise (crisp) nonlinear Q-equations. Finally, the uncertainty analysis concludes to an optimization problem. A numerical example is presented to demonstrate this innovative methodology.

Key words: Water distribution system, Uncertainties in design, Resistance to flow, Pipe roughness, Copulas, Fuzzy sets, Extension principle

1. INTRODUCTION

At the design stage of urban water supply and distribution systems several assumptions and projections to future horizons are made. All the values set on the involved parameters are considered constant throughout the operational life of the system. In reality, however, several parameters exhibit significant variability over time. The future water demand and the resistance to flow are among these important uncertain parameters. As known, the variability of the resistance to flow is caused by the changes of the friction coefficient and the internal diameters of the pipes during the life of the system.

This article presents a hybrid fuzzy approach for incorporating these uncertainties in the analysis and design of urban water supply and distribution systems.

2. BASIC NOTIONS

A fuzzy number is a fuzzy set satisfying the properties of convexity and normality. It is defined in the axis of real numbers and its membership function is a piecewise continuous function. For simplicity, a fuzzy number representing the uncertainty in both the pipe roughness and the internal pipe diameters, is a fuzzy triangular number.

An extension of a triangular fuzzy number is the LR fuzzy number with membership function of a non-linear shape (Dubois and Prade 1978). A fuzzy number is of the LR-type if there exist functions L (for left) and R (for right) with:

$$\begin{cases} \mu_A(x) = \begin{cases} L\left(\dfrac{x-\alpha_1}{\alpha_2-\alpha_1}\right) & \text{if } \alpha_1 \le x \le \alpha_2 \\ R\left(\dfrac{\alpha_3-x}{\alpha_3-\alpha_2}\right) & \text{if } \alpha_2 \le x \le \alpha_3 \\ 0 & \text{otherwise} \end{cases} & (1.a) \\ \text{where L and R are two non-decreasing shape functions which satisfy the following equations:} \\ L:[0,1]\to[0,1] \text{ and } R:[0,1]\to[0,1] \\ L(0) = R(0) = 0,\ L(1) = R(1) = 1 & (1.b) \end{cases}$$

The $\mapsto$-cut set of the fuzzy number A (with $0 < \mapsto \le 1$), is the key idea to move from the fuzzy to the crisp sets and it is defined as follows (Klir and Yuan 1995; Zimmermann 1991):

$$\tilde{A}_\alpha = \left\{x \middle| \mu_{\tilde{A}}(x) \ge \alpha,\ x \in \Re\right\}. \tag{2}$$

One can notice that the $\mapsto$-cut set is a crisp set determined from the fuzzy set according to a selected value of the membership function, and reciprocally, a fuzzy set can be derived from a significant number of $\mapsto$-cut sets.

The crisp set including all the elements with non-zero membership function is the 0-cut which is defined as follows (Buckley and Eslami 2002):

$$\tilde{A}_{0^+} = \left\{x \middle| \mu_A(x) > 0,\ x \in \Re\right\} \tag{3}$$

We can now extend the operation of the usual crisp functions, if the inputs are fuzzy sets, based on the extension principle which is briefly presented below.

Let X be a Cartesian product of universe $X = X_1 \times X_2 \times \ldots \times X_n$ and $\tilde{A}_1, \tilde{A}_2, \ldots, \tilde{A}_n$ be defined in the universe sets $X_1, X_2, \ldots, X_n$, respectively. Let f be a (crisp) mapping from X to a universe Y, $y = f(x_1, x_2, \ldots, x_n)$. The mapping f for these particular input sets can now be defined as $\tilde{B} = \left\{\left(y, \mu_{\tilde{B}}(y)\right) \middle| y = f(x_1, x_2, \ldots, x_n), (x_1, x_2, \ldots, x_n) \in X\right\}$, in which the membership function of the image $\tilde{B}$ can be defined (Zimmermann 1991; Tsakiris & Spiliotis 2014) by:

$$\mu_{\tilde{B}}(y) = \sup_{(x_1, x_2, \ldots, x_n) \in f^{-1}(y)} t\left(\mu_{A_n}(x_1), \ldots, \mu_{A_n}(x_n)\right) \tag{4}$$

where f^1 is the inverse image of f and t a fuzzy intersection. Mainly the min intersection which is the intersection of the classical logic is widely used.

The implementation of the extension principle gives the opportunity to use a crisp function in which the input variables are fuzzy numbers (Tsakiris and Spiliotis 2014; Kechagias and Papadopoulos 2007).

In most cases, it is preferable to use $\mapsto$-cuts in the fuzzy analysis. If f is a continuous function in the extension principle, the use of $\mapsto$-cuts can be also extended by determining the $\mapsto$-cuts of the function f (Buckley and Eslami 2002; Buckley et al. 2002). Then, based on the min intersection it holds:

$$\begin{cases} f^{L}\left(\tilde{A}_1,\tilde{A}_2\right)_\alpha = \min\left\{f\left(x_1,x_2\right)\middle| x_1\in\tilde{A}_{1\alpha}, x_2\in\tilde{A}_{2a}\right\}, \\ f^{R}\left(\tilde{A}_1,\tilde{A}_2\right)_\alpha = \max\left\{f\left(x_1,x_2\right)\middle| x_1\in\tilde{A}_{1\alpha}, x_2\in\tilde{A}_{2a}\right\}. \end{cases} \quad (5)$$

In this article concepts from the probability theory, instead of the min-intersection are used and hence, the decision space is reduced (any fuzzy intersection is smaller or equal than the min intersection). In the next section, the relation between copulas and fuzzy intersections will be presented and explained briefly.

As mentioned earlier, instead of the min intersection, several other intersections can be used in the extension principle.

In general, a triangular norm (t–norm for short) (bivariate aggregation function) is a binary operation on the unit interval: $\mathbf{T}\left(\left[0,1\right]\times\left[0,1\right]\rightarrow\left[0,1\right]\right)$ which is associative, symmetric and has neutral element 1.

The above set of axioms constitutes the axiomatic skeleton of fuzzy intersections, T-norms. All functions which satisfy the above axioms are fuzzy intersections (e.g. Klir and Yuan 1995). Among them, one characteristic fuzzy intersection is the min intersection, T_{min} (Eq.6), and the intersection of bounded difference, T_{bd} (Eq.7):

$$T_{min}\left(a,b\right)=\min\left(a,b\right) \quad (6)$$

$$T_{bd}\left(a,b\right)=\max\left(a+b-1,\ 0\right) \quad (7)$$

It holds that every fuzzy intersection has smaller values than the minimum intersection.

3. COPULAS AND FUZZY INTERSECTIONS

Next, the concept of Copulas and their connection with the fuzzy t-norm will be presented in brief.

Definition: A bivariate copula is a function $C:\left[0,1\right]^2\rightarrow\left[0,1\right]$ which satisfies:

$$C\left(x,0\right)=C\left(0,x\right)=0 \text{ and } C\left(x,1\right)=C\left(1,x\right)=x \text{ for all } x\in\left[0,1\right] \quad (8.1)$$

$$C\left(x_1,y_1\right)-C\left(x_1,y_2\right)-C\left(x_1,y_2\right)+C\left(x_2,y_2\right)\geq 0 \text{ for all } x_1,x_2,y_1,y_2\in\left[0,1\right]$$
$$\text{such that } x_1\leq x_2 \text{ and } y_1\leq y_2 \quad (8.2)$$

In statistical analysis, a joint distribution H of a pair of random variables (X, Y) with marginals *F* and *G* respectively, can be expressed by $H\left(x,y\right)=C\left(F\left(x\right),G\left(y\right)\right)$ for each $\left(x,y\right)\in\left[-\infty,\infty\right]^2$, in which *C* is a copula uniquely determined.

Copulas can be used also in case that the input x, y have fuzzy membership functions (that is, *x, y* take values between zero and one) (Beliakov et al. 2014).

From the definition, in case that the inputs are fuzzy sets it holds, that Copulas not necessarily are symmetric or associative. Copulas are monotone, non-decreasing (and thus are aggregation functions) and verify

$$T_{bd}\leq C\leq T_{min} \quad (9)$$

(and thus, are conjunctive functions) (Beliakov et al. 2014).

From the mathematical definition, it is evident that, an associative and commutative copula is a t-norm and a t-norm which satisfies the Eq.8.2, is a copula (Nather 2010).

An interesting family of copulas is the Archimedean family. Among important properties of Archimedean copulas, the symmetry and the associativity are included. In this article, from the Archimedean copulas, the Gumbel-Hougaard copula is selected (e.g. Tsakiris et al. 2016), which belongs to Aczel-Alsina family of t–norms (Beliakov et al. 2014):

$$C\left(x,0\right)=e^{-\left(\sqrt[\theta]{\left(-\ln x\right)^{\theta}+\left(-\ln y\right)^{\theta}}\right)},x,y\in\left[0,\ 1\right],\theta\geq 1 \tag{10}$$

Then, the extension principle based on α-cuts will have the following form:

$$\begin{cases} f^{L}\left(\tilde{A}_1,\tilde{A}_2\right)_{\alpha}=\min\left\{f\left(x_1,x_2\right)\middle|C\left(\mu_1\left(x_1\right),\mu_2\left(x_1\right)\right)\geq a\right\}, \\ f^{R}\left(\tilde{A}_1,\tilde{A}_2\right)_{\alpha}=\max\left\{f\left(x_1,x_2\right)\middle|C\left(\mu_1\left(x_1\right),\mu_2\left(x_1\right)\right)\geq a\right\}. \end{cases} \tag{11}$$

Instead of the individual α-cuts of each parameter, the bivariate boundary of each α-cut is now the curve of copulas with membership function equal to the examined cut. Let for instance, a function with two independent variables. The 0.1-cut according to which the boundaries of the α-cut are examined, by following the min-intersection, will be the rectangular with membership functions greater or equal to 0.1. In the case of Gumbel-Hougaard copulas with $\theta = 2$, the decision space is reduced as can be seen from Fig.1. It should be noted also, that when the parameter θ increases the copulas leads to the min intersection and hence the Eq.11 leads to Eq. 5.

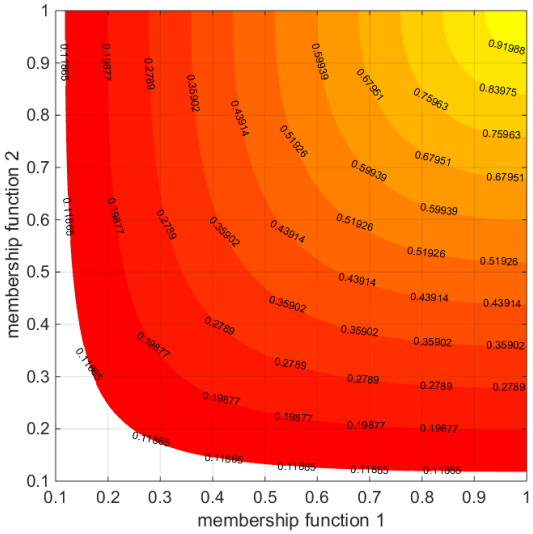

Figure 1. The 0.1-cut for two variables and several bivariate α-cuts based on the Gumbel-Hougaard family of copulas with θ =2

4. UNCERTAINTY IN FUZZY SETS

The **Q**-equations are used to deal with the uncertainties encountered in the looped water distribution systems. To simplify the calculation procedure, the Hazen -Williams equation is used for the calculation of head losses:

$$h_{f,in} = R_{in} Q_{in}^{1.852},\ R_{in} = \frac{10.7\, L_{in}}{C_{in}^{1.852} D_{in}^{4.87}} \tag{12}$$

in which R_{in} is the hydraulic resistance and C_{in} is the Hazen-Williams roughness coefficient. Also, L_{in}, D_{in} are the length and the internal pipe diameter of the branch *i-n*, respectively.

According to the proposed methodology, initially, we determine the resistance of each pipe as fuzzy number based on the extension principle for a certain number of α-cuts:

$$\begin{cases} R_{in}^{\ L}\left(x_{1,in}, x_{2,in}\right)_{\alpha} = \min\left\{ \dfrac{10.7 L_{in}}{x_{1,in}^{1.852}\, x_{2,in}^{4.87}} \,\middle|\, C\left(\mu_1\left(x_{1,in}\right), \mu_2\left(x_{2,in}\right)\right) \geq a \right\}, \\ R_{in}^{\ R}\left(x_{1,in}, x_{2,in}\right)_{\alpha} = \max\left\{ \dfrac{10.7 L_{in}}{x_{1,in}^{1.852}\, x_{2,in}^{4.87}} \,\middle|\, C\left(\mu_1\left(x_{1,in}\right), \mu_2\left(x_{2,in}\right)\right) \geq a \right\}. \end{cases} \tag{13}$$

where $R_{in}^{\ L}, R_{in}^{\ R}$ the left and the right hand side of the resistance at pipe in, $x_{1,in}$ an auxiliary variable which indicates the value of the Hazen-Williams coefficient, $x_{2,in}$ the internal diameter, C a selected copula which will be also a t-norm. Also, μ_1, μ_2 are the membership functions of the Hazen-Williams coefficient and the internal diameter, respectively. In this article by taking concepts from the probability theory instead of the min intersection, the Gumbel-Hougaard copulas with $\theta=2$ is used. For illustration purposes, the Π-shaped membership functions of the internal diameters 0.5 and 0.7m are presented in Fig. 2.

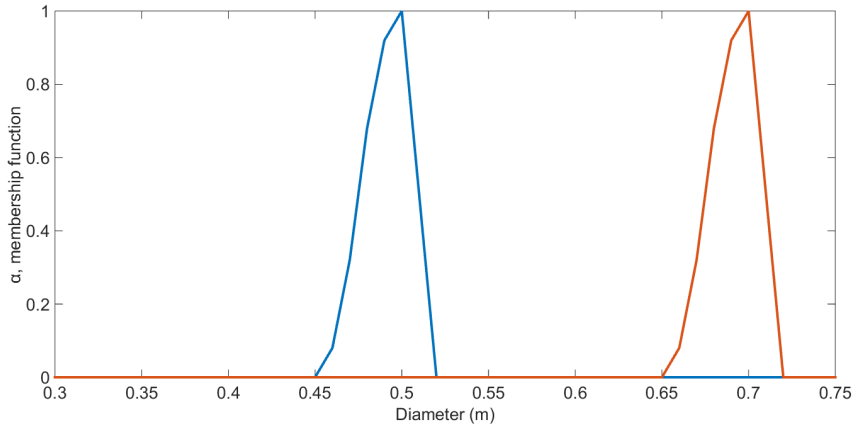

Figure 2. Π-shaped membership functions of the internal diameters of 0.5 and 0.7m.

Alternatively, the resistance can be considered based on initial information or expert knowledge.

Thus, the input variables are fuzzy numbers and the problem is to find the output of the system which will consists also of fuzzy quantities. The system itself is described by a set of precise (crisp) nonlinear equations. In general, this is an ill -constructed problem and several problem depending o each problem itself can be established. Revelli and Ridolfi (2002) proposed the use of an optimisation procedure to determine the minimum and the maximum water flow individually at each branch for each α-cut. Further, Tsakiris and Spiliotis (2017) proposed to produce a simultaneous estimation of all hydraulic variables and their fuzziness. Therefore, an objective function which comprises the weighted sum of the absolute values of the head losses has been proposed. The selection of the weights is based on the principle that each weight is directly proportional to the corresponding flow.

In contrast with the above methodologies, the resistance and its fuzziness for each pipe is determined separately based on a new interpretation of the extension principle with copulas. Thus,

during the analysis, the unique set of parameters with fuzziness is the set of the pipe resistances. Then, an individual solution for each pipe in order to determine the range of the flow for each pipe can be implemented. Alternatively, a global membership function as Spiliotis and Tsakiris proposed can be established:

$$\begin{cases} \min \sum_{in=1}^{L+M-1} \left(\frac{\left| x'_{1,in} \right|}{\left(\sum_{in=1}^{L+M-1} x'_{1,in} \right)} \right) \cdot x'_{2,in} : x_{ni}^{0.852} \left| x'_{1,in} \right| \left(or \ \max \right) \\ \left| \sum_{in}^{in \in I(l)} \pm x'_{2,in} : x_{1,in}^{0.852} \left| x'_{1,in} \right| = 0, \ l = 1,...,L \right. \\ x'_{2,in} \in \widetilde{R}_{in\,\alpha}, \ x'_{1,in} \left(crisp \right) \\ \left| \sum_{in}^{in \in I_1(m)} \pm x'_{1,in} = q_m, \ m = 1,...,M \right. \end{cases} \tag{14}$$

where $\left(\frac{\left| x_{1,in}{}' \right|}{\left(\sum_{in=1}^{L+M-1} x_{1,in}{}' \right)} \right) = w_{in}$ is the weight. It holds: $\sum_{in=1}^{L+M-1} \left(\frac{\left| x_{1,in}{}' \right|}{\left(\sum_{in=1}^{L+M-1} x_{1,in}{}' \right)} \right) = 1.$ (14.a)

In Eq.14, $x_{2,in}'$ is an auxiliary variable which takes values within the corresponding α-cut of the resistance $\widetilde{R}_{in\,\alpha}$ and $x_{1,in}'$ is the flow at pipe *in* (crisp number). The only constraint which comes from fuzzy theory is that the resistance of each pipe must belong to its α-cut. In addition, L is the number of loops and M is the number of nodes. $I_1(m)$ is the set of the pipes that converge to node m and $I(l)$ is the set of the pipes which comprise the loop l.

As mentioned previously, the use of the α-cuts instead of the membership function for corresponding fuzzy sets is adopted. The analysis is based on the crisp Q-equations, whereas as fuzzy inputs, the α-cut sets for the pipe resistances are considered. A minimization problem and a maximization problem is solved to determine the left and the right-hand boundaries of the examined α-cut. The process is repeated for a significant number of α-cuts and thus, the membership function of the water flow in the pipes can be reached.

5. NUMERICAL APPLICATION

Let the system of Fig. 3 which consists of two loops, five branches, and four nodes. The system is the one presented by Revelli and Ridolfi (2002), slightly modified. Larger diameters have been selected to fulfil the constraints of max allowable velocity. The Hazen-Williams equation is used for the calculation of head losses. Furthermore, the uncertainty in this example refers not only to the pipe roughness coefficients (as in the original paper), but also to the internal pipe diameters.

Initially, the fuzzy number which corresponds to the pipe resistance is calculated for a discrete number of α-cuts with respect to Eq. 13 (Fig. 4). Comparing the pipe resistances based on the proposed copula approach (Eq. 13) and the widely-used method of α-cuts and the min intersection (Eq. 5), it can be seen, that the proposed methodology leads to smaller uncertainty for the α-cuts

belonging to the open interval zero-one (Fig. 4).

The proposed global objective function of the weighted sum of the absolute values of the head losses is examined, by considering crisp numbers for the water consumption at the nodes. As mentioned earlier, the selection of each weight is proportional to the magnitude of flow at each branch. The only inputs with fuzziness are the pipe resistances. The results based on Eq. 14 are shown in Figure 5. The membership functions of the water flow at pipes take a significant non-symmetric shape. However, even if a significant fuzziness is considered at the initial variables, the final fuzziness is substantially reduced.

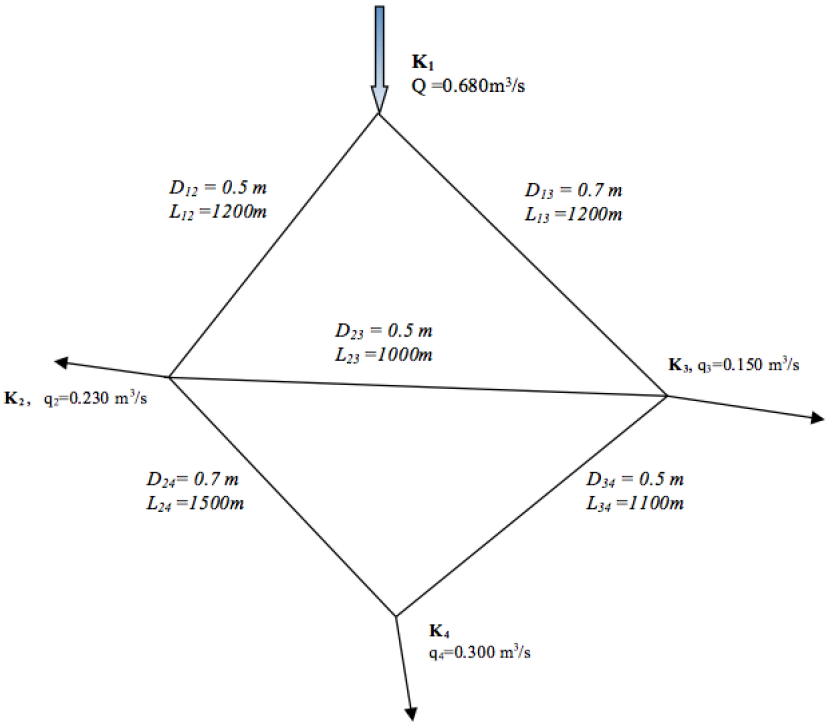

Figure 3. The looped distribution system of the example

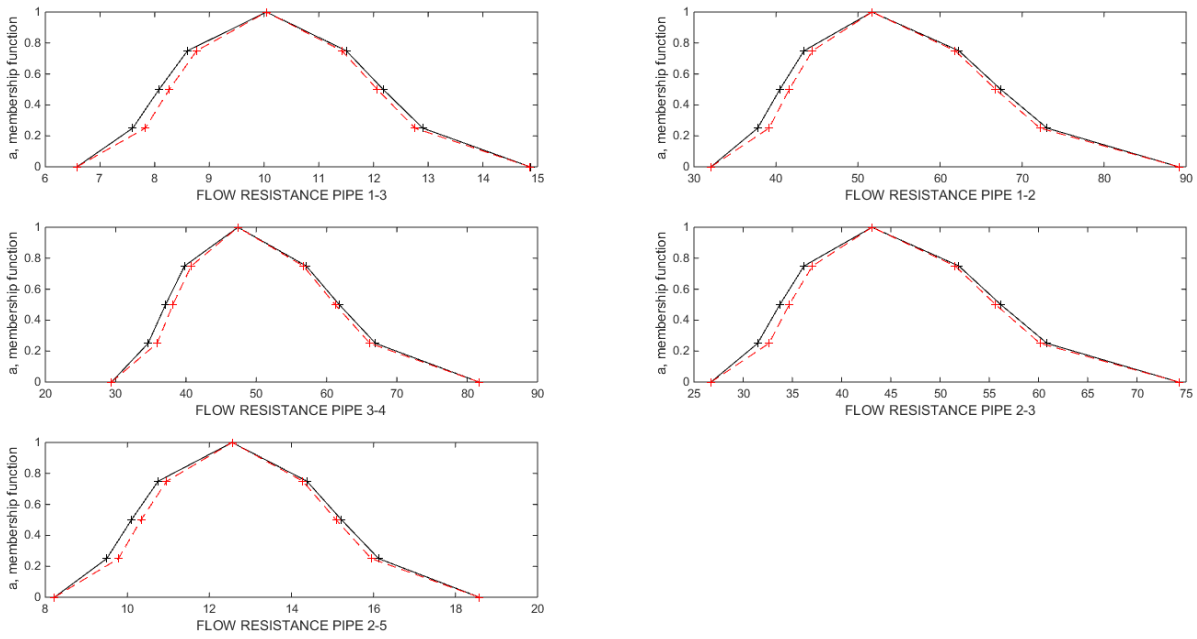

Figure 4. Pipe resistance to flow based on the min intersection (solid line) and the Gumbel-Hougaard copula (dashed line)

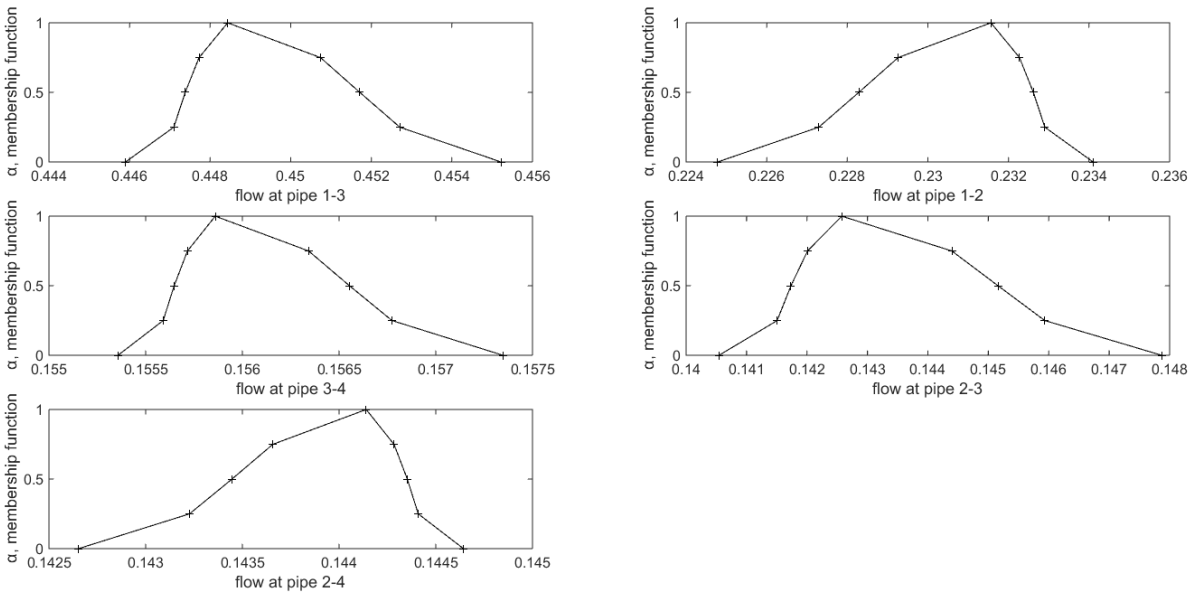

Figure 5. Membership function of flow in each pipe based on the proposed copula approach.

6. CONCLUDING REMARKS

It is concluded that the proposed copula approach used in the design of looped water distribution systems, simplifies the uncertainty analysis and facilitates the incorporation of information related to the resistance to flow. Further, it is observed that the copula approach leads to the reduction of fuzziness when compared to the min intersection approach. The study presented in this paper shows also that the copula approach can be also used in the fuzzy analysis although its origin comes from the probability theory.

REFERENCES

Beliakov, G., Pradera, A. and Calvo T., 2007. Aggregation Functions: A Guide for Practitioners. Springer-Verlag Berlin Heidelberg.

Buckley, J., Eslami, E. 2002. An Introduction to Fuzzy Logic and Fuzzy Sets, Advances in Soft Computing, Volume 13, Springer-Verlag Berlin Heidelberg.

Buckley, J., Eslami, E., Feuring, T. 2002. Solving fuzzy equations, In: J. Buckley, E. Eslami and T. Feuring (Eds), Fuzzy Mathematics in Economics and Engineering, pp.19–46, Springer-Verlag

Dubois, D. and Prade, H. 1978 Operations on fuzzy numbers. International Journal of Systems Science; 9(6), 613-626.

Kechagias, P., Papadopoulos, B. 2007. Computational method to evaluate fuzzy arithmetic operations. Applied Mathematics and Computation; 185(1), 169–177.

Klir, G. & Yuan, B.T. 1995. Fuzzy Sets and Fuzzy Logic Theory and its Applications, Prentice Hall, New York.

Marsden, J., Tromba, A. 2003. Vector Calculus (Fifth Edition), W.H. Freeman and Company, New York.

Näther, W., 2010. Copulas and t-norms: Mathematical tools for combining probabilistic and fuzzy information, with application to error propagation and interaction, Structural Safety; 32, 366–371.

Revelli, R., Ridolfi, L., 2002. Fuzzy approach for analysis of pipe networks. Journal of Hydraulic Engineering; 128(1): 93–101.

Spiliotis, M., Tsakiris, G. 2012. Water Distribution Network Design under Variable Water Demand, Civil Engineering and Environmental Systems; 29(2),107-122.

Tsakiris, G., Kordalis, N., Tigkas, D. Tsakiris, V., and Vangelis, H., 2016. Analysing Drought Severity and Areal Extent by 2D Archimedean Copulas. Water Resources Management; 30(15): 5723–5735

Tsakiris, G. & Spiliotis, M., 2017. Uncertainty in the analysis of urban water supply and distribution systems, Hydroinformatics , (under review)

Tsakiris, G. & Spiliotis, M., 2016. Uncertainty in the analysis of water conveyance systems. International Conference on Efficient & Sustainable Water Systems, "Management toward Worth Living Development", 2nd EWaS 2016, 1-4 June, Chania. Procedia Engineering 162, 340–348.

Tsakiris, G. & Spiliotis, M., 2014. Embankment dam break: Uncertainty of outflow based on fuzzy representation of breach formation parameters. Journal of Intelligent and Fuzzy Systems; 27(5), 2365-2378.

Zimmermann, H. J. 1991 Fuzzy Set Theory and Its Applications. Kluwer Academic Publishers, Dordrecht.

Proceedings of the 10th World Congress of EWRA 'Panta Rhei', 5-9 July 2017, Athens, Greece
© 2017 *European Water Resources Association*

Pressure dependent analysis for managing contaminant propagation in water supply systems

M. Zafari[1*], M. Tabesh[2] and S. Nazif [1]
[1] *School of Civil Engineering, College of Engineering, University of Tehran, Tehran, Iran*
[2] *Center of Excellence for Engineering and Management of Civil Infrastructures, School of Civil Engineering, College of Engineering, University of Tehran, Tehran, Iran*
[*] *e-mail: mohsen.zafari@ut.ac.ir*

Abstract: Since water distribution Network is consisted of different components which are easy to access, they can be contaminated accidentally or deliberately. Therefore, consequence management and withdrawal of contaminant from water distribution network could be a key factor in minimizing the disastrous effects of contaminant propagation on the public health. A number of actions such as contaminant isolation throughout closing valves and opening the hydrants in order to flush out the polluted water were suggested by previous studies to manage the contamination. These response actions lead the network to the critical state which in some nodes, pressure is lower than standard measure. In this situation head driven analysis of water distribution network would be necessary. In this study combination of hydraulic simulation based on head driven analysis method and particle swarm optimization is used for minimizing negative effects of contaminated water to public health as an emergency response after contaminant entrance detection. In addition, the results of consequence management are compared when another kind of hydraulic simulation – demand driven simulation method – is used. The proposed model is applied on network number 3 of EPANET to demonstrate the model applicability in water distribution system and its effectiveness in dealing with contaminant intrusion into the water distribution network.

Key words: Water Distribution Networks, Pressure Driven Analysis, Particle Swarm Optimization, Contaminant Intrusion, Contaminant Propagation

1. INTRODUCTION

Over recent years, there has been much debate about the issue of water safety and what is the best solution to ensure the quality of water. Water distribution networks (WDN) are considered as vulnerable systems to accidental or terrorist attacks because of their dimension and availability of number of nodes. Contaminant intrusion into WDN may lead to many diseases or even human death. Since these systems have significant roles in each society as an infrastructure, suggesting solutions in order to minimize the potential threats is indispensable. Consequence management after detection of contamination is one of the required and major stages to manage the contaminant propagation (U.S. EPA, 2003). Up to now, a few studies have been focused on this stage (Shafeei & Berglund, 2014). Opening hydrants to flush out the contaminated water and valve closure are main solutions that have been recommended by most of them. Although these strategies may reduce the negative effect on public health, considering the proper hydraulic analysis seems to be crucial. On other words, one of the prominent features of consequence management strategy is hydraulic analysis that can influence the reliability of final answer. But majority of previous research focused on optimization modelling and objectives function. Several objective functions have been proposed and effectiveness of them have been indicated. A few numbers of researchers, however, have examined the influence of hydraulic analysis on consequence management.

The aim of this paper is developing a practical method for consequence management in WDNs after recognizing contaminant intrusion. Hydraulic simulation based on HDA is linked with appropriate optimization model to find the optimal hydrants and valves. This could be beneficial for managers of WDN to remove the contaminated water under pressure deficit condition in the

shortest time. In developed model minimizing the total number of contaminated nodes and minimizing the total number of response actions are considered as objective functions. The DDA based model that was proposed before is used to evaluate the approach and examine the effect of hydraulic simulation on optimal answer.

2. PROBLEM STATEMENT AND SOLUTION APPROACH

Three different classes have been introduced to classify the response actions: 1- assessment actions which monitor situation of WDN 2- corrective actions which systematically alter WDN operation to alleviate negative impacts 3- protective actions which should be performed by the public to deteriorate exposure (Rasekh & Brumbelow 2011). This research concentrates on corrective actions and how selection of these actions subjects to hydraulic simulation approach.

Since applying DDA method in valve closure or flushing approaches would result in undesirable solutions for emergency response strategy that some nodes have an inadequate or negative nodal pressure, some DDA based studies have considered a minimal pressure (P^{min}) which answers with nodal pressure less than P^{min} are omitted (Alfonso et al., 2010). However, even consideration of P^{min} does not guaranty optimal solution attainment, because calculated pressure values by DDA approach are lower than HDA (Shirzad et al., 2013). In fact, search space inevitably has been restricted to response actions that do not cause excessively low pressure in the WDN by using DDA method.

To date, limited research has focused on significance of hydraulic simulation approach to selection of emergency response strategy. To address the issue this study develops a HDA based model to find the optimal valves and hydrants to eliminate the contamination from WDN. A previous DDA based study is chosen and the proposed HDA based model is tested on the similar WDN. Identical objective functions and contamination scenario are assumed to compare the results of using two different approaches. Also, the impact of applied hydraulic simulation on ultimate corrective actions is demonstrated.

3. MODEL DEVELOPMENT

Contamination scenario and the hydraulic simulation and optimization approaches are integrated to propose the model that select the proper valves and hydrants to eradicate the contamination from WDN.

Contamination intrusion scenario should be clarified as the input required information for optimization of consequence management operations. This scenario is defined by a set of factors including contaminant mass, location(s) of contaminant intrusion, exact time and day of year which contamination event is triggered, type of the pollutant and the duration of intrusion (Rasekh and Brumbelow, 2013). Since in most of the real occurrences of contamination in WDN the emergency response strategy is identified after verification of contaminant intrusion, local quality test execution and source identification, some initial data needed for contamination scenario are predetermined. Therefore, several researches determine a set of response actions based on source characteristics (Afshar & Najafi, 2014). The proper operational response can be also determined only based on sensors' information (Shafiee & Burglund, 2014) or critical situation (Rasekh and Brumbelow, 2013). Contamination scenario can be determined based on source characteristics (Afshar & Najafi, 2014). The proper operational response can be also determined only based on sensors' information (Shafiee & Burglund, 2014) or critical situation (Rasekh and Brumbelow, 2013). The scenario which is proposed here is identical to the contamination scenario of Afshar and Najafi (2013).

To implement HDA based hydraulic simulation, replacement of head-discharge relationship with fixed nodal outflow in continuity equation is required. The suggested equation by Wagner et al.

(1988) seems to be more realistic (Shirzad et al., 2013). Wagner et al. (1988) equation based on pressure is as follow:

$$\begin{cases} Q_j^{avl} = Q_j^{req} & ; if \quad P_j \geq P_j^{des} \\ Q_j^{avl} = Q_j^{req} \left(\frac{P_j - P_j^{min}}{P_j^{des} - P_j^{min}}\right)^{1/n_j} & ; if \quad P_j^{min} < P_j < P_j^{des} \\ Q_j^{avl} = 0 & ; if \quad P_j \leq P_j^{min} \end{cases} \tag{1}$$

whereas P_j^{min} and P_j^{des} are minimum required and desired pressure in node j respectively, P_j is calculated pressure value at node j, Q_j^{avl} is available outflow at node j, Q_j^{req} is required outflow at node j and n_j is a constant depending on the system situation which varies between 1.5 and 2 (Shirzad et al., 2013). The idea of the applied method is taken from Pathirana (2010) which the minimum required pressure (P^{min}) is presumed zero and the emitter coefficient (K) is defined as illustrated in Equation (2) to replace nodal demand with emitter:

$$\begin{cases} k = Q_j^{req} \times \left(\frac{1}{p_j}\right)^{1/n_j} & ; if \quad P_j \geq P_j^{des} \\ k = Q_j^{req} \times \left(\frac{1}{P_j^{des}}\right)^{1/n_j} & ; if \quad P_j^{min} < P_j < P_j^{des} \\ k = 0 & ; if \quad P_j \leq P_j^{min} \end{cases} \tag{2}$$

Identical formulations with Najafi and Afshar (2013) are used to quantify these objectives as follows:

$$F_1 = \sum_{i=1}^{n} \sum_{t=t_s}^{t_{end}} N(i,t) \ , \ N(i,t) = 1 \ if \ \ C_{i,t} > C_p \ , \ N(i,t) = 0 \ \ otherwise \tag{3}$$

whereas F_1 is the total number of contaminated junctions in all time steps of simulation, i is the consumer node index, n is the total number of consumer nodes, t_s and t_{end} are the beginning and ending time of simulation, $C_{i,t}$ is the contaminant concentration in node i at time t, C_p is the allowed contaminant threshold based on local standards which is equal to 0.01 mg/lit based on Najafi and Afshar (2013) and $N(i,t)$ is a binary variable that is equal to one when the concentration of contaminant is more than allowed threshold in node i at time t and otherwise it is equal to zero.

$$F_2 = \sum_{k=1}^{VA} VA_k + \sum_{j=1}^{HY} HY_j \tag{4}$$

whereas F_2 is the total number of field operations (i.e. valves closure and opening the hydrants), k is the valve index, j is the hydrant index, VA is the total number of valves in WDN, HY is the total number of hydrants in WDN, VA_k is a binary variable that is equal to one when the status of valve k is changed (the initial status of all valves are open) and HY_j is a binary variable that is equal to one when the status of hydrant j is changed (the initial status of all hydrants are close).

Several methods have been proposed to solve multi-objective problems based on PSO (Hu &

Yen; 2015). The approach that presented by Coello et al. (2004) have been demonstrated as a useful and strong tool for solving multi-objective problems. This method is based on using an external repository which keeps a historical record of the non-dominated solutions (i.e. particles). The main parts of external repository are: 1-the archive controller that determines whether a certain particle should be added to the repository or not and 2-the grid that produces well-distributed Pareto fronts. Each particle regarding to its *pbest*, is compared with non-dominated particles which exist in repository in each iteration, then archive members are updated. Finally the members remain in external repository represent the Pareto fronts.

4. RESULTS AND DISCUSSION

EPANET example 3 network (Rossman, 2000) is utilized to evaluate and demonstrate capability of developed model proposed in this study. This network comprises two constant head sources, a lake and a river, three elevated storage tanks, two pumping stations, 117 pipes, 59 consumer nodes and 35 internal nodes (Figure 2). It is assumed that 20 hydrants and 31 valves are available in this WDN, so the total number of decision variables are equal to 51. The situation of decision variables (i.e. valves or hydrants) are coded as binary numbers (0, 1). The valves and hydrants situation in the onset of the procedure are assumed open and closed, respectively. Code 0 represents the steady state of the primary situation of valves or hydrants whereas code 1 represents the alternation in primary state. The outflow of hydrant is presumed constant and equal to 3.473 lit/s (55 gal/min). In EPANET a hydraulic and constituent time step of 15 min was used for a 24-hour simulation period. All of these assumptions are based on Najafi and Afshar (2013).

Contaminant with C_p = 0.01 mg/l is injected with a mass rate of 0.006 kg/s at 9:00 am for a duration of 7 hours. Location of injection is illustrated in Figure 2. Operational responses are performed after finishing the response delay (4 hours) at 1:00 pm and remain unchanged by the end of the contamination withdrawal from the WDN. Response delay is the elapsed time after the contaminant entrance in the WDN until finishing the field operations (valve closure and hydrant opening).

The number of contaminated nodes in which the contaminant concentration were above the acceptable threshold, are determined at each time step (every 15 minutes) after starting the simulation. Total number of contaminated nodes is considered at each simulation by summation of their number in different time steps (F_1). Also, total number of execution of field operations is calculated by using Eq. (6). The Pareto-optimal solution that has been obtained by using DDA based approach (Najafi & Afshar, 2013) is illustrated in Figure 1.

The total number of contaminated nodes are decreased to 464 by performing 14 field operations, while it is equal to 1545 when no response action is employed. Therefore, it seems that execution of field operations reduced the total number of contaminated nodes by near 70%. Regarding the answers, only by closing one valve (Valve 177) substantial reduction in number of field operations is occurred.

Although some answers that is shown in Figure 1 are highly effective in decline the negative impact of contamination, they can lead to escalate the nodal pressure in some junctions. Therefore, these solutions may be impractical due to strong possibility of burst pipes in WDN. Take for example, closing the valves 111 and 173 decrease the total number of contaminated nodes by near 60%, but this answer causes considerable increase in pressure of a tremendous number of nodes that is represented in Figure 2. As shown in this figure, by closing the valves 111 and 173 the upper reaches of these valves experience the pressure above 60 meter (85.7 psi). Accordingly, if the prominence of hydraulic of WDN is ignored and only the quality of water and withdrawal of contamination are considered, some impractical solutions may be proposed that can contribute to wasting time and money. It seems that considering the maximum threshold of pressure which is ignored in most of the previous researches is necessary. This threshold will be considered in the developed HDA based model to make the final solutions more effective.

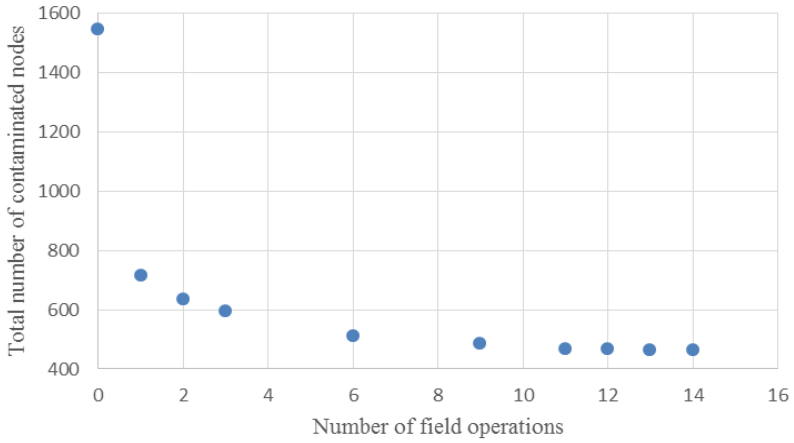

Figure 1. Pareto-optimal solution of the multi-objective optimization by using DDA-based approach (Najafi & Afshar, 2013)

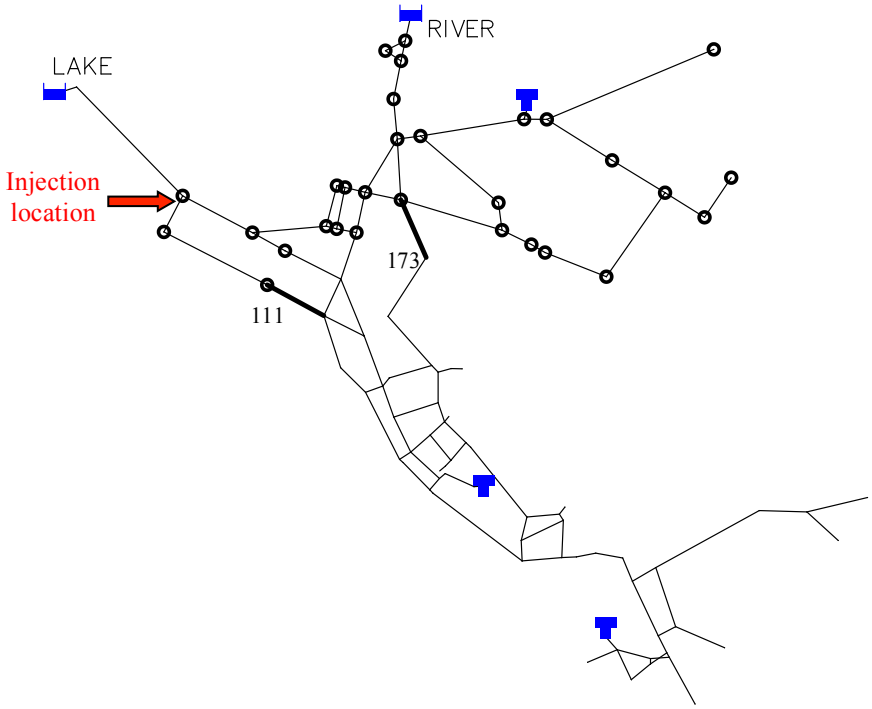

Figure 2. Schematic of EPANET's example 3-The nodes with pressure above 60 m by closing the valves 111 and 173

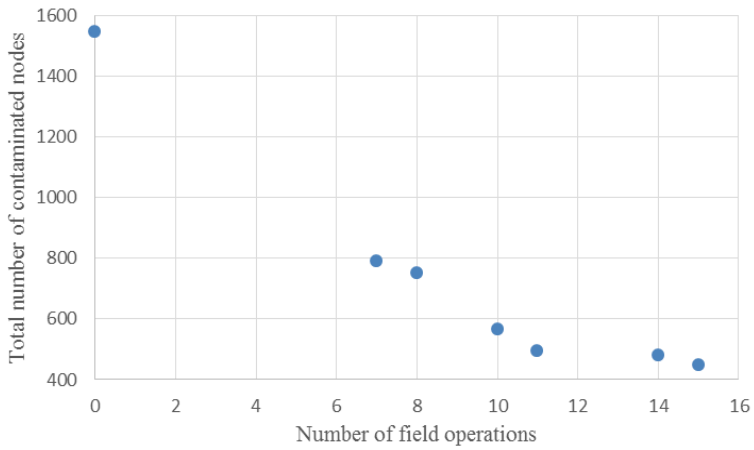

Figure 3. Pareto-optimal solution of the multi-objective optimization by using proposed HDA based approach

The pareto-optimal solution that is acquired by using proposed HDA based approach is shown in Figure 3. The positive constant parameters of PSO (i.e. c_1 and c_2) and the inertia weight were assumed 2 and 1 respectively similar to the main version of PSO (Eberhart & Kennedy, 1995). Also, the number of particles were set equal to 100.

Regarding this figure, it is clear that some over-optimistic and impractical solutions that lead to substantial reduction by only a few field operations are omitted. The total number of contaminated nodes are declined to 448 by performing 15 field operations, while it is equal to 1545 when no response action is employed. It is noteworthy that if the DDA based model is used, this solution will be omitted due to emerging negative pressure in seven nodes of WDN. On other words, the search space is restricted by using DDA based approach, so it is probable that some optimal solutions are not considered. Comparing the answers with answers of Najafi & Afshar (2013), it is obvious that there is a difference between the chosen valves and hydrants. This difference is mainly because of using HDA approach with considering maximum pressure threshold. In fact, some unpractical solutions were omitted due to using maximum pressure threshold, and search space was extended by using HDA based model instead of DDA based approach.

4. SUMMARY AND CONCLUSIONS

Most of the consequence management researches have used the similar response actions such as valves closure for isolating the contaminant and flushing out the polluted water by hydrants opening. However, a few previous studies have considered the significance of their hydraulic simulation approach that may have a major impact on final optimal solutions. This study introduced and tested an effective HDA based approach to find the optimal valves and hydrants and demonstrated the necessity of using HDA method in finding appropriate emergency response actions after intrusion of contamination in WDNs. To substantiate the claim that using DDA method does not guaranty optimal solution achievement the results of developed model was compared with DDA based method. Two important findings that can be reported as a result of this comparison:

1. Corrective actions such as valves closure or opening hydrants may contribute to pressure deficit condition in some junctions of WDN. In this occasion using DDA based model might omit some optimal solutions. Therefore, utilizing DDA based model to find the corrective actions may lead to spending more time compared to using HDA based method. It is noteworthy that minimizing the duration of eliminating contaminant from WDN is absolutely crucial due to importance of public health.
2. Not paying attention to hydraulic of WDN in addition to water quality may cause wasting a great amount of time and money. Take for example, if pressure maximum threshold is not considered, some non-practical response actions might be attained that lead to bursting a number of pipes of WDN.

REFERENCES

Afshar, A., & Najafi, E. (2014). “Consequence management of chemical intrusion in water distribution networks under inexact scenarios.” J. Hydroinf., 16(1), 178-188.

Alfonso, L., Jonoski, A., & Solomatine, D. (2010). “Multiobjective optimization of operational responses for contaminant flushing in water distribution networks.” J. Water Resour. Plann. Manage., 10.1061/(ASCE)0733-9496(2010)136:1(48), 48-58.

Coello, C. A. C., Pulido, G. T., & Lechuga, M. S. (2004). “Handling multiple objectives with particle swarm optimization.” Evol. Comput., IEEE Transactions on, 8(3), 256-279.

Eberhart, R. C., & Kennedy, J. (1995). “A new optimizer using particle swarm theory.” Proc., 6th Int. Symposium on Micro Machine and Human Science (Nagoya, Japan), IEEE Service Center, Piscataway, N.J., 39-43.

Hu, W., & Yen, G. G. (2015). “Adaptive multiobjective particle swarm optimization based on parallel cell coordinate system.” Evol. Comput., IEEE Transactions on, 19(1), 1-18.

Najafi, E., & Afshar, A. (2013). “Consequences Management of Chemical Intrusions in Urban Water Distribution Networks Using the Ant Colony Optimization Algorithm.” J. Water & Wastewater, 82-94.

Pathirana, A. (2010). “EPANET2 desktop application for pressure driven demand modeling.” Proc., 12th Annual Water Distribution Systems Analysis Conference, WDSA, Tucson, Arizona, 12-15.

Rasekh, A., & Brumbelow, K. (2011). “Multi-criteria response planning for water utility contamination events.” Proc., World Environmental and Water Resources Congress 2011, ASCE, California, USA.

Rasekh, A., & Brumbelow, K. (2013). “Probabilistic analysis and optimization to characterize critical water distribution system contamination scenarios.” J. Water Resour. Plann. Manage., 10.1061/(ASCE)WR.1943-5452.0000242, 191-199.

Rossman, L., A., (2000). EPANET2, United States Environmental Protection Agency.

Shafiee, M. E., & Berglund, E. Z. (2014). “Real-Time Guidance for Hydrant Flushing Using Sensor-Hydrant Decision Trees.” J. Water Resour. Plann. Manage., 10.1061/(ASCE)WR.1943-5452.0000475, 04014079.

Shirzad, A., Tabesh, M., Farmani, R., & Mohammadi, M. (2013). “Pressure-Discharge Relations with Application to Head-Driven Simulation of Water Distribution Networks.” J. Water Resour. Plann. Manage., 10.1061/(ASCE)WR.1943-5452.0000305, 660-670.

U.S. Environmental Protection Agency (USEPA). (2003), Response protocol toolbox: Planning for and responding to drinking water contamination threats and incidents, Washington, DC.

Wagner, J., Shamir, U. and Marks, D. (1988), “Water Distribution Reliability: Simulation Methods.” J. Water Resour. Plann. Manage., 10.1061/(ASCE)0733-9496(1988)114:3(276), 276-294.

Proceedings of the 10th World Congress of EWRA 'Panta Rhei', 5-9 July 2017, Athens, Greece
© 2017 *European Water Resources Association*

Evolution of water supply infrastructures of Thessaloniki city, Hellas, through centuries

S. Yannopoulos[1], A. Kaiafa-Saropoulou[2*], E. Gala-Georgila[3] and E. Eleftheriadou[4]
[1] *School of Rural and Surveying Engineering, Faculty of Engineering, Aristotle University of Thessaloniki, GR 54124 Thessaloniki, Greece*
[2] *School of Architecture, Aristotle University, 54124 Thessaloniki, Greece, Cherianon 7, Kalamaria, GR 55133, Thessaloniki, Greece*
[3] *Delfon 195, GR 54655 Thessaloniki, Greece*
[4] *Department of Environment and Hydroeconomy of Thessaloniki, District of Central Macedonia, 26th Oktovriou 64, GR 54627 Thessaloniki, Greece*
[*] *e-mail: minakasar@gmail.com*

Abstract: Thessaloniki city, in the east core of Thermaic gulf, has been continuously inhabited for about 2,330 years. The choice of it' s founding at this specific location is very much attributed to the high availability of water in the wider region. However, the development of Thessaloniki in a big city and the simultaneous increasing population, created an increased need for water, which could not be covered by the water of the wells. Until the 19th century, water needs were met with cisterns, water channels, fountains and water towers in combination with the wells. Moreover, the city was also equipped with large scale and of high expertise water supply projects, which were exploiting the region's water resources in four different places and were transferring water inside the walls. These water transfer works were associated with water distribution systems, with terracotta pipes located beneath roads or following the contour lines. Also, people who lived in the Hellenistic, Roman, Byzantine, Ottoman and newer Hellenic periods gave their own perspective in the problems related to water supply in the city. A review of all these techniques through centuries is presented and commented in this paper.

Key words: Thessaloniki, infrastructures water supply, Hellenistic-Roman-Byzantine-Ottoman and newer Hellenic periods

1. INTRODUCTION

Thessaloniki, was settled in a narrow area between the edge of Hortiatis mountain and the Thermaic Gulf, in a limited area of 250 ha lying between west and east walls, which were developing vertically from the acropolis to the sea. The city had both rich underground aquifers, within the urban grid and good quality water springs in Hortiatis Mountain and the hilly wider region (Figure 1).

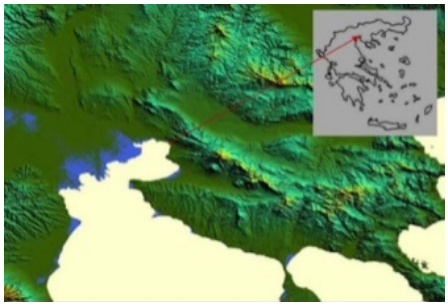

Figure 1. Thessaloniki, Map of the whole area

Soon after the foundation of their new city, the residents used to draw water from underground aquifers, by digging wells. Later on, in parallel with the wells, they constructed four aqueducts, according to advanced hydraulic technologies, through which they carried water to cisterns. From

these water end points, pipe networks, located beneath the roads, were branching all over the city. In modern times, after the liberation in 1912, the city extended extra muros. Thus, new water supply needs have been emerged, which had to be covered based on new hydro-technological achievements. Particularly, after the great fire of 1917 new water sources have been sought and water supply infrastructures have been reorganized, so as to ensure water sufficiency both for the old city center and for all the new neighborhoods which were rapidly expanding. This paper provides valuable insights into the water supply technologies developed in the city of Thessaloniki.

2. THESSALONIKI: SHORT HISTORICAL REVIEW

Thessaloniki was founded in 315 BC by the King of Macedonia Kassandros, who united 26 small agricultural settlements scattered in Mygdonia field. Very soon, the city became one of the most significant cities of the Macedonian Kingdom. It was founded in a limited area with intense downward gradient from Northeast to Southwest, high elevation and steep inclines in the Upper city and more shallow inclines towards the sea (Yannopoulos *et al*., 2015). Through ages its urban profile has been many times renovated, due both to the increasing population, needs and culture of every era. Moreover, series of catastrophic earthquakes, especially during 7th century, and floods changed the ground level in several points within the walls.

One of the most prominent factors for the foundation of the city in this particular area was the adequate quantity and good quality of the water resources rising in Hortiatis Mountain, nearby. Many of these water quantities were "blocked" in underground aquifers, or often appeared in superfluous streams and currents, that were enriched by rain and surplus water altogether flowed with high velocity, crossing the city and eventually discharging into the sea, inner or outer city walls (Yannopoulos *et al*., 2015). Despite all these man-made renewals and the various physical or human-induced disasters mentioned above, the geomorphology of the area maintained its main features inside the city walls over time (Gala-Georgila, 2015). Furthermore, the Hippodamian grid also maintained in general its original plan through ages (Dimitriadis, 1983), so as the superposed horizontal and vertical streets in many cases remained in approximately the same axis with the older ones lying underneath (Egnatia str., Ag. Dimitriou str., Philippou str.). The abundance of aquifers of good quality in specific locations in Hortiatis Mountain, the geomorphology within the city and in the countryside and the almost constant maintenance of the Hippodamian urban plan through centuries, determined the exact locations of the water sources, the aqueducts' routes, their end-points and the development of water distribution networks.

3. DEVELOPMENT OF THE WATER SUPPLY SYSTEM OF THESSALONIKI

3.1 The Hellenistic and Roman periods

There is no doubt that hand-dug wells covered the water demands just after the city's establishment, in the end of 4th century BC. A large number of them have been found in house plans, public places, or even cemeteries, varied in formation of shafts, well-head configuration and size. They were usually stained of circular section, while during the roman period, stone masonry was usually combined with the widespread use of scattered parts of bricks and tiles sometimes all bonded with lime mortar construction.Up till now two square stone made wells of roman times have been recorded in the town. The rectangular shape has been rarely preferred in Byzantine times. On the contrary in Ottoman period all the wells were of circular cross section (Kaiafa, 2014a).

Besides the wells that were in abundance, the city of Thessaloniki, was equipped with more than one water technical project, which had different starting points, Hortiatis, Retziki, Lebet and Anthemounta valley (Galatista) (Gala-Georgila, 2015; Tamiolakis, 1985) (Figure 2). The exact construction dates of these technical water transporting projects remains a nebulous matter, because of the piecemeal architectural remaining. However, bearing in mind that the construction of an

aqueduct was a huge task, usually financed by the Emperor, it is very possible that each of the four aqueducts of Thessaloniki was part of intense building regenerations that took. ace at the turn of 1st century BC, in 2nd century AD or much later at the end of 3rd century AD.

Despite the very few Hellenistic data of a pressurised piping system within the city, the existence of at least one aqueduct before the Roman period, is almost certain, which supplied water to houses, fountains and public baths, just like the one of the 2nd century BC that was located in the NE corner of the city's Agora. During roman period, when the city has been embellished with splendid buildings, increasing water needs are related to the extended use of public baths and latrines, which were playing a major role in the life style and presupposed continuous water flow. In the beginning of the 4th c. AC, Galerius renewed the city by renovating old buildings or constructing new ones, equipping them with advanced hydraulic infrastructure which also expanded all over the urban grid.



Figure 2. Thessaloniki, aqueducts 1. Hortiatis Aqueduct (springs), 2. Retziki Aqueduct (springs), 3. Lebet Aqueduct (springs) 4. Kalamaria Aqueduct (the area SE of the city, remains).

Springs in Hortiatis, nearby the modern village, 600-900 a.s.l., provided the consuming residents of the ancient city with good quality waters at least since Roman era, maybe since 2nd century AD, being probably part of the Antonine's fiscal policy (Kaiafa, 2014b). Water was collected through the qanat of Agia Paraskevi, consisted of two or more underground galleries. Nowadays only its middle Byzantine phase and the renovation of Mourat II are visible. Due to the addition and restorations through centuries in order keep a continuous function until nowadays (1975), almost no evidence of Roman times has been found, except few remains in the lower part of the foundation of the later Ottoman, still standing, water-bridge, the current form of which belongs to the later years of Byzantine and mainly to the Ottoman period. It is very difficult to observe the routing of the Roman phase of Hortiatis aqueduct, though it is unlikely to follow the same way with the Byzantine and Ottoman water-channel, being about 22Km long till the central end point, located probably north of the Byzantine Acropolis (Eptapyrgion) (Gala-Georgila, 2015).

Retziki springs, situated further North, near the church of Agia Triada (Pefka), seem to be a second water collection point, supplying the western side of the city (Figure 2). In the east wider area, at higher level water sources were also used to enrich the lower springs through qanat galleries. Unfortunately, the aqueduct remains over there are so few that neither its construction and its route nor the duration of its function can be clarified. It is assumed though that a water transfer project starting from Retziki springs, 350m a.s.l., was supplying the city even before 2nd century BC. Its presence is indirectly attested in a 2nd century A.D. inscription, referring to the repairing of a water transporting work being in a place name "Altias" (Kaiafa, 2014b). Byzantine archaeological data suggest that its length reached approximately 8 km and its end point is located in the grove of Sykies, near a modern water tank of EYATH S.A. From there the routing of the water till the walls of the city are uncertain. There are two possible alignments, the first of which ended up in the SW part of the Byzantine Acropolis and entered the city from a small gate of the north wall. According to a second view the water conduit met the routing of the third aqueduct of the city, known as Lebet aqueduct. Finally, the remains of an aqueduct bridge that crossed Xiropotamos torrent, very close to the water sources in Retziki, belong to the 15th -16th century AD, as a part of a major renovation (Gala-Georgila, 2015; Tamiolakis, 1985).

The third aqueduct was transferring water from springs located in the area near the present village Eukarpia (Figure 2), which were enriched through qanat, whose exact starting point is not known (Gala-Georgila, 2015). Parts of an open flow aqueduct channel have been found in several spots in the area of Polichni and Stavroupoli, which certify more than one construction phases; the earliest of which are Roman, yet no further information is available so as to have a more exact dating. That is a stone built conduit rectangular in section, covered by stone slabs and a consistent slope of 2‰. The end point was probably located in a cistern in the area of Kallithea, from where the water was branched in the west part of the city.

Moving on, the Roman Emperor Galerius (turn of the 3rd century AD) renovated and improved the hydraulic infrastructures all over the urban grid. The aqueduct which has been built then, simultaneously with the construction of the Palace complex, probably ensured its continuous water supply. Parts of a vaulted stone made water conduit with manholes on its arch, which have been revealed in Toumba, in Pilaia, in the area of American Farm School and at various points in Thermi village, prove the presence of an important and quite extensive aqueduct which laid in Kalamaria valley, southeast of the city of Thessaloniki, in an area where fissured rock aquifers and karstic aquifer discharge ground water through springs. Its beginning is placed either in the Anthemountas valley or near the Thermi dam and the endpoint is located in Thessaloniki, about 150 meters north of Kalamaria's gate in the east city walls, in the area of Evaggelistria (Gala-Georgila, 2015).

The water transfer projects mentioned above were combined with water distribution networks, which were scattered throughout the city. Both Hellenistic and Roman urban grid was undoubtedly favorable to the development of a well-organized network of water distribution. That was consisting mainly of clay pipes with well proofed joints, and more rarely of lead pipes, supplying individual consumers, public buildings and a large number of fountains.

3.2 The Byzantine period

The residency of Constantine the Great in the city during 320-323 AD resulted in the construction of numerous hydraulic infrastructure works. The city flourished over the next two centuries and the population increased at a high pace. Thus, new public buildings and luxurious private residences lead to increased demand for fresh water, which has been covered by water distribution infrastructures (Karydas, 2009). Furthermore, a series of catastrophic earthquakes during the first decades of the 7th century severely damaged the city, resulting in the destruction of public buildings, walls and infrastructures. The constant need of fresh water led to the continuous renewal of the city's water distribution network. Building of large and important cisterns seems to have occurred constantly with reservoirs being found dated to the 7th until 14th centuries. At the same time, successive repair work is evident in cisterns, which indicates that they were abandoned only in case of complete destruction (Gala-Georgila, 2015).

The necessity for water storage, led to the conversion into reservoirs of several important buildings from the Roman and Early Byzantine period, such as the Cryptoporticus in the Roman Forum, the monumental vestibule of the Octagon in the Galerian Complex (Athanassiou *et al*., 2004) and the utilisation of the wall in the Roman Acropolis near the Trigonion area (Marki and Konstantinidou, 2005). The transport of water inside the city was achieved by using masonry stone covered conduits and terracotta pipes with an inner diameter of 10-13cm. The masonry conduits were usually constructed on top of a stable foundation. The side walls were covered with hydraulic mortar, while the bottom was covered using ceramic tiles, stones or slate.

Both the end points of the external aqueducts and the terrain morphology show that the distribution of the water started at the highest points of the city. Water was transported by open flow conduits. Closed terracotta pipes, functioning under pressure, were only utilised to supply water to specific destinations from water towers or reservoirs at a close distance. The flow of water on the highlands, where the gradients can be extremely high in certain parts, was achieved using conduits following the contours of the terrain. The neighbourhoods towards the sea were fed using conduit systems arranged 'vertically' following the streets that were perpendicular to the shoreline.

Reservoirs were usually located at the top of these distribution lines. (Gala-Georgila, 2015). Gradually as the city weakened during the last decades of the 14th century, the water distribution system fell into disrepair.

3.3 The Ottoman period

The city of Thessaloniki was conquered by the Ottomans in 1430. Small scale changes and repairs to the water supply system seem to be occurred immediately after the fall of the city. The Hortiatis aqueduct was repaired and twenty new public fountains were constructed.

During the 16th century the dispersion of the city's population had an important effect on the organisation of the water distribution system, which was very much improved and extended. The incoming water supply was carried by two aqueducts: The Hortiatis aqueduct and the aqueduct of Lembet or Yeni Su, which was constructed by uniting the two earlier byzantine aqueducts of Eukarpia and Retziki (Gala-Georgila, 2015). The main water structures which made up the Ottoman water distribution system were the maksems or taksims and the water towers or suterazisi. The maksems above or below ground were either domed or vaulted buildings containing water tanks with a discharge measuring system or simpler constructions (Dimitriadis, 1983). Known as su terazisi, the water towers had a cistern at the summit from which the water flowed into distribution pipes. These structures helped maintain water pressure and improved water distribution to districts with shallow inclines towards the sea (Gala-Georgila, 2015). The water was conveyed using masonry conduits and terracotta pipes as in the previous periods. The public fountains all over the neighborhoods played a major role.

Over the next few centuries, Thessaloniki experienced great growth, thus the need for fresh water was high, especially considering of the great number of public baths, up to 300. Water needs had been usually ensured by drilling wells, up to 3000, according to the traveller Evlia Tselempi, or building many fountains through the city. According to Thessaloniki contained 300 public baths. During the 19th century the land wall of the city was torn down, a new port was constructed and the infrastructure was modernised. To modernise the water distribution system the 'Ottoman Water Company of Thessaloniki' was founded. The new system utilised pumps and was constructed between the end of the 19th century and the beginning of the 20th century (Tamiolakis, 1985).

3.4 The period from 1912 (independence) to 1939

After the city's liberation from the Ottomans in 1912, the Municipality of Thessaloniki took over the water supply of the city. The three aqueducts of Hortiatis, Retziki and Lebet came to the ownership of the Municipality. Almost immediately, Municipality launched a program of maintenance, repair and improvement of these aqueducts and it took care for their proper operation and exploitation and at the same time, Municipality drilled many boreholes within the city area.

The destruction of the water supply network due to the fire of 1917, the reception of thousands of refugees in 1922 and the rapid expansion of the city outside the walls aggravated the problems of water supply of the city. In order to address this situation, Municipality drilled new boreholes and constructed pumping stations at Rysio, Kadirli (Kalamaria), Papafi, Platanos, etc. In 1926, the municipality replaced the old pipes of water supply, and at the same time expanded and repaired the water supply network of the city. During the period 1915-1939, the Municipality built 18 water tanks in various areas of the city. The purpose of these tanks was primarily to ensure the necessary pressure in the water network and less in storage, since the volume of water that could store each one of them was relative small (Tamiolakis, 1985).

In order to meet the needs, municipality bought water from the private Turkish-Belgian company "Compagnie Ottomane des Eaux de Salonique".

In the period of 1922 – 1930, significant interventions and major infrastructure projects were made in the city. Due to the implementation of the new town planning, significant network pipes that passed through private plots, had to be removed and new pipes had to be constructed in the

limits of the new roads of the city. However, the urban water distribution network of the city was not constructed as a whole, but to meet the water needs of the citizens, it was extended according to the extension of the city. Thus, it was proven the very soon that the network has become inadequate to meet water supply needs because of inadequate sections of the pipelines. Throughout this period, great efforts were made to improve the water supply system with the maintenance of aqueducts, the conduits replacements, the drilling of new boreholes and the construction of reservoirs.

3.5 The water supply system of Thessaloniki after 1939

In 1939, with its establishment, Thessaloniki Water Supply Organization (OYTH) received the water works, which in general (mainly these of Municipality of Thessaloniki) was not in very good condition, since they had not been constructed according to a single plan, but occasionally with the main purpose to meet the current needs of residents. In this way, OYTH confronted significant difficulties in water supply of the city. This situation became hardest with the start of World War II.

In 1949, the conditions became even more difficult with the increase of population due to internal migration and defaults on water bills by users due to the economic impoverishment of the population. From the early 1950s until 1974, the focus was on ensuring the required quantities of water, since the functioning of the urban water distribution network showed satisfactory operation.

The administration of OYTH decided the construction of the pump station of Kalochori and many boreholes were drilled in the wider area, expanding the abstraction of water in the plain of Sindos area, while the aqueduct of Nares in the region of Galikos River was completed. In 1974, it was decided the development of Aravissos sources and of Aliakmonas project and the planning of the urban water distribution network. After the completion of the plans concerning the basic water works, OYTH began the gradual implementation of the construction of reservoirs and major conductors of the water supply network, both to the western and the eastern areas of the city.

Nowadays, according to the contract of 27.7.2001 with the Greek State, EYATH S.A owns or manages facilities which include: a) water abstraction works, b) external aqueducts, boreholes and pipelines, c) pumping stations and tanks and d) the distribution network comprised of pipelines and water meters. EYATH S.A. uses the karst system of aquifers in the Paiko Mountain to supply water to Thessaloniki. Water is abstracted from the Aravissos springs from two natural supply shafts, a spring fitted with a pump and 11 water boreholes which pump water via connecting pipes to the Aravissos aqueduct. The quantity of water obtained from the Aravissos springs ranges from 65,000 m^3/d to 130,000 m^3/d, depending to a large degree on snowfall and rainfall recorded every year (https://www.eyath.gr/).

Also, water is abstracted from the Aliakmonas River in the area known as Varvares around 40 km from the river delta. Water is diverted via a 50 km long free-flowing channel to the Axios River where it reaches the water treatment plant (known as the refinery). Subsequently, the clean drinking water is directed to 75,000 m^3 storage tanks and is distributed via a network of pipes 36 km long to existing water supply tanks at Diavata, Evosmos, Polichni, Neapoli, Vlatades, Toumba and Kalamaria, as well as the Industrial Area of Thessaloniki (Sindos). In the wider area of Axios River (Gefyra, Nea Halkidona, Eleousa, and Agios Athanasios) there are a total of 46 boreholes with ability of pumping around 70,000 m^3/d of water. In case of increased water demand, there are 26 boreholes stand-by in the Kalochori area with ability of pumping around 30,000 m^3/d. From the bed of Galikos River (Narres area) water is abstracted via 3 water collection shafts. The ability of Narres area to collect water varies from 5,000 m^3/d to 25,000 m^3/d depending on rainfall and snowfall recorded each year. The Narres aqueduct is currently out of use and is on stand-by. Moreover, the Agia Paraskevi springs at Hortiatis are used to provide additional water to the Hortiatis Municipal District and as a back up to supply water to the Georgios Papanikolaou Hospital.

Prior to consumption, water is submitted to treatment in the Refinery (Thessaloniki Water Treatment Facility), which lies 2km north of the Sindos Industrial Area close to the Thessaloniki – Edessa National Road. EYATH S.A. is the owner of the facilities, but it has outsourced running to a

third party and supervises how the facilities are run, by sending expert staff from the relevant company division. At present the facilities can treat 150,000 m^3/d and in the future (after the complete integration of plans and works) will reach 600,000 m^3/d (https://www.eyath.gr/). The total water needs come from Aliakmonas River, in a percentage of 50%, from Aravissos springs, 29% and from boreholes, 21%. The average water needs of the city amount to 250,000 m^3/d while the maximum needs (during summer) reach 290,000 m^3/d. EYATH S.A. operates and maintains 34 pumping stations and 21 reservoirs of water storage for the transmission and distribution of drinking water in the Urban Agglomeration of Thessaloniki. The total length of the pipes of the water distribution network is approximately 1,500 km.

4. AUTHORITIES OF WATER SUPPLY MANAGEMENT OF THE CITY WITH TIME

After the liberation from the Ottomans in 1912, the Municipality of Thessaloniki took over the water supply of the city. In 1917, French engineers officers constructed the "Aqueduct of Harilaou" which belonged to the "First Thessaloniki Building Company S.A." This aqueduct functioned with the one of Municipality of Thessaloniki, at the same time. In 1975, the former Thessaloniki Water Supply Organization (OYTH) purchased this aqueduct.

Until 1929, the private Turkish-Belgian "Compagnie Ottomane des Eaux de Salonique" ensured the water supply of the city, in cooperation with the Municipality of Thessaloniki, which had as purpose of providing water at the central part of the city. This company was established in 1888 by entrepreneur Nemlizade Hamdi Efendi with Belgian funds. In October 1929, the company was sold, without the consent of the Greek State in the international company "Energie Industriel", based in Paris and renamed as "Société de Distribution des eaux de Thessalonique".

In 1939, the Thessaloniki Water Supply Organization (OYTH) was founded by the obligatory laws 1563/1939 and 2318/1940. All the rights of the Greek public and of the Municipality of Thessaloniki by concession and of the "Société de Distribution des eaux de Thessalonique" came to the ownership of the OYTH.

In 1997, the two organizations of the city namely the Thessaloniki Water Supply Organization and the Thessaloniki Sewerage Organization converted into anonymous societies (PD 156/1997 and 157/1997) and later, in 1998, the Thessaloniki Water Supply & Sewerage Co. S.A. (EYATH S.A.) was funded from the merger of Thessaloniki Water Supply Organization S.A. (OYTH S.A.) and Thessaloniki Sewerage Organization S.A. (OATH S.A.) (Law 2651/3.11.1998). Its aim is the water supply and water sewerage or other similar services of its area under jurisdiction and beyond, in the frame of integrated use of water resources. The area of jurisdiction is the same as the one of OYTH S.A. and OATH S.A., with the addition of the industrial area of Thessaloniki. EYATH S.A. is responsible for a) water supply of Thessaloniki urban area and b) the collection and conveyance of wastewater to the Wastewater Treatment Plants and their disposal (Yannopoulos *et al*., 2015).

EYATH S.A. is listed on the Athens Stock Exchange. Pursuant to Article 22 of Law 2937/26.7.2001, when the company was listed, the majority of EYATH S.A.'s assets were transferred to a newly established body governed by public law called EYATH Fixed Assets free of consideration. Under a 30-year contract signed on 27.7.2001 by the Greek State, EYATH Fixed Assets and EYATH S.A., were given an exclusive right to provide water supply and sewerage services within its geographical remit. Under that same contract EYATH Fixed Assets was obliged to provide EYATH S.A. with the necessary quantities of water for a fee to meet its consumers' needs, and EYATH S.A. was obliged to ensure the rational use of the water sold and make concerted efforts to ensure a reduction in leaks and water losses as much as possible, by improving and rebuilding the water supply network. The activity of EYATH extends on Urban Agglomeration of Thessaloniki and includes (partially or entirely) the municipalities of Thessaloniki and the Industrial Area of Thessaloniki (Industrial Zone I) in Sindos. EYATH S.A. is responsible for both the external and the internal network of this entire region.

5. EPILOGUE

The observations about water supply technology in the city of Thessaloniki carried out in this study are based on data available from various disciplines including archaeology, history, literature, geology and hydraulic engineering. In order to get a general, final insight into the water supply development of Thessaloniki since its foundation at the end of 4th century BC, it is important to point out a series of factors, which determined the water adequacy of the city ensured by the presence of big water transfer projects and water supply infrastructures. These factors are the location of the city and the urban plan, the physical configuration of the urban area, the ground level alterations due to natural disasters or human actions, the landscape geography, in combination with the rich aquifers beneath the urban grid between the walls, and the rich water sources in specific positions in the wider hilly area. Apart from them, other crucial factors were the rapid development of Thessaloniki in a big city and the simultaneous increasing population, which created an increased need for water.

Thessaloniki was grown according to the Hippodamian plan and was defined by walls with almost steady course both in Roman, Byzantine and Ottoman period. The fact that this urban plan was generally remained through centuries without great alterations was a determining factor for the development of the water supply network within the city since ancient times. Especially as for the Byzantine era, in the Upper city water conduits were laying out following the contour lines of the hill slopes. In contrast, the supply of the inhabited zones towards the south was achieved with subterranean water channel networks laid out along the squared road-grid.

The presence of the rich aquifer in the area is mainly responsible for the large number of hand dug wells, which had an extremely important role during both antiquity, in Byzantine era and especially in Ottoman period, despite the fact that they were composed with urban distribution networks and supplemented by technical works of great scale and high level technology. From all that has been mentioned above four big hydraulic projects are evident in the city, since the Roman era, which have been resulted from thoughtful planning and organised workmanship. The presence of more than one aqueduct, which probably were supplying the city, is unique in Macedonia and was associated with the city's gradual urban expansion, which was a result both of the population increase and the changes of the lifestyle through ages. They were all ambitious projects, renovated many times through ages, in order to achieve continued functioning. All projects originated from the upper, NW part of Thessaloniki, from where branched pipes were supplying the whole city through cisterns or public fountains in central locations. Their existence provides a clear demonstration of the high level of hydraulic engineering expertise of the engineers.

REFERENCES

Athanassiou, F., Malama, V., Miza, M. and Sarantidou, M. (2004) The Construction Phases of the «Octagon» of Galerius' Palace Complex in Thessaloniki, AEMTH 18, 239-254 (in Hellenic).

Dimitriadis, V. (1983) *Topography of Thessaloniki during the Ottoman era, from 1430 to 1912*. Society of Macedonian Studies, Thessaloniki (in Hellenic).

Gala-Georgila, E. (2015) Waterways and Organization of Space in Thessaloniki during the Middle and Late Byzantine periods. Doctoral Dissertation, Aristotle University of Thessaloniki (in Hellenic).

Kaiafa-Saropoulou, A. (2014a) Supplying water in Hellenistic and Roman Macedonia: the art of the wells. 1st IWA Regional Symposium on Water, Wastewater and Environment: Traditions and Culture. Patras, Greece: 557-568.

Kaiafa-Saropoulou, G. A. (2014b) Water management and sanitation technologies in Hellenistic and Roman Thessaloniki. In *10th International Hydrogeological congress,* Vol. 1: 277-286. Thessaloniki.

Karydas, N. (2009) Early Christian houses with triclinium in Thessaloniki - Part II: ten years after, AEMTH Twenty Years, 127-141, Thessaloniki (in Hellenic).

Marki, E. and Konstantinidou, K. (2005) The fortifying Wall of the White Tower and other Fortifications in Thessaloniki, AEMTH 19, 211-220 (in Hellenic).

Tamiolakis, G. (1985) The History of Water Supply of Thessaloniki. University Studio Press, Thessaloniki (in Hellenic).

Vacalopoulos, A. (1983) History of Thessaloniki 316 B.C.-1983, Thessaloniki (in Hellenic).

Yannopoulos, S., Kaiafa-Saropoulou, A., Angelakis, A.N. (2015). Evolution of Sewage Management of Thessaloniki City, Hellas. 3rd National Joint Conference HHA-EEDYP-NSS, December 10-12, 2015, Athens, Greece, pp. 583-598 (in Hellenic).

Proceedings of the 10th World Congress of EWRA 'Panta Rhei', 5-9 July 2017, Athens, Greece
© 2017 *European Water Resources Association*

Water demand management in Europe: Reducing household water consumption in four cities from 1995 to 2015

M. Stavenhagen*, C. Tortajada and J. Buurman
Institute of Water Policy, Lee Kuan Yew School of Public Policy, National University of Singapore
* *e-mail: m.stavenhagen@nus.edu.sg*

Abstract: In many cities urban growth has led to intensified water stress, serious pollution of water resources and increased competition between different water users, including domestic households. An effective strategy to increase both quality and quantity of available water is water demand management. This study examines four European cities which have shown notable success in achieving low domestic water consumption, and attempts to identify what policy instruments were most effective in lowering household water demand and increasing water conservation. The four surveyed cities are: Copenhagen, Denmark; Hamburg, Germany; Tallinn, Estonia; and Zaragoza, Spain. A mixed-methods approach was used consisting of a questionnaire, interviews and review of secondary data and sources of information. We find that a variety of policies and measures are attributed to have lowered the domestic water use, with investments in renovation and maintenance of networks and campaigns for the use of water saving technologies as the most important, closely followed by universal installation of water meters, rapid leak detection, awareness (campaigns) for sustainable use of resources, and municipal regulations. Tariff measures are rarely measured as significant. An important lesson of the study is that water managers should closely examine their own specific situation before designing water demand management policies and measures, as what works or not is very context-dependent.

Key words: urban water demand management, water policy, household water consumption, water conservation, water quality

1. INTRODUCTION

The detrimental impact of increased urban water use on environmental conditions has led to a general rethinking on urban water services (Grafton et al. 2015, OECD 2016). Water is now perceived as a scarce resource and the traditional focus on increasing supply is no longer sufficient to ensure water security and sustainable development of cities. Existing water resources need to be closely managed in terms of both quantity and quality. Water Demand Management (WDM) aiming at more efficient use of existing resources plays an important role in this.

The objective of this study is to compare four European cities that have shown notable success in achieving low per capita domestic water consumption: Berlin, Germany; Copenhagen, Denmark; Tallinn, Estonia; and Zaragoza, Spain. In particular, the goal is to identify the type of water demand management strategies that have been employed, and assess how successful these have been in reducing residential water demand. The assessment is based on information from questionnaires and interviews.

2. WATER DEMAND MANAGEMENT

2.1 Water demand management defined

The simplest definition of WDM is "getting the most from the water we have" (Brooks 2002), i.e. any measure that either reduces the amount of freshwater used, or keeps the water used in the process cleaner than it would otherwise have been. A comprehensive operational definition

proposed by Brooks (2006) defines WDM as any measure – be it administrative, economic, financial, technical, or social – that achieves one or more of the following five things: (1) reducing the quantity or quality of water required to accomplish a specific task; (2) adjusting the nature of the task so it can be accomplished with less water or lower quality water; (3) reducing losses in movement from source through use to disposal; (4) shifting time of use to off-peak periods; and (5) increasing the ability of the system to continue to serve society during times when water is in short supply, i.e. adding resilience to the water system using WDM. Although other definitions of WDM exist (see Gleick 2004, Brown et al. 2009), focus on quantity and quality and an urban utility perspective fits the needs of this study.

2.2 Water demand drivers

One of the strongest water demand drivers for cities is urban growth (Grafton et al., 2015, March & Sauri 2015). In addition, a variety of weather, technological, economic, demographic and cultural factors affect domestic water demand (Parker & Wilby, 2012). Water demand drivers are external factors on which a utility and municipal decision makers have little or no influence. Table 1 gives and overview.

Table 1. Water demand drivers – an overview

Drivers	Impact
1. Demographic and socio-economic factors	
Household income	Available income affects water consumption, though not always in clear ways [2, 3, 4, 5] If the water bill constitutes a small proportion of disposable income, consumption is less sensitive to price, while lower-income households are generally more price responsive [2]
Household size	Water consumption per capita will be higher in smaller households, since some economies of scale cannot be accomplished (e.g. cleaning, washing with full loads, etc.) [2, 6] Indoor water consumption often depends on household size [2, 3, 4]
Age	Higher age leads to lower water use [4] Families with young children or teenagers are high water consumers [1]
2. Settlement structure and property factors	
Housing	Single houses with substantial outdoor areas use significantly more water [2]
Garden	Outdoor use is more sensitive to price changes [2] Landscaping, such as plant species used, e.g. turf grass vs. native species of shrubs and trees in Mediterranean climates [2]
Urban density	Higher population density leads to a lower per capita consumption [4]
3. Environmental factors	
Seasonality	Higher water consumption in the summer due to outdoor use [2, 3, 7]

Sources: [1] Beal et al., 2012; [2] Domene & Sauri, 2006; [3] Inman & Jeffrey, 2006; [4] March & Sauri, 2010; [5] Messner & Ansmann, 2007; [6] Parker & Wilby, 2012; [7] Stoker & Rothfeder, 2014

2.3 Water demand management policies and tools

WDM policies fall into different categories, be they tariff measures such as water price increases or tariff reforms, or non-tariff measures such as application of technological innovations, information campaigns, or regulations and restrictions (Olmstead 2003, Inman & Jeffrey 2006). Effectiveness of the different WDM policies vary depending on the context, see Table 2.

3. WATER DEMAND MANAGEMENT POLICIES IN FOUR CITIES

3.1 Methodology

A mixed method approach combining quantitative and qualitative data was applied to assess and compare the effectiveness of WDM strategies in four cities. A questionnaire was used to obtain information from the utilities on consumption and tariff development over the last 20 years, and

evaluate the relative impact of WDM measures undertaken over the last 10 years. Additionally, semi-structured interviews were conducted with officials from the water utilities and other water experts in all four cities. Further information came from case study reports, sustainability rankings, and academic literature. The cities – Berlin, Copenhagen, Tallinn and Zaragoza – were chosen following the selection criteria: track record of low domestic water use according to OECD (2016) and/or utility data, large urban agglomeration, comparable socio-economic development levels, data availability and willingness to provide information for the questionnaire and in interviews.

Table 2. Overview of effectiveness of WDM policies and tools

Tools	Impact
1. Tariff measures	
Water price	Water consumption tends to be generally price-inelastic, though in some cases higher prices reduce consumption [2, 3, 4, 5, 6, 7]
	"Off-setting effect" of prices: reducing water consumption due to higher price tends to decrease after time, or even rise to a higher level than before the intervention [3]
	Water consumption is price-inelastic up to a threshold (for basic needs, hygiene and cleaning), while any further water quantity is price-sensitive [2, 4]
	Awareness of water price affects water consumption [5]
Tariff structure	Tariff structures such as block pricing reduce water consumption [3, 6]
2. Awareness	
Metering	Metering produces significant water savings due to information, awareness, publicity and faster leakage repairs [1, 2, 3]
	Secretly installing metering has no effect on behaviour [3]
Billing	Frequency of water billing affects water consumption [6]
	Price elasticity may increase by 30% or more when price information is posted on water bills [7]
Public awareness campaigns	Media broadcasts etc. can reduce demand temporarily by 2-5%, though in many contexts effectiveness is unclear [3]
3. Technology	
Water-saving appliances	Significant water savings through introduction of low-flow shower heads, water-efficient toilets, water-saving garden devices, water-efficient appliances etc. [1, 3, 7]
	"Off-setting effect" of water appliances: reduced water consumption dissipates over time [3]
4. Operation & Maintenance	
Leakage	Reducing water network infrastructure leakage is considered one of the most effective WDM measures [3]
5. Regulation and mandatory requirements	
Plumbing codes/ efficiency labelling	Reduced water consumption by 5-10% over 10 years in Australia and US [3]
Restrictions	Mixed effects: reduced water consumption between 25-35% in California and Greece [3], but no effects in one town in Texas [6]
	Restrictions were not followed by more than 50% of customers in drought-affected California [7] and non-compliance was observed in Australia [1]

Sources: [1] Beal et al., 2012; [2] Domene & Sauri, 2006; [3] Inman & Jeffrey, 2006; [4] March & Sauri, 2010; [5] Messner & Ansmann, 2007; [6] Olmstead et al., 2003; [7] Olmstead & Stavins, 2009; [8] Parker & Wilby, 2012; [9] Stoker & Rothfeder, 2014

A caveat in the study is that care should be taken when comparing cities with each other. Water supply data at a city level is not always available, different sources may provide conflicting data and there is no agreement on common definitions of, for instance, household consumption (see also OECD, 2016:19). Similarly, the results of the questionnaires and interviews are self-assessments. Hence, the aim is not so much to compare the performance of the cities (like utilities benchmarking themselves against others), but rather to assess how they achieved a low domestic consumption.

3.2 Results

The four cities have a low domestic water consumption ranging from 113 litres per capita per day (lpcd) in Berlin and 104 lpcd in Copenhagen to 96 lpcd in Tallinn and Zaragoza. For comparison the average of 25 cities in the OECD (2014) study was 182 lpcd in 2012. Furthermore, all cities show clearly decreasing trends, with per capita water demand reductions of 10% (Berlin since 1995), 22% (Copenhagen since 1995), 29% (Zaragoza since 2000) and 31% (Tallinn since 1998).

Water utility officials were asked to assess the impact of thirteen possible WDM measures on reducing water consumption within the last ten years on a scale from 1 (lowest impact) to 5 (highest impact). Large variations exist between cities regarding which WDM measures were regarded as most successful, see Table 3.

Table 3. Impact of WDM measures on water conservation according to water utilities (from 1 – lowest to 5 – highest impact)

		Berlin	Copenhagen	Tallinn	Zaragoza	*Sum*
	Tariff measures					
1	Higher average water price	1	2	2	3	7
2	Changes in tariff structure	1	1	1	**5**	8
	Non-tariff measures					
3	Universal installation of individual water meters	1	3	**4**	**5**	13
4	Greater control of illegal consumption	1	1	**4**	**4**	10
5	Investment in renovation and maintenance of networks	3	**4**	**5**	**5**	17
6	Installing mechanisms for rapid leak detection	2	**4**	**5**	2	13
7	Impact of awareness campaigns and public awareness for sustainable use of resources	1	3	**4**	**5**	13
8	Campaign for the use of water saving technologies (e.g. water-efficient appliances)	3	3	3	**5**	14
9	Federal legislation	2	1	2	-	5
10	Regional legislation	1	2	2	-	5
11	Municipal regulations	1	**5**	2	**5**	13
12	More efficient water use by industry	1	2	**5**	**4**	12
13	More control and more efficient use of water by the local administration	1	**4**	2	**4**	11

Officials in Zaragoza considered nine measures to have had a high impact – defined as a rating of 4 or 5 – while six measures were considered to have had a high impact in Tallinn, and five in Copenhagen. In Berlin, no single measure was considered to have had a high impact, and only two measures were considered medium-impact. The sum of the individual ratings in each city is shown in the last column. The policy with the highest overall rating (at 17) is investment in renovation and maintenance of networks, which three out of four cities considered high impact. The policy with the second-highest overall rating (14) is campaigns promoting water-saving technologies, such as water-efficient appliances for toilets, showers etc. Four other policies share the third-highest overall rating (13): individual water meters; rapid leak detection mechanisms; public awareness campaigns; and municipal regulations. Each of these measures was rated as high impact in two cities. Finally, with slightly lower overall ratings, more efficient water use by industry (12) and by the local administration (11) was also considered as high impact in two cities each.

Although the average price per cubic meter of water has increased in all cities since 1995, only Zaragoza regarded a change in tariff structure as having had high impact on reducing water consumption. No city regarded higher average water prices to have had high impact; the same applies to legislation at the federal or regional level.

4. ANALYSIS OF EFFECTIVE WATER DEMAND MANAGEMENT POLICIES

To assess which WDM policies each city considered most effective in reducing domestic water demand, a two-step approach was taken. First, for each city the main cause for water scarcity is identified. (The demand drivers that were listed in Table 1 apply to a larger or lesser extent for all four cities.) Second, the WDM policies with highest impact for individual cities are evaluated.

4.1 Water challenges

Interestingly, in Berlin, Copenhagen and Tallinn, the primary problem was water pollution.

Exposure to harmful pesticides, industrial waste or sewage threatened existing ground and surface water resources, and indirectly affected the quantity of available water.

Berlin was divided into two administrations after the Second World War. In communist East Berlin, a lack of attention for water quality, coupled with deteriorating, poorly-maintained infrastructure, created problems, which became clearly visible after reunification in 1990. In contrast, West Berlin was an enclave entirely dependent on resources from within its own territory. It needed to pay close attention to water quantity and quality for recycling and reuse, becoming a forerunner in closed water cycle management in the process.

In Tallinn, part of the Soviet Union until 1991, the situation was similar to East Berlin: little treatment of industrial wastewater and sewage, coupled with very low water prices. In both cities, water consumption was high and wastewater treatment poor, threatening available water resources.

In Copenhagen, water is a scarce resource due to the city's location on Zealand island. Water scarcity intensified when chemicals, polluted soil, and pesticides and nutrients from intensive agriculture polluted some of the already stressed ground water wells.

Zaragoza shared some of Copenhagen's problems: the city was already water-stressed – located in a semi-desert climate and dependent on water resources that needed to be transported from far away – when it was hit by severe droughts in the 1990s, leading to a water crisis.

An important observation is that water management has often been reformed as a result of crises, when "policy windows" open (Kingdon, 2011), forcing officials to act. For all four cities, domestic water consumption levels have declined since their respective initial crisis in the 1980s or early 1990s. Hence, the historical context is important when identifying why water (demand) management reforms were first undertaken.

4.2 Water demand management policies and tools

While a variety of WDM policies and tools have been applied to deal with each city's water issues, the individual impact of each policy differs according to where it has been implemented.

Berlin was found to be somewhat of an outlier in this assessment of WDM strategies: household water demand reduced considerably without any particular objective for water conservation from the water utility. While current water demand levels are manageable, the interviewee mentioned that for several reasons less water use might not necessarily be in the utility's best interest. First, there are abundant ground water resources available, as long as these are protected from pollution. Second, from a financial perspective, more water consumed by households means more revenue for the water utility. Third, both supply infrastructure and the sewerage system have been dimensioned according to certain water demand projections and flows; lower flows can lead to hygiene and water quality issues, and has necessitated additional water use by the utility to clean the sewers.

4.2.1 Water infrastructure

Investments in renovation and maintenance of networks are considered among the most effective measures in three cities, Tallinn, Zaragoza, and Copenhagen. A functional and well-maintained water supply network is the basis of efficient water supply. Closely related to this, installing mechanisms for rapid leak detection was considered among the highest-impact policies in Tallinn and Copenhagen. Thus, reducing non-revenue water is regarded as one of the most effective measures in water demand management.

4.2.2 Water conservation campaigns

Awareness campaigns to promote conservation are considered one of the highest-impact policies in Zaragoza and Tallinn. After intensive droughts caused water use restrictions, the municipality of

Zaragoza initiated a water conservation campaign through media coverage and school outreach campaigns, challenging citizens to save 1 billion litres of water. This was achieved within the first year. It also provided guidelines on how to save water and provided subsidized water conservation kits for residents, partnering with citizens to increase their capacity to achieve conservation goals.

4.2.3 Campaigns to introduce water-efficient appliances

Showering and flushing are usually the most water-intensive household activities (not regarding outdoor water use), and thus also carry a high water saving potential. Campaigns to use water-efficient devices, and incentives to replace old and potentially leaking household appliances was applied in all cities, but was considered most effective in Zaragoza and Tallinn. Water users may also be incentivized to purchase water-saving devices following rising water prices; although this was not mentioned in any city as a high-impact policy.

4.2.4 Water meters

The universal installation of individual water meters was considered a high-impact policy in Zaragoza and Tallinn. As has been shown in other regions facing water scarcity (see Table 2), giving direct and household-specific feedback about their water consumption increases users' awareness, and leads to reduced demand. In Tallinn, it also led to a new market for water water-saving appliances.

4.2.5 Municipal regulations

Copenhagen and Zaragoza both considered municipal regulations one of the policies with the highest impact. In Copenhagen, the water utility cooperates closely with the municipality beyond water supply and sanitation services, e.g. by upgrading the city's stormwater infrastructure to address climate change. In Zaragoza, water services are provided by the municipality, through departments that are part of the broader municipal administration.

No city regarded regional or national policies as effective to reduce water demand. However, Berlin, and Tallinn both mentioned the European Water Framework Directive as useful to improve their water management, due to common objectives and monitoring of water quality standards. They also mentioned how the focus on water quality led to lower water demand over time, since WDM often addresses water quality and quantity at the same time (see Brooks 2006).

4.2.6 Water prices and tariffs

Zaragoza is the only city that considers a change in water tariff structure as among its highest-impact water policies. The new block tariff system is highly progressive, with water prices per cubic meter in the high-usage block more than five times higher than for the primary "subsistence" quantity block. No city regarded prices to be of high impact, although prices have risen in all municipalities, quite significantly in some circumstances, e.g. more than 800% since 1995 in Tallinn.

Despite rising water prices since 1995, the water consumption rates of Berlin, Copenhagen and Tallinn have either plateaued or risen slightly since 2012. One reason might be an inelasticity of water demand up to a certain threshold: water demand for basic needs (such as hygiene, cleaning, cooking etc.) will remain constant, while additional non-essential water demands are more price-sensitive (Domene & Sauri 2006, March & Sauri 2010). Another possibility might be that an "off-setting effect" of prices has set in (Inman & Jeffrey 2006). In this case, users in these cities have

been accustomed to prices, adjusting their demand to previous levels (or higher) and not focusing on additional costs of their consumption. Prices might have lost their signalling function.

6. CONCLUSION

Residential water demand has significantly reduced in all four cities, and a variety of different WDM policies is credited to have had a high impact on water conservation over the last decade. These include: water network infrastructure investments and leakage control; water conservation campaigns and increased use of water-efficient appliances; the universal application of individual water meters; and municipal regulations.

Since several of these policies reinforce each other, creating awareness among users for water scarcity and incentives for conservation, a package of several inter-related policies seems to lead to the best results. In the study, the cities with a comparatively larger number of high-impact policies also featured the lowest residential water consumption.

Further research on urban WDM strategies might take advantage of the increasing usage of smart water meters to address existing data limitations in household water use, for two reasons. First, the accuracy and availability of household water data will most likely increase. Second, the ability of smart meters to identify and measure specific water uses (e.g. showering, washing machines etc.) will provide more precise and detailed data, providing valuable insights on how to fine-tune WDM policies to more effectively target desired behavioural changes at the household level.

An important lesson from the study is that urban water managers must closely examine their own specific water problems before designing and implementing the "right" WDM policies. The specific water demand drivers, socio-economic status of the city's residents, their water usage patterns, and experiences with previous policy tools (e.g. to avoid off-setting behaviour) need to guide urban municipal choice of water policy reforms. As Grafton et al. (2015) point out, "the pathways [towards sustainable water management] may, and indeed should likely, be different with different barriers and hurdles encountered… There is no one-size-fit-all solution to the transition process within or between countries and urban areas."

REFERENCES

Interviews conducted with officials from: Berliner Wasserbetriebe (BWB), Berlin; HOFOR, Copenhagen; A/S Tallinna Vesi, Tallinn; and the Municipal Water Office of the city of Zaragoza.

Beal, C., Makki, A., Stewart, R., 2012. Identifying the drivers of water consumption: A summary of results from the South East Queensland residential end use study. Science Forum and Stakeholder Engagement: Building Linkages, Collaboration and Science Quality. http://www.urbanwateralliance.org.au/publications/forum2012/index.html#presentations (accessed 7 April 2017)

Brooks, D. B., 2002. Water: Local-Level Management. Ottawa: International Development Research Centre.

Brooks, D. B., 2006. An Operational Definition of Water Demand Management. International Journal of Water Resources Development, 22:4, 521-528.

Brown, R. R., Keath, N., Wong, T. H. F., 2009. Urban water management in cities: historical, current and future regimes. Water Science & Technology, 59(5), 847-855.

Domene, E., Sauri, D., 2006. Urbanisation and Water Consumption: Influencing Factors in the Metropolitan Region of Barcelona. Urban Studies, 43:9, 1605-1623.

Gleick, P., 2002. Soft Water Paths. Nature, 418 (25/07/2002).

Grafton, Q., Daniell, K.A., Nauges, C., Rinaudo, J.-D., Chan, N.W.W., 2015. Understanding and Managing Urban Water in Transition. Springer Netherlands.

Inman, D., Jeffrey, P., 2006. A review of residential water conservation tool performance and influences on implementation effectiveness. Urban Water Journal, 3:3, 127-143.

Kingdon, J.W., 2011. Agendas, alternatives and public policies, 2nd edn. Boston, MA: Longman.

March, H., Saurí, D., 2010. The Suburbanization of Water Scarcity in the Barcelona Metropolitan Region: Sociodemographic and Urban Changes Influencing Domestic Water Consumption. The Professional Geographer, 62:1, 32-45.

Messner, F., Ansmann, T., 2007. Wassernutzung der privaten Haushalte in Leipzig: Enflussfaktoren der Wassernachfrage und Bedeutung der individuellen Wahrnehmung diesers Faktoren duch die Wassernutzer. Ergebnisse einer Haushaltbefragung in der Stadt Leipzig, UFZ Berich, Helmhotz-Zentrum fuer Umweltforschung, No. 1/2007. Working Paper. https://www.econstor.eu/bitstream/10419/57852/1/700396047.pdf (accessed 7 April 2017)

OECD, 2014. Survey on Water Governance for Future Cities: City Profiles. http://www.oecd.org/gov/regional-policy/water-governance-in-cities-city-profiles.htm (accessed 7 April 2017)

OECD, 2016. Water Governance in Cities. OECD Studies on Water; OECD Publishing, Paris.

Olmsteadt, S., Hanemann, M., Stavins, R.N., Kennedy, J.F., 2003: Does Price Structure Matter? Household Water Demand Under Increasing-Block and Uniform Prices. Working Paper. https://www.researchgate.net/publication/228916287_Does_Price_Structure_Matter_Household_Water_Demand_Under_Increasing-Block_and_Uniform_Prices (accessed 7 April 2017)

Olmsteadt, S.M., Stavins, R.N., 2009. Comparing price and nonprice approaches to urban water conservation. Water Resources Research, 45, W04301.

Parker, J.M., Wilby, R.L., 2013. Quantifying Household Water Demand: A Review of Theory and Practice in the UK. Water Resource Management, 27, 981-1011.

Stoker, P., Rothfeder, R., 2014. Drivers of urban water use. Sustainable Cities and Society 12, 1–8.

Proceedings of the 10th World Congress of EWRA 'Panta Rhei', 5-9 July 2017, Athens, Greece
© 2017 *European Water Resources Association*

Impact of water pricing policy and climate change on future water demand in Volos, Greece

N. Mylopoulos, C. Fafoutis*, S. Sfyris and A. Alamanos
Laboratory of Hydrology and Aquatic Systems Analysis, Department of Civil Engineering, University of Thessaly, Pedion Areos, 38334 Volos, Greece
* *e-mail: fafoutis@uth.gr*

Abstract: The aim of this study is the water demand forecasting in the city of Volos and the evaluation of various parameters affecting it, such as water price, temperature and rainfall. Time series data of water consumption levels and the number of water meters from 2007 to 2012 were collected from databases of Water Utility of Volos, while raw data concerning rainfall and temperature were retrieved from weather stations in the city of Volos. Furthermore, the elasticities of the parameters introduced in the scenarios were available from previous survey conducted by the University of Thessaly. Those elasticities indicate the grade each parameter affects the water consumption, such as the water price and climatic conditions (temperature and rainfall). Subsequently, nine scenarios were created by altering one or more parameters and via the proposed forecasting model (prediction equation), using the specific water consumption and the number of water meters. Estimations of future water demand for the years 2013-2024 under different pricing policies and climate change scenarios were performed using the WEAP model. Then, a scenario comparison was conducted in order to export more conclusions referring to the future consumption. The results of this study prove that rational water pricing can lead to remarkable water conservation.

Key words: Water demand forecasting, elasticity, water consumption, water pricing

1. INTRODUCTION

It is obvious that problems connected with water resources and their exploitation in combination with the general environmental problems have been continuously increased. The situation is expected to be sharpened still more in the near future due to the impacts from climate change (reduction of rainfalls and intensity of extreme meteorological phenomena) (IPCC, 2001; IPCC, 2007). Besides, in Greece, water resources management is based in most regions in the management of its natural offer taken water demand for granted. This confrontation is ineffective, and leads with mathematic certainty to an economic and environmental impasse, having as a main characteristic the exhaustion of water resources (Brundtland, 1987). The causes of crisis of water differ from country to country and from region to region depending on natural, economic, social and political conditions that prevail in each study area. However, the more systematic approach could recognize the existence of common characteristics (Serageldin, 1995).

This study aims to simulate and forecast the urban water demand in the city of Volos, as a function of all the factors mentioned above, under various scenarios, in order to propose sustainable solutions and alternative management policies.

2. STUDY AREA

Volos is the capital of the prefecture of Magnesia (Central Greece) with a population of approximately 144,420 inhabitants. Volos has a Mediterranean climate with an average annual temperature of 16.4 °C and 504 mm of annual rainfall. The Municipal Water Utility of Volos is responsible for the urban water supply in the city. Also, the Industrial Area is under the Municipal Water Utility of Volos. The water needs are covered by 5 springs and 40 wells, and the water is

collected in 8 reservoirs.

The city faces problems of water adequacy, mainly due to the leakages, which are estimated to be above the 40% of the total supplied water. Furthermore, major environmental issues arose the last decades, such as, the systematically extraction of the non-renewable ground water, the contamination of ground water due to lixiviation of agricultural fertilizers, chemicals and heavy metals and the salinisation of the ground water creating many environmental problems on the quantity and the quality of the water resources (Mylopoulos and Mentes, 2005).

The broader study area was divided into five main sectors. Sectors 1, 2 and 3 cover the former municipality of Volos, whereas sector 4 the former municipality of Nea Ionia. Finally the last sector covers the Industrial Area.

3. METHODOLOGY

3.1 Development of the water demand forecasting model

The methodology is a classical process with a prediction equation used in various similar studies (Fafoutis, 2008; Alamanos and Betsios, 2014), where the future water demand depends on the number of water meters, the specific water consumption per capita per day in the base year and one or more of the following parameters: water pricing, temperature and rainfall.

The prediction equation used in the forecasting model is:

$$Q_y = N \cdot q^* \cdot (X_{1,y}/X_{1,b})^{\beta 1} \cdot (X_{2,y}/X_{2,b})^{\beta 2} \ldots (X_{i,y}/X_{i,b})^{\beta i} \quad (1)$$

where:

Q_y : the residential water consumption for month m
N : the number of water meters
q^* : the specific consumption per capita per day in the base year
d_m : the number of days in each month
$X_{i,y}$: the value of parameter i in the year of prediction y
$X_{i,b}$: the value of parameter i in the base year b
β_i : the elasticity of parameter i

3.2 Data used

Time series data of water consumption levels and the number of water meters, in each consumption sector of the city from 2007 to 2012, were collected from databases of the Water Utility (Water Utility of Volos, 2011), while raw data concerning rainfall and temperature were retrieved from meteorological stations in the city of Volos.

The elasticity of a parameter indicates the grade that affects the water consumption. When the elasticity is positive, the water demand increases when the value of the parameter increases also. However, when the elasticity is negative, an increase of the value of the parameter leads to a decrease in water demand.

The elasticities of the parameters introduced in the scenarios were available from a previous survey conducted by the University of Thessaly (Bonaros, 2014), where the elasticity of water pricing, temperature and rainfall were estimated -0.524, 0.109 and -0.026 respectively.

3.3 Scenario Analysis

For the purposes of the study, nine scenarios were developed and simulated. Analysis was formulated using the following assumptions: in all scenarios the water meters have a steady increase

in the forecasting period, according to the trendline equation, which was originated from the data referring to the number of water meters in the years 1994-2012. Moreover, the specific consumption per capita per day in the base year was considered that remains constant through the forecasting years and was calculated by dividing the total annual consumption to the residents and the days of the base year.

The base year used is 2012 and projections of water consumption levels are made for years 2013 and 2024 under nine different scenarios (water pricing policy and climate change scenarios):

Scenario 1: price of water is stable from 2012 to 2024
Scenario 2: increase in water price so that the real price of water will remain stable and equal to the real price of water in 2012
Scenario 3: drought for years 2012 and 2024 (10% increase of temperature and 20% decrease of rainfall every four years)
Scenario 4: wet weather conditions for years 2012 and 2024 (10% decrease of temperature and 20% increase of rainfall every four years)
Scenario 5: 5% increase of the real price of water every four years (base year 2012)
Scenario 6: 10% increase of the real price of water every four years (base year 2012)
Scenario 7: 20% increase of the real price of water every four years (base year 2012)
Scenario 8: 20% increase of the real price of water every four years and wet weather conditions (10% decrease of temperature and 20% increase of rainfall every four years)
Scenario 9: the real price of water is stable from 2012 to 2024 and drought (10% increase of temperature and 20% decrease of rainfall every four years)

All scenarios were simulated using the WEAP software (Water Evaluation And Planning system), which supports the analysis of various scenarios for integrated water resources management and helps design the policy of their exploration.

In this study, the schematic of the city was set up first. Then, the supply sources (groundwater), the reservoirs and the demand sites for each water sector of the city were placed. Finally, all the above components were connected (transmission link) and the data of each component of the schematic were imported in the WEAP software (Figure 1).

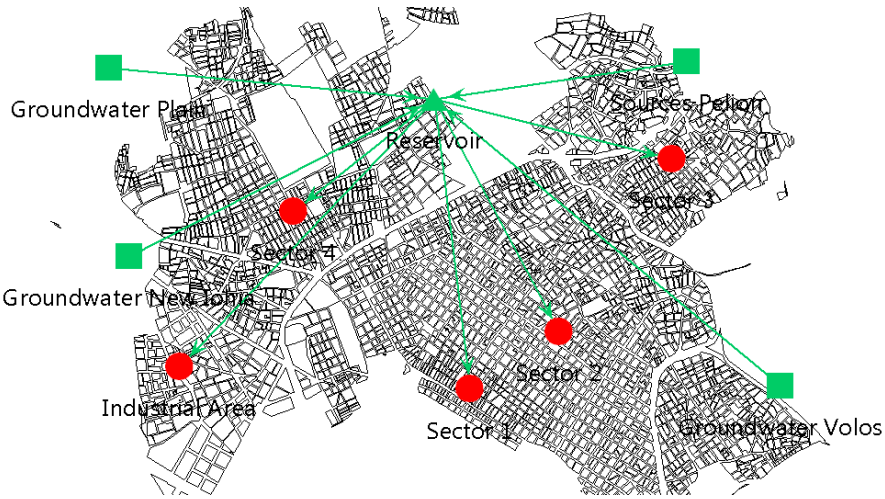

Figure 1. WEAP schematic

4. RESULTS AND DISCUSSION

4.1 Valuation

The water demand of the city of Volos, for each scenario, resulted from the forecasting model is presented in Figure 2.

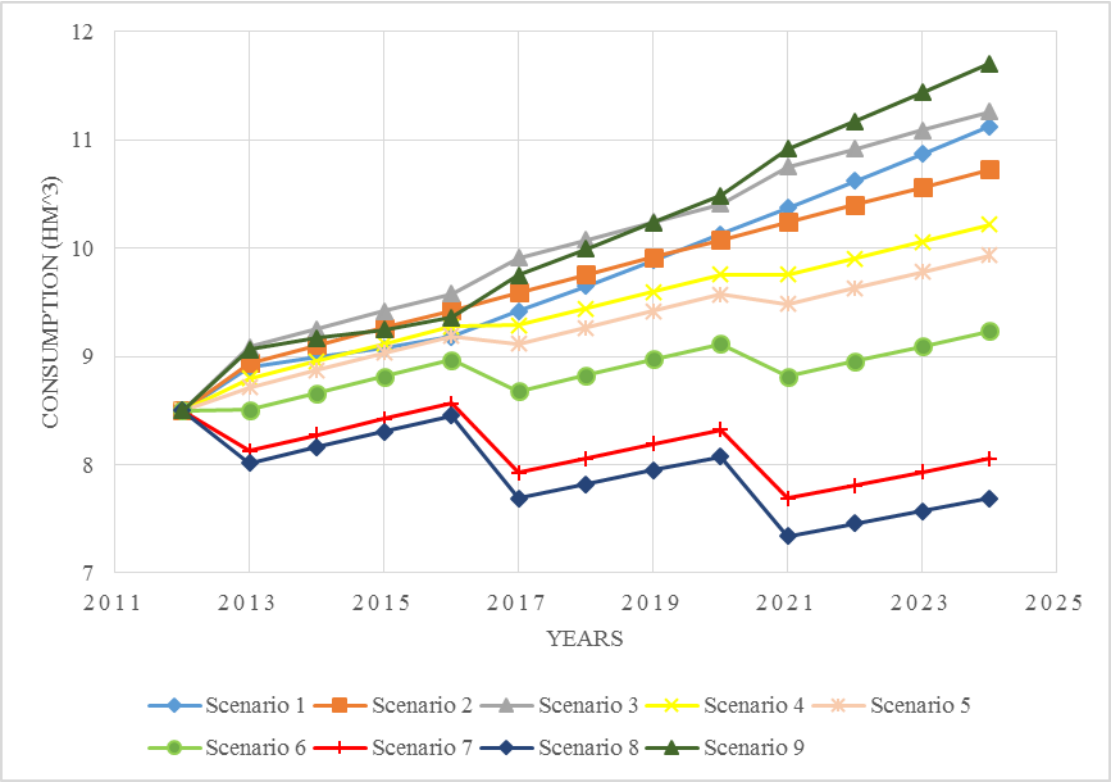

Figure 2. Total water consumption (m3) for years 2013-2024 under scenarios 1-9

It is evident that there are notable differences in water demand levels under the nine different scenarios. Important increases in water consumption levels appear under scenarios 1, 2, 3, and 9. Only under scenarios 7 (where the real price of water increases 20% every four years) and 8 (where the real price of water increases 20%, the temperature decreases 10% and the rainfall increases 20% every four years) there is a decrease in water consumption. Under scenarios 4, 5 and 6 water demand increases at lower scales in relation to the increase noticed under scenarios 1 and 9.

If the average annual water supply of the years 2007-2012, is assumed until 2024 and an average of 40% network losses is applied for the same time period, then the water balance can be calculated for every prediction scenario.

The findings mentioned above are fully justified: the water balance of scenario 1 is in line with the predictions of the continuous deterioration of the available water resources. Thus, the necessity of reducing the water losses is proved to be immediate. Regarding the water balance of the other scenarios, compared to scenario 1 (do-nothing), it is observed that the increasing water price has a positive impact on the water balance (scenarios 5, 6 and 7), otherwise the unmet demand will be significant (scenarios 2 and 9). The results of scenarios 3, 4 and 8 were as expected, due to their extreme climate changes.

4.2 Comparison

4.2.1 Water pricing policies

The scenarios referring to water pricing policies are 1,2,5,6 and 7. In these scenarios the water demand levels are affected by the real price of water, besides the increase of water meters that affect all scenarios studied (Figure 3).

Scenario 1 simulates the future demand by assuming that no pricing measures are taken by the Municipal Water Utility of Volos. The differences in water demand levels, by comparing scenarios 2,5,6,7 with scenario 1, are caused exclusively by the changes of the real price of water. Therefore, it is obvious how the real price of water eventually affects the future water consumption.

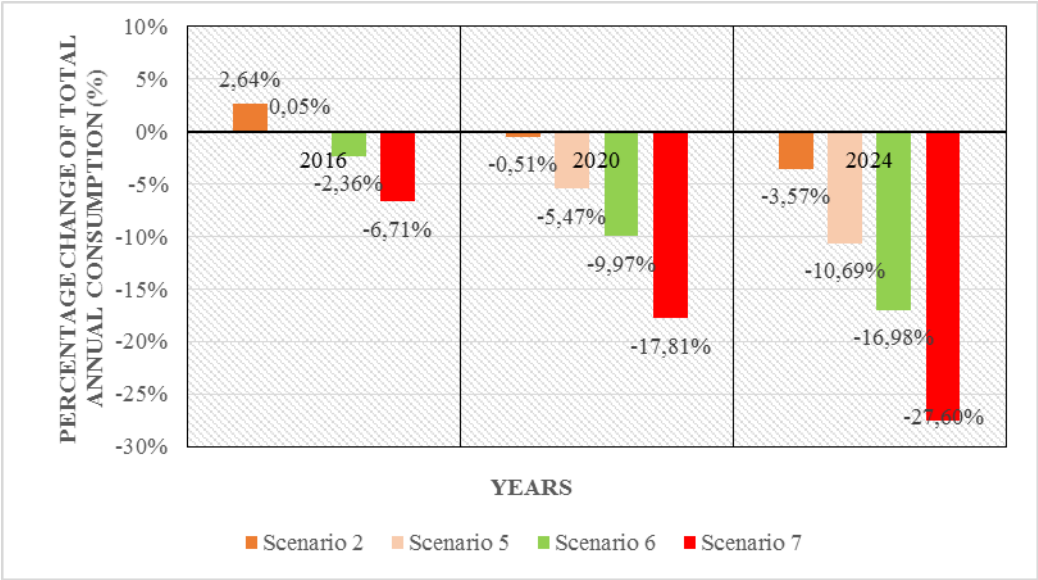

Figure 3. Percentage change (%) of total annual consumption every four years under scenarios 2,5,6,7 compared to scenario 1

So, if in the upcoming years the Water Utility will not be able to provide larger amounts of water, and at the same time the water meters (number of consumers) increase, a water pricing policy, similar to scenario 7, will result in a total water consumption remaining almost stable until 2020 and then reducing until 2024.

If the amounts of water available in the upcoming years are larger than today, a water pricing policy corresponding to scenarios 5 and 6 should be adopted, because one of the basic principles of water resources sustainable management is the water demand management and not the ongoing supply increase (supply management).

Furthermore, the pricing policies of scenarios 1 and 2 must definitely not be adopted, since the water consumption level provided is very high and trying to cover this requirement, it will have very negative impact on the environment.

Hence, it is necessary to adopt a pricing policy, where the real price of water will increase in upcoming years as part of the water demand management.

4.2.2 Climate change scenarios

The climate change scenarios are 3 and 4. By comparing them, it is investigated how the climatic conditions eventually affect the future water consumption. Scenarios 3 and 4 examined the assumptions of drought and wet conditions for the upcoming years respectively, using as base scenario the pricing policy described in scenario 2 (where the real price of water remains constant and equal with that of 2012 for the forecasting period). In scenario 2 the future consumption is affected only from the increase of water meters, while in scenarios 3 and 4 the future consumption is affected additionally from the climate changes (Figure 4). Therefore, the differences in the future consumption levels are due to the changes in temperature and rainfall.

From this comparison, it is clear that the climate changes will not affect critically the levels of future consumption, although very extreme changes in temperature and rainfall are assumed, that are hardly possible to be verified.

The climate change scenarios differ from pricing policies scenarios, discussed so far, since here the changes in the parameters affecting them are independent of the human factor. Nevertheless, the results are very useful, since for example in case of drought, the consumption that will come up, requires a proper demand management policy, rational pricing and public awareness and information policy in order to cover it.

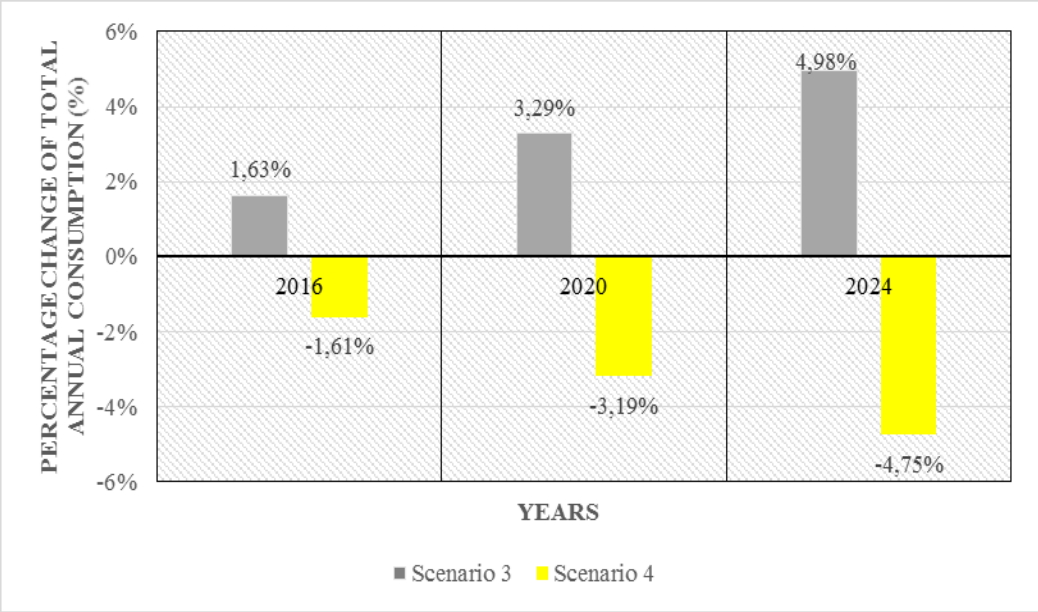

Figure 4. Percentage change (%) of total annual consumption every four years under scenarios 3 and 4 compared to scenario 2

5. CONCLUSIONS

The study attempts to propose policies in order to cover the future water consumption and cost-effectiveness, under various future conditions, in the city of Volos. Different scenarios focusing on water pricing and climate change were investigated.

The selected prediction equation shows that the effect of elasticities on the future water demand is significant, since they indicate the exponential change of each parameter. The fact that the equation allows changing each parameter separately while keeping the others constant, shows the impact of each variable on the total future consumption.

The study did not intend to define a new equation or methodology, but to simulate the condition of water supply and demand in the city of Volos. That led to the conclusion that demand increases dramatically. The exploitation of the water resources was proved insufficient, and a large number of wells are being used, damaging the aquifer. A large quantity of water is not being billed, and it shows an increasing trend after 2009.

Water pricing is proved to be a very important financial tool for the water demand management, since it is the only factor perceived directly by the consumers and is compatible with the principles of the Sustainable Water Resources Management and the Water Framework Directive 2000/60/EC (WFD, 2000; Fafoutis, 2008). This is also reinforced by the results of scenario 5, where a small price increase leads to significant water savings. In any case, the Water Utility of Volos should adopt a water policy directed towards to the water demand management, the reduction of the losses and the implementation of rational water pricing, in order to achieve water conservation and sustainable use.

REFERENCES

Alamanos, A., Betsios A., 2014. Water Demand in Skiathos city-Alternative scenarios predicting future consumption. Senior thesis. 196 pages. Department of Civil Engineering, University of Thessaly.

Bonaros, B., 2014. Research to find the demand curve of the water and the estimation of natural resources in the city of Volos. Senior thesis, 102 pages. Department of Civil Engineering, University of Thessaly.

Brundtland, G.H., 1987. World Commission on Environment and Development *Our Common Future*. Oxford University Press, 1987.

Fafoutis C., 2008. Integrated approach to water demand management in the residential sector - costing according to the full value. PhD thesis. Department of Civil Engineering, University of Thessaly.

Intergovernmental Panel on Climate Change, (IPCC), 2001. Climate Change 2001 - The Scientific Basis. Contribution of Working Group I to the Third Assessment Report of the Intergovernmental Panel on Climate Change (IPCC). Houghton, J. T., Ding, Y., Griggs, D.J., Noguer, M., van der Linden, P. J., and D. Xiaosu (Eds.). Cambridge University Press, UK.

Intergovernmental Panel on Climate Change, (IPCC), 2007. Climate Change 2007: The Physical Science Basis, in: Contribution of Working Group I to the Fourth Assessment Report of the Intergovernmental Panel on Climate Change. Edited by: Solomon, S., Qin, D., Manning, M., Chen, Z., Marquis, M., Averyt, K. B., Tignor, M., and Miller, H. L. Cambridge University Press, Cambridge.

Mylopoulos, N., A. Mentes, 2005. A sustainable framework for water resources management in an urban watershed: the case of Volos, Greece. Urban Water Journal, 2 (1), 13-22.

Serageldin, I., 1995. Water Resources Management: A new Policy for a Sustainable Future.

Water Evaluation And Planning System. Stockholm Environment Institute (SEI). www.weap21.org.

Water Utility of Volos, 2011. The existing water supply situation in the new municipality Volos. Directorate Planning and Development, Planning and Development Department.

WFD, 2000. Directive 2000/60/EC of the European Parliament and of the Council of 23 October 2000 establishing a framework for Community action in the field of water policy. Official Journal of European Communities, 22 October 2000.

Proceedings of the 10th World Congress of EWRA 'Panta Rhei', 5-9 July 2017, Athens, Greece
© 2017 *European Water Resources Association*

Domestic water demand forecasting for Makkah, Saudi Arabia

M.F.M. Abushammala[1*] and A.K. Bawazir[2]
[1] *Department of Civil Engineering, Middle East College, Knowledge Oasis Muscat, PB No 79, Al Rusayl 124, Sultanate of Oman*
[2] *Civil & Electrical Projects Contracting Company LTD (CEPCO), P.O. Box 8234, Jeddah 21482, Kingdom of Saudi Arabia*
[*] *e-mail: eng_abushammala@yahoo.com*

Abstract: The prediction of water demand is important in countries that have less water resources. Water demand forecasts assist water utility managers in taking decisions on additional supply acquisition, treatment infrastructure, water use restrictions, water conservation impacts, price elasticity and demand management. The aim of this paper is to develop an Artificial Neural Network (ANN) models for predicting annual and monthly domestic water demand in Makkah city, Saudi Arabia. The variables that were selected for development the water demand prediction models were: household area (m^2), city population, average personal income, average maximum temperature, and average number of visitors. This data between the years 2002 and 2012 were collected from the relevant sources. The number of dataset was eleven on annual basis and 132 on monthly basis. An ANN approach using feed forward backpropagation was developed to predict monthly and annual domestic water demand in relation to the selected variables. The study revealed that the ANN water demand models can predict monthly and annually water demand with a mean square error (MSE) between 0.0006 and 0.0002, and models' efficiency (E) between 0.97348 and 0.94626. In conclusion, it is suggested that a further development of the proposed ANN models are required to generalize and apply the proposed models to other cities in Saudi Arabia.

Key words: Makkah, water demand, artificial neural network, prediction, domestic water, water consumption

1. INTRODUCTION

A successful management of the water utility requires a careful balance of available water supply to meet the required water demand. Water demand forecasts help water utility managers to take decisions regarding additional supply, water treatment extension, water use restrictions, water conservation impacts, price flexibility and demand management (Billings & Jones, 2008). There are several factors that could impact water demand, including population, employment, technology, weather, climate, price, infrastructure efficiency, conservation programs, socioeconomics, and water awareness. However, many of these variables are difficult to quantify and have a high degree of uncertainty (Billings & Jones, 2008). It has been suggested that the threat of increasing water demand greatly outweighs other consequences of climate variability including variations in the hydrologic cycle in defining the status of global water systems (Vorosmarty et al., 2000). Therefore, it is absolutely necessary to increase the skill and usability of current water demand modelling efforts.

Extensive studies in water demand have been conducted since the 1960's with a primary focus on aggregate municipal demand or residential demand. Most research on water demand use an economic modelling approach that attempts to utilize water price and socio-economic variables such as covariates in statistical models for water demand (Arbués et al., 2003). Many studies have emphasized the use of price elasticities and income for water demand forecasting (Katzman, 1977). Such econometric models have been used to forecast water demand and have been expanded to incorporate price and incomes using traditional and generalized least squares technique (Katzman, 1977; Malla & Gopalakrishnan, 1997; Babel et al., 2007). Multiple regression models to analyze sustainable water consumption (Coles & Simiu, 2003) have been developed and recently socioeconomic indicators have been incorporated into these models (Babel et al., 2007). Discrete/continuous choice models have been created and found to have increased price elasticity

when used (Hewitt & Hanemann, 1995). Most recently, a study was conducted by Ajbar & Ali (2015) to predict water demand in Makkah city, Saudi Arabia using Artificial Neural Network.

The main water resources in Saudi Arabia are divided into four categories namely underground, surface, desalinated, and treated wastewater. The main source of surface water in the south-western region is the rainfall. Dams are used to store surface water in some regions of the Kingdom. The Ministry of Water and Electricity (MOWE) built approximately 230 dams in the country to store runoff water (Al-Zahrani, 2009). According to Al-Ibrahim (1990), underground water is classified into renewable and non-renewable resources, where approximately 30% of the non-renewable resource has been utilized in 1995 (Al-Turbak & Al-Dhowalia, 1996).

This paper mainly aims at predicting the monthly and annually water demand in Makkah city, Saudi Arabia. The proposed annual water demand model could be utilized for future development plans consideration; especially capital expenditures and water quantities. However, the monthly water demand model is important for municipal authorities to improve monthly water production quantities.

2. METHODOLOGY

2.1 Makkah City, case study

Makkah city is situated in the Southern part of Saudi Arabia, about 70 km from Jeddah, and 277 m above the sea level; exactly at 21°25′0″N 39°49′0″E. The total area is over 1,200 km^2. The city population in 2012 was about 1.7 million, whereas visitors during Hajj period are more than triple this number every year. It has an extremely arid climate, with warm temperature in winter, which range from 18 °C at night to 30 °C in the afternoon, and summer temperatures range between 30 °C to 40 °C, and some rains between November and January.

2.2 Data collection

The following variables were selected for the development of water demand prediction models: household area (m^2) (Schleicha & Hillenbrand, 2009), city population (Ajbar & Ali, 2015), average personal income (Vorosmarty et al., 2000; Ajbar & Ali, 2015), average maximum temperature (Ajbar & Ali, 2015), and average number of visitors (Ajbar & Ali, 2015; Griffin & Chang, 1990). The data between the years 2002 and 2012 were collected from the relevant sources. The selection of these variables in this period of time was limited by the historical data availability. The data on water demand and consumption were collected from the Ministry of Water and Electricity. The data on household area, population, personal income, and number of visitors was collected from the Ministry of Planning and Pilgrimage. Data on the temperature was available from the local weather authority. The data was monthly for the following parameters: domestic water demand (m^3), visitors (capita), and temperature (°C), while the yearly data was collected for the household area (m^2), personal income (USD), and population (capita) parameters.

2.3 Development of ANN models

MATLAB mathematical software version 7.11.0 (R2010b) was used as a tool to develop Artificial Neural Network (ANN) models for the prediction of Makkah city's water demand (m^3) on monthly and yearly basis. Initially, the data was set between 0 and 1 in order to achieve minimum mean square error (MSE) estimation.

The following subsections describe the methods and algorithms used during models development.

2.3.1 Database description

The collected dataset was divided into input and target matrixes. The input variables for predicting the yearly water demand as a target were household area, city population, average personal income, average maximum temperature, and average number of visitors per year. While, for predicting the monthly water demand as a target, the input variables were household area, city population, and average personal income on yearly basis, as well as maximum temperature and number of visitors on monthly basis. The number of dataset was eleven annually and 132 on monthly basis. Initially, the entire dataset was randomized to prevent the biases and to create representative sections of the datasets for training and testing (Abushammala et al., 2014). Subsequently, the dataset was divided into training and testing subsets. In ANN modelling, one fifth of the dataset was used in the testing stage due to its smaller size.

2.3.2 Basic considerations

In this study, a feedforward (newff) network with an input layer, a hidden layers, and an output layer was used. The log-sigmoid transfer function (logsig) was used between all layers at all developed networks. According to Sablani (2007), there are two modes for learning a network; a supervised and an unsupervised. The supervised back-propagation is the most popular training algorithm (Abrahart et al. 2004; Rene & Saidutta, 2008). Therefore, scaled conjugate gradient (trainscg) back-propagation algorithm was used in this study for training the networks. The training process between both input and expected output was repeated until the performance error decreased to an acceptable level, and the internal connection weights were modified in response to the computed error. For a single iteration, the error is calculated and the summed errors from overall neurons are divided by the size of data used in the training process to estimate average MSE. The maximum number of training epoch, the performance error goal, and the momentum factor were set to be 104, 10-4, and 0.92, respectively (Abushammala et al., 2015).

3. RESULTS AND DISCUSSION

3.1 Selection of Training Algorithm

Five backpropagation training algorithms were used to determine the best training algorithm for the gathered data. For all algorithms, a three-layered approach with a log-sigmoid transfer function (logsig) at a hidden layer and an output layer was used. In addition, 20 and 4 neurons were used in the hidden layers respectively for the monthly and annually basis as initial values for all backpropagation algorithms. The momentum was a constant 0.92 for all the algorithms used. The testing phase results with different backpropagation training algorithms are provided in Table 1. Compared to other backpropagation algorithms, Levenberg-Marquardt (trainlm) was the best algorithm, producing the lowest MSE, and was associated with the highest efficiency (E) value in the testing phase which has been calculated according to Abushammala et al. (2014). Using the Levenberg-Marquardt algorithm resulted in a decrease of up to 10 % of the MSE produced compared with using the Powell-Beale conjugate gradient algorithm, which was the algorithm that produced the second lowest MSE (Table 1). Subsequently, the Levenberg-Marquardt algorithm was considered for training the final ANN water demand model for both basis.

3.2 Optimization of Neuron Numbers

Optimization of neural network neuron numbers is an important task in developing the best ANN model. Therefore, the optimum network neuron numbers were investigated in the current study for

both monthly and annual ANN models to improve the estimation performance of both models. The number of hidden layer chosen was one, similar to the initial ANN structure. The Levenberg-Marquardt backpropagation training algorithm was used for training different ANN models with different neuron numbers at hidden layer. The neurons number in the hidden layer was varied between 15 and 25 for the monthly model, while number of neurons in the hidden layer of the yearly model varied between 2 and 4. The optimal number of neurons in the hidden layer for both models was chosen based on the lowest MSE, and the highest *E* value in the testing stage.

Table 1. Comparison of backpropagation algorithms

Backpropagation algorithms	Function	MSE	*E*
Levenberg-Marquardt backpropagation[a]	trainlm	0.0009	0.7384
Scaled conjugate gradient backpropagation	trainscg	0.0011	0.6969
BFGS quasi-Newton backpropagation	trainbfg	0.0066	0.6535
One step secant backpropagation	trainoss	0.0105	0.6197
Powell-Beale conjugate gradient backpropagation	traincgb	0.0010	0.7194

[a] *Best training algorithm*

The logistic sigmoid transfer function was used at all layers during the training phase, while the value of momentum was a constant of 0.92 (Abushammala et al., 2015). The results show that the 3 neurons in the hidden layer produced smaller MSE and higher *E* value compared with other models on the annual basis (Table 2). However, the monthly model with 15 neurons in the hidden layer produced smaller MSE and higher *E* value in contrast to other models (Table 2).

Table 2. Performance of different models tested in both ANN models with a varying number of neurons in the hidden layer

Models	Training stage		Testing	
	MSE	E	MSE	E
Annually models				
[5 4 1]	0.00056807	0.97526	0.0042437	0.86425
[5 3 1][a]	0.00060915	0.97348	0.0018152	0.94193
[5 2 1]	0.00058961	0.97433	0.0028277	0.90955
Monthly models				
[27 25 12]	0.00092600	0.75486	0.014561	0.43348
[27 20 12]	0.00017441	0.95383	0.0058722	0.77153
[27 15 12][a]	0.00020299	0.94626	0.0040575	0.84214

[a] *Best neuron number*

Figures 1 and 2 show the optimized ANN structure, the linear regression between the targets of the water demand data and the ANN model outputs in the training phases, the number of epoch during the training phase, and comparison between the real and the predicted values from the ANN for both annual and monthly water demand models. The optimum annual ANN training process took 7 epochs (Fig. 1) to reach the error goal (10^{-6}), while the optimum monthly ANN training process had taken 9 epoch to reach the same error value (Fig. 2).

Figures 1 and 2 show that the target data exhibited slight large variations during the comparison between the target data and the estimated values in the training and the testing phases. However, it was evident that the ANN models' outputs were reasonable and they simulated the target data in both figures.

The correlation coefficient (*R*) value found in this study was relatively higher than some of those reported in the literature; a coefficient of determination of 0.90 for prediction of the quantitative characteristics of water bodies (Palani et al., 2008). However, some previous studies achieved *R* value up to 0.99 (Elmolla et al., 2010). The relatively low values of *R* and *E* of the ANN water demand models obtained by this study might be attributed to data noise, due to the small sample size of the dataset.

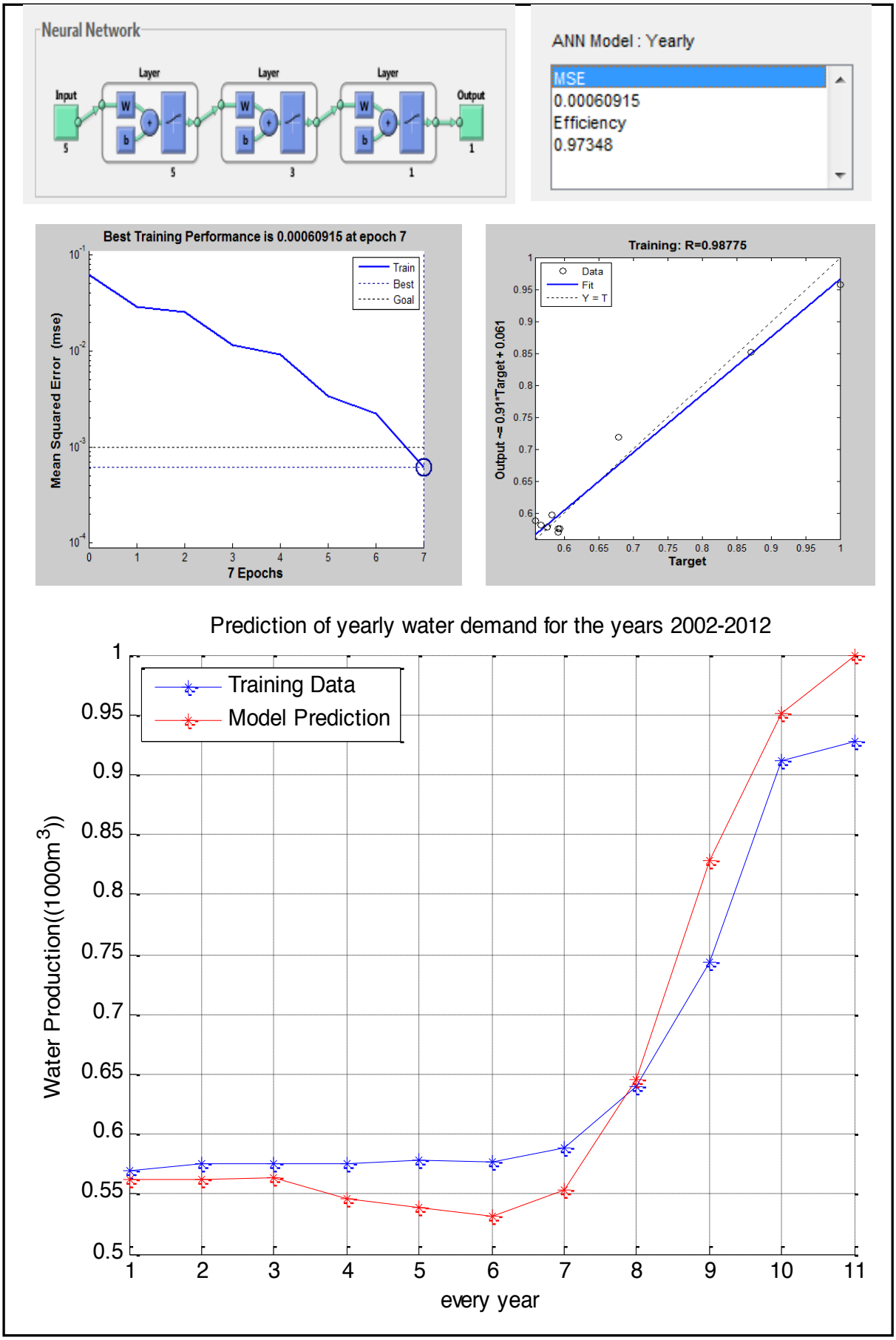

Figure 1. ANN structure, training, and testing performance of the annually model

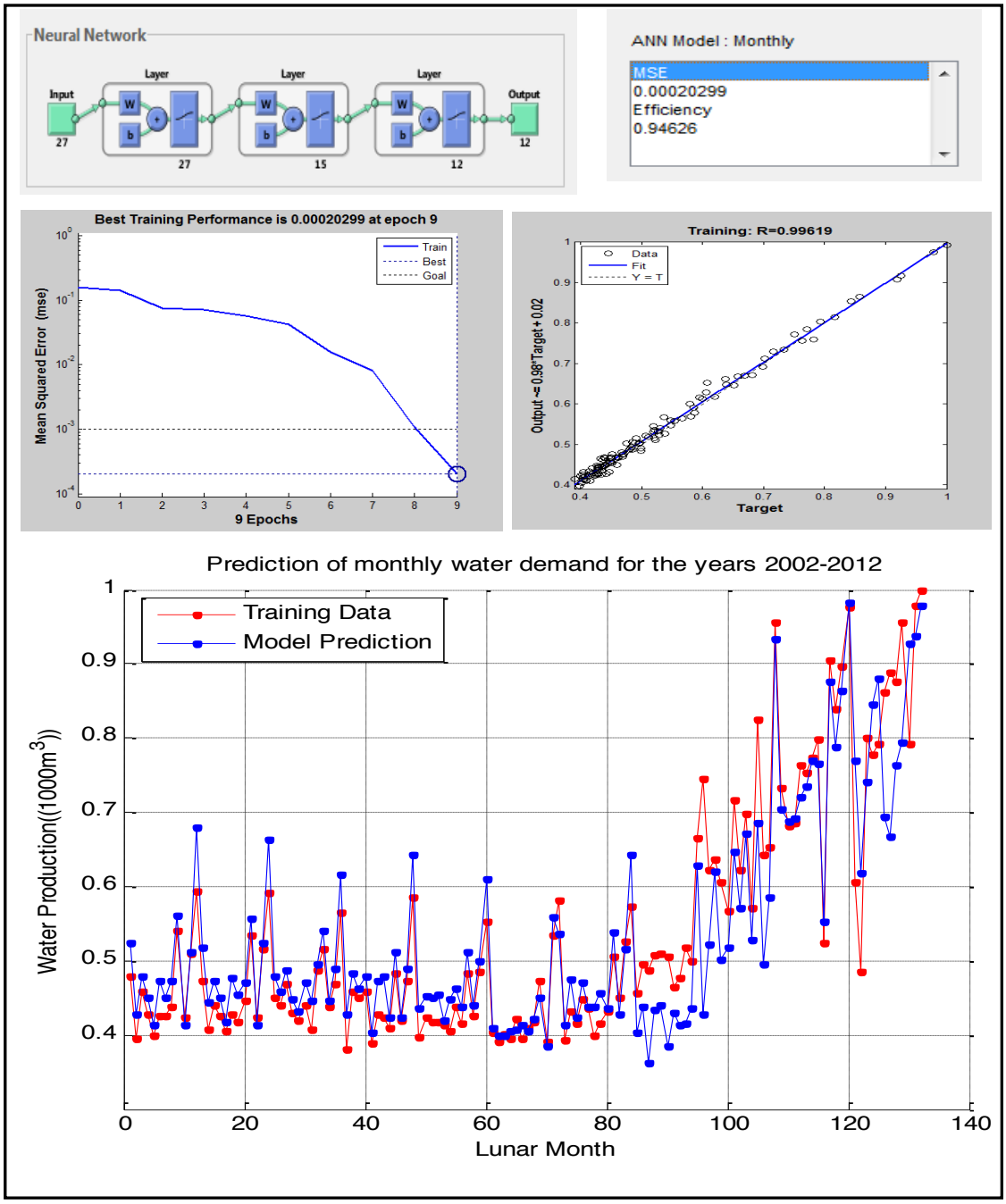

Figure 2. ANN structure, training, and testing performance of the monthly model

4 CONCLUSION

This study aimed to develop a water demand model for predicting monthly and annual water demand in Makkah city, the most visited city in Saudi Arabia for pilgrimage. The analysis of historical data (2002-2012) revealed that most of the selected variables in this study were positively influenced by the water demand. The data also demonstrates a steady annual increment in the water demand; 1888 m^3 in 2002 to 18888 m^3 in 2012. The main conclusions of the study were as follows:

1. The selected variables in this study were all important at different levels for prediction of water demand in Makkah city.
2. ANN prediction models developed in the current study can be used for monthly and yearly water demand estimation in Makkah city and could be optimised and could even be used in other cities in the country.

ACKNOWLEDGEMENT

The authors are grateful to the Ministry of Water and Electricity (MOWE), Ministry of Planning and Pilgrimage, and the weather authority for providing the data needed to complete this research.

REFERENCES

Abrahart, R.J., Kneale, P.E., See, L.M., 2004. Neural networks for hydrological modeling. London: Taylor and Francis Group plc.

Abushammala, M.F.M, Basri N-E.A., Elfithri, R., Younes, M.K., Irwan, D., 2014. Modeling of methane oxidation in landfill cover soil using an artificial neural network. Journal of Air and Waste Management Association: 64: 150-9.

Abushammala, M.F.M., Basri, N-E.A., Younes, M.K., 2015. Landfill Methane Oxidation: Predictive Model Development. Journal of Applied Sciences: 15: 283-288.

Ajbar, A., Ali, E.M., 2015. Prediction of municipal water production in touristic Mecca City in Saudi Arabia using neural networks. Journal of King Saud University-Engineering Sciences: 27: 83-91.

Al-Ibrahim, A.A., 1990. Water Use in Saudi Arabia: Problems and Policy Implications. Journal of Water Resources Planning and Management (ASCE): 116: 375-388.

Al-Turbak, A.S., Al-Dhowalia, K.H., 1996. Contribution of Treated Wastewater in Solving Water Shortage Problems in Saudi Arabia (in Arabic), King Saud University. Symposium on Wastewater Treatment Technology and Reuse, Riyadh: 14-33.

Al-Zahrani, K.H., 2009. Sustainable Development of Agriculture and Water Resources in the Kingdom of Saudi Arabia, Conference of the International Journal of Arts and Sciences: 1: 3-37.

Arbués, F., García-Valiñas, M.A., Martínez-Espiñeira, R., 2003. Estimation of residential water demand: a state of the art review. The Journal of Socio-Economics: 32: 81-102.

Babel, M.S., Das Gupta, A.D., Pradhan, P., 2007. A multivariate econometric approach for domestic water demand modeling: An application to Kathmandu, Nepal. Water Resources Management: 21: 573-589.

Billings, R. B., Jones, C. V., 2008. Forecasting Urban Water Demand, Second Edition. American Water Works Association, Denver, CO.

Coles, S., Simiu, E., 2003. Estimating Uncertainty in the Extreme Value Analysis of Data Generated by a Hurricane Simulation Model. Journal of Engineering Mechanics: 129: 1288-1294.

Elmolla, E.S., Chaudhuri, M., Eltoukhy, M.M., 2010. The use of artificial neural network (ANN) for modeling of COD removal from antibiotic aqueous solution by the Fenton process. Journal of Hazardous Materials: 179: 127-134.

Griffin, R.C., Chang, C., 1990. Pre-test analyses of water demand in thirty communities. Water Resources Research: 26: 2251-2255.

Hewitt, J.A., Hanemann, W.M., 1995. A Discrete/ Continuous Choice Approach to House hold Water Demand under Block Rate Pricing. Land Economics: 71: 173-192.

Katzman, M.T., 1977. Income and price elasticities of demand for water in developing countries. Water Resources Bulletin: 13: 47-57.

Malla, P.B., Gopalakrishnan, C., 1997. Residential water demand in a fast-growing metropolis: the case of Honolulu, Hawaii. International Journal Water Resources Development: 13: 35-51.

Palani, S., Liong, S.Y., Tkalich, P., 2008. An ANN application for water quality forecasting. Marine Pollution Bulletin: 56: 1586-1597.

Rene, E.R. Saidutta, M.B., 2008. Prediction of BOD and COD of a refinery wastewater using multilayer artificial neural networks. Journal of Urban and Environmental Engineering: 2: 1-7.

Sablani, S.S., 2007. Artificial neural network modeling. In Handbook of food and bioprocess modeling techniques, ed. Sablani, S.S., Datta, A.K., Rehman, M.S. Mujumdar, A.S. London: Taylor & Francis Group, LLC: 375-403.

Schleicha, J. Hillenbrand, T., 2009. Determinants of residential water demand in Germany. Ecological economics: 68: 1756-1769.

Vorosmarty, C.J, Green, P., Salisbury, J., Lammers, R.B., 2000. Global Water Resources: Vulnerability from Climate Change and Population Growth. Journal of Science: 289: 284-288.

Proceedings of the 10th World Congress of EWRA 'Panta Rhei', 5-9 July 2017, Athens, Greece
© 2017 *European Water Resources Association*

The role of rainwater harvesting on providing vegetation water requirement in arid and semi-arid regions

M.T. Dastorani[1*], B. Kouhzad[1], A. Sepehr[1] and A. Talebi[2]
[1] *Faculty of Natural Resources and Environment, Ferdowsi University of Mashhad, Iran*
[2] *Faculty of Natural Resources, Yazd University, Yazd, Iran*
[*] *e-mail: dastorani@um.ac.ir*

Abstract: Water harvesting Knowledge has an ancient history. From old times, people, specially, occupants of arid lands whose access to water was limited, invent different ways to collect and conserve water. Today, many of these methods are reclaimed and introduced as Indigenous Knowledge. There are many case studies in different branches of water harvesting and new methods based on Indigenous Knowledge have been presented. These studies especially in our country, which is situated in the desert belt, are of importance. Present study was carried out in a watershed near Mashhad in Iran. Given that Mashhad city is situated in a semi-arid zone in Khorasan Razavi, therefore, is in a good situation for this study. Selected area located in Dehbar district, south of Mashhad contains different parts with various slopes. Basic meteorology data were collected and essential soil properties were measured in soil lab. Based on references, experiences and the local characteristics, it was tried to choose the best structures for the area. Negarim microcatchment and absorbing Banequet was chosen for both of slopes. During nine months, after each precipitation, soil sampling was done with six time repeating process. Soil moisture was calculated after each time. Using basic data and soil information, Changing Procedure of soil moisture was studied. Graph analysis showed that in total, both structures performances were 20% better than the control plots. At the end of precipitation period, loosing moisture in control plots is about two times more than the structures, an average of 30%. The acquired results confirm the success of tested structures on utilization of soil moisture.

Key words: Harvesting, Arid lands, Negarim Microcatchment, Absorbing Banquet, soil moisture

1. INTRODUCTION

In arid and semi-arid areas, rainfall is low and unpredictable with unsuitable timing. Majority of rainfall is transformed into runoff due to several factors including lack of vegetation and high intensity. Furthermore, in these areas evaporation is very high which would make the low level of rainfall unavailable. That's why various systems for collecting and utilization of water has been frequently used since old times(Laura, 2004). Available records in rainwater harvesting field shows that after widespread drought in Africa that caused serious damage to the crops, in 1970's and 1980's general attention focused on water harvesting which led Evanari et al (1971), to use these methods for the first time in Palestine desert (with the average precipitation of 90 mm per year) that resulted in increased food production. Boers and Ben Asher (1982), executed water harvesting systems including farming contours, surface runoff storagein underground reservoirs, construction of regional microcatchments to improve soil moisture and water storage in small turkey nest farms in the Negev Desert. Hatibu and Mahoo (1999), did a comprehensive study on the usage of water harvesting systems for the recovery of soil moisture within a field in Tanzania. Martinez et al (2016), studied indigenous knowledge of structures such as microcatchments, contour bunds, Bankettes and rock bunds. The purpose was to evaluate the effect of a modified model for these water harvesting structureson the hydrological regime of soil and vegetation without damaging interference in the region's ecosystem. The result of these findings ultimately led to presentation of Modipe software model. The application of this model is to estimate the most efficient structure for the land according to local conditions. In a study, Razzaghi (2011), investigated the positive impact of Meskat reclamation systems and Zey pitting holes on increasing moisture retention in the region,

improving the efficiency of agricultural production and restoring the pastures in Libya. Hosseini et al (2005), assessed and monitored soil moisture retention in the Bankettes using statistical tests, to compare them with the natural conditions in a 5 month study in Taleghan, Iran. Results showed the positive effect of Bankette structure in increasing soil moisture. Tabatabaei_yazdi et al (2010), attempted to estimate rainwater harvesting potential for using in rainfed supplemental irrigation inKhorasan Province of Iran with arid and semi-arid climatic conditions, and stated about 70% increase in production outputs. Gebretsadic (2009), managed to grow native plant species with no irrigation and only using water stored in Negarim Microcatchmentsconstructed at the project site, in a three-year time period in a case study in dry cold heights of Austria.Studies on the effects of diamond and crescent microcatchment systems on soil moisture and seedlings survival in Azadshahr region of Golestan province in Iran showed that in a 5 year period, soil moisture increased, and seedlings grown under rainfed conditions, while seedlings in observation areas did not survive, so the systems aresuitable locations to store moisture and seedlings grown under rain fed conditions while seedlings in observation plot did not survive (Shahini and Roughani, 2012). Studies on diamond microcatchments on the east of Golestan province of Iran in Maravetape area showed that insemi-arid conditions in this area, rainfed Olive gardens can be created. Establishing an insolation nylon system in the collecting area of these systems, increased the runoff volume in the planting areas of olive seedlings three times more than the annual rainfall of the area (Shahini and Roughani, 2013).

Present study tried to assess the effects of few rainwater harvesting systems on soil moisture increase and also moisture remaining time period to supply vegetation water requirement in arid and semiarid areas near Mashhad in north east of Iran.

2. MATERIALS AND METHODS

2.1 Location of the study

Since the study was to evaluate the effect of water harvesting systems in arid and semi-arid, the area under study selected in Khorasan Razavi province of Iran, about 10 km distance from the Mashhad city, and in south of Torghabeh county, Dehbar watershed, with 59°, 22' and 27" E longitude, and 36°, 13' and 31" N latitude. This area is a part of Binalud highlands in terms of topography. Figure (1) shows a view of related study area inside Dehbar watershed.

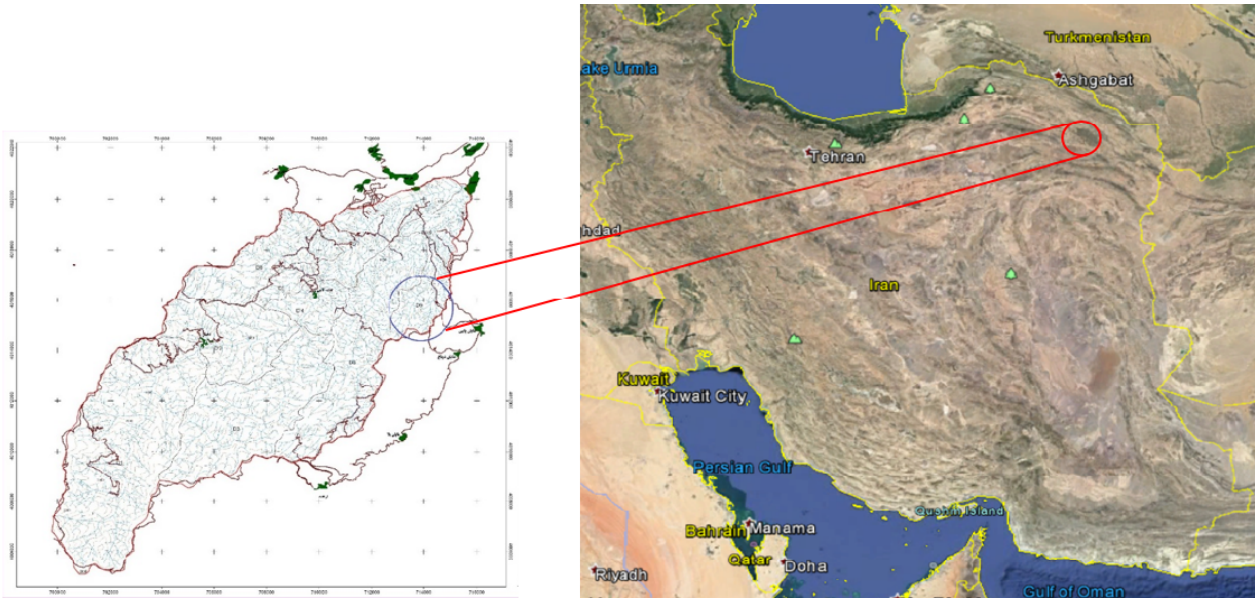

Figure 1. Study area location

2.2 Research data and methodology

On the selected hillside of the case study, the slope of the area was measured and two places were selected for construction of the systems one in upstream part with 2.4% land slope and the other one in downstream part with 22 % land slope. From geological point of view, the study area is situated in Mashhad geological sheet which is a part of Binalud structural zone, containing gray to black Teriassic aged Mashhad slits and Filits in rotation with Shale, sandstone and JurassicConglomerate. Important characteristics of soil including texture, pH, EC, Lime percent, Porosity, Organic materials,Bulk density and True density weremeasured in lab for both chatchment areas and infiltration pits of the structures in two depths of (0-15) and (15-30) cm. The results of these assessment showed that based on pH, regional soils are in the category of low alkaline soils. Also the salinity is in low level, and texture is loam and clay loam in all collected soilsamples. Soil Lime percentage and organic materials are low as well. In terms of porosity, bulk density and true density, the soils are classified in agricultural average condition.

To collect precipitation data, Rain gauge graphs of Mashhad synoptic meteorological station were used. By extracting information from these graphs and unite conversion, the amount, Intensity and duration of precipitation events were calculated for the nine-months study duration.

According to initial investigation for constructing the structures, it was decided that each structure had to be built in both slopes with an observation (control) area for each one. Selected sides for each microcatchment was 3.33 meters preparing about 10 m^2 runoff collecting area. The area of infiltration pits was selected 1 m^2so the rate of catchment area to cultivated area is about 10.Infiltration pits were situated in the lowest part of each microcatchment to ease the runoff flow from all parts of the catchment. Figure 2 shows the constructed microcatchments in this research. Each microcatchmet contains two parts: catchments area where provides the runoff, and the cultivated area where receives the runoff collected in catchment area.



(a)



(b)

Figure 2. A view of the constructed Negarim Microcatchment (a) and Bankette (b) structures

To study the soil moisture process, after each precipitation, from all the runoff collecting areas and also infiltration pits in both slopes (2.4% and 22%) and in two depth (0-15 and 15-30 cm) soil samples were collected and the moisture content was measured. For each precipitation event, sampling had 5 repeats (with three days time intervals). Therefore, in every sampling round, 20 samples were collected and transferred to the lab.To review and assess the soil's hydrological condition and completing the needed data for evaluation, Curve Number (CN) had to be calculated. Due to the results of soil texture, soil hydrological group was estimated as group C. In field visits, pasturelands hydrological condition was estimated as poor with less than 50% vegetation cover. Also, precedencesoil moisture status was calculated using the results of precipitation monitoring. Using these information, curve numbers were calculated as are shown in Table (1).

Table 1. Rainfall events and Curve Number calculation

Sampling date	Cumulative precipitation of last 5 days	Total precipitation	Precedence moisture condition	Curve Number
2014.10.14	1.6+5.0+0+0+1.3	7.9	1	72
2014.11.6	3.1+7.7+7.1+1.0+8.7	6.18	2	86
2014.11.26	0+0+0+2.6+9.2	1.9	2	86
2014.12.24	1.1+0+9.3+2.40	2.9	2	86
2015.1.11	2.2+2.8+9.20+0	14	2	86
2015.2.16	5.0+5.15+0+2.1+6.2	8.19	2	86
2015.2.19	9.4+9.0+0+5.0+5.15	8.21	3	94
2015.2.22	3.1+10+3+9.4+9.0	1.20	3	94
2015.3.7	1.0+3.10+5.1+0+1.1	13	3	94
2015.3.10	3.10+1.0+7+0+0	4.17	3	94
2015.3.27	6.6+7+0+0+4.0	7.7	3	94
2015.3.31	6.6+7+0+0+0	6.13	3	94
2015.4.5	0+0+0+3.2+2.3	5.5	3	94
2015.5.8	0+0+3.4+1.1+9.12	3.18	2	86

3. RESULTS AND DISCUSSION

3.1 Calculation of runoff and infiltration

For each structure in each rainfall, the amount of runoff and infiltration was calculated. According to table (2), result of these assessment showed that in the first months of sampling, about half of the occurred precipitation forms the total runoff and infiltration and the other half has been lost from the area in different shapes of waste especially evapotranspiration. Due to low precipitation amount and intensity and high potential of evapotranspiration, soil moisture in the first three months of sampling was very low. Increase in the rainfall events in winter months and it's continuity affects the infiltration and runoff percentage positively. The aim of monitoring the rates of runoff and infiltration is to analyze soil moisturechanging procedure during the sampling time period.

Table 2. The calculation of runoff and infiltration in structures

Sampling dates	Negarim Upstream catchment		Bankette Upstream catchment		Negarim Downstream catchment		Bankette Downstream catchment		Total
	Q(mm)	W(mm)	Q(mm)	W(mm)	Q(mm)	W(mm)	Q(mm)	W(mm)	Q+W
2014.10.14	1.2	0.56	0.95	0.6	1.05	0.58	1.1	0.57	6.61
2014.11.6	0.7	0.66	1.5	0.63	1.2	0.64	1.2	0.64	7.17
2014.11.26	0.8	0.92	0.8	0.92	0.7	0.93	0.7	0.93	6.7
2014.12.24	1.2	0.44	1.2	0.44	2.4	0.4	2.4	0.4	8.88
2015.1.11	2.5	0.76	2.6	0.76	2.7	0.75	2.7	0.75	13.52
2015.2.16	2.9	0.68	3	0.62	3.1	0.62	3	0.62	14.54
2015.2.19	0.28	0.79	3	0.67	3.2	0.68	2.8	0.7	12.12
2015.2.22	3.1	0.51	3	0.52	3.2	0.51	3.1	0.51	14.45
2015.3.7	2.7	0.54	2.7	0.54	2.8	0.53	2.8	0.53	13.14
2015.3.10	2.9	0.53	3	0.53	3.2	0.52	3.2	0.52	14.4
2015.3.27	2.7	0.41	2.7	0.41	0.27	0.62	0.27	0.62	8
2015.3.31	2.9	0.89	3.2	0.86	0.36	1.1	3.3	0.86	13.47
2015.4.5	0.27	0.47	0.27	0.47	1.1	0.4	1.1	0.4	4.48
2015.5.8	2.5	1.32	2.6	1.31	2.8	1.3	2.8	1.3	15.93

3.2 The effect of the proposed structures on the soil moisture process

To investigate the usefulness of implemented techniques in the soil moisture, sampling occurred

regularly after each rainfall event with five repeats every three days to calculate bulk and volumetric moisture. Using these data provided the possibility to evaluate and compare of changes in soil moisture volume during a crop year in study and the related observation areas. According to figure (3) and (4), this study showed that there is an average of 25% difference in moisture retention, between Negarim Microcatchment infiltration pits and the related observation area for the of 2.4% slope site. This difference reaches 30% in the 22 % slope site. There wasn’t a meaningful difference between the moisture content of (0-15) and (15-30) depths. Also, the difference in moisture content between Absorbing bankette infiltration pit and the related observation area in 2.4% and 22 % slopesites were respectively 27% and 31 %. There wasn’t a meaningful difference between depths here either. Study shows that in the beginning of sampling in Autumn, where amount, intensity and duration of the rainfall events were relatively low and the soil was dry (due to hot summer with no rainfall), moisture change processis mild. The increase in rainfall intensity,duration and occurrences in Febraury and March made a stable moisture period in infiltration pits which followed by 30% increase in soil moisture of both structures while moisture increase in observation areas were only about 15 % in average. These results show an agreement with those reported by the case studies of Martinez et al (2004), Martinez (2008), Hosseini et al (2005), Gebretsadic (2009), Razaghi (2011), Shahini and Roghani (2012), Shahini and Roghani (2013), Sadeghzadeh et al (2013), Rehman et al (2014). Also in all of these studies the common method for determining soil moisture were TDR or bulk moisturemeasurement like this study.

To verify the effect of structures on runoff harvesting, two statistical hypothesis tests (0 and 1 tests) were used. In the first Test, zero hypothesis (H0), absence of significant difference in moisture between infiltration pits and observation area and in one hypothesis (H1), Existence of significant difference in moisture between infiltration pits and observation area was considered.

According to the results,there is no difference between moisture average of catchments areas and the related observation areas in significant level of 1% and 5% in both structures with same slope and depth.So it can be safely said that there is a harmony between catchments and the related observation areas. Test results between infiltration pits of both structures and the related observation areas show significant difference in moisture average in significant level of 1% and 5% in both depths and slopes, means differences in moisture retention between infiltration pits and the observation areas are impressive and the structures functions are successful. Studies of Hosseini et al (2005), Razzaghi et al (2011), Shahini and Roghani (2012), Shahini and Rorhani (2013), Sadeghzade et al (2013) and Rehman et al (2014) who used hypothesis tests to prove the significance of their results, also found the same results.



Figure 3. Moisture content comparison between catchment and infiltration areas of both structure

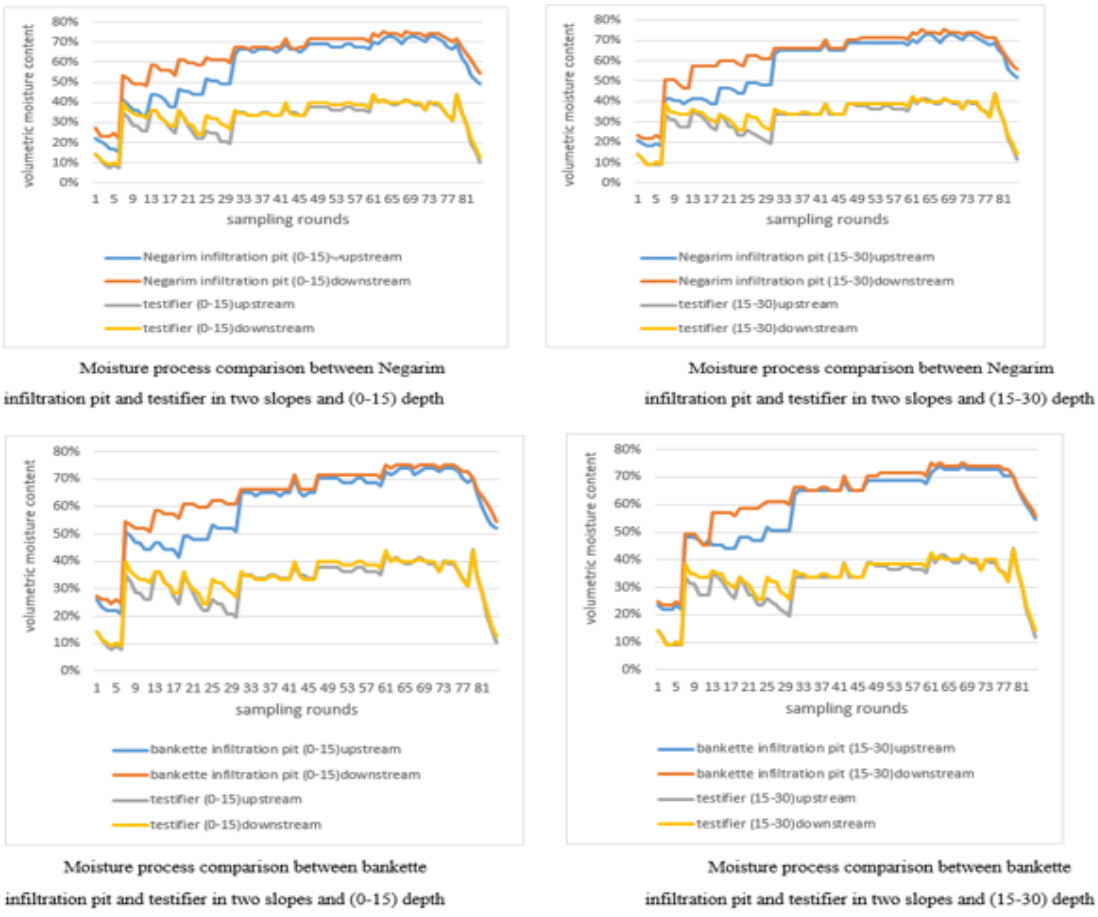

Figure 4. Moisture content comparison of infiltration pits of both structures with the related observation plot in both slopes

4. CONCLUSIONS

In overall, the performance of both structures used in this research is much better than the observation areas. In 2.4 % slope area, absorbing Bankette was better than the Negarim microcatchment by the average of 2%. This difference in 22% slope area is only 1%. Sampling depth did not have a significant effect on the results. Also, the average performance of both structures in comparison to the observation areas is by about 10% higher. This difference reaches 30% in winter rainfall events. In the last few rainfalls, moisture decrease process in structures is about 10% in average, while the observation areas lost about 30% of soil moisture during the same time period.By examining the performance of the structures, it can be said that using water harvesting methods, is a non-aggressive approach in the recovery of soil moisture in local scale, which has an impressive effect on soil moisture storage especially in short time periods with relatively low expenses. Using these methods on longer periods of time (more than two years) can also help the vegetation recovery and soil fertility. Also this study proves the success of both of the structures provided and tested. Using similar methods and promoting them as native case studies would help the development of scientific resources and information in water harvesting and management. Using this case study especially for longer periods of time can also improve soil fertility and green coverage in addition to soil moisture increase as well as aquifer recharge, which would present a chance to improve the water and agricultural condition on arid and semi arid regions.

REFERENCES

Boers, T.M., and BenAsher, J. 1982. A review of rainwater harvesting. In Agric. Water Management, 5(1):145158.

Caffrey, P and Farmer, A. 2014. Profiles of Agricultural Management Practices. ARCC, 6(2):32-41

Evenari, M, Shana, L and Tadmor, N H. 1971. The Neger, the challenges of a desert. Havard University Press. Cambridge, Mass, 25(3):269-282

Gebretsadic, W.2009. Evaluation of The Adaptability and Response of Potential Indigenous Trees to Water Harvesting in the Rehabilitation of Kuriftu Lake atchment. Ms. Thesis. University of Natural Resources and Applied Life Sciences (BOKU), Vienna, Austria, 4(3):143-162

Hatibu, N. and Mahoo, H. 1999. Rainwater harvesting technologies for agricultural production: A case for Dodoma, Tanzania. Sokoine University of Agriculture, Department of Agricultural Engineering and Land Planning, 17(3):161-171

Hosseini, M, Karami, A and Atapourfard, A. 2005. Bankette impact on controlling runoff and soil moisture retention. The second conference of water harvesting and soil and water resources management. Kerman. Iran (in Persian).

Laura R, 2004. Water farms: a review of the physical aspects of water harvesting and runoff enhancement in rurallandscapes. Technical Report04/6, CSIRO Land and Water, Canberra ACT.

Martinez de Azagra, A.,Mongol, J., Rojo, L., 2004. Oasification: a forest solution to many problems of desertification, invest agrar, 13(3): 437- 442.

Martinez de Azagra, A., 2008. Complete version of MODIPE, second reunion for hydrologic forestry. (Spanish), 4(2): 123-145.

Razzaghi, M. 2011. Rain Water Harvesting Systems is a Way for Water Conservation. International Journal of Water Resources and Arid Environments 1(4): 72 84.

Rehman, O, Rashid, M, Kausar, R, Alvi, S .2014. Microcatchment Techniques For Efficient Utilization Of Stored Rain Water In Gullied Lands. International Journal of Agriculture and Crop Sciences, 18(1):19-49

Sadeghzade Reyhan M, Zare haghi D and Neyshabouri M. 2013. Evaluation of rain water harvesting, soil moisture and seedling growth. Journal of Soil and Water Science, 23 (4): 203 to 214 (in Persian).

Shahini G. and Roughani M. 2012. Micro catchment used in the creation of tree cover in arid and semi-arid. Proceedings of the Third National Conference on combating desertification and sustainable development of wetlands in the Iranian desert, 25 to 26 September, Arak (in Persian).

Shahini Gh and Roughani M. 2013. Role of contours Micro catchments on the establishment of Olive Branch area on the slopes of Golestan province. The Sixth National Conference of watershed management and soil and water resources management, Kerman, Iran (in Persian).

Tabatabaei Yazdi J, Haghayeghi moghadam A, Ghodsi M and Afshar H. 2010. Rainwater harvesting for supplemental irrigation of dryland wheat in Mashhad. Journal of water and soil (Agricultural Sciences and Technology, 24 (2): 198 to 207 (in Persian).

Proceedings of the 10th World Congress of EWRA 'Panta Rhei', 5-9 July 2017, Athens, Greece
© 2017 *European Water Resources Association*

Robustness and vulnerability assessment of water networks by use of centrality metrics

A. Agathokleous[1], C. Christodoulou[1] and S.E. Christodoulou[1,2*]
[1] *Nireas International Water Research Center, University of Cyprus, 1 Panepistimiou Avenue, Aglantzia, Cyprus*
[2] *Department of Civil and Environmental Engineering, University of Cyprus, 1 Panepistimiou Avenue, Aglantzia, Cyprus*
[*] *e-mail: schristo@ucy.ac.cy*

Abstract: The reliability of a water distribution network (WDN) is a function of several time-invariant and time-dependent factors affecting its components and connectivity, most important of which have been shown to be the network's topology, its operating pressure, the type of key components (such as the diameter, length, material and age of water pipes) and the network's historical performance (such as the number of previously observed failures in the network). In terms of network topology, this attribute even though generally thought as time-invariant it actually is time-dependent, as the paths in a water distribution network change over time based on the hydraulics in the network (water demand and water pressure/flow alter the way water flows in the piping network). The work described herein examines the time-dependent nature of a WDN topology and by means of a betweenness centrality index (BC) method demonstrates the effect of topology on the network's vulnerability / reliability. The importance of the BC index is demonstrated by use of a case-study water distribution network operated under both normal and abnormal conditions. The proposed method is also coupled with spatial mapping to indicate areas of concern in the network, and with a decision support system to assist in prioritizing actions to improve on the network's robustness and resilience.

Key words: Network robustness; Vulnerability assessment; Pipe breakage

1. INTRODUCTION

One of the biggest challenges faced by water authorities is the management of their WDN, especially in light of the increasing network complexity and of the increasing rate of pipe deterioration. As a result, it is becoming increasingly important to being able to assess the network reliability and resilience to catastrophic events by use of management tools. The management system of a well-organized WDN includes decision support systems (DSS) to assess the pipeline system condition and the extent of damage due to pipe failures. The development of these tools requires installation within the network of monitoring devices and sensors, hydraulic simulation models, extended database, geographical in-formation systems (GIS) and mathematical models that simulate the behavior of the WDN through time (Figure 1).

The development of an integrated tool for condition assessment of WDNs is an expensive, time consuming and multi-faceted procedure which, despite its complexity, most times fails to reflect in great detail the actual real-time behavior of network operation. Further, the development, operations and maintenance of the underlying hydraulic and mathematical tools require specialized knowledge, not typically found within the water agencies, and analysis of real-time WDN operational data that hinder the applicability of the models. These aforementioned difficulties give rise to the need for an automated early-stage appraisal system of a WDN's vulnerability, based on the WDN's topological characteristics, which could then be easily amended with additional information for a more holistic vulnerability model. Such information are the hydraulic characteristics and past network performance under normal and abnormal operating conditions (Agathokleous 2015).

The goal of the research work presented herein is the development of a model that: (a) it is cost efficient; (b) its use does not require hydraulic and mathematical knowledge and advanced software skills; (c) it does not require operational data beyond the topography of the WDN; (d) it can lead to reliable conclusions within a short time; (e) it can also be used as a management tool for designing

the operation mode of a WDN.

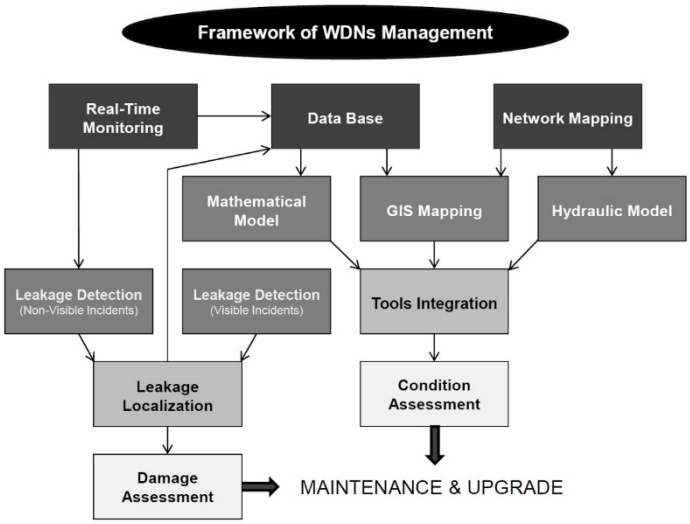

Figure 1. Schematic framework of a WDN management system.

The paper proposes a model based on the principle that the sections of a WDN which are hubs and support large segments of the pipeline system, are subject to stresses whose size is of greater intensity and frequency relative to other network sections, thus being more vulnerable to failure. The importance of each node, relative to the other nodes, with regards to its contribution to the provided network service is computed factoring in the topology of the WDN as described by a betweenness centrality (BC) metric. Finally, for validating the applicability and accuracy of the proposed model, the deduced by the model spatial risk levels (BC weighted graph) are compared to corresponding maps created by the use of actual WDN failure data (pipe bursts).

1.1 Case-study network

The case-study network utilized in the analysis is a District Metered Area (DMA) from the WDN of the city of Nicosia (Cyprus). The studied DMA (DMA6) is divided into 4 sub-district metered areas (Sub-DMAs) and it is remotely monitored through a supervisory control and data acquisition (SCADA) system across the DMA, which continually collects and transmits operational information. All leakage incident data reports since 2003 had been maintained in a specially designed database. The data utilized for verification / validation purposes of the proposed model, covers the time period from 01/01/2003 to 31/12/2010 and includes 548 incidents associated with water mains (WM).

2. STATE OF KNOWLEDGE

2.1 Condition assessment models for WDNs

To date, several mathematical models simulating the operations and condition of WDNs have been developed. Initial research efforts were based on the development of a single-objective mathematical model expressing the failure pattern or system reliability, while subsequent studies expanded the work by presenting multi-objective failure models. More recent efforts focused on the development of models simulating WDN behavior. Finally some recent research activities focused on abnormal operating conditions due to exogenous factors that affect the condition of the network.

Kleiner and Rajani (2001) provide an overview of the mathematical models related to structural deterioration of the WDNs, with the different models grouped into classes according to the

governing equations and the types of data that are required for the implementation of each model. Michaud and Apostolakis (2006) presented a scenario-based methodology for the ranking of the elements of a WDN, based on multi-attribute utility theory and a graph theory-based network analysis algorithm. The researchers modelled the system as a network and evaluated the consequences of the failure of each of the network's elements to the supply level, considering the capacity of the elements' connection to the available resources.

Christodoulou (2010) presented a framework for a risk-based integrity-monitoring strategy for the management of WDNs, based on a combination of artificial neural network, parametric and nonparametric survival analysis. In their work, Martinez-Rodriguez et al. (2011) noted that the concept of reliability had been introduced in an attempt to quantitatively measure the possibility of maintaining an adequate service for a given period, and that numerous researchers had considered reliability as a measure of redundancy. A methodology presented by Aydin (2014) uses performance criteria (resiliency, reliability and vulnerability) for evaluating sustainability indices for each node, in terms of nodal pressure and water age. This calculation identifies problematic nodes individually. Shuang (2014) evaluated the nodal vulnerability of WDNs under cascading failures, by use of monitored pressures in different nodes and flows in different pipes which are then used to estimate the network topological structure and the consequences of nodal failure.

In the works of Christodoulou and Fragiadakis (2014) and Fragiadakis et al. (2016) a methodology was presented for the seismic and hydraulic assessment of the reliability of WDNs based on general seismic assessment standards, localized historical records of critical risk-of-failure metrics, and hydraulic simulations using adapted EPANET models. Agathokleous and Christodoulou (2016) investigate the effects of IWS on the condition and breakage rate of WDN, by studying the change in the rate of occurrence of failures before, during and after IWS periods, using statistical and survival analyses. The researchers concluded that IWS practices negatively affect the vulnerability of WDNs.

2.2 Betweenness centrality (BC)

The centrality metric is the most widely used indicator for identifying important nodes of a network based on topological characteristics. Centrality is given in terms of a real valued function for each network node (vertices of a graph), and the resulting values provide a ranking which identifies the most important nodes (Bonacich 1987, Borgatti 2005). The ease in calculation of the centrality metric depends on the net-work size (number of vertices and edges), the connectivity of vertices (number of edges linked on each vertex, directed / undirected edges and connected / disconnected vertices) and the weights as-signed to the edges (Opsahl et al. 2010).

BC is an indicator for identifying the vertices of a network that have high contribution to the transfer of items within the network, and it is equal to the degree of which a vertex falls on the shortest path between the other vertices (Freeman 1977). Mathematically, the BC of a vertex, u, is defined by (Anthonisse 1971):

$$C_B(u) = \sum_{s \neq u \neq t} \frac{\sigma_{st}(u)}{\sigma_{st}} \quad (1)$$

where σ_{st} is the total number of shortest paths from vertex s to vertex t and $\sigma_{st}(u)$ is the number of those paths that pass through u.

3. ANALYSIS, RESULTS & DISCUSSION

3.1 Pipeline system of DMA6 and vulnerability during continuous water supply

The WDN in study is first analyzed topologically, with BC metrics computed for every node in

the network and geographically mapped. The result of the analysis is then spatially mapped using a weighted graph, showing the levels of the BC index across the case-study DMA (Figure 2a).

The areas of high BC values (shown in red) indicate the nodes through which a high number of origin-to-destination paths passes, when considering only the topology of the network. As expected, BC numbers are lower on the periphery of the network, and increase towards its center.

The WDN in study is then analyzed under normal (continuous water flow) operating conditions (data period before March 2008). For this, the continuous water supply (CWS) mode, the BC metrics are computed in conjunction with the underlying hydraulic model for the DMA. That is, the hydraulic model and the deduced nodal pressures and pipe water flows in essence dictate the origin-to-destination paths for every calculation and thus affect the BC computation. As with the previous case, the result of the analysis is then spatially mapped by use of a heatmap, showing the levels of the BC index across the case-study DMA (Figure 2b).

A comparison between Figures 2a and 2b shows the difference in the spatial allocation of the nodal BC indices and of the resulting network vulnerability, when the hydraulic behavior of the DMA under continuous water supply operations is considered. Now the BC values are higher along major water mains, as the deduced water flows at the nodes along these pipes create more water pathways passing through these nodes. Noteworthy is also the fact that the change in network vulnerability (Figure 2b) is actually obtained by opening/closing 9 valves (nodes) in the original network (Figure 2a). This change in vulnerability indicates the effects of hydraulics on the network performance.

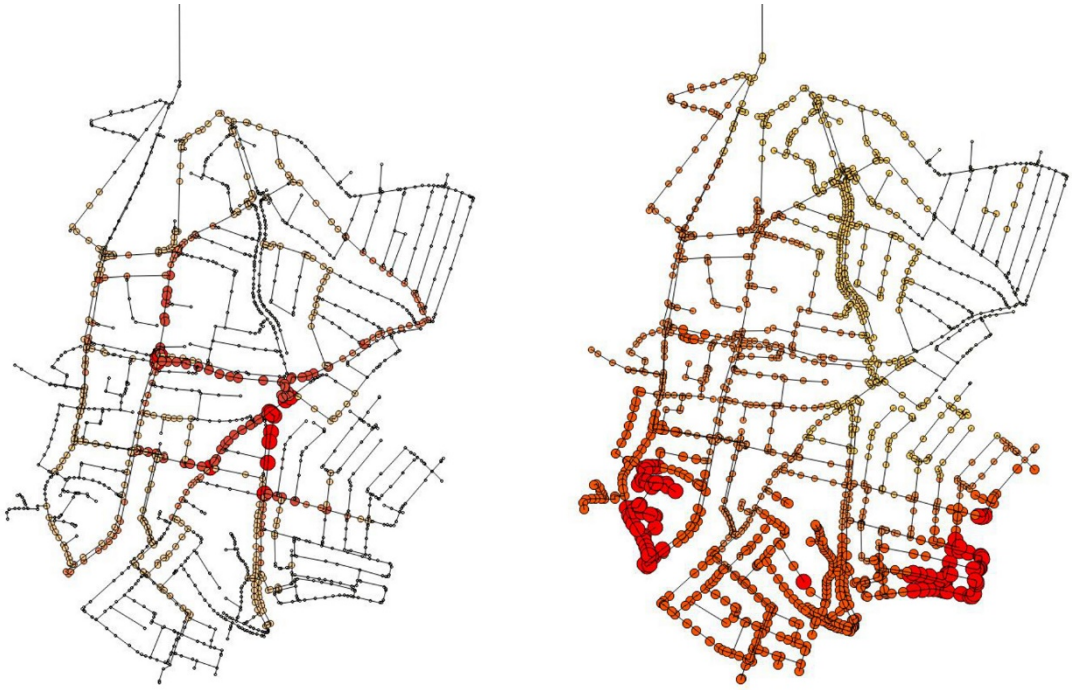

(a) *(b)*

Figure 2. Betweenness centrality weighted graph for: (a) Network topology, (b) Continuous water supply (CWS) operations.

3.2 Vulnerability heatmap of intermittent water supply (IWS)

When in abnormal operating conditions (such as IWS operations), the network in study exhibits a different behaviour, with the BC indices varying compared to the ones deduced for the CWS operations (Figure 2b). Under IWS operations (data period after March 2008), the DMA in study is subdivided into four sub-DMAs, each receiving water for 12 hours every 48 hours. During this operation mode the BC indices change, depending on which sub-DMA is active (Figure 3) and how

the varying water flow affects the water pathways and the origin-destination pairs in the network.

As with the CWS case (Figure 2b), the BC metrics are computed in conjunction with the underlying hydraulic model for the sub-DMA, and the deduced water flows in the piping network dictate the origin-to-destination paths in the network, thus affecting the computation of the nodal BC indices.

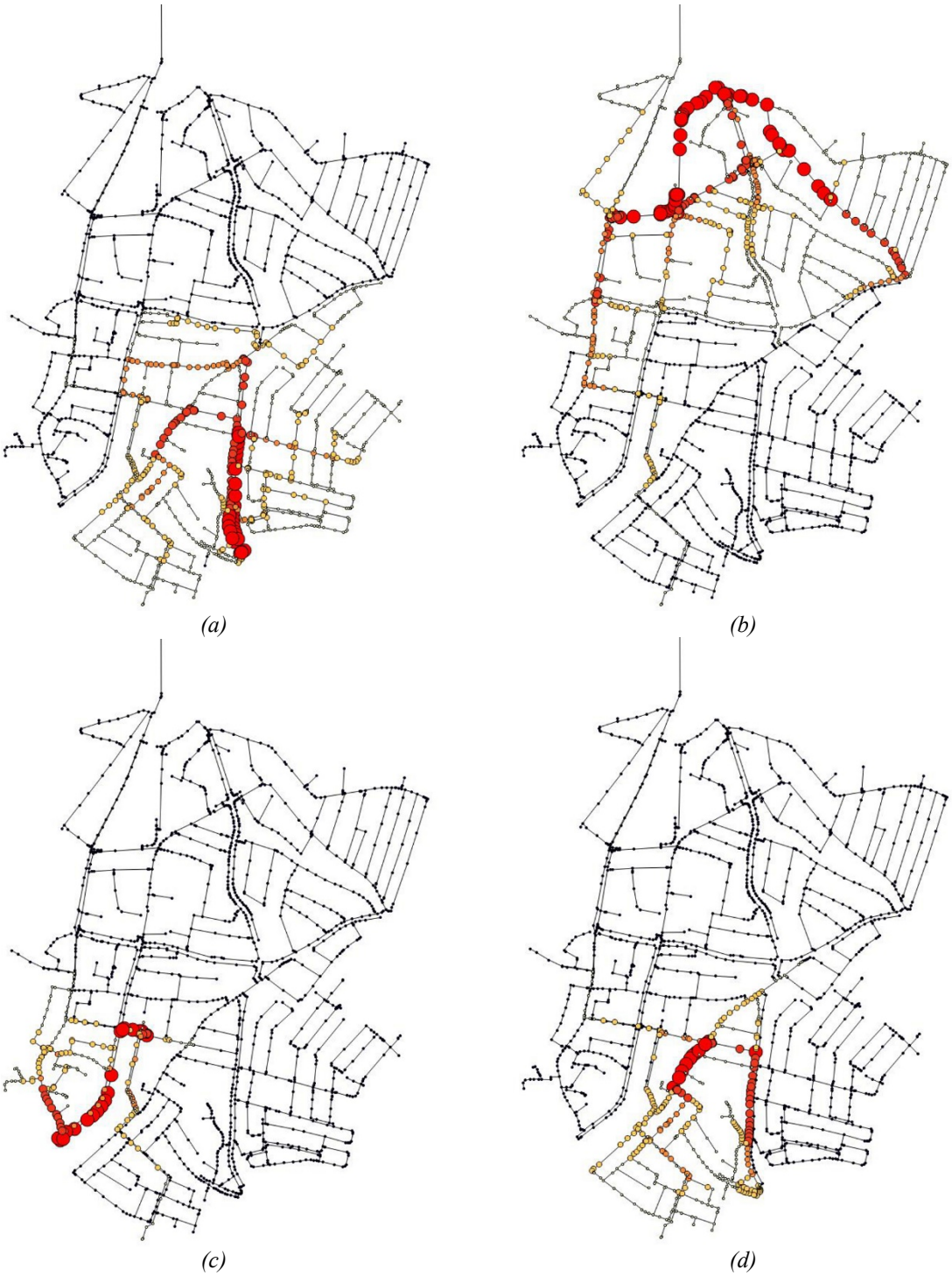

Figure 3. Betweenness centrality weighted graph for the intermittent water supply operation. (a) Sub-DMA 6A, (b) Sub-DMA 6B, (c) Sub-DMA 6C, (d) Sub-DMA 6D.

3.3 Spatial distribution of the failure incidents

The results of shifting in the BC indices as a result of the change in the water supply operations (from CWS to IWS) can be seen in Figure 4, depicting the failure incidents in the WDN in study

during the time periods of CWS and IWS. Figure 5 illustrates the heat-maps generated using the failure incidents number, presented by Figure 4.

As can be seen in Figure 5, the spatial distribution of the failure incidents changes as the mode of operations changes, and the centre of gravity shifts as the failure incidents cluster around regions of high BC indices.

This spatial shift and the observed clustering can be attributed to the 'reorganization' of the WDN, as evidenced by the BC weighted graphs, stemming from the changes in water flow/pressure across the network.



(a) (b)

Figure 4. Failure incidents (pipe breaks) in studied WDN: (a) during CWS operations (before March 2008); (b) during IWS operations (after March 2008).



(a) (b)

Figure 5. Heat-maps of failure incidents (pipe breaks) in studied WDN: (a) during CWS operations (before March 2008); (b) during IWS operations (after March 2008).

4. CONCLUSION

The work presented herein provides evidence of the links between the behavior of a WDN under varying operating conditions, the BC indices of the network's nodes, and the network's vulnerability. Given these links, WDN operators can forecast a WDN's behavior under several scenarios and plan for them, optimizing the behavior of the WDN and minimizing its vulnerability against endogenous and exogenous threats, without the need for dynamic hydraulic models. Furth research work is currently under way to link the observed fragility of a WDN with its BC characteristics, using a larger dataset (higher number of incidents, and longer time periods).

ACKNOWLEDGMENT

The work presented herein is part of research initiatives funded by the University of Cyprus's "Post-Doctoral Researchers" program. Special thanks are also extended to Nicosia's Water Board for providing operational data on its network.

REFERENCES

Agathokleous, A., 2015. Sensor-Based Sustainable Management of Urban Water Distribution Networks Utilizing Survival Analysis Modeling. Thesis (Ph. D.); University of Cyprus, Nicosia, Cyprus.

Agathokleous, A., Christodoulou, S., 2016. The Impact of Intermittent Water Supply Policies on Urban Water Distribution Networks. Proc., 2nd EWaS International Conference; Crete, Greece, 1-4 June.

Anthonisse, J., 1971. The rush in a directed graph. Technical Report BN 9/71, Stichting Mathematisch Centrum Amsterdam, Netherlands.

Aydin, N. Y., Mays, L., Schmitt, T., 2014. Sustainability Assessment of Urban Water Distribution Systems. Journal of Water Resources Management; 28(12): 4373-84.

Bonacich, P., 1987. Power and centrality: A family of measures. American Journal of Sociology; 92(5): 1170-1182.

Borgatti, S. P., 2005. Centrality and network flow. Social Networks; 27(1): 55-71.

Christodoulou, S. E., 2010. Water Network Assessment and Reliability Analysis by Use of Survival Analysis. Journal of Water Resources Management 25(4): 1229-38.

Christodoulou, S. E., Fragiadakis M., 2014. Seismic Reliability Assessment of Water Distribution Networks - Extending the ALA Guidelines. Proc., 9th IWA World Water Congress & Exhibition; Lisbon, Portugal, 21-26 September.

Fragiadakis, M., Xanthos, S., Eliades D. G., Gagatsis A., Christodoulou S. E., 2016. Graph-Based Hydraulic Vulnerability Assessment of Water Distribution Networks. Proc., Critical Information Infrastructures Security (edited by Panayiotou, C. G., Ellinas, G., Kyriakides, E., Polycarpou, M. M.); 8985:81–87.

Freeman, L. C., 1977. A set of measures of centrality based on betweenness. Sociometry; 40(1): 35-41.

Kleiner, Y., Rajani, B., 2001. Comprehensive review of structural deterioration of water mains: Statistical models. Urban Water; 3(3): 131-150.

Martínez-Rodríguez, J. B., Montalvo, I., Izquierdo, J., Pérez-García, R., 2011. Reliability and Tolerance Comparison in Water Supply Networks. Journal of Water Resources Management; 25(5): 1437-48.

Michaud, D., Apostolakis, G. E., 2006. Methodology for Ranking the Elements of Water-Supply Networks. Journal of Infrastructure Systems; 12 (4): 230-42.

Opsahl, T., Agneessens, F., Skvoretz, J., 2010. Node centrality in weighted networks: Generalizing degree and shortest paths. Social Networks; 32: 245-251.

Shuang, Q., Zhang, M., Yuan, Y., 2014. Node Vulnerability of Water Distribution Networks under Cascading Failures. Journal of Reliability Engineering & System Safety; 124: 132-41.

Proceedings of the 10th World Congress of EWRA 'Panta Rhei', 5-9 July 2017, Athens, Greece
© 2017 *European Water Resources Association*

The role of domestic rainwater harvesting systems in storm water runoff mitigation

I. Gnecco*, A. Palla and P. La Barbera
Department of Civil, Chemical and Environmental Engineering, University of Genova, Genoa, Italy
* *e-mail: ilaria.gnecco@unige.it*

Abstract: The role of Domestic Rainwater Harvesting (DRWH) systems in storm water runoff mitigation is investigated at the urban block scale by implementing a hydrologic-hydraulic model able to predict the outflow hydrographs together with the hydraulic behaviour of the DRWH at high time resolution. The hydrologic behaviour of an urban block equipped with DRWH systems has been continuously simulated over 26-years of rainfall records. The modelling is undertaken using EPA SWMM; the DRWH is implemented in the model by using a storage unit linked to the building water supply system and to the drainage network. In order to quantify the impact of DRWH systems on improving the hydrologic performance of the urban block, the peak and volume reduction are evaluated with respect the "do nothing" scenario. Although the reduction ratios are limited for exceedance rainfall events (high-intensity and short-duration), the installation of DRWH systems at the urban catchment scale contributes to satisfactory increase the hydrologic performance of the storm water drainage network. At the same time, the modelling results point out that the widespread implementation of rainwater harvesting systems at the urban catchment scale noticeably affects the quali-quantity aspects of urban water management; indeed these storage tanks contribute to reduce the use of potable water and to limit overflow discharges and drainage system failures.

Key words: rainwater harvesting; storage tank, storm water control; SWMM

1. INTRODUCTION

Rainwater Harvesting (RWH) systems are recognized as a widely accepted solution to save water in buildings. The installation of rainwater harvesting systems, as well as the use of water saving devices, are supported by the European legislation (EU, 2009). Domestic RWH (DRWH) consists of the small-scale concentration, collection, storage and use of rainwater coming from rooftops and other impervious surfaces. Rainwater can be used to replace drinking water for many uses in the house such as the flushing of toilets and the garden watering (USEPA, 2004).

RWH systems may also play an important role in mitigating the impact of urban storm water due to the increase of imperviousness in urban areas (Burns et al., 2015): according to the Low Impact Development (LID) principles and applications aimed at promoting storage, infiltration and evapotranspiration (Palla and Gnecco, 2015), RWH may contribute to increase at-source retention and detention of storm water. Then, catchment scale implementation of rainwater tanks may help to reduce frequency, volume and peaks of storm water runoff in urban drainage systems (see e.g. Palla et al., 2017).

In this framework, the main objective of this paper is to investigate the role of DRWH systems in storm water runoff mitigation at the urban block scale by implementing a hydrologic-hydraulic model able to predict the outflow hydrographs together with the hydraulic behaviour of the DRWH at high time resolution.

2. METHODS

2.1 The test description

The test site is located in the neighbourhood of Albaro (Genoa, Italy) in the eastern part of the town centre. The test site corresponds to an urban block limited on the four sides by the small road network leading into the internal lots and two/three-storey buildings. The block area is about 0.6 ha and was urbanized in the sixties with 4 buildings and a private green area. The analysis of land use data reveals that 57% of the urban block is covered with impervious surfaces and that rooftops account for 33% of the total areas.

The precipitation regime of the study area is analysed based on rain data collected at the raingauge station of Villa Cambiaso (44.3986N; 8.9633E) located in the vicinity. Rainfall data are available since 1990 with 1-minute resolution. The statistics of the annual rainfall depth as well as the rainfall-event characteristics are typical of the Mediterranean area: the average and standard deviation values of the annual rainfall depth are respectively 1340 mm and 372 mm, the rainfall-event depth and Antecedent Dry Weather Period (ADWP) are higher than 14 mm and 1.5 days, on average.

The management of storm water is separated from the sewer system and addressed according to the traditional approach; in particular the separate sewer system consists of three pipes located below the street network without any LID source control solutions (such as green roofs, permeable pavements, rainwater harvesting systems) installed in the area.

The installation of a DRWH system for each building of the urban block is here assumed as hypothetic scenario for planning and design purposes according to an integrated storm water mitigation strategy.

In each DRWH system, the roof runoff is collected in the corresponding storage tank and pumped directly to the point of use while the overflow is directly conveyed to the downstream drainage network. The water demand to be supplied by rainwater is limited to the toilet flushing and is assumed to occur at a constant daily rate. The toilet flushing demand per person is assumed of 40 l/d (UNI/TS 11445, 2012).

In the present test site, the tanks are designed according to the simplified method as indicated in the Italian guideline UNI/TS 11445 (2012). This method is based on the evaluation of two terms: the annual inflow, Q, and the annual rain water demand, D. In particular, the annual inflow is evaluated by multiplying the collected area with the annual runoff depth and the latter is determined by multiplying the annual rainfall depth with the discharge coefficient of the corresponding collected area equal to 0.8 for a pitched roof. The storage volume of the tank is then assumed as the 6% of the minimum value between the inflow and the water demand on annual basis.

In order to define the water demand conditions in the selected urban block, and consequently to design the proposed DRWH systems a survey was carried out in May 2016 to investigate the actual number inhabitants for each building. Based on the survey, the four buildings are classified as 4-flat house (2 units), 6-flat house (1 unit) and condominium (1 unit) characterized, respectively, by the following numbers of inhabitants of 16, 24 and 32.

In Table 1, the main characteristics of each building in terms of roof area and number of inhabitants are reported together with the main characteristics of each DRWH system including the annual rain water demand, the demand fraction (D/Q), the tank capacity (S) and the storage fraction (S/Q). Note that the demand and storage fractions are dimensionless indexes that allow comparing the performance of different RWH systems (Palla et al., 2011).

2.2 The DRWHS modelling and performance indexes

The hydrologic-hydraulic modelling is undertaken using EPA SWMM 5.1.007 (Rossman, 2010).

In the present study, the DRWH systems are simulated in SWMM as hydraulic nodes using the *storage unit* objects. The inflow of the storage unit is the subcatchment outflow connected to the DRWH system. The storage outflows consist in the rainwater supply and the overflow that are implemented respectively as a pump linked to the building water supply and a weir section linked to the drainage network. Note that the building water supply system is schematized by an outfall section. In order to reproduce the daily rainwater-demand pattern, specific control rules (clock time rules) are defined to activate the pumps.

Table 2. Main characteristics of the building (number of inhabitants, roof area) and DRWH system (annual water demand, demand fraction, tank capacity, storage fraction) for the three typologies of residential units

	Inhabitant number (-)	**Roof area (m^2)**	**Annual water demand (m^3/y)**	**Demand fraction (-)**	**Tank capacity (m^3)**	**Storage fraction (-)**
4-flat house	16	420	234	0.51	14	0.03
6-flat house	24	420	350	0.77	21	0.05
Condominium	32	680	467	0.64	28	0.04

The study area in the current configuration ("do nothing scenario") is implemented in the model by means of 12 subcatchments, 6 junctions, 6 conduits and 1 outfall. The subcatchments are characterized by single land use type and homogenous properties according to the required high-spatial discretization. Compared to the current condition, the DRWH scenario includes 4 storage units (1 for each building), 4 weirs (1 for each tank), 8 pumps (2 for each DRWH), and 4 outfalls representing the water-supply system in the buildings. The geometry of each tank is designed according with the available surface area in the vicinity of the building and by considering an effective water depth in the tank of 2 m. Further details on the model configuration are provided elsewhere (Palla et al., 2017).

Finally, the modelling scenarios (relating to the "do nothing" and DRWH configurations) concern continuous simulation performed over 26-years at 1-minute time interval; as for the initial condition of the DRWH systems, the tanks are assumed initially empty as is generally recommended (Mitchell, 2007).

In order to assess the role of DRWH systems in storm water runoff mitigation two hydrologic performance indexes are defined: the peak and volume reduction rates, namely *PR* and *VR*, respectively. The hydrologic performance indexes are evaluated at the event scale. For each rainfall event, the peak reduction is calculated as the relative percentage difference between the outflow peaks of the "do nothing" and DRWH scenarios; the volume reduction is similarly evaluated.

3. RESULTS

3.1 The system performance

The system performance is evaluated with respect to the entire simulation period by means of two dimensionless indexes commonly used in the literature (e.g. Palla et al., 2011): the water saving efficiency and the rainwater overflow ratio.

Figure 1 reports the water saving efficiency and overflow ratio for the three typologies of residential buildings. Results highlights excellent performance in terms of water saving efficiency whose value is almost equal to 0.8 in all cases. Further, it can be noticed that the water saving efficiency value slightly increases with the increasing of the corresponding *D/Q* (or *S/Q*), since in the present study case *S/Q* corresponds to the 6% of the *D/Q* according to the simplified method of the Italian guidelines. The opposite behaviour is observed for the overflow ratio values that decrease from 0.66 to 0.59.

3.2 The hydrologic performance

Results of the continuous simulation (26-year long) provide a fully characterization of the hydrologic-hydraulic behaviour of the investigated catchment together with each DRWH system (i.e. the water depth in the tank, the supplied rainwater discharge, the inflow and the overflow rates) at 1-minute time resolution. Based on the simulation results, it emerges that the mean values of peak (*PR*) and volume (*VR*) reduction rates, evaluated for the 2125 rainfall events, are respectively equal to 0.33 and 0.26, while the maximum values are 0.65 for peak and 0.51 for volume.

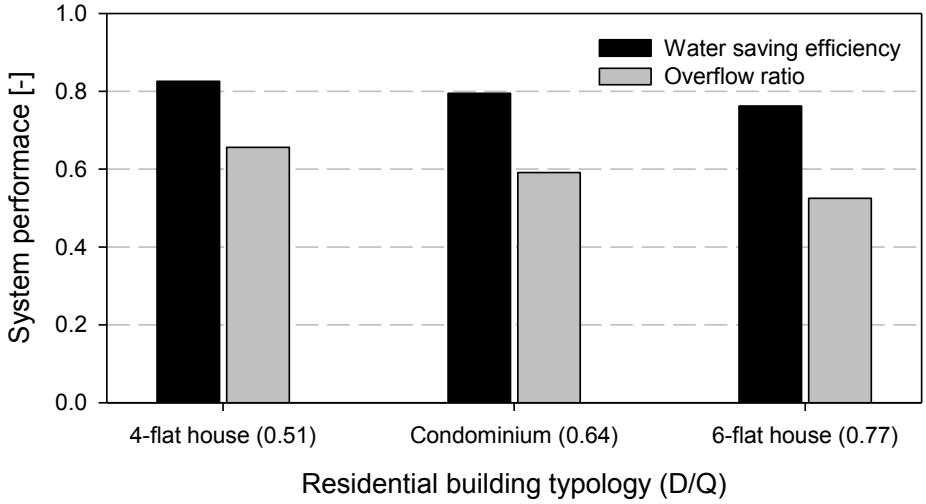

Figure 1. The water saving efficiency and overflow ratio for the three typologies residential buildings.

As an example, Figure 2 illustrates the hydrologic response of the urban block simulated for three rainfall events: the 20 September 2002, the 6 December 2006 and the 4 November 2011 events, respectively. In detail, each graph reports the hyetograph and the corresponding hydrographs simulated for the reference and the DRWH scenarios. The selected rainfall events differ in terms of rainfall event features thus resulting in different hydrologic performance at the catchment scales, in order to provide a picture of the impact of DRWH systems on the urban block hydrologic response. The 20 September 2002 rainfall event (see Figure 2) is characterized by a total rainfall depth and duration respectively of 52.6 mm and 1 h (2-year return period event) while the maximum rainfall intensity over 10 minutes is 146 mm/h (5-year return period event) and the ADWP is 18 hours. Being classified among the medium-to-high-frequency event, the DRWH systems contribute significantly to improve the hydrologic performance of the urban block thus resulting in *VR* of 0.205 and *PR* of 0.341. The 6 December 2006 rainfall event (see Figure 2) is characterized by a total rainfall depth and duration respectively of 60.6 mm and 3.2 h (less than 2-year return period event) while the maximum rainfall intensity over 10 minutes is 104 mm/h (2-year return period event) and the ADWP is less than 2 hours. Due to the limited ADWP the volume reduction is limited (*VR* = 0.011), on the contrary, the storage tanks are effective on the peak reduction (*PR* = 0.092). Finally, the 4 November 2011 rainfall event (see Figure 2) is characterized by a total rainfall depth and duration respectively of 301 mm and 8.4 h (300-year return period event) while the maximum rainfall intensity over 10 minutes is 191 mm/h (15-year return period event). Such event is included among the flash flood events occurring in Genoa (Italy), thus it is expected that any source control system such as DRWH tank, is ineffective in mitigate the catchment hydrologic response (*VR* = 0.002 and *PR* = 0.009).

Aiming at pointing out the influence of precipitation regime, the 2125 rainfall events are classified based on the following characteristics on event basis: the rainfall depth, the maximum rainfall intensity over 10 minutes (corresponding to the time of concentration of the urban block) and the ADWP. In particular, five classes characterised by a constant frequency of about 0.2 are defined.

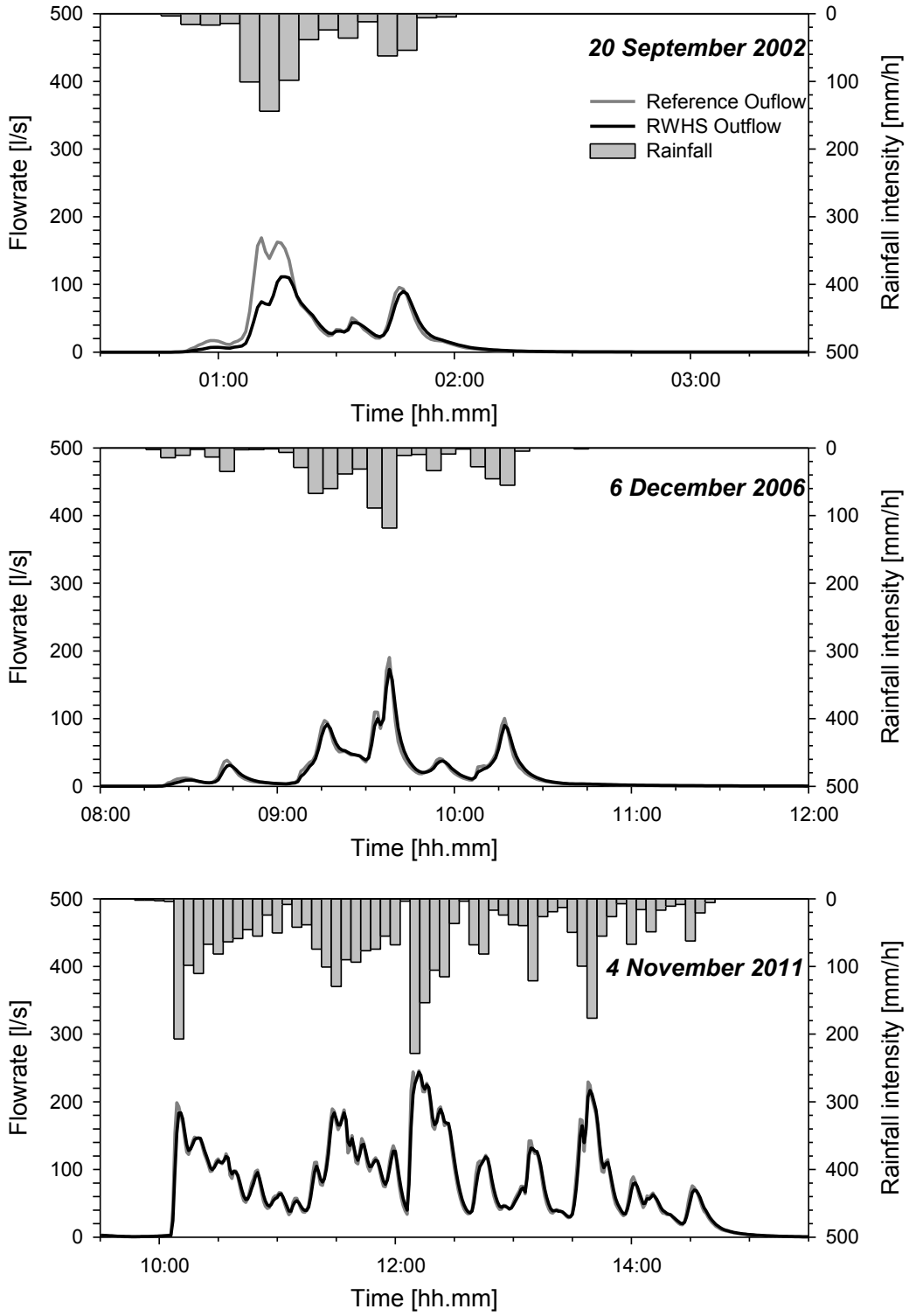

Figure 2. The hyetograph, the corresponding hydrographs simulated for the reference and the DRWH scenarios are plotted for three rainfall events (the 20 September 2002,the 6 December 2006, and the 4 November 2011 events).

Figure 3 shows the non-parametric distribution of the volume (hatched box) and peak (grey box) reduction rates for each class of the investigated rainfall event characteristics: ADWP (a); depth (a); maximum intensity over 10 minutes. Looking at data reported in Figure 3, it clearly emerges that high values of the ADWP (greater than 42 hours) reveal the highest performance both in terms of peak and volume reduction rate respectively equal to 0.5 and 0.4, on average. Indeed in such cases, the status of the DRWH tanks (only partially full) contributes to enhance the storm water runoff mitigation. Results confirm that for rainfall events with total depth exceeding 20 mm, the hydrologic performance decreases below 0.2 (in terms of both the median and mean values).

Focusing on rainfall intensity, events characterized by the maximum rainfall intensity under 25 mm/h show that the hydrologic performance ranges between 0.25 and 0.35 while it slightly decreases for high-intensity event.

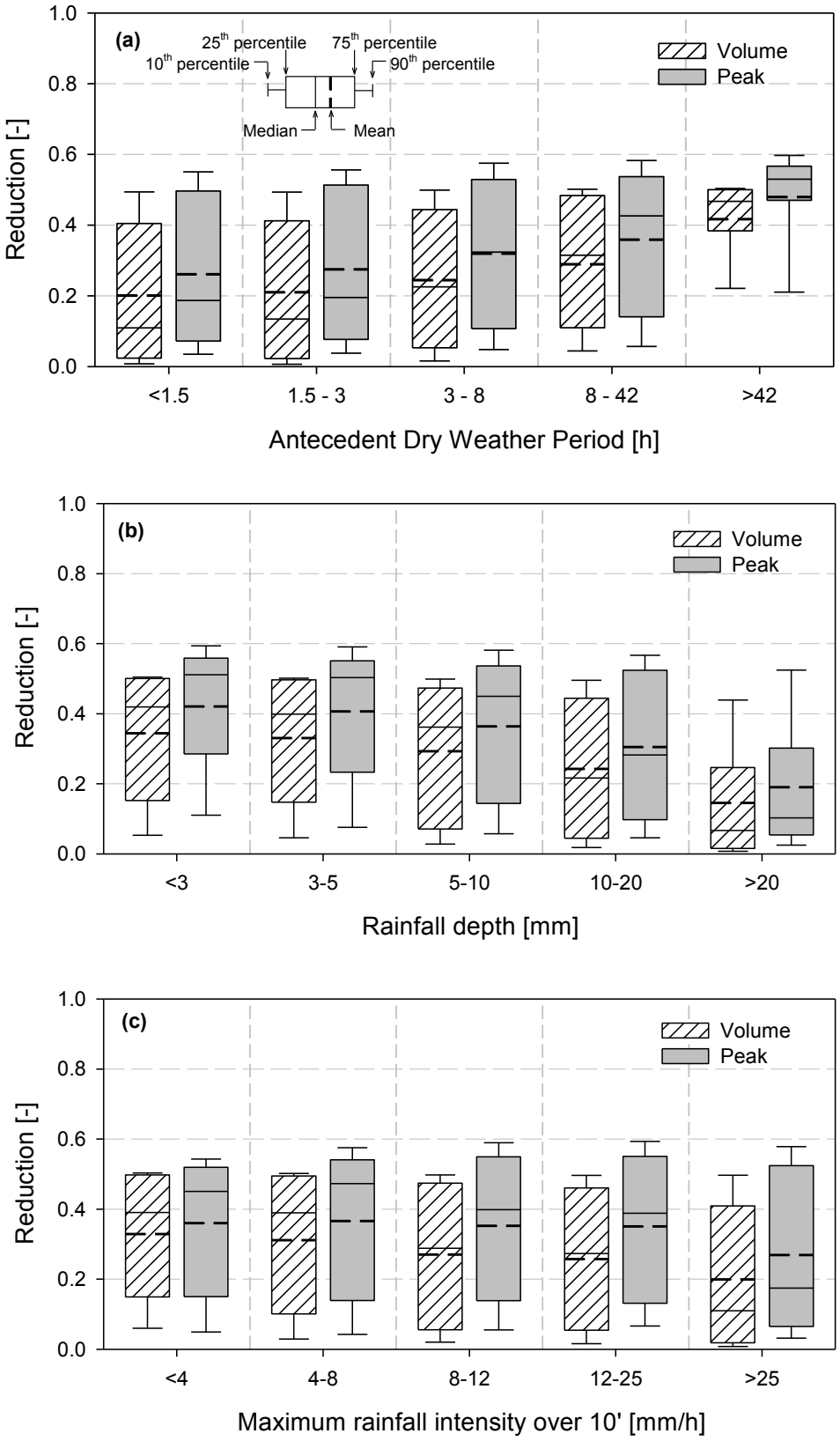

Figure 3. Box-plots of the volume (hatched box) and peak (grey box) reduction rate with respect to the following rainfall event characteristics: antecedent dry weather period (a); depth (a); maximum intensity over 10 minutes.

4. CONCLUSIONS

The hydrologic behaviour of the investigated urban block equipped with DRWH systems has been continuously simulated over 26-years of rainfall records using the EPA SWMM model. In order to quantify the impact of the DRWH systems on improving the hydrologic performance of the urban block, the peak and volume reduction are evaluated on event-basis with respect the “do nothing” scenario. Simulation results point out that the peak and volume reduction rate evaluated for the 2125 rainfall events are respectively equal to 0.33 and 0.26, on average. With reference to the influence of precipitation regime, ADWP greater than 42 hours are associated to the highest hydrologic performance (on average) while the rainfall depth seems to limit the hydrologic performance at least when the total depth exceeds 20 mm.

The present results point out that the widespread implementation of rainwater harvesting systems at the urban catchment scale noticeably affects the quali-quantity aspects of urban water management. In detail, the DRWH systems operate as source control solutions thus contributing to limit overflow discharges and drainage system failures; reducing the amount of runoff volume that need to be treated before discharging into the receiving water bodies and finally diminishing the use of potable water.

REFERENCES

Burns, M.J., Fletcher, T.D., Duncan, H.P., Hatt, B.E., Ladson, A.R., Walsh, C.J. 2015. The performance of rainwater tanks for stormwater retention and water supply at the household scale: an empirical study. Hydrol. Process. 29: 152–160.

Campisano, A., Gnecco, I., Modica, C., Palla, A. 2013. Designing domestic rainwater harvesting systems under different climatic regimes in Italy. Water Sci. Technol. 67: 2511-2518.

European Commision. 2009. Study on water performance of buildings. Reference report 070307/2008/520703/ETU/D2.

Mitchell, V.G. 2007. How important is the selection of computational analysis method to the accuracy of rainwater tank behaviour modelling? Hydrol. Process. 21: 2850-2861.

Palla, A., Gnecco, I., La Barbera, P. 2017. The impact of domestic rainwater harvesting systems in storm water runoff mitigation at the urban block scale. J. Environ. Manage. 191:297-305.

Palla, A., Gnecco, I. 2015. Hydrologic modeling of Low Impact Development systems at the urban catchment scale. J. Hydrol. 528: 361-368.

Palla, A., Gnecco, I., Lanza, L.G. 2011. Non-dimensional design parameters and performance assessment of rainwater harvesting systems. J. Hydrol. 401: 65-76.

UNI/TS 11445. 2012. Rainwater harvesting systems for non-potable uses. Design, installation and maintenance, UNI Ente Italiano di Unificazione, (In Italian).

USEPA. 2004. Guidelines for Water Reuse, EPA Report 625-R-04-108, US Environmental Protection Agency, Washington, DC, USA.

Proceedings of the 10th World Congress of EWRA 'Panta Rhei', 5-9 July 2017, Athens, Greece
© 2017 *European Water Resources Association*

Water efficiency indicators studies and energy applied to real water distribution system of south of Minas Gerais - Brazil

F.G.B. Silva*, F.R. Soares, M.R. Andrade and D.O. Sant´Ana
NUMMARH, Institute of Water Resources – IRN, UNIFEI – Federal University of Itajubá, Brasil
* *e-mail: ffbraga.silva@gmail.com*

Abstract: The indicators applied to water distribution systems help in its diagnosis and support the management actions. Hydraulic and energy-related indicators can relate energy consumption, input flow, pressures and demand to identify systems and tools to minimize energy costs and maximize hydraulic reliability. This study was carried out in a real system, in a city of the south of Minas Gerais, Brazil. With the available data, the main water and energy efficiency indicators were calculated based on Alegre al. (2014). Among those main parameters, the value of PH4 - Utilization of pumping capacity, 98.4%, Op23 - Water losses per branch, 55.90 m³ / branch /year, Op 24 - Water losses per pipeline length, 8.57 m³ / km Of conduit/days. Op26 - Apparent water volume loss at system entry, 0.65%. The results indicate that the system as a whole has a reasonable behavior compared to other case studies regarding water and energy efficiency.

Key words: Water Distribution Systems, Indicator, Leakage, efficiency hydric

1. INTRODUCTION

Around the world, water and energy crises have recently taken place in the national and international media. The subject is important and worrying because it is two basic elements of the daily life of the population, water, and energy.

In this work, the focus is the water distribution systems losses at and the pumping stations energy, we will relate are mainly due to the existing losses and the inadequate operation, involving control of pressure levels, pump operation among others factors.

The method used is the study of the network either by visiting the sanitation companies or by hydraulic and electrical measurements parameters, thus generating some indicators for a better understanding and diagnosis of the system.

The author´s calculated important indicators for a better hydroelectric management of the sector under study taking into account the measures of flow, pressure, level, elevation of altimetry and electricity consumed.

Indicators are important tools that in the case of its application in water distribution systems have large applicability since they can diagnose systems and compare it with others. This allows managers to find problems and set up changes that can allow the water and energy best uses and so financial gains.

We will study in water distribution system of a mountainous city in the south of Minas Gerais, Brazil.

The indicators made calculated in the literature. However, some authors stand out in the field of study.

According to Alegre, et. al. (2004), the performance indicator (ID) is an instrument commonly used to test water distribution parameters at companies. His work specifies various indicators, wich highlighting the following items:

a) Indicators of water resources, Human resources indicators, Infrastructure indicators, Operational indicators, Service Quality Indicators , Economic and Financial Performance Indicators.

b) Another important and current document on Brazilian studied indicators was the SNIS (2015), which presents an extensive range of information and indicators capable of providing a comprehensive view to get consistent assessments of service performance across the country.

Cabrera, et. Al. 2010 proposed work on the water balance and the energy-water in water distribution system. The analysis allowed us to represent all the energy of the system, which shows the importance the energy balance. This balance aims to get performance indicators and test the system from the energy point of view, thus identifying improvement actions to improve the efficiency of the system.

Vilanova, MRN (2012) presented work which had the initiative to develop a set of indicators of hydraulic and energy efficiency, allowing to compare the current situation of an optimal condition system, referring to components, physical and operational, more relevant in the hydraulic and energy context. The best condition to give the lowest energy and water consumption, taking into account the limits and operational requirements of the studied system. In this context, it four indicators were proposed: optimum pumping operation indicator, hydraulic energy recovery indicator, available hydraulic load indicator and water efficiency indicator.

2. METHODOLOGY

With the choice of the municipality in a study developed a partnership. With the help of professionals from the water supply company, he defined a target sector, whose main need is the sectorization.

Propose the following studies from here:

- Determination of topographic dimensions using GPS equipment;
- Obtaining flow data using ultrasonic flowmeters;
- Compression data;
- Survey of the energy data of the pumps.

For this, before the field work, several trainings were carried out with the GPS equipment, flow and pressure meters, besides their calibrations and laboratory measurements.

Figure 1 illustrates the work done. Step 1 begins with the search for cities with the desired profile, where the company of interest forms a partnership and its place was near the region South of Minas Gerais, Brasil. In step 2, the longest and most laborious; Develops several trainings with the equipment. Also in this step he collected the field data. In step 3, the analysis of data from the field campaigns took place, as well as the establishment of indicators with their respective calculations.

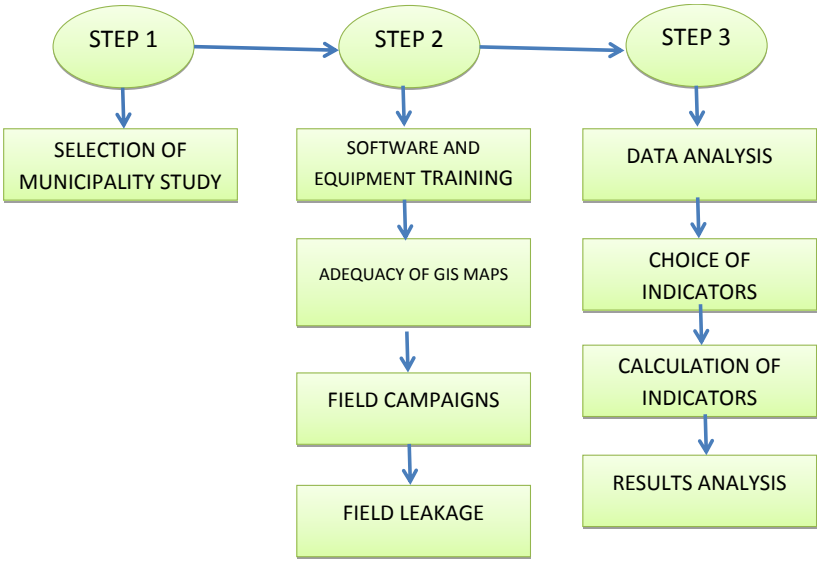

Figure 1. Workflow of work (Adapt Soares, 2016)

The Figure 2 (Goulart, 2015), generated through the EPANET program, express well-defined topographic zones and help define nodes to receive the pressure meters. The node choices were important because they were low, medium and high-pressure regions.

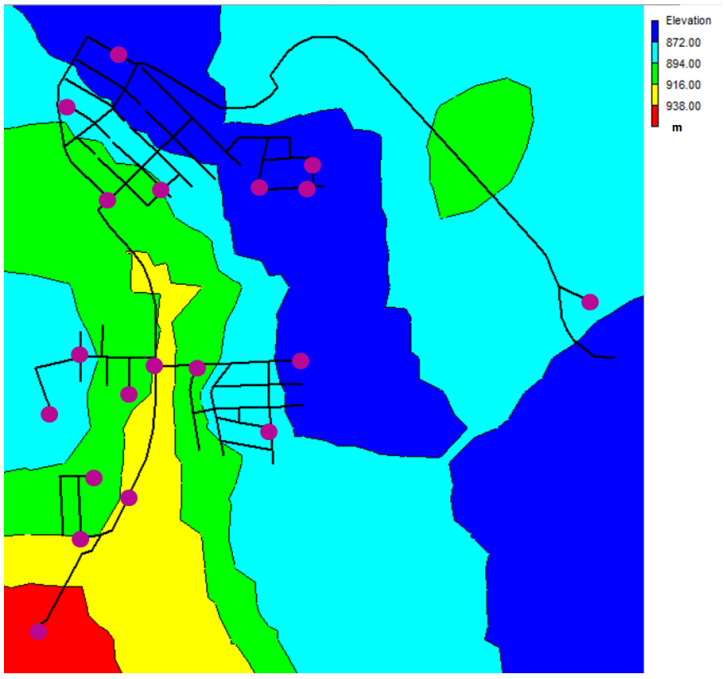

Figure 2. Location of the nodes of the houses that received the pressure gauges, Goulart, T. D. C. (2015)

2.1 Indicators choices

Evaluating the current literature, made an analysis to choose the indicators used. Alegre et. al. (2004) was the main reference consulted and shows several existing indicators and method of calculation.

The focus indicators of this work follow:

A) Ph4 - Pumping capacity utilization (%).

B) Ph5 - Standard energy consumption (kWh / m³ / 100m).

C) Ph6 - Reactive energy consumption (%).
D) Ph8 - Valve density (n / km).
E) Ph 14 - Automation Degree (%).
F) Ph15 - Remote control Degree (%).
G) WR1 - Use of water resources inefficiency (%).
H) Op23 - Water losses per branch (m³ / branch / year).
I) Op 24 - Water losses per pipeline length (m³ / km / day).
J) Op26 - Apparent water volume loss at system entry (%).
K) Op 27 - Actual losses per branch (l / branch / day).
L) Op 28 - Losses by length of conduit (l / km of conduit/day).
M) Op29 - Leakage infrastructure indicator.
N) Fi46 - Financial indicator of water not billed in terms of volume (%)
O) Op39 - Water indicator not measured (%).
P) Minimum loss indicator (l / extension / day).

3. RESULTS

A) Ph4 - Utilization of pumping capacity (%).

Figure 3 it is possible to observe the values of the daily consumption in kWh referring to the pumps of the reservoir R3, during the week of the field campaign. The ordinate chart represents consumed energy.

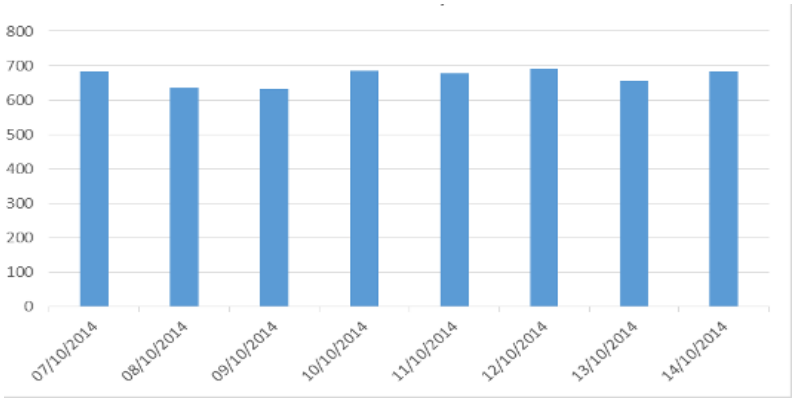

Figure 3. Daily energy consumption, with a maximum consumption of 683,297 kWh on 12/10/2014 (Soares, 2016)

Figure 4 shows the power in kW used by the pumps of the reservoir. In ordinate present power demand in KW.

The two charts are of high relevance, as its shows the pump consumptions, values used to calculate the Ph4 indicator.

$$Ph\ 4 = D\ 2 / (C\ 7 \times 24) \times 100 \quad (1)$$

D2 - Maximum daily energy consumption for pumping (kWh)), ie the number of hours of engine operation on the day of greatest energy consumption during the reference period X nominal power.

D2 = 683,297 kWh x 28,55% (value proportional to the sector).

D2 = 195.08 kWh.

C7 - Maximum pumping capacity of lifting stations (kW).

C7 = 28.77 kW x 28.55% (value proportional to the sector).

C7 = 8.21 kW.

Ph4 = 98.9%.

Thus, it was concluded that 98.9% of the pumping capacity was used on the day of greatest energy consumption.

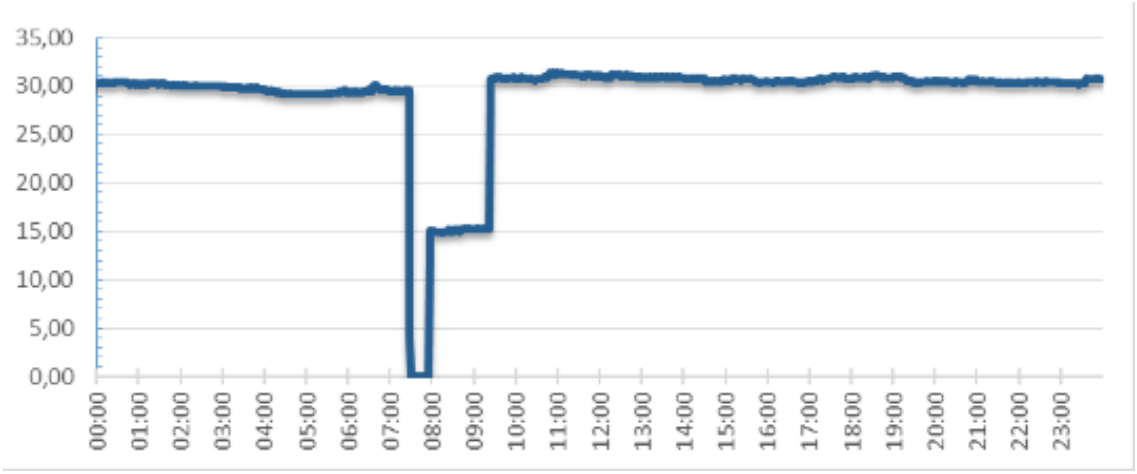

Figure 4. Curve giving an average power of 28.77 kW. (Soares,2016)

B) Ph5 - Standard energy consumption (kWh / m³ / 100m)

$$Ph5 = D1 / D3 \quad (2)$$

D1 - Energy consumption in pumping.

D3 - Uniformity factor (m³x100m) ie the volume pumped in the period x gauge height / 100.

H - Total lifting height (gauge) of the system [m].

D3 = 54,39 x 125,43 / 100 = 68,22 (m³x100m).

Ph5 = 0,40 kWh/m³/100 m.

C) Ph6 - Consumption of reactive energy

$$Ph6 = D4 / D1 \times 100 \quad (3)$$

D1 - Energy consumption in pumping.

The average reactive energy consumption measured by the contracted company was 33401,702 kVar / min or 2004102,12 kVar / hour

D4 - Consumption of reactive energy, according to contracted company was on the average equal to 5780,22 kVar.

D1 - Energy consumption for pumping at the lift station. 655 kWh.

where kWh and kVar are equivalent and their admission ratio.

Ph 6 = 30.59%.

The result of Ph6 by more than 30% shows that the excessive spending of this reactive energy increases the energy invoice at the end of the month, generating a considerable financial loss.

D) Ph8 - Valve density (n / km)

$$Ph8 = C22 / C9 \quad (4)$$

C22 - Sectional valves. 8 records.

C9 - Length of distribution network (km). 8,698 km.

Ph8 = 8.698 / 8 = 1.08 records per km.
This indicator verifies the ability to isolate a sector if it needs to intervene in the network.

E) Ph 14 - Automation degree (%)

$$Ph14 = C16 / C15 \times 100 \quad (5)$$

C15 - Control unit. 2 units.
C16 - Unit with automatic control. 2 units.
Ph14 = 100%. That is, the sector was fully automated.

F) Ph15 - Remote control rating (%)

$$Ph15 = C17 / C15 \times 100 \quad (6)$$

C15 - Control unit. 2 units.
C17 - Unit with remote control. 0 units.
Ph15 = 0%. That is, there is no system-wide remote control in the industry that would help monitor the real-time industry.

G) WR1 - Use of water resources inefficiency

$$WR1 = A19 / A3 \times 100 \quad (7)$$

A19 - Actual losses (m³). 26599,61 m³ / year.
A3 - Water in the system inlet (m³). 95795,61 m³ / year.
WR1 = 27.77%.
This indicator reveals the inefficiency in the use of water resources in the sector under study, which was around 27.77%.

H) Op23 - Water losses per branch (m³ / branch / year)

$$Op23 = (A15 \times 365 / H1) / C24 \quad (8)$$

A15 - Water losses (m³). 27225.18 m³ / year = 74.59 m³.
C24 - Number of extensions (nº) .487 extensions.
H1 - Reference period (day).
Op23 = 55.90 m³ / branch / year.

I) Op 24 - Water losses per pipeline length (m³ / km / day)

$$Op24 = (A15 / H1) / C8 \quad (9)$$

A15 - Water losses (m³). 27225.18 m³ / year = 74.59 m³.
C8 - Length of the conduits (Km). 8,698 km.
H1 - Reference period (day).
Op24 = 8.57 m³ / km of conduit / day.

According to Alegre et. al (2014) this indicator is applied because it has a density of extensions greater than 20 / Km (in this case they gave 56 extensions per Km).

J) Op26 - Apparent water volume loss at system entry (%)

$$Op26 = A18 / A3 \times 100 \quad (10)$$

A3 - Water at the system inlet (m³). 95795,61 m³ / year.
A18 - Apparent losses (m³). 625.87 m³ / year.
Op26 = 0.65%.

K) Op 27 - Actual losses per branch (l / branch / day)

$$Op27 = A19 \times 1000 / (C24 \times H2 / 24) \quad (11)$$

A19 - Actual losses (m³). 26599.31 m³ / year = 72.87 m³ / day.
C24 - number of extensions (number). 487 extensions.
H2 - System pressurizing time. Same as 24 h.
Op27 = 149.63 l / extension / day.

L) Op 28 - Losses by length of conduit (l / km of conduit / day)

$$Op28 = A19 \times 1000 / C8 \times H2 / 24 \quad (12)$$

A19 - Actual losses (m³). 26599.31 m³ / year = 72.87 m³ / day.
C8 - Length of the conduit. 8,698 km.
H2 - System pressurizing time. Same as 24 h.
Op28 = 8377.80 l / km of conduit / day.

According to Alegre et. al. (2004), this indicator does not apply because it has a density of extensions greater than 20 / Km (in this case they gave 56 extensions per Km).

M) Op29 - Leakage infrastructure indicator

$$Op29 = Op27 / (18 \times C8 / C24 + 0.7 + 0.025 \times C25) / (D34 / 10) \quad (13)$$

Op27 - Actual losses per branch. 149.63 l / extension / day.
C8 - Length of conduits. 8,698 km.
C24 - Number of extensions. 487 extensions.
C25 - Average length of extensions. 4m (estimated).
D34 - Average operating pressure. 31.3 mca = 306.76 kPa.
Op29 = 4.36
Well maintained systems tend to have values close to 1.

N) Fi46 - Financial indicator of water not billed in terms of volume

$$Fi46 = A21 / A3 \times 100 \quad (14)$$

A3 - Water in the system inlet. 95795,61m³ / year
A21 - Unbilled water. (2016). 27,225.18 m³ / year
Fi46 = 28.42%
That is, 28.42% is the volume of unbilled water.

O) Op39 - Water indicator not measured

$$Op39 = (A3-A8-A11) / A3 \times 100 \quad (15)$$

A3 - Water in the system inlet. 95795,61m³ / year.
A8 - Billed consumption measured. 68570,43 m³ / year.
A11 - Unbilled consumption measured. 0.
Op39 = 28.4

4. CONCLUSIONS

In this paper performance indicators of water distribution systems. The application studied a city in the southern of Minas Gerais, Brazil. This city is within the research of NUMMARH - Nucleus of Simulation Modeling in Environment and Hydric Resources of the Federal University of Itajubá, Brazil. The indicators applied to a real system used as main reference the work of Alegre et. The main conclusion of this work is the usefulness of this tool as a method to analyze the behavior of different systems. Because the indicators studied provided much information on the hydraulic structure under study. The NUMMARH group is currently studying other cities and intends to propose new indicators in future studies.

ACKNOWLEDGMENTS

The paper authors thanks FAPEMIG - Foundation for Research Support of Minas Gerais for the support in particular to the PPM Project - Researcher of Minas Gerais, in particular to PPM 00755-16 and the Brazilian Ministry of Science and Technology for the *REDECOPE FINEP* Project. Ref. 0983/10 -"Development of Efficient Technologies for Hydroenergetic Management in Water Supply Systems"

REFERENCES

Alegre, H., Hirner, W., Baptista, J. M. e Parena, R. 2004. “Performance indicator for water supply services” – IWA (series technical guides).

Cabrera, E.; Pardo, M. A.; Cobacho, R.; Cabrera Jr, E.. 2010. Energy Audit of Water Networks. Journal of Water Resources Planning and Management. V. 136, pp. 669-677. .

Goulart, T. D. C. 2015. "Enhancement Studies of Calibration Model Employing Genetic Algorithm and Application in Water Distribution Network of Cambui (MG)". UNIFEI-MG.

Hernández, E.; Pardo, M.A.; Cabrera, E.; Cobacho, R..2010. Energy assessment of water networks, a case study. Water Distribution System Analysis. Tucson, Arizona, EUA. Setembro, 2010.

SNIS. 2015. “National sanitation information system” www.snis.gov.br

Soares, F. R. 2016 Comparative study of the energy hydro efficiency indicators in water distribution systems - analysis of municipal municipalities of the south of minas gerais.

Vilanova, M. R. N.2012. "Development and evaluation of hydraulic and energy efficiency indicators for water supply systems as a tool to support decision making". 2012. 316 f. Thesis (Ph.D. in Mechanical Engineering) - Faculty of Engineering of Guaratinguetá, Paulista State University, Guaratinguetá.

Proceedings of the 10th World Congress of EWRA 'Panta Rhei', 5-9 July 2017, Athens, Greece
© 2017 *European Water Resources Association*

Relationship between Hazen-William coefficient and Colebrook-White friction factor: Application in water network analysis

M. Niazkar[1], N. Talebbeydokhti[2] and S.H. Afzali[3*]
[1] *Department of Civil and Environmental Engineering, Shiraz University, Shiraz, Iran*
[2] *School of Engineering, Department of Civil and Environmental Engineering, Head of Environmental Research and Sustainable Development Center, Shiraz University, Shiraz, Iran*
[3] *School of Engineering, Department of Civil and Environmental Engineering, Shiraz University, Shiraz, Iran,*
[*] *e-mail: afzali@shirazu.ac.ir*

Abstract: Although Darcy-Weisbach (D-W) equation has been accepted as a standard resistance equation in pressurized flow, some researchers and engineers still prefer to utilize Hazen-Williams (H-W) equation for analyzing water distribution networks (WDNs) in practice. The main difference between roughness coefficients of these two resistance equations is that D-W friction factor varies with Reynolds number of flow field while H-W coefficient is usually considered as a fixed value for a specific material. In this paper, discrepancies between solving three pipe networks using these two resistance equations are investigated. These networks were solved using two hydraulic solver named gradient algorithm and finite element method assuming different values for roughness values. In order to compare the results, equivalent friction factors based on these two resistance equations were required to be used. In this regard, several methods for computing equivalent roughness values were selected from the literature. The first category uses Reynolds number and pipe diameter data for converting D-W friction factor to H-W coefficients and vice versa. On the other hand, the second one is exclusively a function of pipe diameter. The obtained results demonstrate that errors of solving networks with H-W coefficients are not significant in comparison with the results obtained by the D-W equation. More importantly, the method, which only exploits pipe diameter for roughness conversion, is appeared to be not reliable for some cases considered in this paper.

Key words: Resistance equation, Darcy-Weisbach friction factor, Hazen-William coefficient, water distribution system, turbulent flows

1. INTRODUCTION

Hazen-William (H-W) and Darcy-Weisbach (D-W) formulas are two of the most common resistance equations in pressurized flow. Although the application of the former one is quite widespread in practice, especially in United States, the latter one has much more reasonable background and acceptability in academic literature (Travis and Mays, 2007; Elhay and Simpson, 2011). The empirical H-W equation utilizes a crisp coefficient (C_{HW}) for each type of pipe material. However, the friction factor (f) of the dimensionally-consistent D-W equation is a function of material properties (absolute roughness, ε) and Reynolds number (Re) in turbulent flows, the most common flow regime in water networks. In spite of numerous applications of these resistance equations in water distribution network (WDN) problems, only a few studies investigated the accuracy of such applications (Lion, 1998; Christensen et al., 2000; Bombardelli and Garcıa, 2003; Uribe et al., 2015). In this regard, much more studies are required to be conducted focusing on the application of these crucial equations and also relationships between C-W and D-W equations in pipe network analysis.

In this paper, the discrepancies between solving three sample pipe networks using these two resistance equations are investigated. Moreover, the performance of different available relationships between C_{HW} and f in analyzing water networks are studied. These analyses are conducted in the whole range where the C-W equation is valid. Furthermore, two different hydraulic solvers are utilized to determine the performance of different relations for WDN analysis. The results overall indicate that application of C-W equation and the relationships converting C_{HW} to f, which considers

both pipe diameter and Reynolds for conversion, yield to closer results to when D-W friction factor is used. Moreover, C-W equation with relationship converting to D-W friction factor, which exclusively takes into account pipe diameter for the conversion, should be used with more caution.

2. RELATIONSHIPS BETWEEN H-W AND D-W COEFFICIENTS

The H-W and D-W resistance equations relate head loss (h_L) of a typical flow through an arbitrary pipe (Eq. 1).

$$h_L = \frac{10.67L}{C_{HW}^{1.852} D^{4.87}} Q^{1.852} = \frac{8fL}{\pi^2 g D^5} Q^2 \tag{1}$$

where L is pipe length, π is pi number, g is gravitational acceleration, D is pipe diameter, and Q denotes pipe flow rate. In Eq. 1, the first and second right hand-side terms are H-W and D-W equations, respectively. The multiplier 10.67 in H-W equation is only valid when D and L are substituted in SI values (Larock et al., 2000).

As implied in Eq. 1, different resistance equations are supposed to yield into a unique head loss for a specific flow. Since different resistance equations have different multipliers and exponents for involving parameters, the aforementioned closure requires use of equivalent flow resistance coefficients.

In essence, relationships in which convert C_{HW} to equivalent f may be classified into three major groups. The first category includes relations that require pipe diameter and flow Reynolds number for this conversion; whereas the second category exclusively utilizes pipe diameter information. The equations of the first category include Liou's (1998) and Locher's (2000) equations while Travis and Mays' (2007) equation can be classified in the second category. These equations are shown in Eq. 2 to Eq. 4, respectively.

$$f = 133.80 C_{HW}^{-1.85} \mathrm{Re}^{-0.148} D^{-0.0158} \upsilon^{-0.148} \tag{2}$$

$$f = 1016.610 C_{HW}^{-1.85} \mathrm{Re}^{-0.148} D^{-0.0158} \tag{3}$$

$$\varepsilon = D(3.320 - 0.021 C_{HW} D^{0.01})^{2.173} \exp(-0.04125 C_{HW} D^{0.01}) \tag{4}$$

The third category may be relations which directly relate C_{HW} to ε and vice versa without requiring any pipe-diameter information. For instance, Eq. 5 and Eq. 6 are the examples of such equations which are obtained using Excel-embedded regression tools (Niazkar and Afzali, 2016) based on available and reliable data including C_{HW} and their equivalent ε (Liou, 1998; Valiantzas, 2008; Uribe et al., 2015) listed in Table 1. As shown, the range of applicability of these equations are $100<C_{HW}<150$ and $0.0015\text{mm}<\varepsilon<1.5200\text{mm}$.

$$C_{HW} = -348.15\varepsilon^6 + 1436.1\varepsilon^5 - 2132\varepsilon^4 + 1315.9\varepsilon^3 - 224\varepsilon^2 - 85.538\varepsilon + 149.32 \qquad R^2 = 0.94 \tag{5}$$

$$\varepsilon = 2\times10^{-7} C_{HW}^5 - 0.0002 C_{HW}^4 + 0.0396 C_{HW}^3 - 5.0397 C_{HW}^2 - 5.0397 C_{HW}^2 + 319.04 C_{HW} - 825.6 \qquad R^2 = 0.95 \tag{6}$$

3. APPLICATION AND RESULTS

Calculating flow roughness is one of the inevitable steps in WDN analysis. Since this analysis requires iterations where flow rate and Reynolds number may change in each iteration, those flow resistance coefficient, which varies with flow regime variation, should be revised in each iteration of such analyses. In this research, the impact of resistance equation selection on pipe network

analysis is the main focus. The most common resistance equations, i.e., H-W and D-W equations, are utilized for this purpose. Two hydraulic solvers, invariantly called gradient algorithm and finite element method (FEM), are used to solve three sample pipe networks selected from the literature. For each network, five scenarios described later in this paper are considered and in each one, the network was solved assuming twenty two C_{HW} with their equivalent ε selected from the literature (Liou, 1998; Valiantzas, 2008; Uribe et al., 2015). In each WDN analysis, similar pipe material was assumed for all pipes. In other words, it was assumed that all pipes have the same C_{HW} while different values of C_{HW}, ranging from 100 to 150 (Table 1), were utilized in different WDN analyses. This range includes a variety of different pipe materials in practice since proper application of H-W equation is for $100<C_{HW}<160$ (Diskin, 1960).

Table 1. Equivalent C_{HW} and ε used in D-W friction factor calculation

Item	Pipe materials	C_{HW}	ε(mm)	Reference
1	Uncoated, new cast iron	120	0.2781	Liou (1998)
2	Uncoated, new cast iron	129	0.1643	Liou (1998)
3	Uncoated, new cast iron	121	0.3007	Liou (1998)
4	Coated, very straight, no specials	144	0.0579	Liou (1998)
5	Coated, Bonn service main, new	114	0.8534	Liou (1998)
6	Coated, Bonn service main, new	111	1.0363	Liou (1998)
7	Coated, well laid, new cast iron	146	0.0488	Liou (1998)
8	Coated, well laid, new cast iron	145	0.0570	Liou (1998)
9	Coated, Danzing main, new cast iron	131	0.2846	Liou (1998)
10	Uncoated, new cast iron	115	0.9498	Liou (1998)
11	Coated, straight, no special, new	140	0.1598	Liou (1998)
12	Coated, Rochester main, new cast	129	0.3109	Liou (1998)
13	Coated, Rosemary siphon, new cast	142	0.0975	Liou (1998)
14	Coated, Edinburgh main, new cast	112.3	1.3411	Liou (1998)
15	Coated sheet iron, riveted	133	0.0908	Liou (1998)
16	Tuberculated Rosemary siphon, cast	112	1.4630	Liou (1998)
17	Cleaned Rosemary siphon, cast iron	142	0.1097	Liou (1998)
18	Exposy coasted steel	145	0.0280	Valiantzas (2008)
19	Plain steel, new	130	0.2030	Valiantzas (2008)
20	Concrete	100	1.5200	Valiantzas (2008)
21	PVC	150	0.0015	Uribe et al. (2015)
22	Cast iron	140	0.1000	Uribe et al. (2015)

In order to assess the performance of C-W equation and the available relationships between C_{HW} and f, each pipe network was solved for five different scenarios under steady-state condition. These scenarios are presented as following:

1. In the first scenario, the implicit Colebrook-White (C-W) formula is used in the process of analyzing sample network. Since this formula is generally accepted as a standard equation for computing D-W friction factor in the literature, the results of this scenario is considered as the benchmark solution.
2. The C-W equation is considered as flow resistance equation in the second scenario. In order to provide a rational comparison, equivalent C_{HW} listed in Table 1 are used for each pipe material in this scenario.
3. Liou's (1998) equation is used to convert C_{HW} to f. Since this equation requires pipe diameter and Reynolds number for conversion, it is used in each iteration of hydraulic solvers. Finally, it is emphasized that the D-W equation is used as the resistance equation in this scenario.
4. The fourth scenario is similar to the third one except that in this scenario, Locher's (2000) equation is used instead of Liou's (1998) equation.
5. Unlike the third and fourth scenarios, the second type of relationships between C_{HW} and f, i.e., Travis and Mays's (2007) equation, is utilized in this scenario. Since the second category

relates ε with C_{HW} by using only pipe diameter information, there is no need to use this equation in each iteration of WDN analysis whereas f is evaluated based on absolute roughness and Reynolds number in each iteration.

It should be noted that unknown hydraulic heads are calculated considering H-W equation in the second scenario in both gradient algorithm and FEM while D-W equation is used in other scenarios. Furthermore, C_{HW} is converted to equivalent f in the main calculation in the three last scenarios. As hydraulic head values are computed in the hydraulic solvers in these scenarios, flow rate are computed using H-W and D-W equations in FEM and gradient algorithm, respectively. These h-based methods are coded in MATLAB and Excel spreadsheet and the details of steps of these methods and their codes can be found in Niazkar and Afzali's (2017a) paper for interested readers. Finally, the root mean square error (RMSE) and mean absolute relative error (MARE) are used to compare the hydraulic heads obtained in different scenarios with that of the first scenario. These evaluation criteria are shown in Eq. 7 and Eq. 8, respectively.

$$RMSE = \sqrt{\frac{\sum_{i=1}^{N}(h_{i,1} - h_{i,j})^2}{N}} \qquad \forall j = 2,3,4,5 \tag{7}$$

$$MARE = \frac{1}{N}\sum_{i=1}^{N}\left|\frac{h_{i,1} - h_{i,j}}{h_{i,1}}\right| \qquad \forall j = 2,3,4,5 \tag{8}$$

where $h_{i,1}$ and $h_{i,j}$ are hydraulic head at ith node computed in the first and jth scenario, and N is total number of nodal points in pipe network.

The first pipe network is a small one having seven pipes, six nodes, and a reservoir (Niazkar and Afzali, 2017b). The variation of RMSE computed for the second to fifth scenarios using FEM and gradient algorithm are depicted in Figure 1. As shown, RMSE for the second and third scenarios are close for various C_{HW} while RMSE values for the fourth scenario are sometimes smaller and sometimes larger than the ones calculated for the second scenario. On the other hand, the worst RMSE values are obtained for the fifth scenario for almost all C_{HW} values. This indicates that the method in which uses pipe diameter for converting C_{HW} into equivalent f yield to larger RMSE in comparison with other scenarios.

The second WDN includes 74 pipes, 48 nodes, and two reservoirs (Chin et al. 1978). Figure 2 illustrates RMSE values calculated for different scenarios for different C_{HW} values. According to Figure 2, Travis and Mays' (2007) equation used in the fifth scenario achieved the worst results based on the RMSE values. The discrepancy between hydraulic heads of the first and the fifth scenarios in terms of RMSE is more significant for the lowest C_{HW} values and it decreases with the increase of C_{HW} values. Achieving large RMSE values for the fifth scenario indicates that using relationships between C_{HW} and f which exclusively utilizes pipe diameter for conversion may be unreliable in WDN analysis. Moreover, larger RMSE values overall is achieved when FEM is utilized for solving the second WDN, especially in the fifth scenario.

A real pipe network which consists of 91 pipes, 65 computational nodes, and one reservoir (Arsene and Gabrys, 2014) was solved. The accuracy of different scenarios is compared in Figure 3 for the third network. Based on Figure 3, considered scenarios overall yield to larger RMSE values for C_{HW} values lower than 130 while the accuracy of these scenarios increase for C_{HW} values larger than 130. Although the range of RMSE values depicted in Figure 3 is relatively much lower than the one shown in Figure 2, the fifth scenario in both WDNs result larger RMSE. In Figure 3, the fourth scenario also achieve the highest RMSE for some cases with C_{HW} lower than 130.

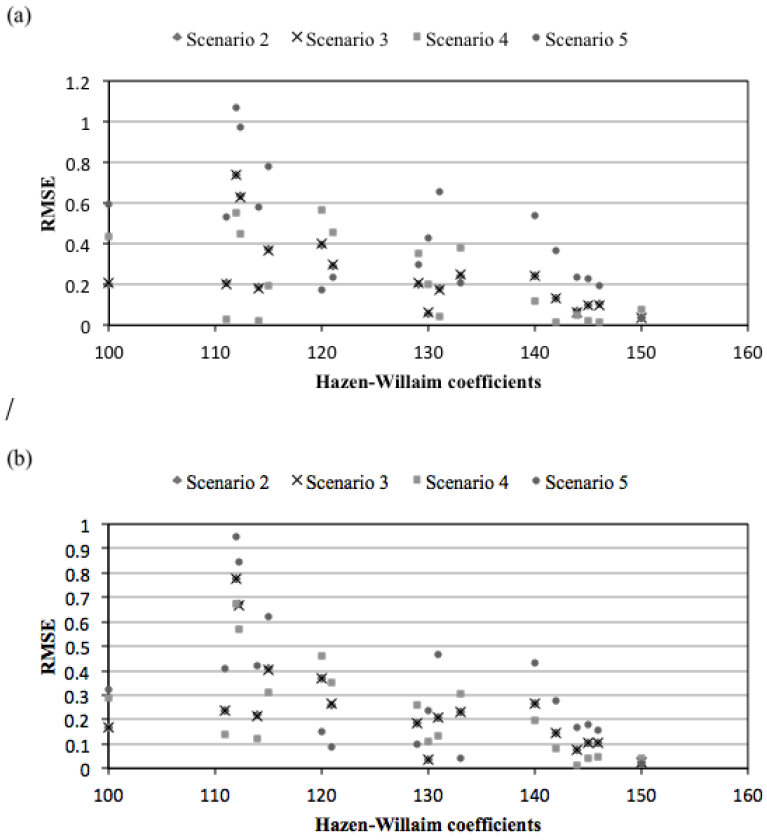

Figure 1. Variation of RMSE for different scenarios computed using (a) FEM and (b) gradient algorithm for the first pipe network.

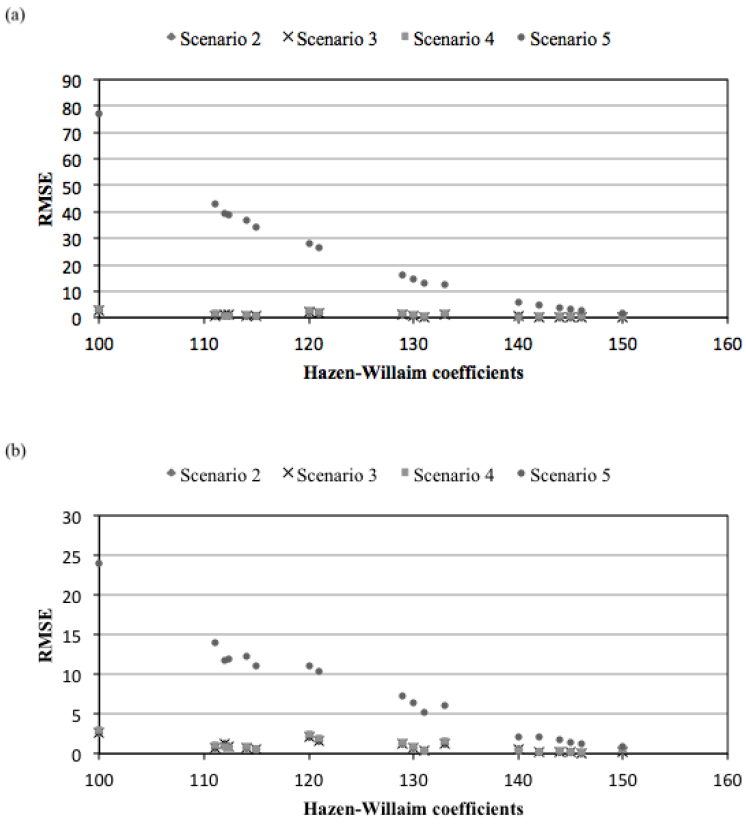

Figure 2. Variation of RMSE for different scenarios computed using (a) FEM and (b) gradient algorithm for the second pipe network.

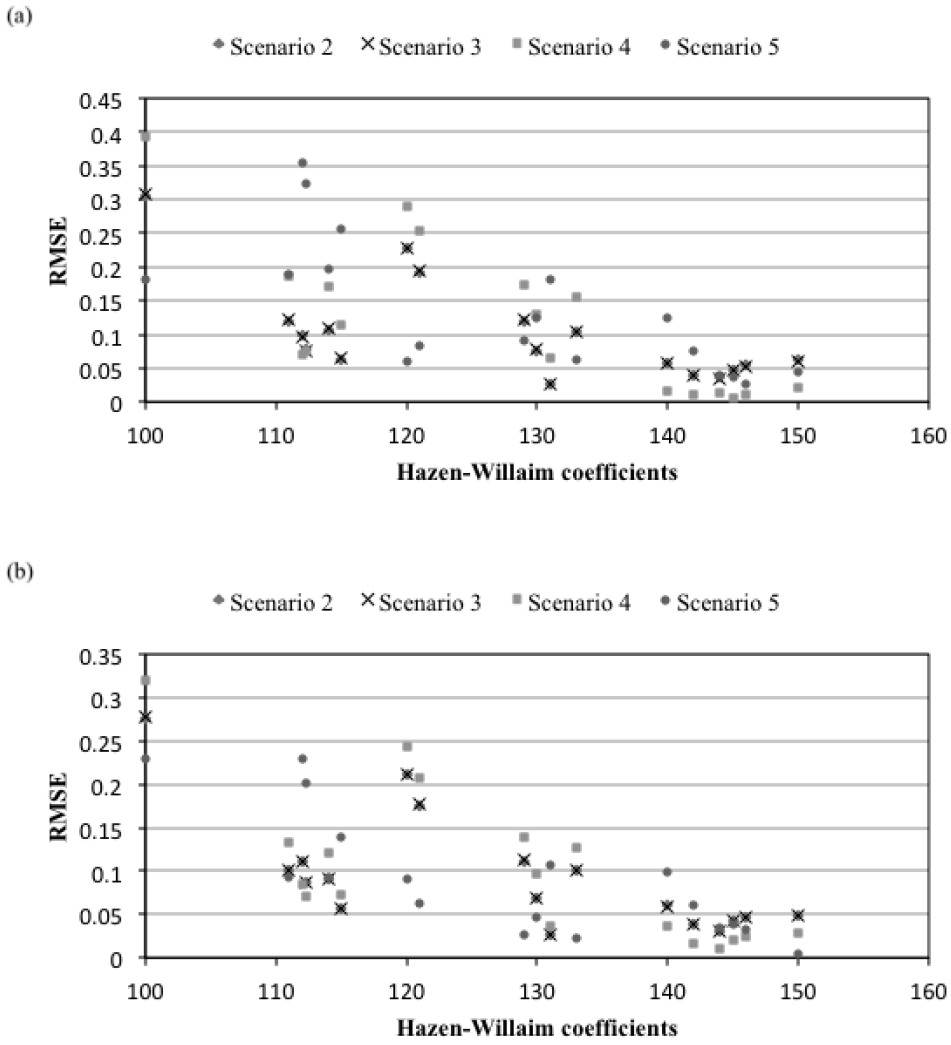

Figure 3. Variation of RMSE for different scenarios computed using (a) FEM and (b) gradient algorithm for the third pipe network.

In order to determine a comprehensive comparison between these scenarios, the average of RMSE and MARE values achieved for different C_{HW} values are computed for each network and each scenario. The average of RMSE values for the three WDNs solved by FEM and gradient algorithm are listed in Table 2. Furthermore, the average of MARE values computed for different scenarios are shown in Figure 4. Table 2 indicates that both h-based methods achieve quite similar average RMSE values for the first and third pipe networks. However, achieved RMSE in the fifth scenario using FEM is approximately three times larger than the one obtained in the same scenario using gradient algorithm. According to Table 2 and Figure 4, solving the three WDNs demonstrates that the second and third scenarios overall achieve the closer results to the first scenario whereas the fifth scenario yield to significant errors, especially for the second network. In other words, solving WDN using H-W equation (second scenario) or using Liou's (1998) equation for converting C_{HW} to f lead to closer results to when D-W equation is utilized. Additionally, application of Travis and Mays's (2007) equation for converting C_{HW} to f in analyzing WDNs causes significant errors for various C_{HW} values, especially in the second network. Since the application of H-W equation and the relationships, which uses both D and Re for converting C_{HW} to f, to WDN analysis yield to results with MARE<0.01 on average, it can be concluded that these equations performs acceptably accurate. On the other hand, solving WDN using relationships, which exclusively uses D for converting C_{HW} to f, are appeared to be unreliable for some cases.

Table 2. Average RMSE values calculated for different scenarios

FEM (average RMSE)	Scenarios			
	2	3	4	5
First network	0.245	0.243	0.220	0.451
Second network	0.871	0.870	1.193	22.352
Third network	0.101	0.101	0.120	0.136
Average	0.405	0.405	0.511	7.646
Gradient algorithm (average RMSE)	**Scenarios**			
	2	**3**	**4**	**5**
First network	0.250	0.249	0.230	0.326
Second network	0.861	0.861	0.986	7.806
Third network	0.094	0.094	0.100	0.090
Average	0.402	0.401	0.439	2.741

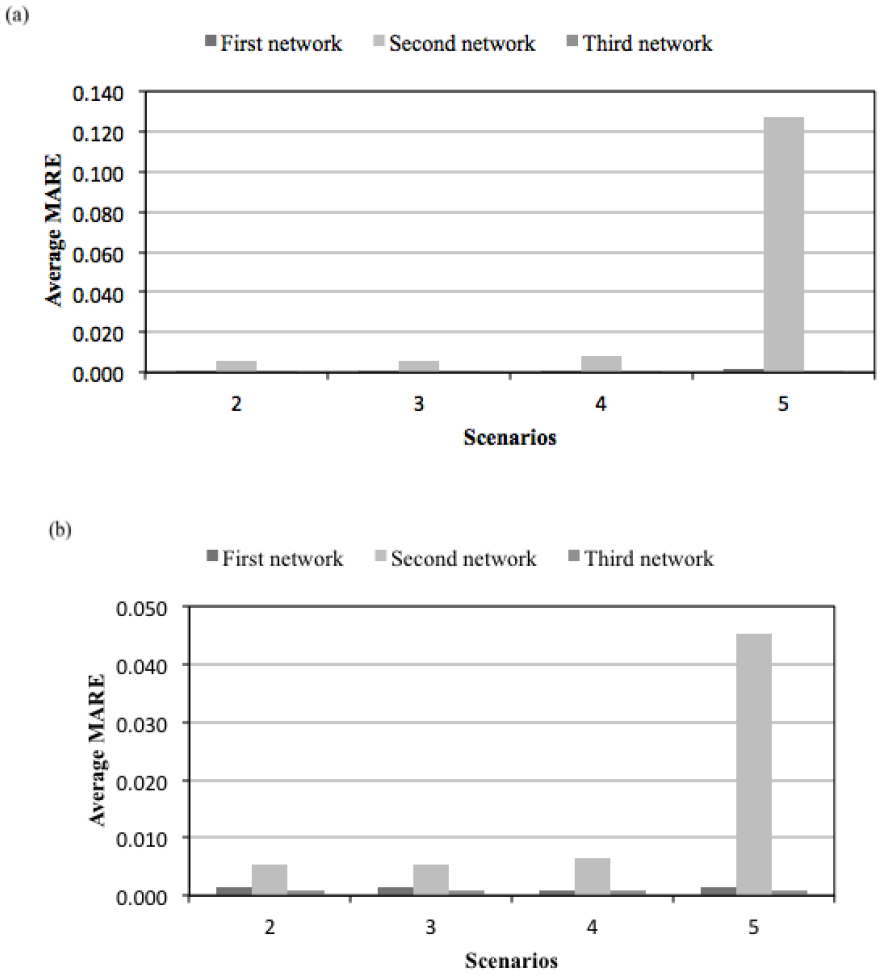

Figure 4. Average MARE values calculated for different scenarios using (a) FEM and (b) gradient algorithm.

4. CONCLUSION

In this research, the application of H-W equation and relationships which convert C_{HW} to f in analyzing WDN is investigated. Regarding the importance of the subject in WDN literature, three pipe networks were solved considering five scenarios for different values of C_{HW} using two h-based hydraulic solvers. Analyzing pipe networks for 660 different cases in this study shows that H-W equation and the relationships, which uses both pipe diameter and Reynolds number for converting C_{HW} to f, overall yield to acceptably close results to when D-W equation is used. However, application of relationship, which uses pipe diameter for converting C_{HW} to f, do not achieve inaccurate results for some cases, especially for lower values of C_{HW}.

REFERENCES

Arsene, C. T., Gabrys, B., 2014. Mixed simulation-state estimation of water distribution systems based on a least squares loop flows state estimator. Appl Math Model.: 38(2): 599-619.

Bombardelli, F. A., Garcıa, M. H. 2003. Hydraulic design of large-diameter pipes. J Hydraul Eng.: 129(11): 839-846.

Chin, K., Gay, R., Chua, S., Chan, C., Ho, S., 1978. Solution of water networks by sparse matrix methods. Int J Numer Meth Eng.: 12(8): 1261-1277.

Christensen, B. A., Locher, F. A., Swamee, P. K. 2000. Limitations and proper use of the Hazen-Williams equation. J Hydraul Eng.: 126(2): 167-170.

Elhay, S., Simpson, A. R., 2011. Dealing with zero flows in solving the nonlinear equations for water distribution systems. J Hydraul Eng.: 137(10): 1216–1224.

Larock, B. E., Jeppson, R. W.,Watters, G. Z. 1999. Hydraulics of pipeline systems. CRC press, New York.

Liou, C. P. 1998. Limitations and proper use of the Hazen-Williams equation. J Hydraul Eng.: 124(9): 951-954.

Niazkar, M., Afzali, S. H., 2016. Streamline Performance of Excel in Stepwise Implementation of Numerical Solutions. Comput Appl Eng Educ.: 24 (4): 555–566. DOI: 10.1002/cae.21731.

Niazkar, M., Afzali, S. H., 2017a. Analysis of water distribution networks using MATLAB and Excel spreadsheet: h-based methods. Comput Appl Eng Educ.: 25 (1): 129-141. DOI:10.1002/cae.21786.

Niazkar, M., Afzali, S. H. 2017b. Analysis of water distribution networks using MATLAB and Excel spreadsheet: Q-based methods. Comput Appl Eng Educ.: 25 (2): 227-289. DOI:10.1002/cae.21796.

Travis, Q. B., Mays, L. W. 2007. Relationship between Hazen–William and Colebrook–White Roughness Values. J Hydraul Eng.: 133(11): 1270-1273.

Uribe, J., Saldarriaga, J., Páez, D. 2015. Effects of the Use of Hazen-Williams Equation on Large WDS Planning Models. In World Environmental and Water Resources Congress: 881-889.

Valiantzas, J. D. 2008. Explicit power formula for the Darcy–Weisbach pipe flow equation: application in optimal pipeline design. J Irrig Drain E-Asce.: 134(4): 454-461.

VII. Agricultural Water Management

Proceedings of the 10th World Congress of EWRA 'Panta Rhei', 5-9 July 2017, Athens, Greece
© 2017 *European Water Resources Association*

Accuracy of daily PM-ET_o estimations with ERA-Interim reanalysis products

P. Paredes[1], D.S. Martins[1,2], J. Cadima[3], C. Pires[2] and L.S. Pereira[1*]
[1] *LEAF Linking Landscape, Environment, Agriculture and Food, Instituto Superior de Agronomia, Universidade de Lisboa, Portugal*
[2] *Instituto Dom Luiz, Faculdade de Ciências, DEGGE, Universidade de Lisboa, Lisboa, Portugal*
[3] *Centro de Estatística e Aplicações da Universidade de Lisboa (CEAUL) and Instituto Superior de Agronomia, Universidade de Lisboa, Portugal*
[*] *e-mail: lspereira@isa.ulisboa.pt*

Abstract: This study assesses the accuracy of estimates of FAO Penman-Monteith daily grass reference evapotranspiration (PM-ET_o) using ERA-Interim reanalysis products with 0.75^ox0.75^o spatial resolution. PM-ET_o requires daily maximum and minimum air temperature, net radiation or sunshine duration, relative air humidity or dew point temperature, and wind speed data. For that, local ET_o estimates from 1979-2013 over 37 weather stations distributed across Continental Portugal were compared with those issued from the nearest reanalysis grid-point to each station. Accuracy was assessed using several statistical indicators. Results show that the PM-ET_o computed with raw reanalysis data clearly underestimates (regression slope $b_0 \leq 1.05$) with RMSE exceeding 1.0 mm day^{-1} in nearly 30% of cases, but with EF generally above 0.50. Using a monthly bias correction improved the performance of estimates, with b_0 usually close to 1.00, RMSE rarely exceeding 0.80 mm day^{-1}, and EF generally above 0.80. These results show that when full local data sets are not available, the PM-ET_o may accurately be computed using daily reanalysis products, thus keeping the ability for the understanding of the physics processes.

Key words: accuracy indicators, FAO Penman-Monteith ET_o, raw reanalysis data, meteorological variables, bias correction

1. INTRODUCTION

Reference crop evapotranspiration (ET_o) is a key variable in both atmospheric and terrestrial branches of the hydrological cycle and plays a major role for agricultural and irrigation water management (Allen et al., 1998).

The FAO Penman-Monteith equation (PM-ET_o) results from the parameterization of the Penman-Monteith equation (Monteith, 1965) for a cool season grass when assuming a crop height of 12 cm, a surface resistance of 70 sm^{-1}, and an albedo of 0.23 (Allen et al., 1998). The PM-ET_o equation was developed to overcome the problems inherent to the existence of numerous methods/equations that compute ET without defining the reference surface, thus to adopt a common definition of reference ET_o (Pereira et al., 2015). The PM-ET_o equation requires maximum and minimum air temperature (T_{max} and T_{min}, ^oC), solar radiation (R_s, MJ m^2 day^{-1}) or sunshine duration (n), air relative humidity (RH, %) and wind speed at 2 m height (u_2, m s^{-1}). Both T_{max} and T_{min} records are available for a good network of stations in most countries, but other variables are often not available or are incomplete. The lack of complete records hampers the computation of PM-ET_o for many locations where the knowledge of ET_o is relevant for agricultural and environmental water management.

The variables required for ET_o estimation may be obtained from global atmospheric reanalysis datasets. The main advantages of reanalysis products are their spatial and temporal consistency over 3 or more decades and free access (Sheffield et al., 2006). Limitations are the coarse spatial resolution of the reanalysis products and the fact that their reliability vary with the climatic variable, locations and time scale. Reanalysis products have been successfully used to assess ET_o at various space and time scales (Srivastava et al., 2013; Martins et al., 2016) though it calls for downscaling

methods on a local-daily basis (Srivastava et al., 2013). Differently, when daily or monthly time scales are used, e.g., using a blended product combining the NCEP/NCAR reanalysis with observation-based datasets (Sheffield et al., 2006) the downscaling is not required as described by Martins et al. (2016).

Aiming at irrigation and water management applications, the objectives of the present study were to assess the performance of the ERA-Interim reanalysis products (Dee et al., 2011) in generating the variables used to compute daily PM-ET_o compared with observations in 37 weather stations in Continental Portugal; 2) to assess the quality of ET_o computed with reanalysis products ($ET_{o\text{-}REAN}$) comparatively to PM-ET_o computed with observations ($ET_{o\text{-}OBS}$); and 3) to use observations for bias correction of the ET_o computed with reanalysis and to assessing the respective accuracy.

2. MATERIALS AND METHODS

2.1 Data

Data from the ERA-Interim (Dee et al., 2011) near-surface global reanalysis dataset was used in this study to estimate PM-ET_o for Continental Portugal. This dataset spans from 1979-present on a 0.75^ox0.75^o lat-long grid and is available at http://www.ecmwf.int/en/research/climate-reanalysis/era-interim. Daily data retrieved included T_{max} and T_{min} (K), wind speed at 10 m height (u_{10}, m s^{-1}), and R_s (W m^{-2}). u_{10} was adjusted for 2 m (u_2) using a logarithmic wind speed profile (Allen et al., 1998). Actual vapour pressure values were estimated using daily data of air temperature and dew point temperature (K). The values of $ET_{o\text{-}REAN}$ were computed by using data from the nearest reanalysis grid-point of each of the 37 weather stations used in the validation (Fig. 1), from which 27 belong to the Instituto Português do Mar e da Atmosfera (IPMA) network and 10 come from the Centro Operativo e de Tecnologia de Regadio. Fig. 1 also presents the time-series interval and the number of days of full observed data availability.

2.2 Reference evapotranspiration estimation

The PM-ET_o equation describes evapotranspiration of a hypothetical grass crop actively growing and adequately watered with height of 0.12 m, a surface resistance of 70 s m^{-1} and an albedo of 0.23 (Allen et al., 1998). At a daily time scale, ET_o (mm day^{-1}) is:

$$ET_o = \frac{0.408\,\Delta\,(R_n - G) + \gamma\,\frac{900}{T_{mean}+273}\,u_2(e_s - e_a)}{\Delta + \gamma\,(1 + 0.34\,u_2)} \quad (1)$$

where R_n is net radiation at the crop surface (MJ m^{-2} day^{-1}), G is soil heat flux density (MJ m^{-2} day^{-1}), T_{mean} is mean daily air temperature at 2 m height (°C), u_2 is wind speed at 2 m height (m s^{-1}), e_s is saturation vapour pressure (kPa), e_a is actual vapour pressure (kPa), e_s-e_a is vapour pressure deficit (kPa), Δ is the slope of vapor pressure curve (kPa $°C^{-1}$), γ is the psychrometric constant (kPa $°C^{-1}$). Daily G is assumed zero (Allen et al., 1998). In this study, e_s was computed as the average of the saturation vapour pressure at T_{max} and T_{min}, $e^o(T_{max})$ and $e^o(T_{min})$. For most stations, e_a was estimated averaging the products $e^o(T_{max})$ RH_{min} and of $e^o(T_{min})$ RH_{max}, i.e., using maximum and minimum daily relative humidity; otherwise, e_a was estimated with the average values of $e^o(T_{max})$ and $e^o(T_{min})$ multiplied by the mean daily relative humidity. Rn was obtained from Rs for all stations but one where it was computed from the daily solar duration (n) using the Angström radiation equation.

2.3 Statistical assessment and bias correction of ET_o computed from reanalysis

Several statistical indicators were used to assess the performance of the reanalysis datasets in

representing the amplitude and time variation of climate variables and of ET_o. The assessment compared the observations O_i with corresponding reanalysis values P_i using the following statistical indicators: i) the coefficient of determination (R^2); ii) the regression coefficient (b_0) of a linear regression forced to the origin (FTO); iii) the Root Mean Square Error (RMSE); iv) the normalized RMSE (NRMSE) by the mean of observations; v) the Percent Bias (PBIAS) is the ratio between reanalysis bias and mean observations, that measures the average tendency of the reanalysis data to be larger or smaller than corresponding observations; and vi) the efficiency of modelling, EF, (Nash and Sutcliff, 1970) that measures the relative magnitude of the mean square error ($MSE=RMSE^2$) and the observed data variance (Legates and McCabe Jr., 1999). A thorough description of these indicators is provided by Martins et al. (2016).

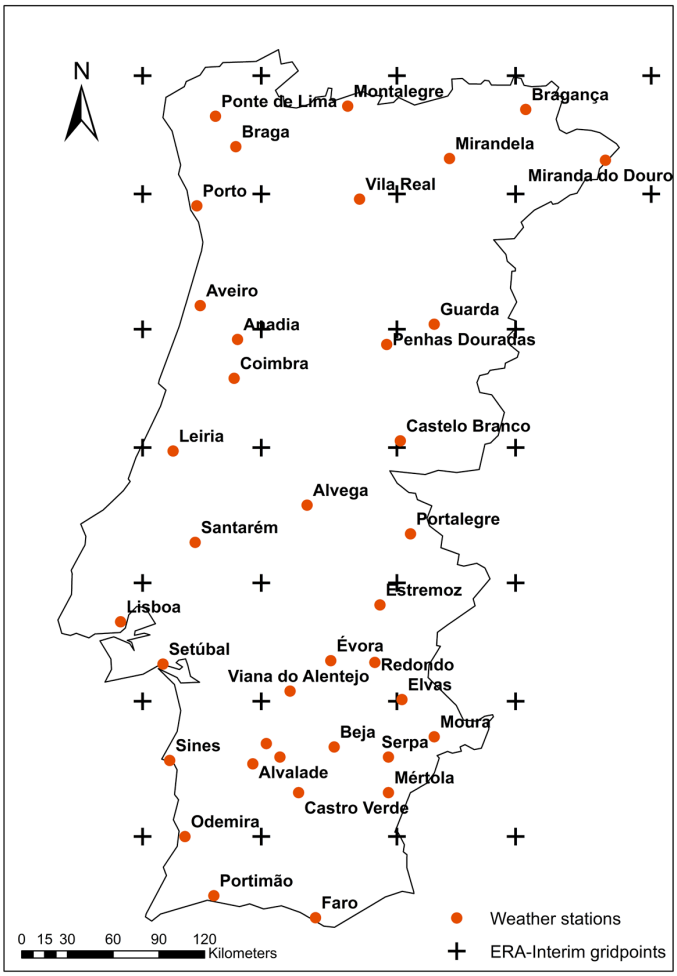

Weather stations locations	Data range	Number of observations
Aljustrel	2001-2013	4174
Alvalade	2001-2013	4189
Alvega	2003-2013	2741
Anadia	2003-2013	2919
Aveiro	2003-2013	3394
Beja	2002-2013	3912
Braga	2003-2013	2339
Bragança	2003-2013	3637
Castelo Branco	2003-2013	3662
Castro Verde	2007-2013	2004
Coimbra	1998-2013	5557
Elvas	1979-2000	7529
Estremoz	2006-2013	2511
Évora	1979-2013	12082
Faro	2003-2013	3752
Ferreira do Alentejo	2001-2013	4127
Guarda	2003-2013	3455
Leiria	2003-2013	1665
Lisboa	2003-2013	3831
Mértola	2003-2013	2481
Miranda do Douro	2009-2013	1578
Mirandela	2003-2013	3240
Montalegre	2003-2013	3107
Moura	2001-2013	3721
Odemira	2002-2013	3852
Penhas Douradas	2003-2013	3233
Ponte de Lima	2000-2009	2319
Portalegre	2003-2013	3847
Portimão	2003-2013	2572
Porto	2003-2013	3627
Redondo	2001-2013	4121
Santarém	2003-2013	3562
Serpa	2006-2013	2327
Setúbal	2003-2013	3134
Sines	2003-2013	3866
Vidigueira	2003-2013	1889
Vila Real	1998-2013	3869

Figure 1. Spatial distribution of the reanalysis grid points (at each 0.75°) and the 37 weather stations in Continental Portugal, including the range of data of the climatic data series and number of observation days with full data sets.

The applied ET_o bias correction at every day t writes as: $ET_{o\_REAN\ 1}(t) = ET_{o\_REAN}(t) - b$, where $b = \overline{ET_{o\_REAN}} - \overline{ET_{o\_OBS}}$ is the difference between the mean values of $ET_{o\text{-}REAN}$ and $ET_{o\text{-}OBS}$ on the month of day t, estimated from all available years. This approach for bias correction aims at being used for real time irrigation scheduling.

3. RESULTS AND DISCUSSION

3.1 Assessing the reanalysis variables

The referred statistical indicators were used to compare all variables used in the PM-ET_o

equation (Eq. 1) obtained by reanalysis or from observations at each of 37 stations (Fig. 1). Table 1 shows the frequency distributions (%) of the statistical indicators in each class for all the weather variables. To facilitate comparisons across different variables, NRMSE was used (Table 1) instead of RMSE.

Table 1. Frequency (%) distributions of the performance indicators for, maximum temperature (T_{max}) and minimum temperature (T_{min}), shortwave radiation (R_s), actual vapour pressure (e_a) and wind speed (u_2) when comparing raw reanalysis products with observed values

	Intervals of R^2	(%)	Intervals of b_0	(%)	Intervals of PBIAS (%)	(%)	Intervals of NRMSE	(%)	Intervals of EF	(%)
T_{max}	]0.95, 1.00]	5.4	]1.30, [	0.0	],-20.0]	35.1	]0.50, 1.00]	0.0	] , 0.00]	13.5
	]0.90, 0.95]	35.1	]1.15, 1.30]	0.0	]-20.0, -10.0]	32.4	]0.30, 0.50]	18.9	]0.00, 0.50]	32.4
	]0.80, 0.90]	43.2	]1.05, 1.15]	0.0	]-10.0, -2.5]	18.9	]0.20, 0.30]	45.9	]0.50, 0.70]	24.3
	]0.70, 0.80]	13.5	]0.95, 1.05]	16.2	]-2.5, 2.5]	0.0	]0.15, 0.20]	21.6	]0.70, 0.80]	10.8
	]0.60, 0.70]	2.7	]0.85, 0.95]	27.0	]2.5, 10.0]	10.8	]0.10, 0.15]	13.5	]0.80, 0.90]	16.2
	]0.50, 0.60]	0.0	]0.70 ,0.85]	43.2	]10.0, 20.0]	2.7	]0.05, 0.10]	0.0	]0.90, 0.95]	2.7
	[0.00, 0.50]	0.0	], 0.70]	13.5	]20.0, [		[0.00, 0.05]	0.0	]0.95, 1.00]	0.0
T_{min}	]0.95, 1.00]	0.0	]1.30, [	37.8	],-20.0]	0.0	]0.50, 1.00]	37.8	] , 0.00]	27.0
	]0.90, 0.95]	5.4	]1.15, 1.30]	35.1	]-20.0, -10.0]	0.0	]0.30, 0.50]	40.5	]0.00, 0.50]	40.5
	]0.80, 0.90]	51.4	]1.05, 1.15]	13.5	]-10.0, -2.5]	5.4	]0.20, 0.30]	16.2	]0.50, 0.70]	18.9
	]0.70, 0.80]	37.8	]0.95, 1.05]	13.5	]-2.5, 2.5]	5.4	]0.15, 0.20]	0.0	]0.70, 0.80]	5.4
	]0.60, 0.70]	5.4	]0.85, 0.95]	0.0	]2.5, 10.0]	5.4	]0.10, 0.15]	2.7	]0.80, 0.90]	5.4
	]0.50, 0.60]	0.0	]0.70 ,0.85]	0.0	]10.0, 20.0]	73.0	]0.05, 0.10]	2.7	]0.90, 0.95]	2.7
	[0.00, 0.50]	0.0	], 0.70]	0.0	]20.0, [	10.8	[0.00, 0.05]	0.0	]0.95, 1.00]	0
R_s	]0.95, 1.00]	0.0	]1.30, [	0.0	],-20.0]	0.0	]0.50, 1.00]	0.0	] , 0.00]	0
	]0.90, 0.95]	0.0	]1.15, 1.30]	0.0	]-20.0, -10.0]	0.0	]0.30, 0.50]	13.5	]0.00, 0.50]	0
	]0.80, 0.90]	64.9	]1.05, 1.15]	43.2	]-10.0, -2.5]	5.4	]0.20, 0.30]	64.9	]0.50, 0.70]	21.6
	]0.70, 0.80]	32.4	]0.95, 1.05]	54.1	]-2.5, 2.5]	18.9	]0.15, 0.20]	21.6	]0.70, 0.80]	27.0
	]0.60, 0.70]	2.7	]0.85, 0.95]	2.7	]2.5, 10.0]	2.7	]0.10, 0.15]	0.0	]0.80, 0.90]	51.4
	]0.50, 0.60]	0.0	]0.70 ,0.85]	0.0	]10.0, 20.0]	24.3	]0.05, 0.10]	0.0	]0.90, 0.95]	0.0
	[0.00, 0.50]	0.0	], 0.70]	0.0	]20.0, [	48.6	[0.00, 0.05]	0.0	]0.95, 1.00]	0.0
e_a	]0.95, 1.00]	0.0	]1.30, [	2.7	],-20.0]	18.9	]0.50, 1.00]	2.7	] , 0.00]	16.2
	]0.90, 0.95]	0.0	]1.15, 1.30]	10.8	]-20.0, -10.0]	27.0	]0.30, 0.50]	13.5	]0.00, 0.50]	35.1
	]0.80, 0.90]	32.4	]1.05, 1.15]	8.1	]-10.0, -2.5]	10.8	]0.20, 0.30]	37.8	]0.50, 0.70]	24.3
	]0.70, 0.80]	35.1	]0.95, 1.05]	21.6	]-2.5, 2.5]	8.1	]0.15, 0.20]	27.0	]0.70, 0.80]	8.1
	]0.60, 0.70]	21.6	]0.85, 0.95]	21.6	]2.5, 10.0]	10.8	]0.10, 0.15]	18.9	]0.80, 0.90]	16.2
	]0.50, 0.60]	10.8	]0.70 ,0.85]	29.7	]10.0, 20.0]	8.1	]0.05, 0.10]	0.0	]0.90, 0.95]	0.0
	[0.00, 0.50]	0.0	], 0.70]	5.4	]20.0, [	16.2	[0.00, 0.05]	0.0	]0.95, 1.00]	0.0
u_2	]0.95, 1.00]	0.0	]1.30, [	32.4	],-20.0]	16.2	]0.50, 1.00]	59.5	] , 0.00]	78.4
	]0.90, 0.95]	0.0	]1.15, 1.30]	5.4	]-20.0, -10.0]	8.1	]0.30, 0.50]	37.8	]0.00, 0.50]	21.6
	]0.80, 0.90]	0.0	]1.05, 1.15]	8.1	]-10.0, -2.5]	5.4	]0.20, 0.30]	2.7	]0.50, 0.70]	0.0
	]0.70, 0.80]	0.0	]0.95, 1.05]	18.9	]-2.5, 2.5]	13.5	]0.15, 0.20]	0.0	]0.70, 0.80]	0.0
	]0.60, 0.70]	8.1	]0.85, 0.95]	10.8	]2.5, 10.0]	0.0	]0.10, 0.15]	0.0	]0.80, 0.90]	0.0
	]0.50, 0.60]	16.2	]0.70 ,0.85]	16.2	]10.0, 20.0]	8.1	]0.05, 0.10]	0.0	]0.90, 0.95]	0.0
	[0.00, 0.50]	75.7	], 0.70]	8.1	]20.0, [	10.8	[0.00, 0.05]	0.0	]0.95, 1.00]	0.0

R^2 is the coefficient of determination of the OLS regression; b_0 is the regression coefficient of the FTO; PBIAS is the Percent Bias; NRMSE is the Normalized Root Mean Square Error; EF is the efficiency of modelling

Results show that the reanalysis-based values were generally not close to the observations, except for R_s. Reanalysis T_{max} ($T_{max\text{-}REAN}$) clearly tended to under-estimate with an FTO slope $b_0 \leq 0.95$ in 83.7% of stations with $R^2 > 0.80$. Only 2.7% of the stations have $R^2 \leq 0.70$. The estimation bias (PBIAS) was small in 29.7% of cases, with PBIAS in the range of -10 to +10%; however, an underestimation bias greater than -20% was observed for 35.1%. The magnitude of the estimation error was generally high, with NRMSE>0.20 in 64.8% of cases. Only 29.7% of stations had EF>0.70, with negative EF values in 13.5% of cases. Results for $T_{min\text{-}REAN}$ (Table 1) show $R^2 > 0.80$ in most cases (56.8%) with only 5.4% of stations having $R^2 < 0.70$; thus, $T_{min\text{-}REAN}$ reasonably reflects the time variability of $T_{min\text{-}OBS}$. $T_{min\text{-}REAN}$ tends to over-estimate, with $b_0 > 1.15$ in most cases; in 13.5% of stations there is no tendency to under- or over-estimation. High positive bias of estimation (PBIAS≥10%) was observed in 83.8% of cases. The magnitude of the estimation error is quite high, with NRMSE>0.30 in 78.3% of stations, and NRMSE<0.10 in 2.7% of cases. The EF

results were relatively poor with EF<0.50 in 67.5% of cases and EF>0.70 in 13.5% of cases.

Results for $T_{min\text{-}REAN}$ in the present study compare in terms of over-estimation and NRMSE, with those reported by Martins et al. (2016) using monthly blended NCEP/NCAR reanalysis for Portugal. Simmons et al. (2010) also reported an over-estimation tendency for T_{min} using monthly ERA Interim. Martins et al. (2016) found no tendency for over or under-estimation of T_{max} but a slightly worse NRMSE relative to the present study.

R_s is arguably the variable from the reanalysis data set that best agrees with observations (Table 1). R^2 were generally good with only 2.5% of cases having R^2<0.60. These results suggest that $R_{s\text{-}REAN}$ reflect the time variability of the observed R_s in the majority of locations. Furthermore, b_0 is generally close to 1.0, with 55% of values within the interval 0.95-1.05 and 42.5% in the interval 1.05-1.15. Estimation bias was small with 72.5% of cases having a PBIAS ranging from -10 to +10% (Table 1), with only 5% of cases having PBIAS>20%. NRMSE was generally >0.20 in most cases. EF was generally higher than 0.70 in most stations, with most values greater than 0.80. These results suggest that $R_{s\text{-}OBS}$ were well estimated by $R_{s\text{-}REAN}$. Similar good results for R_s were reported for Portugal by Martins et al. (2016).

The e_a-$_{REAN}$ results (Table 1) indicate under-estimation, with $b_0 \leq 0.95$ in 56.7% of cases. Most locations present R^2 ranging 0.70-0.90, with <11% of cases having R^2<0.60. The estimation bias ranged -10.0 to +10.0% in 35.1% of cases; the next most frequent interval for PBIAS, representing 27%, was -10 to -20%, so indicating under-estimation. The magnitude of estimation errors was good, with NRMSE<0.20 in 45.9% of cases. Good to acceptable EF results (EF>0.50) were found in 48.6% of cases; however, negative EF values were observed in 16.2% of cases. Few studies are available relative to e_a from reanalysis but most of them show an under-estimation trend (Simmons et al. 2010). Martins et al. (2016) reported no tendency for over- or under-estimation of RH when using the blended NCEP/NCAR reanalysis products for Portugal.

Results in Table 1 relative u_2-$_{REAN}$ show a very high dispersion of values, with R^2<0.50 in most cases. The slope b_0 generally deviates from 1.0, with a considerable over-estimation (b_0>1.30) in 32.4% of cases. $u_{2\text{-}REAN}$ had small estimation bias only in 29.7% of cases. Errors of estimation were very large, with NMRSE>0.5 in most cases. Apparently, there was no gain in using $u_{2\text{-}REAN}$ since EF was generally negative. The results of the present study relative to the low accuracy of $u_{2\text{-}REAN}$ are in agreement with the results reported for the Iberian Peninsula by Lorente-Plazas et al. (2015) and Martins et al. (2016).

3.2 Evaluating ET_o estimates using reanalysis products

Although most variables used to compute PM-ET_o are not well estimated from reanalysis products, the performance of ET_o computed with these reanalysis variables relative to $ET_{o\text{-}OBS}$ is generally good when assessed separately. Figure 2 presents the spatial distribution of the statistical indicators used to compare $ET_{o\text{-}REAN}$, before and after bias correction, with $ET_{o\text{-}OBS}$. As can be seen, $ET_{o\text{-}OBS}$ is acceptably estimated with raw reanalysis variables (Fig. 2a) for most locations but with high spatial variability of results across Portugal. Fig. 2a shows that high R^2 values (R^2>0.80), covered the country well. These results show a strong relationship between O_i and P_i, which means that the time variability of $ET_{o\text{-}OBS}$ is well represented by $ET_{o\text{-}REAN}$; only one case in the northwest presents $R^2 \leq 0.70$.

$ET_{o\text{-}REAN}$ presents no tendency to under or over-estimate $ET_{o\text{-}OBS}$ in 12 locations, mostly located inland; however, a clear tendency to over-estimate occurred in 9 locations in coastal northwest and southeast regions (Fig. 2a). This is most likely due to the overestimation of T_{min}, R_s and u_2 in those locations. Most locations, nearly 60%, present an acceptable PBIAS, within the range -10 to +10%. RMSE is smaller than 0.75 mm day^{-1} in 46% of the stations. A large RMSE (>1.0 mm day^{-1}) occurred in 11 inland locations and the total average RMSE is 0.85 mm day^{-1}. EF results follow a spatial distribution similar to the bias indicators, with EF values >0.50. Thus, EF results indicate that the mean square errors were smaller or much smaller than the $ET_{o\text{-}OBS}$ variance.

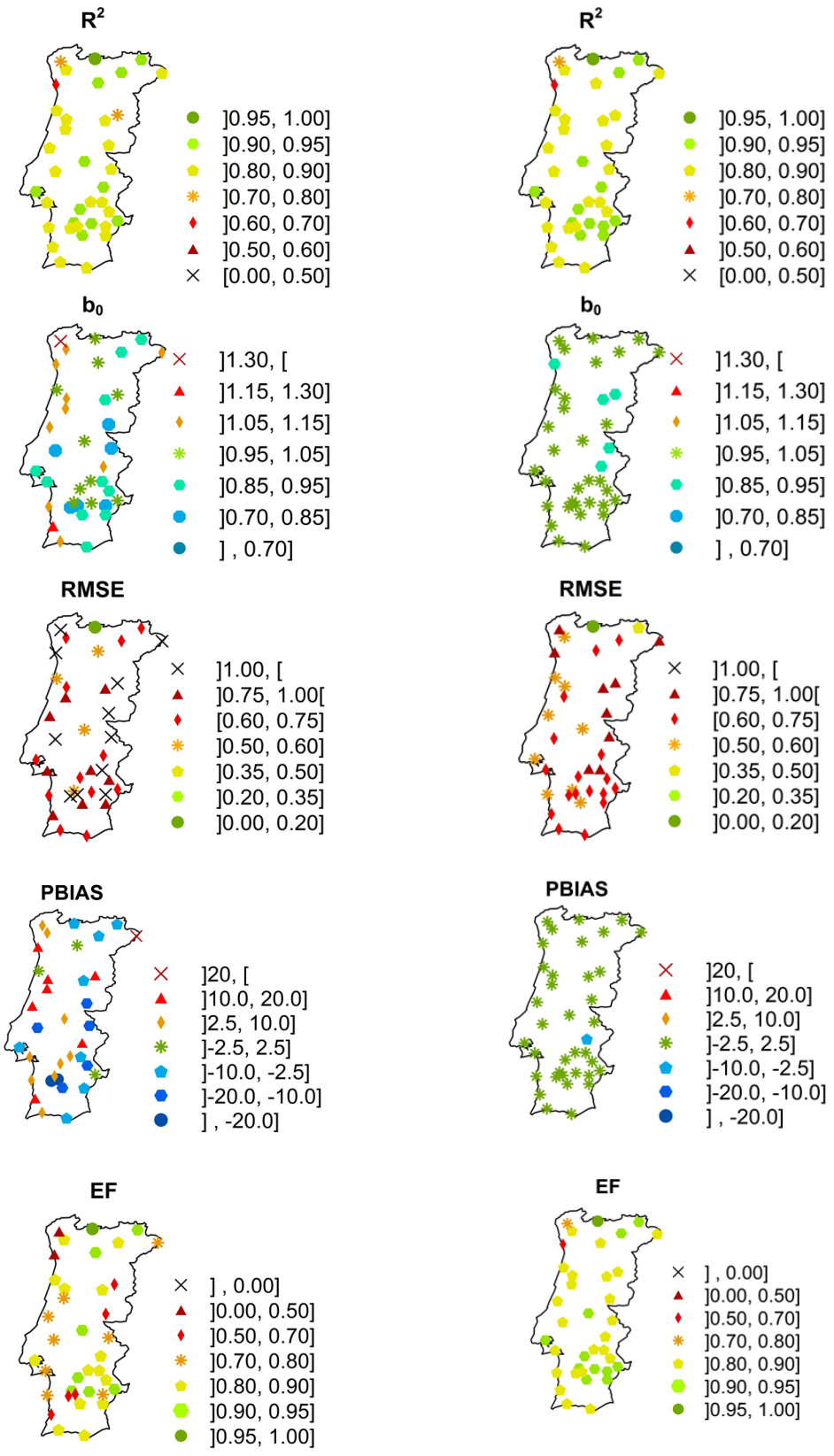

Figure 2. Spatial distribution of the statistical indicators measuring the performance of ET_o estimation using (a) raw reanalysis data and (b) after bias correction

The above described bias correction applied to $ET_{o\text{-}REAN}$ lead to more accurate estimates of ET_o estimations (Fig. 2b) aiming at operational irrigation management. However, this approach is only

possible when observations are available or a previous bias correction has been estimated regionally. Results show a general improvement of all statistical indicators namely in terms of RMSE, which average decreased from 0.85 to 0.68 mm day^{-1} after bias correction. The EF values greatly improved, averaging 0.87, so indicating that MSE were much smaller than the variance of $ET_{o\text{-}OBS}$.

A similar scheme of variance correction was also tested by multiplying the reanalysis results by the ratio $R\sigma = \sigma_{OBS} / \sigma_{REAN}$ between standard deviations of observations (σ_{OBS}) and reanalysis (σ_{REAN}) for the same month, over all the years studied. However, this often produced physically impossible values due to an issue that deserves to be highlighted: in many stations, the variability of reanalysis results was considerably different from that of observed results. For example, in 18% of station-months combinations $R\sigma>1.50$ for both T_{max} and T_{min}, i.e., observed daily variability exceeded the variability of reanalysis estimates by over 50%. For R_s, 22% of station-months exceeded the same ratio threshold of 1.50. For wind-speed, in 14% of station-months $R\sigma>1.50$ whereas in 3% $R\sigma<0.50$. Despite the results, the scheme may be promising after some modifications.

Results for daily $ET_{o\text{-}REAN}$ are coherent with monthly $ET_{o\text{-}REAN}$ obtained by Martins et al. (2016) with blended reanalysis, with locations where no tendency for under- or over-estimation of ET_o are the same in both studies. A similar spatial pattern of RMSE was observed in both studies, but that by Martins et al. (2016) presented lower RMSE values likely due to the lower variance of monthly $ET_{o\text{-}OBS}$. Other studies relative to using reanalysis products for ET_o computations refer to much smaller spatial and time scales than those in the current study (Ishak et al., 2010; Srivastava et al., 2013) and results are not comparable with those above. In a previous study of selected weather stations in Portugal, using temperature only to compute ET_o, Paredes and Rodrigues (2010) found RMSE varying from 0.47 to 0.87 mm day^{-1}, while in the current study RMSE of raw $ET_{o\text{-}REAN}$ ranged from 0.60 to 1.05 mm day^{-1} while bias corrected $ET_{o\text{-}REAN}$ varied from 0.64 to 0.84 mm day^{-1} for the same locations, thus indicating a good accuracy of the ERA-Interim reanalysis products for ET_o computations.

4. CONCLUSIONS

The accurate computation of PM-ET_o is essential for irrigation and water resources management, namely when considering climate change effects. In view of this, the present study assessed the potential of the daily ERA-Interim reanalysis products in reproducing the spatial and temporal variability of the climatic variables used to compute PM-ET_o across Portugal. Results suggest that $T_{max\text{-}REAN}$ and $T_{min\text{-}REAN}$ highly correlate with observations but with a clear tendency for under-estimation of T_{max} and over-estimation of T_{min}. The $R_{s\text{-}REAN}$ revealed good agreement with observations at almost all stations. $e_{a\text{-}REAN}$ and $u_{2\text{-}REAN}$ represented less well $e_{a\text{-}REAN}$ and $u_{2\text{-}REAN}$ and their variability. Despite these limitations, the high values of R^2 and EF indicate that $ET_{o\text{-}REAN}$ adequately explain $ET_{o\text{-}OBS}$ variability. The use of bias correction improved the performance of $ET_{o\text{-}REAN}$

Results show that $ET_{o\text{-}REAN}$ consist of a fair alternative when weather observations are lacking. However, the use of daily reanalysis data should be performed with caution. Based on the current study, the next step is to assess the use of other daily reanalysis products and to improve the use of bias correction.

ACKNOWLEDGEMENTS

The support of FCT, Lisbon, through the Post-Doc grant SFRH/BPD/102478/2014 to the first author, the PhD grant SFRH/BD/92880/2013 to the second author, and the grants attributed to research unit LEAF (UID/AGR/04129/2013) and Pest-OE/MAT/UI0006/2014 is acknowledged.

REFERENCES

Allen RG, Pereira LS, Raes D, Smith M. 1998. Crop Evapotranspiration.Guidelines for Computing Crop Water Requirements .FAO Irrig. Drain. Pap. 56. FAO, Rome, 300 p.

Dee DP et al. 2011. The ERA-Interim reanalysis: configuration and performance of the data assimilation system. Q.J.R. Meteorol. Soc., 137:553–597.

Legates DR, McCabe Jr. GJ. 1999. Evaluating the use of "goodness-of-fit" measures in hydrologic and hydroclimatic model validation. Water Resour. Res. 35:233-241.

Lorente-Plazas R, Montávez JP, Jerez S, Gómez-Navarro JJ, Jiménez-Guerrero P, Jiménez PA. 2015. A 49 year hindcast of surface winds over the Iberian Peninsula. Int. J. Climatol. 35:3007–3023.

Martins DS, Paredes P, Raziei T, Pires C, Cadima J, Pereira LS, 2016. Assessing reference evapotranspiration estimation from reanalysis weather products. An application to the Iberian Peninsula. Int. J. Climatol. DOI:10.1002/joc.4852

Monteith, JL, 1965. Evaporation and Environment. 19th Symposia of the Society for Experimental Biology, University Press, Cambridge, 19:205-234

Nash JE, Sutcliffe JV. 1970. River flow forecasting through conceptual models: Part 1. A discussion of principles. J Hydrol. 10:282-290.

Paredes P, Rodrigues GC 2010. Necessidades de água para a rega de milho em Portugal Continental considerando condições de seca. In: Pereira, LS, Mexia, JT, Pires, CAL (Eds) Gestão do Risco em Secas. Métodos, tecnologias e desafios. Edições Colibri e CEER, Lisboa, pp. 301- 319.

Pereira LS, Allen RG, Smith M, Raes D. 2015. Crop evapotranspiration estimation with FAO56: Past and future. Agric. Water Manage. 147:4-20.

Sheffield J, Goteti G, Wood EF. 2006. Development of a 50-year high-resolution global dataset of meteorological forcings for land surface modeling. J. Climate. 19:3088-3111.

Simmons AJ, Willett KM, Jones PD, Thorne PW, Dee DP. 2010. Low-frequency variations in surface atmospheric humidity, temperature, and precipitation: Inferences from reanalyses and monthly gridded observational data sets. J. Geophys. Res. 115, D01110. doi:10.1029/2009JD012442.

Srivastava PK, Han D, Rico-Ramirez MA, Islam T. 2013. Comparative assessment of evapotranspiration derived from NCEP and ECMWF global datasets through Weather Research and Forecasting model. Atmos. Sci. Lett. 28:4419-4432.

Proceedings of the 10th World Congress of EWRA 'Panta Rhei', 5-9 July 2017, Athens, Greece
© 2017 *European Water Resources Association*

Proving the contribution of a seasonal shallow water table to evapotranspiration

G. Bourazanis[1,2], I. Argyrokastritis[2] and P. Kerkides[2]
[1] *Department of Rural Economy and Veterinary of Regional Government of Laconia, Sparta, Laconia 23100, Greece*
[2] *Laboratory of Agricultural Hydraulics, Department of Natural Resources Development and Agricultural Engineering, Agricultural University of Athens, Ieraodos 75, 11855 Athens, Greece*
[*] *e-mail: gbourazanis@gmail.com*

Abstract: An attempt is made to elaborate on the soil water dynamics in an olive orchard field in Sparta, Laconia. This is a complex process, where soil water moves in all directions, always obeying the appropriate law of flow e.g Darcy's law. Equipped with modern devices and instrumentation we have been able to monitor and detect soil moisture profiles, θ(z,t), during the period of investigation, as well as record all meteorological attributes which could provide the means of estimating atmospheric demands for the olive orchard experimental field. Under certain assumptions, associated with the physical processes of investigation, such as the predominant direction of water flow being the vertical one , the transfer from the moisture profiles' regime to the hydraulic head, h(z,t) field and therefore the subsequent application of Darcy's law, could permit the detection of actual soil water movement, being upwards or downwards , at specific time intervals during the study period. Our basic objective was to investigate the presence of shallow soil water table and moreover its quantitative contribution to the olive trees water needs. The methodology, which could be applied subject to the availability of data, rested on the establishment of two independent conservation principles, the soil surface energy conservation principle and the mass conservation principle of the soil water. It was shown that shallow water table made its presence during the rainy period, and its quantitative contribution to the olive orchard water needs was estimated.

Key words: Seasonal shallow water table, soil moisture profiles, soil hydraulic head profiles, water table contribution to ETc

1. INTRODUCTION

The presence of groundwater at shallow depth from the surface, can provide water to crops contributing significantly to increase their yield in semiarid regions (Sepaskhah, Kanooni, & Ghasemi, 2003) by reducing the requirements for irrigation (Saini & Ghildyal, 1977, Ragab & Amer, 1986, Guitjens, 1990, Ayars & Hutmacher, 1994, while at the same time can cause salinity problems (Rhoades & Loveday, 1990, Hillel, 1998). Experiments on the contribution of groundwater to plant growth have mainly been implemented with lysimeters (Kang, et al, 2001, Stenitzer, et al, 2007, Luo & Sophocleous, 2010, Ghamarnia, et al., 2013).

In this work an attempt is made to determine the movement of soil water in an upward direction contributing to evapotranspiration. Attempting to prove that, two independent methodologies for calculating evapotranspiration were implemented. The first was the FAO-56 method (Allen, et al., 1998) using meteorological data and the second was the water balance method using soil moisture profiles. Furthermore, the relative motion of the water was documented with hydraulic pressure gradient data derived from the soil moisture characteristic curves of the moisture profile at the points where the soil moisture sensors were located.

2. MATERIALS AND METHODS

2.1 Experimental field

The 0.5 ha experimental field (olive orchard) is located about 4 km south of Sparta

(37°22’43.33” N, 22°26’47.10” E). River Evrotas is about 1.5 km east of the experimental field and both are at the same level. During the rainy period, (between December and end of March) a shallow water table is formed due to high precipitation (Bourazanis, Rizos, & Kerkides, 2015). For monitoring this water table, eighteen piezomenters were installed up to 1 m depth. Experimental field’s slope was less than 2/1000 and so it was considered as horizontal.

2.2 Soil moisture measurements

About 1 m away from the central piezometer, seven soil moisture sensors (SMS) were installed to measure soil volumetric water content Θ(%) at 10, 20, 30, 40, 60, 80 and 100 cm depth (figure 2). This was achieved by using ML2 soil moisture sensors (Delta-T, 1999).

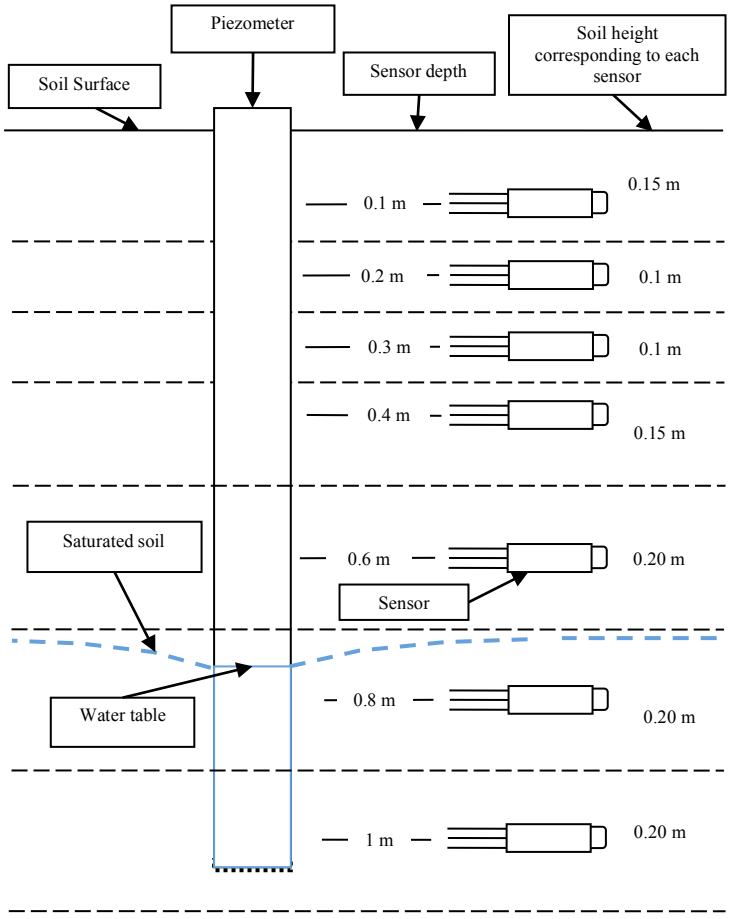

Figure 1. Schematic diagram showing the piezometer & soil moisture sensors installation as well as their positions for the Θ_{si} determinations and the corresponding soil volume.

The considered period 6/06/2014 to 31/08/2014 is chosen when water table was below one meter depth. For calculating water height contained in soil profile it was assumed that each sensor’s measurement corresponds to soil depth intervals presented in Figure 1. The water height in the soil profile is calculated by the equation:

$$I = \sum_{i=1}^{7}(\Theta_{si} * d_{si}) \quad (1)$$

where: I is the total water height, Θ_{si} soil moisture measured by each sensor (i=1-7 with 1st the sensor near the surface and 7th the sensor placed at 1 meter depth) and d_{si} is the soil depth interval corresponding to each sensor (d_{s1}= d_{s4}=15 cm, d_{s2}=d_{s3}=10 cm, d_{s5}=d_{s6}=d_{s7}=20 cm).

2.3 Soil moisture characteristic curves

During the SMS installation and at the same depth, undisturbed soil samples were taken. For determining the soil moisture characteristic curves (SMCC) pressure cells were used (Or & Wraith, 2004, Lu. & Likos, 2002, and Klute, 2006), with a 2.5 bar pressure porous plate. Furthermore the RETC code was used (van Genuchten, Leij, & Yates, 1991) for curve fitting.

2.4 ETc calculations

For calculating evapotranspiration in a daily basis from a reference surface (ETr), meteorological data nearby meteorological station, placed 1.300 m north from the experimental field were used. These data are available at the National Observatory of Athens (NOA) web page (http://penteli.meteo.gr/stations/sparti/). The used data were, air temperature T (^oC), precipitation P (mm) and wind speed u_2 (m s^{-1}). For the calculations the Food and Agricultural Organization (FAO) ETo-Calculation software was used (FAO, 2012).

Daily olive orchards evapotranspiration (ETc) was estimated by the equation ETc=ETr*Kc (Allen, et al., 1998), where Kc is the dimensionless crop coefficient. Crop coefficient values for an olive orchard cultivated in Greece are Kc_{May}=0.40, Kc_{June}=0.45, Kc_{July}=Kc_{August}=0.50 and $Kc_{September}$=0.40 (Papazafiriou, 1991, Papazafiriou, 1999, Papamichail & Babajimopoulos, 2014).

2.5 ETc calculations with the water balance method

ETc for a certain area and a given time period can be calculated with the water balance method (WBM).

$$ET = P + Ir - (SRO + DP) \pm \Delta I \quad (2)$$

where: ET = water height abstracted from the soil profile via evapotranspiration (mm)
P = rainfall height (mm)
Ir = irrigation water applied (mm)
SRO = soil surface runoff (mm)
DP = deeper percolated (mm) and
ΔI = water height calculated as the difference between the soil moisture profile at the beginning and at the end of the considered time period (mm).

Note that all are expressed in height of water (mm).

2. RESULTS

The dataset used for calculating ETr , the Kc values for the considered period and the results are presented in Table 1.

Soil moisture profiles and water height contained in the soil profile at the start and the end of the period are presented in Table 2.

By substituting in equation 2 the results from Tables 2 (P=22.8 mm) and 3 (ΔI=55.5 mm) and by assuming that all the rainfall was effective, and that no soil surface runoff or deep percolation were detected, calculated ETc=32.7 mm. Here it must be mentioned that Ir was zero.

For the same period FAO-56 gave (Table 2) ETc=235.2 mm, meaning that calculated evapotranspiration based on weather and no water shortage conditions, is greater than the amount calculated by the water balance method, namely by 202.5 mm of water, which leads us to the observation that there must be an upward water movement in the soil profile otherwise, this difference is to be attributed to errors of measurement methods, assumptions and conditions imposed. In the remaining an attempt is made to prove that indeed a soil water contribution from below the profile has taken place.

Table 1. ETr Calculation for an olive orchard (1-6-2014 to 31-8-2014)

	P (mm)	T_{mean} (^oC)	T_{max} (^oC)	T_{min} (^oC)	U_2 (m/sec)	ETo (mm/d)	Kc	ETc (mm/d)
2014-06-16	0	23.3	31.4	15.2	1.36	5.7		2.57
2014-06-17	0	24.9	34.9	16.7	1.50	6.6		2.97
2014-06-18	0	23.5	32.9	16.2	1.53	6.1		2.75
2014-06-19	0	24.4	32.2	15.6	2.11	6.4		2.88
2014-06-20	0	23.2	27.3	18.2	2.39	4.7		2.12
2014-06-21	0	23.6	32.3	17.1	2.25	6.4		2.88
2014-06-22	0	24.3	31.8	15.6	2.06	6.3		2.84
2014-06-23	0	24.3	34.4	15.6	1.50	6.5	**0.45**	2.93
2014-06-24	0	25.5	34.8	16.9	1.78	6.7		3.02
2014-06-25	0	28.9	40.3	19.5	2.44	6.6		2.97
2014-06-26	0	30.2	39.7	18.9	2.08	8.2		3.69
2014-06-27	0	28.3	38.4	18.1	2.06	7.9		3.56
2014-06-28	0	27.1	34.1	21	1.97	6.1		2.75
2014-06-29	0	26.1	35.6	17.6	2.00	7		3.15
2014-06-30	0	25.2	34.4	16.6	2.39	7.1		3.20
2014-07-01	0	27.3	37.2	18.9	1.81	7.2		3.60
2014-07-02	0	25.7	35.1	14.7	1.42	6.7		3.35
2014-07-03	0	26.8	36.1	18.4	1.69	6.8		3.40
2014-07-04	0	26.4	34.7	19.8	1.78	6.3		3.15
2014-07-05	0	26.4	34.3	18.9	2.11	6.5		3.25
2014-07-06	0	24.6	34.3	14.5	1.17	6.3		3.15
2014-07-07	0	26.2	35.3	17	1.58	6.6		3.30
2014-07-08	0	28.4	36.9	20.3	1.42	6.5		3.25
2014-07-09	0	29.2	36.8	20.6	2.33	7.2		3.60
2014-07-10	0	28.9	38.2	21.3	2.03	7.2		3.60
2014-07-11	0	26.9	35.3	18.8	2.17	6.9		3.45
2014-07-12	0	25.6	32.2	19.9	2.56	5.9		2.95
2014-07-13	0	26.3	35	16.7	1.69	6.6		3.30
2014-07-14	0	26.3	33.3	20.1	2.47	6.2		3.10
2014-07-15	0	25.6	32.3	19.2	1.92	5.7		2.85
2014-07-16	0	24	30.6	17.6	1.25	5.1		2.55
2014-07-17	0.2	23.8	32.2	17.8	1.17	5.4		2.70
2014-07-18	7	23.7	33.6	18.7	1.81	6.1		3.05
2014-07-19	3.2	22.2	33.1	17.7	1.22	5.6		2.80
2014-07-20	0	24.5	33.4	18.8	1.06	5.4		2.70
2014-07-21	0	26.8	36.5	18.8	1.08	6.1		3.05
2014-07-22	0	27.2	36.5	18.6	1.33	6.4		3.20
2014-07-23	0	25	33.6	16.7	1.44	6		3.00
2014-07-24	0	26.2	33.2	20.6	1.67	5.5		2.75
2014-07-25	1.8	26.3	34.8	21.1	1.50	5.7		2.85
2014-07-26	0	26.9	36.3	20	1.31	6.1		3.05
2014-07-27	0	27.1	36.3	19.1	1.14	6		3.00
2014-07-28	0	27.3	36.2	17.7	0.97	5.9		2.95
2014-07-29	0	28.5	37.3	21.6	1.89	6.6		3.30
2014-07-30	0	28.4	37.6	21.3	1.56	6.4		3.20
2014-07-31	0	27.4	36.2	18.6	1.42	6.2	**0.5**	3.10
2014-08-01	0	27	34.2	21.1	2.19	5.9		2.95
2014-08-02	0	26.2	34.1	18.8	1.92	6.1		3.05
2014-08-03	0	27.6	37.5	20.1	1.47	6.4		3.20
2014-08-04	0	28.8	39.1	20.1	1.39	6.7		3.35
2014-08-05	0	28.9	37.8	21.4	1.67	6.4		3.20
2014-08-06	0	27.3	35.3	20.6	2.11	6.2		3.10
2014-08-07	7	24.3	32.8	18.2	1.83	5.6		2.80
2014-08-08	3.4	24.4	32.2	18.8	1.78	5.4		2.70
2014-08-09	0.2	25.6	34.8	19.1	1.42	5.7		2.85
2014-08-10	0	27.4	37.3	19.7	1.47	6.2		3.10
2014-08-11	0	28.1	38.2	20.5	1.78	6.6		3.30
2014-08-12	0	28.6	38.7	20.3	1.72	6.7		3.35
2014-08-13	0	29.3	39.4	20.4	1.75	6.2		3.10
2014-08-14	0	28.4	39.8	19.3	1.28	6.5		3.25
2014-08-15	0	30.5	41.2	19.3	1.56	7.2		3.60
2014-08-16	0	29.3	37.5	23.1	2.36	6.5		3.25
2014-08-17	0	27.4	35.4	21	2.78	6.4		3.20
2014-08-18	0	25.1	31.8	20.4	1.81	4.9		2.45
2014-08-19	0	25.3	35.6	17.8	1.64	6		3.00
2014-08-20	0	24.5	35.3	15.2	1.22	5.7		2.85
2014-08-21	0	26.7	37.7	16.1	1.42	6.3		3.15
2014-08-22	0	29.5	40.9	20.5	1.22	6.4		3.20
2014-08-23	0	30.9	40.7	18.8	1.44	6.7		3.35
2014-08-24	0	30.1	40.9	19.5	1.42	6.7		3.35
2014-08-25	0	29.3	38.2	19.7	1.61	6.2		3.10
2014-08-26	0	25.7	35.2	15.8	1.31	5.6		2.80
2014-08-27	0	27.1	35.9	20.6	1.58	5.5		2.75
2014-08-28	0	28.2	37.8	20.8	1.83	6.1		3.05
2014-08-29	0	26.6	36	19.1	1.75	5.8		2.90
2014-08-30	0	26.1	34.6	20	1.78	5.3		2.65
2014-08-31	0	24.3	33.9	18.3	1.22	4.9		2.45
	22.8							**235.19**

For each SMS it was possible to determine the soil water pressure head (H) through SMCC assuming that the moisture content values recorded by each sensor belongs to the main drying curve. This was so because there wasn't any addition of water in the soil profile (irrigation, precipitation) for a period of 20 days before the selected date. Table 3 and Figure 2 show clearly the above.

Table 2. Calculating the water height contained in the soil profile at the beginning and at the end of the period

Soil height considered for each sensor (cm)	Sensor depth (cm)	Θ (%)		Water height I (mm)	
		16/06/2014	31/8/2014	16/06/2014	31/8/2014
15	-10	31.78	12.67	47.7	19.0
10	-20	26.04	14.07	26.0	14.1
10	-30	17.69	16.71	17.7	16.7
15	-40	16.49	15.59	24.7	23.4
20	-60	20.43	18.85	40.9	37.7
20	-80	17.32	15.57	34.6	31.1
20	-100	20.68	17.74	41.4	35.5
Water height contained in the soil profile (mm)				**233.0**	**177.5**
ΔI (mm)				**55.5**	

Table 3. Soil water pressure head profiles and calculated water pressure head and hydraulic head gradient profiles at the beginning and at the end of the examined period

H (cm)					**2014-06-16**		**2014-08-31**	
Sensors depth	**2014-06-16**	**2014-08-31**	**ΔZ**	**Depth corresponding to each gradient**	**ΔH/ΔZ**	**Δh/ΔZ**	**ΔH/ΔZ**	**Δh/ΔZ**
-10	-1	-6667						
			10	-15	13.3	14.3	-26.7	-25.7
-20	-134	-6400						
			10	-25	114.1	115.1	-442	-441
-30	-1275	-1980						
			10	-35	21.4	22.4	-25,7	-24,7
-40	-1489	-1723						
			20	-50	-36.95	-35.95	-1,15	-0,15
-60	-750	-1700						
			20	-70	9.2	10.2	-17,5	-16,5
-80	-934	-1350						
			20	-90	-40,65	-39,65	-51,25	-50,25
-100	-121	-325						

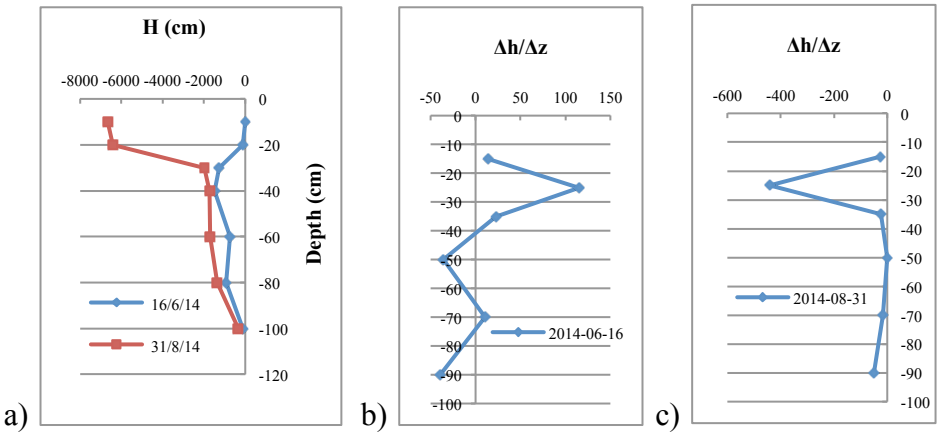

Figure 2. Soil pressure head profiles (a) and hydraulic head gradient profiles at the beginning (b) and at the end (c) of the examined period

2. DISCUSSION - CONCLUSIONS

Trying to interpret these findings we can attribute the difference of the two methodologies (202.5 mm) to:

1. The amount of the effective precipitation taken into account using WBM. Making the hypothesis that the whole precipitation wasn't effective or that there wasn't any precipitation and recalculating the ETc using equation 2 the ETc=55.5mm still appears lower than the ETc calculated by the ETo-56 method (235,19 mm).
2. The event that transpiration of crop plants, with a deep active root zone, still continuous, although the upper soil layer is dry exploiting soil moisture from deeper layers.
3. The contribution of the shallow water table

In any case, the examination of soil water movement and the possible contribution of the water table to ETc is not sufficient since this evidence is indirect. To prove the contribution of the water table to ETc hydraulic head gradients (HHG) must be calculated because this is the driving force of water movement in soil (Poulovassilis, 2010).

Examining soil HHG profile presented in figure 4b (06.16.2014), we see that at depths of -15, -25, -35 and -70 cm the HHG is positive, i.e. the movement of the water is downward, while at -50 and -90 cm, the HHG is negative and so the movement of the water at these depths is upward, resulting to an increase of moisture at -40 and -80 cm respectively. Regarding the figure 4c we see that the HPG in all profile depth is negative which means that water moves upward until the soil surface from which it evaporates. This finding demonstrates that the difference between the two ways of calculating evapotranspiration found is due to upward movement of water, without excluding the removal of moisture from the profile through crop transpiration. It has been reported (Allen, et al., 1998) that olives orchard active rooting depth is 1.2 to 1.7m deep and should therefore be considered equally possible the contribution of transpiration of the crop to the difference between the two ETc results.

In the present study the movement of water within the soil profile and the potential contribution of the shallow water table in evapotranspiration were examined. Initially a comparison between evapotranspiration calculated by using meteorological data (FAO-56) and the water balance method has been made. A difference between these two methodologies results was found, implying possible contribution of the shallow water table to evapotranspiration. Furthermore, an upward movement of water through the soil profile was proven, through the calculation of the hydraulic head gradients We should also bear in mind that olive trees can transpire, exploiting soil moisture from deeper layers, but this cannot diminish the findings of the present study.

REFERENCES

Allen, R. G., Pereira, L. S., Raes, D., & Smith, M. (1998). *Crop Evapotranspiration (guidelines for computing crop water requirements)* FAO Irrigation and Drainage Paper No. 56. Rome, Italy: FAO, Water Resources, Development and Management Service.

Ayars, J. E., & Hutmacher, R. B. (1994). Crop coefficients for irrigating cotton in the presence of groundwater. Irrig Sci , pp. 15:45–52.

Bourazanis, G., Rizos, S., & Kerkides, P. (2015). Soil water balance in the presence of a shallow water table . In EWRA, Proceedings of 9th WORLD CONGRESS *«Water Resources Management in a Changing World: Challenges and Opportunities»*, Istanbul, Turkey 10-13 June 2015.

Delta-T, D. (1999). *User Manual ML2x-UM-1.21*. Cambridge, England: Delta-T.

FAO. (2012). *ETo Calculator, ver. 3.2, Land and Water Digital media Series No 56*. Rome, Italy: FAO.

Ghamarnia, H., Golamian, M., Sepehri, S., Arji, I., & Norozpour, S. (2013). The contribution of shallow groundwater by safflower (Carthamus tinctorius L.) under high water table conditions, with and without supplementary irrigation. Irrig Sci , pp. 31:285–299, DOI 10.1007/s00271-011-0304-2.

Guitjens, J. C. (1990). Alfalfa. In B. A. Stewart, & D. R. Nielsen, *Irrigation of agricultural crops. Agronomy Series 30* (pp 537–568). Madison, WI,: American Society of Agronomy.

Hillel, D. (1998). *Environmental Soil Physics*. New York: Academic Press.

Kang, S., Zhang, F., Hu, X., Jerie, P., & Zhang, L. (2001). Effects of shallow water table on capillary contribution, evapotranspiration, and crop coefficient of maize and winter wheat in a semi-arid region ,. Aust. J. Agric. Res. , pp. 52, 317–327.

Klute, A. (2006). Water retention, Laboratory methods. In A. Klute, *Methods of Soil Analysis Part 1-Physical and Mineralogical Methods*, 2nd Ed., (pp. 635-656). SSSA Book Series 5.

Lu., N., & Likos, W. J. (2002). *Unsaturated Soil mechanics*. John Wiley & Sons INC,.

Luo, Y., & Sophocleous, M. (2010). Seasonal groundwater contribution to crop-water use assessed with lysimeter observations and model simulations. Journal of Hydrology , pp. 389: 325–335.

Or, D., & Wraith, J. M. (2004). Soil water content and water potential relationships. In W. A. Warrick, *Soil Physics Companion* (pp. 49-82). CRC Press.

Papamichail, D. M., & Babajimopoulos, C. S. (2014). *Applied Agricultural Hydraulics*. Thessalonica: Ziti (in Greek).

Papazafiriou, Z. G. (1999). *Crop Water Reqirements*. Thessalonica: Ziti (in Greek).

Papazafiriou, Z. G. (1991). Determination crop coefficients suited to Greek conditions. Progress report on the research program Experimental application of newer irrigation methods (in Greek).

Poulovassilis, A. (2010). *Introduction to irrigation*. Athens, Embrio (in Greek).

Ragab, R. A., & Amer, F. (1986). Estimating water table contribution to the water supply of maize. Agric Water Manag , pp. 11:221–230.

Rhoades, J. D., & Loveday, J. (1990). Salinity in irrigated agriculture . In B. A. Stewart, & D. R. Nielsen, *Irrigation of agricultural crops. Agronomy Series 30* (pp. 1089–1142). Madison, WI: American Society of Agronomy.

Saini, B. C., & Ghildyal, B. P. (1977). Seasonal water use by winter wheat grown under shallow water table conditions. Agric Water Manag , pp. 1:201–298.

Sepaskhah, A. R., Kanooni, A., & Ghasemi, M. M. (2003). Estimating water table contributions to corn and sorghum water use. Agricultural Water Management , pp. 58, 67–79.

Stenitzer, E., Diestel, H., Zenker, T., & Schwartengräber, R. (2007). Assessment of Capillary Rise from Shallow Groundwater by the Simulation Model SIMWASER Using Either Estimated Pedotransfer Functions or Measured Hydraulic Parameters. Water Resour Manage , pp. 21:1567–1584, DOI 10.1007/s11269-006-9113-4.

van Genuchten, M. T., Leij, F. J., & Yates, S. R. (1991). *The RETC code for quantifying the hydraulic functions of unsaturated soils*. Riverside, California.: U.S.D.A.

Proceedings of the 10th World Congress of EWRA 'Panta Rhei', 5-9 July 2017, Athens, Greece
© 2017 *European Water Resources Association*

Temporal variation of reference evapotranspiration and regional drought estimation using SPEI method for semi-arid Konya closed basin in Turkey

A.S. Anli
Ankara University Agricultural Faculty, Ankara, Turkey
e-mail: alperanli@gmail.com

Abstract: Analysis of temporal variation of reference evapotranspiration (ET_0) is of great importance in arid and semi-arid regions where water resources are limited. In this study, temporal variation of reference evapotranspiration (ET_0) with parametric and non-parametric tests and regional drought analysis using SPEI (Standardized Precipitation Evapotranspiration Index) method with L-moment parameter estimation have been carried out in semi-arid Konya closed basin in Turkey. Reference evapotranspiration of concerning closed basin in the basin has been estimated using Penman-Monteith method and one calendar year has been split up multi-scalar periods as 1 month, 3 months, 6 months, 9 months and 12 months. Temporal variation of reference evapotranspiration according to multi-scalar periods has been analyzed through parametric Augmented Dickey-Fuller (ADF) test and non-parametric Mann-Whitney *U* (M-W) test. Significant increasing and little trends for reference evapotranspiration (ET_0) have been detected. According to SPEI method for multi-scalar periods, mild drought has been experienced in general, and however there have been also a significant amount of events where moderate and severe droughts occurred in the basin. When compared with another index RDI (Reconnaissance Drought Index) method using evapotranspiration, it can be said that the SPEI method is particularly sensitive to extreme and severe drought estimates. For estimating regional drought pattern with L-moments for SPEI values, one climatologically homogeneous region has been stated using discordancy, heterogeneity and goodness of fit tests. The best suitable regional distributions for the periods have been found 5-parameter Wakeby distribution. According to Wakeby distribution for homogeneous region, probable regional SPEI quantiles have been estimated various return period.

Key words: reference evapotranspiration, temporal variation, SPEI, regional drought, Konya closed basin

1. INTRODUCTION

In the arid and semi-arid regions where water resources are limited, the temporal variation of the reference evapotranspiration analysis is very important. Reference evapotranspiration is one of the important parameters to calculate the crop water requirement. Konya closed basin is one of the major agricultural regions of our country at the same time that the annual rainfall is extremely low. Surface water resources are extremely limited and only ground water resources are available. But ground water resources are also very deep. Therefore, estimating the water consumption by plants properly and knowing how it changes over time is extremely important in terms of water requirement. The region under the influence of global warming and drought, income expected from agricultural production, the most important factor in achieving estimation and acquisition of water has gained importance. Drought is stated that relationship of water shortage with humidity of a region of its temporary imbalance. The most important factors affecting drought are high temperature, strong wind, low humidity and less than normal precipitation. Many indices to indicate drought developed. These indices are from an arid region benefit in extracting short and sufficient information (Agnew, 1990; Agnew and Warren, 1996). At the same time, these indices are very important to minimize the drought effect and to manage the water resources. Standard Precipitation Index (SPI) only considers precipitation, while Standard Precipitation Evapotranspiration Index (SPEI) and Reconnaissance Drought Index (RDI) consider both precipitation and evapotranspiration (Tsakiris and Vangelis, 2004; Tsakiris and Vangelis, 2005; Tsakiris et al., 2007; Tsakiris, 2010; Unlukara et al., 2010a; Anli, et al., 2011; Vangelis et al., 2013). Time-series analysis such as Mann-Kendall, Mann-Whitney *U*, Augmented Dickey-Fuller and moving average methods are usually

used for temporal changes of climatic parameters by researchers (Unlukara et al., 2010b; Zhang et al., 2010; Yang et al., 2011; Tabari et al., 2012; Ye et al., 2013).

In this study, temporal variation of reference evapotranspiration (ET_0) with parametric and non-parametric tests and regional drought analysis using SPEI (Standardized Precipitation Evapotranspiration Index) method with L-moment parameter estimation have been carried out in semi-arid Konya closed basin in Turkey for planning and management water resources and crop water requirement and partly estimate the capacity of groundwater resources to be important for agricultural water use in the basin.

2. STUDY AREA AND AVAILABLE DATA

One of 26-main river basins in Turkey is Konya closed basin having an area of 53.850 km^2 and its area is about % 7 of Turkey's total area. The basin located in the central Anatolia region is bounded 36º 51' and 39º 29' N latitudes, 31º 36' and 34º 52' E longitudes. The region is characterized by a semi-arid continental climate; summers are hot and dry whereas winters are cold and moist. In terms of the hydrology of the basin, the surface water resources are of little importance as there are only few rivers and creeks. Most of the water is transported as groundwater; therefore, groundwater is of great importance for the water management of the basin. Mean annual total rainfall of the basin which has continental climate is very low when comparing the mean of Turkey (412 mm).

In this study, monthly precipitation, minimum and maximum temperature, relative humidity, wind speed and sunshine data set measured between 1971-2015 were used in Aksaray, Cihanbeyli, Eregli, Karaman, Konya and Nigde meteorological stations in Konya closed basin for calculation of reference evapotranspiration with Penman-Monteith method, standard precipitation evapotranspiration index and estimation of regional SPEI.

3. METHODOLOGY

3.1 Reference evapotranspiration analysis

For calculation of reference evapotranspiration, Penman-Monteith method has been used with CROPWAT software (Allen et al., 1998). The monthly minimum and maximum temperature, relative humidity, wind speed and sunshine values were used to calculate the reference evapotranspiration by the Penman-Monteith method. One calendar year has been split up five multi-scalar periods as 1 month, 3 months, 6 months, 9 months and 12 months (annual). The Penman-Monteith method was able to provide only 6 stations with the exact data required. The Penman-Monteith method is described as follows:

$$ET_0 = \frac{0.408\Delta(R_n - G) + \gamma \frac{900}{T+273} u_2 (e_s - e_a)}{\Delta + \gamma (1 + 0.34 u_2)} \quad (1)$$

ET_0: reference evapotranspiration (mm/day), R_n: Net radiation at the plant surface ((MJ m^{-2} /day), G: Soil heat flux density (MJ m^{-2} / day), T: Average daily air temperature (°C) at a height of 2 m, u_2: Wind speed at 2 m height (m / s), e_s: Saturated vapor pressure (kPa), e_a: Actual vapor pressure (kPA), Δ: The curve of the vapor pressure curve (kPa / ^oC), γ: Psychrometric constant (kPa / ^oC) (FAO, 2013).

3.2 Temporal variation analysis

Temporal variation of the reference evapotranspiration for five multi-scalar periods has been

detected parametric Augmented Dickey Fuller (unit root) test and non-parametric Mann-Whitney *U* test.

Parametric Augmented Dickey Fuller that is a test used to determine whether there is a unit root in the observed series (the series is not stationary) (eq. 2-4).

$$y_t = \rho y_{t-1} + u_t \quad (2)$$

u_t = stochastic error.

$$y_t - y_{t-1} = (\rho-1)\, y_{t-1} + u_t \quad (3)$$

When y_{t-1} is subtracted from both sides of eq. 3, eq. 4 is obtained with $(\rho-1) = y$.

$$\Delta y_t = \delta y_{t-1} + u_t \quad (4)$$

H_o: $\rho=1$, H_1: $\rho<1$

In the case $(\rho-1)= 0$ and $\delta= 0$, the series of y_t have a unit root. In the case $|\rho| < 1$, the series are to be stationary. τ (tau) statistic is used with Monte Carlo simulation technique for detecting the temporal variation. If the absolute τ value is greater than Dickey-Fuller critical tabular values, the time series sample is not stationary (Dickey and Fuller, 1979).

Non-parametric Mann-Whitney U test investigates whether two independent samples come from the same population (Enders, 1995). The hypothesis is stated below:

H_0= two independent samples come from the same population.

H_1= two independent samples do not come from the same population.

The two independent samples (n_A and n_B) are combined and the smallest number is numbered 1. Therefore, the *U* statistic is calculated for detecting the temporal variation with eq. 5:

$$U=n_A n_B + (n_A (n_B+1)/2) - R_A \quad (5)$$

The R_A value in the eq. 4 shows the sum of the orders of the first sample values. The mean and standard deviation of *U* statistic are $\mu_U = (n_A n_B)/2$ and $\sigma_U = (n_A\, n_B\, (n_A+n_B+1)/12)^{1/2}$, respectively. Therefore the Mann-Whitney test statistic is calculated with eq. 6:

$$Z= (U- \mu_U) / \sigma_U \quad (6)$$

The *Z* parameter is compared with the table value (± 1.96) of the standard normal distribution at $\alpha= 0.05$ significance level. If this value is greater than the table value of the standard normal distribution, it is decided that the two samples are not elements of the same population.

3.3 Standard Precipitation Evapotranspiration Index (SPEI) analysis

The SPEI method is an effective drought index that uses precipitation and evapotranspiration amounts together (Vicente-Serrano et al., 2010). In this study, the reference evapotranspiration amounts calculated according to the Penman-Monteith method are indicated on five time scales as 1 month, 3 months, 6 months, 9 months and 12 months. Monthly precipitation amounts are also indicated at the same time scales, and then the difference (D_i series; water surplus or deficit) between the precipitation P_i and evapotranspiration ET_i for the month *i* is calculated using eq. 7:

$$D_i= P_i - ET_i \quad (7)$$

After calculating the D_i series, the frequency distribution showing the best fit for these series was estimated. For this purpose, generalized logistics (GLO), generalized extreme values (GEV), generalized Pareto (GPA), generalized normal (GNO) and Pearson type 3 (PE3) distributions have

been tried with L-moment parameter estimation method (Hosking and Wallis, 1997). Kolmogorov-Smirnov (K-S) test has been used to select the most suitable distribution for D_i series. The probability of each D_i value was calculated using the cumulative distribution function $F(x)$ of the appropriate frequency distribution. With $F(x)$ the SPEI is obtained as the standardized values of $F(x)$ in eq. 8 (Abramowitz and Stegun, 1965):

$$SPEI = W - (C_0 + C_1W + C_2W^2) / (1 + d_1W + d_2W^2 + d_3W^3) \quad (8)$$

$W = (-2ln\ P)^{0.5}$ for $P \leq 0.5$, $P = 1 - F(x)$

$C_0 = 2.515547$, $C_1 = 0.802853$, $C_2 = 0.010328$, $d_1 = 1.432788$, $d_2 = 0.189269$, $d_3 = 0.001308$.

If $P > 0.5$, then P is replaced by $1 - P$ and the sign of the result SPEI is reversed.

RDI (Reconnaissance Drought Index), another important index using evapotranspiration (Tsakiris et al., 2007) were also compared with SPEI results in this study. The classification of the RDI method is almost identical to SPEI. The SPEI and RDI drought categories are given in Table 1.

3.4 Regional SPEI analysis

After calculating the SPEI values for five separate time scales, a regional SPEI analysis was performed for each time scale. After calculating the SPEI values for five separate time scales, a regional SPEI analysis was performed for each time scale. Regionalization has been performed according to the index-storm method with the method of L-moments. The 6 meteorological stations used in the study were considered as one region and the discordancy, heterogeneity and goodness of fit test given in Hosking and Wallis (1997) were performed. Then, regional SPEI values for various return periods (2, 5, 10, 25, 50 and 100 years) were estimated with the regional L-moment algorithm.

For all calculations, the routines written in FORTRAN 77 source codes (L-moments, version 3.04) are used by Hosking (2005). These routines are compiled and run under a main executable program (Anli, 2015).

Table 1. SPEI and RDI drought categories

Drought Category	SPEI & RDI
Non-drought	0 ≤ SPEI & RDI
Mild drought (MiD)	-0.99 ≤ SPEI & RDI < 0
Moderate drought (MD)	-1.49 ≤ SPEI & RDI ≤ -1.0
Severe drought (SD)	-1.99 ≤ SPEI & RDI ≤ -1.5
Extreme drought (ED)	SPEI & RDI ≤ -2.0

4. RESULTS AND DISCUSSION

Monthly reference evapotranspiration amounts were calculated according to the Penman-Monteith method for 6 stations' data series. The monthly reference evapotranspiration amounts were made into 1 month, 3 months, 6 months, 9 months and 12 months periods and their temporal variation were analyzed according to the parametric Augmented Dickey-Fuller and the non-parametric Mann-Whitney U test and have been given table 2 and table 3, respectively.

According to the ADF test statistic and probability values in Table 2, at the 6th month, 9th month and 12th month of Karaman station, there is a unit root in the reference evapotranspiration quantities and the evapotranspiration quantities are not stable over time. Apart from this, the amounts of the evapotranspiration in all the periods of all other stations are stationary.

For this test, the amount of evapotranspiration calculated with the data from the stations is taken as multi-time scale and 3 sub-divisions are allocated within the observation years. Then the variation of these sub-series over time is compared between each other. In Table 3, the reference evapotranspiration amounts obtained from the stations are compared with the time scales of 1, 3, 6, 9 and 12 months (1971-1985) versus (1986-2000), (1971-1985) versus (2001-2015) and (1986-2000) versus (2001-2015) were compared. According to these comparisons, there is an increasing

trend in the reference evapotranspiration quantities in the time scales of the 6, 9 and 12 months of the period of Aksaray station (1971-1985) versus (2001-2015) and in all time scales of (1986-2000) versus (2001-2015). There is a decreasing trend in the reference evapotranspiration quantities in the 12 month time scale of Cihanbeyli station (1971-1985) versus (1986-2000) and in the 9 and 12 month time scales of (1971-1985) versus (2001-2015). The decreasing trend in the 1 and 3-month time scales (1971-1985) versus (1986-2000) period, the increasing trend in the 6, 9 and 12 month time scales (1971-1985) versus (2001-2015) period have been observed. There is also an increasing trend (1986-200) versus (2001-2015) in all time scales. There is an increasing trend in the Karaman station (1986-2000) versus (2001-2015) for 1, 3, 9 and 12 months' time scales. In Konya station (1971-1985) vs (2001-2015), an increasing trend has been observed in all time scales. (1986-2000) versus (2001-2015), there is an increasing trend excluding 9-month time scale. A decreasing trend was observed in the Nigde station (1971-1985) versus (1986-2000) for 6 and 12-month time scales, and in the 9 and 12-month time scaled (1971-1985) versus (2001-2015) periods. According to these results, it can be said that the reference evapotranspiration amounts increased in general and occasionally decreased in time scales. No changes were seen during periods when there were no increasing or decreasing trends.

Table 2. The Augmented Dickey-Fuller test results

ADF	**Aksaray**					**Cihanbeyli**				
	1	**3**	**6**	**9**	**12**	**1**	**3**	**6**	**9**	**12**
Stat	-2.8967	-3.0779	-3.2239	-3.0930	-2.7142	-3.2739	-2.6502	-2.7548	-2.8191	-2.5408
P	0.2229	0.1521	0.0981	0.1462	0.2942	0.0908	0.3192	0.2783	0.2532	0.3620
Result	stationary	stationary	stationary	stationary	stationary	stationary	stationary	stationary	stationary	stationary
	Eregli					**Karaman**				
	1	**3**	**6**	**9**	**12**	**1**	**3**	**6**	**9**	**12**
Stat	-2.5376	-1.3075	-1.8702	-1.9312	-2.2034	-3.2338	-3.1983	-3.9601	-3.9818	-3.6904
P	0.3651	0.8407	0.6231	0.5995	0.4943	0.0967	0.1050	0.0219	0.0210	0.0394
Result	stationary	stationary	stationary	stationary	stationary	stationary	stationary	**non-stat.**	**non-stat.**	**non-stat.**
	Konya					**Nigde**				
	1	**3**	**6**	**9**	**12**	**1**	**3**	**6**	**9**	**12**
Stat	-2.7579	-2.1616	-2.0848	-1.7096	-1.7114	-3.3676	-3.0573	-2.7895	-1.7399	-1.6991
P	0.2799	0.5105	0.5401	0.6852	0.6845	0.0770	0.1602	0.2648	0.6750	0.6909
Result	stationary	stationary	stationary	stationary	stationary	stationary	stationary	stationary	stationary	stationary

When calculating the SPEI values, the probability distribution showing the best fit of the D_i series was determined according to the K-S test. According to the results of K-S test, GEV distribution at 1, 3, 6 and 12 months of D_i series and 9 months of D_i series GPA distribution station provided the best fit at Aksaray. In the Cihanbeyli station, GLO distribution for 1, 6, 9 and 12 month of D_i series and GEV distribution for 3 month of D_i series showed the best fit. The GEV distribution to the D_i series at all time scales at the Eregli and Konya station provided the best fit. The GEV distribution for the 1 and 3 month time scales and the GLO distribution for the other time scales were the best fit at the Karaman station. The GEV distribution for the 1 and 12 month time scales and the GLO distribution at the other time scales were the best fit at the Nigde station. SPEI values were calculated using eq. 8 according to the cumulative probability functions $F(x)$ of the distributions that best fit the D_i series. Drought rates occurred in observation period for time scales according to calculated SPEI and RDI values are given in Table 4.

As seen in Table 4, mild droughts were generally observed for both methods in the basin. In addition, moderate and severe droughts have been observed in some periods. Especially during the observation period at the Nigde station, extreme drought has occurred four times for SPEI methods.

The SPEI method is more sensitive than the RDI method in diagnosing drought, especially severe and moderate drought periods were found more in SPEI method. More mild dry periods have been identified in the RDI method. Extreme droughts are estimated to be almost the same for both methods. As a result; it can be said that both methods are almost close to each other.

Table 3. Mann-Whitney U test results

M-W	Aksaray								
	(1971-1985) vs (1986-2000)			(1971-1985) vs (2001-2015)			(1986-2000) vs (2001-2015)		
Time-Scale	W	P	Trend	W	P	Trend	W	P	Trend
1	215.5	0.5814	No	172.0	0.1611	No	159.5	0.0482	↑
3	234.0	0.1611	No	167.0	0.1029	No	139.0	0.0035	↑
6	209.0	0.8005	No	140.0	0.0041	↑	133.0	0.0014	↑
9	213.0	0.6625	No	144.0	0.0072	↑	134.0	0.0016	↑
12	218.5	0.4907	No	140.0	0.0041	↑	129.0	0.0007	↑
M-W	**Cihanbeyli**								
	(1971-1985) vs (1986-2000)			(1971-1985) vs (2001-2015)			(1986-2000) vs (2001-2015)		
Time-Scale	W	P	Trend	W	P	Trend	W	P	Trend
1	203.0	1.0000	No	178.0	0.2603	No	180.0	0.3012	No
3	233.5	0.1681	No	208.0	0.8362	No	177.0	0.2413	No
6	232.5	0.1827	No	235.5	0.1415	No	205.5	0.9268	No
9	244.5	0.0596	No	248.0	0.0409	↓	207.0	0.8722	No
12	254.0	0.0203	↓	258.0	0.0123	↓	207.0	0.8722	No
M-W	**Eregli**								
	(1971-1985) vs (1986-2000)			(1971-1985) vs (2001-2015)			(1986-2000) vs (2001-2015)		
Time-Scale	W	P	Trend	W	P	Trend	W	P	Trend
1	188.5	0.0282	↓	164.0	0.6833	No	116.5	0.0339	↑
3	198.5	0.0056	↓	120.0	0.0535	No	89.0	0.0003	↑
6	166.0	0.3708	No	115.0	0.0276	↑	107.0	0.0083	↑
9	168.0	0.3123	No	98.0	0.0018	↑	90.0	0.0004	↑
12	162.0	0.5067	No	97.0	0.0015	↑	85.0	0.0001	↑
M-W	**Karaman**								
	(1971-1985) vs (1986-2000)			(1971-1985) vs (2001-2015)			(1986-2000) vs (2001-2015)		
Time-Scale	W	P	Trend	W	P	Trend	W	P	Trend
1	228.0	0.2603	No	181.5	0.3346	No	157.0	0.0366	↑
3	232.0	0.1904	No	183.0	0.3703	No	147.5	0.0115	↑
6	211.0	0.7304	No	180.0	0.3012	No	161.0	0.0565	No
9	221.0	0.4213	No	178.0	0.2603	No	159.0	0.0456	↑
12	226.0	0.3012	No	176.5	0.2322	No	155.0	0.0291	↑
M-W	**Konya**								
	(1971-1985) vs (1986-2000)			(1971-1985) vs (2001-2015)			(1986-2000) vs (2001-2015)		
Time-Scale	W	P	Trend	W	P	Trend	W	P	Trend
1	127.5	0.2040	No	104.5	0.0055	↑	113.5	0.0223	↑
3	132.0	0.3123	No	93.0	0.0007	↑	107.0	0.0083	↑
6	145.0	0.7950	No	90.0	0.0004	↑	113.0	0.0208	↑
9	138.0	0.5067	No	85.0	0.0001	↑	120.0	0.0535	No
12	137.5	0.4884	No	85.0	0.0001	↑	118.0	0.0414	↑
M-W	**Nigde**								
	(1971-1985) vs (1986-2000)			(1971-1985) vs (2001-2015)			(1986-2000) vs (2001-2015)		
Time-Scale	W	P	Trend	W	P	Trend	W	P	Trend
1	232.0	0.1901	No	190.5	0.5812	No	162.0	0.0625	No
3	244.0	0.0627	No	225.0	0.3229	No	179.5	0.2905	No
6	270.5	0.021	↓	238.5	0.1078	No	184.0	0.3950	No
9	175.0	0.2604	No	269.0	0.0026	↓	175.0	0.2064	No
12	290.0	0.0001	↓	279.0	0.0005	↓	177.0	0.2413	No

Table 4. Drought rates for time scales according to SPEI and RDI

SPEI	Aksaray					Cihanbeyli					RDI	Aksaray					Cihanbeyli				
	1	3	6	9	12	1	3	6	9	12		1	3	6	9	12	1	3	6	9	12
ED	-	-	1	-	-	-	1	-	-	-	ED	-	-	1	-	-	-	-	-	-	-
SD	1	3	2	2	3	4	1	2	2	4	SD	1	2	3	3	-	1	1	1	2	2
MD	7	6	4	5	6	3	4	5	4	1	MD	7	3	3	4	8	7	6	4	5	6
MiD	11	10	18	17	16	15	15	14	10	15	MiD	14	20	16	15	12	16	17	17	14	15
SPEI	Eregli					Karaman					RDI	Eregli					Karaman				
	1	3	6	9	12	1	3	6	9	12		1	3	6	9	12	1	3	6	9	12
ED	-	1	-	-	-	-	-	-	-	-	ED	-	1	1	1	1	-	-	-	-	-
SD	-	2	2	2	-	2	4	2	1	1	SD	1	-	-	-	3	2	2	-	-	1
MD	5	3	5	6	6	5	3	5	6	8	MD	6	8	7	6	4	3	6	7	8	5
MiD	14	12	11	10	12	12	14	15	15	11	MiD	14	8	12	10	13	17	13	16	14	15
SPEI	Konya					Nigde					RDI	Konya					Nigde				
	1	3	6	9	12	1	3	6	9	12		1	3	6	9	12	1	3	6	9	12
ED	-	-	-	-	-	1	-	1	1	1	ED	-	-	-	-	-	-	-	1	2	1
SD	3	1	1	2	3	1	2	2	2	2	SD	-	1	2	2	4	1	2	1	2	3
MD	3	8	4	4	3	1	4	4	4	3	MD	2	5	4	3	4	5	3	6	3	3
MiD	10	10	14	13	10	19	14	14	15	17	MiD	20	14	13	12	8	19	18	11	14	14

L-moment method was used for regional analysis of SPEI values and evapotranspiration amounts showed no discordancy according to time scales in one region. In addition, heterogeneity measures are found to be acceptable homogeneous of the basin. The best fit to the SPEI values calculated according to the time scales is ensured by the 5-parameter Wakeby distribution. The regional SPEI values calculated according to these distribution parameters and the regional L-moment algorithm for 2, 5, 10, 25, 50 and 100 year return period are given in table 5.

Table 5. Regional SPEI values for various return period

T_{year}	Time scale				
	1	3	6	9	12
2	0.04	0.01	-0.01	-0.02	-0.01
5	0.91	0.94	0.89	0.90	0.90
10	1.30	1.31	1.27	1.27	1.27
25	1.61	1.57	1.56	1.54	1.55
50	1.75	1.68	1.69	1.65	1.66
100	1.84	1.74	1.77	1.71	1.73

As can be seen from Table 5, it can be said that the drought period will be seen in the short term every 2 and 5 years while the humid period can be seen in the long term.

5. CONCLUSIONS

The study presents an analysis of temporal variation of reference evapotranspiration and the regional drought analysis based on the SPEI which directly influence drought severity. RDI method which use evapotranspiration have only been used in the study for comparison with SPEI results.

It has been observed that the reference evapotranspiration quantities in the study generally increase in time scales, and very few decrease.

Increasing evapotranspiration means increasing plant water demand. Because of this, proper management of water resources should be performed in the basin and pressurize irrigation methods should be applied instead of surface irrigation methods. Limited irrigation practices can also be suggested.

On the other hand, according to SPEI values, it can be said that moderate and severe droughts are occasionally observed in the basin while mild drought is dominant.

The best suitable regional distribution for the SPEI values have been found 5-parameter Wakeby distribution. According to Wakeby distribution for homogeneous region, probable regional SPEI quantiles show that the drought period will be seen in the short term every 2 and 5 years.

REFERENCES

Abramowitz, M. and Stegun, I. A. 1965. Handbook of Mathematical Functions, with Formulas, Graphs, and Mathematical Tables. Dover Publications, 1046 pp.

Agnew, C. T. 1990. Spatial aspects of drought in the Sahel. Journal of Arid Environments 18: 279-293.

Agnew, C. T. and Warren, A. 1996. A framework for tackling drought and degradation: Journal of Arid Environments 33: 309-320.

Allen, R. G., Pereira, L. S., Raes, D. and Smith, M. 1998. Crop Evapotranspiration. (Guidelines for computing crop water requirements), FAO Irrigation and Drainage Paper No. 56.

Anli, A. S. 2015. Regional and Point Precipitation Estimation for 1975-2010 Period over Semi-Arid Central Anatolia Region of Turkey. Fresenius Environmental Bulletin, 24: 2a, 632-643.

Anli, A. S., Polat, H. E. and Semiz, G. D. 2011. Drought analysis for Kirsehir province and its effect of water lands. Proceedings of 2th Water Lands Symposium of Turkey. 22-24 June, Kirsehir, p 22-24 (in Turkish).

Dickey, D. A. and Fuller, W. A. 1979. Distribution of the estimators for autoregressive time series with a unit root. Journal of the American Statistical Association 74: 427–431.

Enders, W. 1995. Applied Econometric Time Series, John Wiley and Sons, UK.

FAO 2013. Database & Software CROPWAT 8. Natural Resources and Environment Department. http://www. fao.org.

Hosking, J. R. M. 2005. Fortran routines for use with themethod of *L*-moments, Version 3.04. Research ReportRC 20525, IBM Research Division, T.C. Watson Research Center, Yorktown Heights, N.Y.

Hosking, J. R. M. and Wallis, J. R. 1997. Regional Frequency Analysis: An Approach Based on *L*-moments. Cambridge University Press: Cambridge, U.K.

Tabari, H., Aeini, A., Talaee, H. and Some'e, S. 2012. Spatial distribution and temporal variation of reference evapotranspiration in arid and semi-arid regions of Iran. Hydrological Processes 26: 500-512.

Tsakiris, G. 2010. Drought management: economics of drought and drought preparedness in a climate change context, Options Méditerranéennes, A95, Turkey; p. 249-257.

Tsakiris, G. and Vangelis, H. 2004. Towards a drought watch system based on spatial SPI. Water Resources Management, 18(1): 1-12.

Tsakiris, G. and Vangelis, H. 2005. Establishing a drought index incorporating evapotranspiration. European Water, 9/10:3-11.

Tsakiris, G., Pangalou, D. and Vangelis, H. 2007. A regional drought assessment based on the reconnaissance drought index (RDI). Water Resources Management, 21(5): 821-833.

Unlukara, A., Yurekli, K., Anli, A. S. and Ors, I. 2010a. Evaluation of the drought of Kayseri province based on RDI (Reconnaissance Drought Index). Research Journal of Agricultural Sciences, 3 (1): 13-17 (in Turkish).

Unlukara, A., Yurekli, K., Anli, A. S. and Ors, I. 2010b. Variation analysis of monthly and annual reference evapotranspiration for Ankara province. I. National Soil and Water Resources Symposium. Proceedings. 1-4 June, Eskisehir, p 16-23 (in Turkish).

Vangelis, H., Tigkas, D., Tsakiris, G. 2013. The effect of PET method in Reconnaissance Drought Index (RDI) calculation. Journal of Arid Environments, 25:357-371.

Vicente-Serrano, S. M., Begueria, S. and Lopez-Moreno, J. I. 2010. A multiscalar drought index sensitive to global warming: The SPEI. Journal of Climate, Volume 23: 1696-1718.

Yang, Z., Liu, Q. and Cui, B. 2011. Spatial distribution and temporal variation of reference evapotranspiration during 1961–2006 in the Yellow River Basin, China. Hydrological Sciences Journal 56(6): 1015-1026.

Ye, X., Li, X., Liu, J., Xu, C. Y. and Ziang, Q. 2013. Variation of reference evapotranspiration and its contributing climatic factors in the Poyang Lake catchment, China. Hydrological Processes, 28 (25): 6151-6162.

Zhang, X., Kang, S., Zhang, L. and Liu, J. 2010. Spatial variation of climatology monthly crop reference evapotranspiration and sensitivity coefficients in Shiyang river basin of northwest China. Agricultural Water Management, 97: 1506-1516.

Proceedings of the 10th World Congress of EWRA 'Panta Rhei', 5-9 July 2017, Athens, Greece
© 2017 *European Water Resources Association*

Calculation of the irrigation water needs spatial and temporal distribution in Greece

K.X. Soulis[1*] and D.E. Tsesmelis[2]
Agricultural University of Athens, Department of Natural Resources Management and Agricultural Engineering, Sector of Water Resources Management, Athens, Greece
[*] *e-mail: soco@aua.gr*

Abstract: Among the vital economic sectors that compete for the scarce water resources in Greece as well as the Mediterranean area, agriculture holds a special position. Agriculture has a dominant role in sustaining the growth of rural areas and at the same time represents the major water consumer. In order to tackle the aforementioned issues, efficient water resources management plans comprising appropriate solutions, best practices, data, and tools are required. However, this effort becomes even more challenging in the case of poorly gauged regions and especially in countries characterized by vast spatial and temporal variability like Greece. Accordingly, this effort presents a methodology for a large-scale evaluation of agricultural water needs for the entire country. The proposed methodology is using an entirely spatially distributed, continuous hydrological model, in order to estimate the spatial distribution of the hydrological balance components, the monthly and yearly mean streamflow values at every point of the studied region as well as irrigation water needs and plants water stress. The model operates as an extension of the ESRI ArcGIS, a GIS software package, in order to facilitate the fully spatially distributed calculation of the hydrological balance components, and at the same time to make use of the advanced capabilities of ArcGIS in managing (editing, analyzing and visualizing) geographical data. The applied methodology produced valuable information concerning agricultural water management, and may act as an effective assessment tool for the evaluation of land use or climate variation impacts and of related adaptation and mitigation strategies.

Key words: Water Resources; Water Demand; Irrigation Needs; GIS; Hydrological Model; Water Balance; Water Stress

1. INTRODUCTION

Agriculture sector has a dominant role in sustaining the growth of rural areas and at the same time represents the major water consumer in Greece as well as the Mediterranean area. Therefore, water conservation in agriculture has recently received much attention in the light of increasing competition for fresh water resources between the various users, especially in semi-arid and arid regions facing limited water availability and at the same time increased water needs (Karavitis et al., 2011, 2014; Soulis et al., 2015a). In order to tackle the aforementioned issues, efficient water resources management plans comprising appropriate solutions, best practices, data, and tools are required. However, this effort becomes even more challenging in the case of poorly gauged regions and especially in countries characterized by vast spatial and temporal variability like Greece as well as for the case of broad area regional studies. In such cases, the estimation of the main water balance components based on meteorological data using a hydrological model seems to be the main feasible alternative (Soulis et al., 2016). This alternative is further facilitated by the development of modern tools such as geographical information systems (GIS), and remote sensing (Soulis and Dercas, 2007, 2010).

Specific scales and purposes require the use of different modelling approaches. Accordingly, hydrological models are categorised according to their spatial and temporal representation, their simulation basis, or their purpose. For example, when their spatial representation is considered, hydrological models can be categorized to "Lumped", which represent a catchment or a sub-catchment as a single entity, e.g. HEC-HMS (US Army Corps of Engineers) and Soil and Water Assessment Tool - SWAT (US Department of Agriculture), and to "Distributed" models, which

divide the catchment into many small entities, e.g. Cascade Two Dimensional model - CASC2D (Ogden, 1997) and Système Hydrologique Européen Transport - SHETRAN (Ewen et al., 2000). Furthermore, the advances in hydrological theory and the constant increment of the available computer power enable the development of more sophisticated hydrological models. For instance, the recent advances in Geo-Information Systems (GIS) and the increased availability of spatial data facilitated the closer integration of GIS and hydrological models (e.g. Efstratiadis et al., 2008; Li and Zhang, 2008; Soulis and Dercas, 2007, 2010).

In this study, a methodology for a large-scale evaluation of agricultural water needs in Greece is presented. The proposed methodology is using a grid based, spatially distributed, continuous hydrological model, in order to estimate the hydrological balance components, the monthly and yearly mean streamflow values at every point of the studied region as well as irrigation water needs and plants water stress in spatially distributed form.

2. MATERIALS AND METHODS

2.1 Hydrological model

In this study, the fully spatially distributed, continuous hydrological model AgroHydroLogos (Soulis and Dercas, 2007, 2010; Soulis, 2013; Soulis et al., 2016) is used in order to estimate the monthly and yearly mean streamflow values at every point of the studied region. AgroHydroLogos was developed as an extension of the GIS software package ArcGIS (ESRI) in order to facilitate the calculation of the hydrological balance components in grid based spatially distributed form and at the same time to make use of the advanced capabilities of ArcGIS in managing, editing, analyzing and visualizing geographical data (Fig. 1). The model calculates, on a daily or on a monthly temporal basis, the main hydrological balance components, such as, soil moisture, direct runoff, deep infiltration, actual evapotranspiration, and base flow. Furthermore, it calculates other important parameters, including plants water stress and irrigation water needs in order to constitute a valuable software tool for agro-hydrological analysis.

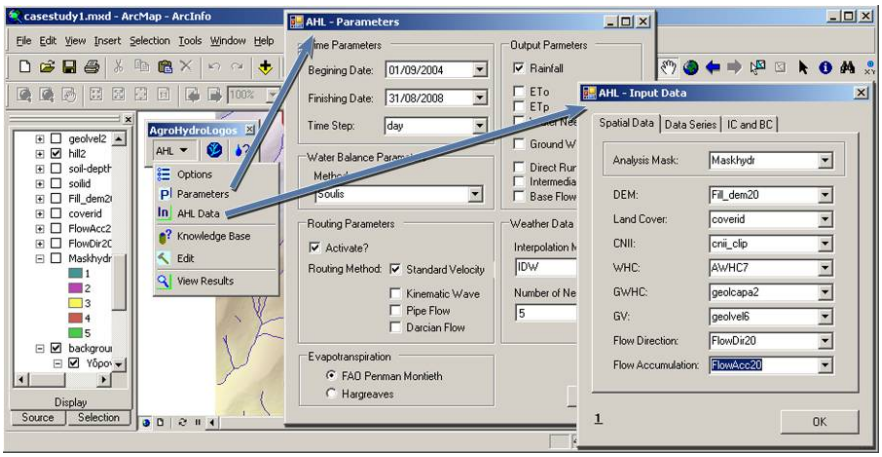

Figure 1. Print screen of AgroHydroLogos main menu and forms.

The main reason behind the selection of AgroHydroLogos simulation model in this study is that it is a grid-based spatially distributed hydrological model. In this way, it was possible to consider the complex vegetation cover and disperse spatial distribution of the various crops in the study area during the estimation of the irrigation water requirements. Furthermore, using a simulation model developed in-house provides more insight and at the same time flexibility in adapting the model to the specific requirements of the present application. Finally, the model has been applied and tested under Greek conditions in previous studies; therefore, the application of the model in an extended

area was facilitated (Soulis et al., 2016).

In this study, the monthly temporal discretization is used. In this case, the estimation of the water balance components is based on the Thornthwaite-Mather (1957) model, which is composed of one soil reservoir and one ground water reservoir. It has only two parameters, i.e. the available water capacity of the soil reservoir at each grid cell ($AWC_{i,j}$) and a retention parameter (a_c). In every temporal step and every grid cell, given the precipitation depth $P_{t,i,j}$, the potential evapotranspiration depth $ET_{p\,t,i,j}$ at the current temporal step as well as the soil water storage depth $S_{t-1,i,j}$ and the surface runoff depth $Q_{t-1,i,j}$, at the previous temporal step, the actual evapotranspiration depth $ET_{a\,t,i,j}$, the surface runoff depth $Q_{t,i,j}$, the ground water recharge depth $Q_{gw\,t,i,j}$, and the soil water storage depth $S_{t,i,j}$ at the current temporal step are calculated as follows:

$$\left.\begin{aligned} S_{\mathrm{t,i,j}} &= S_{t-1,i,j} + P_{t,i,j} - ET_{p\,t,i,j} \\ ET_{a\,t,i,j} &= ET_{p\,t,i,j} \end{aligned}\right\} if \;\; P_{t,i,j} \geq ET_{p\,t,i,j}$$

$$\left.\begin{aligned} Q_{temp\,t,i,j} &= S_{\mathrm{t,i,j}} - AWC_{\mathrm{i,j}} \\ Q_{t,i,j} &= a_c(Q_{t-1,i,j} + Q_{temp\,t,i,j}) \\ S_{\mathrm{t,i,j}} &= AWC_{\mathrm{i,j}} \\ Q_{gw\,t,i,j} &= Q_{temp\,t,i,j} - Q_{t,i,j} \end{aligned}\right\} if \; S_{\mathrm{t,i,j}} \geq AWC_{\mathrm{i,j}}$$

$$\left.\begin{aligned} S_{\mathrm{t,i,j}} &= S_{t-1,i,j} - e^{\frac{P_{t,i,j} - ET_{p\,t,i,j}}{AWC_{i,j}}} \\ ET_{a\,t,i,j} &= P_{t,i,j} + S_{t-1,i,j} - S_{\mathrm{t,i,j}} \\ Q_{t,i,j} &= 0 \end{aligned}\right\} if \;\; P_{t,i,j} < ET_{p\,t,i,j} \qquad (1)$$

The subscript t defines the current temporal step and the subscripts i, j define the current grid cell.

In this application, ET_p is calculated as a function of the reference evapotranspiration (ET_o) and of the land cover characteristics using an adjustment coefficient (K_c) according to FAO (1998) as follows:

$$ET_p = ET_o * K_c \qquad (2)$$

The values of K_c are determined for each grid cell and each month, depending on the vegetation characteristics of each place, based on the model's knowledge base, which contains information for a wide range of land cover types. ET_o is calculated with the Hargreaves method (Hargreaves and Samani, 1985) due to limitations posed by the meteorological data availability (minimum, maximum, and mean temperature values for each time step were available).

Irrigation water needs (*IRR*) are calculated for each of the grid cells belonging to agricultural areas and for each month as the difference between the evapotranspiration rate for standard optimal conditions (equal to $ET_p * S_c$) and the evapotranspiration rate for the actual conditions (ET_a) (Eq. 4). The adjustment coefficient (S_c) is the acceptable ET_p reduction percentage without significant yield reduction (normally $S_c = 0.95$).

$$IRR = ET_p * S_c - ET_a \qquad (3)$$

Base flow is simulated based on the exponential equation proposed by Arnold et al. (1993) and Hattermann et al. (2004), while snow accumulation and snowmelt processes are considered based on the air temperature (Hock, 2003).

Finally, runoff routing through overland flow and through the hydrographical network is performed with a simplified travel time approach described in detail in the study of Soulis (2013).

A more detailed description of the simulation model can be found in the studies of Soulis and Dercas (2007, 2010), Soulis (2013), and Soulis et al. (2016).

2.2 Model setup - Input data

The model applied for a 26-year period and in monthly time basis, from October 1970 to September 1996, and it allowed estimating irrigation water needs all over Greece (national scale, area ≈ 131,940 km²).

The spatial resolution of the hydrological model was set to 300 m x 300 m for the calculation of the hydrological balance, while it was set to equal with the spatial resolution of the DEM (85 m x 85 m) for the runoff routing process. The selection of the spatial resolution resulted as a compromise between the required accuracy and the performance and data storage limitations posed by the size of the study area. A finer spatial resolution designated for the runoff routing process to allow for a more detailed representation of the drainage network. The digital elevation model (DEM) used in the current effort obtained by the Shuttle Radar Topography Mission (SRTM) (Jarvis et al., 2008). The soil data used for the estimation of the Available Water Holding Capacity (AWHC) data layer derived from the European Soil Database (Panagos et al., 2012). The land cover data originated from the CORINE Land Cover (CLC) 2000 and 2012 datasets.

Finally, twenty-two meteorological stations distributed along the study area utilized in this study. The available data were monthly precipitation depth and monthly minimum, maximum, and mean temperature values from 1970 to 1996.

The first year of the simulation period was used as a warm up period in order to initialize the soil moisture spatial distribution, which is an initial condition that is not feasible to be directly estimated.

Table 1. Model validation sites and statistics

ID	Place	Basin Area (km^2)	NSE	Logarithmic NSE	PBIAS (%)
1	Penteli, Attiki	8	0.59	0.80	21.25
2	Alphios, Mesochora	549	0.52	0.75	-24.68
3	Arapitsa, Naousa	129	0.61	0.66	-12.76
4	Faneromeni, Naxos	9	0.72	0.80	14.30
5	Pineios, Thessalia	10,776	0.65	0.82	9.28
6	Evinos	1,083	0.82	0.82	-11.45
7	Mornos	920	0.79	0.86	-0.48
8	Venetikos, Grevena	817	0.78	0.72	-4.64
9	Ladonas	750	0.63	0.50	-22.09
10	Louros	520	-1.97	-6.88	-52.08
11	Aliakmonas	5,005	0.58	0.78	4.74
12	Arachthos	1,820	0.58	0.84	-27.08
13	Vouraikos	184	0.67	0.70	10.58
14	Selinountas	320	-2.28	0.51	79.13
15	Pineios, Ilia	725	0.74	0.60	-1.67
16	Aoos	1,520	0.38	0.67	-39.11
17	Aggitis	1,866	-0.32	-0.56	-16.89

2.3 Calibration – Validation

The calibration and validation of the hydrological model hampered due to the very limited availability of reliable hydrological data as compared to the size of the study region. Therefore, the main calibration parameters of the model as well as the precipitation and temperature grades were adapted based on a trial and error approach using information and hydrometeorological data presented by Koutsoyiannis et al. (2008) and Ministry of Environment and Energy (2015).

Furthermore, the model has been tested for specific parts of the studied region in previous studies (Soulis and Dercas, 2007, 2010).

Model validation was made by comparing the predicted and observed average monthly streamflow rates coming from 17 sites around the study area (Table 1). The corresponding streamflow data obtained from the studies of Koutsoyiannis et al. (2008), Soulis et al. (2015b), Soulis and Dercas (2007), and Papadaki et al. (2015). The performance criteria used were the Nash-Sutcliffe efficiency (NSE), the NSE with logarithmic values (lnNSE), and the percent bias (PBIAS). The model performance was considered satisfactory if NSE and lnNSE > 0.5 and PBIAS < ±25% (Moriasi et al., 2007; Rahman et al., 2013).

3. RESULTS AND DISCUSSION

As previously described, the model applied for a 26-years period and it allowed the estimation of the different water balance components as well as irrigation water needs at a monthly time step all over Greece. Moreover, the model validation results presented in Table 1, indicate that its performance is acceptable in most cases according to the criteria posed and considering the previously described limitations (Moriasi et al., 2007; Rahman et al., 2013).

Based on the above model results the spatial distribution of the 25 years average monthly and yearly values irrigation water needs were calculated.

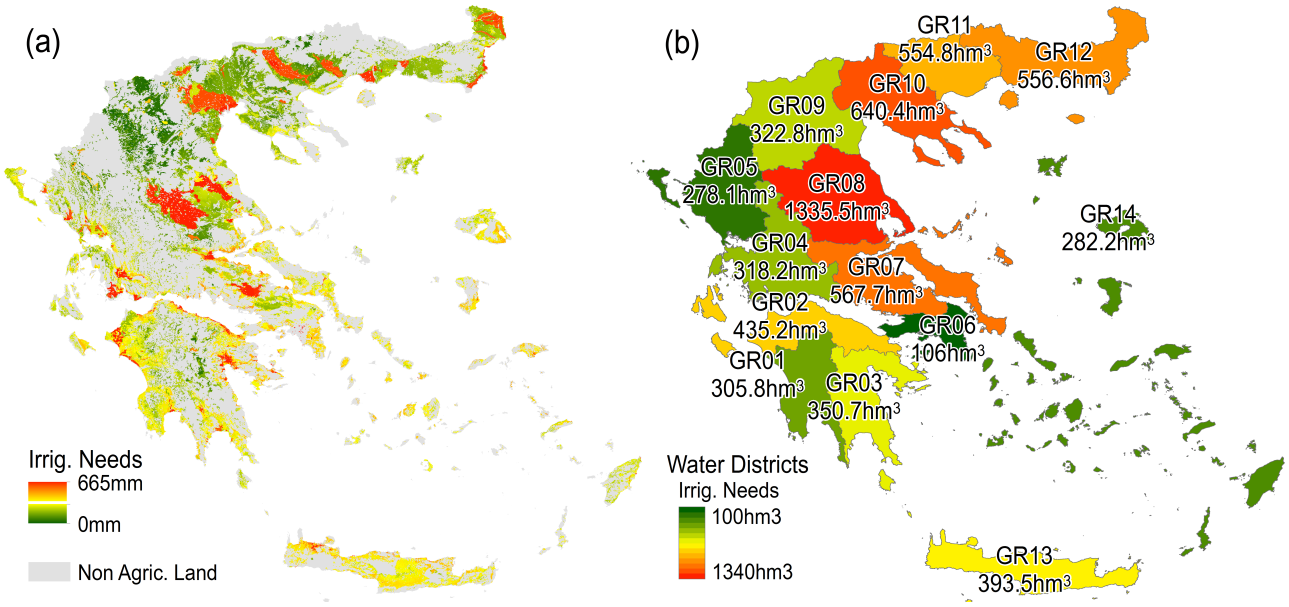

Figure 2. Average annual irrigation water needs depth spatial distribution (a) and irrigation water needs volume per water district (b).

In Fig. 2a the spatial distribution of the average annual irrigation water needs depth is illustrated. As it can be observed, there is a vast spatial variability of the annual irrigation water needs ranging from almost 0 mm to above 650 mm. This variability is mostly a result of the different crop patterns but can be also attributed to the impact to the meteorological conditions of the steep relief, including a massive sierra with a north-south direction dividing the mainland of the country. For example, the three bigger uniform zones of high irrigation water needs are located in the three big plains of the eastern part of the country (Thessaly, Thessaloniki, and Strymonas river valley). In contrast, it can be clearly seen that the irrigation water needs in western Greece are noticeably lower mainly due to the considerable higher rainfall depths prevailing at western Greece. The same findings obtained when the potential irrigation water needs volume for the 14 water districts of Greece considered (Fig. 2b). The obtained results also highlighted the vast temporal variability of irrigation water needs. The average needs for the studied crop covers ranged between 0 mm on

December and 96.5 mm on July. The above findings highlight the ability of the proposed methodology to provide valuable information concerning water resources planning and management as well as to act as an effective assessment tool for the evaluation of land use or climate variation impacts and of related adaptation and mitigation strategies.

Table 2. Estimated irrigation water needs for the studied land cover types for each water district and for the entire study area.

Water District	Permanently irrigated land			Non-irrigated arable land			Vineyards		
	AREA	Irrig. Needs		AREA	Irrig. Needs		AREA	Irrig. Needs	
	Km^2	mm	m^3x1000	Km^2	mm	m^3x1000	Km^2	mm	m^3x1000
GR01	77.7	476	36956	138.3	118	16264	29.7	265	7876
GR02	157.9	481	75905	418.4	126	52573	360.1	258	92803
GR03	41.0	401	16410	149.9	72	10736	11.7	204	2390
GR04	312.6	496	155185	266.2	136	36259	2.4	231	563
GR05	241.9	409	98952	189.1	97	18402	4.4	239	1052
GR06	0.0	0	0	54.0	178	9634	62.0	311	19255
GR07	417.2	513	214099	1257.9	172	216379	12.8	276	3527
GR08	2209.1	496	1094864	2722.4	137	372317	23.1	284	6576
GR09	133.6	380	50796	2724.1	48	129875	14.0	111	1560
GR10	971.5	453	439683	3032.3	110	332277	30.2	247	7472
GR11	1045.8	452	472713	1408.6	97	136142	25.6	259	6608
GR12	871.7	455	396659	2437.7	147	358791	8.4	268	2247
GR13	16.7	329	5509	27.4	176	4828	218.3	244	53264
GR14	0.0	0	0	319.3	174	55613	40.4	277	11176
Total	**6496**	**381**	**3057731**	**15146**	**128**	**1750090**	**843**	**248**	**216368**
Water District	**Fruit trees and berry plantations**			**Olive groves**			**Complex Patterns (crops/natural vegetation)**		
GR01	12.6	478	6024	847.0	266	225073	2121.8	194	412070
GR02	172.8	531	91773	481.7	280	134927	1890.7	210	396199
GR03	255.8	538	137693	649.9	285	185059	1702.4	214	364767
GR04	13.4	528	7079	187.2	291	54567	1570.5	201	315270
GR05	73.5	450	33092	245.2	232	56909	1894.0	165	311623
GR06	7.8	555	4343	51.6	326	16794	755.9	268	202239
GR07	24.4	502	12235	670.8	326	218509	2056.1	243	500021
GR08	98.3	529	51994	88.0	303	26707	1161.8	196	227526
GR09	450.6	423	190716	1.7	127	217	1971.5	109	214717
GR10	4.3	451	1946	149.0	253	37643	1362.6	177	240517
GR11	0.0	0	0	27.4	223	6098	621.6	166	103250
GR12	1.7	476	814	47.9	284	13605	796.1	197	156714
GR13	57.5	514	29536	1915.6	276	528737	1224.2	239	292545
GR14	21.4	470	10073	521.6	288	150380	1978.4	244	482122
Total	**1194**	**460**	**577317**	**5884**	**269**	**1655223**	**21107**	**201**	**4219580**

In Table 2, the calculated irrigation water needs volume for each studied land cover type and for each water district of the study area are presented. It should be noted that the calculated irrigation water volumes are potential values assuming that the entire area is irrigated. In order to provide a more reasonable approximation of the actual irrigation water needs (Fig. 2) estimations of the percentages of each crop cover type that is actually irrigated were used. These estimations based on the irrigated areas statistics provided by ELSTAT (Hellenic Statistical Authority). Comparing the

obtained irrigation needs estimations (Fig. 2) with the estimations included in the master plans on water resource management for the 14 water districts of Greece" (Ministry of Environment and Energy, 2015) it can be seen that the applied efficient and fast automated methodology provides comparable predictions. For example, the estimated irrigation water needs for GR2 in the corresponding master plan are 401.5 hm^3 (present study: 435.2 hm^3), for GR04 are 367 hm^3 (present study: 318.2 hm^3), for GR08 are 1550 hm^3 (present study: 1335.5 hm^3), for GR10 are 527.6 hm^3 (present study: 640.4 hm^3). At the same time the applied methodology on top of being fast and efficient, provides considerable flexibility allowing the investigation of several crop distribution and climate scenarios.

However, the current study also highlighted the limitations of CLC classification for similar studies. The main limitation is that according to the CLC classification the delineation of irrigated crops is difficult. Furthermore, in areas dominated by small fields, which is the case for the current study area, the agricultural areas classified in CLC as "complex" (i.e. annual crops associated with permanent crops, complex cultivation patterns, and agriculture, significant areas natural vegetation) cover a very large part of the total agricultural lands. In this study, the corresponding categories covered 21,107km^2 which is 45% of the total area covered by agricultural lands. Finally, it should be noted that an important limitation is also the scarcity of detailed and reliable soil data in the entire study area.

3. CONCLUSIONS

In this Study, a grid based, spatially distributed, continuous hydrological model is used to make a large-scale evaluation of agricultural water needs in Greece. The model operates as an extension of ESRI ArcGIS utilizing its advanced capabilities in editing, analysing and visualizing geographical data. The applied methodology provided efficient estimations of the spatial distribution of the irrigation water highlighting the vast spatial variability, which is a result of the crop patterns variability, the topography, and the meteorological conditions. The obtained results were comparable with the estimations included in the master plans on water resource management for the 14 water districts of Greece.

The results of this study highlighted the ability of the proposed methodology to provide valuable information concerning agricultural water management and to act as an effective assessment tool for the evaluation of land use or climate variation impacts.

However, the current study also highlighted the limitations of CLC classification for similar studies as well as the limitations posed by the scarcity of detailed and reliable soil data.

REFERENCES

Arnold, J. G., Allen, P. M., Bernhardt, G. A., 1993. Comprehensive surface-groundwater flow model. J. Hydrol. 142: 47-69.

Efstratiadis, A., Nalbantis, I., Koukouvinos, A., Rozos, E., Koutsoyiannis, D., 2008. HYDROGEIOS: A semi-distributed GIS-based hydrological model for modified river basins, Hydrol. Earth Syst. Sci., 12(4): 989-1006.

Ewen, J., Parkin, G., O'Connell, P. E., 2000. SHETRAN: distributed river basin flow and transport modeling system. J. Hydrol. Eng., 5: 250-258.

FAO, 1998. Crop evapotranspiration - Guidelines for computing crop water requirements - FAO Irrigation and drainage paper 56. Food and Agriculture Organization of the United Nations, Rome. Available at http://www.fao.org/docrep/x0490e/x0490e00.htm

Hargreaves, G. L., Samani, Z.A., 1985. Reference crop evapotranspiration from temperature, Appl. Eng. Agr., ASAE 1(2): 96-99.

Hattermann, F., Krysanova, V., Wechsung, F., Wattenbach, M., 2004. Integrating groundwater dynamics in regional hydrological modeling. Environ. Modell. Softw., 19: 1039–1051.

Hock, R., 2003. Temperature index melt modelling in mountain areas. J. Hydrol., 282(1–4): 104–115.

Karavitis, C.A., Alexandris, S., Tsesmelis, D.E., Athanasopoulos, G., 2011. Application of the Standardized Precipitation Index (SPI) in Greece. Water, 3: 787–805. doi:10.3390/w3030787

Karavitis, C. A., Tsesmelis, D. E., Skondras, N. A., Stamatakos, D., Alexandris, S., Fassouli, V., Vasilakou, C. G., Oikonomou, P. D., Gregorič, G., Grigg, N. S., Vlachos, E. C., 2014. Linking drought characteristics to impacts on a spatial and temporal scale. Water Policy, 16: 1172–1197. doi:10.2166/wp.2014.205

Koutsoyiannis, D., Andreadakis, A., Mavrodimou, R., Christofides, A., Mamassis, N., Efstratiadis, A., Koukouvinos, A., Karavokiros, G., Kozanis, S., Mamais, D., Noutsopoulos, K., 2008. National Programme for the Management and Protection of

Water Resources, Support on the compilation of the national programme for water resources management and preservation, 748 pp, Department of Water Resources and Environmental Engineering – National Technical University of Athens, Athens, Greece.

Li, Z., Zhang, K., 2008. Comparison of three GIS-based hydrological models. J. Hydrol. Eng., 13(5): 364-370.

Ministry of Environment and Energy, (2015). Master Plans on Water Resource Management for the 14 water districts of Greece, Ministry of Environment and Energy, Special Secretariat for Water, Available at http://www.ypeka.gr/Default.aspx?tabid=248&language=el-GR

Moriasi, D. N., Arnold, J. G., Van Liew, M. W., Bingner, R., L., Harmel, R. D., Veith, T. L., 2007. Model evaluation guidelines for systematic quantification of accuracy in watershed simulations. Transactions of the Asabe 50(3): 885–900 DOI: 10.13031/2013.23153

Ogden, F. L., 1997. CASC2D Reference Manual. Department of Civil & Environmental Engineering, University of Connecticut, Storrs.

Panagos, P., Van Liedekerke, M., Jones, A., Montanarella, L., 2012. European Soil Data Centre: Response to European policy support and public data requirements. Land Use Policy, 29(2): 329-338.

Papadaki, C., Soulis, K. X., Muñoz-Mas, R., Martinez-Capel, F., Zogaris, S., Ntoanidis, L., Dimitriou, E., 2015. Potential impacts of climate change on flow regime and fish habitat in mountain rivers of the south-western Balkans. Sci. Total Environ., S0048-9697(15)30333-8. doi: 10.1016/j.scitotenv.2015.06.134

Rahman, K., Maringanti, C., Beniston, M., Widmer, F., Abbaspour, K., Lehmann, A., 2013. Streamflow Modeling in a Highly Managed Mountainous Glacier Watershed Using SWAT: The Upper Rhone River Watershed Case in Switzerland. Water Res. Manage. 27(2): 323–339 DOI: 10.1007/s11269-012-0188-9

Soulis K. and Dercas N. 2010, AgroHydroLogos: development and testing of a spatially distributed agro-hydrological model on the basis of ArcGIS, International Congress on Environmental Modelling and Software, Modelling for Environment's Sake, Fifth Biennial Meeting (iEMSs), Ottawa, Canada.

Soulis K.X., Elmaloglou S., and Dercas N., 2015a. Investigating the effects of soil moisture sensors positioning and accuracy on soil moisture based drip irrigation scheduling systems. Agr. Water Manage., 148: 258–268, doi: http://dx.doi.org/10.1016/j.agwat.2014.10.015

Soulis K. and Dercas N., 2007. Development of a GIS-based Spatially Distributed Continuous Hydrological Model and its First Application, Water Int.l, 32(1): 177-192. DOI:10.1080/02508060708691974

Soulis, K. X., 2013. Development of a simplified grid cells ordering method facilitating GIS-based spatially distributed hydrological modeling. Comp. Geosci., 54: 160-163.

Soulis, K. X., Dercas, N. Papadaki, C. H., 2015b, Effects of forest roads on the hydrological response of a small-scale mountain watershed in Greece. Hydrol. Process., doi: 10.1002/hyp.10301

Soulis, K. X., Manolakos, D., Anagnostopoulos, J., Papantonis, D., 2016. Development of a geo-information system embedding a spatially distributed hydrological model for the preliminary assessment of the hydropower potential of historical hydro sites in poorly gauged areas. Renew. Energy, 92: 222-232. doi:10.1016/j.renene.2016.02.013

Thornthwaite, C. W., Mather, J. R., 1957. Instructions and tables for computing potential evapotranspiration and the water balance. Drexel Institute of Technology, New Jersey. Publications in Climatology, 10: 185–311.

Proceedings of the 10th World Congress of EWRA 'Panta Rhei', 5-9 July 2017, Athens, Greece
© 2017 *European Water Resources Association*

Daily transpiration of a single sessile oak measured by the tissue heat balance method

M.S. Ozcelik
Istanbul University, Faculty of Forestry, Department of Watershed Management, 34473, Istanbul, Turkey
e-mail: msaid.ozcelik@istanbul.edu.tr

Abstract: Transpiration is calculated as a component of evapotranspiration for planning water resources in watershed scale. Since the risk of water shortages is quite high for near future because of growing population, this information is important for water conservation and planning studies especially in sub-humid and semi-arid areas of Turkey where vegetation can take up significant amount of water. To present this fact, water consumption of a single full grown sessile oak (*Quercus petraea* (Matt.) Liebl.) was determined in daily basis by the tissue heat balance method in Belgrad Forest, Istanbul. Study period covered one growing season in 2016. The sample tree was 18.5 m in height, 34.5 cm in diameter at breast height. Mean air temperature, humidity, and precipitation were 17.4°C, 76.6 (%) and 368 mm respectively, during the study period. The maximum transpiration was 162.4 kg day-1 in July and the minimum was 0.78 kg day-1 in the first day of April. Total amount of water consumption by this single tree in the whole growing season was 18325 kg. Results of this study revealed that water consumption of the vegetation cover should be taken into account for effective water management in addition to increasing water yield and improving water quality.

Key words: Transpiration, sessile oak, Belgrad Forest, tissue heat balance

1. INTRODUCTION

One of the main ecosystem services provided by forests is fresh water production with high quality for society. On the other hand; forest cover can consume enormous amount of water via transpiration. Since the water demand is increasing due to population growth, industrial developments and agricultural irrigation in Turkey, water resources management with sustainable approach in watershed scale is an important subject both for researchers and decision makers.

The amount of water in an area is directly related to climate, topography of the area and vegetation growing in the site. Vegetation cover is the only component that can be modified by humans in order to increase water yield in the watersheds. Therefore, the knowledge of water consumption rates of tree species and its relation to the atmospheric variables are the primary concerns in watershed management (Özçelik et al., 2016).

The water consumptions of trees via transpiration have been of special interest by researchers from mid-1800's and early studies were mostly conducted in laboratories under restricted conditions without reference to environmental factors (Weaver and Mogensen, 1919). A variety of methods have been put forth such as potometer, tent, lysimeter, watershed water balance, magnetic resonance imaging technics and sap flow methods for measuring transpiration (Özhan, 1982; Renninger and Schafer, 2012). After Huber's pioneer work in 1932, researchers focused on to develop different sap flow technics based on thermal transformation such as tissue heat balance, heat field deformation and heat dissipation. The technics which use heat as a tracer became the most preferred among the researchers interested in measuring tree transpiration in world-wide (Cermak et al., 2004). In fact; sap flow measurements provide interesting information about tree to tree variability within a forest stand and they are the only method in some cases e.g. on stands located on steep slopes, or on small sized plots (Granier et al., 1990, 1996). Moreover, xylem sap flow studies allow partitioning of the total flux to individual trees which may be consisted of different

age, size, social position or species in the stand (Köstner et al., 1996).

Although transpiration of oak species has been examined by researches in a variety of habitats with different goals (Cermak et al., 1982; Breda et al., 1993, 1995; Granier and Breda, 1996; Fenyvesi et al., 1998; Schiller et al., 2003, David et al., 2004; Asbjornsen et al., 2007; Paço et al., 2009; Kanalas et al., 2010; Meszaros et al., 2011, Juice et al., 2015; Yan et al., 2016); transpiration data for oak species growing in Turkey has not examined yet. Therefore, the aim of this study was to investigate daily and total transpiration rates of a single full grown sessile oak (*Quercus petraea* (Matt.) Liebl.) which is one of the18 native oaks of Turkey.

2. MATERIAL AND METHOD

2.1 Study site and sample tree

The study was carried out in Belgrad Forest (41° 09' 48" - 41° 10' 55" N, 28° 57' 27" -28° 59' 27" E). Average annual precipitation was around 1129 mm and mean annual temperature was about 12.3 °C. Precipitation mostly falls between October and April in the site. The warmest month was August while the coldest was February. Snow fall is not common in the site. The climate is sub-humid Mediterranean with mild-rainy winter and hot-dry summer. Parent material was Neogene loamy, the texture was clay loam with medium-good permeability rates and high organic matter (Serengil et al., 2007). The stand was without any understory. The basal area of the stand was 57.78 m^2 and there were about 1500 stems ha^{-1}. Mean tree height was 16 m and mean diameter at breast height was 20.7 cm. One individual full grown sessile oak tree was selected as sample from the stand. The tree was a dominant one with 18.5 m in height and 34.5 cm in diameter at breast height. The highest leaf area index (LAI) of the tree was estimated as 1.42 m^2 m^{-2} in July. The study covered a growing season of 2016 from April 1st to November 15th.

2.2 Environmental data

Two meteorological stations were used for recording meteorological data. One of them was a mini automatic weather station equipped with pluviometer, solar radiation sensor, air humidity and air temperature sensors (EMS Minikin RTHI and EMS Minikin ERI, EMS Brno, Czech Republic) placed at an open field next to the study site while the other one was placed 5 km far away from the study area (GRWS 1000, Campbell Scientific, U.S.A). Air temperature, relative humidity and radiation were measured 5 minute intervals and precipitation was recorded by a tipping bucket rain gauge. Soil moisture was recorded as soil water potential (Ψ, bar) under the forest canopy using calibrated gypsum blocks (Delmhorst Inc, USA) and Microlog SP3 data logger (EMS Brno, CZ). Soil moisture was measured at 25 cm depth from three different points, with 60 minute intervals. Leaf area index (LAI) was estimated by CL-110 plant canopy imager (Bio-science.inc, USA).

2.3 Sap Flow Measurements

A sap flow kit (EMS 81, EMS Brno, CZ) working according to the tissue heat balance method (Cermak et al., 1973, 1982; Kucera et al., 1977) was installed on to tree trunk to determine water consumption of the sample tree. A section of a tree trunk was heated by using electrodes within the trunk with electric current passing through the tissues in the tissue heat balance method. The system consists of four electrodes and thermocouples placed into the tree trunk. The upper three electrodes were heated while the central electrode was not heated and positioned 10 cm below from the others. The temperature difference between the reference and heated part of the tree stem was set to 1 K. The temperature difference (dT) between upper heated electrodes and reference one was measured by needle type thermocouples. Method calculates the heat balance of a defined heated space

according to the equation below (see Cermak et al., 2004):

$$P = QdTcw + dT\lambda \quad (1)$$

where P is input power (W), Q is the sap flow rate (kg s-1), dT is the temperature difference in the measuring points (K), cw is the specific heat of water (J kg-1 K-1) and λ is the coefficient of heat losses from the measuring point (W K-1). Tree trunk was packed with polyurethane foam after installation of the sensors to insulate the temperature field around the sensors from effects of the sun and convective heat loss. Microsoft EXCEL and EMS Mini32 softwares were used to data processing.

3. RESULTS

Results of sap flow measurements showed that the average daily transpiration rate of this single tree was 80.3 kg and varied between 0.78 kg in the first day of growing season and 162.4 kg in July. The total water loss through transpiration in one vegetation period by this tree was 18325 kg. The highest mean daily water consumption was 127.35 kg in July and the lowest was 19.48 kg in November because of the abscission of the foliage (Figure 1). According to the results 57% of the total transpiration occurred in summer months. The mean air temperature, mean air humidity and precipitation was recorded as 17.6 ˚C, 76.6 % and 368 mm respectively in the study period. The soil moisture was contented in April and May with mean -0.2 bar soil water potential (Ψ_{swp}), it started to decrease in June and the minimum Ψ_{swp} was recorded in July as mean -8.33 bar, but there was still available water in the soil. Maximum leaf area index (LAI) was 1.44 m^2 m^{-2} in July.

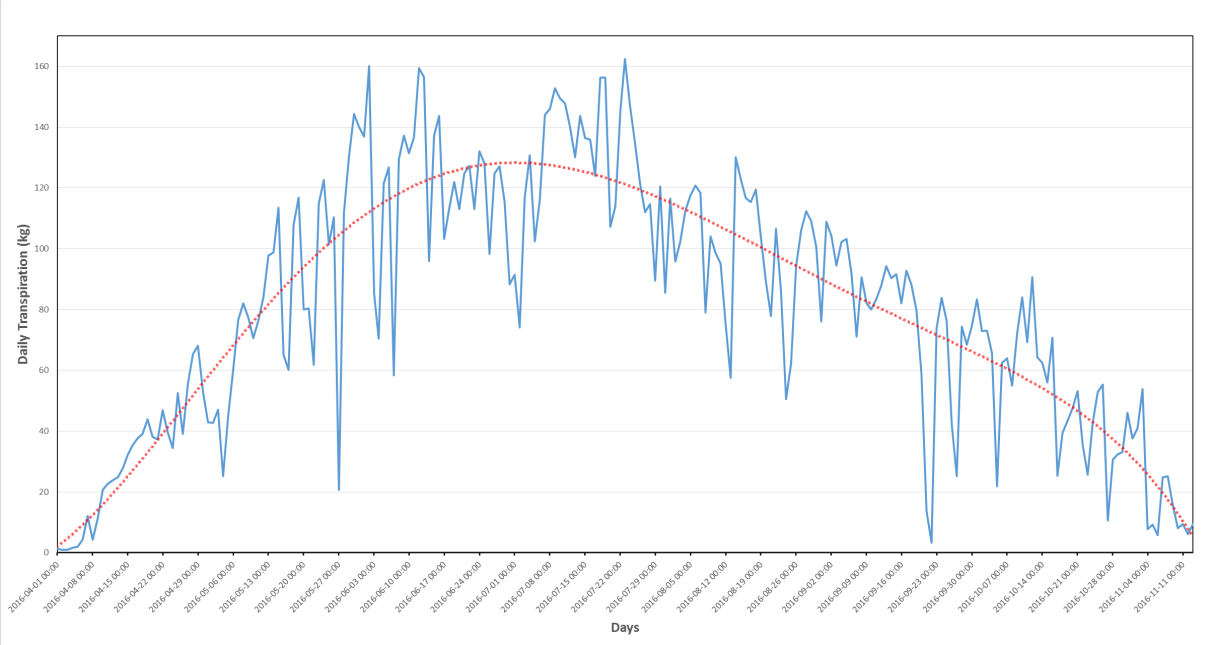

Figure 1. Transpiration trend of the tree in the whole growing season.

4. DISCUSSION AND CONCLUSION

Forest management in an appropriate way relies on maintaining sustainable water in a fresh water producing watershed. In fact, trees have important role on water cycle of terrestrial ecosystems through their effect on forest water use (Aranda et al., 2012). As a result, vegetation cover changes and forestry applications such as thinning and clear cutting can influence water yield in the watersheds (Bosch and Hewlett, 1982; Breda et al., 1995; Stednick, 1996; Lagergren et al.,

2008). To understand this alteration, tree transpiration is monitored by researchers since it is one of the most important factors influencing water yield in the watersheds.

A wide-range of daily maximum tree transpiration rates can be found in literature from 10 kg day-1 to 1180 kg day-1, but it can be said that the general range is between 10 to 200 kg (Wullschleger et al., 1998). Meteorological variations, topography, soil water conditions, tree health, age and diameter, stand characteristics and tree physiology are some of the factors responsible for this variation (Aranda et al., 2012). When the subject is limited by oak species; it can be seen that daily transpiration rates of oak trees were between 10-12 kg and reached up to 400 kg. Breda et al. (1993) recorded 10 kg day-1 maximum transpiration for *Quercus robur* L. in France under water stress. On the other hand Cermak et al. (1982) found 400 kg daily maximum transpiration rate for the same species in a floodplain forest in Czech Republic. Renninger and Schafer (2012) reported 29.2 kg maximum transpiration day-1 for *Q. prinus* L. and 41.6 kg day-1 for *Q. velutina* Lam. According to Wullschleger et al. (2001) the maximum transpiration rates of *Q. alba* L. was 71 kg day-1 while it was only 46 kg day-1 for *Q. rubra* L. in the same site. Considering these studies conducted upon transpiration rates of oak species, it can be said that although the results of this study was compatible with the literature, daily average and maximum transpiration of the sessile oak growing in a sub-humid region of Turkey was higher than most of the other oak species growing under different conditions. This information can be taken as an indicator also for other oak species of Turkey which are covered more than 6.5 million hectares with 18 natural species (Yaltırık, 1984).

It can be concluded based on the transpiration rates of this single tree that water consumption of vegetation cover can reach significant amounts in hot-dry summer months in Turkey, so that this information should be taken in to account in watershed management practises especially conducted in fresh water producing watersheds of the country.

ACKNOWLEDGEMENTS

The author of the study is grateful to Prof. Dr. Kamil Sengonul and Prof. Dr. Ferhat Gokbulak from Istanbul University for their valuable discussions. He is also grateful to Prof. Dr. Jan Cermak from Mendel University and Mr. Jiri Kucera from Environmental Measuring Systems for their help and contribution in both obtaining the sensors and field studies with data evaluating. Financial support was provided by Istanbul University BAP coordination unit, from the projects number 52494 and 52831.

REFERENCES

Abjornsen H, Tomer MD, Gomez-Cardenes M, Brudwig LA, Greenan CM, Schilling K (2007). Tree and stand transpiration in a Midwestern bur oak savanna after elm encroachment and restoration thinning. For Ecol Manag 247: 209-219.

Aranda I, Forner A, Cuesta B, Fernando V (2012). Species-specific water use by forest tree species: from the tree to the stand. Agr Water Manage 114: 67-77.

Bosch JM, Hewlett JD (1982). A review of catchment experiments to determine the effect of vegetation change on water yield and evapotranspiration. J Hydrol 55(1/4): 3–23.

Breda N, Dreyer H, Granier A (1993). Water transfer in mature oak stand (*Quercus petraea*): seasonal evolution and effects of severe drought. Can J For Res 23: 1136-1143.

Breda N, Granier A, Aussenac G (1995). Effects of thinning on soil and tree water relations, transpiration and growth in an oak forest (*Quercus petraea* (Matt.) Liebl. Tree Physiol 15: 295-306.

Cermak J, Deml M, Penka M (1973). A new method of sap flow rate determination in trees. Biol Plantarum 15 (3): 171-178.

Cermak J, Ukehla J, Kucera J, Penka M (1982). Sap flow rate and transpiration dynamics in the full-grown oak (*Quercus robur* L.) in the floodplain forest exposed to seasonal floods as related to potential evapotranspiration and tree dimensions. Biol Plantarum 24 (6): 446-460.

Cermak J, Kucera J, Nadezhdina N (2004). Sap flow measurements with some thermodynamic methods, flow integration within trees and scaling up from sample trees to entire forest stands. Trees 18: 529-546.

David TS, Ferreira MI, Cohen S, Pereira JS, David JS (2004). Constraints on transpiration from an evergreen oak tree in southern Portugal. Agr Forest Meteorol 122: 193-205.

Fenyvesi A, Beres CS, Raschi A, Tognietti R, Ridder HW, Molnar T, Röfler J, Lakatos T, Csiha I (1998). Sap-flow velocities and distribution of wet-wood in trunks of healthy and unhealthy *Quercus robur*, *Quercus petraea* and *Quercus cerris* oak trees in Hungary. Chemosphere 36 (4-5) 931-936.

Granier A, Bobay V, Gash JHC, Saugier B, Shuttleworth WJ (1990). Vapour flux density and transpiration rate comparisons in stand of Maritime pine (*Pinus pinaster* Ait.) in Les Landes forest. Agric For Meteorol 51: 309-319.

Granier A, Breda N (1996). Modelling canopy conductance and stand transpiration of an oak forest from sap flow measurements. Ann Sci For 53: 537-546.

Granier A, Biron P, Breda N, Pontailler JY, Saugier B (1996). Transpiration of trees and forest stands: short and long term monitoring using sap flow methods.

Juice SM, Templer PH, Phillips NG, Ellison AM (2015) Ecosystem warming increases sap flow rates of northern red oak trees. Ecosphere 7 (3): 1-17.

Kanalas P, Fenyvesi A, Kıs J, Szöllösı E, Olah V, Ander I, Meszaros I (2010). Seasonal and diurnal variability in sap flow intensity of mature sessile oak (*Quercus petraea* (Matt.) Liebl. Trees in relation to microclimatic conditions. Acta Biol Hung 61: 115-128.

Köstner B, Biron P, Siegwolf R, Grainer A (1996). Estimates of water vapor flux and canopy conductance of Scots pine at the tree level utilizing different xylem sap flow methods. Theor Appl Climatol 53: 105-113.

Kucera J, Cermak J, Penka M (1977). Improved thermal method of continual recording the transpiration flow rate dynamics. Biol Plantarum 19: 413-420.

Lagergren F, Lankreijer H, Kucera J, Ciencala E, Mölder M, Lindroth A (2008). Thinning effects on pine-spruce forest transpiration in central Sweden. Forest Ecol Manag 255: 2312-2323.

Meszaros I, Kanalas P, Fenyvesi A, Kıs J, Nyıtraı B, Szöllösı E, Olah V, Demeter Z, Lakatos A, Ander I (2011). Diurnal an seasonal chahges in stem radius increment and sap flow density indicate different responses of two co-existing oak species to drought stress. Acta Silv Ling Hung 7: 97-108.

Özçelik MS, Şengönül K, Gökbulak F (2016). Sap flow measurement methods for determining transpiration of forest trees and its importance for watershed management. Turkish Journal of Forestry 17(2): 208-214.

Özhan S (1982). Belgrad Ormanındaki Bazı Meşcerelerde Evapotranspirasyonun Deneysel Olarak Saptanması ve Sonuçların Ampirik Modellerle Karşılaştırılması. Istanbul Üniversitesi Orman Fakültesi Yayınları, Yayın No: 311, Istanbul-Turkiye.

Paço TA, David ST, Henriques MO, Pereira JS, Valente F, Banza J, Pereira FL, Pinto C, David JS (2009). Evapotranspiration from a Mediterranean evergreen oak savannah: The role of trees and pasture. J Hydrol 369: 98-106.

Renninger HJ, Schafer KVR (2012). Comparison of tissue heat balance and thermal dissipation-derived sap flow measurements in ring porous oak and a pine. Front Plant Sci 3: 103.

Schiller G, Unger ED, Moshe Y, Cohen S, Cohen Y (2003). Estimating water use by sclerophyllous species under east Mediterranean climate II. The transpiration of Quercus calliprinos Webb. In response to silvicultural treatments. Forest Ecol Manag 179: 483-495.

Serengil Y, Gökbulak F, Özhan S, Hızal A, Şengönül K (2007). Alteration of stream nutrient discharge with increased sedimentation due to thinning of a deciduous forest in Istanbul. For Ecol and Manag 246: 264-272.

Stednick JD (1996). Monitoring the effects of timber harvest on annual water yield. J Hydrol 176: 79–95.

Weaver J, Mogensen A (1919). Relative transpiration of coniferous and broad-leaved trees in autumn and winter. Botanical Gazette 68(6): 393-424.

Wullschleger SD, Meinzer FC, Vertessy RA (1998). A review of whole plant water use studies in trees. Tree Physiol 18: 499-512.

Wullschleger SD, Hanson PJ, Todd DE (2001). Transpiration from a multi-species deciduous forest as estimated by xylem sap flow techniques. Forest Ecol Manag 143: 205-213.

Yaltırık F (1984). Türkiye Meşeleri Teşhis Kılavuzu. Yenilik Basımevi, Istanbul.

Yan M-J, Zhang J-G, He Q-Y, Shi W-Y, Otsuki K, Yamanaka N, Du S (2016). Sapflow-based stand transpiration in a semiarid natural forest on China's Loess Plateau. Forests 7: 227.

Proceedings of the 10th World Congress of EWRA 'Panta Rhei', 5-9 July 2017, Athens, Greece
© 2017 *European Water Resources Association*

Impact of climate change on water footprint of wheat, rice and potato (case study: Iran)

M. Montaseri* and N.R. Majd
Department of Water Engineering, Urmia University, Iran
* *e-mail: montaseri@hotmail.com*

Abstract: The population growth causes unsustainable global agricultural development especially in arid and semi-arid regions. A new and efficient approach named "water footprint" (including green, blue and grey components) is used by researchers world-wide in order to achieve optimum and sustainable utilization of fresh water resources. Hence in the present study, the water footprints of three agricultural crops (wheat, rice and potato) in all provinces of Iran (31 stations) were calculated for the historical period of 1981-2010. Then the climatic parameters were simulated for two future periods: 2011-2030 and 2045-2065 by the use of the HadCM3 model and the water footprints were also estimated for these two future periods under scenario A2. The results illustrated that, among the considered crops the maximum water footprint belonged to rice and wheat and the minimum amount belonged to potato. The evaluation of water footprint variations in the historical period and the simulated scenarios also showed the highest green water footprint variations in tropical stations and the lowest variation in colder areas. This is explained as follows: the maximum amount of rainfall variations for southern and eastern arid stations of Iran took place during January to March and for the colder areas this was during October up to December. During cold months, no crop cultivation occurs in cold regions but crops are cultivated in hot areas in that period. The blue water footprint variations showed completely different trends being highest for Ardabil, Hamedan, Ghazvin and Rasht and lowest for Bandar-Abbas, Ilam and Tehran.

Key words: Iran, climate change, water footprint, blue water, green water

1. INTRODUCTION

Base consumptive water and water footprint are two variables that vary among different crops. While in this variance, the parameters such as climate, crop productions, people consumption pattern, agriculture practices and water application efficiency have important roles. Therefore there is a need for a new concept in calculation of actual crop water requirement. The water footprint index with considering the direct and indirect water consumptions in three components of blue, green and grey water resources was applied to evaluate the total amount of water consumption in crop production. At a global scale, most of the water use occurs in agricultural production, but there are also substantial water volumes consumed and polluted in the industrial and domestic sectors (WWAP, 2009). So defining a more low water consuming land use pattern in the plain can lead to store more water. To have a better understanding of fresh water resources and its usages, it is important to understand the concept of hidden water. Hoekstra et al. (2011) have shown that visualizing the hidden water use behind products can help in understanding the global character of fresh water and in quantifying the effects of consumption and trade on water resources use. The improved understanding can form a basis for a better management of the globe's freshwater resources. The water footprint is an indicator of freshwater use that looks not only at direct water use of a consumer or producer, but also at the indirect water use (Hoekstra and Chapagain, 2006). Water footprint index is a global index which can be as an indicator of real consumptive water base on region climate condition. At first the mentioned index was presented by Hoekstra (2002) and then this concept was used extensively in the world (Roset et al, 2008; Van Oel et al, 2009; Yu et al, 2010; Chapagain and Hoekstra, 2011; Dumont et al, 2013; Gerbens-Leenes et al, 2013; Herath et al, 2014; Rodriguez et al, 2015; Xu et al, 2015). The water footprint can be regarded as a

comprehensive indicator of freshwater resources appropriation, next to the traditional and restricted measure of water withdrawal (Van Oel et al, 2009). The water footprint of a product is the volume of freshwater used to produce the product, measured over the full supply chain (Hoekstra and Hung, 2005). It is a multidimensional indicator, showing water consumption volumes by source and polluted volumes by type of pollution; all components of a total water footprint are specified geographically and temporally. The objective of the present study is to calculate the green and blue water footprints of 3 agricultural crops (wheat, rice and potato) in all provinces of Iran (31 stations) for the historical period of 1981-2010. In the next step, the climatic parameters were simulated for two future periods: 2011-2030 and 2045-2065 by using of the HadCM3 model and the water footprints were also estimated for these two future periods under scenario A2.

2. STUDY AREA

In this study, Long Ashton Research Station Weather Generator (LARS-WG) downscaled model (Semenov and Barrow 1997) was used to simulate meteorological parameters in two future periods (2011-2030 and 2046-2065) under scenario A2 using HadCM3 model. For this purpose, the daily meteorological data of thirty-one stations in Iran for 30-year period (1981 to 2010) investigated. Figure 1 shows geographical location of 31 selected synoptic stations.

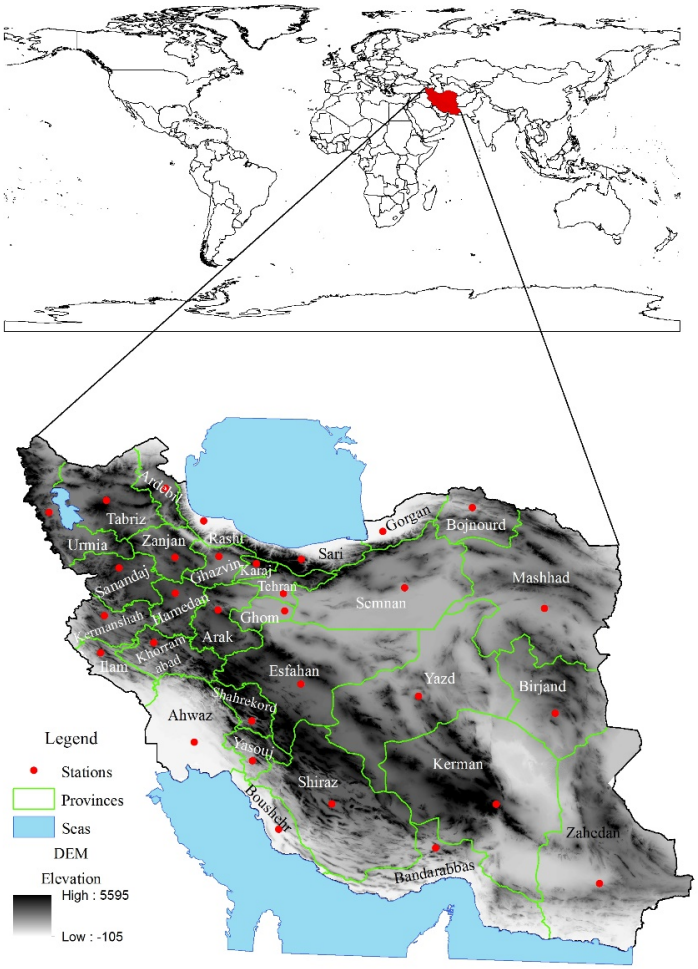

Figure 1. The geographic location of the selected 31 stations

3. METHODOLOGY

The green, blue and grey water footprints of crop production were estimated following the

calculation framework of Hoekstra et al. (2011). The computations of crop evapotranspiration and yield, required for the estimation of the green and blue water footprint in crop production, have been done following the method and assumptions provided by Allen et al. (1998) for the case of crop growth under non-optimal conditions.

The requirement data for evapotranspiration calculation containing minimum temperature, maximum temperature, relative humidity, sunshine hours, wind speed and precipitation in daily scale were obtained from metrological organization.

The FAO Penman-Monteith method has been selected to estimate ETo because it provides very consistent ETo values with actual crop water use, as it has been demonstrated through many years of evaluations reported in the scientific literature. The FAO Penman-Monteith method to estimate ETo is expressed as the equation (1).

$$ET_O = \frac{0.408\Delta(R_n - G) + \gamma \frac{900}{T+273} U_2 (e_s - e_a)}{\Delta + \gamma(1 + 0.34U_2)} \quad (1)$$

where, ETo is reference evapotranspiration [mm day^{-1}], R_n: net radiation at the crop surface [MJ m^{-2} day^{-1}], G: soil heat flux density [MJ m^{-2} day^{-1}], T: mean daily air temperature at 2 meter height [°C], u_2: wind speed at 2 meter height [m s^{-1}], e_s: saturation vapour pressure [kPa], e_a: actual vapour pressure [kPa], $e_s - e_a$: saturation vapour pressure deficit [kPa], Δ: vapour pressure curve slope [kPa $°C^{-1}$] and γ is psychrometric constant [kPa $°C^{-1}$].

The total water footprint of the process of growing crops or trees (WFproc) is the sum of the green, blue and grey components (equation 2).

$$WF = WF_{blue} + WF_{green} + WF_{grey} \quad (2)$$

where, WF_{green} is green water footprint that refers to consumption of green water resources (rainwater insofar as it does not become runoff). WF_{blue} is blue water footprint that, refers to consumption of blue water resources (surface and groundwater) along the supply chain of a product. 'Consumption' refers to loss of water from the available ground/surface water body in a catchment area. Losses occur when water evaporates, returns to another catchment area or the sea or is incorporated into a product. WF_{grey} is grey water footprint that, refers to pollution and is defined as the volume of freshwater that is required to assimilate the load of pollutants given natural background concentrations and existing ambient water quality standards (Hoekstra et al. 2011). The green component in the process water footprint of a growing crop or tree (WF_{green}, m^3/ton) is calculated as the green component in crop water use (CWU_{green}, m^3/ha) divided by the crop yield (Y, ton/ha). The blue component (WF_{blue}, m^3/ton) is calculated in a similar way (equations 3 and 4).

$$WF_{green} = \frac{CWU_{green}}{Y} \quad (3)$$

$$WF_{blue} = \frac{CWU_{blue}}{Y} \quad (4)$$

The grey component in the water footprint of a growing crop or tree (WF_{grey}, m^3/ton) is calculated as the chemical application rate to the field per hectare (AR, kg/ha) times the leaching-runoff fraction (α) divided by the maximum acceptable concentration (c_{max}, kg/m^3) minus the natural concentration for the pollutant considered (c_{nat}, kg/m^3) and then divided by the crop yield (Y, ton/ha) (equation 5).

$$WF_{grey} = \frac{(\alpha * AR)(C_{max} - C_{nat})}{Y} \quad (5)$$

The pollutants generally consist of fertilizers (nitrogen, phosphorus and so on), pesticides and insecticides. One has to consider only the 'waste flow' to freshwater bodies, which is generally a fraction of the total application of fertilizers or pesticides to the field. One needs to account for only the most critical pollutant, that is the pollutant where above calculation yields the highest water volume.

The green and blue components in crop water use (CWU, m^3/ha) are calculated by accumulation of daily evapotranspiration (ET, mm/day) over the complete growing period expressed as the equations (6) and (7).

$$CWU_{green} = 10 * \sum_{d=1}^{lgp} ET_{green} \quad (6)$$

$$CWU_{blue} = 10 * \sum_{d=1}^{lgp} ET_{blue} \quad (7)$$

in which ET_{green} represents green water evapotranspiration and ET_{blue} blue water evapotranspiration. The factor 10 is meant to convert water depths in millimetres into water volumes per land surface in m^3/ha. The summation is done over the period from the day of planting (day 1) to the day of harvest (lgp stands for length of growing period in days). Since different crop varieties can have substantial differences in the length of the growing period, this factor can significantly influence the calculated crop water use.

4. RESULTS AND DISCUSSION

LARS-WG model runs for during studied period (1981-2010) by using daily data of rainfall (mm), temperature (°C) and sunshine hours of 31 synoptic stations. Table 1 shows monthly average of historical data and simulated data under scenario A2 for the three parameters including temperature, rainfall and sunshine hours, respectively.

Simulation of temperature for all stations in future periods will show a rise in temperature, the amount of temperature increase during the period 2046-2065 is higher than the period 2011-2030. Irregular rainfall changes indicate variations in time series which are simulated for future periods. The most precipitation loss and temperature rise will be on the period 2046-2065. Sunshine hours among the studied stations except Rasht station will decrease in the all months. Also it can be seen that there is no significant differences between the scenarios in simulated sunshine hours in both periods.

Figure 2 (a) shows the green and blue water footprints of wheat in historical and two simulated future periods. The green water footprint of wheat is more in the northern and western parts of the country, and the green water footprint is reduced as move to east and center of Iran. However, blue water footprint trend was reversed in the country so that the maximum blue water can be seen in the central and eastern parts of the country. Finally, according to the general terms (crop yield, green and blue water footprints) Khorramabad, Arak, Hamedan and Karaj were selected the best place in the country for cultivation wheat.

Figure 2 (b) shows the green and blue water footprints of rice in historical and two simulated future periods. Rice green water footprint changes shows a decreasing trend from north to south so that the maximum amount of green water is in the North and North West provinces of the country. However the lowest amount of blue water footprint can be seen in these provinces. The highest amount of blue water footprint is obtained in the Central and Western provinces (Ghom,

Kermanshah, Sanandaj and Isfahan). Finally the Northern provinces (Gilan, Mazandaran and Golestan) are introduced as the most suitable place for rice growth and production.

Table 1. Monthly average of historical and simulated data under scenario A2

parameter	time period	Ahwaz	Arak	Ardebil	Bandarabbas	Birjand	Bojnourd	Boushehr
tempe-rature	mean (1981-2010)	26.0	13.7	9.1	26.8	16.4	13.4	25.1
	scenario A2 (2011-2030)	26.7	14.5	9.7	27.5	17.0	14.0	25.7
	scenario A2 (2046-2065)	27.9	15.9	10.9	29.1	18.3	15.3	26.8
rainfall	mean (1981-2010)	226.1	305.2	284.4	179.6	166.7	261.8	260.2
	scenario A2 (2011-2030)	241.0	326.2	286.9	233.2	175.5	284.7	265.5
	scenario A2 (2046-2065)	227.2	316.5	282.2	211.1	165.5	288.3	221.5
sunshine	mean (1981-2010)	8.3	7.8	6.7	8.6	9.1	7.5	8.2
	scenario A2 (2011-2030)	8.3	7.9	6.8	8.7	8.9	7.4	8.4
	scenario A2 (2046-2065)	8.4	7.9	6.8	8.7	8.9	7.4	8.4

parameter	time period	Esfahan	Ghazvin	Ghom	Gorgan	Hamedan	Ilam	Karaj
tempe rature	mean (1981-2010)	16.7	14.1	18.3	17.9	11.1	24.3	15.1
	scenario A2 (2011-2030)	17.3	14.8	18.8	18.4	11.9	25.0	15.7
	scenario A2 (2046-2065)	18.7	16.1	20.2	19.6	13.3	26.4	16.9

parameter	time period	Esfahan	Ghazvin	Ghom	Gorgan	Hamedan	Ilam	Karaj
rainfall	mean (1981-2010)	126.3	324.5	144.9	527.3	324.4	392.3	249.9
	scenario A2 (2011-2030)	134.5	343.1	159.3	546.9	328.2	419.7	268.1
	scenario A2 (2046-2065)	127.9	345.1	156.8	562.6	318.6	406.2	269.2
sunshine	mean (1981-2010)	8.8	8.5	8.2	5.9	7.7	6.5	8.1
	scenario A2 (2011-2030)	8.8	7.9	8.1	5.4	7.6	7.6	8.0
	scenario A2 (2046-2065)	8.9	7.9	8.0	5.3	7.6	7.6	8.0

parameter	time period	Kerman	Kerman	Khorramab	Mashhad	Rasht	Sanandaj	Sari
tempe-rature	mean (1981-2010)	16.1	15.0	16.6	15.1	18.4	13.7	17.5
	scenario A2 (2011-2030)	16.8	15.8	17.3	15.6	19.2	14.5	18.2
	scenario A2 (2046-2065)	18.3	17.1	18.7	16.9	20.6	15.9	19.3
rainfall	mean (1981-2010)	134.5	426.0	481.1	256.3	1339.5	433.1	932.7
	scenario A2 (2011-2030)	149.8	435.3	519.6	270.6	1433.7	412.5	930.6
	scenario A2 (2046-2065)	125.5	432.8	504.4	271.4	1492.4	411.3	977.0
sunshine	mean (1981-2010)	8.9	7.6	7.9	7.9	11.9	7.8	5.3
	scenario A2 (2011-2030)	8.7	7.7	8.0	7.7	9.4	8.1	5.1
	scenario A2 (2046-2065)	8.7	7.7	8.0	7.6	9.3	8.1	5.1

parameter	time period	Semnan	Shahre kord	Shiraz	Tabriz	Tehran	Urmia	Yasouj
tempe-rature	mean (1981-2010)	15.3	11.5	18.4	13.1	18.1	11.4	15.3
	scenario A2 (2011-2030)	15.9	12.1	19.1	13.8	18.8	12.1	15.8
	scenario A2 (2046-2065)	17.2	13.4	20.5	15.2	20.2	13.6	17.2
rainfall	mean (1981-2010)	157.3	326.1	324.0	254.1	240.9	314.2	824.1
	scenario A2 (2011-2030)	162.2	350.8	328.6	259.9	246.6	312.8	847.3
	scenario A2 (2046-2065)	160.0	331.5	275.5	251.2	244.6	296.1	750.3
sunshine	mean (1981-2010)	7.9	8.2	9.2	7.6	7.7	7.9	8.3
	scenario A2 (2011-2030)	8.3	8.5	9.0	7.7	8.1	7.9	8.5
	scenario A2 (2046-2065)	8.3	8.6	9.0	7.7	8.1	8.0	8.6

parameter	time period	Yazd	Zahedan	Zanjan
tempe-rature	mean (1981-2010)	19.8	18.9	11.0
	scenario A2 (2011-2030)	20.4	19.4	11.7
	scenario A2 (2046-2065)	21.8	21.0	13.0
rainfall	mean (1981-2010)	55.9	77.8	293.4
	scenario A2 (2011-2030)	62.0	90.8	295.7
	scenario A2 (2046-2065)	56.4	74.5	295.1
sunshine	mean (1981-2010)	8.6	8.7	7.7
	scenario A2 (2011-2030)	8.9	9.1	7.6
	scenario A2 (2046-2065)	8.9	9.1	9.4

The map of potato Water Footprint changes in the country (figure 2 (c)) indicates high water footprint in the North and South of the country and the coastal areas of the Caspian Sea and the Persian Gulf. The results imply high effect of blue water footprint in the total water footprint of potato in the country. Figure 2 (c) shows high blue water footprint values in the desert areas of Eastern region of Iran.

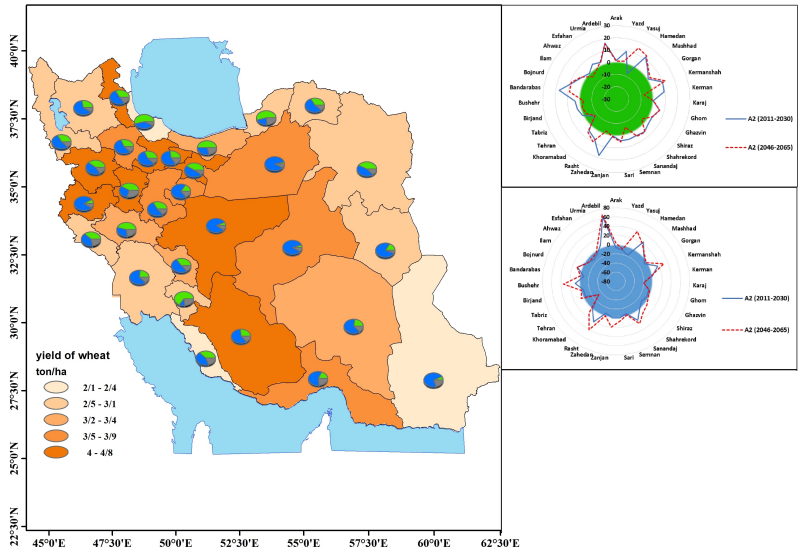

(a)

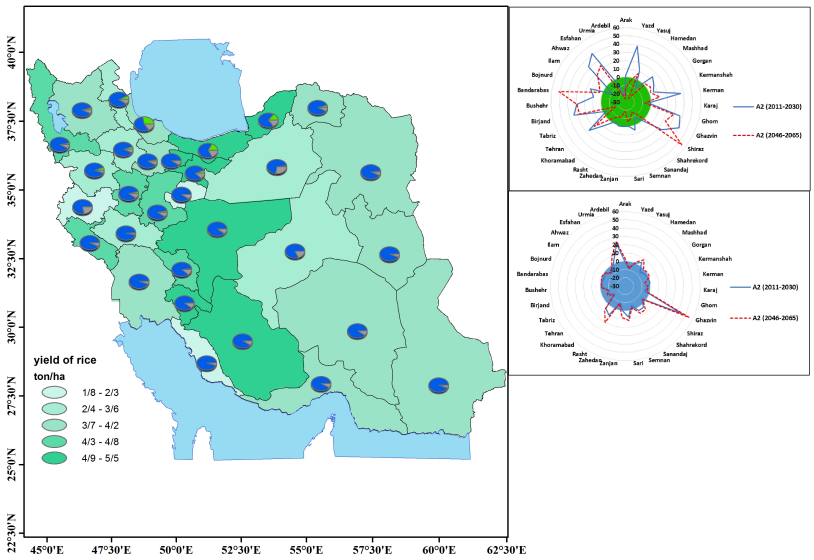

(b)

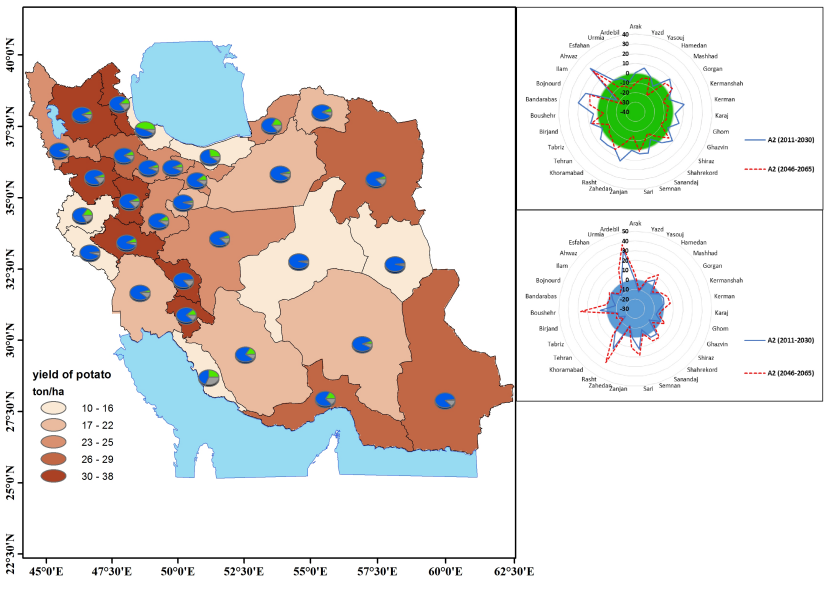

(c)

Figure 2. Green and blue water footprint changes of wheat (a) rice (b) and potato (c) in historical and simulated future periods

5. CONCLUSIONS

The results illustrated that, among the considered crops the maximum water footprint belonged to rice and wheat and the minimum amount belonged to potato. The evaluation of water footprint variations in the historical period and the simulated scenarios also showed the highest green water footprint variations in tropical and the lowest variation in colder areas. This is explained as follows: the maximum amount of rainfall variations for southern and eastern arid stations of Iran took place during January to March and for the colder areas this was during October up to December. During cold months (Oct – Nov – Dec), no crop cultivation occurs in cold regions but crops are cultivated in hot areas in that period. The blue water footprint variations showed completely different trends being highest for Ardabil, Hamedan, Ghazvin and Rasht and lowest for Bandar Abbas, Ilam and Tehran.

The greatest changes of green and blue water footprints will be in the 2011-2030 and 2046-2065 periods respectively because of changes in temperature and precipitation in the mentioned periods. So that precipitation will change more than any other meteorological parameters in 2011-2030 and have significant effects on green water footprint. But in 2046-2065 period temperature changes will be significant and have effective role on crop yield and blue water footprint variations.

REFERENCES

Allen, R.G., Pereira, L.S., Raes, D., Smith, M., 1998. Crop Evapotranspiration – Guidelines for Computing Crop Water Requirements. FAO Irrigation and Drainage Paper 56, FAO, 1998, ISBN 92-5-104219-5.

Chapagain, A. K., Hoekstra, A. Y., 2011.The blue, green and grey water footprint of rice from production and consumption perspectives. Ecological Economics; 70.4: 749-758.

Dumont, A., Salmoral, G., Llamas, M. R., 2013. The water footprint of a river basin with a special focus on groundwater: The case of Guadalquivir basin (Spain). Water Resources and Industry; (1) 60-76.

Gerbens-Leenes, P. W., Mekonnen, M. M., Hoekstra, A. Y., 2013. The water footprint of poultry, pork and beef: A comparative study in different countries and production systems. Water Resources and Industry; (1), 25-36.

Herath, I., Green, S., Horne, D., Singh, R., Clothier, B. 2014. Quantifying and reducing the water footprint of rain-fed potato production, part I: measuring the net use of blue and green water. Journal of Cleaner Production, 81, 111-119.

Hoekstra, A.Y., 2002. Virtual water trade. In: Proceedings of the International Expert Meeting on Virtual Water Trade, Delft, The Netherlands. Value of Water Research Report Series, vol. 12. UNESCO-IHE, Delft, The Netherlands.

Hoekstra, A. Y., Chapagain, A. K., 2006. Water footprints of nations: water use by people as a function of their consumption pattern. In Integrated Assessment of Water Resources and Global Change; 35-48.

Hoekstra A. Y., Chapagain A. K., Aldaya M. M., Mekonnen M. M. 2011. The water footprint assessment manual: Setting the global standard, Earthscan, London, UK.

Hoekstra, A. Y., Hung, P. Q., 2005. Globalization of water resources: International virtual water flows in relation to crop trade. Global Environmental Change; 15(1): 45-56.

Rodriguez C. I., de Galarreta V. R., and Kruse E. E, 2015. Analysis of water footprint of potato production in the pampean region of Argentina. Cleaner Production; 90: 91–96.

Rost, S., Gerten, D., Bondeau, A., Lucht, W., Rohwer, J., Schaphoff, S., 2008. Agricultural green and blue water consumption and its influence on the global water system. Water Resources Research; 44(9).

Semenov, M. A., Barrow, E. M., 1997. Use of a stochastic weather generator in the development of climate change scenarios. Climate Change; 35: 397–414.

Van Oel. P. R., Mekonnen. M. M., Hoekstra. A. Y., 2009. The external water footprint of the Netherlands: Geographically-explicit quantification and impact assessment. Ecological Economics; 69: 82–92.

WWAP. 2009. The United Nations World Water Development Report 3: Water in a changing world, World Water Assessment Programme, UNESCO Publishing, Paris / Earthscan, London.

Xu, Y., Huang, K., Yu, Y., Wang, X., 2015. Changes in water footprint of crop production in Beijing from 1978 to 2012: a logarithmic mean Divisia index decomposition analysis. Cleaner Production; 87: 180-187.

Yu, Y., Hubacek, K., Feng, K., Guan, D., 2010. Assessing regional and global water footprints for the UK. Ecological Economics; 69(5): 1140-1147.

Proceedings of the 10th World Congress of EWRA 'Panta Rhei', 5-9 July 2017, Athens, Greece
© 2017 *European Water Resources Association*

Water buyback in agriculture: What can we expect?

C.D. Perez-Blanco[1,2*] and C. Gutierrez-Martin[3]
[1] *Fondazione Eni Enrico Mattei (FEEM). Isola di San Giorgio Maggiore, 8. 30124 Venice, Italy*
[2] *Centro Euro-Mediterraneo sui Cambiamenti Climatici (CMCC), RAAS Division. Isola di San Giorgio Maggiore, 8. 30124 Venice, Italy*
[3] *Universidad de Córdoba. Campus Rabanales. Ctra N-IV, km 396, Edificio C5. 14014 Córdoba, Spain*
[*] *e-mail: dionisio.perez@feem.it*

Abstract: The reacquisition or buyback of water is an increasingly accepted approach to restore environmental flows threatened by overall location. Reacquisitions are operated through purchase tenders that compensate irrigators who decide to surrender (part of) their right to withdraw water. A major concern in water buyback involves information rents and the extent of the compensation: information asymmetries can lead to agency costs that inflate market prices and hinder buyback welfare enhancing opportunities. The accomplishment of water buyback is therefore conditioned to the ability of the principal to place bids consistent with the shadow price of irrigators. However, methods used to inform buyback programmes to date either rely on ex-post trading data that is not readily available in most regions worldwide; or compensate projected foregone income, and thus ignore the effects that buyback may have on other relevant attributes determining utility. The research hypothesis is that since buyback programmes offer management complexity- and risk-free payments to management complexity- and risk-averse farmers, addressing foregone income may overcompensate sellers. This paper uses revealed preference methods to elicit the parameters of a multi-attribute objective function of irrigators in the overexploited Segura River Basin in SE Spain. Objective functions are used in a series of simulations in which water allocation is progressively constrained to reveal the shadow price of irrigation water using two different compensation measures: i) foregone income, a proxy of the shadow price typically used in the literature; and ii) compensating variation that addresses foregone utility. Results show a relevant gap between the two methods.

Key words: Mathematical programming; water buyback; compensating variation; Spain

1. INTRODUCTION

The reacquisition or *buyback* of water is an increasingly accepted approach to restore the balance in overexploited basins, as shown by the significant investments recently committed to water buyback in areas like Australia's Murray-Darling Basin (AUD 3.1 billion for the period 2009-2024), Spain (EUR 829.9 million for the period 2007-2027) and the US, notably California (USD 547 million during 1987-2011, 55% of which after 2003) (DoEE, 2016; Garrido et al., 2013; GRBA, 2008; Hanak and Stryjewski, 2012). Reacquisitions are operated through purchase tenders that compensate irrigators who decide to surrender (part of) their right to withdraw water. A major concern in water buyback involves information rents and the extent of the compensation (Crase et al., 2012): information asymmetries often lead to agency costs that inflate market prices and hinder the realization of buyback welfare enhancing opportunities. Government agencies (the *principal*) can set in advance price and budgetary thresholds to control for agency costs. The accomplishment of water buyback is therefore conditioned to the quality of the information available, which largely determines the ability of the principal to encourage bids consistent with the shadow price of the potential seller and thus limit agency costs.

Mature water markets in Australia, Chile and the US offer a platform to obtain data on prices and amounts traded for a variety of locations and moments, which can be used to predict responses and adjust bids using econometrics (Zuo et al., 2015). Yet, standard econometrics is not applicable

where formal water markets do not exist or are still in an early stage and *ex-post* trading data is not readily available[††]. This is the case of most regions worldwide –some of which are in the process of, or already implementing buyback programmes (Delacámara and Gómez, 2015). Informing purchase tenders under limited, incomplete or straightaway inexistent trading data demands an in-depth knowledge of, and information on, sellers' motives and behavior, so that their objective function can be obtained to account for the marginal cost of strengthening the water allocation constraint (i.e. the *shadow price*). The Theory of Planned Behavior shows that motives driving behavior can be accurately predicted from a set of assessments based on agent's *beliefs* on the "goodness" or "badness" of an object, which can be in turn normally associated to a particular attribute (Ajzen, 1991). The theory is well supported by empirical evidence (Gómez-Limón et al., 2016), implying that accurate modelling of agents' decisions requires the inclusion of more than one attribute in a multi-attribute utility function –the idea that underpins the development of Multi-Attribute Utility Theory (Keeney and Raiffa, 1993). Yet, methods used to date rely on single-attribute objective functions that compensate projected foregone income, but ignore the effects that buyback may have on other relevant attributes explaining utility, such as risk or management complexity aversion (Heady, 1952). Since buyback programmes offer a payment with no risk or management complexity attached to management complexity- and risk-averse farmers, this approach may overcompensate sellers. This paper relies on Mathematical Programming (MP) methods to elicit the parameters of a multi-attribute objective function that is consistent with economic theory and empirical evidence on farmers' motives and behavior to test this hypothesis. The objective is to enhance the design and performance of water buyback programmes, particularly in areas where *ex-post* trading data is unavailable.

This paper relies on a Revealed Preference Models (RPM) that builds on the methods developed in the seminal work by Gutiérrez-Martín and Gómez (2011) and applies it to the case of agricultural water buyback in the overexploited Segura River Basin in SE Spain. In this version of the model, over 4000 source lines of code have been updated to reduce computational requirements in the calibration procedure, which here is based on a projection method (see Section 2.2). Use of the comprehensive and detailed database recently made available by the Segura River Basin Authority (SRBA, 2014) makes possible to expand the number of agents from 12 to 62, 5x + as compared to previous versions of the model, resulting in more disaggregate and homogeneous units. Calibrated objective functions are used in a series of simulations in which water allocation is progressively constrained and agents have to adapt through crop portfolio decisions (see Section 3). The simulation module captures the changes in income *and utility* resulting from agents' decisions. Buyback prices can be then obtained as the capitalized value of two different compensation measures: i) the foregone income, a proxy of the shadow price typically used in the literature (Martínez-Granados and Calatrava, 2014; Qureshi and Whitten, 2014); and ii) the compensating variation that addresses foregone utility. This allows for comparison between the two compensation methods to test our initial hypothesis of whether conventional estimates based on foregone income overcompensate sellers.

2. METHODS

2.1 Decision-making problem

Irrigators' objective function depends on the attributes they value. The provision of these attributes is in turn mainly determined by the crop mix selected. Consequently, irrigators' decisions are primarily focused on the choice of the crop portfolio that maximizes their objective function,

[††] In these instances, 'prices' do not reflect the interaction between supply and demand in a market environment, rather government charges to (partially) recover regulation, abstraction, transportation and distribution costs (EEA, 2013).

subject to a series of constraints:

$$\underset{x}{\text{Max}}\, U(x) = U(z_1(x);\ z_2(x); z_3(x) \dots\ z_m(x)) \quad (1)$$

$$\text{s.t.:}\quad 0 \le x_i \le 1 \quad (2)$$

$$\sum_{i=1}^{n} x_i = 1 \quad (3)$$

$$x \in F(x) \quad (4)$$

where $x \in R^n$ is the decision variable, a vector that represents the share of the available land dedicated to a particular crop x_i $(i = 1, \dots, n)$, including fallow. In case the same crop can be subject to alternative management techniques (e.g. irrigated and rainfed), each possible combination is treated as an independent crop. Thus every crop has a unique combination of dimensionless attributes z_p $(p = 1, \dots, m)$, which are the variables that agents value and may include, among others, expected profit, risk avoidance and/or management complexities avoidance. Provided attributes are quantifiable, every crop portfolio yields a utility that can be ranked. Rational agents will choose the crop portfolio x^* that maximizes their objective function subject to a series of (quantifiable) constraints, including land availability, water resources, vocation/know-how, agronomic aspects (e.g. crop rotation, including fallow land) and other restrictions (e.g. policy restrictions such as EU Common Agricultural Policy rules), which together define a set of feasible choices $F(x)$. The water resources constraint, of particular relevance for the purpose of this paper, is denoted by:

$$\sum_{i=1}^{n} w_i\, x_i\, ha \le W \quad (5)$$

where w_i is the water requirement of crop x_i, ha is the land allotment and W represents total water availability.

From a positive approach, the optimal solution to the problem above can be obtained *ex-post* observing the cropping decisions actually made by irrigators (x^o). This means that the observed decision is the solution that maximizes the objective function within the domain. RPM can elicit an objective function that is consistent with the domain and observed decisions, which can be used in turn to forecast behavioral responses to key *stimuli*, e.g. reduced water allocation.

2.2 Calibration procedure

Using standard microeconomic theory, the parameters of the objective function can be calculated for a set of attributes equalizing the marginal opportunity cost of trading attribute z_k off for attribute z_p along the welfare's attribute possibility frontier, or *efficient frontier* (the Marginal Rate of Transformation MRT_{z_p,z_k}, the slope of the efficient frontier), and the willingness to give up one unit of attribute z_k in exchange for a unit of attribute z_p (the Marginal Rate of Substitution MRS_{z_p,z_k}, the slope of the indifference curve of the utility function):

$$MRT_{z_p,z_k} = MRS_{z_p,z_k} = -\frac{\partial U/\partial z_p}{\partial U/\partial z_k};\quad \forall p \ne k \quad (6)$$

Irrigators' objective function is calibrated following a procedure in three steps. The model is coded using the General Algebraic Modelling System software (GAMS v21.4) and is available upon request.

2.2.1 Efficient frontier

When making their choices, rational agents face tradeoffs along the *efficient frontier*: crop portfolios with a higher expected profit may display lower risk avoidance, while portfolios avoiding complex management may come at the expense of a lower expected profit. Real world efficient frontiers cannot be represented with a closed mathematical function; nonetheless, provided a sufficient and relevant number of choice alternatives x exists (guaranteed in this case by a large portfolio of 71 crops comprising 80% of irrigated surface), it is possible to represent the efficient frontier using numerical methods. This is done solving an optimization problem that maximizes the value of attribute z_p along the z_k axis within the domain:

$$\underset{x}{\text{Max}}\ z_p(x) \tag{7}$$

$$\text{s.t.: } z_k(x) = c \quad \forall k \neq p \quad c = (0, \dots, 1) \tag{8}$$

$$0 \leq x_i \leq 1 \tag{9}$$

$$\sum_{i=1}^{n} x_i = 1 \tag{10}$$

$$x \in F(x) \tag{11}$$

Note again that attributes are dimensionless with values between zero and one. There is one efficient frontier for every pair of attributes z_p, z_k [‡‡]. The efficient frontier must be convex – otherwise there is no opportunity cost between attributes and the decision becomes trivial.

The position in the two-dimensional space z_p, z_k of the set of points along the efficient frontier is denoted as $\tau_{z_p,z_k}(X^f)$, and the position of one of these points as $\tau_{z_p,z_k}(x^f)$. Analogously, the position of a given crop portfolio x in the space of attributes can be denoted as $\tau_{z_p,z_k}(x)$ and the position of the observed crop portfolio x^o in the space of attributes (i.e. the crop portfolio actually *chosen* by the agent) as $\tau_{z_p,z_k}(x^o)$.

The next problem consists in finding a value along the frontier that can be used as a reference for the calibration of the utility function. For this purpose the MRT_{z_p,z_k} is estimated. Since the solution to agents' decision-making problem is the observed crop portfolio, and agents are rational individuals that aim at maximizing their utility within the domain, the efficient frontier must be close to $\tau_{z_p,z_k}(x^o)$. Therefore the two points that result from *projecting* the position of the observed crop portfolio $\tau_{z_p,z_k}(x^o)$ vertically or horizontally to the efficient frontier, namely $\tau_{z_p,z_k^o}(x^f)$ and $\tau_{z_p^o,z_k}(x^f)$, are also close to each other. $\tau_{z_p,z_k^o}(x^f)$ and $\tau_{z_p^o,z_k}(x^f)$ are obtained solving the problem in equations [6]-[10], setting equation [7] equal to the observed values of the attributes. The MRT_{kp} can be approximated through the slope between the two points. The approximation error and other potential sources of bias in the calibration stage are measured using calibration residuals.

2.2.2 Utility function

The application of the model in this paper relies on a Cobb-Douglas specification for the objective function. As compared to alternative additive or multiplicative-additive functional forms, Cobb-Douglas functions have a decreasing marginal utility for every attribute and guarantee the existence of a global optimum provided the efficient frontier is convex (Inada, 1963). The objective

[‡‡] There are m attributes. Therefore, each set of attributes comprises $t \leq m$ attributes, and $\frac{t!}{2!(t-2)!}$ combinations of two attributes and efficient frontiers.

function in equation [1] is now:

$$U(x) = \prod_{p=1}^{m} z_p(x)^{\alpha_p}; \quad \sum_{p=1}^{m} \alpha_p = 1 \tag{12}$$

The parameters (α) of the Cobb-Douglas objective function can be obtained from the following system of equations:

$$MRS_{z_p,z_k} = -\frac{\partial U/\partial z_p}{\partial U/\partial z_k} = -\frac{\alpha_p}{\alpha_k}\frac{z_k}{z_p} = MRT_{z_p,z_k}; \quad \forall p \neq k \tag{13}$$

$$\sum_{p=1}^{m} \alpha_p = 1 \tag{14}$$

Solving this system for every possible combination of attributes yields an equal number of utility functions, whose parameters are determined by:

$$\alpha_p = \frac{1}{1-\sum_{k=1}^{m}\left(MRT_{p,k}\cdot\frac{z_k}{z_p}\right)} \quad \forall p \neq k \tag{15}$$

Each utility function is then used to solve the problem in equations [1]-[5] to obtain the simulated crop portfolio (x^*) and the corresponding attributes value ($z_p^*; p = 1, \dots, m$).

2.2.3 Goodness of fit

In order to use behavioral models effectively for decision-making, it is of critical importance to use an appropriate level of confidence in their performance. In positive MP methods such as RPM, metrics for performance evaluation are also the very instrument used to reveal the relevant attributes driving agents' behavior. Positive models assume that rational agents choose the crop portfolio that maximizes the provision of the attributes they value, given a number of constraints, and thus that the *relevant attributes* in the model must be those that more accurately represent observed behavior –in other words, those that yield a lower calibration residual/error. Among the available metrics for performance evaluation (see e.g. Bennett et al., 2013), this work relies on the root-mean-square-error, a measure frequently used in economics and environmental research to address the difference between observed and model predicted values. Similar measures have been used in previous applications of RPM (see e.g. Varian, 2012, 2007).

Two calibration residuals are used. The first error is based on the distance between the observed portfolio (x^o) and the simulated crop portfolio (x^*).

$$e_x = \frac{1}{n}\sqrt{\sum_{i=1}^{n}\left(\frac{x_i^o - x_i^*}{x_i^o}\right)^2} \tag{16}$$

The second error assesses the distance between the observed attributes (z^o) and the simulated ones (z^*):

$$e_\tau = \frac{1}{m}\sqrt{\sum_{p=1}^{m}\left(\frac{z_p^o - z_p^*}{z_p^o}\right)^2} \tag{17}$$

An average calibration residual is estimated as the ordinary arithmetic mean of the two metrics above.

$$e = \frac{e_x + e_\tau}{2} \tag{18}$$

The relevant set of attributes is the one that minimizes the average calibration residual. Its corresponding utility function is the one used in the buyback simulation runs.

3. RESULTS

Attributes are selected based on a literature review on the Multi-Attribute Utility Theory (Keeney and Raiffa, 1993) and the Theory of Planned Behavior (Ajzen, 1991), and include measures of profit, risk avoidance and management complexity avoidance. The ordinal utility function ranks alternative decisions and prevents correlation among attributes. The most relevant attributes (z_p) in explaining the behavior of each agent are those displaying a higher parameter value (α_p). In the case of the Segura River Basin, profit is the most relevant attribute in 55 AWDUs, while risk avoidance is the most relevant attribute in 7 AWDUs. Consistent with the literature, both attributes are relevant in explaining the behavior of all the 62 agents in the basin.

The objective functions revealed are then used to assess agents' response to a series of simulations, in which the water allocation constraint W_g is progressively strengthened reducing the allotment from 1% to 50% at 1% intervals ($g = 1, 2, \dots, 50$). The baseline scenario without water reacquisitions used for the calibration of the objective function corresponds to $g = 0$. It is assumed that only surface water, groundwater and resources transferred from outside the basin are purchased; desalinated water and treated wastewater are excluded.

The shadow price of water is estimated in every simulation run both as the foregone income and as the compensating variation that addresses foregone utility. The foregone income (FI_g) is obtained from the change in the variable margin z_1 in two consecutive simulation runs:

$$FI_g = \frac{z^*_{1,g} - z^*_{1,g-1}}{W_g - W_{g-1}} \tag{19}$$

The compensating variation (CV_g) is obtained as follows:

$$CV_g = \frac{e\left(U^*_{g-1}, W_g\right)}{W_g - W_{g-1}} \tag{20}$$

where e is an expenditure function representing the minimum amount of money agents would need to attain the utility level in $g-1$ given a water constraint W_g.

The information above can be used to inform temporary and permanent buyback programmes. A benchmark for temporary reacquisitions can be readily obtained aggregating marginal purchase prices and dividing them by the total amount of water reacquired to obtain an annuity payment. A benchmark for the *permanent* purchase price of water can be estimated as the capitalized value of the shadow prices of water, using the capitalization rate of agricultural land as a reference (GRBA, 2008).

Table 1. Marginal and average water purchase prices and investment costs for selected environmental targets (3.7% capitalization rate)

Target (hm^3)	Balance (hm^3)	Compensating variation			Foregone income		
		Marginal price (EUR/m^3)	Average price (EUR/m^3)	Investment (M EUR)	Marginal price (EUR/m^3)	Average price (EUR/m^3)	Investment (M EUR)
50	-194	1.14	0.58	28.9	2.94	1.33	66.5
100	-144	3.30	1.37	137.2	4.51	2.65	265.2
150	-94	4.42	2.22	332.9	6.91	3.67	550.9
200	-44	6.03	2.89	578.9	9.93	4.73	945.4
250	6	8.81	3.81	952.8	13.90	6.22	1,554.2
300	56	11.63	4.91	1,474.1	16.56	7.78	2,333.2
400	156	21.19	7.87	3,146.5	32.72	11.02	4,408.1
500	256	38.39	11.56	5,781.5	52.77	18.08	9,041.4

Results in Table 1 highlight again the relevant gap in compensation payments between the two methods. The use of a method that accounts for changes in utility instead of changes in income can reduce budgetary pressures (i.e. investment) between 28.5% and 56.4%, depending on the reacquisition target. Results validate the hypothesis of overcompensation in buyback programmes and stress the need for alternative modelling approaches to inform policy design, address agency costs and realize buyback welfare enhancing opportunities.

Even fully accounting for agency costs, buyback programmes can be expensive. The 1980-2012 average water balance in the Segura River Basin is estimated at -244 hm^3/year . A water buyback program that targets the *permanent* purchase of 250 hm^3 has a minimum estimated cost of EUR 952.8 million (compensating variation method). With a lower budget, the *Restoring the Balance in the Murray-Darling Basin* Plan had secured the permanent purchase of 803 hm^3 as at 30 April 2010 (DoEE, 2016). This illustrates the high value of water in the Segura River Basin. A more ambitious target aiming at enhancing environmental flows would demand a minimum investment of EUR 1,474.1 million (300 hm^3 target), EUR 3,146.5 million (400 hm^3 target), EUR 5,781.5 million (500 hm^3 target) or EUR 11,960.3 million (600 hm^3 target) (compensating variation method).

4. DISCUSSION AND CONCLUSIONS

Results are consistent with the (admittedly limited) scientific evidence in the area. By means of a PMP model and using an income compensation approach, Martínez-Granados and Calatrava (2014) find that the annuity payment necessary to buyback 68.7 hm^3 of groundwater rights from irrigators in the western part of the basin[§§] is EUR 0.71/m^3. Using the model presented in this paper and focusing on groundwater resources in the same area, the annuity to achieve the 68.7 hm^3 target is estimated at EUR 0.65/m^3 with the foregone income method (consistent with the PMP single-attribute approach), and EUR 0.35/m^3 with the compensating variation method –suggesting again a bias towards overcompensation in single-attribute approaches.

Water buyback experiences in the Segura River Basin have addressed more modest targets thus far; both in their quantitative and temporary scope (*annual* water purchases). Reacquisitions recovered 2.9 hm^3/year in 2007 and 2008 at an average annuity payment of EUR 0.17/m^3. Tenders targeted farmers in the upper stretches of the basin, in the Albacete Province (NUTS 3), and aimed at maintaining environmental flows in surface water bodies during a severe drought period (*state of emergency*). The annuity that results from applying the methodology above in this specific area[***] to achieve the 2.9 hm^3/year target is lower: EUR 0.10/m^3 and EUR 0.12/m^3 using the compensating variation and foregone income methods, respectively. This simulation accounts for the irrigation restrictions that apply during a state of emergency (-50% of the initial allocation). The difference between the estimated values and the annuity actually paid offers a first estimation of the agency costs incurred. High agency costs can be explained by the limited *ex-post* trading data available, which constrains government agencies to operate with limited information. While literature reports significant trading in the area, mostly beyond the control and supervision of institutions, only 35 formal lease contracts totaling 10.1 hm^3 took place in the Segura River Basin between 2000 and 2005: less than .6% of annual withdrawals (Garrido et al., 2013).

Further research can address the current limitations of the model. Alternative calibration procedures could be used, and results compared, to minimize calibration residuals and correct simulation bias. For example, the calibration procedure could minimize the distance between the position of the observed crop portfolio in the space of attributes and that of the efficient frontier. It is also possible to explore alternative functional forms and/or alternative/complementary attributes in the objective function of the agents to improve accuracy. For example, it could be informative to explore the role of climate, weather and market forecasts on agents' behavior. At this point it is

[§§] This area comprises AWDUs n. 60, 61, 63, 64, 65 and 68. AWDU n. 66 does not use groundwater and is excluded.

[***] This area comprises AWDUs n. 8, 9, 10, 12, 13, 14 and 15. AWDU n. 7 relies on groundwater only and is excluded.

worthy of note the difficulty, if not impossibility, to fully model or interpret the relevant set of attributes, as we are bound by information constraints and our cognitive abilities. As a result, the calibration residual cannot be fully removed. On the other hand, a finite and manageable sample of attributes gives us useful insights for decision-making and more accurate modelling of agents' behavior as compared to alternative approaches.

REFERENCES

Ajzen, I., 1991. The theory of planned behavior. Organ. Behav. Hum. Decis. Process., Theories of Cognitive Self-Regulation 50, 179–211. doi:10.1016/0749-5978(91)90020-T

Bennett, N.D., Croke, B.F.W., Guariso, G., Guillaume, J.H.A., Hamilton, S.H., Jakeman, A.J., Marsili-Libelli, S., Newham, L.T.H., Norton, J.P., Perrin, C., Pierce, S.A., Robson, B., Seppelt, R., Voinov, A.A., Fath, B.D., Andreassian, V., 2013. Characterising performance of environmental models. Environ. Model. Softw. 40, 1–20. doi:10.1016/j.envsoft.2012.09.011

Crase, L., O'Keefe, S., Kinoshita, Y., 2012. Enhancing agrienvironmental outcomes: Market-based approaches to water in Australia's Murray-Darling Basin. Water Resour. Res. 48, W09536. doi:10.1029/2012WR012140

Delacámara, G., Gómez, C.M., 2015. Water trading: An introduction, in: Lago, M., Mysiak, J., Gómez, C.M., Delacámara, G., Maziotis, A. (Eds.), Use of Economic Instruments in Water Policy Insights from International Experience, Global Issues in Water Policy. Springer, pp. 201–207.

DoEE, 2016. Progress of water recovery against 2750GL reduction in surface water SDLs (Report). Department of the Environment and Energy, Canberra (Australia).

EEA, 2013. Assessment of cost recovery through water pricing (Report No. 16/2013). European Environment Agency, Copenhagen (Denmark).

Garrido, A., Rey, D., Calatrava, J., 2013. Water trading in Spain, in: Agriculture and the Environment in Spain: Can We Square the Circle? CRC Press, Taylor & Francis, pp. 205–216.

Gómez-Limón, J.A., Gutiérrez-Martín, C., Riesgo, L., 2016. Modeling at farm level: Positive Multi-Attribute Utility Programming. Omega. doi:10.1016/j.omega.2015.12.004

GRBA, 2008. Plan Especial del Alto Guadiana. Guadiana River Basin Authority.

Gutiérrez-Martín, C., Gómez, C.M., 2011. Assessing irrigation efficiency improvements by using a preference revelation model. Span. J. Agric. Res. 9, 1009–1020. doi:10.5424/sjar/20110904-514-10

Hanak, E., Stryjewski, E., 2012. California's Water Market, By the Numbers, Update 2012 - Techncal Appendix (Report - Appendix No. Update November 2012). Public Policy Institute of California.

Heady, E., 1952. Economics of Agricultural Production and Resource Use, Bailey & Swinfen. ed. Prentice-Hall.

Inada, K.-I., 1963. On a Two-sector Model of Economic Growth: Comments and Generalization. Rev. Econ. Stud. 30, 119–127.

Keeney, R.L., Raiffa, H., 1993. Decisions with Multiple Objectives: Preferences and Value Tradeoffs. Cambridge University Press, Cambridge England ; New York, NY, USA.

Martínez-Granados, D., Calatrava, J., 2014. The role of desalinisation to address aquifer overdraft in SE Spain. J. Environ. Manage. 144, 247–257. doi:10.1016/j.jenvman.2014.06.003

Qureshi, M.E., Whitten, S.M., 2014. Regional impact of climate variability and adaptation options in the southern Murray–Darling Basin, Australia. Water Resour. Econ. 5, 67–84. doi:10.1016/j.wre.2013.12.002

SRBA, 2014. Plan Hidrológico de la Cuenca del Segura 2009-2015 (River Basin Management Plan). Segura River Basin Authority, Murcia (Spain).

Varian, H.R., 2012. Revealed Preference and its Applications*. Econ. J. 122, 332–338. doi:10.1111/j.1468-0297.2012.02505.x

Varian, H.R., 2007. Position auctions. Int. J. Ind. Organ. 25, 1163–1178.

Zuo, A., Wheeler, S.A., Adamowicz, W.L. (Vic), Boxall, P.C., Hatton-MacDonald, D., 2015. Measuring Price Elasticities of Demand and Supply of Water Entitlements Based on Stated and Revealed Preference Data. Am. J. Agric. Econ. aav022. doi:10.1093/ajae/aav022

Proceedings of the 10th World Congress of EWRA 'Panta Rhei', 5-9 July 2017, Athens, Greece
© 2017 *European Water Resources Association*

Sustainability assessment of agricultural production through causal loop diagrams

R. de Vito[1,2*], I. Portoghese[1], A. Pagano[1], R. Giordano[1], M. Vurro[)] and U. Fratino[2]
[1] *Istituto di Ricerca sulle Acque, C.N.R., Italy*
[2] *DICATECh, Politecnico di Bari, Italy*
[*] *e-mail: rossella.devito@ba.irsa.cnr.it*

Abstract: Sustainable management of water resources in agriculture is extremely challenging for both policy-makers and scientists, especially at the local scale, due to multiple, complex, and interconnected loops existing among different issues and actors involved in intensive agricultural system. In such systems, multiple actors are indeed involved in decision-making processes characterized by high complexity of relationships between internal and external factors. Consequently, due to a poor knowledge of the system complexity, management strategies may often be affected by a high uncertain and result ineffective in their impacts. In this context, the proposed work aims at unravelling the complexity behind the sustainability of water use for irrigation purposes. A model based on Causal Loop Diagrams (CLD) was implemented on a reference case study of Southern Italy in order to get a deeper insight into a complex agricultural system. Moreover, a set of sustainability indices based on the concept of "footprint" were implemented in order to quantify the environmental and socio-economic impacts of the agricultural production. The results allow to detect and analyse the feedback mechanisms leading to potential unsustainability and to evaluate the effectiveness of the actions implemented to improve the sustainability.

Key words: Sustainability assessment, Causal loop diagram, Complex system analysis, index-based approach

1. INTRODUCTION

It is well recognized that irrigation practice plays a key economic role for agricultural activities of the Mediterranean area. However, it is likewise recognized that agricultural has the largest environmental impacts not only in term of water consumption but also in term of energy consumption (FAO, 2012; FAO, 2014). As the complexity of the issues related to water resources has increased, there have been extensive studies to combine the concept of sustainability with management issues (Juwana et al. 2012), especially at local scale where the combined action between human activities and external drivers (i.e. climate change and economic development) influence water security (Montanari et al., 2013; McMillan et al., 2016). In the past few decades a growing number of studies were developed based on the results of different index-based approaches used to formulate sustainability policies (Galli et al. 2012; Subagadis et al. 2014; Ozturk 2015). However, due to a poor knowledge of the system complexity, management strategies may often be affected by a high uncertainty and result ineffective in their impacts (Giordano et al. 2013; Portoghese et al. 2013; Giordano et al. 2015; Giordano et al., 2017). With the purpose of supporting the sustainable management of water resources, the present research aims at implementing an integrated methodology in which the results of an index-based approach, capable to evaluate the environmental and socio-economic impacts of the agricultural activities, are coupled with the analysis of the main dynamics affecting the sustainability use of water resources. Particularly, this research work aims to answer the following questions: (i) what are the main drivers and dynamics affecting the sustainable use of water resources? (ii) how an index-based approach may support decision-making in water resources management?

In this framework, a system dynamic (SD) approach is suitable to solve these issues, since problem understanding and framing are key aspects of the SD approach (Setianto et al. 2014), in which the system is considered constituted by sets of interactions among different variables strictly

interviewed (Forrester, 1994; Senge, 1997). SD proved capable to support decision-makers in understanding the structure and behaviours of a complex system based on feedback loops (Sterman 2000) and Causal loop diagrams (CLDs). The proposed methodology has been implemented in a reference case study located in the Apulia region (Southern Italy). The following sections provide a short description of the methodology developed, followed by an application in the case study.

2. MATERIALS AND METHODS

2.1 Study system description

This case study refers to the Capitanata plain, which is located in Apulia region (Southern Italy) within the province of Foggia (covering almost 455,000 ha). Despite the limited water availability, agriculture is a key economic activity in the area and the irrigation practice is essential in supporting agricultural production mainly specialized in cereals (especially durum wheat), vegetables (mainly tomato), olive trees and grapevine. Two irrigation districts are established in the area, (covering approximately 150,000 ha, 126,000 ha of which are served by pressurized irrigation networks), respectively the "Fortore district" on the Northern part and the "Sinistra Ofanto district" on South. Both districts are managed by the local "*Irrigation users organization of Capitanata"* (IUOC) and organized with on-demand supply points equipped with water meters, and pre-paid card devices for each user.

The Fortore district (covering ≈ 104,000 ha) is supplied by the Occhito dam with an average irrigation volume of about 100 Mm^3, far below the actual irrigation demand of the study area. Consequently, irrigation is supplied by the combined use of the surface and ground water source causing an increasing number of uncontrolled withdrawals from the alluvial aquifer through private wells located within farm areas. The limited water availability, coupled with the interaction between different actors significantly affect water use and management, causing environmental and socio-economic impacts associated to agricultural activities, groundwater exploitation, energy consumption and irrigation cost. In this framework, sustainable water management requires a comprehensive knowledge of the main drivers and interactions affecting environmental and socio-economic impacts of the agricultural activities, before undertaking any decision-making process, including policy design.

2.2 Understanding system dynamic

With the purpose of understanding the main drivers of agricultural practices influencing water management, a CLD analysis (Vennix, 1996) of the system was developed using the Vensim PLE ® software, based on the results of semi-structured interviews with the main actors involved in decision-making. Further information of the semi-structured interviews are available in Portoghese et al., (2013) and Giordano et al., (2015).

The CLD of the Capitanata system (Figure 1) demonstrated that mutual influences exist among the actors involved, whose behaviour is influenced by external drivers (i.e. crop market price, CAP subsidies and water availability). The interaction among different water users activates three intertwined dynamics (Figure 1) specifically related to the irrigation water demand (i.e. IWD marked in red), the irrigation water withdrawals (i.e. IWW marked in violet) and the irrigation water cost (i.e. IWC marked in green), which substantially affect the dynamic of the whole system. Another important dynamic is activated within the IWW dynamic, related to the energy consumption (i.e. EC marked in orange) associated to the water withdrawals.

Going further into details, IWD dynamic is mainly related to the crop choice and is influenced by the water availability and market condition (i.e. crop market prices and CAP subsides), which are the main variables contributing to the farmer's crop choice. Two loops are dominant in this

dynamic: a balancing loop (B1 – related to irrigation requirement of crops) and a reinforcing loop (R1 – related to the connection between crops and related profit) which, from a dynamic point of view, can be conceptualized as a "limited to growth" archetype (Vennix, 1996). The IWD dynamic has significant cascading impacts on the other two dynamics. In particular, the IWW module describes the dynamic of water withdrawals from different water sources (i.e. surface and groundwater source) and two loops (B2 and R2 respectively) define the interconnected and interdependent behaviour. When groundwater pumping is more affordable than using the surface water, the use of the aquifer becomes more relevant. As a result, groundwater may be subjected to over-exploitation, and both water quality and quantity may be affected (loop R4). The large amount of water abstracted from groundwater source is also associated to high energy consumption. A reinforcing loop (R3) characterizes the EC module. The IWW dynamic also strongly influences the IWC dynamic, since water withdrawals have important impacts on farmers' costs, which in turn influences the profit in the IWD dynamic (loops B3 and B2).

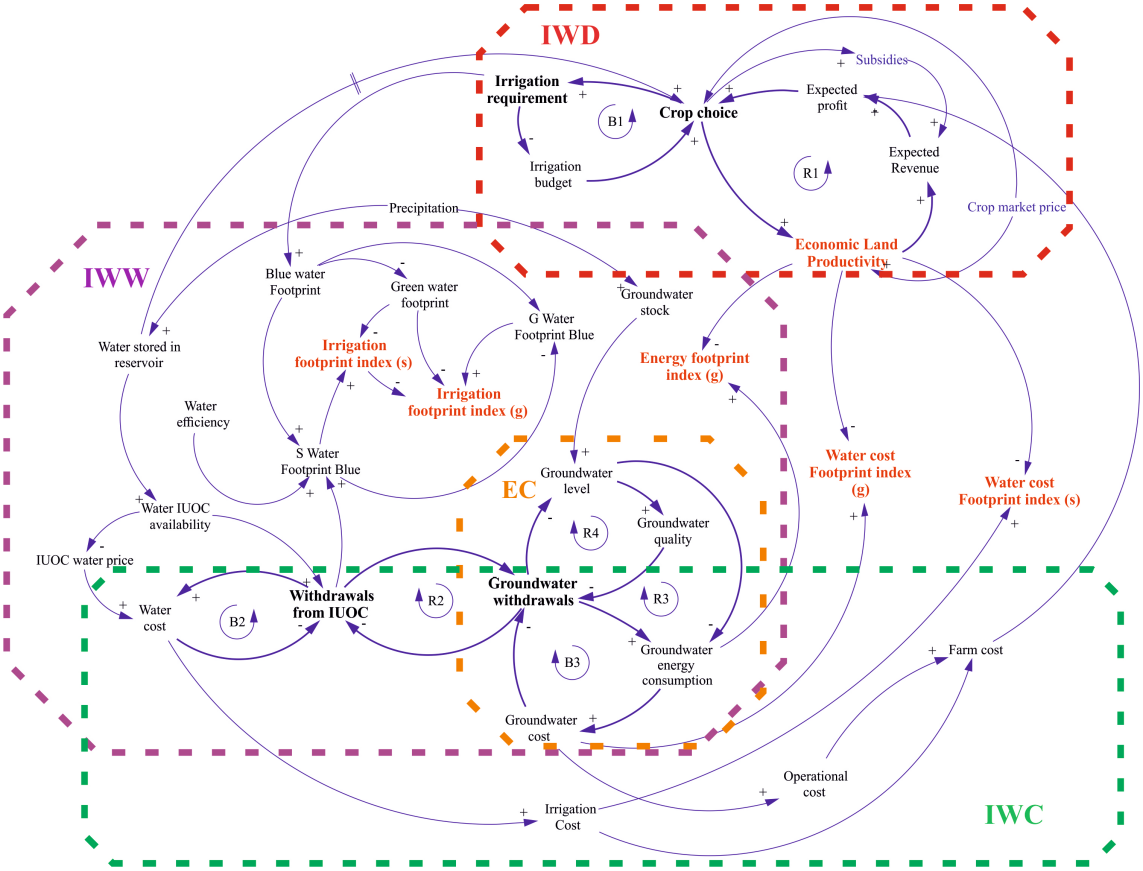

Figure 1. CLD representation of the Capitanata agricultural system. The arrows are marked by a polarity (+ or −) suggesting the type of effect one element has on the other; positive or negative polarity shows whether the variables move on the same or opposite direction. Red variable are the system outputs.

In order to provide a quantitative synthesis of the main dynamics, a set of indices are proposed describing the key aspects of the aforementioned dynamics. These indices are named respectively: *irrigation footprint index*, *energy footprint index* and *water cost footprint index*. The following section provide a brief description of these indices while further details are available in de Vito et al. (2016, under review).

2.3 Irrigation water footprint index (I_w)

The aim of this index is to evaluate the impacts that the IWD dynamic has on the IWW dynamic.

It is based on the concept of *Water Footprint (WF)* introduced by Hoekstra (2003), limiting the analysis only to the green and blue water footprint components. Two different components of I_w were calculated according to Eqs. 1 and 2, distinguishing between surface and groundwater source. The surface component of blue-water footprint *(*SWF_{blue}*)* is computed considering the amount of water abstracted from surface source and the hydraulic efficiency (better describe in the following). Conversely, the groundwater component of the blue-water footprint (GWF_{blue}) is evaluated as the difference between the total blue-water footprint and the surface SWF_{blue}. Both the blue and the green water footprint components were computed through CROPWAT ® software, according to the methodology described by Hoekstra et al. (2011).

$$I_{w\,(s)}\,[-] = SWF_{blue}/\,WF_{green} \tag{1}$$

$$I_{w\,(g)}\,[-] = GWF_{blue}/\,WF_{green} \tag{2}$$

The hydraulic efficiency has been calculated as the product of: (i) c*onveyance efficiency* (i.e. the efficiency related to the water supply network), assumed as 0.87; (ii) f*arm efficiency* (i.e. the efficiency related to the farm management techniques) which was assumed equal to 0.99; (iii) a*pplication efficiency* (i.e. the efficiency related to irrigation methods) which was assumed equal to 0.9.

2.4 Energy footprint index (I_{en})

This index aims to evaluate the impacts that both IWD and IWW have on the EC dynamic. The impact of each crop in terms of energy consumption associated to groundwater abstraction were calculated (Eq. 3) as the ratio between the unit energy consumption for irrigation and the unit economic land productivity of a given crop:

$$I_{en(g)}\,[KWh/€] = E_{a(g)}/E_{lp} \tag{3}$$

Specifically, the economic land productivity (E_{lp}) describes the economic yield of crop production on a unit area (€/ha) calculated as the crop yield (kg/ha) times the crop market value (€/kg).

In the above equation, $E_{a(g)}$ is defined as the product between the energy required to pump a unit volume of water ($E_{w(g)}$, expressed in kWh/m^3), and the volume of water abstracted to irrigate a unit area, expressed in m^3/ha. $E_{w(g)}$ is calculated according to the Eq. 4:

$$E_{w(g)}[KWh/m^3] = H_{t(g)}/(102 * \eta_{(g)} * 3.6) \tag{4}$$

H_t is the hydraulic head [m], composed by the elevation head H_g, the head loss H_p, and the nominal operating pressure of the irrigation system H_e. The pumping efficiency, is identified with η. In our case study we considered: H_g= 40 [m], H_p= 26,5 [m], $\eta_{(g)}$= 0,5.

2.5 Water cost footprint index (I_e)

This index aims to evaluate the influence of IWD and IWW on IWC. It is defined as the ratio between the water costs associated to the agricultural production and the economic land productivity. It can be computed as follows:

$$I_{e(s)}\,[-] = C_{w(s)}/E_{lp} \tag{5}$$

$$I_{e(g)}\,[-] = C_{w(g)}/E_{lp} \tag{6}$$

In the present work, the surface water cost is directly derived considering the water tariff applied by the central authority; groundwater cost is instead computed referring to the variable costs due to the energy consumption, neglecting both additional variable components and fixed costs. This assumption has not substantial implications since the other components could be considered more or less constant values.

3. RESULTS

The sustainability assessment has been carried out between 2000 and 2011 considering the tomato, olive trees and grapevine crops (figure 2 a, b). A comparative analysis is proposed for the normalized indices (figure 2a), which are calculated referring to both surface water and groundwater, clearly showing that in the study area groundwater abstraction has higher environmental impacts but better economic implications.

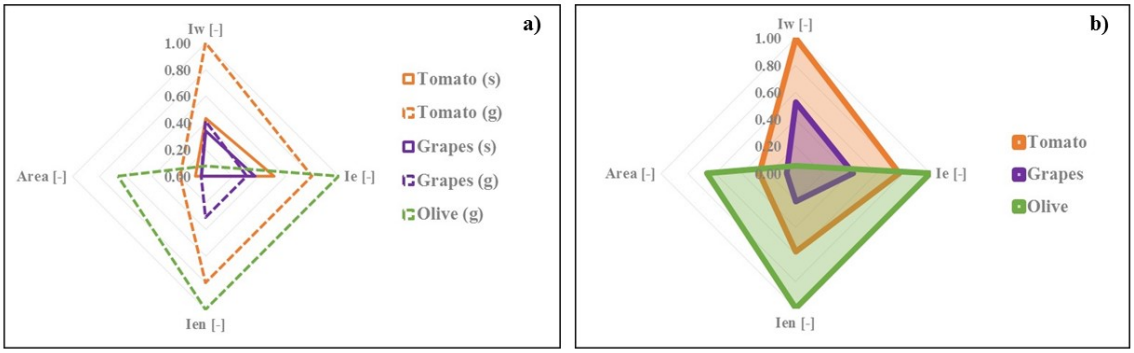

Figure 2. a) normalized indices calculated referring both for surface and groundwater source; b) 'hybrid' configuration depending on the effective ratio between groundwater and surface water.

Going further into details, the olive production has the lowest environmental implications in terms of groundwater exploitation (I_w= 0,21), whereas the low profitability (E_{lp} ≈1200 €/ha) negatively influences both the water-cost footprint index and the energy footprint index. The production of tomato requires instead a large volume of water mainly deriving from groundwater abstraction ($I_{w(s)}$ = 1,14; $I_{w(g)}$ = 2,63). Moreover, it has the higher energy and economic impacts due to the higher cost of water compared with the economic crop value (E_{lp} ≈ 6400 €/ha). Referring to the grapevine it has lower impacts in term of water consumption ($I_{w(s)}$ = 0,89; $I_{w(g)}$ = 1,09) and it represents the most profitable production, due to the high economic value of this crop (E_{lp} ≈ 7900 €/ha). Thus, although the energy consumption and the cost of water are highly relevant, they might be considered 'sustainable' due to their profitability. The same conclusions are supported by a 'hybrid' version of the indices (figure 2b), calculated considering the actual ratio between surface and groundwater volumes used for crop production in the study area. This analysis globally provides significant information of the many different impacts associated to agricultural activities.

Referring to Fig. 1, the I_w index mainly depends on crop choice by farmers, influenced by both water availability and market conditions. Particularly, the market conditions are among the primary causes affecting the unsustainable use of water resources, and this should be carefully taken into account by policy makers. The affordability of groundwater pumping indirectly influences both the I_{en} and I_e. As a result, policy strategies oriented to increase the water tariff in order to discourage water waste may have significant impacts not only in term of water consumption but also in terms of energy consumption and irrigation water cost with cascading effects on the agricultural sector.

4. CONCLUSION

The proposed methodology aims to demonstrate that a deeper insight into the complexity

characterizing agricultural sector can support water management allowing to select the most suitable strategies to guarantee sustainability. Particularly the analysis of costs and benefits related to agricultural activities in a complex area, mainly in terms of water consumption (which is the main environmental impact), but also considering the cascading economic and energetic impacts, is carried out. The limited green water availability is unable to match the crop water requirement and thus large volumes of water for irrigation need to be supplied either by surface water sources or by groundwater. Groundwater withdrawals are often preferred, due to the lower costs and the higher availability, although the impacts of water overexploitation on groundwater could be particularly dangerous and difficult to control. The proposed analysis clearly shows that unsustainability depends on the interaction between different actors, who significantly influence the system's dynamic, conceptualized using three modules (IWD, IWW and IWC). An index-based approach is adopted to summarize the information related to the above dynamics, thus supporting decision-makers in the selection of the most suitable policies for the sustainable management of water resources.

REFERENCES

Bogardi JJ, Dudgeon D, Lawford R, et al (2012) Water security for a planet under pressure: Interconnected challenges of a changing world call for sustainable solutions. Curr. Opin. Environ. Sustain. 4:35–43.

de Vito R, Portoghese I, Pagano A, et al. (2016) An index-based approach for Water-Energy-Food Nexus characterization to assess the local scale sustainability of agricultural productions. Advances in Water Resources (under review)

FAO (2012) Coping with water scarcity An action framework for agriculture and food security.

FAO (2014) Walking the Nexus Talk: Assessing the Water-Energy-Food Nexus in the Context of the Sustainable Energy for All Initiative.

Foley JA (2005) Global Consequences of Land Use. Science (80-) 309:570–574. doi: 10.1126/science.1111772

Forrester JW(1994) System dynamics, systems thinking, and soft or. Syst Dyn Rev 10(2–3):245–25

Galli A, Wiedmann T, Ercin E, et al (2012) Integrating Ecological, Carbon and Water footprint into a "footprint Family" of indicators: Definition and role in tracking human pressure on the planet. Ecol Indic 16:100–112. doi: 10.1016/j.ecolind.2011.06.017

Giordano R, Agostino DD, Apollonio C, et al (2015) Evaluating acceptability of groundwater protection measures under different agricultural policies. Agric Water Manag 147:54–66. doi: 10.1016/j.agwat.2014.07.023

Giordano R, Brugnach M, Pluchinotta I (2017) Ambiguity in problem framing as a barrier to collective actions : some hints from groundwater protection policy in the Apulia Region. Group Decision and Negotiation (in press)

Giordano R, D'Agostino D, Apollonio C, et al (2013) Bayesian Belief Network to support conflict analysis for groundwater protection: The case of the Apulia region. J Environ Manage 115:136–146. doi: 10.1016/j.jenvman.2012.11.011

Gleick PH (2000) The Changing Water Paradigm - A Look at Twenty-first Century Water Resources Development. Water Int 25:127–138. doi: 10.1080/02508060008686804

Hoekstra AY (2003) Virtual Water Trade. Int Expert Meet Virtual Water Trade 12:1–244.

Juwana I, Muttil N, Perera BJC (2012) Indicator-based water sustainability assessment — A review. Sci Total Environ 438:357–371. doi: 10.1016/j.scitotenv.2012.08.093

McMillan H, Montanari A, Cudennec C, et al (2016) Panta Rhei 2013–2015: global perspectives on hydrology, society and change. Hydrol Sci J 6667:1–18. doi: 10.1080/02626667.2016.1159308

Montanari a., Young G, Savenije HHG, et al (2013) "Panta Rhei—Everything Flows": Change in hydrology and society—The IAHS Scientific Decade 2013–2022. Hydrol Sci J 58:1256–1275. doi: 10.1080/02626667.2013.809088

Ozturk I (2015) Sustainability in the food-energy-water nexus: Evidence from BRICS (Brazil , the Russian Federation , India , China , and South Africa) countries. Energy 93:999–1010. doi: 10.1016/j.energy.2015.09.104

Pham L Van, Smith C (2014) Drivers of agricultural sustainability in developing countries: A review. Environ Syst Decis 34:326–341. doi: 10.1007/s10669-014-9494-5

Portoghese I, Bruno E, Vurro M (2010) From regional climate simulations to the hydrological information needed for basin scale impact studies. Adv Geosci 26:25–31. doi: 10.5194/adgeo-26-25-2010

Portoghese I, D'Agostino D, Giordano R, et al (2013) An integrated modelling tool to evaluate the acceptability of irrigation constraint measures for groundwater protection. Environ Model Softw 46:90–103. doi: 10.1016/j.envsoft.2013.03.001

Pretty J, Sutherland WJ, Ashby J, et al (2010) The top 100 questions of importance to the future of global agriculture. Int J Agric Sustain 8:219–236. doi: 10.3763/ijas.2010.0534

Senge PM (1997) The fifth discipline. Meas Bus Excell 1:46–51

Subagadis YH, Grundmann J, Schutze N, Schmitz GH (2014) An integrated approach to conceptualise hydrological and socio-economic interaction for supporting management decisions of coupled groundwater-agricultural systems. Environ Earth Sci 72:4917–4933. doi: 10.1007/s12665-014-3238-1

Vennix, J.A.M., 1996. Group model building: tackling messy problems. System Dynamics Review, 15(4), 379–401.

Proceedings of the 10th World Congress of EWRA 'Panta Rhei', 5-9 July 2017, Athens, Greece
© 2017 *European Water Resources Association*

Estimation of crop water requirements using remote sensing for operational water resources management

J. Tzabiras, M. Spiliotopoulos and A. Loukas*
Laboratory of Hydrology and Aquatic Systems Analysis, Department of Civil Engineering, University of Thessaly, Greece
* *e-mail: aloukas@uth.gr*

Abstract: The overall objective of this work is the development of a District Information System (DIS) which could be used by stakeholders for the purposes of a district day-to-day water management as well as for planning and strategic decision-making. Karla Lake is used in this study, but the overall methodology could be used as a basis for future analysis elsewhere. Surface Energy Balance Algorithm for Land (SEBAL) was used to derive monthly actual evapotranspiration (ET) values from Landsat TM imagery. The methodology was developed using high quality Landsat TM images during 2007 growing season. Monthly ET values are then used as an input to CROPWAT model. Outputs of CROPWAT model are then used as input for WEAP model. The developed scenario is based on the actual situation of the surface irrigation network of the Local Administration of Land Reclamation (LALR) of Pinios for the year of 2007. The DIS is calibrated with observed data of this year and the district parameterization is conducted based on the actual operation of the network. The operation of the surface irrigation network of Pinios LALR is simulated using Technologismiki Works, while the operation of closed pipe irrigation network of Lake Karla LALR is simulated using Watercad. Four alternative scenarios have been tested with the DIS: a) Reduction of channel losses b) Alteration of irrigation methods c) Introduction of greenhouse cultivation and d) Operation of the future Lake Karla network.

Key words: NDVI, SAVI, EVI, EVI2, Evapotranspiration, Landsat, METRIC

1. INTRODUCTION

In many watersheds of the Mediterranean Countries, water resources are presently fully or overcommitted. Demand for water is likely to continue increasing due to population growth as well as increased demand from in-stream users. Irrigators are the largest consumers of fresh water in Mediterranean Countries: either individually or as members of irrigation districts, using up to 80% of all allocated water in some regions. With the increasing water demand of other sectors and environmental constraints, water resources available for agriculture will decrease in the next decades. In this critical context, there is an urgent need to foster the adoption and implementation of alternative irrigation systems and management practices that will allow increased crop water productivity. Hence, the development of an integrated approach to water use and management may be achieved by giving more consideration to the management of water as a resource rather than just the provision of water as a service.

In this paper a principal motivation for the development of a District Information System (DIS) is the harmonization of an on-farm and off-farm irrigation water management that can be used in the region. The main goal is the prior knowledge of farmers' daily scheduling and the integration of the management scenarios in order to develop a strategic long-term decision-making. In this work the DIS has been developed using a GIS-based modeling approach that integrates a generic crop model and a hydraulic model for the distribution and allocation system, using remote sensing information as a key input. The main sub-objectives were: (i) the development of an operational algorithm to retrieve crop evapotranspiration from remote sensing data, (ii) the development of an information system with friendly user interface for the data base, the crop module and the hydraulic module and (iii) the analysis and validation of management scenarios from model simulations predicting the respective behaviour of the on-farm and off-farm systems.

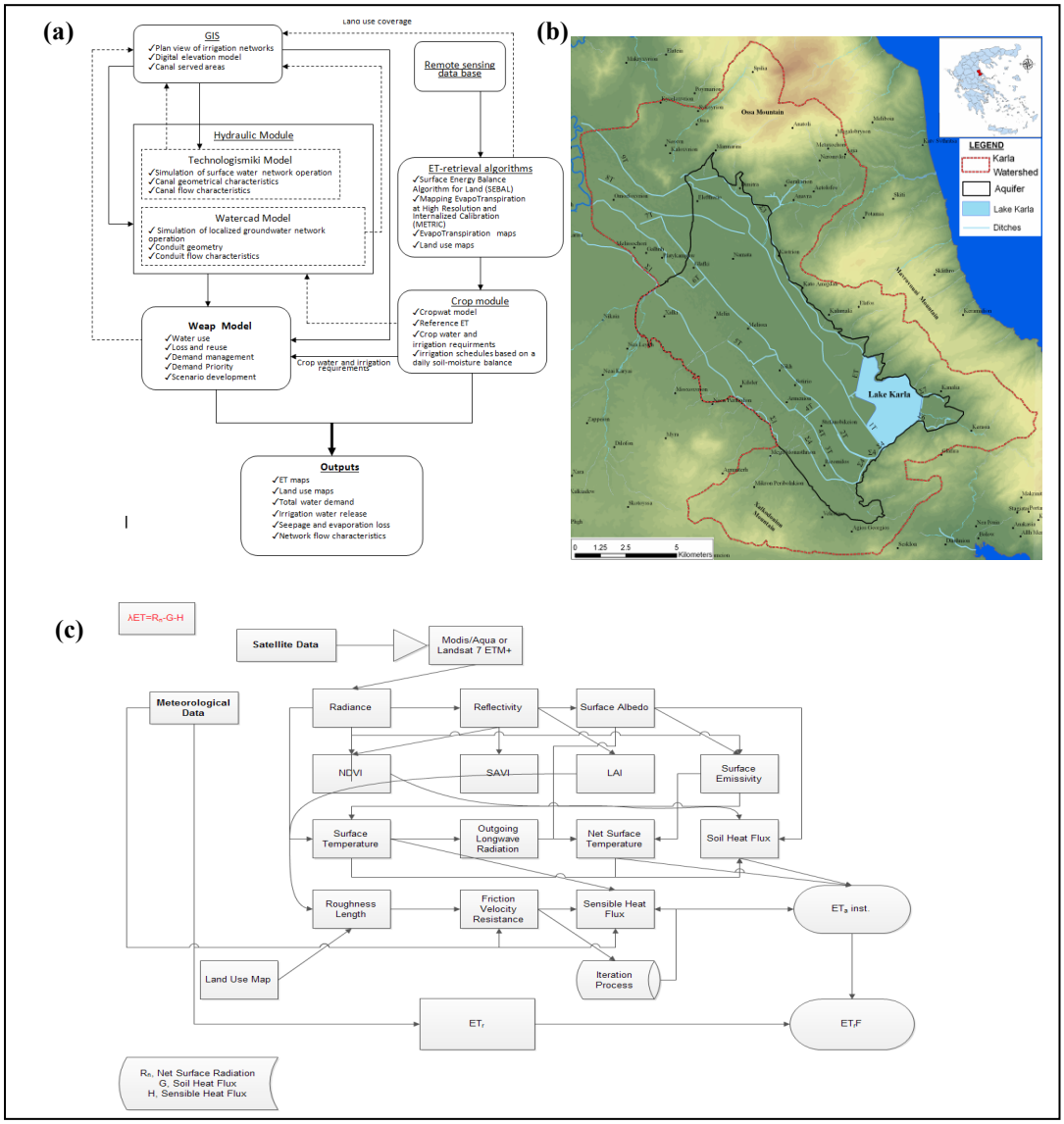

Figure 1. a) General structure of DIS for Lake Karla schemes b) Location of Lake Karla watershed c) SEBAL flowchart

The structure of DIS (Fig. 1a) in this paper consists of the following modules:

a) the WaterCAD model for pressurized networks and b) the Technologismiki Works 2009 for gravity networks,
b) Crop water requirements ETc are calculated using CropWat 8.0
c) The Water Evaluation and Planning System (WEAP) which is a practical tool for water resources planning.

2. METHODOLOGY

Lake Karla basin (Fig.1b) is an intensively cultivated agricultural region lying between latitude 39°20′56′ to 39°45′15′ N and longitude 22°26′10″ to 23°0′27″ E, which is the eastern part of Thessaly, Greece. The climate is typical Mediterranean with an average temperature of 16–17° C and mean annual relative humidity of 67–72 %. The average precipitation is 500–700 mm and occurs mainly in autumn, winter and spring. Most of the aquifer area is plain with an altitude ranging from 45 to 65 m. A great effort has been made on the partial restoration of the former Lake Karla that has been planned to reverse the adverse environmental conditions, caused by the lake drainage. The natural basin of Karla had total extent of 1663 km2 but after the construction of

complimentary works, the drainage area of the restored lake Karla will be 1171 km2 (Loukas et al., 2007). The overall objective of this work is the development of a District Information System (DIS) which could be used by stakeholders for the purposes of a district day-to-day water management as well as for planning and strategic decision-making. The DIS was developed from a GIS-based modeling approach which integrates a generic crop model and a hydraulic model of the transport/distribution system, using land use maps generated by Landsat TM imagery. The main sub-objectives are: (i) the development of an operational algorithm to retrieve crop evapotranspiration from remote sensing data, (ii) the development of an information system with friendly user interface for the data base, the crop module and the hydraulic module and (iii) the analysis and validation of management scenarios from model simulations predicting the respective behavior.

2.1 The remote sensing approach

Surface Energy Balance Algorithm for Land (SEBAL) methodology (Fig. 1c) is proposed for this study, been already used in several studies in many countries around the world with high accuracy (Bastiaanssen 1998a, 1998b, Li et al. 2009). The basic concept in SEBAL is the equation of surface energy balance:

$$LE = \lambda ET = Rn - H - G \quad (1)$$

where LE is the latent heat flux (W/m^2), Rn is net radiation (W/m^2), G is soil heat flux (W/m^2) and H is sensible heat flux (W/m^2). W/m^2 in latent heat flux can easily later converted to mm. Rn can be computed from the land surface radiation balance:

$$Rn = (1-a)RSi + RLi - RLo - (1-\varepsilon o)RLi \quad (2)$$

where a is surface albedo, RSi (W/m^2) is incoming solar radiation, RLi (W/m^2) is incoming long wave radiation, RLo (W/m^2) is outcoming long wave radiation and εo is broad band surface emissivity.

Soil Heat Flux G (W/m^2) can be empirically estimated using a function by Bastiaanssen (2000) which is based on albedo, surface temperature and NDVI:

$$G= \{Ts/a\ (0.0038a+0.0074a2)(1-0.98NDVI4)\}*Rn \quad (3)$$

where Ts is surface temperature in K and NDVI is the normalized difference vegetation index. The third parameter is sensible heat flux (W/m^2):

$$H=pCp(a+bTs)/rah \quad (4)$$

where p is air density (kg/m^3) related with atmospheric pressure, Cp is air specific heat capacity (1004 $Jkg^{-1}K^{-1}$), Ts is surface temperature in K, and rah is aerodynamic resistance to heat transport (sm^{-1}). The definition of the function dT vs. Ts is maybe the most significant philosophy of SEBAL.

dT is the difference between the air temperature very near the surface (at 0.1 m above the zero plane displacement height) and the air temperature at 2m above the zero plane displacement height (Waters et al., 2002). SEBAL methodology suggests linear change in dT with Ts. Equation (4) has two unknown parameters (a and b). This is where initial values from the selection of "cold" and "hot" pixels are used. These pixels serve as a solution for defining dT vs. Ts. "Cold" pixel can be defined as a generally wet, well-irrigated crop surface with full ground cover by vegetation. It is assumed that all energy is used to evaporate water, thus there is no sensible heat flux in this pixel (H=0 and ET=Rn-G). ET at the "cold" pixel is closely predicted by the ET rate from a large expanse of alfalfa vegetation (Bastiaanssen, 1998a). For the selection of "cold" pixel a very moist

terrain has to be found and a pixel with high NDVI, low temperature and low albedo seems to apply this specification. On the other hand, “hot” pixel is defined as a pixel which has low NDVI, high Albedo and high temperature. “Hot” pixel can be defined as a dry, bare agricultural field. It is assumed that all the energy is used to heat the surface in such a way that there is no latent heat flux there (ET=0). In other words, a very dry terrain is selected as a “hot” pixel. It seems that the selection of a “hot” pixel is more difficult than the selection of “cold” pixel because there is a broader range of temperatures for “hot” pixel candidates. After the selection of ”hot” and “cold” pixels the boundary conditions are now ready for solving the H. This is the first estimation of H assuming neutral atmospheric conditions. SEBAL, then, uses an iterative process to correct for atmospheric instability caused by buoyancy effects of surface heating applying Monin-Obukhov theory (Monin and Obukhov, 2002). After the initial computation of H, new values of dT are computed for the “cold” and “hot” pixels and new values of α and β are derived. A corrected value for H is then computed and the stability correction is repeated until H stabilizes. The final step is the calculation of λET from equation (1). The evaporative fraction (ETrF) can be defined as the fraction of the actual ETa by the potential ETr on an instantaneous basis assuming that is constant over the day (Fig. 1c):

$$ETrF = ETa\ inst/ETr \quad (5)$$

2.2 Hydraulic module and WEAP model

The operation of the surface irrigation network of Pinios LALR was simulated using Technologismiki Works. The model was calibrated and flow dividers (square nodes) have been placed at particular network nodes, where the main channels were divided into secondary channels. In these network nodes (flow dividers), the user determines the cut off flow. In this way, the required quantity of water to be diverted, can be altered. In secondary channels, outfalls (triangular nodes) have been placed, where the irrigation water is being pumped directly from farmers, and each outfall corresponds to the water inflow required for the irrigation of crops of the served area. Finally, the irrigation network consists of 816 canals and the primary channels extent at 133.7 km, in total length. The total length of the secondary channels is 330 km and of the main ditches is 102.8 km. Furthermore, the district consists of 375 dividers, 375 outfalls and 70 junctions.

The hydraulic model used for the new Lake Karla district is the WaterCAD model, which is a state-of-the-art software tool primarily for use in the modelling and analysis of water distribution systems. The whole network is fed directly from Lake Karla reservoir by three pumping stations A0, A1 and A2 and the main components are: (a) three distribution pumping stations D3, D4, and D6 (b) two local reservoirs are included in the network for the regulation of pumping stations and (c)two types of water intake (7 l/s and 14 l/s) have been matched with the served zones of the district The network consists of 963 junctions, 1,145 pipes, valves (double activation), 64 air valves and 15 surge valves.

The boundaries of the district area were inserted from the geographical information system and the WEAP model is set up. The water demand nodes (outfalls in the Technologismiki model) are numerous and cannot be imported into WEAP model. Since WEAP model is used only for water resources management, one transmission link includes a relatively large sector of the district. This means that a demand site in WEAP model includes several demand sites of Technologismiki model and the calculated water demand is placed cumulatively in every WEAP model demand site.

3. RESULTS AND DISCUSSION

Four alternative scenarios, were developed to be studied with the DIS:

- Reduction of canal losses (RL)
- Alteration of irrigation methods (IMA)

- Introduction of greenhouse cultivation (GCE)
- Operation of the future Lake Karla network

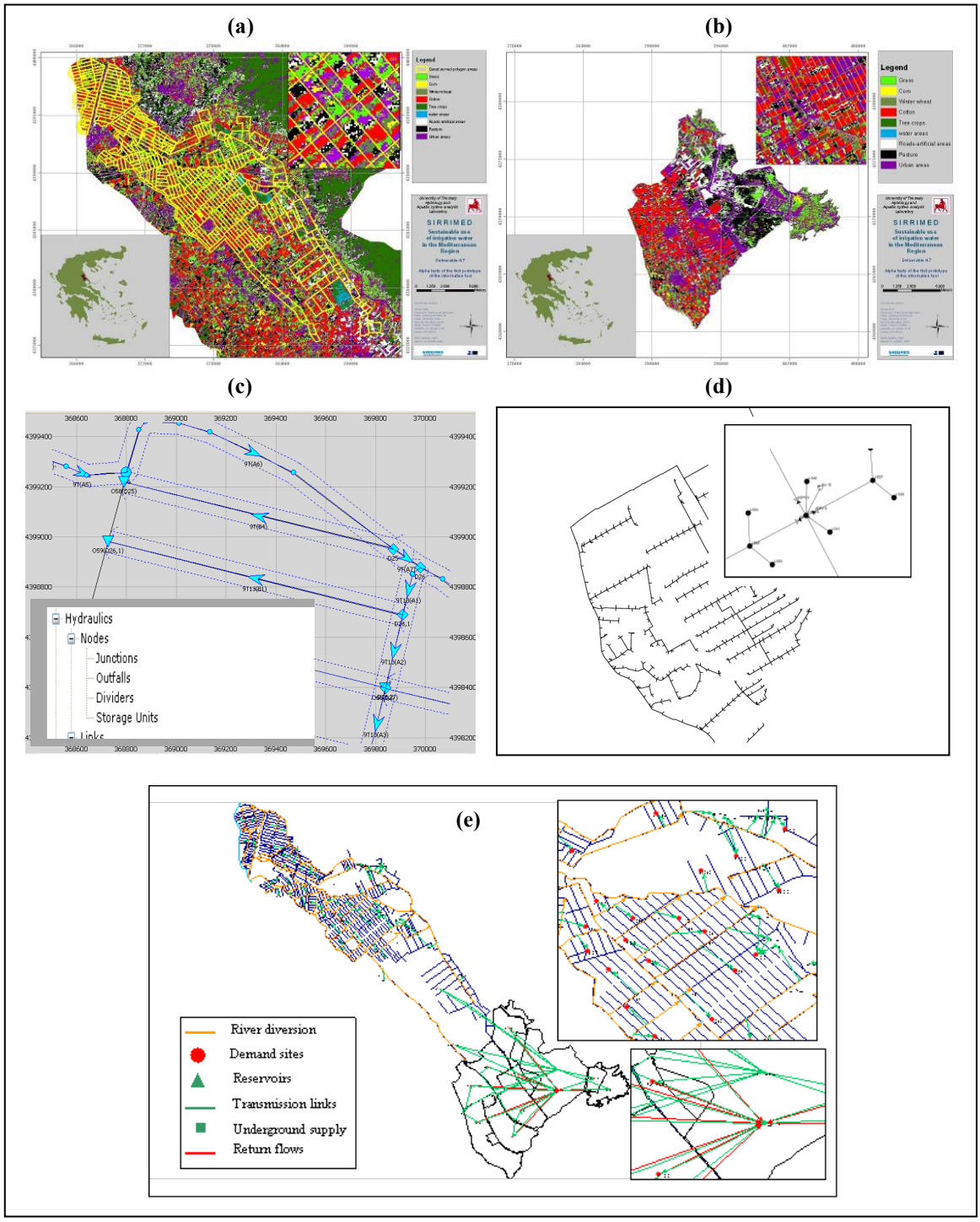

Figure 2. a) Surface irrigation network of LALR Pinios River and land use map b) Land use map of LALR karla area c) Snapshot of Technologismiki model layout of Pinios LALR irrigation network d) Snapshot of WaterCad model layout of Lake Karla LALR irrigation network and e) WEAP model for the existing LALR Pinios network and for the future Lake Karla network

The analysis of the results, in this paper, is conducted for three network conduits, one main ditch (6T(A4)), one primary (9T16(A9)) canal and a secondary one (8T(D54)). It should be mentioned that the results have been calculated for the whole network, but due to time and space limitations a simpler and more comprehensive presentation is made. As mentioned above, there have been two

separate runs of the Technologismiki model, one for steady flow conditions and one for non-steady flow conditions. Two months are selected as representative examples of presenting the results: April (at the beginning of the irrigation period in Greece) and August (where irrigation reaches its maximum). Technologismiki software provides results for the flow rate (m3/s), the flow depth (m), water velocity (m/s), the Froude number and the conveyance capacity of the conduit under study.

The four upper charts of Figure 3 show the variation of flow depth for month April and August at three selected channels, according to the future management scenarios. It is clear that for all cases, the scenario of the reduction of canal losses, creates the conditions for a flow depth decrease, since the canals are supposed to be properly maintained (the Manning coefficient is reduced).

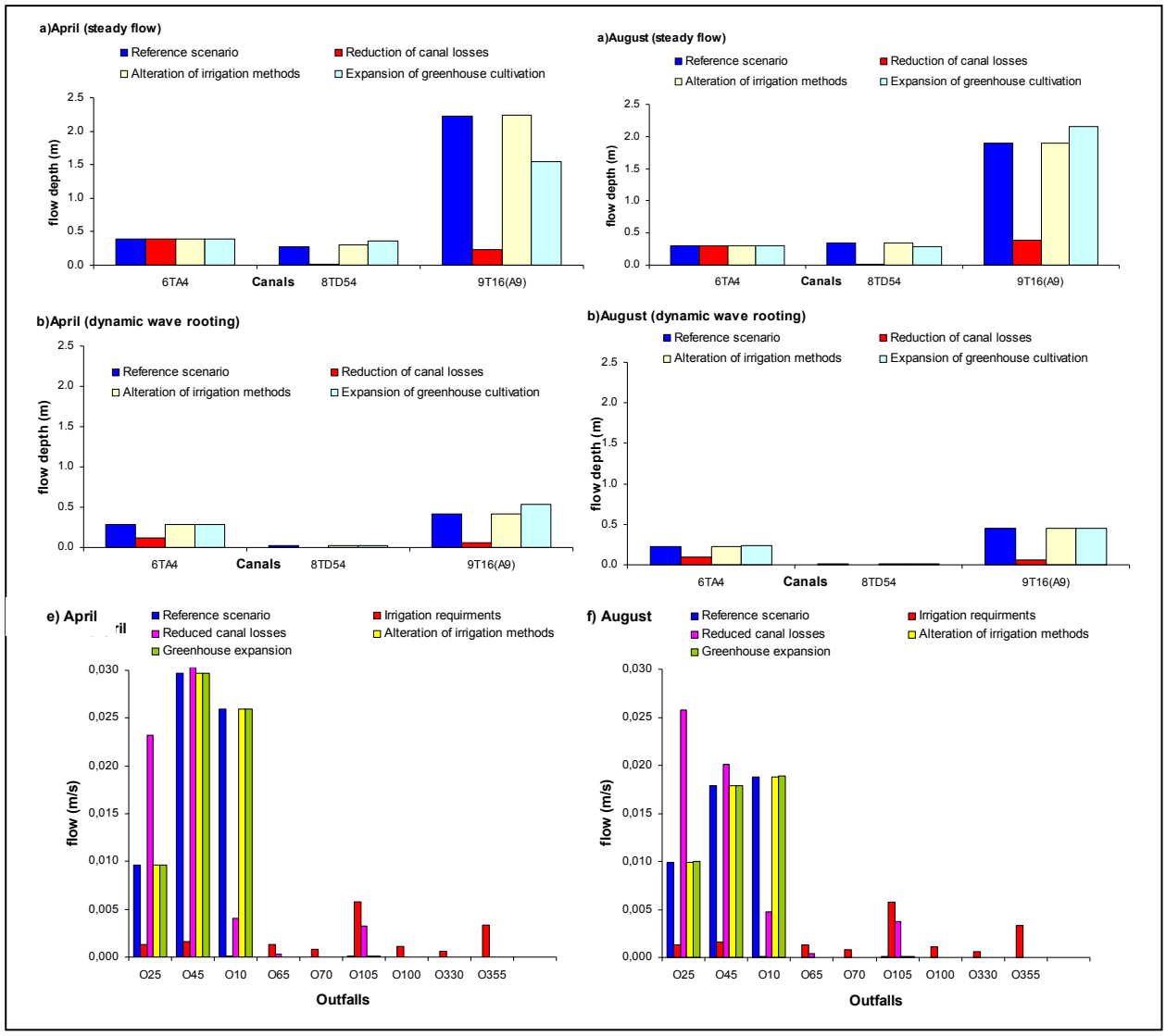

Figure 3. Variation of flow depth according to future management scenarios for a) steady flow and b) dynamic flow rooting and variation of water transferred to outfalls for e) April and b) August (dynamic wave rooting)

Furthermore, the introduction of greenhouse cultivation in some cases, such as for canal 8T(D54), causes an increase in the flow depth. That can be explained by the increased irrigation requirements of greenhouse tomato relatively to cotton for month April. In addition, the scenario of alteration of irrigation methods slightly affects the flow parameters, since the change in conveyance efficiency Df is quite low (5%) and flow rate and consequently flow depth seem not to be highly affected. On the other hand, the variation of flow depth for month August is illustrated at the left of Figure 9. For the scenario of channel losses reduction, as in April, the flow depths of canals

9T6(A9) and 8T(D54) are decreasing compared to the reference scenario. For dynamic wave simulation, the flow depth in August is reduced for all three selected channels. In contrast to April, the scenario of greenhouse cultivation introduction indicates higher flow depth, due to lower water demands than cotton. So the reference scenario and the scenario of alteration of irrigation methods are expected to have lower flow depths.

The charts at the bottom of Figure 3 indicate that when the actual pumping program of Pinios LALR is applied without any control of the network (i.e. for dynamic wave rooting), such as without activation of the dividers, water volume exceeds the irrigation requirements of outfalls O25, O45 and O10, but it is not enough for the outfalls located in the middle and the most remote areas of the irrigation network. This is true for the three future management scenarios and for both months under study (i.e. April and August). The scenario of the reduced canal losses improves the network operation to some extent, since the water in that scenario is reaching outfall O105, but it is still not enough to meet the required irrigation demand. Therefore, the proper network operation is crucial for the sustainable use of the local water resources. Another essential conclusion is that the water supply is not enough. Even when losses are practically annihilated, the water supply does not meet the water irrigation requirements at the most remote outfalls.

4. CONCLUSIONS

This study shows that the DIS is used to simulate the current conditions and the future scenarios. The main outputs of Lake Karla DIS may be evapotranspiration maps and land use maps. Furthermore, flow characteristics of the network are known at every time step. Information about the velocity of the water in a conduit, slopes, depths, Froude numbers, capacity and flow are also extracted by the model. Standard reference evapotranspiration calculations, crop water and crop irrigation requirements as well as design and management of irrigation schemes may be achieved. WEAP model has the ability to provide total water demand, actual water supply and unsatisfied (unmet) water demand. The variation of the unmet demand follows the logical assumption:

- Reduced losses scenario projects the smallest unmet water demand
- Alteration of irrigation methods scenario projects a moderate decrease in unmet water demand
- Expansion of greenhouse cultivation scenario projects increase in unmet water demand due to increased irrigation requirements at winter months
- Operation of new Lake Karla LALR network scenario projects increased unmet water demand, if no groundwater pumping is applied and the water demand is supplied only from the Lake Karla reservoir. This is happening because the Lake Karla aquifer is overused and environmentally degraded with water table drawdown of hundreds of meters in some locations. Thus, pumping of groundwater is posed for the environmental restoration of groundwater. Then, the total water demand is covered by surface water resources.

ACKNOWLEDGMENTS

This work is supported by EFP7's "Sustainable use of irrigation water in the Mediterranean Region" (SIRRIMED). The authors acknowledge Centre for Research and Technology, Thessaly, Greece for the provided meteorological data as well as NASA Warehouse Inventory Search Tool for the provided satellite data. Satellite data are distributed by the Land Processes Distributed Active Archive Center (LP DAAC), located at USGS/EROS, Sioux Falls, SD. http://lpdaac.usgs.gov.

REFERENCES

Bastiaanssen WGM, Menenti M, Feddes RA, Holtslag A.A.M., (1998) “A remote sensing surface energy balance algorithm for land (SEBAL): 1. Formulation” J. Hydrology, 212-213: 198-212.

Bastiaanssen WGM, Pelgrum H, Wang J, Ma Y, Moreno J, Roerink GJ, van der Wal T., (1998) “The Surface Energy Balance Algorithm for Land (SEBAL): Part 2 validation”, J. Hydrology, 212-213: 213-229.

Bastiaanssen, W.G.M., “SEBAL-based sensible and latent heat fluxes in the irrigated Gediz Basin, Turkey”, J Hydrol 229:87-100 (2000).

Li ZL, Tang R, Wan Z, Bi Y, Zhou C, Tang B, Yan G, Zhang X, (2009) “A Review of Current Methodologies for Regional Evapotranspiration Estimation from Remotely Sensed Data”, Sensors 9:3801-3853.

Loukas, A, Mylopoulos, N, Vasiliades, L., (2007) “A modeling system for the evaluation of water resources management strategies in Thessaly, Greece”, Water Resources Management 21 (10), 1673-1702.

Monin, AS, Obukhov, AM, (1954) “Basic laws of turbulent mixing in the surface layer of the atmosphere”. Tr Akad Nauk SSSR Geofiz Inst 24:163–187.

Waters, R, Allen, R, Bastiaanssen W, (2002) “SEBAL. Surface Energy Balance Algorithms for Land. Idaho Implementation. Advanced Training and Users Manual”, Idaho, USA.

Proceedings of the 10th World Congress of EWRA 'Panta Rhei', 5-9 July 2017, Athens, Greece
© 2017 *European Water Resources Association*

Economic productivity of irrigation water and the closure of a river basin in Southern Spain

A. Exposito[1*] and J. Berbel[2]
[1] *Department of Economic Analysis, University of Sevilla, 41018 Sevilla, Spain*
[2] *Department of Agricultural Economics, University of Cordoba, 14014 Cordoba, Spain*
[*] *e-mail: aexposito@us.es*

Abstract: The expansion of irrigated areas in river basins where water resource is scarce usually leads to the closure of the river basin (RB), as a final result of a multiple pressure-response process. This has been the trajectory followed by the Guadalquivir RB, which is the main river in southern Spain. As response to these pressures, farmers have tended to use the resource more efficiently through a modernisation of their irrigation methods and the widespread of deficit irrigation and high-precision techniques. These individual decisions have sought to maximise the economic return to the limited resource (water), provoking changes in crops composition in order to maximize the productivity of irrigated agriculture and the mean productivity per irrigation unit. The analysis carried out in this paper shows a significant increase in irrigation water mean productivity in the period (1989-2005), driven by the creation of new irrigated areas devoted to high value crops and with a dominant use of deficit irrigation strategies, while a second phase (2005-2012) is defined by slower growth in terms of the mean productivity of irrigation water, primarily as a result of a significant reduction in water use per area. Findings show the patterns followed by irrigation water productivity in the analysed case study, which seems to have reached its full capacity.

Key words: irrigation water productivity, agricultural water use, irrigation modernization, river basin management

1. INTRODUCTION

Southern Spain is characterised by a semi-arid climate and an increasing water scarcity. In this context, the Guadalquivir RB has undergone intense transformation in the last 50 years, characterised by a significant growth of irrigated areas, a progressive change in the composition of crops and widespread implementation of water conservation technologies (WCTs).

The aim of this paper is to analyse the impacts on irrigation water productivity generated by those responses (public and private) to the 'closure' process of the Guadalquivir RB observed in recent decades, as no further consumption of water resources is allowed. To this end, the rest of this paper is organised as follows. The next section introduces the theoretical framework regarding the concepts of mature water economies and basin closure process. Subsequently, the case study is briefly described and the fourth section outlines the observed impacts on irrigation water productivity. Finally, this work ends with some concluding remarks.

2. BASIN CLOSURE PROCESS, MATURE WATER ECONOMY AND THE IMPACTS ON THE ECONOMIC PRODUCTIVITY OF IRRIGATION

According to Randall (1981), in the 1980s the Australian water economy entered a 'mature phase' characterised by: (1) inelastic water supply with increasing marginal supply costs (aquifers were already heavily exploited, the best dam locations had been taken and other rivers were protected); (2) high and growing demand (with increasing conflicts among water users); (3) an aging infrastructure which required expensive renovation; (4) a context of increasing negative externalities and (5) a rising social cost of subsidising water use. Randall's framework belongs to public policy and agricultural and environmental economics, so it is focused on national policy and

the instruments recommended are mainly economic in nature (i.e. water pricing or markets).

A different approach comes from the fields of hydrology and agronomy, where the concept of 'basin closure' has been widely used since 2006, focusing in the necessary adaptation processes required to achieve a 'soft landing' for RBs under a closure trajectory. Examples of basin overbuilding and closure are the Jordan River, the Krishna River, the Colorado River, the Yellow River, among others. In this regard, basin closure is defined as an anthropogenic process and the term has been used to describe the situation in a number of basins and aquifers (Molle *et al.,* 2010). An example of this analytical framework can be found in Comair *et al*. (2013), which describe how population growth and increased agricultural demand are contributing to the closure of the Jordan basin.

To the best of our knowledge, the concepts of 'mature water economy' and 'basin closure' have not been fully integrated in the existing literature and they are rarely included together in the same study. An explanation for this may lie in the different levels of analysis of the two analytical frameworks. Randall's 'mature water phase' is defined at national level, with economic and normative instruments defined at this level. Conversely, basin closure is defined in hydrological terms, and economic instruments may be used when the basin belongs mainly to a single country. Nevertheless, as most of the basins listed above are international, finding sustainable solutions entails greater complexity.

We believe that the framework of a 'mature water economy' phase is complementary to the hydrological and ecosystem concept of a 'closed basin', as the solutions to this problem should consider the local situation (natural, social and technical constraints at aquifer or subbasin level), as well as the national policy institutions (the legal framework for managing water resources). Moreover, basin closure status may be seen as a phase beyond a 'mature water economy', indicating the onset of an 'emergency' phase.

In this research paper, we present a case study of a closed basin that has reached the limit where no additional water sources are foreseen, and in which economic instruments (reallocation, volumetric pricing, water rights markets, etc.) and technical strategies (water saving, improved water productivity and water efficiency) have already been widely implemented. Figure 2 represents the closure process of a RB (adapted from Berbel *et al.*, 2013). As WCTs increase irrigation water productivity, the expansion of new irrigated areas consequently leads to increasing pressures on the resource and the basin. In parallel, the extensive modernisation of irrigation systems has enabled widespread use of DI techniques, which have led to a remarkable increase in the economic productivity of irrigated agriculture (Expósito and Berbel, 2016). This in turn affects the characteristics of water demand by reducing the elasticity of demand with respect to the increasing water prices (Expósito and Berbel, 2017). Guadalquivir RB defined by this scenario with increasing pressures on water demand and growing scarcity of the resource,and therefore it can be assumed that the basin has reached a state of closure, with no additional water relevant resources to be consumed.

3. CASE STUDY CHARACTERISATION

The Guadalquivir RB, which is representative of the Mediterranean region, contains 23% of the total irrigated area in Spain (CHG, 2016). The competitiveness of its agriculture, with a focus on high value crops in a context of water scarcity, explains the remarkable expansion in irrigated areas and modernisation of irrigation systems in recent decades, to the point where there are now more than 850,000 hectares of irrigated land. The Guadalquivir is the longest river in southern Spain, with a length of about 650 km and a basin extension of over 57,527 km^2. Land in the basin is divided between forests (49.1 %), agriculture (47.2 %), urban areas (1.9 %) and wetlands (1.8 %). The basin has a Mediterranean climate with an average rainfall of 573 mm, occasional periods of prolonged drought, and an average annual temperature of 16.8ºC.

The current reservoir capacity in the Guadalquivir RB is 8,600 hm^3 and the average water use in the basin amounts to about 3,800 hm^3 per year (CHG, 2016), of which about 3,400 hm^3 goes to

meet the demand of irrigated agriculture (which represents 85% of the total water demand in the basin). The current Guadalquivir Hydrological Plan (2015-2021) declares that the level of the resource consumption has reached its maximum and that no significant supply increases are foreseen in the years to come. Against this backdrop, demand management has become the only available tool to manage water demand in the different socio-economic sectors, including agriculture (Corominas, 2010). Thus, the use of more efficient irrigation techniques plays a key role in achieving water-saving objectives, especially in a context of continuing pressure to increase irrigated areas, despite the explicit administrative moratorium on any further transformation of rain-fed lands into irrigated farmland.

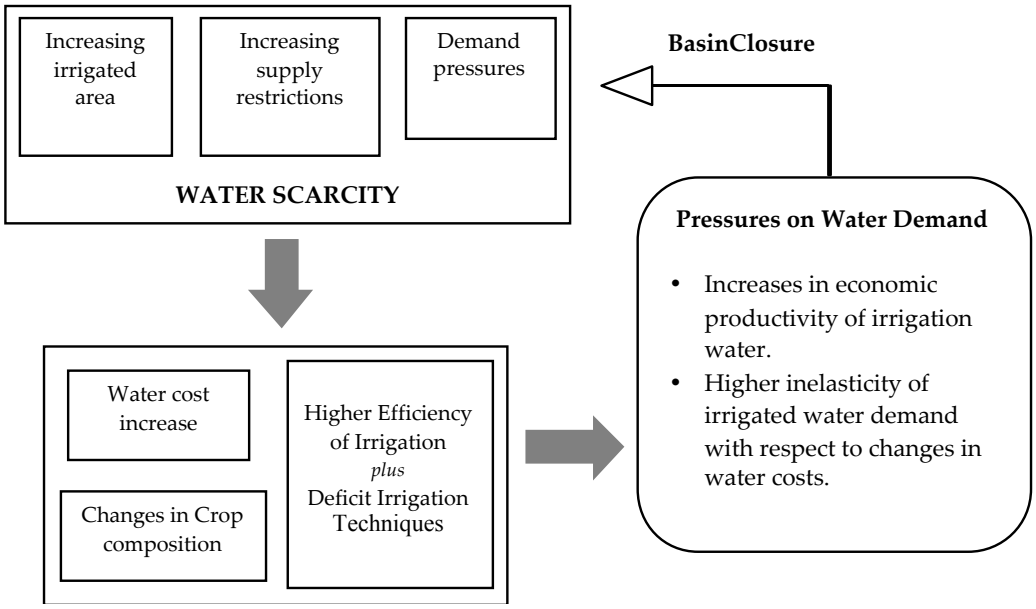

Figure 1. Model of Basin Closure Process.

As shown in Figure 2, the irrigated area in the Guadalquivir basin has increased continuously over the past two decades, mainly through the conversion of rain-fed olive groves into irrigated groves (MAGRAMA, 2015). In 2005, an administrative moratorium was declared on new irrigated areas in the main subbasin (comprising 90 % of the irrigated area), with marginal increases in irrigated areas still allowed in the remaining 10 % of the basin. The impact of this moratorium is reflected in the reduction of the average annual growth rate of irrigated areas, from 9 % in the period 1989-2005 to 0.8 % in the subsequent period.

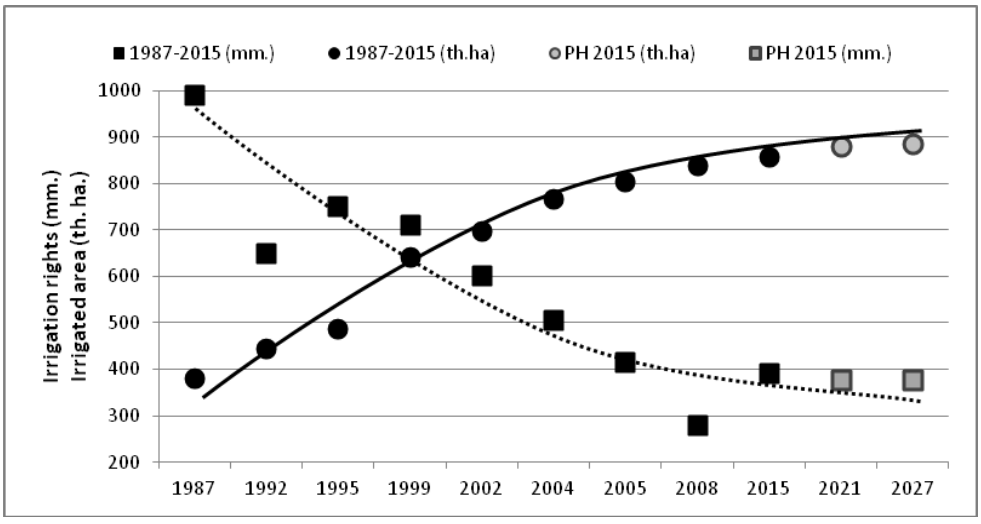

Figure 2. Average irrigation rights and irrigated area.

Farmers have adapted to this reduction in irrigation-water rights by modernising, investing in WCTs and using deficit irrigation (DI) strategies. The modernisation process of irrigation techniques has played a decisive role in the significant increase in irrigation water productivity in recent decades. The fact that the irrigated area in the basin doubled at the same time as a drastic reduction took place in the average irrigation rights per hectare can only be explained by the major investments made in WCTs. In this context, the greater water-use efficiency as an expected effect of irrigation modernisation, along with farmers' increasing commitment to crops with a more efficient water consumption and greater capacity to generate high agricultural yields (i.e. olive groves), have helped the basin to reach high efficiency levels in the use of the scarce water resources available.

The modernisation of irrigated agriculture in the Guadalquivir RB in recent years has been promoted by the regional government through the Andalusian Irrigation Plan (1995-2008) and the Irrigation Agenda H-2015 (CAP, 2010, 2011). The total investment for Andalusia (where the Guadalquivir RB accounts for 85% of the total irrigated area) was estimated at 1.54 billion EUR (of which 59% was publicly subsidised) for 347,234 ha (representing an average investment of 4,438 EUR/ha) in the analysed period. According to Corominas and Cuevas (2017), water efficiency (defined as the amount of water productively used divided by the total water supply) in the modernised areas in the Guadalquivir RB has risen from 0.67 to 0.84. The intense modernisation process in the Guadalquivir RB is reflected in the continuous increase in the surface area of drip-irrigated land in the basin. It is currently the principal irrigation method in the RB, employed in 66% of the total irrigated area, up from 12% in 1989. The comparison at a national level highlights the intense process of modernisation that has taken place in the Guadalquivir RB, which is well ahead of the rest of Spain in this regard. We would argue that the greater degree of mechanisation and modernisation achieved in this RB is reflective of the high level of agronomic development reached, and typical of closed RBs.

The substantial investments made as part of the intense modernisation process in the basin have also resulted in an increase in water costs, both in nominal (50 %) and real terms (12 %), during the last two decades, due mainly to the higher energy-use intensity of drip and sprinkler irrigation techniques and having to resort to deeper or more distant sources. The greater water-use efficiency due to the modernisation of irrigation along with the observed water cost increases have led to significant changes in the composition of major crops cultivated in the basin. Thus, farmers have tended to respond by dedicating more land to high value-added crops that use irrigation water more efficiently, with olive and citrus crops being notable examples. In parallel, the average irrigation water application in the basin fell approximately by 600 m^3/ha between 2005 and 2012, which affected most of the crops but had a particularly notable impact on traditional olive groves, where the use of DI techniques is more widespread. In this regard, ARIS ratios have decreased in major crops of the RB, especially in olive groves (Expósito and Berbel, 2016).

4. IMPACTS ON IRRIGATION WATER PRODUCTIVITY

As a result of the abovementioned responses to the closure process of the Guadalquivir RB, irrigation water productivity has increased dramatically in recent decades. Table 1 shows the yields obtained by rain-fed and irrigated agriculture in terms of Gross Value Added (GVA) in the RB. We assume that the increase in the economic productivity of irrigated agriculture due to improvements in labour and capital factors (improved seeds, machinery, etc.) is incorporated in the productivity of land and estimated by the increase over rain-fed farming productivity. Therefore, mean irrigation water productivity may be estimated as the difference between the estimated economic productivity (in terms of GVA generated per hectare) of irrigated agriculture and that of rain-fed farming.

Results show a relevant increase in the irrigation water mean productivity. However, significant differences are observed between the two analysed periods, 1995-2005 and 2006-2012. In the period 1995-2005, a remarkable expansion of irrigated area occurs in the Guadalquivir RB, with a

153% increase recorded (mainly in woody crops such as citrus and olive groves, which represent about 60% of the total increase in irrigated area in the RB). This expansion of irrigated areas in the basin, along with a 60% reduction in water consumption per hectare as a result of the modernisation of irrigation techniques, explains the significant increase in the irrigation water mean productivity in the period 1995-2005, rising from 0.11 to 0.49 EUR/m^3 (345% increase).

Table 1. Irrigation water mean productivity in the Guadalquivir RB.

				Annual increase rate	
	1989	2005	2012	1989-2005	2006-2012
[1] GVA of irrigation farming (EUR/ha)	1,579	2,653	2,660	4.00%	0.10%
[2] GVA of rain-fed farming (EUR/ha)	416	598	659	2.60%	1.40%
[3] Increase in productivity due to irrigation [3]= [2]-[1] (EUR/ha)	1,163	2,055	2,001	n/a	n/a
[4] Average irrigation water application (m^3/ha)	9,995	4,137	3,392	-3.40%	-2.60%
[5] Irrigation water mean productivity [5] = [3]/[4] (EUR/m^3)	0.116	0.497	0.603	19.30%	3.00%
[6] Irrigated area (ha)	316,646	801,865	845,986	9.00%	0.80%
[7] Rain-fed area (ha)	2,412,091	2,128,952	1,950,853	n/a	n/a

Source: Data for 1989 and 1995 from Carrasco et al. (2010). Own elaboration for 2012. Constant prices (base 2005).

During the period 2006-2012, the average water consumption per hectare decreases by 20%, to approximately 3,400 m^3/ha, while the capacity of irrigated agriculture to generate greater GVA levels than rain-fed agriculture remains largely unchanged (2,001 EUR/ha. in 2012 compared to 2,055 EUR/ha. in 2005). In our opinion, this would seem to indicate that the observed increase in the irrigation water mean productivity (from 0.49 to 0.60 EUR/m^3) in this period can be explained almost exclusively by the higher production efficiency of irrigated farming, which is thus able to generate the same yield levels with lower levels of water consumption.

The capacity of the Guadalquivir RB to increase the agricultural GVA through irrigation tends to level out in terms of GVA per irrigation unit. As a result of the marked expansion of irrigation agriculture in the basin, water resources have become the limiting production factor, in contrast with the traditional model that defines land as the limiting factor. Since the degree of modernisation and efficiency of irrigation techniques in the basin is already high, the ability of irrigated farming to continue generating greater GVA declines, a situation which characterises the current closure of the basin.

Table 2. Productivity of rain-fed and irrigated crops in the Guadalquivir RB, 2012.

Type of crop			[1] Crop GVA/ha (EUR/ha)	[2] Irrigation rights (m^3/ha)	[1]/[2] GVA/irrigation (EUR/m^3)
Cereals	Wheat	rain-fed	431	-	-
	Rice	irrigated	2,451	13,000	0.19
	Corn	irrigated	2,768	6,250	0.44
Industrial	Sunflower	rain-fed	471	-	-
	Cotton	irrigated	1,155	5,600	0.21
	Sugar beet	irrigated	2,726	4,500	0.61
Citrus	Oranges	irrigated	6,300	5,500	1.15
Olive groves	Table olives	rain-fed	1,426	-	-
	Oil-mill olives	rain-fed	1,302	-	-
	Table olives	irrigated	1,755	1,500	1.17
	Oil-mill olives	irrigated	2,500	1,500 – 2,250	1.11 – 1.67

Table 2 shows the 2012 data on GVA per hectare for major irrigated and rain-fed crops, obtained by applying a similar method to that used previously to estimate irrigation water productivity in the basin. Estimates show that the highest GVA-to-irrigation water ratio is achieved by olive and citrus crops. These crops have registered the largest increase in cultivated area over the analysed period,

accounting nowadays for more than 60 % of total irrigated area in the Guadalquivir RB. According to Castillo *et al.* (2017), prices of major crops in the Guadalquivir RB have decreased in real terms in the last two decades, and this reduction in price has not been fully offset by the increase in physical production, meaning that income per hectare has decreased in real terms. Farmers have reacted to this situation by switching from commodity crops (i.e. cereals, sugar beet, and cotton) to higher value crops (i.e. citrus, olive).

5. CONCLUSIONS

The analysis of our case study has clearly revealed how greater resource-use efficiency has led to the expansion of irrigated areas of those crops with higher levels of GVA per irrigation unit (i.e. olive and citrus crops). In our opinion, the declining capacity of irrigated farming in the basin to generate greater GVA per hectare, as shown by the slowing rate of average annual increase in irrigation water mean productivity in the period 2005-2012, would explain the present situation in the Guadalquivir RB. This slow-down in productivity gains reflects the diminishing returns to scale of technical innovation, with DI, crop change and irrigation modernisation reaching the limits of their capacity to create new value, which in turn means that the economic productivity of irrigation water in the basin reaches a plateau.

As described in our research work, the factors driving irrigation water productivity in the Guadalquivir RB are multidimensional by nature:

1) Economic dimension.
   a) Change in crop patterns towards a preponderance of more productive crops.
2) Technical dimension.
   b) Increase in conveyance efficiency (distribution channels).
   c) Water-saving techniques (mainly drip irrigation and high-tech systems).
3) Agronomic dimension.
   d) Implementation of deficit irrigation (DI).
4) Institutional dimension.
   e) Reduction in water rights allocation.

The first three responses (crop pattern change, improved conveyance efficiency and water-saving techniques at farm level) are well documented (e.g. Molden *et al*., 2010; Molle *et al*., 2007). However, the last two responses (extensive use of DI techniques and reduction in water rights allocation) are distinctive features of the Guadalquivir RB and the published evidence on them is scarce; our analysis of these features can therefore be considered one of the main contributions of our analysis.

In our opinion, Guadalquivir can be defined as a closed basin as almost all water resources are allocated to farmers, other economic uses and environmental flows. Additional consumption demands—resulting from the increasing efficiency of irrigation techniques and the widespread use of DI practices with high-productivity crops (i.e. olive, citrus, and almond crops)—will continue to intensify the pressures in the basin. In this context, the Water Authority needs to enforce policy control and ensure good governance to prevent additional consumption demands that cannot be met with the already depleted resources.

In future studies, we plan to expand the microeconomic analysis of the closure process of a river basin by extending the study to other basins with different hydrological and environmental characteristics. Such an analysis would allow us to produce more robust results regarding the evolution of irrigation water productivity at a global basin level, as well as in major crops of the basin. We hope that this paper opens up new avenues for research in the field of water policy and encourages further study of the role of increasing water productivity in the evolution of a river basin.

REFERENCES

Berbel, J.; Pedraza, V.; Giannoccaro, G. (2013). The trajectory towards basin closure of a European river: Guadalquivir. Int. J. River Basin Manag. 11, 111–119.

CAP (2010). Inventario de Regadíos 2008 y su evolución en la última década, Consejería de Agricultura y Pesca, Junta de Andalucía, Sevilla.

CAP (2011). Agenda del Regadío Andaluz H-2015, Consejería de Agricultura y Pesca, Junta de Andalucía, Sevilla.

Carrasco, J.M.; Pistón, J.M.; Berbel, J. (2010). Evolución de la productividad del agua en la Cuenca del Guadalquivir 1989-1995. Economía Agraria y Recursos Naturales. 10(1), 57-67.

Castillo, M; Borrego Marín, M.M.; Berbel, J. (2017). Perspectiva del agricultor sobre el efecto de la modernización de regadíos en la distribución de cultivos. In El impacto de la modernización de regadíos en España; Berbel, J., Gutierrez, C., Eds.; Cajamar Caja Rural; pp. 330-343.

CHG (2016). Plan Hidrológico de la demarcación del Guadalquivir 2015-2021, R. D. 1/2016, Confederación Hidrográfica del Guadalquivir, Sevilla.

Comair, G.F.; Gupta, P.; Ingenloff, C.; Shin, G.; McKinney, D.C. (2013). Water resources management in the Jordan River Basin. Water and Environment Journal, 27(4), 495-504.

Corominas, J. (2010). Los nuevos Planes Hidrológicos de las Cuencas Andaluzas, Observatorio del Agua de la Fundación Botín, Madrid.

Corominas, J.; Cuevas, R. (2017). Análisiscrítico de la modernización de regadíos. In El impacto de la modernización de regadíos en España; Berbel, J., Gutierrez, C., Eds.; Cajamar Caja Rural; pp. 273-307.

Expósito, A.; Berbel, J. (2016). Microeconomics of Deficit Irrigation and Subjective Water Response Function for Intensive Olive Groves. Water, 8(6), 254. doi:10.3390/w8060254

Expósito, A.; Berbel, J. (2017). Why is water pricing ineffective for deficit irrigation schemes? A case study in southern Spain. Water Resour. Manag. 31(3), 1047-1059. doi: 10.1007/s11269-016-1563-8

MAGRAMA (2015). ESYRCE. Informe sobre Regadíos en España, Ministerio de Agricultura, Alimentación y Medio Ambiente, Gobierno de España, Madrid.

Molden, D.; Oweis, T.; Steduto, P.; Bindraban, P.; Hanjra, M. A.; Kijne, J. (2010). Improving agricultural water productivity: Between optimism and caution. Agr. Water Manage. 97(4), 528-535. doi:10.1016/j.agwat.2009.03.023

Molle, F.; Wester, P.; Hirsch, P. (2010). River basin closure: Processes, implications and responses. Agr. Water Manage., 97(4), 569-577.

Molle, F.; Wester, P.; Hirsch, P.; Jensen, J. R.; Murray-Rust, H.; Paranjpye, V.; Pollard, S.; Van der Zaag, P. (2007). River basin development and management. In Water For Food, Water For Life: A Comprehensive Assessment of Water Management in Agriculture; Molden, D., Ed.; London: Earthscan and Colombo, International Water Management Institute; pp. 585-624.

Randall, A. (1981). Property entitlements and pricing policies for a maturing water economy. Aust. J. Agr. Econ., 25.3, 195-220.

Proceedings of the 10th World Congress of EWRA 'Panta Rhei', 5-9 July 2017, Athens, Greece
© 2017 *European Water Resources Association*

Parameterization of "canopy resistance" and estimation of hourly latent heat flux over a crop

A. Margonis[1], G. Papaioannou[1*], P. Kerkides[2] and G. Bourazanis[2]
[1] *National and Kapodistrian University of Athens, Department of Physics, Greece*
[2] *Agricultural University of Athens, Department of Natural Resources Development and Agricultural Engineering, Greece*
[*] *e-mail: gpapaioa@phys.uoa.gr*

Abstract: The objective of this study is to evaluate the estimation of hourly actual evapotranspiration (AET) in olive trees, applying the Penman - Monteith method (PM) either using models which take into account the 'canopy resistance', or its simplified model as proposed by Priestley and Taylor (PT). The evaluation is based on comparisons with experimental measurements of actual evapotranspiration applying the 'Bowen ratio' method (λE). Hourly experimental data, obtained from air temperature, humidity, wind speed and radiation balance measurements, taken at Sparta nearby area (lat 37^0 04′ N, log 22^0 05′ E), during the period from June 2010 up to July 2014 are used. In order to estimate hourly 'canopy resistance', needed in the PM method, the Katerji-Perrier (KP) and the Todorovic (TD) models are applied over olive trees. Canopy resistance (r_c) estimated from KP model is parameterized by a semi-empirical approach which requires a simple calibration procedure, while r_c from TD model is parameterized using a theoretical approach (without a calibration procedure taken place). For estimating λE from minimum data (temperature, humidity and radiation balance) the PT model was also employed, since r_c is not required and the aerodynamic term of PM was taken into account in the dimensionless empirical parameter a of the model. The results show that λE is slightly underestimated when KP and PT models are used and a very good correlation between predictions and experimental measurements exists. These models can be successfully employed for estimating actual evapotranspiration over olive trees. On the other hand, TD model overestimates λE and this can be attributed to some theory assumptions weakness in the model.

Key words: Actual evapotranspiration, canopy resistance, Penman-Monteith method, Katerji-Perrier method, Todorovic method, Priestley and Taylor method

1. INTRODUCTION

The accurate determination of AET at different scales is a common objective for hydrology, the determination of water requirement in irrigated areas and analyzing the impacts of climate change on water resources. Several techniques provide direct measurements of AET, but AET can also be estimated from empirical or mechanistic models, using in situ observed meteorological variables. The most commonly used method is the Penman–Monteith (PM), which is based upon the assumption that all the energy for evaporation is accessible by the plant canopy and that water first has to diffuse through leaves against a surface resistance, before diffusing into the atmosphere against an aerodynamic resistance. Surface resistance is usually difficult to be calculated accurately. Katerji and Perrier (1983) proposed a semi-empirical approach with surface resistance depending on climate variables and the aerodynamic resistance, and requiring in situ calibration of its parameters. A mechanistic model (not requiring in situ calibration) was also developed by Todorovic (1999) with the surface resistance being also a function of climatic variables and aerodynamic resistance.

The PT model (Priestley and Taylor, 1972) can be used for estimating AET, as a simplified form of PM method. The method has successfully simulated AET over grassland, crop fields, and forest ecosystems.

The purpose of this study is to assess the evaluation of AET predictions, obtained from the two modified PM models, with canopy resistance estimated by either the Katerji and Perrier or Todorovic methods and the simplified PM model with zero canopy resistance, as given by the PT method. The evaluation is based on comparisons with measurements of AET, taken over olive trees

during the period June 2010 to July 2014.

2. DATA AND METHODS

2.1 Data

In this study, measurements of temperature, relative humidity and wind speed recorded at 6 and 10m and sunshine duration, total solar- and long wave- radiation taken at 6m, over an olive orchard (of about 4m height) at the rural area of Sparta (Lat. 37° 04′ N, long. 22° 05′E and altitude 0.212 km), during the years 2010, 2011, 2012 and 2014 were used. The data belonging to days with rainfall or irrigation events were removed from the further analysis.

2.2 Methods

2.2.1 Evaluation of hourly actual evapotranspiration

Hourly measured AET was obtained from the Bowen ratio/energy balance (BREB) method by the equation:

$$\lambda E = \frac{A}{1+\beta} \quad (1)$$

where λE is the latent heat flux, A is equal to Rn-G (where Rn is the net radiation and G the ground heat flux) and β is the Bowen ratio given, from the temperature difference T_2-T_1 and the actual vapour pressure difference e_2-e_1 of the air in two heights z_1 and z_2, as follows:

$$\beta = \frac{\rho c_p[T_2-T_1+\Gamma(z_2-z_1)]}{(\rho_\alpha c_p/\gamma)(e_2-e_1)} \quad (2)$$

where Γ is the dry adiabatic lapse rate (^{o}C/m).

Hourly values of all parameters were taken into account after applying Ohmura (1982) criteria for correct β values.

Hourly estimates of AET were calculated by Penman-Monteith method (Allen et al., 1998) as:

$$\lambda E = \frac{\Delta A+\rho c_p D/r_a}{\Delta+\gamma(1+\frac{r_c}{r_a})} \quad (3)$$

where ρ is the air density (kg/m^3), Δ is the slope of the saturation vapour pressure versus temperature function (kPa/^{0}C), γ is the psychrometric constant (kPa/^{0}C) , c_p is the specific heat of moist air (J/kg^{0}C), D is the vapour pressure deficit of the air (kPa), r_c is the bulk canopy resistance (s/m) and r_a is the aerodynamic resistance (s/m).

The resistance r_c according to Katerji and Perrier (1983) (after establishing a linear relationship between the two ratios r_c/r_a and r^*/r_a, where r^* is a climatic resistance) is determined as:

$$\frac{r_c}{r_a} = a\frac{r^*}{r_a} + b \quad (4)$$

where a and b are empirical coefficients and r^* (s/m) is defined as:

$$r^* = \frac{\Delta+\gamma}{\Delta\gamma}\frac{\rho c_p D}{A} \quad (5)$$

By combining Equations (3), (4) and (5), the hourly λE can be written as:

$$\lambda E = \frac{1+\frac{\gamma}{\gamma+\Delta}\frac{r^*}{r_a}}{1+\frac{\gamma}{\gamma+\Delta}(\alpha\frac{r^*}{r_a}+b)}\frac{\Delta}{\Delta+\gamma}A \quad (6)$$

The application of this approach has the advantage of taking into account the set of climatic variables affecting r_c (R_n, D and r_a) but is limited requiring calibration of the coefficients a and b (eq. 4).

Aerodynamic resistance r_a is calculated as:

$$r_a = \frac{ln\frac{z-d}{z_0}ln\frac{z-d}{h_c-d}}{k^2u_z} \quad (7)$$

where z is a reference plane, h_c(m) is the mean height of the crop (m), d(m) is the zero plane displacement equal to $0.67h_c$, k is the von Karman constant, u_z is the wind speed (m/s) at the reference point z and z_0 (m) is the roughness length equal to $0.1h_c$.

In the parameterization of r_c proposed by Todorovic (1999) r_α is as:

$$r_a = \frac{ln\frac{z-d}{z_0}ln\frac{z-d}{z_{0h}}}{k^2u_z} \quad (8)$$

where z_{0h} is the roughness length to the heat flux, equal to $0.1z_0$.

A simplified version of the PM model with r_c=0, was proposed by Priestley and Taylor (1972) as:

$$\lambda E = \alpha\frac{\Delta}{\Delta+\gamma}A \quad (9)$$

where α is the dimensionless Priestley–Taylor parameter. When PT model was employed for estimating AET, calibrated values of α were used, as obtained by inverting eq. 9 and using the calibration set of data.

All the obtained estimates of AET were evaluated by comparisons with the measured AET. The comparisons were based on the results of linear regressions (slope and r^2) and "difference measures" [RMSE, MBE and refined index of agreement (RIA), as proposed by Willmott and Matsura (2005)]

2.2.2 Diurnal and annual variation of actual evapotranspiration and canopy resistance

Average hourly values of AET and r_c from twenty clear days (1-12 July 2011) selected (as ensuring maximum AET values) are used for their diurnal evolution.

Ten days moving average values of hourly values of AET and r_c at 12.00am were used for presenting their annual variation.

3. RESULTS

3.1 Evaluation of hourly actual evapotranspiration

KP model was calibrated for cold and warm period separately, using hourly values of r_c, determined during four clear days of cold period and three clear days of warm period respectively, since 20 values of hourly data have been referred as enough for reliable calibration (Katerji and Rana, 2006). These days were randomly chosen during the year 2011. The calibration yields the

coefficients a and b, from the relation r_c/r_a as a function of r^*/r_a, which was found for cold and warm period separately. The slope, the intercept and the correlation coefficient obtained by linear regression analysis are 0.69, 2.43 and 0.91 respectively, for the cold period and 0.94, 1.37 and 0.99 respectively, for the warm period.

The calibration of the PT model was also carried out for cold and warm period separately, using the same hourly calibration data set. The values of α were determined by the slope obtained by linear regression analysis between measured AET and $\Delta^*A/(\Delta+\gamma)$ and these were 1.005 for the cold period and 1.072 for the warm period.

The results of hourly AET estimated by PM equation, using r_c from the TD and KP methods and PT method presented in Table 1 and Figure 1, demonstrated that the PT model simulates the measured λE very well, while a very good approximation is obtained from the KP model. In contrast, TD model overestimates λE. An analysis during the warm season indicates that the results are better for both the PT and the KP model estimation, while they are worse for the TD model. As water availability decreases, β increases and thus it may be used as an indicator of water stress. The criterion $|b| < 0.3$ is usually used, when applying KP or TD models, in order to exclude water stress situations. When data satisfying the above criteria are used the λE estimates from the TD model seem better (Table1).

3.2 Diurnal and annual variation of actual evapotranspiration and canopy resistance

The diurnal courses of canopy resistance, as estimated by KP and TD methods, ($r_{c,KP}$ and $r_{c,TD}$ respectively), exhibit a similar pattern during the day, as compared to the experimental r_c pattern. The canopy resistance decreases from sunrise, approaching a minimum value at around 8:00 to 10:00 hours and then rises steeply from around 15:00 hours (Figure 2a). The values of $r_{c,TD}$ are always smaller than the corresponding values of the experimental r_c and $r_{c,KP}$, during the day. The estimated values of $r_{c,KP}$ approximate the experimental values r_c very well. The diurnal course of estimated λE_{TD}, λE_{KP}, λE_{PT} and λE shows a bell-shaped curve, similar to that of net radiation (Figure 2b). The evapotranspiration increases sharply after sunrise and takes its maximum value at noon, decreasing later smoothly and then more steeply until the afternoon. Measured and estimated evapotranspiration show an increase at around 13:30 hours coinciding with the maximum value of D.

According to the annual course of the estimated $r_{c,KP}$, $r_{c,TD}$ and the measured r_c , during the warm period, the underestimation of r_c from the TD model is large, while there is a high correlation between $r_{c,KP}$, and r_c. During the cold period, KP model underestimates r_c (Figure 3a). The annual course of estimated λE_{KP}, λE_{PT} and measured λE values traces R_n. By contrast, the annual course of λE_{TD} seems to be particularly affected by the annual course of D (Figure 3b). During the warm period, the overestimation of AET by TD model is large, while there is a high correlation between λE_{KP} and λE. During the cold period KP model underestimates AET.

Table 1. Statistical analysis of hourly evapotranspiration estimations

METHOD	Slope	r^2	RMSE %	MBE %	RIA
All Data					
TD	1.166	0.960	34.545	15.044	0.776
KP	0.920	0.978	19.187	-9.795	0.877
PT	0.927	0.990	14.879	-9.330	0.894
Warm Period Data					
TD	1.245	0.901	36.305	25.781	0.716
KP	0.943	0.957	13.389	-6.393	0.899
PT	0.954	0.969	11.271	-5.361	0.912
All Data (|β|<0.3)					
TD	1.145	0.900	32.350	12.665	0.800
KP	0.901	0.947	19.462	-12.046	0.883
PT	0.910	0.977	14.875	-11.311	0.889
Warm Period Data (|β|<0.3)					
TD	1.222	0.920	33.220	23.144	0.753
KP	0.926	0.973	12.793	-8.445	0.908
PT	0.937	0.984	10.331	-7.381	0.921

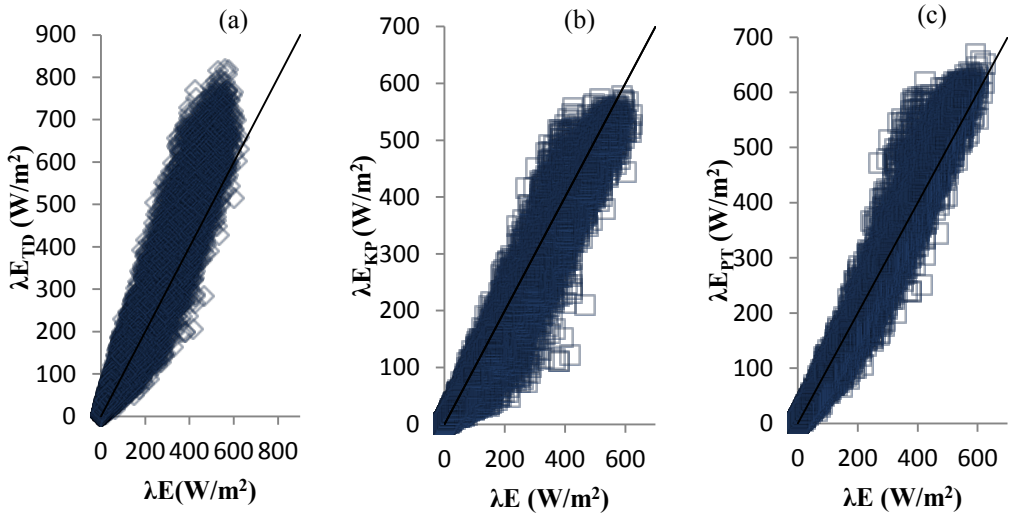

Figure 1. Regression between hourly measured (λE) and estimated AET values by three different methods (a) TD (λE_{TD}), (b) KP (λE_{KP}), (c) PT (λE_{PT})

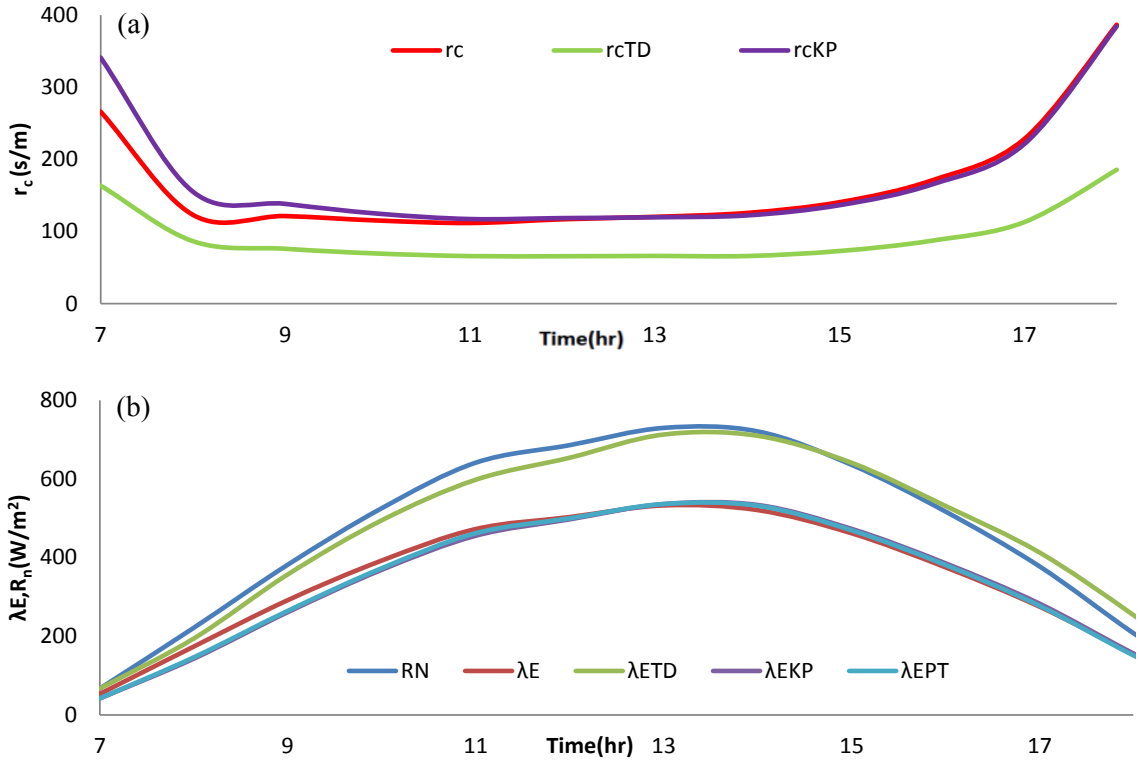

Figure 2. Diurnal course of mean hourly values of (a) measured canopy resistance (r_c), estimated canopy resistance by TD method ($r_{c,TD}$) and the KP method ($r_{c,KP}$) (b) measured (λE) and estimated AET values by three different methods TD (λE_{TD}), KP (λE_{KP}), PT (λE_{PT}) and net radiation, for 12 clear days (1-12 July 2011)

4. DISCUSSION AND CONCLUSIONS

The evaluation of the three methods employed for estimating AET over olive trees on hourly basis, suggested that PT and KP models were the most appropriate (RIA equal to 0.894 or 0.877, respectively) followed by the TD model (RIA=0.776). These results are in agreement with those reported by Shi et al. (2008), when the three methods were used over a forest ecosystem, on a daily scale. The KP model seems to be a reliable model, as demonstrated for a large range of crops, subjected to various water conditions. There are studies proposing the TD model over irrigated

grass, but the model (overestimating up to 30–50%) is not recommended over other crops (Katerji et al, 2011). The disagreement between measured and estimated by the TD model, values of AET (or canopy resistance) is mainly due to the parameterization of r_c by the TD method, through which r_c is mainly a function of water-vapour deficit (D). The variables associated with soil and plant water deficit are not taken into account and as a consequence, r_c value is assumed to be the same for all surfaces, which is not applicable (Katerji et al., 2011).

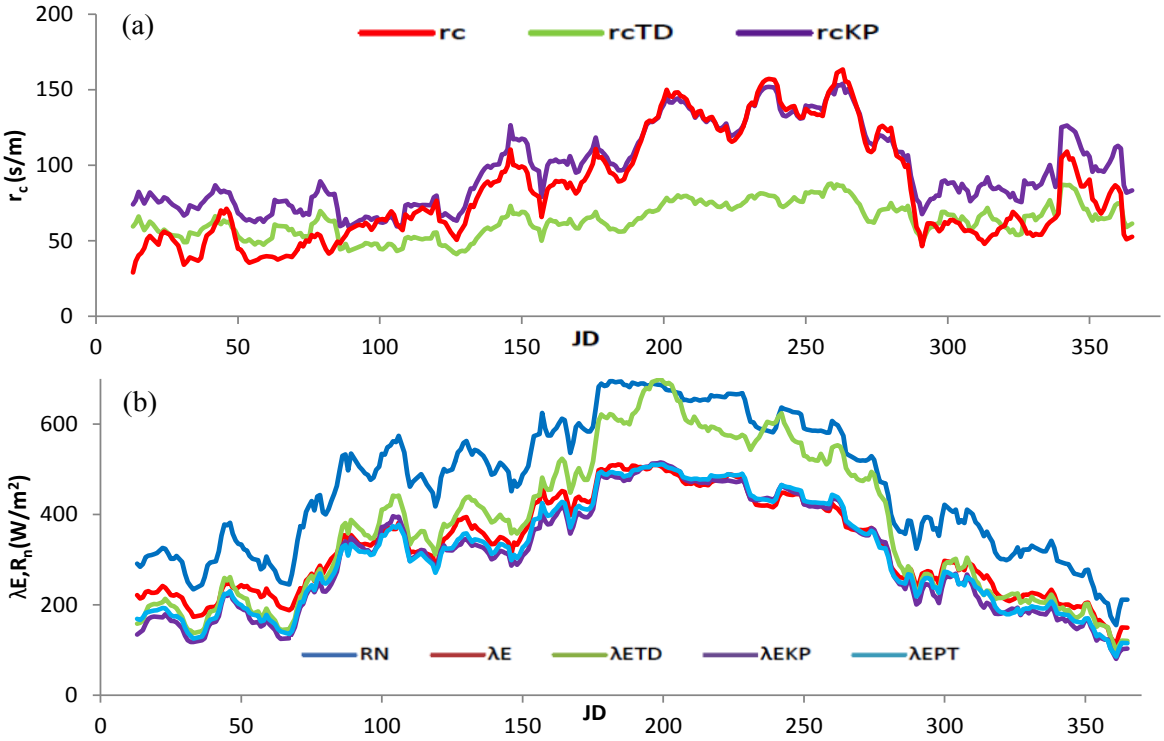

Figure 3. Annual course of mean hourly values of (a) measured canopy resistance (r_c), estimated canopy resistance by TD method ($r_{c,TD}$) and the KP method ($r_{c,KP}$) (b) measured (λE) and estimated AET values by three different methods TD (λE_{TD}), KP (λE_{KP}), PT (λE_{PT}) and net radiation, during the year 2011 at 12.00 am (10 days moving average is shown)

The diurnal courses of estimated and measured latent heat fluxes showed bell-curved shape similar to that of net radiation. Evapotranspiration increased rapidly shortly after sunrise onwards and peaked at noon of solar time, declining first slowly and then more rapidly over the afternoon. However, the TD model significantly overestimated AET at noon, due to the expected high value of the air water-vapor pressure deficit. Similar patterns of daily course of measured AET were also reported over olive orchard (Villalobos et al., 2000; Berni et al., 2009), over alpine grass (Zhu et al., 2014) and over forest ecosystem (Shi et al., 2008). r_c, $r_{c,KP}$ showed similar diurnal evolution. On the contrary, $r_{c,TD}$ was significantly lower than that of r_c and $r_{c,KP}$, during the day, indicating that the TD model is unreliable over olive trees. The observed diurnal evolution of canopy resistance is similar to the ones referred by other studies over olive orchard (Alves and Pereira, 2000; Katerji and Rana, 2006) and the ones published over forest (Shi et al., 2008), irrigated grass (Rana and Katerji, 1994) and alfalfa (Lascano and Evett, 2010).

According to the annual variation of r_c, $r_{c,KP}$ and $r_{c,TD}$, the underestimation from the TD model is large, during the warm period, while there is a high correlation between $r_{c,KP}$ and r_c. Similar results have been published for olive trees (Berni et al., 2009). The annual course of estimated λE_{KP}, λE_{PT} and measured values of λE traces the R_n. By contrast, the annual course of λE_{TD} seems to be particularly affected by the annual course of vapour pressure deficit. During the warm period, the overestimation of AET by TD model is large, while there is a high correlation between λE_{KP} and λE. These results are in agreement with other studies over olive trees (Er-raki et al., 2008; Martinez-Cob et al., 2010).

ACKNOWLEDGEMENTS

The National and Kapodistrian University of Athens, the Greek Ministry of Rural Development and Food and the former Prefecture of Laconia for funding the project are duly acknowledged.

REFERENCES

Allen RG, Pereira LS, Raes D, Smith M. 1998. Crop Evapotranspiration. Guidelines for Computing Crop Water Requirements. FAO Irrigationand Drainage Paper no. 56. FAO: Rome, 300. pp. Alves I, Pereira LS, 2000. Modelling surface resistance from climatic variables. Agricultural Water Management 42: 371–385.

Berni, J.A.J., P.J. Zarco-Tejada, G. Sepulcre-Cantó, E. Fereres, and F. Villalobos. 2009. Mapping canopy conductance and CWSI in olive orchards using high resolution thermal remote sensing imagery. Remote Sensing of Environment 113:2380-2388.

Er-Raki, S., A. Chehbouni, J. Hoedjes, J. Ezzahar, B. Duchemin, and F. Jacob. 2008. “Improvement of FAO-56 Method for Olive Orchards through Sequential Assimilation of Thermal Infrared-Based Estimates of ET.” Agricultural Water Management 95 (3): 309–321.

Katerji N, Perrier A (1983) A modélisation de l’évapotranspiration réelle d’une parcelle de luzerne: rôle d’un coefficient cultural. Agronomie 3(6):513–521

Katerji N, Rana G. 2006. Modelling evapotranspiration of six irrigated crops under Mediterranean climate conditions. Agricultural and ForestMeteorology 138: 142–155.

Lascano RJ, van Bavel CHM and Evett SR (2010). A field test of recursive calculation of crop evapotranspiration. Transactions of the American Society of Agricultural and Biological Engineers 53: 1117–1126.

Martinez-Cob, A., Faci, J.M., 2010. Evapotranspiration of an hedge-pruned olive orchard in a semiarid area of NE Spain. Agric. Water Manage. 97 (3), 410–418.

Ohmura, A., 1982. Objective criteria for rejecting data for Bowen ratio flux calculations. J. Appl. Meteorol. 21 (4), 595–598.

Perrier A. 1975. Etude physique de l’évapotranspiration dans les conditions naturelles. I. Evaporation et bilan d’énergie des surfaces naturelles. Ann. Agron. 26: 1–18.

Priestley CHB, Taylor RJ. 1972. On the assessment of surface heatand evaporation using large-scale parameters. Monthly Weather Review100: 81–92.

Rana G, Katerji N, Mastrorilli M, El Moujabber M (1994) Evapotranspiration and canopy resistance of grass in a Mediterranean region. Theor Appl Climatol 50(1–2):61–71

Shi TT, Guan DX, Wang AZ, Wu JB, Jin CJ, Han SJ, 2008. Comparison of three models to estimate evapotranspiration for a temperate mixed forest. Hydrological Processes 22: 3431–3443.

Todorovic M. 1999. Single- layer evapotranspiration model with variable canopy resistance. Journal of Irrigation and Drainage Engineering—ASCE 125: 235–245.

Villalobos, F.J., Orgaz, F., Testi, L., Fereres, E., 2000. Measurementand modeling of evapotranspiration of olive (Olea europaea L.) orchards. Eur. J. Agron. 13, 155–163.

Willmott CJ, Matsuura K. 2005. Advantages of the mean absolute error (MAE) over the root mean square error (RMSE) in assessing average model performance. *Climate Research* 30: 79–82.

Zhu G F, Su Y H, Li X, et al. 2014a. Modelling evapotranspiration in an alpine grassland ecosystem on Qinghai-Tibetan plateau. Hydrological Process. 28(3): 610–619.

Proceedings of the 10th World Congress of EWRA 'Panta Rhei', 5-9 July 2017, Athens, Greece
© 2017 *European Water Resources Association*

A methodology to determine the productivity - reliability curve as a tool for improving water management in the agricultural sector

A. Chavez-Jimenez[1,2*], A. Granados[2] and L. Garrote[2]
[1] *Institute of Hydraulics, Hydrology and Sanitary Engineering, University of Piura, Peru*
[2] *Department of Civil Engineering: Hydraulics, Energy and Environment, Technical University of Madrid, Spain*
[*] *e-mail: adriadna.chavez@udep.pe*

Abstract: Water scarcity problems may intensify in the future because of the impact of climate change. There are many regions were available water resources are nearly fully allocated. In a scenario of reduction of water availability, the reallocation of water resources may be required and those uses with high consumption and low priority, such as agriculture, could be affected. The decision of reallocation of water uses should be based on the maximization of social welfare. To that end, an assessment of the economic implications of lack of reliability in water use is needed. Water productivity is an often-applied indicator within the agricultural sector. There are studies about the determination of the crop production as a function of irrigation amount and also about the economic evaluation of the water productivities at the basin level. However, this information is not directly applicable to the problem of water reallocation because it does not account for supply reliability. A methodology for determining a Productivity-Reliability (P-R) curve and its application in the Guadalquivir basin (Spain) is presented in this work. The P-R curve represents the average expected value of agricultural production as a function of supply reliability. This curve is based on generally available information such as crop distribution and their market value and also on water availability, which depends on hydraulic infrastructure and water management. The P-R curve is obtained by combining the results of performance simulations of the water resources system in different scenarios and the crop production with the satisfied water supplies.

Key words: Water resources, climate change, agriculture, production, productivity, reliability

1. INTRODUCTION

Water resources distribution is likely to be impacted as a consequence of the climate change. On such scenario some regions of the planet will have to address with either permanent or temporary water scarcity problems. Adaptation and mitigation actions are being prepared for copying with it. Among these actions, the redistribution of the resources among the different uses could be necessary, and those uses with large demand and low priority, as agriculture, would be the most vulnerable (Iglesias et al. 2011). Therefore, the agricultural sector needs tools for improving the water management as a measure for sustainable adaptation to climate change. Hydro-economic models are could help to identify the best management actions for the adaptation to climate change (Molden et al. 2010). Water productivity is a frequently applied indicator which gives an economic view of the use of water (Berbel et al. 2011; Kang et al. 2017). Under a climate change framework water management needs also to take into account water availability, which in turn depends on the natural resources, hydraulic infrastructures and agricultural demands. This study presents a methodology which links production and availability as a tool for improving water management in the agricultural sector. This methodology has been applied to the Guadalquivir basin, in southern Spain.

2. METODOLOGY

The proposed methodology has been devolved in five steps (Figure 1) which were described in the following sub-sections.

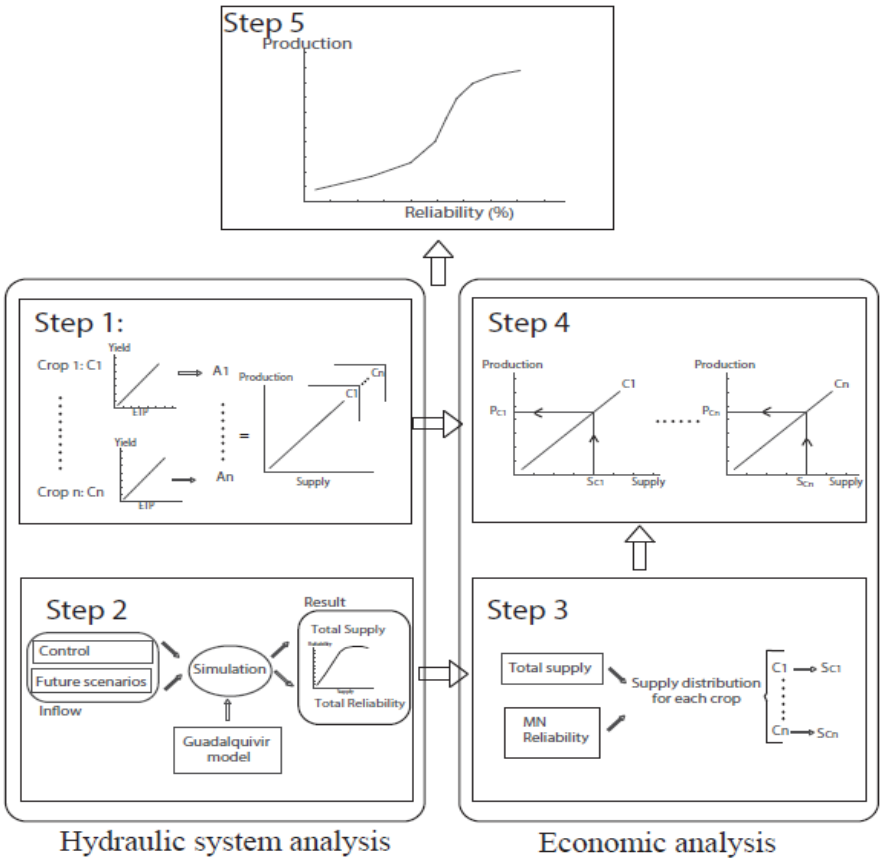

Figure 1. Methodology

2.1 Cropping pattern and Crop Water Production function (CWP function)

The first step consists in the determination of the cropping pattern, CWP functions and market price of the agricultural products.

The cropping pattern indicates the percentage of area that is dedicated to the different crops. It is generally available information, which is shared by river basin authorities and agricultural agencies, either regional or national. The CWP function expresses the relationship between unit yield and crop evapotranspiration (Stewart et al. 1977). Crop production is a complex process which modelling and analysis constitutes a research topic by itself. Water use is analysed as it is a principal factor influencing production (i.e. Berbel et al. (2011) state that 62% of the total production at the Guadalquivir Basin depends on water). CWP functions are obtained in purpose-made research for each crop and region, and they are published in agricultural research journals and books. Among the available CWP functions, those developed for the study region or for one with a similar climate were selected.

The objective of this study requires the computation of the total production for a given supply. Hence a Crop Yield-to-Supply function (CYS function) is obtained by modifying the unit yield (UY_c) and crop evapotranspiration (ETP_c) data from the CWP function into yield (Y_c) and supply (S_c) taking into account the area that is occupied by the crop (A_c). Those adjustments are done using Equations 1 and 2, respectively.

$$Y_c = UY_c \cdot A_c \tag{1}$$

$$S_c = ETP_c \cdot A_c \tag{2}$$

The crop market price (MP_c) and net margin (NM_c) are also available information that is shared in public databases of agricultural markets and agencies.

2.2 Annual supply and reliability

The second step consists in the simulation of the water resources system performance. The objective of this step is determining the supply and reliability. The study is carried out, for a control period based on recorded water resources series and for a set of future scenarios considering climate change under different socio-economic and emissions conditions.

The simulations are done with the OPTIGES model (Andreu et al. 1996), this models simulates the water resources system performance giving back the monthly supplies for each water use.

2.3 Supply distribution among crops

The objective of this step is to allocate the total supply among the different crops. This is necessary since this information is not generally available and is difficult to access for large scale studies. Different angles are considered to distribute the available water resources among users. The first, and simplest, is based on crop water requirements and reliability: supplies cover the full water requirements when reliability is 100%, and they are restricted proportionally to reliability when it is below 100%. The second, and proposed distribution, takes also into account the market price of the agricultural products. In this case, when reliability is equal or over 85% the supplies are distributed proportionally to reliability; while when it is below 85% the proportional distribution is then weighted considering the market price of each product. These rules are represented through Equations 3 to 5:

$$S_{ci} = S_i \cdot F_{1c} \cdot F_{2c} \tag{3}$$

$$F_{1c} = \frac{CW_c}{\sum_{c=1}^{k} CW_c} \tag{4}$$

$$F_{2c} = \frac{(NM_c / \sum_{c=1}^{k} NM_C) \cdot F_{1c}}{\sum_{c=1}^{k} (NM_c / \sum_{c=1}^{k} NM_C) \cdot F_{1c}} \tag{5}$$

where S_{ci} is the supply to crop c during year i, S_i is total supply during the year i, F_{1c} is a factor related to the crop water requirements, CW_c is the water requirement of crop c, F_{2c} is the weighting factor related to net margin, and NM_c is the net margin of crop c.

2.4 Determination of the total production

This step consists in the computation of the total production by applying the S_{ci} values to the CYS function, resulting yield annual values for each crop (Y_{ci}). This process is repeated for each of the n years of the scenario that is analysed. Then Y_{ci} is transformed into production (P_{ci}) by applying the market price (Equation 6).

$$P_{ci} = Y_{ci} \cdot MP_c \tag{6}$$

Finally, the total yield (P_t) for a given scenario is obtained by aggregating the annual production of all crops (Equation 7).

$$P_t = \sum_{c=1}^{k} \sum_{i=1}^{n} P_{ci} \tag{7}$$

2.5 Compilation of the P-R curve

The P-R curve is developed plotting the total production versus the reliability, for each of the analysed scenarios.

3. CASE STUDY: THE GUADALQUIVIR BASIN

The Guadalquivir basin, located in southern Spain (Figure 2), often suffers water scarcity problems because water requirements are in a limit equilibrium with the incoming water resources (Rodríguez Díaz et al. 2007; Chavez-Jimenez et al. 2013). There are almost 3,000,000 ha of cultivated land, with 861,000 ha of irrigated agriculture. The main crops are: olive (oil), wheat, cotton, orange, olive (fruit), rice and corn. Table 1 shows the area occupied by the main crops (MAGRAMA-CHG 2013), their market price (Junta de Andalucía 2014) and their CWP function (see references in Table 1). CWP functions were selected with some criteria based on the similarity of climate of the region where those functions were developed and the Guadalquivir area. Only rice CWP function does not fulfil this requirement, although this crop only represents a 1.4% of the irrigated area in the study basin.

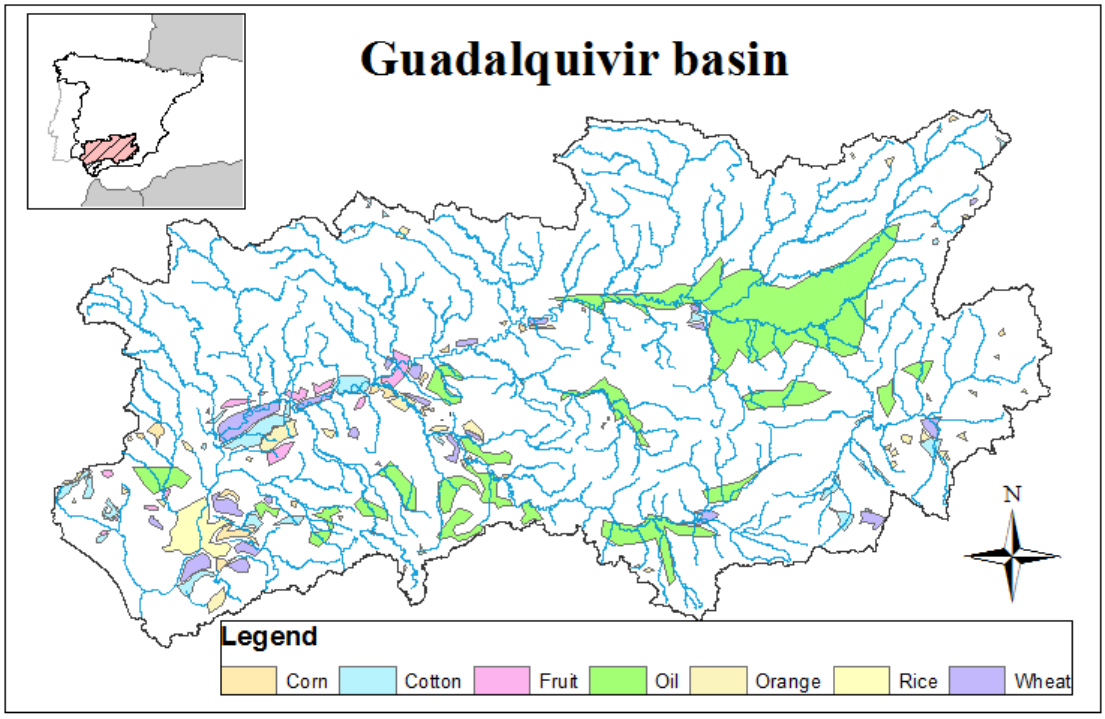

Figure 2. Guadalquivir basin. Location and distribution of the irrigated agriculture

Table 1. Guadalquivir basin. Cultivated area, market price in 2014 and CWP functions of the main crops

Crop	Cultivated area				MP 2014 (€/t)	CWP function (Region where developed; Reference)
	Total		Irrigation			
	(ha)	(%)	(ha)	(%)		
Olive (oil)	1391843	46.8	469099	54.8	366	Y=-6*10^-6*x^2+0.0011x-2.78 (Spain; Moriana and Orgaz, 2003)
Wheat	424424	14.3	67171	16.7	218	Y=-0.00002164*10^2*x^2-0.0378x-6.4335 (Mediterranean; Zhang and Oweis, 1999)
Cotton	135573	4.6	55242	5.4	395	Y=6.05*x+271.81 (Turkey; Dağdelen et al., 2006)
Orange	37984	1.3	37984	1.5	160	Y=0.162x+16 (California; Goldhamer et al., 2001)
Olive (fruit)	33308	1.1	23941	1.3	160	Y=-3*10^-5*x^2+0.063x-16.84 (Moriana and Orgaz 2003)
Rice	35108	1.2	35108	1.4	265	Y=2*10^-9*x^3-9*10^-6*x^2+0.0149x-4.1943 (Bouman et al. 2007)
Corn	17681	0.6	17681	0.7	180	Y=20.949*x-616.92 (Dağdelen et al. 2006)
Sum	**2075923**	**70**	**706229**	**82**		

Water resources studies on the Guadalquivir basin predict that climate change will impact rainfall and water resources. The models predict average reductions ranging from 8 to 70% depending on the model and scenario, and significant increases in their variability (Gonzales-Zeas et al. 2015) This changes will affect the available water resources and scarcity problems increase in magnitude and frequency, being the agricultural sector directly affected and adaptation measures such as water resources reallocation required (Chavez-Jimenez et al. 2015).

This work is based on the analysis of eight scenarios: one representing the control period (1961-1990) and seven representing different climate change projections. The characteristics of these scenarios are shown in Table 2. The performance of the Guadalquivir basin under such scenarios was performed by xxx, using the OPTIGES model, the outputs include series of monthly irrigation supplies and reliability.

Table 2. Characteristics of the control and climate change scenarios

Scenarios	Variation of annual streamflow		Demand (hm^3/yr)	Supply (hm^3/yr)	Reliability (%)	
	Δμ	ΔCV			Mean	Median
Control	-	-	2583.06	2252.38	83	92
DMI1-A2	-47	61		1715.83	52	54
DMI1-B2	-41	-37		1935.25	63	67
DMI2-A2	-50	-50		1847.41	59	57
ETH-A2	-61	93		1286.28	43	46
ICTP-A2	-8	26		1995.70	72	77
MPI-A2	-43	14		1771.41	58	64
SMHI-B2	-44	15		1621.62	55	62

4. RESULTS AND DISCUSSION

The P-R curve for the Guadalquivir basin (Figure 3) has been compiled following the above-described methodology. The production for the control scenario is 1,126 M€/yr, which means a water productivity value of 0.5 €/m^3, considering a 2,252 Mm^3/yr supply served with a mean reliability of the 83%. This value agrees with the results of other studies, i.e. Carrasco et al. (2010) gives the same water productivity value, Rodríguez et al. (2008) gives a lower value of 0.28 €/m^3, and the Guadalquivir River Authority's River Basin Management Plan (MAGRAMA-CHG 2013) indicates that the average productivity is 0.77 €/m^3.

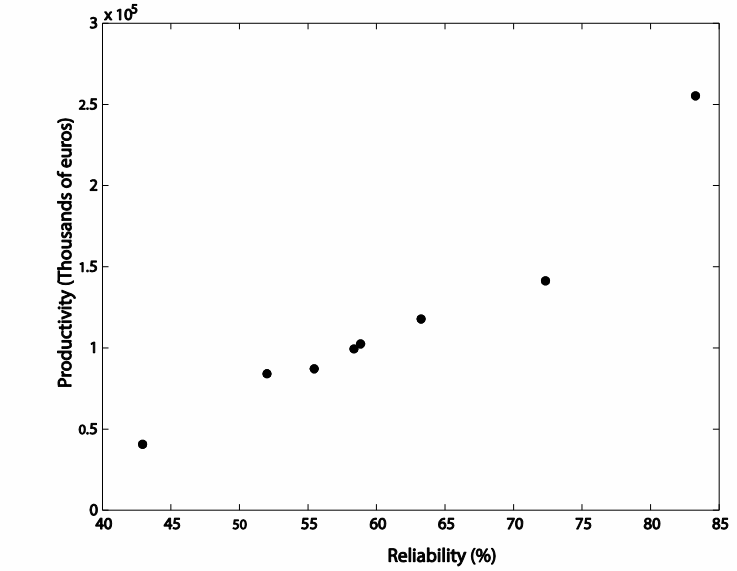

Figure 3. Guadalquivir basin. P-R curve

The production decreases for lower reliabilities. The relation between both variables is not linear; the P-R curve has a sudden drop in production when reliability moves from 80-85% to 70-75%. This drop may be explained through the water requirements during the vegetative cycle. Low reliability supplies imply that the crop do not have enough water to flower and develop the fruit. The worst scenario considered, the ETH-A2, has a strong reduction in reliability with respect to the control period. In such a case the average reliability is 43%, the production is 173 M€/yr and the water productivity is 0.13 €/yr, however 1,286 Mm^3 still being supplied. This result suggests that reallocation of water resources could be done to enhance production.

5. CONCLUSIONS

The proposed P-R curve links together the hydraulic performance and the economic assessment, and may be a useful tool for water resources systems planners and managers. The P-R curve could be determined and compiled with generally available information. This is an important fact, which makes it suitable for its application in large scale analysis, providing a basin or group of basins overview. The P-R curve helps to identify the minimum reliability level beyond which adaptation measures are required. The curve helps to identify the improvement that could be matched with managerial, non-structural measures. Moreover, deeper, structural measures effectiveness (as the increment of the storage capacity, or the introduction of drought resistant crops) could be tested by developing simulated P-R curves.

The P-R curve of the Guadalquivir basin shows that a 10% reduction in the actual reliability would imply a 46% drop of the total production. This highlights the importance of the system management. Significant reduction of the reliability (40%) translates into very large production drops (84%), although supply only reduces 43%. This suggests that reallocation of the available water resources among users should be done if this situation arises.

REFERENCES

Andreu J, Capilla J, Sanchis E (1996) AQUATOOL, a generalized decision-support system for water-resources planning and operational management. J Hydrol 177:269–291. doi: 10.1016/0022-1694(95)02963-X

Berbel J, Mesa-Jurado MA, Pistón JM (2011) Value of Irrigation Water in Guadalquivir Basin (Spain) by Residual Value Method. Water Resour Manag 25:1565–1579. doi: 10.1007/s11269-010-9761-2

Bouman BAM, Lampayan RM, Tuong TP (2007) Water Management in Irrigated Rice : Coping with Water Scarcity.

Carrasco JM, Máximo Pistón J, Berbel J (2010) Evolución de la productividad del agua en la Cuenca del Guadalquivir 1989-2005. Econ Agrar y Recur Nat 10:59–69.

Chavez-Jimenez A, De Lama B, Garrote L, et al (2013) Characterisation of the sensitivity of water resources systems to climate change. Water Resour Manag 27:4237–4258. doi: 10.1007/s11269-013-0404-2

Chavez-Jimenez A, Granados A, Garrote L, Martín-Carrasco F (2015) Adapting Water Allocation to Irrigation Demands to Constraints in Water Availability Imposed by Climate Change. Water Resour Manag 29:1413–1430.

Dağdelen N, Yılmaz E, Sezgin F, Gürbüz T (2006) Water-yield relation and water use efficiency of cotton (Gossypium hirsutum L.) and second crop corn (Zea mays L.) in western Turkey. Agric Water Manag 82:63–85. doi: 10.1016/j.agwat.2005.05.006

Goldhmar D, Arpaia ML, Salinas M (2001) Evaluation of Regulated Deficit Irrigation on Mature Orange Trees Grown Under High Evaporation Demand.

Gonzales-Zeas D, Garrote L, Iglesias A, et al (2015) Hydrologic determinants of climate change impacts on regulated water resources systems. Water Resour Manag. doi: 10.1007/s11269-015-0920-3

Iglesias A, Garrote L, Diz A, et al (2011) Re-thinking water policy priorities in the Mediterranean region in view of climate change. Environ Sci Policy. doi: 10.1016/j.envsci.2011.02.007

Junta de Andalucía (2014) Observatorio de precios y mercados. Consejería de Agricultura, Pesca y Desarrollo Rural.

Kang S, Hao X, Du T, et al (2017) Improving agricultural water productivity to ensure food security in China under changing environment: From research to practice. Agric Water Manag 179:5–17. doi: 10.1016/j.agwat.2016.05.007

MAGRAMA-CHG (2013) Ministerio de Agricultura, Alimentación y Medio Ambiente-Confederación Hidrográfica del Guadalquivir. Plan hidrológico del Guadalquivir 2009-2015.

Molden D, Oweis T, Steduto P, et al (2010) Improving agricultural water productivity: Between optimism and caution. Agric Water Manag 97:528–535. doi: 10.1016/j.agwat.2009.03.023

Moriana A, Orgaz F (2003) Yield responses of a mature olive orchard to water deficits. J Am Sociaty Hortic Sci 128:425–431.

Rodríguez N, Sánchez MT, López J (2008) Un análisis de la eficiencia socioeconómica del agua en el regadío andaluz. Rev Española Estud Agrosociales y Pesq 217:183–208.

Rodríguez Díaz J, Weatherhead E, Knox J, Camacho E (2007) Climate change impacts on irrigation water requirements in the Guadalquivir river basin in Spain. Reg Environ Chang 7:149–159. doi: 10.1007/s10113-007-0035-3

Stewart JI, Cuenca RH, Pruitt WO, et al (1977) Determination and Utilization of water production functions for principal California crops. W- 67 Calif. Contrib. Proj. Rep. University of California, Davis.

Zhang H, Oweis T (1999) Water–yield relations and optimal irrigation scheduling of wheat in the Mediterranean region. Agric Water Manag 38:195–211. doi: 10.1016/S0378-3774(98)00069-9

Proceedings of the 10th World Congress of EWRA 'Panta Rhei', 5-9 July 2017, Athens, Greece
© 2017 *European Water Resources Association*

Water Footprint for cotton irrigation scenarios utilizing CROPWAT and AquaCrop models

M. Zoidou, I.D. Tsakmakis, G.D. Gikas* and G. Sylaios
Laboratory of Ecological Engineering & Technology, Department of Environmental Engineering, School of Engineering, Democritus University of Thrace, 67100 Xanthi, Greece
* *e-mail: ggkikas@env.duth.gr*

Abstract: Water Footprint is a recently-introduced theoretical concept, estimating the amount of water needed to produce each of the goods and services we use. In agriculture, water footprint of a given cultivar is estimated by the water volume of plants' potential evapotranspiration per final crop yield unit. Many studies have been conducted to determine the Water Footprint of various crops in different countries, utilizing various models and datasets ranging from national to regional levels. In this study, we used two FAO agronomic models named CROPWAT and AquaCrop to estimate the annual water footprint of cotton cultivation in Northern Greece for the period 2013 to 2016. Field data obtained from a precision irrigation experiment at farm scale level were used. Both models were executed under full and deficit irrigation strategies. Results showed that there exist substantial differences between the estimations produced by the two models regarding the cotton potential evapotranspiration. Differences were also observed in the case of water footprint estimation by the two models. These differences (about 200 m^3/tn) were more evident under the full irrigation scenario and almost negligible (about 30 m^3/tn) when deficit irrigation was implemented. Lastly, it was confirmed that precision irrigation could contribute significantly to the reduction of cotton water footprint.

Key words: CROPWAT Model, AquaCrop model, Water footprint, Evapotranspiration

1. INTRODUCTION

Nowadays, the agricultural sector is responsible for the consumption of roughly 70% of the total global fresh water withdrawals annually (Tsakmakis et al., 2017). Climate change is expected to exacerbate the pressure in the planet's available water resources with a parallel increase in the irrigation water requirements by up to 70-90% until 2050 (Garrote et al., 2015; Kreins et al., 2015). As a result, the shortage of the existing resources threatens the stability of the agricultural crop production and overwhelms the planet's food security in the near future. One of the potential prospects promising to alleviate the increasing water scarcity is to exploit the irrigation water in a more sustainable way. Water footprint (WF) is a recently-introduced theoretical concept, estimating the amount of water needed to produce each of the goods and services we use (Hoekstra, 2003). In agriculture, the water footprint of a given crop is the ratio of plants potential evapotranspiration divided by the final crop yield. This ratio can be used as an index of irrigation water rational use. The total volume of agricultural water consumed for crop production is the sum of the blue and green water footprints (Hoekstra, 2003; Zeng et al., 2012). Blue water footprint refers to the volume of surface and groundwater consumed (evaporated) during the production of a good or service; green water footprint refers to the rainwater consumed (Hoekstra, 2009). Many studies have been conducted to determine the water footprint of various crops in different countries, utilizing various models and datasets ranging from national to regional levels, providing estimates of the current status (Hoekstra and Mekonnen, 2012; Cao et al., 2014; Chukalla et al., 2015). In this paper two FAO agronomic models are used named CROPWAT and AquaCrop in order to estimate the annual water footprint of cotton in Northern Greece for the period 2013 to 2016, using data obtained from a precision irrigation experiment conducted in the area at farm scale. The models were run for full irrigation and deficit irrigation scenarios and the differences between the two models' estimates, as well as the potential improvement in the Water Footprint under deficit irrigation management, are presented.

2. METHOD AND MATERIALS

2.1 The agronomic models CROPWAT and AquaCrop

The CROPWAT model (FAO, 2009) utilizes the concepts of reference evapotranspiration (ET_o) and crop coefficient, introduced by Allen et al. (1998), in order to estimate the water requirements of a crop for different climate conditions and soil profiles. The model requires: (a) a soil file, where the saturated hydraulic conductivity (K_{sat}) and the available to root zone water content are defined; (b) a crop file, where the duration of the different cultivar development stages, the corresponding crop coefficients (Kc), the planting and harvest dates as well as the yield response factor (YRf) to potential water stresses are imported. Then, the model solves the water balance equation (Allen et al., 1998) utilizing daily ET_o, precipitation and irrigation data as inputs. The most substantial results obtained from CROPWAT simulations are the actual (ET_{cadj}) and potential (ET_c) crop evapotranspiration, effective rainfall and the total gross and net irrigation water. A drawback is that the model is incapable to estimate the final crop production, although it evaluates roughly the reduction in the cultivars potential yield when deficit irrigation is applied.

More recently, FAO introduced the AquaCrop model, a water driven model able to simulate the annual growing cycle of grains, vegetables and root-tuber crops (Raes et al., 2009; Steduto et al., 2009). Similarly to CROPWAT, the model is based partially to the work of Allen et al. (1998), but it also incorporates the relatively novel concept of crop Water Productivity (WP) in order to transform the estimated crop evapotranspiration to final crop yield (Steduto et al., 2007). The data requirements are very similar to those of CROPWAT regarding the climate data, but more detailed information is needed for soil and crop files, making AquaCrop a more sophisticated model. For instance, the soil profile could be divided in up to 5 soil horizons with different hydraulic characteristics each, while the crop file describes details about the cultivar's root maximum depth and growing patterns. Consequently, the output results of AquaCrop except from the water balance data (evapotranspiration, irrigation, rainfall) include information regarding the crop's final dry aboveground biomass and yield.

A key difference between the two models is observed on the crop potential evapotranspiration (ET_c) calculation process. CROPWAT estimates ET_c by multiplying the daily ET_o values with a specific cultivar crop coefficient (K_c), as:

$$ET_c = K_c \times ET_o \tag{1}$$

On the other hand the AquaCrop model calculates the ET_c as the sum of crop potential evaporation (E_c) and crop potential transpiration (Tr_c)

$$ET_c = E_c + Tr_c \tag{2}$$

$$E_c = K_r \times K_e \times ET_o \tag{3}$$

$$Tr_c = K_S \times Kc_{Tr} \times ET_o \tag{4}$$

where: K_r is the evaporation reduction coefficient, fluctuating between 0 and 1, with lower values to occur when insufficient water is available in the soil to respond to the evaporative demand of the atmosphere; K_e is the soil evaporation coefficient being proportional to the fraction of the soil surface not covered by canopy, ranging between 0 – 1; K_s is the soil water stress coefficient (0 – 1); Kc_{Tr} is the crop transpiration coefficient (0 – 1).

The meteorological and soil data used for the models' simulations in the current work were obtained during a precision irrigation project, named FIGARO, carried out in a field located at

Xanthi coastal plain in Northern Greece (41.046°N; 24.892°E; 13 m altitude). The field was cultivated with cotton (*Gossypium hirsutum L.*) from 2013 to 2016 (Tsakmakis et al., 2017). The intensive rainfalls during 2014 cultivation period resulted in no cotton production and thus the data from this season were excluded.

Regarding the crop files, the AquaCrop was calibrated and validated under the deficit irrigation practices which were applied within the FIGARO project. In the case of CROPWAT, crop coefficients and yield response factors proposed by Allen et al. (1998) for the cotton different growing stages were utilized (initial stage K_c=0.15, YRf=0.20; mid-season K_c=1.15, YRf=0.5; harvest K_c=0.5, YRf=0.85), while the corresponding length of each stage was based on the observations of FIGARO project.

Initially the models were executed for deficit irrigation schedules. The amounts of irrigated water and the exact days for these schedules were obtained from FIGARO project. Consequently, an irrigation scenario corresponding to a full irrigation treatment was created. According to it every time the depletion level in the root zone dropped by 1% a theoretical irrigation event was triggered to refill the soil water content back to its field capacity. Then, the models were run again for the three cultivation periods. For both full and deficit irrigation schedules the total gross and total net irrigation amounts were considered to be equal, as the irrigation system utilized was a drip system with negligible losses.

Consequently, utilizing the models results, the green and blue component of crop water requirements (CWR) are calculated by accumulated data on daily crop evapotranspiration ET_c (mm/day) over the complete growing period.

$$CWR_{green} = 10 \times \sum_{d=1}^{lp} ET_{green} \tag{5}$$

$$CWR_{blue} = 10 \times \sum_{d=1}^{lp} ET_{blue} \tag{6}$$

where ET_{green} represents the rainwater lost by evapotranspiration (green water) (mm/d) and ET_{blue} the irrigated and soil water lost by evapotranspiration (blue water) (mm/d) during the cultivation period. The factor 10 is used to convert water depths in millimetres into water volumes per land surface in m^3/ha. The summation is done over the period from the planting day (d=1) to the day of harvest (d=lp; lp is the length of growing period in days).

2.2 Water footprint

The green component of water footprint for growing a crop ($WF_{crop,green}$, m^3/tn) is calculated as the green component in crop water requirements (CWR_{green}, m^3/ha) divided by the crop yield (Y, tn/ha). Similarly, the blue component of water footprint ($WF_{crop,blue,}$ m^3/tn) is defined as the ratio of the blue component in crop water requirements (CWR_{blue}, m^3/ha) against crop yield:

$$WF_{crop,green} = \frac{CWR_{green}}{Y} \tag{7}$$

$$WF_{crop,\mathrm{blue}} = \frac{CWR_{blue}}{Y} \tag{8}$$

The green crop water requirement represents the total rainwater evaporated from the field during the growing period and the blue crop water requirement represents the total irrigation water evaporated from the field. In the case of deficit irrigation scenarios the yield was considered equal

to the annual seed cotton yield measured each year during the FIGARO project. When the full irrigation scenario was implemented, the simulated cotton yield value produced by AquaCrop was used.

The water footprint of the process of growing crops or trees ($WF_{crop,}$ m^3/tn) is the sum of the green and blue components (Hoekstra et al. 2011):

$$WF_{crop} = WF_{crop,green} + WF_{crop,blue} \tag{9}$$

3. RESULTS

The simulation results obtained from the two models are presented in Table 1. For all seasons AquaCrop model estimated a significantly higher crop potential evapotranspiration for both full and deficit irrigation scenarios. This difference was found to be 81 ± 16.4 mm and 159 ± 45.9 mm under full irrigation and deficit irrigation scenarios, respectively. It is noteworthy that the ET_c was found to be the same through the same year in both irrigation scenarios by CROPWAT, while the ET_c under deficit irrigation was always higher according to AquaCrop. These discrepancies between the models are attributed to the different equations utilized by each model during evapotranspiration calculation process (equations 1 to 4). The difference observed between the two irrigation regimes within the same year from AquaCrop are ascribed to the soil evaporation coefficient K_e. The deficit irrigation resulted in lower canopy cover values and larger fractions of non-covered soil surface. As a result the difference between full and deficit irrigation schedule increases as the amount of irrigated water was reduced. In 2016 only 184 mm of irrigated water was applied, raising the difference between full and deficit strategies to 193 mm. In 2013 and 2015 when 227 mm and 303 mm were applied on the field these differences were lowered to 177 and 107 mm, respectively.

Table 1. CROPWAT and AquaCrop water-balance results for each cultivation period.

Year	Parameter	CROPWAT		AquaCrop	
		Full	Deficit	Full	Deficit
2013	Total Rainfall (mm)	142.6	142.6	142.6	142.6
	Effective Rainfall (mm)	3.7	140.9	121.2	141.7
	Efficiency Rain (%)	2.6	98.9	85.0	99.4
	Total Net Irrigation (mm)	720.1	227.0	682.7	227.0
	Potential crop evapotranspiration ET_c (mm)	719.2	719.2	781.5	896.4
	Actual crop evapotranspiration ET_{cadj} (mm)	719.2	508.2	795.7	513.2
2015	Total Rainfall (mm)	195	195.4	148.6	148.6
	Effective Rainfall (mm)	4.1	189.1	121.7	144.0
	Efficiency Rain (%)	2.1	96.8	81.9	96.9
	Total Net Irrigation (mm)	602.3	302.0	583.8	303.0
	Potential crop evapotranspiration ET_c (mm)	601.8	601.8	687.7	708.5
	Actual crop evapotranspiration ET_{cadj} (mm)	601.8	547.8	674.4	541.5
2016	Total Rainfall (mm)	164.8	164.8	164.8	164.8
	Effective Rainfall (mm)	4.0	100.8	135.0	160.0
	Efficiency Rain (%)	2.4	61.2	81.9	97.1
	Total Net Irrigation (mm)	670.2	184.0	649.7	184.0
	Potential crop evapotranspiration ET_c (mm)	669.5	669.5	763.4	862.5
	Actual crop evapotranspiration ET_{cadj} (mm)	669.5	453.4	749.1	491.7

The seed cotton yield at the end of the 2013, 2015 and 2016 cultivation periods was measured at 3.39, 3.97 and 3.55 tn/ha, respectively. The corresponding AquaCrop estimations for these three seasons were 3.28, 3.81 and 3.2 tn/ha. The model seems to perform satisfactorily under deficit irrigation, with a mean deviation from the measured yields equal to 0.21 ± 0.13 tn/ha. Taking into consideration this robust model performance, the simulated potential seed cotton yields in the full irrigation scenario were assumed as reasonable. The estimated yields for the three years were 4.7, 4.2 and 4.5 tn/ha, respectively. Comparing the potential with the measured yields, reductions equal to 27.8%, 5.5% and 27.9% for 2013, 2015 and 2016, respectively, were observed. The

corresponding estimated yield reductions by CROPWAT were 30.4%, 6.5% and 32.6%.

The calculation of the blue, green and total water footprint of the two models are presented in Table 2. For all seasons CROPWAT model estimated a lower green WF for the full irrigation scenario. This mostly attributed to the fact that according to CROPWAT the crop firstly fulfills its water needs with irrigation water and then uses the rain water (Hoekstra et al., 2011). As a result almost 98% of rain water is lost as surface runoff or percolation. On the other hand, AquaCrop uses 98% of rain water for the crop needs, so the estimated green WF is higher than that of CROPWAT. For the full irrigation scenario, AquaCrop estimated lower blue WF values, while for deficit irrigation strategy both models estimated similar blue WF values.

Table 2. Cotton blue, green and total water footprint under full and deficit irrigation scenarios for the three cultivation years.

Year	Parameter (m^3/tn)	CROPWAT		AquaCrop	
		Full	Deficit	Full	Deficit
2013	WF_{green}	7.9	430.6	257.9	433.1
	WF_{blue}	1532.1	693.8	1452.6	693.8
	WF_{total}	1540.0	1124.4	1710.4	1126.8
2015	WF_{green}	9.7	477.8	287.4	363.8
	WF_{blue}	1422.5	763.0	1378.8	765.5
	WF_{total}	1432.2	1240.8	1666.3	1129.4
2016	WF_{green}	8.9	332.8	300.7	528.9
	WF_{blue}	1492.7	608.3	1447.0	608.3
	WF_{total}	1501.6	941.5	1747.7	1137.2

The mean WF_{total} under full irrigation scenario was estimated equal to 1,431 ± 54.6 m^3/tn and 1,708 ± 40.6 m^3/tn by CROPWAT and AquaCrop, respectively. This substantial difference of approximately 200 m^3/tn is a result of discrepancies introduced in the ET_c calculation. However, this difference was found to be considerably lower in the case of deficit irrigation (~ 30 m^3/tn). Moreover, according to AquaCrop, the deficit irrigation strategy has the potential to reduce cotton's WF_{total} more extensively than CROPWAT.

In a similar study, Chapagain and Hoekstra (2004) calculated cotton WF_{total} under full irrigation for different countries around the globe. They estimated values equal to 1,534 m^3/tn for Greece, 1,325 m^3/tn for Spain and 2,320 m^3/tn for Turkey. Their estimations for Greece and Spain were very similar to the findings of the current work.

The deficit irrigation strategy followed in 2015 highlighted its potential to reduce substantially cotton's WF_{total} by 191 m^3/tn and 536 m^3/tn (based on CROPWAT and AquaCrop, respectively). Deficit irrigation managed to save water with only a minor decrease in the seed cotton production (~ 6%).

4. CONCLUSION

In this study we evaluated the rational use of cotton irrigated water in Northern Greece, under full and deficit irrigation strategies, using two widely-used FAO agronomic models and applying the well-known water footprint concept. Under the full irrigation strategy, the CROPWAT model estimated lower Green WF than AquaCrop, but the opposite occurred in the case of blue WF. On the other hand, when deficit irrigation was implemented, the estimated by the two models blue WF was almost similar. As a result, AquaCrop estimated higher WF_{total} values under full irrigation and almost similar results under deficit irrigation strategy. CROPWAT's WF_{total} estimations under full irrigation were comparable to those of a previous study conducted for different countries around the world. The novelty of the present work lies in the fact that AquaCrop model has never been used as a tool to estimate the cotton water footprint.

REFERENCES

Allen, R.G., Pereira, L.S., Raes, D., Smith, M., 1998. Crop evapotranspiration: guide-lines for computing crop water requirements. In: FAO Irrigation and DrainagePaper 56. Food and Agriculture Organization, Rome.

Chapagain, A.K. and Hoekstra, A.Y., 2004.Water footprints of nations.Value of Water Research Report Series No. 16,UNESCO-IHE, Delft, the Netherlands, www.waterfootprint.org/Reports/Report16Vol1.pdf.

Chapagain, A.K. and Hoekstra, A.Y., 2004.Water footprints of nations.Value of Water Research Report Series No. 16,UNESCO-IHE, Delft, the Netherlands, www.waterfootprint.org/Reports/Report16Vol2.pdf.

Chukalla, A. D., Krol, M. S., Hoekstra, A., Y., 2015. Green and Blue water footprint reduction in irrigated agriculture: effect of irrigation techniques, irrigation strategies and mulching. Hydrol. Earth Syst. Sci., 19: 4877-4891.

Garrote, L., Iglesias, A., Granados, A., Mediero, L., Martin-Carrasco, F., 2015.Quantitative Assessment of Climate Change Vulnerability of Irrigation Demands in Mediterranean Europe. Water Resour. Manag., 29: 325-338. doi:10.1007/s11269-014-0736-6

Hoekstra, A.Y., Chapagain, A. K., Aldaya, M. M., Mekonnen, M. M., 2011. The Water Footprint Assessment Manual: Setting theGlobal Standard. Washington, D.C.: Earthscan.

FAO 2009.Cropwat 8.0 for windows user guide. Rome, Italy.

Kreins, P., Henseler, M., Anter, J., Herrmann, F., Wendland, F., 2015.Quantification of Climate Change Impact on Regional Agricultural Irrigation and Groundwater Demand. Water Resour. Manag., 29:3585-3600.doi:10.1007/s11269-015-1017-8

Raes, D., Steduto, P., Hsiao, T. C., Fereres, E., 2009.AquaCrop—The FAO Crop Model to Simulate Yield Response to Water: II. Main Algorithms and Software Description. Agronomy J. 101. doi:10.2134/agronj2008.0140s

Steduto, P., Hsiao, T. C.,Fereres, E., 2007. On the conservative behaviour of biomass water productivity. Irrig. Sci., 25: 189-207.

Steduto, P., Hsiao, T. C., Raes, D., Fereres, E., 2009.AquaCrop—The FAO Crop Model to Simulate Yield Response to Water: I. Concepts and Underlying Principles.Agronomy J. 101. doi:10.2134/agronj2008.0139s

Tsakmakis, I., Kokkos, N., Pisinaras. V., Papaevangelou, V., Hatzigiannakis, E., Arampatzis, G., Gikas, G.D., Linker, R., Zoras, S., Evagelopoulos, V., Tsihrintzis V.A., Battilani, A., Sylaios, G., 2017. Operational Precise Irrigation for Cotton Cultivation through the Coupling of Meteorological and Crop Growth Models. Water Resour. Manag., 31: 563-580.

Proceedings of the 10th World Congress of EWRA 'Panta Rhei', 5-9 July 2017, Athens, Greece
© 2017 *European Water Resources Association*

Mathematical analyses of water management's effects on rice productions: A case study of Mae Kuang Udom Thara Dam, Thailand

C. Likasiri* and E. Duangdai
Department of Mathematics, Faculty of Science, Chiang Mai University, Chiang Mai 50200, Thailand
* *e-mail: chulin.l@cmu.ac.th*

Abstract: This research involves an empirical mathematical model on irrigation water management, rice productions and GDP from rice export. The model is constructed based on a system of linear difference equations to represent the dynamic relationship between water inflows and outflows from Mae Kuang Udom Thara dam, rice productions in the irrigation area, and GDP from rice export. The data used to verify the model are the monthly discharge amounts and the amounts of water flowing into Mae Kuang Udom Thara dam, annual rice productions, and GDP from the rice export sector. All data were collected during 2011-2015. Most of the terms contained in the constructed model have correlation coefficients higher than 0.5. Using the nonlinear optimization to find the parameters minimizing the sum squared error between actual data and solutions from the proposed model, correlation coefficients of water inflow, water outflow, main and second rice crops and GDP from the rice exporter sector are 0.8203, 0.8647, 0.9999, 0.9999, and 0.9659 respectively. According to the correlation coefficients, we can conclude that the model created under our hypotheses can be used to predict water inflow, water outflow, rice production and GDP from the rice export sector since the coefficient correlations of the model solution and the corresponding data are all higher than 0.8.

Key words: water inflow, water outflow, main rice crop, second rice crop, GDP, difference equation

1. INTRODUCTION

Farmland constitutes 41.2 % of Thailand's total area, or about 149 million *rai* (1 *rai*=0.16 ha) (Supasod). Rice producing areas account for some 69 million *rai* and produce, on average, a total of 30 million tons of rice per annum (DAE, TREA). In the year 2014, there were over 3 million rice farmer households nationwide, or 16.3% of total number of households (OAE(a)). During the years 2012-2015, Thailand ranked in the top three of the world's rice exporters (TREA)**.** In 2015 alone, the country exported 173 billion baht's worth of rice, second in value only to rubber that year. Roughly one-fourth of the world's exported rice comes from Thailand; see more details in Table 1 (OAE(b), TREA).

Rice farming requires water from the earliest stages, soil preparation, to right before harvesting. The average rainfall suitable for rice production is 1,400-1,600 millimeters, and anything less will affect both the quality and the quantity of the production (BACPM). In Thailand, around 85% of rice farming takes place during May-October. This main rice crop relies heavily on natural rainfalls. The second rice crop, farmed during November through March, relies on irrigation water (Petchseechoung, 2016)**.** The annual streamflow is 215,000 million cubic meters, but only 72 billion cubic meters is stored, as there are only 85 reservoirs larger than 10,000 rai and 745 reservoirs of 9,000-rai capacity, the remaining 1,000-plus reservoirs being small community reservoirs (Supasod). Crop production is often affected by drought. For example, in the year 2015, drought caused by El Niño led to a decrease in all major agricultural exports (Dhirawiroon, 2015).

Existing literature features models to predict crop production, such as the rice yield prediction model based on artificial neural network (Kunlerd and Seresangtakul, 2014), model to predict rubber production using statistical methodology (Jatuporn and Sukprasert, 2016), crop prediction model for rice production (Koide et. al., 2012), ARIMA model for forecasting areas and rice production (Prabakaran and Sivapragasam, 2014), CERES-Rice model for rice production

(Akinbile, 2013), regression and neural network models for forecasting of crop production (Paswan and Begum, 2013), remote sensing and agrometeorological models for forecasting crop inventory and production (Sharifi, 2000), and seasonal regression model for forecasting crop production (Habyarimana, 2014). However, given that good irrigation management will greatly affect crop production, especially at economic scales, we are interested in models that involve irrigation and crop (in this case, rice, since the study areas are rice farming areas) production, which ultimately affects national GDP.

Table 1. Top 5 rice exporter nations

Unit: million ton	2012	2013	2014	2015
India	10.65	10.57	10.81	10.23
Thailand	6.97	7.05	10.97	9.79
Vietnam	7.73	6.75	6.41	6.61
Pakistan	3.65	3.43	3.32	3.91
USA	3.33	3.40	3.20	3.61

2. DATA COLLECTION

The study area in this research is farmland in Chiang Mai's Doi Saket and San Sai Districts, whose irrigation water comes from Mae Kuang Udom Thara Dam (see figure 1). All data were collected during 2011-2015. The rice production data (in tons) consist of main and second rice crops. The GDP from rice export are collected in million baht and the water inflow and outflow of the Udom Thara Kuang Dam are in million cubic meters.

Rice production data are collected by the Office of Agricultural Economics on an annual basis (OAE(c)). The production of the main rice crop is recorded in November, and that of the second crop in April. GDP of rice in the study area is collected by the National Statistical Office (NSO). We obtained Chiang Mai's GDP data and then calculated the GDP of rice production using the ratio of rice exported in the year 2015. The rice GDP data are also collected on an annual basis and recorded in December.

Water inflow and water outflow data are collected by the Water Watch and Monitoring System for Warning Center, Royal Irrigation Department (RID). We retrieved the data on a monthly basis. All data were normalized by dividing them with their maximum possible value, i.e. 40,000 tons for rice production, 4.5 billion baht for GDP and 115 million cubic meters for water inflow and water outflow.

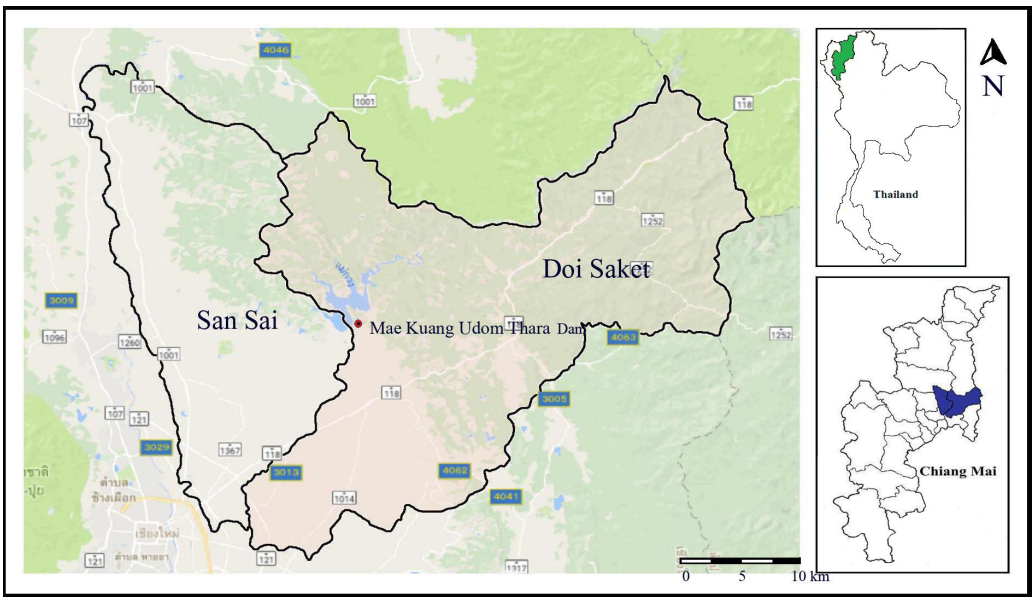

Figure 1. Geography of study area.

3. MAIN RESULTS

3.1 Model constructions

We constructed the model under the following hypotheses:

Let k be the month index and i be the year index.

1) The water inflows in the kth month relates to the water inflows in some previous months.
2) The water outflows in the kth month relates to the water inflows and water outflows in some previous months.
3) Main rice crop production in the ith year relates to the main rice crop production of the previous year, the second rice crop of that year, and water inflows and outflows of some previous months.
4) The second rice crop production in the ith year relates to the main and second rice crop productions of the previous year, and the water inflows and outflows of some previous months.
5) GDP in the ith year relates to the main and second rice crop productions of that year and the GDP of the previous year.

3.2 Variable definitions

Let WI be water inflows, WO be water outflows, MR be main rice crop production, SR be second rice crop production, and G be GDP from rice production.

We are interested in including the terms with medium (0.15-0.49) to high (> 0.5) correlation coefficients in the model. Hence, the correlations between each pair of variables in the hypotheses are studied. Table 2 below shows the correlation coefficients of those inclusion pairs.

Hence, the model should look like this:

$$
\begin{aligned}
WI(k+1) &= \sum_{j=0}^{2} a_j WI(k-j) + a_3 WI(k-11) \\
WO(k+1) &= \sum_{j=0}^{3} b_j WI(k-j) + \sum_{j=0}^{2} c_j WO(k-j) + c_3 WO(k-11) \\
MR(12i+11) &= \sum_{j=2}^{8} d_j WI(12i+j) + \sum_{j=5}^{8} e_j WO(12i+j) + fMR(12(i-1)+11) + gSR(12i+4) \\
SR(12i+4) &= \sum_{j=8}^{12} h_j WI(12(i-1)+j) + \sum_{j=1}^{2} k_j WI(12i+j) + \sum_{j=11}^{12} m_j WO(12(i-1)+j) \\
&\quad + \sum_{j=1}^{2} n_j WO(12i+j) + p_1 MR(12(i-1)+11) + p_2 SR(12(i-1)+4) \\
G(12i+12) &= q_1 MR(12i+11) + q_2 SR(12i+4) + q_3 G(12(i-1)+12)
\end{aligned}
\tag{1}
$$

3.3 Main results

The parameters to minimize the sum squared errors between the actual data and the predicted data can be found with the results shown in Table 3. The correlation coefficients *(r)* of water inflow, water outflow, main rice crop, second rice crop and GDP are 0.8203, 0.8647, 0.9999, 0.9999, and 0.9659 respectively. The sum squared errors of those are 0.6597, 0.2527, 8.0224e-11, 1.1774e-12, and 0.0223 respectively. Since all correlation coefficients are higher than 0.8, we can say that the model (1) with all parameter values as in Table 3 can represent the relationships between water

inflows and outflows (i.e. water irrigations), rice productions and GDP.

Table 2. Correlations between variables under the hypotheses

r	$WI(i+1)$	$WO(i+1)$	$MR(12i+11)$	$MR(12(i+1)+11)$	$SR(12i+4)$	$SR(12(i+1)+4)$	$G(12i+12)$
$\sum_{j=0}^{2} WI(i-j) + WI(i-11)$	0.5333						
$\sum_{j=-1}^{2} WI(i-j)$		0.2608					
$\sum_{j=0}^{2} WO(i-j) + WO(i-11)$		0.3497					
$\sum_{j=2}^{8} WI(12i+j)$			0.4911				
$\sum_{j=5}^{8} WO(12i+j)$			0.6632				
$\sum_{j=8}^{12} WI(12(i-1)+j) + \sum_{j=1}^{2} WI(12(i+1)+j)$					0.7616		
$\sum_{j=11}^{12} WO(12(i-1)+j) + \sum_{j=1}^{2} WO(12(i+1)+j)$					0.5093		
$MR(12i+11)$				0.9397		0.5520	0.5661
$SR(12i+4)$			0.1596			0.2830	0.9719
$G(12i)$							0.6963

Table 3. Parameters to minimize errors between actual data and predicted data

WI	WO	MR	SR	G
$a_0 = 0.9043$	$b_0 = 0.6151$	$d_2 = 0.1520$	$h_8 = -0.5300$	$q_1 = 0.2724$
$a_1 = -0.3283$	$b_1 = -0.3933$	$d_3 = 0.1553$	$h_9 = -0.5020$	$q_2 = -0.5543$
$a_2 = 0.0572$	$b_2 = -0.1766$	$d_4 = 0.1712$	$h_{10} = 1.2598$	$q_3 = 1.5468$
$a_3 = 0.2718$	$b_3 = 0.3785$	$d_5 = 0.2825$	$h_{11} = 0.2352$	
	$c_0 = 0.4614$	$d_6 = 0.1751$	$h_{12} = 0.1930$	
	$c_1 = -0.0089$	$d_7 = 0.3425$	$k_1 = 0.4281$	
	$c_2 = 0.0306$	$d_8 = 0.3599$	$k_2 = 1.1723$	
	$c_3 = 0.1006$	$e_5 = -0.0184$	$m_1 = 0.0883$	
		$e_6 = 0.2858$	$m_2 = -0.7427$	
		$e_7 = 0.1192$	$n_1 = 1.2531$	
		$e_8 = 0.3798$	$n_2 = 1.1236$	
		$f = 0.8397$	$p_1 = 0.2868$	
		$g = -0.1312$	$p_2 = -0.0448$	

3.4 Model prediction

Using the Model, rice productions are predicted in the year 2018. Main rice crop production is projected to be 0.5844, which is equivalent to 23,377.98 million tons, second rice crop production is projected to be 0.2107 (8,428.82 million tons), projected GDP is 0.0457 (205.88 million Baht),

projected water inflow is 0.0289 (3.3272 million cubic meters) and projected water outflow is 0.0213 (2.4547 million cubic meters).

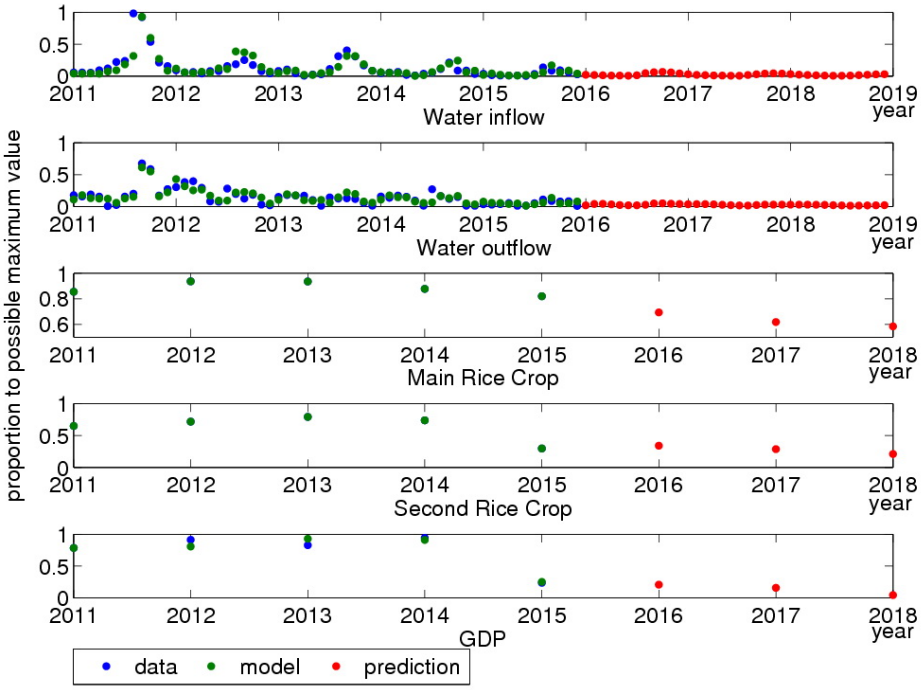

Figure 2. Estimated solutions of model (1)

4. CONCLUSIONS

We are interested in the water management of major dams in Northern Thailand that affect crop productions. The studied dam, Mae Kuang Udom Thara (263 million cubic meter capacity), is one of seven major dams in the region. The other six dams are Bhumibol (13,462 million cubic meters), Sirikit (9,510 million cubic meters), Khwaenoi Bamrungdaen (939 million cubic meters), Mae Ngut Somboon Chon (265 million cubic meters), Kio Kho Ma (170 million cubic meters) and Kio Lom (106 million cubic meters). We focus on rice production for three reasons: 1) rice is the most water-intensive crop in Thailand; 2) most of Thailand's agricultural households are rice farmers; and 3) rice is the country's major export product. We chose this particular dam because most of its irrigation area is farmland. Having verified that this preliminary model can represent the relationships between water irrigations, rice productions and associated GDP, we plan to extend the results to the irrigation of other major dams and to other economic crops including corn, sugarcane, cassava and soybean.

ACKNOWLEDGEMENT

This research is supported by the Department of Mathematics, Faculty of Science, Chiang Mai University. Appreciation is extended to the Centre of Excellence in Mathematics, CHE for providing financial support and to Ms. Wiriya Sungkhaniyom for proofreading.

REFERENCES

Akinbile, C. O., 2013. Assessment of the CERES-Rice model for rice production in Ibadan, Nigeria. Agric Eng Int: CIGR Journal; 15(1): 19-26.

BACPM, Bureau of Agricultural Commodities Promotion and Management. Plant Water Need Data. Available: www.agriman.doae.go.th/home/t.n/t.n1/1Copy_th1.1.html. [Accessed: Mar. 2017].

DAE, Department of Agriculture Extension. Agricultural Land Use. Available: www.agriinfo.doae.go.th/year59/general/land/land59.pdf. [Accessed: Mar. 2017].

Dhirawiroon, S., 2015. Sustainable Drought Solutions. Available: http://www.parliament.go.th/ewtadmin/ewt/parliament_parcy/ewt_dl_link.php?nid=28304. [Accessed: Mar. 2017].

Habyarimana, J. B., 2014. Forecasting crop production: A Seasonal Regression Model Decomposition of MAPE and SMAPE. Journal of Statistical Science and Application; 2: 203-212.

Jatuporn, C., Sukprasert, P., 2016. Forecasting models for rubber production and export quantity of Thailand. Khon Kaen Agr. J.; 44(2): 219-228.

Koide, N., Robertson, A. W., Ines, A. V. M., Qian, J. H., Dewitt, D. G., Lucero, A., 2012. Prediction of rice production in the Philippines using seasonal climate forecasts, Journal of Applied Methorology and Climatology; 52: 552-569.

Kunlerd, A., Seresangtakul, P., 2014. Rice yield prediction model based on Artificial Neural Network, The Tenth National Conference on Computing and Information Technology.

NSO, National Statistical Office, Ministry of Digital Economy and Society, Thailand. National Account. Available: http://service.nso.go.th/nso/web/statseries/statseries15.html. [Accessed: Mar. 2017].

OAE(a), Office of Agricultural Economics, Ministry of Agriculture and Cooperatives, Thailand. Main Rice Crop: Percentages and Numbers of Farming Households by Planted Acreage and Location. Available: http://www.oae.go.th/download/prcai/DryCrop/majorrice2556-57/2.pdf. [Accessed: Mar. 2017].

OAE(b), Office of Agricultural Economics, Ministry of Agriculture and Cooperatives, Thailand. Export Values of Major Agricultural Commodities: 2015-2016. Available: oae.go.th/oae_report/export_import/exp_topten.php?imex=2. [Accessed: Mar. 2017].

OAE(c), Office of Agricultural Economics, Ministry of Agriculture and Cooperatives, Thailand. Agricultural Commodities Production Data. Available: http://www.oae.go.th/ewt_news.php?nid=13577. [Accessed: Mar. 2017].

Paswan, R. P., Begum, S. A., 2013. Regression and Neural Networks Models for prediction of crop production, International Journal of Scientific & Engineering Research; 4(9): 98-108.

Petchseechoung, W., 2016. Rice Industry. Available: https://www.krungsri.com/bank/getmedia/2d2dcc81-eb88-43ed-9945-a90b509e58d7/IO_Rice_2016_TH.aspx. [Accessed: Mar. 2017].

Prabakaran, K., Sivapragasam, C., 2014. Forecasting areas and production of rice in India using ARIMA model, International Journal of Farm Sciences; 4(1): 99-106.

RID, Royal Irrigation Department, Ministry of Agriculture and Cooperatives, Thailand. Dam Water Level Status Report. Available: http://www.thaiwater.net/DATA/REPORT/php/rid_bigcm.php?sdate. [Accessed: Mar. 2017].

Sharifi, M. A., 2000. Crop inventory and production forecasting using remote sensing and agrometorological models: the case of major agricultural commodities in Hamadan Province, Iran. International Archives of Photogrammetry and Remote Sensing; 33: 1364-1372.

Supasod, W.. Water Resource Development Concepts for Agriculture. Available: http://www.rid.go.th/thaicid/_5_article/2549/03Water_Agri.pdf. [Accessed: Mar. 2017].

TREA, Thai Rice Exporter Association. Thai Rice Exporters Association News. Available:http://www.thairiceexporters.or.th/Press%20release/2016/TREA%20Press%20Release%20-%20January%202016%20-%2029012016.pdf. [Accessed: Mar. 2017].

Proceedings of the 10th World Congress of EWRA 'Panta Rhei', 5-9 July 2017, Athens, Greece
© 2017 *European Water Resources Association*

Correction and sensitivity analysis of Hargreaves - Samani model in the estimation of the reference evapotranspiration (case study: Gonabab city in Iran)

A. KhasheiSiuki*, F. Sarvari and M. PourrezaBilondi
Sciences and Water Engineering Dept., University of Birjand, Birjand, Iran
* *e-mail: abbaskhashei@birjand.ac.ir*

Abstract: According to the importance of evapotranspiration in water balance and supplying water requirement of the plant; this research aim to assess the corrective coefficients for Hargreaves-Samani model by using 22 years statistics of meteorological of synoptic station of Gonabad in Iran. The data series containing of 19 years were considered to estimate equations and remaining data (three years) was used to validate equations. Some equations including types of meteorological parameters were estimated by using SPSS software. equations that had better regression results were tested and two equations were selected among them which respectively with root mean squared error of 0.602 and 0.758 and Nash-Sutcliffe coefficient of 0.835 , 0.711 and determination coefficient of 0.858 , 0.776 showed that the close values to FAO Penman-Monteith than the Hargreaves methods. The first equation includes the average, maximum and minimum temperatures, actual hours of sunshine and maximum sunshine hours, the second equation has two parameters of temperature and wind speed in two meters height. In this research the two presented equations were analysed and the results showed that in the first model the evapotranspiration had relatively more sensitivity than the parameters of minimum and maximum temperatures and average temperature and in the second model both parameters of that were sensitive.

Key words: sensitivity analysis, evapotranspiration, corrective coefficient, FAO-Penman-Monteith, Gonabad

1. INTRODUCTION

Combining two separate processes which water has been removed from the soil surface as evaporation and from plant as transpiration, is called evapotranspiration. Because of evapotranspiration is one of basic components of hydrologic cycle, correct determination of that has high importance in water sciences such as hydrologic balance studies and water resources management. Evapotranspiration is estimated in direct methods of lysimeteric (pan evaporation) or indirect methods (empirical equations). In the case that it isn't possible to reach accurate data, FAO Penman Monteith can be used as the standard method to evaluate results of other empirical methods (Qamarnia et al., 2012). The concept of evapotranspiration was propounded in the framework of hydrological, geographical, climatological, biological and agricultural meteorology studies and in order to evaluate dryness periods in the regional, continental and global scales (Gong et al., 2006). The purpose of that was presenting scales or indexes to compare and classify time series' values of meteorological and climatic variables. Using evapotranspiration of reference plant (ETo) has a special and useful place in hydrological, agro-hydrological and also agricultural meteorology discussions and yet many researchers have been conducted about this concept (Lu et al., 2005 & Oudin et al., 2005; Donohoue et al., 2010; Weiss & Menzel, 2008; Pourali Baba and Shiri, 1991). The proper irrigation planning is one of ways to reduce water losses in the fields which its basis is accurate estimation of water requirements of plants. Equations that are used to calculate evapotranspiration of reference plant (ETo) are not suitable for all climatic conditions due to its empirical nature. So it is necessary was corrected the proper equation of each region (Pour Yazdankhah et al., 1991). Estimating evapotranspiration amount of reference plant is considered as one of very important cases in irrigation planning, determining water budget, planning farming

affairs and integrated management of agricultural systems (Pourali Baba & Shiri, 1991).

Based on the latest scientific information available in the world (Allen et al., 1998) the FAO-Penman-Monteith equation (FAO56-PM) is used as reference equation to estimate reference evaporation-transpiration and all models and different estimation equations and their accuracy are evaluated by values from this method (Pourali Baba & Shiri, 1991).

Many researches in all around the world have introduced the Penman-Monteith method as the most accurate method and a standard and valid method to calculate evapotranspiration of the reference plant (Suri, 2005). In another research they have evaluated models of evapotranspiration estimation for semi-arid regions with results of Lysimeter and they have suggested the Penman-Monteith model for these regions such as Karaj (Dehghani Sanij et al., 2004). In this research the basis of measuring the accuracy of all used models will be the reference equation of Penman-Monteith-Fao which this evaluation is formed through using some statistical parameters.

The Hargreaves-Samani method is from the results of Hargreaves and Samani during 1975 to 1982. The mentioned equation has been developed by using 8 years data of Davis California. Different evaluations especially in regions such as Aspendal Australia, Lompoc California, Seabrook New Jersey, Arizona, Damin Haiti and also compared with the corrected Penman method in different regions of Bangladesh show that the above equation presents a good evolution from evapotranspiration of reference plant (Jacovides & Kontoyiannis, 1995).

Some studies have been conducted in this field in Iran too, that it has corrected Hargreaves-Samani method based on the corrected Penman equation and Jensen Hayes for 64 regions of synoptic stations of Iran's Meteorological Organization. Evaluations show that correction of the mentioned equation with reference of Jensen Hayes for Isfahan industrial University station has suitable success (Khajezadeh, 1995; Najafi, 2006).

Hargreaves-Samani method is a simple method which needs few and common data in water resources projects in regions with no complete method statistic but despite suggestion of this model in some regions it doesn’t work in all climates. This issue is consistent according to this the Hargreaves-Samani method is thermal and effect of factors such as relative humidity, wind and sunshine duration and intensity have been not seen in it (Sharifan et al, 2012). In a research that 13 methods of potential evapotranspiration estimation were compared in synoptic station of Ardestan, results of evaluation indexes showed that best method is models of based on temperature and Hargreaves method (Ordibehesht & Samiei, 2013).

Two methods of Hargreaves-Samani and Jensen Hayes have a remarkable importance among different methods of estimation of reference evapotranspiration. Because in addition to they have a suitable relative accuracy in arid and semi-arid regions, also they need few meteorological data compared with other methods (Samani, 2000; Najafi, 2006).

Also with a research that was conducted in Santeh region in Kurdistan respectively Blaney Cradle, pan evaporation and Hargreaves methods have been determinate suitable to estimate evaporation-transpiration (Mirzaei Takhtgahi & Ma'azed, 2006). A research that was conducted to calculate values of monthly ETo in different climatic conditions of Iran showed that Hargreaves-Samani model has suitable accuracy in climatic conditions of warm-wet and cold-arid while this model has weak results in cold-wet climate (Tabari, 2009; Mosaedi & Qbaei Souq, 2013).

Estimation of water requirement is one of the most important stages of designing an irrigation system. Evaluating the effect of meteorology parameters in this estimation in addition to show the sensitivity of estimation models of evapotranspiration of reference plant can estimate water requirement of plants in different climatic conditions. Researches that have been conducted until now show that in various climatic conditions, responses (sensitivity) of evapotranspiration estimation models are not equal to meteorology parameters (Tafazzoli, 2006).

According to researches the sensitivity analysis of different models of ETo estimation especially Penman-Monteith- FAO model, the sensitivity had been relatively during year's days to various meteorology parameters and determination of coefficients (Allen et al., 1998, Estevez et al., 2009, Gong et al., 2006, McCuen, 1974, Qui et al., 1998). As the sample with sensitivity analysis of FAO-Penman-Monteith, thermal Hargreaves, Priestly Taylor, torque and radiant Hargreaves models in

three regions of ocean, subtropical and Mediterranean of France and to evaluate time changes of parameters of radiation, relative humidity, wind speed and temperature showed that time changes of climatic input parameters are strongly affected by type of climate.

Therefore empirical equations with related input data show different uncertainties in different under study regions (Ordibehesht & Samiei 2013; Bois et al., 2006). In another research sensitivity of data of temperature, relative humidity, solar radiation and wind speed were analyzed in standard equation of ASCE Penman- Monteith in 87 automatic stations in Andalusia Spain (Estevez et al., 2009).

Evaluations showed that a few studies have been conducted on correction of Hargreaves equation with above method in arid regions. The purpose of this research was determination of the most suitable correction coefficients for estimation of reference evapotranspiration with Hargreaves-Samani method to be able to use this relation with higher certainty and accuracy in evaporation measuring stations which number of quantitative parameters are measured. of course these coefficients are not constant values but it is introduced an equation including meteorological parameters as the correction coefficient which its value is changed with climatic conditions. This coefficient can be used for climates similar to the case study which is presented here.

2. MATERIALS AND METHODS

Data of this research has been obtained from 22 series meteorological data (1992-2014) of synoptic station of Gonabad. Gonabad city is in the center of Razavi Khorasan in 265 kilometers away of Mashhad; geographically it has longitude of 58 degrees and 41 minutes and latitude of 34 degrees 21 minutes. Gonabad region has arid and desert climate with warm summers and cold winters based on Domarten classification (Sokhanvar et al., 2013). The maximum temperature in this city is 47 degrees above zero in summer and its minimum is 17 degrees below zero in winter. Also the average annual precipitation is 140 mm in this region that it had been in oscillation between 48 to 240 mm in recent years (Sarvari et al, 2013).

From all available statistical period (22 years), 85% of data (19 years) were used for calibration and 15% of that (3 years) for test stage. According to meteorology data after determination of reference evapotranspiration for Hargreaves-Samani method (H.S) and also FAO-Penman-Monteith method (F.P.M); a relation of these two methods were calculated for all statistical data and for each day in calibration stage (k= (ETo F.P.M)/(ETo H.S)).

Then the equations were estimated in SPSS software in a form that in each stage various meteorology parameters such as relative humidity, wind speed, minimum and maximum temperatures and…as independent variables and K relation as the dependent variable, it presented us some equations based on these parameters. After this the obtained equations were multiplied in ETo H.S to obtain ETo values such as F.P.M. In the next stage the new ETos were compared by using F.P.M method as radix by using statistical indexes. Equations that had closer results remained and others were removed (Table 1).

The equations were corrected in test stage in Excel and in linear method and again the statistical indexes were evaluated, two equations that had better results than the H.S method were selected as correction coefficients. The used statistical indexes have been mentioned in Table 1.

In Table 1, N is number of data and Si is the predicted values of evapotranspiration and Q_i is real values of evapotranspiration and S is average of the predicted values of evapotranspiration and Q_i is average of real values of evapotranspiration. In this research the two presented equations were analysed in graph method. In this method the relative changes of independent variable (such as various meteorology parameters) are drawn to relative changes of dependent variables (reference evapotranspiration). The values of changes of independent variable were considered ±50%, ±40%, ±30%, ±20%, ±10% and 0%.

Table 1. The used statistical indexes in equations

Statistical parameter	Formula	Range	Ideal value
RMSE	$\sqrt{\frac{\sum_{i=1}^{N}(Si-Qi)^2}{N}}$	Infinity + to 0	0
R^2	$\frac{[\sum_{i=1}^{N}(Si-\bar{s})(Qi-\bar{Q})]^2}{\sum_{i=1}^{N}(Si-\bar{s})^2\sum_{i=1}^{N}(Qi-\bar{Q})^2}$	1 to-1	1
NS	$1-\frac{\sum_{i=1}^{N}(Si-Qi)^2}{\sum_{i=1}^{N}(Qi-\bar{Q})^2}$	1 to infinity -	1

3.RESULTS AND DISCUSSION

The obtained daily ETo values from H-S method were multiplied in the obtained coefficients in SPSS in order to evaluate the equations and then they compared with obtained daily ETo values from standard method (F-P-M). In Table 2, the first row is related to H-S method and other rows cover estimating equations. It should be noted that the available equations in Table 2 were selected among other equations because they had more desirable statistical results; means less RMSE and more NS than the H-S method. All available equations in Table 2 were corrected again in test stage in linear method and the results were evaluated.

Table 2. The corrected equations in validation period

NS	R^2	RMSE	Equations	Equations Name
-6.24	0.53	1.80	$0.0135\left(0.075*\sqrt{\frac{100\left(\frac{n}{N}\right)}{Tmax-Tmin}}\right)*Ra*\sqrt{Tmax-Tmin}*(Tmean+17.8)$	H-S
0.71	0.77	0.75	$0.5055*\left(ETo\ HS*(0.086Tmean+0.053U_2^2)\right)+0.6387$	FPM-1*
-11.10	0.85	1.49	$0.3674*\left(ETo\ HS(0.067Tmean+0.052U_2^2+RH)\right)+0.9896$	FPM-2*
0.51	0.67	0.91	$0.5706*\left(ETo\ HS(0.066Tmean+0.052U_2^2+1.05RH)\right)+0.4745$	FPM-3*
0.58	0.70	0.86	$0.5489*\left(ETo\ HS(0.075Tmean+0.052U_2^2+1.344RH^2)\right)+0.5107$	FPM-4*
0.66	0.74	0.80	$0.5222*\left(ETo\ HS(0.093Tmean+0.049U_2^2+1.594RH^2-0.036n)\right)+0.5544$	FPM-5*
-21.04	0.04	1.56	$0.0215*(ETo\ HS(0.071Tmax+0.002Tmin^2-2.554*10^{-6}Tmen^4+1.66RH^5+1.281*10^{-5}U_2^6))+2.4851$	FPM-6*
0.83	0.85	0.60	$1.2666*\left(ETo\ HS\left(0.055(Tmax-Tmin)-0.323\left(\frac{n}{N}\right)^{0.5}+0.147\left(\frac{Tmean}{2}\right)\right)\right)+0.1062$	FPM-7*

In Table 2, number of actual hours of sunshine is N, the maximum possible sunshine hours is Tmax, maximum temperature (centigrade grade), Tmin is minimum temperature (centigrade grade), Ra is the radiation entry into the atmosphere (mm/day), Tmean is average temperature (centigrade grade), U2 is wind speed in height of two meters in (meter on second) and RH is relative humidity. It is resulted from statistical results of available equations in Table 3 that FPM-7* equation has the most accuracy. This equation has less RMSE value than the others and although it has less R^2 than some models but due to more NS that has than the other equations the slight difference of its R^2 with other equations can be ignored. The same conditions are applied for FPM-1* equation but it is situated in the second priority with very close difference than the FPM-7* equation. From this

perspective equations of FPM-3*, FPM-4* and FPM-5* are situated in next classes. Equations of FPM-6* and FPM-2* and H-S have the least accuracy than the other equations due to high RMSE and very low R^2 and NS that they have. So two equations of FPM-1* and FPM-7* were presented to correct the Hargreaves-Samani method. According to sensitivity graph of Figures 1 and 2 it is observed that in FPM-7* parameters of maximum and minimum temperatures and average temperature; both parameters of that have more sensitivity means average temperature and wind speed in height of two meters due to high slope that they have. The positive slope of changes of FPM-7* model in front of changes of maximum temperature and average temperature (Tmean) show the direct relationship of the model with these two parameters. The negative slope of changes of FPM-7* model in front of changes of minimum temperature parameter and sunshine hours (N) show the inverse relationship of the model with these two parameters. In other words the evapotranspiration intensity of FPM-7* model is increased by increase of maximum temperature and average temperature and its intensity is reduces by increase of minimum temperature and sunshine hours.

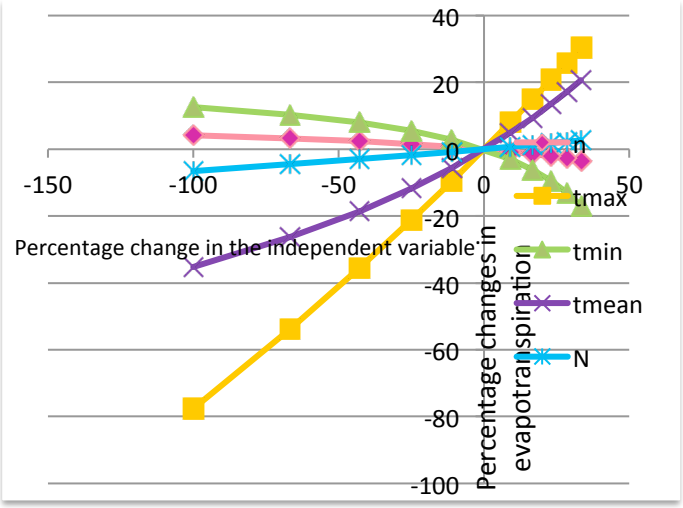

Figure 1. Sensitivity graph of FPM-7 model*

In sensitivity graph of Figure 2, positive slope of changes of FPM-1* in front of temperature changes and wind speed in height of two meters shows the direct relationship of the model with its parameters. In fact whatever these two parameters to be increased the evapotranspiration intensity of the model is increased. The wind speed parameter has more effect on increase of evapotranspiration intensity due to the more slopes that it has.

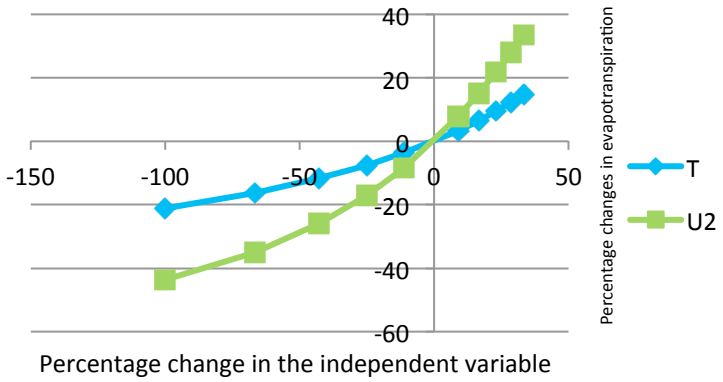

Figure 2. Sensitivity graph of FPM-1 model*

4. CONCLUSION

Using FPM-7* and FPM-1* is suggested instead of Hargreaves-Samani model to calculate water requirement of reference plant in Gonabad region with warm and arid climate, this model can be used in other similar region to this climate. The proposal FPM-7*model has more accuracy than the proposal FPM-1*model but the advantage of proposal FPM-1*model is that needs less data to calculate evapotranspiration. FPM-1*model is sensitive to parameters of wind speed and temperature and it has direct relationship with these two. FPM-7* model is sensitive respectively to parameters of maximum temperature, average temperature, minimum temperature and sunshine hours. Of course this sensitivity is very few about sunshine hours. FPM-1*model has direct relationship with maximum temperature and average temperature and it has inverse relationship with sunshine hours.

REFERENCES

Allen RG, Pereira LS, Raes D, and Smith M ,, 1998. Crop evapotranspiration. Guide lines for computing crop evapotranspiration. FAO Irrigation and Drainage Paper No 56. FAO, Rome.

Beven, K., 1979. A sensitivity analysis of the Penman-Monteith actual evapotranspiration estimates.Journal of Hydrology, 44, 169-190.

Bois, B., Pieri, P., Van Leeuwen, C., Gaudillere, J. P. 2006. Sensitivity analysis of the Penman-Monteith evapotranspiration formula and comparison of empirical methods used in viticulture soil water balance. wwwecole. enitab.fr/people/kees.vanleeuwen/articles/CI- 24.pdf. 1-6.

Dehghani Sanij, H., Yamamoto, T., and Rasiah, V. 2004. Assessment of evapotranspiration estimation models for use in semi-arid environments, Agricultural water management 64: 91-106.

Donohoue, R.J., McVicar, T.R., Roderick, M.L., 2010. Assesing the ability of potential evaporation formulations to capture the dynamics in evaporative demand with a changing climate, Journal of Hydrology, Vol. 386, PP. 186-197.

Estevez J., Gavilan, P., and Berengena, J. 2009. Sensitivity analysis of a Penman-Monteith type equation to estimate reference evapotranspiration in southern Spain. Published online in Wiley InterScience, Hydrol. Process, 23, 3342-3353.

Gong, L., Xu, C. Y., Chen, D., Halldin, S., and Chen, Y. D. 2006. Sensitivity of the Penman-Monteith reference evapotranspiration to key climatic variables in the Chanjing (Yangtze River) basin. Journal of Hydrology, 329, 620-629.

Guyot, G, 1998. Physics of the environment and climate, John Willey, Chichester, USA, 632 pp.

Jacovides C. P. and H. Kontoyiannis. 1995. Statistical procedures for the evaluation of evapotranspiration computing models. Agric. Water Manage. 27, 365-371.

Islami. A, Ghahremani, B. 2013. Sensitivity analysis and uncertainty involved in the estimation of reference evapotranspiration in models with different mathematical structures. Irrigation and Drainage. 1 (7): 79-68.

Lu, J., Sun, G., McNutly, S.G., amatya, D.M., 2005, A comparison of six potential evapotranspiration methods for regional use in the southeastern United States, Journal of American water Resources Association Vol. 41, PP. 621-633.

Khajehzadeh; Gh. 1995. Blaney-Criddle and Hargreaves-Samani modified equations for different regions of Iran. Irrigation and Drainage Master's thesis, University of Shiraz.

McCuen, R.H. 1974. A sensitivity and error analysis of procedures used for estimating evapotranspiration. Water Resources Bulletin, 10 (3), 486-498.

Mirzaei Takhtgahi, H., and Moazed, H. 2006. Comparison of Various Potential Evapotranspiration Estimation Methods, National symposium of Management of Irrigation and Drainage Nets. Ahvaz University of Shahid Chamran, Water Sciences Engineering Faculty.

Mosaedi A. And Ghobaei souq, M 2013. Evaluation of different empirical equations to estimate reference evapotranspiration in different conditions was measured meteorological parameters in several climatic regions of Iran. Soil and Water Conservation Research, 20 (3): 50-27.

Najafi P. 2006. used in the evaluation mode Hargreaves-Samani and Jnsn- Hayes evaporation - transpiration, of alfalfa in. new agricultural science. 2 (5): 68-58.

Ordibehesht, MS,. and M, Samii. 2013. Compare thirteen method to estimate evapotranspiration Ardestān synoptic station. Twelfth National Conference on Irrigation and reduce evaporation, shahid Bahonar University of Kerman, Iran.

Oudin, L., Michel, C., Anctil, F., 2005, Which potential evapotranspiration input for a lumped rainfall-runoff model? Part1- can rainfall-runoff models effectively handle detailed potent.

Pour Ali Baba. and Shiri J .1991. The effect of solar radiation on plant water requirement estimation reference. Third National Conference on Integrated Water Resource Management, Faculty of Agricultural Sciences and Natural Resources of Sari, Iran.

Pouryzdan khah E., Razavipour T., Khaledian. and Rezaei, M. 2012. to determine suitable methods for estimating reference evapotranspiration in the Rasht region. Third National Conference on Integrated Water Resource Management, Faculty of Agricultural Sciences and Natural Resources of Sari, Iran.

Qui, G.Y., Yano, T., Momii, K. 1998. An improved methodology to measure evaporation from bare soil based on comparison of surface temperature with a dry soil Penman-Monteith actual evapotranspiration estimates.Journal of Hydrology,

Qamarnia H., Daei Chin S., Jalili Z., Farmanifard M. And Razdar B. 2012. Comparison of evaporation pan estimate to calculate the reference evapotranspiration (Case Study: Zanjan synoptic station). Third National Conference on Integrated Water Resource Management, Faculty of Agricultural Sciences and Natural Resources of Sari, Iran.

Samani Z. 2000. Estimating solar radiation and evapotranspiration using minimum climatological data. J. Irrig. And Drain. Eng. ASCE. 126(4): 265-267.

Sokhanvar F., Ejtihad e., Vaezi J., Memariani F., Joharchi MR. And the Ranjbar Z 2013. flora, life forms and geographical distribution of plants crescent protected area in Khorasan Razavi province. Taxonomy and Biosystematics publication. 5 (16): 100-85.

Sharifan H., Dehghani A . And Karimi-Rad A. 2012. provide a correction factor for Hargreaves-Samani method to estimate the reference evapotranspiration crops (Case Study: Gorgan station). Soil and Water Conservation Research, 19 (3): 235-227.

Suri, D. 2005. Estimation and Modeling of Potential Evapotranspiration in Different Continental Conditions of Iran, MSc Thesis, Ahvaz University of Shahid Chamran. Water Sciences Engineering Faculty.

Sarvri, F., Khashei Siuki A Ahmadee M. 2013. provided an experimental model of water requirement in order to reduce water stress using rain water harvesting barley (Case Study: Gonabad). The National Conference of rainwater systems, Ferdowsi University of Mashhad, Iran

Tabari, H. 2009. Evaluation of reference crop evapotranspiration equations in various climates, Water Resour. Manage. 24: 10. 2311-2337.

Tafazoli F. 2007. Evaluation of evapotranspiration models sensitivity to radiation daily log all the above. Master's thesis Water Engineering Department, Faculty of Agriculture, University of Bu-Ali Sina.

Weiss, M., Menzel, L., 2008, A global comparison of for potential evapotranspiration equations and their relevance to stream flow modeling in ability of potential evaporation formulations to capture the dynamics in evaporative demand with a changing climate, Journal of Hydrology, Vol. 386, PP. 186-197.

Proceedings of the 10th World Congress of EWRA 'Panta Rhei', 5-9 July 2017, Athens, Greece
© 2017 *European Water Resources Association*

Pollution control by agroforestry systems: A short review

G. Pavlidis[1,2] and V.A. Tsihrintzis[1*]
[1] *Centre for the Assessment of Natural Hazards and Proactive Planning & Laboratory of Reclamation Works and Water Resources Management, School of Rural and Surveying Engineering, National Technical University of Athens, 9 Iroon Polytechniou St., Zografou, 15780, Athens, Greece*
[2] *Laboratory of Chemical Control of Pesticides, Department of Pesticides Control and Phytopharmacy, Benaki Phytopathological Institute, 8 St. Delta St., Kifissia, 14561, Athens, Greece*
[*] *e-mail: tsihrin@survey.ntua.gr*

Abstract: Several mitigation techniques have been proposed for the control of pollution to surface and ground water systems from agricultural activities. Agroforestry, which is the common cultivation of crops and trees, is proposed as one such mitigation technique. Alley crop agroforestry systems have the potential to reduce nitrogen and phosphorus originating from fertilizers; recent studies also exhibit the potential for pesticide removal. It has been previously demonstrated that agroforestry alley crop systems have the potential to remove nitrogen and phosphorus originating from fertilizers excess and recent studies exhibit the potential for pesticides removal. In the present study, the efficiency of agroforestry systems in pollutant reduction is reviewed based on a search comprising a significant number of international studies. A search of relevant international literature was conducted using Scopus, Science Direct and Google Scholar scientific literature search engines, using all relevant keywords for agrochemicals pollution abatement using trees. More than 2000 results were found using various combinations of keywords and the most relevant literature has been extensively studied. From the current knowledge, it can be generally demonstrated that tree roots in agroforestry systems, are able to reduce nitrogen and phosphorus residues in soil from 20% up to 100%, and pesticide transport up to 100%.

Key words: Agroforestry systems, alley cropping, nutrients, fertilizers, herbicides, pesticides, pollution reduction, buffer strips

1. INTRODUCTION

Intensification of agriculture, which started in the last century and still continues, has resulted in degradation of soils, water and the environment in general. Main contributing factors on the environmental impact include the excessive and improper use of agrochemicals (nutrients and pesticides), and the use of motorized agricultural equipment and genetically modified crop species (Gold and Hanover, 1987). Improper agrochemicals management may result in soil deterioration, and non point-source pollution of groundwater and surface water recipients, among other impacts (Reichenberger et al., 2007; DeLonge et al., 2016). Thus, research and determination of protective measures to control agricultural pollution of aquatic systems is deemed necessary. Proposed field application protective measures include vegetated buffer strips, alley crops, and agroforestry systems, among others (USDA, 2004). In the present study, the environmental benefits of agroforestry systems (AFS), i.e., the common cultivation of trees and crops in the same field, in controlling nutrient and pesticide pollution are briefly presented following a detailed scientific literature review.

2. METHODOLOGY

The literature search was conducted using Scopus, Science Direct, Google Scholar and other scientific literature search engines employing appropriate keywords and keyword combinations for agricultural pollution abatement using trees. Representative studies are summarized in this paper.

3. RESULTS

3.1 General environmental and socioeconomic benefits of AFS

The general idea concerning pollution inhibition abilities of AFS lies on the function of tree roots to absorb the pollutants that leach below the rooting zone of alley crops (Figure 1), as a result of the deeper root system of trees. Thus, nutrient recycling takes place and a parallel decrease of fertilizer environmental impacts (Allen et al., 2004; Beaudette et al., 2010; Andrianarisoa et al., 2016; Gikas et al., 2016). AFS can reduce leaching to groundwater and also absorb pollutants from the unsaturated or saturated-low depth zones through their deeper and finer tree roots (Jose, 2009; Andrianarisoa et al., 2016). It is noted that tree roots in AFS do not compete with crops for beneficial nutrients, since, due to their depth, they only absorb the percentage of agrochemicals in the deeper soil layers that may be 60-90% of the applied quantities; depending on the chemical properties of the substance used, this part would otherwise remain in the soil or leach to groundwater (Nerlich et al., 2013).

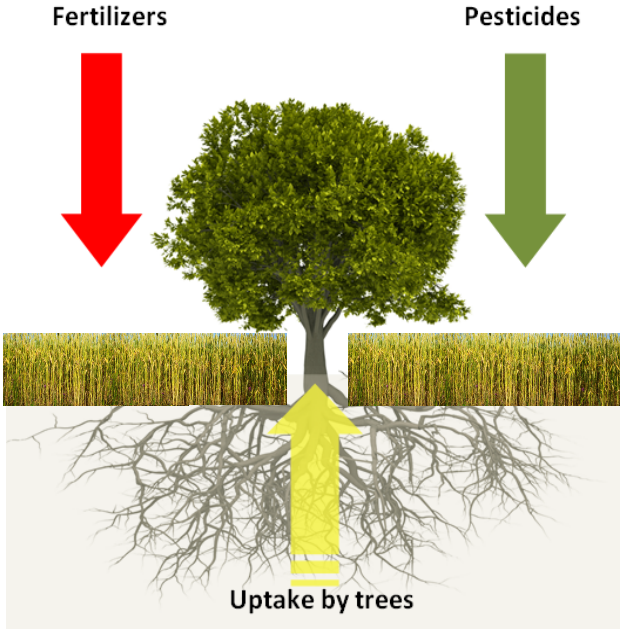

Figure 1. Tree roots in AFS act as pollutant filters

AFS also provide other benefits to farmers and the environment, such as, reduction of runoff, raindrop interception and reduction of soil erosion, reduction of agrochemicals and nutrient recycling, decrease of environmental impacts of fertilizers, soil fertility improvement, increase of use of belowground resources by crops and woody species, weed control, nitrogen fixation, carbon sequestration, improved soil biomass via trees fallow, accelerated mineralization and remediation of soils and shallow groundwaters (Kang, 1997; Alavalapati et al., 2004; Anbumozhi et al., 2005; Lovell and Sullivan, 2006; Bentrup, 2008; Jose, 2009; Calfapietra et al., 2010; Straight, 2012, Tsonkova et al., 2012; Cerdán et al., 2012; Dawson et al., 2014). Regarding water, AFS provide enhanced water infiltration, improved soil water storage, access to lower aquifer water table through tree roots, water quality improvement, reduction of leaching to groundwater, removal of pollutants from unsaturated or low-saturated zone, salinity protection and flood regulation (Gillespie et al., 2000; Jose et al., 2000; Bharati et al., 2002; Huth et al., 2003; Alavalapati et al., 2004; Anbumozhi et al., 2005; Lovell and Sullivan, 2006; Bentrup, 2008; Anderson et al., 2009; Jose, 2009; Calfapietra et al., 2010; Straight, 2012; Tsonkova et al., 2012; George et al., 2012). Agroforestry may also achieve air quality improvement, greenhouse gas reduction, gaseous ammonia reduction and CO_2 recycling, rise and stimulation of soil fauna, micro-climate stabilization, and pollination

(Kang, 1997; Alavalapati et al., 2004; Anbumozhi et al., 2005; Lovell and Sullivan, 2006; Bentrup, 2008; Jose, 2009; Calfapietra et al., 2010; Straight, 2012; Cerdán et al., 2012; Dawson et al., 2014; Bealey et al., 2016). Finally, several socioeconomic effects may arise from AFS implementation, including, among others, high productivity yields, landscape improvement, additional income from timber or fruit production from trees, recreation opportunities, biomass energy production from prunings, reduced fire risk and temperature, and wind moderation (Alavapati et al., 2004; Anbumozhi et al., 2005; Lovell and Sullivan, 2006; Bentrup, 2008; Jose, 2009; Calfapietra et al., 2010; Cerdán et al., 2012; Tsonkova et al., 2012; Dawson et al., 2014; Cadoux et al., 2015).

Typical AFS tree species include the following genera: *Populus* and *Salix, Eucalyptus, Betula, Alnus, Robinia and Nothofagus* (Ceulemans and Deraedt, 1999; Mitchell et al., 1999; Karacic et al., 2003; Calfapietra et al., 2010), *Juglans* (Gold and Hanover, 1987), *Prunus, Pinus, Fraxinus, Juniperus* and *Quercus* (Reisner et al., 2007; Schultz et al., 1995). Apart from crop-tree combination, important parameters concerning the efficiency of nutrient reduction are also the soil type, the hydrogeological profile of the area and the prevailing climatic conditions (Nair, 2004; Köhler et al., 2006). In the following section, the efficiency of various AFS on pollution abatement potential is presented through previous applications performed worldwide.

3.2 Efficiency of pollution reduction of agrochemicals

Many AFS applications have been presented in the worldwide literature in the last three decades, with AFS systems mostly found in American, African and European continents, either as cultivating techniques or integrated into crop and land management policies (Duchemin and Hogue, 2009). Thus, within the context of the present study, previous applications of AFS for pollution abatement were investigated. Till today, the emphasis in the various studies has been given mainly on nutrient uptake, whilst limited number of studies examined the potential for pesticide uptake. Furthermore, the experimental design of most studies till today included only surface runoff as route of environmental exposure to pesticides pollution. Studies reported nitrogen reduction in the range 4.6 to 100% (Schultz et al., 1995; Breman and Kessler, 1997; Allen et al., 2004; Rockwood et al., 2004; Anbumozhi et al., 2005; Borin et al., 2005; Schoonover et al., 2005; Nair et al., 2007; Ryszkowski and Kedziora, 2007; Dougherty et al., 2009; Borin et al., 2010; Udawatta et al., 2010; Wang et al., 2010; Izydorczyk et al., 2013; Nerlich et al., 2013; Andrianarisoa et al., 2016; Gikas et al., 2016; Yang et al., 2016), phosphorus reduction in the range 12 to 100% (Breman and Kessler, 1997; Rockwood et al., 2004; Borin et al., 2005; Schoonover et al., 2005; Nair et al., 2007; Borin et al., 2010; Wang et al., 2010; Izydorczyk et al., 2013; Nerlich et al., 2013; Gikas et al., 2016) and pesticide/herbicide reductions in the range 40 to 100% (Schultz et al., 1995; Popov et al., 2006; Otto et al., 2008; Borin et al., 2010; Passeport et al., 2014).

Following the previous findings, it is hard to determine which plants take up higher amounts of agrochemical pollutants; however, *Platanus* species, poplar and willow tree species are generally known and have been reviewed for their ability to absorb pollutants, including pesticides and their degradation products, and immobilize them in the woody parts of the tree (Licht and Isebrands, 2005), whilst, the ability of natural pollution abatement systems to retain pesticides is also dependent on the physicochemical properties of the active substance.

4. CONCLUSION AND FUTURE ASPECTS

Based on the reviewed studies, the agroforestry cultivating technique constitutes a novel approach for the achievement of sustainable agriculture, which offers both high crop yields and environmental protection. Previous studies demonstrate the ability of tree roots in AFS to reduce nitrogen and phosphorus groundwater leaching up to 97.7 and 90% for nitrogen and phosphorus, respectively, and up to 100% for surface runoff attenuation. The respective reduction of pesticides was also observed in levels up to 100% for several herbicides and fungicides, however, only surface

runoff has been examined till today. Agroforestry systems, as a pollution reduction technique, consist a new research sector, particularly for pesticides attenuation, as there is lack in scientific information. It certainly deserves further research and experimental or field observations in order to offer practical benefits to agriculture, the environment, and in extension to human health and welfare, particularly in the Mediterranean region.

ACKNOWLEDGMENTS

The authors acknowledge funding of the research from IKY and Siemens through the Research Scholarship Program "Research Projects for Excellence IKY/SIEMENS", Grant No. 2603.

REFERENCES

Alavalapati, J., Shrestha, R., Stainback, G., Matta, J., 2004. Agroforestry development: An environmental economic perspective. Agroforestry Systems;61:299-310.

Allen, S.C., Jose, S., Nair, P.K.R., Brecke, B.J., Nkedi-Kizza, P., Ramsey, C.L., 2004. Safety-net role of tree roots: evidence from a pecan (Carya illinoensis K. Koch)–cotton (Gossypium hirsutum L.) alley cropping system in the southern United States. Forest Ecology and Management;192(2-3):395-407.

Anbumozhi, V., Radhakrishnan, J., Yamaji, E., 2005. Impact of riparian buffer zones on water quality and associated management considerations. Ecological Engineering;24(5):517-23.

Anderson, S.H., Udawatta, R.P., Seobi, T., Garrett, H.E., 2008. Soil water content and infiltration in agroforestry buffer strips. Agroforestry Systems;75(1):5-16.

Andrianarisoa, K.S., Dufour, L., Bienaimé, S., Zeller, B., Dupraz, C., 2015. The introduction of hybrid walnut trees (Juglans nigra×regia cv. NG23) into cropland reduces soil mineral N content in autumn in southern France. Agroforestry Systems;90(2):193-205.

Bealey, W.J., Dore, A.J., Dragosits, U., Reis, S., Reay, D.S., Sutton, M.A., 2016. The potential for tree planting strategies to reduce local and regional ecosystem impacts of agricultural ammonia emissions. J Environ Manage;165:106-16.

Beaudette, C., Bradley, R.L., Whalen, J.K., McVetty, P.B.E., Vessey, K., Smith, D.L., 2010. Tree-based intercropping does not compromise canola (Brassica napus L.) seed oil yield and reduces soil nitrous oxide emissions. Agriculture, Ecosystems & Environment;139(1-2):33-9.

Bentrup, G., 2008. Conservation buffers: design guidelines for buffers, corridors, and greenways, General Technical Report, National Agroforestry Center: Department of Agriculture, Forest Service, Southern, SRS-109, Research Station:110.

Bharati, L., Lee, K.H., Isenhart, T.M., Schultz, R.C., 2002. Soil-water infiltration under crops, pasture, and established riparian buffer in Midwestern USA, Agroforestry Systems;56:249–257.

Borin, M., Vianello, M., Morari, F., Zanin, G., 2005. Effectiveness of a buffer strip in removing runoff pollutants from a cultivated field in North-East Italy. Agricultural Ecosystems and Environment;105:101–114.

Borin, M., Passoni, M., Thiene, M., Tempesta, T., 2010. Multiple functions of buffer strips in farming areas. European Journal of Agronomy;32(1):103-11.

Breman, H. and Kessler, J., 1997. The potential benefits of agroforestry in the Sahel and other semi-arid regions. European Journal of Agronomy;7:25–33.

Cadoux, S., Sauzet, G., Valantin-Morison, M., Pontet, C., Champolivier, L., Robert, C., et al., 2015. Intercropping frost-sensitive legume crops with winter oilseed rape reduces weed competition, insect damage, and improves nitrogen use efficiency. Ocl;22(3):D302.

Calfapietra, C., Gielen, B., Karnosky, D., Ceulemans, R., Scarascia Mugnozza, G., 2010. Response and potential of agroforestry crops under global change. Environ Pollut;158(4):1095-104.

Cerdán, C.R., Rebolledo, M.C., Soto, G., Rapidel, B., Sinclair, F.L., 2012. Local knowledge of impacts of tree cover on ecosystem services in smallholder coffee production systems. Agricultural Systems;110:119-30.

Ceulemans, R. and Deraedt, W., 1999. Production physiology and growth potential of poplars under short-rotation forestry culture, Forest Ecology and Management;121(1-2):9-23.

Dawson, I.K., Leakey, R., Clement, C.R., Weber, J.C., Cornelius, J.P., Roshetko, J.M., et al., 2014. The management of tree genetic resources and the livelihoods of rural communities in the tropics: Non-timber forest products, smallholder agroforestry practices and tree commodity crops. Forest Ecology and Management;333:9-21.

DeLonge, M.S., Miles, A., Carlisle, L., 2016. Investing in the transition to sustainable agriculture. Environmental Science & Policy;55:266-73.

Dougherty, M.C., Thevathasan, N.V., Gordon, A.M., Lee, H., Kort, J., 2009. Nitrate and Escherichia coli NAR analysis in tile drain effluent from a mixed tree intercrop and monocrop system. Agriculture, Ecosystems & Environment;131(1-2):77-84.

Duchemin, M., Hogue, R., 2009. Reduction in agricultural non-point source pollution in the first year following establishment of an integrated grass/tree filter strip system in southern Quebec (Canada). Agriculture, Ecosystems & Environment;131(1-2):85-97.

George, S.J., Harper, R.J., Hobbs, R.J., Tibbett, M., 2012. A sustainable agricultural landscape for Australia: A review of interlacing carbon sequestration, biodiversity and salinity management in agroforestry systems. Agriculture, Ecosystems & Environment;163:28-36.

Gikas, G.D., Tsihrintzis, V.A., Sykas, D., 2016. Effect of trees on the reduction of nutrient concentrations in the soils of cultivated areas. Environ Monit Assess;188(6):327.

Gillespie, A.R., Jose, S., Mengel, D.B., Hoover, W.L., Pope, P.E., Seifert, J.R. et al, 2000. Defining competition vectors in a temperate alley cropping system in the midwestern USA: 1. Production physiology. Agroforestry systems;48(1):25-40.

Gold, M. and Hanover, L.W., 1987. Agroforestry systems for the temperate zone, Agroforestry Systems;5:109-121.

Huth, N.I., Carberry, P.S., Poulton, P.L., Brennan, L.E., Keating, B.A., 2003. A framework for simulating agroforestry options for the low rainfall areas of Australia using APSIM, European Journal of Agronomy;18:171-185.

Izydorczyk, K., Fratczak, W., Drobniewska, A., Cichowicz, E., Michalska-Hejduk, D., Gross, R. and Zalewski, M., 2013. A biogeochemical barrier to enhance a buffer zone for reducing diffuse phosphorus pollution-preliminary results, Ecohydrology and Hydrobiology, Vol. 13, pp.: 104-112.

Jose, S., Gillespie, A.R., Seifert, J.R., Mengel, D.B., Pope, P.E., 2000. Defining competition vectors in a temperate alley cropping system in the mid-western USA. 3. Competition for nitrogen and litter decomposition dynamics. Agroforestry Systems;48: 61–77.

Jose, S., 2009. Agroforestry for ecosystem services and environmental benefits: an overview. Agroforestry Systems;76(1):1-10.

Kang, B.T., 1997. Alley cropping-soil productivity and nutrient recycling, Forest Ecology and Management;91:75-82.

Karacic, A., Verwijst, T., Weih, M., 2003. Above-ground woody biomass production of short-rotation Populus plantations on agricultural land in Sweden. Scandinavian Journal of Forest Research; 18:427-437.

Köhler, K., Duynisveld, W.H.M., Böttcher, J., 2006. Nitrogen fertilization and nitrate leaching into groundwater on arable sandy soils. Journal of Plant Nutrition and Soil Science; 169(2):185-95.

Licht, L. and Isebrands, J.G., 2005. Proceedings of the joint IEA bioenergy task 30 and task 31 workshop on sustainable bioenergy production systems: environmental, operational and social implications Linking phytoremediated pollutant removal to biomass economic opportunities, Biomass and Bioenergy;28(2):203–218

Lovell, S.T., Sullivan, W.C., 2006. Environmental benefits of conservation buffers in the United States: Evidence, promise, and open questions. Agriculture, Ecosystems & Environment;112(4):249-60.

Mitchell, J.K., Walker, S.E., Hirschi, M.C., Cooke, R.A.C., 1999. Nitrate losses under various cropping systems, Proceedings of the 1999 IUGG 99, the XXII General Assembly of the International Union of Geodesy and Geophysics; Birmingham, UK; 18 - 30 July; Code 55779. 1999;257:33-39. IAHS-AISH Publication.

Nair, V.D. and Graetz, D.A., 2004. Agroforestry as an approach to minimizing nutrient loss from heavily fertilized soils: The Florida experience, Agroforestry Systems;61:269–279.

Nair, V.D., Nair, P.K.R., Kalmbacher, R.S., Ezenwa, I.V., 2007. Reducing nutrient loss from farms through silvopastoral practices in coarse-textured soils of Florida, USA. Ecological Engineering;29(2):192-9.

Nerlich, K., Graeff-Hönninger, S., Claupein, W., 2012. Agroforestry in Europe: a review of the disappearance of traditional systems and development of modern agroforestry practices, with emphasis on experiences in Germany. Agroforestry Systems;87(2):475-92.

Otto, S., Vianello, M., Infantino, A., Zanin, G., Di Guardo, A., 2008. Effect of a full-grown vegetative filter strip on herbicide runoff: maintaining of filter capacity over time. Chemosphere;71(1):74-82.

Passeport, E., Richard, B., Chaumont, C., Margoun, C., Liger, L., Gril, J-J. and Tournebize, J., 2014. Dynamics and mitigation of six pesticides in a "Wet" forest buffer zone. Environmental Science and Pollution Research, Vol., 21, pp.: 4883-4894.

Popov, V.H., Cornish, P.S., Sun, H., 2006. Vegetated biofilters: The relative importance of infiltration and adsorption in reducing loads of water-soluble herbicides in agricultural runoff. Agriculture, Ecosystems and Environment;114(2-4):351-359.

Reichenberger, S., Bach, M., Skitschak, A., Frede, H.G., 2007. Mitigation strategies to reduce pesticide inputs into ground- and surface water and their effectiveness: a review. Sci Total Environ;384(1-3):1-35.

Reisner, Y., de Filippi, R., Herzog, F., Palma, J., 2007. Target regions for silvoarable agroforestry in Europe. Ecological Engineering; 29(4):401-18.

Rockwood, D.L., Naidu, C.V., Carter, D.R., Rahmani, M., Spriggs, T.A., Lin, C. et al., 2004. Short-rotation woody crops and phytoremediation: Opportunities for agroforestry?, Agroforestry Systems; 61:51–63.

Ryszkowski, L. and Kedziora, A., 2007. Modification of water flows and nitrogen fluxes by shelterbelts, Ecological Engineering;29(4):388-400.

Schoonover, J.E., Williard, K.W.J., Zaczek, J.J., Mangun, J.C., Carver, A.D., 2005. Nutrient attenuation in agricultural surface runoff by riparian buffer zones in Southern Illinois, USA. Agroforestry Systems;64(2):169-80.

Schultz, R.C., Colletti, J.P., Isenhart, T.M., Simpkins, W.W., Mize, C.W., Thompson, M.L., 1995. Design and placement of a multi-species riparian buffer strip system, Agroforestry Systems;29:201-226.

Straight, R., 2012. Shade Coffee Production Enjoys Resurgence. Inside Agroforestry: Many paths to success; 21(1):4-5.

Tsonkova, P., Böhm, C., Quinkenstein, A., Freese, D., 2012. Ecological benefits provided by alley cropping systems for production of woody biomass in the temperate region: a review. Agroforestry Systems;85(1):133-52.

Udawatta, R.P., Garrett, H.E., Kallenbach, R.L., 2010. Agroforestry and grass buffer effects on water quality in grazed pastures. Agroforestry Systems; 79(1):81-7.

United States Department of Agriculture (USDA), 2004. Agroforestry Working Trees for Water Quality. USDA and National Agroforestry Center, Lincoln, NE.

Wang, L, Tang, L., Wang, X., Chen, F., 2010. Effects of alley crop planting on soil and nutrient losses in the citrus orchards of the Three Gorges Region. Soil and Tillage Research;110(2):243-50.

Yang, L., Ding, X., Liu, X., Li, P., Eneji, A.E., 2016. Impacts of long-term jujube tree/winter wheat–summer maize intercropping on soil fertility and economic efficiency—A case study in the lower North China Plain. European Journal of Agronomy;75:105-17.

Proceedings of the 10th World Congress of EWRA 'Panta Rhei', 5-9 July 2017, Athens, Greece
© 2017 *European Water Resources Association*

Spatial interpolation of potential evapotranspiration for precision irrigation purposes

N. Malamos[1*], I.L. Tsirogiannis[2], A. Tegos[3], A. Efstratiadis[3] and D. Koutsoyiannis[3]
[1] *Department of Agricultural Technology, Technological Educational Institute of Western Greece, Amaliada, Greece*
[2] *Department of Agricultural Technology, Technological Educational Institute of Epirus, Arta, Greece*
[3] *Department of Water Resources and Environmental Engineering, School of Civil Engineering, National Technical University of Athens, Zographou, Greece*
[*] *e-mail: nmalamos@teimes.gr*

Abstract: Precision irrigation constitutes a breakthrough for agricultural water management since it provides means to optimal water use. In recent years several applications of precision irrigation are implemented based on spatial data from different origins, i.e. meteorological stations networks, remote sensing data and in situ measurements. One of the factors affecting optimal irrigation system design and management is the daily potential evapotranspiration (PET). A commonly used approach is to estimate the daily PET for the representative day of each month during the irrigation period. In the present study, the implementation of the recently introduced non-parametric bilinear surface smoothing (BSS) methodology for spatial interpolation of daily PET is presented. The study area was the plain of Arta which is located at the Region of Epirus at the North West Greece. Daily PET was estimated according to the FAO Penman-Monteith methodology with data collected from a network of six agrometeorological stations, installed in early 2015 in selected locations throughout the study area. For exploration purposes, we produced PET maps for the Julian dates: 105, 135, 162, 199, 229 and 259, thus covering the entire irrigation period of 2015. Also, comparison and cross validation against the calculated FAO Penman-Monteith PET for each station, were performed between BSS and a commonly used interpolation method, i.e. inverse distance weighted (IDW). During the leave-one-out cross validation procedure, BSS yielded very good results, outperforming IDW. Given the simplicity of the BSS, its overall performance is satisfactory, providing maps that represent the spatial and temporal variation of daily PET.

Key words: irrigation; potential evapotranspiration; agrometeorological stations; bilinear surface smoothing; spatial modelling

1. INTRODUCTION

Potential evapotranspiration (PET) is a crucial parameter of several applications in hydrological modelling, irrigation and environmental studies. Especially, precision irrigation requires daily or even hourly PET estimates in order to increase the efficiency of water use through optimization procedures that include the use of sensors along with extensive soil, water and crop data. A significant concept for precision irrigation design is the spatial variability of the PET since the well-established FAO Penman-Monteith model (Allen *et al.* 1998), but also alternative frameworks (Tegos *et al*. 2015) provide point estimates.

In the present study, spatial interpolation of PET estimates based on measurements from agrometeorological stations placed in an irrigated plain of Greece is investigated in daily scale. In this context, daily PET maps for the characteristic day of each month for the 2015 irrigation period were produced, using the well-known Inverse Distance Weighting (IDW) and the recently introduced non-parametric bilinear surface smoothing (BSS) methodology (Malamos and Koutsoyiannis 2016a). Furthermore, comparison and cross validation against the calculated FAO Penman-Monteith PET for each station, were performed between the two methods, in order to evaluate the performance of BSS.

2. MATERIALS AND METHODS

2.1 Study area and meteorological stations network

The study area was located at the plain of Arta (453.29 km^2, the biggest of the region), at the Region of Epirus at the north west coast of Greece. It is part of the Arachthos and Louros hydrological basins and borders with Amvrakikos Wetlands National Park. The local climate is of Mediterranean type, characterized by dry and hot summers and rainy and moderately cool winters.

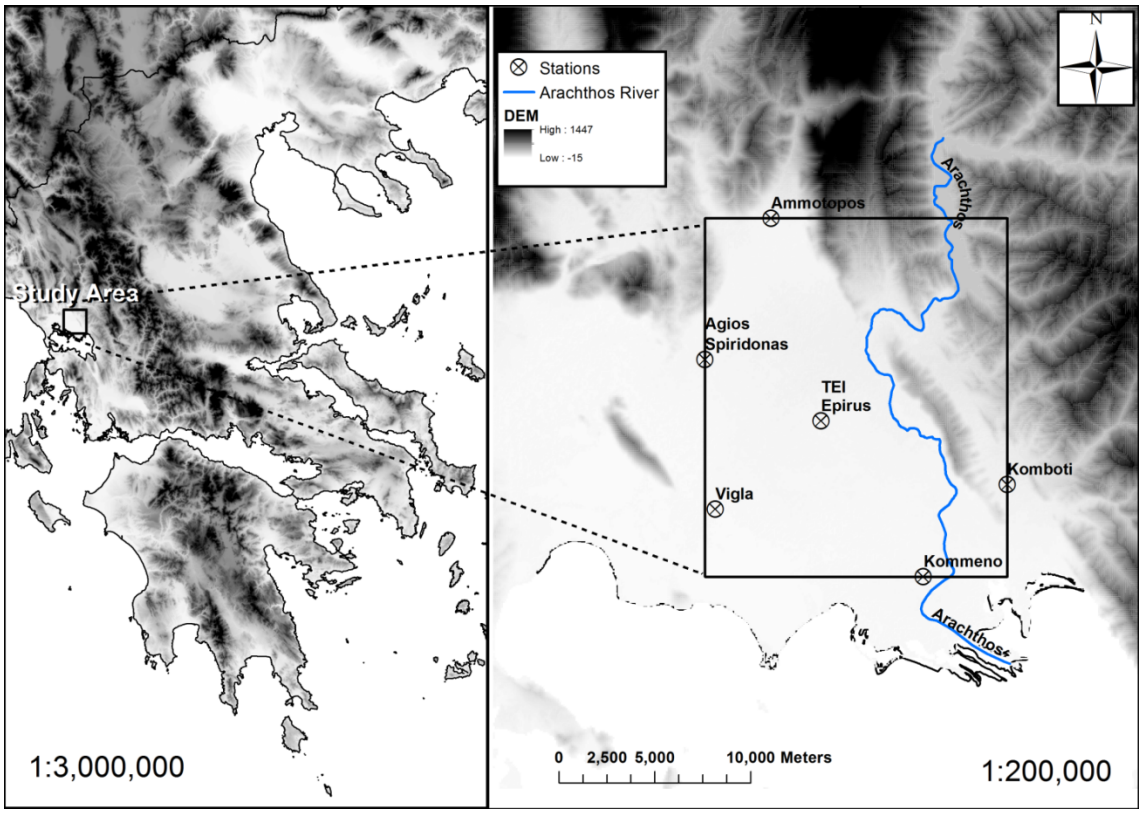

Figure 1. The Arta plain along with the study area and the agrometeorological stations network

Irrigation in the area is performed by means of surface irrigation, sprinkler irrigation and drip systems in proportions of about 40%, 40% and 20% respectively (Tsirogiannis and Triantos, 2009), with a continuous diminution of surface irrigation. The vast majority of farmers irrigate based on experience and inherited practical advices. As water is plentiful and cheap, most farmers over irrigate using water by the old open canal scheme that covers part of the plain and from numerous boreholes.

An agrometeorological stations network of six fully equipped weather stations was installed in early 2015 for the implementation of IRMA_SYS project (Malamos *et al.* 2016 - http://arta.irrigation-management.eu/) in order to monitor evapotranspiration related parameters. The data from the six meteorological stations are available at http://openmeteo.org/ under Database Contents License v.1.0 for individual measurements and Open Database License v.1.0 for the data series as they are published at Open Data Commons (http://opendatacommons.org/).

The analysis extend (mask) boundaries were defined by the coordinates of the outermost stations according to each one of the four cardinal directions. This was mandatory in order to ensure that the PET estimates adjacent to the boundaries of the study area are obtained from interpolation rather than extrapolation. The maps were produced using a 500 × 500 m grid for practical and computational reasons, covering an area of approximately 294.8 km^2 inside the plain of Arta.

2.2 The Penman-Monteith equation for potential evapotranspiration

The Penman-Monteith (PM) equation for estimating potential evapotranspiration from a vegetated surface, as formalized by Allen *et al.* (1998), is:

$$\mathrm{PET} = \frac{1}{\lambda} \frac{\Delta(R_n - G) + \rho_\alpha c_\alpha (v_a^* - v_a)/r_a}{\Delta + \gamma(1 + {}^{r_s}/_{r_a})} \quad (1)$$

where PET is the daily potential evapotranspiration; R_n is the net incoming daily radiation at the vegetated surface; G is the soil heat flux; ρ_a is the mean air density at constant pressure; c_a is the specific heat of the air; r_a is an aerodynamic or atmospheric resistance to water vapour transport for neutral conditions of stability; r_s is a surface resistance term; $v_a^* - v_a$ is the vapour pressure deficit of the air, defined as the difference between the saturation vapour pressure v_a^* and the actual vapour pressure v_a; λ is the latent heat of vaporization; Δ is the slope of the saturation vapour pressure curve at specific air temperature; and γ is the psychrometric constant. Given that the typical time scale of the PM equation is daily, all associated fluxes are expressed in daily or mean daily units.

Apart from the site location, expressed in terms of latitude, φ, the PM equation requires air temperature, humidity, solar radiation and wind speed data for calculating the model variables R_n, v_a^*, v_a, and Δ.

2.3 Spatial interpolation methods

The mathematical framework of Bilinear Surface Smoothing (Malamos and Koutsoyiannis 2016a), suggests that fit is meant in terms of minimizing the total square error among the set of original points $z_i(x_i, y_i)$ for $i = 1,\ldots, n$ and the fitted bilinear surface, that in matrix form, can be written as:

$$p = \|\boldsymbol{z} - \hat{\boldsymbol{z}}\|^2 \quad (2)$$

where $\boldsymbol{z} = [z_1,\ldots, z_n]^T$ is the vector of known applicates of the given data points with size n (the superscript T denotes the transpose of a matrix or vector) and $\hat{\boldsymbol{z}} = [\hat{z}_1,\ldots, \hat{z}_n]^T$ is the vector of estimates with size n.

The details of the method including the algorithms and derivations of the equations are available at (Malamos and Koutsoyiannis 2016a).

The parameters required to implement the methodology, are the segments of the bilinear surface, i.e. mx, my and the smoothing parameter λ. These parameters can be estimated by transforming the smoothing parameter λ in terms of tension: τ_λ whose values are restricted in the interval [0, 1), for both directions i.e. $\tau_{\lambda x}$ and $\tau_{\lambda y}$ (Malamos and Koutsoyiannis 2016a). This transformation provides a convenient search in terms of computational time and is based on the generalized cross-validation (GCV - Craven and Wahba 1978) methodology. Thus, for a given combination of segments mx, my, the minimization of GCV results in the optimal values of $\tau_{\lambda x}$, $\tau_{\lambda y}$. This can be repeated for several trial combinations of mx, my values, until the global minimum of GCV is reached.

On the other hand, the Inverse Distance Weighting (IDW) method was implemented as a quick interpolator capable to address the characteristics of the study area regarding the limited number of meteorological stations. IDW is a straightforward and non-computationally intensive method (Burrough and McDonnell 1998). The IDW implementation for producing the PET maps of the study area was performed by means of ESRI's ArcGIS environment.

3. RESULTS AND DISCUSSION

In order to evaluate the performance of the BSS methodology for spatial interpolation of daily PET, we interpolated the Penman-Monteith PET values acquired at the stations locations (Table 1)

using both BSS and IDW for the characteristic day of each month for the 2015 irrigation period as presented in Figures 2 and 3.

Table 1. Penman-Monteith PET values at the locations of each of the six stations

Julian dates	PM PET (mm)					
	Agios Spiridonas	Vigla	Ammotopos	TEI of Epirus	Kommeno	Kompoti
105	3.4	3.2	3.4	3.2	3.2	3.1
135	4.1	4.4	4.5	4.4	4.5	4.1
162	4.8	4.4	5.2	4.9	5.5	5.4
199	6.2	5.2	6.7	6.4	6.1	6.3
229	4.6	4.7	5.0	4.7	4.9	4.8
259	3.8	3.4	3.8	3.7	3.6	3.6

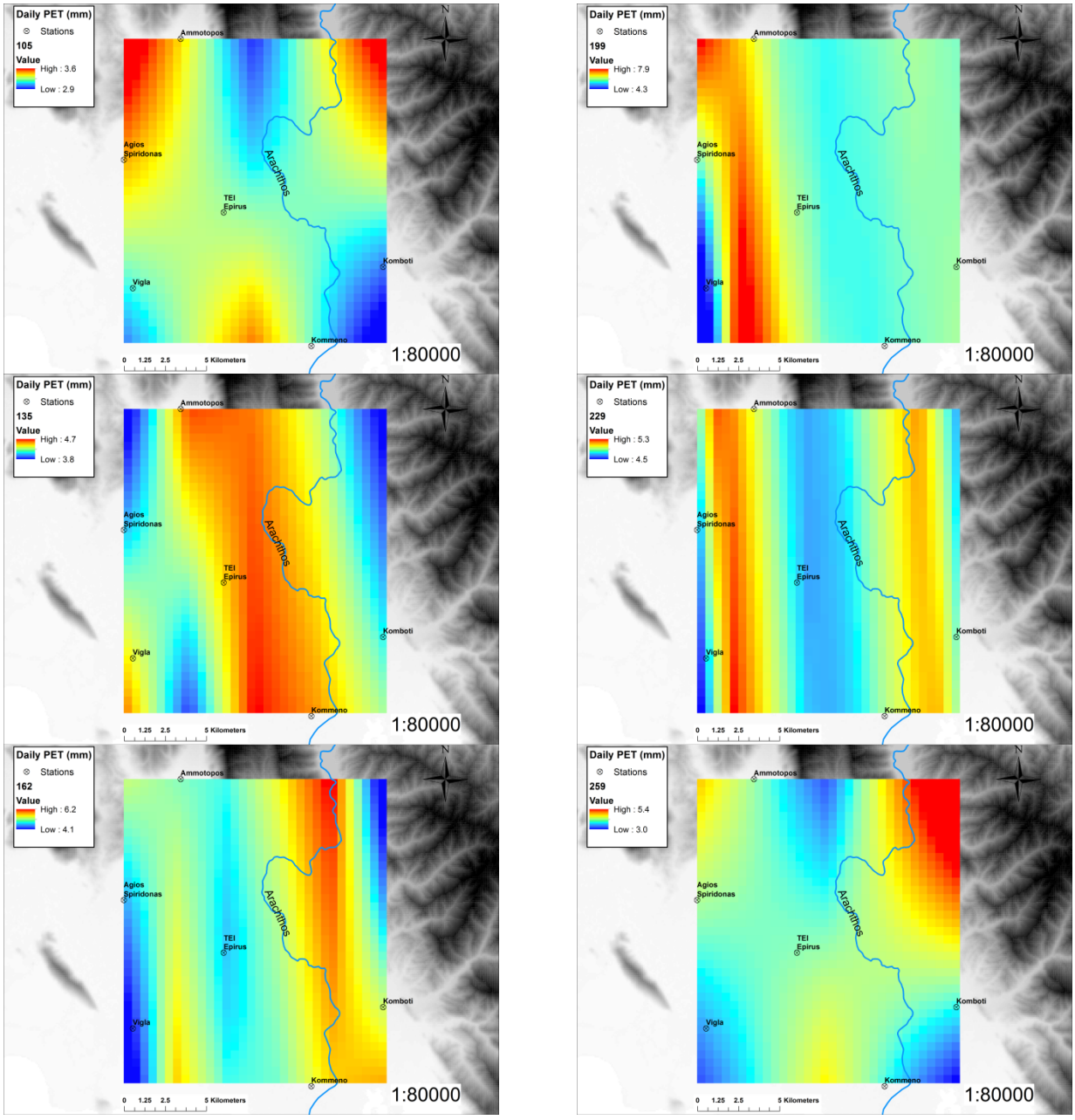

Figure 2. BSS PET maps for Julian dates 105, 135, 162, 199, 229, 259 of year 2015

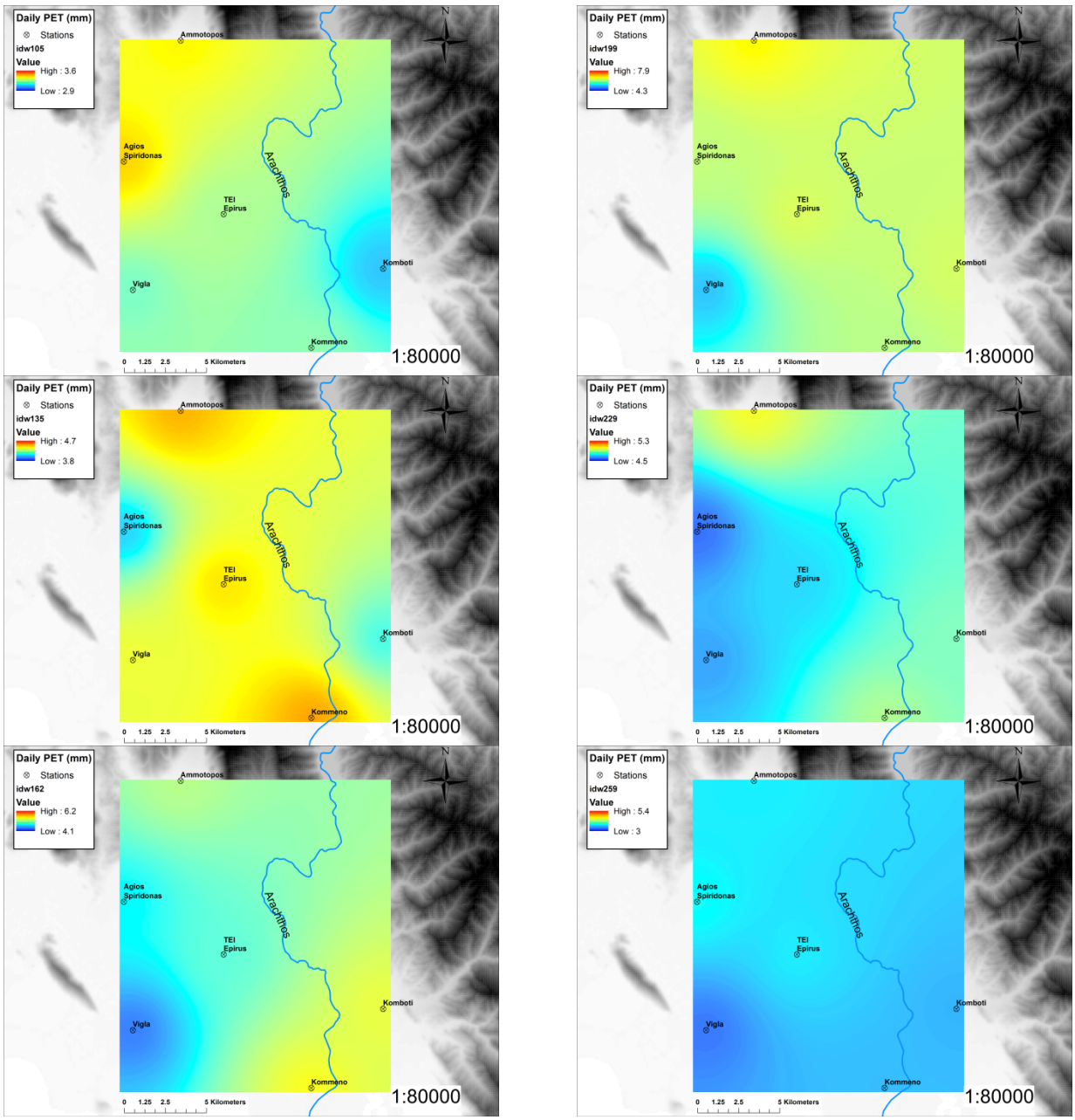

Figure 3. IDW PET maps for Julian dates 105, 135, 162, 199, 229, 259 of year 2015

From the comparison of the produced maps it is obvious that the BSS modelled PET values, have wider range than those of IDW, thus producing very plausible interpolation surfaces that respect the variation due to terrain, avoiding the characteristic IDW's bull's eye shaped artefacts.

Considering BSS's implementation, the global minimum of GCV for each day was reached by implementing it for different numbers of segments mx and my ($1 \leq mx \leq 15$ and $1 \leq my \leq 15$, while $m + 1 \geq 6$) and minimizing GCV for each one, by altering the adjustable parameters.

The results of the above procedure are presented in Table 2, along with the corresponding mean square error values. It is obvious that the BSS implementation resulted in very small mean square error values, respecting the estimated PM PET values at the stations locations. We note that there is no need to present the corresponding mean square error values for the IDW at the given data points i.e. the stations locations, since it is an exact method of interpolation so its results respect the data points exactly.

Also, the above criteria of performance may not be representative with respect to the validity of the interpolation results in other locations, except for those incorporated in the interpolation procedure. So, an alternative technique was implemented for the evaluation of the bilinear surface

smoothing method efficiency, in terms of performing a leave-one-out cross validation procedure of the two methods. The procedure was implemented in MS-Excel® and included a loop in which the PET values at the location of each station were estimated using the remaining five as the input dataset to each one of the two interpolation methods. In this way, we acquired a total of six, one for every day, PET estimates at the stations locations which were compared against the already acquired daily PM PET values. We should note that BSS was implemented using the previously obtained parameter values as presented in Table 2.

Table 2. BSS optimal parameter values and performance indices

Julian dates	mx	my	$\tau_{\lambda x}$	$\tau_{\lambda y}$	Mean square error	Global minimum GCV
105	2	3	0.902	0.154	1.75×10^{-5}	2.93×10^{-3}
135	4	5	0.003	0.765	1.42×10^{-5}	3.76×10^{-3}
162	5	4	0.99	0.001	1.13×10^{-5}	4.95×10^{-3}
199	6	12	0.76	0.019	7.42×10^{-5}	3.15×10^{-2}
229	14	6	0.201	0.001	3.77×10^{-6}	6.35×10^{-4}
259	2	6	0.784	0.067	2.47×10^{-5}	5.11×10^{-3}

The performance of each method was evaluated by using statistical criteria such as: mean bias error (MBE), mean absolute error (MAE), root mean square error (RMSE), mean square error (MSE) and modelling efficiency (EF) which is calculated on the basis of the relationship between the observed and predicted mean deviations (Malamos and Koutsoyiannis 2016b). As Table 3 states, BSS clearly outperformed IDW in all circumstances, apart from the EF and RMSE criteria at the Kompoti station. In this case, both methods failed to provide satisfactory estimates of PET values. An explanation to this behaviour is the fact that the Kompoti station is placed on the east side of the study area close to the mountains (see Figure 1) so when it is missing, the available information is inadequate to describe the orography effects, thus resulting in insufficient estimates.

Table 3. Performance of BSS and IDW against PM PET values in the leave-one-out cross validation procedure

	Agios Spiridonas		Vigla		Ammotopos		TEI of Epirus		Kommeno		Kompoti	
	BSS	IDW	BSS	IDW	BSS	IDW	BSS	IDW	BSS	IDW	BSS	IDW
MBE (mm)	0.0	0.8	0.0	0.4	0.0	0.4	0.0	0.1	-0.5	1.6	-1.7	1.7
MAE (mm)	0.1	0.8	0.1	0.4	0.0	0.4	0.1	0.1	0.5	1.6	1.7	1.7
RMSE (mm)	0.1	0.8	0.2	0.5	0.1	0.4	0.1	0.1	0.8	1.6	1.9	1.7
EF	0.99	0.18	0.95	0.47	1.00	0.85	0.99	0.98	0.44	-1.55	-2.02	-1.44

4. CONCLUSIONS

Two different approaches for spatial interpolation of daily potential evapotranspiration were implemented using data from six meteorological stations located in the plain of Arta, at the Region of Epirus. Both approaches were implemented for the characteristic day of each month for the 2015 irrigation period, i.e. Julian dates: 105, 135, 162, 199, 229 and 259. The objective was to evaluate the performance of bilinear surface smoothing (BSS) method against the inverse distance weighting (IDW) method. The comparison against the estimated values of the FAO Penman-Monteith (PM) PET for each station showed that BSS yielded very good results with very small mean square error values, respecting the given PM PET values.

Also, a leave-one-out cross-validation procedure per station was used for validating the performance of both spatial interpolators. Thus we acquired a total of six, one for every day, PET estimates at the stations locations which were compared against the already acquired daily PM PET values. During this cross validation procedure BSS clearly outperformed IDW in almost every case,

respecting the variation of the terrain and also avoiding the characteristic IDW’s bull's eye shaped artefacts. Given the simplicity of the BSS methodology, its overall performance is satisfactory, providing maps that represent the spatial and temporal variation of daily PET, thus granting the necessary tools for implementing precision irrigation on daily or finer time scale.

REFERENCES

Allen, R.G., Pereira, L.S., Raes, D., Smith, M., 1998. Crop evapotranspiration - Guidelines for computing crop water requirements - FAO Irrigation and drainage paper 56. FAO, Rome.

Burrough, P.A. and McDonnell, R.A., 1998. *Principles of Geographical Information Systems*. New York: Oxford University Press.

Craven, P. and Wahba, G., 1978. Smoothing noisy data with spline functions - Estimating the correct degree of smoothing by the method of generalized cross-validation. *Numerische Mathematik*, 31 (4), 377–403.

Malamos, N. and Koutsoyiannis, D., 2016a. Bilinear surface smoothing for spatial interpolation with optional incorporation of an explanatory variable. Part 1: Theory. *Hydrological Sciences Journal*, 61 (3), 519–526.

Malamos, N. and Koutsoyiannis, D., 2016b. Bilinear surface smoothing for spatial interpolation with optional incorporation of an explanatory variable. Part 2: Application to synthesized and rainfall data. *Hydrological Sciences Journal*, 61 (3), 527–540.

Malamos, N., Tsirogiannis, I.L., and Christofides, A., 2016. Modelling irrigation management services: the IRMA_SYS case. *International Journal of Sustainable Agricultural Management and Informatics*, 2 (1), 1–18.

Tegos, A., Malamos, N., and Koutsoyiannis, D., 2015. A parsimonious regional parametric evapotranspiration model based on a simplification of the Penman–Monteith formula. *Journal of Hydrology*, 524, 708–717.

Tsirogiannis I., Triantos S., 2009. Survey of irrigation practice in Arta and development of web tools for irrigation management. National Conference of the Greek Society of Agricultural Engineers, Thessaloniki, 8-10/10/2009, 51-58 (in Greek).

Proceedings of the 10th World Congress of EWRA 'Panta Rhei', 5-9 July 2017, Athens, Greece
© 2017 *European Water Resources Association*

The effect of Yazd wastewater on forage quantity and quality of *Atriplex lentiformis*

A.A. Karimian* and M. Ebrahimi
Faculty of Natural Resources, Yazd University, Yazd, Iran
* *e-mail: akarimian@yazd.ac.ir*

Abstract: Municipal wastewater is a major source of water in arid regions. The study on the production of forage crops using wastewater is very important. In this study examines the effects of municipal wastewater on forage quantity and quality of *Atriplex lentiformis*. This experiment includes a completely randomized design with 3 irrigation treatments (100% drinking water, 50% drinking water + 50% wastewater, 100% wastewater) in 10 replicates for 4 months. The results showed that 100% wastewater treatment increased leaf fresh and dry weight to stem ratio of *Atriplex lentiformis* ($p<0.05$), But had no significant effect on height of this plant. In the wastewater treatment, quality characteristics such as percent crude protein increased and decreased total ash. The percentage of NDF and ADF, dry matter digestibility, metabolic energy, crude fiber, digestible energy and total digestible nutrients were not affected by irrigation treatment. According to this survey results, 100% wastewater treatment, is the best treatment for irrigate this species. In total it seems that due to water scarcity in arid region, the use of wastewater not only to compensate for the shortage of water resources to forage production but is also effective in improving forage quality.

Key words: *Atriplex lentiformis,* Municipal wastewater, Forage Quantity, Forage Quality

1. INTRODUCTION

Effect of sewage irrigation on yield and quality of forage plants has been studied by several researchers. (Paliwal, et al, 1998, Ali Nejad Jahromy, et al, 2012, Yadav, et al 2002) The impact of wastewater on the nutritive value and digestibility of Rye grass showed that the amount of soluble carbohydrates of feed in the first period of cutting to the third period, was 3 to 6 times higher (Ben-Gadelia et al, 2001). The nutritional value of Bahyagras (*Paspalum notatum* Flugge.) Were examined under irrigation with sewage and result showed that wastewater increased the protein content of forage, while no significant difference was observed in digestibility (Adjei and Rechcigl, 2002). In another study increased forage crude protein of sorghum, irrigated by sewage water, but other quality parameters such as dry matter digestibility, digestible energy and cell wall percent had no significant change (Jalali, et al, 2010). Increase soil nutrients under irrigation whit wastewater, and easier access to macro and micronutrients of sewage water will be increase of plant growth (Moradmand, 2008). Generally, in the production of forage plants not only performance of dry mater but the quality of forage is also important. The main criteria in determining the quality of forage is crude protein, digestibility and percent of cell wall (Wilson, 1994). In this case digestibility is special importance because it is directly related to the amount of energy and nutrients received by the animals'(Tilley, and Terry,. 1963)

The aim of this study was to evaluate quantitative and qualitative characteristics of *Atriplex lentiformis* forage under sewage irrigation.

2. MATERIAL AND METHODS

The process of this research was conducted in the greenhouse of College of Natural Resources, University of Yazd. This study was done as a completely random design with three irrigation

treatment included (drinkable water 100%, drinkable water 50% + sewage water 50% and sewage water 100%) in 10 replicate during 4 month. watering performed by Manual sprinklers regularly every 2 days until germination and after that water at field capacity and the same amount was given to plants. After 4 month some quantitative characteristic such as leaf fresh and dry weight to stem ratio, total weight (leaves + stem) and height and qualitative characteristics such as percent of crude protein (CP), soluble carbohydrates (SC), total ash decreased, *Neutral detergent fiber* (NDF), *acid detergent fiber* (ADF), dry matter digestibility (DMD), metabolic energy (ME), crude fiber (CF), digestible energy (DE) and total digestible nutrients (TDN) were determined. For data analyses was used SPSS software and one-way Anova. Data normality was tested using the Kolmogorov-Smirnov. Average were compared with Duncan test at the 5% level.

3. RESULTS

3.1 Soil properties before applying irrigation

Soil properties used for planting before applying irrigation has been shown in Table 1.

Table 1. Characteristics of the soil before irrigation treatments

Soil texture	N (%)	Cd	Pb (mg/kg)	P	Mg	Ca	Na (meq/lit)	K	EC (dS/m)	pH
Sandy lom	0.12	3.36	2.46	62	2.3	25.77	11.21	0.6	2.61	7.46

3.2 Quantitative characteristics of Atriplex lentiformis

3.2.1 Fresh and dry leaf to stem ratio

The effect of irrigation treatment (sewage 100%, drinkable water 100%, and sewage 50% and drinkable water 50%) on dry leaf to stem ratio was significant at the 1% level. But the total weight (leaves + stem) and height of *Atriplex lentiformis* was not significant (Table 2).

Table 2. Analysis of variance effect of different irrigation treatments on quantity Atriplex lentiformis

Source	df	Mean Square			
		Total Weight	Height	Leaf to Stem Ratio(Wet)	Leaf to Stem Ratio(Dry)
Treatment	2	4.91^{ns}	35.62^{ns}	1.67^{*}	0.18^{ns}
Error	27	1.93	67.07	0.08	0.23
Total	29				

*ns: no significant difference at 5% level, *: significant at 5% and **: significant at 1%*

Wastewater treatment 100%, in compare to other treatments had maximum amount of leaf to stem ratio in both wet and dry (Figure 1).

3.3 Qualitative characteristics of Atriplex lentiformis

The effect of irrigation on the percentage of crud protein and total ash were significant differences. Soluble carbohydrates (SC) neutral detergent fiber (NDF), acid detergent fiber (ADF), dry matter digestibility (DMD), metabolism energy (ME), crude fiber (CF), digestible energy (DE) and total digestible nutrients (TDN) were not affected by different irrigation treatments (Table 3).

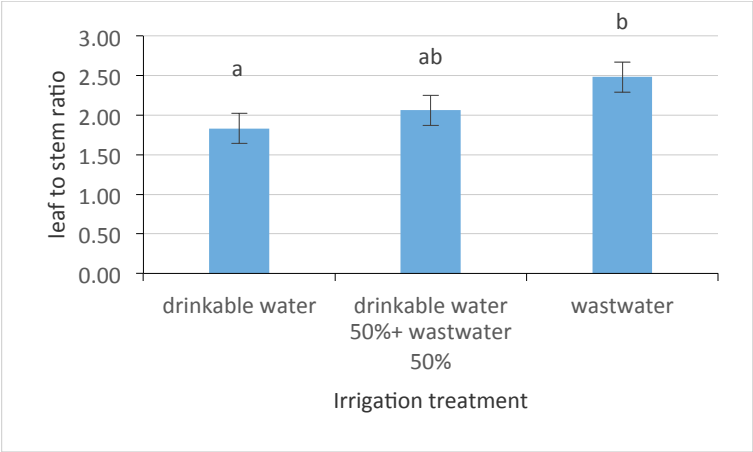

Figure 1. Comparison of the effect of irrigation on fresh and dry leaf to stem ratio of Atriplex lentiformis according to Duncan test at 5% level

Table 3. Analysis of variance effect of different treatments on Atriplex lentiformis forage quality.

Source	df	Mean Square								
		CP	CF	DE	ME	Ash	WSE	DMD	TDN	ADF
Treatment	2	10.91^{*}	0.69^{ns}	1.49^{ns}	0.14^{ns}	0.61^{**}	0.41^{ns}	4.87^{ns}	4.43^{ns}	3.35^{ns}
Error	6	3.95	2.09	4.02	0.19	0.04	0.86	6.67	11.05	8.35

ns: no significant difference at 5% level, *: significant at 5% and **: significant at 1%

3.4 Crude protein

Mean comparison showed that crude protein in the sewage water 100% compare to drinkable water100% had the highest value.

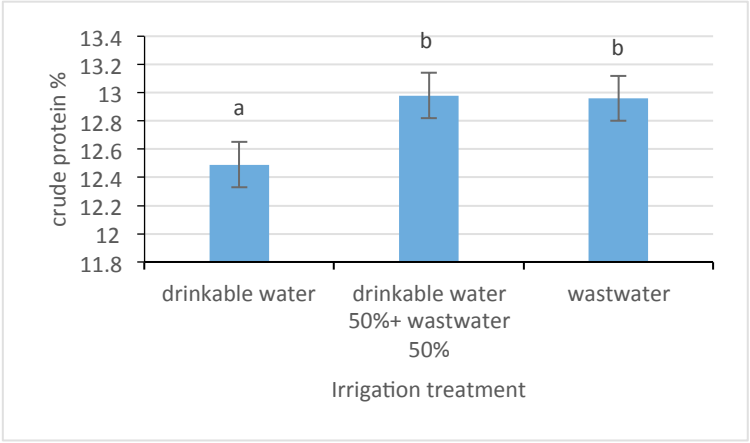

Figure 2. Comparison of the effect of irrigation on the percentage of crude protein of Atriplex lentiformis according to Duncan test at 5% level.

3.5 Total Ash

The highest amount of total ash in drinkable water 100% and the lowest waste water 100% was observed (Figure 2).

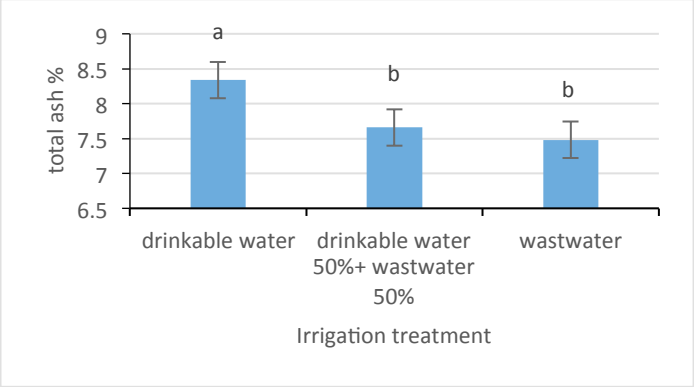

Figure 3. Comparison of the effect of irrigation on the percentage of total ash of Atriplex lentiformis according to Duncan test at 5% level.

4. DISCUSSION AND CONCLUSION

Sewage increased leaf to stem ratio in state of the wet. Although leaf to stem ratio, is a Quantity parameter but it has an impact on quality. Increase leaf to stem ratio, is due to the increasing number and leaf area to stem ratio. Using wastewater for irrigation cause to facilitate Foliation and increased the number of leaves and consequently increasing plant photosynthesis (Myers, et al, 1996).

Sewage increased the percentage of crude protein and reduced total ash of *Atriplex lentiformis*. It may be because of large quantities of organic matter to inorganic materials in plant. High crude protein concentration can be attributed to the presence of adequate amounts of nitrogen in wastewater. Adjei, and Rechcigl, 2002 Reported that wastewater increase the protein content of forage. There was no significant change in cell wall in different treatments. Plant cell walls increased as a result of exposure to biotic and abiotic stresses. So it seems that in this study, plants haven't been faced with stress in different ratios of sewage and drinkable water. Therefore, it seems in situations where there is limited water resources in arid regions if proper treatment, the use of wastewater not only to compensate the shortage of water resources for feed produce but is also effective in improving forage quality.

REFERENCES

Adjei, M.B., and Rechcigl, J.E. 2002. Bahiagrass production and nutritive value as affected by domestic wastewater residuals. Agronomy Journal. 94: 1400-1410.

Ali Nejad Jahromy, H., Mohammad Khani, A., and Salehi, M.H. 2012. Effect of municipal sewage sludge on growth and yield and accumulation of lead and cadmium of Shahrekord *Melissa oficinalis*. Journal of Science and Technology of Agriculture and Natural Resources, Water and Soil Sciences. 16(60): 173-185.

Ben- Ghadelia, D., Soloman, R., Miron, J., Yosef, E., Zomberg, Z., and Kipnis, T. 2001. Effect of water salinity on composition and in vitro digestibility of winter annual ryegrass grown in Arava desert. Journal of Animal Feed Science and Technology. 91: 139-147.

Jalali, A., Galavi, M., Ghanbari, A., Ramroudi, M., and Yousefolahi, M. 2010. The effect of irrigation with treated wastewater and urban and performance of heavy metals in forage sorghum (*Sorghum bicolor* L.). Journal of Science and Technology of Agriculture and Natural Resources, Water and Soil Sciences. 52(5): 15-24.

Moradmand, M., 2008. The effect of irrigation with treated wastewater of Shahrekord on growth and yield of pepper and elements concentrations in their tissues. M.Sc. thesis, Soil Science Engineering, Faculty of Agriculture, University of Shahrekord. 143p.

Myers, B.J., Theiveyanath, S.O., Brian, N.O., and Bond, W.J. 1996. Growth and water use of *Eucalyptus grandis* and *Pinus radiata* plantation irrigated with effluent. Journal of Tree Physiuol. 16: 211-219.

Paliwal, K., Karunaichamy, K.S.T.K., and Anonthavalli, M. 1998. Effect of sewage water irrigation on growth, performance, biomass and nutrient accumulation in *Hardwickia binata* under nursery conditions. Journal of Ioresource Technology. 66: 105-111.

Tilley, J.M.A., and Terry, R.A. 1963. A two- stage technique for the In Vitro digestion of forage crops. Journal of British Grassland Society. 18: 104-111.

Wilson, J.R., 1994. Cell wall characteristics in relation to forage digestion by ruminants. Journal of Agricultural Science Cambridge. 122: 173-182.

Yadav, R.K., Goyal, B., Sharma, R.K., Dubey, S.K., and Minhas, P.S. 2002. Post irrigation impact of domestic sewage effluent on composition of soils, crops and ground water-A case study. Journal of Environment International. 28(6): 481-486.

Proceedings of the 10th World Congress of EWRA 'Panta Rhei', 5-9 July 2017, Athens, Greece
© 2017 *European Water Resources Association*

Spatial and temporal assessment of potential soil erosion over Greece

A.P. Kazamias* and M. Sapountzis
Aristotle University of Thessaloniki, School of Forestry and Natural Environment, Laboratory of Mountainous Water Management and Control, Thessaloniki, Greece
* *e-mail: kazamias.petros@gmail.com*

Abstract: Soil erosion is considered as one of the most important environmental problems in the Mediterranean region threatening soil and water resources. The main purpose of this study is to investigate the spatial and seasonal distribution of potential soil loss across Greece. The Revised Universal Soil Loss Equation (RUSLE) model is applied at monthly time-step in a geographic information system (GIS) framework using freely available gridded data and remote sensing derived products. The rainfall erosivity (R-factor) is estimated using long-term monthly average precipitation from the CHELSA high-resolution gridded climate data set. The soil erodibility factor (K-factor) is estimated using ISRIC-World Soil Information SoilGrids250m global gridded maps of soil properties and classes. The cover management factor (C-factor) and the topographic factor (LS-factor) are assessed using remote sensing data. Time-series normalized difference vegetation index (NDVI) data from the Moderate Resolution Imaging Spectroradiometer (MODIS) are used for the C-factor and the digital elevation model (DEM) from Advanced Spaceborne Thermal Emission and Reflection Radiometer (ASTER) is used for the LS-factor. The average annual soil erosion over Greece is estimated at 4.75 t $ha^{-1}yr^{-1}$. About, 12.33% of the Greek territory is observed with soil erosion rates higher than 10 t $ha^{-1}yr^{-1}$, mainly located in high relief areas. Autumn and winter months are the most erosive, demonstrating high rainfall erosivity (R-factor) and vegetation cover (C-factor) values. Finally, 4 out of the 46 Greek River Basins (RBs) are found with average soil erosion rates greater than 15 t $ha^{-1}yr^{-1}$. The results of this study further confirm the seasonality of soil erosion under Mediterranean climate and vegetation conditions.

Key words: Soil erosion, RUSLE, GIS, Remote sensing, Greece

1. INTRODUCTION

Soil erosion is considered as one of the most important environmental problems across the earth as it threatens soil fertility, water resources and agriculture productivity (Rahman et al., 2009). The semiarid Mediterranean regions are particularly vulnerable to erosion because of major land-use changes over the last decades and the long dry periods followed by intensive and erosive rainfalls (Van Der Knijff et al., 1999). Monitoring soil erosion in situ is very costly and usually limited to small experimental sites. The development of many empirical and physical soil erosion models coupled with remote sensing and GIS allowed the assessment of soil erosion risk across a wide range of spatiotemporal scales (Millward and Mersey, 1999; Wu and Wang, 2007). Among these models, the most widely used are the empirical USLE-family models (USLE/RUSLE) because of their simplicity, robustness and efficiency (Xiaosong et al., 2011).

Several studies have been conducted in the Greek territory for soil erosion risk assessment at local/regional scales, but none of them at country-scale. The majority of these studies estimated the potential annual soil loss without taking into account the intra-annual temporal variability of vegetation and rainfall, two important factors affecting soil erosion processes. Some recent studies explored soil erosion at monthly or seasonal time-step (Alexandridis et al., 2015; Panagos et al., 2012) and their findings suggest this approach as much more consistent for estimating the potential annual soil erosion. The objective of this study is to assess and map the spatial distribution of soil erosion over Greece at a monthly time-step and identify River Basins prone to soil erosion.

2. MATERIAL AND METHODS

2.1 Study area

Greece is a Mediterranean country, located in southeastern Europe (34° - 42° N, 19° - 28° E), covering an area of 131,957 km^2 with a coastline stretching for 15,000 km. It has a typical Mediterranean climate characterized by mild, wet winters and dry, hot summers. The complex topography of Greece and particularly the Pindos mountain range crossing Greece from NW to SE contribute to the spatial heterogeneity of climate. The average annual precipitation ranges from more than 2000 mm in the mountainous areas of northwest Greece to less than 400 mm in Attica basin of central Greece and western Cyclades (Nastos et al., 2016). According to CORINE Land Cover 2012 (CLC2012) of the European Environment Agency (EEA, Copenhagen, 2012; http://www.eea.europa.eu) 69.2% of the Greek territory is covered by forest and semi-natural vegetation (shrublands and grasslands), followed by agricultural areas which cover 23.1%, artificial surfaces cover 3.5%, water bodies and wetland cover 1.9% and finally other land cover types comprise 2.2% of the total area. Following the implementation of the EU Water Framework Directive (WFD) Greece was divided into 46 River Basins (RBs).

2.2 Soil erosion prediction by RUSLE

The Revised Universal Soil Loss Equation (RUSLE) model was developed by Renard et al. (1997) as a revision and update on the Universal Soil Loss Equation (USLE) by Wischmeier and Smith (1978). The RUSLE function (Eq.1) incorporates five different factors related with climatology, pedology, topography, land cover and land management for the calculation of soil loss.

$$A = R \times K \times LS \times C \times P \quad (1)$$

where A is the average annual soil loss (t ha^{-1} yr^{-1}), R is the rainfall erosivity factor (MJ mm ha^{-1} h^{-1} yr^{-1}), K is the soil erodibility factor (t ha h ha^{-1} MJ^{-1} mm^{-1}), L is the slope length factor (dimensionless), S is the slope steepness factor (dimensionless), C is the vegetation cover factor (dimensionless), P is the conservation practice factor (dimensionless).

In the present study, RUSLE has been adopted in a Geographical Information System (GIS) framework to predict annual soil erosion on a pixel-by-pixel basis (Eq.2), where the monthly soil loss ($A_{monthly}$) values were computed for each month of the year 2013 (Eq.3).

$$A_{annual} = \sum_{j=1}^{J=12} (A_{monthly})j \quad (2)$$

$$A_{monthly} = R_{monthly} \times K \times LS \times C_{monthly} \times P \quad (3)$$

Two factors, the rainfall erosivity (R-factor) and the vegetation cover (C-factor) were calculated with different data for each month, while soil erodibility (K-factor) and slope length and steepness (LS-factor) were assumed constant for the entire year. The conservation practice (P-factor) was assigned the value of 1 because there were no reliable data to define its value. Each factor of the RUSLE model was calculated in raster format. In order to have consistent results all raster layers were projected to the Universal Transverse Mercator (UTM) Zone 34N projection system and were resampled to the same pixel size of 250 m x 250 m. Also, artificial surfaces, water bodies and wetlands were masked out from the produced soil loss raster maps. The study was supported by SAGA GIS 2.1.2, ESRI ArcGIS 10.0 and R programming language.

2.3 RUSLE input data

2.3.1 Rainfall erosivity factor (R)

The rainfall erosivity factor (R) measures the erosive force of a specific rainfall in a particular location (Morgan, 2004). In the present study, long-term average monthly precipitation data from the CHELSA climate data set (Karger et al., 2016) were used to calculate monthly R-factor values, following Eq.4,5 developed by Arnoldus (1980). CHELSA is a high resolution (30 arcsec, ~1 km) gridded climate data set providing mean monthly temperature and precipitation values for the time period 1979-2013 for the earth's land surface areas.

$$R_{annual} = \sum_{i=1}^{I=12} (R_{monthly})i \quad (4)$$

$$R_{monthly} = 1.735 \times 10^{\left(1.5 \log_{10}\left(\frac{p_i^2}{P}\right) - 0.08188\right)} \quad (5)$$

where R_{annual} is the annual rainfall erosivity (MJ mm ha^{-1} h^{-1} yr^{-1}), $R_{monthly}$ is the monthly rainfall erosivity (MJ mm ha^{-1} h^{-1}), p_i is the monthly rainfall (mm) and P is the annual rainfall (mm).

2.3.2 Soil erodibility factor (K)

Soil erodibility depends on many soil properties such as soil texture, aggregate stability, shear strength, infiltration capacity, organic content and chemical composition (Morgan, 2004). In practical terms, the soil erodibility factor is a quantitative annual value defining the resistance of soil to both detachment and transport. In the present study, the soil erodibility factor (K) was calculated using Eq.6 suggested by Renard et al. (1997), which is based on the geometric mean particle size and requires the percentage of sand, silt and clay contents. The soil texture information were derived from ISRIC-World Soil Information SoilGrids250m (Hengl et al., 2016), a dataset with global gridded soil information based on machine learning techniques. Three raster layers at 250 m resolution with clay content (weight %), silt content (weight %) and sand content (weight %) of topsoil (15 cm depth) were downloaded from http://soilgrids.org. Combining the above three raster layers, the geometric mean particle size was derived for each grid cell (Eq. 7). Afterwards, the K-factor was estimated for each grid cell (Eq. 6):

$$K = 0.0034 + 0.0405 \times \exp\left[-0.5\left(\frac{\log D_g + 1.659}{0.7101}\right)^2\right] \quad (6)$$

$$D_g = \exp(0.01 \sum f_i \ln m_i) \quad (7)$$

where K is the soil erodibility factor (t ha h ha^{-1} MJ^{-1} mm^{-1}), D_g is the geometric mean particle size for each particle size class (clay, silt, sand), f_i is the corresponding particle mass fraction for each particle class in percent and m_i is the arithmetic mean of the diameter limits for each particle size class (mm) based on the USDA classification. The m_i values for each soil particle class are the following: for clay 0.0010 mm, for silt 0.0026 mm and for sand 1.025 mm.

2.3.3 Topographic factor (LS)

The slope length factor (L) and slope steepness factor (S) are generally lumped together as the topographic factor (LS), reflecting the effect of terrain morphology and topography on soil erosion processes (Lou et al. 2004). In this work, the LS-factor was computed in the System for Automated

Geoscientific Analyses (SAGA) GIS software using the Module LS factor and following the algorithm developed by Desmet and Govers (1996). The LS-factor calculation required a digital elevation model (DEM) which was derived from the Advanced Spaceborne Thermal Emission and Reflection Radiometer (ASTER) with a cell size of 30 m.

2.3 Vegetation cover factor (C)

The vegetation cover factor (C) reflects the effect of cropping and management practices on soil erosion rates in agricultural areas and the effect of natural vegetation on reducing soil erosion in forested areas(Renard et al., 1997; Wischmeier and Smith, 1978). The C-factor gets values between 0 and 1; values closer to 0 indicate dense vegetation, while values closer to 1 are for bare soil. Several methodologies are proposed in the bibliography for calculating C-factor at regional scale by incorporating vegetation indices derived from satellite images. In the present study, monthly C-factor maps were produced from monthly Normalized Difference Vegetation Index (NDVI) products following Eq.8 proposed by Van Der Knijff et al. (1999):

$$C = \exp\left[-a\frac{NDVI}{(b-NDVI)}\right] \quad (8)$$

where a and b are unitless parameters that determine the shape of the curve relating NDVI and C-factor values.

Van Der Knijff et al. (1999) suggested that this scaling approach gives better results than assuming linear relationship. Also, the values of 2 and 1 were selected for the parameters a and b, respectively (Gitas et al., 2009; Kouli et al., 2009; Van Der Knijff et al., 1999). The monthly NDVI products were calculated from the 16-day MODIS NDVI (MOD13Q1) composites for the year 2013. The resulting monthly C-factor maps have the same spatial resolution as the MODIS NDVI composites, namely 250 m pixel size.

3. RESULTS AND DISCUSSION

3.1 RUSLE factors

For the period 1979-2013, the average rainfall erosivity over Greece was found to be 372.2 MJ mm ha^{-1} h^{-1} yr^{-1}, with values ranging from 80.86 to 1316.37 MJ mm ha^{-1} h^{-1} yr^{-1}. From the spatial distribution of the R-factor (Figure 1D), it can be clearly denoted that the Pindos mountain range affects the values of R-factor, acting as a boundary between western and eastern Greece. High values were observed in the western part of Greece, the Ionian Islands, western Crete and some islands located in the south-eastern Aegean Sea, while low values were found in the eastern and northern Greek mainland. Concerning the temporal variability of rainfall erosivity, the highest values were observed during the winter period and late autumn. The highest monthly rainfall erosivity rates were observed in December, with values ranging from 19.96 to 464.95 MJ mm ha^{-1} h^{-1} and a mean value of 112.07 MJ mm ha^{-1} h^{-1}. The lowest monthly rainfall erosivity rates were observed during the summer period, ranging from 0 to 2.59 MJ mm ha^{-1} h^{-1}.

The soil erodibility values for Greece ranged from 0.0025 to 0.045 t ha h ha^{-1} MJ^{-1} mm^{-1}, with a mean value of 0.038 t ha h ha^{-1} MJ^{-1} mm^{-1} and standard deviation (SD) of 0.0024 t ha h ha^{-1} MJ^{-1} mm^{-1} (Figure 1C).

The topographic factor (LS) values ranged from 0 to 16, with a mean value of 2.86 and standard deviation (SD) of 2.47 (Figure 1B). The highest values for LS-factor occurred in the steep hillslopes of Pindos mountain range and on Mount Olympus.

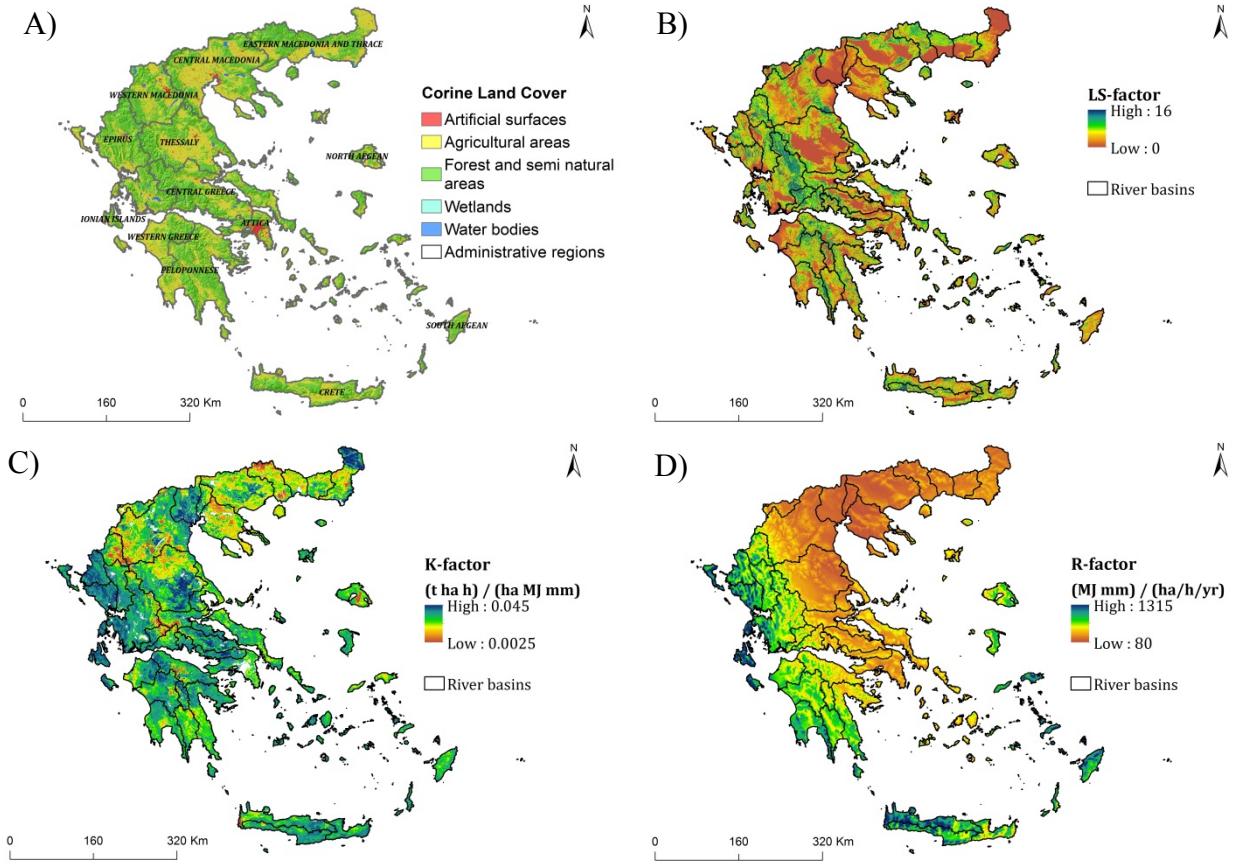

Figure 1. A) Land cover map (CLC2012) with the 13 administrative regions of Greece, B) LS-factor map of Greece, C) K-factor map of Greece, D) R-factor map of Greece.

The highest C-factor values were observed during the winter months (December, January, February) ranging from 0.187 to 0.439, with a mean value of 0.246. Similar high values were found in autumn (September, October, November) and March with mean C-factor values in the range of 0.163 for each month. The lowest values were noticed in spring and summer period (April-August) with mean C-factor values close to 0.1.

3.2 Monthly and annual potential soil loss

The boxplots in Figure 2 depict the distribution of potential monthly soil loss for Greece. The highest values were observed in December with a mean soil loss of 1.78 t $ha^{-1}m^{-1}$ (SD=5.92), whereas the lowest monthly soil loss rates were observed during summer months (June, July and August) with mean values of 0.1 t $ha^{-1}m^{-1}$ (SD=0.020). The contribution of each season to annual soil loss is the following: winter (December, January, February) with 63.1%, autumn (September, October, November) with 26.19%, spring (March, April, May) with 10.39% and summer (June, July, August) with 0.32%.

The estimated annual soil loss for Greece ranged from 0.1 to 148.16 t $ha^{-1}yr^{-1}$, with an average value of 4.75 $ha^{-1}yr^{-1}$. The potential annual soil erosion was subdivided into 6 classes and the resulting map is illustrated in Figure 3A**.** Approximately 77.56% of the Greek territory is classified as either very low (0-1 t $ha^{-1}yr^{-1}$) or low (1-5 t $ha^{-1}yr^{-1}$) potential soil erosion risk, 10.11% as moderate (5-10 t $ha^{-1}yr^{-1}$) and 9.95% as high (10-20 t $ha^{-1}yr^{-1}$) and very high (20-50 t $ha^{-1}yr^{-1}$). Finally, only 2.38% of the investigated area is prone to severe erosion (> 50 t $ha^{-1}yr^{-1}$). The areas with severe erosion rates were located across the Pindos mountain range and in Crete Island, due to high rainfall erosivity and large LS-factor values.

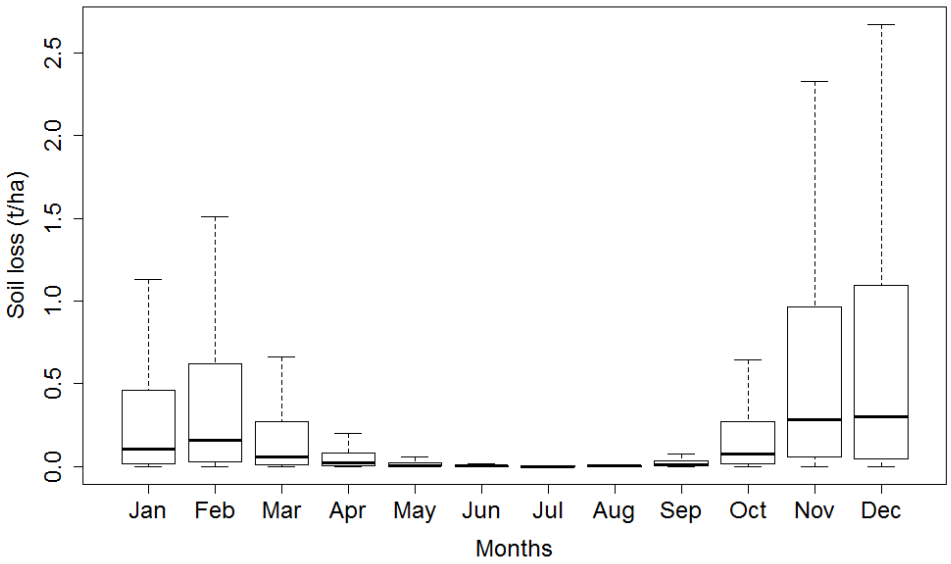

Figure 2. Boxplots showing the monthly distribution of soil loss.

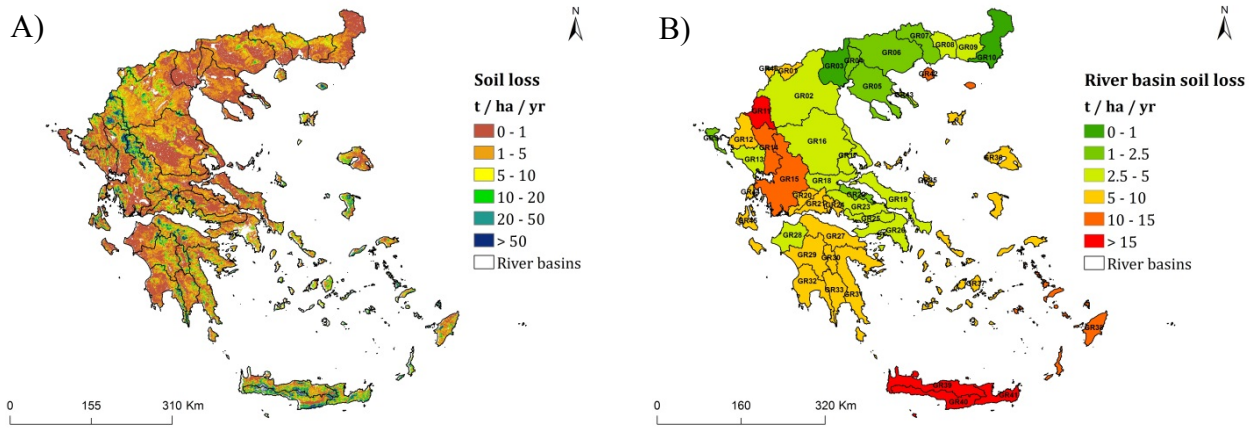

Figure 3. A) Spatial distribution of potential annual soil erosion for Greece, B) Map of average potential annual soil erosion for every river basin in Greece (labels correspond to RBs EU-code).

The final objective of this study was to quantify potential soil erosion rates across all Greek River Basins. In Figure 3B the average potential annual soil erosion values of each River Basin are classified into 6 classes. Half of the river basins, located in Eastern Macedonia, Central Macedonia, Western Macedonia, Thessaly, Central Greece and Attica, have average soil erosion rates lower than 5 t ha^{-1} yr^{-1}. River basins located in the western part of the Pindus mountain range, in North/South Aegean and in the Peleponnese region show higher average soil erosion rates with values ranging from 5 to 15 t $ha^{-1}yr^{-1}$. Finally, four river basins are prone to high erosion rates (>15 t $ha^{-1}yr^{-1}$), Aoos (GR11) and all three RBs in Crete Island (GR39, GR40 and GR41).

4. CONCLUSIONS

The present study was a first attempt to estimate the spatial and temporal distribution of potential soil erosion in Greece and identify River Basins prone to soil erosion risk. The average annual soil erosion was found to be 4.75 $ha^{-1}yr^{-1}$, of which almost 90% was produced during autumn and winter seasons of the year. These results follow the seasonal pattern of rainfall erosivity (R-factor) and vegetation cover (C-factor), which both showed high values in autumn and winter, and low values

in summer and spring. These findings have also been confirmed in other studies conducted in the Mediterranean region (Karydas and Panagos, 2016; Panagos et al., 2014, 2012). The spatial distribution of soil erosion in Greece confirmed the findings of many other studies suggesting that soil movement is mainly controlled by topography, and furthermore, that soil loss results from the RUSLE model are strongly correlated with steep slopes and the topographic factor (Ali and De Boer, 2010; Kouli et al., 2009; Prasannakumar et al., 2012).

It must be noted that the quantitative assessment of soil loss using an empirical model like RUSLE with coarse resolution datasets as inputs has great uncertainty. Nevertheless, the spatial and seasonal distribution of soil erosion across Greece seems to be accurately simulated, leading in the identification of River Basins with high erosion rates. These results can be used for effective environmental policy management and the implementation of mitigation measures to protect agricultural and urban areas.

REFERENCES

Alexandridis, T.K., Sotiropoulou, A.M., Bilas, G., Karapetsas, N., Silleos, N.G., 2015. The effects of seasonality in estimating the C-factor of soil erosion studies. L. Degrad. Dev. 26, 596–603.

Ali, K.F., De Boer, D.H., 2010. Spatially distributed erosion and sediment yield modeling in the upper Indus River basin. Water Resour. Res. 46.

Arnoldus, H., 1980. An approximation of the rainfall factor in the Universal Soil Loss EquationDe Boodt, M., Gabriels, D. (Eds.), Assessment of Erosion. Wiley, New York, pp. 127–132.

Desmet, P.J.J., Govers, G., 1996. A GIS procedure for automatically calculating the USLE LS factor on topographically complex landscape units. J. Soil Water Conserv. 51, 427–433.

Gitas, I.Z., Douros, K., Minakou, C., Silleos, G.N., 2009. Multi-Temporal Soil Erosion Risk Assessment in N . Chalkidiki Using a Modified Usle Raster Model. EARSeL eProceedings 8, 40–52.

Hengl, T., Mendes De Jesus, J., Heuvelink, G.B.M., Gonzalez, M.R., Kilibarda, M., Blagotí, A., Shangguan, W., Wright, M.N., Geng, X., Bauer-Marschallinger, B., Guevara, M.A., Vargas, R., Macmillan, R.A., Batjes, N.H., Leenaars, J.G.B., Ribeiro, E., Wheeler, I., Mantel, S., Kempen, B., 2016. SoilGrids250m: Global Gridded Soil Information Based on Machine Learning, PLOS One.

Karger, D.N., Conrad, O., Böhner, J., Kawohl, T., Kreft, H., Soria-Auza, R.W., Zimmermann, N., Linder, H.P., Kessler, M., 2016. Climatologies at high resolution for the Earth land surface areas. arXiv:1607.00217. [Physics] 1–19.

Karydas, C.G., Panagos, P., 2016. Modelling monthly soil losses and sediment yields in Cyprus. Int. J. Digit. Earth 9, 766–787.

Kouli, M., Soupios, P., Vallianatos, F., 2009. Soil erosion prediction using the Revised Universal Soil Loss Equation (RUSLE) in a GIS framework, Chania, Northwestern Crete, Greece. Environ. Geol. 57, 483–497.

Millward, A. a, Mersey, J.E., 1999. Adapting the RUSLE to model soil erosion potential in a mountainous tropical watershed. Catena 38, 109–129.

Morgan, R.P.C., 2004. Soil Erosion and Conservation, 3rd ed. Wiley-Blackwell.

Nastos, P.T., Kapsomenakis, J., Philandras, K.M., 2016. Evaluation of the TRMM 3B43 gridded precipitation estimates over Greece. Atmos. Res. 169, 497–514.

Panagos, P., Christos, K., Cristiano, B., Ioannis, G., 2014. Seasonal monitoring of soil erosion at regional scale: An application of the G2 model in Crete focusing on agricultural land uses. Int. J. Appl. Earth Obs. Geoinf. 27, 147–155.

Panagos, P., Karydas, C.G., Gitas, I.Z., Montanarella, L., 2012. Monthly soil erosion monitoring based on remotely sensed biophysical parameters: a case study in Strymonas river basin towards a functional pan-European service. Int. J. Digit. Earth 5, 461–487.

Prasannakumar, V., Vijith, H., Abinod, S., Geetha, N., 2012. Estimation of soil erosion risk within a small mountainous sub-watershed in Kerala, India, using Revised Universal Soil Loss Equation (RUSLE) and geo-information technology. Geosci. Front. 3, 209–215.

Rahman, M.R., Shi, Z.H., Chongfa, C., 2009. Soil erosion hazard evaluation-An integrated use of remote sensing, GIS and statistical approaches with biophysical parameters towards management strategies. Ecol. Modell. 220, 1724–1734.

Renard, K.G., Foster, G., Weesies, G., McCool, D., Yoder, D., 1997. Predicting soil erosion by water: a guide to conservation planning with the Revised Universal Soil Loss Equation (RUSLE). Agric. Handb. No. 703.

Van Der Knijff, J.M., Jones, R.J. a., Montanarella, L., 1999. Soil Erosion Risk Assessment in Italy 54.

Wischmeier, W., Smith, D., 1978. Predicting rainfall erosion losses: a guide to conservation planning. Agric. Handb. No. 537 163.

Wu, Q., Wang, M., 2007. A framework for risk assessment on soil erosion by water using an integrated and systematic approach. J. Hydrol. 337, 11–21.

Xiaosong, L.I., Bingfang, W.U., Hao, W., Jin, Z., 2011. Regional soil erosion risk assessment in Hai Basin. J. Remote Sens. 15, 372–387.

Proceedings of the 10th World Congress of EWRA 'Panta Rhei', 5-9 July 2017, Athens, Greece
© 2017 *European Water Resources Association*

Water availability and requirements for precision agriculture in vulnerable agroecosystems

N.R. Dalezios[1,2], N. Dercas[2], N.V. Spiropoulos[3] and E. Psomiadis[2]
[1] *Department of Civil Engineering, University of Thessaly, Volos, Greece*
[2] *Department of Natural Resources Management and Agricultural Engineering, Agricultural University of Athens, Athens, Greece*
[3] *SIGMA Geotechnologie, Munich, Germany*
[*] *e-mail: dalezios.n.r@gmail.com*

Abstract: Agriculture is strongly influenced by the availability of water. Crop yields are affected by variations in climatic factors, like temperature and precipitation, and the frequency and severity of extreme events, like droughts. The aim of this paper is to present the water availability and requirements in vulnerable agriculture. This information contributes to precision agriculture for effective crop monitoring and irrigation management. A drought-prone area characterized by vulnerable agriculture is selected, namely Thessaly in central Greece. Water availability is assessed through rainfall frequency analysis for climate variability impacts. Crop water requirements are considered by estimating crop evapotranspiration (ET) through the combined use of WV-2 satellite images with ground-truth data. The satellite-based ETcsat is produced by using the reference ETo from FAO method, meteorological data and Kc extracted from NDVI utilizing the Red and NIR bands. Based on precipitation frequency analysis, evidence of precipitation reductions is shown. The results justify the importance of water availability for vulnerable agriculture and the need for drought monitoring in the Mediterranean basin as part of an integrated climate adaptation strategy. The results also justify the combined use of WV-2 satellite images with ground-truth data for monitoring crop ET and the incorporation into the precision agriculture methodology has proven to be very useful for optimal agricultural production.

Key words: water availability, evapotranspiration, vulnerable agriculture, rainfall frequency, drought, precision agriculture

1. INTRODUCTION

Agriculture significantly depends on climate resources and, specifically, is strongly influenced by water availability. Moreover, climate variability has significant impact on agricultural production at local, regional, as well as global scales. Climate change is expected to modify rainfall, evaporation, runoff and soil moisture storage patterns. Similarly, variability of seasonal precipitation pattern is also significant (Dalezios, 2011). Crop yields are affected by variations in climatic parameters, such as temperature and precipitation, and the frequency and severity of extreme events, like droughts, floods, severe rainstorms and hail (Dalezios (ed.), 2017). Several regions, such as the entire Mediterranean basin, are characterized by vulnerable agriculture due to the combined effect of reduced precipitation and temperature increases in areas already coping with water scarcity (Dalezios et al., 2016). Agricultural production risks could become an issue in the Mediterranean region as mainly droughts and heatwaves are likely to increase the incidence of crop failure (Dalezios et al., 2009). As yield variability increases, the food supply is at increasing risk. Specifically, the predicted increase in extreme weather events is expected to increase yield variability and to reduce average yield (Alexandrov and Hoogenboom, 2000). In particular, in the European Mediterranean region, cereal yields are likely to be reduced due to limited water availability, heat stress and the short duration of the grain-filling period.

Irrigation has always been significant for crop production in most Mediterranean countries mainly due to high evapotranspiration rates and restricted rainfall inputs. The demand for irrigation water is projected to rise in a warmer climate, increasing the competition between agriculture and urban, as well as industrial, water users (Olesen and Bindi, 2002). More water is expected to be required per unit area under drier conditions, and peak irrigation demands are also predicted to rise due to more severe heat waves. Precision

agriculture is a rather recent approach to address the issues of water availability and needs for effective crop water and fertilizer monitoring in vulnerable agroecosystems (Dalezios et al., 2012).

The objective of this paper is to present water availability and water requirements in vulnerable agroecosystems in the Mediterranean region by using precision agriculture methods in order to achieve optimal crop water monitoring and irrigation management. A drought-prone area characterized by vulnerable agriculture is selected, namely Thessaly in central Greece. At first, the study area is presented showing the need for vulnerability assessment, which affects agriculture and its sustainability. Water availability is considered through drought assessment and rainfall frequency analysis. Specifically, mainly agricultural droughts affect sustainability of agriculture and may result in environmental degradation of a region, which is one of the factors contributing to the vulnerability of agriculture. In this paper, the adjusted Vegetation Health Index (VHI) is used for the detection of agricultural drought and its impacts (Dalezios et al., 2014). Crop water requirements are also considered within the precision agriculture framework by estimating crop evapotranspiration (ET) through the combined use of WV-2 satellite images with ground-truth data sets (Psomiadis et al., 2016; Dercas et al., 2017). The satellite-based ETcsat is produced by using the reference ETo from FAO-56 Penman-Monteith equation based on meteorological data (Allen et al., 1998), and Kc extracted from NDVI utilizing the Red and NIR satellite bands.

2. STUDY AREA AND DATA SETS

2.1 Study Area

The study area is the region of Thessaly, located in central Greece, with a total area of 14,036 Km^2. Thessaly has a highly variable landscape with high mountains surrounding the plain, which is the largest in the country (Figure 1). Thessaly is characterized by vulnerable agriculture, due to water deficit for agriculture and the occurrence of extreme hydrometeorological events, such as hail and droughts. Mean annual precipitation over Thessaly is about 700mm, unevenly distributed in space and time, varying from about 400mm at the central plain to more than 1,850mm at the western mountain peaks (Dalezios et al., 2014). At the Thessalic plain the mean annual precipitation has been reduced over the last decades about 20% (Dalezios, 2011) and ranges between 250 to 500mm.

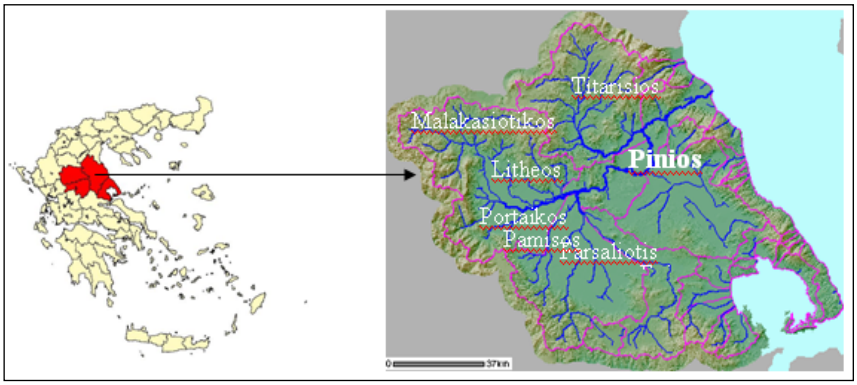

Figure 1. Geophysical map of Thessaly.

The Thessalic plain constitutes the main agricultural area of the country, with cotton being the major crop, however, wheat, sugar beets, maize, barley, horticulture, fruits, olive trees and recently energy crops are also cultivated. Since rainfall is, in general, rare from June to August, the resulted water deficit is replaced by irrigation in order to satisfy crop water needs. The amount of water used for irrigation purposes accounts for about 96% of the total water consumption.

2.2 Data sets

Data used in this study include daily values of temperature and precipitation covering a period of 46 years (1955-2000) from the meteorological station of Larissa. The precipitation data were divided into nine classes ranging from light to heavy and extreme precipitation events, and the number of precipitation events per class was calculated. The temperature trend for the period 1955-1975 is declining, whereas for the period 1976-2000 is increasing (Bampzelis et al., 2006). Thus, the time series is divided in two periods, namely 1955-1975 and 1976-2000. Since the duration of the two periods was different, the precipitation frequencies were normalized.

For the VHI estimation, a time series of 10-day Brightness temperature (BT) images was used extracted from Channels 4 and 5 for 20 consecutive hydrological years (October 1981 - September 2001) with resolution 8x8 km2 provided by NOAA. Similarly, a time series of 10-day Normalized Difference Vegetation Index (NDVI) extracted from Channels 1 and 2 for 20 consecutive hydrological years (October 1981 - September 2001) with resolution 8x8 km^2 provided by NOAA.

3. WATER AVAILABILITY

Annual precipitation is expected to decrease, then problems in the agriculture sector may come first from extreme events in water scarcity, e.g., long droughts, rather than from the decrease in average water availability. In the Mediterranean region, average yields are expected to decrease, but most of the concern is about the recurrence of extreme droughts with disastrous consequences.

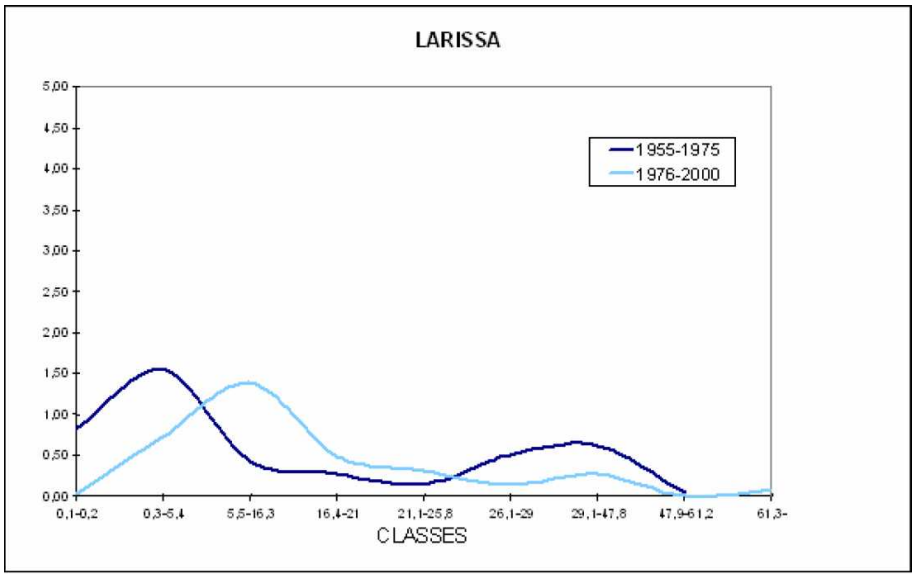

Figure 2. Precipitation Frequency analysis for Larissa station (from Dalezios, 2011).

Studies show increase in drought frequency for almost most parts of Europe. The regions most prone to drought risk increase are the entire Mediterranean basin and some parts of central and eastern Europe, where the projected irrigation water demand has increased (Giorgi et al., 2004). Changes in precipitation extremes in Europe agree that the intensity of daily precipitation events will predominantly increase also over many areas, whereas means are likely to decrease. The number of wet days in Europe is projected to decrease, which leads to longer dry periods except in the winters of western and central Europe.

For the impacts of climate variability and change to water availability, the trends of precipitation and evapotranspiration rates are investigated. Precipitation time series from Larissa station are used to delineate changes in the range and frequency of daily precipitation for two separate periods in the data set (Bampzelis et al., 2006). The frequency analysis results show that in Thessaly, there were indications of a shift towards higher precipitation intensities for the second period (after 1975). In

particular, precipitation of a slightly greater volume but less frequent was observed in the Larissa station for the period 1955-1975 compared to the latest period (1976-2000) (Figure 2). This fact indicates a trend for precipitation episodes with less total amounts, but of increased intensity causing floods and greater loss of water. Reduction of precipitation inputs and decline of water availability could adversely affect future crop production in the region and consequently the local economy.

For the quantification of agricultural drought, one of the most reliable and widely used indices is applied, namely VHI. The computation of VHI is based on satellite data of temperature and the NDVI. The VHI is a combination of the Vegetation Condition Index (VCI) and the Temperature Condition Index (TCI), both derived from NOAA/AVHRR satellite data (Kogan, 1995). VCI and TCI, as well as VHI, as properly adjusted, have been successfully applied for the detection of agricultural drought and for monitoring agricultural crops (Dalezios et al., 2014). The Vegetation Health Index (VHI) represents overall vegetation health and is used for drought mapping and crop yield assessment. The five classes of VHI that represent agricultural drought, as well as no drought conditions, are illustrated in Table 1. Specifically, from Table 1 it is evident that drought severity is decreasing with increasing VHI values, i.e. class 1 refers to extreme drought with VHI values less than 10, whereas for VHI values greater than 40 there is no drought. VHI is expressed by the equation:

$$VHI = 0.5 * (VCI) + 0.5 * (TCI) \quad (1)$$

In VHI computation, an equal weight has been assumed for both VCI and TCI, since moisture and temperature contributions during the vegetation cycle are not specified. Similarly, VCI and TCI vary from zero, for extremely unfavorable conditions, to 100, for optimal conditions.

Table 1. VHI drought classification scheme (from Kogan, 1995).

VHI values	Vegetative drought classes	Drought class numbers
<10	Extreme drought	1
<20	Severe drought	2
<30	Moderate drought	3
<40	Mild drought	4
>40	No drought	

The results consist of VHI estimation on a monthly basis for a period of 20 years (1981-2001) using satellite data and are shown in Table 2, which presents the cumulative areal extent of monthly VHI values throughout the warm season. Specifically, the initial four VHI severity classes of the analysis are merged into two in Table 2, namely extreme (class 1) and severe (class 2) drought into one class, and moderate (class 3) and mild (class 4) drought into another class, respectively. The reason for merging classes is the small number of pixels in each class in order to develop a sizeable data set for fitting models. The results indicate that drought occurs every year during the warm season starting in May with increasing severity and areal extent throughout the warm season with the maximum occurring in September. The majority of pixels is accumulated between mild to moderate drought severity classes indicating a significant decrease in the number of pixels from mild to extreme drought classes for all the months. The above findings justify the new scientific trend to develop and use composite drought indices for regional drought assessment and monitoring (Dalezios et al., 2016).

Table 2. Cumulative areal extent (number of pixels) of monthly VHI values (from Dalezios et al., 2014)

Class	1981	1982	1983	1984	1985	1986	1987	1988	1989	1990	1991	1992	1993	1994	1995	1996	1997	1998	1999	2000	2001
1&2	188	105	66	37	242	107	49	150	205	306	7	20	33	0	77	89	10	40	33	68	52
3&4	1136	1443	1634	1157	1820	1767	1394	1737	1533	2045	942	1255	1201	773	1005	1428	1407	1312	1450	1604	1059

4. WATER REQUIREMENTS

Precision agriculture is a dynamically developing field of agricultural science, which is based on geoinformatics. Monitoring water needs for agriculture based on precision agriculture methods requires a combination of field observations, such as crop characteristics, crop water requirements, as well as micro-meteorological data, such as daily air temperature, wind speed, humidity, and precipitation in order to calculate reference evapotranspiration (ET_o). High resolution satellite data are also used to analyze the spatial distribution and variability of crop coefficient (K_c) and crop evapotranspiration (ET_c) (Dalezios et al., 2011) and contribute through processing and analysis to decision support at field level (Dalezios et al., 2012).

4.1 Study area and data set

Two adjacent agricultural fields of cotton (1.8 ha) and corn (1.4 ha), respectively, were used during the growing season of 2015 in Thessaly, Central Greece (Figure 3a). Three diachronic WorldView-2 (WV-2) scenes were analyzed in bundle format (one 0.5m panchromatic channel and eight 2m multispectral channels in 16-bit digital format) due to excellent spatial and spectral information content. The acquisition dates were June 13, July 29 and Sep 2, 2015, respectively. Valuable ground field data were also acquired approximately the same dates, as above.

4.2 Image pre-processing

The methodological approach includes image filtering and pre-processing. Four WV-2 scenes were atmospherically, radiometrically and geometrically corrected (Lanzl and Richter, 1991; Updike and Comp, 2010). Several algorithms are in general used for removing the atmospheric effects on the data and the radiance values are converted to reflectance values. Various levels of input data are used to drive atmospheric models, ranging from detailed atmospheric profiles acquired by radiosondes to standardised models representative of general latitudinal areas. As atmospheric conditions are subject to spatiotemporal variability and no precise data related to them at the time of data acquisition are normally available, standardised atmospheric models are used, such as those provided by ATCOR3 model developed by DLR, Munich Germany, calibrating the data and converting the Digital Number (DN) values of each WV2 image to Top of Atmosphere (TOA) and ground reflectance through the Geomatica software (Dercas et al., 2017; Lanzl and Richter, 1991). This procedure was fulfilled utilizing the Digital Elevation Model (DEM) of the area, geographic longitude/latitude and the weather conditions that were present at the image acquisition time. The geometric registration was based on two different approaches: geocoding using image-to-GCPs and image-to-image as a master-to-slave approach (Spyropoulos, 1999). The first WV-2 acquired on May 17, corrected using 10 GCPs. All the other images orthorectified on the first image using image-to-image registration.

4.3 Image processing

Image processing involves the computation of the Chlorophyll and NDVI indices using Red, RedEdge, NIR(1) and NIR(2) of WV-2 channels (Figure 3b) and Red, RedEdge and NIR of ground sensor, principal component analysis and clustering leading to the production of thematic maps. This is the first attempt with new bands, especially with NIR(2) of WV-2, which is less influenced by atmosphere. The indices were applied onto 2m multispectral data and on pan-sharpened 0.5m data. Pan-sharpening is a digital synthesis, whereas the 2m multispectral channels are merged with the 0.5m panchromatic channel to generate another set of multispectral channels that preserve the spectral information, but in higher spatial feature space of 0.5m, thus enhancing the information integrity and clarity. In conjunction with field and meteorological data, as well as models, the

imagery was used to calculate reflectance, NDVI, fractional cover, crop coefficient (K_c) and crop evapotranspiration (ET_c) maps over the 100 km^2 image coverage.

4.4 Estimation of ET_o

Reference evapotranspiration (ET_o) is estimated by the FAO Penman-Monteith method using conventional meteorological data, which is consistent with actual crop water use data (Allen *et al.*, 1998):

$$ET_0 = \frac{0.408(R_n - G)\Delta + \gamma(\frac{900}{T_{mean} + 273})u_2(e_s - e_a)}{\Delta + \gamma(1 + 0.34u_2)} \quad (2)$$

where: T_{mean} is mean temperature (^oC), and u_2 is wind speed at 2 m height.

4.5 Estimation of K_c

The crop coefficient (K_c) is developed from NDVI indices of WV-2 channels and Red, RedEdge and NIR of ground sensor. The K_c integrates the effect of features that distinguish a typical field crop from the grass reference, which has a homogenous appearance and covers completely the ground. The values of K_c are influenced by crop type, climate, soil evaporation and crop growth stages (Allen et al., 1998). In FATIMA, the following relationship was developed (Dercas et al., 2017):

$$K_c = 1.33 * (Red\ NDVI) + 0.21 (R^2 = 0.92) \quad (3)$$

4.6 Estimation of crop evapotranspiration ET_c

Crop Evapotranspiration ET_c is the evapotranspiration from disease-free, well-fertilized crops, grown in large fields, under optimum soil water condition and achieving full production under the given climatic conditions (Allen et al., 1998). In FAO method, ET_c is calculated as follows:

$$ET_c = K_c * ET_0 \quad (4)$$

where ET_o is calculated by ground based observations. The satellite-based ET_{csat} is produced by using the reference ET_o from FAO-56 Penman-Monteith equation derived from meteorological data (Allen et al., 1998) and Kc extracted from NDVI utilizing the Red Edge and second NIR bands of WV-2, respectively. If there is not available a full data set for the use of Penman-Monteith equation, several other empirical equations could be employed, such as Hargreaves or Turk models, among others.

4.7 Results and discussion

The results are summarized in Figures 3 and 4. In particular, Figure 3a shows the crops' location within the selected field and Figure 3b shows the Red Edge NDVI. Figure 4 shows the plot of the estimated mean K_c values for cotton during the growing season of 2015 from equation (3) and the corresponding ET_{csat} from equation (4).

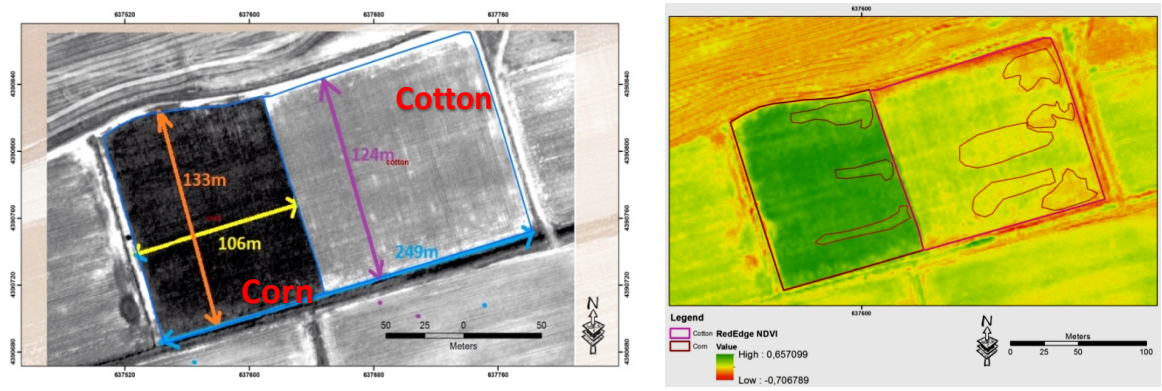

Figure 3. (a) The shape and area of the two selected crops, (b) The Red Edge NDVI (from Psomiadis et al., 2016).

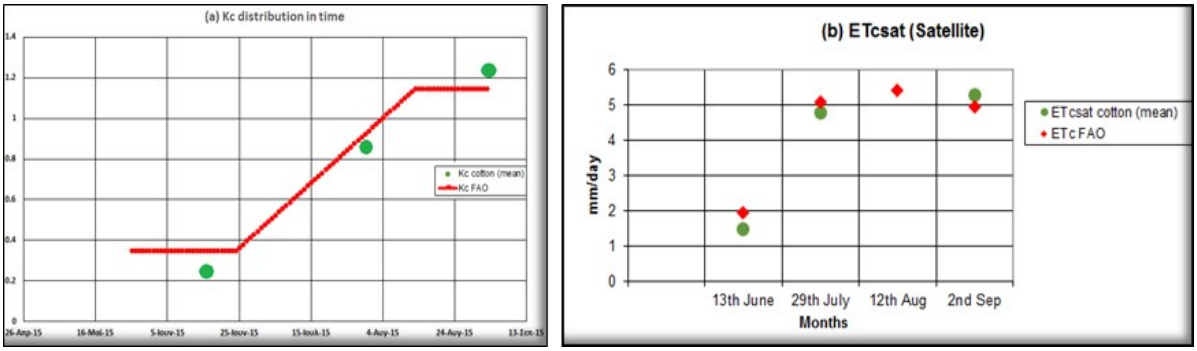

Figure 4. Temporal comparison (a) Kc and (b) ETcsat from WV-2 and ETc produced by FAO for cotton field in 2015 (from Dercas et al., 2017).

Figure 4 shows that both mean K_c (Figure 4a) and mean ET_{csat} (Figure 4b) follow the same pattern with increasing trend throughout the growing season, as expected. Specifically, ET_{csat} values are very close to ET_c FAO (Figure 4b), which is a promising sign for the new WV-2 approach. Moreover, the behavior of cotton Kc mean values based on Red and NIR spectral bands of WV–2 data, as compared with the Kc values from FAO for 2015, follows almost the same distribution pattern. Indeed, Kc is dependent on the type of satellite data and cannot be applied in a generic way. Spatial and spectral resolution are the key components of any sensor, which is used for Kc extraction. Sensors with different bandwidth of Red, Red Edge and NIR spectral bands create heterogeneous results. Additionally, the type and size of fields, such as small size farms or land fragmentation, plays a role on the satellite data and thus on the Kc equation to be used.

5. SUMMARY AND CONCLUSIONS

Climatic projections indicate increases in temperature and decreases in precipitation, combined with the more frequent occurrence of extreme events, such as drought, in the Mediterranean region. Agriculture is expected to be most influenced by the adverse impacts of climate change and variability, with high probability of crop production reductions, due to less availability of water for irrigation. The results of the frequency analysis show that there was a shift towards higher precipitation intensities for the second period (after 1975) indicating a trend for precipitation episodes with less amounts, but of increased intensity causing floods and greater loss of water. Moreover, in order to reduce the risk of climate change impacts on agriculture, comprehensive methodologies need to be developed, integrating the results of studies on drought and evapotranspiration assessment and monitoring, for the formulation of cost-effective mitigation measures and adaptation strategies. The results indicate that drought occurs every year during the warm season with increasing severity and areal extent with the maximum occurring at the end of

summer. The majority of pixels is accumulated between mild to moderate drought severity classes indicating a significant decrease in the number of pixels from mild to extreme drought classes for all the months.

The comparison of WorldView-2 (WV-2) satellite data and field measurements has shown that the utilization of WV-2 is definitely a useful tool for precision or operational farming, allowing not only the extraction of crop area, but also the derivation of useful parameters, such as ETc from Kc, which is derived from satellite data and can be used for the estimation of crop water and fertilization needs. The results of the applied methodology justify the combined use of WV-2 satellite images with ground-truth data set for monitoring ET_c in different crops.

ACKNOWLEDGEMENTS

Conventional meteorological data were obtained by the Hellenic National Meteorological Service. Satellite data were provided by NASA. Research was funded by the INTERREG Illb PRODIM project, EU FP6 PLEIADES project and currently by HORIZON2020 FATIMA project.

REFERENCES

Allen, R.G., Pereira, L.S., Raes, D., Smith, M., 1998. Crop evapotranspiration: Guidelines for computing crop requirements. Irrigation and Drainage Paper No. 56, FAO, Rome, Italy, 300p.

Alexandrov, V.A. and Hoogenboom, G., 2000. The impact of climate variability and change on crop yield in Bulgaria. Agricultural and Forest Meteorology, 104: 315-327.

Bampzelis, D., Chatzipli, A., Dadali, O. and Dalezios, N.R., 2006. Frequency analysis of precipitation characteristics in different climate zones for Greece. In: Proceedings of the 3rd HA1CTA International Conference: Information Systems in Sustainable Agriculture, Agroenvironment and Food Technology. Editors: Dalezios and Tziortzos, Publisched by EC, Luxenbourg, 20-23 September, Volos, Greece, 887-895.

Dalezios, N.R. (editor), 2017. Environmental Hazards Methodologies for Risk Assessment and Management. Publisher: IWA, London UK, 534pp.

Dalezios, N.R., N. Dercas and S. Eslamian, 2016. Water Scarcity Management: Part 2: Satellite-based Composite Drought Analysis. I.J.H.S.T. (accepted, in press).

Dalezios, N.R., A.Blanta, N.V.Spyropoulos and A.M. Tarquis, 2014. Risk Identification of Agricultural Drought in Sustainable Agroecosystems. NHESS: 14, 2435-2448.

Dalezios, N.R., N.V. Spyropoulos, A. Blanta and S. Stamatiades, 2012. Agrometeorological remote sensing of high resolution for decision support in precision agriculture. 11th International Conference on Meteorology, Climatology and Atmospheric Physics. Athens, 29 May – 1 June 2012, 51-56.

Dalezios, N.R., 2011. Climatic change and Agriculture: Impacts-Mitigation-Adaptation. Scientific Journal of GEOTEE. Vol. 27, January, 13-28.

Dalezios, N.R., A. Mplanta, C. Domenikiotis, 2011. Remotely Sensed Cotton Evapotranspiration for irrigation Water Management in Vulnerable Agriculture of Central Greece. JITAG. J of Information Technology Agriculture. Vol.4, No 1, 1-14.

Dalezios N.R., Z. Gkagkas, C. Domenikiotis, E. Kanellou and A. Mplanta, 2009: Climate Change and Water for Agriculture: Impacts-Mitigation-Adaptation. Proceedings, EWRA Conference on Water Resources Conservancy and Risk Reduction under Climatic Instability, Techn. Univ. of Cyprus (TUC), sponsored by EWRA and TUC, Limassol, Cyprus, 25-27 June (in the CD).

Dercas, N., N.V. Spyropoulos, N.R. Dalezios, E. Psomiadis, A. Stefopoulou, G. Madonanakis and N. Tserlikakis, 2017. Comparing cotton crop evapotranspiration using diachronic very high spatial resolution satellite data and ground measurements. 9th Intern. Conf. on Sustainable Water Resources Management, 18-20 July, Prague, Czech Republic (accepted, to be presented).

Giorgi, F., Bi, X. and Pal, J., 2004. Mean interannual and trends in a regional climate change experiment over Europe: Climate Change scenarios (2071-2100). Climate Dynamics, 23: 839-858.

Kogan, F.N., 1995. Application of vegetation index and brightness temperature for drought detection, Advances in Space Research, 15, 91-100.

Lanzl F, Richter R (1991) A fast atmospheric correction algorithm for small swath angle satellite sensors. ICO topical meeting on atmospheric, volume, and surface scattering and propagation, Florence, Italy, August 1991.

Olesen, J.E. and Bindi, M., 2002. Consequences of climate change for European agricultural productivity, land use and policy. European Journal of Agronomy, 16: 239-262.

Psomiadis, E., N. Dercas, N.R. Dalezios and N.V. Spyropoulos, 2016. The role of spatial and spectral resolution on the effectiveness of satellite-based vegetation indices. Proc. of SPIE, Edinburgh, UK, 26-29 Sep, Vol. 9998 99981L-1-13.

Spyropoulos VN, 1999. The benefits of high-resolution earth imagery in agriculture – The Ikonos system and its applications to agri-environment schemes. 1st workshop on the management and monitoring of agri-environment schemes. Joint Research Center (JRC) Ispra, Italy, 23–24 Nov 1999.

Updike T. and Comp C., 2010. Radiometric use of WorldView-2 Imagery. Technical Note, DigitalGlobe, 1601 Dry Creek Drive Suite 260 Longmont, Colorado, USA, 80503.

Proceedings of the 10th World Congress of EWRA 'Panta Rhei', 5-9 July 2017, Athens, Greece
© 2017 *European Water Resources Association*

Modelling sustainable smart islands using harmony search: A water-energy nexus initiative in Greece

I. Kougias[1,2*], S. Szabo[1], A. Nikitas[2] and N. Theodossiou[3]
[1] *European Commission, Joint Research Centre, Directorate for Energy, Transport and Climate: Renewables and Energy Efficiency Unit, 21027 Ispra, Italy*
[2] *University of Huddersfield, Huddersfield Business School, Department of Logistics, Operations, Hospitality and Marketing, Queensgate, Huddersfield HD1 3DH, UK*
[3] *Aristotle University of Thessaloniki, Department of Civil Engineering, Division of Hydraulics & Environmental Engineering, 541 24 Thessaloniki, Greece*
[*] *e-mail: Ioannis.Kougias@ec.europa.eu*

Abstract: The islands of the Aegean Sea in Greece represent a unique example for the water and energy interrelation. A great number of them are not interconnected to the main power grid and independent local grids produce power mainly using imported fossil fuels (e.g. heavy oil, diesel). Equally important, water resources' scarcity is an additional challenge, especially during the high-demand, summer months. Thus, in many arid islands potable water is transported from the mainland by means of sea transport, at a significant cost. This approach apart from the additional cost of fuel and water transport also imposes significant economic and environmental impact to these idyllic touristic locations. Seasonal variability in power demand and drinking water consumption, fuel price volatility as well as a growing touristic development, impose some additional complexity. The present study analyses specific island grids of the Aegean Sea. Selected islands are analysed as case studies over a 20-year period (2016-–2036). The developed energy modelling exercise uses a Harmony Search Algorithm (HSA) in its core. The aim is to investigate whether deployment of renewable energy sources (RES) to existing energy production could lead to a cleaner, sustainable system, decrease the current burden to the government budget and support local resources. The aim is to examine whether increased share of RES, battery storage, desalination and their combination could reduce islands reliability on imports, reduce its cost and potentially eliminate the current non-sustainable and heavily subsidized status quo.

Key words: Water energy nexus; sustainable development; energy modelling; renewable energy; optimization; harmony search

1. INTRODUCTION - THE DISPARITY BETWEEN MAINLAND AND ISLAND ELECTRIFICATION IN GREECE

Islands' electrification in Greece has always been a challenge due to the various technical and economic constraints. The complexity of the issue is accentuated from the islands' high number, their sparseness as well as the significant seasonal variability of electricity demand due to the fact that are popular tourist destinations. This issue was addressed in the main Ionian Islands through interconnections to the mainland Greek grid. Corfu is connected through a high voltage (HV) connection, while an additional HV cable connects the mainland to Lefkada, Kefalonia, Zakynthos and again to the mainland. The aforementioned interconnections are part of a plan realized since the 60's that extended the islands' connectivity. It included 13 connection projects during the 60's, 20 and 22 projects in the 70's and the 80's respectively, and additional 10 from 1991 until recently.

The ongoing project of interconnecting the Cyclades, an island group of the Aegean Sea, to the main grid was signed in 2014. Its first phase is expected to be completed by the end of 2017 with an overall budget of €240 million. It will interconnect four islands to the mainland through a 220 km cable. The second phase has a smaller budget (€40 million), is expected to start in 2018 and 47.6 km of cable will create new links and upgrade existing interconnections in more Cycladic islands. It is important to note that some islands are grouped together and are electrified by the same power system.

1.1 Fossil fuel subsidies

Contrary to the islands of the Ionian Sea, the majority of those of the Aegean Sea are not connected to the main power grid. Accordingly, electricity is produced locally by autonomous systems based on thermal power stations. The latter use (low sulphur) heavy oil in the bigger islands, while smaller systems use diesel as fuel. The cost of electrifying Greece's islands through fossil fuel powered stations is significantly high. The recent (March 2017) tender of the Public Power Corporation foresees €311 million for 940.000 metric tons of heavy oil and additional €286 million for 350 million litres of diesel, with a large share of it directed to power systems in non-interconnected islands. This significant cost is subsidized and shared by all mainland consumers, through a levy in electricity bills.

The ongoing interconnection of the Cyclades is expected to lead to annual savings of €100 million, while the planned interconnections of Crete will reduce the cost of fuel subsidies by another €300 million every year. Equally important these projects will result in significant reductions of greenhouse gas (GHG) emissions and improvements of islands' air quality, since the carbon intensity of the central grid is significantly lower than that of autonomous power plants. They will also make more feasible a mobility paradigm shift, dictated by the vision of low carbon societies, since more affordable electricity could enable the uptake of electric vehicles, which are ideal for the short-distance trips taken in the majority of the small to medium Greek islands (i.e. a single charge could facilitate even the longest trip the island could offer). Moreover, interconnections will allow higher penetration (Patsialis et al., 2016) of renewable energy sources (RES) and utilization of islands' wind and solar energy potential.

1.2 Alternative electrification pathways

The present research focuses on alternative electrification pathways for those islands that are not foreseen to be interconnected in the small- and medium-term. It aims to highlight prime locations where energy autarky could be achieved based on RES. In doing so the research designs sustainable energy portfolios through an optimization process. Their implementation is favoured by recent technological breakthroughs and significant cost reductions of RES systems. Thus, the research question focuses on analysing whether the least cost energy portfolio contains high share of RES. Comparison of sustainable portfolios to extended interconnections is outside the scope of the present study.

Efforts for the design of sustainable energy portfolios at the islands has a long history; already in 1983 the first European commercial wind park was developed on the island of Kythnos (five 15 kW turbines) (GWEC and IRENA, 2012). This is due to the high cost of electricity production in these islands. Shipping the fuel to such remote locations leads to electricity cost several times higher than that of the main grid. Indicatively, in 2015 the average full production cost was higher than €300/MWh in several islands, while the average variable cost reached €200/MWh in many cases.

1.3 Water and energy interrelation: a nexus approach

The climate in these islands is characterized by a continuous dry and hot period, and very low precipitation. Thus, local water resources are not sufficient to cover the needs and water is often imported from the mainland with water carrier ships or produced locally in desalination plants. Ten of the Aegean islands have literally no local water resources nor operational desalination plants. Patmos is one of those islands and this is the reason it was selected as a case study.

Between 2006 and 2014 €71 million were spent in water transport for these islands (€5.5 million in 2014), although the required water quantities are relatively low. Just for the summer of 2015 168000 m^3 were transported to the ten islands at a cost of €1.7 million (equal to €10.4/m^3). The Secretariat General for the Aegean and Island Policy of the Ministry of Maritime Affairs, Islands

and Fisheries has published a tender for the transport of 320000 m^3 for 2017. The foreseen budget is €4.09 million, equal to €12.77/m^3 (Ministry of Maritime Affairs, Islands and Fisheries, 2016).

The option of desalination is also hindered by the particularly high cost of electricity and the limitation of the existing aged energy infrastructure. Desalination is an energy-intensive process and electricity constitutes ≈20% of the total cost. In that sense, sustainable and low-cost electricity (Kougias et al., 2016a, b) could also mitigate water scarcity, showing the close water and energy interrelation on islands.

2. METHODOLOGY

For the optimization exercise we selected five islands that are not foreseen to be connected to the mainland by sea-cable. They cover a wide spectrum of electricity consumption that ranges between 15 GWh/year up to 800 GWh/year. Selected islands also have a different drinking water status: Rhodes has abundant local water resources, sufficient to provide to neighbour islands. Patmos stands on the opposite extreme: it does not have an operational desalination plant and drinking water is transported from the mainland. The remaining three islands face different degree of water stress, depending on desalination production (if any) and their local water resources.

2.1 Optimization Process

The present research included the design and development of an ad hoc optimization model to process energy information of selected islands that served as case studies. The model uses a metaheuristic algorithm in its core, the music-inspired Harmony Search Algorithm (HSA) (Kougias and Theodossiou, 2013a). HSA has been successfully used in various engineering problems, including applications covering water and energy interrelation (Kougias and Theodossiou, 2013b), (Kougias et al., 2016c). Independent runs analysed scenarios of the energy portfolio for each of the selected islands. The aim was to simulate future needs and the required investments on new energy capacity. The model optimized the future power capacity installations for each system, on a 20-year horizon (from the baseline 2016 until 2036). For each island numerous runs were performed with the optimum solution the algorithm converged representing the most advantageous option found in terms of overall cost. Naturally, accepted solutions need to satisfy the various constraints. The main model's constraint ensures that suggested portfolios can cover the electricity demand and the various losses, throughout the studied period.

2.2 Model Formulation

2.2.1 Decision Variables

The model's decision variables represent additions of power capacity that need to be implemented over the studied time frame. This includes investments in solar PV and wind RES systems (variables X_1 and X_2), conventional fossil fuel based systems (variable X_3). Moreover, the model investigates the battery storage option (variable X_4) and optimizes the duration of operation of fossil systems to minimize fuel consumption (variables X_5 and X_6). Naturally, initial values of the decision variables correspond to those of the baseline year 2016.

2.2.2 Objective function

The objective function quantifies the required investment of each energy portfolio (installation and operation cost) for the whole period in net present values (NPV).

$$Total\ cost(j) = Capital\ cost(j) + Operation\ cost(j) + CO_2\ tax(j) \quad (1)$$

where, *j*: analysed year; *Capital cost*: cost of new capacity additions; *Operation cost*: fuel cost; *CO_2 tax*: carbon tax.

Incoming and outgoing cash flows of Equation 1 over the studied period (2016-2036) were transformed into NPV at a discount rate equal to 3%. The efficiency of the different systems and capacity factors were based both on the previous work of the authors (Szabó and Jäger-Waldau, 2008) technology-specific analyses (Šúri et al., 2005) and developments reported in (IRENA, 2012).

2.2.3 Model parameters

The energy Systems' capital cost was estimated for solar PV at €1.1/Wp (Jäger-Waldau, 2016), for wind at 1.3/Wp, for conventional systems at €0.9 million/MW, and battery storage cost at €0.12/MWh. The fluctuation of oil price hinders estimations of operation cost of heavy oil- or diesel-fuelled power stations. The model run a fuel-price scenario that takes into account recent low diesel prices (€40/barrel) and incorporates the increasing trends the oil market has experienced since. The highest oil price in the studied time frame is considered to be €100/barrel. The fossil fuel stations' decommissioning was also taken into account, since aged equipment will be needed either to be phased out or retrofitted.

In order to study the battery storage option, the model distinguishes day from night electricity consumption (Szabó et al., 2015). We assume that two thirds of the consumption takes place during the day (16-hours), while the remaining one third is night consumption (8-hours). We also assume that battery storage exclusively covers night demand. In that sense batteries charge from the daily produced solar PV electricity and provide the stored electricity at night. Thus, batteries provide electricity when solar PV systems cannot; conventional systems cover peak-loads and support the night operation, while PV and wind systems reduce oil/diesel consumption by providing base-load.

3. RESULTS

The following section presents the outcome of the optimization exercise for the selected five islands. It presents economically advantageous energy portfolios that involve the minimum possible capital and operational cost for the analysed 20-year time frame. It is interesting to note that in all five cases conventional production appears to decrease steadily, with the aging fossil fuel equipment not being replaced.

3.1 Rhodes

During the last two decades the electricity demand in Rhodes island has more than doubled: from 393.2 GWh in 1996 to 764.6 GWh in 2010 and 816.6 GWh in 2016. Figure 1 shows the optimal energy strategy, as estimated by the HAS-based model. Projections suggest a rapid reduction on fossil-based production between 2016 and 2022, followed by a mild one. After 2028 oil-fuelled production steadily converges to the very low share of 2036.

Notable is the significant share of wind in the final (2036) production. In terms of installed capacity the model converged to almost 6× the current capacity. This illustrates the favourable conditions of Rhodes that hosts one of the best wind potentials in Greece. Our analysis has not taken into account land limitations, i.e. whether it is possible to increase up to that extent the number of installed wind farms. Grid limitations, as far as the absorption of extended variable power is concerned, is and additional issue that exceeds the targets of the present exercise.

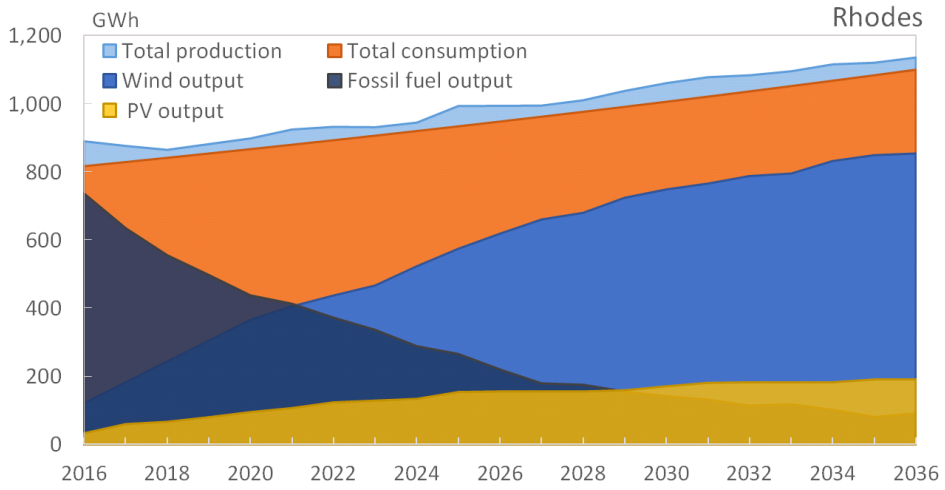

Figure 1. Optimal projection of electricity production for Rhodes.

3.2 Lesvos

The output for Lesvos is illustrated in Figure 2. The power mix evolves similarly to Rhodes, with wind capacities taking over. Solar PV installations increase almost linearly in the early period and have a moderate development rate in the 2026-2036 period.

So far high-enthalpy geothermal fields, similar to those of Milos Island, have not been explored in Lesvos. However, there is evidence that multiple medium-temperature geothermal fields could potentially provide energy in favourable terms (Koroneos et al., 2004). Our analysis did not consider this technology due to the increased degree of uncertainty as far as its cost is concerned.

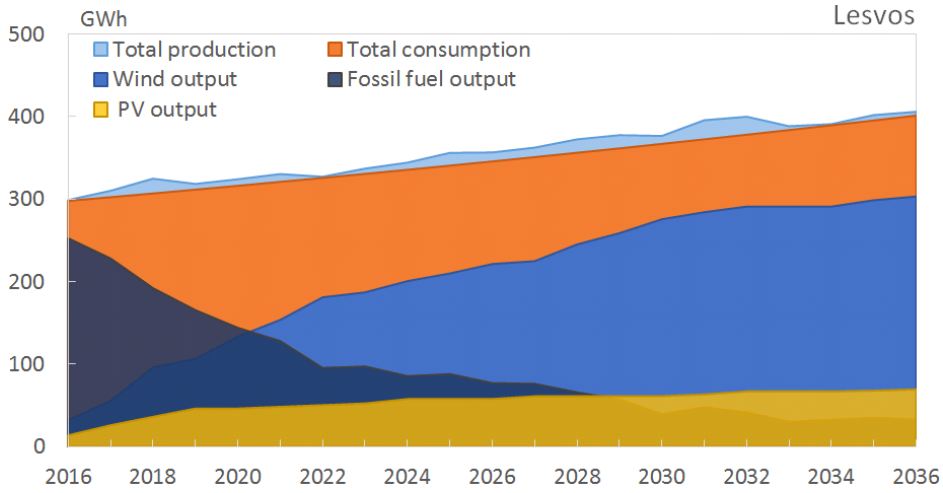

Figure 2. Optimal projection of electricity production for Lesvos.

3.3 Chios

For Chios the modelling results also suggest steadily abandoning fossil-based electricity in favour of RES (Figure 3). Solar PV systems appear to take a bigger role in that case and eventually contributing more than 25% of the 2036 consumption. It is interesting to note that Chios has desalination plants (in Tholos and Miligkas) with a total potential of 5000 m^3/day (Ministry of Environment and Energy, 2015).

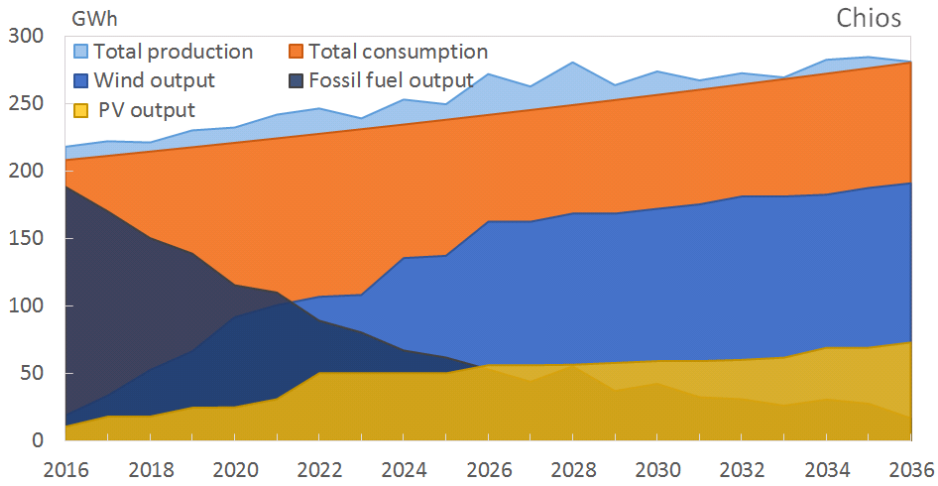

Figure 3. Optimal projection of electricity production for Chios.

Spikes in the production curve (e.g. 2026, 2028) illustrate the effect of power capacity installations in independent small systems. It is likely that the produced electricity will excess the sum of consumption and losses, at least for a short period, until the demand increases and bridges the gap. Similarly to Lesvos, there is evidence in Chios for potential geothermal energy production (Dotsika et al., 2016).

3.4 Karpathos-Patmos

Karpathos and Patmos –although different in size– have significantly lower consumption than the previously analysed islands. Karpathos has an excellent wind potential and the model converges to higher share of wind compared to Patmos.

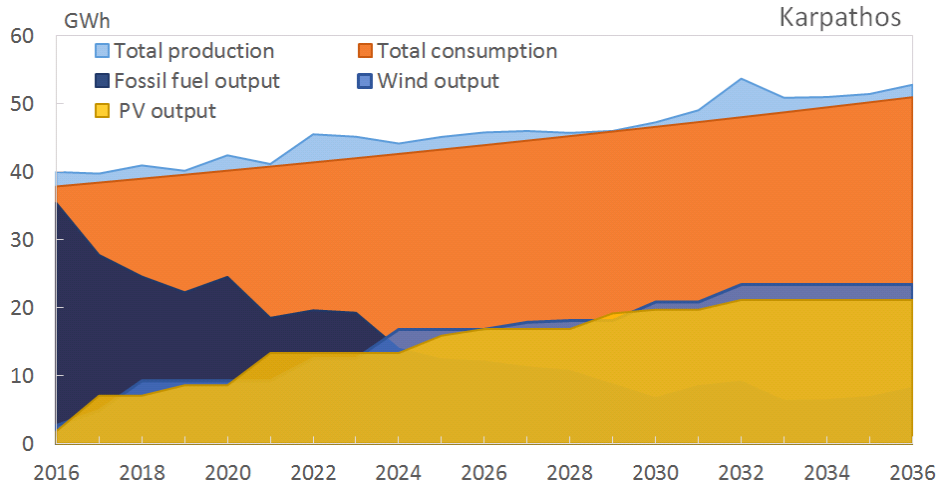

Figure 4. Optimal projection of electricity production for Karpathos.

However, in both cases the share of solar in the final consumption is as high as wind. This is different from the previous cases (Figures 1-3) and shows PV's suitability on smaller islands. Wind units have a large capacity and require larger investments. Modular PV systems' installation is flexible allowing gradual increase of the capacities and distribution of the investment over a period of time. This is favourable particularly in power systems with relatively low consumption, because large capacities' installation "all at once" is more difficult to be recouped.

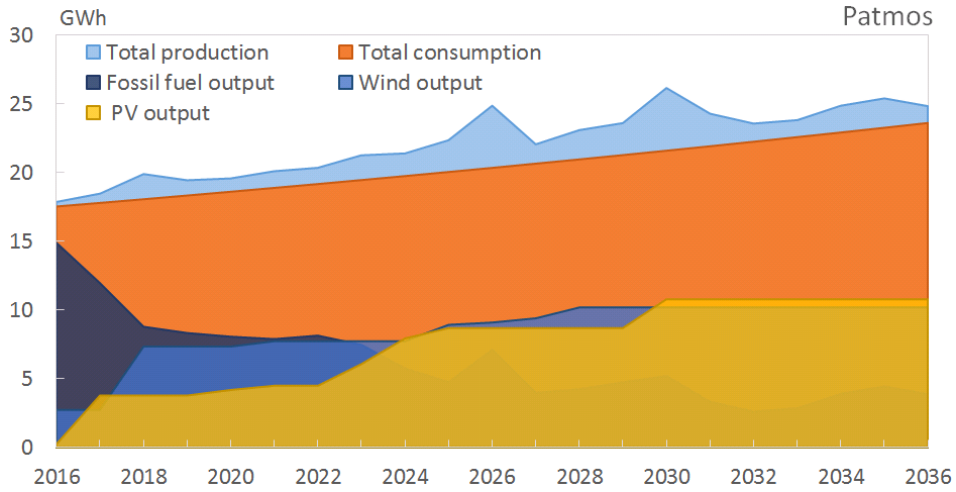

Figure 5. Optimal projection of electricity production for Patmos.

4. CONCLUSIONS

The unique situation of the Greek electricity system presents a great burden for the households as it means an extra charge in their electricity bills on one hand, but can be a good opportunity to become exemplar in sustainable energy on the other. From security, environmental and climate point of view the present status on relying dominantly on heavy oil and diesel generation in meeting the island demand is the least optimal.

Another pathway that a more efficient energy production approach could open is adopting electro-mobility which, in principle, is ideal for short-distanced inner-island trips. The electrification of cars is a measure reducing significantly environmental impacts from transport since electric propulsion is energy efficient, does not cause local emissions and reduces noise (Altenburg et al., 2012). A potential scenario of introducing an electric vehicle (EV) fleet as a distributed energy storage system that would increase the participation of renewables could be particularly appealing for the isolated island systems studied. A system as such that was piloted through simulation methods in a comparable system (i.e. the island of Tenerife) showed very promising results in increasing the renewable share in the electricity mix of the island and reducing CO2 emissions, the total cost of electric generation and the oil internal market (Díaz et al., 2015). Electric biking is another electro-mobility initiative that could be adopted because of its added potential to contribute to increased bicycling. E-biking is suitable for altitude differences and make longer distance biking accessible for more people; thus it can potentially transform cycling from a non-issue currently, despite a consistently rising tourist-driven demand for it in Greek islands, to a viable door-to-door mobility solution for these areas that would be embraced even from the locals.

The analysis presented in the present work shows that remote islands of Greece could leave behind this deadlock by scaling up indigenous electricity sources. The model shows that RES can cover the demand and represent the least cost energy generation option for the analysed islands. Maintaining the present system costs hundred millions cross-subsidy from all the electricity consumers of Greece. Ongoing connection projection will decrease this burden but will not vanish it.

When we compare the overall modelled costs (Table 1) it appears that the transformation would cost only half of the 20-year cumulative cross-subsidy for each island. The transition includes the installation of new capacities, storage and fuel costs. It is also visible that the cost savings are larger for the islands with higher population as the model identifies better opportunities to attain the economies of scale. The e-mobility options also favours the relatively more populated islands, as they have bigger car-fleets, so having the critical threshold for creating the necessary infrastructure (e-fuel stations). Therefore prioritizing the bigger islands not included in interconnection plans could be a cost optimal approach in converting the islands' present electricity generation to the

sustainable power portfolio.

Table 1. Energy portfolios' outlook for the analysed islands and average cost of electricity of the modelled transformation

Island	Installed capacity (MW) in 2016	Modelled capacity (MW) in 2036	Actual Elec. Consumption (MWh) in 2016	Modelled Elec. Consumption (MWh) in 2036	Modelled avg. cost €/MWh
Rhodes	301.4	510.1	889741	1135754	46.3
Lesvos	110.5	195.7	298936	405876	45.8
Chios	85.8	153.2	218272	281324	49.6
Karpathos	20.3	27.7	39970	52793	55.1
Patmos	7.95	12.6	17861	24828	52.7

REFERENCES

Altenburg T, Bhasin S, Fischer D. Sustainability-oriented innovation in the automobile industry: advancing electromobility in China, France, Germany and India. Innovation and Development, 2012, 2(1), 67-85.

Díaz AR, Ramos-Real FJ, Marrero GA, Perez Y. (2015). Impact of electric vehicles as distributed energy storage in isolated systems: The case of Tenerife. Sustainability, 2015, 7(11), 15152-15178.

Dotsika E, Leontiadis I, Poutoukis D, Cioni R, Raco B. Fluid geochemistry of the Chios geothermal area, Chios Island, Greece. Journal of volcanology and geothermal research, 2006, 154(3), 237-250.

Global Wind Energy Council (GWEC) and International Renewable Energy Agency (IRENA) (2012), 30 Years of Policies for Wind Energy: Lessons from Greece, 2012, 1–10.

International Renewable Energy Agency (IRENA). Renewable Energy Country Profiles; Special Edition on Islands; IRENA: Masdar City, United Arab Emirates, 2012.

Jäger-Waldau A. PV Status Report 2016; Publications Office of the EU: Luxembourg, 2016, 1–84.

Koroneos C, Michailidis M, Moussiopoulos N. Multi-objective optimization in energy systems: the case study of Lesvos Island, Greece. Renewable and Sustainable Energy Reviews, 2004, 8(1), 91-100.

Kougias I, Bódis K, Jäger-Waldau A, Moner-Girona M, Monforti-Ferrario F, Ossenbrink H, Szabó S. The potential of water infrastructure to accommodate solar PV systems in Mediterranean islands. Solar Energy, 2016b, 136, 174-182.

Kougias I, Bódis K, Jäger-Waldau A, Monforti-Ferrario F and Szabó S. Exploiting existing dams for solar PV system installations. Prog. in Phot.: Res. and Appl., 2016a, 24(2), 229-239.

Kougias I, Karakatsanis D, Malatras A, Monforti-Ferrario F and Theodossiou N. Renewable energy production management with a new harmony search optimization toolkit. Clean Tech. and Env. Policy, 2016c, 18(8), 2603-2612.

Kougias I, Theodossiou N. Multiobjective pump scheduling optimization using harmony search algorithm (HSA) and polyphonic HSA. Water Resources Management, 2013b, 27, 1249–1261.

Kougias I, Theodossiou, N. Application of the Harmony Search optimization algorithm for the solution of the multiple dam system scheduling. Optimization & Engineering, 2013a, 14(2), 331–344.

Ministry of Environment and Energy (YPEKA). Economic analysis of water use in the islands of the Aegean Sea (in Greek language), 2015.

Ministry of Maritime Affairs, Islands and Fisheries - Secretariat General for the Aegean and Island Policy of the. Declaration of international competition for the transport and delivery of drinking water in arid islands for the period from 1/1/2017 to 31/12/2017, 2016, 30 November.

Patsialis T, Kougias I, Kazakis N, Theodossiou N, Droege P. Supporting Renewables Penetration in Remote Areas through the Transformation of Non-Powered Dams. Energies, 2016, 9(12), p.1054

Súri M, Huld TA, Dunlop ED. PVGIS: A web-based solar radiation database for the calculation of PV potential in Europe. Int. J. Sustain. Energy, 2005, 24, 55–67.

Szabó S, Jäger-Waldau A. More competition: Threat or chance for financing renewable electricity? Energy Policy, 2008, 3, 1436–1447.

Szabó S, Kougias I, Moner-Girona M, and Bódis, K. Sustainable energy portfolios for small island states. Sustainability, 2015, 7(9), pp.12340-12358.

Proceedings of the 10th World Congress of EWRA 'Panta Rhei', 5-9 July 2017, Athens, Greece
© 2017 *European Water Resources Association*

Multi-objective optimization for irrigation deficit through cascade reservoirs

M.U. Rashid[1], S.S. Haider[2], M. Latif[1] and N.A. Raja[1]
[1] *Department of Civil Engineering, University of Management and Technology, Lahore, Pakistan*
[2] *Department of Architecture, University of Management and Technology, Lahore, Pakistan*
[*] *e-mail: usman.rashid@umt.edu.pk*

Abstract: Reservoirs play a strategic role in the rapid monetary growth of the world by providing numerous benefits. However, the reduction in appropriate sites along with environmental and social apprehensions has resulted in curtailment of new reservoirs around the world in 21st century. There is a potential of benefits available from existing reservoirs which have not been capitalized. To move forward in this context, the optimized benefits from reservoirs must be attained. Reservoirs operation optimization considering sediment evacuation (RESOOSE), a recently developed model which combines multiple reservoirs operation and sediment evacuation with Genetic Algorithm based optimization module, had been used in the study. The objective function of optimizing the irrigation deficits was developed. The RESOOSE model was then applied to optimize the irrigation deficits of Tarbela and Diamer Basha Reservoirs in Pakistan. The average annual irrigation shortages, sediment evacuation, hydropower and flood damages of existing rule curves had been computed as 6.9 billion m^3, 21.534 million m^3, 36.9 billion Kw and 616.2 million US$ which were used as constraints. The irrigation shortages had been minimized by optimized rule curves without reducing these benefits from existing values. The optimized operation of the selected multiple reservoirs reduce the irrigation shortages to 5.95 billion m^3 (13.7% reduction). The study suggests change in existing operation of Tarbela and Diamer Basha Reservoirs due to enhanced benefits. Reducing irrigation deficits will certainly help in achieving the objective of exploiting the potential benefits of from cascade reservoirs.

Key words: Tarbela, Diamer Basha, Optimization, Multi-objective, Genetic Algorithm, RESOOSE Model, Irrigation Deficit, Irrigation Shortage

1. INTRODUCTION

Reservoirs have significant role for rapid economic growth of any country as they are used for storing and providing water for hydroelectric power (HEP), irrigating land and reducing floods. Due to social and environmental concerns like population augmentation, land use management etc., the availability of suitable sites for building a reservoir is becoming scarce with the passage of time. Therefore, the need to conserve the existing reservoirs by enhancing their useful life, along with building new ones is gaining a worldwide primary attention. According to (White 2010; WCD 2000) the process of building new dams was initiated in 1950s, reaching its peak in 1970s at the average rate of two dams (commissioned) per day. Till year 2003 almost 33,100 reservoirs with overall storage capacity of 6700 km^3 have been constructed.

The reservoir life and capacity is severely affected by the sediment deposition. Flow characteristics and sediment load governs the degree of severity a reservoir have to face during its life. The common methods of sediment management are soil conservation and flushing (full and partial drawdown) while others include sediment routing through sluicing and watershed protection measures (Rashid et al. 2014). Though the sedimentation rate is different worldwide (0.1 to 2.3%), it causes the annual storage loss of 1% which corresponds to the loss of US$ 9 billion per year.

To capitalize on profit (net benefit) and curtailing irrigation losses there is a need to develop an efficient cascade reservoirs system which itself is a complex process. The primary constraints for a typical reservoir operation are related to its releases and storages indexes, developing conservation equation and ensuring dams' safety (see Chen and Chang 2007 for details). One of the primary functions of a reservoir is to control damages caused by the flood because floods are directly related

with the safety of human lives and have lasting impacts on the socio economic growth of an area. With the marked improvement in simulation and modelling techniques, real time optimal flood control methods and operations were devised and implemented to various reservoirs built in USA and China (Wang et al. 2013). The implementation of a hydro model for the modelling of Tarbela reservoir in Pakistan has also resulted in HEP increase along with several other irrigation benefits. The model also helped in proposing several curative measures to minimize the effect of sedimentation deposition at Tarbela.

Khan et al. (2012) developed an optimization model ROSSE and applied to optimize the rule curves of Tarbela Reservoir for minimizing the irrigation shortages, flood damages and maximizing the hydropower benefits. ROSSE model has capability to handle only single reservoir. The optimized rule curves minimize the irrigation shortages by 24%. Genetic Algorithm regarding reservoir operation policy optimization was modeled, simulated and implemented to various reservoirs in India. These models used inflows and time as input parameters to simulate releases. Several researchers have developed various models on GA to compute multi reservoir optimal operation. E-g, Multidimensional GA was developed and implemented to perform the optimal operation on the multiple reservoirs located in Chi River Basin, Thailand. Chang et al. (2003) formulated two separate models (i-e, for simulation and flushing) which are used in the sediment flushing optimization of Tapu Reservoir in Taiwan. Because of compound water-sediment relationships and for the lengthy simulation times, the models of such type should be simplified.

Wardlaw and Bhaktikul (2004) discussed and compared the linear programming (LP) with GA approach and concluded various advantages of GA over LP like robust optimization, less processing time and , excellent handling of constraints. Various reservoirs were optimized on the similar footprints to meet the irrigation and socio-environmental needs. In northern Iran, Sefidrub reservoir was optimized using GA which resulted in 37 million ton evacuation of sediments keeping same power efficiency (Hajiabadi and Zarghami 2014). Combined Simulation GA Optimization model was used to optimize the operation of Nam Oon reservoir in Thailand (Suiadee and Tingsanchali 2007).

Several researchers have studied the issue of optimization of a reservoir in detail. Labadie (2004) proposed that optimization of multiple reservoirs instead of single a reservoir would result in better overall efficiency. The reservoir optimization approach should be multidimensional, nonlinear; must be able to accommodate and deal with the time dependent changes (dynamic in nature) and probabilistic characteristics of reservoir systems. Genetic algorithm optimization techniques have been most commonly used in Asia (including China, India, Iran, Taiwan etc.) with perceptible success in reducing the damages caused by flood along with the increase irrigation, storage and HEP increase (Wardlaw and Sharif 1999; Ranjithan 2005).

The objectives of the study is to minimize the irrigation shortages without reducing the hydropower, sediment evacuation, flood damages reduction benefits by optimization the rule curves of cascade reservoirs. RESOOSE model was applied to Tarbela and Diamer Basha Reservoirs for computing the optimized rule curves.

2. RESERVOIRS OPERATION OPTIMIZATION CONSIDERING SEDIMENT EVACUATION (RESOOSE) MODEL

The flow chart of RESOOSE model is shown in Figure 1. It has four interconnected modules which are Optimization, Sediment Evacuation, Reservoir Operation and Hydropower. The model has capabilities of optimizing the multiple reservoirs operation considering sediment outflow. It is user-friendly and has GUI. It has been coded and developed using MATLAB. It has also four main forms which are used to specify the input data including objective function, variables, GA parameters, bounds, hydrological data, preliminary rule curves for starting simulation and termination criteria to stop the optimization process. The existing models having optimizing and sedimentation capabilities handle only single reservoir. The RESOOSE model is different in the manner as it handles multiple reservoirs for multi-objective optimization.

Genetic Algorithm (GA) technique has been used for optimization module in RESOOSE model that emerges from biological evolution process i.e. mutation, selection, inheritance and cross-over. GA, being newest optimization technique, has been used worldwide successfully for optimization of reservoirs. Some of its capabilities are vigorous technique of optimization, constraints handling and less execution time. Reservoir operation is important central module of this model that is based on conservation equations and computes releases and storage at each time step. The basis of sediment module is Tsinghua equation (IRTCES 1985) to calculate sediments outflow and actual sediments rating curves to calculate sediment inflow to reservoirs. The elevation capacity curve also updates after deposition and outflow of sediments every year. Further details of RESOOSE Model can be viewed from Rashid et al. (2015).

The reservoir operation and sediment evacuation modules of RESOOSE Model were successfully calibrated and verified against observed water levels, discharges and elevation-storage capacities of Tarbela and Chashma Reservoirs on Indus Basin. Moreover, optimization module of MATLAB, used in RESOOSE Model, has been dully verified by the developer Mathworks (Rashid et al. 2015; Mathworks 2013a Mathworks 2013b).

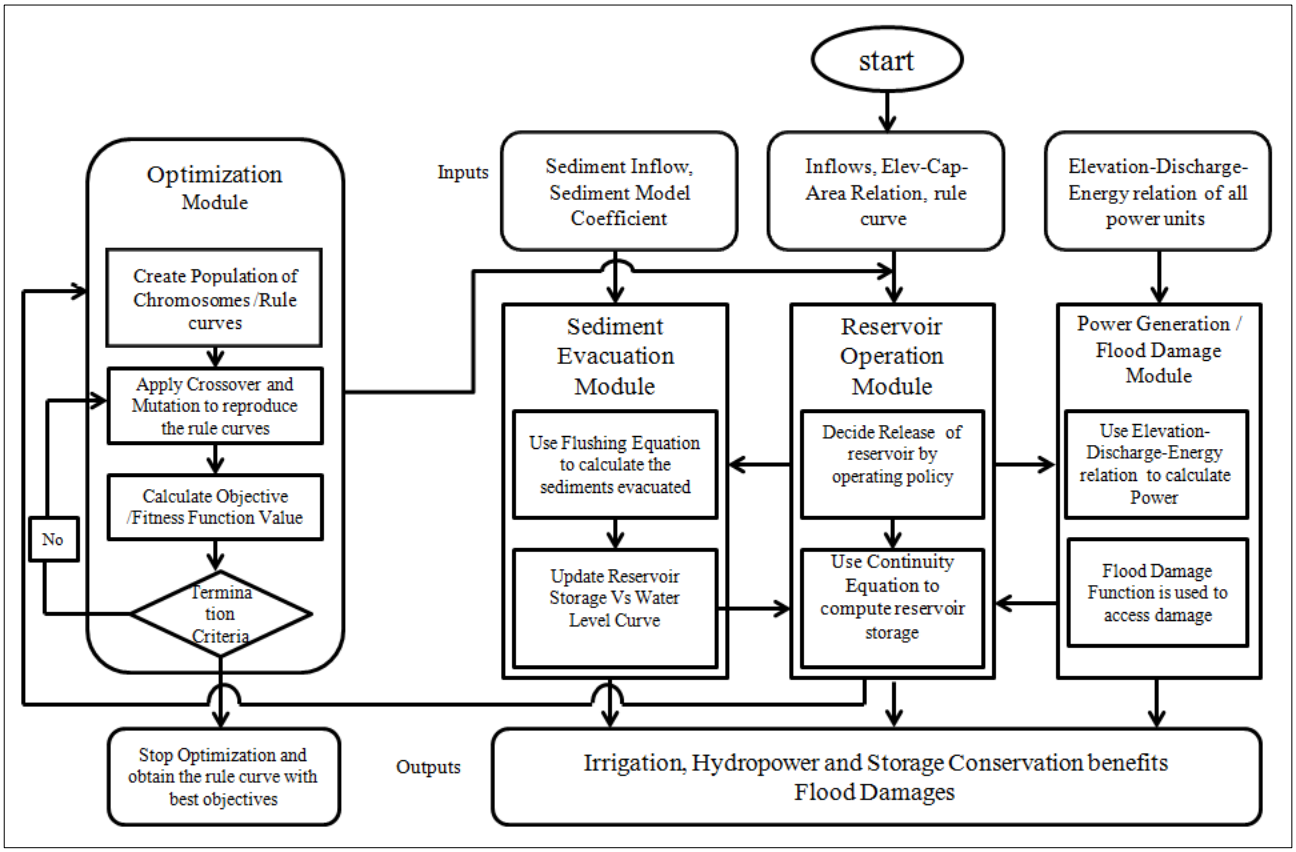

Figure 1. Flow Chart of RESOOSE Model

3. APPLICATION OF RESOOSE MODEL TO CASE STUDY RESERVOIRS

The case study reservoirs selected for optimizing the irrigation shortages are Tarbela (1.43 BCM storage capacity) and Diamer Basha (1.07 BCM storage capacity) on Indus River in Pakistan. Tarbela is one of the largest Dams of Pakistan which was commissioned in 1974 located 65 km North-west of Islamabad. Diamer Basha Dams is located about 315 km upstream from Tarbela Dam. Its proposed completion is in year 2020 published by Water and Power Development Authority (WAPDA) Pakistan. The prominent characteristics of the reservoirs are mentioned in Table 1 (WAPDA 2012; WAPDA 2008).

3.1 Objective Function

RESOOSE Model has capability to optimize the rule curves for several objective functions including maximizing the irrigation, hydropower and sediment evacuation and minimizing the irrigation shortages and flood damages of cascade reservoirs. This manuscript focuses on optimizing the rule curves for minimizing irrigation deficits. The objective function thus developed is as follows:

$$\text{Objective Function} = \text{Minimize} \sum_{n=1}^{years} \sum_{t=1}^{36} [\mathrm{D} - \mathrm{R}]_{t,n} \text{ if } \mathrm{R} < D \quad (1)$$

where D is the demand in a time step‘t’ whereas R is the releases form downstream reservoir through conjunctive operation of cascade reservoirs (in this manuscript Diamer Basha upstream and Tarbela downstream reservoir on Indus River) . Both irrigation demand and reservoir releases are in m^3 and time step in the study is 10 daily as it is standard practice in Pakistan that for whole irrigation system the demands and releases are computed in 10 daily time step.

3.2 Constraints

The constraints considered for optimizing rule curves of the cascade reservoirs are as follows:

Constraint 1: Lower Rule Curve (LRC) ≤ Upper Rule Curve (URC) for all times steps in simulation

Constraint 2: Maximum Conservation Level (MCL) ≥ Rule Curves ≥ Minimum Operating Level (MOL) For Diamer Basha and Tarbela Reservoirs MOL is 1060 m and 420.3 m (As of 2013) respectively, whereas MCL is 1160 m and 472.5 m respectively

Constraint 3: Hydropower benefits of optimized rule curves ≥ current rule curves while minimizing the irrigation deficit

Constraint 4: Sediment Evacuation benefits of optimized rule curves ≥ current rule curves while minimizing the irrigation deficit

Constraint 5: Flood damages reduction by optimized rule curves ≥ current rule curves while minimizing the irrigation deficit

Table 1. Salient Feature of Tarbela and Diamer Basha Reservoirs

Sr. No.	Feature	Diamer Basha Reservoir	Tarbela Reservoir
1	Type	Roller Compacted Concrete dam	Rock and Earth fill dam
2	Catchment Area	153,200 km^2	169,650 km^2
3	Commissioning year	2020 (proposed)	1974
4	Reservoirs Length	105 km	88 km
5	Reservoirs Area	120.9 km^2	250 km^2
6	Gross Storage	10 BCM	14.34 BCM
7	Live Storage	7.90 BCM	11.94 BCM
8	Spillways	1	2
9	Power Capacity	4500 MW	3478 MW

The hydropower, sediment evacuation and flood damage reduction benefits of current rule curves are 36.902 Billion kWh, 21.534 million m^3. The flood damage of existing rule curves are 616.19 million US$/year. The flood damages have been computed using regression analysis major flood damages of Pakistan. Flood damage function, derived from peak flows during historical floods of Indus River and its tributaries in Pakistan from 1976-2010 and damages they occurred. The flood damage function is as follows:

$$C_f = 0.272Q_m - 1861.50 \quad (2)$$

where C_f is flood damage in million US$ and Q_m is maximum instantaneous flow in m^3/s.

3.3 Data Required

A long time (1975-2014) series of data for both Diamer and Basha Reservoirs i.e. inflows, outlows, levels, irrigation demand, rule curves, hydropower capacities, spillways and tunnel capacities of dams, sediment inflows and outflows, sediment characteristics (gradation curves) and major flood damages of Indus River of Pakistan was used to study their stochastic effects.

Pakistan's whole water resources system is administered by 'WAPDA' which is responsible for its development, operation, management of flood, hydropower production along with its allocation. Indus River System Authority (IRSA) regulates flows among the country's provinces by WAPDA with precedence to primary irrigation. The systems and concerned authorities work for smooth distribution of water among country without dispute. The irrigation demands for conjunctive operation of case study reservoirs are shown in Figure 2.

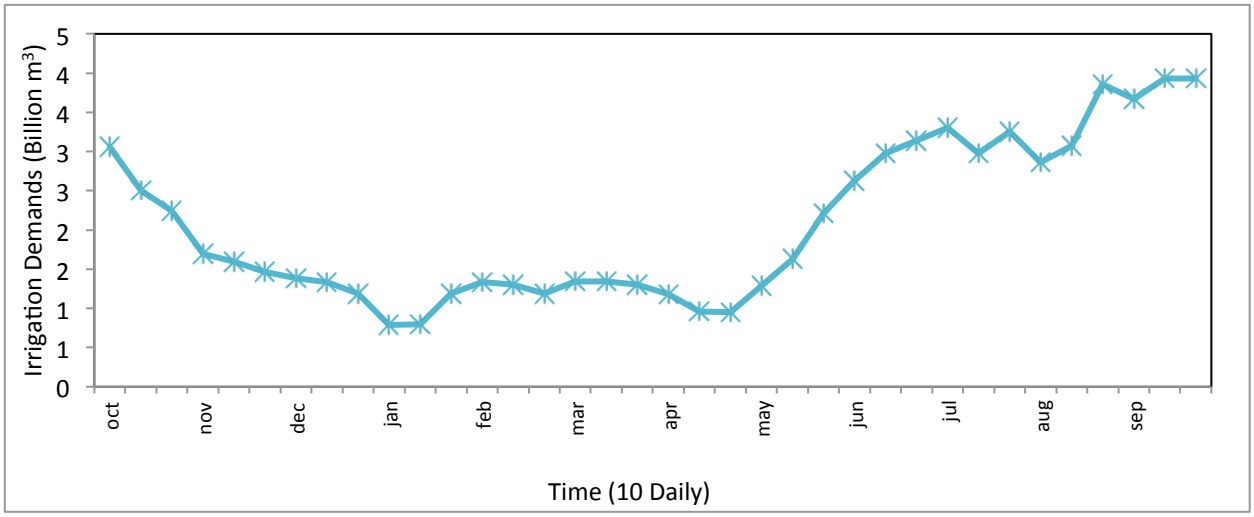

Figure 2. Irrigation Demands for Case Study Reservoirs (Billion m^3)

4. RESULTS AND DISCUSSION

The optimization of objective function i.e. minimizing irrigation shortages through conjunctive operation of cascade reservoirs (Tarbela and Diamer Basha) is shown in table 2. The optimized rule curves along with optimized irrigation shortages are shown in Figure 3 and existing rule curves along with its irrigation shortages are shown in Figure 4. The average annual irrigation shortages, sediment evacuation, hydropower and flood damages of existing rule curves have been computed as 6.9 billion m^3, 21.534 million m^3, 36.9 billion Kw and 616.2 million US$. The current irrigation shortages of Tarbela and Diamer Basha Reservoirs have been reduced to 5.95 BCM by optimized rule curves (13.7 % Reduction) in the current study. The optimized rule curves have achieved this reduction in irrigation shortages with reducing the flood damages reduction, hydropower and sediment evacuation benefits of current rule curves.

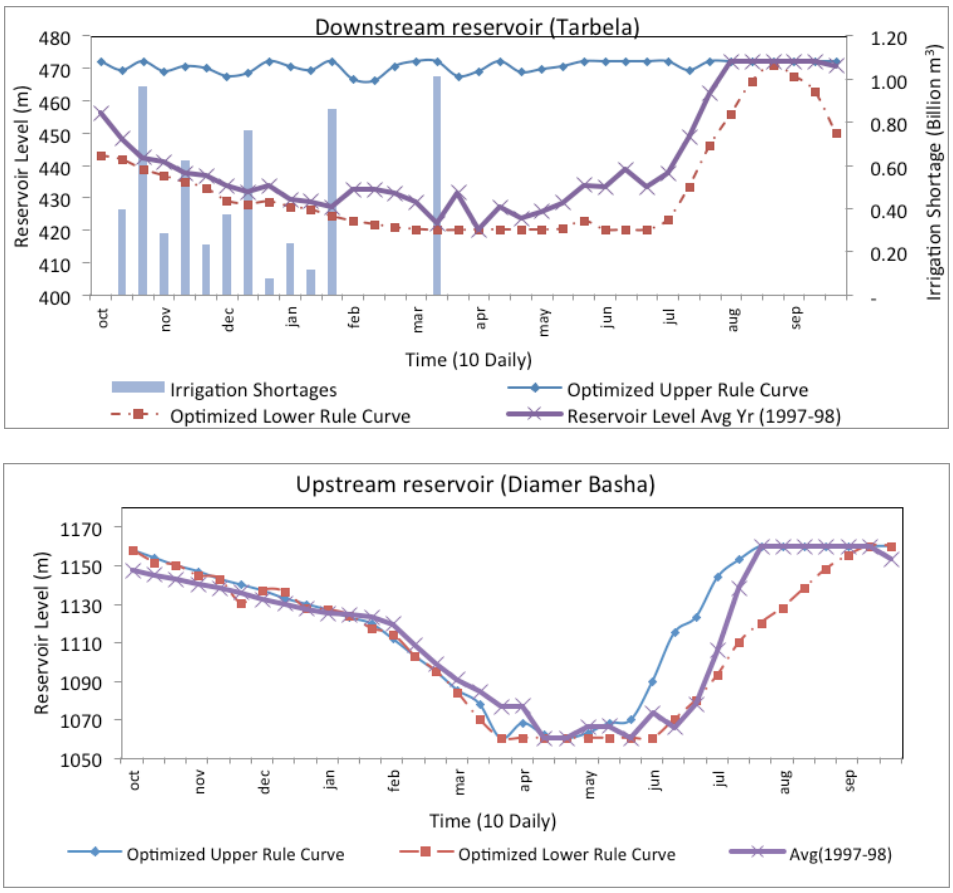

Figure 3. Optimized Rule Curves of Diamer Basha & Tarbela Reservoirs and Irrigation Shortages (Billion m3)

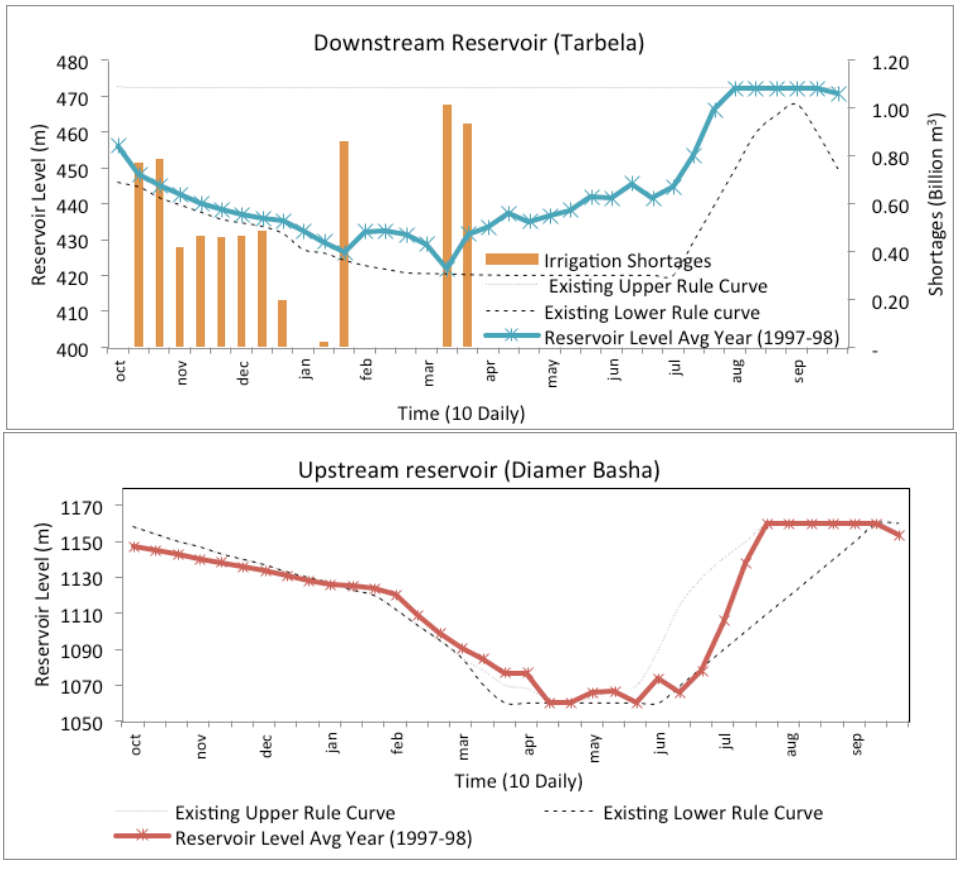

Figure 4. Existing Rule Curves of Diamer Basha and Tarbela Reservoirs and Irrigation Shortages (Billion m^3)

Table 2. Optimization results for Tarbela and Diamer Basha Reservoirs

Rule Curves	% reduction of objective function w.r.t. current rule curves	Irrigation shortages (Billion m^3/year)	Annual Benefits			Trapping Efficiency
			Power (Billion Kw)	Sediment (Million m^3)	Flood damages (Million US$)	
Optimized Rule Curves	13.7%	5.95	36.95	21.754	613.6	82%
Existing rule curves*	-	6.90	36.902	21.534	616.19	87%

** The existing rule curve of Diamer Basha Reservoir is taken from the Reports (WAPDA 2012; WAPDA 2008)*

5. CONCLUSIONS AND RECOMMENDATIONS

1. The study successfully applied the RESOOSE model to optimize the cascade reservoirs rule curves for minimizing the irrigation shortages.
2. It has been demonstrated for Tarbela and Diamer Basha Reservoirs that the irrigation deficits can be reduced by ensuring the current level of hydropower, sediment evacuation and flood damages.
3. The optimized rule curves have reduced the irrigation shortages from 6.9 Billion m^3 to 5.95 Billion m^3 (13.7% reduction) of Case study Reservoirs.
4. After successful application of RESOOSE Model to Case study Tarbela and Diamer Basha reservoirs, it is recommended that their operational/proposed rule curves may be revised to meet the irrigation demands and for achieving the objective of exploiting the potential benefits of from cascade reservoirs.

REFERENCES

Chang FJ, Lai JS, Kao LS (2003) Optimization of operation rule curves and flushing schedule in a reservoir. Hydrological Processes 17(8): 1623-1640.

Chen L, Chang FJ (2007) Applying a real-coded multi population genetic algorithm to multi reservoir operation. Hydrological Processes 21(1): 688-698.

Hajiabadi R, Zarghami M (2014) multi-objective reservoir operation with sediment flushing: case study of Sefidrud Reservoir. Water Resources Management, Published online October 2014. DOI:10.1007/s11269-014-0806-9.

IRTCES (1985) Reservoir sedimentation Manual. "International research and training centre on erosion and sedimentation (IRTCES)", The Tshingua University, Beijing, China

Khan NM., Babel MS, Clemente RS, Tingsanchali T, Loung HT (2012) "Reservoir Optimization-Simulation with a Sediment Evacuation Model to Minimize Irrigation Deficits". Water Resources Management 26(11): 3173-3193.

Mathworks (2013a) MATLAB capabilities: verification, validation and test of available tools. Web http://www.mathworks.com/. Accessed 29.06.2013.

Mathworks (2013b) Advantages and Optimization capabilities of MATLAB computer language. Web http://www.mathworks.com/products/matlab/. Accessed 29.07.2016.

Ranjithan SR (2005) Role of evolutionary computation in environmental and water resources systems analysis. Journal of Water Resources Planning and Management 131(1):1-10.

Rashid MU, Shakir AS, Khan NM (2014) Evaluation of sediment management options and minimum operation levels for Tarbela Reservoir, Pakistan. Arabian Journal of Science and Engineering 39(4): 2655-2668.

Rashid, M. U., A.S. Shakir, N. M. Khan, A. Latif & M. M. Qureshi. (2015) Optimization of Multiple Reservoirs Operation with Consideration to Sediment Evacuation. Water Resources Management 29(7): 2429–2450.

Suiadee W, Tingsanchali T (2007) A combined simulation genetic algorithm optimization model for optimal rule curves of a reservoir: a case study of the Nam Oon Irrigation Project, Thailand. Hydrological processes 21(23): 3211-3225.

Wang F, Valeriano OC, Sun X (2013) Near real-time optimization of multi-reservoir during flood season in Fengman Basin of China. Water Resources Management 27(12): 4315-4335.

WAPDA (2008) Reservoir Operation and Sediment Transport Study: Diamer Basha Dam Project, Pakistan. Published by WAPDA. Web http://www.wapda.gov.pk. Accessed 1.10.2012.

WAPDA (2012) Design Report of Diamer Basha Dam Project, Pakistan. Published by WAPDA. Web http://www.wapda.gov.pk. Accessed 1.10.2015.

Wardlaw R, Bhaktikul K (2004) Comparison of genetic algorithm and linear programming approaches for lateral canal scheduling. Irrigation and Drainage Engineering 130(4): 397-414.

Wardlaw R, Sharif M (1999) Evaluation of genetic algorithm for optimal reservoir system operation. Journal of Water Resources Planning and Management 125: 25–33.

WCD (2000) Dams and development: A new framework for decision-making by World Commission on Dams. Earthscan Publications Ltd., London and Sterling, Va.

White WR (2010) A review of Current Knowledge World Water: Resources, Usage and the Role of Man-Made Reservoirs. FR/R0012, Foundation for Water Research Allen House, Liston Road, Marlow.

Proceedings of the 10th World Congress of EWRA 'Panta Rhei', 5-9 July 2017, Athens, Greece
© 2017 *European Water Resources Association*

Irrigation with highly saline water: A new innovative water treatment system evaluated for vegetable production in greenhouse

A. Gertsis* and K. Zoukidis
Perrotis College, American Farm School, Marinou Antypa 54, str. P.O.Box 23, GR 55102 Thessaloniki, Greece
* *e-mail: agerts@afs.edu.gr*

Abstract: Good quality irrigation and potable water became items of scarcity in the recent years. In agricultural production, irrigation represents one of the major inputs and challenges for farmers survival. Recently the deterioration in quality and quantity of water is a major social and economical issue globally for food , feed and other agricultural production ouputs. Modern technological advances offer some possibilities for desalinized water use or reverse osmosis water for irrigation; however, the cost is still very high and not sustainable in large scales. Research projects with alternative systems including, ultrasound and electromagnetic technologies are under evaluation with promising outcomes. A new water treatment system using alternate low frequencies (ultrasounds) was evaluated in long term studies with various plant species, some very salinity sensitive, under greenhouse conditions. This paper presents data from the lettuce and celery only plant species, although results were similar for other vegetable species. The MAXGROW system provided very satisfactory results when used to irrigate a number of vegetable species with high electrical conductivity (ca. 8 to 12 dS/m) irrigation water. Results from long term evaluation have shown that vegetable yield was not affected adversely and in most cases it was increased. The effect of treated saline water by the system on soil properties was not shown to be adverse as compared with regular EC water qualities used in the study.

Key words: MAXGROW, water treatment, ultrasound, vegetables, saline water, sonication

1. INTRODUCTION

The scarcity of fresh water in arid and other regions necessitates use of saline water as a valuable alternative input for crop irrigation. Saline water has an agricultural potential but it is necessary to develop special management techniques and use of special water technologies, to obtain optimal yield and maintain high quality of commercial products. Field experiments, which were carried out in a pear orchard, had shown that by using saline water through subsurface drip irrigation (SDI) reasonable yields can be obtained (Gideon et al., 2002). Saline water use for agricultural production offers several additional benefits: (1) re-use (instead of disposal as with fresh water) during the entire year, with minimal environmental risk of groundwater deterioration (Oron, 1993); and (2) a premium market price for the fruits and vegetable products because of a high content of total soluble solids and an extended shelf life, due to the adaptation of the plant to the stressful growing conditions (Mizrahi & Pasternak, 1985)

Salinity is one of the major abiotic stresses that adversely affect crop productivity and quality. About 20% of irrigated agricultural land is adversely affected by salinity (Flowers and Yeo, 1995). Progress in breeding for salt-tolerant crops has been hampered by the lack of understanding of the molecular basis of salt tolerance and lack of availability of genes that confer salt tolerance. Most crop plants are susceptible to salinity even when ECe is _3.0 dS m^{-1} which in terms of osmotic potential is less than –0.117 MPa (osmotic potential =0.39 x ECe). At these salinity levels, the predominant cause of crop susceptibility appears to be ion toxicity rather than osmotic stress (Chinnusamy et al., 2005). Throughout the world, water scarcity is being recognised as a present or future threat to human activity and as a consequence, a definite trend to develop alternative water resources such as desalination can be observed. The most commonly used desalination technologies are reverse osmosis (RO) and thermal processes such as multi-stage flash (MSF) and multi-effect distillation (MED) (Fritzmann et al., 2007). Little information is available about the ability of

horticultural crops to detoxify reactive oxygen species and to synthesize compatible solutes and hence on the potential contribution of these mechanism to induce salt tolerance in horticultural crops (Paranychianakis and Chartzoulakis, 2005).

The U.S. Geological Survey (8) Gleick, 1996) found that 96.5% of Earth's water is located in seas and oceans and 1.7% of Earth's water is located in the ice caps. Approximately 0.8% is considered to be fresh water. The remaining percentage is made up of brackish water, slightly salty water found as surface water in estuaries and as groundwater in salty aquifers. Water shortages have plagued many communities, and humans have long searched for a solution to Earth's meager fresh water supplies. Thus, desalination is not a new concept; the idea of turning salt water into fresh water has been developed and used for centuries (Greenlee et al., 2009**).** Most of the technologies used to treat saline irrigation water are expensive and nof financial viable for large area irrigation.

There is not adequate information on simple and yet effective technologies to utilize saline water and sustain crop productivity. The objective of this study is to evaluate in a long-term and in various crop species and substrates, the efficiency of the MAXGROW technology system, using highly saline irrigation water (treated and untreated) and its effects in crop productivity and in substrates chemical properties, mainly pH and Electrical Conductivity (EC).

2. NEW WATER TREATMENT SYSTEMS

2.1 Water treatment systems

Use of ultrasound (US) in water treatment was reviewed by Gibson et al. (2008). They reported a critical review of ultrasound application for wastewater treatment is presented with emphasis on disinfection. Much of the work in this area remains at the laboratory scale. As a result, there is a need for fundamental information regarding the effect of sonication on the kinetics of disinfection and interaction of ultrasound with suspended particles. Such information is necessary for process engineering, design, and scale-up of ultrasound systems. A more recent review was reported by Doosti et al. (2012) where they stated that "one of the innovate technologies that was used for improvement of water treatment process is application of ultrasound (US) waves having a frequency of 20,000 Hz (20 kHz) or above, that is called "*sonication*". The results show this technique could improve the water treatment process environmentally. The most experiments are carried out in laboratory scale due to its cost. Ultrasound is longitudinal wave with a frequency above 20 kHz (Leighton, 1994). This frequency is above the sonic range (20 Hz to 20 kHz) at which humans can hear and below the mega-sonic region (>600 kHz) (Deymier et al., 2004; Wong, 2002). In US waves, energy is transmitted by the vibration of the molecules in the environment where the wave is being spread (Bello et al., 2005).

2.2 The MAX GROW system

The MAX GROW is an electronic water treatment system (Figure 1) using multiple transmissions of low radio frequencies to tackle the problems caused by saline water. It works by generating up to million vibrations per second and it differentiates the mineral salts to produce safe, easily removed by-forms. waves in constantly altered frequencies. It transmits radio waves in constantly variable frequencies which are programmed automatically, virtually every tenth of a second from the device itself based on a mathematic algorithm. These waves dissolve totally the large molecules of calcium carbonate ions in water (http://www.salinitysolution.com/en/).

3. METHODOLOGY

The study is a long-term assessment and the first set of yield results are presented herein. The

experiment was set in a greenhouse, using 15-liter black PE pots filled with three "substrates": 1. a sandy loam soil 2. a mixture of medium size pumice with a composted material (a commercial product by BIOSOLIDS) in a volume/volume ratio of 4:1 and 3. BIOSOLIDS material only (in these pots celery is only currently evaluated; other species will be followed up). Within each substrate, four irrigation water qualities treatments were used (each treated and untreated by the device): a mixture of sea water with regular water with an Electrical conductivity (EC) of ~8.0 dS/m initially and ~ 12 dS/m later in another growth cycle and regular irrigation water with an EC ~0.8 dS/m. Four lines of 20 pots each per substrate were formed, with the following arrangement: Line A= High salinity water treated with the MAXGROW device irrigation, Line B= Regular salinity water Treated with the MAXGROW device irrigation, Line C= (High *salinity* water, Non Treated with the MAXGROW device irrigation and Line D= regular salinity water, Non Treated with the MAXGROW device. There were 160 total pots, for the first two substrates and 48 pots for the BIOSOLIDS only substrate, with 20 and 12replications for each of the imposed treatments for the first two and the BIOSOLIDS substrates, correspondingly (Figure 2).



Figure 1. The electronic water treatment system (MAXGROW) used in the study.



Figure 2. The plot plan in the greenhouse.

Five vegetable species were selected for being sensitive to salinity and were used in a number of production cycles:

1. Green onions (*Allium cepa*), 2. Spinach (*Spinacia oleracea*), 3. Arugula (*Eruca sativa)* 4. Radishes (*Raphanus sativus*) and 5. Celery (*Apium graveolens*) were planted in the BIOSOLIDS

substrate only, since it is a perennial crop species and will be used for at least 4 growing seasons (for leaf cutting only). All substrates received appropriate and minimum fertilizer and no pesticides were used. At maturity/harvesting stage for each species, the fresh yield was harvested and weighted. Substrate chemical properties affecting crop yield measured included pH and ECs (using 1:1 v/v ratio of dionized water and substrate), in the beginning (before any water treatment), and at the end of each cycle of plants grown. Therefore, a continuous set of substrate measurements was completed to monitor the long term variation. The presented values include the grand average for the entire period. Additional agronomic measurements were taken (relative leaf chlorophyll levelplant height, etc.). This paper presents data from the lettuce and celery only plant species, although results were similar for the other four species.

Means comparisons using Student's *t* test was performed using JMP 8 statistical software (www.jmp.com), within each main and secondary treatment.

4. RESULTS AND DISCUSSION

4.1 Yield results

The four species used received minimum chemical fertilizer and no chemical pesticides were used. Therefore, the production system was considered a "low input" system to test the possible salinity effects; in other words, a "crash test" scenario was performed. The data analyses for yield are presented in Table 1, pooled across all treatments and separately for each of the two substrates and each plant species within each, and for the four water irrigation type treatments (saline & regular EC water, which was treated or non-treated by the MAXGROW system).

The saline water treated with the MAXGROW device increased statistically the yield in many cases, while it was in almost all cases on the higher yielding edgeIn the sandy loam substrate, the saline water treated produced the highest yields in all four crop species (spinach, radish, green onions and arugula), while in the Pumice+Compost substrate the yield was among the top in all crop species but not as high and significant as in the sandy loam substrate. The real cause of this is not clear yet, but it is hypothesized that the system provides a high level of break-down of macromolecules of various salts, making them more transportable through the plant cell membrane system. This hypothesis can be further tested using sophisticated microscopy techniques and additional validation studies, which are in progress.

In addition to yield measurements, some preliminary sensory characteristics were prematurely evaluated from a panel of 10 people and the general consensus was that the crops irrigated with saline water had a more "spicy+salty" and pleasant taste compared with those irrigated with regular water. The panel's opinion was based on the taste of the "control" plants considered to be the plants irrigated with "regular water non-treated".

Yield from the two lettuce varieties and two seasons harvestings (2015 & 2016) are shown in Tables 1 & 2, across the two substrates. Results had shown that the High EC-treated water quality outyielded the other irrigation qualities and was statistically significant higher in many cases, proving the system's efficiency, in both years.

The yield of celery plants from two sets of leaf harvesting, is shown in Table 3. Both yield sets were not statistically significant, while the High-EC treated irrigation provided numerically higher mean yield from all other water qualities. The organic substrate (BIOSOLIDS) used to produce celery, is not a typical growing medium and was used in this study as a exceptional medium for plant growth. The high percent of its organic matter (45-60%) has probably "buffered" some effects of the water salinity. This study is followed up for more harvestings (not reported in here), to further validate the effect shown in the first cycle.

Table 1. Vegetable yield (g/pot fresh weight) data (Two lettuce varieties) across the two substrates (2015 season)

Oneway Analysis of Lettuce COS- By Water quality				
Water quality				Mean
High EC treated	A			131,6
Low C Not Treated)	A	B		112,4
Low EC Treated	A	B		105,1
High EC not Treated		B		98,2

Oneway Analysis of Lettuce Salad -By Water quality		
Water quality		Mean
Low EC Not Treated	A	164,3
Low EC Treated	A	156,7
High EC not Treated	A	144,8
High EC Treated	A	140,3

Table 2. Vegetable yield (g/pot fresh weight) data (Two lettuce varieties) across the two substrates (2016 season)

Oneway Analysis of Lettuce variety COS -By Water quality				
Water quality				Mean
High EC Treated	A			185,7
Low EC Not Treated	A	B		185,1
High EC not Treated		B	C	143,8
Low EC Treated			C	129,8

Oneway Analysis of Lettuce variety Salad by Water quality				
Water quality				Mean
High EC Treated	A			237,5
Low EC Treated	A	B		195,7
Low EC Not Treated		B		170,7
High EC not Treated		B		165,4

Table 3. Celery yield data (g/pot- fresh leaves) for two growth cycles (sets)

Water Quality			Set#2
Low EC-Non Treated		A	110.3
High EC-Treated		A	107.9
Low EC-Treated		A	92.2
High EC-Non Treated		A	89.4
			Set #1
Low EC –Non Treated		A	152.7
High EC- Treated	A		150.6
High EC –Non Treated		A	145.8
Low EC -Treated	B		79.3

4.2 Substrate pH & EC results

The results of sequential sampling and analyses during the period of data collection of pH and EC changes in the three substrates as affected by the four "water qualities" within each Substrate, are shown in Table 4. The long term grand average of each substrate property was used to compare the means. In general, the pH was statistically affected by irrigation water quality. The High EC – treated water resulted in the lower pH in all three substrates.

The EC of the substrates was also affected (increased) by the High EC treated water, although the levels were not in the range of representing potential problems in crop productivity in all three substrate and, remained in all cases lower than the physiological critical level of 4 dS/m, through the entire measuring period. The results indicate that the MAXGROW system was effective in keeping the EC in within crop productivity limits for optimal growth. These results are compatible with the yield results presented in the previous section and further verify the effect of the system. In all Tables below, treatments not connected by same letter are statistically significant, using Student's *t* test.

Table 4. The effect of water quality in pH and EC on each substrate

Oneway Analysis of pH Grand average By WATER QUALITY – SUBSTRATE=BIOSOLIDS		
Water Quality		Mean
Low EC-Non Treated	A	7,390
High EC-Non Treated	A	7,360
Low EC-Treated	B	7,180
High EC-Treated	B	7,170

Oneway Analysis of pH Grand average By WATER QUALITY - SUBSTRATE=Pumice + BIOSOLIDS	
Water Quality	Mean
Low EC-Treated	7,478
High EC-Treated	7,346
High EC-Non Treated	7,331
Low EC-Non Treated	7,324

Oneway Analysis of pH Grand average By WATER QUALITY - SUBSTRATE=Sandy loam soil	
Water Quality	Mean
Low EC-Non Treated	7,525
Low EC-Treated	7,498
High EC-Non Treated	7,456
High EC-Treated	7,396

Oneway Analysis of EC (dS/m) Grand average By WATER QUALITY - SUBSTRATE=BIOSOLIDS	
Water Quality	Mean
High EC-Treated	1,718
High EC-Non Treated	1,456
Low EC-Non Treated	0,806
Low EC-Treated	0,716

Oneway Analysis of EC (dS/m) Grand average By WATER QUALITY - SUBSTRATE=Pumice + BIOSOLIDS	
Water Quality	Mean
High EC-Non Treated	1,694
High EC-Treated	1,560
Low EC-Treated	1,074
Low EC-Non Treated	0,993

Oneway Analysis of EC (dS/m) Grand average By WATER QUALITY - SUBSTRATE=Sandy loam soil	
Water Quality	Mean
High EC-Treated	1,950
High EC-Non Treated	1,266
Low EC-Treated	0,979
Low EC-Non Treated	0,863

5. CONCLUSIONS

This phase of the study provided adequate data for comparisons between highly saline and regular water (treated and untreated with the MAXGROW system) used for irrigation of vegetable species. The results have shown that the saline water treated by the MAXGROW technology in many cases increased yield and the some increase was statistically significant. Therefore, this technology can be efficiently used to irrigate the vegetable species using high EC (salinity) lever irrigation water. The effects on substrate properties (pH and EC) were shown to be minimal and not exceeded the critical limits for crop growth and productivity. The long term effects on the examined and other crop species are under continuous evaluation, for further validation of the trends and results shown in this phase. Also, the level of salinity will be progressively increased in follow-up studies, to test the "limits" of the system. The benefits of the device can be translated in positive economic outputs for the farmerswithout any adverse effects on substrates or soils. The short and long term benefits are expected to be substantial, in terms of the reduction of fresh water supplies for irrigating crops or use of high EC irrigation water for efficient irrigation.

ACKNOWLEDGMENTS

The authors express their sincere gratitude to the MAXGROW Salinity Solution Ltd.,

(http://www.salinitysolution.com/en/) for the equipment and technical support provided for the studies.

REFERENCES

Bello ARC, Angelis DF, Domingos RN. 2005. Ultrasound Efficiency in Relation to Sodium Hypochlorite and Filtration Adsorption in Microbial Elimination in a Water Treatment Plant. Brazilian Archives of Biologyand Technology, 48: 739-745

Chinnusamy, V., A. Jagendorf, and Jian-Kang Zhu. 2005. Understanding and Improving Salt Tolerance in Plants. Crop Sci. 45:437–448 (2005).

Deymier PA, Vasseur JO, Khelif A. 2004. Second-order sound field during megasonic cleaning of patterned silicon wafers: Application to ridges and trenches. Journal of Applied Physics 90, 4211-4218

Doosti, M.R., R. Kargar, M.H. Sayadi. 2012. Water treatment using ultrasonic assistance: A review. Proceedings of the International Academy of Ecology and Environmental Sciences, 2012, 2(2):96-110

Flowers, T.J., and A.R. Yeo. 1995. Breeding for salinity resistance in -pyrroline-5-carboxylate synthetase crop plants. Where next? Aust. J. Plant Physiol. 22:875–884

Fritzmann C., J. Löwenberg, T. Wintgens and T. Melin (2007) State-of-the-art of reverse osmosis desalination. Desalination 216 (2007) 1–76

Gibson, John H., Darrell Hai Nien Yong, Ramin R. Farnood, and Peter Seto. 2008. A Literature Review of Ultrasound Technology and Its Application in Wastewater Disinfection. *Water Qual. Res. J. Can. 2008 · Volume 43, No. 1, 23-35*

Gideon, O., Yoel DeMalach, Leonid Gillerma, Itsik David and Susan Lurie. 2002. Effect of Water Salinity and Irrigation Technology on Yield and Quality of Pears. Biosystems Engineering (2002) 81 (2), 237}247

Greenleea Lauren F., Desmond F. Lawlerb , Benny D. Freemana , Benoit Marrotc and Philippe Moulin (2009 Reverse osmosis desalination: Water sources, technology, and today’s challenges. water research 43 (2009) 2317–2348

Leighton TG. 1994. The Acoustic Bubble. Academic Press, San Diego, USA

Maas, E. V. and G. Hofman (1997). Crop salt tolerance-current assessment. Journal Irrigation and Drainage Engineering Division, ASCE, 103, 115-134

Mizrahi, Y and Pasternak D (1985). Effect of salinity on quality of various agricultural crops. Plant Soil, 89, 301}307

Wong KYK. 2002. Ultrasound as A Sole or Synergistic Disinfectant in Drinking Water. Master Thesis. Worcester Polytechnic Institute, USA

Proceedings of the 10th World Congress of EWRA 'Panta Rhei', 5-9 July 2017, Athens, Greece
© 2017 *European Water Resources Association*

Irrigation water pricing in the countries of the OECD – Modern trends and critical review: The Greek case

I. Giannopoulou[1], E. Eleftheriadou[2*] and S. Yannopoulos[1]
[1] *Faculty of Engineering, School of Rural and Surveying Engineering, Aristotle University of Thessaloniki, 54124, Thessaloniki, Greece*
[2] *Department of Environment and Hydroeconomy of Thessaloniki, Region of Central Macedonia, 546 29, Thessaloniki, Greece*
[*] *e-mail: e.eleftheriadou@pkm.gov.gr*

Abstract: During the last decades, due to urbanization and rapid industrial development, water demand has increased enormously resulting in a substantial decrease of the annual renewable water resources per citizen. In addition, water prices do not depict the real value of water, thus misleading consumers to underestimate its real value. Hence, the planning of water pricing techniques is a crucial step for water supply companies and local societies, in order to achieve effective allocation of the restricted water resources to the consumers. In the 90's several movements by economists brought up the issue of "setting the price right", as a tool to produce economic motives to the water users. The main cause of the unwise water consumption in the irrigation sector, that represents 70% of the global consumption, is the underpricing of irrigation water, while it is widely accepted that proper pricing policy is the basic factor for the conservation of the operational competence of water irrigation systems. The current study focuses on the modern trends across the countries of the OECD concerning water management in agriculture, the pricing of the irrigation water and also the reforms observed in the pricing policies. In addition, the Greek case is presented, where a new legislative framework is under way, introducing general rules of estimating water costs and water pricing of the water services. In order to manage water in a more efficient way, the OECD countries should adopt strategies that promote sustainable irrigation water management and take into account climate change, implementing policies that should be easily adopted, according to national or local demands.

Key words: water pricing, water cost, pricing policies, irrigation, OECD, Greece

1. INTRODUCTION

During the 90's economologists had already pointed out the necessity of treating water as an economic good and especially referred to "setting the price right" in order to create economic motives for the water users. (World Bank, 2004; Molle and Berkoff, 2007). But it was after many decades that the water managers shifted from satisfying the offer to managing the demand, which Winpenny (2004) defined as "doing better with what we have".

Full cost of water is comprised by three main components (Toan, 2016): i) the full supply cost, ii) the full economic cost and iii) the full cost, comprised of the full economic cost and the environmental externalities. Many water experts consider that the underpricing of irrigation water is the main reason for the continually increasing water demand in the irrigation sector, which represents approximately 70% of water use globally (FAO, 2011).

According to the World Water Council, water users do not appreciate water being provided free of charge or at a low price and tend to waste it. In addition, underpricing the value of water gives the impression to the consumers that the real value of water is as low as its price. Hence, the planning of water pricing techniques is a crucial step for water supply companies and local societies, in order to achieve effective allocation of the restricted water resources to the consumers. Particularly, in the irrigation sector, proper pricing policy is the basic factor for the conservation of the operational competence of water irrigation systems. Sandra Postel (Postel, 1992) supports that the value of water is systematically being underestimated resulting in its long-term over-consumption. Water pricing is the main factor that can induce proper water allocation and according to Dinar and Subramanian (1997), in cases where water prices do not reflect its value, then water

users receive the wrong information, whereas environmentalists believe that water pricing can function towards reduced water abstractions and the protection of ecosystems.

Managing water resources in the agricultural sector is a very complicated process as it covers a wide range of irrigation systems, climatic conditions, source types (surface, underground waters) (IWMI, 2007), different property rights systems, cultural and social conditions, all these within state borders or even between countries (OECD, 2009).

In the agricultural sector, water resources management refers mainly to irrigation in order to ensure steady water supply during the productive period, to flood, drainage and drought management and also to restoration and conservation of ecosystems.

All OECD countries have developed strategic policies for the confrontation of the general issues of water resources management and concerning agriculture they share a common vision through a long-term plan for sustainable water resources management that includes:

- The adaptation of the agricultural sector to climatic change, as the impacts on the agricultural income and on the achievement broader goals of rural development.
- Protection of the ecosystems that are within agricultural areas.
- Balancing water uses among different productive sectors.
- Improving water use efficiency.

In the present paper the modern trends in the OECD countries are examined regarding water management in agriculture, water pricing of irrigation water and any reforms that have been realized in water costing. The paper also presents an overview on the irrigation situation and focuses on irrigation water pricing in Greece.

2. MODERN TRENDS IN THE OECD COUNTRIES

The Organisation for the Economic Co-operation and Development (OECD) was created in 1961 when an agreement was signed between 18 European countries, USA and Canada. Today OECD has 35 Member countries, but also holds synergies with emerging economies, such as the People's Republic of China, India, Brazil and many others. The organisation's purpose is not to set rules, but to encourage cooperation among its members and to provide consultation services for the establishment of governmental policies.

During the period of 2002-2004, water use in irrigation in OECD countries, represented 44% of the total water use, while in eight of them irrigated agriculture consumed water in a percentage above 55% (Greece 83%, Mexico 77%, Turkey 75%, Japan 66%, Spain 60%, Portugal 52%, New Zealand 57%, Australia 55%). In the majority of the countries, there is a great difference between supply and demand resulting in numerous conflicts among irrigation and other uses, but also with the environment (Giannopoulou and Yannopoulos, 2015).

An increase of water use for irrigation is observed in four countries (Greece, Korea, New Zealand and Turkey) mainly due to an increase in the irrigated land, while the opposite is observed in other countries, as in Australia and Mexico. The latter decrease is due to a combination of factors that vary across countries, but mostly due to the improvement of water use efficiency, to the safeguarding of the water amount for environmental needs and the shrinking of the agricultural sector in Europe (OECD, 2010a).

For certain countries, as Greece and Turkey, irrigation holds the lead role in agriculture and the increase of irrigation water demand in the last decades is far higher than in other sectors. However, in countries such Australia, Korea, Mexico, Portugal and Spain, this increase was lower compared to other sectors.

The increase in irrigation water productivity was realized through the use of more efficient irrigation techniques (such as drip irrigation) and the implementation of water saving applications. In general, the average rate of water use per hectare was decreased by 7% during the period of 1990-2004, whereas in most cases the agricultural production presented an increase. For example, in USA during the 90’s, irrigation water productivity increased while at the same time, irrigation

amounts per hectare decreased by 7% (Hutson *et al*., 2004).

The use of modern irrigation technologies, has gained ground against traditional ones and in countries as Australia, France, Greece, Italy, Spain more than 25% of the irrigated land is served by modern irrigation systems. Moreover, irrigation efficiency has been promoted by the reinforcement of irrigation channels against leakages and the upgrading of the irrigation techniques, such as measuring the soil moisture and estimating precisely the optimal water amount needed.

Over-exploitation of water resources for meeting irrigation demands is often detrimental to ecosystems, as it reduces water quantities below the environmental thresholds in rivers, lakes and wetlands, affecting also leisure activities, fisheries and other uses of the ecosystems. It should be noted that agriculture is a substantial and increasing diffuse pollution source in many OECD countries and imposes many threats in cases where drinking water demands are met by groundwater sources.

3. PRICING POLICY IN OECD

Until the 80's, in most OECD countries irrigation water management was focused on ensuring the essential water quantities. Great emphasis was placed on the infrastructure in order to satisfy the demand and to collect the maximum amount of water (Pahl-Wostl, 2008). A critical turn point in water management was achieved in the International Conference on Water and the Environment in Dublin in 1992, where the 4th principle on the economic value of water states that "*Managing water as an economic good is an important way of achieving efficient and equitable use, and of encouraging conservation and protection of water resources*" (ICWE, 1992). This is also emphasized in the Earth Summit in Rio, where water is introduced as an economic good.

In the OECD countries, water pricing policies are based on (Tsur, 2005):

- Volumetric charges of the water consumed.
- The water-production relation, thus water pricing is connected to the production.
- The irrigated area, where it can also be connected with the type of cultivation, the irrigation method, seasonality and/or other factors.
- Multi-rate volumetric methods, where pricing differs according to the amount of water consumed.
- Two- part tariff, where the users are charged a fixed annual amount plus a constant marginal price per unit.
- Betterment levy, where water pricing is based on the irrigated area taking into account the increase in land value due to the irrigation.
- Water markets, with great variations across countries.

According to FAO (FAO, 2004), there are substantial inter-state differences on water costs and cost mechanisms, depending on various factors, such as type of sources, water deficiency, technology of irrigation systems and socio-economic targets. In general, OECD countries have different reasons for imposing water costs, such as cost recovery or for improving allocation and protection of water resources (Dinar and Subramanian, 1997). Moreover, increases in irrigation water do not take place simultaneously in the OECD countries, as in the cases of domestic or industrial costs, while charges are substantially lower compared to other economic sectors.

In most OECD countries large-scale irrigation projects have been built with public capital grants (Berbel *et al*., 2007). Moreover, the OECD raises awareness that subsidies are often harmful to the environment as they can result in increased levels of waste and emissions (Toan, 2016). However, it has been observed that subsidies are very common, especially in developed countries and consequently have caused negative issues, such as water resources depletion and environmental degradation.

Currently, there is a tendency across the OECD countries, for gradually shifting water costs towards the users, in order to maintain the economic sustainability of the water supply infrastructure. The reforms in water policy should be developed as an integrated part of a broader

reform framework that includes institutional changes in water allocation methods and introducing cost recovery for water supply while adopting water policy in the long-term central governmental decision-making (OECD, 2010a). The OECD recognizing the difficulties for countries to move towards full cost recovery, promoted the concept of "*sustainable cost recovery*" by finding the right balance between water revenues, the so-called "3Ts" (tariffs, taxes and transfers).

It should be noted that in the recent years there is a substantial progress on the water pricing sector for irrigation. Many countries have made remarkable efforts in order to re-examine the pricing of water infrastructure and to calculate the portions of cost recovery (OECD, 2010b).

The most adverse motive affecting irrigation in the European countries is the water charge per hectare and only in few irrigated areas other policies, such as per volume or other variable, are implemented. Despite the common recognition that volumetric rate systems should be implemented, there is a general lack of such policy implementation.

4. REFORMS IN WATER COSTING TECHNIQUES IN OECD

In the majority of the OECD member states there is a tendency to change water costing methods towards the increase of the imposed costs to the consumers, in order to ensure economic sustainability of the water supply systems. The OECD has concluded in certain factors that could reinforce a future implementation of water pricing reforms:

- ceasing of the subsidies for the construction of irrigation works;
- wide acceptance that irrigation is not the basic factor for the promotion of agricultural development;
- a certain degree of inter-sectoral competition regarding insufficient water resources;
- the common perception that water pollution and environmental degradation can be confronted only by reducing the total water consumption;
- the implementation of economic reforms towards the decrease of the state participation in commercial activities.

More specifically, according to OECD (2010a), the reforms of water policies should be developed as an integrated part of a broader reform framework that incorporates institutional changes on water allocation patterns, water property rights, full cost recovery and a stable mechanism for financing water supply infrastructure. Moreover, certain issues that should be taken into account and can promote such reforms are (OECD, 1999):

- the cancellation of any water diversion projects, unless they are fully financed by the new end-users;
- the systematic estimation of water supply cost, that corresponds to each user or group of users;
- the definition of the percentage of the total expenses, that can be imposed to the farmers;
- the confrontation of drought conditions for farmers, that cannot meet the high water prices and the owners of historic water rights;
- the definition of the environmental cost in combination with the penalties of the users, that pollute the resource;
- the public consultation that will convince farmers of the positive effects of the reforms, such as the higher level of water supply reliability.

Water property rights, in most OECD countries, involve a complicated set of rules, where water is allocated among users and environmental needs based on quantities rather than on costs. As water conflicts among users are getting more intense, policies should be more robust and strict in order to achieve a more equitable allocation depending on economic, environmental and efficiency criteria. Some progress has been achieved in the last years on water pricing of irrigation water and some countries have presented remarkable efforts on re-examining water pricing and cost recovery in the irrigation sector.

5. THE GREEK CASE

The agricultural sector in Greece is a substantial contributor of the state's economy, even if its role has been weakened in the last years. More specifically, its contribution to the GDP in the beginning of the 90's until 2004 was reduced from 14% to 7%, while the employment rate in agricultural activities reduced from 22% to 17% (OECD, 2008), resulting in 13,5% in 2014.

The increased water use and the intensity of irrigation is quite alarming, as nearly half of the water used for irrigation comes from groundwater aquifers and in many coastal regions sea-water intrusion is observed (OECD, 2000). Moreover, losses in the water systems are quite common, reaching 45-50%, due to leakages, infiltration and evaporation.

Water charges are based on the irrigated area and not on the volumetric consumption and independently of the cultivation type, the season or the irrigation method. Hence, there is a general lack of motivation that would guide farmers towards water saving measures. Only recently and in a few areas water charges are shifted towards the volumetric consumption, due to bad experiences of water droughts during the summer months.

The estimation of the abstracted water volumes from aquifers is a hard task as a substantial part of the irrigated area is served by private boreholes or wells. The environmental cost of the exploitation of the aquifers, abstractions and possible pollution, is neglected, whereas there is a complete lack of mechanisms for cost recovery and penalties imposition in cases of over-consumption.

In the summer of 2016, a new legislation (Common Ministerial Decision) on the estimation of water cost and pricing was placed under public consultation, in order to promote sustainable water use in all sectors. The aim was to set general rules on water cost and pricing estimation and to set the methods and processes for cost recovery of the water services for various uses.

According to the draft text, water cost is comprised of three components: i) *the financing cost*, ii) *the environmental cost* and iii) *the resource cost*. The estimation process of the financing cost takes into account four parameters:

- the capital cost;
- the operating cost, that includes all the essential expenses for the operation of the water services infrastructure comprising of fixed and variant costs;
- the maintenance cost, that includes all the expenses for the expendable materials and labor;
- the management cost and other costs, connected to the management of the responsible water agency.

The environmental cost is defined on a water body level or on a group of water bodies and is derived from the cost estimation of the Complementary Programme of Measures of the River Basin Management Plans (RBMPs), that aim at achieving "good" water quality. In order to estimate the environmental cost, at least one of the following conditions should be met: a) surface water bodies with ecological status below "good", b) surface water bodies with chemical status below "good", c) surface water bodies with ecological and/or chemical status "unknown", and d) groundwater water bodies that are characterized with "bad" chemical status.

The resource cost is estimated in a similar way through a different set of Complementary Programme of Measures, that aim at water saving and rational management of water resources. The prerequisite conditions that have to be met are either: i) groundwater with "bad" quantity status or ii) not meeting the demands, due to irrational water management.

The relevant governmental authority notifies each year at the end of October, the water agencies of the environmental and the resource cost per cubic meter, while the financing cost will be estimated by the water agencies themselves.

Specifically, the irrigation water pricing is based on a mixed charging system comprised of two parts: i) a fixed charge, according to the cultivated area and ii) a variable charge per water unit (volumetric charge per cubic meter of water consumption). In cases where volumetric quantities of water cannot be registered, the variable charge will be realized based upon estimations of the

quantities used, made by the water provider agencies.

This new legislative framework has received a lot of negative criticism for facing water pricing with a pure economic direction and from the comments received during the public consultation it is evident that the public perceives it as an effort of the government to increase water costs, even if the relevant minister supports that water pricing will not be depicted on water costing. Moreover, the new ministerial decision is accused of providing a legal base for promoting water agencies, without categorizing them in "good" and "bad" water managers. It is also believed that the exception of cases where volumetric charges are not feasible, typically perpetuates the current policy, where charges are not connected to the actual consumption.

6. CONCLUSIONS

Water management in the OECD countries covers a wide range of agricultural systems and climatological conditions, abstractions from various sources, as surface and ground waters and in some cases use of precipitation water, recycled waste and desalinated water. Such management should function in a wide range of different political, legal, cultural frameworks involving various sectors, such as agriculture, environment, energy and others.

Water pricing is an efficient way of improving water allocation techniques and encouraging water users towards water resources conservation. When water prices reflect accurately the economic value of water, then water users are given the proper information in order to choose the amount of water and the use that provides them the highest interest. Thus, water pricing may influence water use efficiency, in an individual or in a social level. In practice, water pricing systems can be implemented in order to satisfy a variety of demands, for example fixed taxes of water supply could be shifted to other sectors if needed (Giannopoulou and Yannopoulos, 2015).

The OECD countries should adopt strategies that promote sustainable irrigation water management, that:

- Recognize the complexity and the diversity of water resources management in agriculture.
- Strengthen the institutions and water property rights.
- Ensure that water costs reflect the full supply cost.
- Promote an integrated policy covering various sectors as agriculture, urban water use, energy and environment.
- Take precaution measures that support agriculture in relation to climatic change and the consequences of climatic variability.
- Confront lack of knowledge and information in water resources management.

It is anticipated that future agricultural policies will be affected to a large extent by climate change and variability and encompassing seasonality factors, such as alterations of the precipitation yearly-rate or of the snow-melting. These policies should be easily adopted, according to national or even local demands. The great variability of catchments should be taken into account during policy building, in combination with the heterogeneity of water sources, the allocation of water resources, the relation between water quantity and quality, while establishing also the necessary balance with the complicated institutional regulations and the water property issues.

It is widely accepted that water resources management in the OECD countries should undergo substantial alterations in order to provide better services with a minimum cost to the society and to overcome any uncertainties of the future availability of water resources. Sustainable water resources management in the agricultural sector is under the responsibility of the relevant management bodies and the end-users that should secure an efficient and equitable allocation among sectors while achieving the social, environmental and economic goals.

REFERENCES

Berbel J., Calatrava J., Garrido A., 2007. Chapter 13. Water Pricing and Irrigation: A Review of the European Experience. In: F. Molle and J. Berkoff (eds.), Irrigation Water Pricing: The gap between theory and practice, CABI, Wallingford, the United Kingdom, pp. 295-327.

Dinar A., Subramanian A., 1997. Water Pricing Experiences: An International Perspective. In: A. Dinar and S. Subramanian (eds.), Water Pricing Experiences: An International Perspective. World Bank Technical Paper No. 386, pp. 1-12.

FAO, 2004. Water charging in irrigated agriculture: An analysis of international experience. FAO Water Reports 28. Rome, Italy.

FAO, 2011. The State of the World's Land and Water Resources for Food and Agriculture (SOLAW) – Managing Systems at Risk. Food and Agriculture Organization of the United Nations, Rome and Earthscan, London, UK.

Giannopoulou I., Yannopoulos S., 2015. Irrigation Water Pricing in the countries of the OECD – Modern trends and Perspectives. In: Cartography of Mind, Soul and Knowledge. Oblation to Myron Myridis, Emeritus Professor, School of Rural and Surveying Engineering, Aristotle University of Thessaloniki, pp. 934-958.

Hutson S.S., Barber N.L., Kenny J.F., Linsey K.S., Lumia D.S., Maupin M.A., 2004. Estimated use of water in the United States in 2000. Reston, Va., U.S. Geological Survey Circular 1268.

ICWE, 1992. The Dublin Statement on Water and Sustainable Development. International Conference on Water and the Environment. (accessed at: http://www.wmo.int/pages/prog/hwrp/documents/english/icwedece.html, March 2105).

IWMI (International Water Management Institute), 2007. Water for Food, Water for Life: A Comprehensive Assessment of Water Management in Agriculture. IWMI, Columbo, Sri Lanka.

Molle F. and Berkoff J., 2007. Chapter 2. Water pricing in irrigation: mapping the debate in the light of experience. In: F. Molle and J. Berkoff (eds.), Irrigation Water Pricing: The gap between theory and practice, CABI International, Wallingford, UK, pp. 21-93.

OECD, 1999. Agricultural Water Pricing in OECD Countries. Document ENV/EPOC/GEEI(98)11/FINAL, OECD, Paris, France.

OECD, 2000. Environmental Performance Reviews: Greece. Paris, France. (accessed at: www.oecd.org/env, March 2014)

OECD, 2008. Environmental Performance of Agriculture in OECD countries since 1990. Greece Country Section. Paris, France, pp. 210-211 & 313-323.

OECD, 2009. Managing Water for ALL: An OECD Perspective on Pricing and Financing.OECD Publishing, Paris, France.

OECD, 2010a. Sustainable Management of Water Resources in Agriculture. OECD Publishing, doi: 10.1787/9789264083578-en. (accessed at: www.sourceoecd.org/agriculture/9789264083455, June 2015).

OECD, 2010b. Agricultural Water Pricing_EU and Mexico. (accessed at: http://www.oecd.org/eu/45015101.pdf., March 2015)

Pahl-Wostl C., 2008. Requirements for adaptive water management. In: C. Pahl-Wostl, P. Kabat and J. Moeltgen (eds.), Adaptive and Integrated Water Management: Coping with Complexity and Uncertainty. Springer Publishing, Berlin, Germany, pp. 1-22.

Postel S., 1992. Last oasis: facing water scarcity. W.W. Norton & Co., New York, USA.

Toan T.D., 2016. Water pricing policy and subsidies to irrigation: a Review. Environmental Processes; 3: 1081-1098.

Tsur Y., 2005. Economic aspects of irrigation water pricing. Canadian Water Resour. J., 30(1): 31-46.

Winpenny J., 1994. Managing Water as an Economic Resource. Routledge and Overseas Development Institute, London, UK.

World Bank, 2004. World Bank water resources sector strategy: strategic directions for World Bank engagement. World Bank, Washington, DC.

Proceedings of the 10th World Congress of EWRA 'Panta Rhei', 5-9 July 2017, Athens, Greece
© 2017 *European Water Resources Association*

Irrigation of walnut trees in the vicinity of Hisareyn - Gölcük / Kocaeli, Turkey

F. Dokmen[1*], Y. Ahi[2] and D.D. Koksal[2]
[1] *Kocaeli University, The Vocational School of Food & Agricultural,Campus of Arslanbey, Kartepe-Kocaeli, Turkey*
[2] *Namık Kemal University, Faculty of Agricultural, Department of Biosystem Engineering, Tekirdağ, Turkey.*
[*] *e-mail: funda.dokmen@kocaeli.edu.tr*

Abstract: Walnut trees as well as their fruits represent an important sector of the agricultural industry. Walnut is a valuable fruit species and its cultivation contributes significantly to the economy in Turkey. Turkey with its 13.2 billion walnut trees is so important in terms of walnut cultivation among other countries in the world. There are many problems about irrigation during the growing period of walnut. Walnut trees need irrigation during the growing period. Irrigation is a key-factor for walnut cultivation. Generally, application of irrigation is recommended from the beginning of April until the end of October. Irrigation methods change according to orchard's soil characteristic and climatic conditions of the cultivation area. In this study, irrigation methods and water resources were investigated in the walnut orchards located in the vicinity of Hisareyn-Gölcük/Kocaeli in Turkey. Irrigated and non-irrigated walnut orchards were compared. Double ring infiltrometer test has been performed for the purpose of determining the soil infiltration rate. According to physical observations and the determination of soil characteristics, irrigation methods were assessed with the purpose of determining the most suitable ones for walnut orchard irrigation in the area.

Key words: Infiltration, irrigation, orchards, productivity, walnut

1. INTRODUCTION

In the recent years, walnut cultivation has been steadily increasing in Turkey, due its high economic value. Turkey is among the native lands for walnut cultivation. It has over 4.5 million walnut trees as a result of the cultivation done so far. Due to its walnut production of nearly 120 thousand tons, Turkey ranks third in the world in this sector (Anonymous, 2016).

Walnut trees can easily adapt to various soil and climate conditions. Although it takes a long time to grow, walnut is one of those fruit species which is most common over the world, with its cooling requirement of 400-1800 hours. In general, walnut trees adapt more easily to valleys that are sun-drenched in the summer and moderately warm in winter, secured from the wind. Since Turkey is on a geographical location where climate transitions are influential, the choice of plants and orchard systems of cultivators vary. In certain regions of our country, late frosts in the spring are among the most important factors which cause inefficiency in the walnut trees. Among the other most important factors are irrigation and the correct choice and application of the irrigation method.

Walnuts require a cool enough weather in winter and autumn to satisfy the need for cooling and a temperature of 25-35 ^{0}C in spring and summer which is enough to support normal growth and maturing. A total minimum yearly precipitation of 500 mm is sufficient for walnut cultivation. However, it is important that it is regular. Especially in the summer, there should be enough water and humidity in the soil.

If the precipitation in winter is not enough to wet the soil at least 180 cm deep, irrigation must be applied during the winter as well in order to make up for the water and humidity deficiency.

They grow well in deep soils which do not retain water, with a groundwater level of not more than 2.5-3 meters. The pH value of the soil should be around 6-7 without any problems of soil alkalinity or saltiness. The soil should be well-drained, rich in organic matter and well-aired. The level of water retention capacity of the soil is of additional importance for cultivation; the higher it

is, the better. According to studies, the yearly water demand of walnut trees is around 750-1500 mm. Some researchers and also FAO studied about crop yield response to water relation to irrigation of walnut trees (Goldhamer et al. 1982; Golhamer et al. 1984; Fulton et al. 2003; Chauvin et al., 2005; FAO, 2012; Goldhamer and Beede, 2015).

2. MATERIAL AND METHODS

The study has been performed in the walnut orchards in the town of Hisareyn within the district of Gölcük, located in the city of Kocaeli. All of the orchards where walnuts were cultivated had been set up according to the cultivators' own knowledge and experiences. While some of the orchards were set up on the plain, the others were set up on high lands within the forest land, approximately 300-500 m above sea level.

The research area is 13 km from the city of Kocaeli and 7 km from the district of Gölcük. The climate of the district is under the influence of Black Sea climate, but it also shows climate properties of the Marmara Region. When average climatic values measured throughout many years (1950 - 2015) are studied, it is seen that the average temperature has been 23.8 ^{0}C and the highest average temperature has been measured in July as 29.6 ^{0}C. The lowest average temperature has been measured in January as 3.3 ^{0}C. Average number of rainy days has been the highest in January with 17.4 and the lowest in August with 5.2. Total monthly precipitation has been recorded to be the highest in December with the average being 110.0 kg m^{-2} and the lowest in July with the average being 37.1 kg m^{-2} (Anonymous, 2017).

The local walnut orchards have been visited and the problems they face in irrigation have been identified. The cultivation sites have been photographed.

Soil samples have been taken and analysed according to Blake (1965) and Benami ve Diskin (1965). Soil texture was measured with a hydrometer as explained in Bouyoucos (1962).

In addition, samples have been taken from the water sources used in irrigation and irrigation water quality analyses have been performed in the laboratory, according to Ayyıldız, 1990.

The actual value of water logging speed of the soil (infiltration) needed for the preparation of the irrigation system has been identified (Criddle ve ark., 1956) by double ring infiltrometer measurements as ranging between 8 mm h^{-1} and 50 mm h^{-1}, depending on local soil properties.

3. RESULTS

The walnut species cultivated in the research area are Yalova 1, Yalova 3, Yalova 4, Şebin and Bilecik as the local species and Chandler, Pikan and Fernor as the foreign species. The most important reason why the foreign species are preferred in the area is that they provide high efficiency, high quality fruits that are full inside with thin shells and therefore also yield high incomes.

The size of the walnut orchards in the research area vary between 5 and 10 decars. The young trees in the orchards are generally planted within 9x9 m and 10x10 m spaces. As well as orchards where spring water is used, there are also certain walnut orchards where the cultivation is done without any irrigation. Non-irrigated orchards are mostly the cultivation sites set up within the forest land (Figure 1).

According to the laboratory results, the soil texture in the research area walnut orchards can be classified as either loamy or sandy-loamy. Average water retention capacity is 26.94 mm.

And according to the results attained in the analyses, the irrigation water quality is moderately salty and low in sodium which is considered class 2 irrigation water and the pH value of the waters is on a neutral level, varying between 7-7.50.

Flood irrigation and wetting the whole orchard are methods commonly used in irrigation. The number of orchards where drip irrigation method is used is very low and they are set up without a project, according to the cultivators' own knowledge and experiences. Therefore, the cultivators are

unable to reach the desired efficiency levels with these irrigation systems.

Walnut is a fruit species which responds very well to drip irrigation. Thus, the walnut cultivators in the research area were advised to make use of the drip irrigation method. The purpose of the drip irrigation method is to apply at once, a low amount of irrigation water, only to the area where the plant roots grow with the help of a pressure pipe and drippers so as not to cause a tension resulting from a deficiency in humidity. With this system a wet surface is created only along the plant rows without wetting the whole cultivation site and the ground between the rows remains dry. When irrigation is applied this way, the benefits obtained from the irrigation water are maximized. And the water loss due to evaporation is minimized. In addition, since the setup cost for the drip irrigation system is lower in comparison with other irrigation systems and that it saves water and has a positive influence on keeping the fertile soil in cultivation gardens, it should be a preferred choice among cultivators (Figure 2). The plots were irrigated by drip irrigation. Irrigation was taken by a pump from a water tank near the experimental site.



Figure 1. Walnut orchards in the research area

It is of great importance that irrigation water reaches all of the roots of walnut trees. Therefore when the irrigation system is being set up, it is a must that the irrigation project is prepared in a wat that enables the irrigation water to reach the capillary roots that are spread over the crown projection areas of the trees.



Figure 2. Drip irrigation in the walnut orchard

4. CONCLUSION

With their wide branches and wide leaves, walnut trees require a lot of water. Especially during the two years following the planting of the young plant, regular irrigation is needed. The growth in spring and meeting the water needs of the plants during the periods when the trees grow fruits and

when the meaty parts of the fruits are forming are very important. If the trees are unable to get enough water during this period, growth and vegetation will slow down and decreases in quality and efficiency will be seen due to the inability of the fruits to form enough meat. Although walnuts are drought tolerant, irrigation yields higher efficiency.

The irrigation to be applied after the fruit has reached a sufficient size helps the meaty part of the fruit to grow and fill in the hard shell. Therefore, in contrast to many other fruit species, irrigation throughout the growing period plays an important role in walnut gardens.

Therefore in the irrigation of walnut gardens:

- Cultivators must get technical counselling for a science-based walnut cultivation while they are setting up their orchards.
- Irrigation must be applied when walnut trees are forming leaves and blossoming in the spring.
- Generally, irrigation must be started at the beginning of April and continued through October.
- In dry years, irrigation must be applied in autumn and winter as well.
- Irrigation must be applicable during fertilization and through a drip irrigation system,
- When the fruit size reaches the size of a marble,
- When the meaty parts of the fruits are growing,
- 15 days prior to the harvest,
- And at least once immediately after the harvest.

ACKNOWLEDGEMENT

This study is supported by Scientific Research Projects Unit (BAP-2015/013) of Kocaeli University and Vision 2023 of Gölcük Municipality of Kocaeli, Turkey. Authours would like to thank to Scientific Research Projects Unit (BAP) of Kocaeli University and Vision 2023 of Gölcük Municipality of Kocaeli,Turkey.

REFERENCES

Anonymous, 2016. Devlet İstatistik Enstitüsü (Recorder of Goverment Statistics Institue) (www.die.gov.tr), Ankara.

Anonymous, 2017. T.C. Orman ve Su İşleri Bakanlığı, Meteoroloji Genel Müdürlüğü Kayıtları (Recorder of Meteorology General Directory), Ankara.

Ayyıldız, A. 1990. Sulama Suyu Kalitesi ve Tuzluluk Problemleri (Problems of Salinity and Irrigation Water Quality), Ankara Üniversitesi, Ziraat Fakültesi Ders Kitabı, 344, Ankara.

Benami, A., Diskin, M.H. 1965. Design of Sprinkler Irrigation, Lowdermilk Faculty of Agricultural Engineering. Instıtute of Technology. Haifa. Israel.

Blake, G.R. 1965. Bulk Density Methods of Soil Analysis, Am. Soc. Agron. 9, 374-377, Winconsin. USA.

Bouyoucos, G. J., 1962. Hydrometer method improved for making particle-size analysis of soils. Agron. J. 53: 464 – 465.

Chauvin, W., Ameglio, T., Pruner, J.P., Soing, P. 2005. Irrigation of Walnut Tress Managing The Water Potential, ISHS Acta Horticulture 705: V International Walnut Symposium (http://www.actahort.org/books/705/705_69.htm)

Criddle, W.D., Davis, S., Pair, C.H., Shockley, D.G. 1956. Methods for Evaluation of Irrigation Systems. USDA Agric. Handbook. 82 pp., Washington D.C.

FAO, 2012. Crop Yield Response to Water, FAO Irrigation and Drainage Paper 66, ISSN 0254-5284, Rome, Italy.

Fulton, A., Salinas, M., Montoro, A., Goldhamer, D. 2003. Evaluation of Trunk or Scaffold Shrinkage in Walnut as an Indicator of Orchard Water Status. An annual research report submitted to the California Walnut Board for 2003

Goldhamer, D.A., T.M. DeJong, D. Ramos, R. Beede, S. Sibbett. 1982. Water Use Requirements of Normal and High Density Walnuts. An annual research report submitted to the California Walnut Board for 1982.

Goldhamer, D.A., R. Kjelgren, R. Beede, T.M. DeJong, D. Ramos. 1984. Water Use Requirements of High and Conventional Density Walnuts under Localized Irrigation. An annual research report submitted to the California Walnut Board for 1984.

Goldhamer, D.A., Beede, R.H. 2015. Walnut Irrigation Management: Past and Future Methods. http://www.cekings.ucanr.edu /files/19470.pdf

Proceedings of the 10th World Congress of EWRA 'Panta Rhei', 5-9 July 2017, Athens, Greece
© 2017 *European Water Resources Association*

Soil water electrical conductivity determination based on the salinity index concept

G. Kargas*, P. Mougiou, A. Petsetidi and P. Kerkides
Department of Natural Resources Development and Agricultural Engineering, Agricultural University of Athens, Greece
* *e-mail: kargas@aua.gr*

Abstract: The dielectric devices can provide simultaneously and for the same spot of soil, measurements of the apparent soil dielectric permittivity (ε_s) and bulk soil electrical conductivity (σ_b). For the prediction of the electrical conductivity of the soil solution (σ_p), the method based on the concept of salinity index (X_s) is proposed. In the standard method X_s is defined as the partial derivative of the bulk soil electrical conductivity (σ_b) with respect to the apparent dielectric permittivity (ε_s). The evaluation of this approach is made by measurements with a dielectric sensor (i.e the WET) in different porous media at different levels of electrical conductivity of the moistening KCl-solution (EC_i). From the results it is shown that the relationship between the σ_b and ε_s is strongly linear for σ_p and σ_b values up to 7.4 and 1.74 dS m^{-1} respectively. The salinity index model performance at predicting σ_p values is satisfactory with RMSE values lying between 0.84-2.04 dS.m^{-1} for the maximum electrical conductivity values of the moistening KCl-solution (EC_i).

Key words: soil salinity, bulk electrical conductivity, apparent dielectric permittivity, dielectric sensor

1. INTRODUCTION

The soil salinity assessment is mainly based on measurements of the electrical conductivity of the saturated paste extract, (EC_e) which has been established as the standard method (U.S. Salinity Laboratory, 1954). However, the σ_p is a better index of soil salinity than the EC_e since the plant roots actually experience the solute concentration of the soil solution. The extraction of soil solution is often impractical and can only be implemented at quite high values of soil moisture (θ). To overcome this difficulty in the determination of σ_p indirect methods have been proposed which are based on the determination of both θ and σ_b. Bulk soil electrical conductivity could be regarded as the combined effect of the electrical conductivity of the soil solution and solid phase, as well as, the interaction between these. A direct consequence of the above is that σ_b is related to σ_p, θ and the soil characteristics (e.g. through porosity, clay content, inert or charged solid surfaces etc.).

Until some decades ago, σ_b was generally measured by the Wenner device or the four electrodes method (Corwin, 2002; Corwin and Hendrickx, 2002). The development of the dielectric sensors, allowing simultaneous, automatic σ_b and ε_s measurements in the same spot made the σ_p estimation easier and contributed substantially in the study of salt movement in soils. A number of models, in which σ_b, θ and σ_p or σ_b, ε_s and σ_p are related to each other, were proposed (Amente et al., 2000; Hilhorst 2000; Malicki and Walczak, 1999; Mualem and Friedman, 1991; Rhoades et al., 1976). The relationship σ_b-ε_s has been shown to be linear for ε_s>6.2 (Kargas and Kerkides 2010, 2012).

Malicki and Walczak (1999) introduced the term of soil salinity index (X_s) describing soil salinity status, as one of many application of the TDR technique. The salinity index was defined as the partial derivative of σ_b with respect to ε_s (equation 1) and appeared independent of the moisture content. The two variables from which the salinity index was calculated were determined by TDR.

$$X_s = \frac{\partial \sigma_b}{\partial \varepsilon_s} \tag{1}$$

In practice, Xs is obtained through the appropriate expression, (valid for σb>0.08 dS m-1 and εs>6.2)

$$X_s = \frac{\sigma_b - 0.08}{\varepsilon_s - 6.2} \tag{2}$$

where σ_b=0.08 dS.m^{-1}and ε_s=6.2 is the point where the lines $\sigma_b\left(\varepsilon_s;\sigma_p\right)$converge.

Salinity index is generally independent of θ, for the range θ>0.12 cm^3 cm^{-3} up-to saturation, where corresponding ε_s values are usually larger than 6.2, but it has been shown that this is practically true for θ>0.2 cm^3 cm^{-3} (Wilczek et al., (2012)). Malicki and Walczak (1999) reported that salinity index depends mainly on σ_p and soil texture.

The σ_p can be calculated for mineral soils if salinity index and the slope ($l = \frac{\partial X_s}{\partial EC_i}$) of the salinity index and the electrical conductivity of the wetting solution (EC_i) are known. It has been shown that *l* can be estimated from an empirical relationship based on sand content.

The proposed relationship for σ_p estimation is

$$\sigma_p = \frac{Xs}{l} = \frac{\sigma_b - 0.08}{\left(\varepsilon_s - 6.2\right)\left(0.0057 + 0.00007S\right)} \tag{3}$$

where S (sand content) is expressed in % on a mass basis.

Wilczek et al., (2012) applied the model of Malicki and Walczak (1999) with data obtained by an FDR technique. In an attempt to minimize the effect of the bulk electrical conductivity on ε_s, they measured the real part of the dielectric permittivity in an operating frequency range 380-440 MHz.

The WET dielectric sensor has the capacity to predict the water content through the ε_s, of the soil. It can also measure the σ_b, through the imaginary part of the relative dielectric permittivity and the temperature of the soil (Delta –T Devices Ltd, 2007).

The objective of the present work is to evaluate the soil solution electrical conductivity σ_p, predicted by the Malicki and Walczak model. To this end, WET sensor measurements were made in four different soils using four different levels of the electrical conductivity of the moistening solution.

2. MATERIALS AND METHODS

2.1 WET sensor

All measurements in the present study were taken with a WET sensor, a capacitance dielectric sensor which operates at a frequency of 20 MHz. The sensor consists of three metal rods, 6.8 cm long, 3 mm in diameter, and spaced 1.5 cm apart. The volume sampled is cylindrical, 6.8 cm long, with a diameter of 10 cm for a total volume of about 500 mL (Delta-T Devices Ltd., 2007). The central rod is covered by a coating material except at the tip, which acts as a soil temperature meter. The sensor was connected to an HH2 moisture meter. The sensor detects the changes of the 20 MHz electromagnetic signal and sends this information to the HH2, which calculates the capacitance, conductance and temperature of the material between the rods (i.e. the soil). The capacitance and conductance are used to determine the ε_s and σ_b using built-in calibration files. In addition to soil temperature, the calculated outputs are θ and σ_p, the latter based on the model of Hilhorst (2000).

Soil water content is calculated from ε_s using a simple regression formula that relates θ to ε_s

$$\theta = a\sqrt{\varepsilon_s} - b \quad (4)$$

where *a* and *b* are fitting parameters. Since the WET sensor outputs ε_s, the calibration consists of fitting the coefficients *a* and *b,* the values of which are known to vary with soil type. Texture based values suggested by the manufacturer are, for inorganic soils in general, *a* = 0.099 and *b* = 0.178; for organic soils and sands, *a* = 0.119 and *b* = 0.167; and for clays, *a* = 0.091 and *b* = 0.182 (Delta-T Devices Ltd., 2007).

2.2 Measurements in soils

Four porous materials were used that were air dried and put through a 2 mm sieve. The characteristics of soils are given in table 1. The attained bulk densities for the four soils (1,2,3, and 4) tested were:1.44, 1.25,1.38, 1.52 g cm^{-3} respectively.

Table1. Physicochemical characteristics of tested soils.

SOILS	Sand %	Silt %	Clay %	pH	Organic matter %	$CaCO_3$ %	Cation Exchange Capacity ($mmol_c/kg$)	Saturation extract EC_e ($dS\ m^{-1}$)
1	57.0	26.5	16.5	7.31	0.58	0.00	9.39	2.40
2	35.8	36.0	28.2	7.48	1.87	0.41	15.47	1.21
3	51.8	30.0	18.2	7.02	1.56	0.00	9.73	1.10
4	67.8	16.0	16.2	7.22	0.23	0.00	8.69	1.28

The dry soil samples were moistened with KCl-solution of known electrical conductivity (EC_i=0.28, 1.2, 3 and 6 dS m^{-1}) to predetermined moisture contents, from dry until almost saturated with constant steps of $\Delta\theta$=0.05 cm^3 cm^{-3}. This could easily be achieved since the volume of the soil sample is estimated from its dry mass and its bulk density and therefore the volume of soil solution to be gradually added is also known. Moistening of the soil samples was achieved by adding the predetermined volume of the solution and thoroughly mixing the sample for achieving uniform moisture as a whole. This was repeated for each one of the KCl-solutions' electrical conductivity. For each soil type, around 30 soil columns were prepared. After equilibrating for 24 h in air-tight conditions the measurements were taken with the WET sensor been inserted vertically in the centre of the surface of each column. The θ was calculated using equation (4). σ_p-values were calculated with the Malicki and Walczak model (equation 3). When reaching saturation, the soil sample after equilibrating for 24 h in air-tight conditions, was placed in a Buchner funnel where the soil solution was extracted through the application of suction and σ_p was measured by a conductivity meter.

Optimal values for *a* and *b* could be determined for each soil by linear regression between measured θ (θ_m) and $\sqrt{\varepsilon}_s$ using all θ_m values for the four salinity levels.

3. RESULTS AND DISCUSSION

3.1 Measured dielectric properties of soils

Figure 1 illustrates the relationship between ε_s and θ_m for the four porous media and at four salinity (EC_i) levels. Also, the results obtained by the Topp equation (Topp et al., 1980) are shown (solid line) as a reference. From these it is obvious that ε_s values of the soils were larger than those of the Topp equation, especially at larger θ_m values. The different responses compared to Topp's equation demonstrated the need for individual calibration equations for each porous medium (Seyfried and Murdock, 2001).

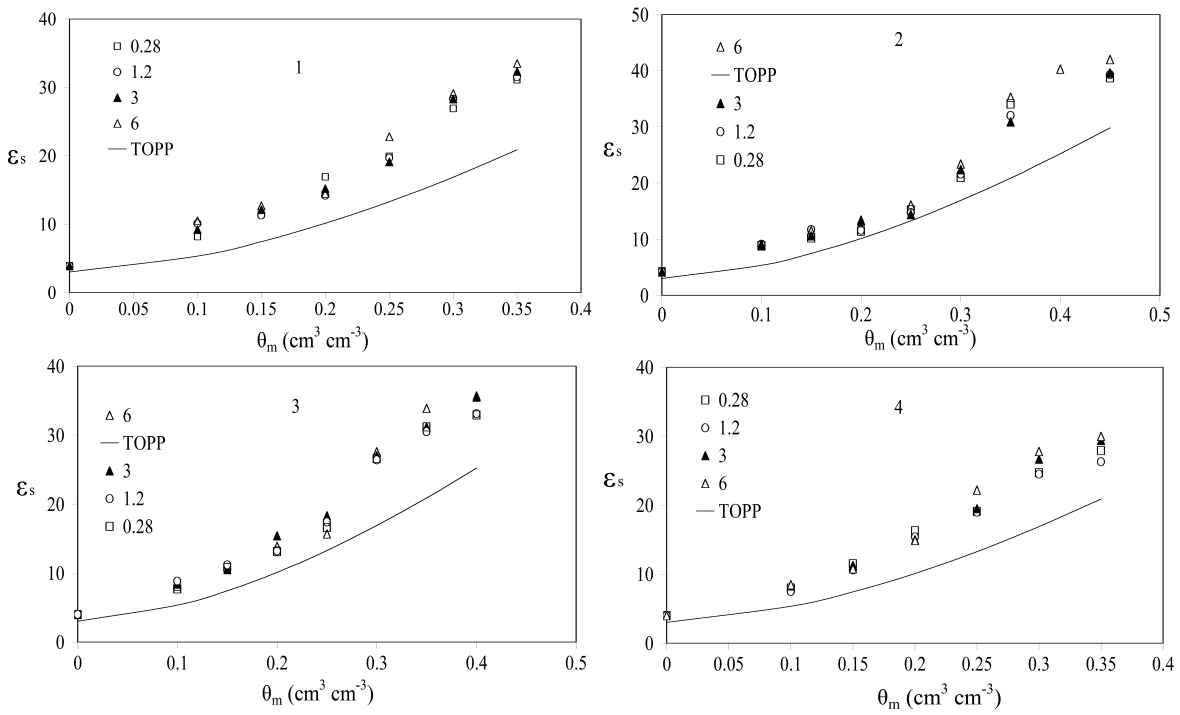

Figure 1. The relationship ε_s-θ_m for the WET sensor in 1,2,3 and 4 soils for various salinity levels (dS m^{-1}) (symbols). The relationship according to Topp et al., (1980) is also shown as a solid line.

The relationship between the θ_m and the square root of the apparent dielectric permittivity is strongly linear for all soils and salinity levels (EC_i) (Kargas et al., 2014). The slopes of the linear relationship were 0.09, 0.091, 0.091 and 0.092 and the intercepts 0.173, 0.16, 0.156 and 0.171 for 1,2,3 and 4 soils with R^2=0.982, 0.967, 0.966 and 0.984 respectively. These values corresponding to EC_i=6 dSm^{-1}. Maximum σ_b values in the case EC_i=6 dS m^{-1} when the soils are saturated, are 1.63, 1.74, 1.56, and 1.38 dS m^{-1} for the 1,2,3 and 4 soils. The corresponding values of the parameters *α* and *b*, however, do not coincide with those suggested for inorganic soils by the manufacturer. For all porous media the *α* and *b* values, are lower. The very close to each other values, of *α* and *b* parameters of the four soils tested are due to their similar particle size distribution, as is shown in Table 1.

3.2 Estimation of soil solution electrical conductivity (σ_p)

In Table 2 the measured values of σ_p at the maximum θ_m attained for every soil and EC_i tested are presented. Maximum θ_m values attained were 0.35, 0.45, 0.40 and 0.35 cm^3 cm^{-3} for 1,2,3 and 4 soils respectively. The difference between EC_i and σ_p is anticipated to be larger for low EC_i values when the σ_p value of the soils before adding the moistening solution is rather significant. More specifically, the largest difference was found in the soil 1, with EC_i of 0.28 dS m^{-1} the σ_p at the maximum θ_m attained was 3.65 dS m^{-1}.

Table 2. The values of σ_p (dS m^{-1}) at the maximum θ attained for the four ECi in the four soils tested.

EC_i (dS m^{-1})	1	2	3	4
	σ_p (dS m^{-1})	σ_p (dS m^{-1})	σ_p (dS m^{-1})	σ_p (dS m^{-1})
0.28	3.65	1.67	1.29	1.76
1.20	3.94	2.54	2.14	2.39
3.00	6.01	4.18	3.76	3.76
6.00	7.40	6.40	6.60	6.60

In order to test the concept of salinity index introduced by Malicki and Walczak (1999) the σ_b

versus ε_s values were plotted for all moistening solutions (Figure 2, left panel). The relationship σ_b-ε_s is valid for volumetric soil moisture θ>0.1 cm^3 cm^{-3} (Malicki and Walczak, 1999). The relationship $\sigma_b = f(\varepsilon_s; EC_i)$ is strongly linear ($0.99<R^2<0.999$) for all soils and salinity levels up to 6 dS m^- and is independent of water content. Similar results were obtained by Wilczek et al., (2012) using the FDR technique.

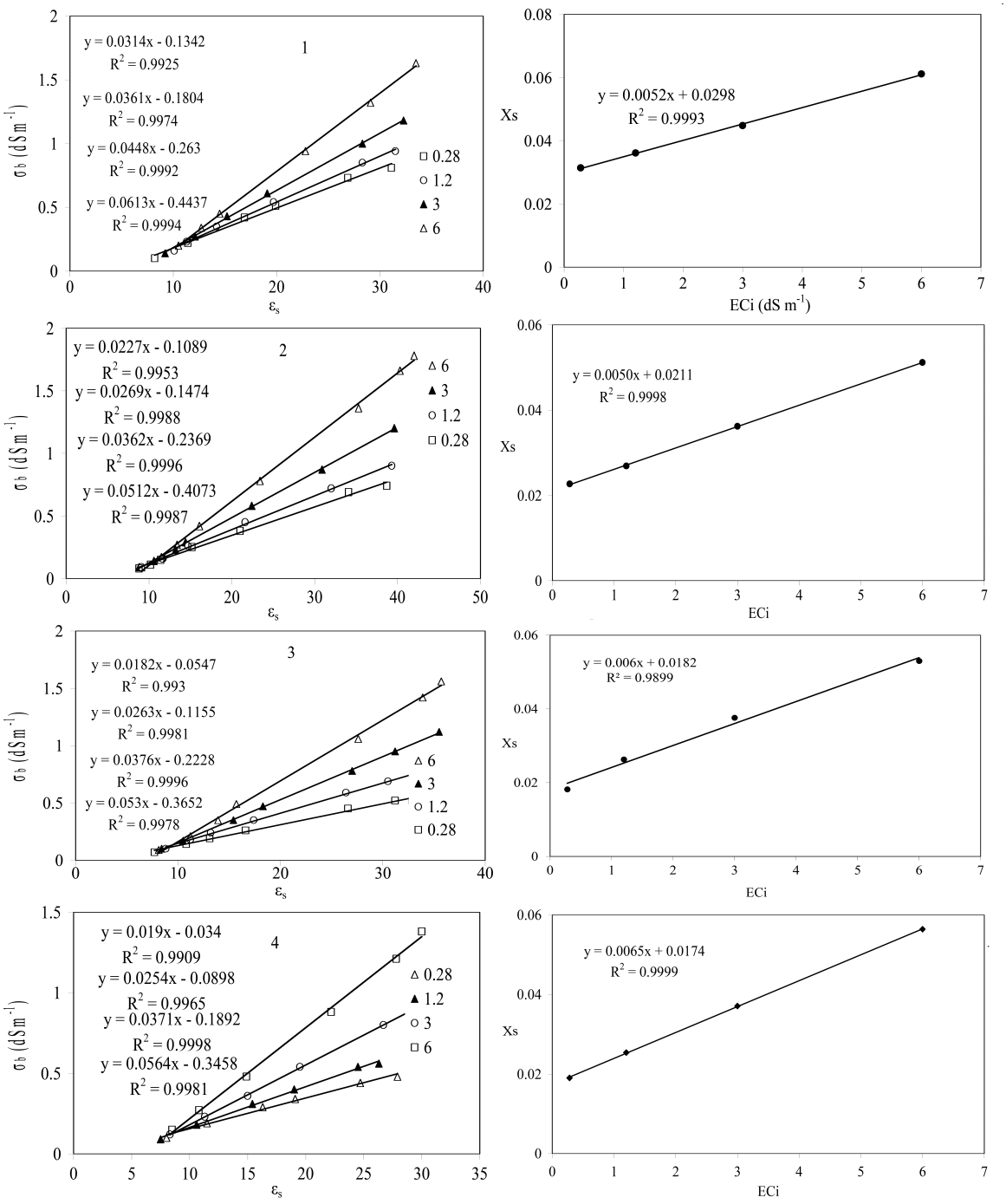

Figure 2. On the left: The relationship between the σ_b vs ε_s for all porous media and salinity levels. On the right: The relationship between salinity index X_s and EC_i for all porous media and salinity levels.

From the results (Figure 2, left panel) it is apparent that the salinity index, with data obtained by the WET sensor, depends on soil salinity. More specifically in all four soils tested, the increase of EC_i resulted in an increase of the salinity index and also for the same value of EC_i there were small differences in the values of the salinity index for the soils examined except for soil 1. These small differences may be attributed to the slight differences in the soils' particle size distribution.

In Figure 2 (right panel) the relationship between the salinity index and EC_i, for the soils tested, is shown. From the results one may notice that this relationship is strongly linear ($R^2 \geq 0.989$). The slopes of the linear relationships have magnitudes very different to those reported by Malicki and Walczak (1999) (their legend Figure 2) for similar soil types. For example the magnitude of the slope for the soil 1 (Sandy Loam) is 0.0052, while the respective value of Malicki and Walczak (1999) for the loamy sand is 0.011. This difference can be attributed to the relatively low operating frequency of the WET sensor compared to TDR.

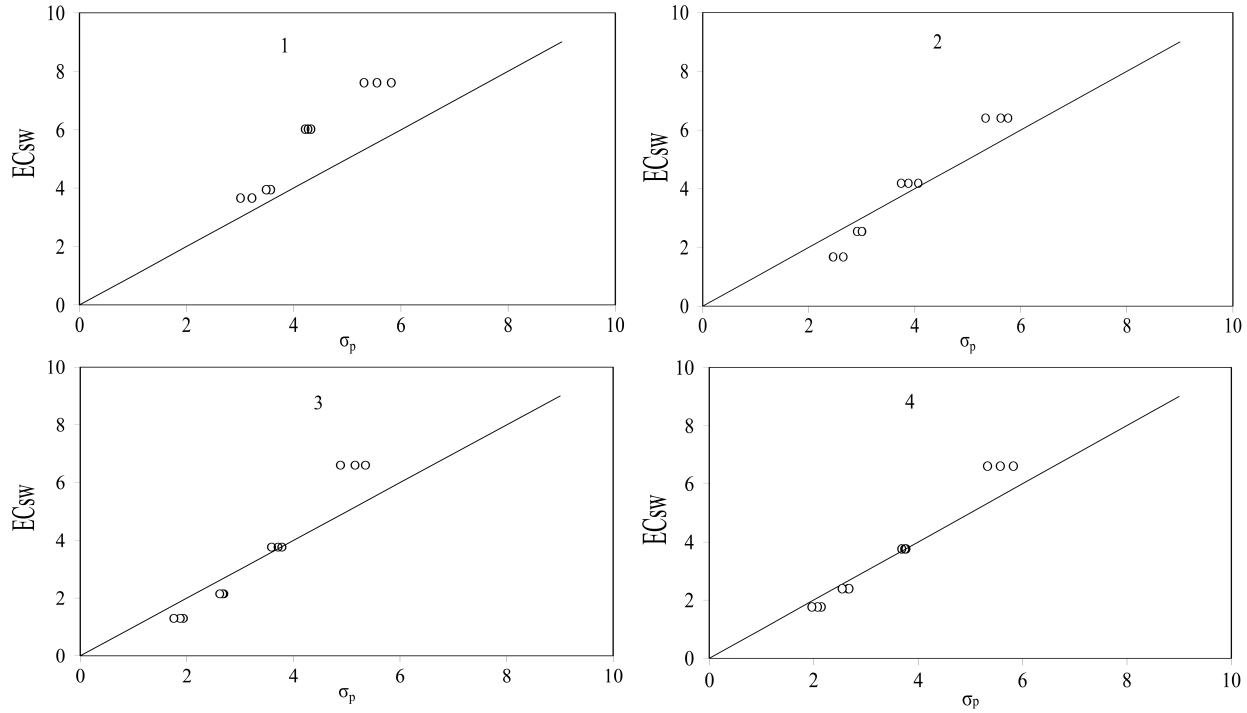

Figure 3: The relationship between actual σ_p values (EC_{sw}) (dS m^{-1}) (Vertical axis) and the predicted ones (Horizontal axis) according to the model of Malicki and Walczak (open circles, equation 3) (dS m^{-1}).

Comparing the σ_p of the Malicki-Walczak model (equation 3) to the actual σ_p values (Figure 3) it appears that the model overestimates σ_p up to a threshold of σ_p values (around 4 dS m^{-1}). Above this threshold (4 dS m^{-1}), the model in all cases underestimates σ_p values. This underestimation becomes larger with increasing of σ_p. More specifically for soil 1 when measured σ_p=6.01 dS m^{-1} RMSE was 1.74 while for σ_p=7.6 it was 2.04 dS m^{-1}. This underestimation could be attributed to the large ε_s values predicted by the WET sensor compared to TDR (Figure 1).

Generally the Malicki-Walczak model performs better for θ higher than 0.25 cm^3 cm^3. Thus it appears that the WET response to salinity is more reliable when the mobile water phase is dominant.

4. CONCLUSION

It was found that the measured WET- ε_s values depend on soil type and are larger than those of the Topp equation. Also the relationship between the volumetric water content (θ_m) and the square root of the apparent dielectric permittivity is strongly linear.

The salinity index approach, as this was introduced by Malicki and Walczak, making use of TDR data, is applicable, even when data are collected by the WET sensor. The relationship $\sigma_b = f(\varepsilon_s; EC_i)$ is strongly linear for all soils and salinity levels with maximum σ_b around 2 dS m^{-1}. The Malicki-Walczak model approaches quite reliably σ_p for σ_p<4 dS m^{-1} while above this value, it underestimates σ_p.

REFERENCES

Amente G, Baker M. and C. Reece 2000. Estimation of soil electrical conductivity from bulk soil electrical conductivity in sandy soil. Soil Sci. Soc. Amer. Journal 64:1931-1939.

Corwin D. 2002. In Methods of soil analysis, Part 4-Physical Methods. Published by Soil Science Society of America, pp 1287-1289.

Corwin D.and Hendrickx J. 2002. In Methods of soil analysis, Part 4-Physical Methods. Published by Soil Science Society of America, pp 1282-1287.

Delta –T Devices 2007. User manual for the WET sensor (type WET-2). Delta –T Devices Ltd. 128. Low road Burwell Cambridge CB5 OEJ. UK, www:http://www.delta-t.co.uk.

Hilhorst M.A. 2000. A pore water conductivity sensor. Soil Sci. Soc. Amer. Journal 64: 1922-1925.

Kargas G. and Kerkides p. 2010. Evaluation of a dielectric sensor for measurements of soil water electrical conductivity. Journal of Irrigation and Drainage Engineering 136(8):553-558.

Kargas, G., Kerkides P. 2012. Comparison of two models in predicting pore water electrical conductivity in different porous media. Geoderma 189:563-573.

Kargas, G., Kerkides P. and M.S. Seyfried. 2014. Response of Three Soil Water Sensors to Variable Solution Electrical Conductivity in Different Soils. Vadose zone Journal doi:10.2136/vzj2013.09.0169 September 2014, v. 13.

Malicki M. and R. Walczak, 1999. Evaluating soil salinity status from electrical conductivity and permittivity. Eur. Journal soil science 50:505-514.

Mualem Y. and S. Friedman, 1991. Theoretical prediction of electrical conductivity in saturated and unsaturated soil. Water Resour. Res. 27:2771-2777.

Rhoades J, P. Ratts and R. Prather, 1976. Effects of liquid-phase electrical conductivity, water content, and surface conductivity on bulk soil electrical conductivity. Soil Sci. Soc. Amer. Journal 40:651-655.

Seyfried, M. S., and M. D. Murdock. 2001. Response of a new soil water sensor to variable soil, water content, and temperature. Soil Science Society of America Journal 65: 28-34.

Topp, G.C., J.I. Davis and A.P. Annan. 1980. Electromagnetic determination of soil water content: measurements in coaxial transmission lines. Water Resources Research. 16:574-582.

Wilczek A., Szyplowska A., Skierucha W., Ciesla J., Pichler V. and Janik G. 2012. Determination of soil pore water salinity using an FDR sensor working at various frequencies up to 500 MHz. Sensors 12:10890-10905.

U.S. Salinity Laboratory Staff, 1954. Diagnosis and improvement of saline and alkali soils. USDA Agric. Handb. 60. U.S. Gov. Print. Office, Washington, DC.

Proceedings of the 10th World Congress of EWRA 'Panta Rhei', 5-9 July 2017, Athens, Greece
© 2017 *European Water Resources Association*

Assessing the vulnerability of water for agricultural use to climate change: The case of Cyprus

D. Charchousi[1*], M.P. Papadopoulou[1], K. Spanoudaki[2], D. Alexakis[3], C. Giannakopoulos[4] and A. Karali[4]
[1] *Laboratory of Physical Geography and Environmental Impacts, School of Rural and Surveying Engineering, National Technical University of Athens, Athens, Greece*
[2] *Institute of Applied and Computational Mathematics, Foundation for Research and Technology-Hellas, Heraklion, Crete, Greece*
[3] *Laboratory of Reclamation Works and Water Resources Management, School of Rural and Surveying Engineering, National Technical University of Athens, Athens, Greece*
[4] *Institute for Environmental Research and Sustainable Development, National Observatory of Athens, Athens, Greece*
[*] *e-mail: charchousi@gmail.com*

Abstract: Agriculture is an economic sector highly affected by climate change, since it is directly dependent on climatic variables (e.g. precipitation) and the availability of surface and groundwater resources for irrigation. Climate change impacts on hydrological variables can affect agricultural production. Water availability changes and water quality deterioration necessitate the development of adaptation measures. The present study focuses on the quantification of climate change effects on groundwater resources availability in Cyprus. Climate change impacts on agriculture are analysed in terms of groundwater availability (quantity) and quality (salinity) in an important agricultural region in Cyprus. The Kiti aquifer in Larnaca is a coastal aquifer facing saltwater intrusion. Groundwater pumping for irrigation purposes has caused significant salinization of groundwater resources in the area. In order to assess climate change effects on the availability of freshwater resources, groundwater flow and salinity transport at Kiti aquifer are estimated using SEAWAT, a 3D variable-density simulator of groundwater flow coupled with solute transport. Available meteorological and hydrogeological data are used to calibrate and validate the numerical model. Further in-situ groundwater elevation and quality measurements have also been performed in 2016 to assess the current state of groundwater resources. In order to estimate aquifer's response to climate change, projections for climatic variables, for the period 2016-2060 have been produced using the RCA4 Regional Climate Model of the Swedish Meteorological and Hydrological Institute, forced by the IPCC RCP 4.5 and 8.5 scenarios. The predictions of the climatic model have been used as forcing for the groundwater model to quantify climate change impacts on groundwater availability and quality and to assess the vulnerability of existing agricultural practices to climate change. As it is evident from the analysis of the two climate change scenarios under current cultivation and irrigation practices, a decrease in groundwater levels of 3-4m is estimated resulting in groundwater table deterioration to certain areas close to 10 m below sea level.

Key words: water availability, Kiti aquifer, groundwater flow, salt water intrusion, climate change, irrigation, SEAWAT

1. INTRODUCTION

Agriculture is an economic sector vulnerable to climate change, as it is highly dependent on climatic conditions (precipitation, temperature, soil moisture, humidity) and on the availability of surface and groundwater resources for irrigation purposes. Climate change may not necessarily have only detrimental effects to agriculture, as for instance the prolonged growing seasons due to raising temperature (Gornall et al., 2010). However, extreme events as floods and extended periods of drought, as well as insufficiency in irrigation water availability caused by climate change can be threatening for agricultural productivity (USDA, 2015; FAO, 2008).

During the recent decades, climate change impacts on water resources quality and quantity have been extensively studied. However, most of research has been focused on impacts to surface water, due to the fact that these water bodies' vulnerability to climate change is more obvious and direct than on groundwater (BGR, 2008; Green et al., 2011). The majority of previous research works concerning climate change impacts on groundwater resources focus mainly on the changes on quantity, due to changes on precipitation and evapotranspiration rate, rather than the quality

(Meixner et al., 2016).

Although groundwater quality is also affected by climate change, there are much fewer studies reporting its effects (Green et al., 2011). Thermal-hydrological-geochemical processes that affect water quality is expected to be altered due to climate change (Glassley et al., 2003). For instance, potential decrease on groundwater recharge and the consequent groundwater level depletion could affect nitrate concentration on pumping water (Stuart et al., 2011). Moreover, a decrease on surface water resources availability will also cause among others further overexploitation of the aquifers and in consequence salinization and seawater intrusion problems will be worsen in coastal areas (Green et al., 2011).

The present study focuses on agriculture vulnerability to climate change due to likely changes on groundwater resources. Increased temperature and decreased precipitation have already caused numerous issues on the agricultural sector during the recent years in Cyprus. Climate change is expected to cause greater problems on groundwater quality and quantity in the future, such as increased water demand for irrigation, decreased water availability and deterioration of water quality (CYPADAPT, 2013). The aim of the present study is to assess climate change impacts on groundwater used for irrigation in Cyprus. Groundwater availability is studied not only in terms of quantity but also of quality, as Cyprus is facing serious salinization problem in its coastal areas. An important agricultural area in Cyprus, Kiti has been selected as pilot area in this study to estimate vulnerability of water used in agriculture to climate change.

2. CASE STUDY

Agriculture is an important sector of Cyprus economy. The most important crops produced in Cyprus are cereals (wheat, barley), vegetables and other perennial crops, such as grapes and bananas and olives. Agriculture is the most water-intensive sector in Cyprus, followed by the domestic sector (Papadaskalopoulou et al., 2015). Agriculture in Cyprus is vulnerable to water availability and in spite of the various measures encouraged by the government, the irrigation needs cannot be always met, as some of the measures such as crop rotation cannot be easily and immediately adopted (CYPADAPT, 2013).

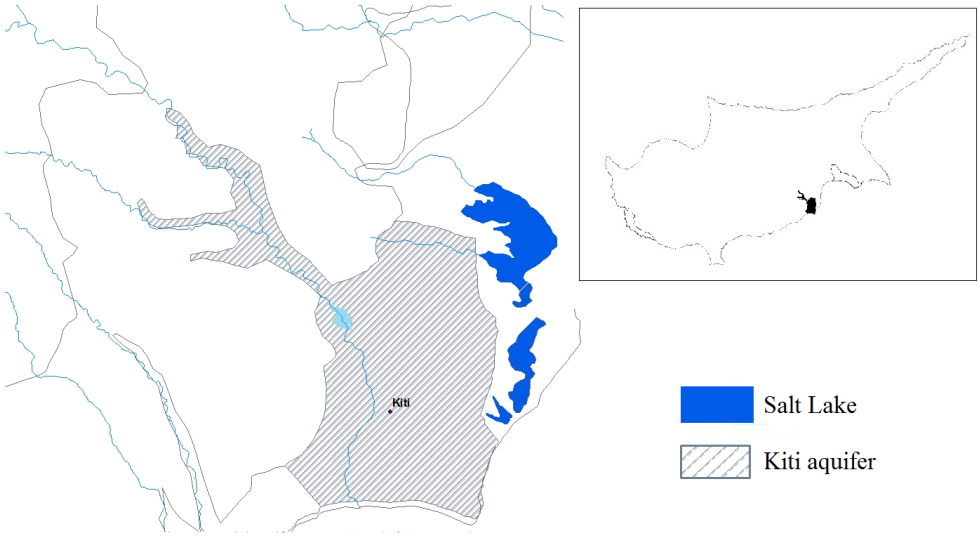

Figure 1. Kiti pilot aquifer

Kiti aquifer, known as CY-3 groundwater system, is located in South Cyprus, in Larnaca district (Fig. 1). The area is mostly agricultural, but in its coastal parts tourism is rapidly developed. A significant part of irrigation needs in Kiti area are covered by the Southern Conveyor Project. The limited precipitation observed during the recent years has led to diminished direct natural recharge

of Kiti aquifer. As reported by the Water Development Department, the most productive parts of the aquifer have faced salinization and they have been abandoned and also the less productive parts are depleted and borehole yields have dramatically dropped (WDD and FAO, 2002).

3. MODELLING CLIMATE CHANGE IMPACTS ON GROUNDWATER RESOURCES

In this section, an attempt to assess the impacts of future climate changes on water for agricultural use in Cyprus based on the climate projections imposed by RCP4.5 and RCP8.5 scenarios for the period 2030-2060 is being made. In particular, the study focuses on irrigation water sustainability assessment in Kiti pilot aquifer, based on the groundwater flow and contaminant transport simulation using SEAWAT algorithm.

3.1 Conceptual model development

As Kiti aquifer is a typical case of salinization problem in Cyprus, SEAWAT algorithm is used to simulate seawater intrusion impacts on Kiti coastal aquifer. SEAWAT is a coupled version of MODFLOW 2000 (Harbaugh et al., 2000) and MT3DMS (Zheng and Wang, 1999), used in order to simulate the variable density effects on transient groundwater flow (Langevin et al., 2007).

Kiti pilot area is crossed by Tremithios river. In 1964, Kiti dam was constructed for recharge purposes. The aquifer at its western part is in hydraulic connection with the Tremithios river alluvial deposits (WDD and FAO, 2002). At its north-east boundary the aquifer neighbours with two salt lakes, while its south and south-east boundaries is the shoreline (Fig.1). The aquifer system is layered. The impervious base of the aquifer consists mainly of Pliocene marls. The sediments of the aquifer consist of Pleistocene marine terrace deposits such as silts, gravel and sands, whereas the aquifer sediments along the Tremithios riverbed consist of river alluvial deposits (WDD and FAO, 2002; Milnes and Renard, 2002).

3.2 Numerical model development

The model developed has been calibrated for hydraulic conductivity, specific yield, porosity and dispersivity. The transient calibration was performed for the hydrological years 2008-2009 and 2009-2010. Observed head well measurements and chloride concentrations for the period 2006-2016 have been used for model validation. During the analysis, field measurements were performed in two selected locations in Kiti aquifer for validation purposes. Groundwater level has been monitored in June 2016 and water samples were collected in agreement with the sampling and storing methods described in Stamatis et al. (2011). Estimation of Cl^-, NO_3^-, SO_4^{2+}, Na^+, K^+, Mg^{2+} and Ca^{2+} concentrations was performed by an ion chromatography system (Dionex ICS-3000) at the Laboratory of Reclamation Works and Water Resources Management NTUA. The pH and conductivity values were determined immediately after collection with a portable meter (PT-370 pH meter, CON 5 conductivity meter). The elevated Cl^-, SO_4^{2+}, Na^+ and K^+ concentrations in groundwater as well as the observed high conductivity values (Table 1) denotes an input of seawater intrusion into Kiti groundwater system. The obtained pH values of collected water samples indicate the slightly alkaline nature of groundwater in the area.

Figure 2 shows typical groundwater level contours in Kiti aquifer for September 2009 (end of dry period) and March 2010 (end of wet period). Based on the simulation results, chloride concentrations relative to that of seawater (seawater chloride concentration is taken equal to 22 g/L, i.e. relative chloride concentration at the sea boundary is 1) for September 2009 are observed. The extent of seawater intrusion in the area is evident from both groundwater levels and chloride concentrations in the aquifer.

Table 1. Values of water quantity and quality parameters (in-situ measurements and sampling June 2016)

Well Name	Water table m amsl	Cl^- mg/L	NO_3^- mg/L	SO_4^{2-} mg/L	Na^+ mg/L	K^+ mg/L	Mg^{2+} mg/L	Ca^{2+} mg/L	Cond. µS/cm	pH
Detection Limit		**1**	**0,5**	**1**	**0,05**	**0,05**	**0,05**	**0,05**		
H4110-0331	4,14	708,6	99,7	199,5	194,1	6,5	107,7	181,0	3.010	7,17
H4110-0378	0,62	1.706,2	<0,5	370,6	311,8	5,9	270,6	366,2	5.090	7,23

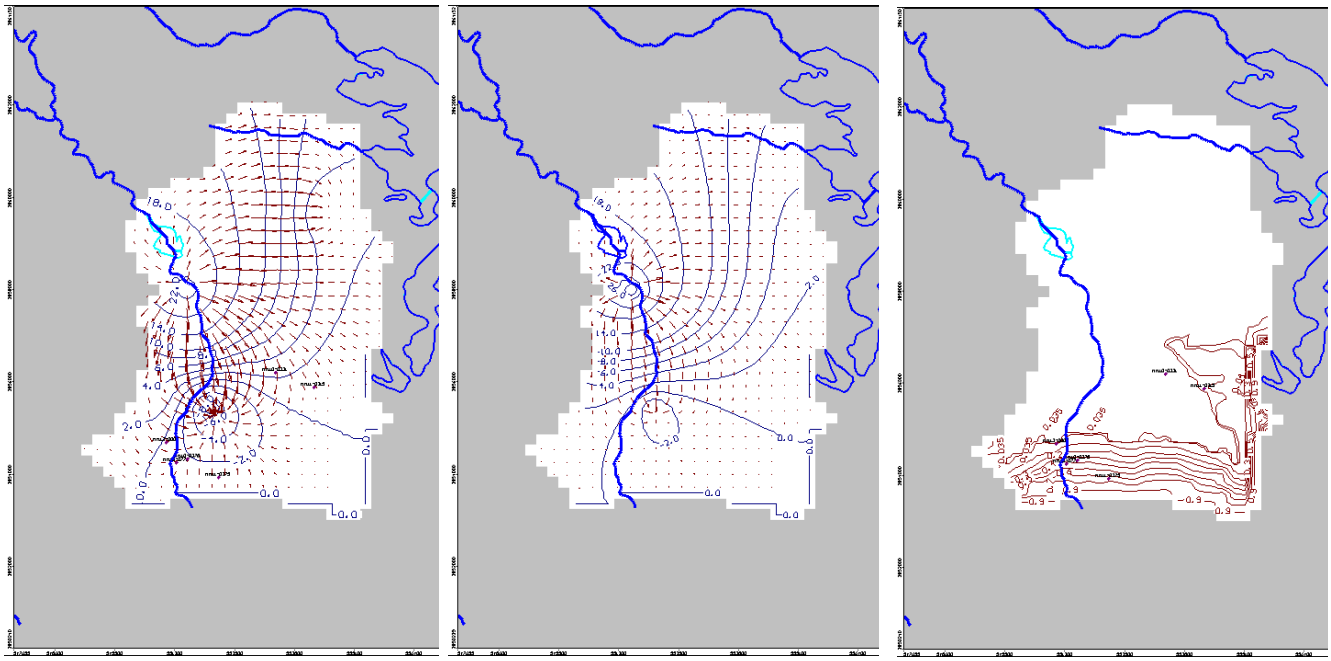

(a) (b) (c)

Figure 2. Results of numerical simulations: (a) groundwater level, September 2009; (b) groundwater levels, March 2010; (c) relative chloride concentrations, September 2009 (concentration observation wells are also shown)

3.3 Climate change projections

Climate change projections for the area were based on the RCA4 Regional Climate Model of the Swedish Meteorological and Hydrological Institute (SMHI) (Strandberg et al., 2014 and references therein) driven by the Max Planck Institute for Meteorology model MPI-ESM-LR (Popke et al., 2013). The model has a horizontal resolution of 12km^2 and was developed within the framework of EURO-CORDEX (Coordinated Downscaling Experiment - European Domain). Future model projections were based on two new IPCC scenarios, namely the RCP4.5 and the RCP8.5.

RCP4.5 is a stabilization scenario where total radiative forcing is stabilized before 2100 by the employment of a range of technologies and strategies for reducing greenhouse gas emissions (Clarke et al., 2007). Radiative forcing in RCP4.5 peaks at about 4.5 W/m^2 (~540 ppm CO_2) in year 2100 (Thomson et al., 2011). RCP4.5 is comparable to the SRES scenario B1 with similar CO_2 concentrations and median temperature increases by 2100 according to Rogelj et al. (2012).

RCP8.5 is characterized by increasing greenhouse gas emissions over time, representative for scenarios in the literature leading to high greenhouse gas concentration levels. RCP8.5 assumes a high rate of radiative forcing increase, peaking at 8.5 W/m^2 (~940 ppm CO_2) in year 2100 (Riahi et al., 2011).

4. RESULTS AND DISCUSSION

Several groundwater flow and quality simulation runs have been performed in order to assess aquifer response to climate change. Future precipitation predictions derived from the RCA4

Regional Climate Model have been used as inputs to the groundwater model, in order to assess the climate change impacts on groundwater quality and quantity.

Kiti groundwater level ensemble contour maps for the IPCC RCP 4.5 and 8.5 scenarios for the end of the dry period of 2059-2060 hydrological year (September 2060) and the projected relative chloride concentrations are shown in Figure 3 (a) and 3 (b) respectively. As it is evident from the analysis of the two examined climate change scenarios for the area -under current cultivation and irrigation practices, a decrease in groundwater levels of 3-4 m, resulting in a drop of groundwater table to certain areas close to 10 m below sea level. Predicted relative chloride concentrations also show an approximately 1.5 fold increase, indicating the need for additional mitigation measures.

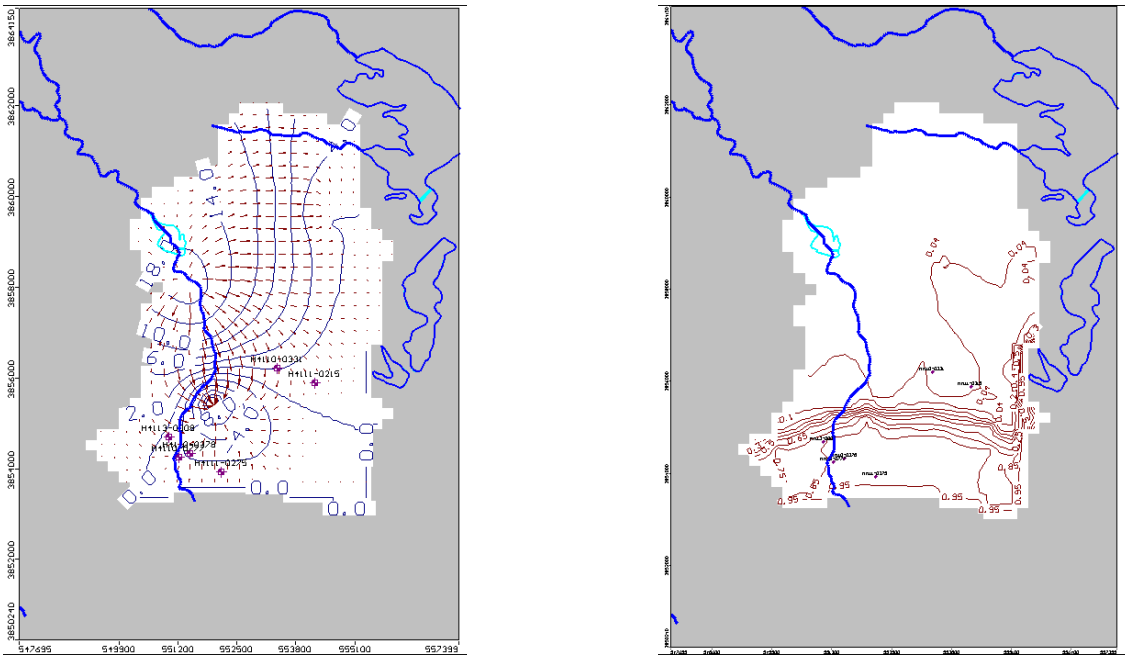

(a) (b)

Figure 3. Kiti aquifer – Ensemble groundwater simulation results: (a) groundwater level and (b) relative chloride concentrations, under the IPCC RCP 4.5 and 8.5 climate change scenarios - Hydrological year 2059-2060, end of dry period

5. CONCLUSIONS

Optimal groundwater management should be considered as an adaptation option to maintain and improve agricultural productivity under future climate change conditions. Climate change seems to be critical for groundwater sustainability. To improve water and food efficiency, adaptation measures for groundwater quality and quantity sustainability such as crop restructuring, use of recycled water and fertigation practices should be adopted.

ACKNOWLEDGEMENTS

The authors would like to acknowledge the European financial instrument for the Environment, LIFE, for the financial support in the framework of the ADAPT2CLIMA project LIFE14 CCA/GR/000928.

REFERENCES

BGR, 2008. Groundwater and Climate Change: Challenges and Possibilities. Available online: www.bgr.bund.de

Clarke, L., J. Edmonds, H. Jacoby, H. Pitcher, J. Reilly, R. Richels, 2007. Scenarios of Greenhouse Gas Emissions and Atmospheric Concentrations, Sub-report 2.1A of Synthesis and Assessment Product 2.1 by the U.S. Climate Change Science Program and the Subcommittee on Global Change Research. Department of Energy, Office of Biological & Environmental Research, Washington, 7 DC., USA, 154 pp.

CYPADAPT, 2013. Assessment of past responses to adapt to the adverse climate change impacts in Cyprus. Deliverable 2.3, project CYPADAPT LIFE10 ENV/CY/000723. Available online: cypadapt.uest.gr

FAO, 2008. Climate change, water and food security. FAO Water Report 36. Rome.

Glassley, W.E., Nitao, J.J., Grant, C.W., Johnson, J.W., Steefel, C.I., Kercher, J.R., 2003. The impact of climate change on vadose zone pore waters and its implication for long-term monitoring. Computers & Geosciences 29: 399–411.

Gornall, J., Betts, R., Burke, E., Clark, R., Camp, J., Willett, K., Wiltshire, A., 2010. Implications of climate change for agricultural productivity in the early twenty-first century, Phil. Trans. R. Soc. B 365: 2973–2989. doi:10.1098/rstb.2010.0158

Green, T. R., Taniguchi, M., Kooi, H., Gurdak, J.J., Allen, D.M., Hiscock, K.M., Treidel, H., Aureli, A., 2011. Beneath the surface of global change: Impacts of climate change on groundwater. Journal of Hydrology 405 (3–4): 532-560.

Harbaugh, A.W., Banta,E.R .,Hill,M.C., McDonald,M.G., 2000. MODFLOW-2000, the U.S. Geological Survey Modular Ground-Water Model-User guide to modularization concepts and the ground-water flow process, U.S. Geological Survey Open-File Report 00-92. 121 pages. Available online: www.usgs.gov

Langevin, C.D., Thorne, D.T., Jr., Dausman, A.M., Sukop, M.C., and Guo, Weixing, 2007, SEAWAT Version 4: A Computer Program for Simulation of Multi-Species Solute and Heat Transport: U.S. Geological Survey Techniques and Methods Book 6, Chapter A22, 39 p.

Meixner, T., Manning, A.H., Stonestrom, D.A., Allen, D.M., Ajami, H., Blasch, K.W., Brookfield, A.E., Castro, C.L., Clark, J.F., Gochis, D.J., Flint, A.L., Neff, K.L., Niraula, R., Rodell, M., Scanlon, B.R., Singha, K., Walvoord, M.A., 2016. Implications of projected climate change for groundwater recharge in the western United States. Journal of Hydrology 534: 124–138.

Milnes, E. and Renard, P., 2002. Assessment of Seawater Intrusion versus Mass Return Flow from Irrigation in the Kiti Coastal Aquifer System (Southern Cyprus) Based On Field Investigations and Three-Dimensional Finite Element Simulations. 17th Salt Water Intrusion Meeting, Delft, The Netherlands, 6-10 May 2002.

Papadaskalopoulou, C., Katsou, E., Valta, K., Moustakas, K., Malamis, D., Dodou, M., 2015. Review and assessment of the adaptive capacity of the water sector in Cyprus against climate change impacts. Resources, Conservation & Recycling 105: 95-112.

Popke, D., Stevens, B., Voigt, A., 2013. Climate and climate change in a radiative-convective equilibrium version of ECHAM6, J. Adv. Model. Earth Syst., 5(1), 1–14, doi:10.1029/2012MS000191.

Riahi, K., Rao, S., Krey, V., Cho, C., Chirkov, V., Fischer, G., Kindermann, G., Nakicenovic, N., Rafaj, P., 2011. RCP8.5—A scenario of comparatively high greenhouse gas emissions, Clim. Chang., 109, 33–57, doi:10.1007/s10584-011-0149-y.

Rogelj, J., Meinshausen, M., Knutti, R., 2012. Global warming under old and new scenarios using IPCC climate sensitivity range estimates, Nat. Clim. Chang.,2, 248–253, doi:10.1038/nclimate1385.

Stamatis, G., Alexakis, D., Gamvroula, D., Migiros, G., 2011. Groundwater quality assessment in Oropos–Kalamos basin, Attica, Greece. Environmental Earth Sciences 64 (4): 973-988.

Strandberg, G., Bärring, L., Hansson, U., Jansson, C., Jones, C., Kjellström, E., Kolax, M., Kupiainen, M., Nikulin, G., Samuelsson, P., Ullerstig A., Wang, S., 2014. CORDEX scenarios for Europe from the Rossby Centre regional climate model RCA4, REPORT METEOROLOGY AND CLIMATOLOGY No. 116, 2014, Swedish Meteorological and Hydrological Institute. Norrköping, Sweden.

Stuart, M.E., Gooddy, D.C., Bloomfield, J.P., Williams, A.T., 2011. A review of the impact of climate change on future nitrate concentrations in groundwater of the UK, Science of the Total Environment 409: 2859–2873.

Thomson, A. M., Calvin, K.V., Smith, S.J., Kyle, P., Volke, A., Patel, P., Delgado-Arias, S., Bond-Lamberty, B., Wise, M.A., Clarke, L.E., Edmonds, J.A., 2011. RCP4.5: A pathway for stabilization of radiative forcing by 2100, Climatic Change, 109 ,77–94, doi:10.1007/s10584-011-0151-4.

USDA, 2015. Brown, M.E., Antle, J.M., Backlund, P., Carr, E.R., Easterling, W.E., Walsh, M.K., Ammann, C., Attavanich, W., Barrett, C.B., Bellemare, M.F., Dancheck, V., Funk, C., Grace, K., Ingram, J.S.I., Jiang, H., Maletta, H., Mata, T., Murray, A., Ngugi, M., Ojima, D., O'Neill, B., Tebaldi, C. Climate Change, Global Food Security, and the U.S. Food System. 146 pages.

WDD and FAO, 2002. Reassessment of the island's water resources and demand - Assessment of groundwater resources of Cyprus. Ministry of Agriculture, Natural Resources and Environment, Republic of Cyprus. Available online: www.moa.gov.cy

Zheng, C., Wang, K., 1999. MT3DMS - A modular three dimensional multispecies transport model for simulation of advection, dispersion and chemical reactions of contaminants in groundwater systems. Contract report SERD99-1, U.S. Army Corps of Engineers.

Proceedings of the 10th World Congress of EWRA 'Panta Rhei', 5-9 July 2017, Athens, Greece
© 2017 *European Water Resources Association*

Utilizing earth observation systems towards the implementation of Nexus approach for achieving sustainable water management at a river basin scale

G. Zalidis[1,2]
[1] *Aristotle University of Thessaloniki, School of Agriculture, Laboratory of Remote Sensing, Spectroscopy and GIS, 54124 Thessaloniki, Greece*
[2] *Interbalkan Environment Center, Loutron 18, 57200, Lagadas, Greece*
e-mail: zalidis@agro.auth.gr

Abstract: Information derived from Earth Observation systems can act as a catalyst for an enhanced and holistic understanding of processes in the Earth system, the development and effectiveness of policies and the monitoring of sustainable use of water resources at river basin scale. In this context, they can facilitate the intensification of agricultural production, while taking into account the principles of a low-input sustainable agriculture that can monitor functional properties related to energy and water use efficiency. The current approach puts major emphasis on utilizing existing in situ networks and develop infrastructure strategies, bridging them with new technologies (e.g. unmanned platforms, advanced sensory systems), in order to monitor agro-environmental directives and providing outcomes more efficient and targeted for the implementation of the Sustainable Development Goals, at different temporal and spatial scales and in a holistic fashion. An approach of integrating water, energy and agricultural production at the watershed level was implemented in the framework of transboundary territorial projects at the Strymon and Nestos watersheds. Via a series of indicators, inputs and outputs to the system were quantified and the efficiency of using energy and water-soil resources as related to food production has been evaluated. The results of those projects indicated the necessity of implementing the Nexus approach in dynamic systems regarding water resources. This necessity is highlighted by existing GEO Initiatives, EO in-situ networks and their data integration with spaceborne data aiming at developing the strategic planning and the road map to implementation of nexus approach on management of natural resources.

Key words: river basin, nexus approach, Earth Observation, low-input agriculture

1. INTRODUCTION

It is widely acknowledged that the combined pressures, such as the growth in world's population, the overexploitation of natural resources, the urbanization and the globalization, the increase in agricultural production, the excessive application of fertilizers and chemicals, the intensive livestock operations, the disposal of high volumes of untreated wastewater and solids and the climate change, have resulted in an enhancing number of environmental problems (Dou et al. 2009). These generally take the form of pollution, depletion or degradation of water, air and soil. Soil erosion, water salinity and pollution, desertification, forest depletion and coastal degradation are accounted for the major environmental problems in developing countries. Consequently, threats posed to social-ecological systems at all levels, such as to water bodies, soils, food chain, energy availability and people's and livestock's health should be taken into account for a more integrated management approach.

Therefore, the importance and necessity of managing natural resources is evident and has encouraged the development of a range of approaches and methodologies. Conventional thinking on natural resource management often encourages a technical approach to problem solving (Groot & Maarleveld, 2000; Ramirez, 1999; Uphoff, 1992). The process is usually linear with clearly defined steps: (1) creating a goal statement, (2) assessing constraints or problems and opportunities for achieving the goal, (3) identifying ways to solve problems, (4) selecting the "best" way and (5) finally implementing the solution. However, practitioners who approach resource management in

this top-down manner often exclude the interconnection and interdependence of the three sectors: water, energy and food security.

This can be achieved through a “NEXUS” approach. The term “NEXUS” in Latin describes the act of tying together or something which binds. In connection with environmental resource management, the term "NEXUS" was introduced for the first time during the 1980's, notably in a project by the UN University (Food-Energy Nexus programme; Sachs & Silk, 1990) and was established in the Bonn in 2011 Conference (https://www.water-energy-food.org/about/bonn2011-conference). This concept is gaining interest since it is closely related to the Sustainable Development Goals (SDGs) that were developed in Rio in 2012 (Ringler et al., 2013). Assets of a more integrated approach, combining these three sectors would likely be: economic efficiency, resource efficiency, improved livelihood options and public health. Yet it may have negative consequences on communities, to commodity prices, to sub-optimal infrastructure design and environmental degradation (Bazilian et al., 2011). Such an approach can result in improved water, energy, and food security by integrating “management and governance across sectors and scales”, reducing trade-offs, and building synergies, overall promoting sustainability and a transition to green economy (Hoff, 2011). The interdependencies of water, energy and food can be visualized as follows (Figure 1).

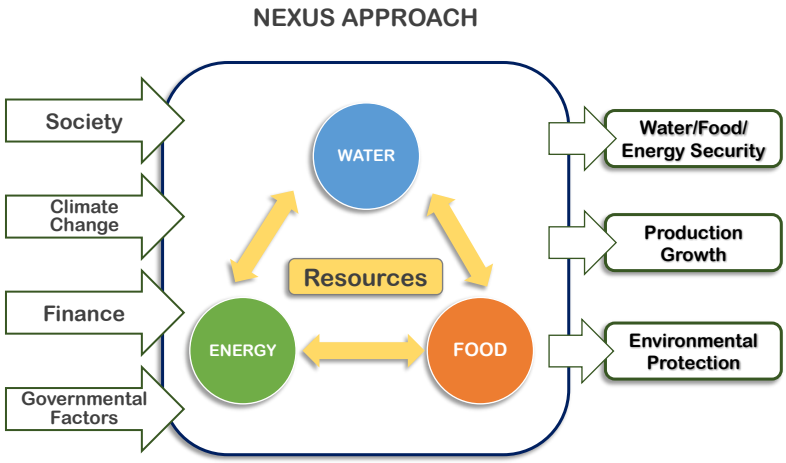

Figure 1. “The water, energy and food security nexus”

The "NEXUS" approach highlights the interdependence of water, energy and food security and the natural resources that underpin that security – water, soil and land. Based on a better understanding of the interdependence of water, energy and climate policy, this new approach identifies mutually beneficial responses and provides an informed and transparent framework for determining trade-offs and synergies that meet demand without compromising sustainability. In addition, a "NEXUS" approach means that when governments and industries determine policies in one sector—whether it is energy, agriculture or water—they take into account the implications in other sectors. Similarly, policy and planning processes within each sector would account for different scales, from local to transnational (Bird *et al.,* 2014).

The potential of Earth Observation techniques in the management of land and water resources has been widely acknowledged (Bastiaanssen et al., 2005). The implementation of new technologies can provide constant data, such as crop evapotranspiration (ETc), suitable for mapping crops and irrigated areas and monitoring changes with satisfactory accuracy and in a cost-effective way (D’Urso et al., 2010).

The "NEXUS" approach and its challenges have not been consistently and comprehensively addressed before. The case study described below provides a first overview of that managerial approach in Greece, in a river basin scale through spaceborne and in situ measurements. However, it should be recognized that further work will be needed so as to develop a solid data and knowledge base upon which a more efficient resources management approach is going to be built.

2. CASE STUDY

This survey was a first attempt to combine some major factors that influence the Water - Energy - Food Security "NEXUS" in a river basin level in Greece. The experiments were conducted, in the framework of the cross-border European Territorial Cooperation Project - AGROLESS, at the Strymon and Nestos watersheds, Northern Greece, which aimed to establish common reference strategies for the implementation of reduced input agricultural practices in the cross-border area of Greece – Bulgaria with the use of the concept of site-specific crop management, optimum profitability, sustainability and protection of land resources. The pilot applications that were undertaken were the following:

Pilot application 1: The application concerns the development of a fully controlled system of hydrofertilization with the ability to control both water quantity and fertilizer applied in the field via a digital decision support system. The pilot area faces serious environmental water deficit problems and precise irrigation will be a crucial factor for the sustainability of the local water bodies and ecosystems.

Pilot application 2: Pilot fields have been selected to cover a wide range of crops and include asparagus, pomegranate, kiwi, vine and corn. The pilot fields have been selected at various locations with the criterion of representing the major crops in the targeted area in terms of crop variety, management practices, climatic and soil conditions. Furthermore, the cooperation, willingness and open-minded approach of the farmers that cultivate the pilot crops have also been taken into account while selecting the pilot crops (Figure 2).



Figure 2. Study area of Strymon and Nestos watersheds, Northern Greece

A series of steps were taken into account in order to apply agriculture of less inputs, regarding the main axes of "income" or the "input energy" inside an agricultural field which are Fertilization, Irrigation and Plant protection.

Firstly, soil mapping used to identify zones of variability regarding the different needs on managerial practices. Soil mapping was held by detailed soil sampling, 0-30cm and by the use of more time-effective and innovative technology that involved methods, such is scanning of soils with the use a Veris MSP3 system. The samples were measured in i-BEC's certified chemical laboratory, which assessed the physical (concentrations of Sand, Silt and Clay) and chemical

parameters (nitrates, pH, organic matter, electrical conductivity, potassium and calcium carbonate) of the samples. Then, a robust protocol (Ben Dor et al., 2015) was used to measure the reflectance of each soil sample in the vis-NIR (350-2500 nm) region in a laboratory. Statistical models were developed which correlated the input spectra with the soil's properties. The best results (i.e. correlation coefficient greater than 0.6) were achieved for the physical parameters, for the Soil Organic Matter and for the calcium carbonates. Secondly, the Nitrogen content of corn leaves was estimated using vis-NIR spectroscopy. Approximately 60 corn leaves were sampled from two different fields. The Nitrogen content was measured using the Kjeldahl method in i-BEC's chemical laboratory. The SPECIM v10-e hyperspectral push broom camera was used, capturing the 400-1000 nm range to capture a hyper- spectral image of the corn plantations. The statistical models generated achieved a correlation coefficient of 0.72 in an independent testing set.
The Veris MSP3 Soil EC, Organic Matter, and pH Mapping System collected geo-referenced soil electrical conductivity (EC), soil reflectance, and soil pH measurements as it was pulled across the field by a tractor.

Remote sensing provided valuable information on various parameters that were acquired by air-photographs or satellite images, without field visits or with minimum sampling locations. It was used for mapping crop yield and soil fertility parameters, monitoring soil moisture content, determining fertilization applications in the spatial domain, monitoring crop growth, monitoring water use and irrigation requirements, detecting crop diseases, mapping weed and insect infestations.

The ultimate goal of the soil sampling and analysis was the creation of a continuous surface model (raster surface) for each fraction of soil (sand, silt and clay) using spatial interpolation, and subsequent classification by USDA. Based on the results of this classification in three soil horizons, the field was divided into two distinct zones and along with other factors it was decided to implement differentiated fertilization inputs in each zone with autonomous hydrofertilizing networks, so that each zone is completely and independent in the inflow of irrigation water and nitrogen fertilizer.

Reduced-input agriculture was based on the application of farming practices in accordance with the soil variations of the field plot. The application of agrochemicals (such as fertilizers) and other inputs (such as irrigation water) was based on the actual needs of the field, in an economically and environmentally friendly way. Unlike traditional agricultural practices, precision farming, manages field plot variability. Zoning the field was accomplished in accordance with the properties of the soil and was a prerequisite for the accurate application of spatially differentiated practices.

In the experimental corn crop field plot, zoning configuration of the hydrofertilizing system took place. The goal of the configuration was to apply hydrofertilization to the crop at the right time, the right place and in adequate quantity in accordance with the needs of the crop.

Fertilization practice (in terms of quantity, space and time of application) was defined by an algorithm that was developed after a series of experiments of nitrogen fertilization in corn and also by using the N-sensor of YARA which measured and recorded the corn condition in “real time”. The customization of fertilization will apply for the nitrogen needs, since nitrogen is the main limiting factor in the development of the crop.Precision irrigation was based in identifying and quantifying the variability i.e. spatial and temporal variability that was existed in soil and crop conditions within a field and between fields. Various components of the soil-crop-atmosphere continuum were measured in real-time conditions so as to provide precise and/or real- time control of irrigation applications and consequently minimum energy consumption.

A telemetric meteorological station was installed at the experimental field plot with a real-time data collection centre for all meteorological data. Based on the data, the crop evapotranspiration (ETc) and effective rainfall, the crop irrigation needs were accurately calculated. For an exact determination of the ability of soil to retain and provide water, soil moisture sensors were installed, one for each plot. The soil moisture sensors were installed at a depth to meet the profile of the root system.

Moreover, energy indicators (eg energy to produce, to supply water, to transport, green house

gases, etc.) were measured and ffinally a relational database was developed as an organized collection of geographic data designed to incorporate, store, update, manage, analyze and properly allocate information. All the spatial data both in vector and raster format which are included in the database will be presented through a WebIMS application.

3. DISCUSION

Until now, only isolated case studies were conducted. In order to approach NEXUS managerial strategy, the evaluation of the above findings will be done in future in conjunction with energy indicators and food security indicators (eg availability, productivity, health care, nutrition etc). Since water, energy and food sectors are interlinked in numerous ways, their interaction is considered complex and an integrated approach to assess the synergies among the three above sectors is of high difficulty. Thus, to move from a sectoral approach to a holistic approach, an efficient scientific framework is needed. The comprehension of the interconnection and interdependencies that link the three sectors will lead to an effective and sustainable managing system of the above watershed area.

The use of new technologies such as Earth observation systems which include satellite and in situ data, can provide geospatially consistent data and information for monitoring the progress of W–E–F issues at basin and national scales. Through them an up – to - date database will be created that should include various parameters such as physical and socio-economic data.

The impacts to water, energy, and food security that arise from climate change and regional political and economic factors need to be studied towards an establishment of effective practices and guidelines within the framework of sustainable development goals.

Apart from scientists, environmental managers and stakeholders it is also important for policymakers' to understand the role of the water, energy and food nexus in order to design sustainable policies and strategies. NEXUS approach not only emphasizes the interrelation of resources but considers also the cycle from research to implementation. Including "NEXUS" approach in integrated management strategies for a river basin, in Greece for the first time, could evaluate the condition of the water resource while also will provide an integrated resources management and future decision making at national level. Compared to an Integrated Water Resource Management approach, the water energy food ecosystems nexus approach concurrently considers multiple sectors and their evolution. This offers the opportunity to better involve key economic sectors—energy and agriculture in particular—in the dialogue over transboundary water resource uses, protection and management.

ACKNOWLEDGMENTS

Project "AGRO_LESS: Joint reference strategies for rural activities of reduced inputs" (B3.11.02), of the European Territorial Cooperation Programme Greece-Bulgaria 2007-2013.

REFERENCES

Bastiaanssen, W. G. M., Allen, R. G., Pereira, L. S., Smith, M., Raes, D., Wright, J. L., & Others. (2005). SEBAL Model with Remotely Sensed Data to Improve Water-Resources Management under Actual Field Conditions. Journal of Irrigation and Drainage Engineering, 131(February), 2. http://doi.org/10.1061/(ASCE)0733-9437(2005)131

Bazilian, M., Rogner, H., Howells, M., Hermann, S., Arent, D., Gielen, D., et al. (2011). Considering the energy, water and food nexus: Towards an integrated modelling approach. Energy Policy, 39(12), 7896–7906. http://doi.org/10.1016/j.enpol.2011.09.039

Ben Dor, E., Ong, C., & Lau, I. C. (2015). Reflectance measurements of soils in the laboratory: Standards and protocols. Geoderma, 245–246. http://doi.org/10.1016/j.geoderma.2015.01.002

Bird, J., Dodds, F., McCornick, P. G., & Shah, T. (2014). Water-food-energy nexus.

Dou, Z., C.F. Ramberg, J.D. Toth, Y. Wang, A.N. Sharpley, S.E. Boyd, C.R. Chen, D. Williams, and Z.H. Xu, 2009. Phosphorus speciation and sorption –desorption characteristics in heavily manured soils. Soil Sci. Soc. Am. J. 73: 93-101.

D'Urso, G., Richter, K., Calera, A., Osann, M. A., Escadafal, R., Garatuza-Pajan, J., … Vuolo, F. (2010). Earth Observation products for operational irrigation management in the context of the PLEIADeS project. Agricultural Water Management. doi: 10.1016/j.agwat.2010.08.020

Groot, A., & Maarleveld, M. (2000). Demystifying facilitation in participatory development. IIED.

Hoff, H. (2011). Understanding the Nexus. Background paper for the Bonn2011 Nexus Conference: Stockholm Environment Institute, (November), 1–52.

Ramirez, R. (1999). Participatory learning and communication approaches for managing pluralism: implications for sustainable forestry, agriculture and rural development.

Ringler, C., Bhaduri, A., & Lawford, R. (2013). The nexus across water, energy, land and food (WELF): Potential for improved resource use efficiency? Current Opinion in Environmental Sustainability, 5(6), 617–624. doi: 10.1016/j.cosust.2013.11.002

Sachs, I., & Silk, D. (1990). Food and energy: strategies for sustainable development. United Nations University Press.

Uphoff, N. T. (1992). Local institutions and participation for sustainable development. Citeseer.

Proceedings of the 10th World Congress of EWRA 'Panta Rhei', 5-9 July 2017, Athens, Greece
© 2017 *European Water Resources Association*

Evaluation of the water footprint and water use efficiency in a high density olive (*Olea europea* L.) grove system

A. Gertsis*, K. Zoukidis and A. Mavridis
Perrotis College, American Farm School, Marinou Antypa 54, str. P. Thessaloniki, Greece
* *e-mail: agerts@afs.edu.gr*

Abstract: Modern approaches in sustainable agricultural production management require holistic approaches and evaluation of the water use efficiency and water footprint. The irrigation water scarcity due to overuse and quality deterioration due to increased salinity levels, represent significant obstacles in sustainable agricultural systems. Systems that promote and evaluate less-inputs and more efficient production are strongly considered lately. This study presents results of two years from an olive grove, planted in high density linear systems adapted for mechanical harvesting. The grove was established in 2011 in Thessaloniki, Greece, for long term evaluation of the effects of major production inputs in olive yield and olive oil quantity and quality. The experimental design includes three planting densities (medium, high and super high density; 500, 1000 and 1670 trees/ha, correspondingly), two commonly used worldwide olive oil varieties/clones adapted for mechanical harvesting (Koroneiki and Arbequina), grown under two irrigation levels (conventional and 50% less) and two fertility levels (conventional and 50% less) with a foliar split application in the fertility treatments. Results from the two years (2015 & 2016) on water use efficiency (WUE) and water footprint (WF) are presented in this paper. The results indicated that increase in WUE and decrease in WF was achieved with management approaches such as planting density at least for the measured period and tree age. Additional efforts to minimize water use and increase WUE are in progress.

Key words: Olive grove, water footprint (WF), water use efficiency (WUE), high density olive

1. INTRODUCTION

1.1 Irrigation water utilization – an agronomic approach

The use of water in agriculture (both in crop and animal production systems) represents a very significant portion of the "fresh water" deposits in Earth and is under strong monitoring globally in the last decades. Particular use by crop species varies greatly and there are no common procedures to calculate crop water use and water use efficiencies. Water use efficiency (WUE) and water productivity (WP) are two different terms. However, they seem to cause some confusion and different interpretation among agronomists and engineers. WUE is the percent of water supplied to the plant that is effectively taken up by the plant, i.e., that was not lost to drainage, bare soil evaporation or runoff. In the general agronomic approach, the crop WUE is meant to be the ratio of total water used by crops over the total economic yield achieved at field conditions, which is very close to be considered as the WP. In the context of this study, the agronomic approach will be used, since the emphasis is on how much total water was provided to the field (total of rainfall and irrigation) and how much economic product was output. This is a simple but more realistic approach.

Physiological based Water-use efficiency (WUE) refers to the ratio of water used in plant metabolism to water lost by the plant through transpiration. Two types of water-use efficiency are referred to most frequently: photosynthetic water-use efficiency (also called intrinsic or instantaneous water-use efficiency), which is defined as the ratio of the rate of carbon assimilation (photosynthesis) to the rate of transpiration, and water-use efficiency of productivity (also called integrated water-use efficiency), which is typically defined as the ratio of biomass produced to the

rate of transpiration.

Increases in water-use efficiency are commonly cited as a response mechanism of plants to moderate to severe soil water deficits, and has been the focus of many programs that seek to increase crop tolerance of drought e.g. project AZORT (http://www.cespevi.it/azort/azort.html). However, there is some question as to the benefit of increased water-use efficiency of plants in agricultural systems, as the processes of increased yield production and decreased transpiration water loss (that is, the main driver of increases in water-use efficiency) are fundamentally opposed (Bacon, 2004).If there existed a situation where water deficit induced lower transpiration rates without simultaneously decreasing photosynthetic rates and biomass production, then water-use efficiency would be both greatly improved and a desired trait in crop production.

Water productivity is the amount of beneficial output per unit of water depleted. In its broadest sense, it reflects the objectives of producing more food, and the associated income, livelihood and ecological benefits, at a lower social and environmental cost per unit of water used (Molden et al., 2007). Usually, water productivity is defined as a mass (kg), monetary ($) or energy (calorific) value of produce per unit of water evapotranspired (Kijne et al., 2003; Molden et al., 2010). They reported a range of WP for table olives of 1-3 kg/m^3.

1.2 Water footprint

Water is one of the most important commodities/natural goods on earth. However, continuous, multidisciplinary pressures through time, like climate change, water consumption and pollution, promote today, more than ever before, issues of sustainable water availability, use and management (Hoekstra et al., 2012). Although there are substantial water volumes consumed and polluted in the industrial and domestic sectors (WWAP, 2009), there are accumulated difficulties in the water-agriculture framework, such as the expected, increasing number of global population of more than 9 billion people by 2050 (Alexandratos et al., 2012). Additionally, the demanding needs for delivering successfully the four Fs (Food, Fibre, Fuel and Feed) of agriculture in the future, constitute a framework of establishing enhanced, holistic approaches to confront with these global challenges and to support better water balance (equilibrium) in nature as agriculture accounts for up to 70% of global water withdrawals (Calzadilla et al., 2010; FAO, 2015).

Towards that perspective, the combination of Water Footprint (Hoekstra, 2003) with GIS (Geographic Information Systems) applications can provide significant benefits. The concept of "Water Footprint-WF" defines the total volume of freshwater that is used to produce the product (Hoekstra et al., 2009). It provides a framework to analyse the link between human consumption and the appropriation of the globe's freshwater. The water footprint of a product is defined by three components

i) the *blue water footprint* which refers to the volume of surface and groundwater consumed (evaporated) as a result of the production of a good;
ii) the *green water footprint* which is referred to the rainwater consumed, and,
iii) the *grey water footprint* of a product which refers to the volume of freshwater that can be associated with the production of a product over its full supply chain.

The blue water footprint refers to consumption of blue water resources (surface and ground water) along the supply chain of a product. The green water footprint refers to consumption of green water resources (rainwater stored in the soil as soil moisture). The grey water footprint is defined as the volume of freshwater that is required to assimilate the load of pollutants based on existing ambient water quality standards (Hoekstra et al., 2009).

The enhanced approach of geospatial analytics can provide extraction of information in multiple levels, while examining several aspects of crop-related parameters with water use at international, national and local scale.

It is important to comprehend that spatial analysis of large areas demonstrate a low spatial resolution and they limit the accuracy of the results (Hoekstra et al., 2011). Towards enhanced spatial resolution and better analysis of the spatial factors that influence the Water Footprint can be

facilitated through the use of a Geographic Information System (GIS), providing a lot of benefits, such as the spatial factors related with climatic conditions, or/and precipitation (Fig. 1). Also, GIS gives us the capacity to easily calculate the WF of a case studied area (regional WF) by multiplying the WF of the specific crop by the aggregated size of the fields in the region of study. Additionally, GIS allows different approaches of geospatial modelling relating the impact of changes in agricultural practices with spatial distributions of different crops, with demographic data and estimated simulation of future climatic models affecting severely evapotranspiration ,e.g., model Prudence (Christensen et al., 2007) for 2070-2100 in relation to 1961-1990 period, enabling spatial time series analysis (Fig. 2) and helping significantly in cost-benefit analysis of the implementing practices, so as to reduce water consumption and increase efficiency (Thorp et al., 2015; Singh, 2016) .

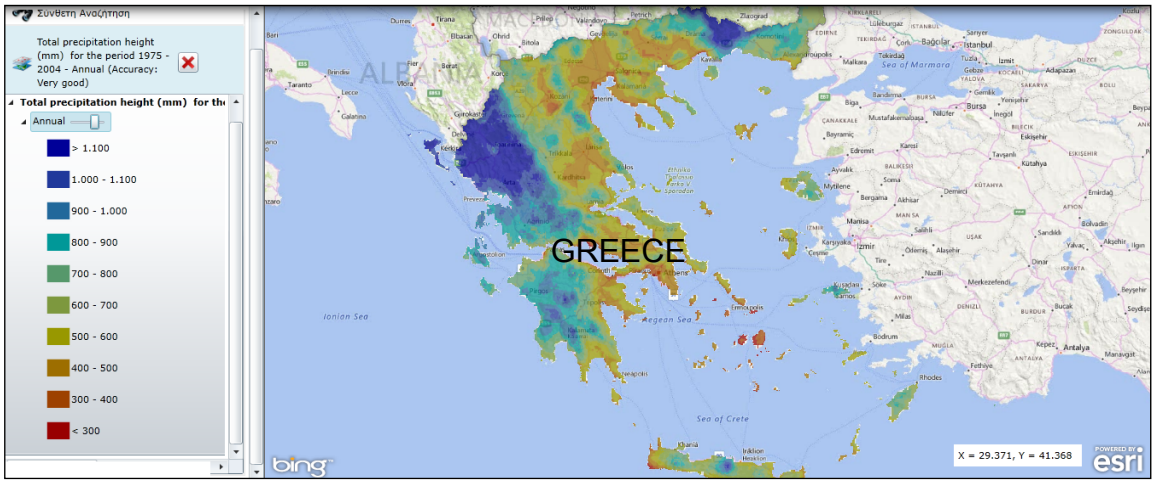

Figure 1. Total precipitation height (mm) in Greece for the period 1975-2004 provided by the Web-GIS portal of the project Geoclima (Source: www.geoclima.eu)

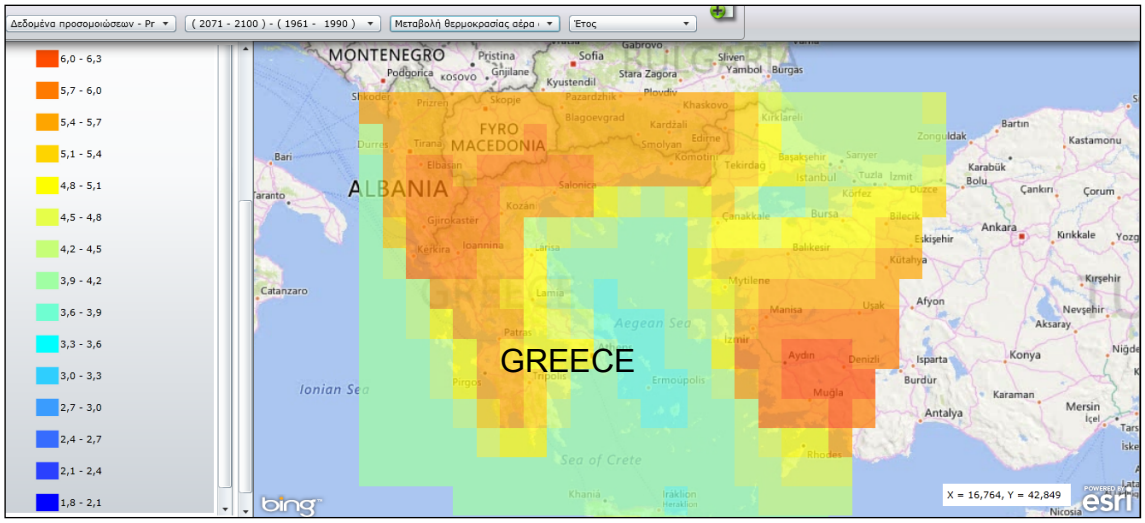

Figure 2. Estimation of maximum temperature change (^{o}C) at 2 meters height in Greece for the period 2071-2100 in relation to the period 1961-1990, based on the climatic model PRUDENCE, provided by the Web-GIS portal of the project Geoclima (Source: www.geoclima.eu)

2. NEW OLIVE PRODUCTION SYSTEMS

The worldwide trend in olive (*Olea europea* L.) production systems for olive oil, is in establishing high to super-high density systems adapted to mechanical harvesting and, is evident in

all olive producing countries and in newcomers. These systems require higher levels of management and cautious use of major production inputs. One main advantage is the significantly lower harvesting cost due to modern technologies available in fully mechanical harvesting, since the main production cost (over 80-90% of the total cost) is the manual harvesting of olives.

3. MATERIALS AND METHODS

The Educational-Research-Demonstration olive grove (N40^o 34’ 13.42” and E22^o 59’ 12.25”) was established in late 2011 in Perrotis College, American Farm School of Thessaloniki, Greece (Fig. 3) and includes the following treatments: two varieties (Koroneiki and Arbequina), three planting densities acronym Super-High Density (SHD), High density (HD) and Medium (MD) density and included 1670, 1000 and 500 trees/ha, correspondingly, two irrigation levels (conventional irrigation and 50% less) and two fertilization levels (conventional fertilization and 50% less). The first year of mechanical and manual harvesting was in 2014. A number of trees from each treatment are harvested manually and the rest by a special olive harvester (Gregoire G120 model). The olive grove aims to evaluate in a long term all possible effects of the above treatments on olive production and olive oil, of the new high density systems.

The total amount of irrigation plus the rainfall in each growing season will be used to estimate WUE based on total water provided to the field and the olive yield produced. The climatic data were collected by a nearby located automatic weather station (Davis Vantage Vue, http://www.davisnet.com/solution/vantage-vue/). The average yield for each planting density across all within treatments values and varieties will be presented.



Figure 3. The Educational-Research-Demonstration olive grove in Perrotis College, American Farm School of Thessaloniki, Greece

4. RESULTS AND DISCUSSION

4.1 Water use efficiency

Table 1 presents the calculated WUE for all three planting densities as an average across all other treatments. The trend shown is in close agreement but lower, when adjusted, with other

conventional olive production systems. Since all the trees are young in age (< 6 years), the WUE was affected by the planting density and so, the SHD system produced the highest WUE as compared with the HD and the MD (Medium) density. A simple linear model used to extrapolate the expected WUE for the next 4 years and high yields observed in some treatments, produced the results shown in Table 2. It appears that WUE is increased yearly, under "average" weather conditions, that are considering the average of the three years used to measure the WUE. The variability in climate among the three years used was high enough to justify the rationale of using this "average" for modelling purposes.

Hijazi et al. (2014) reported from an olive grove in Syria, WUE values ranging from 0.4 to 2.1 kg/m^3 for a range of irrigation systems. Average production of fruits was 8.53 tons/ha or 48 kg/tree and a planting density of 180 trees/ha. Using drip irrigation, WUE increased from 1.3 kg/m^3 to 2.36 kg/m^3 compared with surface irrigation. These values are for conventional planting systems and older trees (18 years old) and are comparable to the high density systems of the presented study under drip irrigation, considering approximately similar tree age and yields/ha. Therios (2008) reports that the olive tree is very efficient in its use of water. It requires 312 g water to produce 1 g dry matter or converted to equivalent of 3, 2 kg/m^3, whereas other evergreen plants such as *Citrus* and *Prunus* species require 400 and 500 g, respectively. Nuberg and Yunusa (2003) reported for Australia the WUE range for two years ranged from 0.4 to 2.1 kg/m^3.

A statistical approach based on linear regression models with very high R^2 (0.95-0.98) and using "hypothesized future individual tree yields" resulted in simulated WUE for the three planting densities as shown in Table 2. The hypothesized yields were within the high range achieved in 2016 season. The WUE for the next 5 years, assuming three-year average total rain and irrigation levels, ranged from 0,65 to 3,58 kg/m^3. These values appear realistic but they may vary among the planting densities, not necessarily exhibiting a linear relationship. The SHD olive systems have an advantage during the first 4-8 years, due to higher population per unit area and, therefore, more efficient use of water and fertilizer inputs; however, the yield of the SHD systems was reported to level-off or slightly decreasing after 8-10 years. In this later period, the HD systems may have an overall advantage in WUE. This is a speculation not yet reported.

Table 1. Agronomic Water Use Efficiencies of the three planting densities (SHD-HD-MD).

Year	Average yield/ tree (kg)	Total rain (mm)	Total irrigation SHD (mm)	Total irrigation HD (mm)	Total irrigation MD (mm)	Average yield SHD (kg/ha)	Average yield HD (kg/ha)	Average yield MD (kg/ha)	WUE SHD (kg/m^3)	WUE HD (kg/m^3)	WUE MD (kg/m^3)
2016	4,5	353	65	39	20	7515	4500	2250	1,797	1,148	0,604
2015	3,2	458	40	24	12	5344	3200	1600	1,074	0,664	0,341
2014	1,6	418	32	19	10	2672	1602	800	0,594	0,366	0,187

Table 2. Simulated WUEs for the three planting densities (SHD-HD-MD for future yearly expected tree yields.

Yield (kg/tree)	Total water SHD (mm)	Total water HD (mm)	Total water MD (mm)	YIELD SHD (kg/ha)	YIELD HD (kg/ha)	YIELD MD (kg/ha)	WUE SHD kg/m^3	WUE HD kg/m^3	WUE MD kg/m^3
4,5	418	392	373	7515	4500	2250	1,80	1,15	0,60
3,2	498	482	470	5344	3200	1600	1,07	0,66	0,34
1,6	450	437	428	2672	1602	800	0,59	0,37	0,19
5	455	437	424	8350	5000	2500	1,93	1,23	0,65
6	455	437	424	10020	6000	3000	2,35	1,50	0,79
7	455	437	424	11690	7000	3500	2,76	1,77	0,93
8	455	437	424	13360	8000	4000	3,17	2,03	1,07
9	455	437	424	15030	9000	4500	3,58	2,30	1,22

4.2 Water footprint (WF)

The calculations for the WF are shown in Table 3 for each of the three planting densities. The blue water footprint is considered as the amount of surface and groundwater consumed (evaporated and transpired) for the production of olives.

The green water footprint is considered as the effective rainwater amount consumed and is approximately equal to 80% of the seasonal rainfall. The grey water footprint of a product refers to the volume of freshwater that can be associated with the production of a product over its full supply chain. It the case of our study, the full supply chain is very near (<400 m) to the olive grove, in the facilities of the Krinos Olive Center of Perrotis College-AFS, where all production is processed, bottled and distributed to consumers. Since no pesticides and fungicide were used in all three years and only one herbicide application was used in the last two years in the lines only, the Grey water affect is considered negligible. Therefore, it is approximated as equal to zero. The Green WF is taken equal for each planting density, considering the rainfall factor.

Results from Salmoral et al. (2011) show more than 99.5% of the water footprint of one liter of bottled olive oil is related to the olive production, whereas less than 0.5% is due to the other components such as bottle, cap and label. Over the studied period, the green water footprint in absolute terms of Spanish olive oil production represents about 72% in rain fed systems and just 12% in irrigated olive orchards. Blue and grey water footprints represent 6% and 10% of the national water footprint, respectively. It is shown that olive production in Spain is concentrated in regions with the smallest water footprint per unit of product.

Table 3. The three components of the water footprint (WF) calculated for the average of the olive grove for each planting density.

WF component	SHD	HD	MD
Blue WF	273	262	254
Green WF	328	328	328
Grey WF	~0	~0	~0
Total WF	**601**	**590**	**582**

5. CONCLUSIONS

It appears that olive trees in super high density systems, utilized better than the lower density systems the total water in the field and have a higher WUE. This long-term study will produce in the next years, additional data to further evaluate the interaction of WUE and Total Fertilizer Use Efficiency (TFUE), in an effort to increase the WUE of the systems evaluated. The WF of olive is relative small, if production and processing units are close. The SHD systems did not have much higher WF from the lower density systems, proving again their highest overall water efficiency. This study reports only the average trend for the three planting densities across all other treatments.

REFERENCES

Alexandratos N., Bruinsma J., 2012. World agriculture towards 2030/2050: the 2012 revision. ESA Working paper No. 12-03. Rome, FAO.

Bacon, M. 2004. Water Use Efficiency in Plant Biology. Oxford: Blackwell Publishing Ltd.

Calzadilla A., Rehdanza K., Tol R. S. J., 2010. The economic impact of more sustainable water use in agriculture: a computable general equilibrium analysis. J. Hydrol. 384, 292–305. doi: 10.1016/j.jhydrol.2009.12.012.

Christensen, J.H. Christensen, O.B. 2007. Climatic Change 81(Suppl 1): 7. doi:10.1007/s10584-006-9210-7

Descheemaeker, K., Stuart W. Bunting, Prem Bindraban, Catherine Muthuri, David Molden, Malcolm Beveridge, Martin van Brakel, Mario Herrero, Floriane Clement, Eline Boelee, and Devra I. Jarvis. 2013. Chapetr 8. Increasing Water Productivity in Agriculture. IN © Managing Water and Agroecosystems for Food Security (ed. E. Boelee) CAB International 2013.

Hijazi, A., M. Doghoze, N. Jouni, V. Nangia, M. Karrou, and T. Oweis. 2014. Water requirement and water-use efficiency for olive trees under different irrigation systems. 7th International Conf. on Water Resources in the Mediterranean Basin, Oct 10-12, Marrakech, Morocco.

Hoekstra, A. Y., 2003. Virtual water trade. Proceedings of the International Expert Meeting on Virtual Water Trade, IHE Delft, ED : A.Y Hoekstra. Value of Water Research Report Series N°12 Delft, The Netherlands.

Hoekstra A. Y., Chapagain A. K., Aldaya M. M., Mekonnen M. M. 2011. The Water Footprint Assessment Manual: Setting the Global Standard. London: Earthscan

Hoekstra, A.Y., Mekonnen, M.M., 2012. The water footprint of humanity. PNAS 2012 109(9): 3232-3237; doi: 10.1073/pnas.1109936109.

Kijne, J.W., Barker, R., and Molden, D. (eds) (2003) Water Productivity in Agriculture: Limits and Opportunities for Improvement. Comprehensive Assessment of Water Management in Agriculture Series 1. CAB International, Wallingford, UK in association with International Water Management Institute (IWMI), Colombo.

Mekonnen, M.M., Hoekstra, A.Y., 2010. The green, blue and grey water footprint of crops and derived cropproducts. Value of Water Research Report Series No. 47, UNESCO-IHE, Delft, the Netherlands.

Molden D, Oweis T, Steduto P , Bindraban P, Hanjra MA , Kijne J. 2010a. Improving agricultural water productivity: Between optimism and caution. Agricultural Water Management 97: 528–535.

Nuberg, Ian and Isa Yunusa. 2003. Olive water use and yield – monitoring the relationship. RIRDC Publication No 03/048 RIRDC Project No UA-47A

Salmoral, G, M. M. Alday, D. Chico, A. Garrido and M. R. Llamas. 2011. The water footprint of olives and olive oil in Spain. Spanish Journal of Agricultural Research 2011 9(4), 1089-1104

Singh A. 2016. Managing the water resources problems of irrigated agriculture through geospatial techniques: An overview. Agric. Water Management 174, 2–10. 10.1016/j.agwat.2016.04.021

Shtull-Trauring, E., Aviani, I., Avisar, D., & Bernstein, N. 2016. Integrating High Resolution Water Footprint and GIS for Promoting Water Efficiency in the Agricultural Sector: A Case Study of Plantation Crops in the Jordan Valley. Frontiers in Plant Science, 7, 1877. doi: 10.3389/fpls.2016.01877

Thorp K. R., Hunsaker D. J., French A. N., Bautista E., Bronson K. F. 2015. Integrating geospatial data and cropping system to analyze spatial seed cotton yield, water use. Precision Agriculture 16, 532–557. doi: 10.1007/s11119-015-9393-x

WWAP (World Water Assessment Programme), 2009. The United Nations World Water Development Report 3: Water in a Changing World. WWAP, UNESCO Publishing, Paris, and Earthscan, London.

Proceedings of the 10th World Congress of EWRA 'Panta Rhei', 5-9 July 2017, Athens, Greece
© 2017 *European Water Resources Association*

Regulation and mitigation services of forests as the components of urban resilience

B. Uygur Erdogan
Istanbul University, Faculty of Forestry, Department of Watershed Management, 34473, Istanbul, Turkey
e-mail: uygurb@istanbul.edu.tr

Abstract: Urbanization has been an unavoidable situation due to human expansion worldwide. However, urban sprawl causes degradation of natural resources and loss of their services. As a consequence of this, urban ecosystems can not be able to adapt themselves rapidly to these changes and create opportunities to face up to new circumstances. Therefore, sustainably managing urban ecosystems for providing important ecosystem services become more crucial to meet several public demands in the context of both human well-being and resilience of urban ecosystems. In this perspective, the role of green areas or forests in urban ecosystems becomes prominent in terms of providing ecosystem services. The objective of this study was to determine the forest contribution to the resilience of Istanbul by providing water quality regulation and flood mitigation services. Kağıthane watershed which is located on the European side of Istanbul was selected as study site where the pressure has been increasing over the years. 11 sub-watersheds were studied and land use types in the watersheds were classified into four groups as forest, rangeland, agricultural and urban areas. Both water quality regulation and flood mitigation services were quantified by using mathematical equations based on field measurement. Additionally, a scoring method was developed to determine the relevant capacity of each land use type. Results revealed that forested sub-watersheds had high potential while urbanized sub-watersheds have low potential for providing these services. Therefore, adaptive management approaches should integrate the ecosystem services into planning in the context of urban resilience.

Key words: Ecosystem services, water quality regulation, flood mitigation, forests, urban resilience

1. INTRODUCTION

Human being and environment have been related to each other in the context of being a part of the same ecosystem. However, this relation is based upon the dependence of human well-being on ecosystems' services and processes (Ehrlich and Ehrlich, 1981; De Groot et al., 2002). Eventually, this supply-demand balance between humans and ecosystems has become a crucial issue in terms of ecosystem vulnerability and sustainability in a changing environment. Population increase, rapid urbanization and human activities such as land use changes can be mentioned as the main reasons of degradation of ecosystems and loss of their services. As a result of alteration and degradation of ecosystems, approximately 60 % of ecosystem services have been destroyed or used in unsustainable manner worldwide (MEA, 2005). Additionally, more than half of the world population is expected to live in cities by 2030 (UN, 1997). Therefore, degradation of ecosystems and services is going to be more severe even if the cities and urban systems couldn't be planned and managed sustainably through their services. Also planning urban systems by the lack of service conservation causes more vulnerable urban systems to environmental disasters such as floods, droughts, water scarcity (Peters et al., 2004). However, urban systems as the complex social-ecological systems (Pickett et al., 2001) require to be resilient to all these disturbances (Alberti et al., 2003; McPhearson et al., 2014) in the context of providing human well-being (Tzoulas et al., 2007). The key components of building the resilience of urban systems have been stated as ecosystem services in previous studies (Bolund and Hunhammar, 1999; Jansson, 2013). Additionally, green spaces and infrastructures along with forests in urban ecosystems became prominent in the process of providing urban ecosystem services. Beside these, the land and its use have been indicated as the main factors in terms of generating and providing ecosystem services

(Bolund and Hunhammar, 1999) and supporting biodiversity to promote ecosystem resilience in urban areas (Colding, 2007). Thereby, to moderate land use change impacts, ecosystem service based approaches and management strategies have begun to make sense in the process of conserving biodiversity, ecosystems and services in urban planning. On the other hand, quantification of ecosystem services has been highlighted in case of integration into management plans (Daily et al., 2009; Logsdon and Chaubey, 2013).

Objective of this study was to determine contribution of forest to the resilience of Istanbul by providing water quality regulation and flood mitigation services among the hydrological services. To gain this goal, the relationship between different land use types and hydrological services in watershed scale was investigated and discussed. The effects of land use types on selected hydrological services were investigated by quantification of these services in the watershed. Furthermore, this study was implemented to estimate a practical ecosystem services based approach for urban planners to incorporate hydrological services into management plans in the context of urban resilience.

2. MATERIAL AND METHOD

2.1 Material

Kağıthane watershed which is one of three important watersheds on the European side of Istanbul was selected as the study site (39º - 45º N and 41º - 45º E). The watershed has 179 km^2 area and drains into the Golden Horn. Upland of the watershed is covered by forests while lowland is occupied by residential areas. Average annual precipitation ranges between 800 and 1120 mm. The main parent materials of the region are Neogen Belgrad and Carboniferous formations while clay schists and alluvial zones can be seen locally in some parts of watershed (Çokoyoğlu, 2008).

This watershed was selected as study area because within the borders of it, there is a forest called Belgrad which had provided fresh water to the city approximately for 300 years from 17th to 20th century (Çolak and Kırca, 2015) whereas it has been used just for recreational facilities for a long time.

2.2 Method

Water quality regulation and flood mitigation services were examined in this study. For the first step of this quantification methodology, the study site was divided into 11 sub-watersheds based on land use types by using ArcGIS (Figure 1a). Thus, any effect on these hydrological services throughout the watershed can be determined by using this study scale because of being regional services (Brauman et al., 2007). For spatial analysis, land use types were classified in four groups as forest, rangeland, agricultural and urban areas by using CORINE 2006 as base maps (Figure 1b).

The second step of this quantification methodology was to develop mathematical equations based on field measurements for both water quality regulation and flood mitigation services. Additionally, a scoring method was developed to determine the relevant capacity of each land use type. The quantification methods implemented for selected hydrological services were detailed below separately.

2.2.1 Water quality regulation service

Estimation of water quality regulation service depends on indicators identifying the pollution or quality of water. In this study, pH, electrical conductivity (EC) (µS/cm), turbidity (NTU), dissolved oxygen (DO) (mg/l) and total suspended solid particles (TSSP) (mg/l) were selected as physical water quality parameters to analyze and quantify. Except for total TSSP, water quality parameters

were analyzed with the WTW Multiline P4 Universal Meter (WTW, Weilheim, Germany) in the field. Stream waters were sampled for TSSP and analyzed by evaporation procedure in the laboratory. Since it was not a monitoring study, streams were sampled once for analyzing the water quality parameters.

Relations between water quality parameters and land use types were determined according to coefficients based upon land use intensities and value of water quality parameters by using a mathematical equation which was developed as;

$$Y = a * X_1 + b * X_2 + c * X_3 + d * X_4 \quad (1)$$

where,

X_1, X_2, X_3, X_4 : Forest, rangeland, agricultural land and urban area as a percentage of total sub-watershed (%)

a, b, c, and d: Estimated coefficients for water quality parameters

Y: pH, electrical conductivity, turbidity, dissolved oxygen and total suspended solid particles.

Estimated coefficients for water quality parameters were the coefficients for each land use type at the same time. Additionally, that provide a way to change the scale from single point to watershed. Also, this model was validated in other watersheds for the reliability of the coefficients. This model was calibrated in 27 sub-watersheds and validated in other 10 as a part of project involved Kağıthane watershed.

After computing new coefficients of each watershed related to their land use types, water quality parameters were assessed by a simple scoring method, which was aimed to determine the ranges of parameters (Serengil, 2010).

2.2.2 Flood mitigation service

Flood mitigation service was investigated based on Soil Conservation Service Curve Number Method (SCS-CN) and the results were used in a mathematical model. Therefore, to assess the curve numbers (CN) for different lands in the sub-watersheds, soil-cover characteristics such as permeability and cover type were determined according to field data of soil and spatial analysis, respectively. To study permeability, soil samples were collected from sub-watersheds. Permeability was calculated according to the Darcy Law (Frevert et al., 1959) whereas texture was determined by Bouyoucos Hydrometer method (Irmak, 1954). An average value of these soil properties was calculated for each sub-watershed in order to determine the hydrologic soil group (HSG) of soil samples along with the land use intensities to be used while specifying CN. Other than these soil and land use properties, flood mitigation service was linked to rainfall characteristics of the study site. Hereby, the rainfall more than 50 mm in 24 h was accepted to be a storm leading to flood (Fu et al., 2013). Due to daily precipitation data from the meteorological station in the study site, the single storms and their duration were determined. Based on these data, the amount of flood water mitigated by an ecosystem per year can be estimated as the difference between storm and runoff (Fu et al., 2013):

$$Flood\_mit = P\_ev - \left(\frac{P_{ev} - 0.2S}{P_{ev} + 0.8S}\right)^2 \times storm\ days \quad (2)$$

where Flood_mit is flood mitigation (mm); P_{ev} is single-event rainfall (mm); storm days is the number of stormy days and S is the amount of rain water (mm) retained by the ecosystem before runoff occurs which was as following (NRSC, 2004):

$$S = \frac{25400}{CN} - 254 \quad (3)$$

where CN is curve number which is a coefficient taking a value varying between 0 and 100 related to site conditions such as land use, rainfall intensity and soil permeability (NRSC, 2004).

As it was mentioned above, CNs for all soil samples were determined according to the land use types and soil properties for all sub-watersheds. On the other hand, to determine CN for each sub-watershed, weighted CN was calculated as (SCS, 1971):

$$Weighted\ CN = \sum a \times CN/100 \quad (4)$$

where Weighted CN is the curve number represents the whole watershed; a is the intensity of land use type.

Overall, the last step of this quantification methodology for both water quality regulation and flood mitigation services was to show the capacities of each land use types for the services they provide. Therefore, a classification based on a matrix which has a scale consisting of: 0 = no relevant capacity, 1 = low relevant capacity, 2 = relevant capacity, 3 = medium relevant capacity, 4 = high relevant capacity and 5 = very high relevant capacity was used in order to determine the capacities (Burkhard et al., 2012). As a consequence of these computations water quality regulation and flood mitigation services were mapped in watershed scale.

3. RESULTS

Size of the selected 11 sub-watersheds varied between 332.37 and 3908.50 ha consisting of different land use types such as forest, rangeland, agricultural and urban areas. Some of these sub-watersheds included only one land use type while some included more than one. Thus, percentage of each land use types was changed in the sub-watersheds.

3.1 Results of water quality regulation service

Results of field surveys and laboratory analyses showed that the water quality parameter values were changed from site to site depending on land use types. Therefore, as a result of using these measured values as inputs of implemented mathematical equation, the coefficients for both water quality parameters and land use types were estimated. So that, after implementing the mathematical equation with these coefficients which was used to link the land use types with these water quality parameters in watershed scale, the values of selected water quality parameters have changed related to land use types of sub-watersheds as expected.

Results showed that forest dominated sub-watersheds (SW-3 and SW-4) (95 % - 94 % forested) had the lowest EC (427 µS/cm) and TSSP (0.384 – 0.350 mg/l, respectively) whereas lowest forested sub-watersheds (SW-5 and SW-8) (non-existence forest) had the highest EC (1294 - 1305 µS/cm, respectively) and TSSP (1830 – 1843 mg/l, respectively) among the 11 sub-watersheds. 99 % - 100 % urbanized sub-watersheds that had the highest value of TSSP. Also, in the same sub-watersheds (SW-5 and SW-8), highest values for turbidity were estimated with the values of 215.02 – 217.90 NTU, respectively. In another sub-watershed (SW-7) which was 50 % urbanized had highest values of EC (848 µS/cm); TSSP (1.088 mg/l) and turbidity (111.52 NTU) after these urbanized sub-watersheds (SW-5 and SW-8). Beside all these, pH values varied between 7.18 and 8.16 while DO changed between 4.76 and 8.06 in all sub-watersheds.

Scoring all these values according to the range scale provided to obtain the map of water quality parameters in watershed scale. When examining the scores of water quality parameters, 2 was considered as the minimum while 8 was the maximum score in the sub-watersheds (Figure 1c). Following that, the scoring map has been transformed to the ecosystems' capacity map which shows service provision capacity of ecosystems by using Burkhard's capacity classification (Burkhard et al., 2012). The classification of ecosystems' capacity in the sub-watersheds varied from no relevant capacity to high relevant capacity. When the land use types and capacities were

analyzed together, results showed that forested sub-watersheds had high relevant capacity whereas urbanized sub-watersheds had relevant capacity to provide water quality regulation service (Figure 1d).

3.2 Results of flood mitigation service

The hydrologic soil groups were determined based on soil properties and existing HSG were A, B, C and D group. According to the hydrologic soil groups and land use types in the sub-watersheds, the Curve Numbers (CN) were varied between 30 and 98. Additionally, representing each sub-watershed with one CN was done by modifying CN to weighted CN related to land use types. Thus, the Curve Numbers (CN) were changed between 32 and 98.

After implementing the mathematical equation by using these weighted CN for each sub-watershed, the amount of rain water retained before runoff was calculated. Results showed that the land use types either ecosystems in sub-watersheds retained rain water with values varied between 7 % - > 76 %. The amount of retained rain water was minimum (7-16 %) in urbanized sub-watersheds while it was maximum (> 76 %) in forest dominated sub-watersheds (Figure 1e). When these results were evaluated by the Burkhard's capacity classification, results revealed that urbanized sub-watersheds had low relevant capacity whereas forested sub-watersheds had high relevant capacity to provide flood mitigation service (Figure 1f).

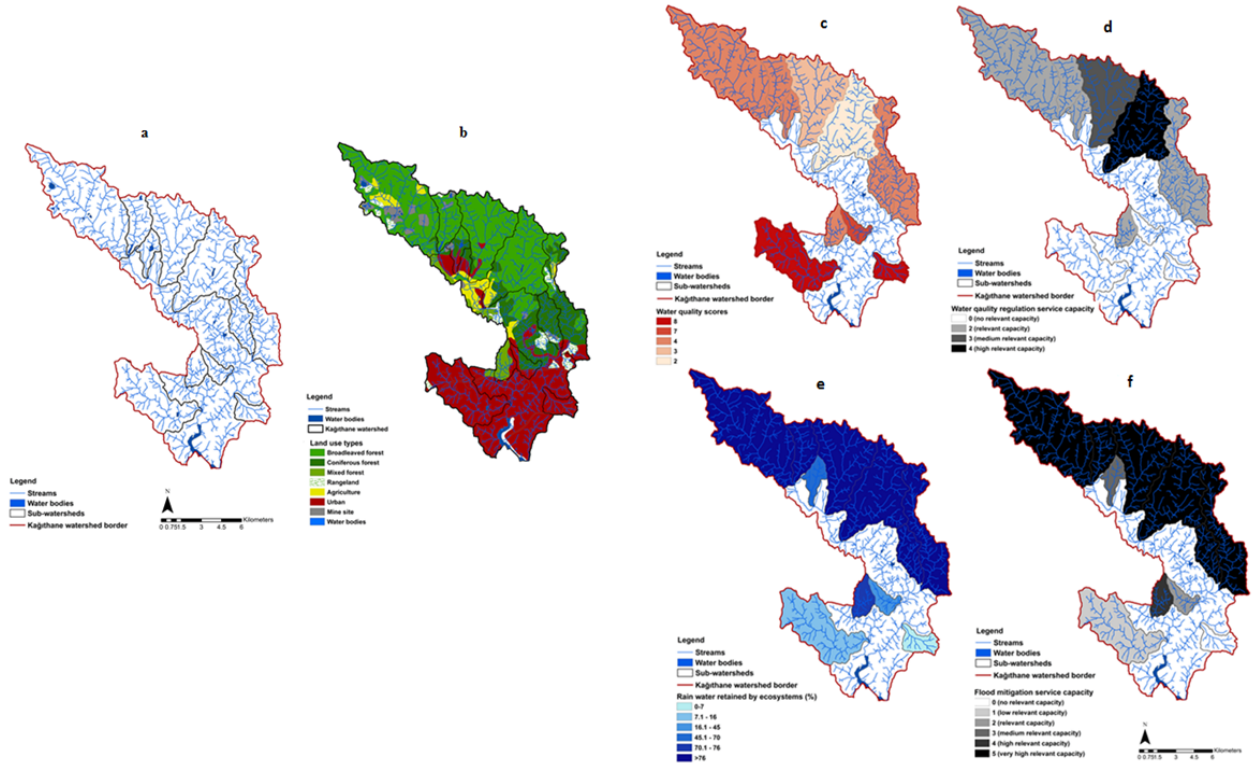

Figure 1. (a) Sub-watersheds, (b) Land use types in study site and (c) Scores of water quality parameters, (d) Water quality mitigation service capacities of sub-watersheds, (e) The amount of retained rain water and (f) Flood mitigation service capacities of sub-watersheds.

4. DISCUSSION

Results of this study indicated that water quality regulation and flood mitigation services were affected by land use types and that was ranked as altering regional hydrological ecosystem services by changing the way of land use (Jin et al., 2015), modifying the ecosystem services by conversion

of lands (Costanza et al., 1997; DeFries and Eshleman, 2004). Forest was determined as the most effective land use type in case of providing these hydrological ecosystem services. Also, the role of forests on hydrological processes is well documented in many studies. However, forests (Carvallo-Santos et al., 2014) and vegetation types (Brauman et al., 2007) were considered as the main components of provisioning hydrological services among the multiple ecosystem services such as providing wood, clean air, recreation, nutrient cycling, disturbance control and resilience to climate change (WRI, 2002). Moreover, Brauman et al (2007) mentioned forests as the ecosystems which improve water quality in a catchment by filtering toxics, nutrients, sediments and other substances from water through the root systems (Hanson et al., 2011) and forest floor (Eisalou et al., 2013). On the other hand, forests and vegetation types are also play a significant role on water flow regulation by consuming water through transpiration (Brauman et al., 2007); intercepting, absorbing water and decreasing peak flows during heavy rainfall (Hanson et al., 2011). Indeed, the results of this study for both hydrological ecosystem services consistent with these inferences in terms of determining the capacity of forest ecosystems. In contrast, urbanized sub-watersheds had the lowest capacities to provide these services because of the imperviousness. Additionally, the increased impermeable surfaces make cities more vulnerable to floods (Gomez-Baggethun et al., 2013). However, conversion of these vulnerable cities into resilient ones in the context of human well-being has been related to green spaces, green infrastructures, parks and forests, green streets and their services in these cities (Bolund and Hunhammar, 1999; Sandstr˝m, 2002). For instance, Bolund and Hunhammar (1999) aimed to analyse the impacts of urban ecosystems (street trees, lawns/parks, urban forests, cultivated land, gardens and blue areas) on the life of citizens in Stockholm and they concluded that urban ecosystems contribute to the quality of life by providing services such as air filtration, micro climate regulation, noise reduction, rainwater drainage and recreational values to citizens. Another study carried out by Cheisura (2004) showed that urban parks and nature provide many social services in addition to being the main components for city sustainability. Collier et al (2013) mentioned urban green spaces as a tool to improve the urban resilience and sustainability. Therefore, the contribution of green areas to the resilience should be considered by urban planners in terms of planning and designing urbans based up on human well-being.

5. CONCLUSION

This study focused on determining the forest contribution to the resilience of Istanbul by providing water quality regulation and flood mitigation services in watershed scale. However, it has concluded that forested sub-watersheds had the highest capacity to provide these services. So, this should be accepted as an ingredient of planning the resilient cities. As a consequence of this, the urban greens should be managed in terms of both ecosystem and human health while the urban systems are going to be planned and designed for future. So, integrating ecosystem services to both environmental and urban plans becomes a necessity. Thus, ecosystems should be planned in the context of conservation of their services. On the other hand, quantification of ecosystem services leads to define possible utilization of ecosystems that provides sustainable human well-being. Therefore, as the recent study indicated basic quantification models should be improved for each ecosystem service to insert them in plans.

ACKNOWLEDGEMENTS

The author would like to thank Prof. Dr. Yusuf Serengil from Istanbul University for his consultancy. Also, the study was supported by TUBITAK with the project number 112Y096.

REFERENCES

Alberti M., Marzluff, J.M., Shulenberger, E., Bradley, G., Ryan, C., Zumbrunnen, C. 2003. Integrating humans into ecology: opportunities and challenges for studying urban ecosystems. BioScience, 53 (12): 1169-1178.

Bouland P. and Hunhammar S. 1999. Ecosystem services in urban areas. Ecological Economics, 29, 293-301.

Brauman K.A., Daily G,C., Ka'eo Duarte T., Mooney H.A. 2007. The nature and value of ecosystem services: an overview highlighting hyrologic services. The Annual Review of Environment and Resources, 32, 67-98.

Burkhard B., Kroll F., Nedkov S., Müller F. 2012. Mapping ecosystem service supply, demand and budgets. Ecological Indicators, 21, 17-29.

Carvallo-Santos C., Honrado J.P., Hein L. 2014. Hydrological services and the role of forests: Conceptualization and indicator-based analysis with an illustration at a regional scale. Ecological Comlexity, 20, 69-80.

Chiesura A. 2004. The role of urban parks for the sustainable city. Landscape and Urban Planning, 68, 129-138.

Colding J. 2007. Ecological land-use complementation for building resilience in urban ecosystems. Landscape and Urban Planning, 81, 46-55.

Collier M.J., Nedović-Budić Z., Aerts J., Connop S., Foley D., Foley K., Newport D., McQuaid S., Slaey A., Verburg P. 2013. Transitioning to resilience and sustainability in urban communities. Cities, 21-28.

Costanza R., D' Arge R., De Groot R., Farber S., Grasso M., Hannon B., Naeem S., Limburg K., Paruelo J., O' Neil R.V., Raskin R., Sutton P., Van Den Belt M. 1997. The value of the world's ecosystem services and natural capital. Nature, 387, 253-260.

Çokoyoğlu S., 2008. Alibey ve Kağıthane havzalarında arazi kullanımı ve sorunlarının 50 yıllık değişimi, Yüksek Lisans Tezi, İstanbul Üniversitesi Fen Bilimleri Enstitüsü, 82 s. İstanbul.

Çolak A. and Kırca S. 2015. Belgrad Ormanı'ndan Taksim'e: Hayaldeki su. Atlas Dergisi, 268.

Daily G.C., Polasky S., Goldstein J., Kareiva P.M., Mooney H.A., Pejchar L., Ricketts T.H., Salzman J., Shallenberger R. 2009. Ecosystem services in decision making: time to deliver. Frontiers in Ecology and Environment, 7 (1): 21-28.

De Groot, R.S., Wilson, M.A., Boumans, R.M.J., 2002. A typology for the classification, description and valuation of ecosystem functions, goods and services, Ecological Economics, 41, 393-408.

DeFries R., Eshleman K.N. 2004. Land-use change and hydrologic processes: a major focus for the future. Hydrological Processess, 18, 2183-2186.

Ehrlich P.R. and Ehrlich A.H., 1981. Extinction: The causes and consequences of the disappearance of species, Random House, New York.

Eisalou H.K., Şengönül K., Gökbulak F., Serengil Y., Uygur B., 2013. Effects of forest canopy cover and floor on chemical quality of water in broad leaved and coniferous forests of İstanbul, Turkey, Forest ecology and Management, 289, 371-377.

Frevert K.R., Schwab G.O., Edminster T.W., Barnes K.K. 1959. Soil and water conservation engineering. John Wiley and sons. Inc. New York Chapman and Hall, Ltd. London.

Fu, B., Wang, Y.K., Xu, P., Yan, K., 2013. Mapping the flood mitigation services of ecosystems- A case study in Upper Yangtze river basin, Ecological Engineering, 52, 238-246.

Gómez-Baggethun E., Gren Å., Barton D.N., Langemeyer J., McPhearson T., O'Farrell P., Anderssson E., Hamstead Z., Kremer P. 2013. Urban ecosystem services. In: Elmqvist, T., et al. (Eds.), Cities and Biodiversity Outlook: Urbanization, biodiversity and ecosystem services: Challenges and opportunities. Springer, Netherlands, 175-251.

Hanson C., Talberth J., Yonavjak L. 2011. Forests for water: Exploring payments for watershed services in the U.S. South. World Resources Institute Issue Brief 2, 1-16.

Irmak A. 1954. Arazide ve laboratuvarda toprağın araştırılması metodları. İÜ Yayın no: 599, Orman Fakültesi Yayın no: 27, Halk Bankası matbaası, İstanbul.

Jansson Å. 2013. Reaching for a sustainable, resilient urban future using the lens of ecosystem services. Ecological Economics, 86, 285-291.

Jin G., Wang P., Zhao T., Bai Y., Zhao C., Chen D. 2015. Reviews on land use change induced effects on regional hydrological ecosystem services for integrated water resources management. Physics and Chemistry of the Earth, 89-90, 33-39.

Logsdon R.A. and Chaubey I. 2013. A quantitative approach to evaluating ecosystem services. Ecological Modelling, 257, 57-65.

McPhearson T., Hamstead Z.A., Kremer P. 2014. Urban ecosystem services for resilience planning and management in New York City. 2014. Ambio, 43, 502-515.

Millennium Ecosystem Assessment. 2005. Ecosystems and human well-being: wetlands and water synthesis. ISBN 1-56973-597-2, World Resources Institute, Washington DC.

NRSC (Natural Resources Conservation Service), 2004. Estimation of direct runoff from storm rainfall. National Engineering Handbook, Part 630, Chapter 10, USDA, Washington D.C.

Peters D.P.C., Pielke R.A., Bestelmeyer B.T., Allen C.D., Munson-McGee S., Havstad K.M. 2004. Cross-scale interactions, nonlinearities, and forecasting catastrophic events. Proceedings of National Academy of Science. USA, 101 (42): 15130-15135.

Pickett S.T.A., Cadenasso M.L., Grove J.M., Nilon C.H., Pouyat R.V., Zipperer W.C., Costanza R. 2001. Urban Ecologıcal Systems**:** Linking terrestrial ecological, physical, and socioeconomic components of metropolitan areas. Annual Review of Ecology and Systematics, 32, 127-157.

Sandstr˝m U.G. 2002. Green infrastructure planning in urban Sweden. Planning Practice & Research, 17: 4, 373-385.

Serengil Y., İnan M., Yurtseven İ., Kılıç Ü., Uygur B. 2012. Stream corridors as indicators of watershed land use: A case study in İstanbul. IUFRO Landscape Ecology Conference, Bosque, 33 (3): 345-352.

Soil Conservation Service (SCS), 1971. *Hydrology*, National Engineering Handbook, Supplement A, Section 4, Chapter 10, USDA, Washington D.C.

Tzoulas K., Korpela K., Venn S., Yli-Pelkonen V., Ka´zmierczak A., Niemela J., James P. 2007. Promoting ecosystem and human health in urban areas using green infrastructure: A literature review. Landscape and Urban Planning, 81, 167-178.

UN. 1997. Urban and rural areas 1996. UN, New York United Nations publications.
World Resources Institute. 2002. World resources 2000-2001: People and ecosystems: Fraying web of life. ISBN: 1-56973-443-7, 10 G St., NE, Washington, DC.

Proceedings of the 10th World Congress of EWRA 'Panta Rhei', 5-9 July 2017, Athens, Greece
© 2017 *European Water Resources Association*

Wastewater treatment and reuse for irrigation as alternative resource for water safeguarding in Souss-Massa region, Morocco

M. Malki[1*], L. Bouchaou[1], I. Mansir[1], H. Benlouali[2], A. Nghira[3] and R. Choukr-Allah[2]
[1] *Applied Geology and Geo-Environment Laboratory, Faculty of Sciences, Ibn Zohr University, BP 8106 Agadir, Morocco*
[2] *Salinity and Plant Nutrition Laboratory, Hassan II Institute of Agronomy and Veterinary Medicine, BP773 Agadir, Morocco*
[3] *Souss-Massa-Drâa Hydraulic Basin Agency, Agadir, Morocco*
[*] *e-mail: malki.mouna@gmail.com*

Abstract: The Souss-Massa basin river is an arid area located in Southern Morocco. The region is characterized by a very intensive agriculture. However, water resources overexploitation, succession of drought years and several sources of pollution constitute major challenges for compatibility between securing the existing activity and safeguarding the groundwater. In order to cope with water scarcity and attenuate the impacts on groundwater, policy makers encourage the reuse of treated wastewater as a substitute resource for agricultural practices. In fact, the Biological System in Tiznit based on Anaerobic, facultative and maturation lagoons is an effective treatment technology leading to a good quality effluent that complies with WHO guidelines to be used without restriction for irrigation. This successful practice in the south of Morocco demonstrates that water reuse can be reliable, commercially viable, socially acceptable, environmentally sustainable and safe. In this particular project, cereals, cooked vegetables, fodder crops (namely alfalfa) and fruit trees were irrigated. In this paper, costs, benefits, and added-value impacts of wastewater treatment reuse as alternative resources are presented. The case of the wastewater treatment plant of Tiznit is presented as a successful experience in the region on wastewater reuse with the irrigation of about 430 ha of several crops.

Key words: over pumping, water scarcity, water reuse

1. INTRODUCTION

Water is a major challenge for sustainable development, particularly in arid areas with modest water resources and increasing freshwater demand, caused by the population growth and the high demand of industrial and agricultural sectors. With climate change constraints and high anthropogenic pressure, the reuse of industrial and domestic wastewater can contribute to water resources safeguarding and reversing environmental damage from raw sewage discharges (Amraoui et al., 2010). In fact, greater water consumption is directly associated with increased wastewater generation that requires adequate treatment to prevent health risks and environmental degradation. For that reason, the field of wastewater treatment is experiencing a continuous development and the reuse of treated wastewater is considered as a good alternative resource, of varied uses, for water safeguarding, particularly in areas with high demand and low availability of natural resources.

Treated wastewater is nowadays world widely used for agricultural irrigation, industrial reuse, groundwater recharge, and potable water supply (Asano, 1998). However, it has been largely used in agriculture to its socio-economic implications, fertilization supply, and sustainable availability (Candela et al., 2007; Singh et al., 2011; Ribasl et al., 2010).

At Morrocan scale, treated wastewater reuse is adopted in some regions for different uses. We have for instance, the Gharb region (North-West Morocco) where the treated wastewater is used to recharge the aquifer in order to cope with sea water intrusion caused by overexploitation of groundwater. In the Kenitra Region, treated wastewater is used to irrigate forest Eucalyptus trees for dunes fixation and wood production (El Oualja, 2013). As well, at Marrakesh and Bensliman cities, treated wastewater is used to irrigate golf course. (Choukr-Allah,2013).

In Souss-Massa region as well, arid area with persistent water scarcity, the development of

reclaimed domestic wastewater reuse projects has recently emerged as a potential nonconventional resource to satisfy the increasing water demand (Choukr-Allah and Hamdy, 2005).

2. PRESENTATION OF STUDY AREA AND PROBLEMATIC

Souss-Massa, Southwestern Morocco, extends over 12,000 km^2 and is divided into Souss plain (4.150 km^2), Massa plain (1,600 km^2) and the Mountainous areas of high-Atlas and anti-Atlas (6,250 km^2) (figure 1). Climate is arid in the West and becomes semi-arid towards the east. Rainfalls are rare and irregular in time and space with an average precipitation of 250 mm/year in the plain and 500 mm/year in the mountain. And the evaporation is high with a potential superior than 2000 mm/year (Bouchaou et al., 2008).

In the last decades, the region has known a fast urbanization coupled with the expansion of economic activities, raising the pressure on the limited water resources on the area. In fact, Souss-Massa region is largely depending on agriculture for social and economic development which requires huge quantities of water. Indeed, total water resources of Souss_Massa basin river are estimated at 816 Mm^3, while total water demand is estimated at 1076 Mm^3, from which 90 to 95% are used in irrigated agriculture (Tagma et al., 2009). This has led to a water deficit exceeding 260 Mm^3 (Hirich and al. 2015). As a result, the aquifer has undergone a reduction of the piezometric level from 0.5 to 2.5 m/year causing saline intrusion in coastal areas, water quality degradation and threats to environmentally interesting areas (F.A.D, 2012).

3. WASTEWATER MANAGEMENT IN SOUSS MASSA RIVER BASIN

3.1 Wastewater collect

Although surface water resources in the Souss Massa basin are good on average, the streams water quality is considered critical downstream the urban discharges, and groundwater resources quality is ranging from good in the Souss water table to very poor in Tiznit and Chtouka water tables. The degradation of water resources has been induced by domestic, industrial and agricultural pollution (ABHSM, 2006).

According to the investigations conducted by the hydraulic basin agency of Souss-Massa in 2007, the urban area of Agadir is generating annually over 11872 tons of BOD_5, which represent about 68% of the total domestic pollution load of Souss-Massa Region.

Moreover, the industrial sector is participating as well to the total pollution load with about 71% of potential polluting industries located at the provinces of Chtouka-Ait Baha and Inezgane Ait Melloul (Cement plant and food industry). Taroudant city counts about 24% with the largest organic pollution load producted by the dairy industry (82% of BOD_5 and 77% of COD). The provinces of Tiznit and Agadir-Ida-Outanane register the lowest values with respectively 4% and 1% of potential polluting industries.

Agricultural pollution in Souss-Massa basin is mainly related to farming practices and livestock. Nitrate pollution resulting from agriculture depends on the practice of fertilization, irrigation mode and the use of pesticides (Malki et al., 2016 a&b). Consequently, to assess the agricultural pollution load, it is required to define varieties of crops in the area, quantities of applied fertilizers and pesticides, type of soil as well as the number of livestock.

In one hand, the spatial distribution of nitrate concentrations in the Souss-Massa basin makes evident the relation between nitrate pollution and the different agricultural practices. The figure 1 shows clearly that the irrigated areas with practices involving intensive use of nitrogen compounds, are registering high nitrate concentration (>50 mg/L). In addition, nitrate pollution is also affected by type and soil texture. Nitrate leaching is higher in shallow soils with light texture as it is the case of Chtouka and Massa's soil (sandy texture with a low clay content). The agricultural pollution load

based on the leached nitrogen amounts was estimated by the ABHSM to about 1511 Tons of nitrates per year.

In the other hand, the Province of Taroudant has registred a remarkable increase in livestock activity with an important pollution load evaluated by the agency to 1.04903 million kg/year of SM, 563353 kg/year OM, 63338 Kg/year N and 14433 Kg/year generated in 2007.

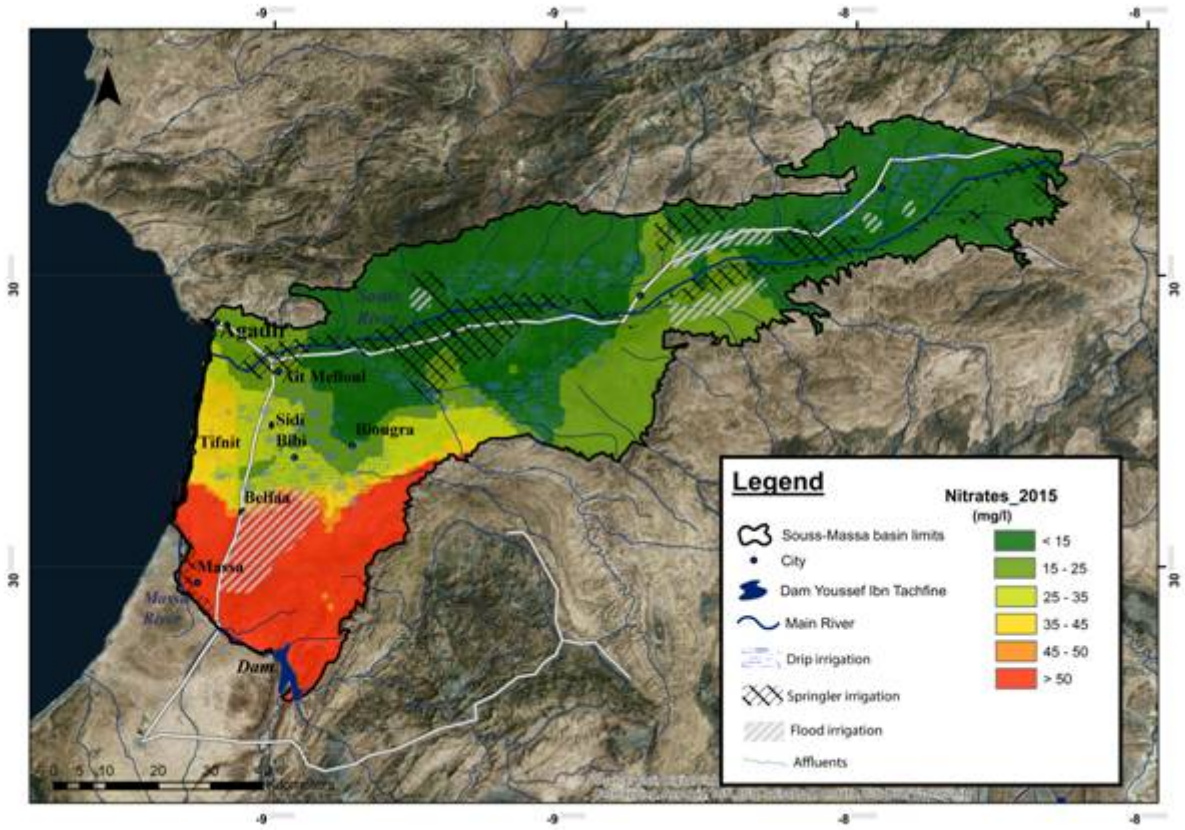

Figure 1. Spatial distribution of $N0_3$ contents related to irrigation mode used in Souss-Massa basin (Malki et al., 2016c)

3.2 Wastewater treatment

Liquid sanitation is a concern for both water managers and users. The region contains 6 main sewage treatment plants: 2 purification plants per infiltration percolation on sand and 4 sewage treatment plants by natural lagoon (figure 2). There are also special treatment plants such as Agadir-Massira airport plant, the station of Douar-Oulad-Mimoun in Chtouka, the plant of COPAG in Taroudant, and several other similar stations spread over different douars and communes of the region. As regards industrial wastewater, RAMSA has required manufacturers to set up a treatment system at the source and separate the brines before being discharged into the sewerage networks. Additionally, several sewage treatment plants are under construction in the Souss-Massa region, notably in Aourir and Anza.

The following table presents the important characteristics of the main sewage treatment plants of Souss-Massa region.

However, connection to the sanitation network remain relatively low in some cities such as Taroudant and Ouled Taima along with small centers like Massa, Sidi Ifni, Biougra, Ouled Barhil, etc., where only a part of the population (63% to 85% of Taroudant and Ouled taima population, respectively) are connected to the sanitation canal. The cities do not have an appropriate management of sewage, and wastewater is directly rejected without any treatment.

Table 1. Characterization of Main sewage treatement plants of Souss-Massa Region

Station name	Total Capacity	Purification rate	1st treatment	2nd treatment	Additional information
Bensergaou *(Fig. 2a)*	750 m^3/day	98 %	anaerobic lagoons	percolation infiltration	Infiltration through a sand filter
M'zar *(Fig. 2b)*			• Anaerobic phase • Capacity 75 000 m^3/day • Purification rate 60%	• Infiltration percolation • Capacity 10 000 m^3/day • Purification rate 96 to 99%	• Third treatment UV • Capacity of 30 000 m^3/day • Reduction of 1000 FC per 100 ml.
Drarga	650 m^3/day	98%	Infiltration-percolation	Infiltration-percolation	Tertiary treatment in a reed bed
Biougra *(Fig. 2c)*		21 000 Equivalent Habitant	Natural lagooning		
Ait Iaazza	200 L / s		Natural lagooning		
Tiznit *(Fig. 2d)*	5800 m^3/day		Natural anaerobic lagoon	Natural anaerobic in facultative basin	Tertiary treatment (12.21 days retention time in the maturation pond)

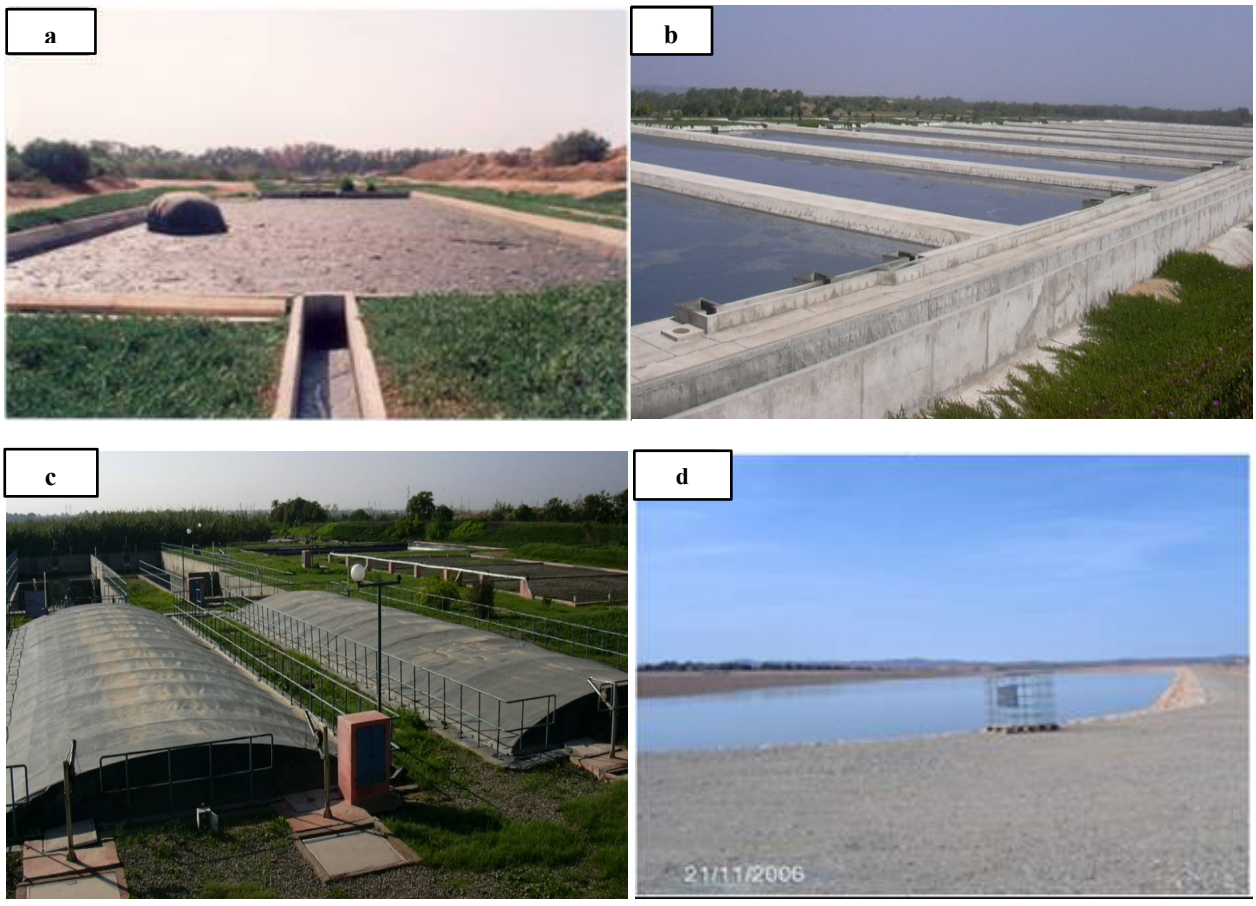

Figure 2. Treatment plant of (a) Bensergaou, (b)M'zar , (c) Biougra and (d) Tiznit. (Daoudi, 2011)

4. TREATED WASTEWATER REUSE IN SOUSS-MASSA REGION.

4.1 Potential of treated wastewater reuse in Souss-Massa region

The potential of treated wastewater is estimated to 50 Mm^3/year from which 60% is produced in Agadir (Choukr-allah et al., 2005).

Treated wastewater by Ben Sergao station is used for irrigation of golf courses and landscapes.

In Ait Melloul city, reuse is adopted for silviculture by the irrigation of 400ha of Argan forest using about 4 Mm^3/year of treated wastewater produced by the M'zar station (Benzine, 2012). As well, in Drarga city, the reuse is adopted for the irrigation of about 16 ha of some cereals, forage and vegetable crops using the drip irrigation system, recording an increase in the yield of the irrigated crop, which indicates the efficiency of treated wastewater reuse. This increase is mainly resulting from more supply of nitrogen, since the treated wastewaters contain already some fertilizing elements and allow the farmer to save fertilizes inputs (Choukr-Allah, 2003).

4.2 Wastewater reuse in agriculture: case study of Tiznit pilot project

Tiznit city is characterized by an arid climate with low and irregular rainfall coupled with prolonged drought sequences. The average rainfall is 150 mm/year. In this context, the protection of the resource becomes a priority concern in development programs, and the treatment and reuse of treated wastewater in agriculture is thus presented as a key solution. This allows exploiting a resource with additional water available at all times. Reducing operating costs by minimizing chemical fertilizer is also to consider (DPA, 2009).

4.2.1 Technical aspects

The wastewater treatment is located in the West side of Tiznit city, Southern part of Morocco (figure 1). It extends over 39 hectares and was first operated in 2006. The total cost of the plant was 41 Million MAD (3.8 Million Euros). Part of the cost (70%) was supported by ONEP through a German cooperation and the rest was paid by the municipality who offered the land (Daoudi, 2011).

For the implementation of this project, several steps have been taken. A monitoring committee was first created; led by the DPA. An agreement between all stakeholders, including the health department, was developed with well-defined responsibilities. Most of the farmers will use drip irrigation as a suitable technique to irrigate their crops, because of the water quality and low volume of water available. The government will subsidize 100% of the investment needed for drip irrigation system. 9 Million MAD (about 1 Million USD) was invested in the reuse project to pump the effluent to the irrigated areas and install the irrigation network. The hydro-agricultural development is funded by the Agricultural Development Fund (Choukr-allah, 2003)

The treatment plant was designed for an average flow of 4900 m^3 for the first phase and 5800 m^3 for the second phase. It is a natural lagoon system using a primary treatment (3.1 days retention time in an anaerobic basin), and secondary treatment (24.3 days retention time in a facultative basin), and a tertiary treatment (12.21 days retention time in the maturation pond).

Two locations are using the treated wastewater of Tiznit Plant. Downstream of the plant (Attbane) where treated wastewater could be conveyed by gravity, and in the upstream (Doutourga) where the effluent is pumped using a pumping station. The farmers of the areas were organized in agricultural irrigation associations in order to facilitate awareness programs on the best practices for reusing treated wastewater. The total of the farmers plots were 665 with average size of 0.65 ha (Chourk-allah et al. 2005).

The cropping system is based on fruit crops (olives & Pam trees), Cereals (Wheat & barley), vegetable crops and forage crops (Beans, cauliflower, Artichoke, alfalfa).

4.2.2 Qualitative evaluation

The quality of treated wastewater by Tiznit plant complies with the Moroccan standard laying down the specific limit values for domestic waste. According to the DPA directives for the classification of crops, this treated wastewater can be reused in irrigation for category B (Irrigation of cereal, industrial or fodder crops, pastures and fruit trees) and category C (Localized irrigation of

Category B crops in the absence of exposure of workers and public).

4.2.3 Added values of Tinzit pilot project

Within the Tiznit area, wastewater reclamation and reuse has contributed to the food security of the region by producing several crops for several years using treated wastewater. In Morocco, the inclusion of wastewater reuse in its National Water Strategy since 2000 signaled the placing of a high priority on the value of reclaimed water. The high-quality treated wastewater coming out of the treatment plant and being used to irrigate alfalfa and olive trees demonstrates the safe and effective use of reclaimed water in irrigating high-value crops.

This demonstrates that the reuse of treated wastewater in the region of Tiznit is reliable, commercially viable, socially acceptable, environmentally sustainable and safe. The direct beneficiaries from this project and its expansion are the farmers and society, whose income, standards of living and economic status were remarkably elevated, almost reducing unemployment and poverty.

The productivity of the lands irrigated with reclaimed water was substantial. In fact, the processed wastewaters bring fertilizing nutrients and save inputs and increase the yield of the crops.

5. CONCLUSION

Water is playing a central role in curbing poverty and supporting economic development and stability of several regions of Morocco. The water imbalance is becoming more severe throughout the years, worsened by climate change in the country. As a result, the government of Morocco implemented various projects in order to satisfy water demands by integrating wastewater reuses as an additional water resource. The local agriculture extension service provided a great support to the dissemination of the best practices for the reuse of treated wastewater and the precautions to prevent any health risks for the farmers and the consumers, as well as for the protection of the soil and groundwater deterioration.

The high competition between water use sectors are leading to the use of marginal water in Agriculture. Non-treated wastewater reuse is a common practice since 1980; because of the increasing water demand, the succession of dry seasons and increasing aquifer salinity. It is estimated that Tiznit, by the year 2020, will reuse 100% of the treated wastewater in the Agriculture sector.

REFERENCES

ABHSM, 2006. Pdaire: Étude de révision du plan directeur d'aménagement intégré des ressources en eau des bassins du Souss Massa, ABHSM, AGADIR

Amraoui F., Chlaida M. et Moutaib Z. (2010), Les eaux usées du grand Casablanca : Possibilité de traitement et de réutilisation en agriculture urbaine

Asano, T. (Ed.). (1998). Wastewater Reclamation and Reuse: Water Quality Management Library (Vol. 10). CRC Press.

Benzine L. (2012). Réutilisation des eaux usées épurées dans le bassin de Souss Massa. Journée de sensibilisation sur Les Potentialités et Perspectives de la Réutilisation des Eaux Usées Dans la Région du Sous Massa, Complexe Horticole d'Agadir,

Bouchaou, L., Michelot, J. L., Vengosh, A., Hsissou, Y., Qurtobi, M., Gaye, C. B., ... & Zuppi, G. M. (2008). Application of multiple isotopic and geochemical tracers for investigation of recharge, salinization, and residence time of water in the Souss–Massa aquifer, southwest of Morocco. Journal of Hydrology, 352(3), 267-287.

Candela, L., Fabregat, S., Josa, A., Suriol, J., Vigués, N., & Mas, J. (2007). Assessment of soil and groundwater impacts by treated urban wastewater reuse. A case study: Application in a golf course (Girona, Spain). Science of the Total Environment, 374(1), 26-35.

Choukr-Allah R (2003). Municipal wastewater reclamation and reuse: Moroccan experiences. In: hamdy A (ed) Advanced short course on sewage: treatment-practices-management for agriculture use in the Mediterranean countries Cairo, Egypt, 1993. pp 301-310

Choukr-Allah R. (2005) Wastewater treatment and reuse in Morocco: situation and perspectives. In: El Gamal F. (ed.) LNe, Bogliotti C. (ed.) , Guelloubi R. (ed) Options Méditerranéennes : Série B. Etudes et Recherches, vol 53. CIHEAM, Bari, Italy, pp 271- 287

Choukr-Allah R. (2013). Interventions to increased efficiency and effectiveness of treated wastewater reuse in Agriculture in the Mediterranean Region Paper presented at the International Conference on: Sustainable Water Use for Securing Food Production in the Mediterranean Region under Changing Climate, Agadir, Morocco, March 10 - 15, 2013,

Daoudi M. 2011. Optimisation De La REUE Dans L’agriculture : Cas De Tiznit. Séminaire international sur la reutilisation des eaux usees traitées dans la région arabe, RABAT 06 Juin 2011

DPA, (2009) Direction provinciale de l’agriculture de Tiznit, Direction epuration et reutilisation des eaux usees de la ville de tiznit a des fins agricoles pour l’irrigation des périmètres de Doutourgua et Attbane.

F.A.D, 2012 French Agency for Development (2012). Water demand management in the Mediterranean countries - Case study of Morocco. (Translated from French).

Hirich, A., Choukr-Allah, R., Rami, A., & El-Otmani, M. (2015). Feasibility of Using Desalination for Irrigation in the Souss Massa Region in the South of Morocco. In Recent Progress in Desalination, Environmental and Marine Outfall Systems (pp. 189-203). Springer International Publishing.

Malki, M., Bouchaou, L., Hirich, A., Ait Brahim, Y. and Choukr-allah, R. 2016b. Impact of agricultural practices on groundwater quality in intensive irrigated area of Chtouka-Massa, Morocco. Science of the Total Environment 574 (2017) 760–770

Malki, M., Choukr-allah, R., Bouchaou, L., Ait Brahim, Y., Hirich, A., et al., 2016a. Evolution of groundwater quality in intensive agricultural zone: case of Chtouka-Massa Aquifer, Morocco. Arab. J. Geosci. 9, 566.

Malki, M., Choukr-allah, R., Bouchaou, L., Hirich, A., Ait Brahim, Y. et al. 2016c. Assessment of Groundwater Quality: Impact of Natural and Anthropogenic Contamination in Souss-Massa River Basin. (eds.), The Souss-Massa River Basin, Morocco, Hdb Env Chem.

Tagma, T., Hsissou, Y., Bouchaou, L., Bouragba, L., & Boutaleb, S. (2009). Groundwater nitrate pollution in Souss-Massa basin (south-west Morocco).African Journal of Environmental Science and Technology, vol. 3, pp.10.

Proceedings of the 10th World Congress of EWRA 'Panta Rhei', 5-9 July 2017, Athens, Greece
© 2017 *European Water Resources Association*

Bioenergy water footprints, comparing first, second and third generation feedstocks for bioenergy supply in 2040

P.W. Gerbens-Leenes
Center for Energy and Environmental Studies, Faculty of Science and Engineering, University of Groningen, Groningen, The Netherlands
e-mail: p.w.leenes@rug.nl

Abstract: Freshwater is important for energy. Energy scenarios show increasing energy use, combined with increasing bioenergy shares. Bioenergy derives from *first (*food crops*), second (*energy crops or agricultural residues) and *third (*algae*) generation feedstocks*. There is an ongoing debate about the competition between energy and food crops. Energy crops have no direct competition with food, but an indirect one, using the same natural resources, like water. Crop residues seem a good alternative for food or energy crops. This paper gives water footprints (WFs) of first, second and third generation bioenergy (m^3/GJ). Next, it compares WFs of future energy demand using different bioenergy feedstocks. WFs of energy from residues is smallest, WFs of energy crops largest. Bioenergy from algae has the largest blue WF. From a resource-use point of view, impacts of green WFs on the environment are smaller than impacts of blue WFs. Comparing different bioenergy feedstocks, residues are most favorable. With increasing bioenergy production, impacts on freshwater also increase. It is expected that increased production of *first generation biofuels* heavily contributes to global water scarcity. For *third generation bioenergy*, the application of algae would substantially increase the global blue WF. Comparing IEA scenarios, the greenest scenarios have the largest WFs, due to large contribution of bioenergy (especially in the case of energy crops and algae). Feedstocks with a relatively small WF are crop residues. The potential is enormous, but large challenges remain concerning technical possibilities to convert residues into energy carriers in combination with the possibility that not all residues are available for bioenergy.

Key words: Water footprint; Bioenergy; First, second and third generation biofeedstocks

1. INTRODUCTION

Freshwater is an important resource to provide energy, especially bioenergy (Gerbens-Leenes et al., 2009; IEA, 2012). The most recent World Energy Outlook energy scenarios show an increase of total energy use, in combination with an increase of the share of renewables, especially of bioenergy (IEA, 2016). The IEA has developed three different energy scenarios for 2040 that all show an increase of total energy demand, but are based on different energy mixes (IEA, 2016). These scenarios are the current policies scenario (annual bioenergy use 77 EJ), the new policies scenario (annual bioenergy use 79 EJ) and the 450 scenario (annual bioenergy use 97 EJ). Bioenergy that derives from biomass needs large amounts of water in agriculture and forestry. Freshwater is a scarce resource, because most of the world's water is saltwater, only 2.6% is freshwater of which the largest part is stored in ice (Speidel et al., 1988). Agriculture, industry and domestic supply, with different quality standards for freshwater, are the main users. In 2000, agriculture accounted for 70% of total water withdrawals, industry for 20% and domestic withdrawals for 10% (Shiklomanov, 2000). Humans influence surface water distribution, for example by building large dams (Pekel et al., 2016) for hydropower, water storage for irrigation in agriculture, or flood control. The impacts of agriculture on freshwater availability are very large, because that sector uses large amounts of freshwater.

Biomass is a renewable energy feedstock, providing bioenergy carriers, like the biofuels bioethanol or biodiesel that are mainly applied for transportation, but also electricity, when used in a power plant, or heat when burned in a stove. Bioenergy includes the so termed first, second and

third generation bioenergy (Gerbens-Leenes et al., 2014). *First generation bioenergy* is energy from food crops. There is an ongoing debate about the competition between crops for energy and crops for food. *Second generation bioenergy* is energy from either energy crops or from agricultural residues. When energy crops are applied for energy, there is no direct competition with food, but an indirect one over the natural resource input, like water. Crop residues, leftovers from agriculture, seem a good alternative for food or energy crops. *Third generation bioenergy* includes energy from algae. The aim of this paper is to give an overview of water footprints (WFs) of first, second and third generation bioenergy (m^3 per GJ) and to show the consequences of a large scale introduction of bioenergy in the global energy system on water resources for 2040. The main research questions are:

- What is the average global consumptive (green, blue and grey) WF of first, second and third generation bioenergy types?
- What is the consumptive WF of the IEA 450 scenario for 2040 for first, second and third generation bioenergy types?

The next section, Section 2, gives the method and data sources applied for the assessment. Section 3 shows the main results. Section 4 provides a discussion on the limitations of the study. Finally, Section 5 concludes summarizing the main findings. This paper is based on earlier research into the WFs of first, second and third generation bioenergy. It compares WFs of different feedstocks from these earlier studies and the consequences for water if these feedstocks are applied on a global scale in the near future.

2. METHOD AND DATA

The six major crops that are relevant for biofuels are sugar cane, maize, cassava, oil palm, rape and soybean (Fischer et al., 2009). These crops use 338 million hectares of agricultural land or 22% of the total cultivated land area. Part of these crops is applied for biofuels, 25 million hectares of agricultural land or 1.6% of the total cultivated land area. Figure 1 shows the production chain of bioenergy. The biomass that forms the input for bioenergy includes food crops, residues from food crops, wood and other crops grown for energy purposes, such as miscanthus. Food crops, such as sugar cane, generate the so termed first generation bioenergy. The residues of food crops are the input for the so termed second generation bioenergy. The energy crops also generate second generation bioenergy. Algae form the input for third generation bioenergy. The bioenergy not only includes the biofuels, such as ethanol and biodiesel, but also electricity and heat.

For the overview of the WF of first, second and third generation bioenergy types, data on WFs of first generation biofuels were derived from Mekonnen and Hoekstra (2010). The most important crops that form the feedstock for bioethanol were included: sugar beet, sugar cane, potato, cassava, maize, barley, rye, paddy rice and wheat, as well as the main crops for biodiesel: palm oil, rapeseed and soybean. For second generation bioenergy, the study included residues from sugar beet, soybean, sugar cane, cassava, maize, wheat, paddy rice and rapeseed, as well as the energy crop miscanthus and the wood types pine and eucalyptus. Data on second generation bioenergy were derived from the study of Mathioudakis et al. (2017) into the WF of second generation bioenergy. The study also includes the WF of firewood. Data were derived from Mekonnen et al. (2015). For third generation bioenergy, bioenergy from algae, the study derived data on WFs of algae energy from Gerbens-Leenes et al. (2014).

When bioenergy is generated from food crops, carbohydrates or oils are extracted from the crop. These extraction yields can be used as food, or applied as the feedstock for the biofuels ethanol and biodiesel. The conversion is rather straightforward, because the crops already contain carbohydrates for ethanol or oil for biodiesel. Figure 2 shows that bioenergy can also be generated from residues or energy crops. The conversion is often more difficult and demands sophisticated technology (Cuellar and Straathof, 2015). When second generation bioenergy is produced, such as the biofuels bioethanol or pyrolysis oil, lignocellulosic feedstocks like straws, wood and stalks are converted to

fuel in processes like pyrolysis or fermentation. Pyrolysis is a thermochemical conversion process decomposing lignocellulosic biomass between 300 and 400°C, generating heat, volatile gases, pyrolysis oil and solid carbon (Basu, 2013). Pyrolysis oil has a relatively large oxygen content, larger than oil extracted from an oilseed crop, and therefore the energy content of pyrolysis oil is smaller than the energy content of first generation oils (Lehto et al., 2013). Biochemical conversion is a process in which bacteria or enzymes break down biomass molecules into smaller molecules (Basu, 2013). Another way of generating bioenergy is to convert the biomass directly into heat, or indirectly into electricity.

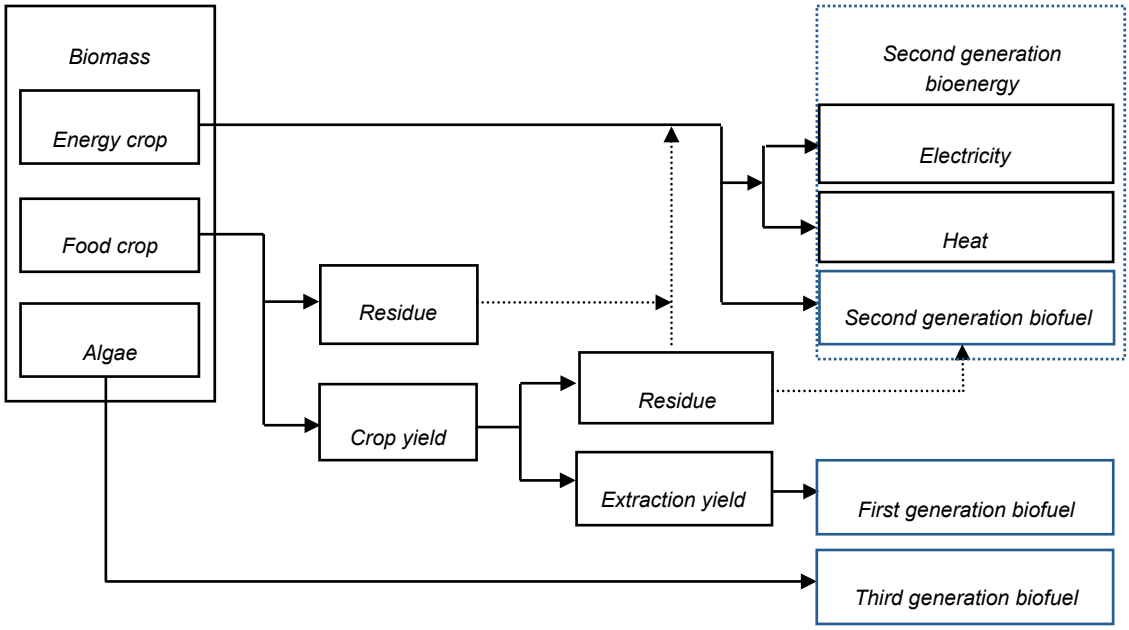

Figure 1. Production chain bioenergy generating first, second and third generation biofuels and bioenergy (electricity and heat)

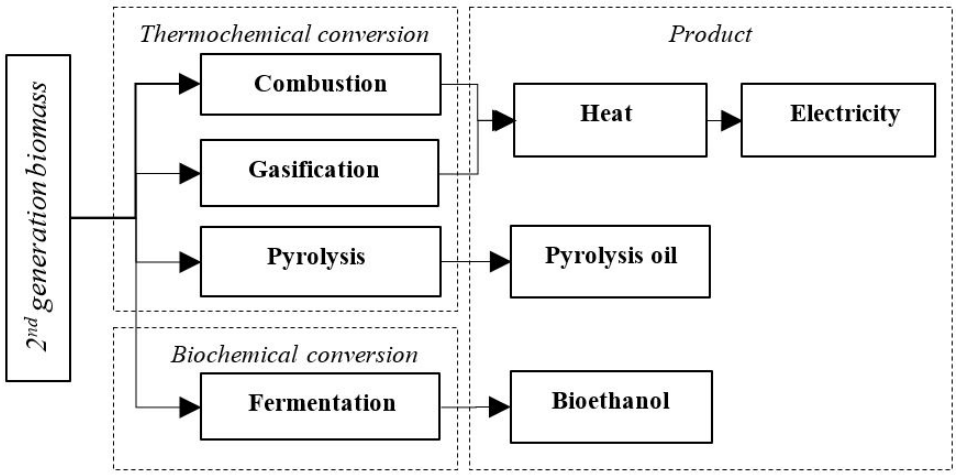

Figure 2. Conversion routes for second generation biomass feedstock

To estimate the WF related to future biomass use, the study calculated the global water consumption related to bioenergy use in 2040 based on the IEA scenarios (IEA, 2016). The IEA developed three different scenarios, the current policies scenario (annual bioenergy use 77 EJ), the new policies scenario (annual bioenergy use 79 EJ) and the 450 scenario (annual bioenergy use 97 EJ). For the estimation, the study combined bioenergy use according to the 450 scenario with average data on the WFs of first, second and third generation bioenergy. The total WF (WF_{total}, m^3/y) is estimated as:

$$WF_{total} = \sum_{s} \left(E \times WF[s] \right) \quad (1)$$

where E is the bioenergy demand (GJ/y) of the 450 scenario, and $WF[s]$ the average WF per unit of bioenergy produced from bioenergy source s (m^3/GJ). Next, the results were compared with the global average WF between 1996 and 2005. Data on the global average WF were derived from Hoekstra and Mekonnen (2012).

3. RESULTS

Figure 3 shows the global average water footprint (WF) of first generation biofuels in m^3 per GJ bioethanol or biodiesel. All WFs are dominated by the green WF, i.e. water from precipitation. The blue WF, i.e. water from irrigation, is relatively large for sugar cane, paddy rice and wheat. The grey WF is relatively large for potato and rapeseed. Figure 3 also shows that, in general, the WF of bioethanol is smaller than the WF of biodiesel. For bioethanol, total WFs range between 50 and 180 m^3 per GJ, for biodiesel total WFs are between 150 and 350 m^3 per GJ.

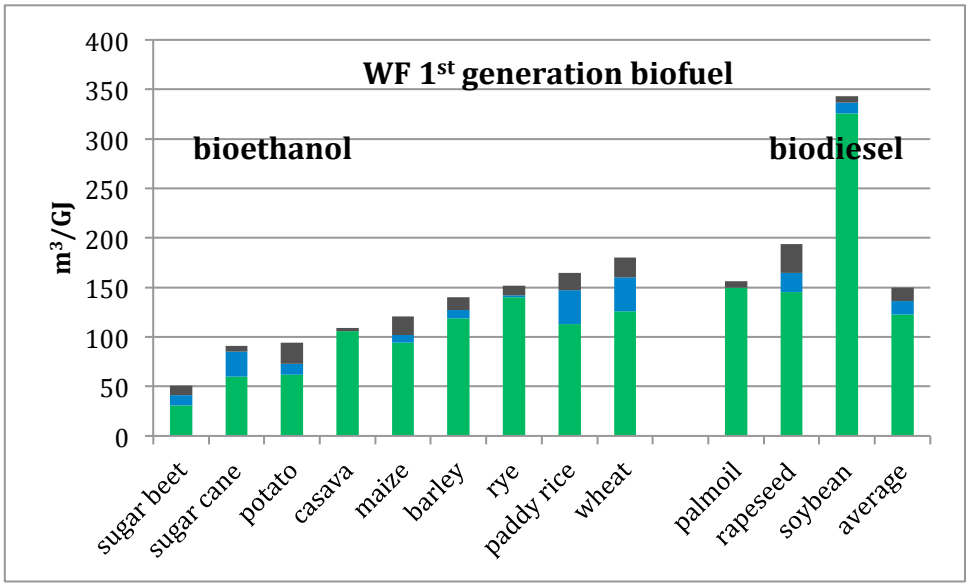

Figure 3. Global average water footprint of first generation biofuel in m^3 per GJ ethanol or per GJ biodiesel

Figure 4 shows the WF of second generation biofuels from residues in m^3 per GJ (average bioethanol and biodiesel). As could be expected, the WFs are also dominated by the green WF. Sugar beet shows the smallest WF, 7 m^3 in total, rapeseed has the largest total WF, 37 m^3. When Figure 4 is compared to Figure 3, we find that WFs for second generation biofuel from residues are much smaller than WFs of first generation biofuels. For sugar beet, for example, the difference is a factor of 7, for rapeseed a factor of 6.

Figure 5 shows the WF of second generation biofuel from energy crops in m^3 per GJ (average bioethanol, biodiesel and heat). The WF is only green. Especially the WF of bioethanol or biodiesel derived from pine is large, 350 m^3 per GJ, the WF of heat from firewood is relatively small and ranges between 19 and 100 m^3 per GJ with an average value of 60 m^3 per GJ.

Figure 6 gives an overview of WFs of first, second and third generation biofuels. First and second generation biofuels from residues are dominated by their green WF, but also have a blue and grey one, while second generation biofuels from energy crops only have a green WF and third generation biofuels from algae only have a blue WF. The WFs of biofuels from residues are smallest. The green WF of biofuel from energy crops is much larger than green WFs of the other biofuels. For biofuels from algae, the blue WF is largest.

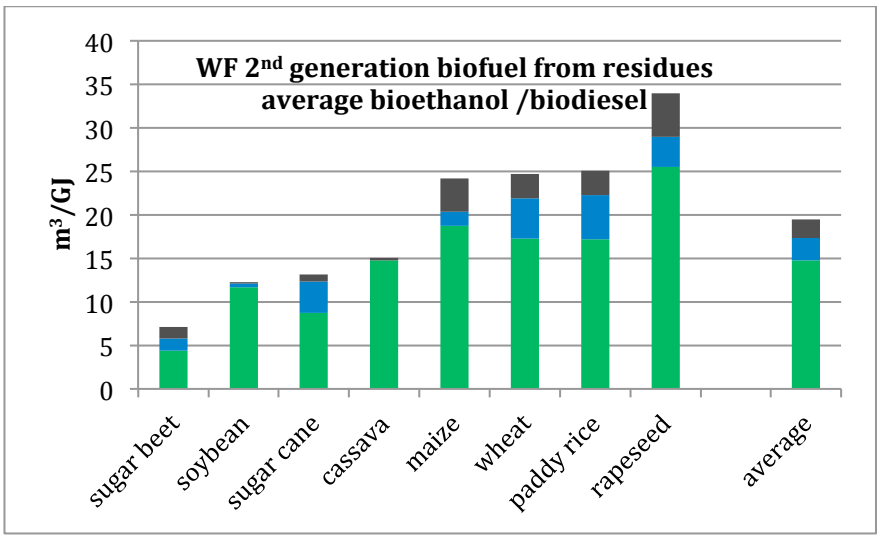

Figure 4. Water footprint of second generation biofuel from residues in m^3 per GJ (average ethanol and biodiesel)

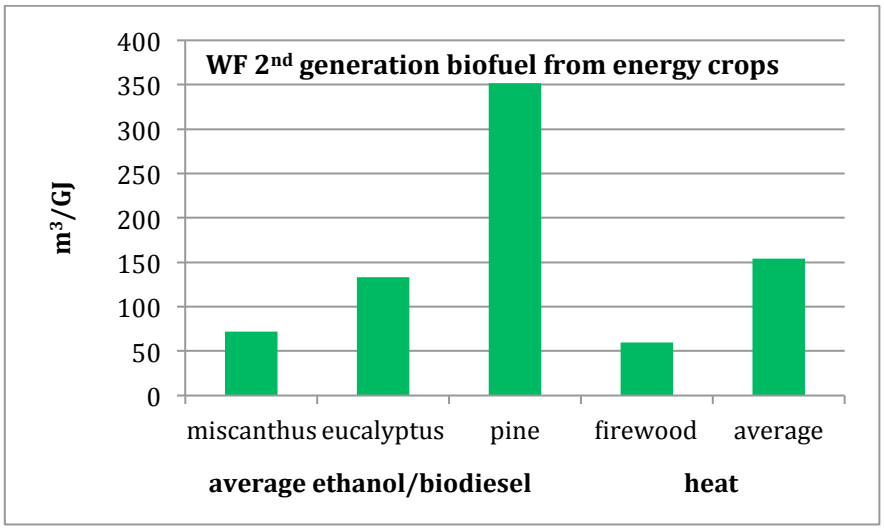

Figure 5. Water footprint of second generation biofuel from energy crops in m^3 per GJ (average ethanol, biodiesel and heat)

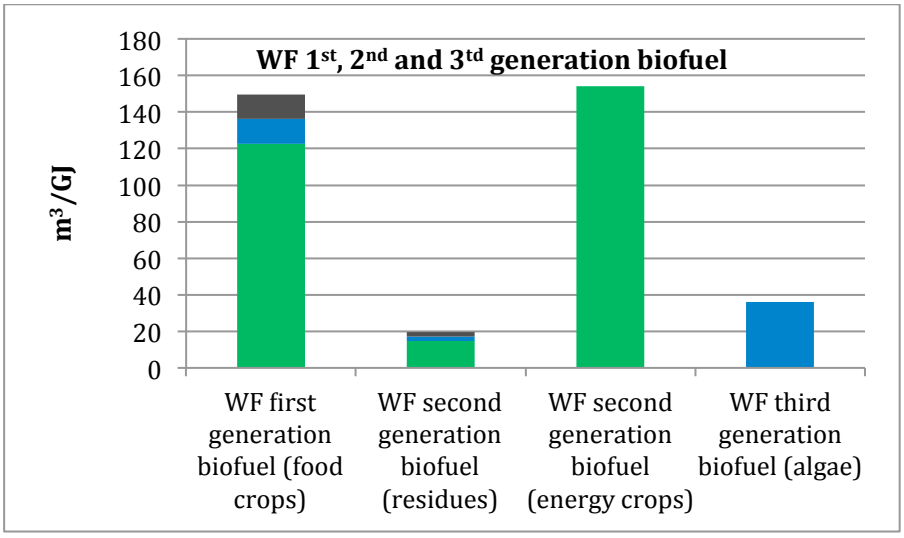

Figure 6. Overview of water footprints of first, second and third generation biofuel

Figure 7 shows the global WF of bioenergy in the IEA New Policies Scenario for 2040 together with the global average WF for the period 1996-2005. Between 1996 and 2005, the global average WF was 9,087 Gm^3 per year, of which 74% was green, 11% blue and 15% grey. This WF is completely dominated by agriculture, 92%. Crops require 7,400 Gm^3 per year and pasture 900 Gm^3 per year. Part of the crops is applied for energy purposes, for example sugar cane in Brazil is partly used as a feedstock for ethanol.

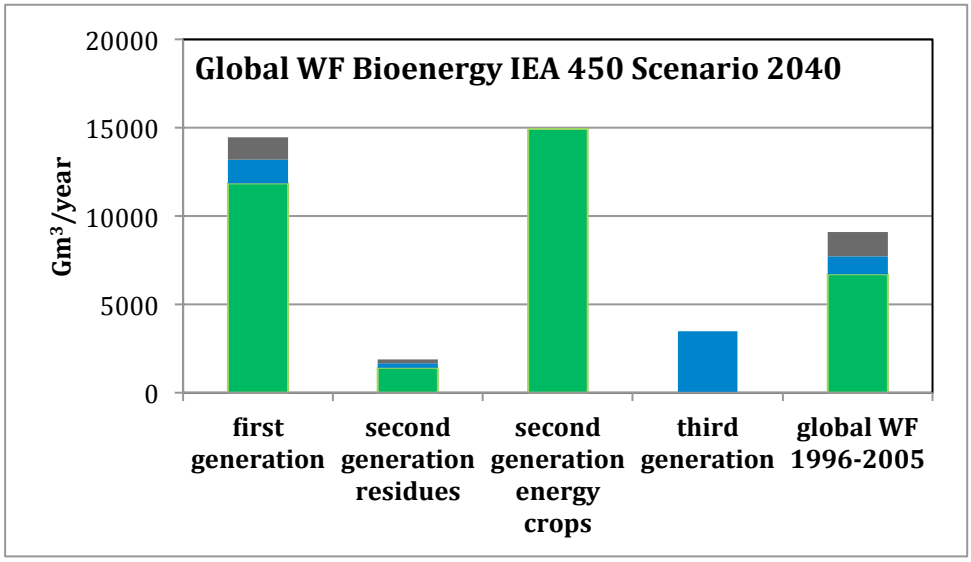

Figure 7. Global water footprint of first generation bioenergy, second generation bioenergy from residues, second generation energy crops and third generation bioenergy in the IEA 450 Scenario for 2040 and the average global water footprint in the period 1996-2005

In many regions of the world, water was already a scarce resource between 1996 and 2005. With the introduction of bioenergy in the IEA 450 scenario, the WF of bioenergy will exceed the global average WF from the end of the 20th and the beginning of the 21st century. When energy crops are applied, the green WF will exceed the average global green WF. For the third generation bioenergy, especially the blue WF might be problematic. The only option would be to use residues for bioenergy.

4. DISCUSSION

- The WFs of bioenergy were derived from existing literature. It is possible that when more detailed data become available, the WFs also change. However, large differences exist between the energy feedstocks, i.e. WFs of first generation feedstocks are much larger than WFs of second generation feedstocks from residues. Also, this WF contains not only a green component, but also a blue WF component related to irrigation and a grey one related to pollution. The WFs of second generation energy crops, like wood or miscanthus are relatively large. However, they only contain the green component. The data for the third generation feedstocks, algae, have been based on a limited amount of studies. Although other research might show more sustainable options to produce algae, the WF of algae feedstock is based on the application of blue water that has a larger impact on water scarcity than green water.
- Another issue is that the IEA scenario's with a large bioenergy contribution might not be realistic. Large contribution of bioenergy, as shown in this paper, requires a lot of fresh water that for some scenarios even exceeds present global water consumption. This might cause feedback mechanisms that cause a decrease of the use of bioenergy. Also, the energy mixes or total energy production might be different due to factors like shale gas development,

population characteristics or other growth scenarios than assumed by the developers of the IEA scenarios.

- The scenario using algae as a feedstock has a WF that is smaller than the WFs of scenarios using first generation feedstocks or second generation energy crops; however the WF is completely blue. Blue water use is even larger than present blue water use. This might also not be realistic. Another issue is the enormous land use related to algae production (Gerbens-Leenes et al., 2014) making this scenario problematic.
- The scenario applying crop residues is favorable in terms of WFs. The WFs of the residues were based on a WF recalculation in which the total WF of a specific crop was reallocated over the crop yield and the crop residue. This means that the total WF for agriculture does not increase. From this point of view, this scenario using residues is possible. However, this scenario depends on the availability of residues and the possibility to convert them into bioenergy. Globally the availability is huge (Montforti et al., 2013), but there are still technical challenges for the conversion into bioenergy and it is uncertain whether all these residues are really available for energy purposes.

5. CONCLUSIONS

When WFs of first, second and third generation bioenergy are compared, residues are the most favourable bioenergy feedstocks in terms of water use. The total WF does not increase when residues are applied for energy purposes. When crops are grown specifically for energy, food crops or energy crops, the WFs are large. Food crops have a green, blue and grey WF, while energy crops, such as miscanthus, are dominated by a green WF. The 450 IEA scenario for 2040 shows that when bioenergy from food crops is applied, the WF of the bioenergy exceeds the present global WF. Today, there is already water scarcity in many river basins. Therefore, the use of food crops for bioenergy is probably impossible. The use of bioenergy crops has a large demand for green water, also exceeding the present global green WF. For the third generation feedstock, algae, the blue WF exceeds the present blue WF. Using energy crops or algae for large scale energy supply might not be realistic from a water perspective. Only the use of residues for energy does not increase the WF, because all water was already allocated to the crops and the assessment has been based on a WF reallocation. The question remains whether the residues are really available for energy purposes.

ABBREVIATIONS

EJ Exajoule
GJ Gigajoule
IEA International Energy Agency
WF Water footprint

REFERENCES

Basu, P., 2013. Biomass gasification, pyrolysis and torrefaction: practical design and theory. Elsevier Science, San Diego, USA.

Cuellar, M.C., Straathof, A.J.J, 2015. Biochemical conversion: biofuels by industrial fermentation. In: De Jong, W., Van Ommen, J.R. (eds.), Biomass as a Sustainable Energy Source for the Future: Fundamentals of Conversion Processes. John Wiley & Sons, New Jersey, USA, pp. 403.

Fischer, H., Hizsnyik, E., Prieler, S., Shah M., Van Velthuizen, H., 2009. Biofuels and food security. International Institute for Applied Systems Analysis, Laxenburg, Austria.

Gerbens-Leenes, P.W., Hoekstra, A.Y., Van der Meer, T.H., 2009. The water footprint of bioenergy. Proc. Natl. Acad. Sci. 106, 10219–10223.

Gerbens-Leenes, P.W., Xu, L., De Vries, G.J., Hoekstra, A.Y., 2014. The blue water footprint and land use of biofuels from algae. Water Resour. Res. 50, 8549–8563.

IEA, 2012. World energy outlook 2012. International Energy Agency. Paris, France.

IEA, 2016. World energy outlook 2016. International Energy Agency. Paris, France.

Hoekstra, A.Y., Mekonnen, M.M., 2012. The water footprint of humanity. Proc. Natl. Acad. Sci. 109(9), 3232−3237.

Lehto, J., Oasmaa, A., Solantausta, Y., Kytö, M., Chiaramonti, D., 2013. Fuel oil quality and combustion of fast pyrolysis bio-oils. VTT Technol., 87, 79.

Mathioudakis, V., Gerbens-Leenes, P.W., Van der Meer, T.H., Hoekstra, A.Y., 2017. The water footprint of second-generation bioenergy: A comparison of biomass feedstocks and conversion techniques. J.Clean.Prod. 148, 571-582.

Mekonnen, M.M., Hoekstra, A.Y., 2010. The green, blue and grey water footprint of crops and derived crop products. Value of Water Research Report Series No. 47, UNESCO-IHE, Delft, the Netherlands. http://www.waterfootprint.org/Reports/Report47-WaterFootprintCrops-Vol1.pdf

Mekonnen, M.M., Gerbens-Leenes, P.W., Hoekstra, A.Y., 2015. The consumptive water footprint of electricity and heat: a global assessment. Environ. Sci. Water Res. Technol. 1, 285–297.

Monforti, F., Bódis, K., Scarlat, N., Dallemand, J.-F., 2013. The possible contribution of agricultural crop residues to renewable energy targets in Europe: A spatially explicit study. Renew. Sustain. Energy Rev. 19, 666–677.

Pekel, J.F., Cottam, A., Gorelick, N., Belward, A.S., 2016. High-resolution mapping of global surface water and its long-term changes. Nature. Letter. doi:10.1038/nature20584

Shiklomanov, I.A. 2000. World water resources and water use: present assessment and outlook for 2005. In F. Rijberman, ed. World water scenarios: analysis (Chapter 12). World Water Vision.

Speidel, D.H., Ruedisili, L.C., Agnew, A.F., 1988. Perspectives on Water: uses and abuses. Oxford University Press, New York, USA.

VIII. Groundwater Hydrology and Contamination

Proceedings of the 10th World Congress of EWRA 'Panta Rhei', 5-9 July 2017, Athens, Greece
© 2017 *European Water Resources Association*

Space-time modelling of aquifer level using novel geostatistical tools

E.A. Varouchakis*, P.G. Theodoridou and G.P. Karatzas
School of Environmental Engineering, Technical University of Crete, Greece
* *e-mail: evarouchakis@gmail.com*

Abstract: Space-time geostatistical approaches can improve the reliability of dynamic groundwater level models in areas with limited spatial and temporal data. Space-Time Residual-Kriging (STRK) is a reliable method for spatiotemporal interpolation that can incorporate auxiliary information. STRK is applied to combine the estimated trend and interpolated residuals for the final prediction of the groundwater level, while the uncertainty of estimations is determined using the STRK variance. The method though leads to an underestimation of the prediction uncertainty. Therefore, STRK variance is not usually applied for de-trended data that involve complex spatiotemporal trend functions. Spatiotemporal trend is approximated using a combined component based on a physical law that governs groundwater flow in an aquifer under pumping conditions. A Bayesian approach based on the bootstrap idea is employed to determine the uncertainty of the spatiotemporal model parameters (trend and covariance) and estimations. This stochastic modelling approach produce multiple realizations, rank the prediction results with respect to specified criteria, and captures the range of the uncertainty. The interdependence of the spatiotemporal residuals is modelled using a new space-time variogram based on the product-sum approach that involves the hydraulic conductivity anisotropic ratio within the exponential function. The proposed methodology is applied to predict spatiotemporal groundwater level fluctuations and to investigate the uncertainty of estimations at a sparsely gauged basin on the island of Crete, Greece.

Key words: space-time geostatistics, space-time variogram, Bayesian analysis, uncertainty, groundwater level

1. INTRODUCTION

Geostatitstical analysis has an important role in groundwater resources management, as with a limited dataset the aquifer level spatial or spatiotemporal distribution can be represented. Previous research has shown that the estimation of a spatial trend, that incorporates auxiliary information (e.g., topographic and geomorphologic features), improves the predictions of groundwater level (e.g. Varouchakis and Hristopulos, 2013). Therefore, the introduction of a spatiotemporal trend model for space-time geostatistical analysis of groundwater level would be an interesting approach to improve spatiotemporal predictions. The spatiotemporal trend applied in this work was approximated by involving a product of temporal and spatial components. The temporal trend was captured by using an exponentially weighted moving average filter whereas, for the spatial term a physical law, that governs the groundwater flow under pumping conditions, was applied. The latter is based on Thiem's equation for an unconfined aquifer.

The correlation of spatiotemporal residuals was modelled using the product-sum space-time variogram based on a modified exponential variogram component. Up to now, spatiotemporal covariance functions for groundwater level applications have not been established. However, spatiotemporal covariance functions that are based on physical ground have been developed and are mostly applied in atmospheric pollution and synthetic data. Such as, the Cressie-Huang models (Cressie and Huang, 1999), Gneiting's non-separable models (Gneiting, 2002), a series of non-separable models based on physical laws and dynamic rules reviewed in Kolovos et al. (2004) and non-separable models expressed through the spectrum density function instead of the direct covariance function (Porcu et al. 2008).

The space-time Residual Kriging (STRK) method was applied to combine the estimated trend and residuals for the final prediction of the groundwater level. The spatiotemporal trend variance

was investigated due to the complex nature of its calculation. The variance of the trend component is based on the predictors at the prediction location, the variance of the exponential weighted moving average filter for the temporal trend, and the variance of the Thiem's equation parameters. The aforementioned variance terms are necessary to be determined in order to calculate correctly the STRK estimations variance. Therefore, the Bayesian approach based on the bootstrap idea as described in Pilz and Spöck (2007) was applied for the characterization of the prediction uncertainty. This approach considers the uncertainty of the spatiotemporal trend parameters and of the estimated spatiotemporal covariance function.

The main objective of this study was to develop a new covariance function for groundwater level applications and to test its efficiency on spatiotemporal analysis. The second objective was the approximation of the water table spatiotemporal trend by developing a function that has a physical background. Finally, the third objective was the calculation of spatiotemporal uncertainty that has not been approached before with a methodology based on classical Bayesian analysis.

2. METHODOLOGY

Space-time geostatistical analysis and predictions proceed as follows: 1) approximation of the spatio-temporal trend, 2) Space-time variogram calculation of the residuals, 3) application of space-time residual kriging (STRK) for the prediction of fluctuations and trend at the desired locations, and 4) estimation of prediction accuracy. The above steps are presented next in detail.

A random field can be decomposed in trend and fluctuations. Therefore, the initial geostatistical analysis step is to approximate the spatiotemporal trend of the field data. The spatiotemporal trend approximation involves the separate temporal and spatial trend removal. For the first the exponentially weighted moving average filter (Pham 2006) was used on the mean bi-annual groundwater level at wells with available field data. This model was selected because it can provide discrete estimates of future groundwater level trends based on the previous period trend value and the groundwater level value of the desired estimation time step.

The spatial trend approximation is based on a physical law that governs the groundwater flow under pumping conditions. The analytical solution of a system of multiple wells in an unconfined aquifer was included in the spatial trend modeling. This component of the trend is based on Thiem's equation of an unconfined aquifer. The equation describes the relationship between the steady-state radial inflow at a pumping well and the drawdown,

$$H^2(\mathbf{s}) = H_0^2(\mathbf{s}) + \frac{1}{\pi K}\sum_{i=1}^{n} Q_i \ln\left(\frac{r_i}{R_i}\right), \quad r_i < R_i, \quad i = 1\ldots,n \tag{1}$$

where, $H(\mathbf{s})$ is the estimated hydraulic head, $H_0(\mathbf{s})$ is the initial hydraulic head before abstraction, K is the hydraulic conductivity, n is the number of wells (i=1…,n), $r_i = \| \mathbf{s} - \mathbf{s}_i \|$ is the distance of the estimation point from the i-th well, Q is the pumping rate, and R_i is the well's radius of influence. The pumping wells contributing in the equation are those whose distance from the estimation point does not exceed their radius of influence. When pumping tests are not available, R_i is determined using empirical equations, subject to available hydrogeological field data, i.e.,

$$R_i = 575\, s_{w,i} \sqrt{\hat{H}_{0,i}\, K_i} \tag{2}$$

where $s_{w,i}$ is the drawdown at the well face (m), K is the hydraulic conductivity around the pumping well and $\hat{H}_{0,i}$ (m) is the initial saturated thickness. The bottom of the saturation zone can be determined from geological cross-sections whereas, the top is obtained from the available head

measurements. The initial saturated thickness is herein assumed to follow the linear trend function. The variables $s_{w,i}$ and K are not known at every well so uniform values were used. The optimal $s_{w,i}$ is determined from a linear regression analysis of the mean annual groundwater levels of a 30 year period. The K value was determined from recent pumping test at selected wells (Varouchakis 2016).

The spatiotemporal trend was then obtained by multiplying the spatial with the temporal trend and dividing by the reference spatial trend to retain the original units. The spatiotemporal residuals are calculated simply by subtracting the groundwater level of each well at a specific time step from the corresponding spatiotemporal trend. The temporal trend remains constant for every time step while the spatial, varies according to the application of Thiem's law.

Groundwater level is part of the aquifer's saturation zone and describes the water table variation. Hydraulic conductivity is an important parameter that determines both groundwater flow and level in the saturation zone. It is an anisotropic parameter that usually varies significantly in the vertical direction. Therefore, the anisotropic ratio of the average hydraulic conductivity can be applied as a scale factor in front of the theoretical variogram model to control the fitting to the experimental variogram of the groundwater levels. According to hydrogeological literature, hydraulic head is defined by a differentiable function. Therefore, we apply an exponential variogram to describe the spatial and temporal dependence of the groundwater level residuals.

The experimental space-time variogram of the residuals is calculated using the method of moments and then modelled with a theoretical spatiotemporal variogram function. Herein, we apply the product-sum spatiotemporal variogram by means of the exponential variogram functions:

$$\gamma_{z_{s,t}}(\mathbf{r}) = \frac{K_z}{K_{x,y}}\sigma_z^2\left[1-\exp\left(-\frac{|\mathbf{r}_{s,t}|}{\xi_{s,t}}\right)\right] \tag{3}$$

where σ is the variance, ξ is a characteristic length, $\mathbf{r}$ is the lag vector in space and time and the K fraction is the anisotropic ratio. The product-sum variogram combines the use of separate spatial and temporal variograms under a non-separable function.

The product-sum space-time variogram (De Cesare et al., 2001; De Cesare et al., 2002) model is a generalization of the product and the sum model. It is defined as:

$$C_{ST}(\mathbf{r}_s, r_t) = k_1 C_S(\mathbf{r}_s) C_T(r_t) + k_2 C_S(\mathbf{r}_s) + k_3 C_T(r_t) \tag{4}$$

C_S, C_T are purely spatial and temporal covariance models with $k_1 > 0$, $k_2 \geq 0$, $k_3 \geq 0$. In terms of the variogram, the above equation is expressed as:

$$\gamma_{ST}(\mathbf{r}_s, r_t) = \left(k_1 C_S(0) + k_3\right)\gamma_T(r_t) + \left(k_1 C_T(0) + k_2\right)\gamma_S(\mathbf{r}_s) - k_1\gamma_S(\mathbf{r}_s)\gamma_T(r_t) \tag{5}$$

where γ_S, γ_T are purely spatial and temporal variogram models.

Then, the space-time Residual Kriging (STRK) method is applied as it combines a trend function for the data, obtained by an appropriate model, with the interpolation of the residuals. In order though to consider the estimations uncertainty of the whole proposed approach based on STRK, kriging variance and parameters uncertainty, the empirical Bayesian bootstrapping method was applied to perform a certain number of realizations.

Therefore, aquifer level and predictions uncertainty maps are developed to present the groundwater level distribution in the aquifer under study based on the spatiotemporal interdependence of the available data.

3. RESULTS

The proposed spatiotemporal geostatistical approach was applied to groundwater level data from the Mires aquifer in Crete, Greece. The dataset consists of bi-annual observations from 11 wells for the period 1981 to 2008. The spatiotemporal analysis considers the period 1981-2007 while, the last two periods were retained for the model validation.

Following the proposed spatiotemporal trend analysis, the space-time variogram of the residuals is applied. The fitting of the experimental variogram to the proposed spatiotemporal model is presented in Figure 1.

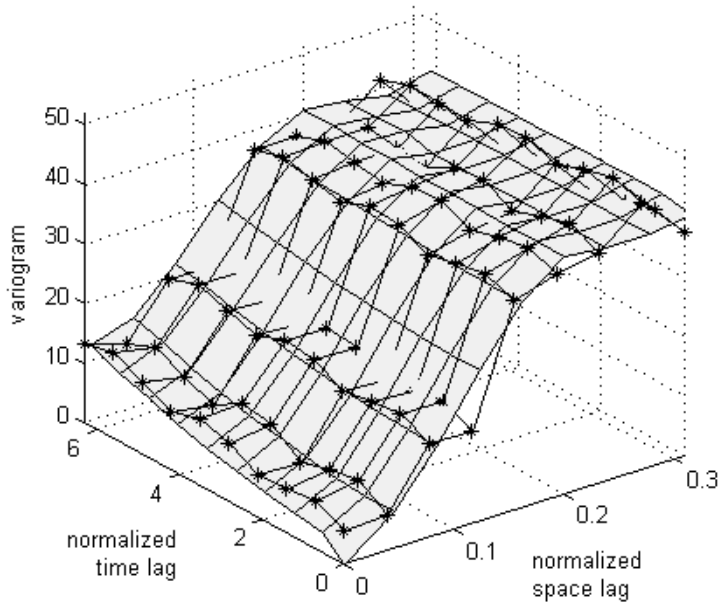

Figure 1. Space-time variogram fitting of the product-sum model to the experimental variogram.

The respective parameters of the variogram are: $\sigma_z^2 = 43.16$, $\xi_r = 0.27$ (≈ 3 km), $\xi_\tau = 0.94$ (≈ 12 months). The hydraulic conductivity anisotropic ratio for the study area was based on the available hydrogeological information that it decreases in the vertical direction by an order of magnitude compared to the horizontal direction.

Next, a validation process is applied to identify the efficiency of the estimations. The validation results are presented in terms of the Mean Absolute Relative Error (MARE) and the Mean Absolute Error (MAE) (Table 1). The first column presents the groundwater level estimation error for the wet period of hydrological year 2007-2008 while the second the estimation error for the dry period.

Table 1. Cross validation results of STRK methodology.

Cross Validation Metrics	2007-08 Wet period	2007-08 Dry period
MARE	0.11	0.14
MAE (m)	1.18	1.41

Finally, the interpolation maps (Figure 2) are derived using STRK with Bayesian bootstrapping. Results are presented for the wet period as they deliver lower validation error compared to those for the dry period.

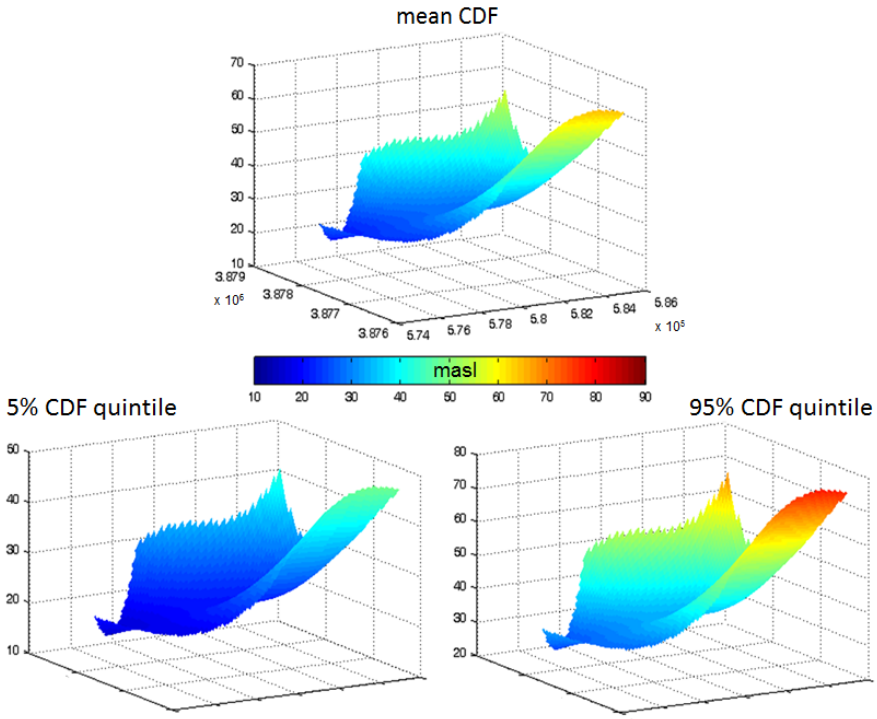

Figure 2. Estimation of the aquifer level (meters above sea level, masl) and of the uncertainty of predictions: 2007-08 Wet Period, at the levels of 5% and 95 %, CDF denote the cumulative distribution function.

4. DISCUSSION AND CONCLUSIONS

Reliable spatiotemporal modelling of the groundwater level is crucial for groundwater resources management, as it provides information for groundwater level spatiotemporal variability. STRK combined with the appropriate spatiotemporal trend and dependence functions provides a flexible and accurate approach for the stochastic modeling of groundwater level in sparsely gauged basins. This work presented an integrated approach for the interpolation of groundwater level data in sparsely monitored basins. The approach uses a new spatiotemporal trend model which involves the product of a temporal and of a spatial trend function. The product of temporal and spatial trend components is not new; however, the use of the exponentially weighted moving average filter for the temporal trend and of a spatial component based on a physical law that governs groundwater flow is.

The proposed physically based scaling factor provides a more stable theoretical variogram with an excellent fit to the experimental variogram leading to optimal parameter calculation for the prediction process with STRK. Therefore, the proposed variogram is a flexible new model for the estimation of the interdependence of groundwater level space-time data. In addition, STRK using the modified variogram structure provided accurate results. The incorporation of auxiliary information based on physical laws (e.g., Thiem's law) in the trend improves the interpolation accuracy by 26% compared to the plane space-time ordinary kriging. Finally, it was clearly identified that the Bayesian Bootstrap methodology provides a straightforward numerical framework for assessing the uncertainty of the spatiotemporal model parameters and of the groundwater level predictions.

REFERENCES

Cressie, N., Huang, H. C., 1999. Classes of Nonseparable, Spatio-Temporal Stationary Covariance Functions. J. Am. Stat. Assoc.; 94: 1330-1340.

De Cesare, L.D., Myers, D.E., Posa, D., 2001. Estimating and modeling space-time correlation structures. Stat. Probabil. Lett.; 51: 9-14.

De Cesare, L.D., Myers, D.E., Posa, D., 2002. FORTRAN programs for space-time modeling. Comput. Geosci.; 28: 205-212.

Gneiting, T. (2002). Nonseparable, stationary covariance functions for space-time data. J. Am. Stat. Assoc.; 97: 590-600.

Kolovos, A., Christakos, G., Hristopulos, D. T., Serre, M. L., 2004. Methods for generating non-separable spatiotemporal covariance models with potential environmental applications. Adv. Water Resour.; 27: 815-830.

Pham, H., 2006. Springer Handbook of Engineering Statistics, London: Springer-Verlag.

Pilz, J., Spöck, G., 2008. Why do we need and how should we implement Bayesian kriging methods. Stoch. Env. Res. Risk A.; 22: 621-632.

Porcu, E., Mateu, J., Saura, F., 2008. New classes of covariance and spectral density functions for spatio-temporal modelling. Stoch. Env. Res. Risk A.; 22: 65-79.

Varouchakis, E. A., Hristopulos, D. T., 2013. Improvement of groundwater level prediction in sparsely gauged basins using physical laws and local geographic features as auxiliary variables. Adv. Water Resour.; 52: 34-49.

Varouchakis, E.A., 2016. Integrated water resources analysis at basin scale: a case study in Greece. J. Irrig. Drain. E-ASCE; 142(3), 05015012.

Proceedings of the 10th World Congress of EWRA 'Panta Rhei', 5-9 July 2017, Athens, Greece
© 2017 *European Water Resources Association*

Artificial neural networks and particle swarm optimization based model for the solution of groundwater management problem

S. Gaur*, A. Dave, A. Gupta, A. Ohri, P.K.S. Dikshit and S.B. Diwedi
Department of Civil Engineering, Indian Institute of Technology (BHU), Varanasi, India
* *e-mail: shishir.gaur@gmail.com*

Abstract: Fulfilling the growing water demand, at domestic, industrial and agriculture level, is the most challenging task and groundwater plays the most important role for achieving this demand. In this scenario, proper management of groundwater resources is the most required act, as unmanaged groundwater extraction may cause shrinking of aquifer, sea water intrusion and water quality problems. The simulation-optimization approach is the most efficient way to solve any ground management problem where complex numerical models simulate the groundwater flow and/or contamination transport. The optimization model employs simulation for achieving the values of the groundwater head, velocity, concentration etc. This repeated use of the flow model increases the computational burden extensively and takes several hours to converge the final solution. In this study, Artificial Neural Network (ANN), Bagged Decision Trees (BDT) and Particle Swarm Optimization (PSO) models were developed and coupled for the management of groundwater resources. The Analytic Element Method (AEM) based flow model was developed and used to generate the dataset for the training and testing of the ANN model. These developed ANN-PSO & BDT-PSO models were applied to minimize the pumping cost of the wells. The results show that the ANN model can reduce the computational burden significantly and it is able to analyze different scenarios as well.

Key words: Groundwater Modeling, Groundwater management, Artificial Neural Network, Analytic Element Method, Particle Swarm Optimization

1. INTRODUCTION

The groundwater management problems are addressed by simulation-optimization approach. In the simulation-optimization process, simulation model is repetitively called by optimization model for generating head values of groundwater along with the velocity, concentration etc. The repetitive use of simulation models increases the computational burden extensively and it requires several hours to get the final solution. Different researchers (Rogers and Dowla, 1992; Johnson and Roger, 1995; Coppola et al., 2003;Singh et al., 2004) applied ANN modeling to substitute the numerical models. They applied ANN and optimization algorithm to solve different hydrological management problems and found this combination to be more fast and robust. ANN has been applied in the different areas of hydrology such as rainfall-runoff modeling, groundwater management, stream flow forecasting, ground-water modeling, water quality, water management policy, precipitation forecasting, hydrologic time series and reservoir operations, it was found that ANN based optimization model needs very less computational time and it is more flexible in comparison of mathematical programming methods. Arndt et al. (2005) approximated the results of finite-element based simulation model through ANN-computed predictions. The Study concluded that the value of the objective function at the simulation based optimal solution was only 1% better than the optimal solution obtained by the ANN. Nikolos et al. (2008) performed the study, by coupled ANN and differential evolution algorithm, to substitute the finite-element numerical model for water resource management problems. The study also concluded that the use of ANN as an approximation model could significantly reduce the computational burden and provide solutions very close to the optimal ones.

This paper examines the applicability of ANN-PSO & BDT-PSO based models to minimize the pumping cost of the wells, where the ANN & BDT model have been developed as a substitute of

AEM based groundwater simulation model. Both ANN & BDT models were trained and tested through dataset generated by AEM model. The results of ANN-PSO & BDT-PSO model have been compared with AEM-PSO model by applying both models on real field data for the aquifer of Dore river basin, France.

2. METHODOLOGY AND STUDY AREA

The presented study incorporates the strength of both the artificial neural networks and the optimization algorithms to solve the well field management problems. Intially, the groundwater flow model has been developed using analytic element method. Further, three scenarios have been taken by considering the set of four, five and six wells and AEM model has been used to compute the groundwater head with the given random discharges and co-ordinates for those set of wells. The random discharges of the wells have been generated for each scenario by using a random number generator that generates uniform random pumping rates within the range from $120m^3$/hr to $280m^3$/hr. Co-ordinates of the pumping wells have also been generated within the limit of study area by random number generator. Finally, the dataset for the training of ANN & BDT has been developed. The location and discharges of the wells have been taken as input and the groundwater head at the periphery of the well has been taken as output for ANN & BDT model. The database so generated is employed in training and testing the ANN's for all possible input ranges. Thus, the developed ANN & BDT models are integrated with PSO and used as a proxy simulator to AEM-PSO model for evaluation of the cost function. A penalty function method is used to handle the constraints in the optimization function. The optimal number of wells is determined by comparing the total cost of the system for all the 3 scenarios. Finally, the recommended management solution is validated using the AEM-PSO model. The major steps involved in the above procedure are explained in the following sections.

In the present study Dore river catchment, France has been taken as the study area. The developed models have been applied to fulfill the water demand of the city Thiers which is one of the major city of Loire region, France. The study area lies between $45^0$54'N to 46^0N latitude and $3^0$25'E to $3^0$29'10"E longitude. The average annual rainfall recorded at the rain gauge station of the basin is 780 mm. The major part of the area is covered by fluvial quaternary sediments underlain by marls and clay. The elevation of the bottom impervious layer of aquifer varies from 254 to 258 m from Mean Sea level (MSL). The location of the different hydrological features and other required data has been extracted from the geological maps 1/50,000 provided by BRGM (National Service for Geological Survey). Total 12 piezometric measurements are available in the study area, which shows the hydraulic gradient in the North direction.

3. OBJECTIVE FUNCTION AND CONSTRAINTS

The objective of the study is to minimize the total cost for the new pumping wells. The different parts of the cost function have been defined below.

(a) Well Installation Cost: the well construction have five separate steps. These include drilling, installing the casing, installing the well screen, installing the filter pack, grouting and well development. In the simplest form the well installation cost can be expressed as,

$$C_{wi} = A_1 N_w \tag{1}$$

where A_1 is the total cost for single well installation which includes the cost of drilling, casing, well screen, filter pack, sealing and well development; N_w*is* the total number of wells. In the above equation all the wells have been considered of the same depth and diameter. Therefore the cost of each well has been taken constant and the total cost can be calculated by multiplying the installation cost of one well by number of wells.

(b) Piping Cost: In this study, piping length has been considered from wells to reference location only and all pipes have been considered with the same diameter and material. The piping cost can be given as

$$C_{pn} = A_2 \sum_{i=1}^{N_w} L_i \tag{2}$$

where L_i = pipe length for i^{th} well and A_2 = total cost for the development of per meter pipe network which includes the cost of earthwork, cost of pipes, joining separate pipe sections together by welding, applying an outer insulation, and lowering the pipeline into the trench.

(c) Pumping Cost: The major factors that influence the pumping cost depends upon the volume of the water to be pumped, weight density of the water, hydraulic head, efficiency of the pump and energy cost (Sharma and Swamee, 2006; Moradi et al, 2003). Total cost of pumping ($C_p$in euros) consists of the cost of pump units (C_{pu} in euros) and the capitalized electricity cost (pumping cost) (C_{pE} in euros) including the annual repair and maintenance cost and hence can be expressed (Swamee and Sharma, 1990a; Swamee, 1996) for a single well as

$$C_{pi} = C_{pu} + C_{pE} = k_P \frac{\gamma Q H}{\eta} + \frac{8.76 R_E \gamma Q H r_T}{\eta} \tag{3}$$

$$\text{where, } r_T = \frac{(1+r)^T - 1}{r(1+r)^T} \tag{4}$$

γ = weight density of the fluid (N/m^3); H = pumping head (m), which is equal to the head from water table in aquifer to the height of storage tank including head losses in pipes; η= combined efficiency of the pump and the prime mover; R_E = the cost of the electricity per kilowatt-hour (euros/kwh); r = the rate of interest expressed as "euros per euros per year" (euros/euros/year), T= life of the project in years. For the long life of the project (T→∞) Equation (4) gives $r_T=1/r$. The same pump unit was adopted for each well, therefore it was not included in the optimization function. Thus the total pumping cost can be expressed as

$$C_p = \sum_{i=1}^{N_w} \left(\frac{8.76 R_E \gamma Q_i H_i r_T}{\eta} \right) \tag{5}$$

where Q_i is the potential discharge from i^{th} well. i = 1, 2…….. N_w. As the well installation cost is constant for all the wells, it is not included in optimization process but is used to calculate the overall cost of the pumping system. Thus, the objective function for this problem is as follows,

$$Minimize \left\{ \sum_{i=1}^{N_w} \left(A_2 L_i + \frac{8.76 R_E \gamma Q_i H_i r_T}{\eta} \right) \right\} \tag{6}$$

subject to

$$Q_{i,\min} < Q_i < Q_{i,\max} \tag{6a}$$

$$\sum_{i=1}^{N_w} Q_i > Q_{total} \tag{6b}$$

$$h_i > h_{i,\min} \tag{6c}$$

$$(x_i, y_i) \neq A_i \tag{6d}$$

$$\sqrt{\left(x_i - x_j\right)^2 + \left(y_i - y_j\right)^2} \geq S_{w,\min} \tag{6e}$$

where $Q_{i,min}$ and $Q_{i,max}$ are the minimum and maximum discharge limit for i^{th} well, $h_{i,min}$ = minimum allowable head of groundwater at i^{th} well, $S_{w,min}$ = minimum distance between any pair of wells; x_j and y_j are co-ordinates of remaining well i.e. $i \neq j$.

The first constraint has been taken as to limit the drawdown of the groundwater under permissible limit.

$$h_i > 253 \text{ m} \tag{7}$$

where $h_i$is the minimum water head on the periphery of the ith well and i = 1, 2…., N_w.

The second constraint is related to the minimum water discharge from all the wells. This constraint has been fixed on the basis of minimum water demand of the area and taken as 820 m^3/hr, and hence

$$Q_{tot} > 820 \text{ m}^3/\text{hr} \tag{8}$$

The third constraint prescribes the maximum and minimum discharge limits of the single well. On the basis of aquifer properties and availability of pumps, the discharge limit has been selected as follows

$$120 \text{ m}^3/\text{hr} < Q_i < 280 \text{ m}^3/\text{hr} \tag{9}$$

The forth constraint incorporates the minimum distance between the wells. By considering the local practices and to provide the protective zone around the wells a minimum distance of 100 m between any two wells has been considered.

4. MODEL DEVELOPMENT

AEM is a computational method based upon the superposition of analytical expression to represent the two dimensional vector fields. Each type of analytic element can simulate different types of geohydrological features (extraction wells, rivers, infiltration areas, aquifer inhomogeneities and other features). In this study, ground water flow model based on Analytic element theory is developed by MATLAB 7.0 and applied on the case study (Gaur et al., 2011).

The ANN structures are generally capable of identifying complex nonlinear relationship between input and output data sets (Maier and Dandy, 2000; ASCE Task Committee on Application of Artificial Neural Networks in Hydrology, 2000a). It can be considered as a universal function approximator. To design the architecture of ANN, a trial-and-error procedure suggested by various researchers (Atiya and Ji 1997; Morshed and Kaluarachchi 1998) have been used in this study. The back-propagation with Levenberg-Marquardt (L-M) technique was used to train the ANN model. The sigmoid transfer functions ‘tansig’, log-sigmoid ‘logsig’ and linear ‘purelin’ have been chosen for transfer functions of both the hidden layer and the output layer.

Only one hidden layer has been used. Similar to the neural networks, the decision trees are popularly used for various machine learning applications. The individual decision trees are highly sensitive to noise in its training dataset. The trees that grow very deep may learn a highly irregular pattern, but they are sensitive to overfitting thus, lead to low bias, but very high variance. Rather than taking output from just a single tree, the output from multiple trees can be taken. But training

multiple trees from same dataset could give strongly correlated trees or may even give the same tree. To avoid this problem Bagging Technique is used.

Bagging or Bootstrap aggregating (proposed in 1994 by Leo Beriman) is a machine learning technique used to improve accuracy and stability of machine learning algorithms. In order to improve the accuracy of decision trees, it combines results from different trees trained using randomly generated dataset. Thus, the trees get de-correlated. Given a training dataset of samples N, bagging generates $\mathcal{M}$ new datasets of size S, by taking samples from dataset uniformly with replacement.Now $\mathcal{M}$ decision trees are trained for these new $\mathcal{M}$ datasets and output is decided by the average of all the trees. This same concept of sample bagging can be extended on the features also thus rather than selecting all the features at the same time only a fraction of features can be selected to further avoid correlation. The performance of both the models has been measured by calculating the value of the coefficient of correlation (R) and Normalized Root Mean Squared Error (NRMSE). The plots of all wells are similar therefore graph of only well 1 has been shown here. Figure 1 shows the plot between NRMSE and number of neurons. The optimum number of neurons was taken as 39 for 15 input features in ANN model. Whereas, figure 2 shows plot between NRMSE and number of trees. The optimum number of trees was found out to be 105, in BDT model, for the 15 input features model. In this model, fraction of data used by each tree (considering replacement) from the data present in the training set was also varied.

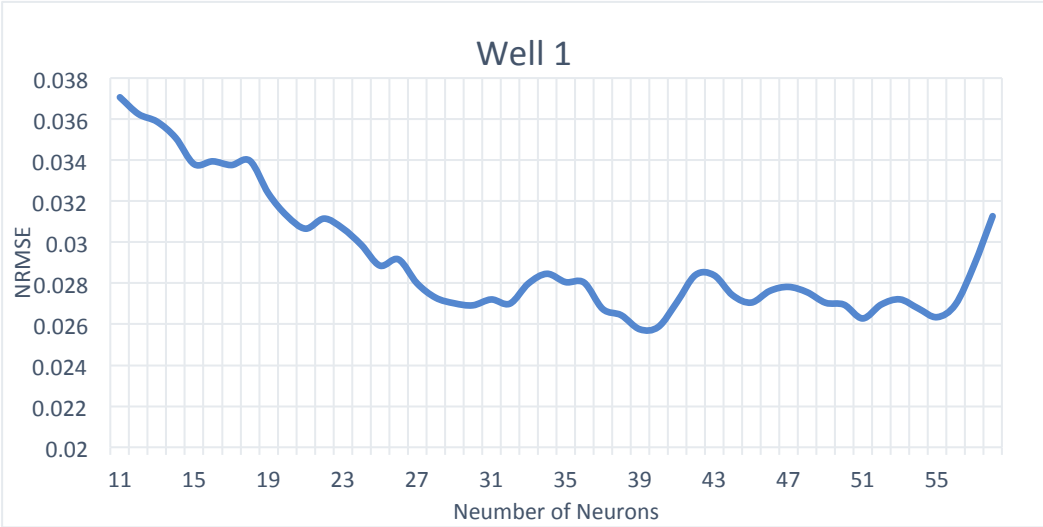

Figure 1. Shows plot of NRMSE v/s Number of Neurons.

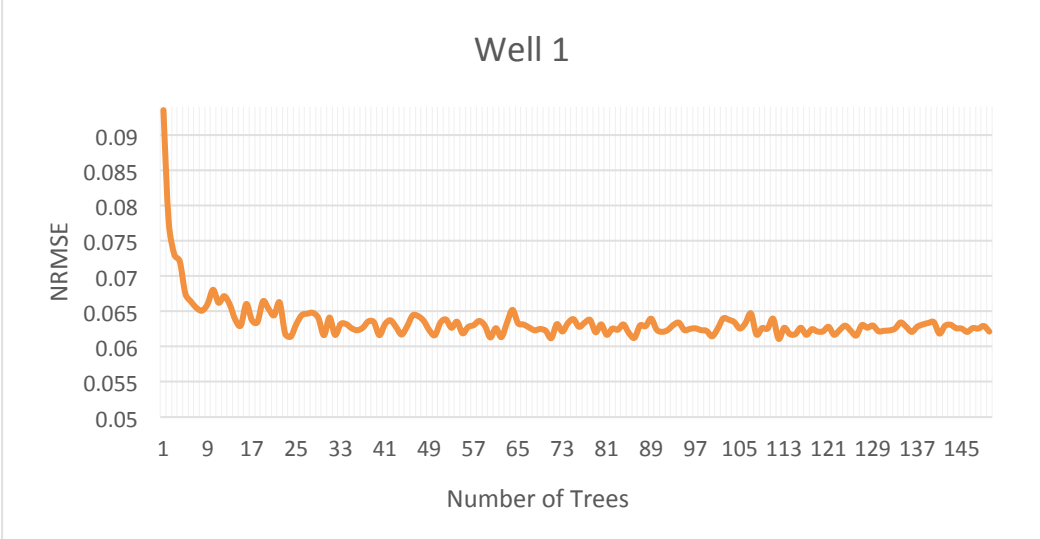

Figure 2. Shows plot of NRMSE v/s Number of Trees.

5. MODEL APPLICATION

The ANN and BDT models were developed and trained for a specific area which had the highest probability for occurrence of well. This specific area was obtained from the results of the AEM-PSO model. The training and testing dataset for both the models have been generated with the help of AEM model. In this process, 2000 set of random discharge and location of wells, i.e. pumping patterns, were generated by random number generator. Further AEM model was used to compute the groundwater head for generated data set. Therefore, 15 input variables,which consist of coordinates (x, y) and the discharge (Q) of all the five wells, and corresponding groundwater head were used for the training and testing of ANN and BDT models. Finally, to minimize the cost of all five wells, PSO has been combined with ANN and BDT models. Two modifications have been done to overcome this problem and increase the efficiency & accuracy of these models.

Firstly, the velocity term of PSO models has been modified to deal with the decision variable of the well coordinate. The decimal number values generated by the velocity term generally increase the iteration of PSO models exceptionally, especially in the case of optimal location. To deal with this problem, restrictions have been put on velocity term for integer number and 'units position' rounded up to 5 or 10 accordingly. This implies that from each previous location, new search location will be at least 5 m away. The number of iterations got reduced significantly due to this modification. An examination has been done on a set of 5 wells.It was observed that the modified model got converged in less than 1000 iterations whereas the normal AEM-PSO took more than 2500 iterations to converge the model.

Secondly, modifications were done in ANN model to improve its accuracy and efficiencies. Additional input features were introduced in the models which consisted of the distances of the concerning well from the remaining wells. From the results obtained, significant improvements were seen in the model as the NRMSE value was found to be lower than the previous case. It was also observed that with the increase in the number of input features from 15 to 19, the number of neurons in the hidden layer required for the ANN model reduced notably. It was observed that the optimum no. of neurons was 36 for 19 input features ANN model. The similar trends were observed in case of BDT model. The number of trees required for the model decreased with the increase in the number of input features. For BDT model with 19 parameters, optimum number of trees was found out to be 85.

Three different scenarios have been developed for finding out the optimal well location and discharges. The increment in the number of wells has also been done in a systematic way from one scenario to the other. In each scenario, total 15 (4+5+6) neural networks are constructed, one ANN for each well. The coefficient of correlation (R) and NRMSEare used to measure the performance of the developed ANN and BDT. It is discovered that as the number of pumping patterns increase, the coefficient of correlation for both the ANN model and BDT model increases, however, after a certain limit the accuracy remains almost constant. It is observed that even though the pumping patterns increase beyond a certain value, the coefficient of correlation does not further increase. Thus, 1400 and 1150 pumping patterns have been found suitable for the 15 input features and 19 input features model, respectively .The integration of these developed models is done with PSO model to further determine the optimal pumping cost for the considered problem. In the first stage, Models have been operated for 1000 iterations, but they converged after 842, 935, and 984 iterations for the set of 4, 5, and 6 wells respectively. The PSO models are said to converge if its objective function value does not change for 50 iterations. The models have been operated for 1000 iterations in the second stage but it converged after 753, 793 and 923 iterations for the set of 4, 5, and 6 wells respectively.

A total of fifteen runs have been done for each set of wells. Out of these runs the value that comes out to be minimum, has been considered as the optimal solution. It is further found that the set of five wells is likely to get more optimal rates in comparison of the set of four and six wells. The optimal cost by AEM-PSO, ANN-PSO and BDT-PSO models is shown in Figure 3.

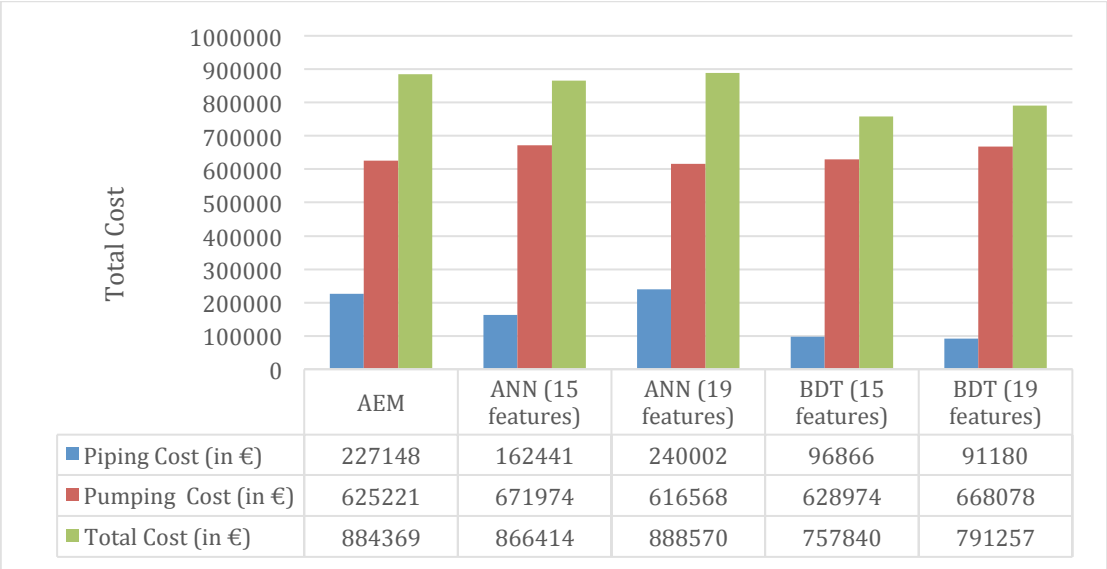

	AEM	ANN (15 features)	ANN (19 features)	BDT (15 features)	BDT (19 features)
Piping Cost (in €)	227148	162441	240002	96866	91180
Pumping Cost (in €)	625221	671974	616568	628974	668078
Total Cost (in €)	884369	866414	888570	757840	791257

Figure 3. Optimal cost by AEM-PSO, ANN-PSO and BDT-PSO Models

Final optimal cost by ANN-PSO model for the set of five wells is 888570 Euros for 19 input features model comprising of 616,568 Euros for pumping, 240,002 Euros for piping, 20,000 Euros for well installation and 12,000 Euros for pumping unit and that for BDT-PSO model is 791,257 Euros for 19 input features model comprising of 668,078Euros for pumping, 91,180 Euros for piping, 20,000 Euros for well installation and 12,000 Euros for pumping unit. It has been found that the total length of all pipes, from reference location by ANN-PSO (19 input features) is 5% more than the total length found by AEM-PSO model. It can be concluded from the results that the 19 input features ANN-PSO model is capable to produce the results near to AEM-PSO model whereas the results from other three models are inferior to the result of AEM-PSO model.

The major advantage of the ANN-PSO model that has been found is that it reduces the computational time. Where the AEM-PSO model approximately takes 5-6 hours for 700 iterations of model convergence, ANN-PSO model takes only 4-5 minutes and BDT-PSO takes 10-12 minutes (when run in intel core i7 processor) for the same number of iterations.

6. SUMMARY AND CONCLUSIONS

In this study, the AEM based simulation model was approximated to ANN & BDT models which were later combined with PSO algorithm to minimize the pumping well cost. The cost of ANN-PSO model is found to be 2% more and 0.5% less (in case of 15 & 19 input parameters respectively) than the cost obtained from AEM-PSO model. Whereas the cost of BDT-PSO model is found to be nearly 14% less and 10% less (in case of 15 & 19 input parameters respectively) from the cost of AEM-PSO model. Even though cost in case of BDT-PSO model is minimum, it is not in accordance with the AEM-PSO model as it fails to account interference. The result obtained from ANN-PSO models was found close to the result of AEM-PSO model with the error of 1%. Whereas, the results obtained by BDT-PSO models were found to be more inferior to the results of AEM-PSO model with error of 10%. It was found that number of iterations for the convergence of ANN-PSO models is less in comparison to the BDT-PSO. This ANN model for the area was successful in accounting well interference and also required fewer amounts of data for training.

REFERENCES

ASCE Task Committee on Application of Artificial Neural Networks in Hydrology. 2000a. Artificial neural networks in hydrology. I: Preliminary concept. Journal of Hydrologic Engineering; 5-2; 115–123.

Atiya, A., Ji, C., 1997. How initial conditions affect generalization performance in large networks. IEEE Trans on Neural Network; 8; 2; 448-451.

Coppola, E., Poulton, M., Charles, E., Dustman, J., 2003. Application of Artificial Neural Networks to complex groundwater management problems. International Association for Mathematical Geology; 12; 4; 303–320.

Gaur, S., Chahar, B.R., Graillot, D., 2011. Analytic Elements Method and Particle Swarm Optimization based Simulation-Optimization Model for Groundwater Management, Journal of hydrology; 402 (3-4), 217-227.

Johnson, V.M., Rogers, L.L., 1995. Location analysis in ground-water remediation using neural networks. Ground Water; 33; 5; 749-758.

Maier, H.R., Dandy, G.C., Neural networks for the prediction and forecasting of water resources variables: a review of modelling issues and applications. Environmental Modelling and Software; 15; 1; 101-123.

Math Works Inc..2001. MATLAB V R2009a, Apple Hill Drive, Natick, Massachusetts, USA.MathWorks, Inc., 2001. MATLAB. 3 Apple Hill Drive, Natick, Massachusetts, USA.

Morshed, J., Kaluarachchi, J.J., 1998a. Application of artificial neural network and genetic algorithm in flow and transport simulations. Advances in Water Resources; 22; 2; 145-158.

Moradi, J.M., Marino, M.A., Afshar, A., 2003. Optimal design and operation of irrigation pumping station. Journal of Irrigation and Drainage Engineering; 129; 3; 149 154.

Nikolos, I.K., Stergiadi, M., Papadopoulou, M.P., Karatzas, G.P., 2008. Artificial neural networks as an alternative approach to groundwater numerical modelling and environmental design. Hydrological Processes; 22; 3337–3348.

Rogers, L.L., Dowla, F.U., 1992. Groundwater remediation optimization with artificial neural networks and the genetic algorithm (abstract). Eos. Trans. AGU, Fall Meeting; 73; 43; 186.

Rogers, L.L., Dowla, F,U., 1994. Optimization of groundwater remediation using artificial neural networks with parallel solute transport modeling. Water Resources Research; 30; 2; 457–481.

Sharma, A.K., Swamee, P.K., 2006. Cost Considerations and General Principles in the Optimal Design of Water Distribution Systems. ASCE Conference Proceeding; 247; 85.

Singh, R.M., Datta, B., Jain, A., 2004. Identification of unknown groundwater pollution sources using artificial neural networks. Journal of Water Resource Planning and Management; 130-6; 506-514.

Swamee, P.K., 1996. Design of multistage pumping mains. Journal of Transportation Engineering; 122; 1; 1–4.

Swamee, P.K., Sharma, A.K., 1990a. Decomposition of large water distribution systems. Journal of Environmental Engineering; 116; 2; 269–283.

Proceedings of the 10th World Congress of EWRA 'Panta Rhei', 5-9 July 2017, Athens, Greece
© 2017 *European Water Resources Association*

Vulnerability of groundwater to pollution using three different models in Halabja Saidsadiq basin, Iraq

T.O. Abdullah[1], S.S. Ali[2], N.A. Al-Ansari[3*] and S. Knutsson[3]
[1] *Department of Geology, University of Sulaimani, Kurdistan Region, NE. Iraq and Department of Civil, Environmental and Natural Resources and Engineering, Division of Mining and Geotechnical Engineering, Lulea University of Technology, Sweden*
[2] *University of Sulaimani, Kurdistan Region, NE Iraq*
[3] *Department of Civil, Environmental and Natural Resources and Engineering, Division of Mining and Geotechnical Engineering, Lulea University of Technology, Sweden*
[*] *e-mail: nadhir.alansari@ltu.se*

Abstract: Halabja Saidsadiq Basin (HSB) is one of a major basin of Iraq in terms of groundwater reservoirs. Intensive agricultural practices and economic revolution are widespread and located close to groundwater wells, which pose imminent threats to these resources. Therefore, the most effective and realistic solution is to prevent the contamination of groundwater through. The present study targets the computation of the vulnerability of groundwater reservoirs of the study area. Three methods have been examined, namely DRASTIC, VLDA and COP to model a map of groundwater vulnerability for contamination. The standard DRASTIC vulnerability maps classified the basin of four vulnerability index zones: very low (34%), low (13%), moderate (48%) and high (5%). The VLDA model also classified the area into four categories as well: low (2%), moderate (44%), high (53%) and very high (1%).Four vulnerability classes were recognized based on COP model including very low, low, moderate and high vulnerability classes with coverage areas of (1%, 37%, 2% and 60%) respectively. After constructing every vulnerability map, it required to be confirmed in order to estimate the validity of the theoretical sympathetic of current hydrogeological conditions. In this study, nitrate concentration analysis was selected as a contamination indicator to validate the result. Considerable variations in nitrate concentration on dry to wet seasons had been renowned. Consequently, it points toward that groundwater in the HSB are capable to receive the contaminant due to suitability of overlies strata in terms of geological and hydrogeological conditions. Based on this confirmation, the result exemplifies that the degree and distribution of vulnerability classes acquired using VLDA model is more sensible.

Key words: Vulnerability, DRASTIC, VLDA, COP, Nitrate concentration, Halabja Saidsadiq Basin (HSB)

1. INTRODUCTION

The Halabja and Saidsadiq Basin (HSB) is one of the most important basins in terms of water groundwater aquifers. The concentration of economic, agricultural and social activities within the basin makes it of great importance to the region. The improvement in the economy, its development and comprehensive agricultural activities are extensive and are located near groundwater wells, posing imminent threats to these resources. From the perspective of these developments, there is an expansion of human quantities that make a line to live in this basin and the surrounding areas. This is forcing increasing attention to water, which has placed significant weight on water resources. Therefore, groundwater pollution is of particular concern as groundwater resources are the main source of water for drinking, agriculture, irrigation and industrial activities.

Groundwater vulnerability is a measure of how easy or how hard it is for pollution at the land surface to reach a productive aquifer. The vulnerability studies can provide valuable information about stakeholder working on preventing further deterioration of the environment (Mendoza & Barmen, 2006). To simplify the identification of the groundwater state and to resist the pollutants in the reservoirs, several methods were recommended such as DRASTIC, VLDA, COP, GOD, SINTACS, etc. These different methods are offered under the form of numerical excerpt systems based on the negotiation of the different factors affecting the hydrogeological system (Attoui and Bousnoubra 2012).

In HSB, different vulnerability models have been applied previously; while it is very important to confirm the calculated vulnerability model reflecting the real vulnerability system in the region. Therefore, the primary objective of the present study is to compare the vulnerability map of three different models, DRASTIC, VLDA and COP, to choose a more reasonable model to be applied in the area to protect groundwater from pollution.

2. STUDY AREA

The study basin is located in the northeastern part of Iraq (Figure 1), geographically it is located between the latitude 35” 00 00" and 35" 36’ 00" N and the longitude 45” 36’ 00" and 46” 12’ 00" E. The entire study area is about 1278 square kilometers and its population of about 190,727 in early 2015. Ali (2007) divided this basin of two sub-basins including Halabja- Khurmal and Said Sadiq sub-basins. Nearly 57% of the studied area is an arable area due to its suitability for agriculture (Statistical Dtectorate, 2014).

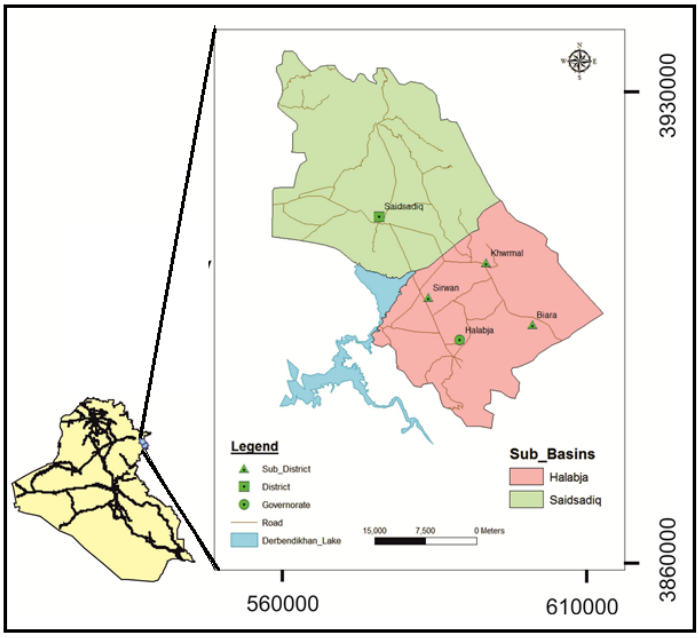

Figure 1. Location map of study basin.

2.1 Geology and hydrogeological setting

Geologically, the studied area is located within Western Zagros Fold-Thrust Belt. Structurally, it is located within the High Folded zone, imbricated, and thrusted zone. Different geological formations were exposed to the basin, these formation consists of limestone, dolomitic limestone and conglomerate which have an effective role in the vulnerability system in the basin. Alluvial (Quaternary) deposits are the most important unit in the area in terms of hydrogeological characteristics and water supply. The thickness of these deposits as observed by (Abdullah et al, 2015 a) of about nearly 300 m.

Hydrogeologically, different groundwater aquifers exist in the area based on its geological origin, Table 1. The mountain series, which surround the basin of the northeast and southeast, are characterized by high depth of groundwater, while toward the center and the southeastern part, the groundwater level has a relatively lower depth. A groundwater movement is usually from high elevated areas at the north and northeast and south and southeast towards southwest or generally toward the reservoir of Derbandikhan Dam.

Table 1. Type of aquifers in the study basin.

Aquifer type	Geological formation	Thickness (m)	References
Intergranular	Quaternary deposits	more than 300	Abdullah 2015 a
Fissured	Balambo,Kometan	250	Ali,2007
Fissured-Karstic	Avroman	200	Jassim and Goff,2006
	Jurassic formation	From 80 to 200	
Non-Aquifer (Aquitard)	Qulqula	more than 500	Jassim and Goff,2006
	Shiranish	225	
	Tanjero	2000	

3. METHODOLOGY

To study groundwater vulnerability in this basin, three different models were applied with the aid of GIS technique. The first applied model is DRASTIC, which is consist of seven physical parameters .The most important parameters that control groundwater contamination comprise to be the depth to water (D), Net recharge (R), Aquifer media (A), Soil media (S), Topography (T), Impact of vadose zone media (I), and Hydraulic conductivity (C).These parameters are weighted from one to five based on their relative significance of contributing to the contamination potential. Each parameter characterized by different rating and weighting to value. The achieving index is a qualified measure of vulnerability to contamination; areas with a higher index value are more vulnerable than those with a lower index. The standard DRASTIC index (DI(w-r)) calculated is based on the following equation, (Aller et al,1987):

$$DI = D_W D_r + R_W R_r + A_W A_r + S_W S_r + T_W T_r + I_W I_r + C_W C_r \quad (1)$$

where:
DI is the DRASTIC Index, (D, R, A, S, T, I and C) are the seven parameters
w is the weight parameter and r is the rate of the parameter as recommended by (Aller et al, 1987).

The second applied model is VLDA, principally it reflect lithology of vadose zone (V), pattern of land use (L), groundwater depth (D), and aquifer characteristics (A), (Zhou et al, 2012). In addition, consistent weight can be assigned to each of the four indexes depending on its impact on groundwater vulnerability.

The vulnerability comprehensive assessment index (DI) is the sum of the above-mentioned weighted four indexes, as computed conferring to the following formula, (Zhou et al, 2012):

$$DI = \sum_{j=1}^{4} (\mathrm{Wij Rij}) \quad (2)$$

where DI is the comprehensive assessment index , Wij is the weight of the jth comprehensive assessment index of the ith sub-system, Rij is the value of the jth assessment index of the ith subsystem; 4 is the quantity of indexes.

The slighter the DI signifier to the lower vulnerability of the groundwater system and the better the stability will be. For evaluating the groundwater vulnerability, the new corresponding weights in HSB were proposed using sensitivity analysis method (Abdullah 2015 b). According to the result of sensitivity analysis, the proposed weights used for VLDA model measured as 8.2, 4.8, 5.2 and 4.8, and after normalization, the weight is 0.357, 0.209, 0.226 and 0.209, respectively, (Abdullah 2016a).

The third applied model is COP; its abbreviation comes from the three initials of factors namely flow Concentration (C), Overlying layers (O) and Precipitation (P) (Vias et al., 2006). The hypothetical basis of this strategy, as indicated by the European Approach (Daly et al., 2002) and (Goldscheider and Popescu, 2004), it is to evaluate the ordinary protection for groundwater (O variable) controled by the properties of overlying soils and the unsaturated zone, and also to measure how this assurance can be adjusted by diffuse, infiltration (C factor) and the climatic conditions (P Factor – precipitation). The COP-Index map was computed from equation 3

(Abdullah et al., 2016b; Vias et al., 2006):

COP Index Map= C*O*P (3)

4. RESULT AND CONCLUSIONS

After the weighted scores were attained for all parameters in each model, the GIS technique was used to combine all layers. The Standard DRASTIC models to reveal four zones of vulnerability index to comprise very low, low, moderate and high vulnerability index, Figure 2. The moderate and very low vulnerability zones which covering an area of 48% and 34% of the whole studied area respectively. The moderate vulnerability zone occupies two different areas; the first zone is the area of mountains surrounding the studied basin comprises the fissure and karstic aquifer. While the second area comprise the Quaternary deposits surrounding the area of Derbandikhan Lake in the southwest of the basin. Furthermore, the zone with low vulnerability comes in the third sequence and occupies 13% of the overall surface of the basin. The zone with high vulnerability indexes cover only 5% of the total area and located in the centre of the basin, this area is characterized by the area of high water table level and of fractured limestone type of an aquifer.

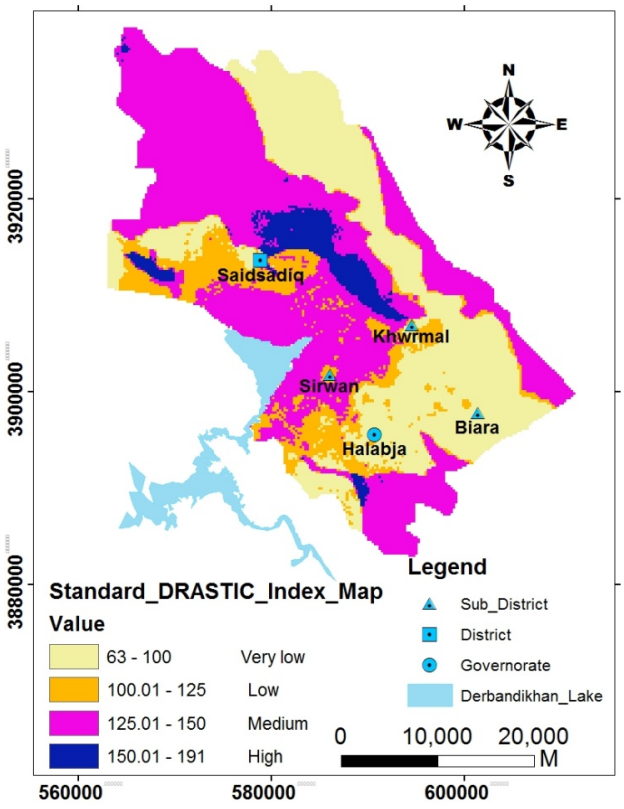

Figure 2. DRASTIC Vulnerability Index Map of HSB

The vulnerability outcome based on VLDA model, reveals that a total of four ranges of vulnerability indexes had been distinguished ranging from low to very high, with vulnerability indexes (2.133-4 , >4-6, >6-8 and > 8), Figure 3. The area of low and very high vulnerability zone of 2% and 1% of whole study area respectively. The High vulnerability classes occupied most of the mountains area that surrounding the basin and the central part of HSB. This vulnerability zone covered an area of 53% of whole area. Finally, medium vulnerability zones to cover an area of 44% of all studied area and positioned southeast and northwest. Both high and moderate vulnerability class that occupied most of the studied basins refer to the exhaustive human activities, good water yield property and lithological composition of an aquifers.

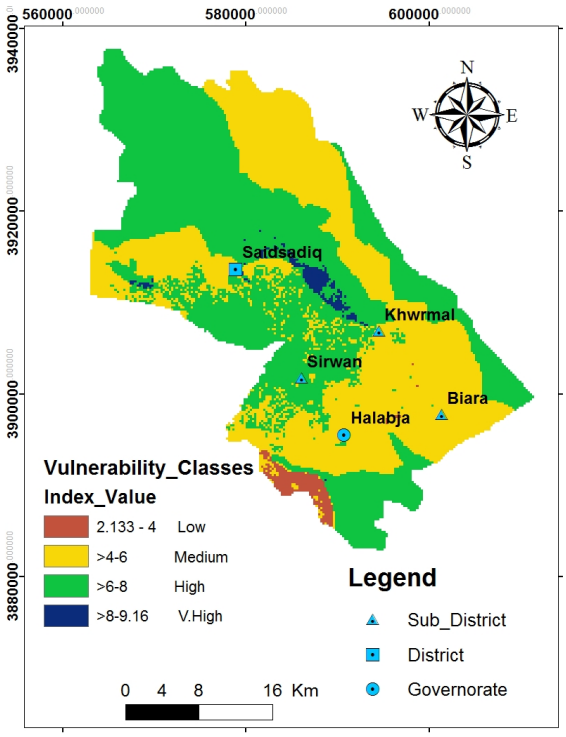

Figure 3. VLDA Vulnerability Index Map of HSB

Four classes of vulnerability ranging from very low to high are branded depending on the COP model, Figure 4. High vulnerability zones which cover an area of 60% of the whole HSB, geologically includes the area of a fissure and slight karstic carbonate rocks. While, low vulnerability class comes in the second order and occupy 37% of the whole area, this area mostly characterized by alluvial deposits. The zone with moderate and very low vulnerability classes cover only 2% and 1% of the total area respectively.

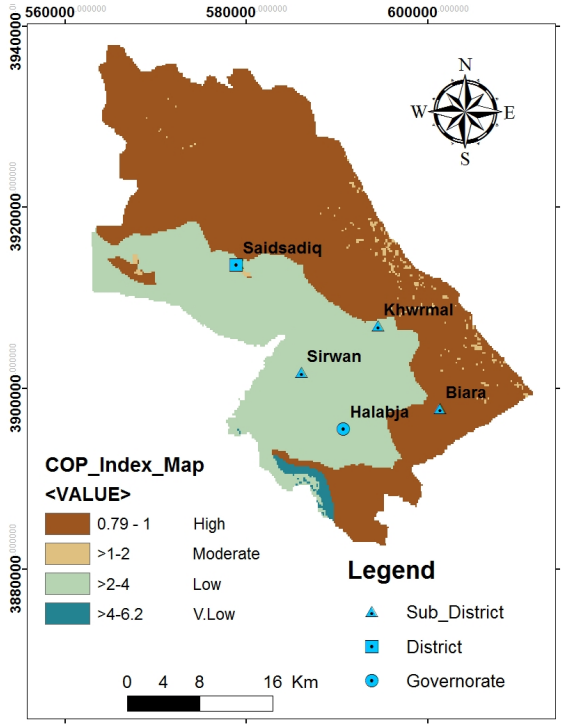

Figure 4. COP Vulnerability Index Map of HSB

4.1 Validation of the result

The significant dissimilarity has been illustrious from all applied models. So validation of vulnerability maps for these three models became obligatory, therefore nitrate concentration analysis has been selected. Nitrate as a pollution indicator can be supportive to distinguish the evolution and changes of groundwater quality. In the particular study case, the nitrate differences between two following seasons (dry and wet) were analyzed from (30) watering wells. The result illustrates considerable variations in nitrate concentration on dry to wet seasons, Figure 5. Based on this validation, it can be confirmed that HSB is capable of receipt the contaminant due to suitability in geological and hydrogeological conditions. Based on this verification, the degree and distribution of level of vulnerability acquired using VLDA model are more sensible than that attained from the standard DRASTIC and COP models. With increasing nitrate concentration the vulnerability rates increased too, because land to use patterns is considered being one of the most effective factors of VLDA model and this parameter dose not included in DRASTIC and COP models.

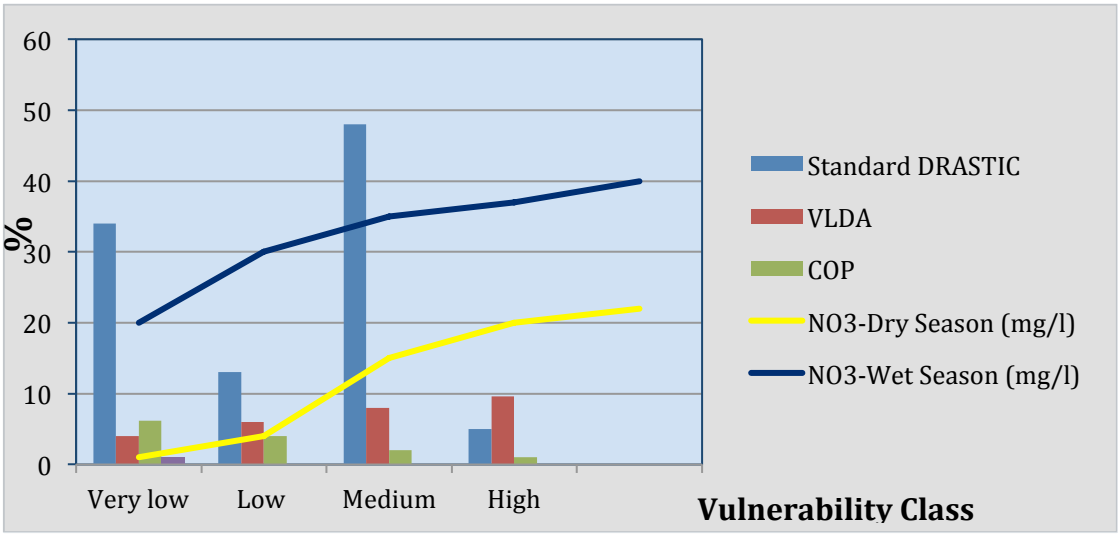

Figure 5. Comparison of all applied models with nitrate concentration.

5. CONCLUSION

Three different methods particularly standard DRASTIC, VLDA and COP have been applied to assess the potential vulnerability of HSB to groundwater contamination. The values of the standard DRASTIC vulnerability indexes ranged between (63 and 191), the VLDA indexes with values ranging from (2-9), the values of the COP indexes ranged between (1-6). The higher index value for both DRASTIC and VLDA models means higher vulnerability category, while the lower index value of COP model means higher vulnerability class.

The vulnerability classes are elucidated in Table 2, all models to clarify four vulnerability classes. DRASTIC and COP models comprises (very low to high), while VLDA model embraces (low to very high).The significant dissimilarity has been illustrious from all applied models. Therefore, validation of achieved vulnerability maps becomes compulsory. Nitrate as a pollution indicator from agricultural processes can be supportive to distinguish the evolution and changes of groundwater quality. The result illustrates considerable variations in nitrate concentration on dry to wet seasons. So it can be concluded that groundwater in HSB is capable of receiving the contaminant. Based on this verification, Figure 5 demonstrates that the degree and distribution of level of vulnerability acquired using the VLDA method is more sensible than that attained from

both standard DRASTIC and COP methods.

Table 2. Result of index ratio for all applied models.

Vulnerability class	DRASTIC rate %	VLDA rate %	COP rate %
Very low	34	0	1
Low	13	2	37
Medium	48	44	2
High	5	53	60

REFERENCES

Aller L., Bennett T., Lehr JH., Petty RH, and Hackett G.,1987. DRASTIC: a standardized system for evaluating groundwater pollution potential using hydrogeologic setting. USEPA report 600/2-87/035, Robert S. Kerr Environmental Research Laboratory, Ada, Oklahoma74820, 252 p.

Ali S. S.,2007. Geology and hydrogeology of Sharazoor - Piramagroon basin in Sulaimani area, northeastern Iraq. Unpublished PhD thesis, Faculty of Mining and Geology, University of Belgrade, Serbia. 317P.

Attoui B, Kherci N, Bousnoubra H.,2012. State of vulnerability to pollution of the big reservoirs of groundwater in the region of Annaba-Bouteldja (NE Algeria). Geographia Technica. 2:1-13.

Abdullah T. O. , Ali S.S., Al-Ansari N.A. and Knutsson S.,2015a. Effect of agricultural activities on groundwater vulnerability: Case study of Halabja Saidsadiq Basin, Iraq. Journal of Environmental Hydrology 23(10).The open access electronic journal found at http://www.hydroweb.com/protect/pubs/jeh/jeh2015/AnsariGW.pdf

Abdullah, T.O., Ali, S.S., Al-Ansari, N.A. and Knutsson, S.,2015b. Groundwater Vulnerability Mapping using Lineament Density on Standard DRASTIC Model: Case Study in Halabja Saidsadiq Basin, Kurdistan Region, Iraq. Engineering, 7, 644-667. http://dx.doi.org/10.4236/eng.2015.710057.

Abdullah, T.O., Ali, S.S., Al-Ansari, N.A. and Knutsson, S.,2016a. Assessing the vulnerability of groundwater to pollution using DRASTIC and VLDA models in Halabja Saidsadiq Basin, NE - Iraq.. Journal of Civil Engineering and Architecture 10 (2016) 1144-1159, doi: 10.17265/1934-7359/2016.10.006.

Abdullah, T.O., Ali, S.S., Al-Ansari, N.A. and Knutsson, S.,2016b. Groundwater Vulnerability Using DRASTIC and COP Models: Case Study of Halabja Saidsadiq Basin, Iraq. Engineering, 8, 741-760. http://www.scirp.org/journal/PaperInformation.aspx?PaperID=71681.

Daly D, Dassargues A, Drew D, Dunne S, Goldscheider N, Neale S, Popescu C, Zwhalen F .,2002. Main concepts of the "European Approach" for (karst) groundwater vulnerability assessment and mapping. Hydrogeol J 10(2):340–345.

Goldscheider, N. and Popescu, C.,2004. The European Approach. In: Zwahlen F (ed) Vulnerability and risk mapping for the protection of carbonate (karst) aquifers. European Commission, Brussels, pp 17–21.

Huang T, Pang Z, Edmunds W.,2012. Soil profile evolution following land-use change: Implications for groundwater quantity and quality. Hydrol. Process 27(8):1238-1252.

Jassim S.Z. and Guff J.C.,2006. Geology of Iraq. Jassim (Eds) D. G. Geo Survey. Min. Invest. Publication. 340p.

Mendoza JA, and Barmen G., (2006): Assessment of groundwater vulnerability in the Rio Artiguas Basin, Nicaragua. Environmental Geology 50: 569_580.

Statistical Directorate in Sulaimaniyah,2014.Archive Department.

Vias J.M.,Andreo B., Perles M.J. , Carrasco I., Vadillo P. and Jim'enez P.,2006. Proposed method for groundwater vulnerability mapping in carbonate (karstic) aquifers: the COP method. Application in two pilot sites in Southern Spain. Hydrogeology Journal (2006) 14: 912–925. DOI 10.1007/s10040-006-0023-6.

Zhou J. , Li Q. ,Guo Y. , Guo X. , Li X., Zhoa Y. and Jia R.,2012. VLDA model and its application in assessing phreatic groundwater vulnerability: a case study of phreatic groundwater in the plain area of Yanji County, Xinjiang, China. Environmental Earth Science Journal Vol.67 .pp. 1789-1799.

Proceedings of the 10th World Congress of EWRA 'Panta Rhei', 5-9 July 2017, Athens, Greece
© 2017 *European Water Resources Association*

Artificial intelligence and regression analysis in predicting ground water levels in public administration

G.N. Kouziokas[1*], A. Chatzigeorgiou[2] and K. Perakis[1]
[1] *University of Thessaly, School of Engineering, Department of Planning and Regional Development, Volos, Greece*
[2] *University of Macedonia, Department of Applied Informatics, Thessaloniki, Greece*
[*] *e-mail: gekouzio@uth.gr*

Abstract: Water level prediction of ground water can be considered as a very important tool in water resources management. This research implements artificial neural network models in order to build the optimal forecasting models for predicting the water levels and regression analysis in order to evaluate the prediction accuracy. In this research, an Artificial Neural Network Perceptron is applied in order to construct forecasting models for predicting water levels of ground water. The developed models are then compared each other in order to find the optimal one according the best performance that will lead to the most accurate predictions. Several topologies were tested in order to discover the best forecasting model. The different predictive models were constructed by implementing different number of the nodes in the hidden layers, also by testing different number of the hidden layers. The results showed an increased prediction accuracy of the developed Artificial Neural Network Models. This research is aiming at providing the scientists and engineers with the optimal prediction models in order to be used for forecasting the water levels of ground water with increased accuracy compared to other prediction techniques and methods. The developed forecasting models can provide accurate predictions of water levels of ground water which can be very valuable for the public administrators and stakeholders in water resources management.

Key words: Artificial intelligence; Neural networks; Environmental management; Public Administration; Water level prediction

1. INTRODUCTION

Groundwater levels monitoring is of high importance in public administration and in environmental management and planning, since water is highly connected with the quality of human life and the health of the natural environment (Jacobs & Holway, 2004; Kemper, 2004).

Groundwater levels forecasting can play a significant role in public management and planning since the authorities will have the opportunity to take the appropriate measures in order to prevent the rapid decrease of the groundwater levels and to protect the public health (Davies et al. 2001; Howard et al., 2006; Schmoll, 2006).

Information technology and especially artificial intelligence have been applied in various fields of environmental management and public administration the last years (Kouziokas, 2016a, 2016b, 2016c, 2016d; Metaxiotis et al., 2003). Artificial neural networks have been also used as a predictive method by some researchers in order to forecast groundwater levels (Adamowski & Chan, 2011; Daliakopoulos et al., 2005; Giustolisi & Simeone, 2006; Sreekanth et al., 2009).

Giustolisi & Simeone (2006), have studied groundwater level predictions by using artificial neural networks and a multi-objective strategy. The results have showed satisfactory prediction results by using a linear model in short time forecasting and a nonlinear model in distant time predictions.

Adamowski & Chan (2011), have used artificial neural networks and coupling discrete wavelet transforms for predicting groundwater levels. The developed prediction models have provided very accurate groundwater level forecasts in a monthly basis.

Sreekanth et al. (2009), have used artificial neural networks to develop prediction models to predict groundwater levels in the Maheshwaram watershed. The results have showed better prediction results than the conventional forecasting methods.

In this research, artificial intelligence and regression are used for forecasting groundwater levels. The levels of groundwater were chosen to be predicted, since groundwater resources are associated with public health and are considered of high importance. Artificial neural network models are developed in order to build the optimal forecasting model. The developed forecasting models can provide predictions of groundwater levels which can be used by the public administrators in water resources management and planning. The research methodology, the discussion and the results are described in the next sections.

2. THEORETICAL BACKGROUND

2.1 Artificial neural networks

Artificial Neural Networks (ANNs) were utilized in this research in order to construct and compare forecasting models regarding groundwater predictions. Artificial Neural Networks are computing systems that their construction simulates the neural structure of the human brain (Basheer & Hajmeer, 2000; Suykens et al., 2012). Artificial Neural Networks process the input data and the information traverses the neural network connections so as to produce the output values according to the input. Their advantage is that they can be used also at non-linear relationships between the input and the output (Almeida, 2002; Poznyak et al., 1999; Zhang et al., 1998).

2.2 Feed Forward Multilayer Perceptron

In this research, a Feedforward Multilayer Perceptron (FFMLP) was used in order to construct the artificial neural network prediction models. FFMLP is implemented in this study, since several studies have showed that Feed Forward Multilayer Perceptron is the most suitable regarding problems that have to deal with time series forecasting (Kouziokas et al., 2016a, 2016b; Tang & Fishwick, 1993; Zhang et al., 2001). In a Feed Forward Multilayer Neural Network, the neurons are connected only forward. The neural network layers have connections to the next layers, but they do not have any connections backwards (Blum & Li, 1991; Hornik, 1991; Hornik et al., 1989). Figure 1 shows the topology of a typical feed forward neural network, where *n* is the number of neurons in the input layer, *k* is the number of neurons in the hidden layer and *o* is the number of neurons in the output layer. I_1, I_2, …,In are the input values and O_1, O_2, .., On are the output (predicted) values.

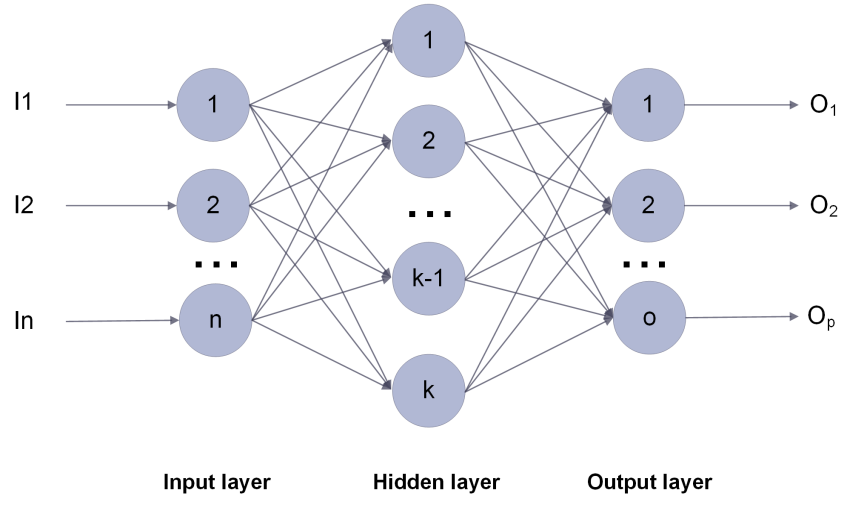

Figure 1. A typical feedforward neural network. n is the number of neurons in the input layer, k is the number of neurons in the hidden layer and o is the number of neurons in the output layer.

2.3 Levenberg Marquardt Algorithm

The Levenberg Marquardt algorithm was selected as a training algorithm for the Feed Forward Multilayer Neural Network, since it produced better results than the other training algorithms.

The Levenberg Marquardt algorithm is considered as one of the fastest learning algorithms compared to other algorithms (Marquardt, 1963). In this research, the Levenberg Marquardt algorithm yield better outputs than the most common algorithms that were tested (Resilient Backpropagation, BFGS Quasi-Newton, Scaled Conjugate Gradient) by using different neural network topologies.

The Levenberg Marquardt algorithm combines the steepest descent algorithm and the Gauss-Newton algorithm. The Levenberg Marquardt algorithm can be used for solving non-linear least-squares problems (Liu, 2010; Lourakis, 2005).

3. RESEARCH METHODOLOGY

The research methodology that was followed, consists of five stages: data collection and preparation, neural network prediction models development, comparison of the developed neural network models so as to discover the optimum one according to the performance, testing the optimum developed neural network model in groundwater forecasting and finally assessing the forecasting results by using RMSE error and linear regression.

Firstly, groundwater and climate data were collected and prepared so as to feed the artificial neural network models. In the second stage, artificial neural network prediction models were developed by testing different topologies, learning algorithms and transfer functions in order to construct the optimal neural network forecasting model. In the next phase, a comparison of the constructed neural network models was performed, in order to find the optimum model according to the performance results. In the next stage, optimum developed neural network model was tested in groundwater forecasting. In the last stage, the forecasting results were evaluated by using Root Mean Squared Error (RMSE) and linear regression. Figure 2 shows an overview of the stages of the followed research methodology.

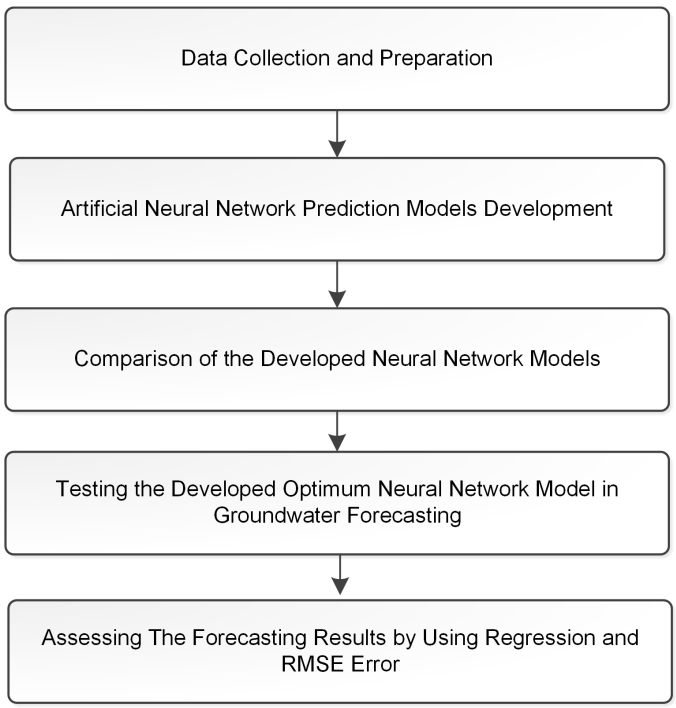

Figure 2. Overview of the research methodology.

4. RESULTS

4.1 Data collection and preparation

Groundwater data were retrieved from the official website of the United States Geological Survey (USGS) for the Montgomery country in Pennsylvania (https://www.usgs.gov). The climate data were retrieved from the official website of Pennsylvania State Climatologist office. Data regarding the daily values of the average temperature, the average relative humidity and the precipitation were pre-processed in order to be used as inputs in the developed Artificial Neural Network Models.

Groundwater data were collected for the Montgomery County Observation Well in Pennsylvania of USA. The data were collected and prepared (checked for incoherencies, duplicates, etc.) for the 365 days of the year 2014.

Figure 3 shows the values of the mean daily groundwater level (feet below the land surface) for the year 2014 for the Montgomery County Observation Well.

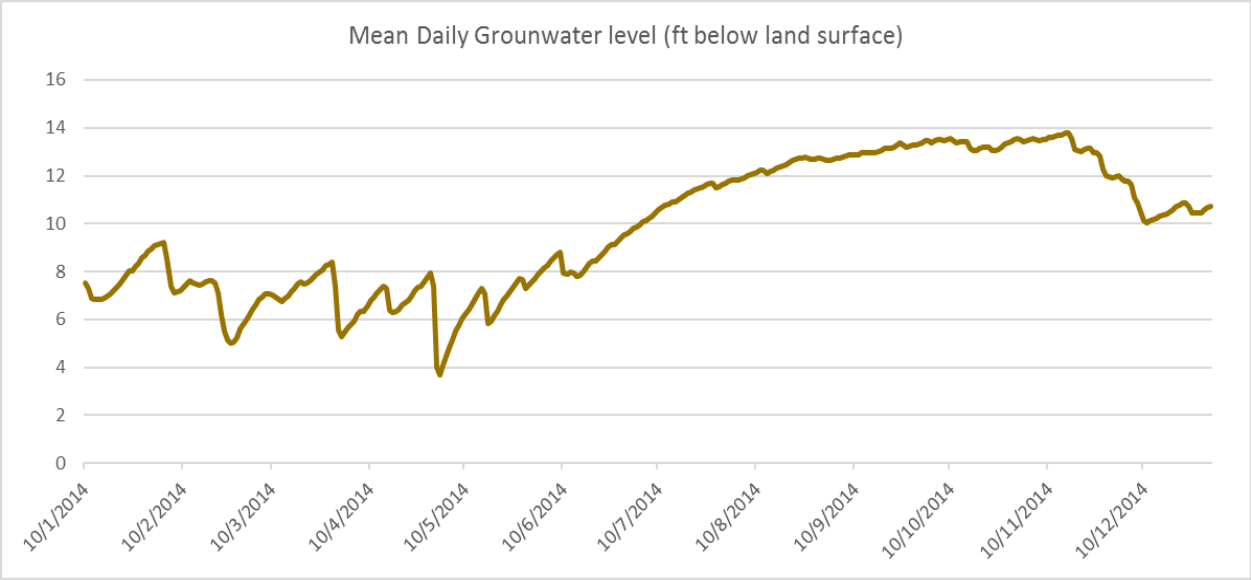

Figure 3. Daily groundwater level (feet below the land surface).

4.2 Artificial neural network models

The artificial neural network models were developed by using as input parameters several factors that influence the groundwater levels such as Average Temperature (AT), Average Relative Humidity (ARH), precipitation (PRE) (includes drizzle and rainfall) and the depth to groundwater level (DGL) below land surface.

The data was divided into three different parts. 70% of the primary data was used as the training set, 15% for the validation set and 15% for the test set. The training data set was used in order to train the neural network with historical data of the input factors. The validation set was used so as to assess the performance of the developed artificial neural network models.

4.3 Optimum neural network model implementation

The optimum forecasting model was developed by comparing the performance of the different neural network models that were investigated. Multiple neural network topologies were tested regarding the number of the hidden layers (one to two hidden layers), the number of the neurons of

every hidden layer (one to fifty neurons) and the most common transfer functions for the hidden layers and also the most common learning algorithms.

The most common transfer functions that were tested for the hidden layers are the following: Tanh-Sigmoid Transfer Function (TSTF), Log-Sigmoid Transfer Function (LSTF) and Linear Transfer Function (LTF).

The most common training algorithms that were tested for training every neural network model were: Levenberg Marquardt (LM), Resilient Backpropagation (RB), Scaled Conjugate Gradient (SCG), BFGS Quasi-Newton (BFGS-QN).

The optimal neural network model was the one where the training algorithm was Levenberg Marquardt (LM) algorithm. The optimum model was evaluated according to the minimum Root Mean Squared Error (RMSE) among all the other constructed models. The Root Mean Squared Error (RMSE) of the optimal model was found to be 0.0742.

According to the results, the topology of the optimal neural network model consists of 22 neurons in the first hidden layer and 25 neurons in the second hidden layer. The transfer function of the first hidden layer is Tanh-Sigmoid Transfer Function (TSTF) and the transfer function of the second hidden layer is Tanh-Sigmoid Transfer Function (TSTF).

The linear regression analysis was utilized to evaluate the forecasting accuracy of the optimal artificial neural network model. The R value was used which shows the linear relationship between the outputs and the targets. If the R value is one, then it shows that there is an exact linear relationship between the predicted values (outputs) of the network and the target values (inputs) of groundwater levels.

The R value of the predicted and the actual groundwater levels was 0.99775. This R value shows that the predictions of the groundwater levels produced by the optimal forecasting model are very precise for the selected region.

5. CONCLUSIONS AND DISCUSSION

This research utilizes artificial intelligence and regression analysis in forecasting groundwater levels which is very vital in public administration, in natural resources management and in water management. In this paper, several artificial neural network models were developed by testing several parameters regarding the topology of the neural network and also the training algorithms and the transfer functions of the hidden layers.

The optimal artificial neural network model was developed by taking into consideration several factors that affect the groundwater levels. These parameters were used as input values in order to forecast the groundwater levels. Also, several neural network topologies were tested in order to find the optimum one according to their performance.

Compared to other researches this study have used artificial neural networks in combination with regression analysis by utilizing different input variables and a wider range of learning algorithms and topologies of ANNs by investigating also several factors that improved the performance of the optimal forecasting model.

The results showed a very precise prediction accuracy of the groundwater levels compared to other researches that have used artificial neural network for groundwater predictions (Adamowski & Chan, 2011; Giustolisi & Simeone, 2006; Sreekanth et al., 2009).

The developed optimal neural network forecasting model and the groundwater predictions can be very useful to the authorities in public and water management and also in taking proactive measures so as to apply effective management strategies in order to minimize the rapid losses of the amount of the water resources.

This research could contribute to the prevention of natural water loss which is very vital and could have negative impact on human health by adopting the appropriate water management strategies and is aiming at providing scientists and engineers with prediction models in order to be used for forecasting the water levels of groundwater with increased prediction accuracy.

ACKNOWLEDGEMENTS

United States Geological Survey (USGS) website for retrieving the groundwater data.

REFERENCES

Adamowski, J., & Chan, H. F. (2011). A wavelet neural network conjunction model for groundwater level forecasting. Journal of Hydrology, 407(1), 28-40.

Almeida, J. S. (2002). Predictive non-linear modeling of complex data by artificial neural networks. Current opinion in biotechnology, 13(1), 72-76.

Basheer, I. A., & Hajmeer, M. (2000). Artificial neural networks: fundamentals, computing, design, and application. Journal of microbiological methods, 43(1), 3-31.

Blum, E. K., & Li, L. K. (1991). Approximation theory and feedforward networks. Neural networks, 4(4), 511-515.

Daliakopoulos, I. N., Coulibaly, P., & Tsanis, I. K. (2005). Groundwater level forecasting using artificial neural networks. Journal of Hydrology, 309(1), 229-240.

Davies, H., Rosen, M. R., & White, P. A. (2001). Groundwater and health. Groundwaters of New Zealand, 253-272.

Giustolisi, O., & Simeone, V. (2006). Optimal design of artificial neural networks by a multi-objective strategy: groundwater level predictions. Hydrological sciences journal, 51(3), 502-523.

Hornik, K. (1991). Approximation capabilities of multilayer feedforward networks. Neural networks, 4(2), 251-257.

Hornik, K., Stinchcombe, M., & White, H. (1989). Multilayer feedforward networks are universal approximators. Neural networks, 2(5), 359-366.

Howard, G., Bartram, J., Pedley, S., Schmoll, O., Chorus, I., Berger, P. (2006). Groundwater and public health. Protecting groundwater for health: managing the quality of drinking-water sources. London, International Water Association Publishing, 3-19.

Jacobs, K. L., & Holway, J. M. (2004). Managing for sustainability in an arid climate: lessons learned from 20 years of groundwater management in Arizona, USA. Hydrogeology Journal, 12(1), 52-65.

Kemper, K. (2004). Groundwater—from development to management. Hydrogeology Journal, 12(1), 3-5.

Kouziokas, G. N. (2016a). Artificial intelligence and crime prediction in public management of transportation safety in urban environment. Proceedings of the 3rd Conference on Sustainable Urban Mobility (pp. 534-539). Volos: University of Thessaly Greece.

Kouziokas, G. N. (2016b). Geospatial Based Information System Development in Public Administration for Sustainable Development and Planning in Urban Environment. European Journal of Sustainable Development, 5(4), 347-352.

Kouziokas, G. N. (2016c). Technology-based management of environmental organizations using an Environmental Management Information System (EMIS): Design and development. Environmental Technology & Innovation, 5, 106-116. doi:http://dx.doi.org/10.1016/j.eti.2016.01.006.

Kouziokas, G. N. (2016d, September). An Information System for Monitoring Environmental Indicators in Public Management for Sustainable Development. Paper presented at the 11th International Scientific Conference eRA-11, Piraeus University of Applied Sciences, Piraeus.

Kouziokas, G. N., Chatzigeorgiou, A., & Perakis, K. (2016a, June). Applying Levenberg Marquardt Algorithmin Feedforward Neural Network Models for Predicting Crime in Public Management. Paper presented at the International Conference on Computational and Informational Sciences and Engineering, University of Thessaly, Portaria, Volos.

Kouziokas, G. N., Chatzigeorgiou, A., & Perakis, K. (2016b, September). Predicting Environmental Data in Public Management by Using Artificial Intelligence. Paper presented at the 11th International Scientific Conference eRA-11, Piraeus University of Applied Sciences, Piraeus, Greece.

Liu, H. (2010, August). On the levenberg-marquardt training method for feed-forward neural networks. In 2010 Sixth International Conference on Natural Computation (Vol. 1, pp. 456-460). IEEE.

Lourakis, M. I. (2005). A brief description of the Levenberg-Marquardt algorithm implemented by levmar. Foundation of Research and Technology, 4, 1-6.

Marquardt, D. W. (1963). An algorithm for least-squares estimation of nonlinear parameters. Journal of the society for Industrial and Applied Mathematics, 11(2), 431-441.

Metaxiotis, K., Ergazakis, K., Samouilidis, E., & Psarras, J. (2003). Decision support through knowledge management: the role of the artificial intelligence. Information Management & Computer Security, 11(5), 216-221.

Poznyak, A. S., Yu, W., Sanchez, E. N., & Perez, J. P. (1999). Nonlinear adaptive trajectory tracking using dynamic neural networks. IEEE Transactions on Neural Networks, 10(6), 1402-1411.

Sreekanth, P. D., Geethanjali, N., Sreedevi, P. D., Ahmed, S., Kumar, N. R., & Jayanthi, P. K. (2009). Forecasting groundwater level using artificial neural networks. Current science, 96(7), 933-939.

Schmoll, O. (2006). Protecting groundwater for health: managing the quality of drinking-water sources. World Health Organization.

Suykens, J. A., Vandewalle, J. P., & de Moor, B. L. (2012). Artificial neural networks for modelling and control of non-linear systems. Springer Science & Business Media.

Tang, Z., & Fishwick, P. A. (1993). Feedforward neural nets as models for time series forecasting. ORSA journal on computing, 5(4), 374-385.

Zhang, G. P., Patuwo, B. E., & Hu, M. Y. (1998). Forecasting with artificial neural networks: The state of the art. International journal of forecasting, 14(1), 35-62.

Zhang, G. P., Patuwo, B. E., & Hu, M. Y. (2001). A simulation study of artificial neural networks for nonlinear time-series forecasting. Computers & Operations Research, 28(4), 381-396.

Proceedings of the 10th World Congress of EWRA 'Panta Rhei', 5-9 July 2017, Athens, Greece
© 2017 *European Water Resources Association*

Ground water risk management using dynamic bayesian networks and PROMETHEE method

A. Roozbahani*, E. Ebrahimi and M.E. Banihabib
Department of Irrigation and Drainage Engineering, College of Aburaihan, University of Tehran, Iran
* *e-mail: roozbahany@ut.ac.ir*

Abstract: The aquifers are considered as the best and most accessible source of fresh water. In recent years, they have been faced with severe water withdrawal in Iran, therefore some plains was considered as forbidden plains that it means the water withdrawal from these aquifers is unauthorized. Given such a critical situation in aquifers, the need for management of groundwater resources in the form of tools such as monitoring the level of the aquifers and developing the restoring scenarios is essential. Then for this purpose, A Decision Support System-DSS has been developed in this paper based on Prediction of groundwater level and Multi Criteria Decision Making methods (MCDM). Due to the flexible and simple structure, a probabilistic Dynamic Bayesian Networks (DBNs) has been used for monthly groundwater level prediction under uncertainties. After analyzing the obtained results, some applicable groundwater management scenarios such as artificial recharge and irrigation system change as well as relative criteria such as economic, social and technical attributes have been defined for decision making procedure. After elicitation of decision makers' opinions about criteria's relative importance and performance, among the MCDM methods, PROMETHEE-II technique has been applied to ranking the scenarios regarding their efficiency in restoring the Birjand aquifer in Iran which has a critical groundwater resource condition. The results show the ability of the proposed DSS in planning and management of groundwater resources, reducing the risk of aquifer level declining by applying short term management scenarios and predict its effects on rehabilitation.

Key words: Bayesian Networks, Groundwater Management, MCDM, PROMETHEE-II, DSS

1. INTRODUCTION

The water crisis affects the aquifers and made critical situation in most of the countries in arid and semi-arid regions especially in Iran. Although aquifers contain low percentage of water on the earth, but often have fresh water resources and high quality and access to them is as easy as possible that this could lead to a massive water withdrawal from the country's aquifers and groundwater levels are falling. As a result, some plain was considered as forbidden plains that it means the water withdrawal from these aquifers is unauthorized and illegal that has made the serious tensions in water management. Birjand plain as one of the banned plains in Iran, in recent years has been faced with a sharp drop in groundwater level, which requires management practices by integrating predictive tools such as Bayesian Networks (BN); a tool with which we can improve the effectiveness of the proposed management scenarios to predict the aquifer water level. Management scenarios could include reducing water withdrawals from the aquifer, preventing unauthorized wells and so on**.**

Given the critical situation of water resources and lack of efficiency in removing all stress management scenarios in Birjand, the need to apply Multi Criteria Decision Making (MCDM) in this area is necessary**.**In fact by using these methods, depending on socioeconomic status and geographical nature of the region, the best management scenario can be proposed. Therefore, in this study, the practical scenarios will be used to remove water stress in Birjand and by applying Dynamic Bayesian Network (DBN) tools, impacts of management scenarios on improving groundwater will be investigated and risk management will be performed on the plain.

It is important to mention that in the recent years, due to the flexible and simple structure, Bayesian Networks has been used in different water related problems, especially about the

hydrological predictions. Many researchers use it to better understand and model the complex issues of artificial intelligence(Charniak, 1991; Heckerman et al, 1995; Jensen, 1996); groundwater management (Henriksen et al, 2007; Olalla et al, 2007;Farmani et al, 2009);Irrigation and agricultural systems modeling (Batchelor and Cain, 1999); Integrated natural resource management (Borsuk et al, 2004; Hamilton et al, 2007; Johnson et al, 2009; Alameddine et al, 2010) and River basins modeling (Kragt et al, 2009; Merritt et al, 2010; Holzkämper et al, 2012; Madadgar et al.2014).

Also a lot of researches have been done in the field of application of MCDM technique in water resources systems. For example Geng and Wardlaw (2013) applied a MCDM approach in a river basin in China, in order to integrate different purposes in planning, applied management and decision making. In their research a variety of measures based on economic, social and environmental and management scenarios were developed. Compromise planning (CP) based on the distance from the ideal solution was used in the mentioned study. Dabral et al. (2014) using spatial integration and multi criteria decision making, determined the proper locations for artificial recharge of aquifers in India. Azarnivand et al. (2015)presented some Strategic options to restore Urmia Lake basin in Iran through the matrix of strength - weakness - opportunity – threat (SWAT)and ranked them by fuzzy analytic hierarchy process (FAHP) based on sustainable development criteria. According to the description provided, the main innovations of the research include:

- Develop a model to predict groundwater level with the help of probabilistic Bayesian Networks
- Develop an integrated decision support system (DSS) based on predicting the future condition with the Dynamic Bayesian Network and taking into account the economic and social parameters for ranking scenarios to help revive the Birjand aquifer in Iran, using a practical MCDM technique, namely, PROMETHEE-II.

2. METHODOLOGY

2.1 Dynamic Bayesian Network

This research is focused on models that belong to the class of probabilistic graphical models, with their one prominent member, Dynamic Bayesian Networks (DBNs) (Dean and Kanazawa, 1989). BNs are widely used practical tools for knowledge representation and reasoning under uncertainty in equilibrium systems. BNs are probabilistic graphical models that offer compact representations of the joint probability distribution over sets of random variables (Molina et al. 2013).A BN consists of three main elements: a set of variables that represent the factors relevant to a particular environmental system or problem; the relationships between these variables that quantify the links between variables and the set of conditional probability tables (CPTs) that quantify the links between variables and are used to calculate the state of nodes. The first two elements form a Bayesian Diagram and the addition of the third forms a full structure. A BN can be run as a standalone network, but it is possible to link together a number of networks to produce an Object-Oriented Bayesian Network (OOBN) model (Koller and Pfeffer, 1997). OOBNs are based on the Object-Oriented Programming paradigm (OOP) and thus adopt the same attributes used in OOP languages. OOBNs can be utilized in two ways. First, they can be used for time slicing for problems in which processes take place over multiple time periods (Kjaerulff, 1995). This is how DBNs are built. Because BNs are not intended for transient analysis, time slicing provides one way to generate predictive simulations. This is the method that has been adopted for the current study where networks representing different time domains are linked to outputs nodes to produce a dynamic probabilistic model for monthly groundwater level prediction.

Figure 1 is an overview of the concept of dynamic Bayesian Networks. DBN model is a stationary Markov process under the influence of components and changes that are repeated over

time.A dynamic Bayesian Network is a way to expand of Bayesian Network to model the probability distribution of random variables.

A DBN is defined as a pair of BNs ($B_1, B_{\rightarrow}$), where B_1 is a BN represents the initial distribution of Z_1 and $B_{\rightarrow}$ is two time slice BN (2TBN), that defines the transition distribution $P(Z_t|Z_{t-1})$ using a Directed Acyclic Graph (DAG) as follows(Murphy, 2002):

$$P(Z_t|Z_{t-1}) = \prod_{i=1}^{N} P(Z_t^i \Big| P_a(Z_t^i)) \quad (1)$$

where Z_t^i is ith node in time of t and $P_a(Z_t^i)$ is parent of Z_t^i in the graph.

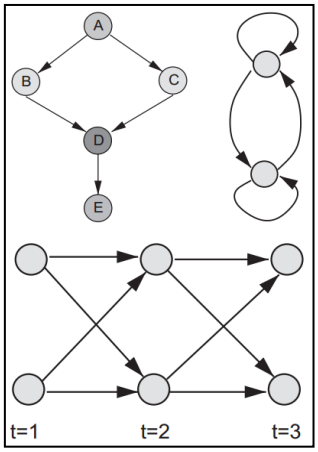

Figure 1. Top left: A simple Bayesian Network. Top right: Network with two feedbacks that they interact with each other; this is not a Bayesian Network. Bottom: time-dependent dynamic Bayesian Networks

2.2 Multi Criteria Decision Making (MCDM)

The first stage in each MCDM problem is to determine the following issues (Roozbahani et al. 2012):

- Identification of the decision makers and stakeholders
- Selection of the criteria and their relative weights
- Selection of the alternatives

After that, selection of a proper method to rank these alternatives is necessary. As it was mentioned before, PROMETHEE-II method has been selected in this paper for purpose of groundwater management. This method has been briefly described in the following section.

2.2.1 PROMETHEE-II

The PROMETHEE family of outranking methods is one of the most recently developed MCDM methods. ROMETHEE is an outranking method for a finite set of alternative actions. It often works based on conflicting criteria. PROMETHEE is also a quite simple ranking method in the concept and application compared with the other methods for multi-criteria analysis (Brans et al., 1986). The implementation of the PROMETHEE II requires the two following additional types of information:

1. The weights of criteria: Determination of the weights is an important step in most multi criteria methods. PROMETHEE II assumes that the decision-maker is able to weight the criteria appropriately, at least when the number of criteria is not too large (Macharis et al. 1998).

2. The preference functions: This function translates the difference between the evaluations of two alternatives into a preference degree ranging from zero to one for each criterion. To facilitate the association of a preference function to each criterion, the developers of the PROMETHEE method have proposed six types of preference functions which have performed satisfactorily for many real world applications. Each shape depends on up to three thresholds: indifference threshold, preference threshold and gaussian threshold.

The method, which was developed first for single DM case, consists of the following steps:

Step1: Determination of deviations based on pair-wise comparison between each set of two alternatives a and b:

$$d = g_j(a) - g_j(b) \tag{2}$$

where $g_j(a)$ and $g_j(b)$ are the values of criterion j for alternatives a and b, respectively.

Step2: Estimation of preference functions $p_j(a,b)$:

$$p_j(a,b) = H(d_j(a,b)) \tag{3}$$

Step 3: Calculation of an overall or global preference index as follows:

$$\pi(a,b) = \sum_{j=1}^{n} w_j p_j(a,b) \tag{4}$$

where $\pi(a,b)$ varies from 0 to 1 and expresses the degree of which alternative a is preferred over b based on all the criteria (n). w_j is the relative weight of jth criterion.

Step 4: Calculation of outranking flows as follows:

The leaving flow**:**

$$\varphi^{+}(a) = \sum_{b \in A} \frac{\pi(a,b)}{n-1} \tag{5}$$

The entering flow:

$$\varphi^{-}(a) = \sum_{b \in A} \frac{\pi(b,a)}{n-1} \tag{6}$$

Step 5: Calculation of net outranking flow/PROMETHEE II complete ranking as follows:

$$\varphi(a) = \varphi^{+}(a) - \varphi^{-}(a) \tag{7}$$

where $\phi(a)$ denotes the net outranking flow for each alternative. A scenario with highest value of net flow represents the best scenario.

3. CASE STUDY AND RESULTS

3.1 Study Area

Birjand catchment basin in the Loot Desert in Iran is located 485 km south of Mashhad and in

the East on Iran. The climate is dry and in recent years due to uncontrolled withdrawal of water from aquifers, the region is faced with declining groundwater levels. According to the water level, the average water level drawdown in the Birjand aquifer during last 50 years has been 0.4 meters per year and aquifer deficit volume is about 10.75 million cubic meters. The general direction of groundwater flow, from East to West and from the north and south sides toward the center of the aquifer is in progress**.** Figure 2 shows the study area along the piezometric network.

For DBN modeling regarding the explicit input data, Necessary Path Condition (NPC) method with 5% confidence level as well as Estimation-Maximization(EM) method was conducted for calibration of BN's structure and parameters, respectively**.** The calibration period includes 12 years of historical data record (1997 to 2008) and validation data includes a period of 5 years (2009 to 2013) with monthly time step. In this paper, six predictors have been used to predict the groundwater level in the next month (WTT): Rainfall (Rain), Temperature (T), Evaporation (ET), Recharge and discharge in the current month as well as groundwater table in the current month (WT). Also by defining 10 different scenarios for sensitivity analysis to predict the groundwater level in the next month, uncertainties related to the effect of predictive parameters have been investigated. The final selected DBN structure has been shown in Fig. 3.

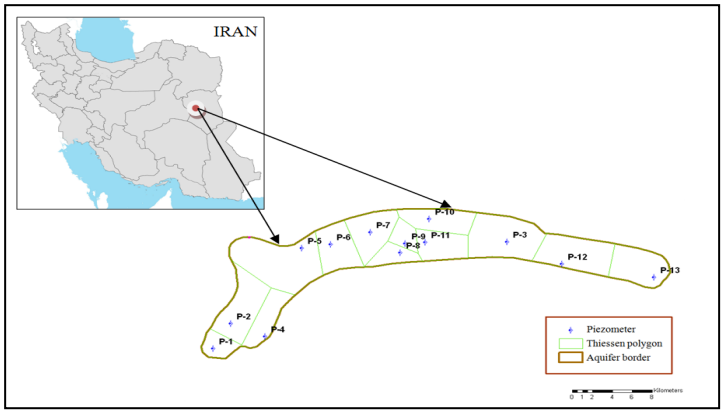

Figure 2. Thiessen network of Birjand aquifer

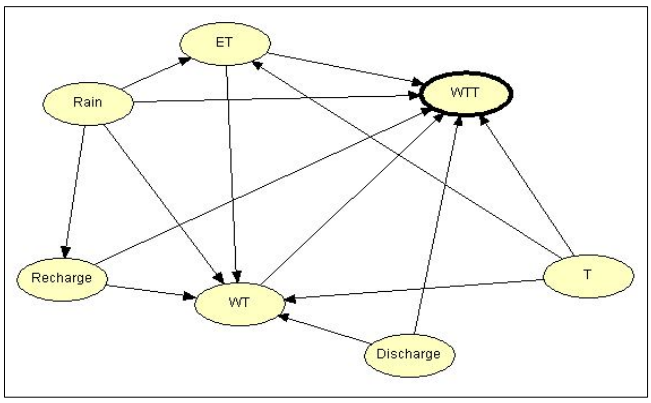

Figure 3. Selected BN structure for groundwater level prediction

Values of the coefficient of determination (R^2) and Root Mean Square Error (RMSE) for superior prediction scenario (Fig. 3) per 13 piezometers were obtained and the accuracy of piezometers is shown in Table 1.

Since groundwater hydrograph is an appropriate tool to evaluate the prediction accuracy, using it, is more desirable to show the efficiency of DBN Model**.**Therefore the amount of groundwater hydrograph was calculated during the five years of validation period. As can be seen in Figure 4, Bayesian Networks has been able to predict with reasonable accuracy.

Table 1. Accuracy of water level prediction in 13 piezometers

Piezometer No.	R^2	RMSE (m)
1	0.12	1.43
2	0.43	0.44
3	0.06	0.41
4	0.97	1.94
5	0.96	2.66
6	0.99	0.77
7	0.99	0.82
8	0.87	0.84
9	0.98	0.63
10	0.98	0.20
11	0.18	3.58
12	0.79	2.09
13	0.16	2.13

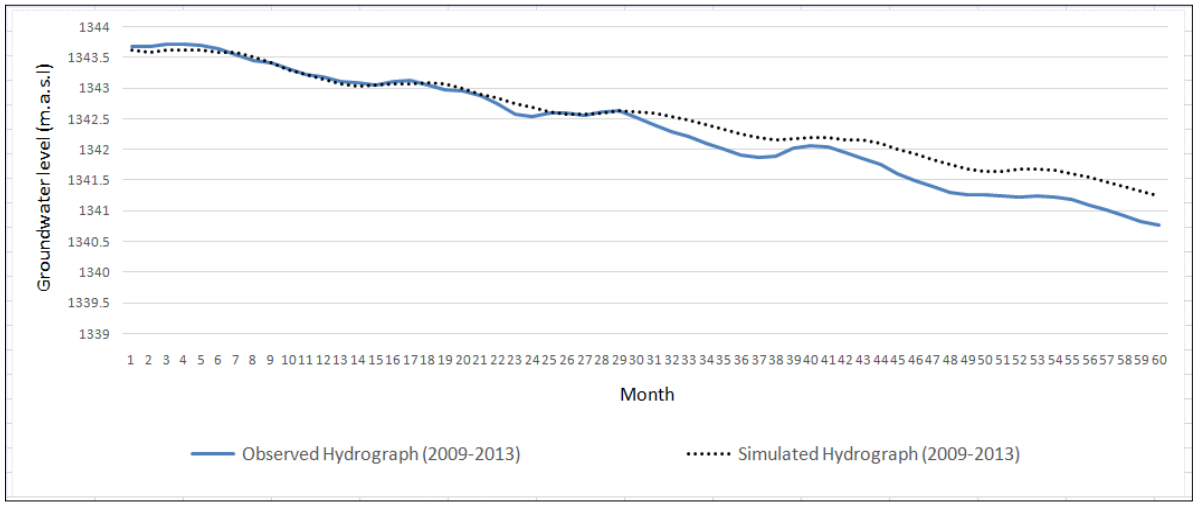

Figure 4. Comparison of observed and predicted groundwater in Birjand plain

3.2 Decision making scenarios for aquifer restoration

The rehabilitation scenarios which are recommended for the plain should suit climatic conditions, geographical potentials of this region and have the operational capability. The scenarios proposed in this research, with research and study and use of the viewpoints of local decision makers in the field of water resources in the study area, were obtained. These scenarios include the following:

S1: Change in surface irrigation to pressurized irrigation systems; S2: Removal of unauthorized wells; S3: Improvement of artificial recharge projects; S4: Installation of smart water meters**.**

3.3 Decision criteria and their values

To conduct the MCDM method, a number of criteria defined in this study based on the existing studies and interview with 20 researchers, professors and decision makers. These criteria have been listed as follows:

C1: Socio-cultural acceptance and participation of stakeholders; C2: Efficiency of applying of scenarios in improvement of the aquifer's water level; C3: Cost of implementation; C4: Ease of implementation. The final decision matrix of the current study is shown in Table 2. In addition, relative weights of four criteria obtained by AHP method (Saaty, 1980) can be seen in this table.

Table 2. Decision matrix of alternative

Scenario	Criteria			
	C1 (w=0.28)	C2 (w=0.30)	C3 (w=0.33)	C4 (w=0.09)
A1	5.7	21	32513	4.9
A2	4.3	12	389	6.7
A3	6.6	21	5400	5.5
A4	5.5	17	16775	5.7

3.4 Data analysis and ranking results

In order to use MCDM method, the precedence orders and preference of criteria have been imposed in the criteria for each decision maker and then their ranking results obtained by PROMETHEE-II, are aggregated to find the group ranking of alternatives. Table 3 shows the final net flows and complete rankings. According the ranking, scenario 3 (Artificial recharge projects) and scenario 2 (The removal of unauthorized wells) have obtained the first and second highest ranks, respectively which must be considered by decision makers in short and long term management in this area. The the efficiency of applying of scenario 3 in improvement of groundwater level in the end of 2015 is shown in Figure 5 and compared with the condition that no risk management strategy has been implemented in the study area (current trend continue). As it can be viewed in this figure, this scenario can increase the water level up to 21 cm from current situation.

Table 3. Final ranking results

Rank	Scenario	Net flow
1	S3	0.52
2	S2	-0.07
3	S1	-0.21
4	S4	-0.24

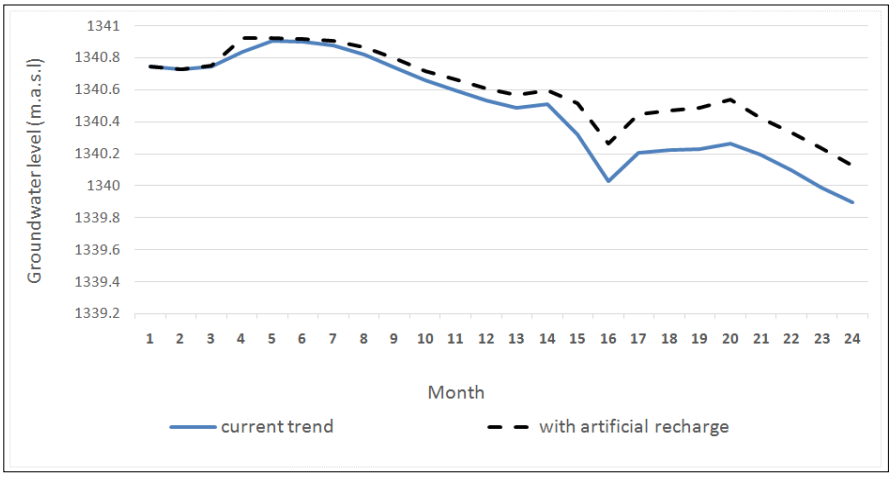

Figure 5. Effect of implementation of selected scenario in groundwater level improvement (2014-2015)

4. CONCLUSION

In this paper, we introduced a comprehensive DSS for groundwater risk management by integration of DBN and MCDM techniques. The capabilities of this framework were evaluated in one of important and under stressed aquifers in Iran. Time dependent Bayesian model which aims to reduce the uncertainty and predict the monthly groundwater level was able to simulate the effects of different management scenarios on improving the groundwater level. To prioritize these scenarios, after presenting the results of the Bayesian Network, four appropriate criteria were determined.

Based on these criteria, scenarios were evaluated using PROMETHEE-II as one of the most applicable MCDM techniques. In fact, the decision matrix with four criteria and four scenarios was obtained and then MCDM PROMETHEE method was performed and scenario of optimization of artificial recharge plans was chosen as the best management scenario in the study area. By analyzing the results presented in this study, it is observed that by applying risk management methods and taking into account the conditions prevailing in each region, not only we can obtain the best scenario management, but also the impact of management scenarios on groundwater levels can be easily calculated by DBN rather than existing groundwater models such as MODFLOW. The approach proposed in this study as a Decision Support System, can be utilized by managers and users of water resources systems to reduce water shortage crisis in other similar study areas that are under stressful conditions from water resources point of view**.**

REFERENCES

Alameddine, I., Cha, Y. K., Reckhow, K. H., 2010. An evaluation of automated structure learning with Bayesian Networks: an application to estuarine chlorophyll dynamics. Environmental Modelling and Software. 26: 163–172.

Azarnivand, A., Madani, F.S.H., Banihabib, M.E. 2015. Extended fuzzy analytic hierarchy process approach in water and environmental management (case study: Lake UrmiaBasin,Iran). Environ Earth Sci. 73: 13–26.

Batchelor, C., Cain, J., 1999. Application of belief networks to water management studies. Agricultural Water Management. 4: 51–57.

Borsuk, M., Stow, C., Reckhow, K., 2004. A Bayesian network of eutrophication models for synthesis, prediction, and uncertainty analysis. Ecological Modelling. 173: 219–239.

Brans, J., Vincke, P., Mareschal, B., 1986. How to select and how to rank projects: the PROMETHEE method. European Journal of Operational Research. 24(2): 228–238.

Charniak, E., 1991. Bayesian Networks without tears. Artificial Intelligence Magazine. 12: 50–63.

Dabral, S., Bhatt B., Joshi, J.P., Sharma, N. 2014. Groundwater suitability recharge zones modelling - A GIS application. ISPRS - International Archives of the Photogrammetry, Remote Sensing and Spatial Information Sciences. XL-8: 347-353.

Dean, T., Kanazawa, K., 1989. A model for reasoning about persistence and causation. Computational Intelligence. 5 (2): 142–150.

Farmani, R., Henriksen, H.J., Savic, D., 2009. An evolutionary Bayesian belief network methodology for optimum management of groundwater contamination. Environmental Modelling and Software. 24: 303–310.

Geng, G., Wardlaw, R., 2013. Application of Multi-Criterion Decision Making Analysis to Integrated Water Resources Management. Water Resour Manage. 27:3191–3207.

Hamilton, G. S., Fielding, F., Chiffings, A. W., Hart, B. T., Johnstone, R. W., Mengersen, K., 2007. Investigating the use of a Bayesian Network to model the risk of Lyngbyamajuscula bloom initiation in Deception Bay, Queensland, Australia. Human and Ecological Risk Assessment: An International Journal. 13: 1271–1287.

Heckerman, D., Mamdani, A., Wellman, M., 1995. Real world applications of Bayesian Networks. Communication of the ACM. 38: 24–26.

Henriksen, H.J., Rasmussen, P., Brandt, G., Bulow, D.V., Jensen, F.V. 2007. Public participation modelling using Bayesian Networks in management of groundwater contamination. Environmental Modelling and Software. 22: 1101–1113.

Holzkämper, A., Kumar, V., Surridge, B. W. J., Paetzold, A., Lerner, D.N., 2012. Bringing diverse knowledge sources together – a meta-model for supporting integrated catchment management. Journal of Environmental Management. 96: 116–127.

Jensen, F., 1996. An Introduction to Bayesian Networks. Springer-Verlag D, Heidelberg.

Johnson, S., Fielding, F., Hamilton, G., Mengersen, K., 2009. An integrated Bayesian Network approach to Lyngbya majuscula bloom initiation. Marine Environmental Research. 69: 27–37.

Kjaerulff, U., 1995. dHugin: a computational system for dynamic time-sliced Bayesian Networks. Int. J. Forecast. 11: 89–111.

Koller, D., Pfeffer, A., 1997. Object-oriented Bayesian Networks. In: Proceedings of the Thirteenth Annual Conference on Uncertainty in Artificial Intelligence UAI-97, Providence, Rhode Island.

Kragt, M. E., Newham, L. T. H., Jakeman, A. J., 2009. A Bayesian Network approach to integrating economic and biophysical modelling.18th World IMACS/MODSIM Congress. 13–17 July,Cairns, Australia.

Macharis, C., Brans, J., Mareschal, B., 1998. The GDSS PROMETHEE procedure: a PROMETHEE-GAIA based procedure for group decision support. Journal of Decision Systems. 7: 283–307

Madadgar, S., Moradkhani, H., 2014. Spatio-temporal drought forecasting within Bayesian Networks. Journal of Hydrology. 512: 134–146.

Merritt, W. S., Ticehurst, J. L., Pollinoa, C., Fu, B. 2010. The Value of using Bayesian Networks in Environmental Decision Support Systems to support natural resource management. In: International Congress on Environmental Modelling and Software Modelling for Environment's Sake.5th Biennial Meeting, Ottawa, Canada.

Molina, J. L. Velázquez, D. P. Aróstegui, J. L. G. Velázquez, M.P., 2013. Dynamic Bayesian Networks as a Decision Support tool for assessing Climate Change impacts on highly stressed groundwater systems. Journal of Hydrology. 479: 113–129.

Murphy, K. p., 2002. Dynamic Bayesian Networks: Representation, Inference and Learning. PHD.Thesis, University of California, Berkeley, USA.

Olalla, F. M. D. S., Dominguez, A., Ortega, F., Artigao, A., Fabeiro, C., 2007. Bayesian Networks in planning a large aquifer in Eastern Mancha Spain. Environmental Modelling and Software. 22: 1089–1100.

Roozbahani, A., Zahraie, B., Tabesh, M., 2012. PROMETHEE with Precedence Order in the Criteria (PPOC) as a New Group Decision Making Aid: An Application in Urban Water Supply Management. Water resources management. 26(12): 3581-3599.

Saaty, T. L., 1980. The Analytic Hierarchy Process. McGraw-Hill, New York.

Proceedings of the 10th World Congress of EWRA 'Panta Rhei', 5-9 July 2017, Athens, Greece
© 2017 *European Water Resources Association*

Analytical solutions to groundwater flow around wells using discharge potential

S. Korkmaz
Uludağ University, Department of Civil Engineering, 16059 Bursa, Turkey
e-mail: skorkmaz06@gmail.com

Abstract: In general, potential flow describes the flow vector field as the gradient of some scalar potential function. Various definitions of potential function have been used in literature. In this study, the discharge potential was used to solve the problem of groundwater flow around wells. The advantage of discharge potential is that it is applicable to combined confined and unconfined groundwater flow. When the discharge potential satisfies Laplace's equation, potential theory is applicable. When two or more discharge potentials each satisfy Laplace's equation, their sum also satisfies it which means that the principle of superposition can be implemented. Using the latter, solutions to various groundwater flow problems were made. One advantage of analytical solution using discharge potentials is that the size of the computation domain does not influence the solution unlike numerical methods such as finite differences in which the entire boundary condition surrounding the computation domain has to be specified. When using the method presented, however, specifying an observed head at one single point is enough to reach a solution in the case of an infinitely large aquifer. For presentation of the results of two-dimensional flow problems, flownets were drawn by interpolation from discrete values of potential function and stream function.

Key words: groundwater, potential flow, discharge potential, well

1. INTRODUCTION

There are many numerical and analytical methods for solving the problem of groundwater flow around wells. Most widely used numerical methods are finite differences and finite element. With the ongoing advance in computing technology, it has become possible to calculate the groundwater head on very fine grids. For example, MODFLOW (McDonald and Harbaugh 1988) and MIKE-SHE (Refsgaard and Storm 1995) are among the most widely used software for numerical modelling of groundwater flow. However, the question of how to impose the boundary conditions of an infinite aquifer still remains a challenge in such numerical approaches. It is usually overcome by modelling an extensive aquifer which leads to additional computation time. This constitutes one important drawback in numerical solutions.

On the other hand, there are useful analytical relations to solve some common groundwater flow problems. For example, Thiem (1906) introduced a basic equation to solve for the transmissivity of a confined aquifer that is pumped by a fully penetrating well. Theis (1935) presented the well function to be used for the interpretation of unsteady pumping data in confined aquifers. Kruseman and de Ridder (1990) and Lohman (1972) presented methods for finding aquifer parameters from aquifer tests.

In this study, an analytical method involving discharge potentials was used to solve the problem of groundwater flow around wells. The concept of discharge potential was first introduced by Strack (1981a, 1981b). Haitjema (1995) used it as a basis for the analytical element method in which hydrogeological features are represented by elements like line sinks or line doublets. The advantage of using discharge potential is that it satisfies Laplace's equation and the potential theory is applicable.

2. METHODOLOGY

Two main equations describing groundwater flow are specific discharge derived from Darcy's Law (Darcy 1856) and the continuity equation. For a 3-dimensional flow in a homogeneous and isotropic medium:

$$q_x = -K\frac{\partial h}{\partial x} \tag{1a}$$

$$q_y = -K\frac{\partial h}{\partial y} \tag{1b}$$

$$q_z = -K\frac{\partial h}{\partial z} \tag{1c}$$

where q_x, q_y, q_z are specific discharges in x, y and z directions; K is the hydraulic conductivity; and h is the hydraulic head in the aquifer. Most of the time the aquifer is assumed to be homogeneous and isotropic in the horizontal plane. If it is anisotropic in the 3-D domain then K_x, K_y, and K_z should be used to represent hydraulic conductivities in x, y and z directions respectively. When employing the Dupuit-Forchheimer assumption the vertical flow component defined in Eq.(1c) can be ignored. The continuity equation is defined as:

$$\frac{\partial q_x}{\partial x} + \frac{\partial q_y}{\partial y} = 0 \tag{2}$$

Combining Eqs.(1a)-(1b) and (2) gives

$$\frac{\partial^2 h}{\partial x^2} + \frac{\partial^2 h}{\partial y^2} = 0 \tag{3}$$

which is the Laplace's equation. For a confined aquifer, the discharge vector in x-direction can be written as follows:

$$Q_x = -Kb\frac{\partial h}{\partial x} = bq_x \tag{4}$$

where b is the thickness of the confined aquifer. If Eq.(2) is multiplied by b, the continuity equation can be written in terms of the discharge vector:

$$\frac{\partial Q_x}{\partial x} + \frac{\partial Q_y}{\partial y} = 0 \tag{5}$$

Now, a discharge potential $\Phi(x, y)$ can be defined as in the following:

$$\Phi = Kbh \tag{6}$$

so that

$$Q_x = -\frac{\partial \Phi}{\partial x} \text{ and } Q_y = -\frac{\partial \Phi}{\partial y} \tag{7}$$

If Eq.(7) is combined with Eq. (5), the following Laplace's equation is obtained:

$$\frac{\partial^2 \Phi}{\partial x^2} + \frac{\partial^2 \Phi}{\partial y^2} = 0 \tag{8}$$

Generally, potential flow describes the flow vector field as the gradient of some scalar potential function. In this case, the discharge vector field Q_x and Q_y are equal to the negative of gradient of

the discharge potential $\Phi(x, y)$. For the solution of a groundwater flow problem in a confined aquifer Eq.(8) can be used instead of Eq.(3) provided that the boundary conditions are defined in terms of $\Phi(x, y)$.

Solution of groundwater flow problem in an unconfined aquifer is always more complicated than that in a confined aquifer due to the unknown position of the phreatic surface. Specific discharges are defined in the same manner as in a confined aquifer. However, the discharge vector is defined as:

$$Q_x = -Kh\frac{\partial h}{\partial x} = hq_x \tag{9}$$

In order for Q_x to be related to the discharge potential as in Eq.(7), the discharge potential should be chosen as:

$$\Phi = \frac{1}{2}Kh^2 \tag{10}$$

while Eqs. (7) and (8) remain valid for unconfined aquifer.

2.1 One-dimensional groundwater flow

The solution of a 1-D flow problem with Dirichlet boundary conditions on both sides of the flow domain yields the following result for both confined and unconfined aquifers in terms of $\Phi(x, y)$:

$$\Phi = \frac{\Phi_2 - \Phi_1}{L}x + \Phi_1 \tag{11}$$

where Φ_1 and Φ_2 are boundary conditions defined using Eq.(6) for a confined aquifer and Eq.(10) for an unconfined aquifer. Similarly, in order to reach the solution in terms of $h(x, y)$ the left-hand side of Eq.(11) is replaced by Eq.(6) for a confined aquifer and by Eq.(10) for an unconfined aquifer.

2.2 Combined confined and unconfined flow

A confined aquifer with Dirichlet boundary conditions (known head) on both sides may become extremely drained so that the hydraulic head along a portion of the aquifer falls below the confining layer causing unconfined flow conditions at that portion. This situation creates combined confined and unconfined flow. In order for Eq.(11) to be valid for such a case, the discharge potential should be continuous everywhere in the flow domain. At the interface of confined and unconfined flow conditions the value of h is equal to b. Using the above presented definitions of discharge potential at the interface is computed as $\Phi_i = Kb^2$ for confined flow and $\Phi_i = \frac{1}{2}Kb^2$ for unconfined flow, therefore the function is discontinuous at the interface. To overcome this issue, the discharge potential for confined flow is modified as follows (Strack 1981a):

$$\Phi = Kbh - \frac{1}{2}Kb^2 \tag{12}$$

As a result, to solve the combined confined and unconfined flow problem, Eq.(12) should be used for confined portion and Eq.(10) for unconfined portion. Both equations will yield the same result at the interface which is $\Phi_i = \frac{1}{2}Kb^2$. The additional constant at the right-hand side of Eq.(12) does not affect the solution. As a result, the solution given in Eq.(11) will be valid.

2.3 Two-dimensional groundwater flow

The potential function, $\Phi(x, y)$, can be calculated anywhere in the domain in a 2-D flow problem. Using discrete values of potential function, equipotential contours can be drawn. The values of contours will decrease in the flow direction. As $\Phi(x, y)$ satisfies the Laplace's equation, the potential theory is applicable. There exists also a stream function, $\Psi(x, y)$, which satisfies the Laplace's equation. $\Phi(x, y)$ and $\Psi(x, y)$ are related to each other as in the following Cauchy-Riemann equations:

$$\frac{\partial \Psi}{\partial x} = -\frac{\partial \Phi}{\partial y} \tag{13a}$$

$$\frac{\partial \Psi}{\partial y} = \frac{\partial \Phi}{\partial y} \tag{13b}$$

Similarly, contours of stream function can also be drawn using discrete values of stream function in the flow domain. These contours represent streamlines. Streamlines are tangential to flow vectors and intersect the equipotentials perpendicularly. Streamlines have the values of stream function. The difference between the values of two streamlines represent the flow rate passing in between the two. Usually the results of such problems are presented using flownets. If the flownet is formed of squares:

$$\Delta Q = |\Delta \Phi| = |\Delta \Psi| \tag{14}$$

2.3.1 Flow around a pumping well

Flow around pumping wells are solved using polar coordinate system on r-α plane in which the origin is at the center of well. When there is one single pumping well in an infinitely large aquifer, the pumping rate Q is equal to the total discharge from the aquifer towards the well. If Q is the total flow rate abstracted from the well then:

$$Q_r = \frac{-Q}{2\pi r} \tag{15}$$

where r is the radial distance measured outwards from the well, Q_r is the flow rate towards the well per unit width of the aquifer at a distance r from the well. Negative sign indicates the direction towards the well. The discharge potential is introduced as follows:

$$Q_r = -\frac{d\Phi}{dr} \tag{16}$$

In order to solve for $\Phi(r)$ observation at one single point is required, such as

$$\text{at } r = r_0 \quad \Phi(r_0) = \Phi_0 \tag{17}$$

Integrating Eq.(16) with respect to r gives

$$\Phi = \frac{Q}{2\pi} \ln r + c \tag{18}$$

and using the boundary condition in Eq.(17) gives

$$\Phi = \frac{Q}{2\pi} \ln \frac{r}{r_0} + \Phi_0 \tag{19}$$

In order to form a flownet, streamlines should be drawn. In this case streamlines can be drawn with equal angles and all pointing to the well. Therefore,

$$\Psi = \frac{Q}{2\pi}\alpha \tag{20}$$

where α is measured from +x axis in between $-\pi<0<\pi$. In *x*-*y* coordinate system:

$$\Psi = \frac{Q}{2\pi}\tan^{-1}\frac{y}{x} \tag{21}$$

2.3.2 Flow around multiple pumping wells

When there is more than one pumping well, the superposition principle is applied to solve for $\Phi(r)$. Individual solutions for two wells on two identical aquifers are given below:

$$\Phi_1 = \frac{Q_1}{2\pi}\ln r_1 + \mathrm{c}_1 \tag{22a}$$

$$\Phi_2 = \frac{Q_2}{2\pi}\ln r_2 + \mathrm{c}_2 \tag{22b}$$

where r_1 and r_2 are radial distances measured outwards from well 1 and well 2 respectively. If these two wells are on the same aquifer, the solutions in Eq.(22) can be superposed:

$$\Phi = \frac{Q_1}{2\pi}\ln r_1 + \frac{Q_2}{2\pi}\ln r_2 + c_3 \tag{23}$$

When the boundary condition in Eq.(17) is used:

$$\Phi = \frac{Q_1}{2\pi}\ln\frac{r_1}{r_0^{(1)}} + \frac{Q_2}{2\pi}\ln\frac{r_2}{r_0^{(2)}} + \Phi_0 \tag{24}$$

where $r_0^{(1)}$ and $r_0^{(2)}$ are the distances of the boundary condition from well 1 and well 2 respectively. The stream function is calculated in a similar manner:

$$\Psi = \frac{Q_1}{2\pi}\alpha_1 + \frac{Q_2}{2\pi}\alpha_2 \tag{25}$$

in which α_1 and α_2 are angles measured from +x axis originating at respective wells.

2.3.3 Pumping well in a uniform flow field

The problem of pumping well and a uniform flow field is similarly solved using the superposition principle. The potential function of a uniform flow Q_0 in +x direction is solved using the relation given in Eq. (7):

$$Q_0 = -\frac{\partial\Phi}{\partial x} \tag{26}$$

Integrating Eq.(26) gives

$$\Phi = -Q_0 x + c \tag{27}$$

and the stream function is

$$\Psi = -Q_0 y \tag{28}$$

Superposing Eqs. (27) and (18) gives

$$\Phi = -Q_0 x + \frac{Q}{2\pi} \ln r + c \tag{29}$$

And superposing Eqs. (28) and (20) gives

$$\Psi = -Q_0 y + \frac{Q}{2\pi} \alpha \tag{30}$$

3. APPLICATION

The following example problems were solved using the methods described above.

3.1 Combined confined and unconfined flow

A confined aquifer has a length of L=500 m, a thickness of b=20 m and a hydraulic conductivity of K=0.001 m/s. In a dry season it becomes extremely drained so that the boundary conditions are $h(0)$=30 m and $h(500)$=5 m where the second boundary condition indicates a head lower than the thickness of the aquifer. The solution in terms of discharge potential is calculated from Eq.(11). The interface potential is calculated as $\Phi_i = \frac{1}{2} K b^2 = 0.2$ and heads are computed from Eq.(12) if $\Phi > \Phi_i$ and from Eq.(10) if $\Phi < \Phi_i$. The result is illustrated in Fig.1 in terms of heads. The interface is at x=258 m and unconfined flow occurs at the right-hand side of the interface. The non-linear head distribution of unconfined flow is clearly visible in Fig.1.

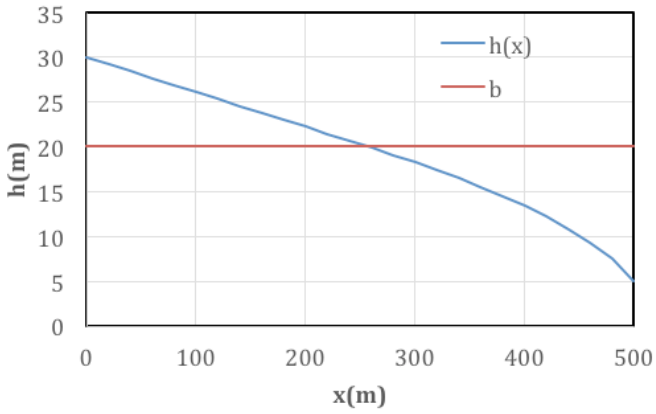

Figure 1. Example solution for combined confined and unconfined flow.

3.2 Flow around multiple pumping wells

Two pumping wells are drilled on an infinitely large unconfined aquifer with a hydraulic conductivity of K=0.01 m/s. Pumping rates are Q_1=30 m^3/s and Q_2=35 m^3/s. The first well is located at (x, y)=(150, 300) and the second one at (x, y)=(350, 100). An observation well is located at (x, y)=(400, 300) and measures a groundwater head of h_0=80 m. The solution is computed from

Eqs.(24) and (25). The potential at the observation well is calculated as $\Phi_0 = \frac{1}{2}Kh_0^2 = 32$. $\Phi(x, y)$ and $\Psi(x, y)$ are calculated over a domain of 500 m x 500 m with Δx=5 m and Δy=5 m intervals. The contour plot of equipotentials and streamlines are shown in Fig.2. It is also possible to create a plot of groundwater heads by conversion from Φ(x, y) to h(x, y) using Eq.(10). Lines emerging from wells towards –x direction are called branch cut. The continuity equation (Eq. 5) is non-zero at the wells which means that the Laplace's equation is not valid at the wells. As a result, flow into the wells exists in –x direction creating a jump in streamline values which is equal to the value of flow rate.

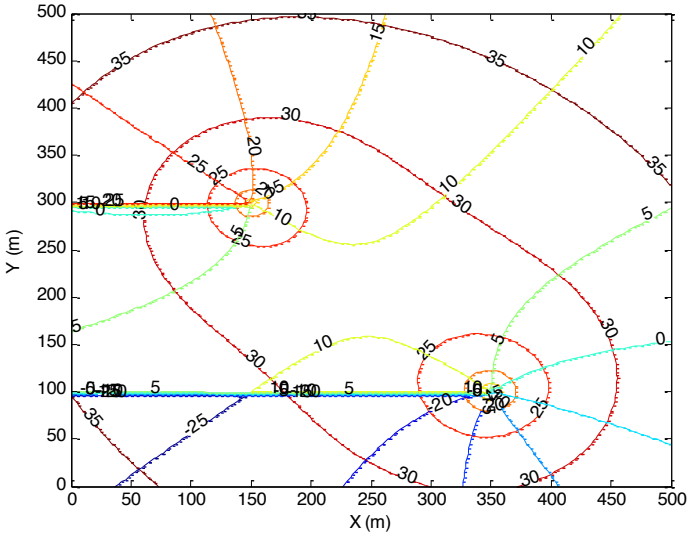

Figure 2. Contour plot of equipotentials and streamlines for two pumping wells in an unconfined aquifer.

3.3 Pumping wells in a uniform flow field

In this example, a uniform flow of Q_0=0.04 m^2/s in +x direction is superposed to the above problem. Solution is made by modifying Eqs.(29) and (30) for two wells. The flownet is depicted in Fig.3. The capture zone of the well on the left-hand side is significantly reduced due to the uniform flow in +x direction.

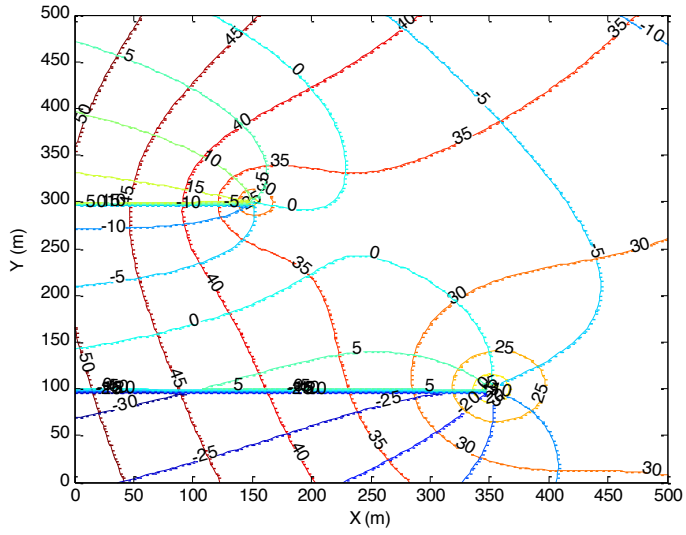

Figure 3. Contour plot of equipotentials and streamlines for two pumping wells in an unconfined aquifer with a uniform flow in +x direction.

4. CONCLUSION

Analytical solutions to several groundwater flow problems were made using the discharge potential. This brings the advantage of linear governing equations for both confined and unconfined flows. It is even possible to obtain a single continuous solution for combined confined and unconfined flow in the same aquifer. In 2-D flows, a flownet composed of equipotentials and streamlines can be drawn. Capture zones of wells and flow directions in the aquifer are easily demonstrated. From equipotentials it is possible to obtain the groundwater heads. As the governing equation is linear, the superposition principle can be applied to various cases, such as, multiple pumping wells and pumping wells in a uniform flow field. One important advantage of this method over numerical methods is that the solution is independent of the size of the computation domain, that is, infinite aquifer can be modelled without any concern for boundary conditions. Known head value at one single point such as a measurement at an observation well is sufficient to reach a solution.

REFERENCES

Darcy, H., 1856. “Les Fontaines Publiques de la Ville de Dijon”, Dalmont, Paris.

Haitjema, H.M. 1995. *Analytic Element Modeling of Groundwater Flow*. Academic Press, CA.

Kruseman, G.P., and de Ridder N.A. 1990. *Analysis and Evaluation of Pumping Test Data*. (2nd ed.), Publication 47, Intern. Inst. for Land Reclamation and Improvement, Wageningen, The Netherlands, 370 p.

Lohman, S.W., 1972. “Ground-Water Hydraulics”, U.S. Geological Survey Professional Paper 708.

McDonald, M. G., and Harbaugh, A. W., 1988. “A modular threedimensional finite-difference ground-water flow model.” *Techniques of water-resources investigations*, U.S. Geological Survey, Denver, 586.

Refsgaard, J. C., and Storm, B. J., 1995. “MIKE SHE.” *Computer models of watershed hydrology*, V. P. Singh, ed.,Water Resources Publications, Littleton, CO, 809–846.

Strack, O. D. L., 1981a. “Flow in aquifers with clay lamina. I. The comprehensive potential”. *Water Resourc. Res*.,17, 985-992.

Strack, O. D. L., 1981b. “Flow in aquifers with clay lamina. II. Exact solution”. *Water Resourc. Res*., 17, 993-1004.

Theis, C. V., 1935. "The relation between the lowering of the piezometric surface and the rate and duration of discharge of a well using ground-water storage". *Transactions American Geophysical Union*, 16, 519–524.

Thiem, G., 1906. *Hydrologische methoden* (in German). Gebhardt, Leipzig.

Proceedings of the 10th World Congress of EWRA 'Panta Rhei', 5-9 July 2017, Athens, Greece
© 2017 *European Water Resources Association*

Management of coastal hydrosystems through the application of free and open source software tool FREEWAT

M. Perdikaki[1,2], C. Pouliaris[1,2], I. Borsi[3], R. Rossetto[4] and A. Kallioras[1,2]
[1] *Lavrion Technological & Cultural Park of NTUA, Greece*
[2] *National Technical University of Athens, School of Mining & Metallurgical Engineering, Greece*
[3] *TEA SISTEMI Spa, Pisa, Italy*
[4] *Sant'Anna School of Advanced Studies, Institute of Life Sciences, Pisa, Italy*
[*] *e-mail: mperdikaki@metal.ntua.gr*

Abstract: FREEWAT is an open source and public domain GIS integrated modelling environment for the simulation of water quantity and quality in surface water and groundwater with an integrated water management and planning module. It involves the integration of: (i) Observation-Analysis Tool (OAT) that combines a number of time-series processing functionalities for statistical analysis of observations and help prepare model input data; (ii) AkvaGIS that involves hydrochemical and hydrogeological Analysis Tools and (iii) Groundwater Flow (MODFLOW-2005) and Transport modeling modules. FREEWAT platform will be applied in a typical Mediterranean environment that hosts a naturally occurring –and today degraded– coastal wetland with the characteristics of a distinct ecosystem linked to a typical coastal hydrogeological system of a semi-arid region; and therefore can serve as a model for similar systems world-wide. The geo-hydrological setting of the area involves a multi-layer aquifer system consisting of (i) an upper un-consolidated formation of depositional unit dominated mostly by fluvial sediments and (ii) the surrounding and underlying karstified marbles; both being linked to the investigated wetland and also subjected to seawater encroachment.

Key words: Groundwater modelling, Open source public domain GIS integrated GW modelling, Marathon coastal hydrosystem, water resources management

1. INTRODUCTION

Water framework directive as well as its daughter directives, consider integrated water resources management as a matter of ample priority for the European Union Member States. Water resources simulation is widely accepted as a crucial pillar in the management process, by means that it provides a sophisticated tool for stakeholders, decision and policy makers.

FREEWAT is an open source and public domain GIS integrated modelling environment for the simulation of water quantity and quality in surface water and groundwater with an integrated water management and planning module. FREEWAT aims at promoting water resource management by simplifying the application of the Water Framework Directive and other EU water related Directives.

It provides an integration of existing software modules for water management in a single environment into the GIS based FREEWAT platform and supports their application in an innovative participatory approach gathering technical staff and relevant stakeholders (in primis policy and decision makers) in designing scenarios for the proper application of water policies. The open source characteristics of the platform allow to consider this an initiative "ad includendum" (looking for inclusion of other entities), as further research institutions, private developers etc. may contribute to the platform development.

The core of the FREEWAT platform (Figure 1) is the SID&GRID (Rossetto et al. 2013) framework in its version ported to the QGIS desktop (Borsi et al., 2013). FREEWAT is conceived as a composite plugin for the well-known GIS open source desktop software QGIS. As composite plugin, it is designed as a modular ensemble of different tools: some of them can be used

independently, while some modules require the preliminary execution of other tools. In this framework, the following tool classifications can be defined:

- Tools for the analysis, interpretation and visualization of hydrogeological and hydrochemical data and quality issues, also focusing on advanced time series analysis, embedded in akvaGIS module.
- Simulation of models related to the hydrological cycle and water resources management: flow models, transport models, crop growth models, management and optimization models (also related to irrigation management and rural issues).
- Tools to perform model calibration, sensitivity analysis and uncertainty quantifications.
- Additional tools for general GIS operations to prepare input data, and post-processing functionalities (module OAT – Observation and Analysis Tool).

The modelling environment is based on the well-known codes of the MODFLOW family (USGS)– basically used for analysis of groundwater systems. The version integrated in FREEWAT is the MODFLOW One Water Hydrologic Model (MODFLOW-OWHM; Hanson et al., 2014), aiming at performing simulations of systems where conjunctive use of surface- and ground-water is of concern. It also includes a specific module to run management decisions and evaluate different irrigation scenarios, which is coupled to a crop growth module for simulating crop yield.

Along to this, simulation of solute transport in aquifers may be performed by means of the MT3DMS code (Zheng, 2010), including density dependent capabilities using the SEAWAT code (Langevin et al., 2007).

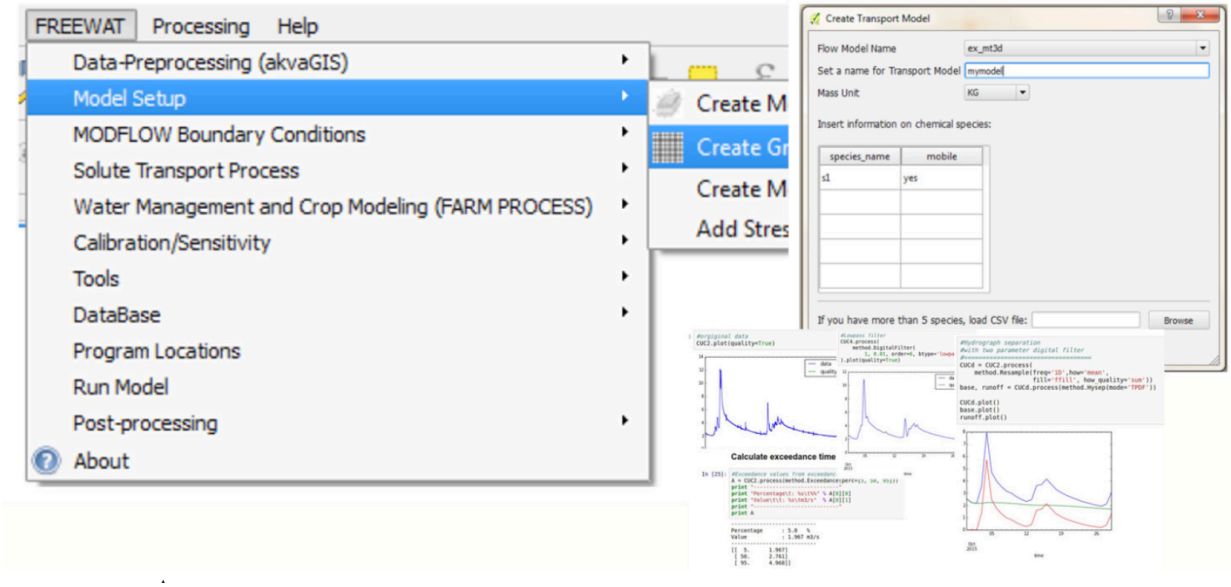

Figure 1. Example of the FREEWAT main menu with some graphs produced using the OAT module.

The modelling framework is completed by including GUIs (Figure 2) to run automated codes (Poeter et al., 2014) for assessing sensitivity analysis, calibration and uncertainty evaluation of hydrologic models (Foglia et al., 2007).

A set of tools to facilitate the management of a large number of physical and chemical parameters, to ensure compliance with standard regulatory guidelines (with a special focus on requirement deriving from the Groundwater Directive), is included via the akvaGIS module (developed by the IDAEA-CSIC).

Finally, the FREEWAT platform is improved by adding the following modules:

1. aquifer-lake interaction (integration of the MODFLOW – LAK7 package, USGS);
2. a tool for time-series analysis in data processing for model calibration (Observations Analysis Tool - OAT).

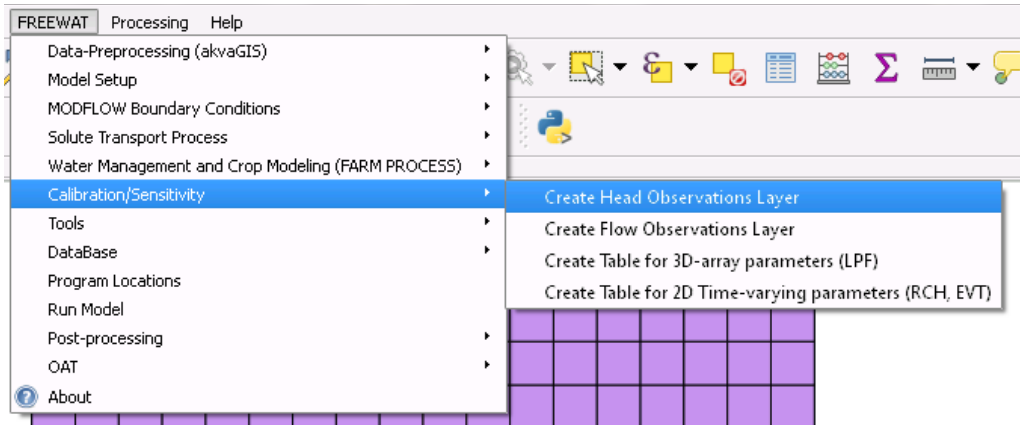

Figure 2. Example of the Model Data Object of observation heads.

This paper presents an application of the FREEWAT platform in a coastal unconsolidated aquifer that is hydraulically connected to the Mediterranean Sea. It provides the information used for the development of the conceptual model, based on a series of hydrogeological data, as well as the application of groundwater flow simulation under steady state conditions.

2. CASE STUDY DESCRIPTION

2.1 General setting and condition.

Marathon plain (40 km^2), located at the NE of Attica (Greece), is characterized as a typical Mediterranean environment that involves a naturally occurring –and presently degraded– coastal wetland with the characteristics of a distinct ecosystem linked to a typical coastal hydrogeological system of a semi-arid region. The area faces severe surface and groundwater degradation issues due to recent human activities.

2.2 Hydrogeological characteristics

The geo-hydrological setting of the area involves a multi-layer aquifer system that consists of (i) an upper unconsolidated formation dominated mostly by alluvial deposits and (ii) the surrounding and underlying karstified marble units (Figure 3). Both aquifers are subjected to intensive pumping conditions due to agricultural activities in the largest part of the plain. As a result, seawater intrusion affected the groundwater within both formations; however more it is more pronounced in the upper unconsolidated layer.

3. MODELING TOOL APPLICATION

The mathematical model of the unconsolidated aquifer of Marathon plain, was applied through the FREEWAT platform.

3.1. Conceptual model of Marathon plain

For the simulation of the unconsolidated aquifer, the conceptual model of Marathon plain took into consideration geological, hydrogeological, hydrological, geophysical data (existing and recently collected field data), as well as geographical information such as land cover, land use, DEM.

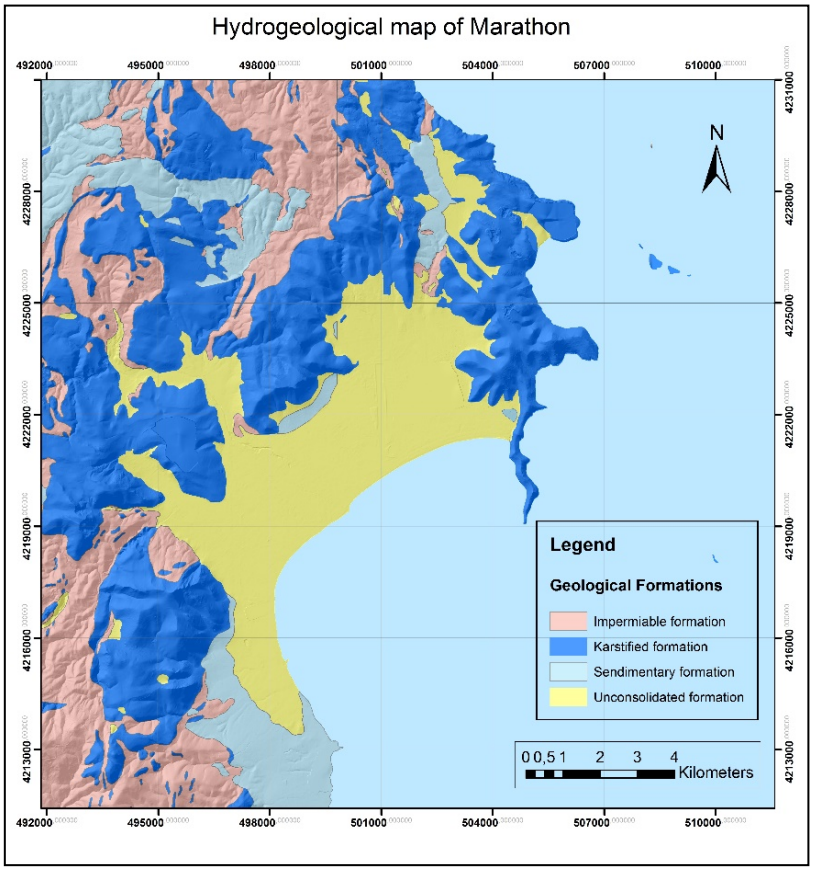

Figure 3. Hydrogeological map of study area.

The natural boundaries of the system are the karstified marbles at the northern and western part of the plain, the coastline at the southern part, while at the east the study area includes a coastal wetland that is hydraulically disconnected to the underlying alluvial aquifer layer. The system discharges into the Mediterranean Sea, while water that is pumped from a number of shallow and deeper groundwater wells -used for agricultural purposes- is considered another significant loss from the system. The unconsolidated formation is recharged mainly through: (i) direct infiltration from precipitation; (ii) the lateral inflows from the surrounding karstified marbles; (iii) by irrigation return inflows; and (iv) the karstic spring of *Makaria* which is a major discharge point of the local marble unit at the NE part of the area.

3.2. Simulation the granular aquifer through the FREEWAT platform

The granular system of Marathon plain was simulated using MODFLOW 2005 (Harbaugh, 2005) in the FREEWAT platform while the aquifer was simulated considering the available data of the year 1998. The model was run under steady state conditions for a stress periods of 5 months. The top and bottom parts of the aquifer were defined from a series of geophysical surveys that conducted in the study area during previous research by Melissaris and Stavropoulos (1999). The initial head was calculated from a piezometric map of May 1998 (Melissaris and Stavropoulos, 1999) and the model was calibrated using the piezometric map of October 1998 (Melissaris, Stavropoulos, 1999). For the temporal discretization of the simulated aquifer, a grid was created with cell size of 100×100 m^2; whereas the hydraulic conductivity of the unconsolidated formation ranges from 10^{-6} to 10^{-5} m/sec (Siemos, 2010). The aquifer was considered to be homogenous and isotropic so the hydraulic conductivity was used for the entire formation is 2 m/day (equals to 2.3×10^{-5} m/sec) and was estimated by “trial and error” methods.

The boundary conditions of the case study are presented in Table 1.

Table 1. Assigned boundary conditions

Boundary	Type of Boundary Condition	Quantity	Unit
Rainfall	Recharge(RCH)	$4.4x10^{-5}$	m/day
Nothern & Southern Marble	General Head (GHB)	2	m
Makaria spring	General Head (GHB)	2.5	m
Coast	Constant Head (CHD)	0	m
Swamp	Constant Head (CHD)	0	m
Wells	Well(WEL)	-100	m/day

The direct infiltration from precipitation was calculated from meteorological data of this period, while the total amount of rainfall from May to September 1998 was 34 mm and the direct infiltration from precipitation was considered as 20% of the precipitation. Finally this volume was equally assigned to the entire surface of the model (4.4×10^{-5} m/day).

The surrounding karstified marbles were represented as a general head boundary taking into consideration the piezometric level at the contact zone between the unconsolidated aquifer and the marbles in question. This boundary condition is considered a result of the diffuse flow that corresponds to the fractured porosity of the marble unit. Pumping volume has been estimated at 2×10^{6} m^3/year (Siemos, 2010), and refers to the irrigation needs of the area corresponding to the agricultural activities at the period of investigation.

The following figure shows a step of the procedure to construct the model in QGIS using the FREEWAT plugin.

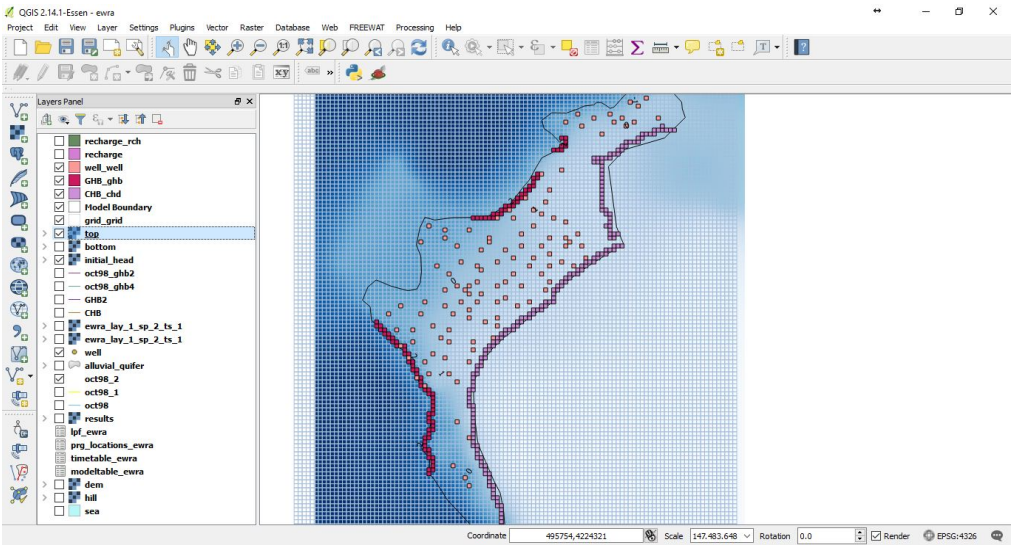

Figure 4. Construction of the mathematical model of Marathon plain using QGIS and FREEWAT.

The results of the simulation were visualized using the post-processing tool of FREEWAT and other tools of QGIS (Figure 5).

4. CONCLUSIONS

This study presents the application of FREEWAT platform in a coastal aquifer system in the Mediterranean region. FREEWAT is an open source and public domain GIS integrated modelling environment for groundwater simulation and data processing. The coastal area of Marathons was selected as a case study for the application of FREEWAT platform, to simulate the groundwater flow of the alluvial aquifer layer. The study area is a typical Mediterranean coastal site that is hydraulically connected to the sea, while the groundwater resources are exclusively used for irrigation purposes. The model calibration was based on a series of geological, hydrogeological, hydrologic and geographical data that were collected from previous studies as well as during this

present research. Freewat platform was proved an efficient and flexible tool for the realization of the groundwater simulation of the study area, while as being integrated within a GIS environment, it provided additional capabilities to this exercise.

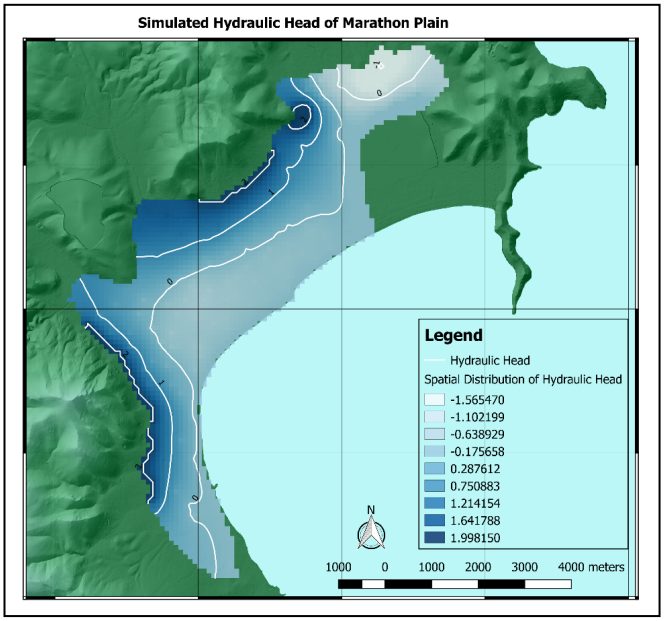

Figure 5. Results of simulation for the granular aquifer of Marathon.

ACKNOWLEDGMENTS

This paper is presented within the framework of the project FREEWAT, which has received funding from the European Union's Horizon 2020 research and innovation programme under Grant Agreement n. 642224. This paper content reflects only the authors' views and the European Union is not liable for any use that may be made of the information contained therein.

REFERENCES

Borsi, I., Rossetto, R., Schifani, C., Hill, M.C. (2013). Modelling unsaturated zone flow and runoff processes by integrating MODFLOW-LGR and VSF, and creating the new CFL, Journal of Hydrology, 488, pp. 33-47.

Foglia, L., Mehl, S.W., Hill, M.C., Perona, P., Burlando, P. (2007): Testing alternative groundwater models using cross validation and other methods, Ground Water, Vol. 45:5, pp. 627-641.

Hanson R.T., Boyce S.E., Schmid W., Hughes J.D., Mehl S.M., Leake S.A., Maddock T., Niswonger R.G. (2014). One-water Hydrologic Flow Model (MODFLOW-OWHM), U.S. Geological Survey, Techniques and Methods 6–A51, 120 p.

Harbaugh, A.W., 2005, MODFLOW-2005, the U.S. Geological Survey modular ground-water model -- the Ground-Water Flow Process: U.S. Geological Survey Techniques and Methods 6-A16.

Langevin, C.D., Thorne, D.T., Jr., Dausman, A.M., Sukop, M.C., and Guo, Weixing, 2007, SEAWAT Version 4: A Computer Program for Simulation of Multi-Species Solute and Heat Transport: U.S. Geological Survey Techniques and Methods Book 6, Chapter A22, 39 p.

Melissaris P., Stavropoulos X. (1999). Hydrogeological assessment of the coastal plain of Marathon, Attica. Report submitted to the Ministry of Agriculture, Department of Land Reclamation, Athens.

Poeter, Eileen P., Mary C. Hill, Dan Lu, Claire R. Tiedeman, and Ste en Mehl, 2014, UCODE_2014, with new capabilities to de ne parameters unique to predictions, calculate weights using simulated values, estimate parameters with SVD, evaluate uncertainty with MCMC, and More: Integrated Groundwater Modeling Center Report Number: GWMI 2014-02.

Rossetto, R., Borsi, I., Schifani, C., Bonari, E., Mogorovich, P., Primicerio, M. (2013) SID&GRID: Integrating hydrological modeling in GIS environment. Rendiconti Online Società Geologica Italiana. Volume 24, 2013, Pages 282-283

Siemos N. (2010). Evaluation of water resources in Attica & Islands of Argosaronic Gulf, Inst. of Geological and Mineral Exploration, Athens, p. 148.

Zheng, C., 2010. MT3DMS v5.3, a modular three-dimensional multispecies transport model for simulation of advection, dispersion and chemical reactions of contaminants in groundwater systems, Supplemental User's Guide. Technical Report prepared for US Army Corps of Engineers, 51 p.

Proceedings of the 10th World Congress of EWRA 'Panta Rhei', 5-9 July 2017, Athens, Greece
© 2017 *European Water Resources Association*

Modifying SINTACS method to assess groundwater vulnerability and pollution risk to nitrate

G. Busico[1], N. Colombani[2], E. Cuoco[1], M. Mastrocicco[1*], M. Sirna[1] and D. Tedesco[1]
[1] *DISTABIF, University of Campania "Luigi Vanvitelli", Via Vivaldi 43, 81100 Caserta, Italy*
[2] *BIGEA, University of Bologna, Via Selmi 3, 40126 Bologna, Italy*
[*] *e-mail: micol.mastrocicco@unina2.it*

Abstract: Groundwater as a source of water supply and ecological asset has drawn a growing attention in order to meet the increasing demand of water resources due to fast demographic growth and urbanization, and to economic and agricultural activities intensification. In particular, the assessment of agrochemicals losses from cultivated land and the potential of groundwater contamination, especially from nitrogen species, is a serious issue to effectively meet the measures established in the European Water Framework Directive (Directive 2000/60/EC). The use of indices, describing the intrinsic and the specific groundwater vulnerability are widespread methods to characterize areas affected by non-point agricultural sources. In the present study, the SINTACS method was applied in order to estimate the intrinsic vulnerability of the aquifer underlying the Campanian Plain, an intensively cultivated and densely populated coastal plain located in Southern Italy. Nitrogen losses from the top soil were estimated based on climatic, soil and topographic data using LOS indices. By combing the SINTACS and the LOS indices in a GIS environment, the specific vulnerability of the local unconfined aquifer to nitrogen losses was calculated. Results show that the inclusion of an estimate of the potential percolation of nitrogen species below the agricultural fields, can improve the vulnerability classification of the study area allowing a more detailed and targeted management of groundwater resources and a wiser allocation of land use.

Key words: vulnerability indices, N leaching, GIS, Non-point source pollution

1. INTRODUCTION

Groundwater is considered an important resource to guarantee human and environmental needs, but it is increasingly affected by diffuse and punctual sources of pollution (Morris et al. 2003). The use of nitrogen (N) fertilizers is one of the most widespread non-point sources of pollutant (Mastrocicco et al. 2009; Puckett et al. 2011). Treatment of groundwater pollution is often unpractical, so groundwater vulnerability assessment is a valuable tool for the implementation of agrochemicals management strategies to prevent groundwater pollution. A wide variety of methods has been developed in the past decades to assess groundwater vulnerability (Foster 1987; Gogu and Dassargues 2000; Kazakis and Voudouris 2015). These methods can be broadly grouped in two main categories: (i) process-based mathematical models which are powerful tools to predict pollutants fate but need a the large number of input data; (ii) overlay indices methods based on ratings and weights which can be easily applied at regional scale via GIS because they require less and more accessible data. Although, the indices methods are often strongly affected by subjectivity.

In this study, a combined method was used by applying indices of low data requirements, which can describe separately the vulnerability of the topsoil and of the aquifer system. After applying the SINTACS method (Civita and De Maio 2004) to an unconfined aquifer to gain its vulnerability, in order to estimate the potential pollution risk due to agricultural practice within the same area, the LOS indices (Aschonitis et al. 2012; 2013) were calculated to obtain the vulnerability of the topsoil (30 cm) to nitrogen losses.

The separate analysis and combination of the aforementioned compartments can provide a more robust and detailed description of the response of the whole hydrogeological systems to pollution.

2. SITE DESCRIPTION

The Campanian Plain, which covers approximately 1400 Km^2 with a population of more than 1 million inhabitants, shows an heterogeneous land use: the urban area covers approximately 30% of the territory, the agricultural land is about 40% (where a variety of different crops are cultivated) and forests and pastures occupy the remaining 30% of the territory, mainly in the mountainous area.

The Campanian Plain is limited by Massico Mountain and Roccamonfina Volcano to the North, by the carbonatic ranges of Maggiore, Tifatini and Avella Mountains to the Est and by the volcanic systems of Phlegrean Fields and Vesuvio to the South. While on its western side, the Campanian Plain overlooks the Tyrrhenian Sea. The geological evolution of the Campanian Plain begun in the upper Pliocene and proceeded in the Quaternary with a critical extensive-tectonic stress, which brought to a large graben development. The tectonic stretching allowed the development of important volcanic centres (Roccamonfina, Phlegrean Fields and Somma-Vesuvio) in the most depressed areas at the graben borders. Such geological conditions lead to the accretion of thick continental, marine and volcanic deposits (Ortolani and Aprile 1985; Romano et al. 1994). The deepest unit is made by marine clays and sands with an upper limit between -90 m and -20 m above sea level (a.s.l.). The overlying unit is composed by Phlegrean volcano-clastic and volcanic sediments, constituted by pyroclastic sands and cinerites reworked in subaqueous environment. The Campanian Ignimbrite emission took place in different eruptive events (Civetta et al. 1997) and consisted in the emplacement of a pyroclastic rock layer formed by a trachytic-phonolithic flow. The Holocenic sediments, outcropping in the middle of the plain, are irregular successions of clays, silts and peat beds (Barra et al. 1996), while toward the coast dunes and sandbars parallel to coast are present. In the Southern part of the plain, the outcropping unit is an irregular succession of pozzolans, cinerite and sandy pyroclastite due to the Phlegrean activity.

3. MATERIALS AND METHODS

The Underground Digital Terrain Model (UDTM) was obtained by the interpretation of 447 stratigraphic surveys. From the analysis of the UDTM, the predominant units of the unsaturated zones are the Ignimbrite Campana and the Pre-Ignimbrite, which were demonstrated to be an important flow barrier to prevent pollutants migration toward the aquifer (Bruno and Godio 1997).

The water depth, measured in 1000 monitoring wells, ranges from 1 m to more than 70 m.

The effective infiltration was calculated multiplying the recharge for texture coefficient derived from the type of soil cover, identified using the thematic map “Lands of Campania” (Gennaro 2002). The recharge was calculated subtracting the actual evapotranspiration to the recorded rainfall using the climatological data of 6 meteorological stations, covering the period 2006-2016. To calculate the volumes of evapotranspiration the Penman–Monteith formula was applied (Allen et al. 1998). The resulting effective infiltration in the study area ranges from 85 to 348 mm.

Concerning the types of aquifer, in the northern area a calcareous aquifer, fractured and/or karstified, can be found, while in the rest of the study area, the aquifer is hosted by alluvial and volcanic deposits.

The hydraulic conductivity for the limestone formation is generally high, ranging from $1x10^{-3}$ m/s to $5x10^{-5}$ m/s, while the volcanic complex has a medium to low permeability with values ranging from $1x10^{-5}$ m/s to $5x10^{-7}$ m/s (Allocca et al. 2007).

The slope of the topographic surface is mild (0-1%) in the coastal area and in the centre of the plain, but moving inland the slope gradually increase, from 15-20% in the piedmont area up to 45% in the mountains.

SINTACS, established for hydrogeological, climatic and impact settings typical of the Mediterranean countries (Civita and De Maio 2004), was applied to evaluate groundwater vulnerability of the study area on the base of the aforementioned data. The acronym SINTACS stands for the seven parameters included in the method: Soggiacenza (depth to water), Infiltrazione efficace (effective infiltration), Non saturo (vadose zone), Tipologia della copertura (soil cover),

Acquifero (aquifer), Conducibilità idraulica (hydraulic conductivity), Supeficie topografica (slope of topographic surface). The rating assigned to each parameter is multiplied for a weight, to describe the environmental impact or the particular hydrogeological situation.

The form of the equation is the following:

$$I_{SINTACS} = \sum_{J=1}^{7} P_J W_J \tag{1}$$

where P_J is the rating of each parameter and W_J is the corresponding weight.

According to the description of the seven parameters taken into consideration by the SINTACS method and the ratings proposed by Civita and De Maio (2004), the vulnerability assessment in the study area was developed in GIS environment and all the seven parameters were arranged in raster format, with a regular grid of 200×200 m (Fig. 1).

In order to obtain the intrinsic vulnerability of the area, on the base of the aforementioned data, the ratings of the seven parameters were multiplied by the string of weights proposed by Civita and De Maio (2004) for the "Severe Impact" scenario, which emphasize the role of the first, second and forth parameter among all the others.

The LOS indices (Aschonitis et al. 2012) estimate the intrinsic vulnerability of agricultural land to water and nitrogen losses in the top 30 cm of soil. LOS indices, calibrated via multiple regression analysis using the GLEAMS model (de Paz et al. 2002), quantify (i) the annual losses of the percolated water beneath the root zone (LOSW-P), (ii) the annual losses of the surface runoff (LOSW-R), (iii) the annual losses of N leaching beneath the root zone (LOSN-PN) and (iv) the annual losses of N through the surface runoff (LOSN-RN).

In the study area to estimate the annual N losses, on the base of the aforementioned data, the LOSN-PN map (Fig. 2) was calculated according to the following formula:

$$\text{LOSN-PN} = \left\{ \begin{matrix} -0.1536\sqrt{\text{OM}} + 2.6981\sqrt{\text{T}} + 0.0439\sqrt{\text{Ks}} \\ -0.2046\sqrt{\text{S}} + 0.0471\sqrt{\text{PCP}} - 0.2515\sqrt{\text{PE}} \\ -0.0116\sqrt{\text{IR}} \end{matrix} \right\}^2 \tag{2}$$

where LOSN-PN is the amount of N losses beneath the top 30 cm of the soil profile (kg/ha/ year), OM is the organic matter (%) and T is the mean annual temperature (°C), Ks is hydraulic conductivity (mm/day), S is the surface slope (%), PCP is the total annual precipitation (mm/year), PE is the total annual potential evapotranspiration (mm/year), IR is the total annual irrigation amount (mm/year).

The SINTACS and LOSN-PN maps were then combined to gain the potential impact to groundwater resources due to N percolation below the top soil (Fig. 3), according to Uricchio et al. (2004).

4. RESULTS AND DISCUSSION

For the study area, the intrinsic vulnerability ranges from 85 to 205. These values were then divided into 4 intervals of vulnerabilities: from 85 to 115 a low vulnerability class was identified, from 115 to 145 a medium vulnerability class was identified, from 145 to 175 very high vulnerability class was identified and from 175 to 205 very high vulnerability class was identified (Fig. 1).

According to the SINTACS classification, the most vulnerable area of the Campanian Plain coincides with the coastal area where the modern and relict dune systems are located; while the less vulnerable portions of the territory are located in the foothills in the North eastern and southern part of the study area (Fig. 1).

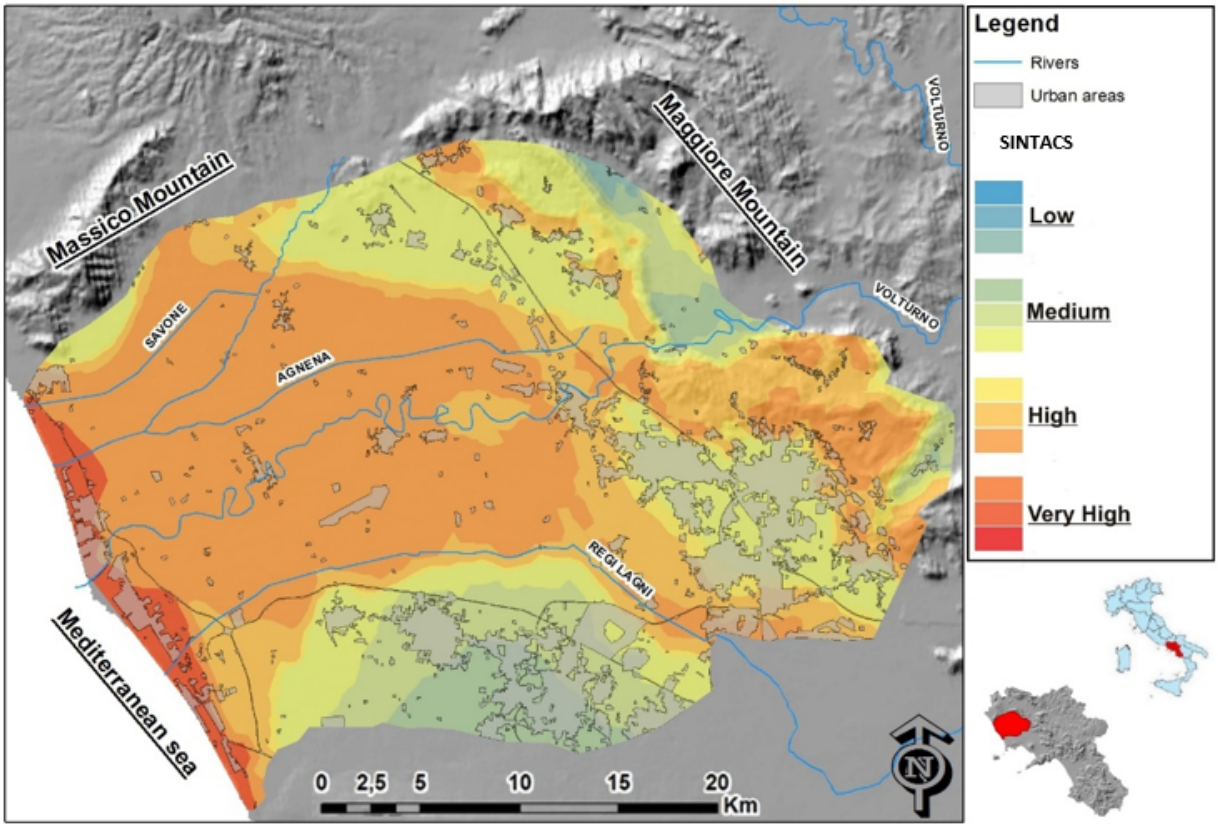

Figure 1. SINTACS map for the Campanian Plain

On the other hand, the annual losses of N leaching beneath the root zone, calculated according to the LOSN-PN index, range from 4 up to 54 kg-N/ha/year (Fig. 2). Also in this case, as with the SINTACS classification, the zone that shows the highest value of leaching is the coastal area. High values of leaching characterize even the southern portion of the study area, which was instead classified as a low vulnerability zone. Small values of N leaching are calculated for the mountainous area at the North eastern and eastern part of the study area. While the North eastern portion also falls in the a low vulnerability area, the eastern portion of the territory was classified as a medium to highly vulnerable area.

Combining the SINTACS and LOSN-PN maps, the potential impact to groundwater resources due to N percolation below the top soil was calculated and represented in Figure 3. The combination of the two indices shows that the coast is still the most endangered portion of the study site but the area interested by a very high impact is wider than the one calculated with the SINTACS method. The same happen in the southern part of the study area, where the specific vulnerability to N leaching is higher than the intrinsic vulnerability of the aquifer. The latter was in fact classified as medium according to the SINTACS method. On the contrary, the mountainous area shows a low specific vulnerability to N leaching either in the North eastern part either in the eastern part of the territory, which was instead classified as highly vulnerable according to the SINTACS method, thus giving a substantial widening of the low vulnerability area. The central portion of the territory does not show a remarkable change in its classification among the SINTACS and the combined method.

5. CONCLUSIONS

This study verifies the suitability of combining different vulnerability indices in the assessment of the potential threat to groundwater resources due to N leaching in an intensively populated and cultivated area in southern Italy.

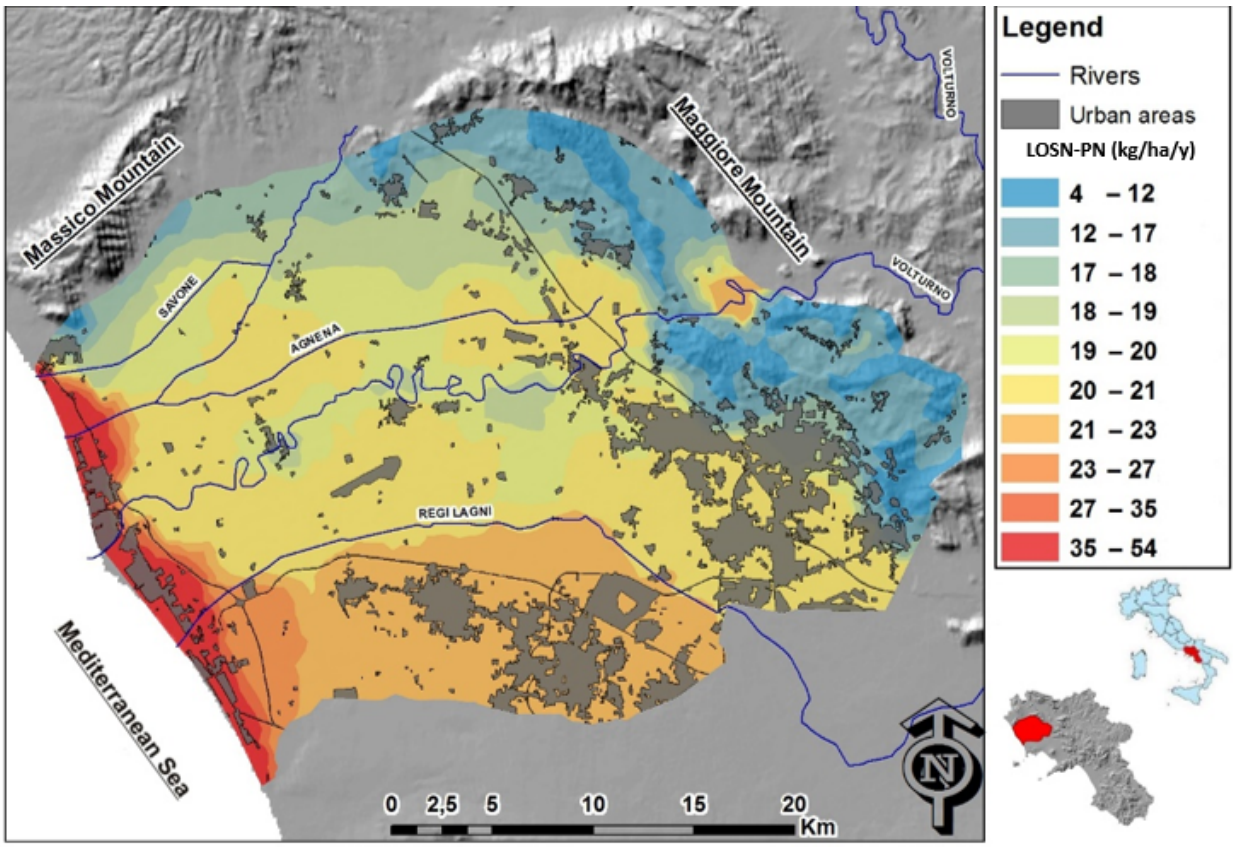

Figure 2. LOSN-PN (kg-N/ha/year) for the Campanian Plain

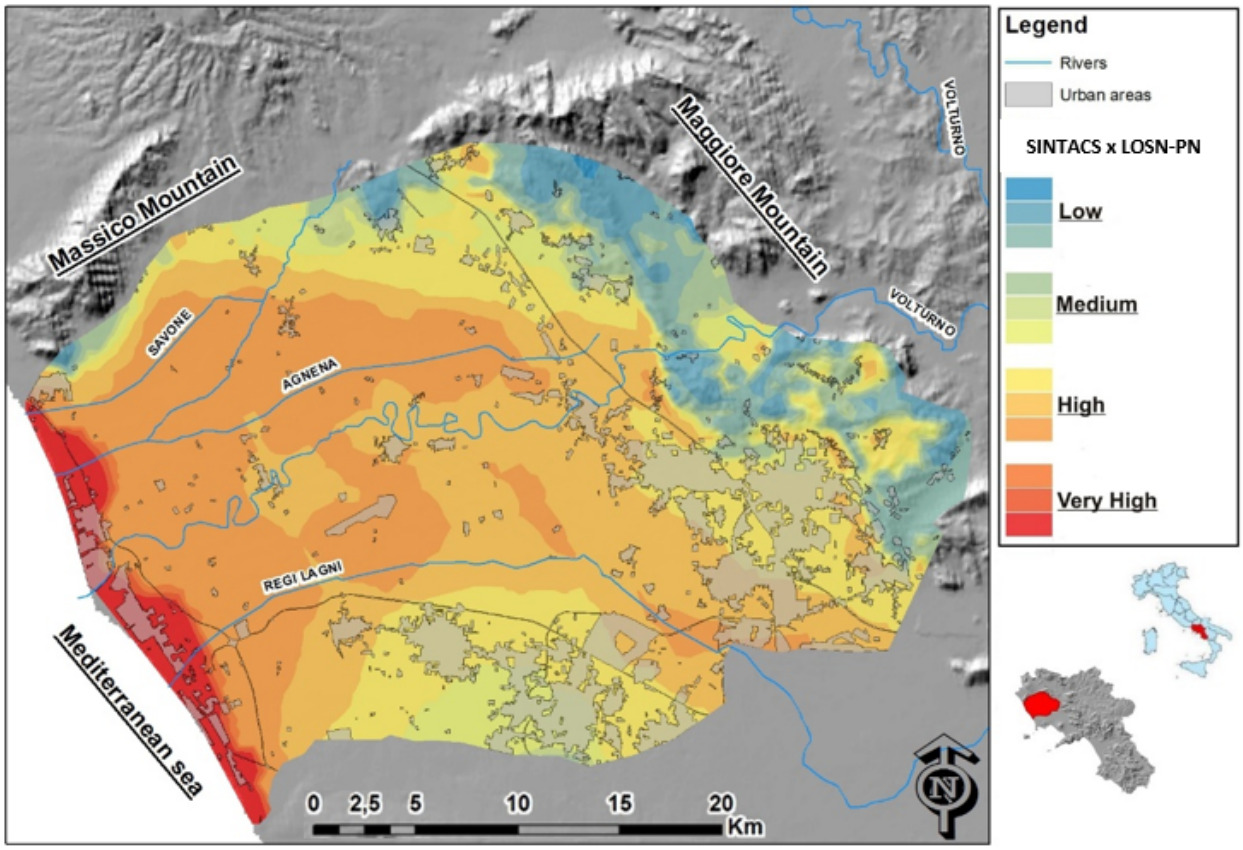

Figure 3. Combination of the SINTACS and LOSN-PN indices for the Campanian Plain.

The SINTACS method was applied to gain the intrinsic vulnerability map for of the local unconfined aquifer while the LOS method was applied to gain the potential percolation of N below the topsoil.

The specific vulnerability to N losses, resulting from the combination of the two indices in a GIS environment, returns a more reliable representation of the distribution of the vulnerable zones in the study area, allowing a more detailed and targeted management of land use at the ground surface and a better allocation and exploitation of the groundwater resources.

The ease with which it is possible to dispose of the basic input parameters to calculate both the SINTACS and the LOS methods, suggests that the proposed method is widely applicable to many other regions and environments, aiming to create a sustainable water management plan, flexible land use allocation, and define groundwater quality protection zones in unconfined aquifers.

Despite these positive aspects, it's worth to note that the combined application of these two indices could be further improved by the inclusion of the processes involved in the transport, transformation and attenuation of reactive nitrogen species from the topsoil towards the underlying unconfined aquifer.

REFERENCES

Allen, R. G., Pereira, L. S., Raes, D., Smith, M., 1998. Crop evapotranspiration – Guidelines for computing crop water requirements. Food and Agriculture Organization of the United Nations, FAO, Rome, Italy.

Allocca, V., Celico, F., Celico, P., De Vita, P., Fabbrocino, S., Mattia, C., Monacelli, G., Musilli, I., Piscopo, V., Scalise, A. R., Summa, G.and Tranfaglia, G., 2007. Carta Idrogeologica dell'Italia Meridionale. Istituto Poligrafico e Zecca dello Stato.

Aschonitis, V. G., Mastrocicco, M., Colombani, N., Salemi, E., Kazakis, N., Voudouris, K., Castaldelli, G., 2012. Assessment of the intrinsic vulnerability of agricultural land to water and nitrogen losses, via deterministic approach and regression analysis. Water Air & Soil Pollution; 223(4): 1605-1614.

Aschonitis, V. G., Salemi, E., Colombani, N., Castaldelli, G.and Mastrocicco, M., 2013. Formulation of indices to describe intrinsic nitrogen transformation rates for the implementation of best management practices in agricultural lands. Water Air & Soil Pollution; 224(3): 37-49.

Barra, D., Romano, P., Santo, A., Campajola, L., Roca, V., Tuniz, C., 1996. The versilian transgression in the Volturno river plain (Campania, southern Italy): paleoenvironmental history and chronological data. Il Quaternario; 9 (2): 445-458.

Bruno, P. P. G., Godio, A., 1997. Environmental risk assessment of a shallow aquifer in "Piana Campana" (Italy): a field comparison between seismic refraction and reflection methods. European Journal of Environmental and Engineering Geophysics; 2: 61-76.

Civetta, L., Orsi, G., Pappalardo, L., Fisher, R. V., Heiken, G., Ort, M., 1997. Geochemical zoning, mingling, eruptive dynamics and depositional processes. The Campanian Ignimbrite, Campi Flegrei Caldera, Italy. Journal of Vulcanology and Geothermal Research; 75: 183-219.

Civita, M., De Maio, M., 2004. Assessing and mapping groundwater vulnerability to contamination: The Italian "combined" approach. Geofisica internacional-mexico; 43(4): 513.

De Paz, J. M., Ramos, C., 2002. Linkage of a geographical information system with the GLEAMS model to assess nitrate leaching in agricultural areas. Environmental. Pollution; 118: 249–258.

Foster, S. D. D., 1987. Vulnerability of soil and groundwater to pollutants. In: W. Van Duijvenbooden and H.D. Waegeningh (eds). Proceedings of TNO Committee on Hydrogeological research; 38: 69-86.

Gennaro, A., 2002. I sistemi di terra della Campania. SELCA, Firenze. pp 63.

Gogu, R. C. and Dassargues, A. (2000). Current trends and future challenges in groundwater vulnerability assessment using overlay and index methods. Environmental Geology; 39(6): 549 - 559.

GWD 2006/118/EC. Directive of the European Parliament and of the council on the protection of groundwater against pollution and deterioration. 12/12/2006.

Kazakis, N. A., Voudouris, K. S., 2015. Groundwater vulnerability and pollution risk assessment of porous aquifers to nitrate: modifying the drastic method using quantitative parameters. Journal of Hydrology; 525: 13-25.

Mastrocicco, M., Colombani, N., and Palpacelli, S., 2009. Fertilizers mobilization in alluvial aquifer: laboratory experiments. Environmental Geology; 56(7): 1371-1381.

Morris, B. L., Lawrence, A. R. L., Chilton, P. J. C., Adams, B., Calow, R. C. and Klinck, B. A., 2003. Groundwater and its susceptibility to degradation: a global assessment of the problem and options for management. Early warning and assessment report series 03-3. United Nations Environment Programme, 126 pp.

Ortolani, F., Aprile, F., 1985. Principali caratteristiche stratigrafiche e strutturali dei depositi superficiali della Piana Campana. Boll. Soc. Geol. It., 104 (2), 195-206, 7 figg., Roma.

Puckett, L. J., Tesoriero, A. J.and Dubrovsky, N. M., 2011. Nitrogen Contamination of Surficial Aquifers - A Growing Legacy. Environmental Science and Technology; 45: 839-844.

Romano, P., Santo, A., Voltaggio, M., 1994. L'evoluzione geomorfologica del Fiume Volturno (Campania) durante il tardo Quaternario (pleistocene medio-superiore- Olocene). Il Quaternario; 7(1): 41-59, Napoli.

Uricchio, V. F., Giordano, R., Lopez, N., 2004. A fuzzy knowledge-based decision support system for groundwater pollution risk evaluation. Journal of Environmental Management; 73: 189-197.

Proceedings of the 10th World Congress of EWRA 'Panta Rhei', 5-9 July 2017, Athens, Greece
© 2017 *European Water Resources Association*

Application of head-guided zonation method to delineate groundwater vulnerability zones in a data-scarce catchment

D.K.S.Y. Klaas[1,2], M.A. Imteaz[1] and A. Arulrajah[1]
[1] *Department of Civil & Construction Engineering, Swinburne University of Technology, Melbourne, VIC, Australia*
[2] *Department of Civil Engineering, Politeknik Negeri Kupang, Indonesia*
[*] *e-mail: dklaas@swin.edu.au*

Abstract: Developing a reliable groundwater model which often requires an extensive and costly subsurface profiling is a real challenge in data-scarce. In this study the Head-Guided Zonation (HGZ) methodology was applied on the recharge area of Oemau Spring in Rote Island, Indonesia, which is under potential risk of contamination from land use changes. The methodology involves calibrating a groundwater model using the HGZ method in parameterisation step. Using distribution of hydraulic gradient, HGZ method aims to represent distribution of subsurface parameters, such as hydraulic conductivity and specific yield, in areas where geologic data is scarce. This study shows that the HGZ method can be effectively used to calibrate a physically-based groundwater model. The results from reverse particle-tracking simulation were used to develop vulnerability zones.

Key words: vulnerability zones, groundwater contamination, model calibration, particle tracking, karst aquifer

1. INTRODUCTION

Estimation of contaminant migration can be used as a predictive tool to draw vulnerability zones which delineate influence areas categorised by simulated travel distance and time of particles moving through the model domain. However, developing a reliable groundwater model which often requires an extensive and costly subsurface profiling is a real challenge in data-scarce areas such as those in developing countries (e.g. Li, et al., 2009; Candela, et al., 2014). Consequently, choosing the most appropriate and adaptable method in parameterising a groundwater model is important to overcome data limitation and realistically represent a complex subsurface system. The aims of this study were to develop, calibrate and validate a physically-based groundwater model using the Head-Guided Zonation (HGZ) method; and to develop groundwater vulnerability zones based on the result of particle-tracking simulation.

2. METHODOLOGY

2.1 Study area

Rote Island (Figure 1) with a total area of 1,223 km^2 is situated in the southernmost part of Indonesia (located between latitudes 10°25'00"S ~ 11°00'00"S and longitudes 121°49'00"E ~ 123°26'00"E). The community relies entirely on karst springs for their domestic and agricultural purposes. Nevertheless, provision of freshwater from karst springs in Rote Island is presently under threat from human activities due to rapid population increase and land use change, particularly in the recharge area of Oemau Spring (ORA). The rapid change in land use in ORA could potentially result in substantial and immediate effects on the water quality of the spring. Geologically, the subsurface of ORA is dominated by carbonate formations featured as karst landscape with Holocene coralline limestones (63.93%), Bobonaro formations (27.83%) – mainly consist of a

mixture of carbonate rocks and scaly clay, and alluvium deposits (8.25%). Governed by a monsoonal climate, ORA has mean annual precipitation of 1000 - 2300 mm and humidity between 75 and 92%.

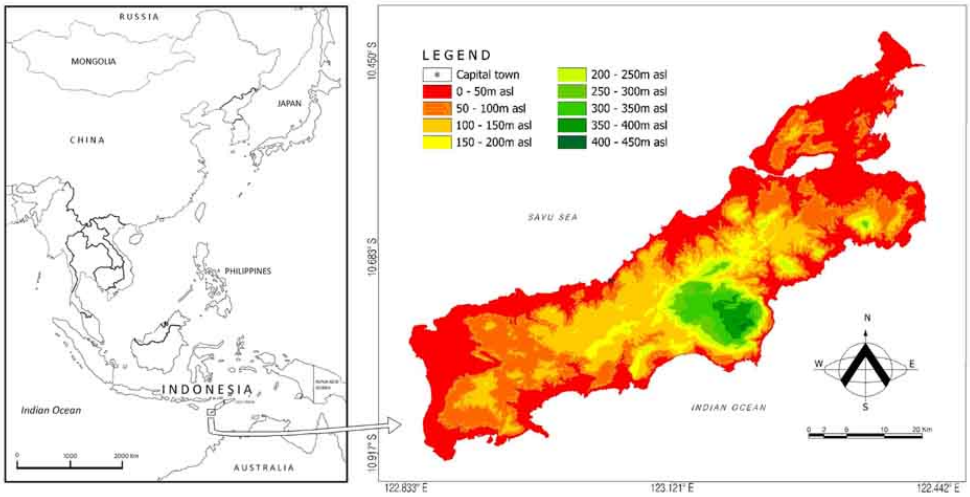

Figure 1. Study area: Indonesia, Rote Island.

2.2 Model development and analysis

This study employed MODFLOW (McDonald and Harbaugh et al., 1988) to perform groundwater flow simulations under both steady-state and transient conditions. Using Groundwater Modeling System (GMS) suite (BYU, 2014), the conceptual model was set up as one horizontal layer and discretised into 50 x 50 m grid cells (Figure 2). Recharge package, RCH (Harbaugh *et al*., 2000) was employed to simulate recharge calculated using water balance method (Bras, 1990). Penman-Monteith (Allen et al., 1998) and SCS-CN (Viessman and Lewis, 1995) methods were used to calculate evapotranspiration and surface runoff respectively. Seven dug wells were selected as observation wells to provide the basis for groundwater simulations. Two model boundaries were assigned: (1) no-flow boundary assuming no flux flowing through the surface-water divides, and (2) specified head boundary (Dirichlet) at downstream using Time-Variant Specified-Head.

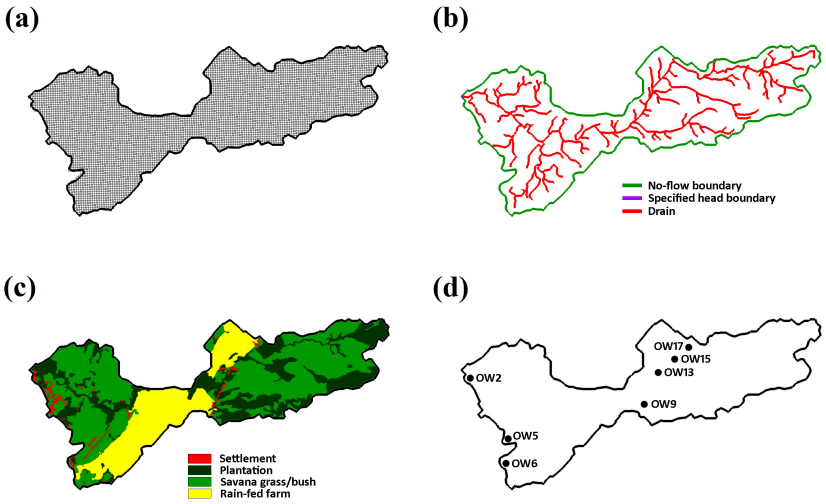

Figure 2. Conceptual model and boundary conditions of the groundwater models showing (a) Model grid; (b) Source and sinks; (c) Recharge; and (d) Observation wells

3. FINDINGS

3.1 Zone delineation using HGZ method

The HGZ principally employs available groundwater level data to divide the area of interest into several zones of piecewise constant. It assumes that each zone has the same hydogeologic characteristics represented by similar hydraulic gradient of groundwater flow. Hydraulic gradients between groundwater heads were calculated to delineate the zones after drawing groundwater contours from the interpolation of groundwater level data recorded from the seven dug wells in ORA (Fetter, 2001; Hudak, 2005). Based on the hydraulic gradient calculation the model domain was divided into three zones. The selected zones resulted in six parameters to be calibrated (each zone represents two parameters; hydraulics conductivity and specific yield).

3.2 Model calibration and validation

The negative bias values of ME_h of -0.57 and -0.09 m in both steady-state and transient calibrations respectively suggest a relatively minor underestimations of simulated heads by the model. In transient validation the head is slightly overestimated by 0.19 m. In both transient calibration and validation, the model performances were considered acceptable with $RMSE_h$ values of 0.46 and 0.48 respectively, indicating an overall well calibrated and validated model.

3.3 Delineation of vulnerability zones

The delineation of vulnerability zones are based on the time and pathlines taken by hypothetical particles travelling through the simulated model to arrive at the spring. The reverse particle-tracking method in MODPATH (version 5) computed the particles travelling through the simulated subsurface pathlines trajectories. In the simulation, pathlines were tracked backwards through times by computing values of velocity vector based on the flow rates at every grid cell. Figure 3a illustrates the zones of influence and their corresponding travel time produced by reverse particle-tracking simulation. It shows the maximum distance particles can travel in 3 years which is around 6.5 km from the Oemau spring. Figure 3b shows the developed vulnerability zones, in which the zonation is categorised into three different zones.

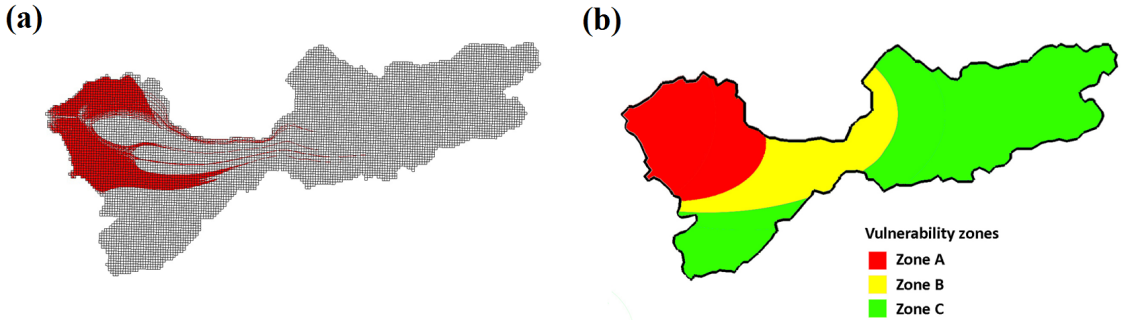

Figure 3. Development of vulnerability zones showing (a) zone of influence using reverse particle-tracking simulation, and (b) proposed vulnerability zones based on the result of particle-tracking simulation.

4. CONCLUSIONS

This study shows that the HGZ method can be successfully used to calibrate a physically-based groundwater model. Using the result of particle-tracking simulation (travel time and pathline

trajectory) and the potential risk of current human activities to water quality at Oemau Spring, three zones of vulnerability were developed. The proposed vulnerability zones can be used by the regional decision makers to protect the spring from contamination and to ensure provision of safe and good quality water from Oemau Spring. It is worth noting that the HGZ method is considered valid for a homogenous and anisotropic groundwater system, such as karst aquifer. Therefore, this method can be recommended to be applied in other areas characterised by similar hydrogeological settings.

REFERENCES

Allen, R.G., Pereira, L.S., Raes, D. and Smith, M. (1998) Crop evapotranspiration - Guidelines for computing crop water requirements, 333p.

Bras, R.L. (1990) Hydrology: An introduction to hydrologic science, Addison-Wesley, Reading, Massachusetts, USA.

BYU (2014) Groundwater Modeling System (GMS) version 9.2.9., Environmental Modeling Research Laboratory, Brigham Young University, Provo, USA.

Candela, L., Elorza, F.J., Tamoh, K., Jiménez-Martínez, J. and Aureli, A. (2014) Groundwater modelling with limited data sets: the Chari–Logone area (Lake Chad Basin, Chad). Hydrological Processes 28(11), 3714-3727. http://dx.doi.org/10.1002/hyp.9901.

Fetter, C.W. (2001) Applied hydrogeology, Prentice-Hall, Upper Saddle River, New Jersey, USA.

Harbaugh, A.W. (2005) MODFLOW-2005, the U.S. Geological Survey modular ground-water model, the Ground-Water Flow Process, 253p.

Harbaugh, A.W., E.R., B., Hill, M.C. and McDonald, M.G. (2000) MODFLOW-2000, the U.S. Geological Survey modular ground-water model: user guide to modularization concepts and the ground-water flow process, 127p.

Hudak, P.F. (2005) Principles of hydrogeology, CRC Press LLC, Boca Raton, Florida, USA.

Li, H.T., Brunner, P., Kinzelbach, W., Li, W.P. and Dong, X.G. (2009a) Calibration of a groundwater model using pattern information from remote sensing data. Journal of Hydrology 377(1–2), 120-130. http://dx.doi.org/http://dx.doi.org/10.1016/j.jhydrol.2009.08.012.

McDonald, M. and Harbaugh, A. (1988) A modular three-dimensional finite-difference groundwater flow model, U.S.G.S., Book 6, Chapter A, 1258 p.

Panagopoulos, G. (2012) Application of MODFLOW for simulating groundwater flow in the Trifilia karst aquifer, Greece. Environmental Earth Sciences 67(7), 1877-1889. http://dx.doi.org/10.1007/s12665-012-1630-2.

Poeter, E.P. and Hill, M.C. (1997) Inverse models: A necessary next step in ground-water modeling. Ground Water 35(2), 250-260. http://dx.doi.org/10.1111/j.1745-6584.1997.tb00082.x.

Scanlon, B.R., Mace, R.E., Barrett, M.E. and Smith, B. (2003) Can we simulate regional groundwater flow in a karst system using equivalent porous media models? Case study, Barton Springs Edwards aquifer, USA. Journal of Hydrology 276(1–4), 137-158. http://dx.doi.org/http://dx.doi.org/10.1016/S0022-1694(03)00064-7.

Viessman, W. and Lewis, G.L. (2003) Introduction to hydrology, Pearson Education, Upper Saddle River, NJ, USA.

Proceedings of the 10th World Congress of EWRA 'Panta Rhei', 5-9 July 2017, Athens, Greece
© 2017 *European Water Resources Association*

Impact of land-use change on a multilayer aquifer in south-eastern coast of Caspian Sea

I. Karimirad, K. Ebrahimi* and S. Araghinejad
Department of Irrigation & Reclamation Engineering, Faculty of Agricultural Engineering and Technology, College of Agriculture and Natural Resources, University of Tehran, Karaj, Iran
* *e-mail: ebrahimik@ut.ac.ir*

Abstract: Human activities through land-use changes affect different parts of ecosystem such as geo-hydrological processes. Multilayer aquifer of Golestan province in South-eastern coast of Caspian Sea located in an agricultural zone. This paper demonstrate historical land-use changes and evaluate its impact on confined and phreatic layers of the aquifer. In order to trace land-use changes, three land-use maps of 1984, 2005 and 2013 were used. Data recorded in 33 piezometers and 43 monitoring wells were used to study groundwater dynamics in each layer. According to geological formation and groundwater flow direction, recharge areas of confined and phreatic aquifers determined and land-use changes in each one assessed, using GIS software. Results presents considerable land-use changes in mountainous area and ignorable changes in the plain. Both domestic and agricultural consumption have significant impact on phreatic layer but only influence of agricultural wells on confined layer approved. Also the results show threat of saltwater intrusion from Caspian Sea and fossil brine from north part of the plain in confined and phreatic layers, respectively, in case of continuing the land-use change trend. In mountainous district, forest and rangeland areas decreased and residential and agricultural areas increased that according to SCS method altogether higher CN value and reduce recharge rate. Mountainous district lost 12 percent of forests and rangelands that totally added to agricultural area. After all the confined aquifer which recharge only in mountainous area, is more affected by changes in land-use.

Key words: Confined Aquifer, GIS Software, Golestan Province, Phreatic aquifer, SCS method

1. INTRODUCTION

Demand for water and land resources expand with the increase of human activities in arid and semi-arid regions, resulting in ecological and environmental concerns (Adamat et al., 2003). With the rapid population increase and the associated demand on land resources, it is now incumbent upon policy makers and land-use planners to adopt preventive and restorative measures (Sakieh et al., 2015). Land use is an indicator of human interaction with nature. Therefore, it is necessary to discover and monitor land use changes in order to either protect the environment or ensure sustainable development (Pandian et al., 2014). Land use change generally is assumed to cause changes in hydrological dynamics of catchments as well (Huismann et al., 2009).

Groundwater system's formations are usually layered due to their geomorphologic origins. Grouping of the layers is based on their hydraulic properties, not on their geological ages (Cheng, 2000). The existences of multilayer aquifers including phreatic and confined layers, cause complexity in hydrodynamic of the aquifer, because of dissimilar recharge zones and different impressibility from human activities (Karimirad et al., 2015). Land use change pattern reflects the rate of change in groundwater recharge (Mishra et al., 2014). The increase in impervious areas has a major impact on groundwater and is a major concern over the past years to those who are involved in groundwater studies (Mishra et al., 2014). Special attention should be given to the effect of land-use changes on the hydrological cycle and the protection of groundwater systems, especially discharge and recharge areas (Batelaan et al., 2003).

Assessing the impacts of land cover change on hydrological regimes has been done by Germer et al. (2010) showed influence of land-use change and proved that deforestation for pasture may

increase runoff volumes over wide regions of Amazonia. Fathian et al. (2016) evaluated the impact of changes in land use and climate variability on surface water in the eastern subbasins of Lake Urmia basin and deduced stream flow are more sensitive to changes in land cover than climatic variables. Zhang et al. (2016) assessed hydrological impacts of land use change in the headwater region of the Heihe River Basin, northwest China. Land use changes were dominated by the expansion of built-up lands (18.29%) and a decrease in farmlands (-17.08%) induced slight reductions in surface runoff, groundwater discharge and stream flow. Salmani et al. (2012) assessed the impact of land use changes on hydrological regime Ghazaghli watershed, Golestan province, IRAN using SWAT. They estimated if build-up areas remain approximately constant, agricultural lands increase by 30% and forests and rangelands decrease 5% and 26%, respectively, groundwater flow would decrease one percent and surface flow would increase up to 17 percent. Singh et al. (2010) studied an alluvial and hilly terrain in India, to trace land-use and land-cover changes during years 1989, 2000 and 2005. They showed the quantity of groundwater increased with the help of natural and artificial recharge due to increased area of fallow land. Baker and Miller (2013) investigated land cover and land use changes in Kenya's Rift Valley between years 1986, 1995 and 2003 using SWAT. The results showed land use changes caused corresponding increases in surface runoff and decreases in groundwater recharge.

Flow dynamics of multilayer aquifers has been studied by bakker (1999) or Zhou and Li (2011). Also some researchers studied impact of climate change on multilayer aquifers, but the entire groundwater system has been dealt as a unified water body like La Plana de La Galera or Seine multi-layer aquifers that were investigated by Stigter et al. (2014) and Habets et al. (2015), respectively. Boy-Roura et al. (2013) assessed vulnerability of a multi-layered aquifer in the Osona region, northeast Spain to nitrate pollution and declared potential nitrate infiltration in the confined layers is less probable, since their recharge area lay in distant forested part of the region with no agricultural activity. But, none of them compare the impact of land use change on phreatic and confined aquifers, simultaneously, in a multilayer groundwater system. Therefore this paper aims to investigate the impacts of land use change on Golestan multilayer aquifer.

2. METHODS AND MATERIALS

Multilayer aquifer of Golestan province of IRAN in South-eastern coast of Caspian Sea located in an agricultural zone. The annual average rainfall of the area is 550 mm, with a climate classified according to De-Martonne method as semi-arid in the north and semi-humid in the south and southwest (Mostafazadeh and Sheikh, 2012). The alluvial multilayer aquifer has about 4720 Km^2 area and its average elevation is 63 m above mean sea level. The confined layer beneaths the phreatic one and spreads across the phreatic layer except about 400 Km^2 in southern part. The aquifer is extended from the Caspian Sea in the west to the city of Kalale in the East for about 130 kilometers and from the Eastern Alborz Mountains in the south to ancient Great Wall of Gorgan in the north for about 35 Km Position of the rain gauges, observational wells, piezometric wells and also multi-layer aquifer's district are illustrated in Figure 1. Northern part of phreatic layer (1402 Km^2) contains saline water due to Caspian Sea water intrusion and fossil brine dissolution (Kankash-Omran, 2013). The confined aquifer is abstracting all over the plain but according to groundwater flow direction and topography of the area, it is only recharging across its southern and south-eastern boundary. While, the phreatic aquifer recharges all over the plain and mountainous area.

In the present paper, trend analysis performed using long-term monthly precipitation data of 19 gauges in time period of 1976 to 2013 which have a good distribution over the studied area. Also 19 observational wells located in the phreatic aquifer with the time period of 38 years (the same period as the precipitation data) and 19 piezometric wells within the confined aquifer with 14-year time period (2000-2013) are used in groundwater trend analysis. Trend significance determined by Mann-Kendall test (Mann 1945) and its amount and aspect (ascending or descending) calculated using Sen's slope value. Land use maps prepared using Landsat TM images that were captured in

1984, 2005 and 2013. Landsat TM/ETM+ spectral data are frequently used for LULC classification on regional scales due to their relatively lower cost, longer history and higher frequency of archives (Manandhar et al., 2009).

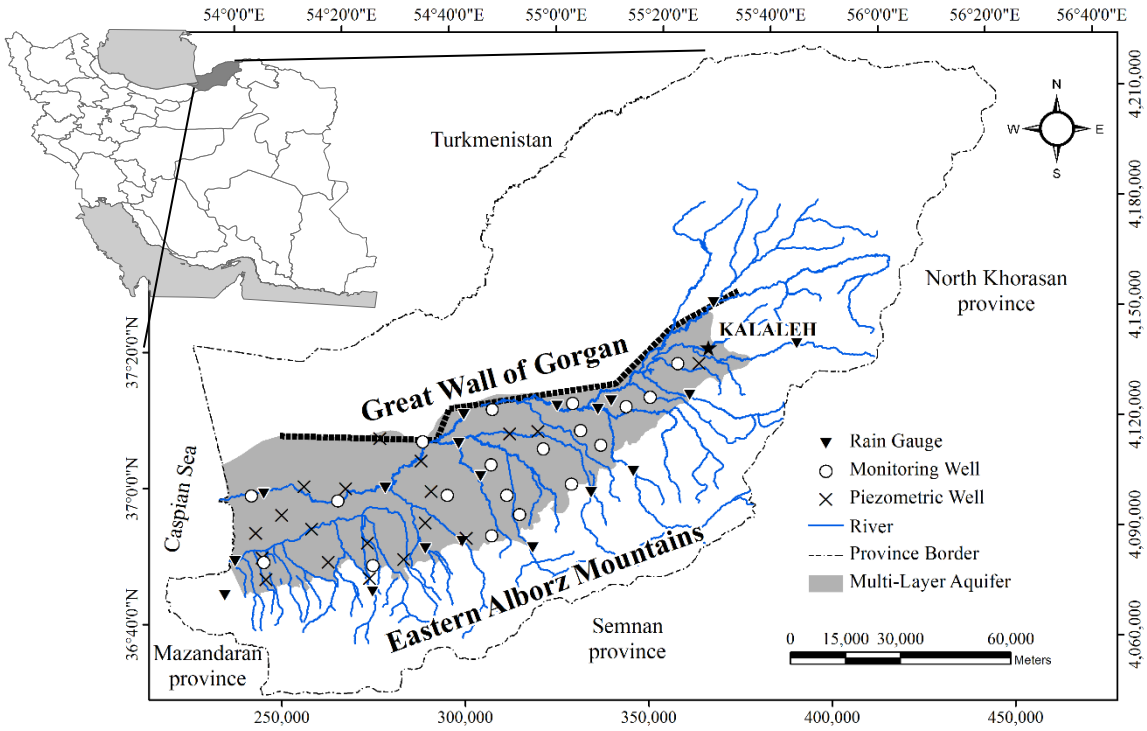

Figure 1. Location of multilayer aquifer of Golestan province, selected rain gauges, observational and piezometric wells

In order to evaluate impact of land use changes on each layer's recharge area SCS (Soil Conservation Service) method was applied. This method generates Curve Number (CN) values integrating land use/land cover and hydrologic group of soil to determine precipitation lost (Cronshey et al., 1986). S in this method indicates potential maximum retention after runoff begins and can be representative for infiltration, therefore in the paper this parameter used to compare groundwater natural recharge rate.

3. RESULTS

Mann- Kendall test at 95 percent confidence level and Sen's slope values show there is no significant trend in precipitation data (Table 1). But Piezometric level of confined aquifer declining at the rate of 12 mm per month. This is while the rate of water level changes in the phreatic aquifer is only one mm per year over the whole time period (38 years). In other words, the piezometric level of the confined aquifer during these years has dropped more than two meters. It is worth mentioning during the same period with the confined aquifer data (last 14 years), the water level of the phreatic aquifer has no trend.

As the next step, water table contours were drawn in Arc GIS software and flow lines of phreatic aquifer that are perpendicular to them established (Figure 2- left). The same procedure was applied on piezometric level contours for confined aquifer (Figure 2- right). According to groundwater flow direction and geological formation, recharge areas of each aquifer determined. Phreatic layer recharge area (PLRA) consists of all Gorganrud and Gharesoo water basin including whole aquifer area (11,150 Km^2 within solid black border). But confined layer recharge area (CLRA) southern mountainous portion of the region (3,837 Km^2 netted area).

Table 1. The results of Mann- Kendall trend test

Time series	P-Value	test result	Sen's Slope
precipitation	0.1982	No trend	
Phreatic aquifer water level	0.0000	Trend	-0.001
Confined aquifer piezometric level	0.003	Trend	-0.012

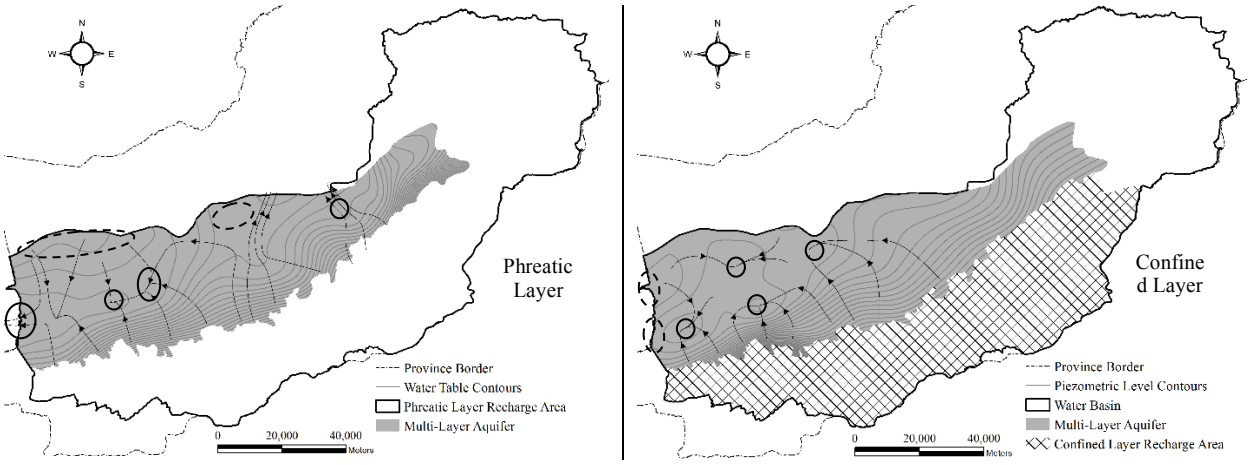

Figure 2. Water table (left) and piezometric level (right) contours, flow lines, PLRA, CLRA, discharge and recharge areas

Since the divergent flow lines represent recharge and converging ones indicate intensive abstraction (Stuyt et al., 2005), several recharge (dashed ellipsoids) and discharge (solid ellipsoids) areas detected over the plain. In phreatic aquifer there are four major discharge areas that from east to west include Gonbad-e Kavus city nearby, two agricultural zones and aquifer discharge to Caspian Sea. It is notable that Gonbad-e Kavus is the second greatest city of the province located at the edge of the aquifer. Also right dashed ellipsoid relates to Voshmgir dam lake that is recharging the aquifer and left one reveals fossil brine development into the aquifer. Confined aquifer has some major recharge and discharge areas too that all distinguished intense abstractions are in agriculture land use. Also seawater intrusion is more dominant in confined layer so that at two sections located in estuary of Gorganrud and Gharesoo. Caspian Sea is recharging the aquifer.

Figure 3 demonstrate land use maps in years 1984, 2005 and 2013 and Table 2 presents land use areas within PLRA, CLRA and multi-layer aquifer area (MLAA). As it can be seen, CLRA is mostly forested with inconsiderable but growing build-up areas. In general forest land use is decreasing continually and build-up areas are increasing dramatically. But changes in agriculture and rangelands aren't the same during time periods so that between years 1984 and 2005 agriculture lands increased and rangeland areas reduced and from 2005 to 2013 changes are vise versa. Anyway, these changes show sum of degraded forest and rangeland land uses added to agriculture. All above mentioned trends in land use changes are the same in both PLRA and CLRA.

Transition matrix of different land uses in PLRA, CLRA and MLAA are presented in Table 3, Table 4 and Table 5, respectively. The greatest transition from 1984 to 2005, all over the region, was the conversion of forest to agriculture. Also in the time period between 2005 and 2013 the conversion of forest and agriculture to rangeland in mountainous area and agriculture to build-up area in the plain were dominant.

After all, in order to estimate groundwater recharge, CN values calculated using land use types and soil hydrologic groups (Figure 4-a).

Then S calculated using SCS method and specific values (divided by area) presented in Figure 4-b. Accordingly, groundwater natural recharge over the multi-layer aquifer remain nearly constant whereas confined and phreatic layers are recharging by precipitation 18.12 and 12.40 percent, respectively, less than 30 years ago. It is worth mentioning that both S and R change rate in the last period is almost two times of the first period (-39 m^3/ha/year versus -22 m^3/ha/year for S and 20 m^3/ha/year versus 10 m^3/ha/year for R).

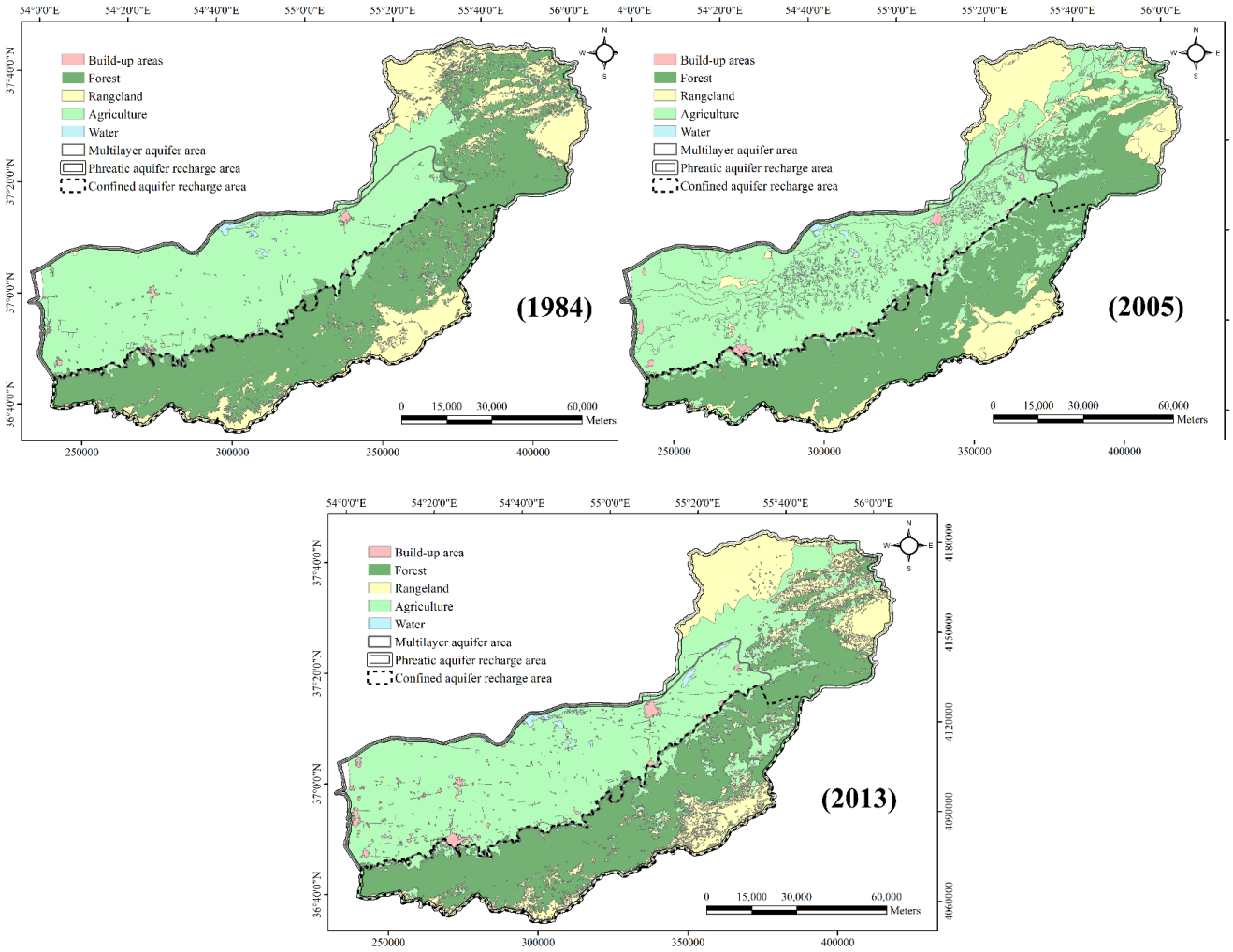

Figure 3. Land use maps in 1984, 2005 and 2013

Table 2. Land uses areas of PARA, CARA and MLAA in 1984, 2005 and 2013 (Km^2)

Year	1984			2005			2013		
Region	PLRA	CLRA	MLAA	PLRA	CLRA	MLAA	PLRA	CLRA	MLAA
Build-up area	39	0	38	66	6	59	173	10	154
Forest	4285	2886	103	3710	2798	36	3424	2635	50
Rangeland	1912	758	3	1556	525	46	2051	728	0
Agriculture	4860	192	4184	5781	514	4199	5420	463	4099
Water	44	1	43	45	0	42	75	2	72

Table 3. Transition matrix of different land uses (Build-up area (BA), Forest (F),Rangeland (R), Agriculture (A), Water (W)) within PLRA in 1984, 2005 and 2013 (Km^2)

	Year	1984-2005					2005-2013					1984-2013				
	To	BA	F	R	A	W	BA	F	R	A	W	BA	F	R	A	W
First year	BA	22	0	1	17	0	45	2	0	19	0	36	0	0	3	0
	F	4	3291	206	782	1	3	3133	346	224	1	8	3338	211	725	2
	R	0	360	1234	317	0	5	62	1337	144	2	4	52	1814	41	0
	A	40	56	110	4630	22	121	226	367	5008	48	125	33	26	4636	40
	W	0	0	0	21	21	0	1	0	21	23	0	0	0	11	33

Table 4. Transition matrix of different land uses within CLRA in 1984, 2005 and 2013 (Km^2)

	Year	1984-2005					2005-2013					1984-2013				
	To	BA	F	R	A	W	BA	F	R	A	W	BA	F	R	A	W
First year	BA	0	0	0	0	0	1	2	0	3	0	0	0	0	0	0
	F	3	2530	54	300	0	2	2441	215	137	1	4	2572	31	278	1
	R	0	226	462	70	0	2	47	451	21	0	2	35	695	25	0
	A	3	40	5	144	0	6	144	62	301	1	4	27	1	159	0
	W	0	0	0	1	0	0	0	0	0	0	0	0	0	0	1

Table 5. Transition matrix of different land uses within MLAA in 1984, 2005 and 2013 (Km^2)

	Year	1984-2005					2005-2013					1984-2013				
	To	BA	F	R	A	W	BA	F	R	A	W	BA	F	R	A	W
	BA	22	0	1	16	0	44	0	0	16	0	36	0	0	3	0
Firs	F	1	33	0	69	0	0	28	0	8	0	2	45	0	56	0
t	R	0	0	0	3	0	1	0	0	43	2	0	0	0	3	0
year	A	36	3	45	4076	21	109	21	0	4011	46	117	5	0	4022	39
	W	0	0	0	21	21	0	0	0	19	23	0	0	0	11	32

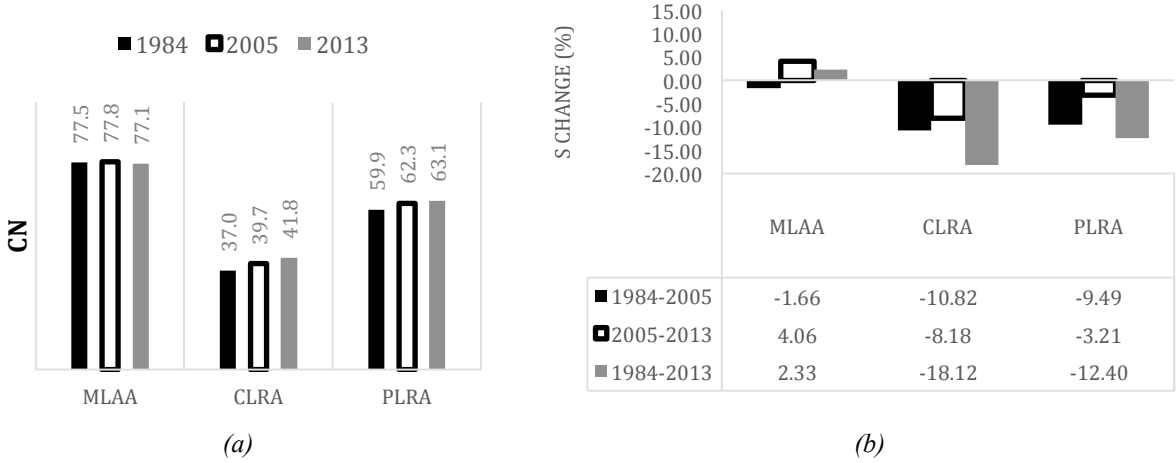

Figure 4. SCS method results including: a) CN values and b) specific S changes within MLAA, CLRA and PLRA in different periods of time

4. CONCLUSIONS

Detecting no significant trend in time series of precipitation can prove that human activities caused negative trend and decline of the confined aquifer piezometric level that necessitate consumption management of this section to prevent critical irreversible situations of the plain subsidence. Phreatic layer is both negatively and positive affected by current aquifer area land use, because is over- exploited through residential and agricultural areas and recharged by dam reservoirs. In addition this layer threatened by fossil brine development from northwest boundaries. On the other hand, confined layer is over-exploited through agricultural wells and threatened by Caspian Sea water intrusion.

Generally, deforestation of mountainous areas to cultivate them and urbanization of the plain are the most serious concerns of the region in terms of land use change, because of accelerating rate of deforestation in past years and build-up areas that become fourfold. Changing trend of agriculture and rangelands land uses probably caused by wet seasons occurred just before 2005 and subsequent growth in cultivated lands and then by several droughts occurred between 2005 and 2013 that created barren lands due to insufficient water resources (Karimirad et al., 2015).

Finally, all land use changes led groundwater natural recharge to be nearly constant over the multi-layer aquifer whereas confined and phreatic layers are recharging significantly less than 30 years ago and confined layer is more impressed with an alarming trend that is consistent with Karimirad et al. (2015).

REFERENCES

Adamat A. L., Foster R. A. N., Baban S. M. J., 2003. Groundwater vulnerability and risk mapping for the Basaltic Aquifer of the Azraq Basin of Jordan using GIS, Remote Sensing and DRASTIC. Appl. Geogr.; 23: 303-324.

Baker, T. J., Miller, S. N., 2013. Using the Soil and Water Assessment Tool (SWAT) to assess land use impact on water resources in an East African watershed. Jurnal of Hydrol.; 486: 100-111.

Bakker, M., 1999. Simulating groundwater flow in multi-aquifer systems with analytical and numerical Dupuit-models. Jurnal of Hydrol; 222(1): 55-64.

Batelaan, O., De Smedt, F., Triest, L., 2003. Regional groundwater discharge: phreatophyte mapping, groundwater modelling and impact analysis of land-use change. Jurnal of Hydrol.; 275(1): 86-108.

Boy-Roura, M., Nolan, B. T., Menció, A., Mas-Pla, J., 2013. Regression model for aquifer vulnerability assessment of nitrate pollution in the Osona region (NE Spain). Jurnal of Hydrol; 505: 150-162.

Cheng, A. H., 2000. Multilayered Aquifier Systems: Fundamentals and Applications. CRC Press; p: 169.

Cronshey, R., McCuen, R., Miller, N., Rawls, W., Robbins, S., Woodward, D., 1986. Urban hydrology for small watersheds—TR–55: Washington. DC, US Dept. of Agriculture, Soil Conservation Service, Engineering Division, Technical Release, 55, 164.

Fathian, F., Dehghan, Z., Eslamian, S., 2016. Evaluating the impact of changes in land cover and climate variability on streamflow trends (case study: eastern subbasins of Lake Urmia, Iran). International Journal of Hydrology Science and Technology; 6(1): 1-26.

Germer, S., Neill, C., Krusche, A. V., Elsenbeer, H., 2010. Influence of land-use change on near-surface hydrological processes: undisturbed forest to pasture. Journal of hydrology; 380(3): 473-480.

Habets, F., Viennot, P., Thierion, C., Vergnes, J., Ait-Kaci, H., Caballero, Y., Ackerer, P., Amraoui, N., Augeard, B., Besson, F., De Dreuzy, J. R., Longuevergne, L., Martin, E., Morel, T., Regimbeau, F., Thiery, D., Soubeyroux, J. M., 2015. Combined effect of climate change and groundwater abstraction on multi-layer and alluvial aquifers in France. Our Common Future under Climate Change (CFCC) Conference: International scientific conference.

Huismann, J. A., Breuer, L., Bormann, H., Bronstert, A., Croke, B. F. W., Frede, H. G., Graff, T., Hubrechts, L., Jakeman, A. J., Kite, G., Leavesley, G., Lanini, J., Lettenmaier, D. P., Lindstrom, G., Seibert, J., Sivapalan, M. G., Viney, N. R., Willems, P., 2009. Assessing the impact of land use change on hydrology by ensemble modelling (LUCHEM) III: scenario analysis. Adv. Water Resour.; 32: 159–170.

Kankash-Omran Consulting Engineers Co., 2013. Updating report on water balance of gharesoo and gorganrood rivers drainage basin. (In Persian)

Karimirad, I., Ebrahimi, K., Araghinejad, S., 2015. Investigation of Climate Variability Impacts on Multilayer Aquifers (Case Study: Gorgan Plain). Journal of Water Management and Irrigation; 5(2): 261-275. (In Persian)

Manandhar, R., Odeh, I. O., Ancev, T., 2009. Improving the accuracy of land use and land cover classification of Landsat data using post-classification enhancement. Remote Sensing; 1(3): 330-344.

Mann, H. B., 1945. Nonparametric tests against trend. Econometrica: Journal of the Econometric Society: 245-259.

Mishra, N., Khare, D., Gupta, K., Shukla, R., 2014. Impact of land-use change on groundwater—a review. Adv Water Resour. Protect.; 2: 28-41.

Mostafazadeh, R., Sheikh, V., 2012. Rain-Gauge Density Assessment in Golestan Province Using Spatial Correlation Technique. Journal of Watershed Research; 24(4): 79-87. (In Persian)

Pandian, M., Rajagopal, N., Sakthivel, G., Amrutha, D. E., 2014. Land use and land cover change detection using remote sensing and GIS in parts of Coimbatore and Tiruppur districts, Tamil Nadu, India. International Journal of Remote Sensing & Geoscience; 3(1): 15–20.

Sakieh, Y., Salmanmahiny, A., Jafarnezhad, J., Mehri, A., Kamyab, H., Galdavi, S., 2015. Evaluating the strategy of decentralized urban land-use planning in a developing region. Land Use Policy; 48: 534-551.

Salmani, H., Mohseni, S. M., Rouhani, H., Salajegheh, A., 2012. Evaluation of Land Use Change and its Impact on the Hydrological Process in the Ghazaghli Watershed, Golestan Province. Journal of Watershed Management Research; 3(6): 43-60. (In Persian)

Singh, S., Singh, C., Mukherjee, S. 2010. Impact of land-use and land-cover change on groundwater quality in the Lower Shiwalik hills: a remote sensing and GIS based approach. Open Geosciences; 2(2): 124-131.

Stigter, T. Y., Nunes, J. P., Pisani, B., Fakir, Y., Hugman, R., Li, Y., Tome, S., Ribeiro, L., Samper, J., Oliveira, R., Monteiro, J. P., Silva, A., Tavares, P. C. F., Shapouri, M., Cancela da Fonseca, L., El Himer, H., 2014. Comparative assessment of climate change and its impacts on three coastal aquifers in the Mediterranean. Journal of Regional environmental change; 14(1): 41-56.

Stuyt, L. C. P. M., Dierickx, W., Beltrán, J. M., 2005. Materials for subsurface land drainage systems (No. 60). Food & Agriculture Org.

Zhang, L., Nan, Z., Xu, Y., Li, S., 2016. Hydrological impacts of land use change and climate variability in the headwater region of the Heihe River Basin, Northwest China. PloS one; 11(6): e0158394.

Zhou, Y., Li, W., 2011. A review of regional groundwater flow modeling. Journal of Geoscience frontiers; 2(2): 205-214.

Proceedings of the 10th World Congress of EWRA 'Panta Rhei', 5-9 July 2017, Athens, Greece
© 2017 *European Water Resources Association*

Hydrochemical and qualitative assessment of natural water spring in southern Italy

S. Gaglioti[1], E. Infusino[2], T. Caloiero[3*] and G. Callegari[3]
[1] *Research Consultant, Pizzo (VV), Italy*
[2] *University of Calabria, Department of Environmental and Chemical Engineering (DIATIC), Rende (CS), Italy*
[3] *Institute for Agricultural and Forest Systems in the Mediterranean, National Research Council of Italy, Rende (CS), Italy*
[*] *e-mail: tommaso.caloiero@isafom.cnr.it*

Abstract: Groundwater represents a natural resource of great socio-economic importance for the entire southern Italy, where it is used for both irrigation and drinking purposes. Knowledge of the complex hydrogeological environment, of the chemical composition of waters and of the interpretation of geochemical maps allows the definition of flow domain, groundwater quality and degradation processes affecting the aquifers. The present paper offers a large qualitative assessment of water springs falling within the Crati river basin in Calabria, southern Italy, which is the largest basin in the region with an area of 2447.7 km^2 and a complex lithology. 190 samples of water springs, located over 300 m a.s.l., were collected and analysed. For each sample, physical (i.e. pH, water temperature, conductivity) and chemical parameters, such as major cations (Ca^{2+}, Mg^{2+}, Na^{+}, K^{+}) and major anions (SO_4^{2-}, Cl^{-}, HCO_3^{-}), were evaluated. The physical and chemical tests allowed the characterization of the hydrochemical facies of the sampled waters by means of the Langelier-Ludwig diagram. Moreover, the relationship between water temperature and altitude of the water springs has been assessed as well as the one between conductivity and altitude. Due to the extension of the basin, the investigated area was split into 5 sub-areas, with different hydrochemical behaviour. Results showed a good quality status of the water springs, where the hydrochemical facies of bicarbonate-alkaline type is predominant, and allow us to identify the chemical and physical behaviour of groundwater in relation with the several lithologies present in the sub-areas.

Key words: groundwater, water springs, Langelier-Ludwig diagram, Crati river basin

1. INTRODUCTION

Groundwater is affected by sources of natural and artificial origin. Safe drinking water is the basic need for every citizen. About 80% of the diseases in the world and one-third of the deaths in the developing countries are caused by contaminated water (WHO 2004). If water is suitable for drinking, it can also be safe for all other purposes. Usually, groundwater is safer than surface water in normal conditions, as it is naturally protected from the contamination caused by the infiltration of recharge water through soil cover. However, soils can be contaminated as a result of human activities. On the other hand, toxicity of minerals present in soils and rocks can also be caused by groundwater contamination following geochemical processes. Thus, fresh infiltrating recharge water can affect the quality of pure groundwater (Subba Rao 2008). In view of the rapid changes in groundwater due to the influences of natural and artificial sources, the examination of the quality of groundwater has been the issue of a great number of research papers (e.g., Appelo & Postma 2005; Fantong et al. 2009; Subramani et al. 2010; Ako et al. 2012). The most commonly used method to describe the constraints of groundwater evolution is the hydrochemical approach.

The present study is the first of its kind in the study area that attempts to evaluate groundwater quality in the Crati river basin in Calabria, southern Italy, by collecting and analysing 190 samples of water springs. In fact, although the Calabria region, and in particular the Crati basin, is an area characterized by several water springs and where groundwater is a prime source for drinking, only few studies, and for a small number of water springs, have been conducted in the past years to evaluate groundwater quality and degradation processes affecting these aquifers (Apollaro et al. 2006; Cantasano et al. 2013).

2. DATA AND METHODS

The Crati river Basin is the largest basin in the Calabria region (Figure 1), with an area of 2447.7 km^2 and a perimeter of about 320 km. The maximum and average altitudes are 2258 m a.s.l. and 597 m a.s.l. respectively. The 95-km long Crati River rises in the Sila Mountains at 1742 m a.s.l. and flows into the Ionian Sea.

It is a basin characterised by a typically Mediterranean climate, presenting sharp contrasts due to its position within the Mediterranean Sea and to its orography. Specifically, warm air currents coming from Africa and high temperatures affect the eastern sector, leading to short and heavy rainfall. The western side, instead, is affected by western air currents which cause temperatures to be milder and higher precipitation amounts on the mountains than on the other side. Cold and snowy winters and fresh summers with some precipitation are typical of the inner areas of the basin (Caloiero et al. 2016). From a geological point of view (Figure 1), the Crati Basin is bounded by the crystalline rocks of the Sila Massif to the east, by the crystalline and sedimentary rocks of the Coastal Chain to the west and south, and by the carbonatic rocks of the Pollino Massif to the north. The basement of the Crati Graben consists of Paleozoic granitoids and metamorphic rocks (gneiss, amphibolite, shale, schist and phyllite) belonging to the Alpine and Hercynian Chains. The Basin is L-shaped and has been divided into a N-S oriented Crati and an E-W oriented Sibari sub-basins (Colella et al. 1987).

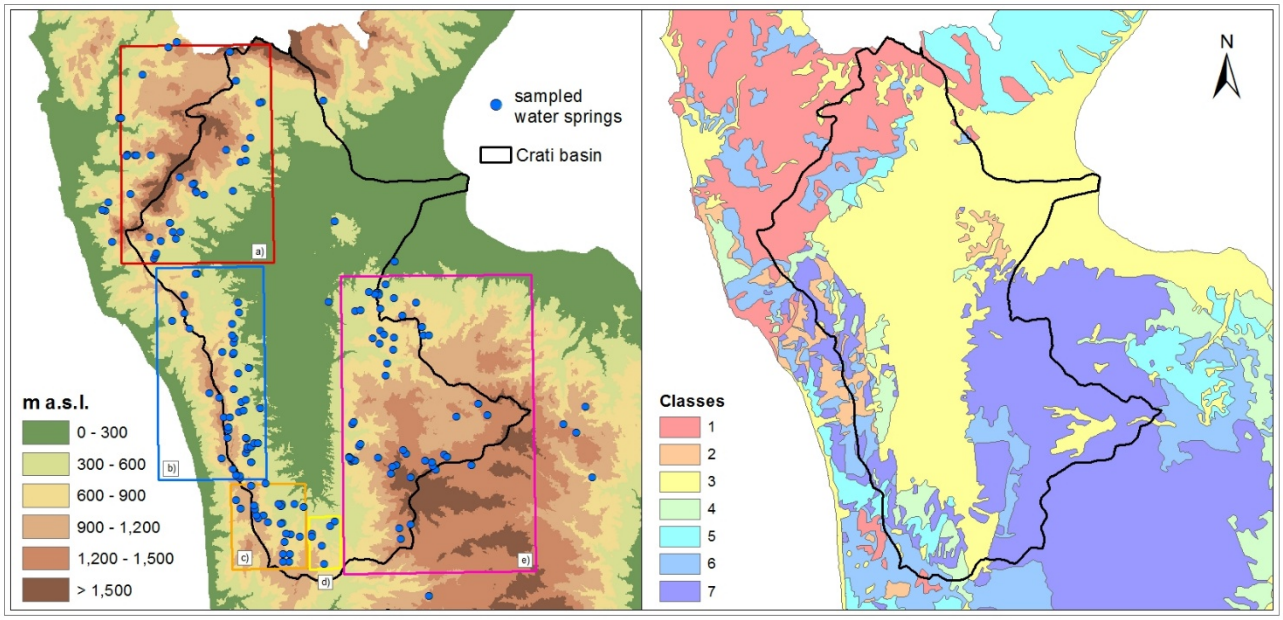

Figure 1. Crati river basin with water springs and sub-zones (left) and lithological map of the basin (right). Lithological units are grouped in seven classes: 1) limestones and dolostones; 2) metamorphic rocks at places with ophiolites; 3) sand, clay and gravel; 4) clayely and marly terranes; 5) flysch; 6) sandstones, conglomerates, limestones banks; 7) metamorphic rocks.

Due to its extension, as well as its geomorphological and hydrogeological properties, the investigated area was divided into 5 sub-areas, a) Pollino Massif, b) Coastal Chain, c) Mt. Cocuzzo, d) Serre Area, e) Sila Plateau (Figure 1), whose sampled waters have different hydrochemical behaviour.

The sampling of the 190 water springs has been conducted between February 2016 and May 2016, when the maximum discharges of the sources is usually recorded (Cantasano et al. 2013).

The physical parameters (i.e. temperature, pH and specific electrical conductivity compensated at 20°C), have been determined in situ using portable pH meter and conductivity meter. While the chemical parameters, such as major cations (Ca^{2+}, Mg^{2+}, Na^{+}, K^{+}) and major anions (SO_4^{2-}, Cl^{-},

HCO_3^-), were evaluated according to acknowledged laboratory standard methods (APHA 2002). The analysis conducted allowed us to determine the so-called *hydrochemical facies* for all the water spring samples, by means of the well-known Langelier – Ludwig (LL) squared diagram (Langelier & Ludwig 1942). This diagram allows the water classification by placing each sample point in one of the four sectors in which it is divided: First Sector chloride-sulphate alkaline-earth waters; Second Sector chloride-sulphate alkaline waters; Third Sector bicarbonate-alkaline waters; Fourth Sector bicarbonate alkaline-earth waters. The ions concentrations have been expressed in mEq/l. Moreover, further investigation has been conducted from the analysis of the diagrams which represent the comparison between the elevation of the water springs and two physical parameters such as temperature and conductivity.

3. RESULTS AND DISCUSSION

3.1 Langelier – Ludwig squared diagram

By evaluating ions concentration, for each sub-area a specific LL diagram has been obtained and the different hydrochemical facies have been investigated. Figure 2 shows the five different LL diagrams obtained, and a global overview of the spatial distribution of the LL classification within the Crati River basin.

On the basis of the different lithologies, significant results have been obtained for each sub-area.

In the Coastal Chain, the majority of the samples fall within the fourth sector with a random distribution revealing a high variability of the chemical and physical characteristics which can be due to a mixing effect between different types of water (Cantasano et al. 2013). This behaviour is typical of a strong lithological inhomogeneity as well as an important faults system running through the area.

As to what concerns the Sila Plateau area, from the analysis of the LL diagram, the water samples mainly fall within the first and the fourth sector, according to two different groups, thus evidencing water springs rich in Sodium and Potassium and, at the same time, poor in Calcium, Magnesium and alkalinity. This is a typical behaviour of aquifers flowing into intrusive magmatic or plutonic rocks, which also give waters some acid character.

In the Mt. Cocuzzo area results showed samples homogeneously grouped mostly in the fourth sector, very close to the lower right vertex of the diagram. This signals the presence of hard waters coming from deep aquifers, which are rich in Calcium and Magnesium. These two ions contribute to the high conductivity which has been detected in some water samples found in a restricted area.

The Pollino Massif area showed quite a similar behaviour with the Mt. Cocuzzo area. In fact, the majority of the samples fall within the fourth sector, due to waters particularly rich in Bicarbonates, Calcium and Magnesium. The alkaline character of these aquifers is due to a prolonged contact with limestones, dolostones, gypsum and anhydrite. In the west side of the Pollino Massif, only few waters springs showed a chloride-sulphate alkaline-earth character, probably due to some sea aerosols transport.

In the Serre area, all the water samples fall within the fourth sector and, as in the case of the Mt. Cocuzzo area, this is related to the presence of hard waters coming from deep aquifers rich in Calcium and Magnesium.

From the spatial distribution of the results obtained through the LL squared diagrams it can be observed that the bicarbonate alkaline-earth type emerged as predominant in each analysed area. In particular, it must be noted that these water springs are located at the highest elevations, very close to the basin borders.

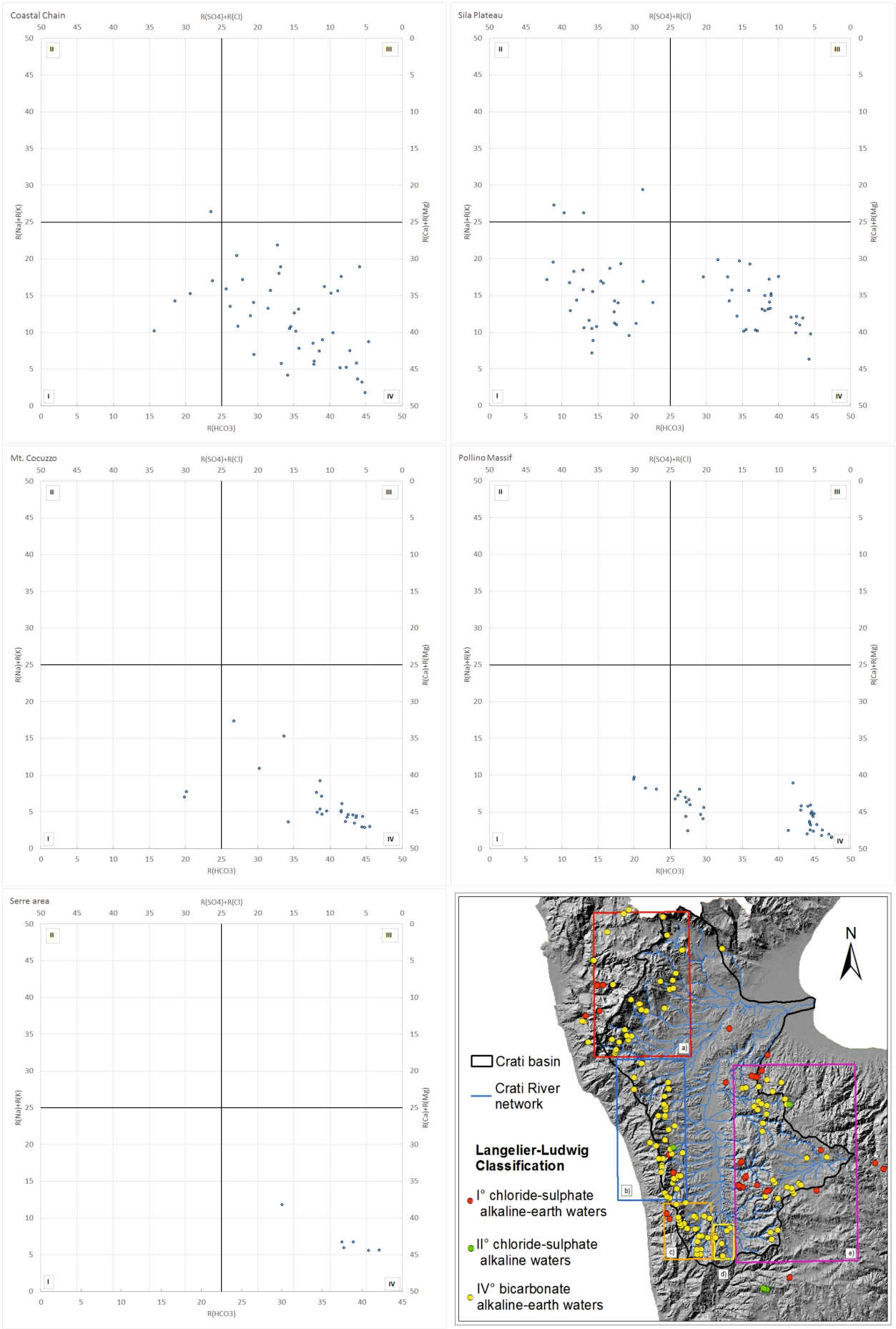

Figure 2. Langelier – Ludwig squared diagram for each area and spatial distribution of the results.

3.2 Relationship between water springs conductivity and elevation

From the analysis of relationship between water springs conductivity and altitude, some general information about the aquifers behaviour and their interaction with external phenomena can be evidenced (Figure 3).

In the Mt. Cocuzzo area, the sample points showed high variability with altitude, with some of the water springs clearly differing from others for their high conductivity values (maximum value in all the Crati river basin equal to 1185 µS/cm). In particular, this group is placed on a sulphurous-chalk lithological bedrock, which can explain the high conductivity values.

In the Coastal Chain, a slight downward behaviour of the conductivity with elevation has been detected, and three different water springs groups can be identified, probably due to the presence of several aquifers at different depths.

An almost homogeneous behaviour has been identified in the Pollino Massif, where limestone and dolostone make waters more conductive but the depth of these waters does not allow a remarkable interaction with precipitation.

The Sila Plateau area showed the most interesting results. In fact, in this area the highest water springs (1674 m a.s.l.) and the lowest conductivity value (45 µS/cm) have been found. This result may be indicative of the presence of relatively shallow aquifers, which are affected by rainfall (Infusino et al. 2006) and infiltration into the soil. Moreover, as the altitude decreases, the rainfall decreases too but the infiltration path and, consequently, the amount of dissolved salts brought in solution increase: that's why more conductive water springs have been found at the lowest altitude (Wilcox et al. 1956; Powell et al. 1985).

In the Serre area, no relationship between water springs conductivity and elevation has been evidenced.

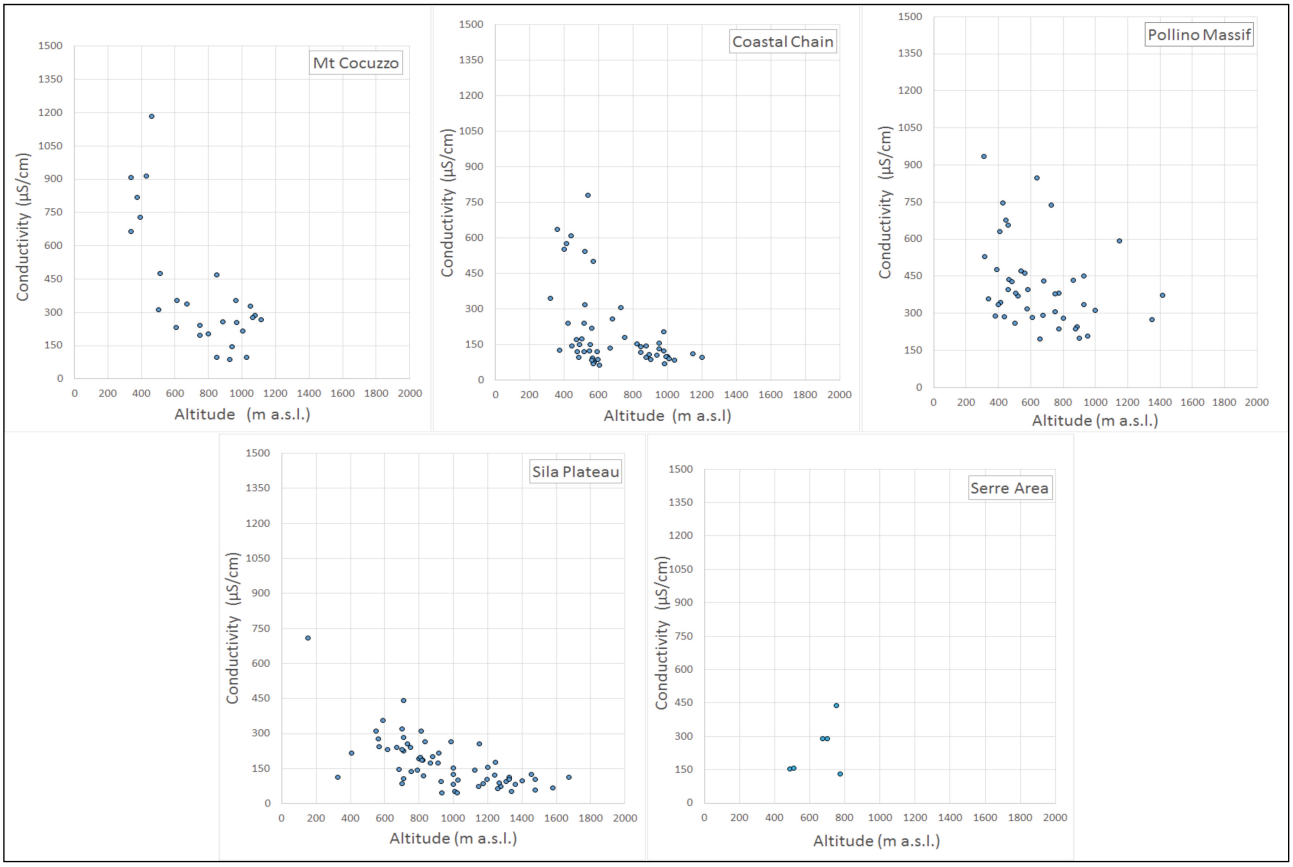

Figure 3. Relationship between water springs conductivity and elevation

3.3 Relationship between water springs temperature and elevation

Further information can be derived from the analysis of the diagrams which represent the comparison between the temperature and the elevation of the water springs, expressed as m a.s.l. (Figure 4). In fact, water spring temperature is influenced by many factors such as the season of the year in which the samples have been collected, the latitude and the elevation of the water springs. This latter relationship strictly depends on the depth of the aquifer. Indeed, elevation impacts on soil temperature in the same way as it does on air temperature. Moreover, water spring temperature is also linked to air temperature, with solar radiation, and finally with the geothermal gradient (Celico 1986).

As a result, in the Pollino Massif and in the Mt. Cocuzzo areas a homogeneous distribution of the temperatures with elevation can be observed. This is a typical behaviour of the deep groundwater aquifers which are not influenced by air temperature and show an almost constant temperature. On the contrary, in the Coastal Chain, in the Sila Plateau and in the Serre areas a marked reduction of the water springs temperature with elevation has been detected, which means superficial aquifers whose water temperature is influenced by air temperature.

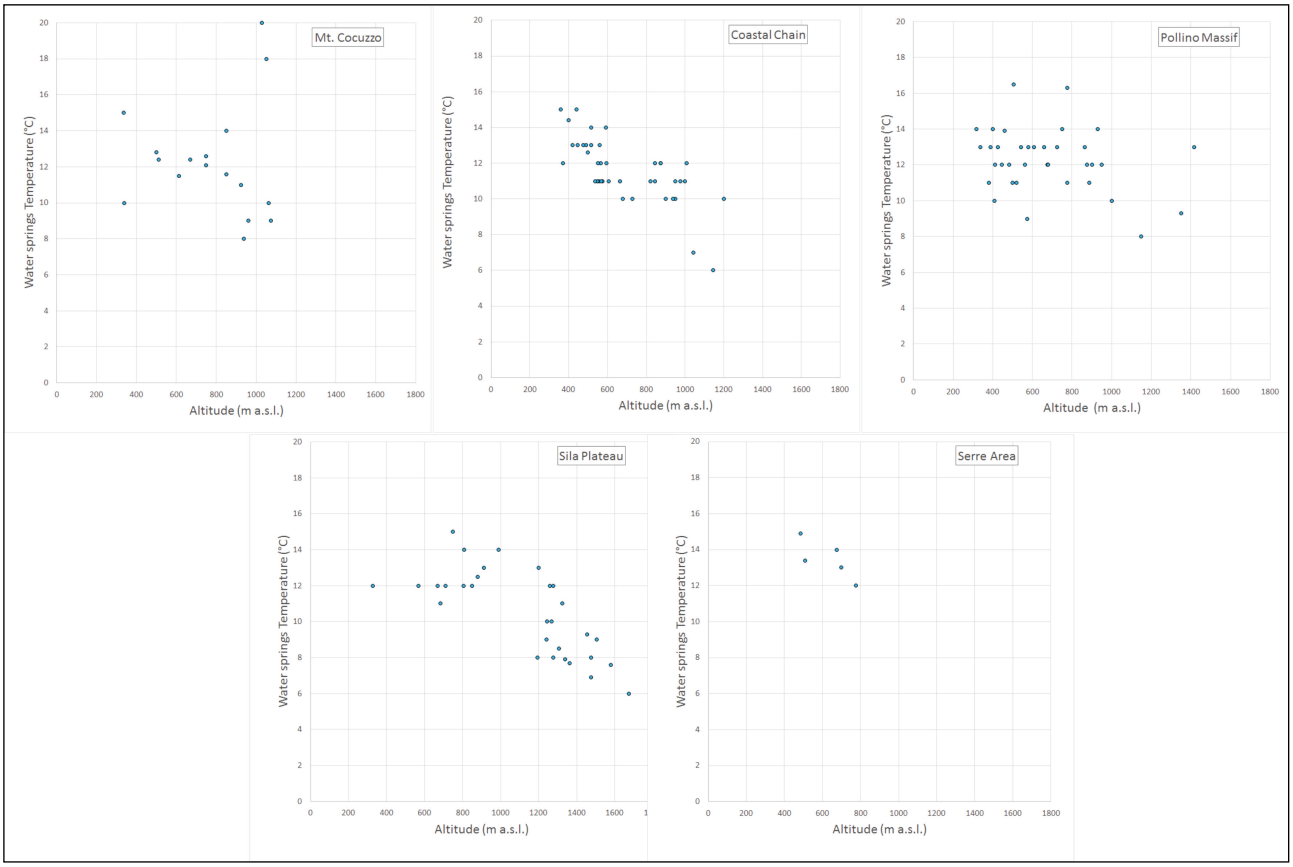

Figure 4. Relationship between water springs temperature and elevation

4. CONCLUSIONS

The present study is the first of its kind in the study area that attempts to evaluate groundwater quality in the Crati river basin in Calabria, southern Italy, by collecting and analysing 190 samples of water springs. The analysis of the major chemical and physical parameters allowed us to offer a global overview of the hydrochemical facies of the natural water springs in the five sub-areas in which the basin has been divided. As a result, the bicarbonate alkaline-earth and the chloride-sulphate alkaline-earth water types were the most detected, with very few occurrences of chloride-

sulphate alkaline type. Moreover, the bicarbonate alkaline-earth water types were detected at the highest elevations, very close to the basin borders.

From the analysis of the relationship between water springs conductivity and altitude, some general information about the aquifers behaviour and its interaction with external phenomena has been evidenced. In the Coastal Chain, Mt. Cocuzzo and Sila Plateau areas a downward behaviour of the conductivity with elevation has been detected. In particular, the most interesting results have been detected in the Sila Plateau area where, due to the presence of relatively shallow aquifers, the highest water springs and the lowest conductivity value have been found.

Finally, in the Coastal Chain, in the Sila Plateau and in the Serre areas a marked reduction in water springs temperature with elevation has been detected, probably due to the presence of superficial aquifers.

REFERENCES

Ako, A.A., Shimada, J., Hosono, T., Kagabu, M., Ayuk, A.R., Nkeng, G.E., Takem, G.E.E., Takounjou, A.L.F., 2012. Spring water quality and usability in the Mount Cameroon area revealed by hydrogeochemistry. Environ. Geochem. Hlth; 34:615–39.

APHA., 2002. Standard Methods for the Examination of Water and Wastewater. American Public Health Association, Washington, DC.

Apollaro, C., Artusa, C., Franco, C., De Rosa, R., Polemio, M., Virga, R., 2006. Geochemical studies of springwater in the Vaccuta and Abatemarco river basins (north-western Calabria, Italy). IJEGE; 2:59-75.

Appelo, C.A.J., Postma, D., 2005. Geochemistry, groundwater, and pollution. Rotterdam: Balkema Publishers.

Caloiero, T., Sirangelo, B., Coscarelli, R., Ferrari, E., 2016. An Analysis of the Occurrence Probabilities of Wet and Dry Periods through a Stochastic Monthly Rainfall Model. Water; 8:39.

Cantasano, N., Ietto, F., Callegari, G., Froio, R., Infusino, E., 2013. Assessment of the spring water quality in the municipal area of Chiaravalle Centrale (CZ, Italy). L' Acqua; 3:69-76.

Celico, P., 1986. Prospezioni geochimiche. In: Prospezioni idrogeologiche, Liguori Editore, pp. 307–357.

Colella, A., De Boer, P.L., Nio, S.D., 1987. Sedimentology of a marine intermontane Pleistocene Gilbert-type fan-delta complex in the Crati Basin, Calabria, southern Italy. Sedimentology; 34:721–736.

Fantong, W.Y., Satake, H., Ayonghe, S.N., Aka, F.T., Asai, K., 2009. Hydrogeochemical controls and usability of groundwater in the semi-arid Mayo Tsanaga River Basin: Far North Province, Cameroon. Environ Geol.; 58:1281–1293.

Infusino, E., Callegari, G., Frega, G., 2006. Deposizioni atmosferiche nell'area urbana di Cosenza in Calabria. Proc. XXIII Giornata dell'ambiente 2005, Rome, Accademia dei Lincei, 227:145.

Langelier, W.F., Ludwig, H.F., 1942. Graphical methods for indicating the mineral character of natural waters. JAWWA; 34:335.

Powell, J.D., Larson, J., 1985. Relation Between Ground-Water Quality and Mineralogy in the Coal-Producing Norton Formation of Buchanan County, Virginia. U.S.G.S. WSP 2274.

Subba Rao, N., 2008. Factors controlling the salinity in groundwaters from a part of Guntur district, Andhra Pradesh, India. Environ. Monit. Assess.; 138:327–341.

Subramani, T., Rajmohan, N., Elango, L., 2010. Groundwater geochemistry and identification of hydrogeochemical processes in hard rock region, Southern India. Environ Monit Assess; 162:123–137.

WHO, 2004. Guidelines for Drinking Water Quality (vol. 2). Health Criteria and other supporting information. Geneva.

Wilcox, J.C., Holland, W.D., Mcdougald, J.M., 1956. Relation of elevation of a mountain stream to reaction and salt content of water and soil. Can. J. Soil Sci.; 1:11-20.

Proceedings of the 10th World Congress of EWRA 'Panta Rhei', 5-9 July 2017, Athens, Greece
© 2017 *European Water Resources Association*

Mechanism of controlling seawater intrusion at coastal aquifers using subsurface barrier

R. Shafiee, S.S. Mehdizadeh* and A.S. Gooya
Civil Engineering Group, Islamic Azad University, Central Tehran Branch, P.O. Box 13185, Tehran, Iran
* *e-mail: Saj.Mehdizadeh@iauctb.ac.ir*

Abstract: One of cases that threaten groundwater in coastal aquifers is seawater intrusion (SWI). Inserting subsurface barrier (SB) is known as a way of preventing SWI. In this study, we attempted to achieve the optimum indexes for SB characteristics including longitudinal position, height, thickness and its hydraulic conductivity. Numerous scenarios have been defined and the finite difference dispersive SEAWAT model has been used. The positive impact of SB is evaluated by measuring the salt wedge toe retrogression, freshwater volume increase and the reduction of trapped salt wedge dimension over time. The results indicated that inserting the SB closer to shoreline control the SWI more efficient due to dilution of larger trapped wedge behind it. The results also illustrated that the more the height of SB approaches to 5% salinity contour the more efficient it will be. It is also shown that changing the thickness of SB had the least effect on SWI controlling but by reducing its permeability, its performance in short term and long term will have an effective improvement. Therewith, analyzing the performance of SB in aquifer with presence of extraction well demonstrate that even though SB can act successfully in reducing the salinity of extracted water, it cannot eradicate it entirely. Turning over of saline flow form above the barrier and reaching the salt wedge behind it, is found to be the reason. Eventually, the results show that constructing a SB is not a short-term method for controlling SWI and its effects are more significant in long period.

Key words: Coastal aquifer, Seawater intrusion, subsurface barrier, Transition zone

1. INTRODUCTION

Researches on controlling seawater intrusion (SWI) in coastal aquifers had a tremendous growth in the past decade but are mostly limited to all methods rather than constructing subsurface barrier (SB) (i.e. Cheng et al., 2000; Mantoglou, 2003; Mantoglou et al., 2004; Mantoglou and Papantoniou, 2008; Park et al., 2009; Abd-Elhamid and Javadi, 2011). Luyun-Jr et al, (2009) did a numerical and experimental research on controlling SWI in an unconfined coastal aquifer using SB. Based on their experiments, low height barriers can remove the salt wedge faster while the height needs to be determined properly as constructing a low height barrier might not be helpful for special cases. These researchers in 2011 investigated the effect of the recharge well and retaining walls location on salt wedge receding. Their results showed that the closer the recharge well to salt wedge, the better performance it has in removing the salt from aquifer and the further it goes, the weaker it becomes. Using a liner equation, they also proved that salt wedge would recede more when the barrier was built deeper and closer to ocean. At this study, we have distinguished the SB and retaining walls. Walls generally begin from the surface of aquifers, and it does not necessarily stretches to the bottom of the aquifer.

Kaleris and Ziogas (2013) evaluated the effects of retaining walls on saltwater dynamic movements and protecting groundwater extraction in coastal areas of Greece, based on SUTRA dispersive model. They concluded that the wall proper performance happens when the wall is constructed in a depth of more than 60% of the aquifers height and is located closer than twice the aquifer's height. They also found that constructing a retaining wall is more effective in heterogeneous aquifers and the greatest impact on SWI occurs when the hydraulic conductivity of the barrier is less than 10% of the hydraulic conductivity of the whole aquifer. Review of previous studies indicates that the SB impact on the increase or decrease rate of saltwater and freshwater

volume, optimum geometrical parameters of a barrier, the flow path lines near the barrier and finally analyzing the efficiency of SB while well is pumping water, is not investigated yet. Therefore, in this study, using SEAWAT dispersive model, a two-dimensional saturated homogeneous unconfined aquifer is simulated for different longitudinal position, height, thickness and hydraulic conductivity of SB to investigate reduction of salinity over time. The impact of constructing SB on thickness of transition zone is also provided in this study. Finally, the simultaneous performance of well and the barrier is investigated and the influence of the barrier on decreasing the salinity of extracted water has been analyzed.

2. MATERIALS AND METHODS

2.1 Large-scale aquifer

The chosen large-scale aquifer in this study is an unconfined, homogenous and two-dimensional aquifer that is similar to the aquifer presented by Lu et al., (2013). The simulated area, according to Figure 1, includes 430 m of landward and 70 m of seaward boundary. The height of the aquifer is 48 m and the sea section and the land section is divided by a coastal line with a 0.1 slope. The concentration of seawater in the ocean is 35 Kg/m^3 and the freshwater constant head (H_f:[L]) and seawater constant head (H_s:[L]) are respectively 46.2 and 45 m at vertical side of the aquifer. The aquifer bed assumed as no-flow boundary condition.

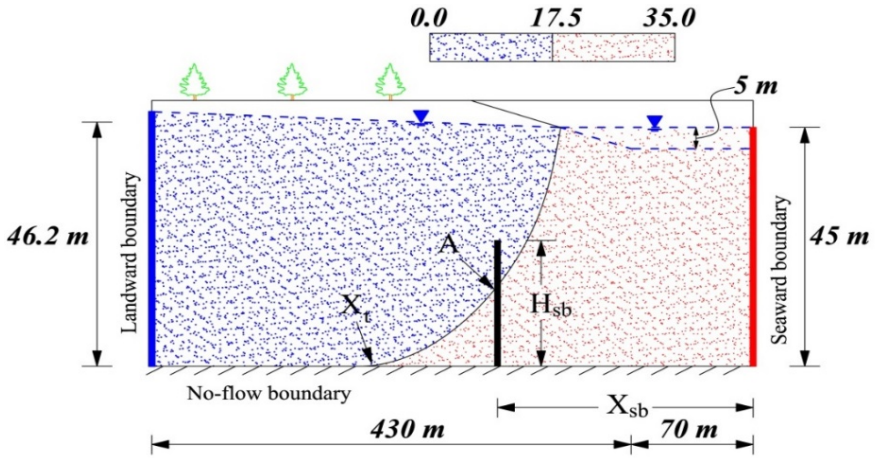

Figure 1. Dimensions and specifications of simulated aquifer

2.2 SEAWAT model settings

SEAWAT simulates SWI in aquifers by solving groundwater flow equation using MODFLOW model, and contaminant transport equation using MT3DMS model. The governing equations of groundwater flow and contaminants can be found in many recent studies (e.g. Langevin et al, 2008) and it is not expressed here for brevity. The aquifer is assumed homogenous, isotropic, and hydraulic conductivity equals to 8.64 m/d. Porosity is set to be 0.4 for each cell and the longitudinal dispersivity is considered 1 m through aquifer. The cell dimensions are assumed 1.0 m in length (ΔX) and 0.5 m in height (ΔZ). The model is first simulated for sufficiently long time to reach to steady condition. Then the SB is placed at desired location and the aquifer is simulated for 85 years at transient state. Specific yield (S_y) and specific storage (S_s) is respectively 0.25 and 0.0008 m^{-1} and time steps are set to 5 days for both flow and transport equations.

14 different scenarios are defined which are similar in time, boundary and initial conditions but differ at SB specifications. These specifications include (1) the distance between SB and the ocean (X_{sb}), (2) the height of SB (H_{sb}), (3) its width (W_{sb}) and (4) its hydraulic conductivity (K_{sb}). These specifications became dimensionless by dividing them with length and height of the aquifer according to Table 1. The average groundwater level is chosen as the height of the aquifer (H: [L]).

Table 1. Specifications of simulated scenarios

Scenario	Ksb (m/d)	Kr:Ksb/Kh	Wsb (m)	Wr:Wsb/H	Hsb (m)	Hr: Hsb/H	Xsb (m)	Xr:Xsb/L
Ts-1	0.00864	0.001	2	0.04	23.5	0.52	203	0.41
Ts-2	0.00864	0.001	2	0.04	23.5	0.52	248	0.50
Ts-3	0.00864	0.001	2	0.04	23.5	0.52	303	0.61
Ts-4	0.00864	0.001	2	0.04	12.5	0.27	248	0.50
Ts-5	0.00864	0.001	2	0.04	18.5	0.41	248	0.50
Ts-6	0.00864	0.001	2	0.04	22.5	0.49	248	0.50
Ts-7	0.00864	0.001	4	0.09	22.5	0.49	248	0.50
Ts-8	0.00864	0.001	6	0.13	22.5	0.49	248	0.50
Ts-9	0.0864	0.010	2	0.04	22.5	0.49	248	0.50
Ts-10	0.000864	0.0001	2	0.04	22.5	0.49	248	0.50
Ts-11	0.08640	0.010	2	0.04	12.5	0.27	294	0.59
Ts-12	0.00864	0.001	4	0.09	12.5	0.27	248	0.50
Ts-13	0.00864	0.001	4	0.09	17.5	0.38	248	0.50
Ts-14	0.00864	0.001	2	0.04	12.5	0.27	294	0.59

2.3 The methods of scenarios comparison

In most of recent studies on SWI problem, the thickness of transition zone is used according to following equation:

$$W_t = \frac{A_t}{L_t} \quad (1)$$

where W_t indicates the thickness of the zone [L], A_t indicates its area [L^2] and L_t indicates the length of it [L]. Considering 5% to 95% of sweater as transition zone threshold, this area will gradually decrease due to dilution over time by freshwater. The shape of the transition zone over time demonstrates that because of drastic changes and the irregularity of its area behind the barrier, W_t cannot be an appropriate index to compare the scenarios. In this study, the receding rate of salt wedge toe (X_t: [L]) and the height reduction of the trapped salt wedge (A: [L], see figure 1) with $0.5C_s$ criterion (C_s: sea salinity concentration) are two selected indexes for investigating SWI that have been dimensionless, using the following equations:

$$RR = 100\times\left(\frac{X_{t0}-X_{ti}}{X_{t0}}\right) \quad (2)$$

$$A_r = 100\times\left(\frac{A_0-A_i}{A_0}\right) \quad (3)$$

where X_{t0} is the length of salt wedge toe before construction of SB, X_{ti} is the length of salt wedge toe at time i. RR is the receding percentage of salt wedge toe at the same time, A_0 is the height of $0.5C_s$ salinity contour before construction of the barrier at its position. A_i is the similar height at time i and finally A_r is the decrease percentage of mentioned height.

3. RESULTS AND DISCUSSION

3.1 Longitudinal distance of SB from sea

Three scenarios including Ts-1 (the barrier is located at right one-third side of the transition zone), Ts-2 (the barrier is located at the middle of the transition zone) and Ts-3 (the barrier is located at left one-third side of the transition zone) were evaluated in this section according to following graphs.

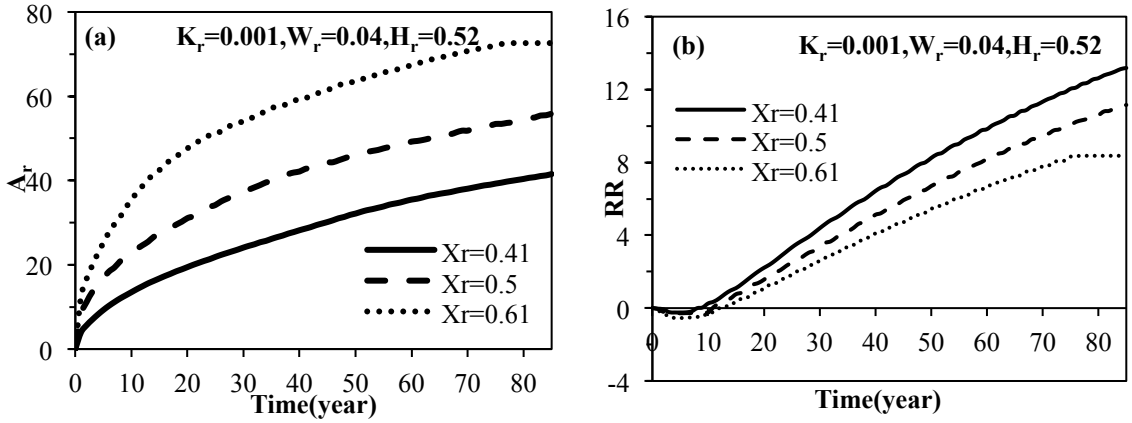

Figure 2. The impact of different longitudinal location of SB on (a) A_r and (b) RR dimensionless parameters

According to above comparison, in terms of SB distance from coastline, the closer the SB is to the ocean, the better performance achieved both in long-term and short-term. However, by constructing the barrier closer to the ocean, the W_t will not decrease. The W_t was 8.5, 8.1 and 6.9 m after 85 years as respectively SB getting further from ocean. The thicker transition zone for closest SB scenario to coastline is not a disadvantage as more dilution of the salt wedge that is trapped behind the barrier occurs at this scenario.

3.2 Optimal height of SB

Considering the fact that the aim of constructing a SB is to protect the aquifer against SWI with concentrations more than 1.75 kg/m^3, the H_{sb} is defined for Ts-6, Ts-5 and Ts-4 scenarios respectively lower, same and higher than 1.75 kg/m^{3}salinity contour height at the location of barrier. Scenario Ts-12 and Ts-13 follow the same rules and H_{sb} is respectively less and equal to 1.75 kg/m^3 salinity contour but the SB is thicker in these two scenarios.

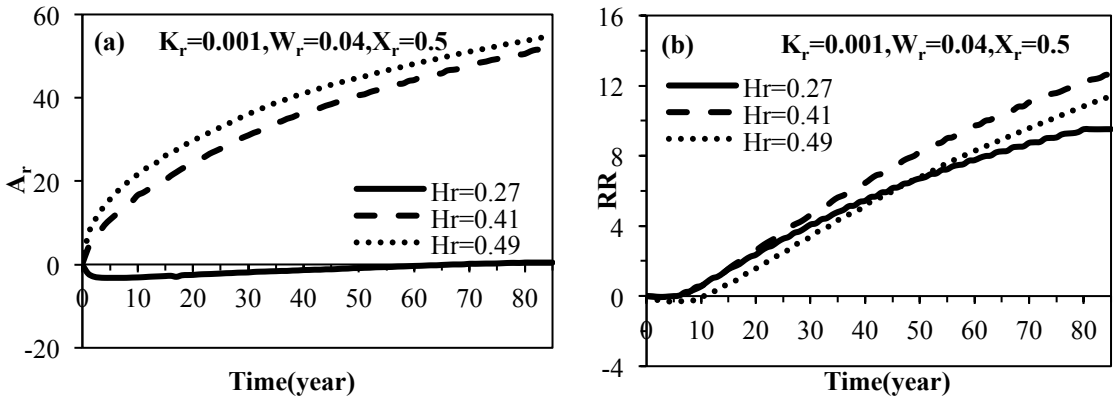

Figure 3. The effect of different H_{sb} on (a), A_r and (b) RR dimensionless parameters

According to above graphs, increasing H_{sb}, disconnects the sweater flow available in front and behind of the barrier and consequently leads to sever reduction of A point height. This condition is partly true for salt wedge receding rate and the scenarios with higher H_{sb} performed better. Before constructing the SB, the saltwater flow direction is first toward the transition zone and then turns toward the sea. By constructing the barrier, saltwater flow near the salt wedge toe still tends to turn toward the sea. However, by increasing the barrier's height, the trapped brackish flow behind the barrier starts to spin as they contacted the barrier and finally they are obliged to pass a longer path in order to reach the ocean. The velocity reduction and flow slow motion results in larger salt plume behind the SB and occupies a larger area of the aquifer at initial years.

3.3. Thickness and hydraulic conductivity of SB

There is no tangible difference in barrier performance when W_{sb} is changed. Obviously, the thicker SB could potentially provide better results but its requirement of more space than the narrow ones can slightly reduce the freshwater volume. It is clear that the less permeable scenarios are significantly more successful. Increasing or decreasing K_{sb} has a direct impact on flow transmission through the barrier body and leakage across the body of barrier will diminish its efficiency.

3.4. The influence of SB on improving salinity of extracted water

Since one of the main goal of constructing SB is improving the quality of extracted water, in the last part of this study the salinity of arbitrary placed well is measured for selected scenarios. For real similarity, both fully and partially penetrated well are modeled. It is found that the salinity of abstracted water has decreased considerably specially for fully penetrated well as it gets closer to coastline. The salinity changed from 9.8 kg/m^3 to 2.7 kg/m^3 (i.e. 72% decay rate) after ten years for fully penetrated case. Nonetheless, the progress has stopped after almost ten years and SB could not completely convert the extracted brackish water to freshwater. Similar desalinated trend occurred for water of partially penetrated well but slower than the fully penetrated scenario. The partially penetrated well had initially 1.1 kg/m^3 salinity but after 10 and 85 years, respectively it reduced with 27% and 92% decay rate.

4. CONCLUSION

SB is known recently an effective solution to prevent SWI. In this study, dispersive SEAWAT model is used to introduce optimum parameters for SB including longitudinal position, barrier height, thickness and its hydraulic conductivity. The simulated large-scale aquifer is assumed two-dimensional homogeneous aquifer. The simulation results demonstrated that constructing SB would widen the transition zone. That is because SB prevents routine movement of saline water around toe position to be discharged to the sea. The flow velocity consequently reduces around the toe and eventually leads to diffused flow directions. It is also found that inserting SB closer to shoreline controls SWI more efficiently. That is due to greater trapped saline water behind the SB lost its connection with sea and gradually is diluted by freshwater. The results also indicate that if the height of SB approaches to 5% concentration contour line and if it was shorter from this contour respectively in long and short time more efficient SWI controlling will be achieved. Higher SB increases mixing zone thickness at early times. It is shown that changing thickness of SB has the minimum effect on SWI controlling but generally more thickness leads to better SWI controlling. It is concluded that as the hydraulic conductivity decreased, the operation of SB is improved due to major disconnection of flows at both side of SB. Constructing SB improves the salinity of abstracted water too. It is found that proximity of well and SB pulls seawater toward well screen

and cannot completely retard the trapped salt wedge. It is finally advised that constructing SB should be considered as long-term remediation activity for aquifers expose to SWI.

REFERENCES

Abd-Elhamid, H.F., Javadi, A.A., 2011. A Cost-Effective Method to Control Seawater Intrusion in Coastal Aquifers. Water Resource Management 25, 2755-2780.

Anwar, H.O., 1983. The effect of a subsurface barrier on the conservation of freshwater in coastal aquifers. Water Research. 17 (10), 1257–1265.

Cheng, AH-D., Halhal, D., Naji, A., Ouazar, D., 2000. Pumping optimization in saltwater-intruded coastal aquifers. Water Resources Research, 36(8), 2155-2165.

Kaleris, V., and Ziogas, A. 2013. The effect of cutoff walls on saltwater intrusion and groundwater extraction in coastal aquifers. Journal of Hydrology 476. 370-383

Langevin, C.D., Thorne Jr, D.T., Dausman, A.M., Sukop, M.C., Guo, W., 2008. SEAWAT Version 4: A computer program for simulation of multi-species solute and heat transport: U.S. Geological Survey Techniques and Methods, Book 6, Chap. A22, 39 pp., http://pubs.usgs.gov/tm/tm6a22/.

Lu, C., Chen, Y., Zhang, C., Luo, J., 2013. Steady-state freshwater–seawater mixing zone in stratified coastal aquifers. Journal of Hydrology 505, pp. 24-34.

Luyun Jr, R., Momii, K., Nakagawa, K., 2009. Laboratory-scale saltwater behavior due to subsurface cutoff wall. Journal of Hydrology 377, 227-236.

Luyun Jr., R., Momii, K., Nakagawa, K., 2011. Effects of recharge wells and flow barriers on seawater intrusion. Ground Water 49 (2), 239–249.

Mantoglou, A., 2003. Pumping management of coastal aquifers using analytical models of saltwater intrusion, Water Resources Research, 39, 1335, doi:10.1029/2002WR001891, 12.

Mantoglou, A., Papantoniou, M., Giannoulopoulos, P., 2004. Management of coastal aquifers based on nonlinear optimization and evolutionary algorithms. Journal of Hydrology 297, 209-28.

Mantoglou, A., Papantoniou, M., 2008. Optimal design of pumping networks in coastal aquifers using sharp interface models. Journal of Hydrology 361, 52-63.

Park, N., Cui, L., Shi, L., 2009. Analytical design curves to maximize pumping or minimize injection in coastal aquifers. Ground Water 47 (6), 797-805.

Sugio, S., Nakada, K., Urish, D.W., 1987. Subsurface seawater intrusion barrier analysis. Journal of Hydraulic Engineering– ASCE 113 (6), 767–779.

Proceedings of the 10th World Congress of EWRA 'Panta Rhei', 5-9 July 2017, Athens, Greece
© 2017 *European Water Resources Association*

Long term monitoring of aquifer salinization processes in a physical analog model

N. Colombani[1*], B.M.S. Giambastiani[1] and M. Mastrocicco[2]
[1] *Department of Biological Geological and Environmental Sciences, University of Bologna, V. Selmi 3, 40126 Bologna, Italy*
[2] *Department of Environmental, Biological and Pharmaceutical Sciences and Technologies, University of Campania "Luigi Vanvitelli", Via Vivaldi 43, 81100 Caserta, Italy*
[*] *e-mail: nicolo.colombani2@unibo.it*

Abstract: A long-term experiment on an unconfined shallow aquifer physical analog model was performed to study the salinization processes in finely graded sandy-silty sediments. The unconfined shallow aquifer was reconstructed within a laboratory large tank (4x8x1.4 m) equipped with 26 standard piezometers. The sediments (~35 m^3) pertaining to a crevasse splay deposit of the paleo-Po river system were sourced in March 2004 from an unconfined alluvial aquifer near Ferrara (Northern Italy). In July 2013, 600 l of NaCl saline solution (35 g/l) was injected in the aquifer physical analog model and the fate and transport of the saline solution was monitored since nowadays. The system was subjected to high evaporation rates, which caused the upper soil salinization in presence of saline groundwater. The movement of the saline solution was monitored in time and space with both fully screened piezometers and high resolution multi-level coring (every 5 cm). The results highlighted how the saline front migrated within the aquifer physical model in response to different boundary conditions: lateral input of water from irrigation canals, sprinkler irrigation and evaporation, all in controlled conditions. This study aims to elucidate the processes of soil salinization in reclaimed agricultural lands characterized by highly saline groundwater.

Key words: soil salinization; saline groundwater; evaporation; low permeability

1. INTRODUCTION

In the following decades, the increase of surface water resources losses as a result of widespread pollution and of the increasing water demand for economic development, will drive a progressive stress on shallow groundwater bodies, especially in coastal areas (Kundzewicz & Döll 2009). Like various low-lying coastal areas around the Europe (Feseker 2007; Oude Essink et al. 2010), the Po river Delta shallow coastal aquifer was found to be affected by autonomous salinization caused by the upward flux of saline and hypersaline groundwater (Colombani et al. 2016a). Thus, soil salinization mechanisms have to be rigorously quantified using controlled conditions, by using long term laboratory apparatus. Large tank experiments can be extremely useful to infer long term changes in groundwater and aquifers matrix (Werner et al., 2016). This can be achieved accelerating the groundwater flow conditions as typically can be done in column experiments, but using standard monitoring techniques like standard monitoring wells and accounting for soil's heterogeneities (Lee et al. 2008; Mastrocicco et al. 2011). In this study, a three years long experiment was performed in a physical analog model to quantify the foreseeable impacts of climate change on the unconfined aquifer of the Po Delta. This was achieved modifying the boundary conditions and monitoring piezometric heads and salinity using multi-level sampling (MLS) devices.

2. MATERIALS AND METHODS

The experiment was performed in a physical analog model (4 m wide by 8 m long and 1.4 m deep) located in the Hydrogeology Laboratory at the Scientific and Technological Pole of the

University of Ferrara. The physical analog model was filled with 42 m^3 of unconsolidated material (35 m^3 of natural sediments and 7 m^3 of gravel), by means of a bulldozer equipped with a 2-ton tilting shovel mounted on a 8-m-long telescopic crane.

An external reservoir (constant head) was connected to the tank via three inflow pipes. Twenty-six piezometers were installed using a hand driven auger, on the base of a semi-regular monitoring grid. A complete description of the tank set-up can be found in Mastrocicco et al. (2011). Groundwater levels were measured using an electric contact phreatimeter and salinity was measured converting electrical conductivity and temperature collected data. Core samples were collected several times along the maximum salinity gradient of the physical analog model. Core samples were taken every 5 cm by mean of a micro auger equipment. Soil water content was measured gravimetrically and pore water salinity was measured extracting with ultrapure water the water-soluble fraction from the sediment samples, using a sediment to water weight ratio of 1:5.

The experiment started in July 2013, here an input of 600 L of saline water (35 g/l) was provided from the constant head at the end of the model. Then, the boundary conditions were left unaltered for 8 months (until February 2014) to monitor the salinization of the physical analog model. From February 2014 to February 2016 the physical analog model was no more supplied with water and left under bare evaporation conditions. From February 2016 a freshwater (0.35 g/l) constant head was provided. Finally, from May 2016 to June 2016 three different irrigation rates were applied (1, 5 and 10 mm/h for 24 hours each) on the physical analog model ground surface and then monitored until October 2016.

3. RESULTS AND DISCUSSION

The long term experiment here described tried to resemble the possible scenario of a portion of the unconfined aquifer, which could occasionally be salinized by irrigation canals affected by seawater ingression as reported by different authors as a mean of aquifer salinization (Feseker 2007; Oude Essink et al. 2010; Colombani et al. 2016a). The movement of the saline wedge was extremely slow sue to the low hydraulic conductivity of the sediments. In fact, after 6 months from the injection, the saline wedge had just travelled a maximum distance of 2 m from the injection boundary (Fig. 1). The contour maps of figure 1 show that the saline wedge moved preferentially in zone characterized by a higher hydraulic conductivity values. In addition, saline front did not behave as sharp interface, but was rather diluted, indicating a relatively large dispersion coefficient both in the longitudinal and transversal direction. While the vertical dispersivity seems less pronounced. This behaviour was due to the intra-well artificial mixing that led to a biased saline distribution within the monitoring wells (Britt, 2005; Colombani et al., 2016b). In fact, Figure 1 shows the vertical salinity distribution observed in the monitoring wells in the saltwater wedge was quite different from the pore water vertical salinity distribution.

Another aspect that is appreciable only employing MLS, is the top soil salinization. In the right chart of Figure 2, is apparent an accumulation of salts in the top soil even in absence of saline groundwater, this was due to continuous evaporation since 2006, when the physical analog model was assembled and continuously flushed with freshwater (Mastrocicco et al., 2011).

Moreover, that changing the boundary conditions increased the top soil salinity in time due to evaporation processes combined with high capillary rise of the sediments. A high top soil salinity was found at the end of the desiccation period (February 2016) in the zones reached by saline groundwater. Salinity higher than 15 g/L was found in surficial samples collected below Y coordinate of 1.5 m (see Fig. 1). Consequently, when irrigation was supplied a sudden salinity increase was observed in all the monitoring wells up to Y coordinate of 2.0 m. However, given that the physical analog model was almost completely desiccated, the first two irrigation events did not produce any groundwater head increase. On the contrary, the third irrigation event produced a sharp rise in the water table, but since the irrigation rate was excessive, surface run-off and ponding occurred, spreading the saline water in an area larger than the one affected by the saltwater wedge.

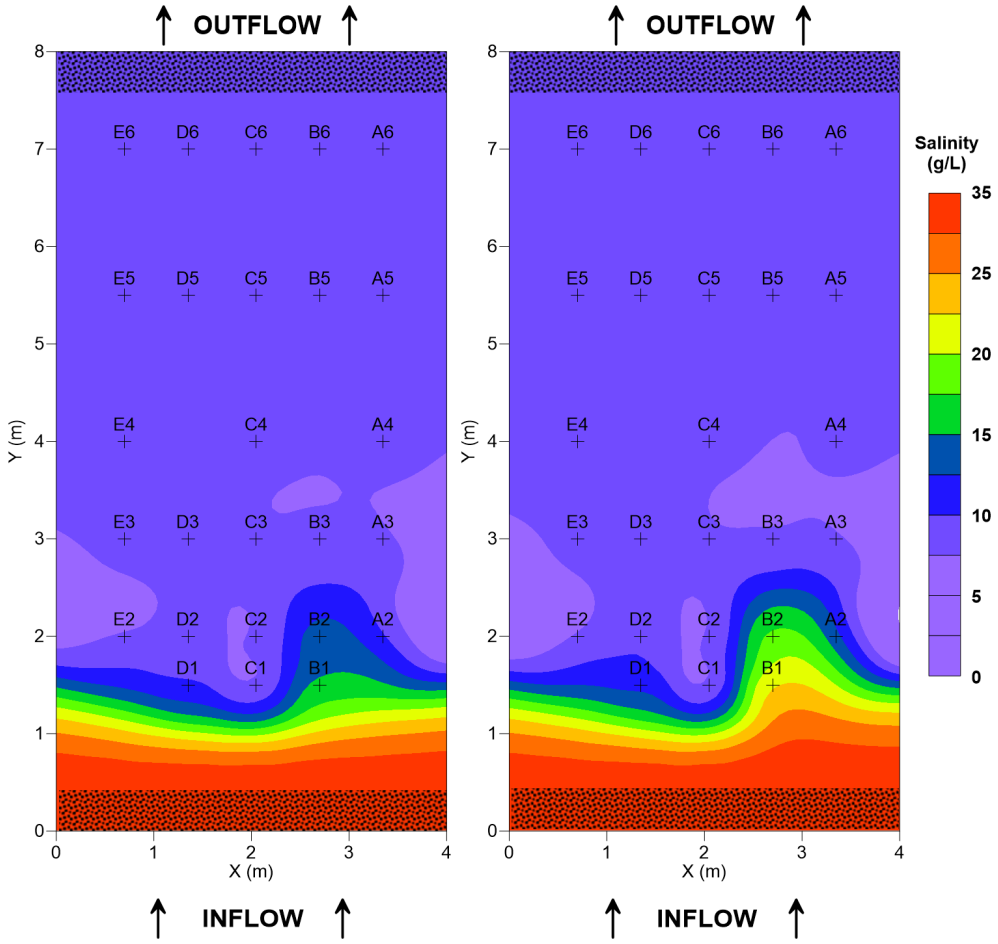

Figure 1. Upper left panel: groundwater salinity contour map at the water table in February 2014. Upper right panel: groundwater salinity contour map at the model bottom in February 2014.

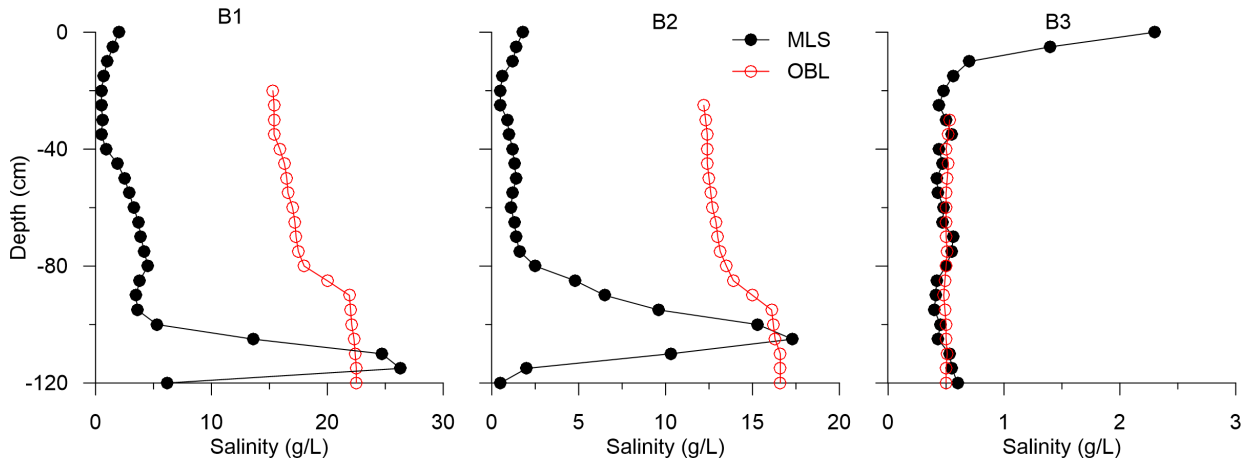

Figure 2. Vertical pore water salinity distribution (MLS) and open borehole logs (OBL) vertical groundwater salinity distribution of three selected points in February 2014.

More information is given in Table 1, where the salinity of monitoring wells is reported for each irrigation event. As can be seen from table 1, the last irrigation event produced a salinity increase respect to the background value of 0.3 g/L. In fact, a salinity increase of 1-2 g/L in many observation wells even beyond the Y coordinate of 4.0 m. On the contrary, since the inflow boundary was set up with freshwater from February 2016, the salinity in the monitoring wells near to the inflow decreased nearly to background values (Table 1).

Table 1. Salinity in monitoring wells at the end of the monitoring period (10/10/2016).

i.d.	**Salinity (g/L)**	i.d.	**Salinity (g/L)**
A2	0.76	C4	1.02
A3	1.32	C5	3.64
A4	7.00	C6	2.36
A5	3.19	D1	2.80
A6	1.43	D2	1.17
B1	0.59	D3	0.85
B2	0.97	D5	1.19
B3	1.11	D6	1.71
B5	2.97	E2	3.74
B6	3.82	E3	5.36
C1	0.81	E4	0.92
C2	1.02	E5	3.71
C3	2.76	E6	2.16

Finally, given that sprinkler irrigation often produce surface run-off and ponding (Gillies & Smith, 2005), this mechanism could be a mean to spread salt contamination in large areas at the border of the saltwater wedge or near salinized water canals and rivers (Da Lio et al., 2015).

4. CONCLUSIONS

A three years long experiment was performed in an aquifer physical analog model to study the lateral and vertical migration of saline groundwater. Vertical and lateral saltwater migration was affected by heterogeneities of sediment grain size, creating preferential pathways and stagnant zones. The monitoring wells did not captured the vertical distribution of salinity due to artificial mixing within the monitoring wells and this can be a source of bias when attempting to build up a robust conceptual model of saltwater intrusion. The top soil salinization increased in time due to evaporation processes combined with high capillary rise of the sediments. The irrigation practices like sprinklers can eventually increase the areas of salt contamination if the top soil salinity is carried along the agricultural fields via surface run-off.

REFERENCES

Britt, S. L., 2005. Testing the in-well horizontal laminar flow assumption with a sand-tank well model. Ground Water Monit. Remed.; 25(3): 73-81.

Colombani, N., Osti, A., Volta, G., Mastrocicco, M., 2016a. Impact of climate change on salinization of coastal water resources. Water Resour. Manage.; 30(7): 2483-2496.

Colombani, N., Volta, G., Osti, A., Mastrocicco, M., 2016b. Misleading reconstruction of seawater intrusion via integral depth sampling. J. Hydrol.; 536: 320-326.

Da Lio C., Carol E., Kruse E., Teatini P., Tosi L., 2015. Saltwater contamination in the managed low-lying farmland of the Venice coast, Italy: an assessment of vulnerability. Sci. Tot. Environ.; 533: 356-369.

Feseker, T., 2007. Numerical studies on saltwater intrusion in a coastal aquifer in northwestern Germany. Hydrogeol. J.; 15(2): 267-279.

Gillies, M. H. & Smith, R. J., 2005. Infiltration parameters from surface irrigation advance and run-off data. Irrig. Sci.; 24(1): 25-35.

Kundzewicz, Z. W. & Döll, P., 2009. Will groundwater ease freshwater stress under climate change? Hydrological Sci. J.; 54(4): 665-675.

Lee, E. S., Woo, N. C., Schwartz, F. W., Lee, B. S., Lee, K. C., Woo, M. H., Kim, J. K., Kim, H. K., 2008. Characterization of controlled-release KMnO 4 (CRP) barrier system for groundwater remediation: a pilot-scale flow-tank study. Chemosphere; 71(5): 902-910.

Mastrocicco, M., Colombani, N., Palpacelli, S., Castaldelli, G., 2011. Large tank experiment on nitrate fate and transport: the role of permeability distribution. Environ. Earth Sci.; 63(5): 903-914.

Oude Essink, G. H. P., van Baaren, E., S., de Louw, P., G. B., 2010. Effects of climate change on coastal groundwater systems: a modeling study in the Netherlands. Water Resour. Res.; 46: W00F04.

Werner, A. D., Kawachi, A. and Laattoe T., 2016. Plausibility of freshwater lenses adjacent to gaining rivers: Validation by laboratory experimentation. Water Resour. Res.; 52: 8487-8499.

Proceedings of the 10th World Congress of EWRA 'Panta Rhei', 5-9 July 2017, Athens, Greece
© 2017 *European Water Resources Association*

A three dimensional modeling approach to groundwater management in Paharpur canal command area, Dera Ismail Khan, Pakistan

A. Khan[1*], A. Qadir[2], M. Zafar[1] and T. Khan[1]
[1] *Department of Earth and Environmental Sciences, Bahria University, Shangrilla Road, E-8, Islamabad, Pakistan*
[2] *Department of Geology, University of Haripur, Hattar Road, Haripur, Khyber Pakhtunkhwa, Pakistan*
[*] *e-mail: aneela00@yahoo.com*

Abstract: The main aim of this study was to analyze the groundwater flow system in Paharpur Canal Command Area, Dera Ismail Khan using 3D numerical groundwater flow modeling. The groundwater flow system in the area was modeled using MODFLOW 4.2. The model was run for both steady and non-steady state conditions. The area was modeled with a grid of 171 columns and 399 rows with three layers assigned on the basis of the varying hydraulic conductivity values. The upper 100 meter of the unconfined aquifer was modeled. The steady state model was simulated and then calibrated for the year 1980 using PEST. Non-steady state simulation was carried out from the year 1980 to 2010 to evaluate the effects of groundwater abstraction on the water table depths and flow direction. The groundwater model developed has resulted in better understanding of the groundwater flow of the study area. Water logged zone have also been identified with the aid of the model. Groundwater management of the area can be effectively carried out with the support of the model developed.

Key words: Groundwater, modeling, MODFLOW, calibration, water logging

1. INTRODUCTION

Fresh water is essential component of all forms of life and it is mainly obtained from two sources, i.e. surface water and groundwater (McMurry and Fay, 2004). Groundwater is an exceedingly important freshwater resource and its ever-increasing demand for agriculture, domestic and industrial use in Pakistan ranks it as of strategic importance (Amin, 2012). Agriculture is the largest sector of Pakistan's economy. It accounts for about 70 percent of the export earnings (PWP, 2001). The uncontrolled and unregulated use of groundwater leading to the overdraft of aquifers and salt-water intrusion has emerged in many areas of the Indus Basin, Pakistan (Kijne, 1999). The secondary salinization associated with the use of poor quality groundwater for irrigation has further compounded the problem. The phenomenon of water logging and salinity is widespread in many agricultural areas all around the globe where it causes several socio-economic and environmental losses. In irrigation command areas, Groundwater models such as MODFLOW have been widely employed in general groundwater studies including water-logging problems (McDonald and Harbaugh, 1988).

Although research on climate change in Pakistan is still in its infancy, there is evidence that future changes in climate will have adverse effects on agricultural production (Hussain and Hanif, 2013). Hence Groundwater modeling is an important tool to provide guidance for management of groundwater particularly in the areas where the hydrological cycles are predicted to be accelerated due to climate change (Mall et al., 2006).

This paper is a part of the study aimed to analyze the groundwater flow system in Paharpur Canal Command Area. Numerical three dimensional finite difference steady and non-steady state flow models were prepared for the unconfined aquifers using MODFLOW version 4.2. The overall objective of the current work was to determine in detail the groundwater movement and access the interaction of the groundwater aquifers with the Paharpur Canal and Indus River. In non-steady state simulations, the effect of pumping wells on the groundwater flow and depth were determined.

2. STUDY AREA

The Paharpur Canal Command Area is located on the north eastern side of Dera Ismail Khan (Figure 1). Dera Ismail Khan is the southern most of the districts in the Khyber Pakhtunkhwa Province of Pakistan. Paharpur Canal Command Area falls within longitude 70° 55' to 71° 18' East and latitude 31° 45' to 32° 25' North (WAPDA, 1980). Chashma Barrage is on the northern side and to the south is the City of Dera Ismail Khan. The Paharpur Canal forms the western boundary. The Paharpur Canal emerges from the Chashma Barrage and ends near the south of Dera Ismail Khan City at Kotla Qaim Shah (Naqvi, 1977). The eastern boundary is formed by the Indus River. Agriculture is the principle source of income in Dera Ismail Khan District (Hussain and Hanif, 2013).

Physiographically the area consists of active flood-plains, meandering flood-plains and piedmont plains (WAPDA, 1980). Most part of the district is a dry alluvial plain (Qadir et al., 2014). The climate of Dera Ismail Khan is semi-arid (Naqvi, 1977). About 60% of the rainfall occurs in July and August in the monsoon season. Clay, silt and gravel of late Pleistocene to Holocene age constitutes the unconsolidated sediments of the study area. At a greater depth the unconsolidated sediments in the area consists of clay. This clay section is overlain by deposits of Holocene age and consists of sand dune and alluvium which is more than 300 m thick (Hood et al., 1970). This alluvium constitutes the unconfined aquifers in the area. The alluvium mostly consists of sand with clay, silt and gravel in subordinate amount.

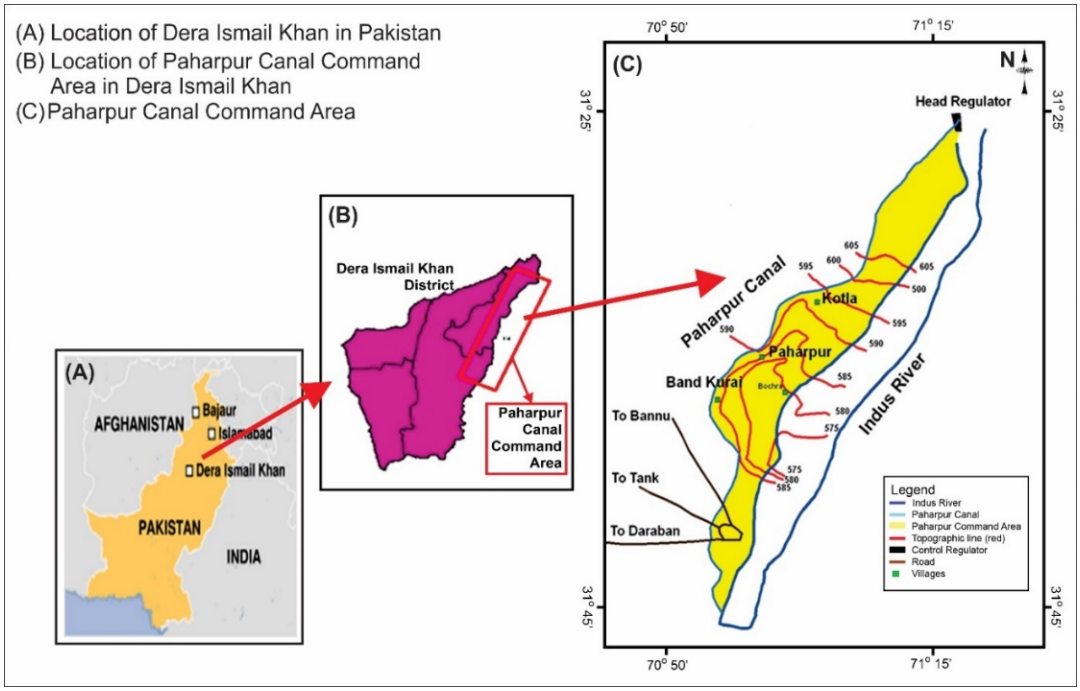

Figure1. Location of Paharpur Canal Command Area in Dera Ismail Khan, Pakistan.

3. METHODOLOGY

The methodology followed the standard procedures adopted from Anderson and Woesnner (1992), starting with the hydrogeologic model conceptualization. Then the modeling software is selected. The next step involves the numeric model development and its simulation. After that model calibration is executed. It consists of changing the values of input parameters in an attempt to match field conditions. Sensitivity analysis is carried out on the calibrated model to deduce how changes in each parameter affect the model results. Final step comprises the analysis of the model results.

4. MODEL DESIGN FOR THE PAHARPUR CANAL COMMAND AREA

The boundaries of the model were determined by using a base map created in Global Mapper. MODFLOW imported the base map from Glober Mapper in .dxf format. MODFLOW developed by the USGS, is a computer program using the finite-difference method to describe the movement principle of groundwater flow. The modeled region has a total area of about 2,727 km^2. The block centered grid consists of square cells of 171 × 399 grid cells, 0.04 km^2 each. The thickness of alluvium in this area is approximately 300 meters (Hood et al., 1970). Top 100 meters of this alluvium was modeled. This portion has been divided into three layers on the basis of varying permeability. The horizontal and vertical hydraulic conductivities were assigned to the three layers. Initial hydraulic head distributions for the model were obtained from the test holes and test wells drilled and installed by Water and Power Development Authority (WAPDA). The latitude and longitude of the wells together with their groundwater table elevation values were imported in the model. The Paharpur Canal consists of five distributaries. These include the Takarwah, Kot Hafiz, Rakh, Girsar and Rakh Mangan distributaries (WAPDA, 1980). Stream boundary conditions have been applied to the Paharpur and its five distributaries. Indus River was assigned the constant head boundary. The discharge rates along the Indus River were gathered from Indus River System Authority (IRSA). The annual average rainfall for the year 1980 is 239.3 mm per year, obtained from the Mianwalli Observatory. According to the report by Amin, 7% of the precipitation in the area contributes to the recharge. Therefore, recharge value of 16.75 mm per year was assigned to the first layer of the model. An evapotranspiration value of 1,350 mm per year as calculated from the Thornthwaite equation was assigned to the model. The elevation values of the modeled region were obtained from the elevation contour map of the area cartographed by WAPDA and then the depth to the static water level values is subtracted from the elevation values obtained. The resultant calculations are used as initial prescribed hydraulic heads for the initial specification of the head values.

5. MODEL CALIBRATION AND SENSITIVITY ANALYSIS

After the model has been designed and the initial parameters and boundary conditions have been assigned, the model is run and executed. The study area model had been executed using Slice Successive Over Relaxation method (SSOR).

The purpose of the calibration of a groundwater flow model is to demonstrate that the model can response field measured heads and flows (Anderson and Woessner, 1992). The calibration of the model had been carried out using PEST (acronym for parameter estimation). The hydraulic heads generated by the steady state simulation were used to calibrate the model with the measured hydraulic heads in the field. The hydraulic heads (measured in the year 1980) from twenty four wells were used to calibrate the model. Recharge and hydraulic conductivity values of the three layers were chosen for the calibration purpose. The scatter diagram after calibration is shown in the Figure 2.

During calibration, PEST calculates the composite sensitivities for all the estimated parameters (Doherty, 2005). In the study model, the hydraulic conductivities of the first layer (kx-1, ky-1 and kz-1) have higher sensitivity than the sensitivities of the hydraulic conductivities of the second (kx-2, ky-2 and kz-2) and third (kx-3, ky-3and kz-3) layer. The model is highly sensitive to ky-1. These sensitivities are calculated only for the estimated parameters.

6. GROUNDWATER BEHAVIOUR (1980 – 2010)

6.1 Steady state model

Equipotential head map of the first layer of the steady state model for the year 1980 is shown in

the figure 3A. The general movement of the groundwater as indicated by the equipotential contours is from north east towards the south. In the upper and lower parts of the modeled area, the water is dominantly moving from the Indus River towards the Paharpur Canal as indicated by the direction of the velocity vectors. However, in the central part of the model area there is some localized movement of the groundwater towards the Indus River.

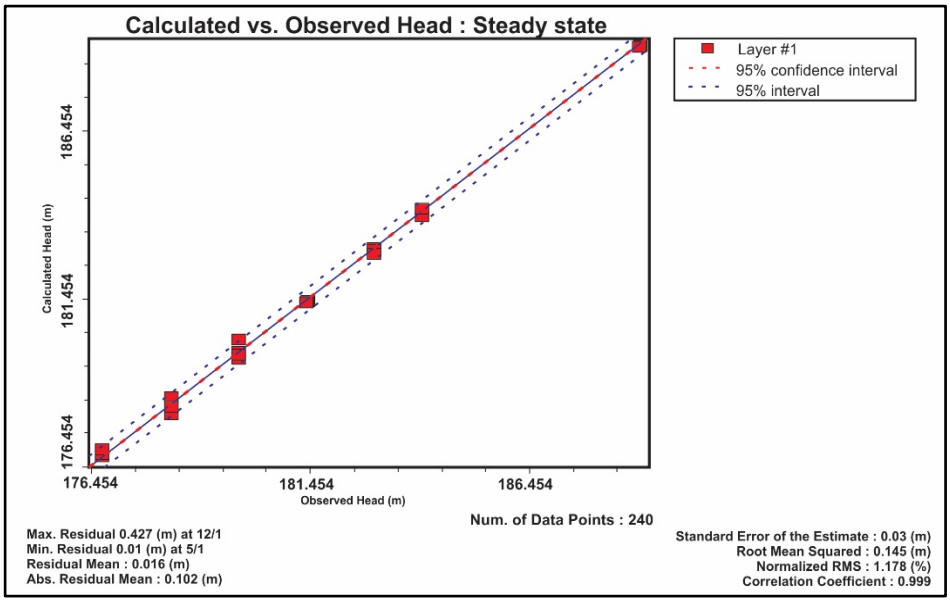

Figure 2. The steady state calibration results of the groundwater flow model.

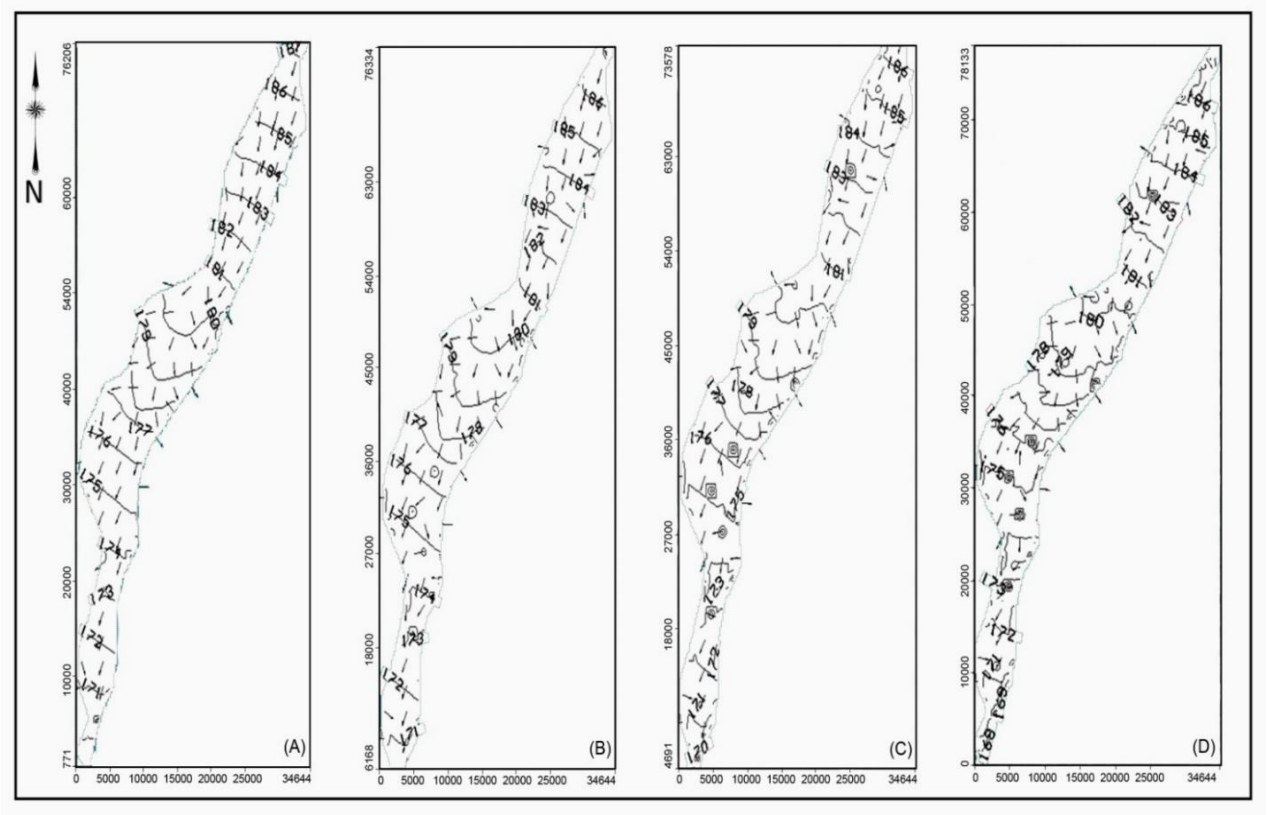

Figure 3. The equipotential map of the years 1980, 1990, 2000 and 2010, (A–D) for layer 1. Equipotential contours of 1m interval.

The water table depth map for the steady state simulation is shown in figure 4A. In the upper and central parts of the area the water table ranges between 0 to 4 meters therefore in these areas water

logging problems are being encountered. Water logging can lead to salinization in the area. In the southern part the water table ranges from 5 to 7 meters below the surface.

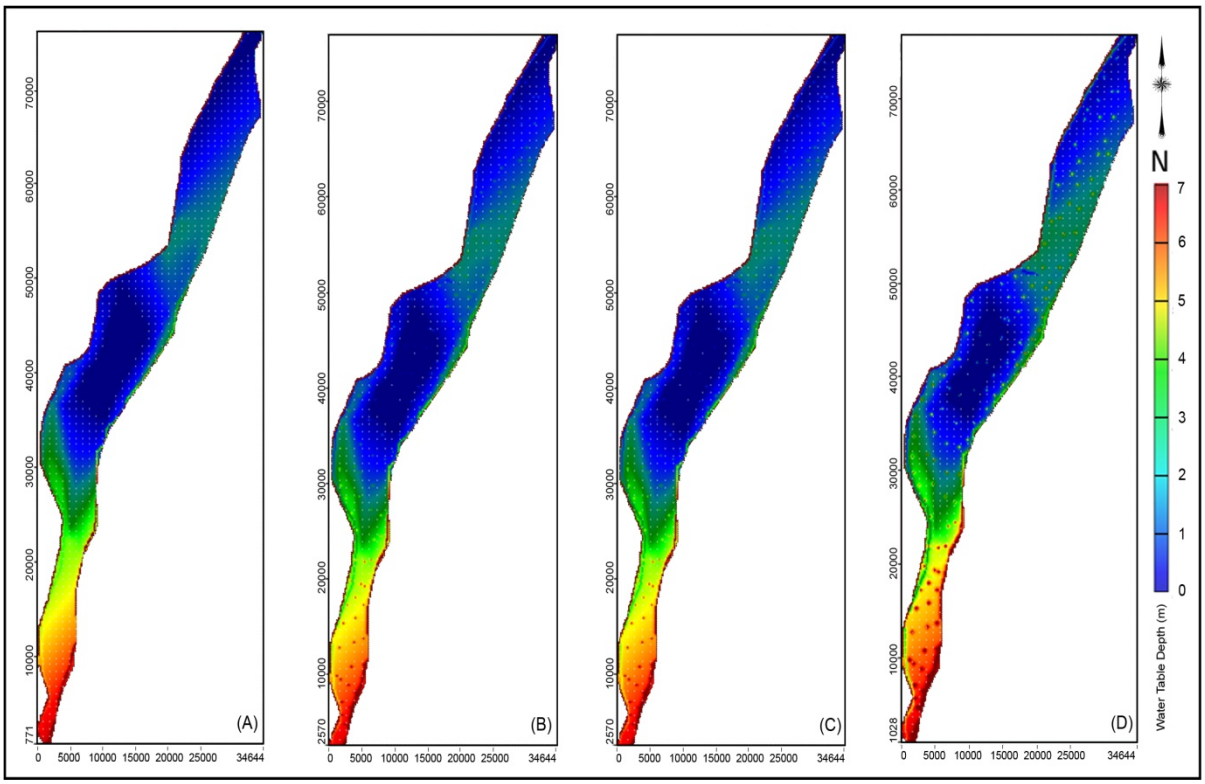

Figure 4. The water table depth maps of the years 1980, 1990, 2000 and 2010, (A–D), showing the changes in the water table depth.

6.2 Non-steady state model

The transient model is built from the year 1980 to 2010 to see the influence of pumping on the groundwater flow and its level. Each year here represents a stress period. Each stress period comprises of two time steps, one time step represents six months. Cumulative discharge has been assigned to the pumping wells in the modeled area.

The dominant groundwater flow direction during the non-steady simulation is the same as in the steady state simulation, i.e. from north to south (Figure 3). However, there have been localized changes in the groundwater flow directions as a result of pumping wells. By analyzing the equipotential contour maps we see that the drawdowns are becoming more pronounced with time.

By analyzing the successive water table graphs it is inferred that the depth of the groundwater is increasing across the modeled region as a result of pumping (Figure 4). There has been a significant change in the water depth in the water logged regions in the upper and central parts of the study area. The areas formerly shown with the dark blue color have been replaced by relatively light blue color as the non-steady simulation proceeds.

In the southern parts of the modeled area the water depth has also increased as indicated by increase in the red zone and reduction in the yellow zone. Hence there is an overall decline in the water depth as a result of pumping.

7. GROUNDWATER BUDGET

Mass balance computation involves the identification and quantification of all flows in and out

of the aquifer. The calculated mass balance components include pumping from wells, recharge, evapotranspiration, river losing and gaining, changes in storage, stream leakage and constant head boundary. On the basis of groundwater budget analysis of the system, it is inferred that the aquifer recharge is lesser than the discharge (Figure 5). Thus we can deduce that the depth to the groundwater is increasing with time.

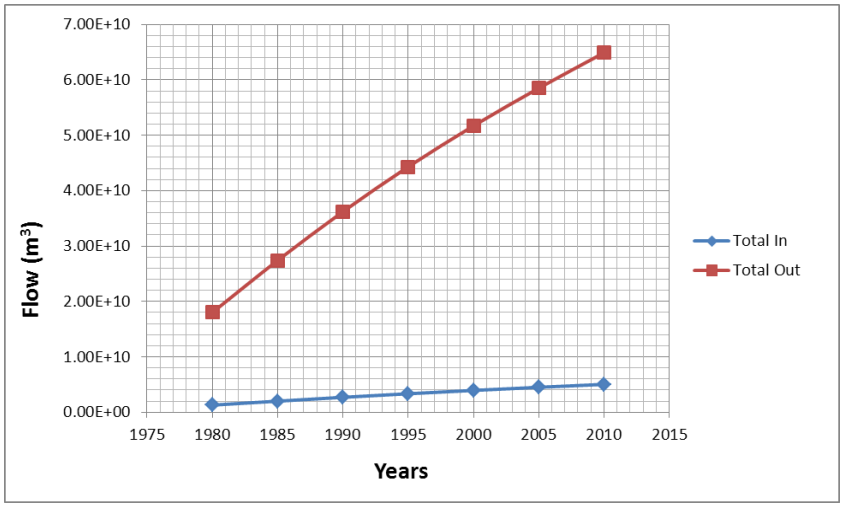

Figure 5. The groundwater budget analysis of the Paharpur Canal Command Area groundwater flow model simulation.

8. CONCLUSIONS

From the groundwater model developed we deduce that on long term basis the heavy pumping of groundwater will result in the decline of water table in the study area. However it would be useful for the areas facing the water logging problem.

The results of the study will be useful to predict the sustainability of the groundwater resources of the study area in the coming era of climatic changes and to evaluate possible management actions. Water logging and salinity can be improved by various water management practices. Hence future subsurface water conditions in the area can be forecasted and appropriate measures can be foreseen with the aid of this model.

REFRENCES

Amin, M. Pakistan's Groundwater Reservoir and its Sustainability. Member Water, WAPDA, 705-WAPDA-House Lahore, Pakistan.

Anderson, M. P., and Woessner, W., 1992. Applied Groundwater Modeling. Acad. Press, San Diego, USA.

Doherty, J., 1995. PEST: A unique computer program for model-independent parameter optimisation.

Hood, J.W. et al., 1970. Water Resources and related Geology of Dera Ismail Khan District, West Pakistan, with reference to the availability of Ground water for development, U.S.G.S., Water supply paper, D.C., U.S.A.

Hussain, S. and Hanif, M., 2013. Climate Change Scenarios and Possible Adaptation Measures: The Livelihoods Programme Hindukush Districts Chitral and DI Khan - Khyber Pakhtunkhwa, Pan Graphics (Pvt) Ltd. Islamabad.

Kijne, J. W., 1999. Improving the productivity of Pakistan's irrigation: The importance of management choices. Colombo, Sri Lanka: International Water Management Institute.

Mall, R.K., Gupta, A., Singh, R., Singh, R.S. and Rathore, L.S., 2006. Water Resources and Climate Change: An Indian Perspective. Curr. Sci., 90: 12, 25. June.

McDonald, M. G., and Harbaugh, A. W., 1988. A modular three-dimensional finite-difference groundwater flow model. Techniques of Water-Resources Investigations 06-A1, USGS.

McMurry, J. and Fay, R.C., 2004. Hydrogen, Oxygen and Water, 4th Ed. In: K.P. Hamann (ed.) McMurry Fay Chemistry. Pearson Education, New Jersey. pp. 575-599.

Naqvi, A. H. S., 1977. Groundwater conditions in Hydro. Sec. Plan. Direc. Groundwater Projects WAPDA. Groundwater Supply, 2, 10–20. Paharpur Area Dera Ismail Khan District N.W.F.P.

PWP, 2001. Supplement to the framework for action (FFA) for achieving the Pakistan water vision 2025-Civil society response to FFA. Islamabad, Pakistan: Pakistan Water Partnership.

Qadir, A., Ahmad, Z., Khan, T., Zafar, M., 2014. Causes and effects of temporal groundwater level change in the alluvial aquifer of Dera Ismail Khan area, Pakistan. Journal of Himalayan Earth Sciences Volume 47, No. 2, pp. 185-191.

WAPDA, 1980. Command Area Development Project, Drainage Component, Chashma Right Bank Canal Stage-1.

Proceedings of the 10th World Congress of EWRA 'Panta Rhei', 5-9 July 2017, Athens, Greece
© 2017 *European Water Resources Association*

Hydrogeological and hydrochemical regime of fissured rocks in Pelion massif (E. Thessaly)

E. Dikarou[1], G. Migiros[1], G. Stamatis[1], K. Serelis[1] and A. Solomonidou[2]
[1] *Institude of Mineralogy-Geology, Agricultural University of Athens, Iera Odos 75, 11855 Athens, Greece*
[2] *NASA Jet Propulsion Laboratory, Caltech, Pasadena, California, USA*
[*] *e-mail: gel_dikarou@hotmail.com*

Abstract: The massif of Eastern Thessaly is structured by formations of the Pelagonian zone. There, an extensive nappe of transformed and in places intensely layered formations composting of schists and gneisses with alternating marbles and interference ophiolitic formations, is composed. The aforementioned nappe is characterized by heterogeneity in terms of the permeability of individual formations. The large number of springs, identified and registered in this study, suggests the presence of an underground communication network, which forms preferred flow pathways for the circulation of water through a dense network of tectonic fissures, which in turn follows the directions of the main fractural system (30 ^{O} N- 40 ^{O}E, 30 ^{O}N- 40 ^{O}W). Concerning the way the springs are being expressed, we distinguish those of zonodi development along the slope and then follow the fracture and those that exhibit a linear array along the inclination of the slope. The springs, in their entirety, are characterized by low value electrical conductivity and remarkable seasonal and regional variations in their supplies (5 - 40 m^3 / h), indicating shallow aquifers of limited capacity. The performed hydrochemical analysis of major, trace, and rare earth elements, revealed the host rock. The waters of the Pelion springs are characterized as moderately alkaline and by low TDS values with three dominant hydrochemical types: i. Mg - Ca- HCO_3 (reflecting the effect of gneiss-schistolithic background), ii. Ca -HCO_3 (indicating the effect of carbonate rocks), and iii. Ca - Na - HCO_3 - Cl (revealing the effect of the dissolution of Na-Bearing minerals and transported marine aerosols).

Key words: Pelagonian, schists, fissured rocks, springs, hydrochemistry, Pelion massif

1. INTRODUCTION

Fissured or fractured rocks are present in many areas in the Hellenic domain, but mainly in the geotectonic zones of the Internal Hellenides (Mountrakis, 1985; Ferriere, 1982; Katsikatsos et al., 1986; Krasny, 2002; Meyer & Pilger, 1963). In addition, they are related to the metamorphic rocks and ophiolites of various areas (e.g. Katsikatsos et al. 1986). As mentioned by Stournaras (2007), these rocks have been one of the main goals of hydrogeological research, as they have been previously suggested as impervious rocks or aquitards. Whereas, a new approach to their hydrogeological regime proved that these formations contain much more water than have been exploited for. Concerning their hydrogeological behaviour, they are regarded as heterogeneous media, due to the fact that their secondary porosity and permeability resulting by weathering and fracturing vary in all scales and directions. Its storage capacity is lower than of porous media and karst formations; however they can yield groundwater of sufficiently good quality for drinking purposes and may host significant water resources (Barrocu, 2005). This is nicely shown in the area of Pelion where tectonic deformation plays fundamental role in the hydrogeological regime thus, groundwater flows mainly through fractures that constitute the main infiltration pathways.

This study provides an estimate of the hydrogeological and hydrochemical status of the Pelion groundwaters. The objectives of this work are: a) the identification of the groundwater chemical composition, as well as, the main factors and mechanisms that control its direction flow; and b) the correlation between the all scales tectonic deformation of the area, and the spatial distribution of the springs.

2. STUDY AREA

2.1 Geomorphological setting

The study area includes 268 km^2 , located in the Pelion Mountain, bounded by NE of Horefto, SE of Mylopotamos, SW of the Prophet Elijah and by NW of the city of Volos. Pelion Mount presents a diverse terrain, characterized as flat to semi-mountainous and mountainous. The area is covered by dense vegetation and rugged terrains, mainly in the mountainous parts. The main drainage network paths are outlined by the main watershed, bordered by the ridge of Pelion with general direction NW-SE. The drainage network is characterized by significant alignments, which indicates major morphological gradients and V type riverbeds. In the northeastern part of the Pelion ridge, the main streams flow towards the NE into the Aegean Sea, while in the SW part, towards the southwest into the Pagasitikos Gulf. In this study, using the topographical maps of the Hellenic Military Geographical Service (HMGS) (scaled 1: 5,000) and the ArcGIS software capabilities (Figure 1) the drainage network density was calculated *(Dd)* as 2,55 km^{-1}, a significant low value that suggests increased groundwater flow opposed to surface. This is the result of: i. the increased secondary porosity due to dense fractured network appeared in the crystalline metamorphic host rocks, creating preferred pathways for the underground flow; ii) the thick weathered soil, which facilitates the infiltration and iii) the dense vegetation which complicates the surficial flows.

2.2 Geological and Tectonic Structure

The study area belongs to the Pre-Upper-Cretaceous tectonic nappe of the Pelagonian zone and it comprises two main formations (Katsikatsos et al. 1987, Figure 1):

- A Paleozoic – Lower Mesozoic ortho and para metamorphic rock complex, consisting of amphibole (mainly glaucophane) schists, calc-epidote and quartz schists, mica (mainly muscovite and chlorite) schists and gneisses, quartzites and phyllites. In the upper layers, intercalations of thick-bedded coarse-crystalline marbles are locally occurred. It has a thickness of about 3.000m (Katsikatsos et al. 1977).
- Middle Triassic – Upper Jurassic Marbles, forming the normal upward evolution of the Paleozoic formations (Katsikatsos et al 1977), consisting of medium bedded karstic and bituminous marbles with local horizontal intercalations of calcite-muscovite schists with cipolin. In the lower members, interpolation of dolomitic marbles and crystalline dolomites are observed (Katsikatsos et al. 1977). The upper layers are mostly thin bedded with muscovite, epidote and chlorite schists' intercalations. They have a maximum thickness of 500m (Katsikatsos et al. 1977).

In particular, during the tectonic placement of the Pre-Upper-Cretaceous nappe a greenschist facies of metamorphism took place. Afterwards, these rocks during post-Cretaceous and pre-Eocene period went through another metamorphic episode of high pressure – low temperature conditions (7-8 kbar, 320-360°C) in the glaucophane facies (Ferriere 1982, Katsikatsos et al. 1986). At the same time, measurements on mylonites' fabrics, shown that 54 Myrs until 15Myrs ago, ductile deformation occurred and affected the Pelion Massif (Lips et al. 1999) which resulted in the formation of an Oligocene-Early Miocene ductile domal structure (anticline) in the Pelion Massif, with a NW-SE axis of folding. This structure is supposed to be responsible for Pelion high altitudes (Ferriere 1977, Lips et al. 1999, Figure 1).

Additionally, in the Pelion area three sets of faults are observed (Papanikolaou; 2008, Figure 1):

- A system of E-W mostly normal trending faults.
- NE-SW mostly strike slip trending faults (Ferriere 1982) parallel to the stretch direction.
- NW-SE to NNW-SSE trending faults, formed from an older extensional stress field associated to the Miocene-Lower Pliocene NE-SW extension.

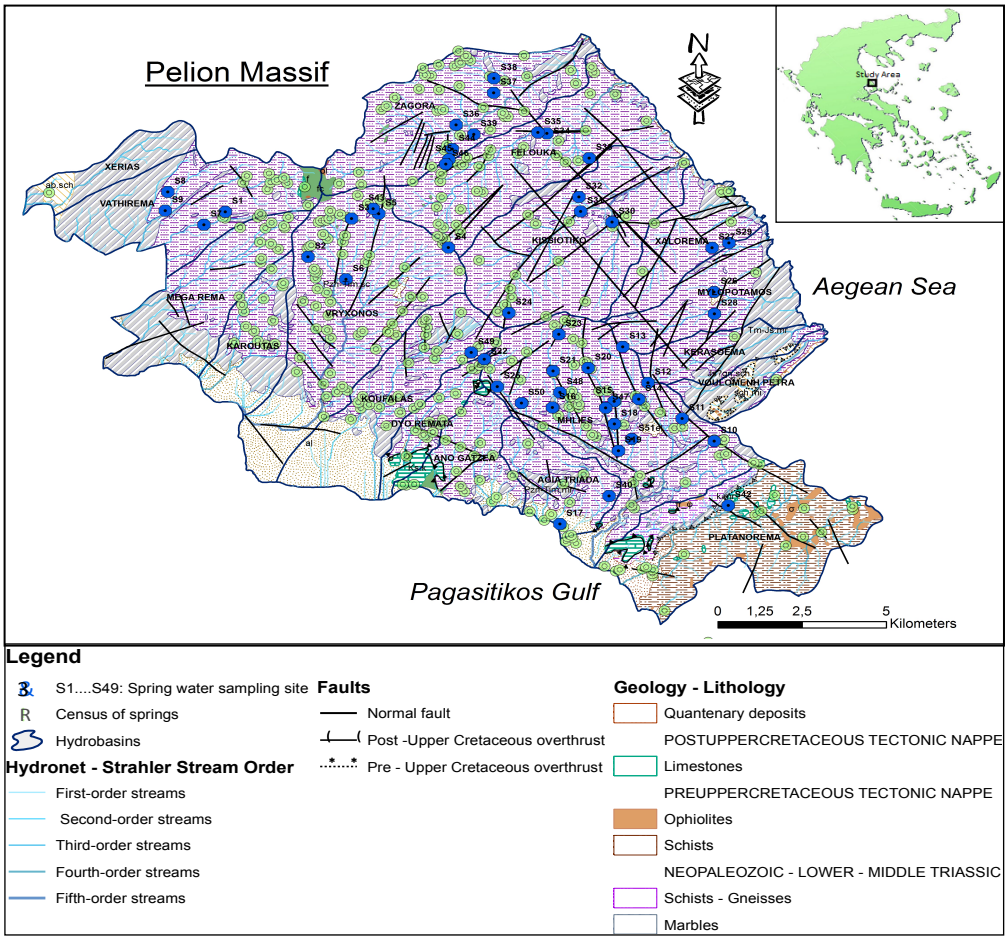

Figure 1. A simplified geological map of the Pelion Massif also showing the spring water sampling sites (Modified by Katsikatsos et al 1987).

2.3 Hydrogeological characteristics

The study area is covered by schists and gneisses, which are considered to be impervious and with negligible primary porosity and hydraulic conductivity. However, considerable quantities of water are discharged through a well scattered and dense network of springs. This happens because water resides mainly through fractures or fractured zones, known as secondary porosity (Tam et al. 2004). The groundwater flow is closely controlled by the regional tectonic structure. It is mainly stored in fractures and crushed zones and circulates with hydrodynamic terms through a network of high hydraulic conductivity zones (Tam et al. 2004).

The storage capacity of fractured or as called fissured rocks, is lower than the porous media and the karstic formations, however it can host significant quantities of good quality water for drinking purposes (Stournaras 2008). In the Pelion area, where high rates of annual precipitation have been recorded (Papanikolaou 2008), (~1200mm at 700m elevation), metamorphic bedrocks are recharged only from direct rainfall percolation, as there is no significant inflow from the adjoining hydrogeological basins. Schists are characterized as heterogeneous media (Papanikolaou, 2008). In particular, they are divided into hard-rocks where quartz, amphiboles and epidote is the main mineral composition, exposing higher permeability rates, and soft-rocks where clay minerals prevail, displaying low permeability. The presence of mica acts as a hydrologic barrier (Papanikolaou, 2008), blocking the fissures and impede any percolation process. However, the large number of well scattered springs implies that the presence of clayish schists is limited (Papanikolaou, 2008). Additionally, the presence of thick soil due to strongly weathered schists, promotes the infiltration processes. Some intercalations of Middle Triassic – Upper Jurassic thick-bedded marbles occur locally within the schists and the gneisses. In the SE and the NW part of the

area these formations are aligned to the coastline, discharging water towards the Aegean Sea and the Pagasitikos Gulf respectively. Finally, we came to three different permeability features in the study area. The marbles which are of high permeability (>40%) hosting significant quantities of water, covering about 16% of the study area, the hard-rock schists of medium permeability (~25-30%) occupying the largest part of the area (~70%), and finally the soft rock clay-rich schists of low permeability (<17%) that are of limited extent.

2.3.1 Springs

In the area of Pelion forty-nine (49) spring water samples have been collected during December 2010 until June 2012. The fieldwork data, concerning the physical and chemical properties of spring waters, in combination with the study of the geological structure, came up with interesting results regarding the fissured rocks permeability, the surficial and subsurficial water flow paths and the springs' distribution. The vast majority of the springs are located within the schists and gneisses, while a few others, known as contact springs, occur near the boundaries with the overlying marbles, hosting highest quantities of water. The large number of well scattered springs implies that water recharge and percolation occurs mainly through the fracture network that forms preferential flow paths (Papanikolaou 2008). Springs are widely distributed from 150 up to 1350m height, but most of them are located above 500 meters. They are characterized by high seasonal discharge rates ranging from a few m^3/h up to 150 m^3/h, while most of them provide approximately 5 to 20 m^3/h rates (Papanikolaou 2008). During summer, springs in higher elevations experience a significantly higher drop in the discharge rates compared to springs in lower elevations, suggesting that there is a time delay mechanism (Papanikolaou 2008). Aquifers in the study area are hosted in shallow depths and are of limited capacity with short residence times that according to Papanikolaou (2008) estimations not exceed a couple of years. They receive water by regional underground flow through the fractured network with additionally important in situ recharge by precipitation, surface water circulation and fresh water from higher altitudes (V. T. Tam et al. 2004). Concerning the behavior of the well scattered springs in space and time, there are these who show up along the slope and then follow the fracture and those that exhibit a linear array along the inclination of the slope. Moreover, they are classified as linear sequentially charging springs, where the one feeds the other from up to downstream, so that springs in higher elevations recharge the ones in lower elevations, reinforcing the estimation of sequential filling springs and the presence of an underground fractured network.

3. MATERIALS AND METHODS

3.1 Sampling, preparation and fieldwork

The spring sampling sites were recorded in the field using a Garmin eMap Geographical Positioning System (GPS). Portable instruments were used in order to measure in situ the physicochemical parameters, such as temperature T (^{0}C) and Electrical Conductivity (EC) (WTW/LF-330), pH (WTW/330i) values and discharge rates Q·l/s (Flow Probe FP101/Global Water). For the pH and EC measurements, the electrodes were calibrated daily with reference buffer solutions.

Water collected spring samples were placed into precleaned polypropylene containers and rinsed three times with sample water before final collection. Each water sample was then divided into two subsamples (Gamvroula 2012). One set of subsamples was vacum filtered through 0.45-μm pore size membrane filters and kept refrigerated in 1,000 mL container for major ions analysis and the second set of 49 subsamples was filtered with sterile 0.22-lm disposable syringe filter and acidified to pH< 2 with 1 mL of ultrapure HNO_3 and stored in 100-mL container for trace element analysis

(Gamvroula 2012). Each container was completely filled with water, noticing that no air bubbles were trapped within it.

All possible precautions were taken during collection and handling of water samples to minimize contamination. During fieldwork, all the water subsamples were stored in an iced cooler, while at the laboratory, the refrigerator's was maintained between 2 and 4 ^{o}C.

3.2 Hydrochemical analysis

Dissolved ions, including NH^{4+}, NO^{3-}, PO_4^{3-}, SO_4^{2-} and SiO_2 were measured photometrically for the non-acidified samples using a HACH DR 3000 apparatus, Ca^{2+} and Mg^{2+} by atomic absorption spectroscopy (AAS/GBC 908 AA), bicarbonate (HCO_3^-) with a HACH digital titrator on the non-acidified water subsamples and Na^+ and K^+ with a flame photometry (INTECH/ 1382) at the Laboratory of Geology of the Agricultural University of Athens (Gamvroula 2012). Titration methods were used to measure Cl^- and total hardness (H_{total}), using Titriplex-Losung A 0.1 M $AgNO_3$ and 0.1 M HCl, respectively (Hoell 1979). The charge-balance error for major ionic species, calculated by the software package AQUACHEM, did not exceed 5%.

Traces to ultra-trace concentrations of elements were determined on the acidified subsamples by Inductively Coupled Plasma Mass Spectrometry (ICP-MS) at the ACME Analytical Laboratories Ltd, Vancouver, Canada (ISO 9002 Accredited Co.). The standard solutions were diluted in ultrapure water (resistivity 18.3 MΩ at 25°C) prepared with a water purification system (Zeneer Power I) supplied by Human Corporation.

4. RESULTS – DISCUSSION

4.1 Groundwater quality

As water flows from higher altitudes to lower, it follows a longer path within the metamorphic rocks, thus it gradually enriches its chemical composition as the leaching surface increases. Higher number of dissolved solids is obtained as more ions are disrupted from the minerals' surface and enriches the water solvent, increasing its conductivity. The relative abundance of various elements in groundwater mainly depends on their chemical mobility (Singhal 2010).

Springs emerged from schists are characterized by low EC values (mean value 199 μS/cm), low TDS values (mean value 197mg/l) revealing poor mineralization (Pazand 2014), relatively low total hardness values (mean 2,42 meq/l **)** and moderate alkaline character (mean PH value 7,5). The fact is that spring water from higher altitudes characterized by significantly low ions dissolution, because water flow path and residence time are limited. Most physical and chemical parameters are increased downwards, by the constant input of warmer surficial waters.

A scatter distribution of the spring water samples on Piper diagram revealed three typical hydrochemical types: i. the Ca-Mg-HCO_3, indicating the influence of schists and gneisses; ii. the Ca-HCO_3, displaying the marbles influence and iii. the normal geo-alkaline Ca-Na-Cl-HCO_3 revealing the effect of the dissolution of Na-bearing minerals such as glaucophane and albite (with significant high concentrations of Na^+ from 3 up to 60 mg/l), while the corresponding high Cl^- values (5 to 130 mg/l) indicate the influence by transported marine aerosols. Ca^{2+} concentrations' range from 1,7 up to 88,7 mg/l, values higher than 40mg/l indicate the influence of carbonate minerals while passing through marbles or through the weathering, enriched with clastic carbonate materials, soil.

The hydrochemical composition of the spring water samples are statistically analysed and part of the results are shown on Table 1 (the full table is available for distribution from the author upon request).

Table 1. Statistical summary of the hydrochemical analysis of the 49 spring water samples of the Pelion Massif.

Parameters	Units	Springs (n=45) Metamorphic Rocks L-M Triassic Schists *(Pzn- Tim.sc)*			(n=2) Metamorphic Rocks L-M Triassic Marbles *(Pzn- Tim.mr)*			(n=1) Mica schists Eoellenic Tectonic Nappe *(Sch-mi)*	(n=1) Eluvial mantle Holocene *(el)*
		Min	Max	Mean	Min	Max	Mean		
Temperature	**^{o}C**	5,5	15,6	10,6	8,3	10,2	9,3	15,6	10,8
pH		6,2	8,2	7,5	6,8	7,9	7,4	7,8	7,6
El. Conductivity	**µs/cm**	27,2	578	213,7	177	192	185	421	198
TDS	**mg/l**	30,9	518,3	195	127,8	172,2	150	464,8	118
Total Hardness	**meq/l**	0,22	6,04	2,4	1,6	2,0	1,8	5,52	1,88
Carbonate Hard.	**meq/l**	0,2	5,3	2	1,85	2,0	1,93	4,68	1,88
Permanent Hard.	**meq/l**	0	1,51	0,35	0	0,25	0,13	0,84	0
Ca^{2+}	**mg/l**	1,7	88,7	39,9	30,5	32,4	31,5	63,42	34,4
Mg^{2+}	**mg/l**	0,7	29,8	4,9	1,5	2,2	1,9	29,83	1,96
Na^{+}	**mg/l**	3,0	60,7	8,9	4,7	5,1	4,9	19,48	4,85
K^{+}	**mg/l**	0,2	3,4	0,6	0,32	0,36	0,34	1,23	0,32
HCO_3^{-}	**mg/l**	12,2	323,3	129,6	97,6	134,2	115,9	280,6	115,9
Cl^{-}	**mg/l**	5,0	130,0	16,1			7	31	6
SO_4^{2-}	**mg/l**	0,3	25,7	10,5	5,8	16,2	11	15,4	10,6
NO_3^{-}	**mg/l**	2,2	11,0	4,7	2,8	3,4	3,1	8,6	4,9
NH_4^{+}	**mg/l**	0,1	0,8	0,5	0,1	0,3	0,2	0,7	0,6
PO_4^{3-}	**mg/l**	0,1	0,7	0,3	0,1	0,5	0,3	0,2	0,5
SiO_2	**mg/l**	3,5	13,4	6,9	5,8	8	6,9	12,7	6,6
Mn	**ppm**	0,0001	0,005	0,0004	0,0026	0,00006	0,00133	0,0008	0,00005
Zn	**ppm**	0,002	0,05	0,01	0,0116	0,0104	0,011	0,13	0,005
Ni	**ppm**	0,0002	0,006	0,0004			0,0002	0,0002	0,0002
Cu	**ppm**	0,0001	0,002	0,0006	0,0003	0,0005	0,0004	0,0006	0,0003
Cr	**ppm**	0,0005	0,004	0,0009			0,0005	0,0007	0,0005
Cd	**ppm**	0,0001	0,0004	0,0002			0,0011	0,0013	0,0014

4.2 Correlation between tectonic deformation and springs spatial distribution

In fractured media, tectonic structure plays a primary role in the groundwater circulation. The fact is that surficial and subsurficial water will try to find the easier pathway to flow, and this is through the secondary porosity that fractures provoke.

This fracturing pattern is characterized by heterogeneity and changes spatially and in all scales. In the microscopic scale, the clay/platy minerals of the schists' recrystallized perpendicular to the applied stresses (Papanikolaou 2008), forming foliation features towards the NE and the SW, promoting flow parallel to these directions. In the mesoscopic scale, two main directions of fractures are observed, the intrabedded longitudinal NE-SW fractures and the transverse NW-SE trending fractures (Papanikolaou 2008). The tectonic discontinuities drain water both within the host rocks (e.g. schists and gneisses) and from side blocks (e.g. Triassic marbles of high permeability), creating natural infiltration pathways. In the macroscopic scale, three sets of faults, several kilometres long, are observed. Two of them are NE-SW trending (N 030° ± 10° and N 050° ± 10°), forming a 20° angle of tectonic wedge and the transverse third set is NW-SE trending (N320^{o} ±5°). They dominate the surficial flow by forming preferential pathways to the water, thus at the eastern limb of the Pelion mega-anticline water flows towards the NE and towards the SW at the western limb. Springs are aligned to the faults and show up where the hydraulic head of the aquifer intersects the weakened surface.

5. CONCLUSIONS

The aim of this study was to estimate the hydrogeological and hydrochemical status of the fissured media of the Pelion massif. The groundwater flow is closely controlled by the regional tectonic structure. The large number of well scattered springs implies that water recharge and percolation occurs mainly through preferential flows paths that fractures create. Springs show up along the slope and then follow the fracture or a linear array along the inclination of the slope. The ones of higher elevations recharge those in lower, reinforcing the estimation of sequential filling springs and the presence of an underground well developed fractured network. The spring water chemical analysis came up with remarkable results concerning their composition as well as their chemical differentiation via altitude with regard to the petrochemical composition of the schists' and gneisses' metamorphic bedrock. This comparative analysis will be the goal of the next work. In conclusion, the hydrochemical progress of a water body is considered to depend mainly on the direction and the regional groundwater flow conditions.

REFERENCES

Barrocu, G., 2005. Groundwater investigation planning and management in fissured rocks. 7th Hellenic Hydrogeological conference: 55-68. Athens.

Ferriere, J. 1977. Le secteur meridional du "massif metamorphique de Thessalie". Le massif du Pelion et ses environ. Proceedings of the VI Colloquium on the Geology of the Aegean region: 291-309.

Ferriere, J. 1982. Peleogeographies et Tectoniques Superposees dans les Hellenides Internes au Niveau de l' Othrys et du Pelion (Grece). These Univ. des Sciences et Techniques de Lille, p. 1-970.

Gamvroula, D., Alexakis, D., Stamatis, G. Diagnosis of groundwater quality and assessment of contamination sources in the Megara Basin (Attica, Greece). Saudi Society of Geosciences 2012.

Hoell, K. 1979. Wasser: Untersuchung, Beurteilung, Aufbereitung, Chemie, Bakteriologie, Virologie, Biologie. Walter de Gruyter, Berlin.

Katsikatsos, G., Migiros, G., Triantafphyllis, M. and Mettos, A. 1986: Geological structure of Internal Hellenides (E. Thessaly-SW Macedonia-Euboea-Attica-Northern Cyclades Islands and Lesvos). IGME, Geol. and Geoph. Res., Special Issue, p. 191-212.

Katsikatsos, G., Papadeas, G., Mylonakis, I., and Triantaphylus, E. 1987. IGME 1:50000 geological sheet Zagora – Syki.

Kaveh, Pazand, Ali Reza, Javanhir. Rare earth element geochemistry of spring water, north western Bam, NE Iran. Appl Water Sci (2014) 4: 1-9.

Krasny, J. and Sharp, J.M. 2007. Hydrogeology of fractured rocks from particular features to regional approaches: State of the art and future challenges. Groundwater in fractured rocks. Volume edited by Krasny J. and Sharp, 4-27 J. Taylor and Francis Group, London, UK.

Papaniklaou, I., Migiros, G. 2008. Brittle deformation and hydrogeologival pattern of the Eastern Pelion Area (Tsangarada). 8th International Hydrogeological Congress of Greece. 1: 347-360. Athens.

Singhal, B.B.S., Gupta, R.P. 2010. Applied Hydrogeology of Fractured Rocks. Second Edition. Springer Netherlands.

Stournaras, G. 2007. Water, Environmental dimension and path. Tziola publications. Athens.

Stournaras, G., Migiros, G., Stamatis, G., Evelpidou, N., Botsialas, K., Antoniou, V., Vassilakis, E. Groundwater in fractured rocks. Chapter 8. p. 133-149. Taylor & Francis Group, London, UK. 2007.

Tam, V. T., De Smedt, F., Batelaan, O., Dassargues, A. 2004: Study on the relationship between lineaments and borehole specific capacity in a fractured and karstified limestone area in Vietnam. Hydrogeology Journal (2004) 12; p. 662–673.

Proceedings of the 10th World Congress of EWRA 'Panta Rhei', 5-9 July 2017, Athens, Greece
© 2017 *European Water Resources Association*

Updated groundwater vulnerability evaluation at a coastal aquifer system in NE Greece

G. Eminoglou[1], I. Gkiougkis[1], A. Kallioras[2] and F.-K. Pliakas[1*]
[1] *Engineering Geology Laboratory, Civil Engineering Department, Democritus University of Thrace, 67132 Xanthi, Greece*
[2] *Engineering Geology and Hydrogeology Laboratory, School of Mining Engineering and Metallurgy, National Technical University of Athens, 157 80 Athens, Greece*
[*] *e-mail: fpliakas@civil.duth.gr*

Abstract: This paper presents the updated vulnerability assessment of Xilagani - Imeros aquifer system in the coastal plain region of Rhodope Prefecture, NE Greece, in the framework of the groundwater management in the region. Information regarding the geological and geomorphological environment, as well as data concerning the hydrologic and hydrogeological regime of the study area are stated. The paper presents the application of DRASTIC and GALDIT vulnerability indexes procedures and the design of easy to use vulnerability maps in order to identify the parts where there is a serious potential for groundwater resources qualitative degradation due to agricultural pollution (DRASTIC approach) or seawater intrusion (GALDIT approach). The research is based on the results of hydrogeological studies in the study area for the year 2015 compared to the year 2006, including field hydrogeological measurements and chemical analyses in the laboratory, as well as the design of groundwater piezometric maps and hydrochemical maps. It is worth mentioning that DRASTIC index values for the year 2015 do not differ substantially compared to the corresponding values for the year 2006. Instead, increase of GALDIT index values is recorded for the year 2015 indicating worsening of the groundwater salinization status due to seawater intrusion.

Key words: DRASTIC GALDIT Vulnerability index, Coastal hydrogeology, Groundwater pollution, Seawater intrusion, Coastal aquifer management

1. INTRODUCTION

This paper refers to the assessment of the updated groundwater vulnerability of the Xilagani – Imeros coastal aquifer system, at the SW part of Rhodope Prefecture, NE Greece. The research is based on the results of previous hydrogeological studies in the study area (Sakkas et al., 1998; Pliakas et al., 2001; Pliakas et al., 2004; Pliakas et al., 2007). The paper presents the application of DRASTIC and GALDIT vulnerability indexes procedures and the design of easy to use vulnerability maps in order to identify the parts where there is a serious potential for groundwater resources qualitative degradation due to agricultural pollution (DRASTIC approach) or seawater intrusion (GALDIT approach) for the year 2015 compared to the year 2006.

DRASTIC method is a familiar method developed in the US Environmental Protection Agency (USEPA) by Aller et al. (1987) and this method has been applied in several regions by different researchers (Sener et al. 2009). Pedreira et al. (2015) mention that DRASTIC standardized model (Aller et al. 1987) targets the groundwater protection through the evaluation of the groundwater pollution potential in any hydrogeological scenery. The final product is addressed to decision makers, administrators and authorities to support the assessment of the groundwater vulnerability to different sources of contamination.

Recinos et al. (2015) note that Chachadi and Lobo Ferreira (2001) realized the necessity for developing a numerical ranking system to assess the general seawater intrusion potential of each hydrogeological setting. GALDIT vulnerability index (Lobo Ferreira et al., 2005; Chachadi and Lobo-Ferreira, 2005) involves measurable parameters which can be synthesized to provide an efficient tool for mapping the seawater intrusion potential of a coastal aquifer. Once the GALDIT

index has been computed, it is possible to identify areas that are more likely to be susceptible to seawater intrusion than other areas. The higher the vulnerability index, the greater the seawater intrusion potential. Pedreira et al. (2015) point out that GALDIT indicator model is applied to an area of interest using its hydrogeological information and choosing ratings related to the specific conditions within the area, regarding seawater intrusion. Thus, it is possible to delineate zones that are more prone to seawater encroachment than other areas.

2. DESCRIPTION OF THE STUDY AREA

The plain area of Xilagani – Imeros has mild morphologic characteristics with low elevation, extended between Lissos River and the western foot of Ismaros Mount, whereas Thracian Sea covers the southern boundaries of the area (Figure 1). The geological environment of the study area includes recent sediments originated from Lissos River -and some other branches of the same river- overlying Neogene deposits or Paleogene deposits of Rhodope massif (Pliakas et al., 2004).

The main cultivation type of the area is cotton, while the southern part of the area of investigation is not arable due to groundwater salinization. There are 55 groundwater wells (about 10 of them abandoned), with mean depth of 70 m and mean pumping rate of approximately 40 m^3/h, while at the northern parts of the site the groundwater wells present pumping rates of approximately 60 to 70 m^3/h (Pliakas et al., 2004, Pliakas et al., 2007).

According to Kallioras et al. (2011), the aquifer system of the study area contains clay materials and appears in the form of successive layers composed of clay-sands and sands with a width ranging from 1 to 10 m, with many interferences of clay layers. Relevant hydrogeological studies of the semi-confined aquifer of the study area (Sakkas et al., 1998; Pliakas et al., 2001; Pliakas et al., 2004; Pliakas et al., 2007) have shown 4 distinct main geoelectrical formations categorized according to the values of their specific electrical resistivity, as follows (ASCE, 1987, Kallergis, 2000): coarse grained sand (>40 Ohm×m), fine grained sand (25-40 Ohm×m), clay-sand materials (15-25 Ohm×m), clay (<15 Ohm×m), while the dominance of clay and clay-sand materials throughout the whole extent of the study site is very distinct (the positions of the relevant geoelectric sounding measurements and their section axes are shown in Figure 1 upper). According to these studies, the groundwater level gradually increases from October to March, due to natural recharge from direct infiltration from precipitation (at parts of the aquifer where it appears semi-confined or unconfined), percolation from Lissos River and lateral inflows from the NE part of the study area where there is a hydraulic connection with the mountainous zone (Figure 1 lower). During the period between April and October the groundwater level appears below the mean sea level fact which is attributed to the overpumping conditions for irrigation purposes.

The evaluation and assessment of the qualitative characteristics of the study aquifer involved the determination of certain chemical parameters, such as Na^+, K^+, Ca^{2+}, Mg^{2+}, Cl^-, HCO_3^-, SO_4^{2-}, PO_4^{3-}, NO_3^-, NO_2^-, and certain physicochemical parameters such as alkalinity P, alkalinity M, total hardness and pH (July 2015). The majority of the groundwater samples of the investigated aquifer (Figure 1 upper), according to specific standards and drinking water limits (Government Gazette-GG 630, 26-4-2007, GG 2075, 25-9-2009, GG 3322, 30-12-2011, Kallergis, 2000), are characterized as non-potable, as the concentrations of Cl^- (163-1,400 mg/L), Na^+ (175-680 mg/L), K^+ (5-27 mg/L), Ca^{2+} (32-497 mg/L), Mg^{2+} (16-256 mg/L) are above the quality standards. The values of electrical conductivity range between 1,133-4,750 μS/cm, where the higher values of electrical conductivity appear within the southern (coastal) part of the study site, fact which imposes the argument of seawater intrusion conditions.

3. APPLICATION OF DRASTIC AND GALDIT METHODS

DRASTIC has been the most commonly used for mapping aquifer vulnerability in porous aquifers (Aller et al., 1987). The DRASTIC method considers seven parameters, which taken

together, provide the acronym (Panagopoulos et al., 2006; Sener et al., 2009). These are depth to groundwater (D), net recharge (R), aquifer media (A), soil media (S), topography (T), influence of the vadose zone (I) and hydraulic conductivity (C). Each parameter is subdivided into ranges and is assigned different ratings in a scale of 1 (least contamination potential) to 10 (highest contamination potential). This rating is scaled by a pesticide and DRASTIC weighting factors ranging between 1 (least significant) and 5 (most significant).

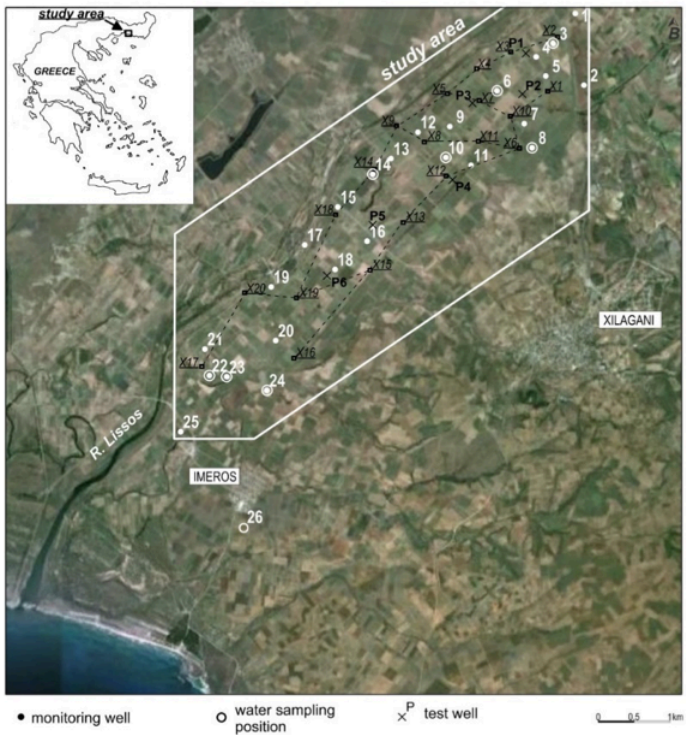

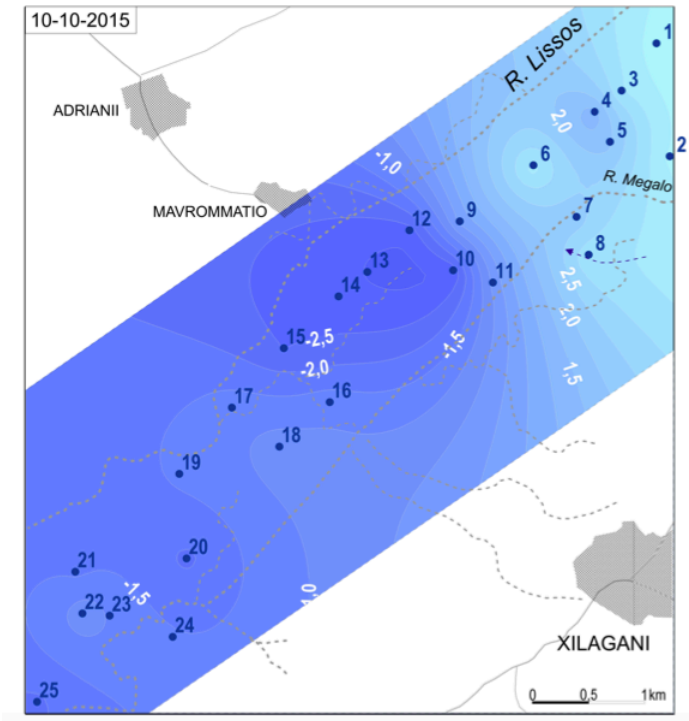

Figure 1. Upper: Study area, positions of monitoring wells, test wells and geoelectric sounding measurements and their section axes (Kallioras et al., 2011). Lower: Piezometric map (m a.s.l.) (10-10-2015) (dotted line: main groundwater recharge axis).

The linear additive combination of the above parameters with the ratings and weights was used to calculate the DRASTIC Vulnerability Index (DVI) as given below (Aller et al., 1987; Sener et al., 2009):

$$DVI = DrDw + RrRw + ArAw + SrSw + TrTw + IrIw + CrCw \quad (1)$$

where r is the rating for corresponding ranges and w the weight for each parameter.

The calculation of Pesticide DVI (considering S, T, I, C parameters with different weights compared to the original DRASTIC method) included the values of all parameters in every single investigated groundwater well (Table 1). The results from the application of DRASTIC vulnerability index have been linked with GIS, for the design of a vulnerability map (DVI – 2015) in order to identify the parts where there is a serious potential for groundwater resources qualitative degradation (Figure 2 upper - left). Additionally, nitrate distribution map has been designed (nitrate ions in mg/L, July 2015) (Figure 2 upper - middle), where it is revealed that the NE part of the study area where increased nitrate concentrations are present coincides with the areas of high vulnerability based on the application of DVI (DVI >160).

Pesticide DVI values range from 119 to 183 in 2006, while from 115 to 179 in 2015 (Table 1). In both approaches, DVI values are higher in the northern parts of the study area, and gradually decrease towards the southern parts. In 2015, there is an upward trend in the southern wells (Figure 2 upper - left, Figure 2 upper - right).

The development of GALDIT index (GVI) is aiming the assessment of aquifer vulnerability to sea-water intrusion in coastal aquifers (Lobo Ferreira et al., 2005). The most important factors controlling seawater intrusion were found to be the following: Groundwater occurrence (aquifer type; unconfined, confined and leaky confined); Aquifer hydraulic conductivity; Depth to groundwater Level above the sea; Distance from the shore (distance inland perpendicular from shoreline); Impact of existing status of sea water intrusion in the area; and Thickness of the aquifer, which is being mapped. The acronym GALDIT is formed from the highlighted letters of the previous parameters. According to Kallioras et al. (2011), these factors, in combination, are determined to include the basic requirements needed to assess the general seawater intrusion potential of each hydrogeological setting. A numerical ranking system to assess seawater intrusion potential in hydrogeological settings has been devised using GALDIT factors. The system contains three significant parts: weights, ranges, and ratings. Each GALDIT factor has been evaluated with respect to the other to determine the relative importance of each factor. Each of the six indicators has a pre-determined fixed weight that reflects its relative importance to seawater intrusion. The GALDIT Index is then obtained by computing the individual indicator scores and summing them as per the following expression:

$$GVI = \sum_{i=1}^{6} \{(W_i)R_i\} / \sum_{i=1}^{6} W_i \quad (2)$$

where Wi is the weight of the ith indicator and Ri is the importance rating of the ith indicator.

Once the GALDIT-Index has been computed, it is therefore possible to classify the coastal GALDIT Vulnerability Index, GVI, was calculated according to the values of each parameter in every single groundwater well (Table 1). The results from the application of GALDIT vulnerability index were linked with GIS in order to design vulnerability maps for the study area with respect to the potential for aquifer contamination due to seawater intrusion (Figure 2 lower - left, GVI - 2015). Revelle coefficient was also calculated and distributed throughout the entire study area, so that the Revelle distribution map (July 2015) is correlated against the vulnerability map from the application of GALDIT VI (Figure 2 lower - middle). It was concluded that at the SW part of the study area (with a direction towards the shoreline) there is a coincidence between the zone of high vulnerability based of GALDIT VI (GVI > 7.5) and the high Revelle coefficient.

Low GVI values are observed in 2015 at the NE part of the study area, which become moderate

at the area of the wells 6, 7, 8, as in 2006, with significant increase especially south of the area of the wells 15 and 16. GVI values have increased from 2006 to 2015, in 2006 ranging from 4.5 to 8.5 with an average value of 6.9, while in 2015 from 4.5 to 9 with an average value of 7.1 (Figure 2 lower - left, Figure 2 lower - right).

Table 1. [A]: DRASTIC Vulnerability Index (DVI) rating and weighting values for the various hydrogeological parameter settings. [B]: GALDIT Vulnerability Index (GVI) rating and weighting values for the various hydrogeological parameter settings (10-10-2015).

[A]: 2015 – Pesticide DVI: 115-179						
D (m) [1]	R (mm) [2]	A	S	T (%)	I	C (m/s)
2.2-8.4	32.9-41.1	clay - sandy deposits	clay - sandy material	0.1-1.2	clay - sandy deposits	1×10^{-6}-1×10^{-4}
Dr	Rr	Ar	Sr	Tr	Ir	Cr
4-10	1-2	6-9	4-6	9-10	4-9	2.5-7.5
Dw	Rw	Aw	Sw	Tw	Iw	Cw
5	4	3	5	3	3	2
	Vulnerability:	Very high	High	Moderate	Low	Very low
	DVI:	>160	140-160	120-140	100-120	<100

[B]: 2015 – GVI: 4.5-9.0					
G	A (m/s)	L (m) [3]	D (m)	I (Revelle) [4]	T (m)
semi-confined aquifer	1×10^{-6}-1×10^{-4}	-3.2-3.7	3263-10790	0.7-10.9	7-27
R1	R2	R3	R4	R5	R6
10	2.5-7.5	2.5-10	2.5-10	2.5-10	7.5-10
W1	W2	W3	W4	W5	W6
1	3	4	4	1	2
		Vulnerability:	High	Moderate	Low
		GVI:	≥ 7.5	5 – 7.5	< 5

[1]: 10-10-2015, [2]: infiltration: 10% of mean annual rainfall (Kallioras et al., 2010) (2011-2014: 411.9 mm), [3]: 10-10-2015, [4]: July 2015

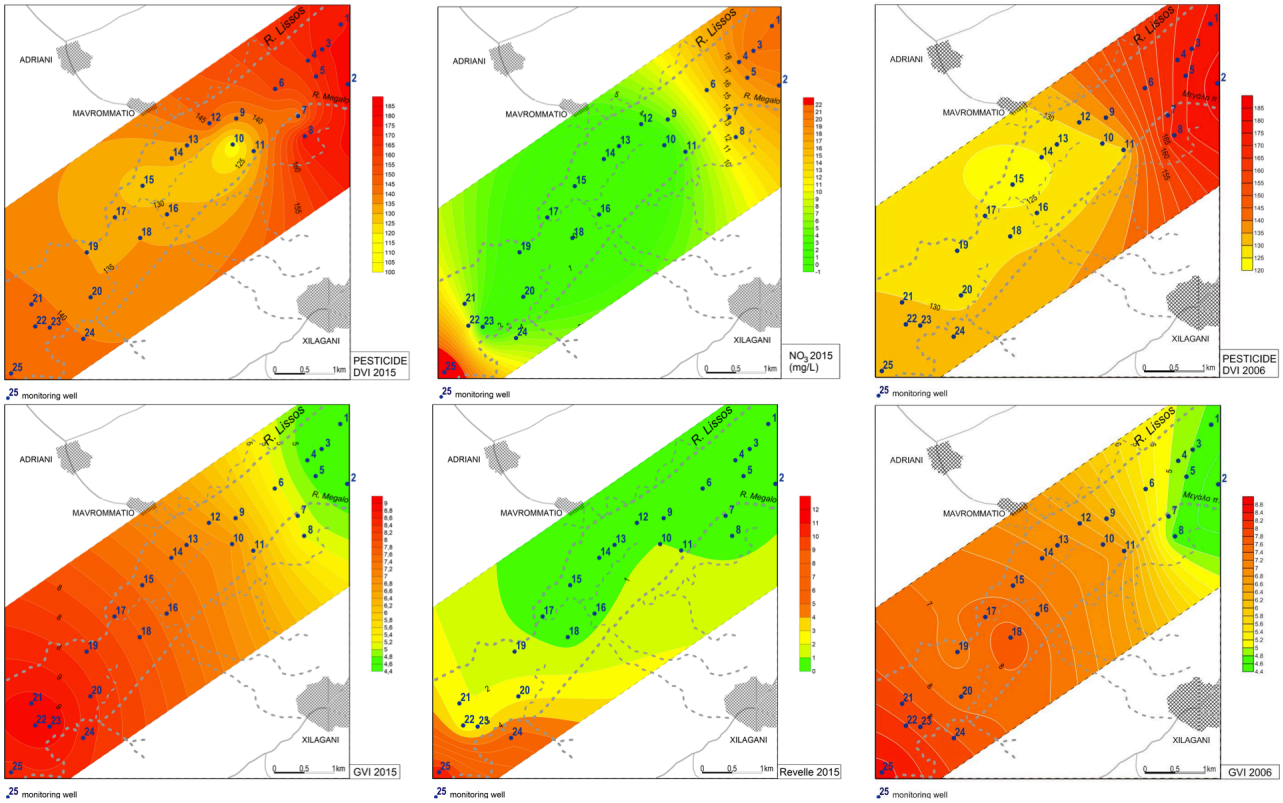

Figure 2. Upper left: Pesticide DRASTIC aquifer vulnerability map (DVI values) (2015). Upper middle: distribution of nitrates (NO_3^-) concentrations map (2015). Upper right: Pesticide DRASTIC aquifer vulnerability map (DVI values) (2006, Kallioras et al., 2011). Lower left: GALDIT aquifer vulnerability map (2015). Lower middle: Distribution of Revelle values map (2015). Lower right GALDIT aquifer vulnerability map (2006, Kallioras et al., 2011).

4. CONCLUSIONS

The updated vulnerability assessment of Xilagani - Imeros aquifer system in the coastal plain region of Rhodope Prefecture, NE Greece, is presented in this paper. The research included the analysis and interpretation of DRASTIC and GALDIT vulnerability indexes spatial distribution with respect to the spatial distribution of nitrate concentration and Revelle coefficient values, respectively, for the year 2015. It is worth mentioning that DRASTIC index values for the year 2015 do not differ substantially compared to the corresponding values for the year 2006. Instead, increase of GALDIT index values is recorded for the year 2015 indicating worsening of the groundwater salinization status due to seawater intrusion.

Margane (2003) states that DRASTIC method is a popular approach to groundwater vulnerability assessments because it is relatively inexpensive, straightforward, and uses data that are commonly available or estimated and produces an end product that is easily interpreted and incorporated into the decision-making process. On the other hand, Pedreira et al. (2015) mention that GALDIT index is a relative tool and it does not exclude the need for more detailed field investigations.

REFERENCES

Aller, L., Bennett, T., Lehr, J. H., Petty, R. J., Hackett, G., 1987. DRASTIC: a standardized system for evaluating ground water pollution potential using hydrogeologic settings. EPA-600/2-87-035, EPA, Washington, DC

ASCE, 1987. Ground Water Management. 3rd Edition, ASCE Manuals and Reports on Engineering Practice No 40, New York

Chachadi, A. G., Lobo-Ferreira, J. P., 2001. Seawater intrusion vulnerability mapping of aquifers using the GALDIT method. COASTIN, 4: 7-9.

Chachadi, A. G., Lobo-Ferreira, J. P., 2005. Assessing aquifer vulnerability to sea-water intrusion using GALDIT method: Part 2 - GALDIT Indicators Description, Fourth Inter-Celtic Colloquium on Hydrogeology and Management of Water Resources, Portugal, 11–14, July 2005, CD of Proceedings.

Kallergis, G., 2000. Applied – Environmental Hydrogeology. Volume B, published TCG, Athens, 345p (in Greek).

Kallioras, A., Pliakas, F., Diamantis, I., 2010. Simulation of groundwater flow in a sedimentary aquifer system, subjected to overexploitation. Water, Air, & Soil Pollution, Springer, 211(1-4): 177-201.

Kallioras, A., Pliakas, F., Skias, S., Gkiougkis, I., 2011. Groundwater vulnerability assessment at SW Rhodope aquifer system in NE Greece. Advances in the Research of Aquatic Environment, Environmental Earth Sciences, Springer, 2: 351-358

Lobo-Ferreira, J. P., Chachadi, A. G., Diamantino, C., Henriques, M. J., 2005. Assessing aquifer vulnerability to seawater intrusion using GALDIT method: Part 1 Application to the Portuguese Aquifer of Monte Gordo. Fourth Inter-Celtic Colloquium on Hydrogeology and Management of Water Resources, Portugal, 11–14, July 2005, CD of Proceedings.

Margane, A., 2003. Guideline for Groundwater Vulnerability Mapping and Risk Assessment for the Susceptibility of Groundwater Resources to Contamination. Technical Cooperation Project Management, Protection and Sustainable Use of Groundwater and Soil Resources in the Arab Region. Technical Cooperation no: 1996.2189.7. ACSAD Damascus, BGR Hannover, 184 pp.

Panagopoulos, G.P., Antonakos, A. K., Lambrakis, N. J., 2006. Optimization of the DRASTIC method for groundwater vulnerability assessment via the use of simple statistical methods and GIS. Hydrogeol J. 14: 894-911.

Pedreira, R., Kallioras, A., Pliakas, F., Gkiougkis, I., Schuth, C., 2015. Groundwater vulnerability assessment of a coastal aquifer system at River Nestos eastern Delta, NE Greece, Environmental Earth Sciences, Springer, 73: 6387–6415.

Pliakas, F., Diamantis, I., Kallioras, A., Petalas, C., 2004. Study of the progress of seawater intrusion within a plain area of Rhodope Prefecture. Proceedings of the 10th International Congress of the Geological Society of Greece, Thessaloniki, Greece, 15-17/4/2004, 2057-2066 (in Greek).

Pliakas, F., Diamantis, I., Petalas, C., Panilas, S., 2001. Feasibility study of artificial recharge application to Rhodope plain areas aquifers in Thrace, Greece. A first approach. Proceedings of the 9th International Congress of the Geological Society of Greece, Athens, Greece, 26-28/9/2001, 5: 1923-1932 (in Greek).

Pliakas, F., Mouzaliotis, A., Kallioras, A., Diamantis, I., 2007. Hydrogeological assessment of the salinization problem of Xilagani – Imeros aquifer system in SW plain area of Rhodope Prefecture, Greece. Proceedings of the 11th International Conference of the Geological Society of Greece, Athens, Greece, 24-26/5/2007, 2: 536-547.

Recinos, N., Kallioras, A., Pliakas, F., Schuth, C., 2015. Application of GALDIT index to assess the intrinsic vulnerability to seawater intrusion of coastal granular aquifers. Environmental Earth Sciences, Springer, 73: 1017–1032.

Rupert, M. G., 1999. Improvements to the DRASTIC groundwater vulnerability mapping method. U.S. Geological Survey Fact Sheet FS-066-99, USGS, Reston, VA.

Sakkas, I., Diamantis, I., Pliakas, F., et al., 1998. Groundwater artificial recharge study of Xanthi – Rhodope aquifers. Research Project for the Greek Ministry of Rural Development and Food. Sections of Hydraulics and Geotechnical Engineering, DUTH, Department of Civil Engineers DUTH, Xanthi, Greece (in Greek).

Sener, E., Sener, S., Davraz, A., 2009. Assessment of aquifer vulnerability based on GIS and DRASTIC methods: a case study of the Senirkent-Uluborlu Basin (Isparta, Turkey). Hydrogeology J., 17: 2023–2035.

Proceedings of the 10th World Congress of EWRA 'Panta Rhei', 5-9 July 2017, Athens, Greece
© 2017 *European Water Resources Association*

Use of remote sensing and electrical resistivity tomography to determine Tidsi spring recharge and underground drainage

M. Hssaisoune[1,2*], S. Boutaleb[1], L. Bouchaou[1], M. Benssaou[1] and T. Tagma[3]
[1] *Laboratory of Applied Geology and Geo-Environment, Faculty of Science, Ibn Zohr University, Agadir, Morocco*
[2] *Earth sciences department, faculty of sciences and technologies, Sultane Moulay Slimane University, Beni Mellal, Morocco*
[3] *Hassan 1er University, Settat, Morocco*
[*] *e-mail: m.hssaisoune@usms.ma*

Abstract: The Souss plain, located in southwestern Morocco, is characterized along its southern edge by the emergence of several springs - Tidsi, Tioute and Tiare springs - flowing from the Calcareous Anti-Atlas Mountains' with low but constant rates despite successive drought years. This study was focused on Tidsi spring and aims to understand its hydrogeological functioning by determining the recharge area and underground drainage coming from Anti-Atlas Mountains. To reach these objectives, a remote sensed image (Landsat TM+) has been processed in order to map the geostructural mega-lineaments passing through the study area in order to better know the regional fracturation. Then, a geophysical investigation using 2D electrical resistivity tomography has been carried out to study the underground relationships between these mega-lineaments to assess their importance in Tidsi spring's recharge. Satellite image processing shows that Anti-Atlas Georgian limestones are well fractured. The lineation follows three corridors. The major lineaments' directions are in order of importance as follows: NW-SE, E-W and rarely NE-SW, respectively. These results were confirmed by field observations which indicate N20°, N50°, N90°, N130°, N160° lineament directions. Tomography pseudosections reveal the existence of two deep subvertical low-resistivity discontinuities. They show also the link of some lineaments with deep fractures leading to recharge of Tidsi spring. These results allow proposing hydrological behaviour of groundwater from Anti-Atlas Mountains which takes into account for both flows through subvertical faults and karstic fractures.

Key words: Souss plain, Tidsi spring, remote sensing, electrical resistivity tomography, Karstic fractures

1. INTRODUCTION

In the Middle Souss region, the three Tidsi's springs from Anti-Atlas Mountains are considered as a vital resource capable of supplying drinking and irrigation water for Tidsi village (figure 1). However, the hydrogeological functioning of these springs concerned the heads of Souss-Massa Basin Agency, those of Ministry of Energy, Mines, Water and Environment and also the non-governmental organizations (NGO) of the region.

Indeed these sources represent an alternative resource to the overexploitation of other aquifer systems such as the shallow aquifer of the Souss and also a permanent supply water recharge of this aquifer. The isotopic analysis (Bouchaou et *al.,* 2008) show that the recharge area of Tidsi spring is located at the high elevation ranges from 800 to 1200 m.a.s.l. thus exceeding the elevation of Tidsi calcareous plateau which is around 500 m.a.s.l.

Remote sensing and geophysical prospecting can be used to determine the unknown water origin of these springs and in future to cartography the high vulnerability perimeter of this spring's (Boutaleb et *al.,* 2009; Qarqori et *al.,* 2009; Sirieix et *al.,* 2014). The processing and interpretation of remote sensed image (Landsat TM +) will make it possible to detect the geostructural mega-lineaments passing through Georgian limestone plateau, in order to detect the regional fracturation. Geophysical investigation using 2D electrical resistivity tomography will make it possible to specify the characteristics of deep lineaments (Dahlin, 2001; Travelletti et *al.,* 2011).

This aims of this study is to understand the hydrogeological functioning of Tidsi springs by determining the recharge area and underground drainage coming from Anti-Atlas Mountains.

2. STUDY AREA AND METHODS

2.1 Study area

The Souss Basin, whose the Tidsi region as an integral part, is located in the middle western of Morocco (Figures 1.a and 1.b) limited by Anti-Atlas and High Atlas mountains in the South and in the North, respectively, Atlantic ocean in the West and Siroua massif in the east.

Tidsi is one of the most important rural districts in Taroudant province occupied by more than 5000 people (Haut-Commissariat au Plan, 2014), with touristic, agricultural and artisanal competences. The region has a typical arid climate with an average rainfall ranging from 250 to 300 mm/year and an annual mean temperature ranges between 14 and 18°C in the Anti-Atlas and can reach 20°C in the plain.

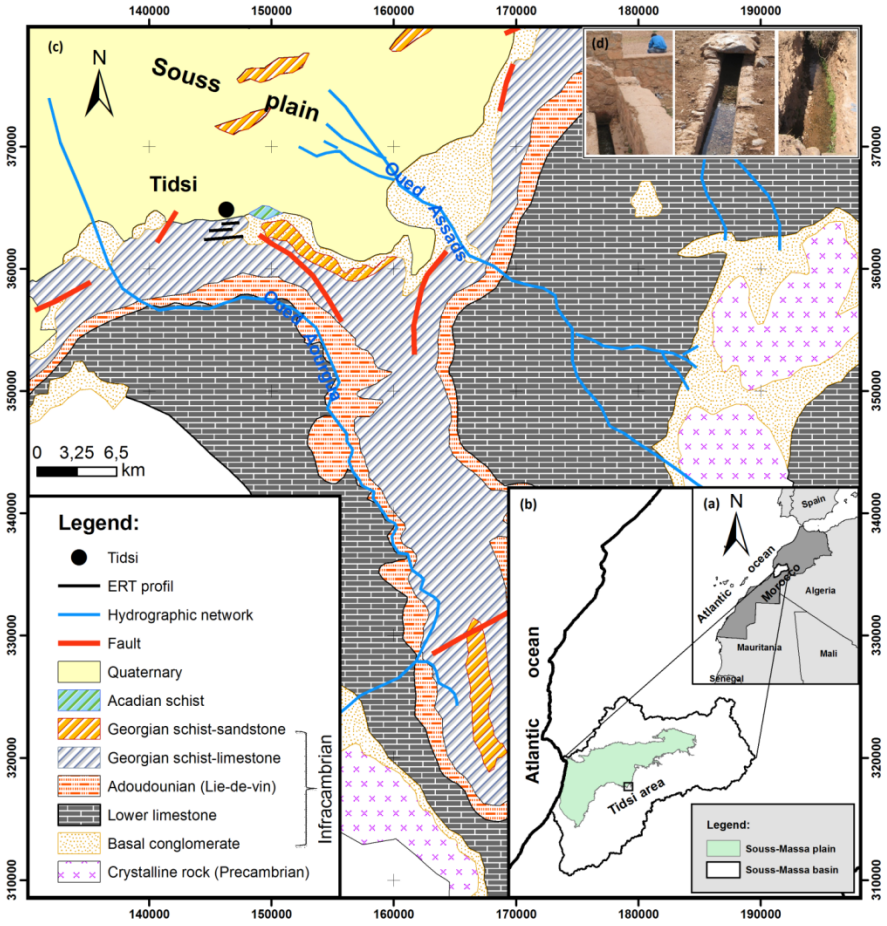

Figure 1. Geographic and geologic situation of study area: (a) Overview of study area at national scale, (b) Location of the Souss-Massa basin and Tidsi area, (c) simplified geological map of Tidsi area and (d) field photographs of Tidsi springs

From geological point of view the Tidsi area is characterised by the Plio-Quaternary sediments (sands, gravels, and lacustrine limestone) in the Souss plain with a Paleozoic schistose basement. The Anti-Atlas Mountains are characterized by Paleozoic formations (carbonate, schist and conglomerate) and Precambrian crystalline formations (Figure 1c). The Paleozoic formations are affected by hercynian deformation with a low intensity.

2.2 Methods

To reach the objectives of this study, a remote sensed image (Landsat TM+) has been processed in order to map the geostructural mega-lineaments passing through the study area in order to better know the regional fracturation. The mathematical processing of the Landsat TM+ satellite image of the Tidsi region was performed by applying the vertical Sobel matrix by integrating mathematical algorithms. The 7 x 7 directional filters were applied in the N-S, E-W, NW-SE and NE-SW directions to the satellite image covering the Tidsi region.

Then, a geophysical imaging was carried out mainly by Electrical Resistivity Tomography (ERT). Resistivity data were acquired by a Syscal R1 and a multi-electrode Lund system imaging using a Wenner array configuration of 48 electrodes and 5 m spacing, reaching a depth of about 50 m.

3. RESULTS AND DISCUSSIONS

The lineaments in satellite images are characterized by rectilinear or curvilinear elements that can be perceived on the surface and which reflect deeper phenomena such as faults, fractures or geological contacts.

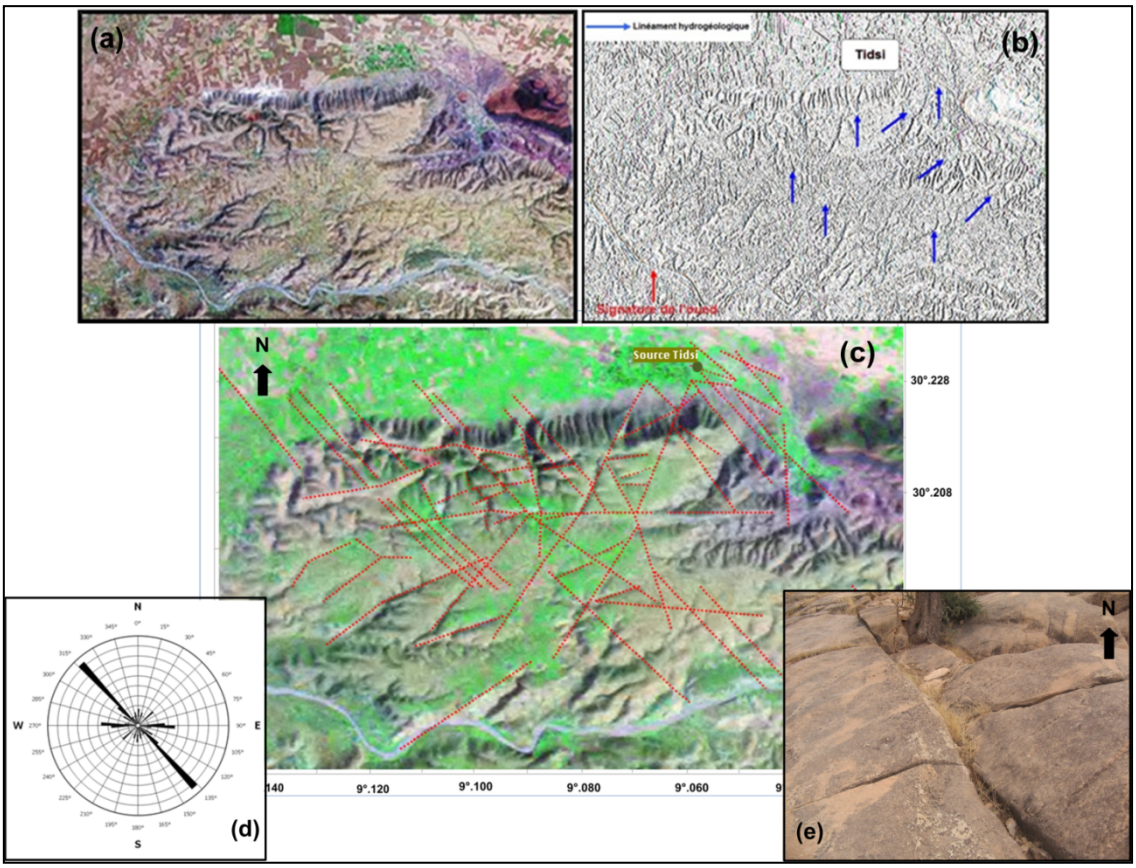

Figure 2. Remote sensed image: (a) Raw Landsat TM+ satellite image of the Tidsi region, (b) results of mathematical processing of the Landsat TM+ satellite image by applying vertical Sobel matrix, (c) synthetic map of the major lineaments of the Tidsi region, (d) major lineaments directions frequency and (e) field photograph of limestone fractures.

The results of remote sensed image (Figures 2c, 2d and 2e) indicate that the lineation follows three corridors. The major lineaments' directions are in order of importance as follows: NW-SE, E-W and rarely NE-SW, respectively. These results were confirmed by field observations which indicate N20°, N50°, N90°, N130°, N160° lineament directions (Figure 2e).

The NW-SE lineaments' are well represented in the center of limestone plateau and in SE part of Tidis springs with a kilometric extension.

The results of geophysical investigation are represented as pseudosections of measured apparent resistivity, calculated apparent resistivity and inverse model resistivity section (Figures 3, 4 and 5). Tree 2D resistivity high resolution images have been obtained allowing detecting, delineating important fractures and also to hydrogeological characterization of the underground relationships between these mega-lineaments to assess their importance in Tidsi spring's recharging.

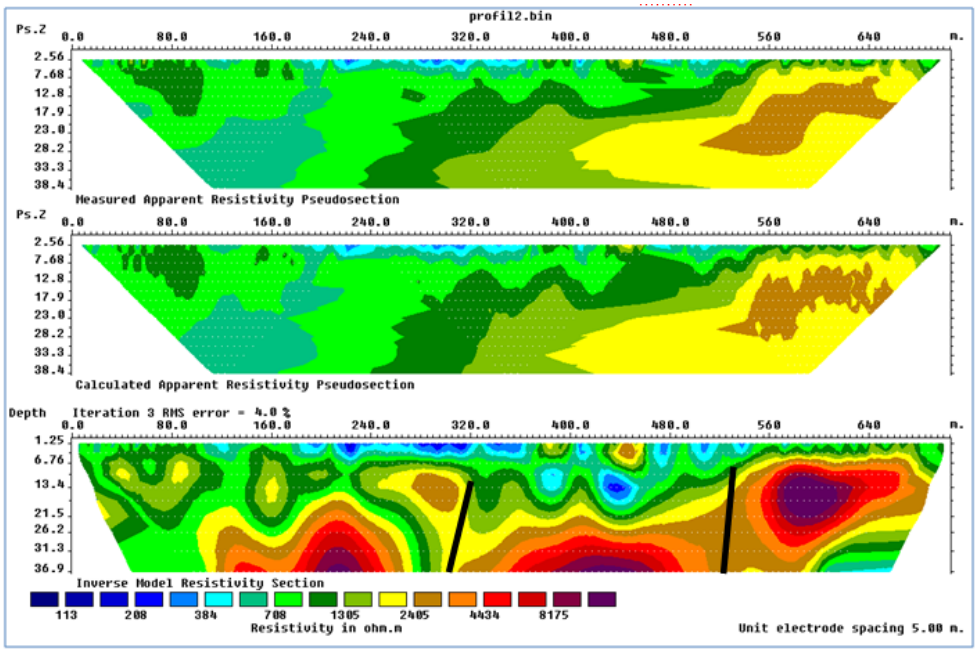

Figure 3. The result of mathematic inversion model of profile Tidsi 1

The 2D pseudosection of profile Tidsi 1 (Figure 3), show that the limestone mass with high resistivity (from 4000 ohm.m to more than 8000 ohm.m) is not lateraly continuous. This electrical discontinuity suggests the passage of faults draining waters that cause the low values of resistivity to the right of conducting anomalies. The latter are probably correspond to the passage of the geological faults or lineaments that drained water to the Tidsi springs. It is important to note that the limestone formations with high resistivity values are found mainly in east of the profile and in the west part the surface deposit characterized by the presence of clays and plio-quaternary formations caused the low resistivity which overcome these limestones.

The Tidsi 2 tomographic profile confirms the existence of the two faults already detected in the first profile Tidsi1. These two faults are encountered at the respective measuring stations 250 m and 370 m (Figure 4). The first anomaly is at the center of the line connecting the anomaly of the Tidsi1 profile and the location of the Tidsi source. This profile confirms the hypothesis of the feeding of the source by the hydrogeological lineament.

Tidsi 3 profile shows the continuity of the fault in the direction of the source (figure 5). Indeed, a clearly visible conductive anomaly centered in line with the measuring station 240 m is shown and appears to be aligned with respect to the location of the two other conducting anomalies of the two previous profiles Tidsi 1 and Tidsi 2.

The projection of the tomographic profiles on the satellite image of the Tidsi region allowed us to accurately locate the location of the fault that appears to be the source of the Tidsi source and to map it (Figure 6).

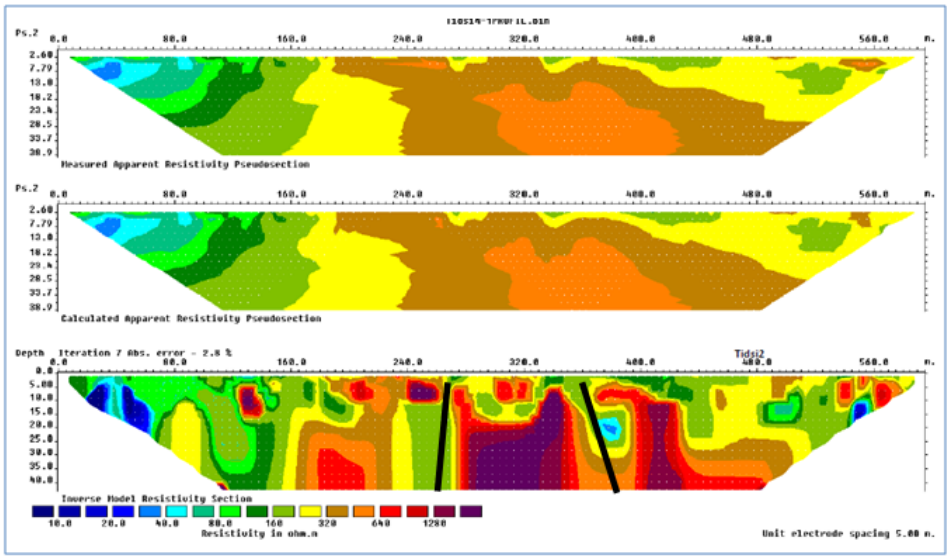

Figure 4. The result of mathematic inversion model of profile Tidsi 2

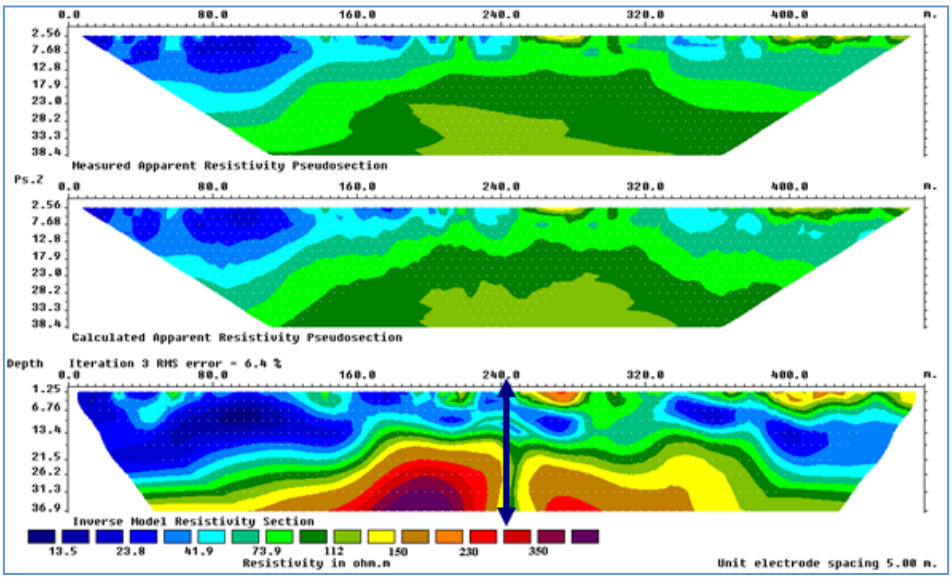

Figure 5. The result of mathematic inversion model of profile Tidsi 3

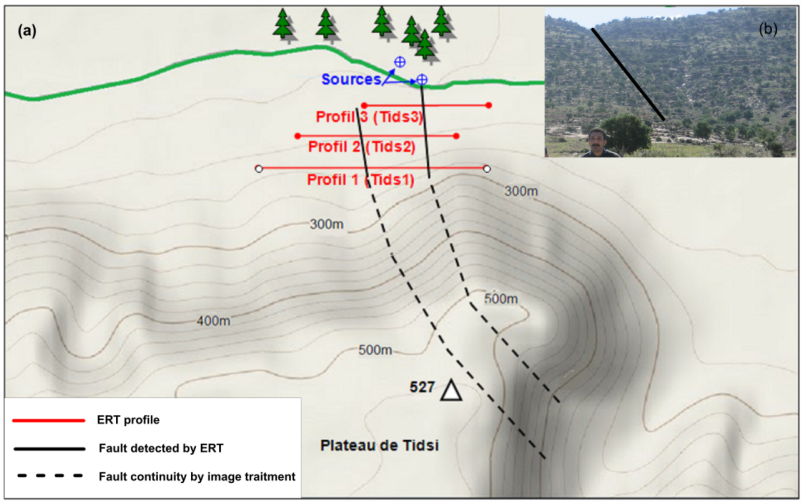

Figure 6. (a) Projection of faults detected by ERT and its continuity on the topographical map of Ait Baha (1/100 000) and (b) field trip photograph fault in Tidsi springs area.

4. CONCLUSION

The use of remote sensing allows determining the major lineaments' directions, these ones are in order of importance as follows: NW-SE, E-W and rarely NE-SW, respectively.

Electrical tomography has confirmed the connection of some lineaments with the deep fractures which are corridors of water circulation. The technique of identifying lineaments by satellite imagery followed by a validation by geophysics seems adapted to study the aquifers of fractured limestone basement.

The coupling between the different types of geological, hydrogeological, remote sensing and geophysical results, related to the Tidsi source region, shows that Georgian limestones are affected by faults that are, perhaps, transport of high altitudes water to the Tidsi area.

REFERENCES

Bouchaou L, Michelot JL, Vengosh A, et al., 2008. Application of multiple isotopic and geochemical tracers for investigation of recharge, salinization, and residence time of water in the Souss–Massa aquifer, southwest of Morocco. J Hydrol. 2008;352:267–287.

Boutaleb S., El Hammichi F., Tabyaoui H., Bouchaou L. and Dindane K., 2009. Determination of the preferential flows in a karstic area (Tafrata, Morocco): Contribution of satellite SAR ERS-1 and Landsat ETM+ data and of the geophysical prospection. Revue des Sciences de l'Eau 22(3), pp 407-419. ISSN : 1718-8598.

Dahlin T., 2001. The development of DC resistivity imaging techniques. Computers and Geosciences, 27, 1019-1029.

Haut-Commissariat au Plan (HCP) 2014. Recensement de la population et d'habitation du Maroc 2014. www.hcp.ma.

Qarqori KH., Rouai M., Moreau F., Saracco G., Hermitte D., Boualoul M., Dauteuil O., Biessy G., AND Sahbi H., 2009. Electrical Resistivity Tomography of the Karstic Aquifer of Bittit spring (Middle Atlas, Morocco). Geophysical Research Abstracts, Vol. 11, EGU2009-8225, 2009 EGU General Assembly 2009

Sirieix C., Riss J., Rey F., Pretou F.& Lastennet R., 2014. Electrical resistivity tomography to characterize a karstic Vauclusian spring: Fontaine d'Orbe (Pyrénées, France). Hydrogeology Journal, pp 1-14. DOI 10.1007/s10040-013-1095-8 Springer-Verlag Berlin Heidelberg.

Travelletti J., Sailhac P., Malet J.-P. , Grandjean G. AND Ponton J., 2011. Hydrological response of weathered clay-shale slopes: water infiltration monitoring with time-lapse electrical resistivity tomography

Proceedings of the 10th World Congress of EWRA 'Panta Rhei', 5-9 July 2017, Athens, Greece
© 2017 *European Water Resources Association*

Environmental impacts of urbanization in hydrogeological systems

A. Mitropapas[1*], A. Panagopoulos[2], G. Karatzas[3] and A. Kallioras[1]
[1] *National Technical University of Athens, School of Mining Engineering and Metallurgy, Athens, Greece*
[2] *Hellenic Agricultural Organisation (HAO)-General Directorate of Research, Soil and Water Resources Institue, Thessaloniki, Greece*
[3] *School of Environmental Engineering, Technical University of Crete, Polytechneioupolis, Chania 7310, Greece*
[*] *e-mail: mitropapas@metal.ntua.gr*

Abstract: The impact of urban areas growth is a rather complex research topic in the field of hydrogeology. Urbanization significantly affects the natural water cycle, both in terms of quantity and quality, recognized as a challenge with scientific approaches which should be extended to different spatial and temporal scales. The analysis and interpretation of these hydrosystems is a difficult and complicated task influenced by many factors. Urban groundwater resources management is an issue of paramount importance that becomes a necessity in the case of Attica, Greece. Urban aquifers are considered very sensitive ecosystems that are subject to several stresses being mainly of anthropogenic origin. Due to the great heterogeneity of the related infrastructures -such as underground structures and water supply/sewage/stormwater systems - the water balance of groundwater may vary greatly in spatial terms within the urban environment, highlighting that the main contributor to recharge and discharge clearly differ from those in natural systems. Buildings, roads, and other surface infrastructure create an impermeable covering that alters all parts of the hydrological cycle. So it is clear, that the investigation of urban hydrosystems and the thorough evaluation of hydrological processes related to the hydrological cycle of urban groundwater, required modern approaches both in terms of developing new modelling approaches (holistic) and new monitoring techniques of hydrological processes with state of the art technologies. The urban aquifer system of Attica can be used as a reference site that incorporates multi-disciplinary environmental problems and highlights the need for an Integrated Urban Water Management (water supply-drainage-sewage systems).

Key words: Urban Hydrogeology, Urbanization, Groundwater, Monitoring technologies

1. INTRODUCTION

1.1 Urban Hydrogeology

Urbanization is a rather complex research topic in the field of hydrogeology with ecological, economic and social implications (Schirmer, Leschik and Musolff, 2013). The increasing urbanization conditions are a global challenge in the management of water resources in urban areas, both environmental and economic and social tasks. Today, approximately 50% of the world population lives in urban areas and according to the United Nations (2008), by 2050 these numbers are going to rise significantly (Schirmer, Leschik and Musolff, 2013; United Nations, 2008). This trend would result in additional environmental pressures not only in the water balance of sensitive hydrologically areas, such as those of the Mediterranean basin but also would have negative impact on the quality of air, soil and urban water resources (Schirmer, Leschik and Musolff, 2013;Diamond and Hodge, 2007).

Urbanization significantly affects the natural water cycle, both in terms of quantity and quality, recognized as a challenge with scientific approaches which should be extended to different spatial and temporal scales. Urban aquifers are considered very sensitive ecosystems that are subject to several stresses being mainly of anthropogenic origin.

1.2 Quantitative issues

Groundwater recharge in urban areas is one of the most significant and complex task. Surface coverings such as buildings, roads and other impermeable units, result in maximizing runoff and minimizing infiltration into the groundwater and consequently the natural recharge of aquifers is reduced (Lerner, 1990). Nevertheless, urban recharge is often as high, or higher than pre-urbanization rates (Lerner, D. 2002), and this happens because of subsurface infrastructures. Infrastructures such as water supply pipe-network, storm drainage, sewage system generate large amounts of recharge through leakages (Vázquez-Suñé, E., Carrera, J., Tubau, I., Sánchez-Vila, X. and Soler, A., 2010). Run off is often carried in storm sewers or artificial waterways, so significant amounts of storm water leaked from sewers into the groundwater system. Another hydrological pathway of recharge in urban areas is the over-irrigation of parks and gardens especially in summer season when used large amounts of water.

Estimation of recharge in urban areas is a difficult task and depends on many factors. Landuse and surface cover influence the quantification of recharge and show us the need of conduction of many surveys such as remote sensing, aerial photography and geophysics.

1.3 Qualitative issues

In terms of qualitative impacts on the underlying urban aquifer systems, significant contaminant loads may result from in-situ sanitation, sewer leakage, industrial chemicals, and disposal of liquid effluents and solid wastes (mainly leachates from uncontrolled landfills). In many cases, groundwater contamination from increased heavy metals concentration has been reported as a result of extended flooding conditions of urban surfaces and consequent infiltration.

1.4 General introduction to the case study

The metropolitan area of Athens, Greece, will be used as a reference site to investigate the quantitative impacts of intense urbanization on the underlying aquifer system of the area. In the beginning of 20th century, Athens had a population of some tens of thousands of residents, being a megacity today with a population that exceeds 5million people. This tremendous expansion of the city's population, greatly affected the underlying aquifer systems in terms of both its groundwater quality as well as its quantity.

2. CASE STUDY DESCRIPTION

2.1 Geographical setting

Attica region is situated at the southeastern part of Greece. Attica basin ($412km^2$) is surrounded by the mountain of Aigaleo to the west, Parnitha to the north, Pentelicus to the northeast, Hymettus to the east and the Saronic Gulf to the southeast. It is a typical coastal hydrogeological system of a semi-arid region, where a significant rise of population has been noticed the last decades. From 1971 to 2011, according to the numbers of Hellenic Statitstical Authority the population of the central part of the Region of Athens has been three times higher (from 867.000 to 3.000.000). The following figure shows a map of the study area including information with respect to its hydrographic network and morphologic relief.

With respect to its climate, Athens metropolitan region is a semi-dry area with a mean annual rainfall of approximately 390mm (Koutsoyiannis and Baloutsos, 2000) to app. 1000mm on the highest altitutes of the mountainous zone, while 50-100 rainy days are recorded as an average annual. It contains a poorly developed river network that is dominated by streams of ephemeral

flow, whereas the area is subject to an urban heat island phenomenon that affects temperature and in turn other atmospheric properties over Athens. The mean annual temperature varies between 16°C to 18°C, depending on the altitude as well as the distance from the coast, while the annual atmospheric temperature range is app. 16°C.

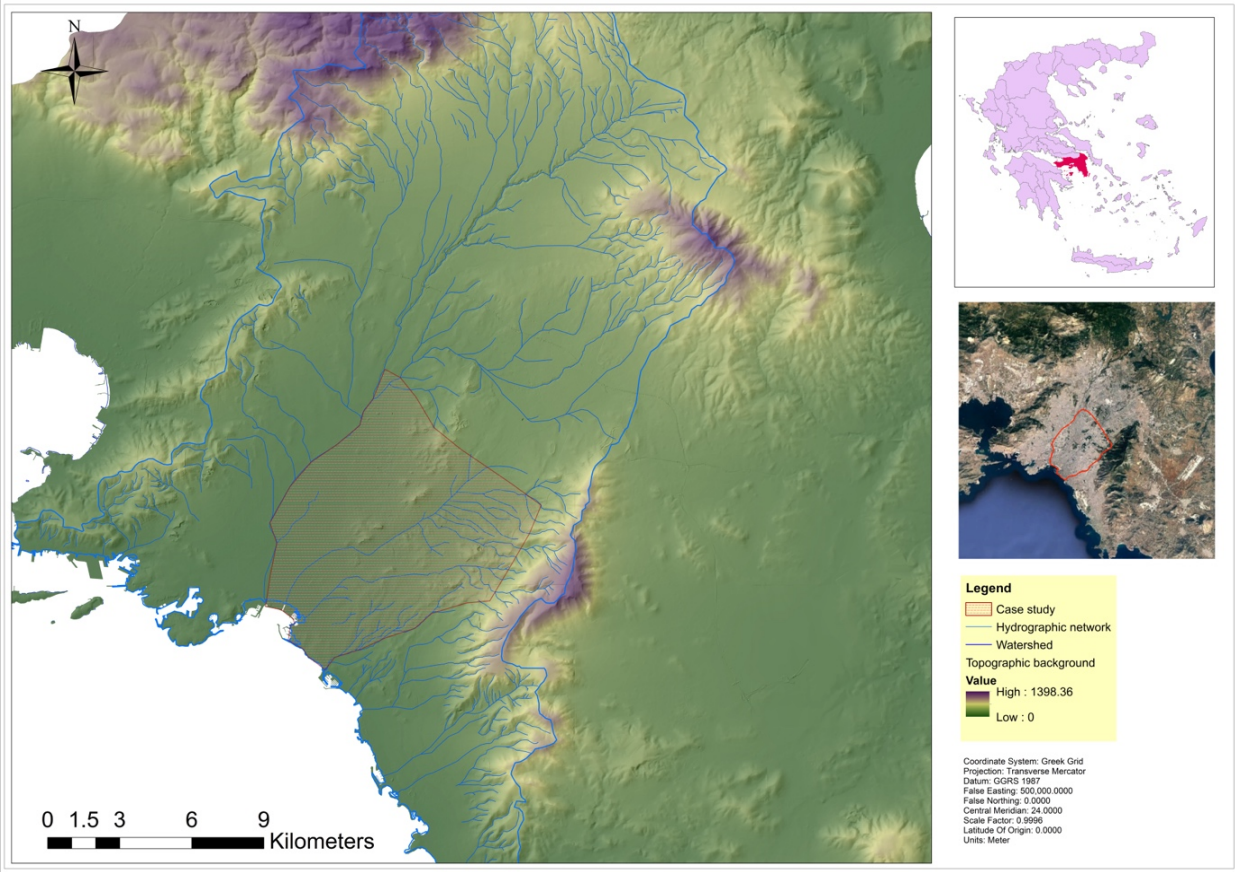

Figure 1. Study area, hydrographic network and morphological relief of Attica Region.

2.2 Geological setting

The geological structure of the study area is dominated by alpine and post alpine formations. The geological basement of Attica consists of "Athens schist", marbles and limestones whereas the upper layers consist of Neogene (marls, clays, sandstone, conglomerates) and Quaternary deposits (Bathrellos et al., 2007).

2.3 Hydrogeological setting

The hydrogeological setting of area involves a multi-layer aquifer-system that consists of an upper unconsolidated formation dominated mostly by Quaternary deposits (alluvial and human deposits) and secondly the surrounding kasrtified marble units (Figure 2). The conceptual hydrogeological model of the underground hydrosystem of the metropolitan area of Athens involves a highly complicated karstified system of the mountainous zone (dual porosity due to fractures and large karstic conduits), that surrounds the underlying unconsolidated aquifer system of Kifissos river. The underlying aquifers are recharged by the river through its natural watercourse (mainly within its northern upstream part); while the southern part of the aquifer system is artificially and incidentally recharged by leakages from the stormwater/wastewater/water supply networks (combined with lateral recharges from the karst systems, direct infiltration from precipitation and irrigation return flows from urban green areas).

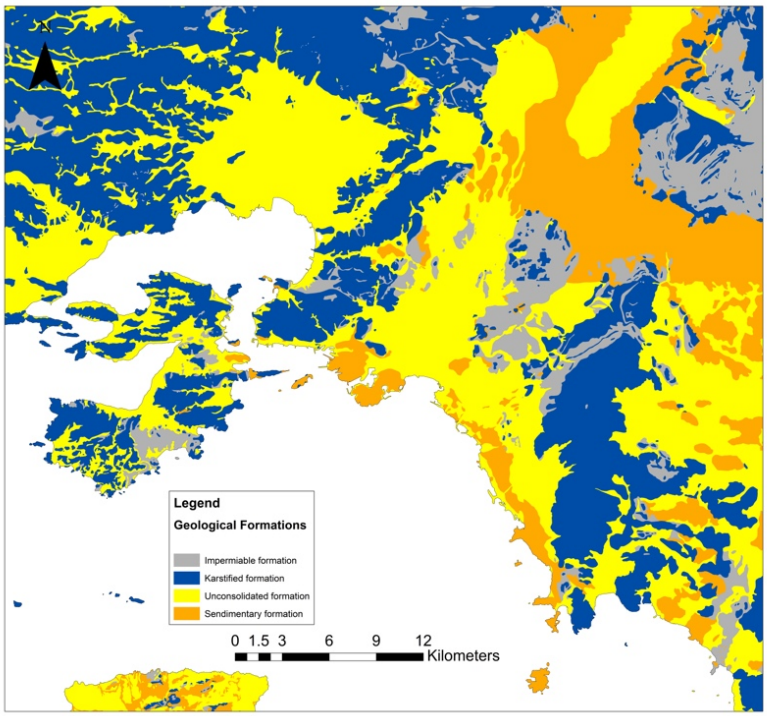

Figure 2. Hydrogeological map of study area

Figure 3 shows an up-to-date thorough inventory of over 2000 groundwater wells (public and/or private) that is based on previous research (Koumantakis et al., 1997) as well as on current research activities.

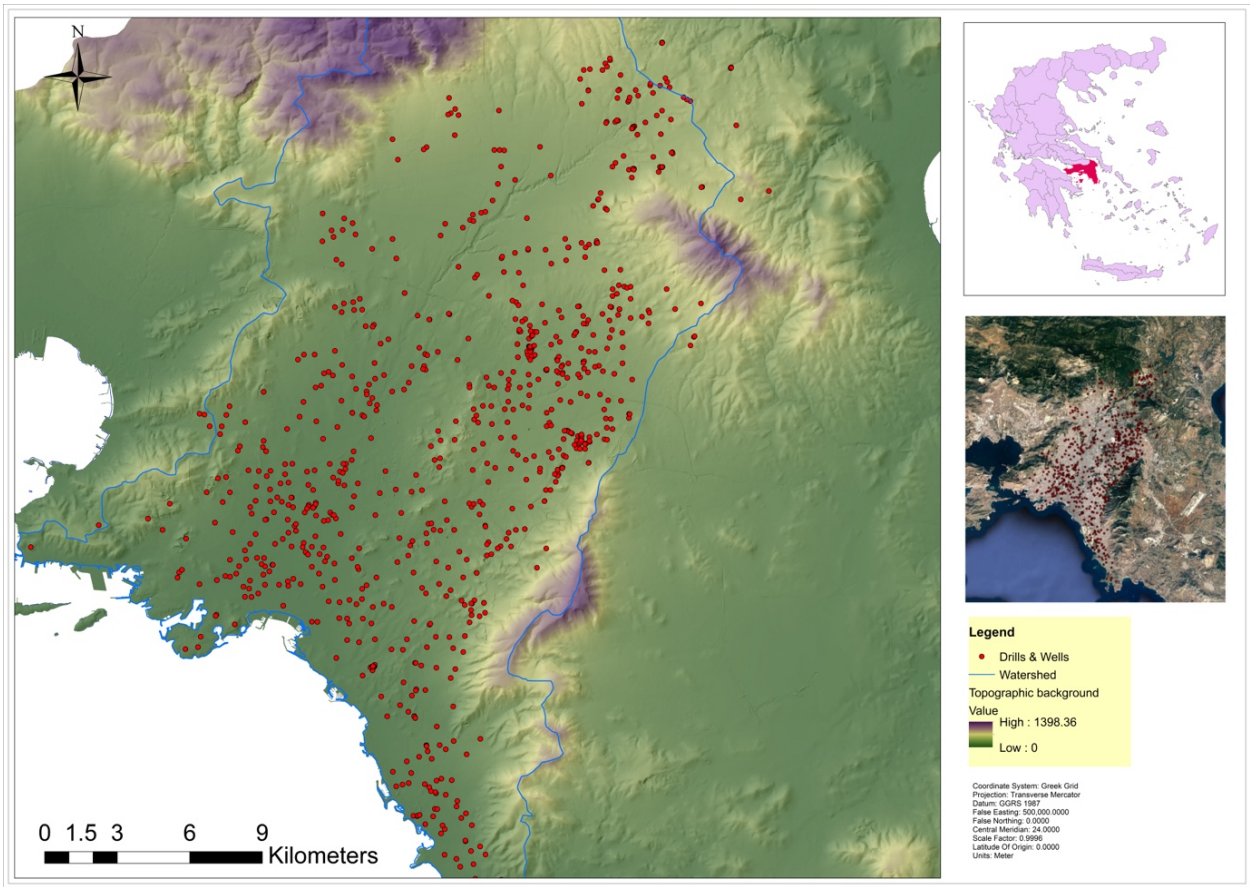

Figure 3. Map with drills and wells

The current monitoring network consists of approximately 70 drills and 10 wells (Figure 4) that focuses on the lower aquifer layer as well as on the upper unconsolidated layer in the vicinity of Kifisos River.

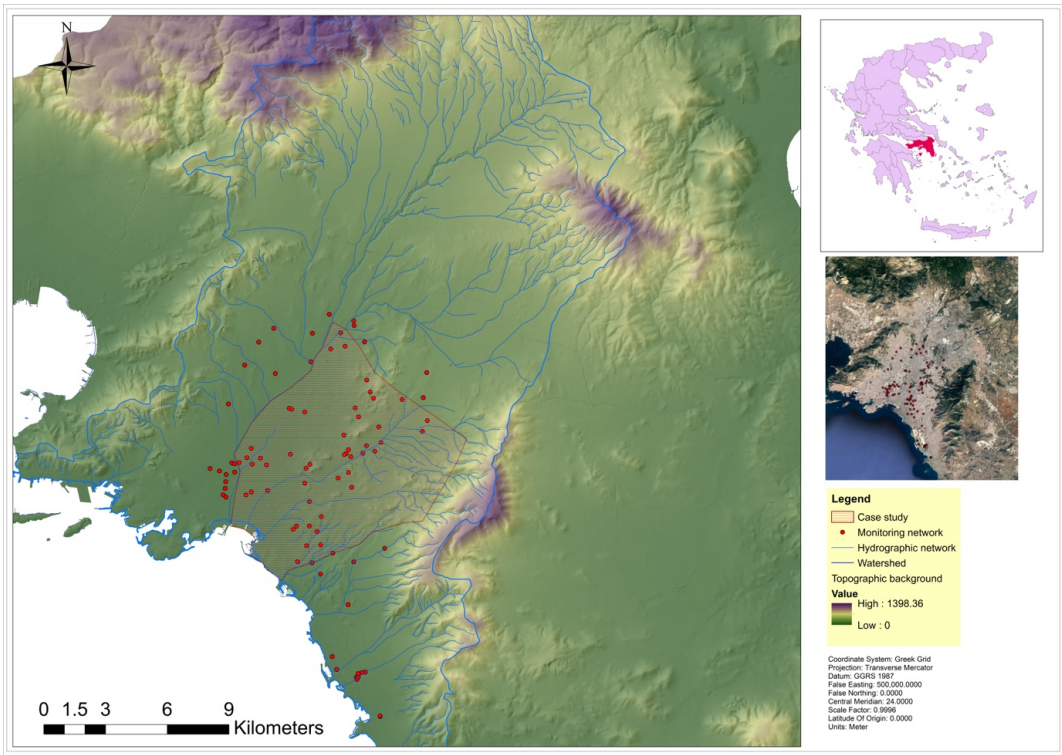

Figure 4. Map of monitoring network for the study area of Athens.

The piezometric conditions of the study area were investigated through a wide measuring campaign that took place for first time in 1996, from app.140 measuring points (mainly groundwater wells and boreholes) as shown in Figure 5.

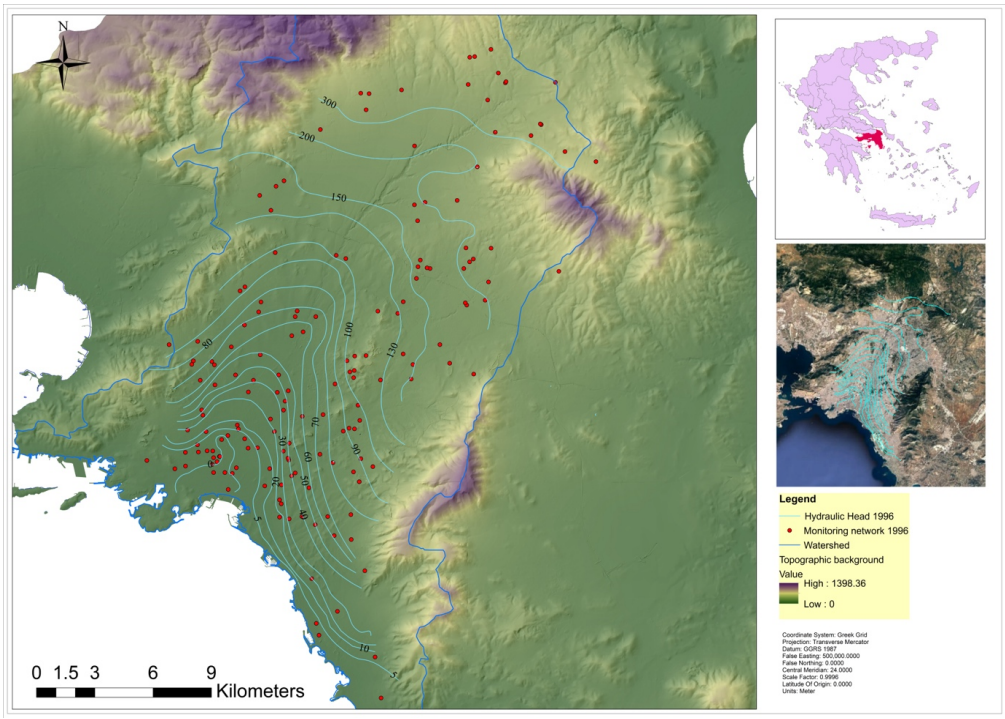

Figure 5. Piezometric conditions of the study area of Athens in October 1996 (groundwater level data source: Koumantakis et al., 1997).

After 20 years, in October 2016, a new measuring campaign took place from app. 80 measuring points which are evenly distributed throughout the entire study area (Figure 6).

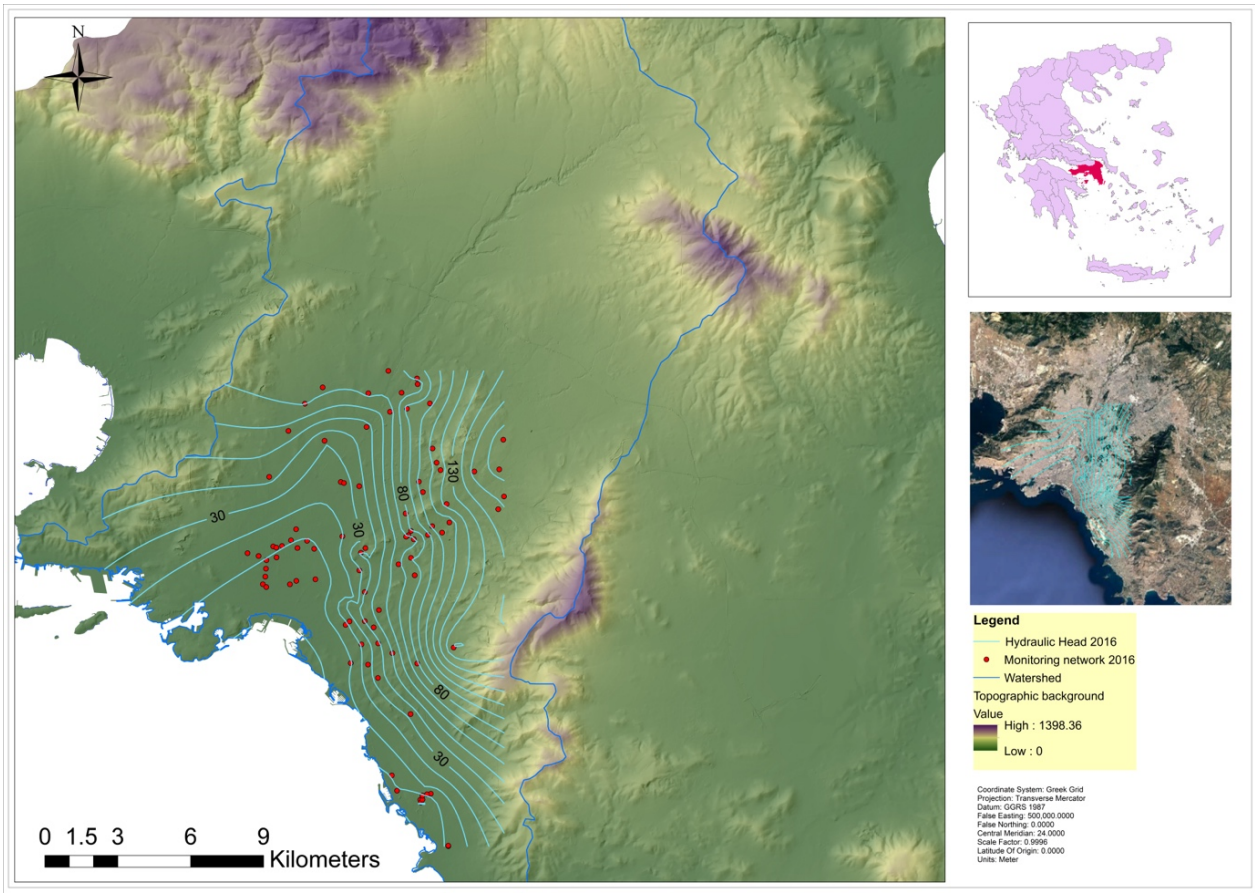

Figure 6. Piezometric conditions of the study area of Athens in October 2016.

Figures 5 and 6 show that the groundwater hydrology of the investigated aquifer has not changed significantly during the last decades, mainly as a result of unchanged exploitation conditions. A major discharge axis towards the Mediterranean Sea is noted, while lateral recharge from the surrounding karstic aquifer systems is also evidence from the above maps.

3. CONCEPTUAL MODEL

3.1 Conceptual approach analysis

This study focuses on the quantitative characteristics and how these influence the entire water balance of the underlying aquifer system. All the components of the hydrological cycle are subject to substantial changes within an urban environment. The water balance of groundwater may vary greatly in spatial terms within the urban environment, highlighting that the main contributor to recharge and discharge clearly differ from those in natural systems. Underground structures and water supply/sewage/stormwater systems, surface coverings such as buildings, roads and other surface infrastructure create new paths to the conceptualization of hydrologic processes. For example, leakages through the three kind of systems in a city. Leakages consist a significant contributor to the recharge of the aquifer. All the above are illustrated in the following figure (Figure 7).

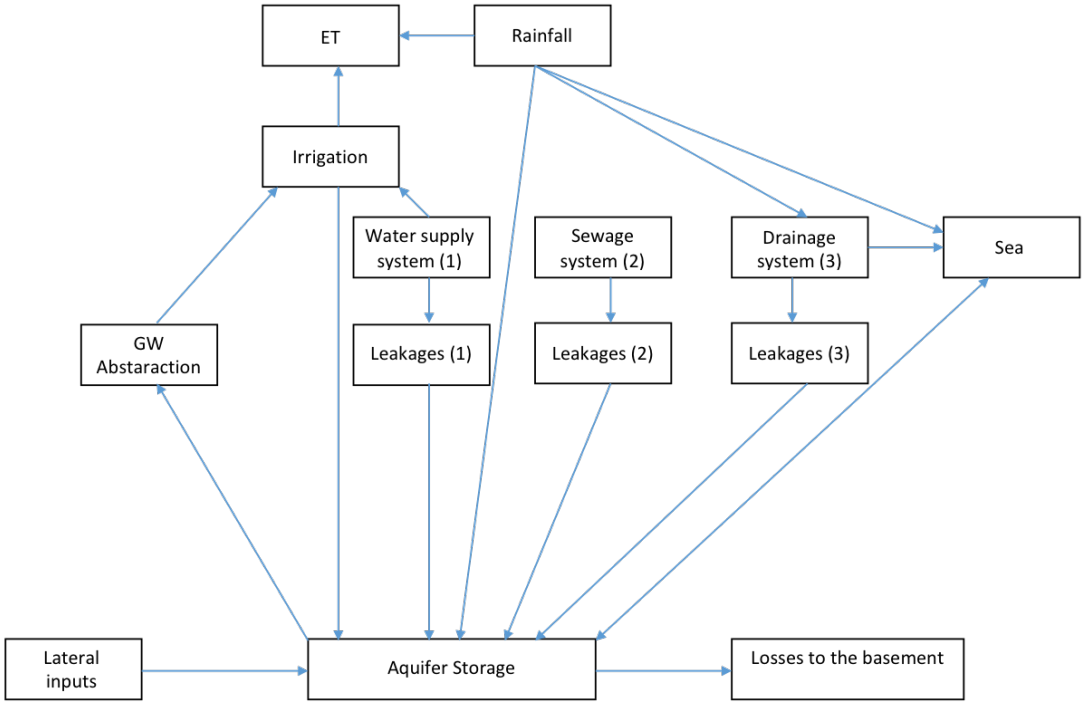

Figure 7. Conceptualization of hydrologic processes in the aquifer system of Athens metro.

3.2 Conceptual model

With respect to the geological setting, Athens basin is dominated by alpine (marbles, schists, limestones and sandstones) and post-alpine rocks (Neogene and loose Quaternary formations). Carboniferous and Quaternary formations are the most common aquifer layers in Athens Basin mainly in its western and northern parts. The upper layer involves Neogene deposits, having a thickness of approximately 60-80 meters; being the most exploited aquifer layer of the study area. The uppermost layer consists of Quaternary deposits (mainly alluvial sediments). The thickness of this layer ranges from a few meters to 30 meters and it has a direct interaction with most of city's infrastructure elements. The conceptualization of the urban groundwater budget and hydrogeological cycle of Athens is illustrated in the following figure (Fig 8).

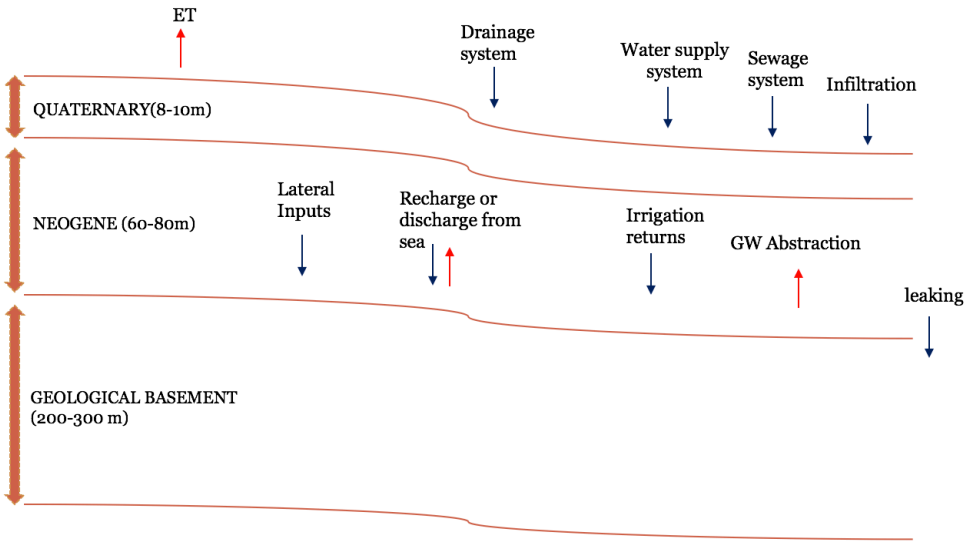

Figure 8. Conceptualization of urban groundwater budget and hydrogeological cycle

4. CONCLUSIONS

The impact of urbanization in the aquifer system through changes that recorded in hydrological processes at all hydrological zones (superficial, saturated and unsaturated) is the basic research topic in this study. Specifically, this research aims to develop new methods of quantification of recharge and new monitoring technologies with three basic axis (i) the influence of landuse (built up areas, green areas), (ii) the artificial recharge through leakages (water-supply system, storm and sewage system) and (iii) the effect of local cone of depression of groundwater as a result of underground structures and green areas. The urban hydrosystem of Attica will be used as a reference site that incorporates multi-disciplinary environmental problems and highlights the need for an Integrated Urban Water Management (water supply-drainage-sewage systems) (Boukhemacha et al., 2015).

REFERENCES

Bathrellos, G., Skilodimou, H., Kelepertsis, A., Alexakis, D., Chrisanthaki, I. and Archonti, D. (2007). Environmental research of groundwater in the urban and suburban areas of Attica region, Greece. Environmental Geology, 56(1), pp.11-18.

Boukhemacha, M., Gogu, C., Serpescu, I., Gaitanaru, D. and Bica, I. (2015). A hydrogeological conceptual approach to study urban groundwater flow in Bucharest city, Romania. Hydrogeol J, 23(3), pp.437-450.

Diamond, M. and Hodge, E. (2007). Urban Contaminant Dynamics: From Source to Effect. Environmental Science & Technology, 41(11), pp.3796-3800.

Koukis, G. and Sabatakakis, N. (2000). Engineering geological environment of Athens, Greece. Bulletin of Engineering Geology and the Environment, 59(2), pp.127-135.

Koutsoyiannis, D., Baloutsos, G. (2000). Analysis of a long record of annual maximum rainfall in Athens, Greece, and design rainfall inferences. Nat. Hazards, 22, pp. 29–48.

Koumantakis et al. (1997). Hydrogeological assessment and groundwater exploitation in the basin of Athens metropolitan area, Technical Report for the Ministry of Environment, Urban Planning and Public Works, Athens Organization, 1995-1997.

Lerner, D. (1990). Groundwater recharge in urban areas. Atmospheric Environment. Part B. Urban Atmosphere, 24(1), pp.29-33.

Lerner, D. (2002). Identifying and quantifying urban recharge: a review. Hydrogeology Journal, 10(1), pp.143-152.

Salvadore, E., Bronders, J. and Batelaan, O. (2015). Hydrological modelling of urbanized catchments: A review and future directions. Journal of Hydrology, 529, pp.62-81.

Schirmer, M., Leschik, S. and Musolff, A. (2013). Current research in urban hydrogeology – A review. Advances in Water Resources, 51, pp.280-291.

United Nations (2008). World urbanization prospects: the 2007 Revision. Population division of the department of economic and social affairs of the United Nations Secretariat, New York.

Vázquez-Suñé, E., Sánchez-Vila, X. and Carrera, J. (2004). Introductory review of specific factors influencing urban groundwater, an emerging branch of hydrogeology, with reference to Barcelona, Spain. Hydrogeol J, 13(3), pp.522-533.

Vázquez-Suñé, E., Carrera, J., Tubau, I., Sánchez-Vila, X. and Soler, A. (2010). An approach to identify urban groundwater recharge. Hydrol. Earth Syst. Sci., 14(10), pp.2085-2097.

Proceedings of the 10th World Congress of EWRA 'Panta Rhei', 5-9 July 2017, Athens, Greece
© 2017 *European Water Resources Association*

A two-dimensional analytical model for tide-induced groundwater fluctuation in leaky aquifers

M.-H. Chuang[1] and H.-D. Yeh[2]
[1] *Department of Urban Planning and Disaster Management, Ming-Chuan University, Taoyuan, Taiwan*
[2] *Institute of Environmental Engineering, National Chiao Tung University, Hsinchu, Taiwan*
[*] *e-mail: hdyeh@mail.nctu.edu.tw*

Abstract: Tide-induced groundwater head fluctuations in coastal leaky aquifer systems are complicated and difficult to quantify. Yet, the prediction of groundwater fluctuations may be a crucial work in dealing with the problems of groundwater resources management or contamination remediation in coastal aquifers. This study develops a two-dimensional analytical model for describing the groundwater flow in an *L*-shaped leaky aquifer bounded by a river and the ocean with an arbitrary included angle and subject to the effect of tidal fluctuations. The solution of the model is developed in Cartesian coordinates based on the methods of finite sine transform and Hankel transform. On the basis of the analytical solution, the groundwater fluctuations induced by the joint effect of estuarine and oceanic tides are examined. In addition, the influences of physical parameters such as aquitard leakage (L), included angle (Φ), damping coefficient (K_{er}) and separation coefficient (K_{ei}) on the groundwater fluctuations in the confined aquifer are investigated and discussed. The analysed results indicate that those parameters have significant impacts on the head fluctuations in the *L*-shaped coastal leaky aquifer system. The results also show that the effect of L on the normalized amplitude and phase lag of the groundwater fluctuations increases with Φ, but the joint effect of K_{er} and K_{ei} on both parameters decreases as Φ increases.

Key words: analytical model, coastal leaky confined aquifer, groundwater fluctuations, *L*-shaped aquifer

1. INTRODUCTION

The dynamic behavior of groundwater flow in tidal aquifers subject to the tidal effect has received much attention in recent decades. The propagation of the tidal waves along an estuary results in amplitude decay and phase change with distance (Sun, 1997). Tide-induced head fluctuations in a 2-D coastal aquifer system subject to the effects of both oceanic and estuarine tides is therefore complicated. Sun (1997) presented an analytical solution derived from a 2-D transient groundwater flow equation with an estuarine tidal boundary. The predicted head fluctuations in a confined aquifer from his solution showed good match as compared with those of the finite different solutions. Tang and Jiao (2001) displayed a 2-D analytical solution for groundwater head distribution in a coastal leaky confined aquifer. Both the works of Sun (1997) for 2-D groundwater flow in a confined aquifer and Jiao and Tang (1999) for 1-D groundwater flow in a leaky confined aquifer can be considered as special cases of Tang and Jiao (2001). Their solution was also tested against the results obtained from implicit finite difference approximations. Li et al. (2002) developed an analytical model to describe tidal groundwater head fluctuations in an *L*-shaped aquifer, which is bounded by two water-land boundaries with a right angle. The solution of the model is derived using the methods of complex transform and the Green's function.

To our knowledge, the existing solutions for *L*-shaped aquifers are only applicable for the case that the river is perpendicular to the ocean. Yet, the intersection for a river entering the sea in a natural coastline may form an acute or obtuse angle. The objective of this paper is to develop a 2-D analytical model for describing groundwater head fluctuations in a coastal leaky aquifer system with any degree of included angle between the river and the ocean. The solution of the model is developed based on the methods of finite sine transform and Hankel transform along with the transformation between the polar coordinates and Cartesian coordinates. This solution can be used

to assess the effects of the oceanic tides and estuarine tides on the groundwater head fluctuations. In addition, the solution can also be used to explore the impacts of leakage and included angle on the head fluctuations and investigate the dynamic groundwater response to various scenarios for the leakage and bending angle of the coastline in tidal leaky confined aquifers.

2. MODEL SETUP AND BOUNDARY CONDITIONS

Consider a coastal leaky aquifer system with an unconfined aquifer on the top, a confined one at the bottom, and an aquitard in between. Figure 1 shows a cross-section view of the conceptual model for an L-shaped aquifer bounded by a river and the ocean with an included angle Φ. The x-axis is horizontal along the seashore while the y-axis is perpendicular to the x-axis and positive toward inland with an angle of $|90 - \Phi|$ between the axis and the river. The joint effect of tidal fluctuations from the ocean and the estuary on the groundwater flow of the confined aquifer is considered. The groundwater fluctuations in the unconfined aquifer is negligible as compared with that in the confined aquifer. These two aquifers, however, interact with each other through the leakage of aquitard. The bottom of the confined aquifer is impermeable. Assume that the aquifer is homogeneous and the thickness of the unconfined aquifer is very large as compared with the magnitude of the tidal fluctuations, therefore allowing linearization of the flow equation for the unconfined aquifer. The flow velocity in the confined aquifer is essentially horizontal, and there is a vertical leakage through the aquitard.

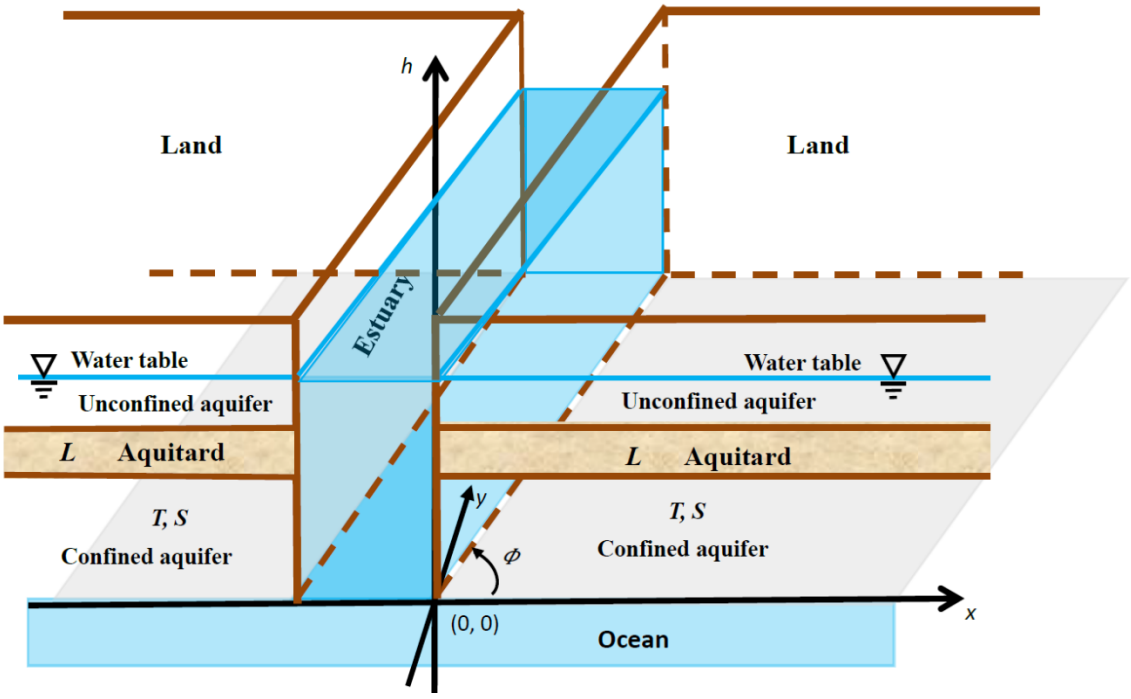

Figure 1. A cross-section view of two-dimensional conceptual model in a leaky anisotropic aquifer system with an arbitrary included angle (Φ) in Cartesian coordinates (x, y).

In addition, the aquitard storage is assumed negligible and the leakage is linearly proportional to the difference in heads of the unconfined and confined aquifers (Li and Jiao, 2001). The initial groundwater head at time $t = 0$ in the entire system is uniform and equals h_m, which is a distance from the groundwater head to a convenient reference. When $t > 0$, h_m in the unconfined aquifer remains constant all the times (Jiao and Tang, 1999). Under these assumptions the governing equation for describing the head fluctuations in the confined aquifer ($x > y\cot\phi, y > 0$) can be written as:

$$T\left(\frac{\partial^2 h}{\partial x^2}+\frac{\partial^2 h}{\partial y^2}\right)=S\frac{\partial h}{\partial t}+L(h-h_m) \tag{1}$$

where $h(x, y, t)$ is the hydraulic head; T and S are the transmissivity and storativity, respectively. The leakage L is defined as the ratio of the hydraulic conductivity of the aquitard to its thickness.

The tidal boundary condition for the ocean is written as

$$h(x,0,t)=h_m+A\cos(\omega t+c) \tag{2a}$$

where $h(x,0,t)$ is the hydraulic head at $y = 0$, i.e., along the seashore, A is the amplitude of the tidal fluctuations, ω is the tidal speed, c is the phase shift, and h_m is the hydraulic head from the datum and commonly assumed to be zero for convenience in the development of analytical solution. Also, $\omega = 2\pi/ t_0$ where t_0 is the tidal period. The estuarine tidal boundary condition is written as

$$h(y\cot\phi,y,t)=h_m+Ae^{-K_{er}y\csc\phi}\cos(\omega t+K_{ei}y\csc\phi+c) \tag{2b}$$

where $h(y\cot\phi,y,t)$ is the hydraulic head along the river bank. The K_{ei} is a separation coefficient defined as the change of phase with distance and K_{er} is a damping coefficient of tidal amplitude (Sun, 1997).

The remote boundary conditions for Eq. (1) at the inland sides in the x- and y-directions are expressed, respectively, as

$$h(x\to\infty,y,t)=0 \tag{2c}$$

and

$$h(x,y\to\infty,t)=0 \tag{2d}$$

3. ANALYTICAL SOLUTION

The method of separation of variables is employed first to develop the solution of the model consisted of Eqs. (1) and (2). Let $\bar{h}(x,y)$ be a complex function of the real variables x and y, and assume as

$$h(x, y, t) = \bar{h}(x,y)A\ \mathrm{Re}\,(e^{i\omega t+c}) \tag{3}$$

where $i=\sqrt{-1}$ and Re denotes as the real part of the complex expression.

Substituting Eq. (3) into Eq. (1) and dividing the results by $Ae^{i\omega t+c}$ yields

$$\frac{\partial^2\bar{h}}{\partial x^2}+\frac{\partial^2\bar{h}}{\partial y^2}-(\bar{L}+i\omega\bar{S})\bar{h}=0 \tag{4}$$

where $\bar{L}=L/T$ and $\bar{S}=S/T$. The tidal boundary conditions of Eqs. (2a) and (2b) can therefore be expressed, respectively, as

$$\bar{h}(x,0)=1 \tag{5a}$$

and

$$\overline{h}(y\cot\phi, y) = \mathrm{Re}(e^{-K_e y\csc\phi}) \tag{5b}$$

where $K_e = K_{er} + iK_{ei}$ and the remote boundary conditions of Eqs. (2c) and (2d) respectively become

$$\overline{h}(\infty, y) = 0 \tag{5c}$$

and

$$\overline{h}(x, \infty) = 0 \tag{5d}$$

By changing the Cartesian coordinates (*x, y*) to the polar coordinates (r, θ), Eq. (4) can be written as

$$\frac{\partial^2 H}{\partial r^2} + \frac{1}{r}\frac{\partial H}{\partial r} + \frac{1}{r^2}\frac{\partial^2 H}{\partial \theta^2} = S_L H \tag{6}$$

where $r = \sqrt{x^2 + y^2}$, $\theta = tan^{-1}(y/x)$, $S_L = \overline{L} + i\omega\overline{S}$, and $H(r, \theta)$ is the hydraulic head expressed in the polar coordinates. Likewise, the tidal boundary conditions, Eqs. (5a) and (5b), can be respectively transformed to the polar coordinates as

$$H(r, 0) = 1 \tag{7a}$$

and

$$H(r, \phi) = \mathrm{Re}(e^{-K_e r}) \tag{7b}$$

and the transformed remote boundary conditions are

$$H(\infty, \theta) = 0 \tag{7c}$$

and

$$H(0, \theta) = 1 \tag{7d}$$

The solution for Eq. (6) subject to the boundary conditions, Eq. (7), developed in the polar coordinates is presented as follows.

Applying the finite sine transform to Eqs. (6) and (7) results in (Yeh and Chang, 2006)

$$\frac{\partial^2 \overline{H}}{\partial r^2} + \frac{1}{r}\frac{\partial \overline{H}}{\partial r} - \frac{\mu_n^2}{r^2}\overline{H} + [1 - (-1)^n e^{-K_e r}]\frac{\mu_n}{r^2} = S_L \overline{H} \tag{8}$$

Then the Hankel transform $\widehat{f}(u) = \int_0^\infty rf(\mathrm{r})J_v(ur)dr$ is adopted to eliminate the *r* coordinate in Eq. (8). The result can be obtained as:

$$\widehat{\overline{H}}(u, n) = \frac{\mu_n}{u^2 + S_L}\int_0^\infty \{\frac{[1 - (-1)^n e^{-K_e r}]}{r}\} J_{\mu_n}(ur)dr \tag{9}$$

where $J_{\mu_n}(\cdot)$ is the Bessel function of the first kind of order μ_n and $\mu_n = n\pi/\phi$ with n = 1, 2, 3, ….

Taking the inverse Hankel transform $f(\mathrm{r}) = \int_0^\infty u\,\widehat{f}(u)J_v(ur)dr$ first and then the inverse finite sine transform to Eq. (9), the solution of hydraulic head in the polar coordinates can be obtained as:

$$H(r,\theta) = \frac{2}{\phi}\sum_{n=1}^{\infty}\sin(\mu_n\theta)\int_0^\infty u_p[1-(-1)^n u_k]\,\mathrm{d}u \tag{10a}$$

with

$$u_p = \frac{uJ_{\mu_n}(\mathrm{ur})}{u^2 + S_L} \tag{10b}$$

$$u_k = \frac{(\sqrt{u^2 - K_e^2} - K_e)^{\mu_n}}{u^{\mu_n}} \tag{10c}$$

By changing the polar coordinates to the Cartesian coordinates, Eq. (10) can then be transformed as

$$\bar{h}(x,y) = \frac{2}{\phi}\sum_{n=1}^{\infty}\sin[\mu_n tan^{-1}(y/x)]\int_0^\infty u_c[1-(-1)^n u_k]\,\mathrm{d}u \tag{11}$$

Substituting Eq. (11) into Eq. (3), the solution for the hydraulic head $h(x, y, t)$ in the confined aquifer written in the Cartesian coordinates can then be denoted as

$$h(x, y, t) = A\mathrm{Re}\{\frac{2e^{i\omega t+c}}{\phi}\sum_{n=1}^{\infty}\sin[\mu_n tan^{-1}(y/x)]\int_0^\infty u_c[1-(-1)^n u_k]\,\mathrm{d}u\} \tag{12a}$$

where

$$u_c = \frac{uJ_{\mu_n}(\mathrm{u}\sqrt{x^2+y^2})}{u^2 + S_L} \tag{12b}$$

4. RESULTS AND DISCUSSION

In this section several hypothetical cases given in Jiao and Tang (1999) and Li et al. (2002) are adopted to investigate the effects of leakage (L), included angle (Φ), damping coefficient (k_{er}), and separation coefficient (k_{ei}) on the head fluctuations in the leaky confined aquifer. The values of aquifer parameters in the case studies are: L in the range of 0.001 to 0.01 /hour, $k_{er} = k_{ei}$ ranging from 10^{-6} to 10^{-4}, T = 50 m^2/hour, S = 0.0001, $\omega = 0.2618$ rad/hour, and $h_m = 0$. The amplitude of head fluctuations is normalized as $h_A = |h|\ /A$ and the phase lag is defined as $ph = \tan^{-1}(-1\times \mathrm{Im}(h)/\mathrm{Re}(h))$ in which Im denotes the imaginary part of the complex expression.

The curves of h_A and ph of the head fluctuations versus Φ for various values of L are plotted in Figure 2. This figure displays the joint effect of L and Φ happened at (x, y) = (212.1m, 212.1m) (i.e., (r, θ) = (300 m, 45°)) for T = 50 m^2/hour, S = 0.0001, $K_{er} = K_{ei} = 10^{-5}$ /hour, and L ranging from 0.001 to 0.01 /hour. The figure indicates that h_A decreases significantly but ph increases slightly when increasing Φ from 50° to 120° and L < 0.01/hour. The figure, on the other hand, indicates that both h_A and ph decrease apparently as L increases. Obviously, both L and Φ have significant impact on the groundwater fluctuations in the leaky confined aquifer.

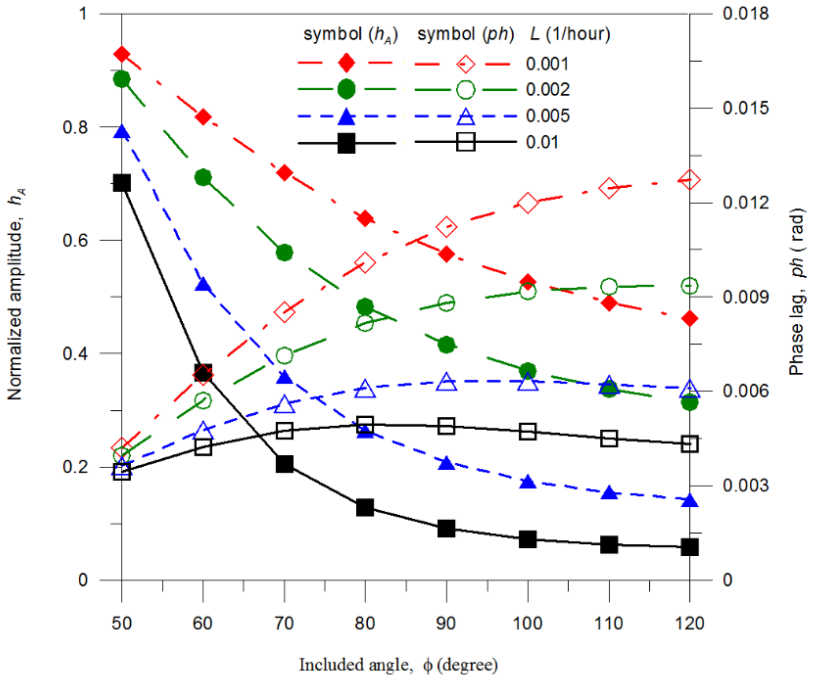

Figure 2. The curves of h_A and ph of the head fluctuations versus Φ happened at $\theta = 45^o$ for $T = 50\ m^2$/hour, $S = 0.0001$, with various leakages at $r = 300m$

The curves of h_A and ph of head fluctuations versus Φ for various values of k_{er} and k_{ei} are plotted in Figure 3. This figure displays the joint effects of Φ, k_{er}, and k_{ei} occurred at $(r, \theta) = (3000\ m, 45^o)$ for $T = 50\ m^2$/hour and $S = 0.0001$ with various values of k_{er} and k_{ei} . The figure shows that h_A decreases markedly but ph increases significantly as Φ increases from 50° to 120° for $L = 0$. This figure, however, indicates that h_A decreases but ph increases as k_{er} $(= k_{ei})$ increases from 10^{-6} to 10^{-4} for Φ in the range between 50° and 120°. As indicated in the figure, the k_{er} and k_{ei} also have significant influences on the groundwater fluctuations in the estuarine leaky confined aquifer. Figures 2 and 3 displays the effect of L on the h_A and ph of the groundwater fluctuations increases as Φ increases. In contrast, the effect of K_{er} and K_{ei} decreases with increasing Φ.

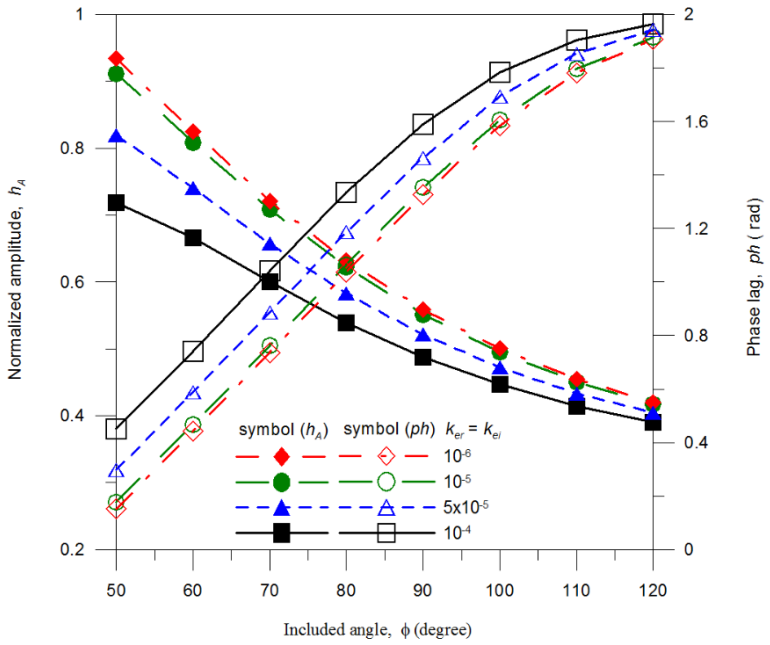

Figure 3. The curves of h_A and ph of the head fluctuations versus Φ happened at $\theta = 45^o$ for $T = 50\ m^2$/hour, $S = 0.0001$, with various values of K_{er} and K_{ei} at $r = 3000m$.

5. CONCLUDING REMARKS

A new two-dimensional analytical model has been presented to describe the groundwater level fluctuations in an *L*-shaped leaky confined aquifer bounded by a river and the ocean with an arbitrary included angle. The solution of the model expressed in Cartesian coordinates is developed by applying first the finite sine transform and then the Hankel transform. This solution is used to explore the influences of the leakage, included angle, damping coefficient, and separation coefficient on the tidal responses in *L*-shaped leaky aquifer systems. The results display that the normalized amplitude of the groundwater fluctuations decreases markedly but the phase lag of the groundwater fluctuations increases slightly as the included angle increases. On the other hand, both the normalized amplitude and phase lag decrease apparently as the leakage increases. In addition, the normalized amplitude decreases but phase lag increases as the damping and separation coefficients increase. Obviously, these four parameters including the leakage, included angle, damping coefficient, and separation coefficient all have significant impacts on the groundwater level fluctuations in a tidal leaky confined aquifer system.

ACKNOWLEDGMENTS

This study was partly supported by the Taiwan Ministry of Science and Technology under the grants MOST 104-2621-M-130 -003 and 105-2221-E-009 -043-MY2.

REFERENCES

Jiao, J. J., Tang, Z. H., 1999. An analytical solution of groundwater response to tidal fluctuation in a leaky confined aquifer, Water Resour. Res.: 35(3): 747-751.

Li, H., Jiao, J. J., 2001. Analytical studies of groundwater-head fluctuation in a coastal confined aquifer overlain by a semi-permeable layer with storage, Adv. Water Resour.: 24: 565-573.

Li, H., Jiao, J. J., Luk, M., Cheung, K., 2002. Tide-induced groundwater level fluctuation in coastal aquifers bounded by L-shaped coastlines, Water Resour. Res.: 38(3): 1024.

Sun, H., 1997. A two-dimensional analytical solution of groundwater response to tidal loading in an estuary, Water Resour. Res.: 33(6): 1429-1435.

Tang, Z., Jiao, J. J., 2001. A two-dimensional analytical solution for groundwater flow in a leaky confined aquifer system near open tidal water, Hydrol. Process.: 15(4): 573-585.

Yeh, H. D., Chang, Y. C., 2006. New analytical solutions for groundwater flow in wedge-shaped aquifers with various topographic boundary conditions, Adv. Water Resour.: 29(3): 471-480.

Proceedings of the 10th World Congress of EWRA 'Panta Rhei', 5-9 July 2017, Athens, Greece
© 2017 *European Water Resources Association*

Pumping optimization in coastal aquifers: Comparison of sharp interface and density dependent models

G. Kopsiaftis*, V. Christelis and A. Mantoglou
Laboratory of Reclamation Works and Water Resources Management, School of Rural and Surveying Engineering, National Technical University of Athens, Zografou, 15780, Greece
* *e-mail: gkopsiaf@central.ntua.gr*

Abstract: Seawater intrusion in coastal aquifers can be simulated using models of different accuracies, depending on the application and the required approximation level. In the present work, two seawater intrusion models of different complexities are employed to calculate the optimal pumping rates in coastal aquifer management problems. The first model simulates variable-density flow and salt transport processes and utilizes SEAWAT code. It is considered a time-intensive numerical model which hinders the implementation of simulation-optimization routines in coastal aquifer management. The second model coarsely approximates seawater intrusion by considering the sharp interface approach. The sharp interface model is faster compared to the variable density models, yet, it may introduce errors in the prediction of seawater intrusion since it neglects dispersion mechanisms. In this study, we investigate the potential of three sharp interface model variations to produce satisfactory approximations of the variable density based optimization. A pumping optimization problem is solved for an unconfined coastal aquifer with multiple pumping wells. The efficiency and effectiveness of the sharp interface models are compared to the optimal solutions and the computational time from the SEAWAT based optimization, which is used as benchmark. Results are further analysed based on the capability of the sharp interface models to produce feasible solutions for the SEAWAT based optimization.

Key words: Sharp interface models, SEAWAT, pumping optimization, coastal aquifer, seawater intrusion

1. INTRODUCTION

Seawater intrusion simulation is mainly based on two modelling approaches, the sharp interface models and the variable density and salt transport models. The latter emulate the dispersion zone between freshwater and saltwater and are considered more realistic than the sharp interface assumption, however, at increased computational cost (Werner et al., 2013). As a result, the coupling of variable density models with optimization algorithms for coastal aquifer management may lead to impractical computational times. On the contrary, the sharp interface models have been widely used in problems of pumping optimization of coastal aquifers due to their simple formulation and their fast runtimes (e.g. Mantoglou et al., 2004; Mantoglou and Papantoniou, 2008; Christelis et al., 2012; Karatzas and Dokou, 2015).

However, sharp interface models tend to overestimate seawater intrusion and thus may lead to a significant underestimation of the maximum allowable pumped groundwater. In this work, we perform a comparison between sharp interface and variable density models based on the optimal solutions obtained for a single-objective pumping optimization problem of coastal aquifers. First, optimization is performed based on the variable density model to obtain a benchmark solution and computational time. Then, we utilize the corresponding sharp interface model which is based on the single potential formulation of Strack (1976), to solve the same optimization problem. The sharp interface model is also employed using the density correction approach proposed by Pool and Carrera (2011) and that of Lu and Werner (2013). The objective is to identify if the corrected sharp interface models could provide reasonable approximations of the variable density optimal solutions while offering a much cheaper-to-run approach for coastal aquifer management.

2. MATERIAL AND METHODS

2.1 Variable Density Model

Variable density models consider that freshwater and seawater are mixed due to the hydrodynamic dispersion mechanism. In the simplified approach adopted in the current study, viscosity and thermal effects are neglected and density depends only on concentration. SEAWAT numerical solves the coupled flow and solute-transport equations, which are expressed as follows (Guo and Langevin, 2002):

$$-\nabla\cdot(\rho\mathbf{q})+\rho_s q_s=\rho S_f\frac{\partial h_f}{\partial t}+n\frac{\partial\rho}{\partial C}\frac{\partial C}{\partial t} \tag{1}$$

where ρ is the fluid density **q** is the specific discharge vector, ρ_s is the density of water entering from a source or leaving through a sink, q_s is the volumetric flow rate per unit volume of porous medium representing sources and sinks, S_f is the specific storage, h_f is the freshwater head, n is porosity and C is the solute concentration. It should be noted that $\rho = \rho(P,C)$, where P is the fluid pore pressure and

$$\frac{\partial C}{\partial t}=\nabla\cdot(\mathbf{D}\cdot\nabla C)-\nabla\cdot(\mathbf{v}C)-\frac{q_s}{n}C_s \tag{2}$$

in which **D** is the hydrodynamic dispersion tensor, **v** is the fluid velocity vector and C_s is the solute concentration of water entering or leaving through sources and sinks respectively. It should be noted that no solute reactions are considered.

An additional set of equations is required, to describe the relation between the fluid density and velocity and solute transport. Darcy equations serve this purpose, which could be expressed as:

$$q_x=-K_{fx}\left(\frac{\partial h_f}{\partial x}\right),\quad q_y=-K_{fy}\left(\frac{\partial h_f}{\partial y}\right),\quad q_z=-K_{fz}\left(\frac{\partial h_f}{\partial z}+\frac{\rho-\rho_f}{\rho}\right) \tag{3}$$

in which q_x, q_y, q_z are the specific discharge components in the principal directions, K_{fx}, K_{fy}, K_{fz} are the freshwater hydraulic conductivity components in the same directions, and ρ_f is the freshwater density.

For incompressible fluids, water density is related to solute concentration through the following equation:

$$\rho=\rho_o\left(1+\frac{\alpha}{(C_s-C_o)}(C-C_o)\right) \tag{4}$$

where ρ_o is the freshwater density, α is the density difference ratio and C_o, C_s are reference and maximum concentration respectively. In the current paper we consider C_o= 0 kg/m^3 and C_s= 35 kg/m^3.

The density ration has the following form:

$$\alpha=\frac{\rho_s-\rho_o}{\rho_o} \tag{5}$$

where ρ_s is the maximum seawater density.

2.2 Sharp interface model

Sharp interface models are simplified approximation of the coastal aquifer physical processes, since they neglect density variability in space, due to mixing between freshwater and saltwater. In the current study a steady state sharp interface model is employed, which assumes that horizontally-flowing freshwater floats above static saltwater (Essaid, 1999). The position of the interface is estimated using Ghyben-Herzberg approximation. Figure 1 presents vertical cross-sections for an unconfined coastal aquifer, where a sharp interface separates freshwater from saltwater.

As shown in the figure, there are two distinct zones in the aquifer. In zone 1 the aquifer behaves as an unconfined while in zone 2 a freshwater lens floats above the static saltwater layer. In zone 1 fresh groundwater is pumped by *M* fully penetrating pumping wells. Variable d [L] represents the depth from sea level to the aquifer base and variable ξ(x,y) [L] is the freshwater depth from sea level to the interface. Variable τ represents the point in the cross-section where the interface intersects the base of the coastal aquifers. Point τ is usually called "toe" of seawater wedge and comprises a typical measure of the extent of seawater intrusion.

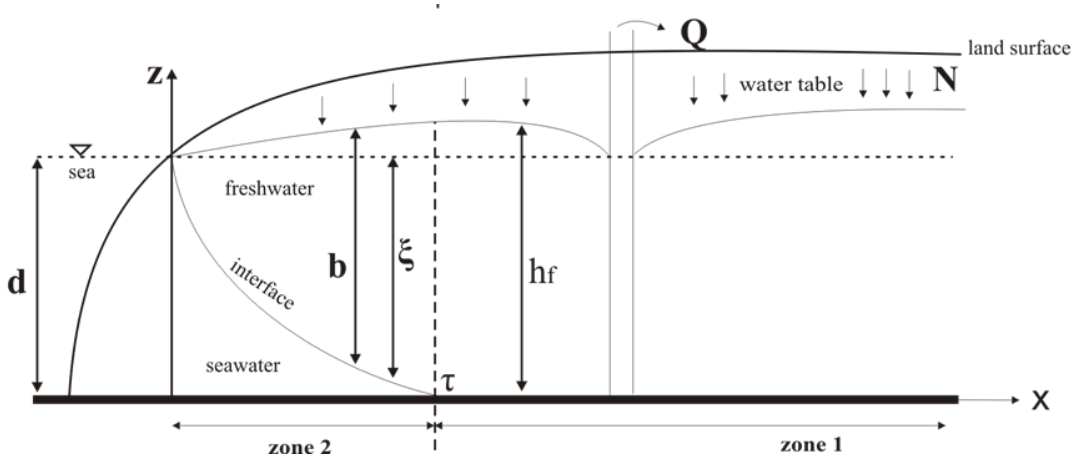

Figure 1. Schematic vertical cross-sections of an unconfined coastal aquifer based on the sharp interface approximation.

In the case of the unconfined aquifer, a groundwater recharge rate N [LT^{-1}] replenishes the aquifer. Variable $b = b(x, y)$ [L] is the total freshwater depth where in zone 1 $b = h_f$ and in zone 2 $b(x, y) = h_f - d + \xi(x, y)$, where $h_f(x, y)$ [L] is the freshwater head with reference to the impermeable aquifer base. The Ghyben-Herzberg relation links the hydraulic head h_f with depth ξ through the density ratio ε as $(1/\varepsilon)(h_f - d) = \xi(x, y)$. The following differential equations govern the steady state flow, based on the single potential formulation, which are applicable in both zones of the aquifer (Strack 1976, Mantoglou 2004):

$$\frac{\partial}{\partial x}\left(K\frac{\partial \phi}{\partial x}\right)+\frac{\partial}{\partial y}\left(K\frac{\partial \phi}{\partial y}\right)+N-Q(x,y)=0, \quad \text{unconfined interface flow} \tag{6}$$

where ϕ [L^2] is the flow potential and K [LT^{-1}] is the aquifer's hydraulic conductivity. The distributed pumping rate $Q(x, y)$ [L^3T^{-1}] is expressed as: $Q(x,y)=\sum_{j=1}^{M} Q_j\,\delta\left(x-x_{wj}, y-y_{wj}\right)$ where (x_{wj}, y_{wj}) are the coordinates of a pumping well *j* with rate Q_j and $\delta\left(x-x_{wj}, y-y_{wj}\right)$ is the Dirac delta function. In the case of unconfined aquifers, the flow potential of Strack (1976) is defined as (Cheng and Ouazar, 1999):

$$\left.\begin{aligned} \phi &= \frac{1}{2}\left[h_f^2 - (1+\varepsilon)\varepsilon^2\right], \quad \text{zone 1} \\ \phi &= \frac{(1+\varepsilon)}{2\varepsilon}\left(h_f - \varepsilon\right)^2, \quad \text{zone 2} \end{aligned}\right\} \tag{7}$$

At the location of the toe, the potentials have the following values for each coastal aquifer type (Cheng and Ouazar, 1999, Mantoglou 2004):

$$\phi_\tau = \left[\frac{\varepsilon(\varepsilon+1)}{2}\right] d^2 \tag{8}$$

Depending on the complexity of the problem, equation (6) may be solved analytically or numerically (Mantoglou 2003). Here, a numerical solution is employed following Mantoglou et al. (2004). In the present paper the academic version of HydroGeoSphere code (HGS) (Therrien and Sudicky, 1996, Graf and Therrien, 2005, Therrien et al., 2006) is used to simulate sweater intrusion for the sharp interface model.

2.3 Sharp interface model modifications

Two additional modifications of the sharp interface model, described in the previous section, are employed in the current study, to test their applicability and usefulness within a pumping optimization framework.

The first modification is an empirical correction for this sharp interface model to better match the corresponding results of the variable density model, proposed by Pool and Carrera (2011). Practically, a specific modified density ratio for the sharp interface model is calculated based on the aquifer depth B and the transverse dispersivity value α_T defined in the variable density model as follows:

$$\varepsilon^* = \varepsilon\left[1 - \left(\frac{a_T}{B}\right)^{1/6}\right] \tag{9}$$

where ε is the saltwater-freshwater density ratio defined as $\varepsilon = (\rho_s - \rho_f)/\rho_f$, with ρ_s being the saltwater density and ρ_f the freshwater density.

The second modification was introduced by Lu and Werner (2013), who proposed that the exponent $1/6$ in equation (9) should be changed to $1/4$.

3. PUMPING OPTIMIZATION FRAMEWORK

The main objective of pumping optimization in coastal aquifers is to maximize the well pumping rate, while protecting the aquifer from extended seawater intrusion. The extend of seawater intrusion is expressed as the distance between the well location and a specific critical iso-surface. In the case of variable density models the 0.5 kg/m^3 isochlore is selected, while in the case of the sharp interface models the interface between freshwater and saltwater is used as a critical iso-surface. In both cases a constraint is set to prevent the critical iso-surface from reaching or overrunning the wells at the base of the aquifer. This is a nonlinear constraint, which is expressed as follows:

$$\left.\begin{array}{l}\text{maximize: } \sum_{i=1}^{M} Q_i \\ \text{subject to: } x_{ri} \le x_{wi}, \forall i \in (1,2,...,M)\end{array}\right\} \quad (10)$$

where Q_i is the pumping rate of the i well, M is the total number of wells, $x_{ri} = x_{ri}(Q_1, Q_2, ..., Q_M)$ and x_{wi} is the distance of the critical surface and the well from the coast respectively. In this formulation the pumping rates are the decision variables of the optimization. Although the objective function in (10) is linear, the overall optimization problem is nonlinear due to the nonlinear dependence of the constraints on the decision variables (Kourakos and Mantoglou 2009).

4. APPLICATION AND RESULTS

A rectangular shaped hypothetical unconfined aquifer is used to apply the optimization framework using both the variable density model and the sharp interface model (Figure 2). The hypothetical aquifer is an abstraction of a real unconfined coastal aquifer located at the Greek Island Kalymnos. The size of the aquifer is 7000 m×3000 m×25 m. The inland boundary is a specified flux boundary, while the remaining boundaries and the aquifer bottom are considered impermeable. The aquifer is anisotropic and recharge is distributed uniformly. Table 1 outlines the basic model parameters. The aquifer is pumped by ten wells, which are also depicted in Figure 2.

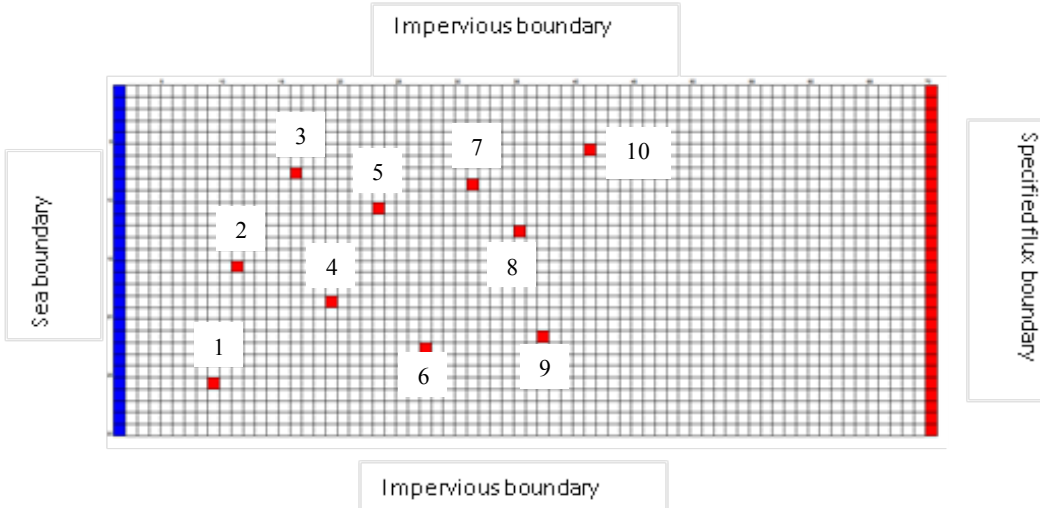

Figure 2: The rectangular shaped unconfined aquifer with the boundary conditions and the well locations.

Table 1. Basic model parameters

Parameters	Values
K_x	100 m/d
K_y	100 m/d
K_z	1 m/d
Longitudinal dispersivity	50 m
Transverse dispersivity	5 m
Vertical dispersivity	0.5 m
Density ratio	0.025
Recharge	8.22×10^{-5} m/d
Lateral inflow	3696 m^3/d

The evolutionary annealing-simplex algorithm (Efstratiadis and Koutsoyiannis, 2002), which is a probabilistic heuristic global optimization technique, is used to calculate the maximum allowed pumping rates, based on the optimization framework described in Section 3. Table 2 contains the optimized pumping rates for the seawater intrusion models used in the current study.

Table 2. Optimised pumping rates (m^3/d)

Seawater Intrusion Model	Well number										Total
	1	2	3	4	5	6	7	8	9	10	
Variable Density	1.9	0.7	999.3	134.8	919.6	746.0	377.9	636.0	25.2	675.0	4516.6
Sharp Interface (Strack)	0.0	92.9	1000.0	0.00	999.4	0.0	5.7	480.3	0.7	167.8	2746.8
Sharp Interface (Pool & Carrera)	3.0	0.0	216.6	397.9	249.6	496.8	1000.0	605.6	748.2	999.8	4717.4
Sharp Interface (Lu & Werner)	0.0	0.3	60.7	3.2	777.6	35.2	718.6	985.2	920.2	999.2	4500.2

The results indicate that the Strack sharp interface model, as expected, overestimated the seawater penetration and provided a much lower optimal solution compared to the other seawater intrusion models. Interestingly, the total amount of the allowable pumped water calculated using the Lu and Werner (2013) modification, is similar to the variable density results, however, with a different distribution among the wells. The optimal solutions obtained with the sharp interface models were further evaluated using the more accurate variable density model. Both modified sharp interface models provided an optimal pumping rate distribution which violated the constraints and resulted in a non-feasible optimal solution (Figure 3).

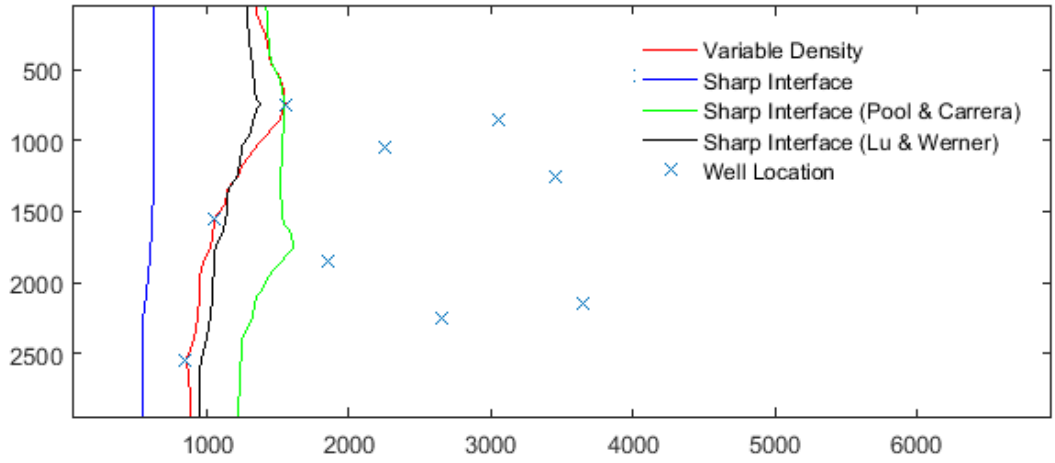

Figure 3. Presentation of the 0.5 kg/m3 iso-chlore at the aquifer bottom, using the optimal pumping rates from each seawater intrusion model.

5. CONCLUSIONS

In the current paper an effort was made to couple several seawater intrusion models with an optimization module. The objective of the study was to examine if the simplified sharp interface models could replace the time consuming and complex variable density model in the optimization process. The results indicated that the sharp interface model introduced by Strack (1976) significantly underestimates the maximum allowed pumping rates. Regarding the modified sharp interface models, despite the fact that none of them led to a feasible solution, the results are promising and could potentially substitute the variable density model in the optimization procedure. The differences in the model solutions could be attribute to the fact that sharp interface models tend to have abrupt behavior near the critical pumping rates. Further study, could clarify the differences of the models in several levels of the pumping rates, in order to cope with the non-feasible solution problem.

REFERENCES

Cheng, A.D. and Ouazar, D., 1999. Analytical solutions. In Seawater intrusion in coastal aquifers—concepts, methods and practices (pp. 163-191). Springer Netherlands.

Christelis, V., Kopsiaftis, G., Mantoglou, A., 2012. Coastal aquifer management under drought conditions considering aquifer spatial variability. IAHS-AISH Publication 293-297.

Efstratiadis, A. and Koutsoyiannis, D., 2002, July. An evolutionary annealing-simplex algorithm for global optimisation of water resource systems. In Proceedings of the Fifth International Conference on Hydroinformatics (pp. 1423-1428).

Essaid, H.I., 1999. USGS SHARP Model. In Seawater Intrusion in Coastal Aquifers—Concepts, Methods and Practices (pp. 213-247). Springer Netherlands.

Graf, T. and Therrien, R., 2005. Variable-density groundwater flow and solute transport in porous media containing nonuniform discrete fractures. Advances in water resources, 28(12), pp.1351-1367.

Guo W., Langevin C.D., 2002. User's guide to SEWAT: A Computer Program for Simulation of Three – Dimentional Variable – Density Ground - Water Flow, BOOK 6, Chapter A7, Techniques of Water – Resources Investigations of the U.S. Geological Survey, 7-18.

Karatzas, G. P., Dokou, Z., 2015. Optimal management of saltwater intrusion in the coastal aquifer of Malia, Crete (Greece) using particle swarm optimization, Hydrogeol J 23(6):1181-1194.

Kourakos, G. and Mantoglou, A., 2009. Pumping optimization of coastal aquifers based on evolutionary algorithms and surrogate modular neural network models. Advances in Water Resources, 32(4), pp.507-521.

Lu, C. and Werner, A.D., 2013. Timescales of seawater intrusion and retreat. Advances in Water Resources, 59, pp.39-51.

Mantoglou, A., 2003. Pumping management of coastal aquifers using analytical models of saltwater intrusion. Water resources research, 39(12).

Mantoglou, A., Papantoniou, M. and Giannoulopoulos, P., 2004. Management of coastal aquifers based on nonlinear optimization and evolutionary algorithms. Journal of Hydrology, 297(1), pp.209-228.

Mantoglou, A., Papantoniou, M., 2008. Optimal design of pumping networks in coastal aquifers using sharp interface models. J Hydrol 361:52–63.

Pool M., Carrera J., 2011. A correction factor to account for mixing in Ghyben-Herzberg and critical pumping rate approximations of seawater intrusion in coastal aquifers. Water Resources Research 47: W05506, doi:10.1029/2010WR010256.

Strack, O.D.L., 1976. A single-potential solution for regional interface problems in coastal aquifers. Water Resources Research, 12(6), pp.1165-1174.

Therrien, R. and Sudicky, E.A., 1996. Three-dimensional analysis of variably-saturated flow and solute transport in discretely-fractured porous media. Journal of Contaminant Hydrology, 23(1-2), pp.1-44.

Therrien, R., McLaren, R.G., Sudicky, E.A. and Panday, S.M., 2006. HydroGeoSphere. Groundwater Simulations Group, University of Waterloo, Waterloo, Canada.

Werner, A. D., Bakker, M., Post, V. E. A., Vandenbohede, A., Lu, C., Ataie-Ashtiani, B., Simmons, C. T., Barry, D. A., 2013. Seawater intrusion processes, investigation and management: Recent advances and future challenges. Adv Water Resour 51:3-26.

Proceedings of the 10th World Congress of EWRA 'Panta Rhei', 5-9 July 2017, Athens, Greece
© 2017 *European Water Resources Association*

Towards sustainable management of groundwater: A case study of semi-arid area, Iraqi Kurdistan region

M. Nanekely[1*], M. Scholz[1,2] and S. Qarani Aziz[3]
[1] *Civil Engineering Research Group, School of Computing Science and Engineering, University of Salford,UK*
[2] *Division of Water Resources Engineering, Faculty of Engineering, Lund University, P.O. Box 118, Lund 221 00, Sweden*
[3] *Department of Civil Engineering, College of Engineering, Salahaddin University-Erbil, Iraq*
[*] *e-mail: m.a.a.nanekely@edu.salford.ac.uk*

Abstract: In this paper, Erbil province the capital of Iraqi Kurdistan has been chosen as a representative case study for a large number of provinces in semi-arid areas, lacking imbalance between water demands and supply. Climate change is expected to bring adverse impact on water availability, which would intensify the pressure on water resources and increases the environmental concerns. Sustainable water use and prudent management prefer the rational water use and to preserve groundwater exploitation. The study aims to develop a framework considering sustainability aspects. A total of twenty wells have been selected among ninety-nine observation wells across the province along a period of 16 years from 2000 to 2015 to assess water level depression. The groundwater level had been falling nearly by half, this highlights the issues that the groundwater level has been significantly affected by; impacts of the non-sensible usages of groundwater, dry spell periods, mismanagement of water resources, and unsustainable planning. Urban areas and suburbs were more exposed to water insecure than outskirts The results also suggest that the management of water resources and drainage systems would get worse if there was not adoption on a clear policy to manage it by relying on a robust framework based on sustainability concepts.

Key words: Groundwater depletion; Sustainability; Water Management; Climate change; Framework

1. INTRODUCTION

Groundwater has a substantial role in agriculture, water supply and health, and the elimination of poverty in both urban and rural areas, thus, it is regarded as a vital and the sole resource in most of the studied semi-arid regions. Currently, Iraq is dramatically disturbed by complex political and socio-economic problems, in its northern part, i.e. the Kurdish-inhabited region, fast urbanization and economic expansion are visible everywhere. Monitoring and water management schemes are necessary to prevent aquifer over-exploitation in the region. Artificial recharges with temporary runoff water, construction of subsurface dams and several other aquifer management and regulation measures have been designed, and some implemented, in order to improve the water situation (Stevanovic and Iurkiewicz 2009).

Recently, the World Economic Forum 2017 within its global risk report has pointed out that Environment-related risks also stand out in this year's global risk landscape. The major risk interconnections of Global Risks Perception Survey (GRPS) involve environmental risks, the most frequently cited of these being the pairing of "water crises" as well as "failures to climate change mitigation and adaptation". The World Bank expects that water stress could cause extreme societal overstrain in regions like the Middle East, where the economic effects of water scarcity could reach at risk 6% of gross Domestic Product (GDP) by 2050 (Heijden et al., 2015).

Population growth associated with accelerated social and economic activities and developments as well as expanding irrigated areas for agriculture purposes are main drivers for an ever increasing demand for water worldwide (Wada et al., 2010). On the other hand, climate change has put additional pressure on water resources in arid and semiarid areas, which are naturally facing water shortages. Dragoni and Sukhija (2008) have pointed out the importance of understanding the impact of climate change and variability on the availability and sustainability of surface and

groundwater resources. The need and the necessity for groundwater studies in water-scarce areas are crucial for sustainable management of water resources. Warner (2007) has underlined that there is a need to asses and understand climatic change and variability over long period to better plan and manage groundwater resources, while taking into account the increasing pressures on groundwater resources due to population growth, industrial, agricultural, and ecological needs.

Furthermore, literatures indicated that research has started to focus more on understanding the impacts of climate variability and alteration on groundwater quantity and quality, these impacts remain poorly understood (Green et al., 2007). Groundwater-residence time scales can range from days to tens of thousands of years or more, which delays and disperses the effects of climate and challenges efforts to detect responses in the groundwater to climate variability (Chen et al., 2004). Moreover, human activities, such as groundwater pumping and resulting loss of storage and capture of natural discharge, are often on the same time scale as some climate variability and change, which makes it difficult to distinguish between human and climatic stresses on groundwater (Hanson et al., 2004). Therefore, the need and the necessity for groundwater studies in semiarid areas are considered as a mainstay of sustainable water management, as it has always taken into account as one of water resources that ought to be reliable and supportive for surface water resources in the purpose of agricultural irrigation uses, livestock's watering, and domestic water supplies in developing countries.

1.1 Groundwater depletion

Famiglietti (2014) have said that ''Groundwater depletion the world over poses a far greater threat to global water security than is currently acknowledged'', therefore, semi-arid regions as part of the global scale are also threatened by the diminution of groundwater availability.

In areas that are exposed to water shortages, and that have large groundwater aquifer; the groundwater often used as an alternative source of water supply. Groundwater overuse or continuing depletion occurs, whenever the abstractions of groundwater surpass its repletion (Wada et al., 2010).

The groundwater levels in the study area strongly declined in the drought period of 2006-2009. Several sources in the area indicate that groundwater pumping in the study area intensified during the last years. It is likely that the total pumping rates exceed recharge rates over large areas, as groundwater tables are declining. Mulder (2013) says a negative residual term was found of about 10 mm per year.

The total global groundwater depletion is quite substantial, totalling an estimated 39 (±10) % of the global yearly groundwater abstraction, 2 (±0.6) % of the global yearly groundwater recharge, 0.8 (±0.1) % of the global yearly continental runoff and 0.4 (±0.06) % of the global yearly evaporation. This makes groundwater over□abstraction a term of the global water balance that cannot be neglected (Wada et al., 2010). Moreover, studies on semiarid regions have seen the semi-arid regions are not excluded while the crisis is being exacerbated by the over-demand for water. Continued groundwater depletion will be unsustainable, with potentially dire consequences for the economic and food security (Famiglietti et al., 2011). The global groundwater depletion has been increasing since the 1960 and is likely to increase further in the near future, while the increase of impoundment by dams has been tapering off since the 1990s (Chao et al., 2008).

1.2 Groundwater replenishment

Ebrahimi et al., (2016) have estimated that irrigation water has more contribution than rainwater to recharge the ground in arid and semi-arid areas by one-third. On the other hand, the groundwater can be recharged by municipal wastewater, but still there are some uncertainties in terms of health risk considerations, and have limited the use of reclaimed disposed urban wastewater for groundwater recharging, this based on the groundwater recharge criteria.

1.3 Groundwater and surface water interaction in semiarid regions

The interactions between groundwater and surface water are complex. To understand these interactions in relation to climate, landform, geology, and biotic factors, a sound hydro-geo-ecological framework is needed. Surface-water and groundwater ecosystems are viewed as linked components of a hydrologic continuum leading to related sustainability issues. the mechanisms of interactions between groundwater and surface water (GW–SW) as they affect recharge–discharge processes are comprehensively to be understood, and also the ecological significance and the human impacts of such interactions.

Despite commendable efforts to craft solutions to meet required surface water allocations, consideration of the ability of groundwater withdrawals to meet current and future demands remain dormant. The heightened awareness of the rates of groundwater depletion will reinforce urgent discussion on conjunctive management solutions required to ensure a sustainable water future (Castle et al., 2014).

1.4 Sustainable management of groundwater

Sustainable groundwater use should be established by management institutions in concert with regional stakeholders, while taking into account hydrologic, environmental and political constraints. Multidisciplinary studies supported by reliable data and integrated water resources modelling are desired ends in the basin, but full integration of the disciplines must await future researches (Al-Azawi and Ward 2017).

Securing future groundwater availability involves a multi-spectrum of efforts, including minimising net losses from the underground reservoir, managing groundwater as an integrated part of the hydrologic cycle, developing infrastructure based on an understanding of the natural hydrologic system, using water wisely and efficiently, and allocating and monitoring water fairly for human as well as environmental and ecological needs (Sheng 2013).

1.5 Climate change impact on groundwater resources

'Climate change is the most severe problem that we are facing today—more serious even than the threat of terrorism' said the UK government chief scientific adviser (King 2004). Researchers have become convinced that water supplies forced by global climate model in semi-arid regions. Studies show that up to 60% of the climate-related trends of river discharge, winter air temperature, and snow-pack's during the second half of last century are human-induced. It is expected that water shortages, lack of storage capability to meet seasonally changing river flow, transfer of water from agriculture to urban uses, and other critical impacts of climate variations (Sheng 2013).

In arid and semiarid regions such as the study area, people live in drought most the time. In addition to impacts of groundwater pumping, a prolonged drought period can further lower groundwater level to the point at which shallow wells may go dry and it intensifies the issue much more.

2. MATERIALS AND METHODS

Groundwater water levels observed at ninety-nine observation wells across the case study area. Data were made available by the Ministry of Agriculture and Water Resources in the Kurdistan Region of Iraq. Twenty observation wells have been chosen out of the total (i.e. ninety-nine). The selection was based on the availability of a complete set of monthly readings of water level between 2000 and 2015. The groundwater level observed in 2000 has considered as a reference level to examine the changes in water level observed in the investigated observation wells. Figure (1) shows boundary of the appointed observation wells across the study area.

Microsoft Excel (2010) has been used to prepare the tables and charts, also the trends of groundwater level, as well as ArcGIS v.10.2 has been used to make interpolations and spatially distribution of the data. The data were arranged and tabulated based on what have been collected and consisted of; well code and IDs, the district that the well situated, coordinates, well depth, geological formation, groundwater basin, and monthly readings of groundwater level. Monthly readings along the 16 years have been converted to mean annually readings, then the differences of the first and last readings were found to check whether been regressed or not.

3. RESULTS AND DISCUSSION

3.1. Groundwater data analysis

The data of groundwater levels have been managed as the time series along studied period verse the depression of water in the wells. The values of trends' slope has been calculated, based on this a spatial distribution map of groundwater depression has been prepared.

3.2. Results obtained from the groundwater study

Results show that the fall in groundwater level was between 11% and 88% with respect to the reference water level. The average fall was almost 42% and the standard deviation nearly 25%. This points out that the level of groundwater has been significantly decreased; this because of the combined impact of the non-rational utilisation of groundwater, impacts of dry-spell periods (1999-2001 and 2007-2008), the lack of groundwater recharge, and mismanagement in surface-water and groundwater interactions.

Findings have also highlighted the future potential risk of the combined effect on irrigated agriculture areas, livestock's' watering, as well as domestic water supply. Moreover, the notable drop observed in groundwater level between 2000 and 2015 has underlined that the ground water level at some sites has reached a critical level indicating that the utilisation of groundwater has to be carefully treated and sustainably managed. The preliminary results are in line with what has been stated in the report of (Dizayee and Johnson 2016) that the present exploitations of groundwater in the Erbil basin is unsustainable and a significant attention should be paid to the sustainable use of groundwater and the necessity of healthy management of groundwater.

A spatial distribution map has been prepared, Figure (1), this has been set based on the regression slope (b-value) trends for the selected observation wells. The regression values give a general indication that the groundwater level in all wells have significantly dropped, the values of declination ranged from 0.05 to 5.8, by focusing on this map, it can be perceived the that urban and suburb areas were most affected than peri-urbans.

From what have been reviewed and studied, a schematic diagram (Figure 2) has been developed demonstrating the main drivers that cause a serious degradation in groundwater levels in arid and semi-arid areas. Overexploitation of groundwater, population growth associated with a notable increase in water demands, and climate change and variability contribute significantly to groundwater decline. Illegal abstraction of groundwater, weakness in application of existing regulations and legislations, and delay in updating the current regulations and legislations are the main features of the non-rational utilisation of groundwater. Reduction in annual precipitation, increase in temperature and evapotranspiration rates and successive droughts have increased the dependency on groundwater, particularly in areas where there is a shortage in surface water. The fall in the annual amount of precipitation decreases groundwater aquifer replenishment, resulting in decreasing groundwater levels as the withdrawal rate exceeds recharge. Major uncertainty still surrounds the detailed effects of climate change on groundwater replenishment. This may attribute to the limited research on the impacts of climate change on groundwater.

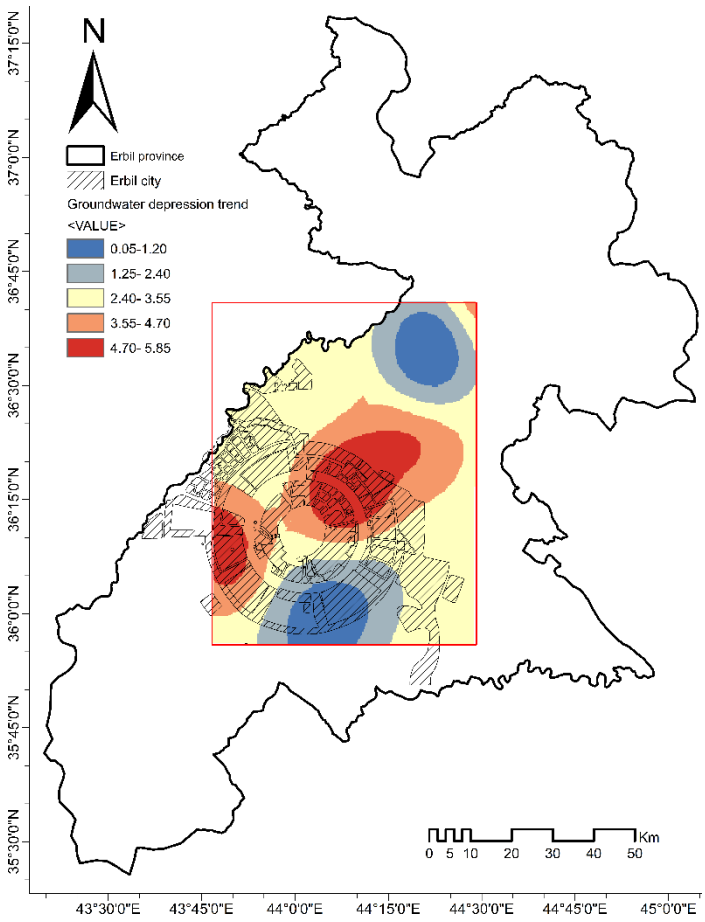

Figure 1. The depression trend in the selected twenty observation wells

Despite that the study area is characterised by highly infiltrative and Karstified ground, the water levels of the aquifers in Northern Iraq are very responsive to changes in rainfall regimes (Mulder 2013), but the direct effect of climate change on groundwater resources depends upon the change in the volume and distribution of groundwater recharge. Less precipitation in winters and warmer summers lead to notable deficits in groundwater recharge. However, aquifers are recharged more effectively by prolonged steady rain, which continues into the spring, rather than short periods of intense rainfall (Groundwateruk 2016).

The effects of climate change on groundwater across Erbil province include: (a) a long-term decline in groundwater storage, and (b) increased frequency and severity of groundwater droughts. These effects critically have impacts on; the socio-economic conditions of the local communities, groundwater-related impacts on water supplies, livestock's watering, and on ecosystems that depend on groundwater such as wetlands, ecosystems in streams fed by groundwater, hanging valleys and swamps, limestone cave systems, and springs.

4. CONCLUSIONS

This study seeks to help the stockholders as planners, decision-makers, and community's by developing a framework to tackle the problems that these areas have been encountering in groundwater depletion. The study has adopted an approach whereby initiating from specific elements and induced toward the thorough form of the framework, which highlighted a number of aspects; sustainability; regulations and legislations pertaining the sustainable water management; socio-economics situation; climate change; and eco-system issues, which are derived from the themes that have become concerned by hydro-policy-makers and who interested in sustainable drainage systems. The shortage is coming from over-abstraction of the groundwater, poor-

management of water resources, population growth, and increase in global temperature.

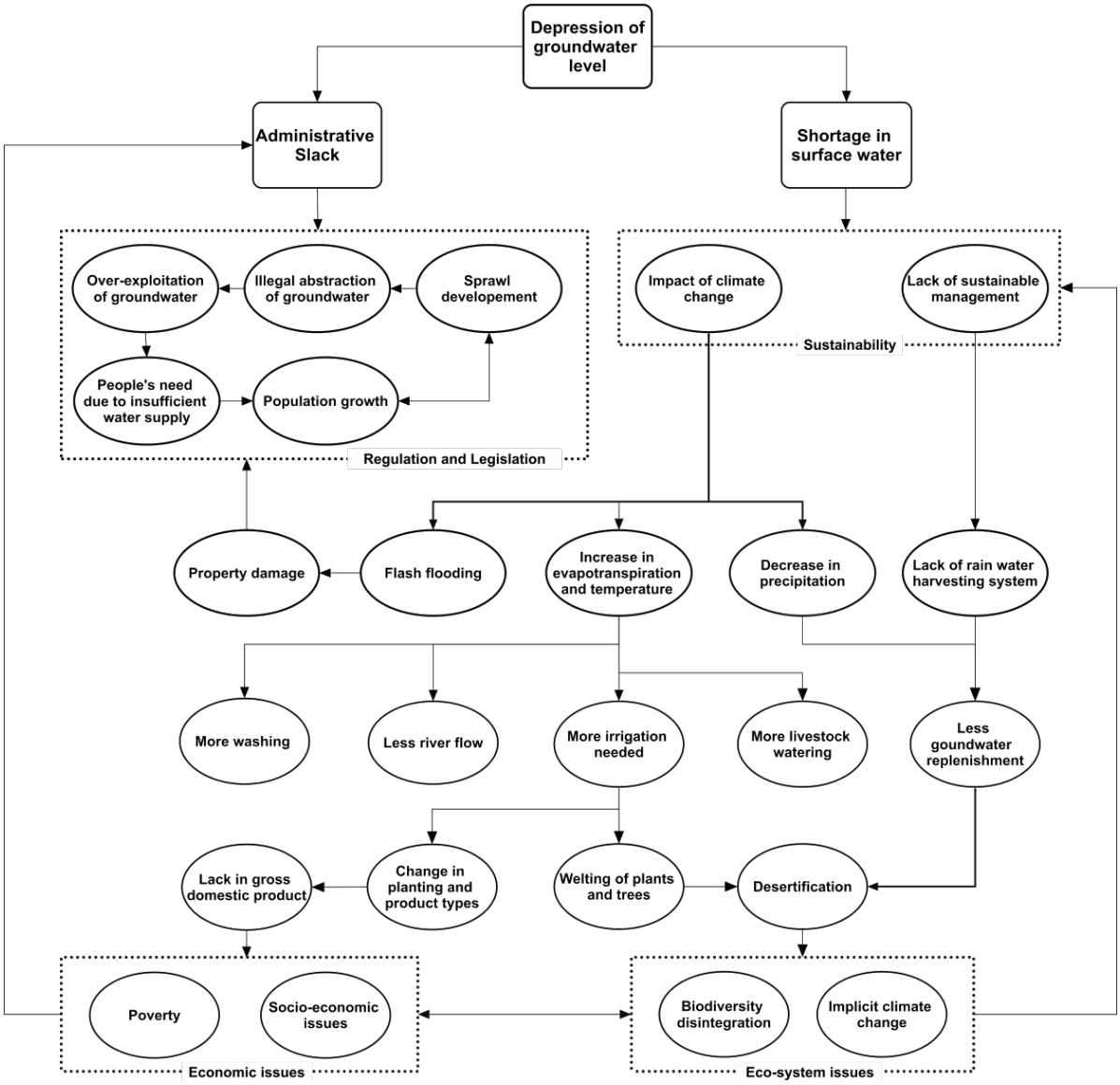

Figure 2. A schematic diagram of interrelated aspects framework for sustainable groundwater management

Urban and suburb developments are the most affected areas than peri-urbans and outskirts, which need an official posture toward the retrogressive situation. The necessity of mighty management of groundwater is essential through sustainable use of groundwater. The semi-arid regions are most vulnerable to groundwater depletion due to the intensify stress on water demand for multi purposes, this because of the lack of legislations, recurring drought periods, living levels, and non-sustainable strategies.

Understanding the potential effects of climate variability, as well as repletion situation on groundwater availability and quality, is more complex than with surface water, and needs more comprehensive studies. Therefore, there is a need to develop a robust framework that be based on sustainability concepts to manage water resources and drainage systems as an interrelated components for maintained groundwater.

REFERENCES

Al-Azawi, Ali A. Obeed, and Frank A. Ward. “Groundwater use and policy options for sustainable management in Southern Iraq.” International Journal Of Water Resources Development 33, no. 4 (2017): 1-21.

Castle, Stephanie L., Brian F. Thomas, John T. Reager, Matthew Rodell, Sean C. Swenson, and James S. Famiglietti. “Groundwater depletion during drought threatens future water security of the Colorado River Basin.” Geophysical Research Letters 41, no. 16 (2014): 5904-5911.

Chao, B. F., Y. H. Wu, and Y. S. Li. “Impact of artificial reservoir water impoundment on global sea level.” Science 320, no. 5873 (2008): 212-214.

Chen, Zhuoheng, Stephen E. Grasby, and Kirk G. Osadetz. “Relation between climate variability and groundwater levels in the upper carbonate aquifer, southern Manitoba, Canada.” Journal of Hydrology 290, no. 1 (2004): 43-62.

Dizayee, R., and B. Johnson. “The Michael and Sally McCracken Annual-Student Research Symposium.” Texas Christian University Web site. 18 September 2016. http://www.srs.tcu.edu/previous_posters/Geology/2014/105.

Dragoni, W., and B. S. Sukhija. “Climate change and groundwater: a short review.” Geological Society, London, Special publication 288, no. 1 (2008): 1-12.

Ebrahimi, Hydar, Reza Ghazavi, and Haji Karimi. “Estimation of Groundwater Recharge from the Rainfall and Irrigation in an Arid Environment Using Inverse Modelling Approach and RS.” Water Resources Management 30, no. 60 (2016): 1939-1951.

Famiglietti, J. S. “The global groundwater crisis.” Nature Climate Change 4, no. 11 (2014): 945-948.

Famiglietti, J. S., et al. “Satellites measure recent rates of groundwater depletion in California's Central Valley.” Geophysical Research Letters, 2011: 38.

Green, Timothy R., Makoto Taniguchi, and Henk Kooi. “Potential impacts of climate change and human activity on subsurface water resources.” Vadose Zone Journal 6, no. 3 (2007): 531–532.

Groundwateruk. Raising awareness of groundwater. 19 September 2016. http://www.groundwateruk.org /Groundwater_resources_climate_change.aspx (accessed January 08, 2017).

Hanson, R.T., M.W. Newhouse, and M.D. Dettinger. “A methodology to assess relations between climatic variability and variations in hydrologic time series in the southwestern United States.” Journal of Hydrology 287, no. 1-4 (2004): 252–269.

Heijden, Kitty van der, Betsy Otto, and Andrew Maddocks. Beyond conflict, water stress contributed to Europe’s migration crisis. 3 November 2015. http://www.wri.org/blog/2015/11/beyond-conflict-water-stress contributedeurope% (accessed February 10, 2017).

King, David A. The American Association for the Advancement of Science. 2004. http://science.sciencemag.org/ (accessed January 5, 2017).

Mulder, Gert. Observing groundwater depletion in Northern Iraq from space: A comparitive study between catchment hydrology and the GRACE satellite mission. Doctoral dissertation, TU Delft: Delft University of Technology, 2013.

Sheng, Zhuping. “Impacts of groundwater pumping and climate variability on groundwater availability in the Rio Grande Basin. Ecosphere.” Ecosphere 4, no. 1 (2013): 1-25.

Stevanovic, Zoran, and Adrian Iurkiewicz. “Groundwater management in northern Iraq.” Hydrogeology journal 17, no. 2 (2009): 367-378.

Wada, Yoshihide, Ludovicus P. H. van Beek, Cheryl M. van Kempen, Josef W. T. M. Reckman, Slavek Vasak, and Marc F. P. Bierkens. “Global depletion of groundwater resources.” Geophysical research letters 37, no. 20 (2010): 1-5.

Warner, S. D. “Climate change, sustainability, and ground water remediation—the connection.” Ground Water Monitoring and Remediation 27, no. 4 (2007): 50–52.

Proceedings of the 10th World Congress of EWRA 'Panta Rhei', 5-9 July 2017, Athens, Greece
© 2017 *European Water Resources Association*

Assessing groundwater use in irrigation districts with multiple resources (MIGRAD)

D. Zingaro, I. Portoghese*, A. Pagano, R. Giordano and M. Vurro
National Research Council Water Research Institute, UOS Bari, Italy
* *e-mail: ivan.portoghese@cnr.it*

Abstract: A water allocation model at farm-scale was developed to interpret water allocation patterns in an intensive agricultural district of Southern Italy, supplied by groundwater and surface waters (from reservoir) with variable costs and distinct management regimes. The model aims at evaluating the impact of farm-scale water costs on water resources management and groundwater conservation at district scale. Semi-structured interviews were carried out involving local stakeholders to define (i) the relationship between irrigation source selection and water tariff applied by the irrigation district, and (ii) the conjunctive use of groundwater based on water cost convenience. It was demonstrated that farmers' choice depends on the ratio between volumetric water tariff and the groundwater pumping cost at farm-scale. The results also demonstrated that a restrictive water tariff policy applied during drought periods produced an increase in the groundwater use instead of reducing the water consumption. The model allowed to analyze the drivers influencing farmers' behaviour, thus assessing the effectiveness of water protection policies, specifically those related to water tariff.

Key words: water allocation criteria, integrated water management for irrigation, groundwater use, multi-resources water supply system

1. INTRODUCTION

Water resources management needs to taking into account for interests related to sharing an increasingly limited resource (Portoghese et al. 2013). Therefore, an increasing level of conflict between different water users and uses is observed, particularly in the Mediterranean area (Jury and Vaux, 2007), due to water scarcity problems and climatic conditions (Portoghese et al. 2015). Therefore, integrated water resource management (IWRM) requires methods and tools to define how different water managers and users perceive the water resources and behave consequently (Giordano et al. 2013), based on the assessment of the impacts on water resources (Bouwer, 2000). Sustainable management of water resources for irrigation requires the use of integrated approaches (Bouwer, 2000), since agriculture represents the most impacting activity on water resources (Giordano et al. 2013).

Assuming a competitive and unregulated water extraction regime, the temporal and spatial variability of external drivers results in inefficient pricing and misallocation of resources (Katic and Grafton, 2012). Consequently, it is necessary to define an adequate design of economical instruments, such as energy and irrigation water pricing, to help limiting water overexploitation.

The purpose of this study is to evaluate the impact of farm-scale water costs on water resources management and groundwater exploitation at district scale. The selection of specific water sources by farmers is analyzed as a function of both energy- and water-related drivers, considering a water supply system serving multiple users through multiple resources.

The case of Capitanata plain (Southern Italy), characterized by intensive groundwater use for agriculture (Guyennon et al. 2016), is investigated.

2. MATERIALS AND METHODS

2.1 Study Area

The case study is characterized by favorable climate conditions for intensive agriculture. The cultivated area is approximately 500,000 ha. The irrigation network is available approximately on 150,000 ha, but only 126,000 ha are supplied by means of two irrigation schemes with on-demand pressurized networks (Lamaddalena, 2004): (a) the Fortore system, on the Northern part, serving an area of 110,000 ha, and the Sinistra Ofanto system, on the South, serving approximately 40,000 ha. Surface water use for irrigation in both districts is managed by the Consorzio di Bonifica della Capitanata (CBC) which is a governing and technical body ruled by farmers' representatives. Significant alluvial aquifers underling the Capitanata plain are heavily exploited for irrigation through private wells used to increase available volumes under water scarcity conditions.

The Fortore system is an example of conjunctive use of surface water (SW) and groundwater (GW) for irrigation, with significant complexity for water resources management.

Cropping patterns are among the major drivers of irrigation needs and, consequently, of water resources exploitation. To perform a simple but significant assessment of cropping pattern changes (within the irrigated area), a specific subset of crops was selected. Only crops having higher water-requirement and/or covering a wider surface were taken into account with their temporal variabilities (according to data by the Italian Statistical Service), namely: Industrial Tomato (190-300 km^2), Grape (285-442 km^2), Olive (525-550 km^2), Peach (28-44 km^2) and Vegetables (22-31 km^2). A regional land use map (dated 2011) was used to characterize the spatial location of crops. For the sake of simplicity, the "average hectare" approach was adopted to describe the variability of cropping patterns.

2.2 Description of the main dynamics

An interview-based approach was adopted to define how different water managers and users perceive the water resources and behave consequently, under the assumption that past behaviours can be used to predict the future evolution. Semi-structured interviews involving both local farmers and members of the CBC were used (Giordano et al., 2013; Giordano et al., 2015).

Farmers' behaviour was investigated mainly to define the relationship between irrigation source selection and water tariff. The irrigation source selection depends on multiple externalities (Irrigation demand, Climate, SW Tariff, Pumping cost, etc.) which jointly influence the farmers' behaviour. The impact of these conditions on groundwater resources exploitation, considering the withdrawals needed to fulfil the irrigation demand, was analysed. Moreover, the impact on GW is indirectly related to the "market conditions" of crop products; in fact, in case of high market price for irrigated products, farmers prefer to increase the irrigated land regardless of SW availability. In such conditions, farmers perceive GW as an easily accessible resource without control by regional authority.

On the other side, the CBC has mandate to implement a water policy aiming at equitably fulfilling farmers' irrigation needs at reasonable costs, and guaranteeing the recovery of operational costs for the consortium. Consequently, the behaviour of CBC managers was analysed concerning their year-by-year decision on the SW tariff, which depends on water availability in the reservoir at the beginning of the irrigation season and on other variables (e.g. economic conditions, expected irrigation water demand, climate).

The tariff plan has increasing unit prices (SW_{price}) according to specific volume thresholds with a minimum tariff corresponding to the first slot, which guarantees a basic water allocation (BWA). The other thresholds are meant to gradually decrease accessibility to SW use, thus imposing a constrain to over-consumption of water for irrigation. An 'Accessibility degree' is defined to generalize the scheme used for the tariff plans, mainly depending on the first threshold, ranging

from (1) in drought years, to (4) in normal conditions. The records of the applied irrigation tariffs were provided by CBC except for the years between 1993 and 1999. In this period, the tariff plans were defined generalizing the decision rules adopted by the CBC (see Section 2.3.3 for further details).

2.3 Water Source Selection model

The proposed model has been developed taking into account different sub-models. The global structure is represented in the following diagram (Fig. 1), while the following subsections provide a more detailed analysis of the single sub-models.

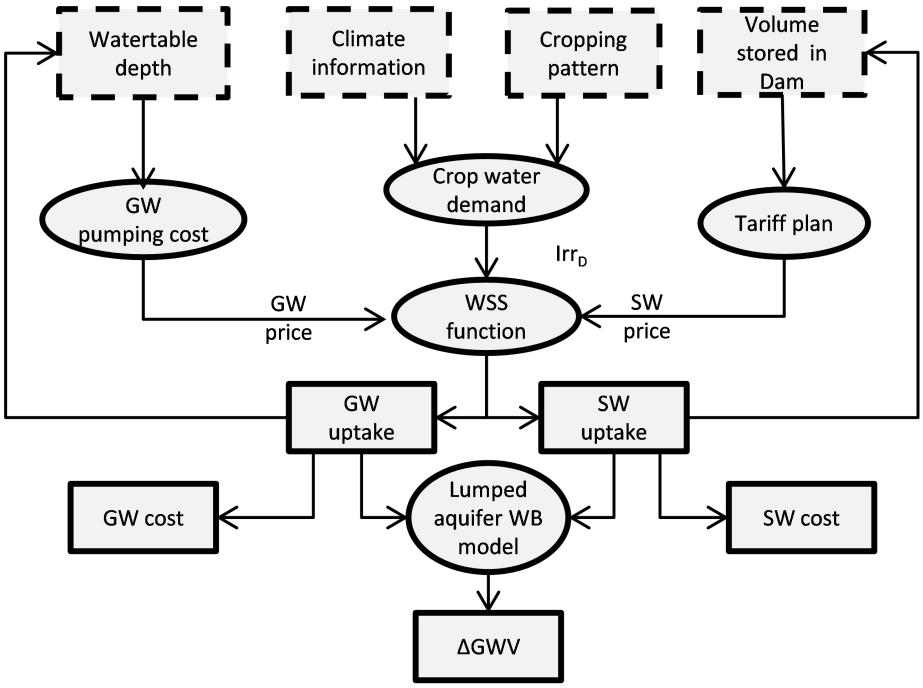

Figure 1. Conceptual model. The rectangles with dashed line are model inputs. The rectangles with continuous line are model outputs. Ellipses identify specific submodels.

2.3.1 WSS (Water Source Selection) function

The behaviour of farmers with respect to water use for irrigation depends on energy and water pricing. The selection of water source for irrigation, particularly, aims at reducing production costs.

The developed model is able to define the fraction of irrigation demand that is satisfied from consortium irrigation network (*%SW*), which is estimated as a function of unit cost ratio (*CR*) between unit SW_{price} and GW_{price} (explained in details in the following) for unit volume. The model equation (1) has the following structure:

$$\%SW = (Y)\, CR^2 - 2CR_M(Y)\, CR + SW_M + (CR_M^2)\, (Y) \quad (1)$$

where: $Y=((SW_m-SW_M))/((CR_m-CR_M)^2)$; SW_m, is *%SW* value when *CR* is minimal (i.e. SW_{price} is minimal assuming a constant GW_{price}); SW_M, is *%SW* value when *CR* is maximum (i.e. SW_{price} is the highest assuming a constant GW_{price}); CR_m is the value of *CR* when SW_{cost} is minimal; CR_M is the value of *CR* when SW_{price} is maximum.

This function simulates the attitude of farmers to prefer groundwater source (*%GW*) as the SW_{price} gets higher.

2.3.2 GW pumping cost

The pumping cost per unit volume of water (GW_{price}) is defined by means of the following equation (2):

$$P = H_{tot}/(367{,}2\ \eta)\ [\mathrm{kWh/m^3}] \quad (2)$$

where: $H_{tot} = H_1 + H_2$ [m] is the total head given by the sum of water table depth (H_1) below the soil surface and the required hydrant pressure (H_2), and η is the pump efficiency.

Finally, the Groundwater pumping cost (GW_{price}) is estimated as a product between P and c, where c is unit energy cost. In our case study we considered the following values: H_1= 40 [m], H_2= 26,5 [m], η= 0,5 and c= 0,22 [€/kWh]. The resulting average GW_{price} is 0,08 [€/m^3]. Additional costs such as maintenance and depreciation are neglected for the purposes of the present work.

2.3.3 Tariff plan

The CBC defines a tariff plan for SW on yearly basis, based on the volume stored in the reservoir in March. Then, considering the available tariff plans in the period 2000-2012, and the strategies selected under similar hydrological conditions, four different types of tariff were identified, and associated to a water 'accessibility degree'. A linear correlation between the accessibility degree and the water volume in March (R^2=0,97) allows assigning the expected tariff plan as a function of the volume stored in the dam in other years. This linear function has been adopted to predict the SW tariffs in the years with no official data.

2.3.4 Crop water demand

The irrigation demand is variable according to the seasonal climate variability and to the cropping patterns. CROPWAT 8.0 was used to estimate the monthly irrigation demand (Irr_d) throughout the period of interest with the "average hectare". Hydraulic soil properties (mean spatial values) and crop properties (crop coefficients K_c, crop yield, etc.) were considered as well. Particularly, the most suitable K_c coefficients for evapotranspiration calculation were attributed according to the FAO database. The efficiency of irrigation systems was estimated considering drip irrigation (efficiency set to 0,9). An additional reduction coefficient was applied to take into account both deficit irrigation techniques (e.g. for olives) and the practice of reducing irrigated areas to have higher unit water volumes available from the SW system.

3. RESULTS AND DISCUSSION

3.1 Parameterization and validation of the WSS function

The parameters of WSS function were defined as follows. In case of years with limited water availability (2000, 2007 and 2008) SW_M=0 e SW_m=1, which means that SW is accessed up to the BWA. While, in case of 'average' climatic conditions, when the reservoir is full and the irrigation season can be performed regularly, SW_m=0.9 and SW_M=0.1. The resulting function defines the source selection criteria, depending on the irrigation demand and tariff thresholds, and quantifies the preference for groundwater source (*%GW*), when the SW_{price} increases. The validation of the WSS model has been performed comparing the simulated and measured irrigation volumes withdrawn from the reservoir. Measured values were modified considering the conveyance efficiency (0,87 as in Guyennon et al., 2016) to take into account the water losses in the pressurized network. The results of this comparison show a good agreement (R^2=0,91), proving a reliable

reconstruction of farmers' behaviour under different tariff and/or climate conditions.

3.2 Modelled water allocation

The model was applied in the case study for the period 1993-2012, evaluating the monthly uptake volumes provided by the SW irrigation system and by farm-scale GW pumping. For each irrigation season, starting from the cumulated monthly Irr_d, the *CR* was calculated and then both GW and SW uptakes estimated by means of the WSS function. Therefore, the monthly uptakes provided by both available irrigation sources were estimated.

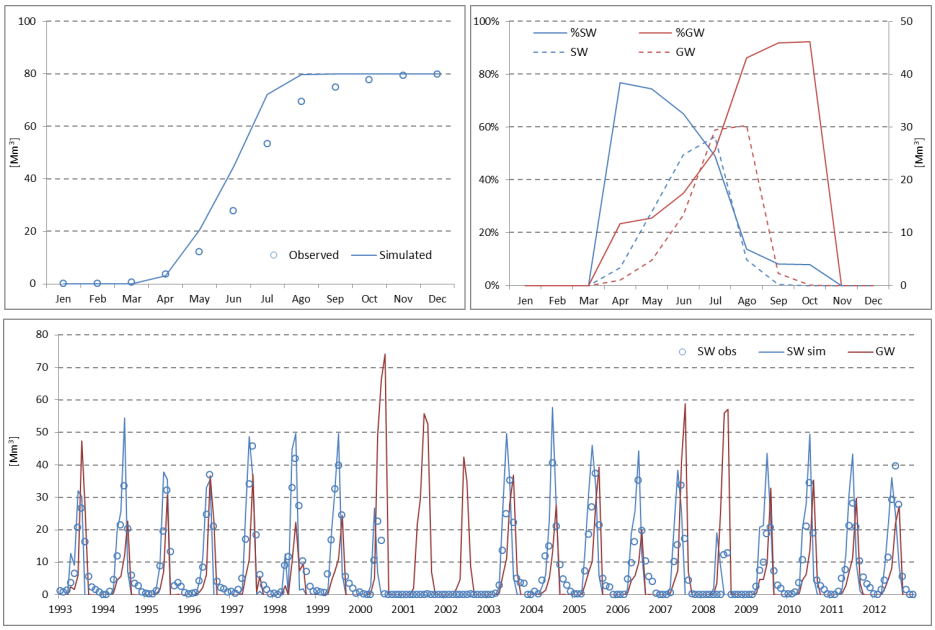

Figure 2. Upper panel on the left: Cumulative monthly mean of SW uptake. Upper panel on the right: Average monthly of the percentage and absolute values (dashed and continuous line respectively) of the SW and GW. Bottom panel: monthly GW and SW uptakes.

The model results are shown in Fig. 2 in terms of variability of SW and GW uptakes, according to the variations of climate and cropping patterns, and compared with observed SW uptakes. As expected, SW uptakes change according to both SW availability and tariff accessibility. The years with the highest percentage of the GW uptake were 2001 and 2002 ($\%GW$ = 100%), due to the failure of the SW system caused by severe drought conditions. GW exploitation was also high in 2000, 2007 and 2008 ($\%GW_{mean}$= 76%) due to the limited SW availability. During the years with regular irrigation season, the average fraction of GW uptake was lower ($\%GW_{mean}$=40%). Conversely, in such conditions, the SW supply is able to cover approximately 60% of the whole irrigation demand. Considering the effects of water tariff plans on water accessibility, the restrictive tariff plans applied under drought conditions produce a marked increase in the groundwater use, rather than reducing the overall water consumption.

Concerning the irrigation costs from one year to the other, variations are explained in terms of Irr_d and tariff plan (SW_{price}). However, even when irrigation costs increase, the negative effect on farmer's economy is limited and masked by other policies affecting farmers' behaviour on water use (Giannoccaro and Berbel, 2011).

3.4 Impacts of water price and Irr_d on GW volume

Understanding the impacts of changes in both Irr_d and tariff plans on agricultural production and groundwater exploitation is essential for ensuring the sustainability of groundwater resources. To

jointly analyse the dynamics of groundwater volume and irrigation-water consumptions, a simplified water balance of the study area has been implemented (Guyennon et al. 2016) throughout the period of interest using a System Dynamics (SD) approach in order to account for the complex network of interaction (i.e. feedbacks and delay mechanisms) influencing the system dynamic evolution. Conceptual GW stock and flow equations were implemented using STELLA®. Among GW outflows, irrigation uptakes from private wells are introduced using the WSS function. Adopting the historical records of climate, cropping patterns and SW tariffs, the groundwater balance was simulated in terms of GW volume variability. The simulation allowed to investigate the sensitivity of GW storage to climate and SW tariff variations, including other variabilities occurred in crops and water management. Groundwater table depth measurements by the regional monitoring network (Passarella et al. 2016) were converted into GW volume changes and plotted in Fig.3 as spatially averaged values, to validate model results.

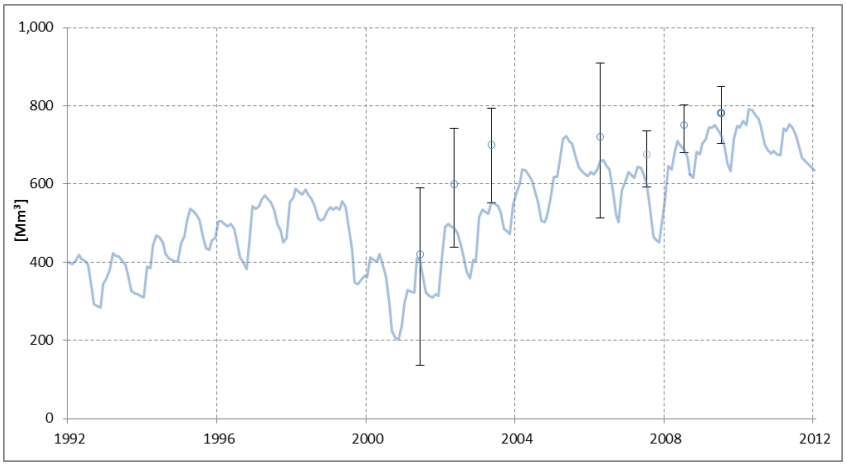

Figure 3. Simulated GW volume at monthly time-scale. Observations are reported like spatial median (Blue circles) with associated error bars.

The comparison in Fig. 3 shows that: (i) the whole period under investigation corresponds to a GW recharge period, since GW volume increased significantly (+55% from 2002 to 2012), due to higher rainfall; (ii) during drought years, SW accessibility is low (e.g. 2001, 2002, 2008) and GW volume depletion is more evident than in regular irrigation seasons; (iii) between 2005-2012 aquifers seem to reach a new dynamic equilibrium. These results highlight how climate variations combined with SW pricing have stronger negative impacts on GW storage during droughts that should properly addressed.

4. CONCLUSIONS

A farm-scale water allocation model has been developed to investigate the dynamics of water resources exploitation at district scale. An interview-based modelling approach was useful to understand interconnections between the water management authority, farmers and physical system. SW tariff policies and climatic conditions were identified as the main drivers of GW sustainability. The developed WSS function helped explaining how GW uptakes may depend on the evaluation of economic convenience performed by farmers: particularly in the case study, SW supply is preferred to GW source until their cost ratio (*CR*) is below 1,5. More specifically, farmers respond to restrictive SW pricing policies by increasing GW uptake to reduce their production costs related to irrigation practice. During persistent recharge periods (2002-2012), an increase in SW accessibility was highlighted by higher %SW volume. Conversely, during drought periods, SW supply was reduced but %GW increased. Therefore, in such conditions, an effective decrease of GW uptakes may be achieved only through reduction of the irrigation demand (e.g. supporting a reduction of the irrigated land by means of subsidies).

The present study underlined that a feasible integrated management of GW resources requires to take into account various interactions among decision-makers, policies and climatic conditions (Giordano et al. 2015). More in detail, the key aspects to be considered are: (i) the main variables related to Irr_d, both direct (environmental) and indirect (e.g. cropping pattern mainly related to agriculture subsidies and SW accessibility), (ii) the behaviours of various stakeholders at different levels and (iii) GW response under different conditions impacting on GW recharge and exploitation.

AKNOWLEDGEMENT

This research is co-funded by the FCRP foundation under the grant n. 3329/2015 for the MIGRAD Project.

REFERENCES

Bouwer, H., 2000. Integrated water management: emerging issues and challenges. Agric. Water Manag.; 45: 217–228.

Giannoccaro, G., Berbel, J., 2011. Influence of the Common Agricultural Policy on the farmer's intended decision on water use. Spanish J. Agric. Res.; 9: 1021–1034.

Giordano, R., D'Agostino, D., Apollonio, C., et al., 2013. Bayesian Belief Network to support conflict analysis for groundwater protection: The case of the Apulia region. J. Environ. Manage.; 115: 136–146.

Giordano, R., D'Agostino, D., Apollonio, C., et al., 2015. Evaluating acceptability of groundwater protection measures under different agricultural policies. Agric Water Manag.; 147: 54–66.

Guyennon, N., Romano, E., Portoghese, I., 2016. Long-term climate sensitivity of an integrated water supply system: The role of irrigation. Sci Total Environ.; 565: 68–81.

Jury, W.A., Vaux, H.J., 2007. The Emerging Global Water Crisis: Managing Scarcity and Conflict Between Water Users. Adv. Agron.; 95: 1–76.

Katic, P.G., Grafton, R.Q., 2012. Economic and spatial modelling of groundwater extraction. Hydrogeol J.; 20: 831–834.

Lamaddalena, N., 2004 Modern Irrigation Schemes and Impact on Drought Mitigation. OPTIONS méditerranéennes, Series B, n°48; 265: 245–265.

Passarella, G., Barca, E., Sollitto, D., et al., 2017. Cross-Calibration of Two Independent Groundwater Balance Models and Evaluation of Unknown Terms: The Case of the Shallow Aquifer of "Tavoliere di Puglia" (South Italy). Water. Resour. Manage.; 31(1): 327-340.

Portoghese, I., D'Agostino, D., Giordano, R., et al., 2013. An integrated modelling tool to evaluate the acceptability of irrigation constraint measures for groundwater protection. Environ. Model Softw.; 46: 90–103.

Portoghese, I., Vurro, M., Lopez, A., 2015. Assessing the Impacts of Climate Change on Water Resources: Experiences From the Mediterranean Region. Managing Water Resources under Climate Uncertainty: Examples from Asia, Europe, Latin America, and Australia. Springer International Publishing, Cham, 177–195.

Proceedings of the 10th World Congress of EWRA 'Panta Rhei', 5-9 July 2017, Athens, Greece
© 2017 *European Water Resources Association*

Using groundwater flow simulation of the Chania Plain area to propose a proper irrigation plan

C. Goumas[1], Z. Dokou[1], G.G. Morianou[1], N.N. Kourgialas[1,2] and G.P. Karatzas[1*]
[1] *School of Environmental Engineering – Technical University of Crete, Polytechnioupolis, 73100 Chania, Greece*
[2] *Hellenic Agricultural Organization (H.A.O.-DEMETER), National Agricultural Research Foundation (N.AG.RE.F.) - Institute for Olive Tree, Subtropical Crops and Viticulture - Agrokipio, 73100 Chania, Greece*
[*] *e-mail: karatzas@mred.tuc.gr*

Abstract: The objective of this work was the simulation of groundwater flow at the aquifer of the Chania plain area in Crete, Greece. This area is dominated by irrigated olive and citrus trees with high water demands during the dry period. In the present study, the three-dimensional Princeton Transport Code (PTC) model was employed in combination with the pre-post processor model ArgusOne, which has been developed specifically to simulate groundwater flow and solute transport. PTC employs a unique splitting algorithm for solving the fully three-dimensional equations, which significantly reduces the computational burden. For the model calibration, a simulation time of two years (1998 - 2000) was considered. The model was calibrated using hydraulic head data. In order to quantify the accuracy of the calibration process, a statistical analysis was performed between the simulation results and the corresponding groundwater field data. In addition, for the study area, the irrigation needs in a yearly basis were estimated based on a common irrigation amount for olive and citrus trees (period between May to September). Finally, using the simulation results the effects of saltwater intrusion are discussed and a proper irrigation plan is proposed based on crop requirements.

Key words: groundwater flow; irrigation wells; PTC model

1. INTRODUCTION

Aquifers are the primary source of freshwater for both human needs and crop production. For the majority of the agricultural production areas, groundwater is remaining the ultimate source of freshwater, since it is generally less prone to pollution compared to surface water. Aquifers are constantly recharged by rainwater seepage and continuously feed reservoirs (Siebert et al., 2010).

The water resources around the world are under increasing pressure due to the rapid population and economic growth. As a result of the continuous increase in the water demand for human and agricultural needs, an accurate mapping and characterization of the aquifers is necessary. For an accurate aquifer characterization and simulation, an extensive analysis is needed with field-testing and data gathering.

The application of finite difference and finite element methods to groundwater flow equations has allowed complex and real world systems to be simulated (Bear and Verrujit, 2012). Numerical simulation models have provided a framework for conceptualizing and evaluating aquifer systems (Gorelick, 1983). Various numerical models have been developed for groundwater simulations, such as the Finite Element subsurface FLOW system (FEFLOW) (Diersch, 2005), the Groundwater Modeling System (GMS) (Xiaobin, 2003) and USGS MODular groundwater Flow model MODFLOW (McDonald and Harbaugh, 1988), etc.

In the present study, the well-known Princeton Transport Code (PTC), a groundwater flow and contaminant transport simulator (Babu et al., 2002), was used to simulate the dynamics of a freshwater coastal aquifer located at the Chania Plain. The simulation of groundwater resources leads to effective irrigation management plans that can enhance the agricultural productivity especially in small Mediterranean agricultural watersheds (Kourgialas et al., 2015).

2. STUDY AREA

The study area is the Chania Plain domain, located in the Chania Prefecture in western Crete, Greece. The study area extends from the White Mountains (Lefka Ori) to the coastline, including the city of Chania and the river basins of Tavronitis and Keritis, with coordinates 35.4° to 35.5° North latitude and 23.8° to 24.1° East longitude. The coastline of the Chania Prefecture is over 350 km long and the study area has a total catchment of 2320 km^2 (Figure 1). Agriculture is a significant part of the area's economy, and agricultural land occupies a large portion of the area (600 km^2) from which 105 km^2 are considered as irrigation land (Nikolaidis and Karatzas, 2010). The climate is sub-humid Mediterranean with humid and relatively cold winters and dry and warm summers. The average annual precipitation is about 665 mm of which over 95% occurs between October and May (Chartzoulakis et al., 2001).

The main geological formations in the study area, are classified based on their permeability (Figure 1) (Nikolaidis and Karatzas, 2010):

- Granular non-alluvial deposits of small to very small permeability (P3)
- Granular alluvial deposits of ranging permeability (P1)
- Miocene deposits of moderate to low permeability (P2)
- Karstic formations of high to moderate permeability (K1)
- Impermeable formations of small to very low permeability (A1 & A2)

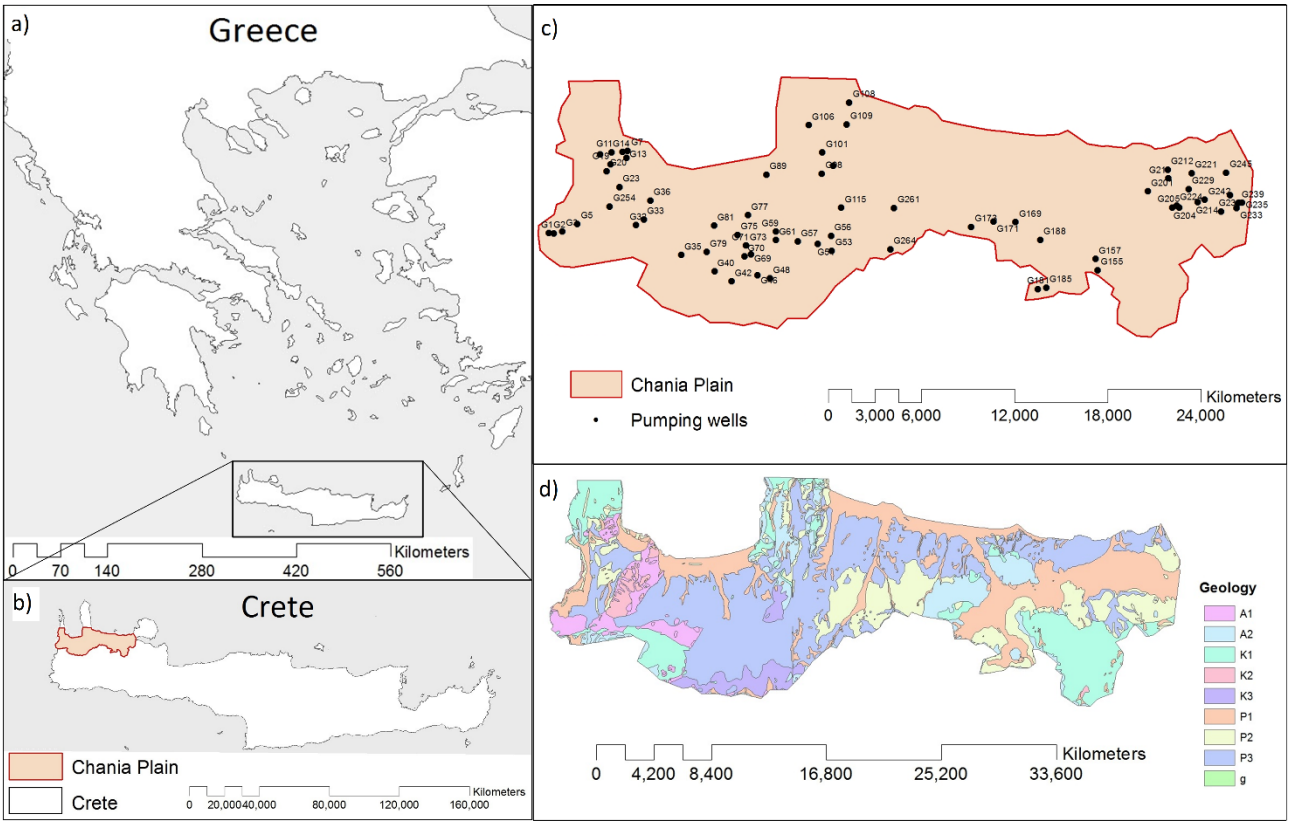

Figure 1. Location of Chania Plain: a) Greece, b) Crete, c) Chania Plain with the pumping well locations and d) the hydrogeology, of the study area.

3. MATERIALS & METHODS

3.1 Princeton Transport Code (PTC) model set-up

In order to simulate groundwater flow in the study area, the Princeton Transport Code (PTC) model was applied. PTC is a plug-in extension for the ArgusONE graphical pre- and post-processor

software suite. PTC uses a system of partial differential equations to calculate groundwater flow according to hydraulic head h (Eq. 1), using a combination of finite-element and finite-difference methods, and groundwater Darcy velocity in three-dimensions x, y and z (Eq. 2, 3 and 4, respectively):

$$\frac{\partial}{\partial x}\left(K_{xx}\frac{\partial h}{\partial x}\right)+\frac{\partial}{\partial y}\left(K_{yy}\frac{\partial h}{\partial y}\right)+\frac{\partial}{\partial z}\left(K_{zz}\frac{\partial h}{\partial z}\right)-S\frac{\partial h}{\partial t}+Q=0 \quad (1)$$

$$V_x=-K_{xx}\frac{\partial h}{\partial x} \quad (2)$$

$$V_y=-K_{yy}\frac{\partial h}{\partial y} \quad (3)$$

$$V_z=-K_{zz}\frac{\partial h}{\partial z} \quad (4)$$

The above system of equations is a result of combining Darcy's law and Conservation of Mass Law. The PTC model has also the ability of contaminant transport calculations (Babu et al. 2002).

The PTC – ArgusONE model has been designed to be fully compatible with GIS (Geographical Information System) files. The model domain outline, the polygons describing the area geological formations with corresponding hydraulic conductivities, the well locations, the initial heads and the pumping rates were imported into the model using shapefiles. An important parameter needed to be determined is the aquifer depth. From the ground survey data presented by Lionis and Perleros (2001), a bottom layer with a depth of 100 m below sea level was considered. A brief description of the model input parameters is given in Table 1.

Table 1. Model input

Parameter	Model input
Mesh Type	Triangular
Water table iterations	50
Convergence Criterion	0.0001
Number of Layers	3
Number of Stresses	4
Total Stress time	180 days
Total Time steps per stress	40
Total Simulation Time	720 days

The simulation time was set to two years based on the available data for the time period from April 1998 to April 2000. According to the hydrogeological study presented by Lionis and Perleros (2001), the bottom layer of the aquifer comprises mostly of limestone, the middle layer of marls and the upper layer consists of the geological formations presented in the hydrolithologic map of Figure 1. The hydraulic conductivity values used were 0.015 m/d for granular non-alluvial formations, 100 m/d for granular alluvial deposits (mainly located near the coastline), 0.15 m/d for miocene deposits, 86.4 m/d for karstic formations and 0.00024 m/d for flysch deposits (impermeable formations).

A Dirichlet boundary condition (BC) of fixed hydraulic head equal to 100 m was applied along the coastline to simulate the sea boundary. At the southern boundary of the region, Neumann conditions (specified flux) were applied in order to represent the in-flows from the mountains and from aquifers adjacent to the model domain (constant flows 1 and 2 in Figure 2). Pumping wells were also represented by Neumann boundary conditions with zero pumping rates during wet seasons (all the wells are used for irrigation purposes) and 114,492 m^3/d during dry seasons (in total). The pumping well locations are presented in Figure 2. The finite element mesh generated for the area consisted of 6275 triangular elements (Figure 2).

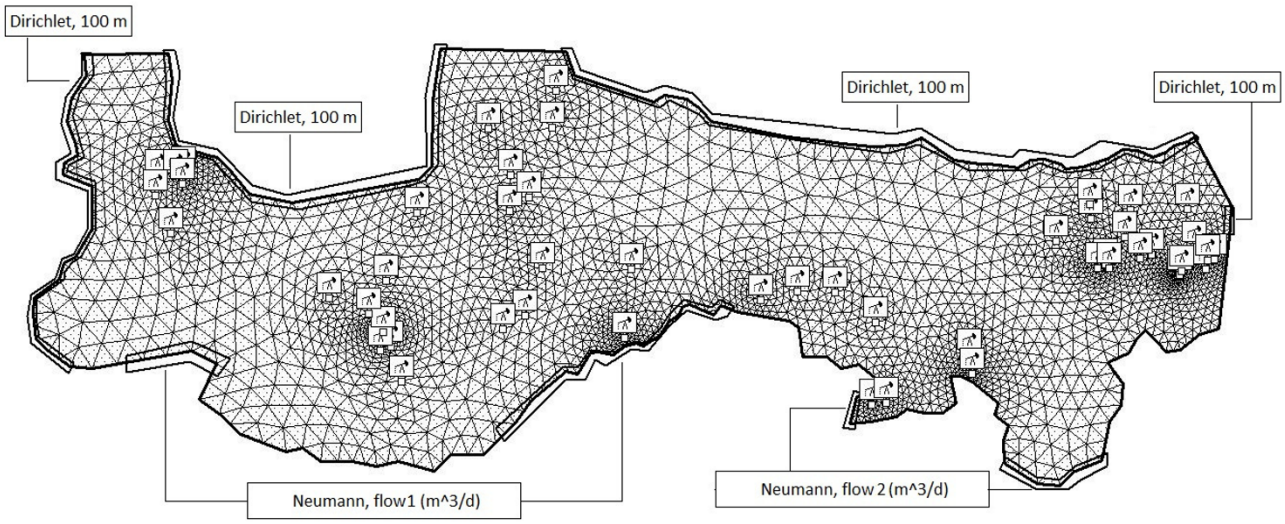

Figure 2. Model domain with the lateral in-flows.

3.2 Calibration process

A calibration processs was performed estimating the groundwater flows from the adjacent basins (south boundary conditions) and comparing the measured hydraulic head values with the observed heads from well-data. The model was calibrated for the time period Apr. 1998 – Apr. 2000 based on the available hydraulic head data of 70 wells. Two statistical indicators were employed in order to determine the fit of the model results to the observed measurements. These indicators were the Root Mean Square Error (RMSE) and the coefficient of determination (R^2). Values of RMSE close to zero indicate a perfect fit. Regarding the coefficient R^2, a value equal to 1 indicates a perfect fit between simulated and observed data (Abramowitz and Stegun, 2012).

4. RESULTS

4.1 Calibration results

The calibration was performed manually by adjusting the inflows from the southern boundaries until the model results were in good agreement with the observed data (hydraulic heads). The calibration values with the best match between field data and simulation results were equal to 5000 m^3/d and 1750 m^3/d for flow 1 and equal to 200 m^3/d and 70 m^3/d for flow 2, for the wet and dry periods, respectively.

During the calibration process, the majority of the wells show a good agreement between simulated and observed values while few wells had not such a good agreement. This behavior was explained considering that some wells must be pumping water from a separate, impermeable or leaky aquifer, which is not included in the present model. In addition, it was observed that in the area marked by the circle in Figure 3, the geological formations of moderate permeability (P2) are dominating and the hydraulic conductivity value inserted into the model was too low to adequately represent the real conditions. Therefore, during the calibration process the hydraulic conductivity value of the porous formation P2 was increased to 20 m/d, in order to succeed a better much between simulated and observed hydraulic head values. Both modifications to the formations' hydraulic conductivities were within the typical values of such formations found in the literature.

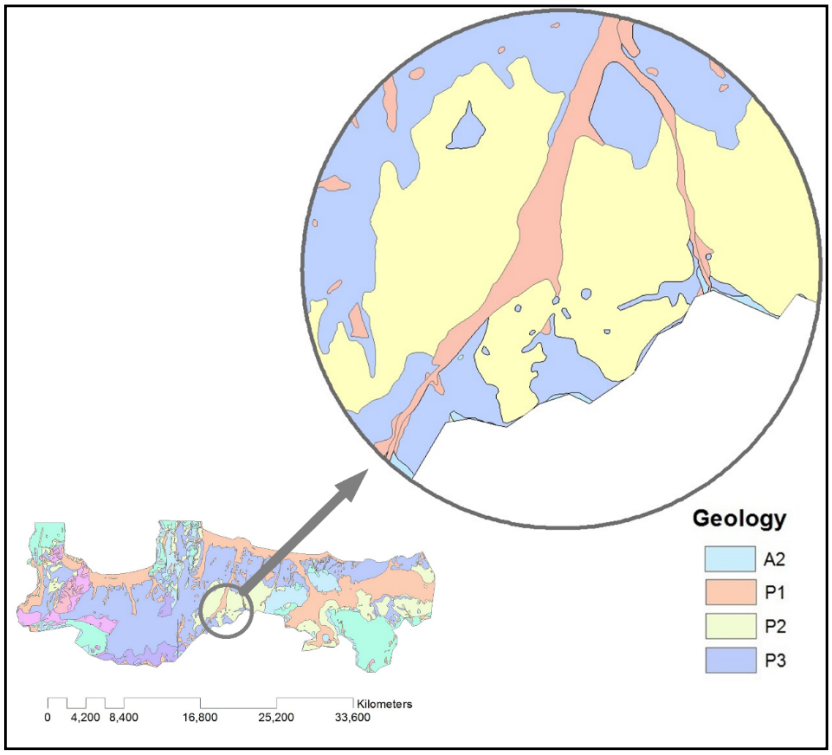

Figure 3. Area of higher hydraulic conductivity

The good correlation between field measurements and the simulation results is shown in Figure 4, for the calibration period. Moreover, in this figure a statistical indicator is presented verifying the good agreement. The correlation coefficient (R^2) is approximately equal to 0.987, the Root Mean Squared Error (RMSE) is equal to 3.3, an acceptable value according to Anderson et al. (2015).

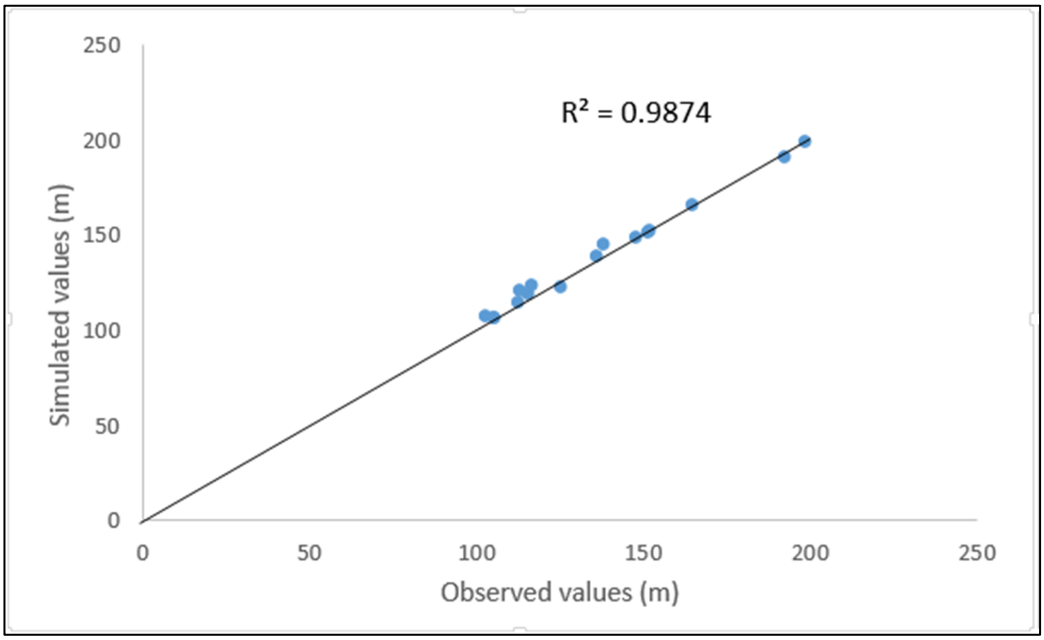

Figure 4. Observed vs. Simulated hydraulic heads values, and the 1:1 line.

4.2 Two-dimensional maps model results

The PTC model results are shown in **Error! Reference source not found.**Figure 5 for the dry and the wet season, respectively.

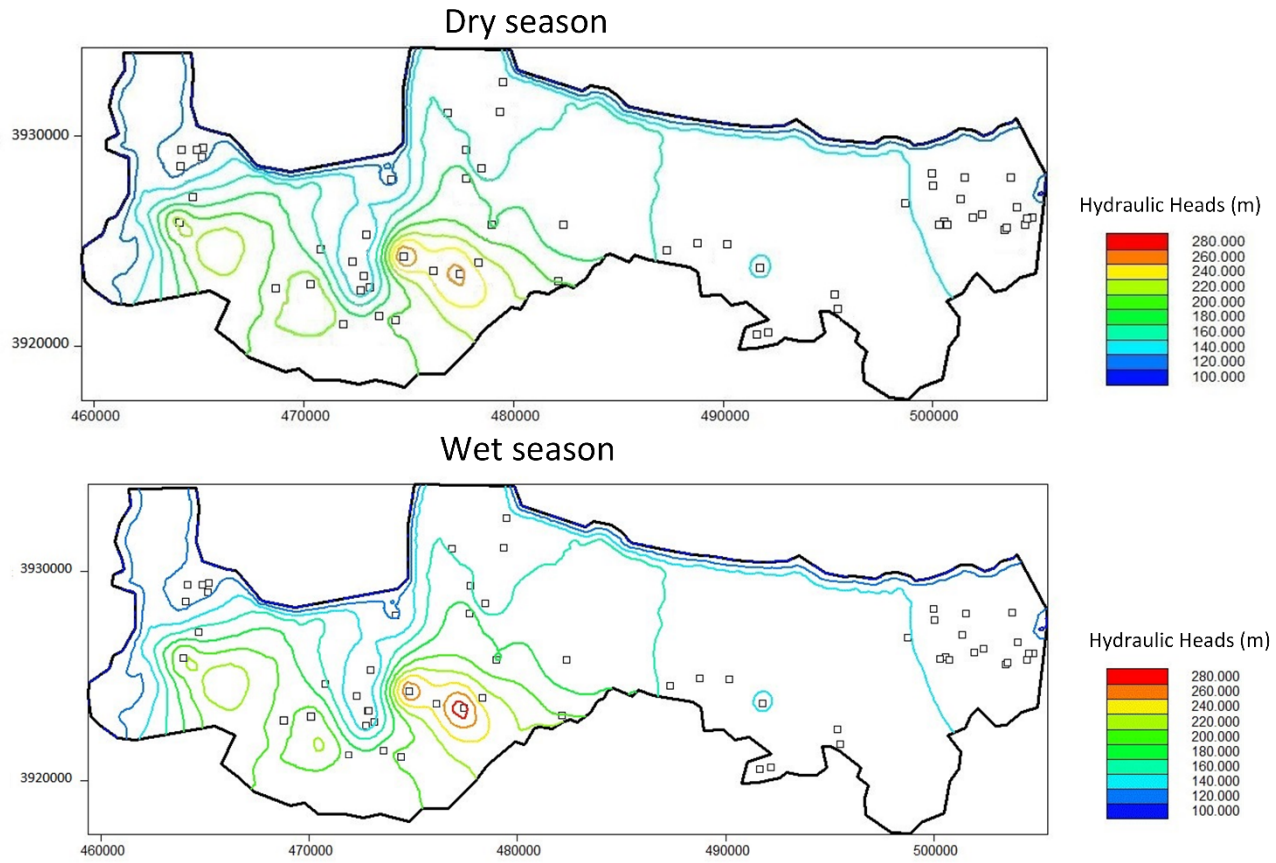

Figure 5. Simulated hydraulic heads for the dry and the wet season

Based on Figure 5 it can be easily verified that all pumping locations, remain safe from saltwater intrusion (saltwater interface at 102.5 m based on Ghyben-Herzberg equation for a given aquifer depth of 100 m) for both wet and dry seasons. The wells located in the western part of the region, near the coastline, could be potentially affected in the future, in the case of an extended dry period with increase pumping rated. It is also observed, that the hydraulic heads do not decrease significantly during dry season. This is partly due to the short time period of modelling, as well as the large domain area. Thus, one may presume that the pumping wells do not pose a significant threat to the aquifer regarding saltwater intrusion. More detailed modeling focused on a local scale might reveal local problems due to saltwater intrusion that cannot be captured by this large scale model.

For the study area, an appropriate common irrigation amount for olive and citrus trees (period between May to September) is around 250 mm and 450 mm per 10^3 m^2 of agricultural land, respectively (Kourgialas and Karatzas, 2015). From the irrigated land of 105 km^2, in the study area, 70% consists of olive trees while the rest of citrus. Thus, the irrigation needs in a yearly basis can be estimated to be $18*10^6$ m^3 and $14*10^6$ m^3 for olive and citrus trees, respectively. Taking into consideration the above findings (with the total irrigation needs to be $32*10^6$ m^3/year, while water abstraction for irrigation to reach $42*10^6$ m^3/year) the proposed modeling approach could be used by local authorities in order to organize a proper groundwater abstraction irrigation plan for a sustainable agricultural and urban development.

5. CONCLUSIONS

In the present work, a simulation of the groundwater flow in the Chania Plain aquifer was performed using the Princeton Transport Code. The data used for model calibration was from April 1998 until April 2000. Based on the simulation results, at the west side of the domain the hydraulic

heads are higher, verifying the correct placement of the majority of the pumping wells. In addition, there was insignificant differentiation between the wet and dry stresses, despite the increase of pumping rates during the dry period. Therefore, the pumping wells do not affect significantly the hydraulic characteristics and the behaviour of the aquifer's physical system.

Due to high irrigation demands in the Chania Plain there is a large number of pumping wells in order all agricultural needs to be satisfied. The effectiveness of the model development is significant, allowing the local authorities to properly control the pumping effects at any well location, by means of running additional model scenarios in order to avoid potentially harmful well placements.

REFERENCES

Abramowitz M., and Stegun I.A., 2012. Engineering statistics Handbook.3.3.24 NISTSEMATECH E-Handbook of Statistical Methods (accessed February 2014), National Institute of Science and Technology

Anderson, Mary P, Woessner, William W. and Hunt, Randall J., 2015. Applied Groundwater Modeling: Simulation of Flow and Advective Transport, Academic Press, 2nd edition

Babu, D.K, Pinder, G.F., Niemi, A., Ahlfeld, D.P. and Stothoff, S.A., 2002. Chemical Transport by Three-Dimensional Groundwater Flows, argusone.com

Bear, J., and Verruijt, A., 2012. Modeling groundwater flow and pollution (Vol. 2). Springer Science & Business Media.

Chartzoulakis, K. S., Paranychianakis, N. V., and Angelakis, A. N., 2001. Water resources management in the island of Crete, Greece, with emphasis on the agricultural use. Water Policy, 3(3), 193-205.

Diersch, H. J. G., 2005. FEFLOW finite element subsurface flow and transport simulation system. Inst. for Water Resources Planning and System Res., Berlin.

Gorelick, S. M., 1983. A review of distributed parameter groundwater management modeling methods. Water Resources Research, 19(2), 305-319

Kourgialas, N. N., Karatzas, G. P., and Morianou, G., 2015. Water management plan for olive orchards in a semi-mountainous area of Crete, Greece. Global Nest Journal, 17(1), 72-81.

Kourgialas, N.N., and Karatzas, G.P., 2015. A modeling approach for agricultural water management in citrus orchards: Cost-effective irrigation scheduling and agrochemical transport simulation. Environmental Monitoring and Assessment, 187:462, DOI 10.1007/s10661-015-4655-7.

Nikolaidis, N., and Karatzas, G.P., 2010. Water resources management plan for the Keritis, Therissou and Koiliaris basins.

Lionis, M., and Perleros, B., 2001. Hydrogeological study for Chania area (KA 9481721). Ministry of Agricultural, Directorate of Hydrogeology. Athens (in Greek).

McDonald, M. G., and Harbaugh, A. W., 1988. A modular three-dimensional finite-difference ground-water flow model.

Siebert, S., Burke, J., Faures, J. M., Frenken, K., Hoogeveen, J., Döll, P., and Portmann, F. T., 2010. Groundwater use for irrigation–a global inventory. Hydrology and Earth System Sciences, 14(10), 1863-1880.

Xiaobin, Z., 2003. Groundwater modeling system (GMS) software. Hydrogeology and Engineering Geology, 5, 53-55.

Proceedings of the 10th World Congress of EWRA 'Panta Rhei', 5-9 July 2017, Athens, Greece
© 2017 *European Water Resources Association*

Sustainable use of groundwater for irrigated agriculture: A case study of Punjab, Pakistan

G.Z. Hassan* and F.R. Hassan
Irrigation Research Institute (IRI), Government of the Punjab, Irrigation Department, Library Road Old Anar kali Lahore, 54000, Pakistan
* *e-mail: zakirjg@gmail.com*

Abstract: Irrigated agriculture in Pakistan contributes 22% to GDP, 66% to foreign exchange, over 90% to food production, employs 45% of country's labor force and ranks the country as 8th largest food producer in the world. Nature has blessed Pakistan with plenty of water resources and specially a large groundwater reservoir of more than 300 m depth. Pakistan is 4th largest user of groundwater after India, USA & China. In Punjab Province, 40 MAF of groundwater are being extracted through 1.2 million tube-wells annually. Groundwater is contributing about 45% crop-water requirements and thus has gained the vital potential in irrigated agriculture. Besides irrigation uses groundwater is the major source of drinking, industrial and commercial requirements and has boosted up the cropping intensity from 60% in 1947 to 160-170% in 2015 to meet ever increasing demand of food and fiber. A monitoring network of about 3000 piezometers has been installed to observe the groundwater potential (quantity and quality) in the Province at grid of 6x6 km. Data so observed since 2006 have been analyzed using latest tools of groundwater modeling and GIS. Under recent study some recommendations have been formulated for sustainable use of groundwater for irrigated agriculture. It has been observed that over all groundwater reservoir is depleting, quality of groundwater is deteriorating reducing the crop yields and fertile land and major source of groundwater recharge is seepage from canal network. Recharge of aquifer using flood water and rainfall harvesting are two major structural interventions for sustainable use of groundwater.

Key words: Groundwater, Punjab, Pakistan, quality, irrigated agriculture, piezometers, groundwater recharge, flood, salinity

1. BACKGROUND

World population is expected to increase by 45% in the next thirty years. Groundwater is the world's most extracted raw material with withdrawal rates currently in the estimated range of 982 km^3/year. Out of total earth's water, 99 % is unusable for human beings while only 1 % is usable. Out of this usable (1%), 99% comes from groundwater while nearly 1 % world's groundwater is fresh and is accessible for consumption. Pakistan is 4th largest user of groundwater after India, USA and China. Pakistan is blessed with a plenty of water resources including a large groundwater reservoir underlying the Indus Basin. The extent of this large and highly transmissive aquifer is about 297,200 km^2 with a length of 1,900 km, but this natural resource is under serious threats and need immediate measures for its sustainable utilization. In Pakistan, over 90% drinking water and 100% industrial water comes from groundwater. Groundwater has helped in increasing cropping intensity from 60% in 1947 to 150% or even more in 2015. In Pakistan, current per capita water availability (1200 m^3/person) is low, which puts us in the category of a high water stress countries on the globe. UNESCO has predicted that by 2020 water shortage will be a serious worldwide problem. Without improved efficiencies, agricultural water consumption is expected to increase by about 20% globally by 2050 WWAP (2012). Groundwater quality depends on the climatic parameters, nature of the surface flow, topography, extent of seepage and irrigation with amendment practices. Groundwater in the Indus basin contributes around 35% to the total water available for agriculture and water quality of the 60 percent area is marginal to brackish World Bank (1997) and Ahmad and Rashida (2001).

Pakistan is the 8th largest food producing country and economy heavily relies on agriculture sector which accounts for a quarter of its GDP and employs two-fifths of total labor force. The agriculture mainly depends on the Indus River System (IRS) for 90% of its irrigation needs, which is also a source of generation of about 30% energy of the country. Pakistan's agricultural performance is closely linked with the supply of irrigation water. This natural resource is being utilized for drinking, agricultural, industrial, livestock, commercial and other uses and is continuously under threat. The other most obvious uses of water for people are drinking, cooking, bathing, cleaning, and for some watering family food plots.. Irrigated agriculture contributes over 90% of Pakistan's food production. Agriculture sector generates over 60% of foreign exchange. It is the second largest sector, accounting for over 22% of GDP, and remains by and far the largest employer, absorbing 45% of the country's total labor force. Around 63% of country's population living in rural areas is indirectly or directly linked with this sector for their livelihood. While on the other, it is a large market for industrial products such as fertilizer, pesticides, tractors and agricultural implements. According to Kaldor's (1978) two-sector model, agricultural and industrial sectors supply inputs to each other and provide market for their outputs but differ in a number of ways. The agricultural sector has disguised unemployment and produces consumer goods for competitive markets, while industrial sector produces investment goods which are sold in imperfectly competitive markets at mark-up prices. According to Duranton (1998), in order to transform from agriculture sector to industrial sector a significant increase in the agricultural sector productivity is necessary. On the demand-side, the growth in agricultural production increases agricultural income which leads to increase in the demand for industrial products; whereas on the supply side, the increase in the agricultural productivity shifts human resources from the agricultural to the industrial sector Jorgenson (1967). Chebbi (2010) evaluated the role of agriculture in economic growth and dealings with other sectors. Johansen's multivariate approach has been used to study the co-integration with the other sectors in its country economy and he deeply analyzed how to overcome the problems of spurious regression. The annual groundwater pumpage has increased from 4 billion m^3 in 1959 to around 60 billion m^3 in 1999-2000. About 79 % area in Punjab and 28% area in Sindh provinces has fresh groundwater suitable for agriculture Afzal (1999) and Bhutta (1999). In Punjab province about 40-50% crop water requirements are being met from groundwater through about 1.2 million tubewells installed by the farmers. Groundwater quality in the Punjab province is deteriorating with the passage of time and sweet water is becoming rare and out of reach of the common farmers who are dependent on groundwater for their livelihood. (Hassan et al, 2014).

The IBIS is the largest integrated irrigation system in the World. Historically IBIS has been fed through run of river supplies derived from Indus and its five major tributaries. For supplying water to Pakistan's irrigation network (the largest manmade canal system in the world) the Indus Basin Project (IBP) was designed and constructed to replace the waters of Eastern Rivers. Any reduction in those waters will put Pakistan's agriculture, food security and economy at great risk. Hassan et al, (2013) during a study found that pollution in surface water bodies is affecting the groundwater quality in the underlying aquifer in Lahore city. They recommended to allow/arrange minimum flow in the River at least to meet the requirements of dilution of pollutants and to treat the wastewater before throwing it into the river. Domestic and industrial effluents contain organic and inorganic pollutants, which deeply percolate to groundwater. Flow in Ravi River especially during the winter is remarkably insufficient to dilute and wash off wastewater pollution (Hassan et al, 2016). Pakistan is bestowed with a largest contiguous irrigation canal network, major part of which lies in Punjab Province. This network was started to be constructed by British during early nineteen century. The continuous expansion of the irrigation system over the past century significantly altered the hydrological balance of the Indus River Basin (IRB) in Pakistan (Hassan and Bhutta, 1996). This also posed severe impacts on aquifer equilibrium. From the above discussion it has been concluded that economy of Pakistan is agri-based for which water resources are required on sustainable basis to feed the ever increasing population of the country.

2. EXPERIMENTAL SETUP AND DATA ANALYSIS

For monitoring of groundwater round about 3000 piezometers have been installed at different location scattered in whole province as depicted in Figure 1.

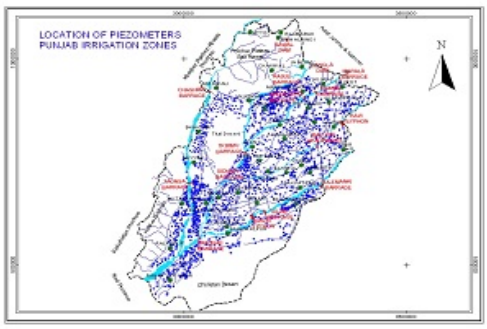

Sr. No.	GW Monitoring Units	Total No of Piezometers	Area (km²)
1.	Bahawalpur	607	23100
2.	DG Khan	464	12138
3.	Faisalabad	559	15626
4.	Lahore	320	18195
5.	Multan	587	22735
6.	Sargodha	421	10814
7.	Thal	248	13929
	Total	3206	116537

Figure 1. Piezometric network in Punjab province

Groundwater levels have been measured using water level indicator from the piezometers biannually (premonsoon and postmonsoon). The observed data have been analyzed to visualize the aquifer behavior in the study area. (IRI, 2009) and (IRI, 2013) conducted a field survey and investigation study by installation of sixty exploratory boreholes in the field at various critical sites in Punjab to explorer the groundwater quality and soil stratification to observe the impact of surface drains and other potential threats for groundwater. Wherein it was observed that surface water bodies especially drains are playing a vital role in contamination of groundwater. A study was conducted for groundwater investigation in Faisalabad area using Groundwater water Model (MODFLOW) where tile drainage and surface drainage networks are functional and groundwater is brackish for which one of the causes is heavy industrial pollution in the area (IRI, 2012). Map Showing the Doabs of Punjab Province and depth to watertable data at selected points in different Doabs over the period of 2011-15 have been plotted to depict the fluctuations of groundwater levels which have been shown in Figures 2.



Map Showing the Doabs of Punjab Province

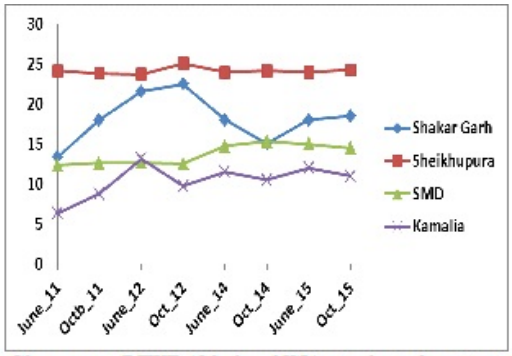

Changes in DTWT (ft below NSL) at selected points in Rechna Doab (2011 to 2015)

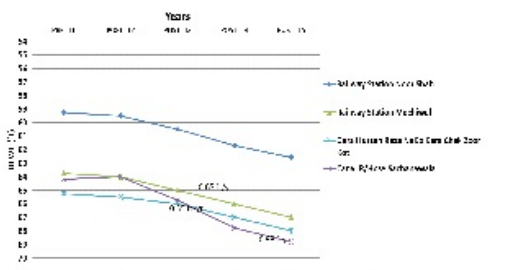

Changes in DTWT (ft below NSL) at selected points in Bari Doab (2011 to 2015)

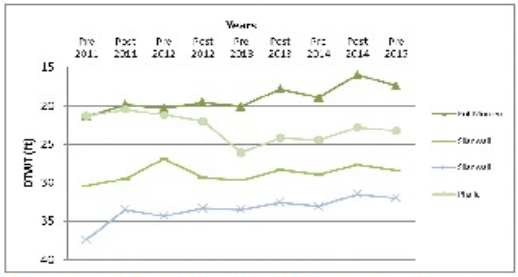

Changes in DTWT (ft below NSL) at selected points in Chaj Doab (2011 to 2015)

Figure 2. DTWT at selected points in different Doabs over the period of 2011-15

In Chaj Doab (bounded by Chenab River on the south-east and Jhelum River on the north-west) groundwater deeper than 20 feet showed nearly constant rise of 1.7 to 2.2 feet per year. During years 2011-2015, water levels in the Chaj Doab rose from 0.3 to 2.6 ft per year with average 0.9 ft. Groundwater level is in rising trend. Flood water contributes significantly towards recharging the aquifer average rise in Chaj doab during flood 2014 is 0.77 ft/season. Total recharge of GW during flood season 2014 in Chaj Doab is 1.20 MAF. Recharge potential in Chaj doab during October 2010 and June 2012 were found out as 4.32 and 4.675 MAF respectively IRI (2016). The area under depth to watertable more than 30 feet was 95 Km^2 in pre-monsoon 2011 which decreased to 30 Km^2 in post-monsoon 2011 and it further decreased to 2.65 Km^2 in post-monsoon 2015 in Chaj Doab area as shown in Figure 3.

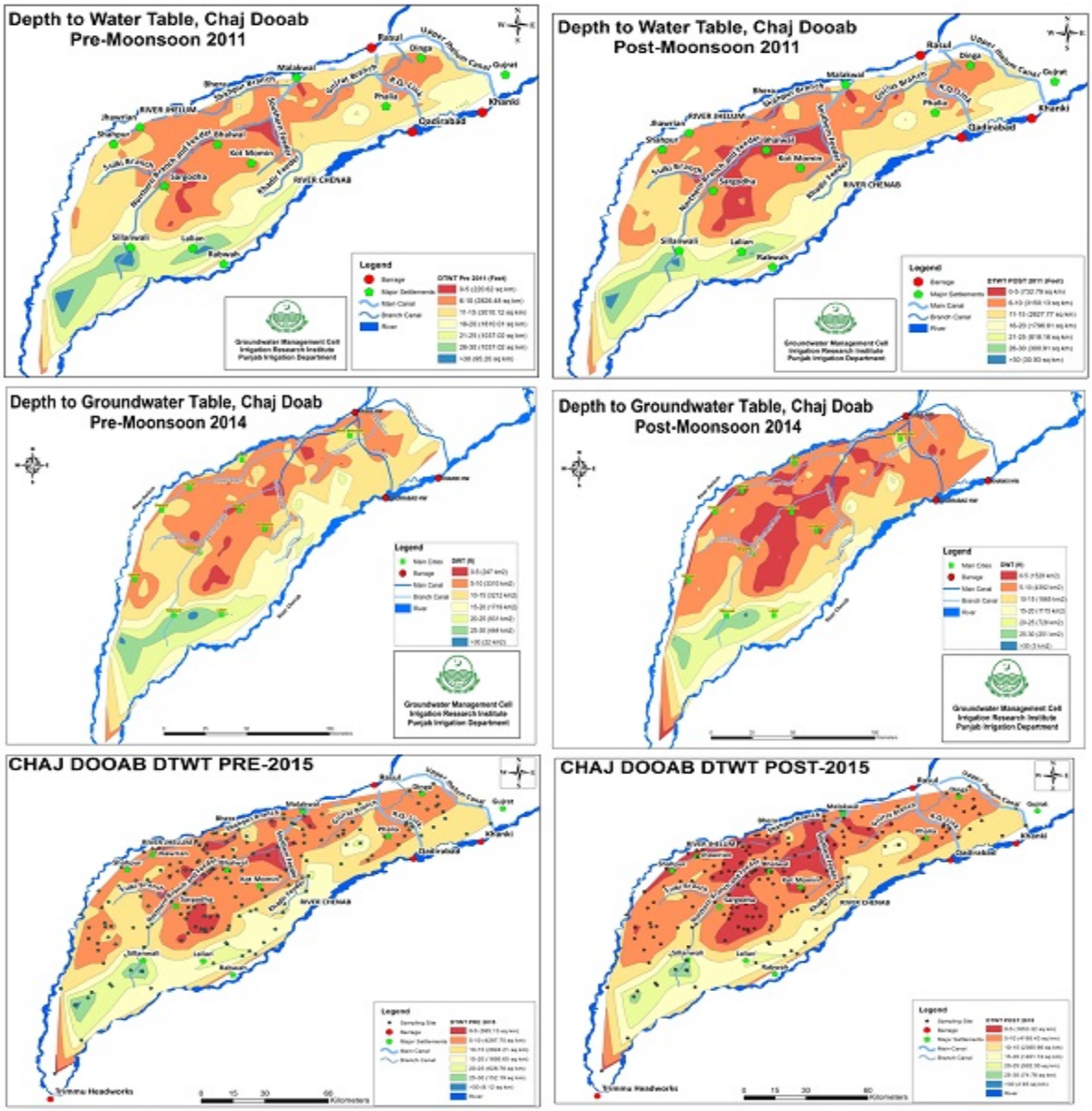

Figure 3. DTWT situation in Chaj Doab premonsoon and postmonsson (2011, 2014 and 2015)

Groundwater levels are falling at an average rate of 1-2 ft/year in some areas of Rechna Doab (bounded by two rivers, on the south and east by the Ravi River while on the North and West by the Chenab River) is showing in figure 4. Recharge potential in Rechna doab during October 2010 and June 2012 were found out as 15.80 and 16.381MAF respectively. Flood water contributes significantly towards recharging the aquifer average rise in Rechna doab during flood 2014 is 2.57 ft/season. Total recharge of GW during flood season 2014 in Rechna Doab is 1.90 MAF IRI (2015).

Research study carried out in Lower Bari Doab Canal (LBDC) has indicated that by increase of depth to water table from 40 ft. to 70ft the cost of pumping per acre-feet has increased 125% as showing Figure 4.

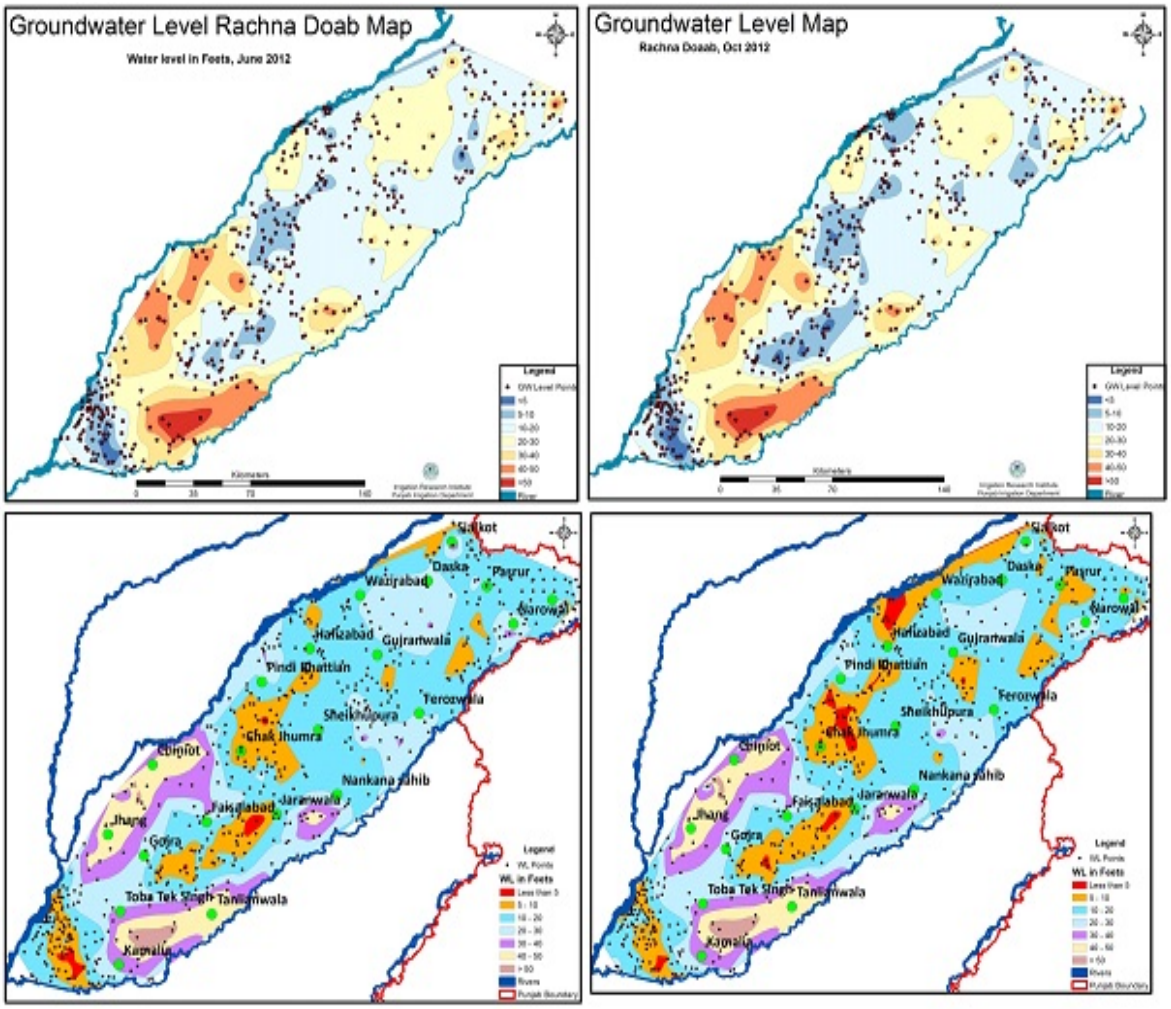

Figure 4. DTWT situation in Rechna Doab pre-monsoon and post-monsoon (2012 and 2014)

3. CONCLUSIONS

From the analysis of data collected it has been observed that unplanned excessive pumpage, lack of awareness and capacity of stakeholders, lack of regulatory framework and spatial/temporal uncertainty in surface water due to climatic changes (droughts and floods) are the major challenges for groundwater management in Punjab. In Chaj Doab the watertable are showing rising trends with an average rate of 0.9 ft/year and quality is deteriorating with the passage of time. In the Rechna Doab area it is been observed the average depleting rate is 1-2ft/year and over exploitation in certain areas is causing intermixing of fresh and saline water leading to overall groundwater quality. Groundwater in Bari doab is under the worst conditions where water table has gone below 50-60 ft in certain areas and cost of pumpage has increased more than 100 times. In urban areas due to increase in population and reduction in recharge to infrastructural development groundwater in under tremendous pressure. For example in Lahore city (provincial capital) groundwater has fallen even more than 100 ft below the natural surface and average annual rate of groundwater depletion is 2.54 ft. Direct energy intensity has risen 80% (from 1 to 1.8 MJ per kg of crop produced) in Punjab between 1995-2010. Use of groundwater in irrigated agriculture consumes 30 times more energy as compared to surface water. It has been observed that flood water plays a significant role in

recharging the aquifer. For example during flood 2014, 2.57 ft rise in water table has been observed in Rechna doab.

4. RECOMMENDATIONS

Management of groundwater can be accomplished by adopting suitable measures both on demand as well as on supply side. Some mitigation measures for groundwater management are:-

- Creating additional surface storages, improving canal operations for timely deliveries, improving application and delivery efficiencies to reduce the pressure on groundwater, increasing the water productivity are the major management options.
- Rain water harvesting and groundwater recharge particularly in south Punjab.
- Aquifer recharge using flood water by flood plain management and building retention reservoirs along rivers.
- Sewerage, agricultural and industrial effluents must be treated and recycled it will avoid groundwater pollution as well.
- Legislation for regulating the groundwater abstraction and IWRM are required.
- Awareness raising and capacity building of stakeholders about groundwater management must be ensured
- The capacity of groundwater institutions be developed to perform key functions of planning, research and providing information/technical support at regional level as well as local level.
- Adopting the drought-tolerant and low delta crops where water is scarce or unreliable
- Subsidy on SMART energy and water use and defining groundwater entitlements.

REFERENCES

Afzal, M. 1999. Water for agriculture. Paper for water Vision Pakistan.

Ahmad, S., Rashida, M. 2001. Indus basin irrigation system water budget and associated problems. J. Engineering and Applied Sciences.; 20 (1): 69-75.

Bhutta, M. N. 1999. Vision on water for food and agriculture: Pakistan's perspective. Regional South Asia Meeting on Water for Food and Agriculture Development. New Delhi.

Chebbi, E. H. 2010. Agriculture and economic growth in Tunisia. Emerald Group Publishing Limited.; (Vol. 2 no. 1): 63-78.

Duranton, G. 1998. Agricultural Productivity, Trade, and Industrialization. Oxford Economic Papers.; 50: 220-236.

Hassan, G. Z., Bhutta, M. N. 1996. A Water Balance Model to Estimate Groundwater Recharge in Rechna Doab Pakistan., Printed in Netherlands.; 10: 297-317,.

Hassan, G. Z., Shabir, G., Hassan, F. R., Akhtar, S. 2013. Impact of Pollution in Ravi River on Groundwater underlying the Lahore City. 72nd Annual Session of Pakistan Engineering Congress, Lahore, Pakistan.; Paper 749: 355-380.

Hassan, G. Z., Hassan, F. R., Akhtar, S. 2014. Environment Threats to Groundwater in Lahore Area., Pakistan Engineering Congress, Lahore Pakistan.; World Environment Day: 68-97.

Hassan, G. Z., Hassan, F. R., Akhtar, S. 2016. Environmental Issues and concerns of Groundwater in Lahore. Proceedings of the Pakistan Academy of Sciences.; Life and Environmental Science 53(3) 163-178 (2016), ISSN 2518-4261 (print), ISSN 2518-427X (Online): 163-178.

IRI (Irrigation Research Institute). 2009. Research Studies on Artificial Recharges of Aquifer in Punjab. Government of the Punjab, Irrigation Department, Irrigation Research Institute: Research Report No IRR-Phy/552.

IRI. 2012. Groundwater Investigation for Sustainable Water Supply to FDA City Housing Scheme, Faisalabad. Government of the Punjab, Irrigation Department, Irrigation Research Institute, Lahore, Pakistan: Research Report No IRR-Phy/577.

IRI. 2013. Research Studies on Artificial Recharges of Aquifer in Punjab. Government of the Punjab, Irrigation Department, Irrigation Research Institute, Lahore, Pakista: Research Report No IRR-Phy/579.

IRI. 2015. Groundwater Behavior in Rechna Doab, Punjab, Pakistan. Groundwater Management Cell, Irrigation Department, Irrigation Research Institute, Lahore, Pakistan: Research Report No IRR-GWMC/101.

IRI. 2016. Challenges and Opportunities for Sustainable use of Groundwater in Chaj Doab, Punjab, Pakistan. Groundwater Management Cell, Irrigation Department, Irrigation Research Institute, Lahore, Pakistan: Research Report No IRR-GWMC/102.

Jorgenson, D. 1967. Surplus Agricultural Labor and Development of a Dual Economy. Oxford Economic Papers 19: 288-312.

Kaldor, N. 1978. Further Essays on Economic Theory. In M. Baskin (ed.) Economics and Human Welfare.; Essay in Honor of Tibor Scitovsky. New York: Academic Press.

World Bank. 1997. Staff Appraisal Report. Pakistan National Drainage Program. Rural Development Sector Management Unit, South Asia Region.

WWAP (United Nations World Water Assessment Program). 2012. Managing Water under Uncertainty and Risk.; The United Nations World Water Development Report 4 Paris: UNESCO. http://www.unesco.org/new/en/natural-sciences/environment/water/wwap/wwdr/wwdr4-2012/

Proceedings of the 10th World Congress of EWRA 'Panta Rhei', 5-9 July 2017, Athens, Greece
© 2017 *European Water Resources Association*

Physics-based and data-driven surrogate models for pumping optimization of coastal aquifers

V. Christelis* and A. Mantoglou
Laboratory of Reclamation Works and Water Resources Management, School of Rural and Surveying Engineering, National Technical University of Athens, Athens, Greece
* *e-mail: vchrist@survey.ntua.gr*

Abstract: Data-driven surrogate models have been widely used in pumping optimization of coastal aquifers. However, their efficacy has not been previously compared to physics-based surrogate modelling techniques. In this work, we utilize a set of sharp interface models of different complexity to investigate the performance of a variable-fidelity optimization framework against a data-driven approach. In particular, the numerical solution of sharp interface flow represents the available high-fidelity seawater intrusion model. Furthermore, several analytical models represent lower-fidelity approximations for simulating seawater intrusion. To statistically assess the performance of the surrogate-based methods against the high-fidelity optimal solution, we utilized a total of 30 independent optimization runs for each approach. The results indicate that the analytical models which poorly approximate the numerical sharp interface model had also limited skills to approximate the high-fidelity optimal solution. On the other hand, the surrogate-based optimization frameworks that were developed by using either the most accurate analytical model or the data-driven surrogate model were in good agreement with the high-fidelity optimization results. It was also observed that the variable-fidelity optimization algorithm required fewer evaluations with the high-fidelity model in order to converge to the optimal solution. Moreover, the set of these seawater intrusion models could be conveniently used for further development and testing of variable-fidelity optimization frameworks in coastal aquifer management.

Key words: seawater intrusion; pumping optimization; surrogate modelling; variable-fidelity optimization

1. INTRODUCTION

A common optimization problem in water resources is the calculation of maximum groundwater abstraction from coastal aquifers, subject to constraints that control seawater intrusion (SWI) (Singh, 2014). The optimal search space is typically explored using evolutionary algorithms due to their ability to handle the non-convex nature of these problems (Ketabchi and Ataie-Ashtiani, 2015). However, evolutionary algorithms require a large number of function evaluations to converge and their combination with numerical models of SWI significantly increases the overall computational cost (Mantoglou and Papantoniou 2008). In order to obtain optimal solutions within reasonable computational times, several studies in coastal aquifer management have applied surrogate modelling techniques (e.g. Kourakos and Mantoglou, 2009; Papadopoulou et al., 2010; Sreekanth and Datta, 2011; Christelis and Mantoglou, 2016a; Roy and Datta, 2016).

The majority of these studies have employed various data-driven surrogate models which are based on function approximation techniques and are built upon the input-output relations of the original computer models (Razavi et al., 2012b). Another competent approach for surrogate-based optimization (SBO) is the development of physics-based surrogate models and their use in the so-called variable-fidelity optimization framework (Robinson et al., 2006). Variable-fidelity SBO utilizes models which simulate the physical process at different fidelity levels and consequently at different computational complexity and cost (Forrester et al., 2008). The scope is to use the efficient low-fidelity (LF) models for most of the objective and/or constraint function evaluations and use the complex high-fidelity (HF) model only to correct or enhance the LF models towards the HF response. Physics-based surrogate models have been widely applied in other engineering fields (e.g. Bandler et al., 1994; Gano et al., 2004; Koziel et al., 2008; Koziel and Leifsson, 2016). However,

their use is limited in water resources optimization (Asher et al., 2015). Sreekanth and Datta (2015), in their recent review paper, do not report any similar applications specifically developed for coastal aquifer management.

In the present work, we investigate the favourable and disadvantageous aspects of using physics-based surrogate modelling techniques for a single-objective pumping optimization problem of coastal aquifers. Several LF models are employed to approximate the HF model response for the calculation of optimal pumping rates. The variable-fidelity approach is embedded within the operations of an evolutionary algorithm. The results obtained from the variable-fidelity SBO are compared against the direct optimization with the HF model and a data-driven SBO method.

2. METHODS

2.1 The fidelity concept in SWI modelling

In general, two broad levels of fidelity can be defined in SWI modelling. First, the variable-density and solute transport numerical models which provide a realistic, HF representation of coastal aquifer processes at increased computational cost (Dokou and Karatzas, 2012; Werner et al., 2013). Second, the sharp interface assumption which represents a LF approximation of coastal aquifer flow since it neglects the mixing of freshwater with seawater (Cheng et al. 1999). However, a much wider taxonomy of fidelity levels can be realized either within the same model formulation (e.g. grid resolution, convergence criteria or dimensionality), or among the different mathematical formulations of the available SWI models. For example, several sharp interface models of varying accuracy have been developed in the literature to simulate SWI (e.g. Mantoglou 2003; Pool and Carrera, 2011; Koussis et al. 2012; Koussis et al. 2015).

Due to the exploratory nature of our study, we employ the SWI models presented in Mantoglou (2003), which are based on the sharp interface theory and the single-potential formulation of Strack (1976). They provide a convenient mathematical model that has been widely used in the development of simulation-optimization routines (e.g. Mantoglou et al., 2004; Mantoglou and Papantoniou, 2008; Christelis et al., 2012; Kourakos and Mantoglou, 2015; Karatzas and Dokou, 2015). Our analysis follows the comparisons performed by Mantoglou (2003) for sharp interface models of different fidelity, in the case of finite-size coastal aquifers.

2.2 SWI models

Consider the finite-sized, coastal aquifer of rectangular shape presented in Figure 1.

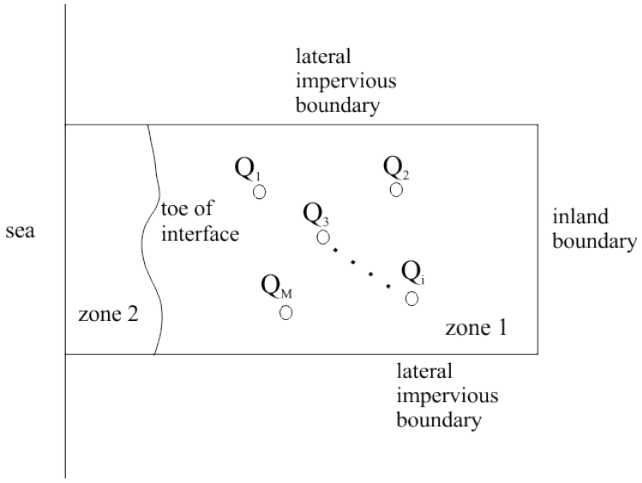

Figure 1. Plan view of a coastal aquifer of finite size pumped by M wells.

Besides the coastal fixed head boundary three other boundaries exist which affect flow. The two lateral no-flow boundaries and an inland constant flux boundary. Seawater is considered to be static and aquifer flow is horizontal and steady-state. In zone 1 unconfined flow is assumed and the aquifer is replenished by distributed groundwater recharge N while in zone 2 a freshwater lens floats above the static saltwater layer. The aquifer is pumped by M wells and a "toe" of the sharp interface between freshwater and saltwater is formed. As the groundwater abstraction from the pumping wells increases, the "toe" advances further inland. Based on the single-potential formulation of Strack (1976), the following differential equation governs the entire flow domain:

$$\frac{\partial}{\partial x}\left(K\frac{\partial \phi}{\partial x}\right)+\frac{\partial}{\partial y}\left(K\frac{\partial \phi}{\partial y}\right)+N-Q\left(x,y\right)=0 \tag{1}$$

where ϕ is the flow potential (Strack, 1976) and K is the aquifer's hydraulic conductivity. The distributed pumping rate $Q\left(x,y\right)$ is expressed as: $Q\left(x,y\right)=\sum_{j=1}^{M} Q_j\,\delta\left(x-xw_j,y-yw_j\right)$ where (xw_j,yw_j) are the coordinates of a pumping well j with rate Q_j and $\delta\left(x-xw_j,y-yw_j\right)$ is the Dirac delta function.

Mantoglou (2003) developed fast analytical SWI models for solving equation (1), by using the method of images, in the case of finite-sized coastal aquifers with homogeneous hydraulic parameters. A general expression of the derived analytical model for unconfined coastal aquifer flow is presented below:

$$\begin{aligned}
\phi\left(x,y\right)=&\frac{q}{K}x+\frac{N}{K}x\left(L-\frac{x}{2}\right)+\\
&+\sum_{j=1}^{M}\frac{Q_j}{4\pi K}\ln\left[\frac{\left(x-x_j\right)^2+\left(y-y_j\right)^2}{\left(x+x_j\right)^2+\left(y-y_j\right)^2}\right]+\sum_{j=1}^{M}\frac{Q_j}{4\pi K}\ln\left[\frac{\left(x-x_j\right)^2+\left(y+y_j\right)^2}{\left(x+x_j\right)^2+\left(y+y_j\right)^2}\right]+\\
&+\sum_{j=1}^{M}\frac{Q_j}{4\pi K}\ln\left[\frac{\left(x-x_j\right)^2+\left[y-\left(2b-y_j\right)\right]^2}{\left(x+x_j\right)^2+\left[y-\left(2b-y_j\right)\right]^2}\right]+\sum_{j=1}^{M}\frac{Q_j}{4\pi K}\ln\left[\frac{\left(x-x_j\right)^2+\left[y+\left(2b-y_j\right)\right]^2}{\left(x+x_j\right)^2+\left[y+\left(2b-y_j\right)\right]^2}\right]+\\
&+\sum_{j=1}^{M}\frac{Q_j}{4\pi K}\ln\left[\frac{\left(x-x_j\right)^2+\left[y-\left(2b+y_j\right)\right]^2}{\left(x+x_j\right)^2+\left[y-\left(2b+y_j\right)\right]^2}\right]+\sum_{j=1}^{M}\frac{Q_j}{4\pi K}\ln\left[\frac{\left(x-x_j\right)^2+\left[y+\left(2b+y_j\right)\right]^2}{\left(x+x_j\right)^2+\left[y+\left(2b+y_j\right)\right]^2}\right]+\\
&+\sum_{j=1}^{M}\frac{Q_j}{4\pi K}\ln\left[\frac{\left(x-x_j\right)^2+\left[y-\left(4b-y_j\right)\right]^2}{\left(x+x_j\right)^2+\left[y-\left(4b-y_j\right)\right]^2}\right]+\sum_{j=1}^{M}\frac{Q_j}{4\pi K}\ln\left[\frac{\left(x-x_j\right)^2+\left[y+\left(4b-y_j\right)\right]^2}{\left(x+x_j\right)^2+\left[y+\left(4b-y_j\right)\right]^2}\right]+\\
&\sum_{j=1}^{M}\frac{Q_j}{4\pi K}\ln\left[\frac{\left(x-x_j\right)^2+\left[y-\left(4b+y_j\right)\right]^2}{\left(x+x_j\right)^2+\left[y-\left(4b+y_j\right)\right]^2}\right]+\sum_{j=1}^{M}\frac{Q_j}{4\pi K}\ln\left[\frac{\left(x-x_j\right)^2+\left[y+\left(4b+y_j\right)\right]^2}{\left(x+x_j\right)^2+\left[y+\left(4b+y_j\right)\right]^2}\right]+\\
&+\cdots
\end{aligned} \tag{2}$$

where the term $\frac{q}{K}x$ represents ambient flow and the term $\frac{N}{K}x\left(L-\frac{x}{2}\right)$ accounts for surface accretion for an aquifer of length L (Mantoglou, 2003). As the number of additive terms in equation (2) is increased, the analytical model better approximates the numerical solution of equation (1) (for details see Mantoglou, 2003). Based on the above and by following Mantoglou (2003), we define 5 models of different fidelity for simulating SWI:

- LF1: the analytical model considers only the coastal boundary assuming semi-infinite dimensions.
- LF2: the analytical model considers the coastal boundary and the two lateral no-flow boundaries.
- LF3: the analytical model considers the coastal boundary, the two lateral no-flow boundaries and the inland boundary.
- LF4: the analytical model is the same with LF3 in terms of boundary conditions, but, uses more reflections for the real pumping wells to increase the accuracy of the flow solution.
- HF: the numerical solution of equation (1), using a groundwater flow code, represents the available HF simulation.

Obviously, the computational times produced by the above models are not significant since the sharp interface approximation is considered. However, they represent a hierarchy of model fidelity and complexity for simulating SWI and are utilized as a paradigm for investigating physics-based surrogate modelling techniques in coastal aquifer management.

2.3 Pumping optimization frameworks

The following optimization problem is solved in order to control SWI and calculate maximum groundwater abstraction:

$$\begin{aligned} &\min -\sum_{i=1}^{M} Q_i \\ &s.t.\ x_i^{toe}\left(Q_1, Q_2, \ldots Q_M\right) < xw_i, \forall i = 1,2,\ldots M \\ &\quad Q_{\min} \le Q_i \le Q_{\max}, i = 1,2,\ldots M \end{aligned} \tag{3}$$

The first line of the constraint functions formulate a nonlinear optimization problem (Mantoglou et al., 2004) while $Q_{\min}$ and $Q_{\max}$ define the lower and upper limits of pumping rates, respectively. The variable x^{toe} is the horizontal distance of the toe from the coast as a function of the pumping rates Q_i and xw is the horizontal distance of the wells from the coast. In order to honour the constraints, the "toe" of the interface is not allowed to reach the pumping wells. The above constrained optimization problem is transformed to an unconstrained formulation where the nonlinear constraints are embedded in the objective function using penalty terms as follows:

$$\min f\left(\mathbf{Q}\right) = \begin{cases} -\sum_{i=1}^{M} Q_i, \; if\ \forall i = 1,2\ldots M; x_i^{toe}\left(Q_1, Q_2, \ldots Q_M\right) < xw_i \\ M_v \sum_{i=1}^{Mv}\left[\max\left(\left(x_i^{toe} - xw_i\right), 0\right)\right]^2, if\ \exists i = 1,2\ldots M;\ x_i^{toe}\left(Q_1, Q_2, \ldots Q_M\right) \ge xw_i \end{cases} \tag{4}$$

Here, the evolutionary annealing-simplex (EAS) algorithm (Efstratiadis and Koutsoyiannis, 2002; Rozos et al. 2004; Tsoukalas et al., 2016) was employed to solve the optimization problem defined in equation (4). One of the advantages of EAS algorithm is that rather few parameters must be previously set. These are the initial population length m, two annealing schedule controlling parameters λ and ψ, a mutation probability p_m and a convergence criterion ε. The global exploration of the optimal search space is ensured for initial populations in the order of $m = 8 * D$, where D denotes the dimensionality of the decision variable vector (Kourakos and Mantoglou 2009). The other EAS parameters were set to $\lambda = 0.95$, $\psi = 2$, $p_m = 0.1$ and $\varepsilon = 10^{-4}$. All calculations, pre- and post-processing of the data were implemented in MATLAB environment.

Three different optimization frameworks are proposed in order to calculate the optimal solution for a problem with $M = 10$ pumping wells. The first, denoted as EAS-HF, is to combine the HF model with the EAS algorithm and solve a direct optimization problem without the use of surrogate models. This corresponds to the HF approach where the most complex and computationally expensive model is used. The second, demoted as EAS-VF, is the variable-fidelity approach that we develop in this paper.

Let the vectors $\mathbf{G}_{HF}(\mathbf{Q})$ and $\mathbf{G}_{LF}(\mathbf{Q})$ represent the x^{toe} calculations for the M pumping wells, of the HF and the LF model respectively. Where $\mathbf{Q}$, is a decision variable vector of pumping rates proposed by EAS-VF algorithm. The LF models approximate the location of the interface "toe" with errors comparative to the HF model (see Mantoglou, 2003). However, the LF models offer a faster, less complex approach in order to calculate the optimal pumping rates. Since the LF and the HF models share the shame physics, we apply a variable-fidelity SBO framework similar to the concept of implicit space mapping (ISM) developed by Bandler et al. (2004). In general, the ISM method proposes an optimization scheme where fixed parameters of the HF model are iteratively adjusted in the LF model in order to minimize the differences between the HF and LF models. A similar optimization scheme was developed by Christelis and Mantoglou (2016b) which corrects the density ratio of a LF sharp interface model and adjusts its response towards that of a variable-density and salt transport model. Although not explicitly formulated in their work, that approach has also some similarities with the ISM technique.

In this case, we select the hydraulic conductivity K fixed for the HF model F5, but, it is utilized as a black-box parameter subject to calibration in the LF models. Thus, an unconstrained optimization sub-problem is also defined where an optimal value K is calculated based on the following minimization:

$$\min_{K} g(K) = \sqrt{\frac{\left(\mathbf{G}_{HF}(\mathbf{Q}) - \mathbf{G}_{LF}(\mathbf{Q},K)\right)^2}{M}} \tag{5}$$

Note that problem (5) is based on function evaluations with the LF model. Thus, if the latter is not significantly faster than the HF model, then it will add considerable cost to the primary optimization problem (equation 4). In order to further enhance the alignment between the HF and the LF models a relation is also established between the vector $\mathbf{Q}$ and the optimal value K, by using a data-driven model. In this study, we employ a cubic radial basis function (RBF) model which predicts an optimal value $\widehat{K}$, given a proposed vector $\mathbf{Q}$ from the EAS-VF algorithm. Thus, the x^{toe} calculation from the enhanced LF model is given by:

$$\widehat{\mathbf{G}}_{HF} = \mathbf{G}_{LF}\left(\mathbf{Q},\widehat{K}\right) \tag{6}$$

In summary, the EAS-VF algorithm steps are the following:

1. Define the initial population of the EAS algorithm and other required parameters.
2. Create a sampling design of points $\mathbf{Q}$ and of size n and evaluate the HF model.
3. Find the best objective function value from step 2 and add the related vector $\mathbf{Q}$ to the initial population.
4. For each evaluated point from step 2, solve problem (5) and create an archive for the optimal K values and the related points $\mathbf{Q}$.
5. Train the RBF model on the archived multidimensional inputs $\mathbf{Q}$ and optimal values K.
6. Run EAS algorithm using the physics-based surrogate model (equation 6).
7. If a better current optimum is found with the physics-based surrogate model, evaluate the related $\mathbf{Q}$ with the HF model. Solve problem (5) and store $\mathbf{Q}$ and optimal K to the archive.
8. Are the EAS convergence criteria met? If yes provide optimal solution, else go to step 5.

For step 2 of EAS-VF we use a Latin Hypercube Sampling technique (Mckay et al. 2000) in the order of $2*D+1$. The third optimization approach, denoted as EAS-RBF, is a data-driven SBO approach which utilizes cubic RBF models for replacing the HF model and it is also embedded in the EAS algorithm (Christelis and Mantoglou, 2016a).

3. RESULTS AND CONCLUSIONS

The above optimization frameworks were tested for 30 independent trials due to the stochastic nature of EAS algorithm. The distribution of optimal solutions for all methods is demonstrated in Figure 2.

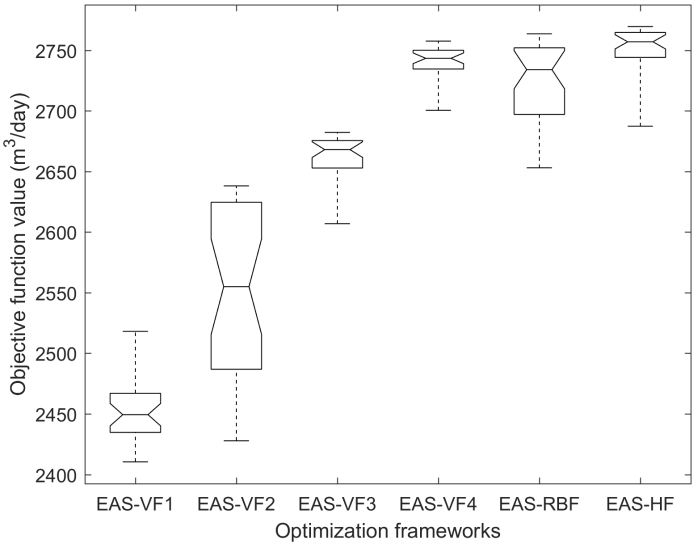

Figure 2: Boxplots of the distribution of best optimal values among the different optimization frameworks .

Results indicate that among the variable-fidelity optimization frameworks EAS-VF1, EAS-VF2, EAS-VF3 and EAS-VF4, only the one developed with the most accurate model LF4 provides a good agreement with the EAS-HF solutions. Thus, the differences between the HF and the other LF models could not be adequately reduced using the EAS-VF framework. The RBF-EAS results are also in good agreement with the HF-based optimization. RBF-EAS found a better maximum solution compared to the EAS-VF4, however, it has a less symmetrical distribution of optimal values and a lower median than EAS-VF4. Furthermore, none of the box plot notches of the SBO methods appear to overlap with those of the EAS-HF approach. This is an indication that the optimal SBO results may have a different "true" median from the EAS-HF algorithm. Note that despite the simplicity of the flow equation (1), the response of the constraint functions is markedly non-smooth and non-linear close to the region of optimal solutions (see Mantoglou, 2003). That is, the objective function receives increased penalty values even with small perturbations around the optimal solutions. As a result, the particular HF-based optimization problem is not an easy task for SBO strategies.

In terms of computational gains, it is worth mentioning the median of the number of HF evaluations required for EAS algorithm to converge. The EAS-HF has a median of 7322 HF runs, the EAS-VF4 has a median of 153 HF runs and the RBF-EAS has a median of 271 HF runs. Interestingly, the variable-fidelity SBO framework EAS-VF4 used almost half of the HF runs to converge among the 30 trials comparative to the data-driven approach RBF-EAS.

The results indicate that the developed variable-fidelity SBO method required a LF model which is in good agreement with the HF model in order to approximate the HF-based optimization results. Further research is underway on different correction and enhancement methods for the development of variable-fidelity SBO strategies in coastal aquifer management.

REFERENCES

Asher, M. J., Croke, B. F. W., Jakeman, A. J., Peeters, L. J. M., 2015. A review of surrogate models and their application to groundwater modelling. Water Resour Res 51(8):5957-5973.

Bandler, J. W., Biernacki, R. M., Chen, S. H., Grobelny, P. A., Hemmers, R. H., 1994. Space mapping technique for electromagnetic optimization, IEEE T MicrowTheory 42(12):2536-2544.

Bandler, J. W., Cheng, Q. S., Nikolova, N. K., Ismail M. A., 2004. Implicit space mapping optimization exploiting preassigned parameters. IEEE T. Microw.Theory, 52(1):378-385.

Cheng, A. H. D., Ouazar, D., 1999. Analytical solutions. J Bear, A.H.-D Cheng, S Sorek, D Ouazar, I Herrera (Eds.), Seawater Intrusion in Coastal Aquifers—Concepts, Methods and Practices, Kluwer Academic Publishers, Dordrecht.

Christelis, V., Kopsiaftis, G., Mantoglou, A., 2012. Coastal aquifer management under drought conditions considering aquifer spatial variability. IAHS-AISH Publication 293-297.

Christelis, V., Mantoglou, A., 2016a. Pumping optimization of coastal aquifers assisted by adaptive metamodeling methods and radial basis functions. Water Resour Manage doi:10.1007/s11269-016-1337-3.

Christelis, V., Mantoglou, A., 2016b. Coastal aquifer management based on the joint use of density-dependent and sharp interface models. Water Resour Manage 30(2):861-876.

Dokou, Z., Karatzas, G. P., 2012. Saltwater intrusion estimation in a karstified coastal system using density-dependent modelling and comparison with the sharp-interface approach. Hydrolog Scis J 57(5):985–999.

Efstratiadis A, Koutsoyiannis, D., 2002. An evolutionary annealing-simplex algorithm for global optimization of water resource systems, Proceedings of the Fifth International Conference on Hydroinformatics, Cardiff, UK, International Water Association Publishing 2:1423-1428.

Forrester, A. I. J., Sóbester, A., Keane, A. J., 2008. Engineering design via surrogate modelling-A practical guide. Wiley, New York.

Forrester, A. I. J., Keane, A. J., 2009. Recent advances in surrogate-based optimization. Prog Aerosp Sci 49:50-79.

Gano, S., Sanders, B., Renaud, J.,2004. Variable fidelity optimization using a kriging based scaling function. In 10th AIAA/ISSMO Multidisciplinary analysis and optimization conference (p. 4460).

Karatzas, G. P., Dokou, Z., 2015. Optimal management of saltwater intrusion in the coastal aquifer of Malia, Crete (Greece) using particle swarm optimization, Hydrogeol J 23(6):1181-1194.

Ketabchi, H., Ataie-Ashtiani, B., 2015. Evolutionary algorithms for the optimal management of coastal groundwater: A comparative study toward future challenges. J Hydrol 520:193-213.

Koziel, S., Bandler, J. W., Madsen, K., 2008. Quality assessment of coarse models and surrogates for space mapping optimization, Optim Eng, 9(4):375-391.

Koziel, S., Leifsson. L., 2016. Simulation-Driven Design by Knowledge-Based Response Correction Techniques, New York, Springer.

Kourakos, G., Mantoglou, A., 2009. Pumping optimization of coastal aquifers based on evolutionary algorithms and surrogate modular neural network models. Adv Water Resour 32(4):507-521.

Kourakos, G., Mantoglou, A., 2015. An efficient simulation-optimization coupling for management of coastal aquifers. Hydrogeol J 23(6):1167-1179.

Koussis, A.D., Mazi, K., Destouni, G., 2012. Analytical single-potential, sharp-interface solutions for regional seawater intrusion in sloping unconfined coastal aquifers, with pumping and recharge. J Hydrol 416-417:1-11

Koussis, A.D., Mazi, K., Riou, F., Destouni, G., 2015. A correction for Dupuit–Forchheimer interface flow models of seawater intrusion in unconfined coastal aquifers. J. Hydrol., 525:277-285.

Mantoglou, A., 2003. Pumping management of coastal aquifers using analytical models of saltwater intrusion. Water Resour Res 39(12):1335.

Mantoglou, A., Papantoniou, M. Giannoulopoulos, P., 2004. Management of coastal aquifers based on nonlinear optimization and evolutionary algorithms. J Hydrol 297(1–4):209–228.

Mantoglou, A., Papantoniou, M., 2008. Optimal design of pumping networks in coastal aquifers using sharp interface models. J Hydrol 361:52–63.

McKay, M. D. Beckman, R. J., Conover W. J., 2000. A comparison of three methods for selecting values of input variables in the analysis of output from a computer code. Technometrics, 42(1):55-61.

Papadopoulou, M. P., Nikolos, I. K., Karatzas, G. P., 2010. Computational benefits using artificial intelligent methodologies for the solution of an environmental design problem: saltwater intrusion. Water Sci Technol 62(7):1479-1490.

Pool, M., Carrera, J., 2011. A correction factor to account for mixing in Ghyben-Herzberg and critical pumping rate approximations of seawater intrusion in coastal aquifers. Water Resour Res 47(5).

Razavi, S., Tolson, B. A., Burn, D. H., 2012a. Numerical assessment of metamodelling strategies in computationally intensive optimization. Environ Modell Softw 34:67-86.

Razavi, S., Tolson, B. A., Burn, D. H., 2012b. Review of surrogate modelling in water resources. Water Resour Res 48(7).

Robinson, T., Willcox, K., Eldred, M., Haimes, R.. 2006. Variable-fidelity optimization for variable-complexity design. In 11th AIAA/ISSMO multidisciplinary analysis and optimization conference (p. 7114).

Roy, D. K., Datta, B., 2016. Fuzzy C-Mean Clustering Based Inference System for Saltwater Intrusion Processes Prediction in Coastal Aquifers. Water Resour Manage doi:10.1007/s11269-016-1531-3.

Rozos, E., Efstratiadis, A., Nalbantis, I., Koutsoyiannis, D., 2004. Calibration of a semi-distributed model for conjunctive simulation of surface and groundwater flows. Hydrol Sci J 49(5): 819-842.

Singh, A., 2014. Optimization modelling for seawater intrusion management. J Hydrol 508:43-52.

Sreekanth, J., Datta, B., 2011. Comparative evaluation of Genetic Programming and Neural Network as a potential surrogate models for coastal aquifer management. Water Resour Manage 25:3201-3218.

Sreekanth, J., Datta, B., 2015. Review: Simulation-optimization models for the management and monitoring of coastal aquifers. Hydrogeol J doi:10.1007/s10040-015-1272-z.

Strack, O. D. L., 1976. A single-potential solution for regional interface problems in coastal aquifers. Water Resour Res 12 (6):1165–1174.

Tsoukalas, I., Kossieris, P., Efstratiadis, A., Makropoulos, C., 2016. Surrogate-enhanced evolutionary annealing simplex algorithm for effective and efficient optimization of water resources problems on a budget. Environ Modell Softw, 77:122-142.

Werner, A. D., Bakker, M., Post, V. E. A., Vandenbohede, A., Lu, C., Ataie-Ashtiani, B., Simmons, C. T., Barry, D. A., 2013. Seawater intrusion processes, investigation and management: Recent advances and future challenges. Adv Water Resour 51:3-26.

Proceedings of the 10th World Congress of EWRA 'Panta Rhei', 5-9 July 2017, Athens, Greece
© 2017 *European Water Resources Association*

Phreatic / confined flows in polygons: Dupuit-Forchheimer model versus potential solutions

A.R. Kacimov[1*], A. Al-Maktoumi[1] and Y.V. Obnosov[2]
[1] *Department of Soils, Water and Agricultural Engineering, Sultan Qaboos University, Oman*
[2] *Institute of Mathematics and Mechanics, Kazan Federal University, Kazan, Russia*
[*] *e-mail: anvar@squ.edu.om*

Abstract: Analytical and numerical (HYDRUS2D and MODFLOW) solutions for steady unconfined Darcian flows with accretion and leakage in a single aquifer is obtained for domains bounded by trigons (in particular common triangles) and polygons that allows modeling catchment-scale groundwater flows. Strack's comprehensive potential obeys the 2-D Poisson equations, which assumes the Dupuit-Forchheimer vertical averaging of the head. Along the lateral boundaries in 2-D flows and leaky layer in 1-D flow, Robin's condition models clogging of river/wadi banks and beds. In a layered aquifer, confined flows are decoupled into two types of analytic elements: highly-low permeable strata with 1-D and essentially 2-D seepage, correspondingly. The conjugation between these fragments is based on a "seepage shear" condition. This leads to a boundary condition along the interfaces between the two types of commingled strata, which is similar to Kirkham-Brock's one. The method of hodograph is used for two types of 2-D potential flow fragments: arbitrary triangles and trapezia. By routines of computer algebra, the complex potential and physical domain are parametrized via an auxiliary variable. Deviation from trivial 1-D approximations in 2-D fragments are found. Implications for groundwater quality, dissolution of the porous skeleton of the strata and soil erosion by suffusion, as triggered by an intricate "winding" of flow paths between the strata, are discussed.

Key words: Seepage refraction, hodograph, leaky layer, infiltration, numerical simulations

1. INTRODUCTION

In groundwater hydrology and geotechnical/reservoir engineering, steady Darcian flows through saturated porous materials often involve a basic analytic element of a stratified domain consisting of two rectangular horizontal layers OB_1B_2C and OCC_1O_1 of contrasting hydraulic conductivities, K_1 and K_2, sandwiched between an impermeable bedrock and caprock (Fig.1).

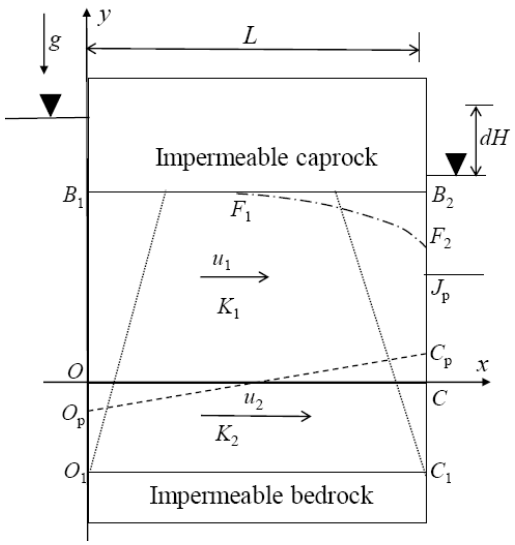

Figure 1. Two-layered aquifer.

If the inlet O_1OB_1 and outlet C_1CB_2 are vertical and "fully submerged" under the corresponding left-right river levels, then flow in both strata of Fig.1 is strictly horizontal and not commingled. The Darcian velocities $u_1=K_1\ dH/L$ and $u_2=K_2\ dH/L$ do not depend on each other and there is no cross-flow from one layer to another. Then the stream tubes are rectangles, with the stremalines parallel to the interface.

In aquifers, soils, earth dams and even laminated porous chemical reactors the ideal conceptualization of Fig.1 does not realize and gravity, multiple external inputs (leakage through aquitards, infiltration-evaporation, unsaturated zones, among others) distort the 1-D flow regimes and then gravity, Darcian resistance and capillarity make complicated topology of water fluxes and fields of state variables (pore pressure, velocity, moisture content, temperature, concentration of dissolved solutes) as investigated in Polubarinova-Kochina (1977), Strack (1989) and Toth (2009).

In this paper, we study one-phase water/moisture flows in rigid aquifers and the following physical perturbations of the trivial 1-D flows in Fig. 1:

a) The interface OC can be tilted (a dashed line O_pC_p in Fig.1);
b) The inlet and outlets (dotted lines O_1B_{1p} and C_1B_{2p}) can be non-vertical;
c) The water level in the rivers of Fig.1 can drop beneath the bedrock (for example, point B_2 drops to point J_p) such that a phreatic surface F_1F_2 (dashed-dotted line) and seepage face F_2J_p are formed;
d) The confining upper and lower rocks can be slightly permeable and accretion or losses from layers 1 and 2 can take place as infiltration or leakage;
e) The segments O_1B_1 and C_1B_2 can be "clogged" by a thin layer of low-permeable sediments.

The impact of perturbation a) has been addressed in Kacimov and Obnosov (1995, 1997, 2000, 2012), Kacimov et al. (1999) as the problem of refraction (conjugation) of two 2-D confined flows. In refraction, the normal component of the Darcian velocity vectors and pore pressures across O_pC_p are continuous but the velocity components tangential to the interface jump. Only in view types of tilted interfaces O_pC_p exact analytical solutions are possible. Therefore, simplified analytical analysis of perturbations b)-e) calls for benchmarking with numerical solutions. Our main assumption is: the substratum of conductivity K_2 or clogging of the riverbank is thin and flow there is 1-D and either along or across the layer.

2. TWO-DIMENSIONAL FLOW IN TRIANGULAR SEEPAGE-FACED DOMAIN WITH THIN "SHEARING" SUBSTRATUM

In this section we consider a special case of a two-layered conduit in Fig. 1: a relatively low permeable triangle OBC and a highly-permeable subjacent trapezium O_1OCC_1 (Fig.2a). The segment BC_1 is a seepage face. We introduce Cartesian coordinates xOy, the abscissa axis coinciding with the interface. The trapezium (Fig.2b) has a small thickness d and the upper base OC of a size $L = H(\cot\pi\alpha + \cot\pi\gamma)$. The middle line of the trapezium is L_1, $L_1>L$. We assume that flow in the trapezium is 1-D, horizontal (along the layer) and not affected by flow in the triangle. This assumption holds if $K_2>>K_1$. In the superjacent triangle, flow is 2-D and is influenced by the "seepage shear" in the trapezium (see Kacimov, 2006).

We approximate the sides O_1O and C_1C of the trapezium in Fig. 2b as vertical segments (in reality they are not) and C_1C as a constant head outlet (although this line is a seepage face). Then from Darcy's law the velocity in the trapezium can be approximated as:

$$u_2 = K_2 H_0 / L_1 \tag{1}$$

The triangle OBC, G_z, has angles $\alpha\pi$, $\beta\pi$ and $\gamma\pi$ (clearly, $\alpha+\beta+\gamma=1$), and height $H=H_0-d$. We consider the case $\beta<\pi/2$. Davison (see Khristianovich et al., 1938) studied flow in triangular cores assuming that OC in Fig.2a is a no-flow boundary. In this paper, the boundary condition along OC

is determined from the refraction condition of two commingled flows: a 2-D in G_z and approximate 1-D in the subjacent trapezium. The horizontal component u_1 of the velocity vector $V_1(u_1,v_1)$ in G_z obeys the following conjugation boundary condition along *OC* (Polubarinova-Kochina, 1977):

$$u_1 / K_1 = u_2 / K_2 \tag{2}$$

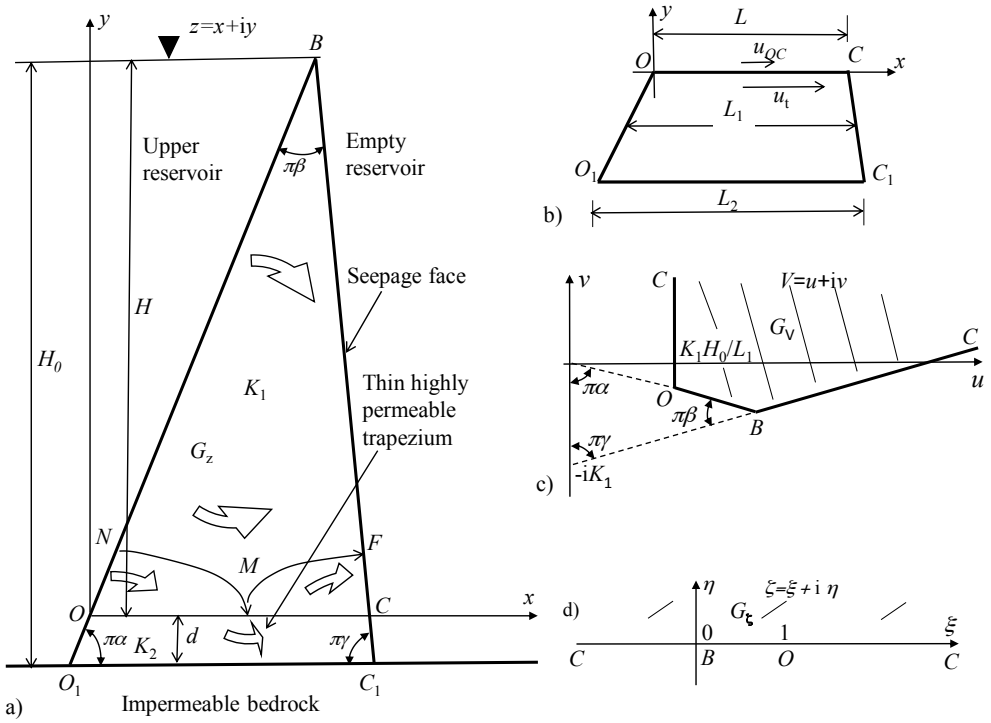

Figure 2. Vertical cross-section of flow through two commingles porous fragments (a), trapezoidal substratum (b), hodograph domain for 2-D flow in triangle, auxiliary complex plane (d).

From Eqs. (1) and (2) the horizontal component of velocity along the bottom of the triangle is:

$$u_{OC} = K_1 H_0 / L_1 \tag{3}$$

This condition is analogous to the Kirkham-Brock boundary condition of a constant vertical component of velocity at the bottom of a porous flow domain with a very low-permeable underlay (Kacimov and Obnosov, 2015).

For flow in the triangle G_z, we introduce a complex physical plane $z=x+iy$ and complex potential $w=\phi+i\psi$ ($\phi=-K_1 h$, $h=p+y$, h is the total hydraulic head and p is the pressure head). A complexified Darcian velocity is $V=u+iv$ (we drop the subscript "1"). The hodograph domain G_V in Fig. 2c is a trigon whose angles are determined as in Polubarinova-Kochina (1977). According to Eq. (3), the vertical ray *OMC* passes through the point $V_M=\text{const}=K_1H_0/L$. The domain G_ω, $\omega=\mathrm{d}w/\mathrm{d}z$, is a mirror image of G_V with respect to the horizontal axis. We map conformally G_ζ, the upper half of an auxiliary ζ-plane, onto G_z (see Fig.2d) by the Schwartz-Christoffel transformation:

$$z(\zeta) = -c_1 e^{i\pi\alpha} \int_1^{\zeta} \tau^{\beta-1}(1-\tau)^{\alpha-1}\,\mathrm{d}\tau = c_1 e^{i\pi\alpha} \int_0^{1-\zeta} \tau^{\alpha-1}(1-\tau)^{\beta-1}\,\mathrm{d}\tau \tag{4}$$

The positive mapping constant c_1 in eqn. (4) is determined by the condition $z(0)=H(\cot\pi\alpha+i)$ as:

$$c_1 = \frac{H}{\sin \pi\alpha} / \int_0^1 \tau^{\beta-1}(1-\tau)^{\alpha-1} \mathrm{d}\tau = \frac{H}{\sin \pi\alpha B(\alpha,\beta)}$$

Then Eq. (4) upon integration becomes:

$$z(\zeta) = e^{\mathrm{i}\pi\alpha} \frac{H\,\mathrm{B}(1-\varsigma;\alpha,\beta)}{\sin \pi\alpha\,\mathrm{B}(\alpha,\beta)} \tag{5}$$

Here $\mathrm{B}(\alpha,\beta)$ is the Euler beta function and $\mathrm{B}(z;\alpha,\beta)$ is the incomplete beta function. At point *C* the width $L = z(\infty) = H(\cot \pi\alpha + \cot \pi\gamma)$.

The boundary conditions for an analytic function ω=dw/dz=u- iv are:

BC: v=$\cot \pi\gamma$ u - K_1
OB: $v = -\cot \pi\alpha$ u
OC: u=$K_1 H_0 / L_1$

wherefrom we get:

$$V_B = u_B + \mathrm{i}v_B = \frac{K_1}{\cot \pi\alpha + \cot \pi\gamma} - \mathrm{i}\frac{K_1 \cot \pi\alpha}{\cot \pi\alpha + \cot \pi\gamma} = -\mathrm{i}e^{\mathrm{i}\pi\alpha} K_1 \frac{\sin \pi\gamma}{\sin \pi\beta},$$

$$V_O = u_O + \mathrm{i}v_O = \frac{K_1 H_0}{L_1} - \mathrm{i}\frac{K_1 H_0}{L_1} \cot \pi\alpha = -\mathrm{i}e^{\mathrm{i}\pi\alpha} \frac{K_1 H_0}{L_1 \sin \pi\alpha}.$$

Similarly, taking into account that $B = \mathrm{i}e^{-\mathrm{i}\pi\alpha} K_1 \sin \pi\gamma / \sin \pi\beta$, we map G_ζ onto G_ω by the Schwartz-Christoffel integral:

$$\omega(\varsigma) = \mathrm{d}w / \mathrm{d}z = -\mathrm{i}e^{-\mathrm{i}\pi\alpha} \left(c_2 \int_0^\varsigma \tau^{-\beta}(1-\tau)^{-\alpha} \mathrm{d}\tau - \frac{K_1 \sin \pi\gamma}{\sin \pi\beta} \right) \tag{6}$$

where the positive mapping constant c_2 has to be found from the given position of point $O = \omega(1) = \mathrm{i}e^{-\mathrm{i}\pi\alpha} K_1 H_0 / (L_1 \sin \pi\alpha)$ in G_ω. Then Eq. (6) upon integration transforms to:

$$\mathrm{d}w / \mathrm{d}z = -\mathrm{i}e^{-\mathrm{i}\pi\alpha} \frac{K_1 \sin \pi\gamma}{\sin \pi\beta} \left(\frac{H_0}{H} \frac{\mathrm{B}(\varsigma;1-\beta,1-\alpha)}{\mathrm{B}(1-\beta,1-\alpha)} \left(1 - L / L_1\right) - 1 \right) \tag{7}$$

From Eqs. (5) and (7) we get:

$$w(\zeta) = \int_1^\varsigma \frac{\mathrm{d}w}{\mathrm{d}z} \frac{\mathrm{d}z}{\mathrm{d}\varsigma} \mathrm{d}\varsigma = -\frac{e^{\mathrm{i}\pi\alpha} H}{\sin \pi\alpha\,\mathrm{B}(\alpha,\beta)} \int_1^\varsigma \frac{\mathrm{d}w}{\mathrm{d}z} \varsigma^{\beta-1}(1-\varsigma)^{\alpha-1} \mathrm{d}\varsigma$$

$$w(\zeta) = \mathrm{i}\frac{\gamma K_1}{\pi} \left[\left(1 - L / L_1\right) H_0 \int_1^\varsigma \frac{\mathrm{B}(t;1-\beta,1-\alpha)}{t^{1-\beta}(1-t)^{1-\alpha}} \mathrm{d}t - H\,\mathrm{B}(1-\beta,1-\alpha)\,\mathrm{B}(1-\varsigma;\beta,\alpha) \right] \tag{8}$$

where w_O=w(1)=0. Therefore, the flow rate through *OB* is:

$$\psi_B = \mathrm{Im}\, w(0) = K_1\left[H\frac{\sin\pi(\alpha+\beta)}{\sin\pi\alpha\sin\pi\beta} - \frac{\gamma}{\pi}\left(1 - L/L_1\right)H_0\int_0^1 \frac{\mathrm{B}(t;1-\beta,1-\alpha)}{t^{1-\beta}(1-t)^{1-\alpha}}\mathrm{d}t\right] \tag{9}$$

i.e. ψ_B depends linearly on L/L_1.

We used Eq. (7) for plotting the magnitude of the Darcian velocity vector along *OC* in Fig.2. If this vector is oriented from the triangle into the substratum and the hydraulic gradient exceeds a safe limit (Polubarinova-Kochina, 1977 suggested this limit to be 1) an internal erosion across the interface takes place. This insidious phenomenon (suffusion) is much more difficult to combat than a common "visible" erosion along BC_1 (see Yakimov and Kacimov, 2017). In Fig. 2, a separatrix *NMF* divides flow into a part which passes through the first medium only and a "winding" part which dives into and re-emerges from the substratum. This topology is of concern in evaluations of groundwater quality which depends on the residence time of water particles within a specific hydrostratigraphic unit.

3. ONE-DIMENSIONAL DUPUIT-FORCHHEIMER FLOW IN LEAKY AQUIFER WITH ACCRETION

In this section we consider perturbation c). Without any loss of generality, we assume the water levels in both rivers of Fig.1 below the caprock and being constant, h_L (Fig.3). The caprock is slightly permeable and infiltrates with a given intensity of $N>0$ that recharges the phreatic surface *BC*. The horizon H=const>0 in Fig.3 is determined by a constant total hydraulic head H in the deeper aquifer which supplies water through a leaky layer. Due to symmetry the watershed between the two rivers is considered as the *Oy* axis.

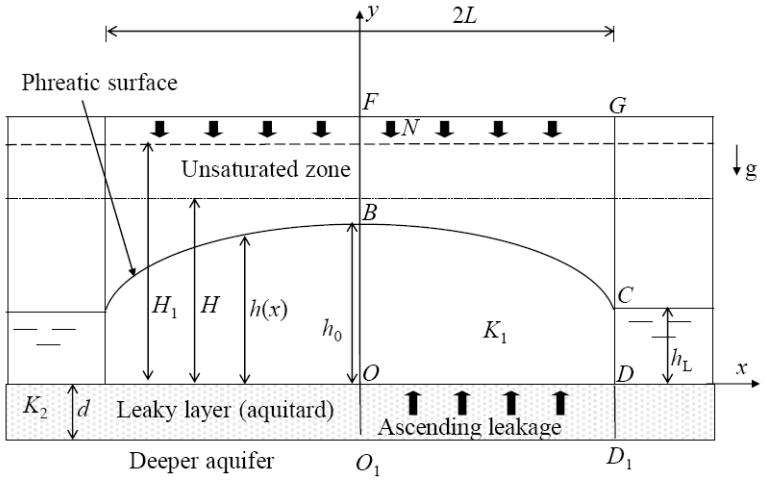

Figure 3. Vertical cross-section of phreatic flow with leaky layer and infiltration.

Recently, Strack (2017) and Ausk and Strack (2015) investigated stratified aquifers similar to one in Fig.3 using the Dupuit-Forcheimer model. In this model, flow is vertically averaged that results in the following boundary-value problem for an ordinary differential equation (ODE):

$$\begin{aligned} &K_1\frac{\mathrm{d}}{\mathrm{d}x}\left(h\frac{\mathrm{d}h}{\mathrm{d}x}\right) = \frac{K_2}{d}(h-H) - N, \quad 0 \le x \le L, \\ &h(L) = h_L, \qquad \frac{\mathrm{d}h}{\mathrm{d}x}(0) = 0, \end{aligned} \tag{10}$$

where *h(x)* is the saturated thickness measured from *OD* in Fig.3. Leakage from a deeper aquifer is counted through the Robin boundary condition (the first term in the RHS of eqn.(10)). We introduce

$\omega = \sqrt{K_2 / (\mathrm{K}_1\, dH_1)}$, H_1=H+Nd/K_2, the maximum water table height is h_0. Dimensionless variables are: $(h^*, h_0^*, h_L^*, x^*, L^*) = (h/H_1, h_0/H_1, h_L/H_1, \omega x, \omega L)$. We drop the superscript "*" for the sake of brevity. Then Eq. (10) becomes a nonlinear ODE:

$$\frac{\mathrm{d}}{\mathrm{d}x}\left(h\frac{\mathrm{d}h}{\mathrm{d}x}\right) = h - 1. \tag{11}$$

We followed Rybakova and Emikh (1966) and linearised Eq. (10) by multiplying it by $(h+1)/(2h_a)$ where $h_a = (h_0 + 1)/2$. The resulting linear ODE is integrated as:

$$h^2 = 1 - (1 - h_L^2)\frac{\cosh(x/\sqrt{h_a})}{\cosh(L/\sqrt{h_a})}. \tag{12}$$

At x=0 Eq. (12) reads:

$$h_0^2 = 1 - (1 - h_L^2)\frac{1}{\cosh[L/\sqrt{(h_0+1)/2}]} \tag{13}$$

which is a nonlinear equation with respect to h_0. We solved Eq. (13) by computer algebra and compared the results with the solution of the non-linear Eq. (11), which dates back to Boussinesq (see Polubarinova-Kochina, 1977). We showed that the water tables in the two cases practically coincide.

We also used HYDRUS2D FEM code (Šimůnek et al., 2008) and simulated a transient saturated-unsaturated flow governed by the Richards equation. We selected a rectangular domain O_1FGDD_1 (Fig. 3) of sizes $2L$=20 m and $|OF|$=2 m. This rectangle is composed of a thin silty clay layer O_1ODD_1 of conductivity K_2=0.48 cm/day, d= 20 cm, and an overlying coarser layer $OFGD$, a sandy loam with K_1 = 106 cm/day, 180 cm thick. The initial condition in terms of the pressure head is p_0=-100 cm. The flow domain discretization was 20 and 10 layers in x- and z- directions. The boundary conditions for the right half of the flow domain in Fig. 3 are: a constant total head h_L=60 cm along CD, no flux along O_1OF and D_1D, vertical infiltration flux N=2 cm/day along FG, seepage face condition along CG, and constant positive pressure head p=80 cm along O_1D_1. The Van Genuchten-Mualem soil properties are selected for both strata from the Soil Catalogue of HYDRUS.

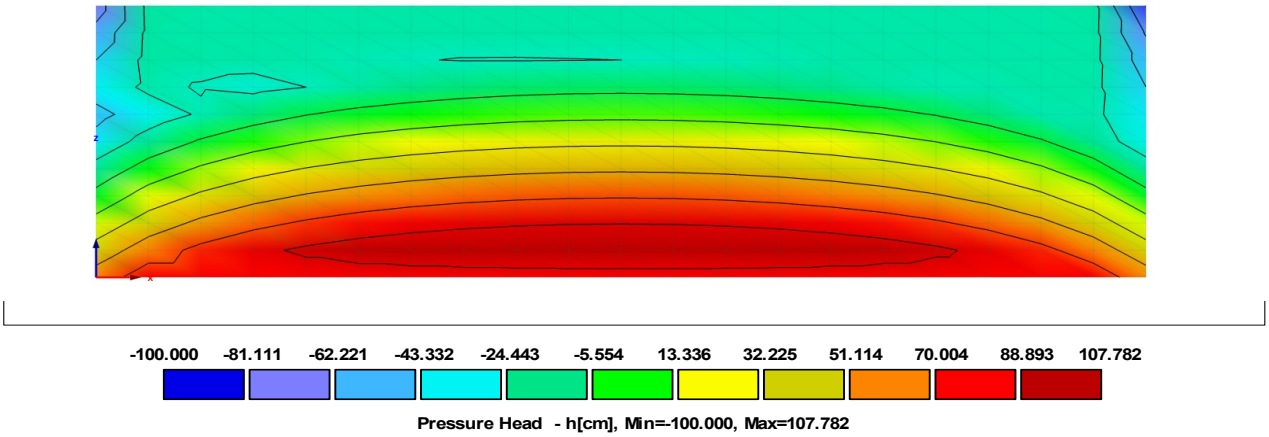

Figure 4. HYDRUS2D calculated pore pressure head in a vertical cross-section of Fig. 3.

HYDRUS2D gives distributions of $p(x,y,t)$ (Fig. 4), moisture content, $m(x,y,t)$, velocity magnitude, $V(x,y,t)$ and its horizontal $u(x,y,t)$ and vertical $v(x,y,t)$ components. Simulations were run for 40 days and steady-state flow established in about 20 days that was monitored at a set of observational nodes within the rectangles. HYDRUS2D-computed steady-state h_0 is almost the same as in the analytical solution, Eq. (12). The Dupuit-Forchheimer model does not, obviously, predict the vertical variation of the total head $h(x,y)$ or $V(x,y)$, as HYDRUS2D or the potential model in Section 2 do. From Fig.4 we see that at steady state conditions there is a distinct maximum of the pore pressure $p(0,y)$= 108 cm just above point O in Fig. 3. Similarly to Section 2, we checked that the hydraulic gradient at the interface between the fine substratum and coarser layer is within the suffusion limit.

4. TWO-DIMENSIONAL DUPUIT-FORCHHEIMER FLOW IN A TRIANGULAR AQUIFER WITH ACCRETION AND CLOGGED RIVER BANKS.

In Section 3 the groundwater mound was symmetric with respect to the discharge outlets (parallel rivers) and in the "leaky" substratum (aquitard) of Fig.4 flow was 1-D vertical posited in eqn. (10). The discharge boundary may have a polygonal shape that corresponds to islands, promontories, meandering rivers, among others. In this Section, we model 2-D Dupuit-Forchheimer flow with accretion on the phreatic surface in the same triangular domains as in Kacimov et al. (2016), with the following difference: along the river banks (the triangle boundary) the Robin rather than Dirichlet's boundary condition holds. In other words, flow through clogged river banks is normal to the triangle sides and the flux is proportional to the head difference in the aquifer (unknown and varying along the triangle sides) and river (fixed and known).

A numerical solution has been obtained by a MODFLOW-based FDM (Simcore Software, 2012). A regular triangular domain was considered. All external boundaries of the triangle are constant head river boundaries. The hydraulic head in the river (triangle's exterior) is 9 m whereas the initial head in the aquifer (triangle's interior) is 10 m, the triangle height is 300 m, K_1 =10 m/day for the aquifer and K_2= 1 m/day for the clogging layer of the river bank, the recharge rate N=0.09 m/day, aquifer's porosity =0.35, and the aquifer thickness is 20 m. The grid cells are uniform in the x- and y- directions: $dx = dy$ = 3 m away from the triangle sides. The grid is refined to $dx = dy$ = 1m as the triangle boundary is approached. This results in a mesh of 134 rows and 150 columns, the total number of active cells is 46503 with a volume of 930060 m^3. The Preconditioned Conjugate Gradient (*PCG*2) solver has been selected for solving the flow equation with a convergence criterion of 0.001.

The MODFLOW calculated water table surface is shown in Fig. 5a and the head distribution line at a cross section A-A` is presented by Fig. 5b.

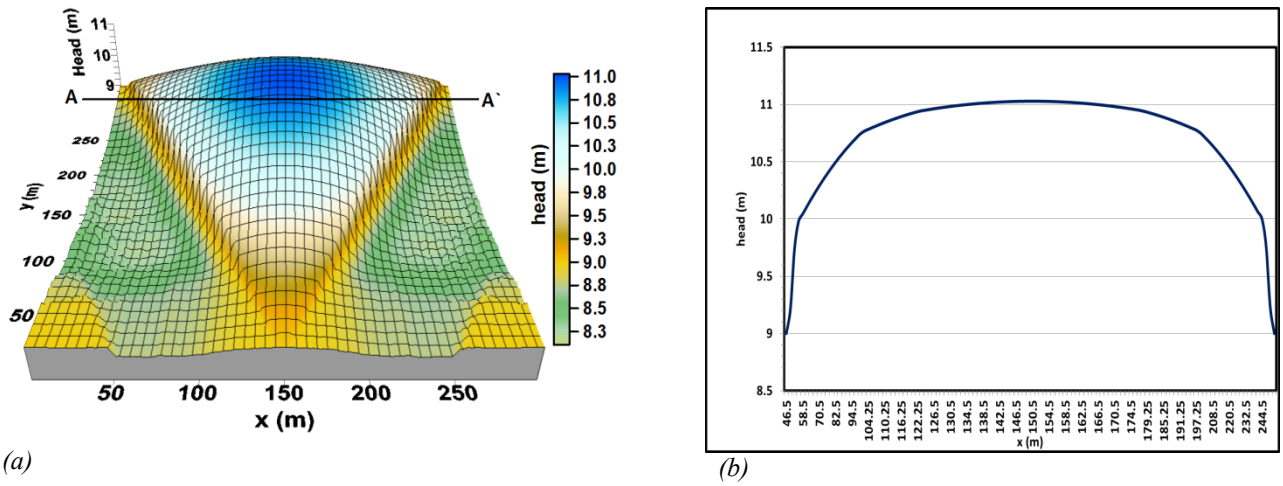

(a) (b)

Figure 5. (a) MODFLOW calculated 3-D water table surface; (b) water table across the cross-section A-A`.

MODFLOW simulation results illustrate that the clogged riverbank induces a water table mound with a maximum at the centre of the triangle significantly higher than that for the constant head bank (Kacimov et al., 2016). The low permeability "cake" of the river-bank causes a steep hydraulic gradient at the aquifer-riverbank interface (*dh/dx=0.175*), a lower than 0.02 gradient elsewhere in the domain (with a minimum reaching a value of 0.0001 across cells at the apex of the mound.

5. CONCLUDING REMARKS

Analytical and numerical solutions obtained for steady-state or asymptotic steady-state limits of transient saturated or saturated-unsaturated flows, if juxtaposed, provide insight of a complex topology and field values of groundwater characteristics: total head, pore pressure, and Darcian velocity in aquifers of polygonal geometry, both in a vertical and planar cross-sections. The corresponding simulations are indispensable tools in water resource management.

REFERENCES

Kacimov A.R. 2006. Analytical solution and shape optimisation for groundwater flow through a leaky porous trough subjacent to an aquifer. Proc. Royal Soc. London A, 462, 1409-1423.

Kacimov A.R., Obnosov Yu.V. 1995. Groundwater flow in a medium with periodic inclusions. Fluid Dynamics, 30(5), 758-766.

Kacimov A.R., Obnosov Yu.V. 1997. Analytic solution to a problem of seepage in a checker- board massif. Transport in Porous Media, 28 (1), 109-124.

Kacimov A.R., Obnosov Yu.V. 2000. Two-dimensional seepage in porous media with heterogeneities. J. Geochemical Exploration, 69-70, 251-255.

Kacimov A., Kayumov I., Al-Maktoumi A. 2016. Rainfall induced groundwater mound in wedge-shaped promontories: the Strack-Chernyshov model revisited. Advances in Water Resources, 2016, 97, 110-119.

Kacimov A.R., Obnosov Yu.V., Yakimov N.D. 1999. Groundwater flow in a medium with a parquet-type conductivity distribution. J. Hydrology, 226, 242-249.

Kacimov A.R., Obnosov Yu.V. 2012. Analytical solutions for seepage near material boundaries in dam cores: the Davison-Kalinin problems revisited. Applied Mathematical Modelling, 36, 1286–1301.

Kacimov A.R., Obnosov Yu.V. 2015. An exact analytical solution for steady seepage from a perched aquifer to a low-permeable sublayer: Kirkham-Brock's legacy revisited. Water Resources Research, 51, 3093–3107.

Khristianovich, S.A., Mikhlin S.G. and Davison B.B. 1938. Some New Problems of Continuum Mechanics. Moscow-Leningrad, Akad. Nauk SSSR (in Russian).

Polubarinova-Kochina, P.Ya. 1977. Theory of Ground-water Movement. Nauka, Moscow (in Russian).

Rybakova S.T., Emikh V.N. 1966. On the problem of horizontal perfect drainage with a leaky layer. Izv. An SSSR Mekhanika Zhidkosti i Gaza, N3, 161-165 (in Russian).

Simcore Software, 2012. Processing MODFLOW: an integrated modeling environment for the simulation of groundwater flow. Transport React. Process.

Šimůnek J., Van Genuchten M.T., Šejna, M. 2008. Development and applications of the HYDRUS and STANMOD software packages and related codes. Vadose Zone J., 7(2), 587–600.

Strack O. D. L. 1989. Groundwater Mechanics. Prentice-Hall, Englewood Cliffs.

Strack O.D. 2017. Vertically integrated flow in stratified aquifers. J. Hydrology (in press).

Strack O.D.L., Ausk B.K. 2015. A formulation for vertically integrated groundwater flow in a stratified coastal aquifer. Water Resources Research, 51(8), 6756-6775.

Toth, J. 2009. Gravitational Systems of Groundwater Flow- Theory, Evaluation, Utilization. Cambridge University Press, Cambridge.

Yakimov N.D., Kacimov A.R. 2017. Darcian flow under/through a leaky cutoff-wall: Terzaghi-Anderson's seepage problem revisited. International J. for Numerical and Analytical Methods in Geomechanics, DOI: 10.1002/nag.2668

Proceedings of the 10th World Congress of EWRA 'Panta Rhei', 5-9 July 2017, Athens, Greece
© 2017 *European Water Resources Association*

Comparison of SGD rate between northern-southern coastlines of the Persian Gulf using RS

M. Farzin[1*], A. Nazari Samani[1], S. Feiznia[1], G.A. Kazemi[2] and I. Golzar[3]
[1] *Department of Arid and Mountainous Regions Reclamation, University of Tehran,Karaj, Iran*
[2] *Private Consultant, Unit 7, Blook 45, Amir Abad, Abadan, Iran*
[3] *Department of Environmental Engineering, Islamic Azad University, Science and Research Branch, Tehran, Iran*
[*] *e-mail: m.farzin@ut.ac.ir*

Abstract: Submarine Groundwater Discharge (SGD) is defined as any subsurface flow of water from the land into the sea. In this research, we have tried to use remote sensing technique to determine the potential areas for SGD in southern coastlines of the Persian Gulf - around Bahrain where submarine freshwater springs have long been known- and a section in northern Persian Gulf coastline opposite to Bahrain. For this purpose, first necessary corrections (atmospheric, radiometric, and geometric) were made on the obtained Landsat 8 data in 2016 across the study area. Then, by mapping sea surface temperature (SST) and standard temperature anomaly (STA), probable anomalous areas caused by SGD into the coastlines of the Persian Gulf were identified and mapped. Results show that although 29 submarine freshwater springs are known to exist around Bahrain, thermal anomalies in northern coastlines of the Persian Gulf are much more than that of the southern coastlines; we could not detect significant thermal anomaly around and near Bahrain. Therefore, it is likely that the rate of SGD into north of the Persian Gulf is considerably high and much more than in the southern Persian Gulf. The approach implemented in this study can be used for any coastal regions that may have an interaction with coastal aquifers especially for other parts of the Persian Gulf coastlines.

Key words: SGD, Submarine Spring, Remote Sensing, Persian Gulf

1. INTRODUCTION

Submarine Groundwater Discharge (SGD) is defined as any subsurface flow of water from the land into the sea. A significant component of water cycle, SGD is highly important for management of coastal areas for at least three reasons including chemical and ecological effects of SGD, loss of fresh water resources through SGD, and geotechnical aspects of coasts, e.g. slope instability (Burnett et al, 2006). A predecessor of SGD, Submarine Freshwater Discharge (SFD) has been known for many centuries; for example, phenomenon of the submarine karstic springs was recognized as early as in the first century BC (Ford and Williams, 2007). Because of the difficulty in assessing and understanding, both SGD and submarine freshwater springs were neglected for many years. In fact, the term SGD which was previously known as SGWD, has appeared in the literature in the early 1970's or even before. During the years, a variety of techniques have been implemented to measure SGD including seepage meters, seawater temperature survey using marine navigations, thermal remote sensing and TIR, seawater electrical conductivity surveys, geochemical tracers, hydrological and hydrogeological modeling, water budget calculations, geophysical methods, and radioisotopes that have been presenting several references about these.

Thermal remote sensing is one of the most effective methods for identifying SGD sites. It has been demonstrated that thermal remote sensing is a powerful tool for pre-screening the whole area (Schubert et al, 2014) and detecting the SGD potential sites in order to narrow down the field survey locations (Hennig et al, 2015). This technique is based on thermal gradient between incoming groundwater and the ambient sea water. Landsat data is one of the best datasets in this regard.

In this paper we have tried to use thermal remote sensing technique for assessing areas with likely SGD potential in southern coastlines of the Persian Gulf - around Bahrain where submarine

freshwater springs are very well known - as well as a section of the northern Persian Gulf that is located on the opposite side to Bahrain. This research is a part of a larger study to locate submarine freshwater springs in the northern Persian Gulf area.

2. MATERIAL AND METHOD

2.1 Study Area

Persian Gulf is a semi-enclosed marginal sea, 200–300 km wide, with a mean depth of 35 m and a total volume of 6000 km^3 located in the south of Iran and is connected to the Oman Gulf through the narrow Strait of Hormuz. The study area is a rectangle located on two sections of the southern and northern coastlines of the Persian Gulf (Fig. 1). The southern section is situated around Bahrain with 29 submarine freshwater springs that are known for long time (Al Bassam and Tiro, 2011). The northern section is located on a part of Iranian shorelines opposite to Bahrain where there is no scientific report of submarine springs.

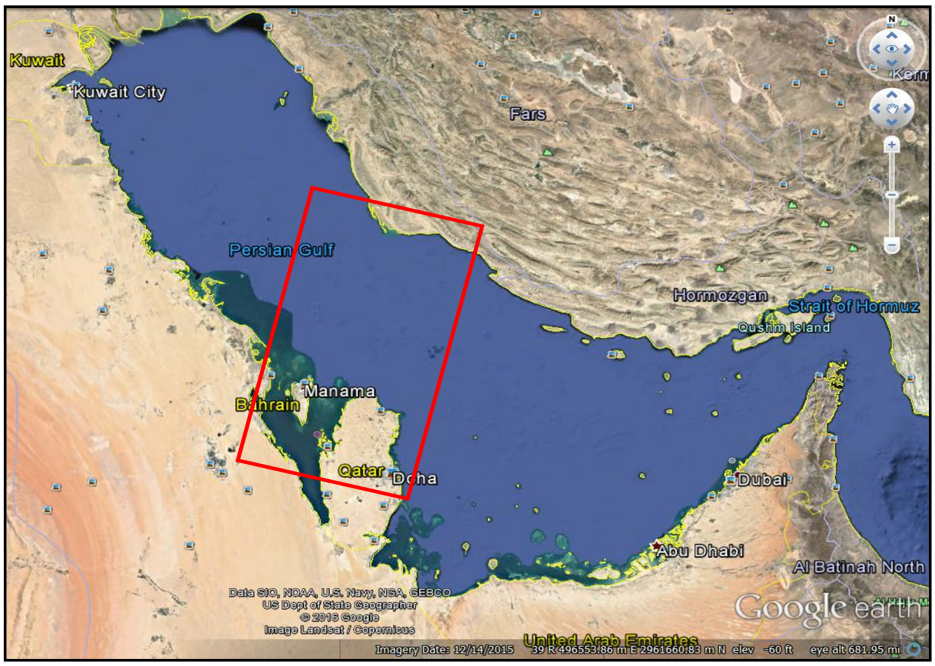

Figure 1. The location of the study area in southern Iran and Bahrain.

2.2 Method

The feasibility of using temperature as a groundwater tracer was recognised in the early 1900's (Anderson, 2005). It has also been demonstrated that remote sensing methods have applicability for recognising temperature difference between surface water bodies and discharging groundwater (Wilson and Rocha, 2016). In this study, we have used Landsat 8 thermal data. Landsat 8 satellite was successfully launched on February 11, 2013, carrying two sensors on-board: (1) the Operational Land Imager (OLI) and (2) the Thermal Infrared Sensor (TIRS) with two spectral bands in the long wave infrared region (LWIR). To achieve the goal, first, necessary corrections (atmospheric, radiometric, and geometric) were made on Landsat 8 data in 2016 (February, March, May, October) across the study area. Then, according to the metadata of the bands for Landsat 8 (thermal constant, rescaling factor value, etc.) as shown in Table 1, Sea Surface Temperature (SST) was mapped using the Formulas 1-4.

Table 1. Metadata of Landsat 8 bands (USGS, 2016)

	Band 10	Band 11
Native Resolution	100 m	100 m
K1	774.89	480.89
K2	1321.08	1201.14
M_L	3.3420E-04	3.3420E-04
A_L	0.10000	0.10000

The digital numbers of Band 10 were converted to the brightness temperature by using the metadata. These were first converted to radiance by following relation:

$$L_\lambda = M_L * Q_{cal} + A_L \quad (1)$$

where, L_λ is top of atmosphere spectral radiance, M_L is band-specific multiplicative rescaling factor, Q_{cal} is digital number, and A_L is band-specific additive scaling factor.

For acquisition of brightness temperature, the following relation was used:

$$BT = K_2/\ln(K_1/L_\lambda + 1) \quad (2)$$

Then, SST was mapped by following formula:

$$SST = BT/\ln \varepsilon * (BT/\rho) * w + 1 \quad (3)$$

$$\rho = hc/s \quad (4)$$

where, ε is emissivity which is 0.989 for sea water (Srivastava et al. 2009; Wilson and Rocha, 2016); w is radiance emitted wavelength; h is Planck's constant ($6.626*10^{-34}$ JS); c is speed of light ($2.998*10^8$ m/s) and s is Boltzmann's constant ($1.38*10^{-23}$ J/K).

To recognize where on the SST map anomalous thermal arrangements potentially reveal groundwater inputs, and to allow comparisons across image frames, thermal anomaly (TA) and standardised thermal anomaly (STA) maps were created using formulas 5-6 (Wilson and Rocha, 2016):

$$TA = Tp - \check{T} \quad (5)$$

where, TA represents temperature anomaly (°C), Tp is the temperature value specific to each pixel in the scene (°C), and $\check{T}$ is the average temperature value for the sea surface (°C).

$$STA = TA/\sigma \quad (6)$$

where, STA (dimensionless) represents standardised thermal anomaly, TA is temperature anomaly and σ is standard deviation.

Finally, using SST and STA maps, probable anomalies caused by submarine groundwater discharge into coastlines of the Persian Gulf were identified and mapped. All calculations were carried out by using ENVI 5.3 and Arc Map 10.3.1 software.

3. RESULT AND DISCUSSION

Figures 3-6 depict STA maps for the study area.

Available multi-national oceanographic observations for the Persian Gulf region are limited, because investigations have been undertaken by individual countries in their own coastal waters (Moradi and Kabiri, 2015). So far, use of remote sensing in Persian Gulf area have been limited to environmental purposes, habitat mapping, coastal and hydro-biological processes, and variability of SST and Chlorophyll-a (Al-Ghadban, 2004; Alsahli et al. 2012; Moradi and Kabiri, 2015) with no

research about SGD. Satellite remote sensing allows information on SST to be mapped at moderate resolution, over large areas and long periods of time; by analysing these maps we have identified and recognized the potential SGD zones.

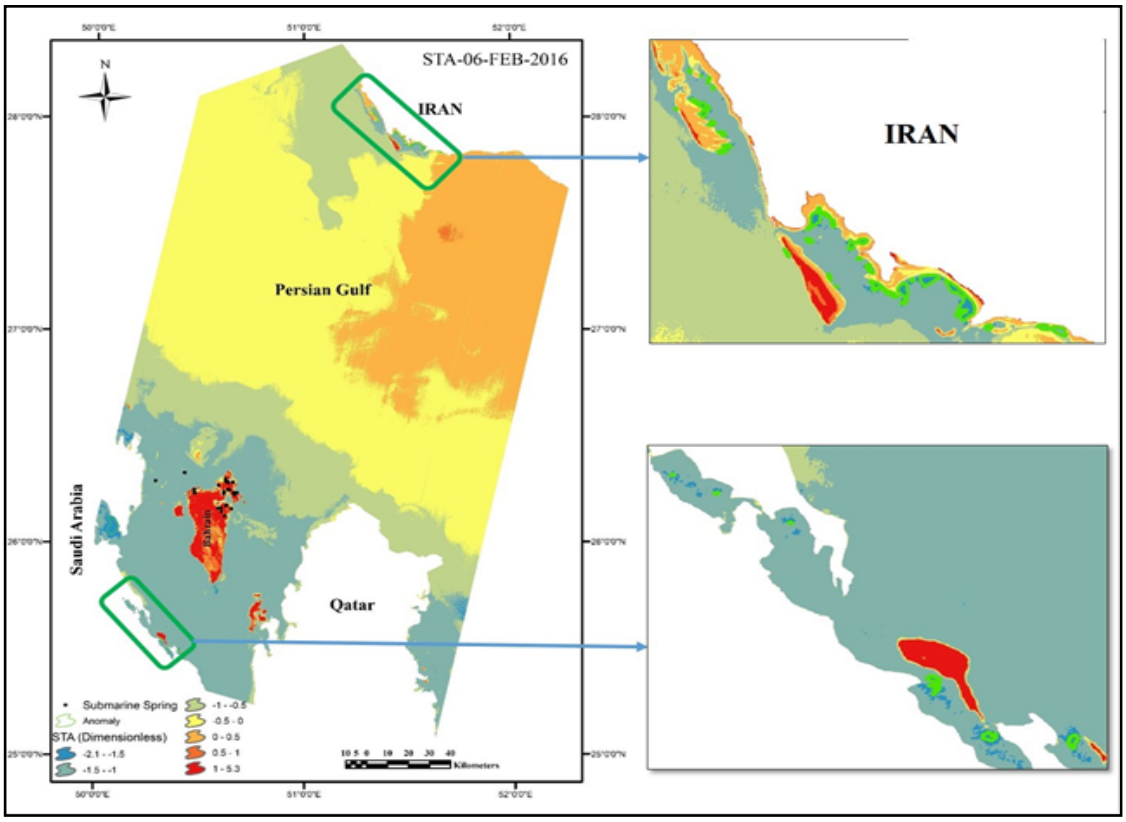

Figure 2. STA Map based on 06-FEB-2016 data with anomalies boundary and the location of springs.

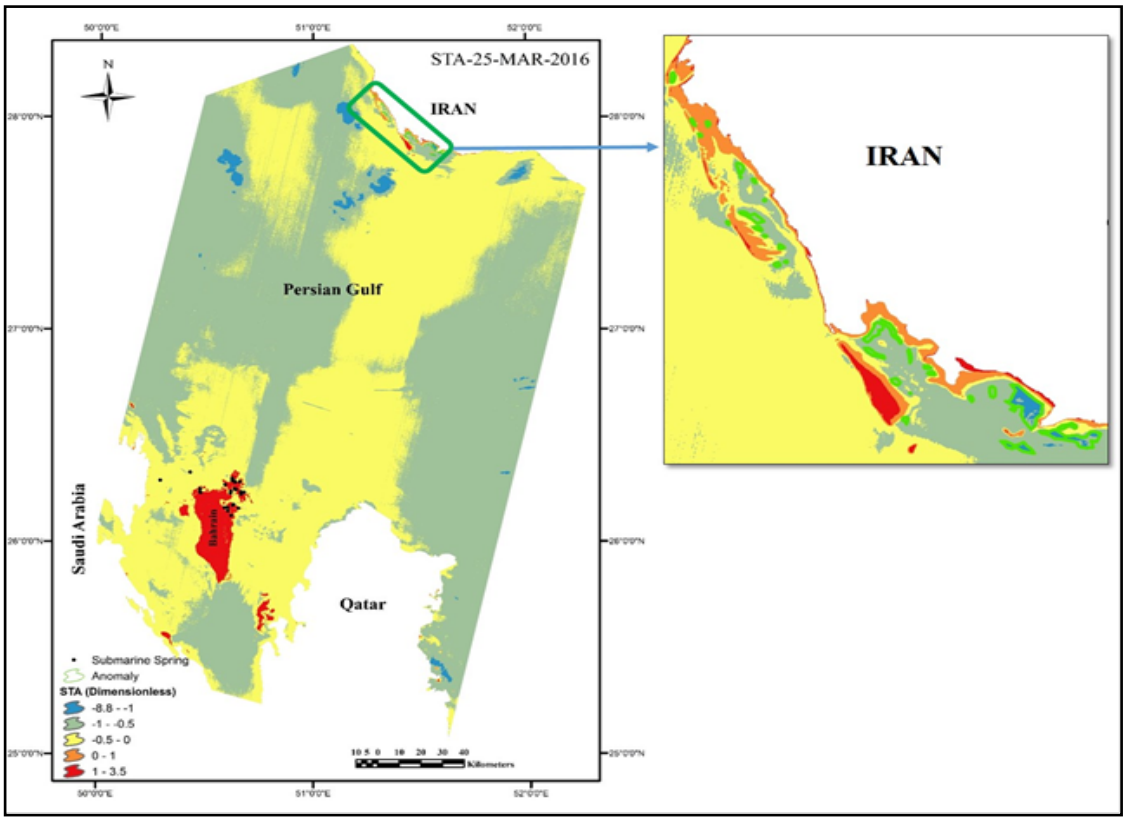

Figure 3. STA Map based on 25-MAR-2016 with anomalies boundary and the spring sites.

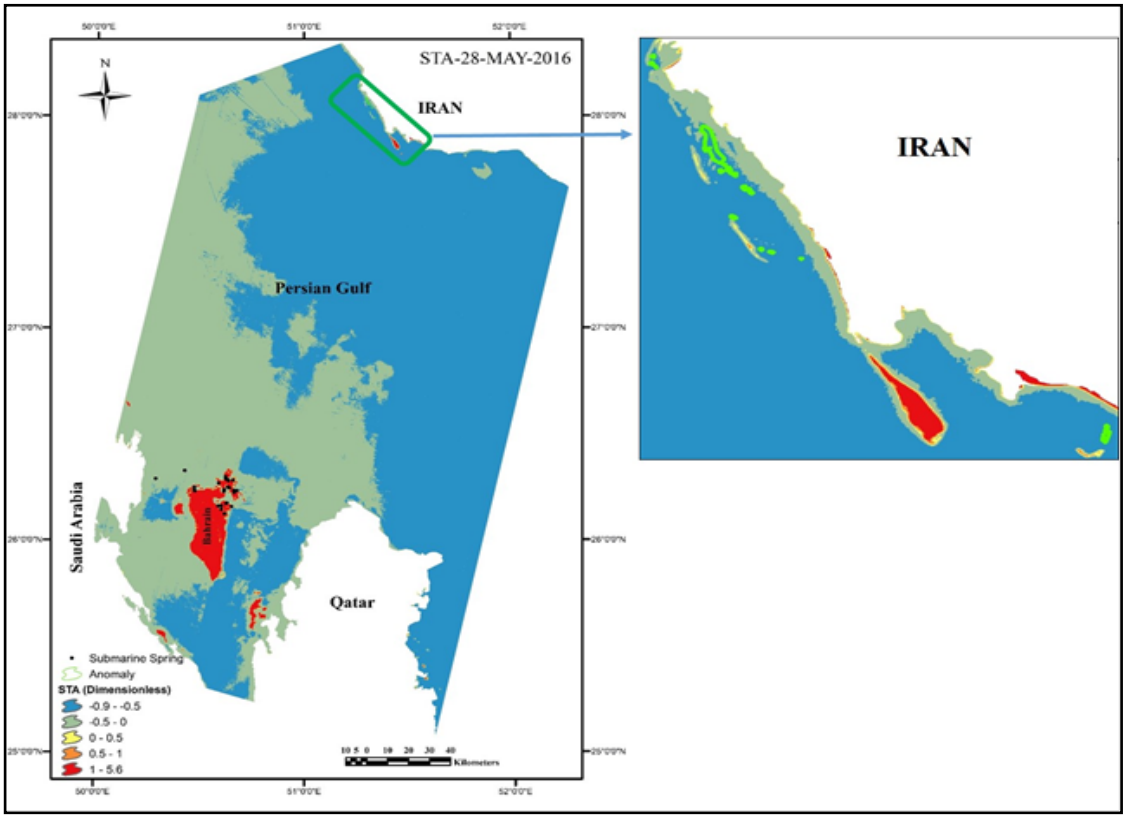

Figure 4. STA Map based on 28-MAY-2016 with anomalies boundary and the location of springs.

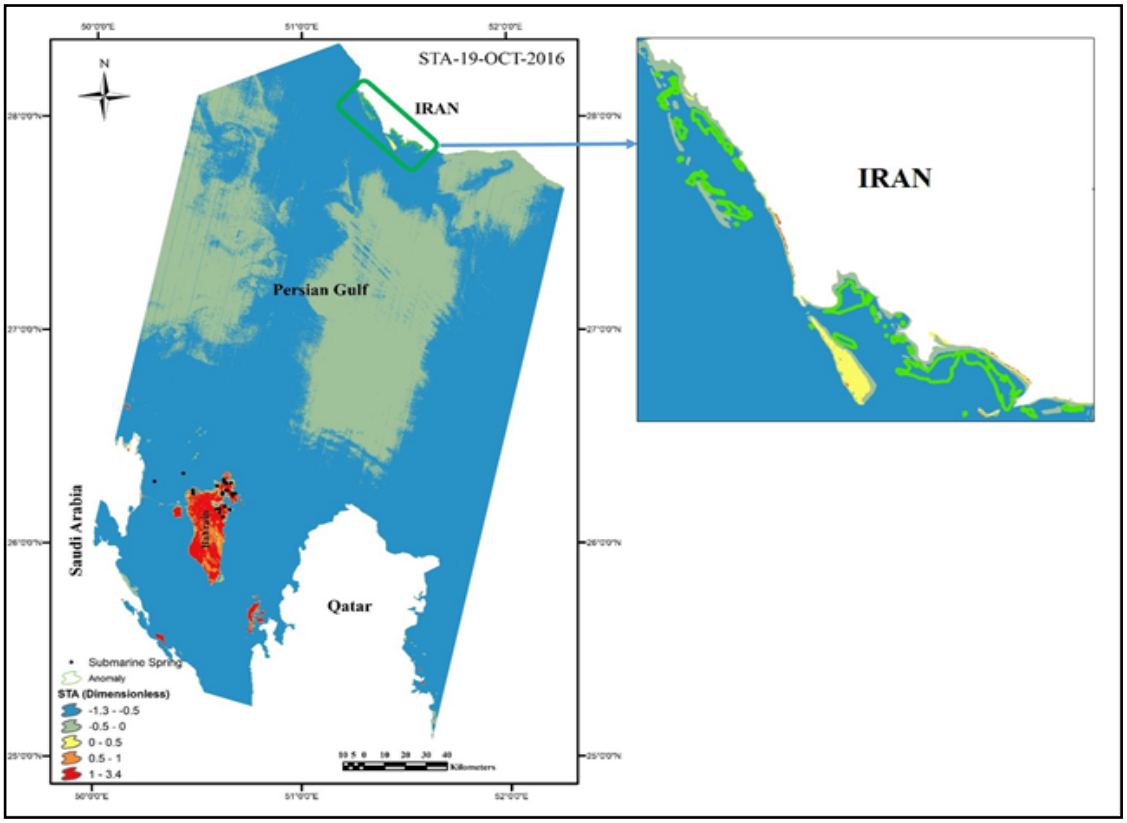

Figure 5. STA Map based on 19-OCT-2016 data with anomalies boundary and the location of springs.

It has been stated that estimation of groundwater discharge into Persian Gulf using traditional techniques including seepage meters and piezometers is problematic because the flow is often

patchy and diffuse (Lee and Cherry, 1978). The artesian springs are the first report on seepage into the Persian Gulf (Judd and Hovland, 2007). Willams (1946) and Fromant (1965) have reported freshwater discharge from narrow fractures into the shallow sea around Bahrain islands (south of the Persian Gulf). It is reported that Bahraini pearl-fishers could survive on the sea for long times by collecting freshwater from submarine springs (Chapman, 1981). There are 29 submarine freshwater springs in Bahrain's water (Al Bassam and Toro, 2011); Umm Jarajir is the most important spring with 10 meter depth. Total discharge rate of this specific spring has not been studied as yet, nevertheless it seems to discharge a substantial volume of the water. Despite the very high potential of SGD into northern coastlines than the southern coastlines of the Persian Gulf including more rain, presence of significant Karstic formations in nearby, several faults and lineaments, etc., there are no reports or scientific article about this region as yet. Hence, we have tried to demonstrate the importance of northern coastlines of the Persian Gulf in presenting probable SGD using thermal remote sensing at moderate resolution.

As can be seen from figures 2 to 5, in spite of presence of 29 submarine freshwater springs around Bahrain (south of the Persian Gulf), thermal anomalies on northern coastlines of the Persian Gulf are much more than the southern coastlines so that considerable anomaly was not detected around and near Bahrain.

4. CONCLUSION

The anomalies show the localized abrupt changes or discontinuities that result from disturbance events that we believe this events on coastlines of the Persian Gulf are related to SGD. In addition, the lands leading to the northern coastlines have different conditions from the other side of the Persian Gulf including more rain, more suitable geological settings, and steeper hydraulic gradient that are prone to appearance of submarine springs on the northern coastlines than the southern coastlines. Therefore, we can conclude that most probably the rate of SGD in north of the Persian Gulf is very high and much more than the south. So, the coastal aquifers may have active interactions with the sea in this regions that may significantly impact water chemistry, water quality, biology and ecology; which, unfortunately, has been ignored as yet. This approach can be used for any coastal regions that may have an interaction with coastal aquifers especially on the other Persian Gulf coastlines.

REFERENCES

Al Bassam, A. A., Tiro, E. H. M., 2011. Using remote sensing and GIS for submarine freshwater springs exploration as a plausible water source in Saudi Arabia. Sixth National GIS Symposium in Saudi Arabia April 24 – 26, 2011 Le Meridian, Al-Khobar – Eastern Province.

Al-Ghadban, A. N., 2004. Assessment of suspended sediment in Kuwait Bay using Landsat and SPOT images. Kuwait journal of science & engineering; 31 (2): 155-172.

Alsahli, M. M., Alsahli, M. M., Price, K. P., Buddemeier, R., Fautin, D. G., Egbert, S., 2012. Mapping spatial and temporal distributions of Kuwait SST using MODIS remotely sensed data. Appl. Remote Sensing J; 2 (2): 1–16.

Anderson, M. P., 2005. Heat as a groundwater tracer. Groundwater; 43 (6): 951–968.

Burnett, W. C., Aggarwal, P. K., Bokuniewicz, H., Cable, J. E., Charette, M. A., et al, 2006. Quantifying submarine groundwater discharge in the coastal zone via multiple methods. Science of the Total Environment; 367: 498–543.

Chapman, R. E., 1981. Geology and water: An introduction to fluid mechanics for geologists. Springer Netherlands press, 228 p.

Ford, D., Williams, P., 2007. Karst Hydrogeology and Geomorphology. John Wiley & Sons press, Chichester, West Sussex, England. 562 pp.

Fromant, A. C., 1965. The water supplies of Bahrain. Journal of the Institute of Water Engineers; 19: 579–85.

Hennig, H., Mallast, U., Merz, R., 2015. Multi-temporal thermal analyses for submarine groundwater discharge (SGD) detection over large spatial scales in the Mediterranean. Geophysical Research Abstracts; 17: EGU2015-4929.

Lee, D. R., Cherry, J. A., 1978. A field exercise on ground water flow using seepage meters and mini-piezometers. J. Geol. Educ; 27: 6–10.

Judd, A., Hovland, M., 2007. Seabed Fluid Flow: The Impact on Geology, Biology and the Marine Environment. Cambridge University Press, 475p.

Moradi, M., Kabiri, K., 2015. Spatio-temporal variability of SST and Chlorophyll-a from MODIS data in the Persian Gulf. Marine Pollution Bulletin; 98 (1-2): 14–25.

Schubert, M., Scholten, J., Schmidt, A., Comanducci, J. F., Pham, M. K., Mallast, U., Knoeller, K., 2014. Submarine Groundwater Discharge at a Single Spot Location: Evaluation of Different Detection Approaches. Water; 6: 584-601.

Srivastava, P. K., Majumdar, T. J., Bhattacharya, A. K., 2009. Surface temperature estimation in Singhbhum Shear Zone of India using Landsat-7 ETM+ thermal infrared data. Advances in Space Research; 43: 1563–1574.

USGS, 2016. Landsat 8 (L8) Data Users Handbook, Version 2.0, March 29, 2016, LSDS-1574. 106p.

Williams, M. O., 1946. Bahrain: port of pearls and petroleum. National Geographic; 89: 194–210.

Wilson, J., Rocha, c., 2016. A combined remote sensing and multi-tracer approach for localising and assessing groundwater-lake interactions, International Journal of Applied Earth Observation and Geoinformation; 44: 195–204.

Proceedings of the 10th World Congress of EWRA 'Panta Rhei', 5-9 July 2017, Athens, Greece
© 2017 *European Water Resources Association*

Groundwater flow simulation in confined aquifer by meshless element free Galerkin method

T. Pathania* and A.K. Rastogi
Department of Civil Engineering, Indian Institute of Technology Bombay, Mumbai, India
* *e-mail: tineshpathania07118@gmail.com*

Abstract: In groundwater management problems, the flow behaviour of the aquifer system is analysed by solving the governing equations analytically or using numerical techniques. Numerical techniques such as finite difference method (FDM) and finite element method (FEM) are in use for many decades for solving complex flow problems as these cannot be addressed by analytical methods. In the recent years, meshless methods have been effectively used in solving the groundwater problems. These methods do not require mesh formation resulting in lesser computational cost and time as compared to mesh based methods. The element free Galerkin (EFG) method is one of the efficient and accurate meshless method for the complex flow problems. This method uses moving least square (MLS) approximation for obtaining the shape functions which lack the Kronecker delta function property. Therefore, presently the Dirichlet boundary conditions are imposed using the Lagrange multiplier method. The present study simulates the groundwater flow in a hypothetical heterogeneous and anisotropic confined aquifer using EFG method. The aquifer system is imposed with both Dirichlet and Neumann boundary conditions. The numerical outputs of the EFG model in MATLAB are verified with the groundwater head values obtained from the FEM simulation. The satisfactory results of the EFG model shows the efficacy of the present method.

Key words: Element free Galerkin method, groundwater flow simulation, meshless method, moving least square approximation

1. INTRODUCTION

Groundwater is relatively pure and a convenient source of drinking water in many parts of the world. The increasing population and rapid growth of industrial sectors worldwide have raised the major problems of depletion of the groundwater table and contamination of the groundwater resources. The solution to these problems demands for proper management of the groundwater resources. Groundwater modeling plays a crucial role in predicting the spatial and temporal distribution of the groundwater in the aquifer system with the help of available analytical and numerical techniques. The analytical solutions are based on fundamental laws of nature and thus have been used only for obtaining the solution of simplified groundwater flow problems. The mesh based numerical techniques of FDM and FEM have been extensively used in solving the complex groundwater problems. These methods initially divides the whole problem domain into meshes/grids or elements connected together by field nodes in a well-defined manner (Liu and Gu 2005). This mesh formation procedure leads to higher computational cost and time in simulating the groundwater flow in aquifer systems. In last few decades, new methods which do not require meshing have been developed and are known as meshless methods. In these methods, the field nodes are scattered on the problem domain and its boundaries to represent the whole problem. Also, there is no connectivity among the field nodes as prerequisite in meshbased methods.

The application of meshless methods in groundwater problems have been used in very few studies. Park and Leap (2000) presented the solution procedure of the meshless EFG method for modeling the groundwater flow in confined aquifer domains. In their study the Dirichlet boundary conditions has been imposed using the coupled EFG-FEM technique as MLS approximation in EFG model do not satisfy Kronecker delta property. Praveen Kumar and Dodagoudar (2009) used the EFG method for estimating the contaminant distribution in the unsaturated zones of porous media. The EFG outputs were verified with the published experimental results and FEM solutions. Meenal

and Eldho (2011) used the meshless Point Collocation method (PCM) with multiquadric radial basis function for simulating the groundwater flow in unconfined aquifers. The efficacy of the developed model was ensured by verifying its outputs with analytical and FEM solutions. Swathi and Eldho (2014) used the Galerkin equivalent of Meshless Local Petrov-Galerkin (MLPG) method with exponential radial basis function for solving the unconfined aquifer problems. The results of this method on comparison with available analytical and numerical solutions were found to be satisfactory.

The EFG model developed by Belytschko et al. (1994) employs the use of MLS approximation for approximating the unknown function and thus, the Dirichlet boundary conditions requires special treatment. In the available literature, the existing techniques for implementing the Dirichlet boundary conditions in EFG method includes Lagrange multiplier method (Belytschko et al. 1994), modified variational principles (Lu et al. 1994) and coupled EFG-FEM technique (Belytschko et al. 1995). The results obtained by using Lagrange multipliers are very accurate (Park and Leap 2000). Therefore in the present study the Lagrange multiplier method is used to implement the Dirichlet boundary conditions. The main objective of this study is to test the efficacy of the EFG method in simulating the groundwater flow in a confined aquifer system by comparing its outputs with FEM solutions.

2. ELEMENT FREE GALERKIN METHOD

The EFG method is a meshless method based on the Galerkin weak form defined over the global problem domain (Liu and Gu 2005). This technique uses MLS approximation in the Galerkin weak form to develop a set of linear algebraic equations. It also requires a set of background cells for performing the numerical integration of integral form obtained from the Galerkin method. It is performed using the Gauss quadrature scheme over these cells. The present study uses the cubic spline weight function for evaluating the EFG shape functions from MLS approximation of unknown head. The EFG shape functions and its derivative are computed using the procedure given in Praveen Kumar and Dodagoudar (2009).

2.1 EFG discretization of governing equation

The governing equation for the two dimensional groundwater flow in a heterogeneous and anisotropic confined aquifer is given as (Bear 1979)

$$\frac{\partial}{\partial x}\left[T_x \frac{\partial h}{\partial x}\right] + \frac{\partial}{\partial y}\left[T_y \frac{\partial h}{\partial y}\right] = S\,\frac{\partial h}{\partial t} + Q_w\,\delta(x - x_i)(y - y_j) - q \tag{1}$$

The initial conditions used are written as

$$h(x, y, 0) = h_0\,(x, y) \quad x, y \in \Omega \tag{2}$$

The boundary conditions used for the groundwater flow problems are represented as

$$h(x, y, t) = h_D\,(x, y, t) \qquad x, y \in \Gamma_S \tag{3}$$

$$T\,\frac{\partial h}{\partial n} = q_B\,(x, y, t) \qquad x, y \in \Gamma_E \tag{4}$$

where $h(x, y, t)$ is the piezometric head (m), T_x and T_y are the transmissivities in x and y directions respectively (m^2/d), S is the storage coefficient, Q_w is a source or sink function ($-Q_w$= source, + Q_w= sink) (m^3/d/m^2), δ is the Dirac delta function with the property that when $x = x_i$ and $y = y_j$

then $\delta = 1$ otherwise 0, Ω is the flow region, Γ is the boundary region ($\Gamma_S \cup T_E = \Gamma$), $\partial/\partial n$ is the normal derivative, q is the known recharge rate ($m^3/d/m^2$), $h_0(x,y)$ is the initial head in flow region (m), $h_D\ (x,y,t)$ is the known head value at the Dirichlet boundary (m), $q_B(x,y,t)$ is the known inflow rate at the Neumann boundary ($m^3/d/m^2$).

In EFG method initially the trial solutions $\hat{h}(x,y,t)$ is defined as $\hat{h}(x,y,t) = \sum_{I=1}^{n} h_I(t)\,\phi_I(x,y)$, where h_I and ϕ_I are the unknown head and EFG shape function at node I respectively, and n is the number of nodes in the domain of influence of point of interest.

The weak integral form of the governing groundwater flow equation [Eq. (1)] is represented as (Praveen Kumar and Dodagoudar 2009)

$$\int_{\Omega} \left(\frac{\partial}{\partial x}\left[T_x \frac{\partial h}{\partial x}\right] + \frac{\partial}{\partial y}\left[T_y \frac{\partial h}{\partial y}\right] - S\frac{\partial h}{\partial t} - Q_w + q \right) \delta h^T \, d\Omega = 0 \tag{5}$$

Using Green's theorem, Eq. (5) can be simplified to following expression

$$\int_{\Gamma_E} \left(T_x \frac{\partial h}{\partial x} n_x\right) \delta h^T \, d\Omega - \int_{\Omega} \left(T_x \frac{\partial h}{\partial x} \delta\left(\frac{\partial h^T}{\partial x}\right)\right) d\Omega + \int_{\Gamma_E} \left(T_y \frac{\partial h}{\partial y} n_y\right) \delta h^T d\Omega - \int_{\Omega} \left(T_y \frac{\partial h}{\partial y} \delta\left(\frac{\partial h^T}{\partial x}\right)\right) d\Omega$$
$$- \int_{\Omega} S\frac{\partial h}{\partial t} \delta h^T \, d\Omega - \int_{\Omega} Q_w \delta h^T \, d\Omega + \int_{\Omega} q \delta h^T \, d\Omega = 0 \tag{6}$$

On rearranging the terms in Eq. (6)

$$\int_{\Omega} \left(T_x \frac{\partial h}{\partial x} \delta\left(\frac{\partial h^T}{\partial x}\right)\right) d\Omega + \int_{\Omega} \left(T_y \frac{\partial h}{\partial y} \delta\left(\frac{\partial h^T}{\partial x}\right)\right) d\Omega + \int_{\Omega} S\frac{\partial h}{\partial t} \delta h^T \, d\Omega$$
$$= \int_{\Gamma_E} \left(T_x \frac{\partial h}{\partial x} n_x + T_y \frac{\partial h}{\partial y} n_y\right) \delta h^T \, d\Omega - \int_{\Omega} Q_w \delta h^T \, d\Omega + \int_{\Omega} q \delta h^T \, d\Omega \tag{7}$$

On using the Lagrange multiplier method for implementing the Dirichlet boundary conditions and Eq. (4) in Eq. (7), it can be written as

$$\int_{\Omega} \left(T_x \frac{\partial h}{\partial x} \delta\left(\frac{\partial h^{\mathrm{T}}}{\partial x}\right)\right) d\Omega + \int_{\Omega} \left(T_y \frac{\partial h}{\partial y} \delta\left(\frac{\partial h^{\mathrm{T}}}{\partial x}\right)\right) d\Omega + \int_{\Omega} S\frac{\partial h}{\partial t} \delta h^{\mathrm{T}} \, d\Omega$$
$$= q_B \int_{\Gamma_E} \delta h^{\mathrm{T}} \, d\Omega - \int_{\Omega} Q_w \delta h^{\mathrm{T}} \, d\Omega + \int_{\Omega} q \delta h^{\mathrm{T}} \, d\Omega - \int_{\Gamma_S} \delta \lambda^{\mathrm{T}} (h - h_D) d\Gamma - \int_{\Gamma_S} \lambda \, \delta h^{\mathrm{T}} \, d\Gamma \tag{8}$$

where λ is a Lagrange multiplier for incorporating the Dirichlet boundary conditions and it is defined as (Liu and Gu 2005)

$$\lambda = \sum_{K=1}^{n_\lambda} N_K(s) \lambda_K \qquad x, y \in \Gamma_S \tag{9}$$

where n_λ is the number of nodes used for this interpolation, s is the arc length along the boundary, λ_K and $N_K(s)$ are the Lagrange multiplier and shape function at node K on the Dirichlet boundary respectively.

In EFG method, the source/sink terms are also distributed to the neighbouring nodes in the domain of influence of point under consideration and it is represented as

$$Q_w = \sum_{I=1}^{n} Q_w\, \phi_I(x,y)\,, \qquad q = \sum_{I=1}^{n} q\, \phi_I(x,y), \tag{10}$$

Therefore, using the trial solution, and Eqs. (9) and (10) in Eq. (8) gives

$$\begin{aligned}\int_{\Omega} \left(T_x \frac{\partial \phi_I(x,y)}{\partial x} h_I^{t+\Delta t}\right) \frac{\partial \phi_J(x,y)}{\partial x} \delta h_J \, d\Omega + \int_{\Omega} \left(T_y \frac{\partial \phi_I(x,y)}{\partial y} h_I^{t+\Delta t}\right) \frac{\partial \phi_J(x,y)}{\partial y} \delta h_J \, d\Omega \\ + \int_{\Omega} S \left(\phi_I(x,y) \frac{\partial h_I}{\partial t}\right) \phi_J(x,y)\, \delta h_J \, d\Omega \\ + \int_{\Gamma_S} \delta (N_K \lambda_K)^{\mathrm{T}} \left(\phi_I(x,y) h_I^{t+\Delta t} - h_D\right) d\Gamma + \int_{\Gamma_S} (N_K \lambda_K)\, \phi_J(x,y) \delta h_J \, d\Gamma \\ = q_B \int_{\Gamma_E} \phi_J(x,y) \delta h_J \, d\Omega \; - \int_{\Omega} (Q_w - q) \phi_I(x,y) \phi_J(x,y)\, \delta h_J \, d\Omega\end{aligned} \tag{11}$$

where $I, J = 1,2,3, \ldots \ldots \ldots n$.

The Eq. (11) can also be written as

$$\begin{aligned}\int_{\Omega} \left(T_x \frac{\partial \phi_I(x,y)}{\partial x} \frac{\partial \phi_J(x,y)}{\partial x} h_I^{t+\Delta t}\right) \delta h_J \, d\Omega + \int_{\Omega} \left(T_y \frac{\partial \phi_I(x,y)}{\partial y} \frac{\partial \phi_J(x,y)}{\partial y}\, h_I^{t+\Delta t}\right) \delta h_J \, d\Omega \\ + \int_{\Omega} \left(S \frac{\partial h_I}{\partial t} \phi_I(x,y) \phi_J(x,y)\right) \delta h_J \, d\Omega \\ + \int_{\Gamma_S} \delta \lambda_K{}^{\mathrm{T}} \left(N_K{}^{\mathrm{T}} \phi_I(x,y) h_I^{t+\Delta t} - N_K{}^{\mathrm{T}} h_D\right) d\Gamma + \int_{\Gamma_s} (N_K \lambda_K)\, \phi_J(x,y) \delta h_J \, d\Gamma \\ = q_B \int_{\Gamma_E} \phi_J(x,y) \delta h_J \, d\Omega \; - \int_{\Omega} (Q_w - q) \phi_I(x,y) \phi_J(x,y)\, \delta h_J \, d\Omega\end{aligned} \tag{12}$$

The above integral form considers local numbering system for all the nodes in the local domain of influence. On transforming it from local to global in Eq. (12), it gives the following matrix form

$$\left[\left(\left[K^{(1)}\right] + \left[K^{(2)}\right]\right)\left\{h_I^{t+\Delta t}\right\} + [P]\left\{\frac{\partial h_I}{\partial t}\right\} + [G]\{\Lambda\} - \{f\}\right] \delta H^{\mathrm{T}} + \left[[G^{\mathrm{T}}]\left\{h_I^{t+\Delta t}\right\} - \{V\}\right] \delta \Lambda^{\mathrm{T}} \tag{13}$$

where

$$\{H^T\} = [h_1 \;\; h_2 \;\; h_3 \;\; \cdots\cdots h_N]\,, \tag{14a}$$

$$\{\Lambda^T\} = [\lambda_1 \;\; \lambda_2 \; \lambda_3 \;\; \cdots\cdots\cdots \lambda_{nt}] \tag{14b}$$

where N is the total number of nodes in the flow domain and nt is the total number of field nodes on the Dirichlet boundaries. The column vector $\left\{h_I^{t+\Delta t}\right\}$ gives the unknown nodal head values at time $t + \Delta t$. The elements of the global matrices $\left[K^{(1)}\right]$, $\left[K^{(2)}\right]$, $[P]$ and $[G]$ are computed as

$$K_{IJ}^{(1)} = \int_{\Omega} \left(T_x \frac{\partial \phi_I(x,y)}{\partial x} \frac{\partial \phi_J(x,y)}{\partial x}\right) d\Omega\,, \qquad K_{IJ}^{(2)} = \int_{\Omega} \left(T_y \frac{\partial \phi_I(x,y)}{\partial y} \frac{\partial \phi_J(x,y)}{\partial y}\right) d\Omega \tag{15a}$$

$$P_{IJ} = \int_{\Omega} S\, \phi_I(x,y) \phi_J(x,y) d\Omega\,, \qquad G_{KJ} = \int_{\Gamma_S} N_K \phi_J(x,y) d\Gamma \tag{15b}$$

Also, the elements of global vectors $\{f\}$ and $\{V\}$ are computed as

$$f_J = q_B \int_{\Gamma_E} \phi_J(x,y) d\Omega - \int_{\Omega} (Q_w - q)\phi_I(x,y)\phi_J(x,y)\,\delta h_J\, d\Omega \ , \quad V_K = \int_{\Gamma_S} {N_K}^{\mathrm{T}} h_D d\Gamma \qquad (15c)$$

where $I, J = 1,2,3, \ldots \ldots \ldots N$, $K = 1,2,3, \ldots nt$ and $Q_w = q_w/a$, q_w is the pumping or recharge rate (m^3/d) and a is the nodal area (m^2). Since both δH and $\delta \Lambda$ are the arbitrary values, the Eq. (13) can be satisfied only if

$$\left([K^{(1)}] + [K^{(2)}]\right)\{h_I^{t+\Delta t}\} + [P]\left\{\frac{\partial h_I}{\partial t}\right\} + [G]\{\Lambda\} - \{f\} = 0 \qquad (16)$$

$$[G^{\mathrm{T}}]\{H\} - \{V\} = 0 \qquad (17)$$

The time derivative term in Eq. (16) is discretized using forward finite difference discretization (Pinder and Gray 1977; Wang and Anderson 1982) and it is expressed as

$$\frac{\partial h_I}{\partial t} = \frac{h_I^{t+\Delta t} - h_I^t}{\Delta t} \qquad (18)$$

Both the Eqs. (16) and (17) can be collectively written in the following matrix form

$$\begin{bmatrix} K^* & G \\ G^{\mathrm{T}} & 0 \end{bmatrix} \begin{Bmatrix} H^* \\ \Lambda \end{Bmatrix} = \begin{Bmatrix} F \\ V \end{Bmatrix} \qquad (19)$$

where

$$K_{IJ}^* = K_{IJ}^{(1)} + K_{IJ}^{(2)} + P_{IJ}\frac{1}{\Delta t}\,, \qquad H_I^* = h_I^{t+\Delta t}, \qquad F_I = f_I + P_{IJ}h_J^t\frac{1}{\Delta t} \qquad (20)$$

The Eq. (19) represents the resultant system of equations obtained from the EFG method on utilizing the Lagrange multiplier method. However, the number of unknowns are increased by the size of $\{\Lambda\}$. On solving, Eq. (19) gives the nodal head values in the whole problem domain at time $t + \Delta t$.

3. NUMERICAL PROBLEM AND RESULTS

In the present study a two dimensional confined aquifer problem (Sharief 2007) consisting of three different zones (Figure 1) is selected. The aquifer area 1800 m × 1000 m with storativity = 0.004 has Dirichlet boundaries on the west (h = 100 m) and east (h = 95 m) sides whereas northern and southern boundaries are considered as impervious (no flow) boundaries. The transmissivity values for the three different zones in the x and y directions are T_x = 500 m^2/d and T_y = 300 m^2/d, T_x = 400 m^2/d and T_y = 250 m^2/d, and T_x = 250 m^2/d and T_y = 200 m^2/d respectively. The aquifer is recharged through the two aquitards lying between the northern nodes 6 to 24 and 42 to 60 with recharge rates 0.00024 and 0.00012 m/d respectively. A pond with seepage rate of 0.009 m/d is also located in the problem domain. The aquifer region consists of three pumping wells (PW) at nodes 26, 29 and 46 extracting groundwater at the rate of 200, 500 and 700 m^3/d respectively. It also contains a recharge well (RW) located at node 17 with injection rate of 800 m^3/d. Three observation wells are located in aquifer system at the nodes 21, 34 and 51.

In the simulation of groundwater flow by EFG method the aquifer domain is discretized using 60 nodes with nodal spacing of 200 m in both the x and y directions. The total 45 (9×5) number of background cells are used in the whole domain for the global integration with each cell size = 200 m × 200 m. In each cell 4 × 4 gauss points are used for the numerical integration by Gauss

quadrature scheme. The steady state analysis is used for obtaining the initial head distribution in the flow domain as shown in Figure 2. For this analysis all pumping and recharge wells are non-operational which are active during the transient flow analysis. The time step size (Δt) of 1 day is chosen for the system simulation and the total simulation time is 10000 days.

The flow behaviour in this aquifer system has been studied by Sharief (2007) using FEM method (60 nodes and 90 elements) and the available results are used for the verification of the present model.

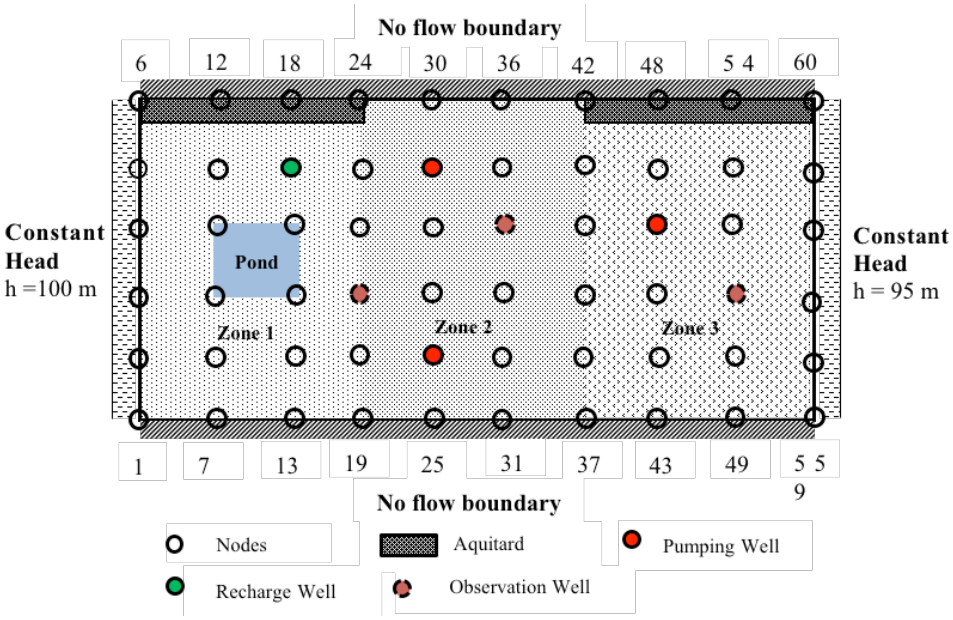

Figure 1. Meshless discretization of confined flow domain (Adapted from Sharief 2007).

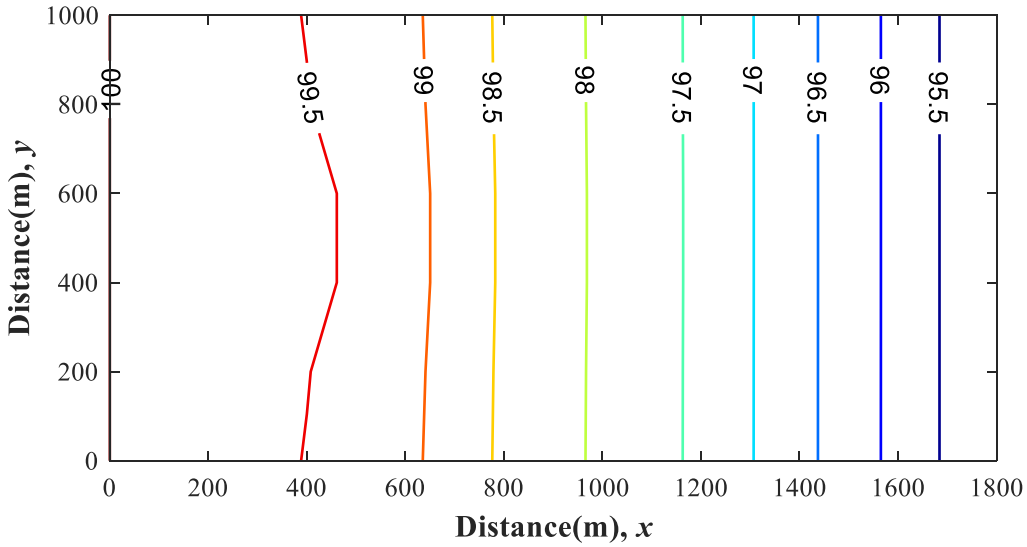

Figure 2. Steady state head distribution.

On fine tuning of the scaling parameter (Praveen Kumar and Dodagoudar 2009) within the range, d_{max}= 1~4 the value of 1.1 in EFG method gives the appropriate solution for this groundwater problem. The groundwater head distribution obtained from the EFG simulations at the end of the simulation period of 10000 days is shown in Figure 3. The comparison of head values at the observation wells after 10000 days by EFG simulations with the FEM solutions of Sharief are shown in Table 1. The EFG outputs are closely matching with the available FEM results. The effect of pumping and recharge wells at the observation wells in the flow region after 10000 days is also

presented in Table 2. It is found that the head value increases when only the recharge well is active and it decreases when three pumping and the recharge well are active. However, it goes down significantly by 1.31 m due to pumping for observation well at node 34 as it is surrounded by all pumping wells.

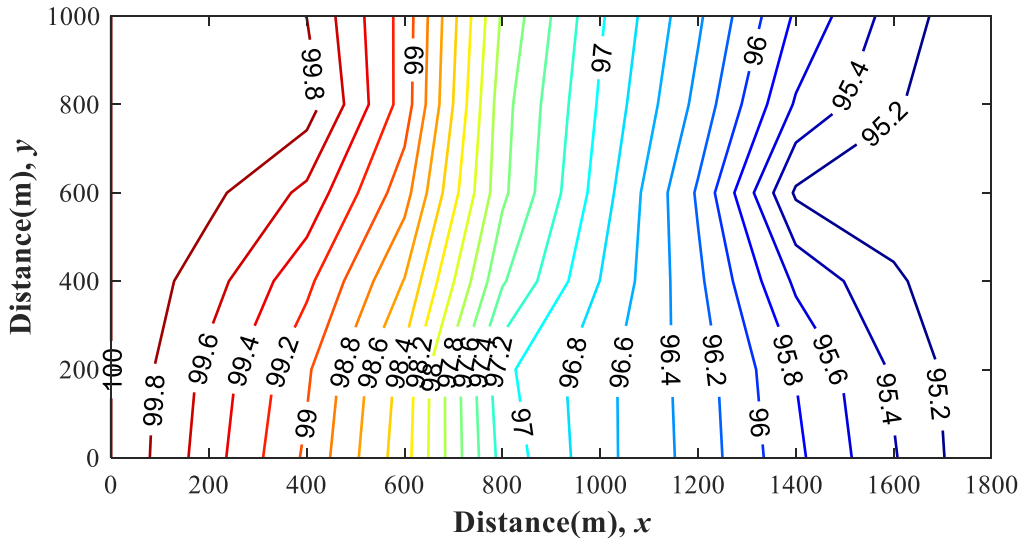

Figure 3. Head distribution in the flow region after 10000 days.

Table 1. Comparison of head distribution after 10000 days

Node No	Head in m (FEM)	Head in m (EFG)	Percentage Difference
21	98.20	98.59	0.396
34	97.10	96.90	0.206
51	95.25	95.23	0.021

Table 2. Effect of pumping and recharge wells at observation wells

Node No	Both PW and RW Inactive (m)	Only RW Active (m)	Both PW and RW Active (m)	Increase in Head due to RW (m)	Decrease in Head due to PW (m)
21	99.08	99.45	98.59	0.37	0.86
34	97.81	98.21	96.90	0.40	1.31
51	95.81	95.91	95.23	0.10	0.68

In this study an attempt is also made to run the EFG simulations with different time step sizes which are chosen as 5, 10, 20, 40 and 80 days respectively. The study found that the head values at three observation wells for Δt = 1 day were same as for sixteen fold increase in time step size. This suggests the robustness and stability of the EFG scheme.

4. CONCLUSIONS

In the present study an EFG discretization of a two dimensional groundwater flow model is presented. A MATLAB code is developed for the EFG model. The EFG shape functions derived from the MLS approximation do not obey Kronecker delta property. Thus, the Dirichlet boundary conditions are incorporated accurately using the Lagrange multiplier method. The elimination of the mesh generation procedure in pre-processing in this meshless method saves computational cost and time. However, the increased size of the resultant matrix in EFG method using Lagrange multipliers makes it computationally expensive. The EFG model is applied to a known problem (Sharief 2007)

and its outputs are verified with his FEM results. The percentage difference between the groundwater head values predicted by the EFG and FEM simulations is less than 0.4 %. The EFG technique was found to be a stable numerical scheme as it gave the same head values for larger time step sizes. Therefore the present study suggests the application potential of meshless EFG method in simulating real field aquifers which are important for groundwater management.

REFERENCES

Bear, J. (1979). Hydraulics of groundwater, McGraw Hill Publishing, New York.

Belytschko, T., Lu, Y.Y., and Gu, L. (1994). "Element free Galerkin methods." International Journal for Numerical Methods in Engineering, 37, 229–256.

Belytschko, T., Organ, D., and Krongauz, Y. (1995) "Coupled finite element-element–free Galerkin method". Computational Mechanics, 17, 186-195.

Dolbow, J., and Belytschko, T. (1998). "An introduction to programming the meshless element free Galerkin method." Archives of Computational Methods in Engineering, 5(3), 207–241.

Liu, G. R., and Gu, Y. T. (2005). An introduction to meshfree methods and their programming, Springer, The Netherlands.

Lu, Y.Y., Belytschko, T., and Gu, L. (1994). A New Implementation of the Element Free Galerkin Method. Comput. Methods. Appl. Mech. Engrg., 113, 397-414.

Meenal, M., and Eldho, T. I. (2011). "Simulation of groundwater flow in unconfined aquifer using meshfree point collocation method." Eng. Anal. Bound. Elem., 35(4), 700-707.

Park, Y.-C., and Leap, D. I. (2000). "Modeling groundwater flow by the element free Galerkin (EFG) method." Geosciences Journal, 4(3), 231-241.

Pinder, G.F., and Gray, W.G. (1977). Finite element simulation in surface and subsurface hydrology, Academic Press, New York.

Praveen Kumar, R., and Dodagoudar, G. R. (2009) "Meshfree analysis of two dimensional contaminant transport through unsaturated porous media using EFGM." Int. J. Numer. Meth. Biomed. Engng., 26, 1797–1816.

Rastogi, A. K. (2012). Numerical groundwater hydrology, Penram International Publishing Pvt. Ltd., Mumbai, India (Reprint).

Sharief, S.V.M. (2007). "Groundwater remediation strategies using FEM-GA simulation-optimization models." PhD Thesis, Department of Civil Engineering, Indian Institute of Technology Bombay, Mumbai, India.

Swathi, B., and Eldho, T. I. (2014). "Groundwater flow simulation in unconfined aquifers using meshless local Petrov-Galerkin method." Eng. Anal. Bound. Elem., 48, 43–52.

Wang, H., and Anderson, M. P. (1982). Introduction to groundwater modeling finite difference and finite element methods, W.H. Freeman and Company, New York.

IX. Legislation and Policies

Proceedings of the 10th World Congress of EWRA 'Panta Rhei', 5-9 July 2017, Athens, Greece
© 2017 *European Water Resources Association*

Sustainable restoration of the Urmia lake: History, threats, opportunities and challenges

M. Soudi[1], H. Ahmadi[1], M. Yasi[2] and S.A. Hamidi[3]
[1] *Department of Water Engineering, University Urmia, Urmia, Iran*
[2] *Department of Irrigation & Reclamation Engineering, University of Tehran, Karaj, Iran*
[3] *Department of Physics, College of Natural Sciences and Mathematics, Indiana University of Pennsylvania, USA*
[*] *e-mail: soudi_mina@yahoo.com*

Abstract: The natural and human-induced processes are currently major threats to aquatic ecosystems and water bodies, all over the world. Urmia Lake, the world's second largest saline lake, is located in the Northwest of Iran, is being drying up mainly due to the mismanagement of water use in the basin and the reduction of inflow to the lake. The lake water level has rapidly declined since the mid-1990s. Construction of more than fifty dams and diversion structures, along with the effects of climate change, are the main causes. Construction of a 15 km long causeway in the middle of the lake is an additional cause, which eliminates the natural circulation in the lake. The situation has turned to critical over the past two decades, and the need for restoration is an urgent priority for the region. The contribution of the ten principal rivers for flowing water into Urmia Lake is considered an ultimate solution to this crisis. However, the most challenges for any restoration plan are to be public awareness and general knowledge on the environmental values of the lake to local communities. This paper addresses the major causes to the desiccation of Urmia Lake, and presents an overview on the restoration plan and strategies that have been setup for the next years. Major threats and challenges are also highlighted in terms of the public awareness and community benefits in order to secure the feasibility of the plan for preservation of this internationally recognized wetland at a sustainable environmental status.

Key words: Causeway Urmia Lake, Restoration plan, Water management, Drought, Lake Causeway

1. INTRODUCTION

The Urmia Lake Basin is one of the most valuable ecosystems that is located in the northwest of Iran, between the provinces of West and East Azerbaijan. As an endorheic or terminal lake, water leaves the lake only by evaporation. So it is a closed-basin and the only outlet is evaporation (UNEP, 2012), but the inlets consist of precipitation, rivers, runoff flow and groundwater inflow (Ghaheri, 1999).

Because of its unique natural and ecological features, such as existence of exclusively a kind of Artemia (Urmiana Artemiana) as an exclusively parthenogenetic population (Barigozzi et al., 1987), this hypersaline lake was declared as a Wetland of International Importance by the Ramsar Convention in 1971 (Ramsar Site) and in 1976 as designated a UNESCO (UNESCO Site) Biosphere Reserve (ULRC, 2015a).

Since 1979 a dike type causeway gradually has been constructed in the middle of the lake and divided the lake into north and south parts, where connects the city of Urmia (West Azerbaijan Province) to city of Tabriz (East Azerbaijan Province) and limits the exchange of water within just 1.25 Km long opening that covered by a bridge (Teimouri, 1998). Results of hydrodynamic numerical modeling of Urmia Lake reveal that flow regime have been effected by wind input as a climate and hydrologic factor, but river discharge, evaporation and rainfall were main parameters affecting salinity distribution in the lake models. Therefore, the causeway has no significant effect on the lake flow and salinity regime (Zeinoddini et al., 2009). However, the influence of the causeway on salinity difference between north and south parts as well as on exchanging of flow between these two parts is unassailable, and needs much more hydrodynamic studies to have a better knowledge about it. The location of Urmia Lake and the causeway as well as mouth of its

major input rivers are shown in Figure 1.

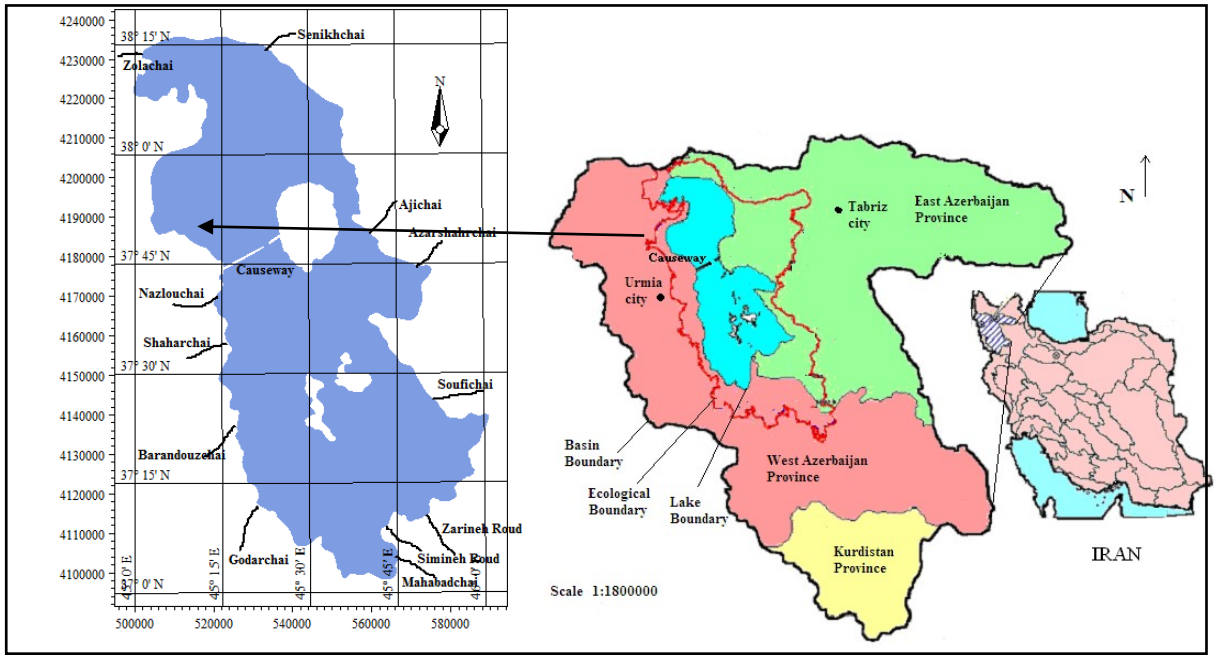

Figure 1. Study site: (a) General shape of Urmia Lake with input rivers and location of Causeway, (b) The location of Urmia Lake Basin in Iran

2. CAUSES AND CONSEQUENCE OF DRYING

During the last two decades (since 1995) some parameters severely have been declined the water level of Urmia Lake. Based on precipitation measurement stations in the lake basin, the average of the basin precipitation from 1995 to 2013 has been decreased about 18 percent, about 68 millimeters (ULRC, 2015a). Investigations result by Hassanzadeh et al., (2011) revealed that four dams (Alaviyan, ZarinehRoud, Mahabad and Nahand) have been responsible for 25% of the lake level reduction, while climate change and overuse of surface water is the cause of 65% of the lake level reduction in the recent years. The remained 10% is caused by lower precipitation on the lake.

Nonetheless, reduction of the water level of the lake through the two recent decades, whether in monthly or yearly scales was more harsh and different than changes of precipitation and temperature anthropogenic factors impacts rather than natural variability. (Jalili et al., 2016 a; Jalili et al., 2016 b; Zoljoodi and Didevarasl, 2014).

Furthermore, last assessment of water demand in the Urmia Lake Basin revealed that 70 percent consumption of renewable water resources of the basin. Whereas according to stable development index of United Nations Commission, the amount of secure and acceptable consumption of renewable water resources have been determined between 20 and 40 percent. Therefore, 30 percent overuse from the Urmia Lake Basin (because of development of agriculture) has effected stability of the water resources of the basin (ULRC, 2015a).

In the Urmia Lake Basin, population growth leads to increasing in the need for food as well as demand for water (Khatami and Berndtsson, 2013). Agriculture activities in the basin consume about 90 percent of water of the whole basin and more than 60 percent of the renewable water. Based on recently published data by Ministry of Energy (MOE), in 2011 annual water volume consumption for agriculture purpose was 4.3 MCM. In spite of that, agriculture consist of 30 percent of whole basin incomes (ULRC, 2015a). It seems that developing industrial activities in Urmia Lake basin can decrease, depending on the economy of the region to agriculture and may decrease water demand.

Drop in the lake water level increase the salinity of the lake. Artemia Urmiana tolerate a salinity

range of 40 to 250 g/l (Csavas, 1996) so continuation of this trend in recent years treat the life of Artemia, and confront it with extinction danger. Since Artemia is the main food resources of birds, especially flamingos, which spawn in the basin, a severe decrease in number of birds have been occurred (Abbaspour et al., 2012).

Furthermore, drying of Urmia Lake leaves the majority of the lake converted by salt, especially in southern part. Based on experience from Aral Sea, this change leads to numerous problems in the ecosystem and the climate of the area such as salt storm and subsequently refractory diseases for child and other health hazards (Zetterstrom, 1999).Unfortunately converting the lake to an active region of saline dusts can be threatening significantly the population of the lake basin.

In Figure 2, some examples of consequences of drop in the Urmia Lake water level are shown. Other impacts are rising of the lake bed level and change it to flatter bed because of settling salts. Basis on satellite images and Remote Sensing observations bed level of the Lake 4 up to 108 centimeter has increased since 2013 to 2015 (WRI, 2015).



(a) *(b)* *(c)*

Figure 2. Examples of consequence of drying the Urmia Lake; a: desertification in Jabalkandi region (south -western part of UL, in January 2014); b: salt storm; c: disappearing of birds.

3. ADMINISTRATIVE ACTION PLANS OF URMIA LAKE RESTORATION NATIONAL COMMITTEE

Management and structural policies have been proposed for the restoration of the lake by Urmia Lake Restoration National Committee (ULRC). While these programs have had benefits and defects, so professional investigation of cost to benefit of projects is essential. Mentioned action plans consist of below actions (ULRC, 2015b).

I. Reduction of inflow volume in watercourses ending to the Urmia Lake.
   - Connecting two major rivers, ZarinehRoud and SiminehRoud, for facilitating water delivery into the lake.
   - Dredging of SiminehRoud, Godarchai, Mahabadchai and Ajichai Rivers

II. Increase in input water volume to the lake by extrication of stored water of the constructed dams

III. Inspection of illegal overusing of surface and ground waters.

IV. Protection actions for decreasing to salt storm disasters

V. Inter basin water transfers plans
   - from Zaab River subbasin
   - from Silve Dam in Southern part of the lake

VI. Increasing the efficiency of irrigation water by using new irrigation methods.

Some of the mentioned action plans have high cost such as dredging of major rivers and inter basin water transfers plans. So those restoration plans so far have had multi millions dollars expenses for government but implementation process is slow and the efficiency of them in restoration of the lake water level is a matter of question (Khatami and Berndtsson, 2013).

Transferring of water from other basins to Urmia Lake, because of long distance between two basins have had much more expenses, and also cause problems for the water balance and ecosystem of the other basins. Thus, inter basin water transfer plans are expensive and time consuming, and at least cannot be considered as a short term solution.

4. MAIN FINDINGS AND IMPLICATIONS

Results of the sensitivity analysis of different parameters declared that the lake is highly sensitive to river input, so that the water development projects implementation in the Urmia Lake Basin will disturb the lake ecosystem (Abbaspour et al., 2012).

Japan International Cooperation Agency, JICA et al., (2016), in collaboration with Water Resources Management Company (WRMC) and MOE have been modeled the projects effect and the hydrological cycle of Lake Urmia Basin by MIKE-SHE and GETFLOWS numerical models respectively.

Based on the result of the MIKE-SHE model, the water level of Urmia Lake was simulated for the condition that the selected hydrological situation will continuously occur every year from the beginning to the end of the sequential simulation. The results of sequential simulation are summarized in Figure 3. As a result, it can be seen that only the Project 3 (P3) can achieve the target water level (1,274.1 m), even though all projects except No. 1 have the possibility to recover the lake water level to some extent (JICA et al., 2016). It seems that there is essential to design an appropriate dams operation schedule.

From the result of the simulation, it became clear that the river inflow volumes of approximately 2,050 MCM is necessary for around 10 years to adjust the in target water level. However, in case of the project prepare of over 2,100 MCM/year, the water level will also rise to more than the target water level of 1,274.1 m in the future. Other studies estimate inflow volumes as 3085 MCM of inflow per year for restoration of the lake (Abbaspour and Nazaridoust, 2007). Thus, to adjust the water level to the target, after the achievement of the target water level, the total river inflow volume should be controlled to approximately 2,100 MCM/year (JICA et al., 2016).

If all projects are implemented, the river inflow volume will increase to approximately 3,177 MCM/year and the lake water level is likely to rise to around 1,276.78 m (higher than the target water level). In this case, it takes around 6 years to reach the target water level (1,274.1 m) (JICA et al., 2016).

If all projects are implemented, the river inflow volume will increase to approximately 3,177 MCM/year compared with Project No. 1 (maintenance status quo) and the lake water level is likely to rise to around 1276.78 m (higher than the target water level). In this case, it takes around 6 years to reach the target water level 1274.1 m (JICA et al., 2016).

One of the solutions proposed for reducing the salt content of Urmia Lake is using desalination techniques, but desalination in hypersaline waters is a hight cost projects. A better strategy would be better to allow more fresh water through several rivers reaching the lake to reduce salinity and improve aquatic life rather than creating fresh water through reverse osmosis and distillations processes (Karbasi et al., 2010). Fortunately, authorities of the Ministry of Energy have agreed with this policy.

Among varies restoration plans, its seem be better to allow the rivers flow to reach the lake for reducing salinity and increasing aquatic life rather than creating fresh water through reverse osmosis and distillations processes (Karbasi et al., 2010). During dry seasons, Southern part of the Urmia Lake was dry in the last two years (Figure 4). An emergency action was to release 136 MCM water from three reservoir dams (Bukan, Sarough, and Hassanlou) to the lake during February and March 2015. In 2016, extra precipitation over the Urmia Lake Basin resulted in the overflow of flood flows from the most of the basin dams to the lake. So, the lake water level approached to 1270.55 m in February 15, 2016. Figure 5 shows the effectiveness of natural water inflows on the lake surface area. At the same time, other actions such as dredging of the rivers mouths, connecting ZarinehRoud and SiminehRoud Rivers, and controlling the illegal overuse of surface waters facilitated the recovery of the lake.

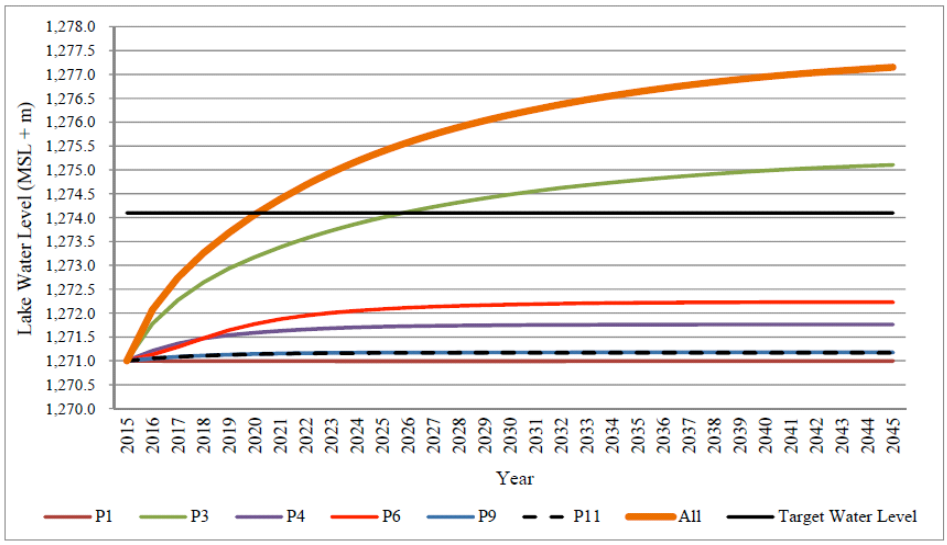

Figure 3. Project Effects (Change of Yearly Average Water Level).
P1: Prohibition against any increase of water use (maintenance of status quo). P 3: Stop of whole water supply. P 4: Water Transmission from Zab River to Urmia Lake Basin. P 6: Controlling and reducing water consumption in agriculture section. P 9: transferring Rivers' water into the body of the Lake. P 11: Transferring from Aras River in West Azerbaijan merely into Urmia Lake. Including No.3, 4, 9, 11 (in this case No.6 contain in No.3) (JICA et al., 2016).

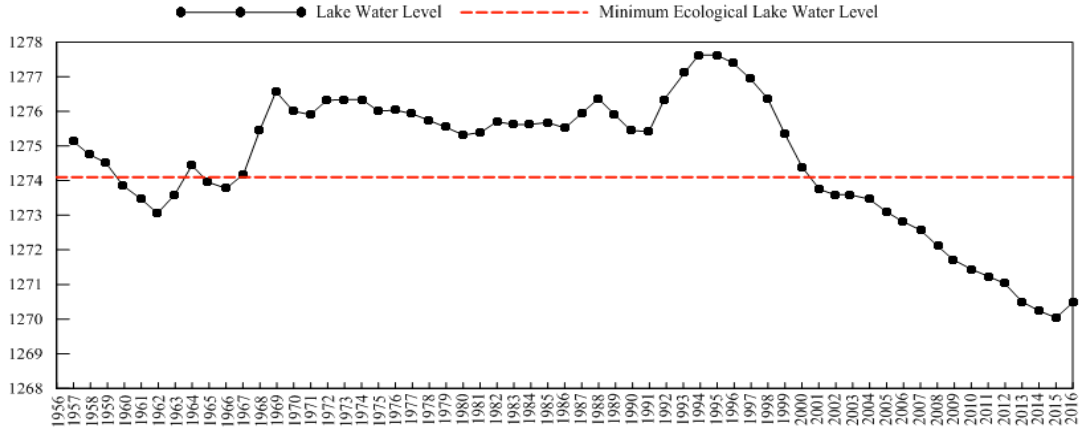

Figure 4. Urmia Lake surface trend for last 60 years

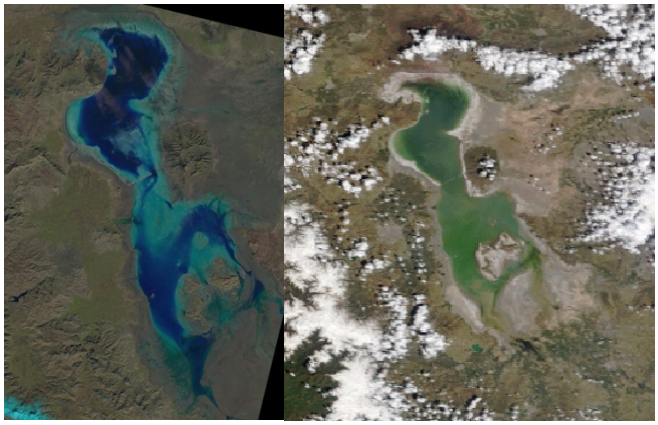

(a) Before *(b) After*

Figure 5. A satellite image of the storage water extrication action effects in the Urmia Lake, captured on (a) November 28, 2015 (showing the extent of dried regions (white) in the Southern part; and (b) February 15, 2016. Image Source:https://earthexplorer.usgs.gov/

5. CONCLUSIONS

Traditional water management will soon result in the drying crisis of Urmia Lake, an internationally registered hyper-saline wetland, in Iran. The most priority is an action plan to deliver in-basin surface waters into the lake. The restoration of the lake demands the action plan for supplying and delivering water from the ten major rivers around the lake, in the order of 20% to 40% of potential annual flows from these rivers. The revision of the current water allocation for agricultural uses, emergency plan to reduce 40% of irrigation water, to lease farmers' water-rights, to prevent illegal water intakes from the rivers, to release 30 to 40% of reserved water from 13 large dams around the lake, and to perform river improvement works to facilitate water delivery are necessary for saving the Urmia Lake. Long life and sustainable solution is to increase the rivers environmental flow allocations from existing 10% to 20% to 40% of their potential annual flows. The change in the volume of water regulation in the 13 operating dams, and the reduction of possible storage of water in the 11 under-construction dams are to be considered for the future restoration of the Urmia Lake.

In recent years the southern part of the lake was completely dried out. This part of the lake is wide and shallow, and as a consequence of the drying, crystallized salt has been deposited on the lake bed. The lake bed has risen, and thereby strategies such as more discharge from dams may not be effective. Because by discharge of stored fresh water in the dams in the southern part of the lake a large quantities of fresh water will be released on a crystalized salt bed and this will waste a lots of water by evaporation.

Therefore it is important to develop models to study the effects of dams' release in different parts of the lake. A multi-purpose multi-disciplinary project is underway by authors to develop numerical framework to study the hydrodynamic behavior of the lake under the natural drivers as well as different restoration strategies to analyze the effectiveness of these efforts and predict the future of this precious natural body of water. The output of this research will be useful to improve our understanding about the future plans and also effective operation of dams and management of water resources.

REFERENCES

Abbaspour, M. and Nazardoust, A. (2007). Determination of environmental water requirenments of Lake Urmia, Iran, an ecological approach. International Journal of Environmental Studies, 64(2): 161-169.

Abbaspour, M., Javid, A. H., Mirbagheri, S. A., Givi, F. A. and Moghimi, P. (2012). Investigation of lake drying attributed to climate change. International Journal of Environmental Science and Technology, 9(2): 257-266.

Barigozzi C, Valsasnini P, Ginelli E, Badaracco G, Plevani P. and Baratelli L. (1987). Further data on repetitive DNA and speciation in Artemia, Artemia Research and Applications, 1: 103-105.

Csavas, I. 1996. Current status of aquaculture industry and outlook highlight of resources, In Proc. of I.M.O.A. Seminar, Taipei, Taiwan, 41–52.

Ghaheri, M., Baghal-Vayjooee, M. and Naziri, J. (1999). Lake Urmia, Iran: A summary review, International Journal of Salt Lake Research, 8. 1: 19-22.

Karbassi, A.R., Nabi Bidhendi, G., Pejman, A. and Esmaeili Bidhendi, M. (2010). Environmental impacts of desalination on the ecology of Lake Urmia, Journal of Great Lakes Research, 36: 419–424

Hassanzadeh, E., Zarghami, M., Hassanzadeh, Y. (2011). Determining the main factors in declining the Urmia Lake level by using system dynamics modeling, Water Resource Management, 26(1): 129-145.

Jalili S., Hamidi S. A. and Ghanbari R. N. (2016). Climate variability and anthropogenic effects on Lake Urmia water level fluctuations, northwestern Iran, Hydrological Sciences Journal, 3: 1-1.

Jalili, S., Hamidi, S. A., Morid, S., & Ghanbari, R. N. (2016). Comparative analysis of Lake Urmia and Lake Van water level time series. Arabian Journal of Geosciences, 9(14), 644.

Japan International Cooperation Agency (JICA)., Ministry of Energy (MOE). and Water Resource Management Company (WRMC). (2016). Data collection Survey on Hydrological Cycle of Lake Urmia Basin in the Islamic Republic of Iran. Draft final report 1.

Khatami, S. and Berndtsson, R. (2013). Urmia Lake Watershed Restoration in Iran: Short- and Long-Term Perspectives, Proccedings of the 6th International Perspective on Water Resources and the Environment (IPWE).

Ramsar (no date). Ramsar Site List. Accessed 24 January 24, 2012 at: http://www.unesco.org/mabdb/br/brdir/directory /biores.asp?mode=gen&code=IRA+07.

Teimouri. B., (1988). Urmia golden gate highway (known as Martyr Kalantari Highway) after two decades of uncertainty. Sanat Haml-o Naql (Transportation Industry)., 173:18-23.

UNEP. G. (2012). The drying of Iran's Lake Urmia and its environmental consequences. J. Environ. Dev. 2012;2 :128-37.

UNESCO (no date). UNESCO-MAB Biosphere Reserves Directory. 24 January 24, 2012 at: http://www.unesco.org/mabdb /br/brdir/directory/biores.asp?mode=gen&code=IRA+07.

Urmia Lake Restoration Committee. (2015a). Urmia Lake drying reasons and probable treats. http://ulrp.sharif.ir/sites/default/ files/field/files/01%20Urmia%20Lake% (In Persian).

Urmia Lake Restoration Committee. (2015 b). Restoration plan of Urmia Lake review of approved solutions, administrative situation and progress projects., http://ulrp.sharif.ir/sites/default/files/field/files/02%20Urmia%20Lake%.... (In Persian).

Water Research Institute. (2015). Bathymetry of Lake Urmia and investigation of its sedimentation rate from 2013-2015 by remote sensing technology and field survey, (In Persian).

Zeinoddini, M., Tofighi, M. and Vafaee, F. (2009). Evaluation of dike-type causeway impacts on the flow and salinity regimes in Urmia Lake, Iran, Journal of Great Lakes Research, 35(1), 13-22.

Zetterstrom, R. 1999. Child health and environmental pollution in the Aral Sea region in Kazakhstan. Acta Paediatrica Supplement, 429: 49-54.

Zoljoodi, M. and Didevarasl, A. (2014). Water-Level Fluctuations of Urmia Lake: Relationship with the Long-Term Changes of Meteorological Variables (Solutions for Water-Crisis Management in Urmia Lake Basin), Atmospheric and Climate Sciences.

Proceedings of the 10th World Congress of EWRA 'Panta Rhei', 5-9 July 2017, Athens, Greece
© 2017 *European Water Resources Association*

Measuring sustainable delivery of water, sanitation and hygiene services at the household level: Does the measure matter?

R. Giné-Garriga* and A. Pérez-Foguet
Department of Civil and Environmental Engineering (DECA), Engineering Sciences and Global Development (Esc&GD), Barcelona School of Civil Engineering, Universitat Politècnica de Catalunya, Barcelona, Spain
* *e-mail: ricard.gine@upc.edu*

Abstract: Water, sanitation and hygiene (WaSH) are at the very core of sustainable development. As we embark on a new round of global goals to follow the 15 year Millennium Development Goals period, namely the Sustainable Development Goals, a top priority is to address a coherent framework for monitoring these services. In coming years, the sector will witness the development of a variety of multidimensional monitoring measures, albeit from different perspectives. This paper reviews three different multidimensional approaches that are increasingly adopted to determine the level of service delivered at the household. At the global level, a ladder approach to monitoring has been promoted by the WHO/UNICEF Joint Monitoring Programme. Alternatively, the use of aggregated indicators is widespread, as they are adequate to capture and simplify the complexity inherent in services delivery. Finally, the Alkire & Foster methodology for multidimensional poverty measurement has been extensively used for pro-poor targeting. We adapt this method to capture a set of direct household-related water and sanitation deprivations that batter a person at the same time. Taking the international post-2015 monitoring framework as a reference point, this article analyses these measures and their outcomes. For illustrative purposes, one small town in Mozambique is selected as initial case study. We conclude that multidimensional measures are needed to provide a complete picture of the context in which the WaSH services are delivered. In consequence, they are useful to report on the SDG monitoring architecture.

Key words: sanitation; Sustainable Development Goals; indicator; multidimensional poverty measurement; identification; monitoring

1. INTRODUCTION

The search for improved metrics to target the neediest has captured the attention of researchers and policymakers alike. A key direction for research has been the development of a coherent framework for measuring services delivery from a multidimensional perspective, and recent efforts have identified several multidimensional measures. Some of them have been applied to assess water, sanitation and hygiene (WaSH) services in rural contexts (Flores Baquero et al. 2013; Giné Garriga and Pérez Foguet 2013). However, there is no consensus on how best to profile WaSH-related poverty across dimensions. Specifically, though it is widely accepted that there are complementary ways of profiling poverty and that each dimension is important to be accounted for in such an exercise, the literature shows two significant challenges that discourage the empirical use of these conceptually attractive measures.

First weakness involves how the basic input data are combined. For new dimensions to provide significantly additional information, they should not be strongly correlated with the rest. This would imply that there are no synergies or conflicts among them, which appears to be quite an unrealistic assumption (Nardo et al. 2005). In case independence is assumed, then it may be meaningful to either aggregate them or define a welfare function over multiple dimensions. Other related issue is the choice of weights to reflect the relative importance given to the dimensions. A conventional practice is the selection of weights following consultation with experts (Flores Baquero et al. 2016), but they are often singled out for their arbitrariness (Booysen 2002). Alternatively, multivariate techniques present an empirical and more objective option. However, statistical weights do not always reflect the priorities of decision-makers (Nardo et al. 2005), and they are data-specific. No

weighting system is therefore above criticism. There are also many aggregating techniques available for constructing a composite. In linear aggregation rules, compensability among parts is implicit (Nardo et al. 2005). In poverty measures, a complete compensability may not be desirable as different dimensions are equally legitimate. A non-compensatory logic might be necessary: multi-criteria analysis entails full non-compensability, and the use of a geometric aggregation emerges as an in-between solution.

Second flaw relates to the method for identifying the poor, which remains understudied. Most attempts either leave identification unspecified or select criteria that seem reasonable over two dimensions, but become less tenable when additional dimensions are used (Alkire and Foster 2011). In an attempt to address this weakness, Alkire and Foster introduced an intuitive approach to identifying the poor at the person / household level, namely the M0 or Adjusted Headcount Ratio. It uses a 'dual cut-off' identification system that gives clear priority to those suffering multiple deprivations, and shows at a glance the incidence, intensity and depth of poverty. There are four properties of this methodology that have helped make it useful in practice (Alkire and Foster 2011; Alkire and Foster 2016). First, M0 is robust when using ordinal or cardinal variables as it classifies the individuals' achievements into ''deprived" and ''non-deprived". Second, by adjusting the incidence of multidimensional poverty by the intensity, the measure satisfies the condition of dimensional monotonicity (Alkire and Foster 2011): both if an additional person becomes poor and if a person already considered as multidimensionally poor becomes poor in additional dimension(s), M0 will increase. Third, the measure is decomposable by population subgroups, meaning that the M0 of the overall society can be obtained as the population-weighted sum of subgroup poverty levels (subgroups need to be mutually exclusive and collectively exhaustive of the population). Subgroup Decomposability enables poverty comparisons across subgroups, facilitating regional analysis and targeting. Fourthly, after identification, M0 can be broken down by indicator. The overall M0 can be expressed as the weighted sum of the proportion of the total population who has been identified as poor and is deprived in each indicator (weights referring to the relative weight of each indicator). Analogous to the population subgroup decomposability, Dimensional Breakdown enables analysis of the contribution of deprivations in each indicator to overall poverty.

In order to contribute further to the ongoing debate about improved monitoring and reporting methods, the purpose of this study is to compare three multidimensional approaches that are widely adopted to assess the level of service delivered at the household. A ladder approach has been promoted by the WHO/UNICEF Joint Monitoring Programme (JMP) (Joint Monitoring Programme 2015a), who has been officially mandated to monitor progress towards the water and sanitation SDG targets. The use of aggregated indicators is widespread, as they are adequate to capture and simplify the complexity inherent in services delivery (Giné Garriga and Pérez Foguet 2010; Giné Garriga and Pérez Foguet 2013). Finally, the Alkire & Foster methodology for multidimensional poverty measurement has been extensively used for pro-poor targeting (Alkire and Foster 2011). We adapt this method to capture a set of direct household-related water and sanitation deprivations that batter a person at the same time. These three multidimensional measures and their outcomes are analysed and compared. For the sake of simplicity, however, this paper focuses on the issue of sanitation and hygiene. A case study from a small town in Mozambique has been selected for illustrative purposes.

2. METHODS

In terms of method, the three measures are founded on a common theoretical background. There is broad consensus at the international level that SDG targets for WaSH should take into account the normative criteria enshrined in the Human Rights to Water and Sanitation (Joint Monitoring Programme 2015b). In keeping with this goal, the quality of sanitation services may be described on the basis of the contents of the Human Right to Sanitation (HRtS) (United Nations General Assembly 2010). We adopt this approach herein, and each normative criterion of the HRtS is understood as a "poverty" dimension. Available indicators are consequently classified in five

different categories - availability, physical accessibility, quality and safety, affordability and acceptability. Table 1 presents the proposed list of indicators. Each indicator is assessed against four different levels of service, namely good service level, intermediate, poor and no level of service (Giné-Garriga et al. 2017).

Table 1. Sanitation descriptors based on human right normative content: imensions, indicators

Normative Criteria of the HRtS (Y)	**Indicator (X)**
Availability	Type of sanitation facility - Sanitation ladder
	Toilet facility location
Physical Accessibility	Safety and security while accessing the sanitation facility
	Safety and security while using the sanitation facility
	Continuity of use of the latrine
	Suitability of use of the latrine
Quality and Safety	Sanitary conditions of the latrine
	Latrine condition standards
	Hand washing facility and soap in the vicinity of the latrine
	Hygienic practices in the latrine
	Safe management and disposal of human urine and faeces
Affordability	Affordability of sanitation services
Acceptability	Conditions of privacy in the latrine
	Conditions of comfort in the latrine
	Cultural-related issues

2.1 The Sanitation Index

Index construction relies on a step-by-step procedure initially suggested by OECD-JRC (Nardo et al. 2005), which was adopted by Giné Garriga and Pérez-Foguet (Giné Garriga and Pérez Foguet 2010) to estimate a Water Poverty Index (WPI), and which was subsequently applied to different conceptual frameworks (Flores Baquero et al. 2013; Giné Garriga and Pérez Foguet 2013). Specifically, we have applied in this study the same method as Flores et al (Flores Baquero et al. 2016). That is, the five index dimensions are calculated as the arithmetic average of raw indicators:

$$Y_j(Av, PA, Q, Aff, Acc) = \frac{\sum_{i=1,2,3...} X_{j,i}}{n_j} \quad (1)$$

where j are the values of each normative criterion (Y) for a particular household, Xi refers to indicator i of the criterion j, and nj is the total number of indicators of criterion j.

In next stage, the different dimensions of the index are aggregated into one single value. As regards the weighting technique, the choice of weights reflects the expert opinion. With regard to the aggregation process, we have opted for a weighted multiplicative function to avoid compensability among the different dimensions - different rights-based criteria are equally legitimate (United Nations Economic and Social Council 2002). The index can be calculated by applying the following formula:

$$SI = \prod_{j=Av,PA,Q,Aff,Acc} Y_j^{w_j} \quad (2)$$

where SI is the value of the sanitation index for a particular household, Yj refers to dimension j of the index, and wj is the weight applied to that dimension.

2.2 The Sanitation Service ladder

To monitor progress towards the sanitation target of the SDGs, the JMP recommends using a 'service ladder' approach. In particular, a five-rung ladder is proposed to differentiate between improved facilities that are safely managed, those that are not correctly managed, and those of an otherwise improved type that are shared by more than one household. The ladder also distinguishes between unimproved facilities and households practicing open defecation. In practical terms, the proposal seeks to progressively realise the HRtS by firstly extending access to the unserved, secondly moving people up the 'service ladder', and thirdly eliminating inequalities in access (Joint Monitoring Programme 2015b).

In accordance with this monitoring strategy, this study adopts a ladder approach to measure progressive realization of the HRtS, albeit from a multidimensional perspective. Taking the set of indicators listed in Table 1 as a starting point, the level of service is determined through applying a conservative interpretation of the descriptors included in each criterion. For instance, the service level of a household with access to improved sanitation which is located in the immediate vicinity is categorized as "intermediate"; to enjoy a good level of service, the latrine should be located inside the household. In turn, the overall service level is given by the worst-performing criteria. Overall, moving up the ladder would necessarily mean that the different elements of all criteria have been fulfilled. Numerically, the level of service can be formulated as:

$$SSL = \min_{j=Av,PA,Q,Aff,Acc}^{n_j} X_{j,i} \tag{3}$$

where SSL is the level of sanitation service for a particular household, and Xi refers to dimension j of the index.

2.3 A Sanitation Adjusted Headcount Ratio

The Adjusted Headcount Ratio (or M_0) assesses the nature and intensity of poverty at the individual level by considering overlapping deprivations suffered at the same time, with poor people being those who are multi-dimensionally poor (Alkire and Foster 2011). The M_0 can be used as an analytical tool to identify the most vulnerable people, show aspects in which they are deprived and the extent of their poverty, and help to reveal the interconnections among deprivations. This can enable policy makers to target resources and design policies more effectively. Application of this method is detailed elsewhere (Alkire and Foster 2011); briefly, the steps for identification and aggregation of households include:

1) Defining the case study
2) Defining the dimensions and corresponding set of indicators which will be considered in the multidimensional measure (Table 1). Data for all indicators need to be available for the same household; otherwise the household is removed from the dataset.
3) Setting the poverty lines (deprivation cut-offs) for each indicator, namely the level of achievement considered sufficient in order to be non-deprived in each indicator. Applying the cut-off to identify whether each household is deprived or not in each indicator.
4) Selecting the weights for contribution of each indicator to the overall metric, such that these sum to one (equal weights among indicators are assumed for simplicity).
5) Counting the number of deprivations for each household, i.e. creating the weighted proportion of deprivations for each household, this can be called its deprivation score.

6) Determining the poverty cut-off "k", namely the proportion of weighted deprivations a household needs to experience in order to be considered multidimensionally poor. Obtaining the set of poor households "N_P" by identifying each household as multidimensionally poor or not, according to the selected poverty cut-off. In practice, it is useful to calculate the measure for several values of k, and then perform robustness checks of the cut-off (Table 3).
7) Computing the proportion of people who have been identified as multidimensionally poor in the population. This is the headcount ratio H, also called the incidence of multidimensional poverty.
8) Computing the average share of weighted indicators in which poor people are deprived. This entails adding up the deprivation scores of the poor, and dividing them by the total number of poor people. This is the intensity of multidimensional poverty, A.
9) Computing the M_0 measure as the product of the two previous partial indices: $M_0 = H \cdot A$. Analogously, M_0 can be obtained as the sum of the weighted deprivations that the poor (and only the poor) experience, divided by the total population.

In short, a clear advantage of this methodology is that it captures both the incidence (number of sanitation poor people) as well as the intensity (how sanitation poor they are).

3. RESULTS AND DISCUSSION

In this section, we compare the results obtained by applying the three approaches described above to assess the level of sanitation poverty at the dwelling. Specifically, we aim to determine how these measures reveal sanitation-related deprivations and whether they are useful to target the sanitation poor. To do this, we exploit data from a household-based survey conducted in 2011 in the municipality of Manhiça, in southern Mozambique.

To begin with, Table 2 presents the proportion of households that meet a specific level of service per each criterion. The differences between the index and the ladder approach stem from the method employed to construct the monitoring tool, and they are particularly linked to the issue of compensability between indicators and dimensions. They are of minor significance at the dimension level, but they are substantial for the aggregated values. For instance, index values show that 17.29% of households have no service at all, half of them (51.38%) access to poor level of service; and roughly one third (31.32%) enjoy an intermediate service level. The aggregated figures that describe the sanitation service level through a ladder approach show that population percentages with access to poor and intermediate level of service are 79.25% and 3.46%, respectively.

As regards the Alkire and Foster approach, the M_0 is computed by setting two different deprivation cut-offs - namely "intermediate service level" and "good service level" – and various multidimensional poverty cut-offs k. The multidimensional headcount ratio H provides an insight into the incidence of poverty. Table 3 shows that it logically decreases with both the deprivation cut-off (i.e. the poverty line) and the poverty cut-off k. By way of example, taking as a deprivation score reference an intermediate service level, 57.4% of households in Manhiça would be targeted as sanitation poor if the cut-off k is 0.6 or higher. However, if the reference level of service is taken as "good", then the percentage of poor amounts to 99.3%. It is worth noting that the multidimensional headcount ratio H does not satisfy the dimensional monotonicity property, and so it does not change if any of the poor households become deprived in an additional dimension. This limitation is overcome by the Adjusted Headcount Ratio M_0. One may be also interested in knowing how sanitation poor the poor people are or the intensity of multidimensional poverty (A). In previous examples, poor people are deprived, on average, in 75% and 87.3% of the dimensions, respectively.

In terms of interpretation, it is worth mentioning that increasing the poverty cut-off hinders the definition of poverty alleviation measures. In a similar way, it is difficult to interpret the line between the poor and the non-poor for low deprivation scores ($k \leq 0.4$). This is consistent with the high degree of sanitation poverty shown in Table 2 for improved levels of service. For instance, the ladder approach shows that only 3.46% of households enjoy an intermediate level of service, while

the headcount ratio if the deprivation cut-off is 0.2 shows that 96.5% of households are considered as sanitation poor. Another illustrative example is that households with no sanitation service in Table 3 - namely those who defecate in the open, 17.29% of households – might be considered to be equivalent to those poor households who are deprived in all the dimensions (k=1), i.e. 17.4% of households.

Table 2. Sanitation Poverty: i) The Sanitation Index; ii) The Sanitation Service ladder

	Availability		Physical Access		Quality and Safety		Affordability		Acceptability		Overall Sanitation Service Level	
	HH	%	HH	%	HH	%	HH	%	HH	%	HH	%
The Sanitation Index												
Good Service	64	5.21	596	50.30	1	0.08	5	0.47	243	19.77	0	0.00
Intermediate Service	268	21.81	410	34.60	268	21.97	719	68.22	694	56.47	317	31.32
Poor Service	722	58.75	4	0.34	776	63.61	155	14.71	117	9.52	520	51.38
No Service	175	14.24	175	14.77	175	14.34	175	16.60	175	14.24	175	17.29
The Sanitation Service ladder												
Good Service	64	5.21	596	50.30	0	0.00	5	0.47	243	19.77	0	0.00
Intermediate Service	266	21.64	0	0.00	119	9.75	719	68.22	694	56.47	35	3.46
Poor Service	724	58.91	414	34.94	926	75.90	155	14.71	117	9.52	802	79.25
No Service	175	14.24	175	14.77	175	14.34	175	16.60	175	14.24	175	17.29
Missing Data	0		44		9		175		0		217	
Total HH	1229		1229		1229		1229		1229		1229	

Table 3. Adjusted Headcount Ratio adapted to sanitation in Manhiça, Mozambique, for two deprivation cut-offs and five multidimensional poverty cut-offs k

	Poverty line: Intermediate Service Level					Poverty line: Good Service Level				
	k=0,2	k=0,4	k=0,6	k=0,8	k=1	k=0,2	k=0,4	k=0,6	k=0,8	k=1
N	1012	1012	1012	1012	1012	1012	1012	1012	1012	1012
$N_{P,K}$	977	887	581	259	176	1012	1012	1005	906	466
H	0,965	0,876	0,574	0,256	0,174		1	0,993	0,895	0,460
A	0,590	0,629	0,750	0,936	1,000		0,870	0,873	0,903	1,000
M_0	0,569	0,551	0,430	0,240	0,174		0,870	0,867	0,808	0,460

Finally, it might be interesting to analyse the composition of multidimensional poverty by considering the percentage contribution of each dimension to overall poverty. It can be seen in Table 4 that the poor in Manhiça exhibit the highest deprivation levels in quality and safety of sanitation facilities, followed by the availability of infrastructure. These results are coherent with sanitation-related priorities shown in Table 2. A dimensional breakdown of poverty may reveal different underlying structures of poverty, which in turn could suggest different policy responses. In Manhiça, for instance, policy attention should be directed to improve the quality of latrines, by e.g. reviewing the construction standards of toilets and/or providing a basic handwashing facility in or near sanitation infrastructure.

Table 4. Contribution of deprivation of each dimension to multidimensional poverty for an "intermediate level of service" and five different poverty cut-offs.

	K=0,2	K=0,4	K=0,6	K=0,8	K=1
Availability, Contribution	27,71%	28,57%	26,08%	21,37%	20,00%
Physical Access, Contribution	18,16%	18,24%	20,29%	20,13%	20,00%
Quality and Safety, Contribution	32,99%	31,54%	26,68%	21,37%	20,00%
Affordability, Contribution	11,32%	11,51%	13,96%	18,98%	20,00%
Acceptability, Contribution	9,83%	10,14%	12,99%	18,15%	20,00%

4. CONCLUSIONS

This paper presents three measures that can help the effective allocation of resources by making possible the targeting of those with the greatest sanitation needs; they can help address SDGs strategically and monitor impacts of policy intervention. These multidimensional measures can be adapted to the local and national level using indicators and weights that make sense for the municipality or the country, they can also be adopted for national poverty eradication programs, and they can be used to study changes over time.

In summary, achieved results demonstrate that applying a multidimensional analysis of poverty provides a number of advantages. Notably, they focus on the level of service and are based on data related to the normative content of human rights obligations related to sanitation, as opposed to deriving information through accessibility variables (e.g. access to improved infrastructure). Another virtue of the proposed methods is their decomposability. Because the data used as input are at micro-level (households), these tools allow for a wide range of analysis focusing on sub-groups (e.g. wealth, geographic clusters, etc.). Finally, by calculating the contribution of each dimension to multidimensional poverty provides information that can be useful for revealing the configuration of deprivations, which can help with policy targeting.

REFERENCES

Alkire S, Foster J (2011) Counting and multidimensional poverty measurement. J Public Econ 95:476–487. doi: 10.1016/j.jpubeco.2010.11.006

Alkire S, Foster J (2016) Dimensional and Distributional Contributions to Multidimensional Poverty. Oxford

Booysen F (2002) An Overview and Evaluation of Composite Indices of Development. Soc Indic Res 59:115–151. doi: 10.1023/a:1016275505152

Flores Baquero O, Gallego Ayala J, Giné Garriga R, et al (2016) The Influence of the Human Rights to Water and Sanitation Normative Content in Measuring the Level of Service. Soc Indic Res 1–24. doi: 10.1007/s11205-016-1374-6

Flores Baquero O, Jiménez A, Pérez Foguet A (2013) Monitoring access to water in rural areas based on the human right to water framework: a local level case study in Nicaragua. Int J Water Resour Dev 29:605–621. doi: 10.1080/07900627.2012.757017

Giné-Garriga R, Flores-Baquero Ó, Jiménez-Fdez de Palencia A, Pérez-Foguet A (2017) Monitoring sanitation and hygiene in the 2030 Agenda for Sustainable Development: A review through the lens of human rights. Sci Total Environ 580:1108–1119. doi: 10.1016/j.scitotenv.2016.12.066

Giné Garriga R, Pérez Foguet A (2013) Unravelling the Linkages Between Water, Sanitation, Hygiene and Rural Poverty: The WASH Poverty Index. Water Resour Manag 27:1501–1515. doi: 10.1007/s11269-012-0251-6

Giné Garriga R, Pérez Foguet A (2010) Improved Method to Calculate a Water Poverty Index at Local Scale. J Environ Eng 136:1287–1298. doi: 10.1061/(asce)ee.1943-7870.0000255

Joint Monitoring Programme (2015a) Progress on Sanitation and Drinking Water: 2015 update and MDG assessment. Geneva / New York

Joint Monitoring Programme (2015b) JMP Green Paper: Global monitoring of water, sanitation and hygiene post-2015. New York and Geneva

Nardo M, Saisana M, Saltelli A, et al (2005) Handbook on Constructing Composite Indicators: Methodology and User Guide. OECD, Paris

United Nations Economic and Social Council (2002) The right to water. General Comment No. 15. Resolution E/C.12/2002/11. 18.

United Nations General Assembly (2010) The human right to water and sanitation. Resolution A/RES/64/292

Proceedings of the 10th World Congress of EWRA 'Panta Rhei', 5-9 July 2017, Athens, Greece
© 2017 *European Water Resources Association*

Water market and its effects on the sustainable management of water resources in Chile

Nicole Kretschmer[1,2*], Ricardo Oyarzun[1,2], Pablo Alvarez[3], Jose Arumi[4]
[1] *Departamento Ingeniería de Minas, Universidad de La Serena, Chile*
[2] *Centro de Estudios Avanzados de Zona Arídas (CEAZA), La Serena, Chile*
[3] *Departamento de Agronomía, Universidad de La Serena, Chile*
[4] *Facultad de Ingeniería Agrícola, Universidad de Concepcíon, Chile*
[*] *e-mail: nkretschmer@userena.cl*

Abstract: A simple definition of sustainability is that sustainable use of water requires the maintenance of a desired flow of benefits to a particular group or place undiminished over time, without reducing benefits to other users, including ecosystems. Thus water plays an integral role in ecosystem support, economic development, community well-being and cultural values. Water availability is influenced by both, natural and anthropogenic factors, including climatic variability. Within this framework, the consequences of a private water management system (due to private water rights) crossed by and linked to the market itself is being analyzed and evaluated, focusing on the case of Chile since the 1981 water code was introduced. It shows how water rights since then have evolved in terms of, extraction point, permanency and execution of rights, analyzing not only water allocation issues but also sustainability concepts. Thus, the main question being addressed is: How does the Water Market facilitate or hinder sustainable water management? Did mobility induced by the water code of 1981 generated territorial development including expansion of agricultural area as well as changes in crop patterns and thus provoked economic development in some areas, but limited water access to others, leading to unsustainable water use? Preliminary results of two different catchments are being presented: The highly regulated basin of the Limarí River in the semi-arid north of Chile, and the Diguillín River catchment in the south of Chile, with a different climate and diverse management issues, including inter-basin water transfer.

Key words: Sustainable Water Management, Private Water Rights, Water Markets, Chile, Remote Sensing, Modelling

1. INTRODUCTION

The scope of sustainability assessment of integrated water resource management (IWRM) and its evolution in Chile has been described in detailed by Kretschmer and others (2012). In the legal political framework, catchment management issues are mainly expressed through the national water politics, based on the water code of 1981. It defines water as a national good of public use, driven by the application of economic market principles (Bauer, 2011). This allows the transfer of property rights for water use, as well as water volumes to be traded on the spot market (Alvarez et al, 2006).

The main user in the catchments under study is the agricultural sector; the river associations which are represented by the users are responsible for the allocation of water. The catchments are different in size, climate and water resource systems; here mainly the constructed water control facilities are influencing the water management possibilities in addition to the distribution of water rights.

The Limarí River basin (11,666 km², spanning 30º 10' to 31º 20' S and 70º 15' to 71º 45' W) is part of the semi-arid northern macro zone, where the average precipitation is ca. 90 mm/year (DGA, 2015). In contrary the catchment of the Diguillín River (36º 45'to 37º 15' S and 71º 48' to 72º 24' W) is a sub-catchment of the Itata River basin (11,326 km2) of the southern macro zone (moderate climate), with an average precipitation of 1,850 mm/year (macro zone: 2,420 mm/year, DGA, 2015). Climate conditions favour agriculture in both cases. It is influenced by El Nino Southern Oscillation (ENSO) which can cause multi-year periods of drought prone conditions in the north and much less water availability in the south.

The objective of the current work is to investigate in these two catchments with different climate if current and future water management, dependent on water rights and changes based on the regulations of the water market, allows a sustainable management of water resources.

2. LIMARÍ RIVER BASIN

The water allocation of the Limarí basin is more complex than the Diguillín sub basin, based on water rights and considering a system with three reservoirs with a total capacity 1.000 MCM. Water is being allocated since 1972 among the legally connected organisations of the La Paloma system, which started its operation after the termination of the main reservoir, La Paloma (750 MCM). This incorporates nine organisations, as well upstream and downstream users. Only four organisations of upstream catchments are independent.

Impacts of possible future changes in the Limarí basin have been look at, simulating the water allocation and analyzing reliabilities of supply with different scenarios. These results are further used to evaluate the resulting regulated flows in terms of the required minimal ecological flows (Qeco).

2.1 Methodology

For basin simulation the WRAP Modelling System (**W**ater **R**ight **A**nalysis **P**ackage, developed at the Texas A&M University; Wurbs, 2010) is being used. WRAP is a river-reservoir system water allocation model. Primary objective of the model is to provide capabilities for assessing hydrologic and institutional water availability and reliability within the framework of a priority –based water rights (Wurbs, 2006). We used the model to evaluate water supply feasibility associated with alternative water resource development projects, water use scenarios and regulatory requirements.

The presented results emerged from basin simulation of different scenarios (S) with different target setups and future developments in two upper independent catchments: S1 is a representation of the average real allocation data; S20 assigns upstream as well as downstream of the reservoirs the maximum volumes according to the water rights to be distributed; S21 simulates upstream real allocation data (which is in general less than legally possible), based on allocation rules of the river association and downstream using the actual legal data and maximum amounts agreed upon within a common operation rule inside the Paloma system; S22 further includes the total future use of two independent upstream sub-catchments with the construction of new upstream reservoirs. Simulations were done with previously generated natural flow data of 65 years.

Reliabilities have been calculated for meeting water supply in any randomly selected future month: The period reliability is based on counting the number of periods of the simulation during which the specific demand target is either fully supplied (firm yield) or a specific percentage of the demand is met; Volume reliability is the percentage of the total target demand amount that is actually supplied.

Furthermore the impact caused by altered allocation patterns between legally defined volumes and actually average supplied data is demonstrated through indicators of a shortage metrics. Shortage represents failures to fully meet water supply diversion requirements (Wurbs et al, 2010).

To further evaluate the support provided for the ecosystem by the prevailing water management the legal required Qeco are evaluated with the resulting remaining stream flows. All standards developed so far by the National Water Authority (DGA) are based on hydrological patterns. They are expressed as percentage of annual or monthly mean flows or flow frequency distribution with no limnological considerations. In 2002 the DGA released a manual of standards (DGA, 2002), were Qeco is presented as one permanent and continuous value over the whole year. Regarding the manual of 2008 (DGA, 2008), the establishment of Qeco for all new water use rights is required as well for those, which are being processed and water rights which are already established, but which are transferred to another extraction point. Furthermore the seasonal variation of the streamflow is

considered by calculating Qeco based on the natural monthly flow regime. More recently the Chilean Water Code underwent changes (Regulation 'decreto' No14/2012) in favor for a minimum ecological flow: the monthly variability is maintained, nevertheless a higher percentage of mean flows is being required.

The analysis was done comparing the modelled monthly streamflows of each month of the whole sequence with the monthly theoretical requirements of Qeco. Since in the basin all surface water rights were approved before these regulations came into force, the minimum flows cannot be claimed legally until a change of extraction point is being requested by the user. The results are expressed as monthly failures in percentage of the total months considered.

2.2 Results and conclusions of allocation model

Only some main outcomes possibly influencing the sustainability of the system are presented.

The real distribution of water from the Cogoti reservoir (150 MCM) in the scenario S1 sums up in average to 55 MCM annually, versus 40 MCM annually in the scenarios S20, S21 and S22, which reflect the official operational rule of the common La Paloma system.

The resulting shortage metrics of the allocation from the Cogoti reservoir (representing the weakest sub-catchment within the system), shows much higher values of vulnerability and severity when allocating the average volumes of the last decades compared to the assigned volume which were agreed upon with all organisations; here all indicators are close to cero, demonstrating almost no shortage. The actual management clearly facilitate an unsustainable use and thus it provokes higher vulnerability for its users. The system is designed to be able to allocate sufficient water for three consecutive years (in total 320 MCM/year) in case of drought conditions and when all associations comply with the achieved agreements.

To evaluate the consequences on supply security subject to changes of assignation, and new reservoirs, we furthermore calculated the annual yields of the existent reservoirs. The highest annual yields of the main reservoir La Paloma varied within the different scenarios between 236 MCM (S20) and 256 (S21). Scenario S21 resulted in the most allocated volumes evaluating the 85% volume and period reliability.

The simulation without allocating additional streamflow of the downstream river, yields only in a maximum of 215 MCM annually distributed (85% reliability) and thus only reaches about 89 % of the volume stipulated in the operational rule (240 MCM). In fact this is just a theoretical yield since most of the time downstream river flow supports the reservoir in water supply. Including the natural river water in the downstream area, the downstream users received in average 41.1 MCM /year (16%) additional surface water. These results show that especially a newly arising demand of downstream users to change their extraction point into the reservoir might provoke a hazardous disequilibrium of the system. Moreover, decision making should be based on various simulations, including more water scarce years as being witnessed in the last decade.

The behaviour of the yields of the three system reservoirs is different analysing the scenarios S21 and S22. The 85% volume and period reliability of the Recoleta reservoir (100 MCM) is almost equal in both scenarios (48 MCM annually), since it is independent of the changes upstream of the Cogoti reservoir. The common operational rule indicates an annual use of 40 MCM, thus it counts with a reserve and could be provided to other areas. In contrast the yield of the Paloma reservoir drops almost to the same amount in volume as the Cogoti reservoir in scenario S22, about 10 MCM/year. For the La Paloma reservoir this implies less than 4%, on the contrary for the Cogoti reservoir the allocated volume drops about 24% to 35 MCM, which denotes a much higher impact. This shows that not even with the 85% reliability the legal annual target for Cogoti (40 MCM) might be supplied under this future scenario.

Nevertheless the 85% reliability yields of all reservoirs in scenario S22 sum up to around 335 MCM/year compared to scenario S21 with 355 MCM/year. The operation rule indicates the average release of 320 MCM/ year; thus even with the decrease of supply reliabilities, still the whole system provides the assigned volume with more than 85% reliability; the challenge is to find an agreement

in between the organisations to a reallocation inside the system.

2.3 Qeco evaluation

When evaluating the minimum required flow in the Limarí basin, none of the historical and recent legal requirements for Qeco can be satisfied in total, neither in the present nor in future scenarios. The analysis with the requirement of 2008 results in higher satisfaction than using the more recent regulation of 2012 (Figure 1). The legislation of 2012 puts more attention to the high flow events, and less to the average or water poorer years; thus for this semi-arid catchment the regulations of 2008 are more suitable. Nevertheless forcing the fulfilment even of Qeco 2008 in the evaluated control points (CP) would also result in severe shortages in the supply of the water rights. The percentage of failure per sub-catchment is the average percentage of failure of all CP considered in one sub-catchment.

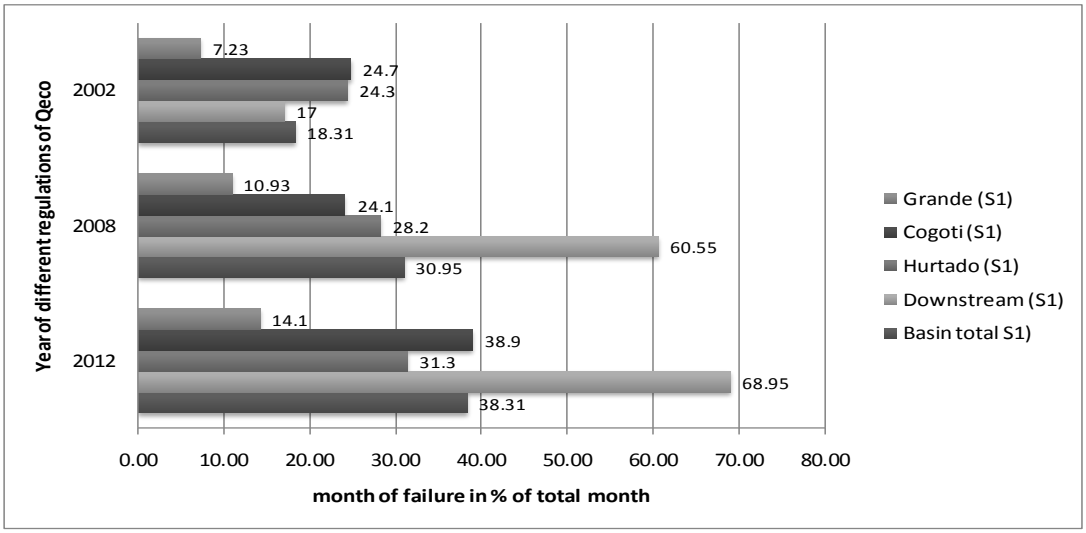

Figure 1. Percentage of monthly failure per sub-catchment with the different legal requirements in scenario S1 (Kretschmer, 2015)

As expected the maximum failures result from the most recent legislation of 2012. The failures reach 38% in the total basin, as average of all sub-basins. The downstream basin shows the maximum percentage of failure with the regulations of 2012 and 2008. The smallest failures occur in the sub-catchment of the Grande River (upstream catchment) with 11% considering the regulation of 2008. As explained before the legislation of 2008 is considered as a good indicator for a monthly Qeco in the region, with an average failure of 31% in total.

Additionally winter and summer month were analysed separately and according to the water management structures in the basin the results are different in the upper unregulated sub-catchments and in the lower regulated. The unregulated sub-catchments result in more failures in summer month: in the main Grande River the failures are more than double during the summer. In contrast failures in the lower regulated catchment are higher in winter month since less water is diverted in winter.

In case more extraction points are changed from the downstream areas into the reservoir in the future will provoke further failures of meeting Qeco downstream.

3. DIGUILLIN RIVER CATCHMENT

Whereas in the Limarí basin changes in water rights and volumes can occur within one association or among the association which are part of the La Paloma system, in the case of the

Diguillín River sub-catchment an inter-basin water transfer (channel Laja-Diguillín) is the only possibility to divert higher volumes. The Diguillín River catchment itself is unregulated (without reservoir) until now, and thus changes in water management is limited without new water sources. Necessary changes for water management in the catchment of the Diguillín River were legally initiated with an agreement between the Chilean Water Work Division (DOH) and the river association of the Diguillín River in 1998. The agreement defines the benefits for the river association of the project between the lake Laja (part of the Laja River basin) and the Diguillín River catchment (part of the Itata River basin). The new system allocates water from the lake Laja to the Diguillín catchment. The project started in 1993, but first volumes were diverted in 2001. The official termination and inauguration of the conveying channels (three stretches, in total 61 km) took place in 2002. Since then diverted volumes are steadily increasing. The maximum volume agreed upon is expected to be diverted in 2021. Works for new irrigation networks are still ongoing. Additionally the planned reservoir in the sub-catchment of the Diguillín River as part of the project is still missing, too.

This example shows, that greater modifications in water management are long term changes and it needs almost on generation to be implemented (here 24 years). But on the other hand it demonstrates that even within the rigid legal framework far-reaching alterations of catchment management, including inter-basin water transfers, can be achieved. Nevertheless this inter-basin transfer system is only possible since it is based on water rights (here 65m3/sec in the irrigation period), which possess the state represented with the DOH in the lake Laja. The objective is to generate new irrigated areas (until the end of the Project are approximately 25,000 ha), as well as an increase of irrigation security from 60% to 85% for about 20,340 ha of the association of the Diguillín River.

3.1 Methodology

The goal of a preliminary analysis was to evaluate if changes aimed for with the new inter-basin transfer system in the last 16 years can be detected and quantified with the analysis of MODIS satellite images.

For analysis the MODIS images MOD09A1 (here daily images of January between 2000 and 2016) were used to calculate the *Normalized Difference Vegetation Index* (NDVI) and further the standard deviations (SD) between years of each pixel, for detection of changes in land use; higher pixel values represent changes. Considering the different time periods of termination of the different stretches of the conveying system the different SD of the NDVI were calculated for each part and analysed. The MODIS images had been masked with all areas of potential agricultural land, excluding forests, scrubs and urban areas. Preliminary results had then been discussed with stakeholders of the area and could thus be corrected to finally define the ranges of SD representing new agricultural lands. Herewith new agricultural areas could be digitized and the resulted areas are almost equal to the size of areas announced by the DOH, which is the state partner association of the user association of the Diguillin River.

3.2 Preliminary results and conclusion

Analysing the results of SD including all images from 2000 until 2016, in the area of influence changes in land use can be observed easily (Figure 2).

The changes of the influence of the new conveying channel system Laja –Diguillín are highlighted with circles. Not only the users of the Diguillín river catchment receive benefits, but also areas which until now did not had access to surface water are and will be used for agricultural purposes (left hand side of the channel stretch Huepil-Diguillín). Of interest is to analyse the area between the Temuco Creek and Diguillín River, upstream of the new channel system. New agricultural land could be cultivated and further changes along the river can be noticed, too

(changes to more permanent crops based on higher irrigation security). Especially the upstream area marked with a circle shows the positive impact provoked by indirect benefits (users can use more water upstream, since downstream users are receiving additional water from lake Laja). With that the management of the Temuco Creek changed to a more sustainable use, too.

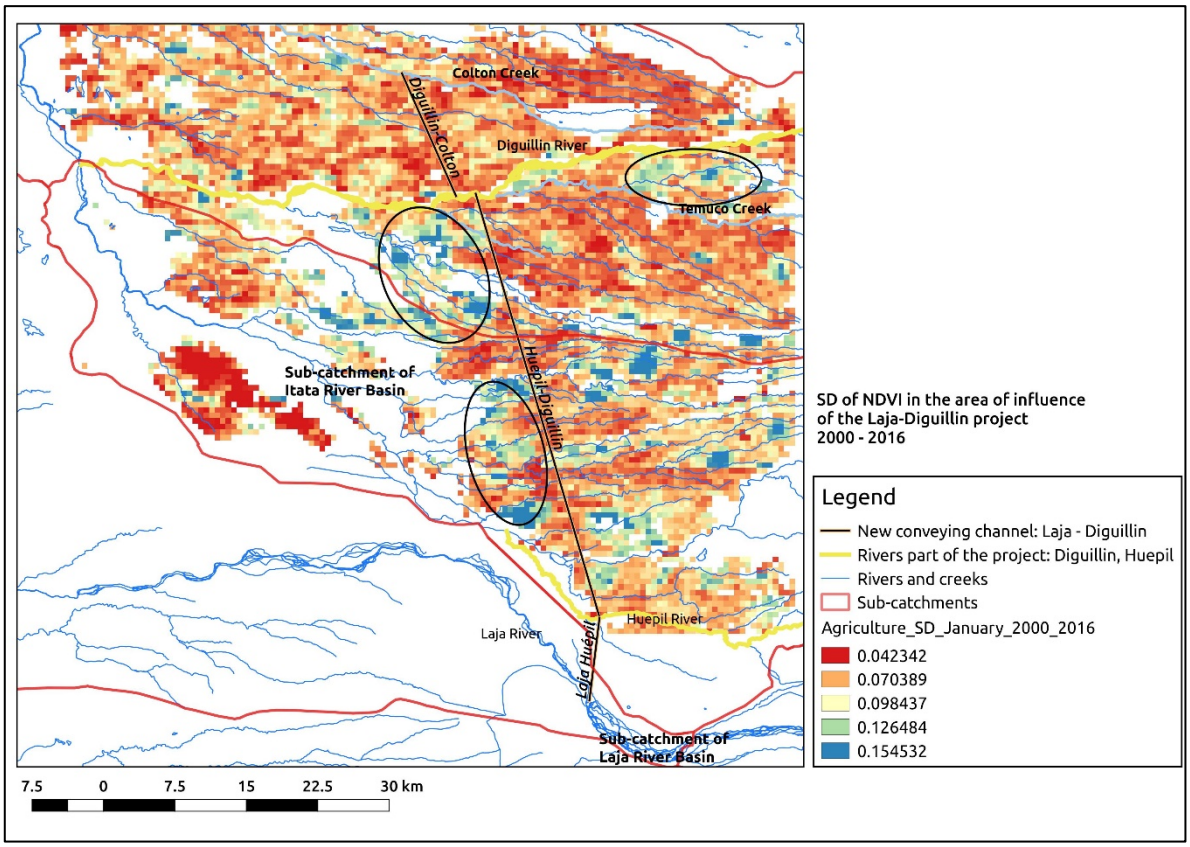

Figure 2. Standard deviation (SD) of the calculated NDVI of all Januarys between 2000-2016

Calculation of different SD considering different time frames and further classification resulted in 1,165 ha of new agricultural land use of the influence of the channel Diguillin-Colton since 2014 (which before did not had access to surface water). In the other stretch (Huepil-Diguillín) a total of 4,145 ha of new agricultural area between 2000 and 2016 could be classified. These results show that the analysis of MODIS data can be used for these catchment to identify the benefits over a longer time frame.

The project, evaluating the sustainability of water management in the Limarí and Diguillín River catchments is still in execution and financed by CONICYT, FONDECYT 2016 Postdoctoral Grants, Project Number: 3160200.

REFERENCES

Alvarez P., Kretschmer N., Oyarzún R, 2006. Water management for irrigation in Chile: causes and consequences: Kongress der Wasser Berlin 2006: Integrated water resources management in Africa, Asia and Latinamerica}

Bauer C., Schlager E,.2011. 1.02 - Governing Water: Institutions, Property Rights, and Sustainability, In Treatise on Water Science, edited by Peter Wilderer, Elsevier, Oxford, 2011, Pages 23-33, ISBN 9780444531995, http://dx.doi.org/10.1016/B978-0-444-53199-5.00003-8.

Decreto N.14 del 22 de mayo de 2012, Ministry of Environment (Ratified July19th 2013)

DGA, 2002. Manual de Normas y Procedimientos para la Administración de Recursos Hídricos, Dirección General de Recursos Hídricos, Departamento de Administración de Recursos Hídricos, Ministerio de Obras Publicas, República de Chile, Santiago 31. Mayo 2002

DGA, 2008. Manual de Normas y Procedimientos para la Administración de Recursos Hídricos, S.I.T. No 156; Dirección General de Recursos Hídricos, Ministerio de Obras Publicas, Republica de Chile, Santiago 17. Diciembre 2008

DGA, 2015. Atlas del agua, Chile 2016, Direccion general de aguas, Deciembre 2015

Kretschmer N, 2015. Impacts of the existing water allocation scheme on the Limarí watershed – Chile, an integrative approach, PhD Dissertation, Universität Stuttgart.- Stuttgart: Institut für Wasser-und Umweltsystemmodellierung, Heft 242

Kretschmer, N., Wendt, A., Oyarzún R, 2012. Watershed management: Its scope, a general analysis of its situation in Chile, and one approach to deal with it integrating environmental, political and social issues; in: Chile: Environmental, Political and Social Issues, page 69 -90, e-book, Novapublisher, INC 2012

Wurbs, R.A, 2006. Methods for Developing Naturalized Monthly Flows at Gauged and Ungauged sites, Journal of Hydrologic Engineering, Vol.11, No.1 , 1.January 2006

Wurbs, R.A., 2010. Water Rights Analysis Package (WRAP) Modeling System Reference Manual, Technical Report 255, Texas Water Resources Institute, First Edition August 2003, Last Edition 2010

Wurbs, R.A., Hoffpauir R.J., Olmos H.E., Salazar A., Kim T.J., Schnier S.T.,2010. Conditional Reliability, Sub-Monthly Time Step, and Flood Control Features of WRAP, Technical Report 284, Texas Water Resources Institute, March 2010 Draft.

Proceedings of the 10th World Congress of EWRA 'Panta Rhei', 5-9 July 2017, Athens, Greece
© 2017 *European Water Resources Association*

Prototype observatory facilitating integrated coastal zone management at municipal level

N. Kokkos, V. Kaplakis, V. Pissinaras and G. Sylaios*
Laboratory of Ecological Engineering & Technology, Department of Environmental Engineering, Democritus University of Thrace, 67100 Xanthi, Greece
* *e-mail: gsylaios@env.duth.gr*

Abstract: The ICZM Observatory of Kavala Municipality has been developed within the framework of Mare Nostrum Project to aid the day-to-day operations of the Municipality, aiming to collect, analyze and process historic, present and forecasted ICZM datasets from various sources. The Observatory follows the well-known DPSIR context (Drivers, Pressures, States, Impacts and Responses) of the European Environmental Agency. Municipal geo-spatial data, environmental data from previous reports, EU and national environmental legislation and institutional information, results from coupled operational models and climate change scenarios have been incorporated in the system. Data are presented in a well-structured layer-basis on a web-GIS environment. A well-designed interface allows the user to enter the Observatory and select the following options: a) Land Development and Uses; b) Environmental Datasets; c) Legislative and Institutional Framework; and d) Toolkit for Public Participation. The system is expected to aid decision-makers at Municipal, Regional and National level to formulate policies on ICZM matters; to provide reliable datasets to scientists and engineers, improving the preparation of technical studies and applications; to engage active citizens and the broader public into coastal zone issues, raising their awareness for coastal environmental and landscape protection; to promote the distribution of information among coastal managers, stakeholders and the general public, especially on issues affecting current and future activities and investments.

Key words: ICZM Observatory, coastal management and planning, web-GIS, operational numerical models, public participation, Kavala Municipality

1. INTRODUCTION

Kavala Municipality is located at the Northern coastline of the Aegean Sea, in proximity to the Bulgarian and Turkish borders. The area is dynamic, affected highly by the Black Sea Water influence, and local contributors, as transboundary rivers (Nestos River) washing out pollutants and suspended matter, local urban developments, industrial complexes, intense agriculture and mariculture activities and touristic blooming. Recent environmental assessment (Sylaios et al., 2015) exhibited that the area is affected by:

- coastal erosion, related to river damming and water abstraction for agriculture,
- eutrophication incidents, related to land-based sources of nitrogen and phosphorus compounds,
- heavy metals and PAHs pollution, related to offshore oil exploitation activities,
- coastal salinization and seawater intrusion along the rivers course, associated to intense coastal drillings and freshwater abstractions for agriculture,
- pressure for touristic expansion even to the most remote beaches of the coastline,
- marine litter, especially plastics, as a result of beach-bar activities,
- alien species invasion, related to area's tropicalization and climate change impacts,
- severe floods under extreme rainfall events and long periods of droughts,
- coastal biodiversity reduction due to overfishing and pollution.

At the same time, new perspectives for developments along the coastal zone regularly arise, as the prospect for an LNG terminal, at the eastern part of Kavala Municipality coastline, the

expansion of the existing oil and gas exploitation activities, the pressure induced by local, national and international coastal tourism after loosening borders regulations.

The ICZM Observatory of Kavala Municipality is expected to formulate a unit operating within the framework of Municipality's daily functions, aiming to collect, analyze and process historic, present and forecasted ICZM datasets from various sources. The role of Kavala Municipality ICZM Observatory in the overall Municipal functioning and the broader Kavala coastline management is shown schematically in Figure 1.

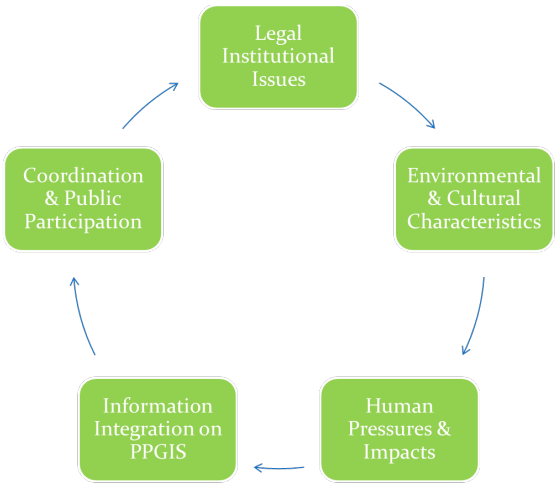

Figure 1. The role of ICZM Observatory of Kavala Municipality.

2. METHOD

2.1 The conceptual framework

The conceptual framework of the ICZM Observatory of Kavala Municipality will follow the well-known DPSIR context (Drivers, Pressures, States, Impacts and Responses) of the European Environmental Agency.

Driving Forces are divided into primary and secondary forces. The ICZM Observatory reports on the issues forcing the coastal zone of the Municipality, as the population (number, age structure), the land development and use, transport (number of persons and quantity of goods transported by road and water), industry (types of plants, resource types), agriculture (types of crops, fertilisers used), landfills (type, age), sewage systems (types, length), and non-industrial sectors.

Pressures exerted on the coastal environment as a result of production and consumption processes. The ICZM Observatory reports on pressures affecting the coastal zone of the Municipality, as emissions (per driving force for numerous compounds), divided into direct emissions to air, water and soil and indirect emissions to air, water and soil, production of waste and noise, hazards and risks.

State refers to monitoring results of the present conditions, that is, the quality of the various environmental compartments (air, water, soil, biota, etc.) in relation to the functions that these compartments fulfil. The ICZM Observatory systematically collects existing data from various sources (Democritus University, Kavala Technological University, public services, etc) on the parameters describing the state of the present coastal environment, as air, water and soil quality, ecosystems, and human health.

Impacts refer to the changes observed in the physical, chemical or biological state of the environment. They determine the quality of the coastal ecosystems and the welfare of human beings having environmental or economic attributes.

Responses represent the policies formulated to minimize the impacts of pressures occurring as a result of driving forces.

The above framework is expected to provide a better context for the integration of different types

of datasets, allowing the consideration not only for environmental but also for socio-economic and regulatory aspects of the ecosystem. Such tool enables the coupling of sound scientific knowledge and advice with the responsive local, regional and national decisions, aiming to enhance the effectiveness of management actions. The application of this approach may follow either a descriptive and rather static pathway, reporting socio-economic and environmental datasets and indicators, or a more dynamic perspective, explaining the temporal behavior of the coastal ecosystem, using the results of numerical models.

The ICZM Observatory of Kavala Municipality follows both approaches, i.e.,

- the collection and presentation of all available primary datasets,
- the production and illustration of environmental and socio-economic indicators,
- the dynamic perception of short-term environmental prognosis using interlinked numerical models, and
- the utilization of long-term (up to 2100) meteorological forecasts to assess the impact of climate change.

All the above are publicly-available through the ICZM Observatory's web-GIS system which can be accessed at the following link: http://dkavalas.maps.arcgis.com/apps/PublicGallery/index.html?appid=f3c948945d1f488991c9de8b6960e82d

2.2 Policy and legislation in the ICZM observatory

All policy and legislation documents referring on issues and activities related to the Kavala Municipality coastal zone were collected, clustered at categories and sub-categories according to their subject and inserted in the webGIS system. Particular emphasis was placed on Environmental Legislation (EU and national), covering all issues related to water, soil, biota, environmental impacts of human activities, etc. The aim of the "Policy and Legislation" module of the ICZM Observatory of Kavala Municipality is to allow the easy and user-friendly access to legal documents related to the management and protection of the coastal zone of civil services, organizations, private firms, developers and the broad public. These documents draft the legal and institutional framework of coastal zone management in Greece, having the coastline of Kavala Municipality as a pilot case study.

For the moment a total of 77 documents have been uploaded on the web-based GIS tool of the ICZM Observatory of Kavala Municipality, classified in the following categories: Water Resources Management (19 legal documents), Environmental Permitting Regulations (37 documents), Solid Waste Management (6 documents), Coastal Zone Protection (4 documents), Port Authority Organization and Regulations (5 documents), and Financing Development and Environmental Protection Projects (6 documents).

2.3 Socio-economic indicators in the ICZM observatory

A series of environmental and socio-economic indicators were imported in the webGIS system of the ICZM Observatory as reported by various sources (Eurostat, OECD, ESPON, etc.). More specifically, the indicators used to describe the various components of the coastal environment are the following: Physical, Chemical, Geological, Biological, Demographic, Social, Economic, and Governance.

For instance, demographic indicators report on parameters as the coastal population density (inh/sq m), the mean annual population change, the share of employment in Agriculture and Fisheries, the temporal change of employment in Agriculture and Fisheries, etc. Environmental indicators report on parameters as the climate change potential indicator, the renewable resources potential indicator, the natural environment indicator, the air quality indicator, and the financing environmental investments indicator. Eutrophication indicators report on the load of nitrogen and

phosphorus per km of coastline length, the load of heavy metals per km of coastline length, etc.. Finally, fisheries indicators include the total level of catch or landings per year, the proportion of by-catch as a percentage of the total catch, and fishing mortality.

2.4 Operational numerical models in the ICZM observatory

The ICZM Observatory of Kavala Municipality is equipped with a series of modern numerical models, interlinked between them to provide short-term prognostic results. The basic model is the meteorological model TAPM, utilizing information for initial and boundary conditions downloaded from NOAA/GFS. This meteorological model offers short-term predictions on several meteorological parameters for the next five days. Precipitation predicted by the meteorological model is then used from the hydrological model SWAT 2009 (Neitsch et al., 2011), to determine the levels of streams and torrents discharging along the Kavala Municipality coastal zone. Freshwater outflux among with winds and air temperature variability are imported as boundary conditions to the coastal hydrodynamic model ELCOM (Hodges and Dallimore, 2001) to reproduce the predicted flow field along the coastline. ELCOM model is forced from the open ocean boundary through the myOcean model datasets, thus utilizing Copernicus Program products. Further, the water column flow field, the stratification-mixing patterns and the primary production expressed as chlorophyll-a concentration are forecasted by the 1-D model PHYTO (Sharples, 1999). Finally, the wind speeds and directions produced by the meteorological model as short-term forecasts are imported on a three-nested grids wave model (SWAN, Booij et al. 1999) to produce the wave characteristics predicted along Kavala Municipality.

2.5. The webGIS Architecture of the ICZM Observatory

The ICZM Observatory of Kavala Municipality consists of three interlinked components: the geo-spatial databases, the application server and the user interface (Figure 2). All information is stored on a Geodatabase and with the use of a GIS application (ESRI ArcGIS) a series of Maps is produced. Maps, data and reports are made available to the broader public through the Map Viewer environment in connection with a Web-GIS interface.

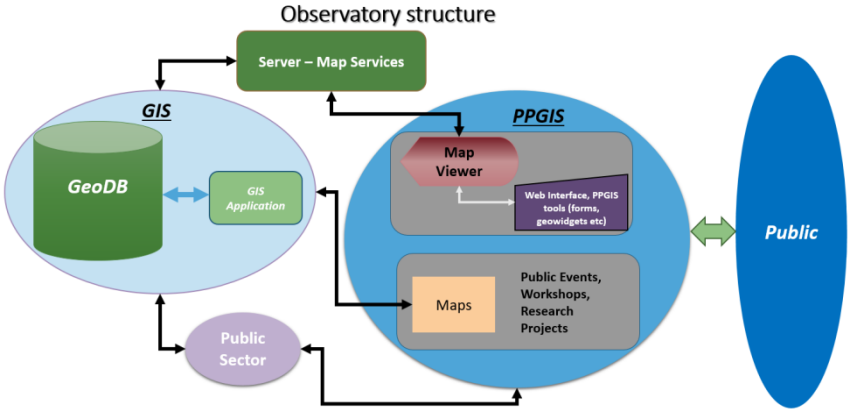

Figure 2. The webGIS architecture of the ICZM Observatory of Kavala Municipality based on innovative Spatial Data Infrastructure components.

Municipal geo-spatial data have been digitized and organized into layers made readily available through the Observatory. This layered structure consists of: a) digitized base maps (topographic, bathymetric, geologic, soil, land uses maps), b) administrative borderlines (regional, municipal and departmental borders), c) urban and rural planning maps (General Urban Plan, future spatial plans), d) municipal acts (building permits, building blocks, urban pedestrian streets, dangerous and illegal

buildings, coastal setbacks, port authority zone and infrastructure, etc), e) public networks (electricity, optical fibers, telecommunication networks, water and sewerage pipelines, large industrial facilities, planned municipal works along the shoreline, etc.), f) locations of public interest (schools, social service facilities, sport facilities, parks and open spaces, areas of historic and cultural significance, etc.). All information was stored on the Geodatabase and with the use of a GIS application (ESRI ArcGIS) a series of Maps may be produced. Maps, data and reports are made available to the broader public through the Map Viewer environment in connection with a Web-GIS interface.

3. RESULTS

The user enters the system through the link provided above and has the ability to follow one of the four presently available options.

- Land Development and Uses
- Environmental Datasets
- Legislative and Institutional Framework
- Toolkit for Public Participation

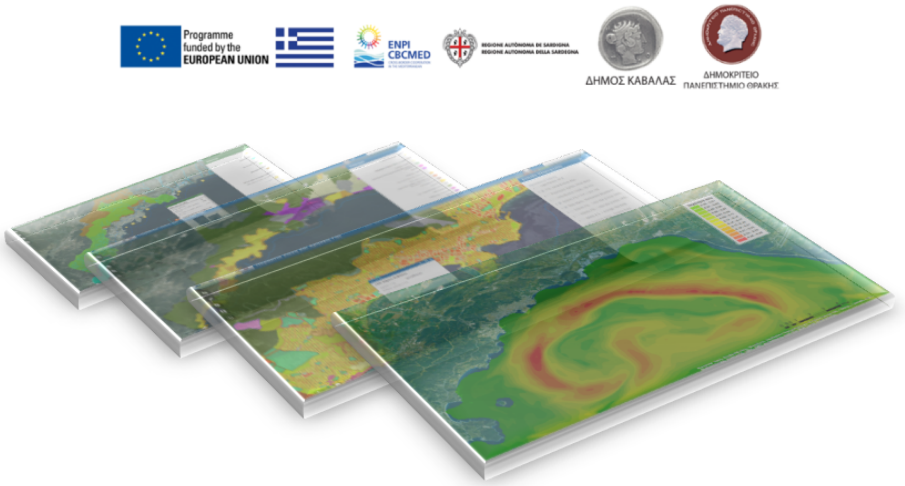

Figure 3. The WebGIS user interface showing the various options the user may follow.

An example of the web-application interface is presented in Figure 4, in which the Kavala Municipality General Urban Plan is shown. The user has the opportunity to select from a variety of features as Basemap Gallery or to present different GIS layers (e.g., Municipal Boundaries, Coastline, Coastal Zone, Settlements, etc). Further, several fields, as the location, the regional authority, the supervising agency, the areal coverage, the Ministerial Decision and others appear after clicking on each digitized element.

In another example the implementation of SWAN model results in the ICZM Observatory of the Kavala Municipality can give an overview of both the average and maximum wave heights and their direction and therefore demonstrate the most vulnerable area to extreme waves. Figure 5 illustrates the propagation of waves (significant wave height and direction) along the main touristic beaches of Kavala Municipality. SWAN model is coupled to TAPM meteorological model and short-term wave predictions may be produced.

4. CONCLUSIONS

The ICZM Observatory of Kavala Municipality has been initiated through Mare Nostrum

Program (Alterman et al. 2016). It is aimed to improve the overall management of the coastal zone in the area, by upgrading the operational capacity of the Municipality, on a day-to-day basis and under extreme events; by promoting best practices in spatial planning and urban development and uses; by approaching a diverse spectrum of stakeholders and presenting in an explicit manner the institutional and legal framework of the coastal zone, and by advancing the organization and interrelation of existing data of diverse nature (demographic, social, economic, environmental, planning, etc.) collected from different sources.

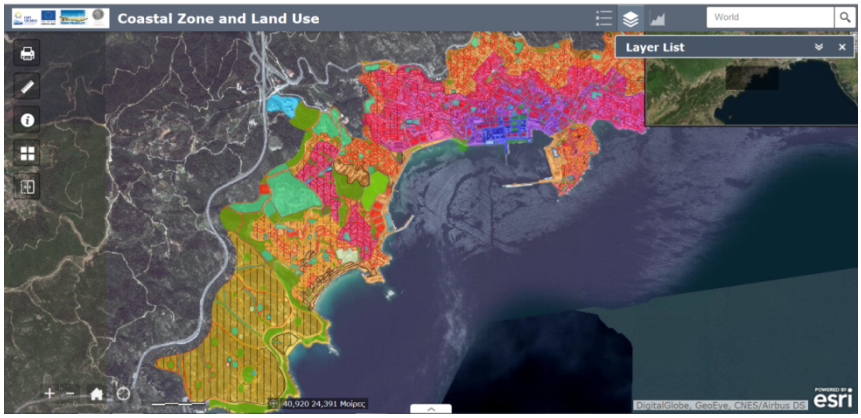

Figure 4. WebGIS interface showing the General Urban Plan along the coastal zone of the Kavala Municipality.

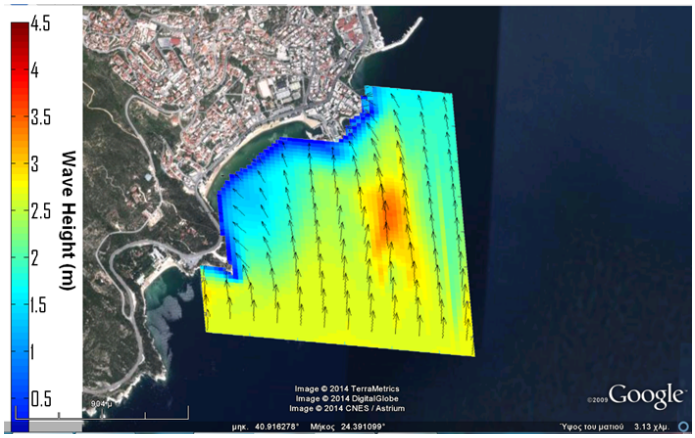

Figure 5. Indicative wave propagation towards Kalamitsa Bay, as produced by SWAN model application, coupled with the meteorological TAPM model.

REFERENCES

Alterman, R., Carmon, D., Pellach, C., Boral, R., Teschner, N., Lalenis, K., Sylaios, G., et al., 2016. Bridging the Legal Institutional Gap in the Mediterranean Coastline Management. Mare Nostrum Project Final Report, 175 p.

Booij, N., Ris, R.C., Holthuijsen, L.H., 1999. A third-generation wave model for coastal regions. 1. Model description and validation. Journal of Geophysical Research; C104: 7649–7666.

Hodges, B., Dallimore, C., 2001. Estuary and Lake Computer Model: ELCOM Science Manual Code Version 2.0.0. Cent. Water Res., Univ. Western Australia, Perth.

Neitsch, S.L., Arnold, J.G., Kiniry, J.R., Williams, J.R., 2011. Soil and water assessment tool theoretical documentation. Texas Water Resources Institute.

Sharples, J., 1999. Investigating the seasonal vertical structure of phytoplankton in shelf seas. Marine Models Online; 1: 3–38.

Sylaios, G., Kokkos N., Pisinaras, V., Anastasiou, S., Koutrakis, E., Kallia, A., Zoidou, M., Tsakmakis, I., Vidoris, P., Gikas, G., Zoras, S., Melidis, P., Tsihrinztis, V.A., Mertzanidis, I., 2015. The ICZM Observatory of Kavala Municipality, including updated PPGIS and Toolkit. Mare Nostrum Project Technical Report D8.5. 170 p.

Proceedings of the 10th World Congress of EWRA 'Panta Rhei', 5-9 July 2017, Athens, Greece
© 2017 *European Water Resources Association*

Legislative framework for drinking water (re)sources monitoring in the Adriatic region

B. Karleusa[1*] and B. Matic[2]
[1] *Faculty of Civil Engineering, University of Rijeka, Rijeka, Croatia*
[2] *Jaroslav Černi Institute for the Development of Water Resources, Belgrade, Serbia*
[*] *e-mail: barbara.karleusa@uniri.hr*

Abstract: The Strategic project Networking for Drinking Water Supply in Adriatic Region (acronym DRINKADRIA) co-financed by the European Union through the program IPA Adriatic CBC 2007–2013 evaluated various aspects for cross-border drinking water resources management and protection in the Adriatic region, e.g., climate and land use change impact, monitoring and protection legal and policy framework, increased demand during touristic season, etc. Seventeen partner institutions from eight countries across the Adriatic region (Italy, Slovenia, Croatia, Bosnia and Herzegovina, Montenegro, Serbia, Albania and Greece) participated in project implementation. Due to complexity of cross–border drinking water (re)sources management the legal framework pertaining to drinking water sources monitoring at national and regional level is analysed based on data and information provided by partners. All legal acts and descriptions in English are uploaded on the DRINKADRIA project shared platform. This paper provides legal framework evaluation synopsis, underline the identified gaps, and provide comparison of monitoring practices with respect to cross-border drinking water sources in the Adriatic region. Given the differences in national legal framework it is concluded that the protocol for cross-border monitoring of water resources used for human consumption should be defined on bilateral (trilateral) level among countries instead as a unified protocol for the whole Adriatic area. However, the basic framework and common structure of the protocol is proposed.

Key words: legal framework, drinking water resources management, cross-border, transboundary, Adriatic region

1. INTRODUCTION

While management of water supply systems is a broad domain well addressed by professionals and researchers the issue of cross-border water supply systems is not so recognized (Altran et al., 2014). The Strategic project Networking for Drinking Water Supply in Adriatic Region (acronym DRINKADRIA), with total budget of 6,600,000 EUR, main goal was to develop a foundation for strategies and procedures that would secure cross-border water supply with specific emphasis on drinking water resources management in trans-boundary context, climate change and specific socio-economic aspects of the Adriatic region (Karleuša, 2016a). Seventeen partner institutions from eight countries across the Adriatic region (Italy, Slovenia, Croatia, Bosnia and Herzegovina, Montenegro, Serbia, Albania and Greece) participated in project implementation (Figure 1).

In addition to evaluation of various significant aspects of cross–border drinking water resources management and protection within the project area (climate and land use change impact, monitoring and protection legal and policy framework, increased demand during touristic season, etc.) several guidelines for protocols development are proposed to contribute in sustainable cross–border drinking water resources management, e.g., *Guidelines for the improvement of drinking water protection zones delineation in the Adriatic region* (Brenčič and Čenčur Curk, 2016), *Guidelines for long term Cross-Border Water Supply Planning* (Vidmar and Matić, 2016), etc.

Drinking water resources and supply management at the national level is extremely complicated and when it comes to cross-border level it is multiplied as stated by Kanakoudis et al., 2015.



Partner	Institution name	Country
LB	CATO – Area Council for Eastern Integrated Water Service of Trieste	IT
FB1	VERITAS SpA	IT
FB2	Optimal Territorial Area Authority n.3 Marche Centro – Macerata	IT
FB3	CNR-IRSA	IT
FB4	Water Utility of Nova Gorica	SLO
FB5	University of Ljubljana	SLO
FB6	Region of Istria	CRO
FB7	Water Utility of Istria	CRO
FB8	University of Rijeka	CRO
FB9	Croatian Geological Survey	CRO
FB10	The Jaroslav Černi Institute for the Development of Water Resources	SRB
FB11	Water Supply and Sewarage Association of Albania	AL
FB12	Hydro-Engineering Institute of Sarajevo	BIH
FB13	P.C. Utility Neum	BIH
FB14	Public Utility "Vodovod i kanalizacija" Nikšić	MNE
FB15	Region of Ionian Islands	GR
FB16	University of Thessaly	GR

Figure 1. Participating countries and partners of DRINKADRIA project (Altran et al., 2016)

Cross-border water supply systems are not typical in Europe and majority of them occurred in regions where the wars have occurred in last 100 years together with major political changes (Vidmar and Matić, 2016). Based on Banovec et al. (2016) specifics regarding differences in legislation and different agencies are even more evident in case of countries involved in DRINKADRIA project.

One of Project activities was to analyse the possibility to define a common protocol for water (re)sources monitoring in the Adriatic area. This paper provides legal framework evaluation synopsis, underline the identified gaps, and presents main monitoring practices comparison findings with respect to cross-border but also cross-regional (between regions within one country) drinking water (re)sources in the Adriatic region.

2. EXISTING LEGAL FRAMEWORK OVERVIEW

Adriatic region countries diversity, types of drinking water sources, intention to address both cross-border and cross-regional monitoring practices resulted in template development for data and information collection. Due to complexity of cross–border and cross–regional drinking water (re)sources management the legal framework pertaining to drinking water sources monitoring at national and regional level was analysed based on data and information provided by partners during the project implementation (Karleusa, 2016b). As presented in Figure 2 collection and analyses of legal framework relevant for protocol development at EU and national level (including legislation on regional level in countries where existing) is considered in evaluation. Also the stage of implementation of EU legislation in national legislation in countries that are not member of EU was analysed.

2.1 EU legislation

The legal framework for water resources monitoring activities in EU is provided in *Water Framework Directive (WFD, 2000/60/EC)*. *Drinking Water Directive (DWD, 98/83/EC)*, on the quality of water intended for human consumption addresses the quality of water for human consumption and *Groundwater Directive (GWD, 2006/118/EC)* which underline groundwater quality and quantity standards and introduces measures to prevent over abstraction and limit pollutants discharge into the groundwater.

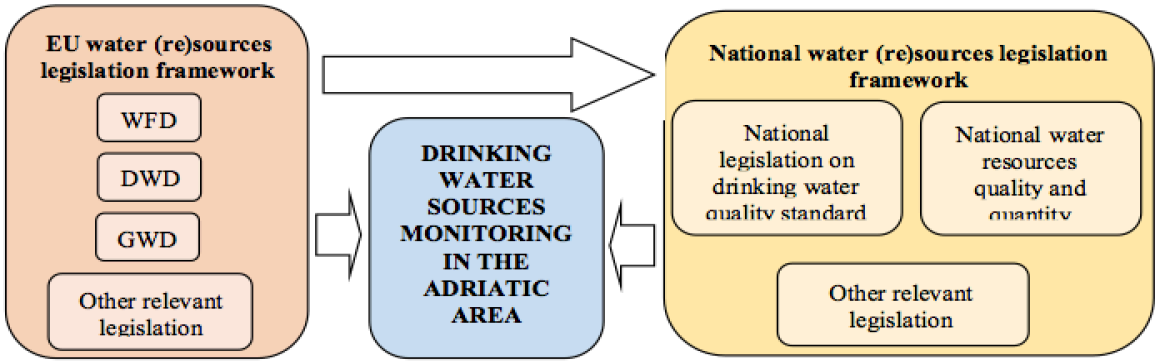

Figure 2. Approach applied in legal framework analysis relevant for protocol development at EU and national level

2.2 National legislation

The overview and analyses of most important national and regional legislation regarding water (re)sources monitoring in Adriatic area in all partner countries is based on reports submitted by project partners' during year 2015 (Karleuša, 2016b).

The Italian legislation, on the national level, concerning the quality of surface and groundwater intended for human consumption basically derives from the application of EU Drinking Water Directive according to the: *Legislative Decree no. 31*, *Implementation of EU Drinking Water Directive 98/83/EC on the quality of water intended for human consumption* and *Legislative Decree no. 27*, *An integration/modification of the previous Legislative Decree, no. 31/2001*; *Legislative Decree no. 152*, but also *Environmental Code* (that is a unified text of law that takes into account several aspects connected to Environmental quality and actions; among other aspects: Environmental Impact Assessment (EIA), Water management and pollution prevention, Waste management and Contaminated soils remediation, Air protection and pollution prevention, Compensation claims against environmental damages) and *Legislative Decree no. 30, Implementation of EU Groundwater Directive.*

Slovenian legislation dealing with drinking water monitoring, the surface and groundwater quality monitoring is presented in six regulations. The legislation is on the national level. On the top of the hierarchy there is the *Water act* and below are specific regulations: *Regulations on drinking water*, and depending on the type of water resource: *Decree on ground water status* and *Regulations on ground water monitoring*, *Decree on surface water status* and *Regulations on surface water status*.

Water legislation in Croatia functions within a legal framework comprised of several regulations. The legislation is on the national level. On the top of the hierarchy is the *Water act* and below are specific regulations: *Act on water intended for human consumption, Regulations on parameters compliance and analysis methods for water intended for human consumption*, and *Decree on water quality standard* both for surface and ground water.

The Greek legislation dealing with the surface and groundwater quality, monitoring and drinking water is presented in several regulations: *National Law 3199/2003 for the "Protection and management of water"*, *Joint Ministerial Decision (JMD) Y2/2600/01 regarding the water quality for human consumption*, *Ministerial Decision 1811 for the determination of the maximum allowable concentrations of pollutants in groundwater*, *JMD 140384 Determination of the national stations network for monitoring the quality and quantity of the water systems*, and *JMD 51354/2641/E103/2010 for the determination of the Environmental quality standards for the concentrations of pollutants in surface waters*.

In Bosnia and Herzegovina (B&H) surface and ground water quality requirements are regulated differently on the national and the entity (regional) level (Federation of Bosnia and Herzegovina (FB&H) and Republic of Srpska). Quality of ground water intended for human consumption is

under the authority of the Bosnia and Herzegovina (on national level), and is regulated according to: *Regulations on drinking water safety* and *Regulations on natural mineral and natural spring water*.

Quality of the surface water under the authority of the FB&H is regulated by: *Water Act*, *Regulations on dangerous and harmful substances in water*, *Regulations on classification of waters and coastal sea waters within the borders of Former Socialist Republic of Bosnia and Herzegovina*, *Regulations on watercourse categorization*, *Decision on characterization of surface and ground waters, reference requirements, and parameters for the assessment of water status and water monitoring.*

Additionally, in the FB&H the *Decision on characterization of surface and ground waters, reference, requirements, and parameters for the assessment of water status and water monitoring* deals with the quality of ground water but only in the terms of determination of the water quality status, pollution pressures, quantity and similar parameters necessary for the issuing of management plan for river basins and is in line with the WFD, 2000/60/EC recommendations.

Quality of the surface water under the authority of the Republic of Srpska is regulated by *Water Act* and *Regulations on classification and categorization of watercourses*.

For Montenegro legislation at the national level significant for drinking water comprises of *Water act*, *Regulations on the hygienic quality of drinking water*, *Regulations on methods for determining and maintaining sanitary protection zones for drinking-water sources and restrictions in the related zones,* and *Law on communal activities*.

In Serbia drinking water and water resources quality monitoring legal framework includes number of acts and by-laws, namely, *Water act*, *Act on sanitary observation*, *Drinking water supply sources management and protection act*, *Environmental protection act* and *Act on amendments and additions to the Act on environmental protection*, *Act on public health*, *Regulations on drinking water sanitary standards*, *Regulations on surface water ecological and chemical status parameters and groundwater chemical and quantitative status parameters.*

Water Framework Directive is not operative in Albania in 2015, but the *Law on integrated management of water resources* and some other Decisions of the Council of Ministers (DCM) were supposed to be updated in 2015 were written in compliance with this directive. Albania legislation dealing with the surface water, groundwater and drinking water quality monitoring was presented in several laws and regulations: *Law no. 1. 111/2012, Integrated management of water resources*, *DCM no. 1189, to the rules and procedures for the drafting and implementation of a national program of environmental monitoring*, *DCM no. 246, for determination of the environmental quality standards for surface waters*, *DCM no. 1304, The approval of the regulation on the water supply and sewage services in the service area of the water-joint stock supply and sewage utilities*, *DCM no. 145, for the approval of the Hygiene and health regulation for the control of drinking water quality, the design, construction and supervision of systems of drinking water supply*.

3. THE MAIN OUTPUTS AND DATABASE

Since Italy, Slovenia, Croatia and Greece are EU members their national drinking water and water resources quality legislation is in compliance with the WFD (2000/60/EC), DWD (98/83/EC) and GWD (2006/118/EC).

In Bosnia and Herzegovina, Serbia, Montenegro and Albania the level of EU legislation transposition and implementation differs from country to country.

Monitoring legislation referring to water quality for human consumption in Bosnia and Herzegovina is in accordance with Drinking water directive although B&H is not member of EU. Croatia has two regulations that cover jointly the DWD. There are minor differences between national legislative acts regarding monitoring the quality of water for human consumption in Italy, Slovenia, Croatia and B&H. Montenegro, Serbia and Albania have their own legislation relevant for the monitoring of the water quality for human consumption. The proposal for the Regulation on Drinking Water Quality in Albania which integrates DWD (98/83/EC) norms and regulation (2015), is under the approval process.

In Serbia WFD requirements are transposed into Water act and by-laws (existing and those that are still pending to be approved). Water Framework Directive is not operative in Albania, but the Law on integrated management of water resources and some other DCM updated recently are developed in compliance with this Directive. The most complex structure of legislation is found in the Bosnia and Herzegovina (B&H). The surface and ground water quality requirements are regulated differently on the national and entity level (FB&H and Republic of Srpska).

From analyses of national legislation for water (re)sources monitoring in DRINKADRIA countries it can be concluded that there are more particularities and differences with respect to monitoring of water quality intended for human consumption.

The analyses of national legal framework, because of the domain complexity and discrepancy among national legal framework resulted in conclusion that the more specific protocol for cross-border drinking water sources monitoring should be defined on bilateral (trilateral) level among countries instead as a unified protocol for the whole Adriatic area. However, based on outcomes and identified gaps, the guideline framework and common structure of the protocol was proposed within the Project outputs (Karleuša, 2016b).

The bi/tri-lateral protocol for monitoring activities on cross-border water resources used for drinking water supply should include:

- relevant institutions in countries involved;
- the procedure for exchange of results from monitoring at the national and other levels of monitoring between relevant institutions of both (all three) countries;
- the procedure for planned monitoring programmes exchange or even the preparation of joint monitoring programmes;
- the procedure to enable the access to monitoring locations in the neighbour country;
- the procedure of sample collection;
- the monitoring methods for both (all three) countries that should be standardized and comparable;
- the procedures regarding data and information use and publication;
- the procedure of covering additional monitoring costs;
- human resources and capacities development;
- other that might address cross-border water resources used for human consumption management.

The DRINKADRIA project shared platform (http://drinkadria.fgg.uni-lj.si/) is organised to provide different tools that help in capitalisation of new knowledge and results from the Project assuring the DRINKADRIA project sustainability (Matić, 2016; Matić B. and Miletić-Radić M., 2016). On shared web platform an application for searching water (re)sources monitoring legislative acts in Adriatic region was created (http://drinkadria.fgg.uni-lj.si/water-resources/legislation-water-sources-monitoring/). It is designed as a database from which is possible to find legal acts from EU and from each project country and access the act/decree/regulation in the original language and if available in English language (Figure 3). For national acts/decrees/regulations there is a short description of the content in English language.

5. CONCLUSION

Because of the domain complexity and discrepancy among national legal framework for drinking water monitoring in eight DRINKADRIA project countries evaluation of national data resulted in conclusion that the more specific protocol for cross-border drinking water sources monitoring should be defined on bilateral (trilateral) level among countries instead as a unified protocol for the whole Adriatic area. However, based on outcomes and identified gaps, the guideline framework and common structure of the protocol was proposed within the Project outputs. The next step should be the preparation of bilateral (trilateral) protocols between countries

that share cross-border water resources used for human consumption with all specifics regarding national legislation.

The other relevant output of the Project is the *Legislation on water source monitoring database*, which consists of legislative acts from EU and from each project partner country with the possibility to access to the act/decree/regulation in the original language and if available in English language with a short description of the content in English language. It is expected that this database will be updated thought future projects in which DRINKADRIA project partners, with the help of the developed network of institutions and professionals, will participate.

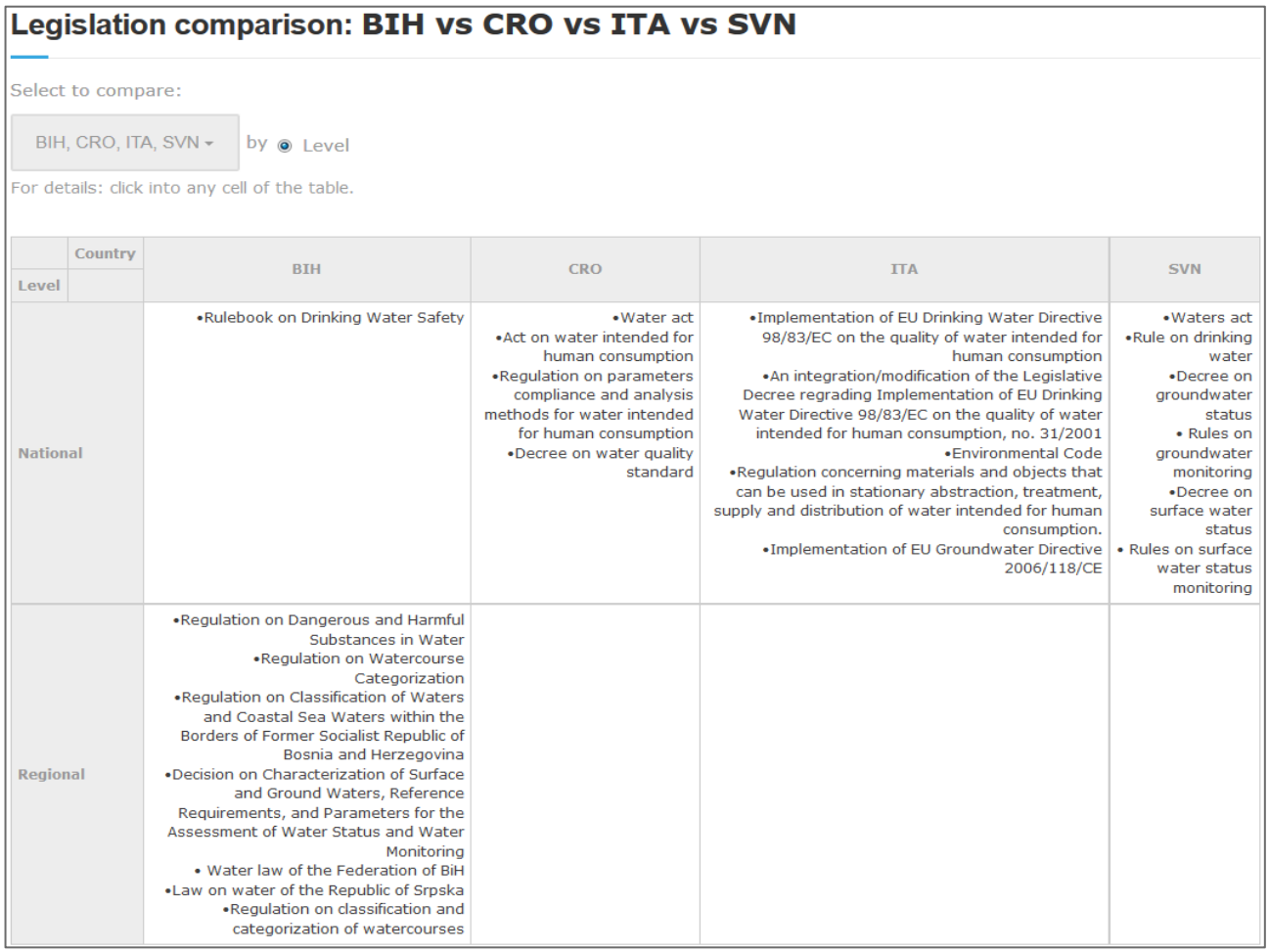

Legislation comparison: BIH vs CRO vs ITA vs SVN

Select to compare:

BIH, CRO, ITA, SVN ▾ by ◉ Level

For details: click into any cell of the table.

Level \ Country	BIH	CRO	ITA	SVN
National	•Rulebook on Drinking Water Safety	•Water act •Act on water intended for human consumption •Regulation on parameters compliance and analysis methods for water intended for human consumption •Decree on water quality standard	•Implementation of EU Drinking Water Directive 98/83/EC on the quality of water intended for human consumption •An integration/modification of the Legislative Decree regrading Implementation of EU Drinking Water Directive 98/83/EC on the quality of water intended for human consumption, no. 31/2001 •Environmental Code •Regulation concerning materials and objects that can be used in stationary abstraction, treatment, supply and distribution of water intended for human consumption. •Implementation of EU Groundwater Directive 2006/118/CE	•Waters act •Rule on drinking water •Decree on groundwater status • Rules on groundwater monitoring •Decree on surface water status • Rules on surface water status monitoring
Regional	•Regulation on Dangerous and Harmful Substances in Water •Regulation on Watercourse Categorization •Regulation on Classification of Waters and Coastal Sea Waters within the Borders of Former Socialist Republic of Bosnia and Herzegovina •Decision on Characterization of Surface and Ground Waters, Reference Requirements, and Parameters for the Assessment of Water Status and Water Monitoring • Water law of the Federation of BiH •Law on water of the Republic of Srpska •Regulation on classification and categorization of watercourses			

Figure 3. DRINKADRIA shared web platform – list of relevant legislative documents for Bosnia and Herzegovina (BIH), Croatia (CRO), Italy (ITA), and Slovenia (SVN), (http://drinkadria.fgg.uni-lj.si/water-resources/legislation-water-sources-monitoring/, accessed 30.01.2017)

ACKNOWLEDGMENTS

The research for this paper and the preparation of this paper was financially supported by the EU IPA Adriatic Cross-Border Cooperation Programme 2007-2013 (DRINKADRIA project) and the University of Rijeka (research project 13.05.1.3.08 - Development of new methodologies in water and soil management in karstic, sensitive and protected areas).

REFERENCES

Altran, E., Banovec, P., Brenčič, M.,Corbatto, K., Cossettini, P., Čenčur Curk, B., Čohilj, M., Della Sala, S., Džajić Valjevac, M., Gartner, M., Guduraš, D., Hvalič, M., Kanakoudis, V., Karleuša, B., Lisjak, R., Masciopinto, C., Matić, B., Miana, P., Miletić – Radić, M., Nardi, D., Papadopoulo, A., Perovic, M., Piccolotti, A., Radman, I., Romano, E., Silvoni, R., Tsitsifli, S., Vidmar, V.,

2016, DRINKADRIA Layman's report, URL: http://www.drinkadria.eu/fileadmin/user_upload/Layman_-_final_version/Drinkadria_Laymans_Report_WEB.pdf, (accessed February 13, 2017).

Altran, E., Banovec, P., Toscano, P., Karleuša, B., 2014. Challenges in the Management of Cross-border Water Supply Systems - The DRINKADRIA project, Water Ideas 2014, Conference proceedings, Bologna, 22-24 October 2014.

Brenčič, M., Čenčur Curk, B., 2016. DRINKADRIA project deliverable 4.4: Drinking water protection zones in the Adriatic region – state of the art and guidelines for the improvement of the present status, URL: http://drinkadria.fgg.uni-lj.si/capitalization_sustainability/project-outputs/, (accessed February 15, 2017).

Karleuša, B., 2016. About DRINKADRIA Project. Proceedings of International Symposium: Cross-Border Water Management, 29th January 2016, Rijeka, Croatia, 13-22.

Karleuša, B., 2016. DRINKADRIA project deliverable 4.3: Common protocol for water resources monitoring activities in the Adriatic region - Project Report and Annexes, URL: URL: http://drinkadria.fgg.uni-lj.si/capitalization_sustai
nability/project-outputs/, (accessed January 30, 2017).

Primož, B., Domadenik, P., Guduraš, D., Cilenšek, A. and Vidmar, V. 2016. DRINKADRIA project deliverable 5.3: Long term cross-border water supply planning and regional drinking water supply economics model, URL: http://drinkadria.fgg.uni-lj.si/capitalization_sustainability/project-outputs/, (accessed February 2, 2017).

Vidmar, V., Matić, B., 2016. DRINKADRIA project deliverable 5.2: Guidelines for Long term Cross Border Water Supply Planning URL: http://drinkadria.fgg.uni-lj.si/capitalization_sustainability/project-outputs/, (accessed February 2, 2017)

Matić, B., 2016. DRINKADRIA project deliverable 3.4: Synopsis report on Capitalization processes, URL: http://drinkadria.fgg.uni-lj.si/capitalization_sustainability/project-outputs/, (accessed February 1, 2017).

Kanakoudis, V., Papadopoulou, A., Tsitsifli, S., Altran, E., Cencur-Curk, B., Karleusa, B., Matic, B., 2015. DRINKADRIA project - from an idea to policy recommendation - A common approach development, towards water resources management and supply, across Adriatic Sea countries, Proceedings of 9th World Congress EWRA 2015, 10-13 June, Istanbul, Turkey.

Matić, B., Miletić-Radić, M. 2016. DRINKADRIA project capitalization and sustainability and connection with good practice of dissemination and communication activities, International Symposium: Cross-Border Water Management, 29th January 2016, Rijeka, Croatia, 23-38.

Proceedings of the 10th World Congress of EWRA 'Panta Rhei', 5-9 July 2017, Athens, Greece
© 2017 *European Water Resources Association*

Ecological flows and the Water Framework Directive implementation: An effective coevolution?

Vanessa Ramos[1*], Nuno Formigo[2], Rodrigo Maia[1]
[1] *Department of Civil Engineering, University of Porto, Portugal*
[2] *Department of Biology, University of Porto, Portugal*
[*] *e-mail: vmr@fe.up.pt*

Abstract: The Water Framework Directive (WFD) is the first piece of European environmental legislation addressing hydromorphological modifications and impacts on water bodies. Accordingly, in those water bodies where the hydromorphological pressures are having an impact on the ecological status, action is needed to achieve WFD objectives. Ecological flows appeared as one of the answers to this challenge. Due to their importance, Member States (MS) have been looking to integrate ecological flows in the River Basin Management Plans (RBMPs) and Programmes of Measures (PoMs). More than 16 years after WFD adoption, the study aims to provide a systematic review of the use of ecological flows within the WFD implementation and they contribution to the achievement of that environmental objectives. Based on analysis of official documentation reporting the progress of WFD and ecological flows implementation, as well as, the answers of MS contact points and country experts to understand how this topic has been assessed. Even though an evolution on this theme can be perceived, some challenges still arise, namely a clear and common definition and a methodology for ecological flows calculation. These difficulties are related with the lack of a common approach to these issues, since there is no standard solution for the problems present in MS. More efforts are required, namely in the: i) the development of a verifiable link between ecological flow regimes and biological indicators and ii) the implementation of an ecological flow regime and the assessment of its effects in the water bodies status.

Key words: Water Framework Directive, Ecological flows, Water bodies status

1. INTRODUCTION

Water managers around the world, pressed by stakeholders and water policies, are increasingly aware of the importance of preventing freshwater ecosystems degradation, which indirectly support people through the provision of ecosystem services (Acreman and Ferguson 2010; Acreman et al. 2014b). Amongst others, environmental flows appear as a possible answer to this challenge. A globally and widely used definition for describing environmental flows is "the quantity, timing and quality of water flows required to sustain freshwater and estuarine ecosystems and the human livelihoods and well-being that depend on these ecosystems" (Brisbane Declaration 2007). This definition recognizes and highlights the importance of flow temporal variability to sustain structure and functions of riverine ecosystems. Hence, within this concept, the link between hydrology and ecological condition has a key role.

This definition has been evolving accordingly to scientific knowledge and debate. Initially, environmental flows (or ecological flows) were usually defined as minimum flows, because they were considered the limiting factor to achieve a healthy ecosystem (Acreman et al. 2014b). In the 1980s, scientific community recognised that not only minimum flows dictate the structure and functions of riverine ecosystems (Bunn and Arthington 2002), but also that the temporal patterns of flows were fundamental (Arthington 2012). The idea is that too much flow in the wrong period of the year can have negative consequences such as having too little flow (Acreman et al. 2014a).

Even though some scientific advances have been perceived, namely related with the definition of flow-ecology relationships (i.e. between water flows and ecosystem state), attempts to implement environmental flows have raised several questions, for example, related with who should decide the

target condition of the ecosystem (Poff et al. 2010; Acreman et al. 2014b).

In the European Union, all water bodies should achieve at least good water status/potential (European Commission 2000). This goal was introduced with the adoption of the Water Framework Directive (WFD), one of the most influential pieces of European legislation. WFD is implemented through several 6 year cycles, through River Basin Management Plans (RBMPs) and the associated Programme of Measures (PoMs), for each European Member State. The WFD does not explicitly refers the term environmental flow (or ecological flow), although it expresses that action is needed in those situations where the hydromorphological pressures are having an impact on the ecological status, interfering with the capacity to achieve WFD objectives (European Commission 2012a). In 2012, the European Commission, EC (European Commission 2012b), stated that there is a need to "*put quantitative water management on a much more solid foundation, namely the identification of the ecological flow, i.e., the amount of water required for the aquatic ecosystem to continue to thrive and provide the services we rely upon. Fundamental to this is the recognition that water quality and quantity are intimately related within the concept of 'good status'. However, there is no EU definition of ecological flow, nor a common understanding of how it should be calculated"*. To address this gap, the EC proposed, within a CIS (Common Implementation Strategy) working group, the development of a Guidance Document (European Commission 2012b, 2015a, b).

In this context, the main goal of this study is to understand how the inclusion of ecological flows has been evolving in the context of WFD implementation.

2. RESEARCH DESIGN

To achieve the main goal of this paper, the authors designed a questionnaire (see link: www.goo.gl/geqLCp) to evaluate: a) if ecological flows were included in the 1st RBMPs and 2nd RBMP, and b) some key aspects related with the definition, implementation and monitoring of ecological flows in the 2nd RBMPs. The two first questions of the questionnaire were related to the inclusion of ecological flows within the 1st RBMPs (Question 1 – Q1) and the 2nd RBMPs (Q2). The other questions, related with the 2nd RBMP, have the goal to assess: a) the sites selected to assess ecological flows (Q2.1), b) if MS have legislation or guidelines to guide the definition of ecological flow regimes (Q2.2), c) the methodologies applied to assess ecological flows (Q2.3), d) the temporal application of ecological flow regimes (Q2.4), e) if the defined ecological flow regimes are ecologically relevant, in other words, if the defined regime show a clear relation/connection between flow and biology (Q2.5), f) the inclusion of ecological flow regimes into the Programme of Measures (Q2.6), g) if the defined ecological flow regimes are being implemented and their effects are being evaluated (Q2.7), h) which metrics have been used to assess ecological flow effects (Q2.7.1). After contacting the Environment Water Team (Env-Water Team) of the EC, the questionnaire was sent to Member States contact points of the WFD CIS Working Group Ecological Status (WG ECOSTAT). In total, thirty questionnaires were sent (three for Belgium representatives from Flanders, Wallonia and Brussels-Capital Region, and one for each of the remaining twenty-seven EU Member States). Figure 1 present those countries that answered the questionnaire.

To enhance knowledge about the inclusion of ecological flows within the 1st RBMPs, an analysis of official European documentation was performed. Until now, four implementation reports (IR) were published (Maia 2017). Within the presented work, a special detail was given to the 3rd IR and 4th IR. The 3rd IR presents a review of the progresses in the implementation of WFD, based on information reported by MS. The 4th IR focused on the Programmes of Measures.

The next section (3) provides the obtained results. Firstly (section 3.1), considerations about the results assessed in the official European documentation was presented. Then (section 3.2), a special focus was given to the guidance document developed by a CIS working group (EC, 2015). Finally, (section 3.3) questionnaire results were presented.

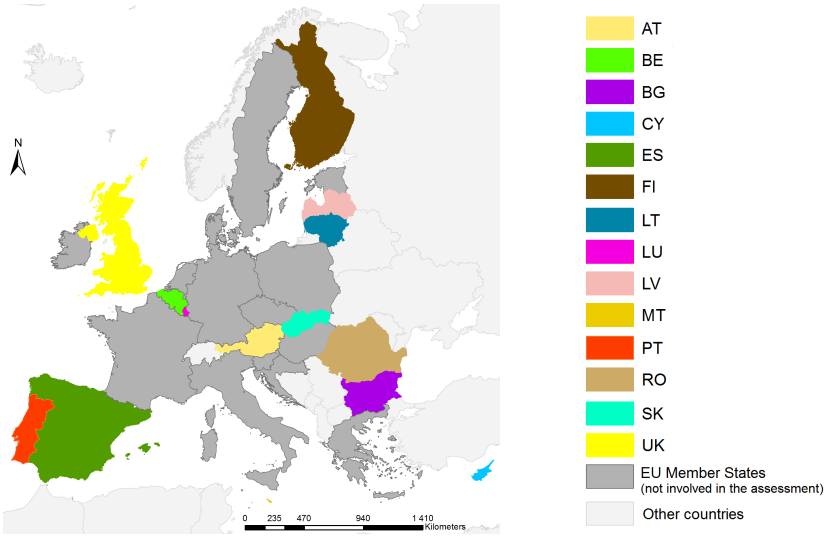

Figure 1. Countries involved in the assessment of ecological flows progress.

3. EVALUATION OF ECOLOGICAL FLOWS IMPLEMENTATION WITHIN WFD

3.1 First WFD implementation cycle – WFD official documentation

Concerning the 1st RBMPs, official documentation about the progress in the implementation of WFD was evaluated. Through the analysis of the 3rd implementation report, some relevant aspects about ecological flows integration within the 1st RBMPs were noticed.

In 43% of the countries, the RBMPs refer the existence of (national/regional) guidelines or regulations to define an ecological flow regime. Nevertheless, since this question was not a specific requirement for reporting, other countries may also have some guidelines or regulations. In a questionnaire filled by MS (within the CIS Workshop on Water Management, Hydropower & WFD in 2011), countries were asked to report if there is relevant legislation to ensure ecologically based flow at hydropower plants (Table 1).

Table 1. Legislation used to ensure ecologically based flow at hydropower plants (adapted from 3rd IR).

There is relevant legislation	**There is no legal requirement but there is relevant recommendation**		**No legal requirement or recommendation but defined in individual cases**	**Generally, no legislative means**	**No information about these countries**
National level	**National level**	**Regional level**			
Austria, Bulgaria, Spain, Lithuania, Latvia, Romania	Slovakia, United Kingdom, Portugal	United Kingdom	Belgium, Luxembourg	Finland	Cyprus, Malta

Regarding methods for the definition of an ecological flow regime, several methods were used (Figure 2), being the static definition of minimum ecological flows the most frequently applied method.

The European Commission, made several recommendations for the 2nd and 3rd RBMPs of the overall European countries, such as: 1) the methodologies used to assess ecological flow regimes should be clearly referred, 2) it would be important to define more standardised methods and the development of a common understanding for setting ecological flow, 3) monitoring programmes should target river stretches where ecological flows are applied to enhance our knowledge about the effects of ecological flows on the biological elements used to assess WFD impacts should be crucial

of their relation, 4) the establishment of ecological flows for all European water bodies is necessary, also to deal with water scarcity and drought situations.

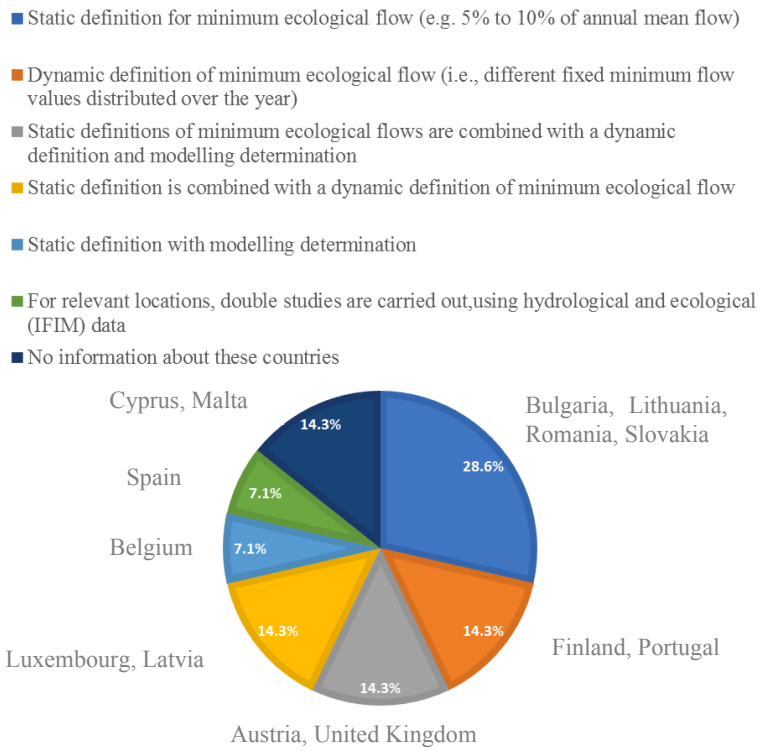

Figure 2. Methods used for the definition of an ecological flow regime (based on the 3rd IR).

The 4th IR was developed by the European Commission with the aim to provide an overview of the progress made by MS in the development and implementation of Programmes of Measures under the WFD, enabling the Commission to understand what are the strengths and weaknesses of the implementation of WFD, in the different MS. This document also provides recommendations for each Member State to fill the gaps within the 2nd RBMPs. Regarding those measures related with the improvements in ecological flow regimes and/or establishment of minimum ecological flow, the 4th IR indicates that most of the countries had not completed the process or did not even started it. EU Commission make some recommendations about this topic, for some of the assessed countries: 1) Austria and Finland should conduct a review of hydropower permits as restoration measures and the establishment of an ecological flow downstream of hydropower plants will be necessary to achieve good surface water status; 2) Bulgaria, Spain and Latvia should develop a proper methodology to establish a link between ecological flows and the good ecological status as well as to guarantee that ecological flows are applied through a review of the permits. Moreover, the Commission asked Spain to "avoid presenting the maintenance of ecological flow in new dams as an ecological benefit of the dam, while they should be considered as a mitigation measure", 3) Romania the indication was that this country should "further develop and analyse ecological flow using the information on ecological status and the information available under the Common Implementation Strategy (CIS)".

3.2 Guidance nº 31 – Ecological flows in the implementation of the Water Framework Directive

The assessment of progress of WFD, made it clear that actions should be taken to boost several topics within the WFD agenda. In this context, in 2012, the Commission prepared the Blueprint to Safeguard Europe's Water resources which "outlines actions". One of the main objective is to ensure that people, the economy and the environment have sufficient quantity of good quality water

available. In fact, the "Blueprint" recognizes that water quality and quantity are intimately linked with the concept of "good status", enhancing the importance of an EU-wide acknowledgement of the ecological flows role. In this context, the "Blueprint" proposed the development of a guidance document, within the WFD common implementation strategy (CIS), regarding ecological flows. The idea was that the recommendations of this guidance could be applied in the 2nd and 3rd RBMPs. A CIS Working Group presented the guidance, in 2015, with the main goal to support a shared understanding of ecological flows and ways to use them in the RBMPs. The document covers several aspects, such as: 1) a working definition of ecological flows in the context of WFD, 2) steps in the WFD cycle where eflows are relevant, and 3) lessons learned from case studies that have been developed in several EU-MS. Nevertheless, the document highlights that it "does not offer a full protocol for the implementation of Eflows in water bodies, nor is it intended to lead to uniform implementation of eflows". In fact, MS are encouraged to "make best use of the shared understanding of eflows in all steps of the WFD process" while should to consider the site-specific eflows implementation (related with several aspects, namely the national or regional legislation, specific environmental values or ecosystem services).

In the guidance, the CIS Working Group choose to adopt the term of "ecological flows", that within the context of the WFD, is defined as: "an hydrological regime consistent with the achievement of the environmental objectives of the WFD in natural surface waters bodies as mentioned in Article 4(1)." It should be emphasized that, within this definition, according to Article 4(1), the environmental objectives refer to: 1) non-deterioration of the existing status, 2) achievement of good ecological status in natural surface water body, 3) compliance with any standards and objectives for protected areas. The provided definition provided is referred as a "working definition of ecological flows" that did not cover those ecological flows that should be implemented in heavily modified water bodies and/or those qualified for an exemption. For those water bodies, ecological requirements "are to be derived taking into account technical feasibility and socio-economic impacts on the used that would be affected by the implementation of ecological flows". Throughout the document several recommendations were provided:

- Ecological flows consideration should be included in national frameworks. The national frameworks should include ecological flows: 1) that consider all flow components of the natural flow regime (and not only the minimum flows), 2) defined considering their link with biological requirement according to the objectives of WFD and Birds and Habitat Directives (BHD);
- MS should develop methods for the classification of ecological status based on metrics more sensitive to hydrological pressures, considering the relationship between hydrology, morphology and the biological impacts. The idea is to use metrics that are appropriately sensitive to hydrological alteration;
- A suitable definition and implementation of ecological flows require the monitoring of hydrology to get a full picture of hydrological alterations and the associated impacts on habitat/morphology and biology, to support the achievement of ecological flows. The results from monitoring will enable the assessment of the effectiveness of flow restoration actions (as part of the programme of measures);
- The selection of the most suitable method to define ecological flows is influenced by the resources availability (such as monitoring data) and on severity in the pressures;
- The programmes of measures should guarantee the implementation of ecological flows (through incorporation in basic measures, controls on surface and groundwater abstractions, impoundments and other activities that impact hydromorphology, through the authorization process and regular review of permits);
- The assessment of costs associated with the implementation of ecological flows should not be used to change the ecological flows developed based on technical/scientific process.
- Public participation on ecological flows should be developed in all the phases of the WFD planning process, from its design, implementation plan and effective implementation follow-up.

3.3 Questionnaires completed by country representative experts

In this section, questionnaire results are presented and a discussion about them is performed. Figure 3, shows which countries incorporated ecological flow assessment within the 1st and 2nd RBMPs (Q1 and Q2). It is important to notice that, for the overall analysis, once the three Belgium representatives provided identical answers, no distinction was made between them, and the results are presented as "Belgium".

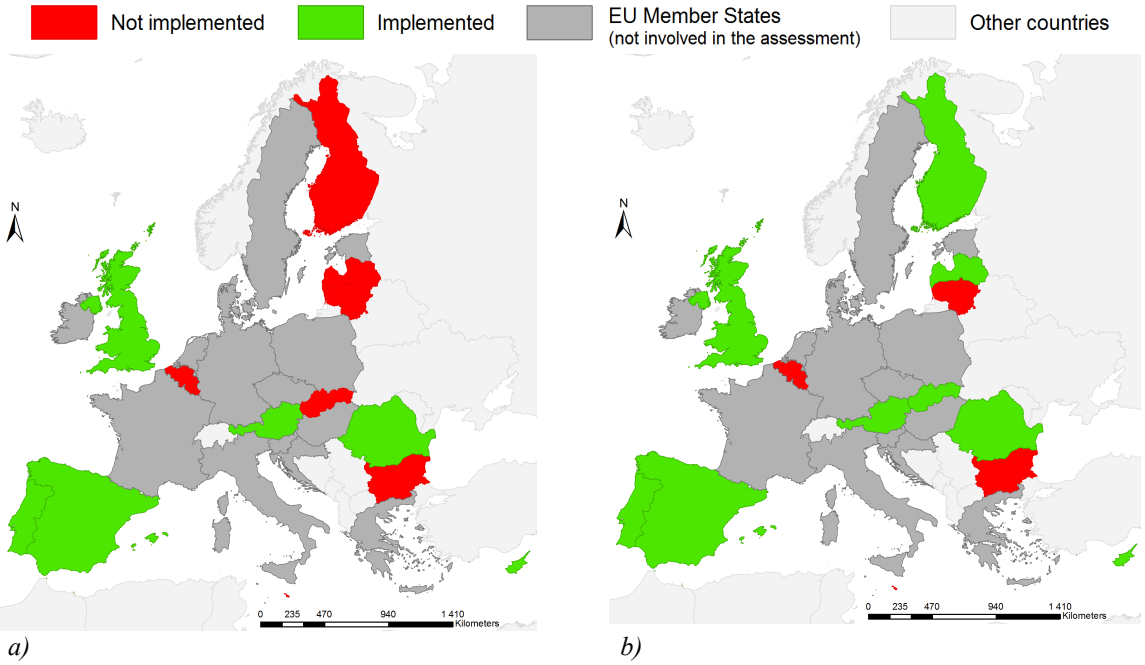

Figure 3. Status of ecological flow assessment integration within the a) 1st RBMPs and b) 2nd RBMPs.

Comparing Figure 3a) and Figure 3b), it is possible to notice a progression in the integration of ecological flows assessment in RBMPs, since some countries started to include this topic within the 2nd RBMPs. Nevertheless, it is possible to notice that some countries still did not include ecological flows in their assessments: Belgium, Luxembourg, Lithuania, Bulgaria and Malta. Hence, from now, these countries will not appear in the evaluation of the remaining questions, which are related with the way ecological flows are considered in the 2nd RBMPs. Hence, the countries evaluated from now on will be nine.

One of the firsts steps for the definition of ecological flows is the selection of locations for which the ecological flows will be determined (Q2.1). Some years ago, the definition and implementation of ecological flows was perceived as a measure to mitigate downstream effects of dams (being frequently applied only to those locations). Currently, a global "sense of urgency has arisen" (Poff et al. 2010) to implement ecological flows for wider locations for their inclusion into basin-wide and regional water-resources planning (Dyson et al. 2003; Poff et al. 2010). Taking this into consideration, this study tried to identify the differences between European MS in terms of ecological flows definition. Table 2, presents a list of the locations for which MS had defined ecological flows.

Through the analysis of Table 2, it is possible to verify that there is a balance between those countries that already define ecological flows for the whole RBDs and those that are still focused in the development of ecological flows only for downstream dams.

Most of the countries reported (Q2.2) to have a national legislation (Austria, Bulgaria, Spain, Latvia, Portugal, Romania, United Kingdom) that provides guidance for the definition of ecological flow regimes and their inclusion in the RBMPs. Finland refers that they have a regional legislation as well as Latvia. Portugal refer the existence of a national guideline (Alves and Bernardo 2002). None of the countries reported the existence of regional legislation/guidelines.

*Table 2. Ecological flows location (**A** – only for downstream dam's river stretches, **B** – for several rivers affected by different types of pressures, **C** – for the whole River Basin District (RBD, i.e. for their main rivers and tributaries).*

Country	A	B	C
Austria			■
Cyprus	■		
Spain		■	
Finland		■	
Latvia	■		
Portugal	■		
Romania			■
Slovakia	■		
United Kingdom			■

Legend: ■ Applicable

Another important factor to assess was the ecological flow methods (Q2.3) used for the definition of ecological flow regimes within RBMPs. Table 3 presents these results.

Table 3. Ecological flows methods.

	Hydrological	Hydraulic	Habitat Simulation	Holistic
Country	Cyprus, Spain, Latvia, Romania, Slovakia, United Kingdom, Portugal	-	Spain	Austria, Finland, United Kingdom

It is possible to notice that hydrological methods are the most commonly used methods to define ecological flow regimes. To assess the evolution in the implementation of ecological flows, a parallelism is made with the methods referred in Figure 2 and Table 3. Hydrological methods and hydraulic methods range the methods: a) static definition for minimum ecological flow (e.g. 5% to 10% of annual mean flow), b) dynamic definition of minimum ecological flow (i.e. different fixed minimum flow values distributed over the year), c) static definition is combined with a dynamic definition of minimum ecological flow. On the other hand, habitat simulation methods range: a) static definitions of minimum ecological flows are combined with a dynamic definition and modelling determination, b) static definition with modelling determination, c) for relevant locations, double studies are carried out, using hydrological and ecological (IFIM) data. Based on this parallelism it is possible to notice that Austria, Finland and United Kingdom showed an increase in the complexity of the methodologies used (changed for holistic methods). The other countries seem to use the same types of methodologies used in the 1st RBMPs.

Ecological flows are required to sustain freshwater ecosystems. Ecosystems needs would depend on the hydrological patterns, in other words, their value should change accordingly with the type of year (Q2.4).

As expected, most of the countries (67% - Finland, Latvia, Portugal, Romania, Slovakia, United Kingdom) had defined ecological flows for normal years, without considering the definition of a specific regime for drought years. This could be related to the type of methodology used, as well as, with a lack of understanding of the effects of droughts on freshwater ecosystems.

One of the recommendations of the European Commission is that ecological flows should be ecologically relevant. In other words, it would be expected that the defined ecological flows present a clear relation/connection with biological elements, which are the main elements used to assess water bodies status (Q2.5). Table 4 show the answers reported by each country.

Through the examination of Table 4, it is possible to notice that most of the countries defined ecological flows regimes that provide some insights (qualitative information) about the link between ecological flow regime and biological indicators.

As stated before, ecological flows are used as a measure to sustain freshwater ecosystems. Hence, their inclusion within the Programmes of Measures (Q2.6) of the RBMPs should be essential for the implementation of ecological flow regimes. All the countries reported inclusion of this topic, within the Programmes of Measures.

*Table 4. Ecological flows and their link with biological indicators (**A** – there is a distinguishable link, **B** – some insights (qualitative information) are provided about this link, **C** – no clear connection is provided).*

Country	A	B	C
Austria	■		
Cyprus		■	
Spain		■	
Finland		■	
Latvia			■
Portugal		■	
Romania			■
Slovakia			■
United Kingdom		■	

Legend: ■ Applicable

The implementation of ecological flows and the monitorization of their effects on biological is crucial to gain knowledge for further adjustments (Q2.7). Hence, it was considered relevant to understand if MS are not only implementing ecological flows but also monitoring its effects.

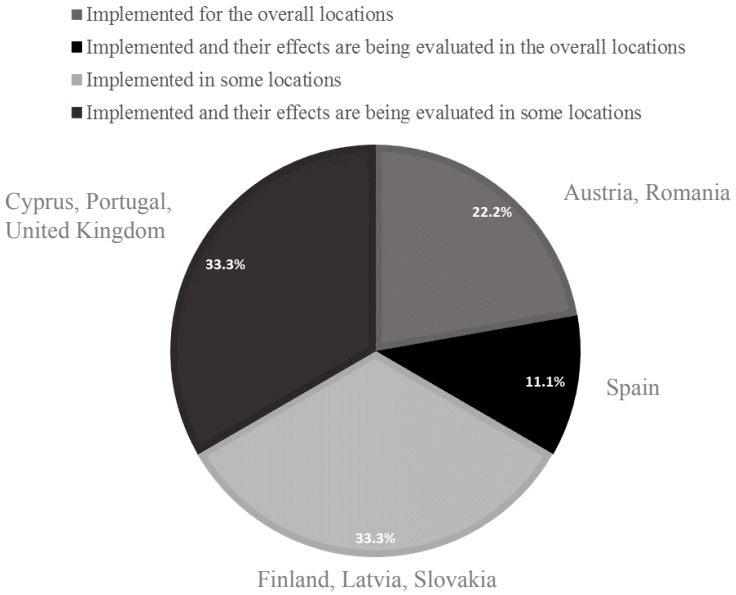

Figure 4. Status of ecological flows implementation and evaluation of their effects.

As expected, most of the countries had already implemented ecological flows only for some locations. Only four countries (Cyprus, Portugal, United Kingdom, Spain), are evaluating the ecological effects of the ecological flows regimes. The evaluation of the effects of ecological flows (Q7.1) is based on monitoring programs focused on the ecological quality assessment (considering biological, physicochemical, specific pollutants and hydromorphological elements) and chemical status, under the provisions of the WFD). This evaluation is complemented by the evaluation of other relevant aspects, namely those expected to help clarify relations between the mitigation measure and the ecological outcomes such as detailed hydromorphological characterizations. United Kingdom use ecological indicators of severe water resources pressures. Cyprus referred that no specific indices are used to evaluate effects of ecological flows, they used the national indices used to assess water bodies.

5. CONCLUSIONS

Through this study is was possible to evaluate the overall status of ecological flow definition and

implementation within the RBMPs. It was possible to conclude that, even though, countries show an overall progression through the comparison between the 1st and 2nd RBMPs, MS should enhance their knowledge and efforts about this subject. Moreover, it was possible to understand that few countries incorporated the recommendations provided in the CIS guidance document. Although, some countries highlight that actions have been taken to take into consideration this document for the 3rd implementation cycle. The difficulties could be related with the timing of this document, that was developed very close to the deadline for adoption of the 2nd RBMPs.

Based on the analysis of the official documents and answers to the questionnaire, it was possible to conclude that countries use different methods to define ecological flow regimes. Moreover, most of the methodologies do not seem to be necessarily linked to the achievement of WFD environmental objectives. In the 1st RBMPs most of the countries used a static definition for minimum ecological flows, which do not encompass the multiple aspects of an ecological flow regime. Within the 2nd RBMPs, most of the countries are using hydrological methods, without trying to understand the relation between ecological flow regimes and biological elements, i.e. the achievement of WFD environmental objectives. To gain knowledge about this relation, monitoring programmes should be implemented to understand the effects of ecological flows on the biological quality elements. This will provide evidence about relation between flow and biological elements, as well as, on how to manage ecological flows to achieve WFD environmental objectives. An overall conclusion is that it will be important to put together efforts to enable the development of a common and standardised method for setting ecological flows. In fact, these recommendations were highlighted by European Commission after the assessment of 1st RBMPs, although this necessity seems to persist within the 2nd RBMPs. This method should be of regional applicability (i.e. river basin district), taking in consideration site-specific characteristics. Indeed, the establishment of ecological flows for all water bodies could be used to enhance the achievement of WFD environmental objectives, as well as to deal with drought effects.

ACKNOWLEDGEMENTS

The first author gratefully acknowledges for the PhD research grant provided by a protocol between FEUP and EDP - Produção de Energia, S.A. The authors are grateful to all those Member State contact points of the WG ECOSTAT and country representative experts that agreed to answer the questionnaire about ecological flows within the WFD implementation (Austria – Gisela Ofenböck, Belgium – François Darchambeau, Sofie Bracke, Wim Gabriels, Bulgaria – Marin Marinov, Cyprus – Gerald Dörflinger, Spain – Carmen Coleto, Finland – Marko Jarvinen, Lithuania – Audrone Pumputyte, Luxembourg – Nora Welschbillig, Latvia – Jānis Šīre, Tatjana Kolcova, Portugal – Sofia Batista, Romania – Otilia Mihail, Slovakia – Emilia Mišíková Elexová, United Kingdom – Peter Pollard, Malta – Annabelle Zammit). Thanks, are also due to the Environment Water Team of the European Commission, on behalf of Dr. Daniel Calleja Crespo (Director-General for Environment), for providing the contacts of country representative experts. Finally, the authors would like to thank Dr. Eleftheria Kampa from the Ecologic Institute (Berlin-Germany).

REFERENCES

Acreman M, Arthington AH, Colloff MJ, et al (2014a) Environmental flows for natural, hybrid, and novel riverine ecosystems in a changing world. Front Ecol Environ 12:466–473. doi: 10.1890/130134

Acreman MC, Ferguson AJD (2010) Environmental flows and the European Water Framework Directive. Freshw Biol 55:32–48. doi: 10.1111/j.1365-2427.2009.02181.x

Acreman MC, Overton IC, King J, et al (2014b) The changing role of ecohydrological science in guiding environmental flows. Hydrol Sci J 6667:1–18. doi: 10.1080/02626667.2014.886019

Alves MH, Bernardo JM (2002) Caudais ecológicos em Portugal. Minstério das Cidades, Ordenamento do Território e Ambiente, Lisboa, Portugal

Arthington AH (2012) Environmental Flows. Saving Rivers in the Third Millennium, Freshwater. University of California Press, Berkeley

Brisbane Declaration (2007) Environmental Flows are Essential for Freshwater Ecosystem Health and Human Well-Being.

Bunn SE, Arthington AH (2002) Basic principles and ecological consequences of altered flow regimes for aquatic biodiversity. Environ Manage 30:492–507. doi: 10.1007/s00267-002-2737-0

Dyson M, Bergkamp M, Scanlon J (2003) Flow: The Essentials of Environmental Flows. Gland, Switzerland, Cambridge

European Commission (2000) Directive 2000/60/EC of the European Parliament and of the Council of 23 October 2000 establishing a framework for Community action in the field of water policy. Off J Eur Parliam L327:1–82. doi: 10.1039/ap9842100196

European Commission (2012a) Commission Staff Working Document. European Overview (2/2). Accompanying the document Report from the Commission to the European Parliament and the Council on the Implementation of the Water Framework Directive (2000/60/EC). River Basin Management Plans.

European Commission (2012b) Communication from the Commission to the European Parliament, the Council, the European Economic and Social Committee and the Committee of the Regions. A Blueprint to Safeguard Europe's Water Resources.

European Commission (2015a) Ecological flows in the implementation of the Water Framework Directive : guidance document n°31.

European Commission (2015b) Policy Summary of Guidance Document No. 31. Ecological flows in the implementation of the Water Framework Directive.

Maia R (2017) The WFD implementation in the European Member States. Water Resources Management (in revision).

Poff NL, Richter BD, Arthington AH, et al (2010) The ecological limits of hydrologic alteration (ELOHA): a new framework for developing regional environmental flow standards. Freshw Biol 55:147–170. doi: 10.1111/j.1365-2427.2009.02204.x

Proceedings of the 10th World Congress of EWRA 'Panta Rhei', 5-9 July 2017, Athens, Greece
© 2017 *European Water Resources Association*

Underground taming of floods in the Ganges basin: Technologies, institutions and policies

V. Ratna Reddy[1*], S.K. Rout[1] and P. Pavelic[2]
[1] *Livelihoods and Natural Resource Management Institute, Hyderabad, India*
[2] *International Water Management Institute, Vientiane, Lao PDR*
[*] *e-mail: vratnareddy@lnrmi.ac.in*

Abstract: A technological approach for protecting flood prone locations through using excess flood water for recharge and storage in the depleted aquifers and using it for protecting dry season agriculture has been conceived and termed as under-ground taming of floods for irrigation (UTFI). UTFI as a total package deals with conjunctive water resources management, with specific foci in terms of flood, surface water, groundwater and irrigation management. This paper makes an attempt to assess the institutional and policy options for sustainable UTFI management in the Ram Gaga sub-basin of Ganges in Uttar Pradesh, India where UTFI testing is underway. While UTFI technically addresses various anomalies at scale, appropriate institutional arrangements are required to address sustainability of the interventions. Absence of any institutional arrangements is identified as one of the constraints for adopting UTFI. There appears to be clear demand for institutional evolution, though it needs to be introduced externally. Given the substantial socio-economic benefits (impacts), public and private sector agencies (banks, CSR initiatives) could support the collective initiatives. This requires strengthening of existing institutions fostered with new ones. Creating appropriate policy environment is critical in this regard. Promotion and strengthening the NGO sector in the region would go a long way in bridging this gap.

Key words: Floods, droughts, resilience, payments for environmental services, participatory learning, social regulation, Ganges basin

1. INTRODUCTION

Managing supply of and demand for water resources at the river basin level is amongst the most critical policy issues for the governments of South Asia (Moench and Dixit, 2004). In most river basins situations of water scarcity and abundance coexist although they are divided by time and / or space. Monsoon floods are common in some of the drought-prone regions, i.e., rainy season excess water and dry season scarcity of water (time dimension). Similarly, while some (down-stream) locations experience flooding, others (up-stream) face water shortages (space dimension). These anomalies make the local communities highly vulnerable in the rural and peri-urban areas (Molden, et. al., 2014). Enhancing the resilience of the local communities through appropriate agricultural water management interventions, viz., technological, institutional and policy, is critical for sustaining the livelihoods of these communities.

An approach using excess flood water for recharge and storage in the depleted aquifers and using it for protecting dry season agriculture has been conceived and termed as under-ground taming of floods for irrigation (UTFI) (Fig. 1). UTFI is a new approach to implementing Managed Aquifer Recharge (MAR) and fosters the much-needed principles of conjunctive use management of water resources (Pavelic, et. al., 2012). The potential for such an intervention is estimated to be quite good in the Ganges basin (Brindha and Pavelic, 2016; Amarasinghe, et. al., 2016). This however requires a unified approach that considers both the supply (MAR infrastructure) as well as demand side interventions (institutions for managing MAR infrastructure). Of late, 'bottom-up' voluntary social regulation, participatory learning, etc., along with market-based instruments like payments for environmental services (PES) when integrated with the traditional 'control and command' regulations are observed to be more effective in dealing with sustainable resource management

(Iraldo, et. al., 2014). The political economy factors also play a critically important role in adopting institutional arrangements embedding appropriate regulatory instruments.

This paper makes an attempt to assess the institutional and policy options for sustainable UTFI management in the Ram Ganga sub-basin of Ganges in western Uttar Pradesh, India where UTFI testing is underway (Pavelic, et. al., 2015). Specific objectives included:

i. Assess the location specific institutional strengths and weaknesses in the study area,
ii. Identify appropriate institutional modalities for sustainable UTFI management, and
iii. Suggest potentially viable governance arrangements and policies for UTFI implementation and scaling up.

1.1 Approach

In total, 10 potential locations (villages) were studied for UTFI implementation in the Ram Ganga sub-basin. In one of the villages, namely Jiwai Jadid, UTFI interventions have been established during 2015 with the involvement of local communities and officials. The sample villages represent both up-stream, down-stream locations within the sub-basin. Both qualitative and quantitative research was used to elicit information. Focus Group Discussions (FGDs) and Key Informant Interviews (KII) were used as part of the qualitative research. Household information was collected from a representative (socioeconomic groups) sample of 30 households from each village using a structure questionnaire was collected. That is, institutional assessment is based on a total of 300 sample households spread over 10 villages. Care was taken to minimise the strategic bias.

Table 1. Sample Villages and Sampling Details

Village	Block	Location	No. of HHs (2011 census)	No. of FGDs conducted	No. of KIIs	No. of Sample HHs
Kumharia Kalan	Suar	Upstream	321	1	3	30
Mankara	Bilaspur	Upstream	315	1	3	30
Ashokpur	Chamaraua	Upstream	249	1	3	30
Patti Ashokpur	Chamaraua	Upstream	220	1	3	31
Azim Nagar	Saidnagar	Upstream	311	1	3	30
Mursaina	Sadar	Upstream	342	1	3	30
Moh.Nagar Nankar	Milak	Downstream	263	1	3	30
Jiwai Jadid	Milak	Downstream	313	5	10	31
Narkhera	Milak	Downstream	418	1	3	30
Sihari	Milak	Downstream	532	1	3	30
Total	NA	NA	3284	14	37	302

Note: FGD= Focus Group discussion; KIIs= Key Informant Interviews; HH = households. Upstream and downstream are the locations relative to the intervention village (Jiwai Jadid).

2. ANALYSIS

2.1 Profile of the Sample Region and Villages

Size of the sample villages ranges between 110 households to 600 households. Household size varies between 5.7 and 6.2 with an average of 5.9, which is relatively higher (Census, 2011). Proportion of female population is below 50 per cent in all the sample villages. It may be noted that the demographic profiles do not vary much between up-steam (US) and down-stream (DS) villages.

Majority (90 percent) of the farmers are small and marginal (< 1 Hectare). Average farm size is higher in the DS, which is not usual. Access to water is more evenly distributed, as the extent of irrigation is almost 100 percent in most cases. The social composition is dominated by backward (OBC) communities which account for about 50 percent of the total population with other communities (OC) and scheduled caste (SC) are equally divided.

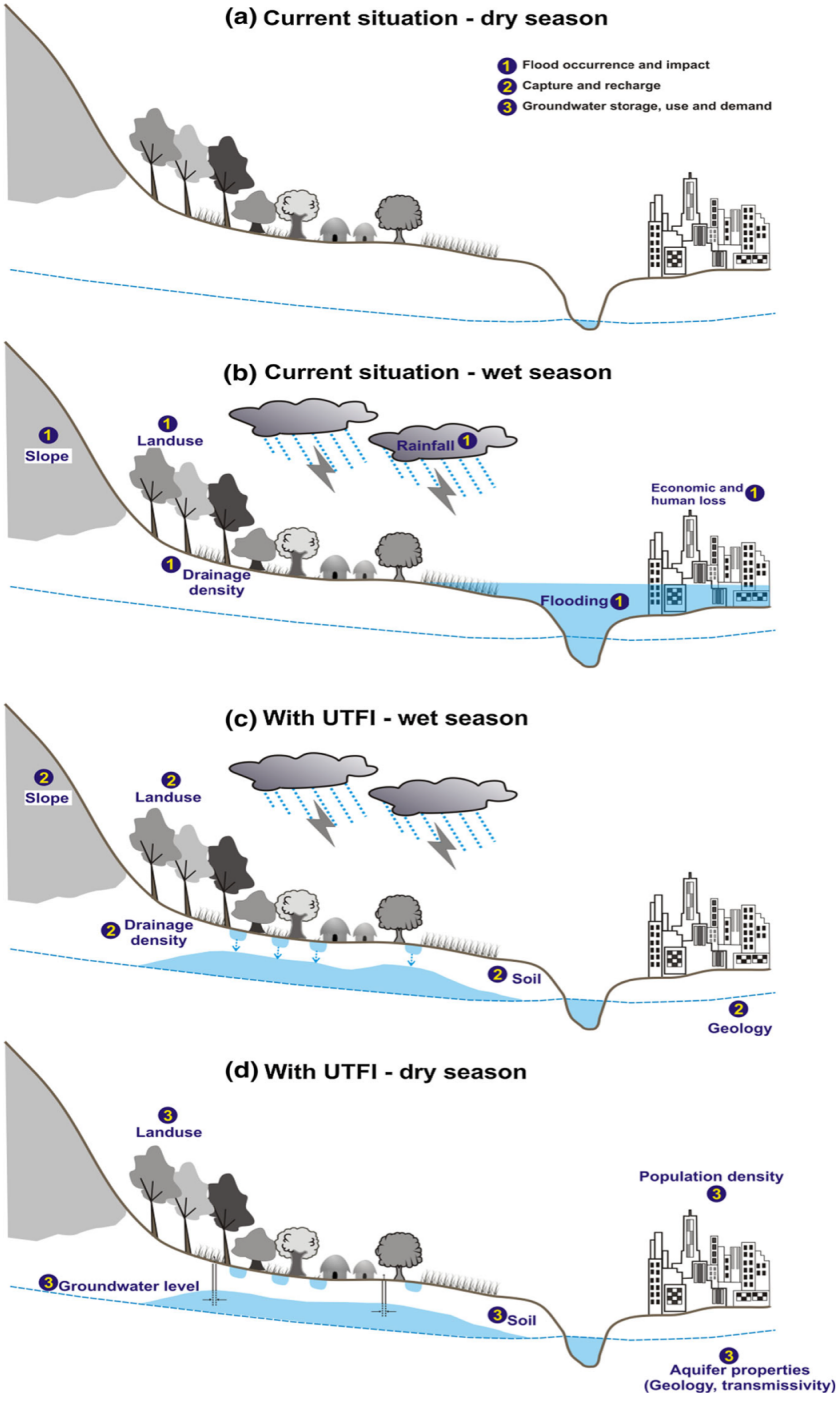

Figure 1. Schematic illustration of UTFI (Source: Brindha and Pavelic, 2016).

Predominant occupation in the sample villages is agricultural, as cultivators and agriculture labour together considered dependent on agriculture. Occupational structure varies widely between US and DS (Table 2). Dependence on non-agriculture wage occupations is more in US (30 percent) when compared to DS (17 percent). The contribution of agriculture and livestock together accounts for 54 percent of the household income. Their contribution is more in downstream while the contribution of labour is more in upstream. Labour contributes 40 percent of the household income.

In the case of irrigation infrastructure, 73 percent of the households have bore wells. Due to the relatively scarce groundwater situation in US villages, larger proportion (76 percent) of households have bore wells with higher depth and lower area irrigated per well. In both the locations, number of households appear to have more than one well in all the villages i.e., average number of wells per household is 1.2.

Table 2. Occupational Distribution and Source wise Income of the Sample Households.

Name of the Village	Cultivation +Livestock	Agrl. +Non-agrlLabour	Non-Agrl. Wage Labour	Total
Occupation				
Upstream	66 (64)	30 (32)	4 (4)	100 (100)
Downstream	81 (81)	17 (16)	3 (3)	100 (100)
Overall	72 (70)	25 (25)	3 (5)	100 (100)
Income				
Upstream	59854 (54)	44728 (40)	6425 (05)	111008 (100)
Downstream	76688 (61)	41807 (33)	7237 (06)	125733 (100)
Overall	59854 (54)	44728 (40)	6425 (05)	111008 (100)

Note: Figures in brackets are percentage of sample population.
Source: Sample Survey.

Collective choice institutions are not a strong characteristic of the region. There are no community driven initiatives or institutions one can refer to in the sample villages. No instances of systematic collective action even in extreme situations of severe flooding, though people come together to overcome the situation. Though one can observe the presence of self-help groups (SHGs) in some villages, they are not effective. There are no farmer groups in the sample villages. The only institution that is functional is the Panchayati raj institutions. Thus, it is a big challenge to design and promote new institutional entities for UTFI management.

2.2 Floods: Intensity and impacts

Five main impacts due to floods are identified by the households. These include: inundation of residential areas, farm lands, crop losses, livestock losses, loss of employment and health impacts. Of these, monetary losses due to inundation are not reported (Table 3). It is estimated that an average household loses about Rs. 8000 (US$ 123) during moderate floods and about Rs. 16000 (US$ 246) during severe floods. While the loses range between Rs. 7000 (US$ 107) and Rs. 14000 (US$ 214) in the upstream villages, households in downstream incur losses to the tune of Rs. 20000 (US$ 308) during severe flooding. As a proportion of household income, it is 5 to 10 percent during moderate and severe floods respectively in the upstream and 8 to 14 percent in the downstream. Flood losses account for 3 to 7 percent of large and medium farmers household income, while they account for 6 to 18 percent in the case of small and marginal farmers, depending on the intensity of floods.

2.3 Household Resilience and Adaptation

No planned community efforts for flood management are evident in the sample villages. Participants in general tend to adapt individually to the flood related problems. Flood related adaptation strategies are mostly construction of dams and flood barriers by the government, which are helping in reducing flood incidence. But, there are no specific interventions or strategies at the village level, such as rehabilitation centres.

Table 3. Extent of Total Losses due to Floods across Economic Category of Households (Rs. / Household)

Location of the Village	Economic Category	Crops		Livestock		Employment		Health		Total	
		MF	SF	MF	SF	MF	SF	MF	SF	MF	SF
Upstream	LL	--	--	1840	3648	3000	5600	250	400	5090	9648
	SMF	1325	3062	2810	5442	1600	3000	260	580	5995	12084
	LMF	11486	18171	720	1440	2000	3800	--	--	14206	23411
	All	1822	3802	2538	4932	2600	4800	259	564	7219	14098
Downstream	LL	--	--	3805	6378	3000	5400	1000	1250	7805	13028
	SMF	3798	7421	4858	7839	2800	5200	490	1030	11946	21490
	LMF	7200	14400	2130	3194	2800	5200	--	--	12130	22794
	All	4406	8667	4104	6610	2000	3800	575	1233	11085	20310

Note: Figures in brackets are percentage to respective household income.

Many households whose houses were damaged during past floods have now constructed their new houses on elevated land or by raising plinth levels to stay above the past flood levels. Agricultural areas suffered more damage than the houses because of the lower level of the farms and almost all the farmland in the village had been damaged by the floods. However, participants admitted that they did not undertake any protective measures to safeguard their farms from floods. Though most villages have access to communication systems there is little information available relating to flood forecasts. When asked if any members from the participants' family had ever attended a disaster/flood training program or if they had ever received information on flood preparedness, not a single participant responded affirmatively. However, almost all the participants believed that such training should be provided. And, climate change and water stress is also perceived as a livelihood threat in the near future.

Income diversification seems to be a major strategy adopted by the households in response to floods. Households with diverse sources of income were more resilient to flood impacts than those with single source of income. Important strategies include creation of employment, education, skill development, land development and reclamation, improving rural infrastructure and credit support. Social infrastructure such as health and education are part of long-term recovery process, while cheaper credit, debt relief and rebuilding of physical infrastructure are of extreme importance.

Preferred interventions vary from providing food security and input subsidies to institutional credit depending on the economic status of the household. While SC and ST households (lowest social category) prefer the provision of food grains and support for agricultural inputs, households belonging to other communities prefer assistance for agricultural inputs, provision of food grains and assistance for crop losses in the same order of priority. Awareness levels are low, especially in the non-intervention villages, as far as the need for natural resource management interventions like UTFI.

2.4 Institutional dynamics

Sustainable management of UTFI interventions poses number of opportunities and challenges. Opportunities are in the form of evolving new institutional arrangements that are more comprehensive in dealing with natural resource management dilemmas. It is observed that learnings from some of the existing institutions like watershed management, water user associations, participatory groundwater institutions would help designing appropriate institutions. Instruments such as payments for environmental services and participatory learning could be integrated for achieving financial sustainability, equity and social acceptability.

Despite being a naturally endowed region, communities are relatively poor due to small land holdings. As a result wage employment contributes substantially to the household income along

with agriculture and livestock. Downstream villages are better off due to better access to water. Unlike the widely-held belief that strong social capital is associated with economic backwardness, social capital as well as the presence of voluntary sector are weak in this region, which is unique.

Flood impacts are substantial in terms of income losses across the households. Impacts are disproportionately born by the socioeconomically vulnerable sections. Higher magnitude of flood impacts in the downstream villages is also associated with water stress during summer months. The contrast is more conspicuous in the upstream villages emphasising the need for UTFI interventions.

In the context of UTFI, user / stakeholder groups could be formed viz., UTFI management committee (UMC) that is similar to or under the FPOs with broader objectives, which can get support from higher-level institutions. Given the wider scale of benefits awareness building is prerequisite. Awareness campaigns need to be designed in the local context and folk tradition. There appears to be lot of space and potential for non-governmental organisations (NGO), hence requires concerted policy support. This would help bridging the gap between the communities and the public and private financial institutions.

While UTFI management requires the involvement of number of departments and institutions such as irrigation, groundwater, watershed, etc., they need to be integrated with the UMC / FPO as and when they evolve. At present, maintenance of UTFI structures were taken up under the Mahatma Gandhi National Rural Employment Guarantee (MGNREG) programme. The gram panchayat (GP) should play an overarching role of guiding and monitoring the CBOs, including UMC. At present, GP is only the active institutional anchor present at the village level. A nuanced assessment of organising the local communities to manage UTFI (say UMC) and other CBOs is needed to identify and strengthen the drivers of collective strategies in the region. This along with the design of appropriate instruments for sustainable management of UTFI interventions would be taken up.

2.5 Summing up

The observations presented here provide some insights and directions for future work on scaling up.

- There is strong interest in the UTFI activities though there are some apprehensions regarding reduction in flooding. While UTFI technically addresses such anomalies at scale, appropriate institutional arrangements along with awareness building are required.
- Absence of any institutional arrangements is identified as one of the constraints for adopting flood mitigation and recovery mechanisms. There appears to be clear demand for institutional evolution, though it needs to be introduced externally with policy support.
- Given the substantial socio-economic benefits, public and private sector agencies could support the collective initiatives. Promotion of NGO sector would go a long way in bridging this gap.

ACKNOWLEDGEMENTS

This work was financially supported by the CGIAR Research Program on Climate Change, Agriculture and Food Security (CCAFS). Thanks are due to Brindha Kartikeyan, Prasun Gangopadhyay and Navneet Sharma for their support in selecting the field sites and conducting field work.

REFERENCES

Amarasinghe Upali Ananda, Lal Muthuwatta, Lagudu Surinaidu, Sumit Anand, and Sharad Kumar Jai (2016), “Reviving the Ganges Water Machine: potential”; *Hydrology and Earth System Sciences*., 20, 1085–1101.

Brindha K and Paul Pavelic (2016); “Identifying priority watersheds to mitigate flood and drought impacts by novel conjunctive water use management”, Environ Earth Sci (2016) 75:399 DOI 10.1007/s12665-015-4989-z.

Iraldo Fabio, Francesco Testa and Irene Bartolozzi (2014), An application of Life Cycle Assessment (LCA) as a green marketing tool for agricultural products: the case of extra-virgin olive oil in Val di Cornia, Italy, *Journal of Environmental Planning and Management*, 57:1, 78-103, DOI: 10.1080/09640568.2012.735991.

Pavelic Paul, Kriengsak Srisuk, Phayom Saraphiromb, Suwanchai Nadee, Kewaree Pholkern, Sumrit Chusanathas, Sitisak Munyou, Theerasak Tangsutthinon, Teerawash Intarasut, Vladimir Smakhtin (2012),"Balancing-out floods and droughts: Opportunities to Utilize flood water harvesting and groundwater storage for agricultural development in Thailand", *Journal of Hydrology*, Vols. 470–471 (pp 55–64).

Pavelic P.; Brindha K.; Amarnath G.; Eriyagama N.; Mutuwatte L.; Smakhtin V.; Gangopadhyay P.; Malik R.P.S.; Mishra A.; Sharma B.R.; Hanjra M.A.; Reddy V. Ratna; Mishra V.K.; Verma C.L.; Kant L (2015); Controlling floods and droughts via underground storage: From concept to pilot implementation in the Ganges Basin, IWMI Research Report No. 165.

Moench Marcus and Ajaya Dixit (2004), Adaptive Capacity and Livelihood Resilience: Adaptive Strategies for Responding to Floods and Droughts in South Asia; The Institute for Social and Environmental Transition, International, Boulder, Colorado, U.S.A. and the Institute for Social and Environmental Transition, Nepal.

Molden D. J, Vaidya R. A, Shrestha A. B, Rasul G, Shrestha M. S (2014), “Water infrastructure for the Hindu Kush Himalayas”. *International Journal of Water Resources Development* :1–18. And, Nepal Santosh,

Wolfgang-Albert Flügel and Arun Bhakta Shrestha (2014), Upstream-downstream linkages of hydrological processes in the Himalayan region, *Ecological Processes*, 3:19 (http://www.ecologicalprocesses.com/content/3/1/19).

Proceedings of the 10th World Congress of EWRA 'Panta Rhei', 5-9 July 2017, Athens, Greece
© 2017 *European Water Resources Association*

Environmental crimes in the water sector

L. Segato[1*], W. Mattioli[1], N. Capello[1] and M. Migliorini[2]
[1] *RiSSC - Research Centre on Security and Crime, Italy*
[2] *SiTI - Istituto Superiore sui Sistemi Territoriali per l'Innovazione, Italy*
[*] *e-mail: lorenzo.segato@rissc.it*

Abstract: Water stress is creating unprecedented tensions between freshwater users, with inter-connected risks (World Bank, 2016). Freshwater, the "blue gold", is becoming an attractive target for criminals, but the attention of Law Enforcement Agencies and criminologists on water within environmental crimes is only recent. Crimes against water remain difficult to assess, detect and prosecute, because legislations and policies on freshwater vary from Country to Country, data are inconsistent and not standardised, water-related crimes are often recoded under other offences – like fraud, corruption, theft, forgery/counterfeiting of documents, terrorism, or other crimes against heath or the environment. Offences range from water pilfering to tampering, from corruption in water services to cyber or terrorist attacks to water physical and digital infrastructures. The probability and impact of these threats can be high, but need to be assessed to develop effective countermeasures. Unlike any other known crime, water crimes are aggravated through their additional cost and impact on the environment and cost to future generations. Being part of a wider study, this paper provides the definitions of water crimes and water related crimes, and a tentative inventory of different offences against water, based on case studies collected in five European Countries, and on UNODC International Classification of Crime for Statistical Purposes (ICCS).

Key words: Water crime, freshwater, corruption, environmental crimes, risk, threat, criminology

1. INTRODUCTION

1.1 Water Stress[†††]

The assumption concerning secure supply of freshwater for the planet – even only for Europe – is false. Water covers more than 70% of the planet, but 97% is salted and held in the oceans, 2% is freshwater locked in snow and ice (e.g. glaciers), leaving less than 1% accessible for human requirements, distributed unequally.

Only 9 countries share 60% of the total amount of freshwater, while 873 million people lack access to safe drinking water (United Nations, 2012). By the year 2025, 1.8 billion people will live in places and under conditions in which water is "scarce" (see e.g. Johns, 2010; Arsenault, 2012; Ciampi, 2013). The global consumption of water is doubling every 20 years, more than twice the rate of human population growth; within the next three decades, demand for water from agriculture could increase by 50%, and for urban uses by between 50% and 70%; by 2035, the energy sector is projected to consume 85% more water (World Bank, 2014). These increased strains will create unprecedented conflicts between different water uses, and inter-connected risks between them (World Bank, 2016).

1.2 Risk and Threats

The progressive reduction in the quantity and quality of freshwater have major consequences for

[†††] *Water stress occurs when the demand for water exceeds the available amount during a certain period or when poor quality restricts its use. Water stress causes deterioration of freshwater resources in terms of quantity (aquifer over-exploitation, dry rivers, etc.) and quality (eutrophication, organic matter pollution, saline intrusion, etc.).*

health, business success and security; the harms and risks to water supply are associated with multiple causes that include economic growth, global warming, but also crime. The reduced availability of freshwater, the tensions in trans-boundary basins, the strategic relevance for public safety and State security, widespread corruption and corporate interests, unequal distribution of resources, and large scale investments in highly corrupted Countries, are drivers for criminal opportunities. Freshwater is becoming a "hot product" attractive for criminals (Clarke, 1999), potentially exposed to illicit interests of individuals, companies, terrorists and organized crime. Both physical and logical water management infrastructures are exposed to cyber and traditional terrorist threat (Europol, 2014; ENISA, 2014).

Nevertheless, crimes against water remain difficult to assess, detect and prosecute, especially because legislations and policies on freshwater vary from Country to Country; data are inconsistent or not comparable, water crimes are often recoded under other offences – like fraud, corruption, theft, forgery/counterfeiting of documents, terrorism, or other crimes against heath or the environment; and academic and law enforcement interest in water crime issues (White, 2003, Bricknell, 2010; Brisman *et al.,* 2016) is very recent.

The paper is divided as follows: after a general introduction (§ 1) about the importance of water and the growing illicit interests on it, showing the urgent need to consider the nature, dynamics and impacts of water crimes, the paper focuses on the environmental crimes (§ 2), with a focus on the water sector (§ 3). Chapter § 4 relies on some considerations about the targets and the contribution of the Water Crimes Project to this emerging crime that is presently under-researched.

2. ENVIRONMENTAL CRIMES

2.1 Defining Environmental Crimes

There is no precise definition of environmental crimes. UNODC International Classification of Crime for Statistical Purposes (ICCS) defines crime as: "*the punishable contravention or violation of the limits on human behaviour as imposed by national criminal legislation*", but an act against the environment can be criminalized under very different legal provisions in different countries, or may be considered a criminal offence in one country but not in another.

The EU Directive 99/2008 on the protection of the environment through criminal law acknowledges the rise in environmental offences, but it "obliges Member States to provide for criminal penalties in their national legislation in respect of serious infringements of [*a list of*] provisions of Community law on the protection of the environment". Member States shall criminalise at least 9 conducts that influence the environment, namely causing (or likely to cause) "death or serious injury to any person or substantial damage to the quality of air, the quality of soil or the quality of water, or to animals or plants", and only "when unlawful and committed intentionally or with at least serious negligence" (art 3).

In general terms, "Environmental crime" is often understood to describe illegal activities harming the environment and aimed at benefitting individuals or groups or companies from the exploitation of, damage to, trade or theft of natural resources, including serious crimes and transnational organized crime (UNEP/INTERPOL, 2016).

2.2 Types and scale of Environmental Crimes

For years, five areas have been considered of major importance about environmental crime: illegal trade in wildlife; illegal logging and its associated timber trade; illegal, unreported and unregulated fishing; illegal trade in controlled chemicals (including ozone-depleting substances) and illegal disposal of hazardous waste (INTERPOL, 2012); references about "water" were missing.

More recently, new types of environmental crime have been considered, no longer restricted to iconic wildlife and rare wood species alone: a recent report of UNEP/INTERPOL (2016) points out that the term "environmental crime" covers not only the illegal trade in wildlife (Europol, 2013), but

also forestry, illegal logging (UNICRI, 2014) and fishery crimes, illegal dumping of waste including chemicals, smuggling of ozone depleting substances, surface water pollution (Eurojust, 2014) and illegal mining (UNEP/INTERPOL, 2014).

Second only to the trade in drugs and weapons, environmental crime is considered the largest illegal business in the world (UNEP/INTERPOL, 2016). INTERPOL estimates that global wildlife crime is worth billions of dollars a year; the World Bank states that illegal logging costs developing countries $15 billion in lost revenue and taxes. In the mid-1990s around 38,000 tons of CFCs were traded illegally every year – equivalent to 20 per cent of global trade in CFCs and worth $500 million; and in 2006 up to 14,000 tons of CFCs were smuggled into developing countries (EIA, 2008). No data are available on water crimes.

2.3 Causes and consequences of Environmental Crimes

The root causes of environmental crimes vary greatly: they are primarily the low risks and high profits in a permissive environment because of poor governance and widespread corruption, minimal budgets to police, prosecution and courts, inadequate institutional support, political interference and low employee morale, minimal respect to local communities. The situation is especially critical on support to prosecution and courts/the judiciary in many developing countries.

Unlike any other known crime, environmental crimes are aggravated through their additional cost and impact on the environment and cost to future generations. Deforestation, dumping of chemicals and illegal fisheries causes loss of ecosystem services such as clean air and clean water, extreme weather mitigation, food security and even health and wellbeing. They also deprive governments of much-needed revenues and undermine legal businesses. An additional by-product of environmental crime is that it undermines peace. The UN Security Council has recognized the serious threat to security posed by environmental crime, with UN reports pointing to armed groups and potentially even terrorists sustained through the spoils of this rising criminal industry.

Environmental crime has become one of the world's most profitable organised criminal activities and has a significant impact not only on the environment, but on society and the economy in general, and that it has been identified as an emerging threat in the Serious and Organised Crime Threat Assessment (SOCTA) 2014-2017 (EU Council, 2016).

Some of the consequences of environmental crime are irreversible. The economic, environmental and health impacts of illegal trade can be sufficiently important to disrupt whole economies and ecosystems, undermining legal and environmentally sustainable activities and reducing future options for the use of resources. There can be spill over effects, with indirect consequences. For instance, in fragile states illegal trade can undermine the rule of law and can fuel armed conflict. Any serious attempt to tackle illegal trade in environmental goods would benefit from a systematic evaluation of the impacts (OECD, 2012).

Moreover, environmental crimes are a catalyst for corruption (EIA, 2008): in the same way that criminals perceive these crimes as an easy option, so individuals in corporate or official positions of authority and power view environmental crime as a chance to cash in. Examples of institutionalized corruption are: signing and forging import and export certificates; facilitating the transport of illicit goods and 'turning a blind eye'. Far more serious, and yet just as common, is the complicit, long-term involvement of individuals from the police, army, government and intergovernmental organizations. Furthermore, corruption may be preventing the true cost and extent of environmental crime from being properly assessed or effectively addressed.

3. ENVIRONMENTAL CRIMES

3.1 A growing interest (and related issues) on Water Crimes

In global terms, the topic of "crimes against water" is considered as an emerging global issue (INTERPOL, 2012) and "water management" as an emerging environmental crime (INTERPOL,

2016), but several factors influence negatively the intelligence capacity, and data collection for systematic analysis of the phenomenon. The main cause is the absence of a common legal definition of "water crimes" and "water security". A consequence is that – when reported to the police or public prosecutor office – water crimes are often recoded under other offences – like fraud, corruption, trafficking, falsification of documents, terrorism, with the only significant exception of pollution. The absence of a specific legal framework discharge the information about "water" in data collection mechanisms, hindering the capacity of a systematic analytical approach.

To date, there is no idea about the number and the impact of offences against water.

Another problem is that water may be either the environmental resource damaged by a crime (e.g. surface water pollution, or fraudulent water quality reporting); the object of a crime (e.g. water theft or corruption on the part of private companies related to the economic control/exploitation of water); or the means of the crime (e.g. intentional flooding or the deliberate poisoning of a water supply).

This paper describes the research activity attempting to define water crimes and to classify all crimes related to freshwater (according to the EU Directive 60/2000). Researchers have applied some existing crime classification systems, to understand if they can identify and collect information on water crimes and, eventually, to understand how to overcome existing limits.

Firstly, the UNODC ICC system has been tested. Water crimes and water related crimes might fall into the following ICCS Level 1 categories:

10 (acts against the natural environment)
1 (acts leading to death or intending to cause death)
2 (acts leading to harm or intending to cause harm to the person)
7 (acts involving fraud, deception or corruption)
9 (acts against public safety and state security)
5 (acts against property only)

The main problem of using ICCS approach is that the information about "water" is lost in the data collection process, apart from category 10012: "acts that cause the pollution of degradation of water", which includes "Water pollution is the direct or indirect introduction of substances or energy into a body of water, water utilities or marine environment (including estuaries), resulting in harm to living resources, hazards to human health, hindrances to marine activities including fishing, impairment of the quality of sea water and reduction of amenities. (Organisation for Economic Cooperation and Development. Marine Pollution. Web: http://stats.oecd.org/glossary /detail.asp?ID=1596)" (UNOCD, 2015).

Information about the type of water (e.g. fresh water, marine water), the service stage involved (e.g. impoundment, treatment, abstraction), or the intended use (e.g. agricultural, for human consumption, recreational) are not accounted for into the ICCS system, even in the disaggregating variables about the event, the victim, the perpetrator or other data description/inclusion, making impossible to use ICCS as it is for analysing water crimes.

The adoption of a universal working definition of "water crime" must include all and only the meaningful forms of offences against waterbodies, based on – but not necessarily limited to – the descriptions deriving from criminal law of different countries. For this paper, the following working definition will be used:

WATER CRIME can be defined as any punishable contravention or violation of the limits on human behaviour as imposed by national criminal legislation, against surface, and ground water, or against water services. Water crime definition includes also any intentional act that can potentially harm or damage the water.

WATER RELATED CRIME can be defined as any punishable contravention or violation of the limits on human behaviour as imposed by national criminal legislation, which uses surface, and ground water, or water services, as a mean for committing other crimes.

3.2 Types of Water Crimes

Typical water crimes go from the pilfering of water from pipelines, to illegal waste management by a factory, up to marine pollution by oil spills (in a very inclusive definition of water crimes). In general, water crimes can reduce the freshwater through acts against water quantity, or quality, or its accessibility or availability.

Water theft includes the illegal acquisition of natural water through pumping, impoundment or diversion of water from irrigation channels, river systems, dams or ground water courses, damaging or removing water meters and physically connecting to water distribution pipes as well as stealing aid tanks (The Global Initiative, 2014). More than this, elaborate smuggling of water with complex network chains and water mafias has recently emerged: smuggling modes vary and among others include the development of illegal pipelines, illegal truck deliveries as well as the co-optation of water regulators complicit in licensing fraud and broader government acquiescence to illegal water delivery. Illegally sourced and smuggled water is used for personal consumption, agriculture, industry, and sometimes for other illegal activities, such as the production of illegal narcotics.

Other examples of different types of water crimes identified by the European Union (2016) include: river and marine pollution, manipulation of sampling methods to avoid treatment costs, fraud and illegal trafficking of water, terrorism and cyber threats to water management operations, illegal waste discharges from factories, and unauthorized consumption from the water network.

Researchers have collected and analysed 86 relevant case studies from 4 European Countries (Italy, Spain, Slovenia and Hungary). The seven main water threats detected are: corruption, organised crime, and cyber-attack in the water sector, water pollution, water theft, water fraud, and water terrorism.

3.3 Causes and consequences of Water Crimes

Water security is weakened by gaps and loopholes in different legislations, and exposed to criminal activities by individuals, companies, and criminal groups. The "blue gold" (Barlow, 2001) has become in time an opportunity and a product for criminals, driven by perceptions of low risk and high profit, attracting the greater interest of organized crime groups (UNEP, 2012).

There are many factors that can influence the risk, and the impact of water crimes. For instance: urbanization, population growth, environmental degradation, water pollution, climate change and increased living standards. As surface water depletes, there is increased pressure for ground water usage, which is more difficult to regulate for use, abuse, and theft (Felbab-Brown, 2015). Four main risk factors are the water price, the certainty of water availability, the demand of water, and the investments in the water sector.

The cumulative impact of water crimes has the potential to jeopardize the sustainability of water resources. For example, over-extraction of coastal groundwater can have detrimental effects for terrestrial, freshwater and coastal marine ecosystems that rely on water flows through creeks and rivers (Poff & Zimmerman, 2010; Vörösmarty *et al.*, 2010).

Water contamination can be associated with depletion of underground and surface water sources, degradation of soil, contamination of surface and ground water through fertilizer/ chemical or effluent run off from farm land, destruction of wildlife habitat, and reduction of biodiversity.

Recent weather events all around the planet have given rise to enhanced concerns about the impact and consequences of toxic chemicals and hazardous waste materials being swept up in flood waters and polluting freshwater systems. The storage of legacy mining waste, stockpiling of tires, repositories for chemical wastes and so on are indirectly implicated in water-related crime insofar as how this occurs may violate relevant regulatory regimes and thus contribute to greater harm than might normally be expected.

3.4 Risk and threats on Water Crimes

Water security is among the top global risks in terms of development impact (WEC, 2016), but remains a challenge for many countries today coping with complex water issues that cut across economic sectors (World Bank, 2016).

Corruption plays a significant role in water smuggling: petty bribes to government officials and water suppliers are used to falsify meter readings, avoiding disconnections, and concealing illegal connections. The rising demand for water only serves to reinforce these corrupt practices and enforce a sense of discretionary power among officials, consequently weakening a country's rule of law (The Global Initiative, 2014).

Whereas the scope of corruption varies substantially across the sector and between different countries and governance systems, estimates by the World Bank (2016) suggest that 20% to 40% of water sector finances are being lost to dishonest and corrupt practices.

Furthermore, both physical and logical water management infrastructures are exposed to cyber and traditional terrorist threat (Europol, 2014; Enisa, 2014). Recent terrorist events around the globe highlight that the possibilities of intentional poisoning of freshwater supply also need to be considered carefully and seriously as part of the water crimes. This involves not only analysis of broad counter-terrorism strategies, but examination of the geographical, social and economic contexts within which water supply (its quantity and quality) is managed and monitored. Finally, it should be considered the potential threat of water crimes to national and international security, financial wellbeing, and human health in a period witnessing rapid economic, social and environmental change.

According to INTERPOL (2016) the international trend is similar in the areas of wildlife crime, illegal logging and timber trade, illegal fishing and the illegal trade in chemicals or hazardous wastes.

Another risk factor is that in general, criminal penalties for environmental crimes are relatively light. Important offences risk being excluded from the categories of organized or serious crimes for which reinforced legal tools and law enforcement resources are usually provided (UNODC, 2015).

4. CONCLUSIONS

Water is one of the most basic human needs and is indispensable to almost all economic activities, including agriculture, energy production, industry, and mining (World Bank, 2013). Nowadays, water is under unprecedented pressure as growing populations and competing economic sectors demand more of it leaving insufficient water to meet human needs, as well as sustaining the environmental flows that keep our ecosystems healthy. Crime is emerging as one of the future threats to freshwater availability.

Groundwater reserves are depleting in many places, leaving current and future generations with close to no buffer against increased climate variability, and, without effective regulation and suppression of water crimes, the sustainability, long-term viability, and inclusive and equitable use of water cannot easily be achieved (Felbab-Brown, 2015). To date, awareness, intelligence and studies on water security appear more focused on critical infrastructures, and more developed in other part of the world than in Europe, where this type of environmental crimes has never been systematically analysed. Water demand (and price) is expected to increase by 55% worldwide between 2000 and 2050, bringing water very attractive for criminals and criminal organizations. In fighting environmental crimes, a strong regulatory regime and effective prevention mechanisms, including anti-corruption measures, may be just as important as criminal law tools. Environmental crime is a haven for corruption at all levels and unless corrupt officials are tackled efforts to combat environmental crime will be impeded - a fact that should be acknowledged within cross-cutting resolutions on environmental crime within the United Nations and within the UN Convention against Corruption (EIA, 2008), and this is particularly true for crimes against water.

International criminal law conventions (or a single convention) could be conceived to have

comparable obligations of criminalization and an extension of criminal jurisdictions ensuring that no safe havens remain for the offenders (ISSC, 2010).

Based on this background, the research project "Water Crimes" has developed a tentative definition of water crimes and water related crimes, is building the first Inventory of water crimes, based on several case studies. The authors wish to thank the European Commission – Internal Security Fund for the support to the Water Crimes Project (2016-2017).

REFERENCES

Arsenault C, 2012. Risk of Water Wars rises with scarcity. http://www.aljazeera.com/indepth/features/2011/06/201162219314723165 3.html

Barlow M, 2001. Blue Gold. The Global Water Crisis and the Commodification of the World's Water Supply. Revised Edition. National Chairperson, Council of Canadians.

Bricknell S, 2010. Environmental Crime in Australia. Research and Public Policy Series, 109, Water Theft: 103-114. Australian Institute of Criminology, Canberra, Australia

Brisman A, McClanahan W, South N, 2016. Water Security, Crime and Conflict. Criminology and Criminal Justice, International and Comparative Criminology. Oxford Handbook Online.

Ciampi M, 2013. 'Water Divide' in the Global Risk Society. International Review of Sociology, 23 (1): 243-260.

Clarke RV, 1999. Hot products: understanding, anticipating and reducing demand for stole goods. Policing & Reducing Crime. Police Research Series, 112. London.

Environmental Investigation Agency (EIA), 2008. Environmental Crime. A threat to our future.

European Union Agency for Network And Information Security (ENISA), 2014. National cyber security strategy list. http://www.enisa.europa.eu/activities/Resilience-and-CIIP/national-cyber-securitystrategies-ncsss/national-cyber-security-strategies-inthe-world

European Union Council, 2016. Council Conclusions on countering environmental crime

Felbab-Brown V. 2015. Water Crimes: a global crisis on the rise. https://www.brookings.edu/on-the-record/water-crimes-a-global-crisis-on-the-rise/

INTERPOL, 2012. Environmental Crime. International Criminal Police Organization. http://www.INTERPOL.int/Crime-areas/Environmental-crime/Environmental-crime

INTERPOL, 2016. Environmental Crime. http://www.INTERPOL.int/Crime-areas/Environmental-crime/Environmental-crime

Johns C, 2010. Editor's Note. In Special Issue: "Water: our thirsty world". National Geographic, 217 (4): 4.

OECD, 2012. Illegal Trade in Environmentally Sensitive Goods. OECD Trade Policy Studies.

Poff N, Zimmermann J, 2010. Ecological responses to altered flow regimes: a literature review to inform the science and management of environmental flows. Freshwater Biology, 55: 194-205.

The Global Initiative, 2014. Water, water everywhere: charting the growth of organized water theft, in Analysing Organised Crime.

United Nations Office on Drugs and Crime (UNODC), 2015. International classification of crime for statistical purposes (ICCS). Wien, Austria.

Vörösmarty C, McIntyre P, Gessner M, Dudgeon D, Prusevich, A, Green P, Gidden S, Bunn S, Sullivan C, Liermann C, 2010. Global threats to human water security and river biodiversity. Nature, 467: 555-561.

White RD (Ed.), 2009. Environmental crime: a reader. Cullompton: Willan Publishing.

World Bank, 2013. Water Resources Management: Sector Results Profile. http://www.worldbank.org/en/results/2013/04/15/water-resources-management-results-profile

World Bank, 2016. High and Dry. Climate Change, Water, and the Economy. Water Global Practice.

Proceedings of the 10th World Congress of EWRA 'Panta Rhei', 5-9 July 2017, Athens, Greece
© 2017 *European Water Resources Association*

Grounded theory methodology and public participation in water management

Z. Srdjevic[1*], N. Funamizu[2], B. Srdjevic[1] and R. Bajcetic[3]
[1] *University of Novi Sad, Faculty of Agriculture, Department of Water Management, Novi Sad, Serbia*
[2] *Hokkaido University, Graduate School of Engineering, Sapporo, Japan*
[3] *Public Water Management Company 'Vode Vojvodine', Novi Sad, Serbia*
[*] *e-mail: srdjevicz@polj.uns.ac.rs*

Abstract: Water resources are under increased the pressure in almost all parts of the world. In such circumstances, it is also common to have conflicts between different water sectors (for instance, tourism vs environmental use; municipal and industrial supply vs agricultural water use, etc.), and interest groups. In most cases, related problems could be efficiently solved through the public participation and involvement of stakeholders. Traditional public participation in water management is mostly focused on the problem solving, rather than on other important contexts such as: stakeholders' understanding of the problem; motivation (willingness) to participate; preferences; understanding the solving methodology; and expectations that participatory process will lead to desired solution(s). Approach that has been proven to successfully take into account most of these concerns in managing water related participatory problems is known as Grounded Theory Methodology (GTM). In this paper authors use GTM to analyse data collected within the previous study of stakeholders' selection and prioritization in managing water resources of the Krivaja River basin in Serbia. Extensive data sets include detail information about stakeholders, description of the catchment characteristics, and perception of public participation provided by questionnaires distributed and collected within six months period. Results obtained by GTM are compared with similar case studies from developing as well developed countries.

Key words: public participation, water management, Krivaja River, grounded theory methodology

1. INTRODUCTION

Public participation (PP) as concept was introduced in 1992, when 178 Governments adopted the Rio Declaration on Environment and Development (UN, 1992) where it is stated that "Environmental issues are best handled with participation of all concerned citizens, at the relevant level." In 1993 public participation was identified as one of seven key elements for the long-term environmental programme for Europe (UNECE, 1993). Since then PP approach became requirement in decisions related to environmental management; one of best known examples of that requirement related to water management is EU Water Framework Directive (EC, 2000).

Although there are many examples of successful application of PP in water management, recent studies show that there are still some unresolved issues that cause unwanted results such are lack of official guidance documentation (Ijjas and Botond, 2004, Challies et al., 2016), lack of coordination between different frameworks that can result in unrelated participatory procedures (Albreht, 2016), lack of communication between different sectors working on water management (UNECE, 2013), highly variable participation in the planning process (Benson et al., 2014), or rather poor performance of PP and lacking in continuity (Slavikova and Jilkova, 2011).

The reason of unwanted results of PP in water management can be found in traditional public participation approach which is mostly focused on the problem solving, rather than on other important contexts such as: meaning of PP to stakeholders; stakeholders' interpretation of PP; stakeholders' understanding of the problem; motivation (willingness) to participate; preferences; understanding the solving methodology; and expectations that participatory process will lead to desired solution(s). Approach that has been proven to successfully take into account most of these

concerns in managing water related participatory problems is known as Grounded Theory Methodology (GTM). It is defined as 'an inductive, theory discovery methodology that allows the researcher to develop a theoretical account of the general features of a topic while simultaneously grounding the account in empirical observations or data' (Martin & Turner, 1986). GTM method was successfully used in many cases related to PP in environmental management (i.e. Reed, 2008; Rault and Jeffrey, 2008; Wesselink et al., 2011; Aggestam, 2014; Waylen et al., 2015; Vente et al., 2016).

Here we used GTM to better and deeper understand attitudes, views and preferences of stakeholders participating in the management of water resources of the Krivaja River basin in Serbia. Obtained results are compared with similar case studies from developing as well developed countries.

2. BRIEF DESCRIPTION OF THE GROUNDED THEORY METHODOLOGY

The Grounded Theory Methodology is qualitative research methodology defined by Glaser and Strauss (1967), whose aim is to develop theories grounded in data systematically gathered, compared and analysed; thus, GTM should 'explain as well as describe' (Corbin and Strauss, 1990). Although data for grounded theory can come from various sources (interviews, government documents, observations, books), their collection and analysis must be done according to specific canons and procedures given and described in detail in (Corbin and Strauss, 1990). In other words, as Knigge & Cope (2006) state, the grounded theory seeks to find rigorous, verifiable and explicit ways to draw conclusions.

Urquhart et al. 2010 provided "four distinctive characteristics of the grounded theory method:

1. The main purpose of the grounded theory method is theory building.
2. As a general rule, the researcher should make sure that their prior – often expert – knowledge of the field does not lead them to preformulated hypotheses that their research then seeks to verify – or otherwise. Such preconceived theoretical ideas could hinder the emergence of ideas that should be firmly rooted in the data in the first instance.
3. Analysis and conceptualization are engendered through the core process of joint data collection and constant comparison, where every slice of data is compared with all existing concepts and constructs to see if it enriches an existing category (i.e. by adding/enhancing its properties), forms a new one or points to a new relation.
4. 'Slices of data' of all kinds are selected by a process of theoretical sampling, where the researcher decides on analytical grounds where to sample from next."

Figure 1 illustrates application of GTM developed for the analysis of public participation perception in water management in Jordan and Singapore (Al-Najar et al., 2013).

3. CASE STUDY

Serbia is candidate country for the EU and one of the first negotiation chapters that is opened is financially demanding Chapter 27 – Environment. Among other alignments required within the Chapter 27, full implementation of Water Framework Directive 2000/60/EC is also foreseen, including introduction of public participation in water management decisions. Experiences of other counties show that introducing PP is long and challening process since it is entirely different mode of governance (Mostert, 2003). We believe that this process can be accelerated if public fully understand the process i.e. if public awareness of water importance is raised, various stakeholders are identified and involved, awareness of the public's rights and of the public authorities' obligations are raised, access to information is assured, etc.

Although Serbian legislation still does not recognize nor regulate public participation in water management, we conducted study based to GTM to assess perception of public participation within

stakeholders involved in managing water resources of the Krivaja River basin in Serbia (Figure 2). It is selected as a case study because it is multifunctional and multipurpose system, with complex decision - making process characterized by the conflict interests of different parties: government, local authorities in municipalities, responsible water management companies, ecologists, public bodies etc. The conflicts are presently sharpened because of the lack of funding, improper legislation or absence of precise water policies, low efficiency in collecting water taxes, difficulties in motivating societal delegates to participate in management, etc. Today, water in Krivaja River basin is managed by public water management company Vode Vojvodine, and three smaller water management companies: Severna Backa, Krivaja and Backa.

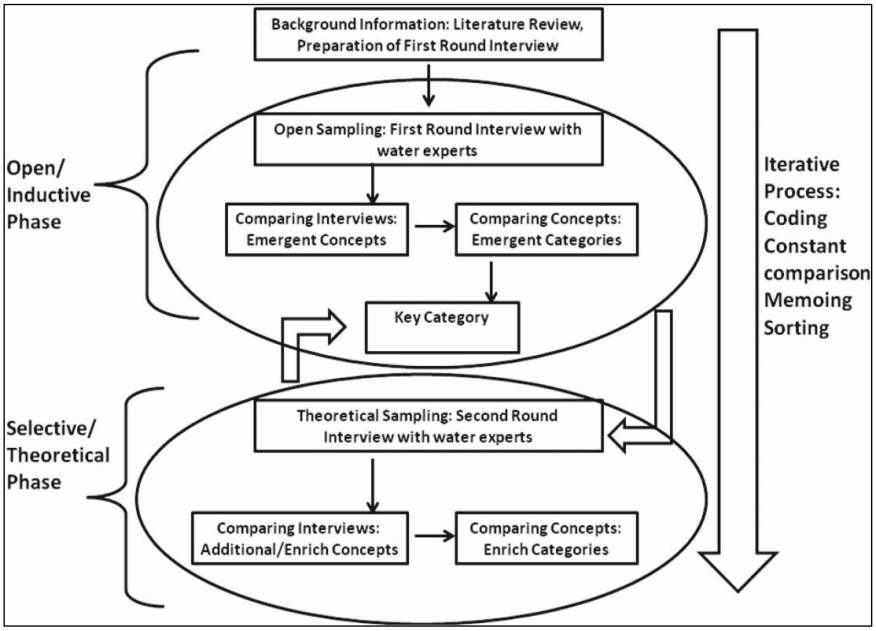

Figure 1. Process of GTM (Al-Najar et al., 2013).

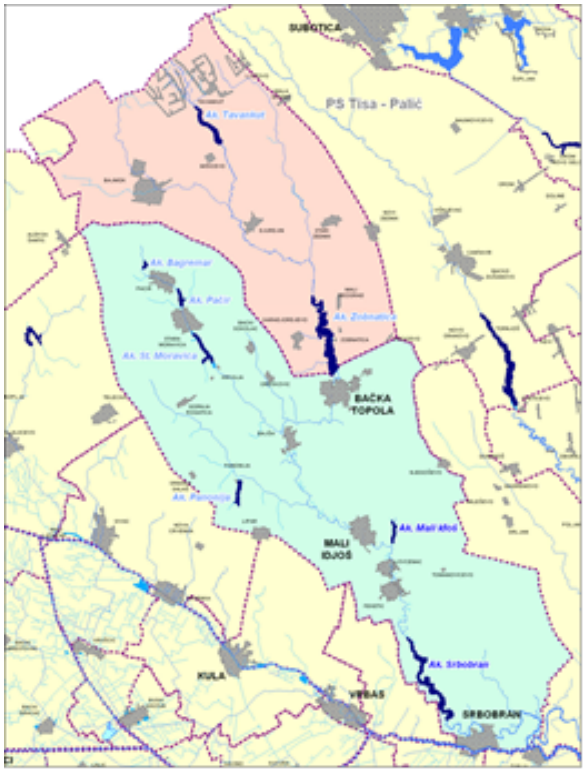

Figure 2. Krivaja River basin, Serbia, with reservoirs (existing, and to be build).

Eight major stakeholders' groups and their sub-groups were identified for Krivaja River basin (Bajčetić et al., 2015):

1. users (irrigation, industry, fishing ponds, tourism),
2. government (ministries and provincial secretariats),
3. water sector (public water management company and regional water management companies),
4. scientific community (university and research institutes),
5. local authorities,
6. non-governmental organizations,
7. citizen's associations, and
8. general public.

3.1 Collection of data and implementation of GTM

Semistructured interviews, regular mail and e-mail were used to distribute questionnaires to

- 110 legal entities (20 responses received)
- 30 individuals (5 responses)
- public institutions: state institutions, ministries, provincial secretariats, local governments, water management companies, academic bodies, etc. (35 responses), belonging to 8 major stakeholders' groups and their sub-groups as identified in (Bajčetić et al., 2015).

Extensive qualitative and quantitative data sets included questions regarding detail information about stakeholders, catchment characteristics, perceived level of water scarcity, existing pricing policy, legal and institutional framework, fairness, perceived level of responsibility of authorities and other stakeholders, importance of different groups in managing waters, involvement of public in decision making process, etc. were collected within six months period.

Using the GTM, we grouped the types of problems and challenges related to PP and recognized as most important or mentioned within the questionnaires, and categorised statements of respondents to four main categories: why PP (scarcity problems, intersectoral cooperation); who should be involved in PP of Krivaja River water management; level of involvement; way of involvement (efficient water use or direct involvement in decision making process). Second set of questionnaires is then sent to quantitatively assess perception of those four categories.

3.2 Results and comparison with other countries

According to responses, there are scarcity of water, especially in vegetation period. Also, intersectoral cooperation is not satisfactory if views of non-governmental organizations/citizen's associations and citizents are considered.

Figure 3 shows that respondents believes that, in average, highest level of participation in water management regarding planning demands, financing, infrastructure planning and management (decision-making process) should have sector of fishing/outdoor activities, ministries and provincial secretariats and public water management company and regional water management companies. Non-governmental organizations/citizen's associations and citizents are considered as least important to be involved in PP.

If compared with perception of PP in other countries given in (Rault and Jeffrey, 2008) and (Al-Najar et al., 2013), there are more similarities of our results with results obtained in developing countries in distinction between officials and non-officials attitudes and views, objectives of PP and justification of introducing PP.

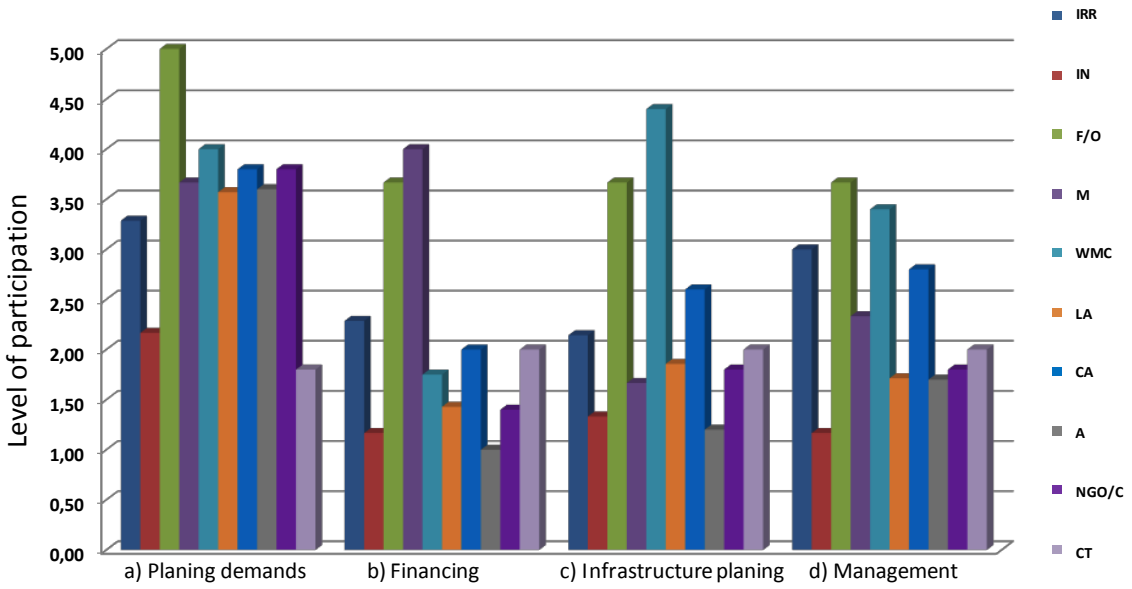

Figure 3. Perception of level of participation in different management issues.
Note: IRR – irrigation sector; IN – industry; F/O - fishing ponds/outdoor activities; M - ministries and provincial secretariats; WMC - public water management company and regional water management companies; LA - local authorities; CA – county authorities; A – academia; NGO/C - non-governmental organizations/citizen's associations; and CT – citizens.

4. CONCLUSIONS

Introduction of PP in water management is long and challenging process aimed to solve complex environmental, economic and societal problems and increase sustainability of decisions. It requires time and effort in order to inform the public and raise wider awareness about the importance of water management, increase willingness of different sectors to participate, change mentality and way of thinking, make processes more democratic and transparent, improve communication between sectors, setting mechanisms, set the legal framework, etc.

Data obtained from 60 respondents and analysed with GTM proved that there is a long road infront of Serbia in order to introduce and fully implement PP, similar to most of developing countries with adolescent democracy.

ACKNOWLEDGEMENTS

This work was supported in part by the Matsumae International Foundation that provided 3-months fellowship for Dr. Zorica Srđević's stay at the Hokkaido University, and by the Ministry of Education, Science and Technological Development of Serbia under the grant 174003 (2011-2016) - Theory and application of Analytic hierarchy process (AHP) in multi-criteria decision making under conditions of risk and uncertainty (individual and group context).

REFERENCES

Aggestam, F., 2014. Wetland restoration and the involvement of stakeholders: an analysis based on value-perspectives. Landscape Research 39:680-697.

Albrecht, J., 2016. Legal framework and criteria for effectively coordinating public participation under the Floods Directive and Water Framework Directive: European requirements and German transposition. Environmental Science & Policy 55 (2): 368–375.

Al-Najar, F.O., Ushijima, K., Funamizu, N., 2013. The perception of the public participation approach applied to water management in Jordan. Water Policy 15:1078–1093.

Bajčetić, R., Srđević, B., Srđević, Z., Blagojević, B., Zoranović, T., 2015. Participativno odlučivanje o prioritetima raspodele voda u slivu reke Krivaje u Vojvodini. Vodoprivreda 47 (273-278): 287-293. (in Serbian).

Benson, D., Fritsch, O., Cook, H., Schmid, M., 2014. Evaluating participation in WFD river basin management in England and Wales: Processes, communities, outputs and outcomes, Land Use Policy 38: 213-222.

Challies, E., Newig, J., Thaler, T., Kochskämper, E., Levin-Keitel, M., 2016. Participatory and collaborative governance for sustainable flood risk management: An emerging research agenda, Environmental Science & Policy 55 (2): 275–280.

Corbin, J.M., Strauss, A. L., 1990. Grounded theory research: Procedures, canons, and evaluative criteria. Qual Sociol 13: 3-21.

De Vente, J., Reed, M. S., Stringer, L. C., Valente, S., Newig, J., 2016. How does the context and design of participatory decision making processes affect their outcomes? Evidence from sustainable land management in global drylands. Ecology and Society 21(2):24.

European Commission, 2000. Directive 2000/60/EC of the European Parliament and of the Council of 23 October 2000 establishing a framework for Community action in the field of water policy [Water Framework Directive], Official Journal of the European Communities L 327: 1–72.

Glaser, B.G., Strauss, A.L., 1967. The discovery of grounded theory. Chicago: Aldine.

Ijjas, I., Botond. K., 2004. Participation and Social Learning in the Implementation of the WFD in Agricultural Water Management: Stakeholder Workshops Report. AWP5 Report of the Harmonicop Project. http://www.harmonicop.info/_files/_down/Hungarian%20National%20SH%20Workshop%20Report.pdf

Martin, P. Y., Turner, B. A., 1986. Grounded Theory and Organizational Research. Journal of Applied Behavioral Science 22(2): 141 – 157.

Mostert, E., 2003. The challenge of public participation. Water Policy 5(2):179-197.

Rault, P. K., 2008. On the appropriateness of public participation in Integrated Water Resources Management: some grounded insights from the Levant. The Integrated Assessment Journal 8(2):69–106.

Reed, M. S., 2008. Stakeholder participation for environmental management: A literature review Biological Conservation 141(10):2417–2431.

Slavíková, L., Jílková, J., 2011. Implementing the Public Participation Principle into Water Management in the Czech Republic: A Critical Analysis. Regional Studies 45(4): 545-557.

UNECE, 1993. United Nations Economic Commission for Europe, Second Ministerial Conference “Environment for Europe” in Lucerne, Switzerland (see: www.unece.org/env/efe/historyofefe/history.en2011_2.html)

UNECE, 2013. United Nations Economic Commission for Europe, Guide to Public Participation under the Protocol on Water and Health, available at: http://www.unece.org/fileadmin/DAM/env/water/publications/PWH_public_participation/GuidePublicParticipationPWH_WEB_EN.pdf

United Nations, 1992. Text of the Rio Declaration, available at: www.un.org/documents/ga/conf151/aconf15126-1annex1.htm

Urquhart,C., Lehmann, H., Myers, M.D., 2010. Putting the ‘theory’ back into grounded theory: guidelines for grounded theory studies in information systems. Info Systems J 20:357–381.

Waylen, K.A., Blackstock, K.L., Marshall, K.B., Dunglinson, J., 2015. Participation–Prescription Tension in Natural Resource Management: The case of diffuse pollution in Scottish water management. Environmental Policy 25(2):111–124.

Wesselink, A., Paavola, J. 2011. Rationales for public participation in environmental policy and governance: practitioners' perspectives. Environment and Planning A 43:2688-2704.

Proceedings of the 10th World Congress of EWRA 'Panta Rhei', 5-9 July 2017, Athens, Greece
© 2017 *European Water Resources Association*

The Non-Conventional Water Resources (NCWR) programme in north Mediterranean

M. Antonakopoulou, K. Toli, V. Constantianos, and M. Scoullos
Global Water Partnership - Mediterranean Secretariat (GWP-Med)
* *e-mail: mariela@gwpmed.org*

Abstract: Water is a key input for life, socio-economic growth and ecosystem stability. The Mediterranean countries face severe water - related challenges, due to pressures on limited fresh water resources, linked to climate change and variability, as well as unsustainable water use and small catchment areas specially encountered in the islands of the region. The use of non conventional water resources can be a solution towards local water security and climate change adaptation as it can cover needs for secondary uses, without putting further stress on the available resources. In this context, the Global Water Partnership – Mediterranean (GWP-Med) developed the multi-stakeholder programme "*The Non-Conventional Water Resources (NCWR) Programme in North Mediterranean"* bringing together, national and local authorities in Greece, Malta, Cyprus and Italy and is supported by The Coca-Cola Foundation. The Programme aims, through an integrated approach, to promote the use of non conventional water resources in insular communities, towards water security and climate change adaptation at community level. The Programme showcases replicable and cost – effective pilot applications of NCWR, through its technical pillar. It also supports educational activities for teachers and students with the use of dedicated material and special trainings for local technicians on the application of modern NCWR systems. Moreover, it raises awareness on smart NCWR applications and efficient water use solutions as well as promotes capacity-building activities for stakeholders, mostly critical for the development of resilient economies. Since 2008, the Programme has implemented more than 90 small and medium scale applications of NCWR systems in 32 islands in 3 Mediterranean countries.

Key words: non conventional water resources (NCWR), climate change adaptation, multi-stakeholder partnership, rainwater harvesting, greywater recycling, educational activities, technical trainings, awareness raising, capacity building

1. INTRODUCTION

Water has a multidimensional concept, as it is not only limited to its physical measure, but encompasses other qualitative, environmental and socio-economic dimensions (FAO, 2003). It is the key element for improved livelihoods and economies, sustainable development and well-functioning ecosystems and its efficient use can benefit multiple sectors including health, environment, energy, agriculture, industry, tourism and other. Water is also the fundamental medium through which climate impacts are felt, such as changes in rainfall patterns and other extreme phenomena like droughts and floods, which link the climate system to the environmental and socio – economic systems.

The Mediterranean region is a water scarce region and ranks among the most water stressed regions in the world. Water resources in the region are at high-level risk and threatened by climatic factors and anthropogenic influences. The increasing pressures on natural freshwater has led to the depletion of aquifers, salinisation, desertification, drought and flooding (European Union, 2012). Part of the region currently faces an enduring economic crisis, socio-political instability and conflicts often under dramatic conditions (Lelieveld et al., 2012). Migration flows put further stress on water resources in the transition and destination countries (GWP-Med, 2017).

Moreover, the Mediterranean region consists of myriad of islands, each with a combination of water resource, ecological, development and management pressures. These encounter water scarcity due to small catchment areas and limited fresh water sources while extreme flash floods are observed particularly in urban and peri-urban centers, as a result of climate change and poor urban design. The increase in water demand due to the needs of rapid, and often uncontrolled, urban

development have also put local water and food security at risk, with social and economic implications for the local populations and the ecosystems they support.

All factors mentioned above have increased the urgency for the identification of opportunities for climate resilient development and for the implementation of effective water management actions, to secure living environments and economic development in the Mediterranean region. These actions require the development of more innovative sustainable water management tools which combine past and present technical knowledge. Consequently, the non conventional water resources are growing in importance and significantly increase local water availability. These non conventional sources of water represent complementary supply sources that are substantial and can be reused for domestic and agricultural uses (Holst-Warhaft et al., 2010).

In this context, *The Non-Conventional Water Resources (NCWR) Programme in North Mediterranean* promotes through an integrated approach the sustainable management of water resources. It emphasizes on promoting a new water culture and the use of non conventional water resources (NCWR) such as rainwater, storm water and greywater aiming to increase water availability at local and national level in a sustainable and cost-effective way.

2. THE NON CONVENTIONAL WATER RESOURCES PROGRAMME

The Global Water Partnership – Mediterranean (GWP-Med), the regional partnership for the Mediterranean of the intergovernmental organisation Global Water Partnership (GWP), acknowledging the water scarcity and climate change challenges, as well as the potential of the use of NCWR in the region, developed the multi-stakeholder programme "*The Non-Conventional Water Resources (NCWR) Programme in North Mediterranean*". The Programme, which started in 2008 in Greece and then expanded to Malta (2011), Cyprus (2013) and Italy (2017), brings together the GWP-Med, the local and/or national authorities of the target countries and the Coca-Cola System in the respective countries. It also engages civil society partners and a number of specialised NGOs at national/local levels, including the Mediterranean Information Office for Environment, Culture and Sustainable Development (MIO-ECSDE), the Mediterranean Educational Initiative for Environment and Sustainability (MEdIES) and Nature Trust Malta (NTM). The Programme is primarily supported by The Coca-Cola Foundation grants, with various contributions also from the partners.

2.1 Aim and objectives

The Programme aims to advance the use of non conventional water resources through an integrated approach, as a sustainable solution for local water security and climate change adaptation.

The Programme's specific objectives are to:

- Showcase NCWR applications that can be replicated at local level in the Mediterranean.
- Train teachers and educate students on NCWR, and increase awareness on sustainable water use.
- Enhance the capacity of the local authorities on the management of NCWR.
- Train local technicians on the application of modern NCWR systems and materials, and build their capacity to install and/repair such systems and share their expertise at local level.
- Promote multi-stakeholder partnerships for local NCWR initiatives.
- Promote knowledge and sharing of experiences on aspects of integrated approaches to NCWRM.
- Advance regional dialogue among Mediterranean countries on how to advance the use of NCWRM.

2.2 Main pillars of the Programme

The Programme focuses on the following pillars of action:

A. *Non conventional water resources pilot applications*: these include infrastructure works for the application of NCWR technologies, such as the installation of new and reinstatement of existing NCWR systems, mainly rainwater harvesting (RWH), stormwater retention & greywater reuse systems, in selected public buildings and areas.
B. *Educational and training activities* on NCWR and sustainable water use, which include hands-on activities for students and teacher trainings; and training seminars for local technicians on NCWR technologies.
C. *Awareness raising & Capacity building* on smart NCWR applications and sustainable water use solutions to enhance public participation and strengthen the capacity of the participating authorities and beyond.

2.2.1 NCWR pilot applications

The Programme focuses on the demonstration of innovative and cost-effective solutions for the use of rainwater, the management of stormwater and the reuse of greywater.

Rainwater harvesting has been a traditional practice for water supply, especially in water scarce islands and areas. Elaborate water harvesting, conveyance and storage systems, from as early as the Bronze Age, can be found in the Minoan civilisation in Greece (c.a. 3500 BC) (Larry et al., 2013). With supportive technologies including simple processes and infrastructure, rainwater can be used in household and communities for secondary uses (UNEP,2006). It is a cost-effective solution that contributes to climate change adaptation.

Stormwater management is an effective way for adapting, to increased water demand and variability in rainfall patterns (M. Qadir, et al., 2006). The decentralised nature of rainwater harvesting and storm water management, allows the owners to benefit from direct management of water demand and supply (MED, 2006).

Greywater recycling is the practice of treating and reusing wastewater generated from bathroom sinks, bath tubs and clothes washing machines. The treated greywater is used for secondary uses in households, communities and industries, increasing water availability and decreasing wastewater load of sewerage systems. Recycling greywater on site reduces groundwater pumping as well as wastewater transportation. Greywater recycling is a sustainable way to manage water resources and can be cost-effective in the long term.

NCWR pilot applications are designed and implemented by GWP-Med, with the support of the local and/or national authorities. All applications incorporate the local water needs and are usually of small/medium size. The applications are applied in public spaces such as schools, football fields, administration buildings, and other open spaces. The public spaces are indicated by the local authorities and further technical studies are undertaken by the Programme to ensure the feasibility of the applications.

The selection of the NCWR systems is decided upon agreement between GWP-Med and the local and technical authorities, as the latter are responsible to safeguard the operation and maintenance of the systems. In all cases, the systems applied are custom made, relying on the technical specification of the building or area and the local water needs. The systems also hold substantial replication potential. Some of the innovative technologies used, are further analysed.

Rainwater harvesting systems

Underground applications of rainwater harvesting systems involve the installation of modular water tanks, made of recycled polypropelene, a high resistance material, which allows for many underground applications, while the surface can be used as park or parking lot (Fig. 1). Each module is comprised of the three-dimensional fittings of cubiform cells that have a 95% capacity.

The practical reasons that led to the choice of this tank include its:

- cost effectiveness compared to concrete and other systems
- free of maintenance type
- easy, on-the-spot assembly
- free of space restrictions.

For above ground installations, metallic tanks have been installed in many project sites, as they are appropriate for the use requested. Collected water in most cases is used for irrigation or animal husbandry.

Greywater recycling systems

The greywater recycling technologies (Fig. 2), applied by the Programme, include: (i) a patented system, based on coagulation and sedimentation; (ii) a membrane bioreactor treatment system. The first consists of a medium scale system of 3 tanks. A special chemical is added, for the removal of pathogens, solids and organics. Clean water is then used for irrigation and toilet flushing. The second one is a compact system. Its main technology for the efficient removal of contaminants, is ultrafiltration. The treated water is also disinfected and safely used for secondary uses.

The practical reasons that led to the choice of this systems include:

- low capital and operating costs
- high quality of the treated water
- easy operation

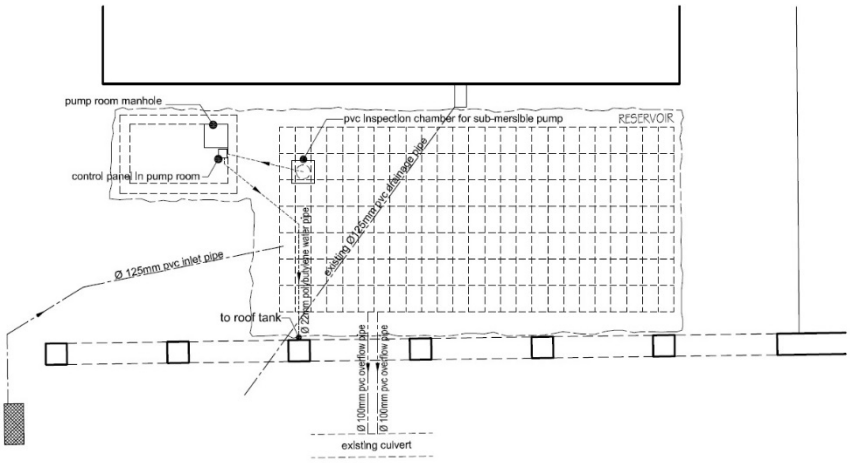

Figure 1. As - built drawing of an underground RWH modular tank. It is connected to the roof tank and then rainwater is used for toilet flushing; Gharb school, Gozo, Malta, 2012.



Figure 2. (a) Greywater recycling system, treated water is used for field irrigation, football club in Cyprus, 2015 (left); (b) Greywater recycling system with ultrafiltration installed in the national swimming pool in Malta, 2016 (right)

2.2.2 Educational and training activities

Educational activities for the educational community

The educational component of the Programme aims to educate people and create a new water culture. The educational programme is designed with the ambition to raise awareness and sensitise the educational community on water related challenges of the region and to familiarise them with the concept of non conventional water resources. A dedicated educational programme is developed for the needs of each project country and includes the following:

- *Teacher's Resource Pack*, specifically directed to teachers of primary and secondary education. The pack presents simple teaching methods about water issues, to be used in class. It contains special activities, methodological tips, worksheets, references and information (MEdIES, 2010-16).
- *Teacher training sessions* on the Resource Pack and the methodology used to: strengthen their teaching skills, develop new methods and carry out special hands-on activities to educate students on the water related aspects and the use of NCWR. The trainings are organised in collaboration with the Ministry of Education of each country (MEdIES, 2010-16).
- *Hands-on activities for students*. These activities include interactive games, exercises, experimental and discovery – based activities for students to learn about water and ways to save it, and get more familiar with the NCWR. The activities are adapted according to the age of the students.

The Programme through the educational activities has successfully reached out to more than 27.500 students while a total number of approximately 4.300 teachers have been trained in the training sessions. The teachers and the students participate in the activities with great enthusiasm, especially when applied in insular communities where they often experience reduced water availability.

Technicians' trainings

Technical trainings are organised in the framework of the Programme, aiming to enhance local expertise in the project countries. Local technicians, engineers, architects and professionals in the construction business are trained on how to install applications of modern NCWR systems, building their own capacity to install and/or repair such systems. It has been observed that the trainings are inspiring and the local technicians and engineers are very keen in further developing their knowledge on the application of NCWR. The urgency for NCWR systems is well acknowledged by the participants, thus opportunities for new green jobs are increasing.

2.2.3 Awareness raising activities

The Programme secures systematic communication of its messages and results and includes continuous awareness raising campaigns, use of communication tools, development of informational and publicity material as well as knowledge-sharing material at local and national level. Awareness is also raised during events, through the distribution of water saving devices which save up to 50% of the water consumption in each faucet (European Union, 2011). This action is implemented in collaboration with the local authorities.

One of the well-established communication actions of the Programme is the social media campaign which runs every year during the week leading to the World Water Day (22 March) and highlights how NCWR can be utilised at household and community level. In addition to local and national publicity, part of the outreach of the Programme is realised through Mediterranean and international GWP-Med's and GWP's established capacities.

One of the priorities of the Programme is also to engage stakeholders and local authorities, to create and strengthen existing multi-stakeholder partnerships and enable the identification of new opportunities, towards sustainable planning and management of water resources (GWP, 2012). The Programme through capacity building workshops and dialogue activities succeeds to reinforce the involvement of local authorities and related stakeholders in participatory processes for sustainable water resources management, emphasizing on the use of NCWR.

3. RESULTS AND DISCUSSION

Over the years, the Mediterranean islands have encountered various local and global challenges namely economic crisis, socio-political instability, conflicts and large-scale migratory movements, climate change, changing water consumption patterns and urbanisation. The *NCWR Programme in the Mediterranean* has since 2008 delivered tangible results, through: (i) technical interventions which utilise NCWR and reuse water for non-potable uses, addressing the needs and priorities set by the local and the national authorities; (ii) education for sustainable development; (iii) building capacity at technical and management level of NCWR; and (iv) raising awareness at local, national and international level. The results of the Programme are summarised in Table 1.

Table 1: Results of the Programme for the period 2008 - 2017

Outcomes in numbers / Project country	Islands	NCWR applications	Installed Capacity (m3)	Annual Water yield (m3)	Beneficiairies	Students	Teachers	Technicians
Greece	29	62	99.969	256.105	54632	12754	2807	210
Malta	2	16	11.273	16.684	53110	13316	1228	55
Cyprus	1	16	28	3830	32121	1500	279	30
Total	32	94	111.270	276.619	139863	27570	4314	295

Since its initiation in 2008, the Programme has expanded to 32 Mediterranean islands in 3 countries, while activities have commenced in a fourth country, attracting local and high-level political interest as well as engaging water related stakeholders. It has encouraged local populations to embrace the activities with their practical capacities (e.g. input to the local water balance, risk management, landscaping of public spaces, etc.) contributing directly to improving local livelihoods. More than 90 pilot rainwater harvesting, greywater reuse and small desalination systems have been implemented and until today, save approx. 275,000 m^3 of water annually. The Programme has demonstrated new and innovative technologies, where possible, while replication of these applications is already practiced by local authorities and, in some cases, individuals. Teachers and students enthusiastically participate in the educational activities, and have gained from the specialised material produced and trainings conducted.

The NCWR Programme is not only well established among partners with shared values, but is also globally acknowledged as a showcase, presented in different conferences, fora and meetings as well as being awarded as “best practice” in the World Water Forum in Korea in 2015. The Programme was ranked 2nd globally at the Water Showcase World Final of the 7th World Water Forum among 115 water showcases. This success for the NCWR Programme is a solid proof of international recognition by the global water community for its practical contribution towards water security and climate change adaptation at local level Mediterranean islands.

3.1 Instructive lessons learned

The involvement of the local authorities in the Programme implementation, by contributing to the NCWR applications, increases ownership. This ensures the sustainability of the demonstration applications delivered to the islands and contributes to the Programme’s objective to promote

NCWR practices as a sustainable way for water availability. Awareness raising of targeted groups and general public can create the acceptance of NCWR at local level and facilitate the expansion of this cost-effective method at domestic and community level. Demonstrating the water saving potential of the use of NCWR and the tangible addition to the local water budget in a cost-effective and sustainable manner, can affect national policies to integrate the use of NCWR in the water resources planning, as is the case of Malta and the new National Water Management plan (2015). Multi-stakeholder partnerships, including the private sector, can successfully promote local NCWR initiatives. Experience with this type of applications has created pivotal knowledge that can be shared with other water scarce communities in the Mediterranean and beyond (Toli, 2015).

3.2 Replicability and transferability

The Programme offers site-specific practical applications of NCWR systems utilising both innovative and conventional technologies available in the countries. It can thus be expanded and replicated in other water scarce areas in the Mediterranean and beyond. Its innovation lies in its holistic approach. The infrastructure works offer both tangible results (rainwater or greywater to be reused) and act as demonstration applications of locally appropriate technologies. The educational activities target the young generation, creating a new water culture of sensitised and responsible consumers. Awareness raising activities target the general public, drawing their attention to critical water challenges and offering easy and cost-effective solutions to address these at domestic, community, local and regional level. Starting from one country the Programme has already expanded to four countries, while demand for replication has been expressed by other Mediterranean countries who face water scarcity issues and urge to advance the use of NCWR, e.g. Cyprus, Lebanon, Tunisia, etc. (Toli, 2015).

3.3 Sustainability

NCWR is a cost-effective method, as investment for infrastructure is inexpensive. The use of innovative materials and techniques enables the long-term operation of NCWR systems with minimal operational and maintenance costs. Sustainability of applications is secured through agreements with the beneficiaries to maintain the systems. Supporting local, and in cases remote, communities to respond to water security challenges through sustainable solutions is of distinctive added value for improving the inhabitants' livelihoods (Toli, 2015).

3.4 The way forward

The Programme driven by the global urban agenda, has already embarked on new activities in cities in the project countries, aiming to highlight the potential of NCWR to increase green/blue infrastructure in cities and contribute to resilience and improved livelihoods. Moreover, the Programme will continue to search for new partnerships and opportunities in the South Mediterranean region, towards achieving solutions with an emphasis on the water-related Sustainable Development Goals.

REFERENCES

AMCOW, CDKN, GWP, 2012. Water Security and Climate Resilient Development. Technical Background Document
de Châtel F., Gail Holst-WarhaFt and Tammo Steenhuis, 2014. Water Scarcity, Security and democracy: a Mediterranean Mosaic.
European Union, 2011. Water scarcity and desertification: Background note in view of the Europe 2020 MP Survey
European Union, 2012. Current water resources in Europe and Africa. Ispra, Italy
FAO, 2003, Review of world water resources by country. Rome, Italy.
GWP-Med, 2017. http://www.gwp.org/en/GWP-Mediterranean/WE-ACT/Programmes-per-themes/water-employment-migration/

GWP-Med, Greece, Malta, Cyprus, 2008 – 2017. http://www.gwp.org/NCWR/
GWP, The IWRM Toolbox, http://www.gwp.org
Joint Mediterranean EUWI/WFD Process, 2007. Mediterranean Water Scarcity and Drought Report
Lelieveld, J., Hadjinicolaou, P., Kostopoulou, E. et al., 2012. Climate change and impacts in the Eastern Mediterranean Middle East. Journal of Climatic Change; Volume 114, Issue 3 pp 667–687
Mays L, George P. Antoniou and Andreas N. Angelakis, 2013. History of Water Cisterns: Legacies and Lessons. Water
MED Joint Process WFD /EUWI, 2006. Water scarcity drafting group document: water scarcity management in the context of wfd.
MEdIES, Cyprus, 2016. http://www.medies.net/articles.asp?cID=8&aID=1099
MEdIES, Greece, 2012. http://www.medies.net/staticpages.asp?aID=630&overRideCategory=1
MEdIES, Greece, 2016. http://www.medies.net/articles.asp?cID=8&aID=1061
MEdIES, Malta, 2013. http://www.medies.net/articles.asp?cID=8&aID=819
Qadir M., B.R. Sharma, A. Bruggeman, R. Choukr-Allah, F. Karajeh, 2006. Non-conventional water resources and opportunities for water augmentation to achieve food security in water scarce countries; AGRICULTURAL WATER MANAGEMENT 87 (2007)2–22
Toli K., GWP-Med, 2015. http://gwp.org/globalassets/global/toolbox/case-studies/americas-and-caribbean/cs_464_mediterranean_nwrm.pdf
UNEP, 2009. Rainwater harvesting: a lifeline for human well-being

Proceedings of the 10th World Congress of EWRA 'Panta Rhei', 5-9 July 2017, Athens, Greece
© 2017 *European Water Resources Association*

Towards 3D modelling of public law restrictions in water bodies

D. Kitsakis[1*] and I. Papageorgaki[2]
[1] *Lab. of Photogrammetry, School of Rural and Surveying Engineering, National Technical University of Athens, Greece*
[2] *Lab. of Reclamation Works and Water Resources Management, School of Rural and Surveying Engineering, National Technical University of Athens, Greece*
[*] *e-mail: dimskit@yahoo.gr*

Abstract: Water bodies constitute a vital resource both for human activities and biodiversity. In order to serve public benefit and contribute to the efficient management and protection of water bodies, Public Law imposes restrictions (PLRs) on land which, given the 3D spatial component of the physical attributes related to water bodies, require to be defined and managed taking into account their vertical extent. Physical factors that affect the integrity of a water body include, inter alia, hydrology, geomorphological characteristics, substrate (bottom composition), riparian zones, tidal effects for estuaries. In this paper, a 3D GIS-based model is developed, in order to present 3D PLRs applying to water bodies according to Greek legal framework, based on EU legislation, taking into account regulations such as on waste water, surface or groundwater protection and wetlands. During the analysis, spatial tools are employed in order to transpose literal descriptions, qualitative and quantitative water bodies' characteristics to 3D volumes, while conflicts and malfunctions that depict the complexity of water body related legislation are presented. The outcomes of this research can be used to present the 3D volumes defined by the implementation of water bodies' related PLRs as well as the contribution of 3D PLR modelling in water bodies' protection and efficient management.

Key words: 3D Modelling, Public Law Restrictions (PLRs), Water Basins, GIS

1. INTRODUCTION

Natural environment is highly affected by human activities. Given their impact, along with the need of environmental protection and accommodation of, steadily growing, public needs, legislation imposes restrictions on land in order to secure public benefit and to support sustainable management. Despite the 3D characteristics of land implied in legislation, definition of Public Law Restrictions (PLRs) on land as well as on maps is based on 2D space, excluding the 3D information. Considering the complexities and overlapping activities on land that result in overlapping Rights, Restrictions and Responsibilities (RRRs), exploitation of 3D representations would contribute to address complications in land protection and management (Kitsakis and Dimopoulou, 2016).

Public Law Restrictions (PLRs) apply to a great variety of fields including urban planning, mineral activities, archaeology, groundwater, pollution, environment, aviation, infrastructures, utilities and constructions; Givord (2012) numbers more than 150 laws, regulations and ordinances regulating contemporary life in Switzerland. Currently, PLR cadastres have been established, or initiatives towards recording PLRs in centralised databases are taken, in various countries especially in Europe (CLRKEN, 2015).

In the field of water management, there is an extensive regulatory framework, originating both from national and EU legislation, aiming to the protection of water bodies, including surface waters and groundwater. Further restrictions that are not directly related but impact on water bodies need to be taken into account. Such restrictions apply to 3D space, while are descriptively defined in relative legal documents. The development of management methodologies able to handle the legislation and the physical characteristics of the water bodies in the same system is required. The quantity of surface water/groundwater available also constitutes a simple exponent of the ability of the system to respond to the rapidly increasing needs. Velázquez et al. (2010), investigate surface water/groundwater interaction and definition of related components using 17 hydrological models.

Each proposed solution is very sensitive to hydrological components such as surface flow, geomorphological heterogeneities in landscapes, soil characteristics, and hydrogeological components. Uncertainty and lack of information in groundwater systems constitute the main reasons that aforementioned characteristics cannot precisely simulate a real aquifer. Therefore, the need of applying PLRs to groundwater has to take advantage of surface hydrology, where transferring hydrological information is possible (Papageorgaki and Nalbantis, 2016).

This paper aims to develop a 3D GIS-based model as a decision support system for surface and groundwater resources management. A framework that can handle 3D physical characteristics and 3D PLRs that apply to water bodies, based on Greek and relative EU legislation is proposed. This approach is more focused on legislation regulating water bodies than hydrological characteristics, aiming to present the need of their compromising and adjustment, towards effective, both water and land, management. Legal restrictions applying to 3D space are modelled in 3D and presented through exploiting GIS spatial analysis, topology and tools, to contribute to effective visualisation and management of water bodies and land.

2. MATERIALS AND METHODS

2.1 Public law restrictions on water bodies

Water constitutes a vital asset for human life and biodiversity. On the other hand, the needs of human activities affect water resources either on water quality, through pollution of surface or groundwater, or by depletion of water reserve (Winter et al., 1998). Considering the lack of water supplies, water protection, both by means of environmental protection and for the accommodation of public needs on water supply, requires to be ensured. This need, mostly addressing issues of water supply and conflict resolution, is evident by water "regulations" in ancient Middle East civilisations such as Mesopotamian civilisations, Israel and Egypt (Ellickson and Thorland, 1995; Postel, 1999).

In Europe, most of environmental legislation and water bodies' regulations derive from European Union Regulations and Directives, transposed to national legislation. Directive 2000/60/EC constitutes the cornerstone of water body protection also complemented, inter alia, by directives on Bathing Water, Drinking Water, Environmental Impact Assessment, Urban Waste Water Treatment, Nitrates and Habitats (Annex VI, part A). Depending on each Directive's field, characterizing and management of water bodies is based on 3D characteristics, e.g. elevation, or on characteristics that impact on water movement and storage in 3D (e.g. porosity, above or underlying water bodies geological types and stratification or substrate types). Furthermore, measures on water protection involve vertical limitations, e.g. restrictions in drilling depth, or specifications regarding constructions' liner thickness to preserve pollutants away from groundwater through leaching (Council Directive 1999/31/EC). Characteristic regulations on water bodies are presented below.

The EU Water Framework Directive (WFD 2000/60/EC) defines g*roundwater* as "…water below the surface of the ground in the saturation zone and in direct contact with the ground or subsoil", *aquifer* as "a subsurface layer or layers of rock or other geological strata of sufficient porosity and permeability to allow either a significant flow of groundwater or the abstraction of significant quantities of groundwater" and *body of groundwater* as "a distinct volume of water within an aquifer or aquifers" (Art. 2, Sec. 2, 11, 12 respectively). These definitions involve 3D characteristics, also implying their relation with hydrogeological characteristics such as porosity and permeability. Annex II requires identification of the "general character of the overlying strata in the catchment area from which groundwater body receives its recharge" (Sec. 2.1), while stratification as well as geological and hydrogeological characteristics of the groundwater bodies are required for their further characterisation (Sec. 2.2). This is also clarified in groundwater characterisation technical report (2004), which additionally sets geological boundaries ahead of hydraulic ones regarding delimitation of upper and lower ground water bodies' boundaries. Relative

stipulations also apply to surface waters e.g. lake parts of different depth (Fig. 1). Mapping and location of boundaries of surface and groundwater water bodies are required to be included in river basin management plans (Annex VII). Relative characteristics are presented in 2D maps, which may only present regions where overlapping groundwater or surface water bodies exist, while further geographical features of each water body along with their interrelation, except of horizontal overlapping, cannot be clearly presented.

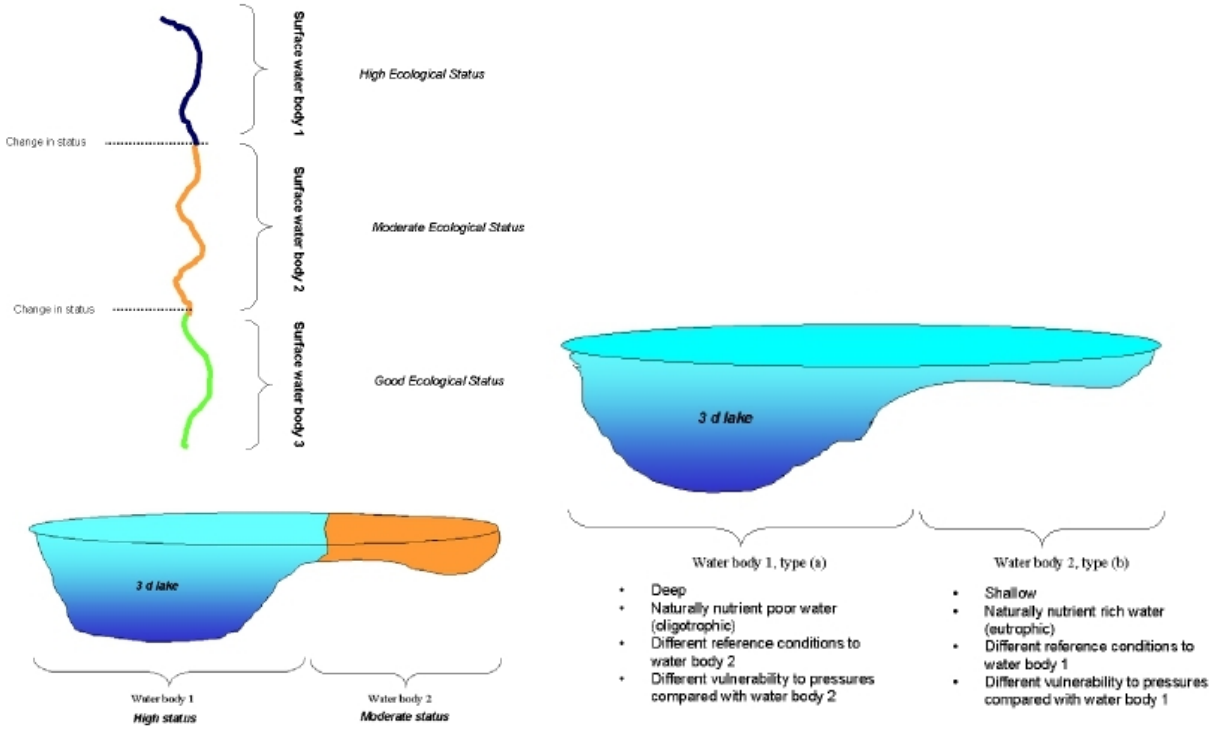

Figure 1. Identification of water bodies according to differences in status (European Commission, 2003).

The EU Directive 2006/118/EC on the protection of groundwater against pollution and deterioration provides for "measures to prevent input into groundwater of any hazardous substance" (Sec. 1.a). Section 2, stipulates that impact on groundwater chemical status with diffuse sources of pollution should be taken into account, whenever technically possible. 3D mapping of diffuse sources of pollution and interrelation of them with geological soil characteristics requires considerable resources; therefore such an approach could apply to distinct cases on specific land uses and land types.

Similarly, Directive 2008/105/EC, provides for the establishment of an "...inventory, including maps, if available, of emissions, discharges and loses of priority substances and pollutants" (Art. 5, Sec.1). Although mapping of this inventory is optional and no provision for 3D representation of its content is made, given the 3D characteristics of the recorded data, as well as their interrelation with soil characteristics, e.g. permeability, 3D mapping of such data would contribute to accurate delineation of areas at risk, providing for effectiveness on ensuring environmental, and especially, water quality.

2.2 Study area

This paper examines water body regulations applying to Western Sterea Ellada RBD (GR04) in western Greece (Fig. 3), based on the Water Framework Directive 2000/60/EC RBD classification. To ensure efficient implementation of the WFD, the river basin management plans (RBMPs) and the accompanying Programmes of Measures are necessary for each RBD. The Western Sterea Ellada RBD is about 10,199 km^2 in size, including the River Basins of Acheloos, Evinos and

Mornos river and Lefkada island. The largest part of the study area is mountainous with major outbreaks in eastern part, as Pindos mountain is the eastern border of the RBD with a max ground elevation of 2,489 m. Flat plains and lowland are located south. The average annual precipitation ranges from 800 to about 1,000 mm in lowland and reaches 1,400 mm in semi-mountainous areas, whilst at high altitudes exceeds 1,800 mm. Geologically, it is an alluvial plain, and its formation is the result of the erosion to which the surrounding geologic formations have been subjected while the eroded soil material has been deposited in the plain.

2.3 3D Public Law Restrictions on study area

In this section, laws defining requirements ensuring the quantity and the quality of surface water and groundwater, applying to the study area are presented. Joint Ministerial Order 145116 (Official Gazette, 354 B, 8/3/2011) defines measures on *treated waste water reuse* based, inter alia, on directives 2000/60/EC, 91/271/EEC and 2006/118/EC. Article 5, on aquifer recharge, requires preparation of hydrogeological assessment considering aquifer's depth, geological stratification and hydraulic conductivity along with recharge depth, ensuring prevention of effluent filtration to groundwater (Sec. 3). Art. 8 on disposing treated liquid waste on ground water bodies through percolation requires examination, inter alia, of aquifer's depth, geological stratification and hydraulic conductivity of each geological stratum, recharge depth and abstraction in the vicinity of recharge area (Sec. 1.a.1).

Joint Ministerial Order 43504 (Official Gazette, 1784 B', 20/12/2005), based on the Directive 2000/60, defines *water use license* categories, their content, type, duration and procedures required for their issuing. It also regulates documentation required for construction works related to exploitation of water sources. Article 6 defines three types of water use licenses requiring definition of land ownership status along with survey plans presenting areas of water use, building footprints, coordinates of water abstractions within 500 m radius in Hellenic Geodetic Reference System (HGRS87) and planar coordinates of starting and ending point of construction works. Furthermore, depending on license type, a report presenting geological and hydrogeological conditions of the water use area, or a geological map describing qualitative and quantitative characteristics of water resources before and after construction works is required. Stipulated documentation is mainly 2D based however, involves a number of components with 3D aspects or impact on water bodies' characteristics in 3D space. Furthermore, given that planar coordinates are already required to be recorded, introduction of Z recording to survey plans would provide for 3D data of water use areas with small impact on required survey operations, which combined with 3D hydrogeological data may result in accurate definition of water use areas and their specifications. Further combination with other Public Law restrictions that may apply in the area, e.g. environmental or archaeological restrictions, allows for unambiguous representation of 3D space involved, thus allowing efficient land management and decision making.

By Decision 1285 (Official Gazette 1326 B', 8/7/2008), Heads of Epirus and Aetolia-Acarnania Regions in Greece, *prohibitive and restrictive measures are defined for the protection of surface and groundwater*. Decision is based, inter alia, on Directives 97/11/EC, 96/61/EC, 98/83/EC and 2000/60/EC. Extensive water abstraction construction works, as well as of point source water abstraction construction works are explicitly defined in 3D, involving their depth characteristics along with soil hydrogeological features.

Part II defines prohibitions on water abstraction and relative works in the vicinity of a number of objects, e.g. power-lines, national road network etc, also stipulating minimum, planar, distances in metres. Part III, stipulates restrictive measures for aquifer protection in cases of water supply, agriculture and industrial use, which are explicitly defined in 3D or imply 3D characteristics (Sec. 3). Indent (i) provides for drillings' isolation through 10-30 metres depth of pipes' enclosure, or up to the depth of the closest impermeable geological stratum, while indent (ii) requires for sealing the vicinity of water abstraction.

2.4 GIS-based Model

The diagram of the proposed framework is shown in Figure 2. Applied methodology is implemented as following.

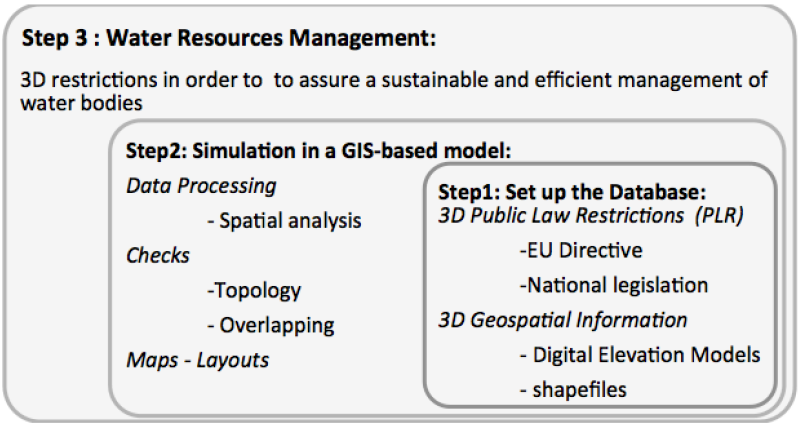

Figure 2. Diagram of the proposed framework.

The 3D spatial characteristics of study area and the descriptive PLRs are imported as features in a geodatabase (step 1). Analysis (step 2) involved description of spatial relationships between surface water/groundwater and water quality with 3D PLRs at regional scale, in order to model the water quantity and quality from a local water body with different types of soils, as each geological stratum allows or not water to flow through it according to its characteristics. Validation of the topology was run at this stage. For example, once water is absorbed from a soil type, that holds water longer and does not drain well, the water pollution extends slowly to deeper zones. The process is repeated for each water body contributing to sustainable management decision making, based on analysis' exports.

3. RESULTS AND DISCUSSION

Preceding examination of legal regulations depicts that implementation of 3D PLRs can contribute to clarification of the legal status and restrictions applying to surface areas, involving 3D characteristics. Therefore, the surface area can be characterized as area with high priority management. In Figure 3 (left), surface areas where 3D PLRs apply are presented, while in Figure 3 (right) an example of the 3D model of stratified PLRs that apply to water bodies (lakes situated on geological stratum of different soil characteristics), based on geological stratums' depth, is presented.

Aforementioned cases present that 3D representation of regulations on water bodies contributes to the clarification of the complexities deriving from the combination of topography, geological characteristics, and descriptions of regulative measures based on mathematical models and qualitative characteristics. Literal description of water body regulations extending to 3D space introduces ambiguities that inhibit efficient water bodies' protection and management, also impeding land management. 2D maps can prove useful in case of extended areas that share similar characteristics in terms of hydrogeological and soil characteristics. However, they cannot accurately and unambiguously depict differentiations deriving from geological stratification, while they cannot be interrelated with other, horizontally overlapping but applying to different height level, PLRs.

Transition from descriptive regulations, based on geological or hydrological characteristics, as well as qualitative characteristics to 3D volumes constitutes a challenge towards introduction of 3D PRLs on water bodies (Kitsakis & Dimopoulou, 2016), under an interdisciplinary approach, considering that each restriction may be defined by combination of regulations (Givord, 2012).

Dependence of environmental regulations on the type of each development's characteristics impedes definition of specific and uniform environmental restrictions within a region, thus leading to different interrelations between water bodies' and relative environmental PLRs (Kitsakis and Dimopoulou, 2016). Furthermore, technical issues such as hardware requirements along with 3D data management and querying techniques need to be addressed.

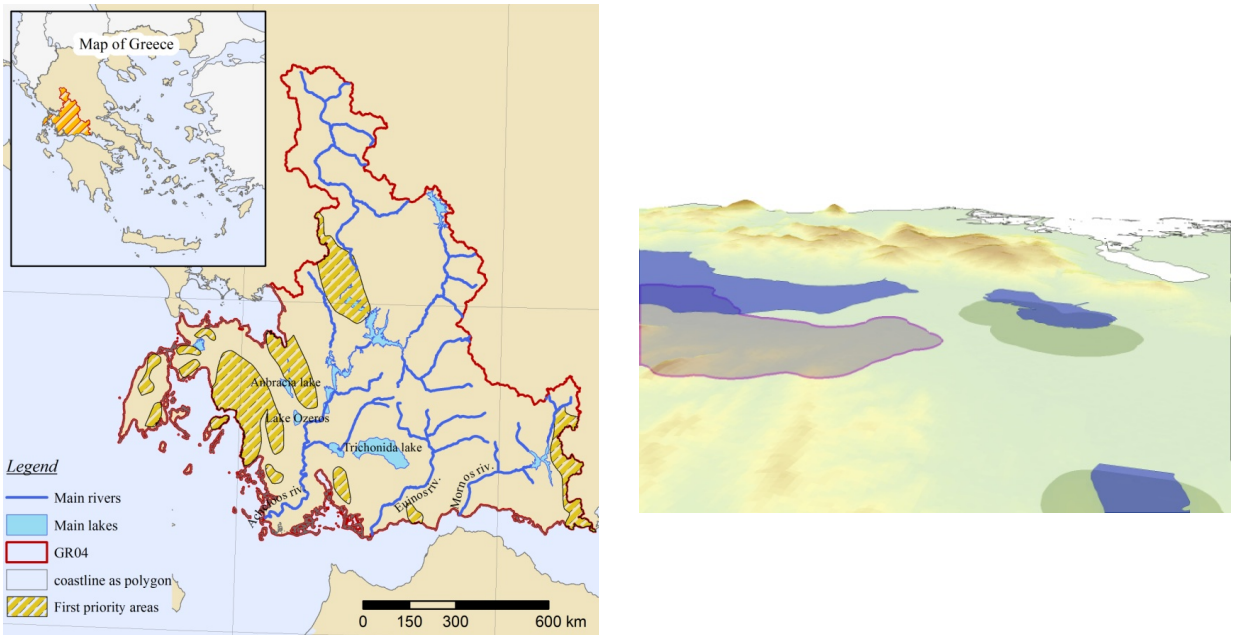

Figure 3. (Left) The spatial distribution of 3D PLRs in the study area. (Right) Stratification of PLRs depending on geological stratum soil characteristics (blue: lake, green: geological stratum 1, purple: geological stratum 2)

4. CONCLUSIONS

From preceding analysis, the following conclusions can be drawn:

- Intense exploitation of land, along with the need of securing public benefit has resulted in the need of applying vertical restrictions on land use, deriving from Public Law.
- Water bodies are defined and managed using characteristics with direct 3D components, e.g. depth, or components that are not described in 3D, e.g. geomorphological and hydraulic characteristics, which however impact on water bodies' protection and management in 3D space.
- Legislation defines water bodies using 3D stipulations, while also providing various restrictions in 3D space, for their protection and management, taking into account aforementioned direct or implied 3D characteristics. However, such regulations are either literally described or presented in 2D maps.
- Mapping and presentation of PLRs in 3D allows clarification of ambiguities regarding their extent in 3D space, thus leading to efficient, both water bodies' and land, protection and management.
- Modelling of the impact of non 3D components in 3D space involves quantification of qualitative characteristics, or "translation" of geological or hydraulic features to 3D volumes.

REFERENCES

CLRKEN. 2015. Results of the questionnaire in preparation for the CLRKEN Workshop in Nov. 2015.
Ellickson, R. C., & Thorland, C. D., 1995. Ancient Land Law: Mesopotamia, Egypt, Israel. Chi.-Kent L. Rev., 71, 321.
European Commission, 2003. Identification of water bodies. Technical report.

European Commission, 2004. Groundwater body characterisation. Technical report.

Givord, G., 2012. Cadastre 3D des restrictions de droit public à la propriété foncière. M.Sc thesis, Conservatoire National des Arts et Métiers École Supérieure des Géomètres et Topographes.

Kitsakis, D., and Dimopoulou, E., 2016. Possibilities of Integrating Public Law Restrictions to 3D Cadastres. 5th International Workshop on 3D Cadastres, (pp. 25-46). Athens, Greece.

Papageorgaki, I. and Nalbantis, I., 2016. Classification of drainage basins based on readily available information. Water Resources Management, pp.1-16.

Postel, S., 1999. Pillar of Sand: Can the Irrigation Miracle Last?, W.W. Norton Company (A Worldwatch Book), New York.

Velázquez, J.A., Anctil, F., and Perrin, C., 2010. Performance and reliability of multimodel hydrological ensemble simulations based on seventeen lumped models and a thousand catchments. Hydrology and Earth System Sciences, 14(11), pp.2303-2317.

Winter, T., Harvey, J., Franke, L., and Alley, W., 1998. Ground water and Surface water A single resource U.S geological Survey circular 1139. Denver, Colorado: U.S. Department of the Interior.

Proceedings of the 10th World Congress of EWRA 'Panta Rhei', 5-9 July 2017, Athens, Greece
© 2017 *European Water Resources Association*

A road map for resolving conflicts in dam's administration: The case of Peiros - Parapeiros dam in Greece

M.V. Podimata[1] and P.C. Yannopoulos[2]
[1] *Special Secretariat for Water, Ministry of Environment and Energy, Greece*
[2] *Department of Civil Engineering/School of Engineering/ University of Patras, Rion Patras, Greece*
[*] *e-mail: mpodim@upatras.gr*

Abstract: Conflicts regarding water management pose particular challenge for negotiation. Especially, large scale water development projects, like dams, are often the source of conflict over political, institutional, economic, environmental and many other issues. A negotiation resolution of such a water dispute may face many difficulties because of the great variety and number of positions or/and interests about water resources among stakeholders. The present study aims to present a realistic analysis of conflict experiences which stem from the case study of Peiros - Parapeiros Dam (Greece). It aims to capture the broad spectrum of the possible intentions of the four main users of the Dam; three municipalities and one industrial area. It analyses the dynamics of the users, as well as their strategies and interventions across them and predicts the path of negotiations by creating improved programming that responds to the relations among the four main water users. The analysis is based on graph theory (GT), conflict analysis (CA), data envelopment analysis (DEA), principal component analysis (PCA) and fuzzy logic (FL). The model applied is the Evolutionary Model of Multilateral Negotiations (EMMN). The study intends to help identifying practical solutions via a flexible negotiation support system (NSS). The findings of the model may furnish insights into the resolution of Peiros Parapeiros Dam Conflict and may contribute in reducing negotiating time and cost for decision makers in a broader way.

Key words: dam conflicts, water conflict management, negotiations, Asterion reservoir, policy making, decision making

1. INTRODUCTION

Dams, as many other large-scale water development projects, have often been the source of conflict among institutional and stakeholder groups involved. In such cases, the majority of arising conflicts is associated to water allocation issues, operational matters, legitimate concerns, administrational issues, etc. The deployment of conflict resolution tools and building consensus are critical issues of discussion and pose particular challenges for decision makers and practitioners. This paper presents a comprehensive approach to (a) understand the dynamics of conflicts on a dam construction project and (b) predict the outcome of negotiations between water users. A case study methodology is adopted. Qualitative and quantitative data were gathered from consultations processes taken place prior to the operation start of Peiros – Parapeiros Dam (PPD), in North Peloponnisos Peninsula (Greece). The applied model is the Evolutionary Model for Multilateral Negotiation (EMMN). The paper intends to demonstrate the utility of negotiation support systems (NSS) in exploring coalitions and building consensus. The following analysis is based on graph theory (GT), conflict analysis (CA), data envelopment analysis (DEA), principal component analysis (PCA) and fuzzy logic (FL). A sensibility analysis is conducted to quantify the impact of "weight power" on multilateral negotiations.

The remainder of the paper is organized as follows. Section 2 consists of a brief literature review of studies on dam conflicts around the world and makes a short introduction of PPD and the arising conflicts. The EMMN is described in Section 3. The model application follows in Section 4 where the results are presented. Section 5 concludes the paper.

2. DAMS AND CONFLICTS

2.1 Overview

Dams, by design, alter the natural flow regime and with it the surrounding society and environment. Hence, dams provoke significant impacts on society, economy and environment. Moreover, by default, dams pose a common property problem which is a critical potential for conflict. Therefore, dams are associated with several types of conflicts.

In literature, various works on conflict and negotiation over shared waters have been published over the years. Narrowing down the topic, there is an extended discussion with empirical evidence and case studies over dam conflicts. One of the earliest studies in the context is that of Rogers (1969), who analyzed the disputes between India and Pakistan about the water of Ganges and Brahmaputra rivers by using techniques of linear programming and game theory. Game theory has been successfully employed to explore and model dam conflicts by adding insights into potential for cooperation (Dinar et al. 2013). In the coming years, game theory and many hybrid methods have been applied to different conflict situations in the construction and operation of large dams and reservoirs (Young et al. 1982; Lund and Palmer 1997; Mahjouri and Ardestani 2011; Lee 2012; Suttinon et al. 2012). A growing body of research examines policy and institutional arrangements (Awakul and Ogunlana, 2002; Mahato and Ogunlana, 2011), like the present work which uses a game-rooted model, EMMN.

2.2 Peiros – Parapeiros dam conflict

Peiros – Parapeirtos Dam (PPD) is located in the northernmost of Peloponnisos peninsula in Greece and about 30 km SW from Patras city. It collects water from the Peiros River and the Parapeiros River and its purpose is to provide water to Patras Municipality (PM), to industrial area of Patras (IAP) and to other two smaller municipalities adjacent to the reference area; Erymanthos Municipality (EM) and Western Achaia Municipality (WAM). The whole project is comprised by a low concrete diversion dam on the Peiros River that diverts water via a tunneled pipeline to a high embankment dam across the Parapeiros River. There is a daedalus water supply network carrying raw water to the water treatment plant of Patras city and treated water (elaborated by a treatment plant next to the storage dam) to the other two municipalities and IAP. Still, PPD is under construction. The up-coming completion of works will bring a new main source of water to more than 1,200,000 residents and visitors throughout the NW Peloponnisos Peninsula. In full operation of the project (target year 2035), the served population is estimated to 2,300,000 inhabitants (Demetrakopoulos et al, 2013).

PPD has generated many conflicts in regional level. One example of conflict concerns the height of compensation fees during land expropriation, as some court disputes are still continued. These conflicts have delayed the project and affected adversely the total cost. However, nowadays with the up-coming PPD completion, conflicts mostly focus on institutional issues. The aforementioned four main users (three municipalities and an industrial area), which are called Decision Makers (DM), have to decide how they are going to manage and operate the new reservoir that stores water behind the dam. Still, there is no corresponding consensus about the technical and financial management of the dam and its accompanying projects The continuous consultations between institutions and users' representatives have revealed that the formation of a joint agreement is not an easy task to be accomplished, due to arising disputes and conflicting preferences regarding dam's jurisdiction/supervision, legal status of dams' commissioner and obligations regarding operational cost of the dam. That fact slows down the completion of project works and jeopardizes the operation of the dam by provoking delays in expected benefits for the community of the broader region (Podimata and Yannopoulos, 2015b).

In 2012 negotiations started among PM, EM WAM and IAP regarding the jurisdiction of the

dam and the legal representation of the authority responsible for the reservoir's management. The negotiation continued in 2013 and 2014, but they failed since there were competing views on the appropriate organizational and funding scheme of the dam's administrator. After a comprehensive survey and reviewing roundtable discussions during that meeting and the official announcements of involving parties in PPD conflict, five major scenarios were conducted, described in Table 1. The same table ranks each scenario from most (1) to least preferred (5), illustrating the preference ranking of each DM (Podimata and Yannopoulos, 2015a).

Table 1. PPD jurisdiction scenarios and preference ranking

Scenario	Details	Preference ranking			
		PM	EM	WAM	IAP
Sc1	The three municipalities should manage PPD by their own, without any IAP's participation in decision-making processes	2	1	1	5
Sc2	All four major users of the dam (three municipalities along with IAP) should be charged with managing PPD and implementing associated regulations for its operation.	4	2	2	1
Sc3	Municipality of Patras should exclusively manages PPD.	3	5	5	4
Sc4	PPD is a public project. The state should undertake the PPD management in financial and technical level (e.g. in a state-owned enterprise form).	1	3	4	3
Sc5	The administration of PPD should be undertaken by an independent organization, following purely private-economic patterns but incorporating representatives from government authorities, municipalities and IAP	5	4	3	2

3. EVOLUTIONARY MODEL FOR MULTILATERAL NEGOTIATIONS

3.1 Model overview

The Evolutionary Model for Multilateral Negotiations (EMMN) is a novel negotiation support system for modeling and analyzing conflicts among multiple participants. It was developed at the University of Waterloo (Canada) by Sheikhmohammady (2009) –original formulation– and by Sheikhmohammady et al. (2012). EMMN examines DM's preferences by pair-wise comparisons and provides priority sequences of preference statements, which are combined with the power of DM during negotiations processes and their building support intention to form coalitions with other DM.

Each conflict-game consists of (adapted from Sheikhmohammady 2009):

- a set of DM $N=\{1,2,\ldots,n\}$,
- a set of alternative agreements $A=\{a_1,a_2,\ldots,a_j,\ldots a_q\}, j\in[1,q], q\in \mathbb{N}$ alternatives,
- a set of preference rankings P_i over A for each DM. The preference relation follows the binary relation pattern of GMCR II. It is assumed that all preferences are transitive,
- a set of power weights of the negotiating parties $W=\{w_1,w_2,\ldots,w_n\}$
- a set of possible coalitions among DM $|C|=\sum_{k=1}^{n}\binom{n}{k}=\sum_{k=1}^{n}\frac{n!}{k!(n-k)!}=2^n-1$
- a set of negotiation states $S=\{s_1,s_2,\ldots,s_j,\ldots s_q\}, j\in[1,q], q\in, \mathbb{N}$. Each state consists of an alternative and a non-empty subset of DM, who support that alternative as the outcome of the negotiation, e.g. state $s(a_j,C)$ stands for the negotiation state a_j (where $a_j\in A$), which is supported by a group of DM, $C\subseteq N, C\notin\emptyset$. Remark that the set of all mathematically possible states are $|S|=q(2^n-1)$. Note also that a negotiation state $s(a_j,C)$ is feasible if $\sum_{i\in C} w_i \geq T(a_j)$,

where $T(a_j) > 0$ is a threshold number standing for the minimum strength of a coalition to consolidate an agreement.

Table 2. EMMN algorithms (adapted from Sheikmohammady, 2009)

Movement Type (Details)	State Criteria	Likelihood of movements (L)	Fuzzy categories
Preferential Improvement (PI)	$(a_j, C) \rightarrow (a_q, C), \quad a_q \succ a_j, \quad i \in C$	$L_{PI} = \begin{Bmatrix} 1 & P_i(a_j) - P_i(a_q) > 1 \quad i \in C \\ 0 & \text{otherwise} \end{Bmatrix} + \begin{Bmatrix} 1 & \text{if } \lvert C \rvert > 1 \\ 0 & \text{otherwise} \end{Bmatrix}$	$L_{PI} = \begin{cases} 0 & \text{possible} \\ 1 & \text{likely} \\ 2 & \text{very likely} \end{cases}$
Agglomeration (AG)	$(a_j, C) \rightarrow (a_j, C'), \quad C \subset C'$ a_j acceptable for all $i \in (C' - C)$	$L_{AG} = \begin{Bmatrix} 1 & \text{if } (a_j, C') \text{ is feasible} \\ 0 & \text{otherwise} \end{Bmatrix} + \begin{Bmatrix} 1 & \text{if } P_i(a_j) = 1 \text{ , for } \forall i \in C' - C \\ 0 & \text{otherwise} \end{Bmatrix}$	$L_{AG} = \begin{cases} 0 & \text{possible} \\ 1 & \text{likely} \\ 2 & \text{very likely} \end{cases}$
Disloyalty (DL)	$(a_j, C) \rightarrow (a_q, D), \quad C \neq D, C \cap D \neq \{\}, \quad a_q \succ a_j$ (a_k, D) is feasible for all $i \in D$	$L_{DL} = \begin{Bmatrix} 1 & \text{if } (a_j, C) \text{ is infeasible} \\ 0 & \text{otherwise} \end{Bmatrix} + \begin{Bmatrix} 1 & \text{if } P_i(a_q) \leq Acc_i \text{ , for } \forall i \in D \\ 0 & \text{otherwise} \end{Bmatrix}$	$L_{DL} = \begin{cases} 0 & \text{possible} \\ 1 & \text{likely} \\ 2 & \text{very likely} \end{cases}$
Strategic Disimprovement (SD)	$(a_j, C) \rightarrow (a_q, D), \quad C \neq D, C \cap D \neq \{\}, \quad a_q \prec a_j$ (a_j, C) *is infeasible and* (a_q, D) *is feasible*	$L_{SD} = \begin{Bmatrix} 1 & \text{if } P_i(a_q) \leq Acc_i \quad \text{for } \forall i \in C \cap D \\ 0 & \text{otherwise} \end{Bmatrix} + \begin{Bmatrix} -1 & \exists i \in C \cap D \quad \therefore a_k \text{ is iniquely worst for } i \\ 0 & \text{otherwise} \end{Bmatrix} + \begin{Bmatrix} 1 & \text{if } P_i(a_q) = 1 \text{ for } \forall i \in D - C \\ 0 & \text{otherwise} \end{Bmatrix}$	$L_{SD} = \begin{cases} -1 & \text{unlikely} \\ 0 & \text{possible} \\ 1 & \text{likely} \\ 2 & \text{very likely} \end{cases}$

Preferential Improvement (PI): Move to a more preferred alternative
Agglomeration (AG): Join a coalition since new state is acceptable to all DM
Disloyalty (DL): Move from a coalition to other coalition more preferred
Strategic Disimprovement (SD) :Move from infeasible coalition to a less preferable but feasible coalition

4. MODEL APPLICATION

4.1 Calibrating power asymmetries

During negotiation processes, it is crucial to address player's power asymmetries and dynamics. However, the concept of power is multidimensional, complex and not always quantitative. Authors calculated DM's relative power by applying a Multiple Criteria Decision Analysis (MCDA) model and comparing one's side strength factors to the others, such as population dynamics, geographical criteria, water release rates and organizational status. Seven criteria were considered to be influential elements of DM capabilities in negotiations about PPD for the estimation of DM's power weights. These criteria are the following: (a) Population served by dam's operation, (b) Territorial jurisdiction of the dam, (c) Territorial jurisdiction of the formed watershed, (d) Water release rate, (e) Coverage rate of water supply needs, (f) Administrative capacity, and (g) Other administrative characteristics.

All criteria were scaled appropriately in order to compare the data in a fair manner. The conducted scales were a) linear (analogue mode), b) logarithmic (boosts weak DM) and c) powered (debilitates weak DM). The analysis showed that power ranking follows a stable pattern; i.e. PM and IAP are the dominant DM and the other two municipalities follow. Data Envelopment Analysis method (DEA), a linear programming technique proposed by Charnes et al. (1978), was applied to find out a) the relative importance of each criterion utilized for assessing DM power's weight and b) the most favorable set of relative weights for each DM. After applying Principal Components Analysis (PCA) over power weight criteria, the analysis showed that the first principal component for all cases is the population criterion, which is a quite logical assumption. PCA also showed that C6 and C7 (territorial criteria) are highly correlated, in all cases. The power rating of each DM in negotiation skills, scaled by DEA, is presented in Table 3.

Table 3. DM's power weights scaled by DEA

DM	Linear weight	Logarithmic weight	Power weight
PM	68,53	64,57	73,45
EM	49,12	40,56	66,58
WAM	51,38	42,38	67,16
IAP	67,08	66,28	72,28

4.2 Indentifying negotiation states

Relying on the above mentioned information, the sum of possible coalitions, is: $C = \sum_{k=1}^{n} \binom{n}{k} = \sum_{k=1}^{n} \frac{n!}{k!(n-k)!} = 2^n - 1 \xrightarrow{n=4} C = 15$. Noting that there are 4 DM and 5 options for each one of them, $|S| = q\left(2^n - 1\right) = 5(2^4 - 1) = 75$ potential negotiation states were examined. Table 4 lists the negotiation states. An adjacency matrix of size 75 × 75 was used, whose (i, j) entry is $(0,1)$ meaning non-connected i^{th} (or, respectively, connected) vertex to j^{th} vertex was used in order possible movements of involved DM from each state to another to be investigated. Considering that only unanimous agreements are feasible, the power threshold for any alternative in the analogue mode of the aforementioned scale was set $T(a_j) > 236$. Note that this index represents the minimum sum of DM's weights in Table 3. The case of coalition between a bold and weak DM was also analyzed. In that case the power threshold was set $T(a_j) > 116$, which presents the minimum sum of EM and IAP weights.

Table 4. Negotiation States

ID	Scenario	DM	ID	Scenario	DM	ID	Scenario	DM
1	SC1	PM	26	SC1	C{PM,WAM}	51	SC1	C{PM,EM,WAM}
2	SC2	PM	27	SC2	C{PM,WAM}	52	SC2	C{PM,EM,WAM}
3	SC3	PM	28	SC3	C{PM,WAM}	53	SC3	C{PM,EM,WAM}
4	SC4	PM	29	SC4	C{PM,WAM}	54	SC4	C{PM,EM,WAM}
5	SC5	PM	30	SC5	C{PM,WAM}	55	SC5	C{PM,EM,WAM}
6	SC1	EM	31	SC1	C{PM,ΒΙΠΕ}	56	SC1	C{PM,EM,ΒΙΠΕ}
7	SC2	EM	32	SC2	C{PM,ΒΙΠΕ}	57	SC2	C{PM,EM,ΒΙΠΕ}
8	SC3	EM	33	SC3	C{PM,ΒΙΠΕ}	58	SC3	C{PM,EM,ΒΙΠΕ}
9	SC4	EM	34	SC4	C{PM,ΒΙΠΕ}	59	SC4	C{PM,EM,ΒΙΠΕ}
10	SC5	EM	35	SC5	C{PM,ΒΙΠΕ}	60	SC5	C{PM,EM,ΒΙΠΕ}
11	SC1	WAM	36	SC1	C{EM,WAM}	61	SC1	C{PM,WAM,ΒΙΠΕ}
12	SC2	WAM	37	SC2	C{EM,WAM}	62	SC2	C{PM,WAM,ΒΙΠΕ}
13	SC3	WAM	38	SC3	C{EM,WAM}	63	SC3	C{PM,WAM,ΒΙΠΕ}
14	SC4	WAM	39	SC4	C{EM,WAM}	64	SC4	C{PM,WAM,ΒΙΠΕ}
15	SC5	WAM	40	SC5	C{EM,WAM}	65	SC5	C{PM,WAM,ΒΙΠΕ}
16	SC1	IAP	41	SC1	C{EM,IAP}	66	SC1	C{EM,WAM,IAP}
17	SC2	IAP	42	SC2	C{EM,IAP}	67	SC2	C{EM,WAM,IAP}
18	SC3	IAP	43	SC3	C{EM,IAP}	68	SC3	C{EM,WAM,IAP}
19	SC4	IAP	44	SC4	C{EM,IAP}	69	SC4	C{EM,WAM,IAP}
20	SC5	IAP	45	SC5	C{EM,IAP}	70	SC5	C{EM,WAM,IAP}
21	SC1	C{PM,EM}	46	SC1	C{WAM,IAP}	71	SC1	C{PM,EM,WAM,IAP}
22	SC2	C{PM,EM}	47	SC2	C{WAM,IAP}	72	SC2	C{PM,EM,WAM,IAP}
23	SC3	C{PM,EM}	48	SC3	C{WAM,IAP}	73	SC3	C{PM,EM,WAM,IAP}
24	SC4	C{PM,EM}	49	SC4	C{WAM,IAP}	74	SC4	C{PM,EM,WAM,IAP}
25	SC5	C{PM,EM}	50	SC5	C{WAM,IAP}	75	SC5	C{PM,EM,WAM,IAP}

4.3 EMMN outcome

Testing the unanimous agreement scenario (when $T(a_j) > 236$), the model predicts 256 possible

movements from initial to subsequent negotiation states, in total of 5,625 cases (=75×75 combinations). The model identifies all the preferable movements (90), the agglomeration ones (117), the disloyalty ones (28), the strategic disimprovements (21) and their associated likelihoods. EMMN predicts 5 states where there aren't any movements away from them (stable states). It also calculates 8 states where there is no movement to them but there are very likely movements from these states to others (non desirable states). The model outcome showed that state with ID 72 and 74 get the highest score. Hence, we interpret that this negotiation model predicts as most likely outcomes the coalition about a) the joint operation of the dam by all users (Sc.2) and b) the exclusive state control of the dam (Sc.4). Figure 1a visualizes a normalized path of negotiation process which illustrates the possible moves from each state to another (adjacency graph).

In the second case (when $T(a_j) > 116$), the results of the model give a more complex picture of the negotiation processes with 397 allowable movements; a predictable fact since the number of feasible states was increased. EMMN predicts alike results regarding stability and disinterest presented in Table 8, with the exception of adding state with ID 59 which is characterized as stable and feasible. EMMN gives highest score on state with ID 51. State with ID 67 follows and states with ID 72 and 74 are subsequent. Hence, we interpret that Sc.1 and Sc.2 with 3-membered coalitions are most likely outcomes of the negotiation process. The corresponding adjacency graphs are presented in Figure 1(b).

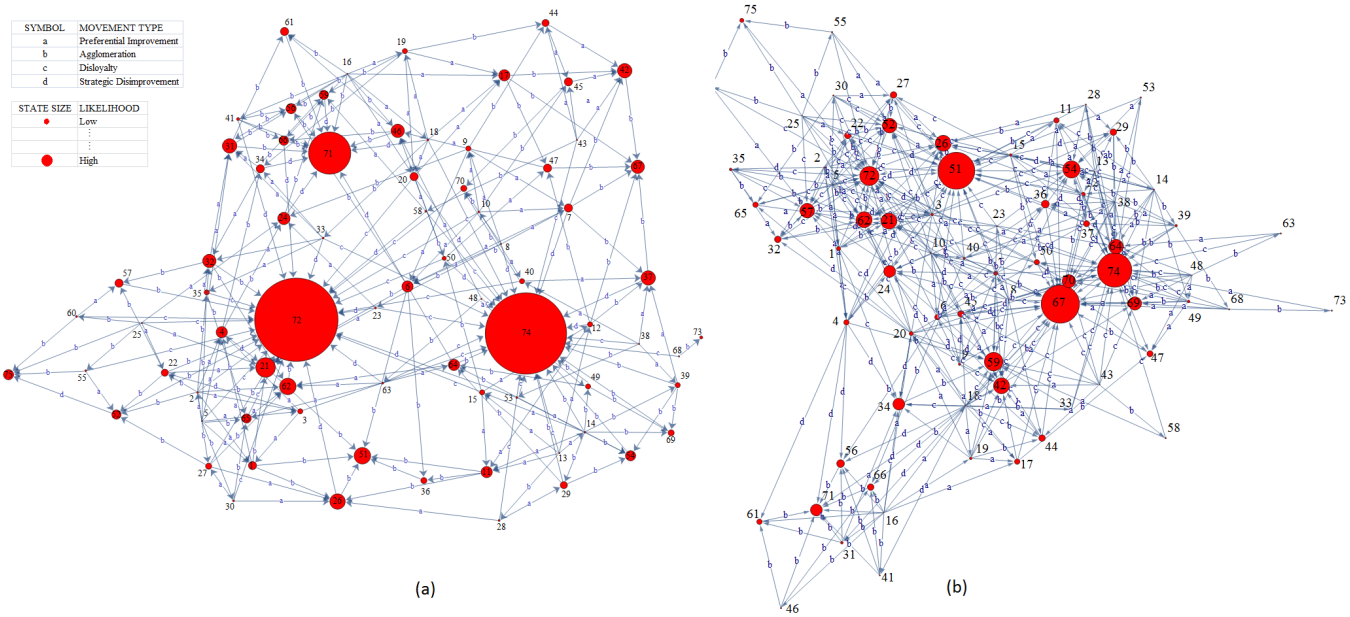

Figure 2. EMMN normalized adgacency graphs

5. CONCLUSIONS

The paper explores the case of Peiros-Parapeiros Dam (PPD) currently being built in Greece and reviews the experience of conflicts over PPD jurisdiction. Finding joint agreements and finding confidence-building cooperation schemes (cooperative arrangements) are thorny issues. This paper analyzes the positions of involving parties and examines possible states of conflict resolution by using the evolutionary model for multilateral negotiations (EMMN). The model application reveals the pathway of negotiations and illustrated how negotiation processes could evolve. Joint operation of the dam by all users (Sc.2) seems to be the prevalent model outcome in both cases conducted. However, the results of the model depend strongly on the power threshold value. Power threshold evaluation requires an in-depth knowledge of a DM's profile in order to model asymmetry in negotiations. That's why authors paid attention to power ranking with DEA incorporation, PCA inclusion and three-leveled scaling. Lessons yielded by PPD conflict may offer “how to” ideas to

investigate multistakeholder partnerships and coalitions that reduce conflicts which would otherwise retard the wider development effectiveness of large dams.

REFERENCES

Awakula, P., Ogunlana, S. O., 2002. The effect of attitudinal differences on interface conflicts in large scale construction projectsQ The case of the Pak Mun Dam project. Envir. Impact Assessment Review; 22: 311-335.

Charnes, A., Cooper, W.W., Rhodes, E., 1978. Measuring the efficiency of decision making units. European Journal of Operational Research; 2(6): 429-444.

Demetrakopoulos, A. K., Dimas, A. A., Kaleris, B. K, Yannopoulos, P. X., Manariotis, I. D., Chasiakos, A., Podimata M., Lepidas, F., 2013. Dam operator of the water project "Water supply of Patras city, Patras Industrial Zone and Northwest settlements of Achaia prefecture via the Peiros and Parapeiros Rivers". University of Patras, Patras, pp.136 (in Greek).

Dinar, A., Dinar, S., McCaffrey, S., McKinney, D., 2013. Bridges Over Water Understanding Transboundary Water Conflict, Negotiation and Cooperation, 2nd edn. World Scientific Publishing.

Lee, C. S., 2012. Multi-objective game theory models for conflict analysis in reservoir watershed management. Chemosphere; 87(6): 208-613.

Lund, J. R, Palmer, R. N. 1997 Water Resource System Modeling for Conflict Resolution. Water Resources Update; 108:70-82.

Mahato, B. K., Ogunlana, S. O., 2011. Conflict dynamics in dam construction project: A case study. Built Enviornment Project and Asset Management; 1(2): 176-194.

Mahjouri, N., Ardestani, M., 2011. Application of cooperative and non-cooperative games in large-scale water quantity and quality management: a case study. Environ Monit Assess; 172(1-4): 157-169

Podimata, M., Yannopoulos P.C., 2015a. Evaluation of decision making and negotiation processes under uncertainties regarding the water management of Peiros-Parapeiros Dam, in Achaia Region (Greece). HS7.6 / Using Models for Decision Support and Long Term Planning under Climate and Environmental Uncertainty EGU 2015, Vienna 12-17 April, 2015.

Podimata, M., Yannopoulos P.C., 2015b. Simulation of negotiations over the institutional management of Peiros – Parapeiros Water Project. National Joint Consortium of Hellenic Hydrotechnical Association (HHA) – Greek Committee for Water Resources Management (EEDYP) – Hellenic Water Association (HWA) on Integrated Water Resources Management in new era, Athens 10-12 December, 2015 (in Greek).

Rogers, P., 1969. A Game Theory Approach to the Problems of International River Basins. Water Resources Research; 5(4): 749-760

Sheikhmohammady, M., 2009. Modelling and Analysis of Multilateral Negotiations. PhD Dissertation, University of Waterloo.

Sheikhmohammady, M., Hipel, K. W., Kilgour, D. M., 2012. Formal Analysis of Multilateral Negotiations over the Legal Status of the Caspian Sea. Group Decis Negot.; 21(3): 305-329.

Suttinon, P., Bhatti, A. M., Nasu, S., 2012. Option Games in Water Infrastructure Investment. J Water Res Plan-ASCE; 138(3): 268-276.

Young, H. P., Okada, N., Hashimoto, T., 1982 Cost Allocation in Water Resources Development. Water Resour Res; 18(3): 463-475

Proceedings of the 10th World Congress of EWRA 'Panta Rhei', 5-9 July 2017, Athens, Greece
© 2017 *European Water Resources Association*

A perspective to wastewater legislation in European Countries and Turkey

H.T. Gultas[1*], A.H. Orta[2] and Y. Ahi[2]
[1] *Biosystem Engineering Department, Agriculture and Natural Sciences Faculty, Bilecik Şeyh Edebali University, 11230, Bilecik, Turkey*
[2] *Biosystem Engineering Department, Agriculture Faculty, Namık Kemal University, 59030, Tekirdağ, Turkey*
[*] *e-mail: huseyingultas@bilecik.edu.tr*

Abstract: Factors such as intense industrialization, population growth, pollution due to the resulting over-consumption, ill-judged approaches to water policy and water management, inefficient irrigation techniques and global climate change increase the competition for water resources even more day by day. This entails the use of alternative water resources. In many countries, as well as in Turkey, the emphasis placed on the use of treated wastewater is growing. In its worldwide projections until the year 2030, United Nations' water-related goals for sustainable development are to achieve the reuse of water in greater quantities and to increase the use of safe treated wastewater. According to the model developed for the potentials of reusing wastewater of European countries, Turkey ranks as the 4th among 31 countries in the projection for the year 2025. In the relevant legislation in our country, there are parts that encourage the use of treated wastewater in areas as irrigation water. Although there are some serious obstacles against the reuse of water in Europe, European countries have started updating the legislation and seeking ways to increase the safe reuse of wastewater through intense efforts, especially during the years 2014-2016, for it are known that safe and healthy reuse of water can be provided in other areas. In this study, the legal legislation and operation concerning the reuse of wastewater both in our country and in European countries is evaluated. It is aimed to present the approaches toward the reuse of wastewater in both their positive and negative aspects.

Key words: Legislation, water recycling, water pollution regulations, projections

1. INTRODUCTION

Water is the fundamental element for the survival of humankind and is very valuable. Since the early 2000's, worldwide incidents and the resulting changes are posing serious problems to humanity's access to resources. Water resources are among the most important factors that are affected by these problems. These changes can be described as the rapid and unbounded population growth, mass migrations, intense demands for people's food supply, the anomalies seen in the timing and duration of yearly precipitation, the rise in the rate of increase of atmosphere temperature, etc. All these elements which, pose a threat to sustainable use of resources, are causing a decrease in the world's available water supply. This is of critical importance as quality and quantity constantly vary in terms of agricultural irrigation that uses up almost 70% of the available water supply. Ultimately, this can lead to consequences that have economic, social and even political impact. By transferring the share of agricultural irrigation to meeting the water demands of cities and the industry, which they believe, will provide high yield and benefits, public authorities are forcing users to look for new water sources (Winpenny et al., 2010).

The matters of maintaining the sustainable use of water resources and the use of different water sources for meeting the rising demands are being evaluated and researched. Water has a character that is prone to rapid negative influence that results in the deterioration of its quality parameters. Therefore, when fresh water supplies are taken into account, it can be said that they can rapidly become undrinkable and unavailable. However, it is believed that by way of treating with proper techniques the polluted water sources that are unfit neither for people's drinking water needs, nor for industrial use or by using them directly in agricultural irrigation, the demands can be satisfied. Scientists and institutions are performing many studies concerning such practices and their possible outcomes. There are certain points to be taken into account and noted concerning the use of

untreated wastewater or of treated wastewater (Sanz and Gawlik, 2014). Different water sources such as these can be used for agricultural irrigation purposes or for the irrigation of green areas.

These points lead to the conclusion that the use of such water resources must be thoroughly examined, researched and subjected to severe inspection and its use should be defined with laws.

2. METHODOLOGY

Since this study is an areal assessment on a macro level, the information and resources used as scientific material are based on the legal regulations of European countries and of Turkey on the matter. In this study, the European Framework Directive on Water which deals with water sources and wastewater reuse in European countries has been examined; as well as the agricultural and recreational use of treated wastewaters and the related legal regulations and the perspectives on the matter in general. In this context, Turkey's attitudes towards the issue and the studies carried out on the European Water Framework Directive and the use of treated wastewater have been investigated. Possibilities for the utilization of relevant regulations and resources have been investigated and the findings have been reported in the Results section.

3. RESULTS AND DISCUSSION

3.1 The reuse of treated wastewater and the concerning legislations in European Countries

European countries, which can be said to have been in a good condition in terms of water sources until the end of the previous century, used not to face severe drought, floods or serious scarcity in drinking or utility water too often. Today, however, almost 11% of the European continent and the 17% of the inhabitant populations are faced with the problem of water shortage (scarcity) (EC, 2015). In addition to this, the developments which allow us to use domestic and industrial water sources in the best ways and highest levels possible have inversely proportional negative effects on the environment and water sources (Akkaya et al., 2006). On top of these matters, especially in the countries on the Mediterranean belt including Turkey, the irregularity in the distribution and intensity of precipitation has caused the option of diversifying the water sources already being used to be taken into consideration.

One of the sources that could possibly be used is utilizing the organic domestic wastewater in particular, in order to be reused for the purpose of agricultural or recreational, and even domestic use (Angelakis et al., 1999; Mesropyan et al., 2016). In the United Nations Sustainable Development Goals (SDG6) it has been prescribed to increase the reusability of treated wastewater until 2030. It is possible that this could even be beneficial. However, among the issues that require attention, its possible effects on the environment and human health come first. For poorly treated waters or waters that fail to meet certain standards could pose serious hazards for human health, particularly by way of entering into the food chain.

The aforementioned reasons have forced the countries to take measures and many legal arrangements have been made as a result of the legislations that have been adopted. Among the various directives concerning the protection and management of water sources in the European countries, the most important one is the European Water Framework Directive (WFD), which was issued in the year 2000, by the number 2000/60/EC. WFD has taken effect for the purpose of forming a framework for integrated water management throughout Europe (Moens, 2003; Blöch, 2005). Including all water sources, European Water Framework Directive offers a holistic approach to the protection of water sources and the opportunity for source rehabilitation and sustainable use. It is expected to have long-term effects. On the level of river basins where water management is not limited by political borders, new approaches concerning management style, water pricing and the "polluter pays" principle (Gelgeç, 2012).

Having started in early 90's, the studies have continued with the establishment of a new

Environment-Water mission unit within the European Union Commission in 1996. It has been deemed favorable to discuss and make plans for the future of water sources in Europe not only in the context of wastewater or reusability, but also in an integrated fashion. And the result of the efforts that were made toward this purpose was the European Water Framework Directive.

With the intention of making legal arrangements concerning the use of treated wastewater and bringing certain standards to its use throughout Europe, The European Wastewater Directive was introduced by the European Union Council in 1991, issued by the number 91/271/EEC. This directive has been replaced by the directive that goes by the number 98/15/EC in 1998, with the goal of making some arrangements. Having a binding effect on the European countries, it includes observations on the methods to be used in the treatment of wastewater, on the necessary standards and on the desired properties of the water to be discharged. Yet another directive is the Nitrates Directive which goes by the number 91/676/EEC, introduced in order to prevent agricultural nitrates from getting mixed with waters, causing pollution and any possible future pollutions.

However, the legislations and directives concerned have not been influential in increasing the Reuse of Treated Wastewater to the desired levels. Therefore, a need for new arrangements has arisen. For this purpose, in a new circular economy package introduced in December 2015 by the European Union Commission, what needs to be done in order to encourage and support the reuse of treated wastewater all over Europe has been laid out in the form of an Action Plan. According to this Plan; 1) an integrated water use and management program will be implemented within the framework of the legislations adopted by the European Commission. For example; as a measure to address water scarcity and in order to achieve good status under the Water Framework Directive, and in the investment to be made in the treatment of effluents as required by the Urban Wastewater Treatment Directive. For this purpose, within the framework of the criteria specified in WFD for the reuse of wastewater in an integrated manner, certain regulations were adopted within the Joint Implementation Strategy for the Water Framework Directive, under the heading of the planning and management of water use, to be put into effect cooperatively by the European Commission, Member Countries and other partners. These regulations were issued in July 2016. In the light of studies carried out in the European Union and some other countries, ways for a better wastewater use which takes into account the environmental and socio-economical factors as well. 2) As it was decided that no consistent and comprehensive legislation exists within the European Union, Member Countries and other users had to come up with their own legislations. The use on the European region has not reached the desired levels as this situation caused too many conflicting legal arrangements to be made. The Commission has decided to make efforts for specifying water quality parameters for reuse on the lowest level possible, from the beginning of 2017 on. It was agreed that the Joint Research Center and an independent scientific committee for the Health, Environment and Emergency Risks (SCHEER) establish cooperatively the parameters concerning public health, which cause much concern. 3) In the context of reuse in industrial activities, efforts are already being made within the framework of Industrial Emissions Directive, issued by the number 2010/75/EU. 4) Several working groups have been formed in the recent years for supporting the reuse of treated wastewater in Europe and in order to make efforts towards this goal (Industrial Water Reuse and Recycling (InDuRe), Water and Irrigated Agriculture Resilient Europe (WIRE), Real Time Water Quality Monitoring (RTWQM), Verdygo – modular and sustainable wastewater treatment) (EC, 2015).

When legal arrangements which have already been made and those that are planned to be implemented are considered, it can be said that there is a strong will within the European Union to increase the Reuse of Treated Wastewater, that especially in the south of Europe, the countries within the Mediterranean Basin are faced now with a serious problem of drought and water scarcity and that intense efforts are directed to solving these problems.

3.2 Reuse of treated wastewater in Turkey and the relevant legislations

In Turkey, within the scope of liabilities specified under the "Environment" section of the

"National Program for the Undertaking of European Union Requirements," issued in 2001 and updated in 2003, joint efforts by the participation of relevant organizations and institutions are being made for fitting the environmental legislation of Turkey to the European Union legislation. Among the things to be done within the scope of conforming to the Water Framework Directive (WFD), is to revise the existing legislation concerning water management, to overcome the conflicting points and to make the necessary legal arrangements for this purpose.

Within this framework, certain legal arrangements have been made in terms of conformity and forming a country-specific legislation. The Water Pollution Regulation, which goes by the number 25687, was issued in 2004. The purpose of the Regulation was to determine the legal and technical basis necessary for preventing water pollution in conformity with the sustainable development goals, in order to protect the country's potential of ground water and surface water sources and to help it be utilized in the best ways possible. Later, in 2006, the number 26047 issued the Urban Wastewater Regulation. Correspondingly, in 2010, the number 27527 issued the Technical Procedure Statement for Wastewater Treatment Facilities. With this statement, certain parameters such as the criteria concerning the design of urban wastewater treatment facilities, the technologies to be preferred and the criteria for the discharge of treated wastewater, etc. have been standardized (Özbay and Kavaklı, 2008).

Despite the legislation that was adopted, even the number of wastewater treatment facilities is way under the desired rate. Wastewater treatment facilities are sufficient to meet the needs of only approximately 45% of the country's population. And the existing treatment facilities are mostly located on the western and southern regions of the country (Arslan-Alaton et al., 2005). Approximately the halves of these facilities are adequate only for pre-treatment and the treatment of wastewater itself is a serious problem. For these reasons and due to the fact that water sources are only relatively adequate for now, the reuse of treated wastewater consists only of a few pilot projects and scientific studies. In conclusion, when Turkey is concerned, it can be said that there is still much to be done both for the treatment of wastewater and the reuse of treated wastewater.

4. CONCLUSIONS

Since the beginning of the century, the need for water in Continental Europe, especially in the countries that are located on the Mediterranean belt, including Turkey, has increased due to factors such as the irregularities in the timing and intensity of precipitation, the heavy increase in the populations resulting from mass migration, the increase in the industrial water use due to the increased use of technology, etc. For these reasons, alternative sources to be offered for utilization are being considered continually. According to some of United Nations reports, the issues of wastewater management and water quality have cross-linkages with a range of other water- and non-water issues, not least in respect of the water, energy and food nexus. It has also been acknowledged that wastewater management clearly plays a role in achieving future water security in a world where water stress will increase (UN-Water, 2015).

As specified in the legislation, one of these alternative sources is treated wastewater. The very limited number of alternative sources that can be utilized so quickly and easily turns the attention to the reuse of wastewater after treatment. When the legislation adopted in the European Union and Turkey is examined and evaluated, it is seen that serious efforts are directed to dealing with issues concerning both water and the reuse of treated wastewater and that it is considered in detail in terms of health, environment and socio-economical factors. These considerations generally result from the concerns related to possible problems to be faced in the treatment, the criteria to be adopted for the process and the possibility of the discharged water to pose a threat to the public through the product chain. The different uses of reclaimed water lead to different pathways by which reclaimed water enters the environment. It is important to look at both the initial receiving environment for reclaimed water and the final location (USEPA, 2012). Health, environment and other sensitive factors must be considered while making legal regulations about wastewater treatment or usage.

In conclusion; it is possible to claim that reuse of treated wastewater and the legislations

concerning it in the European Union and in Turkey are improving. Within the framework of the plans and projections that are made, efforts are directed towards both designating the legislations and establishing environment and human health-safe utilization criteria.

REFERENCES

Angelakis, A.N., Morocos de Monte, M.H.F., Bontoux, L., Asano, T., 1999. The status of wastewater reuse practice in Mediterranean Basin: Need for guidelines. Wat. Resources 33(10): 2201-2217.

Akkaya, C., Efeoğlu, A., Yeşil, N., 2006. Avrupa Birliği su çerçeve direktifi ve Türkiye' de uygulanabilirliği. TMMOB Su Politikaları Kongresi, Ankara.

Arslan-Alaton, İ., Gürel, M., Eremektar, G., Övez, S., Tanık, A., Orhon, D., 2005. Türkiye' de sürdürülebilir atıksu yönetimi: Mevcut durum, karşılaşılan sorunlar ve çözüm önerileri. Arıtılmış Evsel Atıksuların Tarımsal Sulamada Kullanılması Çalıştayı, Ankara.

Blöch H., 2005. European Union legislation on wastewater treatment and nutrients removal. In Proceedings of IWA Specialized Conference on Nutrient Management in Krakow, Poland, 18-21.09.2005.

EC, 2015. Water reuse - An action plan within the circular economy. European Commission, Water Department, Brussels.

Gelgeç, T., 2012. Türkiye Su Mevzuatı ve Değişen Su Paradigması. Namık Kemal Üniversitesi Fen Bil. Enst. Yüksek Lisans Tezi, 46 sayfa, Tekirdağ.

Mesropyan, E., Mkrtchyan, V., Hovsepyan, A., 2016. A new solution to municipal wastewater treatment in Armenia. European Water 53: 71-75.

Moens, R.P., 2003. Su Çerçeve Direktifi' nin Türkiye' de Uygulanması, Uygulama El Kitabı. Project No: 105774, Doc. No: 13/99047338/MJH, Vol. F1.

Özbay, İ., Kavaklı, M., 2008. Türkiye' de ve diğer ülkelerde arıtılmış atıksuların geri kazanım uygulamalarının incelenmesi. Çevre Sorunları Konferansı, Kocaeli.

Sanz, L.A., Gawlik, B.M. 2014. Water REuse in Europe: Relevant Guidelines Needs for and Barriers to Innovation. E.U. J.R.C. Institute Environment and Sustainability, p. 51.

UN-Water, 2015. Wastewater management. A UN Water Analyticsal Brief. UN Water Publications.

USEPA, 2102. Guidelines for water reuse. (EPA/600/R-12/618) United States Environmental Protection Agency, USA.

Winpenny, J., Heinz, I., Koo-Oshima, S., 2010. The Wealth of Waste: The Economics of Wastewater use in Agriculture. Food and Agriculture Organization of the United Nations. Water Reports No: 35.

